  Bull. Chem. Soc. Jpn., 54, 1—4 (1981)

The Reduction of Sulfuric Acid by Hydrogen on Activated Carbon Impregnated with Copper Sulfate

Akira KATAGIRI,* Kiyoshi WATANABE,† and Shiro YOSHIZAWA**

Department of Chemistry, College of Liberal Arts and Sciences, Kyoto University, Yoshida, Sakyo-ku, Kyoto 606

*** Department of Industrial Chemistry, Faculty of Engineering, Kyoto University, Yoshida, Sakyo-ku, Kyoto 606*

(Received August 27, 1979)

The reduction of sulfuric acid has been studied for the purpose of the regeneration of activated carbon, which is used as an acceptor of sulfur dioxide from exhaust gas. When activated carbon impregnated with sulfuric acid was heated in a hydrogen atmosphere, sulfuric acid was reduced to sulfur dioxide by carbon in the temperature range from 200 °C to 350 °C. When copper sulfate was added, the sulfuric acid was reduced to sulfur dioxide, mainly by hydrogen, in the temperature range from 190 °C to 270 °C. At 227 °C, for example, the rate of reduction by hydrogen was nine times greater than the rate of reduction by carbon. Copper sulfate was sufficiently effective in an amount of one-fifth of the sulfuric acid in moles, indicating that copper in some form participates in the catalytic reaction.

Activated carbon can be used as an acceptor of sulfur dioxide from exhaust gas emitted by the combustion of fossil fuels. When exhaust gas which contains sulfur dioxide, oxygen, and water vapor is passed through a column of activated carbon, the sulfur dioxide is catalytically oxidized on carbon, according to Eq. 1, to sulfuric acid, which is then accumulated in the micropores of carbon:

$$SO_2 + 1/2O_2 + H_2O \longrightarrow H_2SO_4. \quad (1)$$

The kinetics and mechanism of this reaction have been investigated by several groups of workers.[1-10] Since the rate of the reaction decreases as the amount of sulfuric acid increases, the sulfuric acid must be removed periodically in order to recover the catalytic activity of carbon. Several methods have been proposed for this purpose. One of them is to remove the sulfuric acid as sulfur dioxide by heating it in an inert gas, where the following reaction takes place:[1,2]

$$H_2SO_4 + 1/2C \longrightarrow SO_2 + 1/2CO_2 + H_2O. \quad (2)$$

This method has the advantage that sulfur dioxide is obtained in a concentration high enough to be used directly for a sulfuric acid plant. However, it has the disadvantage of consuming the carbon. Another method is to reduce the sulfuric acid to elemental sulfur by the following two steps:[11,12]

$$H_2SO_4 + 3H_2S \longrightarrow 4S + 4H_2O \quad (3)$$

$$3H_2 + 3S \longrightarrow 3H_2S. \quad (4)$$

Reactions 3 and 4 proceed at 150 °C and 540 °C respectively. In this method, 3 mol of hydrogen are needed per mol of sulfuric acid in the over-all reaction.

Another process has also been investigated, in which a copper-alumina absorbent is used as an acceptor of sulfur dioxide and is regenerated by hydrogen.[13,14] Reactions 5 and 6 occur in the absorption step at 400 °C, and Reaction 7 occurs in the regeneration step at 400 °C. In this process, 2 mol of hydrogen are needed per mol of sulfur dioxide recovered.

$$Cu + 1/2O_2 \longrightarrow CuO \quad (5)$$

$$CuO + SO_2 + 1/2O_2 \longrightarrow CuSO_4 \quad (6)$$

$$CuSO_4 + 2H_2 \longrightarrow Cu + SO_2 + 2H_2O \quad (7)$$

† Present address: Research Laboratories of Osaka Soda Co., Ltd., 9 Otakasu-cho, Amagasaki 660.

The reduction of sulfuric acid by hydrogen (Eq. 8) is even more favorable, because only 1 mol of hydrogen is consumed per mol of sulfur dioxide recovered.

$$H_2SO_4 + H_2 \longrightarrow SO_2 + 2H_2O \quad (8)$$

Although Reactions 2 and 8 are both thermodynamically possible, the second one can be conducted preferentially if an appropriate catalyst is used. The aim of the present work is to test the catalytic effect of copper on this reaction.

It has previously been reported[3,5] that, when Reaction 1 takes place on activated carbon at temperatures from 50 °C to 140 °C, the concentration of sulfuric acid formed is the equilibrium one which depends upon the water-vapor concentration in the gas phase. For example, 73 wt% H_2SO_4 is formed at 100 °C at the water-vapor concentration of 6 vol %. In such an acidic medium and in the presence of oxygen, copper would exist in the form of sulfate. Thus, copper sulfate was used as the catalyst component in this work.

Experimental

Apparatus and Procedure. Granular activated carbon, which had been impregnated with sulfuric acid with or without copper sulfate, was heated in a stream of nitrogen or hydrogen at a constant or linearly increasing temperature, while the evolved gas was analyzed.

The apparatus used is shown in Fig. 1. A Pyrex tube, 23 mm in inner diameter, was used as a reactor; in it an activated carbon sample (13 g) was packed to a length of 9 cm. The reactor was placed in an electric heater. The temperature of the catalyst was controlled so as to increase at the rate of 2 °C/min using a chromel–alumel thermocouple and a temperature-programming unit. In some experiments, the temperature was kept constant. The flow rate of the gas was kept constant at 100 cm^3/min.

Preparation of Samples. Commercially available activated carbon (4 mmϕ × 6 mm, cylindrical, BET surface area 1170 m^3/g), made from coconut shell, was used for all the experiments. The activated carbon was impregnated under reduced pressure with an aqueous sulfuric acid containing 20 g of H_2SO_4 per 100 cm^3, or with a solution containing 20 g of H_2SO_4 and 20 g of $CuSO_4 \cdot 5H_2O$ per 100 cm^3, and then dried at 100 °C for 2 h. These samples contained 0.76 mmol of H_2SO_4 per g of carbon and, if added, 0.15 mmol of $CuSO_4$ per g of carbon. Other samples containing

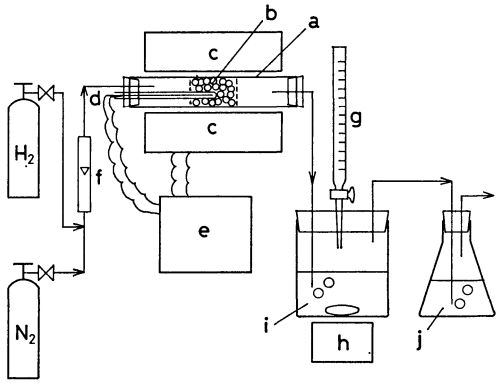

Fig. 1. Experimental apparatus.
a: Reactor (Pyrex), b: activated-carbon, c: electric heater, d: thermocouple, e: temperature-programing unit, f: flow meter, g: buret (1 mol dm^{-3} NaOH), h: magnetic stirrer, i: 6 wt% H_2O_2 solution, j: 0.025 mol dm^{-3} $Ba(OH)_2$ solution.

different amounts of copper sulfate were also prepared.

Analysis of Evolved Gas. The amount of sulfur dioxide evolved was measured as a function of the time, according to the method reported by Kamino *et al.*[2] The outflow gas from the reactor was passed through a 6 wt% hydrogen peroxide solution, and the solution was titrated at appropriate intervals with a standard solution of sodium hydroxide, using a mixed solution of Methyl Red and Methylene Blue as an indicator.††

The total amount of carbon dioxide evolved was determined as follows: after the removal of the sulfur dioxide, the outflow gas was introduced into a 0.025 mol dm^{-3} barium hydroxide solution, in which carbon dioxide was absorbed. The solution was made free from barium carbonate by filtration, and then it was titrated with 0.1 mol dm^{-3} hydrochloric acid. The amount of carbon dioxide absorbed was calculated from the decrease in the concentration of barium hydroxide during each run.

The formation of hydrogen sulfide was checked qualitatively by introducing the outflow gas directly into a silver nitrate solution and looking for a black precipitate of Ag_2S. The formation of elemental sufur was checked by visual inspection, because even a small amount of sulfur could be detected by means of a yellowish-white deposit at the outlet of the reactor. To confirm the results of the above tests, the gravimetric determination of hydrogen sulfide and elemental sulfur was also done by a method described elsewhere.[15]

Results and Discussion

Activated carbon containing 0.76 mmol of H_2SO_4 per g of carbon was heated in a stream of nitrogen or hydrogen under an increasing temperature, while the amount of sulfur dioxide evolved was measured. As is shown by Curves a and b in Fig. 2, which represent the cumulative amount of sulfur dioxide as a function of the increasing temperature, the evolution of sulfur dioxide occurred in the temperature range from 200 °C to 350 °C. This temperature range

†† As the color of this indicator changes from purple to green at pH 5.4, neither carbon dioxide nor hydrogen sulfide, if present, affects the results of titration.

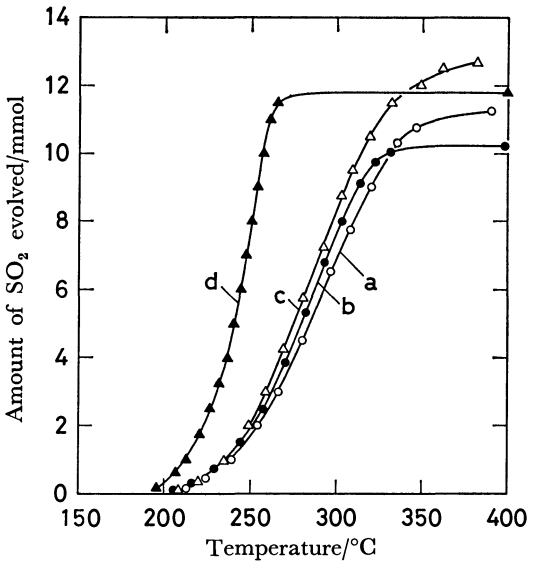

Fig. 2. Relationships between amount of SO_2 evolved and temperature under different conditions.
Atmosphere; ○,△: N_2, ●,▲: H_2, addition of $CuSO_4$; ○,●: None, △,▲: 0.15 mmol/g-carbon, heating rate: 2 °C/min.

TABLE 1. THE AMOUNTS OF SO_2 AND CO_2 EVOLVED

Experimental conditions		Evolved gases/mmol	
Atmosphere	$CuSO_4$	SO_2	CO_2
H_2	Not added	12.0	5.03
N_2	Added[a]	11.6	5.44
H_2	Added[a]	10.0	1.20

Temperature range: Room temperature—400 °C. Heating rate: 2 °C/min. a) 0.15 mmol/g-carbon.

is in good agreement with that reported for Reaction 2 by other workers.[1,2] Curves c and d show similar results for activated carbon containing 0.76 mmol of H_2SO_4 and 0.15 mmol of $CuSO_4$ per g of carbon. In the case of the nitrogen atmosphere (Curve c), the evolution of sulfur dioxide took place in almost the same temperature range as above. In the case of the hydrogen atmosphere (Curve d), the evolution of sulfur dioxide began at 190 °C and was completed at 270 °C. We supposed that Curves a, b, and c correspond to Eq. 2, and Curve d, to Eq. 8. To verify this supposition, the amounts of sulfur dioxide and carbon dioxide evolved were determined in the same runs. The results are shown in Table 1. The mole ratio of CO_2/SO_2 was about 0.5 in the cases in which an activated carbon sample not containing copper sulfate was heated in the hydrogen atmosphere, and in which a sample containing copper sulfate was heated in the nitrogen atmosphere. These results indicate that Reaction 2 took place almost exclusively. On the contrary, the mole ratio of CO_2/SO_2 was much smaller when the sample containing copper sulfate was heated in the hydrogen atmosphere, indicating that Reaction 8 took place predominantly. Hydrogen sulfide and elemental sulfur were not detected in any of the above cases.

The amounts of carbon dioxide and sulfur dioxide

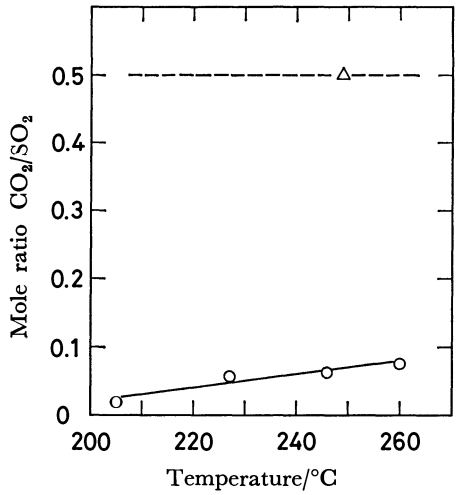

Fig. 3. Mole ratio CO_2/SO_2 in the evolved gas at constant temperatures (The broken line shows the mole ratio expected from Eq. 2).
Amount of $CuSO_4$ added: 0.15 mmol/g-carbon, atmosphere; △: N_2, ○: H_2.

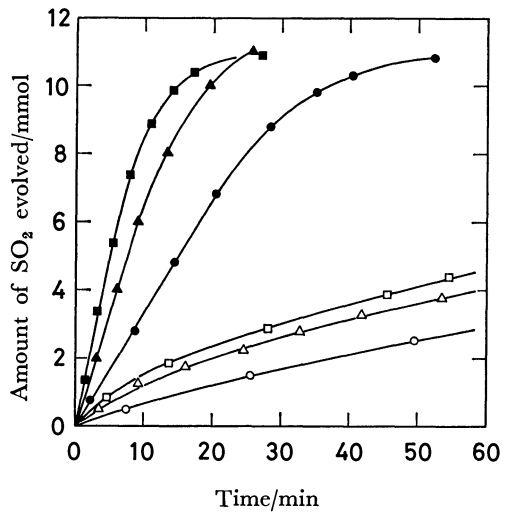

Fig. 4. Relationships between amount of SO_2 evolved and time at constant temperatures.
○,△,□: Without addition of $CuSO_4$, ●,▲,■: with addition of $CuSO_4$ (0.15 mmol/g-carbon), temperature; ○: 224 °C, △: 244 °C, □: 253 °C, ●: 221 °C, ▲: 244 °C, ■: 250 °C.

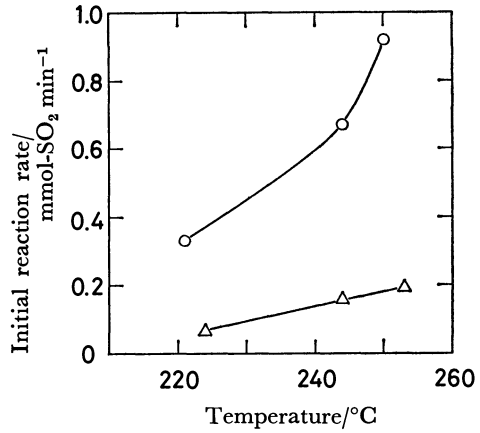

Fig. 5. Initial reaction rates with and without addition of $CuSO_4$.
△: Without addition of $CuSO_4$, □: with addition of $CuSO_4$.

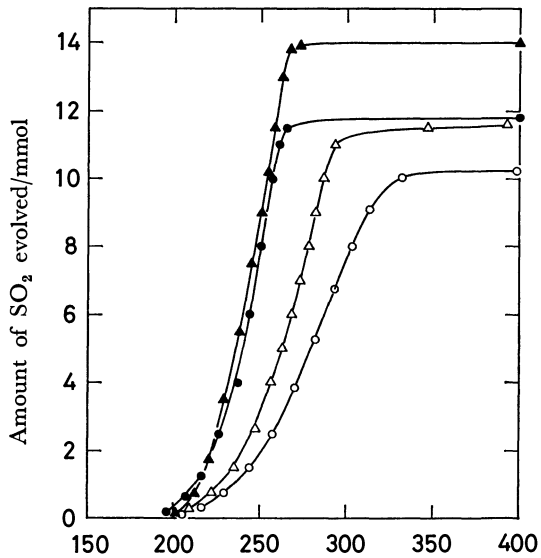

Fig. 6. Relations between amount of SO_2 evolved and temperature for different amounts of $CuSO_4$ added.
Amount of $CuSO_4$ added (mmol/g-carbon); ○: 0, △: 0.015, ●: 0.15, ▲: 0.52, heating rate: 2 °C/min.

evolved were also measured at constant temperatures, using activated carbon samples which contained copper sulfate. Figure 3 shows the mole ratio of CO_2/SO_2 which was obtained when the sample was heated in the nitrogen or hydrogen atmosphere. In the case of the nitrogen atmosphere, the mole ratio was 0.5, as would be expected from Eq. 2. The mole ratio was much smaller in the case of the hydrogen atmosphere, but increased slightly with an increase in the temperature. This indicates that the rate of Reaction 2 increases more rapidly with an increase in the temperature than that of Reaction 8. Since the reduction of sulfuric acid is considered to proceed only according to Eqs. 2 and 8, of the total amount of sulfuric acid the fraction which is reduced by carbon is simply twice the mole ratio of CO_2/SO_2. At 227 °C, for example, the contribution of Reaction 2 to the total amount of sulfuric acid reduced was 10%, and that of Reaction 8 was 90%.

The rate of reduction of sulfuric acid was also studied at constant temperatures. Figure 4 shows the cumulative amount of sulfur dioxide, which was evolved at constant temperatures, as a function of the time. Figure 5 shows the initial reaction rate, which was determined from the initial slope of the curve in Fig. 4. The rate of the evolution of sulfur dioxide was much higher in the presence of copper sulfate than in its absence at the same temperatures. The Arrhenius plot of the initial reaction rate gives the apparent activation energies of 83 kJ/mol in the absence of copper sulfate and 73 kJ/mol in its presence. These values are regarded as approximately corresponding

to Reactions 2 and 8 respectively, and they indicate that the contribution of Reaction 2 should increase as the temperature increases. This conclusion is consistent with the result that the mole ratio of CO_2/SO_2 increases with an increase in the temperature, as is shown by the solid line in Fig. 3. Judging from the values of the activation energy, the transport processes are not the rate-determining steps in either reaction.

The effect of the amount of copper sulfate was also studied, using activated carbon impregnated with a constant amount of sulfuric acid, but with different amounts of copper sulfate. It may be seen from Fig. 6 that the addition of 0.15 mmol-$CuSO_4$/g-carbon is sufficient for Reaction 8 to occur under these conditions. This amount of copper sulfate is about one-fifth that of the sulfuric acid in moles. Therefore, it is supported that copper in some state has a cataytic effect on Reaction 8.

Concluding Remarks

It was found that sulfuric acid is reduced by hydrogen on activated carbon with copper sulfate at temperatures from 190 °C to 270 °C. A succeeding paper will describe metals other than copper as catalysts, and will discuss the catalytic mechanisms.

References

1) H. Dratwa, H. Jüntgen, and W. Peters, *Chem. -Ing. -Tech.*, **39**, 949 (1967).
2) Y. Kamino, S. Onitsuka, and K. Yasuda, *Bull. Jpn. Petrol. Inst.*, **14**, 1 (1972).
3) H. Kuronuma, K. Urano, and R. Kiyoura, *Kōgyō Kagaku Zasshi*, **74**, 1972 (1971).
4) H. Kuronuma, K. Urano, and R. Kiyoura, *Kōgyō Kagaku Zasshi*, **74**, 1976 (1971).
5) K. Yamamoto and M. Seki, *Kōgyō Kagaku Zasshi*, **74**, 1576 (1971).
6) K. Yamamoto, M. Seki, and K. Kawazoe, *Nippon Kagaku Kaishi*, **1972**, 1046.
7) I. Sugiyama, K. Kawazoe, K. Yamamoto, and M. Seki, *Nippon Kagaku Kaishi*, **1972**, 1052.
8) K. Yamamoto, M. Seki, and K. Kawazoe, *Nippon Kagaku Kaishi*, **1973**, 1268.
9) A. Katagiri, C. Inazumi, Z. Takehara, and S. Yoshizawa, *Nippon Kagaku Kaishi*, **1975**, 1471.
10) A. Katagiri, M. Kiyono, Z. Takehara, and S. Yoshizawa, *Nippon Kagaku Kaishi*, **1975**, 1705.
11) F. J. Ball, S. L. Torrence, and A. J. Repik, *J. Air Pollution Control Assoc.*, **22**, 20 (1972).
12) G. N. Brown, S. L. Torrence, A. J. Repic, J. L. Stryker, and F. J. Ball, *Chem. Eng. Prog.*, **68** [8], 55 (1972).
13) D. H. McCrea, A. J. Forney, and J. G. Myers, *J. Air Pollution Control Assoc.*, **20**, 819 (1970).
14) F. M. Dautzenberg, J. E. Nader, and A. J. J. van Ginneken, *Chem. Eng. Prog.*, **67** [8], 86 (1971).
15) A. Katagiri, K. Watanabe, and S. Yoshizawa, *Bull. Chem. Soc. Jpn.*, **54**, 5 (1981).

  Bull. Chem. Soc. Jpn., 54, 5—7 (1981)

The Reduction of Sulfuric Acid by Hydrogen on Various Metal-Carbon Catalysts

Akira KATAGIRI,* Kiyoshi WATANABE,† and Shiro YOSHIZAWA**

Department of Chemistry, College of Liberal Arts and Sciences, Kyoto University, Yoshida, Sakyo-ku, Kyoto 606

*** Department of Industrial Chemistry, Faculty of Engineering, Kyoto University, Yoshida, Sakyo-ku, Kyoto 606*

(Received September 17, 1979)

The reduction of sulfuric acid, which is formed on the activated carbon catalyst in the course of removing sulfur dioxide from exhaust gas, was investigated. The platinum, palladium, silver, and copper on activated carbon were found to be catalytically active in the reduction of sulfuric acid by hydrogen, while manganese, iron, cobalt, nickel, and zinc were found to be inactive. The copper–carbon catalyst is favorable, because sulfuric acid was reduced selectively to sulfur dioxide on it at temperatures from 190 °C to 270 °C. On the platinum–carbon catalyst, the reduction occurred at a relatively low temperature (140 °C to 200 °C), but hydrogen sulfide and elemental sulfur were formed in addition to sulfur dioxide. It is concluded from thermodynamic calculations that catalytically active metals were in the metallic state on activated carbon under the present reaction conditions. An electrochemical mechanism is proposed for the reaction.

In the course of removing sulfur dioxide from exhaust gas by using the activated carbon catalyst, sulfuric acid is formed and accumulated on the catalyst. As a method for removing the sulfuric acid and regenerating the catalyst, Reaction 1 seems to be suitable,

$$H_2SO_4 + H_2 \longrightarrow SO_2 + 2H_2O \quad (1)$$

because the sulfur dioxide obtained can be used directly for sulfuric acid production. However, other side reactions such as Reactions 2, 3, and 4, may possibly occur. For example, the standard Gibbs energy change, ΔG°, for reactions 1, 2, 3, and 4 at 500 K

$$H_2SO_4 + 1/2C \longrightarrow SO_2 + 1/2CO_2 + H_2O \quad (2)$$

$$H_2SO_4 + 3H_2 \longrightarrow S + 4H_2O \quad (3)$$

$$H_2SO_4 + 4H_2 \longrightarrow H_2S + 4H_2O \quad (4)$$

are −133.0 kJ/mol, −110.8 kJ/mol, −271.5 kJ/mol, and −311.8 kJ/mol respectively.[1] It was reported in a previous paper[2] that, when copper sulfate was added, Reaction 1 took place on activated carbon, with only a small consumption of carbon due to Reaction 2. It was suggested that copper in a certain state exerts a catalytic effect on Reaction 1 selectively. In the present paper, experimental results on several metals other than copper as a catalyst component are described, and a possible mechanism of the catalysis is discussed.

Experimental

Apparatus and Procedure. Granular catalysts were heated in a stream of hydrogen under the condition of a linearly increasing temperature, and the gas thus evolved was analyzed. The apparatus used was described in the previous paper.[2] A Pyrex tube 23 mmϕ in inner diameter was used as the reactor, in which catalyst was packed to a length of *ca.* 9 cm. The amount of catalyst packed in was *ca.* 13 g in the case of activated carbon and *ca.* 15 g or 20 g in the case of activated alumina. The catalyst temperature was controlled so that it increased at the rate of 2 °C/min. The flow rate of hydrogen was held constant at 100 cm³/min. Under these conditions it was easy to follow the amount of sulfur dioxide evolved, and the linearity of the temperature with the time was relatively good.

Preparation of Catalysts. Commercial activated carbon (4 mmϕ × 6 mm cylindrical) made from coconut shell was used for these experiments. The activated carbon was impregnated with aqueous sulfuric acid, together with or after the addition of each metal component, and then dried at 100 °C for 2 h. Manganese, iron, cobalt, nickel, copper, and zinc were added to the carbon by impregnating it with a mixed solution of sulfuric acid and the respective sulfates. Platinum, palladium, and silver were added to the carbon in advance by impregnating it with aqueous solutions of hexachloroplatinic(IV) acid, palladium(II) chloride, and silver nitrate respectively, and by then heating it in a hydrogen atmosphere at 400 °C, where these salts were reduced to metals. The content of the metal or the metal ion was controlled so as to be *ca.* 9 mg/g carbon in all cases. In the case of the copper–carbon catalyst, this amount was sufficient as a catalyst component.[2] The amount of sulfuric acid was *ca.* 0.8 mmol/g carbon. This amount was chosen on the basis of the practical data in a pilot-plant test performed by Kamino *et al.*,[3] where 0.7—1.6 N m³ of sulfur dioxide was adsorbed by 57 kg of activated carbon per hour.

Activated alumina (3 mmϕ spherical) was also used in place of activated carbon. In this case, the metal content was *ca.* 8 mg/g alumina, and the amount of sulfuric acid impregnated was *ca.* 0.7 mmol/g alumina.

Analysis of Gas Evolved. The amount of sulfur dioxide in the outflow gas from the reactor was determined by passing the gas through a hydrogen peroxide solution and by titrating the solution at appropriate intervals with a sodium hydroxide solution.[2] The total amounts of hydrogen sulfide and of elemental sulfur evolved were determined gravimetrically in the other runs, as follows: the outflow gas from the reactor was introduced directly into an acidic solution of silver nitrate, in which silver sulfite, silver sulfide, and elemental sulfur were precipitated. After the filtration of these precipitates, the silver sulfite was removed by washing with an aqueous ammonia solution, and then the elemental sulfur was dissolved in carbon disulfide. The weight of the remaining silver sulfide was measured, from which the amount of hydrogen sulfide evolved was calculated. Since solid sulfur was also deposited at the outlet of the reactor, it was dissolved in carbon disulfide and the solution thus obtained was put together with the former one. After the evapolation of the solvent, the weight of the solid sulfur was measured.

† Present address: Research Laboratories of Osaka Soda Co., Ltd., 9 Otakasu-cho, Amagasaki 660.

Results and Discussion

Activated carbons containing sulfuric acid and various metals or metal sulfates were heated in a stream of hydrogen under the condition of an increasing temperature, while the amount of sulfur dioxide evolved was followed. The results are shown in Fig. 1. When platinum, silver, palladium, or copper was added to activated carbon, the evolution of sulfur dioxide was observed in a lower temperature range than in the case of simple activated cabon. These metals are considered to catalyze Reaction 1. In the cases of platinum–, silver–, and palladium–carbon catalysts, the contribution of Reaction 2 must be smaller, if there is any at all, than in the case of the copper–carbon catalyst, because the rate of this reaction depends upon the temperature, but not upon the presence of metal.[2] When manganese, iron, cobalt, nickel, or zinc was added, the evolution of sulfur dioxide was observed in the same temperature range as in the case of simple activated carbon. In these cases, it was likely that not Reaction 1, but Reaction 2 took place exclusively. A comparison of the total amount of sulfur dioxide evolved was rather difficult because of the poor reproducibility of the initial amount of sulfuric acid impregnated. However, the curve for the platinum–carbon catalyst in Fig. 1 differs apparently from the others, indicating that sulfur dioxide was not the only product. In fact, a yellow deposit was observed at the outlet of the reactor in this case.

In order to see whether carbon in itself plays any role in Reaction 1, similar experiments were carried out by using activated alumina in place of activated carbon. Figure 2 shows the results on copper–alumina and copper–carbon catalysts, as well as on simple activated alumina and activated carbon. The evolution of sulfur dioxide took place on the copper–alumina catalyst in a temperature range *ca.* 100 °C higher than in the case of the copper–carbon catalyst. This fact indicates that carbon also participates in the catalysis in Reaction 1. A similar result was obtained for the platinum–alumina catalyst, where the evolution of sulfur dioxide occurred mainly in the temperature range from 300 °C to 450° C. Incidentally, the total amount of sulfur dioxide evolved was almost the same in Fig. 2, although the initial amount of sulfuric acid on the alumina catalysts was about 1.3 times larger than that on the carbon catalysts.

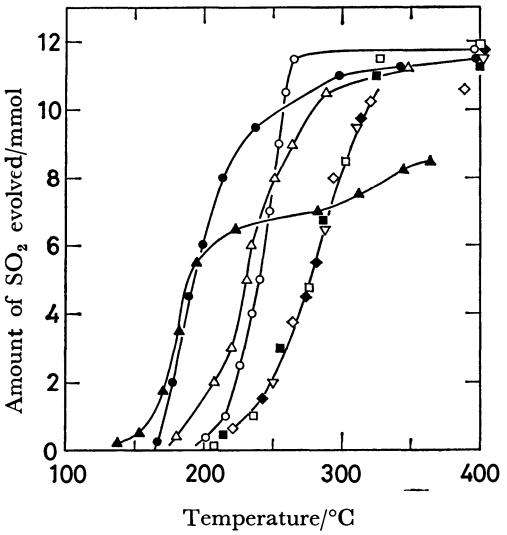

Fig. 1. Relations between amount of sulfur dioxide evolved and temperature for various metal–carbon catalysts.
Metal or metal sulfate added; ▽: $MnSO_4$, □: $FeSO_4$, ■: $CoSO_4$, ◇: $NiSO_4$, ○: $CuSO_4$, ◆: $ZnSO_4$, ●: Ag, △: Pd, ▲: Pt. Weight of packed catalyst: 13 g.

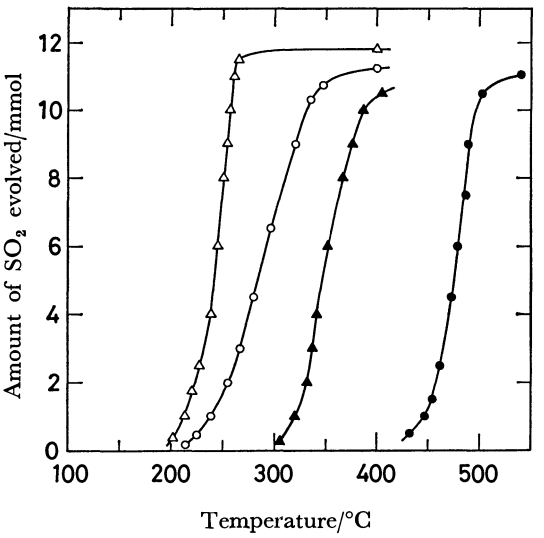

Fig. 2. Relations between amount of sulfur dioxide evolved and temperature for copper–alumina (▲), copper–carbon (△), simple alumina (●), and simple carbon (○) catalysts. Weight of packed catalyst ▲,●: 20 g, △,○: 13 g.

Since it is possible that sulfuric acid is reduced by hydrogen to elemental sulfur and further to hydrogen sulfide, the amounts of these products were determined in the cases of the platinum–, silver–, and copper–carbon catalysts and the copper–alumina catalyst. As is shown in Table 1, a considerable amount of hydrogen sulfide was formed on the platinum–carbon catalyst, together with a small amount of elemental sulfur. On the silver–carbon catalyst, a small amount of hydrogen sulfide was formed. To the contrary, neither of these products was detected in the case of the copper–carbon catalyst. Considerable amounts

Table 1. The amounts of SO_2, S, and H_2S evolved

Catalyst	Weight of packed catalyst	Evolved gases/mmol		
	g	SO_2	S	H_2S
Platinum–carbon[a]	13	8.5	0.3	3.5
Silver–carbon[a]	13	10.0	0.0	0.2
Copper–carbon[a]	13	10.5	0.0	0.0
Copper–alumina[b]	15	6.0	0.8	4.1

Temperature range: a) Room temperature to 400 °C. b) Room temperature to 500 °C. Heating rate: 2 °C/min.

of hydrogen sulfide and elemental sulfur were formed on the copper–alumina catalyst, which is used in commercial plants of the flue-gas desulfurization process (Shell Process).[4,5] This catalyst seems to be suitable for the purpose of recovering elemental sulfur in combination with the Claus process.

In order to infer the actual state of each metal component under the reaction conditions, the standard Gibbs energy change, ΔG°, for Reaction 5 was calculated from the thermodynamic data.[1]

$$M_{2/n}SO_4 + H_2 \longrightarrow (2/n)M + H_2SO_4 \quad (5)$$

Here, "n" indicates the ionic valence of the metal, M. As is shown in Table 2, the values of ΔG° calculated for silver and copper have a negative sign. This suggests that these metals exist in the metallic state under the present reaction conditions. There is no doubt that platinum and palladium are also in the metallic state, though the necessary data are not available. The other metals in Table 2 have positive values of ΔG°, indicating that these metals exist as sulfates. It is probable that catalytically active metals are in the metallic state, while inactive metals are in the ionic state.

Table 2. The standard Gibbs energy change, ΔG° (kJ/mol), for Reaction 5

$M_{2/n}SO_4$	Temperature/K			
	300	400	500	600
$MnSO_4$	267.4	272.2	276.2	280.2
$FeSO_4$	135.1	141.3	146.6	152.0
$CoSO_4$	70.9	76.5	82.0	88.0
$NiSO_4$	87.4	91.4	95.2	99.5
$CuSO_4$	−29.1	−24.7	−21.2	−17.5
$ZnSO_4$	182.7	188.3	193.2	198.3
Ag_2SO_4	−71.5	−63.1	−55.5	−47.8

It may be noted in Fig. 1 that, when the added metal has a lower hydrogen overvoltage, the evolution of sulfur dioxide takes place in the lower temperature range. Thus, the sequence of hydrogen overvoltage at 25 °C,[6] Pt<Pd<Ag<Cu, agrees substantially with the sequence of the temperature range in which the reaction occurs, Pt<Ag<Pd<Cu.†† Considering that the hydrogen overvoltage is a measure of the electrocatalytic activity of metal in the hydrogen-evolution reaction, and that sulfuric acid is a liquid electrolyte at temperatures below 337 °C, the following electrochemical mechanism is proposed for Reaction 1:

$$H_2 \longrightarrow 2H^+ + 2e^- \quad (6)$$

$$H_2SO_4 + 2H^+ + 2e^- \longrightarrow SO_2 + 2H_2O. \quad (7)$$

Thus, the anodic reaction Eq. 6, proceeds on metal, and the cathodic reaction, Eq. 7, on cabon. Reaction 7 is the reverse of that proposed in the catalytic oxidation of sulfur dioxide on activated carbon.[7,8] When the added metal has a low hydrogen overvoltage, Reaction 6 is catalyzed by the metal: therefore, the total reaction, Eq. 1, can occur at a relatively low temperature. In contrast, alumina has no electric conductivity; therefore, Reaction 7 cannot proceed on alumina. Probably, then the catalytic reduction of sulfuric acid on the copper- or platinum–alumina catalyst occurs by another mechanism.

The standard electromotive force of the hypothetical cell composed of Reactions 6 and 7 is calculated as 0.689 V at 500 K. If the overvoltage for Reaction 6 on the catalyst surface is greater than 0.689 V at 500 K, it is impossible for these reactions to occur at this temperature. This is the case with the simple activated carbon. Thus, one of the present authors has previously investigated the kinetics of Reaction 6 at various electrodes in the eutectic melt of lithium chloride and potassium chloride in relation to the hydrogen–chlorine fuel cell;[9] he found that the overvoltage at the carbon electrode was greater than 0.84 V at 773 K. At the temperature of 500 K, the overvoltage must be much greater. This may be the reason why Reaction 1 does not take place on the simple activated carbon.

It has been reported that sulfur dioxide, hydrogen sulfide, and elemental sulfur were produced in the electrolysis of concentrated sulfuric acid at moderately high temperatures, and that the distribution of the products depended strongly on the temperature.[10,11] Besides, the kinetics and mechanism of the electrode reaction are possibly dependent on the electrode potential. In the catalytic reduction of sulfuric acid in the present work, also, it is probable that the distribution of the products is determined by the reaction temperature and the local potential on the catalyst surface, both of which are dependent on the electrocatalytic activity of the metal added.

Conclusion

It is concluded that the copper–carbon catalyst is the best for the purpose of recovering sulfur dioxide from the reduction of sulfuric acid by hydrogen. This catalyst is not likely to be poisoned by sulfide formation, because copper on carbon may become ionic in the oxidizing atmosphere in the step of sulfuric-acid formation, and then be reduced to metal in the reduction step, cyclically.

†† Palladium seems to be out of order in these two sequences. This may be ascribed either to the specific temperature dependency of its activity, or to the discrepancy of the mechanisms of hydrogen-electrode reaction on it at low and high temperatures.

References

1) I. Barin and O. Knacke, "Thermochemical Properties of Inorganic Substances," Springer-Verlag (1973).
2) A. Katagiri, K. Watanabe, and S. Yoshizawa, *Bull. Chem. Soc. Jpn.*, **54**, 1 (1981).
3) Y. Kamino, S. Onitsuka, K. Yasuda, and S. Inoue, *Bull. Jpn. Petrol. Inst.*, **14**, 135 (1972).
4) D. H. McCrea, A. J. Forney, and J. G. Myers, *J. Air Pollution Control Assoc.*, **20**, 819 (1970).
5) F. M. Dautzenberg, J. E. Nader, and A. J. J. van Ginneken, *Chem. Eng. Prog.*, **67**[8], 86 (1971).
6) N. Kameyama, "Denkikagaku No Riron Oyobi Ōyō," Maruzen (1963), Vol. 1.
7) A. Katagiri, Z. Takehara, and S. Yoshizawa, *Denki Kagaku*, **41**, 430 (1973).
8) A. Katagiri, C. Inazumi, Z. Takehara, and S. Yoshizawa, *Nippon Kagaku Kaishi*, **1975**, 1471.
9) S. Yoshizawa, Z. Takehara, and H. Katsuya, *Denki Kagaku*, **32**, 519 (1964).
10) H. Hoffmann, *Z. Elektrochem.*, **27**, 442 (1921).
11) F. Beck, *Electrochim. Acta*, **17**, 2317 (1972).

Polarized Absorption Spectra of Indole and Benzimidazole

Izumi MAKI, Kichisuke NISHIMOTO,* Masa-aki SUGIYAMA,†
Hiroshi HIRATSUKA,† and Yoshie TANIZAKI††

Department of Chemistry, Faculty of Science, Osaka City University, Sumiyoshi-ku, Osaka 558
† *Department of Chemistry, Tokyo Institute of Technology, Meguro-ku, Tokyo 152*
†† *Department of Materials Science and Technology, Technological University of Nagaoka, Niigata 949-54*

(Received October 16, 1979)

The polarization spectra of indole, 3-indolebutyric acid, and benzimidazole have been measured and analyzed by means of MO theory taking Σ-Π interaction into consideration. Induced transition moment due to Σ-Π interaction can be assigned to each σ-bond (both direction and magnitude) pictorially. The effect of hetero atom on the electronic absorption spectra can be interpreted reasonably. Agreement between experimental and calculated results is satisfactory.

In previous papers[1,2] the effects of Σ-Π interaction on π-π* transition energy and on the transition moment in a conjugated system were formulated with use of the partitioning technique,[3] Σ-Π interaction being shown to have an important effect upon the excited singlet states. The effect can be neglected for the triplet states, since it arises from the exchange interaction between σ- and π-electrons. The calculated oscillator strength was reduced to almost one-half of the reference one evaluated by the conventional π-electron approximation (P-P-P method). The MO-CI method based on the π-electron approximation usually gives too large transition moments.

Our aim is to elucidate the effect of substituent or hetero atoms in a large conjugated system on the direction and magnitude of the transition moment in view of Σ-Π interaction. The transition moment of π-π* transition is important in weak intermolecular interaction, exciton interaction in the solid state or in enzyme systems, and in optical properties of molecules, such as optical activity, CD and MCD spectra.

A photoabsorbed tryptophan in an enzyme which has indole residue as its functional group interacts with a distant tryptophan in the same enzyme. The origin of such long distance interaction (*ca.* R=30 Å) is thought to be an exciton interaction. Comprehensive studies[4-6] have been made on electronic spectra of indole which is an active part of tryptophan.

We have determined the direction of transition moment of indole, 3-indolebutyric acid, and benzimidazole and compared the result with that of MO-CI calculation taking Σ-Π interaction into consideration. By our method the induced transition moment caused by Σ-Π interaction can be decomposed into individual σ-bonds which are mostly localized. The decomposition of the induced moment will help to clarify the general feature of Σ-Π interaction in a molecule.

Experimental

Materials. Indole, 3-indolebutyric acid, and benzimidazole (guaranteed, Tokyo Kasei Co., Ltd.) were purified by repeated recrystalization from ethanol or a mixed ethanol–water solution. PVA (polyvinyl alcohol) powder (Koso Chemical Co., Ltd., average polymerization degree 1400) was used for preparation of the film. Preparation of the PVA film and details of dichroism were reported.[7]

Measurement. Dichroic spectra of indole and 3-indolebutyric acid in the stretched PVA films were measured with a Simadzu QV-50 spectrophotometer equipped with a Glan-Thompson polarizer available for the region over 220 nm. The dichroic spectra of benzimidazole, whose maximum corresponding to the intense band at 220 nm of indole is at 205 nm, were measured with a Simadzu UV-200S automatic recording spectrophotometer available for the region over 190 nm.

In the dichroism analysis, the stretched ratio Rs indicates the degree of deformation of the PVA structure, the dichroic ratio Rd the ratio of optical densities ($D_{\parallel}/D_{\perp}$) at a given wavelength, and $D_{\parallel}$ and $D_{\perp}$ are the densities for the incident polarized light the electric vector of which is parallel and perpendicular, respectively, to the stretching direction of the film.

Rd can be expressed as a function of Rs and a parameter r, which is defined as the ratio of two components (μ_a and μ_b) of a transition moment of an electronic transition. μ_a and μ_b are the components parallel and perpendicular, respectively, to an orientation axis (OA) peculiar to the molecule.[7] The angle of the transition moment against OA, which will be referred to as the orientation angle, can be obtained using the Rd and Rs values. The apparent orientation angles for the bands are indicated along the Rd curve in Figs. 1 and 2.

Theoretical

A report was given on an improvement of the P-P-P method considering Σ-Π interaction, which was

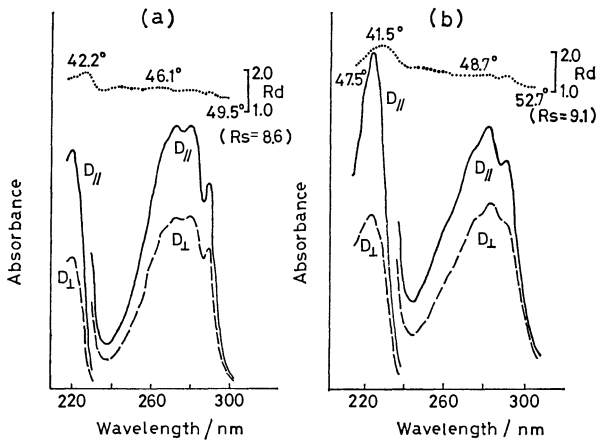

Fig. 1. Dichroic spectra of (a) indole and (b) 3-indolebutyric acid in the stretched PVA film.

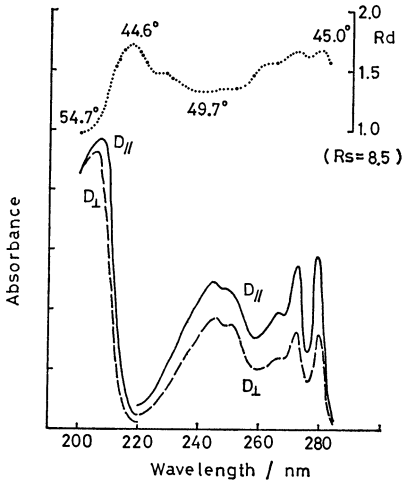

Fig. 2. Dichroic spectra of benzimidazole in the stretched PVA film.

found to be satisfactory for the calculation of electronic spectra of conjugated systems, particularly for the calculation of transition moments.[1]

A physical picture is given of the effect of Σ-Π interaction on the transition moment. The transition moment, $\tilde{\boldsymbol{m}}$, can be expressed by

$$\tilde{\boldsymbol{m}} = \boldsymbol{m}_0 + \Delta\boldsymbol{m} \tag{1}$$

$$\Delta\boldsymbol{m} = \frac{1}{\sqrt{2}\varepsilon}\sum_{i\alpha}\sum_{\mu} C_{i\alpha}d_{i\mu}d_{\alpha\mu}\sum_{\mathrm{AB}}\boldsymbol{r}_{\mathrm{A}}B_{\mathrm{AB}}\gamma_{\mathrm{B}\mu}, \tag{2}$$

where $\boldsymbol{m}_0$ is the transition moment obtained by the conventional P-P-P calculation, $\Delta\boldsymbol{m}$ the correction term due to the Σ-Π interaction, and ε the energy parameter. In Eq. 2, $C_{i\alpha}$ is the variation parameter associated with the configuration, $|{}^{\alpha}_{i}>$, and $d_{i\mu}$ the μ-th AO coefficient of the i-th MO. $\Delta\boldsymbol{m}$ can be decomposed into the individual A–B σ-bond polarization, $\Delta\boldsymbol{m}_{\mathrm{AB}}$, as follows.

$$\Delta\boldsymbol{m} = \sum_{\mathrm{A>B}}\Delta\boldsymbol{m}_{\mathrm{AB}}$$

$$\Delta\boldsymbol{m}_{\mathrm{AB}} = (\boldsymbol{r}_{\mathrm{A}}-\boldsymbol{r}_{\mathrm{B}})B_{\mathrm{AB}}(X_{\mathrm{B}}-X_{\mathrm{A}}), \tag{3}$$

where

$$X_{\mathrm{B}} = \frac{1}{\sqrt{2}\varepsilon}\sum_{i\alpha} C_{i\alpha}d_{i\mu}d_{\alpha\mu}\gamma_{\mathrm{B}\mu} \tag{4}$$

and $\boldsymbol{r}_{\mathrm{A}}$ is the position vector of the atom A. Equation 4 can be rewritten as

$$X_{\mathrm{B}} = \frac{1}{\sqrt{2}\varepsilon}\sum_{\mu} Y_{\mu}\gamma_{\mathrm{B}\mu}, \tag{5}$$

where Y_{μ} is defined by

$$Y_{\mu} = \sum_{i\alpha} C_{i\alpha}d_{i\mu}d_{\alpha\mu}, \tag{6}$$

Y_{μ} represents the component of the transition density (CTD) at μ-th atom. When π-π^* transition takes place, Y_{μ} is produced at μ-th atom, creating an induced charge, X_{B}, on the atom B. In Eq. 3, the vector $(\boldsymbol{r}_{\mathrm{A}}-\boldsymbol{r}_{\mathrm{B}})$ indicates the A-B σ-bond given by the structural formula. $(X_{\mathrm{B}}-X_{\mathrm{A}})$ gives the difference between the induced charge of atom A and that of atom B. B_{AB} plays the role of projection operator whether a σ-bond exists or not between the atoms A and B.

MO-CI calculations have been carried out for indole, 3-methylindole and benzimidazole. As regards their geometry, it is assumed that all molecules consist of regular hexagons and pentagons, in which each C–C and C–N bond length is 1.40 Å. Values for the valence-state ionization potentials, I, and electron affinities, A, of the carbon and nitrogen atoms are taken as follows.

$I(\mathrm{C}) = 11.16\,\mathrm{eV}$ $\quad A(\mathrm{C}) = 0.03\,\mathrm{eV}$

$I(\mathrm{N}^{+1}) = 14.12\,\mathrm{eV}$ $\quad A(\mathrm{N}^{+1}) = 1.78\,\mathrm{eV}$

$I(\mathrm{N}^{+2}) = 26.70\,\mathrm{eV}$ $\quad A(\mathrm{N}^{+2}) = 9.26\,\mathrm{eV}$

The two center core integrals $\beta_{\mu\nu}$ are calculated by the variable β method:[8]

$$\beta_{\mu\nu}(\mathrm{C\text{-}C}) = -1.90 - 0.51\,P_{\mu\nu}\ \mathrm{eV}$$

$$\beta_{\mu\nu}(\mathrm{C\text{-}N}) = -2.09 - 0.53\,P_{\mu\nu}\ \mathrm{eV}.$$

In the CI calculation, all possible singly excited configurations are included.

Results and Discussion

Determination of Orientation Axis. Indole and 3-indolebutyric acid show very similar spectra (Figs. 1(a) and 1(b)). From a comparison of the *R*d curves, we see that the absorption in the range 240—300 nm consists of two bands with different polarizations. Let us denote the bands for the long and short wavelength side by bands (I) and (II). The apparent orientation angles are 49.5° (I) and 46.1° (II) for indole, and 52.7° (I) and 48.7° (II) for 3-indolebutyric acid, both orientation angles increasing with the substituent effect. On the other hand, the apparent angle for a third band (III) at *ca.* 220 nm decreases from 42.2° to 41.5°. Such changes suggest that the orientation axis rotates and approaches the polarization direction of the third band away from those of the first and second transitions. Thus, the polarization direction of bands I and II is on one side of the orientation axis of the molecule and that of band III on the opposite side.

In dichroism analysis, when an absorption band is isolated from the others, the *R*d value for the band should be constant in the band region. However, the value for band III (max. 224 nm) of 3-indolebutyric acid, for example, is not constant but decreases from maximum at 230 nm toward the short wavelength for the band region observed. The decrease in *R*d indicates that band IV penetrates into the band III region. The orientation angle for band III would become smaller than 41.5° if no penetration takes place.

The same situation is considered for band III of indole; the true orientation angle should be less than 42.2°. Since bands I and II overlap each other, their specific orientation angles should be >49.5° and <46.1° for indole and >52.7° and <48.7° for 3-indolebutyric acid, respectively.

Figure 2 shows the dichroic spectra and *R*d curve for benzimidazole. From a comparison of Fig. 2 with Figs. 1(a) and 1(b), we see that bands, I and II (Fig. 2) are isolated from each other and correspond

to bands I and II of indole, respectively, and also band III of benzimidazole corresponds to that of indole. The apparent orientation angles for I(45°) and III(44.6°) of benzimidazole are nearly equal to each other and differ from that of II(49.7°), suggesting that their transition moments are on one side of the orientation axis of the molecule while band II is on the opposite side, in contrast to the case for indole. This indicates that the direction of the transition moment of band I of indole has been moved from one side to the other of the orientation axis by the substituent effect of aza-nitrogen at the 3-position of indole molecule.

The orientation axis of molecule can be determined by a comparison of the experimental orientation angles of band polarizations and the calculated absolute angles of corresponding transition moment.

In the dichroism analysis, the induced orientation axis (OA) of molecule in the stretched PVA substrate is assumed to take a specific direction in the molecular plane. Let us denote the angle between OA and the molecular coordinate axis X by $\theta_{OA}(X)$, where $-90° \leqq \theta_{OA}(X) \leqq 90°$ ($\theta_{OA}(X)$ is defined as positive for anticlockwise direction). If we denote the theoretically calculated angle of the moment of the n-th singlet transition (S_n) against the X-axis by $\theta_n(X)$, and the angle of S_n against OA by $\theta_n(OA)$, we have

$$\theta_n(OA) = 90° \pm (90° - |\theta_n(X) - \theta_{OA}(X)|), \quad (7)$$

where the signs + and − are taken for negative and positive values, respectively. $\theta_n(OA)$ should be compared with the experimental orientation angle $\theta_N(OA)$ of the band number N corresponding to the n-th transition.

We can now determine the absolute angle $\theta_{OA}(X)$ of the orientation axis against the X axis of the molecule in the stretched PVA substrate. The relation between $\theta_n(OA)$ and $\theta_{OA}(X)$ for indole is shown in Fig. 3(a) where the lower limit $\theta_I(OA) > 49.5°$ and upper limits $\theta_{II}(OA) < 46.1°$ and $\theta_{III}(OA) < 42.2°$ are added. For $\theta_{OA}(X)$ satisfactory conditions are as follows: $\theta_I(OA) > 49.5°$ in the range −36.2°—44.8°, $\theta_{II}(OA) > 46.1°$ in the range from 43.5° to −44.3° through 90°, and $\theta_{III}(OA) < 42.2°$ in the range $-38.6° \leqq \theta_{OA}(X) \leqq 45.8°$. The orientation axis (OA) associated with the indole molecule should be restricted to a common direction for which the three conditions are satisfied simultaneously. Such an angle $\theta_{OA}(X)$ (44°±1°) can be found in the range 43.5°—44.8° (Fig. 4(a)).

In the same way, the orientation axis of the 3-indolebutyric acid molecule can be determined to be $\theta_{OA}(X) = 39° \pm 1°$, making use of the calculated result for methyl derivative of indole instead of the 3-(3-carboxypropyl) derivative.

In the case of benzimidazole, the range of angle $\theta_{OA}(X)$ which satisfies the experimental conditions is 5°—29° (Figs. 3(b) and 4(b)). The range is dependent on the experimental data for bands I and IV the orientation angles of which are $\theta_I(OA) \leqq 45°$ and $\theta_{IV}(OA) > 54.7°$, respectively. However, band IV greatly overlaps band III of $\theta_{III}(OA) < 44.6°$ (Fig. 2). If band IV is isolated from band III, it will have

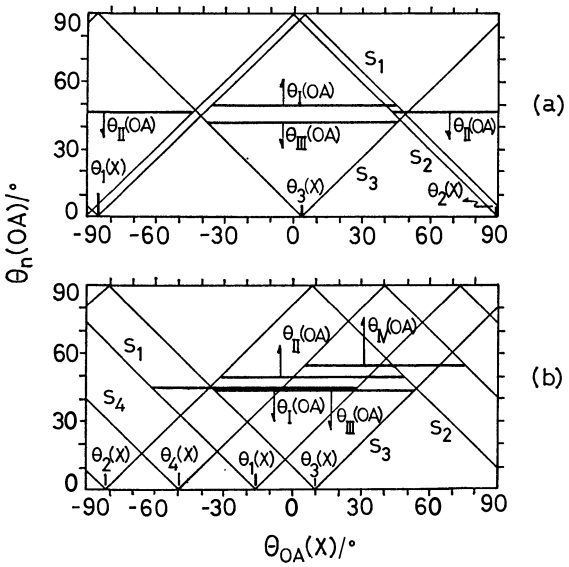

Fig. 3. The angle-relation between the moment of n-th transition (S_n) and the orientation axis (OA) of molecule when the angle of OA to the molecular axis (X) varies in the range −90°—90°.
The abscissa represents the angle of OA to X, $\theta_{OA}(X)$, and the ordinate the angle of the moment of S_n to OA, $\theta_n(OA)$. The horizontal lines indicate the experimental orientation angles (lower or upper limit) of the band number N, $\theta_N(OA)$, which are compared with the theoretical values $\theta_n(OA)$. The allowed angles of $\theta_N(OA)$ are as follows. (a) indole: $\theta_I(OA) > 49.5°$, $\theta_{II}(OA) < 46.1°$, $\theta_{III}(OA) < 42.2°$. (b) benzimidazole: $\theta_I(OA) \leqq 45°$, $\theta_{II}(OA) > 49.7°$, $\theta_{III}(OA) < 44.6°$, $\theta_{IV}(OA) > 54.7°$.

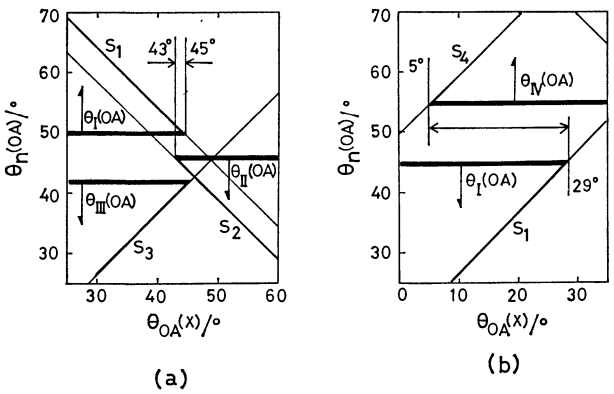

Fig. 4. Angle-relation of $\theta_n(OA)$ and $\theta_{OA}(X)$ of (a) indole and (b) benzimidazole. See the illustration of Fig. 3.

an angle much larger than 54.7°. This will make the lower limit of $\theta_{OA}(X)$ shift from 5° toward 29° (Fig. 4(b)). Since the first peak of band I is considered to be pure electronic transition because of its isolation from band II, the value $\theta_I(OA) = 45°$ would be reliable and the angle of $\theta_{OA}(X)$ may be *ca.* 29°.

The directions of OA of indole, 3-indolebutyric acid and benzimidazole determined experimentally are given in Table 1. $\theta_{OA}(X)$ is the absolute angle of OA against the molecular X(long) axis. The

Table 1. Experimental orientation angle θ_N(OA) of band N, calculated orientation angle θ_n(OA) of n-th transition and determined direction θ_{OA}(X) of orientation axis OA of indole, 3-indolebutyric acid and benzimidazole

N	θ_N(OA) (θ_n(OA))		
	Indole	3-Indolebutyric acid	Benzimidazole
I	>49.5° (50.3°)	>52.7° (53.5°)	≦45° (45°)
II	<46.1° (45.6°)	<48.7° (47.3°)	>49.7° (71°)
III	<42.2° (40.4°)	<41.5° (34.5°)	>44.6° (19°)
IV	≫42.2°	≫41.5°	≫54.7° (79°)
θ_{OA}(X)[a]	44°±1°	39°±1°	*ca.* 29°

a) The angle against the X-axis of the molecule. See Figs. 4 and 5. For determination of θ_{OA}(X) for 3-indolebutyric acid, the calculated results for 3-methylindole were used.

Table 2. Excitation energies and oscillator strengths of π-π^* singlet states of indole, benzimidasole, and 3-methylindole

Compound	Calculations		Experimental[a]	
	E/eV	f	E/eV	log(ε/l mol^{-1} cm^{-1})
Indole	4.48	0.024	4.1	≈3.2
	4.78	0.061	4.3	3.7
	6.02	0.886	5.5	4.5
	6.33	0.114		
	6.50	0.111		
3-Methylindole[b]	4.48	0.024	4.1	≈3.0
	4.81	0.067	4.3	3.7
	6.02	0.922	5.6	4.5
	6.40	0.077		
	6.52	0.124		
Benzimidazole[c]	4.58	0.012	4.5	3.7
	5.05	0.086	5.0	3.7
	6.15	0.858	6.0	4.4
	6.51	0.249		
	6.72	0.046		

a) In aqueous solution. b) Experimental values are for 3-indolebutyric acid. c) pH of aqueous solution *ca.* 10.

geometrical relation of OA and the transition moments of S_n are shown in Fig. 5. Agreement between experimental and calculated results is satisfactory. In the case of indole the calculated angles of S_1 and S_2 are 50.3° and 45.6°, respectively. However, the angles observed are 49.5° and 46.1°, respectively, showing that the partial overlapping of the two bands makes the respective transition directions (absolute angles) approach each other (apparent angles). Similarly, the orientation angle of S_3 transition turns toward that of S_4 because of overlapping. The calculated and experimental results agree (Fig. 5).

Substituent Effect on the Electronic Transition Moment. The calculated π-π^* transition energies and oscillator strengths of indole, 3-methylindole, and benzimidazole are summarized in Table 2. Agreement between calculated and experimental results is satisfactory. The calculated transition moments, $\boldsymbol{m}_0$ and $\tilde{\boldsymbol{m}}$, and oscillator strengths, f_0 and f, of these molecules are summarized in Table 3. The directions of $\boldsymbol{m}_0$ and $\Delta\boldsymbol{m}$ are almost opposite each other, f being considerably reduced. It is of interest to study the effect of the methyl group on the transition moment of the methyl substituted systems. The induced σ-polarization of indole and that of 3-methylindole are illustrated in Figs. 6 and 8, respectively. In the case of 3-methylindole, a large induced σ-bond polarization is found

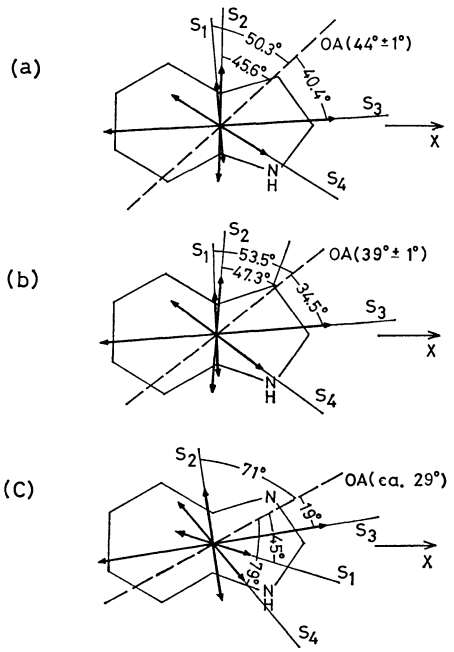

Fig. 5. Calculated transition moments (S_n) and orientation axis (OA) of (a) indole, (b) 3-indolebutyric acid and (c) benzimidazole. X means the molecular long axis.

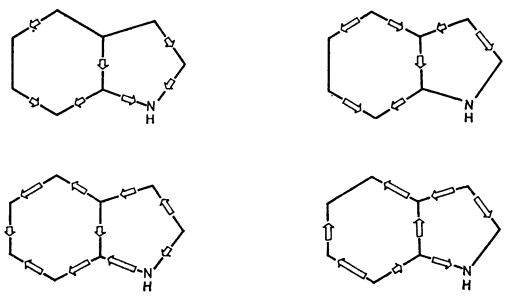

Fig. 6. The divided induced σ-polarization, $\Delta\boldsymbol{m}_{AB}$'s, of indole.

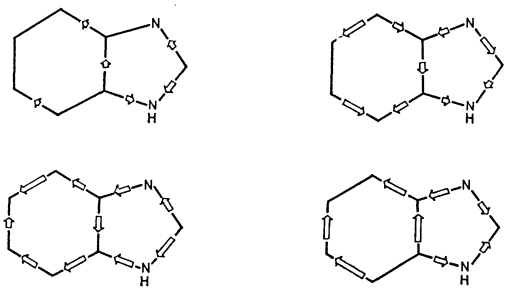

Fig. 7. The divided induced σ-polarization, $\Delta\boldsymbol{m}_{AB}$'s, of benzimidazole.

Table 3. Calculated transition moments and oscillator strengths of indole, benzimidazole, and 3-methylindole

States[a]	Transition moments[b] m_0/eÅ x	m_0/eÅ y	Δm/eÅ x	Δm/eÅ y	$\tilde{m}$/eÅ x	$\tilde{m}$/eÅ y	Oscillator strengths[c] f_0	f	f/f_0	θ/° [d]
				Indole						
S_1	−0.029	0.392	0.010	−0.144	−0.019	0.248	0.061	0.024	0.39	−85.7
S_2	−0.004	0.587	0.007	−0.204	0.003	0.383	0.144	0.061	0.42	89.6
S_3	1.697	0.113	−0.403	−0.031	1.294	0.082	1.524	0.886	0.58	3.6
S_4	0.491	−0.341	−0.105	0.102	0.386	−0.238	0.198	0.114	0.58	−31.7
S_5	0.071	0.704	−0.018	−0.269	0.052	0.434	0.286	0.111	0.39	83.2
				Benzimidazole						
S_1	0.216	−0.067	−0.052	0.019	0.164	−0.048	0.020	0.012	0.60	−16.4
S_2	−0.096	0.682	0.024	−0.248	−0.072	0.435	0.210	0.086	0.41	−80.6
S_3	1.642	0.367	−0.398	−0.150	1.244	0.217	1.523	0.858	0.56	9.9
S_4	−0.560	0.726	0.133	−0.221	−0.427	0.505	0.479	0.249	0.52	−49.8
S_5	−0.263	0.340	0.055	−0.154	−0.208	0.185	0.108	0.046	0.43	−41.7
				3-Methylindole						
S_1	−0.026	0.383	0.016	−0.134	−0.011	0.249	0.058	0.024	0.41	−87.5
S_2	0.009	0.589	0.017	−0.190	0.026	0.399	0.146	0.067	0.46	86.3
S_3	1.727	0.094	−0.408	0.010	1.319	0.105	1.575	0.922	0.59	4.5
S_4	−0.376	0.370	0.073	−0.154	0.303	−0.216	0.156	0.077	0.49	35.6
S_5	0.048	0.722	−0.006	−0.257	0.042	0.465	0.299	0.124	0.41	83.2

a) Singlet states are placed in order of increasing the energy. b) x and y indicate components of the transition moment. c) f_0 and f are calculated by using $\boldsymbol{m}_0$ and $\boldsymbol{m}$, respectively. d) Angles of $\boldsymbol{m}$ from the molecular long axis shown in degrees are defined as positive for anticlockwise direction.

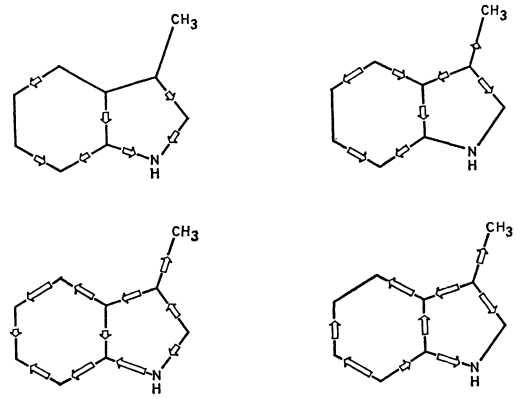

Fig. 8. The divided induced σ-polarization, $\Delta \boldsymbol{m}_{AB}$'s, of 3-methylidole.

at C–CH_3 σ-bond, but its oscillator strength and the direction of transition moment of the π-π^* excitation are almost the same as those of indole. It is thus concluded that in an alkyl derivative, the induced σ-bond polarization appearing at C–C (alkyl) σ-bond differs at each excited state. However, it has no appreciable effect on the direction of the transition moment of the π-π^* excitation. For determination of the direction of transition moment, the alkyl substituted molecule is often used instead of the parent molecule because of its larger orientation in the adsorption on the PVA film or in crystallization. The theoretical results support the pertinence of such experimental prescription. The induced σ-polarization are shown in Figs. 6—8 where, for the sake of simplicity, the π-π^* transition moments are omitted. The gross features of the induced σ-bond polarizations of each molecule considered resemble each other.

References

1) I. Maki, K. Kitaura, and K. Nishimoto, *Bull. Chem. Soc. Jpn.*, **50**, 1720 (1977).
2) I. Maki, K. Kitaura, and K. Nishimoto, *Bull. Chem. Soc. Jpn.*, **51**, 410 (1978).
3) P. O. Löwdin, "Perturbation Theory and Its Application in Quantum Mechanics," ed by C. H. Wilcox, Wiley, New York (1966).
4) E. Lippert, *Adv. Mol. Spectrosc.*, **1**, 443 (1962).
5) M. Sun and P. S. Song, *Photochem. Photobiol.*, **25**, 3 (1977).
6) Y. Yamamoto and J. Tanaka, *Bull. Chem. Soc. Jpn.*, **45**, 1362 (1972).
7) Y. Tanizaki and H. Hiratsuka, *J. Spectrosc. Soc. Jpn.*, **25**, 205 (1976); Y. Tanizaki and S. Kubodera, *J. Mol. Spectrosc.*, **24**, 1 (1967).
8) K. Nishimoto and L. S. Forster, *Theoret. Chim. Acta*, **3**, 407 (1965).
9) K. Ohno, *Theoret. Chim. Acta*, **2**, 219 (1964).
10) G. Klopman, *J. Am. Chem. Soc.*, **86**, 4550 (1964).

Catalytic Activity of Highly Dispersed Palladium. I. The Mechanism of Cyclohexene Hydrogenation and the Role of ZrO_2 Support

Bu Yong Lee,* Yasunobu Inoue, and Iwao Yasumori

Department of Chemistry, Tokyo Institute of Technology, Ookayama, Meguro-ku, Tokyo 152

(Received December 19, 1979)

The hydrogenation of cyclohexene vapor on dispersed palladium was studied in the pressure range of 10—40 Torr† at temperatures between 283 and 323 K. Palladium was impregnated on ZrO_2 and α-Al_2O_3 over the wide range of 0.03 to 2.1 wt%, and the percentage exposed was varied from 13 to 96% for Pd/ZrO_2 and from 2 to 15% for Pd/α-Al_2O_3. The hydrogenation activity, V_g, per unit of weight of the Pd dispersed on ZrO_2, exhibited a sharp maximum at 0.05 wt%, but the turn-over frequency, V_s, per exposed atom around this maximum remained almost constant, which shows the reaction to be structure-insensitive. The value of V_s for Pd/ZrO_2 at 301 K was larger than those for Pd/α-Al_2O_3 and Pd bulk metal by one order of magnitude. The ZrO_2 carrier affected the catalytic behavior of palladium; the reaction orders with respect to the hydrogen and cyclohexene pressures changed to 0.73 ± 0.04 and 0.64 ± 0.04 respectively from the corresponding values, 0.97 ± 0.03 and 0.07 ± 0.04 for Pd/α-Al_2O_3 and Pd metal. The deuterium distributions in the reactant and product molecules in the reaction with D_2 suggested that the hydrogenation on Pd/ZrO_2 and Pd/α-Al_2O_3 proceeds *via* the associative mechanism; the slow step is assumed to be the reaction of the surface cyclohexyl radical with the adsorbed hydrogen atom. The poisoning due to preadsorbed CO decreased the catalytic activities of Pd/ZrO_2 and Pd/α-Al_2O_3 almost linearly with the amounts of surface CO and caused a complete deactivation at about a half coverage of the surface Pd atoms, irrespective of the percentage exposed. On the basis of these results, the structure-insensitivity of the cyclohexene hydrogenation on Pd and the carrier effect of ZrO_2 are discussed.

In order to get a fundamental understanding of heterogeneous catalysis by metals, the effect of the surface structure on the activity has been extensively studied using metals dispersed on supports[1] as well as their single crystals.[2] It appears that attention has been forcused on the shapes and size distributions of metal crystallites in connection with their activity, while supports have simply been regarded as inert matrices. Recently, however, it has been pointed out that the peculiar catalytic activity might be induced by the interactions between metal particles and support; this has been known as the "support effect."[3] In this regard, the oxides of Group IV_a metals have exerted noteworthy effects as supports or promotors of the catalytic hydrogenation.

Maxted and Ali[4] reported that palladium metal loaded on ZrO_2, ThO_2, and TiO_2 exhibited not only a higher activity for the liquid-phase hydrogenation of cyclohexene than that of the unsupported metal, but also its maximum in activity at a definite concentration of Pd, depending on the respective supports. Recently, Fujimoto *et al.*[5] showed that the addition of ThO_2 to the silica-supported Pd catalyst markedly increased the activity for the hydrogenation of CO. These positive effects of the oxides are of particular interest, but they have not yet been analyzed in detail.

Since the influence of the oxides on the catalytic behavior of Pd seems to become smaller as the size of metal crystallites increase, distinct evidence of the support effect can be obtained by the use of catalysts in a state of high dispersion or with a large percentage exposed. In the present study, the first one of this series, ZrO_2 was taken as a potentially interesting support on which palladium metal was dispersed over a wide range of surface concentrations and the hydrogenation of cyclohexene was studied. The reaction on α-Al_2O_3-supported and bulk metal palladium was also examined for comparison. Both supported catalysts were characterized by CO chemisorption and X-ray diffraction methods, and the percentage exposed was determined. Although most of the works on cyclohexene hydrogenation over Pd blacks[6] and Pd/Al_2O_3[7] have been carried out in the liquid phase, we studied the reaction in the gas phase because of easier kinetic analysis. The kinetics was supplemented by the results of an examination of the deuterium distributions in the product and reactants in the reaction with D_2.

The relationship between the percentage exposed and the turnover frequency enables us to inspect the effect of the surface structure upon the catalytic behavior, but it is not sufficient for us to evaluate the surface density of active sites. Accordingly, the poisoning due to preadsorbed CO was applied to the present catalyst system in order to evaluate the density and, further, to study the nature of the active sites, which may change through the interaction with carries.

Experimental

Catalysts. Palladium supported on zirconia or α-alumina was prepared by the impregnation method at room temperature. Both supports were washed with 0.1 mol dm^{-3} nitric acid and then rinsed thoroughly with ion-exchanged water. The surface area, as evaluated by the BET method using nitrogen, were 38.5 m^2/g for ZrO_2 and 3.8 m^2/g for α-Al_2O_3. The impregnation of palladium was carried out by adding, drop by drop, an aqueous solution of palladium nitrate, in a concentration of about 13 g/l, to a batch of the supports which were slowly being stirred. The addition was stopped at the incipient wetness of the support, and then the catalysts were dried in air at 393 K for 12 h. The concentration of Pd was thus widely changed, *i.e.*, from 0.03 to 2.1 wt% for Pd/ZrO_2 and from 0.05 to 2.1 wt% for Pd/α-Al_2O_3. Palladium metal powder was prepared by reducing $PdCl_2$ with an aqueous solution of $NaBH_4$.

In order to determine the conditions which provide a

† 1 Torr=133.322 Pa.

catalytic activity as stable and high as possible, the influence of the reduction temperature on the catalytic activity of Pd/ZrO_2 and $Pd/\alpha\text{-}Al_2O_3$ was investigated up to 875 K; reduction at 523 K was found to be a suitable treatment. The catalyst activity was also examined at the same temperature as a function of the reduction time for up to 5 h, but no significant difference was observed after 1 h. Thus, a fresh catalyst was subjected to pretreatment by oxidation with 20 Torr of oxygen at 523 K for 1 h, followed by reduction with 20 Torr of hydrogen at 523 K for 1 h and then evacuation for 1 h at the same temperature. This series of treatments was also employed prior to each kinetic run.

Kinetics of Reaction. The gas-phase hydrogenation of cyclohexene was carried out by using a closed circulation system with a volume of 450 ml. The cyclohexene was degassed, subjected several times to a trap-to-trap distillation, and then transferred to the reaction system. The pressure decrease during the course of the reaction was followed by means of a glass Bourdon gauge. A gas chromatographic analysis verified that cyclohexane was the only product under the present experimental conditions and that the rate of the pressure decrease corresponded exclusively to the rate of cyclohexane formation. The hydrogenation was studied in the pressure range of 10—40 Torr at temperature between 283 and 323 K. The reaction with deutrium was carried out under exactly the same conditions as those used in the hydrogenation. After the reduction, the cyclohexene and cyclohexane were separated gas chromatographically by the use of a 6 m column of Celite-545, with Dinonyl phthalate added, and then analysed by means of a mass-spectrometer, Hitachi RMU-7M, at an ionization voltage of 15 eV. The mass patterns including isotope peak (^{13}C) and the isotope effect on the ionization were corrected.[8] The hydrogen, hydrogen deuteride, and deuterium were analysed by means of gas chromatograph.[9] In order to determine the percentage exposed of palladium atoms, the adsorption of CO was employed at 301 K in a static system with a volume of 150 ml after the catalysts had been treated in the same manner as that employed in the kinetic study. X-Ray diffraction was also applied to the catalysts.

Material. Zirconia of an extra pure grade was obtained from the Koso Chemical Co., and α-alumina, from the Shimadzu Seisakusho, Ltd. Cyclohexene of an extra pure grade, purchased from Yoneyama Chemical Industries, Ltd., was distilled *in vacuo* and found to be gas chromatographically pure. Hydrogen (99.99% pure) and deuterium (containing less than 0.5% HD) were obtained from Takachiho Kagaku Kogyo and were purified through a molecular-sieve trap cooled to 80 K.

Results

Figure 1 shows the variation in the catalytic activity, V_g, (molecule min^{-1} g Pd^{-1}) of Pd/ZrO_2 and $Pd/\alpha\text{-}Al_2O_3$ for the hydrogenation of cyclohexene with different Pd contents. The Pd/ZrO_2 catalyst was characterized by a marked rise in the activity with an increase in the Pd content and by a maximum at 0.05 wt%, whereas $Pd/\alpha\text{-}Al_2O_3$ shows only a slight increase around 0.2 wt%. A comparison between the highest activities showed that the activity per gram of Pd dispersed on ZrO_2 was about 170 times greater than that of Pd on $\alpha\text{-}Al_2O_3$. Kinetic studies were carried out for most of these catalysts; the results thus obtained are summarized in Tables 1 and 2.

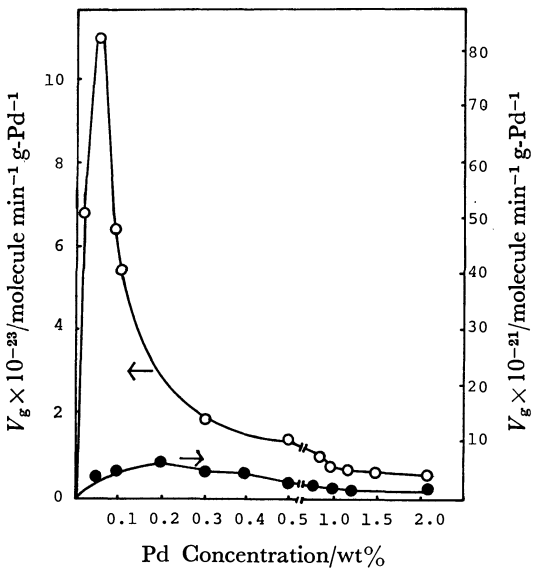

Fig. 1. Change in catalytic activity V_g with Pd content.
Unless otherwise stated, the following conditions were used: P_h=40 Torr, P_e=40 Torr, reaction temp=301 K.
○: Pd/ZrO_2, ●: $Pd/\alpha\text{-}Al_2O_3$.

It should be noted that, for a series of each kind of catalyst, the reactions gave almost the same activation energy and pressure dependence, irrespective of the Pd concentration, but there were significant differences in these kinetic parameters between the reaction on Pd/ZrO_2 and $Pd/\alpha\text{-}Al_2O_3$; the activation energy for the reaction on Pd/ZrO_2 was, on the average, higher by about 13 kJ mol^{-1} than for $Pd/\alpha\text{-}Al_2O_3$ and Pd bulk metal. The reaction orders with respect to the partial pressures of hydrogen and cyclohexene were, respectively, 0.73±0.04 and 0.64±0.04 for Pd/ZrO_2, whereas the corresponding values were 0.97±0.03 and 0.07±0.04 for $Pd/\alpha\text{-}Al_2O_3$ and Pd bulk metal.

The detailed analysis of the reaction was performed by using deuterium as a tracer, and the deuterium distributions in gaseous cyclohexene, cyclohexane, and hydrogen were investigated. The results are summarized in Table 3. Neither hydrogenation nor exchange reaction of cyclohexene with D_2 occurred on either of the supports, ZrO_2 and $\alpha\text{-}Al_2O_3$, under the present experimental conditions. The reaction of cyclohexene with D_2 or with H_2+D_2 on Pd/ZrO_2 and $Pd/\alpha\text{-}Al_2O_3$ demonstrated that considerable amounts of cyclohexene [D_1] and [D_2] were formed at a conversion of from 8 to 10%. Equilibration among H_2, HD, and D_2 in the gas phase proceeded completely in the case of $Pd/\alpha\text{-}Al_2O_3$; the values of K, defined as the P_{HD}^2/P_hP_D radio, were 3.1—4.2(±0.4) in the $C_6H_{10}+D_2$ system and 3.5—3.7(±0.3) in the $C_6H_{10}+H_2+D_2$ system. In the reaction using the Pd/ZrO_2 catalyst, however, although appreciable amounts of HD and H_2 were produced, the equilibrium among them did not hold; the K's were 0.6—0.8 (±0.2) in the $C_6H_{10}+D_2$ system and 1.2—1.3(±0.1) in the $C_6H_{10}+H_2+D_2$ system. As for the product, cyclohexane, a distribution ranging from [D_0] and

Table 1. Kinetic parameters of cyclohexene hydrogenation and CO adsorption on Pd/ZrO_2

Pd wt%	V_g[a] Molecule / min g-Pd	CO[b] Molecule / g-Pd	D(%)[c]	V_s / s^{-1}	Reaction order[d] m	n	Activation energy[e] E_a / kJ mol^{-1}
0.03	6.8×10^{23}	4.48×10^{21}	(79.2)	2.5	0.75	0.60	48.1[g]
0.05	11.0	5.47	(96.6)	3.3	0.71	0.66	51.5
0.08	6.4	3.77	(66.6)	2.8	0.71	0.60	46.1
0.1	5.3	3.68	(65.0)	2.4	0.68	0.68	49.4
0.3	1.7	1.33	(23.5)	2.1	0.75	0.62	47.7
0.5	1.4	0.84	(14.8)	2.8	0.76	0.60	51.1
0.7	1.1	0.78	(13.8)	2.4	0.78	0.60	49.8
1.0	0.7	0.76	(13.4)	1.5	0.70	0.60	47.7
1.2	0.7	—	—	—	0.75	0.60	50.2
1.5	0.6	—	—	—	0.73	0.65	46.1
2.1	0.4	0.57	(10.1)[f]	1.2	0.70	0.60	46.1

a) P_h=40 Torr, P_e=40 Torr; reaction temperature=301 K. b) Saturated adsorption at 301 K. c) Percentage exposed (%), evaluated on the assumption that a CO molecule adsorbs on a Pd atom. d) $V=kP_h^mP_e^n$. e) Temperature range=283—323 K. f) X-Ray diffraction gave a value of 9.7%. g) ±1.5 kJ/mol.

Table 2. Kinetic parameters of cyclohexene hydrogenation and CO adsorption on Pd/α-Al_2O_3 and Pd metal

Pd wt%	V_g[a] Molecule / min g-Pd	CO[b] Molecule / g-Pd	D(%)[c]	V_s / s^{-1}	Reaction order[d] m	n	Activation energy[e] E_a / kJ mol^{-1}
0.05	3.9×10^{21}	—	—	—	0.95	0.0	35.2[g]
0.1	4.4	5.7×10^{20}	(10.1)	0.13	0.97	0.0	31.0
0.2	6.4	8.4	(15.0)	0.12	1.00	0.0	33.5
0.3	4.0	—	—	—	1.00	0.0	35.2
0.4	3.8	—	—	—	1.00	0.0	38.5
0.5	2.1	—	—	—	1.00	0.0	38.1
0.7	1.9	1.7	(2.8)	0.19	1.06	0.1	33.9
1.0	0.7	—	—	—	1.00	0.0	36.9
1.3	0.7	—	—	—	1.00	0.0	33.5
2.1	0.8	1.3	(2.2)[f]	0.10	1.00	0.1	38.5
Pd Black	7.8×10^{19}	1.4×10^{19}	—	0.09	1.00	0.0	32.7

a), b), c), d), e): See Table 1. f) X-Ray diffraction gave a value of 2.5%. g) ±1.5 kJ/mol.

$[D_5]$ was observed in the reactions using the respective catalysts, but there was a tendency for Pd/ZrO_2 to provide a higher concentration of cyclohexane $[D_0]$.

Figure 2 shows the isotherms of CO adsorbed at 301 K on 0.05 wt% Pd/ZrO_2 and ZrO_2. Carbon monoxide was introduced up to 60 Torr, and then, after the evacuation at the same temperature for 20 min, the adsorption was repeated under the same conditions. As may be seen from Fig. 2, the amount of CO adsorbed on Pd/ZrO_2 in the second run was much the same as that on the ZrO_2 surface, on which only the reversible adsorption took place. Thus, the difference between the first and second runs gave the amount of irreversible adsorption on the surface of metallic palladium. By assuming that an exposed Pd atom can accommodate one carbon monoxide molecule,[10] the number of Pd atoms exposed was evaluated. Tables 1 and 2 involve the percentage exposed and also the hydrogenation activity per exposed atom, *i.e.*, the turn-over frequency V_s, represented in terms of molecule s^{-1} exposed Pd $atom^{-1}$. It should be noted that the change in V_s was rather small throughout the whole range of Pd loading. The V_s at 0.05 wt% was only twice as large as that at 1.0 wt%. However, the V_s on Pd/ZrO_2 was 20 to 30 times higher than those on Pd/α-Al_2O_3 and Pd bulk metal.

The poisoning effect of CO was examined at 301 K. A known amount of CO was preadsorbed on a bare Pd surface after the pretreatment, after which the catalyst was evacuated for 20 min and the reaction gas was introduced. Figure 3 shows the change in the activity with the increase in the fraction of CO coverage, which was defined as the ratio of the amount of CO adsorbed to that at saturation. In all cases of 0.05, 0.3, and 1.0 wt% Pd/ZrO_2 catalysts as well as of 0.2 wt% Pd/α-Al_2O_3 studied, an almost linear decrease in the activity occurred with the increase in the fraction of the surface occupied by CO, and zero activity was attained at around θ=0.45 when the lines were extrapolated.

Table 3. Deuterium distributions in the reactions of cyclohexene with D_2 or H_2+D_2 on Pd/ZrO_2 and $Pd/\alpha\text{-}Al_2O_3$

Catalysts		0.05 wt% Pd/ZrO_2				0.2 wt% $Pd/\alpha\text{-}Al_2O_3$			
Conversion (%)		$D_2+C_6H_{10}$[a] 8	15	$D_2+H_2+C_6H_{10}$[b] 8	15	$D_2+C_6H_{10}$[a] 10	17	$D_2+H_2+C_6H_{17}$[b] 10	17
Cyclohexane	D_0(%)	28	22	32	41	9	17	19	10
	D_1	37	34	40	44	19	26	22	24
	D_2	23	28	21	13	34	31	35	43
	D_3	8	8	6	2	16	16	21	19
	D_4	3	3	1	0	10	10	1	3
	D_5	2	2	0	0	6	0	0	0
	D_6	0	1	0	0	3	0	0	0
	D_7	0	0	0	0	2	0	0	0
	D_8—D_{12}	0	0	0	0	0	0	0	0
Cyclohexene	D_0	79	69	94	81	79	82	98	80
	D_1	10	16	3	6	10	8	1	6
	D_2	4	11	3	6	5	6	1	6
	D_3	3	2	0	5	4	2	0	5
	D_4	2	1	0	2	2	1	0	3
	D_5	1	0	0	0	0	0	0	0
	D_6—D_{10}	0	0	0	0	0	0	0	0
H_2(%)		8	5	27	30	2	2	13	20
HD		19	17	35	36	25	22	45	48
D_2		73	78	38	34	73	76	42	32

Reaction temp=301 K, a) $P_D=P_e=40$ Torr, b) $P_H=P_D=20$ Torr, $P_e=40$ Torr.

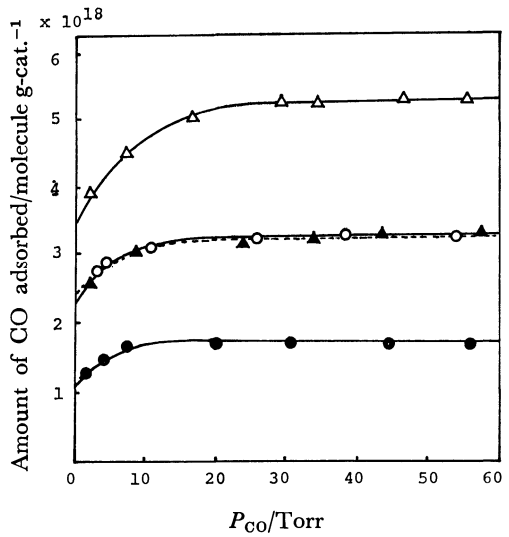

Fig. 2. Adsorption of CO on 0.05 wt% Pd/ZrO_2 and ZrO_2.
△: Total adsorption of CO, ▲: reversible adsorption of CO, ○: adsorption on ZrO_2, ●: irreversible adsorption of CO.

Discussion

It is a feature of the cyclohexene hydrogenation on Pd/ZrO_2 that the high activity appears in a narrow range of Pd concentrations, as is shown in Fig. 1. Such a drastic change in the activity contrasts with the results on $Pd/\alpha\text{-}Al_2O_3$. This maximum activity was also observed in the liquid-phase hydrogenation.[4] The measurement of the CO-adsorption on Pd/ZrO_2, however, revealed that the fraction of Pd exposed per unit weight of the metal varied with the amount of Pd loading in a manner parallel to the change in the activity. Accordingly, the turn-over frequency, V_s, was rather constant around the maximum of activity (V_g) and then gradually decreased to about a half of the value with an increase in the Pd content. A similar relation between V_g and V_s was also observed in the case of $Pd/\alpha\text{-}Al_2O_3$, but the value of V_s for $Pd/\alpha\text{-}Al_2O_3$ was smaller by one order of magnitude than that for Pd/ZrO_2, irrespective of the Pd content. The small variation in V_s as well as the similarity in the kinetic parameters over the wide range of percentage exposed suggests that the hydrogenation of cyclohexene is "structure-insensitive" in character and that the sharp maximum in V_g is attributable to the highest density of active sites. The slight fall in V_s with the decrease in the percentage exposed may be due to the decrease in the virtual site density; the steric hindrance between adsorbed cyclohexene molecules may become more distinct on the smooth surfaces of larger particles, or the stoichiometry between the adsorbed CO and the Pd atom may vary with the percentage exposed. From the amount of CO chemisorbed on 0.05 wt% Pd/ZrO_2, the average diameter of Pd particles was calculated to be about 17 Å, provided that the particles are spherical. This estimation indicates that, as a primary effect, the ZrO_2 surface has a high capability of dispersing Pd metal as very fine particles or crystallites which possess a high density of active sites.

Since the surface density of the active site varies in proportion to the percentage exposed of Pd atoms,

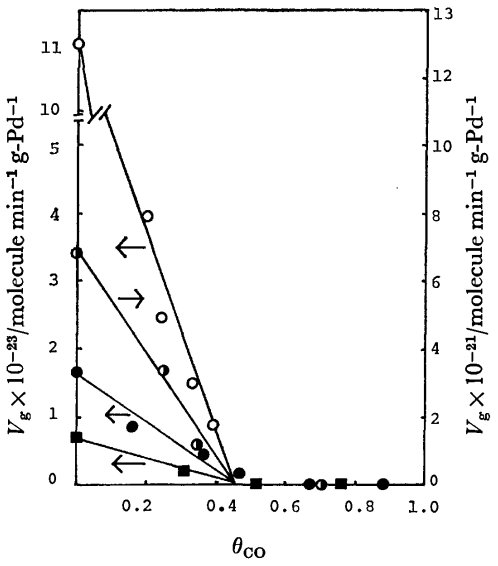

Fig. 3. Poisoning effect of adsorbed CO on cyclohexene hydrogenation.
○: 0.05 wt% Pd/ZrO_2, ●: 0.3 wt% Pd/ZrO_2, ■: 1.0 wt% Pd/ZrO_2, ◑: 0.2 wt% Pd/α-Al_2O_3.

the poisoning due to preadsorbed CO permits us to evaluate the density. As may be seen from Fig. 3, a nearly linear relationship exist between the decline in the activity and θ_{CO}, and the zero activity was brought about at $\theta_{CO}=0.45$ for all the Pd/ZrO_2 and Pd/α-Al_2O_3 catalysts examined. This coincidence of CO coverage where the activity vanishes suggests that the topography of the active sites is similar for Pd particles dispersed on both ZrO_2 and α-Al_2O_3.

There are clear differences in the pressure dependence and activation energy between the reactions on the Pd/ZrO_2 and Pd/α-Al_2O_3 catalysts, but the general features of wide distributions in the reactant and product were rather analogous in both cases and suggest that the hydrogenations proceed via the associative mechanism described by the following pathway;

$$H_2(g) \underset{k_{-1}}{\overset{k_1}{\rightleftarrows}} 2H(a) \quad (1)$$

$$C_6H_{10}(g) \underset{k_{-2}}{\overset{k_2}{\rightleftarrows}} C_6H_{10}(a) \quad (2)$$

$$C_6H_{10}(a) + H(a) \underset{k_{-3}}{\overset{k_3}{\rightleftarrows}} C_6H_{11}(a) \quad (3)$$

$$C_6H_{11}(a) + H(a) \underset{k_4}{\rightarrow} C_6H_{12}(g) \quad (4)$$

were k_i and k_{-i} denote, respectively, the rate constants of the forward and reverse reactions at the ith step. The changes in the fractions of the surface covered with hydrogen atoms, θ_H, cyclohexene, θ_e, and cyclohexyl radicals, θ_y, as functions of the time are described as:

$$\frac{d\theta_h}{dt} = 2k_1P_h\theta_v^2 - 2k_{-1}\theta_h^2 - k_3\theta_h\theta_e + k_{-3}\theta_y\theta_v - k_4\theta_h\theta_y \quad (5)$$

$$\frac{d\theta_e}{dt} = k_2P_e\theta_v - k_{-2}\theta_e - k_3\theta_e\theta_h + k_{-3}\theta_y\theta_v \quad (6)$$

$$\frac{d\theta_y}{dt} = k_3\theta_e\theta_h - k_{-3}\theta_v\theta_y - k_4\theta_y\theta_h, \quad (7)$$

where θ_v denotes the fraction of the vacant surface and is equivalent to $(1-\theta_h-\theta_e-\theta_y)$. The wide deuterium distributions in cyclohexane permit us to assume that Step 3 is in pseudo-equilibrium; thus, the following relationship;

$$K_3\theta_e\theta_h = \theta_y\theta_v \quad (8)$$

is obtained, where $K_3=k_3/k_{-3}$. The employment of the steady-state approximation on the adsorbed hydrogen atoms and cyclohexene molecules, *i.e.*, $d\theta_h/dt=d\theta_e/dt=0$, and the insertion of Eq. 8 into Eqs. 5 and 6 lead to;

$$2k_1P_h\theta_v^2 - 2k_{-1}\theta_h^2 - k_4\theta_y\theta_h = 0 \quad (9)$$

$$k_2P_e\theta_v - k_{-2}\theta_e = 0. \quad (10)$$

Solving the set of Eqs. 8, 9, and 10, we can obtain these expressions for θ_y and θ_h in a steady state;

$$\theta_y = K_2K_3P_e\theta_h \quad (11)$$

and;

$$\theta_h = \frac{\sqrt{2k_1P_h}}{[(1+K_2P_e)\sqrt{2k_{-1}+k_4K_2K_3P_e}+(1+K_2K_3P_e)\sqrt{2k_1P_h}]}, \quad (12)$$

where $K_1=k_1/k_{-1}$. Accordingly, the rate of cyclohexene hydrogenation, V_g, is given by;

$$V_g = k_4\theta_y\theta_h = \frac{2k_1k_4K_2K_3P_hP_e}{[(1+K_2P_e)\sqrt{2k_{-1}+k_4K_2K_3P_e}+(1+K_2K_3P_e)\sqrt{2k_1P_h}]^2}. \quad (13)$$

In order to examine the validity of the derived equation for the observed pressure dependences, Eq. 13 is transformed into;

$$\sqrt{\frac{P_h}{V_g}} = \sqrt{\frac{1}{(2k_1k_4K_2K_3)P_e}}[\sqrt{2k_1P_h}(1+K_2K_3P_e) + (1+K_2P_e)\sqrt{2k_{-1}+k_4K_2K_3P_e}], \quad (14)$$

which provides a linear relationship between $(P_h/V_g)^{1/2}$ and $P_h^{1/2}$ under the condition of a constant P_e. A similar transformation of Eq. 13 with respect to the cyclohexene pressure gives;

$$\sqrt{\frac{P_e}{V_g}} = \sqrt{\frac{1}{(k_4K_1K_2K_3)P_h}}\left[(1+K_2K_3P_e)\sqrt{K_1P_h} + (1+K_2P_e)\sqrt{1+\frac{k_4K_2K_3}{2k_{-1}}P_e}\right], \quad (15)$$

which can not be used for the examination of the pressure dependence. Considering that the desorption of hydrogen is still much faster than the hydrogenation, *i.e.*, $2k_{-1}\theta_h^2 > k_4K_2K_3P_e\theta_h^2$, one can expand the second term in brackets in Eq. 15 as:

$$(1+K_2P_e)\sqrt{1+\frac{k_4K_2K_3P_e}{2k_{-1}}} = \left[1+\left(K_2+\frac{k_4K_2K_3}{4k_{-1}}\right)P_e+\frac{k_4K_2^2K_3}{4k_{-1}}P_e^2+\cdots\right]. \quad (16)$$

Accordingly, Eq. 15 is rewritten in an approximate form:

$$\sqrt{\frac{P_e}{V_g}} = \sqrt{\frac{1}{(k_4K_1K_2K_3)P_h}} \times\left[1+\sqrt{K_1P_h}+\left(1+K_3\sqrt{K_1P_h}+\frac{k_4K_3}{4k_{-1}}\right)K_2P_e\right]. \quad (17)$$

It follows, therefore, that a linear relationship of $(P_e/V_g)^{1/2}$ *vs.* P_e exists under the condition of a constant P_h. As for the hydrogenation on Pd/α-Al_2O_3, in which gaseous hydrogen molecules are in equilibrium with the adsorbed hydrogen atoms, the rate equation was simplified to:

$$V_g = \frac{k_4K_1K_2K_3P_hP_e}{\{1+\sqrt{K_1P_h}+K_2P_e+K_2K_3P_e\sqrt{K_1P_h}\}^2}. \quad (18)$$

It is apparent that this equation provides relationships similar to those described above for the hydrogen- and cyclohexene-pressure dependences. Figure 4 shows good linear plots of the observed values for the above-mentioned relationships, which verifies the validity of Eqs. 13 and 18, and hence the mechanism proposed. The assumption that one of the reactions other than Step 4 is a slow process leads to an unsatisfactory conclusion in explaining the observed pressure dependence and isotope distribution. When Gonzo and Boudart[11] studied the hydrogenation of cyclohexene on γ-alumina-supported Pd in the gas and liquid phases, they observed no appreciable difference in the mechanism of reaction between these systems. They showed that the rate-determining step is the addition of a hydrogen atom to the cyclohexyl species,

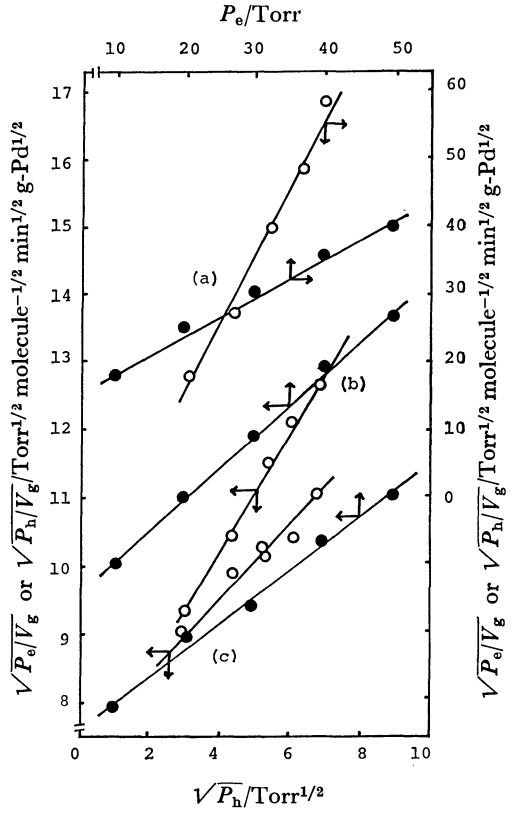

Fig. 4. Plots of $\sqrt{P_h/V_g}$ *vs.* $\sqrt{P_h}$ and $\sqrt{P_e/V_g}$ *vs.* P_e. ○: $\sqrt{P_h/V_g}$ *vs.* $\sqrt{P_h}$ (P_e=40 Torr), ●: $\sqrt{P_e/V_g}$ *vs.* P_e (P_h=40 Torr), reaction temp=301 K. (a): 0.2 wt% Pd/α-Al_2O_3, (b): 1.0 wt% Pd/ZrO_2, (c): 0.08 wt% Pd/ZrO_2.

which accords with the present conclusion. The value of the turn-over frequency, 3.3 s^{-1} at 301 K (P_h=P_e=40 Torr) on 0.05 wt% Pd/ZrO_2 was close to the value, 3.4 s^{-1}, obtained by correcting their data[11] to the present reaction conditions.

These characteristic features of the hydrogenation by Pd/ZrO_2, *viz.*, the high V_s value and the different kinetics as compared to those on Pd/α-Al_2O_3 and Pd bulk metals, are certainly associated with carrier effects caused by ZrO_2. If one assumes the dispersed state of metal to be a spherical particle, the percentages exposed of 96% (0.05 wt% Pd/ZrO_2) and 13% (2.1 wt% Pd/ZrO_2) correspond to particle sizes of about 17 and 140 Å in diameter respectively. As is shown in Table 2, there is evident lack of variation in the kinetic behavior through the whole range of the percentage exposed, while the CO-poisoning results clearly show that almost all the surface atoms exposed are responsible for the catalytic hydrogenation. Thus, these facts lead to two plausible models: a long-range influence caused by the ZrO_2 substrate strongly affects the character of the dispersed metal particles, irrespective of their size, and, alternatively, Pd metal aggregates with a specific morphology are formed on the ZrO_2 surface, thus increasing the fraction of active interface between the metal and the carrier. In a special case, a small fraction of ZrO_2 might be embedded in the crystallites of Pd metal. The latter situation appears to produce noteworthy interaction.

As has been described, the general feature of the Pd/ZrO_2 catalyst was a homogeneous distribution of the active sites over almost the entire surface. However, it was found that the reaction orders with respect to the hydrogen and cyclohexene pressures shifted to 1.0 and 0.1 respectively when the 0.05 wt% Pd/ZrO_2 catalyst was poisoned by adsorbed CO so severely that more than 93% of the catalytic activity was lost. For the reaction on the 0.3 wt% Pd/ZrO_2 catalyst poisoned to the same extent, however, the hydrogen order remained unchanged, though the cyclohexene order was attenuated to 0.35. Although a detailed study will be needed to confirm whether such reaction-order shifts occur gradually with an increase in the amount of adsorbed CO or only in the extreme case of an almost complete deactivation, the almost linear relationships observed in Fig. 3 indicate that the latter is more plausible. The variations in the kinetic behavior are presumably caused by the electronic effect of preadsorbed CO upon the state of palladium-surface atoms rather than by the geometrical blocking of active sites by the CO, so as to put more restriction on the adsorption of hydrogen compared to that of cyclohexene. The finding that the change in the kinetic parameters of the hydrogenation on the catalysts with higher percentages exposed is more prominent gives support to this consideration. It should be noted that the shifts in the kinetic parameters occurred in an opposite direction from those caused by the ZrO_2 substrate. The adsorption of CO on the Pd (111) surface was found to increase the work function by 1.02 eV,[12] indicating an electron transfer from the Pd surface to CO. By taking the present results together with this face into

consideration, we can predict that ZrO_2 works as an electron donor.

In order to confirm this view, it is necessary to examine the effect of added ZrO_2 to Pd upon the catalytic properties, and therefore the analysis of these sytems by X-ray photoelectron spectroscopy seems to be essential. These studies are now in progress by using $Pd+ZrO_2$ dispersed on inactive substrates such as α-Al_2O_3.

References

1) A. D. O. Cinneide and J. K. A. Clarke, *Catal. Rev.*, **7**, 213 (1973).
2) G. A. Somorjai, *Catal. Rev.*, **7**, 1 (1973); *Adv. Catal.*, **26**, 1 (1977).
3) G. M. Schwab, *Adv. Catal.*, **27**, 1 (1978).
4) E. B. Maxted and S. I. Ali, *J. Chem. Soc.*, **1961**, 4137.
5) K. Fujimoto, H. Hashimoto, and T. Kunugi, *J. Jpn. Petrol. Inst.*, **21**, 135 (1978).
6) V. I. Spitsyn, A. A. Balandin, and L. I. Barsova, *Russ. J. Phys. Chem.*, **42**, 184 (1968).
7) A. S. Hussey and G. P. Nowack, *J. Org. Chem.*, **34**, 439 (1969).
8) J. Turkevich, L. Frieman, E. Solomon, and F. M. Wrightson, *J. Am. Chem. Soc.*, **70**, 2638 (1948); J. Turkevich, *Discuss. Faraday Soc.*, **10**, 46 (1951).
9) S. Ohno and I. Yasumori, *Bull. Chem. Soc. Jpn.*, **41**, 2227 (1969).
10) M. Boundart, *Adv. Catal.*, **20**, 153 (1969).
11) E. E. Gonzo and M. Boudart, *J. Catal.*, **52**, 462 (1978).
12) H. Conrad, *Surf. Sci.*, **43**, 462 (1974).

The Gibbs Energies, Enthalpies, and Entropies of the Dilution of Aqueous Sodium Chondroitin-4-sulfate and -6-sulfate

Masakatsu YONESE,* Hideya TSUGE, and Hiroshi KISHIMOTO

Faculty of Pharmaceutical Sciences, Nagoya City University, Tanabe-Dori, Mizuho-ku, Nagoya 467

(Received January 29, 1980)

The osmotic coefficients of a solvent, ϕ, in aqueous solutions of sodium chondroitin-4-sulfate (NaChS-A) with a relatively low molecular weight and -6-sulfate (NaChS-C) with various molecular weight were measured by means of vapor-pressure osmometry. The molar Gibbs energes of dilution, $\Delta_{\mathrm{dil}}G$, were determined from the thermodynamic analysis of the ϕ values. The molar entropies of dilution, $\Delta_{\mathrm{dil}}S$, were calculated through the substitution of the molar dilution enthalpies, $\Delta_{\mathrm{dil}}H$, which had been measured previously, into $\Delta_{\mathrm{dil}}G$. These thermodynamic quantities of dilution were discussed by taking Manning's limiting law into consideration. The concentration and temperature dependencies of the observed $\Delta_{\mathrm{dil}}H$ agreed well quantitatively with those of the electrostatic $\Delta_{\mathrm{dil}}H$ calculated by Manning's limiting law, when the distance between the neighboring charges of the polyion, b, was assumed to be 4.8 Å, whereas the observed $\Delta_{\mathrm{dil}}G$ and $\Delta_{\mathrm{dil}}S$ values did not agree quantitatively with the theoretical ones based on electrostatic interactions. From a comparison of the experimental $\Delta_{\mathrm{dil}}S$ values with the theoretical ones, the non-electrostatic dilution entropy was evaluated and discussed.

Chondroitin-4-sulfate and -6-sulfate, whose repeating units are composed of *N*-acetyl-D-galactosamine-4- and -6-sulfates, together with D-glucuronic acids, respectively, are known to be important components of mammalian connective tissues and are expected to interact specifically with the ions in biological environments according to their polyelectrolyte nature. To elucidate their behavior as biopolyelectrolytes, we have previously investigated their physicochemical properties in simple aqueous solutions with various counter-cations, such as osmotic coefficients,[1] partial molar volumes,[2] and the enthalpies of dilution.[3]

This paper concerns the Gibbs energies, enthalpies, and entropies of the dilution of sodium chondroitin-4-sulfate (NaChS-A) with a relatively low molecular weight and -6-sulfate (NaChS-C) with various molecular weights. The Gibbs energies were determined from the thermodynamic analysis of the osmotic coefficients measured by vapor-pressure osmometry. Since the enthalpies had been measured in a preceding work,[3] the entropies of dilution were calculated through the substitution of the enthalpies into the Gibbs energies. These thermodynamic quantities of dilution were discussed by taking Manning's limiting law[4] into consideration.

Experimental

Materials. Sodium chondroitin-4-sulfate (NaChS-A) was obtained commercially from the Seikagaku Kogyo Co., Ltd. (Tokyo, Japan); its average molecular weight $\overline{M}$, was 2.0×10^4. Four kinds of sodium chondroitin-6-sulfate (NaChS-C) with different molecular weights were used, two of them being commercial ones from the Seikagaku Kogyo Co., Ltd. ($\overline{M}=6.5\times10^4$ and 7.3×10^4), and the others having been offered by the Kaken Yakukako Co., Ltd. (Tokyo. Japan) ($\overline{M}=5.7\times10^4$ and 1.1×10^4). Their molecular weights were determined by viscosity measurements.[5,6] Distilled and deionized water was used for the preparation of aqueous ChS salt solutions.

Osmotic Coefficient. The osmotic coefficients were measured by means of vapor-pressure osmometry using an Hitachi-Perkin-Elmer Model 115 Molecular Weight Apparatus.[1] Aqueous sodium chloride solutions were used as reference solutions, and their osmotic coefficients, ϕ', were obtained from the literature.[7] When the solvent vapor pressure of a reference electrolyte solution is equal to that of a polyelectrolyte solution, the osmotic coefficient of the polyelectrolyte, ϕ, is given by

$$\phi = \frac{\nu' m' \phi'}{\nu_{\mathrm{p}} m_{\mathrm{p}}}, \tag{1}$$

where ν' and ν_{p} are the total numbers of cations and anions produced by the dissociation of NaCl and the polyelectrolyte, and where m' and m_{p} are the molalities of NaCl and the polyelectrolyte respectively. The factors of the denominator, ν_{p} and m_{p}, can be written as follows;

$$\nu_{\mathrm{p}} = Z/Z_{\mathrm{g}} + 1 \tag{2}$$

and;

$$m_{\mathrm{p}} = 2m/Z, \tag{3}$$

where Z, Z_{g}, and m are the stoichiometric charge number per polymer, the charge number of a counter ion, and the molality of the polymer on a repeating unit basis (mol kg^{-1}) respectively. Then,

$$\phi = \frac{\nu' m' \phi'}{(Z/Z_{\mathrm{g}}+1)(2m/Z)}. \tag{4}$$

Results and Discussion

The Osmotic Coefficients of NaChS Salts. Figures 1, 2, and 3 show the linear relationships between the ϕ values and polymer concentrations for various ChS samples at 298.15, 310.15, and 323.15 K respectively. They also show that the ϕ values depend on the polymer molecular weights; that is, higher-molecular-weight samples have smaller ϕ values. However, ϕ seems to approach a definite value with the increase in the molecular weight.

The Calculation of the Gibbs Energies, Enthalpies, and Entropies of Dilution. The molar Gibbs energy of dilution per repeating unit containing two ionized groups, $\Delta_{\mathrm{dil}}G$, from the initial concentration, m_{i}, to the final concentration m_{f}, ($m_{\mathrm{i}} \gg m_{\mathrm{f}}$), can be written as follows;

$$\Delta_{\mathrm{dil}}G = 2(1/Z+1/Z_{\mathrm{g}})RT\ln(a_{\pm,\mathrm{f}}/a_{\pm,\mathrm{i}}) \tag{5-a}$$

$$= 2(1/Z+1/Z_{\mathrm{g}})\,RT\ln\left(\frac{2m_{\mathrm{f}}\gamma_{\pm,\mathrm{f}}/Z}{2m_{\mathrm{i}}\gamma_{\pm,\mathrm{i}}/Z}\right), \tag{5-b}$$

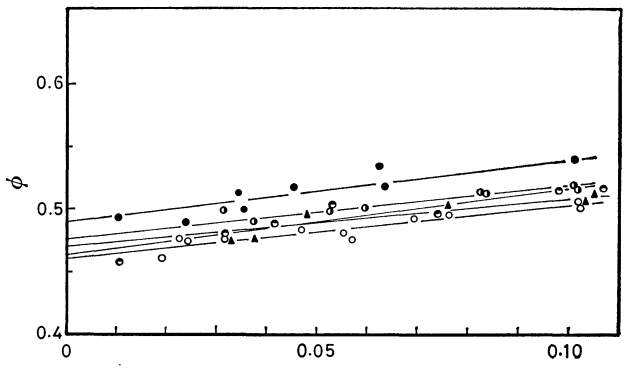

Fig. 1. Osmotic coefficients (ϕ) *vs.* concentration of NaChS-A and -C at 298.15 K.
◑: NaChS-A ($\bar{M}=2.0\times10^4$), ●: NaChS-C ($\bar{M}=1.1\times10^4$), ○: NaChS-C ($\bar{M}=5.7\times10^4$), ▲: NaChS-C ($\bar{M}=6.5\times10^4$), ◓: NaChS-C ($\bar{M}=7.3\times10^4$).

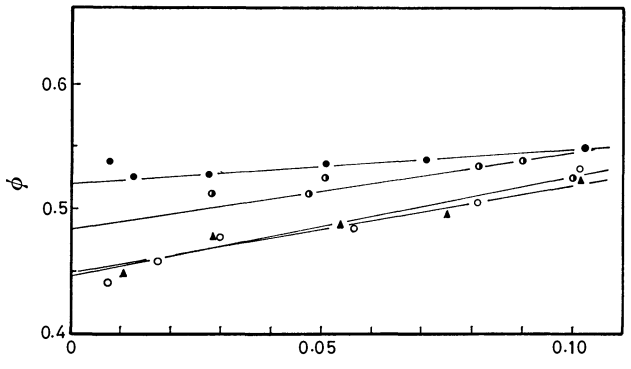

Fig. 2. Osmotic coefficients (ϕ) *vs.* concentration of NaChS-A and -C at 310.15 K.
Symbols are the same as in Fig. 1.

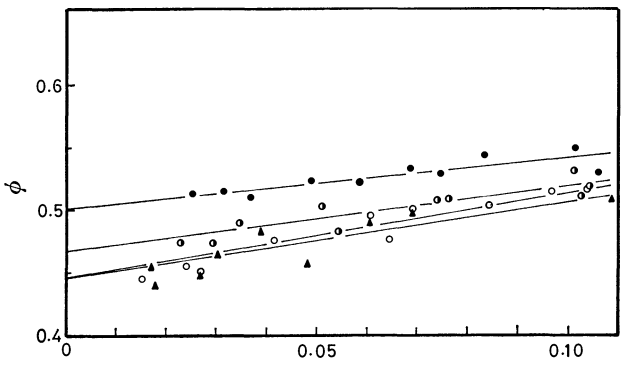

Fig. 3. Osmotic coefficients (ϕ) *vs.* concentration of NaChS-A and -C at 323.15 K.
Symbols are the same as in Fig. 1.

where $a_\pm$ and $\gamma_\pm$ are the mean activity and the mean activity coefficient of a polyelectrolyte respectively. To obtain $\Delta_{dil}G$ from the relation between m and ϕ, the mean activity coefficients in Eq. 5-b were calculated by means of the Gibbs-Duhem equation:

$$\ln(\gamma_{\pm,f}/\gamma_{\pm,i}) = (\phi_f-\phi_i) + 2\int_{m_f}^{m_i}\frac{1-\phi}{\sqrt{m}}d\sqrt{m}. \quad (6)$$

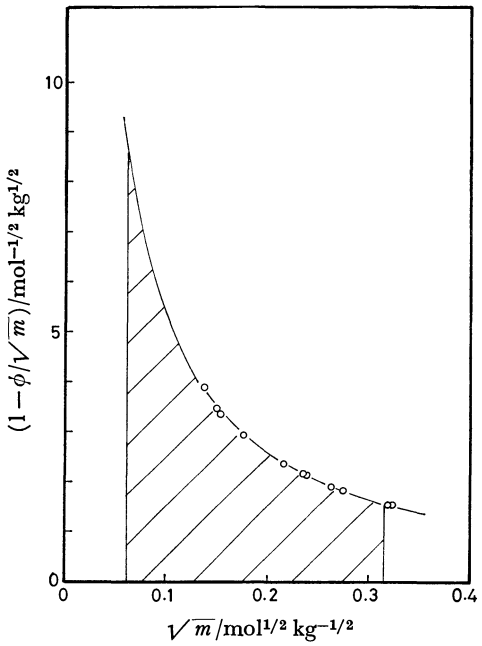

Fig. 4. Graphic integration of Eq. 3 at 310.15 K.
Sample: NaChS-C ($\bar{M}=1.1\times10^4$).

In calculating $\int_{m_f}^{m_i}\frac{1-\phi}{\sqrt{m}}d\sqrt{m}$ by graphic integration, the relations between ϕ values and m were assumed to be linear for the extrapolation of ϕ to the lower-m region. An example of the graph for integration is shown in Fig. 4.

When the experimental results of the molar dilution enthalpies per repeating unit, $\Delta_{dil}H$, in the previous paper[3] are used with the $\Delta_{dil}G$ thus obtained, the molar entropies of dilution, $\Delta_{dil}S$, can be obtained from Eq. 7:

$$\Delta_{dil}S = (-\Delta_{dil}G+\Delta_{dil}H)/T. \quad (7)$$

Table 1 shows $\Delta_{dil}G$, $\Delta_{dil}H$, and $\Delta_{dil}S$ values from $m_i=0.10$ and 0.08 mol kg^{-1} to $m_f=3.85\times10^{-3}$ mol kg^{-1}. These quantities can be divided into non-electrostatic and electrostatic terms, as expressed by Eq. 8.[3,8] The former is the contribution from the dilution of a polyelectrolyte solution in a hypothetical reference state in which all the ions are discharged and is indicated by the superscript "o," while the latter is the contribution from the electrostatic interaction of polyions with counterions and is indicated by the superscript "el."

$$\Delta_{dil}G = \Delta_{dil}G^{el} + \Delta_{dil}G^{o} \quad (8\text{-a})$$

$$\Delta_{dil}H = \Delta_{dil}H^{el} + \Delta_{dil}H^{o}, \quad (8\text{-b})$$

and

$$\Delta_{dil}S = \Delta_{dil}S^{el} + \Delta_{dil}S^{o}. \quad (8\text{-c})$$

According to Manning's limiting law, $\Delta_{dil}G^{el}$, $\Delta_{dil}H^{el}$, and $\Delta_{dil}S^{el}$ per mol of the repeating disaccharide unit can be evaluated as follows in the case of $\xi\geq1.0$:[3]

$$\Delta_{dil}G^{el} = -(RT/\xi)\ln(m_i/m_f) \quad (9\text{-a})$$

$$\Delta_{dil}H^{el} = (RT/\xi)\left(1+\frac{Td\varepsilon}{\varepsilon dT}\right)\ln(m_i/m_f), \quad (9\text{-b})$$

and

TABLE 1. THE VALUES OF $\Delta_{dil}G$, $\Delta_{dil}H$, AND $\Delta_{dil}S$ FOR NaChS-A AND -C

	Sample	$\bar{M}$	298.15 K	310.15 K	323.15 K
$\Delta_{dil}G$/kJ mol^{-1}	NaChS-A	2.0×10^4	−8.25	−8.80	−8.86
			−7.59	−8.09	−8.14
	NaChS-C	1.1×10^4	−8.65	−9.25	−9.37
			−7.97	−8.56	−8.65
		5.7×10^4	−7.69	−8.30	−8.59
			−7.09	−7.60	−7.87
		6.5×10^4	−8.06	−8.63	−8.67
			−7.48	−7.88	−7.96
		7.3×10^4	−7.97	—	—
			−7.32	—	—
$\Delta_{dil}H$/kJ mol^{-1}	NaChS-A	2.0×10^4	−1.69	−2.59	−3.00
			−1.79	−2.76	−2.62
	NaChS-C	1.1×10^4	−1.58	−2.59	−2.57
			−1.83	—	−2.23
		5.7×10^4	−1.84	−2.86	−2.87
			−1.85	—	−2.57
$\Delta_{dil}S$/J mol^{-1} K^{-1}	NaChS-A	2.0×10^4	22.0	20.0	18.1
			19.5	17.2	17.1
	NaChS-C	1.1×10^4	23.7	21.5	21.0
			20.6	—	19.9
		5.7×10^4	19.6	17.5	17.7
			17.6	—	16.4

The upper values for each sample: $m_i=0.10$ mol kg^{-1}. The lower values for each sample: $m_i=0.08$ mol kg^{-1}. $m_f=3.85\times10^{-3}$ mol kg^{-1}.

$$\Delta_{dil}S^{el} = (2R/\xi)\left(1+\frac{T\mathrm{d}\varepsilon}{2\varepsilon\mathrm{d}T}\right)\ln(m_i/m_f), \qquad (9\text{-c})$$

where R is the gas constant, T is the absolute temperature, ε is the permittivity of the solvent (water), and ξ is the charge density parameter, which is defined by:

$$\xi = e^2/4\pi\varepsilon kTb, \qquad (10)$$

where e is the elementary charge, k is the Boltzmann constant, and b is the distance between the neighboring charges of a polyion.

In a preceding paper,[3] treating the dilution enthalpy of NaChS, we assumed implicitly that the non-electrostatic enthalpy of dilution, $\Delta_{dil}H^{\circ}$, is negligible; then, so as to fit the theoretical values obtained from Eq. 9-b with the experimental $\Delta_{dil}H$ values over as wide range of temperatures and concentrations as possible, we selected $b=4.8$ Å, which was in agreement with the value estimated from the X-ray diffraction measurement of NaChS film. The fit between the experimental $\Delta_{dil}H$ and theoretical $\Delta_{dil}H^{el}$ values at 298.15 K is illustrated in Fig. 5. In this paper, we continued to use 4.8 Å as b for the reason mentioned above and calculated the values of $\Delta_{dil}G^{el}$ and $\Delta_{dil}S^{el}$ from the initial concentration, *i.e.*, 0.10 and 0.08 mol kg^{-1}, to the final concentration of 3.85×10^{-3} mol kg^{-1} at various temperatures, using Eqs. 9-a and -c. The results are tabulated in Table 2, along with the $\Delta_{dil}H^{el}$ values calculated in the preceding paper.

The Evaluation of Non-electrostatic Terms. By substituting the above-mentioned electrostatic quantities, which were evaluated according to Manning's law, and the experimental over-all quantities of dilution into Eqs. 8-a, -b, and -c, we obtained the non-

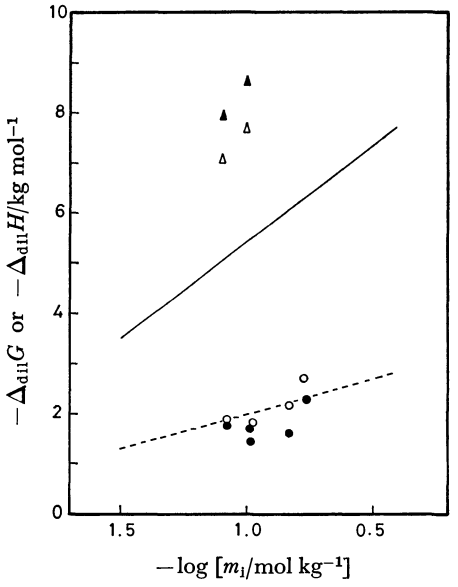

Fig. 5. $\Delta_{dil}G$ and $\Delta_{dil}H$ estimated from the Manning's limiting law for NaChS-C having two different molecular weights at 298.15 K.
△: Observed $\Delta_{dil}G$ ($\bar{M}=5.7\times10^4$), ▲: observed $\Delta_{dil}G$ ($\bar{M}=1.1\times10^4$), ○: observed $\Delta_{dil}H$ ($\bar{M}=5.7\times10^4$), ●: observed $\Delta_{dil}H$ ($\bar{M}=1.1\times10^4$), ——: $\Delta_{dil}G^{el}$ calculated from Eq. 9-a, – – – –: $\Delta_{dil}H^{el}$ calculated from Eq. 9-b.

electrostatic contributions of dilution, $\Delta_{dil}G^{\circ}$ and $\Delta_{dil}S^{\circ}$, shown in the upper and middle sections of Table 3. Also, the values of $\Delta_{dil}S^{\circ}$ can be calculated from $-\Delta_{dil}G^{\circ}/T$ when $\Delta_{dil}H^{\circ}$ is considered to be zero. The values thus calculated, as tabulated in the lower section of Table 3, reflect only the difference in experimental ϕ or $\Delta_{dil}G$ values between samples of different molecular weights, while the values in the middle column involve additionally the differences in the experimental $\Delta_{dil}H$ between different samples.

Next, we will examine the effect of polymer-chain

Table 2. The values of $\Delta_{dil}G^{el}$, $\Delta_{dil}H^{el}$, and $\Delta_{dil}S^{el}$, as calculated from Manning's limiting law

	298.15 K	310.15 K	323.15 K
$\Delta_{dil}G^{el}$/kJ mol^{-1}	−5.43	−5.60	−5.68
	−5.06	−5.18	−5.29
$\Delta_{dil}H^{el}$/kJ mol^{-1}	−2.02	−2.44	−2.90
	−1.90	−2.27	−2.70
$\Delta_{dil}S^{el}$/J mol^{-1} K^{-1}	11.4	10.1	8.6
	10.6	9.4	8.0

The distance between the neighboring charges of the polyion, b, is 4.8 Å. The upper values: $m_i=0.10$ mol kg^{-1}. The lower values: $m_i=0.08$ mol kg^{-1}. $m_f=3.85\times10^{-3}$ mol kg^{-1}.

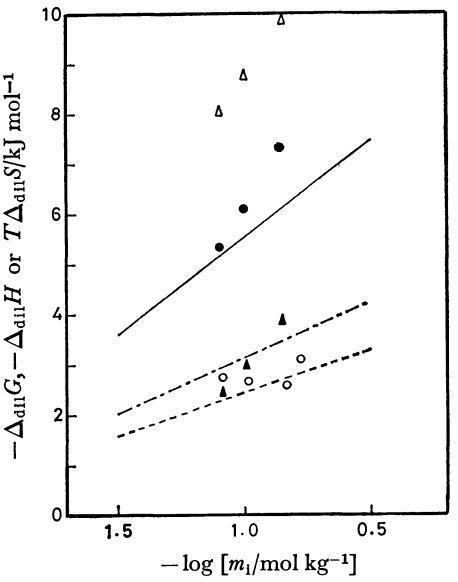

Fig. 6. Thermodynamic quantities of dilution of NaChS-A at 310.15 K.
△: Observed $\Delta_{dil}G$, ○: observed $\Delta_{dil}H$, ●: $T\Delta_{dil}S$ calculated from Eq. 7, ▲: $T\Delta_{dil}S^{\circ}$ calculated from Eqs. 7,8-c, and 9-c, ——: $\Delta_{dil}G^{el}$ calculated from Eq. 9-a, ----: $\Delta_{dil}H^{el}$ calculated from Eq. 9-b, —·—: $T\Delta_{dil}S^{el}$ calculated from Eq. 9-c.

Table 3. The values of $\Delta_{dil}G^{\circ}$ and $\Delta_{dil}S^{\circ}$ for NaChS-A and -C

	Sample	$\overline{M}$	298.15 K	310.15 K	323.15 K
$\Delta_{dil}G^{\circ}$/kJ mol^{-1}	NaChS-A	2.0×10^4	−2.82	−3.20	−3.18
			−2.53	−2.91	−2.84
	NaChS-C	1.1×10^4	−3.22	−3.69	−3.69
			−2.91	−3.38	−3.36
		5.7×10^4	−2.26	−2.74	−2.91
			−2.03	−2.42	−2.58
		6.5×10^4	−2.63	−3.07	−2.98
			−2.42	−2.71	−2.67
		7.3×10^4	−2.54	—	—
			−2.27	—	—
$\Delta_{dil}S^{\circ}$/J mol^{-1} K^{-1} a)	NaChS-A	2.0×10^4	10.6	9.9	9.5
			8.9	7.8	9.1
	NaChS-C	1.1×10^4	12.3	11.4	12.4
			10.0	—	11.9
		5.7×10^4	8.2	7.4	9.1
			7.0	—	8.4
$\Delta_{dil}S^{\circ}$/J mol^{-1} K^{-1} b)	NaChS-A	2.0×10^4	9.5	10.4	9.8
			8.5	9.4	8.8
	NaChS-C	1.1×10^4	10.8	11.9	11.4
			9.8	10.9	10.4
		5.7×10^4	7.6	8.8	9.0
			6.8	7.8	3.0
		6.5×10^4	8.8	9.9	9.2
			8.1	8.7	8.3
		7.3×10^4	8.5	—	—
			7.6	—	—

The upper values for each sample: $m_i=0.10$ mol kg^{-1}. The lower values for each sample: $m_i=0.08$ mol kg^{-1}. $m_f=3.85\times10^{-3}$ mol kg^{-1}. a) Calculated from Eqs. 7 and 8-c. b) Calculated by assuming $\Delta_{dil}H=\Delta_{dil}H^{el}$ or $\Delta_{dil}S^{\circ}=-\Delta_{dil}G^{\circ}/T$.

length on these thermodynamic quantities. As may be seen in Table 1, the polymers with lower molecular weights have larger values of $-\Delta_{dil}G$ and $\Delta_{dil}S$ than the higher-molecular-weight polymers. As compared with the differences in $-\Delta_{dil}G$ and $\Delta_{dil}S$ between samples of different molecular weights seems to be negligible. Therefore, the magnitudes of electrostatic $\Delta_{dil}H^{el}$, $\Delta_{dil}G^{el}$, and $\Delta_{dil}S^{el}$ can be considered to be approximately invariant with the change in the chain length of the polymer. This situation explains the agreements between the corresponding values of $\Delta_{dil}S^{\circ}$ in the middle and lower sections of Table 3. After all, the effects of the chain length on various thermodynamic quantities can be concentrated in $\Delta_{dil}S^{\circ}$. The discussion of $\Delta_{dil}G^{\circ}$ can, then, be reduced to that of $\Delta_{dil}S^{\circ}$. The values of $\Delta_{dil}S^{\circ}$ increase significantly with the decrease in the chain length in Table 3. We cannot explain it clearly in this stage, but can only suggest that the effect of the chain length on $\Delta_{dil}S^{\circ}$ is attributable to the problem of the conformation of ChS. With respect to the value of $\Delta_{dil}S^{\circ}$ of a sufficiently long chain, the discussion is very important because of the comparatively large value of $\Delta_{dil}S^{\circ}$ in $\Delta_{dil}G^{\circ}$. However, in order to elucidate the nature of $\Delta_{dil}S^{\circ}$ more clearly, the structural study of ChS in solution, including that of the solvent, is considered to be necessary.

References

1) M. Yonese, H. Tsuge, and H. Kishimoto, *Nippon Kagaku Kaishi*, **1978**, 108.
2) H. Tsuge, M. Yonese, and H. Kishimoto, *Nippon Kagaku Kaishi*, **1978**, 609.
3) H. Tsuge, M. Yonese, and H. Kishimoto, *Bull. Chem. Soc. Jpn.*, **52**, 2846 (1979).
4) G. S. Manning, *J. Chem. Phys.*, **51**, 924 (1969).
5) M. B. Mathews, *Arch. Biochim. Biophys.*, **61**, 367 (1956).
6) M. Nakagaki and K. Ikeda, *Bull. Chem. Soc. Jpn.*, **41**, 555 (1968).
7) R. A. Robinson, and R. H. Stokes, "Electrolyte Solutions," Butterworths, London (1959), p. 481.
8) G. E. Boyd and D. P. Wilson, *J. Phys. Chem.*, **80**, 805 (1976).
9) S. Arnott, J. M. Guss, D. W. L. Hukins, and M. B. Mathews, *Science*, **180**, 743 (1973).
10) D. H. Isaac, and E. D. T. Atkins, *Nature (London), New Biol.*, **244**, 252 (1973).

Studies of the Generation of Excited Singlet Products in the Oxidation of the -CO-CH- Containing Molecules. The Chemiluminescence of Acylcarbazoles

Isao KAMIYA* and Takashi SUGIMOTO

Department of Chemistry, College of General Education, Nagoya University, Chikusa-ku, Nagoya 464

(Received February 19, 1980)

Direct chemiluminescence emissions have been found from the air oxidation of 3-acyl-9-methyl- (**1**), 3,6-diacyl-9-methyl- (**2**), and 9-acylcarbazoles (**3**) due to the generation of an excited singlet state of monocarboxylate ions (from **1** and **2**) and the carbazole anion (from **3**). The relative intensities *vs.* the reaction time for the luminescent reaction of 3-isobutyryl-9-methylcarbazole could be interpreted by a reaction scheme involving consecutive reactions. Using this reaction scheme, the values of the decomposition rate of intermediates at 30, 40, and 50 °C were determined to be 0.19, 0.42, and 0.98 min^{-1} respectively, which were comparable to the values reported for the decomposition rates of isolated dioxetanes giving excited singlet products.

In the course of our studies, we have established the generation of excited triplet carbonyl products from the air oxidation of various simple ketones with a -CO-CH- group, such as 3-methyl-2-butanone and isopropyl phenyl ketone in alkaline aprotic solvents.[1] We further succeeded in observing the direct chemiluminescence (CL) due to the generation of excited singlet products in the air oxidation of such -CO-CH- containing molecules as 9,10-diisobutyrylanthracene and 9,10-dipropionylanthracene.[2] For the luminescent reaction of the -CO-CH- containing molecules (simple ketones and diacylanthracenes), a reaction pathway involving the cleavage of a dioxetane intermediate was discussed as a possible mechanism.

Two different paths have been reported for the thermolysis of isolated dioxetanes. Simple dioxetanes decompose by homolytic cleavage to afford excited products, mainly in triplet states.[3] On the other hand, complex dioxetanes, which give high yields of excited singlet products, decompose by means of the intermolecular electron-transfer mechanism,[4] which is conceptually similar to the CIEEL mechanism.[5]

Thus, it seems likely that the difference in the state of the excited products is due to the different decomposition paths of the dioxetane intermediates: one (produced from simple ketones) gives an excited triplet product, and the other (from diacylanthracenes), an excited singlet product.

In order to test the validity of, and to broaden the scope of, the luminescent reaction mechanism, we have further examined some acylcarbazoles which contain the -CO-CH- group and a fluorescence moiety for the direct CL by air oxidation under the same experimental conditions. In the present paper, we will report the CL emission features observed from the acylcarbazoles and the kinetic evidence for the reaction path involving a dioxetane intermediate in the luminescent reaction of 3-isobutyryl-9-methylcarbazole.

Results and Discussion

3-Acyl-9-methylcarbazoles. When 0.2 cm^3 of a solution of potassium *t*-butoxide (*t*-BuOK) in *t*-butyl alcohol (2×10^{-2} mol dm^{-3}) was added to 2 cm^3 of an aerated solution of 3-isobutyryl-9-methylcarbazole (**1a**) in *N,N*-dimethylformamide (DMF) or dimethyl sulfoxide (DMSO) (1.0×10^{-4} mol dm^{-3}), there appeared a CL emission in the UV region. The CL spectrum measured in a DMF solution had a peak at 370 nm; thus, it was similar to the fluorescence spectrum of the 9-methylcarbazole-3-carboxylate ion (**4**), one of the reaction products, measured in an alkaline DMF solution, as is shown in Fig. 1. Even when the concentration of **1a** was raised to 1.0×10^{-3} mol dm^{-3}, no change in the spectral distribution was observed (*cf*, 3,6-diisobutyryl-9-methylcarbazole below).

9-Methyl-3-propionylcarbazole (**1b**) and 3-acetyl-9-methylcarbazole (**1c**) also exhibited similar CL emissions. However, the carbazole **1b** showed a weaker emission with an intensity one 30th of that from **1a**, and **1c** the weakest (one 1000th). These results indicate that the intensity of the CL emission is much affected by the nature of the C-H bond adjacent to the carbonyl group; it increases in the order of primary<secondary<tertiary. The order of the CL intensity is consistent with those observed in simple ketones and diacylanthracenes. The following reaction scheme, involving the cleavage of a dioxetane intermediate which is produced by the oxygenation of the anion formed by the loss of a proton from the

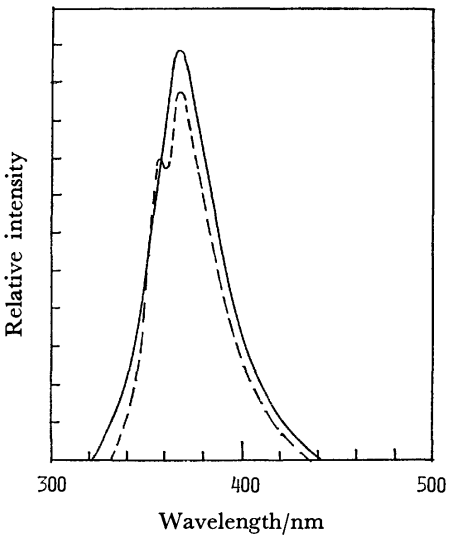

Fig. 1. Chemiluminescence spectrum of **1a** in DMF (solid curve), and fluorescence spectrum of **4** measured in an alkaline DMF solution (broken curve).

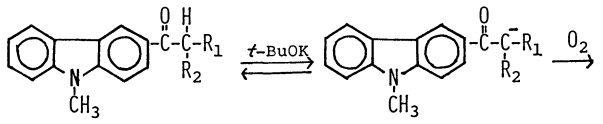

1a : $R_1 = R_2 = CH_3$
1b : $R_1 = CH_3$, $R_2 = H$
1c : $R_1 = R_2 = H$

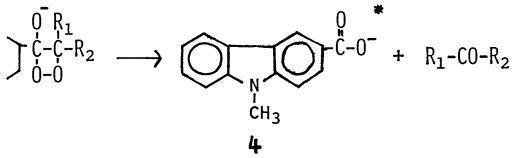

4

α-carbon atom, seems plausible in explaining the emission feature and the emitting product, **4**.

Recently, an intense CL emission arising from the base-induced oxidation of 3-(alkoxycarbonylamino)-benzofuran-2(3*H*)-ones, which contain a –CO–CH– group, has been reported by Lofthouse *et al.*, who also proposed an analogous reaction scheme involving a dioxetane intermediate for the luminescent reaction.[6]

The change in the concentrations of the reactant, **1a**, and the product, **4**, with the reaction time at 30, 40, and 50 °C in the luminescent DMF system [2 cm^3 of a **1a** solution in DMF (1.0×10^{-4} mol dm^{-3}) + 0.2 cm^3 of a *t*-BuOK solution in *t*-butyl alcohol (2×10^{-2} mol dm^{-3})], as measured by high-performance liquid chromatography, are illustrated in Figs. 2a, 2b, and 2c respectively.[7] Each figure shows that the concentration of **1a**, [**1a**], decreases rapidly to a certain value [**1a**]$_\infty$; thereafter, it is kept almost constant because of the extremely slow decrease, probably due to the consumption of *t*-BuOK and dissolved oxygen. In the rapid decay stage, the plots of log ([**1a**]—[**1a**]$_\infty$) *vs.* the reaction time (t) being almost straight lines, the decomposition of **1a** was found to obey a pseudo-first-order reaction with respect to ([**1a**]—[**1a**]$_\infty$), although a slight deviation arose at the final decay stage. From the slopes of the lines, the apparent rate constants (k) at 30, 40, and 50 °C were determined to be 0.22, 0.26, and 0.43 min^{-1} respectively.

The change in the relative intensities of the CL emission (I_R) with the reaction time, measured under the same experimental conditions, are illustrated by a solid curve in each of figures (2a—2c), where the values of I_R are taken to be normal at the maximum intensity. The figure of the emission curve suggests very strongly that the luminescent reaction arises from the following kinetic scheme involving consecutive reactions:

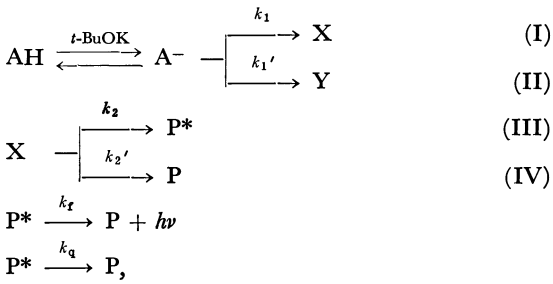

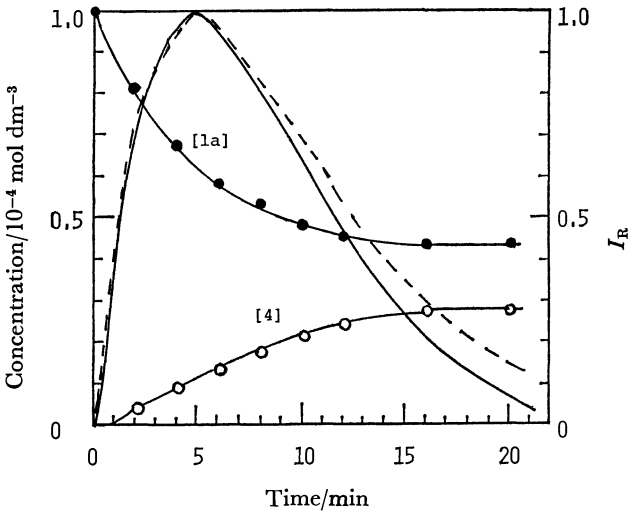

Fig. 2a. Changes in the concentrations of **1a** ([**1a**]) and **4** ([**4**]) with reaction time (t) in DMF at 30 °C, and relative intensities of CL emission (I_R) *vs.* t: observed I_R, solid curve; calculated I_R, broken curve.

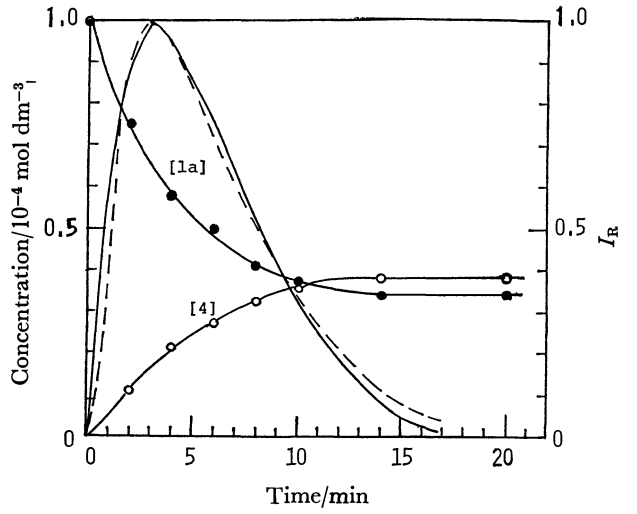

Fig. 2b. Changes in [**1a**] and [**4**], and I_R-t curves in DMF at 40 °C.

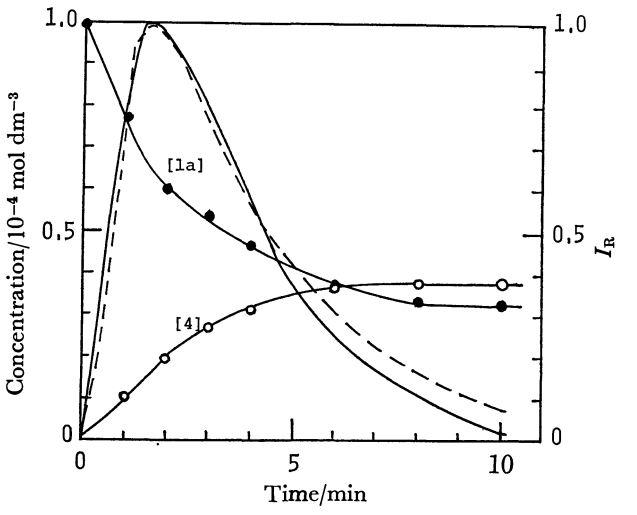

Fig. 2c. Changes in [**1a**] and [**4**], and I_R-t curves in DMF at 50 °C.

where AH=**1a**, X=dioxetane intermediate, Y=other product, and P=**4**.

Assuming that competitive decomposing reactions (III and IV) obey the first-order reaction,[8] and recalling the finding that the competitive reactions of I and II also obeyed a pseudo-first-order reaction with respect to ([AH]−[AH]∞), we can write the CL intensity (I) at the initial stage as:

$$I = k_1k_2\Phi_f\{([AH]_0-[AH]_\infty)/(k_d-k)\} \times\{\exp(-kt)-\exp(-k_dt)\}$$
$$= \alpha\beta\Phi_f([AH]_0-[AH]_\infty)\{kk_d/(k_d-k)\} \times\{\exp(-kt)-\exp(-k_dt)\}, \quad (1)$$

where $[AH]_0$ is the initial concentration of **1a**, $k_1+k'_1=k$, $k_2+k'_2=k_d$, $\alpha=k_1/k$, $\beta=k_2/k_d$, and $\Phi_f=k_f/(k_f+k_q)$. Putting t_m as the time required to reach the maximum of $I(I_m)$, we can derive the following equations:

$$k_d\exp(-k_dt_m) = k\exp(-kt_m), \quad (2)$$

and:

$$I_m = \alpha\beta\Phi_f([AH]_0-[AH]_\infty)\{kk_d/(k_d-k)\} \times\{\exp(-kt_m)-\exp(-k_dt_m)\}.$$

Therefore,

$$I_R = I/I_m = \{\exp(-kt)-\exp(-k_dt)\}/ \{\exp(-kt_m)-\exp(-k_dt_m)\}.$$

From the CL emission curves shown in Figs. 2a—2c, t_m being found to be 5.0, 3.0, and 1.5 min at 30, 40, and 50 °C respectively, the values of k_d at these temperatures can be calculated from Eq. 2 to be 0.19, 0.42, and 0.98 min^{-1} using the values of k determined above.

Taking the values of k, k_d, and t_m, we can calculate the values I_R by means of the following numerical equations:

30 °C; $I_R = \{\exp(-0.22t)-\exp(-0.19t)\}/ \{\exp(-0.22\times5)-\exp(-0.19\times5)\}$
$= \{\exp(-0.22t)-\exp(-0.19t)\}/(-0.054)$

40 °C; $I_R = \{\exp(-0.26t)-\exp(-0.42t)\}/0.174$

50 °C; $I_R = \{\exp(-0.43t)-\exp(-0.98t)\}/0.295$.

The dotted curves in Figs. 2a—2c illustrate the curves of I_R *vs.* t calculated from the above equations. The curves of I_R thus calculated are in fairly good agreement with those of the observed I_R values (solid curves) at these temperature except at the final stage, where the reactions of I and II obey the first-order reaction no longer.

It should be noted that the values of k_d (for example, 0.42 $min^{-1}=7.0\times10^{-3}$ s^{-1} at 40 °C) are comparable to the values reported for the decomposition rates of isolated dioxetanes (6.5×10^{-3} s^{-1} for the **7** dioxetane in DMF at 25 °C,[9a] 7.6×10^{-3} s^{-1} for **8** in benzene at 65 °C,[9b] 4.6×10^{-3} s^{-1} for **9** in CH_2Cl_2 at 25 °C,[9c] and 2.96×10^{-3} s^{-1} for **10** in decane at 79 °C[9d]).[10]

The activation energy for the decomposition of X (the competitive reactions of II and IV) was estimated to be 68 kJ mol^{-1} from the Arrhenius plot of k_d.

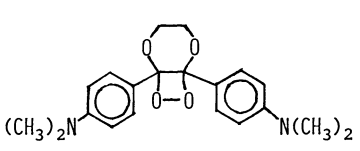

7 8

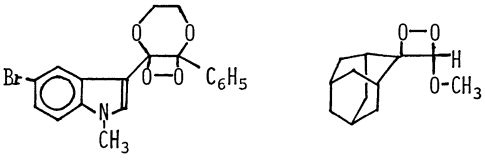

9 10

Analogous values have been obtained for the decomposition of dioxetanes (82.4 kJ mol^{-1} for **7** and 87.9 kJ (21 kcal) mol^{-1} for **8**[9a,9b]).

Using the value of 1.28×10^{-2} proposed by Lee *et al.*[11] for the efficiency of the CL emission from a standard luminol solution in DMSO (1.26×10^{-6} mol dm^{-3}), the efficiencies of CL from the **1a** solution in DMF [Φ_{CL}=quantity of total light (mol) emitted from 1 dm^3 of the solution/([AH]$_0$−[AH]$_\infty$)] at 30, 40, and 50 °C were determined to be 3.5×10^{-4}, 4.2×10^{-4}, and 5.7×10^{-4} respectively from the ratio of the total light emitted from the luminol solution to the total measured light from the **1a** solution.[12] From Eq. 1, Φ_{CL} can be written as:

$$\Phi_{CL} = \int I dt/([AH]_0-[AH]_\infty) = \alpha\beta\Phi_f.$$

The value of $\alpha=k_1/(k_1+k'_1)$ is given by [**4**]∞ (the final concentration of **4**)/([AH]$_0$−[AH]∞) and was found to be almost unchanged in the temperature range between 30 °C and 50 °C, since the values of [**4**]∞/([**1a**]$_0$−[**1a**]∞) were obtained to be 0.51, 0.58, and 0.57 at 30, 40, and 50 °C respectively. As Φ_f is not so varied with the temperature, the effect of the temperature on Φ_{CL} may be mainly attributed to the temperature dependence of β ($=k_2/(k_2+k'_2)$, which is itself presumably due to the difference in activation energy between the reaction of III (k_2) and the reaction of IV (k_2'),[13] since there has been found a difference in activation energy between a higher-energy path leading to an excited product and a lower-energy path leading to a product in a grand state in the decomposition of dimethyldioxetane.[14]

3,6-Diacylcarbazoles. 3,6-Diisobutyryl-9-methylcarbazole (**2a**) also gave rise to CL emission with an intensity comparable to that from **1a**. Figures 3a and 3b illustrate the changes in the spectral distribution with the reaction time observed when 0.2 cm^3 of *t*-BuOK solution in *t*-butyl alcohol (2×10^{-2} mol dm^{-3}) was added to 2 cm^3 of **2a** solution in DMSO in two different concentrations (1.0×10^{-3} mol dm^{-3} and 1.0×10^{-4} mol dm^{-3}). The figures indicate that the spectrum of the CL emission from **2a** varies during the course of the reaction. In a solution with a high **2a** concentration, the apparent emission was, at the initial stage, composed of one intense peak at 440 nm with a spectral distribution similar to that of the fluorescence of **2a**. During the course of the reaction,

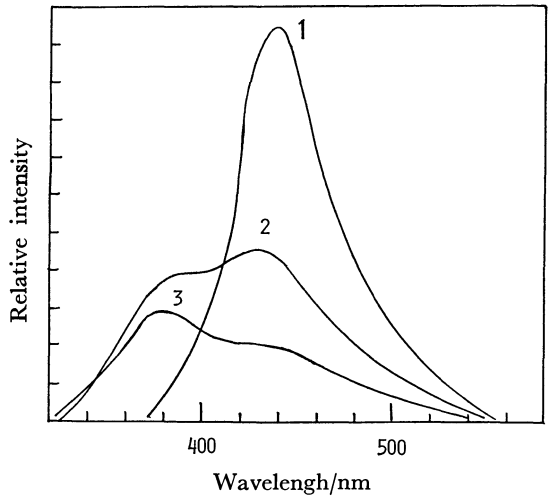

Fig. 3a. Change of CL spectrum of **2a** with reaction time in a DMSO solution of high **2a** concentration (1.0×10^{-3} mol dm^{-3}).
1→2→3.

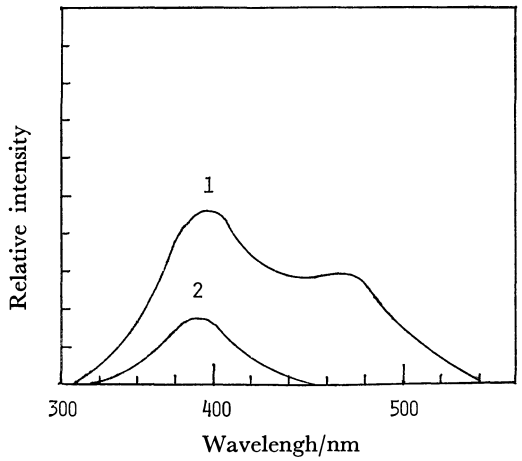

Fig. 3b. Change of CL spectrum of **2a** with reaction time in a DMSO solution of low **2a** concentration (1.0×10^{-4} mol dm^{-3}). 1→2.

the intensity of the peak gradually decreased with a blue shift, and simultaneously a new peak appeared at about 370 nm. In a solution with a low **2a** concentration, the spectrum had two peaks at the initial stage; these peaks also varied with a blue shift until only one peak, at 370 nm, was observed. Thus, it seems likely that a portion of the excited product emits UV light (370 nm), while the other portion of the excited product transfers energy to unoxidized **2a**, thereby exciting **2a** to emit fluorescence (440 nm).

9-Methyl-3,6-dipropionylcarbazole, whose C–H bond adjacent to the carbonyl group is secondary, showed a much weaker emission than **2a**, and 3,6-diacetyl-9-methylcarbazole, which possesses a primary C–H bond, exhibited a very weak emission. From the finding that the emission from the exctied product showed a peak at 370 nm, it seems likely that excited singlet 3-acyl-9-methylcarbazole-6-carboxylate ions (**5**) are generated from the air oxidation by the same mechanism as that proposed for **1a**. In the reaction systems, **5** may be successively oxidized, since the final product was the 9-methylcarbazole-3,6-dicarboxylate ion, which showed a greenish fluorescence with a peak at 450 nm. However, it seems unlikely that the CL emission arises from the oxidation of **5**, since no emission peak at 450 nm was observed in the luminescent reactions.

3,6-Diisobutyrylcarbazole and the lower homologues gave an oxidation product which showed fluorescence with a peak at 470 nm, but an extremely weak emission was observed from its oxidation. This is probably because the luminescent reaction is debased by competitive processes brought about by the hydrogen atom at the 9-position of the carbazole. A similar debasement has been oberved in the oxidation of 9-isobutyrylanthracene.[2]

9-Acylcarbazoles. 9-Isobutyrylcarbazole (**3a**) and 9-propionylcarbazole (**3b**) exhibited CL emission with intensities one 50th of those from **1a** and **2a**. An extremely weak emission was exhibited by 9-acetylcarbazole (**3c**). The spectrum of the fluorescence from the spent reaction solution in DMSO, as measured with exciting at 340 nm, and the roughly estimated spectral distribution of the CL emission from **3a** (because of low intensity) are illustrated in Fig. 4, together with the fluorescence spectrum of

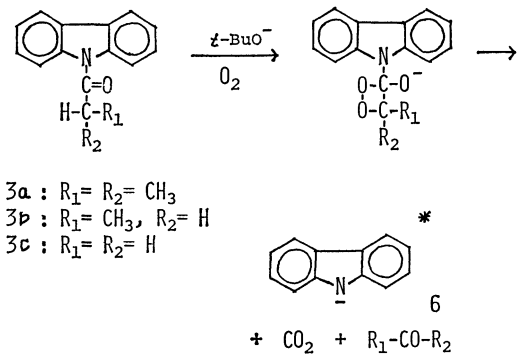

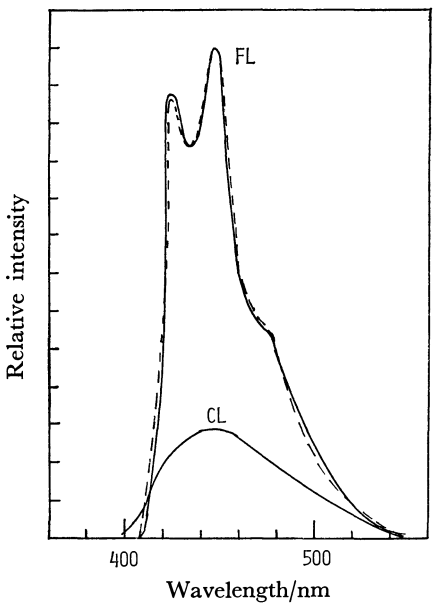

Fig. 4. Spectral distribution of CL emission from **3a** (CL), fluorescence spectrum of the spent reaction solution (FL), and fluorescence spectrum of **6** measured in an alkaline DMSO solution (broken curve).

the carbazole anion (**6**) measured in an alkaline DMSO solution with exciting at 340 nm. The figure shows that the CL spectrum is analogous to the fluorescence of the product, which is very similar to the fluorescence of **6**. Carbazole was isolated, and acetone was also obtained as 2,4-dinitrophenylhydrazone from the oxidation products. These results are interpreted by the reaction scheme shown in the previous page, leading to the generation of an excited-singlet carbazole anion *via* a dioxetane intermediate.

Summarizing the results of the present study, we conclude that excited-singlet products are surely generated in the air oxidation of molecules containing a –CO–CH– group and a fluorescence moiety in alkaline aprotic solvents. The emission features and emitting products generated by oxidation suggest that dioxetanes may be the critical intermediates in giving excited-singlet products. Work is now in progress to search for other –CO–CH– containing molecules which exhibit CL in high yields.

Experimental

The elemental analyses were conducted at the Analytical Section, Meijo University, Nagoya.

*The Preparation of 3-Acyl-9-methylcarbazoles (**1a—c**).* Aluminium chloride (11.0 g) was added, in small portions, into a vigorously stirred solution of 9-methylcarbazole[15] (15.0 g) and isobutyryl chloride (11.0 g) in benzene (300 cm^3) at 5—8 °C over a 30-min period. The mixture was stirred at that temperature for an additional 30 min and then at 25—30 °C for 24 h. Thereafter the mixture was poured onto crushed ice (400 g). The benzene layer, after being separated from the aqueous solution, was participated by water, aqueous sodium hydrogencarbonate, and water as usual. The benzene solution was concentrated to about 50 cm^3 and placed in a silica-gel column (Wako Gel C-100, 5×45 cm). The column was eluted first by a 1:1 mixture of benzene and hexane (1.5 dm^3) to remove the unchanged starting material. The column was then eluted by benzene. The subsequent evaporation of the eluate gave an oily residue, which was crystallized from ethanol to give colorless needles (45% yield) of 3-isobutyryl-9-methylcarbazole (**1a**); mp 64.5—66 °C (from ethanol) (Found: C, 81.56; H, 6.69; N, 5.43%. Calcd for $C_{17}H_{17}NO$: C, 81.24; H, 6.82; N, 5.57%).

Similar treatments of 9-methylcarbazole with propionyl chloride or acetyl chloride gave, respectively, 9-methyl-3-propionylcarbazole (**1b**) [25% yield, mp 83.5—84.5 °C (from ethanol) (Found: C, 80.73; H, 6.17; N, 5.75%. Calcd for $C_{16}H_{15}NO$: C, 80.98; H, 6.37; N, 5.90%)] and 3-acetyl-9-methylcarbazole (**1c**) [50% yield, mp 99—100 °C (from methanol) (Found: C, 80.86; H, 5.70; N, 6.09%. Calcd for $C_{15}H_{13}NO$: C, 80.69; H, 5.87; N, 6.27%)].

The Preparation of 3,6-Diacyl-9-methylcarbazoles. 9-Methylcarbazole (20 g) was added, in small portions, to a vigorously stirred mixture of aluminium chloride (60 g) and isobutyryl chloride (40 g) in nitrobenzene (200 cm^3) at 0 °C. The resulting solution was stirred in an ice-bath for 6 h and then at 20—25 °C for 2 d. The solution was subsequently poured onto crushed ice (500 g), and the aqueous layer was discarded. The nitrobenzene solution, after being participated by water, was subjected to steam distillation to remove the solvent. The oily residue was extracted with benzene (2×200 cm^3). The extract was concentrated to about 150 cm^3 and fractionated on a silica-gel column (5×50 cm), eluted by a mixture of ethyl acetate and benzene (1:9). The evaporation of the eluate and subsequent crystallization from acetone gave colorless needles (82% yield) of 3,6-diisobutyryl-9-methylcarbazole (**2a**); mp 128—129.5 °C (from ethanol) (Found: C, 78.60; H, 7.18; N, 4.15%. Calcd for $C_{21}H_{23}NO_2$: C, 78.47; H, 7.21; N, 4.36%).

The replacement of isobutyryl chloride by propionyl or acetyl chloride in the foregoing reaction gave 9-methyl-3,6-dipropionylcarbazole [66% yield, mp 196—197 °C (from ethanol) (Found: C, 77.92; H, 6.52; N, 4.62%. Calcd for $C_{19}H_{19}NO_2$: C, 77.79; H, 6.53; N, 4.77%)] and 3,6-diacetyl-9-methylcarbazole [59% yield, mp 198—199 °C (from ethanol) (Found: C, 75.70; H, 5.61; N, 5.21%. Calcd for $C_{17}H_{15}NO_2$: C, 75.87; H, 5.97; N, 5.53%)] respectively.

The Preparation of 3,6-Diacylcarbazoles. Carbazole (10 g) was added, in small portions, into a vigorously stirred solution of isobutyric anhydride (10 g) and aluminium chloride (15 g) in nitrobenzene (150 cm^3) at 0—5 °C. The resulting dark green solution was stirred at 4—5 °C for 12 h and then added to ice-cold 0.5 mol dm^{-3} hydrochloric acid (300 cm^3). The nitrobenzene solution was separated from the aqueous layer and submitted to steam distillation to remove the solvent. The residual solid was dissolved in ethyl acetate and fractionated on a silica-gel column (4.5×50 cm), eluted by ethyl acetate–benzene (2:3). The evaporation of the eluate and subsequent crystallization from ethyl acetate gave yellow needles (26% yield) of 3,6-diisobutyrylcarbazole; mp 203.5—204 °C (Found: C, 78.14; H, 6.82; N, 4.96%. Calcd for $C_{20}H_{21}NO_2$: C, 78.14; H, 6.89; N, 4.56%).

3,6-Dipropionylcarbazole [36% yield, mp 238—240 °C (from ethyl acetate) (Found: C, 77.19; H, 5.98; N, 4.76%. Calcd for $C_{18}H_{17}NO_2$: C, 77.39; H, 6.13; N, 5.01%)] and 3,6-diacetylcarbazole [11% yield, mp 236—237 °C, dec (from ethyl acetate) (Found: C, 76.57; H, 5.04; N, 5.35%. Calcd for $C_{16}H_{13}NO_2$: C, 76.47; H, 5.22; N, 5.57%)] were similarly synthesized from carbazole and the appropriate acid anhydride.

*The Preparation of 9-Acylcarbazoles (**3a—c**).* A mixture of potassium carbazole (5.0 g), isobutyryl chloride (10 g), and sodium carbonate (5 g) was heated under reflux for 2 h. The mixture was then added to water (50 cm^3), and the product was extracted with ether (2×100 cm^3). The extract, after washing with sodium hydrogencarbonate and water, was evaporated to give an oily residue, which was then fractionated on a silica-gel column (3.4×40 cm), eluated by a 1:1 mixture of hexane and benzene. The eluate was evaporated and subsequently crystallized from methanol to give colorless needles (80% yield) of 9-isobutyrylcarbazole (**3a**); mp 43—44.5 °C (Found: C, 81.01; H, 6.19; N, 6.01%. Calcd for $C_{16}H_{15}NO$: C, 80.98; H, 5.90; N, 6.37%).

9-Propionylcarbazole (**3b**) [85% yield, mp 90.5—91 °C (from methanol) (Found: C, 80.69; H, 5.67; N, 6.27%. Calcd for $C_{15}H_{13}NO$: C, 80.69; H, 5.87; N, 6.27%)] and 9-acetylcarbazole (**3c**) [60% yield, mp 67—68.5 °C (from methanol) (Found: C, 80.14; H, 5.09; N, 6.53%. Calcd for $C_{14}H_{11}NO$: C, 80.36; H, 5.30; N, 6.69%)] were similarly obtained from potassium carbazole and propionyl or acetyl chloride respectively.

*The Isolation of 9-Methylcarbazole-3-carboxylic Acid and 9-Methylcarbazole-3,6-dicarboxylic Acid from the Oxidation Products of the 3-Isobutyryl or 3,6-Diisobutyryl Precursor (**1a** or **2a**).* 3-Isobutyryl-9-methylcarbazole (500 mg) in DMF was added to *t*-BuOK (4.0 g) in DMF (250 cm^3), after which the mixture was stirred under oxygen at 25 °C for 2 h. Water (100

cm^3) was added to the mixture, and the resulting solution was evaporated to dryness under reduced pressure. The residue was dissolved in water (150 cm^3), and a small amount of an insoluble material was removed by extraction with benzene (2×50 cm^3). The solution was brought to boil, adjusted to pH 2—3 with hydrochloric acid, and then chilled. The colorless needles (385 mg, 86% yield) of 9-methylcarbazole-3-carboxylic acid melted at 258—259 °C (from water) (Found: C, 74.59; H, 4.67; N, 6.09%. Calcd for $C_{14}H_{11}NO_2$: C, 74.65; H, 4.92; N, 6.22%).

3,6-Diisobutyryl-9-methylcarbazole, on air oxidation in a way similar to that described above, yielded 9-methylcarbazole-3,6-dicarboxylic acid (95% yield), which did not melt below 300 °C (Found: C, 66.70; H, 4.33; N, 5.23%. Calcd for $C_{15}H_{11}NO_4$: C, 66.91; H, 4.12; N, 5.20%).

Measurements of the CL Intensity and Fluorescence Spectra. A 2-cm^3 aerated solution of the acylcarbazoles in DMF or DMSO was placed in a quartz cell, which was kept at a constant temperature by means of a thermostatically controlled cell holder. The CL intensity was measured immediately after adding 0.2 cm^3 of a solution of *t*-BuOK in *t*-butyl alcohol (2×10^{-2} mol cm^{-3}) into the solution of the reactant on a Hitachi MPF-2A fluorescence spectrophotometer, with the exciting source turned off. The fluorescence spectra were measured on the same apparatus.

Measurements of the Changes in the Concentrations of Reactant and Product in CL Reaction of ***1a*** *by High-performance Liquid Chromatography.* We took 0.2-cm^3 aliquots of the reaction solution out at regular intervals and immediately added them to a solution of phosphoric acid in methanol (2×10^{-3} mol dm^{-3}, 0.2 cm^3) to stop the oxidation. A 25-mm^3 aliquot of the solution was subjected to high-performance liquid chromatography using a JASCO Trirotar on a JASCO SS-10-ODS-A reverse-phase column (4.6×250 mm), using methanol as the elution solvent (1.0 cm^3/min). The eluate containing the unchanged reactant (**1a**) and product (9-methylcarbazole-3-carboxylic acid, **4**) was detected on a JASCO UVIDEC-100-II UV spectrometer at 285 nm, and the retention times and the quantities of **1a** and **4** were determined by calculating the areas of the peaks with a Intelligent 5000 E integrator.

The authors wish to thank Mr. Nobuhiko Honda for his technical assistance. The present work was partially supported by a Grant-in-Aid for Scientific Research No. 354136 from the Ministry of Education, Science and Culture.

References

1) I. Kamiya and T. Sugimoto, *Bull. Chem. Soc. Jpn.*, **50**, 2442 (1977); I. Kamiya, *ibid.*, **50**, 2447 (1977).

2) I. Kamiya and T. Sugimoto, *Chem. Lett.*, **1978**, 335; *Photochem. Photobiol.*, **30**, 49 (1979).

3) W. H. Richardson, F. C. Montgomery, M. B. Yelvington, and H. E. O'Neal, *J. Am. Chem. Soc.*, **96**, 7525 (1974); K. A. Horn and G. B. Schuster, *ibid.*, **100**, 6649 (1978). L. B. Harding and W. A. Goddard, III, *ibid.*, **99**, 4520 (1977).

4) F. McCapra, I. Beheshti, A. Burford, R. A. Hann, and K. A. Zaklika, *J. Chem. Soc., Chem. Commun.*, **1977**, 944; K. A. Zaklika, A. L. Thayer, and A. P. Schaap, *J. Am. Chem. Soc.*, **100**, 4916 (1978).

5) "Chemically Initiated Electron-exchange Luminescence": J.-y. Koo and G. B. Schuster, *J. Am. Chem. Soc.*, **99**, 6107 (1977); G. B. Schuster, *Acc. Chem. Res.*, **12**, 366 (1979).

6) G. J. Lofthouse, H. Suschitzky, B. J. Wakefield, and R. A. Whittaker, *J. Chem. Soc., Perkin Trans. 1*, **1979**, 1634.

7) Analogous curves showing the increasing concentration of **4** were also obtained by monitoring the increasing fluorescence intensity at 370 nm (the peak of the fluorescence of **4**).

8) It has been reported that the decomposition of various isolated dioxetanes obey the first-order reaction (see Ref. 9).

9) a) K. A. Zaklika, T. Kisse, A. L. Thayer, P. A. Burns, and A. P. Schaap, *Photochem. Photobiol,*. **30**, 35 (1979); b) A. L. Baumstark and T. Wilson, *Tetrahedron Lett.*, **1976**, 2397; c) H. Nakamura and T. Goto, *Photochem. Photobiol.*, **30**, 27 (1979); d) E. W. Meijer and H. Wynberg, *Tetrahedron Lett.*, **1979**, 3997.

10) From the kinetic data, the intermediate X seems relatively stable at a low temperature if it is isolated. However, the oxidation of the carbazole does not proceed appreciably at a low temperature. Thus, it may be difficult to isolate X from the luminescent systems employed here.

11) J. Lee, A. S. Wesley, J. F. Ferguson, III, and H. H. Seliger, "Bioluminescence in Progress," ed by F. H. Johnson and Haneda, Princeton Univ. Press (1966), p. 35. See also: W. Adam, G. A. Simpson, and F. Yany, *J. Phys. Chem.*, **78**, 2559 (1974).

12) When light is detected by the signal of an electrophotometer, the total light intensity per unit volume from a chemiluminescent solution is given by $T=G\int S_t dt$, where G is the instrumental factor and where S_t is the magnitude of the signal measured over the emission band at time t and is experimentally determined by the graphical integration of the spectral distribution curve, corrected for the wavelength response of the photomultiplier.

Assuming that the ratio of S_t to the magnitude of the signal at the peak of the emission spectrum ($I(\lambda_m)_t$), $\sigma=S_t/I(\lambda_m)_t$, is kept constant during the reaction, we can write: $T=G\sigma\int I(\lambda_m)_t dt$. $\int I(\lambda_m)_t dt$ is experimentally determined by the graphical integration of the $I(\lambda_m)_t$ *vs.* t-curve. Thus, $\Phi_{CL}=G\sigma\int I(\lambda_m)_t dt/[M]$ for a solution ([M] is the concentration decrement of M), and $\Phi'_{CL}=G\sigma'\int I'(\lambda'_m)_t dt/[M']$ for the other solution, so that:

$$\Phi_{CL}=\Phi'_{CL}\sigma[M']\int I(\lambda_m)_t dt/\sigma'[(M]\int I'(\lambda'_m)_t dt.$$

13) Assuming that $k_2=A\exp(-E_a/RT)$, $k'_2=A'\exp(-E_a'/RT)$ and $A\sim A'$, we can write that $1/\beta-1=\exp(\Delta E_a/RT)$, where $\Delta E_a=E_a-E_a'$ is the difference in activation energy between Reactions III(E_a) and IV(E_a'). If ΔE_a is tentatively taken to be 10 kJ mol^{-1} with reference to the value reported for dimethyldioxetane (13—14 kJ mol^{-1}),[14] the β values are calculated to be 1.8×10^{-2}, 2.1×10^{-2}, and 2.4×10^{-2} at 30, 40, and 50 °C respectively. The ratio of the β values (1.0:1.2:1.3) is roughly agreeable to that the observed Φ_{CL} values (1.0:1.2:1.6).

14) G. B. Schuster, B. Dixon, J.-y. Koo, S. P. Schmidt, and J. P. Smith, *Photochem. Photobiol.*, **30**, 17 (1979); S. P. Schmidt and G. B. Schuster, *J. Am. Chem. Soc.*, **102**, 306 (1980).

15) T. S. Stevens and S. H. Tucker, *J. Chem. Soc.*, **123**, 2140 (1923).

Spectral Behavior of 3,6-Substituted Aminoacridine Dyes with Emphasis on the Perturbation of the Exonuclear Amino Groups

Kiwamu YAMAOKA,* Sumihare NOJI, and Mamoru YOSHIDA
Faculty of Science, Hiroshima University, Higashisenda-machi, Hiroshima 730
(Received April 7, 1980)

The optical absorption spectra of several derivatives of Proflavine (PF) and Coriphosphine O (CP) were measured in aqueous solutions at 25 °C. The effect of the perturbation of one or both of the exonuclear amino groups on the spectral behavior was studied in order to explore the relationship between the spectra and the chemical structures of the symmetric 3,6-disubstituted acridine dyes which can bind to various polyelectrolytes, often showing metachromasy. The metachromatic spectra of the complexes between 3,6-diaminoacridine dyes and polyanions were reproduced reasonably well when one of the two amino groups of PF was converted to an acylamino group. A similar result was observed when the amino group of CP was acetylated. In these cases, the spectra show two absorption bands of nearly equal intensity on both sides of the single peak of PF and CP in the visible region. These results are indicative of the close similarity in chemical structures between the monacylamino PF and the PF bound to the electron-rich sites of polyanions.

The symmetric 3,6-diaminoacridine dyes and their derivatives, such as Proflavine (PF), Trypaflavine (TF), and Acridine Orange (AO), show a deceptively simple absorption band in the visible wavelength region. Yet, a recent work has clearly shown that the spectral feature of this band is quite complex, actually consisting of two orthogonally polarized component bands with vibrational structures.[1] The visible spectra of those dyes are all metachromatic, exhibiting large hypo- and hypsochromic changes in solutions in the presence of various polyelectrolytes.[2] Because of this striking metachromatic behavior, the bathochromic change of the spectra has long been ignored, in spite of an early mention of the importance of the long-wavelength absorption component band associated with the dye-polymer complexes.[3] The pure spectra of TF bound to various polymers have indeed shown a long-wavelength band in addition to the short-wavelength band, their intensity being about equal.[4]

In contrast with the above cases, substitution on the 10- and/or 9-position of the acridine nucleus affects the absorption spectrum of acridine itself only slightly.[5] For example, 10-methylacridinium and 9-aminoacridinium both show a visible spectrum in which the short-axis polarized transition (the ^1L_a band) is well separated from the long-axis polarized transition (the ^1L_b band).[1,6,7] These two acridines also bind to some polymers,[8–12] but they show no appreciable metachromatic effect. The bound-dye spectra have revealed that both the short- and long-axis polarized bands shift toward the red slightly with a concomitant decrease in intensity.[11,12] Thus, introduction of amino groups into the 3- and 6-positions of acridine appears to be responsible for the large metachromatic spectra of dye–polymer complexes.

In the course of the study of spin-labeled acridine dyes, attachment of a nitroxide radical to one of the 3,6-amino groups of PF altered the visible spectrum of PF in such a way that the original peak was split into two bands.[13] Interestingly, the spectral profile of this monosubstituted-PF (slPF) resembled the spectra of TF bound to various polyions.[4] This remarkable change of slPF, however, disappeared and a PF-like simple spectrum was restored when both amino groups of PF were coupled with the radicals.[14] These results are suggestive of three possibilities: (1) The nitroxide radical effects the spectral splitting of the mother compound PF. (2) Conjugation of the newly produced acylamino group with the acridine ring perturbs the π-electron system. (3) Lowering of molecular symmetry from a C_{2v} to a less symmetric C_s group increases the separation between the short- and long-axis polarized components of the visible band. The present work was undertaken for the purposes of (1) discriminating these points, and (2) exploring the relation between the spectra of 3,6-substituted diaminoacridine dyes, in which an amino group or groups are perturbed, and the bound-dye spectra of dye-polymer complexes. For this purpose, the absorption spectra of a number of closely related acridine dyes were determined and correlated.

Experimental

Materials. Proflavine (PF), 3,6-diaminoacridinium chloride **1a**, was purified according to Albert.[5] Monoacetylated Proflavine (AcPF), 3-acetamido-6-aminoacridinium chloride **1b**,[15] and diacetylated Proflavine (Ac_2PF), 3,6-diacetamidoacridinium chloride **1c**,[16] were prepared by a standard acetylation procedure. Preparations of monopyrrolidinylated Proflavine (slPF), 6-amino-3-(1-oxy-2,2,5,5-tetramethyl-3-pyrrolidinyl-carbonylamino)acridinium chloride **1d**,[13,17] and dipyrrolidinylated Proflavine (sl_2PF), 3,6-bis(1-oxy-2,2,5,5-tetramethyl-3-pyrrolidinyl-carbonylamino)-acridinium chloride **1e**,[14,17] were described in detail elsewhere. Coriphosphine O (CP), 3-amino-6-dimethylamino-2-methylacridinium chloride **2a**, was purchased from Chroma Gesellschaft, Schmid & Co. and was purified by the silica gel thin layer chromatography, with an eluent system of 1-butanol–acetic acid–water (4:1:5). Acetylated Coriphosphine O (AcCP), 3-acetamido-6-dimethylamino-2-methylacridinium chloride **2b**, was prepared by acetylating CP with an acetic acid–acetic anhydride mixture at 118 °C. Crude AcCP was purified in a manner similar to CP. All chemical structures of dyes **1a** to **2b** are shown in Fig. 1.

Measurements. Absorption spectra were measured on a Hitachi model EPS-3T recording spectrophotometer at 25 °C. Optical titration of each dye was carried out to determine the pK-value, usually at the wavelength of maximum absorption in a concentration range of 5×10^{-5} M (1 M = 1 mol/l) in the presence of 1.0×10^{-2} M Tris buffer. The pH values were controlled by adding either 0.05 M

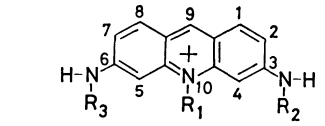

(1)

1a: $R_1, R_2, R_3 = -H$ (PF)

1b: $R_1, R_3 = -H$; $R_2 = -\overset{\overset{O}{\|}}{C}-CH_3$ (AcPF)

1c: $R_1 = -H$; $R_2, R_3 = -\overset{\overset{O}{\|}}{C}-CH_3$ (Ac$_2$PF)

1d: $R_1, R_3 = -H$; $R_2 = -\overset{\overset{O}{\|}}{C}-$ (slPF)

1e: $R_1 = -H$; $R_2, R_3 = -\overset{\overset{O}{\|}}{C}-$ (sl$_2$PF)

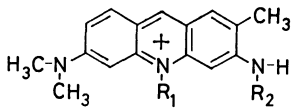

(2)

2a: $R_1, R_2 = -H$ (CP)

2b: $R_1 = H$; $R_2 = -\overset{\overset{O}{\|}}{C}-CH_3$ (AcCP)

Fig. 1. Chemical formulas of acridine dyes utilized in this work.

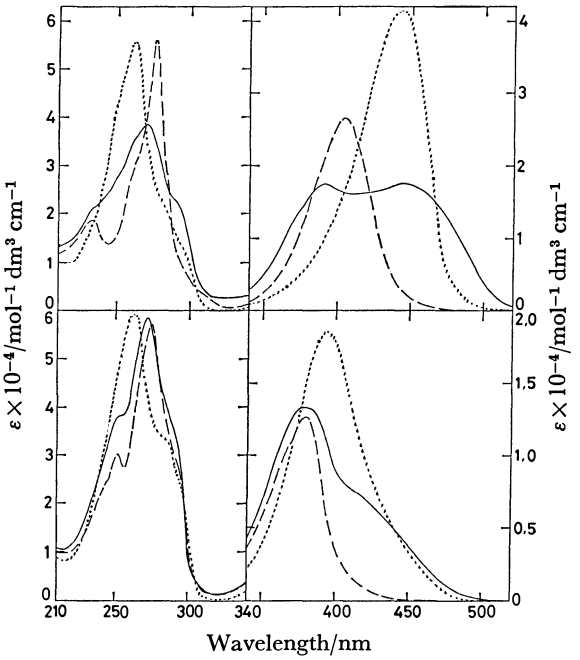

Fig. 2. Absorption spectra of AcPF and Ac$_2$PF in aqueous solutions.
The protonated forms in a pH range of 4—5 are shown in the upper half and the base forms in a pH range of 10—11 are in the lower half. AcPF (——) and Ac$_2$PF (— —). PF (·····) is also shown for comparison.

HCl or 0.05 M NaOH; no precipitate of dye occurred. The molar absorption coefficient ε was expressed in M^{-1} cm^{-1}. The pH was determined with a Hitachi-Horiba F-7 pH meter.

Results and Discussion

Absorption Spectra of Acetylated Proflavines. The absorption spectra of mono- and diacetylated Proflavines, AcPF and Ac$_2$PF, are shown in Fig. 2, together with the spectrum of PF for comparison. In the upper half, the spectra of the protonated forms of these dyes are given. The spectrum of AcPF shows two absorption bands of nearly equal intensity in the visible wavelength region. Each band clearly consists of some subbands, probably the vibrational structure, which are more pronounced in organic solvents. Close examination indicates that these two bands are separated unevenly with respect to the original single peak at 444 nm of PF, *i.e.*, the longer-wavelength band is almost unshifted but the shorter-wavelength band is shifted by 50 nm toward the blue. It is quite interesting to note that a further acetylation of the remaining amino group of AcPF results in a simple spectral profile in the visible wavelength. This spectrum of Ac$_2$PF rather resembles that of PF, although their intensity and peak position differ from each other greatly. The UV spectra of these protonated dyes also vary with the degree of acetylation in such a way that the major peak at 262 nm of PF moves toward the long wavelengths.

In the lower half of Fig. 2, the spectra of the deprotonated (neutral or base) forms are shown. Again the effect of the perturbation of the exonuclear amino groups on the spectra is quite remarkable. Just as the removal of the proton from the 10-position gives rise to the hypo- and hypsochromic changes for PF, a very similar effect appears for the base forms of AcPF and Ac$_2$PF. The visible bands of the base forms are located in the 370—390 nm region regardless of the substituents at the 3- and 6-positions. The spectral behavior of the basic AcPF is most interesting, *i.e.*, the longer-wavelength peak diminishes to be just a shoulder near 410—420 nm, while the shorter-wavelength band remains. The visible and UV spectra of the base forms of PF and Ac$_2$PF are again similar to each other.

The results in Fig. 2 clearly show three points: The nonsymmetric substitution of either the 3- or 6-position of PF by an acetyl group gives rise to a new spectral feature, *i.e.*, the appearance of two absorption maxima. The symmetric substitution of both the 3- and 6-positions of PF reverts to the original feature of the single peak. Finally, the removal of a proton from the 10-position affects the spectral profiles hypso- and hypochromically.

Absorption Spectra of Spin-labeled Proflavines. The absorption spectra of mono- and dipyrrolidinylated Proflavines, slPF and sl$_2$PF, are shown in Fig. 3, together with the spectrum of PF for comparison. These protonated PF derivatives (upper half) behave surprisingly similarly to their acetylated counterparts. The visible spectrum of slPF shows two bands of about equal intensity, *i.e.*, the longer-wavelength band is

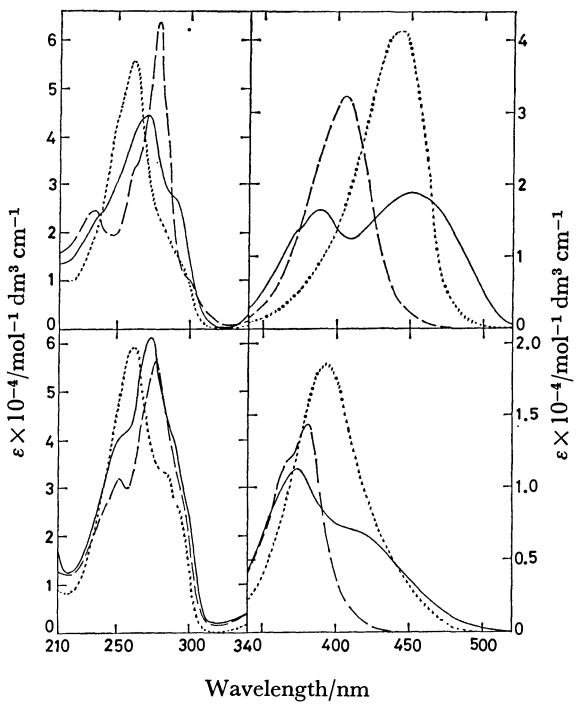

Fig. 3. Absorption spectra of slPF and sl_2PF in aqueous solutions.
The protonated forms in pH 4—5 are in the upper half and the base forms in pH 10—11 are in the lower half. slPF (——) and sl_2PF (— —). PF (·····) is also shown for comparison.

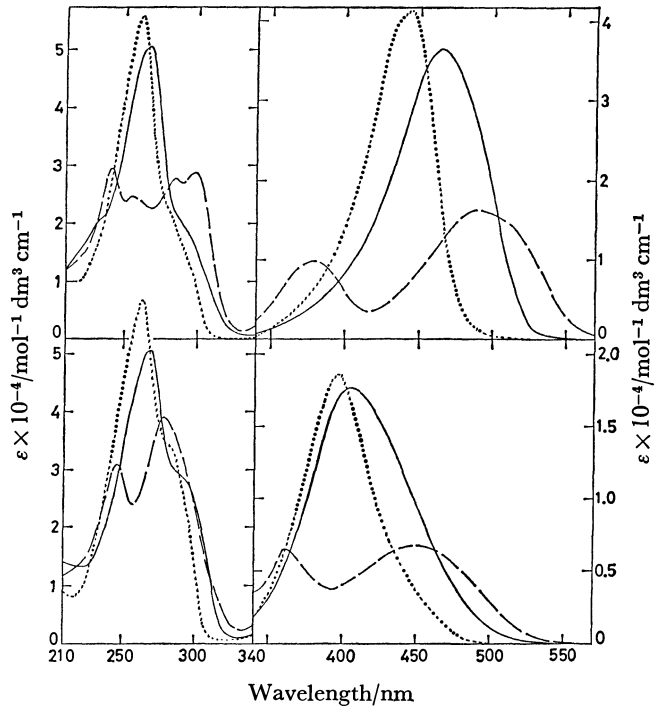

Fig. 4. Absorption spectra of CP and AcCP in aqueous solutions.
The protonated forms in the pH range of 4—5 are in the upper half and the base forms in the pH range of 10—11 are in the lower half. CP (——) and AcCP (— —). PF (·····) is also shown for comparison.

at 450 nm, but the shorter-wavelength band is further apart by 60 nm from the peak of PF. The spectrum of sl_2PF, which is obtained by substitution of the remaining amino group of slPF, reverts to the simple spectrum of PF. The UV spectra of slPF and sl_2PF behave just like those of AcPF and Ac_2PF. It should be noted that the free nitroxide radical absorbs light very weakly, showing the maximum absorption at 398 nm (ε=8.6, absorbance=0.18 at 21 mM in aqueous solution). The results in Figs. 2 and 3 exclude the contribution of the radical to the observed spectra of slPF and sl_2PF in the visible wavelength region.

The spectra of the deprotonated forms of PF, slPF, and sl_2PF are shown in the lower half of Fig. 3. The removal of a proton from the 10-position affects each spectrum in the very same way as in the case of the acetylated counterparts. Comparison of the data in Fig. 3 with those in Fig. 2 clearly indicates that the simultaneous substitution of two amino groups on the 3,6-positions by either acetamido or pyrrolidinyl radical groups results in the spectral feature closely related to that of PF itself. This is conceivable in the sense that the substitution at both positions retains the molecular C_{2v} symmetry for all PF, Ac_2PF, and sl_2PF. Yet, it is surprising to see that the conversion of each exonuclear amino group to an acylamino group restores the original band structure.

Absorption Spectra of Coriphosphines. Now, a question arises: Is the appearance of two bands of nearly equal intensity in the visible region due to the perturbation of one of the two exonuclear amino groups ? Alternatively, does the breakdown of molecular symmetry from the C_{2v} to the C_s point group result in two bands instead of one ? The answer is given in Fig. 4, where the absorption spectra of CP and its acetylated derivative, AcCP, are shown. The structure of CP differs from PF in that a methyl group is attached at the 2-position of the acridine nucleus and one of the amino groups is substituted by the dimethylamino group (Fig. 1). Hence, the molecular symmetry of CP is lower than the C_{2v} and may be considered to be C_s. Yet, the absorption spectrum of CP is close to that of PF, showing a single band at 465 nm in the visible region.

The spectrum of AcCP clearly shows two absorption bands at 490 nm and 381 nm, just as the cases of AcPF (Fig. 2) and slPF (Fig. 3). Results in Fig. 4 at once ascertain that the lowering of the symmetry of PF as such does not cause the splitting of the single peak into two peaks of nearly equal intensity. This view is further supported by the acetylation of the amino groups of CP. The base forms of CP and AcCP behave similarly to the deprotonated PF dyes, as is shown in the lower half of Fig. 4. A noticeable difference is that the longer-wavelength peak of AcCP remains as a distinct peak even when the proton is removed from the 10-position, In conclusion, it is most probably the acylation of one, but not both, of two amino groups on the 3,6-positions that results in the new spectral feature, *i.e.*, the development of two bands.

Comparison of Optical Properties of Dyes ***1a—2b.*** Since systematic studies of the effect of the substitution of particular groups on the spectra of the 3,6-disub-

TABLE 1. SPECTRAL PROPERTIES AND pK-VALUES OF DYES **1a—2b**

Dyes	pK	$\varepsilon \times 10^{-4}$/mol^{-1} dm^3 cm^{-1} ($\lambda_{max}$)[a] in water	
		Cationic form	Base form
PF	9.11[b]	4.15(444)	1.86(395)
AcPF	8.20±0.09	1.75(446), 1.74(392)	0.65(420), 1.33(377)
Ac_2PF	6.25±0.03	2.67(405)	1.27(381), 0.99(365)
slPF	7.98±0.03	1.88(452), 1.64(389)	0.67(420), 1.13(375)
sl_2PF	5.88±0.04	3.23(406)	1.44(381), 1.14(365)
CP	9.85±0.05	3.64(465)	1.76(405)
AcCP	8.38±0.02	1.61(490), 0.99(381)	0.67(450), 0.65(362)

a) The value in the parentheses is the peak or shoulder wavelength in nm. b) This value is taken from Ref. 19.

stituted acridine dyes are few, it is appropriate to compare their spectral properties. The data are summarized in Table 1. In the concentration range covered in this work, the Beer-Lambert law holds for each dye in aqueous and ethanolic solutions. Thus, the possibility that the changes in all spectra result from dye-aggregation can be excluded. The pK-values were determined for dyes **1a—2b** by optical titration. It is clear from Table 1 that conversion of amino groups to acylamino groups decreases the pK-value in the order of unsubstituted>monosubstituted>disubstituted. This is in conformity with other cases,[5] and the electron-donating tendency of an amido group may be responsible for it. The pK-value of 6.25 for AcPF is in good agreement with a previously reported value of 6.2.[18]

The symmetric 3,6-disubstituted Ac_2PF and sl_2PF should belong to the C_{2v} group as PF and, consequently, their apparently simple visible band should contain the long- and short-axis polarized bands.[1] It would be helpful to identify the directions of the polarization of the two clearly visible absorption bands for AcPF and slPF. However, these transition moments are no longer polarized along the short- and long-axes in a molecular plane under symmetry considerations. Individual transition moments may be determined by the film dichroism method.[1]

All dyes examined in this work bind to sodium polyphosphate, exhibiting the hypso- and hypochromic effects. It is worth noting that the pure spectra of TF bound to various polyelectrolytes are very close to the spectra of AcPF and slPF, each of which contains an exonuclear acylamino group. This apparent similarity suggests that one of the two amino groups of PF or TF in the dye-polymer complexes may be electronically affected by the electron-rich polymer sites such as $-COO^-$, $-SO_3^-$, and $-PO_2^-$– by still unclarified reasons. In this connection, the interaction of AcPF and other dyes described in this work with polyions should be studied to obtain the pure spectra of the bound dyes.[19] Molecular orbital calculations capable of taking into account the substitution effect on the exonuclear groups should also be carried out to elucidate these profound spectral changes on a more quantitative and systematic basis.

Conclusion

The absorption spectra of the symmetric 3,6-disubstituted acridine dyes show a single band in the visible wavelength region regardless of the bulkiness of the substituents (PF, Ac_2PF, and sl_2PF). Conversion of an amino group to an acylamino substituent gives rise to the spectrum which shows two bands of nearly equal intensity. This spectrum resembles the pure spectrum of a 3,6-diaminoacridine bound to various polyelectrolytes. The mere decrease of the molecular symmetry from C_{2v} to C_s cannot result in such a drastic spectral change. The π-electron system of the acylamino group at either the 3- or 6-position must interact with the π-electron system of the acridine nucleus by conjugation.

References

1) Y. Matsuoka and K. Yamaoka, *Bull. Chem. Soc. Jpn.*, **52**, 3163 (1979); **53**, 2146 (1980).
2) J. A. Bergeron and M. Singer, *J. Biophys. Biochem. Cytol.*, **4**, 433 (1958).
3) K. Yamaoka and R. A. Resnik, *J. Phys. Chem.*, **70**, 4051 (1966).
4) K. Yamaoka and M. Takatsuki, *Bull. Chem. Soc. Jpn.*, **51**, 3182 (1978); M. Takatsuki and K. Yamaoka, *ibid.*, **52**, 1003 (1979); Other references are cited therein.
5) A. Albert, "The Acridines," St. Martin's Press, New York (1966), Chaps. 10 and 11.
6) V. Zanker and G. Schiefele, *Z. Elektrochem.*, **62**, 86 (1958).
7) J. Yoshino, T. Hoshi, T. Masamoto, H. Inoue, and K. Ota, *Nippon Kagaku Kaishi*, **1972**, 2227.
8) A. R. Peacocke and J. N. H. Skerrett, *Trans. Faraday Soc.*, **52**, 261 (1956).
9) K. Yamaoka and R. A. Resnik, *Biopolymers*, **8**, 289 (1969).
10) K. Yamaoka, *Biopolymers*, **11**, 2537 (1972).
11) K. Yamaoka and M. Masujima, *Biopolymers*, **17**, 2485 (1978).
12) K. Yamaoka, M. Takatsuki, and K. Nakata, *Bull. Chem. Soc. Jpn.*, **53**, 3165 (1980).
13) K. Yamaoka and S. Noji, *Chem. Lett.*, **1976**, 1351.
14) K. Yamaoka and S. Noji, *Chem. Lett.*, **1979**, 1123.
15) A. Albert and W. H. Linnell, *J. Chem. Soc.*, **1936**, 1614.
16) L. Benda, *Ber.*, **45**, 1787 (1912).
17) S. Noji and K. Yamaoka, *J. Sci. Hiroshima Univ. Ser. A*, **44**, 101 (1980).
18) G. Löber and G. Achtert, *Biopolymers*, **8**, 595 (1969).
19) M. Takatsuki and K. Yamaoka, *J. Sci. Hiroshima Univ. Ser. A*, **40**, 387 (1976).

Kinetic Studies on Intramolecular Excimer Formation in Dinaphthylalkanes

Shinzaburo Ito,* Masahide Yamamoto, and Yasunori Nishijima
Department of Polymer Chemistry, Kyoto University, Sakyo-ku, Kyoto 606
(Received April 9, 1980)

Various dinaphthylalkanes in which two naphthyl groups are separated by three carbon atoms were prepared, and intramolecular excimer formation was investigated. All rate constants in Förster's kinetics were determined by the steady state and time-resolved fluorescence measurements. A large difference in the association rate constant was observed with variation of molecular structure. The results suggest that intramolecular excimer formation is directly controlled by the rotational relaxation processes of the molecules from their neighboring conformations to the excimer conformation. A large formation rate (7.9×10^8 s^{-1} at 25 °C) was observed for *meso*-2,4-dinaphthylpentane, the rate for the *racemo* isomer being found to be one tenth of that for the *meso* isomer. This indicates that the isotactic sequence in vinyl aromatic polymers plays an important role in the intramolecular excimer formation.

Excimer is an excited dimer existing only in the excited state by the attractive interaction between an excited chromophore and one in the ground state. It turns unstable in the ground state due to the steric hindrance between chromophores. The formation of intermolecular excimers is thus expected to be controlled by the mutual diffusion of chromophores. Verification of the diffusion controlled process has been carried out mainly using pyrene molecule as a chromophore.[1,2]

The formation of intramolecular excimers is considered to be governed by the micro-structures of molecules to which chromophores are attached. It seems that there are two controlling factors for the intramolecular excimer formation: (a) conformational changes of the molecule which corresponds to the mutual diffusion process in the case of intermolecular excimer formation, and (b) the geometrical arrangement of two chromophores in an excimer state which is determined by the micro-structure of the molecule. Concerning (b), Hirayama proposed the $n=3$ rule for the intramolecular excimer formation.[3] The results indicate that the most favorable arrangement of chromophores is a symmetrical parallel sandwich arrangement which can be formed specifically in a compound having a molecular structure in which two aromatic groups along the alkane chain are separated by three carbon atoms.

This paper deals with (a), the relationship between the micro-structures of molecules and their rotational relaxation processes within the lifetime of a chromophore. A naphthalene chromophore seems to have fairly strict arrangements in the excimer state,[4] its emission properties being favorable for detection in spectroscopic analyses. The photophysical characteristics are useful for investigating the rotational relaxation processes. In order to clarify the problem (a), quantitative study on various model compounds by the time-resolved fluorescence method, is necessary. Advance in the time-resolved technique for photoluminescence measurements enables us to determine the rate constants of the kinetic scheme including the intramolecular excimer formation process.[5-9] We have investigated various dinaphthylalkanes satisfying the $n=3$ rule,[3] under photostationary and transient conditions. The individual rate constant of photophysical processes was determined. From the results, the relationship between the molecular structure and its conformational relaxation is discussed. The compounds examined are regarded as the dimeric model compounds of vinyl polymers. Their photophysical behavior provides useful information on the intramolecular excimers in polymer systems.

Experimental

Materials. 1,3-Di(2-naphthyl)propane (1,3-DNPr) was synthesized by the procedure of Chandross and Dempster.[4] The other sample were prepared by as follows.

1,3-Di(2-naphthyl)butane (1,3-DNBu): 1,3-Di(2-naphthyl)-1-propanone, obtained as an intermediate product in the synthesis of 1,3-DNPr, was reacted with methylmagnesium iodide in ether solution. The oily product was purified by a column chromatography on silica gel. 2,4-Di(2-naphthyl)-2-butanol thus obtained was reduced in acetic acid solution by addition of zinc dust and hydrochloric acid. The product was chromatographed on silica gel with hexane–dichloromethane (4:1): mp 65—66 °C; IR (KBr) 3050, 2950, 2930, 2850, 1630, 1600, 1510, 815, 740, and 475 cm^{-1}; NMR (CS_2) $\delta=1.35$ (3H, d, $J=6.5$ Hz), 1.90—2.16 (2H, m), 2.52—2.96 (3H, m), and 7.06—7.74 (14H, m). Found: C, 92.69; H, 7.18%. Calcd for $C_{24}H_{22}$: C, 92.86; H, 7.14%.

1,3-Di(2-naphthyl)pentadecane (1,3-DNPd) and 1,3-di(2-naphthyl)-5-phenylpentane (1,3-DN-5-PhPe) were synthesized by the same method as that for 1,3-DNBu, 1-bromododecane and 1-bromo-2-phenylethane being used for 1,3-DNPd and 1,3-DN-5-PhPe, respectively, instead of methyl iodide. 1,3-DNPd: IR (KBr) 3050, 2930, 2850, 1630, 1600, 1510, 815, 740, and 475 cm^{-1}; NMR (CS_2) $\delta=0.75$—0.95 (3H, m), 1.17 (20H, s), 1.54—1.83 (2H, m), 1.92—2.18 (2H, m), 2.50—2.80 (3H, m), and 7.05—7.76 (14H, m). Found: C, 90.67; H, 9.82%. Calcd for: $C_{35}H_{44}$; C, 90.46; H, 9.54%. 1,3-DN-5-PhPe: IR (KBr) 3050, 2930, 2850, 1630, 1600, 1510, 815, 740, 695, and 475 cm^{-1}; NMR (CS_2) $\delta=1.85$—2.22 (4H, m), 2.30—2.82 (5H, m), and 6.85—7.80 (19H, m). Found: C, 92.87; H, 6.99%; M^+, 400. Calcd for $C_{31}H_{28}$: C, 92.95; H, 7.05%; M, 400.

2,4-Di(2-naphthyl)pentane (2,4-DNPe): 1,3-Di(2-naphthyl)-2-propen-1-one, obtained in the course of the synthesis of 1,3-DNPr, was reacted with methylmagnesium iodide in the presence of a trace amount of cuprous chloride, and the product was extracted with benzene. After benzene had been removed, the residue was recrystallized from carbon tetrachloride to give colorless crystalline 1,3-di(2-naphthyl)-1-butanone: mp 148—150 °C. The ketone was reacted again with methylmagnesium iodide in ether solution. The product, 2,4-dinaphthyl-2-pentanol, was reduced by the same method as that for 1,3-DNBu. The residual oil was purified by a column chromatography on silica gel.

The oily product consists of *meso* and *racemo* isomers (*ca.* 1:2). The isomers were separated by a recycle gel permeation chromatography. After seventy cycles, fractionated samples were used for measurements. The purity of the isomers was found to be 85% for both isomers by the methyl proton resonance in NMR spectra. Emission intensity was corrected by this proportion of isomers. 2,4-DNPe: IR (KBr) 3050, 2950, 2920, 2860, 1630, 1600, 1505, 815, 740, and 475 cm^{-1}; NMR (CS_2) for *meso* isomer, $\delta=1.35$ (3H, d, $J=7$ Hz), 1.7—2.3 (1H, m), 2.5—2.95 (1H, m), and 7.16—7.80 (7H, m), NMR (CS_2) for *racemo* isomer, $\delta=1.24$ (3H, d, $J=6.8$ Hz), 1.96—2.18 (1H, m), 2.42—2.85 (1H, m), and 7.18—7.80 (7H, m). Found: C, 92.53; H, 7.48%; M^+, 324. Calcd for $C_{25}H_{24}$: C, 92.54; H, 7.46%; M, 324.

Measurements. Tetrahydrofuran (THF) was used as a solvent, which was purified by vacuum distillation after preliminary distillation over sodium metal. The concentration of samples was adjusted to *ca.* 10^{-4} mol dm^{-3} at which the intermolecular excimer formation is negligible. The sample solutions were deaerated by freeze-thaw cycles at 10^{-5} mmHg.† Absorption spectra were obtained with a Shimadzu UV-200S spectrophotometer, and fluorescence spectra with a Shimadzu spectrofluorophotometer model RF-502 in which the spectra were corrected for the instrumental response. The quantum yields of emission were determined relative to that of quinine sulfate in 1 mol dm^{-3} sulfuric acid, whose reported quantum yield is 0.51.[7] The decay curves of fluorescence were directly measured using a pulse fluorometer, TRW instrument model 31B or a single photon counting technique (Ortec Inc., 9200 nanosecond fluorescence spectrometer). The monomer and excimer fluorescence were separated by a suitable combination of filters. A quartz dewar equipped with a thermocouple was used for low temperature measurements.

Results and Discussion

Structural formulas of dinaphthylalkanes are summarized in Fig. 1. The alignment of aromatic groups favorable for intramolecular excimer formation can be achieved when two adjacent aromatic groups are separated by three carbon atoms of alkane chain. Hence, effective intramolecular excimer formation can be expected in these compounds. Absorption spectra for these samples are nearly the same and similar to those of 2-ethylnaphthalene (MNEt) corresponding to the monomeric unit. This indicates that there is no specific interaction between naphthyl groups in the ground state, each chromophore behaving like an isolated naphthalene unit. Figure 2 shows the fluorescence spectra of three typical compounds at −20 °C. They consist of two emission bands. The structured shorter wavelength band and the broad longer wavelength band are assigned to the monomer fluorescence and intramolecular excimer fluorescence, respectively. Relative fluorescence intensities of these bands differ considerably with sample. Although the molecular structures of these samples are very much alike as a common dimer unit, they show different efficiency in excimer formation. This can be attributed to the conformational relaxation processes after excitation of chromophores, from identity of the absorption and emission bands on the spectra of these samples.

† 1 mmHg=133.322 Pa.

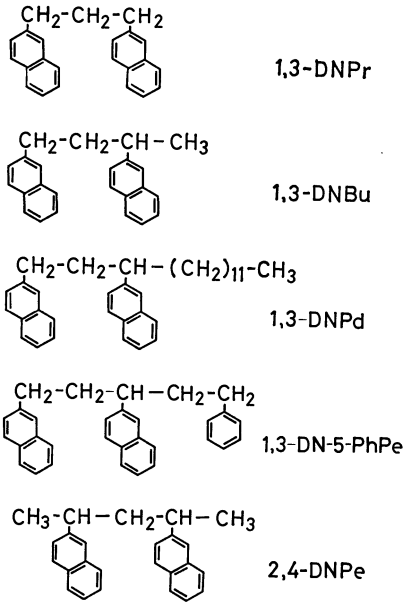

Fig. 1. Structures of dinaphthylalkanes studied in this work.

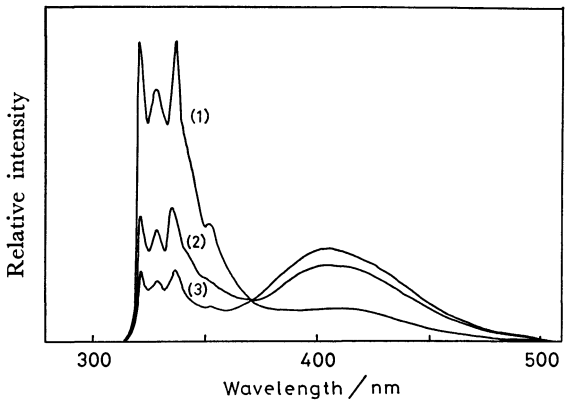

Fig. 2. Fluorescence spectra of the solutions of three typical compounds in THF at −20 °C.
(1): 2,4-DNPe (*rac*), (2): 1,3-DNPr, (3): 2,4-DNPe (*meso*).

The ratios of quantum yield (Φ_D) of excimer fluorescence to that of monomer fluorescence (Φ_M) for all samples at various temperatures are given in Table 1. Figure 3 shows the temperature dependence of Φ_M and Φ_D for three typical samples. Below −100 °C, fluorescence spectra of all samples are almost the same as those of MNEt. There is no indication of interaction between the naphthalene groups in the excited state when the molecular motion is suppressed. With rise in temperature, the monomer fluorescence is quenched steadily with increase in the excimer fluorescence. This shows that intramolecular excimer formation is governed by the conformational changes of the molecules. Some remarks are given concerning Table 1. (1) The compounds having alkyl substituents at one side of the dimer unit such as 1,3-DNBu, 1,3-DNPd, and 1,3-DN-5-PhPe, show the same efficiency of excimer formation, the efficiency being independent of the kind of substituent. (2) 1,3-DNPr

Table 1. Ratios of the quantum yield of excimer fluorescence to that of monomer fluorescence

Temp/°C	1,3-DNPr	1,3-DNBu	1,3-DNPd	1,3-DN-5-PhPe	2,4-DNPe (*meso*)	2,4-DNPe (*rac*)
0	2.6	3.2	3.6	3.6	5.2	0.59
−20	1.4	1.7	2.0	2.0	3.3	0.27
−40	0.61	0.83	0.89	0.98	1.9	0.10
−60	0.22	0.33	0.35	0.38	0.87	0.05

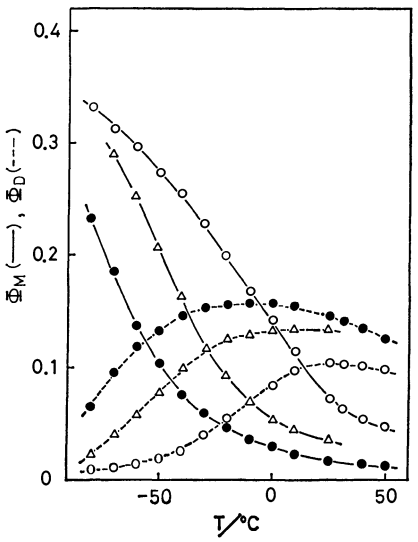

Fig. 3. Temperature dependence of quantum yields, Φ_M and Φ_D.
○: 2,4-DNPe (*rac*), △: 1,3-DNPr, ●: 2,4-DNPe (*meso*).

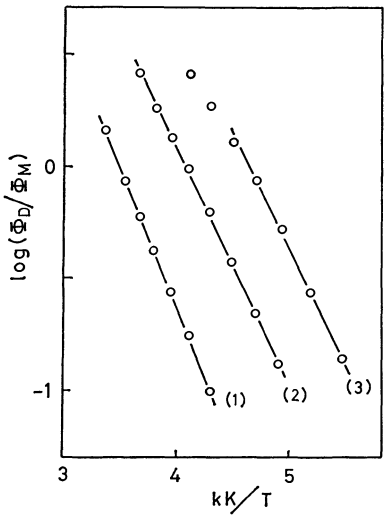

Fig. 4. Arrhenius plots of the ratio, Φ_D/Φ_M.
(1): 2,4-DNPe (*rac*), (2): 1,3-DNPr, (3): 2,4-DNPe (*meso*).

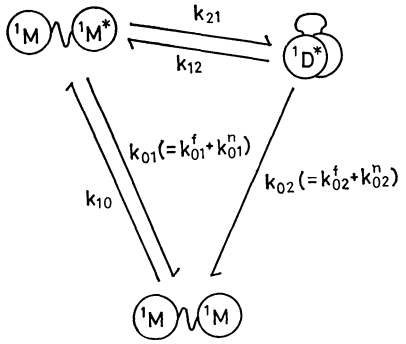

Fig. 5. Photophysical kinetic scheme of the energy dissipation processes. ^{1}M, ^{1}M*, and ^{1}D* represent the ground state of monomer, the excited singlet state of monomer, and the intramolecular excimer, respectively.

shows lower efficiency than that of 1,3-DNBu. (3) The highest efficiency of excimer formation is observed for 2,4-DNPe(*meso*), but its isomer 2,4-DNPe(*rac*) gives the lowest efficiency among the measured compounds. The effect of molecular configuration for intramolecular excimer formation appears typically in these isomers. This large difference in excimer formation for 2,4-DNPe between (*meso*) and (*rac*) is similar to the result of the steady state observation for diphenylpentanes.[10]

The activation energy, E_a, for the excimer formation process can be obtained in the low temperature region by the equation

$$\Phi_D/\Phi_M = K \exp(-E_a/RT),$$

where K is a constant. The plots are shown in Fig. 4. In all samples except for 2,4-DNPe(*rac*), E_a was found to be 4.8—5.3 kcal/mol.†† 2,4-DNPe(*rac*) gives a somewhat larger value of E_a, 5.5 kcal/mol. The activation energy required for intermolecular excimer formation of MNEt in THF was found to be 3.2—3.4 kcal/mol.[11] The larger activation energies of intramolecular excimers indicate methylene chain restriction in the conformational changes. Somewhat larger activation energy for 2,4-DNPe(*rac*) suggests that some other conformational restraints in the excimer formation process are imposed on this compound. Although the activation energies for *meso*- and *rac*-diphenylpentanes were reported by Bokobza *et al.*[10] to be 2.0 and 4.6 kcal/mol, respectively, no such large difference was found for the two isomers of 2,4-DNPe in the present investigation.

The scheme of photophysical kinetics including the intramolecular excimer formation process is given in Fig. 5. However, it is not clear which process causes the difference in the efficiency of excimer formation for these compounds. For the sake of clarification, all the rate constants in the kinetic scheme should be determined by the time-resolved measurements. Rise and decay curves of the excimer emission after excitation by a pulse with a half-width of about 2.5 ns, are

†† 1 cal=4.184 J.

Table 2. Intramolecular excimer formation rate constants and their activation energies

Temp/°C	$k_{21}/10^7$ s^{-1}					
	1,3-DNPr	1,3-DNBu	1,3-DNPd	1,3-DN-5-PhPe	2,4-DNPe (*meso*)	2,4-DNPe (*rac*)
50						17
25	21	28	29	29	79	8.7
0	12	17	17	17	41	3.6
−20	4.8	7.0	7.0	7.1	17	
−40	1.9	2.6	2.8	2.9	7.8	
−60	0.7	1.0	1.0	1.0	3.3	
E_a/kcal mol^{-1}	5.1	5.2	5.3	5.3	4.8	5.5

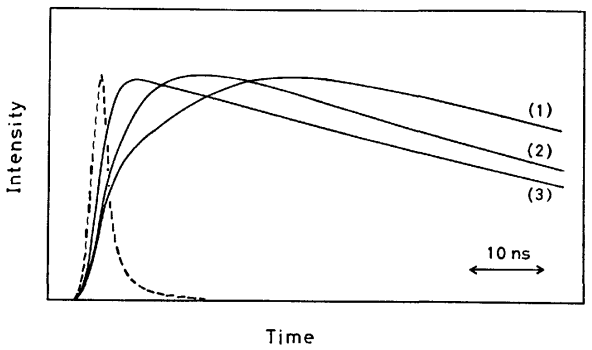

Fig. 6. Rise and decay curves of the intramolecular excimer fluorescence in THF at 25 °C.
(1): 2,4-DNPe (*rac*), (2): 1,3-DNPr, (3): 2,4-DNPe (*meso*). The broken line is the excitation light pulse.

shown in Fig. 6 for three typical samples at 25 °C. On the assumption that the actual lifetime of the monomer emission in the absence of the excimer formation process is equal to the lifetime of MNEt under the same conditions, all the rate constants given in Fig. 5 can be determined by analysis of the transient curves and the quantum yields, Φ_M and Φ_D.

The theoretical response functions $I_M(t)$ and $I_D(t)$, for the monomer and excimer fluorescence, are derived by

$$I_M(t) = C_M(e^{-\lambda_1 t} + Ae^{-\lambda_2 t}),$$
$$I_D(t) = C_D(e^{-\lambda_1 t} - e^{-\lambda_2 t}),$$

where C_M, C_D, A, λ_1, and λ_2 are given as functions of the rate constants,[1] and

$$\lambda_{1,2} = [k_{01}+k_{21}+k_{02}+k_{12} \mp \{(k_{01}+k_{21}-k_{02}-k_{12})^2 + 4k_{21}k_{12}\}^{1/2}]/2,$$
$$A = (k_{01}+k_{21}-\lambda_1)/(\lambda_2-k_{01}-k_{21}).$$

The value of A is too large to be estimated accurately from the monomer fluorescence decay curve in the intramolecular excimer systems. On the assumption mentioned above, the rate constants, k_{01}^f and k_{01}^n are determined by measurement of the quantum yield and lifetime of MNEt. The other rate constants, k_{21}, k_{12}, k_{02}^f, and k_{02}^n are then obtained from the observed values, λ_1, λ_2, Φ_M, and Φ_D, by using the following relations,

$$\Phi_M = k_{01}^f(k_{02}+k_{12})/\lambda_1\lambda_2,$$
$$\Phi_D = k_{02}^f k_{21}/\lambda_1\lambda_2,$$

Table 3. Kinetic rate constants at 25 °C

$k_{01}^f/10^7$ s^{-1}	0.49
$k_{01}^n/10^7$ s^{-1}	1.3
$k_{02}^f/10^7$ s^{-1}	0.16—0.22
$k_{02}^n/10^7$ s^{-1}	0.8 —1.2
$k_{12}/10^7$ s^{-1}	2.6 —0.8

$$\lambda_1 + \lambda_2 = k_{01} + k_{21} + k_{02} + k_{12},$$
$$\lambda_1\lambda_2 = (k_{01}+k_{21})(k_{02}+k_{12}) - k_{21}k_{12}.$$

The rate constant k_{21} values measured at various temperatures are given in Table 2, other rate constants at 25 °C for all the samples being summarized in Table 3. There is an appreciable difference in the pseudo-1st order rate constant k_{21} values of the association process among these compounds, although little change is seen in the other rate constants. It is apparent that the marked increase of the excimer formation efficiency observed in the steady state measurements is due to the large values of the association rate constant k_{21}.

The observed compounds seem to have the same geometrical alignment of the naphthyl groups in the excimer state. We might conclude that the rate constant k_{02} does not vary so much with sample. There is no considerable change in the dissociation rate constant k_{12}, although somewhat a larger value is obtained for 2,4-DNPe(*meso*). The value of k_{12} for the intermolecular excimers in concentrated solution of MNEt in THF is given by

$$k_{12} = A\exp(-E_d/RT),$$

where A, E_d, and R are the Arrhenius factor, the activation energy of the dissociation process, and the gas constant, respectively. The values for A and E_d were found to be 4.4×10^{15} s^{-1} and 7.7 kcal/mol, respectively. A much smaller value is obtained for k_{12} in the case of the intramolecular excimer than in the case of the intermolecular excimer. This is due to the binding effect of the methylene chain. The binding energy of the excimer state seems to be the same in the compounds we studied because of a similar molecular structure in the dimer unit. Therefore, it is understandable that there is no appreciable difference in the value of k_{12}. The methyl group of 2,4-DNPe(*rac*) should be situated in an unstable gauche position in the excimer conformation. However, the

unstable energy is too small to affect the dissociation rate constant.

For the association rate constant k_{21}, the compounds 1,3-DNBu, 1,3-DNPd, and 1,3-DN-5-PhPe show the same value. This indicates that the association rates are determined only by the configuration of the common dimer units, and the conformations in the dimer units are not much influenced by the substituent groups of the 3-position for these model compounds. This indicates that the rate of conformational relaxation in the terminal dimer units is not strongly affected by the increase of mass or chain length of these substituent groups. The effect of molecular weight on the rotational relaxation times was reported, *e.g.*, by the measurement of fluorescence depolarization,[12,13] ^{13}C NMR,[14] and ESR.[15] The results indicate that the relaxation time of molecular motions increases with increasing molecular weight. However, no such changes were observed in the case of intramolecular excimer systems. The observed rate constants of intramolecular excimer formation reflect the local segment motions of the end group of the molecule with respect to the molecular coordinate system. It seems that the molecular size of the alkane chain such as pentadecane, is too small to cause changes in the local segment motion and the local environment around the end groups.

Large differences in the association rate constants for 1,3-DNPr, 1,3-DNBu, and 2,4-DNPe(*meso*) and (*rac*) are observed (Table 2). First, let us discuss the results for 2,4-DNPe(*rac*) which gives the smallest value of k_{21}. The rate of intramolecular excimer formation is controlled by the internal rotational motion of the molecule from the equilibrium conformation in the ground state to the excimer one. From the analysis of NMR spectra,[16–18] we know that the preferred conformation for *racemo* dimers is situated at tt, indicating a planar conformation for the alkane chain. In order to reach the excimer conformation from the tt conformation, it is necessary to carry out an unfavorable conformational cange, $g^+ \rightleftarrows g^-$ with respect to the naphthyl groups. This seems to be the cause of the small values of k_{21} and the somewhat larger value of E_a for 2,4-DNPe(*rac*). Secondly, there are considerable differences in 1,3-DNPr, 1,3-DNBu, and 2,4-DNPe(*meso*). These differences are due to the equilibrium distribution of conformations at the ground state, whose distribution determines the initial positions of the naphthalene chromophores immediately after their excitation. Particularly, the population of the neighboring conformation to the excimer conformation seems to play an important role in the excimer formation rate (Fig. 7). The results are interpreted as follows: In 1,3-DNPr where $R_1=R_2=H$, the planar conformation with respect to the naphthyl groups (a) is most stable, the fraction of the neighboring conformation such as (b) not being large. In 1,3-DNBu where $R_1=H$ and $R_2=CH_3$, the neighboring conformation (b) becomes favorable owing to the steric hindrance of the methyl group. In 2,4-DNPe(*meso*) where $R_1=R_2=CH_3$, the conformational distribution seems to be predominantly in the neighboring conformation (b). According to the analysis of NMR

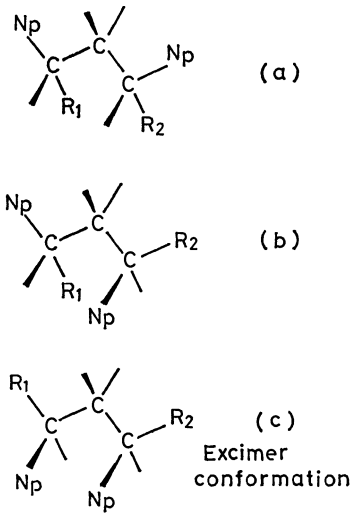

Fig. 7. Stable conformations of (a) 1,3-DNPr, (b) 1,3-DNBu and 2,4-DNPe (*meso*), and (c) the excimer conformation. Np: 2-naphthyl.

spectra for *meso*-diphenylpentane,[16–18] all other conformations have no appreciable fractions. The observed k_{21} values of the three compounds increase in this order. Thus, the association rate constants reflect the population of the neighboring conformation to the excimer state (c), and the rotational motion from this neighboring one to the excimer state.

The compounds we studied can be regarded as model compounds of poly(2-vinylnaphthalene) (PVN), which shows efficient intramolecular excimer formation.[7] 2,4-DNPe(*meso*) is considered to be a model compound of the isotactic sequence in PVN, the large value of k_{21} indicating the important role of isotactic sequence in the intramolecular excimer formation in vinyl aromatic polymers.

The authors wish to thank Dr. Yoshiteru Sakata, Osaka University, for the separation of the isomers of 2,4-DNPe by a recycle gel permeation chromatography. This work was supported by a Grant-in-Aid for Special Project Research on Photophysiology No. 411204 from the Japanese Ministry of Education, Science and Culture.

References

1) J. B. Birks, D. J. Dyson, and I. H. Munro, *Proc. R. Soc. London, Ser. A*, **275**, 575 (1963).
2) R. Speed and B. Selinger, *Aust. J. Chem.*, **22**, 9 (1969).
3) F. Hirayama, *J. Chem. Phys.*, **42**, 3163 (1965).
4) E. A. Chandross and C. J. Dempster, *J. Am. Chem. Soc.*, **92**, 3586 (1970).
5) G. E. Johnson, *J. Chem. Phys.*, **61**, 3002 (1974).
6) P. A. Avouris, J. Kordas, and M. A. El-Bayoumi, *Chem. Phys. Lett.*, **26**, 373 (1974).
7) S. Ito, M. Yamamoto, and Y. Nishijima, *Rep. Prog. Polym. Phys. Jpn.*, **19**, 421 (1976).
8) C. David, M. Piens, and G. Geuskens, *Eur. Polym. J.*, **12**, 621 (1976).
9) K. A. Zachariasse, W. Kühnle, and A. Weller, *Chem. Phys. Lett.*, **59**, 375 (1978).
10) L. Bokobza, B. Jasse, and L. Monnerie, *Eur. Polym.*

J., **13**, 921 (1977).
11) B. K. Selinger reported the activation energy for 2-methylnaphthalene in ethanol: 2.8 kcal/mol (*Aust. J. Chem.*, **19**, 825 (1966)). But, the activation energy for MNEt in THF was found to be 3.2—3.4 kcal/mol in this work.
12) M. Uchida, Doctral Thesis, Kyoto University, Kyoto, 1977.
13) S. Murase, Y. Suzuki, M. Yamamoto, and Y. Nishijima, *Rep. Prog. Polym. Phys. Jpn.*, **21**, 405 (1978).
14) A. Allerhand and R. K. Hailstone, *J. Chem. Phys.*, **56**, 3718 (1972).
15) A. T. Bullock, G. G. Cameron, and P. M. Smith, *J. Phys. Chem.*, **77**, 1635 (1973).
16) F. A. Bovey, F. P. Hood, E. W. Anderson, and L. C. Snyder, *J. Chem. Phys.*, **42**, 3900 (1965).
17) H. Pivcova, M. Kolinsky, D. Lim, and B. Schneider, *J. Polym. Sci., Polym. Symp.*, **22**, 1093 (1969).
18) T. Moritani and Y. Fujiwara, *J. Chem. Phys.*, **59**, 1175 (1973).

Molecular Structures of the Reduced 1,2,4-Triazine Derivative and Its Reaction Product with Electron-deficient Acetylene

Hiroshi Ayato,* Isao Tanaka, Takashi Yamane, Tamaichi Ashida, Tadashi Sasaki, Katsumaro Minamoto, and Katsuhiko Harada

Department of Applied Chemistry, Faculty of Engineering, Nagoya University, Chikusa-ku, Nagoya 464

(Received April 9, 1980)

The molecular structures of 3-methylthio-2-methyl-5,6-diphenyl-2,5-dihydro-1,2,4-triazine (**1**) and its reaction product with dimethyl acetylenedicarboxylate, 5,6-bis(methoxycarbonyl)-2-methyl-1-methylthio-4,8-diphenyl-2,3,7-triazabicyclo[3.3.0]octa-3,6-diene (**2**), were determined by the X-ray method. The former belongs to the triclinic system $P\bar{1}$, with $Z=2$, $a=10.776(2)$, $b=10.203(2)$, $c=8.556(1)$ Å, $\alpha=105.44(2)$, $\beta=104.94(2)$, and $\gamma=60.31(2)°$; the latter belongs to the orthorhombic system $Pca2_1$, with $Z=4$, $a=18.166(2)$, $b=7.444(2)$, and $c=16.080(2)$ Å. Both structures were solved by the direct method. The final R-factors are 0.075 for **1** and 0.048 for **2**. In Compound **1** the dihydrotriazine ring is in the boat form, while in Compound **2** both of the *cis*-fused five-membered rings are in the envelope form.

Unlike the well-studied oxidation reaction of 1,2,4-triazines, the reduction chemistry here is still not completely established. Paudler has suggested that 1,2,4-triazines undergo covalent hydration across the N(4)–C(5) bond,[1] and Neuenhoeffer has shown that they can act as dienes in the Diels-Alder reaction.[2] Therefore, the reduced compound of 3-methylthio-5,6-diphenyl-1,2,4-triazine with $NaBH_4$ would be methylated by methyl iodide to give **1′**, and the reaction of **1′** with dimethyl acetylenedicarboxylate (DMAD) would produce **2′**.[3]

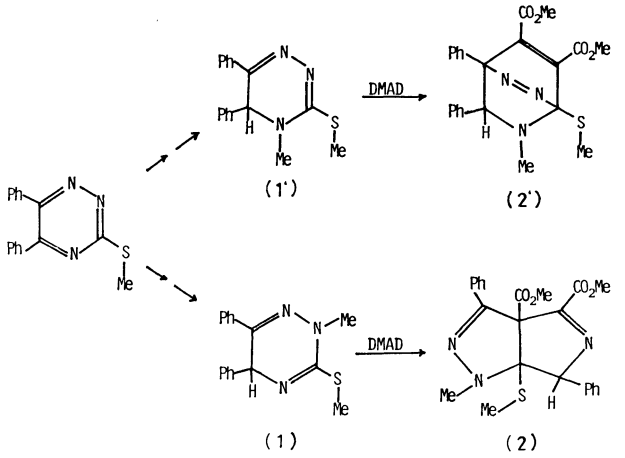

The present X-ray study was attempted in order to confirm the structures of those reaction products; it showed that they were **1** and **2** instead of **1′** and **2′**. The detailed descriptions of their structures will be given in this paper.

Experimental

Compound 1. The intensity data were collected on a Rigaku automated four-circle diffractometer at the Ultra High Intensity X-Ray Diffraction Laboratory of this university, using graphite-monochromatized Mo $K\alpha$ radiation. The ω-2θ scan method with the scan speed of 8°/min (2θ) was applied. A total of 2749 independent reflections up to 50° (2θ) were collected. The crystal used for the experiment had the dimensions of $0.3\times0.3\times0.2$ mm³.

Crystal Data: $C_{17}H_{17}N_3S$, $P\bar{1}$, $a=10.776(2)$, $b=10.203(2)$, $c=8.556(1)$ Å, $\alpha=105.44(2)$, $\beta=104.94(2)$, $\gamma=60.31(2)°$, $V=778.76$ Å³, $Z=2$, $d_{obsd}=1.25$, $d_{calcd}=1.260$ g cm^{-3}, μ(Mo $K\alpha$) = 2.042 cm^{-1}.

Compound 2. The intensity data were collected on a Hilger & Watts four-circle diffractometer at the Faculty of Science, Nagoya University, using Ni-filtered Cu $K\alpha$ radiation. The ω-scan method for $2\theta\leqq80°$ and the ω-2θ scan for $80°\leqq2\theta\leqq114°$ were applied, and 1528 independent reflections were obtained. The crystal dimensions were $0.4\times0.2\times0.4$ mm³.

Crystal Data: $C_{23}H_{23}N_3O_4S$, $Pca2_1$, $a=18.166(2)$, $b=7.444(2)$, $c=16.080(2)$ Å, $V=2174.46$ Å³, $Z=4$, $d_{obsd}=1.33$, $d_{calcd}=1.336$ g cm^{-3}, μ(Cu $K\alpha$) = 15.71 cm^{-1}.

Structure Determination and Refinement

The intensity data of both compounds were corrected for Lorentz and polarization effects, but not for absorption. Both structures were solved by the *MULTAN* program[4] and refined by the block-diagonal least-squares procedure with the *HBLS V* program.[5] All the hydrogen atoms were located on the difference Fourier map. In the refinement, the function minimized was $\Sigma w(|F_o|-|F_c|)^2$, with $w=(\sigma^2(F)+a|F_o|+b|F_o|^2)^{-1}$ for $|F_o|>0$ and $w=c$ for $|F_o|=0$, where $\sigma(F)$ is the standard deviation based on the counting statistics. The thermal parameters of three hydrogen atoms in the *S*-methyl group of **1** were fixed at 8.0 Å² throughout the refinement, but all the others were subjected to the refinement. The final R-factors were 0.075 for **1** and 0.048 for **2**. The atomic scattering factors were taken from the International Tables for X-Ray Crystallography.[6] All the calculations were carried out on a FACOM 230-75 computer at Nagoya University. The final atomic parameters are given in Tables 1 and 2.[7]

Results and Discussion

Compound 1. The bond lengths and angles are shown in Fig. 1, together with the atom-numbering system. The estimated standard deviations are 0.003—0.005 Å for the bond lengths and 0.2—0.4° for the angles. The equations of the best planes are listed in Table 3. A stereoscopic view of the molecule, as drawn by the *ORTEP II* program,[8] is shown in Fig. 2.

The dihydrotriazine ring is folded at N(2) and C(2) to take a boat form, with the dihedral angle between Plane (I) (N(2), N(1), C(3), C(2), and C(12)) and Plane (II) (N(2), C(1), N(3), C(2), and S) of 146.5°. The phenyl ring bonded to C(2) is in an

Table 1. Atomic parameters and estimated deviations of (**1**)

(a) Non-hydrogen atoms ($\times 10^4$ for the positional parameters and $\times 10^2$ for the thermal parameters).

Atom	x	y	z	B_{eq}/Å^2 a)	Atom	x	y	z	B_{eq}/Å^2 a)
S	5124(1)	2883(1)	3810(1)	543	C(8)	5700(2)	8342(2)	2900(2)	493
N(1)	8921(1)	2101(1)	3256(1)	402	C(9)	6687(2)	8478(2)	4233(2)	484
N(2)	7759(1)	2594(1)	4067(1)	426	C(10)	7850(2)	7197(2)	4735(2)	495
N(3)	6061(1)	3778(1)	1903(1)	354	C(11)	8037(2)	5754(2)	3899(2)	421
C(1)	6395(2)	3153(2)	3150(2)	378	C(12)	9840(2)	2202(2)	1094(2)	377
C(2)	7195(2)	4056(2)	1618(2)	332	C(13)	9797(2)	3085(2)	82(2)	492
C(3)	8658(2)	2761(2)	2037(2)	345	C(14)	10914(2)	2519(3)	−833(3)	654
C(4)	8167(2)	1725(3)	5389(2)	651	C(15)	12043(2)	1100(3)	−731(3)	698
C(5)	3523(2)	3896(3)	2470(3)	707	C(16)	12101(2)	225(2)	270(3)	600
C(6)	7058(1)	5605(2)	2557(2)	310	C(17)	11018(2)	758(2)	1180(2)	470
C(7)	5882(2)	6917(2)	2055(2)	412					

a) The equivalent isotropic temperature factor as defined by W. C. Hamilton (*Acta Crystallogr.*, **12**, 609 (1959)).

(b) Hydrogen atoms ($\times 10^3$ for positional parameters and $\times 10$ for thermal ones).

Atom	Bonded to	x	y	z	B/Å^2	Atom	Bonded to	x	y	z	B/Å^2
H(1)	C(2)	704(1)	409(1)	46(1)	10(3)	H(10)	C(9)	653(1)	948(1)	481(2)	30(4)
H(2)	C(4)	743(2)	225(2)	605(2)	51(6)	H(11)	C(10)	862(2)	724(2)	573(2)	41(5)
H(3)	C(4)	911(2)	180(2)	610(3)	68(7)	H(12)	C(11)	886(2)	482(2)	423(2)	36(5)
H(4)	C(4)	828(2)	65(2)	488(2)	59(6)	H(13)	C(13)	901(1)	412(2)	0(2)	25(4)
H(5)	C(5)	270(2)	397(3)	284(3)	80a)	H(14)	C(14)	1074(2)	322(2)	−153(2)	50(6)
H(6)	C(5)	358(2)	341(3)	145(3)	80a)	H(15)	C(15)	1274(2)	70(2)	−138(2)	53(6)
H(7)	C(5)	350(2)	488(3)	260(3)	80a)	H(16)	C(16)	1286(2)	−81(2)	28(2)	50(5)
H(8)	C(7)	516(2)	680(2)	109(2)	30(4)	H(17)	C(17)	1097(2)	17(2)	193(2)	30(4)
H(9)	C(8)	488(2)	924(2)	250(2)	43(5)						

a) These parameters were fixed.

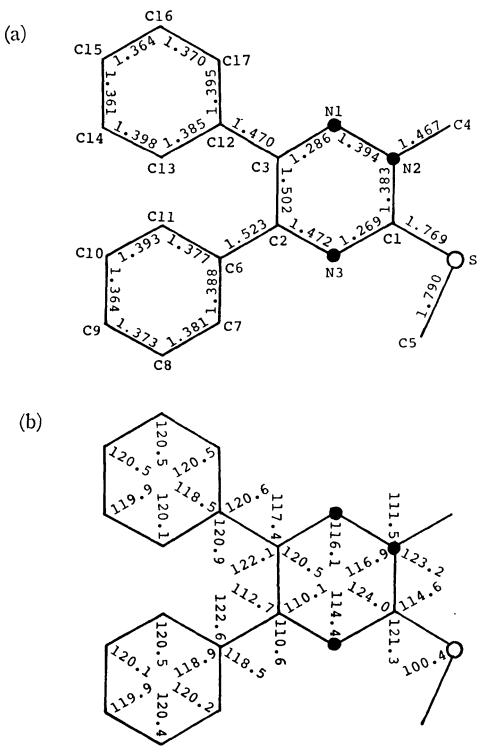

Fig. 1. Bond lengths and angles of **1**. (a) Bond lengths (l/Å), and (b) bond angles (ϕ/°).

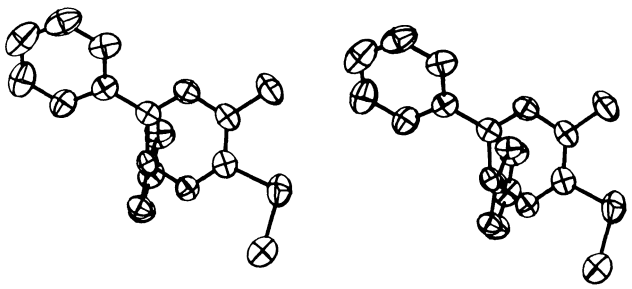

Fig. 2. A stereoscopic veiw of **1**. The atoms are represented by thermal ellipsoids drawn at the 50% probability level.

axial position with the torsion angle (C(3)–C(2)–C(6)–C(11)) of 14.1°, so that it can avoid close interaction with the C(3)-phenyl group.

The N(1)–C(3) and C(1)–N(3) double-bond lengths are 1.286 Å and 1.269 Å respectively. The N(3)–C(2) bond length is compatible with the single-bond distance, while the N(2)–C(1) bond length of 1.383 Å is significantly shorter and the N(1)–N(2) of 1.394 Å is shorter than the single-bond distance of 1.44 Å.[9] These shortenings and the coplanarity of the C(3)-phenyl group and Plane (I) are due to the delocalization of the π-electrons and lone-pair electrons of N(2). The sp^2 character of the N(2) atom is further evidenced by the planar arrangement of the bonded atoms, as is indicated by the sum of the bond angles, 351.6°. The C(1)–S bond, 1.769 Å, is shorter than the normal

TABLE 2. ATOMIC PARAMETERS AND ESTIMATED STANDARD DEVIATIONS OF (2)

(a) Non-hydrogen atoms ($\times 10^4$ for the positional parameters and $\times 10^2$ for the thermal parameters).

Atom	x	y	z	B_{eq}/Å^2	Atom	x	y	z	B_{eq}/Å^2
S	3460(1)	6042(1)	4590(1)	374	C(9)	2932(2)	1909(7)	1833(3)	399
O(1)	3913(1)	2685(4)	3520(2)	401	C(10)	2633(3)	401(7)	1450(4)	453
O(2)	4654(1)	3852(4)	2544(3)	405	C(11)	1896(3)	265(9)	1303(4)	552
O(3)	3573(2)	5346(9)	901(3)	778	C(12)	1440(3)	1686(10)	1545(4)	520
O(4)	4649(2)	6727(5)	993(2)	468	C(13)	1724(2)	3171(8)	1939(4)	431
N(1)	2299(2)	6055(5)	2839(3)	382	C(14)	2233(3)	8586(9)	3767(5)	593
N(2)	2668(2)	7376(5)	3257(3)	401	C(15)	2709(3)	4449(8)	4669(4)	531
N(3)	4113(2)	8199(5)	2446(2)	339	C(16)	4669(2)	8306(6)	3838(3)	337
C(1)	3554(2)	5392(6)	2798(3)	272	C(17)	4691(3)	9115(7)	4620(4)	435
C(2)	2752(2)	4885(6)	2554(3)	279	C(18)	5334(3)	9098(7)	5081(4)	482
C(3)	3403(2)	6762(6)	3508(3)	309	C(19)	5973(3)	8308(8)	4762(3)	492
C(4)	3959(2)	8315(6)	3339(3)	304	C(20)	5957(2)	7576(9)	3983(5)	520
C(5)	3916(2)	6661(6)	2178(3)	279	C(21)	5308(2)	7547(7)	3509(3)	384
C(6)	4045(2)	3812(5)	3014(3)	274	C(22)	4028(2)	6170(6)	1278(3)	333
C(7)	5181(2)	2400(8)	2676(5)	528	C(23)	4801(3)	6222(8)	123(4)	603
C(8)	2484(3)	3300(6)	2089(3)	331					

(b) Hydrogen atoms ($\times 10^3$ for positional parameters and $\times 10$ for thermal ones).

Atom	Bonded to	x	y	z	B/Å^2	Atom	Bonded to	x	y	z	B/Å^2
H(1)	C(4)	368(2)	940(6)	348(4)	15(10)	H(13)	C(15)	268(4)	395(8)	530(5)	48(18)
H(2)	C(7)	564(4)	260(11)	233(6)	61(20)	H(14)	C(15)	279(3)	337(10)	425(5)	46(17)
H(3)	C(7)	495(3)	112(11)	253(6)	58(21)	H(15)	C(15)	221(3)	516(7)	453(5)	34(14)
H(4)	C(7)	531(3)	233(11)	329(7)	60(21)	H(16)	C(17)	418(3)	980(7)	487(4)	34(14)
H(5)	C(9)	349(2)	179(8)	196(4)	24(12)	H(17)	C(18)	529(3)	969(7)	566(4)	30(13)
H(6)	C(10)	300(3)	−77(8)	129(5)	36(15)	H(18)	C(19)	646(2)	838(7)	513(4)	25(12)
H(7)	C(11)	165(3)	−86(9)	104(5)	44(16)	H(19)	C(20)	641(2)	704(9)	371(4)	32(15)
H(8)	C(12)	86(3)	155(8)	142(4)	32(14)	H(20)	C(21)	531(2)	690(9)	290(4)	33(14)
H(9)	C(13)	137(3)	427(8)	210(5)	37(15)	H(21)	C(23)	533(2)	673(8)	8(5)	32(13)
H(10)	C(14)	175(3)	885(8)	347(4)	36(15)	H(22)	C(23)	439(3)	677(10)	−21(5)	50(17)
H(11)	C(14)	253(5)	955(7)	388(6)	57(19)	H(23)	C(23)	477(3)	478(7)	8(4)	33(14)
H(12)	C(14)	209(3)	802(10)	439(5)	46(17)						

TABLE 3. BEST PLANES OF (1)

(a) Equations ($X=ax+0.4953by-0.2578cz$, $Y=0.8687by-0.1595cz$, $Z=0.9529cz$)

Plane (I): N(1), N(2), C(2), C(3), C(12)
$0.5504X+0.5556Y+0.6232Z-7.8915=0$

Plane (II): S, N(2), N(3), C(1), C(2)
$0.0230X+0.7858Y+0.6180Z-3.6336=0$

Plane (III): C(2), C(6), C(7), C(8), C(9), C(10), C(11)
$0.7898X+0.1161Y-0.6023Z-7.0700=0$

Plane (IV): C(3), C(12), C(13), C(14), C(15), C(16), C(17)
$0.5904X+0.2788Y+0.7574Z-7.9449=0$

(b) Dihedral angles (ϕ/°) between the planes
(I)—(II) 146.5 (I)—(IV) 162.2 (II)—(III) 105.2

(c) Displacements ($\delta/10^{-3}$ Å) of atoms from the planes

(I)		(II)		(III)		(IV)	
N(1)	−32	S	−28	C(2)	12	C(3)	14
N(2)	26	N(2)	11	C(6)	−10	C(12)	−9
C(2)	−6	N(3)	62	C(7)	−10	C(13)	−9
C(3)	−5	C(1)	8	C(8)	6	C(14)	1
C(12)	18	C(2)	−52	C(9)	5	C(15)	11
C(4)[a]	42	C(4)[a]	99	C(10)	1	C(16)	1
		C(5)[a]	−180	C(11)	−4	C(17)	−9

a) Atoms not included in the best-plane calculations.

C–S single-bond length of 1.81 Å, with a small amount of double-bond character. Consequently, the C(5) atom deviates from Plane (II) by only 0.18 Å, and a short contact, 2.893 Å, occurs between C(5) and N(3). Such a shortening is also observed in 2-(methylthio)benzothiazole,[10] in which the C–S bond length is 1.77 Å.

Compound 2. The bond lengths and angles are shown in Fig. 3, together with the atom-numbering system. The estimated standard deviations are 0.006—0.012 Å for the bond lengths and 0.3—0.8° for the angles. The equations of the best planes are listed in Table 4. A stereoscopic view of the molecule is shown in Fig. 4.

The molecule consists of two central *cis*-fused five-membered rings and six peripheral side groups directly bonded to them. Each of the five-membered rings is in the envelope form. In one five-membered ring, C(1), C(2), N(1), and N(2) are coplanar (Plane (I)), including C(8) of the phenyl group, while in the other ring, C(1), C(5), N(3), and C(4) are coplanar (Plane (II)) with C(22) of the methoxycarbonyl group. These two planes form an angle of 107.7°. The C(3) atom is out of these planes by 0.47 Å and 0.39 Å respectively.

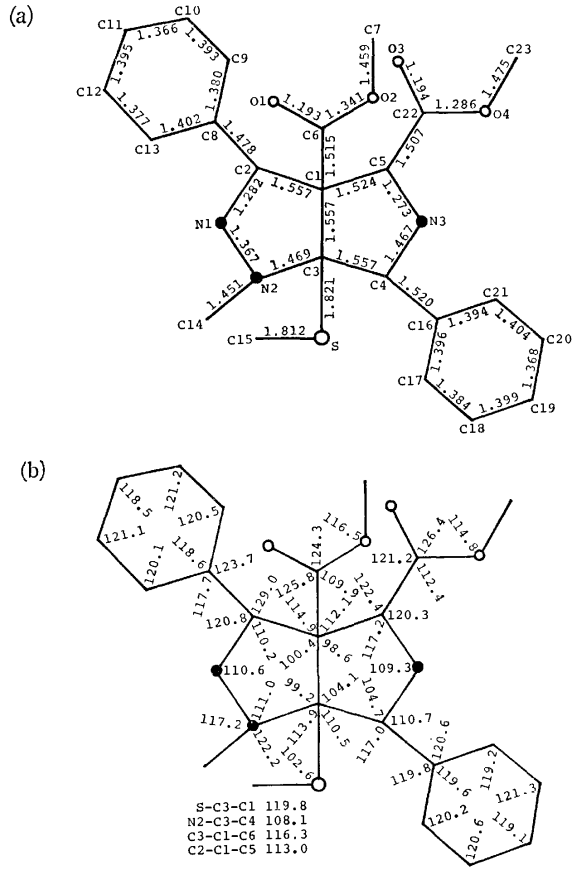

Fig. 3. Bond lengths and angles of **2**. (a) Bond lengths (l/Å), and (b) bond angles (ϕ/°).

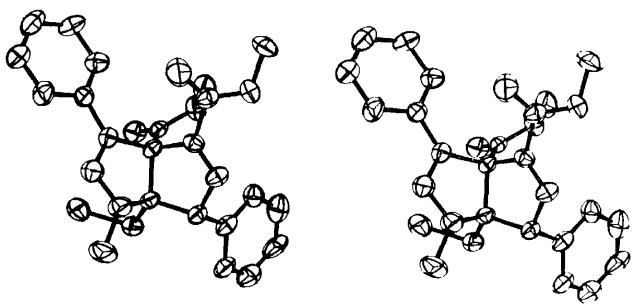

Fig. 4. A stereoscopic view of **2**. The atoms are represented by thermal ellipsoids drawn at the 50% probability level.

Plane(I) and the C(2)-phenyl group are almost coplanar (the dihedral angle is 174.9°), while the dihedral angle between Plane (II) and the C(5)-methoxycarbonyl group is 140.9°, the latter being also roughly planar. As is shown in Fig. 4, three groups, methylthio, C(1)-methoxycarbonyl and C(4)-phenyl, which protrude from the fused ring to the same side, take conformations so as to avoid close interactions among the six peripheral groups.

It may be worth noting the short bond lengths of C(2)–C(8) and N(1)–N(2) compared with the corresponding single ones.[9] These observations and the coplanarity described above suggest that the delocalization of π-electrons occurs between the C(2)-phenyl ring and N(2) *via* C(2) and N(1). The sp^2 character of the N(2) atom is found in this compound as well as in Compound **1**, and the sum of the bond angles around the N(2) atom is 350.4°.

Table 4. Best planes of (**2**)

(a) Equations ($X=ax$, $Y=by$, $Z=cz$)

Plane (I): N(1), N(2), C(1), C(2), C(8)
$0.0858X+0.5174Y-0.8515Z+1.2001=0$

Plane (II): N(3), C(1), C(4), C(5), C(22)
$0.8989X-0.3803Y+0.2175Z-5.2673=0$

Plane (III): C(2), C(8), C(9), C(10), C(11), C(12), C(13)
$0.1263X+0.4457Y-0.8862Z+1.3175=0$

Plane (IV): C(4), C(16), C(17), C(18), C(19), C(20), C(21)
$0.2534X+0.8772Y-0.4078Z-5.0666=0$

Plane (V): O(1), O(2), C(1), C(6)
$0.4590X+0.5501Y+0.6977Z-8.3121=0$

Plane (VI): O(3), O(4), C(5), C(22)
$0.4305X-0.8585Y+0.2785Z+0.2193=0$

(b) Dihedral angles (ϕ/°) between the planes

(I)—(II)	107.7	(I)—(III)	174.9	(I)—(V)	105.7
(II)—(IV)	101.4	(II)—(V)	110.8	(II)—(VI)	140.9

(c) Displacements (δ/10^{-3} Å) of atoms from the planes

(I)		(II)		(III)	
N(1)	4	N(3)	17	C(2)	70
N(2)	2	C(1)	12	C(8)	−6
C(1)	0	C(4)	−11	C(9)	−12
C(2)	−14	C(5)	−3	C(10)	12
C(8)	2	C(22)	−11	C(11)	16
				C(12)	−6
				C(13)	−2

(IV)		(V)		(VI)	
C(4)	5	O(1)	1	O(3)	1
C(16)	10	O(2)	0	O(4)	1
C(17)	−16	C(1)	2	C(5)	1
C(18)	1	C(6)	−3	C(22)	−2
C(19)	15	C(7)[a]	8	C(23)[a]	50
C(20)	−11				
C(21)	−4				

a) Atoms not included in the best-plane calculations.

The authors would like to express their thanks to Prof. Jiro Tanaka of Nagoya University for his very kind permission to use the diffractometer.

References

1) W. W. Paudler and L. K. Chen, *J. Heterocycl. Chem.*, **7**, 767 (1970).
2) H. Neunhoeffer and H. W. Fruhauf, *Ann. Chem.*, **758**, 125 (1972).
3) T. Sasaki, K. Minamoto, and K. Harada, *Heterocycles*, **10**, 93 (1978).
4) G. Germain, P. Main, and M. M. Woolfson, *Acta Crystallogr., Sect. A*, **27**, 368 (1971).
5) T. Ashida, "The Universal Crystallographic Computing System-Osaka," The Computation Center, Osaka University (1973), p. 55.
6) "International Tables for X-Ray Crystallography," The Kynoch Press, Birmingham (1974), Vol. IV, p. 72.
7) The F_o and F_c tables and anisotropic temperature factors are available at the Office of the Editor of the Bulletin of the Cemical Society of Japan as Document No. 8037.
8) C. K. Johnson, "ORTEP II," Report ORNL-3794, Oak Ridge National Laboratory, Tennessee (1971).
9) "International Tables for X-Ray Crystallography," The Kynoch Press, Birmingham (1968), Vol. III, p. 270.
10) P. J. Wheatley, *J. Chem. Soc.*, **1962**, 3636.

Isobaric Thermogravimetry of the Gas Encapsulation with Molecular Sieves A

Tetsuo TAKAISHI, Yujiro KAMEI,† Atsushi YUSA,† and Tatsuo OHGUSHI*

School of Material Science, Toyohashi University of Technology, Toyohashi 440

† *Komatsu Electronics Metals Co., Hiratsuka 254*

(Received April 22, 1980)

The isobaric gas sorption with (Na,Ca)–A and (K,Ca)–A zeolites was measured gravimetrically in temperature ranges of −160——40 °C for O_2 and N_2, and of room temperature—200 °C for n-C_4H_{10}. The sorption hysteresis, *i.e.*, the gas encapsulation was observed. The maximum point, in the temperature rising branch of the isobar, was located at about −90 °C for N_2 and in the range 120—170 °C for n-C_4H_{10}, and shifted to the lower temperature side with the increasing content of calcium for n-C_4H_{10}. The observed results are explained in terms of an incomplete blocking action of cations on window sites. This incompleteness was amplified by bivalent cations introduced onto other sites than the window sites, and the sieving character of the ion-exchanged zeolite was delicately modified.

The unit cell of zeolite A is a cube with a side-length of about 1.2 nm, at the center of which there exists a nearly spherical cavity accommodating sorbed molecules. This cavity is surrounded by six 8-membered oxygen rings, which costitute windows to the cavity. In commercial molecular sieves 3A and 4A, all of these windows are blocked by K^+ and Na^+, respectively.[1] The molecular sieving characters of these zeolites are primarily determined by the size of the aperture of the *partially-blocked* windows. The effective size of the aperture, however, depends upon temperature. At higher temperatures, a situation is realized that larger molecules, which are not sorbed at lower temperatures, are able to be sorbed. If the temperature is lowered after such molecules being sorbed at higher temperatures, the windows are closed and the sorbed molecules are encapsulated.[2]

Usually the encapsulation process requires high temperature and pressure, in order to ensure a reasonable rate and amount of sorption. However, the encapsulation may be realized at not so much high temperatures and pressures as usual, if the rate of sorption is increased by some means. This is a problem of the present work.

Experimental

The block diagram of measuring system used is shown in Fig. 1(a). A Cahn RG-type electro-balance was used which was drastically improved in the authors' laboratory to be bakable at 180 °C.[3] The pressure of adsorbed gas was measured with a MKS Baratron type-210 diaphragm gauge, and controlled within ±0.5% of the preset value with a Granville-Phillips type-216 automatic pressure controller by adding some manual operations. A main pumping system consisted of a sorption-pump and an ion-spattering pump of a capacity of 50 $l\,s^{-1}$. Apart from gas handling system, the apparatus was free from grease or oil, and a back-ground pressure of 10^{-5} Pa was easily attained in a few hours by a mild baking-out.

The leg of the balance and cryostat are shown in Fig. 1(b). Radiation heating from the upper part of the apparatus and disturbance due to convection were reduced by a copper shield, S, which acted at the same time as a gasket for conflat flange. A sheath IC junction, J, was fixed on the lowest conflat flange by copper wire.

The temperature of the sample was rised or lowered at approximately constant rates, in a similar manner to the

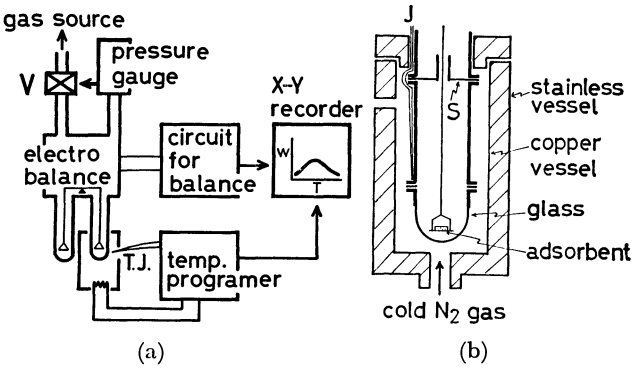

Fig. 1. Apparatus for isobaric thermogravimetry of gas sorption.
(a) Main system: V, Granville-Phillips type-216 automatic pressure controller, (b) details of the leg of balance-chasis for sorbent: thick line, made of stainless steel; thin line, made of glass.

usual thermo-gravimetry. Low temperatures were realized by cooling with cold nitrogen gas supplied from a liquid nitrogen reservoir by electric heating, and controlled within ±0.5 °C of a preset value. Before the sorbate gas was introduced, 10 Pa of He gas was introduced to facilitate the rapid temperature equilibration.

Powdery zeolites of given composition were prepared by a method described in the preceding papers.[4,5] These zeolites were pressed in a form of disc, 13 mm in diameter and about 500 mg in weight. Prior to sorption experiments, zeolite samples were carefully dehydrated, at 390—400 °C for about 100 h, the residual pressure being 10^{-5} Pa or so. This dehydration condition was far better than that in conventional sorption experiments. Sorbate gases, N_2, O_2, and n-C_4H_{10} (supplied from Takachiho Chemical Co.), had nominal purities better than 99.9, 99.8, and 99.7%, respectively, according to mass-spectroscopic analyses and were used after further drying with 13 X zeolite.

Results

(Na, Ca)–A Zeolites. The sorption isobar was measured for n-C_4H_{10} and N_2 with $(Na_{12-2x}Ca_x)$–A zeolite, in which $x=1.93$. According to the preceding paper,[5] this zeolite is classified as 4A in their molecular sieving characters. The temperature was rised or lowered at a constant rate from −155 to −50 °C for N_2 at a constant pressure of 9.3×10^3 Pa,

while for n-C_4H_{10} from room temperature to 200 °C at 8.3×10^3 Pa. The temperature was not rised above 200 °C for fear of cracking and polymerization of n-C_4H_{10}. The form of sorption isobar depended upon the rate of temperature rise. Representative curves for $(Na_{12-2x}Ca_x)$–A are shown in Fig. 2, which shows that the rate of sorption is so low that equilibrium is not attained at 200 °C.

The effect of the composition to the form of the isobar was studied, results being shown in Fig. 3. The peak, in the temperature rising branch, shift to the lower temperature side with the increasing content of calcium. The shift was remarkable for n-C_4H_{10}, but not so for N_2.

(K,Ca)–A Zeolites. The molecular sieving action of $(K_{12-2x}Ca_x)$–A zeolite drastically changes in the neighbourhood of $x=4$.[4] This tendency was further studied in detail by the present method. Sorption isobars for O_2 and N_2 are shown in Fig. 4. Large amounts of N_2 and O_2 were sorbed, virtually without an activation energy, into $(K_{3.58}Ca_{4.21})$–A at −196 °C, so that this zeolite may be classified as 5A. On the other hand, $(K_{4.30}Ca_{3.85})$–A sorbed very small amounts of these gases, being classified as 3A. A diagram in the lower part of Fig. 4 shows that a small amount of sorption took place even at −196 °C without any activation energy, and that some of windows were in the state of "open" against to O_2 and N_2. In the terminology of percolation theory, however, the percolatable fraction of cell is less than 0.03.

As for n-C_4H_{10}, quite different features were observed as shown in Fig. 5; namely, the peak appeared in the isobar with $(K_{4.30}Ca_{3.85})$–A. This means that n-C_4H_{10} was allowed to pass through the window blocked by K^+ at temperatures higher than 100 °C.

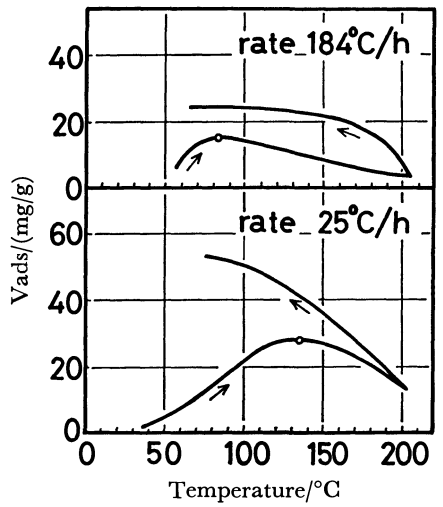

Fig. 2. Sorption isobar and the rate of temperature change.
Zeolite: $(Na_{8.14}Ca_{1.93})$–A, gas: n-C_4H_{10} at constant pressure of 8.3×10^3 Pa (=62 Torr), ○: maximum point in the temperature rising branch.

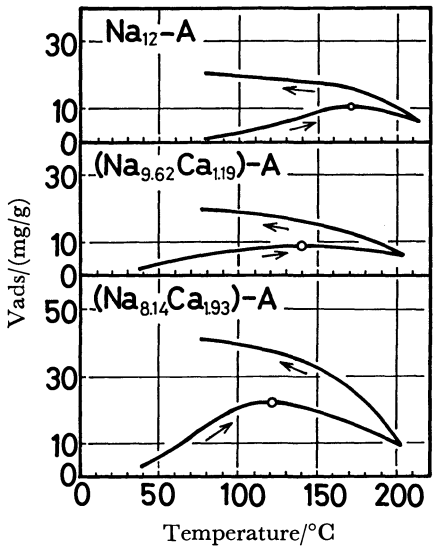

Fig. 3. Effect of the zeolite composition to the sorption isobar of n-C_4H_{10}.
Pressure: 8.3×10^3 Pa (=62 Torr), rate of temperature change: 68 °C h^{-1}, ○: maximum point in the temperature rising branch.

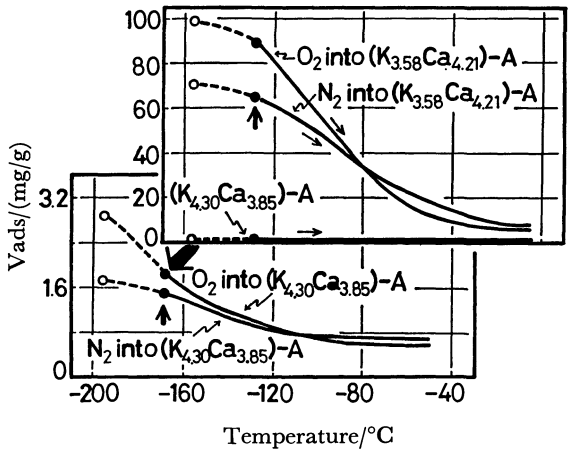

Fig. 4. Sorption isobar of N_2 and O_2 with (K,Ca)–A zeolites.
The continuous temperature rise start from the point designated by arrows; ○: measured by dipping in a liquid nitrogen bath, $P(O_2)=1.6\times10^4$ Pa (=120 Torr), $P(N_2)=9.3\times10^3$ Pa (=70 Torr), rate of temperature change, 50 °C h^{-1} for O_2, 100 °C h^{-1} for N_2.

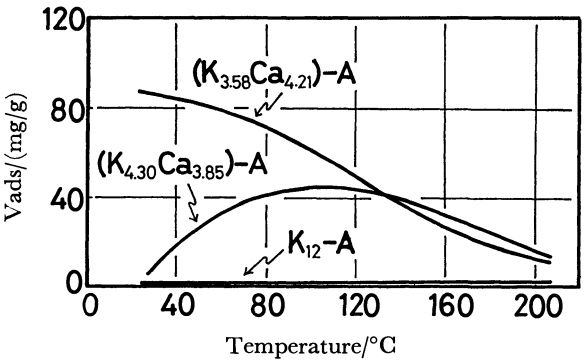

Fig. 5. Sorption isobar of n-C_4H_{10} with (K,Ca)–A zeolites.
Rate of temperature rise: 68 °C h^{-1}, pressure: 8.3×10^3 Pa (=62 Torr).

Discussion

Let us outline, for a better understanding of the sieving action, the structure of dehydrated zeolite A and cation distribution in it. Figure 6 shows its framework and cation sites. Abbreviations are used as the α-site for the site near the plane of the 8-membered oxygen ring, the β-site for the site near the center of the 6-membered oxygen ring, and the γ-site for the site near the center of the 4-membered oxygen ring. At the center of the unit cell, there exists a large cavity, named the α-cage, which is nearly spherical with a diameter of 1.14 nm and can accomodate visiting gas molecules. The 8-ring constitutes a window to the cavity, and the sieving character of zeolite A is determined by the state of the 8-ring, that is, whether the α-site is unoccupied or occupied by a cation and by what kind of cation. On the other hand, the occupancy factor on the β- and γ-sites does not directly influence the sieving character. The distribution of cations is determined by their affinities to these sites. The γ-site has a very weak affinity for all cations. Na^+ and bi-valent cations like to reside on the β-site than the α-site, while reverse is the case with K^+, Rb^+, and Cs^+.[4-10] Let us express the composition as $(M^{I}_{12-2x}M^{II}_{x})$–A, where M^{I} and M^{II} are uni- and bi-valent cations, respectively. If M^{I} is Na, one open window (unoccupied α-site) per unit cell is produced at $x=2$, while if M^{I} is K, Rb, or Cs, at $x=5$.

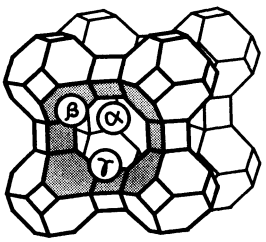

Fig. 6. Structure and cation sites of dehydrated zeolite A.

According to the percolation theory, the sieving character drastically changes in a narrow range of the concentration of the open window arround a critical value say, one per unit cell. The applicability of the theory has quantitatively been proved with (Na,Ca)–A system. In the preceding paper, the percolation theory was applied to sorptions of N_2 at 90 K and *n*-butane at 323 K with (K,Ca)–A system.[4] Then, it was concluded that there exists the third kind of window, named the conditionally-opened window, through which N_2 cannot pass at 90 K but *n*-butane, a larger molecule, can at 323 K. The 6th Ca^{2+} in Ca_6–A occupies the α-site and constitutes a conditionally-opened window.[4] Some fraction, not all, of windows blocked by K^+ also constitute conditionally-opened windows in (K,Ca)–A with a higher Ca-content.[4] This is further proved to be true by the present experiment with $(K_{4.30}Ca_{3.85})$–A.

Let us now present a model for the conditionally-opened window, of which the effective aperture-size markedly increases in a temperature range, 90—400 K. This is done by using the form of the potential surface experienced by the window-blocking cation. Here are taken into consideration potentials due to the framework and exchangeable cations but not that due to co-existing sorbed molecules. In K_{12}–A, the potential $\Phi(0)$ is to have such a sharp valley as shown in Fig. 7(a), the amplitude of thermal oscillation of the blocking K^+ is very small. A large energy may be required to push K^+ ion aside and make a way for a visiting molecule. Hence, the blocked window behaves as a perfectly closed one as far as the present temperature range concerns. In the conditionally-opened window in $(K_{12-2x}Ca_x)$–A, the blocking cation is easily displaced at a moderate temperature, and the potential $\Phi(x)$ is to have a very gentle curvature at its valley, as schematically shown in Fig. 7(b). In the figure, ξ denotes the distance of the shift of the potential minimum from the window plane, η the decrease of the potential at its minimum point, and $\Delta\rho$ the increase in the curvature of the potential surface at its valley. Values for ξ, η, and $\Delta\rho$ depend upon the distribution of cations, especially upon those in the neighborhood of the concerned K^+. If $\Phi(x)$ has a higher symmetry, ξ may be very small or zero. This is the case with Ca_6–A as shown by Firor and Seff.[11] Such a high symmetry is realized only in limitted cases with favourable compositions. With an unfavourable composition, the local configuration of cations arround a given α-site differs from site to site, so that ξ is small for some K^+ while large for others. The value of η influences the stability of the crystal but does not its sieving character which is a main concern in the present work, and is not further discussed. The larger the values for ξ and/or $\Delta\rho$, the smaller the activation energy for the passage of a visiting molecule, as can be seen from Fig. 7(b).

A window with a too large ξ behaves as a pseudo-open window. Its concentration may increase with the increasing x, except at some special values of x where $\Phi(x)$ has a high symmetry. The critical point in the percolation theory must be located at such a composition that the sum of concentrations of the open and pseudo-open windows is 1 p.u.c. This is the reason why the critical point in (K,Ca)–A system is located not at 5 but at 4.2 or so.[4]

There is another conceivable model for the activated sorption process. Breck and Smith proposed the activation of the vibration of breathing mode of the 8-ring.[2] This is unacceptable, since the framework is very rigid and one has never observed a high Debye-Waller factor of the framework. The present model, on the other hand, is in harmony with the structural observation due to Seff and his coworkers; that is, there exist loosely bound and/or displaced M^{I} cation on the α-site in (K,Zn)–A, and (Cs,Ca)–A.[12,13]

There might occur some fear that the residual water molecule influences both of the sieving character and structure. Comparing the present and previous results, one find some discrepancies in the amounts of sorption with samples of the same origine, especially with $(K_{3.58}Ca_{4.21})$–A.[4] This is attributed to the difference in the degree of dehydration. The

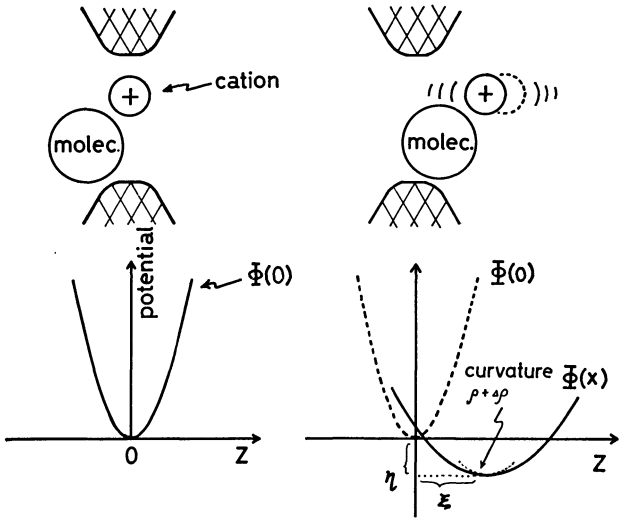

(a) (b)

Fig. 7. Model for the conditionally-opened window, and the potential experienced by the cation.
(a) Side view of the 8-ring window. Perfectly closed window. (b) Conditionally-opened window. The window aperture is increased with increasing ξ and $\Delta\rho$. $\Phi(x)$: The potential experienced by the window-blocking cation at composition $(M^{I}_{12-2x}M^{II}_{x})$–A, ξ: the distance of the shift of the potential minimum from the window plane, η: the decrease of the potential at the minimum point, $\Delta\rho$: the change in the curvature.

critical point slightly shifts to the lower Ca-content side. On the other hand, the main feature of the curve of composition *vs.* sorption capasity is not so much changed that the applicability of the present model is affected. However, the use of a clean vacuum system is essential to determine the exact value for the critical composition.

Previously, the window size was controlled solely by the kind of cation blocking the window. Now, one can finely control it by changing the form of the potential experienced by the blocking cation, that is, by changing $\Delta\rho$ and ξ values. This indirect method may be named as the cation-loosening one, though this name has a drawback that it does not include the effect of ξ. The cation-loosening can be adopted as an effective mean in tailoring molecular sieve. An example of the success in the tailoring is a highly selective sorption of PH_3 from SiH_4 with (K_4Zn_4)–A, though this was accomplished before the recognition of the method. Other examples of the tailoring are encapsulation of Kr into (K,M^{II})–A and H_2 into (Cs,M^{II})–A. These will be reported in the succeeding papers.[14,15]

The present paper was in part supported by a Grant-in-Aid for Research from the Ministry of Education of the Japanese Government, Contract No. 443001.

References

1) D. W. Breck, W. G. Eversole, R. M. Milton, and T. B. Read, *J. Am. Chem. Soc.*, **78**, 5963 (1956).
2) D. W. Breck and J. V. Smith, *Sci. Am.*, **200**, 85 (1959).
3) T. Takaishi, A. Yusa, Y. Ogino, and S. Ozawa, *J. Chem. Soc., Faraday Trans. 1*, **70**, 671 (1964).
4) T. Ohgushi, A. Yusa, and T. Takaishi, *J. Chem. Soc., Faraday Trans. 1*, **74**, 613 (1978).
5) A. Yusa, T. Ohgushi, and T. Takaishi, *J. Phys. Chem. Solids*, **38**, 1233 (1977).
6) T. Takaishi, Y. Yatsurugi, A. Yusa, and T. Kuratomi, *J. Chem. Soc., Faraday Trans. 1*, **71**, 97 (1975).
7) L. V. C. Rees and T. Berry, "Proc. Conf. Molecular Sieves," Soc. Chem. Ind., London (1968), p. 149.
8) I. E. Maxwell and A. Baks, *Adv. Chem. Ser.*, **121**, 87 (1973).
9) T. B. Vance, Jr., and K. Seff, *J. Phys. Chem.*, **79**, 2136 (1975).
10) M. Nitta, K. Ogawa, and K. Aomura, *J. Chem. Soc., Faraday Trans. 1*, **72**, 2893 (1976).
11) R. L. Firor and K. Seff, *J. Am. Chem. Soc.*, **100**, 3091 (1978).
12) N. V. Raghavan and K. Seff, *J. Phys. Chem.*, **80**, 2133 (1976).
13) V. Subramanian and K. Seff, preprint.
14) T. Takaishi and K. Itabashi, unpublished data.
15) T. Takaishi and K. Itabashi, unpublished data.

The Crystal and Molecular Structure of Grayanotoxin XVI Hemihydrate

Akio FURUSAKI,* Shinsei GASA, Ryūzō IKEDA, and Takeshi MATSUMOTO
Department of Chemistry, Faculty of Science, Hokkaido University, Sapporo 060
(Received April 30, 1980)

The molecular structure of grayanotoxin XVI, $C_{22}H_{34}O_6$, has been confirmed by means of an X-ray crystal analysis of its hemihydrate. The crystals are orthorhombic, with eight formula units in a unit cell with dimensions of $a=17.503$, $b=37.933$, and $c=6.371$ Å; the space group is $P2_12_12_1$. 4180 unique intensity data were collected on a four-circle diffractometer with LiF-monochromated Cu $K\alpha$ radiation. The structure was solved by the Monte Carlo direct method, using the 30 strongest reflections as the starting set, and was refined by the block-diagonal least-squares method. The final R value was 5.5%. The present analysis has revealed that the crystal used comprises about four parts of grayanotoxin XVI (6-*O*-acetylgrayanotoxin II) and one part of 10,20-dihydrograyanotoxin XVI. The molecules of the major component exist in two different conformations: One has the chair B-ring, and the other the twist-chair B-ring. About two-fifths of the molecules of the latter type are replaced at random by the molecules of the minor component.

Grayanotoxin (hereafter G) XVI is one of the physiologically-active diterpenes isolated from *Leucothoe grayana Max.*[1] On the basis of the chemical evidence, the **1** structure was proposed for this toxic substance. The main purposes of the present study were to confirm **1** and to test the effectiveness of the Monte Carlo direct method, a new phase-determining procedure.[2]

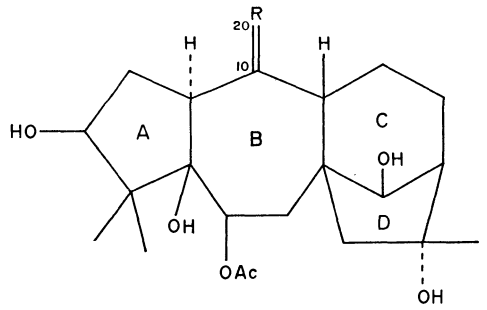

1: R = CH_2 2: R = CH_3, H

Experimental

Single crystals of G XVI hemihydrate were obtained as colorless needles from an ethanol–water solution. A sample with dimensions of about $0.1\times0.3\times0.6$ mm^3 was used for the X-ray measurement. The crystal data are summarized in Table 1. The cell dimensions and reflection intensities were measured on a Rigaku four-circle diffractometer using Cu $K\alpha$ radiation ($\lambda=1.5418$ Å) monochromatized with an LiF crystal. The intensity measurement was made by the θ-2θ continuous-scan technique at a 2θ scan rate of 2° min^{-1}; the background was measured for 30 s at each end of the scan range. The intensities were corrected for the Lorentz and polarization factors, but not for the absorption or extinction effect. In the range of 2θ values up to 140°, 4180 unique structure factor amplitudes above the $\sigma(F)$ level were selected for the structure determination.

Table 1. The crystal data

Formula	$C_{22}H_{34}O_6\cdot0.5\,H_2O$
Formula weight	403.5
Crystal system	Orthorhombic
Space group	$P2_12_12_1$
Cell dimensions	$a=17.503(6)$ Å
	$b=37.933(11)$ Å
	$c=6.371(3)$ Å
	$V=4230$ Å^3
Z	8
D_x	1.267 g cm^{-3}
μ (Cu $K\alpha$)	7.14 cm^{-1}

Structure Determination

The present structure containing 57 independent non-hydrogen atoms was solved by means of the Monte Carlo direct method.[2] The 30 strongest reflections were chosen as the starting set. In order to extend the tentative-phase set derived from successively-generated random numbers, 12 cycles of the tangent procedure were performed using 932 $|E|$ values above 1.30; during the first 5 cycles, the phases of the starting reflections were kept constant. Since the 261st phase set showed a low R_K value of 34.4% ($R_K=\Sigma||E_o|-k|E_c||/\Sigma|E_o|$),** 8 additional cycles of the tangent procedure were carried out; the R_K value was reduced to 27.6%. An E-map calculated with 864 phases clearly revealed the locations of all the non-hydrogen atoms except one. The computing time required for the phase determination was about 54 min on a FACOM 230-75 computer. This shows that the Monte Carlo direct method is still effective even for structures composed of more than 50 independent non-hydrogen atoms.

The 56 atomic positions obtained from the E-map were refined by the block-diagonal-matrix least-squares method with isotropic temperature factors. A difference Fourier map revealed that the remaining atom, C(A20), was distributed statistically between two positions in the ratio of about 3 to 2. Since close re-examination of the NMR spectrum demonstrated the presence of the dihydrograyanoid **2**, these two atomic positions, named C(A20a) and C(A20b) respectively, were assigned to the methylene carbon atom in **1** and the methyl carbon atom in **2** respectively. The whole structure thus obtained was refined by the least-squares method with anisotropic temperature factors; 0.6 and 0.4 times the atomic scattering factors of carbon were used for the C(A20a) and C(A20b)

** The second lowest of the R_K values for the 261 sets was 37.3%.

atoms respectively. After all hydrogen atoms, except those attached to the randomly-distributed carbon atom, had been located in a second difference Fourier map, further least-squares refinement was repeated including these hydrogen atoms with isotropic temperature factors. The following weighting scheme was used:

$$W=1/\{\sigma(F)^2 \exp(AX^2+BY^2+CXY+DX+EY)\},$$

where $X=|F_o|$ and $Y=\sin\theta/\lambda$. The A, B, C, D, and E coefficients are constants which were determined from the $(\Delta F)^2$ values. In this manner, the R value reached 5.5%. The atomic parameters are listed in Table 2. The tables of the anisotropic temperature factors and of the observed and calculated structure factors are kept at the Chemical Society of Japan (Document No. 8038).

All the calculations were performed on a FACOM 230-75 computer at the Hokkaido University Computing Center, using our own programs. Random numbers were generated by calling a function RANDOM in the program library of the Computing Center. The atomic scattering factors were taken from the International Tables.[3]

Results and Discussion

Chemical Structure. The skeletons of the two independent G XVI molecules, A and B, are shown in Fig. 1, where each atom is represented as a thermal ellipsoid enclosing a 50% probability. Table 3 gives the bond distances and angles, and Fig. 2 shows the torsion angles in the tetracyclic systems. The C(A10)–C(A20a) and C(A10)–C(A20b) distances are almost equal, lying nearly midway between the accepted distances for C=C and C–C bonds. However, the projected angle of C(A9)–C(A10)–C(A20a) onto the plane normal to the C(A1)–C(A10) bond is significantly different from that of C(A9)–C(A10)–C(A20b) (see Fig. 3). Although these projected angles, 160 and 137°, deviate from their respective standard values of 180 and 120° by about 20°, they indicate that the C(A10)–C(A20a) and C(A10)–C(A20b) bonds are oriented roughly in the directions of the sp^2 and sp^3 hybrid orbitals on the C(A10) atom respectively, the C(A20b) atom being on the β side of the molecule. Since the apparent thermal motion of the C(A10) atom is greater than that of any other atom in the B-ring, the unusual distances and directions of these

Table 2. The final atomic parameters and estimated standard deviations

(1) The non-hydrogen atoms.

Atom	$x(\times 10^4)$	$y(\times 10^5)$	$z(\times 10^4)$	B_{eq}[a]/Å^2	Atom	$x(\times 10^4)$	$y(\times 10^5)$	$z(\times 10^4)$	B_{eq}/Å^2
O(A1)	−143(2)	29412(7)	5843(5)	4.91	O(B1)	−819(2)	54556(6)	250(4)	4.65
O(A2)	−491(2)	22523(5)	5107(4)	3.44	O(B2)	−395(2)	49412(5)	3281(3)	3.41
O(A3)	−1786(1)	20713(6)	2542(4)	3.20	O(B3)	−1105(1)	42765(5)	3391(4)	3.00
O(A4)	−2207(2)	19330(8)	−651(5)	5.02	O(B4)	−1342(2)	37691(6)	1713(5)	5.01
O(A5)	−288(1)	16382(5)	−2494(4)	3.31	O(B5)	800(2)	37245(6)	688(5)	4.14
O(A6)	263(2)	9729(6)	−2350(5)	4.39	O(B6)	1890(2)	34799(7)	3265(5)	4.33
C(A1)	179(2)	24642(8)	1922(5)	3.03	C(B1)	266(2)	47926(8)	−48(5)	3.11
C(A2)	309(2)	28657(8)	2318(7)	4.29	C(B2)	−27(3)	50500(9)	−1736(6)	3.87
C(A3)	−347(2)	29887(8)	3661(6)	3.73	C(B3)	−823(2)	51553(8)	−1110(5)	3.69
C(A4)	−1017(2)	27449(7)	3078(5)	2.98	C(B4)	−1136(2)	48359(8)	91(5)	3.24
C(A5)	−597(2)	23795(7)	3005(5)	2.53	C(B5)	−439(2)	47260(7)	1455(5)	2.77
C(A6)	−1004(2)	20946(7)	1741(5)	2.64	C(B6)	−415(2)	43441(7)	2167(5)	2.75
C(A7)	−674(2)	17244(7)	1867(5)	2.81	C(B7)	240(2)	42433(8)	3627(5)	3.00
C(A8)	143(2)	16505(7)	1148(5)	2.65	C(B8)	1066(2)	42540(8)	2827(5)	3.05
C(A9)	768(2)	18245(8)	2545(5)	3.12	C(B9)	1383(2)	46378(9)	2608(6)	3.92
C(A10)	840(2)	22288(10)	2496(8)	4.86	C(B10)	966(2)	49003(9)	1196(6)	3.80
C(A11)	1547(2)	16509(9)	2077(6)	3.96	C(B11)	2243(2)	46234(11)	2163(9)	5.16
C(A12)	1713(2)	16345(10)	−300(7)	4.02	C(B12)	2477(2)	43381(12)	565(8)	5.12
C(A13)	1030(2)	14930(8)	−1558(5)	3.35	C(B13)	2093(2)	39816(10)	978(6)	3.99
C(A14)	340(2)	17331(7)	−1177(5)	2.62	C(B14)	1232(2)	40453(8)	793(5)	3.12
C(A15)	237(2)	12406(8)	1167(5)	3.45	C(B15)	1578(2)	40551(10)	4452(6)	3.82
C(A16)	738(2)	11322(8)	−733(6)	3.56	C(B16)	2173(2)	38412(10)	3234(6)	3.92
C(A17)	1340(3)	8565(9)	−269(7)	4.79	C(B17)	2980(3)	38396(14)	4097(9)	5.74
C(A18)	−1663(2)	27731(10)	4657(7)	4.35	C(B18)	−1856(2)	49235(10)	1336(7)	4.59
C(A19)	−1318(2)	28474(8)	910(6)	3.85	C(B19)	−1335(2)	45493(10)	−1543(6)	4.22
C(A20a)	1569(4)	23878(19)	2310(14)	5.05	C(B20)	1185(3)	52349(11)	1261(10)	5.82
C(A20b)	1303(6)	23275(34)	4211(32)	8.07	C(B21)	−1485(2)	39748(8)	3096(6)	3.38
C(A21)	−2332(2)	19915(9)	1179(7)	3.91	C(B22)	−2098(2)	39270(11)	4662(8)	4.98
C(A22)	−3104(2)	19915(13)	2213(9)	5.39	O(W)	−397(2)	35663(8)	−2030(5)	5.52

a) $B_{eq}=8\pi^2(u_1^2+u_2^2+u_3^2)/3$, where u_i is the root-mean-square deviation in the ith principal axis of the thermal ellipsoid.

TABLE 2. (Continued)

(2) The hydrogen atoms.

The atomic coordinates are multiplied by 10^3.

Atom[a)]	x	y	z	B/Å^2	Atom	x	y	z	B/Å^2
H(A1)	4(2)	243(1)	45(6)	2.9(7)	H(B2b)	26(2)	522(1)	−196(7)	4.0(8)
H(A2a)	27(3)	298(1)	87(8)	5.0(9)	H(B3)	−113(2)	520(1)	−242(7)	3.9(8)
H(A2b)	77(3)	287(1)	329(10)	6.3(11)	H(B6)	−46(3)	420(1)	89(8)	4.8(9)
H(A3)	−50(2)	322(1)	347(6)	3.1(7)	H(B7a)	14(2)	400(1)	419(6)	2.9(6)
H(A6)	−102(2)	218(1)	34(6)	2.7(6)	H(B7b)	18(3)	440(1)	504(9)	5.4(10)
H(A7a)	−99(2)	158(1)	86(6)	2.5(6)	H(B9)	133(2)	473(1)	420(6)	3.3(7)
H(A7b)	−73(2)	163(1)	330(7)	4.4(8)	H(B11a)	242(2)	485(1)	146(7)	4.6(9)
H(A9)	63(2)	173(1)	409(7)	4.2(8)	H(B11b)	253(3)	458(2)	344(10)	6.6(12)
H(A11a)	197(3)	176(1)	282(8)	5.0(9)	H(B12a)	229(3)	445(1)	−63(8)	4.7(9)
H(A11b)	153(2)	141(1)	256(7)	3.8(8)	H(B12b)	306(3)	431(1)	57(8)	5.5(10)
H(A12a)	186(3)	187(1)	−95(8)	4.8(9)	H(B13)	224(2)	382(1)	−7(7)	3.8(8)
H(A12b)	219(3)	149(1)	−71(8)	4.9(9)	H(B14)	110(2)	416(1)	−50(6)	2.6(6)
H(A13)	117(3)	147(1)	−316(8)	5.3(10)	H(B15a)	126(2)	390(1)	537(6)	3.4(7)
H(A14)	46(2)	197(1)	−141(6)	2.9(6)	H(B15b)	185(3)	422(2)	536(10)	6.9(12)
H(A15a)	−24(2)	113(1)	86(7)	4.0(8)	H(B17a)	296(3)	373(1)	559(8)	5.3(10)
H(A15b)	46(2)	116(1)	252(6)	3.1(6)	H(B17b)	316(3)	407(1)	429(8)	5.1(9)
H(A17a)	114(3)	66(1)	11(8)	4.8(9)	H(B17c)	328(4)	363(2)	333(11)	7.9(14)
H(A17b)	166(3)	90(1)	84(8)	5.5(10)	H(B18a)	−210(3)	474(1)	194(9)	6.3(11)
H(A17c)	161(2)	83(1)	−141(7)	4.2(8)	H(B18b)	−226(3)	503(2)	37(11)	7.5(14)
H(A18a)	−206(3)	264(1)	446(8)	5.2(10)	H(B18c)	−173(2)	508(1)	228(6)	3.5(7)
H(A18b)	−180(4)	300(2)	476(12)	8.2(15)	H(B19a)	−170(3)	465(2)	−252(11)	7.3(13)
H(A18c)	−151(4)	269(2)	613(11)	8.1(15)	H(B19b)	−162(3)	436(1)	−90(8)	5.3(10)
H(A19a)	−147(2)	307(1)	103(7)	3.9(8)	H(B19c)	−87(3)	446(1)	−219(8)	4.6(9)
H(A19b)	−174(3)	270(1)	40(8)	4.8(9)	H(B20a)	92(2)	542(1)	57(7)	3.9(8)
H(A19c)	−93(3)	283(1)	−23(8)	4.7(9)	H(B20b)	165(4)	531(2)	213(11)	7.4(13)
H(A22a)	−325(3)	227(2)	241(10)	7.5(13)	H(B22a)	−247(3)	379(2)	427(10)	7.3(13)
H(A22b)	−298(5)	188(2)	346(14)	10.0(19)	H(B22b)	−237(4)	415(2)	499(13)	9.2(17)
H(A22c)	−343(4)	186(2)	140(11)	7.6(14)	H(B22c)	−185(6)	382(3)	590(16)	11.5(23)
H(OA1)	−22(4)	316(2)	643(13)	9.2(17)	H(OB1)	−65(2)	563(1)	−44(7)	4.7(9)
H(OA2)	−43(3)	242(1)	576(8)	5.1(9)	H(OB2)	−47(3)	518(1)	282(8)	5.4(10)
H(OA5)	−41(3)	180(1)	−316(8)	5.1(9)	H(OB5)	105(3)	361(1)	155(8)	4.7(9)
H(OA6)	−8(3)	111(1)	−254(10)	6.5(12)	H(OB6)	220(3)	335(1)	285(10)	6.3(11)
H(B1)	37(2)	456(1)	−80(6)	3.1(7)	H(OWa)	−73(5)	365(2)	−127(15)	10.5(20)
H(B2a)	−3(2)	492(1)	−297(7)	3.9(8)	H(OWb)	0(3)	360(1)	−133(8)	5.0(9)

a) The hydrogen atoms are denoted by the number of the carbon atom to which they are attached, suffixed by a, b, or c where necessary.

two bonds may be due partly to the disordering of the C(A10) atom.

It is thus concluded that, although about three-fifths of the A molecules correspond to compound **1**, the remaining A molecules correspond to compound **2**.*** Since the B molecules having no disordering correspond to **1**, it follows that the present crystal as a whole contains about one-fifth of **2**. This unexpected contaminant is the first 10,20-dihydrograyanoid to be obtained from *Leucothoe grayana Max.*

Molecular Geometry. As Table 3 shows, all the bond distances are normal except for the randomly-distributed C(A20) atom. There is no great difference between the two crystallographically-independent molecules of G XVI.

The five-membered A-rings in both of the molecules take similar envelope forms; the C(4) atom deviates remarkably from the mean plane for the other four atoms onto the α side of the molecule.† Although this conformation makes the O(1)H and O(2)H hydroxyl groups 1,3-diaxial, it is stabilized by the formation of the intramolecular hydrogen bond, O(2)H···O(1) (see Table 4).

The difference between the A and B molecules can be most clearly seen for the conformations of their central seven-membered B-rings; the B-ring of the former has the twist-chair form with an approximate two-fold rotation axis through the C(A10) atom, while that of the latter adopts the chair form with an approximate mirror plane through the C(B6) atom. According to Hendrickson's calculations,[4] cycloheptane prefers the twist-chair conformation. In Hendrickson's

*** Unless otherwise stated, "A molecules" will mean solely molecules of **1** in the description given below.

† The atomic name, C(i), is used when the description is valid for both of the A and B molecules.

Table 3. The bond distances (l/Å) and angles (ϕ/°), with their standard deviations
The standard deviations given in parentheses refer to the last decimal position.

(1) The bond distances.

	Mol. A	Mol. B		Mol. A	Mol. B		Mol. A	Mol. B
C(1)-C(2)	1.560(4)	1.541(5)	C(6)-C(7)	1.521(4)	1.524(4)	C(12)-C(13)	1.536(5)	1.533(6)
C(1)-C(5)	1.557(4)	1.582(5)	C(6)-O(3)	1.463(4)	1.461(4)	C(13)-C(14)	1.533(4)	1.530(5)
C(1)-C(10)	1.507(5)	1.515(5)	C(7)-C(8)	1.526(4)	1.534(5)	C(13)-C(16)	1.553(5)	1.540(6)
C(2)-C(3)	1.506(6)	1.503(6)	C(8)-C(9)	1.558(4)	1.564(5)	C(14)-O(5)	1.428(4)	1.434(4)
C(3)-C(4)	1.539(5)	1.534(5)	C(8)-C(14)	1.552(4)	1.546(5)	C(15)-C(16)	1.551(5)	1.531(5)
C(3)-O(1)	1.447(5)	1.432(4)	C(8)-C(15)	1.564(4)	1.564(5)	C(16)-C(17)	1.513(5)	1.516(6)
C(4)-C(5)	1.570(4)	1.554(5)	C(9)-C(10)	1.539(5)	1.528(5)	C(16)-O(6)	1.456(5)	1.457(4)
C(4)-C(18)	1.517(5)	1.526(6)	C(9)-C(11)	1.543(5)	1.533(6)	C(21)-C(22)	1.503(6)	1.476(6)
C(4)-C(19)	1.529(5)	1.545(5)	C(10)-C(20a)	1.417(8)	1.326(5)	C(21)-O(3)	1.327(4)	1.336(4)
C(5)-C(6)	1.524(4)	1.519(4)	C(10)-C(20b)	1.411(18)		C(21)-O(4)	1.207(5)	1.203(5)
C(5)-O(2)	1.435(4)	1.424(4)	C(11)-C(12)	1.543(6)	1.541(7)			

(2) The bond angles.

	Mol. A	Mol. B		Mol. A	Mol. B
C(2)-C(1)-C(5)	104.9(3)	105.3(3)	C(14)-C(8)-C(15)	100.7(2)	101.5(3)
C(2)-C(1)-C(10)	115.3(3)	117.6(3)	C(8)-C(9)-C(10)	117.9(3)	119.3(3)
C(5)-C(1)-C(10)	116.1(3)	110.9(3)	C(8)-C(9)-C(11)	109.3(3)	109.4(3)
C(1)-C(2)-C(3)	106.5(3)	107.0(3)	C(10)-C(9)-C(11)	110.4(3)	112.6(3)
C(2)-C(3)-C(4)	104.9(3)	104.6(3)	C(1)-C(10)-C(9)	122.2(3)	121.3(3)
C(2)-C(3)-O(1)	108.6(3)	111.6(3)	C(1)-C(10)-C(20a)	114.8(4)	120.5(4)
C(4)-C(3)-O(1)	110.2(3)	109.2(3)	C(1)-C(10)-C(20b)	118.2(6)	
C(3)-C(4)-C(5)	100.4(2)	102.2(3)	C(9)-C(10)-C(20a)	120.0(4)	117.9(4)
C(3)-C(4)-C(18)	111.4(3)	112.4(3)	C(9)-C(10)-C(20b)	107.2(6)	
C(3)-C(4)-C(19)	109.1(3)	107.5(3)	C(9)-C(11)-C(12)	111.9(3)	114.1(3)
C(5)-C(4)-C(18)	115.5(3)	114.6(3)	C(11)-C(12)-C(13)	112.3(3)	112.9(4)
C(5)-C(4)-C(19)	111.1(3)	111.4(3)	C(12)-C(13)-C(14)	108.9(3)	106.2(3)
C(18)-C(4)-C(19)	108.9(3)	108.5(3)	C(12)-C(13)-C(16)	112.8(3)	115.2(3)
C(1)-C(5)-C(4)	103.9(2)	103.3(2)	C(14)-C(13)-C(16)	102.2(3)	102.5(3)
C(1)-C(5)-C(6)	108.6(2)	108.1(2)	C(8)-C(14)-C(13)	101.9(2)	101.6(3)
C(1)-C(5)-O(2)	111.7(2)	111.2(3)	C(8)-C(14)-O(5)	109.8(2)	112.0(3)
C(4)-C(5)-C(6)	115.0(2)	116.4(3)	C(13)-C(14)-O(5)	111.3(2)	112.9(3)
C(4)-C(5)-O(2)	109.3(2)	110.2(2)	C(8)-C(15)-C(16)	108.5(3)	108.1(3)
C(6)-C(5)-O(2)	108.4(2)	107.5(2)	C(13)-C(16)-C(15)	102.5(3)	103.2(3)
C(5)-C(6)-C(7)	116.7(3)	116.3(3)	C(13)-C(16)-C(17)	116.5(3)	115.2(3)
C(5)-C(6)-O(3)	107.2(2)	107.7(2)	C(13)-C(16)-O(6)	108.3(3)	107.9(3)
C(7)-C(6)-O(3)	106.4(2)	104.6(2)	C(15)-C(16)-C(17)	115.1(3)	116.9(4)
C(6)-C(7)-C(8)	120.7(2)	119.9(3)	C(15)-C(16)-O(6)	109.8(3)	105.1(3)
C(7)-C(8)-C(9)	114.1(3)	112.9(3)	C(17)-C(16)-O(6)	104.4(3)	107.9(3)
C(7)-C(8)-C(14)	117.2(3)	116.3(3)	C(22)-C(21)-O(3)	111.2(4)	111.8(3)
C(7)-C(8)-C(15)	106.2(2)	107.9(3)	C(22)-C(21)-O(4)	126.0(4)	124.5(3)
C(9)-C(8)-C(14)	107.7(2)	109.6(3)	O(3)-C(21)-O(4)	122.9(3)	123.7(3)
C(9)-C(8)-C(15)	110.0(3)	107.7(3)	C(6)-O(3)-C(21)	117.4(3)	119.1(2)

computed twist-chair form (hereafter HTC), substituents at the 2a, 2'a, 3a, and 3'a positions sustain strong steric repulsions (see Fig. 4(a)). For the O(A2)H and C(A14)H groups situated at the 3a and 3'a positions, however, no unusually-close contacts are observed: for example, O(A2)···H(A7b), 2.66(4) Å; O(A2)···H(A9), 2.87(4) Å; C(A14)···H(A1), 2.89(3) Å; C(A14)···H(A6), 3.08(3) Å; H(A14)···H(A1), 2.23 (5) Å. This relief of the steric hindrance may be explained from the remarkable flattening of the B-ring, due mainly to the conformational transmission[5] at the *trans* A/B- and *cis* B/C-junctions. The magnitudes of the C(A10)-C(A1)-C(A5)-C(A6) and C(A7)-C(A8)-C(A9)-C(A10) torsion angles, 85.0 and 68.8°, are much smaller than the corresponding value for HTC, 97°; hence, the axial nature of the C(A5)-O(A2) and C(A8)-C(A14) bonds is remarkably decreased.

The occurrence of the chair B-ring should be noted in two respects: (1) The chair cycloheptane is less stable than the twist-chair cycloheptane by 2.16 kcal/mol;[4] (2) the bulky C(B14)H group is placed at a very hindered position on the chair B-ring. In Hendrickson's computed chair form of cycloheptane

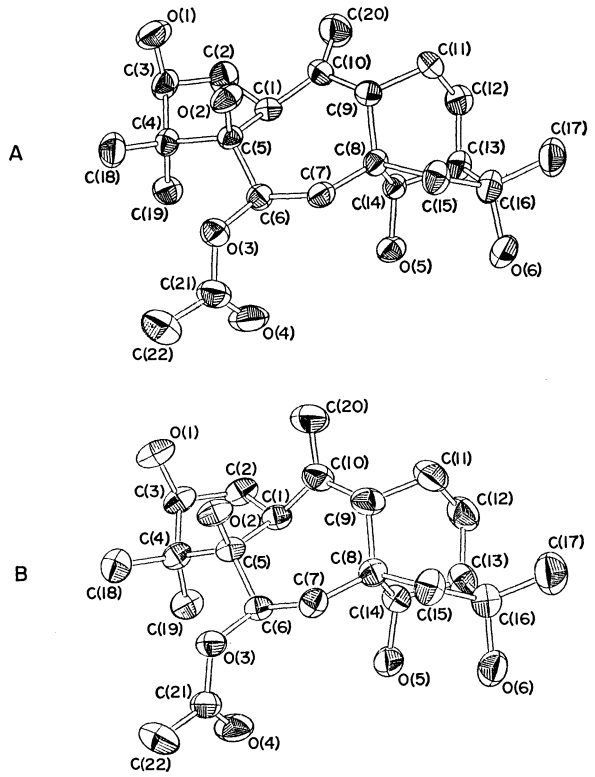

Fig. 1. Perspective views of the A and B molecules. For the sake of clarity, the C(A20b) atom was omitted.

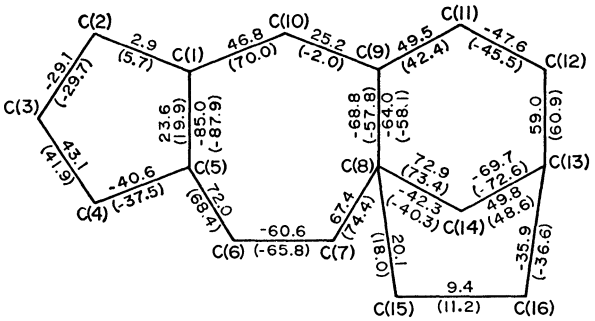

Fig. 2. The torsion angles (ϕ/°) of the A-, B-, C-, and D-rings. Only the torsion angles relevant to atoms which form the same ring are given in the ring. The values for the B molecule are given in parentheses.

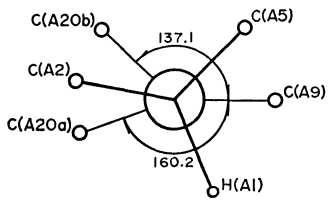

Fig. 3. The projected angles (ϕ/°) onto the plane normal to the C(A1)–C(A10) bond.

(hereafter HC), the 3a-3'a interaction is the severest, and stronger than the 2a-3'a and 2'a-3a interactions in HTC (see Fig. 4(b)). The 3a-3'a repulsion between the C(B14)H group and the H(B1) atom is relieved mainly by the closing of the C(B6)–C(B7)–C(B8)–C(B9) and C(B7)–C(B8)–C(B9)–C(B10) torsion angles. The magnitudes of these torsion angles are

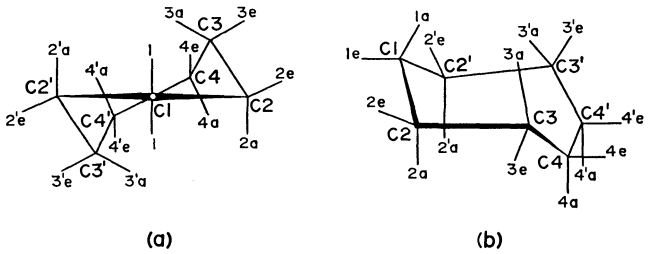

Fig. 4. Hendrickson's (a) twist-chair and (b) chair forms of cycloheptane.

smaller than the corresponding values for HC, 92 and 71°, by about 18 and 13° respectively. Since these torsion angles are opposite in sign, this shows a remarkable decrease in axiality of the C(B8)–C(B14) bond.[6] In spite of such a relief of the 3a-3'a repulsion, the C(B14)H group is still hindered severely: C(B1)···C(B14), 3.344(4) Å; C(B1)···H(B14), 2.82(3) Å; H(B1)···C(B14), 2.66(4) Å; H(B1)···H(B14), 1.98(5) Å.

The exocyclic methylene group in the B molecule, C(B20)H_2, sustains great steric repulsions from the two methylene groups, C(B2)H_2 and C(B11)H_2: H(B20a)···H(B11a), 2.24(7) Å; H(B20b)···H(B2b), 2.12(6) Å. As will be shown by the projected angle of C(B1)–C(B10)–C(B9) onto the plane normal to the C(B10)=C(B20) double bond, 173.1°, these steric repulsions probably push the C(B20)H_2 group away from the C(B1)–C(B10)–C(B9) plane to the β side of the molecule. In the G II molecule having the severe H(20a)···H(11a) interaction of 1.92(5) Å,[7] the C(9)–C(10)–C(20) bond angle is greater than the C(1)–C(10)–C(20). In the B molecule, the relation is reversed: C(B9)–C(B10)–C(B20), 117.9°; C(B1)–C(B10)–C(B20), 120.5°. Further, the C(B2)–C(B1)–C(B10) bond angle is expanded from the corresponding angle in G II, 113.3°, to 117.6°, while the C(B5)–C(B1)–C(B10) bond angle is reduced from 119.5° for G II to 110.9°. These changes in bond angle can be explained on the basis of the strong H(B20b)···H(B2b) repulsion.

The six-membered C-rings in both of the A and B molecules take the chair conformation, but are much deformed by three main causes: (1) the three-bond bridge, C(8)–C(15)–C(16)–C(13); (2) the conformational transmission at the *cis* B/C-junction; (3) the steric repulsion between the C(14)H group and the H(1) atom.

In both the A and the B molecules, the form of the five-membered D-ring is intermediate between the envelope form characterized by the mirror plane through the C(14) atom and the half-chair form characterized by the two-fold rotation axis through the C(15) atom. Although the D-ring is forced to take the envelope form by the existence of the chair C-ring, it is probably deformed by the C(11)H_2···C(17)H_3 repulsion and the O(5)···O(6) hydrogen bonding. In the A molecule, the O(6)H group donates its proton to the O(5)H, while in the B molecule, the latter donates to the former (see Table 4).

Crystal Structure. The crystal structure viewed along the c axis is shown in Fig. 5. There are six kinds of intermolecular hydrogen bonds; the details

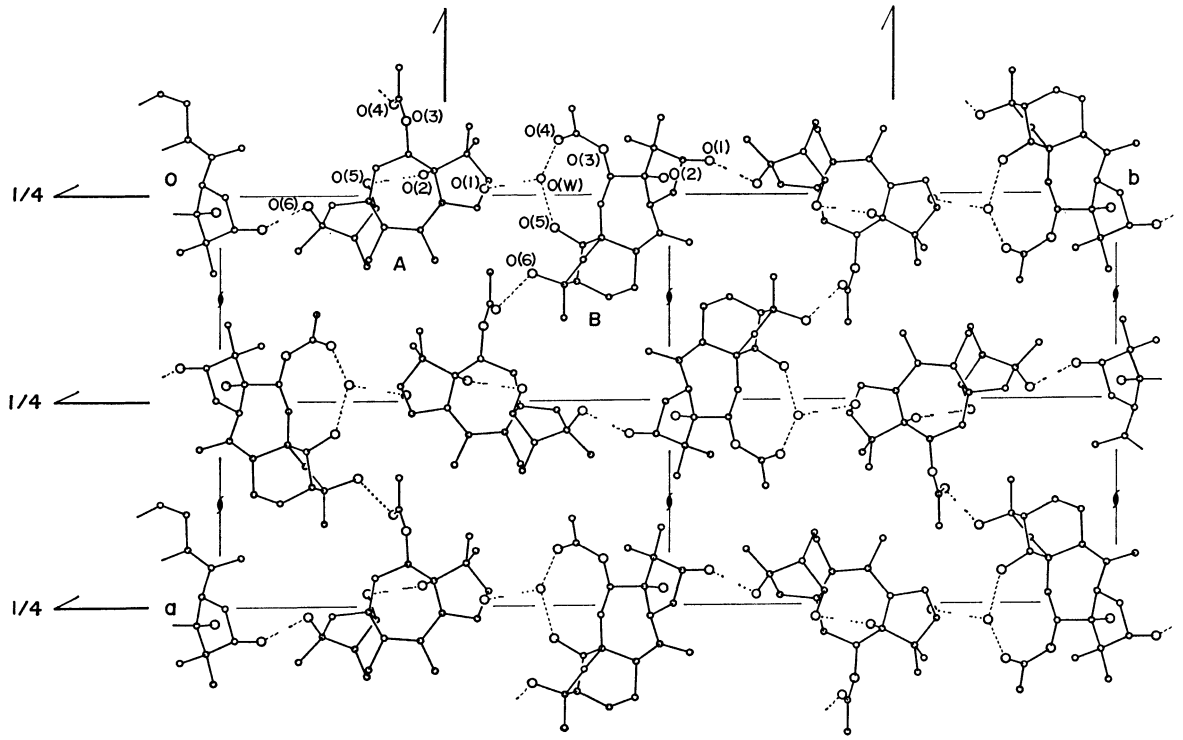

Fig. 5. The crystal structure viewed along the c axis.

Table 4. The hydrogen bonds, X-H···Y

X	Y	X···Y (l/Å)	H···Y (l/Å)	X-H···Y (ϕ/°)
(1) Intramolecular				
O(A2)	O(A1)	2.724(3)	2.04(4)	148(5)
O(A6)	O(A5)	2.703(3)	2.05(5)	139(5)
O(B2)	O(B1)	2.844(3)	2.05(5)	141(4)
O(B5)	O(B6)	2.683(4)	1.89(5)	159(4)
(2) Intermolecular				
O(A1)	O(W)[b]	2.767(4)	1.85(7)	172(7)
O(A5)	O(A2)[c]	2.809(3)	2.04(5)	168(5)
O(B1)	O(A6)[d]	2.866(4)	2.03(5)	166(4)
O(B6)	O(A4)[e]	2.779(4)	2.04(6)	156(6)
O(W)	O(B4)[a]	3.002(5)	2.23(9)	158(8)
O(W)	O(B5)[a]	2.784(4)	1.96(5)	168(5)

The symmetry codes are as follows: a) x, y, z (given in Table 2); b) x, y, $1+z$; c) x, y, $-1+z$; d) $-x$, $1/2+y$, $-1/2-z$; e) $1/2+x$, $1/2-y$, $-z$.

of the hydrogen bonds are given in Table 4. Each water molecule donates its protons to the O(B4) carbonyl and O(B5) hydroxyl oxygen atoms of the same B molecule, and it accepts the proton from the O(A1)H hydroxyl group of the neighboring A molecule. The couples of the A and B molecules connected through such mediation of the water molecule are further held together by the remaining three hydrogen bonds, forming a three-dimensional hydrogen-bonded structure.

References

1) S. Gasa, R. Ikeda, N. Hamanaka, and T. Matsumoto, *Bull. Chem. Soc. Jpn.*, **49**, 835 (1976).
2) A. Furusaki, *Acta Crystallogr., Sect. A*, **35**, 220 (1979).
3) "International Tables for X-Ray Crystallography," The Kynoch Press, Birmingham (1974), Vol. IV.
4) J. B. Hendrickson, *J. Am. Chem. Soc.*, **83**, 4537 (1961).
5) R. Bucourt, *Bull. Soc. Chim. Fr.*, **1962**, 1983; **1963**, 1262.
6) R. Bucourt, "The Torsion Angle Concept in Conformational Analysis," in "Topics in Stereochemistry," ed by E. L. Eliel and N. L. Allinger, John Wiley & Sons, New York (1974), Vol. 8, pp. 162—165.
7) A. Furusaki, N. Hamanaka, and T. Matsumoto, *Bull. Chem. Soc. Jpn.*, **53**, 764 (1980).

  Bull. Chem. Soc. Jpn., 54, 55—59 (1981)

The Reactions of NH Radicals with Ethylene and Propene in the Liquid Phase

Takashi KITAMURA, Shigeru TSUNASHIMA,* and Shin SATO

Department of Applied Physics, Tokyo Institute of Technology, Ookayama, Meguro-ku, Tokyo 152

(Received May 15, 1980)

The photolysis of hydrogen azide was studied in liquid ethylene, propene, and the mixture with ethane at the temperature of Dry Ice–methanol. The products observed were aziridine (0.18), ammonia (0.16), and nitrogen (1.0) from the ethylene solution and 2-methylaziridine (0.33), allylamine (0.12), ammonia (0.17), and nitrogen (1.0) from the propene solution. The values in parentheses show the yields relative to that of nitrogen. The relative yields were independent of the concentration of hydrogen azide in the range of 0.8—8×10^{-2} mol dm^{-3}. The reaction of NH($a^1\Delta$) radicals with olefin consists of three processes: the addition to double bond, the insertion into the C–H bond, and the deactivation to the $^3\Sigma^-$ state. The branching ratios and the relative rate constants of the reactions of NH($a^1\Delta$) radicals with ethylene, propene, and ethane were estimated.

Since NH is isoelectronic with O and CH_2, it is expected that the reactions of NH will be similar to those of O and CH_2. In spite of many investigations, the reactions of NH are not understood well. The main reason is that most studies failed to detect the NH-containing products. Recently, we found the amine formation in the photolysis of hydrogen azide in liquid ethane, propane, and isobutane at the temperature of Dry Ice–methanol by treating the products with NaOH.[1,2] The amine formation was explained by the insertion reaction of the singlet NH($a^1\Delta$) into the C–H bond of paraffin. If the singlet NH reacts with the olefin like the singlet O or CH_2 reacts with, then the formation of aziridine, the product of NH added to the double bond of ethylene, can be expected.

Many investigations in the gas phase failed to detect the aziridine formation.[3-6] Jacox and Milligan photolyzed a mixture of hydrogen azide and ethylene in the Ar matrix at 4 K and detected aziridine by infrared absorption spectroscopy. No kinetic study, however, was given.[7]

The photolysis of hydrogen azide was studied in liquid ethylene and propene at the temperature of Dry Ice–methanol in order to investigate the reactivity of NH radicals to olefin.

Experimental

The experimental methods were essentially the same as those described in the previous papers.[1,2] Hydrogen azide was prepared *in vacuo* by heating a mixture containing sodium azide and an excess amount of stearic acid; it was used after having been dried with phosphorus pentaoxide and degassed at −120 °C. Pure grade ethylene (Yokohama Chemicals Co.), ethane, and propene (Takachiho Shoji Co.) were used after the low temperature distillation. The mixture of hydrogen azide (8—80 μmol) and hydrocarbon (≈10 mmol) was prepared in a quartz tube of 8 mm o.d. and liquefied at the temperature of Dry Ice–methanol. The amount of the solution was about 1 cm^3. The solution was irradiated with a medium pressure mercury lamp (Toshiba H-400P) through a filter (Toshiba UV 27) which cut off the light shorter than 250 nm.

After the irradiation, non-condensable products at the temperature of liquid nitrogen were analyzed with a combination of a Toepler pump, a gas burette, and a CuO furnace at 300 °C. The solvent hydrocarbon was evacuated at a temperature lower than −80 °C. Less volatile products, including unreacted hydrogen azide, were passed through a trap packed with NaOH coated glass wool. The products thus obtained were analyzed with GLC, using a column packed with Amine 220 on NaOH coated Celite 545 (Gasukuro Kogyo Co., 5 m in length) at 40 °C. For the identification of the products, a mass spectrometer was used.

Results

The products observed in the ethylene solution of hydrogen azide were nitrogen, ammonia, and aziridine. Beside these products, small peaks of unidentified products were observed on the gas chromatogram. These peaks were too small to be analyzed. Neither methane nor hydrogen formation was observed. The products observed in the propene solution were nitrogen, ammonia, 2-methylaziridine, and allylamine.

To check the validity of the present analytical method, known amounts of ammonia and aziridine were added to the ethylene solution of hydrogen azide. After having been passed through the NaOH trap, less volatile parts were analyzed with GLC. Figure 1 shows the amounts of aziridine and ammonia recovered as functions of those introduced in the solution. The recovery was almost 100%.

Figures 2 and 3 show the relative yields of the products obtained in the ethylene and propene solutions, respectively, as functions of the concentration of hydrogen azide. The relative yields of the products

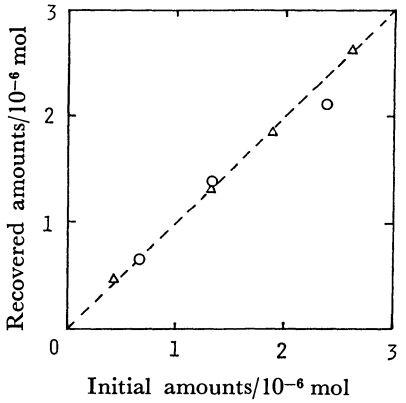

Fig. 1. The amounts of aziridine and ammonia recovered from the ethylene solution of hydrogen azide against the amounts introduced in the solution.
○: Aziridine, △: ammonia.

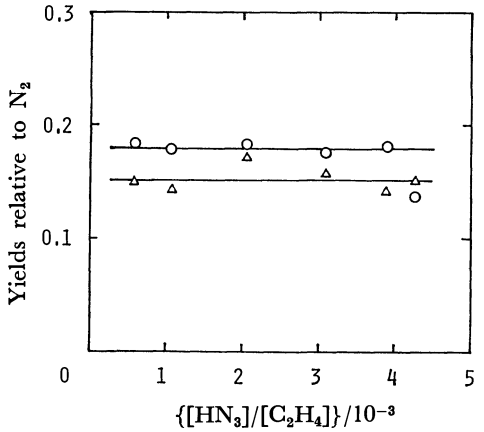

Fig. 2. Relative yields of the products as functions of the $[HN_3]/[C_2H_4]$ ratio obtained in the photolysis of the ethylene solution of hydrogen azide.
○: Aziridine, △: ammonia.

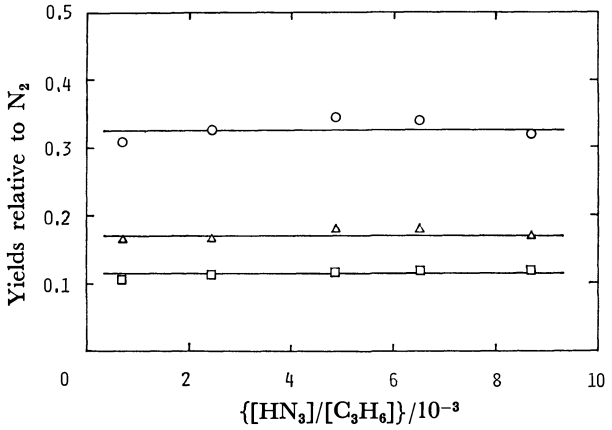

Fig. 3. Relative yields of the products as functions of the $[HN_3]/[C_3H_6]$ ratio obtained in the photolysis of the propene solution of hydrogen azide.
○: 2-Methylaziridine, □: allylamine, △: ammonia.

were independent of the concentration of hydrogen azide. The yields of aziridine and ammonia were 0.18 ± 0.02 and 0.16 ± 0.02 times that of nitrogen in the case of ethylene. In the case of propene, the yields of 2-methylaziridine, allylamine, and ammonia were 0.33 ± 0.02, 0.12 ± 0.01, and 0.17 ± 0.01 times that of nitrogen.

When the mixture of ethylene and ethane were used as the solvent, the ethylamine formation competed with the aziridine formation. Figure 4 shows the relative yields of the products obtained in the mixture of ethane, ethylene, and hydrogen azide, as functions of the mole fraction of ethylene. In this case, the $[HN_3]/([C_2H_4]+[C_2H_6])$ ratio was kept constant at 2.0×10^{-3}.

When ethylene was added to the propene solution of hydrogen azide, the aziridine formation competed with the formations of 2-methylaziridine and allyl amine, as is shown in Fig. 5. In this case, the $[HN_3]/([C_2H_4]+[C_3H_6])$ ratio was 2.5×10^{-3}.

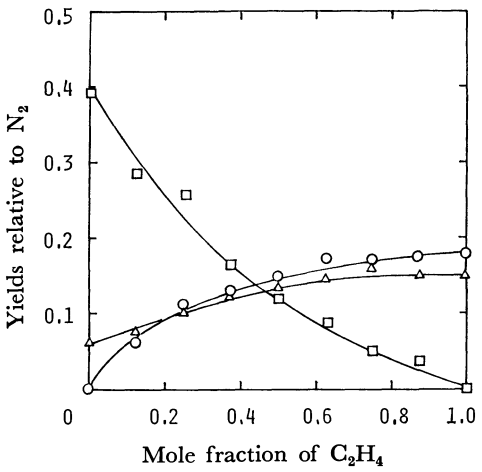

Fig. 4. Effect of ethylene on the photolysis of the ethane solution of hydrogen azide as functions of the mole fraction of ethylene.
○: Aziridine, △: ammonia, □: ethylamine.

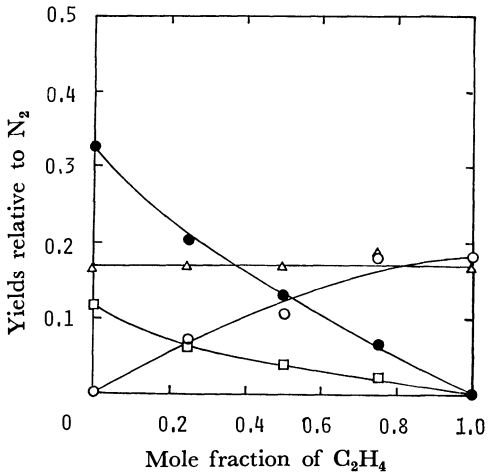

Fig. 5. Effect of ethylene on the photolysis of the propene solution of hydrogen azide as functions of the mole fraction of ethylene. The $[HN_3]/([C_2H_4]+[C_3H_6])$ ratio is 2.5×10^{-3}.
○: Aziridine, ●: 2-methylaziridine, □: allylamine, △: ammonia.

Discussion

Reaction Mechanism. In previous papers,[1,2] the amine formation in the photolysis of hydrogen azide in liquid paraffin was explained by the insertion of $NH(a^1\Delta)$ into the C–H bond of paraffin. As was shown in Fig. 4, when ethylene was added to the ethane solution of hydrogen azide, the ethylamine formation decreased and the aziridine formation increased. In the case of propene, the allylamine/2-methylaziridine ratio was independent of the concentration of hydrogen azide, as is shown in Fig. 3. These results suggest that aziridine is formed by the addition of the singlet NH to the double bond of olefin. To explain the results obtained, the following reaction mechanism was considered:

$$HN_3 + h\nu \longrightarrow {}^1NH + N_2 \qquad (1)$$

$$^1NH + Ol \longrightarrow \text{aziridine} \qquad k_a \qquad (2)$$

$$\longrightarrow \text{amine} \qquad k_1 \qquad (3)$$

$$\longrightarrow {}^3NH + Ol \qquad k_d \qquad (4)$$

$$^3NH + HN_3 \longrightarrow NH_2 + N_3 \qquad (5)$$

$$NH_2 + HN_3 \longrightarrow NH_3 + N_3 \qquad (6)$$

$$N_3 + Ol \longrightarrow OlN + N_2. \qquad (7)$$

Here, ^1NH and ^3NH represent the NH radicals in the $a^1\Delta$ and $X^3\Sigma^-$ states respectively. Ol means olefin used. In the case of propene, allylamine is a possible insertion product. The insertion into the vinylic C–H bond will give vinylamine, which is known to be an unstable compound at room temperature; therefore, the vinylamine, even if formed, will not be detected.

In the case of paraffin, Reaction 8 was assumed for the reaction of N_3:[1,2]

$$N_3 + N_3 \longrightarrow 3\,N_2. \qquad (8)$$

Since olefin is known as a radical scavenger, Reaction 7 is assumed instead of Reaction 8. The product OlN will give a polymer.[8]

As shown in Figs. 2 and 3 and in the previous papers,[1,2] the relative yield of ammonia in the olefin solution was larger than that in the paraffin solution and was independent of the concentration of hydrogen azide. The following reactions might be considered for the ammonia formation:

$$^1NH + RH \longrightarrow NH_2 + R \qquad (9)$$

$$^3NH + RH \longrightarrow NH_2 + R \qquad (10)$$

$$NH_2 + RH \longrightarrow NH_3 + R. \qquad (11)$$

Here, RH denotes an hydrocarbon molecule. If these reactions are taken into the mechanism, it is necessary to assume that the rate of the abstraction by ^1NH or ^3NH from ethylene is almost the same as that from propene and faster than that from paraffin including isobutane. This assumption is not acceptable, since olefin is known as a radical scavenger and the rate is faster than that of the hydrogen atom abstraction. The rate of the abstraction is known to depend on the strength of the C–H bond included.

Another possible mechanism for the ammonia formation is a molecular hydrogen abstraction from hydrocarbon:

$$^1NH + C_2H_4 \longrightarrow NH_3 + C_2H_2, \quad \Delta H = -200\ \text{kJ mol}^{-1}. \qquad (12)$$

Reaction 12 can successfully explain the concentration dependence of the ammonia formation. If Reaction 12 occurred in the case of ethylene, we should also consider the similar reaction in the case of paraffin:

$$^1NH + C_2H_6 \longrightarrow NH_3 + C_2H_4, \quad \Delta H = -240\ \text{kJ mol}^{-1}. \qquad (13)$$

By the inclusion of Reaction 13 in the mechanism, the concentration dependence of the ammonia formation should have an intercept. This was not the case, as was shown in the previous paper.[2] There is no reason to assume that Reaction 12 is important in the case of olefin while the similar reaction is not important in the case of paraffin. Thus it may be concluded that a reaction such as Reaction 12 is not important.

The remaining sources of ammonia are Reactions 5, 6, and 14:

$$^1NH + HN_3 \longrightarrow NH_2 + N_3. \qquad (14)$$

In fact, Reaction 14 has been considered to be important in the case of paraffin to explain the result that the relative yield of amine decreased with an increase in the concentration of hydrogen azide.[2] In the case of olefin, Reaction 14 should not be important, since the relative yield of aziridine or amine is constant for the change in the concentration of hydrogen azide. Thus, the remaining sources of ammonia are Reactions 5 and 6.

In the case of paraffin, Reaction 15 has been considered to explain the material balance and the concentration dependence of the ammonia formation:

$$NH_2 + NH_2 \longrightarrow N_2H_4. \qquad (15)$$

If Reaction 15 is included in the mechanism, the relative yield of ammonia should linearly increase with an increase in the concentration of hydrogen azide. In the case of olefins, however, this is not the case, as is shown in Figs. 2 and 3. That is, the rate of Reaction 15 is negligibly small in the olefin solution.

As was discussed above, it was necessary to ignore Reactions 14 and 15 to explain the results obtained with the olefin solution. In the case of paraffin, the rate of Reaction 14 has been considered to depend on the solvent.[2] Although the detailed interaction is unknown, the solvent effect seems to be the only way to explain the difference in the hydrogen azide concentration dependence of ammonia formation in paraffin and in olefin solutions.

Cornell *et al.* assumed the reactions of triplet NH with ethylene to explain the formation of HCN, CH_3CN, H_2, and CH_4 in the photolysis of a mixture of hydrogen azide and ethylene in the gas phase at room temperature:[4]

$$^3NH + C_2H_4 \longrightarrow CH_3CN + H_2$$
$$\longrightarrow HCN + H + CH_3. \qquad (16)$$

If Reaction 16 is included in the mechanism, the H_2 and CH_3CN formations should be observed. However, these were not found, as shown in the Results section. An intermediate of Reaction 16 may be a vibrationally excited aziridine in the triplet state, which may be efficiently deactivated to the ground state under the present experimental conditions:

$$^3NH + C_2H_4 \longrightarrow \text{aziridine}. \qquad (17)$$

A similar addition reaction to the double bond of olefin has been considered in the cases of triplet O and CH_2.[9–12] If Reaction 17 is included in the mechanism, the relative yield of ammonia should increase while that of aziridine should decrease with an increase in the concentration of hydrogen azide, because of the competition between Reactions 5 and 17. This is not the case, as shown in Figs. 2 and 3. That is, the addition reaction, if it occurred, should be negligible compared with Reaction 5. In the case of O atoms, the addition rate of the triplet oxygen has been measured to be about two orders of magnitude slower than that of the singlet O atoms at room temperature.[10] In the case of NH radicals, Cornell

et al. estimated the rate of Reaction 16 to be about 10^7 dm^3 mol^{-1} s^{-1} at room temperature.[4] Recently, McDonald *et al.* have determined the rate constant for the reactions of the singlet NH with ethylene to be 2.3×10^{10} dm^3 mol^{-1} s^{-1} at room temperature.[13] That is, the rate of triplet NH is about three orders of magnitude smaller than that of the singlet NH. If Reaction 17 has some activation energy, the rate will become smaller under the present experimental conditions.

Material Balance. From the above reaction mechanism, the following relations are expected to hold between the amounts of the products:
for ethylene;

$$N_2 = \text{aziridine} + 3 \text{ ammonia}, \quad (18)$$

for propene;

$$N_2 = \text{2-methylaziridine} + \text{allylamine} + 3 \text{ ammonia}. \quad (19)$$

Using the values shown in Figs. 2 and 3, the (aziridine+3 ammonia)/N_2 and the (2-methylaziridine+allylamine+3 ammonia)/N_2 ratios can be estimated to be 0.67 ± 0.08 and 0.96 ± 0.04 respectively. In the case of propene, the ratio is close to unity, while the ratio in the case of ethylene is considerably smaller than unity. That is, about 30% of NH-containing products are missing in the case of ethylene. Similar results have been obtained in the case of paraffin, and hydrazine was assumed to be the missing product (Reaction 15). In the case of ethylene, however, the hydrazine formation was ignored, as was discussed in the previous section. It is necessary to consider another mechanism for the missing products. This point will be discussed later.

In the case of paraffin, hydrogen formation has been observed. This was explained by assuming that about 9% of the photodissociation of hydrogen azide leads to the formation of hydrogen atom and N_3:[2]

$$HN_3 + h\nu \longrightarrow H + N_3 \quad (20)$$

$$H + HN_3 \longrightarrow H_2 + N_3. \quad (21)$$

In the presence of an excess amount of olefin, the scavenging of hydrogen atoms by olefin may be more important than Reaction 21. This explains the absence of hydrogen formation in the olefin solution:

$$H + Ol \longrightarrow R, \quad (22)$$

where R denotes a C_2H_5 or C_3H_7 radical. There is a possibility that the reaction of R affects the total yield of nitrogen. The following reactions can be considered for the reactions of alkyl radicals:

$$R + N_3 \longrightarrow RN_3 \quad (23)$$

$$R + R \longrightarrow \text{products} \quad (24)$$

$$R + HN_3 \longrightarrow RH + N_3. \quad (25)$$

If Reaction 23 is important, the nitrogen formation is not affected and Eqs. 18 and 19 still hold. If Reaction 24 is important, Reaction 20 has to be taken into account for the formation of nitrogen. The correction is about 9%. If Reaction 25 is important, the correction of 18% is necessary for the yield of nitrogen. Although it is difficult to decide which reaction is important under the present experimental conditions, the correction of 18% is too large for the case of propene.

Relative Rate Constant. Assuming the above reaction mechanism, the following rate constant ratios can be estimated by using the yields of products shown in Figs. 2 and 3.

$$k_{ae}/k_{de} = \text{aziridine/ammonia} = 1.1\pm0.2 \quad (26)$$

$$k_{ap}/k_{dp} = \text{2-methylaziridine/ammonia} = 1.9\pm0.1 \quad (27)$$

$$k_{ip}/k_{dp} = \text{allylamine/ammonia} = 0.67\pm0.04 \quad (28)$$

$$k_{ap}/k_{ip} = \text{2-methylaziridine/allylamine} = 2.9\pm0.3, \quad (29)$$

where subscripts a, i, and d stand for the addition, insertion, and deactivation reactions of the singlet NH with ethylene (e) or propene (p) respectively.

From the results shown in Fig. 5, the relative rate constant of the reaction of the singlet NH with ethylene to that with propene can also be estimated. Using the steady-state treatment, Eqs. 30, 31, and 32 can be obtained for the relative yields of the products:

$$\text{aziridine}/N_2 = k_{ae}c/k_e X \quad (30)$$

$$\text{2-methylaziridine}/N_2 = k_{ap}c/k_p\ (1-X) \quad (31)$$

$$\text{allylamine}/N_2 = k_{ip}c/k_p\ (1-X), \quad (32)$$

where $X=k_e[C_2H_4]/(k_e[C_2H_4]+k_p[C_3H_6])$. The symbol c means $(N_2-2\,NH_3)/N_2$, which was almost independent of the fraction of ethylene, as is shown in Fig. 5. k_e and k_p are the sum of the rate constants for the addition, insertion, and deactivation of the singlet NH with ethylene and propene respectively.

In order to estimate the k_e/k_p ratio, a weighted mole fraction, X′, is introduced, which is defined as follows:

$$X' = f[C_2H_4]/(f[C_2H_4]+[C_3H_6]), \quad (33)$$

where f is a weighted factor. If $f=k_e/k_p$, then $X=X'$. Assuming a value for f, the values of X' can be calculated for any mole fraction of ethylene. If the f factor is equal to k_e/k_p, the plots of the left-hand-side of Eqs. 30, 31, and 32 against X' should give straight lines for each product. Such plots are made by varying the f factor until good linearities can be obtained for every product. When the f factor was assumed to be 1.6, good linearities could be obtained, as are shown in Fig. 6; that is, $k_e/k_p=1.6$.

A similar relative rate constant for the reaction of the singlet CH_2 with ethylene and propene has been estimated to be 0.77 in the gas phase.[9] For the singlet O, 2.2/6.0=0.37 has been reported.[10] The trend in the reactivity of the singlet NH is in the opposite direction to those of the singlet O and CH_2; the ratio for NH is larger than unity, while those for O and CH_2 are smaller than unity. No proper interpretation can be found for this anomaly at present.

From the slopes of the straight lines in Fig. 6, the k_{ae}/k_e, k_{ap}/k_p, and k_{ip}/k_p ratios can be estimated to be about 0.30, 0.48, and 0.17 respectively. Combining these values with those estimated from Eqs. 26—29, the k_{de}/k_e and k_{dp}/k_p ratios can be estimated to be 0.27 and 0.25 respectively. These values are listed in Table 1. Although the $(k_{ap}+k_{ip}+k_{dp})/k_p$ ratio is close to unity, the $(k_{ae}+k_{de})/k_e$ ratio is only 0.57. That is, some reaction path is missing in the case of ethylene. The extent of the missing reaction cor-

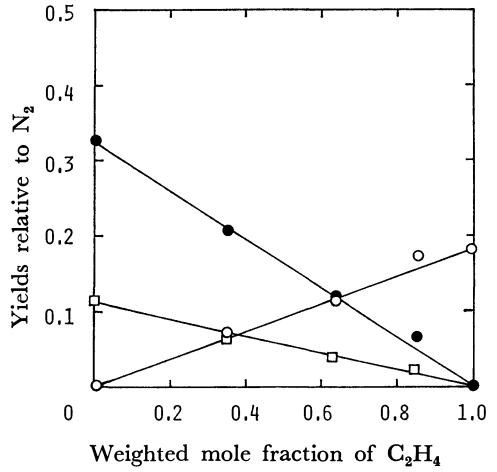

Fig. 6. Plots for Eqs. 30, 31, and 32 as functions of the weighted mole fraction of ethylene.
○: Aziridine, ●: 2-methylaziridine, □: allylamine. $f=1.6$ (see Text).

TABLE 1. VALUES OF RELATIVE RATE CONSTANTS

	C_2H_4		C_3H_6	
Addition	[1.00][a]	(0.30)[b]	1.0	(0.48)
Insertion				
Vinyl[c]	1.43	(0.43)	0.21	(0.10)
Allyl	0	0	0.35	(0.17)
Deactivation	0.90	(0.27)	0.52	(0.25)
Total	3.33	(1.00)	2.08	(1.00)

a) The rate of aziridine formation in the ethylene solution is assumed to be unity. b) The values in parenthese show the relative values for each olefin, assuming the total rate to be unity. c) Values estimated on the assumption that the missing reaction is the insertion into the vinylic C–H bond.

responds to the amount of the missing NH-containing products, which was disscussed in the previous section. The missing product might be vinylamine, since this compound is known to be unstable at room temperature.

The following relations can also be obtained by using the steady-state treatment:

$$\text{2-methylaziridine/aziridine} = k_{ap}[C_3H_6]/k_{ae}[C_2H_4] \quad (34)$$

$$\text{allylamine/aziridine} = k_{ip}[C_3H_6]/k_{ae}[C_2H_4]. \quad (35)$$

The k_{ap}/k_{ae} and k_{ip}/k_{ae} ratios were estimated to be 1.0 ± 0.1 and 0.32 ± 0.05 respectively, using the results shown in Fig. 5. The rate of the addition to the double bond of ethylene is almost equal to that of propene. The relative rate constants are summarized in Table 1.

From the results shown in Fig. 4, it is possible to estimate the relative rate of the insertion into the C–H bond of ethane to the addition to the double bond of ethylene.

$$^1NH + C_2H_6 \longrightarrow C_2H_5NH_2 \quad (36)$$

When competition between Reactions 36 and 2 is considered, the following relation can be obtained:

$$\text{ethylamine/aziridine} = k_{36}[C_2H_6]/k_{ae}[C_2H_4]. \quad (37)$$

The k_{36}/k_{ae} ratio is estimated to be 0.82 ± 0.05. Since ethane has 6 C–H bonds, the addition reaction is about $6/0.82=7.3$ times faster than the insertion reaction per C–H bond. This value can be compared with 3 $k_{ap}/k_{ip}=8.6$, *i.e.*, the addition reaction is 8.6 times faster than the insertion into the allylic C–H bond of propene. In the case of the singlet O, DeMore estimated this ratio to be $0.37/0.071=5.2$ in the Ar solution at 87 K.[11] For the singlet CH_2, this ratio was larger than 10, depending on the source of the CH_2.[12] The ratio obtained with the singlet NH is between the ratios obtained with the singlet O and CH_2.

Table 1 shows that the branching ratio for the deactivation (Reaction 4) by ethylene is almost the same as that by propene and slightly larger than that by paraffin.[2] In this article, Reaction 4 followed by Reactions 5 and 6 is assumed to be responsible for the ammonia formation. However, Reaction 9, the hydrogen atom abstraction from hydrocarbon by the singlet NH, is indistinguishable from Reaction 4 only from the kinetics. If Reaction 9 should be considered instead of Reactions 4 and 5, the branching ratio for the deactivation would be that of Reaction 9. In this case, it is necessary to assume that the rate of the abstraction from ethylene is faster than those from propene and from paraffin, as was discussed already.

References

1) S. Tsunashima, M. Hotta, and S. Sato, *Chem. Phys. Lett.*, **64**, 435 (1979).
2) S. Tsunashima, J. Hamada, M. Hotta, and S. Sato, *Bull. Chem. Soc. Jpn.*, **53**, 2443 (1980).
3) J. L. Brash and R. A. Back, *Can. J. Chem.*, **43**, 1778 (1965).
4) D. W. Cornell, R. S. Berry, and W. Lwowski, *J. Am. Chem. Soc.*, **88**, 544 (1966).
5) W. C. Richardson and D. W. Setser, *Can. J. Chem.*, **47**, 2725 (1969).
6) R. S. Konar, S. Matsumoto, and B. deB, Darwent, *Trans. Faraday Soc.*, **66**, 1698 (1970).
7) M. E. Jacox and D. E. Milligan, *J. Am. Chem. Soc.*, **85**, 278 (1963).
8) K. Ishizaki and S. Sato, *Bull. Chem. Soc. Jpn.*, **47**, 2597 (1974).
9) S. Kryzanowski and R. J. Cvetanović, *Can. J. Chem.*, **45**, 665 (1967).
10) O. Kajimoto and T. Fueno, *Chem. Phys. Lett.*, **64**, 445 (1979).
11) W. B. DeMore, *J. Phys. Chem.*, **73**, 391 (1969).
12) J. N. Butler and G. B. Kistiakowsky, *J. Am. Chem. Soc.*, **82**, 759 (1960).
13) J. R. McDonald, R. G. Miller, and A. P. Baronavski, *Chem. Phys.*, **30**, 133 (1978).

Steady-state and Picosecond Studies of Energy Transfer between Dyes with Closely Located S_1-Levels. Rhodamine-6G and 3,3′-Diethylthiacarbocyanine Iodide in Acetone Solution

Yoshihumi KUSUMOTO,* Hiroyasu SATO,** Kazuto MAENO, Shuichi YAHIRO, and Nobuaki NAKASHIMA***

Chemical Institute, College of Liberal Arts, Kagoshima University, Korimoto, Kagoshima 890

***Chemistry Department of Resources, Faculty of Engineering, Mie University, Tsu 514*

****Institute for Molecular Science, Okazaki 444*

(Received May 26, 1980)

Lasing wavelengths and fluorescence spectra were measured for a mixed dye system containing various concentrations of Rhodamine 6G (Rh-6G) and 3,3′-diethylthiacarbocyanine iodide (DTC), which have very closely located S_1 levels, in acetone at room temperature. A new way of confirming the occurrence of energy transfer is presented on the basis of the reabsorption effect. It was found that most of the pump power absorbed by Rh-6G is transferred to DTC. A study of the fluorescence decay by a picosecond laser revealed that the energy transfer is essentially governed by the Förster mechanism. The observed fluorescence decay data agree fairly well with the R_0 value of 73.2 Å calculated from the spectral overlap.

Dye lasers have made a great progress over a wide wavelength region ranging from the ultraviolet (UV) to the infrared (IR). Hildebrand[1] and Lin[2] reported near-IR dye laser emission from several polymethine dyes directly pumped by UV nitrogen laser radiation (λ=337.1 nm). However, it is difficult to obtain efficient laser emission in longer wavelength regions (*e.g.*, near-IR), from nitrogen-laser pumped dye solutions, mainly because of very small absorption at 337.1 nm. A means to overcome the difficulty is the excitation of a dye laser through energy transfer processes for some dye mixture systems excited by 337.1-nm radiation of a nitrogen laser.[3-9] The energy transfer process with the use of a proper mixture of dyes can provide a means of extending the wavelength region in which lasing is achieved.

In the dye mixture systems studied so far, the fluorescent levels of donor and acceptor are widely separated (over 1800 cm^{-1}),[3-9] and thus there is little ambiguity in the lasing species. In a system of a donor and acceptor with closely located energy levels, however, it is difficult to identify the lasing species. Investigation of such a system seems to be important in connection with the intermolecular energy transfer in photosynthetic pigments, considering that several forms of chlorophyll with slightly different absorption maxima are operative in the primary energy-transfer process in photosynthesis.[10] In this connection, we have studied the energy transfer mechanism. The intermolecular singlet-singlet electronic energy transfer was found to proceed by at least three mechanisms: the resonance, exchange, and trivial mechanisms.[11] In order to differentiate various mechanisms contributing to energy transfer in dye laser systems, the study of fluorescence decay curve with a picosecond laser seems to be effective.

In this paper, we report the lasing behavior and energy transfer mechanism of the system 3,3′-diethylthiacarbocyanine iodide (DTC) as an acceptor and Rhodamine 6G (Rh-6G) as a donor in acetone at room temperature. The S_1 levels of both dyes are closely located. Some results have been reported.[12]

Experimental

Rh-6G (laser-dye grade; Eastman Kodak Co.), DTC (laser-dye grade; Dojindo Lab.), and acetone (spectrograde or guaranteed grade) were used without further purification.

The nitrogen and dye laser system and the spectrofluorometer were constructed in our laboratory. The nitrogen laser was similar to the one described by Basting *et al.*[13] and Maeda and Miyazoe.[14] The dye solution in a quartz spectrofluorometer cell with a square section 1×1 cm^2 was transversely pumped by 337.1-nm radiation from a pulsed nitrogen laser with an output peak power of *ca.* 500 kW at the nitrogen pressure *ca.* 60 Torr. No mirrors were employed, lasing being conducted between the side walls of the dye cell.

The dye lasing wavelengths and fluorescence spectra were measured with a Nalumi RM-21 500-mm grating monochromator equipped with an EMI 6256S photomultiplier. For the fluorescence spectra, the sample degassed in 9 mm diam. pyrex tubes was excited by an Ushio USH-500D 500-W super-high-pressure mercury arc lamp, Toshiba V-V40 and UV-39 filters being used to select 436-nm light.[15] For the fluorescence decay curves, the sample in a quartz spectrofluorometer cell was pumped with the second harmonic (530 nm) of a Nd^{3+}: YAG laser, the decays being measured with a Hamamatsu C979 streak camera. The donor emission was selected with a Nihon-Shinkukogaku IF-W interference filter (λ_{max}=560 nm). The time-sale of the streak camera was fully calibrated. The width of the exciting pulse was *ca.* 26 ps. The results of three shots on the same sample were averaged. All measurements were made at room temperature. Other experimental details have been reported.[9,16]

Results and Discussion

Spectra. The absorption and fluorescence spectra of Rh-6G and DTC are shown in Fig. 1. The good spectral overlap between the Rh-6G fluorescence and DTC absorption suggests the possibility of energy transfer from Rh-6G to DTC. Since the peak wavelengths of the fluorescence spectra are close to each other for these dyes, the emission in a mixture of the two dyes can not be concluded to originate from the acceptor (DTC).

Confirmation of Energy Transfer by Reabsorption Effect. Since we observed no lasing for DTC by itself, it may follow that the excitation energy is effectively transferred from Rh-6G to DTC when the laser emission in the mixtures originates from DTC. The lasing wavelengths and fluoresence spectra of the Rh-6G-DTC dye mixture system were measured at various donor concentrations for a fixed acceptor concentration. The plot of peak wavelengths (λ_{max}) in the laser emission (L) and fluorescence (F) *versus* donor concentration [D] is shown in Fig. 2, together with the concentration dependence of the λ_{max}-values in L and F of Rh-6G alone in acetone. The λ_{max}-values in L and F of the dye mixture are independent of concentration while those in the Rh-6G only system shift to longer wavelengths with increasing concentration because of the reabsorption effect. This indicates that the emission in the dye mixture originates essentially from DTC.

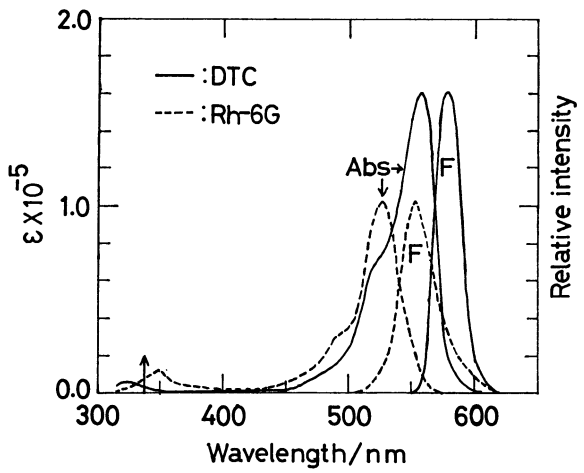

Fig. 1. Absorption (Abs) and fluorescence (F) spectra for the Rh-6G and DTC dyes separately.
Absorption path length: 1 mm. Concentration: Rh-6G, 5×10^{-5} M for Abs and 1×10^{-5} M for F; DTC, 5×10^{-5} M for Abs and 1.5×10^{-5} M for F; in acetone. The arrow on the abscissa refers to the 337.1-nm excitation wavelength.

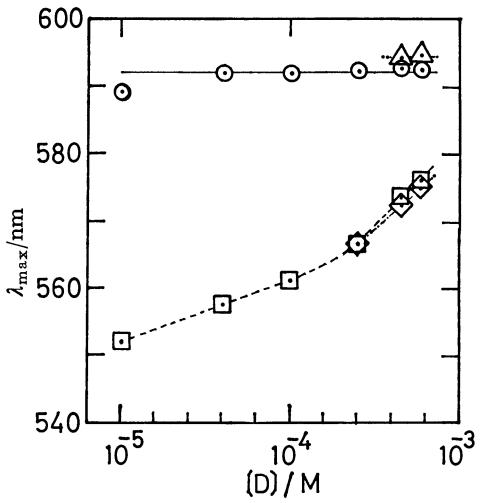

Fig. 2. Plots of the λ_{max}-values in the laser emission (L) and fluorescence (F) *versus* the Rh-6G concentration [D] for a fixed DTC concentration (1.5×10^{-4} M).
▲ and ⊙: L and F of Rh-6G-DTC dye mixture system, respectively; ◈ and ⊡: L and F of Rh-6G alone, respectively. It was not possible to obtain laser action from Rh-6G alone as well as from the mixture in the low concentration range under our experimental conditions.

We measured the λ_{max}-values of L and F in the dye mixture system at various acceptor concentrations for a fixed donor concentration. The results are shown in Fig. 3 together with the concentration dependence of λ_{max} in F of DTC in acetone. The λ_{max}-values in F of both the dye mixture and the DTC-only system agree, showing a shift due to the reabsorption effect as in the case of the Rh-6G. The λ_{max}-values in L of the dye mixture system show a concentration dependence similar to those of F mentioned above. The results show that the laser emission in the dye mixture system originates essentially from DTC at least within the concentration range studied. Most of the excitation energy absorbed by Rh-6G is transferred to DTC as a useful pump power, *viz.*, pumping by excitation transfer is efficient.

We carried out an experiment with dye mixtures containing coumarin 2 as donor and coumarin 1 as acceptor in ethanol at room temperature and at 77 K over a wide range of concentration. The S_1 levels of both dyes are more closely located than the Rh-6G-DTC system. We have confirmed on the basis of the reabsorption effect that in this system the energy transfer from coumarin 2 to coumarin 1 occurs at 77 K.[17]

Fluorescence Decay Behavior. Rh-6G-only and DTC-only System: Fluorescence was monitored at 560 nm and 580 nm for Rh-6G and DTC, respectively. An exponential decay was observed in each case with

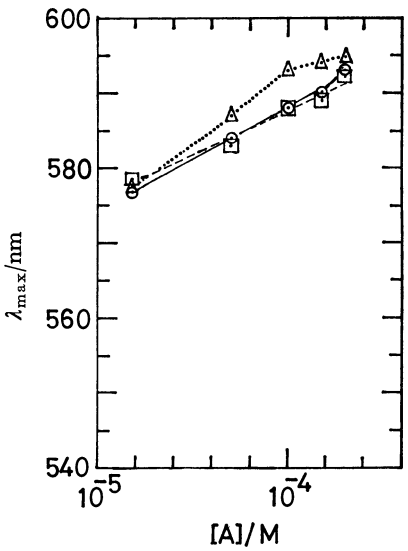

Fig. 3. Plots of the λ_{max}-values in L and F *versus* the DTC concentration [A] for a fixed Rh-6G concentration (5×10^{-4} M).
▲ and ⊙: L and F of Rh-6G-DTC dye mixture system, respectively; ◙: F of DTC alone.

lifetime of 2.6 ns (Rh-6G 1.0×10^{-5} M)[18]† and 130 ps (DTC 2.0×10^{-6} M). The latter is in good agreement with the predicted value of Roth and Craig.[19]

Rh-6G Plus DTC System: Fluorescence was monitored at 560 nm. The λ_{max}-values in F of Rh-6G and DTC are 552 nm (10^{-5} M) and 590 nm (10^{-4} M), respectively. The experimental decay curves indicate that the initial part ($t\lesssim400$ ps) suffered from a serious overlap of the DTC-fluoresence. Since the initial part ($t\lesssim30$ ps) was influenced by the exciting pulse duration, only the later part of the decay was used for the analysis. The following holds for the Förster-type time-dependent fluorescence decay of the donor in the presence of a large number of acceptor molecules:[20,21]

$$I_Q(t) = I_Q(0)\exp\{-t/\tau_D - 2([A]/C_0)(t/\tau_D)^{1/2}\} \quad (1)$$

where $C_0=(7.65/R_0)^3$. R_0, critical transfer distance, is given by the formula

$$R_0^6 = \frac{9000(\ln 10)\phi_D\kappa^2}{128\pi^5 Nn^4}\int f_D(\bar{\nu})\varepsilon_A(\bar{\nu})d\bar{\nu}/\bar{\nu}^4. \quad (2)$$

In these formulas, τ_D is the fluorescence lifetime of the donor in the absence of energy transfer, ϕ_D the fluorescence quantum yield of the donor, N Abogadro's number, n reflactive index of the media, f_D the spectral distribution of the donor fluorescence normalized to one (in units of quanta on a wavenumber scale), and ε_A the molar decadic extinction coefficient of the acceptor. The average value of κ^2, an orientation factor, is 2/3 when the molecules are free to rotate at a rate much greater than that of transfer, and 0.475[22] when the orientation of the donor and acceptor is random but the rate of rotation is much smaller than that of transfer. From Eq. 1 and the fluorescence decay in the absence of the acceptor

$$I_F(t) = I_F(0)\exp(-t/\tau_D), \quad (3)$$

we have the linear relationship:

$$\ln[I_Q(t)/I_F(t)] = \ln[I_Q(0)/I_F(0)] - 2([A]/C_0)\tau_D^{-1/2}t^{1/2}. \quad (4)$$

The values of C_0 and R_0 can be calculated from the spectral overlap of fluorescence band of Rh-6G and absorption band of DTC to be 1.14×10^{-3} M and 73.2 Å, respectively. The value of the orientation factor κ^2 was assumed to be 2/3 in this calculation (*vide infra*). In Fig. 4, $\ln[I_Q(t)/I_F(t)]$ is plotted against $t^{1/2}$, the number of data points being restricted for the sake of clarity. The straight line in the figure has the slope calculated with the values given above. The experimental points representing the later part of decay seem to fit the line although the data points are scattered because of the small intensity of $I_Q(t)$. This suggests that the energy transfer in the present dye laser system takes place essentially through the process of nonradiative resonance transfer of the Förster type. A large R_0 value is due to a large spectral overlap, which is in turn caused by the closely located S_1 levels of the dyes.

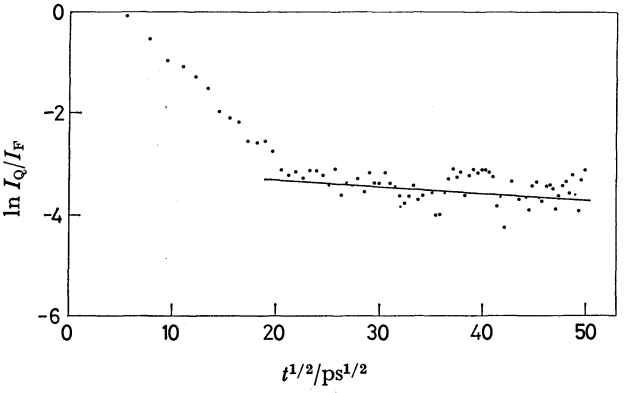

Fig. 4. $\ln[I_Q(t)/I_F(t)]$ plotted as a function of $t^{1/2}$. $I_Q(t)$: Rh-6G 1×10^{-5} M, DTC 9×10^{-5} M, $I_F(t)$: Rh-6G 1×10^{-5} M. The slope of the straight line was calculated with $R_0=73.2$ Å.

The Förster theory assumes that the rate of translational diffusion is small enough to preclude a significant perturbation of the random distribution of distances between D and A during the course of measurement.[11d,11e] On the basis of picosecond-absorption spectroscopic studies Rehm and Eisenthal[23] stated that the Förster theory gives a good description of singlet-singlet energy transfer between Rh-6G (donor) and malachite green (acceptor) in glycerol even up to the earliest time (20 ps). Porter and Tredwell[21] carried out similar studies with a picosecond laser and streak camera system on the same pair in a low viscosity solvent (ethanol), showing that the Förster theory is applicable up to a limiting time resolution of 10 ps. They showed that translational diffusion does not distort the kinetics of the energy transfer system at a viscosity of 1.2 cP.†† The significant changes in the intermolecular distances during energy transfer can be precluded because of the relationship[11c]

$$R_0 \gg [2(D_D+D_A)\tau_D]^{1/2}, \quad (5)$$

where D_D and D_A are the diffusion coefficients of the donor and acceptor, respectively. In our case, the viscosity of the solvent (0.32 cP) is *ca.* 4-fold smaller than in their case; the diffusion coefficient of Rh-6G would be *ca.* 4 times larger, assuming the Stokes-Einstein relation $D=kT/(6\pi\eta b)$.[11b] The coefficient for DTC is unknown. However, the size and charge of the molecule are comparable to those of Rh-6G indicating that the value of the coefficient should be similar. Thus, $[2(D_D+D_A)\tau_D]^{1/2}$ would be *ca.* 45 Å, twice as large as in the case of Porter and Tredwell. Our value of R_0, 73.2 Å is much larger.

Gösele *et al.*[24] reported that an expression formally analogous to Eq. 1 can be obtained for the time-dependent fluorescence intensity even when diffusion governs the fluorescence quenching effects. In the diffusion-governed kinetics, instead of R_0^3, should be used $r_{AD}^2 D^{1/2}\tau_D^{1/2}$ multiplied by a constant with a value close to 2, where r_{AD} is a certain collision distance and D the sum of D_A and D_D (the quantity α in their formulas is replaced by R_0^6/τ_D). According to these authors, the quenching effects are controlled by diffusion and by long-range energy transfer when $Z_0=R_0^3/(2r_{AD}^2 D^{1/2}\tau_D^{1/2})\ll1$ or $Z_0\gg1$, respectively. For the case where the long-range energy transfer is

† 1 M=1 mol dm^{-3} in this paper.

†† 1 cP=10^{-3} kg m^{-1} s^{-1} in SI units.

dominant, we have $R_0 \gg r_{AD}$ and hence $R_0^2 \gg 2^{1/2} r_{AD}^2$. When we multiply the left and right sides of the inequality 5 by R_0^2 and $2^{1/2} r^2{}_{AD}$ respectively, we obtain the relation $Z_0 \gg 1$. Thus, the relation $Z_0 \gg 1$ is equivalent to inequality 5.

Birks[11c] and Birks and Georghiou[25] observed the donor fluorescence decay of phenanthrene in the absence and presence of acridine in six solvents of viscosity η=64.6 cP (cyclohexanol) to 0.4 cP (heptane). Their results were compared with the relations of Förster[20], Yokota and Tanimoto[26], and Voltz *et al.*,[27] the last being developed from diffusion theory and extrapolates to Stern-Volmer kinetics.[11c] A mean value of R_0=25.5 Å was obtained from the spectroscopic data. At η=64.6 cP, where $\sqrt{2D\tau_D} < R_0$, the donor decay follows Förster kinetics. At η<3.7 cP where $\sqrt{2D\tau_D} > 3R_0$, the decay was exponential, following Stern-Volmer kinetics. At intermediate viscosities, where the decay was non-exponential but more rapid than predicted by the Förster relation, the decay agreed with the Yokota-Tanimoto relation within experimental error. The Voltz relation predicted a more rapid decay than that observed.

In our case, R_0 is much larger than $\sqrt{2D\tau_D}$. In the Yokota-Tanimoto relation, the second term in the exponent of Eq. 1 is multiplied by

$$B = [(1+10.87x+15.50x^2)/(1+8.743x)]^{3/4} \quad (6)$$

with $x = D\alpha^{-1/3}t^{2/3} = DR_0^{-2}\tau_D^{1/3}t^{2/3}$. The slope of the $\ln[I_Q(t)/I_F(t)]$ *vs.* $t^{1/2}$ plot is not constant but dependent on $t^{1/2}$ because of the presence of B. For our case with $D = 1\times10^{-5}$ cm^2 s^{-1}, R_0=73.2 Å, and τ_D=2.6 ns, the slope calculated by means of the Yokota-Tanimoto relation increases in absolute value with $t^{1/2}$. The experimental points in Fig. 4 show no such tendency. The slope is constant and time-independent, indicating that the Förster kinetics is applicable, although the viscosity of the solvent is very low. If we compare our results with those of Birks and Georghiou,[25] we find the following: (1) a larger R_0 value, R_0=73.2 Å instead of 25.5 Å, (2) a larger b value, large dye molecules instead of small molecules phenanthrene and acridine and (3) a smaller τ_D value, τ_D=2.6 ns instead of $\tau_D \approx 60$ ns. Each of the effects (1), (2), and (3) diminishes the boundary value of η for diffusion-dominated kinetics, *i.e.*, a value of η which satisfies $\sqrt{2D\tau_D} = 3R_0$. The value becomes smaller by a factor of $(73.2/25.5)^2 \approx 8$ than that of Birks and Georghiou if we take (1) into consideration.

The energy transfer seems to follow the Förster mechanism, although some contribution of diffusion controlled process can not be entirely ruled out.

Bojarski and Dudkiewicz[28] proposed the concentration effects on orientation factor κ^2 by considering the concentration-dependent ratio of rotation time (τ_r) and time of the excitation energy localization $\tau_1 = [\sum_D k_{D^*D} + \sum_A k_{D^*A} + k_F + k_q]^{-1}$, where k_{D^*D} and k_{D^*A} denote the rate constant of long-range nonradiative electronic excitation energy transfer due to the dipole-dipole interaction between an excited donor (D*) and an unexcited donor (D) and that between D* and an acceptor (A), respectively, and k_F and k_q those for emission and internal conversion, respectively. They assumed the value of κ^2 to be a function of $a = \tau_r/\tau_D$ and $\gamma = [A]/C_0$. The deviation of κ^2 from the value of rapid rotation is important when $\gamma \geq 1$ for $a \lesssim 0.1$. For a larger a, it becomes prominent from a smaller γ. They reexamined the data of Porter and Tredwell[21] and concluded that the small systematic change in C_0 can be caused by the change in κ^2. In the case (P. and T.) (τ_r=320 ps. τ_D=4200 ps, a=0.0762) the acceptor concentration is very high (10^{-2}—10^{-3} M), the values of γ being in the range 3.05—0.33. In our case, the value of τ_r should be smaller than that in more viscous ethanol (320 ps). With τ_D=2600 ps, the value of a would be *ca.* 0.1. Since $\gamma = 9\times10^{-5}/1.14\times10^{-3} = 0.079$, the deviation of the value of κ^2 from the value of rapid rotation can be neglected. The value $\kappa^2 = 2/3$ seems to be reasonable.

Concluding Remarks. A new method has been worked out for confirming the occurrence of energy transfer on the basis of the reabsorption effect. Rh-6G, with a high fluorescence quantum yield (0.83 or 0.92)[18] and a good spectral overlap characteristics with DTC, can be used as an efficient donor for lasing of DTC even though DTC has a very low fluorescence quantum yield (0.048).[19] The energy transfer occurs by a nonradiative process of the Förster-type. French *et al.*[10] found that the absorption bands of chloroplasts can be considered as a superposition of bands associated with several chlorophyll forms. A very efficient energy transfer occurs among them, their S_1 levels being very close. The dyes we used have very closely located S_1 levels. A combination of these dyes can be considered as a model system of chloroplasts. Occurrence of resonance energy transfer is possible for these dyes even in dilute solutions (below 10^{-3} M) mainly due to good spectral overlap characteristics, *i.e.*, a large value of R_0. Further experiments on the energy transfer of these dyes in micellar systems are in progress.[29-30]

This work was partly supported by a Grant-in-Aid for Special Project Research on Laser Spectroscopy No. 221626 from the Japanese Ministry of Education, Science and Culture.

References

1) O. Hildebrand, *Opt. Commun.*, **10**, 310 (1974).
2) C. Lin, *IEEE J. Quantum Electron.*, QE-**11**, 61 (1975).
3) C. E. Moeller, C. W. Verber, and A. H. Adelman, *Appl. Phys. Lett.*, **18**, 278 (1971).
4) F. B. Dunning and E. D. Stokes, *Opt. Commun.*, **6**, 160 (1972).
5) A. Dienes and M. Madden, *J. Appl. Phys.*, **44**, 4161 (1973); C. Lin and A. Dienes, *J. Appl. Phys.*, **44**, 5050 (1973).
6) I. B. Berlman, M. Rokni, and C. R. Goldschmidt, *Chem. Phys. Lett.*, **22**, 458 (1973).
7) S. A. Ahmed, J. G. Gergely, and D. Infante, *J. Chem. Phys.*, **61**, 1584 (1974).
8) E. Weiss and S. Speiser, *Chem. Phys. Lett.*, **40**, 220 (1976).
9) Y. Kusumoto, H. Sato, and K. Maeno, *Sci. Rept. Kagoshima Univ.*, **26**, 151 (1977).
10) C. S. French, *Proc. Natl. Acad. Sci. U. S. A.*, **68**, 2893 (1971); C. S. French, J. S. Brown, and M. C. Lawrence,

Plant Physiol., **49**, 421 (1972).
11) a) N. J. Turro, "Molecular Photochemistry," Benjamin, New York (1967); b) A. A. Lamola, "Energy Transfer and Organic Photochemistry," ed by P. A. Leermakers, A. Weissberger, A. A. Lamola, and N. J. Turro, Interscience, New York, N. Y. (1969), p. 17; c) J. B. Birks, "Photophysics of Aromatic Molecules," John Wiley, New York (1970), Chap. 11; d) R. G. Bennett, *J. Chem. Phys.*, **41**, 3037 (1964); e) R. G. Bennett and R. E. Kellogg, *Photochem. Photobiol.*, **7**, 571 (1968); f) N. J. Turro, *Pure Appl. Chem.*, **49**, 405 (1977).
12) Y. Kusumoto, H. Sato, K. Maeno, and S. Yahiro, *Chem. Phys. Lett.*, **53**, 388 (1978).
13) D. Basting, F. P. Schäfer, and B. Steyer, *Opto-electron*, **4**, 43 (1972).
14) M. Maeda and Y. Miyazoe, *Jpn. J. Appl. Phys.*, **13**, 827, (1974).
15) The Rh-6G and DTC dye samples studied were decomposed by continuous irradiation by 365-nm light selected with a Toshiba UV-DIA filter.
16) M. Sumitani, N. Nakashima, K. Yoshihara, and S. Nagakura, *Chem. Phys. Lett.*, **51**, 183 (1977).
17) Y. Kusumoto and H. Sato, Unpublished results.
18) K. A. Selanger, J. Falnes, and T. Sikkeland, *J. Phys. Chem.*, **81**, 1960 (1977), and references therein. Data for fluorescence lifetime of Rh-6G in solution reported are diverse.
19) N. J. L. Roth and A. C. Craig, *J. Phys. Chem.*, **78**, 1154 (1974).
20) Th. Förster, *Ann. Phys.*, **2**, 55 (1948); Th. Förster, *Z. Naturforsch.*, **4a**, 321 (1949).
21) G. Porter and C. J. Tredwell, *Chem. Phys. Lett.*, **56**, 278 (1978).
22) I. B. Berlman; "Energy Transfer Parameters of Aromatic Compounds," Academic Press, New York (1973), p. 28.
23) D. Rehm and K. B. Eisenthal, *Chem. Phys. Lett.*, **9**, 387 (1971).
24) U. Gösele, M. Hauser, U. K. A. Klein, and R. Frey, *Chem. Phys. Lett.*, **34**, 519 (1975).
25) J. B. Birks and S. Georghiou, *Chem. Phys. Lett.*, **1**, 355 (1967); *J. Phys. B. (Proc. Phys. Soc.) Ser. 2*, **1**, 958 (1968).
26) M. Yokota and O. Tanimoto, *J. Phys. Soc. Jpn.*, **22**, 779 (1967).
27) R. Voltz, G. Laustriat, and A. Coche, *C. R. Acad. Sci. Paris*, **257**, 1473 (1963); *J. Chim. Phys.*, **63**, 1253 (1966); R. Voltz, J. Klein, F. Heisel, H. Lami, G. Laustriat, and A. Coche, *J. Chim. Phys.*, **63**, 1259 (1966).
28) C. Bojarski and J. Dudkiewicz, *Chem. Phys. Lett.*, **67**, 450 (1979).
29) Y. Kusumoto and H. Sato, *Chem. Phys. Lett.*, **68**, 13 (1979).
30) H. Sato, Y. Kusumoto, N. Nakashima, and K. Yoshihara, *Chem. Phys. Lett.*, **71**, 326 (1980); and references therein.

  Bull. Chem. Soc. Jpn., 54, 65—68 (1981)

Thermodynamic Studies of Thallium Halide Formation in Nonaqueous Solvents

Yukio Sasaki,* Masao Takizawa, Kisaburo Umemoto,** and Niro Matsuura**

Tokyo Institute of Polytechnics, Iiyama, Atsugi, Kanagawa 243-02

***Department of Pure and Applied Science, College of General Education, The University of Tokyo, Komaba, Meguro-ku, Tokyo 153*

(Received May 29, 1980)

The differences in the order of stability among halide ions for metal halogeno-complexes in nonaqueous solvents and water are examined by means of the thermodynamic constants for the formation of thallium halides of transfer from water to *N,N*-dimethylformamide (DMF) and propylene carbonate (PC). The thermodynamic constants for the formation of thallium halides were calculated from the solubility products of thallium halides. The differences in the order of stability for thallium halides were found to be dependent mainly on the enthalpy changes for the formation of thallium halides of transfer from water to DMF and PC, while the enthalpy changes of transfer for thallium halides are themselves largely influenced by the enthalpy changes for halide ions of transfer from water to DMF and PC.

In previous papers,[1-4] the formation of metal halogeno-complexes was investigated potentiometrically in dimethyl sulfoxide, *N,N*-dimethylformamide, and propylene carbonate. The order of stability for metal halogeno-complexes (halogeno-cadmium, -lead, -copper and -zinc complexes[5]) among halide ions in nonaqueous solvents was found to be different from that in water. The classification of metals according to their complexation with halide ions is shown in Table 1. The solid line indicates the classification by Ahrland[6] in water, while the broken line indicates the classification obtained by our studies in nonaqueous solvents.[7] The stability of the halogeno-complexes on outside metals of the triangle in Table 1 decreases in the order of $Cl^->Br^->I^-$. However, the stability on inside metals is the reversed order; $I^->Br^->Cl^-$.

The purpose of the present paper is to elucidate the reason for differences in the stability on metal halogeno-complexes in *N,N*-dimethylformamide, propylene carbonate, and water from the thermodynamic constants for the formation of thallium halides.

Experimental

Materials. The purification of *N,N*-dimethylformamide (DMF) and propylene carbonate (PC), the preparation and purification of tetraethylammonium perchlorate, and the preparation of the saturated thallium amalgam have been described elsewhere.[8,9] The tetraethylammonium halides and thallium(I)perchlorate($TlClO_4$) were obtained commercially and were purified by recrystallization with water–ethanol or ethanol–ethyl acetate mixtures. The electrolytes were dried in a vacuum oven for 2 d in the temperature range of 60—70 °C.

Procedure. The solubilities of thallium(I)halides (TlX) were determined by means of potentiometric titration. A solution of 10^{-3} mol dm^{-3} of $TlClO_4$ was titrated with a solution of 5×10^{-2} mol dm^{-3} of TlX. The indicator electrode was a saturated thallium amalgam electrode, while the reference electrode was an aqueous saturated calomel electrode (SCE) equipped with a nonaqueous salt bridge.[9] The experimental device is shown in Fig. 1. The potential of the cell was measured on a Hewlett-Packard Model 34703A ohm meter. Each temperature was controlled to an accuracy of 0.1 °C.

Results and Discussion

The titration curves for Tl^+ with Cl^- in PC at 10, 20, and 25 °C are shown in Fig. 2. One well-defined equivalent point at $C_{Cl^-}/C_{Tl^+}=1$ (mol ratio) was found in each titration curve (Fig. 2). The precipitation

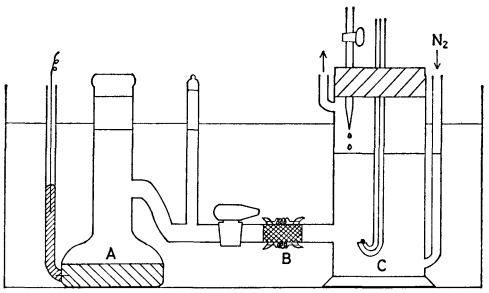

Fig. 1. Experimental device.
A: SCE, B: salt bridge composed of DMF–water mixture containing 0.5 mol dm^{-3} tetraethylammonium perchlorate and aqueous solution containing 1 mol dm^{-3} NaCl,[5] C: thallium amalgam electrode.

Table 1. Classification of metals according to their complexation with halide ions

Cr	Mn	Fe	Co	Ni	Cu	Zn	Ga	Ge	As
Mo	Tc	Ru	Rh	Pd	Ag	Cd	In	Sn	Sb
W	Re	Os	Ir	Pt	Au	Hg	Tl	Pb	Bi

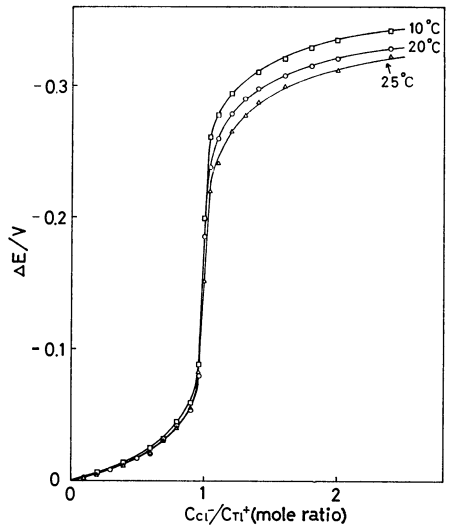

Fig. 2. Potentiometric titration curves for Tl^+ with Cl^- in PC at 10, 20, and 25 °C.
ΔE: potential shift caused by addition of Cl^-, tetraethylammonium perchlorate: 0.1 mol dm^{-3}.

appeared in the range from 10 to 30 °C soon after halide ions were added. This fact shows that the precipitation of TlX occurred as is shown in Eq. 1. In previous papers,[10] it was confirmed that the

$$Tl^+ + X^- = TlX. \quad (1)$$

Nernst equation was obeyed in DMF and PC containing $TlClO_4$ in the range from 1×10^{-4} to 2×10^{-3} mol dm^{-3}. The solubility products of TlX, assuming no complex formation of Tl^+ with Cl^-, and using the activity coefficients of TlX in DMF and PC,[10] were calculated from the titration curves on the basis of the Nernst equation. The order of the solubility products of TlX in DMF and PC is; TlI>TlBr>TlCl. The enthalpy changes ($\Delta H^\circ_{(TlX)}$) for the formation of TlX were obtained graphically from the slope of the log K_{s0} *vs.* $1/T$ plot (Vant Hoff plot, Eq. 2), where the K_{s0}

$$\log K_{s0} = \frac{\Delta H^\circ_{(TlX)}}{2.303R}\frac{1}{T} + \text{const.} \quad (2)$$

are solubility products. Figure 3 shows the plots of log K_{s0} *vs.* $1/T$ in DMF, PC, and water. The solubility products in water were obtained by means of the solubilities quoted from the literature.[11,12] The order of the solubility products in water is the reverse of that DMF and PC, as is shown in Fig. 3. The values of log K_{s0} for TlX in DMF and PC at 25 °C are given in Table 2. The values of log K_{s0} in DMF are in fair agreement with those of the literature.[10,13] However, the log K_{s0} values in PC are not in agreement with those of Salomon.[14] It is presumed that this disagreement arises from the use of the lithium–lithium halides reference electrode, since lithium metal may react with PC.[13]

The free-energy changes ($\Delta G^\circ_{(TlX)}$) for the formation of TlX can be correlated to log K_{s0} with the temperature in Eq. 3, and

$$\Delta G^\circ_{(TlX)} = 2.303RT \log K_{s0} \quad (3)$$

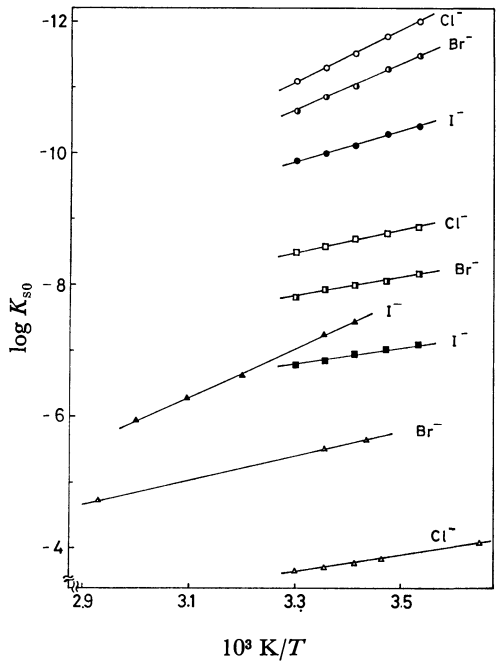

Fig. 3. Plot of log K_{s0} *vs.* $1/T$ for thallium halides in DMF, PC, and water.
(□◨■): DMF, (○◑●): PC, (△◭▲): water.

Table 2. Logarithms of solubility products for TlX at 25 °C

Solvent	TlX	log K_{s0}
DMF	TlCl	−8.58 −8.58[a] −9.0±0.5[b]
	TlBr	−7.94 −8.13[a]
	TlI	−6.86 −7.06[a]
PC	TlCl	−11.31 −11.30[a] −12.39[c] −10.6[d] −12.4±0.5[b]
	TlBr	−10.84 −10.96[a] −12.66[c] −12.0[d]
	TlI	−9.99 −9.84[a] −12.22[c] −11.4[d]

a) Ref. 10. b) Ref. 13. c) Ref. 14. d) F. G. K. Baucke and C. W. Tobias, *J. Electrochem. Soc.*, **116**, 34 (1969). Approximate data obtained by emission spectroscopy.

Table 3. Thermodynamic constants for formation of thallium halides in DMF, PC, and water at 25 °C

Solvent	TlX	$\Delta G^\circ_{(TlX)}$ / kJ mol^{-1}	$\Delta H^\circ_{(TlX)}$ / kJ mol^{-1}	$T\Delta S^\circ_{(TlX)}$ / kJ mol^{-1}
DMF	TlCl	−48.98	−30.51	+18.46
	TlBr	−45.33	−29.38	+15.95
	TlI	−39.14	−26.86	+12.28
PC	TlCl	−64.51	−77.33	−12.82
	TlBr	−61.85	−70.40	−8.55
	TlI	−56.98	−46.62	+10.36
Water	TlCl	−21.34	−26.30	−4.97
	TlBr	−31.43	−34.57	−3.13
	TlI	−41.36	−71.05	−29.69

the entropy changes ($T\Delta S^\circ_{(TlX)}$) were calculated from the $\Delta H^\circ_{(TlX)}$ and $\Delta G^\circ_{(TlX)}$. These thermodynamic

constants in DMF and PC were compared with those in water. The thermodynamic constants in DMF, PC, and water at 25 °C are given in Table 3. The thermodynamic constants in water, in the same manner as with DMF and PC, were obtained graphically. In Table 3, the order of the stability of TlX with $\Delta G^\circ_{(TlX)}$ in DMF and PC is found to be TlCl>TlBr>TlI, while it is TlI>TlBr>TlCl in water. Accordingly, the results in DMF and PC do not give support to the classification of the thallium ion obtained by Ahrland.[6] The reason for difference in stability in nonaqueous solvents and water was investigated by means of the thermodynamic constants for the formation of TlX of the transfer from water to DMF and PC. These constants, $\Delta G^\circ_{tr(TlX)}$, $\Delta H^\circ_{tr(TlX)}$ and $T\Delta S^\circ_{tr(TlX)}$, are listed in Table 4. From the values of $\Delta G^\circ_{tr(TlX)}$, it is manifest that TlCl becomes the most stable compound among the TlX compounds. The differences in $\Delta H^\circ_{tr(TlX)}$ and $T\Delta S^\circ_{tr(TlX)}$ between TlCl and TlI are -48.40 and -18.54 kJ mol^{-1} for transfer from water to DMF, and -75.46 and -47.90 kJ mol^{-1} for transfer from water to PC, respectively. Therefore, it was found that the enthalpy changes in transfer from water to DMF and PC contribute much to the free-energy changes of the transfer.

The thermodynamic constants, $\Delta G^\circ_{tr(TlX)}$, $\Delta H^\circ_{tr(TlX)}$ and $T\Delta S^\circ_{tr(TlX)}$, were compared with those of halide ions (X^-) for transfer from water to DMF and PC. These constants, ΔG°_{tr}, ΔH°_{tr}, and $T\Delta S^\circ_{tr}$, with crystal ionic radii of X^-, are given in Table 5. The ΔG°_{tr} were calculated by the use of the medium effects[10,15] in Eq. 4.

$$\Delta G^\circ_{tr} = 2.303RT \log_m \gamma_I \quad (4)$$

Table 4. Thermodynamic constants for formation of thallium halides of transfer from water to DMF and PC at 25 °C

Transfer	TlX	$\Delta G^\circ_{tr(TlX)}$ / kJ mol^{-1}	$\Delta H^\circ_{tr(TlX)}$ / kJ mol^{-1}	$T\Delta S^\circ_{tr(TlX)}$ / kJ mol^{-1}
From water to DMF	TlCl	−27.64	−4.21	+23.43
	TlBr	−13.89	+5.19	+19.08
	TlI	+2.22	+44.19	+41.97
From water to PC	TlCl	−43.18	−51.03	−7.85
	TlBr	−30.41	−35.83	−5.42
	TlI	−15.62	+24.43	+40.05

The ΔH°_{tr} are available in the literature.[16,17] The ΔG°_{tr} shown in Table 5 is the greatest positive value for Cl^-, which has the smallest ionic radius and the most strongly solvated anion in water, DMF and PC[18,19] among the X^- compounds. The fact shows that Cl^- is the most unstable anion for transfer from water to DMF and PC. Therefore, it is considered that the free-energy changes for the formation of TlX, $\Delta G^\circ_{tr(TlX)}$, are greatly influenced by the free-energy changes of X^-, ΔG°_{tr}, for transfer from water to DMF and PC. From a comaprison of ΔH°_{tr} with $T\Delta S^\circ_{tr}$ among the X^-, it can be seen that the values of ΔH°_{tr} contribute much to those of ΔG°_{tr}. Accordingly, it may be concluded that the differences shown in Table 1 in the order of stability for metal halogeno-complexes in DMF, PC, and water depend mainly on the enthalpy changes ($\Delta H^\circ_{tr(TlX)}$) for the formation of TlX, and that the $\Delta H^\circ_{tr(TlX)}$ are greatly influenced by the enthalpy changes (ΔH°_{tr}) of halide ions.

References

1) Y. Sasaki, M. Takizawa, and N. Matsuura, *Nippon Kagaku Kaishi*, **1976**, 1414.
2) Y. Sasaki, M. Takizawa, K. Umemoto, and N. Matsuura, *Nippon Kagaku Kaishi*, **1977**, 983.
3) N. Matsuura, M. Takizawa, and Y. Sasaki, *Nippon Kagaku Kaishi*, **1975**, 2238.
4) N. Matsuura, M. Takizawa, and Y. Sasaki, *Nippon Kagaku Kaishi*, **1976**, 1495.
5) M. Aihara and S. Misumi, *Bull. Chem. Soc. Jpn.*, **46**, 1674 (1973).
6) S. Ahrland, *Acta Chem. Scand.*, **10**, 723 (1956).
7) Y. Sasaki, M. Takizawa, K. Umemoto, and N. Matsuura, unpublished data.
8) N. Matsuura, K. Umemoto, M. Waki, Z. Takeuchi, and M. Omoto, *Bull. Chem. Soc. Jpn.*, **47**, 806 (1974).
9) N. Matsuura, K. Umemoto, and Z. Takeuchi, *Bull. Chem. Soc. Jpn.*, **47**, 813 (1974).
10) N. Matsuura and K. Umemoto, *Bull. Chem. Soc. Jpn.*, **47**, 1334 (1974).
11) L. G. Sillen, "Stability Constants Supplement No. 1," Special Publication 25, The Chemical Society, London (1971).
12) R. C. Weast, "Handbook of Chemistry and Physics," 53rd ed, Rubber Co., Cranwood Parkway, Cleveland, Ohio (1972).
13) J. C. Synnott and J. N. Butler, *Anal. Chem.*, **41**, 1890 (1969).

Table 5. Thermodynamic constants for halide ions of transfer from water to DMF and PC at 25 °C

Transfer	X^-	r(A)[a]	$\log_m \gamma_I$	ΔG°_{tr} / kJ mol^{-1}	ΔH°_{tr} / kJ mol^{-1}	$T\Delta S^\circ_{tr}$ / kJ mol^{-1}
From water of DMF	Cl^-	1.81	+6.51	+37.15	+21.17	−15.98
	Br^-	1.96	+4.35	+24.81	+4.10	−20.71
	I^-	2.20	+1.56	+8.91	−12.30	−21.21
From water of PC	Cl^-	1.81	+5.36	+30.58	+26.40	−4.18
	Br^-	1.96	+3.31	+18.87	+13.56	−5.31
	I^-	2.20	+0.47	+2.68	−3.26	−5.94

a) Crystal ionic radii.

14) M. Salomon, *J. Phys. Chem.*, **73**, 3299 (1969); M. Salomon, *J. Electroanal. Chem.*, **26**, 319 (1970).
15) A. J. Bard, "Electroanalytical Chemistry," Marcell Dekker, New York and Basel (1975), Vol. 8.
16) C. V. Krishnan and H. L. Friedman, *J. Phys. Chem.*, **73**, 3934 (1969).
17) J. F. Coetzee and C. D. Ritchie, "Solute-solvent Interactions," Marcell Dekker, New York and Basel (1976), Vol. 2.
18) R. F. Rodewald, K. Mahendran, and R. Fuchs, *J. Am. Chem. Soc.*, **90**, 6698 (1968).
19) R. Fuchs and K. Mahendran, *J. Org. Chem.*, **36**, 730 (1971).

  Bull. Chem. Soc. Jpn., 54, 69—72 (1981)

The Crystal Structure of [*N*-(*t*-Pentyloxycarbonyl)-L-prolyl]-L-alanylglycine

Yasuyuki YAMADA, Isao TANAKA,* and Tamaichi ASHIDA

Department of Applied Chemistry, Faculty of Engineering, Nagoya University, Chikusa, Nagoya 464

(Received May 29, 1980)

The crystal structure of the title compound was determined by the X-ray method. The space group is $P2_1$, with $a=18.741(3)$, $b=12.602(1)$, $c=9.553(1)$ Å, $\beta=118.46(2)°$, and $Z=4$. The structure was determined successfully by the vector-space-search method, using a dimer structure of Boc–Pro–Val–Gly–OH as a rigid group. The final R value was 0.075 for 2025 non-zero reflections. Two independent molecules related by a pseudo two-fold axis are linked by β-sheet-type hydrogen bonds. This kind of dimerization commonly occurs in all the Boc–Pro–X–Gly–OH peptides except Boc–Pro–Leu–Gly–OH. The packing similarity of these peptides is discussed.

A series of structure analyses of the [*N*-(*t*-butoxycarbonyl)]-L-prolyl-X-glycine (Boc–Pro–X–Gly–OH, X; any amino acid residue) type oligopeptides have shown that these peptides take either one of two conformations, a folded or an extended one. The folded conformation of Boc–Pro–Leu–Gly–OH[1] is designated as the β-turn structure[2] because of the presence of a 4-1-type intramolecular hydrogen bond. On the other hand, the extended conformation of Boc–Pro–Ile–Gly–OH[3] and Boc–Pro–Val–Gly–OH,[4] both with a branched side chain at the C^β carbon, is characterzied by the formation of β-sheet-type intermolecular hydrogen bonds. These analyses, therefore, seem to illustrate the fact that a slight difference in the side chain results in the complete change of the main-chain folding.

The present study is concerned with the crystal analysis of peptides containing an alanyl residue at the X site. The alanyl residue having only a methyl group as a side chain seems to exert the least steric effect on the main-chain folding. We could expect, therefore, to get some clue as to whether or not the branched structure at the C^β atom has some definite effect on the main-chain folding. Crystals of [*N*-(*t*-butoxycarbonyl)]alanyl peptide, Boc–Pro–Ala–Gly–OH, however, contained four molecules in an asymmetric unit, furthermore, they were twinned. Therefore, we gave up trying to analyze it; as an alternative, [*N*-(*t*-pentyloxycarbonyl)-L-prolyl]-L-alanylglycine (Poc–Pro–Ala–Gly–OH) was studied.

Experimental

The synthesis was performed by first preparing the [*N*-(*t*-butoxycarbonyl)alanyl]glycine benzyl ester (Boc–Ala–Gly–OBzl), followed by the conventional removal of the Boc group and the addition of N-protected proline Poc–Pro–OH, leading to Poc–Pro–Ala–Gly–OBzl. After the removal of the benzyl group by catalytic reduction, the aimed peptide was crystallized from an ethylacetate solution. The crystal data are given in Table 1.

Table 1. Crystal data

Molecular formula	$C_{16}H_{27}O_6N_3$
Molecular weight	357.40
Space group	$P2_1$
Cell constants	$a=18.741(3)$ Å
	$b=12.602(1)$ Å
	$c=9.553(2)$ Å
	$\beta=118.46(2)°$
Density obsd	1.21 g/cm³
calcd	1.20 g/cm³ (for $Z=4$)

A crystal with dimensions of 0.14 mm × 0.07 mm × 0.06 mm was used for the X-ray experiment. A Hilger & Watts four-circle diffractometer equipped with Ni-filtered Cu K_α radiation was used for the data collection. The ω-2θ step scanning mode was adopted. Data were collected up to $2\theta=100°$ for total 2169 reflections, of which 2025 were non-zero. Lorentz and polarization corrections were applied, but no absorption correction was made.

Structure Determination

The direct method was first applied, but did not give reasonable results. The vector-space-search program RICS was next applied on the assumption that the molecule has either a β-turn or an extended conformation.[4] The extended model, 20 atoms of Boc–Pro–Val–Gly–OH excluding the N-terminal and side-chain carbons, seemed to be probable, but the partial structure tangent refinement based on these atomic coordinates did not converge properly. It was further assumed that two independent molecules exist as a dimer, as is observed in Boc–Pro–Ile–Gly–OH[3] and Boc–Pro–Val–Gly–OH.[4] This assumption was quite reasonable in view of the similar packing pattern of the two previously analyzed peptides. The phases calculated from the 40 atoms thus obtained easily led to the whole structure. All the H atoms were located on the difference Fourier map.

The structure was refined by the block-diagonal least-squares program HBLS V.[5] The function minimized was $\Sigma\omega(|F_o|-|F_c|)^2$, where the weights, ω, were unity for all the non-zero reflections and zero for the zero reflections. The final R value was 0.097 for all the reflections and 0.075 for the non-zero reflections. The atomic scattering factors were taken from the International Tables for X-Ray Crystallography.[6] The final positional parameters are given in Tables 2 and 3.† The isotropic temperature factor, $B=4.4$ Å², was assigned to all the hydrogen atoms.

Discussion

The structure of Poc–Pro–Ala–Gly–OH is charac-

† The F_o and F_c tables and anisotropic temperature factor table are kept as Document No. 8109 at the Chemical Society of Japan.

TABLE 2. THE ATOMIC POSITIONAL PARAMETERS, WITH THEIR e.s.d.'s IN PARENTHESES ($\times 10^4$)

	X	Y	Z	B_{eq}/Å^2 a)
O(1)A	4436(3)	6399(6)	10922(7)	5.2
O(2)A	5758(3)	6571(6)	12799(7)	5.6
O(3)A	4713(3)	4313(6)	9165(7)	5.7
O(4)A	2378(4)	4363(5)	3984(8)	6.3
O(5)A	1179(4)	2280(6)	937(8)	6.3
O(6)A	1294(4)	2200(8)	3367(9)	8.1
N(1)A	5387(4)	6328(6)	10199(8)	4.2
N(2)A	3618(4)	4989(6)	7085(8)	4.6
N(3)A	2927(4)	2756(6)	4661(9)	4.9
C(1)A	3912(10)	4800(20)	12500(25)	13.9
C(2)A	4253(9)	5850(20)	13142(17)	12.1
C(3)A	4355(14)	7704(20)	12720(32)	16.6
C(4)A	3185(8)	6767(14)	10709(19)	9.8
C(5)A	4072(7)	6660(12)	11932(14)	7.2
C(6)A	5230(5)	6428(8)	11413(11)	4.6
C(7)A	4760(5)	6159(8)	8534(10)	4.1
C(8)A	5223(7)	6277(11)	7635(12)	6.8
C(9)A	6097(7)	6150(22)	8851(15)	13.5
C(10)A	6213(5)	6381(9)	10395(12)	5.5
C(11)A	4382(5)	5080(9)	8322(10)	4.6
C(12)A	3168(5)	3990(8)	6745(11)	5.2
C(13)A	2524(7)	4039(12)	7237(15)	7.5
C(14)A	2804(5)	3750(7)	5016(10)	4.3
C(15)A	2492(6)	2370(9)	3041(12)	5.5
C(16)A	1585(5)	2298(7)	2494(12)	5.3
O(1)B	10520(3)	−138(6)	8990(7)	5.0
O(2)B	11433(3)	−333(6)	11617(7)	6.0
O(3)B	9628(3)	1919(6)	9377(8)	6.4
O(4)B	6979(4)	1899(6)	4716(8)	6.5
O(5)B	5514(4)	3982(6)	2162(8)	6.3
O(6)B	6779(4)	3979(7)	2461(8)	7.3
N(1)B	10103(4)	−61(6)	10788(7)	4.1
N(2)B	8538(4)	1258(6)	7260(8)	4.7
N(3)B	7371(4)	3540(7)	5730(8)	5.5
C(1)B	11142(32)	1392(34)	7461(70)	35.6
C(2)B	11696(12)	380(22)	8840(28)	16.1
C(3)B	11381(12)	−1516(15)	8874(21)	12.1
C(4)B	10459(13)	−496(18)	6532(16)	15.2
C(5)B	11052(7)	−416(10)	8314(14)	6.4
C(6)B	10727(5)	−204(8)	10549(10)	4.6
C(7)B	9270(5)	101(8)	9515(11)	4.6
C(8)B	8776(6)	64(10)	10398(14)	6.4
C(9)B	9345(8)	154(23)	12046(16)	13.8
C(10)B	10166(6)	−91(10)	12332(12)	5.5
C(11)B	9163(5)	1142(8)	8730(11)	4.9
C(12)B	8406(5)	2259(8)	6376(12)	5.1
C(13)B	8683(7)	2128(13)	5161(15)	8.2
C(14)B	7510(6)	2518(8)	5560(11)	4.9
C(15)B	6554(6)	3955(9)	4755(11)	5.6
C(16)B	6322(6)	3968(9)	2994(11)	5.6

a) The equivalent isotropic temperature factor as defined by W.C. Hamilton (*Acta Crystallogr.*, **12**, 609 (1959)).

TABLE 3. HYDROGEN POSITIONAL PARAMETERS, WITH THEIR e.s.d.'s IN PARENTHESES ($\times 10^3$)

	x	y	z	Bonded to
H(1)A	403(5)	423(9)	1341(11)	C(1)A
H(2)A	411(5)	448(8)	1159(11)	C(1)A
H(3)A	327(5)	487(8)	1182(11)	C(1)A
H(1)B	1149(5)	196(9)	739(11)	C(1)B
H(2)B	1072(5)	146(8)	782(11)	C(1)B
H(3)B	1104(5)	89(8)	635(11)	C(1)B
H(4)A	483(5)	580(8)	1372(11)	C(2)A
H(5)A	395(5)	613(9)	1387(11)	C(2)A
H(4)B	1193(5)	61(9)	1006(11)	C(2)B
H(5)B	1224(5)	7(8)	884(11)	C(2)B
H(6)A	407(5)	790(9)	1330(11)	C(3)A
H(7)A	429(5)	824(8)	1191(11)	C(3)A
H(8)A	491(5)	772(8)	1346(11)	C(3)A
H(6)B	1161(6)	−166(8)	823(11)	C(3)B
H(7)B	1091(5)	−194(8)	850(11)	C(3)B
H(8)B	1169(5)	−152(8)	1023(11)	C(3)B
H(9)A	282(5)	677(8)	1142(11)	C(4)A
H(10)A	298(5)	604(8)	1002(11)	C(4)A
H(11)A	312(5)	736(8)	981(11)	C(4)A
H(9)B	1076(5)	−57(8)	590(11)	C(4)B
H(10)B	1019(5)	5(9)	611(11)	C(4)B
H(11)B	994(5)	−118(8)	622(11)	C(4)B
H(12)A	436(5)	671(8)	822(11)	C(7)A
H(12)B	907(5)	−51(8)	858(11)	C(7)B
H(13)A	522(5)	695(9)	723(11)	C(8)A
H(14)A	512(5)	584(8)	681(11)	C(8)A
H(13)B	853(5)	−56(8)	1035(11)	C(8)B
H(14)B	832(5)	55(8)	1006(11)	C(8)B
H(15)A	649(5)	657(8)	849(11)	C(9)A
H(16)A	632(5)	541(8)	892(11)	C(9)A
H(15)B	915(5)	−17(8)	1288(11)	C(9)B
H(16)B	934(6)	90(9)	1247(11)	C(9)B
H(17)A	652(5)	707(9)	1074(11)	C(10)A
H(18)A	666(5)	586(8)	1141(11)	C(10)A
H(17)B	1031(5)	−75(9)	1288(11)	C(10)B
H(18)B	1060(5)	44(8)	1321(11)	C(10)B
H(19)A	340(5)	562(8)	643(11)	N(2)A
H(19)B	824(6)	61(8)	679(11)	N(2)B
H(20)A	354(6)	343(8)	731(11)	C(12)A
H(20)B	874(5)	286(8)	710(11)	C(12)B
H(21)A	274(5)	408(8)	851(11)	C(13)A
H(22)A	221(5)	329(8)	702(11)	C(13)A
H(23)A	208(5)	471(8)	661(11)	C(13)A
H(21)B	922(5)	182(8)	547(11)	C(13)B
H(22)B	862(5)	269(8)	454(11)	C(13)B
H(23)B	837(5)	146(8)	433(11)	C(13)B
H(24)A	329(5)	228(8)	539(11)	N(3)A
H(24)B	770(6)	383(8)	661(11)	N(3)B
H(25)A	271(5)	162(8)	304(11)	C(15)A
H(26)A	257(5)	290(8)	225(11)	C(15)A
H(25)B	646(5)	471(8)	516(11)	C(15)B
H(26)B	616(6)	348(8)	510(11)	C(15)B
H(27)A	58(5)	214(9)	30(11)	O(5)A
H(27)B	526(5)	413(9)	88(10)	O(5)B

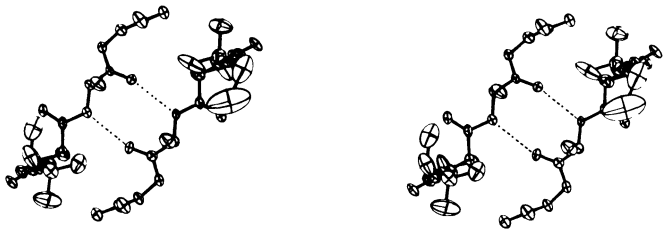

Fig. 1. ORTEP drawing of the dimer structure of Poc–Pro–Ala–Gly–OH *via* β-sheet type hydrogen bonds.

terized by dimer formation with a pair of β-sheet-type hydrogen bonds. The ORTEP drawing[7] of the dimer, viewed along a pseudo-twofold rotation axis, is given in Fig. 1. The bond lengths, bond angles, and torsion angles are shown in Fig. 2. Some abnormal bond lengths in the pentyloxy group may be ascribed to its extremely large thermal motion.

Among the Boc(Poc)–Pro–X–Gly–OH type peptides, those which have Ala, Val, and Ile at the X position crystallize with a similar packing pattern. The crystal-lattice transformation of the alanyl peptide by $a'=a+c$, $b'=b$, and $c'=c$ clearly shows the close relationship between the crystal packings of the alanyl and valyl peptides. Although the space group of the isoleucyl peptide, $P2_12_12$, differs from those of the valyl and alanyl peptides, $P2_1$, the former crystal packing is still close to the latter. That is to say, although the alanyl and valyl peptides are devoid of the twofold axis, there still remains a pseudo-twofold rotation symmetry. The packing similarity is illustrated in Fig. 3, in which dotted lines are drawn in the alanyl and valyl peptide crystals in order to coincide with the unit cell of the isoleucyl peptide.

The similarity of the molecular packing is again obvious in Table 4, which shows the hydrogen-bonding system. No significant difference in the hydrogen-bonding pattern is observed for the two independent molecules (A) and (B); the patterns differ only in the point in which the C-terminal of the molecule interacts with water for the two independent molecules (A) and (B) of Boc–Pro–Val–Gly–OH. Thus, the hydrogen-bonding patterns of three peptides, Boc–Pro–Ile–Gly–OH, Boc–Pro–Val–Gly–OH, and Poc–Pro–Ala–Gly–OH, differ only in the interactions with water molecules, the β-sheet-type hydrogen bonds being completely reserved. The lack of a strict twofold axis in the alanyl and valyl dimer should, therefore,

Table 4. The hydrogen-bond networks in the Boc(Poc)-Pro-X-Gly-OH system

Donor	Acceptor	Distance/Å
	(Boc-Pro-Ile-Gly-OH)	
Gly COOH	Pro C=O	2.60(1)
Ile NH	Ile C=O	2.83(1)
Gly NH	Boc C=O	2.87(1)
Water	Boc C=O	2.80(3)
	(Boc-Pro-Val-Gly-OH)	
Gly(A) COOH	Pro(B) C=O	2.619(8)
Val(A) NH	Val(B) C=O	2.949(7)
Gly(A) NH	Water	2.911(12)
Water	Boc(B) C=O	2.920(10)
Gly(B) COOH	Pro(A) C=O	2.582(9)
Val(B) NH	Val(A) C=O	2.922(7)
Gly(B) NH	Boc(B) C=O	2.942(8)
Water	Boc(A) C=O	2.760(11)
	(Poc-Pro-Ala-Gly-OH)	
Gly(A) COOH	Pro(B) C=O	2.60(1)
Ala(A) NH	Ala(B) C=O	2.86(1)
Gly(A) NH	Poc(A) C=O	2.91(1)
Gly(B) COOH	Pro(A) C=O	2.56(1)
Ala(B) NH	Ala(A) C=O	2.85(1)
Gly(B) NH	Poc(B) C=O	2.84(1)

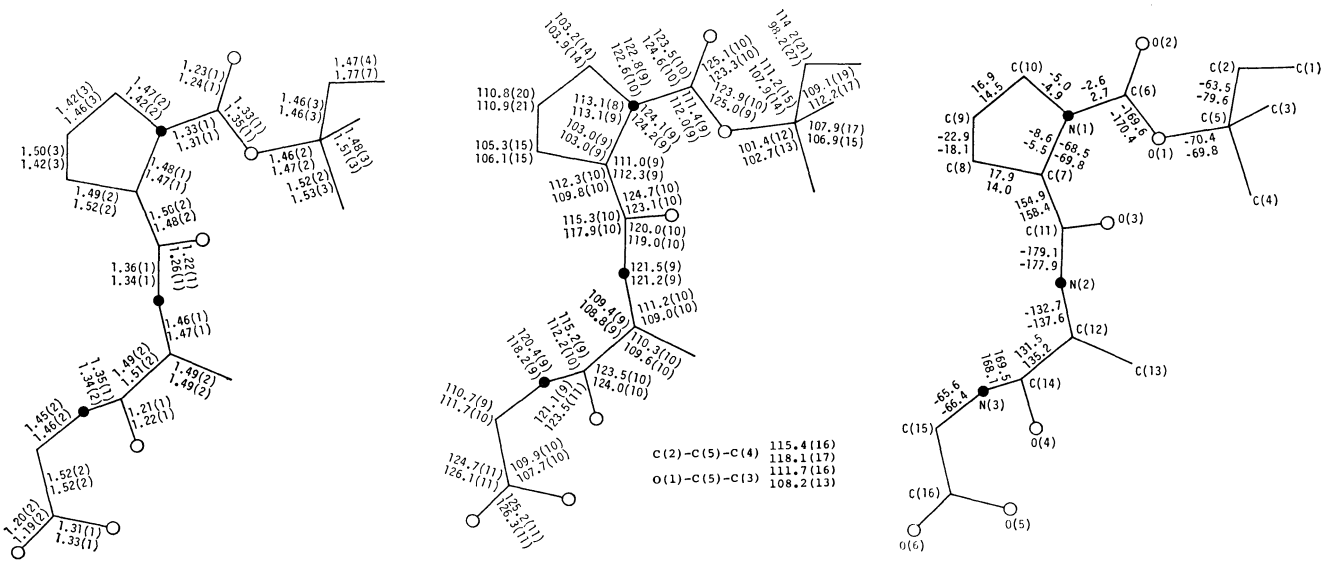

(a) (b) (c)

Fig. 2. (a) Bond lengths (Å), (b) bond angles (°), and (c) torsion angles (°) with atom numbering system. Upper figures are for (A) and lower for (B) molecule.

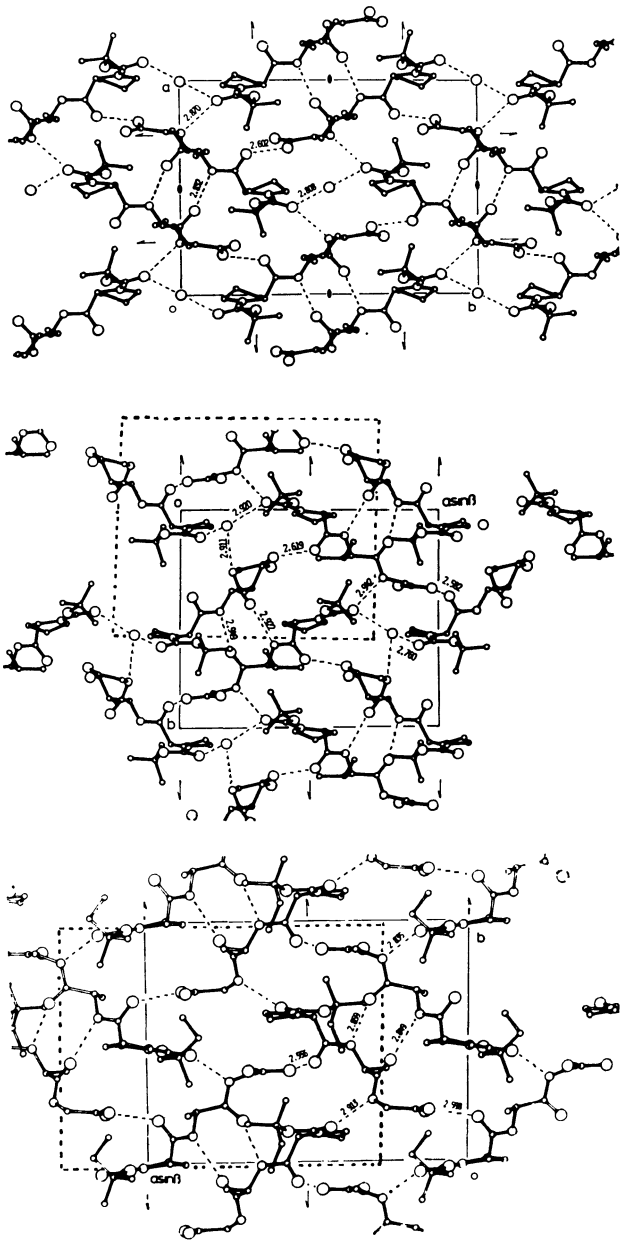

Fig. 3. The comparison of the crystal structures of Boc–Pro–Ile–Gly–OH (top), Boc–Pro–Val–Gly–OH (center), and Poc–Pro–Ala–Gly–OH (bottom). Dotted lines in valyl and alanyl peptide crystals are drawn in order to coincide with the unit cell of isoleucyl peptide.

be attributed to inter-dimer interactions at the C-terminal.

Boc–Pro–Leu–Gly–OH is special in terms of its molecular interaction as well as its molecular conformation. In other words, all three substances besides the leucyl peptide are stabilized by the intermolecular hydrogen bonds, whereas the leucyl peptide is stabilized by the intramolecular one. The dimer structure of the alanyl peptide implies that the C^{β} branched side-chain structure of the valyl and isoleucyl residues is not the only reason for them not to take a β-turn structure, and that the intermolecular interaction emerges as the more important stabilization factor.

No appropriate reason has been given for the uniqueness of the leucyl peptide, but on the basis of these crystal structure analyses, together with other examples, Z–Gly–Pro–Leu–Gly–Pro–OH[8] and Z(*p*-Br)–Gly–Pro–Leu–Gly–OH,[9] we may conclude that there is a stronger tendency for the leucyl residue to be involved in the third site of the β-turn.

References

1) T. Ashida, I. Tanaka, Y. Shimonishi, and M. Kakudo, *Acta Crystallogr., Sect. B*, **33**, 3054 (1977).
2) C. M. Venkatachalam, *Biopolymers*, **6**, 1425 (1968).
3) Y. Yamada, I. Tanaka, and T. Ashida, *Acta Crystallogr., Sect. B*, **36**, 331 (1980).
4) I. Tanaka and T. Ashida, *Acta Crystallogr., Sect. B*, **36**, 2164 (1980).
5) T. Ashida, UNICS-Osaka, The Computation Center, Osaka Univ. 55—61 (1973).
6) "International Tables for X-Ray Crystallography," Birmingham, Kynoch Press (1974), Vol. IV.
7) C. K. Johnson, ORTEP. Oak Ridge National Laboratory Report ORNL-3794 (1965).
8) S. Bando, N. Tanaka, T. Ashida, and M. Kakudo, *Acta Crystallogr., Sect. B*, **34**, 3447 (1978).
9) T. Ueki, T. Ashida, M. Kakudo, Y. Sasada, and Y. Katsube, *Acta Crystallogr., Sect. B*, **25**, 1840 (1969).

Chiral Mesophases of 12-Hydroxyoctadecanoic Acid in Jelly and in the Solid State. II. A New Type of Mesomorphic Solid State

Taro TACHIBANA,* Tomoko MORI, and Kayako HORI
Department of Chemistry, Ochanomizu University, Otsuka, Bunkyo-ku, Tokyo 112
(Received June 18, 1980)

A new type of chiral solid mesophase was obtained by evaporating the solvents from solutions or jellies of chiral 12-hydroxyoctadecanoic acid (12HOA). The mesomorphic solids exhibited some optical properties characteristic of a helicoidal mesophase: (1) spherulitic or Schlieren texture under a polarizing microscope, (2) reflective circular dichroic band, and (3) induced circular dichroic spectra with a single sign due to achiral molecules added to the solid. From the circular dichroic and X-ray studies, it was concluded that the helicoidal mesophase structure exists locally as small domains with a chiral smectic structure within the mesomorphic solids. Microscopic observation revealed that, upon heating, the transition of the mesomorphic solid to the crystalline solid occurred. This process was studied by differential scanning calorimetry. Formation of a variety of helicoidal systems from chiral molecules such as 12HOA and polypeptides was regarded as a phenomenon characteristic of chiral assemblies of amphiphilic molecules.

In the preceding paper,[1] we described a chiral mesomorphic system which occurs in jellies of 12-hydroxyoctadecanoic acid (12HOA) with a solvent such as benzene or carbon tetrachloride. The jellies were shown to be composed of a number of small ordered domains with a supramolecular helicoidal structure such as has been found in the chiral smectic phase. In the course of the investigation, we have found that solids prepared by evaporating the solvents from the jellies showed liquid crystalline textures under a polarizing microscope, and that they exhibited enantiomeric circular dichroism (CD) similar to that observed for the jellies.[2] Further, the solids yielded almost the same X-ray diffraction patterns as those of the crystalline powder. These results indicate that much of the original structure of the jelly is retained in the mesomorphic solid: the solid also is composed of a number of small ordered domains with a chiral structure, which is probably a chiral smectic type.

Mesomorphic solids with a chiral structure were first found for a synthetic polypeptide, poly (γ-benzyl L-glutamate) (PBG), by Samulski and Tobolsky.[3] They reported that it forms stable solid films with a liquid crystalline local structure when the films are made by casting from solutions. This was evidenced from the X-ray study and the swelling experiment. Tachibana and Oda[4] found that solid films prepared from some samples of poly (γ-methyl D(L)-glutamate) (PMG) exhibit iridescent colors due to the selective reflection of circularly polarized light of one sense. Hatano *et al.*[5] observed an induced circular dichroism (ICD) for achiral molecules such as pyrene or acridine orange buried in solids of PMG. All these observations were attributed to the presence of the cholesteric (chiral nematic) phase in the solid films of PBG or PMG. The chiral solid mesophases have been hitherto known only for synthetic polypeptides and other biopolymers,[6] and their mesomorphic behavior was associated with the structure of polymer molecules. However, the chiral solid mesophase of 12HOA is different from that of the above-mentioned polymers in that the former is made up of a low-molecular-weight compound; it is probably a chiral smectic phase. The present paper will deal with the structure and properties of the newly found mesomorphic solid state.

Experimental

Materials. Crystalline samples of chiral 12HOA used were the same ones as in the preceding paper.[1] The solvents used were of reagent grade and further purified by standard methods. The samples of chiral 12HOA in the mesomorphic solid state were (1) apparently amorphous solids obtained by freeze-drying jellies or concentrated solutions, and (2) translucent solid films cast from solutions on quartz plates at room temperature. For freeze-drying, jellies (conc. of 12HOA, 50—100 mmol l^{-1}) were previously frozen at −40 °C in a deep-freezer, and solutions (0.6 mol l^{-1}) in 1-pentanol or 1-hexanol were frozen with liquid nitrogen.

Methods. The apparatus and procedure were essentially the same as those described in the preceding paper.[1] The CD of 12HOA in the solids obtained from jellies and from solutions were measured by a Nujol mull method after the solids had been powdered. The Nujol mull was enclosed between two flat quartz plates in the form of a thin layer. The CD spectra were not modified by varying the content of samples in a Nujol mull. The CD of 12HOA in the solid film state was measured on films formed by evaporation of the solvent from the solution on a quartz plate. The linear dichroism contribution to the observed CD signal was eliminated by rotating the sample around the light beam.[7] Thermal studies were made by the use of a DSC-2 Perkin-Elmer differential scanning calorimeter. The temperature scale was calibrated using the mp of indium supplied by the Perkin-Elmer Corp. The heat of transition was calibrated using the area under the fusion peak of indium and its known enthalpy of fusion (3.26 kJ mol^{-1}). IR spectral change with temperature was recorded on a JASCO IR-G infrared spectrophotometer with a controlled heating apparatus.

Results and Discussion

Formation of Mesomorphic Solids. Chiral 12HOA dissolves readily in cyclohexane, aromatic solvents, and chlorinated solvents such as carbon tetrachloride, chloroform, dichloromethane, and chlorobenzene, and these solutions set into jellies above a certain concentration. The jellies exhibit the optical properties characteristic of the helicoidal mesophase.[1,2] Ap-

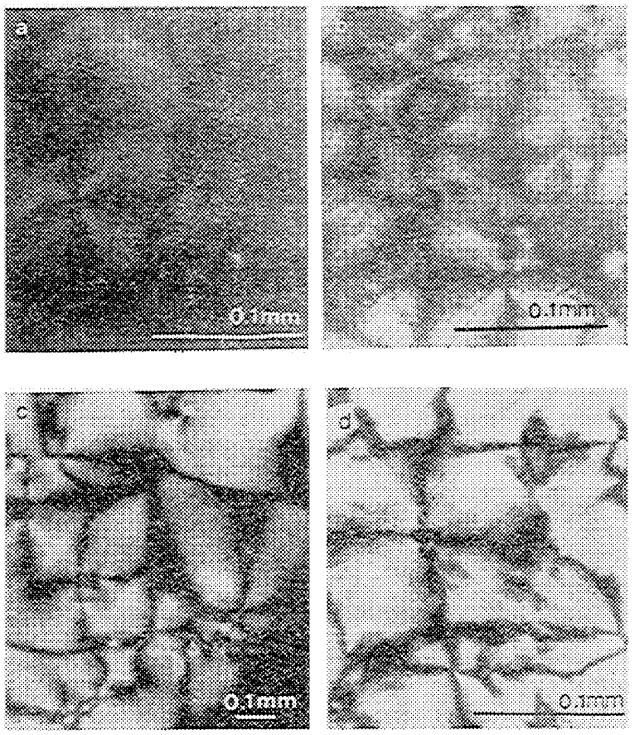

Fig. 1. Typical textures under a polarizing microscope. (a): Spherulitic texture of a CCl_4-jelly (35.2 mmol l^{-1}), (b): spherulitic texture of a solid film made from CCl_4-jelly (35.2 mmol l^{-1}), (c): schlieren texture of a CCl_4-jelly (318 mmol l^{-1}), (d): schlieren texture of a solid film made from CCl_4-jelly (318 mmol l^{-1}).

parently amorphous solids were obtained by freeze-drying the jellies, and solid films were made by casting from the jelly-forming solutions at room temperature. These solids dissolved readily in solvents for the crystalline solid. Visual observation by means of polarizing microscopy showed that these solids displayed, between crossed polarizers, the same spherulitic or Schlieren texture as did the original jellies, irrespective of solvents used, of the supporting material such as quartz, glass, potassium bromide, or calcium fluoride, and of the surface-treatment. The texture was more strikingly observed with the solid films. Figure 1 shows typical examples of the texture. The spherulitic domains in the solid films showed negative birefringence, as did that in the original jellies. These observations demonstrate that the texture in the original jellies was retained, on drying, in the solids, suggesting that the solid formed from the jellies have the same mesomorphic structure as was present in the original jellies.

On the other hand, solutions of chiral 12HOA in normal alcohols with the numbers of carbon atoms from two to seven did not form jellies; but another interesting phenomenon was observed. A drop of each hot concentrated solution of chiral 12HOA in alcohols was placed between two glass plates for microscopic use, allowed to come to room temperature, and continuously observed under a polarizing microscope. At first, there appeared a number of spherulites, but after a short period they were replaced by many needle-like microcrystals. The change from the spherulites to the crystals was faster when the alcohol used was

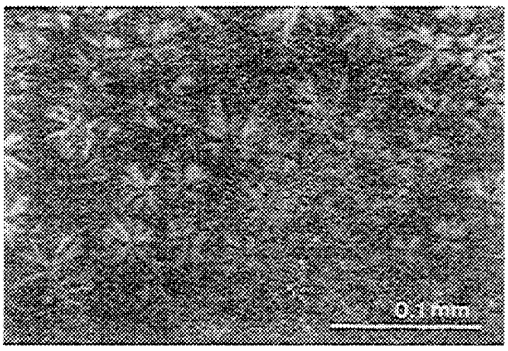

Fig. 2. Spherulites of (*R*)-12HOA in a suspension in 1-hexanol under a polarizing microscope.

shorter in hydrocarbon chain. Therefore, it was difficult to separate the spherulites from the solution by evaporation or filtration. However, it was possible to keep the spherulites stable for some time by mixing the thick suspension of the spherulites with Nujol immediately after occurrence of the spherulites. Figure 2 presents spherulites of (*R*)-12HOA, which were precipitated from 1-hexanol. The spherulites showed birefringence with an optically negative sign, as observed for spherulitic textures in jellies with other solvents such as benzene or carbon tetrachloride. Apparently amorphous solids from alcoholic solutions of chiral 12HOA were obtained by freeze-drying a 1-pentanol or 1-hexanol solution of chiral 12HOA. As will be described later, this solid also is a mesomorphic state.

Circular Dichroism in the Mesomorphic Solids. As described in the preceding paper, jellies of chiral 12HOA with benzene or carbon tetrachloride exhibit a weak but definite CD band in a range of wavelengths in which they absorb no light; the sign is negative for the (*R*)-enantiomer and positive for the (*S*)-enantiomer. The observed CD has been ascribed to the preferential reflection of circularly polarized light of one sense by the jellies in which there are a number of ordered domains with a supramolecular helicoidal structure. Mesomorphic solids of 12HOA prepared by freeze-drying the jellies also were found to exhibit a definite, but broad CD band around 550 nm with negative sign for the (*R*)-enantiomer and positive sign for the (*S*)-enantiomer, while the crystalline powder of chiral 12HOA in Nujol mull showed no CD peak except that due to the molecular absorption ($\approx$200 nm). Figure 3 shows a typical example of the CD spectra of the mesomorphic solids of both enantiomers. Jellies of chiral 12HOA with various solvents exhibited a CD band in a longer wavelength region with an increase in the refractive index of the solvent used. However, mesomorphic solids prepared from the jellies exhibited a CD band in almost the same region of wavelength, 520—580 nm, irrespective of the kind of the solvent used. These data are given in Table 1. From these CD results, it is reasonable to consider that the orginal supramolecular helicoidal structure in jellies (probably a chiral smectic structure) is essentially retained in the mesomorphic solids. Thus, the solids can be regarded as a new type of chiral mesomorphic solid state.

On the other hand, the solid films of chiral 12HOA

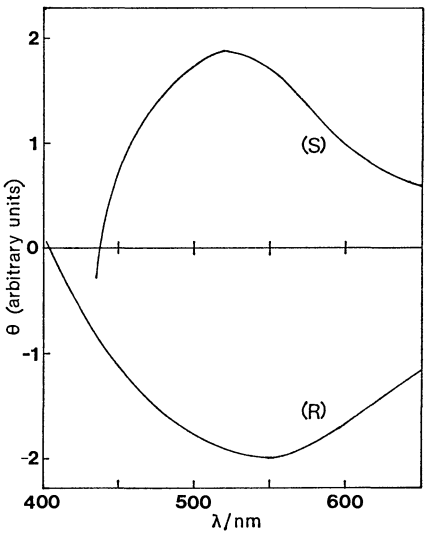

Fig. 3. Enantiomeric CD spectra of the mesomophic solids in Nujol mulls for (*R*)- and (*S*)-12HOA, made from benzene-jellies. The shape of the curve and the location of the peak varied slightly for different samples.

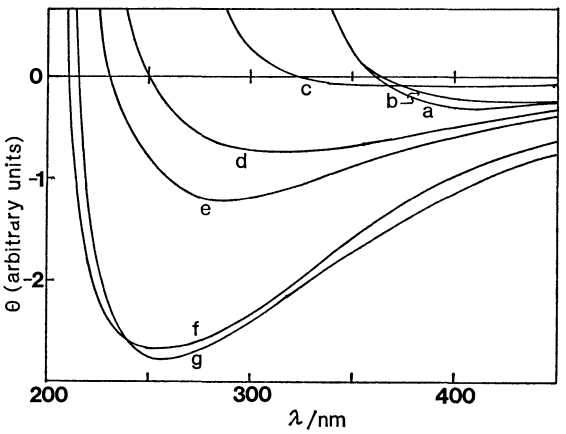

Fig. 4. Changes of CD spectra from a jelly state (128 mmol l^{-1}, with CCl_4) to a solid film state, (a) 5 min, (b) 20 min, (c) 35 min, (d) 40 min, (e) 45 min, (f) 50 min, (g) 80 min after jelly formation.

cast from solutions showed a definite CD band around 250—270 nm with a negative sign for the (*R*)-enantiomer and with a positive sign for the (*S*)-enantiomer, irrespective of the solvents used. Since this result required further investigations, the change of the CD spectrum with drying of the jelly was measured on the films of benzene solution on a quartz plate. The CD change occurred gradually with drying; as the solvent evaporated, the CD increased in its intensity after an initial small decrease and shifted its band maximum from 400 to 250 nm. Figure 4 shows various CD spectra intermediate between the jelly spectrum and the solid film spectrum. This result seemed to be related to a special ordering of the molecules due to some orientational effect at an interface with air or a wall effect of film-supporting plate, but not due to the change of the helical pitch in the supramolecular helicoidal structure, since the CD bands of the solids obtained by freeze-drying locate in a longer wave-

Table 1. The maximal wavelengths of CD of helicoidal mesophase formed from solutions of (*R*)-12HOA in various solvents

	n_D^{20}	λ_{max}/nm		
		Jellies	Solids	
			Freeze-dried	Films
Cyclohexane	1.426	370	520—580	250
CCl_4	1.460	370	520—580	255
Toluene	1.497	490—530	—	255
Benzene	1.501	480	520—550	260
Chlorobenzene	1.524	530—580	530—590	250

The signs of the CD bands were all negative. Jellies or solids were made with solutions ranging in concentration of (*R*)-12HOA from 50 to 100 mmol l^{-1}. Measurements were all made at room temperature.

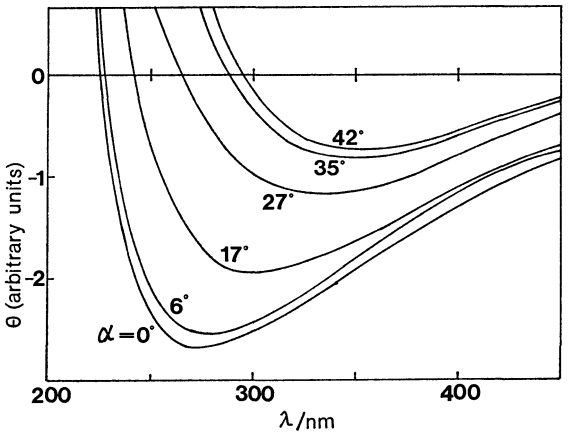

Fig. 5. CD spectra of a solid film for oblique incidence. Here, α denotes the angle between incident beam and normal to the film-supporting plate. Corrections were made for variation of the path length for oblique incidence.

length region than those of the jellies, as shown in Table 1. In order to investigate this possibility, measurements were made on the variation of the CD spectra with the angle, α, between the incident beam and the normal to the film supporting plate. As shown in Fig. 5, the CD spectrum was found to be remarkably dependent on the angle α; the CD intensity decreased and the CD maximum shifted to a longer wavelength side with increasing α. Such a tendency was not observed for the jellies. One can see a striking similarity between the CD spectra in Fig. 4 and those in Fig. 5. This similarity suggests strongly that the CD change shown in Fig. 4 may be explained by the occurrence of an oriented local order in solid films. This deduction was confirmed by the fact that, when the solid films were detached from the quartz plate and crushed to powder, the CD maximum appeared at a wavelength region near to that observed for the amorphous solids obtained by freeze-drying jellies. The details of the alignment in solid films should be examined by using other methods.

Interestingly, both the jellies of (*R*)-12HOA and the solids from them exhibited a CD band with a

negative sign, but suspensions of spherulites of (*R*)-12HOA in alcohols were found to exhibit a positive CD band around 250 nm, regardless of the normal alcohols used. Suspension of (*S*)-12HOA exhibited a negative CD band. Mesomorphic solids from alcohols were obtained by freeze-drying 1-pentanol or 1-hexanol solutions of (*R*)-12HOA, though it was difficult to prepare mesomorphic solid samples by freeze-drying the other alcoholic solutions. The amorphous solids thus obtained exhibited a positive CD band around the same wavelength region as did the suspensions. This CD result indicates that the spherulites in the alcoholic suspensions and the mesomorphic solids from the suspensions have both a supramolecular helicoidal structure, the helical sense of which is opposite to that of a supramolecular helicoidal structure in the mesomorphic solids from the jellies. The chirality of the helicoidal mesophase can be determined by the sign of the reflective CD band; a right-handed (left-handed) helicoidal mesophase reflects right (left) circularly polarized light and transmits left (right) circularly polarized light at the reflective CD band.[8-10] The mesomorphic solids from jellies of (*R*)-12HOA exhibit a negative CD band, and those from alcoholic solutions of (*R*)-12HOA exhibit a positive CD band. This indicates that the circularly polarized light reflected selectively by the solids from jellies is right-handed and that from alcoholic solutions is left-handed. This result leads us to conclude that the screw sense of the supramolecular helicoidal structure in the mesomorphic solids from jellies of (*R*)-12HOA is right-handed and on contrary, that from alcoholic solutions of (*R*)-12HOA is left-handed. Solvent dependence of the chirality of the helicoidal mesophase has already been reported[11] for the cholesteric lyotropic mesophases of polypeptides. The present results show that chiral smectic mesophases of 12HOA also undergo a similar solvent effect.

Induced circular dichroism could be detected for anthracene, which was incorporated into mesomorphic solids from jellies of (*R*)-12HOA. The ICD bands with single negative sign were obtained; these were superimposed on the CD curve of the mesomorphic solids, corresponding to the electronic spectra between 300 and 400 nm. Such ICD characteristics have been reported for jellies of 12HOA,[1,2] and for lyotropic cholesteric liquid crystals of poly(glutamate)[12] and *N*-acyl amino acids,[13] and attributed to a weak interaction between anthracene and the helicoidal systems. The ICD results obtained here also support the assertion that there are helicoidal systems in the mesomorphic solids of 12HOA.

Thermal Behavior. Microscopy with a controlled hot stage showed that, when the solid films were heated, the mesomorphic texture became obscure at about 348 K, followed by the appearance of needle-like microcrystals. Finally the microcrystals melted at 353 K. The microcrystals were stable at room temperature upon cooling and showed no reflective CD bands, indicating the absence of the supramolecular helicoidal structure. This optically observed kinetic behavior was investigated by differential scanning calorimetry (DSC). Figure 6 shows typical thermograms obtained

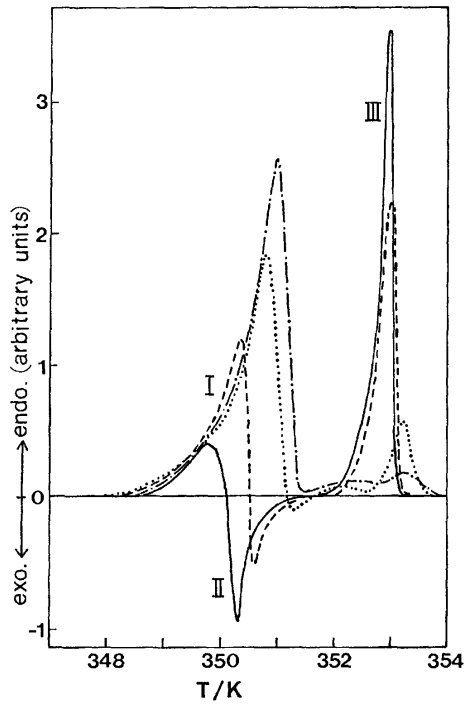

Fig. 6. DSC traces of the mesomorphic solids made from CCl_4-jelly at the various heating rates, ——: 0.31 K min^{-1}, ----: 0.62 K min^{-1}, ·····: 1.25 K min, —·—: 2.5 K min^{-1}.

by heating solid samples made from the carbon tetrachloride-jellies from room temperature to 356 K at four different heating rates. Each DSC trace showed two endothermic peaks, designated as I and III, and one exothermic peak, designated as II. The endothermic peak III occurred at 353 K. The peak III corresponds to the fusion of the needle-like microcrystals observed under a microscope, and occurred very close to the melting point (353.6 K) of the crystalline solids precipitated from solution. The endothermic peak I, which began to appear at 348 K at the appropriate heating rate, indicates a phase transition from the mesomorphic solid to a more disordered solid state. This peak did not recur upon reheating a sample cooled to room temperature from the melt, and the second run showed only the peak at 353 K. This result indicated that the mesomorphic solid state is a monotropic modification which occurs only when it separates out from solution.

It is noticeable that the endothermic peak I was followed by an exothermic peak II within an extremely narrow temperature range. The combination of the DSC result with the microscopic observations would suggest that, upon heating, the mesomorphic solid state transformed into a more disordered solid state at 348 K with an endothermic process (peak I) and that, immediately after the transformation, crystal formation from the disordered solid state occurred with the exothermic process (peak II).

The thermograms for the mesomorphic solids were greatly dependent upon the heating rate, as shown in Fig. 6; those for crystalline samples of 12HOA, however, did not show such dependence. Therefore, the heating rate dependence of DSC traces for the

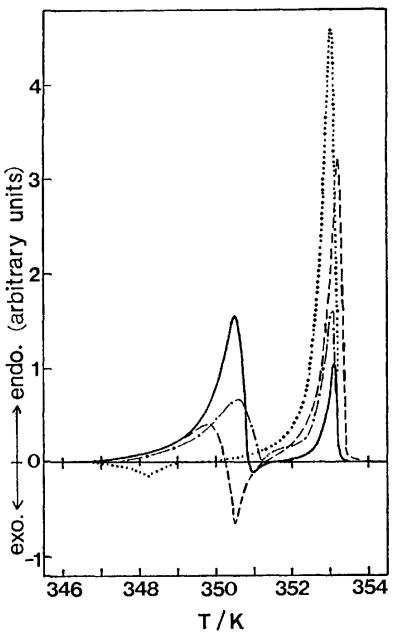

Fig. 10 DSC traces of the mesomorphic solids at a heating rate of 0.31 K min^{-1}.
·····: Made from a cyclohexane-jelly, – – –: made from a benzene-jelly, —·—: made from a 1-pentanol suspension, ——: made from a chlorobenzene-jelly.

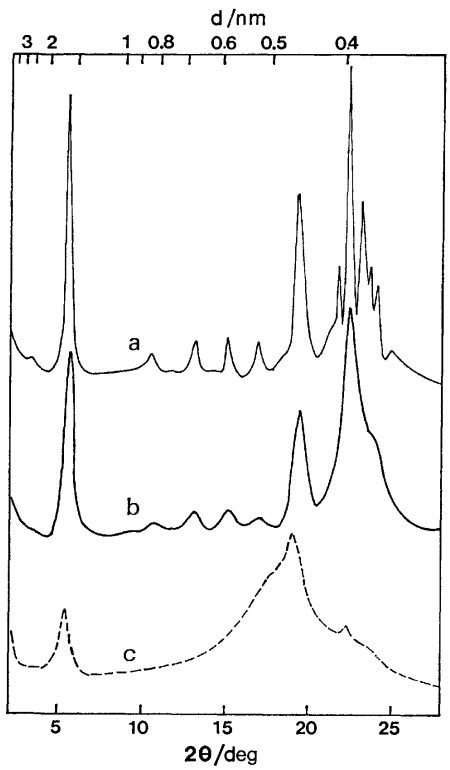

Fig. 11. X-Ray diffraction patterns of (a) powdered crystalline solids, (b) mesomorphic solids from a CCl_4-jelly, (c) jelly (257 mmol l^{-1}, with benzene) (cited from Ref. 1).

vary with the solvents used for preparation of the solids. The DSC trace of the solid from the cyclohexane-jelly was missing the endothermic peak I observed for that from the carbon tetrachloride-jelly. The solid from the chlorobenzene-jelly gave a larger endothermic peak I and a smaller endothermic peak III, in comparison with the endothermic peaks I and III, observed for the solid from the carbon tetrachloride-jelly. The DSC curves with an intermediate shape were obtained for the solids from other jellies and alcoholic solutions. In every case, as the heating rate became faster, the endothermic peak I for the transition of the mesophase to a more disordered phase became higher and the endothermic peak III became lower. When the mesomorphic solids are formed by evaporating the solvents from the jellies or the solutions of 12HOA, the degree of organization of the hydrocarbon chains in the smectic domains probably is different, depending on the solvent used. This may explain the difference in the DSC traces and in the CD spectra of the solids prepared by using various solvents.

X-Ray Diffraction Studies. Figure 11 shows the X-ray diffraction patterns of a powdered sample of the mesomorphic solids and of the crystalline solids, together with that of the benzene-jelly. The mesomorphic solids exhibit the patterns which are very similar to those of the powdered crystalline solids, although each peak in the former is broader than that in the latter. These patterns are composed of comparably sharp peaks corresponding to a long spacing of 4.67 nm (shorter than twice the extended length of 12HOA molecule)[1] and peaks corresponding to short spacings (below 0.46 nm) associated with the interchain packing. This result indicates that there is little difference in short-range-order structure between the mesomorphic solid and the crystalline solid and that, consequently, the mesomorphic solids are composed of a number of small domains with a lamellar structure similar to that in the crystalline solid, though the organization of the alkyl chains in the lamellar structure in the former is less ordered than that in the crystalline solid. Since the lamellar mesophase is a separate phase from the crystalline phase, as evidenced by the thermal studies, it is concluded that the mesophase has a smectic structure, which often forms lyotropic liquid crystals of amphiphilic molecules.

The X-ray examination was also done for the solid films formed by air-drying the benzene-jellies on a sample plate. The diffraction patterns were almost the same as those of the mesomorphic solids obtained by freeze-drying the jellies, except that the patterns from the solid films were missing the reflection peak corresponding to a short spacing of 0.46 nm. The 0.46 nm peak was recovered for the powdered sample obtained by crushing the solid films which were detached from the plate. Therefore, this effect is considered to be attributable to the same orientation effect as has been found in the CD study of the solid films.

Concluding Remarks. Helicoidal Order in Micellar and Polymer Systems: In the present series of papers (I and II), it was described that chiral 12HOA can form lyotropic helicoidal mesophase and solid analogues. This acid and its salt have been found to form helically twisted microfibrils,[17,18] Here it would

Table 2. Similarity of mode in molecular association between PMDG and (*R*)-12HOA

State	Aggregated forms	
	PMDG	(*R*)-12HOA
Dil soln	α-Helix	Chiral micelle
Concd soln and amorphous solid	Helicoidal mesophase (chiral nematic)	Helicoidal mesophase (chiral smectic)
Fibrous state	Helically twisted fibrils (right-handed)	Helically twisted fibrils (left-handed)

be useful to call attention to the helicoidal association of polymer molecules of some polypeptides such as PBG or PMG. That is, these polymer molecules can assemble into a variety of helicoidal forms,[3] *i.e.* (1) helicoidal configuration[3] of single molecule (α-helix), (2) helicoidal (chiral nematic) mesophase in solution above a critical concentration, (3) solid films with helicoidal (chiral nematic) local order, and (4) helically twisted microfibrils.[19] Table 2 illustrates the similarities between 12HOA and PMG with regard to the mode of molecular association. Here a micelle of 12HOA corresponds to the α-helix of a PMG molecule, since the former itself also constitutes a chiral system[20] as does the α-helix. Polypeptides are considered to be amphiphilic in nature since they can form stable monomolecular films at an air-water or oil-water interface. Furthermore, it should be pointed out that both polypeptides and 12HOA are capable of forming the inter- or intramolecular hydrogen bonds. Undoubtedly these common properties of both chiral amphiphiles are responsible for the similarities in the formation of helicoidal assemblies. Chiral 12HOA is a small molecule, but these molecules can link with each other to form "a chiral polymer" by intermolecular hydrogen bonding between the hydroxyl groups; as a result, these "polymer molecules" behave like chiral amphiphilic macromolecules such as polypeptides. The polymer-like behavior of chiral 12HOA that forms jellies with solvents, spherulites or microfibrils are well explained by the formation of the hydrogen-bonded polymers.

The similarity between chiral 12HOA and polypeptides led us to infer that there are some other amphiphiles exhibiting a similar behavior. In fact, this has been shown in several reports. Sakamoto *et al.*[13,21] found that optically active *N*-acyl amino acids such as *N*-lauroyl amino acid form cholesteric mesophase in apolar solvents and form chiral aggregates in polar solvents. They ascribed this result to chiral intermolecular hydrogen bonding. Sato and Hatano[22] found that the nonionic surfactant, "Tween 80" (Atlas Powder Co.) induced CD spectra to an achiral dye solubilized into the micellar solutions. They ascribed this result to the formation of a helicoidal mesophase in concentrated aqueous solution of the surfactant. Kunitake *et al.*[23] observed ICD spectra of a hydrophobic azo dye added to synthetic bilayer membranes of chiral dialkylammonium amphiphiles derived from alanine and glutamic acid. This result seems to suggest that the bilayer membranes constitute a chiral mesomorphic system.

The association behavior of bile acids and their salts also is worthy of remark. Several workers[24,25] have reported ICD results for achiral molecules dissolved in aqueous micellar solutions of sodium deoxycholate, suggesting the fomation of chiral micelles. Ramanathan *et al.*[26] observed that deoxycholic acid formed helical microfibrils when its water suspensions were dried on carbon films and that the helical twist was right-handed. The gelation of sodium deoxycholate solutions also has been often investigated, and the role of hydrogen bonding in the molecular association has been discussed.[27,28] These results seem to suggest that the gels of the deoxycholate can form helicoidal mesophases under a suitable condition, but the evidence has not yet been obtained. All the results observed with these chiral amphiphiles indicate that chiral amphiphiles constitute chiral or helicoidal micellar systems throughout the formation of sequences of intermolecular hydrogen bonds.

In general, amphiphilic molecules exhibit a variety of modes of molecular association, such as micelle, mono- and multilayers, bilayer membrane (liposome), smectic phase, and nematic phase. In addition, when amphiphilic molecules have a chiral structure, they are able to take a preferred orientation in the molecular assemblies, leading to occurrence of chiral assemblies. The resulting assemblies have a different structure from that of assemblies of achiral molecules or racemate molecules. This is reflected in the critical micelle concentration of solution[29] or in the compression curve of monolayers at an air-water interface.[30,31]

In a macroscopic scale observable with a microscope, amphiphiles form thin ribbons or microfibrils. This has been investigated most often with soaps and phospholipids. In some cases, these ribbons or fibrils twist helically regardless of whether the amphiphiles are chiral or not. Then, achiral amphiphiles produce both right-handed and left-handed helices in equal numbers, *e.g.* as have been observed for helical microfibrils from calcium tallowate in grease or from alkali-metal soaps. On the other hand, chiral amphiphiles produce a one-handed helix depending on the chirality of the molecule, though the helical sense is influenced by solvent effects.

The morphology of the assemblies of chiral amphiphilic molecules is of biological interest, since helically twisted lamellae or microfibrils are often encountered in biological systems. The present study suggests that these biological materials form helicoidal mesophases. On this connection, it is instructuve to cite a recent review by Bouligand,[6] who collected examples illustrating that biopolymers assemble into cholesteric liquid crystals or into more or less solid analogues, and that certain fibrous and regularly twisted materials can be considered as polymerized cholesterics.

We wish to thank Miss Y. Onishi for her co-operation in the experimental work, Dr. K. Sakamoto of Central Research Laboratories, Ajinomoto Co., Inc., for his valuable comments, Professor M. Hatano of

Tohoku University for valuable information regarding the signs of CD, and Professor M. Nakazaki of Osaka University for the kind advice concerning the definition of the handedness in a helix. We also are indebted to Professor J. Kumanotani of the University of Tokyo, for giving us the opportunity to use a DSC-2 Perkin-Elmer differential scanning calorimeter.

References

1) T. Tachibana, T. Mori, and K. Hori, *Bull. Chem. Soc. Jpn.*, **53**, 1714 (1980).
2) T. Tachibana, T. Mori, and K. Hori, *Nature*, **278**, 578 (1979).
3) F. T. Samulski and A. V. Tobolsky, "Liquid Crystals and Plastic Crystals," ed by G. W. Gray and P. A. Winsor, Ellis Horwood, Chichester (1974), pp. 175—198.
4) T. Tachibana and E. Oda, *Bull. Chem. Soc. Jpn.*, **46**, 2583 (1973).
5) N. Tsuchihashi, H. Nomori, M. Hatano, and S. Mori, *Chem. Lett.*, **1974**, 823.
6) Y. Bouligand, "Mesomorphic Order in Polymers and Polymerization in Liquid Crystalline Media," ed by A. Blumstein, American Chemical Society, Washington, D. C. (1978), pp. 237—247.
7) F. D. Saeva and G. R. Olin, *J. Am. Chem. Soc.*, **99**, 4848 (1977).
8) This was derived for a helical stacking of birefringent layers (see, *e.g.* E. B. Priestley, *RCA Rev.*, **35**, 584 (1974)).
9) H. Kozawaguchi and M. Wada, *Mol. Cryst. Liq. Cryst.*, **45**, 55 (1978).
10) Right- and left-handed helicoids are defined here as they have been usually for the screw sense; that is, this definition of helical sense is consistent with the usual description that a double-helix of DNA is right-handed. The definition of twist and helical sense adopted by Saeva and Olin (*J. Am. Chem. Soc.*, **78**, 2709 (1976)) is in contrast to our definition.
11) H. Toriumi, Y. Kusumi, I. Uematsu, and Y. Uematsu, *Polymer J.*, **11**, 863 (1979) and references cited therein.
12) F. D. Saeva and G. R. Olin, *J. Am. Chem. Soc.*, **95**, 7882 (1973).
13) K. Sakamoto, R. Yoshida, M. Hatano, and T. Tachibana, *J. Am. Chem. Soc.*, **100**, 6898 (1978).
14) Uzu and Sugiura (*J. Colloid Interface Sci.*, **51**, 346 (1975)) reported the enthalpy of fusion of (*R*)-12HOA crystal to be 8.50 kcal mol^{-1} (35.5 kJ mol^{-1}), which seems to be too small when compared with that of octadecanoic acid (57.5 cal g^{-1}=68.4 kJ mol^{-1}) (W. S. Singleton, T. L. Ward, and F. G. Dollear, *J. Am. Oil Chem. Soc.*, **27**, 143 (1950)).
15) V. Luzzati, H. Mustacchi, and A. E. Scoulios, *Nature*, **180**, 600 (1957).
16) M. Tasumi, T. Shimanouchi, and T. Miyazawa, *J. Mol. Spectrosc.*, **9**, 261 (1962); R. G. Snyder and J. H. Schachtschneider, *Spectrochim. Acta*, **19**, 85 (1963).
17) T. Tachibana and H. Kambara, *Bull. Chem. Soc. Jpn.*, **42**, 3422 (1968).
18) T. Tachibana, S. Kitazawa, and H. Takeno, *Bull. Chem. Soc. Jpn.*, **43**, 2418 (1970).
19) T. Tachibana and H. Kambara, *Kolloid-Z.*, **219**, 40 (1967).
20) T. Tachibana and K. Kurihara, *Naturwissenschaften*, **63**, 532 (1976).
21) K. Sakamoto and M. Hatano, *Bull. Chem. Soc. Jpn.*, **53**, 339 (1980).
22) A private communication from Professor M. Hatano of Tohoku University.
23) T. Kunitake, N. Nakashima, S. Hayashida, and K. Yonemori, *Chem. Lett.*, **1979**, 1413.
24) J. H. Perrin and M. Wilsey, *J. Chem. Soc., Chem. Commun.*, **1971**, 769.
25) J. Gawronski, *Tetrahedron Lett.*, **1976**, 3845.
26) N. Ramanathan, A. L. Currie, and J. R. Colvin, *Nature*, **190**, 779 (1961).
27) G. Sugihara, T. Ueda, S. Kaneshima, and M. Tanaka, *Bull. Chem. Soc. Jpn.*, **50**, 604 (1977).
28) D. G. Oakenfull and L. R. Fisher, *J. Phys. Chem.*, **81**, 1838 (1977).
29) M. Takehara, I. Yoshimura, and R. Yoshida, *J. Am. Oil Chem. Soc.*, **51**, 419 (1974).
30) E. M. Arnett, J. Chao, B. Kinzig, M. Stewart, and O. Thompson, *J. Am. Chem. Soc.*, **100**, 5575 (1978).
31) T. Tachibana, T. Yoshizumi, and K. Hori, *Bull. Chem. Soc. Jpn.*, **52**, 34 (1979).

The Electronic Structures of Condensed Materials Studied by Ultraviolet Photoelectron Spectroscopy

Takashi TAKAHASHI and Yoshiya HARADA*

Department of Chemistry, College of General Education, The University of Tokyo, Komaba, Meguro-ku, Tokyo 153

(Received June 24, 1980)

The solid phase ultraviolet photoelectron spectra of water, carbon disulfide, benzene, *N*-methylaniline, and pentane condensed on a gold substrate at 77 K were measured. The features of the spectra are similar to those of the corresponding gas phase spectra. The difference between the gas and solid phase *IP*'s, the relaxation shift, is nearly constant for each compound studied except for the case of water, where the $3a_1$ molecular orbital state in solid is affected by the hydrogen bonding. The values of the relaxation shift for water, benzene and carbon disulfide are 1.1—1.3 eV, while those for *N*-methylaniline and pentane are 0.6 and 0.7 eV, respectively. The small values for the latter compounds are due to the fact that the molecules are loosely packed in the solids. The mechanisms of the band broadening for the molecular crystal are discussed in relation to the spectrum of solid carbon disulfide. For *N*-methylaniline the spectra of the gas, liquid and solid phases were compared. To our knowledge, this is the first case in which the electronic structures of all the three phases are studied by ultraviolet photoelectron spectroscopy.

The technique of photoelectron spectroscopy provides direct information about the electronic structures of materials in the gas and solid phases. Therefore, it is of considerable interest to investigate the change in the electronic structure due to the phase change by means of photoelectron spectroscopy.

In this work we measured the ultraviolet photoelectron spectra of water, benzene, carbon disulfide, *N*-methylaniline, and pentane in the solid phase and compared them with the corresponding spectra reported for the gas phase. Since all the compounds are liquids at room temperature, they are condensed easily without contamination during exposure. Water, carbon disulfide, benzene, and pentane were chosen as typical organic or inorganic compounds. *N*-methylaniline was studied, because its He I spectrum has been measured in the liquid state[1] and we can compare the electronic structures of all the three phases of gas, liquid, and solid.

Experimental

The samples of benzene, carbon disulfide, *N*-methylaniline, and pentane were distilled twice under vacuum. For the water sample, distilled water was used.

The measurements of the spectra were carried out using an ultra-high vacuum photoelectron spectrometer, which has a preparation and an analyser chamber.[2] The base pressure of the spectrometer was less than 3×10^{-10} Torr. The He I (21.22 eV), Ne I (16.85 and 16.67 eV) and Ar I (11.83 and 11.62 eV) resonance lines were used as the exciting sources. For the Ne or Ar doublet, the mean value of the energies was used to analyse the spectra. The resolution of the electron energy analyser was approximately 0.15 eV FWHM (full width at half maximum) in the present experiment.

In the preparation chamber the sample vapour was condensed onto a freshly deposited gold film held at 77 K. The vapour was let in the chamber at a point just above the substrate through a variable leak valve and a copper pipe. The pressure was less than 1×10^{-8} Torr during the condensation. To prevent the sample charging effect the exposure was stopped at intervals to monitor adsorbate peaks. The spectra shown in the following section are those which were measured just before the peak shift caused by the charging sets in.

Results and Discussion

Water (H_2O). Figure 1 illustrates the change in the He I spectra showing the condensation of water on a gold film at 77 K. To obtain the ionization potential (*IP*), the kinetic energy, E_K, of the electrons was determined by taking the zero of kinetic energy as the low energy cutoff of each spectrum† and then the relation $IP=h\nu-E_K$ was used. This method gives the work function of gold to be 4.9 eV, which is in good agreement with the value, 4.9—5.1 eV, recommended by Eastman.[3]

In Fig. 1 the features of the spectra at about 11,

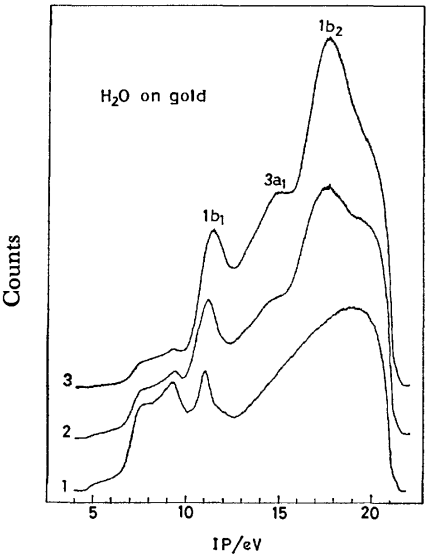

Fig. 1. He I spectra of water condensed on Au at 77 K. (1): Clean gold, (2): H_2O on gold, exposure time, 50 s at 5×10^{-9} Torr, (3): H_2O on gold, exposure time, 100 s at 5×10^{-9} Torr.

† To obtain the cutoff a small shoulder near 0 eV kinetic energy was taken out of consideration, because it is due to stray electrons.

15, and 17.5 eV correspond to the $1b_1$, $3a_1$, and $1b_2$ bands in the spectrum of gas phase water. The large peak between 18 and 21 eV is due to inelastically scattered electrons in the solid film.

As can be seen in Fig. 1, the structures of the spectra between 5 and 10 eV originated from the gold substrate little shift when water molecules are adsorbed. Similar results are observed for all the samples studied and are in contrast with the results observed by Yu *et al.* on a MoS_2 substrate,[4] where the MoS_2 bands gradually shift as coverage increases. They attributed the shift to a dipole between the MoS_2 substrate and the adsorbed molecules. In the case of a metal substrate, the thickness of the electron deficient layer due to the adsorbed gas is much less than the escape depth of photoelectrons. Therefore, the dipole effect may not cause the observable shift of the gold substrate peaks.

In Table 1 the gas phase vertical *IP*'s of water[5] are compared with the solid phase ones. The difference between the gas and solid *IP*'s, the relaxation shift, R ($=IP(\text{gas})-IP(\text{solid})$), mostly corresponds to the polarization energy due to the molecular ion left in the solid after a photoelectron is removed.

TABLE 1. THE VERTICAL IONIZATION POTENTIALS OF GAS AND SOLID WATER TOGETHER WITH THE RELAXATION SHIFTS

Orbital	*IP*(gas)[5] / eV	*IP*(solid) / eV	R[a] / eV
$1b_1$	12.62	11.3	1.3
$3a_1$	14.78	15.0	−0.2
$1b_2$	18.55	17.6	1.0

a) $R=IP(\text{gas})-IP(\text{solid})$.

Atkinson *et al.* have also measured the He I spectrum of water adsorbed on gold and found the structures at 6.3, 10.2 and 12.6 eV below the Fermi level of gold.[6] Adding 4.9 eV for the work function of gold, we have 11.2, 15.1, and 17.5 eV for the ionization potentials of solid water, which are in good agreement with the values obtained in the present experiment (Table 1).

In Table 1 the relaxation shift of the $3a_1$ state is negative. As was pointed out by Campbell *et al.*,[7] on solidification of water, the $3a_1$ molecular orbital state is predominantly affected by the hydrogen bonding because of its orbital geometry, and appears considerably perturbed in the solid state spectrum. Therefore, the negative value of the relaxation shift for the $3a_1$ state may be due to the stabilization of the $3a_1$ orbital caused by the hydrogen bonding and also to the change in the band shape.

Benzene (C_6H_6). Figure 2 shows the He I spectra of benzene condensed on the gold substrate. The characteristic features of the solid spectrum shown in the figure are summarized in Table 2 together with the corresponding features of the gas phase spectrum.[8,9] Since the e_{2g} and $a_{2u}(\pi)$ bands are not well resolved in the gas phase spectrum, they are observed as a single band at 10.7 eV in the solid phase

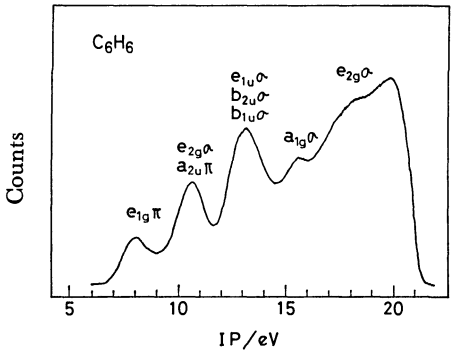

Fig. 2. He I spectrum of benzene condensed on Au at 77 K.

TABLE 2. THE VERTICAL IONIZATION POTENTIALS OF GAS AND SOLID BENZENE TOGETHER WITH THE RELAXATION SHIFTS

Orbital	*IP*(gas)[8,9] / eV		*IP*(solid) / eV	R[a] / eV
$1e_{1g}\pi$	9.24		8.1	1.1
$3e_{2g}$	11.49	11.8[b]	10.7	1.1
$1a_{2u}\pi$	12.3			
$3e_{1u}$	13.8			
$1b_{2u}$	14.7	14.3[b]	13.1	1.2
$2b_{1u}$	15.4			
$3a_{1g}$	16.85		15.5	1.3_5
$2e_{2g}$	19.2		—	—

a) $R=IP(\text{gas})-IP(\text{solid})$. b) Centre of the bands.

spectrum (Fig. 2). Similarly the band at 13.1 eV is correlated to the e_{1u}, b_{2u}, and b_{1u} bands in the spectrum of the gas.

As shown in Table 2, the relaxation shift of solid benzene is 1.1—1.3 eV, which is in good agreement with the corresponding values obtained by Yu *et al.* (1.0 eV)[4] and Grobman and Koch (1.15 eV).[10]

The observed relaxation energies for naphthalene,[10] anthracene[10] and naphthacene[11] are 1.1, 1.2, and 1.0—1.3 eV, respectively. Thus the relaxation energy is essentially constant for the aromatic molecules, benzene to naphthacene. This means that the value of the relaxation energy for polycyclic aromatic crystals depends on the molecular packing, irrespective of the size of the molecules.

Carbon Disulfide (CS_2). Figure 3 shows the He I, Ne I and Ar I spectra of carbon disulfide condensed on the gold substrate. The peak positions in the spectra are the same for the three different excitation sources.

In Table 3 the vertical *IP*'s of solid carbon disulfide obtained from Fig. 3 are compared with those of the gas.[8] The relaxation shift for each band is 1.2—1.3 eV, being nearly constant as in the case of benzene.

It is worthwhile to note that the width of each band in the solid spectra is fairly constant and also does not depend on the excitation energy (Fig. 3). Subtracting the background emission due to the secondary electrons, we obtained the FWHM's (full width at half maximum) of the π_g, π_u, σ_u, and σ_g bands to be 0.8_5, 0.9_5, 0.8_0, and 0.9_0 eV, respectively. On the other hand, the corresponding FWHM's estimated

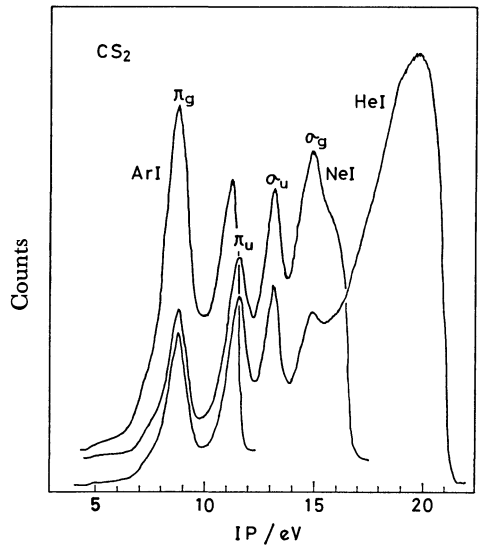

Fig. 3. He I, Ne I, and Ar I spectra of carbon disulfide condensed on Au at 77 K.

Table 3. The vertical ionization potentials of gas and solid carbon disulfide together with the relaxation shifts

Orbital	IP(gas)[8]	IP(solid)	R[a]
	eV	eV	eV
π_g	10.10	8.8	1.3
π_u	12.84	11.6	1.2
σ_u	14.48	13.2	1.3
σ_g	16.20	14.9	1.3

a) $R=IP(\text{gas})-IP(\text{solid})$.

from the envelope of the vibrational structure of the gas phase spectrum are very different and are 0.10, 0.27, 0.03, and 0.03 eV, respectively.[8] The small FWHM values for the σ_u and σ_g bands in the gas spectrum are due to the fact that each of these bands consists of the strong 0-0 peak with the very weak vibrational progression.

In order to interpret the difference in the bandwidth between the solid and gas phase spectra, it is necessary to know the mechanisms of broadening of the solid state bands. Since, as described above, the bandwidth in the solid spectra little depends on the excitation energy, the width of the upper state in solid (conduction bandwidth) is considered not to make large contribution to the broadening of the bands in contrast to the cases of metals or ordinary semiconductors. For the molecular crystal such as solid carbon disulfide, possible dominant mechanisms of the broadening are:[12] (a) the polarization energy dispersion due to the lattice vibrations in the neutral state, (b) the energy loss of the photoelectrons during their transport to the surface as a result of the excitations of the intramolecular vibrations of neutral molecules, and (c) the difference in the ionization potential between the surface and the bulk. The FWHM of the solid band expected from the mechanism (a) may be a few tenth of a relaxation energy R.†† Therefore, it is possible in the present case that the

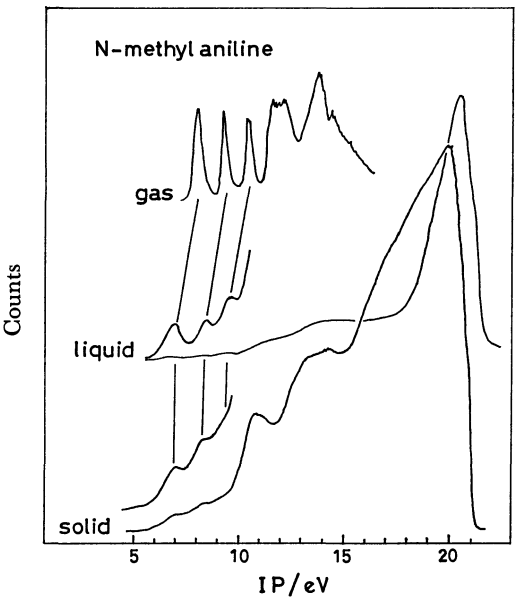

Fig. 4. He I spectra of *N*-methylaniline in the gas,[8] liquid[1] and solid phases.

Table 4. The vartical ionization potentials of gas, liquid, and solid *N*-methylaniline together with the relaxation shifts

Orbital	IP(gas)[13]	IP(liquid)[1]	IP(solid)	R_1[a]	R[b]
	eV	eV	eV	eV	eV
π_4	7.65	7.1	7.0	0.5_5	0.6_5
π_3	9.05	8.6	8.4	0.4_5	0.6_5
n	10.20	9.8	—	0.4	—
σ	11.5	—	(11.0)	—	(0.5)

a) $R_1=IP(\text{gas})-IP(\text{liquid})$. b) $R=IP(\text{gas})-IP(\text{solid})$.

mechanisms (b) and (c) also contribute to the bandwidth ($\approx$0.9 eV) which amounts to about 70% of the relaxation energy (1.2—1.3 eV). The fact that the FWHM's of the solid phase bands are nearly constatnt irrespective of those of the gas phase bands suggests that the mechanism (b) involving the energy loss due to the intramolecular vibrations makes considerable contribution to the broadening of the solid bands.

N-*Methylaniline* ($C_6H_5NHCH_3$). Figure 4 shows the He I spectrum of *N*-methylaniline condensed on the gold substrate together with the spectra in the gas[8] and liquid[1] phases. To our knowledge, *N*-methylaniline is the first compound whose ultraviolet photoelectron spectrum has been measured in all the three phases of gas, liquid, and solid. As is seen in Fig. 4, the bands are more diffuse in the order of gas, liquid and solid, the order of increasing intermolecular interaction.

Table 4 gives the vertical *IP*'s of *N*-methylaniline in the three phases together with the relaxation shifts, R_1 and R for the liquid and solid phases. In the table we find that the value of R_1 (0.4—0.5 eV) is

†† For example, in the case of solid naphthacene, the estimated FWHM due to the machanism (a) is 0.3 eV, the relaxation energy being *ca.* 1.2 eV.[12]

not much different from that of R ($\approx$0.6 eV). Since the relaxation shift is mostly due to the polarization energy of the neutral molecules surrounding a molecular ion, the small difference between the two sets of values suggests that no large change in the intermolecular distance arises on going from liquid to solid.

Pentane (C_5H_{12}). Figure 5 shows the He I spectrum of pentane condensed on the gold substrate. Since the gas phase spectrum of pentane is diffuse and its band assignment has not been well established, we compared the positions of prominent features of the gas phase spectrum[14] with those of the solid phase one (Table 5).

As is shown in Table 5, the relaxation shift of pentane is 0.7 eV, which is small compared with those of the other samples studied (1.1—1.3 eV), except for the case of *N*-methylaniline (0.6 eV). The molecule of pentane is chain-like and has freedom of rotation about its CC single bonds. When such molecules are solidified, especially at low temperature, they are expected to be loosely packed in solid. This may be the reason why pentane shows a small relaxation shift. In the case of *N*-methylaniline, its large substituent of the benzene ring may hinder a close packing of molecules in solid, also leading to a small relaxation shift.

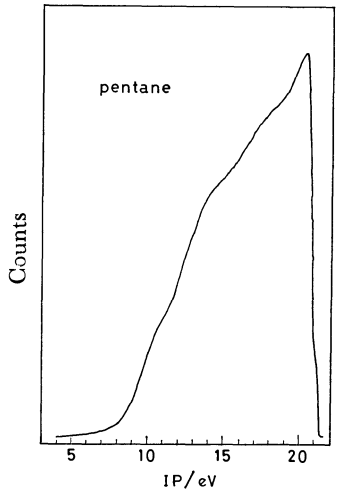

Fig. 5. He I spectrum of pentane condensed on Au at 77 K.

TABLE 5. THE PROMINENT FEATURES IN THE SPECTRA OF GAS AND SOLID PENTANE TOGETHER WITH THE RELAXATION SHIFTS

E(gas)[14] / eV		E(solid) / eV	R[a] / eV
10.8 11.4 12.05	11.1[b]	10.4	0.7
15.1		(14.4)	(0.7)

a) $R=E(\text{gas})-E(\text{solid})$. b) Centre of the overlapping features.

The authors are grateful to Kazuhiko Seki and Naoki Sato, The Institute for Molecular Science, for their helpful discussion.

References

1) L. Nemec, H. J. Gaehrs, L. Chia, and P. Delahey, *J. Chem. Phys.*, **66**, 4450 (1977).
2) Y. Harada, T. Takahashi, S. Fujisawa, and T. Kajiwara, *Chem. Phys. Lett.*, **62**, 283 (1979).
3) D. E. Eastman, *Phys. Rev. B*, **2**, 1 (1970).
4) K. Y. Yu, J. C. McMenamin, and W. E. Spicer, *Surf. Sci.*, **50**, 149 (1975).
5) K. Siegbahn, *J. Electron Spectrosc. Relat. Phenom.*, **5**, 1 (1974).
6) S. J. Atkinson, C. R. Brundle, and M. W. Roberts, *Faraday Discuss. Chem. Soc.*, **58**, 62 (1974).
7) M. J. Campbell, J. Liesegang, J. D. Libey, R. C. G. Leckey, and J. G. Jenkin, *J. Electron Spectrosc. Relat. Phenom.*, **15**, 83 (1979).
8) D. W. Turner, C. Baker, A. D. Baker, and C. R. Brundle, "Molecular Photoelectron Spectroscopy," Wiley, London (1970).
9) E. Lindholm, *Faraday Discuss. Chem. Soc.*, **54**, 200 (1972).
10) W. D. Grobman and E. E. Koch, "Photoemission from Organic Molecular Crystals," in "Photoemission in Solids," ed by L. Ley and M. Cardona, Springer, Berlin (1979), Vol. 2, Chap. 5, pp. 261—298.
11) K. Seki, H. Inokuchi, and Y. Harada, *Chem. Phys. Lett.*, **20**, 197 (1973).
12) K. Seki, Y. Harada, K. Ohno, and H. Inokuchi, *Bull. Chem. Soc. Jpn.*, **47**, 1608 (1974).
13) J. P. Maier and D. W. Turner, *J. Chem. Soc., Faraday Trans. 2*, **69**, 521 (1973).
14) D. F. Brailsford and B. Ford, *Mol. Phys.*, **18**, 621 (1970).

Study of Phase Transfer Catalysis by Layered Scintillation Method

Taketoshi HIDESHIMA,* Misao MORINAGA,† and Hideo KIMIZUKA††

College of Arts and Sciences, Chiba University, Yayoi-cho, Chiba 260

† *Otsuka Chemical Co. Ltd., Naruto, Tokushima 772*

†† *Department of Chemistry, Faculty of Science, Kyushu University, Hakozaki, Fukuoka 812*

(Received June 25, 1980)

The static and kinetic feature of the reaction of sodium cyanide with 1-bromoalkanes in the presence of various phase transfer catalysts was investigated in the oil/water system by using a layered scintillation method and the mechanism of catalytic action was discussed. From the measurement of equilibrium constants for both reactions of hexadecyltrimethylammonium cyanide with 1-bromooctane and of sodium cyanide with hexadecyltrimethylammonium bromide in organic phase, it was pointed out that the latter reaction was responsible for the advance of overall reaction. It was also found that majority of the phase transfer catalysts exist in the oil phase. It was suggested that an uptake reaction of cyanide ion from the aqueous phase at the interface is essential and that the reaction process does not follow a simple model proposed by Starks *et al.*

It is well known that the presence of a small quantity of phase transfer catalyst such as hexadecyltrimethylammonium bromide remarkably promotes the reaction of 1-bromooctane in the organic phase with sodium cyanide in the aqueous solution, although the reaction does not take place even after two weeks boiling in the absence of the catalyst. The mechanism of this reaction has been considered by Starks *et al.* as follows:[1)]

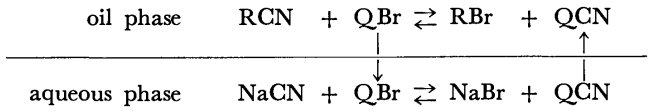

where QBr denotes quaternary ammonium bromide. It has been postulated that the circulation of the catalyst between the two phases dominates. On the other hand, a few papers against this simple model have also been presented.[2–4)]

In the preceding papers,[5–8)] a new technique using liquid scintillation counter has been devised for the study of the interaction in the oil/water system. This method has been proved to be very useful for the direct measurement of the dynamic and static interaction including the interfacial accumulation as well as the oil-water partitioning of radioactive species.

In this paper, the application of this method to the reaction of various 1-bromoalkanes with sodium cyanide in the presence of the phase transfer catalysts is described from both views of kinetics and statics and the mechanisms of catalytic action is briefly discussed.

Experimental

The procedure for measurement was described elsewhere.[5,6)] The pH of the aqueous solution was adjusted at 9.0 with Menzel's buffer solution. The experiments were carried out at 20±1.5 °C except for the case otherwise described.

Materials. In this study, 1-bromobutane, 1-bromohexane, 1-bromooctane, 1-bromodecane, 1-bromododecane, 1-bromohexadecane, bromobenzene, and 1-bromonaphthalene were used as reagents in organic phase. In these, 1-bromooctane was purified by fractional distillation. Quaternary ammonium bromides used here as the phase transfer catalysts were tetramethylammonium bromide(Me_4NBr), tetraethylammonium bromide(Et_4NBr), tetraprorylammonium bromide(Pr_4NBr), tetrabutylammonium bromide (Bu_4NBr), trimethylvinylammonium bromide(Me_3VNBr), benzyltriethylammonium bromide($BeEt_3NBr$), hexadecyltrimethylammonium bromide(CTAB), ethyldimethylhexadecylammonium bromide($CEtMe_2NBr$), and hexadecylpyridinium bromide(CPydBr). Most of these reagents were commercial ones and were used without further purification unless otherwise stated. Radioactive sodium cyanide-^{14}C obtained from New England Nuclear was used as a nucleophilic agent for the displacement reaction, and it was diluted to a suitable specific activity 9.16 Ci/mol with nonradioactive sodium cyanide of guaranteed grade. Radioactive and nonradioactive hexadecyltrimethylammonium cyanide(CTACN) were prepared from CTAB by using anion exchange resin in the CN form. Radioactive [methyl-^{14}C] hexadecyltrimethylammonium bromide(CTAB-^{14}C) was purchased from The Radiochemical Center, England. 2,5-Diphenyloxazole (PPO) and 1,4-bis-(5-phenyloxazolyl)benzene (POPOP) obtained Packed Instrument Co., Ltd. were used as scintillators.

Procedure. Layered Scintillation Method: The scintillator solution without a reactant (ST) was prepared by dissolving 2 g PPO and 0.125 g POPOP into 1000 cm^3 of a toluene solution containing 10 vol% 1-butanol. The scintillator solution with a reactant(ST(R)) was prepared by dissolving a given amount of bromoalkanes in ST.

First, 10 cm^3 of ST(R) or ST was layered on 10 cm^3 of the aqueous solution of cyanide ion labeled with ^{14}C, and the time course of increase in the amount of radioactive substance entering into the scintillator phase was measured by a liquid scintillation counter, Beckman LS-100.

After the reaction reached equilibrium, 0.5 cm^3 of the aqueous solution and 5 cm^3 of the scintillator solution were taken from each phase. The concentration of the radioactive substance in each phase was determined by the standardization procedure as follows; 0.5 cm^3 of the radioactive aqueous solution was mixed with 5 cm^3 of ST, 5 cm^3 of ST(R) (or ST) and 10 cm^3 of methanol. 5 cm^3 of the scintillator solution was mixed with 0.5 cm^3 of nonradioactive solution of cyanide ion having the same composition as the radioactive one, 5 cm^3 of ST and 10 cm^3 of methanol. Since the quenching efficiencies are the same for these standardized solutions, we can determine the partition coefficient of the total radioactive cyanide from the ratio of the counts of the two standardized solutions. The partition coefficients measured in this study were as follows:

1) $$K_{CN} = \frac{[CN]_o}{[CN]_w} = \frac{[NaCN]_o + [QCN]_o}{[NaCN]_w + [QCN]_w}$$

(Partition coefficient of cyanide ions in the absence of a 1-bromoalkane and in the presence of the catalyst)

2) $K^{R}_{CN} = \dfrac{[CN]_o + [RCN]_o}{[CN]_w}$

$= \dfrac{[NaCN]_o + [QCN]_o + [RCN]_o}{[NaCN]_w + [QCN]_w}$

(Partition coefficient of cyanide ions in the presence of a 1-bromoalkane and catalyst)

3) $K^{R}_{NaCN} = \dfrac{[NaCN]^{R}_{o}}{[NaCN]_w}$

(Partition coefficient of sodium cyanide in the absence of catalyst and in the presence of a 1-bromoalkane)

4) $K_{NaCN} = \dfrac{[NaCN]_o}{[NaCN]_w}$

(Partition coefficient of sodium cyanide in the absence of both the catalyst and a 1-bromoalkane)

5) $K_{QCN} = \dfrac{[QCN]_o}{[QCN]_w}$

(Partition coefficient of CTACN in the absence of a 1-bromoalkane when QCN is used in place of the mixture of NaCN and QBr)

6) $K^{R}_{QCN} = \dfrac{[QCN]_o + [RCN]_o}{[QCN]_w}$

(Partition coefficient of CN in the presence of a 1-bromoalkane when QCN is used in place of the mixture of NaCN and QBr)

7) $K_Q = \dfrac{[Q]_o}{[Q]_w} = \dfrac{[QCN]_o + [QBr]_o}{[QCN]_w + [QBr]_w}$

(Partition coefficient of Q^{+}-^{14}C)

In these equations the subscripts o and w, and superscript R refer to oil and aqueous phase and the reactant, respectively.

Potentiometric Measurement: The concentrations of bromide and sodium ions in the aqueous phase were potentiometrically measured by Horiba N-7 Ion Meter with the aid of the specific ion electrode for bromide and sodium ions of Activion Halstead and Horiba Ltd., respectively. In some instances, the concentration of cyanide ion was also measured with the cyanide ion electrode of Orion Research Inc.. The experimental conditions were the same as those in the layered scintillation method.

Results

Time Courses of Permeation of Hexadecyltrimethylammonium Ions and Cyanide Ions. The time course of the permeation of hexadecyltrimethylammonium ions from aqueous to organic phase without agitation is shown in Fig. 1. This figure indicates that the time courses of hexadecyltrimethylammonium entering into the organic phase of the systems with and without 1-bromooctane are almost the same and reach equilibrium within 2 h.

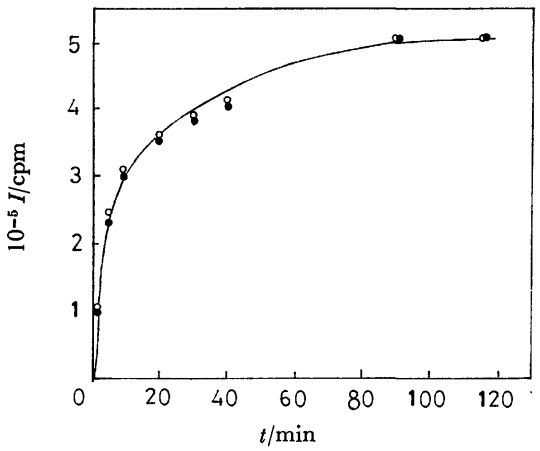

Fig. 1. Time courses of permeations of hexadecyltrimethylammonium ions into scintillator phase. ○: In the absence of 1-bromooctane, ●: in the presence of 115 mM 1-bromooctane. Initial concentration of CTAB is 0.1 mM.

On the other hand, the permeation of cyanide ions is much slower than that of hexadecyltrimethylammonium ions and it takes 20—30 h to reach equilibrium. The time course of increasing counting rate can be expressed by

$$I_\infty - I = I_\infty \exp(-kt) \quad (1)$$

for the system without the displacement reaction of 1-bromoalkane and cyanide ion in the organic phase, while it becomes

$$I_\infty - I = I_{1\infty}\exp(-k_1 t) + I_{2\infty}\exp(-k_2 t) \quad (2)$$

for the system with the displacement reaction, where I denotes the counting rate at a time t, I_∞, $I_{1\infty}$, and $I_{2\infty}$, those at an infinite time and k, k_1, and k_2, the rate constants.

The estimated values of rate constants are summarized in Table 1. In these rate constants, k_1 is thought to be the rate constant for the permeation of cyanide ion into the organic phase, since the value of k_1 is near to that of k for the system without the displacement reaction of 1-bromooctane and cyanide ion. Hence, k_2 may be refered to the rate constant for the displacement reaction in the organic phase. An agitation may cause the increase in k_1.

Partition Coefficients for Various Systems. Table 1 also shows the partition coefficients of cyanide ions

TABLE 1. PARTITION COEFFICIENTS OF CYANIDE IONS AND RATE CONSTANTS

Aqueous phase	NaCN* [a]	NaCN*	NaCN*+CTAB	NaCN*+CTAB	CTACN*	CTACN*
Organic phase	—	$C_8H_{17}Br$	—	$C_8H_{17}Br$	—	$C_8H_{17}Br$
Partition coefficient	0.206 (K_{NaCN})	0.205 (K^{R}_{NaCN})	0.207 (K_{CN})	0.478 (K^{R}_{CN})	0.196 (K_{QCN})	0.568 (K^{R}_{QCN})
Rate constant						
k or k_1/h^{-1}	0.360	0.350	0.358	0.304	0.336	0.308
k_2/h^{-1}	—	—	—	0.162	—	0.0240

a) The asterisk denotes the labeled compound with ^{14}C and initial concentrations of NaCN, CTAB, CTACN, and $C_8H_{17}Br$ are 0.1, 0.1, 0.11, and 115 mM, respectively.

in various systems. The partition coefficients of cyanide ions are small and independent of counter ions since $K_{CN} \simeq K_{NaCN} \simeq K_{QCN}$. It is also found that the direct displacement reaction of NaCN with 1-bromooctane does not take place in the absence of phase transfer catalyst since $K^{R}_{NaCN} = K_{CN}$. The occurrence of displacement reaction is indicated by the result, $K^{R}_{CN} > K_{CN}$, when the phase transfer catalyst CTAB is present. The use of CTACN in the place of the mixture of CTAB and NaCN in the aqueous phase leads to the advance of the displacement reaction in the organic phase to more extent ($K^{R}_{QCN} > K^{R}_{CN}$).

The partition coefficients of hexadecyltrimethylammonium ions, K_Q, are shown in Table 2. Since the partition coefficient of CTA^+ is larger than that of CN^-, it is evident that most of CTA^+ exist in the organic phase. The increase in the concentration of 1-bromooctane leads to the slight decrease of the partition of CTA^+, but in the lower concentration of 1-bromooctane the partition coefficients are the same as that in the absence of 1-bromooctane.

Tables 3 and 4 show the partition coefficients in the systems other than that of 1-bromooctane and CTAB. From these tables, it is found that alkyl bromide with carbon number less than 6 or more than 8, and aryl bromides were not catalyzed by the phase transfer catalysts used in this experiment. Table 3 also indicates that Me_4NBr, Me_3VNBr, $BeEt_3NBr$, and Bu_4NBr are not effective or almost noneffective in the catalytic action. As shown in Table 4, CTAB is effective only in the case of $C_8H_{17}Br$ while $CEtMe_2NBr$ and CPydBr cause the displacement reaction of cyanide with $C_6H_{13}Br$ and $C_8H_{17}Br$ and Et_4NBr, with $C_6H_{13}Br$. The rate constants for these systems are summarized in Table 5. As shown in this table, the time course obey the Eq. 2 except the systems of $C_6H_{13}Br$ with $CEtMe_2NBr$ or Et_4NBr which have smaller partition coefficients than other systems in this table.

Formation Constant. The partition coefficient of cyanide ions increases with the increase in the initial concentration of 1-bromooctane as shown in Fig. 2. Let us define the formation constant of alkanenitrile in the organic phase as

$$K^{o}_{f(RCN)} = \frac{[QBr]_o[RCN]_o}{[QCN]_o[RBr]_o}. \quad (3)$$

Rearranging Eq. 3 we have

$$[RCN]_o = K^{o}_{f(RCN)}[RBr]_o[QCN]_o/[QBr]_o$$
$$= K^{o}_{f(RCN)}([R]_T - [RCN]_o)[QCN]_o/[QBr]_o, \quad (4)$$

where $[R]_T$ is the total concentration of alkyl group.

In the system using CTACN in place of the mixture of NaCN and CTAB, the total concentration of Q, $[Q]_T$, is given as follows:

$$[Q]_T = [QCN]_o(1+K^{-1}_{QCN}) + [QBr]_o(1+K^{-1}_{QBr}). \quad (5)$$

Then,

$$[QBr]_o = \{[Q]_T - [QCN]_o(1+K^{-1}_{QCN})\}/(1+K^{-1}_{QBr})$$
$$= \{[CN]_T - [QCN]_o(1+K^{-1}_{QCN})\}/(1+K^{-1}_{QBr}) \quad (6)$$

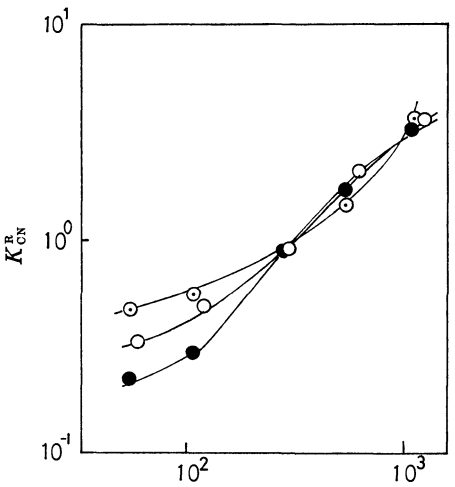

Fig. 2. Plot of partition coefficient *vs.* concentration of 1-bromooctane in the presence of QBr.
○: CTAB, ●: $CEtMe_2NBr$, ⊙: CPydBr. Initial concentrations of NaCN and QBr are all 0.1 mM.

Table 2. Partition coefficient of hexadecyltrimethylammonium ions

$[C_8H_{17}Br]$/mM	0	57.5	115	287	574
Partition coefficient	15.4	15.3	15.9	14.0	12.4

Initial consentration of CTAB-^{14}C is 0.1 mM.

Table 3. Partition coefficients of CN in various systems (1)

R	[RBr]/mM	Partition coefficient				
		Pr_4NBr	Bu_4NBr	Me_4NBr	Me_3VNBr	$BeEt_3NBr$
	0	0.164	0.172	0.190	0.180	0.207
C_4H_9	234	0.155	0.186	0.178	0.155	0.172
C_6H_{13}	236	0.128	0.189	0.190	0.177	0.192
C_8H_{17}	287	0.233	0.277	0.235	0.157	0.174
$C_{10}H_{21}$	242	0.127	0.153	0.167	0.177	0.180
$C_{12}H_{25}$	200	0.135	0.192	0.184	0.169	0.184
$C_{16}H_{33}$	218	0.150	0.278	0.181	0.209	0.214
C_6H_5	239	0.143	0.190	0.200	0.210	0.204
$C_{10}H_7$	238	0.129	0.196	0.182	0.208	0.208

Initial concentrations of NaCN and QBr are all 0.1 mM.

TABLE 4. PARTITION COEFFICIENTS OF CN IN VARIOUS SYSTEMS (2)

R	[RBr]/mM	Partition coefficient			
		CTAB	$CEtMe_2NBr$	CPydBr	Et_4NBr
	0	0.207	0.204	0.293	0.143
C_4H_9	234	0.144	0.196	0.360	0.153
C_6H_{13}	236	0.166	0.716	0.872	0.663
C_8H_{17}	287	0.892	0.870	0.889	0.153
$C_{10}H_{21}$	242	0.138	0.223	0.357	0.155
$C_{12}H_{25}$	200	0.205	0.201	0.362	0.143
$C_{16}H_{33}$	218	0.240	0.301	0.396	0.158
C_6H_5	239	0.139	0.214	0.347	0.233
$C_{10}H_7$	238	0.139	0.214	0.347	0.250

Initial concentrations of NaCN and QBr are all 0.1 mM.

TABLE 5. THE RATE CONSTANTS FOR SYSTEMS WITH THE DISPLACEMENT REACTION

RBr	Catalyst	k_1/h^{-1}	k_2/h^{-1}
$C_6H_{13}Br$	$CEtMe_2NBr$	0.116	—
$C_8H_{17}Br$	$CEtMe_2NBr$	0.086	0.0082
$C_6H_{13}Br$	CPydBr	0.120	0.0104
$C_8H_{17}Br$	CpydBr	0.141	0.0097
$C_6H_{13}Br$	Et_4NBr	0.128	—

The experimental conditions are the same as those of Table 4.

where $[CN]_T$ is the total concentration of CN. In obtaining Eq. 6 the initial condition, $[CN]_T=[Q]_T$, is used. On the other hand, we derive from the equations for K_{QCN} and K^R_{QCN}

$$[RCN]_o = \frac{K^R_{QCN}-K_{QCN}}{K_{QCN}}[QCN]_o = \frac{K^R_{QCN}-K_{QCN}}{1+K^R_{QCN}}[CN]_T \tag{7}$$

and hence, from Eqs. 6 and 7, we obtain

$$(1+K^{-1}_{QBr})[QBr]_o = [QCN]_o(K^R_{QCN}-K_{QCN})/K_{QCN}. \tag{8}$$

Combining Eqs. 4, 7, and 8 gives

$$\frac{[R]_T}{[CN]_T}\cdot\frac{1+K^R_{QCN}}{K^R_{QCN}-K_{QCN}} - 1 = \frac{K^R_{QCN}-K_{QCN}}{K^o_{f(RCN)}K_{QCN}(1+K^{-1}_{QBr})}. \tag{9}$$

Figure 3 shows the plots for the system of CTACN and 1-bromooctane according to Eq. 9, from which the values of $K^o_{f(RCN)}$ are found to be 9.34×10^{-4} at 20 °C and 1.46×10^{-1} at 28 °C, and corresponding free energy, ΔG, 17.0 and 0.48 K J/mol, respectively.

We also estimated an equilibrium constant for the formation of QCN in the organic phase defined as

$$K^o_{f(QCN)} = \frac{[NaBr]_o[QCN]_o}{[NaCN]_o[QBr]_o}. \tag{10}$$

This value can be estimated with the aid of following equations by measuring the concentrations of cyanide, bromide and sodium ion in each phase for the system of NaCN and CTAB without RBr

$$[CN]_o = [NaCN]_o + [QCN]_o \tag{11}$$

$$[Br]_o = [NaBr]_o + [QBr]_o \tag{12}$$

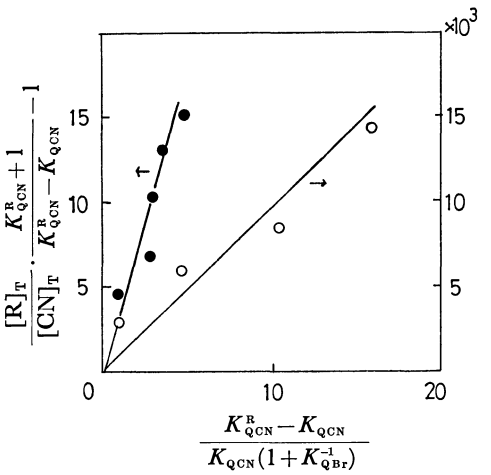

Fig. 3. Plot of Eq. 9 for the system of CTACN and 1-bromooctane.
○: 20 °C, ●: 28 °C. Initial concentration of CTACN is 0.1 mM at 20 °C and 1 mM at 28 °C.

$$[Na]_o = [NaCN]_o + [NaBr]_o \tag{13}$$

and

$$[NaCN]_o(1+K^{-1}_{NaCN}) = [QBr]_o(1+K^{-1}_{QBr}). \tag{14}$$

From the results of potentiometric measurement, the value of $K^o_{f(QCN)}$ for hexadecyltrimethylammonium cyanide was found to be 75 at 28 °C ($\Delta G=-10.8$ K J/mol).

Discussion

Consider the displacement reaction of sodium cyanide with 1-bromooctane occurring in the presence of CTAB. There are four species in the aqueous phase, NaCN, NaBr, QCN, and QBr, which permeate into the organic phase. Majority of CTA^+ ions exists in the organic phase at the equilibrium (Table 3), while the partition coefficient of cyanide ions is small compared to K_Q (Tables 1 and 2). Consequently it is thought that CTA^+ in the aqueous phase permeate into the organic phase mainly in the form of CTAB. Furthermore, as shown in Fig. 1, the permeation rate of CTA^+ into the organic phase is so large that the amount of CTA^+ in the organic phase are saturated rapidly. The mode of permeation does not change even in the presence of 1-bromooctane in the organic phase. On the other hand, the permeation of cyanide ions into the organic phase is much slower than that of CTA^+ and hence we may consider the ionic exchange reaction of CN^- by Br^- at the interface as the counter ion of CTA^+ as was suggested by Makosza *et al.*[2] We have two rate constants for the system with the displacement reaction of 1-bromooctane and CN^- and they are attributed to the permeation of CN^- into the organic phase and the displacement reaction in the organic phase respectively. From these facts, we may conclude that the catalytic action of CTA^+ would proceed rather in the organic phase and not by the circulation between the aqueous and organic phase.

The free energy change for the displacement reaction of 1-bromooctane and CTACN is positive, and hence it is thermodynamically impossible that this reaction

proceed independently. But this reaction may proceed by utilyzing the negative free energy for the displacement reaction between NaCN and CTAB at normal temperature. The free energy change for the overall reaction of NaCN and 1-bromooctane in the presence of CTAB is estimated to be -10.3 kJ/mol at 28 °C, which shows the possibility of the advance of the overall reaction. However, we may consider that the increase in temperature puts forward the displacement reaction of CTACN with 1-bromooctane from the fact that the value of $K^{\circ}_{f(RCN)}$ at 28 °C is larger than that at 20 °C.

The direct reaction of NaCN and 1-bromooctane seems not to advance because of very small reaction rate (Table 1). According to Starks *et al.*, the increase in the ionic radius of cation lowers the activation energy for the displacement reaction.[9] Changing Na^+ to CTA^+ may be essential for the acceleration of displacement reaction.

The authors wish to appreciate to Dr. M. Hayashi for his helpful discussion concerning the result in this work.

References

1) C. M. Starks, *J. Am. Chem. Soc.*, **93**, 195 (1971).
2) M. Makosza and E. Biaeka, *Tetrahedron Lett.*, **1977**, 183.
3) E. V. Dehmlow, M. Slopianka, and J. Heidler, *Tetrahedron Lett.*, **1974**, 2361.
4) E. V. Dehmlow and M. Lissel, *Tetrahedron Lett.*, **1976**, 1783.
5) H. Kimizuka and L. G. Abood, *J. Pharm. Sci.*, **62**, 740 (1973).
6) H. Kimizuka, T. Hideshima, and L. G. Abood, *Mem. Fac. Sci. Kyushu Univ.* Ser. C, **9**(**1**), 143 (1974).
7) T. Hideshima, A. Yamauchi, and H. Kimizuka, *Biochim. Biophys. Acta*, **448**, 155 (1976).
8) T. Hideshima, H. Kimizuka, L. G. Abood, and R. Tanaka, *J. Theor. Biol.*, **65**, 15 (1977).
9) C. M. Starks and C. Liotta, "Phase Transfer Catalysis, Principle and Techniques," Academic Press (1978), p. 31.

Crystal Structures of Mixed Ligand Copper(II) Complexes Containing L-Amino Acids. II. (L-Alaninato)aqua(L-histidinato)-copper(II) Trihydrate

Taizo Ono and Yoshio Sasada*

Laboratory of Chemistry for Natural Products, Tokyo Institute of Technology, Nagatsuta, Midori-ku, Yokohama 227

(Received June 30, 1980)

Copper(II) complex containing L-alanine and L-histidine crystallizes from aqueous solution at pH 7.0. Crystals of (L-alaninato)aqua(L-histidinato)copper(II) trihydrate are monoclinic, space group $P2_1$, $a=10.980(4)$, $b=7.362(3)$, $c=9.700(2)$ Å, $\beta=101.45(3)°$, and $Z=2$. There is some disorder for the location of three water molecules of crystallization. Four coordinating atoms in an approximately planar arrangement around copper are the α-amino nitrogen and imidazole δ-nitrogen of L-histidine, and α-amino nitrogen and α-carboxyl oxygen of L-alanine. They take a *cis* conformation with respect to the amino groups. The axial site is occupied with oxygen atom of water, so that the coordination geometry is square-pyramidal. Similarity and difference are discussed in comparison with the coordination mode in copper complexes containing L-histidine and L-asparagine.

Histidine-containing ternary amino acid copper(II) complexes in serum have attracted wide attention in relation to the copper(II) transport in biological systems, and the preferred second amino acids are asparagine, glutamine and threonine.[1,2] In the previous paper,[3] we have reported the crystal structure of (L-asparaginato)(L-histidinato)copper(II) and its hydrate, in which the coordination mode is the same as that of aqua(L-histidinato)(L-threoninato)copper(II) hydrate.[4] It is interesting to examine the structures of the ternary copper complexes of which the second amino acid is thought less cooperative. We have prepared (L-alaninato)aqua(L-histidinato)copper(II) trihydrate and determined the three-dimensional structure by X-ray analysis.

Experimental

1 mmol of L-alanine (0.0891 g) and 1 mmol of L-histidine (0.1552 g) were dissolved with 10 ml of ion-exchanged water. The solution, into which 1 mmol of copper(II) hydroxide (0.0976 g) prepared by the same manner as in the previous paper was added, turned blue by stirring. After removing the precipitate of copper(II) oxide, small amount of methanol was poured. Blue plate crystals of (L-alaninato)aqua(L-histidinato)copper(II) trihydrate were grown by standing the solution for a few days at room temperatures. Elemental analysis. Found: C, 28.95; H, 5.81; N, 15.28%. Calcd for $C_9H_{22}N_4O_8Cu$: C, 28.61; H, 5.87; N, 14.82%.

Crystal data are: Monoclinic, $a=10.980(4)$, $b=7.362(3)$, $c=9.700(3)$ Å, $\beta=101.45(3)°$. $D_m=1.63$ g cm^{-3} (by floatation), $D_x=1.63$ g cm^{-3}, $Z=2$. Systematic absence, $0k0$ for odd k. Space group, $P2_1$ or $P2_1/m$.

Accurate unit cell dimensions were obtained from a least-squares fit to 2θ data of 18 reflexions measured on a Rigaku automated four-circle diffractometer. Intensity data were collected on the diffractometer with graphite monochromated Mo $K\alpha$ radiation at room temperature. A θ-2θ scan technique was employed, and reflexions for $2\theta \leq 55°$ were recorded. A total of 1746 non-zero reflexions out of 1897 were obtained. Intensities were corrected for the Lorentz and polarization factors but not for absorption and secondary extinction.

Structure Determination

Since this crystal contains L-amino acid, the space group $P2_1/m$ was certainly excluded. The x and z coordinates of a copper atom were obtained from the Harker section in the sharpened three-dimensional Patterson map. Its y coordinate was taken arbitrarily as 0.25. The Fourier map phased with the copper atom has shown a pseudo-symmetry due to a mirror plane at $y=0.25$. Most of atoms in the amino acids were near this plane. Four atoms coordinated to the central copper atom were selected to be in accordance with the stereochemistry of the remaining part of the complex. All the non-hydrogen atoms except for three oxygen atoms of water of crystallization were assigned by successive Fourier syntheses. When the R factor was 0.11, the difference Fourier map showed a disorder about these three water molecules in the space along the two-fold screw axis at

Table 1a. The fractional coordinates ($\times 10^4$) with B_{eq} for the complex

Estimated standard deviations are in parentheses.

Atom	x	y	z	B_{eq}/Å^2 a)
Cu	1951(1)	2501(4)	1467(1)	2.98
C(1)	5075(13)	3568(17)	4986(12)	3.51
C(2)	4373(10)	3155(15)	3414(9)	2.83
C(3)	4776(12)	4518(18)	2409(10)	3.56
C(4)	4337(10)	3984(16)	885(10)	2.80
C(5)	3132(10)	2962(14)	−1016(9)	2.76
C(6)	4956(13)	4233(17)	−204(10)	3.29
N(1)	3033(9)	3215(16)	3297(8)	3.76
N(2)	3218(8)	3175(12)	391(8)	2.60
N(3)	4159(9)	3576(13)	−1367(8)	3.02
O(1)	4387(10)	3763(16)	5850(7)	5.29
O(2)	6188(9)	3664(19)	5201(9)	5.86
C(11)	−329(10)	1507(16)	−149(11)	3.08
C(12)	−634(11)	1477(18)	1351(10)	3.33
C(13)	−1825(11)	2461(35)	1416(12)	4.88
N(11)	462(8)	2141(17)	2345(9)	3.71
O(11)	767(7)	1829(13)	−256(7)	3.77
O(12)	−1162(8)	1212(14)	−1153(8)	4.16
O(1′)	2751(9)	−664(13)	2033(8)	4.42

a) $B_{eq}=8\pi^2(U_1+U_2+U_3)/3$ where U_1, U_2, and U_3 are the principal components of U matrix.

Table 1b. The fractional coordinate ($\times 10^3$), isotropic thermal factors and occupancies for the disordered water molecules

Estimated standard deviations are in parentheses.

Atom	x	y	z	B/Å^2	Occupancy
O(2′)	991(2)	114(4)	648(2)	10.2(6)	0.7
O(3′)	778(3)	102(5)	455(3)	11.9(9)	0.6
O(4′)	189(2)	112(4)	533(3)	10.3(7)	0.6
O(5′)	171(8)	407(15)	570(9)	19.3(33)	0.3
O(6′)	1008(7)	293(17)	641(8)	18.9(31)	0.3
O(7′)	856(4)	480(8)	512(5)	8.9(13)	0.3
O(8′)	790(9)	410(17)	459(10)	13.5(31)	0.2

0, y, 0.5. Seven sites with appropriate occupancies were given for three oxygen atoms. Later stage of refinement was achieved by the full-matrix least-squares. Contributions from hydrogen atoms were not included. The R factor dropped to 0.078 for observed reflexions. Atomic scattering factors used were taken from "International Tables for X-Ray Crystallography."[5] The final atomic parameters are listed in Table 1.[6]

Description of the Structure and Discussion

Figure 1 shows the packing of the molecules in the crystal, the hydrogen bonds being indicated by broken lines. Each complex molecule is connected along b through the axial coordination of the carboxyl oxygen of alanine related by the two-fold screw, which is hydrogen-bonded to the coordinated water in the next complex. α-Carboxyl group of histidine forms two hydrogen bonds, O(2) with water O(1′) of the complex at $1-x$, $0.5+y$, $1-z$ and O(1) with N(3) of imidazole of the complex at x, y, $1+z$. Three-dimensional network is constructed by the bridging coordination of alanine and these hydrogen bonds. The network leaves the cavities along 0, y, 0.5, in which three water molecules take randomly some of seven sites. These random water molecules form hydrogen bonds with the cavity wall and with each other,

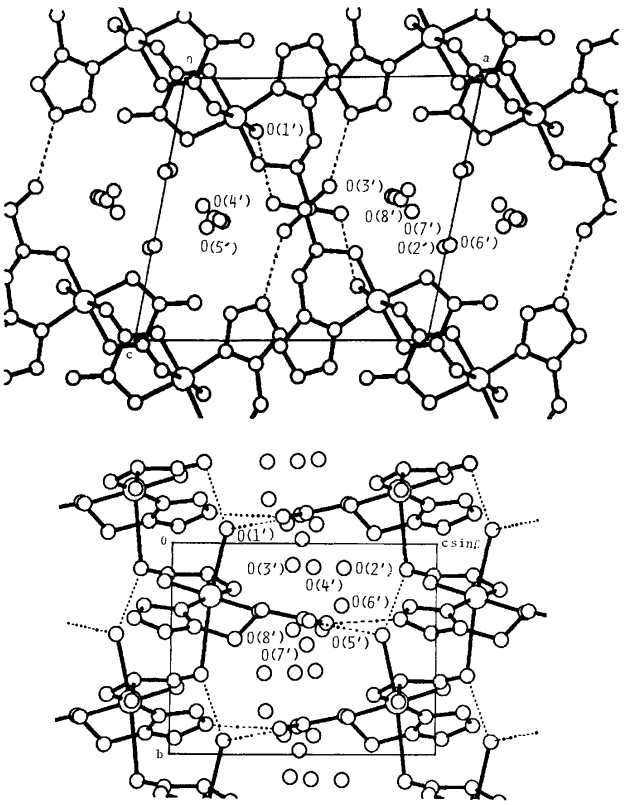

Fig. 1. Crystal structure of (L-alaninato)aqua(L-histidinato)copper(II) trihydrate projected along **b** (upper) and **a** (lower).

although details of the hydrogen bonds of this kind need not be discussed. The possible hydrogen bonds are listed in Table 2. Other than hydrogen bonds, all non-bonded intermolecular distances are normal.

Figure 2 shows the stereo pair of the diagram of the complex. Bond lengths and angles are given in Fig. 3 and Table 3, respectively. L-Alanine molecule coordinates to the central copper through α-amino nitrogen N(11) and α-carboxyl oxygen O(11), while L-histidine links through α-amino nitrogen N(1) and imidazole δ-nitrogen N(2). These four atoms occupy

Table 2. Distances of hydrogen bonds

X at a	Y at	Distance X···Y (l/Å)	X at a	Y at	Distance X···Y (l/Å)
N(1)	O(1) a	2.654(14)	O(2)	O(7′) a	2.755(53)
N(3)	O(1) c	2.763(14)	O(2)	O(8′) a	2.108(108)
O(1′)	O(2) h	2.749(14)	O(12)	O(2′) e	2.781(26)
O(1′)	O(12) f	2.910(13)	O(2′)	O(3′) a	2.687(41)
N(1)	O(4′) a	2.975(31)	O(2′)	O(4′) b	2.634(38)
N(11)	O(7′) h	3.021(53)	O(2′)	O(5′) h	2.908(100)
O(1)	O(3′) g	2.865(34)	O(2′)	O(7′) i	2.690(58)
O(1)	O(5′) a	2.922(97)	O(3′)	O(7′) a	2.934(62)
O(2)	O(3′) a	2.777(34)	O(4′)	O(6′) d	2.768(103)
O(2)	O(4′) g	2.900(31)	O(6′)	O(8′) a	2.805(146)

Code of symmetry-related position

a : x, y, z — d : $-1+x$, y, z — g : $1-x$, $0.5+y$, $1-z$

b : $1+x$, y, z — e : $-1+x$, y, $-1+z$ — h : $1-x$, $-0.5+y$, $1-z$

c : x, y, $-1+z$ — f : $-x$, $-0.5+y$, $-z$ — i : $2-x$, $-0.5+y$, $1-z$

the corners of the planar coordination square, taking a *cis* conformation with respect to the amino groups. The coordination distances, 2.006(10), 1.966(8), 2.000 (10), and 1.961(9) Å, are in agreement with those in the related complexes.[3,7,8] The axial coordination sites are occupied with a water molecule and a carboxyl oxygen of L-alanine in the neighbouring complex as mentioned above. These oxygen atoms, O(1′) and O(12)[a] where superscript a denotes the neighbouring alanine, are at 2.512(9) and 2.864(9) Å from copper, respectively. It has been reported that the in-plane covalent radius of copper is 1.30 Å and the out-of-plane radius is 1.90 Å.[9] If the covalent radius of oxygen is taken as 0.66 Å, Cu–O length should be 2.56 Å which is very close to the value of Cu–O(1′) in the present complex. On the other hand, Cu–O (12)[a] is considerably longer than the expected value. If the fact that the copper atom is 0.09 Å out of the best plane for the equatorial coordinating atoms toward the axial water molecule is also taken into account, it seems that the present complex is five-coordinated square-pyramidal.

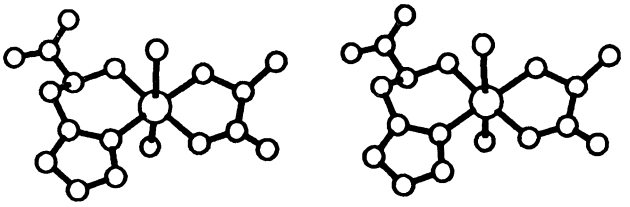

Fig. 2. Stereoview of the structure of (L-alaninato)-aqua(L-histidinato)copper(II).

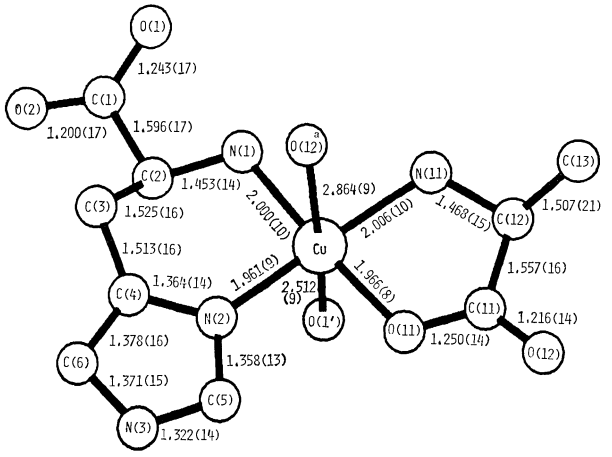

Fig. 3. Bond lengths (*l*/Å) in (L-alaninato)aqua(L-histidinato)copper(II).
Estimated standard deviations in the last digits are in parentheses.

The imidazole ring is planar within the experimental errors, whose mean plane makes a dihedral angle of 4.1(0.4)° with the plane of N(1)–Cu–N(2).

Common feature observed among Cu(ala his), Cu(asn his), its hydrate and Cu(his thr) is a *cis* conformation with respect to the amino groups. In terms of electrostatic repulsion of two carboxyl groups which coordinate to copper at the oblique axial and equatorial positions in the latter three complexes, the *cis* form may be more favourable. In fact, the O···O distances between these carboxyl groups are over 4.0 Å in the observed *cis* form. If the *trans* form were constructed with the same molecular dimensions, short contacts between carboxyl oxygen atoms would be 3.38, 3.25, and 3.15 Å. In the Cu(ala his) complex, however, there is no approach between the carboxyl groups of histidine and alanine. Therefore, the steric hindrance between hydrogen atoms at imidazole moiety and equatorial amino group should be more important. The distances in question were calculated for a hypothetical *trans* form, the smallest being 1.92 and 1.65 Å for Cu(asn his) and its hydrate, respectively.

Table 3. Bond angles (ϕ/°)

N(1)-Cu-N(2)	92.7(4)	C(1)-C(2)-C(3)	109.8(9)
N(11)-Cu-O(11)	82.6(4)	N(1)-C(2)-C(3)	110.4(9)
N(1)-Cu-N(11)	92.8(4)	C(2)-C(3)-C(4)	112.1(10)
N(2)-Cu-O(11)	91.7(4)	C(3)-C(4)-N(2)	123.2(10)
N(1)-Cu-O(11)	175.2(4)	Cu-N(2)-C(4)	127.4(7)
N(2)-Cu-N(11)	169.6(4)	C(3)-C(4)-C(6)	127.2(10)
N(1)-Cu-O(1′)	86.0(4)	N(2)-C(4)-C(6)	109.6(10)
N(2)-Cu-O(1′)	95.6(3)	C(4)-C(6)-N(3)	104.6(10)
N(11)-Cu-O(1′)	93.7(4)	C(6)-N(3)-C(5)	110.3(9)
O(11)-Cu-O(1′)	95.5(3)	N(3)-C(5)-N(2)	109.1(9)
N(1)-Cu-O(12)[a] [a)]	87.6(3)	C(5)-N(2)-C(4)	106.4(9)
N(2)-Cu-O(12)[a]	86.2(3)	Cu-N(2)-C(5)	126.2(7)
N(11)-Cu-O(12)[a]	85.2(4)	Cu-N(11)-C(12)	113.3(7)
O(11)-Cu-O(12)[a]	90.8(3)	N(11)-C(12)-C(11)	108.0(9)
O(1′)-Cu-O(12)[a]	173.4(3)	C(12)-C(11)-O(11)	118.0(10)
Cu-N(1)-C(2)	118.3(7)	C(12)-C(11)-O(12)	118.6(10)
N(1)-C(2)-C(1)	111.0(9)	O(11)-C(11)-O(12)	123.4(11)
C(2)-C(1)-O(1)	115.0(11)	C(11)-C(12)-C(13)	112.4(11)
C(2)-C(1)-O(2)	117.4(11)	N(11)-C(12)-C(13)	114.7(11)
O(1)-C(1)-O(2)	127.6(13)	Cu-O(11)-C(11)	117.5(7)

a) O(12)[a] denotes O(12) in the complex at the symmetry-related position, $-x$, $0.5+y$, $-z$.

These are of course formidable values. In Cu(ala his), the closest approach is 2.06 Å, which may also enough to exclude the *trans* form. It should be added that the *cis* form of the complexes of Cu(asn his) and Cu(his thr) would be further stabilized by the possible ligand-ligand interaction in the solution proposed by Nakahara *et al.*[10,11]

The principal difference between the present and previously reported mixed-ligand complexes is the coordination mode of histidine. In Cu(asn his), its hydrate and Cu(his thr), L-histidine coordinates to copper as a tridentate ligand, while in Cu(ala his) it behaves as a bidentate ligand, that is to say, α-carboxyl group of L-histidine does not coordinate to copper but extends to form the hydrogen bonds with the neighbouring complexes. Neumann *et al.*[1] has reported that mixed-ligand copper complexes, Cu(asn his), Cu(gln his), and Cu(his thr), are preferably formed in serum. These observations can be related to the higher stability of the chelation of histidine as tridentate ligand. Difference in the coordination mode of histidine might be interpreted by pK_a's of the second amino acids, which are 2.34, 2.02, 2.15 and 2.17 for L-alanine, L-asparagine, L-threonine, and L-glutamine, respectively.[12] L-Alanine has distinctly higher pK_a than those of the remaining three amino acids. The high pK_a means the large electron density of carboxyl oxygen. Therefore, it is suggested that amino acid with higher pK_a donates more electron to copper ion, and the electrostatic interaction of copper with axial carboxyl group is not enough to hold the distorted coordination of α-carboxyl group of histidine.

The authors are grateful to Professor Akitsugu Nakahara and his collaborators of Osaka University for their kind advice and to Dr. Akio Takenaka in our laboratory for his assistance in the final refinement and in drawing the diagrams by the computer graphics. Part of the present work was supported by a Grant-in-Aid for Scientific Research from the Ministry of Education, Science and Culture.

References

1) P. Z. Neumann and A. Sass-Kortsak, *J. Clin. Invest.*, **46**, 646 (1967).
2) B. Sarkar and T. P. A. Kruck, "The Biochemistry of Copper," ed by J. Peisach, P. Aisen, and W. E. Blumberg, Academic Press, New York (1966), p. 183.
3) T. Ono, H. Shimanouchi, Y. Sasada, T. Sakurai, O. Yamauchi, and A. Nakahara, *Bull. Chem. Soc. Jpn.*, **52**, 2229 (1979).
4) H. C. Freeman J. M. Guss, M. J. Healy, R-P. Martin, C. E. Nockolds, and B. Sarkar, *Chem. Commun.*, **1967**, 225.
5) "International Tables for X-Ray Crystallography," The Kynoch Press, Birmingham (1974), Vol. IV, p. 72.
6) Table of anisotropic thermal parameters and a list of the observed and calculated structure factors are kept in the office of the Chemical Society of Japan (Document No. 8105).
7) H. C. Freeman, *Adv. Protein Chem.*, **22**, 257 (1967).
8) Freeman[7] suggested that the Cu–N (imidazole) distance is about 2.00 Å, nearly equal to that of Cu–NH_2. But the crystal structures from which he derived this value exhibit some strain to lengthen the Cu–N bonds.
9) A. A. G. Tomlinson, B. J. Hathaway, D. E. Billing, and P. Nicholls, *J. Chem. Soc.*, *A*, 65 (1969).
10) O. Yamauchi, Y. Nakao, and A. Nakahara, *Bull. Chem. Soc. Jpn.*, **48**, 2572 (1975).
11) T. Sakurai, O. Yamauchi, and A. Nakahara, *Bull. Chem. Soc. Jpn.*, **49**, 169 (1976).
12) "Kagaku Binran, Kisohen I," ed by the Chemical Society of Japan, Maruzen, Tokyo (1973), p. 326.

Study of Cationic Surfactant Ion Selective Poly(vinyl chloride) Membrane Electrode Containing Dibenzo-18-crown-6

Tamaki MAEDA, Makoto IKEDA, Mitsuhiro SHIBAHARA, Takahide HARUTA, and Iwao SATAKE*

Department of Chemistry, Faculty of Science, Kagoshima University, Korimoto, Kagoshima 890

(Received July 15, 1980)

Study was made of the potentiometric selectivities of poly(vinyl chloride) membrane with and without dibenzo-18-crown-6. It was found that these membrane electrodes were highly selective for cationic surfactant ions and showed a Nernstian response to surfactant ion such as 1-dodecylpyridinium ion even in the concentration range as low as 10^{-6} mol/dm^3. The selectivity coefficients of inorganic cations, taken with respect to 1-dodecylpyridinium ion, were of the order of 10^{-5} or less, while that of surfactant ion was found to depend not only on hydrophobic alkyl chain length but also on the type of hydrophilic head group. For cationic surfactants with the same hydrocarbon chain length, the membrane without crown ether exhibited the order of selectivity: 1-alkylpyridinium ion > alkyltrimethylammonium ion > alkylammonium ion. In the case of the membrane with crown ether, the selectivity sequence became alkylammonium ion > 1-alkylpyridinium ion > alkyltrimethylammonium ion. For a homologous series of cationic surfactants, the selectivity coefficient increased regularly with increasing alkyl chain length.

A recent study of a number of surfactant ion selective membrane electrodes[1-18] has revealed the utility of such electrodes in the determination of critical micelle concentration[2-4,7,8,15,17,18] as well as in potentiometric titration[1,2,9-14,16] of ionic surfactant solutions. In addition, the use of surfactant ion electrode made it possible to obtain information regarding the surfactant ion activity in solution of ionic surfactant with[5,6] and without[2-4,7,17] interacting polymers.

With the exception of ionic polymer membrane,[17] all of the surfactant ion sensitive membrane electrodes so far studied are composed of either liquid[1-13] or plastic[14-18] membrane, into which is dissolved an ion exchanger made up of a surfactant ion and an oppositely charged organic ion. An ion association complex between cationic and anionic surfactant ions has widely been used as an ion exchanger.[2-7,14,16,17] These electrodes are found to be highly selective for surfactant ion over inorganic ions.[4,12,13] On the other hand, the presence of an interfering surfactant ion is shown to affect appreciably the electrode response to a particular surfactant ion in such a way that the interference increases regularly with increasing hydrocarbon chain length of the interferent.[4,12,13,17]

So far as we know, however, little is known about the selective behavior of surfactant ion sensitive membrane electrode containing electroneutral carriers. It is well known that macrocyclic polyether such as dibenzo-18-crown-6 serves as an electroneutral carrier of membrane electrode sensitive to alkali metal cations, especially to potassium ion.[19-22] Moreover, crown compounds have been found to form complexes with primary alkylammonium ions in aqueous[23] and methanol[24,25] media. It is thus interesting to study whether the crown compound-based membrane electrode responds selectively to cationic surfactant ions. In this paper is described the selective property of cationic surfactant ion sensitive poly(vinyl chloride) (PVC) membrane electrode with and without dibenzo-18-crown-6.

Experimental

Materials. Dibenzo-18-crown-6 (Nakarai Chemicals Ltd.) was recrystallized twice from benzene and dried *in vacuo*. Alkylammonium chlorides with 10, 12 and 14 carbon atoms were prepared from the corresponding alkylamines (purity > 99%, Nakarai Chemicals Ltd.) according to the method of Kolthoff and Strickes.[26] Alkyltrimethylammonium chlorides with 10, 12, and 16 carbon atoms (Tokyo Kasei Kogyo Co. Ltd.) were recrystallized twice from acetone. 1-dodecylpyridinium chloride (Wako Pure Chemical Industry Co. Ltd.) was purified by repeated recrystallization from acetone, then from isobutyl methyl ketone and finally by extraction with ether for 48 h. Tetraalkylammonium chlorides of guaranteed grade and other chemicals of reagent grade were used without further purifications.

Membrane Potential Measurements. The measurements were made with the membranes consisting of 20% PVC and 80% plasticizer, and of 1% dibenzo-18-crown-6, 20% PVC and 79% plasticizer by weight, (abbreviated hereinafter as carrier-free membrane and crown ether membrane). PVC (reported degree of polymerization is 1100) and bis(2-ethylhexyl) phthalate were dissolved into the least amount of tetrahydrofuran and mixed with a tetrahydrofuran solution of dibenzo-18-crown-6. The solution was poured onto a Petri's dish with a cover and allowed tetrahydrofuran to evaporate gradually at room temperature. A resulting membrane of 0.15 mm thickness was fixed to one end of PVC tube of 10 mm diameter by using a tetrahydrofuran solution of PVC as an adhesive. The preparation of carrier-free membrane is the same as that described above, except that dibenzo-18-crown-6 is omitted.

The electrode assembly is shown schematically in Fig. 1. In order to eliminate the leakage of ammonium ion from agar bridge, a double junction was constructed by inserting a small test tube with a pin-hole at the top into PVC electrode. The electrode was rinsed well with distilled water and stored in air when not in use. The selectivity coefficient was determined with the following cell by using the mixed solution method.[27]

Reference electrode (Ag–AgCl) | 1 mol/dm^3 NH_4NO_3 Agar bridge | Reference solution (DPC, 1×10^{-4} mol/dm^3) | PVC membrane | Sample solution (DPC, C_i; Interferent, C_j) | 1 mol/dm^3 NH_4NO_3 Agar bridge | Reference electrode (Ag–AgCl).

Here, C_i denotes the varying concentrations of 1-dodecylpyridinium chloride (DPC) and C_j the constant concentration of interfering ion, respectively. The electromotive force (EMF) (E) of the cell was measured with an accuracy of

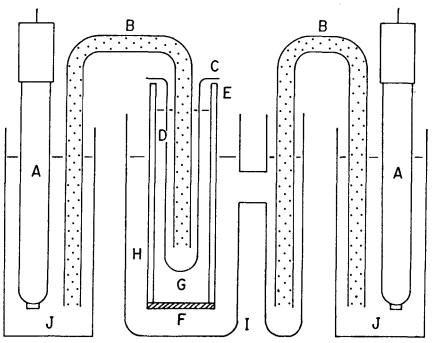

Fig. 1. Schematic diagram of PVC membrane electrode.
A: Reference electrode, B: agar bridge, C: small test tube, D: pin hole, E: PVC tube, F: PVC membrane, G: reference solution, H: sample solution, I: glass cell, J: saturated KCl solution.

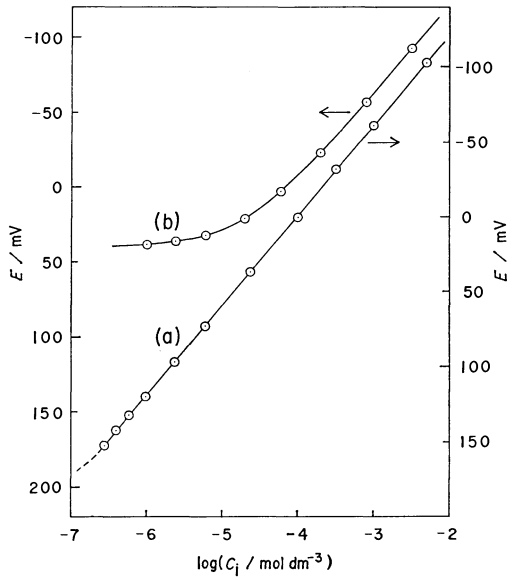

Fig. 2. Plots of EMF (E) of the cell *vs.* the logarithm of 1-dodecylpyridinium chloride concentration (C_i) at 25 °C.
(a): In the absence of interferent, (b): in the presence of 8.0×10^{-5} mol/dm^3 dodecyltrimethylammonium chloride. Arrows indicate the ordinate to be applied.

±0.1 mV, by using a Yokogawa Universal Digital Meter model 2502 connected to a voltage follower amplifier (input impedance $\approx10^{13}\,\Omega$). All measurements were conducted at 25 °C. The PVC membrane was renewed after a series of experiments for a given kind of interferent.

Results and Discussion

It has already been found by Higuchi *et al.*[28] that PVC membrane plasticized with *N,N*-dimethyloleamide or dioctyl phthalate shows a Nernstian response to tetraalkylammonium ions. One might, thus, expect that the carrier-free membrane would also response to cationic surfactant ions. Curve (a) in Fig. 2 shows the typical semilogarithmic plots of EMF of the carrier-free membrane electrode *vs.* DPC concentration in the absence of interferent. In the concentration range below the critical micelle concentration (1.7×10^{-2} mol/dm^3), a linear relation with a slope of 59.6 mV per decade change in DPC concentration was found to hold down to 3×10^{-7} mol/dm^3. The observed slope agrees well with an ideal Nernst slope (59.2 mV at 25 °C), suggesting that the membrane is completely permselective to surfactant ion and 1-dodecylpyridinium ion behaves almost ideally in this concentration range. Similar Nernstian response was also obtained for the crown ether membrane, though a linear relation was confined to the range above 2×10^{-6} mol/dm^3. These electrodes are stable and permit the replicate measurements with surfactant solutions. For example, with the crown ether membrane, the observed slope of 59.3 mV/decade was reproducible to ±0.1 mV over a period of 47 d.

The presence of an interfering ion other than 1-dodecylpyridinium ion, particularly of surfactant ion, affects appreciably the membrane potential. A typical example is given in Fig. 2 by curve (b), which shows the change in EMF of the carrier-free membrane electrode with DPC concentration under constant concentration of dodecyltrimethylammonium chloride. Below a certain DPC concentration, the EMF of the cell tends to deviate gradually from a straight line with a Nernst slope and eventually to level off.

According to the common practice in describing the selectivity of membrane electrode, we calculated the selectivity coefficient, K_{ij}^{pot}, from the following equation,

$$E = E_a - \frac{RT}{F}\ln\frac{a_i + K_{ij}^{pot}a_j}{a_i^\circ}, \qquad (1)$$

where subscript i refers to the primary ion to which the membrane is selective, j to the interfering ion and superscript ° to the reference solution, respectively. E_a is the asymmetric potential of overall cell system and other symbols have their usual meanings. As is shown in Fig. 2, the measurements were made by applying the mixed solution method, *i.e.*, E was followed as a function of the primary ion concentration under the conditions where the concentration of the interfering ion was kept constant. For simplicity, the activity coefficients in Eq. 1 were ignored in the following estimation of K_{ij}^{pot}. In order to estimate the most reliable value of selectivity coefficient, we used a slight modification of graphical curve-fitting method devised by Sillén[29] in the determination of equilibrium constants. Denoting $2.303RT/F$ by S and introducing new variables,

$$X = \frac{C_i}{K_{ij}^{pot}C_j} \qquad (2)$$

and

$$Y = -S\log(1+X), \qquad (3)$$

Eq. 1 may be written as

$$E = E_a + Y - S\log\frac{K_{ij}^{pot}C_j}{C_i^\circ} = Y + D_1. \qquad (4)$$

Furthermore, it follows from Eq. 2 that

$$\log C_i = \log X + \log K_{ij}^{pot}C_j = \log X + D_2. \qquad (5)$$

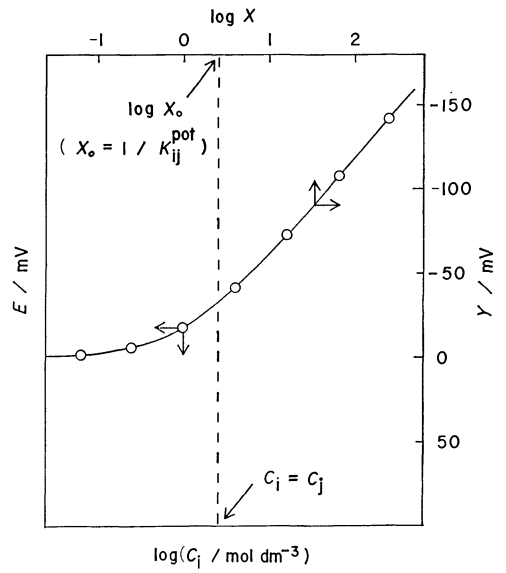

Fig. 3. Determination of the selectivity coefficient by graphical curve-fitting method.
Solid line: Normalizing curve, ○: experimental plots of E *vs.* log C_I. Arrows indicate the coordinates to be applied.

TABLE 1. THE SELECTIVITY COEFFICIENTS (K_{ij}^{pot}) FOR VARIOUS INTERFERENTS AT 25 °C

Interferent (j)	Carrier-free membrane	Crown ether membrane
$C_nH_{2n+1}NH_3^+Cl^-$		
$n=10$	2.2×10^{-3}	2.5×10^{-1}
$n=12$	2.2×10^{-2}	3.3
$n=14$	2.9×10^{-1}	3.6×10
$C_nH_{2n+1}N^+(CH_3)_3Cl^-$		
$n=10$	2.0×10^{-2}	1.7×10^{-2}
$n=12$	2.4×10^{-1}	2.3×10^{-1}
$n=16$	4.2×10	2.2×10
$C_{16}H_{33}N^+C_5H_5Cl^-$	2.1×10^2	1.7×10^2
$(C_nH_{2n+1})_4N^+Cl^-$		
$n=1$	$<10^{-6}$	$<10^{-6}$
$n=2$	9×10^{-6}	7×10^{-6}
$n=3$	8×10^{-4}	5×10^{-4}
Inorganic salts		
NaCl	$<10^{-6}$	2×10^{-5}
KCl	$<10^{-6}$	1×10^{-5}
NH_4Cl	$<10^{-6}$	2×10^{-6}
HCl	$<10^{-6}$	$<10^{-5}$

Under our experimental conditions, both D_1 and D_2 are constant. The comparison of Eq. 4 with Eq. 5 leads immediately to the conclusion that the experimental plot of E against log C_i is shifted by constant D_1 in the ordinate and by D_2 in the abscissa from a plot of Y against log X. As is schematically shown in Fig. 3, therefore, the normalizing curve, in which Y is plotted as a function of log X for the given value of S, may easily be superimposable on the experimental plot of E against log C_i by sliding it both along ordinate and abscissa. The curve-fitting should be made so as to give the best fit of experimental data over the concentration range of C_i studied. This can usually be attained without difficulty. Then one may read the value of log X_o which corresponds to $C_i=C_j$. According to Eq. 5, the value of X_o thus determined is equal to the reciprocal of K_{ij}^{pot}.

The estimated values of selectivity coefficients for various interfering ions are summarized in Table 1, where 1-dodecylpyridinium ion is conventionally taken as the primary ion, i. In some cases in which K_{ij}^{pot} defined above is much larger than unity, the determination of it suffers some experimental limitations, since the presence of even the trace amounts of interfering ion affects significantly the electrode response to 1-dodecylpyridinium ion. For instance with 1-hexadecylpyridinium ion and hexadecyltrimethylammonium ion, the presence of these ions as low as 10^{-6} mol/dm^3 was sufficient to interfere the electrode response to 1-dodecylpyridinium ion. In such cases, therefore, we determined K_{ji}^{pot} and converted it to K_{ij}^{pot} on the basis of the relationship, $K_{ij}^{pot}\cdot K_{ji}^{pot}=1$, which is confirmed to hold for surfactant solutions.[17] It should be noted that inorganic cations and tetraalkylammonium ions with shorter alkyl chain length do not affect appreciably the electrode response to 1-dodecylpyridinium ion. An interesting feature of Table 1 is a marked difference in selectivity sequence for surfactant ions with the same alkyl chain length. The carrier-free membrane gives the selectivity sequence as 1-alkylpyridinium ion>alkyltrimethylammonium ion>alkylammonium ion. In the case of the crown ether membrane, however, the selectivity sequence becomes alkylammonium ion>1-alkylpyridinium ion>alkyltrimethylammonium ion. In fact, the selectivity coefficients of the crown ether membrane for alkylammonium ions are greater than those of the carrier-free membrane by a factor of about 100. This result may reasonably be interpreted in terms of the selective interaction of dibenzo-18-crown-6 with primary alkylammonium ion in membrane phase, since dibenzo-18-crown-6 has been found to form complex in methanol only with primary alkylammonium ion among various organic ammonium ions.[24]

Another important aspect of Table 1 is the regular increase in selectivity coefficient for a homologous series of interfering surfactant ions with respect to the hydrocarbon chain length. A similar trend was already noted both for liquid and plastic membrane electrodes containing an ion association complex.[4,12,13,17] On the basis of an assumption that the mobilities of ions of similar size in membrane phase are comparable with each other, Cutler *et al.*[17] attributed the regular change in selectivity coefficient for a homologous series of surfactant ions to the regular change in partition coefficient of surfactant ion between membrane and aqueous phases.

In the presence of an excess plasticizer, which is the case for the present experiment, the selectivity characteristics of PVC membrane will presumably be described by the theory of liquid membrane electrode. Ciani *et al.*[30] derived the following expression for the

selectivity coefficient of liquid membrane with electrically neutral ligand.

$$K_{ij}^{pot} = \frac{u_{jx}^* k_{jx} K_{jx}}{u_{ix}^* k_{ix} K_{ix}} = \frac{u_{jx}^* k_j K_{jx}^*}{u_{ix}^* k_i K_{ix}^*} \quad (6)$$

In Eq. 6, u represents the mobility, k the partition coefficient and K the association constant. The asterisk refers to the membrane phase and subscript ix to the complexed cation formed between cation i and electrically neutral ligand x.

For a homologous series of surfactant ions, it seems reasonable to assume that the association constant of the complexed cation is independent of hydrocarbon chain length. Moreover, the mobilities of complexed cations will probably be comparable with each other so long as the difference in hydrocarbon chain length remains small. In such cases, therefore, the selectivity coefficient will depend only on the partition coefficient of surfactant ion, and Eq. 6 reduces to

$$\frac{K_{ij}^{pot}}{K_{il}^{pot}} \approx \frac{k_j}{k_l}. \quad (7)$$

The same relationship has already been noted for PVC membrane containing an ion association complex.[17] Equation 7 provides a reasonable explanation for the regular change in K_{ij}^{pot} of the crown ether membrane shown in Table 1, since k is the increasing function of hydrocarbon chain length. In order to check the validity of Eq. 7, we made a tentative calculation of the free energy change, w, for transferring one methylene group from an aqueous medium to the membrane phase. Denoting the number of methylene groups of surfactant ion by n, Eq. 7 can be rewritten as

$$\frac{K_{ij}^{pot}}{K_{il}^{pot}} = \exp\frac{w(n_l - n_j)}{RT}. \quad (8)$$

In Table 2 are given the values of w calculated from Eq. 8 with the data for the crown ether membrane. It is worth noting that the values of w are all similar in magnitude regardless of the type of ionic head group and are close to the free energy change of -3400 J mol^{-1} for transferring one methylene group from an aqueous medium to pure long chain aliphatic alcohols.[31] This observation seems to support the validity of the foregoing treatment based on the theory of liquid membrane.

Examination of Table 1 also shed light on factors which determine the selectivity coefficient of the carrier-free membrane. It can immediately be seen that the quotients of the selectivity coefficients of the carrier-free membrane for a homologous series of surfactant ions are comparable to those of the crown ether membrane. This fact implies that Eq. 7 must also hold, at least experimentally, for the carrier-free membrane. Indeed, the substitution of the selectivity coefficients of the carrier-free membrane into Eq. 8 gives w of $-(2900—3300)$ J mol^{-1} which is in good agreement with those in Table 2. So far as a homologous series of surfactant ions is concerned, therefore, the presence of the electroneutral ligand seems to play a minor role in determining the selectivity characteristics of PVC membrane electrode.

Table 2. The calculated values of w from Eq. 8 with the data for the crown ether membrane at 25 °C

Surfactant	n_j	n_l	$-w$/J mol^{-1}
Alkylammonium ion	12	10	3200
	14	12	3000
	14	10	3100
Alkyltrimethylammonium ion	12	10	3200
	16	12	2800
	16	10	3000
1-Alkylpyridinium ion	16	12	3200
			av. 3100

These membrane electrodes provide a simple means of determining a cationic surfactant ion activity even in the presence of added salts. Under appropriate conditions, it is also possible to estimate the activity of a particular surfactant ion in mixed surfactant solution. Details of the determination of the surfactant ion activity in micellar solution will be reported in a separate paper.

References

1) C. Gavach and P. Seta, *Anal. Chim. Acta*, **50**, 407 (1970).
2) C. Gavach and C. Bertrand, *Anal. Chim. Acta*, **55**, 385 (1971).
3) B. J. Birch and D. E. Clarke, *Anal. Chim. Acta*, **61**, 159 (1972).
4) B. J. Birch and D. E. Clarke, *Anal. Chim. Acta*, **67**, 387 (1973).
5) B. J. Birch, D. E. Clarke, R. S. Lee, and J. Oakes, *Anal. Chim. Acta*, **70**, 417 (1974).
6) I. Satake and J. T. Yang, *Biopolymers*, **15**, 2263 (1976).
7) A. Yamauchi, T. Kunisaki, T. Minematsu, Y. Tomokiyo, T. Yamaguchi, and H. Kimizuka, *Bull. Chem. Soc. Jpn.*, **51**, 2791 (1978).
8) D. Anghel and N. Ciocan, *Colloid Polymer Sci.*, **254**, 114 (1976).
9) N. Ciocan and D. Anghel, *Tenside Detergents*, **13**, 188 (1976).
10) N. Ciocan and D. Anghel, *Anal. Lett.*, **9**, 705 (1976).
11) D. F. Anghel and N. Ciocan, *Anal. Lett.*, **10**, 423 (1977).
12) D. F. Anghel, G. Popescu, and N. Ciocan, *Mikrochim. Acta*, **1977 II**, 639.
13) N. Ciocan and D. F. Anghel, *Fresenius'Z. Anal. Chem.*, **290**, 237 (1978).
14) A. S. Pathan, *Proc. Soc. Anal. Chem.*, **11**, 143 (1974).
15) T. Fujinaga, S. Okazaki, and H. Freiser, *Anal. Chem.*, **46**, 1842 (1974).
16) A. G. Fogg, A. S. Pathan, and D. T. Burns, *Anal. Chim. Acta.*, **69**, 238 (1974).
17) S. G. Cutler, P. Meares, and D. G. Hall, *J. Electroanal. Chem.*, **85**, 145 (1977).
18) J. E. Newbery and V. Smith, *Colloid Polymer Sci.*, **686**, 494 (1978).
19) G. A. Rechnitz and E. Eyal, *Anal. Chem.*, **44**, 370 (1972).
20) O. Ryba, E. Knižáková, and J. Petránek, *Collect. Czech. Chem. Commun.*, **38**, 497 (1973).
21) J. Petránek and O. Ryba, *Anal. Chim. Acta.*, **72**, 375 (1974).

22) M. Mascini and F. Pallazzi, *Anal. Chim. Acta*, **73**, 375 (1974).
23) J. L. Roberts, R. E. McClintock, Y. El-Omrani, and J. W. Larson, *J. Chem. Eng. Data*, **24**, 79 (1979).
24) C. J. Pedersen, *J. Am. Chem. Soc.*, **89**, 7017 (1967).
25) R. M. Izatt, N. E. Izatt, B. E. Rossiter, and J. J. Christensen, *Science*, **199**, 994 (1978).
26) I. M. Kolthoff and W. Strickes, *J. Phys. Colloid Chem.*, **52**, 915 (1948).
27) N. Lakshminarayanaiah, "Membrane Electrodes," Academic Press, New York (1976), p. 124.
28) T. Higuchi, C. R. Illian, and J. L. Tossounian, *Anal. Chem.*, **42**, 1674 (1970).
29) L. G. Sillén, *Acta Chem. Scand.*, **10**, 186 (1956).
30) S. Ciani, G. Eisenman, and G. Szabo, *J. Membr. Biol.*, **1**, 1 (1969).
31) C. Tanford, "The Hydrophobic Effect: Formation of Micelles and Biological Membranes," John Wiley & Sons, New York (1973), Chap. 3.

cm³. The capillary had a capacity of 0.1 cm³ and was graduated to 10^{-3} cm³. The dilatometer was calibrated by using water for which very accurate density data are available at various temperatures.[23] The precision in relative volume change is in the order of 10^{-5}, which is comparable with that in other precision dilatometric studies.[1,7] The purified material was melted and transferred with a syringe to the cell of the dilatometer. The sample in the dilatometer was degassed by repeated melting under vacuum. The whole dilatometer except for the top of the capillary was immersed in a water bath made of glass, so that we could observe color changes accompanying mesomorphic transitions. The well-stirred bath was thermostatted to ±0.01 °C at each temperature. The volume was at first read 15 min after a temperature rise of *ca.* 0.1 °C and every 10 min until it reached a stationary value.

Results

The volume(V/cm³ g^{-1})-temperature(t/°C) relations of COC and CO in the Sm, Ch, and I phases are shown in Figs. 1 and 2, respectively. The volume varies linearly with temperature except in the ranges where transitions and pretransitions occur. The thermal expansivities are 8.34, 8.31, and 7.68×10^{-4} K^{-1} in the Sm, Ch, and I phases of COC, respectively and 10.32, 9.93, and 7.55×10^{-4} K^{-1} in the Sm, Ch, and I phases of CO, respectively. The trend that the lower-temperature phase has a larger expansivity is often found for liquid crystals.

The volume changes in the vicinity of and at the Sm-Ch and Ch-I transitions are complicated by the pretransition anomalies below and above the transition points, as in other cholesteryl esters,[2-4,6-8] while if the nematic(Ne) phase is involved instead of the Ch phase they are usually much less complicated. These anomalies are relatively more pronounced on the side of the Ch phase. A temperature width of 0.5 °C is required for the Sm-Ch transition to be completed and that of 3 to 4 °C for the Ch-I transition. The transition volume ΔV are defined here by the difference between the two straight lines of the related phases and the transition temperatures by a point where $\partial V/\partial t$ has its maximum value. The transition parameters obtained thus are summarized in Table 2. The transition which has a smaller change in the thermal expansivity, has a smaller change in volume in COC, while such a correlation is not found in CO. The present value of $\Delta V_{\text{Sm-Ch}}$(COC)/cm³ mol^{-1}, 0.34[24] is slightly smaller than that given by Lorenz and Stegemeyer,[15] 0.411. The value of $\Delta V_{\text{Sm-Ch}}$(CO)/cm³ mol^{-1}, 0.88 is comparable with that in the literature,[8] 0.92. The value of $\Delta V_{\text{Ch-I}}$(CO), 0.88 cm³ mol^{-1} is larger than that of $\Delta V_{\text{B-I}}$(CO),[8] 0.49 cm³ mol^{-1} because the cholesteric to "blue phase" (B) transition is not included in the latter transition volume.[25] The B phase is regarded here as being included in the pretransition phenomena when the volume change for the Ch-I transition is obtained.

When the volume of COC began rising due to the Sm-Ch transition, the turbidity suddenly increased and was followed by a red or scarlet color. In CO, on the other hand, the change in turbidity was less

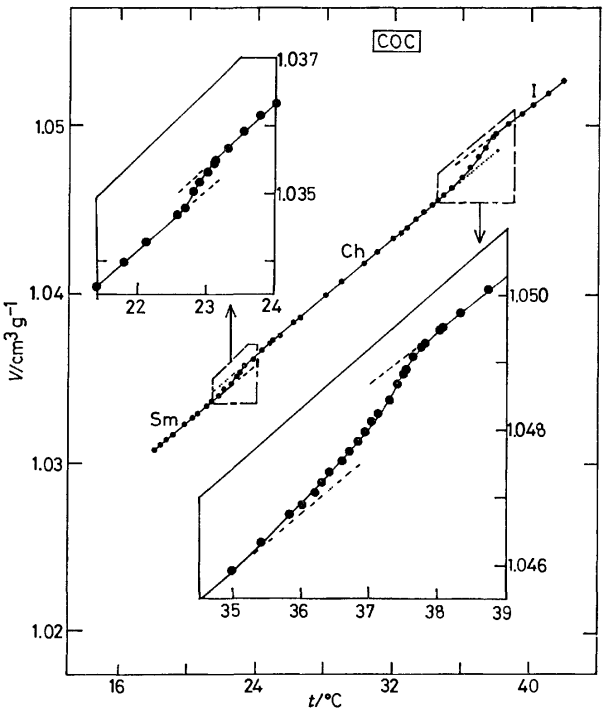

Fig. 1. Volume-temperature relation of COC.

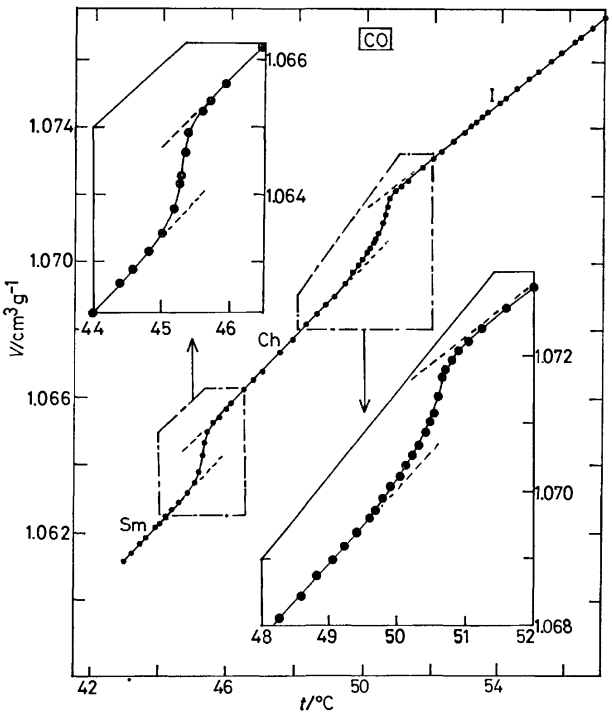

Fig. 2. Volume-temperature relation of CO.

Table 2. Transition parameters for COC and CO

Material	Transition	t_{tr}[a]	ΔV_{tr}[b]
COC	Sm-Ch	22.8	0.34
	Ch-I	37.5	0.66
CO	Sm-Ch	45.4	0.88
	Ch-I	50.7	0.88

a) Transition temperature(°C). b) Transition volume (cm³ mol^{-1}).

drastic and such a color change did not take place. When the volumes of COC and CO began rising due to the Ch-I transition, a blue color appeared together with a sudden increase in transparency; the point is identified with the Ch-B transition and lower by a few °C than the Ch-I transition point. On cooling, however, the blue color survived until 4 to 5 °C below the point found on heating. Thus, the color change had a hysteresis in contrast to the volume change. On heating, the B phase was seen over the pretransition range below the Ch-I transition point.

Discussion

Sm-Ch Transition. Besides the reasons mentioned in the introduction, there are some theoretical reasons why great attention is paid to the order of the Sm-Ch transition. As well known, the thermodynamic criterion for the first-order transition is simply that the first derivatives of the chemical potential with respect to pressure and temperature become discontinuous at a transition point. As seen in Figs. 1 and 2, it is very difficult to find such a discontinuity in the non-linear portion of the V-t relation. The maximum value of $\partial V/\partial t$ is larger in CO than in COC; there is a tendency that the larger the transition volume ΔV the larger the maximum slope $\partial V/\partial t$. The fact that the maximum slope is not infinite but rather small seems to correspond to the finding by Lushington *et al.*[14] that the Sm-Ch peak in the heat capacity-temperature curve is considerably broad and rounded. Thus, it is not easy to decide the transition order solely based on the experimental data; the transition order will be discussed below in view of theory.

Molecular theories based on the mean-field approximation[26-29] indicate that the Sm-Ne transition is allowed to be second order instead of first order for certain values of the potential parameters. McMillan's theory[27] predicts that a second-order transition occurs if the reduced temperature $T_r = T_{Sm\text{-}Ne}/T_{Ne\text{-}I}$ is smaller than $T_r^c = 0.87$; $T_r^c = 0.88$ according to a more refined calculation.[28] The present results in Table 2 give 0.953 and 0.984 as $T_r = T_{Sm\text{-}Ch}/T_{Ch\text{-}I}$ for COC and CO, respectively; similarity in the phase behavior between the Ch and Ne phases is assumed here, as often it is. These values are considerably larger than the critical value of T_r. The difference between T_r and T_r^c is smaller in COC than in CO, corresponding to the relation $\Delta V_{Sm\text{-}Ch}(COC) < \Delta V_{Sm\text{-}Ch}(CO)$. The order of the Sm-Ne transition in CBOOA[30] has been investigated using several different experimental techniques,[31-36] and most of the experimental results[31-34] except some ones[35,36] are in favor of the first-order transition. The reduced temperature for COC, 0.953 is even larger than that for CBOOA, 0.935. Thus, the Sm-Ch transition in COC is more difficult to become second order than at least that in CBOOA is. The comparison of T_r values supports the conclusion that the Sm-Ch transition in COC is weakly first order at atmospheric pressure. Indeed, there is a theory which predicts that the Sm-Ch(Ne) transition is always at least weakly first order.[37]

Ch-I Transition. It is generally accepted that the Ch(Ne)-I transition is first order. The mean-field theories[26-29,38] indicate that the Ne-I transition is always accompanied by a discontinuous change in the long-range orientational order parameter. Since the Ch phase is similar to the Ne phase as mentioned above, the Ch-I transition is also expected to have a discontinuous change in the order parameter. In practice, however, the V-t relations in Figs. 1 and 2 show no clear discontinuity at the Ch-I transition due to the pretransition phenomena, as in the case of the Sm-Ch transition. The volume changes with temperature in the pretransition region of the Ch-I transition are expressed as follows;

$$V = V_{Ch}^n + 8.7\times10^{-4} - 5.9\times10^{-4}(37.56-t)^{1/2} \quad (1)$$

$$V_{Ch}^n = 1.01548 + 8.69\times10^{-4}t \quad (2)$$

for COC and

$$V = V_{Ch}^n + 8.1\times10^{-4} - 6.7\times10^{-4}(50.53-t)^{1/2} \quad (3)$$

$$V_{Ch}^n = 1.01683 + 10.63\times10^{-4}t \quad (4)$$

for CO.[39,40] Here, V_{Ch}^n ($cm^3\,g^{-1}$) denotes the normal volume without the pretransition anomalies, and the constants in Eqs. 1 and 3 are determined by the least-squares fitting of $(V-V_{Ch}^n)^2$ to a function, $a(b-t)$ (a and b, constants). Figure 3 illustrates how Eqs. 1 and 3 fit the experimental data. The anomalous (nonlinear) dependence of the volume on temperature below the transition point can be explained in terms of the Landau-de Gennes theory for the first-order transition.[41,42] The Gibbs free energy G is assumed here to be expanded in powers of a scalar order parameter s as

$$G = G_I + (1/2)As^2 - (1/3)Bs^3 + (1/4)Cs^4, \quad (5)$$

where G_I is the free energy of the isotropic phase.[43] Here, as A is often assumed to have the form $A_1(T-T^*)$ in order to discuss the transition thermodynamics, it is expanded here as

$$A = A_1(T-T^*) + A_2(P-P^*). \quad (6)$$

The coefficients A_1, A_2, B, and C are constants, and T^* and P^* are somewhat below the transition temperature and pressure, respectively. The equilibrium

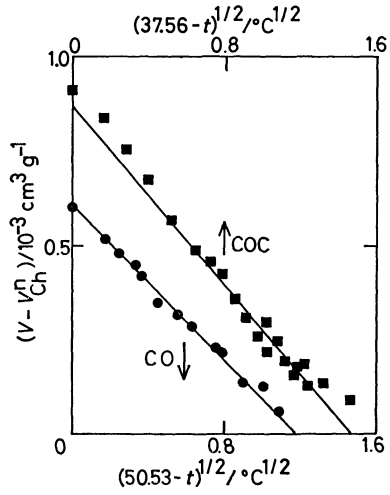

Fig. 3. Fitting of Eqs. 1 and 3 to the pretransition volume data below the Ch-I transition point.

values of s in the Ch phase are obtained as the solutions of the equation $\partial G/\partial s=0$; $s=0$ for the I phase and for the Ch phase

$$A - Bs + Cs^2 = 0. \quad (7)$$

Differentiating Eq. 5 with respect to pressure at constant temperature and taking account of Eqs. 6 and 7, we get

$$V = V_I - A_2B^2/4C^2 + (A_2^2/2C)(P-P^*) + (A_1A_2/2C)(T-T^*) - (A_2B/4^{1/2}A_1^{1/2}C^{5/2}) \times \{[B^2/4A_1C-(A_2/A_1)(P-P^*)]-(T-T^*)\}^{1/2}. \quad (8)$$

If V_I varies linearly with temperature, the equation derived above has the same form as Eqs. 1 and 3 with respect to temperature. If the coefficient B is zero as in the case of the second-order transition, the last term on the right-hand side of Eq. 8 drops, and V becomes a linear function of T. This is not the case, as shown by Eqs. 1 and 3. Thus, the nonlinear behavior of the volume in the pretransition region is explained by the existence of the third term in Eq. 5 which is required for the first-order transition.

References

1) D. Demus, H.-G. Hahn, and F. Kuschel, *Mol. Cryst. Liq. Cryst.*, **44**, 61 (1978).
2) F. P. Price and J. H. Wendorff, *J. Phys. Chem.*, **75**, 2839 (1971).
3) F. P. Price and J. H. Wendorff, *J. Phys. Chem.*, **75**, 2849 (1971).
4) F. P. Price and J. H. Wendorff, *J. Phys. Chem.*, **76**, 276 (1972).
5) F. P. Price and J. H. Wendorff, *J. Phys. Chem.*, **76**, 2605 (1972).
6) F. P. Price and J. H. Wendorff, *J. Phys. Chem.*, **77**, 2342 (1973).
7) D. Armitage and F. P. Price, *J. Appl. Phys.*, **47**, 2735 (1976).
8) D. Armitage and F. P. Price, *J. Chem. Phys.*, **66**, 3414 (1977).
9) D. Armitage and F. P. Price, *Phys. Rev. A*, **15**, 2496 (1977).
10) A. R. Ubbelohde, "The Molten State of Matter," John Wiley & Sons, New York (1978).
11) P. H. Keyes, H. T. Weston, and W. B. Daniels, *Phys. Rev. Lett.*, **31**, 628 (1973).
12) R. Shashidhar and S. Chandrasekhar, *J. Phys. (Paris)*, **36**, Cl-49 (1975).
13) P. Pollmann and G. Scherer, *Chem. Phys. Lett.*, **47**, 286 (1977); *Mol. Cryst. Liq. Cryst.*, **34**, 189 (1977).
14) K. J. Lushington, G. B. Kasting, and C. W. Garland, *Phys. Lett. A*, **74**, 143 (1979).
15) R. Lorenz and H. Stegemeyer, unpublished work cited in Ref. 13.
16) K. Bergmann and H. Stegemeyer, unpublished work cited in Ref. 13.
17) G. G. Maidachenko, *Izv. Vyssh. Ucheb. Zaved., Khim. Tecknol.*, **14**, 1115 (1971); *Chem. Abstr.*, **75**, 141048 (1971).
18) P. Adamskii and A. Dylik-Gromiec, *Mol. Cryst. Liq. Cryst.*, **25**, 281 (1974).
19) W. Elser, J. L. W. Pohlmann, and P. R. Boyd, *Mol. Cryst. Liq. Cryst.*, **36**, 279 (1976).
20) G. W. Gray and M. Hannant, *Mol. Cryst. Liq. Cryst.*, **53**, 263 (1979).
21) G. J. Davis, R. S. Porter, J. W. Steiner, and D. M. Small, *Mol. Cryst. Liq. Cryst.*, **10**, 331 (1970).
22) M. Nakahara, K. Maeda, and J. Osugi, *Bull. Chem. Soc. Jpn.*, **53**, 2499 (1980).
23) G. S. Kell, *J. Chem. Eng. Data*, **12**, 66 (1967).
24) A relatively crude sample was also investigated in order to check the influence of impurities. The volume profile was little changed except for the lower transition point; $\Delta V_{Sm\text{-}Ch}=0.35$ cm^3 mol^{-1} at 20.1 °C
25) It is very delicate to assign a definitive transition volume to the B-I transition from the *V-t* relations in Figs. 1 and 2.
26) K. Kobayashi, *J. Phys. Soc. Jpn.*, **29**, 101 (1970); *Phys. Lett. A*, **31**, 125 (1970); *Mol. Cryst. Liq. Cryst.*, **13**, 137 (1971).
27) W. L. McMillan, *Phys. Rev. A*, **4**, 1238 (1971); **6**, 936 (1972); **7**, 1673 (1973).
28) F. T. Lee, H. T. Tan, Y. M. Shih, and C. W. Woo, *Phys. Rev. Lett.*, **31**, 1117 (1973); *Phys. Lett. A*, **48**, 68 (1974).
29) P. G. de Gennes, "The Physics of Liquid Crystals," Oxford University Press, London (1974), Chap. 7.3.
30) *N*-(4-Cyanobenzylidene)-4-octyloxyaniline.
31) S. Torza and P. E. Cladis, *Phys. Rev. Lett.*, **32**, 1046 (1974).
32) D. Djurek, J. Baturic-Rubcic, and K. Franulovic, *Phys. Rev. Lett.*, **33**, 1126 (1974).
33) W. J. Lin, P. H. Keyes, and W. B. Daniels, *Phys. Lett. A*, **49**, 453 (1974).
34) M. F. Achard, F. Hardouin, G. Sigaud, and H. Gasparous, *J. Chem. Phys.*, **65**, 1387 (1976).
35) K. C. Chu and W. L. McMillan, *Phys. Rev. A*, **11**, 1059 (1975).
36) D. Armitage and F. P. Price, *Mol. Cryst. Liq. Cryst*, **38**, 229 (1977).
37) B. I. Halperin, T. C. Lubensky, and S. Ma, *Phys. Rev. Lett.*, **32**, 292 (1974); B. I. Halperin and T. C. Lubensky, *Solid State Commun.*, **14**, 997 (1974).
38) W. Mair and A. Saupe, *Z. Naturforsch., Teil A*, **13**, 564 (1958); **14**, 882 (1959); **15**, 287 (1960).
39) Similar data analyses were carried out by Chang *et al.*[40] and by Armitage *et al.*[8,9,36]
40) R. Chang and J. C. Gysbers, *J. Phys. (Paris)*, **36**, Cl-147 (1975); R. Chang, *Solid State Commun.*, **14**, 403 (1974).
41) P. Sheng and E. B. Priestley, "Introduction to Liquid Crystals," ed E. B. Priestley, P. J. Wojtowicz, and P. Sheng, Plenum Press, New York (1974), Chap. 10.
42) S. Chandrasekhar, "Liquid Crystals," Cambridge University Press, London (1977), Chap. 2.4.1.

43) The Gibbs free energy density G/V is usually expanded to the fourth power of s. Strictly speaking, therefore, some higher powers had better be included in Eq. 5 because V itself is expressed by a power series of s. For example, $V=V_I+2A_2s^2$ in the present approximation, so that some terms of s^5 and s^6 may be added. For simplicity, however, these higher terms are neglected in the present discussion.

  Bull. Chem. Soc. Jpn., 54, 103—108 (1981)

Molecular Motion in Methylammonium Hexahalotellurates(IV) as Studied by Means of the Pulsed Nuclear Magnetic Resonance

Yoshihiro Furukawa,* Hideko Kiriyama,** and Ryuichi Ikeda†

The Institute of Scientific and Industrial Research, Osaka University, Suita, Osaka 565

† *Department of Chemistry, Nagoya University, Chikusa-ku, Nagoya 464*

(Received February 8, 1980)

Molecular motion in solid $(CH_3NH_3)_2TeX_6$ (X=Cl, Br, and I) was studied by measuring the spin-lattice relaxation time, T_1, of ^1H and ^{35}Cl nuclei in several crystalline phases appearing below room temperature. A deep minimum of the proton T_1 was observed in the low-temperature phase of all the compounds, indicating that the methylammonium ion performs a rapid reorientation as a whole about its three-fold axis. The activation energies, E_a, for the motion of cations are determined to be 7.0, 3.7, and 2.7 kJ/mol for X=Cl, Br, and I respectively. In $(CH_3NH_3)_2TeI_6$, which has the lowest E_a value, the relaxation process associated with the tunneling of the cation is apparent at low temperatures. For all the complexes studied, a shallow T_1 minimum ascribable to the independent rotation of the CH_3 and NH_3 groups in the cation was observed on the high-temperature side of each deep T_1 minimum. The ^{35}Cl T_1 of $(CH_3NH_3)_2TeCl_6$ exhibited a distinct minimum at the lower phase-transition point at 139 K and a discontinuity at the higher one near 230 K. The hindered rotation of the $[TeCl_6]^{2-}$ octahedron occurs in the room-temperature phase, with an E_a value of 48 kJ/mol.

It has been reported that many methylammonium hexahalometallates(IV), $(MA)_2MX_6$ (MA=CH_3NH_3, M=Sn, Pt, Se, Pd, and Pb, and X=Cl, Br, and I), have a rhombohedrally distorted K_2PtCl_6-type structure with the space group $R\bar{3}m$ at room temperature[1] and undergo a structural phase transition at low temperatures.[2,3] Some of them have been studied by means of the halogen nuclear quadrupole resonance (NQR),[2-4] the ^1H nuclear magnetic resonance (NMR),[5] and single-crystal X-ray diffraction in high- and low-temperature phases.[6] It was found that these compounds all have one phase transition similar to one another in nature at temperatures between 103 and 163 K.[3]

On the other hand, methylammonium hexahalotellurates(IV), with crystal structures different from those of the above complexes, also show interesting phase transitions. Kume *et al.* have made halogen NQR and differential thermal analysis (DTA) experiments on $(MA)_2TeX_6$ and found a phase transition at 139 K and an anomaly in the NQR spectra near 230 K for $(MA)_2TeCl_6$, while its hexabromo and hexaiodo analogs gave phase transitions at 158 and 289 K, and at 119 K, respectively.[7] Kitahama and Kiriyama reported the results of their X-ray diffraction study of $(MA)_2TeCl_6$ at various temperatures.[8] According to them, the hexachlorotellurate(IV) has a hexagonal, layered, CdI_2-type structure at room temperature, with the space group $P\bar{3}$ (or $P\bar{3}m1$); the cell constants were $a=7.340$ and $c=7.066$ Å; and $Z=1$. The crystal can be supercooled down to about 105 K without any structural change at both 230 and 139 K. Around 105 K, the crystal is sluggishly transformed to the low-temperature phase (LTP), with an accompanying change in crystal symmetry from $P\bar{3}$ to $R\bar{3}m$. When the temperature is increased from LTP, no structural change was detected by the X-ray study at 139 K,[8] where a clear anomaly was observed by the NQR and DTA measurements.[7] On a further increase in the temperature, the crystal reverts to the room-temperature phase (RTP) near 230 K, even though the DTA study shows no anomaly around this temperature. On the other hand, at room temperature $(MA)_2TeBr_6$ and $(MA)_2TeI_6$ form cubic crystals, presumably belonging to the space group $Fm3m$.[7] In the present investigation, the proton T_1 and the ^{35}Cl NQR T_1 were measured to reveal the nature of the molecular motions in the tellurium complexes. The results thus obtained were compared with those in a similar series of complexes with the rhombohedral structure of the space group $R\bar{3}m$.

Experimental

The proton spin-lattice relaxation time, T_1, was measured at 20 and 60 MHz with a Bruker B-KR 322 s pulsed NMR spectrometer by employing the conventional 180°-*t*-90° pulse sequence. The recovery of nuclear magnetization after the 180° pulse was slightly non-exponential in the vicinity of the temperature of the T_1 minimum. In this case, T_1 value was evaluated from the initial part of the magnetization *vs.* *t* curve. The spin-locking pulse sequence was used for the determination of the rotating-frame spin-lattice relaxation time, $T_{1\rho}$, for $(MA)_2TeI_6$. The NQR T_1 of ^{35}Cl in $(MA)_2TeCl_6$ was determined by the use of a 180°-*t*-90°-*t'*-180° pulse sequence, while its resonance frequency was read directly on a Schomandl ND 100 M frequency synthesizer. A NIC 1074 signal averager was, if necessary, employed in order to increase the signal-to-noise ratio of the ^{35}Cl NQR echo.

The temperature above 77 K was controlled to within ±0.5 K by using an Ohkura EC 61 temperature controller and measured with a copper *vs.* constantan thermocouple. Temperatures below 77 K were obtained by allowing the sample to warm (*ca.* 0.2 K/min) from the temperature of liquid helium and measured with a gold-cobalt *vs.* copper thermocouple.

The samples used were prepared from tellurium dioxide, a methylamine solution, and the corresponding acid of hydrogen halide.[7]

Results and Discussion

Chlorine-35 NQR in $(MA)_2TeCl_6$. The temperature dependence of the ^{35}Cl NQR frequencies,

** Present address: Department of Chemistry, Faculty of Science, Kobe University, 1-1 Rokkodai-cho, Nada-ku, Kobe 657.

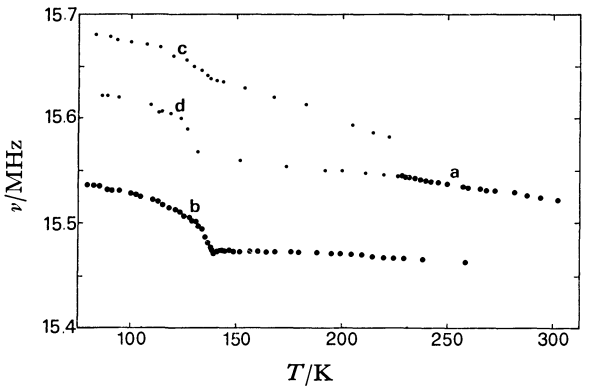

Fig. 1. Temperature dependence of ^{35}Cl NQR frequencies in $(CH_3NH_3)_2TeCl_6$.

as measured by the pulse method, is shown in Fig. 1. The results are in good agreement with those of an earlier work.[7] At room temperature, only a single resonance line, **a**, is observed at 15.52 MHz. When the sample is cooled from room temperature, the **a** line fades out near 230 K. After further cooling down to about 100 K, another line, **b**, is detected, its frequency being 15.54 MHz at 80 K. When the sample is warmed from 80 K, the resonance frequency gradually decreases and gives rise to a small, cusp-shaped anomaly, as in the case of rhombohedral $(MA)_2SnCl_6$, in the vicinity of 139 K.[2,3] On further heating, the **b** line broadens and the **a** line again appears at about 230 K. The former line fades out at about 260 K, while the latter increases in its intensity.

Two additional resonance lines, **c** and **d**, are frequently observed together with the main line, **b**. These extra lines show a temperature dependence similar to that of the **b** line. The intensity of these lines, however, is very weak and varies from sample to sample with the thermal history. Especially, these extra lines are liable to be observed when the sample is cooled from the transition region where both main lines, **a** and **b**, are seen simultaneously in the heating run. Kitahama and Kiriyama observed heavy streaks in the X-ray photographs of LTP with the space group of $R\bar{3}m$, indicating the development of several crystal domains arising from stacking faults in the layered lattice, as well as weak reflections originating from the $P\bar{3}$ phase, which had not been transformed on cooling down to 92 K.[8] The strong NQR line **b** can be attributed to the $R\bar{3}m$ phase, while the weak extra lines may be attributed to some crystal domains associated with the stacking faults and to the unconverted $P\bar{3}$ phase. A similar unusual NQR feature was observed for polytypism found in some compounds with layered structures.[9]

The NQR relaxation time of chlorine-35 in $(MA)_2TeCl_6$ was measured above 80 K. In Fig. 2, the values of T_1 measured on the **a**, **b**, and **c** resonances are identified by different symbols. The T_1 of the **d** resonance could not be measured because of its poor signal intensity and also because of interference from the intense line **b**. The log T_1 *vs.* $1/T$ curve shows an anomalous minimum around the lower

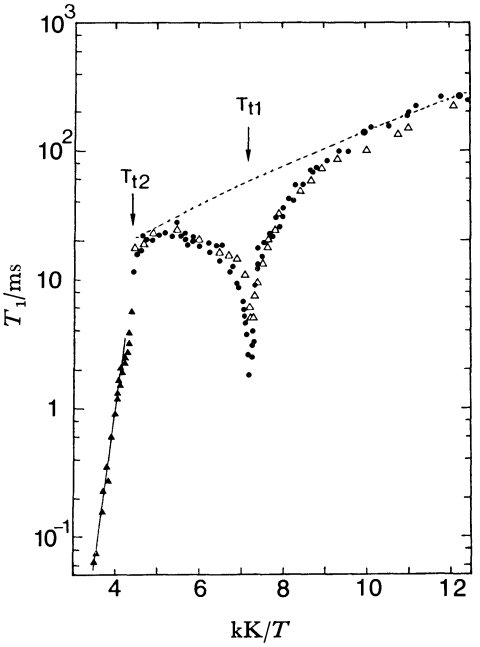

Fig. 2. Temperature dependence of ^{35}Cl NQR spin-lattice relaxation times in $(CH_3NH_3)_2TeCl_6$.
▲: **a**, ●: **b**, △: **c**.

transition temperature (T_{t1}=139 K) and a discontinuous change near 230 K (T_{t2}), where the crystal structure sluggishly changes from $R\bar{3}m$ to $P\bar{3}$ in the heating run.

One can expect the following three processes to interpret the observed relaxation: the usual lattice vibration at low temperatures, the hindered rotation of the $[TeCl_6]^{2-}$ octahedron at high temperatures, and the phase transition around 139 K. The relaxation rate due to the lattice vibration is given by:

$$(T_1)_{vib}^{-1} = aT^2 + b, \quad (1)$$

where a and b are constants.[10] The temperature dependence predicted from this relation is shown in Fig. 2 by the dotted line, which was fitted on the experimental values at 82 and 100.5 K. On the other hand, the T_1 in RTP decreases exponentially with a decrease in the inverse temperature, indicating the occurrence of a hindered rotation of the complex anion. The relaxation due to such hindered rotation is given by $T_1 = C\tau_c$.[11] The correlation time, τ_c, for the rotation is assumed to have this form:

$$\tau_c = \tau_0 \exp(E_a/RT). \quad (2)$$

The constant, C, is 2/3 for the rotation around the C_3-axes of the octahedral anion, which lie on the crystal C_3-axis.[4] The straight line in Fig. 2 is calculated by taking E_a=48 kJ/mol, and $\tau_0 = 1.3 \times 10^{-13}$ s.

The last relaxation process is characterized by the distinct T_1 minimum at T_{t1}. This phenomenon is very similar to those of the halogen NQR T_1 of cubic A_2PtBr_6 ($A=K^+$ and NH_4^+)[12,13] and of rhombohedral $(MA)_2MCl_6$ (M=Sn and Pt).[4] For the former compounds, the T_1 anomaly is interpreted in terms of a softening of the zone-center rotary-lattice mode of the octahedron, which causes a transition from the cubic to the tetragonal phase. A very similar type

of anomalous T_1 change at the transition point was observed in the latter compounds. This anomaly was also explained in terms of a softening of the rotary mode of the complex ion,[4] although no distinct structural change was disclosed on the phase transition.[6] Accordingly, it may be that the T_1 anomaly in the present tellurium complex ion also originates from a softening of the rotary mode of the complex. Quite similary to $(MA)_2SnCl_6$, no structural change was detected at the transition point of the present compound; that is, both LTP and MTP (the middle-temperature phase between T_{t1} and T_{t2}) belong to the same space group, $R\bar{3}m$.[8] One may, therefore, presume that, in the crystals of rhombohedral $(MA)_2MCl_6$, the rotation angle of the octahedral anion at the phase transition is too small to be detected by means of X-ray diffraction.

Proton T_1 *in* $(MA)_2TeCl_6$. The temperature variation of the proton T_1 in $(MA)_2TeCl_6$ gives two different results, depending on the direction of the change in the temperature. Figure 3 shows the results for T_1 as the temperature increases from 4.2 or 77 K. No drastic change was recognized in the log T_1 *vs.* $1/T$ curves at either phase transition point, T_{t1} or T_{t2}, indicating that the motion of the MA^+ ion is almost unaffected by these transitions. By analogy with $(MA)_2SnCl_6$,[5] the deep minimum near $kK/T \approx 15$ is assignable to the reorientation of the MA^+ ion as a whole about its C_3-axis, while the small depression near $kK/T \approx 10$ is assignable to the independent reorientation of the CH_3 and NH_3 groups in the cation. In this system, the spin-lattice relaxation rate for the MA^+ ion is written by:

$$T_1^{-1} = A[\tau_1/(1+\omega_0^2\tau_1^2)+4\tau_1/(1+4\omega_0^2\tau_1^2)] + B[\tau_2/(1+\omega_0^2\tau_2^2)+4\tau_2/(1+4\omega_0^2\tau_2^2)], \quad (3)$$

where $\tau_1 \ll \tau_2$.[5,14] The motional constants, A and B, stand for the contributions to T_1^{-1} from the dipolar interaction modulated *via* the C_3 rotation of the MA^+ ion as a whole, and *via* the independent rotation of the CH_3 and NH_3 groups on the coordinates of the MA^+ ion, respectively. These constants can be determined theoretically from the dimensions of the MA^+ ion[5,14] or experimentally from the T_1 minimum values. The τ_1 symbol is the correlation time for the rotation of the cation as a whole, while τ_2 symbolizes the uncorrelated rotation of the two groups. The preexponential factor, τ_0, and the activation energy, E_a, in the usual Arrhenius relation are determined experimentally.

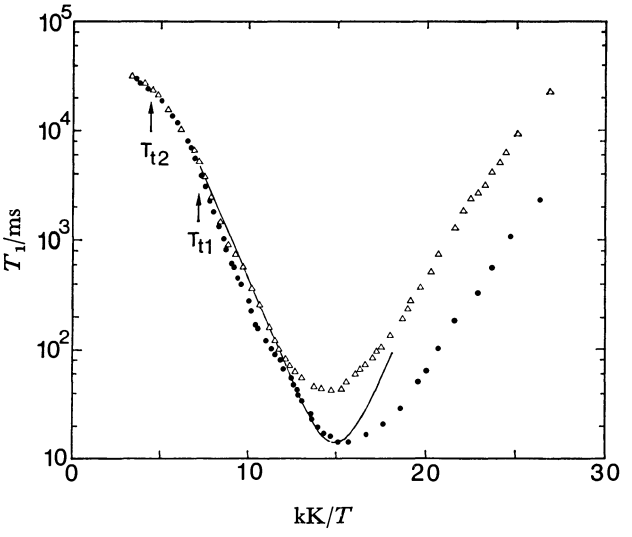

Fig. 3. The spin-lattice relaxation times of protons in $(CH_3NH_3)_2TeCl_6$ measured on heating run from 4.2 or 77 K.
●: 20 MHz, △: 60 MHz.

The experimental points in LTP, however, cannot be fitted to Eq. 3 because the deep T_1 minimum is broad and asymmetric, although all the MA^+ ions are crystallographically equivalent.[8] One possible explanation is that the correlation time is widely distributed because of the stacking faults previously described. The rather long T_1 minimum compared with the theoretical value is consistent with such breadth of the T_1 minimum. Therefore, the activation parameters are evaluated separately from the slopes on the low- and high-temperature sides of the T_1 minimum (Table 1). The T_1 curve simulated by the use of these activation parameters is represented in Fig. 3 by a solid line. The activation energy for the reorientation of the MA^+ ion reflects the intermolecular potential barrier, which is determined partly by the NH···Cl hydrogen bonding and partly by the MA^+···Cl van der Waals force. The E_a values in the Pt, Sn, and Te chloro complexes are 3.6, 4.2, and 6.0 (averaged value) kJ/mol respectively.[5] This order is the same as that of the chlorine ionicity, i, in these complexes, as deduced from ^{35}Cl NQR frequencies, which give i=0.43, 0.66, and 0.67 in that order.[3] This suggests that the former interaction is more effective on the motion of MA^+ ions than the latter one in the present system. The small value of E_a indicates that, in these compounds, the NH···Cl hydrogen bonds are quite weak as compared with that in CH_3NH_3Cl.[15]

When the crystal is cooled down from room temperature, the T_1 behavior is very different from that of the heating process described above. It has been reported that the crystal structure remains unchanged until 105 K on cooling[8] and that the DTA curve shows no heat anomaly in the temperature range of 260—230 K.[7] As can be seen from Fig. 4, the T_1 value at 20 MHz is clearly shortened by about one quarter in the narrow temperature range of 230—222 K. This T_1 anomaly indicates that the motional state of the MA^+ ion abruptly changes at T_{t2}. The T_1 curve between kK/T=4.5—7.5 shows the presence of a new relaxation process superimposed on the rapid reorientations of the CH_3 and NH_3 groups. The long T_1 value of about 4 s observed in this temperature range suggests that the predictable additional motion is, for example, a small-angle tilting of the C_3 axis of the MA^+ ion from its original orientation. This suggestion is supported by the fact that the ^{35}Cl NQR line (**a** in Fig. 1) fades out at 230 K, because such a tilting motion introduces a large fluctuation of the electric-field gradient (EFG) at the chlorine site.[7]

Proton T_1 *in* $(MA)_2TeBr_6$. The temperature

dependence of the proton T_1 at 20 MHz is shown in Fig. 5. The two phase transitions found in the NQR and DTA experiments[7] are marked by discontinuity in the log T_1 *vs.* $1/T$ curve. It is interesting to note that a shallow T_1 minimum near 100 K is clearly observed, because the deep T_1 minimum appears at 44 K, lower by 20 K than that of $(MA)_2TeCl_6$. The T_1 curve in LTP is apparently asymmetric and broad. At the present stage, however, the proton relaxation below 70 K is ascribable to the reorientation of the whole MA^+ ion. The relaxational parameters thus obtained are listed in Table 1. The observed asymmetric T_1 minimum is probably due to the tunneling-assisted relaxation, because of the low rotational barrier of the C_3 reorientation of the cation.[16] As the crystal structures of both LTP and MTP are yet unknown, we cannot, though, rule out the possibility that the presence of two or more nonequivalent MA^+ ions causes the asymmetry of the T_1 curve.

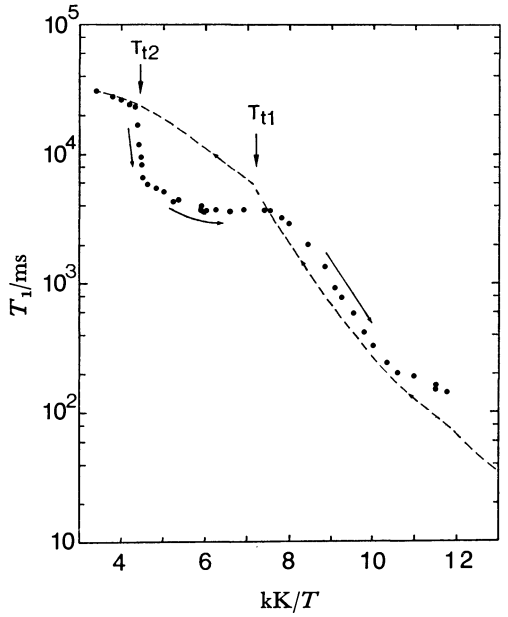

Fig. 4. The spin-lattice relaxation times of protons in $(CH_3NH_3)_2TeCl_6$ measured at 20 MHz on cooling run from room temperature. The broken line shows the data at 20 MHz on heating run.

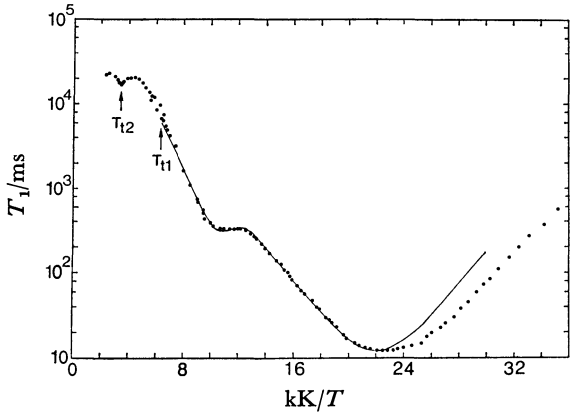

Fig. 5. Temperature dependence of the proton T_1 at 20 MHz in $(CH_3NH_3)_2TeBr_6$.

By using Eq. 3 and assuming that $\omega_0\tau_1 \ll 1$, the data between $kK/T=6$ and 18 were analyzed for the motion specified by τ_2, yielding a T_1 minimum of 430 ms at $kK/T=10.6$ and an activation energy of 9.0 kJ/mol. This process can be assigned to the intergroup dipolar interaction in the cation.[5] The theoretical T_1 minimum due to the independent reorientation is evaluated to be 460 ms, which is in good agreement with the observed value. The E_a value of 9 kJ/mol is reasonable as the internal rotation barrier in the MA^+ ion.[5]

Proton T_1 *and* $T_{1\rho}$ *in* $(MA)_2TeI_6$. The experimental relaxation times for $(MA)_2TeI_6$ are given in Fig. 6, where the log T_1 and log $T_{1\rho}$ are plotted against the inverse temperature, and in Fig. 7, where the log T_1 below 70 K is shown against the temperature. The occurrence of a phase transition was confirmed at 119 K by the discontinuity in both the T_1 and $T_{1\rho}$ curves. There are three temperature regions, characterized by different relaxation processes, for T_1: the linear region of the T_1 curve in RTP, the shallow T_1 minimum in the $kK/T=10$ to 15 region, and the two T_1 minima at very low temperatures. In the series of $(MA)_2MX_6$ (X=Cl and Br), each complex shows a single deep T_1 minimum attributed to the C_3 reorientation of the whole MA^+ ion. The T_1 behavior of $(MA)_2TeI_6$, however, is rather different from that of the foregoing complexes. This is because the T_1 curve in the low temperature rigion yields two T_1 minima, the values of which

Table 1. Motional parameters for $(MA)_2TeX_6$

Compound	A or B[a]/s^{-2}	E_a[b]/kJ mol^{-1}	τ_0/s	Motion
$(MA)_2TeCl_6$	6.2×10^9	7.0 (5.0)	1×10^{-14}	C_3-rotation of MA^+ ion
	—	—	—	independent rot. of CH_3 and NH_3 groups
	—	48	1.3×10^{-13}	hindered rot. of $[TeCl_6]^{-2}$ ion
$(MA)_2TeBr_6$	7.1×10^9	3.7 (3.3)	4×10^{-13}	C_3-rotation of MA^+ ion
	2.1×10^8	9.0	5×10^{-14}	independent rot. of CH_3 and NH_3 groups
$(MA)_2TeI_6$	—	2.7	—	C_3-rotation of MA^+ ion
	2.0×10^8	5.0	3×10^{-12}	independent rot. of CH_3 and NH_3 groups
	—	6.1	—	overall rot. of MA^+ ion

a) The calculated values are $A=10\times10^9$ and $B=1.9\times10^8$ s^{-2} for r(C-H)=1.10, r(N-H)=1.04, r(C-N)=1.47 Å, and all the tetrahedral angles.[4] b) The value in parentheses is estimated from the slope on the low-temperature side of the T_1 minimum.

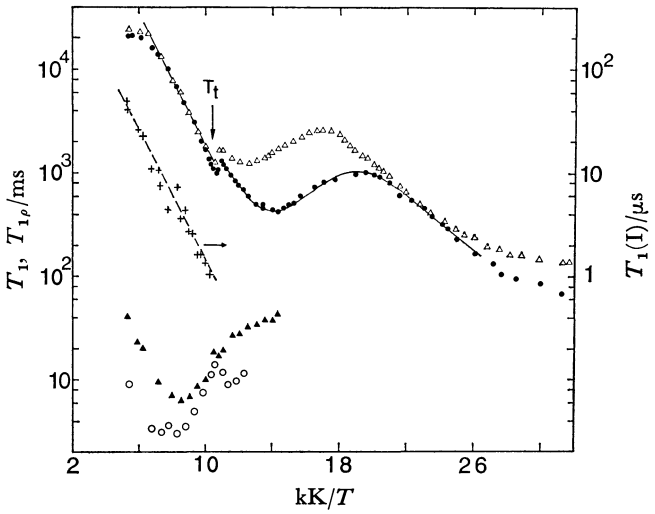

Fig. 6. The spin-lattice relaxation times of protons in $(CH_3NH_3)_2TeI_6$ against kK/T.
●: T_1 at 20 MHz, △: T_1 at 60 MHz, ○: $T_{1\rho}$ at 5 G, ▲: $T_{1\rho}$ at 10 G, and +: T_1(I) calculated from Eq. 5.

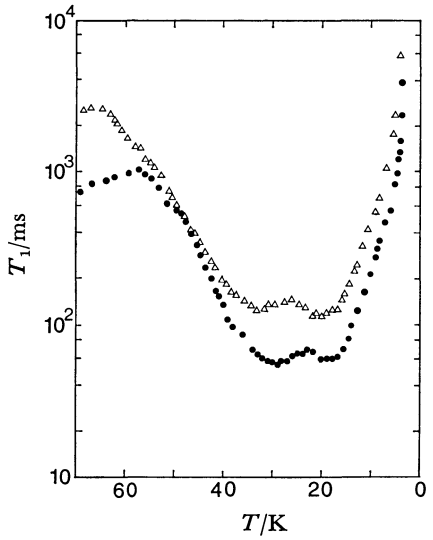

Fig. 7. The spin-lattice relaxation times of protons in $(CH_3NH_3)_2TeI_6$ against T below 70 K.
●: 20 MHz and △: 60 MHz.

are much greater than that expected for the classical C_3 reorientation. The second moment, evaluated from the solid-echo envelope,[17] was 9.5 ± 1.5 G^2 even at 4.2 K. This value is much smaller than the theoretical one of 29.8 G^2 for the MA^+ ion in its stationary state, but close to that for the rapidly reorienting MA^+ ion about its C_3-axis.[5] Additionally, the linear portion of the high-temperature side of the deep T_1 minima gives a very low E_a value of 2.7 kJ/mol. All of these results suggest the existence of tunneling-assisted relaxation in the present system.[18] Considering the transitions among tunneling sublevels in the torsional states of the CH_3 or NH_3 groups, Haupt proposed the following expression of the relaxation rate:[19]

$$T_1^{-1} = AJ(\omega_t \pm n\omega_0) = \frac{A\tau}{1+(\omega_t \pm n\omega_0)^2\tau^2}, \quad (4)$$

where A is a constant, ω_t is the tunnel-splitting frequency, and $n=1$ or 2. If $\omega_t \gg \omega_0$, the relaxation rate due to the intramolecular dipolar coupling associated with $J(\omega_t \pm n\omega_0)$ becomes frequency-independent, while the rate due to the intermolecular one is of the usual BPP type.[20] Therefore, two T_1 minima should be observed, one at $\omega_t\tau=1$ and the other at $\omega_0\tau=0.62$. The T_1 minima in Fig. 7 are frequency-dependent, but to a lesser extent than would be expected from the BPP theory; that is, the ratio, $(T_{1\,\mathrm{min}})^{60\,\mathrm{MHz}}/(T_{1\,\mathrm{min}})^{20\,\mathrm{MHz}}$, which is equal to 3 in the classical dipolar relaxation, is less than 2 in the present case. Although this T_1 behavior can be explained qualitatively in terms of $J(\omega_t \pm n\omega_0)$, it is difficult to deduce the tunneling frequency because two spin systems (CH_3 and NH_3) complicate the problem and because it has not been established that all the MA^+ ions are equivalent in LTP. It is desirable to measure the T_1 and $T_{1\rho}$ of selectively deuterated CH_3ND_3 or CD_3NH_3 salts as well as to determine the crystal structure of LTP.

The activation energy, E_a, for the MA reorientation changes greatly with X in $(MA)_2TeX_6$, as Table 1 shows. The order of the E_a values is the same as that of the electronegativity of halogens in the complex ions. Quite a similar inclination of the E_a value was discussed above for $(MA)_2MCl_6$ with M=Pt, Sn, and Te. Therefore, the differences in the potential barrier among the present tellurium compounds may be determined mostly by the electrostatic interaction between NH_3 groups and halogens in complex ions.

By fitting the experimental points between 110 and 42 K to Eq. 3 ($\omega_0\tau_1 \ll 1$), the shallow T_1 minimum for the motion specified by τ_2 is determined to be 490 ms at 20 MHz. This value is comparable to those of the other MA-compounds and also to the calculated one for the uncorrelated rotation of the MA^+ ion.[5] The E_a value of 5.0 kJ/mol, however, is significantly smaller than those (8—9 kJ/mol) of the others. The difference in E_a seems to be large in contrast with our estimate of a nearly constant energy.[5] Therefore, it may be acceptable to consider that some other relaxation processes, for example, a tunneling or 180° flip of the MA^+ ion, exist in this temperature range in addition to that of the foregoing two motional modes. It may be also plausible to anticipate that the geometry of the MA^+ ion in the present complex is not the same as that in the earlier complexes because of the difference in interionic interactions or packing of the ions in the crystal.

In RTP, the log T_1 value decreases linearly with $1/T$ from room temperature to T_t; the slope of the decrease gives the E_a value of 6.1 kJ/mol. Since the crystal structure is cubic and the proton second moment is only 0.5 G^2 in this phase, this relaxation process is ascribable to the overall reorientation of the dumbbell-like cation.

The observed values of the proton $T_{1\rho}$, on the other hand, behave unusually in RTP. Contrary to the $T_{1\rho}$ expression based on the BPP theory, the $T_{1\rho}$ minimum at the r.f. strength, H_1, of 5 G appeared at a higher temperature than that of the $T_{1\rho}$ at 10 G. Furthermore, on the high-temperature side of both

$T_{1\rho}$ minima, the $T_{1\rho} \propto H_1^2$ relation holds for the six observed $T_{1\rho}$ values in the H_1 range of 2.5—15 G. Such anomalous behavior suggests an intermolecular dipolar relaxation of the second kind between the protons and iodine nuclei.[21] The overall rotation of the MA^+ ion may result in a large fluctuation of the EFG at the site of iodine, in contrast to its C_3 reorientation, which affects the EFG only slightly. This fluctuation shortens the iodine spin-lattice relaxation time $T_1(I)$. Thus, the dipole interaction between the protons and iodine nuclei affects the proton $T_{1\rho}$ through the cross relaxation. This type of relaxation is expressed as follows:[22]

$$T_{1\rho}^{-1} = M_2(\text{H-I})\gamma_H^2 T_1(I)/[1+\omega_1^2 T_1(I)^2], \quad (5)$$

where M_2(H–I) is the proton second moment due to the H–I dipole interaction and where $\omega_1 = \gamma_H H_1$. The value of M_2(H–I) was estimated to be 0.078 G^2 from the $T_{1\rho}$ minimum. Then, the $T_1(I)$ value was obtained by substituting the known parameters into Eq. 5. The results are also included in Fig. 6. It may be noted that the $T_1(I)$ of 50 μs at room temperature shortens with decreasing temperature, while retaining the same slope as that of the proton T_1 above T_t. This finding is strong evidence for the idea that the proton $T_{1\rho}$ is governed by the proton–iodine interaction modulated *via* the overall reorientation of the MA^+ ion. On a lowering of the temperature, the $T_1(I)^{-1}$ becomes large beyond the order of the usual NQR linewidth. This is a reason why the NQR signal fades out below 156 K.[7]

The authors are grateful to Professor Emeritus Ryôiti Kiriyama of Osaka University and Professor Daiyu Nakamura of Nagoya University for their continued interest and encouragement.

References

1) R. W. G. Wyckoff, *Am. J. Sci.*, **16**, 349 (1928).
2) Y. Kume, R. Ikeda, and D. Nakamura, *J. Magn. Reson.*, **20**, 276 (1975).
3) Y. Kume, R. Ikeda, and D. Nakamura, *J. Magn. Reson.*, **33**, 331 (1979).
4) Y. Furukawa, H. Kiriyama, and R. Ikeda, *Bull. Chem. Soc. Jpn.*, **50**, 1927 (1977).
5) R. Ikeda, Y. Kume, D. Nakamura, Y. Furukawa, and H. Kiriyama, *J. Magn. Reson.*, **24**, 9 (1976).
6) K. Kitahama, H. Kiriyama, and Y. Baba, *Bull. Chem. Soc. Jpn.*, **52**, 324 (1979).
7) Y. Kume, R. Ikeda, and D. Nakamura, *J. Phys. Chem.*, **82**, 1926 (1978).
8) K. Kitahama and H. Kiriyama, *Acta Crystallogr., Sect. A*, **34**, S302 (1978).
9) D. Brinkmann and W. Freudenreich, *Z. Kristallogr. Kristallgeom. Kristallphys. Kristallchem.*, **143**, S67 (1976).
10) J. van Kranendonk, *Physica.*, **20**, 781 (1954).
11) M. Goldman, "Spin Temperature and Nuclear Magnetic Resonance in Solids," Oxford Univ. Press, England (1970), Chap. 3.
12) H. M. Van Driel, M. Wiszniewska, B. M. Moores, and R. L. Armstrong, *Phys. Rev. B*, **6**, 1596 (1972).
13) M. Wiszniewska and R. L. Armstrong, *Can. J. Phys.*, **51**, 781 (1973).
14) D. E. Woessner, *J. Chem. Phys.*, **42**, 1855 (1965).
15) S. Albert and J. A. Ripmeester, *J. Chem. Phys.*, **58**, 541 (1973).
16) P. S. Allen and S. Clough, *Phys. Rev. Lett.*, **22**, 1351 (1969).
17) J. G. Powles and J. H. Strange, *Proc. Phys. Soc.*, **82**, 6 (1963).
18) P. S. Allen, *J. Chem. Phys.*, **48**, 3031 (1968).
19) J. Haupt, *Z. Naturforsch., Teil A*, **26**, 1578 (1971).
20) W. Güttler and J. U. Von Schültz, *Chem. Phys. Lett.*, **20**, 133 (1973).
21) R. Blinc, J. Pirš, and S. Žumer, *Phys. Rev. B*, **8**, 15 (1973).
22) N. Bloembergen and P. P. Sorokin, *Phys. Rev.*, **110**, 865 (1958).

Adsorption of *N*-Dodecyl-β-alanine to the Spread Monolayer of Lecithin or Dilaurin

Kazuo Tajima* and Takao Tsutsui

Department of Chemistry, Faculty of Science, Tokyo Metropolitan University, Setagaya-ku, Tokyo 158

(Received May 6, 1980)

The adsorption of *N*-dodecyl-β-alanine (NDA) was studied at the air–solution interface with the spread film of L-α,β-dimyristoyllecithin (DML) or α,α′-dilaurin (DIL). The adsorbed amounts were measured by radiometry using tritium-labelled NDA, combined with surface pressure measurements. Measurements of IR, DSC, and NMR were made in order to determine the bulk properties of amphoteric moieties in the mixture of DML and NDA. For the mixed monolayer of NDA and DML or DIL, the surface composition *vs.* area curves were obtained at various surface pressures. The molecular interaction in monolayer was discussed on the basis of the excess free energy of mixing, which was calculated at various surface pressures and compositions. As a result, the mixing of DIL and NDA in monolayer was ideal at surface pressures less than 5 mN m^{-1}, whereas the mixed monolayer of DML and NDA showed a remarkable condensation in surface molecular area. Such a large condensation at low surface pressure was concluded to be due to the formation of ion pairs between the choline and alanine moieties on the water surface, by referring to the findings obtained by studying the lipid properties in the bulk phase. It was also found that the DML–NDA monolayer near close packing exhibited various types of complicated behavior, depending on the surface compositions. The appreciable differences in the nature of the amphoteric moieties in DML and NDA molecules can explain these findings.

Studies of the monolayer behavior of phospholipids on the surface of surfactant solution are very useful for understanding some of the actions of surfactant on the biomembrane. Nevertheless, few studies on the interaction of membrane lipids with surfactant have been performed, due to some experimental and theoretical restrictions. Studies of mixing in the insoluble lipid films[1] or of binding properties of lipid and metallic ions[2] are more numerous. The thermodynamic approach to analyzing the nature of penetrated films must be based on precise information about the monolayer composition, especially for the penetrated films with the ionic interactions between the polar groups of lipids.[3] Recently, Hendrikx, and Ter-Minassian-Saraga,[4] who studied the adsorption of a cationic surfactant to a lecithin monolayer, found that the mixed monolayer formed a stable two-dimensional micelle on the water surface. The use of ionic surfactant as penetrant, however, would not be convenient for the thermodynamic analysis of the monolayers, because it is almost impossible to distinguish the hydrophobic interaction in the penetrated monolayer with the ionic interaction caused by the surfactant (and/or spread) film ions and their gegen ions.

In the present study, experiments are carried out on the spread monolayer of lecithin and dilaurin into which an ampholytic surfactant is penetrated. By determining the adsorbed amounts by radiometry, attempts are made to elucidate the behavior of the penetrated monolayers as a function of the surface composition or the surface pressure. Further, the work is discussed about the interaction between the polar groups of lecithin and surfactant in monolayer, combined with the observations on their mixtures in the bulk phase.

Experimental

Materials. After the usual purifications, L-α,β-dimyristoylphosphatidyl choline (DML), which had been purchased from Fluka Co., showed a single spot in the TLC analysis. Dilaurin (DIL), *i.e.* glycerol α,α′-dilaurate, was purified by the recrystallization with hexane. *N*-Dodecyl-β-alanine (NDA), *i.e.* 3-(dodecylammonio)propionate, was employed as an ampholytic surfactant. For the radiometry, the alkyl chain in NDA was labelled with tritium.[5] The solution was prepared by using water which was distilled thrice after being refluxed with acidic permanganate solution overnight. Chloroform and hexane were used for the spreading solvent.

Measurements of Surface Properties. Adsorbed amounts of NDA were determined by the radiotracer method. The radioactivity of tritium β-rays at the air–solution interface was detected by a plastic scintillation counter.[6] Equilibrium surface tension was measured by the Wilhelmy plate method. All measurements were made at 30±0.5 °C, above the gel-liquid transition temperature of DML on the water surface.[7] The pH of the solution was at 5.8±0.2 throughout the experiments: at this value NDA[8] and DML[9] in water possess an amphoteric structure.

Preliminary experiments indicated that the surface pressure *vs.* mean molecular area curves which were obtained by the compression method, coincided well with those obtained by the successive additions of spread solution onto the water surface. All the spread monolayers used in present work, then, were formed by the addition method on the solution surfaces at which NDA had already been adsorbed.

Measurements of Bulk Properties. In order to elucidate the polar interaction between DML and NDA in the bulk state, DSC, IR, and NMR measurements were carried out. In the DSC measurements (Rigaku Denki 8056), the lipids were mixed up well in an aluminium DSC pan with chloroform, allowed to stand overnight *in vacuo* to evaporate the solvent, and sealed in nitrogen gas. The measurements were made as a function of mole fraction of NDA. The specimen for the IR measurement (Hitachi EPI G-2) was prepared in the same manner as that used in the DSC analyses. The absorption spectra were taken as functions of the temperature and mole fraction by the Nujol method. The NMR spectra (JEOL FX-100) were also taken for the 0.1 mol dm^{-3} deuteriochloroform solutions of DML, NDA, and their equimolar mixture at 25 °C.

Results and Discussion

Figure 1 shows the relationship between the surface pressure, π, and spread amount, Γ_1, of DML or DIL

monolayer formed on the solution surface of NDA at various concentrations. Figure 2 exhibits the plot of the surface excess, Γ_2, of NDA against the spread amounts of DML or DIL. The subscripts 1 and 2 mean the film-forming substance and surfactant, respectively. In Fig. 2-b, a little hump was observed on the desorption isotherms of NDA at the intermediate region of concentrations, upon spreading small amounts of DML. This means that DML strongly interacts with the adsorbed NDA on the water surface. On the other hand, the isotherms of NDA for the DIL films simply decreased with increasing spread amounts for all concentrations studied. Thermodynamical discussion for these adsorption isotherms will be made elsewhere.

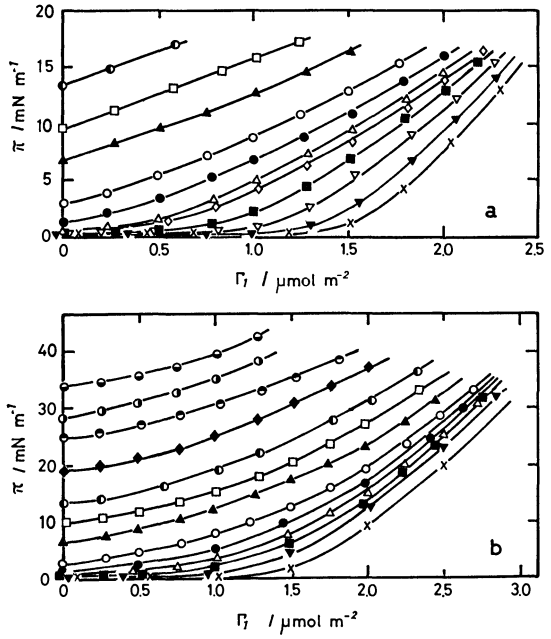

Fig. 1. π *vs.* Γ_1 curves for DIL–NDA (a) and DML–NDA (b) at the following concentrations of NDA ($10^5\ C_2$/mol dm^{-3}).
×: 0, ▼: 0.10, ▽: 0.20, ■: 0.30, ◇: 0.40, △: 0.50, ●: 0.70, ○: 1.0, ▲: 2.0, □: 3.0, ◐: 5.0, ◆: 10, ◓: 20 ◑: 30, ◒: 50.

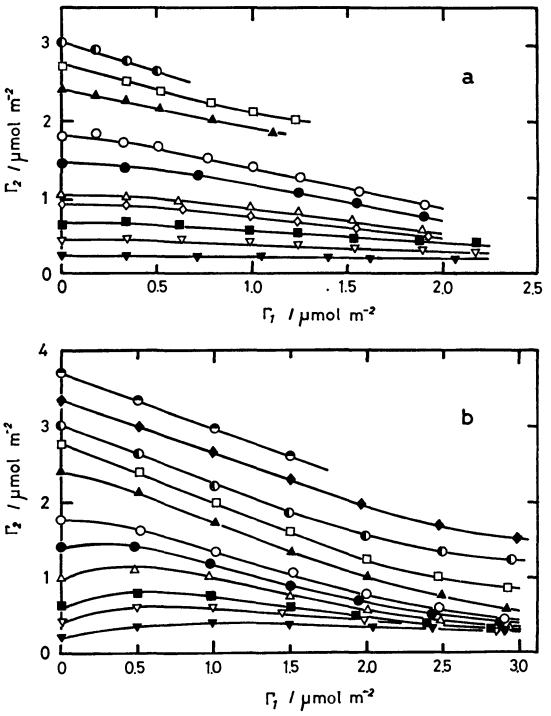

Fig. 2. Γ_1 *vs.* Γ_2 curves for DIL–NDA (a) and DML–NDA (b) at various concentrations of NDA. Signs for each curve are identical with those of Fig. 1 independently of (a) and (b) curves.

Miscibility of Monolayers. Before studying the properties of the penetrated monolayers, the miscibility in monolayer was examined for the DML–NDA and DIL–NDA systems. According to the two-dimensional phase rule,[10] two degrees of freedom are available for one surface phase at constant temperature and pressure in the present systems. Thus the criterion of miscibility is easily made from the relationship in surface pressure and surface fraction at constant total amounts of the monolayers, whose fraction may be chosen by variation in amounts of the spread films and bulk concentration. Here, the surface fraction of NDA, X_2, in the monolayer was obtained by dividing Γ_2 by Γ_t, which was a sum of Γ_1 and Γ_2. The results are shown in Fig. 3. Consequently, the monolayers of both systems were confirmed to be miscible in all surface fractions. In mixing of DML and NDA, there was no indication of the occurrence of a phase separation such as has been observed in mixing of DML and cholesterol on the water surface adsorbed from the dispersed solution.[11]

Area Condensation in Monolayer. The plot of mean molecular area, A, against X_2 in the mixed monolayers of DML–NDA or DIL–NDA is shown at various surface pressures in Fig. 4. The mixing of DIL and NDA in the monolayer was almost ideal at surface pressures lower than 5 mN m^{-1}, but allowed a slight condensation in surface molecular area when surface pressure increased, and approached to the equilibrium spreading pressure of DIL (16.6 mN

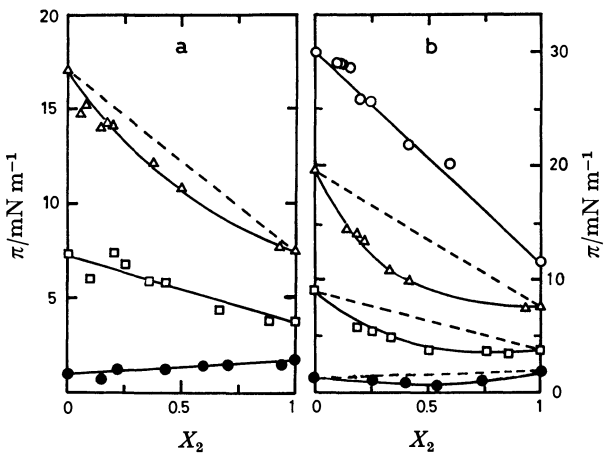

Fig. 3. π *vs.* X_2 curves for DIL–NDA (a) and DML–NDA (b) at the following constant surface excess (Γ_t/μmol m^{-2}).
●: 1.5, □: 2.0, △: 2.5, ○: 3.0,

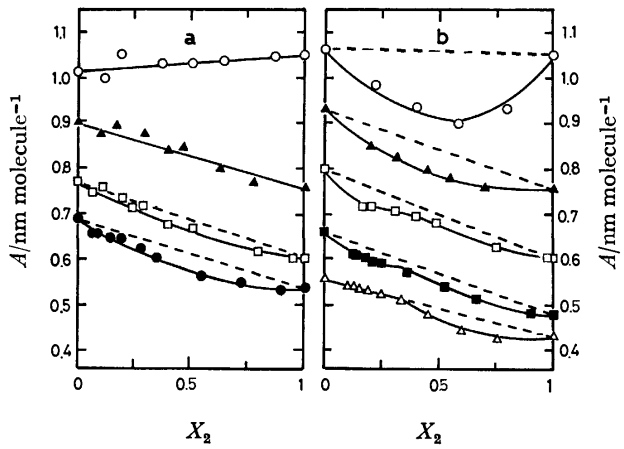

Fig. 4. A *vs.* X_2 curves for the DIL–NDA (a) and DML–NDA (b) monolayers at various surface pressures (π/mN m^{-1}).
○: 2, ▲: 5, □: 10, ●: 15, ■: 20, △: 30.

m^{-1}). Since the mixing of DIL and NDA does not include the process of interionic interaction, the area condensation observed can be considered to arise mainly from the van der Waals interaction in hydrocarbon chains. On the other hand, the mixing in DML and NDA monolayers is likely to depend in a complicated way on the surface pressure and compositions: for instance, there is the remarkable deviation from the additivity in molecular area at low surface pressure, and also a characteristic kink appears at about 0.3 fraction of NDA, as may be seen in Fig. 4-b. Such behavior in mixing cannot be explained without taking into account the interactions between polar groups as well as hydrocarbon chains in the monolayers. Because both the choline moiety in DML and alanine moiety in NDA possess an amphoteric structure under the conditions of the present work, the ionic interaction can be supposed to occur directly between these moieties. In order to confirm the occurrence of such a binding, some experiments were carried out on the mixture of DML and NDA in the bulk phase.

Confirmation of Ionic Binding of DML and NDA in the Bulk Phase. *DSC Analysis*: The endothermic peak at 63.5 °C was found independently of the mole fraction of the mixture. The plot of the heat of transition at 63.5 °C *vs.* the composition is shown in Fig. 5. Since no peaks are observed at 63.5 °C for each single component, the endothermic peak observed seems to be due to the formation of intermolecular compounds in the DML and NDA mixture. The heat of the corresponding transition was endothermically 20.1 kJ mol^{-1} without any medium.

IR Analysis: IR absorption for the ethyl group in the gauche structure of β-alanine appears at 860 cm^{-1}.[12] Thus, the IR spectra for the mixture of DML and NDA were measured at the various temperatures and compositions. The spectra from 780 to 940 cm^{-1} are shown in Fig. 6. For the equimolar mixture the gauche structure almost disappears near the temperature at which the endothermic peak has been found by the DSC measurement. On 68.4% NDA

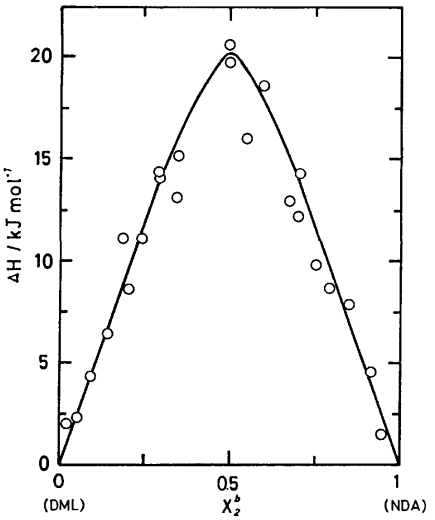

Fig. 5. Heat *vs.* NDA fraction, X_2^b, curve relation to endothermic peaks at 63.5 °C by DSC analysis for DML–NDA mixture.

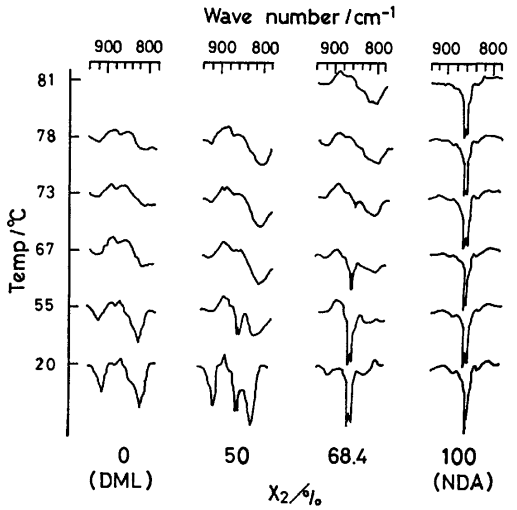

Fig. 6. IR spectra from 780 to 940 cm^{-1} for DML–NDA mixture at various temperatures and compositions.

mixture, however, the corresponding absorption was still observed at 73 °C. This signifies that NDA molecules in more than equimolar quantities exist in the mixture as single molecules. The reason is that the absorption at 860 cm^{-1} for pure NDA remains unchanged while the temperature is increased up to the melting point of NDA, except for the negligible temperature dependence of absorption intensity for each group. It may be concluded that the mixture of DML and NDA converts into an intermolecular compound of 1:1 by heating.

NMR Spectrum: In order to elucidate the contribution of the polar groups to the formation of ionic binding, measurements were made on proton chemical shift for DML, NDA, and their equimolar mixture in the deuteriochloroform solutions. Table 1 shows the proton chemical shift before and after mixing of the DML and NDA solutions. By mixing, $-N^+H_2-$ spectrum of NDA shifted towards the low field, while

TABLE 1. PROTON CHEMICAL SHIFT FOR POLAR GROUPS OF DML, NDA, AND THE EQUIMOLAR MIXTURE IN $CDCl_3$ (ppm) (REFERENCE TMS, 25 °C, 100 MHz)

Groups	DML	NDA	Mixture	$\Delta\delta$[a]
$=N^+H_2$		−8.751	−6.106	+2.65
$-CH_2COO^-$		−2.577	−2.587	−0.01
$\equiv P^-OCH_2-$	−4.118		−4.341	−0.22
$-N^+(CH_3)_3$	−3.340		−3.333	+0.01

a) $\Delta\delta$: Differences of proton chemical shift.

$\equiv P^--O-CH_2-$ spectrum of DML was oppositely shifted towards the high field. However, no difference in chemical shifts was observed for other groups in these compounds within the experimental error (±0.002 ppm). This indicates that the ionic interaction in solution takes place only between the $\equiv P^--O-CH_2-$ group of DML and the $-N^+H_2-$ group of NDA.

From all these experiments, we may conclude that the molecules of DML and NDA, whose polar groups possess both amphoteric structures, form stoichiometrically an intermolecular salt when their mixture is dissolved in a polar solvent or heated up to about 63.5 °C. This may imply the favorable formation of ionic binding with 1:1 of DML and NDA in the penetrated monolayer, provided that the ionic properties of the lipids do not change essentially between the surface and the bulk phases.

Effects of Polar Groups on "Condensing." The condensation at high surface pressure in Fig. 4-b cannot be explained by only the formation of the DML(1):NDA(1) complex as found in the bulk phase. In order to elucidate the unique mixing of DML and NDA in monolayer, one must take into account the difference in the behavior of their polar groups, which depends on the surface pressure and the surface composition. Then the excess free energy of mixing Δg^v, defined by Goodrich,[13] was calculated at 2:1, 1:1, and 1:2 surface compositions at various surface pressures for the DML–NDA and DIL–NDA monolayers. The results are shown in Table 2. A clear difference was found in the mixing behavior of these monolayers. For DML and NDA monolayers, considerably large Δg^v values were appraised even at low surface pressure, compared to those for DIL and NDA monolayer. Since the behavior of hydrocarbon chains in the mixed monolayers is regarded as to be almost

TABLE 2. SURFACE PRESSURE DEPENDENCE OF Δg^v ($-J\,mol^{-1}$) AT CONSTANT SURFACE COMPOSITIONS

π	DML-NDA			DIL-NDA		
$mN\,m^{-1}$	0.33	0.50	0.66	0.33	0.50	0.66
2	134	182	169	0	0	0
5	138	159	154	0	0	0
6	159	87	86	11	12	11
10	218	148	151	96	120	97
15	244	235	235	307	372	307
20	216	325	337			
25	135	421	550			
30	0	543	795			

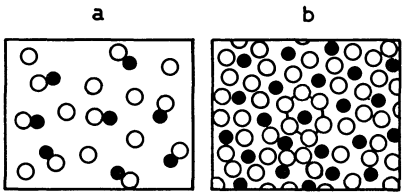

Fig. 7. Schematic representations for mixed monolayer of 2:1 of DML(○) and NDA(●) at low (a) and high (b) surface pressures.

the same between DML–NDA and DIL–NDA, such large values may be considered to be due to the occurrence of ionic binding between DML and NDA in monolayer, as depicted in Fig. 7-a. This consideration coincides with the conclusion obtained in the bulk experiments mentioned above.

The properties of mixed monolayer at high surface pressure are discussed. In the equimolar mixed monolayer at 6 mN m^{-1} the Δg^v values attain a minimum. This is explained by two different origins for the interactive energies caused in mixing: namely, one comes from the ionic binding between polar groups in monolayers and is seen in the low surface density, while the other arises from the condensation between hydrocarbon chains and increases with increasing monolayer density, as may be expected from the Δg^v values for the DIL–NDA system. The surface pressure dependence of Δg^v in the 0.33 fraction monolayer is also interpretable in view of the interaction between the ampholytic moieties of DML and NDA. With increasing film density, the mixed monolayer in all cases is considered to form an ionic network structure which would be more stable rather than remaining in the pair binding of DML(1):NDA(1). Structural formation in monolayer has been also found by Ter-Minassian-Saraga for the mixed monolayer of DML and hexadecyltrimethylammonium chloride.[4] Such a phenomenon turns out to make a unique kink on the A *vs.* X_2 curves in Fig. 4, because the structural monolayer is probably less compressible. A model of mixing at DML(2):NDA(1) composition at high surface pressure is depicted in Fig. 7-b. In DML and cholesterol system, however, the formation of molecular complex of DML(2):CHOL(1) at the surface[11] and bulk[14] phases has been confirmed. Approaching the close packing at about 30 mN m^{-1}, the monolayer which makes a two-dimensional structure becomes so relatively tight and incompressible that the whole system apparently behaves as an ideal one. At 0.66 fraction of NDA the mixed monolayer, however, still keeps the tendency to condense. This is probably because the ionic network structure is gradually broken down by the increases of NDA fraction in the monolayer: the monolayer finally consists of the mixture of DML(1):NDA(1) binding and NDA. Because the dissociation constants of both ampholites at the water surface are $pK_a=3.5$ and $pK_b=3.11$ for NDA[8] and $pK_a=3.32$ and $pK_b=3.55$ for DML[9] at 30 °C, the β-alanine moiety in NDA is considered scarcely to dissociate in water and then to make a hydrated ring structure, compared to the choline moiety in DML. Eventually, NDA molecules in mixed monolayer at

high fraction of NDA tend to be present with the nature like nonionic molecules. Therefore, the maximum condensation occurs at about 0.66 fraction, corresponding to the equimolar mixture of DML–NDA ion pair and NDA. The complicated bahavior in mixing at high surface pressure results from the difference characters in the ampholytic moieties of DML and NDA.

References

1) F. Paltauf, H. Hauser, and M. C. Phillips, *Biochim. Biophys. Acta*, **249**, 539 (1971); D. Ghosh and J. Tinoco, *ibid.*, **266**, 41 (1972).

2) F. Vilallonga, M. Fernandez, C. Rotunno, and M. Cereijido, *Biochim. Biophys. Acta*, **183**, 98 (1969); G, Colacico, *Chem. Phys. Lipids*, **10**, 66 (1973).

3) M. Muramatsu, "Surface and Colloid Science," ed by E. Matijevic, Wiley-Interscience, New York (1973), Vol. 6, p. 137.

4) Y. Hendrikx and L. Ter-Minassian-Saraga, *Adv. Chem. Ser.*, **144**, 177 (1975).

5) T. Okumura, A. Nakamura, K. Tajima, and T. Sasaki, *Bull. Chem. Soc. Jpn.*, **47**, 2996 (1974).

6) K. Tajima, M. Muramatsu, and T. Sasaki, *Bull. Chem. Soc. Jpn.*, **43**, 1991 (1970).

7) N. L. Gershfeld and K. Tajima, *J. Colloid Interface Sci.*, **59**, 597 (1977).

8) A. Nakamura, K. Tajima, and T. Sasaki, *Bull. Chem. Soc. Jpn.*, **48**, 214 (1975).

9) M. M. Standish and B. A. Pethica, *Trans. Faraday Soc.*, **64**, 1113 (1968).

10) D. J. Crisp, "Surface Chemistry," Supplement to Research, Butterworths, London, (1949), pp. 17 and 23.

11) K. Tajima and N. L. Gershfeld, *Biophys. J.*, **22**, 489 (1978).

12) M. Tsuboi and T. Takenishi, "IR Absorption Spectra," Nankoh-Do (1959), Vol. 7, p. 56.

13) F. C. Goodrich, Pro, Intern. Congr. Surface Activity, 2nd, I, 85 (1957).

14) N. L. Gershfeld, *Biophys. J.*, **22**, 469 (1978).

Adsorption of *N*-Dodecyl-β-alanine at the Air-Solution Interface with the Spread Monolayer of Lecithin or Dilaurin. I. Adsorption Isotherms

Takao Tsutsui and Kazuo Tajima*

Department of Chemistry, Faculty of Science, Tokyo Metropolitan University, Setagaya-ku, Tokyo 158

(Received May 28, 1980)

The applicability of the Gibbs adsorption isotherm was examined for the adsorption of *N*-dodecyl-β-alanine (NDA) at the air–solution interface with the spread monolayer of lecithin (DML) or dilaurin (DIL). In order to derive adsorption isotherms, the spread monolayer was treated energetically as a part of the adsorbed monolayer. The isotherms were derived for the following cases: (a) a nonideal mixing of the spread and adsorbed molecules and (b) a nonideal adsorption associated with a conformational change due to the complex formation between monolayer molecules. The isotherm derived for case (a) coincided with the observed isotherm of NDA adsorbed into the DIL monolayer, but deviated from the observed isotherm of NDA adsorbed into the DML monolayer. The DML–NDA isotherm was regarded as to be explained by the isotherm derived for case (b). Further, the applicability of the Pethica's isotherm to the adsorption of NDA in both systems was examined.

Some adsorption isotherms of *N*-dodecyl-β-alanine, which adsorbs at the solution surface with the spread monolayer of lecithin or dilaurin, have been reported in the previous paper.[1] From the radiometrical determination of the adsorbed amount, the properties of both mixed monolayers have been described in detail as a function of suface composition or surface pressure. It was clear that the surfactant remarkably condensed with dilaurin or lecithin in monolayer. For such adsorption systems, however, the adsorbed amount of surfactant is expected to obey the Gibbs adsorption isotherm, such as for adsorption of surfactant at the air–solution interface.[2] Pethica[3] and McGregor and Barnes[4] have derived adsorption isotherms by assuming the accessible area for the adsorbing species in the monolayer. However, they are no unique isotherms applicable to every type of adsorption, because each set has been derived under the particular conditions of the highly condensed film of spread monolayer.

In the present study, attempts are made to elucidate the applicability of the Gibbs adsorption isotherm to the adsorption of surfactant at the air–solution interface with the insoluble film. The derivation of isotherms is achieved for the following cases: (a) a nonideal mixing of the spread and adsorbed molecules, and (b) a nonideal adsorption associated with a conformational change of the monolayer molecules. The interaction in the monolayer is introduced as the excess free energy instead of the partial molar surface area in the isotherm. The validity of the isotherms obtained are tested by comparison with the observed isotherms.

Theory

The Gibbs adsorption isotherm for the air–solution interface with spread film (1) and surfactant (2), is given at a constant temperature, assuming that the water surface is taken as the dividing surface:

$$-\mathrm{d}\gamma = \Gamma_1 \mathrm{d}\mu_1^{\mathrm{s}} + \Gamma_2 \mathrm{d}\mu_2^{\mathrm{b}}, \tag{1}$$

where γ denotes the surface tension and Γ_i and μ_i the relative surface excess per unit area and chemical potential for component i, respectively. Superscripts s and b mean the surface and bulk phases. Since the surface tension can be varied with the amount of spread film independently of the chemical potential of surfactant in the bulk phase, the adsorption of the surfactant is considered only for the solution surface which is covered with a fixed amount of spread film. When the spread and adsorbed monolayers coexist on the solution surface A_t of the surfactant of concentration C_2 at surface pressure π, the effective surface area A_2 available for the adsorption decreases by the surface area A_1 occupied by the spread monolayer. As long as the adsorbed monolayer is present in the same surface pressure, μ_2^{s} is equal to μ_2^{b}, so that the spread and adsorbed monolayers may be related by:

$$\mathrm{d}\mu_1^{\mathrm{s}} = \frac{a_1}{a_2}\mathrm{d}\mu_2^{\mathrm{b}}, \tag{2}$$

where a_i denotes the molar surface area of component i in each monolayer. Therefore, the contribution of spread film to the surface energy may be taken into account as a part of the adsorbed monolayer of the surfactant. Using Eq. 2, Eq. 1 is rewritten for the case of ideal penetration as follows:

$$-\mathrm{d}\gamma = \frac{a^{\mathrm{id}}}{a_2}(\Gamma_1+\Gamma_2)\mathrm{d}\mu_2^{\mathrm{b}}, \tag{3}$$

where $a^{\mathrm{id}}=X_1a_1+X_2a_2$, and X_i is the mole fraction of Γ_i.

If the adsorption is nonideal, the following two cases are taken into account: (a) nonideality in the simple mixing of spread and adsorbed molecules, and (b) nonideality in the case that the standard chemical potentials of the spread and/or adsorbed molecules alter due to the change in the conformation of their polar groups by complex formation, chemical reaction, or denaturation in monolayer.

In Case (a). The surface tension change is defined as follows:

$$\mathrm{d}\gamma = \mathrm{d}\gamma^{\mathrm{id}} + \mathrm{d}\gamma^{\mathrm{v}}, \tag{4}$$

where $\mathrm{d}\gamma^{\mathrm{id}}$ is given by Eq. 3. The $\mathrm{d}\gamma^{\mathrm{v}}$ term is the change of surface tension caused by the nonideal mixing of the spread and the adsorbed molecules. From Goodrich's convention for estimating the excess free energy of mixing,[5] we obtain:

$$\mathrm{d}\gamma^{\mathrm{v}} = \frac{\Delta a}{a}\mathrm{d}\gamma, \tag{5}$$

where $\Delta a=a-a^{\mathrm{id}}$, and a is real molar surface area measured by experiment. Substituting Eq. 5 into 4,

we obtain

$$d\gamma = \left(1-\frac{\Delta a}{a}\right)^{-1} d\gamma^{id} \simeq \left(1+\frac{\Delta a}{a}\right) d\gamma^{id} \quad (6)$$

by neglecting higher terms in the expansion with respect to $\Delta a/a$. For the nonideal adsorption, from Eqs. 3 and 6 we obtain:

$$-d\gamma = \frac{a^{id}}{a_2}(\Gamma_1+\Gamma_2)(d\mu_2^b + d\Delta\xi^v), \quad (7)$$

where $d\Delta\xi^v=(\Delta a/a)d\mu_2^b$. Hence, $\Delta\xi^v$ means the excess free energy arising from the nonideal adsorption of a surfactant. Then $d\Delta\xi^v$ may be equated with $(a_2/a^{id})RTd\ln f^v$ thermodynamically; here f^v is the surface activity coefficient at mixing. When $\Delta a=0$ or $f^v=1$, Eq. 7 is reduced to Eq. 3.

Consequently, when the activity coefficient of surfactant in the bulk phase is assumed to be unity,[6] from Eq. 7 Γ_2 is given by:

$$\Gamma_2 = \frac{\left[\frac{-\partial\gamma}{RT\partial\ln C_2}\right]_{\Gamma_1}}{\left[\frac{a^{id}}{a_2}\right]_{\Gamma_1}+\left[\frac{\partial\ln f^v}{\partial\ln C_2}\right]_{\Gamma_1}} - \Gamma_1. \quad (8)$$

In Case (b). We define an equation similar to Eq. 4 as follows:

$$d\gamma = d\gamma^{id} + d\gamma^v + d\gamma^c, \quad (9)$$

where $d\gamma^c$ denotes the surface tension change caused by an alteration in the molecular structure owing to the complex formation or chemical reaction in the monolayer. The $d\gamma^c$ term can not be experimentally separated from the $d\gamma^v$ term, because both are functions of surface compositions of the film. We assume, in this case, that $d\gamma^v$ defined by Eq. 5 refers only to the nonideal mixing of film-forming molecules, after the complex formation or chemical reaction has been completed. Eventually, we have the following equation, analogous to Eq. 7:

$$-d\gamma = \frac{a^{id}}{a_2}(\Gamma_1+\Gamma_2)(d\mu_2^b + d\Delta\xi^v + d\Delta\xi^c), \quad (10)$$

where $d\Delta\xi^c(=(a_2/a^{id})RTd\ln f^c)$ denotes the change of excess free energy resulting from the alteration in the molecular structure due to complex formation. Finally, the adsorbed amount is estimated by:

$$\Gamma_2 = \frac{\left[\frac{-\partial\gamma}{RT\partial\ln C_2}\right]_{\Gamma_1}}{\left[\frac{a^{id}}{a_2}\right]_{\Gamma_1}+\left[\frac{\partial\ln f^v}{\partial\ln C_2}\right]_{\Gamma_1}+\left[\frac{\partial\ln f^c}{\partial\ln C_2}\right]_{\Gamma_1}} - \Gamma_1. \quad (11)$$

The validity of Eqs. 8 and 11 is experimentally tested later.

Experimental

The monolayer of L-α,β-dimyristoyllecithin (DML) or α,α'-dilaurin (DIL) was formed by spreading on the aqueous solution surface of *N*-dodecyl-β-alanine (NDA), *i.e.* 3-(dodecylammonio)propionate. The adsorbed amount was determined by the radiotracer method, using tritiated NDA. Surface tension was registered by the Wilhelmy plate method. The experiments and procedures to measure the surface excess and surface tension have been reported in the preceding paper.[1] All measurements were made at 30±0.2 °C.

Results and Discussion

Figure 1 shows the plots of surface pressure *vs.* bulk concentration of the surfactant solution at various spread amounts of DIL or DML. Figure 2 exhibits the adsorption isotherms of NDA measured by the

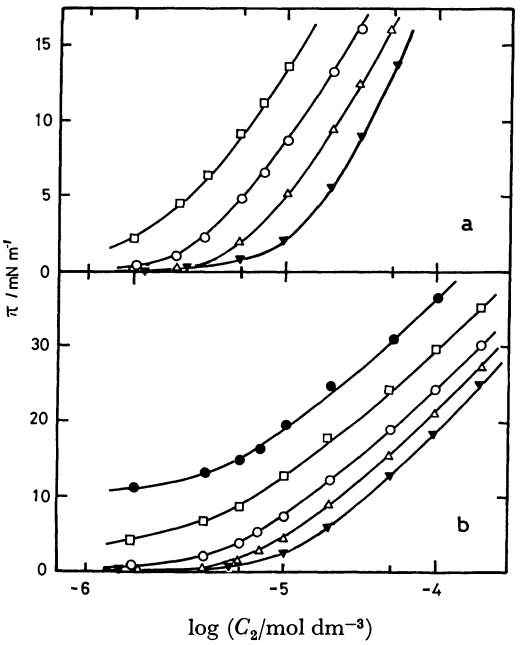

Fig. 1. π *vs.* C_2 curves for DIL–NDA (a) and DML–NDA (b) at various spread amounts (Γ_1/μmol m^{-2}). ▼: 0, △: 0.5, ○: 1.0, □: 1.5, ●: 2.0.

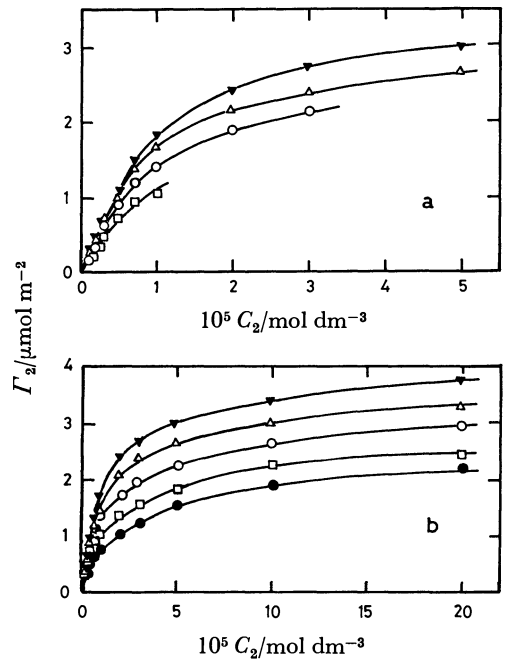

Fig. 2. Adsorption isotherms of NDA measured by the radiometry at various spread amounts (Γ_1/μmol m^{-2}) of DIL(a) or DML(b). ▼: 0, △: 0.5, ○: 1.0, □: 1.5, ●: 2.0.

radiometry at various spread amounts of DIL or DML. Figure 3 shows the π *vs.* Γ curves for each spread film of DIL and DML and for the adsorbed film of NDA. The validity of derived theoretical isotherms for the adsorption systems of DIL–NDA and DML–NDA is tested with using the experimental data shown in Figs. 1, 2, and 3.

DIL–NDA System. In the mixed monolayer composed of DIL and NDA, a contraction of surface area has been reported in Ref. 1 as a function of the surface pressure. The contribution of such a contraction to the surface energy is expressed by $(\partial \ln f^{v}/\partial \ln C_2)_{\Gamma_1}$ in Eqs. 8 and 11, which may be estimated from the concentration dependence of the Goodrich's convention. The comparison of Γ_2 calculated by Eq. 8 with the experimental values is shown in Fig. 4. It was found that the calculated values (solid lines) were in good agreement with the observed ones. Since DIL and NDA molecules have been known to form a simple mixed monolayer without forming any complex,[1] the result in Fig. 4 gives an experimental confirmation of the validity of Eq. 8 or Eq. 11 where $f^{c}=1$. However, these equations are not valid for a mixed film in which the surface pressure of single NDA solutions, π_2°, is lower than that of DIL film alone, π_1°: for instance, in the case where Γ_{DIL} is 1.5 μmol m^{-2} π_1° is 1.0 mN m^{-1} and is equal to that of π_2° at NDA concentration of about 8 μmol dm^{-3}, as may be found from Figs. 1 and 3. Hence, below this concentration (corresponding to the arrow in Fig. 6-a) the calculated value from Eq. 8 or 11 gradually deviates from the observed values, because π_1° in this region is higher than π_2°.

Consequently, Eq. 8 or 11 is valid only in mixed films where π_1° is lower than π_2°, according to the requirement of Eq. 2.

DML–NDA System. Figure 5 shows the comparison of the observed and the calculated values for NDA which adsorbs at the solution surface with various amounts of spread DML. Here, the calculation was made according to Eq. 8, using $(\partial \ln f^{v}/\partial \ln C_2)_{\Gamma_1}$ values obtained for DML system. The predicted isotherm of Eq. 8 does not coincide with the observed one, unlike the findings for DIL system. The reason for this deviation seems to be the following. When NDA molecules adsorb at the solution surface with presence of DML molecules, the DML–NDA ion pair is formed in monolayer,[1] so that the standard chemical potentials of these molecules shift because of the structural changes in their polar groups. Therefore, the adsorption of NDA in the present system is considered to obey Eq. 11, according to the arguments described above. Thus the difference between the observed (signs) and the calculated (solid lines) isotherms in Fig. 5 corresponds to the values of the $(\partial \ln f^{c}/\partial \ln C_2)_{\Gamma_1}$ term in Eq. 11. From this reasoning, we can obtain thermodynamic information about the ion pair formed between the ampholytic moieties of DML and

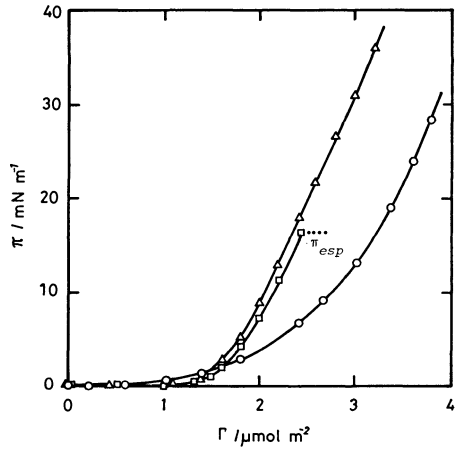

Fig. 3. π *vs.* Γ curves for each spread film of DIL(□) and DML(△) and for the adsorbed film of NDA(○). The curve for the NDA film is calculated from the data in Figs. 1 and 2. π_{esp}: the equilibrium spreading pressure of DIL film (16.6 mN m^{-1}).

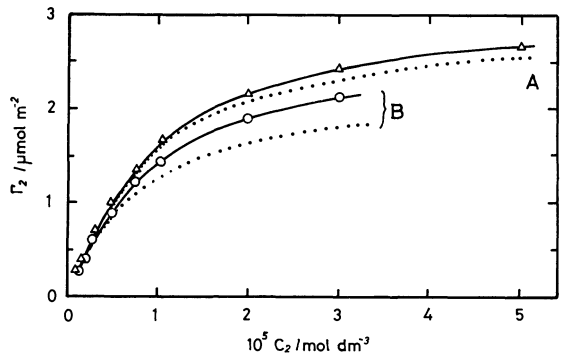

Fig. 4. Test of Eqs. 8 (solid lines) and 12 (dotted lines) at various amounts (Γ_1/μmol m^{-2}) of DIL. Curve A=0.5, curve B=1.0. Observed values are marked by signs.

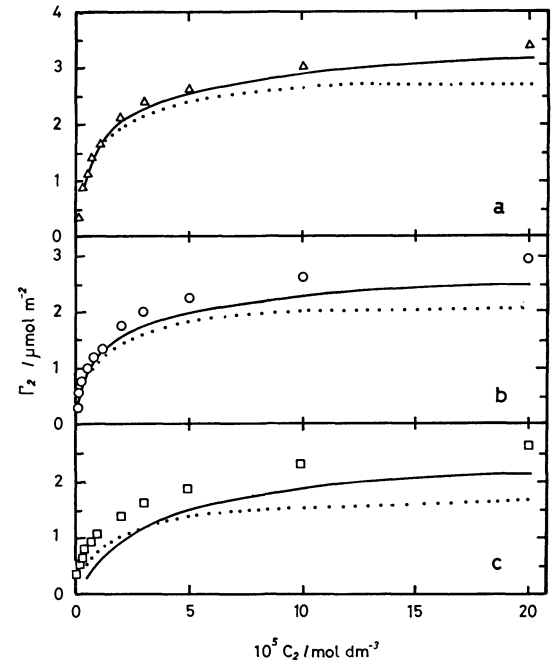

Fig. 5. Test of Eqs. 8 (soild lines) and 12 (dotted lines) at various amounts (Γ_1/μmol m^{-2}) of DML. a: 0.5, b: 1.0, c: 1.5. Observed values are marked by signs.

NDA in monolayer. Further discussion about this will be made elsewhere.

Pethica's Isotherm. Pethica has derived Eq. 12 for the penetration of sodium dodecyl sulfate at the air-solution interface with a fixed amount of cholesterol:[3]

$$d\pi = \Phi RT\Gamma_2 d \ln C_2 \quad (12)$$

where $\Phi = a_1/(a_1 - \bar{a}_1)$, and $\bar{a}_1$ is the partial molar surface area of the monolayer. The Γ_2 values, which have been calculated by Eq. 12 for the DIL-NDA and DML-NDA systems, are shown by the respective lines in Figs. 4 and 5, and compared with the observed values. These dotted lines deviate greatly from the observed isotherms, except for the low concentrations of the surfactant. Since Eq. 12 should be applied to the adsorption of a surfactant into highly condensed monolayer, the adsorption isotherms in such a case are shown in Fig. 6. It is clear that for DIL-NDA system (Fig. 6-a) the predicted isotherm by Eq. 12 follows the observed one at C_2 less than 3 μmol dm^{-3}, whereas the isotherm given by Eq. 8 coincides above 8 μmol dm^{-3}, as indicated by the arrow in Fig. 6-a: *i.e.*, below this concentration the requirement for Eq. 2 is not satisfied. Therefore, Eq. 12 seems to allow the calculation in the adsorption region unsuitable for Eq. 8. On the other hand, in the DML-NDA system the observed values deviate from the isotherm calculated by Eq. 12 as well as by Eq. 8, even though the solution surface is covered with DML film of 2.0 μmol m^{-2}. Hence, Eq. 12 appears not to be useful for the DML-NDA system.

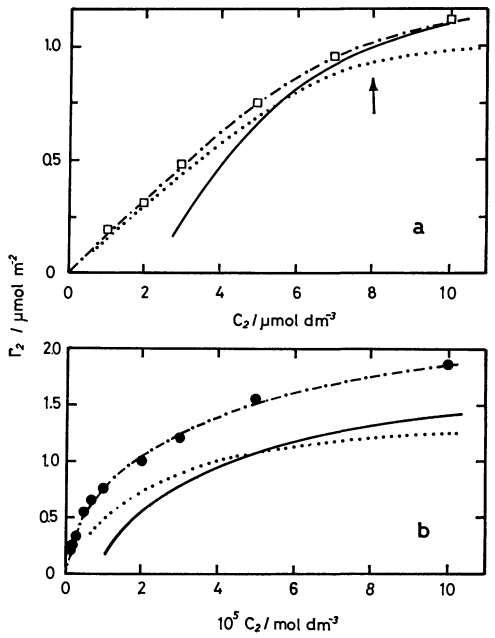

Fig. 6. Comparison of calculated isotherm by Eqs. 8 (solid lines) and 12 (dotted lines) with experimental values (—·□·, —·●—) at spread amount of DIL= 1.5 μmol m^{-2} (a) or of DML=2.0 μmol m^{-2} (b).

In conclusion, Eq. 8, derived for the simple non-ideal adsorption system, could sufficiently explain the observed isotherm for the DIL-NDA system, but could not be applied to the DML-NDA system. Thus, Eq. 11, derived for the complex formation system, was the best one to use for predicting the adsorption of NDA in the DML-NDA system.

References

1) K. Tajima and T. Tsutsui, *Bull. Chem. Soc. Jpn.*, **54**, 109 (1981).
2) K. Tajima, M. Muramatsu, and T. Sasaki, *Bull. Chem. Soc. Jpn.*, **43**, 1991 (1970).
3) B. A. Pethica, *Trans. Faraday Soc.*, **51**, 1402 (1955).
4) M. A. McGregor and G. T. Barnes, *J. Colloid Interf. Sci.*, **54**, 439 (1976).
5) F. C. Goodrich, Proc. 2nd Internat. Congr. Surface Activity, **1**, 85, Butterworths, London (1957).
6) T. Okumura, A. Nakamura, K. Tajima, and T. Sasaki, *Bull. Chem. Soc. Jpn.*, **47**, 2956 (1974).

Crystal Structure and Absolute Configuration of $(-)_{589}$-Tris(2,2′-bipyridine)-cobalt(III) Hexacyanoferrate(III) Octahydrate

Kazunori YANAGI, Yuji OHASHI,* Yoshio SASADA, Youkoh KAIZU,† and Hiroshi KOBAYASHI†

Laboratory of Chemistry for Natural Products, Tokyo Institute of Technology, Nagatsuta, Midori-ku, Yokohama 227

† *Department of Chemistry, Tokyo Institute of Technology, O-okayama, Meguro-ku, Tokyo 152*

(Received May 17, 1980)

The crystal structure and absolute configuration of the title compound, $(-)_{589}$-$[Co(bpy)_3][Fe(CN)_6]\cdot 8H_2O$, has been determined from single-crystal X-ray data. The yellow crystals are triclinic; unit-cell dimensions $a=12.174(3)$, $b=16.742(7)$, $c=10.651(3)$ Å, $\alpha=103.25(3)$, $\beta=104.09(2)$, $\gamma=94.71(3)°$, space group Pl, $Z=2$. The structure was solved by the heavy-atom method and refined to $R=0.076$. The $(-)_{589}$-isomer of $[Co(bpy)_3]^{3+}$ has Δ configuration. The $[Co(bpy)_3]^{3+}$ and $[Fe(CN)_6]^{3-}$ ions have an approximate D_3 symmetry and nearly the same structure as those in other related complexes. All the N atoms in $[Fe(CN)_6]^{3-}$ and the water molecules participate in a three-dimensional hydrogen-bond network.

The absolute configurations of $[Co(bpy)_3]^{3+}$ and tris(1,10-phenanthroline)cobalt(III), $[Co(phen)_3]^{3+}$, have been controversial. Mason and co-workers[1-4] have applied the exciton theory, based on the CD active, long-axis polarized (π, π^*) ligand transition. Hawkins and co-workers[5-7] have proposed an alternative procedure, involving an empirical analysis of both CD and isotropic absorption data of the (d, d*) ligand-field band. The absolute configurations derived by the two methods are not consistent; the former suggests $(-)_{589}$-$[Co(bpy)_3]^{3+}$ to have a Δ configuration, while the latter yields a Λ assignment. The validity of the isotropic absorption analysis has been questioned[8] and the assignment for $(+)_{589}$-$[Co(phen)_3]^{3+}$ has been proposed from the Pfeiffer phenomenon,[9] but the controversy still remains unresolved.

We intend to determine the absolute configuration directly by X-ray analysis, to judge which of the two methods predicts it correctly. Preliminary results of this work have been reported.[10] The absolute configuration thus determined will furnish the basis of the CD theory.

Experimental

The complex of $(-)_{589}$-$[Co(bpy)_3](ClO_4)_3$ was prepared by the method reported,[5] potassium $(+)_{589}$-bistartratoantimonate(III) being used instead of sodium $(+)_{589}$-tartrate.

The crystals of $(-)_{589}$-$[Co(bpy)_3][Fe(CN)_6]\cdot 8H_2O$ were grown by the diffusion method, as shown schematically in Fig. 1. A small glass vessel (A) filled with a solution of $(-)_{589}$-$[Co(bpy)_3](ClO_4)_3$ was placed in the center of a beaker (C). A bent glass pipe with a small opening (B) was filled with a solution of $K_3[Fe(CN)_6]$. Distilled water was poured very carefully down the wall of the beaker until the level was about 1 mm above the opening of the pipe and the vessel. To minimize thermal and photo-racemization, the beaker was kept in the dark at 5 °C. After about 24 h, yellow prismatic crystals were grown on the wall of the central vessel. Found: C, 49.22; H, 3.89; N, 19.28%. Calcd for $[Co(C_{10}H_8N_2)_3][Fe(CN)_6]\cdot 8H_2O$; C, 48.94; H, 4.56; N, 19.02%.

Figure 2 shows the absorption and circular-dichroism spectra in solution, which were recorded on a Simadzu Model MPS-50 spectrometer and JASCO Model ORD/UV-5 spectrometer with CD attachment. These spectra exhibit essentially the same pattern as those of $(-)_{589}$-$[Co(bpy)_3](ClO_4)_3$.[8]

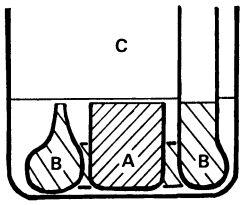

Fig. 1. A schematic drawing of the diffusion method. A small opening of the bent glass pipe is as high as the central vessel.

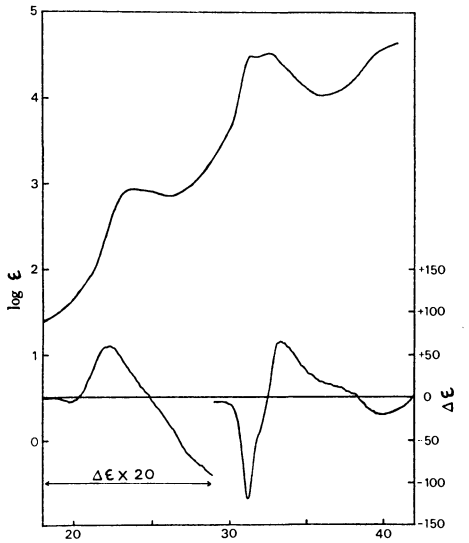

Fig. 2. The absorption (upper curve) and circular dichroism spectra (lower curve) of the $(-)_{589}$-$[Co(bpy)_3][Fe(CN)_6]$ complex in aqueous solution.

The symmetry and approximate cell dimensions of the crystal were determined from oscillation and Weissenberg photographs. The more accurate cell dimensions were obtained by least-squares analysis of 2θ measured on a Rigaku automated four-circle diffractometer. The density was measured by the flotation method in a mixture of carbon tetrachloride and hexane. The crystal data are summarized in Table 1.

Intensity data up to $2\theta \leqq 55°$ were collected on the diffractometer with Mo $K\alpha$ radiation ($\lambda=0.71069$ Å) mono-

Table 1. Crystal data

Formula	$[Co(C_{10}H_8N_2)_3][Fe(CN)_6]\cdot 8H_2O$
F. W.	883.6
Space group	P1
a	12.174(3) Å
b	16.742(7) Å
c	10.651(3) Å
α	103.25(3)°
β	104.09(2)°
γ	94.71(3)°
V	2027(1) Å^3
Z	2
D_m	1.46 g/cm^3
D_x	1.4477(7) g/cm^3
μ(Mo $K\alpha$)	8.3 cm^{-1}

chromated by a graphite. An ω-2θ scan was employed with a scan rate of 4° (2θ) min^{-1}. A total of 6348 independent reflections, ($|F_o| \geqq 3\sigma(|F_o|)$), was used for the structure determination. The intensities were corrected for Lorentz and polarization factors but absorption correction was not applied.

Structure Determination

The positions of the two cobalt and two iron atoms were obtained from the three-dimensional Patterson function. Since the arrangement of these four atoms exhibits a non-crystallographic center of symmetry, the two crystallographically independent complex ions were approximately related to each other by the pseudo inversion center on the first Fourier map. The positions of the atoms in four pyridine rings, which are not related by the pseudo inversion, were selected carefully on the successive Fourier maps.

The structure was refined by the block-diagonal least-squares method. After several cycles of the refinement, sixteen oxygen atoms of the water molecules appeared on a difference map. Further refinement revealed that the eight of sixteen oxygen atoms had the decreased occupancy factors.

The positions of the hydrogen atoms in the 2,2′-bipyridine ligands were obtained from the difference map and refined with the isotropic temperature factors. The hydrogen atoms of water molecules could not be found. The weighting scheme in the final refinement, $w=0.2$ if $|F_o|<13.8$ or $|F_o|>138.1$, $w=(0.000956F_o^2-0.157|F_o|+7.58)^{-1}$ if $13.8 \leqq F_o| \leqq 138.1$, was employed. The final R value became 0.076 for 6348 observed reflections. At the final stage, no peaks higher than 0.58 e Å^{-3} were found on the difference map. Atomic scattering factors including the anomalous terms for Mo $K\alpha$ radiation were taken from the International Tables for X-Ray Crystallography.[11] Final positional parameters and their standard deviations are given in Table 2. A list of the anisotropic thermal parameters and a table of the observed and calculated structure factors are kept in the office of the Chemical Society of Japan (Document No. 8104). The computation was done on a FACOM-HITAC system M-160 computer at this Institute.

Results and Discussion

Absolute Configuration. The intensities of fifteen

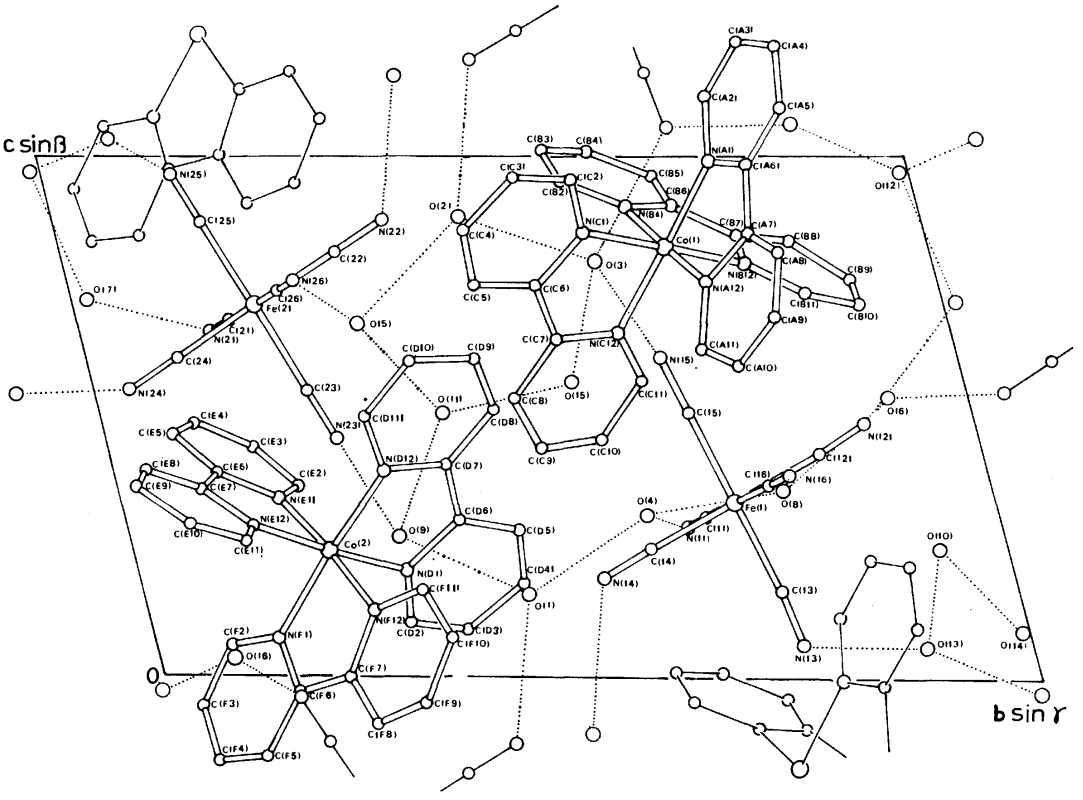

Fig. 3. The crystal structure viewed along the a axis. The hydrogen bonds are represented by dotted lines.

TABLE 2. FRACTIONAL COORDINATES, WITH THEIR STANDARD DEVIATIONS, MULTIPLIED BY 10^4 FOR THE NON-HYDROGEN ATOMS AND 10^3 FOR THE HYDROGEN ATOMS

Atom	x	y	z	B or B_{eq}[a)]	Atom	x	y	z	B or B_{eq}[a)]
Co(1)	7626(1)	7003(1)	8280(2)	25 Å^2	C(E7)	2281(11)	978(7)	3593(11)	36 Å^2
N(A1)	8526(7)	7771(5)	9925(9)	30	C(E8)	2819(13)	373(9)	3938(13)	53
C(A2)	8311(11)	7902(8)	11143(12)	42	C(E9)	3814(14)	215(8)	3611(15)	60
C(A3)	9045(13)	8428(9)	12250(13)	54	C(E10)	4268(12)	735(9)	2916(15)	55
C(A4)	10051(12)	8839(8)	12147(13)	48	C(E11)	3665(10)	1347(8)	2584(12)	39
C(A5)	10276(10)	8731(8)	10947(12)	41	N(E12)	2680(8)	1452(5)	2876(9)	33
C(A6)	9509(9)	8181(7)	9833(11)	31	N(F1)	871(8)	1450(5)	739(9)	32
C(A7)	9667(9)	7977(7)	8513(11)	30	C(F2)	−35(10)	887(7)	585(13)	42
C(A8)	10633(11)	8307(8)	8200(14)	46	C(F3)	−572(12)	349(9)	−606(15)	54
C(A9)	10717(12)	8049(9)	6883(16)	57	C(F4)	−183(14)	391(9)	−1666(15)	64
C(A10)	9806(12)	7490(10)	5963(14)	57	C(F5)	752(13)	953(10)	−1566(15)	61
C(A11)	8897(12)	7138(8)	6302(12)	46	C(F6)	1276(10)	1499(7)	−303(10)	32
N(A12)	8838(7)	7398(5)	7576(9)	29	C(F7)	2251(10)	2152(7)	−1(12)	36
N(B1)	6427(7)	6660(5)	9014(9)	35	C(F8)	2801(13)	2308(9)	−912(15)	56
C(B2)	6339(9)	5993(6)	9528(11)	33	C(F9)	3692(15)	2933(10)	−519(15)	66
C(B3)	5476(11)	5875(8)	10119(13)	50	C(F10)	4037(12)	3424(9)	754(15)	57
C(B4)	4646(12)	6384(8)	10125(15)	49	C(F11)	3436(12)	3224(8)	1659(13)	46
C(B5)	4707(12)	7060(8)	9599(14)	45	N(F12)	2597(8)	2594(5)	1270(9)	31
C(B6)	5598(10)	7183(7)	9037(11)	32	Fe(1)	2500(2)	7040(1)	3367(2)	30
C(B7)	5776(9)	7854(7)	8463(12)	34	C(11)	830(10)	6667(7)	2996(11)	34
C(B8)	5047(12)	8433(8)	8321(15)	65	C(12)	2271(10)	8147(8)	4283(13)	40
C(B9)	5272(12)	9012(9)	7643(14)	67	C(13)	2242(10)	7295(7)	1641(11)	33
C(B10)	6263(11)	9057(10)	7213(15)	54	C(14)	2685(9)	5934(6)	2445(11)	30
C(B11)	6917(10)	8466(8)	7378(12)	37	C(15)	2845(11)	6770(8)	5070(13)	43
N(B12)	6726(7)	7858(5)	7963(8)	31	C(16)	4095(10)	7486(7)	3647(12)	39
N(C1)	8454(8)	6099(6)	8522(10)	28	N(11)	−104(9)	6473(7)	2762(12)	49
C(C2)	9378(10)	6115(7)	9541(12)	30	N(12)	2171(11)	8775(7)	4918(12)	54
C(C3)	9947(12)	5444(8)	9592(14)	43	N(13)	2065(10)	7384(8)	570(11)	53
C(C4)	9554(11)	4714(9)	8550(14)	49	N(14)	2810(8)	5317(6)	1834(10)	41
C(C5)	8613(11)	4671(8)	7497(14)	49	N(15)	3019(12)	6618(8)	6118(12)	65
C(C6)	8089(9)	5387(7)	7534(11)	32	N(16)	5002(10)	7754(9)	3802(14)	71
C(C7)	7122(10)	5450(7)	6459(12)	32	Fe(2)	6727(2)	2104(1)	7114(2)	35
C(C8)	6609(14)	4813(10)	5333(18)	51	C(21)	5096(11)	1758(8)	6846(13)	43
C(C9)	5695(13)	4985(10)	4388(17)	53	C(22)	6571(10)	3188(8)	8130(11)	39
C(C10)	5390(13)	5744(8)	4555(15)	56	C(23)	6399(11)	2475(7)	5479(12)	38
C(C11)	5920(10)	6354(7)	5682(12)	40	C(24)	6859(10)	1058(7)	6054(13)	36
N(C12)	6790(7)	6211(6)	6581(9)	25	C(25)	7082(11)	1721(10)	8734(16)	60
Co(2)	1700(1)	2261(1)	2402(2)	27	C(26)	8340(10)	2434(7)	7413(12)	37
N(D1)	731(7)	3089(5)	2034(9)	30	N(21)	4168(9)	1529(7)	6754(12)	56
C(D2)	−201(10)	2988(8)	1035(12)	42	N(22)	6482(10)	3850(7)	8727(11)	56
C(D3)	−827(10)	3634(8)	893(12)	43	N(23)	6240(13)	2672(7)	4538(11)	66
C(D4)	−451(10)	4405(8)	1823(13)	40	N(24)	6931(10)	430(6)	5359(13)	53
C(D5)	533(10)	4504(7)	2862(12)	35	N(25)	7242(12)	1511(11)	9696(15)	89
C(D6)	1089(9)	3839(7)	2969(11)	32	N(26)	9321(10)	2626(7)	7598(12)	55
C(D7)	2111(9)	3863(7)	4087(11)	32	O(1)	6759(8)	4431(6)	1603(10)	58
C(D8)	2601(11)	4557(7)	5112(12)	40	O(2)	2478(8)	4696(7)	8839(10)	62
C(D9)	3514(11)	4487(7)	6090(12)	42	O(3)	1879(9)	6158(7)	7976(10)	67
C(D10)	3940(10)	3719(8)	6050(12)	42	O(4)	7740(9)	6012(8)	3137(12)	81
C(D11)	3414(10)	3061(7)	4989(11)	37	O(5)	1239(9)	3263(7)	6770(11)	75
N(D12)	2504(8)	3118(6)	3957(9)	36	O(6)	8353(10)	9083(7)	5386(10)	71
N(E1)	821(7)	1823(6)	3394(10)	34	O(7)	2801(11)	161(7)	7221(11)	80
C(E2)	−154(11)	2085(8)	3630(14)	47	O(8)	7199(10)	7602(7)	3616(14)	87
C(E3)	−830(13)	1705(10)	4386(16)	59	O(9)	7357(21)	3094(14)	2676(25)	83
C(E4)	−380(12)	1073(10)	4871(15)	56	O(10)	6214(24)	9229(17)	2439(23)	103
C(E5)	630(13)	813(9)	4643(13)	51	O(11)	9536(29)	3961(19)	5027(29)	129
C(E6)	1227(10)	1201(7)	3888(11)	37	O(12)	2833(24)	9980(15)	9727(21)	97

Table 2. Continued.

Atom	x	y	z	B or B_{eq}[a)]
O(13)	3706(18)	8813(10)	665(20)	59 Å^2
O(14)	7587(23)	9926(16)	902(24)	93
O(15)	9971(24)	5518(18)	5664(28)	106
O(16)	5158(144)	883(87)	345(152)	106
H(A2)	756(8)	752(6)	1107(9)	25(22)
H(A3)	900(12)	833(9)	1280(14)	84(10)
H(A4)	1078(9)	914(7)	1301(11)	43(28)
H(A5)	1121(9)	890(7)	1089(11)	52(28)
H(A8)	1139(7)	885(5)	902(9)	17(20)
H(A9)	1144(11)	828(8)	670(13)	77(10)
H(A10)	984(10)	730(8)	508(12)	66(35)
H(A11)	827(11)	657(8)	580(13)	78(10)
H(B2)	697(9)	563(6)	928(10)	22(25)
H(B3)	558(9)	544(6)	1049(11)	61(28)
H(B4)	406(12)	633(9)	1039(14)	75(10)
H(B5)	401(9)	757(6)	958(10)	39(26)
H(B8)	427(8)	833(6)	891(9)	82(22)
H(B9)	487(8)	953(6)	774(10)	69(24)
H(B10)	639(10)	943(7)	694(12)	51(32)
H(B11)	740(10)	841(8)	712(12)	11(36)
H(C2)	950(8)	661(6)	1035(9)	34(22)
H(C3)	1062(10)	545(8)	1035(12)	52(35)
H(C4)	987(11)	430(8)	845(13)	91(10)
H(C5)	828(9)	411(7)	672(11)	35(29)
H(C8)	694(11)	428(8)	522(13)	22(10)
H(C9)	553(11)	458(8)	382(13)	25(36)
H(C10)	490(9)	595(7)	407(11)	57(29)
H(C11)	549(7)	688(5)	583(8)	67(19)
H(D2)	−48(8)	247(6)	49(9)	23(23)
H(D3)	−145(7)	356(5)	14(9)	16(20)
H(D4)	−83(10)	477(8)	180(13)	65(36)
H(D5)	79(9)	505(6)	348(10)	37(27)
H(D8)	235(8)	509(6)	509(10)	31(25)
H(D9)	376(11)	500(8)	650(13)	76(10)
H(D10)	454(10)	368(7)	653(11)	43(29)
H(D11)	365(10)	245(8)	512(12)	70(35)
H(E2)	−49(7)	268(5)	318(8)	89(18)
H(E3)	−168(12)	209(9)	482(14)	59(10)
H(E4)	−85(10)	69(7)	506(11)	50(31)
H(E5)	102(10)	37(7)	509(11)	48(32)
H(E8)	263(9)	9(7)	431(11)	57(29)
H(E9)	424(9)	−15(7)	379(11)	53(29)
H(E10)	487(10)	71(7)	268(12)	83(32)
H(E11)	395(12)	179(9)	218(14)	10(10)
H(F2)	−37(10)	85(7)	134(11)	58(32)
H(F3)	−127(9)	−3(7)	−46(11)	49(29)
H(F4)	−57(11)	12(8)	−234(13)	78(10)
H(F5)	117(11)	103(8)	−227(13)	80(10)
H(F8)	235(9)	206(7)	−194(10)	33(25)
H(F9)	412(11)	303(8)	−112(13)	76(37)
H(F10)	459(9)	395(7)	107(11)	49(29)
H(F11)	355(9)	357(6)	274(10)	38(26)

a) B_{eq} means the equivalent isotropic temperature factor, defined by $B_{eq}=8\pi^2(U_1+U_2+U_3)/3$ where U_1, U_2, and U_3 are the principal components of U matrix. All the values of B and B_{eq} are multiplied by 10.

Table 3. Relation of $|F|$ in Friedel pairs

h	k	l	$\lvert F_c(hkl)\rvert$		$\lvert F_c(\bar{h}\bar{k}\bar{l})\rvert$	$\lvert F_o(hkl)\rvert$		$\lvert F_o(\bar{h}\bar{k}\bar{l})\rvert$
$\bar{1}$	$\bar{8}$	1	24.8	>	10.8	19.6	>	8.8
1	$\bar{5}$	1	46.0	<	64.0	43.0	<	65.5
3	$\bar{3}$	1	49.6	>	26.0	59.4	>	30.6
$\bar{3}$	3	1	22.0	>	10.8	24.3	>	9.8
1	4	1	54.0	<	73.6	51.5	<	75.1
0	$\bar{5}$	2	34.0	>	23.2	28.0	>	17.2
$\bar{4}$	$\bar{1}$	2	23.6	>	15.2	23.7	>	15.5
2	1	2	20.0	<	46.8	40.0	<	64.1
0	5	2	22.8	>	14.0	25.8	>	16.8
$\bar{7}$	$\bar{12}$	3	21.2	>	11.2	16.2	>	9.9
1	1	3	68.0	>	49.2	58.3	>	43.3
$\bar{4}$	4	3	21.2	>	12.8	22.3	>	14.7
$\bar{2}$	$\bar{7}$	4	25.2	>	15.6	19.2	>	9.1
1	$\bar{4}$	5	20.0	<	30.0	19.2	<	30.5
1	4	7	12.0	<	20.0	9.1	<	17.0

Friedel pairs (hkl and $\bar{h}\bar{k}\bar{l}$), for which differences in intensities were the largest, were measured on the diffractometer using Ni-filtered Cu $K\alpha$ radiation. The observed and calculated structure factors are compared in Table 3, the anomalous scattering terms being taken from the International Tables.[11] All the relations between $|F_c(hkl)|$ and $|F_c(\bar{h}\bar{k}\bar{l})|$ are consistent with those between $|F_o(hkl)|$ and $|F_o(\bar{h}\bar{k}\bar{l})|$, indicating that $(-)_{589}$-$[Co(bpy)_3]^{3+}$ has the Δ configuration.[12]

The Structure of $[Co(bpy)_3]^{3+}$ *and* $[Fe(CN)_6]^{3-}$. The crystal structure viewed along the a axis is shown in Fig. 3, in which the numbering of the atoms is also given. The two crystallographically independent complexes are approximately related by a non-crystallographic inversion center except for the four pyridine rings including N(A12), N(B1), N(E1), and N(F12). The structures of the two crystallographically independent complexes are not significantly different. Both of the $[Co(bpy)_3]^{3+}$ and $[Fe(CN)_6]^{3-}$ ions, which are shown in Fig. 4(a) and (b), have approximate point-group symmetry D_3.

Bond distances and angles in the coordination sphere of $[Co(bpy)_3]^{3+}$ are given in Table 4. The average Co–N distance and N–Co–N angle are 1.93 Å and 83.3°, respectively. These value are in good agreement with those found in $[Co(bpy)_2(NO_3)]^{2+}$ (1.929 Å and 83.27°, respectively),[13] and distinct from those in $[Co(en)_3]^{3+}$ (en: ethylenediamine), (1.978±0.004 Å and 85.4±0.3°, respectively).[14]

For the $[Co(en)_3]^{3+}$ and other trisbidentate complexes with five-membered rings, the following empirical rule has been proposed; those complexes which show prominent positive circular dichroism in the first absorption region possess Δ absolute configuration.[16] The absolute configuration of the present $(-)_{589}$-$[Co(bpy)_3]^{3+}$ complex conflicts with the empirical rule because the prominent positive circular dichroism is found at 22×10^3 cm^{-1} as shown in Fig. 2. The octahedron around the cobalt atom in the $[Co(bpy)_3]^{3+}$ is compared with that of $[Co(en)_3]^{3+}$ [15] in Fig. 5, in which the characteristic values are given.

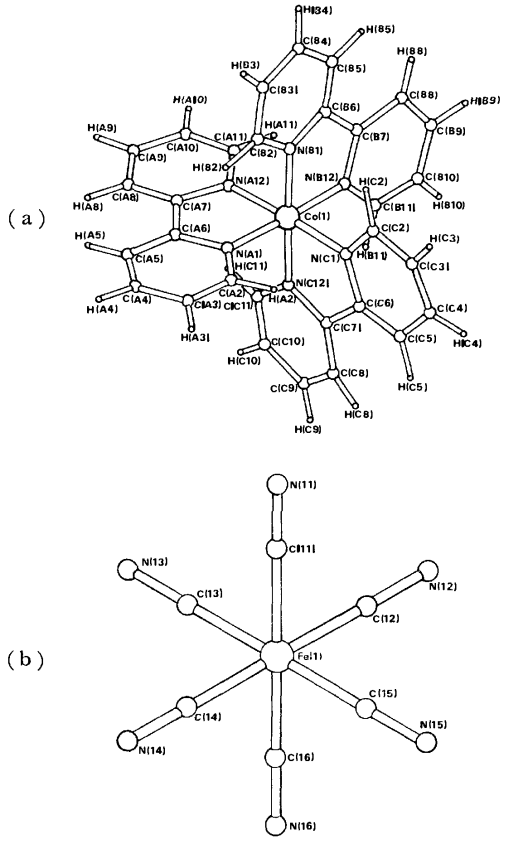

Fig. 4. The molecular structures of $[Co(bpy)_3]^{3+}$, (a), and $[Fe(CN)_6]^{3-}$, (b), viewed along the pseudo three-fold axis. These structures are not significantly different from those of the other crystallographically independent ions.

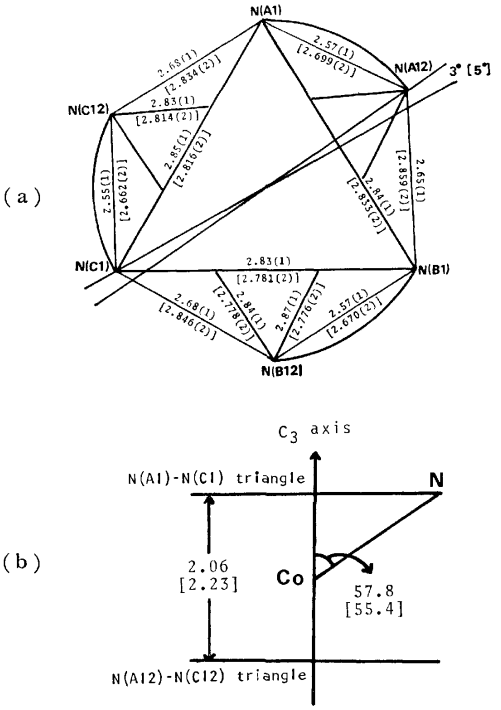

Fig. 5. Comparison of the octahedrons in $[Co(bpy)_3]^{3+}$ and $[Co(en)_3]^{3+}$ (in brackets). (a) Projection down and (b) normal to the pseudo three-fold axis. The values are taken from the present complex including Co(1) and $[Co(en)_3]^{3+}$ in $[Co(en)_3]^{3+}\cdot C_4H_4O_6^{2-}\cdot Cl^-\cdot 5H_2O$.[15]

TABLE 4. BOND DISTANCES(l/Å) AND ANGLES(ϕ/°) IN THE COORDINATION SPHERE OF $[Co(bpy)_3]^{3+}$

	Distances		
Co(1)-N(A1)	1.93(1)	Co(2)-N(D1)	1.94(1)
Co(1)-N(A12)	1.95(1)	Co(2)-N(D12)	1.91(1)
Co(1)-N(B1)	1.92(1)	Co(2)-N(E1)	1.89(1)
Co(1)-N(B12)	1.96(1)	Co(2)-N(E12)	1.95(1)
Co(1)-N(C1)	1.92(1)	Co(2)-N(F1)	1.95(1)
Co(1)-N(C12)	1.91(1)	Co(2)-N(F12)	1.95(1)
	Angles		
N(A1)-Co(1)-N(A12)	82.9(4)	N(D1)-Co(2)-N(D12)	84.1(4)
N(A1)-Co(1)-N(B1)	95.1(4)	N(D1)-Co(2)-N(E1)	94.9(4)
N(A1)-Co(1)-N(B12)	176.9(4)	N(D1)-Co(2)-N(E12)	176.9(4)
N(A1)-Co(1)-N(C1)	95.4(4)	N(D1)-Co(2)-N(F1)	92.7(4)
N(A1)-Co(1)-N(C12)	88.2(4)	N(D1)-Co(2)-N(F12)	88.8(4)
N(A12)-Co(1)-N(B1)	86.7(4)	N(D12)-Co(2)-N(E1)	90.9(4)
N(A12)-Co(1)-N(B12)	94.5(4)	N(D12)-Co(2)-N(E12)	93.5(4)
N(A12)-Co(1)-N(C1)	177.6(4)	N(D12)-Co(2)-N(F1)	175.7(4)
N(A12)-Co(1)-N(C12)	94.8(4)	N(D12)-Co(2)-N(F12)	94.2(4)
N(B1)-Co(1)-N(B12)	83.1(4)	N(E1)-Co(2)-N(E12)	83.1(4)
N(B1)-Co(1)-N(C1)	95.1(4)	N(E1)-Co(2)-N(F1)	92.3(4)
N(B1)-Co(1)-N(C12)	176.6(4)	N(E1)-Co(2)-N(F12)	174.0(4)
N(B12)-Co(1)-N(C1)	87.3(4)	N(E12)-Co(2)-N(F1)	93.3(4)
N(B12)-Co(1)-N(C12)	93.8(4)	N(E12)-Co(2)-N(F12)	93.3(4)
N(C1)-Co(1)-N(C12)	83.5(4)	N(F1)-Co(2)-N(F12)	82.9(4)

These values are not so different between the two octahedrons. It seems difficult to ascribe the opposite sign of the circular dichroism to the slight difference in geometries of the two octahedrons. A more rigorous study is necessary to explain the circular dichroism of the (d, d*) transition.

Bond distances and angles in the bipyridine ligands are listed in Table 5. The average values are given in the final column. There is no significant difference between the corresponding values in the present complex and in other related complexes, such as $[Fe(bpy)_3]^{3+}$,[17] $[Co(bpy)_2(NO_3)]^{2+}$,[13] $[Ni(bpy)_3]^{3+}$,[18,19] $[Ni(bpy)(H_2O)_2]^{2+}$,[20] and $[Cu(bpy)_3]^{2+}$.[21] The average distances of C–N, C–C, and C–C (connecting two pyridine rings) in these complexes are 1.35, 1.40, and 1.48 Å, respectively.

The geometries of the five-membered rings in the $[Co(bpy)_3]^{3+}$, $[Fe(bpy)_3]^{3+}$, and $[Ni(bpy)_3]^{2+}$ complexes are compared in Table 6. The complex of $[Cu(bpy)_3]^{2+}$ is omitted because Jahn-Teller effect distorts its octahedron. The N–M–N angle decreases with the increase of the M–N length. It is noteworthy

Table 5. Bond distances(l/Å) and angles(ϕ/°) in the 2,2′-bipyridine ligands

Atom[a]	bpy A	bpy B	bpy C	bpy D	bpy E	bpy F	Average
			Distances				
N (#1) - C (#2)	1.36(2)	1.35(2)	1.36(2)	1.32(2)	1.36(2)	1.34(2)	1.35(2)
N (#1) - C (#6)	1.37(2)	1.35(2)	1.39(2)	1.37(2)	1.35(2)	1.34(2)	1.36(2)
C (#2) - C (#3)	1.36(2)	1.37(2)	1.37(2)	1.39(2)	1.48(2)	1.35(2)	1.39(2)
C (#3) - C (#4)	1.40(2)	1.41(2)	1.38(2)	1.40(2)	1.38(2)	1.34(2)	1.39(2)
C (#4) - C (#5)	1.35(2)	1.38(2)	1.38(2)	1.39(2)	1.40(2)	1.38(2)	1.38(2)
C (#5) - C (#6)	1.39(2)	1.40(2)	1.38(2)	1.36(2)	1.43(2)	1.40(2)	1.39(2)
C (#6) - C (#7)	1.43(2)	1.46(2)	1.42(2)	1.49(2)	1.45(2)	1.47(2)	1.45(2)
C (#7) - C (#8)	1.40(2)	1.38(2)	1.38(2)	1.37(2)	1.32(2)	1.37(2)	1.37(2)
C (#7) - N (#12)	1.36(2)	1.36(2)	1.39(2)	1.36(2)	1.36(2)	1.33(2)	1.36(2)
C (#8) - C (#9)	1.40(2)	1.40(2)	1.38(3)	1.36(2)	1.37(2)	1.36(2)	1.38(2)
C (#9) - C (#10)	1.40(2)	1.34(2)	1.39(2)	1.42(2)	1.42(2)	1.36(2)	1.39(2)
C (#10) - C (#11)	1.37(2)	1.36(2)	1.34(2)	1.37(2)	1.37(2)	1.42(2)	1.37(2)
C (#11) - N (#12)	1.35(2)	1.32(2)	1.34(2)	1.38(2)	1.33(2)	1.32(2)	1.34(2)
			Angles				
Co(n) - N (#1) - C (#2)	127(1)	127(1)	127(1)	127(1)	125(1)	126(1)	127(1)
Co(n) - N (#1) - C (#6)	115(1)	116(1)	114(1)	113(1)	115(1)	114(1)	115(1)
C (#2) - N (#1) - C (#6)	118(1)	118(1)	119(1)	120(1)	120(1)	120(1)	119(1)
N (#1) - C (#2) - C (#3)	122(1)	122(1)	120(1)	121(1)	123(1)	122(1)	122(1)
C (#2) - C (#3) - C (#4)	120(1)	119(1)	122(1)	119(1)	115(1)	118(1)	119(1)
C (#3) - C (#4) - C (#5)	120(1)	121(1)	120(1)	119(1)	122(2)	122(2)	121(1)
C (#4) - C (#5) - C (#6)	119(1)	116(1)	118(1)	119(1)	120(1)	117(1)	118(1)
N (#1) - C (#6) - C (#5)	122(1)	124(1)	122(1)	121(1)	120(1)	120(1)	122(1)
N (#1) - C (#6) - C (#7)	114(1)	113(1)	114(1)	115(1)	115(1)	115(1)	114(1)
C (#5) - C (#6) - C (#7)	125(1)	123(1)	124(1)	123(1)	125(1)	126(1)	124(1)
C (#6) - C (#7) - C (#8)	123(1)	124(1)	124(1)	124(1)	126(1)	125(1)	124(1)
C (#6) - C (#7) - N (#12)	115(1)	115(1)	114(1)	112(1)	113(1)	115(1)	114(1)
C (#8) - C (#7) - N (#12)	121(1)	120(1)	121(1)	125(1)	121(1)	121(1)	122(1)
C (#7) - C (#8) - C (#9)	119(1)	117(1)	118(1)	118(1)	121(1)	119(1)	119(1)
C (#8) - C (#9) - C (#10)	117(1)	121(1)	121(1)	121(1)	118(1)	122(1)	120(1)
C (#9) - C (#10) - C (#11)	124(1)	120(1)	116(1)	118(1)	118(1)	116(1)	119(1)
C (#10) - C (#11) - N (#12)	118(1)	120(1)	126(1)	123(1)	122(1)	121(1)	122(1)
Co(n) - N (#12) - C (#7)	113(1)	113(1)	114(1)	116(1)	114(1)	114(1)	114(1)
Co(n) - N (#12) - C (#11)	125(1)	125(1)	129(1)	128(1)	126(1)	125(1)	126(1)
C (#7) - N (#12) - C (#11)	121(1)	122(1)	117(1)	116(1)	120(1)	121(1)	120(1)

a) "#" is A, B, C, D, E, or F and "n" is 1 or 2.

Table 6. Distances (l/Å) and angles (ϕ/°) in the five-membered rings of tris 2,2′-bipyridine complexes

	M-N[a]	N-C	C-C	N-M-N[a]	M-N-C[a]	N-C-C
$[Co(bpy)_3]^{3+}$	1.932	1.36	1.45	83.2	115	114
$[Fe(bpy)_3]^{3+}$	1.963	1.36	1.47	82.3	115	114
$[Ni(bpy)_3]^{2+}$	2.089	1.35	1.48	78.6	115	116

a) M means Co, Fe, and Ni atoms.

that the M–N–C angles take a constant value. This indicates that the bipyridine ligand has not a planar conformation; otherwise the M–N–C angle should increase with the increase of the M–N distance. The two rings of each bipyridine ligand in $[Ni(bpy)_3]^{2+}$ are twisted along the connecting C–C bond. The twist angles are reported as 5.8—10.9°.[18] On the other hand, the bipyridine ligands of $[Co(bpy)_3]^{3+}$ have more planar conformations. Two rings of the bipyridine ligand in $[Co(bpy)_3]^{3+}$ are not twisted but slightly bent at the connecting C–C bond. The angles between the normals to the pyridine rings in the six bipyridine ligands are 2.3° to 4.7°. For the $[Fe(bpy)_3]^{3+}$ complex, those angles have intermediate values between those in $[Ni(bpy)_3]^{2+}$ and $[Co(bpy)_3]^{3+}$.

Bond distances and angles in $[Fe(CN)_6]^{3-}$ are given in Table 7. The average Fe–C and C–N distances, 1.94 Å and 1.14 Å, are in good agreement with those in other hexacyanoferrate(III) crystals.[22–26] Although the deviation of each Fe–C bond length from the average value is slightly large, similar distorted octahedrons, characterized by widely varying M–C bond lengths, have been observed in other hexacyanometalate(III) complexes.[22]

Hydrogen Bond. The hydrogen bonding scheme is shown in Fig. 3. All the N atoms of $[Fe(CN)_6]^{3-}$ and the water molecules participate in the hydrogen bonds to form a three-dimensional network through the O–H···N and O–H···O hydrogen bonds. The distances of O···N and O···O and angles of O···O···N and O···O···O are given in Table 8. The $[Co(bpy)_3]^{3+}$ cations are packed in the network with the van der Waals contacts.

The occupancy factors of O(9), O(10), O(11), O(12), O(13), O(14), O(15), and O(16) showed the decreased values from 0.5 to 0.2. The water molecules may be partly lost from the crystal during the data collection, as judged by the fragility of the crystal after the experiment.

Four water molecules, O(2), O(3), O(5), and O(15), are approximately related to O(1), O(9), O(4), and O(11), respectively, by the pseudo inversion center. The other water molecules occupy the positions near the bipyridine ligands which are not related by the pseudo inversion. Preliminary experiments showed that the racemic crystal of this complex has the space

TABLE 7. BOND DISTANCES (l/Å) AND ANGLES (ϕ/°) IN $[Fe(CN)_6]^{3-}$

		Distances	
Fe(1)-C(11)	1.99(1)	Fe(2)-C(21)	1.95(1)
Fe(1)-C(12)	1.96(1)	Fe(2)-C(22)	1.94(1)
Fe(1)-C(13)	1.94(1)	Fe(2)-C(23)	1.94(1)
Fe(1)-C(14)	1.95(1)	Fe(2)-C(24)	1.90(1)
Fe(1)-C(15)	1.93(1)	Fe(2)-C(25)	1.94(2)
Fe(1)-C(16)	1.95(1)	Fe(2)-C(26)	1.94(1)
C(11)-N(11)	1.11(2)	C(21)-N(21)	1.14(2)
C(12)-N(12)	1.15(2)	C(22)-N(22)	1.17(2)
C(13)-N(13)	1.16(2)	C(23)-N(23)	1.11(2)
C(14)-N(14)	1.13(2)	C(24)-N(24)	1.16(2)
C(15)-N(15)	1.15(2)	C(25)-N(25)	1.14(3)
C(16)-N(16)	1.12(2)	C(26)-N(26)	1.17(2)
		Angles	
C(11)-Fe(1)-C(12)	88.8(5)	C(21)-Fe(2)-C(22)	88.8(6)
C(11)-Fe(1)-C(13)	90.2(5)	C(21)-Fe(2)-C(23)	90.7(6)
C(11)-Fe(1)-C(14)	89.8(5)	C(21)-Fe(2)-C(24)	90.9(6)
C(11)-Fe(1)-C(15)	92.7(5)	C(21)-Fe(2)-C(25)	90.2(7)
C(11)-Fe(1)-C(16)	174.7(5)	C(21)-Fe(2)-C(26)	178.7(6)
C(12)-Fe(1)-C(13)	93.4(5)	C(22)-Fe(2)-C(23)	90.3(6)
C(12)-Fe(1)-C(14)	178.5(5)	C(22)-Fe(2)-C(24)	177.6(6)
C(12)-Fe(1)-C(15)	88.6(6)	C(22)-Fe(2)-C(25)	90.7(7)
C(12)-Fe(1)-C(16)	88.2(6)	C(22)-Fe(2)-C(26)	91.3(6)
C(13)-Fe(1)-C(14)	86.5(5)	C(23)-Fe(2)-C(24)	87.4(6)
C(13)-Fe(1)-C(15)	176.5(6)	C(23)-Fe(2)-C(25)	178.7(7)
C(13)-Fe(1)-C(16)	85.6(5)	C(23)-Fe(2)-C(26)	90.6(6)
C(14)-Fe(1)-C(15)	91.6(6)	C(24)-Fe(2)-C(25)	91.7(7)
C(14)-Fe(1)-C(16)	93.2(5)	C(24)-Fe(2)-C(26)	89.0(6)
C(15)-Fe(1)-C(16)	91.6(6)	C(25)-Fe(2)-C(26)	88.5(6)
Fe(1)-C(11)-N(11)	178(1)	Fe(2)-C(21)-N(21)	175(1)
Fe(1)-C(12)-N(12)	174(1)	Fe(2)-C(22)-N(22)	179(1)
Fe(1)-C(13)-N(13)	175(1)	Fe(2)-C(23)-N(23)	178(1)
Fe(1)-C(14)-N(14)	174(1)	Fe(2)-C(24)-N(24)	177(1)
Fe(1)-C(15)-N(15)	177(1)	Fe(2)-C(25)-N(25)	178(2)
Fe(1)-N(16)-N(16)	179(1)	Fe(2)-C(26)-N(26)	179(1)

Table 8. Distances (l/Å) and angles (ϕ/°) of hydrogen bonds

		Distances	
O (1) - N (22)	2.92 (2)	O (6) - O (8)	2.77 (2)
O (1) - O (4)	2.77 (2)	O (7) - N (12)	2.86 (2)
O (1) - O (9)	2.81 (3)	O (7) - N (21)	2.93 (2)
O (2) - N (14)	3.03 (2)	O (7) - O (12)	2.75 (3)
O (2) - O (3)	2.89 (2)	O (8) - N (16)	2.76 (2)
O (2) - O (5)	2.87 (2)	O (9) - N (23)	2.84 (3)
O (3) - N (13)	2.99 (2)	O (9) - O (11)	3.14 (4)
O (3) - N (15)	2.88 (2)	O (10) - O (13)	3.10 (4)
O (3) - O (15)	2.86 (3)	O (10) - O (14)	2.95 (4)
O (4) - N (11)	2.82 (2)	O (11) - O (15)	2.52 (5)
O (4) - O (8)	2.76 (2)	O (12) - O (13)	2.58 (4)
O (5) - N (26)	2.90 (2)	O (12) - O (16)	2.94 (18)
O (5) - O (11)	2.94 (4)	O (13) - N (13)	2.95 (3)
O (6) - N (24)	2.95 (2)	O (16) - N (25)	2.96 (18)
		Angles	
O (4) - O (1) - O (9)	117.7 (7)	N (12) - O (7) - N (21)	110.9 (6)
O (4) - O (1) - N (22)	124.5 (5)	N (12) - O (7) - O (12)	121.6 (8)
O (9) - O (1) - N (22)	105.9 (7)	N (21) - O (7) - O (12)	123.5 (8)
O (3) - O (2) - O (5)	108.2 (5)	N (16) - O (8) - O (4)	116.2 (7)
O (3) - O (2) - N (14)	100.6 (5)	N (16) - O (8) - O (6)	99.8 (6)
O (5) - O (2) - N (14)	135.9 (5)	O (4) - O (8) - O (6)	132.4 (7)
N (13) - O (3) - N (15)	119.3 (5)	N (23) - O (9) - O (1)	119.1 (10)
N (13) - O (3) - O (2)	102.1 (5)	N (23) - O (9) - O (11)	127.3 (9)
O (13) - O (3) - O (15)	130.8 (8)	O (1) - O (9) - O (11)	100.9 (9)
N (15) - O (3) - O (2)	116.3 (5)	O (13) - O (10) - O (14)	106.7 (10)
N (15) - O (3) - O (15)	84.8 (7)	O (5) - O (11) - O (15)	110.6 (14)
O (2) - O (3) - O (15)	103.5 (7)	O (7) - O (12) - O (13)	123.3 (13)
N (11) - O (4) - O (1)	111.8 (6)	O (7) - O (12) - O (16)	81.1 (35)
N (11) - O (4) - O (8)	94.8 (6)	O (13) - O (12) - O (16)	89.1 (35)
O (1) - O (4) - O (8)	139.3 (6)	N (13) - O (13) - O (12)	116.1 (11)
N (26) - O (5) - O (2)	107.9 (5)	O (3) - O (15) - O (11)	113.0 (14)
N (26) - O (5) - O (11)	85.3 (8)	N (25) - O (16) - O (12)	155.1 (66)
O (2) - O (5) - O (11)	103.2 (8)	O (3) - N (13) - O (13)	105.4 (6)
N (24) - O (6) - O (8)	111.8 (6)		

group $P\bar{1}$ and similar unit-cell dimensions to the present crystal; $a=12.374$, $b=16.305$, $c=10.540$ Å, $\alpha=102.76$, $\beta=103.84$, $\gamma=95.48°$. These results indicate the two crystals to be isostructural except for the four pyridine rings and eight water molecules.

References

1) A. J. McCaffery, S. F. Mason, and B. J. Norman, *J. Chem. Soc., A*, **1969**, 1428.
2) S. F. Mason and B. J. Norman, *J. Chem. Soc., A*, **1969**, 1442.
3) B. Bosnich, *Acc. Chem. Res.*, **2**, 266 (1969).
4) S. F. Mason, B. J. Peart, and R. E. Waddel, *J. Chem. Soc., Dalton Trans.*, **1973**, 944.
5) J. Ferguson, C. J. Hawkins, N. A. P. Kane-Maguire, and H. Lip, *Inorg. Chem.*, **8**, 771 (1969).
6) R. G. Bray, J. Ferguson, and C. J. Hawkins, *Aust. J. Chem.*, **22**, 2091 (1969).
7) C. J. Hawkins, "Absolute Configuration of Metal Complexes," Wiley-Interscience, London (1971), Chap. 5.
8) S. F. Mason and B. J. Peart, *J. Chem. Soc., Dalton Trans.*, **1973**, 949.
9) N. A. P. Kane-Maguire and D. E. Richardson, *J. Am. Chem. Soc.*, **97**, 7194 (1975).
10) Y. Ohashi, K. Yanagi, Y. Mitsuhashi, K. Nagata, Y. Kaizu Y. Sasada, and H. Kobayashi, *J. Am. Chem. Soc.*, **101**, 4739 (1979).
11) "International Tables for X-Ray Crystallography," The Kynoch Press, Birmingham (1974), Vol. IV, p. 72.
12) "Nomenclature of Inorganic Chemistry," 2nd ed, IUPAC, London (1970), p. 75.
13) C. W. Reinmann, M. Zocchi, A. D. Mighell, and A. Santro, *Acta Crystallogr., Sect. B*, **27**, 2211 (1971).
14) Y. Saito, "Inorganic Molecular Dissymmetry," Springer-Verlag, Berlin Heidelberg (1979), p. 57.
15) D. H. Templeton, A. Zalkin, H. W. Ruben, and L. K. Templeton, *Acta Crystallogr., Sect. B*, **35**, 1608 (1979).
16) Y. Saito, "Inorganic Molecular Dissymmetry," Springer-Verlag, Berlin Heidelberg (1979), p. 135.
17) B. N. Figgis, B. W. Skelton, and A. H. White, *Aust. J. Chem.*, **31**, 57 (1978).
18) A. Wada, N. Sakabe, and J. Tanaka, *Acta Crystallogr., Sect. B*, **32**, 1121 (1976).
19) A. Wada, C. Katayama, and J. Tanaka, *Acta*

Crystallogr., Sect. B, **32**, 3194 (1976).
20) P. J. C. Tedenac and E. Phillippot, *Acta Crystallogr., Sect. B*, **30**, 2286 (1974).
21) O. P. Anderson, *J. Chem. Soc., Dalton Trans.*, **1972**, 2597.
22) R. C. Elder, G. J. Kennard, M. D. Payne, and E. Deutsch, *Inorg. Chem.*, **17**, 1296 (1978).
23) K. N. Raymond and J. A. Ibers, *Inorg. Chem.*, **7**, 2333 (1968).
24) E. C. Reynhardt and J. C. A. Boeyens, *Acta Crystallogr., Sect. B*, **28**, 524 (1972).
25) N. G. Vannerberg, *Acta Chem. Scand.*, **24**, 2335 (1970).
26) N. G. Vannerberg, *Acta Chem. Scand.*, **26**, 2863 (1972).

  Bull. Chem. Soc. Jpn., 54, 127—129 (1981)

Some Properties of Fluorine-adsorbed Active Carbon

Nobuatsu WATANABE* and Kazuo UENO

Department of Industrial Chemistry, Faculty of Engineering, Kyoto University, Yoshida, Sakyo-ku, Kyoto 606

(Received March 19, 1980)

Properties of fluorine-adsorbed active carbon (FAAC), expected to be a new fluorinating agent, were investigated by means of TG, X-ray diffraction, and ESCA. The fluorine in FAAC was desorbed by heat treatment in a vacuum at temperatures higher than 200 °C. The X-ray diffraction and ESCA measurements suggest that fluorine is inserted between the carbon layer planes of the active carbon, and combines with carbon atoms weakly in comparison with the C–F covalent bond. The reactivity of FAAC against several organic compounds was studied. 1-Butanol, 1-butanethiol, and cyclohexylamine were oxidized. Butyryl chloride was fluorinated to give butyryl fluoride.

Direct fluorination of carbon at temperatures 350—600 °C gives two types of graphite fluoride, identified as polycarbon monofluoride, $(CF)_n$, and polydicarbon monofluoride, $(C_2F)_n$.[1] Some kinds of carbon adsorb a large amount of fluorine at room temperature.[2,3] Active carbon shows 30—50% weight increase when it is exposed to fluorine atmosphere at room temperature.[2] While graphite fluoride is chemically and thermally stable, this fluorine-adsorbed active carbon (FAAC) can oxidize other halogen ions at room temperature,

$$\text{FAAC} + X^- \text{ in aq soln} \longrightarrow C + F^- + \frac{1}{2}X_2 \quad (X=Cl, Br, I)$$

where C is the residual active carbon.[2] Thus FAAC is expected to be a new fluorinating reagent.

In this study, FAAC was prepared in a laboratory scale and studied by thermogravimetry (TG), X-ray diffraction, and X-ray photoelectron spectroscopy (ESCA). Fluorination of several organic compounds with FAAC was examined.

Experimental

Commercial granular active carbon (extra pure) and organic compounds (guaranteed grade) were used without further purification. TG study was carried out with a thermobalance specially designed for use in a fluorine atmosphere.[2]

A schematic diagram of the reactor for fluorination is shown in Fig. 1. The reaction vessel (5) is made of stainless steel, and can be used at desired temperatures with an electric furnace or appropriate coolant. The fluorocarbon oil (Daifluoil, Daikin Kogyo Co.) placed on the mercury column in the manometer (4) prevents fluorine from reacting with mercury. The gas reservoir (3) and all tubings were made of copper.

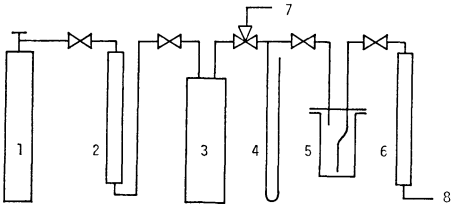

Fig. 1. Schematic diagram of reactor for fluorination. 1: F_2 gas cylinder, 2: HF absorber (NaF pellets heated at 100 °C), 3: gas reservour, 4: Hg manometer, 5: reaction vessel, 6: F_2 absorber (soda-lime pellets), 7: N_2 gas, 8: to vacuum pump.

Results and Discussion

Preparation of Fluorine-adsorbed Active Carbon. FAAC was prepared in the following manner using the apparatus shown in Fig. 1. About 100 g of granular active carbon[4] was placed in the reaction vessel, and heated at *ca.* 150 °C for 2 h in a vacuum to remove water. The vessel was filled with purified nitrogen gas after the active carbon had cooled down to room temperature. Fluorine (0.5 atm) and nitrogen (0.5 atm) were mixed in the gas reservoir. Diluted fluorine was then streamed slowly through the vessel at a flow rate of *ca.* 30 ml/min. The FAAC containing 15—20% fluorine by weight (calculated from the weight increase) was prepared by streaming the gas for 20—30 h. The sample thus obtained had to be washed with nitrogen gas before it was taken out from the reaction vessel. FAAC containing over 20% fluorine would be prepared with further fluorination.

Excessive flow rate of the diluted fluorine sometimes caused explosion in the reaction vessel, or auto-catalytic thermal decomposition of the sample accompanied by a large amount of heat evolution. In the latter case, the sample completely lost the adsorbed fluorine. The reaction vessel should be evacuated as soon as the thermal decomposition takes place, because the inner pressure increases rapidly.

Desorption of Fluorine by Heating. The fluorine adsorbed by FAAC was scarcely desorbed at room temperature even *in vacuo*. This indicates that the fluorine is chemically adsorbed by the active carbon.[2,3] TG was applied in order to study the desorption of

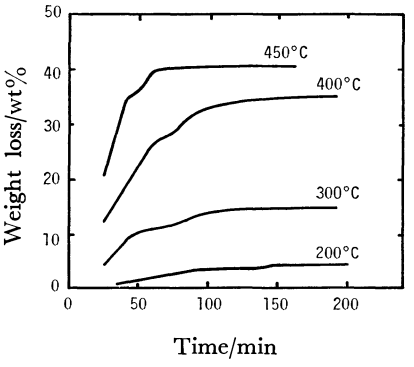

Fig. 2. TG curves for fluorine-adsorbed active carbon at various temperatures in a vacuum.

the fluorine by heating *in vacuo* (Fig. 2). The higher the temperature, the more desorption being observed. The final weight loss at 450 °C corresponds to the desorption of 95% fluorine in FAAC, when no thermal decomposition took place. Various kinds of fluorocarbon were formed in the thermal decomposition of graphite fluoride.[5,6]

Each TG curve was a straight line at first, and then showed slight decrease in the desorption rate, indicating that fluorine is adsorbed heterogeneously. Supposing that the initial desorption rate follows the first order kinetic, the apparent activation energy was calculated to be 28 kJ/mol from the Arrhenius plot of the rate constants. Takenaka[7] found the activation energy for the adsorption of fluorine on graphite to be *ca.* 17kJ/mol. These values are smaller than that for the adsorption of oxygen on graphite.[8] Fluorine might not be combined with carbon covalently like oxides on graphite, but adsorbed weakly on carbon atoms. This was confirmed by ESCA spectra.

Structural Change of Active Carbon by Fluorine Adsorption. The structural change of active carbon was studied by means of X-ray powder diffractometry (Fig. 3). Active carbon has poor regularity as regards carbon layer stacking. Its structure is called turbostratic.[9] A diffused diffraction between 20 and 30° in 2θ corresponds to three to four layers stacked with the same distance of 3.5—3.7 Å (Fig. 3-a). The broad peak disappeared completely when carbon adsorbed fluorine, as shown in Fig. 3-b. However, the regularity of layer packing was recovered by heat treatment at high temperatures such as 300 or 400 °C *in vacuo* because of the desorption of fluorine (Fig. 3-c, d). In the case of graphite, the adsorbed fluorine strained the graphite structure in a direction vertical to the carbon layers, and the stress given to the crystal lattice of graphite was an elastic deformation.[5] The results indicate that the fluorine is not only adsorbed on the surface of the active carbon, but also inserted between carbon layer planes.

ESCA Measurement. In order to elucidate the bonding state of fluorine, FAAC was analyzed by ESCA. In Fig. 4 are shown the spectra for C_{1s}

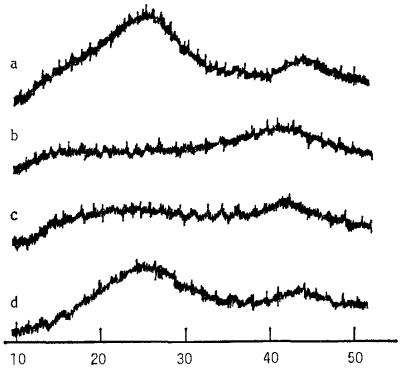

Fig. 3. Variation of X-ray diffraction patterns of fluorine-adsorbed active carbon (FAAC).
a: Original active carbon, b: FAAC, c and d: FAAC after the heat-treatment in a vacuum at 300 and 400 °C, respectively.

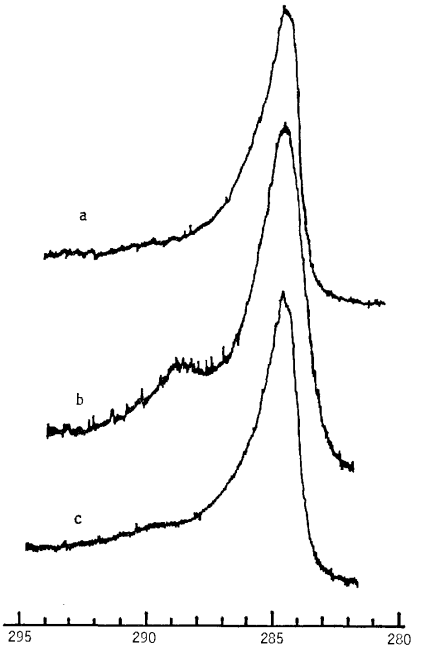

Fig. 4. Variation of ESCA spectra for C_{1s} photoelectron of fluorine-adsorbed active carbon (FAAC).
a: Original active carbon, b: FAAC, c: FAAC after the heat-treatment at 450 °C in a vacuum.

photoelectron of (a) original active carbon, (b) FAAC containing 30% fluorine by weight, and (c) FAAC which is heated at 450 °C for 3 h in a vacuum. The main peak at 284.6 eV corresponds to carbon atoms having no interaction with fluorine.

A new peak appeared at 288.7 eV in the spectrum of FAAC (Fig. 4-b). Since the C–F covalent bond in graphite fluoride has a peak at 290.4 eV,[1] the new peak is due to the interaction between C and F which is weaker than their covalent bond. By heat-treatment, fluorine was desorbed almost completely and a small hump appeared at *ca.* 290 eV, indicating the formation of C–F covalent bond (Fig. 4-c).

A weaker C–F bond was also observed in ESCA spectra of carbon black[3] and natural graphite[15] fluorinated at room temperature. These fluorinated samples have similar oxidizability as FAAC. It is not clear, however, whether the adsorbed fluorine is atom or molecule.

Let us discuss the structure of FAAC and the mechanism of the fluorination of active carbon on the basis of the above results. The composition of FAAC containing 30 wt% of fluorine can be expressed as $C_{3.7}F$. The situation thus differs from the simple adsorption of fluorine on active carbon. FAAC loses the characteristic structure of active carbon. Thus, it is concluded that FAAC is an amorphous solid with no crystallinity, holding fluorine with relatively weak bonding on its layered structure like graphite intercalation compounds. FAAC is similar to the intercalation compound since it permits the reversible insertion and withdrawal of fluorine.

Fluorination of active carbon may be influenced by its structural features rather than surface properties,

Table 1. Reaction of several organic compounds with fluorine-adsorbed active carbon

Run	Substrate	Reaction conditions			Products (Yield/%)
		Solvent	Temp/°C	Time/h	
Oxidation					
1	*n*-BuOH	CCl_4	78	24	$CH_3(CH_2)_2CHO$ (33)
2	*n*-BuSH	CCl_4	78	5.5	Bu-S=S-Bu (10)
3	*cyclo*-$C_6H_{11}NH_2$	—[a]	80	18	*cyclo*-$C_6H_{11}NH_3F$ (20) and oily material
Fluorination					
4	CCl_2=CCl_2	—[b]	250	12	fluorochlorocarbons (50)[c]
5	CCl_2=CCl_2	—[a]	80	21	no reaction
6	$CH_3(CH_2)_2COCl$	CCl_4	75	21	$CH_3(CH_2)_2COF$ (29)[d]
7	$CH_3(CH_2)_2COCl$	CH_3CN	75	21	$CH_3(CH_2)_2COF$ (62)[d]
8	$CH_3(CH_2)_2COCl$	CH_3CN	75	120	$CH_3(CH_2)_2COF$ (90)[d]
No reaction					
9	C_6H_6	—[a]	80	90	
10	*n*-Bu-X (X=Cl, Br)	CCl_4	78	45	
11	C_6H_5-Br	—[a]	100	24	

a) Solvent was the substrate itself. b) Gas phase reaction in a steel reactor ($3\phi \times 30$ cm) heated by an electric furnace. c) Total yield of CF_4, CF_3Cl, CF_2Cl_2, and $CFCl_3$. They were identified by using IR. d) Calculated from the absorption intensity of the C=O band due to COF group.

since the amount of fluorine taken in far exceeds what is expected for the adsorption. The active carbon having looser structure would hold more fluorine than that having rigid structure.

Reactions of Several Organic Compounds with FAAC. *n*-BuOH and *n*-BuSH were oxidized to their corresponding aldehyde and disulfide, respectively (Table 1). The oxidation of cyclohexylamine gave the adduct with hydrogen fluoride and oily material which could not be identified. When the amine was dropped directly to FAAC at room temperature, it burned violently with a red flame and white smoke. Thus, FAAC can oxidize the compound which easily supplies proton.

Hydrocarbons and alkyl halides were inert to FAAC below 100 °C (Runs 5, 9, 10, and 11), and can be used as an inert solvent. However, at a high temperature such as 250 °C, tetrachloroethylene was fluorinated violently with the rupture of C=C double bond, giving various fluorochlorocarbons.

$$CCl_2{=}CCl_2 \longrightarrow CF_4,\ CF_3Cl,\ CF_2Cl_2,\ CFCl_3$$

The carbon-chlorine bonds were also ruptured, $NiCl_2$ being formed on a nickel sample holder in the reactor. Carbon tetrachloride also gave a small amount of fluorochlorocarbons at this high temperature.

It is interesting to know whether FAAC can be used for selective fluorination. As an example, the chlorine in butyryl chloride was substituted by fluorine with FAAC. The reactions in CCl_4 and in CH_3CN were compared with each other. The yield of butyryl fluoride in CH_3CN was about twice that in CCl_4 under the same conditions. Aprotic polar solvent seems to be preferable for the fluorination of acyl chloride. Attempt to use dimethyl sulfoxide as solvent was unsuccessful because DMSO reacted with the acyl chloride.

Such solvent effects can be explained in terms of the surface polarity of active carbon. Its polarity is nearly zero, and it adsorbs nonpolar molecules preferentially.[10] In CH_3CN, the acyl chloride may be attracted by the surface of FAAC on account of its longer alkyl chain than the solvent. On the other hand, in CCl_4, FAAC may be surrounded by the inert solvent, and the reaction rate will slow down.

Even in CH_3CN, however, the reaction rate is regarded to be small (90% yield after 120 h). This may be due to the slow diffusion of active fluorine from the inner part to the surface of FAAC. Thus, fluorination with FAAC is considered to occur on its surface or near it. The polarities of reactant and solvent should be taken into accout. Stirring of the reaction system is indispensable, and crushing of FAAC in dry atmosphere is effective for better yield.

References

1) Y. Kita, N. Watanabe, and Y. Fujii, *J. Am. Chem. Soc.*, **101**, 3832 (1979).
2) N. Watanabe and T. Kawaguchi, *Nippon Kagaku Kaishi*, **1978**, 1082.
3) N. Watanabe, O. Mochizuki, and Y. Kita, *Carbon*, **17**, 359 (1978).
4) When powder active carbon was used as a starting material, only a small amount of graphite fluoride was formed near the gas inlet in the reaction vessel.
5) N. Watanabe and Y. Kita, *Nippon Kagaku Kaishi*, **1975**, 1896.
6) P. Kamarchik Jr., and J. L. Margrave, *J. Therm. Anal.*, **11**, 259 (1977).
7) K. Takenaka, thesis, Kyoto University, 1975.
8) J. J. Tietjen, P. L. Walker Jr., and L. G. Austin, "Chemistry and Physics of Carbon," Marcel Dekker, New York (1966), Vol. 1, pp. 327—365.
9) J. Boscoe and B. Warren, *J. Appl. Phys.*, **13**, 364 (1942).
10) H. Yanai, "Kyuchaku-kogaku Yohron," Kyoritsu Shuppan, Tokyo (1977), p. 11.

Synthetic Inorganic Ion-exchange Materials. XXXI. Ion-exchange Behavior of Tervalent Metals and Rare Earth Elements on Crystalline Antimonic(V) Acid Cation Exchanger

Mitsuo ABE,* Masamichi TSUJI, and Masato KIMURA**

Department of Chemistry, Faculty of Science, Tokyo Institute of Technology, 2-12-1, Ookayama, Meguro-ku, Tokyo 152

(Received March 26, 1980)

The increasing order of ion-exchange selectivity for tervalent metal ions: $Al^{3+} \ll Ga^{3+} \leq Yb^{3+} < Fe^{3+} < La^{3+} < In^{3+}$, was established in 1 mol dm^{-3} nitric acid solution on a crystalline antimonic(V) acid (C-SbA) cation exchanger. Strong correlation was found between the selectivity and the effective ionic radii of these ions. Large separation factors for neighboring ions were obtained, as compared with the commercial ion exchange resin. An effective separation of aluminium(III)-iron(III) ion pairs and a group separation of garium(III) and ytterbium(III) ions from lanthanum(III) ion were performed by using a relatively small C-SbA column (4 cm × 0.4 cm i.d.).

Various antimonic(V) acids behave as cation exchangers and can be prepared in three different species: crystalline, amorphous, and glassy.[1] Among these antimonic(V) acids, crystalline antimonic(V) acid (C-SbA), $Sb_2O_5 \cdot 4H_2O$, has received much attention during the last two decades, owing to its high selectivity for certain elements.[2] The C-SbA exhibits the increasing order of selectivity in microquantities: $Li^+ < K^+ < Cs^+ < Rb^+ < Na^+$ for alkali metals,[3] $Mg^{2+} < Ba^{2+} < Ca^{2+} < Sr^{2+}$ for alkaline earth metals,[4] and $Ni^{2+} < Mn^{2+} < Zn^{2+} < Co^{2+} < Cu^{2+} < Cd^{2+}$ for bivalent transition metals[5,6] in nitric acid media. Effective separations can be achieved for alkali metals,[3,4,7] the pairs of Mg^{2+}–Ba^{2+}, Ba^{2+}–Sr^{2+}, Cs^+–Sr^{2+},[8] and Cd^{2+}–(Zn^{2+}, Cu^{2+}).[5,6] Adsorption reactions for all these ions obey the reversible ion-exchange reactions.[9–11]

Slightly different selectivity was observed on polyantimonic(V) acid (PAA)[12] and hydrated antimony pentoxide (HAP)[13]: $Rb^+ < Cs^+ < Na^+$,[12] $Cs^+ < Rb^+ < NH_4^+ < K^+ < Na^+$,[14] and $Ra^{2+} < Ba^{2+} < Ca^{2+} < Sr^{2+}$.[12]

No systematic study has been carried out for the selectivity of tervalent metals, including rare earth metals, on C-SbA.

On the other hand, the ion-exchange separations of rare earth metal ions are very difficult in nitric acid media, because of the extreme closeness of the chemical properties of individual rare earth elements. Chromatographic separations of rare earth elements on cation exchange resins have been reported by use of complexing agents, such as citrate, lactate, edta and α-hydroxyisobutyrate.[15] In recent years, radioactivation analysis is the only method which allows the determination of each individual rare earth element in high purity metals or rock samples. Even here, more effective mutual separation of rare earth elements may be needed, as well as better separation from the matrix.[16–20]

An improved selectivity for tervalent metal ions has been found on synthetic inorganic ion exchangers such as titanium arsenate,[21] zirconium tungstate,[22] tin(IV) arsenate,[23] and titanium tungstate.[24]

This paper describes the ion-exchange selectivity for micro-amounts of some tervalent metal ions and rare earth metal ions on C-SbA cation exchanger in nitric acid media, and some applications to the chromatographic separation.

Experimental

Chemicals. Antimony pentachloride supplied by Yotsuhata Chemical Co., Ltd., was employed without further purification. Other chemicals (Wako Pure Chemical Industries, Ltd.) were of purity over 99.5%. The water used was prepared by distilling water and then passing it through a mixed bed of anion and cation exchange resins. The water showed a conductivity lower than 3×10^{-5} s cm^{-1}.

Sample Solutions and Determinations. Stock solutions containing 0.1 M (1 M = 1 mol dm^{-3}) metal ion in 0.1 M nitric acid solution were prepared by dissolving weighed amounts of each metal, aluminium, indium, and lanthanum, and iron(III) nitrate nona-hydrate and ytterbium(III) oxide in moderately concentrated nitric acid solution in order to prevent any hydrolysis with warming. The concentration of iron(III) ion was determined gravimetrically as iron(III) oxide.

For the measurement of equilibrated distribution coefficients of garium(III), indium(III), lanthanum(III), and ytterbium(III) ions, aliquots of supernatant solutions were taken into polyethylene capsules and activated together with their standard metal ion solution in known amounts with the TRIGA II reactor at Musashi Institute of Technology (thermal flux, 4×10^{11} n cm^{-2} s^{-1}; fast flux, 6.5×10^{10} n cm^{-2} s^{-1}). The irradiating time was selected by reference to the thermal cross section and the resonance integral of each nuclide.[25] After a cooling time appropriate for each radionuclide, the γ-spectra of the indicator nuclides were analysed with the "GAMA" system using Ge(Li) detector connected to 4096 channel analyser.[26] The indicator nuclide and γ-energy used for determination were as follows: ^{72}Ga, 833 kev; ^{116m}In, 1508 kev; ^{140}La, 1595 kev; ^{175}Yb, 396 kev. Good linearity was obtained for the calibration curve of each metal ion.

The determination of iron(III) or aluminium(III) ions in microamounts was carried out by a Varian-Techtron 1100 atomic absorption spectrometer. For atomization of aluminium, a Varian-Techtron carbon rod atomizer equipped with an automatic sample dispenser was employed.

The emf titration method was employed for the determination of hydrogen ions in sample solution by using 0.1 mol dm^{-3} sodium hydroxide solution.

Preparation of C-SbA as an Ion Exchanger. The procedure was described in an earlier paper.[1]

** Present address: Okamoto Riken Gomu Co., Ltd., 3-27-12 Hongo, Bunkyo-ku, Tokyo 113.

Distribution Coefficients (K_d). C-SbA (0.250 g) was immersed in 25.0 cm³ of a solution containing metal ion of 1×10^{-4} M in a nitric acid solution adjusted to a desired concentration with intermittent shaking at (30±0.1) °C. The K_d values were determined by the following equation:

$$K_d = \frac{\text{Amount of metal ions in exchanger}}{\text{Amount of metal ions in solution}} \times \frac{\text{cm}^3 \text{ of solution}}{\text{g of exchanger}} \ (\text{cm}^3/\text{g}).$$

The concentrations of the metal ions in solid and solution phases were deduced from the differences between the initial and the final concentrations in supernatant solution.

Column Operation. One μmol of garium(III), lanthanum(III), and ytterbium(III) ions preactivated with reactor neutrons was loaded onto the C-SbA column of 4 cm×0.4 cm i.d. pretreated with 0.1 M nitric acid solution. Then, an appropriate eluant was passed through with a flow rate of 0.3 cm³/min. The effluent was collected in test tubes by using a photosensitive drop count-type fraction collector (Ohtake Works, Ltd., Japan), followed by γ-counting with a Ge(Li) detector connected to a Northern 1705 1024 channel analyzer.

Thermal Analysis and X-Ray Study. These were carried out in the manner described previously.[11]

Results and Discussion

The results of the DTA, TGA, and X-ray studies of C-SbA in hydrogen form showed a good agreement with the earlier results.[1,27]

Ion-exchange Selectivity. The time dependence of adsorption for different metal ions showed that the equilibrium was attained within about 20 d for indium(III) and lanthanum(III) ions (Fig. 1). An extremely slow rate of adsorption for iron(III) ion was observed, about 100 d being required. The variety of time dependence from element to element may be considered to reflect the rigid structure of the C-SbA cation exchanger, as described earlier.[9]

The plot of log K_d *vs.* log [HNO_3] showed a linear relationship with a slope of −3, indicating an "ideal" 3:1 ion-exchange reaction (Fig. 2).

The observed K_d values (logarithmic scale) in 1 M nitric acid solution were plotted against the atomic number (Fig. 3 top). The profile parallels the change in the effective ionic radii (EIR)[28] (Fig. 3 bottom).

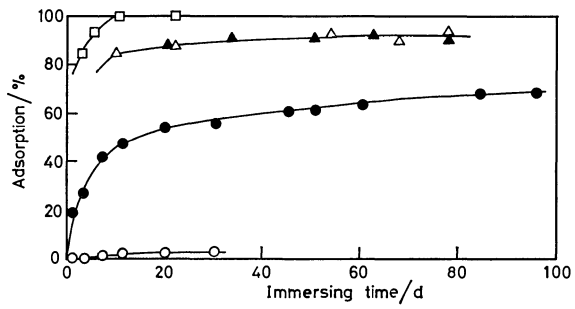

Fig. 1. Time dependence of adsorption of tervalent metal ions on C-SbA.
Ions and concentrations of HNO_3; □: La (0.1 M), △: La (1.0 M), ▲: In (1.0 M), ●: Fe (1.0 M); ○: Fe (4.0 M).

The maximum K_d value was found for ions having about 1 Å of the EIR. Such correlation has been also observed for alkali, alkaline earth, and bivalent transition metal ions, *e.g.*, Na^+ (1.02 Å), Ca^{2+} (1.00 Å), Cd^{2+} (0.95 Å), and Hg^{2+} (1.02 Å). The low K_d values were observed for metal ions having an EIR of about 0.7 Å, *e.g.*, Li^+ (0.74 Å), Mg^{2+} (0.72 Å), and Ni^{2+} (0.700 Å).[5,8-11,29,30] Thus, the ion-exchange reactions are favorable for the ions possessing an EIR of about 1 Å on the C-SbA, if there is a similar situation for the exchange reaction of tervalent metal ions

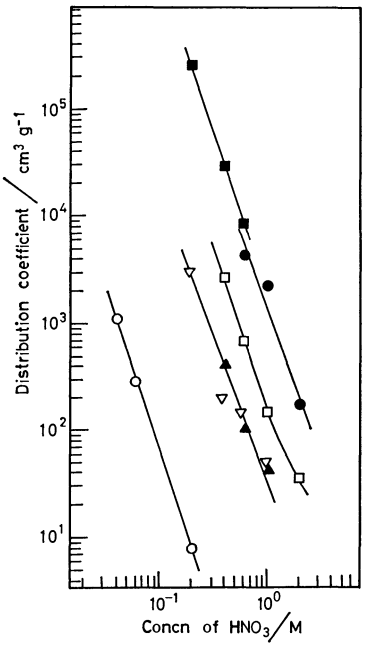

Fig. 2. Distribution coefficients of tervalent metal ions on C-SbA as a function of concentration of HNO_3. Marks, ■: In, ●: La, □: Fe, ▲: Yb, ○: Al, △: Ga.

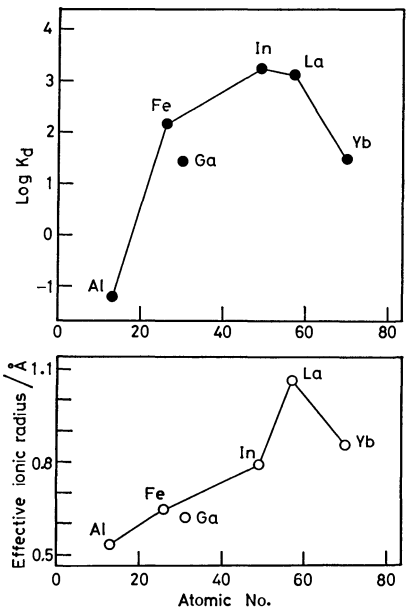

Fig. 3. Relations between changes in K_d values in 1 M HNO_3 and effective ionic radii with atomic number.

on the C-SbA.

In aqueous solution, the cations such as Ni^{2+} and Al^{3+} have an octahedral primary solvation shell.[31] If in the C-SbA the exchanging cations maintain a configuration similar to that in the aqueous solution, the electrostatic forces between ion-exchange sites and the hydrated cations may be less than in the case of partially hydrated or non hydrated cations. A thermodynamic treatment of the ion-exchange reactions reveals that the cations having the EIR of 1.0Å, such as Na^+ and Cd^{2+}, are exchanged as less hydrated cations in the C-SbA with rigid structure than those in aqueous solution.[9,29] If the less hydrated cations are exchanged, the electrostatic force may be increased more than in the case in fully hydrated cations. When a large cation such as Cs^+ is exchanged in the C-SbA, the electrostatic force is less than small cations because of the low electron density for large cations.[30] Therefore we conclude that the C-SbA has an ion-exchange site energetically preferable for the ions with an EIR of about 1 Å.

The C-SbA cation exchanger showed the following selectivity sequence for tervalent metal ions, in increasing order:

$$Al^{3+} \ll Ga^{3+} \leq Yb^{3+} < Fe^{3+} < La^{3+} < In^{3+}.$$

Larger separation factors, $\alpha(A/B)=K_d^A/K_d^B$, were observed on the C-SbA, as compared with those on strong acid-type cation exchange resin[32] (Table 1). The selectivity order for tervalent metal ions on the HAP was found to be in the increasing order: $Fe^{3+}<In^{3+}<Sc^{3+}<Yb^{3+}<Ce^{3+}<Eu^{3+}$ in 1 M nitric acid solution.[13]

Separation of Aluminium(III) and Iron(III) Ions. The separation factor for the pair is very small on organic ion-exchange resin in nitric acid media,[32] and it is difficult to separate them without use of a complexing agent such as ammonium tartrate and citrate. Vydra and Galba[33] have achieved the separation of aluminium(III) from iron(III) ions on hydrous silica by using their hydrolytic products. It is evident from the study of the separation factor for this pair in nitric acid media that their effective separation will be much more favorable on the C-SbA.

When 110 cm^3 of 0.1 M nitric acid solution was used as an eluant, 66% of aluminium(III) ion loaded on the C-SbA was eluted, with a sharp peak followed by a long tail. This may be due to the very slow rate of ion-exchange. It is known that addition of ammonium nitrate improves the elution characteristics for sodium ions.[7] A similar effect was observed for ions studied in the present work, except for iron(III) ion. Therefore a mixed solution of nitric acid and ammonium nitrate was employed for more rapid separation.

When a mixed solution of 0.1 M nitric acid and 0.05 M ammonium nitrate was used as an eluant, aluminium(III) ions were detected from the second fraction and eluted quantitatively with a elution volume of 65 cm^3. More effective elution was achieved by the eluant of a mixed solution of 0.1 M nitric acid and 0.1 M ammonium nitrate: only about a half of the eluant volume was needed for the complete elution (Fig. 4).

Iron(III) ions were not eluted with 70 cm^3 of 0.5 M nitric acid solution. When 6 M nitric acid solution was injected, the iron(III) ions were eluted with a sharp front edge, followed by a strong tailing effect. A mixed solution of 6 M nitric acid and 2 M ammonium nitrate as an eluant showed a similar elution curve. This may be due to a slow rate of ion-exchange for iron(III), as expected from Fig. 1. Thus, 6 M hydrochloric acid was more effective (Fig. 4), owing to the negatively charged chloride complex of the iron(III) ion. Thus, an effective separation was achieved.

Elution Behavior of Garium(III), Ytterbium(III), and Lanthanum(III) Ions. Since separation factors for

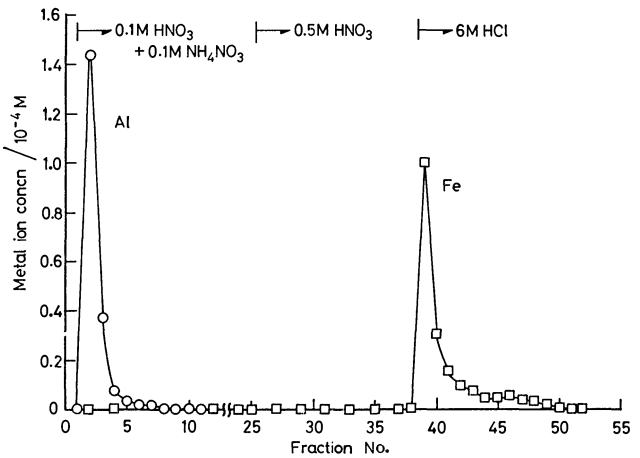

Fig. 4. Separation of Al^{3+}–Fe^{3+} with C-SbA column. One fraction = 5 cm^3. Column size, 4×0.4 cm i.d. Flow rate, 0.3 cm^3 min^{-1}.

TABLE 1. K_d VALUES AND SEPARATION FACTORS (α)[a] OF TERVALENT METAL IONS ON C-SbA IN 1 M HNO_3 SOLUTION

Ion exchanger	Ions	Al	Ga	Yb	Fe	La	In
C-SbA	K_d/cm^3 g^{-1}	6.39×10^{-2}	3.25×10	3.25×10	1.50×10^2	1.34×10^3	1.80×10^3
	α		509	1.00	4.62	8.93	1.34
Ion exchanger	Ions	Fe	Al	Ga	In	Yb	La
Bio-Rad[b] AG50W-X8	K_d/cm^3 g^{-1}	74	79	94	118	193	267
	α		1.0_7	1.1_9	1.2_5	1.6_3	1.3_8

a) Separation factor for neighboring ions. b) Ref. 32.

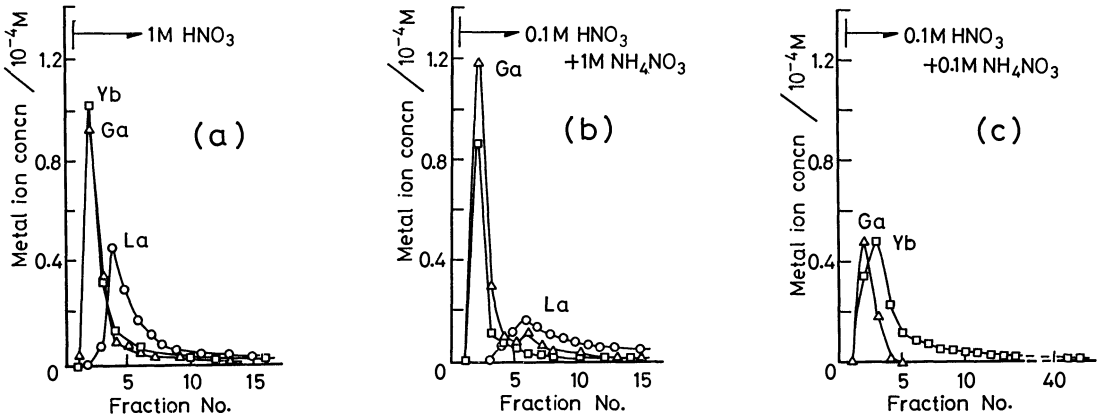

Fig. 5. Elution curves of Ga^{3+}, Yb^{3+}, and La^{3+} with C-SbA column. One fraction=5 cm^3. Column size, 4×0.4 cm i.d. Flow rate, 0.3 cm^3 min^{-1}.

neighboring ions are very small on strong acid-type cation exchange resin in nitric acid media, mutual separations of these tervalent metal and rare earth metal ions can usually be achieved by using aqueous complexing agents or aqueous-organic solvent mixtures.[34] However, even if such a technique is used, much eluant is required for these separations with a large column (*e.g.*, 10 mm i.d.×730 mm h).[18]

On the C-SbA, no ytterbium(III) ions were eluted, but garium(III) ions were partly eluted with 95 cm^3 of a mixed solution of 0.1 M nitric acid and 0.05 M ammonium nitrate. A mixed solution of 0.2 M nitric acid and 0.05 M ammonium nitrate as an eluant showed a similar elution curve for garium(III) ion. A more effective elution was observed for these cations by using a mixed solution containing ammonium nitrate at relatively high concentration (1 M), as in the case of aluminium(III) ions.

Lanthanum(III) ion was not eluted up to 40 cm^3 of 0.5 M nitric-acid solution, and incomplete elution was observed up to 200 cm^3 of the eluant, with a yield of 45%.

Elution peaks with tailings were observed for all elements when 1 M nitric acid (Fig. 5a) and a mixture of 0.1 M nitric acid an 1 M ammonium nitrate (Fig. 5b) were employed as the eluants. The elution order agreed with that of the batch equilibrium data.

The yields up to 16 fractions with 1 M nitric acid solution as an eluant were 95, 89, and 75% for ytterbium(III), garium(III), and lanthanum(III) ions, respectively (Fig. 5a). When a mixed solution of 0.1 M nitric acid and 1 M ammonium nitrate was used as an eluant, these metal ions were eluted with the yields of 70, 65, and 44% for garium(III), ytterbium(III), and lanthanum(III) ions, respectively, up to 13 fractions (Fig. 5b).

The effective group separation was achieved for garium(III) and ytterbium(III) ions from lanthanum(III) ion by using a mixed solution of 0.1 M nitric acid and 0.1 M ammonium nitrate as an eluant (Fig. 5c), while the lanthanum(III) ions adsorbed were completely eluted with a 2 M nitric acid solution. Thus, the C-SbA column can be used repeatedly.

Thanks are due for the assistance by the members of the steering committee of the Radioisotope Laboratory at Tokyo Institute of Technology. The authors wish to express their thanks to Mr. Shogo Suzuki and Dr. Shoji Hirai, Atomic Energy Research Laboratory, Musashi Institute of Technology, for their technical discussions. A part of this work was financially supported by the Japanese Government, The Ministry of Education, under the program for the cooperative use of the TRIGA II reactor installed at Musashi Institute of Technology.

References

1) M. Abe and T. Ito, *Bull. Chem. Soc. Jpn.*, **41**, 333 (1968).
2) M. Abe, *Bunseki Kagaku*, **23**, 1254, 1561 (1974).
3) M. Abe and T. Ito, *Bull. Chem. Soc. Jpn.*, **40**, 1013 (1967).
4) M. Abe, *Bull. Chem. Soc. Jpn.*, **42**, 2683 (1969).
5) M. Abe and K. Kasai, *Sep. Sci. Technol.*, **14**, 895 (1979).
6) M. Abe, *Chem. Lett.*, **1979**, 561.
7) M. Abe, *Sep. Sci. Technol.*, **13**, 347 (1978).
8) M. Abe and K. Uno, *Sep. Sci. Technol.*, **14**, 355 (1979).
9) M. Abe, *J. Inorg. Nucl. Chem.*, **41**, 85 (1979).
10) M. Abe and K. Sudoh, 40th National Meeting of the Chemical Society of Japan, Fukuoka, Oct. 1979, Abstr. I, p. 243.
11) M. Abe and M. Tsuji, *J. Radioanal. Chem.*, **54**, 137 (1979).
12) L. H. Baetsle and D. Huys, *J. Inorg. Nucl. Chem.*, **30**, 639 (1968).
13) F. Girardi, R. Pietra, and E. Sabbioni, *J. Radioanal. Chem.*, **5**, 141 (1970).
14) J. Lefebvre and F. Gaymard, *C. r. Hebd. Séanc. Acad. Sci., Paris*, **260**, 6911 (1965).
15) O. Samuelson, "Ion Exchange Separations in Analytical Chemistry," John Wiley & Sons, New York (1963), pp. 338—352.
16) T. Bereznai, *J. Radioanal. Chem.*, **9**, 81 (1971).
17) E. B. Denechaud, P. A. Helmke, and L. A. Haskin, *J. Radioanal. Chem.*, **6**, 97 (1971).
18) P. Rey, H. Wakita, and R. A. Schmitt, *Anal. Chim. Acta*, **51**, 163 (1970).
19) J. Duffield and G. R. Gilmore, *J. Radioanal. Chem.*, **48**, 135 (1979).
20) R. Dybvzynski, S. Sterlinski, and C. Golian, *J. Radioanal. Chem.*, **16**, 105 (1973).
21) M. Qureshi, H. S. Rathore, and R. Kumar, *J. Chem.*

Soc., A, **1970**, 1986.
22) A. K. De and N. D. Chrowhury, *Chromatographia*, **12**, 448 (1979).
23) M. Qureshi, R. Kumar, and H. S. Rathore, *J. Chem. Soc., A*, **1970**, 272.
24) M. Qureshi and J. P. Gupta, *J. Chem. Soc., A*, **1970**, 2620.
25) R. Van der Linden, F. De Corte, and J. Hoste, *J. Radioanal. Chem.*, **20**, 695 (1977).
26) Y. Murata, S. Hirai, M. Okamoto, and H. Kakihana, *J. Radioanal. Chem.*, **36**, 525 (1977).
27) M. Abe, *Kogyo Kagaku Zasshi*, **70**, 2226 (1967).
28) R. D. Shannon and C. T. Prewitt, *Acta Crystallogr., Sect. B*, **25**, 925 (1969).
29) M. Abe and K. Sudoh, *J. Inorg. Nucl. Chem.*, **42**, 1051 (1980).
30) M. Abe, *Denki Kagaku*, **48**, 344 (1980).
31) J. Burgess, "Metal Ions in Solution," Ellis Horwood Ltd., England (1978), Chap. 5.
32) F. W. E. Strelow, R. Rethemeyer, and C. J. C. Bothma, *Anal. Chem.*, **37**, 106 (1965).
33) F. Vydra and J. Galba, *Z. Anal. Chem.*, **235**, 166 (1968).
34) "Ion Exchange and Solvent Extraction," ed by J. A. Marinsky and Y. Marcus, Marcel Dekker, Inc., New York (1973), Vol. 4, p. 84.

  Bull. Chem. Soc. Jpn., 54, 135—137 (1981)

Formation of Zn-bearing Ferrite by Air Oxidation of Aqueous Suspension

Tadao KANZAKI,* Jun-ichiro NAKAJIMA, Yutaka TAMAURA, and Takashi KATSURA

Department of Chemistry, Tokyo Institute of Technology Ookayama, Meguro-ku, Tokyo 152

(Received April 1, 1980)

Zn-bearing spinel ferrites were obtained by air oxidation of the iron(II) hydroxide suspension of the mole fraction Zn(II) to [Zn(II)+Fe_{total}], r_{Zn}, ranging from 0.029 to 0.33 (except for 0.057) at pH 10.0 and 65 °C, but at r_{Zn}=0.057 only α-FeOOH was formed. The Zn-bearing spinel ferrite obtained at r_{Zn}=0.33 has the normal spinel structure. At pH 8.0, the Zn-bearing spinel ferrite is obtained at r_{Zn}=0.057, but the spinel ferrite is slightly oxidized to γ-Fe_2O_3.

Recently, the conditions for the formation of spinel ferrite from aqueous iron(II) hydroxide suspensions containing other metal ions have been investigated in detail by several workers.[1-4] Kiyama[1] investigated the formation of Mn- and Co-bearing spinel ferrites and reported that, in alkaline suspensions, all the metal ions were incorporated into the spinel ferrites. Katsura *et al.*[2] reported that the oxidized Fe_3O_4–Fe_2TiO_4 solid solution with spinel structure was obtained from the suspension containing titanium(IV) ions. Kaneko *et al.* investigated the formation of Mg-[3] and Cd-[4] bearing spinel ferrites. When the mole fraction of Mg(II) to [Mg(II)+Fe_{total}] or Cd(II) to [Cd(II)+Fe_{total}] in the suspension is below 0.091, almost all the metal ions are incorporated into the spinel ferrite by an oxidation reaction at pH 9.0. When the mole fraction is above 0.091, the excess magnesium(II) produces a basic magnesium(II) sulfate, and the crystalline phases formed from the suspension containing cadmium(II) ion are changed in a complicated way.

In this paper, the reaction conditions for the formation of Zn-bearing spinel ferrite from the suspension containing zinc(II) ion are investigated.

Experimental

Reagents. Chemical reagents of analytical grade were used. A 2 mol/dm³ sodium hydroxide solution was prepared by dissolving sodium hydroxide in distilled water free from carbon dioxide and oxygen. A sulfuric acid solution of 0.856 mol/dm³ zinc(II) sulfate (pH≅3) was prepared from zinc(II) sulfate heptahydrate.

Apparatus. The reaction vessel of the Dewar type used in this study was the same as that employed previously by Kaneko and Katsura.[3]

Procedure. After adding distilled water, zinc(II) sulfate solution, and sodium sulfate to the reaction vessel, nitrogen gas was bubbled into the solution while it was being stirred at 1000 min^{-1} for 1 h to remove the dissolved gases of carbon dioxide and oxygen. Then 12 g of iron(II) sulfate heptahydrate was added to the solution. The resultant volume of the solution was set to 200 cm³, and the total concentration of the sulfate ion was fixed to 65 mmol/200 cm³. pH values were adjusted by using 2 mol/dm³ sodium hydroxide solution and the suspension was let stand for 1 h with stirring under nitrogen at 65 °C (we call this suspension the "initial suspension"). The subsequent procedures were the same as those described by Kaneko and Katsura.[3] The precipitate in this paper means the product obtained by lowering the pH value of the suspension to pH 4.0 with 0.5 mol/dm³ sulfuric acid after the air oxidation. At this pH value, zinc(II) hydroxides and iron(II) hydroxides dissolve completely.

Chemical Analysis. The zinc(II) content was determined by atomic absorption spectrometry after the extraction of an iron with diisopropyl ether. The amounts of iron(II) and iron(III) were determined by the method described by Kaneko and Katsura.[3]

The precipitates were examined by the X-ray powder diffraction method with Fe $K\alpha$ radiation, the electron microscopy, and the Mössbauer spectra measurement at room temperature.

Titration curves were obtained as follows. A sulfuric acid solution containing zinc(II) and/or iron(II) sulfates was titrated with 2 mol/dm³ sodium hydroxide solution at 65 °C. Nitrogen gas was bubbled into the solution during the titration and the values of pH were measured at each point 10 min after the addition of the sodium hydroxide solution.

Results and Discussion

X-Ray Powder Diffraction Patterns, Electron Micrograph, Chemical Composition, and Mössbauer Spectra of the Precipitate obtained by Air Oxidation at pH 10.0. In the X-ray powder diffraction patterns of the precipitate obtained from the suspension of the r_{Zn} values (the r_{Zn} value means the mole fraction of Zn(II) to [Zn(II)+Fe_{total}] in the initial suspension) ranging from 0.029 to 0.33 (except for 0.057), only the peaks for spinel type structure were seen, while at r_{Zn}= 0.057, only the peaks for α-FeOOH were observed. The electron micrographs of the precipitate showed the formation of a spherical or cubic particle of spinel ferrite, except for a needle-like crystal of α-FeOOH for r_{Zn}=0.057. Lattice constants a_0 of the spinel ferrites are plotted against the r_{Zn} values in Fig. 1 (curve A). The lattice constants of completely oxidized samples with spinel type structure are also plotted (curve B). The oxidation of the spinel ferrites was performed by heating at 180 °C in air for 6 h. In the X-ray powder diffraction patterns of the oxidized samples, only the peaks for the spinel type structure were seen. Chemical analyses showed that there was no detectable amount of iron(II) in the oxidized samples. As seen from the curves A and B in Fig. 1, the lattice constants of the spinel ferrites and those of completely oxidized samples increase with increasing the r_{Zn} values. This shows that Fe^{2+} in the spinel ferrite is replaced by Zn^{2+}, and that the amount of Zn^{2+} on the lattice points increases with increasing the r_{Zn} values. Chemical analyses showed that, at the r_{Zn} values ranging from 0.029 to 0.33 (except for 0.057), almost all zinc(II) ions in the initial suspension

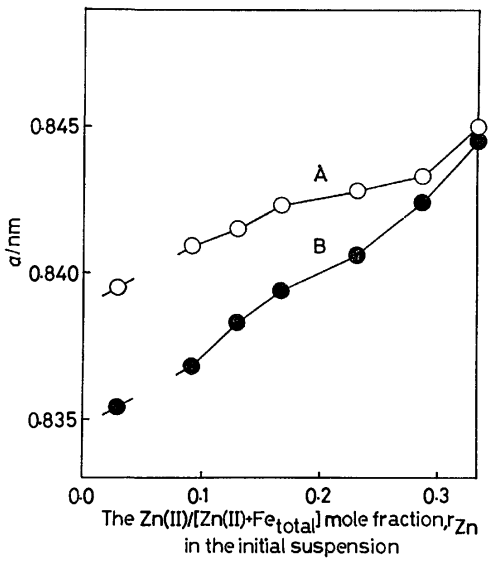

Fig. 1. The relationship between the Zn(II)/[Zn(II)+Fe$_{total}$] mole fraction in the initial suspension and the lattice constants of the spinel ferrite obtained at pH 10.0 or those of the completely oxidized sample with spinel type structure. The curve A: the spinel ferrite, the curve B: the completely oxidized sample, a: the lattice constant.

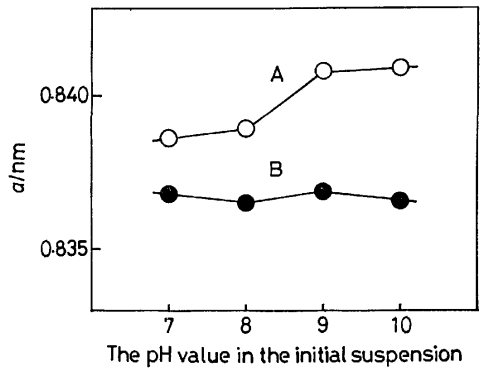

Fig. 2. The relationship between the pH value in the initial suspension and the lattice constants of the spinel ferrite obtained at the Zn(II)/[Zn(II)+Fe$_{total}$] mole fraction of 0.091 in the initial suspension or those of the completely oxidized sample with spinel type structure. The curve A: the spinel ferrite, the curve B: the completely oxidized sample, a: the lattice constant.

(>92%) were taken into the precipitate. The mole fractions of [Zn(II)+Fe(II)] to [Zn(II)+Fe$_{total}$] in the precipitate were 0.30—0.35. These values are close to those of stoichiometric spinel ferrite Fe_3O_4–$ZnFe_2O_4$ (0.333). The lattice constant of the Zn-bearing spinel ferrite at $r_{Zn}=0.33$ (Fig. 1) is very close to that of zinc spinel ferrite $ZnFe_2O_4$ synthesized by the solid state reaction (0.8441 nm).[5]

The Mössbauer spectrum at room temperature of the precipitate obtained at $r_{Zn}=0.33$ showed a quadrupole-split pattern. The isomer shift relative to metallic iron estimated from the quadrupole-split spectrum (0.030 cm s^{-1}) is in good agreement with that of zinc spinel ferrite synthesized by solid state reaction (0.0358 cm s^{-1})[6] within our experimental errors (±0.008 cm s^{-1} as stand. dev.). Thus, the Zn-bearing spinel ferrite obtained at $r_{Zn}=0.33$ and pH 10.0 is concluded to be the zinc spinel ferrite which has the normal spinel structure.

pH *Dependence on the Formation of the Precipitate for* $r_{Zn}=0.091$. In the X-ray powder diffraction patterns of the precipitate obtained by air oxidation of the suspension of $r_{Zn}=0.091$ at pH values ranging from 7.0 to 10.0, only the peaks for spinel type structure were seen, while at pH 11.0 only the peaks for α-FeOOH were observed. The electron micrographs of the precipitate showed the formation of a spherical or cubic particle of spinel ferrite, except for a needle-like crystal of α-FeOOH at pH 11.0. Figure 2 shows the lattice constants a_0 of the spinel ferrites obtained at pH ranging from 7.0 to 10.0 (curve A) and those of the completely oxidized samples with spinel type structure (curve B). As seen from curve B, the lattice constants of the completely oxidized samples are constant within our experimental errors. Chemical analyses showed that almost all zinc(II) ions in the initial suspension (>92%) were taken into the precipitate at the pH values ranging from 7.0 to 10.0, but at pH 11.0, only about 40% of zinc(II) ions were taken in. These results show that, at these pH values, Zn-bearing spinel ferrites which have a constant amount of Zn^{2+} on the lattice points are formed. The mole fractions of [Zn(II)+Fe(II)] to [Zn(II)+Fe$_{total}$] in the precipitate decreased from 0.31 to 0.26 upon decreasing the pH values from 10.0 to 7.0. The lattice constants of the Zn-bearing spinel ferrites obtained at lower pH values, as shown by curve A in Fig. 2, are smaller than those of the spinel ferrites obtained at a higher pH value. These suggest that a Zn-bearing spinel ferrite which is slightly oxidized to γ-Fe_2O_3 is formed at lower pH values. From the electron micrographs, it was shown that the particle size of the Zn-bearing spinel ferrites becomes small at a lower pH value (0.1 and 0.2 μm at pH 7.0 and 10.0, respectively), which seems to cause further oxidation of the spinel ferrites at this lower pH value.

Depression of the Formation of Zn-bearing Spinel Ferrite. As mentioned in a previous section, at $r_{Zn}=0.057$ and pH 10.0 the formation of Zn-bearing spinel ferrite is depressed and α-FeOOH is formed. The depression of the Zn-bearing spinel ferrite was, however, restored, when the pH value in the initial suspension was lowered to pH 8.0, that is, only the peaks for the spinel type structure were seen in the X-ray powder diffraction pattern of the precipitate.

Figure 3 shows the titration curves of the solutions of iron(II) sulfate (curve A), zinc(II) sulfate (curve B) and the mixed solution of zinc(II) and iron(II) sulfates (curve C). Iron(II) sulfate is titrated at pH values around 6.7—8.0 (curve A). However, zinc(II) sulfate is titrated first at pH around 5.5—6.0 (region a—b in curve B), and then around 7.4 (region c—d in curve B). During the titration of zinc(II) sulfate, in the region a—c in curve B, a basic zinc(II) sulfate seems to precipitate, and then in the region c—d, the basic zinc(II) sulfate is converted into $Zn(OH)_2$. The

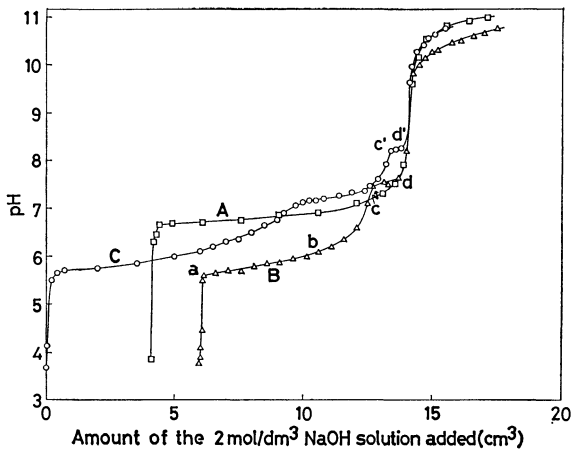

Fig. 3. The titration curves of Fe(II), Zn(II), and Zn(II)+Fe(II) sulfate solutions by 2 mol/dm³ NaOH. The curve A: 1.08×10^{-2} mol Fe(II), the curve B: 8.56×10^{-3} mol Zn(II), the curve C: 8.56×10^{-3} mol Zn(II)+8.53×10^{-3} mol Fe(II). The titration curves of Fe(II) and Zn(II) sulfate solutions are shown from titer of 4.10 cm³ and 6.00 cm³, respectively to compare with that of Zn(II)+Fe(II) sulfate solution. The initial volume of the solutions was fixed to 200 cm³.

point c in curve B represents the addition of 1.5 moles of sodium hydroxide per atom of zinc. Therefore, we can estimate the chemical formula of the hydrolyzed species at this point to be $Zn(OH)_{1.5}(SO_4)_{0.25}$[7] by assuming that the sulfate ion is coprecipitated. In the case of the mixed solution of zinc(II) and iron(II) sulfates, as seen by curve C (Fig. 3), the conversion reaction of the basic zinc(II) sulfate into $Zn(OH)_2$ occurs also at pH around 8.3 (region c'—d' in curve C).

Thus, at pH 8.0 where the depression of the Zn-bearing spinel ferrite formation is restored, the basic zinc(II) sulfate is precipitated in the suspension before air oxidation.

The authors wish to express their thanks to Drs. Masanori Abe and Tadashi Sugihara of Tokyo Institute of Technology for the measurement of the Mössbauer spectra and for helpful discussions.

References

1) M. Kiyama, *Bull. Chem. Soc. Jpn.*, **51**, 134 (1978).
2) T. Katsura, Y. Tamaura, and G. S. Chyo, *Bull. Chem. Soc. Jpn.*, **52**, 96 (1979).
3) K. Kaneko and T. Katsura, *Bull. Chem. Soc. Jpn.*, **52**, 747 (1979).
4) K. Kaneko, K. Takei, Y. Tamaura, T. Kanzaki, and T. Katsura, *Bull. Chem. Soc. Jpn.*, **52**, 1080 (1979).
5) X-Ray Data Card, 22—1012, A.S.T.M.
6) M. Robbins, G. K. Wertheim, R. C. Sherwood, and D. N. E. Buchanan, *J. Phys. Chem. Solids*, **32**, 717 (1971).
7) G. N. Dobrokhotov, *Zh. Prikl. Khim.*, **27**, 1056 (1954); "Stability Constants of Metal-Ion Complexes," ed by L. G. Sillén, The Chemical Society, London (1964), Spec. Pub., No. 17, p. 243.

Oxidation-Reduction Properties of Mixed Oxides in the Cerium-Uranium-Oxygen System

Hiroaki TAGAWA,*,† Takeo FUJINO,* Kenju WATANABE,††
Yumiko NAKAGAWA,†† and Kōji SAITA††
Division of Chemistry, Japan Atomic Energy Research Institute, Tokai-mura, Ibaraki 319-11
(Received April 4, 1980)

The formation and the oxidation-reduction properties of mixed oxides in the Ce–U–O ternary system were examined by means of thermogravimetry and the X-ray diffraction technique. The mixed oxides were prepared by the reactions of CeO_2 with U_3O_8 in air and in hydrogen. The composition of the products heated in air, followed by slow cooling to room temperature, was approximately expressed by this equation: $yCeO_2+(1-y)UO_{2.67}$. By X-ray diffraction, it was shown that the oxides formed at 1100 °C in air were mixtures of $Ce_{0.6}U_{0.4}O_{2.3}$ and α-U_3O_8 in the $y<0.6$ range, while they were in single phases of solid solutions for $y\geq0.6$. When the mixed oxides, MO_{2+x}, where M indicates yCe$+(1-y)$U, were re-heated in air, weight loss due to oxygen liberation was observed above 500 °C, and it was enhanced with a rise in the temperature. The hydrogen reduction of the oxides proceeded in two steps; the first step was the reduction of MO_{2+x} to MO_2 below 600 °C, and the second one was the reduction of MO_2 to MO_{2-x} above 600 °C. The composition of the oxides obtained can be given by this equation: $yCeO_{1.81}+(1-y)UO_{2.00}$. Two separate linear relationships for the lattice parameter of the fluorite-type structure as a function of the cerium content were obtained; one is applicable to the solid solutions with $y\leq0.6$, where the lattice parameter is nearly that of UO_2, and the other to the solid solutions with $y\geq0.4$. The latter obeys Vegard's law between UO_2 and CeO_2. The oxides with $y=0.4$—0.6 were in the two-phase region of the solid solutions.

In the cerium-uranium-oxygen system, it has been shown that there exists a homogeneous region of the solid solution with a fluorite structure. Several workers[1-8] have investigated its composition range, lattice parameter, and thermodynamic properties. A phase diagram of the system at 900 °C was first drawn by Hoch and Furman[4] from the data of Hund[1] and the results of their own quenching experiments. Later, Markin *et al.*[5] constructed a phase diagram between UO_2–U_3O_8 and CeO_2–$CeO_{1.81}$ for temperatures between room temperature and 600 °C using the results obtained by the high temperature X-ray diffraction technique. In spite of their experiments, however, the literature data on the phase relations and the chemical properties seem still to be incomplete.

Cerium is produced in nuclear fuels as one of the fission products of high yields. The knowledge of the Ce–U–O ternary system is, therefore, of basic importance for investigating the irradiation behavior of uranium dioxide fuel in connection with the changes in the phase relations and in the thermodynamic properties caused by accumulated fission products. In addition, cerium is often used in simulation studies of plutonium, a promised fissile material in fast breeder reactor, because of their similar chemical and/or thermodynamic behavior. Therefore, the investigation of this ternary system would contribute to our knowledge of the phase behavior of the Pu–U–O system, too. The physical and chemical properties as well as the phase relations of the Ce–U–O system have, nevertheless, not been systematically studied. In the present experiment, we investigated the formation and the oxidation-reduction properties of the mixed oxide of the Ce–U–O ternary system by means of thermogravimetry and the X-ray diffraction technique. The literature data on the lattice parameter, which were rather scattered, were also re-examined.

Experimental

Materials. CeO_2 of a 99.99% purity was provided by the Shin-etsu Chemical Co. Ltd. The oxide was heated at 1000 °C in air for 3 h before use. U_3O_8 was prepared by heating ammonium diuranate at 900 °C in air for 24 h. Both compounds were weighed so that the cerium contents were 0.10, 0.20, 0.27, 0.40, 0.50, 0.60, and 0.80 atom% in the respective mixtures. Mixing was done in an agate mortar, and the mixtures were compacted at 3×10^8 Pa into cylindrical pellets 10 mm in diameter and about 2 mm thick. The weight of each pellet was about 800 mg.

Apparatus and Procedures. The experiments were mainly carried out by the use of the thermogravimetric technique. The apparatus consists of a Cahn Model-RH electrobalance, a pressure-measurement system, a gas-supply system, and vacuum pumps. The balance was adjusted so as to have a maximum weight change of 500 mg and a sensitivity of 0.01 mg. A fused quartz crucible, 20 mm in height and 18 mm in outer diameter, was suspended from the balance. Then, a quartz reaction tube, 26 mm in outer diameter and 310 mm in length, was connected to the vessel containing the balance. After the reaction system had been evacuated to 10^{-1} Pa, the sample was weighed. The system was then filled with air (or hydrogen in the reduction experiments) and the temperature was raised. Hydrogen from the cylinder was used after having been purified by passage through palladium asbestos heated at 300 °C and through a liquid-nitrogen trap. The weight change due to buoyancy and convection was corrected by using a platinum wire. The sample was weighed again in a vacuum after the reaction.

The temperature of the sample was measured with a Pt/Pt+13%Rh thermocouple placed close to the crucible inside the reaction tube. The furnace temperature was automatically controlled so as to be raised at a constant heating rate or to be held at a desired point. The experiments were made at the heating rate of 2 °C/min.

† Present address: Institute of Environmental Science and Technology, Yokohama National University, Tokiwadai, Hodogaya-ku, Yokohama 240.

†† Department of Chemistry, Tokyo Gakugei University Nukuikita, Koganei, Tokyo 184.

X-Ray Analysis. The samples were finely ground, loaded into capillaries, and then vacuum-sealed. The X-ray photographs were obtained with a Norelco 114.6 mm camera using nickel-filtered Cu $K\alpha$ radiation. The lattice parameters were obtained by least-squares calculations for the diffraction lines at higher angles.

Results and Discussion

Formation of Mixed Oxides in Air. The reaction of CeO_2 with U_3O_8 was examined by heating mixture pellets with various cerium contents from room temperature to 1100 °C in air. After the temperature had been raised to 1100 °C, the sample was held at that temperature for 3 h; then it was slowly cooled. When heated in air, U_3O_8 began to lose oxygen at about 890 °C, and the O/U ratio was lowered from 2.667 to 2.653 at 1100 °C. On the other hand, the weight loss of CeO_2 was not observed up to 1100 °C. For the mixtures of CeO_2 and U_3O_8, it was found that the weight loss occurred at slightly lower temperatures than that of U_3O_8 in any mixing ratio. The weight loss at high temperatures was augmented by y, which suggests a reaction between CeO_2 and U_3O_8, the mixed oxide thus formed being oxygen-deficient compared with the initial bulk composition of the sum of $y\mathrm{CeO_2}+((1-y)/3)\mathrm{U_3O_8}$. While the sample was held at 1100 °C for 3 h, the O/M ratio decreased slightly with time; here, M indicates $y\mathrm{Ce}+(1-y)\mathrm{U}$. The X-ray patterns of these oxides showed that the products were mixtures of α-U_3O_8 and solid solution for $y=$ 0—0.5, and homogeneous solid solutions for $y\geq 0.6$.

Formation of Mixed Oxides in Hydrogen. The reduction of U_3O_8 with hydrogen began at about 330 °C and finished at 630 °C. The product was $UO_{2.000}$. On the other hand, the reduction of CeO_2 with hydrogen began at 550 °C, and then the O/Ce atom ratio gradually decreased with an increase in the temperature. The O/Ce ratio was 1.815 at 1000 °C, and it was hardly changed even after the sample was kept at that temperature for 3 h. As for the mixtures of CeO_2 and U_3O_8, the weight loss began at about 330 °C, the initiation temperature of the reduction of U_3O_8, for any mixing ratio. When the sample was heated further, a plateau appeared on the TG curve around the O/M ratio of 2.02 at temperatures between 600 and 650 °C. Above 650 °C the O/M ratio was seen to decrease again with increasing temperature. This reaction behavior of the CeO_2 and U_3O_8 mixtures in hydrogen atmosphere is very similar to that of the solid solution, as will be stated below.

Hydrogen Reduction of the Mixed Oxides Prepared in Air. Typical TG curves for the reduction of U_3O_8, CeO_2, and the mixed oxides are shown in Fig. 1. The mixed oxides were prepared by heating mixtures of CeO_2 and U_3O_8 at 1100 °C for 3 h in air. As may be seen in the figure, the mixed oxides were reduced to an O/M ratio of nearly two by heating up to 600 °C. Then, the plateau appeared in the temperature range between 600 and 650 °C, after which the specimens were again reduced, but at slower rates. From this fact, it is deduced that the oxides with O/M

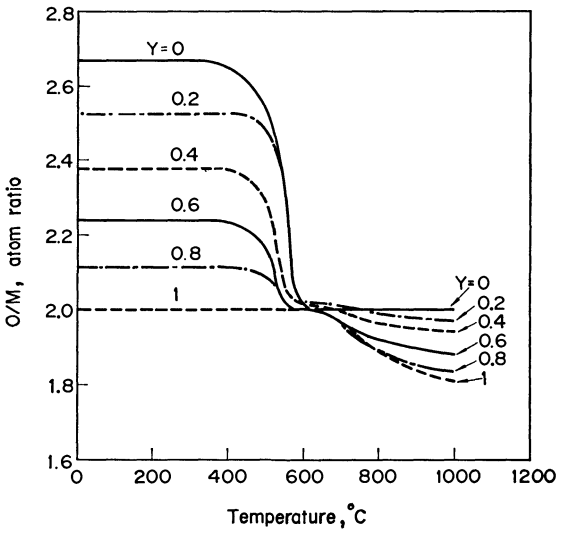

Fig. 1. TG curves for reduction of the mixed oxides MO_{2+x} in hydrogen atmosphere.
Heating rate: 2 °C/min, y: Ce/(Ce+U) ratio.

>2 are reduced more easily than those with O/M<2. This is related to the thermodynamic properties of the solid solution. Thermodynamic studies of $MO_{2\pm x}$ [4,6] show that the curve of the partial molar Gibbs energy of oxygen, $\Delta\overline{G}_{O_2}(MO_{2\pm x})$, against x for any y value changes from a large negative value at O/M<2 to a small negative value at O/M>2 in a sigmoid shape. The large change in $\Delta\overline{G}_{O_2}$ occurs in the vicinity of the stoichiometric composition, O/M≈ 2. As the Gibbs energy of formation of water, $\Delta G^\circ_f(H_2O)$, is close to $\Delta\overline{G}_{O_2}(MO_{\approx 2})$ at temperatures from 600 to 1000 °C, it is reasonable to suppose that the solid solution is readily reduced with hydrogen to the composition with O/M≈ 2. The reduction of the solid solution proceeds by removing the produced water vapor.

The X-ray pattern of the product showed that it was a two-phase mixture with the fluorite-type structure for $0.4\leq y\leq 0.6$, and a single-phase product with the fluorite-type structure for $y\leq 0.3$ and $y>0.6$. The O/M ratio and the lattice parameter of the mixed oxide thus formed are shown in Table 1.

Air Oxidation of the Mixed Oxides Prepared in Hydrogen. Figure 2 shows some typical TG curves for the oxidation of the mixed oxides in air. The mixed oxides used here were prepared by reducing mixtures of CeO_2 and U_3O_8 with hydrogen in situ in a quartz crucible at 1000 °C for 3 h. In a series of experiments to check the completeness of mixing, the reduced pellets were crushed, intimately mixed, and then recompacted into pellets which were used for oxidation. When air was re-introduced into the reaction vessel after evacuation, the sample was slowly oxidized to the O/M ratio of nearly two even at room temperature. This oxidation reaction was accelerated by heating. For the oxidation of UO_2, the formation of U_3O_7 as the intermediate phase was seen on the TG curve. This bend was observed in the oxides of $y=$ 0.1—0.4. Every TG curve for the oxidation of MO_{2-x}

Table 1. Compositions, phases, and lattice parameters of the mixed oxides

y	Oxidized in air at 1100 °C			Reduced in hydrogen at 1000 °C		
	O/M ratio	Phase	Lattice parameter/Å	O/M ratio	Phase	Lattice parameter/Å
0	2.667	α-U_3O_8	a=6.7313 b=11.958 c=4.1451	2.000	UO_2	5.4700
0.10	2.594	α-U_3O_8+s.s.	5.433	1.981	fcc	5.4701
0.20	2.533	α-U_3O_8+s.s.	5.428	1.982	fcc	5.4696
0.27	2.479	α-U_3O_8+s.s.	5.424			
0.40	2.379	α-U_3O_8+s.s.	5.423	1.945	fcc	5.4675(strong) 5.44—5.45(weak)
0.50	2.320	α-U_3O_8+s.s.	5.423	1.914	fcc	5.4683(strong) 5.4412(weak)
0.60	2.24	fcc	5.4269	1.899	fcc	5.4646(weak) 5.4372(strong)
0.80	2.115	fcc	5.4192	1.857	fcc	5.4237
1	2.000	CeO_2	5.4111	1.815	CeO_{2-x}	

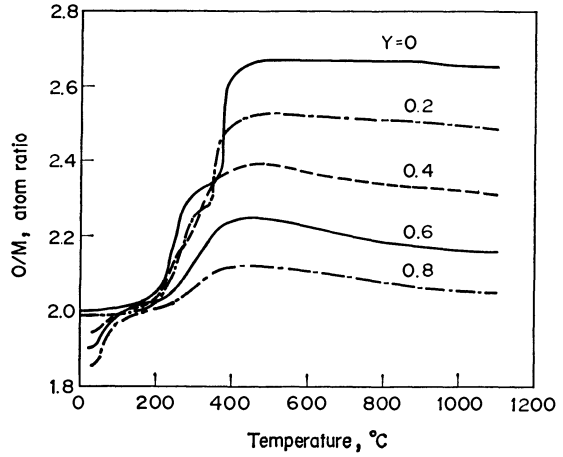

Fig. 2. TG curves for oxidation of the mixed oixdes MO_{2-x} in air.
Heating rate: 2 °C/min, y: Ce/(Ce+U) ratio.

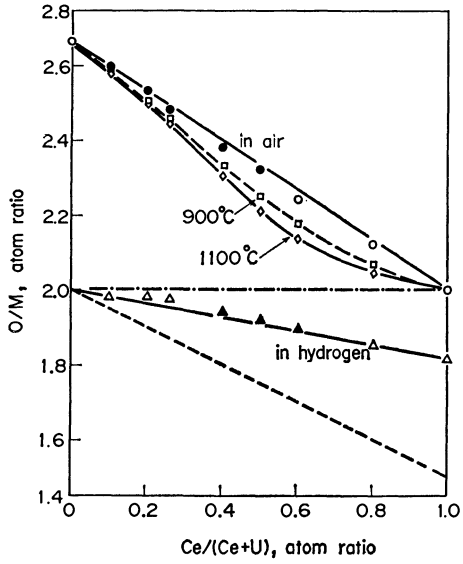

Fig. 3. Variation of the O/M atom ratio of the mixed oxides as a function of cerium concentration.
●: Two-phase mixture below 500 °C in air, ○: single phase below 500 °C in air, □: O/M ratio of the mixed oxides at 900 °C in air,' ◇: O/M ratio of the mixed oxides at 1100 °C in air, △: single phase in hydrogen, ▲: two-phase mixture in hydrogen.

showed a maximum of the O/M ratio at temperatures between 450 and 500 °C. Above 500 °C, the oxides began to lose their oxygen. The decrease in the O/M ratio was enhanced with a rise in the temperature. When the oxides were cooled from higher temperatures than the temperature giving the maximum O/M ratio, the O/M value increased on the line of the heating process up to the maximum O/M ratio, and the value was maintained unchanged on a further lowering of the temperature.

The X-ray pattern of the product revealed that it was a mixture of α-U_3O_8 and the solid solution for $y \leq 0.5$, and was in the single phase of the solid solution for $y \geq 0.6$. For the product of the y values between 0.1 and 0.5, the X-ray intensity of the diffracted α-U_3O_8 lines was weakened with the increase in the cerium content. Although the U_3O_8 phase which was formed accompanying the solid solution has been reported to be in the β modification,[7] it was identified as α-U_3O_8 by the present analysis of the X-ray patterns. The O/M ratio, phase, and lattice parameter for the product slowly cooled from 1100 °C in air are shown in Table 1. It may be seen that the lattice parameter of the cubic fluorite phase remains constant regardless of the cerium content between y=0.1 and 0.5. The products of y=0.6 and 0.8 were found to be in a single phase with the fluorite-type structure, and their lattice parameters were lowered with an increase in the cerium content.

Valence State of Uranium and Cerium in the Mixed Oxides. Figure 3 shows the O/M ratio *vs.* Ce/M ratio for the samples prepared under various reaction conditions. The straight line connecting the circles represents the O/M ratio of the oxides heated in air at 1100 °C, followed by annealing to room temperature. The open circles indicate a single phase, and the filled circles, a two-phase mixture. The other marks represent the

O/M ratio of the samples heated at 900 and 1100 °C in air. The figure shows that the mixed oxide prepared in air is the single phase with a fluorite structure at least below the O/M ratio of 2.24. In the U–O system, the phase diagram shows that the composition range of the fluorite phase extends to O/U=2.25. The O/M ratios of the samples which were obtained by reducing the mixed oxides in a hydrogen atmosphere at 1000 °C for 3 h and then slowly cooling them to room temperature are indicated by △ and ▲ in the same figure, where open and filled marks indicate single-phase and two-phase, respectively. All the oxides prepared in hydrogen had the fluorite structure. The oxides for y=0.4—0.6 consisted of two phases with different lattice parameters. The O/Ce atom ratio of the cerium oxide reduced by hydrogen was 1.815, the same as the ratio reported by Markin *et al.*[5]

For the mixed oxides prepared in air, the O/M ratios of the oxides below 500 °C decrease nearly linearly from 2.667 of U_3O_8 at y=0 to 2.00 of CeO_2 at y=1. This shows that the mean valence state of uranium, +5.33, is not varied by the dissolution of cerium. On the other hand, the O/M ratios of the oxides at 900 and 1100 °C in air are lower than those of the oxides cooled to room temperature. For example, the O/M ratios of the mixed oxides at 900 °C are 2.18 for y=0.6 and 2.07 for y=0.8, the mean valence states of uranium being +4.9 and +4.7 respectively, if cerium is regarded as in the +4 state.

The tendency for the valence state of uranium not to vary or, rather, to be diminished, by the addition or cerium is obviously different from the case of the Sr–U–O system.[9] In this system, the valence state of uranium was raised from +5.33 of U_3O_8 to +6.00 of Sr_2UO_5 with an increase in the content of strontium.

For the mixed oxides prepared in hydrogen, MO_{2-x}, the O/M ratio decreases nearly linearly from 2.00 at y=0 to 1.815 at y=1. This fact shows that the valence state of uranium is +4 and that of cerium is +3.63, neither of which is varied by the Ce/U atom ratio.

Lattice Parameters of the Mixed Oxides. The lattice parameters of the mixed oxides prepared in air and in hydrogen are plotted as functions of the cerium content in Fig. 4, together with the data from the literature.[1–5,7]

The oxide prepared at 1100 °C in air is two-phase mixture for y<0.6. The constant lattice parameter, 5.426 Å, though scattered, indicates that the mixed oxide is in two phases, $Ce_{0.6}U_{0.4}O_{2.3}$+α-U_3O_8. The composition of $Ce_{0.6}U_{0.4}O_{2.3}$ was obtained from Fig. 3 using the intersection between the lattice parameter in the two-phase region of y<0.6, 5.426 Å, and the straight line in the single-phase region of $y\geq$0.6. The lattice parameter of the mixed oxide with $y\geq$0.6 decreases with an increase in the cerium content.

The lattice parameter in the two-phase region of the mixed oxides prepared in air has been determined by many workers.[1–5,7] Although their results are not in complete agreement, it has been found that the lattice parameter has a tendency to increase with a decrease in the y value. On the other hand, the y value at the phase limit of the fluorite solid solution,

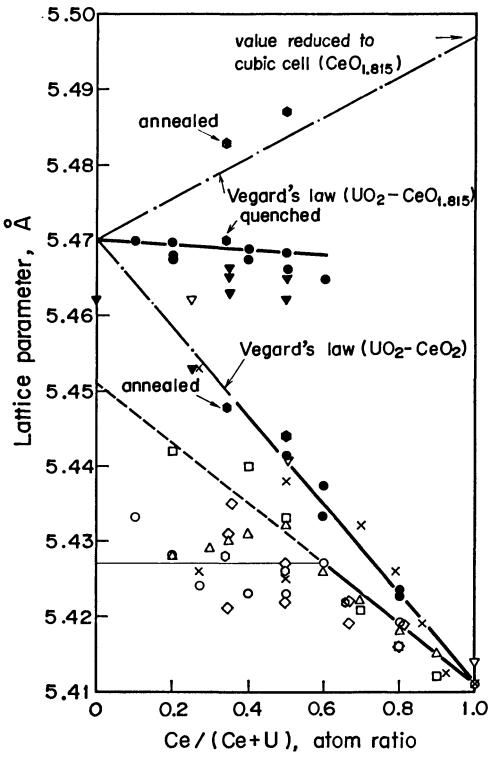

Fig. 4. Lattice parameter of the mixed oxides. □: Hund *et al.*,[1] ◇: Rüdorff and Valet,[2] ×: Zuromsky and Chernock,[3] ▽,▼: Hoch and Furman,[4] ○,●: Markin *et al.*,[5] △: Paul,[7] ○,●: Present work. Open marks and × show the oxides heated in air and filled marks show the oxides heated in hydrogen.

as seen in Paul's results,[7] decreases with a rise in the firing temperature. The lattice parameter value is also varied by the cooling conditions; the value of a quenched sample is larger than that of an annealed one. The difference in the lattice parameters in the literature, therefore, may be caused by the heating and cooling conditions.

The reported values[1,3,7] of lattice parameters in the single-phase region are all in agreement. It is found that the lattice parameter varies linearly against the cerium concentration, except for the results by Hund *et al.*[1] If the line of the lattice parameter *vs.* Ce/(Ce+U) atom ratio is extraporated to y=0, as Rüdorff and Valet[2] have done, 5.451 Å is obtained as the lattice parameter of the cubic uranium oxide. This value is found in the nonstoichiometric region of U_4O_9 the mother structure of which is the fluorite. If the relationship between the lattice parameter and the O/U ratio in U_4O_9 obtained by Lynds *et al.*[10] is applied, the O/U ratio of the extrapolated uranium oxide becomes 2.18. Markin *et al.*[5] obtained oxides with the fluorite-type or U_4O_9-type cubic structure by the partial oxidation of hypostoichiometric oxides, MO_{2-x}, to $MO_{2.25}$ for y<0.4; their lattice parameters are placed on the broken line.

The variation in the lattice parameter of the solid solutions prepared in hydrogen can be shown by two separate lines. One is the line for $y\leq$0.6, with a lower gradient, while the other is the line for $y\geq$0.4,

which follows Vegard's law connecting 5.4700 Å of UO_2 and the 5.4111 Å of CeO_2. The oxides for $y=$ 0.4—0.6 are two-phase mixtures of fluorite structures with different lattice parameters. Markin *et al.*[5] have reported that a two-phase mixture was formed by the phase separation during very slow cooling to room temperature. The lower lattice-parameter values obey Vegard's law. Therefore, it is considered that the oxides with these smaller values correspond to the hypostoichiometric oxides MO_{2-x} formed between UO_2 and $CeO_{2-x'}$, where $2-x'$ is probably much smaller than 1.815.

The larger lattice-parameter values at $y<0.6$ obtained in the present work are in agreement with those by Hoch *et al.*[4] These values are close to the lattice parameter of UO_2. On the other hand, the X-ray pattern of $CeO_{1.815}$ showed the single phase of the fluorite structure with the lattice parameter of 5.4111 Å. The phase diagram of the cerium-oxygen system[11-14] shows that there is a miscibility gap between CeO_2 and $Ce_{11}O_{20}(CeO_{1.818})$. Although $CeO_{1.815}$ has a rhombohedral structure, the psudocubic lattice parameter calculated from the volume of the rhombohedral cell by Brauer and Gingerich[12] and by Ray *et al.*[14] is 5.497 Å. The lattice parameters in the present work are lower than the line of Vegard's law connecting UO_2 and $CeO_{1,815}$, while the data reported by Markin *et al.*[5] are above that line. If our lattice parameters are extrapolated to $y=1$, 5.467 Å is obtained, which corresponds to the $CeO_{1.88}$ of Ray's data.[14]

References

1) F. Hund, R. Wagner, and U. Peetz, *Z. Elekrochem.*, **56**, 61 (1952).
2) W. Rüdorff and G. Valet, *Z. Anorg. Allg. Chem.*, **271**, 257 (1953).
3) G. Zuromsky and W. P. Chernock, USAEC-Report, CEND-147 (1961).
4) M. Hoch and F. J. Furman, "Thermodynamics," IAEA, Vienna (1966), Vol. II, p. 517.
5) T. L. Markin, R. S. Street, and E. C. Crough, *J. Inorg. Nucl. Chem.*, **32**, 59 (1970).
6) T. L. Markin and E. C. Crough, *J. Inorg. Nucl. Chem.*, **32**, 77 (1970).
7) R. Paul, Kernforschungszentrum Karlsruhe Report, KFK-1297 (1970).
8) H. Landspersky, *Jaderná Energie*, **20**, 59 (1974).
9) H. Tagawa, T. Fujino, and J. Tateno, *Bull. Chem. Soc. Jpn.*, **50**, 2940 (1977).
10) L. Lynds, W. A. Young, J. S. Mohl, and G. G. Libowitz, "Nonstoichiometric Compounds," in "Advances in Chemistry Series, 39," ed by R. F. Gould, Am. Chem. Soc., Washington, D. C. (1963), p. 58.
11) D. J. M. Bevan, *J. Inorg. Nucl. Chem.*, **1**, 49 (1955).
12) G. Brauer and K. A. Gingerich, *J. Inorg. Nucl. Chem.*, **16**, 87 (1960).
13) D. J. M. Bevan and J. Kordis, *J. Inorg. Nucl. Chem.*, **26**, 1509 (1964).
14) S. P. Ray, A. S. Nowick, and D. E. Cox, *J. Solid State Chem.*, **15**, 344 (1975).

The Extraction of the Tungsten(VI)-Pyrocatechol Violet Complex with Tridodecylethylammonium Bromide

Yoshio Shijo,* Tokuo Shimizu, and Kaoru Sakai

Department of Environmental Chemistry, Faculty of Engineering, University of Utsunomiya, Ishii-machi, Utsunomiya 321

(Received April 7, 1980)

The extraction equilibria and the fundamental conditions were studied for extracting the tungsten(VI)-Pyrocatechol Violet complex anion in a form of an ionic associate with tridodecylethylammonium salt in carbon tetrachloride. The ternary complex has an absorption maxima at 575 nm in the organic phase. The optimum pH range for the extraction is 4.8—5.6. The distribution ratio and the molar absorptivity are 3.3×10^2 and 4.7×10^4 dm^3 mol^{-1} cm^{-1} respectively. The composition of the ternary complex is estimated to be $WO_2(PV)_2(R_3R'N)_2$. The extraction constant would be:

$$K_{ex}=\frac{[WO_2(PV)_2(R_3R'N)_2]_o}{[WO_2(PV)_2{}^{2-}][R_3R'N^+]^2}.$$

It is given by $\log K_{ex}=13.56$. Many foreign cations can be masked with CyDTA.

The extraction of metal complex anions with quaternary ammonium salts has been successively studied by many workers. Vanadium–4-(2-Pyridylazo)resorcinol,[1] cobalt–4-(2-thiazolylazo)resorcinol,[2] iron–Pyrogallol Red,[3] copper–2-nitroso-1-naphthol-4-sulfonic acid,[4] and magnesium–Xylidyl Blue I[5] complexes have been extracted in the form of the ionic associates with zephiramine. Plutonium–Xylenol Orange,[6] cadmium–8-hydroxyquinoline-5-sulfonic acid,[7] zinc–thiocyanate,[8] and chlorides of many metals[9] have also been extracted with Aliquat 336 (trioctylmethylammonium chloride) in the last two years. Besides, the extraction of metal–pyrocatechol violet(PV) complexes with tridodecylethylammonium bromide (TDEABr) has been studied for extracting copper,[10] tin,[11] aluminium,[12] zirconium,[13] niobium,[14] and iron.[15] Tungsten(VI), as well, is known to react with PV to form a complex, and the absorbance is intensified in the presence of the 1-hexadecylpyridinium cation.[6] Kohara[17] extracted the tungsten(VI)–PV complex in a form of an ionic associate with zephiramine from a 0.6—0.9 mol dm^{-3} hydrochloric acid solution, but the extraction equilibria have not been studied sufficiently. The tungsten(VI)–PV complex has also been extracted with TDEABr in carbon tetrachloride at about pH 5 from a solution containing CyDTA. This extraction system is expected to be selective and sensitive for the spectrophotometric determination of tungsten. In this paper, the extraction equilibria and the fundamental conditions will be discussed for extracting the tungsten(VI)–PV complex with TDEABr.

Experimental

Reagent. A 2.5×10^{-3} mol dm^{-3} tungsten(VI) solution was prepared by dissolving a definite amount of sodium tungstate in a 0.1 mol dm^{-3} sodium hydroxide solution. The solution was diluted as required. A 1×10^{-3} mol dm^{-3} PV solution was prepared by dissolving the Dotite PV in de-ionized water without further purification. TDEABr was prepared by the method described in a previous work.[15] A 5×10^{-3} mol dm^{-3} TDEABr solution was prepared by dissolving TDEABr in purified carbon tetrachloride. A 2 mol dm^{-3} sodium acetate solution was used as a buffer solution. All the other chemicals used were of a guaranteed reagent quality.

Apparatus. A Hitachi 101 spectrophotometer, a Hitachi 200–20 UV-vis. recording spectrophotometer, and a Hitachi Horiba F-7 pH meter were employed.

Standard Procedure. Up to 20 μg of tungsten(VI), a definite amount of 1 mol dm^{-3} sulfuric acid, and 2 cm^3 of a 1×10^{-3} mol dm^{-3} PV solution were mixed in a 100-cm^3 polypropylene beaker. The pH of the solution was adjusted to 5 by the addition of 2 cm^3 of a 2 mol dm^{-3} sodium acetate solution, after which the solution was diluted to 20 cm^3 with deionized water. The solution was transferred into a 35-cm^3 test tube, and 5 cm^3 of 5×10^{-3} mol dm^{-3} TDEABr in carbon tetrachloride were added. The extraction was carried out for 5 min by turning the test tube upside down twice every 5 s. After the phase separation, the organic phase was taken out and centrifuged for 2 min at 3000 min^{-1}. The absorbance of the extract at 575 nm was measured against the reagent blank.

Results and Discussion

Absorption Spectra. The absorption spectra of the ternary complex extracted into carbon tetrachloride and of the tungsten(VI)–PV complex anion in an aqueous solution, and also the absorption spectra of the respective blank solutions, are shown in Fig. 1. The ternary complex and the tungsten(IV)–PV complex anion have absorption maxima at 575 nm and 538 nm respectively. As compared with the corresponding absorption maxima of the complex anion, that of the ternary complex is shifted toward wavelengths longer by 37 nm.

Effect of pH. The aqueous solution containing tungsten(VI) and PV was adjusted to various pH values with the sodium acetate buffer solution, and the extraction was carried out by the above procedure. The results are shown in Fig. 2. The maximum extraction of the ternary complex is reached in the pH range of 4.8 to 5.6. The extract was stable for at least 1 h. PV itself is readily extracted from an aqueous solution.

Organic Solvents. Several kinds of organic solvents were tested in order to achieve a quantitative extraction of the tungsten(VI)–PV complex anion with TDEABr. The ternary complex is extracted in such solvents as carbon tetrachloride, xylene, butyl acetate, and chloroform. The absorbance of the extract was

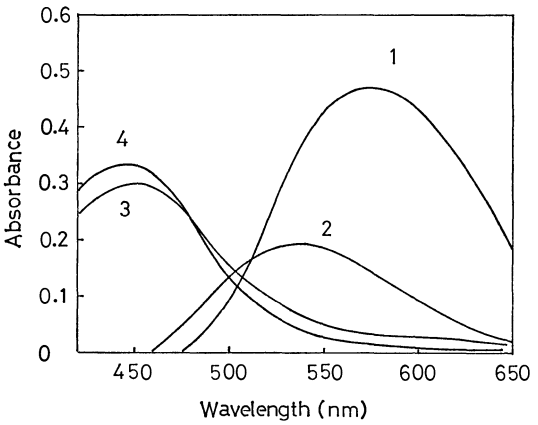

Fig. 1. Absorption spectra of the W–PV–TDEA in carbon tetrachloride and the W–PV complexes in aqueous solution.
pH=5.0, $V_{aq}=20$ cm³, $V_o=5$ cm³, $[TDEABr]_o=5\times10^{-3}$ mol dm⁻³. (1): W–PV–TDEA in carbon tetrachloride $[W]=2.5\times10^{-6}$ mol dm⁻³, (2): W–PV in aq. soln. $[W]=1\times10^{-5}$ mol dm⁻³, (3): PV–TDEA in carbon tetrachloride $[PV]=5\times10^{-6}$ mol dm⁻³, in carbon tetrachloride $[PV]=5\times10^{-6}$ mol dm⁻³, (4): PV in aq soln. $[PV]=2\times10^{-5}$ mol dm⁻³.

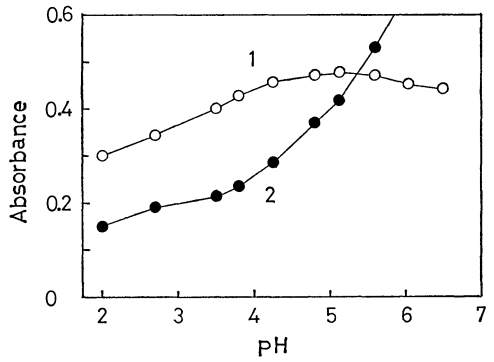

Fig. 2. Effect of pH on the extraction of the W-PV-TDEA complex.
$[W]=2.5\times10^{-6}$ mol dm⁻³, $[PV]=1.25\times10^{-4}$ mol dm⁻³, $[TDEABr]_o=5\times10^{-3}$ mol dm⁻³, 575 nm. (1): W–PV–TDEA, (2): PV–TDEA.

maximal when carbon tetrachloride was used.

The Effect of the Reagent Concentration. The extraction of tungsten(VI) from an aqueous solution containing PV in various concentrations was examined. The optimum concentration range of PV is from 8×10^{-5} mol dm⁻³ to 1.5×10^{-4} mol dm⁻³. The concentration of TDEABr in the organic phase was varied from 1×10^{-4} mol dm⁻³ to 5×10^{-3} mol dm⁻³. The absorbance of the extract was found to be constant in the concentration range from 9×10^{-4} mol dm⁻³ to 5×10^{-3} mol dm⁻³.

Extractability and Molar Absorptivity. An aqueous solution of 20 cm³ containing 18.4 μg of tungsten(VI) and PV was shaken with 5 cm³ of 5×10^{-3} mol dm⁻³ TDEABr in carbon tetrachloride under the optimum conditions. Extraction was repeated for the remaining aqueous phase after the separation of the extract. The extractability of the tungsten(VI) was calculated from the absorbances of the extracts. It was found

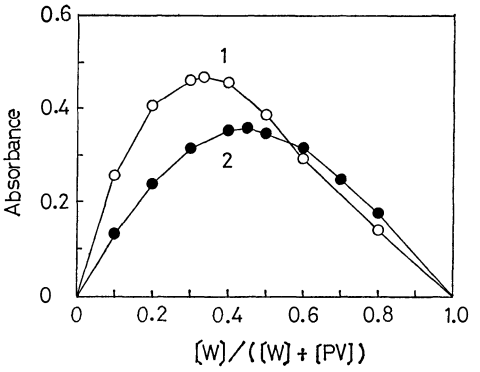

Fig. 3. Continuous variation method applied to the W–PV–TDEA and the W–PV complexes (W:PV).
(1): W–PV–TDEA; $[W]+[PV]=5\times10^{-5}$ mol dm⁻³, $[TDEABr]_o=5\times10^{-3}$ mol dm⁻³ pH=5.0, 575 nm, (2): W–PV; $[W]+[PV]=2\times10^{-4}$ mol-dm⁻³, pH=5.0, 540 nm

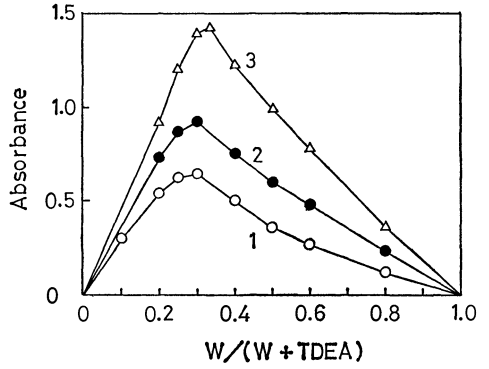

Fig. 4. Continuous variation method applied to the W–PV–TDEA complex (W:TDEA).
W–PV+TDEA=1.5×10^{-6} mol, pH=5.0, (1): 575 nm, (2): 610 nm, (3): 650 nm.

that 98.8% of the tungsten(VI) was extracted by a single extraction. The distribution ratio and the molar absorptivity were 3.3×10^2 and 4.7×10^4 dm³ mol⁻¹ cm⁻¹, respectively. A calibration curve for the determination of the tungsten(VI) was made under the optimum conditions. A good linear relationship was obtained over the concentration range from 1 μg to 20 μg of tungsten(VI) per 5 cm³ of carbon tetrachloride. The coefficient of the variation in ten measurements was 2.4%.

The Composition of the Ternary Complex. Using the continuous-variation method, the mole ratio of tungsten: PV of the ternary complex and of the tungsten(VI)–PV complex anion were found to be 1:2 and 1:1 respectively, as is shown in Fig. 3. The mole ratio of tungsten: TDEA was found to be 1:2, as is shown in Fig. 4. Thus, the composition of the ternary complex was estimated to be $WO_2(PV)_2$–$(R_3R'N)_2$.

Extraction Constant. When the ionic associate of the tungsten(VI)–PV complex anion with the TDEA cation is extracted in the organic phase, the equation representing the extraction equilibria will be:

$$WO_2(PV)_2^{2-} + 2R_3R'N^+ = WO_2(PV)_2(R_3R'N)_{2(o)}. \quad (1)$$

The extraction constant, K_{ex}, is given by:

$$K_{ex} = \frac{[WO_2(PV)_2(R_3R'N)_2]_o}{[WO_2(PV)_2^{2-}][R_3R'N^+]^2}, \quad (2)$$

where the subscript o denotes the organic phase.

The direct determination of each of the component concentrations in Eq. 1 is a difficult problem, because the pure ternary complex can not easily be prepared. The extraction constant, K_{ex}, can, however, be determined by the indirect method, in which the extraction equilibria of the tungsten(VI)–PV complex anion with tridodecylethylammonium 2-naphthalenesulfonate is employed. The corresponding equilibria are written as follows:

$$WO_2(PV)_2^{2-} + 2R_3R'N\cdot NS_{(o)} = WO_2(PV)_2(R_3R'N)_{2(o)} + 2NS^-. \quad (3)$$

The equilibrium constant for Eq. 3 is:

$$K = \frac{[WO_2(PV)_2(R_3R'N)_2]_o[NS^-]_2}{[WO_2(PV)_2^{2-}][R_3R'N\cdot NS]_o^2}, \quad (4)$$

where NS denotes 2-naphthalenesulfonate.

The extraction equilibria of tridodecylethylammonium 2-naphthalenesulfonate may be represented as follows:

$$NS^- + R_3R'N^+ = R_3R'N\cdot NS_{(o)}. \quad (5)$$

The extraction constant for Eq. 5 is:

$$K'_{ex} = \frac{[R_3R'N\cdot NS]_o}{[NS^-][R_3R'N^+]}. \quad (6)$$

Thus, K_{ex}, is given by:

$$K_{ex} = K\times(K'_{ex})^2. \quad (7)$$

The concentration of the $WO_2(PV)_2(R_3R'N)_{2(o)}$ species in Eq. 3 was determined spectrophotometrically as a function of $[NS^-]$, and the value of K was calculated from Eq. 4. The extraction constant, K'_{ex}, in Eq. 6 was also determined by the analogous method from the extraction equilibria between $R_3R'N\cdot NS$ in CCl_4 and the PV anion, the extraction constant of which had already been known. Table 1 shows the value of log K_{ex} calculated from Eq. 7. It is given by

Table 1. Equilibrium extraction data for $WO_2(PV)_2^{2-}$ with $R_3R'N^+$ in carbon tetrachloride at 25 °C

(I=0.005 in an acetate solution and Na_2SO_4 solution) pH=5.0 in an acetate buffer solution (2.0×10^{-3} mol dm^{-3}), $[W]=2.5\times10^{-6}$ mol dm^{-3}, $[PV]=1.25\times10^{-4}$ mol dm^{-3}, $[TDEABr]_o=5\times10^{-3}$ mol dm^{-3}, V_{aq}=20 cm^3, V_o=5 cm^3.

$[NS^-]/10^{-3}$ mol dm^{-3}	log K_{ex}
2.5	13.50
5.0	13.59
7.5	13.56
10	13.59
12.5	13.54
	log K_{ex} = 13.56

All the concentrations in Table 1 show the initial concentrations.

Table 2. Effects of diverse ions on the determination of tungsten(VI)

Ions	Amount added mg	Tungsten(VI) found/μg	Error %
—	—	9.2	0
Be^{2+}	0.1	7.9	−14
Mo(VI)	0.1	18.9	+105
Th^{4+}	0.1	10.4	+13
U(VI)	0.1	10.5	+14
V(V)	0.1	11.6	+26
I^-	10	3.8	−59
SCN^-	10	3.0	−67
ClO_4^-	10	0.6	−93
Citrate	10	0.9	−90
EDTA	10	1.0	−89

log K_{ex}=13.56.

Effect of Foreign Ions. The effect of foreign ions on the determination of 9.2 μg tungsten(VI) was examined upon the addition of 2 cm^3 of 0.05 mol dm^{-3} CyDTA as a masking agent. Portions (0.1 mg) of aluminium, antimony, bismuth, cadmium, cobalt, chromium, copper, gallium, indium, iron, lanthanum, lead, magnesium, manganese, mercury, nickel, tin, and zinc did not interfere, but beryllium, molybdenum, thorium, uranium, and vanadium interfered considerably with the determination of the tungsten(VI). Of the anions tested, 10-mg portions of iodide, thiocyanate, and perchlorate interfered seriously, giving negative errors. Chelating agents, such as EDTA and citrate, also interfered. The main interfering ions are shown in Table 2.

References

1) M. Tajika, H. Hoshino, T. Yotsuyanagi, and K. Aomura, *Nippon Kagaku Kaishi*, **1979**, 85.
2) K. Ueda, *Bull. Chem. Soc. Jpn.*, **52**, 1215 (1979).
3) T. Korenaga, S. Motomizu, and K. Toei, *Anal. Chim. Acta*, **104**, 369 (1979).
4) S. Motomizu and K. Toei, *Bunseki Kagaku*, **27**, 213 (1978).
5) H. Tanaka and H. Watanabe, *Bunseki Kagaku*, **27**, 189 (1978).
6) J. P. Shukla and M. S. Subramanian, *J. Radioanal. Chem.*, **47**, 29 (1978).
7) M. Sugawara and T. Kambara, *Bunseki Kagaku*, **27**, 683 (1978).
8) D. Singh and S. N. Tandon, *J. Inorg. Nucl. Chem.*, **40**, 1803 (1978).
9) V. V. Bagreev, C. Fisher, L. M. Yudushkina, and Yu. A. Zolotov, *J. Inorg. Nucl. Chem.*, **40**, 553 (1978).
10) Y. Shijo, *Bull. Chem. Soc. Jpn.*, **47**, 1642 (1974).
11) Y. Shijo, *Nippon Kagaku Kaishi*, **1974**, 1658.
12) Y. Shijo, *Nippon Kagaku Kaishi*, **1974**, 1912.
13) Y. Shijo, *Bull. Chem. Soc. Jpn.*, **49**, 3029 (1976).
14) Y. Shijo, *Bull. Chem. Soc. Jpn.*, **50**, 1011 (1977).
15) Y. Shijo, *Bull. Chem. Soc. Jpn.*, **50**, 1013 (1977).
16) R. K. Chernova, L. N. Kharlamova, and V. V. Belousova, *Zavod. Lab.*, **44**, 260 (1978).
17) H. Kohara, *Kitakyushu Kogyo Koto Senmon Gakko Kenkyu Hokoku*, **11**, 165 (1978).

The Coordination of the Perchlorate Ion. I. The Crystal and Molecular Structure of Bis(perchlorato)bis(pyrazine-2,3-dicarboxamide)copper(II)

Masao Sekizaki

College of Liberal Arts, Kanazawa University, Marunouchi, Kanazawa 920

(Received April 9, 1980)

Bis(perchlorato)bis(pyrazine-2,3-dicarboxamide)copper(II) has been prepared, and its crystal and molecular structure has been determined by the X-ray diffraction and the infrared spectroscopic methods. The crystals are triclinic with a space group $P\bar{1}$; $a=10.959(4)$, $b=6.970(3)$, $c=7.666(3)$ Å, $\alpha=116.63(3)$, $\beta=78.14(5)$, and $\gamma=97.27(5)°$, and $Z=1$. The refinement of the crystal structure has been carried out by a block-diagonal least-squares method to give $R=0.054$ for 1727 non-zero reflections. The complex is centrosymmetric, with the two bidentate ligand molecules chelating to the copper atom in *trans* positions through the amide oxygen and pyrazine nitrogen atoms to form a square-plane. The two perchlorate ions coordinate weakly to the copper atom through the oxygen atoms from the top and bottom of this plane; thus, an elongated octahedron is formed. The complex molecules are connected to one another by N-O type hydrogen bonds to form a three-dimensional network. The infrared spectrum has been compared with that of the chloride complex. The KBr region clearly show the symmetry depression of the perchlorate ion from T_d to C_{3v} on coordination.

It is well known that a perchlorate ion scarcely coordinates to the transition metal ions. However, it sometimes acts as a unidentate ligand in the presence of organic ligands.[1-4] The present investigation has been carried out in order to ascertain the structure and properties of the coordinating perchlorate ion in the copper(II) complex of pyrazine-2,3-dicarboxamide (abbreviation, pyda) by the spectroscopic and crystallographic methods.*

Experimental

Preparation of the Complexes. Bis(perchlorato)bis(pyrazine-2,3-dicarboxamide)copper(II), [Cu(ClO$_4$)$_2$(pyda)$_2$]: an ethanolic solution of 2.5 g of newly prepared $Cu(ClO_4)_2\cdot 6H_2O$ was added to a hot aqueous solution of 1 g of pyda (Aldrich Chem. Co.). The mixture was, then, cooled slowly. The deep blue crystals precipitated were washed with ethanol. Yield, 1.5 g. Found: Cu, 10.67; N, 18.63; C, 24.23; H, 2.22%. Calcd for $C_{12}H_{12}N_8O_{12}CuCl_2$: Cu, 10.68; N, 18.84; C, 24.23; H, 2.03%.

Pyrazine-2,3-dicarboxamidecopper(II) Chloride, Cu(pyda)Cl$_2$: Three grams of $CuCl_2\cdot 2H_2O$, dissolved in 200 cm^3 of ethanol, were quickly added to 50 cm^3 of a hot aqueous solution of 1 g of pyda. After the filtration of the precipitate instantaneously formed, the solution was slowly cooled to room temperature. The yellowish-green powder thus obtained was washed with ethanol. Yield, 1.2 g. Found: Cu, 21.18; N, 18.28; C, 23.67; H, 2.24%. Calcd for $C_6H_6N_4O_2CuCl_2$: Cu, 21.14; N, 18.64; C, 23.97; H, 2.01%.

Measurement of the Infrared Spectra. A JASCO DS-402G spectrometer and a Hitachi EPI-L spectrometer were used in the 200—4000 cm^{-1} region. The samples were suspended in Nujol and HCB mulls.

Crystallographic Measurement. A crystal of $0.2\times0.1\times0.1$ mm was selected. The intensities were measured on a Philips PW1100 automatic four-circle diffractometer with Cu $K\alpha$ radiation ($\lambda=1.5418$ Å) monochromated by a graphite plate. The θ-2θ scan technique was used at a scan rate of 0.0668°/s in θ, with a scan width of $(1.0+0.3\tan\theta)°$. The intensities of the three reference reflections, monitored every 2 h, remained constant within the limits of experimental error during data collection. Of 1803 independent reflections measured up to $\theta=78°$, 1727 with $|F|>3\sigma$ were used for the structure analysis. No corrections were made for absorption and extinction effects ($\mu r=0.3$). The cell dimensions were refined on the diffractometer by a least-squares method using the 2θ values of 25 reflections.

Crystal Data: $Cu(ClO_4)_2\{C_4N_2H_2(CONH_2)_2\}_2$. F.W.=594.73. Triclinic, $a=10.959(4)$, $b=6.970(3)$, $c=7.666(3)$ Å, $\alpha=116.63(3)$, $\beta=78.14(5)$, $\gamma=97.27(5)°$. $U=511.9(3)$ Å^3. $D_x=1.929$ g cm^{-3}. $Z=1$. Space group $P\bar{1}$. $\mu=47$ cm^{-1} (Cu $K\alpha$ radiation, $\lambda=1.5418$ Å).

Determination and Refinement of the Crystal Structure

The coordinates of the copper and the chlorine atoms were determined from a Patterson map; successive Fourier syntheses gave the approximate skeletal structure. The copper atom occupies the special positions of the triclinic cell. The block-diagonal least-squares refinement was carried out based on 1727 non-zero reflections. The atomic scattering factors were taken from the International Tables for X-Ray Crystallography.[5] After several cycles of refinement with isotropic temperature factors, the R-value became 0.15. Anisotropic temperature factors were, then, introduced for all the non-hydrogen atoms. The R-value was reduced to 0.058. The hydrogen atoms were obtained from the difference-Fourier synthesis. Their positional parameters were refined with isotropic temperature factors of 4.0 Å^2. The final R-value was 0.054.

The final atomic parameters are listed in Table 1. A list of the observed and calculated structure amplitudes has been deposited with the Chemical Society of Japan (Document No. 8108).

The refinement of the structure and the drawing of thermal ellipsoids were carried out with HBLS-IV[6] and ORTEP[7] programs respectively. The other calculations were carried out with programs written by the author. A FACOM 230-75 computer at the Computation Center of Nagoya University and a FACOM M-160 computer at the Data Processing Center of Kanazawa University were used.

* The author has noticed a report on the crystal structure of the same complex. Its conclusion is, however, different from the present one. The details will be discussed later in the present report.

Table 1a. Final parameters of non-hydrogen atoms ($\times 10^4$)

The thermal parameters are in the form: $\exp[-(h^2\beta_{11}+k^2\beta_{22}+l^2\beta_{33}+hk\beta_{12}+hl\beta_{13}+kl\beta_{23})]$.
The estimated standard deviations are in parentheses in this table and the other subsequent tables.

Atom	x	y	z	β_{11}	β_{22}	β_{33}	β_{12}	β_{13}	β_{23}
Cu	0	0	0	41(01)	274(04)	231(03)	−37(03)	−80(03)	366(05)
Cl	−1786(01)	4650(02)	3544(02)	48(01)	133(03)	147(03)	−8(03)	−40(03)	138(05)
N(1)	1738(03)	1004(06)	341(06)	24(03)	136(11)	131(10)	−7(09)	−37(09)	171(17)
C(2)	2214(04)	380(07)	1483(07)	31(04)	106(12)	99(11)	7(10)	−24(10)	119(18)
C(3)	3425(04)	1086(08)	1845(07)	26(04)	157(13)	120(12)	−4(10)	−40(10)	165(20)
N(4)	4103(04)	2343(08)	1052(07)	34(04)	239(14)	190(12)	−51(11)	−63(10)	307(22)
C(5)	3605(05)	2884(10)	−91(09)	43(05)	263(18)	234(17)	−66(14)	−61(13)	392(29)
C(6)	2400(05)	2228(09)	−450(08)	43(04)	186(15)	169(14)	−25(12)	−54(12)	273(23)
C(7)	1231(04)	−979(08)	2198(08)	34(04)	155(13)	124(12)	−22(11)	−46(11)	180(20)
C(8)	4117(05)	653(09)	3170(08)	31(04)	225(16)	177(14)	−1(12)	−52(12)	266(25)
O(7)	167(03)	−1139(07)	1769(06)	28(03)	338(14)	268(12)	−76(09)	−95(09)	516(22)
N(7)	1467(04)	−1962(08)	3178(07)	43(04)	228(14)	227(13)	−56(11)	−95(11)	374(23)
O(8)	3791(04)	−816(08)	3639(07)	52(04)	379(16)	384(15)	−109(12)	−181(12)	641(27)
N(8)	5094(04)	1945(08)	3704(08)	41(04)	286(16)	240(14)	−64(12)	−123(12)	304(25)
O(1)	−659(05)	3484(10)	2847(09)	89(05)	477(22)	357(17)	269(17)	−114(15)	−117(30)
O(2)	−2497(04)	3960(07)	1964(07)	92(05)	256(13)	197(11)	−8(12)	−117(11)	192(20)
O(3)	−2530(05)	4306(08)	5167(08)	102(05)	364(17)	299(14)	−93(14)	−91(13)	542(26)
O(4)	−1466(05)	6890(07)	4239(07)	142(06)	172(12)	201(12)	−124(13)	−29(13)	148(19)

Table 1b. Positional parameters of the hydrogen atoms ($\times 10^3$)

	x	y	z
H–C(5)	417(07)	377(12)	−78(12)
H–C(6)	200(07)	256(12)	−131(12)
Ha–N(7)	86(07)	−290(13)	346(12)
Hb–N(7)	222(07)	−170(12)	356(12)
Ha–N(8)	502(07)	332(12)	492(12)
Hb–N(8)	585(07)	168(13)	300(12)

Results and Discussion

Crystal Analysis. The molecular structure of the complex is shown in Fig. 1, with anisotropic thermal ellipsoids of the non-hydrogen atoms. The bond lengths are also shown in this figure. The bond angles are listed in Table 2.

The complex is centrosymmetric, with two ligand molecules in *trans* positions. Each of the ligand molecules acts as bidentate through one of the pyrazine nitrogen atoms and the oxygen atom of the *ortho* amide group, thus forming a five-membered chelate ring. The four coordinating atoms form a square-plane around the copper atom. The distances of the coordination bonds are similar to those of the other copper amide complexes.[2,8,9]

The oxygen atom of the perchlorate ion lies on the normal line of this plane passing through the copper atom. The distance between the copper and the oxygen atom is 2.495 Å. This value is larger than those of the usual coordination-bond lengths on the square-plane. However it is smaller than those of the other perchloratocopper(II) complexes (2.61 Å for $[Cu(ClO_4)_2(en)_2]$[1] or 2.52 Å for $[Cu(ClO_4)_2(paaH)_2]$,[2] where paaH denotes 2-pyridylacetamide).

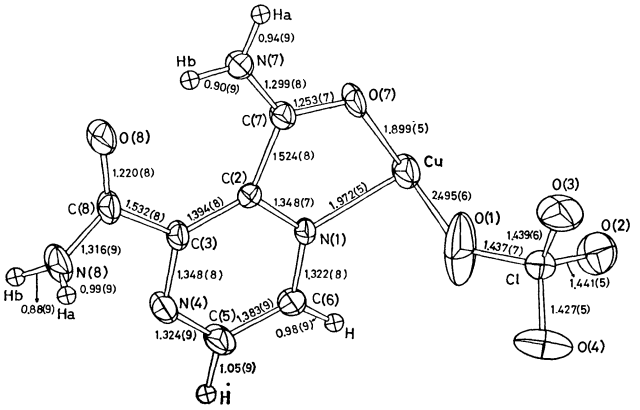

Fig. 1. Structure of the asymmetric unit with the bond lengths (l/Å) and the e.s.d.'s.
Thermal ellipsoids are drawn at 50% probability level. Hydrogen atoms are drawn as spheres with a diameter of 0.2 Å.

Thus, the complex forms a distorted octahedron elongated to the perchlorate oxygen atoms.

The complex molecule is arranged as shown in Fig. 2, with the copper atom occupying the special position of the triclinic unit cell. The hydrogen bonds are listed in Table 3.

The uncoordinated amide group is hydrogen-bonded to that of the neighboring molecule through O(8)···N(8)^{i} to form a column in the [101] direction. The perchlorate ions connect these columns by the hydrogen bonds through O(4)···N(7)^{iv}, O(2)^{ii}···N(8), and O(3)^{ii}···N(8). The van der Waals interactions shorter than 3.2 Å are also observed around the anion. The [101] columns are thus combined with one another by these interactions through the perchlorate ions, thus forming a three-dimensional network.

The perchlorate ion is almost a regular tetrahedron.

Table 2. Bond angles (φ/°)

N(1)-Cu-O(7)	81.9(2)	C(3)-N(4)-C(5)	118.9(6)	C(3)-C(8)-O(8)	121.8(6)
N(1)-Cu-O(1)	87.5(2)	N(4)-C(5)-C(6)	121.5(7)	C(3)-C(8)-N(8)	114.7(6)
O(1)-Cu-O(7)	90.6(3)	C(5)-C(6)-N(1)	119.2(6)	O(8)-C(8)-N(8)	123.5(7)
Cu-N(1)-C(2)	115.0(4)	C(3)-C(2)-C(7)	132.4(5)	O(1)-Cl-O(2)	110.0(4)
Cu-N(1)-C(6)	123.6(4)	N(1)-C(2)-C(7)	109.2(5)	O(1)-Cl-O(3)	110.4(4)
Cu-O(1)-Cl	133.7(4)	C(2)-C(7)-O(7)	116.6(5)	O(1)-Cl-O(4)	108.9(4)
Cu-O(7)-C(7)	116.8(4)	C(2)-C(7)-N(7)	122.7(6)	O(2)-Cl-O(3)	109.4(4)
C(2)-N(1)-C(6)	121.4(5)	O(7)-C(7)-N(7)	120.7(6)	O(2)-Cl-O(4)	110.0(3)
N(1)-C(2)-C(3)	118.3(5)	C(2)-C(3)-C(8)	126.7(5)	O(3)-Cl-O(4)	108.1(4)
C(2)-C(3)-N(4)	120.6(5)	N(4)-C(3)-C(8)	112.7(5)		

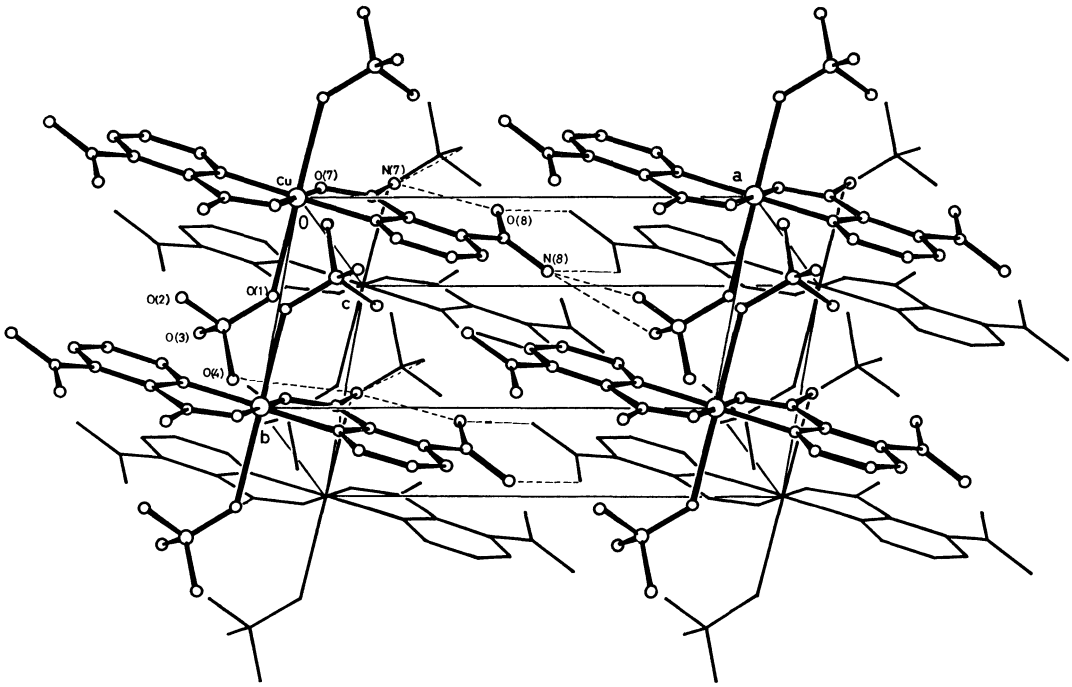

Fig. 2. Crystal structure. Dashed lines exhibit hydrogen bonds.

Table 3. Hydrogen bonds

A·····H———D[a]			A-D(l/Å)	A-H(l/Å)
O(8)	Hb	N(7)[b]	2.618(8)	1.76(9)
O(8)	Ha	N(8)[i]	2.993(8)	2.98(9)
O(2)[ii]	Hb	N(8)	3.164(8)	2.50(9)
O(3)[ii]	Ha	N(8)	3.034(8)	2.71(9)
O(3)	Hb	N(7)[iii]	2.930(8)	2.50(9)
O(4)	Ha	N(7)[iv]	3.239(7)	2.49(9)

a) A, Hydrogen acceptor; D, Hydrogen donor.
b) Key to symmetry operation.

No mark	x	y	z
i	$1-x$	$-y$	$1-z$
ii	$1+x$	y	z
iii	$-x$	$-y$	$1-z$
iv	x	$1+y$	z

The thermal vibrations of the oxygen atoms are larger than those of the other atoms; especially, the coordinated oxygen atom shows a large anisotropy normal to the coordination bond.

Infrared Spectra. The spectrum in the 700—4000 cm^{-1} region has given only poor results because of too many unassignable bands. But that in the 200—700 cm^{-1} region has given important information on the coordination of the perchlorate ion. It is shown in Fig. 3, together with some tentative assignments.[10,11] Those of the free ligand and the chloride complex are also shown for the sake of comparison.

Most of the bands of the free ligand are also observed in both the complexes. On coordination, some new peaks appear; they are marked with e in Fig. 3. Furthermore, the perchlorato complex gives a broad doublet at *ca.* 580 cm^{-1} and two weak bands at 462 and 431 cm^{-1} (marked with f). They must be due to the unidentately coordinating perchlorate ion. Of the four normal vibrations of the free perchlorate ion, two exist in this region (*ca.* 460 and 610 cm^{-1});[12,13] the latter is infrared-active. If the symmetry is lowered to C_{3v} on coordination, the former becomes infrared-active and the latter splits into two bands. The 580 cm^{-1} doublet is assigned a split band, and either of the two bands at 462 and 431 cm^{-1} corresponds to the former.

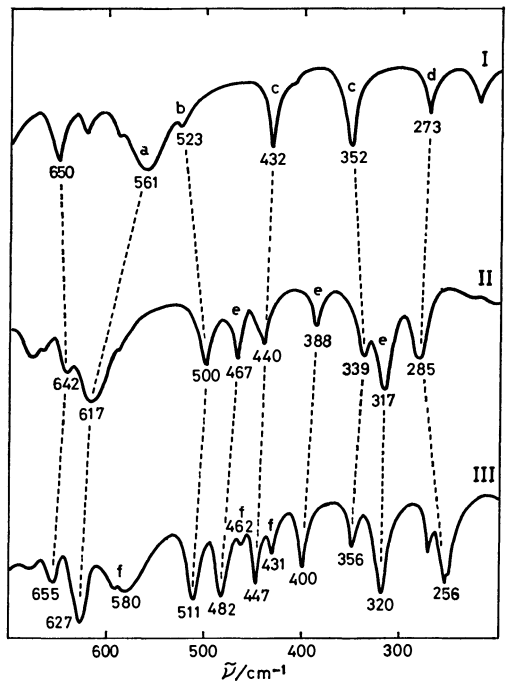

Fig. 3. Infrared spectra of free pyda(I), Cu(pyda)-Cl_2(II), and [$Cu(ClO_4)_2(pyda)_2$] (III).
a: C-O in-plane bending, b: C-O out-of-plane bending, c: pyrazine ring deformation ,d: pyrazine-amide torsion, e: skeletal vibrations due to octahedral coordination, f: normal vibrations of the perchlorate ion.

Comment on the Report by Mondal and Ray[14]

In the course of this investigation, Mondal and Ray reported the crystal structure of the same complex by the photographic method. According to them, the crystal is triclinic with the space group of $C\bar{1}$ and $Z=2$; the structure is square-planar without any coordination of the ClO_4^- ion.

The space group $C\bar{1}$ can be converted to $P\bar{1}$ by means of the following formula on the unit-cell vectors:

$$\boldsymbol{a} = \boldsymbol{c}_r,$$

$$\boldsymbol{b} = (\boldsymbol{a}_r + \boldsymbol{b}_r)/2,$$

and

$$\boldsymbol{c} = (\boldsymbol{b}_r - \boldsymbol{a}_r)/2,$$

where $\boldsymbol{a}_r$, *etc.* are as defined by Mondal and Ray. The lattice constants thus converted are: $a=11.06$, $b=6.80$, $c=7.58$ Å, $\alpha=116.06$, $\beta=76.68$, and $\gamma=97.33°$, which are approximately coincident with the results of the present investigation.

The ClO_4^- ion indeed seems to be non-coordinated, because the atomic parameters given by them certainly show that the anion is far from the complex cation. However the contact between the cation (x,y,z) and the anion $(x-1/2, y-1/2, z)$ is short so that one of the oxygen atoms of the latter approaches the copper atom with the distance of 2.46 Å, which undoubtedly indicates the weak coordination of the anion. Furthermore, although they have stated that there are no hydrogen bonds around the anion, some short contacts are observed between the anion and the neighboring complex molecules. Perhaps they might have forgotten the discussion of the intermolecular interaction in the unit cell of $C\bar{1}$. A set of the XDC[15] converts the positional parameters of the anion so that the anion is near the complex cation. The bond distances and angles less than 2.5 Å calculated by these parameters agree with the results of the present investigation within the limits of experimental error, including the Cu–O weak coordination bond. It is regrettable that, although Mondal and Ray obtained correct data by means of a troublesome photographic method, they gave an incorrect conclusion as to the molecular structure.

The author is grateful to Professor Yoichi Iitaka of the University of Tokyo for the measurements of the intensities with the diffractometer. This work was supported in part by a Grant-in-Aid for Scientific Research No. 354215 from the Ministry of Education, Science and Culture.

References

1) A. Pajunen, *Suomen Kemistilehti, Sect. B*, **40**, 32 (1967).
2) M. Sekizaki, F. Marumo, K. Yamasaki, and Y. Saito, *Bull. Chem. Soc. Jpn.*, **44**, 1731 (1971).
3) M. Sekizaki, K. Yamasaki, and K. Hayashi, *Nippon Kagaku Zasshi*, **91**, 1191 (1970).
4) M. Sekizaki, *Ionics*, Ionics Co., Ltd., Tokyo, **6**, 23 (1980).
5) "International Tables for X-Ray Crystallography," Kynoch Press, Birmingham (1974), Vol. IV.
6) T. Ashida, "Universal Crystallographic Computation Program System (UNICS)," ed by T. Sakurai, The Crystallographic Society of Japan, Tokyo (1967).
7) C. K. Johnson, Oak Ridge National Laboratory Report ORNL-3794 (1965); K. Sasaki, "ORTEP-II(NUNICS)," Library Program of the Computation Center of Nagoya University.
8) M. Sekizaki, *Acta Crystallogr., Sect. B*, **29**, 327 (1973).
9) M. Sekizaki, *Bull. Chem. Soc. Jpn.*, **47**, 1447 (1974).
10) M. Sekizaki and K. Yamasaki, *Spectrochim. Acta, Part A*, **25**, 475 (1969).
11) M. Sekizaki and K. Yamasaki, *Revue de Chimie Minérale*, **6**, 255 (1969).
12) K. Nakamoto, "Infrared Spectra of Inorganic and Coordination Compounds," 2nd ed, Wiley-Intersc. (1970), p. 106.
13) M. Procter, B. J. Hathaway, and P. Nicholls, *J. Chem. Soc., A*, **1968**, 1678.
14) M. Mondal and S. Ray, *Acta Crystallogr., Sect. B*, **33**, 2297 (1977).
15) Cambridge Crystallographic Data Base, TOOL-IR Crystallographic Data Centre (XDC), The University of Tokyo.

Kinetic and Equilibrium Studies on Substitution Reactions of the Chlorobis(β-diketonato)manganese(III) Complexes with Other β-Diketones

Yoshiaki Ito and Shinichi Kawaguchi*

Department of Chemistry, Faculty of Science, Osaka City University, Sumiyoshi-ku, Osaka 558

(Received May 1, 1980)

The $MnCl(\beta\text{-dik})_2$ complexes, where β-dik stands for an anion of acetylacetone, benzoylacetone, and dibenzoylmethane, were confirmed to have the five-coordinate structure in dichloromethane and their adduct formation constants with various donor solvents were measured. Equilibria and kinetics of substitution reactions of $MnCl(\beta\text{-dik})_2$ with other β-diketones were determined by the spectrophotometric method and the mechanism for these reaction is proposed.

The bis(acetylacetonato)halogenomanganese(III) complexes, $MnX(acac)_2$ (X=Cl, Br, and I), were prepared by the reactions of tris(acetylacetonato)-manganese(III) with an equimolar amount of hydrogen halide in organic solvents.[1] They were characterized by measurements of magnetic susceptibility, electronic and infrared spectra, molecular weight, and electric conductivity and were concluded to exist as five-coordinate molecules in noncoordinating solvents but behave as a uni-uni valent electrolyte in methanol. An analogous iron(III) complex, $FeCl(acac)_2$, was confirmed by X-ray analysis to have a square pyramid structure with the chloride anion at the apical position.[2] Although the pseudohalogenomanganese(III) complexes, $MnX(acac)_2$ ($X=N_3$ and NCS), were reported to have a polynuclear chain structure in crystals in which each manganese(III) ion assumes a tetragonally elongated octahedron with the trans-coordinated pseudohalides as the end-to-end bridging ligand,[3,4] they may be five coordinate in solutions of poorly coordinating solvents.[3]

Stults, et al.[5] showed that the $MnX(acac)_2$ complexes are useful in preparing the biologically important Mn(III)-porphyrin[6] in high purity and yield, although the mechanism of the ligand substitution reaction has not been clarified. Kinetic studies on the ligand substitution reactions of five-coordinate complexes have been rather few and to our knowledge, no reports on the reactions of five-coordinate manganese(III) complexes have appeared as yet. This paper is concerned with the substitution reactions of chlorobis(dibenzoylmethanato and benzoylacetonato)-mangangese(III) with acetylacetone, and kinetic and equilibrium data as well as mechanistic discussion are presented.

Experimental

Materials. Acetylacetone (acacH) of the extra-pure grade was distilled twice before use. Benzoylacetone (bzacH) and dibenzoylmethane (dbmH) were recrystallized twice from methanol and dried over silica gel in an evacuated desiccator. Dichloromethane was washed with a 10% aqueous solution of sodium carbonate followed by pure water, dried by means of Linde molecular sieves (Type 3A), and was then distilled through a fractionating column filled with Widmer spirals. Dichloromethane was used immediately after distillation as the solvent for kinetic studies. Diethyl ether was treated with metallic sodium and distilled. Pyridine of the highest grade for spectroscopy was used without further treatment. Methanol was dried by Linde molecular sieves (Type 3A) and distilled. Other organic solvents such as *N,N*-dimethylformamide (DMF), dimethylsulfoxide (DMSO), benzonitrile (PhCN), and acetonitrile (MeCN) were similarly dried and distilled under reduced pressure of nitrogen. Deuterium oxide of 99.75% purity (Merck) was used for the deuteration studies.

Synthesis of Complexes. Bis(acetylacetonato)chloromanganese(III): The complex was prepared by Isobe's method[1] and recrystallized twice from a mixture of dichloromethane and diethyl ether (1:1 by volume) in a dry box under dry nitrogen atmosphere. Found: C, 41.16; H, 4.84%. Calcd for $MnCl(acac)_2=C_{10}H_{14}O_4ClMn$: C, 41.16; H, 4.89%.

Chlorobis(dibenzoylmethanato)manganese(III), $MnCl(dbm)_2$ and Bis(benzoylacetonato)chloromanganese(III), $MnCl(bzac)_2$: Isobe's method was modified a little. Dibenzoylmethane (5.2 g, 23.2 mmol) was added to a solution of $MnCl(acac)_2$ (0.5 g, 1.7 mmol) in dichloromethane (20 cm^3), and the mixture was allowed to stand for about 2 h to deposit the product (0.31 g) in a 33% yield. Recrystallization was performed in an atmosphere of dry nitrogen from an equivolume mixture of dichloromethane and diethyl ether containing six times as many moles of dibenzoylmethane as compared with the complex. Found: C, 66.18; H, 4.15%. Calcd for $MnCl(dbm)_2=C_{30}H_{22}O_4ClMn$: C, 67.11; H, 4.13%. Bis(benzoylacetonato)chloromanganese(III) was also prepared and recrystallized in a similar manner as above. The yield of a crude product was 0.20 g (28.0%). Found: C, 57.89; H, 4.41%. Calcd for $MnCl(bzac)_2=C_{20}H_{18}O_4ClMn$: C, 58.20; H, 4.40%.

Acetylacetonato(dibenzoylmethanato)- and Acetylacetonato(benzoylacetonato)-chloromanganese(III): In an atmosphere of dry nitrogen $MnCl(acac)_2$ (1.0 g, 3.7 mmol) was dissolved in dichloromethane (20 cm^3), and to this solution was added slowly a dichloromethane solution (100 cm^3) of dibenzoylmethane (1.7 g, 7.5 mmol) followed by diethyl ether (100 cm^3). After the reaction for 1 h, a precipitate was filtered and washed with diethyl ether. The yield was 0.60 g (42%). Found: C, 59.54; H, 3.96%. Calcd for $MnCl(acac)(dbm)=C_{20}H_{18}O_4ClMn$: C, 58.20; H, 4.40%. Acetylacetonato-(benzoylacetonato)chloromanganese(III) was also prepared in a similar manner as above to obtain a crude product in a 38% yield. Found: C, 52.38; H, 4.42%. Calcd for $MnCl(acac)(bzac)=C_{15}H_{16}O_4ClMn$: C, 51.38; H, 4.60%.

Both of the mixed β-diketonato complexes were not recrystallized, since they are not stable in solution, but undergo disproportionation reactions. Thus the results of elemental analysis are not satisfactory.

Preparation of Acetylacetone-methylene-d_2. A mixture of

acetylacetone (10 cm^3, 0.0975 mol) and D_2O (30 cm^3, 1.66 mol) was heated under reflux for 4—5 h, and allowed to stand overnight at room temperature. The mixture was extracted three times with 20 cm^3 portions of dichloromethane. The combined extract was subjected to distillation under reduced pressure to leave the deuterated acetylacetone. The ^1H NMR assay of the neat liquid indicates that the deuterium content of the methylene group is 90.2%. When potassium acetylacetonate was added to make the reaction medium basic, the methyl groups of acetylacetone were also deuterated. This product was not used in the following studies.

Measurements. Water contents of organic solvents were determined by means of an MCI digital water microanalyzer CA-01. Absorption spectra were measured with a Hitachi EPS-3T recording spectrophotometer, and infrared spectra in Nujol with a JASCO DS 701G spectrophotometer. A JEOL JNM MH-100 spectrometer was used to obtain ^1H NMR spectra in CD_2Cl_2 with tetramethylsilane as internal reference.

The ligand substitution reactions were followed spectrophotometrically by means of a Union Stopped-Flow Rapid Scan Spectrophotometer RA-1300. The solution reservoir was covered with a polyethylene bag equipped with gloves and filled with dry nitrogen in order to prevent the stock solution from contacting with air.

Results

Addition Reactions of Donor Molecules to the Chlorobis(β-diketonato)manganese(III) Complexes, $MnCl(\beta\text{-dik})_2$, in Solution. Based on the molecular-weight and other data, $MnCl(acac)_2$ has been considered to exist as five-coordinate molecules in noncoordinating solvents.[1] Now the following spectroscopic studies assure that the sixth coordination site of manganese(III) is really left vacant.

The complex is not so stable in dichloromethane solution, but some kind of decomposition proceeds as evidenced by the change of its spectrum with time. However the spectrum shows no change in the coexistence of an excess (*e.g.* ten times molar) amount of free acacH. Under such circumstances, coordination of an acacH molecule to manganese(III) might happen. To a solution of $MnCl(acac)_2$ in dichloromethane (4.00×10^{-4} mol dm^{-3}) containing water at a constant concentration (5.2×10^{-3} mol dm^{-3}) was added acacH to attain various concentrations in the range of $(3.28—21.84)\times10^{-3}$ mol dm^{-3}, but no change in spectrum was observed. Alternatively, the concentration of acacH was kept constant at 9.61×10^{-3} mol dm^{-3} and that of water was varied in the range of $(4.87—49.8)\times10^{-3}$ mol dm^{-3}. The spectrum showed no change, either. These results may be rationalized if the sixth coordination site of $MnCl(acac)_2$ is occupied preferentially by a molecule of either acacH or water at the given concentrations, or alternatively if the complex retains the five-coordinate structure even in the presence of more than fifty times molar excess of acacH and water. In order to find out which of the three possibilities is the case, the following experiments have been performed.

When an increasing amount of DMF was added to a dichloromethane solution of $MnCl(acac)_2$ containing excess amounts of acacH and water, the absorption spectrum varied successively as is seen in Fig. 1, exhibiting a distinct isosbestic point. Thus the coordination of DMF to manganese as is expressed by Eq. 1 is conceivable.

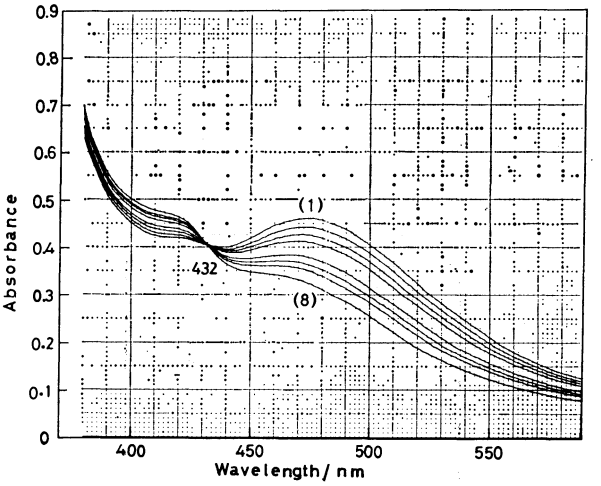

Fig. 1. Absorption spectra of $MnCl(acac)_2$ in dichloromethane at 25.0 °C containing 4.83×10^{-4} mol dm^{-3} complex, 9.80×10^{-3} mol dm^{-3} acacH, and 1.51×10^{-2} mol dm^{-3} H_2O in the absence (curve 1) and presence of DMF at various concentrations: 8.87×10^{-3} (2), 1.77×10^{-2} (3). 2.66×10^{-2} (4), 5.32×10^{-2} (5), 7.10×10^{-2} (6), 8.87×10^{-2} (7), and 1.33×10^{-1} (8) mol dm^{-3}.

$$MnCl(acac)_2X + D \rightleftharpoons MnCl(acac)_2D + X,\ K_{ad}' \quad (1)$$

The equilibrium quotient K_{ad}' is defined by $K_{ad}'=[MD][X]/[MX][D]$, where M and D represent the $MnCl(acac)_2$ moiety and a molecule of donor solvent such as DMF, respectively, and X is either acacH, H_2O, or nil. The observed absorbance per unit path length, A, of the solution is related to the concentration of D by Eq. 2.

$$\frac{1}{\varepsilon_{MX}c_M - A} = \frac{1}{(\varepsilon_{MX}-\varepsilon_{MD})c_M} + \frac{[X]}{(\varepsilon_{MX}-\varepsilon_{MD})c_M K_{ad}'[D]} \quad (2)$$

Here each ε stands for the molar extinction coefficient of the species shown by a subscript, and c_M for the total concentration of the complex. The concentrations of uncoordinated X and D can be approximated by their total concentrations, c, since c_{acacH}, c_{H_2O}, $c_D \gg c_M$. The absorbance at 480 nm was used to calculate the left-hand term of Eq. 2, which was plotted against 1/[D] to result in a good straight line. The slope and intercept of the straight line gave $\varepsilon_{MD}=416$ dm^3 mol^{-1} cm^{-1} at 480 nm and $[X]/K_{ad}'=0.0994$ mol dm^{-3}.

If a water molecule is coordinated to manganese(III) as X, $K_{ad}'(H_2O)$ will be 0.152 since $c_{H_2O}=1.51\times10^{-2}$ mol dm^{-3}. On the other hand, K_{ad}'(acacH) is calculated to be 0.0986 from $c_{acacH}=9.80\times10^{-3}$ mol dm^{-3}. By virtue of these values for the equilibrium quotient of Reaction 1, the absorbance A at various concentrations of X can be calculated from Eq. 3.

$$A = \frac{(\varepsilon_{MX}-\varepsilon_{MD})c_M}{1+K_{ad}'[D]/[X]} + \varepsilon_{MD}c_M \quad (3)$$

The curves in Fig. 2 display the expected change

of A at 480 nm with concentrations of H_2O and acacH as X at a fixed [DMF]. As shown by circles in Fig. 2, the spectra in the 340—700 nm region showed no change under these circumstances, indicating that the coordinated DMF is not replaced at all by H_2O and acacH.

Thus the spectral change depicted in Fig. 1 can not be rationalized by substitution of the H_2O or acacH ligand by DMF, but should be considered to correspond to ligation of DMF at the sixth vacant coordination site according to Eq. 4. Other β-diketonato complexes, $MnCl(bzac)_2$ and $MnCl(dbm)_2$ showed similar behaviors in dichloromethane, indicating that they also reserve the five-coordinate structure in solution.

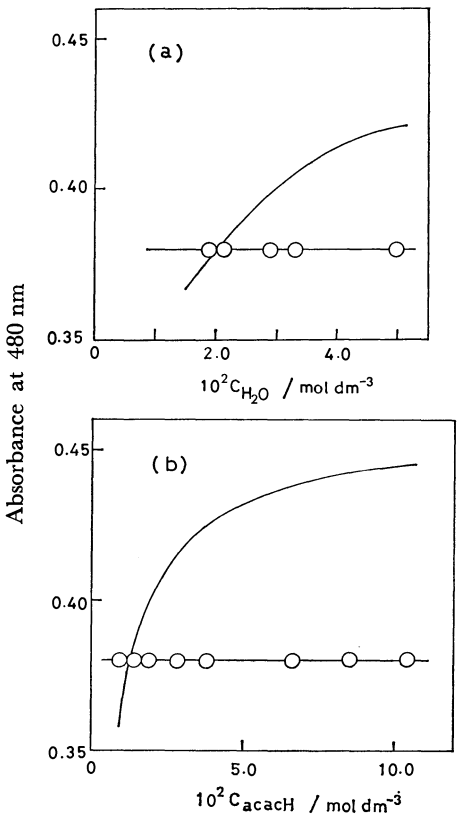

Fig. 2. Dependency of the absorbance at 480 nm of $MnCl(acac)_2$ (4.84×10^{-4} mol dm^{-3}) in CH_2Cl_2 containing DMF (5.84×10^{-2} mol dm^{-3}) on the concentration of (a) water in the presence of acacH (9.62×10^{-3} mol dm^{-3}) and of (b) acacH in the presence of water ($(1.65-2.22)\times10^{-2}$ mol dm^{-3}). Curves represent the calculated values based on the equilibria (1), and circles the observed values.

$$MnCl(\beta\text{-dik})_2 + D \rightleftharpoons MnCl(\beta\text{-dik})_2D \quad (4)$$

$$K_{ad} = [MnCl(\beta\text{-dik})_2D]/[MnCl(\beta\text{-dik})_2][D] \quad (5)$$

Other donor solvents such as pyridine (py), DMSO, methanol (MeOH), MeCN, and PhCN also react with $MnCl(\beta\text{-dik})_2$. The formation constants K_{ad} of these adducts (Eq. 5) were determined in a similar manner as above and are collected in Table 1 together with the molar extinction coefficient of each adduct. The plots of log K_{ad} against the donor number[7] of each solvent gave straight lines (Fig. 3).

When increasing amounts of donor solvents were added to solution of $MnCl(acac)_2$ in dichloromethane, isosbestic points were observed at 434 (py), 431 (DMSO), 432 (DMF), 438 (MeOH), 450 (MeCN), and 447 (PhCN) nm. The reactions of $MnCl(bzac)_2$ with MeOH (432 and 452 nm) and MeCN (426 and 468 nm) also showed two isosbestic points, respectively, while the other donor solvents showed no isosbestic points in the 410—700 nm region. In the case of $MnCl(dbm)_2$, no solvents except MeCN (483 nm) exhibited isosbestic points. These adduct formation reactions are very rapid and could not be followed by the stopped-flow method.

As is exemplified by Fig. 1, a large excess of donor solvents were employed in these experiments, and it was supposed that β-diketone itself might add to $MnCl(\beta\text{-dik})_2$ if a large excess amount was used. Figure 4 shows it is the case in fact. When an increasing amount of acacH was added to a solution of $MnCl(acac)_2$ in dichloromethane, spectral change was observed accompanying an isosbestic point at 443 nm. The resulting spectrum is different from that of $Mn(acac)_3$ and seems to be ascribed to the adduct formed by Reaction 6, although it is not certain whether the acetylacetone molecule is added as a keto or an enol

Table 1. Formation constants (K_{ad}) in dm^3 mol^{-1} and molar extinction coefficients (ε_{ad}) of adducts in dichloromethane at 25.0 °C

$MnCl(\beta\text{-dik})_2 + D \rightleftharpoons MnCl(\beta\text{-dik})_2D$.

D	DN[a]	$MnCl(acac)_2D$			$MnCl(bzac)_2D$			$MnCl(dbm)_2D$		
		K_{ad}	ε_{ad}	(λ/nm)	K_{ad}	ε_{ad}	(λ/nm)	K_{ad}	ε_{ad}	(λ/nm)
py	33.1	102±1	460±13	(480)	310±2	374±1	(500)	374±1	459±1	(530)
DMSO	29.8	28.0±0.6	410±12	(480)	31.4±0.2	366±1	(500)	30.4±0.1	322±2	(530)
DMF	26.6	10.0±0.1	416±5	(480)	11.4±0.1	426±5	(500)	11.4±0.1	390±2	(530)
MeOH	19.0	1.34±0.01	57.4±0.2	(480)	1.12±0.01	144±15	(500)	1.29±0.31	16±6	(530)
MeCN	14.1	0.2444±0.015	569±42	(480)	0.200±0.016	220±24	(520)	0.234±0.005	316±8	(540)
PhCN	11.9	0.258±0.020	594±51	(480)	0.276±0.066	384±115	(500)	0.192±0.060	278±82	(530)
acacH	15.6[b]	0.516±0.008	541±10	(480)	0.46_8[c]			0.44_6[c]		
bzacH	16·4[b]	0.64_8[c]			0.614±0.033	262±18	(540)	0.58_4[c]		
dbmH	17.4[b]	0.86_4[c]			0.84_4[c]			0.822±0.010	164±3	(550)

a) Donor number as defined by Gutmann.[7] b) Determined in this study. c) Calculated. See the text.

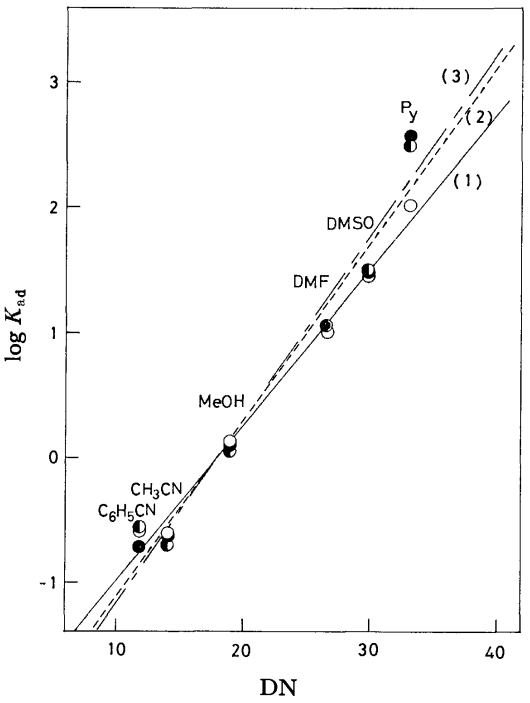

Fig. 3. Formation constants of adducts $MnCl(\beta\text{-dik})_2D$ related to the donor number of addendum D, β-dik being acac (line 1), bzac (2), and dbm (3).

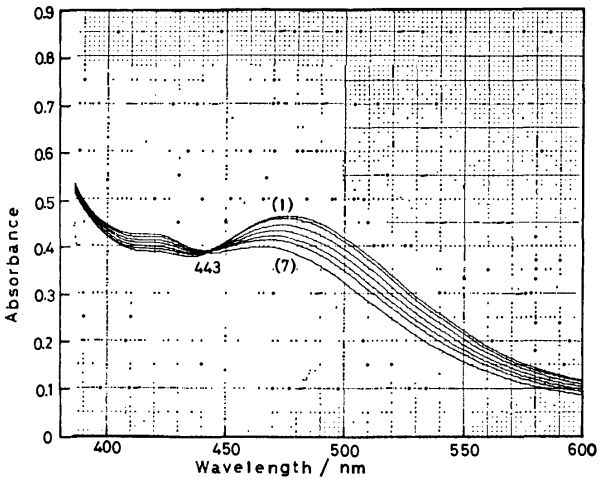

Fig. 4. Absorption spectra of $MnCl(acac)_2$ in dichloromethane at 25.0 °C containing 4.62×10^{-4} mol dm^{-3} complex in the presence of acacH at various concentrations: 9.35×10^{-3} (curve 1), 9.35×10^{-2} (2), 2.23×10^{-1} (3), 4.05×10^{-1} (4), 5.91×10^{-1} (5), 7.97×10^{-1} (6), and 1.17 (7) mol dm^{-3}.

tautomer.

$$MnCl(acac)_2 + acacH \rightleftharpoons MnCl(acac)_2(acacH) \quad (6)$$

The $MnCl(bzac)_2$–(bzacH) and $MnCl(dbm)_2$–(dbmH) systems were also studied in a similar manner. The formation constants of the three kinds of adduct $MnCl(\beta\text{-dik})_2(\beta\text{-dikH})$ were thus determined and listed in Table 1 together with their extinction coefficients at the given wavelengths. The donor number of each β-diketone was estimated by interpolation of the log K_{ad} *vs.* DN plots in Fig. 3, and was in turn utilized to calculate the prospective formation constants of the adducts according to Eq. 7, which are included in Table 1.

$$MnCl(\beta\text{-dik})_2 + \beta\text{-dik'H} \rightleftharpoons MnCl(\beta\text{-dik})_2(\beta\text{-dik'H}) \quad (7)$$

Equilibria for the β-Diketone Substitution Reactions of $MnCl(acac)_2$. Figure 5 shows the absorption spectra of the $MnCl(\beta\text{-dik})_2$ complexes in dichloromethane. When an increasing amount of bzacH or dbmH is added to a $MnCl(acac)_2$ solution containing uncoordinated acetylacetone to stabilize the complex solution, the spectrum changes successively to approach that of $MnCl(bzac)_2$ or $MnCl(dbm)_2$, respectively. The points plotted in Fig. 6 show the observed absorbances at 450 nm as a function of the dbmH concentration added to the solution of $MnCl(acac)_2$ in dichloromethane. These results conform with the following equilibria.

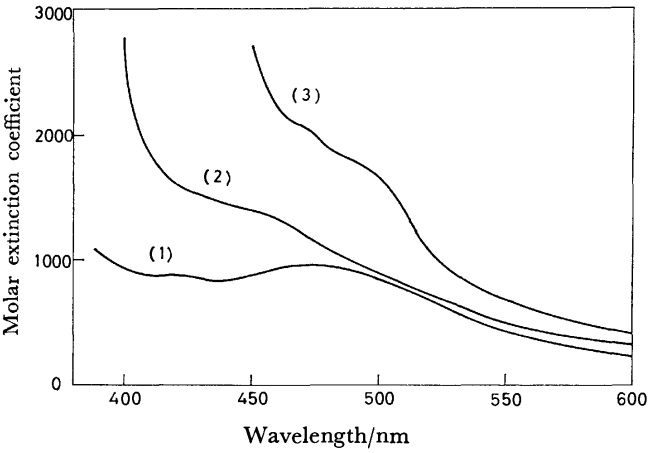

Fig. 5. Absorption spectra of $MnCl(acac)_2$ (curve 1), $MnCl(bzac)_2$ (2), and $MnCl(dbm)_2$ (3) in dichloromethane.

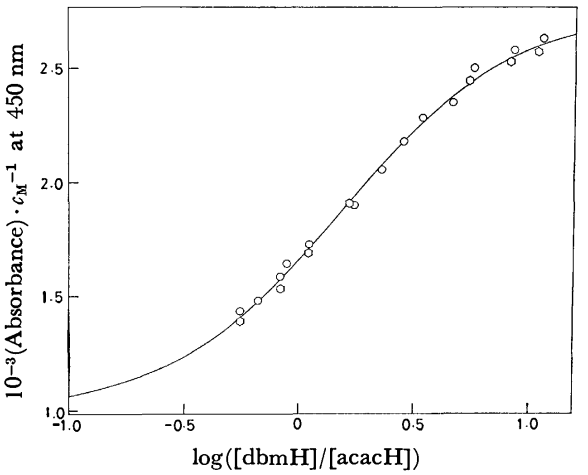

Fig. 6. The absorbance at 450 nm of $MnCl(acac)_2$ solution in dichloromethane at 25 °C as a function of log ([dbmH]/[acacH]), c_M being 2.00×10^{-4} (○) and 2.13×10^{-4} (○) mol dm^{-3}, and c_{acacH} 4.30×10^{-3}. The curve represents the calculated values based on $K_1=0.847$, $K_2=0.401$, and ε for $MnCl(acac)(dbm)=$ 1980 cm^{-1} mol^{-1} dm^3 at 450 nm.

$$MnCl(acac)_2 + \beta\text{-dikH} \rightleftharpoons MnCl(acac)(\beta\text{-dik}) + acacH,\ K_1 \quad (8)$$

$$MnCl(acac)(\beta\text{-dik}) + \beta\text{-dikH} \rightleftharpoons MnCl(\beta\text{-dik})_2 + acacH,\ K_2 \quad (9)$$

The observed absorbance of the reaction mixture is expressed by Eq. 10,

$$A = \varepsilon_{Ma_2}[Ma_2] + \varepsilon_{Mab}[Mab] + \varepsilon_{Mb_2}[Mb_2] = \bar{\varepsilon} c_M, \quad (10)$$

where Ma_2, Mab, and Mb_2 represent $MnCl(acac)_2$, MnCl(acac)(β-dik), and $MnCl(\beta\text{-dik})_2$, respectively. The mean molar absorptivity $\bar{\varepsilon}$ can be calculated by

$$\bar{\varepsilon}_{calcd} = \frac{\varepsilon_{Ma_2} + \varepsilon_{Mab}K_1([\beta\text{-dikH}]/[acacH]) + \varepsilon_{Mb_2}K_1K_2([\beta\text{-dikH}]/[acacH])^2}{1 + K_1([\beta\text{-dikH}]/[acacH]) + K_1K_2([\beta\text{-dikH}]/[acacH])^2}, \quad (11)$$

where K_1 and K_2 are the equilibrium constants for the stepwise substitution Reactions 8 and 9.

$$K_1 = \frac{[Mab][acacH]}{[Ma_2][\beta\text{-dikH}]}, \quad K_2 = \frac{[Mb_2][acacH]}{[Mab][\beta\text{-dikH}]}. \quad (12)$$

Since acacH and β-dikH were used in more than twenty times molar excess than c_M, [acacH] and [β-dikH] may be approximated by the total concentrations c_{acacH} and $c_{\beta\text{-dikH}}$, respectively. A generalized least squares method was applied in order to minimize the error square sum $\Sigma(\bar{\varepsilon}_{obsd} - \bar{\varepsilon}_{calcd})^2$ for the set of constants K_1, K_2, and ε_{Mab}. The constants thus obtained for both the $MnCl(acac)_2$–bzacH and $MnCl(acac)_2$–dbmH systems are listed in Table 2. The solid curve in Fig. 6 representing absorbance calculated for the $MnCl(acac)_2$–dbmH system conforms satisfactorily with the experimental data, supporting presumed participation of the mixed-ligand complex. In fact MnCl(acac)(bzac) and MnCl(acac)(dbm) were prepared and isolated as described in the Experimental section.

Table 2. The equilibrium constants in dichloromethane at 25.0 °C for the substitution reactions of $MnCl(acac)_2$ with benzoylacetone and dibenzoylmethane according to Eqs. 8 and 9

β-Diketone	K_1	K_2	ε(At λ/nm)[a]
bzacH	1.09±0.01	0.43±0.02	1184±10 (434)
dbmH	0.85±0.01	0.40±0.02	1980±20 (450)

a) For the mixed ligand complex MnCl(acac)(β-dik).

Kinetics of the β-Diketone Substitution Reactions of MnCl(β-dik)₂. As is shown in Table 2, the equilibria for the β-diketone substitution reactions of $MnCl(acac)_2$ are rather favorable to the acetylacetonato complex. Thus reactions (13) were studied under the pseudo first order conditions employing excess amounts of acacH.

$$MnCl(\beta\text{-dik})_2 + 2\,acacH \longrightarrow MnCl(acac)_2 + 2\beta\text{-dikH} \quad (13)$$

The spectral change during reactions was recorded over the 405—495 nm region by means of a rapid scan instrument. As was anticipated from the spectra in Fig. 5, no isosbestic point was observed, but the absorbance of the reaction mixture decreased monotonously with time in either case. The progress of reaction was followed spectrophotometrically at an appropriate wavelength by the stopped-flow method.

Figure 7(a) exemplifies a plot of $\ln(A - A_\infty)$ against time for the reaction of $MnCl(dbm)_2$ with acacH in dichloromethane at 25.0 °C which was followed at 450 nm. The observed points in the later stage of reaction fall on a straight line, but those in the earlier stage deviate appreciably from it. This behavior may be rationalized on the assumption that the overall reaction is composed of two consecutive steps (14) and (15), since the existence of the metastable mixed ligand complex was revealed by the foregoing equilibrium studies.

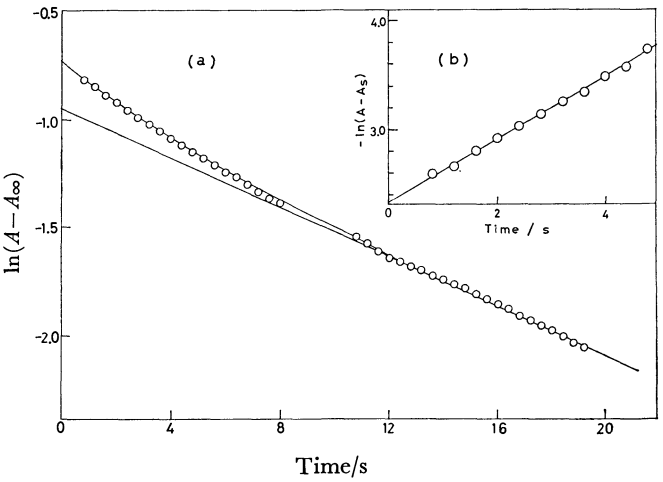

Fig. 7. (a) Pseudo first order plot for the reaction of $MnCl(dbm)_2$ with acetylacetone in dichloromethane at 25.0 °C, c_M, c_{dbmH}, c_{acacH} and c_{H_2O} being 2.47×10^{-4}, 2.47×10^{-3}, 9.74×10^{-2}, and 7.42×10^{-3} mol dm^{-3}, respectively. (b) Linear plot for the earlier part of the above reaction.

$$MnCl(\beta\text{-dik})_2 + acacH \longrightarrow MnCl(acac)(\beta\text{-dik}) + \beta\text{-dikH},\ k_1 \quad (14)$$

$$MnCl(acac)(\beta\text{-dik}) + acacH \longrightarrow MnCl(acac)_2 + \beta\text{-dikH},\ k_2 \quad (15)$$

Under the pseudo first order conditions, the absorbance of a reaction mixture at time t is related to k_1 and k_2 by

$$A - A_\infty = a_1 \exp(-k_1 t) + a_2 \exp(-k_2 t), \quad (16)$$

since A is expressed by Eq. 10 and $A_\infty = \varepsilon_{Ma_2} c_M$, a_1, and a_2 in Eq. 16 being given by

$$a_1 = \frac{(\varepsilon_{Mb_2} - \varepsilon_{Mab})k_1 + (\varepsilon_{Ma_2} - \varepsilon_{Mb_2})k_2}{k_1 - k_2} c_M \quad (17)$$

$$a_2 = \frac{(\varepsilon_{Mab} - \varepsilon_{Ma_2})k_1}{k_1 - k_2} c_M. \quad (18)$$

The later linear part of the $\ln(A - A_\infty)$ *vs.* t plot in Fig. 7(a) gives the slower one of the two rate constants, $k_S = 0.0573\ s^{-1}$, and the ordinate intercept, ln

$a_S=\ln(A_S-A_\infty)=\ln(9.85\times10^{-2})$. Then the values $A-A_S$ were calculated for the absorbance data in the earlier part of reaction and $\ln(A-A_S)$ was plotted against time to result in a straight line in Fig. 7(b). The slope and intercept of this straight line gave the faster rate constant $k_F=0.293\ s^{-1}$ and $\ln a_F=\ln(A_0-A_S)=\ln(3.83\times10^{-1})$. The solid curve in Fig. 7(a) reproduces the calculated values of $\ln(A-A_\infty)$ based on k_S, k_F, a_S, and a_F.

Equation 19 was derived from Eqs. 17 and 18 and utilized to assign k_S and k_F correctly to k_1 and k_2 in Eq. 16.

$$\frac{k_2}{k_1}=\frac{\varepsilon_{Mab}-\varepsilon_{Ma_2}}{\varepsilon_{Ma_2}-\varepsilon_{Mb_2}}\left(\frac{a_1}{a_2}-\frac{\varepsilon_{Mb_2}-\varepsilon_{Mab}}{\varepsilon_{Mab}-\varepsilon_{Ma_2}}\right) \quad (19)$$

If it is assumed that $k_S=k_1$ and $k_F=k_2$, the left-hand side of Eq. 19 becomes 5.1, whereas the right-hand side is -1.7. On the other hand, the reverse assignment that $k_S=k_2$ and $k_F=k_1$ results in fair coincidence between the two values: the left-hand side=0.20 and the right-hand side=0.29. Therefore the latter assignment is reasonable and the pseudo first order rate constants thus obtained will be referred to k_1(obsd) and k_2(obsd) in the following discussion.

The pseudo first order rate constants obtained in dichloromethane at 25.0 °C containing various concentrations of acetylacetone and water are listed in Table 3. When c_{acacH} is maintained constant, k_1(obsd) and k_2(obsd) do not show appreciable change beyond the experimental error even if c_{H_2O} is varried in the 5.87—16.83$\times10^{-3}$ mol dm^{-3} region for MnCl(bzac)$_2$ and in the 1.22—8.16$\times10^{-3}$ mol dm^{-3} region for MnCl(dbm)$_2$. On the other hand both k_1(obsd) and k_2(obsd) increase with c_{acacH} and the slopes of each two straight lines in Figs. 8(a) and (b) give the second order rate constants k_1 and k_2 for the reactions of MnCl(bzac)$_2$ and MnCl(dbm)$_2$ with acacH, respectively. By combining these values with the equilibrium constants listed in Table 2, the second order rate constants for the forward reactions of (8) and (9) were obtained. Table 4 summarizes these rate data.

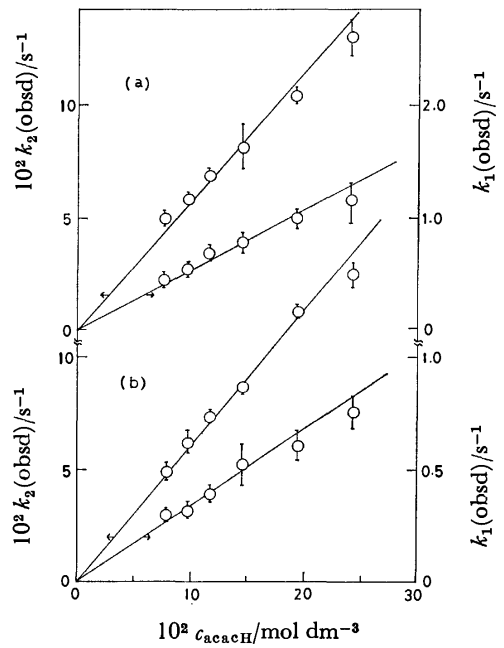

Fig. 8. Dependences on c_{acacH} of k_1(obsd) and k_2(obsd) for the reactions of MnCl(bzac)$_2$ (a) and MnCl(dbm)$_2$ (b) with acacH in dichloromethane at 25.0 °C.

The plots of k_1(obsd) and k_2(obsd) for the reaction of MnCl(dbm)$_2$ with acetylacetone-d_2 (Table 3) against c_{acacH} resulted in straight lines passing through the origin, of which slopes gave $k_1(D)=11.4\pm0.05\ s^{-1}$ and $k_2(D)=0.281\pm0.031\ s^{-1}$. Thus the apparent rate ratios are $k_1(H)/k_1(D)=2.96$ and $k_2(H)/k_2(D)=2.16$. Taking into account the fact that the isotopic purity of the acetylacetone-d_2 used is 90.2%, the kinetic isotope effect is calculated as $k_1(H)/k_1(D)=3.76$ and $k_2(H)/k_2(D)=2.47$. The calculation is based on the assumption that the isotope exchange between acetylacetone-d_2 and water is so slow under the given conditions that the deuterium content of the acetylacetone-d_2 is unaltered during the rate measurements.

Table 3. Pseudo first order rate constants in dichloromethane at 25.0 °C of the substitution reactions of MnCl(β-dik)$_2$ with acetylacetone according to Eqs. 14 and 15

$10^2\,c_{acacH}$ / mol dm^{-3}	$10^3\,c_{H_2O}$ / mol dm^{-3}	$10^2\,k_1$(obsd) / s^{-1}	$10^2\,k_2$(obsd) / s^{-1}
	MnCl(bzac)$_2$[a]		
7.726	8.88	45.4±6.7	4.96±0.31
9.657	9.52	54.2±4.8	5.87±0.21
11.58	9.69	68.5±5.3	6.90±0.22
14.48	9.46	77.9±9.0	8.16±0.98
19.31	8.90	98.0±7.0	10.4±0.5
24.14	8.60	120±23	13.1±0.8
9.730	6.18	55.4±8.8	6.19±0.13
9.730	5.87	65±12	5.73±0.22
9.730	9.17	54±13	5.98±0.35
9.730	12.74	50.2±9.3	6.38±0.50
9.730	16.83	52.6±1.7	5.31±0.27
	MnCl(dbm)$_2$[b]		
7.795	7.90	30.0±2.6	4.91±0.36
9.744	7.42	32.1±3.8	6.19±0.50
11.69	8.88	39.6±3.4	7.29±0.30
14.62	8.14	51.7±9.1	8.60±0.23
19.48	7.92	60.6±6.1	11.99±0.36
24.36	7.94	75.3±7.1	13.64±0.53
9.952	1.22	45.7±0.4	6.00±0.71
9.952	1.48	38.5±8.8	5.85±0.14
9·952	1.42	45.9±1.6	6.26±0.73
9.952	1.47	37.6±3.4	6.1 ±1.3
9.952	4.14	39.2±2.3	6.28±0.19
9.952	8.16	36.6±0.8	6.80±0.28
9.820[c]	5.70	11.6±2.9	3.01±0.72
14.73[c]	5.43	16.2±1.0	3.99±0.27
19.64[c]	5.07	22.2±2.8	5.04±0.43

a) $c_M=2.47\times10^{-4}$ mol dm^{-3} and $c_{bzacH}=3.067\times10^{-3}$ mol dm^{-3} for the former six experiments, and $c_M=2.46\times10^{-4}$ mol dm^{-3} and $c_{bzacH}=3.110\times10^{-3}$ mol dm^{-3} for the latter five experiments. b) $c_M=2.46\times10^{-4}$ mol dm^{-3} and $c_{dbmH}=2.474\times10^{-3}$ mol dm^{-3}. c) Acetylacetone-d_2 was used and $c_{dbmH}=2.472\times10^{-3}$ mol dm^{-3}.

Table 4. Second order rate constants ($dm^3 mol^{-1} s^{-1}$) in dichloromethane at 25.0 °C for the substitution reactions of $MnCl(\beta\text{-dik})_2$ with other β-diketone

$$MnCl(\beta\text{-dik})_2 \xrightarrow[\beta\text{-dik'H}]{\beta\text{-dikH}} MnCl(\beta\text{-dik})(\beta\text{-dik'}) \xrightarrow[\beta\text{-dik'H}]{\beta\text{-dikH}} MnCl(\beta\text{-dik'})_2$$

$MnCl(\beta\text{-dik})_2$	β-dik'H		
	acacH	bzacH	dbmH
$MnCl(acac)_2$		0.634[a]	0.516[a]
$MnCl(bzac)_2$	5.47±0.40		
$MnCl(dbm)_2$	3.38±0.28		
MnCl(acac)(bzac)	0.582±0.041	2.34[a]	
MnCl(acac)(dbm)	0.608±0.029		1.36[a]

a) Calculated value (see text).

Discussion

Addition Equilibria of Donor Molecules to $MnCl(\beta\text{-dik})_2$. As is seen in Figs. 1 and 4, the reaction of $MnCl(\beta\text{-dik})_2$ with a donor slovent in large excess is accompanied by an appreciable change in the absorption spectrum, which suggests some alteration in the coordination sphere. It seems reasonable to suppose that a donor molecule added to $MnCl(\beta\text{-dik})_2$ attains six coordination (Eq. 4). In fact adducts such as $MnCl(acac)_2$(pyridine *N*-oxide),[1] $MnBr(acac)_2$(4-Me-py),[1] $MnBr(acac)_2$(dioxane)$\cdot H_2O$,[1] and $MnNCS(acac)_2(py)$[8] have been prepared and characterized, supporting the existence of addition equilibria represented by Eq. 4 in solution.

The formation constant of adducts, K_{ad}, increases with the donor number of addendum (Table 1), and the $\log K_{ad}$ *vs.* DN plots afford straight lines (Fig. 3) which are reproduced by the following equations based on the least squares treatment, r giving the correlation coeffecient in each case.

$$MnCl(acac)_2: \log K_{ad} = 0.125DN - 2.24 \quad (r=0.994) \quad (20\text{-}1)$$

$$MnCl(bzac)_2: \log K_{ad} = 0.142DN - 2.54 \quad (r=0.981) \quad (20\text{-}2)$$

$$MnCl(dbm)_2: \log K_{ad} = 0.146DN - 2.63 \quad (r=0.984) \quad (20\text{-}3)$$

Such a linear relationship between the adduct formation constant and the donor number of addendum has seldom been noted for five-coordinate complexes. Gutmann found that adduct formation constants of antimony(V) chloride with various donor solvents increase with the donor number.[7] The linear relation is expressed by $\log K_{DSbCl_5}=0.580$ DN-5.44 ($r=0.984$). Carlin and Walker studied the adduct formation of $VO(acac)_2$ with a variety of N- and O-donors in nitrobenzene by the calorimetric and spectroscopic methods, and determined the equilibrium constants as well as thermodynamic functions.[9] Of their data, those for pyridine, piperidine, methanol, and hexamethylphosphoric triamide of which DN values are available satisfy the linear relation: $\log K_{ad}=0.101$ DN-1.94 ($r=0.979$). It is very interesting that both of the slope and intercept show a close resemblance to those in the present system (Eqs. 20) in spite of the difference in the nature of complex and the solvent used. Both of these slopes are much gentle compared with that for $DSbCl_5$, revealing that $VO(acac)_2$ and $MnCl(\beta\text{-dik})_2$ are less sensitive than $SbCl_5$ as the indicator of relative base strength.

Equations 20 were utilized to obtain the DN values of β-diketones based on the observed K_{ad} for $MnCl(\beta\text{-dik})_2(\beta\text{-dikH})$. The DN values were used in turn to calculate K_{ad} for the $MnCl(\beta\text{-dik})_2(\beta\text{-dik'H})$ adducts which can not be determined experimentally since the ligand substitution occurs. As is seen in Table 1, DN of β-diketone increases in the sequence of acacH< bzacH<dbmH and K_{ad} for a given $MnCl(\beta\text{-dik})_2$ also shows the same sequence. The infrared study on $Cu(\beta\text{-dik})_2$[10] and ^1H NMR study on β-diketones[11] show the ability of the aromatic substitutents to supply electron density to the chelate or enolic ring by resonance, and the pK_a values determined in aqueous dioxane (50% by volume) at 25 °C increase in the sequence of acacH(10.28) < bzacH(10.43) < dbmH (11.26).[12] The observed trend of K_{ad} also reflects the electron relasing effect of the phenyl substitutent in bzacH and dbmH. On the other hand, the K_{ad} values for the three $MnCl(\beta\text{-dik})_2$ complexes with a particular β-dikH show a slight decrease in the sequence of $MnCl(acac)_2>MnCl(bzac)_2>MnCl(dbm)_2$. Better β-diketonate ligands seem to suppress the acidity of $MnCl(\beta\text{-dik})_2$.

Water exists as a discrete molecule in benzene,[13] toluene,[14] and cyclohexane[14] solutions, but partially forms a dimer in chlorinated solvents such as chloroform,[13a] 1,2-dichloroethane, and 1,1,2,2-tetrachloroethane.[14] Although the behavior of water in dichloromethane has not yet been reported, the dimerization constants determined in chloroform (0.47) and 1,2-dichloroethane (0.54) at 25 °C[13a] may be used to estimate the degree of dimerization of water in dichloromethane. In the present investigation, the concentration of water has been kept around 10^{-3} mol dm^{-3} and was 5×10^{-2} mol dm^{-3} at most. Under these conditions, the estimated fraction of dimer is less than 2%, and most part of water molecules exist as monomer in dichloromethane. The DN value (18.0) of water was obtained by Gutmann in 1,2-dichloroethane and refers to the monomeric species. Substituting this value into Eqs. 20, we can estimate the adduct formation constants of water with the $MnCl(\beta\text{-dik})_2$ complexes to be 1.02, 1.04, and 0.995 for β-dik=acac, bzac, and dbm, respectively. These figures rationalize the failure of water in affecting the absorption spectrum of $MnCl(acac)_2$ in dichloromethane.

Substitution Equilibria. Most of the equilibrium constants K_1 and K_2 for the substitution reactions of $MnCl(acac)_2$ with benzoylacetone and dibenzoylmethane according to Eqs. 8 and 9 are smaller than 1. This fact might look to contradict the above-mentioned

basicity sequence of the β-diketonate anions: $acac^- < bzac^- > dbm^-$. However it should be noted that Equilibria 8 and 9 involve the β-diketone molecules instead of the β-diketonate anions. The equilibrium constant K_1' for the reaction

$$MnCl(acac)_2 + \beta\text{-dik}^- \rightleftharpoons MnCl(acac)(\beta\text{-dik}) + acac^- \quad (21)$$

will be certainly larger than 1 for $\beta\text{-dik}^- = bzac^-$ and dbm^-, but K_1 is related by K_1' by

$$\log K_1 = \log K_1' - (pK_a \text{ of } \beta\text{-dikH} - pK_a \text{ of acacH}). \quad (22)$$

Since the pK_a values of bzacH and dbmH are larger than that of acacH, $\log K_1$ becomes smaller than $\log K_1'$ by the pK_a difference between the β-diketones.

Mechanism of the Substitution Reactions. Based on the information obtained from the equilibrium and kinetic studies described above, the scheme depicted in Fig. 9 is proposed as a mechanism of substitution reaction of $MnCl(\beta\text{-dik})_2$ with another β-diketone such as acacH. The first step, coordination of an acacH molecule to manganese at the sixth vacant site is evidenced by the equilibrium measurements. Although dbmH exists solely as enol molecules, bzacH and acacH are composed of two tautomers, neat liquids containing 98 and 79% enol, respectively, at 38 °C.[15] The enol content is further increased in inert solvents, and that of acacH was reported to be 87% in chloroform and 96% in carbon tetrachloride at 33 °C.[16] In the present study, acacH and bzacH in dichloromethane at 23 °C were found to contain 83.4 and 97.9% enol, respectively.

The enol tautomer of acetylacetone reacts with the copper(II) ion much faster than the keto form in water and methanol.[17] In the case of thenoyltrifluoroacetone only the enol tautomer was reported to react with nickel(II), cobalt(II), copper(II), and iron(II) in aqueous solution.[18] Although the tautomerization rate is estimated as low as 10^{-5} s^{-1} in aprotic solvents by extrapolation from data in mixed aqueous media,[19] it is difficult to distinguish the contribution of both tautomers in the present case. However mainly the enol tautomer seems to contribute to the overall rate because of its predominant abundance

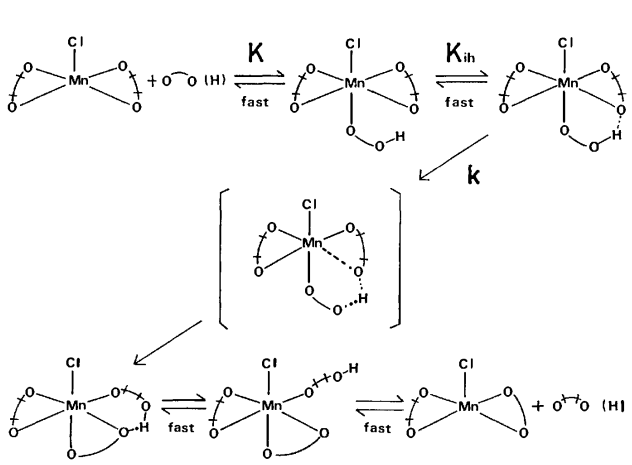

Fig. 9. Proposed mechanism for the ligand substitution reaction of $MnCl(\beta\text{-dik})_2$ with another β-diketone molecule.

and higher deprotonation rate[20] as compared with the keto tautomer. In recent years many kinds of metal complexes containing β-dicarbonyl compounds as a neutral ligand have been prepared.[21] Most of them contain the keto tautomer,[22] but $UO_2(acac)_2(acacH)$,[23] $MnBr_2(acacH)_2$,[24] $[ReCl(CO)_3(bzacH)]_2$,[25] and $PtCl(acac)(acacH)$[26] involve the enol tautomer.

As the second step of the reaction scheme, hydrogen-bonding interaction between the coordinated acacH and a neighboring β-diketonate ligand is presumed. Both ^1H NMR spectra[16] and cryoscopic measurements[27] of acacH in cyclohexane were consistent with intermolecular association. Hydrogen-bonding interaction between the coordinated β-diketonate ligand and various proton donors has also been evidenced by infrared[28] and electronic[29] absorption spectroscopy. X-Ray analysis of $VO(acac)_2(p\text{-}NO_2C_6H_4OH)$ revealed that a p-nitrophenol molecule is linked with one oxygen atom of an acac ligand *via* hydrogen bonding with the OH···O distance of 2.68 Å.[30] Thus the interligand hydrogen bonding presumed in the scheme seems reasonable.

Succeeding intramolecular dissociative interchange, that is, proton transfer from acacH to a leaving β-dik ligand, chelate-ring opening of the β-dik ligand, and chelation of the acac ligand in a synchronous fashion is presumed as the rate-determining step. The observed deuterium isotope effect may be caused by the hydrogen-bonding preequilibrium (K_{ih}) and proton transfer *via* this linkage (k). Thompson and Allred[27] compared the keto-enol equilibria in acetylacetone and acetylacetone-d_2 at various temperatures and concluded that protium forms a stronger hydrogen bond in this system than does deuterium, but the difference is not substantial at ambient temperature. Long and Watson[31] measured the rates of bromination of γ-methylacetylacetone and its γ-deuterio analogue in aqueous solution at 25 °C. The k_H/k_D ratios for the proton transfer from the keto molecule to water and acetate anion were 3.5 and 5.5, respectively, and those for the proton transfer from the enol molecule were also calculated to be 3.4 and 5, respectively. The observed values of k_H/k_D, 3.76 and 2.47 for k_1 and k_2, respectively, for the present system seem to accord with the proposed reaction scheme.

Recently Nishizawa and Saito studied the ligand exchange reaction between $VO(acac)_2$ and acacH-^{14}C in 1,2-dichloroethane.[32] They estimated the donor number of acacH to be 20 by a spectroscopic method, which is a little larger than the value (15.6) obtained in the present study. They also proposed a mechanism which involves the unidentate coordination of acacH to $VO(acac)_2$ ($K_{ad}=0.14$ dm^3 mol^{-1}) as the first step and its chelation associated with the proton transfer to a leaving acac ligand as the rate-determining step, since the observed k_H/k_D value of 1.3 is not so large as to rationalize the assumption of a proton-transfer step as an independent rate-determining step.[32]

Based on the proposed scheme in Fig. 9, the overall rate of reaction is given by Eq. 23.

$$\text{rate} = \frac{kKK_{ih}[acacH]}{1+(1+K_{ih})K[acacH]}[MnCl(\beta\text{-dik})_2] \quad (23)$$

Here $(1+K_{ih})K$ corresponds to K_{ad} of which values are given in Table 1, and $1 \gg (1+K_{ih})K[\text{acacH}]$ under most of the experimental conditions listed in Table 3. Then Eq. 23 is reduced to

$$k_{obsd} = kKK_{ih}[\text{acacH}]. \quad (24)$$

Thus the second order rate constants in Table 4 are composite in reality. The value of K will be large for an entering ligand whose DN is large, while K_{ih} and k will be larger for a more acidic entering ligand. Table 4 indicates that the rate of reaction of $MnCl(acac)_2$ with bzacH is larger than that with dbmH, although K_{ad} for bzacH is smaller than that for dbmH (Table 1). More acidic bzacH seems to have large K_{ih} and k overcompensating for disadvantage in K as compared with dbmH.

On the other hand, the rate of reaction of acacH with $MnCl(bzac)_2$ is a little faster than that with $MnCl(dbm)_2$ at 25.0 °C (Table 4). Since the K_{ad} values are estimated to be comparable for the two systems (Table 1) and K_{ih} seems favorable to more basic dbm ligand, lower rate for $MnCl(dbm)_2$ may stem from the k factor, cleavage of the Mn–O(dbm) bond being a little more difficult as compared with the Mn–O(bzac) bond.

We wish to thank Mr. Junichi Gohda for the elemental analysis and also the Ministry of Education, Science and Culture, for the Grant-in-Aid for Scientific Research (Grant No. 243014).

References

1) K. Isobe and S. Kawaguchi, *Bull. Chem. Soc. Jpn.*, **48**, 250 (1975).
2) P. F. Lindley and A. W. Smith, *Chem. Commun.*, **1970**, 1355.
3) B. R. Stults, R. S. Marianelli, and V. W. Day, *Inorg. Chem.*, **14**, 722 (1975).
4) B. R. Stults, R. O. Day, R. S. Marianelli, and V. W. Day, *Inorg. Chem.*, **18**, 1847 (1979).
5) V. W. Day, B. R. Stults, E. L. Tassett, R. O. Day, and R. S. Marianelli, *J. Am. Chem. Soc.*, **96**, 2650 (1974).
6) L. J. Boucher, *Coord. Chem. Rev.*, **7**, 289 (1972).
7) V. Gutmann, "Coordination Chemistry in Non-aqueous Solutions," Springer-Verlag, Wien (1968); *Coord. Chem. Rev.*, **12**, 263 (1974); **15**, 207 (1975); **18**, 225 (1976).
8) B. R. Stults, V. W. Day, E. L. Tasset, and R. S. Marianelli, *Inorg. Nucl. Chem. Lett.*, **9**, 1259 (1973).
9) R. L. Carlin and F. A. Walker, *J. Am. Chem. Soc.*, **87**, 2128 (1965).
10) K. Nakamoto, Y. Morimoto, and A. E. Martell, *J. Phys. Chem.*, **66**, 346 (1962).
11) R. L. Lintvedt and H. F. Holtzclaw, Jr., *J. Am. Chem. Soc.*, **88**, 2713 (1966); *Inorg. Chem.*, **5**, 239 (1966).
12) J. L. Ault, H. J. Harries, and J. Burgess, *Inorg. Chim. Acta*, **25**, 65 (1977).
13) a) W. L. Masterton and M. C. Gendrano, *J. Phys. Chem.*,**70**. 2895 (1966); b) S. D. Christian, H. E. Affsprung, and J. R. Johnson, *J. Chem. Soc.*, **1963**, 1896.
14) J. R. Johnson, S. D. Christian, and H. B. Affsprung, *J. Chem. Soc., A*, **1966**, 77.
15) G. Allen and R. A. Dwek, *J. Chem. Soc., B*, **1966**, 161.
16) M. T. Rogers and J. L. Burdett, *Can. J. Chem.*, **43**, 1516 (1965).
17) R. G. Pearson and O. P. Anderson, *Inorg. Chem.*, **9**, 39 (1970).
18) M. R. Jaffe, D. P. Fay, M. Cefola, and N. Sutin, *J. Am. Chem. Soc.*, **93**, 2878 (1971).
19) H. Watarai and N. Suzuki, *J. Inorg. Nucl. Chem.*, **36**, 1815 (1974); **38**, 1683 (1976).
20) M. Eigen, W. Kruse, G. Maass, and L. DeMaeyer, *Progr. Reaction Kinetics*, **2**, 285 (1964).
21) *E.g.* Y. Nakamura, K. Isobe, H. Morita, S. Yamazaki, and S. Kawaguchi, *Inorg. Chem.*, **11**, 1573 (1972).
22) *E.g.* S. Koda, S. Ooi, H. Kuroya, K. Isobe, Y. Nakamura, and S. Kawaguchi, *Chem. Commun.*, **1971**, 1321; R. E. Cramer, S. W. Cramer, K. F. Cramer, M. A. Chudyk, and K. Seff, *Inorg. Chem.*, **16**, 219 (1977).
23) J. M. Haigh and D. A. Thornton, *Inrog. Nucl. Chem. Lett.*, **6**, 231 (1970).
24) S. Koda, S. Ooi, H. Kuroya, Y. Nakamura, and S. Kawaguchi, *Chem. Commun.*, **1971**, 280.
25) M. C. Fredette and C. J. L. Lock, *Can. J. Chem.*, **51**, 1116 (1973).
26) D. Gibson, J. Lewis, and C. Oldham, *J. Chem. Soc., A*, **1967**, 72; J. Hillis, J. Francis, M. Ori, and M. Tsutsui, *J. Am. Chem. Soc.*, **96**, 4800 (1974).
27) D. W. Thompson and A. L. Allred, *J. Phys. Chem.*, **75**, 433 (1971).
28) T. S. Davis and J. P. Fackler, Jr., *Inorg. Chem.*, **5**, 242 (1966).
29) A. S. N. Murthy and S. B. Shah, *J. Inorg. Nucl. Chem.*, **40**, 1948 (1978).
30) H. Taguchi, K. Isobe, Y. Nakamura, and S. Kawaguchi, *Bull. Chem. Soc. Jpn.*, **51**, 2025 (1978).
31) F. A. Long and D. Watson, *J. Chem. Soc.*, **1958**, 2019.
32) M. Nishizawa and K. Saito, *Bull. Chem. Soc. Jpn.*, **51**, 483 (1978).

Preparation and Oxidation of Europium(II) Niobium Bronze Eu_xNbO_{3-y}

Kenji Ishikawa, Gin-ya Adachi,* Midori Tanida, and Jiro Shiokawa
Department of Applied Chemistry, Faculty of Engineering, Osaka University, Yamadakami, Suita, Osaka 565
(Received May 2, 1980)

Mixed oxides containing bivalent europium, Eu_xNbO_{3-y} ($0.5<x<1.0$), were synthesized by the solid state reaction of Eu_2O_3, Nb_2O_5, and Nb powder. The structural change of Eu_xNbO_{3-y} from a tetragonal to cubic form takes place at $x=0.65$. The mechanism of oxidation for the bronzes was studied. Each bronze shows different behavior in oxidation, the cubic bronze giving an amorphous phase and the tetragonal bronze complex crystalline products. $EuNbO_4$ was crystallized from both the amorphous and crystalline phases at 950 K and 1070 K, respectively. TG-DTA and magnetic studies indicated that the oxidized phases play an important role in the rate-determining step of oxidation for the bronzes.

Europium (II) niobium bronzes are nonstoichiometric compounds. Fayolle *et al.*[1] reported the preparation of the bronzes. They found a cubic form for a high Eu^{2+} content region and a tetragonal form for a low Eu^{2+} content region. Oxidation of the bronzes has attracted our attention because each phase undergoes changes in different ways. Krylov *et al.*[2] reported on the oxidation of the bronze whose composition is $EuNbO_3$ and concluded that $EuNbO_4$ is an oxidized product of $EuNbO_3$. So far stoichiometry of oxygen of the bronzes has not been considered seriously. However, oxygen content is a very influential factor for understanding the physical and chemical properties of the bronzes, since the valence state of niobium is controlled by the amount of oxygen. We have determined the oxygen content thermogravimetrically, and found that the bronze is described by a general formula, Eu_xNbO_{3-y}. Discussion is given on the oxidation process of the bronze.

Experimental

Reagents. Europium sesquioxide (Shin-etsu Chemical Corp., minimum purity 99.99%), diniobium pentaoxide and niobium metal (Wako Chemical Industries, Ltd., purity 99.99%, and 99.9%, respectively). Europium sesquioxide and diniobium pentaoxide were calcinated at 1000 K for half an hour in the air before being weighed.

Preparative. Mixtures of Eu_2O_3, Nb_2O_5, and Nb with various compositions were ground together in an agate mortar, pressed into pellets and heated in a vacuum (10^{-2} Pa) at 1173 K for 2 h. After cooling, the pellets were ground-ed and pressed into pellets again. They were packed into a Mo box, sealed in a vacuum (10^{-3} Pa) in a silica capsule and heated at 1473 K for 48 h. The reaction was assumed to occur according to the reaction

$$5xEu_2O_3 + a(6x-2)Nb + (5+a-3ax)Nb_2O_5 \longrightarrow 10Eu_xNbO_{3-y}. \quad (1)$$

Niobium metal was taken a times the amount needed to prepared Eu_xNbO_3 in order to compensate slight oxidation loss of the bronzes during the course of synthesis. Reaction conditions and analytical values of the bronzes are summarized in Table 1.

Analytical Method. The atomic ratios (Eu:Nb) in the compounds obtained were determined with a Rigaku Denki energy dispersion type X-ray fluorescent spectrograph unit, "Ultra trace system," having a tungsten target X-ray tube, a stannum second target, and a Si(Li) semiconductor detector. The oxygen content was determined by oxidation of the bronzes in the air. Assuming that the reaction is

$$Eu_xNbO_{3-y} + zO_2 \longrightarrow \frac{x}{2}Eu_2O_3 + \frac{1}{2}Nb_2O_5, \quad (2)$$

y can be determined by means of Eu content (x) and the increase in mass due to oxidation (z). The phase purity and structure type of materials were characterized by X-ray powder data, using a Rigaku Denki "Rotor-flex" diffractometer (Table 2).

Magnetic Measurements. The magnetic susceptibility data of the resulting materials were obtained with a Shimadzu "MB-11" magnetic balance (Table 2).

Thermal Measurements. Differential thermal analysis (DTA) and thermogravimetric analysis (TGA) were carried out in the air at a heating rate of 10 K/min in the tempera-

Table 1. Reaction conditions and analysis of Eu_xNbO_{3-y}

Exp. No.	Reaction mix		Condition		Analytical composition	
	x	a[a]	Temp/K	Time/h	x	y
24	0.50	1.05	1473	48	0.51	+0.02
30	0.55	1.05	1473	48	0.56	−0.01
25	0.60	1.05	1473	48	0.59	−0.01
31	0.65	1.05	1473	48	0.65	0.00
26	0.70	1.05	1473	48	0.70	−0.10
32	0.75	1.05	1473	48	0.72	−0.06
27	0.80	1.05	1473	48	0.79	+0.05
33	0.85	1.05	1473	48	0.85	+0.01
28	0.90	1.05	1473	48	0.89	−0.02
34	0.95	1.05	1473	48	0.91	−0.05
29	1.00	1.05	1473	48	0.97	−0.13

a) Niobium metal was taken a times the amount needed to prepare Eu_xNbO_3.

Table 2. Lattice constants and magnetic properties for Eu_xNbO_{3-y}

Exp. No.	Eu_xNbO_{3-y}		Lattice constants			Magnetic moments	
	x	y	(Cubic) a/Å	(Tetragonal) a/Å	c/Å	Obsd/μ_B	Calcd/μ_B[a]
24	0.51	+0.02		12.355	3.901	5.47	5.69
30	0.56	−0.01		12.363	3.892	5.89	5.97
25	0.59	−0.01		12.361	3.885	5.75	6.14
31	0.65	0.00	3.978			6.24	6.47
26	0.70	−0.10	3.980			6.13	6.69
32	0.72	−0.06	3.985			6.46	6.81
27	0.79	+0.05	4.002			6.77	7.20
33	0.85	+0.01	4.009			7.10	7.47
28	0.89	−0.02	4.012			7.26	7.64
34	0.91	−0.05	4.013			7.43	7.72
29	0.97	−0.13	4.016			7.64	7.95

a) Magnetic moment (calcd) $= \sqrt{x\mu^2(Eu^{2+}) + (Nb^{4+}/Nb)\mu^2(Nb^{4+})}$, $\mu(Eu^{2+}) = 7.94\mu_B$, $\mu(Nb^{4+}) = 1.73\mu_B$.

ture range 300—1173 K. All thermal measurements were performed on a Rigaku Denki DTA "Thermoflex." Powder samples (30—60 mg) were used, alumina powder (99.9%) being employed as a reference. The heat of oxidation for the bronzes was measured with a differential scanning calorimeter (DSC). Measurements were carried out in the air at a heating rate of 10 K/min in the temperature range 300—1173 K. The heat of oxidation was determined from the area beneath a DSC peak. The heat of oxidation of NbO_2 to Nb_2O_5 was used as a standard.[8]

Results and Discussion

X-Ray Data. X-Ray analysis revealed that the samples having europium concentration $x=0.5$—0.65 are of tetragonal symmetry, and those with $x=0.65$—1.0 cubic symmetry (Table 2). A small amount of Eu_3NbO_6 confirmed by the X-ray technique was assigned to a second phase for the slightly oxidized bronzes of high europium concentration ($x>0.9$). Oxidation tendency of the bronzes seemed to increase with x, 1.2 times excess of reducing agent being required for the preparation of single phase bronzes. The niobate Eu_3NbO_6 seems to be formed by the solid state reaction in the bronze of high x. A plot

$$Eu_xNbO_{3-y} \longrightarrow a Eu_3NbO_6 + (1-a)Eu_{\frac{x-3a}{1-a}}NbO_{\frac{3-y-6a}{1-a}} \quad (3)$$

of the lattice constant *vs.* the europium concentration of the cubic phase for $x=0.65$ to 1.0 is given in Fig. 1. Ridgley and Ward[9] reported that the lattice constant for an analogous bronze, Sr_xNbO_3, of cubic symmetry is proportional to x. However, our observation (Fig. 1) does not agree with theirs. The result of X-ray analysis supports the assumption that the solid state reaction (Eq. 3) takes place at high x.

Magnetic Susceptibilities. The magnetic susceptibilities χ_m of the bronzes obey the Curie-Weiss law in the range 77—300 K. The observed and calculated values of effective magnetic moments for the bronzes are summarized in Table 2. The observed moments are close to the calculated values, small lowering of the observed magnetic moments exceeding experimental errors being observed. Europium ions in the starting material are considered to be substantially reduced to the Eu (II) state. However, the reduction power of niobium is not strong enough to reduce all of Eu^{3+} to Eu^{2+},[4] a small amount of Eu^{3+} remaining with Eu^{2+}. The lowering observed in our products would also be interpreted in terms of the reduction power of niobium.

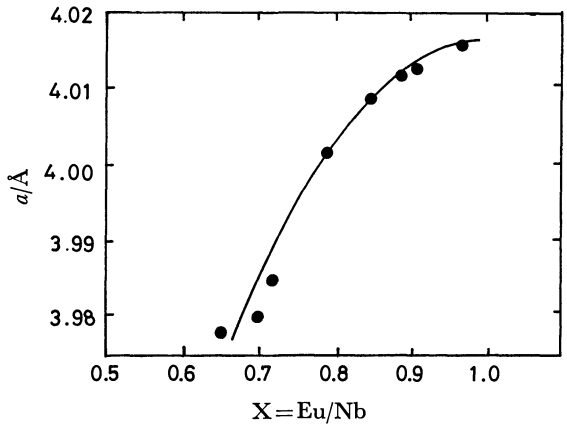

Fig. 1. The variation of lattice constant with europium content in the cubic phase Eu_xNbO_{3-y}.

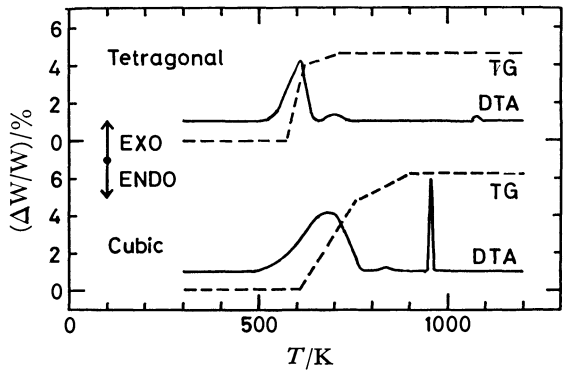

Fig. 2. TGA and DTA curves of $Eu_{0.51}NbO_{2.98}$ (tetragonal) and $Eu_{0.74}MbO_{2.81}$ (cubic).

Thermal Analysis. Typical TGA and DTA

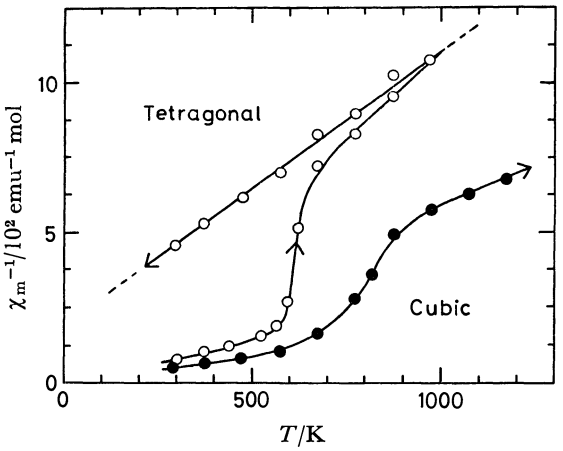

Fig. 3. Inverse magnetic susceptibility *vs.* temperature for $Eu_{0.51}NbO_{2.98}$ (tetragonal) and $Eu_{0.74}NbO_{2.81}$ (cubic).

curves for the tetragonal and the cubic phases are shown in Fig. 2. An abrupt weight gain is observed in the TGA curve for the tetragonal sample at 550—700 K, and a moderate weight gain at 550—900 K for the cubic one. We see that the oxidation proceeds in two steps for both the tetragonal and cubic phases. Magnetic susceptibility measurements were carried out for the same sample in the air in the temperature range 300—1173 K, at a heating rate of 10 K/min (Fig. 3). The magnetic moments of Eu^{2+}, Eu^{3+}, Nb^{4+}, and Nb^{5+} are 7.94, 3.4, 1.73, and 0 μ_B, respectively. The decrease in the magnetic moment is much larger in the oxidation of Eu^{2+} to Eu^{3+} than in the oxidation of Nb^{4+} to Nb^{5+}. From a comparison of the TG-DTA curves (Fig. 2) with the χ_m^{-1} *vs.* T curves (Fig. 3), we see that the initial stage of the oxidation would be due to the oxidation of Eu^{2+}, the second to the oxidation of Nb^{4+}. Figure 3 also shows that the initiating temperature of the oxidation of Eu^{2+} is 550 K for both the tetragonal and cubic phases, the rate of oxidation of Eu^{2+} being larger for the tetragonal phase than for the cubic phase.

The stability of the bronze against oxidation mainly depends on that of Eu^{2+}. The temperature at which oxidation of Eu^{2+} starts is the same for both the tetragonal and cubic phases. The stability of Eu^{2+} to oxidation seems to be of the same order for both bronzes. The rate of oxidation of Eu^{2+} is considered to determine the rate of oxidation of the bronzes. The thermal analyses (TGA and DTA) were carried out for EuO under the same conditions as those for the bronzes. EuO oxidized at 520—580 K, showing that the rate of oxidation of Eu^{2+} in EuO is much greater than that in the bronzes. The oxidation of Eu^{2+} proceeds from the surface to the bulk of the bronze grain. The rate of oxidation of Eu^{2+} in the bulk should be determined by the probability of Eu^{2+} encounter with oxygen. Thus the rate of diffusion of oxygen in the oxidized product layer should control the rate of oxidation of Eu^{2+}.

X-Ray analysis was carried out for the bronzes oxidized at various temperatures. Oxidation of the cubic bronze gave an amorphous phase crystallizing

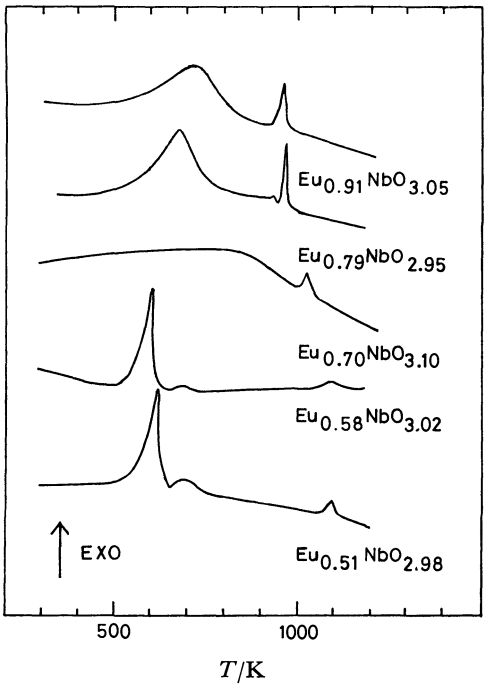

Fig. 4. DTA curves for Eu_xNbO_{3-y}.

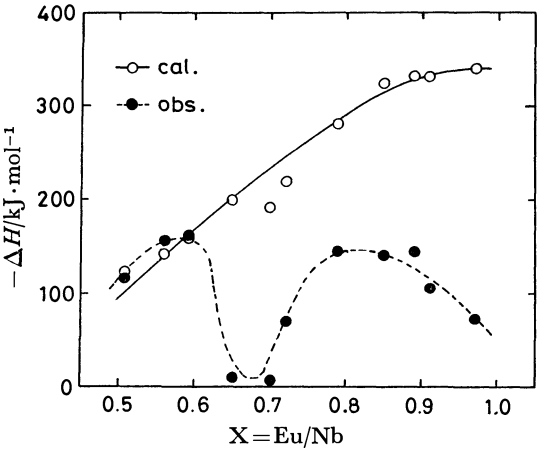

Fig. 5. Heat of oxidation for Eu_xNbO_{3-y}.

at 950 K. On the other hand, the tetragonal phase underwent oxidation giving complex crystalline products which recrystallized at 1070 K. The difference in the rate of oxidation between the tetragonal and cubic phases can be attributed to the difference in the rate of diffusion of oxygen in the layer of the oxidized product. The diffusion coefficient of oxygen for the product obtained by the oxidation of the tetragonal phase should be much larger than that for the amorphous phase resulting from the cubic phase.

On heating the bronzes in the air, $EuNbO_4$ appeared at 1070 K for the tetragonal bronze and at 950 K for the cubic bronze. Exothermic peaks, 950 and 1070 K, due to crystallization are seen in the DTA curves with no weight change (Figs. 2 and 4), suggesting that the amorphous phases are less stable than the crystalline phases. The difference in the stability of the intermediate states affects the heats of oxidation for the bronzes. Figure 5 shows the

observed and calculated heats of oxidation for the bronzes of various Eu^{2+} contents. Both the observed and calculated values show a minimum at $x=0.65$. For the evaluation of the heat of oxidation, the bronze is assumed to be a mixture of EuO, NbO_2, and Nb_2O_5,

$$Eu_xNbO_{3-y} = xEuO + [2(x+1)-1]NbO_2 + (1-x-y)Nb_2O_5. \quad (4)$$

The oxidation reaction is assumed to proceed as follows:

$$Eu_xNbO_{3-y} + \left(\frac{3}{4}x+\frac{y}{2}-\frac{1}{4}\right)O_2 \longrightarrow \frac{x}{2}Eu_2O_3 + \frac{1}{2}Nb_2O_5. \quad (5)$$

The minimum of the heat of oxidation at $x=0.65$ corresponds to the phase transition.

The heats of oxidation for the tetragonal phases are almost equal to the calculated values. The result indicates that the heat of formation for the crystalline phase is close to that for the mixture of Eu_2O_3, and Nb_2O_5 represented by Eq. 4. The heat of transformation from an unknown crystalline phase to the final products, mainly $EuNbO_4$, as well as $EuNb_3O_9$ and $EuNb_5O_{14}$, might be very small. Thermal analysis (TGA-DTA) supports the assumption.

The heat of oxidation for the cubic phases is much lower than that for the calculated ones, a maximum being obtained at $x=0.85$. The result indicates that the heat of formation for the amorphous phase obtained from oxidation of the cubic bronzes is considerably larger than that for the mixture of Eu_2O_3 and Nb_2O_5 shown by Eq. 4. A second cubic phase, Eu_3NbO_6, appears at $x>0.9$. The heat of formation for the existing cubic bronzes, $Eu_xNbO_{3-y}+Eu_3NbO_6$, seems to be smaller as compared with that for single-phased Eu_xNbO_{3-y}, the apparent heat of oxidation decreasing for $x>0.9$. The minimum of the heat of oxidation at $x=0.65$ is due to the difference in stability of these two intermediate phases.

References

1) J. P. Fayolle, F. Studer, G. Desgardin, and B. Raveau, *J. Solid State Chem.*, **13**, 57 (1975).
2) E. I. Krylov, E. M. Elovskikh, G. G. Kasimov, and B. D. Filin, *Zh. Obshch. Khim.*, **44**, 1836 (1974).
3) G. V. Bazuev, O. V. Makarova, and G. P. Shveikin, *Dokl. Akad. Nauk. SSSR.*, **223**, 358 (1975).
4) G. J. McCarthy and J. E. Greedan, *Inorg. Chem.*, **14**, 772 (1975).
5) F. Studer and B. Raveau, *Acta. Crystallogr., Sect. B*, **31**, 2774 (1975).
6) F. Studer, J. P. Fayolle, and B. Raveau, *Mater. Res. Bull.*, **11**, 1125 (1976).
7) G. V. Bazuev, O. V. Makarova, and G. P. Shveikin, *Zh. Neorg. Khim.*, **21**, 3212 (1976).
8) "CRC. Handbook of Chemistry and Physics," The Chemical Rubber. C. O., Cleveland, Ohio (1970—1971), p. D45.
9) D. H. Ridgley and R. Ward, *J. Am. Chem. Soc.*, **77**, 6132 (1955).

  Bull. Chem. Soc. Jpn., 54, 163—169 (1981)

Transition-metal Complexes of Pyrrole Pigments. XVII. Preparation and Spectroscopic Properties of Corrole Complexes†

Yukito Murakami,* Yoshihisa Matsuda, Kazunori Sakata,†† Sunao Yamada, Yasuhiro Tanaka, and Yasuhiro Aoyama

Department of Organic Synthesis, Faculty of Engineering, Kyushu University, Hakozaki, Higashi-ku, Fukuoka 812

(Received May 9, 1980)

Nickel(II), copper(II), and cobalt(III) complexes were prepared with corroles; 2,3,7,8,12,13,17,18-octaethylcorrole (OEC), 2,3,17,18-tetramethyl-7,8,12,13-tetraethylcorrole (MEC), and 8,12-bis[2-(ethoxycarbonyl)ethyl]-2,3,7,13,17,18-hexamethylcorrole (PMC). For the coordination with nickel and copper ions, the corroles acted as dianionic ligands to yield electrically neutral complexes. These complexes exhibited metalloporphyrin-like electronic spectra, while they showed spectra which bear a much closer resemblance to those for metalloporphyrins as the anionic complexes were formed upon addition of alkali. The corroles coordinate to tervalent cobalt as trianionic ligands to form neutral complexes, which were reduced to the corresponding cobalt(II) complexes with sodium hydroborate. These reduced species gave a unique set of g-values ($g_1 \gg g_2 > g_3$) for the complexes of macrocyclic ligands with conjugated double bond system. The plausible coordination geometry as well as the structural properties of the corrole ligands has been discussed.

Corrole (**1**) and tetradehydrocorrin (**2**) are unique macrocyclic tetrapyrroles, having a highly conjugated π-electron system like porphyrin and phthalocyanine. However, the direct linkage between A and D pyrrole rings involved in the former two macrocycles acts to provide a deformation effect on the macrocyclic skeleton so that those rings can not take complete planar structure. A significant structural difference between corrole and tetradehydrocorrin is in orbital hybridization of carbon atoms at 1- and 19-positions. The particular atoms concerned are considered to possess sp^2 hybrid orbitals for corrole while sp^3 for tetradehydrocorrin. Thus, it is interesting to shed light on the unique electronic structure of corrole and the possible consequences of ring deformation in its coordination with transition-metal ions. The synthesis of corrole and its cobalt(III), nickel(II), and copper(II) complexes was reported first by Johnson *et al.*[1,2] However, they did not investigate the electronic structure of these complexes in any detail by spectroscopic means.

Three corroles having different peripheral substituents were employed in the present study; *i.e.*, 2,3,17,18-tetramethyl-7,8,12,13-tetraethylcorrole (MEC), 2,3,7,-8,12,13,17,18-octaethylcorrole (OEC), and 8,12-bis[2-(ethoxycarbonyl) ethyl]-2,3,7,13,17,18-hexamethylcorrole (PMC). The corresponding linear tetrapyrroles, biladiene-ac dihydrobromides, underwent cyclization to afford the corroles under irradiation with visible light. The metal complexes were prepared directly from biladiene-ac's by template reaction as functioned by metal ions. Stereochemistry and electronic structures have been discussed for both ligands and complexes.

Experimental

Electronic absorption spectra were recorded on a Hitachi EPS-2 spectrophotometer at room temperature; chloroform was used as solvent unless otherwise stated. ESR spectra were obtained with a JEOL JES-ME-3 X-band spectrometer equipped with 100-kHz field modulation unit; a standard MgO/Mn(II) sample calibrated with a NMR magnetometer was employed for calibration of the magnetic field. NMR spectra were taken on a Varian A-60 spectrometer for chloroform-*d* solutions; tetramethylsilane being used as an internal reference.

1,19-Dideoxy-2,3,17,18-tetramethyl-7,8,12,13-tetraethylbiladiene-ac dihydrobromide and 1,19-dideoxy-2,3,7,8,12,13,17,18-octaethylbiladiene-ac dihydrobromide were obtained as described previously.[3]

1,19-Dideoxy-8,12-bis[2-(ethoxycarbonyl)ethyl]-2,3,7,13,17,18-hexamethylbiladiene-ac Dihydrobromide. Aqueous ammonia (28%) was added dropwise to a suspension of 3,3′-bis[2-(ethoxycarbonyl)ethyl]-4,4′-dimethyl-5,5′-dicarboxydipyrromethane[4] (5.0 g) and 2-formyl-3,4-dimethylpyrrole[5] (2.65 g) in methanol (200 ml) until a clear solution was obtained. Aqueous hydrobromic acid (47%, 25 ml) was added to the mixture in one portion at 120 °C. After being refluxed for 1 min, the dark red solution was allowed to stand in a freezer for 1 h. The product was recovered, washed with water, methanol, and ether, and then recrystallized from chloroform to give red crystals with green luster; yield 6.9 g (86%), mp>300 °C. UV_{max} ($CHCl_3$): 370, 427, 455, and 518 nm. IR (KBr): 1608 (biladiene skeletal str.) and 1722 cm^{-1} (C=O str.). NMR (CF_3CO_2H): δ 1.38 (6H, t, J=7.0 Hz, $-CH_2CH_2CO_2CH_2C\underline{H}_3$), 2.18, 2.43, and 2.46 (18H, s, $-CH_3$ on pyrrole ring), 2.23—3.27 (8H, m, $-C\underline{H}_2C\underline{H}_2CO_2C_2H_5$), 4.35 (4H, q, J=7.0 Hz, $-CH_2CH_2-CO_2C\underline{H}_2CH_3$), 4.75 (2H, s, $-CH_2-$ at 10-position), 7.66 (2H, s, -CH=), 8.01 (2H, d, J=4.0 Hz, 1- and 19-H), 11.39 (2H, br s, NH), and 11.55 (2H, br s, N^+H).

2,3,17,18-Tetramethyl-7,8,12,13-tetraethylcorrole (MEC). A mixture of 1,19-dideoxy-2,3,17,18-tetramethyl-7,8,12,13-tetraethylbiladiene-ac dihydrobromide (200 mg) and methanol (100 ml) was heated to obtain a homogeneous solution, to which 28% aqueous ammonia (4 ml) was added subsequently. The refluxing green solution was irradiated with a 200-W tungsten lamp for 1 h, and then allowed to stand in a freezer for 2 h. Dark fine crystals were recovered and recrystallized from chloroform–methanol to give purple needles; yield 90 mg (61%). IR (Nujol mull): 3350 cm^{-1} (N–H str.).

Found: C, 79.41; H, 8.15; N, 11.98%. Calcd for $C_{31}H_{38}N_4$: C, 79.77; H, 8.22; N, 12.01%.

The following two corroles were prepared by similar photocyclization of the corresponding biladiene-ac dihydrobromides.

† Contribution No. 579 from this Department.

†† Present address: Kyushu Institute of Technology, Tobata-ku, Kitakyushu 804.

2,3,7,8,12,13,17,18-Octaethylcorrole (OEC): purple needles, yield 19%. IR (Nujol mull): 3345 cm^{-1} (N–H str.). Found: C, 79.38; H, 8.68; N, 11.03%. Calcd for $C_{35}H_{46}N_4$: C, 80.40; H, 8.89; N, 10.72%.

8,12-Bis[2-(ethoxycarbonyl)ethyl]-2,3,7,13,17,18-hexamethylcorrole (PMC): purple needles, yield 51%. IR (KBr): 3360 cm^{-1} (N–H str.). Found: C, 71.90; H, 7.29; N, 9.65%. Calcd for $C_{35}H_{42}N_4O_4$: C, 72.14; H, 7.27; N, 9.61%.

Pyridine(2,3,17,18-tetramethyl-7,8,12,13-tetraethylcorrolato)cobalt(III) [*Co(MEC)Py*] *and (2,3,7,8,12,13,17,18-octaethylcorrolato)cobalt(III)* [*Co(OEC)*] were prepared as described previously.[3]

Pyridine{8,12-bis[2-(ethoxycarbonyl)ethyl]-2,3,7,13,17,18-hexamethylcorrolato}cobalt(III) [*Co(PMC)Py*] was prepared by essentially the same procedure as employed for the preparation of Co(MEC)Py and obtained as purple prisms; yield 43%. IR (Nujol mull): 1603 (pyridine skeletal str.) and 1728 cm^{-1} (C=O str.). Found: C, 67.71; H, 6.08; N, 10.68%. Calcd for $C_{40}H_{44}N_5O_4Co$: C, 66.94; H, 6.18; N, 9.76%.

(2,3,17,18-Tetramethyl-7,8,12,13-tetraethylcorrolato)cobalt(III) [*Co(MEC)*]. A solution of pyridine(2,3,17,18-tetramethyl-7,8,12,13-tetraethylcorrolato)cobalt(III) (100 mg) in chloroform (4 ml) was refluxed for 3 min. Hot methanol (12 ml) was added to the solution, which was subsequently allowed to stand in a freezer for 2 h. Dark precipitates were recovered and washed with methanol to give glittering black prisms; yield 80 mg (92%).

Found: C, 71.43; H, 6.59; N, 11.37%. Calcd for $C_{31}H_{35}N_4Co$: C, 71.24; H, 6.76; N, 10.72%.

(2,3,17,18-Tetramethyl-7,8,12,13-tetraethylcorrolato)nickel(II) [*Ni(MEC)*]. A mixture of 1,19-dideoxy-2,3,17,18-tetramethyl-7,8,12,13-tetraethylbiladiene-ac dihydrobromide (300 mg), nickel(II) acetate tetrahydrate (300 mg), methanol (50 ml), and 28% aqueous ammonia (6 ml) was irradiated with a 200-W tungsten lamp for 20 min. The green solution turned to red and finally to dark brown. The reaction mixture was then allowed to stand at 0 °C overnight, and precipitates were recrystallized from chloroform–methanol (2:1 v/v) to give glittering dark green prisms; yield 100 mg (40%), mp>250 °C.

Found: C, 70.83; H, 6.66; N, 10.66%. Calcd for $C_{31}H_{36}N_4Ni$: C, 71.13; H, 6.95; N, 10.71%.

{8,12-Bis[2-(ethoxycarbonyl)ethyl]-2,3,7,13,17,18-hexamethylcorrolato}nickel(II) [*Ni(PMC)*] was prepared in a manner similar to that employed for the preparation of Ni(MEC): yield 57%, *m/e* 638 (M^+).

(2,3,17,18-Tetramethyl-7,8,12,13-tetraethylcorrolato)copper(II) [*Cu(MEC)*]. A mixture of 1,19-dideoxy-2,3,17,18-tetramethyl-7,8,12,13-tetraethylbiladiene-ac dihydrobromide (315 mg) and copper(II) acetate monohydrate (300 mg) in methanol (150 ml) was stirred at room temperature for 10 min. Precipitates were washed with methanol and recrystallized from chloroform–methanol (2:1 v/v) to give reddish brown needles; yield 50 mg (19%), mp>250 °C.

Found: C, 70.41; H, 6.60; N, 10.55%. Calcd for $C_{31}H_{36}N_4Cu$: C, 70.48; H, 6.88; N, 10.61%.

{8,12-Bis[2-(ethoxycarbonyl)ethyl]-2,3,7,13,17,18-hexamethylcorrolato}copper(II) [*Cu(PMC)*] was prepared by essentially the same procedure as employed for the preparation of Cu(MEC): yield 47%, *m/e* 643 (M^+).

Results and Discussion

Electronic Spectra. Characteristic transition energies and the corresponding molar absorption coefficients (ε) are summarized in Table 1 for the three corrole ligands. The strong absorption bands in the region of 24000—26000 cm^{-1} are presumably due to transitions similar to those observed for porphyrins as B-band. The nature of transitions for the bands in the region of 15000—19000 cm^{-1} is presumably similar to that for Q-bands of porphyrins. The electronic transitions, which result in B- and Q-bands, have not been characterized because multiple transitions with similar energies were observed in these regions due to lower symmetry of the corrole skeleton relative to the porphyrin framework.

The nickel(II) and copper(II) complexes of MEC and PMC were obtained as electrically neutral molecules without additional ligand or counter ion. This fact indicates that the corroles coordinate to nickel(II) and copper(II) as dianionic ligands. The complexes exhibited metalloporphyrin-like spectra, but a number of absorption bands is larger for the corrole complexes than for the corresponding metalloporphyrins. Both nickel(II) and copper(II) complexes of corrole showed much sharper absorption bands upon addition of sodium hydroxide to their DMSO solutions. The characteristic absorption bands are summarized in Table 2 along with molar absorption coefficients for the neutral complexes. The absorption bands for each complex are obviously classified into the following groups: group A, weak bands with transition energy less than 10000 cm^{-1}; group B, bands with intermediate intensity in the region of 10000—20000 cm^{-1}; and group C, very intense bands with high transition energy (greater than 20000 cm^{-1}).

TABLE 1. ELECTRONIC ABSORPTION BANDS FOR CORROLES IN CHLOROFORM AT ROOM TEMPERATURE

Corrole	MEC	OEC	PMC
Absorption maxima/cm^{-1} (ε)	14700^{sh} (1000)	14700^{sh} (1220)	
	16800 (14840)	16800 (19860)	16900 (18800)
	18100 (13280)	18200^{sh} (17160)	18200 (17300)
	18600 (13840)	18600 (19020)	18600 (17200)
			19500^{sh} (8120)
	20000^{sh} (6700)	20000^{sh} (7720)	20000^{sh} (7050)
	20800^{sh} (5040)	21100^{sh} (4780)	20900^{sh} (4720)
	24540 (94800)	24400 (103200)	24600 (106000)
	25100 (116600)	25100 (116200)	25100 (129000)
	30300^{sh} (20800)	30300^{sh} (20600)	30700^{sh} (18200)
	36400^{sh} (14900)	36400^{sh} (15040)	36000^{sh} (14800)

Table 2. Electronic absorption bands for nickel(II) and copper(II) complexes of MEC at room temperature

Complex	Ni(MEC)[a]	[Ni(MEC)]$^-$ [b]	Cu(MEC)[a]	[Cu(MEC)]$^-$ [b]
Absorption maxima/cm^{-1} (ε)	8330^{sh} (574)		10600^{sh} (590)	
	11900 (1310)		11600 (661)	
	15200 (9870)	15600	14900^{sh} (1060)	
	16700 (3840)	17000		
		18000	18200 (10000)	17600
		19000	19800^{sh} (7580)	18800
	23500^{sh} (35300)			
	26000 (42200)	24900	25100 (87700)	24000
	27800 (58800)			
			35800 (26800)	

a) Measured in chloroform. b) Measured in *N,N*-dimethylformamide in the presence of NaOH.

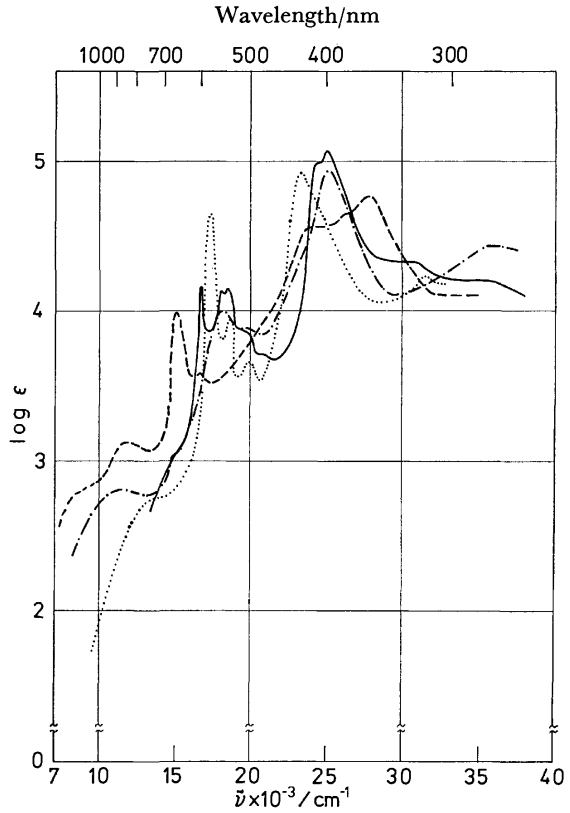

Fig. 1. Electronic absorption spectra of MEC and its metal complexes at room temperature.
——: Metal-free MEC in $CHCl_3$, ----: Ni^{II}(MEC) in $CHCl_3$, —·—: Cu^{II}(MEC) in $CHCl_3$, ·····: Co^{III}(MEC) in pyridine.

The local structure about the central metal may be assumed to be square planar with slight distortion. For such cases, the d-d transitions of nickel(II) and copper(II) are generally expected to appear in the region of 10000—20000 cm^{-1}. The absorption bands classified as group A are, therefore, not attributed to d-d transitions, but rather to charge-transfer transitions. The absorption bands of group B have molar absorption coefficients larger than 1000; they are too large to be assigned to d-d transitions. These bands may be attributed to π-π^* transitions which have similar character as those for the Q-bands of metalloporphyrins. The absorption bands of group C are attributed to transitions from π- to higher π^*-orbitals, corresponding to B-bands of metalloporphyrins. The neutral nickel(II) complex exhibited at least three absorption bands in the B-band region while the corresponding copper(II) complex showed only one band. However, this high energy band for the copper complex is very broad so that it must consist of two or more unresolved absorptions. The corresponding absorption band for the anionic complexes, [Ni(MEC)]$^-$ and [Cu(MEC)]$^-$, is remarkably sharp in a manner as observed for metalloporphyrins.

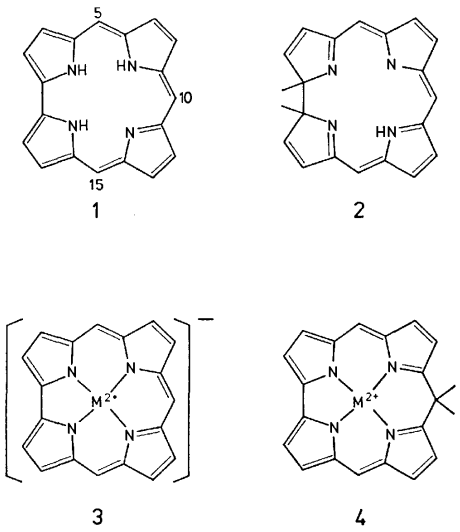

Above observation indicates a large difference in π-conjugation between anionic and neutral complexes. Nine double bonds of the corrole macrocycle (**1**) seem to be conjugated throughout the whole molecule for the anionic complex[6] (**3**) while the protonated structure (the neutral complex) interferes with such a conjugation effect. Structures of the neutral complexes are not established at present, but most plausibly shown by **4**.

Cobalt complexes with the corrole ligands were isolated only in the tervalent cobalt state as Co(corrole) and Co(corrole)Py. We reported previously the following equilibria in solution.[3]

$$n\text{Co(corrole)} \rightleftharpoons [\text{Co(corrole)}]_n \quad (1)$$

$$\text{Co(corrole)} \overset{\text{Py}}{\rightleftharpoons}$$

$$\text{Co(corrole)Py} \overset{\text{Py}}{\rightleftharpoons} \text{Co(corrole)(Py)}_2 \qquad (2)$$

Thus, an absorption spectra for the bis(pyridine) adduct can be obtained directly in the presence of excess pyridine. Electronic spectral data for the cobalt(III) complexes in pyridine are summarized in Table 3. For both complexes, absorption bands in the region of 12000—15000 cm^{-1} are attributed to charge-transfer transitions while higher energy bands are attributed to Q- and B-type transitions.

NMR Spectra. Proton NMR chemical shifts for the selected absorptions of Co(MEC)Py and Co(PMC)Py are listed in Table 4 along with the corresponding data for dicyano(8,12-diethyl-1,2,3,7,13,17,-18,19-octamethyltetradehydrocorrinato)cobalt(III) and dicyano(8,12-diethyl-1,2,3,7,13,17,18,19-octamethyl-AD-bisdehydrocorrinato)cobalt(III) [abbreviated as Co(TDHC)$(CN)_2$ and Co(BDHC)$(CN)_2$, respectively]. The meso-protons at 5-, 10-, and 15-positions and methyl-protons at 2-, 3-, 17-, and 18-positions provide an useful information: these signals shift to lower field in going from Co(BDHC)$(CN)_2$ to Co(TDHC)-$(CN)_2$, Co(MEC)Py, and Co(PMC)Py; those protons involved in the corrole complexes resonate at the lowest field. The result indicates that the significant ring current effect is exercised undoubtedly by the corrole ring on the peripheral protons. The axial pyridine ligand in the corrole complexes is placed in a shielding zone of the ring current, and the pyridine protons resonate at a considerable higher field (δ 5.06—6.30) relative to those in $Co(NH_3)_5Py$ (δ 7.75—8.33 in D_2O).[8]

Table 5 summarizes chemical shifts for metal-free OEC and 2,3,7,8,12,13,17,18-octaethylporphyrin (OEP). OEC exhibits a deshielding effect on the imino-protons and a shielding effect on the meso-protons, but such effects are more pronounced for OEP. This is most plausibly caused by the deviation of the corrole skeleton from ideal planar configuration, which results in reduction of the extent of π-conjugation compared with porphyrins.

Except for the case of OEC, the metal-free corroles showed only broad NMR signals, presumably caused by paramagnetic contamination. This was confirmed by the presence of a sharp ESR signal at $g=2.0$. The paramagnetic species responsible for the observation is presumably radical species of corrole itself generated during photo-cyclization of biladiene-ac's. It is not clear at present whether the formation of such species is influenced by the nature of substituents or simply a matter of slight difference in experimental conditions. The paramagnetic species disappeared upon addition of thiophenol.

ESR Spectra. Copper(II) complexes of the corroles exhibited ESR spectra typical of the planar coordination structure. The X-band ESR spectrum for neutral Cu(MEC) at 77 K is shown in Fig. 2.

Table 3. Electronic absorption bands for cobalt(III) complexes in pyridine at room temperature

Ligand	MEC	OEC
	13300[sh] (530)	12500[sh] (377)
		15200 (1000)
Absorption	17300 (43800)	17200 (56500)
maxima/cm^{-1} (ε)	18500 (8660)	18500 (10800)
	19900 (4520)	19800 (6080)
	23400 (79200)	23500 (11300)

Table 4. Proton NMR chemical shifts for the cobalt(III) complexes of corroles and dehydrocorrins at room temperature[a]

Complex	Medium	δ CH_3 (2, 3, 17, 18)	δ =CH- (5, 15)	=CH- (10)
Co(MEC)Py	CS_2	3.47, 4.30	8.43	8.08
Co(PMC)Py	CS_2	3.31, 3.48, 3.92[b]	9.20	8.99
Co(TDHC)$(CN)_2$[c]	$CDCl_3$	2.36, 2.48	6.99	6.95
Co(BDHC)$(CN)_2$[d]	$CDCl_3$	2.11, 2.29	5.97	5.91

a) Chemical shifts needed for discussion are given. b) One of the three values must be attributed to methyl protons at 7- and 13-positions. c) As for preparation, see: D. Dolphin, R. L. N. Harris, J. L. Huppatz, A. W. Johnson, I. T. Kay, *J. Chem. Soc., C*, **1966**, 30. d) Cited from Ref. 7.

Table 5. Proton NMR chemical shifts for OEC and OEP measured in chloroform-*d* at room temperature

Compound	δ NH	=CH-	CH_3	CH_2
OEC	−2.47	9.39, 9.22[a]	1.75	3.82
OEP	−3.78	10.00	1.89	4.11

a) For 5- and 15-positions, 9.39; for 10-position, 9.22.

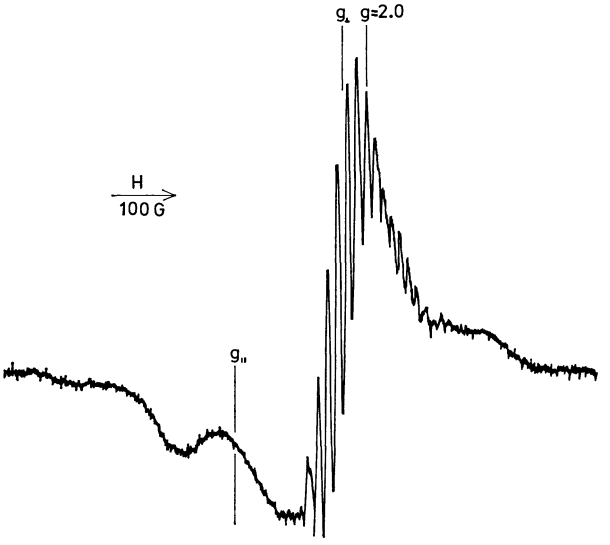

Fig. 2. ESR spectrum of Cu^{II}(MEC) in benzene–xylene (4: 6 v/v) at 77 K.

TABLE 6. SPIN HAMILTONIAN PARAMETERS FOR THE COPPER(II) COMPLEXES OF MACROCYCLIC LIGANDS

Complex	$g_{\parallel}$	$g_{\perp}$	$A_{\parallel}^{Cu} \times 10^4$ / cm^{-1}	$A_{\parallel}^{N} \times 10^4$ / cm^{-1}	$A_{\perp}^{N} \times 10^4$ / cm^{-1}	Medium
Cu(MEC)	2.145	2.021	208	15.8	14.2	Metal-free MEC[c]
Cu(MEC)	2.152	2.030	240	17.3	16.1	Benzene-xylene (4:6 v/v)[d]
Cu(PMC)	2.148	2.023	207	15.6	13.0	Metal-free PMC[c]
Cu(PMC)	2.146	2.030	246	16.9	16.0	Benzene-xylene (4:6 v/v)[d]
Cu(TPP)[a]	2.193	2.071	202	14.5	16.1	Metal-free TPP[c]
Cu(PC)[b]	2.160	2.045	218	18.6	15.5	Metal-free PC[c]

a) Cited from Ref. 9. b) Cited from Ref. 10. c) Measured at 293 K. d) Measured at 77 K.

Spin Hamiltonian parameters for MEC and PMC complexes are summarized in Table 6 along with those for the copper complexes of 5,10,15,20-tetraphenylporphine (TPP) and phthalocyanine (PC). As mentioned earlier, the complexes would possess planar structure with slight rhombic distortion. Rhombic parameters (g_1, g_2, and g_3), however, were not obtained because of the complexity of the spectra in the perpendicular component range. The parameters were evaluated, in any event, for pseudo-tetragonal coordination having C_{4v} local symmetry around the copper atom. Both $g_{\parallel}$ and $g_{\perp}$ for the corrole complexes are significantly smaller than those for the TPP and PC complexes. This observation reflects the deformation of the corrole complexes from planar structure. As mentioned above, the extent of π-conjugation in the neutral complex is much lower than that for metalloporphyrins. In addition, the direct linkage of A and D pyrrole rings stands in favor of such deformation.

A remarkable medium effect on hyperfine splitting constants was observed: the complexes gave larger A-values in frozen solution (benzene–xylene, 4:6 v/v) relative to those for the samples diluted with the corresponding metal-free corroles, while g-values were not affected significantly by the nature of media. The complexes also gave larger A^N-values in frozen solutions compared with those in the solid matrices. These facts suggest that both extent of mixing of 4s orbital with $3d_{x^2-y^2}$ and covalent character of the coordinate bonds are more pronounced in solution state rather than in the matrix of metal-free ligand. Lack of d-d transition energies makes it difficult to evaluate the effect of host structure quantitatively. The neutral copper(II) complexes presumably have a molecular geometry different from those of the corresponding anionic complexes and metal-free ligands. Thus, the neutral complexes are subjected to deformation in the matrices of metal-free corroles which tends to raise the molecular symmetry, while their coordination geometry is less affected in organic solvents. Such deformation is responsible for reduction of the covalency of coordinate bonds and of the mixing of s-orbital with $d_{x^2-y^2}$. Meanwhile, the anionic copper(II) complexes, which have more extensive π-conjugation system relative to the neutral ones, may be stabilized upon protonation to yield the latter complexes because the internal strain provided by the direct A-D linkage is relaxed through such a process (refer to **4**).

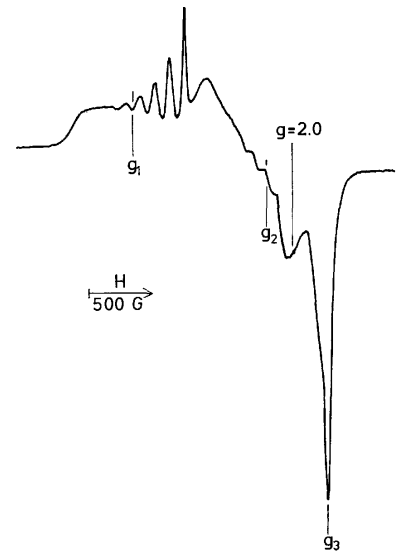

Fig. 3. ESR spectrum of $[Co^{II}(MEC)]^-$ in DMF at 77 K.

The cobalt(II) complexes, generated by reduction of the corresponding cobalt(III) complexes with $NaBH_4$ in *N*,*N*-dimethylformamide(DMF), showed intense ESR signals at 77 K as shown in Fig. 3. The samples did not give such ESR signals at room temperature due to short spin-lattice relaxation time of the low spin d^7 configuration. An ESR spectrum for the pyridine adduct of a reduced cobalt complex was observed upon addition of pyridine to the DMF solution (Fig. 4); except for the appearance of an additional superhyperfine splitting due to the nitrogen nucleus of pyridine, the spectra of both adduct and pyridine-free complex are essentially identical. The spin Hamiltonian parameters for $S=1/2$ and $I=7/2$ were obtained as summarized in Table 7. The spectral feature suggests that the cobalt(II) complexes assume a rhombic symmetry at the coordination site. Since the spectral features of both Figs. 3 and 4 bear a close resemblance to each other as stated above, the spatial arrangement of cobalt and four pyrrole-nitrogen atoms remains practically unchanged regardless of pyridine coordination. Since the superhyperfine splitting shown in Fig. 4 consists of three lines, the coordination of pyridine takes place only at the fifth coordination site; suggesting strongly a pyramidal structure for the original corrole complex with the cobalt atom placed at the top so that pyridine can approach to the metal from only one side of the molecular plane. The

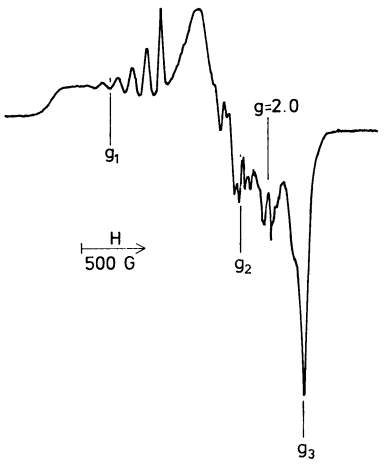

Fig. 4. ESR spectrum of $[Co^{II}(MEC)]^-$ in DMF at 77 K; pyridine was added.

four nitrogen atoms involved in the corrole complexes can not occupy vertices of square even if they are placed on the same plane, because the A and D pyrrole rings are linked directly. The coordination site around the cobalt atom assumes, therefore, C_s local symmetry, distorted from C_{4v}.

The cobalt(II)–corrole complexes provide g-values of $g_1 \gg g_2 > g_3$ as seen in Table 7. Cobalt(II) complexes other than the corrole complexes, given in Table 7, require g-values of $g_1 = g_2 \gg g_3$; local symmetry of C_{4v}. The coordination geometry around the cobalt atom for C_{4v} local symmetry is shown in Fig. 5. Four nitrogen atoms are placed in xy-plane on lines bisecting angles between x and y axes. Therefore, a d-orbital with the largest contribution to σ coordinate bonds is d_{xy} which occupies the highest energy level among d-orbitals. The hole formalism represents the ground

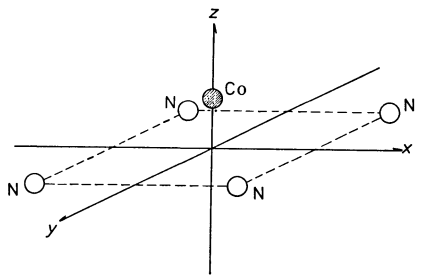

Fig. 5. Coordination geometry around the cobalt atom for C_{4v} local symmetry; four nitrogen atoms are placed in xy-plane while the cobalt atom is displaced upward from xy-plane along z-axis.

state for d^7 configuration by one of the following four configurations: $(d^2_{xy}, d_{x^2-y^2})$, (d^2_{xy}, d_{z^2}), (d^2_{xy}, d_{xz}), and (d^2_{xy}, d_{yz}); the last two configurations are degenerate in C_{4v} while referred to different energy states in C_s. g-Values are represented as shown in Table 8 for the above hole configurations. A relation, $g_{xx} \simeq g_{yy} > g_{zz} = 2$, is obtained for the ground state configuration of (d^2_{xy}, d_{z^2}). Co(II)(TPP) in TPP matrix and Co(II)(PC) diluted with Zn(II)(PC) are included in this category (refer to Table 7). The ground-state configuration can not be established for the corrole complexes on the basis of g-values alone. Nevertheless, either (d^2_{xy}, d_{xz}) or (d^2_{xy}, d_{yz}) is referred to the ground state judging from their coordination geometry. For either of the configurations, the relative magnitude of g-values depends on the energies of excited configurations. Since (d^2_{xy}, d_{xz}) and (d^2_{xy}, d_{yz}) are transformed into each other by interchange of x and y axes, we discuss the situation for the former as the ground state.

Suppose the following correlations are satisfied.

$$E(d_{xy}, d^2_{xz}) \gg E(d^2_{xy}, d_{yz}) \quad (3)$$

TABLE 7. SPIN HAMILTONIAN PARAMETERS FOR THE COBALT(II) COMPLEXES OF MACROCYCLIC LIGANDS AT 77 K

Complex	g_1	g_2	g_3	$A_1^{Co} \times 10^4$ cm^{-1}	$A_2^{Co} \times 10^4$ cm^{-1}	$A_3^{Co} \times 10^4$ cm^{-1}	$A_2^N \times 10^4$ cm^{-1}	Medium
Co(MEC)	3.236	2.263	1.847	181	104			DMF
Co(MEC)Py	3.223	2.206	1.848	180	113		17.2	DMF
Co(PMC)	3.242	2.214	1.841	181	108			DMF
Co(PMC)Py	3.225	2.147	1.854	172	97.9		17.4	DMF
Co(TPP)[a]	2.505[c]		2.034[d]	115[c]		92[d]		metal-free TPP
Co(PC)[b]	2.422[c]		2.007[d]	116[c]		66[d]		Zn(PC)

a) Cited from Ref. 9. b) Cited from Ref. 11. c) Perpendicular component. d) Parallel component.

TABLE 8. REPRESENTATION OF g-VALUES FOR THE GROUND STATE CONFIGURATIONS BASED ON HOLE FORMALISM[a]

Hole configuration for the ground state	Δg_{xx}	Δg_{yy}	Δg_{zz}
$(d^2_{xy}, d_{x^2-y^2})$	$-2\lambda/\Delta E(d^2_{xy}, d_{yz})$	$-2\lambda/\Delta E(d^2_{xy}, d_{xz})$	$8\lambda/\Delta E(d^2_{xy}, d_{x^2-y^2})$
(d^2_{xy}, d_{z^2})	$-6\lambda/\Delta E(d^2_{xy}, d_{yz})$	$-6\lambda/\Delta E(d^2_{xy}, d_{xz})$	0
(d^2_{xy}, d_{xz})	$2\lambda/\Delta E(d_{xy}, d^2_{xz})$	$-2\lambda/\Delta E(d^2_{xy}, d_{x^2-y^2})$ $-6\lambda/\Delta E(d^2_{xy}, d_{z^2})$	$-2\lambda/\Delta E(d^2_{xy}, d_{yz})$

a) ΔE denotes an energy difference between ground state and excited state configurations, the latter being given in parentheses after ΔE; $\Delta g_{ii} = g_{ii} - g_0$.

$$E(d_{xy}^2, d_{x^2-y^2}) > E(d_{xy}^2, d_{yz}) \quad (4)$$

$$E(d_{xy}^2, d_{z^2}) \gg E(d_{xy}^2, d_{yz}) \quad (5)$$

g-Values are interrelated by Eq. 6.

$$g_{zz} \gg g_{yy} > g_{xx} \quad (6)$$

On the other hand, a relationship among g-values is provided by Eq. 8 for an energy correlation given by Eq. 7.

$$E(d_{xy}^2, d_{yz}) \simeq E(d_{xy}^2, d_{z^2}) \quad (7)$$

$$g_{yy} \gg g_{zz} > g_{xx} \quad (8)$$

If (d_{xy}^2, d_{xz}) is referred to the ground state, either of the above conditions [(3), (4), and (5); or (7)] must be satisfied in order to observe the g-value correlation for the present corrole complexes: $g_1 \gg g_2 > g_3$ (refer to Table 7); other ground-state configurations listed in Table 8 are not consistent with this relation.

The cobalt atom is displaced most plausibly from the plane of the four pyrrole-nitrogen atoms to yield a pyramidal geometry as stated earlier. Under such circumstances, d_{xz} and d_{yz} orbitals contribute extensively to the formation of σ-antibonding orbitals. Although strong out-of-plane $p\pi$-$d\pi$ interactions between cobalt and pyrrole-nitrogen atoms may be in favor of the present experimental sequence of g-values, such interactions are expected for all the complexes cited in Table 7. Thus, the π-bonding effect does not explain the difference in interrelation of g-values among these complexes.

Conclusion

Corrole involves a significant internal strain in its macrocyclic skeleton due to the direct linkage between A and D pyrrole rings. This strain may cause deviation of the skeleton from complete planar configuration and consequently results in reduction of the extent of π-conjugation compared to porphyrin. Such an internal strain effect seems to be relaxed to some extent through formation of the bivalent metal complexes, in which corrole acts as a dianionic ligand. The π-conjugation throughout the whole complex molecule is interfered with by the presence of a methylene group at 10-position. Such bivalent metal complexes of neutral charge were transformed into anionic complexes upon losing a proton of 10-position with base.

Corrole is coordinated to the tervalent cobalt as a trianionic ligand. The cobalt(II) complex, generated by reduction of the corresponding cobalt(III) complex with $NaBH_4$, must assume C_s local symmetry at the coordination site; the cobalt atom is placed at the top of a pyramidal structure. Either (d_{xy}^2, d_{xz}) or (d_{xy}^2, d_{yz}) is referred to the ground state configuration (hole) with extensive contribution of d_{xz} and d_{yz} to the formation of σ-antibonding orbitals. The interrelation of experimental g-values ($g_1 \gg g_2 > g_3$) is consistent with such circumstances along with requirement given by (3), (4), and (5); or (7).

References

1) A. W. Johnson and I. T. Kay, *J. Chem. Soc.*, **1965**, 1620.
2) M. Conlon, A. W. Johnson, W. R. Overend, D. Rajapaksa, and C. M. Elson, *J. Chem. Soc., Perkin Trans. 1*, **1973**, 2281.
3) Y. Murakami, S. Yamada, Y. Matsuda, and K. Sakata, *Bull. Chem. Soc. Jpn.*, **51**, 123 (1978).
4) Y. Murakami, K. Sakata, Y. Tanaka, and T. Matsuo, *Bull. Chem. Soc. Jpn.*, **48**, 3622 (1975).
5) G. M. Badger, R. L. N. Harris, and R. A. Jones, *Aust. J. Chem.*, **17**, 1022 (1964).
6) N. S. Hush, J. M. Dyke, M. L. Williams, and I. S. Woolsey, *J. Chem. Soc., Dalton Trans.*, **1974**, 395.
7) Y. Murakami, Y. Aoyama, and S. Nakanishi, *Chem. Lett.*, **1977**, 991.
8) D. K. Lavallee, M. D. Baughman, and M. P. Phillips, *J. Am. Chem. Soc.*, **99**, 718 (1977).
9) J. M. Assour, *J. Chem. Phys.*, **43**, 2477 (1965).
10) C. M. Guzy, J. B. Raynor, and M. C. R. Symons, *J. Chem. Soc., A*, **1969**, 2299.
11) J. M. Assour and W. K. Kahn, *J. Am. Chem. Soc.*, **87**, 207 (1965).

Table 1. Elemental analyses

Complex	Found (Calcd) (%)			
	C	H	N	S
$MoO(tpp)OC_2H_5$	71.67 (71.78)	4.40 (4.32)	7.15 (7.28)	
MoO(tpp)F	70.06 (71.07)	3.91 (3.80)	7.15 (7.53)	
MoO(tpp)Cl	68.27 (69.53)	3.62 (3.71)	7.24 (7.37)	
MoO(tpp)Br	65.98 (65.69)	3.28 (3.51)	6.78 (6.96)	
$MoO(tpp)BF_4$	64.90 (65.13)	3.71 (3.48)	6.90 (6.90)	
$MoO(tpp)N_3$	69.02 (68.93)	3.74 (3.68)	11.31 (12.79)	
MoO(tpp)NCO	70.66 (70.50)	3.72 (3.68)	8.93 (9.14)	
MoO(tpp)NCS	68.96 (69.05)	3.92 (3.61)	8.77 (8.75)	4.02 (4.10)

aratory funnel was used. Each complex was dried *in vacuo* at 100 °C. When the complex was dried *in vacuo* at room temperature, a mixture of MoO(tpp)F and MoO(tpp)F·HF or a mixture of MoO(tpp)Cl and MoO(tpp)Cl·HCl was obtained. The synthesis of the complex, MoO(tpp)Cl, by different method was reported by Ledon *et al.*[6] The visible absorption spectra of the complex, MoO(tpp)Cl, was almost the same as that of Ledon's complex.

The complexes, $MoO(tpp)N_3$ and MoO(tpp)NCO, were prepared in the same manner as described for the synthesis of the halo complexes. The aqueous solution of free acids, HN_3 or HOCN, was freshly prepared by passing the aqueous solution of NaN_3 or KOCN through a column of a cation-exchange resin, Dowex 50W-X8, in the hydrogen-form. Purity of the complexes was confirmed by the elemental analyses (see Table 1).

Trials for the Syntheses of Other TPP Complexes. The synthesis of the iodo complex, MoO(tpp)I, was tried in the same manner as described in the preparation of other halo complexes; the bromo complex, MoO(tpp)Br, was used as a starting material. The IR spectra of the brown crystals thus obtained showed no evidence for the Mo=O bond. The feature of the visible absorption spectrum was different from that of the spectra of other halo complexes.

The synthesis of the perchlorato complex, $MoO(tpp)ClO_4$, was also tried. The visible absorption spectra in dichloromethane of the obtained compound show three peaks in the region of the α and the β bands, suggesting the formation of a complex of a different formula or a mixture containing some other complexes.

ESR Spectra. The ESR spectra of the complexes, MoO(tpp)X, always consisted of six weak lines due to $^{95,97}Mo$ nuclei ($I=5/2$) (abundance *ca.* 25%). The hyperfine structure revealed d^1 Mo(V) state of the central molybdenum atom in all the complexes synthesized. The g-values were found to be 1.967 ± 0.005 for all complexes. A strong central line due to the molybdenum nucleus with $I=0$ was split into nine lines. This superhyperfine structure was assigned to the interaction of the Mo nucleus ($I=0$) with four nitrogen nuclei ($I=1$) of the ligand, TPP. The ESR parameters for several complexes were already reported.[7]

IR Spectra. An intense IR absorption band ascribed to the Mo=O stretching was observed around 935—938 cm^{-1} for each complex, suggesting that synthesized complexes are all oxomolybdenum(V) complexes. The values of ν(Mo=O) are not different among F, Cl, and Br complexes (see Table 2). The BF_4, N_3, and NCO complexes have the absorption peak for the Mo=O stretching in the region of 940 cm^{-1}. The doublet IR bands ascribed to the CN stretching for the complex, MoO(tpp)NCO, were observed at 2060 and 2080 cm^{-1}. The band corresponding to the CN stretching for the complex, MoO(tpp)NCS, was observed at 2075 cm^{-1}. These results suggest that the ligands, NCO^- and NCS^-, in the complexes are coordinated to the central molybdenum atom with N atoms.

Table 2. Absorption peaks in infrared region

Complex	ν(Mo=O)/cm^{-1} (Nujol mull)
$MoO(tpp)OC_2H_5$	904
MoO(tpp)F	938
MoO(tpp)Cl	935
MoO(tpp)Cl[a]	937
MoO(tpp)Br	937
$MoO(tpp)BF_4$	940
$MoO(tpp)N_3$	935
MoO(tpp)NCO	940
MoO(tpp)NCS	950

a) Ref. 6.

Visible Absorption Spectra. The values of λ_{max} and ε_{max} for the electronic spectra of the complexes, MoO(tpp)Br and MoO(tpp)Cl·HCl, were previously reported by the present authors.[7] However, in the detailed characterization of the synthesized complexes, we noticed that the visible absorption spectra of these complexes, especially of MoO(tpp)Br, are very sensitive to impurities in the organic solvents applied.[8] Therefore, the absorption spectra of these complexes were remeasured and corrected. The values of λ_{max} and ε_{max} of the absorption spectra for the complexes in pure dichloromethane are listed in Table 3, suggesting that the complexes, MoO(tpp)X, belong to d-type hyperporphyrin.[1] A typical absorption spectrum is given in Fig. 1. The most intense absorption peak in the visible region, the B or the Soret band, was observed around 460—500 nm, and the other intense bands, the Q or the β and the α bands between

TABLE 3. ABSORPTION PEAKS IN UV AND VISIBLE REGIONS

Complex	λ_{max}/nm ($\varepsilon/10^4$ mol^{-1} dm^3 cm^{-1}) in CH_2Cl_2 at 25 °C					
				Soret	β	α
MoO(tpp)OC_2H_5	320(3.42)	385(sh)		454(15.8)	582(1.51)	622(1.04)
MoO(tpp)F	325(3.70)	370(sh)	390(sh)	463(9.71)	592(1.30)	635(1.04)
MoO(tpp)Cl	337(6.12)	380(sh)	417(2.90)	500(4.17)	627(0.85)	674(0.96)
MoO(tpp)Cl[a]			402(sh)	504(4.1)	632(0.84)	678(0.92)
MoO(tpp)Br	350(6.40)	375, 390(sh)	421(2.63)	508(3.45)	638(0.71)	686(0.86)
MoO(tpp)BF_4	325(4.07)	370(sh)	390(sh)	463(9.82)	591(1.35)	634(1.09)
MoO(tpp)N_3	327(4.17)	369(4.00)	412(3.37)	490(4.34)	616(0.81)	662(0.83)
MoO(tpp)NCO	333(4.76)	360(sh)	413(2.87)	488(4.66)	617(0.85)	664(0.86)
MoO(tpp)NCS	333(5.42)	370(sh)	410(sh)	493(4.55)	622(0.91)	667(0.93)

a) Ref. 6.

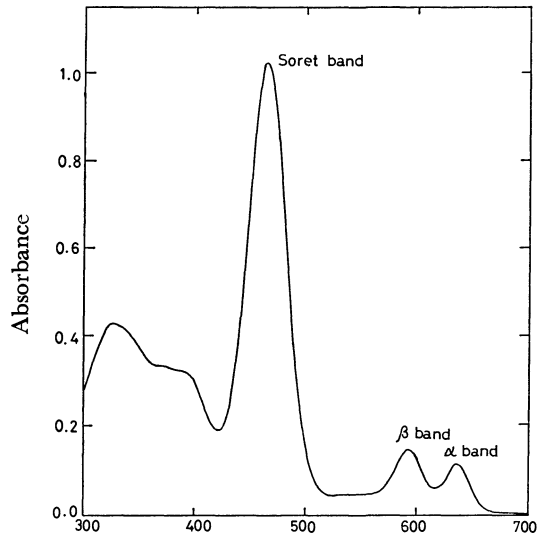

Fig. 1. Absorption spectrum of the complex, MoO(tpp)F, in CH_2Cl_2 at 25 °C. [MoO(tpp)F] = 1.08×10^{-5} mol dm^{-3}.

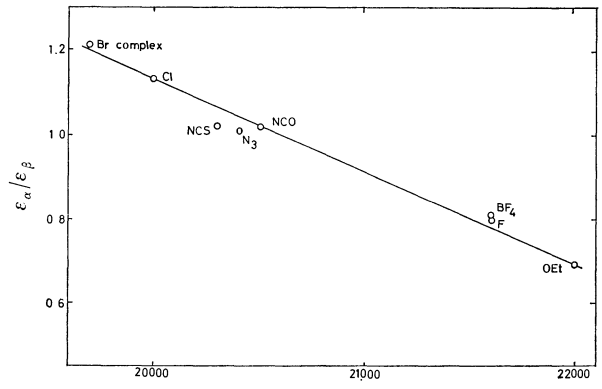

Fig. 2. The correlation between the ratios $\varepsilon_\alpha/\varepsilon_\beta$ and the wavenumbers of the Soret bands in the visible absorption spectra of the complexes, MoO(tpp)X.

550 and 700 nm, respectively. The Soret band would be assigned to charge-transfer (CT) transitions,[1,9] $a_{1u}(\pi)$, $a_{2u}(\pi) \rightarrow e_g(d,\pi)$, and/or the CT transition mixed with a $\pi \rightarrow \pi^*$ transition as assigned for the manganese(III) etioporphyrin complex.[10] The visible absorption spectra of the complexes, MoO(tpp)X, strongly depend on the anionic ligand X^-. Change in the axial ligand X, caused a red shift of the absorption peaks in the visible region relative to those of MoO(tpp)OC_2H_5; the red shift of the Soret band was accompained with the red shift of the α and the β bands. The Soret band and the β band, and the β and the α bands were separated from each other by *ca.* 125 and 40 nm, respectively. The values of the red shift are increased in the order: $X = OC_2H_5 < F \simeq BF_4 < NCO < N_3 < NCS < Cl < Br$.

The red shifts of the visible absorption peaks are also accompanied with the change in the values of ε_{max} of these three peaks; the values of ε_{Soret}, ε_α, and ε_β decreased with increase in the red shift. A linear relationship was observed between the ratio $\varepsilon_\alpha/\varepsilon_\beta$ and the wave number of the Soret band (Fig. 2). This strong correlation between the ratio $\varepsilon_\alpha/\varepsilon_\beta$ and the wavenumber of the Soret band suggests the contribution of the configurational interaction between the transitions for the Soret band and those for the α and the β bands of the complexes, MoO(tpp)X, as suggested for the metalloporphyrins by Gouterman based on his four-orbital model.[11]

Similar red shifts were reported for the complexes, Sn^{IV}(etio)X_2 (etio=etioporphyrin),[12] Mn^{III}(etio)X·H_2O,[13,14] and Zn^{II}(tpp)X^-.[2] The order of the red shifts is F<Cl<Br<I for the Soret bands of these complex series and also F<Cl for the complexes, MoO(oep)X.[1] The intensity ratio $\varepsilon_\alpha/\varepsilon_\beta$ also increased in the same order for Zn(tpp)X^- and in the reversed order for Sn(etio)X_2. Similar reversed relationship between the ratio $\varepsilon_\alpha/\varepsilon_\beta$ and the red shift was previously observed for a series of metalloporphyrins;[1,11] $\varepsilon_\alpha/\varepsilon_\beta$ decreases with increasing red shift of the Soret band for etioporphyrin, octaethylporphyrin, mesoporphyrin IX, and porphyrin IV complexes, but increases for TPP complexes.[2]

The orders of the red shift and of the ratio $\varepsilon_\alpha/\varepsilon_\beta$ for the complexes, MoO(tpp)X, are the same as those for the complexes Zn(tpp)X^- (see Table 4). It is interesting to note that no difference is observed in the spectral behavior between the closed-shell d^{10} zinc(II) porphyrin complexes and the open-shell d^1

Table 4. The orders of the red shift and of the ratio $\varepsilon_\alpha/\varepsilon_\beta$ in the visible absorption spectra of the halo complexes

Complex	Red shift	$\varepsilon_\alpha/\varepsilon_\beta$
Zn(tpp)X^{-}[a]	F < Cl < Br	F < Cl < Br
Sn(etio)X_2[b]	F < Cl < Br	F > Cl > Br
MoO(tpp)X	F < Cl < Br	F < Cl < Br

a) Ref. 2. b) Ref. 12.

oxomolybdenum(V) porphyrin complexes. The order of the red shift for closed-shell metalloporphyrin depends largely on the electronegativity of the central metal atom[12] and on that of the axial ligand X.[2,12] In the series of the halo complexes, MoO(tpp)X (X= F, Cl, and Br), the IR band ascribed to the Mo=O stretching was observed at almost the same frequency 935—938 cm^{-1} and the *g*-values for the complexes were all observed at 1.967±0.005. These data suggest the slight differences in the electronic state of the central molybdenum(V) atom (d^1) in the given complexes. Thus, decreasing electronegativity of the axial halo ligands, X=F, Cl, and Br, should primarily causes the increased electron density in the porphyrin ring *via* the central molybdenum(V) atom, resulting in the red shift and the increase in the ratio $\varepsilon_\alpha/\varepsilon_\beta$. For the NCS, NCO, and N_3 complexes, the correlation of the red shift and the electronegativity of the ligands could not be directly discussed, since the data on the electronegativity of the coordinated ligands, NCS, NCO, and N_3, are not estimated. However, from the order of the red shift, we deduce the order of the magnitude for ligand X to donate electrons to the porphyrin ring through the central moiety O=Mo–X as follows:

$$O{=}Mo{-}OC_2H_5 < O{=}Mo{-}BF_4 \simeq O{=}Mo{-}F < O{=}Mo{-}NCO < O{=}Mo{-}N_3 < O{=}Mo{-}NCS < O{=}Mo{-}Cl < O{=}Mo{-}Br.$$

As in Table 3, the absorption spectra in UV and visible regions of the dichloromethane solutions of the complexes, MoO(tpp)NCS, MoO(tpp)NCO, and MoO(tpp)N_3, give almost the same values of λ_{max} and ε_{max}. This fact indicates that the thiocyanate are the cyanate anions coordinate to the central molybdenum(V) atom *via* N atom as suggested by the data of IR spectra of these complexes. Similar phenomenon was also observed for the complexes, MoO(tpp)BF_4 and MoO(tpp)F; the values of λ_{max} and ε_{max} of the absorption spectra of these complexes are alomst the same (Table 3). These results indicate that in the small ligand it is the donor atom in the ligand coordinated to the central atom that is predominantly responsible for the absorption spectra of the complex, MoO(tpp)X; the values of λ_{max} and ε_{max} in the UV and the visible absorption spectra are primarily determined by the donor atom in the axial ligand X.

Correlation of the Value of ε_{Soret} with the Integrated Intensity of the Sored Band. In connection with the correlation of the red shifts of λ_{max} in the visible absorption spectra of the complex, MoO(tpp)X, with the values of ε_{Soret}, ε_α, and ε_β it was observed that the degree of the broadening of the Soret band is also in the same order as that of the red shift and that the values of ε_{Soret} and the integrated intensity of the Soret band decrease with the red shifts. These facts should be explained in terms of the decrease in the magnitude of transitions in the Soret band with increase in the order of the red shift, though the Soret band becomes broader and less intense with increasing red shift. Relative integrated intensities of the Soret bands of the complexes, MoO(tpp)X, are decreased in the order: F(285)≳BF_4(280)>NCS≃N_3≃NCO(200)>Cl(185)>Br(170).

UV Absorption Spectra. For all complexes, MoO(tpp)X, in dichloromethane a distinct intense absorption band was observed around 330 nm (see Table 3). The order of the red shift of this band with respect to the axial ligand X was found to be the same as that of the red shift of the Soret band, except for the absorption peak of the complex MoO(tpp)N_3. The UV and the Soret bands for the complexes are separated from each other *ca.* 150 nm. The value of ε_{max} of the band, ε_{UV}, increases with the red shifts of the UV band as well as the Soret band, which is in the reversed order of ε_{Soret}; the values of ε_{UV} of the complex are increased in the following order: X=OC_2H_5($\varepsilon_{UV}\times10^{-4}$=3.42)<F(3.70)<$BF_4$(4.01)<$N_3$(4.17)<NCO(4.76)<NCS(5.42)<Cl(6.12)<Br(6.40). Thus the ratio $\varepsilon_{Soret}/\varepsilon_{UV}$ decreases in the order: X=OC_2H_5($\varepsilon_{Soret}/\varepsilon_{UV}$=4.62)>F(2.62)>$BF_4$(2.41)>$N_3$(1.04)>NCO(0.98)>NCS(0.84)>Cl(0.68)>Br(0.54). This tendency is very similar to that of the intensity ratio of the bands V and VI reported for the complexes, Mn^{III}(etio)X·H_2O, in chloroform,[13,14] and for the complexes, MoO(oep)X (X=OCH_3, F, and Cl).[1] The values of ε_{UV} for the complexes, MoO(tpp)Br, MoO(tpp)Cl, and MoO(tpp)NCS, are larger than those of ε_{Soret} for these complexes. Similar relation is observed for $\varepsilon_\alpha/\varepsilon_\beta$ (Fig. 2). These results suggest that the electronic transitions responsible for the three bands, the band around 330 nm, the B band, and the Q band, for the complexes, MoO(tpp)X, are also conjugated with each other, though the assignments of these bands for the given complexes are not yet established.

Comparison of the Visible Absorption Spectra with the IR Spectra. Based on the Raman spectral studies for the complex, $Mo^{V}O$(mec) (mec=2,3,17,18-tetramethyl-7,8,12,13-tetraethylcorrole), it was reported that the strong absorption band observed at 455 nm is largely due to a ligand-metal charge-transfer transition;[15] the intensity of the absorption peak observed at 950 cm^{-1} (Mo=O stretching) in the Raman spectra of MoO(mec) was enhanced to a larger extent than that expected for the core vibrations when the exciting frequency approaches the frequency of the strong band at 455 nm. The Mo=O stretching frequency is also suggested to be a sensitive probe for the surrounding.[3] Therefore it was expected that the peak ascribed to the Mo=O stretching of the complex, MoO(tpp)X, was correlated with the λ_{max} and ε_{max} of the absorption spectra in dichloromethane. However no clear correlation was observed for the complexes, MoO(tpp)-X. The trans effect of an axial ligand X on the frequency of the Mo=O stretching of the complexes,

MoO(tpp)X, must be small except for the complex, $MoO(tpp)OC_2H_5$. The Mo=O stretching for the complex, $MoO(tpp)OC_2H_5$, was observed at the low frequency, 904 cm^{-1}, as shown in Table 2. The M=O stretching was also observed at low frequency for other complexes, $MoO(oep)OCH_3$ (896 cm^{-1}) and $WO(oep)OCH_3$ (901 cm^{-1}).[3] These phenomena could be attributed to the strong π-donor trans effect of alkoxo ligand.[3]

The present work was partially supported by a Grant-in-Aid for Scientific Research No. 464190 from the Ministry of Education, Science and Culture.

References

1) M. Gouterman, "The Porphyrins," ed by D. Dolphin, Academic Press, New York, N. Y. (1978), Vol. III, Part A, Chap. 2.
2) M. Nappa and J. S. Valentine, *J. Am. Chem. Soc.*, **100**, 5075 (1978).
3) J. W. Bucher, "The Porphyrins," ed by D. Dolphin, Academic Press, New York, N. Y. (1978), Vol. I, Part A, Chap. 10.
4) "Inorganic Syntheses," ed by W. C. Fernelius, McGraw-Hill, New York, N. Y. (1946), Vol. II, p. 87.
5) Y. Matsuda, F. Kubota, and Y. Murakami, *Chem. Lett.*, **1977**, 1281.
6) H. Ledon and B. Mentzen, *Inorg. Chim. Acta*, **31**, L393 (1978).
7) T. Imamura, M. Terui, Y. Takahashi, T. Numatatsu, and M. Fujimoto, *Chem. Lett.*, **1980**, 89.
8) The complex assigned to $MoO(tpp)O_2$ in our previous report[7] should be assigned to MoO(tpp)OR. The dichloromethane solution (1% v/v DMSO) of the complex, MoO(tpp)Br, containing a small excess of O_2^-, has two absorption peaks at 444 and 427 nm in the Soret band region. When the solution contains a trace amount of ethanol, the final spectrum of the reaction system agrees with that of the complex, $MoO(tpp)OC_2H_5$. Detailed study of the reaction of the complex, MoO(tpp)X, and O_2^- is now in progress.
9) S. Asher and K. Sauer, *J. Chem. Phys.*, **64**, 4115 (1976).
10) J. A. Shelnuff, D. C. O'Shea, N. T. Yu, L. D. Chenung, and R. H. Felton, *J. Chem. Phys.*, **64**, 1156 (1976).
11) M. Gouterman, *J. Chem. Phys.*, **30**, 1139 (1959).
12) M. Gouterman, F. P. Schwarz, P. D. Smith, and D. Dolphin, *J. Chem. Phys.*, **59**, 676 (1973).
13) L. J. Boucher, *Ann. N.Y. Acad. Sci.*, **206**, 409 (1973).
14) L. J. Boucher, *Coord. Chem. Rev.*, **7**, 289 (1972).
15) N. Ohta, W. Scheuermann, K. Nakamoto, Y. Matsuda, S. Yamada, and Y. Murakami, *Inorg. Chem.*, **18**, 457 (1979).

Note added in proof: When alcohol is absent in the reaction system, the complex, $Mo^{V}O(tpp)NCS$, is reduced by O_2^- to form the complex, $Mo^{IV}O(tpp)$.

Studies on Window Sweep Chronopotentiometry. I. Fundamental Concept, Methodology, and Analytical Application

Yoshikiyo KATO,* Akifumi YAMADA, Norimasa YOSHIDA,†
Kei UNOURA, and Nobuyuki TANAKA
Department of Chemistry, Faculty of Science, Tohoku University, Sendai 980

(Received June 12, 1980)

Window sweep chronopotentiometry, a new galvanostatic method, has been worked out, the electronic circuit of a window sweep chronopotentiograph and digital simulation of the window sweep chronopotentiogram being presented. Analytical application demonstrating the increase in sensitivity of the galvanostatic method for quantitative analysis is presented.

In the galvanostatic method graphical technique has been utilized for the measurement of transition time and the determination of potential-time relationship in an effort to overcome or compensate the double-layer charging.[1-5] The method requires graphical extrapolation which is time-consuming, complicated and inaccurate. The analytical sensitivity of galvanostatic method was limited to 10—100 μM.[6-8]

Derivative chronopotentiometry, reported for transition time measurement,[9-19] is a sensitive electrochemical method, but the frequency response of the derivative circuit has had to be sacrificed for the sake of noise reduction.

Kato *et al.* studied the application of a differential (or subtraction) method to galvanostatic measurement, and developed a sensitive and noise-free method,[20] as application of the differential method. The method, window sweep chronopotentiometry (w. s. chronopotentiometry), is a kind of pseudo-derivative chronopotentiometry.

In this report, the theoretical background, methodology, instrumentation and computer simulation of the method are presented, its analytical application also being reported.

Theoretical

A simplified potential-differential time relationship of reversible and irreversible electrode processes is considered for the cathodic process when only the oxidant is present in the solution.

Reversible Process. Consider the simple first order electrode reaction,

$$\mathrm{Ox} + ne \rightleftharpoons \mathrm{Red}, \tag{1}$$

where Ox and Red indicate the oxidized and the reduced forms, respectively, both being soluble in solution and in electrode. The potential-time relation at constant current can be given[21] by

$$t = \tau[\exp\left\{\frac{nF}{RT}(E-E_{1/2})\right\}+1]^{-2}, \tag{2}$$

with[22]

$$\tau^{1/2} = \frac{nF\pi^{1/2}D_0^{1/2}c_0^\circ}{2j}, \tag{3}$$

where E is electrode potential, $E_{1/2}$ polarographic half-wave potential, τ transition time, t time, D_0 diffusion coefficient, c_0° concentration in the bulk of the solution, and j controlled current density, the other symbols having their usual meanings.

The differential time Δt corresponding to the voltage window ΔE is given by

$$\Delta t = \tau([\exp\left\{\frac{nF}{RT}(E-E_{1/2}-\Delta E)\right\}+1]^{-2} - [\exp\left\{\frac{nF}{RT}(E-E_{1/2})\right\}+1]^{-2}). \tag{4}$$

The peak potential E_p of differential-time potential curve, w. s. chronopotentiogram is obtained by differentiation of Eq. 4 with E.

$$E_p = E_{1/2} - \frac{RT}{nF}\gamma \tag{5a}$$

$$\gamma = \ln[\exp\left\{\frac{nF}{3RT}(-\Delta E)\right\}[\exp\left\{\frac{nF}{3RT}(-\Delta E)\right\}+1]]. \tag{5b}$$

Irreversible Process. The potential-time relation for irreversible electrode reaction is given by[23]

$$j = nFk_c c_0^\circ - \left\{\frac{2}{\sqrt{\pi}}\left(\frac{k_c}{\sqrt{D_0}}+\frac{k_a}{\sqrt{D_R}}\right)\right\}j\sqrt{t} \tag{6}$$

$$k_c = k_s \exp\left\{\frac{-\alpha nF}{RT}(E-E_o)\right\} \tag{7}$$

$$k_a = k_s \exp\left\{\frac{(1-\alpha)nF}{RT}(E-E_o)\right\}. \tag{8}$$

Equation 6 can be written as

$$t = \frac{\pi}{4}\left\{(nFk_c c_0^\circ - j)\Big/\left(\frac{k_c}{\sqrt{D_0}}+\frac{k_a}{\sqrt{D_R}}j\right)\right\}^2. \tag{9}$$

From Eqs. 3 and 9 we get

$$\Delta t = \left\{\frac{\tau^{1/2}-\sqrt{\pi D_0}/2k_c}{1+\sqrt{D_0}k_a/\sqrt{D_R}k_c}\right\}^2 - \left\{\frac{\tau^{1/2}-\sqrt{\pi D_0}/2k_c\exp\left(\frac{nF}{RT}\Delta E\right)}{1+\sqrt{D_0}k_a/\sqrt{D_R}k_c\exp\left(\frac{nF}{RT}\Delta E\right)}\right\}^2. \tag{10}$$

Totally Irreversible Process. The potential-time-current relationship at constant current for a simple first-order totally irreversible electrode reaction 1 can be expressed by[1]

$$\frac{j}{nF} = k_c^\circ\left(c_0^\circ - \frac{2jt^{1/2}}{nF\pi^{1/2}D_0^{1/2}}\right)\exp\left\{\frac{\alpha nF}{RT}E\right\}, \tag{11}$$

where k_c° is the cathodic rate constant at $E=0$. This can be written, after introduction of τ from Eq. 3, as

† Present adress: Kaosekken Tochigi-kenkyusho Bunseki-dainiken, 2606 Akabane, Ichikai-machi, Haga-gun, Tochigi, 321-34.

$$t = \left\{\tau^{1/2} - \frac{\pi^{1/2}D_0^{1/2}}{2k_c^\circ}\exp\left(\frac{\alpha nF}{RT}E\right)\right\}^2. \quad (12)$$

From this we get

$$\Delta t = \left[\tau^{1/2} - \frac{\pi^{1/2}D_0^{1/2}}{4k_c^\circ}\left[\exp\left\{\frac{\alpha nF}{RT}E\right\} + \exp\left\{\frac{\alpha nF}{RT}(E-\Delta E)\right\}\right]\right] \times \frac{\pi^{1/2}D^{1/2}}{4k_c^\circ}\left[\exp\left\{\frac{\alpha nF}{RT}E\right\} - \exp\left\{\frac{\alpha nF}{RT}(E-\Delta E)\right\}\right]. \quad (13)$$

The peak potential can be given by

$$E_p = \frac{RT}{\alpha nF}\ln\left[\frac{2k_c^{\circ\,1/2}\tau^{1/2}}{\tau^{1/2}D_0^{1/2}\{1+1/\exp(\alpha nF\Delta E/RT)\}}\right]. \quad (14)$$

Experimental

All measurements were carried out with a three-electrode cell. A Yanagimoto Type-C dropping mercury electrode (DME) was used as the working electrode, synchronization of DME being made with an electro-mechanical knocker (Horseman Solenoid). A saturated calomel electrode (Hitachi Horiba 2410-05t) was used as the reference electrode, a spiral platinum wire electrode of 9.43 cm^2 in surface area being used as the counter electrode. The solution was deaerated with pure nitrogen and kept under nitrogen atmosphere. The temperature of the solution was kept at 25±0.1 °C. All solutions were prepared in twice distilled water, all chemicals being of analytical grade.

Apparatus. A block diagram and the electronic circuit of the system are shown in Figs. 1 and 2, respectively. When a drop begins to grow, it is held at the potential set by the initial potential source (OA-10). The DME can be also kept free from the potential source by opening the switch G-3 independent of the sequence controller. After the lapse of predetermined period t_m(1—6 s), the sequence controller turns the switch G-3 off. The cell is then disconnected from the potential source (OA-10). Simultaneously switches G-2, G-4, and G-6 are opened, switches G-1 and G-5 being closed.

The balance between the electrode potential and the output of ramp generator(OA-12) is supplied to the window comparator by a follower (OA-2), an adder (OA-3) and/or an inverter (OA-4). The window comparator generates a pulse corresponding to the elapsed time for the change of electrode potential from E to $E-\Delta E$. The output of the TVC, which corresponds to the differential time Δt, is stored on a sample and hold circuit (OA-8). After the lapse of the desired time from t_m the switches G-2, G-3, G-4, and G-6 are closed, switches G-1 and G-5 are opened. Simultaneously the DME knocker dislodges the mercury drop. The measurement cycle is completed and the sequence is repeated. The values of Δt are displayed on an x-y recorder (Riken-denshi F-3EP) as a function of E. The w. s. chronopotentiograph and the x-y recorder were calibrated with a Digital Multimeter (Takedariken TR-6854) and a Digital Counter (Iwasakitsushinki UC-6131).

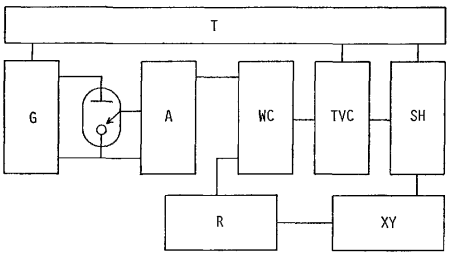

Fig. 1. The block diagram of w. s. chronopotentiograph.
T: sequence controller, G: galvanostat, A: amplifier, WC: window comparator, TVC: time to voltage converter, SH: sample and hold circuit, R: ramp generator, XY: x-y recorder.

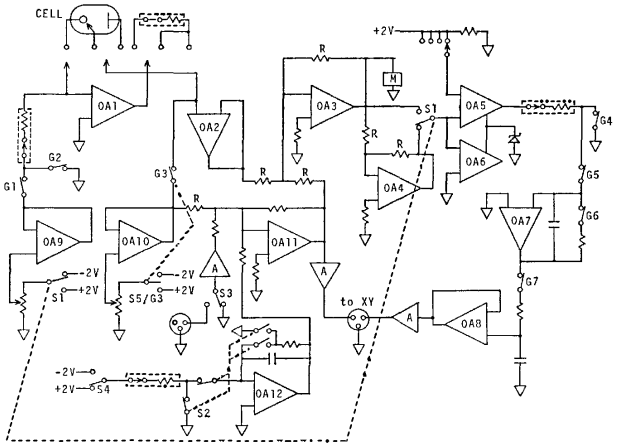

Fig. 2. The circuit diagram of w. s. chronopotentiograph.
G: FET-gate, OA: operational amplifier, S: mechanical swith, M: meter.

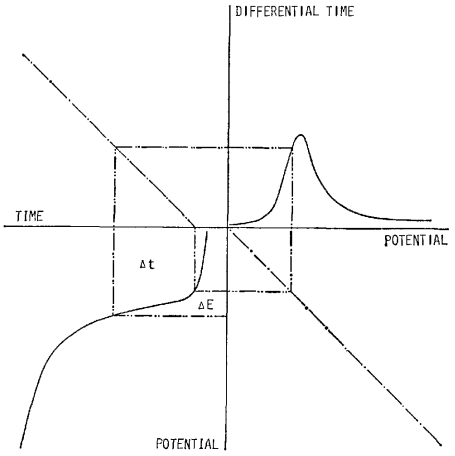

Fig. 3. The schematic diagram of the principle of w. s. chronopotentiometry.

The relation between a w. s. chronopotentiogram and the corresponding conventional chronopotentiogram is given in Fig. 3, the w. s. chronopotentiogram and corresponding conventional chronopotentiogram being shown in the first third quadrants, respectively. The vertical and horizontal axes show differential time and potential, respectively, in the first quadrant, and potential and time, respectively, in the third quadrant. Relations between these quantities are shown by dot-dash-lines.

Results and Discussion

Digital Simulation. W. s. chronopotentiograms were computed on reversible electrode reactions. Change of display with window voltage is shown in

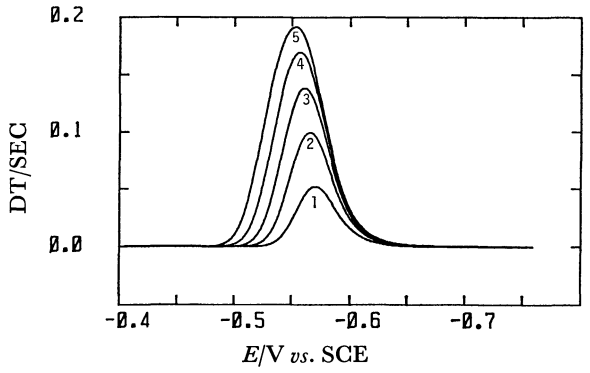

Fig. 4. The w. s. chronopotentiograms simulated with various values of window voltage.
$n=2$, $c_0=1$ mM, $D_0=7.9\times10^{-2}$, $E_0=-0.571$ V. *vs.* SCE, $\Delta E=$(1) 10, (2) 20, (3) 30, (4) 40, (5) 50 mV, temp=25 °C, $t_m=6$ s).

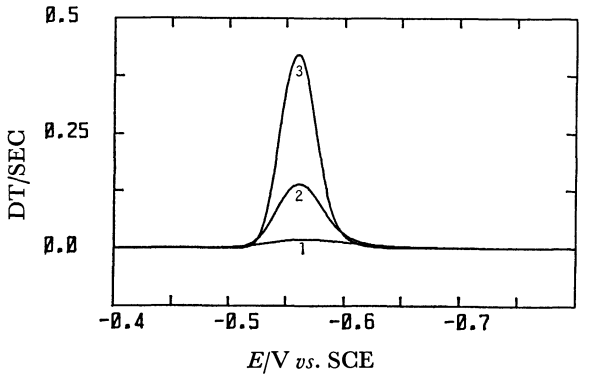

Fig. 5. The w. s. chronopotentiograms simulated with various numbers of electrons. The peak heights are normalized to the case of $n=3$.
$n=$(1) 1, (2) 2, (3) 3, $c_0=1$ mM, $D_0=7.9\times10^{-6}$ cm^2 s^{-1}, $j=1$ mA cm^{-2}, $E_0=-0.571$ V *vs.* SCE, $\Delta E=$ 30 mV, temp=25 °C, $t_m=6$ s.

Fig. 4. The peak potential, peak height, and the half height width of these curves change with the window voltage. In quantitative analysis, a greater window voltage should improve the sensitivity, but, the separability would be reduced.

Change of simulated curves with the number of electrons involved in the electrode reactions is shown in Fig. 5. The peak height and half-height width change markedly with the number of electrons, which can be determined from the peak height and the half-height width.

System Evaluation. For evaluation of the complete system, the reduction of cadmium(II) in a solution of 1 M $NaNO_3$ was studied. The data are shown in Fig. 6 with the corresponding simulated display. Simulation was carried out taking the expansion of mercury drop into consideration. The results are satisfactory, comparable with simulated display. The small difference at the potential over −0.6 V *vs.* SCE is due to the effect of double layer charging.

Effect of Window Voltage. Measurement of the change of w. s. chronopotentiograms with window voltage was carried out by use of 100 μM Cd(II) in 1 M $NaNO_3$. The results are shown in Fig. 7. The dependence of peak potential, peak height, and peak

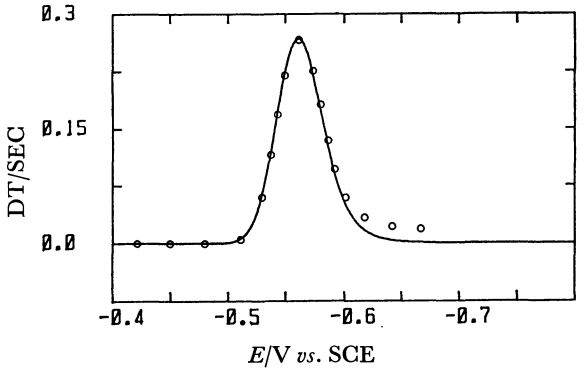

Fig. 6. Experimental data (circle) and the corresponding digital simulation (solid-line) for 1 mM $Cd(NO_3)_2$ in 1 M $NaNO_3$.
$n=2$, $c_0=1$ mM, $D_0=7.9\times10^{-6}$ cm^2 s^{-1}, $j=730$ μA cm^{-2}, $E_0=-0.571$ V *vs.* SCE, $\Delta E=30$ mV, temp= 25 °C, $t_m=6$ s.

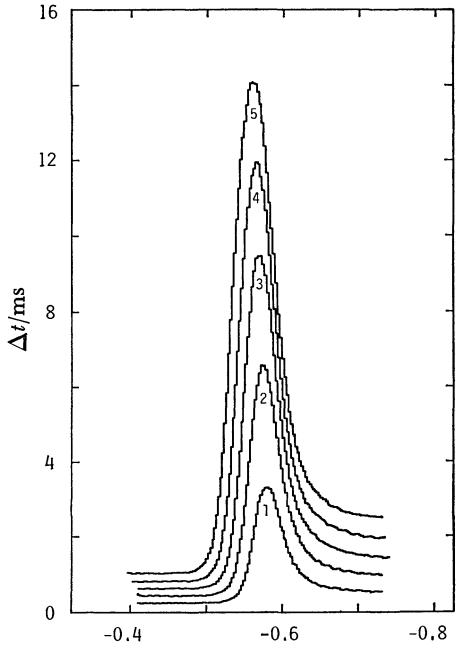

Fig. 7. Effects of voltage window width on w. s. chronopotentiograms of 100 μM $Cd(NO_3)_2$ in 1 M $NaNO_3$ at 25 °C.
$\Delta E=$(1) 10, (2) 20, (3) 30, (4) 40, (5) 50 m V, $j=124$ μA cm^{-2}, $t_m=4$ s.

width on window voltage is in line with expectation.

According to Eq. 5, γ should be a linear function of potential E. Plots for Cd(II)/Cd(Hg) are shown in Fig. 8. The points appear to fall extremely close to the least-square line passing through them. The slope of the line is 13.5 mV and the potential at which γ equals 0 is −0.570 V *vs.* SCE. The results agree with the expected values of slope and potential which are RT/nF and polarographic half-wave potential, respectively.

Effect of the Number of Electrons Involved in Reaction. The w. s. chronopotentiograms of the Tl(I)/Tl(Hg), Cd(II)/Cd(Hg), and Sb(III)/Sb(Hg) are shown in Figs. 9a, 9b, and 9c, respectively, as examples of the

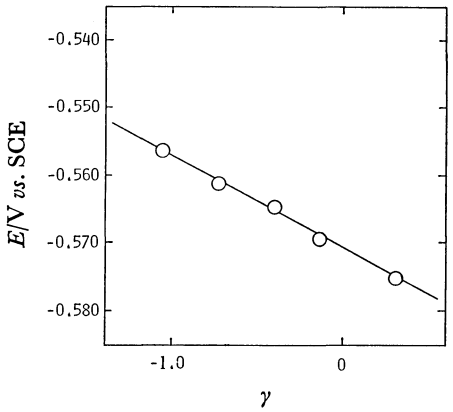

Fig. 8. Plot of electrode potential *versus* values of γ for 100 μM $Cd(NO_3)_2$ in 1 M $NaNO_3$ at 25 °C. $j=124$ μA cm², $t_m=4$ s.

electrode reactions involving one, two and three electrons, respectively.

Irreversible Process. The Zn(II)/Zn(Hg) system was evaluated as an irreversible process. The w. s. chronopotentiogram is shown in Fig. 10. The half-height width of Zn(II)/Zn(Hg) system (112.8 mV) is twice as great as that of the Cd(II)/Cd(Hg) system, which is 59.9 mV and almost equal to the theoretical value 45.5 mV. The peak height of the w. s. chronopotentiogram of Zn(II)/Zn(Hg) system (57 ms) is half as much as that of the Cd(II)/Cd(Hg) system (138.5 ms). The peak height and half height width of w. s. chronopotentiogram would be useful for examining the reversibility of electrode reaction.

Correction of Double Layer Charging. A merit of w. s. chronopotentiometry is the simplicity of procedure for correction in double layer charging. The procedure is suitable for correcting the peak of differential times and the faradaic current for a very dilute solution. The principle of the correction (Fig. 11) is as follows: The charging current density j_c at the potential where electrode reaction occurs is given by

$$j_c = C_{dl}\left(\frac{dE}{dt}\right) \simeq C_{dl}\left(\frac{\Delta E}{\Delta t_{pt}}\right), \quad (15)$$

where j_c is charging current density, C_{dl} differential capacity assumed to be a linear function of potential for the sake of simplicity, dE/dt the gradient of potential-time curve, and Δt_{pt} total peak height. In the absence of electroactive species, the w. s. chronopotentiogram of the solution will be that connected with the solid line. Thus the differential capacity at that potential can be written as

$$C_{dl} = j_t\left(\frac{dt}{dE}\right) = j_t\left(\frac{\Delta t_{pc}}{\Delta E}\right), \quad (16)$$

where j_t is controlled current density and Δt_{pc} charging time. Introducing Eq. 16 into Eq. 15 we get

$$j_c = j_t\left(\frac{\Delta t_{pc}}{\Delta t_{pt}}\right). \quad (17)$$

From this and the relation $j_t=j_c+j_f$ we get

$$j_f = j_t\left(\frac{\Delta t_{pf}}{\Delta t_{pt}}\right), \quad (18)$$

where j_f is the faradaic current density and Δt_{pt} the corrected differential time.

Analytical Application. Analytical application, of w. s. chronopotentiometry, a direct method, and an indirect "enhancement" method, were studied.

Direct Method. The method is based on Eq. 4 which shows the linear relation between $j_f\,\Delta t_{pf}^{1/2}$ and c_i°. A series of measurements were made using cadmium ion to verify the proportionality. The results are shown in Fig. 12. The effects of double layer charging were corrected as regards both current density and time. The corrected points lie very close to the least square line passing through them and origin. The sensitivity of the method seems to be 2—5 μM.

Indirect Method. The signal enhancement of

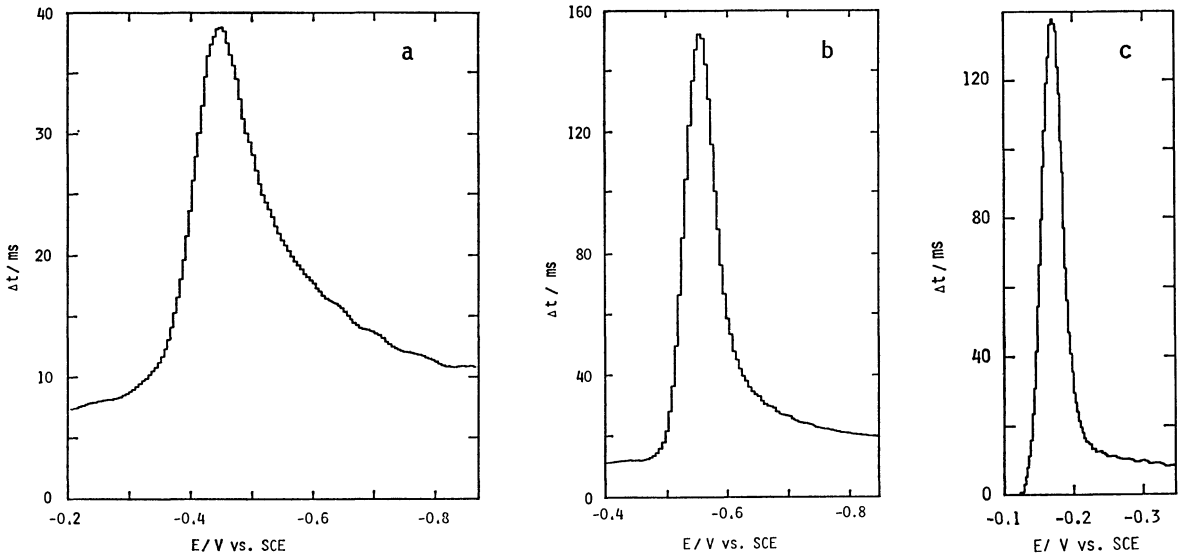

Fig. 9. W. s. chronopotentiograms of (a): 100 μM $TlNO_3$ in 1 M $NaNO_3$ ($j=73.8$ μA cm^{-2}), (b): 100 μM $Cd(NO_3)_2$ in 1 M $NaNO_3$ ($j=124$ μA cm^{-2}), and (c): 120 μM $SbCl_3$ in 1 M HCl ($j=236$ μA cm^{-2}). The measurements were carried out at 25 °C, $t_m=4$ s and $\Delta E=40$ mV.

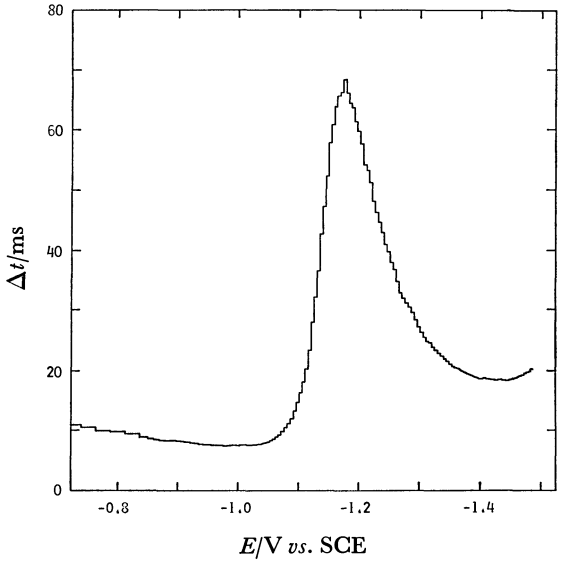

Fig. 10. A w. s. chronopotentiogram of 100 μM $Zn(NO_3)_2$ in 1 M $NaNO_3$ at 25 °C.
j=148 μA cm^{-2}, t_m=4 s, ΔE=40 mV.

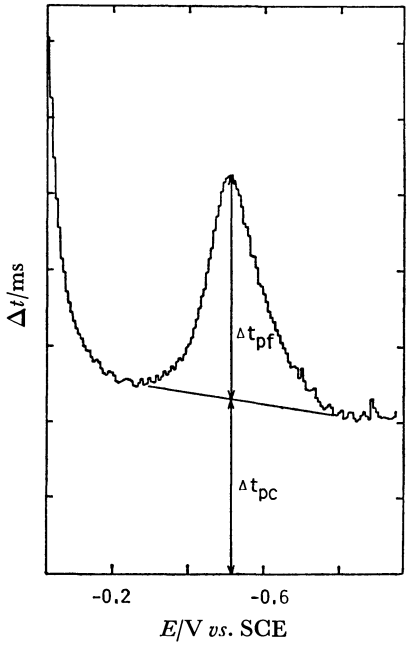

Fig. 11. Correction of w. s. chronopotentiogram for double-layer charging effect.
36 μM $TlNO_3$ in 1 M $NaNO_3$ at 25 °C, j=114.6 μA cm^{-2}, t_m=2 s, ΔE=40 mV.

post-electrolytic substances obtained in the presence of pre-electrolytic ones was utilized for precise determination of trace amount.[24,25] Consider the following electrochemical reactions involving different substances.

$$Ox_1 + n_1e \rightleftharpoons Red_1 \quad (19)$$

$$Ox_2 + n_2e \rightleftharpoons Red_2 \quad (20)$$

Pre-electrolytic substance (reactant Ox_1) is reduced at less cathodic potential less than that of post-electrolytic substance (reactant Ox_2). When Ox_1 and Ox_2 are reduced at sufficiently different potentials, the potential-time curve exhibits two steps, and the w. s. chronopotentiogram two peaks. Since the reduction of Ox_1 and Ox_2 takes place simultaneously after transition time for the reduction of Ox_1, the current efficiency for the reduction of Ox_2 is less than 100%. The transition time and the peak of w. s. chronopotentiogram for the reduction of Ox_2 are greater than would be the case where only the substance

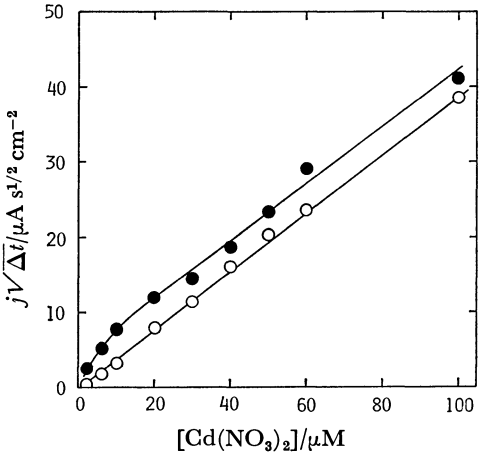

Fig. 12. Plot of $j_f\sqrt{\Delta t_{pf}}$ and $j_t\sqrt{\Delta t_{pt}}$ *versus* concentration of $Cd(NO_3)_2$ in 1 M $NaNO_3$ at 25 °C.
○ for $j_f\sqrt{\Delta t_{pf}}$, ● for $j_t\sqrt{\Delta t_{pt}}$.

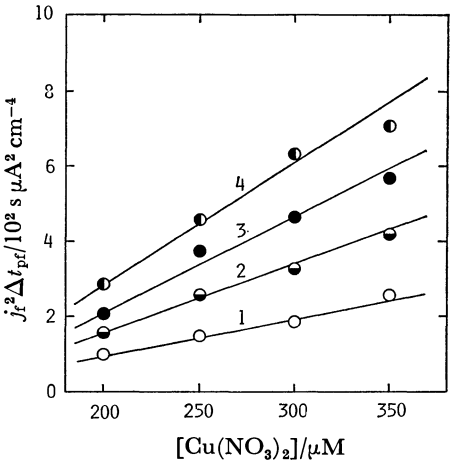

Fig. 13. Plot of $j_f^2\Delta t_{pf}$ for $Cd(NO_3)_2$ versus concentration $Cu(NO_3)_2$ in 1 M KCl at 25 °C.
$[Cd(NO_3)_2]$=(1)4, (2) 6, (3) 8, (4) 10 μM, t_m=8 s, ΔE=40 mV.

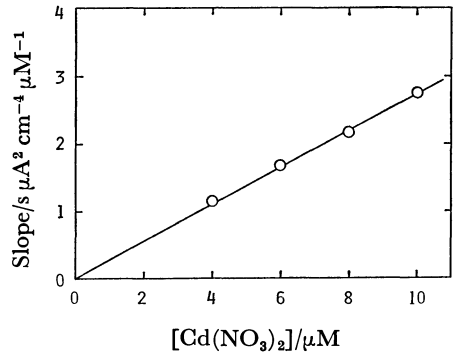

Fig. 14. Plot of the slope of least square line given in Fig. 13 *versus* the concentration of $Cd(NO_3)_2$ in 1 M KCl at 25 °C.

Ox_2 is reduced. Thus the transition time and the peak of w. s. chronopotentiogram for the reduction of Ox_2 depend on the concentration of reactants Ox_1 and Ox_2.

$Cu(NO_3)_2$ was found to be an appropriate pre-electrolytic substance (enhancement reagent), because its polarographic half-wave potential is most positive (0.03 V *vs.* SCE) on mercury electrode. In the presence of $Cu(NO_3)_2$, the enhancement method can be utilized for substances which are reduced at more cathodic potentials than 0.03 V *vs.* SCE.

W. s. chronopotentiograms of Cd(II) were obtained in the presence of various concentrations of $Cu(NO_3)_2$. Figure 13 shows the variation of $j_f^2 \Delta t_{pf}$ of $Cd(NO_3)_2$ with the concentration of $Cu(NO_3)_2$. Figure 14 shows the plots of the slopes of least square lines shown in Fig. 13 as a function of the concentration of $Cd(NO_3)_2$. The curve obtained (Fig. 14) gave an excellent linear relation down to micro molar concentration. For the determination of trace amount, the utilization of enhancement effect improves the sensitivity and accuracy of w. s. chronopotentiometry.

A part of the work was carried out with Grant-in-Aid for Scientific Research No. 472570091668 from the Ministry of Education, Science and Culture.

References

1) P. Delahay and T. Berzins, *J. Am. Chem. Soc.*, **75**, 2486 (1953).
2) P. Delahay and G. Mamantov, *Anal. Chem.*, **27**, 478 (1955).
3) W. H. Reinmuth, *Anal. Chem.*, **33**, 485 (1961).
4) C. D. Russel and J. M. Peterson, *J. Electroanal. Chem.*, **5**, 467 (1963).
5) Y. Takemori, T. Kambara, and I. Tachi, *Z. Phys. Chem. (Sonderheft)*, **1958**, 89.
6) L. Gierst and PH. Mechelynck, *Anal. Chim. Acta*, **12**, 79 (1955).
7) L. Gierst, *Anal. Chim. Acta*, **15**, 262 (1956).
8) J. J. Lingane, "Electroanalytical Chemistry," 2nd ed, Interscience, New York (1958), Chap. XXII.
9) P. E. Sturrock, *J. Electroanal. Chem.*, **8**, 425 (1964).
10) P. E. Sturrock, G. Privett, and A. R. Tarpley, *J. Electroanal. Chem.*, **14**, 303 (1967).
11) D. G. Peters and S. L. Burden, *Anal. Chem.*, **38**, 530 (1966).
12) P. Holmqvist, *J. Electroanal. Chem.*, **68**, 31 (1976).
13) P. Holmqvist, *Anal. Chim. Acta*, **90**, 35 (1977).
14) A. J. Engel and W. C. Purdy, *Anal. Chim. Acta*, **88**, 205 (1977).
15) P. E. Sturrock, W. D. Anstine, and R. H. Gibson, *Anal. Chem.*, **40**, 505 (1968).
16) P. E. Sturrock and B. Vandreuil, *J. Electrochem. Soc.*, **122**, 1311 (1975).
17) P. E. Sturrock, J. Hughey, B. Vandreuil, G. O'brien, and R. H. Gibson, *J. Electrochem. Soc.*, **122**, 1195 (1975).
18) R. H. Gibson and P. E. Sturrock, *J. Electrochem. Soc.*, **123**, 1170 (1976).
19) P. E. Sturrock and R. H. Gibson, *J. Electrochem. Soc.*, **123**, 629 (1976).
20) Y. Kato, A. Yamada, N. Yoshida, and N. Tanaka, *Rev. Polarogr.* (23rd Annual Meeting on Polarography and Electroanalytical Chemistry, November 4th—5th, Osaka), **23**, 62 (1977).
21) Z. Karaoglanoff, *Z. Electrochem.*, **12**, 5 (1906).
22) H. J. S. Sand, *Philos. Mag.*, **1**, 45 (1901).
23) Y. Okinaka, S. Toshima, and H. Okaniwa, *Talanta*, **11**, 203 (1964).
24) T. Berzins and P. Delahay, *J. Am. Chem. Soc.*, **75**, 4205 (1953).
25) C. N. Reilley, G. W. Everett, and R. H. Gibson, *Anal. Chem.*, **27**, 483 (1955).

  Bull. Chem. Soc. Jpn., 54, 181—185 (1981)

The Isolation, Characterization, and Isomerization of *cis*- and *trans*-Bis(benzonitrile)dichloroplatinum(II)

Toshihiko Uchiyama, Yoshio Toshiyasu,† Yukio Nakamura,*
Toshio Miwa, and Shinichi Kawaguchi

Faculty of Science, Osaka City University, Sumiyoshi-ku, Osaka 558
† *Science Education Institute of Osaka Prefecture, Sumiyoshi-ku, Osaka 558*

(Received June 26, 1980)

The reaction of platinum(II) chloride with neat benzonitrile gave bis(benzonitrile)dichloroplatinum(II) as a mixture of cis and trans isomers in variable proportions, depending on the temperature. The geometry of the chromatographically separated isomers was identified on the basis of the dipole-moment and IR data. The ^{13}C NMR spectra in $CDCl_3$ also enabled us to discriminate between isomers in both chemical shift and coupling to the ^{195}Pt of the cyanide carbon, the resonance peak of which was utilized to follow the isomerization. The rate constant (k_c) for the cis-to-trans isomerization was found to be $(3.8\pm0.3)\times10^{-6}$ s^{-1} in $CDCl_3$ at 25 °C, ten times larger than that [$k_t=(2.9\pm0.2)\times10^{-7}$ s^{-1}] of the reverse reaction. The equilibrium between cis and trans strongly favored trans in $CDCl_3$ at 25 °C, whereas in benzonitrile the cis form was the dominant species at room temperature, while the trans form was dominant at higher temperatures.

Bis(benzonitrile)dichloroplatinum(II), $[PtCl_2(PhCN)_2]$, is frequently used as the starting material for the preparation of organoplatinum(II) complexes.[1] The complex was first prepared by Hofmann and Bugge,[2] followed by Ramberg,[3] from potassium tetrachloroplatinate(II) and benzonitrile according to Reaction 1. This preparative method, however requires a long period of over two weeks to obtain the product and gives a poor yield. A more convenient method, starting from platinum(II) chlorides, as represented by Reaction 2, was proposed by Kharasch *et al.*[4] and recommended by Hartley in his review article[1] because of its almost quantitative yield.

$$K_2[PtCl_4] + 2C_6H_5CN \longrightarrow [PtCl_2(C_6H_5CN)_2] + 2KCl \quad (1)$$

$$PtCl_2 + 2C_6H_5CN \longrightarrow [PtCl_2(C_6H_5CN)_2] \quad (2)$$

While the palladium(II) analogue, $[PdCl_2(PhCN)_2]$, has the trans structure,[5] the stereochemistry of $[PtCl_2(PhCN)_2]$, which was obtained from Reaction 1, was ascertained to be cis by Jensen's measurement of the dipole moment in benzene;[6] IR studies in the solid state confirmed this structure.[7] In the present study, we have carried out a detailed examination of the product from Reaction 2 and have found it to be a mixture of cis and trans isomers, the composition of which depends on the reaction temperature. Recently, we briefly reported[8] on the separation of the product into the two isomers and on our isomerization studies by ^{13}C NMR spectroscopy. These results, together with the data on the measurement of the dipole moment, are presented in full below.

Experimental

Commercially available platinum(II) chloride, potassium tetrachloroplatinate(II), and benzonitrile were used without further purification. Dichloromethane over a molecular sieve (type 3A) was decanted, dried further over calcium hydride, and then distilled. The benzene and chloroform which were used as solvents for the measurement of the dipole moment were purified by fractional distillation through a 100-cm column after the usual pretreatment.[9]

Synthesis of ^{13}C*-Enriched Benzonitrile.* Benzoic-carboxy-^{13}C (99%) acid was converted into acid chloride by the usual method.[10] The chloride in benzene was treated with an excess of concentrated aqueous ammonia at 0 °C to give benzamide in an 80% yield. The crude amide (1.76 g) was mixed with 1.6 g of diphosphorus pentaoxide and heated at 200 °C under slightly reduced pressure. The distillate (1.32 g; 88% yield) was used in the preparation of the complex without further purification.

cis- *and* trans-*Bis(benzonitrile)dichloroplatinum(II). Syntheses and Separation by Column Chromatography. (1) Kharasch's Method*:[1,4] When a suspension of $PtCl_2$ (0.255 g) in PhCN (20 cm^3) was stirred at room temperature (26 °C), a clear solution resulted after 7 h. After filtration, a yellow precipitate (0.417 g) was obtained in a 92% yield on the addition of petroleum ether to the filtrate. The chromatographic separation of the crude product through a column ($20\times\phi2$ cm) of silica gel (Merck $60F_{254}$, 70—230 mesh), with CH_2Cl_2 as the eluent, gave *trans*- and *cis*-$[PtCl_2(PhCN)_2]$ in 26 and 58% yields, in this sequence. Found for the trans-isomer: C, 35.1; H, 2.14; N, 5.80%. Mol wt in CH_2Cl_2 at 37 °C, 497. Found for the cis-isomer: C, 35.5; H, 2.12; N, 5.85%. Mol wt, 501. Calcd for $C_{14}H_{10}N_2Cl_2Pt$: C, 35.6; H, 2.14; N, 5.93%. Mol wt, 472. The same procedure was also performed at different reaction temperatures of 60, 100, and 180 °C; this gave increasing trans/cis ratios in this order.

(2) A Slight Modification of Hofmann's Procedure:[2,3] When an aqueous solution (20 cm^3) of $K_2[PtCl_4]$ (0.304 g) was mixed with PhCN (3 cm^3) and then stirred for 4 d at room temperature, the organic layer turned yellow. The yellow precipitate which developed on the interface was collected, washed successively with methanol and ether, and then dried *in vacuo*; yield, 0.220 g; 63%. The filtrate was extracted with CH_2Cl_2, and the extract was concentrated to obtain a yellow product on the addition of petroleum ether; yield, 0.064 g; 18%. While the former product included the cis isomer exclusively, the latter was as a mixture of trans and cis, from which the two isomers were isolated separately by column chromatography as has been described above. The trans/cis ratio was 0.72.

Synthesis of [CN-^{13}C-*Enriched*]-*bis(benzonitrile)dichloroplatinum (II).* The PhCN-[*CN-*^{13}*C*(99%)] (1.3 g) was diluted with unlabeled PhCN (1.3 g), and then $PtCl_2$ (0.363 g) was suspended in the mixture. When the suspension was stirred for 15 h at room temperature, a yellow precipitate gradually increased as the mass of the $PtCl_2$ decreased. The precipitate, with a further crop obtained on the addition

of petroleum ether to the mixture, was collected, washed successively with petroleum ether and ether, and dried *in vacuo*; yield, 0.567 g; 88%. The crude product was separated chromatographically into trans and cis isomers as has been described above.

Rate Determination of cis-trans Isomerization. The *cis*-$[PtCl_2(PhCN)_2]$-$[CN\text{-}^{13}C]$ (60 mg) was suspended in $CDCl_3$ (2 cm^3) in an NMR tube (10 mmϕ) to initiate isomerization. As the reaction proceeded, the solid of the cis isomer gradually dissolved, disappearing completely after 127 h, while the relative concentration of trans to cis in the solution increased slowly and attained an equilibrium of isomerization after *ca.* 70 d. The spectral change in the cyanide-carbon peaks (*vide infra*) of both isomers with time was followed by means of the ^{13}C FT NMR at *ca.* 25 °C and recorded, at appropriate time-intervals, 12 times during the total reaction time of 1675 h. The trans/cis isomer ratio in each set of measurements was determined on the bases of their relative peak areas. The mid-time for the accumulation of spectral data was taken as the time at which a spectrum was measured.

Measurements. The IR spectra (4000—200 cm^{-1}) were measured in Nujol mull with a JASCO DS701G spectrophotometer. The FT ^{13}C NMR spectra were recorded at 25.05 M Hz on a JEOL FX-100 spectrometer. The chemical shifts (δ) are quoted relative to the central peak of chloroform-*d* (δ; 77.1 ppm). The molecular weight was determined with a vapor-pressure osmometer manufactured by Knauer, West Berlin, West Germany.

The measurement of the dielectric constant, ε, was carried out with an apparatus devised by Le Fevre and his collaborators.[11] The specific volume, v, and the refractive index, n, were measured by the usual methods. All the data necessary to calculate the electric dipole moment, μ, were obtained at 25.00±0.02 °C. Benzene and chloroform were used as the solvents. Measurements were made on solutions up to about 0.005 in the weight fraction, w, of solutes.

Results and Discussion

Although $[PtCl_2(PhCN)_2]$ has long been thought to be exclusively cis on the basis of the data of the dipole moment,[6] the isomers of both cis and trans were first isolated separately by column chromatography, as has been shown in the Experimental Section. These isolated isomers are mononuclear in CH_2Cl_2. The trans isomer is eluted from the column prior to the cis and is more soluble in the nonpolar solvents, such as C_6H_6, $CHCl_3$, CH_2Cl_2, and $(CH_3)_2CO$, than the cis, reflecting its geometry. The isomeric composition of the product obtained by Kharasch's method depends on the reaction temperature, the trans/cis ratios being 0.45, 0.69, 4.4, and 5.4 at 26, 60, 100, and 180 °C respectively. Thus, the approximate ΔH of the cis⇌trans isomerization in PhCN is 18 kJ/mol if these values are presumed to give the equilibrium constants at given temperatures.

Determination of cis and trans Configurations by Measurements of the Dipole Moments. As a means of determining the cis and trans configurations of the square-planar metal complexes inert in solution, the measurement of the dipole moment is most useful. In order to confirm the structures of both isomers isolated in the present investigation, we have measured their electric-dipole moments in C_6H_6 and $CHCl_3$ at 25 °C. The symbols I and II are used tentatively for the isomers eluted from the silica-gel column, in this sequence.

Table 1. Polarization data[a] of I and II isomers of $[PtCl_2(PhCN)_2]$

Solvent		I	II
C_6H_6	ε	$2.2726+1.27w$	
	v	$1.1462-0.705w$	
	p_2	0.3711 cm^3	
	P_2	175.2 cm^3	
	μ	0.82D	—
$CHCl_3$	ε	$4.8780-2.80w$	$4.8880+85.5w$
	v	$0.6803-0.208w$	$0.6807-0.222w$
	p_2	0.1455 cm^3	2.1054 cm^3
	P_2	68.7 cm^3	1866.2 cm^3
	μ	—	9.13D[b]
			11.63D[c]

a) The values of the square of the refractive index, n^2; the specific refraction for the sodium D line, r, and the molar refraction, R_D, were determined by employing a $CHCl_3$ solution of I and were then also used in the calculations for II: n^2, $2.0858+1.64w$; r, 0.3260 cm^3; R_D, 153.9 cm^3. b) Value obtained by Halverstadt-Kumler's method.[12] c) Value obtained by Onsager's method.[13]

The polarization data of I and II in C_6H_6 and $CHCl_3$ are summarized in Table 1. The data of II in C_6H_6 are lacking, however, since the solubility was insufficient. The notations p_2 and P_2 in Table 1 represent the specific and the molar polarizations respectively. The dielectric data were analyzed according to the Halverstadt-Kumler method.[12] The calculation of the dipole moments of both isomers was carried out on the following assumptions: 1) the distortion polarization of I is equal to $1.05R_D$; 2) the distortion polarizations of I and II are equal in magnitude, since these complexes have the same composition, $PtCl_2(PhCN)_2$, and 3) chloroform is regarded as nonpolar; since it has a low dielectric constant (4.8 at 20 °C).

The electric-dipole moment of the I isomer was found to be 0.82 D in C_6H_6, but the moment of I in $CHCl_3$ was not calculated since $1.05R_D$ exceeded the P_2 value. On the other hand, the electric-dipole moment of II in $CHCl_3$ was calculated to be 9.13 D. Either value (175.2 or 68.7 cm^3) of the molar polarization of the I isomer in C_6H_6 and $CHCl_3$ in much smaller than that (1888.2 cm^3) of the II isomer in $CHCl_3$, and either is close to the distortion polarization, $1.05R_D$, of I. These results lead to the conclusion that the configurations of the I and II isomers are trans and cis respectively, as is to be expected from the differences in their solubilities and in their elution rates in column chromatography.

Further, we tried to estimate the more exact electric-dipole moment for the cis isomer II by the application of the dielectric theory of polar liquids proposed by Onsager.[13] The value thus obtained, 11.63 D, agrees very closely with the value of 12.5 D in C_6H_6 which was given by Jensen,[6] although we have failed in our

attempt to measure it in the same solvent.

Characterization of the Isomers trans- *and* cis-$[PtCl_2(PhCN)_2]$. *IR Spectra*: The IR spectra of the *trans*- and *cis*-$[PtCl_2(PhCN)_2]$ isomers are very similar to each other except for the bands assignable to the vibrations of ν(C≡N), π(CH) of the phenyl groups, and ν(Pt–Cl). These characteristic bands are shown in Table 2 in comparison with those for *cis*-$[PtBr_2(PhCN)_2]$ and *trans*-$[PdCl_2(PhCN)_2]$, whose configurations were assigned by Walton[7] on the basis of their IR data. As may be seen in Table 2, *trans*-$[PtCl_2(PhCN)_2]$ exhibits a single ν(C≡N) band at 2285 cm^{-1}, while the corresponding band at 2282 cm^{-1} for cis is accompanied by a minor peak at 2290 cm^{-1}. The most remarkable difference in the IR spectra in Nujol is observed in the 800—650 cm^{-1} region. The trans isomer shows two very strong bands at 766 and 688 cm^{-1}, associated with the out-of-plane CH deformation vibrations of the phenyl groups. Each of these bands is split into two well-defined peaks in the spectrum of the cis complex, giving rise to four strong bands at 779, 758, 695, and 684 cm^{-1}. A similar situation was observed in the IR spectra of *cis*-$[PtBr_2(PhCN)_2]$ and *trans*-$[PdCl_2(PhCN)_2]$ listed in Table 1. Thus, these bands are most diagnostic for the determination of the cis- and trans-geometries. In the square-planar complexes of MX_2L_2 (X=halide) type, trans isomers generally exhibit a single ν(MX) band in the IR spectra, while cis isomers generally exhibit two bands. Therefore, the ν(M–X) band has been effectively utilized to identify the configuration of these complexes.[14] In fact, *cis*-$[PtCl_2(PhCN)_2]$ exhibits two bands, at 356 and 350 cm^{-1}, in the region of ν(Pt–Cl), but trans exhibits three bands, at 356, 348, and 310 cm^{-1}. We cannot immediately determine which of these bands is assignable to the ν(Pt–Cl) vibration. Thus, the ν(Pt–Cl) bands are not of diagnostic use in identifying the trans-cis geometry in the present case.

^{13}C *NMR*: The ^{13}C NMR data for the *trans*- and *cis*-$[PtCl_2(PhCN)_2]$ isomers in $CDCl_3$ at 25 °C are listed in Table 3 in comparison with those for free PhCN and *trans*-$[PdCl_2(PhCN)_2]$. In order to detect the cyanide-carbon peaks of very weak intensities, a carbon-13 enriched compound, *cis*-$[PtCl_2(PhCN)_2]$-$[^{13}C\text{-}CN]$, was prepared, and its spectrum was measured.

Both the spectral pattern and the chemical shifts for the isomers were similar to those for free PhCN; this facilitated the assignment of each of the resonances as is shown in Table 3. No significant difference in the chemical shifts between the corresponding peaks of these isomers was observed; only the coupling $^2J(Pt\text{–}C^7)$ of the cyanide carbon to ^{195}Pt showed a serious difference between these isomers. These values for the trans and cis isomers are 289 and 234 Hz respectively, much larger than the corresponding value

Table 2. Characteristic IR bands[a]

$[PtCl_2(PhCN)_2]$ *trans*	$[PtCl_2(PhCN)_2]$ *cis*	*trans*-$[PdCl_2(PhCN)_2]$[b]	*cis*-$[PtBr_2(PhCN)_2]$[b]	Assignments
	2290 sh		2290 sh	ν(C≡N)
2285 s	2282 s	2287 s	2285 s	
766 s	779 s	760 s	773 m-s	π(C–H)
	758 s		754 m-s	
688 s	695 s	678 s	689 m-w	
	684 s		680 s	
356 sh	356 sh	368 s	247 s	ν(M–X)
348 s	350 s		238 s	
310 m				

[c] Not assignable unequivocally.

a) Frequencies in cm^{-1}. b) Ref. 7. c) Not assignable unequivocally.

Table 3. ^{13}C NMR data[a] in $CDCl_3$ at 25 °C

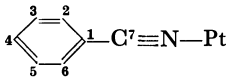

	Free PhCN	$[PtCl_2(PhCN)_2]$ *trans*		$[PtCl_2(PhCN)_2]$ *cis*		*trans*-$[PdCl_2(PhCN)_2]$
	δ	δ	J(Pt–C)	δ	J(Pt–C)	δ
C^1	112.4	109.0	20	109.1		109.0
C^2, C^3	132.0	133.7	8	133.7	3	133.3
C^3, C^5	129.1	129.5		129.6	6	129.4
C^4	132.7	135.4		135.2		135.3
C^7	118.8	116.8	289	115.3	234	122.3

a) Chemical shifts (δ) are quoted relative to the central peak of chloroform-*d* (δ; 77.1 ppm) and converted to values from TMS. Coupling constants (J) in Hz.

of 82 Hz for *trans*-[MePt(*p*-$MeOC_6H_4CN$)L_2]PF_6 (L= $AsMe_3$ or PMe_2Ph),[15] which bears an analogous nitrile ligand. Thus, a rough "NMR trans-influence series"[16] can be drawn as follows: $CH_3 \gg Cl > PhCN$. Because of their long-range interactions, the coupling constants between other carbon atoms and ^{195}Pt are too small for us to evaluate such a trans influence. Also, we could not detect ^{195}Pt satellite bands on C^1 for the cis isomer because of the very weak intensity of the parent peak.

In recent studies, we have found that $[PdCl_2(PhCN)_2]$ reacted with acetylacetone in acetone at room temperature to produce bis(η^3-1-acetyl-2-hydroxyallyl)di-μ-chloro-dipalladium(II), liberating PhCN molecules.[17] On the contrary, no reaction occurred between $[PtCl_2(PhCN)_2]$ and acetylacetone, not even in refluxing acetone, but the complex did react with acetylacetonate carbanions $(CH_3CO)_2CH^-$ in CH_2Cl_2 at room temperature, giving rise to a nucleophilic attack on the cyanide carbons.[18] The C^7-carbon of $[PdCl_2(PhCN)_2]$ is deshielded, exhibiting C^7-resonance at a field (122.3 ppm) lower by 5 to 7 ppm than those for the analogous Pt(II)-complexes, as is shown in Table 3. Therefore, it is unlikely that the above difference in reactivity between the Pd(II) and Pt(II) complexes was brought about by the difference in the shielding effects on the C^7-carbon atoms. No appreciable difference in ν(CN) was observed between the IR spectra of the *trans*-$[MCl_2(PhCN)_2]$, M=Pd(II) and Pt(II), complexes. It seems likely that the difference in the labilities of these two metal centers is mainly concerned with these reaction patterns.

Cis-trans Isomerization Studies by ^{13}C NMR Spectroscopy. In the presence of the cis isomer which remains undissolved, the solution is saturated with the cis isomer of a constant concentration during the reaction. At the initial stage of the reaction, during which the contribution of the reverse reaction to the overall isomerization is regarded as negligible, therefore, the zeroth-order reaction is set up for the cis-to-trans isomerization. In fact, within *ca.* 30 h, the plot of the [trans]/[cis] ratio against the time, t, gave a straight line, as is shown in Fig. 1. The rate constant, k_c, of the cis-to-trans isomerization expressed by Reaction 3 was obtained as:

$$cis\text{-}[PtCl_2(PhCN)_2] \xrightarrow{k_c} trans\text{-}[PtCl_2(PhCN)_2] \quad (3)$$

$(3.8\pm0.1)\times10^{-6}\ s^{-1}$ at 25 °C from the slope of the linear plot drawn by the least-squares method.

After the complete dissolution of the cis isomer, the kinetics can be treated as a reversible first-order reaction as is expressed by Reaction 4. The concentration of each of the cis and trans isomers was calculated from the total amount (60 mg) of the complex

$$cis\text{-}[PtCl_2(PhCN)_2] \underset{k_t}{\overset{k_c}{\rightleftharpoons}} trans\text{-}[PtCl_2(PhCN)_2] \quad (4)$$

used and the [trans]/[cis] ratio. The cis-trans equilibrium was attained at 1516 h after the complete dissolution of the cis isomer. The equilibrium constant, K_e, in Reaction 4 was found to be 13.0 from the data at that time. The $([cis]_t-[cis]_\infty)$ *vs.* t plot is given in Fig. 2. The (k_c+k_t) value was obtained as

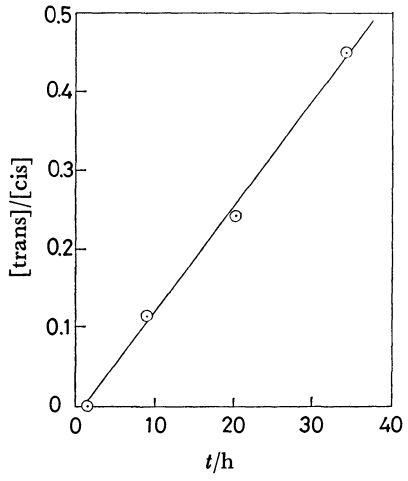

Fig. 1. The [trans]/[cis] *vs.* t plot in the presence of undissolved *cis*-$[PtCl_2(PhCN)_2]$-[^{13}C-*CN*].

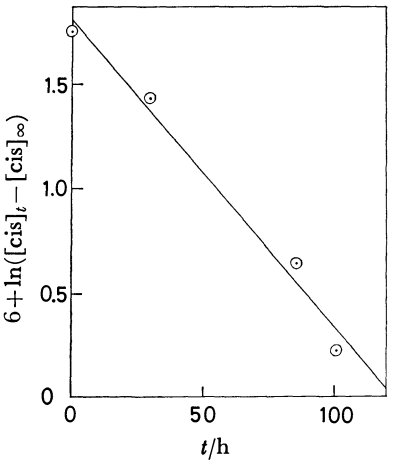

Fig. 2. The $\ln([cis]_t-[cis]_\infty)$ *vs.* t plot for the data obtained after complete dissolution of *cis*-$[PtCl_2(PhCN)_2]$-[^{13}C-*CN*].

$(4.1\pm0.3)\times10^{-6}\ s^{-1}$ from the slope of the straight line drawn by the least-squares method. From this and the K_e values, the rate constants, k_c and k_t, for the forward and the reverse isomerizations were calculated to be $(3.8\pm0.3)\times10^{-6}$ and $(2.9\pm0.2)\times10^{-7}\ s^{-1}$ respectively at 25 °C. The former value is in good agreement with the experimental value in the first step, in which the reverse reaction was ignored.

Considerations of the cis-trans Isomerization Rates. Although *trans*-$[PtCl_2(PhCN)_2]$ has not been prepared, we can find some cases in the literature in which the products obtained from reactions between $[PtCl_2(PhCN)_2]$ and substrates existed eventually in a trans form. For example, Lauhen and Ibers[19] determined the crystal structure of an adduct $[Pt(DISN)_2][PtCl_2(PhCN)_2]$ which had been prepared by mixing stoichiometric quantities of bis(diiminosuccinonitrilo)platinum(II) and $[PtCl_2(PhCN)_2]$ in a $CHCl_3$ solution at the ambient temperature; they found that the latter component has a trans geometry in crystals. Recently Braunstein *et al.*[20] obtained *trans*-(*P*,*N*)-$[Pt\{P(Ph)_2C(Y)=C(Ph)NH\}_2]$ (Y=CO_2Et and CN) by the reactions of $[PtCl_2(PhCN)_2]$ with the Ph_2PCHY

carbanions in THF at 0 °C. In each of these two cases, it is not convincing to argue that *cis*-$[PtCl_2(PhCN)_2]$ was isomerized to the trans form during the prompt reaction, which occurred under quite mild conditions. In fact, the k_c value which was obtained in $CDCl_3$ at 25 °C in the present study is too small to justify the isomerization of *cis*-$[PtCl_2(PhCN)_2]$ to trans in the course of the reactions described above, although k_c is ten times larger than k_t.

The K_e value of 13.0 shows that the equilibrium strongly favors trans in $CDCl_3$ at 25 °C, whereas in PhCN it was found that the cis form is the dominant species at room temperature, but trans at higher temperatures. Therefore, we could prepare the trans isomer in good yields at temperatures above 100 °C by Kharasch's method, although cis was produced exclusively in the preparation at room temperature by Hofmann's method. Contrary to the case in $CDCl_3$, the preference of the cis form in PhCN to trans at room temperature appears probable as behavior in a polar solvent. Walton refers in his paper[7] to the unexpected formation of the trans isomer during the preparation of *cis*-$[PtBr_2(PhCN)_2]$ by Hofmann's method. This might be related to our observation that *trans*-$[PtCl_2(PhCN)_2]$ was included in the filtrate after the isolation of the cis isomer in the preparation according to Hofmann's method.

The authors wish to express their thanks to Professor Yuho Tsuno of Kyushu University for his kindness in supplying the carbon-13 enriched benzoic acid. Thanks are also due to Mr. Junichi Gohda for the elemental analysis. The present work was partly supported by a Grant-in-Aid for Scientific Research (Grant Number 243014) from the Ministry of Education, Science and Culture.

References

1) F. R. Hartley, "The Chemistry of Platinum and Palladium," Applied Science Publishers, London (1973), p. 462.
2) K. A. Hofmann and G. Bugge, *Ber.*, **40**, 1772 (1907).
3) L. Ramberg, *Ber.*, **40**, 2578 (1907).
4) M. S. Kharasch, R. C. Seyler, and F. R. Mayo, *J. Am. Chem. Soc.*, **60**, 882 (1938).
5) J. R. Holden and N. C. Baenziger, *Acta Crystallogr.*, **9**, 194 (1956).
6) K. A. Jensen, *Z. Anorg. Allg. Chem.*, **231**, 365 (1937).
7) R. A. Walton, *Spectrochim. Acta*, **21**, 1795 (1965); *Can. J. Chem.*, **46**, 2347 (1968).
8) T. Uchiyama, Y. Nakamura, T. Miwa, S. Kawaguchi, and S. Okeya, *Chem. Lett.*, **1980**, 337.
9) A. Weissberger *et al.*, "Organic Solvents," Interscience Publishers, New York (1955).
10) A. Murray, III, and D. L. Williams, "Organic Syntheses with Isotopes," Interscience, New York (1958), p. 379.
11) R. J. W. Le Fevre, I. G. Ross, and B. M. Smythe, *J. Chem. Soc.*, **1950**, 276.
12) I. F. Halverstadt and W. D. Kumler, *J. Am. Chem. Soc.*, **64**, 276 (1950).
13) L. Onsager, *J. Am. Chem. Soc.*, **58**, 1486 (1936).
14) K. Nakamoto, "Infrared and Raman Spectra of Inorganic and Coordination Compounds," 3rd ed, John Wiley and Sons, New York (1978), p. 319.
15) M. H. Chisholm, H. C. Clark, L. E. Manzer, J. B. Stothers, and J. E. H. Ward, *J. Am. Chem. Soc.*, **95**, 8574 (1973).
16) T. G. Appleton, H. C. Clark, and L. E. Manzer, *Coord. Chem. Rev.*, **10**, 335 (1973).
17) Z. Kanda, Y. Nakamura, and S. Kawaguchi, *Inorg. Chem.*, **17**, 910 (1978).
18) T. Uchiyama, K. Takagi, K. Matsumoto, S. Ooi, Y. Nakamura, and S. Kawaguchi, *Chem. Lett.*, **1979**, 1197.
19) J. W. Lauher and J. A. Ibers, *Inorg. Chem.*, **14**, 640 (1975).
20) P. Braustein, D. Mutt, Y. Dusausoy, and J. Protas, *J. Chem. Soc., Chem. Commun.*, **1979**, 763.

Table 1. Melting points and analytical results for the complexes[a)]

Complex	Mp/°C[b)]	Found(Calcd) (%)		
		C	H	N
$[PdCl(damf)]_2$*	172(dec)	40.42(40.67)	4.12(4.20)	3.56(3.65)
[Pd(damf)(*S*-pro)]	151(dec)	46.50(46.73)	5.43(5.23)	6.18(6.05)
(+)-$[Pd(damf)(en)]BF_4$[e)]	165(dec)	36.22(36.37)	5.01(4.88)	8.52(8.48)
(−)-$[Pd(damf)(diphos)]PF_6$[d)]	169	52.77(52.52)	4.45(4.52)	1.85(1.57)
(+)-$[Pd(damf)(diars)]PF_6$[e)]	164	47·95(47.81)	3.74(4.12)	1.42(1.43)
(+)-$[Pd(damf)(py)_2]PF_6$[f)]	137—141	41.93(42.33)	4.19(4.17)	6.43(6.44)
(+)-[Pd(damf)(acac)]	119—124	48.15(48.30)	5.21(5.18)	3.22(3.13)
[PdCl(damf)(py)]	148(dec)	46.32(46.59)	4.37(4.78)	6.06(6.04)
[PdBr(damf)(py)]	147	42.54(42.51)	4.19(4.36)	5.54(5.51)
(+)-(*R*)-$[PdCl(S\text{-daef})]_2$**	155	41.92(42.25)	4.65(4.56)	3.89(3.52)
(−)-(*S*)-$[PdCl(S\text{-daef}]_2$**	146—148	42.29(42.25)	4.56(4.56)	3.44(3.52)
(+)-(*R*)-[Pd(*S*-daef)(acac)]**	124—125	49.59(49.43)	5.72(5.45)	3.37(3.04)
(−)-(*R*)-$[Pd(S\text{-daef})(en)]BF_4$	160(dec)	37.58(37.72)	5.20(5.14)	8.45(8.25)

a) Abbreviations used in this paper are as follows; Hdamf=(dimethylaminomethyl)ferrocene, Hdaef=[1-(dimethylaminomethyl)ferrocene, S-Hpro=(S)-proline, en=ethylenediamine, diphos=1,2-bis(diphenylphosphino)ethane, diars=1,2-bis(diphenylarsino)ethane, Hacac=acetylacetone, and py=pyridine. b) dec=decomposition. Molar electric conductances of 10^{-3} mol/dm^3 methanol solutions at 25 °C, Λ/Ω, cm^2/mol. c) 98. d) 104. e) 63. f) 94. * and **: See Refs. 13 and 12, respectively.

sino)ethane by a method similar to the above. Yield, 136 mg (69%). $[\alpha]=+49°$ (*c* 0.10, CH_3OH).

(+)-[Pd(damf)(py)$_2$]PF$_6$. A mixture of 230 mg (0.50 mmol) of (+)-[Pd(damf)(*S*-pro)], 160 mg (2.0 mmol) of pyridine, and 250 mg (1.5 mmol) of sodium hexafluorophosphate in 20 cm^3 of ethanol was heated with stirring for 2 h and filtered. The filtrate was concentrated to *ca.* 2.5 cm^3 and stored in a refrigerator for a few days. Yellow precipitate was collected, washed with ethanol, and dried in air. Yield, 150 mg (46%). $[\alpha]=+194°$ (*c* 0.17, CH_3OH).

[Pd(X)(damf)(py)] (X=Cl and Br). A mixture of 230 mg (0.30 mmol) of $[PdCl(damf)]_2$ and 100 mg (1.3 mmol) of pyridine in 30 cm^3 of dichloromethane was stirred at room temperature for 30 min. The resulting solution was filtered and 10 cm^3 of ethanol was added to the filtrate. Upon concentration yellow crystals (X=Cl) were obtained, which were washed with a small amount of ethanol and dried in air. Yield, 190 mg (68%).

The yellowish brown bromo complex was prepared by metathesis of the chloro complex with excess lithium bromide in hot ethanol. Yield, 73%.

Results and Discussion

A pair of diastereomers of [Pd(damf)(*S*-pro)] are efficiently separated by solubility difference (Fig. 1). In the ^{1}H NMR spectra, the less soluble isomer, (+)-[Pd(damf)(*S*-pro)], in a mixture of chloroform–acetone (1:4) shows sharp signals of the N–CH_3 at 2.87 (s) and 3.09 (s) ppm and that of the C_5H_5 group at 4.23 (s), while the other, (−)-[Pd(damf)(*S*-pro)], at 2.87 (s) and 3.14 (s), and at 4.15 (s), respectively (Table 2). The sharp signals are used as an indication of complete separation of the isomers. The electronic spectra of the two are very similar, while the CD spectra are nearly enantiomeric to each other (Fig. 2). This suggests that the two are a pair of diastereomers resulting from the planar chirality. The geometrical isomer (*trans-N,N*) shown in Fig. 1 is assumed,

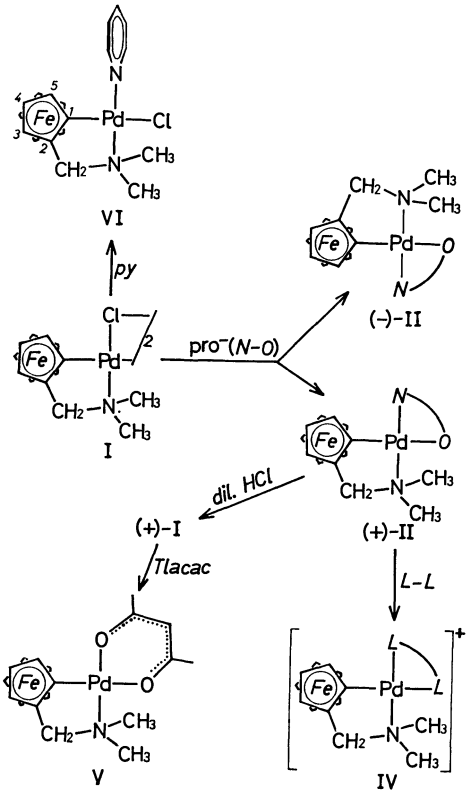

Fig. 1. Cyclo-palladated (dimethylaminomethyl)ferrocene and its derivatives. L–L in IV is en, diphos, diars, or 2py.

since a similar ortho-palladated complex, (*N,N*-dimethylbenzylamine-2*C,N*)(*N*-phenylsalicylideneaminato)-palladium(II)[14] has a *trans-N,N* structure.

A reaction of (+)-[Pd(damf)(*S*-pro)] with dilute hydrochloric acid regenerates the original dimer, (+)-$[PdCl(damf)]_2$. The absorption and CD spectra are

Table 2. Representative signals of ^{1}H NMR spectra of some of the complexes in $CDCl_3$ (δ in ppm from internal TMS)[a]

Complex	$N(CH_3)_2$		Ferrocenyl-H
$[PdCl(damf)]_2$	2.91 s,	3.05 s	4.31 s (C_5H_5)
			4.36[b] (3-H)
			4.00 m (4,5-H)
(+)-[Pd(damf)-(*S*-pro)]	2.87 s,	3.09 s	4.23 s (C_5H_5)
(−)-[Pd(damf)-(*S*-pro)]	2.87 s,	3.14 s	4.15 s (C_5H_5)
(+)-[Pd(damf)-(en)]BF_4	2.68 s,	2.88 s	4.20 s (C_5H_5)
(−)-[Pd(damf)-(diphos)]PF_6	2.46 b,	2.81 b	3.75 s (C_5H_5)
(+)-[Pd(damf)-(diars)]PF_6	2.76 s,	3.09 s	3.79 s (C_5H_5)
(+)-[Pd(damf)-(acac)][c]	2.82 s,	3.03 s	4.18 s (C_5H_5)
			4.25[b] (3-H)
			4.01 m (4,5-H)
[PdCl(damf)(py)]	2.98 s,	3.23 s	4.20 s (C_5H_5)
			4.12 d (3-H)
			3.93 t (4-H)
			3.24 d (5-H)
[PdBr(damf)(py)]	3.01 s,	3.29 s	4.19 s (C_5H_5)
			4.11 d (3-H)
			3.92 t (4-H)
			3.18 d (5-H)

a) s=singlet, d=doublet, t=triplet, m=multiplet, and b=broad. b) Overlapped by the signal of C_5H_5. c) CH_3 of acac resonates at 1.95 s and 1.99 s ppm and methine-H of acac at 5.29 s.

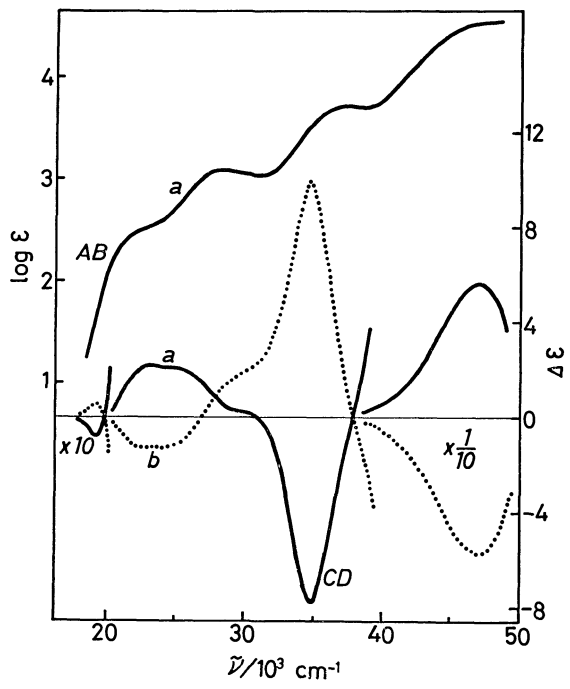

Fig. 2. Absorption (AB) and CD spectra of methanol solutions of a: (+)-[Pd(damf)(*S*-pro)] and b: (−)-[Pd(damf)(*S*-pro)].

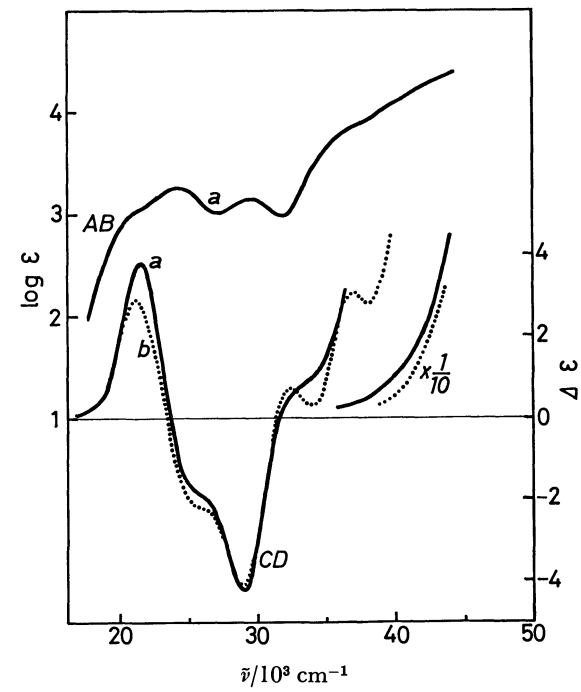

Fig. 3. Absorption (AB) and CD spectra of dichloromethane solutions of a: (+)-[PdCl(damf)]$_2$ and b: (*R*)-[PdCl(*S*-daef)]$_2$.

shown in Fig. 3 together with the CD spectrum of (+)-(*R*)-[PdCl(*S*-daef)]$_2$.[12] The similarlity in CD spectra suggests that (+)-[PdCl(damf)]$_2$ has the same absolute configuration *R* for the ferrocene moiety.

From the separated isomer, (+)-[Pd(damf)(*S*-pro)], the optically active complexes, $[Pd(damf)(L\text{-}L)]^+$ are derived, where L-L are en, diphos, diars, and 2py (Table 1 and Fig. 1). The (+)-[Pd(damf)(acac)] complex was obtained from (+)-[PdCl(damf)]$_2$. Some of the ^{1}H NMR spectral data are given in Table 2.

The CD spectra of (+)-[Pd(damf)(en)]BF_4 and (+)-[Pd(damf)(acac)] are compared with those of (*R*)-[Pd(*S*-daef)(en)]BF_4 and (*R*)-[Pd(*S*-daef)(acac)], respectively (Fig. 4). The absolute configuration of the enantiomer (*S*)-[Pd(*R*-daef)(acac)] has been determined by the X-ray method.[15] The results also show that the absolute configuration of the ferrocene moiety in (+)-[Pd(damf)(en)]BF_4 and (+)-[Pd(damf)(acac)] is *R*. The CD spectra of the other complexes are shown in Fig. 5.

The cyclo-palladated (dimethylaminomethyl)ferrocene complexes change the CD spectra remarkably depending on the kind of ligands (L-L) (Figs. 2—5) and there seems to be no regularity among the spectra. The diphos and diars complexes are a unique pair to give similar spectra. Nevertheless a shoulder absorption observed at *ca.* 22000 cm^{-1} for all the complexes appears to arise mainly from d-d transitions of the iron(II) ion, since the free Hdamf ligand gives a band due to the d-d transitions at 22300 cm^{-1} (ε=107).[16] The CD extremes corresponding to this shoulder (Figs. 2—5) are always positive and the positive extremes seem to be a representative of a (*R*)-ferrocenyl group. A chiral ferrocenylphosphine, (+)-(*R*)-[2-(dimethylaminomethyl)-1-ferrocenyl] diphenylphosphine (VII)

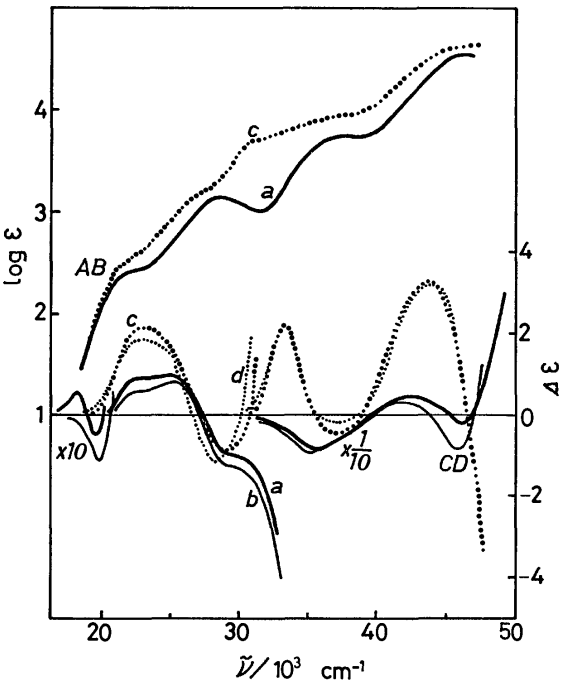

Fig. 4. Absorption (AB) and CD spectra of methanol solution of a: (+)-[Pd(damf)(en)]BF_4, b: (*R*)-[Pd-(*S*-daef)(en)]BF_4, c: (+)-[Pd(damf)(acac)], and d: (*R*)-[Pd(*S*-daef)(acac)].

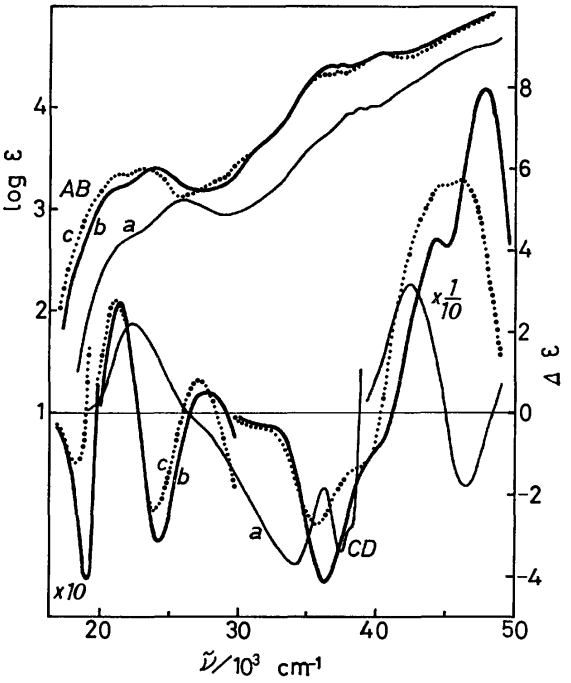

Fig. 5. Absorption (AB) and CD spectra of methanol solutions of a: (+)-[pd(damf)$(py)_2$]PF_6, b: (−)-[Pd(damf)(diphos)]PF_6, and c: (+)-[Pd(damf)-(diars)]PF_6.

has recently been reported to show a positive CD extreme in this region;[10,11] $\Delta\varepsilon = +0.52$ at 21800 cm^{-1}.

The protons of unsubstituted cyclopentadienyl rings of (−)-[Pd(damf)(diphos)]PF_6 and (+)-[Pd(damf)-(diars)]PF_6 resonate at a considerably higher field than those of the other complexes (Table 2). The properly oriented phenyl rings of diphos and diars are expected to bring about the shielding effect by

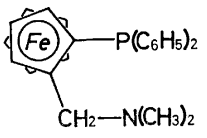

VII

their magnetic anisotropy.[17] In the ^1H NMR spectra of [PdCl(damf)(py)] and [PdBr(damf)(py)] a doublet at a very high field (3.23 (Cl) and 3.18 (Br) ppm) is observed in contrast to those of the other complexes. The doublet can be assigned to 5-H of the substituted cyclopentadienyl ring since this proton should be shielded by the ring current of the coordinated pyridine (Fig. 1, VI), when [PdX(damf)(py)] (X=Cl and Br) has a *trans-N,N, trans-C,X* arrangement like other ortho-palladated complexes, [PdX(C–N)(py)] (C–N= ortho-palladated ligand).[1,18] The structure is supported by appearance of a low frequency ν(Pd–Cl) band at 268 cm^{-1}.[19]

The present work was supported by a Grant-in-Aid for Scientific Research No. 243013 from the Ministry of Education, Science and Culture.

References

1) M. I. Bruce, *Angew. Chem. Int. Ed. Engl.*, **16**, 73 (1977).
2) A. Bahsoun, J. Dehand, M. Pfeffer, M. Zinsius, S.-E. Bouaoud, and G. Le Borgne, *J. Chem. Soc., Dalton Trans.*, **1979**, 547.
3) J. M. Thompson and R. F. Heck, *J. Org. Chem.*, **40**, 2667 (1975).
4) S. Kamiyama, T. Kimura, A. Kasahara, T. Izumi, and M. Maemura, *Bull. Chem. Soc. Jpn.*, **52**, 142 (1979).
5) T. Izumi, K. Endo, O. Saito, I. Shimizu, M. Maemura, and A. Kasahara, *Bull. Chem. Soc. Jpn.*, **51**, 663 (1978).
6) R. A. Holton, *Tetrahedron Lett.*, **1977**, 355.
7) C. H. Chao, D. W. Hast, R. Bau, and R. F. Heck, *J. Organomet. Chem.*, **179**, 301 (1979).
8) D. Marquarding, H. Burghard, I. Ugi, R. Urban, and H. Klusacek, *J. Chem. Research(S)*, **1977**, 82 and references cited therein.
9) W. R. Cullen, F. W. B. Einstein, C.-H. Huang, A. C. Willis, and E.-S. Yeh, *J. Am. Chem. Soc.*, **102**, 988 (1980).
10) K. Yamamoto, J. Wakatsuki, and R. Sugimoto, *Bull. Chem. Soc. Jpn.*, **53**, 1132 (1980).
11) T. Hayashi, T. Mise, M. Fukushima, M. Kagotani, N. Nagashima, Y. Hamada, A. Matsumoto, S. Kawakami, M. Konishi, K. Yamamoto, and M. Kumada, *Bull. Chem. Soc. Jpn.*, **53**, 1138 (1980).
12) V. I. Sokolov, L. L. Troitskaya, and O. A. Reutov, *J. Organomet. Chem.*, **133**, C28 (1977).
13) J. C. Gaunt and B. L. Shaw, *J. Organomet. Chem.*, **102**, 511 (1975).
14) G. D. Fallon and B. M. Gatehouse, *J. Chem. Soc., Dalton Trans.*, **1974**, 1632.
15) L. G. Kuz'mina, Y. T. Struchkov, L. L. Troitskaya, V. I. Sokolov, and O. A. Reutov, *Izv. Akad. Nauk, SSSR, Ser. Khim.*, **1979**, 1528.
16) K. R. Gordon and K. D. Warren, *Inorg. Chem.*, **17**, 987 (1978).
17) K. Tani, L. D. Brown, J. Ahmed, J. A. Ibers, M. Yokota, A. Nakamura, and S. Otsuka, *J. Am. Chem. Soc.*, **99**, 7876 (1977).
18) J. Dehand and M. Pfeffer, *Coordin. Chem. Rev.*, **18**, 327 (1976).
19) T. G. Appleton, H. C. Clark, and L. E. Manzer, *Coordin. Chem. Rev.*, **10**, 335 (1973).

Preparation and Absorption and Circular Dichroism Spectra of Cobalt(III) Complexes with *N,N,N',N'*-Tetrakis(2-aminoethyl)-1,2-ethanediamine, -1,3-propanediamine, -1,4-butanediamine, and -(*R,R*)- and -(*R,S*)- 2,4-pentanediamine

Kazumasa HATA, Myung-Ki DOH,† Kazuo KASHIWABARA, and Junnosuke FUJITA*

Department of Chemistry, Faculty of Science, Nagoya University, Chikusa-ku, Nagoya 464

(Received July 7, 1980)

Cobalt(III) complexes of new sexidentate ligands, *N,N,N',N'*-tetrakis(2-aminoethyl)-1,3-propanediamine (ttn), -1,4-butanediamine (ttmd), and -(*R,R*)- and -(*R,S*)-2,4-pentanediamine (tptn) were prepared and resolved except the *RR*-tptn complex which formed the *Δ*-isomer stereoselectively. The monocyano complexes of *N,N,N',N'*-tetrakis(2-aminoethyl)-1,2-ethanediamine (ten) and ttn, in which the ligands act as a quinquidentate, were also prepared. Absorption and CD spectra of these complexes and the known $[Co(ten)]^{3+}$ complex were compared with one another. The first d-d absorption bands of the sexidentate complexes, $[Co(A)]^{3+}$ are shifted to smaller wave numbers in the order, ttn>ten>ttmd for A, but those of $[Co(CN)(HA)]^{3+}$ are in the reverse order, ten>ttn. The d-d absorption bands of $[Co(RS\text{-tptn})]^{3+}$ which contains one axial methyl group show the remarkable red shift and the hyperchromic effect as compared with those of $[Co(RR\text{-tptn})]^{3+}$ with two equatorial methyl groups.

N,N,N',N'-Tetrakis(2-aminoethyl)-1,2-ethanediamine (ten) can act as a sexidentate ligand to give metal complexes structurally similar to those of ethylenediaminetetraacetate (edta).[1] Emmenegger and Schwarzenbach[2] found that the first absorption band of $[Co(ten)]^{3+}$ shows a remarkable red shift (13 nm) as compared with that of $[Co(NH_3)_6]^{3+}$, and attributed it to the reduction of ligand field strength caused by a strained structure of the complex ion. Muto *et al.*[3] found by the X-ray structure analysis that the coordination octahedron of this complex ion is largely distorted. Similar strain is involved in the structurally related $[Co(edta)]^-$ ion.[4] The strain or distortion in such sexidentate complexes might be diminished or enhanced by changing ring members of the central diamine chelate rings. The strain would also be reduced by opening one chelate ring to form a complex of the type, $[Co(X)(Hten)]^{n+}$ (X=unidentate ligand).

This paper reports the preparation, resolution, and absorption and circular dichroism (CD) spectra of cobalt(III) complexes with sexidentate *N,N,N',N'*-tetrakis(2-aminoethyl)-1,2-ethanediamine (ten), -1,3-propanediamine (ttn), -1,4-butanediamine (ttmd), and -2,4-pentanediamine (tptn) of (*R,R*) and (*R,S*) forms. When the last sexidentate (*RS*)-tptn ligand forms an octahedral complex, one methyl group of the ligand takes necessarily an axial disposition. The complexes of the type, $[Co(CN)(HA)]^{3+}$ (HA=$Hten^+$ and $Httn^+$) in which the hexamine ligands act as a quinquidentate with a free aminoethyl branch are also described in this paper.

Experimental

Preparation of Ligands. All the hexamine ligands were prepared according to a method similar to that for ten reported by Moser and Schwarzenbach.[1]

N-(Phenylsulfonyl)aziridine was prepared from aziridine[5] and benzenesulfonyl chloride by the method of Moser and Schwarzenbach.[1] (*R,R*)- and (*R,S*)-2,4-Pentanediamine (ptn) were obtained by the method of Bosnich and Harrowfield.[6] Other diamines, 1,2-ethanediamine (en), 1,3-propanediamine (tn), and 1,4-butanediamine (tmd) were purchased (Tokyo Kasei) and used without further purification.

Benzene solutions of *N*-(phenylsulfonyl)aziridine (0.33 mol in 100 cm^3) and a diamine (0.058 mol in 10 cm^3) were dried with Na_2SO_4 (4 °C) and molecular sieves 4A 1/16 (room temperature), respectively, for 1 d. To the former solution was carefully added the latter solution dropwise with stirring, the solution being kept at *ca.* 20 °C. The resulting solution was stirred at *ca.* 30 °C for 2 d to give the tetrakis(phenylsulfonyl)derivative. The derivatives from en, tmd, and *RR*-ptn were fine white crystalline products, which were filtered, washed three times with benzene, and dried *in vacuo*, but those from the other diamines were faintly brown colored oily products, and the benzene was removed by evaporating under reduced pressure.

The tetrakis(phenylsulfonyl)derivatives (0.05 mol) were hydrolyzed by heating at 150 °C in a mixture of concd H_2SO_4 (60 g) and water (15 g) for 17 h. Each of the resulting brown solutions was cooled to room temperature, mixed with water (*ca.* 50 cm^3), and adjusted the pH to *ca.* 8 with a concd aqueous KOH solution. After cooling, K_2SO_4

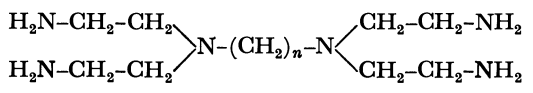

n=2(ten), 3(ttn), and 4(ttmd)

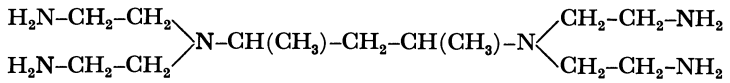

R,R- and *R,S*-tptn

† On leave from the Department of Chemistry, Yeung Nam University, Korea, 1979.

and potassium benzenesulfonate precipitated were filtered off and the precipitate was washed well with ethanol. The filtrate and washings were combined and evaporated under reduced pressure. From the residue the free ligand was extracted with ethanol and the extract was evaporated. This procedure was repeated until the oily ligand was free from potassium benzenesulfonate. All the ligands thus prepared were used for the preparation of complexes without distillation because of their high boiling points. However, all the ligands showed satisfactory ^{1}H NMR spectra in $CDCl_3$ and their metal complexes gave good analytical results.

Preparation of Complexes. *[Co(ten)]$Br_3\cdot 2H_2O$*: Emmenegger and Schwarzenbach[2] first prepared this complex by heating a mixture of ten and $[CoBr(NH_3)_5]Br_2$ over a flame. Yoshikawa *et al.*[7] obtained the complex by stirring an aqueous solution containing the same reactants with active charcoal at room temperature. In the present study, the complex was prepared from *trans*-$[CoCl_2py_4]Cl\cdot 6H_2O$ (py=pyridine)[8] and ten in methanol in the absence of active charcoal.

A methanol solution (50 cm^3) of ten (1 g, 4.3 mmol) was added to a methanol solution (200 cm^3) of *trans*-$[CoCl_2py_4]Cl\cdot 6H_2O$ (3 g, 5.1 mmol). The solution was stirred for several hours at room temperature and then the methanol was evaporated under reduced pressure. The residue was dissolved in 2 dm^3 of water and the pH of the solution was adjusted to *ca.* 3 with hydrochloric acid. This was poured on a column (ϕ5 cm$\times$40 cm) of SP-Sephadex C-25 resin and the product adsorbed was chromatographed with a 0.2 mol/dm^3 Na_2SO_4 solution. To the main red orange eluate was added an aqueous solution of $K_3[Co(CN)_6]$ (*ca.* 2 g). After 1 d, hardly soluble red orange crystals of [Co(ten)]-$[Co(CN)_6]$ formed were filtered, washed with cold water, and then mixed with Dowex 1$\times$8 resin in the bromide form in water in order to convert into bromide. The resin was filtered off and the filtrate was evaporated to *ca.* 3 cm^3 under reduced pressure. The concentrate was mixed with ethanol and stored in a refrigerator for several days to give red orange crystals which were filtered, washed with ethanol and then ether, and air dried.

[Co(ttn)]$Br_3\cdot H_2O$, *[Co(*RR*-tptn)]$Cl_3\cdot 2H_2O$*, *and [Co(*RS*-tptn)]$Cl_3\cdot 2H_2O$*: These complexes were obtained as orange, orange, and red crystals, respectively, by a method similar to that for the ten complex. The *RR*-tptn complex was crystallized by adding acetone instead of ethanol, since the complex is soluble in a mixture of ethanol and water.

[Co(ttmd)]$Br_3\cdot H_2O$: Since the complex contains a seven-membered chelate ring, the reaction was carried out in a dilute solution in order to avoid the formation of polynuclear complexes.[9]

Methanol solutions of *trans*-$[CoCl_2py_4]Cl\cdot 6H_2O$ (1 g in 500 cm^3) and ttmd (0.4 g in 500 cm^3) were simultaneously added to 500 cm^3 of methanol dropwise with stirring over a few hours at room temperature. The resulting solution was stirred for 1 d at room temperature. The methanol was evaporated to dryness under reduced pressure and the residue was dissolved in 2 dm^3 of water. The solution was adjusted to pH *ca.* 3 with hydrochloric acid and poured on a column (ϕ5$\times$40 cm) of SP-Sephadex C-25 resin. By elution with 0.25 mol/dm^3 Na_2SO_4, several bands were eluted from the column, a small amount of high charged species remaining on the top of the column. The red main eluate was rechromatographed by the same method after dilution with water. From the eluate, red crystals of [Co(ttmd)]-$[Co(CN)_6]$ were obtained and converted into bromide by the same method as that for the ten complex.

[Co(CN)(Hten)]$Br_3\cdot 2H_2O$: To a cold (*ca.* 4 °C) aqueous solution (100 cm^3) containing $[Co(ten)]Br_3\cdot 2H_2O$ (0.5 g) and KCN (0.07 g) was added a small amount of active charcoal and the mixture was allowed to stand at *ca.* 4 °C for 5 h with occasional shaking. The active charcoal was filtered off and the filtrate was diluted to 2 dm^3 with water. This was poured on a column (ϕ2.7$\times$60 cm) of SP-Sephadex C-25 resin. The column was thoroughly washed with water and the product adsorbed was eluted with a 0.2 mol/dm^3 Na_2SO_4 solution adjusted the pH to *ca.* 9 with Na_2CO_3. Three bands, yellow, orange, and red orange were eluted in succession, the second orange band being the largest amount. The first yellow and the third red orange bands were presumed from the absorption spectra to involve a dicyano and the starting complexes, respectively. The second orange eluate was diluted ten times with water and the solution was poured again on a small column (ϕ2.7$\times$5 cm) of SP-Sephadex C-25 resin. After the column had been washed with 0.01 mol/dm^3 hydrobromic acid in order to remove Na^+ ions, the complex was eluted with 2 mol/dm^3 hydrobromic acid. The eluate was mixed with acetone and allowed to stand for several days at room temperature to give orange crystals of $[Co(CN)(Hten)]Br_3\cdot 2H_2O$.

[Co(CN)(Httn)]$Br_3\cdot nH_2O$: An aqueous solution (150 cm^3) containing $[Co(ttn)]Br_3\cdot H_2O$ (0.95 g), KCN (0.13 g), and a small amount of active charcoal was stored in a refrigerator (*ca.* 4 °C) for 3 d with occasional shaking. After filtering off the active charcoal, the filtrate was diluted with water to 3 dm^3 and the solution was poured on a column (ϕ2.7$\times$120 cm) of SP-Sephadex C-25 resin. The column was washed with water and the product adsorbed was then eluted with a 0.2 mol/dm^3 Na_2SO_4 solution adjusted the pH to *ca.* 3 with hydrochloric acid. Three orange bands, I, II, and III were eluted in succession. Band I was found to be contaminated with a small amount of the starting complex, so that the eluate was rechromatographed by use of a 0.2 mol/dm^3 Na_2SO_4 solution adjusted the pH to *ca.* 9 with Na_2CO_3 as an eluent, the starting complex being eluted much slower. From bands I and III, orange crystals of $[Co(CN)(Httn)]Br_3\cdot H_2O$ (A) and $[Co(CN)(Httn)]Br_3\cdot 2H_2O$ (B) were obtained, respectively, by the same method as that for the corresponding ten complex. The amount of band II was too small to isolate the complex.

No reaction took place between *[Co(*RR*-tptn)]$Cl_3\cdot 2H_2O$* and KCN even at a higher temperature. Reactions of *[Co(*RS*-tptn)]$Cl_3\cdot 2H_2O$* or $[Co(ttmd)]Br_3\cdot H_2O$ with KCN resulted in decomposition of the complexes to yield cobalt(II) species and other unknown complexes, no mono cyano complexes being found in both reaction products.

Optical Resolution. The $[Co(ttn)]^{3+}$, $[Co(ttmd)]^{3+}$, and *[Co(*RS*-tptn)]$^{3+}$* complexes were resolved by the same SP-Sephadex column chromatographic method as that for $[Co(ten)]^{3+}$ reported by Yoshikawa *et al.*[7]

By elution with 0.2 mol/dm^3 sodium $(+)_{589}$-tartratoantimonate(III), each of $[Co(ten)]^{3+}$, $[Co(ttmd)]^{3+}$, and *[Co(*RS*-tptn)]$^{3+}$* was completely resolved giving two well separated bands of enantiomers. In the case of $[Co(ttn)]^{3+}$, however, the separation of bands was poor, so that the eluate was fractionated into 10 cm^3 and optical purity of each fraction was examined by taking a ratio of CD strength to optical density at 505 nm, the fractions with the ratio of a constant value being collected. The enantiomers eluted faster are $(-)_{589}$-$[Co(ten)]^{3+}$, $(+)_{589}$-$[Co(ttn)]^{3+}$, $(-)_{589}$-$[Co(ttmd)]^{3+}$, and $(-)_{589}$-*[Co(*RS*-tptn)]$^{3+}$*. For each complex, the optically pure fractions were collected, diluted about ten times with water, and poured on a small column of SP-Sephadex C-25 resin. After washing the column with 0.01 mol/dm^3 hydrochloric acid, the complex was eluted with

TABLE 1. ANALYTICAL DATA OF THE NEW COMPLEXES

Complexes	C(%)		H(%)		N(%)	
	Found	Calcd	Found	Calcd	Found	Calcd
$[Co(ttn)]Br_3 \cdot H_2O$	23.44	23.46	5.64	5.73	14.90	14.93
$[Co(ttmd)]Br_3 \cdot H_2O$	24.91	24.98	5.82	5.94	14.36	14.56
$[Co(RR\text{-tptn})]Cl_3 \cdot 2H_2O$	32.64	32.82	7.85	8.05	17.72	17.66
$[Co(RS\text{-tptn})]Cl_3 \cdot 2H_2O$	33.13	32.82	7.88	8.05	17.85	17.66
$[Co(CN)(Hten)]Br_3 \cdot 2H_2O$	22.28	22.24	5.81	5.60	16.28	16.50
$[Co(CN)(Httn)]Br_3 \cdot H_2O$(A)	24.51	24.42	5.63	5.64	16.66	16.62
$[Co(CN)(Httn)]Br_3 \cdot 2H_2O$(B)	24.12	23.70	5.83	5.80	15.63	16.12

ten = $C_{10}H_{28}N_6$, ttn = $C_{11}H_{30}N_6$, ttmd = $C_{12}H_{32}N_6$, tptn = $C_{13}H_{34}N_6$.

2 mol/dm³ hydrochloric acid and the eluate was used for the measurement of CD spectra. The optically active complexes were not isolated because of small amounts. The $\Delta\varepsilon$ values were determined with the aid of ε values of the racemates.

Analytical data of the new complexes are given in Table 1.

Measurements. Absorption and CD spectra were recorded on a Hitachi 323 spectrophotometer and a JASCO J-40 CS spectropolarimeter, respectively. ^1H NMR (D_2O, TMS) and ^{13}C NMR (D_2O, dioxane) were obtained with a JEOL JNM-PMX 60 and a JEOL FX-100 spectrometer, respectively.

Results and Discussion

Absorption Spectra. The ten, ttn, and ttmd Complexes: The $[Co(ten)]^{3+}$, $[Co(ttn)]^{3+}$, and $[Co(ttmd)]^{3+}$ complexes contain a five-, six-, and seven-membered chelate ring, respectively, for the central ditertiary diamine chelate ring. In general, the first absorption band of a tris(diamine)cobalt(III) complex is shifted to smaller wavenumbers as the number of ring members increases. For example, $[Co(en)_3]^{3+}$, $[Co(tn)_3]^{3+}$, and $[Co(tmd)_3]^{3+}$ give the first absorption band at 21400, 20400, and 19900 cm^{-1}, respectively.[10] However, those of the ten-type complexes are shifted to smaller wavenumbers in the order of $[Co(ttn)]^{3+}$, $[Co(ten)]^{3+}$, and $[Co(ttmd)]^{3+}$, the order of the first two complexes being opposite to that expected from the tris(diamine) complexes (Table 2 and Fig. 1). Emmenegger and Schwarzenbach[2] first found the red shift of the first absorption band for $[Co(ten)]^{3+}$ from a comparison with $[Co(NH_3)_6]^{3+}$ (21000 cm^{-1}) and attributed it to a strained structure of the complex ion. The strained structure was confirmed by the X-ray structure analysis on $(+)_{589}$-$[Co(ten)][Co(CN)_6] \cdot 2H_2O$;[3] the six nitrogen donor atoms forms a distorted octahedron, the N–Co–N angles (83.3—102.2°) largely deviating from that of the regular octahedron (90°), and the distortion of the two chelate rings linked meridionally with the central ethylenediamine chelate ring is particularly noticeable. Such a distortion might weaken the ligand field strength to cause the red shift of the first absorption band in $[Co(ten)]^{3+}$. The strain or distortion in $[Co(ttn)]^{3+}$ would be much reduced as compared with that in $[Co(ten)]^{3+}$, since $[Co(ttn)]^{3+}$ containing a six-membered chelate ring gives the first absorption band at a higher wavenumber than that of $[Co(ten)]^{3+}$.

TABLE 2. ABSORPTION AND CD SPECTRAL DATA

Complex	Absorption $\bar{\nu}/10^3$ cm^{-1}(log ε)	CD $\bar{\nu}/10^3$ cm^{-1}($\Delta\varepsilon$)
$(-)_{589}$-$[Co(ten)]^{3+}$	20.5(2.35)	19.6(−3.63)
		22.1(+0.58)
	29.2(2.25)	29.8(−1.04)
	43.7(4.30)	44.0(+11.0)
$(+)_{589}$-$[Co(ttn)]^{3+}$	21·0(1.96)	19.8(+1.62)
		22.1(−0.59)
	29.0(1.95)	27.8(+0.50)
		ca. 35.5(*ca.* +0.3)
	44.0(4.27)	43.3(− 7.0)
$(-)_{589}$-$[Co(ttmd)]^{3+}$	20.0(2.23)	19.2(−1.20)
		21.7(+0.11)
		26.0(−0.25)
	28.3(2.11)	*ca.* 29 (*ca.* −0.1)
		36.6(+1.11)
	46.0(4.16)	40.5(−0.67)
		46.5(−4.52)
$(-)_{589}$-$[Co(RR\text{-tptn})]^{3+}$	20.8(2.07)	19·8(−2.14)
		22.1(+0.56)
	28.7(1.98)	27.5(−0.76)
		37.9(−1.55)
	43.0(4.25)	42.2(+1.55)
		44.8(−0.80)
$(-)_{589}$-$[Co(RS\text{-tptn})]^{3+}$	20.0(2.32)	19.3(−3.38)
		22.0(+0.25)
	28.1(2.20)	26.5(−0.95)
		ca. 29 (*ca.* −0.6)
		37.3(−1.00)
	42.0(4.26)	44.5(−3.10)
$[Co(CN)(Hten))]^{3+}$	22.2(2.13)	
	30.5(2.09)	
	43.9(3.85)	
$[Co(CN)(Httn)]^{3+}$ (A)	21.9(1.98)	
	30.2(1.96)	
	43.7(4.03)	
(B)	21.6(2.10)	
	29.7(2.13)	
	43.5(4.03)	

Dreiding molecular models clearly indicate that $[Co(ttn)]^{3+}$ is much less strained than $[Co(ten)]^{3+}$. In the model of $[Co(ten)]^{3+}$, considerable strains are involved in the three five-membered chelate rings fused in a plane with the cobalt(III) ion as confirmed

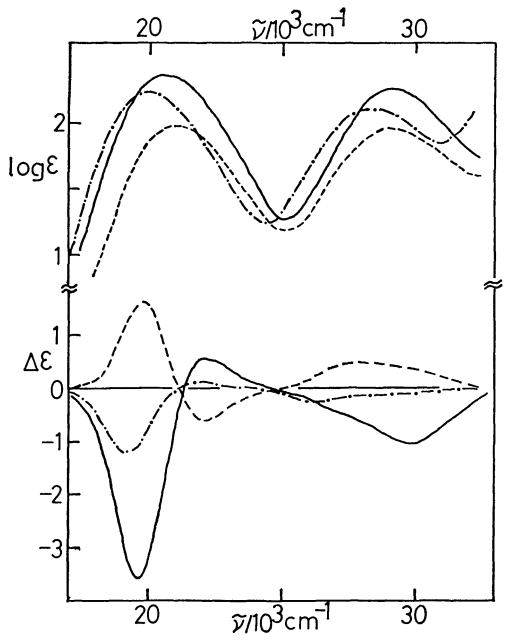

Fig. 1. Absorption and CD spectra of $(-)_{589}$-[Co(ten)]$^{3+}$ (——), $(+)_{589}$-[Co(ttn)]$^{3+}$ (– – –), and $(-)_{589}$-[Co(ttmd)]$^{3+}$ (—·—).

by the X-ray structure analysis. For [Co(ttn)]$^{3+}$, however, neither the corresponding five-six-five-membered chelate rings nor the other chelate rings appear to involve remarkable strain. Thus it is presumed that the reverse order in the first absorption maxima of the two complexes is caused by the strained structure of [Co(ten)]$^{3+}$. On the other hand, [Co(ttmd)]$^{3+}$ shows the first absorption band at the smallest wavenumbers among the three complexes. A molecular model indicates that this complex ion involves no remarkable strain for the skeleton of all the chelate rings, but forms a very crowded structure, some methylene protons coming very close to one another. A crowded complex would expand the molecular volume in order to reduce non-bonded interactions among atoms. The expansion might lengthen the metal-ligand distances to weaken the ligand field strength. In fact, the Co–N distances of [Co(en)$_3$]$^{3+}$,[11] [Co(tn)$_3$]$^{3+}$,[12] and [Co(tmd)$_3$]$^{3+}$ [13] are 1.959—1.979, 1.966—1.999, and 1.986—2.000 Å, respectively, and with an increase in the Co–N distance the absorption maxima are shifted to smaller wavenumbers (*vide infra*).

In contrast with the first absorption band, the second absorption bands are in the usual order of [Co(ten)]$^{3+}$, [Co(ttn)]$^{3+}$, and [Co(ttmd)]$^{3+}$. Accordingly, the energy difference between the first and the second bands becomes larger in [Co(ten)]$^{3+}$ (8700 cm^{-1}) than in [Co(ttn)]$^{3+}$ (8000 cm^{-1}). For a low-spin, octahedral cobalt(III) complex, the energy difference between the first ($^1T_{1g} \leftarrow {}^1A_{1g}$, 10Dq−C) and the second ($^1T_{2g} \leftarrow {}^1A_{1g}$, 10Dq+16B−C) absorption bands is expressed by 16B, where Dq is the parameter of ligand field strength and B and C those of Racah of interelectronic repulsion.[14] The B value is known to be a measure for representing covalent character of the bond between a ligand and a metal ion, the smaller the value the more the covalent character.[15] The B values for the ten and ttn complexes are 544 and 500 cm^{-1}, respectively. Since the values for a series of complexes, [Co(en)$_x$(tn)$_y$(tmd)$_z$]$^{3+}$ [10] are almost constant, 500—506 cm^{-1}, the value of 544 cm^{-1} for [Co(ten)]$^{3+}$ appears to be fairly large and to have relations with the strained structure. Donor atoms in a strained complex would deviate from the regular octahedral coordination sites. The deviation might cause misalignment of the lone-pair orbital of the donor atom to orbitals of the metal ion to decrease the overlap of orbitals between them. The decrease in overlap, or the decrease in covalent character would correspond to an increase in the B value. The [Co(ttmd)]$^{3+}$ complex shows the B value of 519 cm^{-1}. This value indicates that the complex is not so strained as [Co(ten)]$^{3+}$ as the molecular model suggested.

The strain in [Co(ten)]$^{3+}$ would be reduced by forming a quinquidentate complex, [Co(X)(Hten)]$^{n+}$ (X=unidentate ligand), liberating one chelate ring. Emmenegger and Schwarzenbach[2] prepared such complexes with various unidentate ligands. In this study, [Co(CN)(Hten)]$^{3+}$ was newly prepared, since the ttn ligand gave a quinquidentate complex only with a cyanide ion. Although quinquidentate complexes of ten and ttn have two and three possible geometrical isomers, respectively, the cyanide complexes obtained are one and two isomers for ten and ttn, respectively. The structures of the isomers could not be assigned. The structurally related [Co(X)(Hedta)]$^{n-}$ complexes always give only one isomer in which the X ligand occupies the coordination site meridional to the nitrogen atoms of ethylenediamine.[16,17] No corresponding 1,3-propanediaminetetraacetato complex is known, but similar triacetato complexes with H_2O or Cl^- give all of the possible three isomers.[18] In the present quinquidentate complexes, the first absorption band of [Co(CN)(Hten)]$^{3+}$ is observed at a higher wavenumber than those of either isomer of [Co(CN)(Httn)]$^{3+}$ (Table 2 and Fig. 2). The result supports that [Co(ten)]$^{3+}$ is strained and the strain is reduced to a great extent by releasing one chelate ring from the coordination sphere. The ttmd complex gave no monocyano complex.

Reactivity of the sexidentate complexes toward strong bases such as OH^- or CN^- seems to be related with the stability of these complexes expected from the maximum wavenumbers of the first absorption bands. The [Co(ten)]$^{3+}$ complex readily reacts with OH^- [2] or CN^- to yield quinquidentate complexes, opening

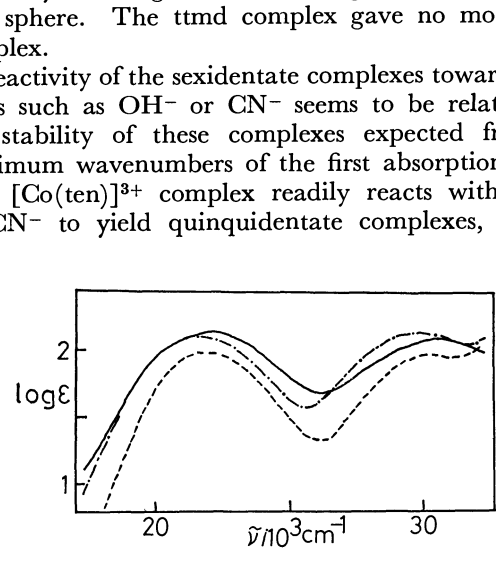

Fig. 2. Absorption spectra of [Co(CN)(Hten)]$^{3+}$ (——), and the two isomers of [Co(CN)(Httn)]$^{3+}$, (A) (– – –) and (B) (—·—).

one chelate ring. The $[Co(ttn)]^{3+}$ complex also gives the mono cyano complex, but the reaction is rather slow as compared with the case of $[Co(ten)]^{3+}$ (Experimental). The ttn complex does not react with OH^-. The $[Co(ttmd)]^{3+}$ complex affords no quinquidentate complex by the reaction with CN^- or OH^-, but gives cobalt(II) species and a small amount of unknown cobalt(III) complexes.

The RR- *and* RS-*tptn Complexes*: The two methyl groups in each *RR*(or *SS*)- and *RS*-ptn chelate ring become equatorial in a λ(or δ)-skew and a chair conformation, respectively.[19] The skeletons of *RR*- and *RS*-tptn ligands in sexidentate complexes should be similar to that of ttn in $[Co(ttn)]^{3+}$, the conformation of the six-membered 1,3-diamine part being in a skew form. When this part forms a chair conformation, both *RR*- and *RS*-tptn ligands can not act as a sexidentate in an octahedral complex. Accordingly, one methyl group in the sexidentate $[Co(RS\text{-tptn})]^{3+}$ complex adopts necessarily an axial disposition. The axial methyl group comes very close to one of the two five-membered chelate rings apical to the six-membered ring and hence $[Co(RS\text{-tptn})]^{3+}$ would be less stable than $[Co(RR\text{-tptn})]^{3+}$. The structurally related ligands, (*R*,*R*(or *S*,*S*))- and (*R*,*S*)-2,4-pentanediaminetetraacetate (ptnta) form stereoselectively Δ(or Λ)-[Co(*RR*(or *SS*)-ptnta)]$^-$ and [Co(Cl)(*RS*-Hptnta)]$^-$, respectively.[20] The *RS*-ptnta in the latter complex functions as a quinquidentate, leaving a free acetate branch, and the six-membered chelate ring forms a chair conformation with two methyl groups disposed equatorially. This indicates that ptnta is not a so strong ligand as it forms a sexidentate complex by overcoming the unstabilization caused by the axial methyl group.

The orange $[Co(RR\text{-tptn})]^{3+}$ and red $[Co(RS\text{-tptn})]^{3+}$ complexes show the first absorption band at 20800 and 20000 cm^{-1}, respectively (Table 2 and Fig. 3). While the maximum wavenumber of the former is nearly the same as that of $[Co(ttn)]^{3+}$, the wavenumber of the latter is as small as that of the crowded $[Co(ttmd)]^{3+}$ complex. Both tptn complexes lose the water of crystallization by heating *in vacuo* without the change of color. Absorption spectra of the complexes do not depend on pH of the solutions. ^{13}C NMR spectra (100 MHz) of the *RR*- and *RS*-tptn complexes in D_2O solutions exhibit seven and twelve (one strong peak due to accidental degeneracy) signals in accordance with the symmetry argument. All the facts lead to the conclusion that both *RR*- and *RS*-tptn ligands act as a sexidentate in the complexes. Thus the red shift of the first absorption band in $[Co(RS\text{-tptn})]^{3+}$ can be attributed to the crowded structure due to the presence of the axial methyl group. On the other hand, the B value (506 cm^{-1}) of this complex is nearly the same as those of $[Co(RR\text{-tptn})]^{3+}$ (493 cm^{-1}) and $[Co(ttn)]^{3+}$ (500 cm^{-1}). This suggests that the red $[Co(RS\text{-tptn})]^{3+}$ complex is not distorted like $[Co(ten)]^{3+}$ and the red shift of the first absorption band is caused by the crowded structure as described for $[Co(ttmd)]^{3+}$. A complex which contains an axial methyl group is known for Λ-β-[Co(ox)(*R*,*R*-2,3″,2-tet)]$^+$ (ox=oxalate ion, *R*,*R*-2,3″,2-tet=(4*R*,6*R*)-4,6-dimethyl-3,7-diazanonane-1,9-diamine), in which the central six-membered chelate ring adopts a chair conformation with one methyl group axial and the other equatorial.[21] This complex, however, shows the first absorption band (19800 cm^{-1}) at a little smaller wavenumber than that of the corresponding *R*,*S*-2,3″,2-tet complex (19920 cm^{-1}), in which the six-membered chelate ring is also in a chair form, but both methyl groups are disposed equatorially.[22] For the *RR*- and *RS*-tptn complexes which contain a skew six-membered chelate ring, the wavenumber difference in the first absorption bands amounts to 800 cm^{-1}.

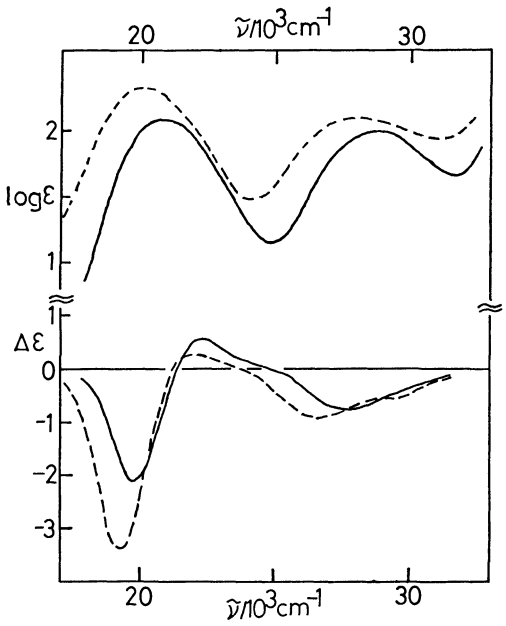

Fig. 3. Absorption and CD spectra of $(-)_{589}$-[Co(*RR*-tptn)]$^{3+}$ (——) and $(-)_{589}$-[Co(*RS*-tptn)]$^{3+}$ (– – –).

Circular Dichroism Spectra. The CD spectra of $(-)_{589}$-$[Co(ten)]^{3+}$, $(+)_{589}$-$[Co(ttn)]^{3+}$, and $(-)_{589}$-$[Co(ttmd)]^{3+}$, all of which were enantiomers eluted faster by SP-Sephadex column chromatography, are compared in Fig. 1. The absolute configuration of $(+)_{589}$-$[Co(ten)]^{3+}$ has been determined by the X-ray method to be Λ.[3] On the basis of the CD pattern in the region of the first absorption band of $(-)_{589}$-Λ-$[Co(ten)]^{3+}$, $(+)_{589}$-$[Co(ttn)]^{3+}$ and $(-)_{589}$-$[Co(ttmd)]^{3+}$ can be assigned to the Λ and Δ configurations, respectively. The strengths of main CD bands in this region decrease with an increase in ring members of the central chelate ring. In the Λ-$[Co(en)_x(tn)_y(tmd)_z]^{3+}$ complexes, the positive CD bands reduce the strength remarkably with an increase in the ring members, the main CD band of Λ-$[Co(tmd)_3]^{3+}$ showing strong negative.[10] The spectral changes in CD among the ten-type complexes appear to be the same case. The CD spectra in the other region are rather complicated and no discussion can be made.

The CD spectra of $(-)_{589}$-$[Co(RR\text{-tptn})]^{3+}$ and $(-)_{589}$-$[Co(RS\text{-tptn})]^{3+}$ are shown in Fig. 3. The $[Co(RR\text{-tptn})]^{3+}$ complex should have the Λ configuration stereoselectively owing to the equatorial preference of the methyl groups.[20] The CD spectrum of

this complex is almost the mirror image of that of $(+)_{589}$-[Co(ttn)]$^{3+}$ in Fig. 1. The result supports the previous assignment for Λ-$(+)_{589}$-[Co(ttn)]$^{3+}$. The $(-)_{589}$-[Co(*RS*-tptn)]$^{3+}$ complex which was eluted faster in column chromatography shows a CD spectral pattern similar to that of $(-)_{589}$-Δ-[Co(*RR*-tptn)]$^{3+}$, indicating the same Δ configuration. The similarlity also supports that the *RS*-tptn ligand acts as a sexidentate in the complex. In the first absorption band, both CD strength and absorption intensity of the *RS*-tptn complex are stronger than those of the *RR*-tptn complex and the values of the dissymmetry factor g ($\Delta\varepsilon/\varepsilon$) are nearly the same (*ca.* 0.017). A similar, but smaller difference is seen in the CD and absorption spectra between Λ-β-[Co(ox)(*R*,*R*-2,3″,2-tet)]$^{+}$ and -[Co(ox)(*R*,*S*-2,3″,2-tet)]$^{+}$.[22] The presence of an axial methyl group in a complex seems to cause the red shift and the hyperchromic effect on the absorption and CD spectra.

The authors wish to thank Dr. T. Ito of Institute for Molecular Science for obtaining ^{13}C NMR spectra. This work was partially supported by Grant-in-Aid for Scientific Research No. 243013 from the Ministry of Education, Science and Culture.

References

1) P. Moser and G. Schwarzenbach, *Helv. Chim. Acta*, **35**, 2359 (1952); **36**, 581 (1953).
2) E. P. Emmenegger and G. Schwarzenbach, *Helv. Chim. Acta*, **49**, 625 (1966).
3) A. Muto, F. Marumo, and Y. Saito, *Acta Crystallogr., Sect. B*, **26**, 226 (1970).
4) H. A. Wiekliem and J. L. Hoard, *J. Am. Chem. Soc.*, **81**, 549 (1959).
5) V. P. Wystrach, D. W. Kaiser, and F. G. Schaefer, *J. Am. Chem. Soc.*, **77**, 5915 (1955).
6) B. Bosnich and J. MacB. Harrowfield, *J. Am. Chem. Soc.*, **94**, 3426 (1972).
7) Y. Yoshikawa, E. Fujii, and K. Yamasaki, *Bull. Chem. Soc. Jpn.*, **45**, 3451 (1972).
8) A. Werner and R. Feenstra, *Ber.*, **39**, 1538 (1906).
9) H. Ogino and J. Fujita, *Bull. Chem. Soc. Jpn.*, **48**, 1836 (1975).
10) M. Kojima, H. Yamada, H. Ogino, and J. Fujita, *Bull. Chem. Soc. Jpn.*, **50**, 2325 (1977).
11) M. Iwata, K. Nakatsu, and Y. Saito, *Acta Crystallogr., Sect. B*, **25**, 2562 (1969).
12) R. Nagao, F. Marumo, and Y. Saito, *Acta Crystallogr., Sect. B*, **29**, 2438 (1973).
13) S. Sato and Y. Saito, *Acta Crystallogr., Sect. B*, **31**, 1378 (1975).
14) Y. Tanabe and S. Sugano, *J. Phys. Soc. Jpn.*, **9**, 753, 766 (1954).
15) C. E. Schaffer and C. K. Jørgensen, *J. Inorg. Nucl. Chem.*, **8**, 143 (1958).
16) G. L. Blackmer and J. L. Sudmeier, *Inorg. Chem.*, **10**, 2019 (1971).
17) K. Ohba and J. Fujita, *Chem. Lett.*, **1978**, 595.
18) M. K. Doh, H. Ogino, J. Fujita, and K. Saito, *Bull. Chem. Soc. Jpn.*, **49**, 469 (1976).
19) F. Mizukami, H. Ito, J. Fujita, and K. Saito, *Bull. Chem. Soc. Jpn.*, **45**, 2129 (1972).
20) F. Mizukami, H. Ito, J. Fujita, and K. Saito, *Bull. Chem. Soc. Jpn.*, **44**, 3051 (1971).
21) S. Yano, A. Fujioka, M. Yamaguchi, and S. Yoshikawa, *Inorg. Chem.*, **17**, 14 (1978).
22) F. Mizukami, *Bull. Chem. Soc. Jpn.*, **48**, 472 (1975).

On Some Mixed Chelates of Nickel(II) Which Are Highly Volatile, Fusible, and Soluble in Nonpolar Solvents

Yoko Saito, Toshio Takeuchi,** Yutaka Fukuda, and Kozo Sone*

Department of Chemistry, Faculty of Science, Ochanomizu University, Otsuka, Bunkyo-ku, Tokyo 112

***Department of Chemistry, Faculty of Science and Technology, Sophia University, Kioi-cho, Chiyoda-ku, Tokyo 102*

(Received July 30, 1980)

It was found that the mixed chelates of nickel(II) with the general formula [Ni(diam)(β-dik)$_2$], where diam means an *N,N*- or *N,N'*-alkylated ethylenediamine and β-dik a β-diketonate anion, are highly volatile, fusible, and often amazingly soluble in nonpolar solvents like CCl_4, benzene, or heptane. Representative data on these properties are presented and their correlations with the structures of the ligands are discussed.

It is very well known that metallic acetylacetonates, and other β-diketonates like hexafluoroacetylacetonates and dipivaloylmethanates, are remarkably volatile, and soluble in a number of organic solvents. These properties have often been applied to the separation of metals by means of gas chromatography and extraction techniques.[1-4]

Recently, Hoshino *et al.* found that a mixed chelate of nickel(II) containing acetylacetonate anion, [Ni tmen (acac)$_2$],*** is highly volatile and can be sublimed at *ca.* 60 °C in a vacuum, when it is formed by the thermal disproportionation of the chelates Ni tmen acac X·nH$_2$O (X=halide ions).[5,6] This interesting observation lead us to a comparative study of the volatilities, melting points, and solubilities of this and related chelates to be reported here.

Experimental

All the chelates studied were prepared according to the literatures,[7-9] sometimes with certain modifications, and their identities were checked by elemental analyses. TG-DTA measurements on them were performed with a Rigaku Denki M8075 instrument in static air (heating rate 5 °C/min, sample weight *ca.* 9 mg, standard:Al_2O_3). Spectral measurements of their solutions in CCl_4, benzene, or heptane (all "Extra Pure") were made with a Hitachi 340 Recording Spectrophotometer from 7 to 25 kK (1 kK=1000 cm^{-1}), using 1 cm quartz cells at room temperature (*ca.* 20 °C).

Table 1. Abbreviations of the ligands

A: Diamines, $R_1R_2N(CH_2)_2NR_3R_4$

R_1	R_2	R_3	R_4	Abbreviation
CH_3	CH_3	CH_3	CH_3	tmen
C_2H_5	C_2H_5	C_2H_5	C_2H_5	teen
CH_3	CH_3	CH_3	H	Me_3en
C_2H_5	C_2H_5	C_2H_5	H	Et_3en
CH_3	H	CH_3	H	*sym*-dmen
C_2H_5	H	C_2H_5	H	*sym*-deen
CH_3	CH_3	H	H	*unsym*-dmen
C_2H_5	C_2H_5	H	H	*unsym*-deen

B: β-Diketonate Anions, $R_1COCHCOR_2^-$

R_1	R_2	Abbreviation
CH_3	CH_3	acac
CH_3	CF_3	tfa
CF_3	CF_3	hfa
$C(CH_3)_3$	$C(CH_3)_3$	dpm

***As to the abbreviations of ligands, *cf.* Table 1.

Results

The chelates prepared are shown in Table 2. As reported formerly,[7-9] the mixed chelates I—XI are all blue to green crystals, and are typical 6-coordinate high-spin nickel(II) complexes.

Melting Points and Volatilities. The TG-DTA data of the mixed chelates studied are classified into three patterns A,B, and C (*cf.* Fig. 1). In the case of A, a sharp endothermic peak is observed on the DTA curve. The fact that this peak corresponds to the melting point of the chelate can be confirmed by visual observation. The chelate then begins to evaporate at a somewhat higher temperature(t_i), where a remarkable drop of the TG curve and a broad endothermic peak on the DTA begins to appear. In some cases t_i is lower than mp, that is, the evaporation begins to occur already in advance of melting.

Nearly quantitative evaporation takes place with some chelates; in such case, the ratio of the final weight (w_f) to the initial weight (w_i) of the chelate, w_f/w_i, is nearly zero. In many cases, however, decomposition of the chelates seems to occur at a later stage of evaporation and the sample remaining in the crucible is converted into a black nonvolatile residue, making the ratio w_f/w_i much higher.

The pattern B is observed when the chelate has water of crystallization. Here two peaks appear on the DTA curve, one corresponding to the dehydration temperature (t_d), and the other to the mp. The TG curve also decreases in two steps, the first of which indicates the quantitative loss of water in the formula.

The pattern C also show two DTA peaks, but here the chelate is anhydrous, and the first peak probably indicates some kind of solid phase transition, which takes place in advance of melting. This temperature is designated as t_t.

All these data are summarized in Table 2, together with those of the simple acetylacetonates of nickel (II) and copper(II).

The volatilities of these chelates can now be studied by taking the temperature at which 25% of the weight of a chelate is lost by evaporation ($t_{1/4}$; *cf.* Table 2),

Table 2. TG-DTA data of the mixed chelates, $Ni(acac)_2$ and $Cu(acac)_2$
As to the meaning of t_i, t_f *etc.*, *cf.* text and Fig. 1.

	Chelate	Pattern	Mp	t_i	t_f	t_d	t_t	w_f/w_i	$t_{1/4}$
I	Ni(teen)(acac)$_2$	A	90	95	322			0.43	180
II	Ni(Et$_3$en)(acac)$_2$·H$_2$O	B	59	112	236	45		0.38	187
III	Ni(*sym*-deen)(acac)$_2$·H$_2$O	B	78	108	216	74		0.21	184
IV	Ni(*unsym*-deen)(acac)$_2$·H$_2$O	B [a]	151	137	216	72, 119		0.65	202
V	Ni(tmen)(acac)$_2$	A	97	114	208			0.067	170
VI	Ni(Me$_3$en)(acac)$_2$·H$_2$O	B	100	104	230	48, 59[c]		0.17	173
VII	Ni(*sym*-dmen)(acac)$_2$·H$_2$O	B	134	118	255	82, 104[c]		0.24	186
VIII	Ni(*unsym*-dmen)(acac)$_2$	A	187	135	230			0.37	204
IX	Ni(tmen)(hfa)$_2$	C	130	80	185		102	0.018	153
X	Ni(tmen)(tfa)$_2$	A	81	114	199			0.013	163
XI	Ni(tmen)(dpm)$_2$	A	162	148	264			0.017	221
	Ni(acac)$_2$	[b]		224	338			0.72	315
	Cu(acac)$_2$	[b]		178	260			0.043	228

a) The DTA curve of this chelate was anomalous, and showed one more strong peak of unknown nature at 157 °C, *i.e.*, just above the mp. This may be related to the high value of w_f/w_i, *i.e.*, the remarkable tendency for thermal decomposition of this chelate. b) Simple sublimation without melting; with Ni(acac)$_2$, much decomposition took place along with it. c) These double peaks may be an indication for stepwise dehydration, *e.g.* by way of hemihydrate formation.

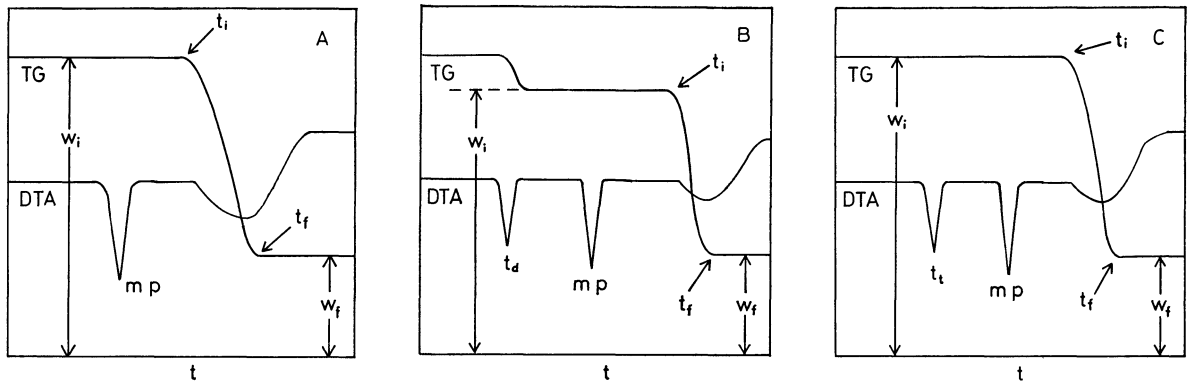

Fig. 1. Typical patterns of the TG-DTA curves (schematic).

and comparing it with those of other chelates.**** The following general trends can be deduced in this way.

1) All the mixed chelates are readily fusible, with melting points which are sometimes much lower than 100 °C. They are also highly volatile, even in static air of 1 atm pressure. In contrast to these observations, the simple acetylacetonates Ni(acac)$_2$ and Cu(acac)$_2$ do not melt by heating, and they are much less volatile (in the case of Ni(acac)$_2$, much part of it is thermally decomposed before sublimation) under the same conditions.

2) Among the mixed chelates with acac and methylated diamines, the volatility increases in the following order of diamines:

$$\text{tmen} \gtrsim \text{Me}_3\text{en} > \textit{sym}\text{-dmen} > \textit{unsym}\text{-dmen}. \quad (1)$$

3) Among the mixed chelates with acac and ethylated diamines, the volatility increases in the following order of diamines:

$$\text{teen} > \text{Et}_3\text{en} \lesssim \textit{sym}\text{-deen} > \textit{unsym}\text{-deen}. \quad (2)$$

4) The volatilities of the *unsym*-dmen and *unsym*-deen chelates are comparable, but among other mixed chelates with acac, those of methylated diamines are slightly more volatile than those of ethylated diamines.

5) Among the mixed chelates containing tmen and various β-diketonate anions, the volatility increases in the following order of β-diketonates:

$$\text{hfa} > \text{tfa} > \text{acac} \gg \text{dpm}.$$

The plot of $t_{1/4}$ in Fig. 2 illustrates these trends.

Solubilities in Nonpolar Solvents. The high volatilities and fusibilities of chelates clearly show that the intermolecular forces acting in their crystals are quite weak. Thus we can expect that they will be soluble in nonpolar solvents. The measurements of their solubilities in C_6H_6, CCl_4, and heptane, which were carried out spectrophotometrically, confirmed this expectation.

From the data in Table 3, we can deduce the following trends:

****Nearly the same trends are observed when we take the temperature at which 5 or 10% of the weight is lost; at these earlier stages of evaporation, the effect of thermal decomposition thus seems to be negligible. The identity of the sublimed chelates with the original ones was also confirmed by their visible and IR spectra.

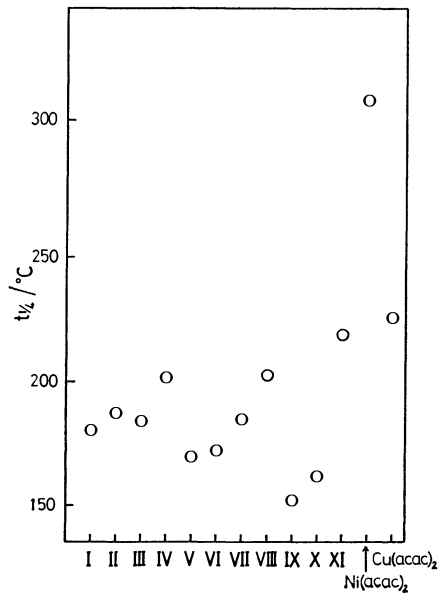

Fig. 2. $t_{1/4}$ values of the chelates. I—XI are those for the mixed chelates (*cf.* Table 2).

Table 3. Solubilities (10^{-2} mol/dm^3, 20 °C) of the mixed chelates, Ni(acac)$_2$ and Cu(acac)$_2$

Chelate	C_6H_6	CCl_4	Heptane
Ni(teen)(acac)$_2$	100	140	55
Ni(Et$_3$en)(acac)$_2$·H_2O	46	65	16
Ni(*sym*-deen)(acac)$_2$·H_2O	13	7.6	0.30
Ni(*unsym*-deen)(acac)$_2$·H_2O	16	7.3	0.30
Ni(tmen)(acac)$_2$	140	100	60
Ni(Me$_3$en)(acac)$_2$·H_2O	130	77	13
Ni(*sym*-dmen)(acac)$_2$·H_2O	33	22	0.60
Ni(*unsym*-dmen)(acac)$_2$	14	14	0.23
Ni(tmen)(hfa)$_2$	39	5.0	1.4
Ni(tmen)(tfa)$_2$	130	64	13
Ni(tmen)(dpm)$_2$	43	28	29
Ni(acac)$_2$	0.97	a)	a)
Cu(acac)$_2$[b]	0.32	—	0.025

a) Too insoluble to measure. b) Taken from Ref. 10.

1) The mixed chelates studied are all highly soluble in typically nonpolar solvents. For example, the solubility of [Ni(*unsym*-dmen)(acac)$_2$] in heptane is 48 g/dm^3, and that of [Ni(tmen)(acac)$_2$] in the same solvent is 220 g/dm^3 (in CCl_4 it is still higher, being 370 g/dm^3!). These figures are very much higher than those of Ni(acac)$_2$ and Cu(acac)$_2$.

2) Among the mixed chelates with acac, there are certain relations between the volatilities and solubilities. For example, in CCl_4 and heptane, the solubility increases with the number of alkyl groups in both the methylated and ethylated diamine series. However, the relation among the chelates with different β-diketonate anions is not clear as yet.

Discussion

All the data obtained show that the intermolecular forces acting among the mixed chelate molecules in crystal are very much weaker than those acting in the crystals of simple acetylacetonates of Ni(II) and Cu(II). This is evidently the consequence of structural differences; it is known that the crystals of Ni(acac)$_2$ is composed of complicated trimeric molecules, and those of Cu(acac)$_2$ contain planar monomeric molecules, in which Cu^{2+} and polar ligand groups are exposed to outer influence.[11,12] Thus we can imagine that a lot of energy is needed to sublime them, or to dissolve them in solvents with nearly no solvating power, because the intermolecular forces in them will be relatively high, and, in the case of Ni(acac)$_2$, energy will also be needed to dissociate the trimer into monomeric gaseous molecules.†

On the other hand, all the mixed chelates studied here are monomeric octahedral, and their polar groups are buried deep under a large number of protruding alkyl (or fluoroalkyl) groups, so that the intermolecular forces acting in them will be essentially weaker than those in Ni(acac)$_2$ or Cu(acac)$_2$. It will be especially weak when the number of alkyl groups on the diamine is large†† (*cf.* the order (1) and (2) mentioned above); however, when their size is too large, the increase of van der Waals force will make the chelate slightly less volatile (*cf.* the $t_{1/4}$ values of the methylated and ethylated complexes). The same effect may be responsible for the lower volatility of the dpm chelate. The higher volatilities of the tfa and hfa chelates are probably due to the partial negative charge on their fluorine atoms, which act to decrease the intermolecular attraction; similar increase in volatility in going from acac to tfa and hfa is already well known among their simple chelates.[1,2]

Our results thus clearly show that the volatility, fusibility, and solubility in nonpolar solvents of a chelate can be drastically augmented by mixed chelate formation with ligands containing bulky groups.

The present work was partially supported by a Grant-in-Aid for Scientific Research No. 347033 from the Ministry of Education, Science and Culture.

References

1) R. W. Moshier and R. E. Sievers, "Gas Chromatography of Metal Chelates," Pergamon Press, Oxford (1965).
2) K. C. Joshi and V. N. Pathak, *Coord. Chem. Rev.*, **22**, 37, (1977).
3) R. E. Sievers and J. E. Sadlowski, *Science*, **201**, 217 (1978).
4) Y. Marcus and A. S. Kertes, "Ion Exchange and Solvent Extraction of Metal Complexes," Wiley-Interscience, London (1969).
5) N. Hoshino, Y. Fukuda, and K. Sone, *Chem. Lett.*, **1979**, 437.

† The occurence of such a dissociation in diphenylmethane solution at 200 °C[13] suggests the monomeric nature of this chelate in gaseous phase.

†† It is possible that, in the mixed chelates containing N–H bonds (*i.e.* those of Me$_3$en, Et$_3$en, *sym*- and *unsym*-dmen and deen), hydrogen bond formation between them and the C–O bonds of neighboring molecules contributes to the intermolecular attraction.

6) N. Hoshino, Y. Fukuda, and K. Sone, *Bull. Chem. Soc. Jpn.* (in press).
7) Y. Fukuda and K. Sone, *J. Inorg. Nucl. Chem.*, **34**, 2315 (1972).
8) Y. Fukuda and K. Sone, *J. Inorg. Nucl. Chem.*, **37**, 455 (1975).
9) Y. Fukuda, R. Morishita, and K. Sone, *Bull. Chem. Soc. Jpn.*, **49**, 1017 (1976).
10) "Inorganic Synthesis," ed by T. Moeller, McGraw-Hill, New York (1957), Vol. V, p. 111.
11) G. J. Bullen, R. Mason, and P. Pauling, *Inorg. Chem.*, **4**, 456 (1965).
12) H. Koyama, Y. Saito, and H. Kuroya, *J. Inst. Polytech. Osaka City Univ.*, **C4**, 43 (1953).
13) J. P. Fackler and F. A. Cotton, *J. Am. Chem. Soc.*, **83**, 3775 (1961).

Kinetic and Equilibrium Studies on the Esterification of Monomeric and μ-Oxo Dimeric Vanadium(V) Complexes with Butyl Alcohols in Chlorobenzene

Akio YUCHI, Yumi YAGISHITA, Shinkichi YAMADA, and Motoharu TANAKA*

Laboratory of Analytical Chemistry, Faculty of Science, Nagoya University, Chikusa-ku, Nagoya 464

(Received August 27, 1980)

Kinetic and equilibrium studies were made on the esterification of the μ-oxo dimeric vanadium(V) complexes with monoanionic bidentate ligands(HL) such as 8-quinolinol, 5-chloro-8-quinolinol, 5,7-dibromo-8-quinolinol, and 4-isopropyltropolone by butyl alcohols (ROH) in chlorobenzene. The stoichiometry and the rate equation are expressed as follows:

$$V_2O_3L_4 + 2ROH \rightleftharpoons 2VO(OR)L_2 + H_2O : K_{DE};$$

$$-\frac{d[V_2O_3L_4]}{dt} = \frac{1}{2} \times \frac{d[VO(OR)L_2]}{dt} = (k_1 + k_2[H_2O])[V_2O_3L_4][ROH].$$

The more basic the bound ligand L^-, the lower the water-independent rate constant k_1 is. For less sterically crowded alcohols, k_1 is higher, giving the reactivity order: $n->i->s->t-$. Water, presumably hydrogen bonded to the terminal oxo group of the complexes, *accelerates* the esterification(k_2 path). The equilibrium constant K_{DE} is linearly correlated with the rate constant k_1. The esterification kinetics of the monomeric complex with 2-methyl-8-quinolinol(HL'), which corresponds to the proposed reactive intermediate in the esterification of the μ-oxo dimeric complexes, is also investigated and found the rate equation to be expressed as

$$-\frac{d[VO(OH)L'_2]}{dt} = \frac{d[VO(OR)L'_2]}{dt} = k_{M,1}[VO(OH)L'_2][ROH].$$

$k_{M,1}$ is 5 times higher than the estimated for the corresponding dimeric complex. Large negative values of ΔS_1^* and $\Delta S_{M,1}^*$ point to an associative nucleophilic attack of alcohol to the vanadium center of both dimeric and monomeric complexes. The difference of the reactivity of complexes and alcohols and the detailed mechanism will be discussed.

With 8-quinolinol(HQ) vanadium(V) forms a *black* water-insoluble complex in weakly acidic media.[1-3] The black solution of this complex dissolved in organic solvents gives rise to a *red* coloration in the presence of alcohols(ROH). This reaction, first ascribed to *cis-trans* isomerization of the complex,[4] was found to be the esterification of the complex with alcohols to give their esters, $VO(OR)Q_2$,[5,6] and has been utilized for the detection and photometric determination of alcohols.[7-14] On the other hand extensive studies on the black complex have given an erroneous composition of $VO(OH)Q_2$.[15-18] Alcohols have been believed to react with this monomeric complex according to the following reaction: $VO(OH)Q_2 + ROH \rightleftharpoons VO(OR)Q_2 + H_2O$.[6,19-22]

Recently we have revealed this black complex to be the oxo-bridged dimer, VOQ_2–O–VOQ_2.[23-25] The crystal structure of the ester has been established by X-ray crystallographic study.[26] Thus the reaction of this dimeric complex with alcohols comes to the stage to be reexamined. In the present paper the esterification of the oxo-bridged dimeric vanadium(V) complexes with 8-quinolinol, 5-chloro-8-quinolinol(H5-Cl-Q), 5,7-dibromo-8-quinolinol (H5,7-Br_2-Q), and 4-isopropyltropolone(H4-Pr-T) by butyl alcohols is investigated from the kinetic and the thermodynamic points of view. The results are compared with the esterification of the *yellow* monomeric complex with 2-methyl-8-quinolinol(H2-Me-Q), $VO(OH)(2\text{-Me-Q})_2$.

Experimental

Materials. All the butyl alcohols were refluxed over freshly ignited calcium oxide, and then with magnesium turnings, and finally distilled. 5-Chloro-8-quinolinol and 5,7-dibromo-8-quinolinol were recrystallized twice from ethanol and acetone, respectively. Chlorobenzene, 8-quinolinol, 4-isopropyltropolone, 2-methyl-8-quinolinol, and ammonium metavanadate were purified as described previously.[23-25]

Vanadium(V) complexes with 8-quinolinol, $V_2O_3Q_4$,[5,6] with 4-isopropyltropolone, $V_2O_3(4\text{-Pr-T})_4$,[25] and with 2-methyl-8-quinolinol, $VO(OH)(2\text{-Me-Q})_2 \cdot 2H_2O$[15] were prepared as described elsewhere. Other complexes with 5-chloro-8-quinolinol, $V_2O_3(5\text{-Cl-Q})_4$, and with 5,7-dibromo-8-quinolinol, $V_2O_3(5,7\text{-}Br_2\text{-Q})_4$ were prepared by mixing dioxovanadium(V) perchlorate solution with the corresponding ligand dissolved in perchloric acid solution and adjusting pH to 4 with ammonia. Found: C, 31.8; H, 1.1; N, 4.2%. Calcd for $V_2C_{36}H_{16}N_4O_7Br_8$: C, 31.85; H, 1.19; N, 4.13%. Found: C, 49.6; H, 2.4; N, 7.3%. Calcd for $V_2C_{36}H_{20}$-

Table 1. Summary of the properties of vanadium(V) complexes

Complex	λ_{max}[a] nm	ν(V=O)[b] cm^{-1}	ν(V-O-V)[c] cm^{-1}
$V_2O_3Q_4$	550	950	715
$V_2O_3(5\text{-Cl-Q})_4$	580	959 (971)[d]	715
$V_2O_3(5,7\text{-}Br_2\text{-Q})_4$	570	970 (945)[d]	720
$V_2O_3(4\text{-Pr-T})_4$	530	950	715
$VO(OH)(2\text{-Me-Q})_2 \cdot 2H_2O$	340	925	—

a) λ_{max} is the wavelength of the absorption maximum in the ultraviolet and visible spectrum. b,c) ν(V=O) and ν(V-O-V) are the wavenumbers of infrared absorption of V=O and V-O-V measured by pottasium bromide disc technique, respectively. d) These absorptions are weak and not assignable.

$N_4O_7Cl_4$: C, 50.03; H, 2.33; N, 6.48%.

Infrared, visible, and ultraviolet spectral data for these complexes are summarized in Table 1. The presence of ν(V-O-V) at near 715 cm^{-1} and absorption near 550 nm indicates the μ-oxo dimeric structure of these complexes. The complex with 2-methyl-8-quinolinol is monomeric because of steric hindrance of methyl group as described previously.[24]

Measurement. All the experiments were performed in a room thermostated at 25±0.5 °C. All the measurements were done using the circulating bath thermostated at each temperature within ±0.1 °C. The volume change of the solvent due to the temperature change was taken into consideration.[27]

Ultraviolet and visible spectra were recorded on a UNION High Sens Spectrophotometer SM-401. A JASCO infrared spectrophotometer A-3 was used for the IR spectral study by potassium bromide disc technique.

Equilibrium study was performed by measuring the absorbance at 480 nm with Zeiss spectrophotometer model 1 PMQ II, after the complete equilibration of the reaction mixtures in stoppered tubes. The reaction was followed spectrophotometrically at 600 nm after the conventional mixing of the reactants.

The water concentration was varied by mixing the dehydrated chlorobenzene ($C_{H_2O}=4\times10^{-3}$ mol dm^{-3}) and the chlorobenzene saturated with water ($C_{H_2O}=2\times10^{-2}$ mol dm^{-3}) at different ratio. The water concentration was checked by the Karl-Fischer method with the coulometric generation of iodine.

Results

Equilibrium. Just dissolved in wet chlorobenzene, vanadium(V) complexes are partially hydrolyzed and give rise to lower species, VO_2L.[25] In the presence of alcohols, furthermore, substitution of the bound ligand by alcohols is also anticipated to yield vanadium(V) alkoxides.[28–30] Actually in the absence of excess ligand, the addition of alcohol causes the color change from black *via* red to yellow, which is characteristic of trialkoxooxovanadium(V), $VO(OR)_3$. To avoid these side reactions an excess amount of ligand (≈0.01 mol dm^{-3}) was added in all experiments. The addition of excess ligand (up to 0.05 mol dm^{-3}) was confirmed to exert no effect on the esterification.

Visible spectra were recorded for complex solutions with different concentrations of alcohols. The time necessary for equilibration at 25 °C is as follows: V_2O_3(4-Pr-T)$_4$ takes 12 h for *n*- and *i*-, 24 h for *s*-, and 48 h for *t*-BuOH; V_2O_3(5-Cl-Q)$_4$ takes 96 h for *n*-BuOH; $V_2O_3Q_4$ takes 120 h for *n*-BuOH. Two distinct isosbestic points near 430 and 530 nm observed for all systems point to the presence of only one equilibrium, which is expressed by Eq. 1.

$$V_2O_3L_4 + 2ROH \rightleftharpoons 2VO(OR)L_2 + H_2O : K_{DE} \quad (1)$$

As the water concentration is large excess and may be regarded as constant, the conditional esterification constant K_{DE}' is given by Eq. 2.

$$K_{DE}' = K_{DE}[H_2O]^{-1} = \frac{[VO(OR)L_2]^2}{[V_2O_3L_4][ROH]^2} \quad (2)$$

The apparent molar absorption coefficient, $\bar{\varepsilon}=\frac{A}{C_V}$, is related with K_{DE}' by Eq. 3.

$$\frac{(2\bar{\varepsilon}-\varepsilon_D)^2}{\varepsilon_E-\bar{\varepsilon}} \times \frac{C_V}{2\varepsilon_E-\varepsilon_D} = K_{DE}'[ROH]^2, \quad (3)$$

where [ROH] is given by

$$[ROH] = C_{ROH} - \frac{2\bar{\varepsilon}-\varepsilon_D}{2\varepsilon_E-\varepsilon_D} \times C_V,$$

and ε_D and ε_E are the molar absorption coefficients of the dimeric vanadium(V) complex and its ester, respectively, and C_{ROH} and C_V are the total concentrations of alcohol and vanadium(V) as a monomeric species, respectively. The logarithm of the left hand side of Eq. 3 being plotted against log[ROH], the straight line with a slope of two and an intercept of log K_{DE}' should be obtained.

In Fig. 1 are shown the results on the systems of V_2O_3(4-Pr-T)$_4$ and $V_2O_3Q_4$ at a fixed water concentration. At different water concentrations the plots gave different straight lines with a slope of two. From

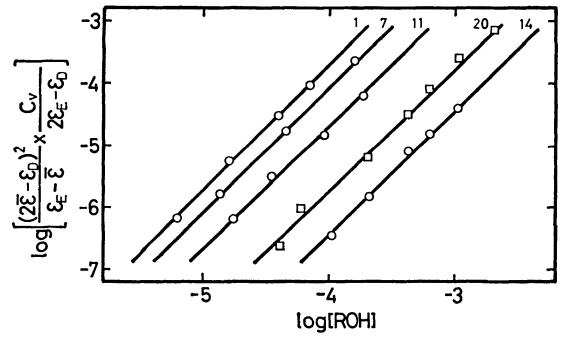

Fig. 1. Determination of the conditional equilibrium constant for the esterification of μ-oxo dimeric vanadium(V) complexes with butyl alcohols. Reaction system: V_2O_3(4-Pr-T)$_4$ (○) with *n*-BuOH(1); *i*-BuOH(7); *s*-BuOH(11); *t*-BuOH(14); $V_2O_3Q_4$ (□) with *n*-BuOH(20). For experimental conditions the same number of Table 2 should be referred.

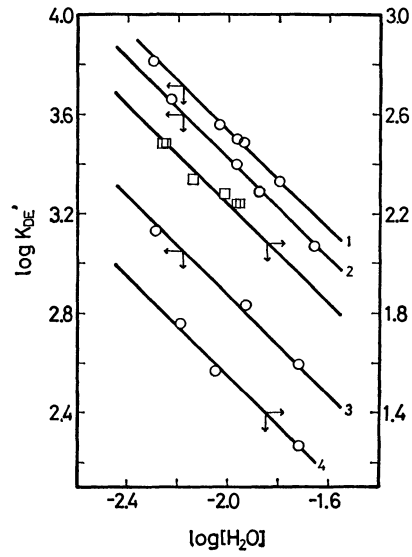

Fig. 2. Determination of the equilibrium constant for the esterification of μ-oxo dimeric vanadium(V) complexes with butyl alcohols. Reaction system: V_2O_3(4-Pr-T)$_4$ (○) with *n*-BuOH (1); *i*-BuOH(2); *s*-BuOH (3); *t*-BuOH(4); $V_2O_3Q_4$ (□) with *n*-BuOH.

Table 2. Conditional equilibrium constants for the esterification of the μ-oxo dimeric complexes with butyl alcohols obtained at various water concentrations at 25 °C

No.	Reaction system	C_V [a] / mol dm^{-3}	C_{HL} [b] / mol dm^{-3}	log [H_2O]	log K_{DE}'
1	V_2O_3(4-Pr-T)$_4$-*n*-BuOH	7.17×10^{-5}	9.80×10^{-3}	−2.30	4.27
2		6.64×10^{-5}	9.87×10^{-3}	−2.04	4.06
3		4.73×10^{-5}	2.83×10^{-3}	−1.97	4.00
4		6.51×10^{-5}	9.80×10^{-3}	−1.94	3.99
5		6.23×10^{-5}	9.95×10^{-3}	−1.80	3.83
6	V_2O_3(4-Pr-T)$_4$-*i*-BuOH	7.06×10^{-5}	9.94×10^{-3}	−2.23	4.16
7		8.48×10^{-5}	1.01×10^{-2}	−1.97	3.90
8		6.13×10^{-5}	1.00×10^{-2}	−1.88	3.79
9		6.32×10^{-5}	9.99×10^{-3}	−1.66	3.67
10	V_2O_3(4-Pr-T)$_4$-*s*-BuOH	6.28×10^{-5}	1.00×10^{-2}	−2.29	3.63
11		6.74×10^{-5}	9.98×10^{-3}	−1.93	3.33
12		6.15×10^{-5}	9.88×10^{-3}	−1.72	3.09
13	V_2O_3(4-Pr-T)$_4$-*t*-BuOH	6.63×10^{-5}	9.83×10^{-3}	−2.19	1.76
14		6.55×10^{-5}	9.83×10^{-3}	−2.05	1.57
15		5.99×10^{-5}	9.88×10^{-3}	−1.72	1.27
16	$V_2O_3Q_4$-*n*-BuOH	5.30×10^{-5}	8.00×10^{-3}	−2.26	2.48
17		4.82×10^{-5}	8.00×10^{-3}	−2.25	2.48
18		5.93×10^{-5}	8.00×10^{-3}	−2.14	2.34
19		5.60×10^{-5}	8.00×10^{-3}	−2.01	2.28
20		5.09×10^{-5}	8.00×10^{-3}	−1.97	2.24
21		5.41×10^{-5}	8.00×10^{-3}	−1.96	2.24
22	V_2O_3(5-Cl-Q)$_4$-*n*-BuOH	4.82×10^{-5}	9.99×10^{-3}	−2.31	2.69

a) Total concentration of vanadium(V) as a monomeric species. b) Total concentration of an excess ligand.

Table 3. Equilibrium and rate constants, and activation parameters for the esterification of V_2O_3(4-Pr-T)$_4$ with butyl alcohols

Alcohol		*n*-BuOH	*i*-BuOH	*s*-BuOH	*t*-BuOH
log K_{DE} [a]		2.03±0.02	1.92±0.02	1.37±0.03	−0.45±0.03
k_1 [b] / mol^{-1} dm^3 s^{-1}	25 °C	5.76×10^{-2}	3.96×10^{-2}	2.95×10^{-2}	2.91×10^{-3}
	30 °C	8.38×10^{-2}	5.87×10^{-2}	4.43×10^{-2}	4.56×10^{-3}
	35 °C	1.22×10^{-1}	8.64×10^{-2}	6.61×10^{-2}	6.89×10^{-3}
ΔH_1^* / kJ mol^{-1}		56±1	57±2	58±2	63±2
ΔS_1^* / J mol^{-1} K^{-1}		−80±3	−81±5	−79±5	−81±5

a) At 25 °C. b) All the values have errors of ±1—3%.

these plots we obtained the conditional equilibrium constants summarized in Table 2. The resulted log K_{DE}' value is plotted against log[H_2O] in Fig. 2. The plots fall along a straight line with a slope of −1 (Eq. 2). This confirms the validity of Eq. 1. The equilibrium constants for the esterification at 25 °C obtained from the intercepts of these plots are summarized in Tables 3 and 4.

Kinetics of the Esterification of the Dimeric Complexes. Kinetics of the esterification was studied with large excess alcohol, so that the back reaction can be neglected. The first-order plot gave a good straight line over 95% conversion.

The rate equation for the dimeric complexes is expressed by Eq. 4,

$$-\frac{d[V_2O_3L_4]}{dt} = \frac{1}{2}\times\frac{d[VO(OR)L_2]}{dt} = k_{0(ROH,HL,H_2O)}[V_2O_3L_4], \quad (4)$$

where $k_{0(ROH,HL,H_2O)}$ is the conditional esterification rate constant involving the concentrations of alcohol, excess ligand, and water. This rate constant was determined from the slope of the first-order plot.

The conditional rate constant was plotted against the alcohol concentration. The results for V_2O_3(4-Pr-T)$_4$ are given in Fig. 3. The plots show the first-order alcohol dependence of $k_{0(ROH,HL,H_2O)}$:

$$k_{0(ROH,HL,H_2O)} = k_{0(HL,H_2O)}[ROH].$$

In each system the ligand was added in a sufficient excess to prevent the formation of the lower complex[25] or alkoxide[28-30] in equilibrium. Addition of the excess ligand was found to exert no effect on the rate. Then,

$$k_{0(ROH,HL,H_2O)} = k_{0(H_2O)}[ROH].$$

Table 4. Equilibrium and rate constants, and activation parameters for the esterification of the μ-oxo dimeric vanadium(V) complexes with *n*-BuOH

Complex		$V_2O_3Q_4$	V_2O_3(5-Cl-Q)$_4$	V_2O_3(5,7-Br_2-Q)$_4$
$\log K_{DE}$[a]		0.25±0.04	0.38±0.04	—
k_1[b] / $mol^{-1}\,dm^3\,s^{-1}$	25 °C	5.90×10^{-3}	0.92×10^{-2}	2.94×10^{-3}
	30 °C	8.42×10^{-3}	1.37×10^{-2}	4.72×10^{-3}
	35 °C	1.19×10^{-2}	2.05×10^{-2}	7.50×10^{-3}
ΔH_1^* / kJ mol^{-1}		52±2	59±1	69±1
ΔS_1^* / J $mol^{-1}\,K^{-1}$		−115±4	−86±3	−63±3
k_2[c] / $mol^{-2}\,dm^6\,s^{-1}$	25 °C	1.24×10^{-1}	0.90×10^{-1}	1.2×10^{-2}
	30 °C	1.54×10^{-1}	1.05×10^{-1}	2.0×10^{-2}
	35 °C	1.78×10^{-1}	1.28×10^{-1}	3.3×10^{-2}
ΔH_2^* / kJ mol^{-1}		24±2	25±2	73±4
ΔS_2^* / J $mol^{-1}\,K^{-1}$		−181±8	−181±8	−30±15

a) At 25 °C. b), c) All the values have errors of ±1—3 and ±3—8%, respectively.

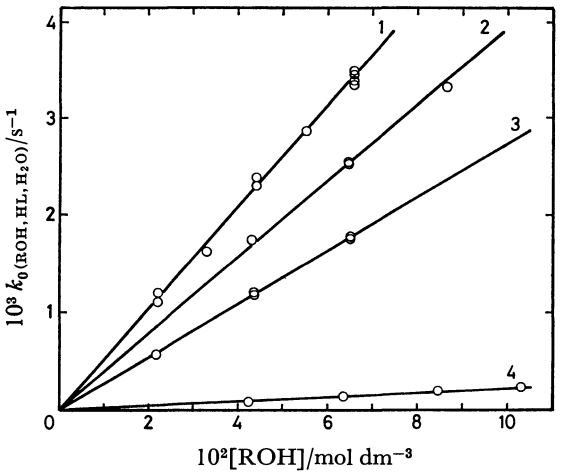

Fig. 3. Plot of $k_{0(ROH,HL,H_2O)}$ for V_2O_3(4-Pr-T)$_4$ *vs.* [ROH]. $C_v=6.73\times10^{-5}$ mol dm^{-3}; $C_{HL}=9.83\times10^{-3}$ mol dm^{-3}; $C_{H_2O}=0.007$—0.020 mol dm^{-3}. ROH: *n*-BuOH(1); *i*-BuOH(2); *s*-BuOH(3); *t*-BuOH(4).

In the absence of the excess ligand enough to prevent the formation of lower species, the esterification proceeds faster. This is attributable to the faster reaction of monomeric VO_2L with alcohol.

Finally $k_{0(H_2O)}$ was plotted against [H_2O]. The results are shown for $V_2O_3Q_4$ with *n*-BuOH in Fig. 4. According to this Figure, $k_{0(H_2O)}$ is rewritten as

$$k_{0(H_2O)} = k_1 + k_2[H_2O].$$

V_2O_3(5-Cl-Q)$_4$ and V_2O_3(5,7-Br_2-Q)$_4$ showed the similar behavior, whereas V_2O_3(4-Pr-T)$_4$ had negligibly small k_2[H_2O] term as compared to k_1.

Thus $k_{0(ROH,HL,H_2O)}$ is expressed by Eq. 5.

$$k_{0(ROH,HL,H_2O)} = (k_1+k_2[H_2O])[ROH] \quad (5)$$

Rate constants at 25, 30, and 35 °C, and activation parameters are summarized in Tables 3 and 4.

Kinetics of the Esterification of the Monomeric Complex. The rate equation for the monomeric 2-methyl-8-quinolinolate complex is expressed by Eq. 6.

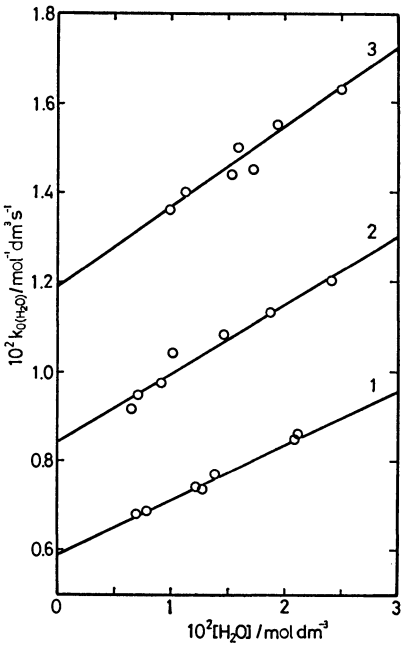

Fig. 4. Plot of $k_{0(H_2O)}$ for $V_2O_3Q_4$ with *n*-BuOH *vs.* [H_2O]. $C_v=5.67\times10^{-5}$ mol dm^{-3}; $C_{HL}=8.00\times10^{-3}$ mol dm^{-3}. At 25 °C(1) ; 30 °C(2) ; 35 °C(3).

$$-\frac{d[VO(OH)(2\text{-Me-Q})_2]}{dt} = \frac{d[VO(OR)(2\text{-Me-Q})_2]}{dt}$$

$$= k_{M,0(ROH,HL,H_2O)}[VO(OH)(2\text{-Me-Q})_2] \quad (6)$$

The kinetic data were analyzed by the treatment similar to that in the case of the dimeric complexes. Despite a very small contribution from the water-dependent path (1—2% acceleration in chlorobenzene saturated with water), the conditional rate constant $k_{M,0(ROH,HL,H_2O)}$ is reasonably expressed by Eq. 7 for *n*- and *i*-BuOH.

$$k_{M,0(ROH,HL,H_2O)} = k_{M,1}[ROH] \quad (7)$$

For *s*- and *t*-BuOH the esterification can not be successfully analyzed because of the concurrent ligand

Table 5. Rate constants and activation parameters for the esterification of VO(OH)(2-Me-Q)$_2$ with butyl alcohols

Alcohol		*n*-BuOH	*i*-BuOH
$k_{M,1}$[a] / mol^{-1} dm^3 s^{-1}	25 °C	2.29×10^{-2}	3.13×10^{-2}
	30 °C	3.13×10^{-2}	4.29×10^{-2}
	35 °C	4.23×10^{-2}	5.65×10^{-2}
$\Delta H_{M,1}^*$ / kJ mol^{-1}		44±1	42±1
$\Delta S_{M,1}^*$ / J mol^{-1} K^{-1}		−128±4	−133±4

a) All the values have errors of ±1—3%.

dissociation reaction in the presence of these alcohols. Rate constants at 25, 30, and 35 °C, and activation parameters are summarized in Table 5.

Discussion

All but 2-methyl-8-quinolinolate complexes have the μ-oxo dimeric structure. No X-ray structural analysis being reported for the μ-oxo dimeric vanadium(V) complex, it was reasonably supposed to have the terminal oxo *cis* to the bridging oxo group from the analogy of many molybdenum(V) complexes[31] and the mixed valence vanadium(IV,V) complex.[32] The strong absorption near 550 nm, which is ascribed to a delocalized three-center pi bond, is characteristic of this configuration.[31] The two oxo groups attached to each vanadium atom in dimeric complexes have a possibility to be *cis* or *trans* to each other. Whereas according to the X-ray structural analysis the ester has the terminal oxo *cis* to the alkoxo group, and these groups are *trans* to the nitrogen atoms of quinoline rings.[26] Thus it will be pertinent to conclude that the rupture of the bridging bond must occur during the esterification of the dimeric complexes and that the *cis* configuration of oxo groups is retained. Since the 2-methyl-8-quinolinolate complex is monomeric because of the steric hindrance of methyl group,[24] the esterification of this complex is the simple nucleophilic substitution reaction of hydroxide by alkoxide group.

Reaction Mechanism. The esterification of the μ-oxo dimeric vanadium(V) complexes is first-order in the alcohol concentration. The reaction involves the water-independent path(k_1 path) and the other path first-order in the water concentration (k_2 path). Since in k_1 path, only one molecule of alcohol is involved in the rate equation, the reactive species VO(OH)L$_2$ must be formed in addition to the final product VO(OR)L$_2$ (Eq. 8). VO(OH)L$_2$ must react rapidly with one more alcohol to yield VO(OR)L$_2$ (Eq. 9).

$$V_2O_3L_4 + ROH \xrightarrow{\text{slow}} VO(OR)L_2 + VO(OH)L_2 \quad (8)$$

$$VO(OH)L_2 + ROH \xrightarrow{\text{fast}} VO(OR)L_2 + H_2O \quad (9)$$

To estimate the bound ligand effect on the reaction rate, log k_1 value is plotted against ΣpK_a, which is the sum of the logarithmic protonation constants of the two ligands coordinated to vanadium and is a measure of electron donation from the ligands to vanadium(V) (Fig. 5). Except the sterically crowded ligand (5,7-dibromo-8-quinolinol), fairly good linear relationship is observed. This implies that the more the coordinated ligand donates, the lower the positive charge on vanadium(V) becomes, resulting in slower esterification. Thus the reaction may be regarded as a nucleophilic attack of alcohol at the vanadium center. However for a given complex (see Table 3) the reactivity of four butyl alcohols does not parallel to nucleophilicity (*t*->*s*->*i*->*n*-), but to sterical freedom (*n*->*i*->*s*->*t*-). Accordingly the difference in reactivity of alcohols mainly stems from the steric factor.

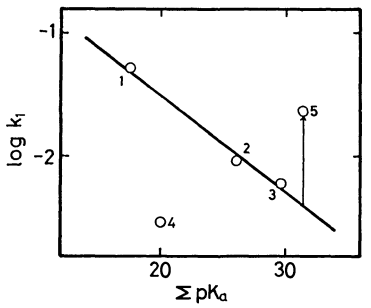

Fig. 5. Correlation of the rate constant for the esterification of vanadium(V) complexes by *n*-BuOH with ΣpK_a of the bound ligand. Complex: 1, V_2O_3(4-Pr-T)$_4$ (Ref. 33); 2, V_2O_3(5-Cl-Q)$_4$ (Ref. 34); 3, $V_2O_3Q_4$ (Ref. 34); 4, V_2O_3(5,7-Br$_2$-Q)$_4$ (Ref. 35); 5, VO(OH)(2-Me-Q)$_2$ (Ref. 34). The pK_a values are taken from the references cited in parentheses. The starting point of an arrow denotes the rate constant for the hypothetical dimeric vanadium(V) complex with 2-methyl-8-quinolinol.

The reactivity of the dimeric complexes is then compared with that of the 2-methyl-8-quinolinolate complex. This complex may be regarded as the proposed reactive intermediate in the esterification of the dimeric complexes (Eq. 8). Although the corresponding dimeric complex with 2-methyl-8-quinolinol has also been synthesized, it is not stable and dissociates to the monomeric complex in wet chlorobenzene.[24] Accordingly the rate constant for the esterification of this unstable dimeric complex is not directly obtained, but it is reasonably estimated by reading the log k_1 value for the ΣpK_a of this ligand (the origin of an arrow in Fig. 5). The experimental rate constant of the monomeric complex (2.29×10^{-2} mol^{-1} dm^3 s^{-1} at 25 °C) is at least 5 times as large as this expected value for the dimeric complex (4×10^{-3} mol^{-1} dm^3 s^{-1} at 25 °C). Thus VO(OH)L$_2$ type complex should be more reactive than the corresponding dimeric complex (Eq. 9). In contrast to the dimeric complexes, the reactivity of alcohols towards the monomeric complex parallels to nucleophilicity (*n*->*i*-).

Exceptionally large negative values of ΔS^* point to an associative mode of activation(S_N2) in both monomeric and dimeric complexes. In the dimeric complexes, ΔH^* is larger with increasing bulkiness of both attacking alcohol and bound ligand, and larger ΔH^* values are always associated with smaller negative ΔS^* values. These findings, taken together

with the reactivity order with alcohols, suggest that steric factor plays an important role in these systems. For the monomeric complex, the smallest ΔH^* values are associated with the negatively largest ΔS^* values.

In the dimeric complexes, due to the other vanadium half-unit linked with the bridging oxo group, the nucleophilic attack of alcohol to vanadium center is sterically hindered and the extra bond-weakening energy is necessary to make alcohol close to vanadium center. The mechanism is explained by a concerted bimolecular reaction, in which a molecule of alcohol attacks associatively the vanadium center and at the same time the bond between vanadium and bridging oxo ligand is weakened. This makes ΔH^* value considerably larger for more sterically crowded system. For a given complex, ΔH^* value increases in the order *n*-<*i*-<*s*-<*t*- and for a given alcohol $V_2O_3Q_4$< V_2O_3(5-Cl-Q)$_4$<V_2O_3(5,7-Br_2-Q)$_4$. The small negative ΔS^* value associated with large positive ΔH^* value suggests that the bond-weakening contribution to the overall activation is more significant as compared to the bond-making, thus the reaction between crowded alcohol and complex becomes less associative. On the other hand in the monomeric complex, alcohol can easily approach to vanadium center without being suffered significant steric hindrance. This makes the reaction more associative. Furthermore since no extra bond-weakening energy is necessary for the activated state, the reactivity order is mainly governed by electronic factor.

Water-dependent Path. The water-dependent rate constant in the esterification of the dimeric complexes, k_2 was constant even in changing the concentration of the excess ligand. Accordingly water must not substitute the bound ligand of the dimeric complexes to yield a reactive lower complex, but it interacts with any site in the complexes such as terminal or bridging oxo group to yield a reactive intermediate. Since a small but definite water-dependent path is observed also in the case of the monomeric complex, the interaction with basic terminal oxo group seems plausible. Moreover, this postulation is supported by the fact that the esterification was much more accelerated in the presence of more acidic substance such as phenol.[36]

As can be seen from the relative changes in k_2 and ΔH_2^* in the presence of water, the acceleration by water becomes higher with increasing ΣpK_a of the bound ligand. That is, the interaction of water is stronger with more basic oxo group in complexes having more basic ligand. The acceleration relative to k_1 (log k_2/k_1: 1.32 for $V_2O_3Q_4$; 0.99 for V_2O_3(5-Cl-Q)$_4$; 0.61 for V_2O_3(5,7-Br_2-Q)$_4$.) is linearly correlated with ΣpK_a. Judging from the extrapolated k_2(0.4) for V_2O_3(4-Pr-T)$_4$, the negligibly small contribution of water-dependent path in the reaction with *n*-BuOH as compared to the k_1 is anticipated and this agrees with our results. In the monomeric complex the same type of acceleration will be anticipated. However the intramolecular hydrogen bonding between terminal oxo and hydroxo groups prevents the formation of a reactive intermediate and the reaction will not be accelerated so much as expected from the estimated k_2 (5.8×10^{-1} mol^{-1} dm^3 s^{-1}). The k_2 path reaction has an energy of activation (ΔH_2^*) less than for the corresponding reaction not involving such an intermediate (ΔH_1^*) by about the heat of formation of the hydrogen bond. Larger negative ΔS_2^* value as compared to ΔS_1^* is also attributable to this pre-equilibrium.

Relationship between K_{DE} *and* k_1. The detailed reaction scheme is expressed as

$$V_2O_3L_4 + ROH \underset{k_{-1}}{\overset{k_1}{\rightleftharpoons}} VO(OR)L_2 + VO(OH)L_2$$

$$VO(OH)L_2 + ROH \underset{k_{EM}}{\overset{k_{ME}}{\rightleftharpoons}} VO(OR)L_2 + H_2O.$$

Then the overall esterification equilibrium constant is equated to

$$K_{DE} = \frac{k_1}{k_{-1}} K_{ME},$$

where $K_{ME}=k_{ME}/k_{EM}$. Using the dimerization constant given by

$$2VO(OH)L_2 \rightleftharpoons V_2O_3L_4 + H_2O : K_{MD}.$$

k_1 is expressed by

$$k_1 = k_{-1}(K_{DE}/K_{MD})^{1/2}.$$

k_{-1} corresponds to the rate constant of the nucleophilic attack of the oxo group in the monomeric complex to the vanadium center of the ester. In this reaction, alcohol accommodated as alkoxide in the ester will not largely affect the rate k_{-1} both electronically and sterically for the complexes with the same bound ligand. Furthermore K_{MD} being constant for the complex with the same ligand, in the reaction system of V_2O_3(4-Pr-T)$_4$ with butyl alcohols log k_1 should be linearly correlated with log K_{DE} with a slope of 1/2 as in Fig. 6. On the other hand, the results obtained in the systems of $V_2O_3Q_4$ and V_2O_3(5-Cl-Q)$_4$ with *n*-BuOH are also well accommodated in the correlation given in Fig. 6. It appears unlikely that k_{-1} and K_{MD} are both constant irrespective of the bound ligand. Thus the linear correlation of log k_1 with log K_{DE} may be resulted from the adequate compensation of k_{-1} and K_{MD} making (log k_{-1}−1/2 log

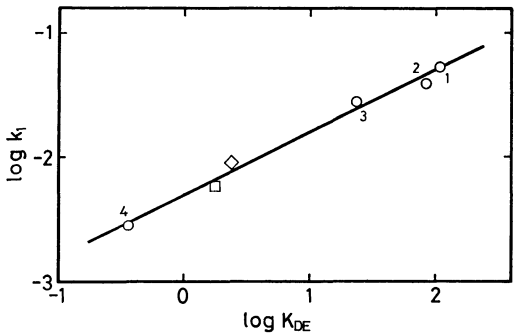

Fig. 6. Correlation of the rate constant for the esterification of the μ-oxo dimeric vanadium(V) complex with its equilibrium constant. Reaction system: V_2O_3(4-Pr-T)$_4$ (○) with *n*-BuOH(1); *i*-BuOH(2); *s*-BuOH(3); *t*-BuOH(4); $V_2O_3Q_4$ (□) with *n*-BuOH; V_2O_3(5-Cl-Q)$_4$ (◇) with *n*-BuOH. The solid line is the straight line with a slope of 1/2.

K_{MD}) constant. In any event, the lower the activation energy for the esterification, the stabler the resulted ester is.

The authors wish to thank the Grand-in-Aid for Scientific Research No. 347029 from the Ministry of Education, Science and Culture.

References

1) R. Montequi and M. Gallego, *Anales Soc. Espan. Fis. Quim.*, **32**, 134 (1934).
2) S. Ishimaru, *J. Chem. Soc. Jpn.*, **56**, 62 (1935).
3) M. Borrel and R. Pâris, *Anal. Chim. Acta*, **4**, 267 (1950).
4) H. J. Bielig and E. Bayer, *Ann. Chem.*, **584**, 96 (1953).
5) A. J. Blair and D. A. Pantony, *Anal. Chim. Acta*, **13**, 1 (1955).
6) A. J. Blair, D. A. Pantony, and G. J. Minkoff, *J. Inorg. Nucl. Chem.*, **5**, 316 (1958).
7) F. Buscarons, J. L. Marin, and J. Claver, *Anal. Chim. Acta*, **3**, 310, 417 (1949).
8) I. Kudo and I. Aoki, *Bunseki Kagaku*, **6**, 791 (1957).
9) S. Maruta and F. Iwama, *Nippon Kagaku Zasshi*, **80**, 1131 (1959).
10) M. Tanaka, *Talanta*, **5**, 162 (1960).
11) M. Pesez and J. Bartos, *Bull. Soc. Chim. Fr.*, **1961**, 1930.
12) M. Stiller, *Anal. Chim. Acta*, **25**, 85 (1961).
13) M. Pribyl and Z. Slovak, *Collect. Czech. Chem. Commun.*, **28**, 848 (1963).
14) P. K. van Gent and J. E. Kerrich, *Analyst*, **90**, 335 (1965).
15) H. Nakamura, Y. Shimura, and R. Tsuchida, *Bull. Chem. Soc. Jpn.*, **34**, 1143 (1961).
16) R. P. Henry, P. C. H. Mitchell, and J. E. Prue, *Inorg. Chim. Acta*, **7**, 150 (1973).
17) L. W. Amos and D. T. Sawyer, *Inorg. Chem.*, **13**, 78 (1974).
18) T. L. Riechel and D. T. Sawyer, *Inorg. Chem.*, **14**, 1869 (1975).
19) P. K. van Gent and E. R. Swart, *J. South. Af. Chem.*, **19**, 85 (1966).
20) D. A. Pantony, *Rec. Chem. Progr.*, **27**, 97 (1966).
21) N. Kurmaiah, D. Satyanarayana, and V. P. R. Rao, *Talanta*, **14**, 495 (1967).
22) M. Tanaka and I. Kojima, *J. Inorg. Nucl. Chem.*, **29**, 1769 (1967).
23) A. Yuchi, S. Yamada, and M. Tanaka, *Bull. Chem. Soc. Jpn.*, **52**, 1643 (1979).
24) A. Yuchi, S. Yamada, and M. Tanaka, *Anal. Chim. Acta*, **115**, 301 (1980).
25) A. Yuchi, H. Muranaka, S. Yamada, and M. Tanaka, *Bull. Chem. Soc. Jpn.*, **53**, 1560 (1980).
26) W. R. Scheidt, *Inorg. Chem.*, **12**, 1758 (1973).
27) "International Critical Tables," McGraw Hill, New York (1928), Vol. 3, p. 29.
28) F. Cartan and C. N. Caughlan, *J. Phys. Chem.*, **64**, 1756 (1960).
29) R. K. Mittal and R. C. Mehrotra, *Z. Anorg. Allg. Chem.*, **327**, 311, **331**, 89 (1964); **355**, 328 (1967).
30) C. N. Caughlan, H. M. Smith, and K. Watenpaugh, *Inorg. Chem.*, **5**, 2131 (1966).
31) E. I. Stiefel, "Progress in Inorganic Chemistry," John Wiley & Sons, Inc. (1977), Vol. 22., p. 1.
32) M. Nishizawa, K. Hirotsu, S. Ooi, and K. Saito, *J. Chem. Soc., Chem. Commun.* **1979**, 707.
33) Y. Oka, M. Yanai, and C. Suzuki, *Nippon Kagaku Zasshi*, **85**, 873 (1964).
34) F. C. Chou and H. Freiser, *Anal. Chem.*, **40**, 34 (1968).
35) V. M. Peshkova, M. I. Gromova, and T. I. Romantseva, *Zh. Anal. Khim.*, **23**, 197 (1968).
36) A. Yuchi, unpublished results.

  Bull. Chem. Soc. Jpn., 54, 207—211 (1981)

The Polarographic Behavior of Bis(acetylacetonato)nickel(II) and Bis(hexafluoroacetylacetonato)nickel(II) in Dimethyl Sulfoxide

Setsuko KUDO,† Akio IWASE,* and Nobuyuki TANAKA**

Department of Chemistry, Faculty of Science, Yamagata University, Koshirakawa-machi, Yamagata 990

***Department of Chemistry, Faculty of Science, Tohoku University, Aoba, Aramaki, Sendai 980*

(Received April 14, 1980)

The d.c. polarographic reduction of $Ni(acac)_2$ and $Ni(hfac)_2$ was studied in detail in dimethyl sulfoxide. Two kinds of tetraalkylammonium perchlorates and sodium perchlorate were used as supporting electrolytes. $Ni(acac)_2$ gave three waves in all the supporting electrolytes, while $Ni(hfac)_2$ gave two waves in the presence of tetraalkylammonium perchlorate. These waves were explained on the basis of the polarographic properties, molecular weights, and conductivities. The electrode reaction mechanism of $Ni(acac)_2$ can be expressed by:

$$Ni(acac)^+ \rightleftharpoons Ni(acac)_2 \rightleftharpoons [Ni(acac)_2]_2 \rightleftharpoons \cdots\cdots \rightleftharpoons [Ni(acac)_2]_p$$

$$\downarrow 2e \qquad \downarrow 2e \qquad \downarrow 4e \qquad \downarrow (2p)e$$

1st wave 2nd wave 3rd wave

where the second wave includes a kinetic current. The first wave of $Ni(hfac)_2$ is due to the reduction of $Ni(hfac)^+$ and $Ni(hfac)_2$ themselves; the second wave corresponds to that of free hexafluoroacetylacetonate.

The nonaqueous electrochemistry of bis(β-diketonato)nickel(II) complexes has been reported by several investigators. Murray and Hiller[1] gave preliminary data on bis(acetylacetonato)nickel(II) in acetonitrile from the standpoint of the supporting-electrolyte effect. The number of electrons participating in the electrode processes, n, is particularly interesting, for certain complexes may partly polymerize even in coordinating solvents. According to the results of Dessy *et al.*,[2] the n value of bis(acetylacetonato)nickel(II) was equal to unity in 1,2-dimethoxyethane. Bond *et al.*[3] presumed a one-electron transfer step for the reduction wave observed in the d.c. polarography of bis(dipivaloylmethanato)nickel(II) in acetone. Recently, Gritzner *et al.*[4] reported on the polarographic and voltammetric behavior of various acetylacetonato and hexafluoroacetylacetonato complexes in acetonitrile. They determined the n value of two for bis(acetylacetonato)nickel(II) coulometrically.

The present paper will report the results of a detailed investigation of the d.c. polarographic reduction of bis(acetylacetonato)nickel(II), $Ni(acac)_2$, and bis(hexafluoroacetylacetonato)nickel(II), $Ni(hfac)_2$, in dimethyl sulfoxide (DMSO).

Experimental

Reagents. Merck analytical reagent-grade DMSO was used without further purification. The content of water was determined with a gas chromatograph. The DMSO contained 0.02—0.06% water.

Sodium perchlorate was dried *in vacuo* for 24 h prior to use. The Nakarai Chemicals tetramethylammonium perchlorate (TMAP) and tetrabutylammonium perchlorate (TBAP) purified for polarography were dried *in vacuo* for 12 h. The Kishida Chemicals nickel(II) perchlorate hexahydrate was brought to a constant weight in a desiccator over magnesium perchlorate.[5] Hexafluoroacetylacetone (Hhfac) from Nakarai Chemicals, Ltd., was used without further purification.

† Present address: Chemical Laboratories, Yamagata Building Service Co., Ltd., Iizuka-machi, Yamagata 990.

Two extra-pure-reagents, $Ni(acac)_2$ and $Ni(hfac)_2$, were obtained from Nakarai Chemicals, Ltd. These compounds were identified as $Ni(acac)_2 \cdot 2H_2O$ and $Ni(hfac)_2 \cdot H_2O$ by elemental analysis.

Potassium acetylacetonate was prepared by the following procedure. Into a solution of 6 cm^3 of acetylacetone (Hacac) in 30 cm^3 of methanol–water (1:1), 2 mol dm^{-3} potassium hydroxide in methanol–water (1:1) was dropwise added until a pH value of 9.0 was reached. The precipitated salt was filtered off and dried *in vacuo*. The analysis of potassium acetylacetonate gave the following results. Found: C, 38.20; H, 5.76%. Calcd for $C_5H_9O_3K$: C, 38.44; H, 5.81%.

Reagent-grade chemicals were used unless otherwise stated.

Apparatus and Procedures. The current-potential curves were obtained with a Yanagimoto Polarograph PA-101 and a Yanagimoto Potentiostat PT-P8.

The polarographic measurements were made at 25.0± 0.2 °C except for the experiments of the temperature effect. An H-type electrolysis cell was used for the measurements. An aqueous SCE-KCl was isolated from the test solution by the use of a compartment with a glass filter (G-4). All the solutions were deaerated with nitrogen gas. Two dropping-mercury electrodes were used. The A electrode had an m value of 1.06_2 mg s^{-1} and a drop time, t_d, of 6.18 s in a deaerated 0.05 mol dm^{-3} TMAP–DMSO solution at −1.0 V and at a height of the mercury reservoir, h, of 47 cm. The B electrode had an m value of 1.24_8 mg s^{-1} and a t_d value of 4.95 s in a deaerated 0.1 mol dm^{-3} TBAP–DMSO solution at −1.0 V and h=45 cm.

In the following sections, i and $\bar{i}$ denote the maximum current and the average current respectively.

The n values were determined on a Yanagimoto Controlled Potential Electrolyzer and a Nikko Keisoku Digital Coulometer NDCM-2.

The conductivities were measured with a Yanagimoto Conductivity Outfit MY-8. The absorption spectra in the visible and ultraviolet regions were obtained with a Spectronic 88-UV Shimadzu-Bausch & Lomb Spectrophotometer at room temperature. The molecular weights were measured in DMSO at 18 °C by cryoscopy, with tris(acetylacetonato)cobalt(III) as the standard material.

Results

Dissolved State of the Complexes in DMSO. Con-

TABLE 1. MOLECULAR WEIGHTS OF $Ni(acac)_2$ IN DMSO AT 18 °C

m/mmol kg^{-1}	Molecular formula	Calcd	Found	Found/Calcd
2.0	$Ni(acac)_2 \cdot DMSO$	335.05	430±50	1.3
3.3	$[Ni(acac)_2 \cdot DMSO]_2$	670.10	650±50	1.0
6.6	$[Ni(acac)_2 \cdot DMSO]_3$	1005.2	1200±200	1.2

TABLE 2. POLAROGRAPHIC DATA OF THE REDUCTION OF $Ni(acac)_2$ AND $Ni(hfac)_2$ IN DMSO

Complex	Supporting electrolyte	$E_{1/2}$/V *vs.* SCE[a]	Slope/mV[b]	i_j/i_t[c]
$Ni(acac)_2$	0.05 mol dm^{-3} $NaClO_4$	−1.12	63	0.15
		−1.33	48	0.15
		−1.64	115	0.70
	0.05 mol dm^{-3} TMAP	−1.22	48	0.21
		−1.44	80	0.41
		−1.83	124	0.38
	0.05 mol dm^{-3} TBAP	−1.25	77	0.49
		−1.46	62	
		−2.00	217	0.51
$Ni(hfac)_2$	0.05 mol dm^{-3} $NaClO_4$	*ca.* −1.0 (Max.)		
	0.05 mol dm^{-3} TMAP	*ca.* −1.0 (Max.)		
		— (Max.)		
	0.05 mol dm^{-3} TBAP	*ca.* −1.0 (Max.)		
		−2.58		
	0.1 mol dm^{-3} TBAP	−1.04	52	
		−2.52	96	

a) The half-wave potentials for $Ni(acac)_2$ were obtained at the concentration of 2 mmol dm^{-3}. b) The slopes of the log-plot analyses for $Ni(acac)_2$ were obtained at the concentration of 5 mmol dm^{-3}. c) The i_j/i_t ratios for $Ni(acac)_2$ were obtained at the concentration of 1 mmol dm^{-3}. The meanings of i_j and i_t are shown in Fig. 1.

ductivity measurements at 25 °C indicate that $Ni(acac)_2$ is little dissociated into ionically-conducting species, while $Ni(hfac)_2$ is dissociated into the 1:1 electrolyte.

The apparent molecular weights of $Ni(acac)_2$ in DMSO are given in Table 1. This complex was polymeric in the concentration range studied here. On the other hand, the cryoscopic results of $Ni(hfac)_2$ were in conflict with the conductance data, showing the molecular weight of undissociated $Ni(hfac)_2 \cdot 2DMSO$. The cryoscopy of $Ni(hfac)_2$ appears to afford no true information; however, the reason for this is not known.

The spectoscopic data indicate that the complexes are of a hexa-coordinate octahedral structure,[6,7] though the cryoscopic data of $Ni(acac)_2$ seem to suggest a penta-coordinate structure.

Reduction of the Complexes in DMSO. Some typical polarograms and polarographic data of the complexes in DMSO are shown in Fig. 1 and Table 2. Sodium perchlorate, tetramethylammonium perchlorate, and tetrabutylammonium perchlorate were used as supporting electrolytes. $Ni(acac)_2$ gave three reduction waves, of which the one at the most negative potential was very irreversible, regardless of the kind of supporting electrolyte used. When TBAP was used as a supporting electrolyte, the first two waves at less negative potentials overlapped; hence, the polarogram of 1 mmol dm^{-3} $Ni(acac)_2$ appeared just like two steps.

$Ni(hfac)_2$ gave two reduction waves in the presence of tetraalkylammonium perchlorate as the supporting electrolyte. When sodium perchlorate was used as the supporting electrolyte, the second wave, at a far

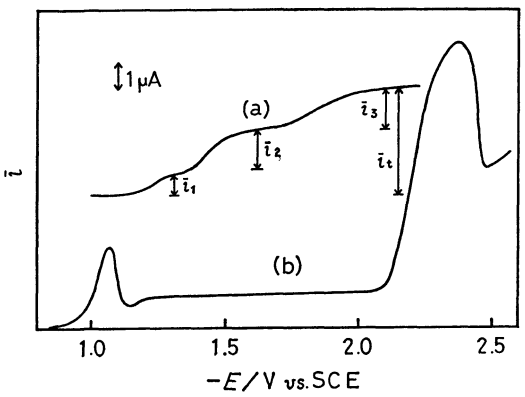

Fig. 1. Polarograms of (a) 3.0 mmol dm^{-3} $Ni(acac)_2$ and (b) 0.5 mmol dm^{-3} $Ni(hfac)_2$ in 0.05 mol dm^{-3} TMAP–DMSO. With the DME (A).

negative potential, overlapped with the sodium-ion reduction. Interestingly, the first wave of $Ni(hfac)_2$ resembled the wave of nickel(II) perchlorate in its polarographic properties. When 0.1 mol dm^{-3} TBAP was chosen as the supporting electrolyte, the maximum at the first wave disappeared and the second wave was a well-defined one (see Fig. 2 and Table 2). The ratio of their heights was equal to 1:4 for the first and the second wave under the controlled drop time. The polarogram of $Ni(hfac)_2$ is compared with that of hexafluoroacetylacetone in Fig. 2. Hexafluoroacetylacetone gave two waves: the first wave is considered to be a hydrogen reduction of the enol form, and the second wave, to be an enolate reduction.[8] The second

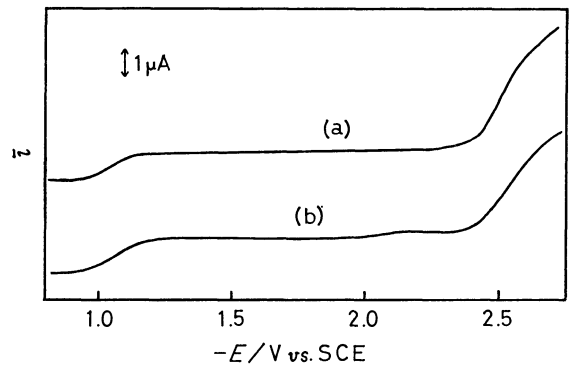

Fig. 2. Polarograms of (a) 0.5 mmol dm^{-3} Ni(hfac)$_2$ and (b) *ca.* 0.9 mmol dm^{-3} Hhfac in 0.1 mol dm^{-3} TBAP-DMSO. With the DME (B).

wave of Ni(hfac)$_2$ appeared at the same potential as that of hexafluoroacetylacetone.

The first limiting currents (i) of Ni(acac)$_2$ and Ni(hfac)$_2$ were proportional to $h^{1/2}$ in all the supporting electrolytes used. The measurements of the current-time (i-t) curve were made in the potential region giving each limiting current of three waves of Ni(acac)$_2$ in 0.05 mol dm^{-3} solution of each supporting electrolyte during the life of a mercury drop. In a TMAP or TBAP solution, the slopes of the plots for log i *vs.* log t were larger than those in a sodium-perchlorate solution. This finding is related to the supporting-electrolyte effect on the total limiting current, $\bar{i}_t$, of Ni(acac)$_2$ to be described later.

All the waves of Ni(acac)$_2$ were not due to the reduction of the ligand, because acetylacetonate itself gave no wave in the potential range observed. The polarographic waves of 1 mmol dm^{-3} Ni(acac)$_2$ were affected by the addition of a small amount of acetylacetonate. The first wave disappeared after the addition of 0.5 mmol dm^{-3} acetylacetonate. The $\bar{i}_t$ decreased as the concentration of acetylacetonate increased. The dependence of the $\bar{i}_t$ on the acetylacetonate concentration suggested the formation of electroinactive Ni(acac)$_3^-$. When 1 mmol dm^{-3} nickel(II) perchlorate was made to react with 1 mmol dm^{-3} potassium acetylacetonate, the polarogram had two waves in the presence of each supporting electrolyte of 0.05 mol dm^{-3}: one was the wave of the nickel ion, and the other was that of Ni(acac)$^+$, which appeared at *ca.* −1.2 V in the TMAP solution. Accordingly, the first wave of Ni(acac)$_2$ corresponds to the reduction of Ni(acac)$^+$.

In Fig. 3 the limiting currents of Ni(acac)$_2$ and Ni(hfac)$_2$ are plotted against their concentrations. In contrast to the linearity of plots for the first wave of Ni(hfac)$_2$, that for the $\bar{i}_t$ of Ni(acac)$_2$ gave curves. The supporting-electrolyte effect on the $\bar{i}_t$ was observed after the correction for the drop time; that is, the $\bar{i}_t$ was low in the presence of tetraalkylammonium perchlorate. This may be explained by the double-layer effect on the reduction rate,[9] judging from the i-t curve data mentioned above.

The plots of the $\bar{i}_j$ and $\bar{i}_t$ values of Ni(acac)$_2$ *vs.*

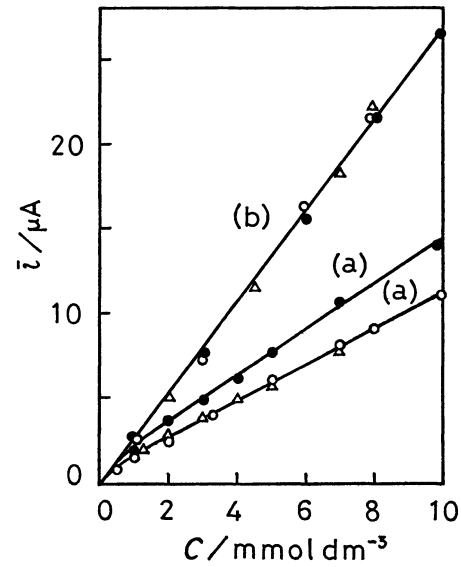

Fig. 3. Dependence of (a) the total limiting current of Ni(acac)$_2$ and (b) the first limiting current of Ni(hfac)$_2$ on the concentration of each complex in DMSO. Supporting electrolyte: (○) TMAP, (△) TBAP and (●) sodium perchlorate. Each in 0.05 mol dm^{-3}. With the DME (A).

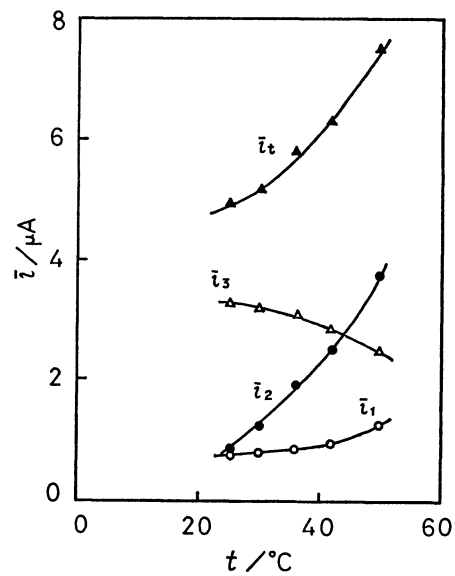

Fig. 4. Effect of temperature on the limiting currents of 3.0 mmol dm^{-3} Ni(acac)$_2$ in 0.05 mol dm^{-3} sodium perchlorate-DMSO. For $\bar{i}_j$ (j=1—3), see Fig. 1. With the DME (A).

the temperature gave the curves shown in Fig. 4. With an increase in the temperature, the $(\bar{i}_1+\bar{i}_2)/\bar{i}_t$ ratio increased and the $\bar{i}_3/\bar{i}_t$ ratio decreased: in a 3 mmol dm^{-3} Ni(acac)$_2$–0.05 mol dm^{-3} sodium perchlorate solution, these ratios were 0.34 and 0.66 respectively at 25 °C, while they were 0.67 and 0.33 respectively at 50 °C.

The controlled potential coulometric experiments were carried out at −1.70 V for 0.5 mmol dm^{-3} Ni(hfac)$_2$ and at −2.30 V for 0.5 mmol dm^{-3} Ni(acac)$_2$

in the presence of 0.05 mol dm^{-3} TMAP. These coulomertic data gave 2.0 and 1.9 respectively as the apparent numbers of electrons per nickel atom.

The effect of water on the polarographic waves was examined below 10%. When 0.05 mol dm^{-3} TMAP was used as the supporting electrolyte, there was no variation in $Ni(acac)_2$ after the addition of 10% water. When 0.05 mol dm^{-3} sodium perchlorate was used as the supporting electrolyte, though, the i_2/i_t ratio increased and the i_3/i_t ratio decreased as the content of water increased in the range of 2—10%. The effect on $Ni(hfac)_2$ was checked in the presence of 0.1 mol dm^{-3} TBAP, for these conditions gave two well-defined waves. The addition of 5% water led to more irreversible waves. Further, the first and second waves shifted a little to more negative and less negative potentials respectively.

Discussion

Many chemists have been interested in the structures of β-diketone chelate compounds in various nonaqueous solvents. They have mainly investigated them by means of NMR, ESR, electronic-spectra, molecular-weight measurements, *etc.* It is well known that the anhydrous $Ni(acac)_2$ exists as a trimer with an octahedral coordination about the nickel(II) in crystals and also in noncoordinating solvents.[7] Yoshida *et al.*[10] have proposed a dimer, $(NiL_2 \cdot H_2O)_2$, for each prevalent form of bis(1,5-dialkyl-2,4-pentanedionato)-nickel(II) monohydrate complexes in noncoordinating solvents, where L represents a β-diketonato anion. Using the rotating-disk-electrode method, Ritzler and Gross[11] have proposed a dimer for the prevalent form of about 1 mmol dm^{-3} $Co(acac)_2$ in propylene carbonate. The present work affords useful information on the molecular association of $Ni(acac)_2$ in DMSO with a great donor-number.

$Ni(acac)_2$ and $Ni(hfac)_2$ in DMSO are involved in the following chemical equilibria:

$$[Ni(acac)_2]_p \rightleftharpoons \cdots \rightleftharpoons [Ni(acac)_2]_2 \rightleftharpoons Ni(acac)_2 \rightleftharpoons Ni(acac)^+ + acac^- \quad (1)$$

$$Ni(hfac)_2 \rightleftharpoons Ni(hfac)^+ + hfac^-, \quad (2)$$

on the basis of the conductance and the molecular-weight data. The degree of the dissociation of $Ni(acac)_2$ to the ions is negligibly small in the absence of a supporting electrolyte, as has been mentioned in the preceeding section.

The polarographic behavior of $Ni(hfac)_2$ is very similar to that of the only species which is diffusion-controlled, judging from the linearity of the limiting current on $h^{1/2}$ and the complex concentration. Further, the apparent diffusion-current constant of the first wave was approximately equal to that of the wave of the nickel(II) ion, which follows a two-electron reduction process to the metal.[12] The n value, determined coulometrically, is consistent with this finding. Both $Ni(hfac)^+$ and $Ni(hfac)_2$ participate, presumably as electroactive species, in the first wave. A comparison between the polarograms of (a) and (b) in Fig. 2 indicates that the second wave of $Ni(hfac)_2$ comes from free hexafluoroacetylacetonate. The complex gave a nickel anodic stripping peak (spike pattern) at −0.1 V in cyclic voltammetry at a platinum electrode; such a peak was also found in nickel perchlorate. This suggests that the ligand is liberated after the reduction of the complex itself at the first wave. Thus, the second wave does not mean the reduction of the only free ligand from the dissociation reaction in the bulk of the solution.

The first wave of $Ni(acac)_2$ does not include the kinetic current due to the preceding chemical reaction, judging from the dependence of the limiting current on $h^{1/2}$. The first wave is due to the reduction of $Ni(acac)^+$, judging from the disappearance of the wave after the addition of acetylacetonate and from the agreement between the half-wave potential of $Ni(acac)^+$ and that of the first wave of $Ni(acac)_2$. However, the i_1/i_t ratio is too large to explain the conductance data. It is, therefore, reasonable to consider the dissociation of $Ni(acac)_2$ to $Ni(acac)^+$ in the bulk of the solution in the presence of a supporting electrolyte. The second and third waves come from the reduction of the monomeric $Ni(acac)_2$ and the polymeric species respectively, judging from the dependence of the i_2 and i_3 on the temperature and from that of the i_t on the complex concentration. Consequently, the electrode reaction mechanism can be expressed by:

$$\begin{array}{ccccccc} Ni(acac)^+ & \rightleftharpoons & Ni(acac)_2 & \rightleftharpoons & [Ni(acac)_2]_2 \rightleftharpoons \cdots \rightleftharpoons & [Ni(acac)_2]_p \\ \downarrow 2e & & \downarrow 2e & & \downarrow 4e \quad\quad \downarrow (2p)e & \\ \text{1st wave} & & \text{2nd wave} & & \text{3rd wave} & \end{array} \quad (3)$$

where the $Ni(acac)_2 \rightleftharpoons Ni(acac)^+ + acac^-$ reaction is so slow that it practically does not proceed in the vicinity of the electrode surface during electrolysis. The i_2/i_3 ratio was dependent on the drop time; the temperature effect on the i_2 can not be interpreted merely by the chemical equilibria shift in the bulk of the solution, so that the second wave includes the kinetic current due to the preceding reaction, the polymeric species$\rightleftharpoons$ $Ni(acac)_2$, in Eq. 3.

The dissolved state is apparently dependent on the nature of the ligands of the complexes. Such behavior of other bis(β-diketonato)nickel(II) complexes will be discussed in the following paper.

References

1) R. W. Murray and L. K. Hiller, Jr., *Anal. Chem.*, **39**, 1221 (1967).
2) R. E. Dessy, F. E. Stary, R. B. King, and M. Waldrop, *J. Am. Chem. Soc.*, **88**, 471 (1966).
3) A. M. Bond, R. L. Martin, and A. F. Masters, *J. Electroanal. Chem.*, **72**, 187 (1976).
4) G. Gritzner, H. Murauer, and V. Gutman, *J. Electroanal. Chem.*, 101, 177 (1979).
5) I. M. Kolthoff and I. B. Reddy, *J. Electrochem. Soc.*, **108**, 980 (1961).

6) J. P. Fackler, Jr., "Progress in Inorganic Chemistry," ed by F. A. Cotton, Interscience Publishers, John Wiley & Sons (1966), Vol. 7, p. 407.
7) F. A. Cotton and J. P. Fackler, Jr., *J. Am. Chem. Soc.*, **83**, 2818 (1961).
8) R. C. Buchta and D. H. Evans, *Anal. Chem.*, **40**, 2181 (1968).
9) P. Delahay, "Double Layer and Electrode Kinetics," Interscience Publishers, New York (1965), p. 205.
10) I. Yoshida, H. Kobayashi, and K. Ueno, *Bull. Chem. Soc. Jpn.*, **45**, 1411 (1972).
11) G. Ritzler and M. Gross, *J. Electroanal. Chem.*, **94**, 209 (1978).
12) C. K. Mann and K. K. Barnes, "Electrochemical Reactions in Nonaqueous Systems," Marcel Dekker, New York (1970), p. 467.

Enzymatic Synthesis of New Pyridine Nucleosides. Clitidine and Its Amide Derivative[1)]

Shuichi TONO-OKA,* Yasuhiko SASAHARA, Akio SASAKI, Haruhisa SHIRAHAMA,†
Takeshi MATSUMOTO,† and Shichiro KAKIMOTO

Institute of Immunological Science, Hokkaido University, Sapporo 060
† *Department of Chemistry, Faculty of Science, Hokkaido University, Sapporo 060*

(Received February 28, 1980)

Two β-NAD-analogs were prepared utilizing a base-exchange reaction catalyzed by pig-brain NADase. These analogs were proved to contain a methyl 1,4-dihydro-4-iminonicotinate and a 1,4-dihydro-4-iminonicotinamide moiety. By successive hydrolytic degradations of these analogs, 1,4-dihydro-4-iminopyridine β-ribosides with 3-carboxyl and 3-carbamoyl groups were prepared in good yields. The former compound was identical with clitidine, a toxic pyridine nucleoside recently isolated from a toadstool. The present synthesis confirmed the 1,4-dihydro-4-imino β-riboside structure of clitidine. Preliminary biological tests showed that the 3-carbamoyl compound was more toxic than clitidine, suggesting that the amide derivative of clitidine is an essential toxic substance in the toadstool.

Recently, Konno *et al.*[2)] have isolated a new pyridine nucleoside, clitidine, as a toxic substance from a toadstool, *Clitocybe acromelalga*. Although the structure, 1-(β-D-ribofuranosyl)-1,4-dihydro-4-iminonicotinic acid (**1**), was assigned to the nucleoside by synthesis, no clear evidence has been given for the 1,4-dihydropyridine form and the β-configuration of the glycosidic linkage.

The pharmaceutical properties of clitidine were investigated in detail[3)] and it was pointed out that its toxicity was relatively weak for a toxic substance from a toadstool. We, therefore, had a doubt whether clitidine itself was a major component of the toxic substance or not. It was assumed that the substance might be an amide form (**2**) in the toadstool.

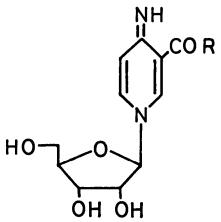

1 R = OH
2 R = NH_2

In order to clarify the ambiguous points, we tried to synthesize these pyridine nucleosides by enzyme-catalyzed reactions. Compared with the chemical synthesis by Konno *et al.*,[2)] which consists of six steps involving a laborious process, the enzymatic synthesis can be performed in three steps with high stereospecificity and good yield of product under mild conditions.

Nicotinamide ribonucleoside[4)] has been prepared by successive enzymatic cleavages of β-NAD. On the other hand, many NAD-analogs[5)] have been prepared by utilizing pig-brain NADase which has β-transglycosidase action along with glycohydrolase activity. These methods were successfully applied to the case of the derivatives of 4-aminonicotinic acid.

The present paper describes details of the preparation of the new NAD-analogs (**4**, **6**), and the degradative synthesis of clitidine (**1**) and its amide derivative (**2**) from the analogs.

Results and Discussion

Preparation of NAD-analogs. When 4-aminonicotinic acid and β-NAD were incubated with pig-brain NADase, only ADP-ribose was produced and no NAD-analog could be detected in which a nicotinamide moiety was replaced by 4-aminonicotinic acid. On the other hand, when methyl 4-aminonicotinate was used as a replacing base, the exchange reaction occurred successfully and yielded the expected analog together with ADP-ribose. These two compounds could be separated and purified by chromatography on DEAE-Sephadex; they provided the ester analog (**4**) and ADP-ribose (**7**) in a ratio of about 2:1. The IR spectrum of **4** showed an ester carbonyl band at 1715 cm^{-1} in place of an amide carbonyl band. The ^{1}H-NMR spectrum also showed an ester methyl group at δ 3.95 (s, 3H) and three protons on the 3,4-disubstituted pyridine ring, together with those of an ADP-ribosyl group (Table 2), indicative of the NAD-analog containing a methyl 4-aminonicotinate moiety.

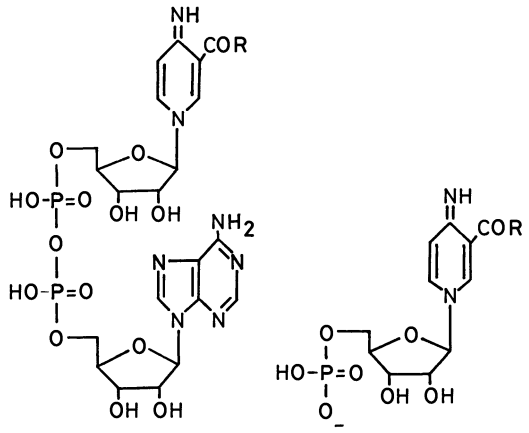

4 R = OCH_3
5 R = OH
6 R = NH_2

10 R = OCH_3
11 R = OH
12 R = NH_2

The formation of a NAD-analog in this base-exchange reaction is considered to proceed in competition with water for an enzyme–ADP-ribose complex

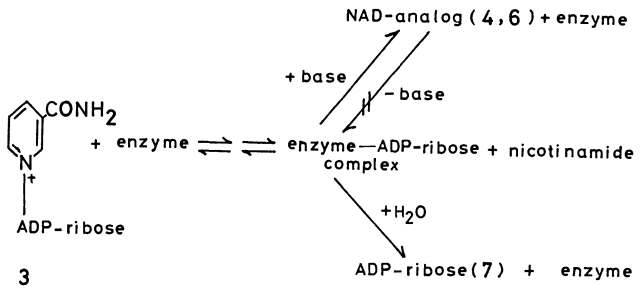

Scheme 1.

(Scheme 1).[6] According to this assumption, a base concentration would have a marked influence on the formation of the analog. In fact, the yield of **4** (based on NAD used) was apparently dependent on the base concentration (Table 1). When NAD was kept at a definite concentration, the yield increased with the concentration of methyl 4-aminonicotinate, becoming almost constant above 25 mM, where the reaction mixture attained a nearly saturated solution of the base. However, the yield was essentially unaffected by the NAD concentrations (Table 1). In the previous communication,[1] the base/NAD in 4:1 ratio has been proved to be useful for this reaction. Accordingly, it was practical to perform the reaction around 7 mM (1 M=1 mol dm^{-3}) NAD and at not less than 25 mM base.

The amide analog (**6**) was also prepared from 4-aminonicotinamide and NAD in a similar manner. In this case, the base concentration could be raised above 45 mM, resulting in a notably higher yield of **6** as compared with that of **4** (Table 1). The ^{1}H-NMR spectrum of **6** showed essentially the same pattern as that of **4** except for the absence of the signal at δ 3.95.

The demethylated analog (**5**) was obtained in 84% yield by treating **4** with 0.2 M NH_4OH at 40 °C for 12 h. In this case, no cleavage of the glycosidic linkage between pyridine and ADP-ribose moieties was observed during the reaction, although NAD was easily cleaved under the same conditions.

The NAD-analogs prepared by Kaplan *et al.*[5] were all susceptible, more or less, to the hydrolase action of NADase. On the other hand, the new analogs (**4**—**6**) were resistant to this action even if they were incubated with NADase for 24 h. These findings show the irreversible formation of the new analogs at the final step (Scheme 1), suggesting the difference in the character of glycosidic linkage between the two kinds of analogs.

Table 1. Effect of the base concentration on the yield of the analogs

Base concn/mM	Yield (%)[a] of analogs			
	4		**6**	
	4 mM NAD	8 mM NAD	4 mM NAD	8 mM NAD
5	23	14	39	32
10	31	40	52	54
15	49	52	65	64
20	55	57	70	73
25	62	63	74	76
30	63	65	76	77
40	—	—	79	78
50	—	—	79	80

a) The yield was estimated on TLC using a thin layer scanner (see Experimental).

Degradation of NAD-analogs. Nucleosides were prepared *via* mononucleotides by hydrolytic cleavages of the analogs obtained above.

By treatment with phosphodiesterase (PDE, optimum pH 9), followed by chromatographic purification, compounds **5** and **6** gave demethyl and amide mononucleotides (**11**, **12**) in quantitative yield, respectively, along with adenylic acid (**13**).

Compound **4** was found to demethylate slowly during the incubation at pH 9, although methyl 4-aminonicotinate itself remained unchanged under the same conditions. Thus, treatment of **4** with PDE resulted in the formation of a mixture of ester mononucleotide (**10**) and **11** in a ratio of about 1:1. On the other hand, treatment of **4** with pyrophosphatase (optimum pH 7) gave **10** predominantly in 85% yield together with a small amount of **11**. Accordingly, it is preferable to use pyrophosphatase for the preparation of **10**, though the reaction rate is slower than for PDE because of the product inhibition[7] by the adenylic acid formed.

Incubation of **11** with 5′-nucleotidase at pH 9, followed by column chromatography, provided the desired nucleoside (**1**) quantitatively; on crystallization from aqueous ethanol it gave white needles: mp 205—207 °C (dec), $[\alpha]_D^{20}=-53.4°$ (H_2O), λ_{max} 271 nm (log ε 4.32, H_2O). The mixed mp of **1** with authentic clitidine was undepressed, and the spectral properties and TLC mobility were also in good agreement with those of the sample.

In a similar manner, an amide nucleoside (**2**) was obtained in nearly quantitative yield by dephosphorylation of **12**. However, unlike the case of **1**, the purification of **2** could not be achieved by the ion exchange chromatography alone owing to concomitance with inorganic salts. In order to remove the impurities, further repeated chromatography on Sephadex G-10 was required and the nucleoside was purified to give a white crystalline mass: mp 145—147 °C (dec), $[\alpha]_D^{20}=-62.8°$ (H_2O), λ_{max} 272 nm (log ε 4.30, H_2O).

Dephosphorylation of **10** was also attempted at pH 8, where the ester moiety remained unchanged. Although the reaction was observed to proceed successfully on TLC, the ester nucleoside could not be obtained, contrary to our expectation, because the ester was readily hydrolyzed during the purification procedures (pH 7).

Some Chemical Aspects of the Compounds Obtained. In the ^{1}H-NMR spectra (Table 2), two anomeric protons of the new analogs (**4**, **6**) appeared as two clear doublets around δ 5.6 (J=5.0 Hz) and δ 6.0 Hz (J=5.5 Hz), separately. Based on the spectral pattern of the mononucleotides (**10**—**12**) and adenylic acid (**13**), the former doublet was assigned to the anomeric proton of the pyridine side. On the other

Table 2. The ^{1}H-NMR spectra of major products and related compounds[a)]

Compd no.	Chemical shifts/δ[b)]							Coupling constants/Hz[c,d)]	
	py-H_2	py-H_5	py-H_6	py-$C_1'H$	ad-H_2	ad-H_8	ad-$C_1'H$	$J_{2,6}$	$J_{5,6}$
3	9.47 s	8.35 dd	9.33 d	6.1 bd	8.42 s	8.59 s	6.1 bd	0.0	6.0
4	8.75 d	6.90 d	8.13 dd	5.64 d	8.08 s	8.32 s	6.00 d	1.5	7.5
6	8.55 d	6.85 d	8.10 dd	5.60 d	8.02 s	8.35 s	6.00 d	1.5	7.5
9	8.71 s	7.75 d	8.63 d	6.0 bd	8.02 s	8.33 s	6.0 bd	0.0	6.0
11	8.73 d	7.03 d	8.25 dd	5.72 d	—	—	—	1.5	7.5
12	8.80 d	7.10 d	8.30 dd	5.65 d	—	—	—	1.5	7.5
13	—	—	—	—	8.10 s	8.50 s	6.05 d	—	—
1	8.70 d	6.92 d	8.10 dd	5.67 d	—	—	—	1.5	7.5
2	8.75 d	6.97 d	8.18 dd	5.65 d	—	—	—	1.5	7.5

a) The spectra were measured in D_2O at 60 MHz, and the abbreviations "py-H_2 and ad-H_2" refer to the protons at C_2 of pyridine and adenine nuclei, respectively. b) The chemical shifts of the ribose protons fell within δ 3.8—4.5 as a broad peak (**4**, **6**) or two broad singlets (**11**, **12**, **1**, **2**). c) The coupling constants were estimated by first-order approximation. d) $J_{H_1'H_2'(py)}$ and $J_{H_1'H_2'(ad)}$ were 5.0 and 5.5 Hz, respectively, for all compounds except for **3** and **9**.

hand, two anomeric protons of the analogs so far prepared including isonicotinic acid-, and 4-methylnicotinamide analogs (**8**, **9**)[8,9] as well as NAD (**3**), which are known to take a pyridinium form, appeared at *ca.* δ 6.0 as a broad doublet.

The coupling constant between H_5 and H_6 on the pyridine nucleus was estimated to be 7.5 Hz for the new compounds, whereas it was 6.0 Hz for the compounds of the pyridinium form. According to Renault *et al.*,[10] the coupling between H_2 and H_3 on the nucleus of 4-aminoquinoline was 8 Hz for the imino form and 5 Hz for the amino form.

In the UV spectra, compounds **4** and **6** showed a strong absorption maximum at 264 nm in spite of the fact that the pyridine bases and ADP-ribose had the maximum at 252 and 259 nm, respectively. As the analogs were cleaved in turn to the nucleoside, a further bathochromic shift was observed from 264 nm to 271 nm or above. In addition, it was reported previously[11] that 4-aminopyridine exhibited the absorption peak at 242 nm in contrast to that of *N*-methyl-1,4-dihydro-4-iminopyridine at 268 nm.

These observations confirmed the 1,4-dihydro-4-imino β-riboside structure of the compounds prepared here.

Toxic Activity and Stability of Nucleosides. LD_{50}-values of clitidine (**1**) and its amide derivative (**2**) were estimated to be 100 and 16 mg/kg by preliminary tests (mice, intraperitoneal).

The carbamoyl group of **2** proved to be quite susceptible to hydrolysis, based on the results from TLC. When treated with boiling water for 5 h, compound **2** was completely hydrolyzed to yield **1**, and with hot water (70 °C) about 70% of **2** was converted to **1**. On the other hand, 4-aminonicotinamide was quite stable under these conditions. Additionally, compound **2** was completely converted to **1** on standing in 0.1 M NaOH at ambient temperature for 24 h, whereas it remained essentially unchanged on standing in water under the same conditions.

These results suggest the possible existence of the amide nucleoside (**2**) in the toadstool and conversion of **2** into **1** during extraction procedures.

Experimental

All melting points were uncorrected. IR and UV spectra were recorded on a Shimadzu IR-27G and a Hitachi 200-20 spectrophotometers, respectively. ^{1}H-NMR spectra were determined on a Hitachi R-20B (60 MHz) spectrometer in deuterium oxide with sodium 2,2-dimethyl-2-silapentane-5-sulfonate as an internal standard. The abbreviations "s, d, dd, br, bs, and bd" denote "singlet, doublet, double doublet, broad, broad singlet, and broad doublet", respectively Optical rotations were measured with a Union PM 101 polarimeter. All the reactions were monitored by TLC on silica gel $60F_{254}$ plates (Merck, 10×10 cm) developed with 2-propanol–0.3% aqueous ammonia (7:3, v/v). The analyses of the chromatograms obtained were performed by a Shimadzu CS-910 scanner equipped with a chromatopack C-R1A. Column chromatographies[12] were carried out on DEAE-Sephadex A-25 connected to LKB Uvicord II (254 nm), unless stated otherwise. β-NAD (Grade III), phosphodiesterase (EC 3.1.4.1, snake venom, Type II), nucleotide pyrophosphatase (EC 3.6.1.9, snake venom, Type II), and 5′-nucleotidase (EC 3.1.3.5, snake venom, Grade IV) were purchased from Sigma Chemical Co.

Pig-brain NADase. The crude enzyme was prepared by the method of Zatman *et al.*[5a] The colloidal supernatant fluid obtained containing about 0.4 U[13] of NADase activity per ml was used without further purification.

4-Aminonicotinic Acid. Prepared from 3-methylpyridine in four steps, and recrystallized from water: mp 318—320 °C (dec) [lit,[14] 330 °C (dec)].

Methyl 4-Aminonicotinate. Prepared by esterification of the above compound, and recrystallized from water: mp 171—173 °C (lit,[15] 174—176 °C).

4-Aminonicotinamide. Prepared from 3-methylpyridine in six steps, and recrystallized from benzene: mp 227—229 °C (lit,[16] 232—234 °C).

Methyl 1,4-Dihydro-4-iminonicotinate Analog of NAD (4). Methyl 4-aminonicotinate (4.8 mmol, 730 mg) and NAD (1.2 mmol, 800 mg, neutralized with 2 M NaOH to pH 7) were incubated with pig-brain NADase (12 U, 30 ml) in 0.1 M Tris-HCl (pH 7.4, 130 ml) at 37 °C for 8 h. After removal of denatured protein by addition of 70% trichloroacetic acid (2 ml), cold acetone (800 ml) was added to the

clear supernatant to give a yellowish hygroscopic powder (720 mg). The crude product thus obtained was dissolved in water (20 ml) and applied to a column of DEAE-Sephadex (HCO_2^--form) (column size; 2.5 cm × 45 cm). The column was eluted with 300 ml portions of 0.02, 0.2, and 0.5 M HCO_2NH_4 (pH 7), successively. The first major component was eluted with the 0.2 M solution. The eluate (70 ml) showing an UV-absorbing peak at 264 nm was collected and lyophilized repeatedly to give **4** (420 mg) as the ammonium salt. An analytical sample of **4** was obtained by further chromatography and drying over P_2O_5 *in vacuo* for 12 h at 40 °C: $[\alpha]_D^{20} = -26.7°$ (*c* 3.22, H_2O); IR (KBr), 3300—2800, 1715, 1655, 1200, 1100, 1065 cm^{-1}; UV (H_2O), λ_{max} 264 nm (log ε 4.27); ^{1}H-NMR (Table 2). Found: C, 35.92; H, 5.13; N, 16.85%. Calcd for $C_{22}H_{29}N_7O_{15}P_2 \cdot 2NH_3$: C, 36.49; H, 4.83; N, 17.41%.

The second major component was eluted with the 0.5 M solution. The eluate (80 ml) showing an UV-absorbing peak at 259 nm was treated in a similar manner to give the product (190 mg), which was identical with authentic ADP-ribose on spectral comparisons.

*1,4-Dihydro-4-iminonicotinamide Analog of NAD (**6**).* 4-Aminonicotinamide (9.3 mmol, 1270 mg) and NAD (2.2 mmol, 1500 mg) were incubated with NADase (16 U, 40 ml) in 0.1 M Tris-HCl (160 ml) for 7 h. The reaction mixture was treated in a similar manner to that described above to give the crude product (1346 mg), which was dissolved in water (30 ml) and applied to a column (HCO_3^--form). The column was eluted with aqueous NH_4HCO_3 (pH 8) in a similar manner to that described above. The first major component was eluted with the 0.2 M solution. The eluate (80 ml) showing a UV maximum at 264 nm was collected and lyophilized repeatedly to give **6** (1035 mg) as the ammonium salt: $[\alpha]_D^{20} = -32.6°$ (*c* 0.37, H_2O); IR (nujol), 3400—2700, 1675, 1580, 1235 cm^{-1}; UV (H_2O), λ_{max} 264 nm (log ε 4.29); ^{1}H-NMR (Table 2). Found: C, 34.25; H, 4.71; N, 19.62%. Calcd for $C_{21}H_{28}N_8O_{14}P_2 \cdot 2NH_3 \cdot H_2O$: C, 34.52; H, 4.93; N, 19.18%.

*Yield Determination of **4** and **6**.* A series of mixtures (1 ml), containing various amounts of methyl 4-aminonicotinate or 4-aminonicotinamide, 4 or 8 μmol of NAD, and NADase (0.12 U) was incubated for 6 h. The aliquots of the reaction mixture were analyzed by TLC using a thin layer scanner with a chromatopack. On the basis of the chromatograms thus obtained, the ratios of the analogs (**4**, **6**) to ADP-ribose (**7**) were evaluated. This method was based on the fact that **4** or **6** and **7** had nearly the same ε-values at 262 nm. The data shown in Table 1 display the averages of three measurements.

*1,4-Dihydro-4-iminonicotinic Acid Analog of NAD (**5**).* Compound **4** (300 mg) was treated with 0.2 M NH_4OH (3 ml) for 12 h at 40 °C. The residue obtained on evaporation of the resulting solution was purified as described for **6** to give **5** (245 mg) as an ammonium salt: $[\alpha]_D^{20} = -31.5°$ (*c* 0.72, H_2O): UV (H_2O), λ_{max} 263 nm (log ε 4.30); ^{1}H-NMR (δ, D_2O), 4.2—4.6 (10H, br, riboses), 5.60 (1H, d, J=5.0 Hz, py-C$_i$H), 6.05 (1H, d, J=5.5 Hz, ad-C$_i$H), 6.80 (1H, d, J=7.5 Hz, py-H$_5$), 8.06 (1H, dd, J=7.5, 1.5 Hz, py-H$_6$), 8.17 (1H, s, ad-H$_2$), 8.43 (1H, s, ad-H$_8$), 8.50 (1H, d, J=1.5 Hz, py-H$_2$). Found: C, 35.02; H, 4.96; N, 15.22%. Calcd for $C_{21}H_{27}N_7O_{15}P_2 \cdot 2NH_3$: C, 35.34; H, 4.63; N, 15.17%.

*1,4-Dihydro-4-iminonicotinic Acid Mononucleotide (**11**).* Compound **5** (539 mg) was incubated with PDE (20 U) in 0.2 M Tris-HCl (pH 9.0, 5 ml) containing $MgCl_2$ (3 mg) at 37 °C for 12 h. In order to reduce the ionic strength, the reaction mixture was diluted with water (250 ml) and applied to a column (HCO_3^--form), followed by successive elution with 200 ml portions of 0.02, 0.2, and 0.5 M NH_4HCO_3 (pH 8). The first major component was eluted with the 0.2 M solution. The eluate (70 ml) showing UV maximum at 268 nm were collected and lyophilized repeatedly to give **11** (260 mg) as the ammonium salt: $[\alpha]_D^{20} = -52.3°$ (*c* 0.65, H_2O); UV (H_2O), λ_{max} 268 nm (log ε 4.31); ^{1}H-NMR (Table 2). Found: C, 35.62; H, 5.07; N, 11.85%. Calcd for $C_{11}H_{15}N_2O_9P \cdot NH_3$; C, 35.97; H, 4.90; N, 11.44%.

Similar treatment of the second major component eluted with the 0.5 M solution gave **13** (255 mg), which was identical with authentic ammonium adenylate on spectral comparisons.

*Methyl 1,4-Dihydro-4-iminonicotinate Mononucleotide (**10**).* Compound **4** (184 mg) was incubated with pyrophosphatase (15 U) in 0.2 M Tris-HCl (pH 7.4, 4 ml) containing $MgCl_2$ (3 mg) for 22 h. The reaction mixture on dilution with water (80 ml) was applied to a column (HCO_2^--form). The column was eluted with aqueous HCO_2NH_4 (pH 7) as described for **11**, followed by lyophilization of the major components eluted with the 0.2 M solution, to give **10** (76 mg) and small amounts of **11** (8 mg). Analytical sample of **10** was obtained by further chromatography and drying over P_2O_5 *in vacuo* for 12 h at 40 °C: $[\alpha]_D^{20} = -50.8°$ (*c* 3.23, H_2O); UV (H_2O), λ_{max} 269 nm (log ε 4.28); ^{1}H-NMR (δ D_2O), 4.00 (3H, s, CO_2CH_3), 4.2 (2H, bs, ribose), 4.45 (3H, bs, ribose), 5.76 (1H, d, J=5.0 Hz, py-C$_i$H), 7.20 (1H, d, J=7.5 Hz, py-H$_5$), 8.47 (1H, dd, J=7.5, 1.5 Hz, py-H$_6$), 9.03 (1H, d, J=1.5 Hz, py-H$_2$). Found: C, 37.47; H, 5.42; N, 10.88%. Calcd for $C_{12}H_{17}N_2O_9P \cdot NH_3$: C, 37.80; H, 5.25; N, 11.02%.

*1,4-Dihydro-4-iminonicotinamide Mononucleotide (**12**).* Compound **6** (750 mg) was incubated with PDE (20 U) in 0.2 M Tris-HCl (pH 9.0, 6 ml) containing $MgCl_2$ (4 mg) for 16 h. The reaction mixture was treated as described for **11** to give **12** (328 mg) as ammonium salt: $[\alpha]_D^{20} = -55.2°$ (*c* 0.85, H_2O); UV (H_2O), λ_{max} 269 nm (log ε 4.30); ^{1}H-NMR (Table 2). Found: C, 35.71; H, 5.40; N, 15.62%. Calcd for $C_{11}H_{16}N_3O_8P \cdot NH_3$: C, 36.07; H, 5.19; N, 15.30%.

*1,4-Dihydro-5-iminonicotinic Acid Ribonucleoside (**1**).* Compound **11** (260 mg) was incubated with 5′-nucleotidase (40 U) in 0.2 M Tris-HCl (pH 9.2, 3.5 ml) containing $MgCl_2$ (8 mg) for 12 h. The mixture was maintained at pH 9 by occasional addition of 0.2 M NaOH. The precipitated phosphate salt was removed by filtration. The filtrate was then diluted with water (60 ml) and applied to a column (HCO_3^--form), which was eluted with 0.02 M NH_4HCO_3. The eluate (60 ml) having UV absorption was lyophilized to give **1** (192 mg) as a white crystalline mass, which on recrystallization from aqueous ethanol gave an analytical sample as white needles: mp 206—208 °C (dec) (lit,[2] 189—191 °C); $[\alpha]_D^{20} = -56.8°$ (*c* 0.75, H_2O); IR (nujol), 3400—3000, 1665, 1580, 1190 cm^{-1}; UV (H_2O), λ_{max} 271 nm (log ε 4.31); ^{1}H-NMR (Table 2). Found: C, 46.39; H, 5.35; N, 9.55%. Calcd for $C_{11}H_{14}N_2O_6 \cdot H_2O$: C, 45.83; H, 5.60; N, 9.72%.

*1,4-Dihydro-4-iminonicotinamide Ribonucleoside (**2**).* Compound **12** (255 mg) was incubated with 5′-nucleotidase (40 U) in 0.2 M Tris-HCl (pH 9.2, 3.5 ml) containing $MgCl_2$ (8 mg) for 10 h. The mixture was maintained at pH 9 during the reaction by occasional addition of 0.2 M NaOH. The resulting mixture was treated as described for **1**, followed by further repeated chromatography on Sephadex G-10 (column size; 2.5 × 100 cm) to give **2** (188 mg) as a white crystalline mass: mp 145—147 °C (dec); $[\alpha]_D^{20} = -62.8°$ (*c* 0.875, H_2O); IR (nujol), 3350—2700, 1675, 1600, 1290 cm^{-1}; UV (H_2O), λ_{max} 272 nm (log ε 4.30); ^{1}H-NMR (Table

2). Found: C, 43.55; H, 6.13; N, 13.88%. Calcd for $C_{11}H_{15}N_3O_5 \cdot 2H_2O$: C, 43.27; H, 6.26; N, 13.76%.

The authors wish to thank Prof. J. K. Seydel, Forschungsinstitut Borstel, West Germany, for his continuing interest and encouragement. They are also grateful to Prof. I. Azuma and Dr. I. Sekikawa for their helpful dicussions and suggestions during this work.

References

1) A part of this work was reported in a preliminary form: S. Tono-oka, A. Sasaki, H. Shirahama, T. Matsumoto, and S. Kakimoto, *Chem. Lett.*, **1977**, 1449.

2) K. Konno, K. Hayano, H. Shirahama, H. Saito, and T. Matsumoto, *Tetrahedron Lett.*, **1977**, 481.

3) I. Ushizawa, N. Katagiri, T. Kato, and N. Taira, *Medicine Biol.*, **94**, 251 (1977).

4) N. O. Kaplan, "Methods in Enzymology," Academic Press, New York (1955), Vol. 2, p. 660.

5) a) L. J. Zatman, N. O. Kaplan, S. P. Colowick, and M. M. Ciotti, *J. Biol. Chem.*, **209**, 467 (1954); b) B. M. Anderson, C. J. Ciotti, and N. O. Kaplan, *ibid.*, **234** (1959); c) P. Walter and N. O. Kaplan, *ibid.*, **238**, 2823 (1963).

6) J. L. Webb, "Enzyme and Metabolic Inhibitors," Academic Press, New York (1966), Vol. II, p. 485.

7) R. C. Nordlie and H. A. Lardy, *Biochem. Biophys. Acta*, **53**, 309 (1961).

8) J. K. Seydel, S. Tono-oka, K. -J. Schaper, L. Bock, and M. Wiencke, *Arzneim. -Forsch.*, **26**, 477 (1976).

9) M. Jarman and F. Searle, *Biochem. Pharmacol.*, **21**, 455 (1972).

10) J. Ranault and J. C. Carton, *C. R. Acad. Sci., Ser. C*, **262**, 1161 (1966).

11) S. F. Mason, *J. Chem. Soc.*, **1960**, 219.

12) Details concerning the reasons for this chromatography have been discussed: S. Tono-oka, A. Sasaki, and S. Kakimoto, *Bull. Inst. Immun. Sci. Hokkaido Univ.*, **38**, 46 (1978).

13) 1 U is the amount of enzyme which will cleave 1 μmol of the corresponding substrate per min.

14) W. Herz and D. R. K. Murty, *J. Org. Chem.*, **26**, 122 (1961).

15) W. C. J. Ross, *J. Chem. Soc., C*, **1966**, 1816.

16) T. Wieland and H. Biener, *Chem. Ber.*, **96**, 266 (1963).

Syntheses of [1]Benzopyrano[4,3-*c*]pyrazoles and -[3,4-*d*]isoxazoles

Tomio SHIMIZU,* Yoshiyuki HAYASHI, Kazunari YAMADA,
Toshiyuki NISHIO, and Kazuhiro TERAMURA
Department of Dyeing, Faculty of Industrial Arts, Kyoto Technical University, Matsugasaki, Sakyo-ku, Kyoto 606
(Received March 31, 1980)

The reaction of 2*H*-1-benzopyran with several 1,3-dipoles gives cycloadducts in good yields. The orientation of the cycloaddition is qualitatively interpreted in terms of FMO theory. These heteropolycyclic compounds were also obtained from hydrazones of 3-aroyl-2*H*-1-benzopyrans, prepared from 3-cyano-2*H*-1-benzopyran.

Interest in the pharmacological activity[1a] and industrially useful chemical properties[2b] of a wide variety of heteropolycyclic compounds, for example, benzopyranopyrazoles,[2] -isoxazoles,[3] and -pyrroles,[4] has considerably increased in the past several years. These compounds have thus far prepared conveniently by intramolecular 1,3-dipolar cycloaddition reactions.[5]

Although the intermolecular reactions of various 1,3-dipoles with polycyclic compounds, such as benzofuran,[6,7] 1-benzothiophene,[6] indene,[7] and 2*H*-1-thiobenzopyran,[8] have been investigated, the reaction with 2*H*-1-benzopyran(**1**) has not been reported. The present paper describes a new, direct synthesis of [1]benzopyrano[4,3-*c*]pyrazoles by the reaction of 2*H*-1-benzopyran with several 1,3-dipoles and the structural determination of the cycloadducts.

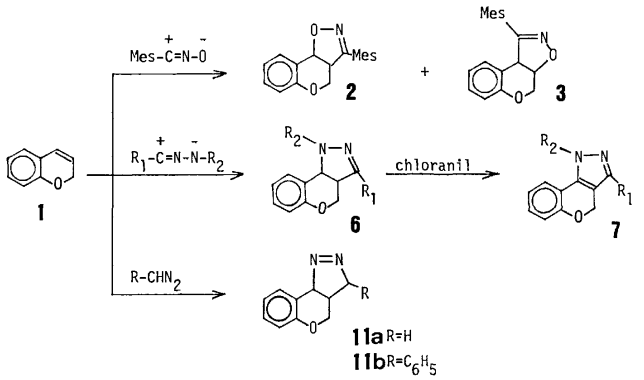

Scheme 1.

Results and Discussion

2*H*-1-Benzopyran(**1**) reacts readily with mesitonitrile oxide (MNO) in refluxing ether for over 4 h. The products are a mixture of the two regioisomers of a simple 1:1 cycloadduct (**2a** and **3a** in 35 and 4% yields respectively). Each regioisomer was isolated and characterized on a crystalline basis (see Table 1). In **3a**, the two benzene rings may lie on planes parallel to each other for steric reasons. Thus, the He proton in the benzopyran benzene ring is shielded and shifts upfield[9] (δ 6.4). While the chemical shift of normal *o*-methyl in the mesityl group usually appears about δ 2.2 (in **2a**, they appear at δ 2.33), one of the *o*-methyl group of **3a** does appear at δ 1.47. This upfield shift can also be ascribed to the shielding effect of the benzopyran benzene ring. One proton doublet at δ 5.6 is only compatible with the methine of benzyl ether (Ha in **2a**) (Table 1).

Benzonitrile oxide(BNO) failed to yield an isolable adduct with **1** under a variety of conditions, and 1,2,5-oxadiazole *N*-oxide (furoxan; a dimer of BNO) was the only isolable compound from the reaction mixture. The difference in the chemical reactivity between BNO and MNO and the regioselectivity of the cycloaddition may be explained in terms of the frontier molecular orbital (FMO) interactions[10] (Scheme 2). BNO has a much higher LUMO (2.19 eV) energy and a lower HOMO (−11.03 eV) energy[10a] than

TABLE 1. YIELDS, MELTING POINTS, AND ANALYTICAL DATA OF **2a** AND **3a**

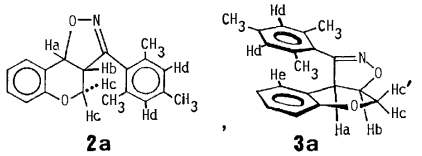

	Yield %	Mp °C	Found(Calcd) (%) C	H	N	NMR (δ) $CDCl_3$
2a	35	140—142	77.6 (77.8)	6.39 (6.48)	4.68 (4.78)	2.23(s, 6H, *o*-CH_3), 2.27(s, 3H, *p*-CH_3), 3.7—4.2(m, 3H, Hb and Hc), 5.6(d, 1H, Ha, J_{ab} = 8 Hz), 6.9(s, 2H, Hd), 6.7—7.6(m, 4H)
3a	4	127—130	77.5	6.46	4.76	1.5(s, 3H, *o*-CH_3), 2.27(s, 3H, *o*-CH_3), 2.37(s, 3H, *p*-CH_3), 4.03(dd, 1H, Hc), 4.40(dd, 1H, Hc'), 4.67(d, 1H, Ha, J_{ab} = 11 Hz), 5.27(dt, 1H, Hb, J_{bc} = 4 Hz), 6.4(d, 1H, He, J = 8 Hz), 6.73(s, 2H, Hd), 6.6—7.35(m, 3H)

TABLE 2. YIELDS, MELTING POINTS, AND ANALYTICAL DATA OF **6**, **7**, AND **14**

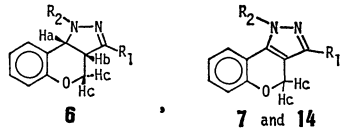

6 **7** and **14**

	R_1	R_2	Method[a]	Yield %	Mp[b] °C	Found(Calcd) (%) C	H	N	NMR (δ)[c]
6a	C_6H_5	C_6H_5	A	41	129—130	81.0	5.32	8.67	3.6—4.6(m, 3H, Hb and Hc), 4.7(d, 1H, Ha, J_{ab}=7 Hz), 6.8—8.0(m, 14H)
			B	75		(80.9)	(5.56)	(8.58)	
6b	C_6H_5	$C_6H_4NO_2$-*p*	A	40	230—233	69.4	4.38	10.5	4.0—4.9(m, 3H, Hb and Hc), 6.17(d, 1H, Ha, J_{ab}= 10 Hz), 6.8—8.0(m, 11H), 8.15(d, 2H, J=9 Hz)
			B	50		(71.2)	(4.61)	(11.3)	
6c	$C_6H_4NO_2$-*p*	C_6H_5	A	51	187—189	71.0	4.48	11.2	3.6—4.9(m, 3H, Hb and Hc), 4.94(d, 1H, Ha, J_{ab}= 8 Hz), 6.7—7.6(m, 9H), 7.7—8.4(m, 4H)
						(71.2)	(4.61)	(11.3)	
6d	$C_6H_4CH_3$-*p*	C_6H_5	A	48	179—180	80.7	5.89	8.22	2.33(s, 3H, CH_3), 3.5—4.5(m, 3H, Hb and Hc), 4.58 (d, 1H, Ha, J_{ab}=7 Hz), 6.67—7.37(m, 11H), 7.57(d, 2H, J=8 Hz)
			B	58		(81.2)	(5.92)	(8.23)	
6e	$C_6H_4CH_3$-*p*	$C_6H_4NO_2$-*p*	A	47	242—244	70.9	4.86	10.8	2.37(s, 3H, CH_3), 3.9—4.85(m, 3H, Hb and Hc), 6.15 (d, 1H, Ha, J_{ab}=10 Hz), 6,66—7,83(m, 10H), 8.13(d, 2H, J=9 Hz)
						(71.7)	(4.97)	(10.9)	
6f	CH_3	$C_6H_4NO_2$-*p*	B	40	209—210	65.5	4.80	13.5	2.15(s, 3H, CH_3), 3.75—4.8(m, 3H, Hb and Hc), 5.97 (d, 1H, Ha, J_{ab}=9 Hz), 6.7—7.7(m, 6H), 8.13(d, 2H, J=9 Hz)
						(66.0)	(4.89)	(13.6)	
7a	C_6H_5	C_6H_5	—	45	140—142	80.1	5.03	8.50	5.5(s, 2H, Hc), 6.6—7.8(m, 14H)
						(81.5)	(4.97)	(8.46)	
7b	C_6H_5	$C_6H_4NO_2$	—	52	236—241	71.2	4.05	10.9	5.5(s, 2H, Hc), 6.6—7.7(m, 11H), 8.16(d, 2H, J=9 Hz)
						(71.5)	(4.09)	(11.4)	
7c	$C_6H_4NO_2$	C_6H_5	—	50	220—224	70.8	4.01	11.2	5.5(s, 2H, Hc), 6.6—7.5(m, 9H), 7.6—8.4(m, 4H)
						(71.5)	(4.09)	(11.4)	
7d	CH_3	C_6H_5	—	38	148—149	77.6	5.45	10.1	2.2(s, 3H, CH_3), 4.58(d, 1H, Hc, J_{cc}=10 Hz), 4.82(d, 1H, Hc), 6.6—7.4(m, 9H)
						(77.8)	(5.38)	(10.7)	
14a	C_6H_5	H	B	72	230[d]				[f]
14b	CH_3	H	B	63	190[e]				[f]

a) A; Prepared by the cycloaddition reaction, B; Prepared by the reaction of **4** with aryl(or tosyl)hydrazines. b) Recrystallized from ethanol. c) **6b**, **6e**, **6f**, **14a**, and **14b** were dissolved in DMSO-d_6, the others were dissolved in $CDCl_3$. d) Lit,[2d] mp 230—233 °C. e) Lit,[2d] mp 197—202 °C. f) The IR and NMR spectra of these compounds were completely identical with authentic specimens.[2d]

pared by the intramolecular 1,3-dipolar cycloaddition reaction of *o*-allyloxyphenyldiazomethane (**10**). This result suggests that the structure of the intramolecular cycloadduct of **10** and the intermolecular cycloadduct of **1** with diazomethane is the same one (**11**), inconsistent with the regioisomers (**12** and **13** respectively).

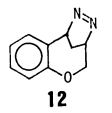

12

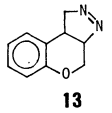

13

The regioselectivity of this reaction may be explained in terms of a dipole-HOMO controlled 1,3-dipolar cycloaddition (see Scheme 2). The treatment of phenyldiazomethane with **1** under similar conditions also gave an oily product, which was found to be compatible with the assigned structure (**11b**, R=C_6H_5). Several attempts to isolate the cycloadducts in the crystalline state were unsuccessful, and it is known that the pyrazolines(**11**) generally exhibit low melting points and are moderately sensitive to heating.[2c]

1 failed to undergo cycloadditions with other 1,3-dipoles, such as phenylazide or diphenylnitrone, under a variety of conditions.

While the 1,3-dipolar cycloadditions reported here gave reasonable yields of polycyclic heterocycles, it is hoped to develop methods of preparing authentic specimens with an unequivocal regiochemistry. In our previous paper,[2d] [1]benzopyrano[4,3-*c*]pyrazoles (**14**) were prepared from the reaction of **9** with Pb(OAc)$_4$ and subsequent treatment with potassium hydroxide. The structures of these pyrazoles were determined by comparison with an authentic specimen, prepared by the reaction of 3-formyl-4-chromanone (**15**) with hydrazine hydrochloride.[9] This latter method is rather cumbersome, however, because the synthesis of **15** involves multistep reactions. We found that the synthesis of **14** from 3-cyano-2*H*-1-benzopyran (**8**) shown in Scheme 3 gave more satisfactory results.

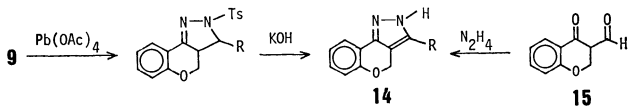

14 **15**

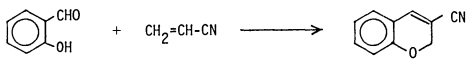

8

Table 3. Yields, melting and boiling points, and analytical data of **4**, **16**, and **17**

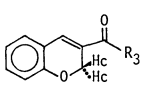

4

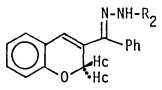

16 and **17**

	R_1	R_2	Yield %	Mp(Bp) °C	Found(Calcd) (%) C	H	N	IR (cm^{-1})	NMR(δ) DMSO-d_6(**16d** and **17b**) $CDCl_3$(Others)
4a	C_6H_5	—	33	(171/4 mmHg)	81.2 (81.3)	5.17 (5.12)	0 (0)	1640(C=O)	5.13(d, 2H, Hc, J=2 Hz), 6.67—7.83(m, 10H)
4b	$C_6H_4CH_3$-*p*	—	22	104 (182/4 mmHg)	81.4 (81.6)	5.60 (5.64)	0 (0)	1640(C=O)	2.5(s, 3H, *p*-CH_3), 5.2(s, 2H, Hc), 6.8—7.9(m, 9H)
4c	CH_3	—	41	(124/2 mmHg)	75.7 (75.8)	5.77 (5.79)	0 (0)	1660(C=O)	2.25(s, 3H, CH_3), 4.87(d, 2H, Hc, J=2 Hz), 6.6—7.3(m, 5H)
16a	C_6H_5	C_6H_5	70	155—158	80.9 (81.0)	5.79 (5.56)	8.66 (8.58)	3320(NH)	5.33(s, 2H, Hc), 5.95(s, 1H), 6.6—7.7(m, 15H)
16b	C_6H_5	$C_6H_4NO_2$-*p*	65	189—192	70.9 (71.2)	4.67 (4.61)	11.0 (11.3)	3300(NH)	5.30(d, 2H, Hc, J=2 Hz), 6.10(s, 1H), 6.7—7.9(m, 12H), 8.07(d, 2H, J=9 Hz)
16c	CH_3	C_6H_5	77	150—151	77.5 (77.3)	6.01 (6.10)	10.6 (10.6)	3350(NH)	1.97(s, 3H, CH_3), 5.2(d, 2H, J=1 Hz), 6.5(s, 1H), 6.6—7.4(m, 10H)
16d	CH_3	$C_6H_4NO_2$-*p*	88	202—204	66.3 (66.0)	4.77 (4.89)	13.8 (13.6)	3320(NH)	2.1(s, 3H, CH_3), 5.1(s, 2H, Hc), 6.67—7.4(m, 7H), 8.05(d, 2H, J=9 Hz), 10.1(s, 1H, NH)
17a	C_6H_5	SO_2-Tol-*p*	55	162—164	68.6 (68.3)	5.09 (4.99)	6.71 (6.93)	3220(NH) 1164(SO_2)	2.4(s, 3H, *p*-CH_3), 5.1(d, 2H, Hc, J=2 Hz), 6.05(s, 1H), 6.65—8.0(m, 14H)
17b	CH_3	SO_2-Tol-*p*	79	184—186	63.4 (63.2)	5.28 (5.30)	8.13 (8.18)	3220(NH) 1150(SO_2)	2.0(s, 3H, CH_3), 2.37(s, 3H, *p*-CH_3), 4.85(s, 2H, Hc), 6.67—8.0(m, 9H), 10.57(s, 1H, NH)

While the synthesis of benzopyrano derivatives using the Wittig reaction is very useful,[13] it is generally difficult to prepare 3-substituted-2*H*-1-benzopyran by this method.[14] A convenient one-step synthesis[16] of **8** (20% yield) is known, it is shown below. A modification of this preparative method was used, since, in our hands, it gave more satisfactory results (40—50% yield) when the reaction mixture was distilled. The **8** was treated with Grignard reagents, and the subsequent hydrolysis of the adducts gave 3-aroyl (or acetyl)-2*H*-1-benzopyrans (**4**). The treatment of **4** with arylhydrazines, *p*-tolylsulfonylhydrazine, or hydroxylamine gave the corresponding arylhydrazones (**16**), *p*-tolylsulfonylhydrazone (**17**), and oxime (**18**) respectively. The yields, melting points, and analytical data for these compounds (**4**, **16**—**18**) are given in Table 3. The treatment of **16** with acetic acid at 110 °C, or the treatment of the mixture of **4** and arylhydrazines with acetic acid at the same temperature, gave cyclized compounds which showed the same physical properties as the **6** prepared by the reaction of **1** with nitrilimines. The treatment of **17** with potassium hydroxide gave cyclized compounds which have the same physical properties as the specimens previously reported.[2d] All attempts to cyclize **18** to **2** failed.

Experimental

Measurements. All the melting and boiling points are uncorrected. The IR spectra were recorded with a Hitachi 215 Infrared Spectrophotometer. The NMR spectra were measured on a Varian T-60A instrument, with TMS as an internal standard.

Materials. 2*H*-1-Benzopyran was prepared by the method of Ide *et al.*[17]

*Preparation of 3-Cyano-2*H*-1-benzopyran(8).* The reaction of salicylaldehyde with acrylonitrile was carried out according to the literature.[16] The reaction mixture was poured into water and extracted with ether several times. A modification of a work-up by distillation *in vacuo* gave **8** (40—50% yield), which solidified in the condenser; bp 105—110 °C/2 mmHg, mp 48—49 °C (from ethanol) (lit,[16] 48—49 °C).

*Preparation of 3-Aroyl(or Acetyl)-2*H*-1-benzopyrans(4).* To an anhydrous ether solution of phenylmagnesium bromide (0.12 mol), we added, drop by drop, an anhydrous ether solution of **8** (0.1 mol) at 10—20 °C. After insoluble materials had thus been precipitated, the mixture was refluxed for 6 h. After cooling, 30% sulfuric acid (100 ml) was added, drop by drop, at 5—10 °C, and then the mixture was refluxed for 2 h. The insoluble material was filtered off using a Celite bed, and the ethereal layer was washed with a 5% sodium carbonate solution and dried over anhydrous sodium sulfate. The subsequent evaporation of the solvent yielded an oily material, which was subsequently distilled *in vacuo* to give **4a** in a 40% yield; bp 171—173 °C/4 mmHg. The spectral data are shown in Table 3.

Reaction of 1 with Mesitonitrile Oxide. A mixture of **1** (8 g, 60 mmol), mesitonitrile oxide (5 g, 31 mmol), and ether (70 ml) was refluxed for 4 d. The subsequent evaporation of the solvent yielded white crystals. Recrystallization from ethanol gave colorless needles of the cycloadduct (**2a**) (mp 140—142 °C, 3.2 g) and then **3a** (mp 127—130 °C, 350 mg). The spectral data are shown in Table 1.

Reaction of 1 with Nitrilimines. To a mixture of **1** (4 g, 30 mmol), triethylamine (4 g, 40 mmol), and benzene (50 ml), we added a benzene solution of hydrazonoyl chlorides (30 mmol), after which the mixture was refluxed for 20 h. The mixture was washed with water, and the subsequent evaporation of the solvent yielded pale yellow crystals. Recrystallization from ethanol gave the cycloadducts (**6**). The spectral data are shown in Table 2.

Dehydration of 6. The dehydration of **6** to **7** was carried out according to the literature.[18]

Reaction of 1 with Diazomethane. To an ether solution of **1** (5 g, 38 mmol), we introduced diazomethane gas (about 0.1 mol) at −15 °C in the dark, after which the mixture was stirred for 4 h at that temperature. Then the mixture was further stirred for 4 d at room temperature. After the evaporation of the solvent, the unreacted 2*H*-1-benzopyran was distilled *in vacuo* (2 mmHg). The NMR spectrum of the residue is completely identical with a previously reported one.[2c]

The Reaction of 4 with Aryl(or p-*Tolylsulfonyl)hydrazines.* An ethanol solution of **4** (20 mmol) and aryl (or *p*-tolylsulfonyl)hydrazines (20 mmol) was refluxed for 6 h. The subsequent evaporation of the solvent yielded a viscous oily material which solidified upon scratching with a glass rod. Recrystallization from ethanol gave colorless needles (**16** or **17**). The spectral data are shown in Table 3. We may also carry out this reaction at room temperature in acetic acid.

The Reaction of 4 with Hydroxylamine. This reaction was carried out in the manner described above.

The Treatment of 4 with Aryl (or p-*Tolylsulfonyl)hydrazines in Acetic Acid.* A mixture of **4** (20 mmol) and aryl (or *p*-tolylsulfonyl)hydrazines in acetic acid (100 ml) was refluxed for 4 h, poured into water, and extracted with benzene. The organic layer was dried over anhydrous sodium sulfate. The subsequent evaporation of the solvent yielded pyrazolines (**6**) in good yields.

The Treatment of 16 with Acetic Acid. A solution of **16** in acetic acid was refluxed for 3 h. The treatment of the reaction mixture in the manner described above yielded pyrazolines (**6**) in good yields.

The Treatment of 17 with Potassium Hydroxide. To a solution of potassium hydroxide (0.4 g, 3 mmol) in 95% aqueous ethanol (50 ml), we added **17** (2 mmol), after which the mixture was stirred for 1 h under refluxing. After the subsequent removal of the solvent from the reaction mixture, the residue was treated with water (50 ml) and extracted with ether (50 ml). The ethereal layer was then dried over anhydrous sodium sulfate. The evaporation of the solvent yielded **14** (about 70% yields).

*Reaction of 3-Benzoyl-2*H*-1-benzopyran with Benzonitrile Oxide (BNO).* To a benzene solution of **4a** (4.7 g, 20 mmol) and α-chlorobenzaldoxime (4 g, 26 mmol), we added a dilute solution of triethylamine (3 ml) in benzene (20 ml) at 5 °C and the mixture was further stirred at room temperature overnight. The mixture was washed with water and the organic layer was dried over sodium sulfate. The evaporation of the solvent yielded **5** in a 30% yield (2.1 g); mp 178—179 °C (from ethanol). NMR ($CDCl_3$) δ: 4.2 (d, 1H, J=11 Hz), 4.95 (d, 1H, J=11 Hz), 6.0 (s, 1H), 6.8—7.8 (m, 12H), and 7.8—8.1 (m, 2H). IR (Nujol): 1680 cm^{-1} (C=O). Found: C, 77.0; H, 4.85; N, 3.88%. Calcd for $C_{23}H_{17}O_3N$; C, 77.7; H, 4.82; N, 3.94%.

References

1) a) R. E. Brown and J. Shavel Jr., U. S. Patent 3624102; *Chem. Abstr.*, **76**, 59618 (1972); b) J. Freedman, U. S. Patent

3553228—3553230; *Chem. Abstr.*, **75**, 5881—5883 (1971).

2) a) H. Meier and H. Heimgartner, *Helv. Chim. Acta*, **60**, 3035 (1977); b) G. Schmidt and B. Laude, *Tetrahedron Lett.*, **1978**, 3727; A. Padwa, S. Nahm, and E. Sato, *J. Org. Chem.*, **43**, 1664 (1977); c) W. Kirmse and H. Dietrich, *Chem. Ber.*, **100**, 2710 (1967); d) T. Shimizu, Y. Hayashi, Y. Nagano, and K. Teramura, *Bull. Chem. Soc. Jpn.*, **53**, 429 (1980).

3) R. Fusco, L. Garanti, and G. Zecchi, *Chim. Ind. (Milan)*, **57**, 16 (1975).

4) a) L. Garanti, G. Padova, and G. Zecchi, *J. Heterocycl. Chem.*, **14**, 947 (1977); b) A. Padwa, P. H. J. Carlsen, and A. Ku, *J. Am. Chem. Soc.*, **99**, 2798(1977); **100**, 3494 (1978).

5) Review: A. Padwa, *Angew. Chem. Int. Ed. Engl.*, **15**, 123 (1976); W. Oppolzer, *ibid.*, **16**, 10 (1977).

6) P. L. Beltrame, M. G. Cattania, V. Radaelli, and G. Zecchi, *J. Chem. Soc., Perkin Trans. 2*, **1977**, 706.

7) P. Caramella, G. Cellerino, K. N. Houk, F. M. Albini, and C. Santiago, *J. Org. Chem.*, **43**, 3006 (1978).

8) L. M. Rossi and P. Trimarco, *Synthesis*, **1978**, 465.

9) F. M. Dean and S. Murray, *J. Chem. Soc., Perkin Trans. 1*, **1975**, 1706.

10) a) K. N. Houk, J. Sims, C. R. Watts, and L. J. Luskus, *J. Am. Chem. Soc.*, **95**, 7301 (1973); K. N. Houk, J. Sims. R. E. Duke, Jr., R. W. Strozier, and J. K. George, *J. Am. Chem. Soc.*, **95**, 7287 (1973); b) K. N. Houk, "Pericyclic Reactions. II," ed by R. E. Lehr and A. P. Marchand, Academic Press, New York (1977); I. Fleming, "Frontier Orbitals and Organic Chemical Reactions," John Wiley & Sons, New York (1976).

11) J. Bastide, N. El Chandour, and O. Henri-Rousseau, *Tetrahedron Lett.*, **1972**, 4225; J. Bastide, O. Henri-Rousseau, and L. Aspart-Pascot, *Tetrahedron*, **30**, 3355 (1974).

12) M. Bonadeo, C. De Micheli, and R. Gandolfi, *J. Chem. Soc., Perkin Trans. 1*, **1977**, 939.

13) E. E. Schweizer, *J. Am. Chem. Soc.*, **86**, 2744 (1964).

14) Recently, a preparation of 3-ethoxycarbonyl-2*H*-1-benzopyran was reported by Ide *et al.*,[15] but this method involves multistep reactions and thus results in a low overall yield.

15) J. Ide, R. Endo, and S. Muramatsu, *Chem. Lett.*, **1978**, 401.

16) H. V. Taylor and M. L. Tomlinson, *J. Chem. Soc.*, **1950**, 2724.

17) J. Ide and K. Iwai, *Chem. Pharm. Bull.*, **11**, 1042 (1963).

18) R. Huisgen, M. Seidel, G. Wallbillich, and H. Knupfer, *Tetrahedron*, **17**, 3 (1962).

19) T. Minato, S. Yamada, S. Inagaki, H. Fujimoto, and K. Fukui, *Bull. Chem. Soc. Jpn.*, **47**, 1619 (1974).

Stereochemical Studies of the Hydrogenation with an Asymmetrically Modified Raney Nickel Catalyst. The Hydrogenation of Acetylacetone

Akira TAI,* Kazuhisa ITO, and Tadao HARADA
Institute for Protein Research, Osaka University, Yamada-Kami, Suita, Osaka 565

(Received April 4, 1980)

The hydrogenation of acetylacetone (I) over asymmetrically modified Raney nickel (MRNi) proceeded, step by step, as follows: acetylacetone (I) $\xrightarrow{\text{Step 1}}$ 4-hydroxy-2-pentanone (II) $\xrightarrow{\text{Step 2}}$ 2,4-pentanediol (III). It was demonstrated that the optical yield of Step 1 and the diastereomer excess of Step 2 are governed by the ratio of the stereo-differentiating reaction site to the non-stereo-differentiating reaction site on the catalyst. The stereochemistry of each step was also discussed based on the mode of the intermolecular hydrogen bondings between the substrate and tartaric acid adsorbed on the catalyst. RNi modified with a mixture of tartaric acid and NaBr (TA–NaBr–MRNi) gave the best result with respect to both Step 1 and Step 2.

In a previous communication, we have briefly reported that the modification of Raney nickel (RNi) with an aqueous solution of tartaric acid (TA) and NaBr gave an excellent catalyst (TA–NaBr–MRNi) for the stereo-differentiating (asymmetric) hydrogenation of acetylacetone (I) to 2,4-pentanediol (III).[1]

Although the hydrogenation of I over various MRNi's has been conducted by our research group[2] and others,[3] and although some important features of the reaction have been reported, the details of the mechanism of the stereo-differentiation have not yet been made clear.

The stereochemical studies of this reaction with the use of the effective enantio-differentiating catalyst (TA–NaBr–MRNi) enable us to obtain clear-cut information for understanding the reaction mechanism of the modified catalyst.

As has been reported,[2] the hydrogenation of I over RNi proceeds by a successive two-step process, as is shown in Scheme 1:

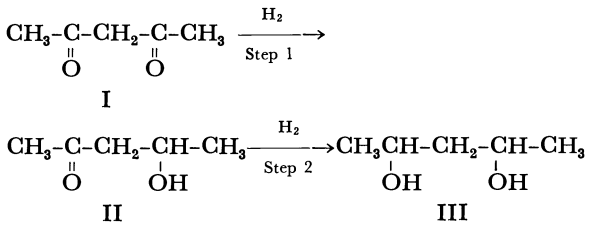

Scheme 1.

In this report, the study of each step will be described first, and then the relation of the two steps will be discussed.

Results and Discussion

Enantioface-differentiating Hydrogenation of I to II. The reaction of Step 1 with an asymmetrically modified catalyst is classified as an enantioface-differentiating reaction.[4] When the hydrogenation of I was stopped at the stage when the consumption of hydrogen reached a 1.1 molar equivalent to I, a mixture of I, II, and III was obtained. The results of the reactions carried out over three types of catalyst (RNi, TA–MRNi, and TA–NaBr–MRNi) are summarized in Table 1. The use of TA–NaBr–MRNi gave a higher optical yield than that of TA–MRNi. A comparable result has been obtained in the hydrogenation of methyl acetoacetate (MAA) to methyl 3-hydroxybutyrate (MHB).[5]

Our recent study[6] has shown that the optical yield of the MAA to MHB reaction is closely related to the ratio of the stereo-differentiating reaction site (the site where the substrate is converted to an optically active product by the aid of TA) to the non-stereo-differentiating reaction site (the site where a racemic product is produced) on the catalysts (hereafter, the abbreviations s.d. and non-s.d. will refer to the stereo-differentiating and non-stereo-differentiating reaction sites respectively). Furthermore, it has also been made clear that the proportion of the s.d. on the catalyst increases in the following order: RNi<TA–MRNi< TA–NaBr–MRNi. The NaBr on TA–NaBr–MRNi is considered to be adsorbed on the non-s.d. and to block the activity of the non-s.d. From the resemblance of the present results to those of MAA to MHB, the s.d. for the hydrogenation of MAA may also be said to function as the s.d. for the hydrogenation of I to II.

As may be found in Table 1, the catalyst giving a higher optical yield gives II in a larger proportion. This fact strongly suggests that both the optical purity and the proportion of II are governed by the ratio of the s.d. to non-s.d. The predominant formation of II in the case of TA–NaBr–MRNi indicates that the rate of Step 2 is appreciably slower than the rate of Step 1 at the s.d. From a comparison of the results with three catalysts (Table 1, Entries 1, 2, and 3), it is also evident that the rate of Step 2 at non-s.d. is higher than that at the s.d. That is, the s.d. and non-s.d. have different kinetics features.

I and MAA give (*R*)-II and (*R*)-MHB respectively in the hydrogenations with the catalyst modified with (*R,R*)-TA. When the structural similarity of I to MAA is taken into account, the mode of enantioface-differentiation of I with TA can be expected to be the same as that of MAA reported before.[7] The mode of the interaction between I and (*R,R*)-TA on the s.d. of the catalyst is shown in Figs. 1a and 1b. As may be found in Fig. 1b, one of the carbonyl groups in I to be hydrogenated comes close to the catalyst surface, with its si-face facing the catalyst, while the other, which remains unchanged, is located far from the catalyst. The considerable optical yield in the

Table 1. Hydrogenation of I to II

	Catalyst	Products (molar %) I	II	III	Optical purity (%) and configuration of II
1	RNi	22	34	44	—
2	(*R,R*)-TA-MRNi	9	60	31	35 (*R*)
3	(*R,R*)-TA-NaBr-MRNi	0	91	9	74 (*R*)
4	(*S,S*)-TA-NaBr-MRNi	0	90	10	73 (*S*)

Table 2. Hydrogenation of II to III

	Catalyst	Substrate	Products (molar %) (*R**,*R**)-III	(*R**,*S**)-III	d.e. (%)
1	RNi	racemic-II	61	39	21
2	RNi	(*R*)-II	49	51	−2[a]
3	(*R,R*)-TA-MRNi	(*R*)-II	64	36	28
4	(*R,R*)-TA-NaBr-MRNi	(*R*)-II	90	10	80
5	(*S,S*)-TA-NaBr-MRNi	(*R*)-II	45	55	−10[a]

a) The sign, (−) indicates excess (*R**,*S**)-III.

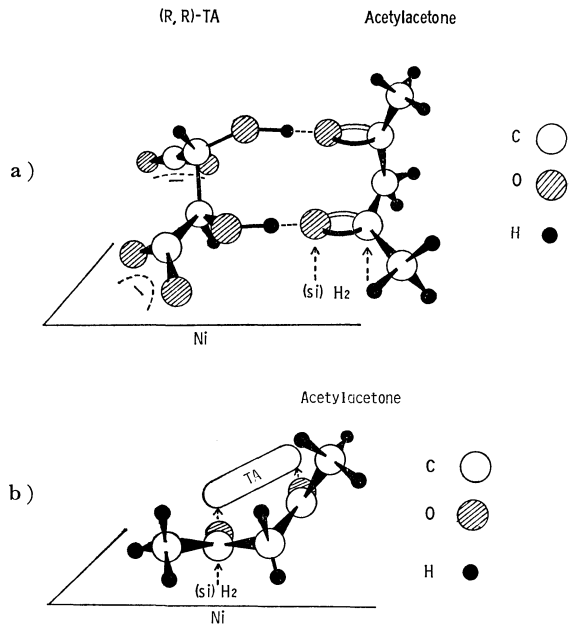

Fig. 1. Schematic representation of the interaction between (*R,R*)-TA and acetylacetone (I) on the catalyst.
a) Front view of coadsorbed species, b) side view of coadsorbed species.

reaction of I to II suggests that almost all of the I which has been adsorbed on the catalyst by interacting with (*R,R*)-TA is hydrogenated to (*R*)-II.

Diastereoface-differentiating Hydrogenation of II to III. 4-Hydroxy-2-pentanone, a substrate of Step 2, is a chiral compound. Therefore, the reaction of II to III is classified as a "diastereoface-differentiating reaction."[4] The efficiency of the reaction is expressed by the diastereomer excess (d.e.$=|(R^*,R^*)-(R^*,S^*)|/\{(R^*,R^*)+(R^*,S^*)\}$) of the product.

The results of the hydrogenation of II over various nickel catalysts are listed in Table 2. In the diastereo-differentiating reaction, the use of either an optically pure substrate or a racemic substrate can be expected to give a product with the same d.e. in principle so long as an achiral reagent or catalyst is used.[4]

In the hydrogenation with an unmodified RNi (Entries 1 and 2, Table 2), however, racemic II produces (*R**,*R**)-III in excess, while (*R*)-II gives (*R**,*R**)-III and (*R**,*S**)-III in almost the same ratio. This unusual result indicates that at least two chiral molecules, such as a substrate and a substrate, or a substrate and a product, are involved in the diastereo-differentiation step of the reaction. From the results presented above, the estimation of the inherent diastereoface-differentiating ability of RNi is found to be impossible. At any rate, a high d.e. is not expected in the reaction of II over unmodified RNi.

Entries 3 and 4, Table 2, show the results of the hydrogenation of (*R*)-II over (*R,R*)-TA–MRNi and (*R,R*)-TA–NaBr–MRNi. When (*R,R*)-TA–NaBr–MRNi was used, (*R*)-II was converted to (*R,R*)-III with 80% d.e.

On the other hand, the use of (*R,R*)-TA–MRNi resulted in the formation of (*R,R*)-III with a considerably low d.e. (28%). This great decrease in the d.e. is attributed to two characteristics of the non-s.d. remaining in the catalyst: 1) the d.e. at the non-s.d. is almost zero, as is expected from the result for RNi (Entry 2, Table 2) and 2) the hydrogenation rate at the non-s.d. is higher than that at the s.d., as has been mentioned in the previous section, so that a large portion of the substrate is hydrogenated at the non-s.d.

As is shown in Entries 4 and 5, Table 2, the hydrogenation of (*R*)-II over (*S,S*)-TA–NaBr–MRNi gave an extremely low d.e., in contrast with the high d.e. of the reaction of (*R*)-II over (*R,R*)-TA–NaBr–MRNi. That is, (*R,R*)-TA–NaBr–MRNi has a much higher diastereoface-differentiating ability than (*S,S*)-TA–NaBr–MRNi toward (*R*)-II. The origin of the high

Table 3. Enantiomer-differentiating hydrogenation of racemic-II

Catalyst		(*R,R*)-TA-NaBr-MRNi	(*S,S*)-TA-NaBr-MRNi
Conversion of hydrogenation (%)		55	43
Recovered-II,	Optical purity (%)	30	29
	Configuration	(*S*)	(*R*)
Hydrogenation products (molar %),			
	(*R,R*)-III	80	77
	(*R,S*)-III	20	23
(*R*,R**)-III,	Optical purity (%)	48	61
	Configuration	(*R,R*)	(*S,S*)

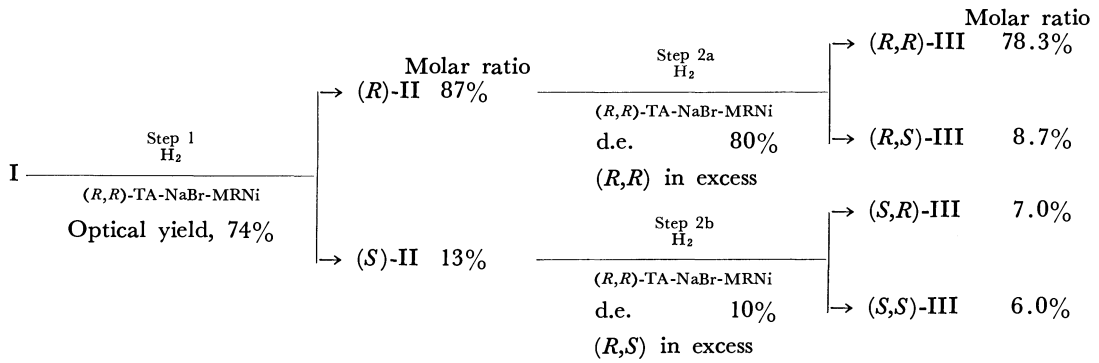

Scheme 2.

d.e. in the combination of *(R)*-II and *(R,R)*-TA–NaBr–MRNi will be explained in the following section.

Enantiomer-differentiating Hydrogenation of Racemic II over TA–NaBr–MRNi. Since II is a chiral compound and TA–NaBr–MRNi is an optically active catalyst, an enantiomer-differentiating hydrogenation could be involved in the course of the reaction of Step 2 if II is a mixture of *(R)*- and *(S)*-II.

As the enantiomer-differentiating reaction and the diastereoface-differentiating reaction are intimately related to each other from the stereochemical viewpoint, a comparison of these two reactions should provide useful information about the stereo-differentiation of the reaction, II to III. In this regard, the partial hydrogenation of racemic II was carried out over *(R,R)*- and *(S,S)*-TA–NaBr–MRNi. The optical purity of the II recovered and the d.e. of the III produced around 50% conversion are listed in Table 3.

As may be found in Table 3, *(R,R)*-TA–NaBr–MRNi hydrogenated *(R)*-II much faster than *(S)*-II. The reaction with *(S,S)*-TA–NaBr–MRNi gave the same results except for the reverse stereochemistry.

The existence of a large enantiomer-differentiation is attributed to the selective adsorption of *(R)*-II on *(R,R)*-TA–NaBr–MRNi, which is brought about by the preferential interaction between *(R)*-II and *(R,R)*-TA. The results in Table 3 also indicate that, if the stereochemistry of II and TA is compatible, thus making for interaction between them, *(R*,R*)*-III is obtained in a high d.e.

From the fact that the hydrogenations of both I and *(R)*-II over *(R,R)*-TA–NaBr–MRNi produce chiral centers with an *R* configuration, the interaction between *(R)*-II and *(R,R)*-TA is expected to be close to that between I and *(R,R)*-TA.

The mode of interaction between *(R)*-II and *(R,R)*-TA is shown in Fig. 2. In this case, two components are brought into a well-fitting interaction by making two hydrogen bondings between them. On the other hand, *(R)*-II and *(S,S)*-TA could not interact well, as is the case of *(R,R)*-TA in any type of arrangemant. The lack of interaction with two hydrogen bondings between TA and II should cause a loss not only of the rigorous stereo-differentiation, but also of the potency of the associative adsorption of II on the catalyst.

From the all discussion presented above, the ratio of diastereomers in the reaction of II to III is governed by both the ratio of s.d. to non-s.d. on the catalyst and the stereochemical compatibility of II and TA.

The Participations of the Enantioface-, Diastereoface-, and Enantiomer-differentiating Reactions in the Process of the I to III Reaction. Based on the data of the separate reactions, I to II and II to III (Entry 3 in Table 1 and Entries 4 and 5 in Table 2), the material balance of the I to III reaction over *(R,R)*-TA–NaBr–MRNi is estimated to be as is shown in Scheme 2. Table 4 shows the proportion of diastereomers and the optical purity of *(R*,R*)*-III observed in the hydrogenation of I to III at a 100% conversion (Entry 2) and those calculated from the figures in Scheme 2 (Entry 3). The good agreement between the observed and calculated values clearly shows that the hydrogenation of the first and second carbonyl group proceeds step by step.

As may be found in Scheme 2, both the enantio-differentiation in Step 1 and the diastereo-differentiations in Steps 2a and 2b serve to give *(R*,R*)*-III with a high optical purity and a high d.e. In the hydrogenation of II to III, the reaction of Step 2a is

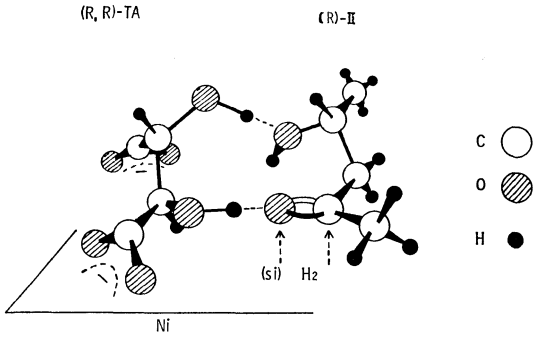

Fig. 2. Schematic representation of the interaction between (*R,R*)-TA and 4-hydroxy-2-pentanone (II).

Table 4. Hydrogenation of I to III over (*R,R*)-TA-NaBr-MRNi

	Conversion %	Hydrogenation products (molar %) (*R*,R**)-III	(*R*,S**)-III	Optical purity of (*R*,R**)-III
1	70	92	8	98
2	100	87	13	86
3	Calculated values based on the data in Scheme 2	84	16	86

expected to proceed predominantly at the early stage of the reaction for the sake of the enantiomer-differentiating reaction with *(R,R)*-TA–NaBr–MRNi, as has been mentioned in the previous section. Therefore, the *(R*,R*)*-III produced at the early stage of the reaction should consist exclusively of *(R,R)*-III.

As is shown in Entry 1, Table 4, the optical purity of *(R*,R*)*-III in the reaction product had reached 98% when the reaction was discontinued at conversion of 70%.

It is evident that the hydrogenation of I to III over TA–NaBr–MRNi is the ideal stereo-differentiating reaction; that is, all three types of the stereo-differentiating reactions, enantioface-differentiation in Step 1, and diastereoface- and enantiomer-differentiations in Step 2, serve to increase the optical purity of *(R*,R*)*-III, the final hydrogenation product.

Experimental

The analytical GLC was carried out with a Shimadzu GC-4A-PF gas chromatograph using a 3 m-5 mm o.d. glass column packed with 15% Ucon 50-HB-2000 on Chromosorb W. The ^{1}H-NMR spectra were taken with a JEOL-FX-100 instrument. The optical rotations were measured with a Perkin Elmer 241 polarimeter.

All the chemicals except for those listed below were obtained from commercial sources and were used without further purification.

The catalysts used in this study were prepared by the method reported before.[5] The THF employed as a solvent of the hydrogenation was prepared as follows: commercial THF was dried over NaH overnight and was then distilled under a nitrogen atmosphere. (*R,R*)- and (*S,S*)-2,4-pentanediol (III) were prepared by the method previously reported.[1] *(R,R)*-III, mp 50.5 °C, bp 111—113 °C/19 mmHg, Found: C, 56.50; H, 11.77%. Calcd for $C_5H_{12}O_2\cdot(0.1\ H_2O)$: C, 56.67; H, 11.62%, $[\alpha]_D^{20}$ −54.5° (*c* 10, ethanol), NMR ($CDCl_3$, TMS) δ, 1.30 (d, J=6.3 Hz, 6H, two $C\underline{H}_3$–CH(OH)–), 1.65 (t, J=6.2 Hz, 2H, –CH(OH)–$C\underline{H}_2$–CH(OH)–) 2.75 (broad signal, 2H, two O$\underline{H}$), 4.23 (m, 2H, two CH_3–$C\underline{H}$(OH)–). The IR spectra of the sample were almost identical to those listed in the literature.[8] The analytical GLC (Ucon/80 °C) showed a single peak. *(S,S)*-III, $[\alpha]_D^{20}$ +54.2° (*c* 10, ethanol). All the other data of this compound were identical to those of *(R,R)*-III. *(R,R)*- and *(S,S)*-2,4-diacetoxypentane (V) were prepared by the treatment of acetic anhydride to III in the presence of pyridine, followed by purification with the preparative GLC of the sample. *(R,R)*-V, $[\alpha]_D^{20}$ −40.5° (*c* 10, ethanol). The analytical GLC (NPGS/80 °C) showed a single peak (retention time 79 min). The NMR spectra (TMS, $CDCl_3$) of V showed signals at δ, 1.22 (d, J=6 Hz, 6H, two $C\underline{H}_3$–CHOAc–), 1.71 and 1.77 (two d, J=7 Hz, 2H, –CH(OAc)–$C\underline{H}_2$–CH(OAc)–), 2.00 (s, 6H, two $C\underline{H}_3C(=O)$–O–), and 4.98 (m, 2H, two –$C\underline{H}$(OAc)–). The NMR spectra were also measured with a solution of V (10 mg) and Eu(hfmc)$_3$ (130 mg) in $CDCl_3$ (0.4 ml). V derived from *(R,R)*-III showed no detectable signal of the antipode. The difference in the chemical shift for acetyl groups (singlet) of *(R,R)*- and *(S,S)*-V was 4 Hz. *(S,S)*-V was obtained from *(S,S)*-III by the procedure described above. All the data were identical with those for *(R,R)*-V except for the value of $[\alpha]_D^{20}$ +40.2° (*c* 10, ethanol). *(R)*- and *(S)*-4-hydroxy-2-pentanone (II) were prepared by the partial oxidation of optically pure *(R,R)*- and *(S,S)*-III as follows: into a slurry of pyridinium chlorocromate (86 g) in 500 ml of CH_2Cl_2, a 40-g portion of *(R,R)*- or *(S,S)*-III, dissolved in 100 ml of CH_2Cl_2, was added all at once, after which the mixture was kept for 2 h with stirring at room temperature. The reaction mixture was then added to dry ether (3 l), and the resulting slurry was kept for another hour under stirring. The slurry was then passed through a column packed with 400 ml of Florisil, and the elute was concentrated under reduced pressure at room temperature. The distillation of the condensate under reduced pressure gave II in a yield of 12 g. *(R)*-II, bp 59—60 °C/20 mmHg, $[\alpha]_D^{20}$ −23.5° (neat), NMR ($CDCl_3$, TMS) δ 1.18 (d, J=0.6 Hz, 3H, $C\underline{H}_3$–CH(OH)–), 2.17 (s, 3H, $C\underline{H}_3$–C(=O)–), 2.56, 2.58 (two d, J=7.1 and 4.70 –C(=O)–$C\underline{H}_2$–CH(OH)–), 4.22 (m, –$C\underline{H}$(OH)–), IR (neat), 3300 (OH) and 1700 cm^{-1} (C=O). The GLC analysis showed a 99% purity. *(S)*-II, $[\alpha]_D^{20}$ +23.4° (neat). All the data of this compound were the same as those of *(R)*-II. A small portion of the sample was treated with acetic anhydride in the presence of pyridine. The resulting 4-acetoxy-2-pentanone (IV) was purified by preparative GLC (Ucon/20 min/100 °C). The analytical GLC (Ucon/85 °C) of the purified sample showed a single peak (retention time, 44 min). The purified IV showed NMR (TMS, $CDCl_3$), δ 1.22 (d, J=6.0 Hz, 3H, $C\underline{H}_3$–CH(OAc)–), 2.00 (s, 3H, $C\underline{H}_3C(=O)$–O–), 2.18 (s, 3H, $C\underline{H}_3C(=O)$–CH_2–), 2.62 and 2.80 (two d, J=7 Hz each, 2H, –CH(OAc)–$C\underline{H}_2$–CH(OAc)–), and 4.95 (m, 2H, –$C\underline{H}$(OAc)–). Racemic II was prepared by the partial hydrogena-

tion of I over racemic-TA–NaBr–MRNi, as will be described below, and the fractional distillation of the product (bp 90—91 °C/38 mmHg).

Partial Hydrogenation of I. Into an autoclave (100-ml capacity), 11.5 ml (0.112 mol) of I, 0.2 ml of acetic acid, and 1.2 g of a catalyst suspended in 23 ml of THF were introduced. Thus, the volume to be occupied by hydrogen became *ca.* 65 ml. (The depression of 1 kg/cm^2 of the hydrogen pressure corresponds to 0.0021 mol of the consumption of H_2 at 100 °C.) After the evacuation of air from the autoclave, H_2 was charged to a pressure of 95 kg/cm^2 at room temperature (this value corresponded to 121 kg/cm^2 at 100 °C), and then heating was commenced. After the temperature of the reaction mixture had become 100 °C, this temperature was maintained until the hydrogen pressure became 58 kg/cm^2 (the consumption of H_2 amounts to 0.135 mol).

The autoclave was quickly cooled in an ice–water bath, and the H_2 was evacuated. After the removal of the catalyst from the reaction mixture, the filtrate was concentrated under reduced pressure to give a crude product. The relative amounts of I, II, and III in the crude product were determined by analytical GLC (Ucon/100 °C). The retention times of I, II, and III (the *(R*,R*)* and *(R*,S*)* isomers were partially resolved into two peaks) were 8, 24, 79, and 84 min respectively. A major portion of the crude product was distilled through a short column (a 5 cm × 10 mm o.d. glass column packed with a small glass helix 3 mm in diameter) under reduced pressure and fractionated into eight fractions. A fraction of pure II (bp 90—91 °C/38 mmHg) was found by the aid of the GLC analysis of each fraction. From the optical rotation of the purified II, the optical yield of the reaction, I to II, was calculated based on the $[\alpha]_D^{20}$ −23.5° (neat) for optically pure *(R)*-II.

Hydrogenation of I to III. The hydrogenation of I was carried out under the same conditions as before until no more consumption of hydrogen was observed. After removing the catalyst from the reaction product by filtration, the filtrate was concentrated under reduced pressure to give a crude product. The ratio of *(R*,R*)*-III to *(R*,S*)*-III in the crude product was determined by analytical GLC (Ucon/85 °C). The retention times of *(R*,R*)*-III and *(R*,S*)*-III were 174 and 189 min respectively. The attempted separation of *(R*,R*)*-III and *(R*,S*)*-III by the preparative GLC failed. However, when they were converted to diacetate (V), the separation by preparative GLC was possible. Thus, the optical purity of *(R*,R*)*-III was evaluated from the optical purity of the *(R*,R*)*-V derived from the crude product.

A 1-g portion of the crude product was converted to V by the method described before. The preparative GLC (NPGS/80 °C) of the crude V gave pure *(R*,R*)*-V. From the optical rotation of the purified *(R*,R*)*-V, the optical purity of *(R*,R*)*-V was calculated based on the $[\alpha]_D^{20}$ −40.5° (*c* 10, ethanol) for optically pure *(R,R)*-V.

Hydrogenation of II to III. The hydrogenation of II was carried out under the conditions described before. After removing the catalyst by filtration, the filtrate was subjected to analytical GLC (Ucon/85 °C). The ratio of *(R*,R*)*-III to *(R*,S*)*-III was evaluated from the peak areas of the corresponding compounds.

Partial Hydrogenation of Racemic II. The hydrogenation of racemic II (0.112 mol) was carried out under the same conditions as above until the consumption of hydrogen became 0.062 mol. After the removal of the catalyst by filtration, the filtrate was concentrated under reduced pressure to give a crude product.

The relative amounts of II, *(R*,R*)*-III, and *(R*,S*)*-III in the crude product were determined by analytical GLC (Ucon/85 °C). A major part of the crude product was distilled through a short column, as mentioned before, under a vacuum, and then fractionated into five fractions. A fraction of pure II (bp 59—60 °C/10 mmHg) was picked out of each fraction by the aid of GLC analysis. The pure II thus isolated from the reaction mixture was subjected to the determination of its optical purity by polarimetry. The optical purity of *(R*,R*)*-III was determined by the procedure previously described.

The authors wish to express their thanks to Professor Yoshiharu Izumi for his helpful suggestions. This work was supported in part by a Grant-in-Aid for Scientific Research No. 403531 from the Ministry of Education, Science and Culture.

References

1) K. Ito, T. Harada, A. Tai, and Y. Izumi, *Chem. Lett.*, **1979**, 1049.
2) T. Tanabe, *Bull. Chem. Soc. Jpn.*, **46**, 1482 (1973).
3) D. Danneels, M. Anteunis, L. van Acker, and D. Tavernier, *Tetrahedron*, **31**, 327 (1975).
4) a) Y. Izumi *et al.*, "Kagaku Sosetsu," Todaishuppan, Tokyo (1974), No. 4; b) Y. Izumi and A. Tai, "Stereodifferentiating Reaction," Kodansha/Academic Press (1977).
5) T. Harada and Y. Izumi, *Chem. Lett.*, **1978**, 1195.
6) T. Harada, A. Tai, M. Yamamoto, H. Ozaki, and Y. Izumi, Proc. 7th Intern. Cong. Catalyst (Tokyo 1980), preprint (A24).
7) A. Tai, H. Watanabe, and T. Harada, *Bull. Chem. Soc. Jpn.*, **52**, 1468 (1979).
8) "The Aldrich Library of Infrared Spectra," 2nd ed (1975), 79E.

Proton Equilibria of a 5-Dimethylamino-1-naphthalenesulfonyl Group Conjugated to Bovine Serum Albumin. I. Effects of The Conjugation on Structural Alternation

Nobuo Ikuta, Joichi Koga,* and Nobuhiko Kuroki

Department of Applied Chemistry, University of Osaka Prefecture, Mozu-Umemachi, Sakai, Osaka 591

(Received May 16, 1980)

The proton equilibria of an optical probe, the 5-dimethylamino-1-naphthalenesulfonyl group, conjugated to bovine serum albumin with various molar ratios to the protein in an acidic solution, were investigated by means of the change in the fluorescence intensity as well as that in the absorbance. Below the molar ratio of 1.7 the apparent pK values for the dimethylamino moiety of the optical probe decreased remarkably with a decrease in the pH of the solution, accompanying conformational changes of the protein caused by the proton binding to the protein. For molar ratios of more than 2.0, the alternation of the higher structure of the protein induced by the conjugation of the probe was detected by ORD measurements, while the pK values of those conjugated probes were lowered at pH's higher than 3.0. For comparison, the probe conjugated with glycine as its free state gave the pK value of 3.99 in an aqueous solution. The shifts of the apparent pK values of the conjugated probe in the protonated protein compared with those for the free probe were, particularly, too large to arise from the Debye-Hückel electrostatic shielding effect. These results are, therefore, interpreted in terms of a change in the short-range interaction in the neighboring residues surrounding the probe.

The interpretation of the ionization of acid-base groups on a protein molecule is complicated in part by the fact that the measurements reflect the composite behavior of a large number of groups. Even in an acidic solution the groups participating in the proton equilibria of acid-base groups on a protein include not only a large number of carboxyl groups, but also imidazole or tyrosine residues in an appreciable number. Their proton equilibria overlap one another, so that a sharp separation cannot be made by means of the potentiometric titration technique.

In order to avoid obscure titration curves, the spectral titration curves are often obtained for tyrosine residues.[1] A useful method for the same purpose is the attachment of an optical probe which has a desirable acidity constant to proteins by means of a covalent linkage.[2-5] The ionization of the probe is usually accompanied by a significant change in both the absorption and emission spectra. It is thus very easy to obtain the titration curve for this group alone. An optical probe of the kind which has been successively employed in protein studies is the 5-dimethylamino-1-naphthalenesulfonyl (DNS) group. Klotz and Fiess[3] reported the proton equilibria of DNS attached chiefly to amino groups on bovine serum albumin (BSA) by means of absorption measurements. Their equilibria indicated a significant difference from those of DNS-amino acid conjugates and were independent of the pH values of the solution in which BSA undergoes a conformational change by ionization. The DNS group conjugated to BSA (DNS-BSA) prepared by them contained 4 to 11 mol of DNS to 1 mol of the protein. There is, therefore, a fear of the alternation of the secondary and tertiary structures of the conjugated protein in their results.

The present investigation was undertaken to see if the proton equilibria of DNS-BSA followed the conformational change on the acid denaturation of the conjugated BSA, the fine structure of which was not grossly altered by the limited degree of conjugation. The degree of protonation of the DNS conjugate was determined from the fluorescent spectra, which have a better sensitivity, in order to measure the quenching by the protonation of the DNS group at a low degree of conjugation.

Experimental

Materials. BSA (crystallized and lyophilized) from the Sigma Chemical Co. (Lot. 17C-8145) and 5-dimethylamino-1-naphthalenesulfonyl chloride (DNS-Cl) from the Tokyo Chemical Co. (Tokyo) were used without further treatment. DNS-glycine conjugate (DNS-Gly) was purchased from the Sigma Chemical Co. (Lot. D-0875). The DNS-L-phenylalanine conjugate (DNS-Phe) was prepared from DNS-Cl and L-phenylalanine according to the method of Gray and Hartley.[6] The stock solution of these conjugates to amino acids were prepared by dissolving the conjugates in ethanol. All the acids, bases, and salts were reagent-grade.

Preparation of DNS-BSA. A solution of BSA was prepared containing 320 mg of protein in 80 ml of 0.1 M Na_2HPO_4 (1 M = 1 mol dm^{-3}). To this cooled solution was added 4 ml of a cold acetone solution containing 0.5—8 mg of DNS-Cl. The mixture was kept in a refrigerator and shaken sometimes for 24 h. The reaction by-products was then removed by dialysis in the cold for 24 h against three successive portions of 0.01 M acetic acid and thereafter for several days against distilled water. The dialysates were monitored for their gradual disappearance. The fluorescence intensity of the dialysate in the final dialysis could not be detected at the maximum sensitivity of the monitoring fluorescence spectrofluorometer. The protein solution was diluted in a volumetric flask and stored in a refrigerator. The stock solution was not used after one month from the time of preparation. The moles of the DNS conjugates to the protein were calculated from the measurement of the absorption at 340 nm using an extinction coefficient of 3.36×10^6 M^{-1} cm^{-1}.[7]

Fluorescence Titration of DNS Conjugate. In order to prevent concentration quenching, a portion of the stock solution of conjugates to BSA or amino acids was diluted with distilled water to give a solution with an optical density of less than 0.1 at 340 nm. To this diluted solution a measured quantity of hydrochloric acid was then added from a micropipet, after which the pH value and the fluorescence spectrum of the solution were measured. The procedure

was repeated with further samples of the solution and different quantities of the acid. Suitable corrections were made for the dilution of the solution by the added acid or base. The pH was measured at 25.0 °C with a Hitachi-Horiba F-7AD pH meter and a 6326-05C combination electrode. The fluorescence emission spectra were measured at the same temperature with a Hitachi Perkin-Elmer MPF-2A fluorescence spectrophotometer. The excitation wavelength (λ_{exc}) was taken at 340 nm. Both the excitation and emission slits were to cover wavelength ranges of 10 nm. Solutions of quinine sulfate in 0.1 M H_2SO_4 were used as the reference in the range of concentration of 10^{-7} to 10^{-5} M.

The protonation of the dimethylamino moiety of the DNS group gave rise to a quenching of the fluorescence of DNS at $\lambda_{exc}=340$ nm, so that the fraction, α, of the DNS group in the basic form was calculated by means of the following equation:

$$\alpha = \frac{\text{(maximum intensity of fluorescence at the pH value of the soln.)}}{\text{(maximum intensity of fluorescence in the basic soln.)}} \quad (1)$$

The emission spectra described in the results were corrected for variations in the detector system by using the known emission spectra of quinine sulfate. In the present experiments, the α values calculated from uncorrected spectra were equal to those from corrected spectra.

Results

Proton Equilibria of Free Probe. The acidity constant of a probe obtained from fluorometric analysis may be evaluated by means of the equilibria containing the components an acid and/or base existing in the excited state. In order to investigate the proton equilibria of the probe conjugates in the ground state, it is necessary to take into account the contribution of the excited probe molecules to the acid dissociation in the ground state. The absorption method is usually employed to determine the proton equilibrium constant in the ground state.

The proton equilibria of DNS conjugated in the ground state may be represented by the following equation:

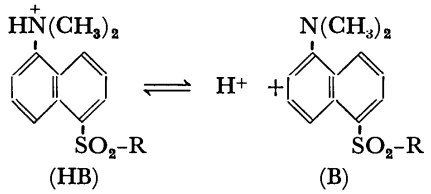

(HB) (B) (2)

When R is replaced by a small molecule such as a glycine residue, $-NHCH_2COOH$, this dissociation can be described quantitatively by the familiar Henderson-Hasselbalch expression:

$$pH = pK_a + \log\frac{\beta}{1-\beta} \quad (3)$$

where pK_a is the apparent acidity constant of the dimethylamino moiety in the DNS group, and β, the fraction of the DNS group in the unprotonated ground state. The absorption spectra of 1.00×10^{-4} M DNS-Gly, as a model of free probes obtained at various pH values, are shown in Fig. 1, where the absorbance is given as a function of the wavelength, λ. The results exhibited isosbestic points at 268 and 304 nm which were identical with those reported for the DNS group conjugated to diaminoethane.[5] The curves corresponding to the highest and lowest pH values in Fig. 1 represent the spectra of the unprotonated (B) and protonated (HB) forms respectively; hence, the fraction of the probe in the protonated ground state, β, is commonly calculated from the amount of the absorption change at each pH value. According to Eq. 3, the plots of the pH values in solution *versus* $\log[\beta/(1-\beta)]$ give a slope of one and a pK_a value which is equal to a pH value at $\log[\beta/(1-\beta)]=0$. For DNS-Gly and DNS-Phe in water, the pK_a values were given as 3.99[8] and 4.00 respectively.

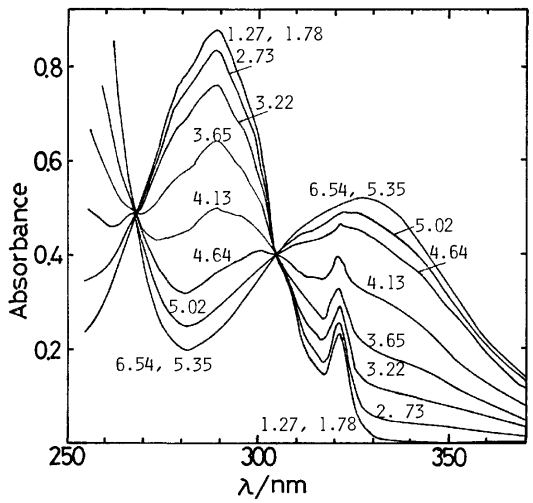

Fig. 1. Absorption spectra of 1.00×10^{-4} M DNS-Gly in water at various pH. Curves are labeled with appropriate pH values. Cell length 1 cm.

The emission spectra of 1.68×10^{-5} M DNS-Gly excited at 340 nm were measured at various pH in water, as is shown in Fig. 2. The spectra were characterized by one band near 590 nm at which the maximum intensity decreased with a decrease in the pH. As is shown in Fig. 1, the absorption at 340 nm was absent in the solution of a lower pH, where all of the dimethylamino moiety of DNS group was protonated. This fact indicates that the DNS molecules are excited only in the unprotonated form when exposed to the light of the 340 nm wavelength. The emission band, therefore, corresponds to the fluorescence from the excited state of the DNS group with the dimethylamino moiety in its unprotonated ground state.

The unprotonated excited molecules, denoted by B*, are treated by the insertion of an additional component in Eq. 2 to give:[9]

$$HB \rightleftharpoons B \rightleftharpoons B^*. \quad (4)$$

The fraction of the unprotonated DNS group in both the excited and ground states make it difficult to estimate from the fluorescence in the above successive equilibrium. The intensity of the emission peak was,

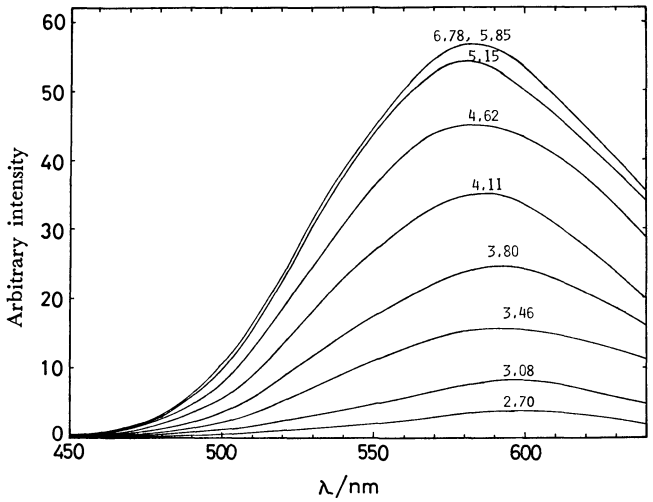

Fig. 2. Corrected emission spectra of 1.68×10^{-5} M DNS-Gly in water at various pH. Curves are labeled with appropriate pH values.

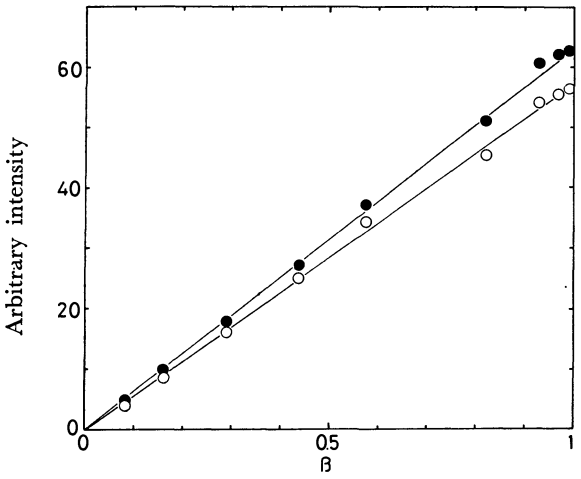

Fig. 3. Maximum intensity of corrected and uncorrected fluorescence spectra of DNS-Gly as a function of the fraction in unprotonated ground state (β). Ordinate scale, I_{max}, is arbitrary intensity of peaks in the corrected (○) and uncorrected (●) spectra.

however, proportional to the fraction of the DNS molecules in the unprotonated ground state (β), as calculated from absorption, as is shown in Fig. 3. The linear relationship implies that the equilibrium between B and HB is scarcely shifted by the processes of excitation and emission between B and B*, which are much faster than those of protonation and unprotonation. Consequently, the fraction of the unprotonated form in the ground state can be calculated from the fluorescence intensity of the DNS group in the same way as from the absorption titration. From the pH value in solution and the α obtained by fluorescence measurement, the pK_a values were obtained as 3.99 and 4.00 for DNS-Gly and DNS-Phe respectively. These values were, as expected, identical with those obtained by the absorption method. Hence, the fraction of the DNS group in the unprotonated form obtained from fluorescence measurements, α, is equal to the β obtained by the absorption method and Eq. 3 can be rewritten as follows:

$$pH = pK_a + \log\frac{\alpha}{1-\alpha}. \quad (5)$$

Proton Equilibria of DNS-BSA Conjugates. The corrected emission spectra of DNS-BSA conjugates with the molar ratio of 1.7 mol of the probe to 1 mol of protein obtained in water as a function of the pH are shown in Fig. 4. The spectra are different from those described before for the free probe. The 580 nm peak of the free probe is remarkably blue-shifted when the DNS group is conjugated to BSA, to 515 nm at high pH values and to 530 nm at low pH values. The large shift is attributable to the hydrophobic environment of the protein at which DNS group is attached. The small red-shift from a high to a low pH corresponds to an energy change of about 0.55×10^3 cm^{-1}, which is slightly larger than that of about 0.48×10^3 cm^{-1} in the case of the free probe. This finding exhibits the effect of the structure change on the environment of the DNS group. The lowering of the quantum yield of the DNS conjugate in unprotonated form with the red-shift may be neglected compared with the quenching by the protonation of the probe. Thus, the proportionality between the fraction of the probe in the unprotonated form and the fluorescence intensity is maintained in DNS-BSA as well as in the free probe, as has been described before. The fraction of DNS conjugates in the unprotonated form can, therefore, be calculated by the same method as in the free probe.

When the DNS group was conjugated to BSA with the molar ratios of 0.9, 2.0, and 2.7 mol of the probe to 1 mol of protein, Eq. 5 was no longer adequate to represent the dissociation over the pH range measured. As is shown in Fig. 5, Henderson-Hasselbalch plots of the DNS-BSA conjugates in aqueous solutions gave three successive straight lines, indicating the three dissociation characteristics, denoted by I, II, and III,

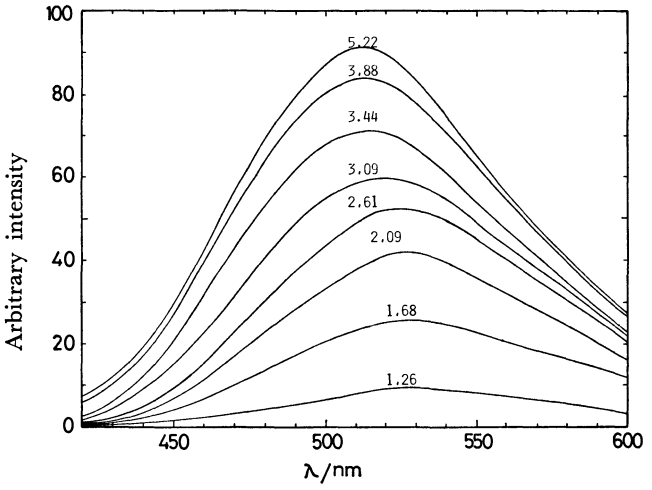

Fig. 4. Corrected emission spectra of 1.08×10^{-5} M solutions of DNS-BSA conjugates with the molar ratio of 1.2 mol probe to 1 mol protein in water at several pH. Curves are labeled with appropriate pH values.

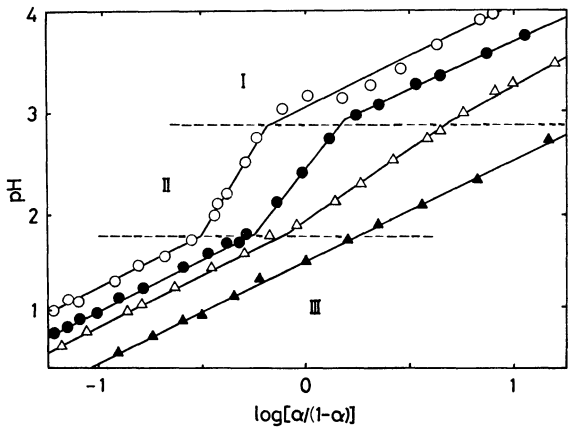

Fig. 5. Henderson-Hasselbalch plots of DNS-BSA conjugates with the molar ratio of 0.9 (○), 2.0 (●), 2.7 (△), and 7.2 (▲) mol probe to 1 mol protein. Two dashed lines divide the plots into three regions denoted by I, II, and III.

in the order of decreasing pH. The slopes were nearly one in I and III, but more than one in II: hence, the apparent pK_a values in both the I and III regions, as calculated from Eq. 5, were almost constant, but those in the II region were not. In the II region it is adjustable to a generalized Henderson-Hasselbalch expression with a parameter, denoted by n, of interaction among dissociation groups in a polyelectrolyte as follows:[10]

$$pH = pK_a + n \log \frac{\alpha}{1-\alpha}. \quad (6)$$

In this study, n may be attributed to the interaction between the DNS group and the other residues in the protein. We should note that the apparent pK_a in the II region obtained from Eq. 6 makes it difficult to discuss quantitatively the proton equilibria of DNS group conjugated to BSA, because the parameter, n, is physicochemically ambiguous in the process of the extension of the simple Maxwell-Portington equation,[11] as described by Katchalsky and Spitnik.[10] The apparent pK_a value in the II region is useless for comparison with the pK_a values in other regions; hence, the value has not been determined. In the case of the DNS-BSA conjugate with the molar ratio of 7.2, Henderson-Hasselbalch plots gave one straight line, from which the constant pK_a and a slope of 1.0 were calculated over the pH range measured. The results of the pK_a values and slopes in each region, summarized in Table 1, show the two following features. Firstly, the pK_a values in the I region are greater than those in the III region except in the case of the molar ratio of 7.4. Secondly, the pK_a values in the I region come close to those in the III region and the slope in the II region decreases to one with an increase in the molar ratio of the conjugates. The former may be attributed to the conformational change on acid denaturation, and the latter to the alternation of the protein by the conjugation of the probe, as was pointed out by Takagi *et al.*[12,13]

The α-helix contents of the DNS-BSA conjugates

Table 1. Apparent pK_a and slope n of DNS-BSA conjugates in water

Molar ratio[a]	Region I		Region II	Region III	
	n	pK_a	n	n	pK_a
0.9	1.0	3.05	3.5	1.0	2.30
2.0	1.0	2.70	2.6	1.0	2.05
2.7	1.0	2.18	1.5	1.0	1.90
7.4[b]	$n=1.0$, $pK_a=1.55$				

a) Moles of dansyl group conjugated to 1 mol of BSA.
b) The regions were indistinguishable in Fig. 5.

were calculated from the ORD measurement with the Moffitt-Yang equation in order to elucidate the alternation of the protein by the conjugation of the probes and the protonation of the ionizable groups in the protein. The α-helix contents of the conjugated proteins with the molar ratios of 0.7 and 5.2 were 46 and 28% in pH 5.0, and 28 and 23% in pH 2.0, respectively. In the unconjugated protein, the α-helix contents were 46% in pH 5.0 and 27% in pH 2.0. It can be seen from the ORD data that both the conjugation of the probe and the binding of the proton to the protein cause a lowering of the α-helix content of the native protein in a neutral solution. Because of the similar α-helix content of the conjugated protein even with the molar ratio of 5.2 in pH 2.0 and 5.0, the constant pK_a obtained for the conjugated protein with the molar ratio of 7.4 should be attributable to the impaired protein, which maintains its structure regardless of the protonation of the protein.

In the case of DNS-BSA, with an average molar ratio below 1.7, it can be seen that the proton equilibria of the DNS group present the same behavior, as is shown in Fig. 6. This finding implies that the BSA conjugated with DNS group with a small molar ratio consists of a conformation which is similar to that of unconjugated BSA, judging from the agreement in α-helix content between the unconjugated BSA and the conjugated BSA with the molar ratio of 0.7.

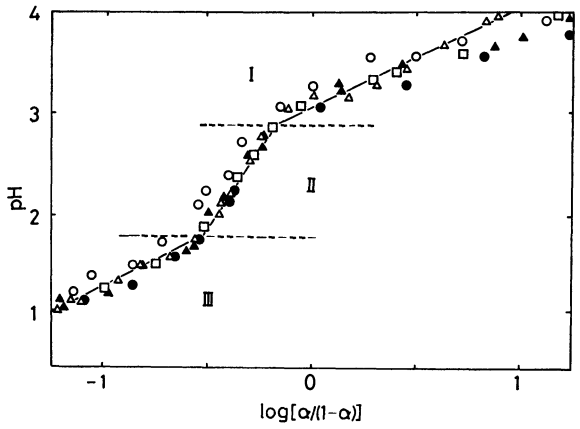

Fig. 6. Henderson-Hasselbalch plots of DNS-BSA conjugates with the molar ratio of 0.3 (○), 0.5 (●), 0.9 (△), 1.6 (▲), and 1.7 (□). Two dashed lines are drawn at the same position of pH values in Fig. 5.

Discussion

BSA undergoes a marked structure change in the region near pH 4, termed "N-F transition," from the normal state (N) to a form (F) having a faster rate of migration in electrophoresis.[14] Futhermore, the protein structure of the F-form is changed into a structure with an expanded form (E) in the region below pH 3.5.[15]

As is shown in Fig. 6, the pH value of the boundary between the I and II regions is 3.0, in agreement with the pH value beginning to occur upon the unfolding by means of the acid expansion. A possible explanation for the agreement may be that, in the I and III regions, the conjugated DNS group exists in two different environments, in the protein of the N- or F-form and in that of the E-form respectively, and that in the II region a transfer of the DNS group proceeds along with the expansion of the protein structure. As has been described in the Results section, the protein conjugated with the molar ratio below 1.7 showed the same behavior on acid denaturation as the unconjugated protein, so the variation in pK_a values against the pH depends only on the effect on the conformational change upon acid denaturation.

The fact that all of the pK_a values obtained for DNS-BSA are smaller than that for DNS-Gly, denoted by pK_o, shows that the protein environment has a profound effect on the ionizing abilities of the dimethylamino moiety. Such an effect can be expressed thermodynamically from the difference between pK_a and pK_o values in the following equation:

$$pK_a = pK_o - 0.434\frac{\Delta G_p}{RT}, \qquad (7)$$

where ΔG_p is the free-energy change resulting from the transfer of the probe from water to a inside of the protein in the solution of a pH value, and where pK_o is estimated for the free probe in the solution which consists of the same solute as in the determination for DNS-BSA; pK_o=3.99 in the present case. The left-hand side in Eq. 7, pK_a, can be calculated from the pH value of a solution and the fraction, α, in Eq. 5; hence, ΔG_p may be estimated. In Fig. 7 the experimental pK_a values are plotted against the pH values in the case of those of DNS-BSA in Fig. 6; the ΔG_p scale at 25.0 °C is indicated on the right-hand side.

If ΔG_p depends only upon the Debye-Hückel electrostatic shielding effect, Eq. 7 can be expressed by the following equation containing Linderstrøm-Lang's parameter:[18]

$$pK_a = pK_o - 0.434\frac{\Delta G_{el}}{RT}\bar{Z}_p, \qquad (8)$$

where ΔG_{el} is the electrical free-energy change for charging an assumed-spherical protein molecule uniformly with a total unit charge and where $\bar{Z}_p$ represents the mean net charge of the protein molecule. Although the values of $\Delta G_{el}/RT$, usually represented by 2ω, may be computed on the basis of the electrostatic theory,[19,20] we shall obtain ω as an experimental parameter and adopt the numerical values for it which have been found by Tanford, Swanson, and Shore to fit the potentiometric titration data.[19] We must also choose values for $\bar{Z}_p$ which are primarily due to a bound or dissociated proton, but which are also influenced by bound salt. In a rough approximation, however, it may be assumed that $\bar{Z}_p$ is equal to the number of protons bound by BSA the values of which can be computed from the data of Tanford, Swanson, and Shore.[19]

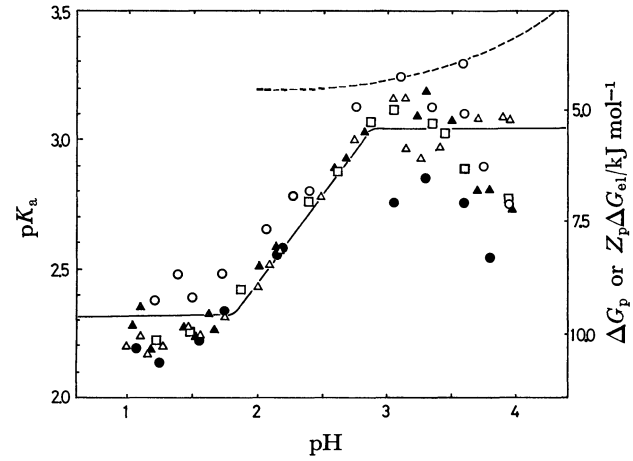

Fig. 7. Apparent pK_a values of DNS-BSA conjugates as a function of pH in aqueous solutions. The pK_a values in symbols and solid line were calculated from the data in Fig. 6 with Eq. 5. BSA conjugates have the molar ratio of below 1.7 mol probe to 1 mol protein. Symbols as in Fig. 6. Dashed line was estimated with Eq. 8 from data of Tanford, Swanson, and Shore.[19]

The calculated results are also illustrated in Fig. 7 for a solution with an ionic strength of 0.03. The experimental curves are shifted greatly from the curves computed on the basis of electrostatic considerations, especially in the lower-pH range. This feature suggests that ΔG_p is constituted not only of ΔG_{el} depending on long-range electrostatic force, but also of the free-energy changes proceeding from several short-range interactions, such as the hydrophobic effect, the hydrogen-bonding, and the alternation of the solvent structure by the intensive electrical field around the protein. Such interactions, resulting from the displacement between the experimental and computed curves, must be greatly changed with the conformational transition accompanying the acid expansion. As Klotz and Fiess have pointed out,[3] the dimethylamino group contributes its pair of electrons to a resonance with the aromatic ring; hence, it cannot be a good acceptor of a hydrogen-bonding. Thus, the difference between ΔG_p and ΔG_{el} is unlikely to involve the contribution of any hydrogen-bonding, and the short-range interactions must arise from some other causes.

Klotz and Fiess,[3] in their study of DNS-BSA similar to this paper, have found that the pK of the dimethylamino group is 1.67 when attached to BSA and 3.99 when attached to glycine. The DNS-BSA conjugates prepared by them, however, have the molar ratio

of 5.9 at which the conjugation causes an alternation of the protein structure because of our results that, at molar ratios of more than 1.7, the normal protein structure no longer maintains its structure, even in a solution near the isoionic point in the I region. They have preferred to interpret their results in terms of a postulated ice-like character of the hydration water in the vicinity of the nonpolar portions of the protein, including the DNS group. Such an environment would tend to stabilize the uncharged form of the dimethylamino group, as the creation of a charged group in place of the uncharged one would require some breakdown of the ice lattice. Thus, the factor of ice lattice is unlikely to contribute to the shift of ΔG_p.

Strauss and Vesnaver,[5] studying the acid-base equilibria of the DNS group conjugated to a copolymer of maleic acid and butyl vinyl ether, have found that the pK values of the dicarboxylate groups and of the dimethylamino group of the probe pass through a maximum as the macromolecule undergoes a transition from a compact to a random-coil conformation. These results have been interpreted in terms of changes in the local solvent surrounding the probe, taking into account both the electrostatic forces due to the negative carboxylate groups and the influence of the nonpolar or hydrophobic butyl groups. The former effect is acid-weakening, and the latter, acid-strengthening, with regard to the $(CH_3)_2NH^+$ group.

In the case of DNS-BSA, BSA can be regarded as a polycation instead of the polyanion studied by Strauss and Vesnaver,[5] so the electrostatic and nonpolar environment effects would reinforce one another, both acting to increase the acid strength of the probe. The integrity of the albumin internal structure may be essential for both the effects, possibly as a consequence of the environment of the DNS group in nonpolar or hydrophobic regions of the intact protein. Such a hydrophobicity would favor the neutral basic form of the dimethylamino group over the ionic acidic form. The cationic charges in $\bar{Z}_p$ neighboring the hydrophobic environment have an intensive electric shielding effect in the inert protein involving the probe compared with that in bulk water.

On account of the hydrophobic residues in the protein, the charges formed by proton binding on the protein are considered to have interesting effects on the pK_a values. The effects of the charges should be investigated further in the proton equilibria of DNS-BSA in aqueous solutions of electrolytes and/or denaturants.

The present work was partially supported by a Grant-in-Aid for Development Research from the Ministry of Education, Science and Culture.

References

1) C. Tanford, *Adv. Protein Chem.*, **17**, 69 (1962).
2) I. M. Klotz and J. Ayers, *J. Am. Chem. Soc.*, **79**, 4078 (1957).
3) I. M. Klotz and H. A. Fiess, *Biochim. Biophys. Acta*, **38**, 57 (1960).
4) P. A. Frey, F. C. Kokesh, and F. H. Westheimer, *J. Am. Chem. Soc.*, **93**, 7266 (1971).
5) U. P. Strauss and G. Vesnaver, *J. Phys. Chem.*, **79**, 1558 (1975).
6) W. R. Gray and B. S. Hartley, *Biochem. J.*, **89**, 59P (1963).
7) B. S. Hartley and V. Massay, *Biochim. Biophys. Acta*, **21**, 58 (1956).
8) The value was identical with the pK_a value reported for DNS-Gly by Klotz *et al.*[3]
9) The protonated form of the DNS group in an excited state should not be included because the energy level of the unprotonated form in an excited state is lower than that of the protonated form in an excited state, judging from the observation of the absorption and emission spectra. This makes the energy transfer from the unprotonated to the protonated form in the excited state very unlikely.
10) A. Katchalsky and P. Spitnik, *J. Polym. Sci.*, **2**, 432 (1947).
11) W. R. Maxwell and J. R. Partington, *Trans. Faraday Soc.*, **33**, 670 (1939).
12) T. Takagi, Y. Nakanishi, N. Okabe, and T. Isemura, *Biopolymers*, **5**, 627 (1967).
13) N. Okabe and T. Takagi, *Biochim. Biophys. Acta*, **229**, 484 (1971).
14) K. Aoki and J. F. Foster, *J. Am. Chem. Soc.*, **79**, 3385 (1957).
15) M. Sogami and J. F. Foster, *Biochemistry*, **7**, 2172 (1968).
16) T. T. Herskovits and Sr. M. Sorensen, *Biochemistry*, **7**, 2533 (1968).
17) R. H. McMenamy, *J. Biol. Chem.*, **240**, 4235 (1965).
18) K. Linderstrøm-Lang, *Compt. Rend. Trav. Lab. Carlsberg*, **15**, 1 (1924).
19) C. Tanford, S. A. Swanson, and W. S. Shore, *J. Am. Chem. Soc.*, **77**, 6414 (1955).
20) G. Scatchard, J. S. Coleman, and A. L. Shen, *J. Am. Chem. Soc.*, **79**, 12 (1957).

Migrated Lupane Derivatives. Boron Trifluoride Etherate-catalyzed Backbone Rearrangement of 3α,4α- and 3β,4β-Epoxy-*D*:*A*-friedo-18β,19α*H*-lupanes and Solvent Effects[1]

Yasushi YOKOYAMA, Yoshihiko MORIYAMA,† Takahiko TSUYUKI, and Takeyoshi TAKAHASHI*

Department of Chemistry, Faculty of Science, The University of Tokyo, Hongo, Bunkyo-ku, Tokyo 113
† *Institute of Chemistry, Kyoto Prefectural University of Medicine, Taishogun, Kita-ku, Kyoto 603*

(Received May 28, 1980)

Backbone rearrangements of 3α,4α- and 3β,4β-epoxy-*D*:*A*-friedo-18β,19α*H*-lupanes catalyzed by boron trifluoride etherate gave 18β,19α*H*-lup-12-en-3-ols, lup-18-en-3-ols, and lup-19-en-3-ols, besides known *D*:*B*-friedo-18β,19α*H*-lup-5-en-3-ols and -5(10)-en-3-ols. *D*:*B*-Friedo-18β,19α*H*-lup-1(10)-en-3α-ol and 3β,10β-epoxy-*D*:*B*-friedo-18β,19α*H*-lupane were also obtained from α- and β-epoxides, respectively. Solvent effects on these reactions were examined.

Acid-catalyzed backbone rearrangements of unsaturated or epoxy triterpenes usually proceed in a reverse direction of their biogenesis,[2] affording a number of migrated triterpenes derived from intermediate cations or their equivalent species corresponding to various biogenetic stages. In previous papers, reports were given on boron trifluoride etherate-catalyzed backbone rearrangement of 3β,4β-epoxyfriedelane (**1**)[3] and 3α, 4α- and 3β,4β-epoxyshionanes (**2** and **3**),[4] migrated friedooleanane and friedobaccharane derivatives being obtained.

So far only a few migrated lupane derivatives have been isolated from natural sources,[5] investigations on these compounds[6,7] not being as extensive as those on migrated oleanane, ursane, and hopane derivatives.[8] In connection with the structural study of guimarenol, formation of *D*:*B*-friedo-18β,19α*H*-lup-5-en-3β-ol from 3β,4β-epoxy-*D*:*A*-friedo-18β,19α*H*-lupane by tratment with boron trifluoride etherate in benzene has been reported.[9] Examination was carried out on the backbone rearrangement of 3α,4α- and 3β,4β-epoxy-*D*:*A*-friedo-18β,19α*H*-lupanes[9] (**4** and **5**) in various solvents catalyzed by boron trifluoride etherate to give a series of migrated lupane derivatives. Solvent effects on the reaction were also examined.

3α,4α-Epoxy-*D*:*A*-friedo-18β,19α*H*-lupane (**4**), derived from friedelin (friedelan-3-one)[7,9] was treated with boron trifluoride etherate in tetrahydrofuran at room temperature until the epoxide (**4**) was consumed. The reaction give a complex mixture, which was separated by preparative thin-layer chromatography (TLC), followed by column chromatography on silica gel impregnated with silver nitrate to afford three compounds **A**, **B**, and **C** in 11, 60, and 5% yields, respectively.

The most polar compound **A** was found to be *D*:*B*-friedo-18β,19α*H*-lup-5-en-3α-ol (**6**) and the less polar compound **B** *D*:*B*-friedo-18β,19α*H*-lup-5(10)-en-3α-ol (**7**) by comparison with authentic specimens.[9]

Spectral data [IR 3400 and 908 cm^{-1}; ^1H NMR δ 3.34 (1H, m) and 5.22 (1H, m)] showed the least polar compound **C**, $C_{30}H_{50}O$, mp 103—109 °C, to be a new alcohol with a trisubstituted double bond. A fragment ion peak at *m/e* 205 in the mass spectrum[10] indicates that the double bond should be located at $\Delta^{1(10)}$ or Δ^7 of a *D*:*A*-friedolupane framework (**a**), $\Delta^{1(10)}$, Δ^5, or Δ^7 of a *D*:*B*-friedolupane framework (**b**), or Δ^5, Δ^7, or $\Delta^{9(11)}$ of a *D*:*C*-friedolupane framework (**c**). Among them, alcohols with the *D*:*A*-friedo-type framework, *D*:*B*-friedo-Δ^7-type framework, and *D*:*C*-friedo-Δ^5-type framework are not feasible on the basis of their formation mechanism. 5-En-3α-ol with the *D*:*B*-friedo-type framework is compound (**6**). Thus compound **C** should be formulated as either *D*:*B*-friedo-18β,19α*H*-lup-1(10)-en-3α-ol (**8**), *D*:*C*-friedo-18β,19α*H*-lup-7-en-3α-ol, or -9(11)-en-3α-ol.

Oxidation of compound **C** with the Jones reagent gave an unsaturated ketone (**9**), $C_{30}H_{48}O$, IR 1710 cm^{-1}. In the ^1H NMR spectrum, allylic methylene protons resonate at δ 2.75 and 3.01 (each 1H, dt, J=21 and J=3 Hz) and an olefinic proton at δ 5.43 (1H, m). Furthermore, another allylic proton resonates at δ 2.35 (1H, m). These observations suggest the existence of a partial structure $-\overset{O}{\overset{\|}{C}}_{(3)}-C_{(2)}H_2-C_{(1)}H=C_{(10)}-C_{(5)}H-$ and *D*:*B*-friedo-18β,19α*H*-lup-1(10)-en-3-one for the unsaturated ketone (**9**). On irradiation at δ 5.43, the signal due to the methylene at $C_{(2)}$ turned into two pairs of double doublet signals (each 1H, J=21 and J=3 Hz), showing that the coupling constant values between the $C_{(1)}$-proton and the $C_{(2)}$-methylene protons are both 3 Hz, and the $C_{(2)}$-protons coupled with the $C_{(5)}$-methine proton with a coupling constant, J=3 Hz. Irradiation of a frequency around δ 2.9 due to the $C_{(2)}$-methylene protons resulted in the change of the signal of $C_{(1)}$-proton to a doublet signal (1H, J=2 Hz). This suggests that the coupling constant between the olefinic proton and the $C_{(5)}$-allylic methine proton is 2 Hz. When the signal around δ 2.35 was irradiated, the signal at δ 5.43 due to the $C_{(1)}$-proton turned to a triplet (1H, J=3 Hz).

Treatment of the β,γ-unsaturated ketone (**9**) with isopropenyl acetate in the presence of *p*-toluenesulfonic acid under reflux gave a conjugated dienol acetate (**10**) [UV 273 nm (ε *ca.* 8000); $C_{32}H_{50}O_2$]. Thus, the structure of *D*:*B*-friedo-18β,19α*H*-lup-1(10)-en-3α-ol (**8**) is given for compound **C**.

Reaction of the α-epoxide (**4**) with boron trifluoride etherate in benzene at room temperature gave *D*:*B*-friedo-18β,19α*H*-lup-5(10)-en-3α-ol (**7**; yield 34%), -5-en-3α-ol (**6**; trace), and an alcohol mixture **D**. The mixture showed two peaks on GLC, but could not

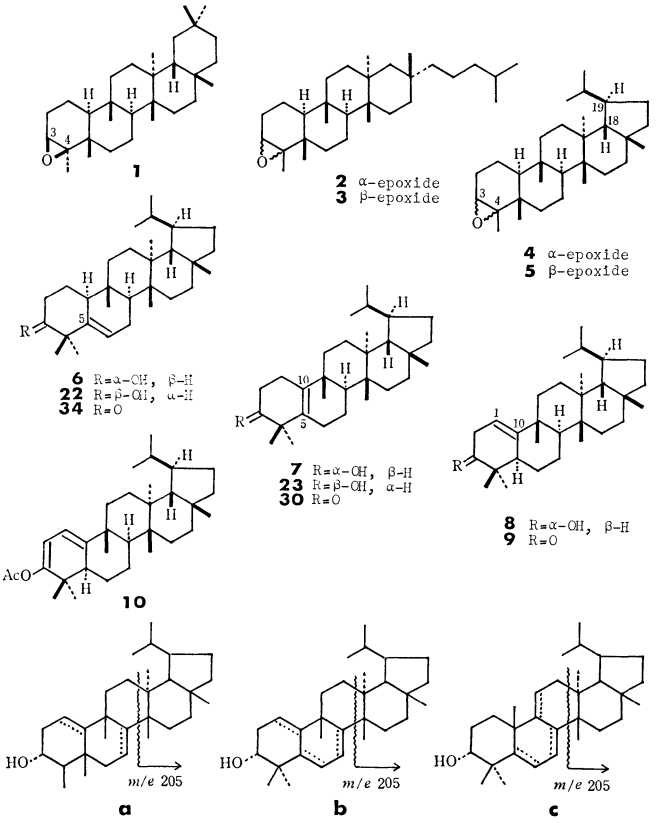

be separated by TLC nor column chromatography. Oxidation of the mixture with the Jones reagent gave the corresponding ketone mixture, which was separable by high performance liquid chromatography (HPLC) to afford three compounds, $\mathbf{D}_1$, $\mathbf{D}_2$, and $\mathbf{D}_3$ in 3, 11, and 6% yields, respectively.

The compound $\mathbf{D}_1$, $C_{30}H_{48}O$, is a ketone with an isolated double bond, the ^1H NMR spectrum showing the presence of two olefinic methyls besides six tertiary methyls. No signal due to olefinic proton was observed. From the fact that germanicol (**11**) was obtained as an ultimate product in friedelane-oleanane rearrangement in benzene,[3b] the compound $\mathbf{D}_1$ should be formulated as lup-19-en-3-one (**12**) in accordance with the ^1H NMR spectral data. The original alcohol in the mixture **D** could be formulated as lup-19-en-3α-ol (**13**).

The compound $\mathbf{D}_2$ showed a molecular ion peak at *m/e* 424.3708 ($C_{30}H_{48}O$) and a prominent peak at *m/e* 218.2004 corresponding to a fragment ion $C_{16}H_{26}^+$. Since Δ^{12}-triterpenes such as β-amyrin (**14**), α-amyrin, and bacchar-12-en-3-one show a prominent peak at *m/e* 218 due to retro-Diels-Alder fragmentation,[11] compound $\mathbf{D}_2$ might be 18β,19α*H*-lup-12-en-3-one (**15**). The proposed structure is supported by its ^1H NMR spectrum; a signal due to an olefinic proton observed at δ 5.21 (t, J=4 Hz) is nearly the same as that (δ 5.20, t, J=4 Hz) of β-amyrin (**14**). The original alcohol should be represented as 18β, 19α*H*-lup-12-en-3α-ol (**16**).

The third compound $\mathbf{D}_3$, $C_{30}H_{48}O$, mp 167—168 °C, was found to be a tetrasubstituted olefinic ketone by its ^1H NMR spectrum which showed the absence of the olefinic proton and the presence of an allylic proton (δ 2.98, 1H, J=6 Hz). The signal resonating at δ 2.98 seems to be central three peaks of a heptet signal due to an isopropyl methine proton on the allylic position. Thus the structure of lup-18-en-3-one (**17**) is suggested for compound $\mathbf{D}_3$.

We prepared a mixture of lup-18-en-3β-yl acetate (**18**) and 18ξ,19ξ*H*-lupan-3β-yl acetate (**19**) from lupeol (**20**) according to the method of Baddeley *et al.*[12] The mixture was treated with lithium aluminium hydride to give an alcohol mixture, which was oxidized with the Jones reagent. The reaction mixture was subjected to separation by HPLC to afford the authentic lup-18-en-3-one (**17**), which was identical with compound $\mathbf{D}_3$. Thus the original alcohol is formulated as lup-18-en-3α-ol (**21**).

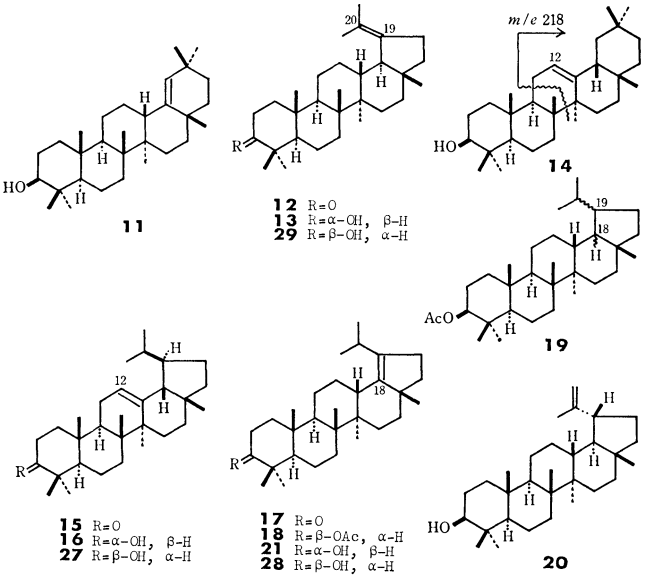

The reactions of 3β,4β-epoxy-*D*:*A*-friedo-18β,19α*H*-lupane (**5**), derived from friedelin,[7,9] with boron trifluoride etherate were investigated under the same conditions as in the case of the α-epoxide (**4**). Treatment of the β-epoxide (**5**) in tetrahydrofuran gave a mixture which was separated into three compounds, **E**, **F**, and **G** in 7, 40, and 11% yields, respectively. The most polar compound **E** and the less polar one **F** were identified as *D*:*B*-friedo-18β,19α*H*-lup-5-en-3β-ol (**22**) and -5(10)-en-3β-ol (**23**) by direct comparison with authentic samples,[9] respectively.

The least polar compound **G**, mp 171 °C, seems to be a fluorohydrin (**24**). Its ^1H NMR spectrum showed a multiplet signal centered at δ 3.68 (1H, $W_{1/2}$=13 Hz) due to a proton on a carbon atom bearing a hydroxyl group. A doublet signal appearing at δ 1.33 (J=24 Hz) indicates the presence of a methyl group attached to a fluorine-bearing carbon atom. The coupling constant value, $J_{F,H}$=24 Hz, is the same as that ($J_{F,H}$= 24 Hz) observed for 4α-fluoroshionan-3β-ol (**25**).[4b] The mass spectrum showed a molecular ion peak at *m/e* 446 (1%) and a characteristic peak at *m/e* 426 (8%) due to $(M-HF)^+$ ion together with a base peak at *m/e* 123. The results together with the fact that a fluorohydrin is often generated by treatment of an

epoxide with boron trifluoride etherate,[3,4b] lead to the conclusion that compound **G** can be formulated as 4α-fluoro-*D*:*A*-friedo-18β,19α*H*-lupan-3β-ol (**24**).

The reaction of β-epoxide (**5**) in benzene gave three products, *D*:*A*-friedo-18β,19α*H*-lupan-3-one (**26**: yield 1%),[9] a fluorohydrin (**24**; yield 13%), and *D*:*B*-friedo-18β,19α*H*-lup-5-en-3β-ol (**22**; yield 9%), other than an alcohol mixture (**27**—**29**) as main products. The mixture, after oxidation with the Jones reagent, was separated by HPLC to afford *D*:*B*-friedo-18β,19α*H*-lup-5(10)-en-3-one[9] (**30**; yield 7%), lup-19-en-3-one (**12**; yield 7%), 18β,19α*H*-lup-12-en-3-one (**15**; yield 31%), and lup-18-en-3-one (**17**; yield 13%).

The reaction of β-epoxide (**5**) in diethyl ether was carried out at 0 °C for 20 min. The reaction mixture was separated by preparative TLC into five compounds. The least polar compound **H** (**31**; yield 22%), $C_{30}H_{50}O$, mp 136—138 °C, showed no characteristic absorption bands in its IR spectrum. A doublet signal at δ 3.72 (1H, J=5.5 Hz), resembling a characteristic signal due to $C_{(3)}$-proton of dendropanoxide (**32**)[3a] (δ 3.75, 1H, d, J=4.8 Hz) and of dihydrobaccharis oxide (**33**)[4b] (δ 3.73, 1H, d, J=5 Hz), was observed in the ^{1}H NMR spectrum. Thus compound **H** was confirmed to be 3β,10β-epoxy-*D*:*A*-friedo-18β,19α*H*-lupane (**31**). The other four compounds were found to be *D*:*A*-friedo-18β,19α*H*-lupan-3-one (**26**; yield 2%), a fluorohydrin (**24**; yield 20%), *D*:*B*-friedo-18β,19α*H*-lup-5-en-3β-ol (**22**; yield 11%), and -5(10)-en-3β-ol (**23**; yield 27%) by spectral data and comparison with authentic specimens.

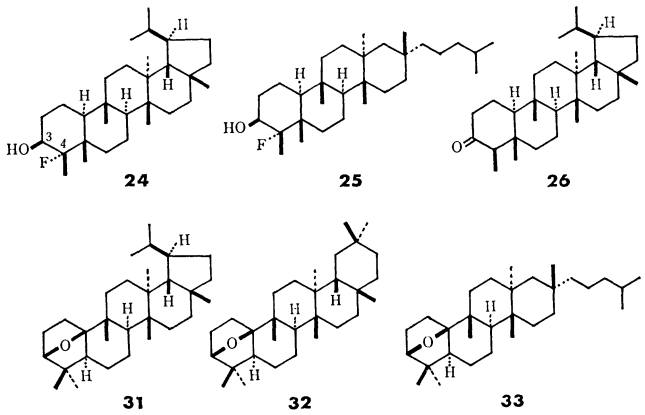

TABLE 1. RELATIVE AMOUNT RATIOS OF PRODUCTS IN THE REACTION OF 3α,4α-EPOXIDE (**4**) WITH $BF_3 \cdot OEt_2$ AT ROOM TEMPERATURE[a]

Solvent	Time / min	5-ene (**6**)	5(10)-ene (**7**)	1(10)-ene (**8**)	12-ene (**16**)	18-ene (**21**)	19-ene (**13**)
Hexane[b]	30	8	18	0	40	24	10
CH_3CN[b]	30	6	13	0	34	13	34
Benzene	60	trace[c]	63[c]	0	20[d]	11[d]	6[d]
CH_2Cl_2[b]	30	3	46	0	29	16	6
DME[b]	30	17	67	12	2	trace	2
Ether[b]	30	15	76	3	2	1	3
THF	45	15[c]	78[c]	7[c]	0	0	0

a) Room temperature, 20—28 °C. b) Determined by small-scale experiments, reaction products being subjected to Jones oxidation. Relative yields of 1(10)-, 12-, 18-, and 19-enes estimated from the peak area of the corresponding ketones on HPLC under the conditions given in General. A mixture containing *D*:*B*-friedo-18β,19α*H*-lup-5-en-3-one (**34**) and -5(10)-en-3-one (**30**) was separated by HPLC and examined by GLC to determine relative yields of 5- and 5(10)-enes. c) Determined by isolation of the product. d) Determined by conversion of the product into the corresponding ketone, isolated by means of preparative HPLC.

TABLE 2. RELATIVE AMOUNT RATIOS OF PRODUCTS IN THE REACTION OF 3β,4β-EPOXIDE (**5**) WITH $BF_3 \cdot OEt_2$ AT ROOM TEMPERATURE[a]

Solvent	Time / min	(**26**)[b]	(**25**)[b]	5-ene (**22**)	5(10)-ene (**23**)	(**31**)	12-ene (**27**)	18-ene (**28**)	19-ene (**29**)
Hexane[c]	60	trace	trace	21	22	0	23	10	24
CH_3CN[c]	60	0	7	11	38	0	27	9	8
Benzene	60	2[d]	4[d]	13[d]	10[e]	0	43[e,f]	18[e,f]	10[e]
CH_2Cl_2[c]	60	0	3	25	33	0	16	14	9
DME[c]	60	0	0	26	67	2	2	1	2
Ether[g]	20	3[d]	25[d]	13[d]	33[d]	26[d]	0	0	0
THF	45	0	19[d]	12[d]	69[d]	0	0	0	0

a) Room temperature, 20—28 °C. b) Determined by GLC before oxidation for small-scale experiments. c) Determined by small-scale experiments, reaction products being subjected to Jones oxidation. Relative yields of 1(10)-, 12-, 18-, and 19-enes estimated from the peak area of the corresponding ketones on HPLC under the conditions given in General. A mixture containig *D*:*B*-friedo-18β,19α*H*-lup-5-en-3-one (**34**) and -5(10)-en-3-one (**30**) was separated by HPLC and examined by GLC to determine relative yields of 5- and 5(10)-enes. d) Determined by isolation of the product. e) Determined by conversion of the product into the corresponding ketone, isolated by means of preparative HPLC. f) Correct data, inverse data in preliminary report (Ref. 1). g) Reaction carried out at 0 °C.

Small-scale experiments using the 3α,4α-epoxide (**4**) or the 3β,4β-epoxide (**5**) (each *ca.* 10 mg) and boron trifluoride etherate (0.1 ml) were carried out in solvents (5—10 ml) such as hexane, dichloromethane, acetonitrile, and 1,2-dimethoxyethane (DME). The results together with those obtained for the reactions in other solvents are summarized in Tables 1 and 2.

Since the rearrangement of **4** and **5** in a solvent with low nucleophilicity proceeds up to the C, D, or E ring,[3,4] highly rearranged products with 12-ene, 18-ene, and 19-ene structures were obtained in the reaction in hexane, acetonitrile, benzene, and dichloromethane. On the other hand, the rearrangement in a solvent with high nucleophilicity, such as diethyl ether or tetrahydrofuran, was interrupted in an early stage to afford *D*:*A*-friedolupane derivatives or *D*:*B*-friedolup-5-ene and -5(10)-ene derivatives. Neither *D*:*C*-friedolup-7-ene nor -8-ene derivative was detected in any solvent. These migratory aptitudes have a strong resemblance to those observed for 3β,4β-epoxyfriedelane (**1**)[3b] of a *D*:*A*-friedooleanane-type rather than those for 3α,4α- and 3β,4β-epoxyshionanes (**2** and **3**)[4b] of a *D*:*A*-friedobaccharane-type. The difference may be due to the existence of the E ring; the fact that the rearrangements of **1**, **4**, and **5** do not stop at the stages giving the *D*:*C*-friedo-type derivatives, but proceed up to the D and E rings, may be explained by release of the intracyclic tension due to the *cis*-fused D/E ring and partly due to 1,3-diaxial methyl groups.

A series of migrated lupanes were thus derived from friedelin. Since the total synthesis of friedelin has been accomplished,[13] the present work constitutes formally the total synthesis of these migrated lupanes.

Experimental

General Procedure. Melting points were measured on a Mel-temp capillary melting point apparatus (Laboratory Devices) and are uncorrected. IR spectra were measured in Nujol mull with a Hitachi EPI-G2 spectrometer or a Hitachi 260-30 spectrometer, UV spectra with a Hitachi 340 spectrophotometer, mass spectra with a Hitachi RMU-6-Tokugata mass spectrometer at 70 eV with a direct inlet system, high resolution mass spectra with a JMS-D300 (JEOL) mass spectrometer, the relative intensity being given in parentheses, and ^{1}H NMR spectra with a Hitachi R-20B (60 MHz) spectrometer, a Varian EM-390 (90 MHz) spectrometer or a JNM-FX-60 FT-NMR (60 MHz) spectrometer (JEOL). Chemical shifts are expressed in δ downfield from TMS as an internal standard and coupling constants in Hz. GLC analysis was carried out on a Shimadzu Gas Chromatograph GC-6A equipped with a hydrogen flame ionization detector (column: Dexsil 300GC, temperature 270—290 °C). Analytical and preparative HPLC were carried out on a Waters Liquid Chromatograph ALC/GPS 202/401 at room temperature with an RI detector (column: μ-Porasil 1/4 (inch)$\times$1 (foot); solvent system: 1.5% diethyl ether–hexane; flow rate: 3 ml/min; pressure: 700 psi). TLC was carried out on Kieselgel 60 GF_{254} (E. Merck) coated in 0.25 mm thickness (for analytical) and in 0.5 mm thickness (for preparative). Wakogel C-200 (Wako) was used for silica gel column chromatography.

Boron Trifluoride Etherate-catalyzed Backbone Rearrangement of 3α,4α-Epoxy-D:A-*friedo-18β,19α*H*-lupane (**4**) in Tetrahydrofuran.* A solution of α-epoxide[9] (**4**; 84.0 mg) in tetrahydrofuran (20 ml) was treated with freshly distilled boron trifluoride etherate (0.5 ml) at room temperature for 45 min. A saturated aqueous sodium hydrogencarbonate solution (5 ml) was added, stirring being continued for 30 min. The usual work-up gave a mixture, which was separated by preparative TLC (developed with benzene–diethyl ether, 19:1) to afford *D*:*B*-friedo-18β,19α*H*-lup-5(10)-en-3α-ol[9] (**7**; 50.0 mg) and crude 1(10)-en-3α-ol (**8**) and 5-en-3α-ol[9] (**6**). The crude alcohol (**8**) was further purified by column chromatography on silica gel impregnated with 25% silver nitrate. Elution with benzene gave pure **8** (4.3 mg). The crude alcohol (**6**) was subjected to further separation by preparative TLC (developed with benzene–diethyl ether, 19:1) to give pure **6** (9.6 mg). **8**: mp 103—109 °C (crystallized from methanol); IR 3400 and 908 cm^{-1}; ^{1}H NMR ($CDCl_3$) δ 0.63, 0.82, 1.01, 1.10 (each 3H, s), 0.89 (6H, d, J=6 Hz; (C$\underline{H}_3$)$_2$CH–), 0.96 (6H, s), 3.34 (1H, m, $W_{1/2}$=7 Hz), and 5.22 (1H, m, $W_{1/2}$=8 Hz); MS *m/e* (%) 426 (M^+; 41), 408 (100), and 205 (40); Found: *m/e* 426.3847. Calcd for $C_{30}H_{50}O$: M, 426.3860.

D:B-*Friedo-18β,19α*H*-lup-1(10)-en-3-one (**9**).* The Jones reagent (one drop) was added to a solution of **8** (7.0 mg) in acetone (5 ml) at 0 °C, and the reaction mixture was stirred at 0 °C for 20 min. The usual work-up gave a residue (6.9 mg), which was purified by preparative TLC (developed with benzene) to afford *D*:*B*-friedo-18β,19α*H*-lup-1(10)-en-3-one (**9**; 4.1 mg), mp 215—218 °C (crystallized from acetone); IR 1710 cm^{-1}; ^{1}H NMR ($CDCl_3$) δ 0.8—0.95 (9H, 3$\times$$CH_3$), 0.96, 0.99, 1.01, 1.08, 1.15 (each 3H, s), 2.35 (1H, m), 2.75 (1H, dt, J=21 and J=3 Hz), 3.01 (1H, dt, J=21 and J=3 Hz), and 5.43 (1H, m, $W_{1/2}$=9 Hz); MS *m/e* (%) 424 (M^+; 55), 205 (100), and 123 (86); Found: *m/e* 424.3710. Calcd for $C_{30}H_{48}O$: M, 424.3705.

3-Acetoxy-D:B-*friedo-18β,19α*H*-lupa-1(10),2-diene (**10**).* A mixture of **9** (0.7 mg), isopropenyl acetate (2 ml), and *p*-toluenesulfonic acid (catalytic amount) was refluxed for 10 h. The usual work-up gave a residue, which was purified by preparative TLC (developed with benzene) to give 3-acetoxy-*D*:*B*-friedo-18β,19α*H*-lupa-1(10),2-diene (**10**; 0.1 mg), UV_{max} (dioxane) 273 nm (ε *ca.* 8000); MS *m/e* (%) 466 (M^+; 4) and 123 (100); Found: *m/e* 466.3822. Calcd for $C_{32}H_{50}O_2$: M, 466.3811.

Boron Trifluoride Etherate-catalyzed Backbone Rearrangement of 3α,4α-Epoxy-D:A-*friedo-18β,19α*H*-lupane (**4**) in Benzene.* A solution of α-epoxide (**4**; 30.1 mg) in benzene (15 ml) was treated with boron trifluoride etherate (0.3 ml) at room temperature for 1 h. A saturated aqueous sodium hydrogencarbonate solution (10 ml) was added, stirring being continued for 20 min. The usual work-up gave a mixture, which was subjected to separation by preparative TLC (developed with benzene–diethyl ether, 9:1) to afford *D*:*B*-friedo-18β,19α*H*-lup-5(10)-en-3α-ol (**7**; 10.1 mg), -5-en-3α-ol (**6**; trace), and a mixture (9.7 mg) of alcohols. This mixture, dissolved in acetone (5 ml), was oxidized with the Jones reagent (one drop) at 0 °C, and the solution was stirred at 0 °C for 1 h. After the usual work-up, the reaction mixture was purified by preparative TLC (developed with benzene) to give a mixture (7.7 mg) of 3-oxo compounds. The mixture was separated by preparative HPLC into lup-19-en-3-one (**12**; 1.0 mg), 18β,19α*H*-lup-12-en-3-one (**15**; 3.2 mg), and lup-18-en-3-one (**17**; 1.8 mg). **12**: mp 174—177 °C (crystallized from acetone); IR 1712 cm^{-1}; ^{1}H NMR ($CDCl_3$) δ 0.77, 0.91, 0.95, 1.06 (each 3H, s), 1.01 (6H, s; 2$\times$$CH_3$), 1.53 and 1.55 (each 3H, s; >C=C(C$\underline{H}_3$)$_2$); MS *m/e* (%) 424 (M^+; 65) and 257 (100); Found: *m/e* 424.3711. Calcd for $C_{30}H_{48}O$: M, 424.3705. HPLC R_t=28.8 min.

15: mp 152.5—153 °C (crystallized from acetone); IR 1710 cm^{-1}; ^1H NMR ($CDCl_3$) δ 0.77, 0.87 (each 3H, d, J= 6 Hz), 0.94, 1.01 (each 3H, s), 1.07, 1.13 (each 6H, s; 2× CH_3), and 5.21 (1H, t, J=4 Hz); MS *m/e* (%) 424 (M^+; 100) and 218 (88); Found: *m/e* 424.3708. Calcd for $C_{30}H_{48}O$: M, 424.3705. HPLC R_t=31.3 min. **17**: mp 167—168 °C (crystallized from acetone); IR 1710 cm^{-1}; ^1H NMR ($CDCl_3$) δ 0.82—1.05 (21H; 7×CH_3), and 1.07 (3H, s); MS *m/e* (%) 424 (M^+; 100); Found: *m/e* 424.3691. Calcd for $C_{30}H_{48}O$: M, 424.3705. HPLC R_t=32.2 min.

Preparation of Lup-18-en-3-one (17). A mixture[12] (32.4 mg) of lup-18-en-3β-yl acetate (**18**) and 18ξ,19ξ*H*-lupan-3β-yl acetate (**19**) was dissolved in tetrahydrofuran (20 ml), and treated with lithium aluminium hydride (51 mg) under reflux for 2 h. The usual work-up gave a mixture (34.0 mg) of lup-18-en-3β-ol and 18ξ,19ξ*H*-lupan-3β-ol. A portion (17 mg) of this mixture was dissolved in acetone, a drop of the Jones reagent being added at 0 °C. After the reaction mixture had been stirred for 50 min, the usual treatment gave a residue, which was subjected to separation by preparative HPLC to afford lup-18-en-3-one (**17**; 8.9 mg).

*Boron Trifluoride Etherate-catalyzed Backbone Rearrangement of 3β,4β-Epoxy-*D:A*-friedo-18β,19α*H*-lupane (5) in Tetrahydrofuran.* A solution of β-epoxide[9] (**5**; 31.2 mg) in tetrahydrofuran (15 ml) was treated with freshly distilled boron trifluoride etherate (0.3 ml) at room temperature for 45 min. The same work-up as in the case of α-epoxide (**4**) gave a mixture, which was separated by preparative TLC (developed with benzene–diethyl ether, 9:1) to give *D:B*-friedo-18β,19α*H*-lup-5(10)-en-3β-ol[9] (**23**; 12.4 mg) and a mixture (7.3 mg) of 5-en-3β-ol[9] (**22**) and 4α-fluorohydrin (**24**). The mixture was subjected to separation by column chromatography on silica gel impregnated with 25% silver nitrate. Elution with benzene gave **24** (3.3 mg) and **22** (2.2 mg). **24**: mp 171 °C (crystallized from methanol); IR 3470 cm^{-1}; ^1H NMR ($CDCl_3$) δ 0.84—0.93 (15H; 5×CH_3), 1.07, 1.25 (each 3H, s), 1.33 (3H, d, J=24 Hz), and 3.68 (1H, m, $W_{1/2}$=13 Hz); MS *m/e* (%) 446 (M^+; 1), 426 (8), and 123 (100); Found: *m/e* 446.3935. Calcd for $C_{30}H_{51}OF$: M, 446.3924.

*Boron Trifluoride Etherate-catalyzed Backbone Rearrangement of 3β,4β-Epoxy-D:A-friedo-18β,19α*H*-lupane (5) in Benzene.* A solution of β-epoxide (**5**; 47.0 mg) in benzene (25 ml) was treated with boron trifluoride etherate (0.3 ml) at room temperature for 1 h. The same work-up gave a mixture, which was subjected to separation by preparative TLC (developed with benzene) to afford *D:A*-friedo-18β,19α*H*-lupan-3-one[9] (**26**; 0.5 mg), 4α-fluoro-*D:A*-friedo-18β,19α*H*-lupan-3β-ol (**24**; 1.5 mg), *D:B*-friedo-18β,19α*H*-lup-5-en-3β-ol (**22**; 4.4 mg), and a mixture (37.2 mg) of alcohols (**27**—**29**). This mixture was dissolved in acetone (10 ml), the Jones reagent (3 drops) being added at 0 °C. The solution was stirred at 0 °C for 15 min. After the usual treatment, the residue was purified by preparative TLC (developed with benzene) to afford a mixture (31.9 mg) of 3-oxo compounds, which was separated by preparative HPLC into *D:B*-friedo-18β,19α*H*-lup-5(10)-en-3-one[9] (**30**; 3.4 mg), lup-19-en-3-one (**12**; 3.5 mg), 18β,19α*H*-lup-12-en-3-one (**15**; 14.5 mg), and lup-18-en-3-one (**17**; 6.2 mg).

*Boron Trifluoride Etherate-catalyzed Backbone Rearrangement of 3β,4β-Epoxy-*D:A*-friedo-18β,19α*H*-lupane (5) in Diethyl Ether.* A solution of β-epoxide (**5**; 41.8 mg) in diethyl ether (20 ml) was treated with boron trifluoride etherate (0.4 ml) for 20 min at 0 °C. A saturated aqueous sodium hydrogencarbonate solution (10 ml) was added, stirring being continued for 20 min. The usual work-up gave a mixture, which was separated by preparative TLC (developed with benzene) to afford 3β,10β-epoxy-*D:B*-friedo-18β,19α*H*-lupane (**31**; 9.0 mg), *D:A*-friedo-18β,19α*H*-lupan-3-one (**26**; 1.0 mg), 4α-fluoro-*D:A*-friedo-18β,19α*H*-lupan-3β-ol (**24**; 8.7 mg), *D:B*-friedo-18β,19α*H*-lup-5-en-3β-ol (**22**; 4.6 mg), and -5(10)-en-3β-ol (**23**; 11.4 mg). **31**: mp 136—138 °C (crystallized from acetone); ^1H NMR ($CDCl_3$) δ 0.84—1.03 (18H; 6×CH_3), 1.67 (6H, s; 2×CH_3), and 3.72 (1H, d, J=5.5 Hz); MS *m/e* (%) 426 (M^+; 79) and 411 (100); Found: *m/e* 426.3861. Calcd for $C_{30}H_{50}O$: M, 426.3860.

*Solvent Effects on the Backbone Rearrangement of 3α,4α-Epoxy-*D:A*-friedo-18β,19α*H*-lupane (4).* Five portions of α-epoxide (**4**; each *ca.* 10 mg) were dissolved in hexane (5 ml), dichloromethane (5 ml), acetonitrile (10 ml), diethyl ether (5 ml), and 1,2-dimethoxyethane (5 ml), respectively, each solution being treated with boron trifluoride etherate (0.1 ml) at room temperature for 30 min. A residue, obtained after the usual work-up, was dissolved in acetone (5 ml) and treated with the Jones reagent (0.1 ml) at 0 °C for 1 h. After purification by preparative TLC (developed with benzene), a mixture of the 3-oxo compounds was examined by HPLC. Since *D:B*-friedo-18β,19α*H*-lup-5-en-3-one[9] (**34**) and -5(10)-en-3-one (**30**) showed the same retention time (R_t=27.3 min) under these conditions, a fraction with R_t=27.3 min was separated by HPLC, the relative amounts of two compounds, **34** (R_t=14.3 min) and **30** (R_t=12.3 min) being examined by GLC.

*Solvent Effects on the Backbone Rearrangement of 3β,4β-Epoxy-*D:A*-friedo-18β,19α*H*-lupane (5).* Four portions of β-epoxide (**5**; each *ca.* 10 mg) were dissolved in hexane (5 ml), dichloromethane (5 ml), acetonitrile (10 ml), and 1,2-dimethoxyethane (5 ml), respectively, each solution being treated with boron trifluoride etherate (0.1 ml) at room temperature for 1 h. A part of the residue, obtained by the usual treatment, was examined by GLC to determine the relative amount ratios of 4α-fluoro-*D:A*-friedo-18β,19α*H*-lupan-3β-ol (**24**; R_t=19.9 min), 3β,10β-epoxy-*D:B*-friedo-18β,19α*H*-lupane (**31**; R_t=9.6 min), and *D:A*-friedo-18β,19α*H*-lupan-3-one (**26**; R_t=16.5 min). The remaining part of the residue was oxidized with the Jones reagent (0.1 ml) in acetone (5 ml) at 0 °C for 1 h, the oxidized product being purified by preparative TLC (developed with benzene). Relative amount ratios of the 3-oxo compounds were estimated in the same way as in the case of α-epoxide (**4**).

The present work was partially supported by a Grant-in-Aid for Scientific Research No. 343008 from the Ministry of Education, Science and Culture.

References

1) A preliminary report was given: Y. Yokoyama, Y. Moriyama, T. Tsuyuki, and T. Takahashi, *Chem. Lett.*, **1980**, 67.

2) *E.g.* E. J. Corey and J. J. Ursprung, *J. Am. Chem. Soc.*, **78**, 5041 (1956); H. Dutler, O. Jeger, and L. Ruzicka, *Helv. Chim. Acta*, **38**, 1268 (1955); G. Brownlie, F. S. Spring, R. Stevenson, and W. S. Strachan, *J. Chem. Soc.*, **1956**, 2419; J. L. Courtney, R. M. Gascoigne, and A. Z. Szumer, *ibid.*, **1958**, 881; R. M. Coats, *Tetrahedron Lett.*, **1967**, 4143; H. W. Whitlock, Jr., and M. C. Smith, *ibid.*, **1968**, 821.

3) a) M. Tori, T. Torii, K. Tachibana, S. Yamada, T. Tsuyuki, and T. Takahashi, *Bull. Chem. Soc. Jpn.*, **50**, 469 (1977); b) M. Tori, T. Tsuyuki, and T. Takahashi, *ibid.*, **50**, 3381 (1977).

4) a) S. Yamada, S. Yamada, K. Tachibana, Y. Moriyama, Y. Tanahashi, T. Tsuyuki, and T. Takahashi,

Bull. Chem. Soc. Jpn., **49**, 1134 (1976); b) K. Tachibana, M. Tori, Y. Moriyama, T. Tsuyuki, and T. Takahashi, *ibid.*, **50**, 1552 (1977).

5) A. G. González, F. G. Jerez, and M. L. Escalona, *An. Quim.*, **69**, 921 (1973); *Chem. Abstr.*, **80**, 24792n.

6) E. Suokas and T. Hase, *Acta Chem. Scand.*, **B28**, 793 (1974).

7) Y. Yokoyama, T. Tsuyuki, Y. Moriyama, T. Murae, H. Toyoshima, and T. Takahashi, *Bull. Chem. Soc. Jpn.*, **52**, 1720 (1979).

8) *E.g.* T. K. Devon and A. I. Scott, "Handbook of Naturally Occurring Compounds," Academic Press, New York and London (1972), Vol. II (Terpenes); "Terpenoids and Steroids," ed by K. H. Overton, The Chemical Society, London, Vol. 1 (1971)-Vol. 8 (1978).

9) Y. Yokoyama, Y. Moriyama, T. Tsuyuki, T. Takahashi, A. Itai, and Y. Iitaka, *Chem. Lett.*, **1979**, 1463; *Bull. Chem. Soc. Jpn.*, **53**, 2971 (1980).

10) *Cf.* H. Hirota, Y. Moriyama, T. Tsuyuki, Y. Tanahashi, T. Takahashi, Y. Katoh, and H. Satoh, *Bull. Chem. Soc. Jpn.*, **48**, 1884 (1975).

11) H. Budzikiewicz, J. M. Wilson, and C. Djerassi, *J. Am. Chem. Soc.*, **85**, 3688 (1963).

12) G. V. Baddeley, J. J. H. Simes, and T. G. Watson, *Tetrahedron*, **26**, 3799 (1970).

13) R. E. Ireland and D. M. Walba, *Tetrahedron Lett.*, **1976**, 1071.

The Reaction of Diazo Ketones in the Presence of Metal Chelates. VIII. The Stereochemistry of the 1,3-Dipolar Cycloaddition of 1-Methoxy-2-benzopyrylium-4-olates to Ethylenic Dipolarophiles

Toshikazu IBATA,* Kimiko JITSUHIRO, and Yoshie TSUBOKURA

Institute of Chemistry, College of General Education, Osaka University, Toyonaka, Osaka 560

(Received May 31, 1980)

1,3-Dipolar cycloadducts were obtained in the reactions of 1-methoxy-2-benzopyrylium-4-olate (**3a**) with ethylenic dipolarophiles, such as dimethyl fumarate, dimethyl maleate, maleic anhydride, *trans*-1,2-dibenzoylethylene, *N*-substituted maleimides, and acenaphthylene. The configuration of the adducts was determined on the basis of the NMR coupling pattern of the methine protons of the adducts in connection with a deuterium experiment. The previously reported structure of the adduct of **3a** with dimethyl fumarate was corrected according to the experimental results obtained using 3-deuterated **3a**. The stereospecificity of the cycloaddition was confirmed in the reactions of dimethyl fumarate, dimethyl maleate, and *trans*-1,2-dibenzoylethylene; this stereospecificity was explained by the concerted ($_{\pi}2_S+_{\pi}4_S$) mechanism. The *exo*/*endo* ratios of the adducts of *N*-substituted maleimides may be explained by the combination of the steric repulsion and π-π interaction of the phenyl ring of **3** and the substituent on the *N*-atom of maleimides. The cycloadditions of 1-methoxy-3-methyl-2-benzopyrylium-4-olate with *N*-substituted maleimides were also explained in a similar manner.

The 1,3-dipolar cycloaddition of pyridinium-3-olate has recently been studied extensively by Katritzky and his co-workers.[1] However, only a few papers are to be found on the reaction of pyrylium-3-olates,[2] which is isoelectronic with pyridinium-3-olate. In the previous papers of this series, we reported the transient formation of 1-methoxy-2-benzopyrylium-4-olate (**3a**: R=H) in the copper chelate-catalyzed decomposition of *o*-methoxycarbonyl-α-diazoacetophenone (**1a**: R=H) *via* an intramolecular carbene-carbonyl reaction.[3] The 2-benzopyrylium-4-olate was found to react as a 1,3-dipole of a type of carbonyl ylide with electron-deficient olefins[3] and acetylenes.[4] In this paper, the stereochemistry of the cycloaddition of **3** will be discussed in detail, using various *cis*- and *trans*-ethylenic dipolarophiles, in order to investigate the mechanism of this reaction.

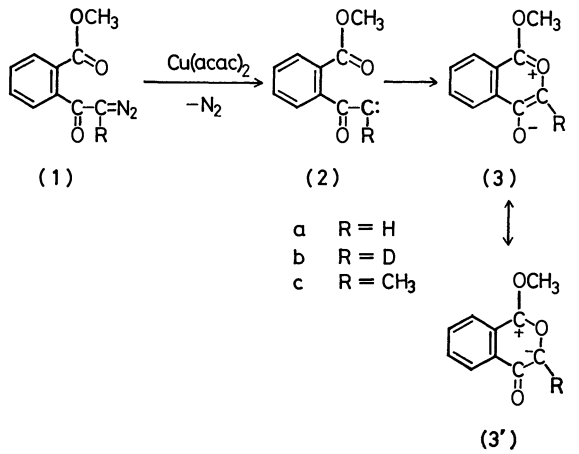

Results and Discussion

The $Cu(acac)_2$ catalyzed decomposition of *o*-methoxycarbonyl-α-diazoacetophenone (**1a**: R=H) in the presence of dimethyl fumarate was reported to give a cycloadduct (**4a**), which was assigned erroneously to 4,7-epoxy-7-methoxy-5-*endo*-6-*exo*-bis(methoxycarbonyl)-1,2-benzocyclohepten-3-one (**4c**).[3] The NMR spectrum of the adduct (**4a**) showed signals of three methine protons, at δ 3.50 (dd), 4.00 (d), and 5.00 (d), besides the three singlets of OCH_3 and a multiplet of aromatic protons (Table 3). The double-doublet signal at δ 3.50 was readily assigned to Hb by reason of its splitting pattern, attributable to the coupling with the adjacent methine protons, Ha and Hc, on its sides. However, for the assignment of the two doublet at δ 4.00 and 5.00, the above data are not sufficient. In order to assign these signals,[4] *o*-methoxycarbonyl-α-diazoacetophenone-α-*d* (**1b**: R=D) was treated similarly in the presence of dimethyl fumarate; a deuterated cycloadduct (**4b**) was thus obtained. The similarity of the structures, **4a** and **4b**, is indicated by the fact that the mixed-melting-point test with **4a** and **4b** does not show any depression (110—111 °C). The IR spectrum of **4b** exhibits a similar pattern almost identical with that of **4a**. In the NMR spectrum of **4b** only two methine protons were observed, δ 4.03 and 3.50, as doublet signals which were coupled each other with J=6.0 Hz. This means that the substitution causes the disappearance of the doublet of **4a** at δ 5.00 and that the double-doublet of **4a** at δ 3.50 is decoupled to form a doublet. Therefore, the signals at 4.00 (d) and 5.00 (d) of **4a** were assigned to Ha and Hc respectively.

The steric relationship between Hb and Hc is determined to be *trans* on the basis of the small value of the coupling constsnt, J_{bc}=1.7 Hz,[6] which indicates an *endo* configuration of Hb. Although the coupling constant, J_{ab}(=6.0 Hz), has a medium value of *cis* and *trans* coupling constants, the steric relationship between Ha and Hb is established as *trans* in comparison with the value of J_{ab} (=9.6 Hz) of the adduct (**4d**) of dimethyl maleate, which has a *cis* configuration of Ha and Hb, as is shown below. The geometry of Hb and Hc of **4d** is confirmed to be *trans* (J_{bc}=2.6 Hz); hence, the configuration of Hb is concluded to be *endo*.

On a large-scale experiment on **1a** with dimethyl fumarate, the major adduct (**4a**) was obtained in a 70% yield, along with a minor product, colorless crystals (mp 115—117 °C, 4% yield). The minor

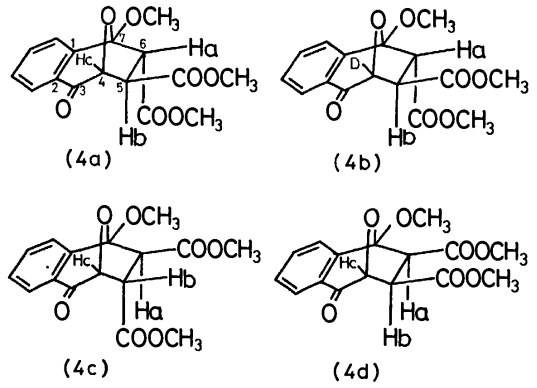

product was characterized as the adduct (**4c**) on the basis of its IR and NMR spectra. The similarity of the IR spectra of **4a** and **4c**, expect for a few differences in the finger-print region, indicates that these adducts are structural isomers different in configuration in the two methoxycarbonyl groups. In **4c**, the geometry between Ha and Hb was deduced to be *trans* (J_{ab}=5.4 Hz), and that of Hb and Hc, to be *cis* (J_{bc}=9.0 Hz). Therefore, the configurations of Hb and Ha are *exo* and *endo* respectively. The fact that the *trans* coupling constants, J_{ab} (6.0 and 5.4 Hz), of **4a** and **4c** are larger than the *trans* coupling constants, J_{bc} (1.7 and 2.6 Hz), of **4a** and **4d** is supported by the inspection of the dihedral angle of a Dreiding Model of the adducts (*trans*-Ha–C–C–Hb, 140°; *trans*-Hb–C–C–Hc, 90°).[7]

When the reaction was carried out in the presence of dimethyl maleate, a 1,3-dipolar cycloadduct (**4d**) was obtained in a 51% yield (mp 145—147 °C); this cycloadduct showed different spectral properties and melting point from the adducts, **4a** and **4c**, described above (Tables 1 and 3). The structure of **4d** was confirmed by a comparison of its IR and NMR spectra with those of an authentic sample synthesized by the esterification of the corresponding dicarboxylic acid, which has been obtained by the hydrolysis of the cycloadduct of 2-benzopyrylium-4-olate (**3a**) with maleic anhydride.

The relation with *trans*-1,2-dibenzoylethylene gave two adducts (**5a** and **5c**). The major adduct (**5a**) showed two doublets, at δ 5.32 and 5.03, and a double-doublet at δ 4.68 (Table 3). These signals were assigned to Ha, Hc, and Hb respectively by comparison with the deuterated adduct (**5b**) in a manner similar to that cited above. The relationships between the neighboring methine protons, Ha-Hb and Hb-Hc, are determined to be *trans* on the basis of the coupling constants (J_{ab}=5.6, J_{bc}=1.8 Hz). The smaller coupling constant J_{ab} (=5.5 Hz) and larger J_{bc} (=8.8 Hz) of the minor adduct (**5c**) show *trans* Ha-Hb and *cis*

Table 1. Yields, melting points, and analytical data of cycloadducts of **3a**

Dipolarophile	Adduct	Yield %	Mp/°C	Found (%) C	H	N	Calcd (%) C	H	N	Molecular formula
Dimethyl fumarate	**4a**	70	111—112	59.89	5.07	—	60.00	5.04	—	$C_{14}H_{16}O_7$
	4c	4	115—117	59.89	5.19	—				
	4b[a]	60	110—111	59.66	4.81	—				
Dimethyl maleate	**4d**[b]	51	145—147	60.27	5.11	—				
1,2-Dibenzoylethylene	**5a**	83	151—152	75.89	4.67	—	76.09	4.42	—	$C_{26}H_{18}O_5$
	5c	6	236—239	76.15	4.26	—				
	5b[a]	70	151—153	76.28	4.25	—				
Maleic anhydride	**7**	48[c]	215—216	57.64	4.06	—	57.54	4.14	—	$C_{14}H_{12}O_7$
N-Phenylmaleimide	**9a**	58	238—239	68.84	4.27	4.18	68.76	4.33	4.01	$C_{20}H_{15}O_5N$
	10a	29	206—207	68.50	4.28	4.00				
N-Ethylmaleimide	**9b**	70	195—197	64.01	5.10	4.77	63.78	5.02	4.65	$C_{16}H_{15}O_5N$
	10b	25	d)							
N-Methylmaleimide	**9c**	61	293—295	62.55	4.64	4.90	62.71	4.56	4.88	$C_{15}H_{13}O_5N$
	10c	33	208—210	62.44	4.52	4.93				
Acenaphthylene	**13**[e]	9	210—212	80.20	4.61	—	80.47	4.91	—	$C_{22}H_{16}O_3$
	14	13	178—179	80.54	4.93	—				

a) An α-deuterated diazo ketone (**1b**) was used. b) Isochromandione (**8**) was obtained as a by-product (18%). c) As a by-product, **8** was obtained in a 14% yield. d) An attempt to purify the *endo* adduct (**10b**) was not successful. e) As a by-product, **8** was obtained in a 14% yield.

Table 2. Yields, melting points, and analytical data of cycloadducts of **3c**

Dipolarophile	Adduct	Yield %	Mp/°C	Found (%) C	H	N	Calcd (%) C	H	N	Molecular formula
N-Phenylmaleimide	**11a**	57	215—217	69.14	4.74	3.66	69.41	4.73	3.86	$C_{21}H_{17}O_5N$
	12a	39	204—206	69.43	4.71	3.72				
N-Ethylmaleimide	**11b**	66	184—186	64.62	5.46	4.22	64.75	5.43	4.44	$C_{17}H_{17}O_5N$
	12b	28	162—163	64.78	5.50	4.35				
N-Methylmaleimide	**11c**	54	229—230	63.56	5.07	4.44	63.78	5.02	4.65	$C_{16}H_{15}O_5N$
	12c	41	191—192	64.03	5.13	4.44				

TABLE 3. SPECTRAL PROPERTIES OF CYCLOADDUCTS OF **3** WITH ETHYLENIC DIPOLAROPHILES

Adduct	NMR (δ, $CDCl_3$)									IR (cm^{-1}, KBr) C=O
	Ha	Hb	Hc	J_{ab}	J_{bc}	OCH_3	OCH_3	OCH_3	Others[a]	
4a	4.00 (d)	3.50 (dd)	5.00 (d)	6.0 trans	1.7 trans	3.45	3.58	3.80		1710, 1734
4b	4.03 (d)	3.50 (d)	—	6.0 trans	—	3.45	3.60	3.82		1710, 1735
4c	3.43 (d)	4.11 (dd)	5.12 (d)	5.4 trans	9.0 cis	3.44	3.60	3.80		1708, 1737
4d	3.57 (d)	3.15 (dd)	5.46 (d)	9.6 cis	2.6 trans	3.44	3.74	3.80		1717, 1753
5a	5.32 (d)	4.68 (dd)	5.03 (d)	5.6 trans	1.8 trans	3.66				1685, 1700
5b	5.34 (d)	4.70 (d)	—	5.6 trans	—	3.64				1685, 1700
5c	4.80 (d)	5.63 (dd)	5.29 (d)	5.5 trans	8.8 cis	3.33				1675, 1705
7[b]	3.80 (d)	3.67 (dd)	5.98 (d)	9.2 cis	2.3 trans	3.44				1710, 1740
9a	3.43 (s)		5.22 (s)	—	0 trans	3.53				1720
9b	3.30 (s)		5.12 (s)	—	0 trans	3.50			1.21 (t, CH_3) 3.63 (q, CH_2)	1710
9c	3.40 (s)		5.10 (s)	—	0 trans	3.50			3.08 (s, CH_3)	1708
10a	3.93 (d)	4.30 (t)	5.20 (d)	9.0 cis	9.0 cis	3.57				1720
10b	3.82 (d)	4.22 (t)	5.10 (d)	9.0 cis	9.0 cis	3.53			0.27 (t, CH_3) 3.07 (q, CH_2)	1705
10c	3.73 (d)	4.17 (t)	5.14 (d)	9.0 cis	9.0 cis	3.53			2.37 (s, CH_3)	1715
11a	3.20 (d)	3.52 (d)	—	8.0 cis	—	3.53			1.73 (s, CH_3)	1710
11b	3.07 (d)	3.38 (d)	—	8.0 cis	—	3.51			1.67 (s, CH_3) 1.23 (t, CH_3) 3.65 (q, CH_2)	1702
11c	3.12 (d)	3.43 (d)	—	8.0 cis	—	3.53			1.70 (s, CH_3) 3.08 (s, CH_3)	1705
12a	3.75 (d)	4.05 (d)	—	10.0 cis	—	3.58			1.87 (s, CH_3)	1720
12b	3.58 (d)	3.88 (d)	—	10.0 cis	—	3.53			1.80 (s, CH_3) 0.30 (t, CH_3) 3.07 (q, CH_2)	1702
12c	3.62 (d)	3.92 (d)	—	10.0 cis	—	3.55			1.83 (s, CH_3) 2.37 (s, CH_3)	1708
13	4.2 (s)		4.90 (s)	—	0 trans	3.25				1703
14	4.3—5.2			c)	c)	3.53				1708

a) Signals of aromatic protons were omitted. b) The NMR spectrum was measured in a $CDCl_3$–pyridine solution.
c) The coupling constant was not determined.

Hb-Hc relationships, which indicate *endo*-Ha and *exo*-Hb configurations.

Reaction with maleic anhydride gave only one adduct in a 48% yield, along with isochroman-1,4-dione (**8**, 14%). The IR spectrum and the results of elemental analysis exhibit that the adduct has a structure (**7**) with two carboxyl groups which were derived from the hydrolysis of the primary adduct (**6**) during the silica-gel-column chromatography. The NMR spectrum of **7** shows doublets at δ 3.80 and 5.98 and a double-doublet at δ 3.67. The coupling constants indicate that the carboxyl groups have the *exo* configuration. The esterification of the adduct (**7**) with diazomethane gave a diester which has the same structure as the adduct (**4d**) obtained by the reaction with dimethyl maleate and the 2-benzopyrylium-4-olate (**3a**). In this case, the absence of an adduct with *endo* carboxyl groups may be attributed to the steric replusion between the anhydride group of the dipolarophile and the carbonyl group of **3a**. The low dipolarophilicity of maleic anhydride caused the by-product formation of lactone (**8**) by the attack

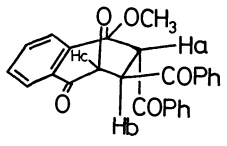
(5a)

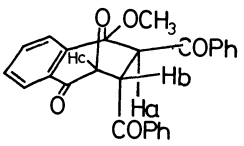
(5b)

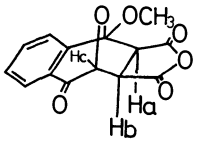
(6)

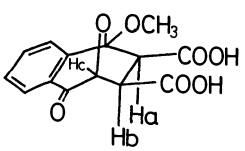
(7)

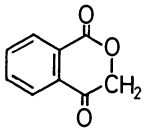
(8)

on 2-benzopyrylium-4-olate (**3a**) of water contained in a benzene solution as an impurity.

N-Phenylmaleimide gave two adducts in yields of 58 and 29%. The major adduct (**9a**) was established to be the *exo* isomer on the basis of its NMR spectrum, which showed singlet signals of methine protons at δ 3.43 and 5.22. From the lack of coupling between Hb and Hc, the configuration of Hb was confirmed to be *endo*. In other words, the *exo* configuration of the adduct (**9a**) was established.[8] Therefore, a singlet at δ 3.43 was assigned to both Ha and Hb, which happened to be equivalent to each other, while a singlet at δ 5.22 was assigned to Hc. The minor adduct (**10a**) shows methine-proton signals at δ 3.93 (d), 4.30 (t), and 5.20 (d), which were assigned to Ha, Hb, and Hc respectively. The coupling pattern, especially the doublet signal (J=9.0 Hz) of Hc, indicates the *endo* structure of the adduct (**10a**).[8] The triplet signal of Hb may be attributed to the same value of the coupling constants, J_{ab} and J_{bc} (=9.0 Hz). The *endo* structure (**10a**) of the minor product was also supported by the abnormal high-field shifts (6.27—6.47 ppm) of two ortho-protons of *N*-phenyl group, which were caused by the shielding effect of the condensed benzene ring. A Dreiding-Model inspection of the *endo* adduct indicates the benzene ring and *N*-phenyl group close to one another.

N-Ethyl- and *N*-methylmaleimides also gave *exo* (**9b**, 70%; **9c**, 61%) and *endo* adducts (**10b**, 25%; **10c**, 33%) respectively. A similar pattern of methine signals was observed in the NMR spectrum of the adducts. The high-field shifts of the *N*-ethyl (δ 0.27, CH_3; 3.07, CH_2) and *N*-methyl signals (δ 2.37) of **10b** and **10c** are explained by the shielding effect of the benzene ring, located close to the *N*-alkyl groups.

Similar results were observed in the reaction of *N*-substituted maleimides with 1-methoxy-3-methyl-2-benzopyrylium-4-olate (**3c**, R=CH_3), which was generated by the $Cu(acac)_2$-catalyzed decomposition of 2-methoxycarbonyl-α-diazopropiophenone (**1c**), yielding *exo* (**11**) and *endo* (**12**) adducts (Table 2). The *endo* adducts show the shielding effect by the benzene ring on the PMR shift of the *N*-methyl, *N*-ethyl, and *N*-phenyl groups (Table 3).

When **1a** was decomposed in the presence of acenaphthylene, two adducts (**13** and **14**) were obtained accompanying lactone (**8**, 14%) in yields of 9 and 13% respectively. The NMR spectrum of **13** has a singlet signal of Hc at δ 4.90 and a broad singlet of two methine protons, Ha and Hb, at δ 4.2. The lack of coupling between Hb and Hc establishes the *exo* structure of the adduct (**13**).[8] Although the multiplet signal of the methine protons of **14** is not sufficient for the determination of the configuration of **14**, it may be identified as *endo* by comparison with the spectrum of **13**.

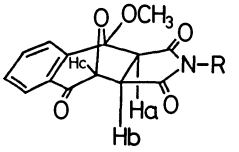
(9)

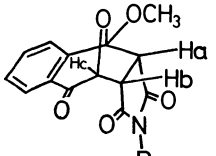
(10)

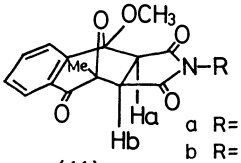
(11)

a R=Ph
b R=C_2H_5
c R=CH_3

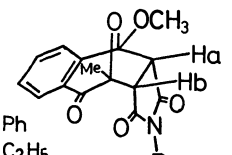
(12)

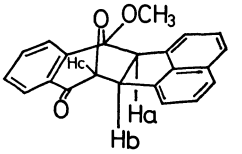
(13)

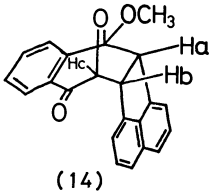
(14)

The stereospecificity of the cycloaddition of the 2-benzopyrylium-4-olate (**3a**) to dimethyl fumarate, dimethyl maleate, and *trans*-1,2-dibenzoylethylene indicates that the cycloaddition proceeds in a ($_{\pi}2_s+_{\pi}4_s$)-type concerted mechanism.[10] In the cycloaddition of *trans* dipolarophiles, such as dimethyl fumarate and *trans*-1,2-dibenzoylethylene, the preferential formation of 5-*endo*-6-*exo* adducts (**4a** and **5a**) to 5-*exo*-6-*endo* adducts (**4c** and **5c**) was explained by the predominance of the transition state (**15a**) over the transition state (**15b**), which contained repulsion between a carbonyl group of dipolarophile and that of 2-benzopyrylium-4-olate. The predominance of the *exo* adducts in the reactions of all the *cis* dipolarophiles except acenaphthylene is explained by the larger stability of the anti-transition state (**16a**) than that of the syn-transition state (**16b**). On the other hand, acenaphthylene showed a reverse tendency to give more *endo* adduct (**14**) than the *exo* isomer (**13**). This might be caused by the π-π interaction[11] between the benzene ring of 2-benzopyrylium-4-olate and the naphthalene moiety of acenaphthylene in the double-layer syn-transition state.[9]

The *endo*/*exo* ratios of the adducts of *N*-substituted maleimides with **3a** and **3c** were found to decrease in the order of *N*-methyl>*N*-phenyl>*N*-ethylmale-

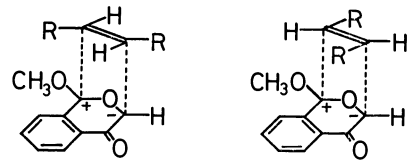

(15a)

(15b)

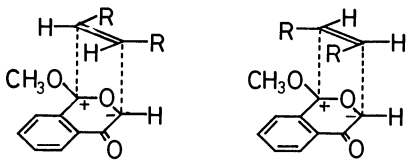

(16a)

(16b)

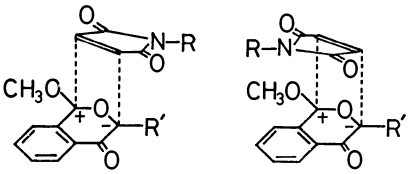

(17a)

(17b)

TABLE 4. THE *endo/exo* RATIOS OF THE ADDUCTS OF MALEIMIDES WITH **3a** AND **3c**

2-Benzopyrylium-4-olate	Maleimide		
	R=Ph	R=C_2H_5	R=CH_3
3a (R′=H)	0.50	0.36	0.54
3c (R′=CH_3)	0.68	0.42	0.76

imide (Table 4). This tendency may be explained by the combination of the steric repulsion and π-π interaction between the benzene ring of 2-pyrylium-4-olate (**3**) and the substituent (R) on the imide nitrogen in the transition state. The steric replusion of *N*-R in the *endo*-transition state (**17b**) may decrease the yield of the *endo* adduct. However, the *endo/exo* ratios are not in the order of the bulkiness of the R group. The π-π interaction of the *N*-phenyl group with the benzene ring of **3** may increase the *endo* yield a little more than the expected value because of its bulkiness and may thus give a value in between those of *N*-methyl- and *N*-ethylmaleimides. The large *endo/exo* ratios of **3c** adducts (**12/11**), in contrast to those of **3a** adducts, may be attributed to the repulsion between the R on the imide-nitrogen and the R′ on the C-3 of **3c** in the *exo* transition state (**17a**), which decreases the yeild of the *exo* adduct slightly (Table 4).

Experimental

All the melting points were measured on a Yanagimoto Melting Point Apparatus and were not corrected. The IR spectra were taken on a Hitachi Spectrometer, model EPI-S2. The ^{1}H-NMR spectra were recorded on a Varian A-60 or EM-360 Spectrometer in a $CDCl_3$ solution; the chemical shifts were described in ppm downfield from TMS as the internal standard (δ scale).

Materials. o-*Methoxycarbonyl-α-diazoacetophenone* (***1a***) was prepared by the procedure described in the previous paper.[3]

o-*Methoxycarbonyl-α-diazoacetophenone-α-d* (***1b***) was synthesized by the reaction of the DCC complex of methyl hydrogen phthalate with deuterated diazomethane, which had itself been prepared by the reaction of *N*-methyl-*N*-nitrosourea with potassium deuteroxide in D_2O.[12] Crude **1b** containing a trace amount of dimethyl phthalate was used without further purification.

o-*Methoxycarbonyl-α-diazopropiophenone* was synthesized by the DCC method using an excess of diazoethane and purified by column chromatography on Al_2O_3 with an activity of 4; viscous liquid, IR (liquid film): 2050 (diazo), 1700 (ester), 1595 cm^{-1} (diazocarbonyl), NMR: 2.57 (s, 3H, CH_3), 3.87 (s, 3H, OCH_3), 7.4—8.1 ppm (aromatic protons).

All the other reagents were purified by recrystallization or distillation before use.

*General Procedure of the Decomposition of **1** in the Presence of Dipolarophiles.* The $Cu(acac)_2$-catalyzed decomposition of **1** was performed according to the procedure described in the previous paper by refluxing a benzene solution of **1** and a 1.2—1.5 molar equivalent of dipolarophile and a catalytic amount of $Cu(acac)_2$ until no more N_2 was evolved.[3] The reaction mixture was separated by silica gel column chromatography, using benzene as the eluent.

*Esterification of Dicarboxylic Acid (**7**).* An ether solution of diazomethane was slowly added to a suspension of 0.10 g of **7** in ether until no more N_2 was evolved. The subsequent evaporation of the ether under reduced pressure yielded 0.11 g of colorless crystals (mp 145—146 °C), later recrystallized from benzene-heptane solution. The IR and NMR spectra were perfectly superimposable on those of **4d** obtained by the reaction of **3a** with dimethyl maleate.

References

1) A. R. Katritzky, N. Dennis, and Y. Takeuchi, *Angew. Chem. Int. Ed. Engl.*, **15**, 1 (1976).
2) a) E. F. Ullman and J. E. Milks, *J. Am. Chem. Soc.*, **84**, 1315 (1962); **86**, 3814 (1964); b) H. E. Zimmerman and R. D. Simkin, *Tetrahedron Lett.*, **1964**, 1847; c) J. W. Lown and K. Matsumoto, *Can. J. Chem.*, **49**, 3443 (1971).
3) K. Ueda, T. Ibata, and M. Takebayashi, *Bull. Chem. Soc. Jpn.*, **45**, 2779 (1972).
4) T. Ibata and K. Jitsuhiro, *Bull. Chem. Soc. Jpn.*, **52**, 3582 (1979).
5) In the previous paper (Ref. 3), the authors made the reverse assignment on the Ha and Hc of the adduct (**4a**).
6) J. W. Lown and K. Matsumoto, *Can. J. Chem.*, **48**, 2215 (1970).
7) M. Karplus, *J. Chem. Phys.*, **30**, 11 (1959).
8) A. R. Katritzky and Y. Takeuchi, *J. Chem. Soc., C*, **1971**, 874.
9) R. Huisgen, *J. Org. Chem.*, **33**, 2291 (1968).
10) R. Huisgen, *Angew. Chem. Int. Ed. Engl.*, **2**, 565 (1963).
11) R. Huisgen, H. Hauk, R. Grashey, and H. Seidl, *Chem. Ber.*, **102**, 736 (1969); T. Ibata, T. Motoyama, and M. Hamaguchi, *Bull. Chem. Soc. Jpn.*, **49**, 2298 (1976).
12) S. M. Hecht and J. W. Kozarich, *Tetrahedron Lett.*, **1972**, 1501.

  Bull. Chem. Soc. Jpn., 54, 245—248 (1981)

Applications of Homogeneous Water-gas-shift Reaction. I. Further Studies of the Hydroformylation of Propene with CO and H_2O

Kazuhisa MURATA* and Akio MATSUDA

National Chemical Laboratory For Industry, Tsukuba Research Center, Yatabe, Tsukuba, Ibaraki 305

(Received June 18, 1980)

Polar ether solutions prepared *in situ* from $Co_2(CO)_8$ and 1,2-bis(diphenylphosphino)ethane (diphos) are active catalysts for the hydroformylation of propene with CO and H_2O. Under the hydroformylation conditions employed, butyl(C_4) or isobutyl alcohols, butyric(C_4) acids, and dipropyl ketones were found to be formed as by-products. A pronounced formation of C_4 alcohols was observed as the reaction temperature was increased; in fact, the catalyst solutions described above actively reduce butyraldehyde to butyl alcohol. The effects of the CO pressure and of the propene concentration on the formation of C_4 aldehydes are also examined. It turns out that the water molecule as well as $Co_2(CO)_8$ and diphos are essential for the formation of catalytic intermediates, which are themselves responsible for the hydroformylation activity.

Recently, we have reported the homogeneous catalysis of hydroformylation with CO and H_2O, in which the $Co_2(CO)_8$–diphos system was used in such polar ether solvents as THF, dioxane, and diglyme with no base.[1]

$$CH_3CH{=}CH_2 + 2CO + H_2O \longrightarrow CH_3CH_2CH_2CHO \text{ or } CH_3\underset{\displaystyle CH_3}{\overset{|}{C}}HCHO + CO_2 \quad (1)$$

The use of CO and H_2O in place of hydrogen is not a racent development. It has been well known, for example, that hydrohydroxymethylation(1′) is catalyzed by the $Fe(CO)_5$–organic tertiary amine system.[2] (Reppe Reaction: The reaction(1′) is more stoichiometric than catalytic.)

$$CH_3CH{=}CH_2 + 3CO + 2H_2O \longrightarrow CH_3CH_2CH_2CH_2OH \text{ or } CH_3\underset{\displaystyle CH_3}{\overset{|}{C}}HCH_2OH + 2CO_2 \quad (1')$$

More recently, special attention has been paid to the possibility of using other transition-metal carbonyl complexes as active catalysts in these reactions, (1) and (1′); a variety of Group 8 metal carbonyl clusters can serve as catalyst precursors in the presence of alkali or amine.[3]

Our catalyst system is considerably different from other ones in that: a) diphos is an essential component, and b) alkali or organic amines are absent.

Also, $Co_2(CO)_8$ is a more conventional catalyst than other metal carbonyl clusters, such as $Ru_3(CO)_{12}$, $Rh_6(CO)_{16}$. Therefore, there is the possibility of developing a novel industrial process. Thus, further studies of our catalyst system were undertaken under reaction conditions more catalytically active than those reported previously.[1]

Experimental

Materials. The propene (Research Grade), diphos, and dioxane used as solvent were obtained commercially and were used with no further purification. The $Co_2(CO)_8$ was prepared by the conventional method. The H_2O was distilled under atmospheric pressure prior to use.

Reaction Procedure. The hydroformylation reactions were carried out in a 100-ml stainless-steel autoclave, in which $Co_2(CO)_8$, diphos, H_2O, and dioxane had been placed. After the vessel was sealed, both propene and CO were introduced. The system was then brought to the desired reaction temperature and pressure by the additional charging of CO under heating. Stirring was then begun, and the reaction took place. The CO pressure was kept constant during the reaction by supplying the gas from a 400-ml pressure storage vessel through a pressure regulator. The reaction temperature was controlled within a range of ±1 °C.

The catalytic reductions of butyraldehyde to butyl alcohol were performed in an identical manner, except for the use of butyraldehyde (25 mmol) in place of propene (25 mmol).

Analysis of Products. Gas analysis was performed at 50 °C with a gas chromatograph using a 6-m Carbowax column. The amount of CO_2 was determined by titration methods. The liquid products other than C_4 acids were analyzed at 100 °C by means of a gas chromatograph equipped with FID using a 6-m column packed with polyethylene glycol adipate. C_4 acid analysis was performed at 150 °C using a gas chromatograph equipped with FID and using a 4-m squalane column. The infrared spectra of catalyst solutions were recorded on a Hitachi type 215 spectrometer.

Results and Discussion

Preliminary Studies Involving the Effect of CO Pressure. The $Co_2(CO)_8$-catalyzed hydroformylation of propene with CO and H_2O was carried out in dioxane solvent, since it was greatly effective for this reaction; only a little hydrogen as a co-product was detected in the dioxane. This reaction can proceed catalytically only in the presence of phosphine; of all the phosphines used, diphos was the most effective. A diphos 1: $Co_2(CO)_8$ 1 ratio was used in order to inhibit the partial decomposition of the catalyst.

In a previous report,[1] the reaction was run at 135 °C for 17 h under an initial pressure of 12 kg/cm^2; C_4 aldehydes (9.2 mmol, *ca.* 37% conversion based on propene) were thus produced with 0.04 mmol of C_4 alcohols, (2), (3). In addition, we have recently found that, under the conditions employed, butyric (C_4) acids (1.0 mmol, (4)) and dipropyl ketones (0.8 mmol, (5)) were formed as by-products in detectable amounts.

$$C_3H_7\text{-}CHO + CO + H_2O \longrightarrow C_3H_7\text{-}CH_2OH + CO_2 \quad (2)$$

$$CH_3CH{=}CH_2 + 3CO + 2H_2O \longrightarrow C_3H_7\text{-}CH_2OH + 2CO_2 \quad (3)$$

$$CH_3CH{=}CH_2 + CO + H_2O \longrightarrow C_3H_7\text{-}COOH \quad (4)$$

$$2CH_3CH{=}CH_2 + 2CO + H_2O \longrightarrow (C_3H_7)_2CO + CO_2 \quad (5)$$

Reaction 4 is a cobalt-catalyzed hydrocarboxylation, which is of little interest to us because it is a well-known example of a Reppe Reaction, which proceeds with no production of CO_2. At 165 °C, CO(50 kg/cm²), 13.0 mmol of C_4 aldehydes was obtained at a 5 h-reaction and few C_4 acids were formed, though a higher CO pressure favored the formation of the acids (Fig. 1). As is shown in Fig. 1, the total amounts of C_4 aldehydes (abbreviated as [aldehydes]) decreased with the increase in the CO pressure, which is analogous to observations in a normal $Co_2(CO)_8$-catalyzed hydroformylation using CO/H_2.[4]

Effect of the Temperature. In normal $Co_2(CO)_8$-catalyzed reactions, the C_4 aldehydes which are formed during the hydroformylation are readily reduced to the corresponding C_4 alcohols at a higher reaction temperature.[5]

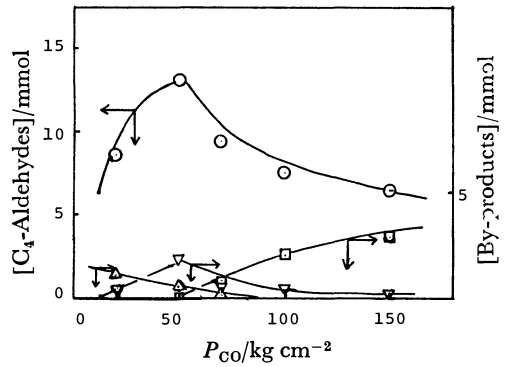

Fig. 1. Effect of CO pressure.
$Co_2(CO)_8$ 2 mmol, diphos 2 mmol, H_2O 60 mmol, dioxane 50 ml, propene 25 mmol, temp 165 °C, time 5 h.
—○—: C_4-aldehydes, —△—: C_4-alcohols, —□—: C_4-acids, —▽—: dipropyl ketones.

The temperature-dependence on the product yields is illustrated in Fig. 2; the reactions were performed using the $Co_2(CO)_8$–diphos system for 5 h under CO (50 kg/cm², const). As one would expect, [aldehydes] rather decreased with the increase in the reaction temperature and there was a pronounced formation of C_4 alcohols. It is not obvious from the data whether the C_4 alcohols are formed step-by-step *via* hydroformylation (1) and then reduction (2), or directly from propene (3). Thus, the possibility of the reduction of butyraldehyde to butyl alcohol with CO and H_2O was tested under the same conditions as those employed in Fig. 2, except that butyraldehyde (25 mmol) was used in place of propene. The reduction (2) occurs, but more slowly than in the hydroformylation of propene; the higher the temperature, the larger the amount of butyl alcohol produced[6] (Fig. 2---,).

Effect of the Propene Concentration. As is shown in Fig. 3, [aldehydes] increased with the initial increase from 25 to 150 mmol of propene, but a further increase of propene resulted in a decrease in the yields. On the other hand, the total amounts of dipropyl ketones ((5), [ketones]) drastically increased, and it turned out, as a result, that the ketones were obtained as the principal products in the reaction of propene with CO and H_2O. Under these conditions, the product molar ratio of 4-heptanone: 2-methyl-3-hexanon: 2,4-dimethyl-3-pentanone was *ca* 1:1.8:0.8; this ratio depends little on the propene concentration.

Generally, dipropyl ketones can be produced under normal oxo conditions in the presence of $Co_2(CO)_8$; the formation of the ketones is favored not only by a high concentration of propene, but also by the use of such hydrogen donors as H_2O, alcohols instead of H_2.[7] Taking into account the fact that H_2O is used as a hydrogen donor in our $Co_2(CO)_8$–diphos system, the findings in Fig. 3 are analogous to those in the normal $Co_2(CO)_8$ system. In the normal system, however, the formation of the ketones does not predominate over that of the aldehydes (or esters,

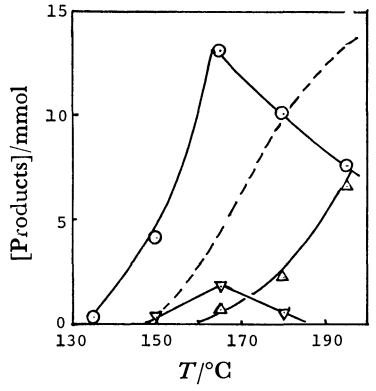

Fig. 2. Effect of temperature.
$Co_2(CO)_8$ 2 mmol, diphos 2 mmol, H_2O 60 mmol, dioxane 50 ml, CO 50 kg/cm², propene 25 mmol, time 5 h.
Marks (○,△,▽): See footnote of Fig. 1, dotted line: reduction of butyraldehyde to butyl alcohol.

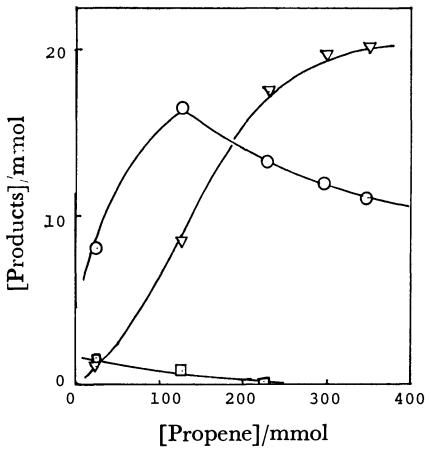

Fig. 3. Effect of propene concentration.
$Co_2(CO)_8$ 2 mmol, diphos 2 mmol, H_2O 60 mmol, dioxane 50 ml, CO 70 kg/cm², temp 165 °C, time 5 h.
Marks (○,▽,□): See footnote of Fig. 1.

acids). In this point, the catalytic behavior of $Co_2(CO)_8$ and that of $Co_2(CO)_8$–diphos was quite different. An obvious explanation cannot be obtained from the data shown in Fig. 3; further work is required.

In recent reports on metal carbonyl (cluster)-catalyzed hydroformylation with CO and H_2O, ketone formation has not been referred to at all.[3] According to our additional experiments, an $RhCl_3$– or $RuCl_3$–Et_3N catalyst system can give dipropyl ketones only as minor product under the conditions shown in Fig. 3. Thus, the $Co_2(CO)_8$–diphos system appears to be more desirable for the exclusive formation of dipropyl ketones from propene; the details will be described in the succeeding paper.[8]

Catalytic Behavior as a Function of Time. The hydroformylation of propene was repeated under the conditions where C_4 aldehydes are predominantly formed, and aliquots of the catalyst solutions were withdrawn from the autoclave at several reaction times and analyzed. The results are illustrated in Fig. 4(○), where an induction period of *ca.* 1 h was observed. In our catalyst system, under the conditions employed, aldol condensation, by which butyraldehyde is converted to C_8 aldehyde, occurs to only a slight extent with the progress of the reaction (see Fig. 4(○,●)), partly because alkali or organic amine is absent in the solution.[9]

The presence of an induction period is of interest in connection with the intermediates present in the catalyst solutions. The period disappears on the pretreatment of the solution ($Co_2(CO)_8$–diphos–dioxane) with both CO (50 kg/cm²) and H_2O (60 mmol) at 165 °C for 1 h in the absence of propene (Fig. 4, □),[10a] whereas it does not disappear on the similar pretreatment of the solution with only CO (Fig. 4, △).[10b] These findings indicate that the H_2O molecule is required for the production of intermediates, which are themselves responsible for the hydroformylation with CO and H_2O. Considering that the catalytic behavior of $Co_2(CO)_8$–diphos system using CO–H_2O is relatively similar to those of normal $Co_2(CO)_8$ using CO–H_2 (Figs. 1, 2, and 3), cobalt carbonyl hydride complexes ($HCo(CO)_m(diphos)_n$, (A))[11] may be probable candidates as the key intermediates necessary for the catalysis of the reaction. Rhodium or ruthenium carbonyl hydrides have already been proposed as intermediates active in hydroformylation using CO–H_2O.[3b]

In the absence of propene, the $Co_2(CO)_8$–diphos system is active in the water-gas-shift reaction (WGSR), thoguh its catalytic activity is *ca.* ten times lower than that of the hydroformylation.[1] Therefore, there is a possibility that the catalytic intermediates which catalyze the hydroformylation participate in the WGSR.[12] In fact, the catalyst solutions derived from the $Co_2(CO)_8$–diphos system show the same absorptions in the metal carbonyl regions in both the presence and absence of propene.[13]

Unfortunately, attempts to isolate (A) were not successful.[14] Also, it is not obvious from our data that the catalytic intermediates, (A), which are necessary for the catalysis of the hydroformylation, are in fact involved in the catalysis of the WGSR. However, undoubtedly, intermediates active in the hydroformylation of propene, as well as in the WGSR, can be formed only from $Co_2(CO)_8$, diphos, and H_2O (Fig. 4).

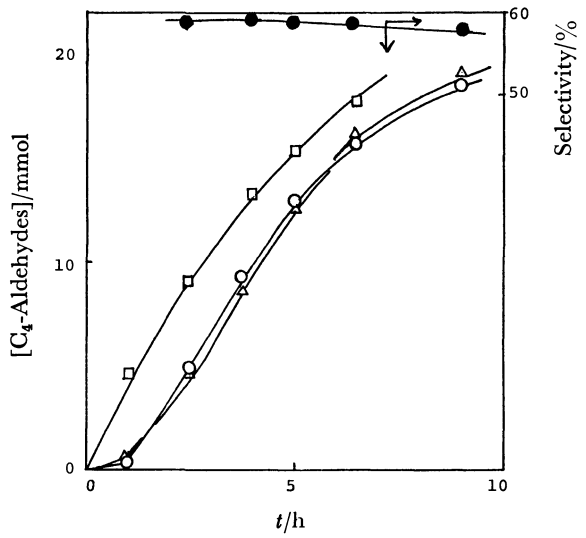

Fig. 4. Cobalt-catalyzed hydroformylation as a function of time.
$Co_2(CO)_8$ 2 mmol, diphos 2 mmol, H_2O 60 mmol, dioxane 50 ml, CO 50 kg/cm², temp 165 °C, propene 25 mmol. Products other than C_4-aldehydes are omitted.
—○—: Standard reaction, —□—: reaction after the pretreatment with CO and H_2O, —△—: reaction after the pretreatment with only CO, —●—: selectivity to linear aldehyde.

References

1) K. Murata, A. Matsuda, K. Bando, and Y. Sugi, *J. Chem. Soc., Chem. Commun.*, **1979**, 785.
2) W. Reppe and H. Vetter, *Justus Liebigs Ann. Chem.*, **582**, 133 (1953).
3) a) H. Kang, C. H. Mauldin, T. Cole, W. Slegeir, K. Cann, and R. Pettit, *J. Am. Chem. Soc.*, **99**, 8323 (1977); b) R. M. Laine, *ibid.*, **100**, 6451 (1978).
4) The catalytic activity rather decreased at a CO pressure of 20 kg/cm² because of the partial decomposition of $Co_2(CO)_8$.
5) B. R. James, "Homogeneous Hydrogenation," Wiley, New York (1973), p. 158.
6) The rate of the reduction of isobutyraldehyde to isobutyl alcohol was approximately the same as that of butyraldehyde under these conditions.
7) I. Wender and P. Pino, "Organic Synthesis *via* Metal Carbonyl," Wiley, New York (1977), Vol. 2, p. 215.
8) K. Murata and A. Matsuda, *Bull. Chem. Soc. Jpn.*, **54**, 249 (1981).
9) The preferential condensation of aldehyde occurs during the ruthenium-catalyzed hydroformylation using CO–H_2O in the presence of KOH.[3b]
10) a) After this pretreatment, propene (25 mmol) was introduced at room temp; the reaction was then carried out under conditions identical with those shown in Fig. 4(○); b) In this run, propene (25 mmol) and H_2O (60 mmol) were introduced at room temp.
11) When either $CH_3CCo_3(CO)_9$ or $Co_4(CO)_{12}$ was used as a catalyst precursor, a longer induction period resulted.

12) Thus, if this is so, the following ideal catalytic cycles, for example, can be surmised in comparison with Heck's mechanism: the intermediates (A) formed during the course of the shift reaction could be trapped by propene (hydride addition), followed by CO insertion, accompanied by the elimination of aldehyde to reform (A). R. F. Heck and D. S. Breslow, *J. Am. Chem. Soc.*, **83**, 4023 (1961).

13) These include ν_{CO} 2062(ms), 2922(m, sh), 1986(s), and 1887(m) cm^{-1}.

14) More recently, we have found that the ^1H-NMR spectrum of an active water-gas-shift catalyst solution consisting of $Co_2(CO)_8$, diphos, H_2O, and dioxane displays a characteristic resonance at δ −17.2. Further studies of this will be discussed elsewhere.

Applications of Homogeneous Water-gas-shift Reaction. II. The Formation of Dipropyl Ketones as Primary Products from CO and H_2O in the Presence of an Excess Amount of Propene. Cobalt-based Catalytic Hydrocarbonylation

Kazuhisa MURATA* and Akio MATSUDA

National Chemical Laboratory For Industry, Tsukuba Research Center, Yatabe, Tsukuba, Ibaraki 305

(Received June 18, 1980)

The hydrocarbonylation of propene with CO and H_2O to give dipropyl ketones occurs predominantly over forming C_4-aldehydes; the catalyst solutions employed are prepared *in situ* from $Co_2(CO)_8$, various phosphines as ligands, and H_2O, a high molar ratio of propene to $Co_2(CO)_8$ of 300/2 being required. Of the several phosphorus ligands examined, 1,2-bis(diphenylphosphino)ethane (diphos) and bis(diphenylphosphino)acetylene are relatively effective for the formation of the ketones (abbreviated as [ketones]). The effects of the reaction variables (CO pressure, temperature, and H_2O concentration) on [ketones] are also examined using the $Co_2(CO)_8$–diphos system; [ketones] increases with the initial increase in CO pressure, but reaches a maximum at *ca.* 100 kg/cm^2 and decreases thereafter. Pronounced decreases of [ketones] are observed when pyridine as well as hydrogen is added to the catalyst solutions.

Hydrocarbonylation, by which dialkyl ketones are produced from olefins, can proceed under oxo conditions by means of a transition-metal catalyst.[1] However, the selectivity of the reaction is significantly low when olefins other than ethene are used;[2] generally, a mixture of ketones, aldehydes, and other oxygenated products is formed. Accordingly, the hydrocarbonylation reaction, despite its potential synthetic value, has scarcely been investigated at all.

We described in our previous papers that the presence of an excess amount of propene under the hydrocarbonylation conditions using CO–H_2O leads to the formation of dipropyl ketones as primary products,[3] and $Co_2(CO)_8$–phosphine system appeared to be much more effective for the ketone formation than other transition-metal catalysts, being especially active for the homogeneous water-gas-shift reaction (WGSR).[4]

In the present paper, further studies of this cobalt catalyzed-hydrocarbonylation will be described, and the catalytic behavior will be compared with that in hydroformylation.

Experimental

The experimental methods are roughly analogous to those described in the preceding paper.[3] The few differences will be outlined below.

The phosphines and pyridine were obtained commercially.

The hydrocarbonylation reactions were performed in a 300 ml stainless-steel autoclave equipped with a vertical agitator. In all runs, the molar ratio of propene to $Co_2(CO)_8$ was kept constant at 300 mmol/2 mmol.

A certain amount of hydrogen was added to a catalyst solution as soon as the solution had been brought to the reaction temperature (Fig. 5). A small amount of pyridine was mixed with the catalyst solutions ($Co_2(CO)_8$–diphos–dioxane–H_2O) before the reactor was sealed (Fig. 6).

Results and Discussion

All of the hydrocarbonylation experiments were carried out for a 5 h-reaction time[5] with the propene/$Co_2(CO)_8$ molar ratio being held constant at 300/2, since the maximum yield of dipropylketones was achieved at this ratio (see Fig. 3 in the preceding paper[3]). $Co_2(CO)_8$ was also used as a catalyst precursor in the dioxane solvent. As is shown in Table 1, THF (Run 1) and the cobalt carbonyl cluster ($CH_3CCo_3(CO)_9$) (Run 2) lead to a reduction in the ketone formation.

Effects of Several Phosphorus Ligand. The results are summarized in Table 1 (Runs 3,4,9—15). The effectiveness of phosphorus ligands in increasing the formation of the ketones ([ketones]) decrease in this order: diphos > $Ph_2PC{\equiv}CPPh_2$ > PPh_3 > $Ph_2PCH_2PPh_2$ > PBu_3 > $Ph_2P(CH_2)_3PPh_2$ > $(PhO)_3P$ > $Ph_2P(CH_2)_4PPh_2$ = $Ph_2As(CH_2)_2PPh_2$.

The effect of the diphos: $Co_2(CO)_8$ ratio on the [ketones] was also examined (Runs 4—8); the most active catalyst appears to be formed with a *ca.* 0.75:1 ratio (Run 5). As we would expect, however, for the <1:1 ratios, the catalyst partially decomposes during the reaction.[6] In the absence of diphos, 6.5 mmol of the ketones were obtained, with the $Co_2(CO)_8$ being completely decomposed.[6,7] (Run 8) Both the order of reactivity and the ratio effect reported here are quite similar to those observed for the hydroformylation using CO–H_2O with a propene/$Co_2(CO)_8$ molar ratio of 25/2.[8] Hereafter, diphos is here used as a ligand.

Effect of CO Pressure. The [ketones] value is remarkably dependent on such reaction variables as CO pressure(P_{CO}), H_2O concentration, and the temperature. Figure 1 illustrates the P_{CO} dependence. The [ketones] value increased with the initial increase in P_{CO}, but nearly reached a maximum as the P_{CO} increased to *ca.* 100 kg/cm^2 decreased thereafter. The C_4 aldehyde formation ([aldehydes]), on the other hand, smoothly decreased with the increase in P_{CO}.

Effect of Temperature. The temperature dependence under 100 kg/cm^2 of P_{CO} is shown in Fig. 2. The [ketones] value increased with an increase in the temperature from 135 °C to 165 °C, but rather decreased at 180 °C, whereas [aldehydes] successively increased; as a result, the selectivity to the ketones drastically decreased (– – –) at 180 °C.

Effect of H_2O Concentration. Figure 3 displays a plot of the product formation as a function of the H_2O added. The [ketones] value reached a maximum

TABLE 1. HYDROCARBONYLATION OF PROPENE USING CO-H_2O CATALYZED BY $Co_2(CO)_8$ WITH SEVERAL PHOSPHORUS LIGANDS

$Co_2(CO)_8$, 2 mmol; phosphine, 2 mmol; dioxane (solvent), 50 ml; propene, 300 mmol; H_2O, 60 mmol; CO 100 kg/cm² (const); time, 5 h; temp, 165 °C.

Run No.	Added phosphine	Products[a] [ketones] mmol	[aldehydes] mmol	[acids] mmol
1	$Ph_2P(CH_2)_2PPh_2$[b]	19.2	10.3	0.7
2	$Ph_2P(CH_2)_2PPh_2$[c]	14.1	8.1	0.6
3	$Ph_2PCH_2PPh_2$	12.9	4.0	1.1
4	$Ph_2P(CH_2)_2PPh_2$	27.0	11.0	0.5
5	$Ph_2P(CH_2)_2PPh_2$ (1.5 mmol)	36.2	—	—
6	$Ph_2P(CH_2)_2PPh_2$ (1.0 mmol)	32.2	—	—
7	$Ph_2P(CH_2)_2PPh_2$ (0.5 mmol)	25.9	—	—
8	none	6.5	2.4	—
9	$Ph_2P(CH_2)_3PPh_2$	12.1	5.9	—
10	$Ph_2P(CH_2)_4PPh_2$	3.9	2.2	—
11	$Ph_2PC{\equiv}CPPh_2$	26.4	12.2	1.1
12	PPh_3	21.6	7.0	0.5
13	PBu_3	12.8	3.9	—
14	$Ph_2As(CH_2)_2PPh_2$	3.9	0.3	—
15	$(PhO)_3P$	5.2	7.7	—

a) [ketones]: 4-heptanone+2-methyl-3-hexanone+2,4-dimethyl-3-pentanone, [aldehydes]: butyraldehyde+isobutyraldehyde, [acids]: butyric acid+isobutyric acid. b) Using THF (50 ml) as the solvent. c) Using $CH_3CCo_3(CO)_9$ as the precursor.

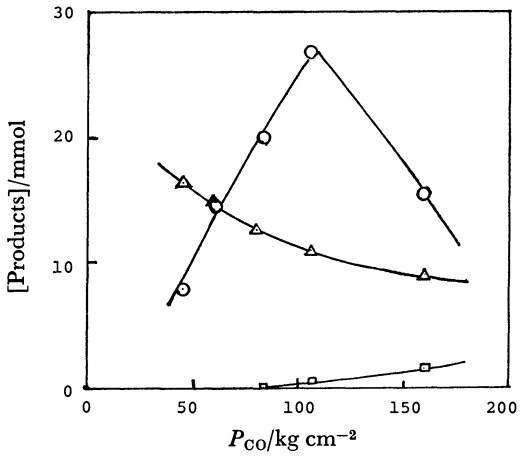

Fig. 1. Effect of CO pressure.
$Co_2(CO)_8$ 2 mmol, diphos 2 mmol, dioxane 50 ml, H_2O 60 mmol, 165 °C, propene 300 mmol, time 5 h.
—○—: Dipropyl ketones, —△—: C_4-aldehydes, —□—: C_4-acids.

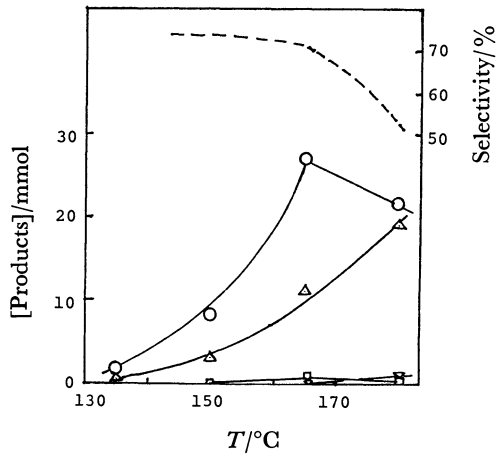

Fig. 2. Effect of temperature.
$Co_2(CO)_8$ 2 mmol, diphos 2 mmol, dioxane 50 ml, H_2O 60 mmol, P_{CO} 100 kg/cm², propene 300 mmol, time 5 h.
—△—: C_4-alcohols, ----: the selectivity; [ketones]/([ketones]+[aldehydes]+[alcohols]+[acids]), other marks: see footnote of Fig. 1.

as the amount of H_2O([H_2O]) increased to *ca.* 120 mmol, and leveled off thereafter. In contrast, [aldehydes] linearly increased with the increase in [H_2O]. Thus, the combined yield (---) increased with [H_2O].

A plot of the product formation as a function of the $Co_2(CO)_8$ concentration, where the diphos/$Co_2(CO)_8$ ratio was kept constant at 1/1, gave results analogous to those shown in Fig. 3.

Catalytic Intermediates. It seems likely that catalytic intermediates(probably $HCo(CO)_m(diphos)_n$, (A)) which catalyze the hydroformylation of propene with CO and H_2O, as has already been described in the preceding paper,[3] also participate in this hydrocarbonylation. In fact, C_4 aldehydes can be formed even during the reaction (Table 1, Figs. 1—3). The influence of phosphorus ligands on the [ketones] value (propene/$Co_2(CO)_8$=300/2, Table 1) is fairly analogous to that on the hydroformylation activity (the ratio=25/2).[8] A smooth increase in the combined yield results when [H_2O] is increased, since the concentration of (A) also increases (Fig. 3). The catalyst solutions active in the hydrocarbonylation have the

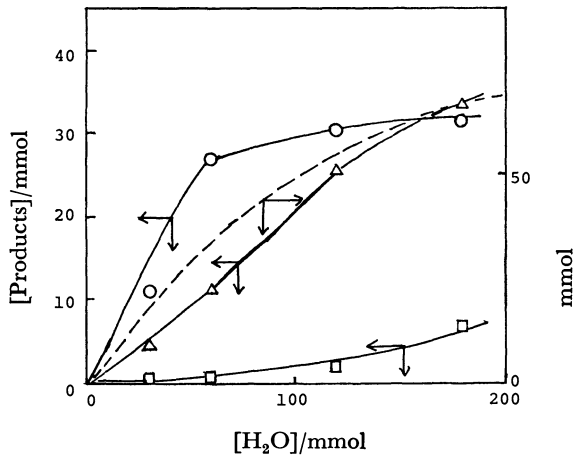

Fig. 3. Effect of H_2O concentration.
$Co_2(CO)_8$ 2 mmol, diphos 2 mmol, dioxane 50 ml, P_{CO} 100 kg/cm², propene 300 mmol, temp 165 °C, time 5 h.
----: A combined yield ([ketones]+[aldehydes]), other marks: see footnote of Fig. 1.

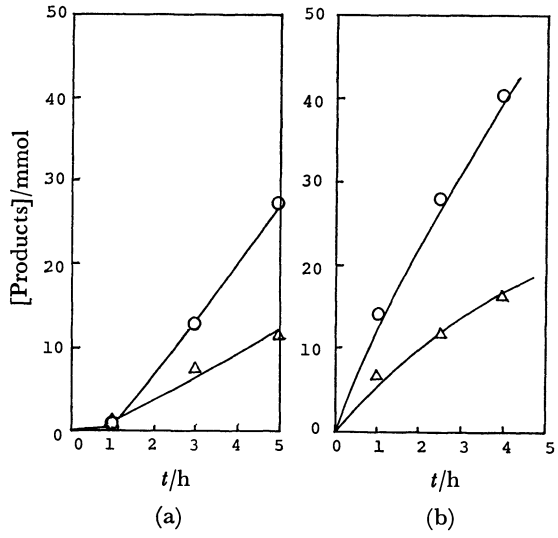

Fig. 4. Cobalt-catalyzed hydrocarbonylation as a function of time.
$Co_2(CO)_8$ 2 mmol, diphos 2 mmol, dioxane 50 ml, P_{CO} 100 kg/cm², H_2O 60 mmol, propene 300 mmol, temp 165 °C.
(a) A standard reaction, (b) a reaction after the pretreatment with both CO (100 kg/cm²) and H_2O (60 mmol) at 165 °C for 1 h, marks (○,△): see footnote of Fig. 1. Other products omitted.

same IR absorptions in the metal-carbonyl region as in hydroformylation. Also, there is an induction period for the ketone formation as well as in the case of aldehydes (Fig. 4a); the period disappears on the pretreatment of the solution ($Co_2(CO)_8$–diphos–dioxane) with both CO (100 kg/cm²) and H_2O (60 mmol) at 165 °C for 1 h in the absence of propene (Fig. 4b).

Thus, if (A) is present, we can postulate the following reaction, which produces acyl complexes (B) as other key intermediates for the hydrocarbonylation as well as hydroformylation. This is analogous to a scheme proposed by Jonassen[9] and Heck[10] with regard

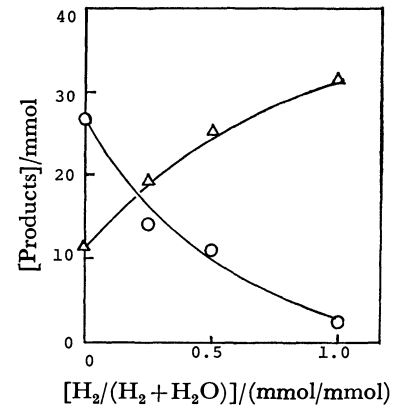

Fig. 5. Effect of added H_2.
$Co_2(CO)_8$ 2 mmol, diphos 2 mmol, dioxane 50 ml, P_{CO} 100 kg/cm², propene 300 mmol, temp 165 °C, time 5 h.
Marks (○,△): See footnote of Fig. 1. Other products omitted.
Total amounts of H_2O and H_2: 60 mmol.

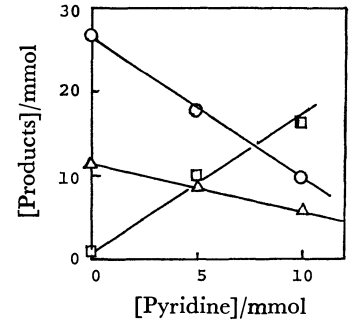

Fig. 6. Effect of added pyridine.
Conditions are the same as in Fig. 5.
Marks (○,△,□): See footnote of Fig. 1.

to these two reactions using a normal $Co_2(CO)_8$ catalyst with CO–H_2.

$$\underset{\text{(A)}}{HCo(CO)_m(\text{diphos})_n} \xrightarrow{CO+CH_3CH=CH_2}$$

$$CH_3CH_2CH_2\text{-}\overset{O}{\overset{\|}{C}}\text{-}Co(CO)_m(\text{diphos})_n$$
(B)

If (B) is rapidly consumed for the formation of C_4 aldehydes (or acids) before the interaction with propene, then the [ketones] value will be diminished. For example, when hydrogen is added to a catalyst solution, a pronounced increase in [aldehydes] results, as is illustrated in Fig. 5, where the total amount of hydrogen donors (H_2O or H_2) was kept constant at 60 mmol, whereas the [ketones] value decreases with an increase in the hydrogen concentration, even at a constant high molar ratio of propene/$Co_2(CO)_8$-(=300/2). A further example was obtained from experiments featuring the addition of a small amount of pyridine; the results are shown in Fig. 6. The rapid reaction of (B) with H_2O takes place, producing C_4 acids (□); as a result, both [ketones] (○) and [aldehydes] (△) decrease. The accelerating effects of pyridine have already been observed on the normal $Co_2(CO)_8$-catalyzed hydrocarboxylation of olefin.[11]

Considering the data described above, it is probable that the intermediates (A) are present. However, because of the possible existence of cobalt carbonyl species different from (B), as is demonstrated by the variations in [ketones] and [aldehydes] with the CO pressure (Fig. 1), the above-mentioned acyl complexes, (B), can be considered only as possible models of the reaction intermediates.

References

1) I. Wender and P. Pino, "Organic Synthesis *via* Metal Carbonyls," Wiley, New York (1977), Vol. 2.
2) G. Natta, P. Pino, and R. Ercoli, *J. Am. Chem. Soc.*, **74**, 4496 (1952).
3) K. Murata and A. Matsuda, *Bull. Chem. Soc. Jpn.*, **54**, 245 (1981).
4) K. Murata and A. Matsuda, *Chem. Lett.*, **1980**, 11.
5) The time is the same as in the hydroformylation.[3]
6) The dissolved cobalt in a 5-h-reaction solution was determined by means of EDTA-titration.

diphos/$Co_2(CO)_8$ (mmol/mmol)	Dissolved Co (mg-atom)
2/2	3.9
1.5/2	2.4
0/2	0

7) Under the conditions employed, no hydrocarbonylation occurs with the resulting metallic cobalt.
8) K. Murata, A. Matsuda, K. Bando, and Y. Sugi, *J. Chem. Soc., Chem. Commun.*, **1979**, 785.
9) J. A. Bertrand, C. L. Aldrige, S. Husebye, and H. B. Jonassen, *J. Org. Chem.*, **29**, 790 (1964).
10) R. F. Heck, *J. Am. Chem. Soc.*, **85**, 3116 (1963).
11) In order to explain these accelerating effects, the following schemes have been proposed:

$$RCOCo(CO)_4 + Py \longrightarrow [RCO\cdot Py]^+[Co(CO)_4]^-$$
$$[RCO\cdot Py]^+[Co(CO)_4]^- + H_2O \longrightarrow RCOOH + [HPy]^+[Co(CO)_4]^-$$
$$[HPy]^+[Co(CO)_4]^- \rightleftharpoons HCo(CO)_4 + Py$$

N. S. Imyanitov and D. M. Rudkovskii, *Zh. Org. Khim.*, **2**, 231 (1966).

Ozonization of Organic Compounds. V. Aromatic Compounds

Tsuneo Saito, Etsuo Niki,* and Yoshio Kamiya

Department of Reaction Chemistry, Faculty of Engineering, The University of Tokyo, Hongo, Bunkyo-ku, Tokyo 113

(Received June 28, 1980)

The ozonization of several aromatic compounds has been carried out at 30 °C in carbon tetrachloride. It was found that three processes proceeded simultaneously; that is, normal and anomalous ozonolyses to give respectively α,β-dicarbonyl and carboxylic compounds and polymerization. Carboxylic acids were the major products. Benzene and hexamethylbenzene gave formic acid and acetic acid respectively, while toluene and 1,3,5-trimethylbenzene gave mixtures of these acids. As the ozonization proceeded, white gummy polymers precipitated, the molecular weight ranged from several hundreds to a few thousands. They contained high concentrations of oxygen which was incorporated into polymer as carbonyl, carboxylic acid, peroxide and/or ether. The polymers were thermally stable below 150 °C.

The interactions of ozone with organic compounds, especially olefins, have been studied quite extensively[1] and this reaction has been applied in preparation and identification of organic compounds. Recently the ozone chemistry has received much attention in the fields of atmospheric oxidation and purification of water. We have previously reported[2] that polypropylene underwent cleavage by ozonization to give lower molecular weight carboxylic acids but that the ozonization of polystyrene brought about crosslinking as well as chain scission, giving rise to broadening of molecular weight distribution.

The ozonization of aromatic ring has also been studied for long time. In 1904, Harries and Weiss[3] found that the ozonization of neat benzene and subsequent hydrolysis gave about 2 equivalents of glyoxal and no hydrogen peroxide. They surmised that the third mole of equivalent of glyoxal reacted with hydrogen peroxide during homolysis to give carbon dioxide and water. Later, in addition to α,β-dicarbonyls, peroxides, and carboxylic acids have been observed as ozonization products from aromatic compounds.[4] Keaveney *et al.*[5] attempted to produce glyoxal from benzene in high yield and they obtained glyoxal in 73 and 52% yields based on ozone absorbed and benzene reacted, respectively. No by-products such as glyoxylic acid, oxalic acid, formic acid, and carbon monoxide were observed. The ozonization of aromatic compounds is not fully understood and much of the data so far obtained are only qualitative.

We have undertaken the study of the ozonization of several aromatic compounds and found that three major processes proceeded simultaneously, that is, normal ozonolysis, anomalous ozonolysis, and polymer formation.

Experimental

Materials. Most of the organic compounds used in this study were those of the highest grade available commercially. They were either used as received or purified when necessary. Ozone was produced in a standard ozone generator, Nippon Ozone Co., Ltd., Model O-3-2, by charging pure oxygen dried beforehand by silica gel.

Procedures. Ozonization was carried out in 100 ml vessel equipped with a condenser. It was started after thermal equilibrium at 30 °C had been reached by bubbling O_3–O_2 gas through the reaction mixture which was stirred with a magnetic stirrer. The gas was introduced at a speed of 100—120 ml/min, the rate of ozone supply being 0.12—0.20 mmol/min.

The amounts of substrate reacted and products formed were measured by gas liquid chromatography and high pressure liquid chromatography. Total amount of peroxides was determined by iodometric titration. Acids were measured by titration and identified by isotachophoretic analysis and liquid chromatography as described previously.[2] Carbon dioxide was also analyzed as previously.[6]

Total yield of carbonyl groups was measured by treating the product solution with a 2 N aqueous hydrochloric acid and by following the consumption of hydrazine spectrometrically, $\lambda_{max}=322$ nm and $\varepsilon=1.10\times10^4$ M^{-1} cm^{-1}.

Polymeric material precipitated from the solution was dissolved into methanol or acetone, dried under vacuum and analyzed. Elemental analysis was carried out at Shonan Analytical Center. Total carbonyl content in the polymer was determined as described above. Double bonds were determined by the Hanus' method.[7] The molecular weight distribution was measured at 40 °C by gel permeation chromatography,[2] Shimadzu-DuPont Model 830. Infrared, ^1H NMR, and ^{13}C NMR spectra were recorded on JASCO spectrometer Model IR-G, Varian EM 360A, and Hitachi NMR Model R-40 respectively.

Thermal decomposition of polymer was performed by dissolving 30 mg dried polymer into 2 ml acetic acid and heating at 150 °C for 2 h in a sealed ampoule under vacuum. The evolved gas was collected by Toepler pump and analyzed by gas chromatography. The solution was analyzed by gas liquid chromatography and gel permeation chromatography.

Results

Table 1 shows the results of ozonization of several aromatic compounds in carbon tetrachloride, a non-participating solvent that does not intreact with carbonyl oxide intermediate. The results in Table 1 show that the reactivities increase in the order of benzene<toluene<1,3,5-trimethylbenzene<hexamethylbenzene in agreement with the previous reports,[4,8–11] suggesting that the attack of ozone to aromatic ring is electrophilic in nature. Since, as shown later, the oxidation of benzylic hydrogens is not important, these reactivities can be taken as those of aromatic ring toward ozone. Runs 4 and 5 show that the rate of ozonization is determined not by concentration of substrate but by ozone dosage. As observed previously,[6] phenols were quite reactive toward ozone and gave similar products as aromatic hydrocarbons.

Runs 1, 2, and 3 show that the ozonization of benzene in carbon tetrachloride gave formic acid as a

TABLE 1. OZONIZATION OF AROMATIC COMPOUNDS IN 50 ml CARBON TETRACHLORIDE AT 30 °C

Run No.	1	2	3	4	5	6	7	8	9	10
Substrate, R	Benzene	Benzene	Benzene	Toluene	Toluene	TMB[f]	HMB[g]	HMB[g]	Phenol	BP[h]
R_0, mmol	11.2	112	225	9.4	94	7.2	9.9	10.0	10.6	5.43
O_3 fed,mmol	2.6	15	37	15	15	15	15	24	15	13
Time/min	21.5	120	307	120	120	120	120	120	120	65
ΔR, mmol				2.4		3.4	4.6	8.9	5.7	4.4
$\Delta R/O_3$ fed, (mol/mol)				0.16		0.23	0.31	0.37	0.38	0.34
Products in mmol										
Peroxide	0.08	0.11	0.17	0.34	0.34	0.67	2.3	4.6	0.19	0.73
Carbonyl[a]			0.17			0.70	3.7	9.3		1.1
Carbonyl[b]	0.20						3.9	9.8		
2,3-Butanedione[c]							0.5	1.6		
Acids[d]	1.2	4.4	15.3	3.9	5.1	5.1	2.4	5.5	2	1.7
Formic acid[e]	1.1	3.6	16.0	4.1	3.9	2.3	0.3	0.5	1.0	0.5
Acetic acid[e]				1.4	1.6	4.3	2.3	5.4		
Other acid[e]			0.6[i]	0.4[j]	0.5[j]	0.5[j]			0.1[j]	0.4[k]
CO_2							1.1			
Polymer, mg		95	333	found	found	found	1004	found	found	found
C, %		34.26	39.94		44.07					
H, %		4.05	4.53		5.00					
O, %		61.69	55.53		50.93					

a) From disappearance of 2,4-dinitrophenylhydrazine determined by UV analysis at 322 nm. b) From weight of 2,4-dinitrophenylhydrazone assuming glyoxal and 2,3-butanedione are formed from benzene and hexamethylbenzene respectively. c) By gas liquid chromatography. d) By titration. e) By isotachophoretic analysis. f) 1,3,5-Trimethylbenzene. g) Hexamethylbenzene. h) *p*-Benzylphenol. i) Glyoxylic acid. j) Not identified. k) Malonic acid.

major product with minor amounts of peroxide and glyoxal. The peroxide must be mostly ozonide, 1,2,4-trioxolane. Glyoxal is further oxidized to glyoxylic acid, but no oxalic acid was found under the present reaction conditions. One of the interesting features of this reaction is the formation of polymeric products. As the ozonization proceeded, white gummy material precipitated from the reaction mixture. The polymer will be discussed in some more detail later in this text.

Similar results were observed with toluene, 1,3,5-trimethylbenzene, hexamethylbenzene, and phenols. Carboxylic acids were obtained as major products, formic and acetic acids from both toluene and 1,3,5-trimethylbenzene, and acetic acid from hexamethylbenzene. Run 4 shows that 34 and 58% of aromatic carbons of toluene yielded formic and acetic acids respectively. Selectivities for formic and acetic acids from 1,3,5-trimethylbenzene based on reacted aromatic carbons are 23 and 42% respectively, and no 2,4,6-trimethylphenol was observed. The higher yields of acetic acid than formic acid from toluene and 1,3,5-trimethylbenzene may partly because of higher reactivity of formic acid toward ozone than acetic acid.[6] Hexamethylbenzene gave carboxylic acid in lower yield than benzene, toluene, and 1,3,5-trimethylbenzene. Interestingly, malonic acid was formed from *p*-benzylphenol roughly as much as formic acid.

The carbonyl compounds formed by the normal ozonolysis are glyoxal, methylglyoxal, and 2,3-butanedione from benzene, 1,3,5-trimethylbenzene, and hexamethylbenzene respectively. 2,3-Butanedione analyzed by gas liquid chromatography was smaller than that estimated from the disappearance of 2,4-dinitrophenylhydrazine (Runs 7 and 8 in Table 1). It is not clear at present if this discrepancy is due to experimental uncertainty or due to the formation of other carbonyl products. It may be noteworthy, however, that the amounts of 2,3-butanedione estimated from 2,4-dinitrophenylhydrazone formed were in good agreement with those analyzed from the disappearance of 2,4-dinitrophenylhydrazine.

Peroxides are one of the important products but their structure is not clear. Most of peroxides could be reduced by triphenylphosphine and dimethyl sulfide.

Quite a small amount of benzaldehyde was observed in the ozonization of toluene. However, little benzyl alcohol was observed even after the treatment with triphenylphosphine, suggesting that little benzyl hydroperoxide was present. Therefore, it may be concluded that oxidation of benzylic hydrogens is not important under the present reaction conditions. Furthermore, hexamethylbenzene was once oxidized in the presence of 2,6-di-*t*-butyl-4-methylphenol, a typical radical scavenger, and no decrease in rate of ozonization of hexamethylbenzene was observed. This suggests that oxidations by free radicals do not play an important role in this ozonization.[12]

It has been reported[10,11,13] that ozonization intermediates oxidize carboxylic acids to corresponding peroxy acids, but no direct evidence for the formation of peroxy acids could be found.

One of the interesting features of the ozonization of aromatic compounds in carbon tetrachloride is the formation of polymeric materials. As mentioned above, white gummy material precipitated as the ozonization proceeded. The ozonization of hexamethyl-

Table 2. Polymer formed in the ozonization of benzene in carbon tetrachloride (Run 3)

Molecular weight	200—4000
Elemental analysis	C 39.94, H 4.53, O 55.53%—$C_3H_4O_3$
Oxygen	17% Carboxylic acid
	28% Carbonyl
	<1% Peroxide (IPA-KI)
	≈54% Dialkyl peroxide, ether
Double bond	none
IR	3250 cm^{-1} (H-bonded OH)
	1725 cm^{-1} (carbonyl)
	950—1110 cm^{-1} (peroxide or ether)
Aromatic hydrogen	none
Thermal decomposition at 150 °C, 2 h: small	

benzene did not give a precipitate, but the presence of polymeric materials was found by gel permeation chromatography. The precipitated polymer was insoluble in carbon tetrachloride and benzene, but partly soluble in chloroform and very soluble in methanol, acetone, tetrahydrofuran, and acetic acid.

The example of gel permeation chromatogram is shown in Fig. 1. The molecular weight of the precipitated polymer ranges from 200 to 4000, while the product solution contained compounds with a molecular weight of a few hundreds. Some data on the polymers are also included in Table 1. The polymer was pale-yellowish white and very deliquescent. In Runs 2 and 3, 95 and 333 mg of polymers precipitated respectively. The ratio of polymer to formic acid on carbon base in these experiments is 1/1.35 and 1/1.44 respectively, suggesting that the polymers are one of the important major products. The analyses of the polymer obtained in Run 3 are summarized in Table 2. It shows that it contains quite a high ratio of oxygen and that 17 and 28% of oxygen incorporated were found as carboxylic and carbonyl oxygen. The hydroperoxidic oxygen was very small. The remaining 55% of oxygen must be peroxidic and/or ether oxygen. No double bond was observed. The ^1H NMR analysis showed the absence of aromatic and methyl hydrogens. The infrared spectrum also showed the absence of aromatic hydrogen but it showed strong absorption at 3250 and 1750 cm^{-1}, which are ascribed to hydrogen-bonded hydroxyl and carbonyl groups respectively. A broad absorption was also observed between 950 and 1100 cm^{-1}, which must be ascribed to peroxide and/or ether linkage in the polymer. ^{13}C NMR analysis also showed the presence of ether, ester, and carboxylic acid.

In order to examine the stability of the polymer, especially of the peroxidic bond possibly involved, thermal decomposition of the polymer was carried out at 150 °C in 2 h in acetic acid under vacuum. Carbon monoxide and carbon dioxide were found by gas analysis and two unknown volatile products were found by gas chromatography, but their formation was small. Little change was observed in the gel permeation chromatogram after thermal treatment, implying that this polymer is thermally stable. Therefore, this polymer is not a dimeric peroxide of the

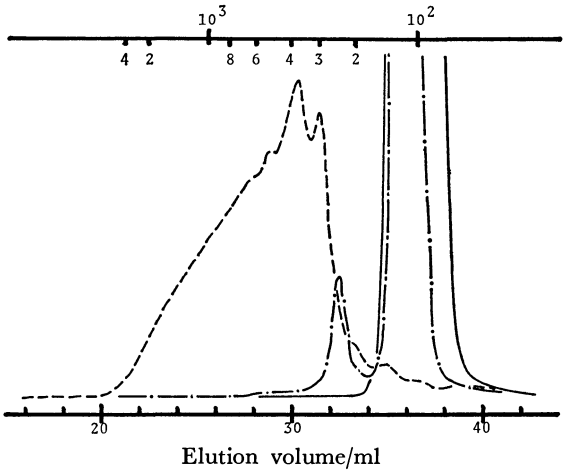

Fig. 1. Gel permeation chromatogram of ozonization products from benzene at 30 °C.
——: Initial solution, —·—: product solution, ----: precipitate.

carbonyl oxides.

It should be noted on the safe handling of the polymeric material. We usually dissolved the precipitate in methanol or acetone and then the solvent was removed and dried under vacuum to obtain a stable polymeric solid. However, once the precipitate was taken out of the reaction mixture and dried directly at room temperature under vacuum, which brought about an explosion. At any time, this polymeric material should be handled with all precautions.

Discussion

As shown above, three processes proceeded competitively in the ozonization of aromatic compounds; they are normal and anomalous ozonolyses and polymer formation. The normal ozonolysis gives α,β-dicarbonyls, whereas the anomalous ozonolysis gives carboxylic acids. The plausible mechanisms are briefly discussed below.

Scheme 1 summarizes the possible major steps in the ozonization of hexamethylbenzene. The primary step is an electrophilic attack of ozone to aromatic ring to yield primary ozonide **1**. Thus the reactivities of polymethylbenzenes increase as observed with increasing number of methyl groups. The primary ozonide **1** is unstable and readily decomposes to give carbonyl group and carbonyl oxide **2**.

The aliphatic double bonds are more reactive than aromatic ring toward ozone and hence **2** must react with ozone to give eventually 2,3-butanedione and carbonyl oxides **4** and **5**. In non-participating solvents, the carbonyl oxide intermediate undergoes either ozonide formation, rearrangement or dimerization and/or polymerization. The latter reactions must become more important with increasing methyl substitution of the aromatic ring due to the decreased 1,3-dipolarophilic and electrophilic character of a ketone carbonyl in comparison to that of an aldehyde carbonyl.[1] For example, Fliszar and coworkers[14] found in the ozonolysis of tetraphenylethylene that no ozonide was

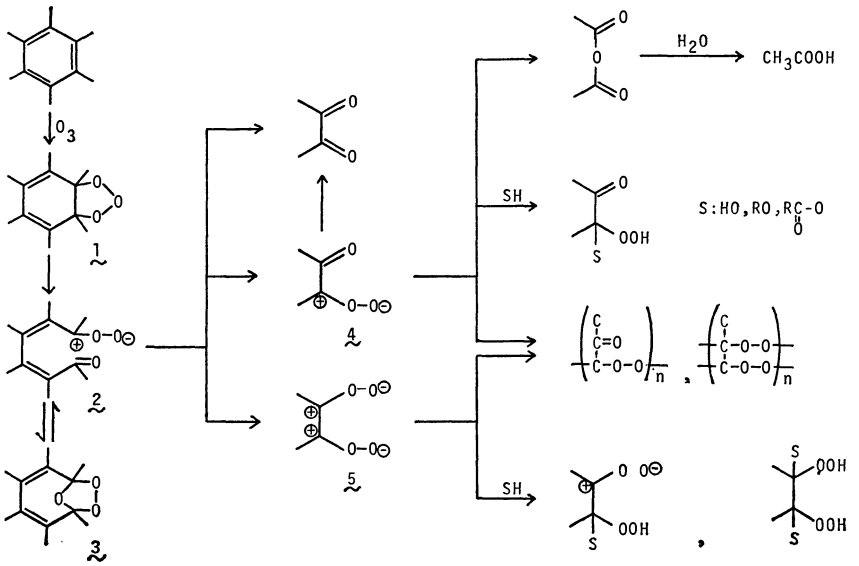

Scheme 1. Major reaction pathways in the ozonization of hexamethylbenzene.

formed but 57% of diphenylcarbonyl oxide dimerized and 43% formed an peroxidic oligomer. The carbonyl oxide may react with itself, aldehyde, ketone, and also primary ozonide.[15]

The participating solvents such as water, alcohol, and carboxylic acid react with carbonyl oxide rapidly and convert it into hydroxy, alkoxy, or acyloxy alkyl hydroperoxides.[1]

The carboxylic acids are anomalous ozonolysis products and formed by the rearrangement of carbonyl oxide or ozonide.[1,16] The detailed machamism is not discussed here, but this anomalous ozonolysis is known to occur with special ease when there are carbonyl groups attached to the double bond as in **4** and when the temperature is relatively high.[16,17]

Thus benzene and hexamethylbenzene give formic and acetic acids respectively, while toluene and 1,3,5-trimethylbenzene give mixtures of formic and acetic acids.

As mentioned already, the polymer formation is one of the characteristic points in the present study. The formation of polymer or oligomers in the ozonization of olefins has been observed in several instances from quite a long time ago[1,18] and several mechanisms have been proposed.[1,15] However, there are only a few cases which describe the polymers from aromatic compounds. Several structures have been proposed for polymeric substances[1] such as open chain polymers of carbonyl oxide with some ether linkages,[14,19,20] polyozonide,[21] and cyclic peroxide.[22] Greenwood and Rubinstein[15] concluded that the alkene ozonization polymer does not have any specific structure and that both the dipolar ion fragment and the aldehyde fragment are incorporated into the polymer in varying ratios.

Our data also show that the polymer contained a high ratio of oxygen as carboxylic, carbonyl, peroxidic, and ether oxygen. Although it is not clearly elucidated, the data in Table 2 imply that the most plausible structure of the polymer from benzene may be written as follows.

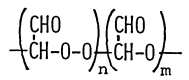

Some of the aldehyde group must be oxidized to carboxylic acid.

Keaveney *et al.*[22] surmised that glyoxal initially formed in the ozonization of benzene underwent condensation to give polymers, especially since such condensations are acid catalyzed.[23] It is difficult to estimate the importance of this process relative to that involving carbonyl oxide.

Finally, in connection with the ozonization of polystyrene,[2] the above results and discussion show that the aromatic ring of polystyrene is cleaved to give carbonyl oxide such as **6** and **7**, which react with other carbonyl oxide or carbonyl group to yield eventually crosslinked polymer.

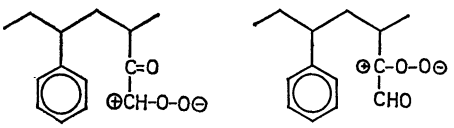

6 **7**

References

1) P. S. Bailey, "Ozonation in Organic Chemistry, Vol. 1, Olefinic Compounds," Academic Press, New York (1978).
2) T. Saito, E. Niki, T. Shiono, and Y. Kamiya, *Bull. Chem. Soc. Jpn.*, **51**, 1153 (1978).
3) C. Harries and V. Weiss, *Ber.*, **37**, 3431 (1904).
4) T. W. Nakagawa, L. J. Andrews, and R. M. Keefer, *J. Am. Chem. Soc.*, **82**, 269 (1960).
5) W. P. Keaveney, R. V. Rush, and J. J. Pappas, *Ind. Eng. Chem. Prod. Res. Dev.*, **8**, 89 (1969).
6) Y. Yamamoto, E. Niki, H. Shiokawa, and Y. Kamiya, *J. Org. Chem.*, **44**, 2137 (1979).
7) F. D. Snell and F. M. Briffen, "Commercial Methods of Analysis," McGraw-Hill, New York (1944), p. 345.
8) P. S. Bailey, *Chem. Rev.*, **58**, 925 (1958).
9) J. Van Dijk, *Recl. Trav. Chim. Pays-Bas*, **67**, 945 (1958).

10) E. Bernatek, E. Karlsen, and T. Ledaal, *Acta Chem. Scand.*, **21**, 1229 (1967).
11) E. Bernatek, H. Hagen, and T. Ledaal, *Acta Chem. Scand.*, **21**, 1555 (1967).
12) Although 2,6-di-*t*-butyl-4-methylphenol is more reactive than hexamethylbenzene toward ozone, the inhibitor concentration was much smaller.
13) However, it is not clear if the peroxy acid is formed from the interaction of ozone with carboxylic acid or from the oxidation of aldehyde formed by normal ozonolysis.
14) S. Fliszar, D. Gravel, and E. Cavalieri, *Can. J. Chem.*, **44**, 67 (1966).
15) F. L. Greenwood and H. Rubinstein, *J. Org. Chem.*, **32**, 3369 (1967), and papers cited therein.
16) Y. Yamamoto, E. Niki, and Y. Kamiya, unpublished work.
17) R. Criegee, "Peroxide Reaction Mechanisms," ed by J. O. Edwards, Interscience, New York (1962), p. 29.
18) For example, C. Harries and R. Seitz, *Ann.*, **410**, 21 (1915); C. Harries and H. Wagner, *ibid.*, **410**, 29 (1915).
19) A. Rieche, R. Meister, and H. Sauthoff, *Justus Liebigs Ann. Chem.*, **553**, 187 (1942).
20) R. Criegee, *Rec. Chem. Prog.*, **18**, 111 (1957).
21) P. S. Bailey and S. B. Mainthia, *J. Org. Chem.*, **23**, 1089 (1958).
22) S. D. Razumovskii, G. A. Niazashvili, I. A. Tutorskii, and Y. N. Yurev, *Vysokomol. Soedin., Ser. A*, **13**, 190 (1971).
23) W. P. Keaveney, R. V. Rush, and J. J. Pappas, *J. Org. Chem.*, **32**, 1537 (1967).

Facile Intramolecular Cyclization Reactions of Aromatic Ethers with Cationoids in Triptycene Systems

Giichi Izumi, Shiro Hatakeyama, Nobuo Nakamura, and Michinori Ōki*

Department of Chemistry, Faculty of Science, The University of Tokyo, Hongo, Bunkyo-ku, Tokyo 113

(Received June 28, 1980)

1,4-Dimethoxytriptycenes were found to give cyclic ethers with unusual ease when a substituent at the bridgehead bears a cationoid center. The easy reaction is attributed to the extreme proximity between the methoxyl group and the cationic center. Mechanisms involving a cyclic oxonium ion and subsequent attack by an anion to produce the cyclic ether and a methyl derivative are discussed.

During the course of other study we have encountered a surprisingly facile ring formation of 1,4-dimethoxytriptycenes if a cationoid center is produced in the 2-position of a 9-substituent. This paper reports such findings and discusses the probable mechanisms of the reaction.

When oxidation of 9-(2-hydroxypropyl)-1,4-dimethoxytriptycene (**1**) was attempted with chromium(VI) oxide in the presence of sulfuric acid, a cyclic ether (**2**) was formed instead of the corresponding carbonyl compound. Expecting that the reaction was caused by the action of an acid which formed a cationoid center, we treated **1** with sulfuric acid and obtained **2** as expected.

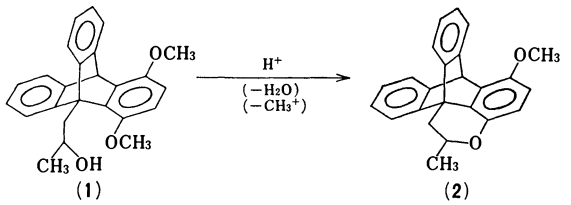

(1) (2)

The reaction is then regarded to proceed *via* an oxonium salt which is formed from the cationoid and the proximate methoxyl group in 1-position. The reaction occurs probably *via* both S_N1 and S_N2 mechanisms, because secondary alcohols undergo other substitution reactions in those fashions[1] and an electron-accepting group in the substituent at the bridgehead should interact strongly with the methoxyl group in the peri-position.[2] If the consideration is valid, 9-allyl-1,4-dimethoxytriptycene (**3**) should give the same product (**2**), when treated with an acid, since addition of a proton to the allyl moiety should produce a cationoid in the 2-position of the 9-substituent. In fact, treating **3** with trifluoroacetic acid gave **2**.

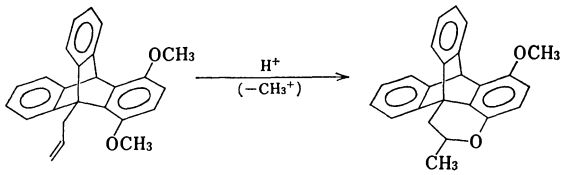

(3) (2)

Being encouraged by the extension, we then proceeded to cationoids which may be developed by a variety of methods. A variety of electrophilic additions to olefins are known to proceed *via* cationoids. We have taken addition of bromine to an olefin as an example.[3] 9-Allyl-1,4-dimethoxytriptycene (**3**) was treated with bromine and was found to give a cyclic ether (**4**).

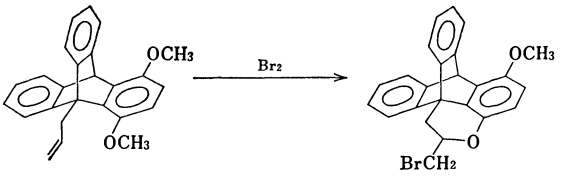

(3) (4)

The facile cyclization is not confined to the propyl derivatives carrying a cationoid in the 2-position. Treating 9-(2-hydroxyethyl)-1,4-dimethoxytriptycene (**5**) with thionyl chloride gave a cyclic ether (**6**). Since the reaction between alcohols and thionyl chloride is known to proceed *via* contact ion pairs,[4] the result was not a great surprise. To our surprise, however, a less cationic species, *p*-toluenesulfonate, cyclized as well: when **5** was treated with *p*-toluenesulfonyl chloride and pyridine at room temperature, the product was **6**. Thus weakly cationic species like sulfonates can react to form cyclic ethers.

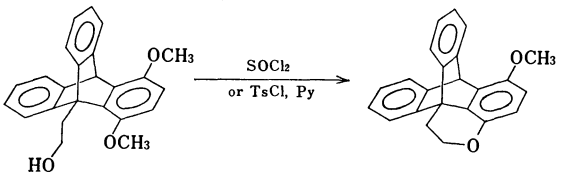

(5) (6)

In order to discuss the mechanism of the reaction, the fate of the methyl group which had been in the methoxyl group must be explored. We ran the reaction of **5** with an excess of thionyl chloride in chloroform-*d* in a sealed tube, expecting that the product from the methyl group must be methyl chloride. The ^1H NMR spectrum of the reaction mixture clearly showed the presence of a sharp signal at δ 3.00 which is ascribable to methyl chloride. The formation of methyl chloride was further confirmed by addition of methanol to the mixture and observing the increase in the intensity of the signal at δ 3.00.

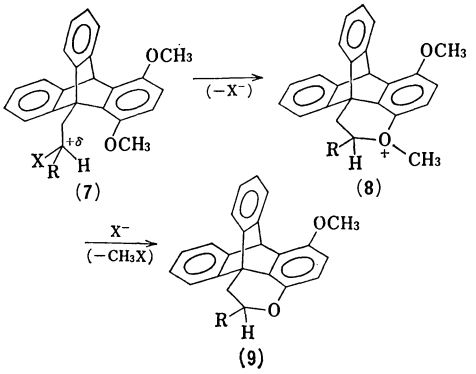

(7) (8) (9)

The mechanism of the reaction may be described now as follows. In the first step a cationoid species (**7**) is formed in the 2-position of the 9-substituent by an electrophilic addition to the olefin or by enhancing the leaving group ability of the substituent. In the second step it cyclizes to an oxonium ion (**8**) which is then attacked by an anion at the least hindered methyl to give the cyclic ether (**9**) and a substituted methane.

The reason for the facile cyclization must be proximate arrangement of the two groups. In other triptycene systems, the substituent in the 9-position and the peri-substituent are known to be well in the sum of the van der Waals radii[5,6] and some very weak interactions were detected.[2,7,8] Therefore, as soon as the cationic species is formed, it interacts very strongly with the methoxyl group in the peri-position, leading to the cyclic oxonium ion (**8**). This postulate is substantiated by the following facts. Although neighboring participation of oxygen[9] in bromination reactions is known to be stronger than that of bromine,[10] the yield of a cyclic ether is only 50—60% when 4-penten-1-ol is treated with bromine and, if it is a 6-membered ring, the yield of a cyclization product drops to 5—10%.[9] Since the cyclic ether formed here is 6-membered, the participation of the oxygen is unusually strong relative to the open-chain compounds, although the entropy factor may contribute to some extent.

The ^{13}C NMR spectrum of 9-allyl-1,4-dimethoxytriptycene (**3**) revealed that there were two detectable conformers at a low temperature. Since it will not be possible to observe conformers about the C_{sp^3}–C_{sp^2} bond in the allyl group, it is natural to assume that the conformers are those involving the restricted rotation about the C_9–C_{allyl} bond: the number of carbon atoms detected by the ^{13}C NMR conforms with this assignment. The competitive bromination of **3** with 9-allyltriptycene (**10**) revealed that a negligible amount of **10** reacted, while the color of bromine faded fast to give **4** as a sole product. This high reactivity of **3** cannot be explained if it reacts in the *ap* conformation because its steric environment is the same as **10** and no strong electronic effect is expected, if any. Rather it will be explained by the neighboring participation of the methoxyl group which facilitates the electrophilic attack.

We conclude that the unusually high reactivity of the methoxyl group toward cationoids is caused by the highly congested state in the triptycene system. The results suggest that the triptycene is a good system to find weak interactions which otherwise are not detectable.

Experimental

*9-Allyl-1,4-dimethoxytriptycene (**3**).* A solution of 2.2 g (0.01 mol) of 9-allylanthracene[11] and 1.1 g (0.01 mol) of *p*-benzoquinone in 10 mL of toluene was refluxed for 1 h. The reaction mixture was cooled. The resulting crystals were collected and washed with ether. The crystals in 20 mL of dioxane were treated with 1.0 g of sodium hydroxide in 10 mL of water and then with dimethyl sulfate under a nitrogen atmosphere. The process was repeated 2—3 times until coloration due to the enolate was not observable on addition of the alkali. The resulting mixture was poured into 500 mL of water. The precipitate was collected, dried, and recrystallized from hexane, mp 235—236 °C. The yield was 80%. Found: C, 84.50; H, 6.06%. Calcd for $C_{25}H_{22}O_2$: C, 84.92; H, 6.24%. ^1H NMR ($CDCl_3$, δ): 3.68 (3H, s), 3.78 (3H, s), 3.9—4.3 (2H, m), 5.0—5.7 (2H, m), 5.88 (1H, s), 5.9—6.4 (1H, m), 6.50 (2H, s), 6.8—7.7 (8H, m). ^{13}C NMR ($CDCl_3$, ppm from TMS): 32.9, 46.0, 54.3, 56.7, 57.1, 109.0, 109.7, 113.7, 122.6, 123.5, 123.8, 133.6, 136.6, 138.1, 145.2, 145.5, 147.2, 148.9.

The signals at 32.9 and 54.3 ppm and many at lower fields split into two peaks in a ^{13}C NMR spectrum at −32 °C. From these, the population ratio was calculated as 0.7. Altough it is not possible to tell which isomer is favored in the equilibrium, the ^1H NMR data suggest that the *ap* isomer is favored: the signal at δ 6.50 splits into two peaks at low temperatures and, if the peak at a higher field corresponds to the $\pm sc$ form as were other compounds of this series,[2] then the ratio $\pm sc/ap$ is 0.7.

*2-Methyl-6-methoxy-7,11b-o-benzeno-7,11b-dihydronaphtho[1,2,-3-de]chroman (**2**).* *a)*: To a solution of 420 mg of 9-(2-hydroxypropyl)-1,4-dimethoxytriptycene, which had been prepared by the Grignard reaction of the corresponding aldehyde,[8] in 20 mL of acetone was added sulfuric acid (0.1 mL H_2SO_4 and 0.2 mL H_2O) and the mixture was stirred at 0 °C for 1 h. The solvent was removed *in vacuo* and the residue was washed with dilute alkali after addition of 30 mL of dichloromethane. The organic layer was evaporated after drying. The product was identical with the substance produced by the action of hydrochloric acid on an adduct from 9-allylanthracene and *p*-benzoquinone followed by methylation (see below).

b): A solution of 1.5 g of an adduct from 9-allylanthracene and *p*-benzoquinone in 50 mL of acetic acid was mixed with 10 mL of cencentrated hydrochloric acid and stirred for 24 h at room temperature. The mixture was poured into 1 L of water and the solid was collected. The solid was treated with aqueous sodium hydroxide and dimethyl sulfate under a nitrogen atmosphere, as was for the preparation of **3**. The product was recrystallized from benzene–hexane, mp 230.3—230.8 °C. Yield 82%. Found: C, 84.57; H, 5.95%. Calcd for $C_{24}H_{20}O_2$: C, 84.68; H, 5.92%. ^1H NMR ($CDCl_3$, δ): 1.65 (3H, d), 3.04 (2H, poorly resolved quartet), 3.73 (3H, s), *ca.* 4.3 (1H, m), 5.85 (1H, s), 6.50 (2H, s) 6.9—7.6 (8H, m).

c): To a solution of 20 mg of 9-allyl-1,4-dimethoxytriptycene (**3**) in 1.5 mL of $CDCl_3$ was added a few drops of trifluoroacetic acid. After standing overnight, the mixture was treated with 10% aqueous sodium hydrogencarbonate. The solvent was evaporated from the organic layer and the product was separated by TLC. The main product was identical with the compound described above.

A ^1H NMR spectrum of the mixture showed broadening of the signal due to dialkoxybenzo protons at δ 6.50, indicating rapid exchange between the aromatic protons and that of trifluoroacetic acid. Thus trifluoroacetic acid-*d* was used to see the exchange: the aromatic proton signal vanished during the reaction. After treatment with aqueous sodium hydrogencarbonate, the ^1H NMR spectrum of the product showed the presence of a deuterium in the methyl in 2-position (broad doublet at δ 1.64 in $CDCl_3$) and the signal due to the dialkoxybenzo protons had an intensity corresponding to one proton only. The position of the deuterium in the diakoxybenzo moiety is not known.

*6-Methoxy-7,11b-o-benzeno-7,11b-dihydronaphtho[1,2,3-de]chroman (**6**).* *a)*: A solution of 0.30 g (8.0 mmol) of

9-(2-hydroxyethyl)-1,4-dimethoxytriptycene (**5**)[2] in 30 mL of dichloromethane was stirred for 30 min with 0.3 mL (40 mmol) of thionyl chloride and then heated under reflux for 30 min. The mixture was treated with aqueous sodium hydroxide and the organic layer was evaporated. Chromatography followed by recrystallization, from benzene-hexane, of the product afforded a pure sample, mp 289.5—290.5 °C, in 95% yield. Found: C, 84.90; H, 5.37%. Calcd for $C_{23}H_{18}O_2$: C, 84.64; H, 5.56%. ^{1}H NMR ($CDCl_3$, δ): 3.15—3.40 (2H, m), 3.78 (3H, s), 4.20—4.50 (2H, m), 5.83 (1H, s), 6.50 (2H, s), 6.9—7.7 (8H, m).

b): A solution of 0.20 g (5.6 mmol) of the alcohol (**5**) in 10 mL of pyridine was mixed with 0.20 g (15 mmol) of *p*-toluenesulfonyl chloride and stirred for 24 h at room temperature. The mixture was mixed with 30 mL of dichloromethane and shaken with dilute hydrochloric acid. The product was identical with the above cyclic ether and was obtained in 92% yield after resrystallization from benzene-hexane. If the reaction was stopped at an incomplete stage, a mixture of **6** and the starting material (**5**) was obtained. The results indicate that the cyclization did not take place by the treatment of the alcohol with hydrochloric acid but it was the sulfonate ester which gave **6**.

*2-Bromomethyl-6-methoxy-7,11b-o-benzeno-7,11b-dihydronaphtho-[1,2,3-de]chroman (**4**).* To a solution of 35.4 mg (0.1 mmol) of **3** in 10 mL of chloroform was slowly added a solution of 15 mg (0.096 mmol) of bromine in 20 mL of chloroform at 0 °C. The reaction proceeded instantaneously as fading of the color indicated. After 1 h, the solvent was evaporated and the residue was purified by chromatography on silica gel, using hexane as an eluent. The product was recrystallized from hexane, mp 195—196 °C. The purity was checked by a ^{1}H NMR spectrum and the molecular constitution by high resolution mass spectroscopy. Found: M^+ 418.0545 and 420.0512. $C_{24}H_{19}O_2Br$ requires M^+ 418.05698 for ^{79}Br and 420.05501 for ^{81}Br. The relative intensities of the peaks were in good agreement with those calculated from the natural abundance of the isotopes. ^{1}H NMR ($CDCl_3$, δ): 2.7—3.6 (2H, m), 3.81 (2H, d), 3.79 (3H, s), 5.84 (1H, s), 6.51 (2H, s), 6.9—7.6 (8H. m).

Competitive Bromination of 9-Allyltriptycene and 9-Allyl-1,4-dimethoxytriptlycene. A solution of 15.5 mg (53 μmol) of 9-allyltriptycene and 18.8 mg (53 μmol) of **3** in 10 mL of chloroform containing 10.7 mg of hexachlorobenzene was treated with 8.4 mg (53 μmol) of bromine in chloroform as above. The disappearance of the starting material was checked by taking the internal standard (C_6Cl_6) in the high pressure liquid chromatography. The decrease in the amount of 9-allyltriptycene could not be detected, whereas **3** reacted completely as far as the detecting device could tell.

We whish to acknowledge the receipt of a Grant-in-Aid for Scientific Research from the Ministry of Education, Science and Culture which supported this work.

References

1) C. K. Ingold, "Structure and Mechanism in Organic Chemistry," Cornell University Press, Ithaca (1953), pp. 306—418.

2) G. Izumi, G. Yamamoto, and M. Ōki, *Chem. Lett.*, **1980**, 969.

3) A neighboring participation by a chloro group was reported during the addition of bromine to allyltriptycenes: S. Hatakeyama, T. Mitsuhashi, and M. Ōki, *Bull. Chem. Soc. Jpn.*, **53**, 731 (1980).

4) D. J. Cram, *J. Am. Chem. Soc.*, **75**, 332 (1953).

5) M. Mikami, K. Toriumi, M. Konno, and Y. Saito, *Acta Crystallogr., Sect. B*, **31**, 2474 (1975).

6) N. Nogami, Ph. D. Thesis, The University of Tokyo (1978).

7) F. Suzuki and M. Ōki, *Bull. Chem. Soc. Jpn.*, **48**, 596 (1975).

8) M. Ōki, G. Izumi, G. Yamamoto, and N. Nakamura, *Chem. Lett.*, **1980**, 213.

9) D. L. H. Williams, E. B. Goetz, and J. E. Dubois, *J. Chem. Soc., B*, **1969**, 517.

10) E. B. Goetz, J. E. Dubois, D. W. Pearson, and D. L. H. Williams, *J. Chem. Soc., B*, **1970**, 1275.

11) D. Mosnaim, D. C. Nonhebel, and J. A. Russel, *Tetrahedron*, **25**, 3485 (1969).

1,3-Dipolar Cycloaddition Reaction of Vinyl Azides with Enamines. Synthesis of Vinyltriazolines and Vinyltriazoles

Yujiro NOMURA,* Yoshito TAKEUCHI, Shuji TOMODA, and Masato M. ITO

Department of Chemistry, College of General Education, The University of Tokyo, Komaba, Meguro-ku, Tokyo 153

(Received July 3, 1980)

Reaction of α- and β-azidostyrene with enamines gave vinyltriazolines regioselectively in moderate yields. 1-Pyrrolidinyl enamines reacted with α-azidostyrene more readily than piperidino or morpholino enamines. β-Azidostyrene was as reactive as azidobenzene while α-azidostyrene was much less reactive. Vinyltriazolines formed from enamines of ketones were deaminated to yield the corresponding vinyltriazoles.

Although considerable amount of studies on vinyl azides has been cumulated[1] since Hassner and Fowler developed the general synthetic method for vinyl azides in 1968,[2] only few examples have hitherto been reported with regard to their reaction as 1,3-dipole: one with methyl propiolate or dimethyl acetylenedicarboxylate (DMAD)[3] and the other with 2-oxoalkylidenetriphenylphosphoranes.[4]

Extensive studies have been cumulated on 1,3-dipolar cycloaddition reaction of aryl azides.[5-10] Sustman and Trill have reported the correlation of the rate of cycloaddition reaction between azidobenzene and various dipolarophiles with the first ionization potentials (IP) of dipolarophiles, rationalizing the dual property of azides,[9] which are known to react readily with both electron-deficient dipolarophiles, such as DMAD, and electron-rich dipolarophiles, such as enamines. Munk and co-workers have examined the reaction of substituted azidobenzenes and enamines and demonstrated the electrophilic character of the azido group towards enamines.[10]

Previously we reported the thermal reaction of vinyl azides with electron-deficient olefins to give vinylaziridines with evolution of nitrogen (Eq. 1),[11] but

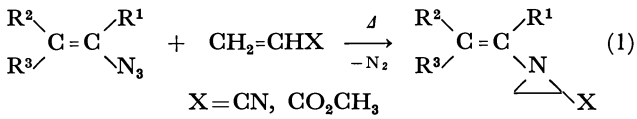

(1)

1,3-dipolar adduct of azide was not isolated. In the course of our further study concerning the 1,3-dipolar reaction of vinyl azides, we have examined the reaction with electron rich olefins, and here we wish to report their reaction with enamines.

Results and Discussion

Reaction of Azidostyrenes with Enamines. Azidostyrenes (**1**) and enamines (**2**) were caused to react at 0 °C without solvent until **1** was completely consumed. The results are summarized in Table 1.

The only product isolated proved to be a 1:1 adduct of azidostyrene and enamine. The structure of the adduct was determined from the spectroscopic inspection. In the case of Entry 4, for example, the two singlet signals at δ 4.85 and 5.36, together with the signals at δ 7.1—7.5, in ^{1}H NMR indicated the existence of 1-phenylvinyl group, the multiplet signals at δ 1.5—1.8 and 2.2—2.6 corresponded to 1-pyrrolidinyl group, and other signals (see experimental) demonstrated the existence of $CH_3\overset{|}{C}H\overset{|}{C}H$-moiety.

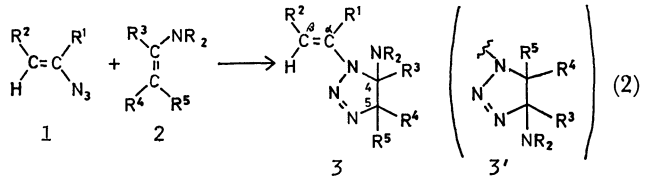

(2)

1a: R^1 = Ph, R^2 = H
1b: R^1 = H, R^2 = Ph

	R^3	R^4	R^5	NR_2
2a	$-(CH_2)_4-$		H	N⟨O⟩
2b	H	C_2H_5	H	N⟨ ⟩
2c	$-(CH_2)_4-$		H	N⟨ ⟩
2d	H	CH_3	H	N⟨ ⟩
2e	H	CH_3	CH_3	N⟨ ⟩
2f	H	C_2H_5	H	N⟨ ⟩
2g	H	C_2H_5	H	N⟨O⟩
2h	C_6H_5	H	H	N⟨O⟩

These results suggested the formation of 1,2,3-triazoline ring by the 1,3-dipolar cycloaddition between the azido group of **1a** and the carbon-carbon double bond of the enamine (**2d**). This was further supported by the ^{13}C NMR spectra of the adducts (Table 2): the two signals at δ 75.9 and 74.2 (both a doublet at off-resonance decoupling condition) corresponded to the two tertiary sp^3 carbons of the triazoline ring neighboring with the nitrogen atom.

The cycloadducts obtained are either 4-amino-Δ^1-1,2,3-triazolines (**3**) or their regioisomers, 5-amino derivatives (**3'**). The mass spectra of the triazolines **3d** and **3f** are summarized in Table 3. Molecular ions (M^+) were not detected in both cases. The peaks at *m/e* 228 and 242 corresponded to M-28 fragments (loss of nitrogen) of **3d** and **3f**, respectively. The peaks at *m/e* 199 corresponded to the further loss of C_2H_5 and C_3H_7 from **3d** and **3f**, respectively. This was rationalized from the β-cleavage of **3** (Fig. 1). The alternative structure **3'** was excluded by the existence of *m/e* 199 fragment becauce the cleavages expected from **3'** would not give this fragment.

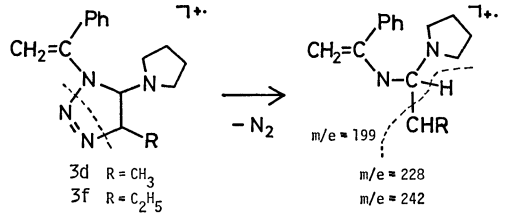

Fig. 1. β-Cleavage to give *m/e*=199 fragment.

TABLE 1. REACTION OF VINYL AZIDES WITH ENAMINES

Entry	Azide	Enamine	Molar ratio (Enamine/Azide)	Reaction time/d[a]	Products	Isolated yield/%
1	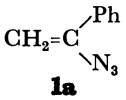 **1a**	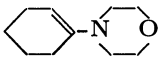 **2a**	1.5	90[b]	**3a** 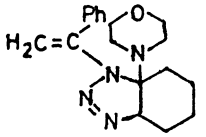	40
2	**1a**	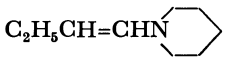 **2b**	1.42	12	**3b** 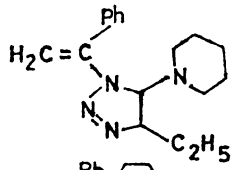	86
3	**1a**	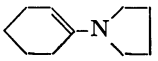 **2c**	1.06	2	**3c** 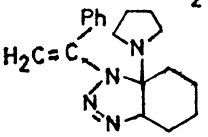	66
4	**1a**	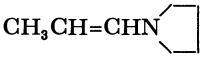 **2d**	2.31	5	**3d** 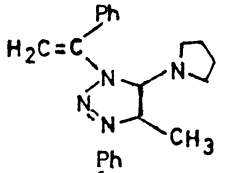	64
5	**1a**	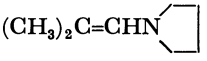 **2e**	1.0	1	**3e** 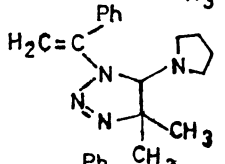	95
6	**1a**	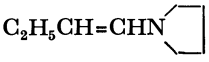 **2f**	1.13	3	**3f** 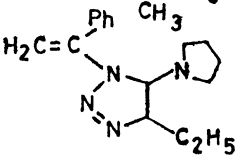	86
7	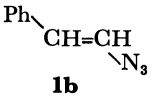 **1b**	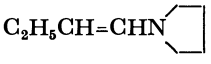 **2g**	1.03	8[b]	**3g** 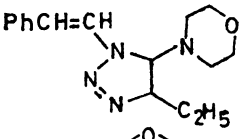	54[d]
8	**1b**	**2a**	1.03	3	**3h** 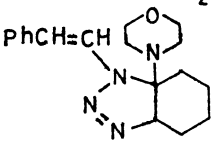	62
9	**1b**	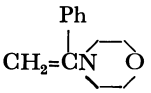 **2h**	1.02	21	**3i** 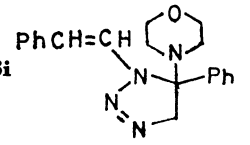	63
10	**1b**	**2e**	1.57	2[c]	**3j** 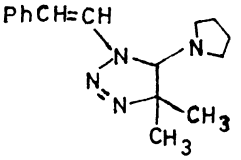	78

a) Reaction time until **1** was completely consumed, unless otherwise noted. b) Some of **1** still remained unchanged. c) Carried out in diethyl ether to avoid uncontrolled reaction. d) Based on consumed **1b**.

The formation of the 4-amino isomers (**3**) is reasonable since the 1,3-dipolar cycloaddition reaction of azides and enamines unexceptionally gives 4-amino-Δ^1-1,2,3-triazolines.[6-10]

The reaction time necessary for the complete consumption of azides could be a measure of relative reactivity of azides and enamines qualitatively (Table 1). The reactivity of enamines towards azides decreased in the order of 1-pyrrolidinyl>piperidino>morpholino (Entry 1—6), which was the same order

Table 2. ^{13}C NMR spectral data of vinyltriazolines (**3**)[a] (δ)

	C-β[b]	C-α[b]	C-4[b]	C-5[b]	Others[c]
3a	97.5 t	144.8 s	80.3 s	73.4 d	15.8 t, 18.1 t, 21.0 t, 24.5 t
3b	98.9 t	146.5 s	79.0 d	78.7 d	10.4 q, 26.2 t
3c	100.5 t	145.6 s	79.8 s	75.3 d	17.7 t, 19.2 t, 25.2 t, 25.8 t
3d	100.2 t	146.2 s	75.9 d	74.2 d	16.9 q
3e	99.7 t	146.8 s	79.5 d	77.4 s	18.7 q, 24.8 q
3f	99.4 t	146.4 s	80.1 d	74.1 d	10.3 q, 24.9 t
3g	107.9 d	125.9 d	77.5 d	77.4 d	9.6 q, 25.4 t
3h	109.3 d	123.9 d	79.2 s	75.7 d	15.4 t, 17.2 t, 23.5 t
3i	110.3 d	125.2 d	84.1 s	76.7 t	
3j	108.3 d	125.8 d	78.5 d	78.2 s	18.5 q, 25.3 q

a) Splitting patterns obtained by off-resonance decoupling. b) See Eq. 2. c) Signals corresponding to phenyl and amino groups were omitted.

Table 3. Fragmentation of vinyltriazoline by electron impact (mass spectral data of **3d** and **3f**)

3d ($R=CH_3$)			**3f** ($R=C_2H_5$)		
m/e	Intensity/%	Fragment[a]	*m/e*	Intensity/%	Fragment[a]
228	13.6	(M)$-N_2$	242	5.6	(M)$-N_2$
			227	19.4	(242)$-CH_3$
213	12.0	(228)$-CH_3$	213	7.9	(242)$-C_2H_5$
199	10.3	(228)$-C_2H_5$	199	12.0	(242)$-C_3H_7$
159	43.9	(228)$-$ 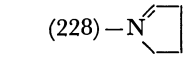	173	35.2	(242)$-$ 
111	81.4	C_3H_5N 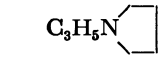	125	29.1	C_4H_7N 
98	Base	C_2H_4N 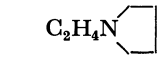	112	Base	C_3H_6N 

a) See Fig. 1.

as was found for the reaction of azidobenzene with enamines.[8,10] From Entries 1 and 8, it seems that β-azidostyrene (**1b**) is much more reactive than the α-isomer (**1a**); indeed, the reactivity of **1b** towards enamines is comparable with that of azidobenzene.[6]

Frontier Molecular Orbital Treatment. Generally, in the case of 1,3-dipolar cycloaddition of electron-rich olefins, the interaction between LUMO of a dipole and HOMO of a dipolarophile is important.[9,12] The lower the energy of LUMO of azide is, and the higher the energy of HOMO of enamine is, the interaction between these orbitals would be greater so that the reaction should proceed faster.

The order of reactivity of enamines towards α-azidostyrene (**1a**), as was described, corresponded to the energy of HOMO of enamines, which is lowered in the order of 1-pyrrolidinyl, piperidino, and morpholino as was estimated by photoelectron spectra (Fig. 2).

The difference in reactivity between the azides (**1a**, **b**) would be rationalized by the difference in the energies of LUMO of **1a** and **1b**. β-Azidostyrene (**1b**), of which the phenyl group is more extensively conjugated with the azido group, would have a lower energy of LUMO than α-azidostyrene (**1a**). The energies of these orbitals estimated by CNDO/2 calculation supported the above trends (Fig. 2). The lower energy of LUMO of **1b** corresponds to its higher reactivity towards enamines.

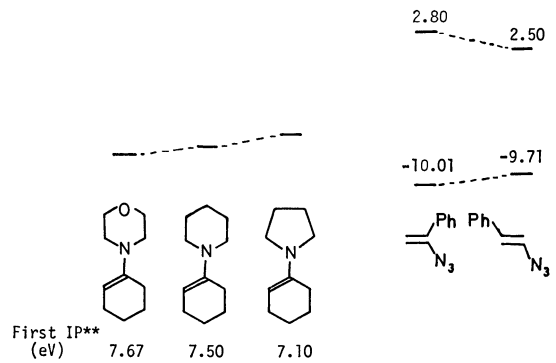

Fig. 2. Energies of frontier orbitals of azides* and enamines.
* Orbital energies (eV) of organic azides were estimated from CNDO/2 calculation.[14] ** Obtained from photoelectron spectroscopy by Domelsmith and Houk.[15]

A possible steric effect, interaction between phenyl group and the amino group in the transition state of the reaction, can also be responsible for the lower reactivity of **1a**.

It is known that the reaction between azides and enamines is dipole-LUMO-controlled reaction, and the orientation should therefore be as shown in Table. 4,

TABLE 4. COEFFICIENTS OF LUMO OF AZIDES ESTIMATED WITH CNDO/2 CALCULATION[14]

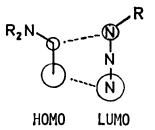

R =	H[13]	Ph	CH_2=CH	CH_2=CPh	PhCH=CH
	0.37	0.263	0.298	0.169	0.165
	0.76	0.495	0.557	0.425	0.462

which is in fact the case.[12] We attempted the calculation of the coefficients of LUMO of various vinyl azides; it seems that the introduction of a vinyl group to the azide does not alter the relative magnitude of the coefficients of LUMO of simple azides such as hydrazoic acid. These results are consistent with the regioselective formation of the 4-aminotriazolines (**3**).

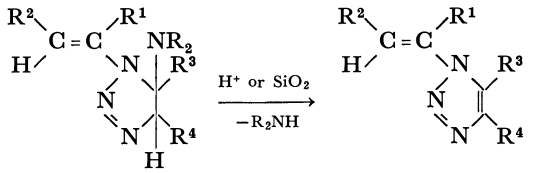

(3)

*Systhesis of Triazoles (**4**) by Deamination of the Aminotriazolines (**3**).* It is known that the 4-alkyl (or aryl)-4-amino-Δ^1-1,2,3-triazolines are easily deaminated by treatment with acid to give the corresponding 1*H*-1,2,3-triazoles.[6] When the aminotriazolines (**3a**,**c**,**h**,**i**) formed from the enamines of ketones were treated with acetic acid at room temperature or eluted through silica-gel column, deamination readily occurred, giving the corresponding triazoles (**4**) in 40—62% yields (Table 5).

Thus, a simple and useful method for the synthesis of vinyltriazoles from vinyl azides, under mild conditions, with high regioselectivity, and in moderate yields, was achieved. The vinyltriazoles like **4** were otherwise difficult to prepare. A known method with α-azidostyrene and 2-oxoalkylidinetriphenylphosphoranes requires much longer time (about a month) and affords the vinyltriazoles in no more than 54% yields.[4]

Experimental

General. Spectroscopic data were obtained with following apparatus: JEOL JNM-MH100 NMR Spectrometer, VARIAN FT-80A FT-NMR System, JEOL JNM-FX90Q FT-NMR System, JASCO DS-403G Grating Infrared Spectrophotometer, HITACHI EPS-3T Recording Spectrophotometer, and HITACHI RMU-6MG Mass Spectrometer.

α- and β-Azidostyrenes were prepared according to Hassner's method.[2] Enamines of ketones were prepared according to the method described in Organic Syntheses.[16] Enamines of aldehydes were prepared according to Mannich's method.[17]

Melting points were determined with microscopic apparatus and uncorrected.

Reaction of Azidostyrenes with Enamines. The azide (**1**) and the enamine (**2**) were mixed and allowed to stand at 0 °C without solvent until the azide was completely consumed, unless otherwise described. The products were purified with alumina column chromatography (eluting with hexane–dichloromethane (1:1)) and/or with recrystallization from an appropriate solvent.[18]

*3a,4,5,6,7,7a-Hexahydro-7a-morpholino-1-(1-phenylvinyl)-1H-1,2,3-benzotriazole (**3a**)*: The mixture of 4.4 g (30 mmol) of α-azidostyrene (**1a**) and 7.5 g (45 mmol) of 4-(1-cyclohexenyl)morpholine (**2a**) was allowed to stand at 0 °C for 90 d. Hexane (10 ml) was added and the precipitates formed were collected and recrystallized from ethanol to give 3.4 g of **3a** as colorless crystals (40% yield); mp 110—111.5 °C (dec); IR (KBr) 1615 cm^{-1} (C=C); ^1H NMR ($CDCl_3$) δ 1.1—2.3 (8H, m), 2.43 (4H, m), 4.61 (1H, t, J=5.5 Hz), 4.72 (1H, s), 5.58 (1H, s), and 7.44 (5H, m); UV_{max} (methanol) 246 nm (ε 7700). Found: C, 69.19; H, 8.01; N, 18.13%. Calcd for $C_{18}H_{24}N_4O$: C, 69.20; H, 7.74; N, 17.93%.

*5-Ethyl-3-(1-phenylvinyl)-4-piperidino-Δ^1-1,2,3-triazoline (**3b**)*: The mixture of 2.0 g (14 mmol) of **1a** and 2.8 g (20 mmol) of 1-(1-butenyl)piperidine (**2b**) was allowed to stand at 0 °C for 12 d. Then the mixture was eluted through alumina column to give 3.9 g of **3b** as faint yellow oil (86% yield): IR (neat) 1615 cm^{-1} (C=C); ^1H NMR ($CDCl_3$) δ 1.06 (3H, t, J=7 Hz), 1.4—1.6 (6H, m), 1.7 (2H, q, J=7 Hz), 2.2—2.6 (4H, m), 4.2—4.4 (2H, m), 4.86 (1H, s), 5.42 (1H, s), and 7.5 (5H, m); UV_{max} (methanol) 240 nm (ε 13000).

*3a,4,5,6,7,7a-Hexahydro-1-(1-phenylvinyl)-7a-(1-pyrrolidinyl)-1H-1,2,3-benzotriazole (**3c**)*: The mixture of 1.0 g (6.9 mmol) of **1a** and 1.1 g (7.3 mmol) of 1-(1-cyclohexenyl)-pyrrolidine (**2c**) was allowed to stand at 0 °C for 2 d. Then the product was eluted through alumina column to give 1.35 g of **3c** as yellowish viscous oil (66% yield): IR (neat)

TABLE 5. DEAMINATION OF AMINOTRIAZOLINES (**3**) TO TRIAZOLES (**4**)

Reactant	R^1	R^2	R^3	R^4	NR_2	Products	Method[a]	Yield/%
3a	Ph	H	$-(CH_2)_4-$			**4a**	B	40
3c	Ph	H	$-(CH_2)_4-$			**4a**	A	46
							B	40
3h	H	Ph	$-(CH_2)_4-$			**4b**	A	54
3i	H	Ph	Ph	H		**4c**	A	62

a) A: Treatment with acetic acid. B: Elution through silica-gel column.

mp 144.5—145.5 °C; IR (KBr) 1650 cm^{-1} (C=C); ^1H NMR ($CDCl_3$) δ 7.3—7.9 (m) and 7.85 (s); UV_{max} (methanol) 281 nm (ε 20000). Found: C, 77.97; H, 5.25; N, 17.16%. Calcd for $C_{16}H_{13}N_3$: C, 77.91; H, 5.30; N, 16.99%.

References

1) G. L'abbé, *Angew. Chem. Int. Ed. Engl.*, **14**, 775 (1975), and references cited therein.
2) A. Hassner and F. W. Fowler, *J. Org. Chem.*, **33**, 2686 (1968).
3) G. L'abbé, J. E. Galle, and A. Hassner, *Tetrahedron Lett.*, **1970**, 303; A. N. Thakore, J. Buchshriber, and A. C. Oehlschlager, *J. Org. Chem.*, **37**, 3213 (1972).
4) P. Ykman, G. Mathys, and G. L'abbé, *J. Org. Chem.*, **37**, 3213 (1972).
5) G. L'abbé, *Chem. Rev.*, **68**, 345 (1968), and references cited therein.
6) R. Fusco, G. Bianchetti, and D. Pocar, *Gazz. Chim. Ital.*, **91**, 849 (1961).
7) M. E. Munk and Y. K. Kim, *J. Am. Chem. Soc.*, **86**, 2213 (1964).
8) R. Huisgen, G. Szeimies, and L. Möbius, *Chem. Ber.*, **100**, 2494 (1967).
9) R. Sustman and H. Trill, *Angew. Chem. Int. Ed. Engl.*, **11**, 838 (1972).
10) N. K. Meilahn, G. Cox, and M. E. Munk, *J. Org. Chem.*, **40**, 819 (1972).
11) Y. Nomura, N. Hatanaka, and Y. Takeuchi, *Chem. Lett.*, **1976**, 901.
12) a) K. N. Houk, *J. Am. Chem. Soc.*, **94**, 8953 (1972); K. N. Houk, J. Sims, C. R. Watts, and I. J. Luskus, *ibid.*, **95**, 7301 (1973); b) K. N. Houk, "Application of Frontier Orbital Theory to Pericyclic Reactions" in "Pericyclic Reactions, Vol. 2," Academic Press, New York (1977), Chap. 4, p. 181.
13) I. Fleming, "Frontier Oribitals and Organic Chemical Reactions," John Wiley and Sons, London (1976).
14) Calculation programme made by Professor Nozomu Ebara *et al.*, based on J. A. Pople and D. L. Beveridge, "Approximate Molecular Orbital Theory," McGraw-Hill, New York (1970). We thank Prof. Ebara for using the programme. Calculation was carried out at The Computer Center of The University of Tokyo.
15) L. N. Domelsmith and K. N. Houk, *Tetrahedron Lett.*, **1977**, 1981.
16) S. Hünig, E. Lücke, and W. Brenninger, *Org. Synth.*, **41**, 65 (1961).
17) C. Mannich, K. Handke, and K. Roth, *Ber.*, **69**, 2106 (1936).
18) The oily triazolines (**3b**, **c**, **e**, **j**) did not crystallize, and the distillation *in vacuo* caused decomposition.
19) Diethyl ether was used as solvent to avoid uncontrolled reaction.

  Bull. Chem. Soc. Jpn., 54, 267—273 (1981)

Dealkylation Reaction of Acetals, Phosphonate, and Phosphate Esters with Chlorotrimethylsilane/Metal Halide Reagent in Acetonitrile, and Its Application to the Synthesis of Phosphonic Acids and Vinyl Phosphates[1)]

Tsuyoshi MORITA,* Yoshiki OKAMOTO, and Hiroshi SAKURAI

The Institute of Scientific and Industrial Research, Osaka University, Yamada-kami, Suita, Osaka 565

(Received July 4, 1980)

A mild and efficient method has been developed for carbon-oxygen bond cleavage using chlorotrimethylsilane/sodium iodide in acetonitrile. It was applied to synthetic transformation under nonaqueous and neutral conditions, such as acetal deprotection and the synthesis of phosphonic acids from the corresponding dialkyl phosphonates *via* methanolysis of their silyl esters. Effectiveness of various kinds of metal or ammonium iodides for this type of dealkylation was examined in the acetonitrile solution by ^{1}H NMR. Satisfactory results were also obtained with lithium or potassium iodide in place of sodium iodide. However, copper(I) or quarternary ammonium iodide was ineffective. Chlorotrimethylsilane/lithium bromide in acetonitrile is effective for selective dealkylation of multifunctional phosphonic esters or dialkyl vinyl phosphates.

Organosilicon compounds have been extensively developed and applied to organic synthesis as reagents, reactive intermediates, and protective groups.[2)] Attention was drawn to a new and efficient method for carbon-oxygen bond cleavage using organosilicon compounds under nonaqueous and neutral conditions, bromotrimethylsilane and iodotrimethylsilane in particular being versatile reagents for synthetic transformation of many functional groups. The chemistry of iodotrimethylsilane has been developed by Olah *et al.*[3)] and Jung *et al.*[4)] with regard to the reactions of carboxylic esters, ethers, acetals, alcohols, carbamates, and sulfoxides. Mckenna *et al.* and Rudinskas *et al.* reported the usefulness of bromotrimethylsilane for the conversion of dialkyl phosphonates into the silyl esters,[5)] sulfoxides into sulfides,[3b)] alcohols into bromides and orthoesters into the corresponding esters.[6)] However, bromotrimethylsilane is of little use for the cleavage of carboxylic esters, ethers, and acetals.

The preparation of bromotrimethylsilane[7)] or iodotrimethylsilane[8)] requires two steps *via* hexamethyldisiloxane from chlorotrimethylsilane, these fuming compounds being easily hydrolyzed in the atmospheric moisture. To overcome the disadvantages inherent in the use of iodotrimethylsilane, two improve methods have been worked out for the preparation of the reagent *in situ* using phenyltrimethylsilane/iodine[9)] or allyltrimethylsilane/iodine[10)] in the presence of carboxylic esters or ethers. The high reactivity of these reagents can be rationalized by the hard and soft acids and base principle,[11)] since they contain both hard acid and soft bases in their molecules. Chlorotrimethylsilane itself is essentially ineffective,[12)] although it is the most easily available reagent and frequently employed as a starting material for many reactive organosilicon compounds in organic synthesis.

In the course of studies on synthesis and biological properties of various phosphonic acids, we have sought a new and mild method for carbon-oxygen bond cleavage in the phosphonic esters with use of the most inexpensive chlorotrimethylsilane itself. In a preliminary communication, we demonstrated that chlorotrimethylsilane/sodium iodide in acetonitrile is an extremely effective reagent for dealkylation of esters, ethers *etc.*[13,14)] Olah *et al.* independently reported a similar use of the reagent in the same reactions.[15)]

In order to avoid an overlap of results, this paper describes the scope and limitation of dealkylation of dialkyl phosphonates and acetals with chlorotrimethylsilane/sodium iodide and the effectiveness of various iodides for this type of reaction. A novel reaction of chlorotrimethylsilane/lithium bromide as a selective dealkylating agent of phsophonic esters having other labile functional groups, and dialkyl vinyl phosphates is also described.

Results and Discussion

Dealkylation of Acetal with Chlorotrimethylsilane/Sodium Iodide. Dealkylation of acetals (**1**) with chlorotrimethylsilane/sodium iodide in acetonitrile was performed under mild and nonaqueous conditions. In most cases, the reaction was virtually complete at 45 °C within 0.5—2.5 h, affording the parent carbonyl compounds (**2**) in one step quantitatively (Eq. 1). The results are summarized in Table 1.

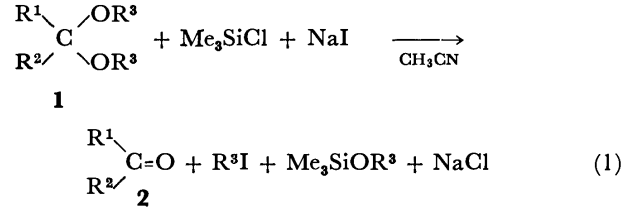

$$\underset{\mathbf{1}}{R^1R^2C(OR^3)_2} + Me_3SiCl + NaI \xrightarrow[CH_3CN]{} \underset{\mathbf{2}}{R^1R^2C{=}O} + R^3I + Me_3SiOR^3 + NaCl \qquad (1)$$

The present method is applicable to both dimethyl and diethyl acetals. However, the case of the ethylene acetal (**1c**) results in relatively poor yield, a similar result being reported on ethylene acetal cleavage with iodotrimethylsilane by Jung *et al.*[4c)] It was found that the acetal cleavage is significantly influenced by the ratio of the reagent to the substrate used. For example, treatment of benzaldehyde dimethyl acetal (**1a**) with 1.5 equiv. of chlorotrimethylsilane/sodium iodide gave a mixture of the acetal (**1a**) and benzaldehyde (**2a**) (14:86) at 45 °C for 0.5 h, in spite of the complete disappearance of the chlorotrimethylsilane signal. The complete conversion of **1a** into **2a** could be achieved by using 2.0 equiv. of the reagent at 45 °C for 0.5 h, the formation ratio of methyl iodide:

Table 1. Acetal dealkylation with chlorotrimethylsilane/sodium iodide

Compound	R^1	R^2	R^3	Temp °C	Time h	Yield[a] of **2** %
1a	Ph	H	Me	45	0.5	88
1b	Ph	H	Et	45	1.5	85
1c	Ph	H	$-CH_2-$	45	2.5	30
1d	$Me(CH_2)_5$	H	Me	45	0.5	91
1e	*p*-$MeOC_6H_4$	H	Me	45	2.5	95
1f	$-(CH_2)_5-$		Me	45	0.5	84
1g	Ph	Me	Me	45	0.5	82

a) Isolated yield. The products were characterized by comparison with authentic samples.

methyl trimethylsilyl ether being 6:1. The results indicate that further dealkylation of the initially formed methyl trimethylsilyl ether occurs competitively.

$$Me_3SiOMe + Me_3SiCl + NaI \xrightarrow[CH_3CN]{} MeI + (Me_3Si)_2O + NaCl \quad (2)$$

A report was given on the useful application of chlorotrimethylsilane/sodium iodide to the conversion of alcohols into iodides *via* their trimethylsilyl ethers.[16]

Effect of Other Iodide. In order to elucidate the effectiveness of various iodides for the dealkylating method using chlorotrimethylsilane, the effect of the salts on the yield was examined, **1a** being selected as a typical substrate and acetonitrile as solvent. The results are summarized in Table 2.

$$\underset{\textbf{1a}}{PhCH(OMe)_2} + Me_3SiCl + MI \xrightarrow[CH_3CN]{} \underset{\textbf{2a}}{PhCHO} + MeI + Me_3SiOMe + MCl \quad (3)$$

We see that the reaction yield is greatly influenced by the kind of salt used, lithium, sodium, and potassium iodide being very effective and giving an excellent yield of **2a** at 45 °C for 0.5 h. However, other salts such as copper(I) or quarternary ammonium iodides are unsatisfactory, the yields of **2a** being invariably lower than 40%, even for the prolonged reaction. This can be explained by the difference in solubility of the chloride (MCl) produced as a by-product in acetonitrile. With the progress of reaction, lithium, sodium, and potassium chloride immediately precipitate, but the ammonium chlorides are highly soluble in the solvent. For the sake of confirmation, we carried out a control experiment in which acetonitrile-soluble phenyltrimethylammonium chloride was added to the acetonitrile solution of chlorotrimethylsilane/phenyltrimethylammonium iodide (entry 9, Table 2). The chloride added prevented the formation of **2a**.[17] The effect of various solvents (carbon tetrachloride, chloroform, or *N,N*-dimethylformamide) on acetal dealkylation using chlorotrimethylsilane/sodium iodide was also examined. Acetonitrile was found to be the most suitable, the reaction in other solvents being slightly slower than that in acetonitrile.

Table 2. Acetal dealkylation with chlorotrimethylsilane in the presence of various iodide salts

Entry	MI	Temp °C	Time h	Yield[a] of **2a** %
1	LiI	45	0.5	100
2	NaI	45	0.5	100
3	KI	45	0.5	100
4	CuI	45	3.0	25
5	Me_4NI	45	3.0	11
6	Bu_4NI	45	3.0	36
7	$PhNMe_3I$	45	3.0	33
8	$PhNMe_3I$	45	5.0	38
9	$PhNMe_3I$[b]	45	3.0	6

a) Determined by ^1H NMR. b) Control experiment: **1a** (7 mmol), Me_3SiCl (14 mmol), $PhNMe_3I$ (14 mmol), and $PhNMe_3Cl$ (7 mmol) in CH_3CN (5 ml).

Dealkylation of Phosphonic Esters with Chlorotrimethylsilane/Sodium or Potassium Iodide. Phosphonic acids were prepared from the corresponding dialkyl esters by acid-catalyzed hydrolytic dealkylation, by refluxing them with 6 mol dm^{-3} hydrochloric acid for several hours. Many multifunctional phosphonic esters are frequently subjected to undesirable reactions under these acidic conditions.[18]

The exothermic reaction of dimethyl phosphonates (**3**) with chlorotrimethylsilane/sodium iodide occurred rapidly at room temperature to give the corresponding bis(trimethylsilyl) phosphonates (**4**) and methyl iodide quantitatively.[19] The dealkylation monitored by ^1H NMR spectroscopy proceeded to completion within 15 min. The rate of dealkylation of dialkyl phosphonates with the reagent decreases according to the bulkiness of the alkyl group in the order: R^2=Me> Et>*i*-Pr.[20] Treatment of the silyl esters (**4**) with methanol at room temperature gave the corresponding

$$\underset{\textbf{3}}{R^1P(O)(OR^2)_2} + 2\,Me_3SiCl + 2\,NaI \xrightarrow[CH_3CN]{} R^1P(O)(OSiMe_3)_2 + 2\,R^2I + 2\,NaCl \xrightarrow[MeOH]{\textbf{4}} \underset{\textbf{5}}{R^1P(O)(OH)_2} \quad (4)$$

$$\underset{\mathbf{3}}{R^1P(OR^2)_2} + 2\,Me_3SiCl + 2\,LiBr \xrightarrow[CH_3CN]{} \underset{\mathbf{4}}{R^1P(OSiMe_3)_2} + 2\,R^2Br + 2\,LiCl \quad (7)$$

The results for several phosphonates are given in Table 4.

Other salts such as KBr, $MgBr_2$, NEt_4Br, and $PhNMe_3Br$ are ineffective. The rate of dealkylation by the present method is slightly smaller than that with bromotrimethylsilane. The dealkylation of phosphonic ester moiety with chlorotrimethylsilane/lithium bromide proceeds with higher functional group selectivity than that with chlorotrimethylsilane/sodium iodide, indicating no cleavage of other functional groups even when a large excess of the reagent is used. Benzyl acetate hardly reacted at all with this reagent at 75 °C for 9 h.

Dealkylation of Dialkyl Vinyl Phosphate with Chlorotrimethylsilane/Lithium Bromide. From our studies on dealkylation of phosphonic and phosphoric ester using bromotrimethylsilane, we find that no C=COP bond cleavage occurs in dialkyl vinyl or dialkyl phenyl phosphates.[25] The C=COP bond cleavage in the hydrolysis of dialkyl vinyl phosphate under acidic or basic conditions occurs predominantly to yield dialkyl phosphate and carbonyl compounds.[26] Hata *et al.* as well as our group have prepared many kinds of unesterified enolphosphates of biologically interest from the corresponding dialkyl esters by means of bromotrimethylsilane.[27] In order to extend our methodology, the reaction of dialkyl vinyl phosphates with chlorotrimethylsilane/lithium bromide in acetonitrile solution was undertaken.

When dialkyl vinyl phosphates (**6**) reacted with chlorotrimethylsilane/lithium bromide in acetontrile, the corresponding bis(trimethylsilyl) vinyl phosphates (**7**) were obtained in high yields.

$$\underset{\mathbf{6}}{R^1OP(OR^2)_2} + 2\,Me_3SiCl + 2\,LiBr \xrightarrow[CH_3CN]{} \underset{\mathbf{7}}{R^1OP(OSiMe_3)_2} + 2\,R^2Br + 2\,LiCl \quad (8)$$

The silyl esters (**7**), treated with methanol at room temperature, were immediately converted into the corresponding phosphates (**8**) which were isolated as anilinium salts. The results are given in Table 5.

$$\mathbf{7} \xrightarrow{MeOH} \underset{\mathbf{8}}{R^1OP(OH)_2} \quad (9)$$

Alcoholysis of the silyl ester (**7a**) was unsuccessful. No desirable anilinium salt of **8a** could be isolated, resulting in the C=COP bond cleavage.

We have developed a mild and versatile method for carbon-oxygen bond cleavage using easily accessible and inexpensive chlorotrimethylsilane/metal halides, and have demonstrated the applicability of this method to synthetic transformation.

Experimental

Boiling points are uncorrected. Melting points were determined on a Yanagimoto micromelting apparatus and are uncorrected. ^1H NMR spectra were obtained with a JNM FX 100 using TMS or DSS as an internal standard, and IR spectra with a Shimadzu IR-400. GLC analyses were performed on a Shimadzu GC-3AF using stainless steel

Table 4. Phosphonic ester dealkylation with chlorotrimethylsilane/lithium bromide

Compound	R^1	R^2	Temp °C	Time h	Yield[a] of **4** %
3a	$PhCH_2$	Me	45—55	1.5	89
3b	$PhCH_2$	Et	70—75	3.0	90
3g	$MeOCOCH_2$	Et	70—75	4.5	87
3i	*t*-$BuOCOCH_2$	Me	45—50	1.5	83
3j	$PhCH_2OCOCH_2$	Et	70—75	4.5	85
3p	$MeOCH_2$	Et	70—75	4.0	88
3r	$(MeO)_2CH$	Me	45—50	1.5	92

a) Isolated yield.

Table 5. Phosphoric ester dealkylation with chlorotrimethylsilane/lithium bromide

Compound	R^1	R^2	Dealkylation conditions: Temp °C	Dealkylation conditions: Time h	Yield[a] of **7** %	Yield[a] of salt of **8** %
6a	$H_2C=CMe$	Et	70—75	3.0	84	—
6b	$Me_2C=CPh$	Et	70—75	3.5	81	93
6c	$Cl_2C=CH$	Me	45—50	1.5	86	95

a) Isolated yield.

columns packed with 25% Silicone DC 550 on Shimalite.

Materials. Commercial chlorotrimethylsilane was dried over CaH_2 and distilled. Acetonitrile and other solvents were dried and distilled by the usual method. Commercial anhydrous inorganic halides were stored in a desiccator. Hygroscopic lithium bromide was dried *in vacuo* at 100 °C just use. All substrates (phosphonic esters, acetals, and phosphoric esters) were prepared by the usual method. All the dialkyl phosphonates (**3a**—**3q**, except **3n** and **3r**) were prepared by the Arbuzov reaction of the corresponding halides with trialkyl phosphite.[18] The phosphonate (**3m**) was prepared from 2-chloro-4,6-dimethoxy-1,3,5-triazine[28] and trimethyl phosphite: yield 80%; viscous oily product; NMR (CCl_4): δ 3.93 (6H, d, J=10.6 Hz, CH_3OP), 4.02 (6H, s, CH_3O); Found: P, 12.31%. Calcd for $C_7H_{12}N_3O_5P$: P, 12.43%. The phosphonate (**3n**) was prepared by the reaction of benzaldehyde with dimethyl phosphonate, followed by acetylation with acetyl chloride in the presence of triethylamine.[18] The phosphonate (**3r**) was prepared from PCl_3 and trimethyl orthoformate.[29] All the phosphates (**6a**—**6c**) were prepared by the Perkow reaction of the corresponding α-halogenocarbonyl compounds with trialkyl phosphite.[26]

General Procedure for Dealkylation of Acetal with Chlorotrimethylsilane/Sodium Iodide. A mixture of acetal (30 mmol), chlorotrimethylsilane (60 mmol), and anhydrous sodium iodide (60 mmol) in dry acetonitrile (15 ml) was heated at 45 °C with stirring, the reaction being monitored by ^1H NMR. When the reaction was completed, the mixture was poured into 5% aqueous solution of $NaHCO_3$ (50 ml), followed by deiodinization with sodium thiosulfate. The resulting organic layer was extracted with ether (50 ml×3), the combined extract being dried over Na_2SO_4. After the removal of low-boiling materials on an evaporator (below 50 °C), the residue was distilled *in vacuo* to afford the pure product.

Effect of Iodide Salts on Dealkylation of Acetal. ^1H NMR analysis was carried out according to the same procedure as that described above. A mixture of benzaldehyde dimethyl acetal (7 mmol), chlorotrimethylsilane (14 mmol), and anhydrous iodide salt (14 mmol) was stirred at 45 °C in dry acetonitrile (5 ml). Conversion of the dimethyl acetal into benzaldehyde was determined by measurement of ^1H NMR spectra of the reaction mixture.

General Procedure for Dealkylation of Dialkyl Phosphonate with Chlorotrimethylsilane/Sodium or Potassium Iodide. Chlorotrimethylsilane (60 mmol) was added dropwise to a mixture of phosphonate (30 mmol) and anhydrous sodium or potassium iodide (60 mmol) in dry acetonitrile (30 ml). The mixture was stirred at 25—35 °C for 15—30 min, the progress of reaction being monitored by ^1H NMR spectroscopy. After complete disappearance of the chlorotrimethylsilane signal, the resulting sodium or potassium chloride was filtered off rapidly and washed with dry ether (20 ml×2). On removing low-boiling materials from the filtrate with an evaporator (below 50 °C), the corresponding silyl esters were obtained as oily residue. The residue was dissolved in methanol (30 ml) containing aniline or cyclohexylamine (60 mmol) and the mixture was concentrated to dryness under reduced pressure to give a white solid, amine salt of phosphonic acid. The crude salts were purified by recrystallization. Some known products were identified by comparison with authenitic samples prepared from dialkyl phosphonates and bromotrimethylsilane.[22] The structures of new compounds were identified by ^1H NMR spectra and elemental analysis.

*Anilinium (Ethoxycarbonylmethyl)phosphonate (Salt of **5h**).* The salt was recrystallized from acetone: yield 85%; mp 134—136 °C; NMR (D_2O): δ 1.27 (3H, t, CH_3C), 4.14 (2H, q, CH_2O), 2.84 (2H, d, J=20.9 Hz, CH_2P), 7.4—7.6 (5H, m, C_6H_5N); Found: C, 46.05; H, 6.29; N, 5.44; P, 11.72%. Calcd for $C_{10}H_{16}NO_5P$: C, 45.98; H, 6.17; N, 5.36; P, 11.86%.

*Anilinium (t-Butoxycarbonylmethyl)phosphonate (Salt of **5i**).* The salt was recrystallized from acetone: yield 77%; mp 115—117 °C; NMR (D_2O): δ 1.46 (9H, s, C_4H_9OCO), 2.74 (2H, d, J=20.8 Hz, CH_2P), 7.4—7.6 (5H, m, C_6H_5N); Found: C, 49.56; H, 6.65; N, 4.95; P, 11.77%. Calcd for $C_{12}H_{20}NO_5P$: C, 49.83 H, 6.97; N, 4.84; P, 10.71%.

*Anilinium (Benzyloxycarbonylmethyl)phosphonate (Salt of **5j**).* The salt was recrystallized from acetone: yield 84%; mp 123—125 °C; NMR (D_2O): δ 2.89 (2H, d, J=20.8 Hz, CH_2P), 5.18 (2H, s, $PhCH_2O$), 7.3—7.6 (10H, m, C_6H_5C, C_6H_5N); Found: C, 55.87; H, 5.50; N, 4.46; P, 8.89%. Calcd for $C_{15}H_{18}NO_5P$: C, 55.73; H, 5.61; N, 4.33; P, 9.58%.

*Anilinium (Ethoxycarbonyl)phosphonate (Salt of **5k**).* The salt was recrystallized from ethanol: yield 85%; mp 143—145 °C; NMR (D_2O): δ 1.28 (3H, t, CH_3C), 4.19 (2H, q, CH_2O), 7.3—7.6 (5H, m, C_6H_5N); Found: C, 44.23; H, 5.89, N, 5.73; P, 12.70%. Calcd for $C_9H_{14}NO_5P$: C, 43.73; H, 5.71; N, 5.67; P, 12.53%.

*Anilinium (Diethylcarbamoyl)phosphonate (Salt of **5l**).* The salt was recrystallized from acetone–ethanol (5/1): yield 88%; mp 142—144 °C; NMR (D_2O): δ 1.10 (3H, t, CH_3C), 1.19 (3H, t, CH_3C), 3.31 (2H, q, CH_2N), 3.69 (2H, q, CH_2N), 7.4—7.7 (5H, m, C_6H_5N); Found: C, 48.32; H, 7.44; N, 10.05; P, 10.95%. Calcd for $C_{11}H_{19}N_2O_4P$: C, 48.18; H, 6.99; N, 10.21; P, 11.29%.

*Anilinium (4,6-Dimethoxy-1,3,5-triazine-2-yl)phosphonate (Salt of **5m**).* The salt was recrystallized from ethanol: yield 91%; dec. 153—155 °C; NMR (D_2O): δ 4.02 (6H, s, CH_3O), 7.3—7.6 (5H, m, C_6H_5N); Found: C, 42.24; H, 4.82; N, 17.82; P, 9.63%. Calcd for $C_{11}H_{15}N_4O_5P$: C, 42.02; H, 4.81; N, 17.83; P, 9.86%.

*Anilinium (α-Acetoxybenzyl)phosphonate (Salt of **5n**).* The salt was recrystallized from methanol: yield 90%; mp 159—161 °C; NMR (D_2O): δ 2.81 (3H, s, CH_3C), 5.82 (1H, d, J=13.0 Hz, CHP), 7.3—7.6 (10H, m, C_6H_5C, C_6H_5N); Found: C, 55.79; H, 5.71; N, 4.24; P, 8.93%. Calcd for $C_{15}H_{18}NO_5P$: C, 55.73; H, 5.61; N, 4.33; P, 9.58%.

*Anilinium (Benzoylmethyl)phosphonate (Salt of **5o**).* The salt was recrystallized from acetone–methanol (10/1): yield 89%; mp 103—104 °C; NMR (D_2O): δ 3.57 (2H, d, J=21.3 Hz, CH_2P), 7.3—8.1 (10H, m, C_6H_5C, C_6H_5N); Found: C, 57.31; H, 5.51; N, 4.81; P, 10.49%. Calcd for $C_{14}H_{16}NO_4P$: C, 57.34; H, 5.50; N, 4.78; P, 10.56%.

*Anilinium (Methoxymethyl)phosphonate (Salt of **5p**).* The salt was recrystallized from acetone: yield 76%; mp 114—116 °C; NMR (D_2O): δ 3.43 (3H, s, CH_3O), 3.59 (2H, d, J=8.5 Hz, CH_2P), 7.3—7.6 (5H, m, C_6H_5N); Found: C, 43.56; H, 6.33; N, 6.37; P, 14.23%. Calcd for $C_8H_{14}NO_4P$: C, 43.84; H, 6.44; N, 6.39; P, 14.13%.

*Anilinium (2,2-Dimethoxyethyl)phosphonate (Salt of **5q**).* The salt was recrystallized from acetone–methanol (10/1): yield 82%; mp 86—88 °C; NMR (D_2O): δ 2.03 (2H, dd, J=18.1 Hz, CH_2P, J=5.9 Hz, $CHCH_2$), 3.36 (6H, s, CH_3O), 7.3—7.6 (5H, m, C_6H_5N); Found: C, 45.28; H, 6.32; N, 5.65; P, 11.52%. Calcd for $C_{10}H_{18}NO_5P$: C, 45.63; H, 6.89; N, 5.32; P, 11.77%.

General Procedure for Dealkylation of Dialkyl Phosphonate with Chlorotrimethylsilane/Lithium Bromide. A mixture of phosphonate (20 mmol), chlorotrimethylsilane (44 mmol for R^2=Me, 56 mmol for R^2=Et) and anhydrous lithium bromide (44 mmol for R^2=Me, 56 mmol for R^2=Et) in dry

acetontrile (15 ml) was vigorously stirred at 45—75 °C for several hours, the reaction being monitored by ^{1}H NMR. When the reaction was completed, the reaction mixture was cooled to room temperature and resulting lithium chloride and the excess of lithium bromide were filtered off. After the removal of low-boiling materials on an evaporator, the residue was distilled under reduced pressure to give the pure trimethylsilyl ester. The products were identified by comparison with authentic samples prepared by use of bromotrimethylsilane.[22]

Bis(trimethylsilyl) Benzylphosphonate (4a). Yield 89%; bp 95—97 °C/0.1 mmHg† (lit,[23] 88—90 °C/0.04 mmHg); IR (neat): 1245 cm^{-1} (P=O); NMR (CCl_4): δ 3.00 (2H, d, J=22.2 Hz, CH_2P), 7.22 (5H, m, C_6H_5C), 0.15 (18H, s, $OSiMe_3$).

Bis(trimethylsilyl) (t-Butoxycarbonylmethyl)phosphonate (4i). Yield 83%; bp 82—84 °C/0.01 mmHg; IR (neat): 1725 (C=O) and 1250 cm^{-1} (P=O); NMR (CCl_4): δ 1.46 (9H, s, C_4H_9O), 2.72 (2H, d, J=22.5 Hz, CH_2P), 0.28 (18H, s, $OSiMe_3$); Found: P, 9.31%. Calcd for $C_{12}H_{29}O_5PSi_2$: P, 9.10%.

Bis(trimethylsilyl) (Benzyloxycarbonylmethyl)phosphonate (4j). Yield 85%; bp 123—125 °C/0.002 mmHg; IR (neat): 1730 (C=O) and 1260 cm^{-1} (P=O); NMR (CCl_4): δ 2.87 (2H, d, J=22.5 Hz, CH_2P), 5.11 (2H, s, $PhCH_2O$), 7.31 (5H, m, C_6H_5C), 0.26 (18H, s, $OSiMe_3$); Found: P, 7.69%. Calcd for $C_{15}H_{27}O_5PSi_2$: P, 8.27%.

Bis(trimethylsilyl) (Methoxymethyl)phosphonate (4p). Yield 88%; bp 123—124 °C/8 mmHg (lit,[23] 73—75 °C/0.02 mmHg); IR (neat): 1250 cm^{-1} (P=O); NMR (CCl_4): δ 3.55 (2H, d, J=8.5 Hz, CH_2P), 3.43 (3H, s, CH_3O), 0.29 (18H, s, $OSiMe_3$).

General Procedure for Dealkylation of Dialkyl Vinyl Phosphate with Chlorotrimethylsilane/Lithium Bromide. Dealkylation of the phosphoric esters (20 mmol) was carried out by the same procedure as that in the case of dialkyl phosphonate. The silyl ester was isolated by distillation *in vacuo*. When the silyl ester (10 mmol) was added to a methanol solution (30 ml) of aniline (20 mmol) and the solution was concentrated to dryness on an evaporator (below 50 °C), anilinium salt was obtained as a white crystalline solid. After recrystallization the structures of the products were characterized by ^{1}H NMR, IR spectra, and elemental analysis.

Bis(trimethylsilyl) 1-Methylethenyl Phosphate (7a). Yield 84%; bp 90—92 °C/8 mmHg (lit,[27] 75—77 °C/1.25 mmHg).

Bis(trimethylsilyl) 2-Methyl-1-phenyl-1-propenyl Phosphate (7b). Yield 81%; bp 110—111 °C/0.01 mmHg; IR (neat): 1680 (C=C) and 1245 cm^{-1} (P=O); NMR (CCl_4): δ 1.70 (3H, d, J=3.0 Hz, CH_3C=COP), 1.88 (3H, d, J=2.4 Hz, CH_3C=COP), 7.2—7.4 (5H, m, C_6H_5C), 0.11 (18H, s, $OSiMe_3$); Found: P, 8.56%. Calcd for $C_{16}H_{29}O_4PSi_2$: P, 8.31%.

Bis(trimethylsilyl) 2,2-Dichloroethenyl Phosphate (7c). Yield 86%; bp 79—81 °C/1 mmHg; IR (neat): 1630 (C=C) and 1245 cm^{-1} (P=O); NMR (CCl_4): δ 6.84 (1H, d, J=5.9 Hz, C=CHOP), 0.30 (18H, s, $OSiMe_3$); Found: P, 9.41. Calcd for $C_8H_{19}O_4PSi_2Cl_2$: P, 9.18%.

Anilinium 2-Methyl-1-phenyl-1-propenyl Phosphate (Salt of 8b). The salt was recrystallized from acetone: yield 93%; mp 142—143 °C; NMR (D_2O): δ 1.71 (3H, d, J=3.1 Hz, CH_3C=COP), 1.75 (3H, d, J=2.2 Hz, CH_3C=COP), 7.3—7.6 (10H, m, C_6H_5C, C_6H_5N); Found: C, 60.16; H, 6.75; N, 4.83; P, 9.85%. Calcd for $C_{16}H_{20}NO_4P$: C, 59.81; H, 6.27; N, 4.83; P, 9.64%.

Dianilinium 2,2-Dichloroethenyl Phosphate (Salt of 8c). The salt was recrystallized from water: yield 95%; dec. 143—147 °C; NMR (CD_3OD): δ 6.9—7.4 (11H, m, C=CHOP, C_6H_5N); Found: C, 44.22; H, 4.58 N, 7.24 P, 8.02; Cl, 18.80%. Calcd for $C_{14}H_{17}N_2O_4PCl_2$: C, 44.34; H, 4.52; N, 7.39; P, 8.17; Cl, 18.70%.

† 1 mmHg=133.3 Pa.

We would like to thank Mr. Syuichi Yoshida for his assistance with dealkylation of acetal. Chlorotrimethylsilane was supplied through the kindness of Shin-Etsu Chemical Industry Ltd.

References

1) This work was presented at the 8th Symposium on Organic Sulfur and Phosphorous Compounds, Tokyo, January 1980.

2) a) P. F. Hudlik, "New Applications of Organometallic Reagents in Organic Synthesis," ed by D. Seyferth, Elsevier, Amsterdam (1976), pp. 127—160; b) E. W. Colvin, *Chem. Soc. Rev.*, **7**, 15 (1978).

3) a) T. L. Ho and G. A. Olah, *Angew. Chem.*, **88**, 847 (1976); b) G. A. Olah, B. G. B. Gupta, and S. C. Narang, *Synthesis*, **1977**, 583; c) T. L. Ho and G. A. Olah, *Proc. Natl. Acad. Sci.*, **75**, 4 (1978).

4) a) M. E. Jung and M. A. Lyster, *J. Am. Chem. Soc.*, **99**, 468 (1977); b) M. E. Jung and M. A. Lyster, *J. Org. Chem.*, **42**, 3761 (1977); c) M. E. Jung, W. A. Andrus, and P. L. Ornstein, *Tetrahedron Lett.*, **1977**, 4175; d) M. E. Jung and P. L. Ornstein, *ibid.*, **1977**, 2659; e) M. E. Jung and M. A. Lyster, *J. Chem. Soc., Chem. Commun.*, **1978**, 315. f) M. E. Jung and M. A. Mazurek, and R. M. Lim, *Synthesis*, **1978**, 588.

5) a) C. E. Mckenna, M. T. Higa, N. H. Cheug, and M. Mckenna, *Tetrahedron Lett.*, **1977**, 155; b) A. J. Rudinskas, T. L. Hullar, and R. L. Salvador, *J. Org. Chem.*, **42**, 2771 (1977).

6) M. E. Jung and G. L. Hatfield, *Tetrahedron Lett.*, **1978**, 4438.

7) W. F. Gilliam, R. N. Meals, and R. O. Sauer, *J. Am. Chem. Soc.*, **68**, 1161 (1946).

8) M. G. Voronkov and Y. I. Khudobin, *Izvest. Akad. Nauk. SSSR, Otdel. Khim. Nauk.*, **1956**, 713; *Chem. Abstr.*, **51**, 1819 (1957).

9) T. L. Ho and G. A. Olah, *Synthesis*, **1977**, 417.

10) M. E. Jung and T. A. Blumenkopf, *Teterahedron Lett.*, **1978**, 3657.

11) T. L. Ho, "Hard and Soft Acids and Bases Principle in Organic Chemistry," Academic Press, New York (1977), p. 171.

12) R. Rabinowitz, *J. Org. Chem.*, **28**, 2975 (1963). This work on dialkyl phosphonate cleavage using chlorotrimethylsilane received little interest owing to the lack of wide applicability.

13) a) T. Morita, Y. Okamoto, and H. Sakurai, *Tetrahedron Lett.*, **1978**, 2523; b) T. Morita, Y. Okamoto, and H. Sakurai, *J. Chem. Soc., Chem. Commun.*, **1978**, 874. This seems to be the first report on dealkylation reaction with use of the reagent.

14) At the same time as that of our preliminary communication,[13] an independent work by Schimidt and Russ appeared describing the condensation of ketones using chlorotrimethylsilane/sodium iodide: a) A. H. Schmidt and Russ, *Chem. Zeitung*, **102**, 26, (1978); b) A. H. Schmidt and Russ, *ibid.*, **102**, 65 (1978).

15) a) G. A. Olah, S. C. Narung, B. G. B. Gupta, and R. Malhotra, *J. Org. Chem.*, **44**, 1247 (1979); b) G. A. Olah, S. C. Narung, B. G. B. Gupta, and R. Malhotra, *Synthesis*, **1979**, 61.

16) Many alkyl silyl ethers derived from primary, secondary, and tertiary alcohols were readily converted into the corresponding iodides quantitatively: T. Morita, S. Yoshida, Y. Okamoto, and H. Sakurai, *Synthesis*, **1979**, 379.

$$ROH \longrightarrow ROSiMe_3 \xrightarrow[CH_3CN]{Me_3SiCl/NaI} RI$$

17) There is probably an equilibrium shifting toward the left

$$Me_3SiCl + I^- \rightleftarrows Me_3SiI + Cl^-$$

The reaction proceeds *via* the formation of a small amount of iodotrimethylsilane (in equilibrium). This seems to be an acceptable explanation. An alternative mechanism was proposed for phosphonic ester dealkylation.[13a] Olah *et al.* pointed out that the active compound formed from chlorotrimethylsilane/sodium iodide in acetonitrile is silylnitrilium iodide, $[CH_3C{\equiv}N^+{-}SiMe_3]\ I^-$.[15a] We believe that the mechanism involves the initial formation of Me_3SiI from Me_3SiCl and NaI, subsequent rapid silylation of CH_3CN by the Me_3SiI, and the dealkylation of organic substrate by silylnitrilium iodide.

18) K. H. Worms and M. Schmidt-Dunker, "Organic Phosphorus Compounds," ed by G. M. Kosolapoff and L. Maier, Wiley, New York (1976), Vol. 7, Chap. 18.

19) After our preliminary communication, the dealkylation of phosphonic esters with iodotrimethylsilane was reported: a) J. Zygmunt, P. Kafarski, and P. Mastalerz, *Synthesis*, **1978**, 609; b) G. M. Blackburn and D. Ingleson, *J. Chem. Soc., Chem. Commun.*, **1978**, 870. Phosphonic ester dealkylation using chlorotrimethylsilane/lithium iodide in CCl_4 was also reported: Y. Machida, S. Nomoto, and I. Saito, *Synthetic Commun.*, **9**, 97 (1979).

20) A similar reactivity was observed for alkyl carboxylate cleavage.[13a]

21) Dialkyl phosphonates having triazine ring were prepared by the Arbuzov reaction of the corresponding chlorides with trialkyl phosphite. However, no report was given on the successful synthesis of their phosphonic acids: W. Hewertson, R. A. Shaw, and B. C. Smith, *J. Chem. Soc.*, **1963**, 1670.

22) T. Morita, Y. Okamoto, and H. Sakurai, *Bull. Chem. Soc. Jpn.*, **51**, 2169 (1978).

23) H. Gross, C. Böck, B. Costisella, and J. Gloede, *J. Prakt. Chem.*, **320**, 344 (1978).

24) C. E. Mckenna and J. Schmidhauser, *J. Chem. Soc., Chem. Commun.*, **1979**, 739.

25) T. Morita, Y. Okamoto, and H. Sakurai, unpubilshed results.

26) E. Cherbuliez, "Organic Phosphorus Compounds," ed by G. M. Kosolapoff and L. Maier, Wiley, New York (1973), Vol. 6, Chap. 15, p. 328.

27) T. Hata, K. Yamada, T. Futatsugi, and M. Sekine, *Synthesis*, **1979**, 189.

28) J. R. Dudley, J. T. Thurston, F. C. Schaefer, D. Holm-Hansen, C. T. Hull, and P. Adams, *J. Am. Chem. Soc.*, **73**, 2986 (1951).

29) H. Gross and J. Freiberg, *Chem. Ber.*, **101**, 1250 (1968).

Aldol Reaction of Aluminium Enolate Resulting from 1,4-Addition of R_2AlX to α,β-Unsaturated Carbonyl Compound. A 1-Acylethenyl Anion Equivalent[1)]

Akira Itoh, Shuji Ozawa, Koichiro Oshima,* and Hitosi Nozaki

Department of Industrial Chemistry, Faculty of Engineering, Kyoto Univesity, Yoshida, Sakyo-ku, Kyoto 606

(Received July 16, 1980)

Organoaluminium reagents R_2AlX (X=SPh, SeMe) easily add to α,β-unsaturated carbonyl compounds in 1,4-fashion. The resulting aluminium enolates react with aldehydes to give aldol adducts in fair to good yields. Formal elimination of HX from the adducts provides α-substituted α,β-unsaturated carbonyl compounds. The overall transformation is an addition of aldehydes to 1-acylethenyl anion equivalent. Diethylaluminium iodide also is found to be an efficient reagent for the same type transformation.

The aldol condensation is one of the most versatile synthetic methods in organic chemistry. Recently, organoaluminium enolates as produced *via* several routes have been utilized as a vast potential agent of the reaction.[2-5)] Conjugate addition of organoaluminium reagents R_2AlX to α,β-unsaturated carbonyl compounds provides another route to aluminium enolates (Scheme 1).[6)] The aldol reaction with an aldehyde component followed by elimination of HX gives α-substituted α,β-unsaturated carbonyl compound **4**. The overall transformation therefore provides an α-carbanion equivalent of the substrate **5** adding to the aldehyde component to form **4**. The sequence gives a solution to the recurring synthetic problem to introduce α-substituent directly to α,β-unsaturated carbonyl compounds.[7)]

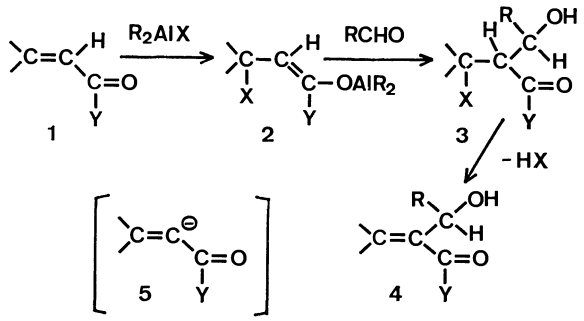

Scheme 1.

Among many candidates for R_2AlX, dimethylaluminium benzenethiolate[8)] (reagent A) and dimethylaluminium methaneselenolate[9)] (reagent B) have been found to be effective (Table 1). Dimethylaluminium benzenethiolate was prepared from trimethylaluminium and thiophenol in dichloromethane and dimethylaluminium methaneselenolate from trimethylaluminium and selenium metal in toluene. These reagents were used directly without isolation. In an attempt to find the suitable solvent for the aldol reaction, the reaction between 2-cyclohexenone and acetaldehyde mediated by Me_2AlSPh was examined in various solvents (solvent, isolated yield of **3**): hexane, 42%; CH_2Cl_2, 43%; toluene, 45%; tetrahydrofuran (THF), 94%. After completion of 1,4-addition of R_2AlX (X=SPh, SeMe) to α,β-unsaturated carbonyl compounds, the reaction mixture was diluted with THF which was found to be the best solvent.

Unfortunately dimethylaluminium benzenethiolate was not effective in the reaction of α,β-unsaturated esters because of sluggishly proceeding 1,4-addition, where a quantity of the corresponding thiocarboxylic *S*-ester was formed[11)] The use of a new ate complex $Me_3Al^-SPhLi^+$ (reagent C) has been found to be much more advantageous possibly due to the increased reactivity of thiolate ion itself as well as of the resulting enolate anion corresponding to **2**.

Erythro and threo ratios of the aldol product **3** have been examined. The aldol product 2-(1-hydroxyethyl)-3-phenylthiocyclohexanone was desulfurized with Raney Ni in ethanol. Analysis of the NMR spectra[12)] revealed that the product was a 1:1 mixture of erythro and threo isomers. Similarly, the aldol products between acetaldehyde and methyl vinyl ketone (run 7) or ethyl acrylate (run 11) were found to be 1:1 and 1:2 mixture of isomers by NMR analysis.[13)]

Spontaneous elimination of phenylthio group in the reaction mixture was observed in run 6. More easily the conversion of **3** to **4** was achieved by the oxidation (sodium periodate for SPh and hydrogen peroxide for SeMe), which facilitates successive elimination[14)] as given in Table 1. Moreover, the overall transformation could be performed in one pot, for instance, the addition of copper(II) chloride and sodium acetate directly to the product in the run 1 without workup afforded the desired compound **4** in 52% yield.

Diethylaluminium iodide[15)] was found to be more effective for the same type transformation. Addition of diethylaluminium iodide to a mixture of aldehyde and α,β-unsaturated ketone in dichloromethane gave α-substituted α,β-unsaturated ketone **4** directly. The whole sequence involving conjugate addition of the iodide, aldol condensation of the resulting aluminium enolate, and elimination of HI element proceeded in one pot. The results are summarized in Table 2.

Tetrahydrofuran was not a suitable solvent for the reaction of Et_2AlI because of the ring cleavage producing 4-iodo-1-butanol. Reaction between ethyl acrylate and acetaldehyde gave the adduct **3** (X=I). Elimination of HI did not proceed spontaneously in this case and treatment with 1,8-diazabicyclo[5.4.0]-undec-5-ene was necessary in order to obtain the product **4**.

Although aldehydes successfully trapped the aluminium enolates in high yields, ketones and other electrophiles such as allyl bromide, acetyl chloride, 2-phenyl-1,3-dioxolane, and cyclohexene oxide failed to react.

Table 1. Reaction between α,β-unsaturated carbonyl compounds and aldehydes by means of Me_2AlSPh or $Me_2AlSeMe$

Run	α,β-Unsaturated carbonyl compound	Reagent[a]	Aldehyde RCHO	**3** Yield %	**4** Yield %[b]
1	2-Cyclohexenone	A	$CH_3(CH_2)_7CHO$	90	71
2	2-Cyclohexenone	A	CH_3CHO	94	92
3	2-Cyclohexenone	B	CH_3CHO	77	77
4	2-Cyclohexenone	A	methacrolein	97	84
5	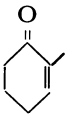	A	CH_3CHO	75	—
6	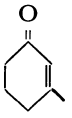	A	CH_3CHO	—	50[c]
7	CH_2=CHCOCH$_3$	A	CH_3CHO	60	57
8	CH_2=CHCOCH$_3$	B	CH_3CHO	55	50
9	2-Cyclopentenone	A	HCHO	56	80[d]
10	2-Cyclopentenone	A	$CH_3(CH_2)_7CHO$	76	60
11	CH_2=CHCOOC$_2$H$_5$	C	CH_3CHO	73	87
12		C	PhCHO	77	74

a) A: Me_2AlSPh, B: $Me_2AlSeMe$, C: Me_3Al–$SPhLi^+$. b) Yields were based on **3**. c) Phenylthio group has been spontaneously eliminated in this case. d) See Ref. 10.

Table 2. Reaction between α,β-unsaturated carbonyl compounds and aldehydes by means of Et_2AlI

Run	α,β-Uusaturated carbonyl compound	Aldehyde RCHO	**4** Yield/%
1	2-Cyclohexenone	CH_3CHO	81
2	2-Cyclohexenone	$CH_3(CH_2)_7CHO$	88
3	CH_2=CHCOCH$_3$	CH_3CHO	61
4	CH_2=CHCOOC$_2$H$_5$	CH_3CHO	62[a]

a) Further treatment with DBU was necessary. See experimental part.

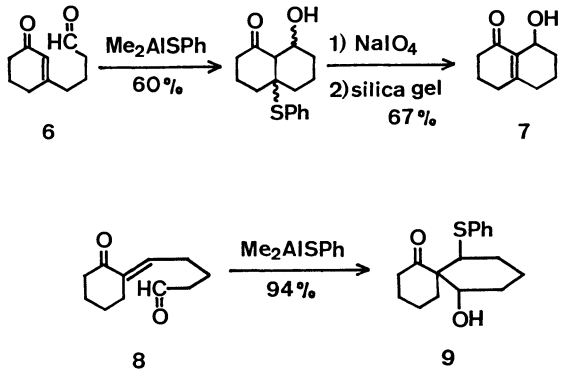

Scheme 2.

Treatment of the α,β-unsaturated carbonyl compounds **6**[16] or **8** with dimethylaluminium benzenethiolate provided an efficient method for the cyclization affording **7** or **9**.

Finally, further synthetic applications of the adduct **10** have been examined (Scheme 3). Treatment of the acetate of **10** with lithium dimethylcuprate(I)[17] afforded **11** in 59% yield. No regio- and stereoisomers were detected. Orthoester Claisen rearrangement[18] of **10** gave a stereoisomeric mixture of **12** in 70% yield. These transformations enable us to introduce a variety of groups on α and β positions of α,β-unsaturated carbonyl compounds.

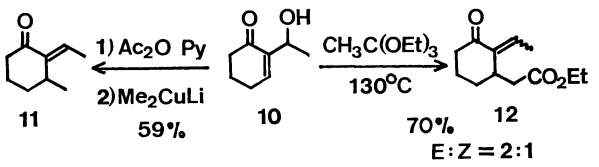

Scheme 3.

Experimental

The infrared spectra were determined on a Shimadzu IR-27-G spectrometer; the mass spectra on a Hitachi RMU-6L machine; the GLPC analyses on a Yanagimoto GCG-550F; and the NMR spectra on a JEOL C-60H or Varian EM-390H spectrometer. The chemical shifts are given in δ in ppm with TMS as the internal standard. Splitting patterns are designated as s, singlet; d, doublet; t, triplet; q, quartet; m, multiplet. The microanalyses were carried out by the staffs at the Elemental Analyses Center of Kyoto University. All experiments were carried out under an atmosphere of dry argon. Tetrahydrofuran was dried by distillation from sodium-benzophenone. Thin layer or thick layer plates were made of E. Merck PF-254, and preparative columns silica gel E. Merck Art. 7734.

2-(1-Hydroxynonyl)-2-cyclohexenone. A solution of thiophenol (0.26 g, 2.4 mmol) in dichloromethane (2.0 ml) was added to a solution of trimethylaluminium in hexane (1.0 M, 2.4 ml, 2.4 mmol) at 0 °C and the mixture was stirred for 20 min. A solution of 2-cyclohexenone (0.19 g,

2.0 mmol) in dichloromethane (2.0 ml) was added at −78 °C and, after 15 min, the resulting white suspension was diluted with THF (10 ml) to give a colorless solution. After additional 5 min, a solution of nonanal (0.34 g, 2.4 mmol) in THF (2.0 ml) was added and stirring was continued for 20 min at −78 °C. The reaction mixture was poured into ice–water and the organic phase was washed with 1 M HCl twice. The aqueous phase was extracted twice with ethyl acetate and the combined organic layers were washed with brine, dried, and freed of the solvent. Purification by column chromatography on silica gel (hexane:ether=2:1) gave 2-(1-hydroxynonyl)-3-(phenylthio)cyclohexanone (0.64 g, 90% yield): IR (neat) 3450, 1700 cm^{-1}; NMR (CCl_4) δ 0.88 (t, J=4.5 Hz, 3H), 1.20—2.40 (m, 22H), 3.46 (m, 1H), 4.00 (m, 1H), 7.20—7.48 (m, 5H); MS *m/e* (%) 238 (2), 220 (7), 206 (24), 140 (13), 135 (16), 125 (100), 110 (98).

The sulfide (0.28 g, 0.72 mmol) was dissolved in 50% aqueous methanol (5.0 ml) and treated with sodium periodate (0.23 g, 1.1 mmol) at 25 °C for 3 d. After purification by column chromatography on silica gel, the obtained sulfoxide was dissolved in toluene (3.0 ml) and heated at reflux for 30 min to give the title compound (0.12 g, 71% yield based on the hydroxy sulfide): bp 185 °C (bath temp, 2 Torr, 1 Torr=133.322 Pa); IR (neat) 3445, 1665, 1653 cm^{-1}; NMR (CCl_4) δ 0.87 (t, J=4.8 Hz, 3H), 1.28 (m, 14H), 1.82—2.07 (m, 2H), 2.24—2.44 (m, 5H), 4.15 (m, 1H), 6.74 (t, J=3.9 Hz, 1H); MS *m/e* (%) 238 (M^+, 3), 221 (3), 220 (11), 141 (13), 136 (18), 126 (100). Microanalysis was performed after trimethylsilylation of the hydroxyl group.[19] Found: C, 69.56; H, 11.01%. Calcd for $C_{18}H_{34}O_2Si$: C, 69.62; H, 11.04%.

2-(1-Hydroxyethyl)-2-cyclohexenone ***10***. Bp 130 °C (bath temp, 2 Torr); IR (neat) 3440, 1665, 1655 cm^{-1}; NMR (CCl_4) δ 1.23 (d, J=6.5 Hz, 3H), 1.96 (m, 2H), 2.36 (m, 4H), 2.69 (bs, 1H), 4.42 (qd, J=6.5 and 1.2 Hz, 1H), 6.80 (td, J=4.1 and 1.2 Hz, 1H); MS *m/e* (%) 141 (9), 140 (M^+, 38), 139 (9), 125 (100), 97 (54). Found: C, 62.07; H, 9.40%. Calcd for $C_{11}H_{20}O_2Si$: C, 62.21; H, 9.49%.[19]

Joining Reaction of 2-Cyclohexenone and Acetaldehyde Mediated by $Me_2AlSeMe$. A mixture of selenium (0.23 g, 2.9 mg-atom), trimethylaluminium (1.0 M hexane solution, 3.0 ml, 3.0 mmol), and toluene (3.0 ml) was refluxed for 2.5 h.[9] The resulting homogeneous solution was diluted with THF (10 ml) and treated with 2-cyclohexenone (0.11 g, 1.1 mmol) at −78 °C. After 70 min, acetaldehyde (0.1 ml, 1.8 mmol) was added and the mixture was stirred for 30 min at −78 °C and for 5 min at 0 °C. Purification by preparative TLC (hexane:ether=1:2) afforded 2-(1-hydroxyethyl)-3-(methylseleno)cyclohexanone (0.20 g, 0.85 mmol) in 77% yield. The selenide (0.20 g, 0.85 mmol) was dissolved in a mixture of dichloromethane (10 ml) and pyridine (0.35 ml, 4.3 mmol) and treated with 30% H_2O_2 (0.55 g, 4.8 mmol) at 25 °C for 30 min to give **10** (91 mg, 77% yield).

2-(1-Hydroxy-2-methyl-2-propenyl)-2-cyclohexenone. IR (neat) 3430, 1664, 1655, 893 cm^{-1}; NMR (CCl_4) δ 1.65 (s, 3H), 2.01 (m, 2H), 2.38 (m, 4H), 2.85 (bs, 1H), 4.75 (s, 1H), 4.82 (s, 1H), 4.95 (s, 1H), 6.78 (t, J=4.2 Hz, 1H); MS *m/e* (%) 166 (M^+, 47), 165 (18), 151 (27), 149 (12), 148 (16), 147 (20), 137 (100); bp 95 °C (bath temp, 2 Torr).[20] Found: C, 65.21; H, 9.08%. Calcd for $C_{13}H_{22}O_2Si$: C, 65.50; H, 9.30%.[19]

2-(1-Hydroxyethyl)-2-methyl-3-(phenylthio)cyclohexanone. IR (neat) 3460, 1703 cm^{-1}; NMR (CCl_4) δ 1.16 (s, 3H), 1.35 (d, J=6.3 Hz, 3H), 1.63—2.55 (m, 7H), 3.66—4.29 (m, 2H), 7.13—7.50 (m, 5H); MS *m/e* (%) 220 (5), 154 (1), 139 (1), 111 (15), 110 (100), 109 (19), 82 (56); bp 140 °C (bath temp, 2 Torr).[20] Found: C, 64.16; H, 8.44%. Calcd for $C_{18}H_{28}O_2SSi$: C, 64.23; H, 8.39%.[19]

2-(1-Hydroxyethyl)-3-methyl-2-cyclohexenone. IR (neat) 3470, 1643, 1625 cm^{-1}; NMR (CCl_4) δ 1.26 (d, J=6.3 Hz, 3H), 1.95 (s, 3H), 1.75—2.05 (m, 2H), 2.25—2.50 (m, 4H), 4.27 (bs, 1H), 4.52 (q, J=6.3 Hz, 1H); MS *m/e* (%) 154 (M^+, 7), 140 (12), 139 (100), 136 (13), 121 (11), 111 (15); bp 94 °C (bath temp, 2 Torr).[20] Found: C, 63.20; H, 9.91%. Calcd for $C_{12}H_{22}O_2Si$: C, 63.66; H, 9.79%.[19]

4-Hydroxy-3-methylene-2-pentanone. IR (neat) 3415, 1665, 1635, 1088 cm^{-1}; NMR (CCl_4) δ 1.23 (d, J=6.6 Hz, 3H), 2.30 (s, 3H), 2.65 (bs, 1H), 4.53 (q, J=6.6 Hz, 1H), 5.98 (s, 2H); MS *m/e* (%) 114 (M^+, 1), 113 (1), 100 (7), 99 (100), 81 (12), 71 (16); bp 45 °C (bath temp, 2 Torr).[20] Found: C, 57.78; H, 9.67%. Calcd for $C_9H_{18}O_2Si$: C, 58.02; H, 9.74%.[19]

2-Hydroxymethyl-2-cyclopontenone. NMR and IR spectra and mp agreed with published data.[7b]

2-(1-Hydroxynonyl)-2-cyclopentenone. IR (neat) 3432, 1686, 1631 cm^{-1}; NMR (CCl_4) δ 0.86 (t, J=5.4 Hz, 3H), 1.29 (m, 14H), 2.33 (m, 2H), 2.56 (m, 2H), 2.87 (bs, 1H), 4.26 (bt, J=5.1 Hz, 1H), 7.32 (bs, 1H); MS *m/e* (%) 224 (M^+, 0.3), 207 (2), 206 (9), 149 (3), 145 (3), 135 (5), 111 (100); bp 124 °C (bath temp, 2 Torr).[20] Found: C, 68.84; H, 10.84%. Calcd for $C_{17}H_{32}O_2Si$: C, 68.86; H, 10.88%.[19]

Ethyl 3-Hydroxy-2-methylenebutyrate. A solution of trimethylaluminium in hexane (1.0 M, 1.2 ml, 1.2 mmol) was added to a solution of lithium benzenethiolate (1.2 mmol, prepared *in situ* from thiophenol and butyllithium at 0 °C) in THF (5.0 ml) at 0 °C. After 1 h, the mixture was cooled to −78 °C and treated with a solution of ethyl acrylate (0.11 g, 1.1 mmol) in THF (1.0 ml) and kept there for 15 min. Acetaldehyde (0.1 ml, 1.8 mmol) was added and the mixture was stirred for 10 min at −78 °C and for 5 min at 0 °C. The crude product was submitted to preparative TLC (hexane:ether=1:1) to afford ethyl 3-hydroxy-2-(phenylthiomethyl)butyrate (0.21 g, 0.81 mmol) in 73% yield. Following the previously described procedure, this hydroxy ester (0.15 g, 0.6 mmol) was subsequently transformed to the title compound (75 mg, 87% yield): IR (neat) 3440, 1713, 1630 cm^{-1}; NMR (CCl_4) δ 1.29 (d, J=6.4 Hz, 3H), 1.32 (t, J=7.2 Hz, 3H), 2.90 (bs, 1H), 4.17 (q, J=7.2 Hz, 2H), 4.50 (q, J=6.4 Hz, 1H), 5.76 (s, 1H), 6.10 (s, 1H); MS *m/e* (%) 129 (51), 101 (75), 99 (44), 98 (34), 97 (21), 83 (100), 73 (37); bp 54 °C (bath temp, 2 Torr).[20] Found: C, 55.61; H, 9.57%. Calcd for $C_{10}H_{20}O_3Si$: C, 55.52; H, 9.32%.[19]

2-(1-Hydroxybenzyl)-2-buten-4-olide. NMR, IR, and mass spectra were found to be in accord with published data.[6]

Desulfurization of 2-(1-Hydroxyethyl)-3-(penylthio)cyclohexanone with Raney Ni. Stirring the hydroxy sulfide (0.11 g) in ethanol (3.0 ml) with Raney Ni W-2 (0.3 g) under hydrogen atmosphere at 25 °C for 14 h followed by preparative TLC isolation (benzene:ethyl acetate=3:1, two developments) gave 2-(1-hydroxyethyl)cyclohexanone (31 mg) in 51% yield. The NMR spectrum (CCl_4) indicated this being a 1:1 mixture of erythro and threo isomers by exhibiting a pair of multiplets at δ 3.82 and 4.13 in a 1:1 ratio as well as a pair of doublets of equal intensities at δ 1.07 (J=6.6 Hz) and 1.09 (J=6.6 Hz).[12]

One Pot Synthesis of ***10***. After successive treatment of 2-cyclohexenone (92 mg, 1.0 mmol) with Me_2AlSPh (1.2 mmol) and acetaldehyde (0.1 ml, 1.8 mmol) in hexane (3.0 ml) and THF (7.0 ml), the reaction mixture was allowed to react with copper(II) chloride (0.68 g, 5.1 mmol) and sodium acetate (0.44 g, 5.3 mmol). The mixture was re-

fluxed for 2 h, poured into water, and filtered through a pad of Celite 545. The organic phase was washed with brine, dried, and freed of the solvent. The residue was submitted to preparative TLC (hexane:ethyl acetate=1:1, two developments) to give **10** (70 mg, 0.50 mmol) in 52% yield.

Joining Reaction of 2-Cyclohexenone and Acetaldehyde Mediated by Et_2AlI. A solution of diethylaluminium iodide in toluene (1.15 M, 1.6 ml, 1.8 mmol) was added to a solution of 2-cyclohexenone (0.12 g, 1.2 mmol) and acetaldehyde (0.10 ml, 1.8 mmol) in dichloromethane (7.0 ml) at 0 °C. After stirring for 20 min at 0 °C, the mixture was diluted with ether and washed with 1 M HCl and brine. Purification by column chromatography on silica gel (hexane:ethyl acetate=3:1) afforded **10** (0.14 g) in 81% yield.

Joining Reaction of Ethyl Acrylate and Acetaldehyde by Means of Et_2AlI. Similar treatment of a solution of ethyl acrylate (0.15 g, 1.5 mmol) and acetaldehyde (0.13 ml, 2.3 mmol) in dichloromethane (7.0 ml) followed by silica gel column chromatography gave ethyl 3-hydroxy-2-(iodomethyl)butyrate (0.44 g, 72% yield): IR (neat) 3470, 1730 cm^{-1}; NMR (CCl_4) δ 1.05 (d, J=6.0 Hz, 3H), 1.33 (t, J=6.9 Hz, 3H), 2.17 (bs, 1H), 2.66 (m, 1H), 3.36 (d, J=6.6 Hz, 2H), 3.90 (m, 1H), 4.18 (q, J=6.9 Hz, 2H); MS *m/e* (%) 272 (M^+, 3), 227 (5), 145 (6), 101 (100), 73 (70), 55 (80). The iodide (0.44 g, 1.1 mmol) was dissolved in benzene (15 ml) and treated with 1,8-diazabicyclo[5.4.0]-5-undecene (0.66 g, 4.3 mmol) at 25 °C for 1 h to give ethyl 3-hydroxy-2-methylenebutyrate (0.12 g, 0.93 mmol) in 86% yield.

10-Hydroxybicyclo[4.4.0]dec-1(6)-en-2-one **7**. A solution of **6**[16] (0.17 g, 1.0 mmol) in THF (2.0 ml) was added to a solution of Me_2AlSPh (3.0 mmol) in hexane (3.0 ml) and THF (9.0 ml) at 0 °C over a period of 40 min. After stirring for additional 20 min, the mixture was poured into ice–water and extracted with ethyl acetate. The cyclized product (0.17 g, 60% yield) was treated with sodium periodate (0.20 g) in 50% aqueous methanol (6.0 ml) at 25 °C for 1 h. The crude sulfoxide was dissolved in ethyl acetate (6.0 ml) and stirred at 25 °C for 9 h in the presence of silica gel (Merck, PF-254, 1.0 g). The reaction mixture was filtered and the filtrate was concentrated. Purification by preparative TLC (ethyl acetate) gave the title compound **7** (67 mg, 40% yield based on the keto aldehyde **6**): IR (neat) 3480, 1655, 1630 cm^{-1}; NMR (CCl_4) δ 1.60—2.40 (m, 11H), 2.99 (m, 2H), 4.42 (bs, 1H); MS *m/e* (%) 166 (M^+, 32), 148 (6), 138 (41), 123 (14), 120 (15), 110 (100). Found: *m/e* 166.0980. Calcd for $C_{10}H_{14}O_2$: M, 166.0992.

5-(2-Oxocyclohexylidene)pentanal **8**. Following the Corey's procedure,[21] 2-[1-hydroxy-5-(2-tetrahydropyranyloxy)pentyl]cyclohexanone was obtained in 54% yield based on cyclohexanone dimethyldrazone. This hydroxy ketone (5.8 g, 20 mmol) was mesylated at 0 °C and the crude mesylate was treated with sodium methoxide (28% solution in methanol, 42 mmol) in methanol at −78 °C. After 12 min at 0 °C, the mixture was diluted with brine and extracted with ethyl acetate. The product was purified by column chromatography on silica gel to give 2-[5-(2-tetrahydropyranyloxy)pentylidene]cyclohexanone (3.7 g) in 68% yield. The tetrahydropyranyl group was removed by treatment with pyridinium *p*-toluenesulfonate (1.5 g) in methanol (45 ml) at 25 °C for 4 h and the product was oxidized with $CrO_3 \cdot 2py$ in dichloromethane to give the title compound **8** in 34% yield: IR (neat) 1724, 1685, 1616 cm^{-1}; NMR (CCl_4) δ 1.59—2.49 (m, 14H), 6.39 (m, 1H), 9.70 (t, J=1.5 Hz, 1H); MS *m/e* (%) 180 (M^+, 21), 162 (13), 152 (12), 124 (70), 93 (63), 81 (54), 79 (63), 67 (100). Found: *m/e* 180.1162. Calcd for $C_{11}H_{16}O_2$: M, 180.1151.

Cyclization of 8 by Means of Me_2AlSPh. The keto aldehyde **8** (94 mg, 0.5 mmol) was treated with Me_2AlSPh (1.5 mmol) as described above to afford **9** (0.14 g, 94% yield): bp 152 °C (bath temp, 3 Torr); IR (neat) 3440, 1702 cm^{-1}; NMR (CCl_4) δ 1.47—2.09 (m, 12H), 2.28—2.47 (m, 2H), 2.93 (bs, 1H), 3.81 (m, 2H), 7.13—7.48 (m, 5H); MS *m/e* (%) 180 (14), 162 (8), 137 (17), 135 (14), 124 (32), 110 (100). Found: *m/e* 290.1329. Calcd for $C_{17}H_{22}O_2S$: M, 290.1339.

(E)-2-Ethylidene-3-methylcyclohexanone **11**: A solution of the acetate of the keto alcohol **10** (0.13 g, 0.7 mmol) in ether (1.0 ml) was added to a solution of lithium dimethylcuparte (0.9 mmol) in ether (3.0 ml) at −23 °C. After 17 min at −23 °C and 5 min at 0 °C, saturated NH_4Cl solution was added and the mixture was filtered. The filtrate was washed with water and brine, dried, and freed of the solvent. Purification by column chromatography on silica gel afforded **11** (57 mg) in 59% yield. The absence of *Z*-isomer was confirmed by the examination of its NMR spectrum.[22]

Ethyl (2-Ethylidene-3-oxocyclohexyl)acetate **12**: A mixture of **10** (0.13 g, 0.9 mmol) triethyl orthoacetate (1.7 ml, 9.2 mmol), and propionic acid (catalytic amount) was heated at 130 °C for 20 min. The mixture was diluted with ethyl acetate and washed with saturated aqueous solution of sodium hydrogencarbonate. The aqueous phase was extracted with ethyl acetate and the combined organic layer was washed with brine, dried, and freed of the solvent. The crude product was submitted to preparative TLC (hexane:ether=1:1, two developments) to give the title compound **12** (*E*-isomer, 89 mg; *Z*-isomer, 45 mg) in 70% yield. The stereochemical assignment was based on the examination of the NMR spectrum.[23]

E-Isomer: Bp 105 °C (bath temp, 0.5 Torr); IR (neat) 1740, 1695, 1620 cm^{-1}; NMR (CCl_4) δ 1.26 (t, J=7.0 Hz, 3H), 1.79 (d, J=7.5 Hz, 3H), 1.70—1.90 (m, 4H), 2.28 (m, 4H), 3.43 (m, 1H), 4.06 (q, J=7.0 Hz, 2H), 6.45 (qd, J=7.5 and 1.2 Hz, 1H); MS *m/e* (%) 211 (5), 210 (M^+, 10), 165 (17), 153 (11), 123 (100), 122 (79), 95 (56). Found: C, 68.50; H, 8.69%. Calcd for $C_{12}H_{18}O_3$: C, 68.55; H, 8.63%.

Z-Isomer: IR (neat) 1740, 1695, 1635 cm^{-1}; NMR (CCl_4) δ 1.24 (t, J=7.0 Hz, 3H), 1.80 (d, J=7.5 Hz, 3H), 1.70—1.94 (m, 4H), 2.30 (m, 4H), 2.69 (m, 1H), 4.05 (q, J=7.0 Hz, 2H), 5.65 (qd, J=7.5 and 1.4 Hz, 1H); MS *m/e* (%) 211 (3), 210 (M^+, 8), 165 (16), 153 (11), 123 (100), 122 (77), 95 (55). Found: C, 68.49; H, 8.68%. Calcd for $C_{12}H_{18}O_3$: C, 68.55; H, 8.63%.

The authors wish to thank the Ministry of Education, Science and Culture, Japan, for the Grant-in-Aid (403022).

References

1) Preliminary account of this work has appeared: A. Itoh, S. Ozawa, K. Oshima, and H. Nozaki, *Tetrahedron Lett.*, **21**, 361 (1980).

2) E. A. Jeffery, A. Meisters, and T. Mole, *J. Organomet. Chem.*, **74**, 373 (1974).

3) J. Tsuji, T. Yamada, M. Kaito, and T. Mandai, *Tetrahedron Lett.*, **1979**, 2257.

4) K. Maruoka, S. Hashimoto, Y. Kitagawa, H. Yamamoto, and H. Nozaki, *J. Am. Chem. Soc.*, **99**, 7705 (1977).

5) H. Nozaki, K. Oshima, K. Takai, and S. Ozawa, *Chem. Lett.*, **1979**, 379.

6) a) T. Mukaiyama, K. Inomata, and M. Muraki,

J. Am. Chem. Soc., **95**, 967 (1973); b) T. Shono, Y. Matsumura, S. Kashimura, and K. Hatanaka, *ibid.*, **101**, 4752 (1979); c) M. Watanabe, K. Shirai, and T. Kumamoto, *Bull. Chem. Soc. Jpn.*, **52**, 3318 (1979).

7) a) D. J. Ager and I. Fleming, *J. Chem. Soc., Chem. Commun.*, **1978**, 177; b) S. J. Branca and A. B. Smith, III, *J. Am. Chem. Soc.*, **100**, 7767 (1978); c) M. A. Guaciaro, P. M. Wovkulich, and A. B. Smith, III, *Tetrahedron Lett.*, **1978**, 4661.

8) N. Davidson and H. C. Brown, *J. Am. Chem. Soc.*, **64**, 316 (1942).

9) A. P. Kozikowski and A. Ames, *J. Org. Chem.*, **43**, 2735 (1978).

10) This product is a key compound for the synthesis of cyclopentenoid antibiotics (see Ref. 7b). The research described here was started to exploit an another versatile route to this compound.

11) T. Cohen and R. E. Gapinsky, *Tetrahedron Lett.*, **1978**, 4319.

12) J-E Dubois and M. Dubois, *Bull. Soc. Chim. Fr.*, **1969**, 3126.

13) D. A. Evans, E. Vogel, and J. V. Nelson, *J. Am. Chem. Soc.*, **101**, 6120 (1979).

14) a) P. A. Grieco and M. Miyashita, *J. Org. Chem.*, **40**, 1181 (1975); b) H. J. Reich, J. M. Renga, and I. L. Reich, *J. Am. Chem. Soc.*, **97**, 5434 (1975).

15) Diethylaluminum iodide was purchased from Aldrich Chemical Co.; E. C. Ashby and S. A. Noding, *J. Org. Chem.*, **44**, 4792 (1979).

16) F. Naef, R. Decorzant, and W. Thommen, *Helv. Chim. Acta*, **58**, 1808 (1975).

17) R. J. Anderson, C. A. Henrick, and J. B. Siddall, *J. Am. Chem. Soc.*, **92**, 735 (1970).

18) W. S. Johnson, L. Werthemann, W. R. Bartlett, T. J. Brocksom, T-t. Li, D. J. Faulkner, and M. R. Petersen, *J. Am. Chem. Soc.*, **92**, 741 (1970).

19) All the hydroxy compounds in Table 1 were transformed to trimethylsilyl ethers in order to obtain analytical samples.

20) Boiling point of the trimethylsilyl ether was recorded.

21) E. J. Corey and D. Enders, *Chem. Ber.*, **111**, 1337, 1362 (1978).

22) M. Bortoluss, R. Bloch, and J. M. Conia, *Bull. Soc. Chim. Fr.*, **1975**, 2722.

23) R. M. Silverstein, C. G. Bassler, and T. C. Morrill, "Spectrometric Identification of Organic Compounds," 3rd ed, John Wiley and Sons, New York, N. Y. (1974), pp. 168—169.

  Bull. Chem. Soc. Jpn., 54, 279—281 (1981)

Fluorination with Xenon Difluoride. 23. Fluorination of Ortho Substituted Aromatic Molecules

Boris Šket and Marko Zupan*

Department of Chemistry and "Jožef Stefan" Institute, Edvard Kardelj University of Ljubljana, Ljubljana, Yugoslavia

(Received March 14, 1980)

The fluorination of 9,10-dihydroanthracene and triptycene with xenon difluoride in the presence of hydrogen fluoride occurred at α and β position with β attack predominating over α attack, while the reaction with acenaphthene resulted in the formation of 2- and 4-fluorosubstituted products, regioselectivity being very little affected by the nature of the catalyst: hydrogen fluoride, boron trifluoride and pentafluorothiophenol. The fluorination of 1,2,3,4-tetrahydro-1,4-methanonaphthalene resulted in the formation of 6-fluoro-1,2,3,4-tetrahydro-1,4-methanonaphthalene, 6,7-difluoro-1,2,3,4-tetrahydro-1,4-methanonaphthalene and rearranged product 1-(2,2-difluoroethyl)indan.

It has been demonstrated that xenon difluoride is a mild fluorinating agent for the fluorination of alkenes, acetylenes, aromatic and heteroaromatic molecules, which has been recently reviewed.[1] It is known that the mechanism of the fluorination of organic molecules with xenon difluoride depends on the following factors: the structure of the molecules, the catalyst used, solvent polarity and temperature, and the formation of free radical intermediates, ion radical intermediates and fluorocarbonium ions has been suggested. It has been demonstrated that the following substrates are convenient catalyst: hydrogen fluoride, hydrogen fluoride–pyridine, trifluoroacetic acid, boron trifluoride etherate, boron trifluoride, pentafluorothiophenol, and bromine.

The electrophilic substitution reactions of ortho substituted aromatic molecules received considerable attention from different points of view.[2] There are three possible attacks of electrophilic agent which leads to α, β, or ipso substituted products. The regioselectivity of the substitution depends on the nature of the substituents on the ortho position. We have recently found[3] that the regioselectivity in fluorination of indan, tetralin, and *o*-xylene with XeF_2 has been explained by differences in the stabilization of carbonium ions A and B (Scheme 1) formed after α and β attack of electrophile. We now report results of further investigations on the effect of the structure of orthosubstituted aromatic molecules on regioselectivity in fluorination reactions with xenon difluoride.

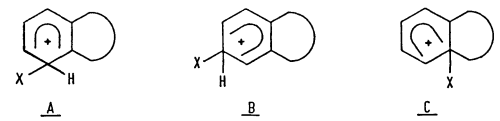

Scheme 1.

Results and Discussion

Under conditions usually used for the fluorination of organic molecules (1 mmol of organic substrate in 2—5 ml of dichloromethane, 1 mmol of xenon difluoride and hydrogen fluoride as catalyst), polymeric materials resulted in the case of 9,10-dihydroanthracene (**1**), triptycene (**4**), and acenaphthene (**7**). We have found that a much higher dilution (50 ml of solvent for 1 mmol of substrate) must be used. The reaction with 9,10-dihydroanthracene (**1**, Scheme **2**) was completed in 20 min and the reaction mixture was isolated by the usual work-up procedure. The crude reaction mixture shows in its ^{19}F NMR two signals: −126 ppm (dd, 39%) and −137.7 ppm (m, 61%). The products were separated by preparative TLC: 2-fluoro-9,10-dihydroanthracene (**2**), and 1-fluoro-9,10-dihydroanthracene (**3**) were isolated. The fluorination of triptycene (**4**) resulted also in the formation of two products: 2-fluorotriptycene (**5**) and 1-fluorotriptycene (**6**), separated by preparative TLC. It can be seen (Scheme 2) that the regioselectivity of the fluorine attack on triptycene is very similar to that in tetralin,[3] while in the case of 9,10-dihydroanthracene a lower regioselectivity was observed. In both cases, the yields of isolated products (**2**, **3**, **5**, and **6**) were considerably lower than those reported for the fluorination of indan or tetralin,[3] which can be ascribed to a significant amount of polymeric materials formed.

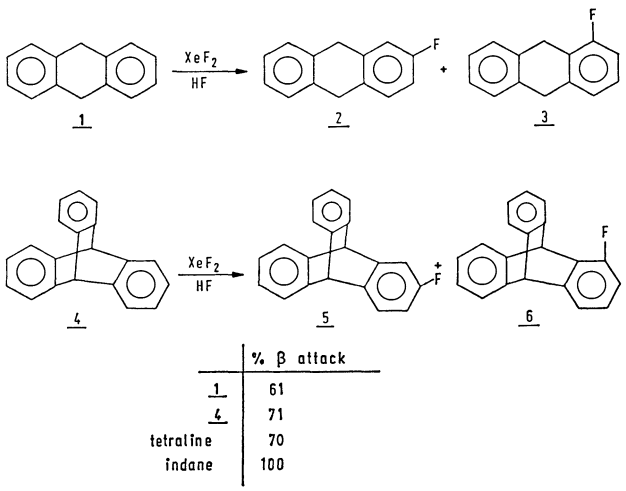

Scheme 2.

The fluorination of acenaphthene (**7**, Scheme 3) must be also carried out in a higher dilution than usual and this resulted in the formation of two products. The structures of the products 3-fluoroacenaphthene (**9**) and 5-fluoroacenaphthene (**8**) were established on the basis of the spectroscopic data, which are in agreement with those in the literature.[5] We have also studied the effect of catalyst (Scheme 3, relative yields) on the regioselec-

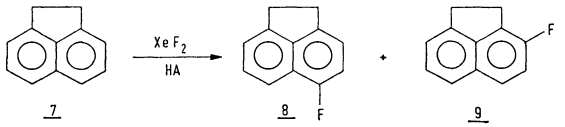

HA	% 8
HF	74
BF_3	74
C_6F_5SH	70

Scheme 3.

tivity of the substitution and found that it is very little influenced. However, it reflected on the yields of products formed. The reaction in the presence of hydrogen fluoride resulted in 50% formation of products **8** and **9**, while the reaction catalyzed by boron trifluoride resulted in only 20% formation of **8** and **9** and was accompanied by a higher amount of polymeric material. The reaction in 50 ml of dichloromethane and in the presence of pentafluorothiophenol was very slow, while the reaction in 10 ml of dichloromethane gave results comparable to those found by HF-catalyzed reaction in a higher dilution (50 ml of dichloromethane).

The fluorination of 1,2,3,4-tetrahydro-1,4-methanonaphthalene (**10**, Scheme 4) resulted in the formation of three products. ^{19}F NMR spectrum of the crude

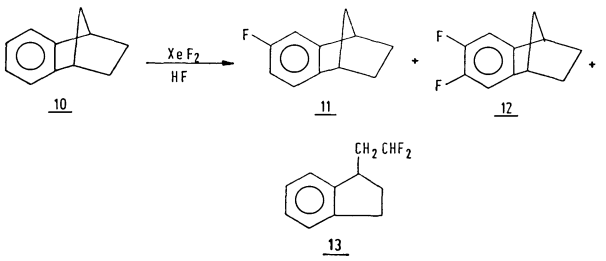

Scheme 4.

reaction mixture shows three signals: −116 ppm (dt, 26%), −118 ppm (m, 63%), and −142.5 ppm (t, 11%). The products were isolated by preparative GLC, and on the basis of spectroscopic data we have established that the lowest signal in ^{19}F NMR corresponds to 1-(2,2-difluoroethyl)indan (**13**); the next signal to 6-fluoro-1,2,3,4-tetrahydro-1,4-methanonaphthalene (**11**), and the last signal to 6,7-difluoro-1,2,3,4-tetrahydro-1,4-methanonaphthalene (**12**).

The mechanism of the fluorination with xenon difluoride is very similar to those already suggested.[3] However, on Scheme 5, three possible pathways which can explain the formation of rearranged 1-(2,2-difluoroethyl)indan (**13**) formed by the fluorination of **10**, are presented. The rearranged product could result from three different intermediates, formed after α, β, or ipso attack, followed by a two-step rearrangement.

Experimental

IR spectra were recorded by using a Perkin-Elmer 727 B spectrometer and ^1H and ^{19}F NMR spectra by JEOL-JNM-PS 100 from CCl_4 or $CDCl_3$ solutions with Me_4Si or CCl_3F as internal reference. Mass spectra and high resolution measurements were taken on a CEC 21-110 spectrometer. Gas liquid partition chromatography was carried out on Varian Aerograph Model 1800 and TLC on Merck PSC Fertigplatten Silica gel F 254 (activated for 3 h at 120 °C before use).

Materials. 9,10-Dihydroanthracene and acenaphthene are commercially available and were crystallized before use. Triptycene[6] and 1,2,3,4-tetrahydro-1,4-methanonaphthalene[7] were synthesized. Hydrogen fluoride and boron trifluoride of Fluka Purum quality were used without further purification. Dichloromethane was purified[8] and stored over molecular sieves. Xenon difluoride was prepared by a photosynthetic method[9] and its purity was higher than 99.5%.

1-Fluoro-9,10-dihydroanthracene (3) and 3-Fluoro-9,10-dihydroanthracene (2). To a solution of 1 mmol of **1** in dichloromethane (50 ml), 1 mmol of xenon difluoride was added at

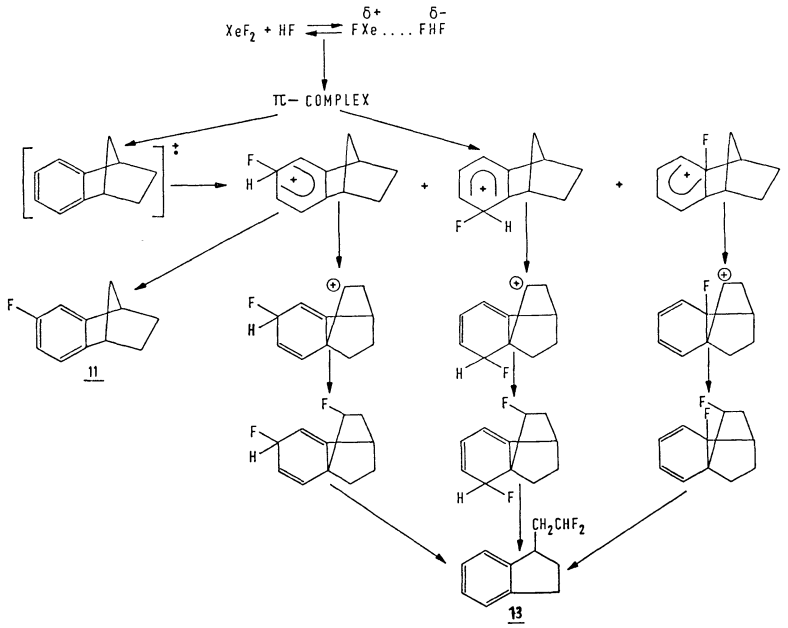

Scheme 5.

25 °C and, under stirring, a catalytic amount of HF was introduced into the reaction mixture. After a few seconds, the colorless solution turned dark blue and xenon gas slowly evolved. After 20 min the gas evolution ceased and the reaction appeared to be complete. The reaction mixture was washed with 10 ml of 5% $NaHCO_3$ aq solution and water, and dried over anhydrous sodium sulfate. The solvent was evaporated *in vacuo*. The crude reaction mixture was separated by preparative TLC (cyclohexane: chloroform=9: 1). 2-Fluoro-9,10-dihydroanthracene (**2**): 42 mg (21%), mp 112—114 °C, NMR spectra: δF=−137.7 ppm, δH=3.2 ppm (broad s, 4H), 7.0—8.1 ppm (m, 7H); mass spectrum: *m/e* 198 (M^+, 100%), 197 (23), 196 (18), 184 (24), 183 (17), 165 (28), 163 (17), 135 (33), 133 (28), 122 (89), 119 (22), 117 (22), 96 (10). Found: C, 84.64; H, 5.29%. Calcd for $C_{14}H_{11}F$: C, 84.82; H, 5.59%. 1-Fluoro-9,10-dihydroanthracene (**3**): 18 mg (9%), mp 76—78 °C, NMR spectra: δF=−126 ppm, δH=3.14 ppm (broad s, 4H), 7.1—8.3 ppm (m, 7H); mass spectrum: *m/e* 198 (M^+, 100%), 197 (23), 184 (21), 183 (24), 135 (35), 133 (22), 123 (25), 122 (64), 109 (72), 96 (25). Found: C, 84.62; H, 5.28%. Calcd for $C_{14}H_{11}F$: C, 84.82; H, 5.59%.

*1-Fluorotriptycene (**6**) and 2-Fluorotriptycene (**5**).* The fluorination and work-up procedure were essentially the same as described for **2** and **3**. The products were separated by preparative TLC (petroleum ether: $CHCl_3$=19: 1). 1-Fluorotriptycene (**6**): 34 mg (12%), mp 243—245 °C, (lit,[10] mp 246—247 °C), NMR spectra: δF=−120 ppm (m), δH=5.4 ppm (d, J=1.5 Hz, 1H), 5.75 ppm (broad s, 1H), 6.6—7.5 ppm (m, 11H); mass spectrum: *m/e* 272 (M^+, 100%), 271 (35), 196 (77), 195 (45), 180 (37), 179 (45), 135 (38), 123 (18), 122 (42), 120 (58), 102 (32), 77 (42), 76 (35). 2-Fluorotriptycene (**5**): 64 mg (23%), mp 228—230 °C (lit,[11] mp 232—234 °C), NMR spectra: δF=−122.25 ppm (m), δH=5.3 ppm (broad s, 2H), 6.6—7.6 ppm (m, 11H); mass spectrum: *m/e* 272 (M^+, 100%), 271 (42), 197 (25), 196 (87), 195 (43), 180 (16), 179 (33), 135 (29), 122 (21), 120 (79), 119 (26), 117 (26), 102 (39), 77 (17), 76 (46).

*3-Fluoroacenaphthene (**9**) and 5-Fluoroacenaphthene (**8**).* To a solution of 1 mmol of **7** in dichloromethane (50 ml in the case of HF, BF_3, and C_6F_5SH catalyzed reaction, and 10 ml in the second experiment catalyzed by C_6F_5SH), 1 mmol of xenon difluoride was added at 25 °C and, under stirring, a trace amount of catalyst (HF or BF_3, and 1 mmol in the case of C_6F_5SH) was introduced into the reaction mixture. After the work-up procedure, the crude reaction mixture was analyzed by ^{19}F NMR, and the relative yields of products **8** and **9** are presented in Scheme 3. We were unable to separate the two isomers, although many different stationary phases in GLC and various solvent systems in TLC were examined. Both isomers were purified by preparative GLC (FFAP-10%, Crom AW, T=120 °C) and the following percentages of the mixture of **8** and **9** were isolated: 50% in the case of HF-catalyzed reaction, 20% in the case of BF_3, and 45% in the case of C_6F_5SH. The reaction mixture shows in its ^{19}F NMR spectrum two signals: δF=126.75 ppm ($\delta F_{1\text{lt}}$=−123.58 ppm for 3-fluoroacenaphthene (**9**)[5] and −134.25 ppm ($F_{1\text{lt}}$=−131.44 ppm for 5-fluoroacenaphthene (**8**)[5]).

*Fluorination of 1,2,3,4-Tetrahydro-1,4-methanonaphthalene (**10**).* The fluorination and work-up procedure were essentially the same as described for **2** or **3**. Products were separated by preparative GLC (FFAP-10%, Crom AW, T=130 °C). 6-Fluoro-1,2,3,4-tetrahydro-1,4-methanonaphthalene (**11**): 52 mg (32%) of volatile liquid product, NMR spectra: δF=−118 ppm (m, J=10.5 Hz and 6 Hz), δH=1.2 ppm (m, 2H), 1.75 ppm (m, 4H), 3.3 ppm (broad s, 2H) and 6.8 ppm (m, 3H); mass spectrum, Calcd for $C_{11}H_{11}F$ *m/e* 162.0844, Found 162.0849, *m/e*: 162 (M^+, 47%), 150 (13), 147 (31), 146 (21), 135 (20), 134 (100), 133 (74), 121 (12), 119 (36), 117 (54), 116 (34), 115 (32), 84 (14), 63 (12), 57 (14). 6,7-Difluoro-1,2,3,4-tetrahydro-1,4-methanonaphthalene (**12**): 13 mg (7%) of volatile liquid product, NMR spectra: δF=−142.5 ppm (*t*, J=9 Hz), δH=1.2 ppm (m, 2H), 1.75 ppm (m, 4H), 3.3 ppm (broad s, 2H), 6.9 ppm (m, 2H); mass spectrum, Calcd for $C_{11}H_{10}F_2$ *m/e* 180.0767, Found: 180.0774, *m/e* 180 (M^+, 26%), 165 (16), 162 (42), 152 (75), 151 (30), 147 (18), 146 (14), 134 (63), 133 (32), 116 (100), 115 (44), 56 (30). 1-(2,2-Difluoroethyl)indan (**13**): 18 mg (10%) of volatile liquid product, NMR spectra: δF=−116.25 ppm (dt, J=60 Hz and 15 Hz), δH=1.8 (m, 2H), 2.31 ppm (tdd, J=15 Hz, 6 Hz and 6 Hz, 2H), 2.85 ppm (t, J=6 Hz, 2H), 3.27 ppm (m, 1H), 5.82 ppm (tt, J=60 Hz and 6 Hz, 1H), 7.05 ppm (m, 4H); mass spectrum: Calcd for $C_{11}H_{12}F_2$ *m/e* 182.0907, Found 182.0896, *m/e*: 182 (M^+, 16%), 117 (100), 116 (16), 115 (36), 91 (16), 51 (15).

We thank Prof. J. Slivnik for the xenon difluoride.

References

1) R. Filler, *Israel J. Chem.*, **17**, 71 (1978).
2) P. B. D. de la Mare, Electrophilic halogenation, Cambridge University Press, Cambridge, (1976); R. B. Moodie and K. Schofield, *Acc. Chem. Res.*, **9**, 287 (1976); G. A. Olah, *ibid.*, **4**, 240 (1971); P. B. D. de la Mare, *ibid.*, **7**, 361 (1974).
3) B. Šket and M. Zupan, *J. Org. Chem.*, **43**, 835 (1978).
4) J. Vaugham, G. J. Welch, and G. J. Wright, *Tetrahedron*, **21**, 1665 (1965).
5) M. J. S. Dewar and J. Michl, *Tetrahedron*, **26**, 375 (1970); R. Fields, "Fluorine-19 Nuclear Magnetic Resonance Spectroscopy," Annual Reports on NMR Spectroscopy, ed by E. F. Mooney, Academic Press, London, (1972), Vol. 5A, p. 167.
6) L. Friedman and F. M. Logullo, *J. Am. Chem. Soc.*, **85**, 1549 (1963).
7) G. Wittig and E. Knauss, *Chem. Ber.*, **91**, 895 (1958).
8) "Technique of Organic Chemistry," ed by A. Weissberger, Interscience, New York, (1955), Vol. 11.
9) S. M. Williamson, *Inorg. Synth.*, **11**, 147 (1968).
10) J. I. Cadogan, J. K. A. Hall, and J. T. Sharp, *J. Chem. Soc., C*, **1967**, 1860.
11) C. E. L. Petersen and A. Berg, *Acta Chem. Scand.*, **25**, 375 (1971).

Excess Thermodynamic Functions of the Systems Cyclohexane+Isomeric Xylenes

Eyunni RAJAGOPAL and Saraswatula Venkata SUBRAHMANYAM*

Department of Physics, SVU Autonomous Post-Graduate Centre, Anantapur 515 003, India

(Received January 7, 1980)

The excess volumes V^E, excess heat capacities C_P^E and excess isothermal compressibilities β_T^E of cyclohexane+isomeric xylenes have been determined at 25, 40, and 50 °C. The results are discussed in the light of Flory's theory.

Studies on the excess thermodynamic functions of binary liquid mixtures throw considerable light in understanding the nature of molecular interactions. In these laboratories we have taken up a systematic study of the thermodynamic behaviour of a large number of binary mixtures containing reasonably simple molecules and test of the applicability of Flory's theory.[1,2] The present paper deals with the studies on the thermodynamic behaviour of the binary mixtures of *o*-xylene, *m*-xylene, and *p*-xylene with cyclohexane which form an interesting series of systems involving similar molecular structures which interact very weakly. The excess volumes V^E, excess heat capacities C_P^E, and the excess isothermal compressibilities β_T^E of the above binary systems have been studied and the results are analysed on the basis of Flory's theory.[3]

Experimental

Analytical reagent grade cyclohexane, *o*-xylene, *m*-xylene, and *p*-xylene were purified according to the standard procedures.[4] The densities of the purified samples determined at 25 °C using bicapillary type pycnometer with an accuracy of 2 in 10^5 are 0.77383, 0.87593, 0.85987, and 0.85673 g cm^{-3} respectively for cyclohexane, *o*-xylene, *m*-xylene, and *p*-xylene. These values are in good agreement with those reported in the literature.[5,6]

The excess volumes were measured directly using a mixing cell with an accuracy of ± 0.002 cm^3 mol^{-1}. The molar heat capacities at constant pressure were measured using an adiabatic calorimeter with an accuracy of $\pm 0.3\%$. Ultrasonic velocity in pure liquids and in binary mixtures was determined using a single crystal variable path interferometer working at 3MHz with an accuracy of $\pm 0.01\%$. The details of the above experimental techniques were discussed in our earlier communications.[1,2] The coefficient of thermal expansion (α) of pure liquids and their mixtures were determined from the experimentally determined density data at an interval of 5 °C in the range 20 to 60 °C.

Results

The experimental results of pure liquids are given in Table 1, along with literature values for comparison. The agreement between the two sets of values is quite good. The experimentally determined excess volume data (as many as a 15 sets of V^E values are obtained at each temperature covering the entire concentration range) of the binary mixtures of *o*-xylene,

Table 1. Pure liquid parameters

Temp / °C	u/ms^{-1}	$10^3\alpha$/K^{-1}	V / cm^3 mol^{-1}	C_P / J K^{-1} mol^{-1}	$\beta_T \times 10^6$ / bar^{-1}	v^* / cm^3 mol^{-1}	T^* / K	p^* / J cm^{-3}
			Cyclohexane					
25	1249.5	1.215	108.762	159.6	112.8	84.30	4723.9	534.88
	(1252.7)[c]			(156.5)[c]				
40	1177.5	1.264	110.796	163.6	129.0	84.47	4754.6	527.67
50	1129.2	1.294	112.185	166.0	141.1	84.66	4783.8	520.09
			o-Xylene					
25	1349.8	0.961	121.200	181.3	81.1	97.77	5348.4	543.12
	(1348.7)[b]	(0.963)[a]		(180.7)[d]				
40	1290.4	0.975	122.981	186.2	89.2	98.18	5423.3	536.95
50	1250.8	0.985	124.191	189.5	95.3	98.46	5472.6	531.30
			m-Xylene					
25	1321.1	1.009	123.470	178.3	87.7	98.81	5204.4	536.03
	(1323.1)[b]	(1.004)[a]		(176.2)[d]				
40	1258.3	1.025	125.403	182.7	97.2	99.26	5278.7	527.10
50	1216.7	1.036	126.693	185.6	104.3	99.58	5329.7	519.64
			p-Xylene					
25	1309.7	1.015	123.930	181.3	89.1	99.08	5188.5	531.59
	(1309.8)[b]	(1.017)[a]		(181.3)[d]				
40	1248.3	1.037	125.851	185.9	98.9	99.43	5247.1	526.18
50	1207.4	1.045	127.167	189.0	105.9	99.80	5305.4	517.74

a) Ref. 6. b) Extropolated value of Ref. 11. c) Ref. 12. d) Ref. 13.

Table 2. Parameters of Eq. 1 and standard deviation of excess volumes

Temp °C	a_0	a_1	a_2	σ / cm mol^{-1}
		Cyclohexane+*o*-Xylene		
25	2.0555	−0.5161	−0.0359	0.003
40	2.1928	−0.8033	0.2606	0.004
50	2.2831	−0.8085	0.4509	0.003
		Cyclohexane+*m*-Xylene		
25	2.5566	−0.5251	0.4050	0.003
40	2.7426	−0.5216	0.0951	0.002
50	2.8206	−0.5563	0.1571	0.003
		Cyclohexane+*p*-Xylene		
25	2.2809	−0.6584	0.5129	0.002
40	2.3667	−0.7375	0.4499	0.004
50	2.4536	−0.7146	0.4356	0.001

m-xylene, and *p*-xylene with cyclohexane were fitted to the equation of the form

$$V^E/x_1x_2 = [a_0+a_1(x_2-x_1)+a_2(x_2-x_1)^2], \quad (1)$$

where x_1 and x_2 are the mole fractions of cyclohexane and xylenes respectively. Values of the coefficients determined using the method of least squares are listed in Table 2. The last column of the table contains values of σ, the standard deviation of the fit in each case. The excess volumes of these systems were studied previously by Reddy *et al.*[8] and Jain *et al.*[7] The accuracy of the experimental excess volumes reported by Reddy *et al.*[8] is ± 0.05 cm^3 mol^{-1}. Further they have studied the *p*-xylene system at 32.5 °C, *m*-xylene system at 34 °C, and *o*-xylene system at 35 °C. In view of this, a direct comparison with the values of the present investigation has not been attempted. The excess volumes of Jain *et al.*[7] are slightly higher than the present ones. However no importance has been given to this discrepancy since Jain *et al.*[7] have not stated the errors involved in their measurements. The results of measurement of u, C_p, α, and β_T of binary mixtures of cyclohexane with isomeric xylenes are presented in Table 3.

Discussion

The experimental excess functions are examined in this section for the binary mixtures in the light of Flory's theory. The excess functions V^E, H^E, and β_T^E are related to the properties of pure components *via* the relations

$$H^E = x_1v_1{}^*p_1{}^*\left(\frac{1}{\tilde{v}_1}-\frac{1}{\tilde{v}}\right) + x_2v_2{}^*p_2{}^*\left(\frac{1}{\tilde{v}_2}-\frac{1}{\tilde{v}}\right) + x_1v_1{}^*\theta_2X_{12}/\tilde{v} \quad (2)$$

$$\beta_T^E = \frac{3\tilde{v}^2(\tilde{v}^{1/3}-1)}{p^*[1-3(\tilde{v}^{1/3}-1)]} - \frac{1}{\tilde{v}}[\phi_1\tilde{v}_1\beta_{T_1}+\phi_2\tilde{v}_2\beta_{T_2}] \quad (3)$$

$$p^* = \phi_1p_1{}^* + \phi_2p_2{}^* - \phi_1\theta_2X_{12} = \frac{T\tilde{v}^{4/3}}{(\tilde{v}^{1/3}-1)}\left[\frac{\phi_1p_1{}^*}{T_1{}^*}+\frac{\phi_2p_2{}^*}{T_2{}^*}\right], \quad (4)$$

where

$$\tilde{v} = \phi_1\tilde{v}_1 + \phi_2\tilde{v}_2 + V^E/(x_1v_1{}^*+x_2v_2{}^*), \quad (5)$$

where v_1 and v_2 are the reduced volumes, $v_1{}^*$ and $v_2{}^*$ are the characteristic volumes, $p_1{}^*$ and $p_2{}^*$ are the characteristic pressures, and β_{T1} and β_{T2} are the isothermal compressibilities of the pure components. $\tilde{v}$, p^*, and θ_2 X_{12} are the reduced volume, characteristic pressure and the interaction energy parameter respectively of the mixture.

The interaction energy parameter of the mixture X_{12} which is a measure of the difference of interaction energy between the unlike pairs and the mean of like pairs, can be evaluated using any experimental excess function. This value of X_{12} can be used to evaluate theoretically the other excess functions. The interaction energy term involves implicitly in the expression for V^E and explicitly in that for H^E. Hence it may appear logical to evaluate X_{12} using H^E rather than V^E data. However in view of the higher accuracy of the experimental V^E data and its availability over comparatively wide temperature and concentration range X_{12} has been evaluated *via* V^E in the present work.

According to Flory's theory at any given temperature X_{12} should be a constant independent of the composition of the mixture. An examination of the data presented in Table 4 indicates that X_{12} is reasonably constant at

Table 3. Properties of binary solutions

x_2	u/ms^{-1}			$10^3\alpha$/K^{-1}			C_p/J mol^{-1}			$10^6\beta_T$/bar^{-1}		
	25 °C	40 °C	50 °C	25 °C	40 °C	50 °C	25 °C	40 °C	50 °C	25 °C	40 °C	50 °C
						Cyclohexane+*o*-Xylene						
0.2502	1265.5	1197.3	1151.8	1.163	1.098	1.038	164.1	168.2	171.5	105.9	118.8	129.5
0.4978	1284.8	1219.1	1175.2	1.185	1.117	1.054	169.3	174.1	177.2	98.8	109.3	118.0
0.7497	1296.4	1240.5	1194.6	1.198	1.129	1.066	175.3	180.0	183.3	91.5	100.7	106.9
						Cyclohexane+*m*-Xylene						
0.2480	1258.9	1189.2	1142.7	1.167	1.128	1.064	163.0	167.5	170.1	107.7	121.2	132.0
0.4989	1274.4	1207.5	1162.7	1.190	1.148	1.082	167.2	172.1	174.9	102.0	114.1	123.4
0.7505	1295.4	1231.0	1187.2	1.213	1.162	1.103	172.8	177.2	180.3	94.7	105.4	116.1
						Cyclohexane+*p*-Xylene						
0.2585	1256.2	1188.6	1143.8	1.168	1.117	1.064	164.2	168.3	171.5	107.9	121.1	131.1
0.4973	1268.7	1201.5	1156.4	1.188	1.140	1.082	169.2	175.9	176.8	102.1	114.4	123.7
0.7463	1273.5	1212.4	1165.4	1.203	1.154	1.099	175.1	179.6	182.9	97.1	107.8	117.1

TABLE 4. COMPARISON OF β_T^E WITH FLORY'S THEORY

T °C	x_2	X_{12} J cm^{-3}	X_{12} mean	$\beta_T^E \times 10^6$/bar^{-1} Exptl	Calcd	C_P^E J K^{-1} mol^{-1}
		Cyclohexane+*o*-Xylene				
25	0.2502	36.59		5.3	3.9	1.1
	0.4978	36.28	35.57	5.4	4.2	1.1
	0.7497	33.85		2.4	2.3	1.4
40	0.2502	38.54		5.8	4.7	1.0
	0.4978	36.30	36.65	5.8	4.6	0.7
	0.7497	35.11		2.6	2.5	0.5
50	0.2502	39.62		6.3	4.2	0.3
	0.4978	36.88	37.69	6.2	4.9	0.5
	0.7497	36.57		1.3	2.7	0.3
		Cyclohexane+*m*-Xylene				
25	0.2480	41.03		1.5	4.5	−1.2
	0.4989	38.78	40.19	3.1	5.9	−1.7
	0.7505	40.75		1.6	3.8	−0.8
40	0.2480	38.09		1.0	4.7	−0.8
	0.4989	38.22	38.13	3.7	7.7	−1.0
	0.7505	38.07		1.3	4.0	−0.7
50	0.2480	38.82		1.7	6.7	−0.7
	0.4989	38.31	38.45	2.5	7.3	−0.8
	0.7505	38.23		2.0	3.6	−0.4
		Cyclohexane+*p*-Xylene				
25	0.2585	36.77		2.0	3.3	−1.0
	0.4973	34.53	35.19	2.3	3.4	−1.2
	0.7463	34.28		2.8	3.4	−0.8
40	0.2585	36.58		3.2	5.8	−1.0
	0.4973	33.04	34.02	1.6	5.8	−0.6
	0.7463	32.45		2.3	3.5	−0.6
50	0.2585	35.62		0.5	6.0	−0.4
	0.4973	33.01	34.13	1.9	6.2	−0.7
	0.7463	33.75		3.4	3.9	−0.3

any particular temperature. Hence the mean value of X_{12} is used to evaluate the excess functions at any given temperature.

The theoretically evaluated excess isothermal compressibilities β_T^E using Eq. 3 are compared with the experimental β_T^E in Table 4. The agreement between the two sets of data is not satisfactory. This disagreement may be attributed to the slight polarity of xylenes. Similar disagreement was also noticed between theoretical and experimental excess parameters of benzene+isomeric xylenes[9] and toluene+isomeric xylenes.[10]

In view of non availability of experimental H^E data for the systems under study at all temperatures and concentrations an attempt is made however to compare the data at 25 °C for equimolar concentrations as can be seen from Table 5. The agreement is not quite good reflecting the inadequacy of Flory's theory in predicting excess functions for these systems under study.

TABLE 5. COMPARISON OF EXPERIMENTAL AND THEORETICAL EXCESS HEATS FOR EQUIMOLAR SOLUTIONS AT 25 °C

System	H^E Calcd	Exptl
Cyclohexane+*o*-Xylene	814	523[a]
Cyclohexane+*m*-Xylene	912	576[b]
Cyclohexane+*p*-Xylene	809	487[a]

a) Evaluated from X_{12} values of Ref. 7. b) Data of Ref. 14.

TABLE 6. COMPARISON OF EXPERIMENTAL AND THEORETICAL EXCESS HEAT CAPACITIES FOR EQUIMOLAR MIXTURES ($x_2 \simeq 0.5$) AT 37.5 °C

System	C_P^E/J K^{-1} mol^{-1} Exptl	Calcd
Cyclohexane+*o*-Xylene	0.7±0.5	1.7±0.8
Cyclohexane+*m*-Xylene	−1.0±0.5	−1.7±0.8
Cyclohexane+*p*-Xylene	−1.3±0.8	−0.9±0.5

Flory's theory is also useful in predicting the excess heat capacities. The excess heat capacities are related to excess enthalpies *via* the relation

$$C_P^E = \left(\frac{\partial H^E}{\partial T}\right)_p \qquad (6)$$

using Eq. 2 excess enthalpies have been evaluated at 25, 40, and 50 °C. $(\partial H^E/\partial T)_P$ has been evaluated using H^E data at 25 and 50 °C which gives the value of C_P^E at 37.5 °C. The value of C_P^E so evaluated at 37.5 °C for the equimolar solutions are compared in Table 6, with C_P^E values obtained by intrapolating the experimental C_P^E data which are given in Table 4. The agreement between experimental and theoretical C_P^E values is quite good.

References

1) S. V. Subrahmanyam and E. Rajagopal, *Z. Phys. Chem.*, **85**, 256 (1973).
2) E. Rajagopal and S. V. Subrahmanyam, *J. Chem. Therm.*, **6**, 873 (1974).
3) a) P. J. Flory, *J. Am. Chem. Soc.*, **87**, 1833 (1965); b) A. Abe and P. J. Flory, *ibid.*, **87**, 1838 (1965).
4) A. Weissberger, "Physical Methods of Organic Chemistry," 2nd ed, Interscience, New York (1955), Vol. VII.
5) E. L. Washington and R. Battino, *J. Phy. Chem.*, **72**, 4496 (1968).
6) a) J. Timmermans, "The Physico-chemical Constants of Pure Organic Compounds," Elsevier, New York (1950); b) J. Singh, H. D. Pflug, and G. C. Benson, *J. Phys. Chem.*, **72**, 1939 (1968).
7) D. V. S. Jain, O. P. Yadav, and V. Arora, *Indian J. Chem.*, **10**, 425 (1972).
8) K. C. Reddy, S. V. Subrahmanyam, and J. Bhimasenachar, *J. Phys. Soc. Jpn.*, **19**, 559 (1964).
9) J. Singh, H. D. Pflug, and G. C. Benson, *J. Phys. Chem.*, **71**, 1227 (1967).
10) S. Murakami, V. T. Lam, and G. C. Benson, *J. Chem. Therm.*, **1**, 397 (1969).
11) "Encyclopedia of Physics Vol. XIII, Acoustics I-Dispersion and Absorption of Sound Waves in Liquids," ed by S. Flugge.
12) E. A. Moelwyn-Hughes and P. L. Thorpe. *Proc. R. Soc. London, Ser. A*, **278**, 574 (1964).
13) J. Williams and F. Danials, *J. Am. Chem. Soc.*, **46**, 903 (1924).
14) G. W. Lundberg, *J. Chem. Eng. Data*, **9**, 193 (1964).

Modified Method for the Determination of Stoichiometry and Formation Constant of Molecular Complexes by Differential Refractometry

Ram SAHAI* and Vinod SINGH
Department of Chemistry, V.S.S.D. College, Kanpur University, Kanpur-208002, India
(Received March 17, 1980)

A modified method has been proposed for the determination of stoichiometry and formation constant of molecular complexes by Job method using differential refractometry. A more adequate model has been presented and has been verified on some strong, moderate, and weak systems in different solvents at 35 °C. The formation constants obtained by this method are in good agreement with the literature values.

Recently we have applied the differential refractometric method[1,2] in Yoshida and Ōsawa's equation[3,4] to determine the stoichiometry and formation constant of molecular complexes which has yielded better results. In Yoshida and Ōsawa's method[5] two experimental sets are essential to calculate the equilibrium constant of a molecular complex. In this communication an attempt has been made to calculate the equilibrium constant of these complexes by using only one experimental set. For this purpose differential refractometry has been applied in Job method and a model has been developed which has been verified on strong as well as on weak molecular complexes.

We realize that in molecular complexes from acceptor, A, and donor, D, when $1:n$ complex is formed, it usually is accompanied by the formation of 1:1, 1:2,---, $1:n-1$ complexes. At this we have,

$$A + nD \overset{K_n}{\rightleftharpoons} AD_n \quad (n>1) \tag{1}$$

and

$$K_n = C_{AD_n}/C_A C_D n = C_{AD_n}/(C_A^\circ - C_{AD_n})(C_D^\circ - nC_{AD_n})^n. \tag{2}$$

Let us assume, V_A and V_D are the volumes of A and D respectively, and $V=V_A+V_D$. Then the total concentration C_T is given by

$$C_T = 1/V(V_A C_A^1 + V_D C_D^1) = 1/V[(V-V_D)C_A^1 + V_D C_D^1], \tag{3}$$

where C_A^1 and C_D^1 represent the concentration of the stock solution of A and D, respectively. From Eq. 2 we have

$$\begin{aligned} C_{AD_n} &= K_n(C_A^\circ - C_{AD_n})(C_D^\circ - nC_{AD_n})^n \\ &= K_n[(1-V_D/V)(C_A^1 - C_{AD_n})] \times [V_D/VC_D^1 - nC_{AD_n}]^2. \end{aligned} \tag{4}$$

Let $V_D/V=v$ and $C_D^1/C_A^1=r$. Then

$$C_{AD_n} = K_n[(1-v)(C_A^1 - C_{AD_n})](vC_A^1 r - nC_{AD_n})^n. \tag{5}$$

To find the maximum value of C_{AD_n} by varying v, we calculate

$$\frac{1}{C_{AD}} \cdot \frac{\partial C_{AD_n}}{\partial v} = \frac{-C_A^1 - \partial C_{AD_n}/\partial v}{(1-v)C_A^1 - C_{AD_n}} + n\frac{rC_A^1 - n\partial C_{AD_n}/\partial v}{vrC_A^1 - nC_{AD_n}}. \tag{6}$$

Setting $\partial C_{AD_n}/\partial v=0$, we obtain

$$C_{AD_n}^{n(r-1)} = rC_A^1[v-n(1-v)]. \tag{7}$$

We chose $r=1$, then

$$v = n/(1+n);\ C_T = C_D^1 = C_A^1. \tag{8}$$

In refractometric measurements, we assumed that the refraction per cm³ of solution is due to the complexed and free acceptor refractions which may be expressed as,

$$\phi = \left(\frac{C_A^\circ - C_{AD_n}}{C_A^\circ}\right)\phi_{CD} + \frac{C_{AD_n}}{C_A^\circ}\phi_{AD}. \tag{9}$$

where $\phi_{CD}=\phi-\phi_D$, and solving Eq. 9 we get,

$$C_{AD_n}/C_A^\circ = \phi_D/(\phi_{AD}-\phi_{CD}). \tag{10}$$

Now assuming $\phi_{AD}-\phi_{CD}=\Delta\phi_{AD}$; the maximum refraction per cm³ of complex which may be calculated from the plot of $\Delta\Omega C_{DA}$ *versus* molar ratio of solutes.† Thus Eq. 10 becomes,

$$C_{AD_n} = \phi_D/\Delta\phi_{AD}C_A^\circ. \tag{11}$$

Therefore, if C_{AD_n} is a maximum, then $\phi_D/\Delta\phi_{AD}C_A^\circ$ would also be maximum at $v=n/(1+n)$. Thus by plotting $\phi_D C_A^\circ$ (or $\phi_D/\Delta\phi_{AD}C_A^\circ$) against X_D (mole fraction of donor), the maximum will occur at $X_D=n/(1+n)$ (Fig. 1). At this point we have,

TABLE 1. EQUILIBRIUM CONSTANT (K_1) DATA FOR SOME STRONG, MODERATE AND WEAK MOLECULAR COMPLEXES AT 35 °C

Complex	Solvent	K_1/dm³ mol⁻¹		
		From Eq. 12	Spectrophotometric method	
			K_1	T/°C
Ethanol–naphthalene	Cyclohexane	2.7±0.2		
Phenol–naphthalene	Cyclohexane	4.0±0.2		
Ph_3N–I_2	Cyclohexane	9.2±1.0	12.5 (9)[a]	26
Tryptophan–chloranil	50% aq ethanol	149.0±10.0	176.0 (10)[a]	25
Dimethyl sulfide–I_2	Heptane	178.0±10.0	200.0 (9)[a]	25
Pyridine–I_2	Heptane	257.0±15.0	290.0 (9)[a]	25
Ph_3As–I_2	CCl_4	714.0±25.0	790.0 (11)[a]	30

a) Number in parentheses indicates the reference number.

† The values of ϕ, ϕ_D, ϕ_A, and $\Delta\Omega C_{DA}$ have been calculated as reported earlier.[6-8]

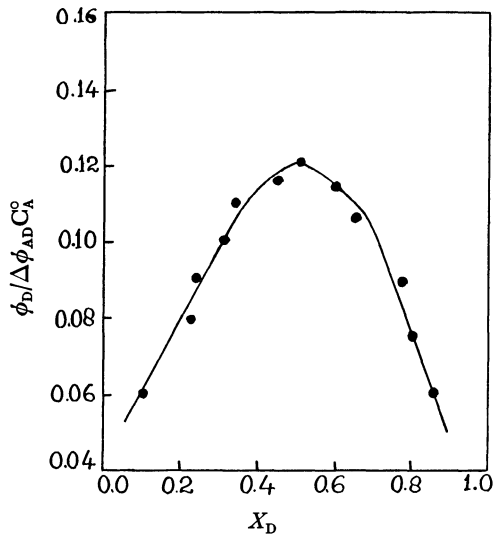

Fig. 1. A plot of X_D *versus* $\phi_D/\Delta\phi_{AD}C_A^\circ$ indicating 1 : 1 stoichiometry of phenol–naphthalene complex.

$$K_n = (\phi_D/\Delta\phi_{AD})/(C_D^\circ)^n(1-\phi/\Delta\phi_{AD})^{n+1} \quad (12)$$

where $C_D^\circ = X_D C_T = n/(1+nC_T)$. Equation 12 has been used to calculate equilibrium constant (K_n) after determining n. Thus the K values calculated for some strong and weak 1 : 1 complexes are listed in Table 1. From this Table it is evident that the K values calculated from Eq. 12 are in good agreement with the spectrophotometric values. The present method involves an experimental simplicity because for one system only one experimental set is sufficient to calculate K but in Yoshida and Ōsawa's and differential refractometric methods, two experimental sets are necessary to get K values.

One of us (VS) is thankful to Kanpur University, Kanpur for providing U. G. C. fellowship. Authors are also thankful to Prof. P. C. Nigam (I. I. T., Kanpur) for providing some experimental facilities.

References

1) R. Sahai and V. Singh, *Indian J. Chem.*, in press.
2) R. Sahai and V. Singh, *J. Solution Chem.*, in press.
3) R. Sahai and V. Singh, *Bull. Chem. Soc. Jpn.*, **53**, 1785 (1980).
4) R. Sahai, V. Singh, and Rekha Verma, *Bull. Chem. Soc. Jpn.*, **53**, 2995 (1980).
5) Z. Yoshida and E. Ōsawa, *Bull. Chem. Soc. Jpn.*, **38**, 140 (1965).
6) R. Sahai, P. C. Pande, and V. Singh, *Indian J. Chem.*, **18A**, 217 (1979).
7) R. Sahai and V. Singh, *Indian J. Pure Appl. Phys.*, **18**, 504 (1980).
8) A. K. Colter and E. Grunwald, *J. Phys. Chem.*, **74**, 3637 (1970).
9) C. N. R. Rao and A. S. N. Murthy, "Spectroscopy in Inorganic Chemistry," Academic Press, New York (1970), Vol. I, p. 107.
10) J. B. Birks and M. A. Slifkin, *Nature*, **197**, 42 (1963).
11) P. C. Pande, Ph. D. Thesis, Kanpur University, Kanpur (1978).

Determination of the Difference in Hard-sphere Volume of Conformational Isomers from Sound Velocity

Masakatsu Aoi and Kiyoshi Arakawa*

Research Institute of Applied Electricity, Hokkaido University, Sapporo 060

(Received April 11, 1980)

Synopsis. The difference in hard-sphere volume of conformational isomers $\Delta V/V$ was determined from sound velocity data by a method proposed on the basis of the Lebowitz theory of solutions. The $\Delta V/V$ values between conformers were found to be 6, 9, 12, 7, and 12% for 1,1,2,2-tetrachloroethane, 1,1,2,2-tetrabromoethane, 1-chloropropane, 1-bromopropane, and ethylcyclohexane, respectively.

We proposed an ultrasonic method suitable for the determination of the difference in hard-sphere volume of conformational isomers ($\Delta V/V$) from sound velocity data,[1] based on the Lebowitz theory,[2] and applied the method to halogenoethanes and cyclohexane derivatives[1b] as typical compounds with conformational isomerism.[3-6]

In order to obtain further information on $\Delta V/V$ of conformational isomers, 1,1,2,2-tetrachloroethane ($CHCl_2CHCl_2$), 1,1,2,2-tetrabromoethane ($CHBr_2CHBr_2$), 1-chloropropane ($CH_3CH_2CH_2Cl$), 1-bromopropane ($CH_3CH_2CH_2Br$), and ethylcyclohexane (*c*-$C_6H_{11}C_2H_5$) have been investigated.

An equilibrium mixture of conformational isomers we studied is considered to be a binary mixture of hard spheres. The formula for isothermal compressibility (κ_T) of the equilibrium mixture was derived from the equation of state for the binary mixture of hard spheres.[2] Details of the procedure for analysis were described in the preceding paper,[1b] notations used here being identical with those in it.

For the case of *c*-$C_6H_{11}C_2H_5$, the relaxation frequency f_r is smaller than the frequency f used for the measurement of sound velocity.[7] In this case, κ_T is expressed by

$$\kappa_T = \left[\frac{RT(1+2\xi)^2}{V(1-\xi)^4} - \frac{2}{V}(\Delta H_v - RT)\right]^{-1}. \quad (1)$$

For CHX_2CHX_2 and $CH_3CH_2CH_2X$[5,8,9] ($f_r \gg f$), κ_T is given by

$$\kappa_T = \left[\frac{RT(1+2\xi)^2}{V(1-\xi)^4} - \frac{2}{V}(\Delta H_v - RT)\right]^{-1} + \frac{V(\Delta V/V)^2}{2RT\{1+\cosh(\Delta G/RT)\}}. \quad (2)$$

$\Delta V/V$ is expressed by

$$\frac{\Delta V}{V} = \frac{N_A}{\xi V}(v_2 - v_1) = \frac{v_2 - v_1}{v_a}, \quad (3)$$

where ξ is packing fraction ($=\rho v_a$), v_a average hard-sphere volume, and v_i hard-sphere volume of the i-th component. Putting the experimental values of κ_T into Eq. 1 or Eq. 2, we determine the magnitudes of v_a, v_1, and $\Delta V/V$. The temperature coefficient α_t of the effective hard-sphere volume was calculated in a similar manner to that reported.[1b]

Table 1. Results for d, v, κ_S, and κ_T

		Temp/°C						
		15	20	25	30	35	40	45
d / 10^3 kg m^{-3}	$CHCl_2CHCl_2$	1.6049_0	1.5969_0	1.5891_4	1.5813_3	1.5734_1	1.5658_5	1.5579_8
	$CHBr_2CHBr_2$	2.9761_8	2.9649_8	2.9537_7	2.9424_5	2.9311_5	2.9199_6	2.9087_0
	$CH_3CH_2CH_2Cl$	0.8984_5	0.8921_8	0.8858_3	0.8795_4	0.8729_8	0.8668_3	0.8601_6
	$CH_3CH_2CH_2Br$	1.3618_9	1.3534_7	1.3450_8	1.3367_6	1.3281_8	1.3196_6	1.3110_6
	c-$C_6H_{11}C_2H_5$	0.7913_8	0.7873_6	0.7832_9	0.7793_0	0.7752_0	0.7711_3	0.7670_6
v / m s^{-1}	$CHCl_2CHCl_2$	1182.5	1166.1	1149.9	1134.1	1118.1	1102.3	1086.5
	$CHBr_2CHBr_2$	1051.3	1039.5	1029.1	1018.4	1007.6	997.2	986.7
	$CH_3CH_2CH_2Cl$	1109.8	1087.3	1066.6	1043.8	1024.1	1002.0	980.5
	$CH_3CH_2CH_2Br$	988.3	970.8	954.3	937.3	920.2	904.1	887.7
	c-$C_6H_{11}C_2H_5$	1312.0	1290.4	1269.1	1248.2	1227.3	1206.3	1185.6
κ_S / 10^{-11} Pa^{-1}	$CHCl_2CHCl_2$	44.56	46.05	47.59	49.17	50.84	52.56	54.37
	$CHBr_2CHBr_2$	30.40	31.21	31.97	32.77	33.60	34.44	35.31
	$CH_3CH_2CH_2Cl$	90.37	94.81	99.23	104.35	109.22	114.90	120.93
	$CH_3CH_2CH_2Br$	75.18	78.40	81.64	85.15	88.92	92.71	96.79
	c-$C_6H_{11}C_2H_5$	73.41	76.27	79.27	82.36	85.64	89.12	92.75
κ_T / 10^{-11} Pa^{-1}	$CHCl_2CHCl_2$	60.25	62.01	63.80	65.63	67.55	69.52	71.56
	$CHBr_2CHBr_2$	42.48	43.42	44.30	45.22	46.18	47.13	48.13
	$CH_3CH_2CH_2Cl$	131.25	136.27	141.28	147.00	152.47	158.74	165.38
	$CH_3CH_2CH_2Br$	105.60	109.23	112.89	116.82	121.01	125.22	129.74
	c-$C_6H_{11}C_2H_5$	94.78	97.88	101.10	104.43	107.93	111.62	115.46

TABLE 2. $\Delta V/V$ AND v_a AND THERMODYNAMIC PARAMETERS AT 25 °C

	$-\Delta V/V$	v_a / 10^{-30} m^3	α [a] / 10^{-3} K^{-1}	C_p / J K^{-1} mol^{-1}	ΔH_v / kJ mol^{-1}	ΔH / kJ mol^{-1}
$CHCl_2CHCl_2$	0.06	95.7_5	0.9874	189.4[b,c]	45.78[d]	−4.60[e]
$CHBr_2CHBr_2$	0.09	114.9_6	0.7649	165.6[b]	70.00[b]	−3.45[e]
$CH_3CH_2CH_2Cl$	0.12	69.3_5	1.4494	132.1[b]	28.49[b]	−1.26[e]
$CH_3CH_2CH_2Br$	0.07	74.2_3	1.2668	140.0[b]	31.92[b,d]	−1.97[e]
c-$C_6H_{11}C_2H_5$	0.12	126.3_0	1.0406	211.8[f]	40.48[b]	7.53[g]

a) Observed values. b) J. A. Riddick and W. B. Bunger, Techniques of Chemistry, Vol. 2, "Organic Solvents," 3rd ed, Wiley Interscience, New York (1970). c) E. W. McGovern, *Ind. Eng. Chem.*, **35**, 1230 (1943). d) J. Laynez and I. Wadsö, *Acta Chem. Scand.*, **26**, 3148 (1972); I. Wadsö, *ibid.*, **22**, 2438 (1968). e) Ref. 3. f) H. M. Huffman, S. S. Todd, and G. D. Oliver, *J. Am. Chem. Soc.*, **71**, 584 (1949). g) Ref. 4.

Experimental

Sound velocity v was measured with an interferometer working at 3 MHz and density d with a pycnometer. The temperature was controlled within ±0.05 °C. Samples were carefully purified before measurements. The accuracy of v is ±0.3 m/s. Adiabatic and isothermal compressibilities (κ_S and κ_T) were estimated from density, sound velocity, and other thermodynamic quantities.

Results and Discussion

Values of d, v, κ_S, and κ_T determined for CHX_2CHX_2, $CH_3CH_2CH_2X$ (X=Cl and Br), and c-$C_6H_{11}C_2H_5$ are summarized in Table 1. The results for v_a and $\Delta V/V$ are given in Table 2, together with values of α, C_p, ΔH_v, and ΔH required for the determination of v_a and $\Delta V/V$. Values of α_t were estimated to be −1.6, −1.3, −2.0, −1.9, and -1.7×10^{-4} K^{-1} for $CHCl_2$-$CHCl_2$, $CHBr_2CHBr_2$, $CH_3CH_2CH_2Cl$, $CH_3CH_2CH_2Br$, and c-$C_6H_{11}C_2H_5$, respectively.

It was found from the negative value of $\Delta V/V$ (Table 2) that the value of v_1 is larger than that of v_2. For CHX_2CHX_2 and $CH_3CH_2CH_2X$, v_1 corresponds to the *anti* form, and to the equatorial form for c-$C_6H_{11}C_2H_5$. Wyn-Jones *et al.*[6] and Christian *et al.*[10] also reported similar results for $CHCl_2CH_2Cl$ by means of the ultrasonic absorption method and the pressure effect of infrared spectroscopy. In the case of CHX_2-CHX_2, the value of $|\Delta V/V|$ for chloro compound is smaller than that for bromo compound, while it is reversed for $CH_3CH_2CH_2X$ and CH_2XCH_2X.[1b]

For c-$C_6H_{11}C_2H_5$, the magnitude of $\Delta V/V$ (12%) is nearly equal to that of c-$C_6H_{11}CH_3$ (11%).[1b] It agrees with the results of c-$C_6H_{11}CH_3$[1b] and c-$C_6H_{11}X$ reported by Christian *et al.*[10] that the equatorial form was found to be larger than the axial one.

Our method is convenient and accurate for the determination of $\Delta V/V$ in conformational isomerism, as compared with the ultrasonic absorption method[6] used so far.

References

1) a) M. Aoi and K. Arakawa, *Bull. Chem. Soc. Jpn.*, **47**, 2639 (1974); b) *ibid.*, **53**, 845 (1980).
2) J. L. Lebowitz, *Phys. Rev. A*, **133**, 895 (1964); K. Tokiwano and K. Arakawa, *Bull. Chem. Soc., Jpn.* **50**, 2217 (1977).
3) N. Sheppard, *Adv. Spectrosc.*, **1**, 288 (1959).
4) E. L. Eliel, N. L. Allinger, S. J. Angyal, and G. A. Morrison, "Conformational Analysis," Interscience Publ., New York (1967), Chaps. 1, 2.
5) J. Lamb, "Physical Acoustics," ed by W. P. Mason, Academic Press, New York (1965), Vol. 2A, Chaps. 4, 5.
6) E. Wyn-Jones and W. J. Orville-Thomas, "Molecular Relaxation Processes," Chem. Soc. Spec. Publ., No. 20 (1966), p. 209; K, R, Crook and E. Wyn-Jones, *J. Chem. Phys.*, **50**, 3445 (1969); K. R. Crook, E. Wyn-Jones, and W. J. Orville-Thomas, *Trans. Faraday Soc.*, **66**, 1597 (1970).
7) J. Lamb and J. Sherwood, *Trans. Faraday Soc.*, **51**, 1674 (1955).
8) K. Krebs and J. Lamb, *Proc. R. Soc. London, Ser. A*, **244**, 558 (1958).
9) J. R. Pellam and J. K. Galt, *J. Chem. Phys.*, **14**, 608 (1946); R. A. Padmanaban, *J. Sci. Ind. Res.*, **19B**, 336 (1960).
10) S. D. Christian, J. Grundnes, and P. Klaboe, *J. Chem. Phys.*, **65**, 496 (1976); *J. Am. Chem. Soc.*, **97**, 3864 (1975).

The Reaction of *cyclo*-Tetraphosphate with L-Valine

Mitsutomo TSUHAKO,* Naoko FUJITA, Akiko NAKAHAMA, Tsuneo MATSUO, Masamitsu KOBAYASHI, and Shigeru OHASHI**

Kobe Women's College of Pharmacy, Motoyamakitamachi, Higashinada-ku, Kobe 658

***Department of Chemistry, Faculty of Science, Kyushu University 33, Hakozaki, Higashi-ku, Fukuoka 812*

(Received March 22, 1980)

Synopsis. *cyclo*-Tetraphosphate (P_{4m}) reacted with L-valine at pH 12 to form a certain phosphorus-containing compound (Compound X). Compound X was obtained in amounts so small as about 3.2% at room temperature after 91 d and about 0.3% at 70 °C after 1 d. Based on the results of paper chromatography, anion-exchange chromatography, and IR spectroscopy, Compound X was proved to be the same orthophosphate derivative of valine, an anion of *N*-(1-carboxy-2-methylpropyl)phosphoramidic acid, as that formed by the reaction of *cyclo*-triphosphate (P_{3m}) with L-valine. The mechanism of the reaction of P_{4m} with L-valine was discussed.

Quimby and Flautt[1] first reported that cyclic phosphates, such as P_{3m}, could be subjected to ring opening with ammonia to form amidophosphates. Since then, the reactions of P_{3m} with alkylamines,[2,3] sodium fluoride,[4] alcohols,[5] and glycine[6] have been actively studied by Feldmann and Rabinowitz. The present authors have already reported that, by the reaction of P_{3m} with L-valine one of the α-amino acids, a P_1-derivative of valine, was produced in the pH range from 10 to 12.[7] Thus, in the present study, the reaction of P_{4m}, one of cyclic phosphates, with L-valine was investigated.

Experimental

Chemicals. Sodium *cyclo*-tetraphosphate tetrahydrate,[8] $Na_4P_4O_{12}\cdot 4H_2O$, was prepared in the following manner: 50 g of diphosphorus pentaoxide was gradually hydrolyzed in 300 cm^3 of cold water, after which the hydrolyzate was neutralized to pH 7 with a cold, concentrated sodium hydroxide solution. Then, by repeating the recrystallization 5 times from water and drying at 40 °C, $Na_4P_4O_{12}\cdot 4H_2O$ was obtained. Reagent-grade L-valine was used without purification.

Reaction between cyclo-*Tetraphosphate and* L-*Valine.* Aqueous solutions of 0.2 mol dm^{-3} of sodium *cyclo*-tetraphosphate tetrahydrate and 0.2 mol dm^{-3} of L-valine were mixed in a volume ratio of 1:1. The pH of the mixture was about 5.97. The solution was adjusted with 6 mol dm^{-3} of a sodium hydroxide solution to pH 12 and then allowed to stand at room temperature and at 70 °C. With the progress of the reaction the pH of the solution was gradually lowered, after which the sodium hydroxide solution was added to maintain the pH 12.

Anion-exchange chromatography, paper chromatography, and IR spectroscopy were carried out by the methods described in a previous paper.[7]

Results and Discussion

Figure 1 shows the anion-exchange chromatograms obtained for the reaction mixtures of P_{4m} with L-valine in a molar ratio of 1:1 after 14 and 91 d at room temperature and at pH 12. In addition to the peaks of ortho-(P_1), pyro-(P_2), tri-(P_3), and tetra-

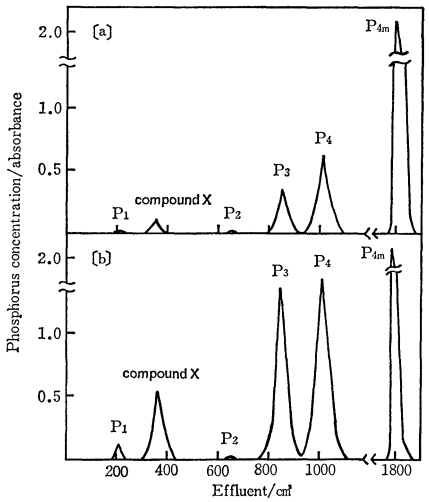

Fig. 1. Elution patterns for the reaction products of P_{4m} with L-valine at room temperature and pH 12. (a) after 14 d, (b) after 91 d.

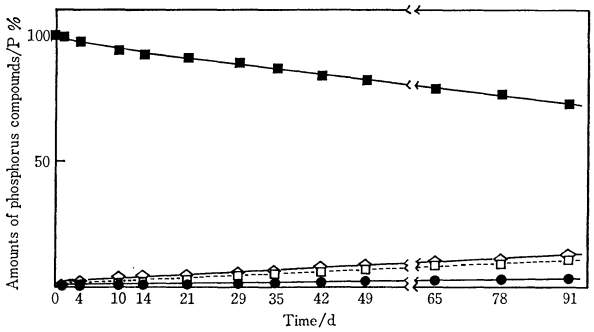

Fig. 2. Change of the amounts of phosphorus compounds in the reaction of P_{4m} with L-valine at room temperature and pH 12.
—●—: P_1-(N)Val, --□--: P_3, —◇—: P_4, —■—: P_{4m}.

phosphate(P_4), the peak of Compound X appeared between those of P_1 and P_2. Though the formation of Compound X was small, it tended to increase gradually with the reaction time. Figure 2 shows the change in the amounts of Compound X, P_3, and P_4, as well as the amount of remaining P_{4m}, determined by means of anion-exchange chromatography. The amounts of P_1 and P_2 formed are omitted here because their amounts were very small (about 0.4 and 0.1% respectively), even after 91 d. The starting material, P_{4m}, decreased gradually with the time, but still about 73% of it remained after 91 d. On the other hand, the yields of P_4, P_3, and Compound X were about 12.5, 11.0, and 3.2% respectively.

Based on the position of the elution peak in the anion-exchange chromatography, and on the results

of paper chromatography, ninhydrin reaction, and IR spectroscopy, Compound X was proved to be identical with the orthophosphate derivative of valine formed by the reaction of P_{3m} and L-valine, *i.e.*, an anion of *N*-(1-carboxy-2-methylpropyl)phosphoramidic acid (P_1-(N)Val), $^{-}O-\overset{\overset{O}{\|}}{P}-NH-\underset{\underset{COO^-}{|}}{CH}-CH\begin{matrix}CH_3\\CH_3\end{matrix}$. Comparing the reaction of P_{4m} and L-valine with that of P_{3m} and L-valine, it was found that, though the same type of phosphate was obtained in both reactions, there were great differences in the yields of the phosphates formed and in the reaction rates.

In the reaction of P_{4m} with L-valine at 70 °C, we obtained the same products as those obtained by the reaction at room temperature, namely P_1, P_2, P_3, P_4, and P_1-(N)Val. Their amounts formed at 70 °C were, however, different from those formed at room temperature. P_3 was predominantly formed at the early stage of the reaction (3—14 d), while P_1 and P_2 were predominant at the later stage (more than 20 d). The formation of P_1-(N)Val was observed immediately after the start of the reaction, but its yield was as low as about 0.3% after 1 d and about 0.1% after 3 d. After 6 d and thereafter, it could not be observed at all. On the other hand, the residual amount of P_{4m} decreased very rapidly, becoming almost zero after 20 d. The fact that, at 70 °C, in spite of the rapid decrease of P_{4m}, P_1-(N)Val was formed in only a very small amount, suggests that the hydrolysis of P_{4m} itself may proceed in preference to the reaction of P_{4m} with L-valine.

It was found that, at room temperature, the reaction of P_{4m} with L-valine is slower than the reaction of P_{3m} with L-valine. This can be understood by analogy with the fact that, in an alkaline solution, the hydrolysis of P_{4m} is slower than that of P_{3m}.

The mechanism of the reaction of P_{4m} with L-valine at pH 12 is summarized in Fig. 3. A phosphorus of P_{4m} may be attacked by the lone pair of the nitrogen of L-valine; consequently, the ring-opening reaction

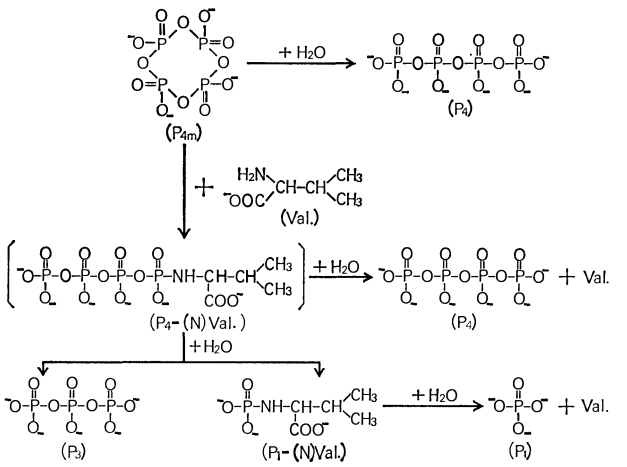

Fig. 3. Mechanism of the reaction of P_{4m} with L-valine.

of P_{4m} may proceed to form a tetraphosphate derivative of valine (P_4-(N)Val), but this compound is very unstable and is immediately hydrolyzed to produce a P_1-(N)Val and P_3. P_2, which is a minor component in the reaction products, may be produced by the hydrolysis of P_3 and P_4.

References

1) O. T. Quimby and T. J. Flautt, *Z. Anorg. Allg. Chem.*, **296**, 220 (1958).
2) W. Feldmann and E. Thilo, *Z. Anorg. Allg. Chem.*, **327**, 159 (1964).
3) W. Feldmann, *Z. Chem.*, **5**, 26 (1965).
4) W. Feldmann, *Z. Anorg. Allg. Chem.*, **338**, 235 (1965).
5) W. Feldmann, *Chem. Ber.*, **100**, 3850 (1967).
6) J. Rabinowitz, J. Flores, R. Krebsbach, and G. Rogers, *Nature*, **224**, 795 (1969).
7) M. Tsuhako, N. Fujita, A. Nakahama, T. Matsuo, M. Kobayashi, and S. Ohashi, *Bull. Chem. Soc. Jpn.*, **53**, 1138 (1980).
8) R. N. Bell, L. F. Audrieth, and O. F. Hill, *Ind. Eng. Chem.*, **44**, 568 (1952).

The Determination of Antimony in Water by Atomic-absorption Spectrophotometry Following Flotation Separation

Susumu NAKASHIMA

Institute for Agricultural and Biological Sciences, Okayama University, Kurashiki, Okayama 710

(Received June 2, 1980)

Synopsis. A flotation method which utilizes an iron(III) hydroxide–surfactant–air system at pH 4 is described for the separation of sub-microgram levels of antimony-(III,V) in water. The antimony content is determined by the generation of stibine, followed by atomic-absorption spectrophotometry with a long absorption cell (60 cm × 1.2 cm i.d.).

From the viewpoints of environmental science and geochemistry, there is an increasing need for a rapid and accurate method for determining low parts per billion (ppb) of antimony in water. At a less than 1 μg dm^{-3} level of antimony in water, a precise direct determination is difficult even by the atomic-absorption spectrophotometry of stibine, which has a high sensitivity.[1-4] Accordingly, the antimony must be concentrated from the water prior to determination.

In previous papers,[5-8] a flotation technique,[9,10] one in which the precipitate of iron(III) hydroxide is floated with the aid of a surfactant and small air bubbles, was used for the pre-concentration of arsenic-(III,V)[5,6] selenium(IV),[7] and tin(II,IV)[8] in water.

The present paper will describe the application of the separation technique mentioned above to the pre-concentration of antimony(III,V), in water and the determination of antimony by atomic-absorption spectrophotometry, following stibine generation.

Experimental

Apparatus. The apparatus employed in this work has all been previously described[5-8] except for the light source, a Hamamatsu TV antimony hollow-cathode lamp.

Reagents. The reagents were the same as those described previously[7,8] except for those mentioned below. The antimony standard solutions were freshly prepared by diluting stock solutions before use. An antimony(III) stock solution (1 mg Sb cm^{-3}) was prepared by dissolving 1.371 g of potassium antimony tartrate hemihydrate in water and then diluting the mixture to 500 cm^3 with water. An antimony(V) stock solution (0.1 mg Sb cm^{-3}) was prepared from the antimony(III) solution by oxidation with a minimum amount of potassium permanganate. A mixed surfactant solution (0.5 mg cm^{-3} for each surfactant) was prepared by dissolving sodium dodecyl sulfate and sodium oleate in 99.5% (v/v) ethanol, with magnetic stirring for sodium oleate. A potassium iodide solution (20% w/v) was prepared by dissolving in water.

Procedure for the Flotation Step. One thousand cm^3 of acidified water is placed in a 1000-cm^3 beaker, and 2 cm^3 of an iron(III) solution (5 mg cm^{-3}) is added. The pH of the solution is adjusted to 4.0±0.2 with an aqueous ammonia solution to precipitate iron(III) hydroxide, and the mixture is stirred for 15 min. After adding 2 cm^3 of the surfactant solution to the beaker, the contents of the beaker are transferred to a flotation cell. Air is passed through at a flow rate of 50 cm^3 min^{-1} from the lower end of the cell for about 2 min to obtain a complete mixing and flotation of the precipitate. Most of the mother liquor is drained from the side arm by opening the cock of the drain pipe. After closing the cock, the residual mother liquor is sucked off through the sintered-glass disk, and the precipitate is washed with 30 cm^3 of water. Four cm^3 of 6 mol dm^{-3} hydrochloric acid is added to the cell to dissolve the precipitate, the filtrate is collected by suction in a 10-cm^3 calibrated flask, the sintered-glass disk is washed with water, the washings are added to the flask, and the mixture is diluted to 9 cm^3 with water. The potassium iodide solution (0.5 cm^3) is added to the flask prior to analysis, and the mixture is diluted to 10 cm^3 with water.

Procedure for the Determination of Antimony. The procedure is similar to that for the determination of tin.[8] A calibration curve is constructed using 2.4 mol dm^{-3} hydrochloric acid solutions containing 1.0 mg cm^{-3} of iron(III), 1.0% of potassium iodide, and 0—0.10 μg cm^{-3} of antimony-(III); this curve is linear within the above range of antimony. The detection limit of antimony was found to be 0.4 ng cm^{-3}.

The atomic-absorption apparatus was operated under the following conditions: wavelength, 217.6 nm; lamp current, 12 mA; gas-flow rates, nitrogen 1.0, hydrogen 1.0, and auxiliary nitrogen 6 dm^3 min^{-1}; spectral bandwidth, 1 nm.

Results and Discussion

The effect of the pH of a 1000-cm^3 solution containing 0.8 μg of antimony(III,V) on the coprecipitation of antimony was investigated. As Fig. 1 shows, satisfactory recoveries of antimony(III,V) were obtained in the pH range of 3.4—7.0. At pH values above 7.5, the efficiency of coprecipitation decreased considerably. When the mixed surfactant solution was used, the surface-foam layer supporting the precipitate of iron(III) hydroxide was stable within the pH range of 3.4—10.1; the pH of 4.0±0.2 was, therefore, used throughout the work.

The presence of up to at least 2.5 mg cm^{-3} of iron-(III) added as a collector did not affect the stibine generation in the presence of potassium iodide.

Table 1 shows the permissible amounts of foreign

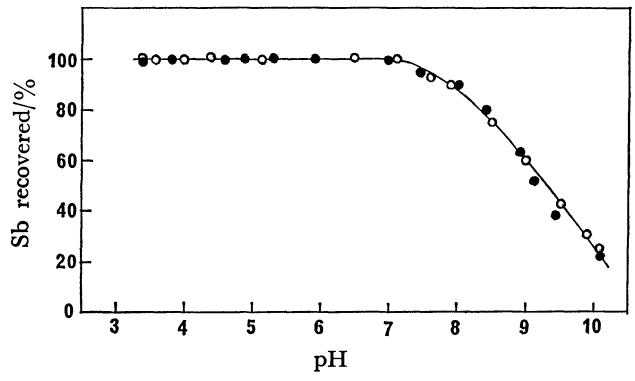

Fig. 1. Coprecipitation of antimony with iron(III) hydroxide as a function of pH.
Solution containing 0.8 μg of Sb and 10 mg of Fe(III), sample volume: 1000 cm^3, ●: Sb(III), ○: Sb(V).

Table 1. Permissible amounts of foreign ions for the determination of antimony[a)]

Ion	Limit [Ion]/[Sb]		Ion	Limit [Ion]/[Sb]		Ion	Limit [Ion]/[Sb]	
Na^+	10000		Zn^{2+}	1000		Se^{4+}	1000	
K^+	10000		Mn^{2+}	1000		Se^{6+}	1000	b)
Ca^{2+}	10000		Al^{3+}	1000		PO_4^{3-}	1000	
Mg^{2+}	10000		Cr^{3+}	1000		Ni^{2+}	800	
Cl^-	10000		Cr^{6+}	1000		Te^{4+}	200	
NO_3^-	10000	b)	Mo^{6+}	1000	b)	Bi^{3+}	100	
SO_4^{2-}	10000		Pb^{2+}	1000	(+)	As^{3+}	30	
SiO_3^{2-}	10000		Hg^{2+}	1000	(+)	As^{5+}	30	
Sr^{2+}	1000		Co^{2+}	1000	(+)	Sn^{4+}	10	
Ba^{2+}	1000		V^{5+}	1000				
Cd^{2+}	1000		Cu^{2+}	1000				

a) Solution containing 1.0 μg of Sb(III) and 10 mg of Fe(III); sample volume, 1000 cm³. b) Maximum concentrations tested. (+): the amounts which give a 10% positive error.

Table 2. Recovery of antimony added to natural surface-water samples[a)]

Sample	Antimony added	Antimony[b)] found	Antimony recovered	Mean recovery
	μg	μg	μg	%
Tap water[c)]	None	0.046±0.004		
	0.300	0.343±0.007	0.297	99
	0.600	0.635±0.012	0.589	98
River water[d)]	None	0.028±0.003		
	0.300	0.309±0.008	0.281	94
	0.600	0.592±0.013	0.564	94

a) Volume of sample, 1000 cm³. b) The mean value of four measurements. c) Laboratory tap water. d) This sample was taken from the Takahashi River, Okayama Prefecture.

ions within a 10% negative or positive error for the determination of 1.0 μg of antimony(III) in 1000-cm³ solutions. As can be seen in Table 1, most foreign ions hardly interfere at all with the determination of antimony(III). In the procedure described here, the addition of potassium iodide overcame suppressive effects by copper(II) and selenium(IV), but did not show much effect on the negative interference by nickel(II). However, when coprecipitation at pH 4 was used, the depressive effect by nickel(II) was found to be largely eliminated in comparison with that which occurs when antimony is directly determined. That is, when the proposed method was used, the value of the permissible amount of nickel(II) increased from 4 to 800 (Ni/Sb in weight) compared with the value permissible in a direct determination. Hydride-forming elements, such as tin(IV), arsenic(III,V), bismuth(III), and tellurium(IV), are coprecipitated with iron(III) hydroxide in the same way as antimony and exert a relatively great effect on the generation of stibine.

The solutions (1000 cm³) containing 0.2—20.0 μg of antimony(III) were analyzed by the procedure described above. The recoveries of the antimony that had been added were greater than 94% in all instances. No blank value was detected throughout the analytical process. The proposed conditions, therefore, appear to be optimal for 1000-cm³ volumes of a solution containing up to 20 μg of antimony(III). The relative standard deviations of ten-times-repeated analyses of the solutions containing 0.4 and 0.8 μg of antimony(III) per 1000 cm³ were 2.7 and 2.4% respectively.

In order to investigate the applicability of this method to surface water, the recoveries of known amounts of antimony(III) added to natural surface water samples were examined by the above procedure. The analyses were carried out on 1000-cm³ aliquots of clear, uncontaminated tap and river waters which had been filtered through 0.45 μm Millipore filters after the addition of hydrochloric acid immediately after sampling. Table 2 indicates that the analytical process gave a satisfactory recovery of antimony from surface waters. The antimony concentrations in the tap and river water samples were low: 0.046 and 0.028 μg dm^{-3} respectively.

The author wishes to thank Professor Atsushi Mizuike and Dr. Masataka Hiraide of Nagoya University for their helpful advice on the flotation technique, and Professor Fuji Morii of Okayama University for her helpful discussions.

References

1) K. C. Thompson and D. R. Thomerson, *Analyst (London)*, **99**, 595 (1974).
2) P. D. Goulden and P. Brooksbank, *Anal. Chem.*, **46**, 1431 (1974).
3) Y. Yamamoto and T. Kumamaru, *Fresenius' Z. Anal. Chem.*, **281**, 353 (1976).
4) T. Kubota and T. Ueda, *Bunseki Kagaku*, **27**, 692 (1978).
5) S. Nakashima, *Analyst (London)*, **103**, 1031 (1978).
6) S. Nakashima, *Bunseki Kagaku*, **28**, 561 (1979).
7) S. Nakashima, *Anal. Chem.*, **51**, 654 (1979).
8) S. Nakashima, *Bull. Chem. Soc. Jpn.*, **52**, 1844 (1979).
9) M. Hiraide and A. Mizuike, *Bunseki Kagaku*, **26**, 47 (1977).
10) M. Hiraide, Y. Yoshida, and A. Mizuike, *Anal. Chim. Acta*, **81**, 185 (1976).

Thermal Behavior of a New Type Molybdenum Oxide Obtained by Oxidation of Molybdenum Powder or Molydenum Trioxide with Hydrogen Peroxide

Yasuhiko KURUSU

Department of Chemistry, Faculty of Science and Technology, Sophia University, 7-1 Kioicho, Chiyoda-ku, Tokyo 102

(Received June 7, 1980)

Synopsis. New molybdenum oxides, Mo-y(yellow) and Mo-b(blue), were obtained by the reaction between molybdenum powder or molybdenum trioxide and hydrogen peroxide. Their reactivity and structure were examined by iodometry, IR, X-ray, and thermal analyses. Mo-y is an acidic oxidant but Mo-b is acidic.

A new type of molybdenum oxide(Mo-y) was obtained by oxidation of molybdenum powder or molybdenum trioxide with 30% hydrogen peroxide. A blue molybdenum compound(Mo-b) was produced by the reaction of molybdenum powder with an inadequate amount of 30% hydrogen peroxide. On the other hand, an excess 30% hydrogen peroxide produced yellow powder(Mo-y). Mo-y and Mo-b have catalytic activity for the dehydration of alcohols, Mo-y being more reactive than Mo-b. Mo-y oxidizes iodide ion, the content of which was determined by iodometry. The result shows that Mo-y has a reactive oxygen. Mo-b does not oxidize iodide ion. In order to investigate the reactivity, the thermal behavior of the active sites of Mo-y was studied. The structural change of Mo-y caused by heating was investigated by means of IR, TG, DTA, and X-ray.

Results and Discussion

Reaction with Hydrogen Peroxide. The reaction scheme is shown in Fig. 1.

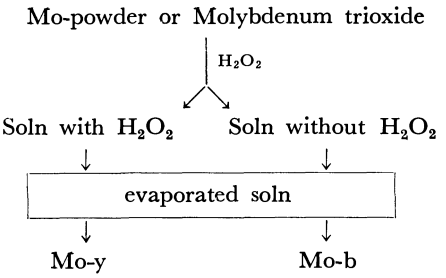

Fig. 1. Reaction path of molybdenum powder or molybdenum trioxide and hydrogen peroxide.

The analysis shows that there is one active oxygen to one atom of molybdenum in Mo-y, indicating the possibility of the existence of a OOH group, while Mo-b has no active oxygen. It seems that Mo-b has OH groups but not a OOH group. Mo-b is synthesized from molybdenum powder but not from molybdenum trioxide. Mo-y, however, is obtained from molybdenum powder or molybdenum trioxide. Glemser and Lutz[1] reported that the structure of molybdenum oxide hydroxide is $MoO_{3-x}(OH)_x$ ($0.5 \leq x \leq 2$). Wilhelmi[2] investigated the MoO_3 and MoO_2 prepared from MoO_3 by reduction with hydrogen at 500 °C and proposed the structure $Mo_4O_{10}(OH)_2$. In this paper, Mo-b is indicated by $MoO_2(OH)_2$ and Mo-y by $MoO_2(OH)(OOH)$.

Differential Thermal Analysis(DTA) and Thermal Gravimetric Analysis(TG). The sample was dried at 30 °C for 72 h under reduced pressure before measurement. DTA and TG curves are shown in Fig. 2. Mo-y showed a gradual decrease in weight up to 200 °C. Above 200 °C, endothermic change takes place with an abrupt decrease in weight, the active oxygen disappearing and Mo-y being transformed into molybdenum trioxide. The weight decrease at 200 °C is calculated from the TG curve to be one mole of water and one gram atom of active oxygen, an endothermic peak was observed and later an exothermic peak, molybdenum trioxide being transformed from amorphous into crystalline form. The weight decrease observed for Mo-b up to 200 °C is calculated to be due to the disappearance of water. The final product was shown to be molybdenum trioxide by IR and X-ray analyses. The DTA curve shows an exothermic peak, the amorphous compound becoming crystalline molybdenum trioxide.

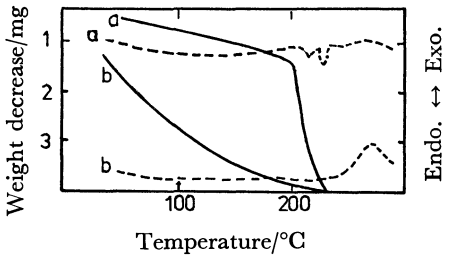

Fig. 2. DTA-TG curves of Mo-y and Mo-b.
a: Mo-y (18.3 mg), b: Mo-b (18.3 mg),
——: TG, ----: DTA, 5 °C/min.

IR Spectrum. For Mo-y, OH stretching frequency and OH deformation vibration were observed at 3450 and 1620 cm^{-1} respectively. The symmetrical terminal Mo–O stretch occurs around 930 cm^{-1} and the antisymmetrical terminal Mo–O stretch at 950 cm^{-1}. The absorption bands are the same as those reported by Mimoun *et al.*[3] and Sotani *et al.*[4] for molybdenum compounds. Absorptions at 980 cm^{-1} are derived from the active oxygen in Mo-y, since the amounts of active oxygen determined by iodometry are associated with the absorbance at 980 cm^{-1} (Fig. 3(A)). The band is assigned to the Mo–O–O stretching vibration. In the case of Mo-b, the region of OH absorption band is the same as that for Mo-y (3400 and 1610 cm^{-1}). The absorption peaks are observed at 970 and 910 cm^{-1}. Probably the band at 930

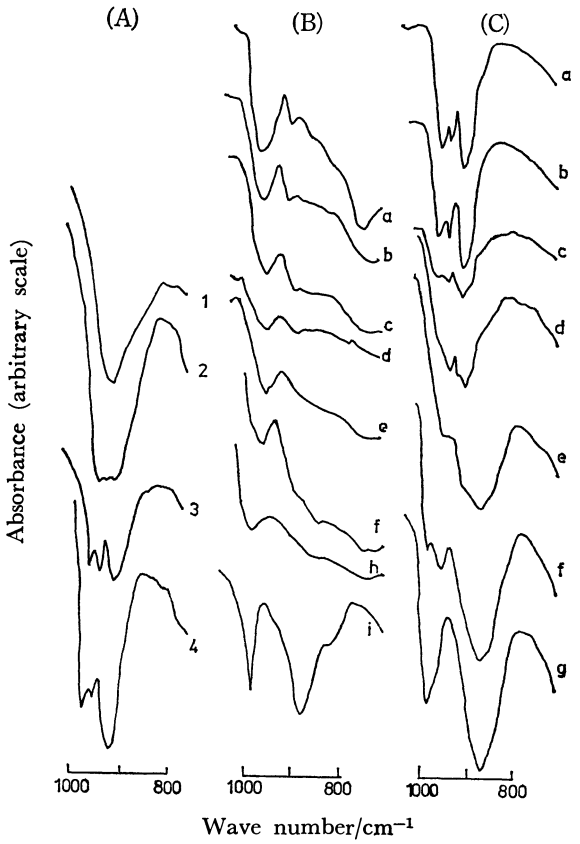

Fig. 3. IR spectra and amount of active oxygen of the molybdenum compound oxidized with hydrogen peroxide (A). Amount of active oxygen (mmol/g); 1: 0.11, 2: 0.13, 3: 3.23, 4: 4.04.
IR spectra of Mo-b(B) and Mo-y(C) at various temperatures of calcination.
a: 30 °C, b: 100 °C, c: 130 °C, d: 160 °C, e: 185 °C, f: 200 °C, g: 220 °C, h: 240 °C, i: 260 °C.

cm^{-1} shifted to the lower wave number region (910 cm^{-1}) owing to the hydrogen bond from absorbed water and the Mo–O bond. The absorption band of the deformation vibration (rocking) mode of the water molecule coordinated with metal was observed at 750 cm^{-1}. Mo-y and Mo-b were dried under reduced pressure in an oven at 30 °C for 72 h. Mo-y treated in the manner described above was calcined under reduced pressure for 1 h at 100, 130, 160, 185, 200, and 220 °C, and Mo-b at 100, 130, 160, 185, 200, 240, and 260 °C. The IR spectra were observed with a KBr tablet. Figure 3(B), (C) show the change of range 1000—800 cm^{-1}. Both compounds turn into molybdenum trioxide above 200—240 °C. The absorption bands of Mo-y at 980, 950 and 930 cm^{-1} assigned to Mo–O gradually decrease by heating up to 200 °C, followed by the disappearance of active oxygen and the appearance of the absorbance of molybdenum trioxide. Upon heating Mo-y, a band was observed at 920 cm^{-1}. It can be assumed that the band at Mo–O shifts to lower wave numbers owing to the increase of polarization of the Mo–O bond. In the case of Mo-b, the Mo–O stretching frequency at 970 cm^{-1} shifts to 990 cm^{-1}. The absorption band at 910 cm^{-1} arising from the Mo–O bond, shifts to 870 cm^{-1}, the band being characteristic of the Mo–O–Mo bond.

X-Ray Analysis. Krebs[5] and Sotani[6] reported on the X-ray analysis of molybdenum oxide, but no report seems to have appeared on the X-ray diffraction analysis of molybdenum oxidized with hydrogen peroxide. The measurement was carried out by the powder method. Mo-b is amorphous, a weak broad diffraction band being observed at 0.307—0.263 nm spacing(d). Mo-y has a high crystallinity and the diffractive band of the spacing at 0.169 nm is very strong. It shows a sheet type structure with 0.619 nm spacing. Molybdenum oxide and molybdenum have 0.53 and 0.567 nm spacing, respectively.[5,6] This difference might arise from the active oxygen in view of the insertion of oxygen between the sheet type structure.

Experimental

Materials. Molybdenum powder (Tokyo Tangusten K.K. Toyama factory: purity 99.985%, diam. 4.2 μm) and hydrogen peroxide (guaranteed reagent 30% Mitsubishi Gas Chemical Co., Ltd.) were used. All other chemicals (Wako Chemicals Co.) were of first grade.

Analysis. Thermal analysis was carried out with a differential thermal gravimetric microbalance (Rigaku TG-DTA), a heating rate of 5 °C/min and static air atmosphere being employed with 18 mg samples in each run. The infrared spectra were obtained with a Hitachi Infrared Spectrophotometer Model 125 on a KBr disk. X-Ray powder patterns were obtained with nickel filtered Cu *K* radiation. Active oxygen was determined by iodometry. EDTA titration[7] was used to measure the content of molybdenum.

Synthesis of Mo-y and Mo-b. Molybdenum powder was added to 30% hydrogen peroxide at 60 °C, a yellow solution being obtained. When the solution became yellow, addition of molybdenum powder was stopped; hydrogen peroxide was then added in order to oxidize the Mo-y satisfactorily. After filtration of unreacted molybdenum powder, the solution was evaporated to give Mo-y as a yellow powder[8]. When molybdenum powder was added to the yellow solution, the color of the solution turned blue. The blue solution was filtered to remove unreacted molybdenum powder, a blue powder being obtained on evaporation of the solution.

This article is gratefully dedicated to Professor Georg Manecke on the occasion of his sixty-fifth birthday.

References

1) O. Glemser and G. Lutz, *Z. Anorg. Chem.*, **264**, 17 (1951).
2) K. A. Wilhelmi, *Acta Chem. Scand.*, **23**, 419 (1969).
3) H. Mimoun, I. S. de Roch, and L. Sajus, *Bull. Soc. Chim. Fr.*, **1969**, 1481.
4) N. Sotani, Y. Saito, M. Taneda, and M. Hasegawa, *Nippon Kagaku Kaishi*, **1974**, 673.
5) B. Krebs, *Acta Crystallogr., Sect. B*, **28**, 2222 (1972).
6) N. Sotani, *Bull. Chem. Soc. Jpn.*, **48**, 1820 (1975).
7) H. Yaguchi and T. Kajihara, *Bunseki Kagaku*, **14**, 785 (1965).
8) Y. Kurusu and N. Ishii, Japan Patent 52-46793 (1977).

Solvent Extraction of Iron(III) in Concentrated Nitric Acid with Several β-Diketones

Tatsuya SEKINE,* Yū KOMATSU,† and Kazuho INABA

Department of Chemistry, Science University of Tokyo, Kagurazaka, Shinjuku-ku, Tokyo 162

† *National Institute for Researches in Inorganic Materials, 1-1 Namiki, Sakura-mura, Niihari-gun, Ibaraki 305*

(Received June 30, 1980)

Synopsis. The solvent extraction of iron(III) in nitric acid (1 to 13.2 mol dm^{-3}) with seven β-diketones into carbon tetrachloride was studied. The extraction curve has a pronounced minimum at from 6 to 7 mol dm^{-3} acid, and the extracted iron(III) species were assumed to be represented by $FeA_a(NO_3)_{3-a}(HA)_n$ (where a and n are from 0 to 3).

The solvent extraction of metal ions with weakly acid chelating extractants(HA) is dependent on the concentration of its dissociated form(A^-), and the distribution ratio increases when the hydrogen-ion concentration is decreased. The extraction of iron(III) with β-diketones such as 2-thenoyltrifluoroacetone (TTA) also shows the above tendency.[1] However, the extractions of metal ions in concentrated acid solutions with weakly acid chelating extractants have also been reported by some authors.[2] For example, titanium(IV) in concentrated hydrochloric acid was extracted with β-diketones.[3] The extractions of zirconium(IV) and hafnium(IV) from concentrated nitric, hydrochloric, and perchloric acid with TTA and *N*-benzoyl-*N*-phenylhydroxylamine are other examples.[4-6] It was also reported that iron(III) was extractable even from concentrated nitric acid with TTA in xylene and that the distribution ratio increased upon an increase in the acid concentration.[7] This extraction was further studied;[8] it was reported that iron(III) was extractable with TTA in xylene both from 10 mol dm^{-3} nitric acid and 10 mol dm^{-3} ammonium nitrate, and that the rate of extraction was higher from the former than the latter. An increase in the rate of the extraction of iron(III) with TTA by the addition of nitrate was also reported and the extraction of the $FeA_2^+NO_3^-$ species was assumed in addition to the FeA_3, although no further details were given.[9]

Experimental

The experiments were carried out at 25±0.3 °C. All the reagents were of an analytical grade. An iron(III) solution prepared by dissolving metallic iron in nitric acid (in some cases, in an acid sodium nitrate solution) and a carbon tetrachloride solution of a β-diketone were placed in a stoppered glass tube, agitated, and centrifuged. Some extractions with TTA was also made by using chloroform as the diluent. In some cases, the iron(III) extracted into the organic phase was agitated with a fresh nitric acid solution and centrifuged. The iron(III) in the organic phase was stripped by a 6 mol dm^{-3} portion of hydrochloric acid. This back-extracted iron(III) and the iron(III) in the equilibrated aqueous phase was determined by atomic absorption, and the distribution ratio was calculated as;

$$D = [\mathrm{Fe(III)}]_{org}/[\mathrm{Fe(III)}]. \quad (1)$$

Results and Discussion

The β-diketones used were as follows: acetylacetone (AA), benzoylacetone(BZA), dibenzoylmethane(DBM), trifluoroacetylacetone (TFA), 2-thenoyltrifluoroacetone (TTA), benzoyltrifluoroacetone(BFA), and hexafluoroacetylacetone(HFA). When the acid concentration was high, the rate of extraction was high; agitation for 1 min was enough to achieve the equiribrium. However, when the acid concentration was lower than 6 mol dm^{-3}, it was low; the extraction of iron(III) in 1 mol dm^{-3} of nitric acid with 0.2 mol dm^{-3} of TTA in chloroform did not reach equilibrium for at least 3 h. In such cases, the distribution ratio at equiribrium was estimated from the extrapolation of the data of the forward extraction from the aqueous phase and of the backward extraction from the organic phase, which had extracted the iron(III) with that β-diketone.

Figure 1 gives the dependence of D on the nitric acid concentration. The extraction with AA was too poor to be determined, and that with HFA was not reproducible for unknown reasons, although its magnitude was between that with TFA and DBM. Judging from these facts, the order of extractability with these β-diketones is: TTA > BFA > TFA > (HFA) > DBM > BZA > AA. As may be seen from Fig. 1, each

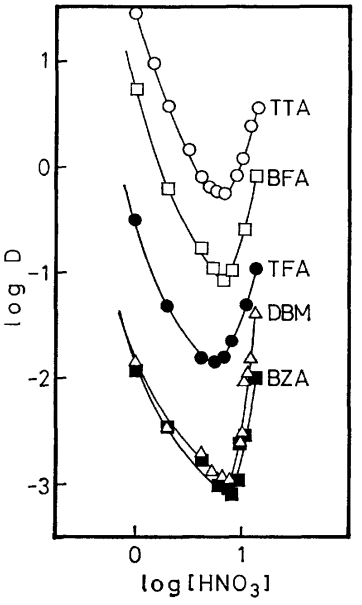

Fig. 1. Distribution ratio of Fe(III) as a function of nitric acid concentration.
Org. phase: CCl_4 initially containing 0.2 mol dm^{-3} of each β-diketone, aq. phase: nitric acid initially containing 5×10^{-4} to 1×10^{-3} mol dm^{-3} Fe(III).

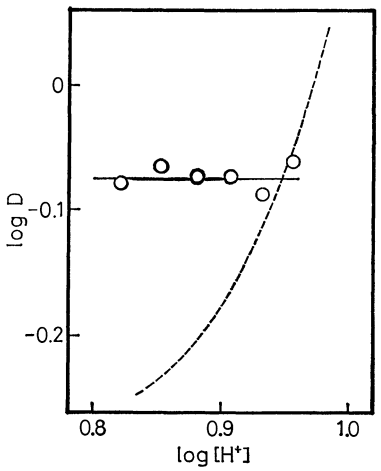

Fig. 2. Dependence of the distribution ratio on H^+ concentration when the aqueous phase was 9.1 mol dm^{-3} (H, Na)NO_3.
Org. phase: CCl_4 containing 0.2 mol dm^{-3} TTA.
The broken line gives the extraction curve when the aqueous phase contains only nitric acid (*cf.* Fig. 1).

extraction curve has a pronounced minimum at about 6 to 7 mol dm^{-3} of the acid. The dependence of the extraction on the β-diketone was determined when the aqueous phase was 13.2 mol dm^{-3} of nitric acid. The slope of the log D *vs.* log $[HA]_{org}$ plot was +3 with TTA, BFA, TFA, and HFA, while it was +2 with DBM and BZA. Figure 2 shows that the extraction with TTA is independent of the hydrogen-ion concentration when the nitrate concentration was 9.1 mol dm^{-3}. The extraction with TTA was also studied by using chloroform as the diluent. It was found that the shape of the curve was rather similar, but the distribution ratio was three to five times higher when the diluent was carbon tetrachloride.

The color of the organic phase which extracted iron(III) from concentrated nitric acid with these β-diketones was similar to that which extracted iron(III) from 1 mol dm^{-3} of nitric acid, except in the case of BZA. The aqueous phase at equiribrium was nearly colorless when the acid concentration was 1 mol dm^{-3} but it was green (TTA and DBM), violet (AA and BZA), pink(BFA and TFA), or colorless (HFA) when the acid was above 6 mol dm^{-3}; the higher the acid concentration, the deeper the color.

Since the ionic concentration in the aqueous phase in Fig. 1 changes with the acid concentration, a quantitative discussion covering all the acid concentration region is difficult. However, since the distribution ratio in Fig. 2 is independent of the hydrogen-ion concentration, the β-diketone in its undissociated form, HA, is assumed to combine with iron(III) nitrate complexes when the nitrate concentration is high. The finding that two molecules of BZA or DBM were enough to extract iron(III) from concentrated nitric acid also seems to support this assumption.

It has been pointed out that the rate of the extraction of iron(III) from acid solutions with the β-diketones as their tris-complexes was low.[10,11] The rate of extraction at low acid concentrations in the present study agrees with this previous finding. The rapid extraction in the concentrated acid region also suggests that type of extraction in this region is different. The observation that an increase in the nitric acid concentration increased the distribution ratio in Fig. 1 may be explained by an increase in the concentration of the iron(III) nitrate complexes (a "salting-out" effect may also contribute). The better extraction when the diluent was carbon tetrachloride than when it was chloroform is similar to the general tendency when solvating-type extractants such as tributyl phosphate are used;[2] this also supports the extraction of the $Fe(NO_3)_3$ complex with two or three molecules of undissociated form β-diketones. Thus, the species extracted from dilute acid solutions should be in the FeA_3 form, but the extracted species should be in the $Fe(NO_3)_3(HA)_n$ (where n is 2 or 3) form from concentrated acid solutions. The extracted species in the intermediate region should be, consequently, mixtures of these two species and the mixed complexes in the form of $FeA_a(NO_3)_{3-a}(HA)_n$ (where a is 1 or 2 and n is smaller than 3). However, an accurate estimation of the composition in the organic phase in this region seems to be difficult because the shape of the absorption curves of the organic phase is not very much affected by the acid concentration, and also because the determination of the molar ratio of Fe^{3+} and NO_3^- in the organic phase by chemical analysis is difficult due to the large amount of nitric acid co-extracted.

We are grateful to Dr. Yoshinori Fujiki of the National Institute for Researches in Inorganic Materials, who encouraged us during this work.

References

1) T. Sekine and T. Tetsuka, *Bull. Chem. Soc. Jpn.*, **45**, 1620 (1972).
2) T. Sekine and Y. Hasegawa, "Solvent Extraction Chemistry," Marcel Dekker, New York (1977); Chap. VII.
3) Y. Komatsu, *J. Inorg. Nucl. Chem.*, **42**, 265 (1980).
4) J. Hála, Proceedings of International Conference of Solvent Extraction Chemistry, Gothenburg, 135 (1966); J. Hála, *J. Inorg. Nucl. Chem.*, **29**, 187 (1967); J. Hála, *J. Inorg. Nucl. Chem.*, **29**, 1317 (1967).
5) J. Hála and D. Pohanková, *J. Inorg. Nucl. Chem.*, **29**, 2983 (1967).
6) J. Hála and J. Smola, *J. Inorg. Nucl. Chem.*, **31**, 1133 (1969).
7) F. L. Moore, W. D. Fairman, J. G. Ganchoff, and J. G. Surak *Anal. Chem.*, **31**, 1148 (1959).
8) C. Testa, *Anal. Chem. Acta*, **25**, 525 (1961).
9) H. Kawamoto and H. Akaiwa, *Chem. Lett.*, **3**, 259 (1973).
10) T. Sekine, J. Yumikura, and Y. Komatsu, *Bull. Chem. Soc. Jpn.*, **46**, 2356 (1973).
11) Y. Komatsu, H. Honda, and T. Sekine, *J. Inorg. Nucl. Chem.*, **38**, 1861 (1976).

Syntheses of Derivatives of N^2-Acetyl-N^3-glycyl-L-2,3-diaminopropionic Acid and Their Hydrolyses by Trypsin

Yoshihiro MINEMATSU, Shinwon KANG, Michinori WAKI,*
Tetsuo KATO, and Nobuo IZUMIYA
Laboratory of Biochemistry, Faculty of Science, Kyushu University 33, Higashi-ku, Fukuoka 812
(Received February 22, 1980)

Synopsis. Amide and ethyl ester of N^2-acetyl-N^3-glycyl-L-2,3-diaminopropionic acid replacing an ethylene group in the side chain of lysine by a peptide bond were synthesized. The susceptibility of each derivative to trypsin was compared with that of the corresponding N^2-acetyl-L-lysine derivative. Each derivative was hydrolyzed by trypsin, but was less susceptible than the corresponding L-lysine derivative.

The specificity of trypsin is restricted. The enzyme hydrolyzes selectively the amide and ester bonds containing a carboxyl group of L-lysine or L-arginine. Several lysine-like derivatives such as L-4-thialysine[1] or L-4-oxalysine[2] are susceptible to trypsin; a methylene group in the side chain of lysine is replaced by a sulfur or oxygen atom. In order to examine the influence of replacement of an ethylene group in the side chain of lysine by a peptide bond, we undertook to synthesize an amide (**1**) and an ethyl ester (**2**) of N^2-acetyl-N^3-glycyl-L-2,3-diaminopropionic acid (Ac-L-A_2pr(Gly)-OH[3]) and to subject them to the action of trypsin. Ac-L-Lys-NH_2 (**3**) and Ac-L-Lys-OEt (**4**) were used for references.

We attempted to synthesize a key intermediate, Ac-L-A_2pr(Z-Gly)-NH_2 (**12**), by the action of methanolic NH_3 on Ac-L-A_2pr(Z-Gly)-OEt (**5**). A crystalline compound (mp 209 °C) was isolated, but the result of elemental analysis was not in line with the calculated value **12**. The structure of the compound with mp 209 °C was determined to be L-2-acetamido-3-[N'-(carbamoylmethyl)ureido]propionamide (**7**) by

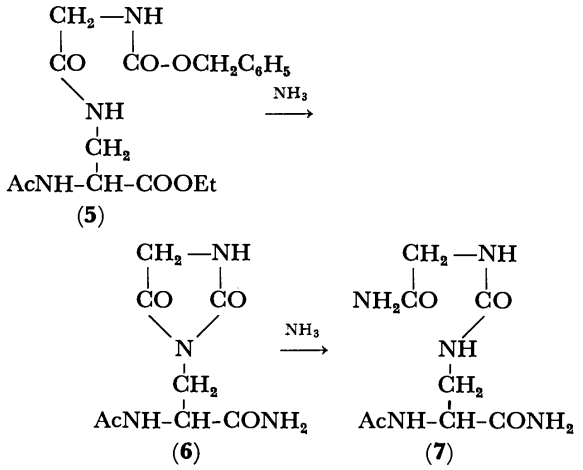

means of nuclear magnetic resonance and infrared spectroscopy. The result of elemental analysis also agreed with the calculated value as **7**. We assume that the starting compound **5** could be converted into an intermediate hydantoin **6** which is subsequently converted into **7**.

The key intermediate **12** was synthesized as follows. Ac-L-A_2pr(Z)-NH_2 (**10**) was prepared from Ac-L-A_2pr(Z)-OEt (**9**) by the action of methanolic NH_3, **10** being transformed into Ac-L-A_2pr-NH_2 (**11**) by hydrogenolysis. Z-Gly-OH was coupled with β-amino group in **11** by the carbodiimide method, the intermediate **12** being obtained in a good yield. Finally, the desired Ac-L-A_2pr(Gly)-NH_2 (**1**) was prepared by hydrogenolysis of **12**. The ester substrate, Ac-L-A_2pr(Gly)-OEt (**2**) was easily prepared from compound **5** by hydrogenolysis.

TABLE 1. OPTIMUM pH AND C_{max} VALUES OF SUBSTRATES BY TRYPSIN AT 30 °C

Substrate	Optimum pH	C_{max}[a]
1	8.0	0.0049
3	7.8	0.37
2	8.2	12.7
4	8.0	246

a) C_{max} values were estimated from $C_{max}=k_3/2.3\,K_m$, where K_m is a Michaelis constant and k_3 a rate constant.[4]

In order to determine the hydrolytic rates of the amide **1** and the ester **2** by trypsin, the effect of pH was measured for the four substrates. The optimum pH values are given in Table 1. For a comparison of the hydrolytic rates, maximum proteolytic coefficients (C_{max})[4] were determined at the optimum pH. Ac-L-A_2pr(Gly)-NH_2 (**1**) is hydrolyzed at *ca.* 1.3/100 times the rate for Ac-L-Lys-NH_2 (**3**), and Ac-L-A_2pr(Gly)-OEt (**2**) at *ca.* 5.2/100 times that of Ac-L-Lys-OEt (**4**). The lysine-like derivative Bz-L-4-thialysinamide is hydrolyzed at 16/100 times Bz-L-Lys-NH_2.[1] Replacement of a methylene group in L-lysine by an atom such as sulfur and that of an ethylene group by a CONH lead to a decrease in the susceptibility for trypsin.

Experimental

All melting points are uncorrected. Homogeneity of each compound was confirmed by TLC carried out on silica gel G (Merck) with various solvent systems, only the R_f value with *n*-BuOH–AcOH–pyridine–H_2O (4:1:1:2, v/v) being presented. Hydrolytic rates were determined by means of a Hitachi amino acid analyzer KLA-5 under the following conditions: flow rate, 30 ml/h; jacket temperature, 55 °C. Trypsin was salt free, crystalline sample from Nutritional Biochemicals Corporation, Ohio, U.S.A. ^{1}H-NMR spectra were measured in DMSO-d_6 with a Hitachi R-20B spectrometer (60 MHz) using tetramethylsilane as an internal standard.

*H-L-A_2pr(Z)-OEt·HCl (**8**·HCl).* *N*-Carboxy anhydride (NCA) of H-L-A_2pr(Z)-OH was synthesized according to the method of Takagi *et al.*[5] The NCA (0.26 g, 1 mmol) was dissolved in ethanolic 1 M HCl (1.7 ml), and the solution

was left to stand at 50 °C for a few min and at room temperature for 2 d. The solvent was evaporated *in vacuo*, and the residue was recrystallized from hot acetone; yield, 0.27 g (89%); mp 165—166 °C; $[\alpha]_D^{20}$ +5.7° (*c* 2, EtOH); R_f 0.77. Found: C, 51.39; H, 6.30; N, 9.24%. Calcd for $C_{13}H_{19}O_4N_2Cl$: C, 51.57; H, 6.33; N, 9.25%.

*Ac-L-A$_2$pr(Z)-OEt (**9**).* Acetic anhydride (0.51 ml, 5 mmol) was added with stirring to a chilled solution of **8**·HCl (0.30 g, 1 mmol) in pyridine (1.6 ml). After being stirred at 0 °C for 30 min and at room temperature for 3 h, the solvent was evaporated. After the residue had been dissolved in EtOAc, the solution was washed with water, dried (Na_2SO_4), and evaporated. The residue was recrystallized from EtOAc–ether; yield, 0.28 g (91%); mp 115—116 °C; $[\alpha]_D^{20}$ +24.2° (*c* 2, $CHCl_3$); R_f 0.90. Found: C, 58.32; H, 6.51; N, 9.09%. Calcd for $C_{15}H_{20}O_5N_2$: C, 58.43; H, 6.54; N, 9.09%.

*Ac-L-A$_2$pr(Z)-NH$_2$ (**10**).* Compound **9** (1 mmol) was dissolved in methanol (6 ml) saturated with NH_3 at 0 °C, and the solution was left to stand at room temperature for 3 d. The solvent was evaporated, and the residue was recrystallized from EtOH–ether; yield, 97%; mp 187—188 °C; $[\alpha]_D^{20}$ −11.7° (*c* 2, DMF); R_f 0.73. Found: C, 55.82; H, 6.07; N, 14.99%. Calcd for $C_{13}H_{17}O_4N_3$: C, 55.90; H, 6.14; N, 15.05%.

*Ac-L-A$_2$pr-NH$_2$·HCl (**11**·HCl).* Compound **10** (0.28 g, 1 mmol) dissolved in ethanolic 0.2 M HCl (5.5 ml) was treated with hydrogen in the presence of Pd black. After the completion of hydrogenolysis, the filtrate from the catalyst was evaporated to dryness: yield of hygroscopic powder (**11**·HCl), 0.18 g (*ca.* 100%); R_f 0.43.

*Ac-L-A$_2$pr(Z-Gly)-NH$_2$ (**12**).* Compound **11**·HCl (0.18 g, *ca.* 1 mmol) and Z–Gly–OH (0.31 g, 1.5 mmol) were dissolved in DMF (8 ml). To the solution were added at 0 °C Et_3N (0.14 ml, 1.0 mmol) and 1-ethyl-3-(3-dimethylaminopropyl)carbodiimide HCl salt (0.29 g, 1.5 mmol). After being stirred at 0 °C for 3 h and at room temperature overnight, the solvent was evaporated. The residue was dissolved in a mixture of H_2O–MeOH (1:1). The solution was put on a column (0.8×3.5 cm) of Dowex 50X8 (H^+ form) and eluted with the same solvent. The eluate was evaporated, and the residue was recrystallized from EtOH–EtOAc; yield, 0.26 g (74%); mp 144—146 °C; $[\alpha]_D^{20}$ −6.4° (*c* 1, EtOH); R_f 0.71. Found: C, 51.40; H, 5.86; N, 16.17%. Calcd for $C_{15}H_{20}O_5N_4 \cdot 3/4H_2O$: C, 51.50; H, 6.19; N, 16.01%.

*Ac-L-A$_2$pr(Gly)-NH$_2$·HCl (**1**·HCl).* This was prepared from **12** (0.35 g, 1 mmol) in the same way as for **11**·HCl; yield of hygroscopic powder, 0.24 g (*ca.* 100%); R_f 0.31.

*Ac-L-A$_2$pr-OEt·HCl (**13**·HCl).* Compound **9** (2 mmol) was hydrogenated in the same way as for **11**·HCl. The residue was recrystallized from DMF–ether; yield, 85%; mp 176—178 °C (dec); $[\alpha]_D^{20}$ −41.8° (*c* 2, EtOH); R_f 0.76. Found: C, 39.90; H, 7.18; N, 13.32%. Calcd for $C_7H_{15}O_3N_2Cl$: C, 39.90; H, 7.18; N, 13.30%.

*Ac-L-A$_2$pr(Z-Gly)-OEt (**5**).* Z–Gly–OH (1.5 mmol) was coupled with **13**·HCl (1 mmol) in the same way as for **12**. The solvent was evaporated, and the residue was dissolved in EtOAc. The solution was washed successively with 4% $NaHCO_3$, 2% HCl, and water, dried, and evaporated. The residue was recrystallized from EtOH–ether; yield, 71%; mp 116—118 °C; $[\alpha]_D^{20}$ −6.1° (*c* 2, EtOH); R_f 0.77. Found: C, 55.78; H, 6.34; N, 11.44%. Calcd for $C_{17}H_{23}O_6N_3$: C, 55.88; H, 6.35; N, 11.50%.

*Ac-L-A$_2$pr(Gly)-OEt·HCl (**2**·HCl).* Compound **5** was hydrogenated in the same way as for **11**·HCl. The residue was recrystallized from 2-propanol–ether; yield, 77%; mp 194—196 °C (dec); $[\alpha]_D^{20}$ −20.2° (*c* 2, EtOH); R_f 0.58. Found: C, 39.89; H, 6.71; N, 15.53%. Calcd for $C_9H_{18}O_4N_3Cl \cdot 1/4H_2O$: C, 39.71; H, 6.85; N, 15.44%.

*Ac-L-A$_2$pr(Gly)-OH (**14**).* 1 M NaOH (0.22 ml) was added to a solution of **2**·HCl (27 mg, 0.1 mmol) in water (0.2 ml). The solution was left to stand at room temperature for 15 min. It was then put on a column of Dowex 50X8 (H^+ form), and the resin was washed with water and eluted with 2 M NH_4OH. The eluate was evaporated; yield of powder, 18 mg (*ca.* 90%); R_f 0.15.

*L-2-Acetamido-3-[N′-(carbamoylmethyl)ureido]propionamide (**7**).* Compound **5** (1 mmol) was treated with methanolic NH_3 (6 ml) in the same way as for **10**. The solvent was evaporated, and the residue was recrystallized from DMF–ether; yield, 94%; mp 208—209 °C; $[\alpha]_D^{20}$ −2.4° (*c* 2, H_2O); R_f 0.76. IR (KBr) 3370, 3210 (NH_2), 3300 (NH), 1610—1670, 1570, 1300 (amide), 1660 (substituted urea CO), 1360 (CH_3) and 1420 cm^{-1} (CH_2); ^{1}H-NMR (DMSO-d_6) δ=7.90 (1H, d, J=7.5 Hz, –CONHCH–), 7.35 (2H, brd s, –CONH$_2$), 7.04 (2H, brd s, –CONH$_2$), 6.29 (1H, t, J=6 Hz, –CONHCH$_2$–), 6.19 (1H, t, J=6 Hz, –CONHCH$_2$–), 4.20 (1H, m, –NHCHCH$_2$–), 3.63 (2H, d, J=6 Hz, –NHCH$_2$CO–), 3.28 (2H, m, –NHCH$_2$CH–) and 1.90 (3H, s, CH$_3$CO–). Found: C, 38.97; H, 6.14; N, 28.32%. Calcd for $C_8H_{15}O_4N_5$: C, 39.18; H, 6.17; N, 28.56%.

*Ac-L-Lys-NH$_2$·HCl (**3**·HCl), Ac-L-Lys-OEt·HCl (**4**·HCl), and Ac-L-Lys-OH (**15**).* These reference compounds were synthesized according to the methods reported.[6-8] R_f values for the 3 compounds were found to be 0.35, 0.76, and 0.28, respectively.

Determination of Hydrolytic Rates. An aliquot (0.2 ml)[9] of trypsin solution in 0.001 M HCl and 0.5 ml of Tris buffer with a certain pH were placed in a 2-ml assay flask containing either an amide or ester substrate in a certain concentration. The solution was made up to 2.0 ml with water, the final concentration of the buffer being 0.1 M. An aliquot sample (0.2 ml) was withdrawn at certain intervals and placed in a flask containing 0.2 M citrate buffer (0.8 ml) at pH 2.2. A portion of the solution was subjected to assay by means of an amino acid analyzer with a 0.6×10 cm column using 0.35 M citrate buffer at pH 5.28.[10] The extent of % hydrolysis at certain intervals was calculated by the amount of either **14** or **15**. The enzymic hydrolysis of the substrates at various intervals followed the first-order kinetics within experimental error.

References

1) S.-S. Wang and F. H. Carpenter, *J. Biol. Chem.*, **243**, 3702 (1968).

2) M. Gorecki and Y. Shalitin, *Biochem. Biophys. Res. Commun.*, **29**, 189 (1967).

3) Other abbreviations used: Bz, benzoyl; Z, benzyloxycarbonyl.

4) N. Izumiya and T. Yamashita, *J. Biochem. (Tokyo)*, **46**, 19 (1959).

5) S. Takagi, H. Tsukatani, and K. Hayashi, *Chem. Pharm. Bull.*, **7**, 616 (1959).

6) K. Daigo, W. T. Brady, and L. J. Reed, *J. Am. Chem. Soc.*, **84**, 662 (1962).

7) S. G. Waley and J. Watson, *Biochem. J.*, **57**, 529 (1954).

8) E. Havinga and C. Schattenkerk, *Tetrahedron, Suppl.* **8**, Part I, 313 (1967).

9) The final concentrations of the enzyme in test solution were as follows: 0.059 mg enzyme *N*/ml for **1**, 0.0091 for **3**, 0.000074 for **2**, and 0.000037 for **4**.

10) Elution volume and relative color intensity were determined as 8.0 ml and 30% for **14** and 8.0 ml and 100% for **15**, respectively.

The Reaction of *cis*-1,2-Dichloroethylene with Borane in Tetrahydrofuran. The Supply of Monochloroborane in a Tetrahydrofuran Solution

Akira ARASE,* Masayuki HOSHI, and Yuzuru MASUDA
Department of Applied Chemistry, Kitami Institute of Technology, Kitami 090

(Received April 25, 1980)

Synopsis. In the reaction of *cis*-1,2-dichloroethylene with borane in THF at 20 °C for 2 h, about 94% of borane was converted to monochloroborane. The resulting solution was stable at 0 °C for several hours.

Monochloroborane (H_2BCl), which has a strongly electronegative chlorine atom, can be expected to show some different properties from borane. For example, the boron atom of H_2BCl adds more selectively to the terminal carbon atom of 1-alkene than does borane.[1,2] The method for the preparation of H_2BCl in a THF solution includes the reaction of hydrogen chloride with BH_3 in THF[3] and the reaction of boron trichloride with BH_3 in THF.[4]

In the course of our study of the reaction using substituted boranes, we needed a less expensive, ready method for the preparation of H_2BCl in a THF solution. It has been reported that, in the hydroboration of alkenyl chloride with BH_3, the boron atom which was once introduced on to a vicinal position of chlorine atom was eliminated rapidly with the chlorine atom to form an olefinic double-bond and H_2BCl. Thus, we tried to prepare H_2BCl in a THF solution utilizing the above elimination reaction.

Polychloroethylenes, bearing chlorine atoms on both doubly bonded carbon atoms, were subjected to the reaction with BH_3 in THF in order to achieve an effective formation of H_2BCl by a β-elimination reaction (1) and to avoid an α-transfer reaction, which would prevent the formation of H_2BCl (1').

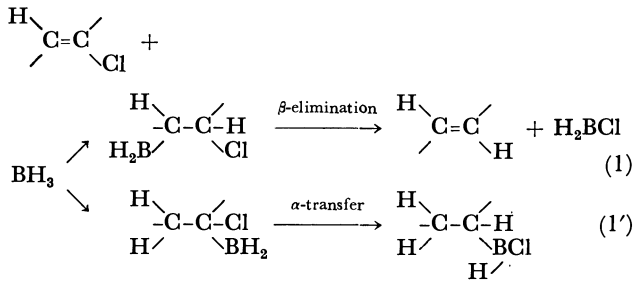

(1)

(1')

Polychloroethylene (4 mmol) was added to BH_3 (2 mmol) in THF at 0 °C, and the solution was stirred at 20 °C. After the reaction, the solution was hydrolyzed. The amounts of residual hydride and chloroborane were estimated by measuring the volume of hydrogen gas evolved and by titrating the hydrochloric acid in the solution with a standardized aqueous 0.1 mol dm^{-3} $NaHCO_3$ solution, using Methyl Orange as the indicator. The results are shown in Table 1.

Tetrachloroethylene and trichloroethylene did not show signs of reaction having occured. However, in the cases of *cis*-1,2-dichloroethylene (*c*-DCE) and *trans*-1,2-dichloroethylene (*t*-DCE), the reaction did proceed. In these cases, it was observed that the hydrogen atom on the boron atom (hydride) was consumed in the reaction, and that nearly an equal amount of hydrochloric acid was formed on the hydrolysis of the reaction mixture. On the other hand, an appreciable amount of vinyl chloride was collected in

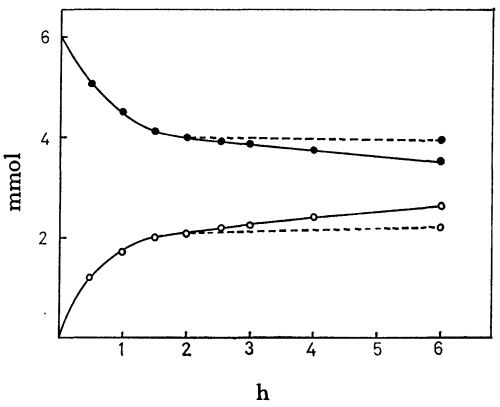

Fig. 1. The amount of hydrogen evolved and hydrochloric acid formed by the hydrolysis in the reaction[a] of *cis*-1,2-dichloroethylene and BH_3 in THF.
●: Hydrogen, ○: hydrochloric acid.
a) 4 mmol of *cis*-1,2-DCE was added to 2 mmol of BH_3 in THF.

Table 1. The reaction of polychloroethylenes or vinyl chloride with BH_3 or H_2BCl in THF at 20 °C

Borane 2 mmol	Chloroethylene 4 mmol	Reaction time h	Hydrogen mmol	Hydrochloric acid mmol
BH_3	Tetrachloroethylene	12	6.00	0
BH_3	Trichloroethylene	12	6.00	0
BH_3	*t*-DCE	2	4.05	2.02
BH_3	*c*-DCE	2	4.01	2.01
BH_3	*c*-DCE	6	3.44	2.52
BH_3	*c*-DCE	6[a]	3.94	2.19
H_2BCl	*c*-DCE	2	4.00	1.98
H_2BCl	Vinyl chloride	2	3.99	1.99

a) After a reaction at 20 °C for 2 h, the reaction temperature was maintained at 0 °C.

a cold trap. As *t*-DCE had the disadvantage in this operation owing to its low boiling property, *c*-DCE was employed for further examinations.

As is shown in Fig. 1, the reaction of the first of the three hydrogen atoms of BH_3 reacted rapidly, but the second and the third did so slowly. When the solution was cooled to 0 °C after a reaction at 20 °C for 2 h, at which point the first hydrogen atom of BH_3 seemed just to have been consumed, the reaction was virtually stopped, as is shown by the dotted line.

The possible reactions which occur upon the addition of *c*-DCE to BH_3 in THF are thought to be as below. However, as is shown in Table 1, H_2BCl

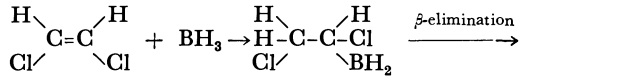

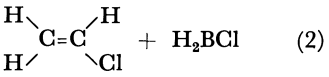

(2)

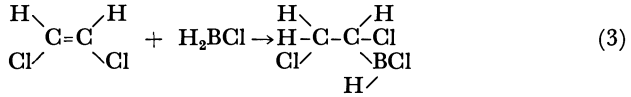

(3)

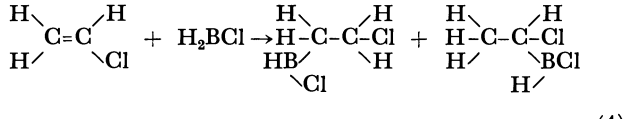

(4)

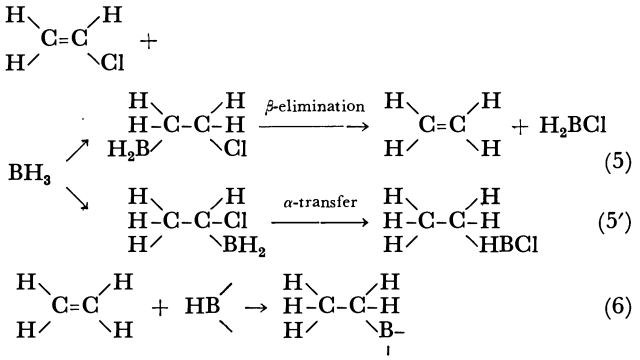

(5)

(5′)

(6)

in a THF solution, prepared from boron trichrolide and BH_3 in THF,[4] hardly reacted with *c*-DCE or vinyl chloride under the same reaction conditions (20 °C, 2 h). Accordingly, the contributions of Reactions 3 and 4 must be negligible. Thus, the source of the hydrochloric acid in the hydrolysed solution is regarded as H_2BCl formed in Reaction 2 and/or 5 and chloroethylborane formed in Reaction 5′. Further, in the reaction of *c*-DCE with BH_3 in THF at 20 °C for 2 h, 0.12 mmol of ethanol was formed by an alkaline–hydrogen peroxide oxidation. This amount corresponds to a 3% loss of the hydride, probably caused by the α-transfer reaction and/or by the hydroboration of ethylene, as is shown in Reactions 5′ and 6. On the other hand, by careful examinations of the reaction mixture and its oxidation product, no compounds were found other than vinyl chloride and ethanol.

These results show that about 94% of BH_3 is converted to H_2BCl in the present reaction. The resulting H_2BCl solution showed nearly the same properties as the H_2BCl solution (THF) obtained by the other established method.[4] For example, the ^{11}B NMR spectrum of the solution showed a triplet at −4.58 ppm (relative to boron trifluoride etherate), with J= 129 Hz (lit,[4] −4.59 ppm, J=131 Hz), and no other signals which should result from BH_3 and H_2BCl[4] were observed. In addition, quite similar results were obtained, both in the yield and in the isomer distribution, on the hydroboration of 1-alkene using such a solution, prepared by a reaction at 20 °C for 2 h.

Experimental

Materials. Commercial tetrachloroethylene, trichloroethylene, *c*-DCE, and *t*-DCE were dried over molecular sieve-5A and distilled before use. BH_3 in a THF solution was prepared as has been described in the literature.[6]

Procedure. A dry, 25-ml flask equipped with a magnetic stirring bar, a septum inlet and an outlet, connected to a cold trap (−70 °C), was flushed with argon. In the flask, 2 mmol of BH_3 in THF was then placed, after which 4 mmol of *c*-DCE was introduced at 0 °C. Then the solution was hydrolyzed with 2 ml of water, and hydrogen evolved was measured by means of a gas meter, connected to an end of the cold trap. On the other hand, hydrogen chloride in the solution was titrated by the use of 0.1 mol dm^{-3} aqueous $NaHCO_3$ solution, using Methyl Orange as the indicator. The solution was then oxidized with alkaline hydrogen peroxide, and the organic layer was analyzed by GLC.

The reaction of vinyl chloride with H_2BCl was examined in a similar manner. In this reaction, a THF solution (5 ml) of vinyl chloride (6 mmol) was added to a THF solution (1.5 ml) of H_2BCl (2 mmol) prepared by the method in Ref. 4.

The ^{11}B NMR spectrum was recorded by means of a Hitachi R-20A spectrometer.

References

1) H. C. Brown and N. Ravindran, *J. Am. Chem. Soc.*, **98**, 1785 (1976).

2) H. C. Brown, N. Ravindran, and S. U. Kulkarni, *J. Org. Chem.*, **44**, 2417 (1979).

3) G. Zweifel, *J. Organomet. Chem.*, **9**, 215 (1967).

4) D. J. Pasto and P. Balasubramaniyan, *J. Am. Chem. Soc.*, **89**, 295 (1967).

5) a) M. F. Hawthorne and J. A. Dupont, *J. Am. Chem. Soc.*, **80**, 5830 (1958); b) P. Binger and R. Köster, *Tetrahedron Lett.*, **1961**, 156; c) D. J. Pasto and S. R. Snyder, O. S. F., *J. Org. Chem.*, **31**, 2773 (1966); d) H. C. Brown and K. A. Kelblysis, *J. Am. Chem. Soc.*, **86**, 791 (1964).

6) G. Zweifel and H. C. Brown, *Org. React.*, Vol. 13, (1963).

Photochemical Reactions of Azidotriazines with Aromatic Substrates

Shigeru TAMURA, Hisao IMAIZUMI, Yoji HASHIDA,* and Kohji MATSUI*

Department of Synthetic Chemistry, Faculty of Engineering, Gunma University, Kiryu, Gunma 376

(Received May 14, 1980)

Synopsis. Triazinylnitrene generated photochemically from 2-azido-4,6-dimethoxy-1,3,5-triazine adds to the aromatic ring of alkylbenzenes and halobenzenes to give *N*-triazinylazepines.

Nitrene Chemistry has been extensively studied and is well established.[1] We have reported that the photolyses of azidotriazines in ketones[2,3] and nitriles[2,4] give 1:1 cycloaddition products of the triazinylnitrene and solvent molecule. In this paper we wish to describe the reactions of triazinylnitrene with several aromatic substrates to give *N*-triazinylazepines.

Results and Discussion

During the course of studies on photocycloadditions of triazinylnitrene to nitriles, we have found that irradiation of 2-azido-4,6-dimethoxy-1,3,5-triazine (**1a**) in phenylacetonitrile (**2d**) with a low-pressure mercury lamp resulted in the formation of *N*-(4,6-dimethoxy-1,3,5-triazin-2-yl)azepine (**3d**) in a 30% yield (Eq. 1). The structure of **3d** was indicated by its elemental

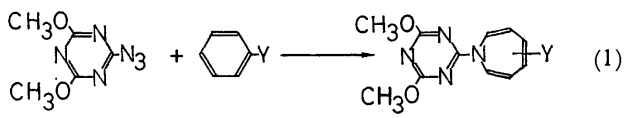

(1)

1a **2** **3**

a: Y=C_2H_5, b: Y=CH_3, c: Y=H, d: Y=CH_2CN, e: Y=Cl, f: Y=F, g=CF_3.

composition and spectral properties. Similar photolyses of azidotriazine (**1a**) in several aromatic substrates also gave *N*-triazinylazepines (**3**); the details are listed in Table 1. Although various azepines have been isolated from the reactions of aromatic substrates with carboxynitrenes,[5-8] sulfonylnitrene,[9] and cyanonitrene,[10] *N*-triazinylazepine is a novel type of the isolable *N*-arylazepine.

Although attempts to determine the isomer distribution were unsuccessful, it is apparent that the *N*-triazinylazepines which were obtained are isomeric mixtures on the basis of the following. For example, the ^{1}H-NMR spectrum of crude triazinylazepine (**3b**) obtained from the reaction with toluene showed singlets at δ 1.85 and 4.00, ascribable to methyl and methoxyl protons respectively. The addition of ^{1}H-NMR shift reagent, however, caused splitting of each peak into two peaks, indicating that at least two isomeric azepines are involved in the crude product. In addition, thermal isomerization of **3b** in acidic solution gave *o*- and *p*-toluidino-1,3,5-triazines in a molar ratio of *ca.* 1:1 (Eq. 2): the ratio was determined by a direct comparison of its ^{1}H-NMR spectrum with those of authentic samples, which were prepared from the reactions of 2-chloro-4,6-dimethoxy-1,3,5-triazine with *o*- and *p*-toluidines.

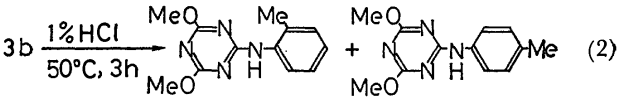

(2)

On the other hand, in the photoreactions of **1a** in anisole, *N*,*N*-dimethylaniline, and acetophenone, no azepine could be isolated as are shown in Scheme 1: the structures of (**4**), (**5**) and (**6**) were determined by spectral properties and mixed-melting-point tests with an authentic sample.[11]

In order to get an insight into a nature of triazinylnitrene, competitive reactions between benzene and monosubstituted benzene were performed (Table 2).

TABLE 1. *N*-TRIAZINYLAZEPINES (**3**)

Azepine	Yield %	Mp/°C(Solvent for recrystallization)	UV λ_{max}/nm	UV $\varepsilon\times10^{-4}$	MS $m/e(M^+)$	^{1}H-NMR, δ[c]	Found(Calcd), (%) C	H	N
3a	40(78)[a]	87—88 (C_6H_6-P.E.[b])	277 235	0.89 0.94	260	1.10(t, 3H), 2.15(q, 2H), 3.98(s, 6H), 5.50—6.50(m, 5H).	60.30 (59.99	6.49 6.20	21.83 21.52)
3b	24(72)	101—102 (P.E.)	276 236	0.95 0.90	246	1.85(s, 3H), 4.00(s, 6H), 5.55—6.40(m, 5H).	58.63 (58.53	5.71 5.73	22.86 22.75)
3c	40(55)	105—106 (C_6H_6-P.E.)	277 234	1.29 1.07	232	3.98(s, 6H), 5.50—6.32(m, 5H).	56.59 (56.88	5.15 5.21	24.02 24.13)
3d	30(35)	107—108 (C_6H_6)	277 209	1.47 1.92	271	3.20(s, 2H), 4.03(s, 6H), 5.40—6.50(m, 5H).	57.38 (57.56	4.80 4.83	25.56 25.81)
3e	20(25)	159—160 (C_6H_6-P.E.)	275 240	1.12 1.49	266	3.95(s, 6H), 5.70—6.50(m, 5H).[d]	49.69 (49.53	4.19 4.16	21.46 21.03)
3f	21(33)	117—118 (P.E.)	271 232	0.84 0.93	250	4.02(s, 6H), 5.50—6.67(m, 5H).	52.41 (52.80	4.47 4.43	22.10 22.39)
3g	15(23)	109—110 (P.E.)	277 231	1.27 1.36	300	4.01(s, 6H), 5.40—7.00(m, 5H).	48.30 (48.01	3.75 3.69	18.79 18.66)

a) Yields in parentheses were determined spectrophotometrically (see Experimental). b) P.E.: Petroleum ether. c) Unless otherwise noted, measurements were performed in $CDCl_3$. d) In DMSO-d_6.

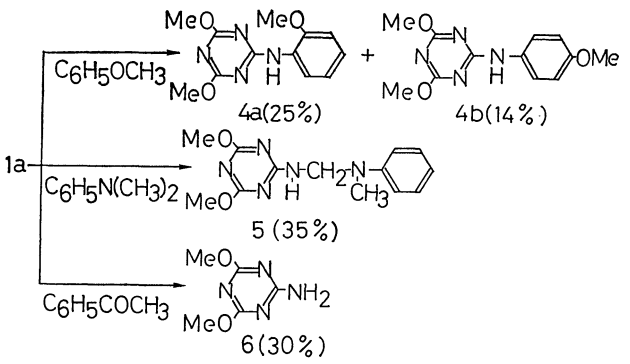

Scheme 1.

TABLE 2. RELATIVE RATES FOR THE REACTIONS OF 4,6-DIMETHOXY-1,3,5-TRIAZINYLNITRENE WITH BENZENES

Aromatic	Relative rate
Ethylbenzene	1.31
Toluene	1.96
Benzene	1.00
Phenylacetonitrile	0.98
Chlorobenzene	0.78
Fluorobenzene	1.10
(Trifluoromethyl)benzene	0.55

The Hammett plots using σ_p-values shows a satisfactory correlation: a least-squares treatment[12] gives an equation, $\log k_x = -0.67\,\sigma_p + 0.07$ with the correlation coefficient (r) of 0.94. The ρ value found is relatively low compared with that in the reaction of ethoxylcarbonylnitrene ($\rho = -1.32$),[13] indicating that the selectivity of triazinylnitrene toward substrate is relatively low. It has been well established[1] that azepines are obtained *via* singlet electrophilic nitrene. Thus, the lower selectivity of triazinylnitrene may be attributed to the electron-withdrawing nature of the triazine nucleus, which enhances the electrophilic reactivity of the nitrene.

On the other hand, the photolysis of 2-azido-4,6-bis(dimethylamino)-1,3,5-triazine (**1b**) in toluene yielded 2-amino-4,6-bis(dimethylamino)-1,3,5-triazine (40% yield), resulting from the hydrogen abstraction by triplet triazinylnitrene.[2] This is easily explained by assuming[2] that, in the photolysis of **1b** bearing highly electron donating dimethylamino groups, the intersystem crossing $^1N \rightarrow {}^3N$ becomes predominant path instead of the reaction of singlet nitrene.

Experimental

Materials. The azidotriazines (**1**) were prepared according to the procedure given in a previous paper.[14]

Irradiation. Let us take as example the photolysis of **1a** in toluene: A solution containing **1a** (2.00 g, 11.0 mmol) in toluene (20 ml) was irradiated for 48 h. After removal of the solvent, the residue was chromatographed on a silica-gel column using benzene–acetone mixture (10:1, v/v) as an eluent to yield crude azepine (**3b**). Recrystallization of crude **3b** from petroleum ether gave 0.65 g of white needles **3b** listed in Table 1.

Irradiations of **1a** in anisole, *N,N*-dimethylaniline, and acetophenone solutions were carried out in the same way to yield **4**, **5**, and **6**, respectively.

4a: mp 135—137 °C; MS *m/e* 262(M^+); ^{1}H-NMR (DMSO-d_6) δ 3.97 (s, 3H), 4.03(s, 6H), 7.00—8.20(m, 4H), 8.85 (s, 1H). Found: C, 55.01; H, 5.36; N, 21.46%.

4b: mp 138—139 °C; MS *m/e* 262(M^+); ^{1}H-NMR($CDCl_3$), δ 3.80(s, 3H), 3.98(s, 6H), 6.80—7.68(m, 4H), 8.35(s, 1H). Found: C, 55.48; H, 5.37; N, 21.56%. Calcd for $C_{12}H_{14}N_4O_3$: C, 54.95; H, 5.38; N, 21.36%.

5: mp 118—119 °C; MS *m/e* 275(M^+); ^{1}H-NMR($CDCl_3$), δ 3.04(s, 3H), 3.98(s, 6H), 5.15(d, 2H), 6.55(t, 1H), 6.70—7.46(m, 5H). Found: C, 56.59; H, 5.92; N, 25.20%. Calcd for $C_{13}H_{17}N_5O_2$: C, 56.71; H, 6.18; N, 25.44%.

Competitive Reactions. After irradiation in a mixed solvent of benzene and monosubstituted benzene (1:1 in volume), known amounts of azobenzene were added into the solution as an internal standard. The products were separated by silica gel TLC using benzene–acetone mixture (20:1, in a typical run) as the developing solvent. From the chromatogram, each product was extracted and diluted with methanol to a fixed volume; then the extinction was measured spectrophotometrically.

References

1) a) "Nitrenes," ed by W. Lwowski, Interscience, New York, N.Y. (1970); b) "The Chemistry of the Azido Group," ed by S. Patai, Wiley, New York, N.Y. (1971), and references cited therein.

2) T. Goka, H. Shizuka, and K. Matsui, *J. Org. Chem.*, **43**, 1361 (1978).

3) R. Kayama, H. Shizuka, S. Sekiguchi, and K. Matsui, *Bull. Chem. Soc. Jpn.*, **48**, 3309 (1975).

4) H. Yamada, H. Shizuka, and K. Matsui, *J. Org. Chem.*, **40**, 1351 (1975).

5) J. W. Baldwin and R. A. Smith, *J. Org. Chem.*, **32**, 3511 (1967).

6) W. Lwowski, T. J. Maricich, and T. W. Mattingly, Jr., *J. Am. Chem. Soc.*, **85**, 1200 (1963).

7) R. J. Cotter and W. F. Beach, *J. Org. Chem.*, **29**, 751 (1964).

8) K. Hafner and C. König, *Angew. Chem.*, **75**, 89 (1963).

9) R. A. Abramovitch and V. Uma, *J. Chem. Soc., Chem. Commun.*, **1968**, 797.

10) F. D. Marsh and H. E. Simmons, *J. Am. Chem. Soc.*, **87**, 3529 (1965).

11) J. Thurston, J. Dudley, D. Kaiser, K. Hechenbleicker, F. Schaefer, and D. Holm-Hansen, *J. Am. Chem. Soc.*, **73**, 2981 (1951).

12) The CH_2CN group was omitted from our calculations, since its substituent constant is unavailable.

13) J. E. Baldwin and R. A. Smith, *J. Am. Chem. Soc.*, **89**, 1886 (1967).

14) R. Kayama, S. Hasunuma, S. Sekiguchi, and K. Matsui, *Bull. Chem. Soc. Jpn.*, **47**, 2825 (1974).

The Reaction of Alkyl 3-Alkoxy-2-bromopropanoate with Triethyl Phosphite

Yoshiki Okamoto,* Tsutomu Tone, and Hiroshi Sakurai

The Institute of Scientific and Industrial Research, Osaka University, Yamadakami, Suita, Osaka 565

(Received June 12, 1980)

Synopsis. Alkyl 3-alkoxy-2-bromopropanoate reacted with triethyl phosphite to give alkyl 2,3-bis(diethoxyphosphinyl)propanoate as the major product.

It is well known that alkyl 2-haloalkanoates react with trialkyl phosphite to give alkyl 2-(dialkoxyphosphinyl)alkanoates by means of an Arbuzov reaction.[1] However, when ethyl 2-bromo-3-ethoxypropanoate(**1**) was treated with triethyl phosphite, the expected product, ethyl 3-ethoxy-2-(diethoxyphosphinyl)propanoate (**2**), was not obtained at all; rather, ethyl 2,3-bis(diethoxyphosphinyl)propanoate(**3**) was obtained as the major product. We now wish to report on these unusual results.

$$ROCH_2CHBrCOOR' + 2P(OR'')_3 \longrightarrow (R''O)_2OPCH_2CH[PO(OR'')_2]COOR' + R''Br + ROR'' \quad (1)$$

The reaction of **1** with three molar equivalents of triethyl phosphite began at 120 °C with the evolution of ethyl bromide, diethyl ether, and ethanol. From the residual mixture, **3**, triethyl phosphate, and ethyl 3-(diethoxyphosphinyl)propanoate(**4**) were obtained by distillation under reduced pressure. The reactions of other alkyl 3-alkoxy-2-bromopropanoates gave similar results, as is summarized in the table.

The yields of **3** were slightly decreased with an increase in the bulkiness of the alkyl group of R and/or R′. Even if an excess amount of triethyl phosphite was used, the yield of **3** did not increase. With an equimolar amount of triethyl phosphite, the yield of **3** was only 12%. In the reaction of **1** with trimethyl phosphite, none of the analogous product could be detected. From this mixture, dimethyl methylphosphonate was isolated almost quantitatively, and **1** was recovered, indicating that the rapid isomerization of trimethyl phosphite to dimethyl methylphosphonate by means of methyl bromide produced from the Arbuzov reaction occurred.

Table 1. Yields of alkyl 2,3-bis(dialkoxyphosphinyl)-propanoates from alkyl 3-alkoxy-2-bromopropanoates(**1**) with trialkyl phosphites

R	R′	R″	Bp/10^{-2} mmHg	Yield/%
CH_3	CH_3	CH_3	—	0[a]
CH_3	C_2H_5	CH_3	—	0[a]
CH_3	CH_3	C_2H_5	130—140	61[b]
C_2H_5	C_2H_5	C_2H_5	138—145	56[b]
n-C_3H_7	CH_3	C_2H_5	130—140	50[b]
i-C_3H_7	CH_3	C_2H_5	131—139	46[b]
n-C_4H_9	CH_3	C_2H_5	130—141	36[b]

a) Methyl or ethyl 2-bromo-3-methoxypropanoate respectively was almost entirely recovered. b) These were contaminated by products from the ester exchange.

The reaction may proceed as is shown in Scheme 1; the unstable intermediate, **2**, which may be formed by the Arbuzov reaction of **1** with triethyl phosphite, immediately eliminates the ethanol to give ethyl 2-(diethoxyphosphinyl)propenoate(**5**), which reacts subsequently with triethyl phosphite to give **3**.

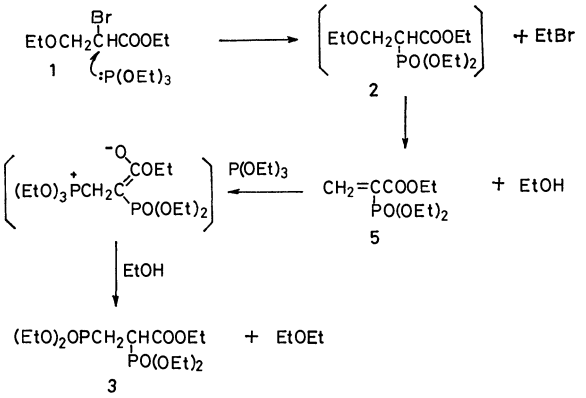

Scheme 1.

A facile elimination of ethanol has been found in the transformation of diethyl 2-(ethoxymethyl)propanedioate into diethyl 2-methylenepropanedioate.[2] When **5** prepared by another method[3] was treated with triethyl phosphite in the presence of ethanol at 110 °C for 0.5 h, **3** was given in a 62% yield.[5]

The formation of ethyl acrylate and **4** may be interpreted as in Scheme 2. The nucleophilic attack of triethyl phosphite may occur at the bromine center to give ethyl acrylate and tetraethoxyphosphonium bromide.[4] The former reacts with triethyl phosphite to give **4**,[5] and the latter decomposes to ethyl bromide and triethyl phosphate. The nucleophilic attack of triethyl phosphite might occur competitively at the carbon adjacent to the ethoxycarbonyl group and at the bromine, giving **3** and **4** respectively. The more nucleophilic diethyl phosphonate anion attacks preferentially at the bromine center to reduce **1** to

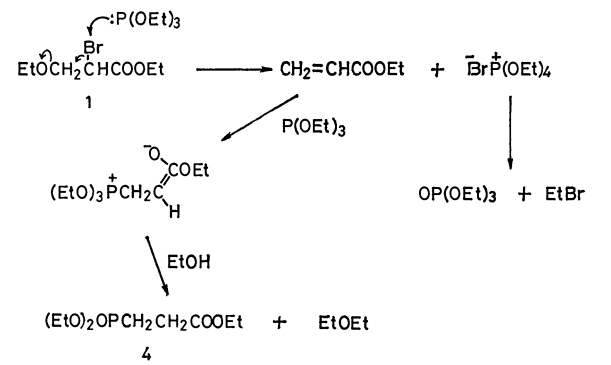

Scheme 2.

ethyl 3-ethoxypropanoate in a high yield at room temperature.

Experimental

*The Reaction of Ethyl 2-Bromo-3-ethoxypropanoate (**1**) with Triethyl Phosphite.* Ethyl 2-bromo-3-ethoxypropanoate (**1**, 15.0 g, 0.067 mol) and triethyl phosphite (33.2 g, 0.21 mol) were placed in a three-necked flask with a gas-inlet tube and a reflux condenser fitted with a tube connected to a trap cooled with Dry Ice–acetone. The mixture was heated at 120—130 °C for 5 h with the bubbling of nitrogen gas, until the evolution of volatile material ceased. The trapped volatile material (6.9 g) was identified as a mixture of ethyl bromide, diethyl ether, ethanol, and a trace amount of ethyl acrylate with GLPC (Shimadzu GC-3AF, a 3 m× 3 mmϕ column packed with 15% PEG 9000 on Uniport B, at 50 °C), but their relative ratio could not be defined with reproducibility. The residual mixture was distilled fractionally to give 1.0 g of a mixture of triethyl phosphate, a trace amount of diethyl ethylphosphonate, 2.1 g of **4** (bp 151—152 °C/1 mmHg,† identified with an authentic sample[6]), and 14.0 g of **3**; bp 138—145 °C/10^{-2} mmHg†. M^+ 374. ^{1}H-NMR (CCl_4) δ=2.40 (2H, m, CH_2), 3.28 (1H, m CH); ^{13}C-NMR ($CDCl_3$–TMS) δ=23.3 (d-d, J_{CP}=140 Hz J_{CCP}=3 Hz, CH_2P), 40.0 (d-d, J_{CP}=127 Hz, J_{CCP}= 3 Hz, CHP); ^{31}P-NMR ($CDCl_3$–85% H_3PO_4) δ=−21.1 (d, J_{PP}=69 Hz, PCH), −27.6 (d, PCH_2).

*The Reaction of Ethyl 2-(Diethoxyphosphinyl)propenoate (**5**) with Triethyl Phosphite.* A mixture of **5** (11.8 g, 0.05 mol), triethyl phosphite (8.3 g, 0.05 mol), and ethanol (9.2 g, 0.2 mol) was heated at 100—110 °C for 2 h in a nitrogen atmosphere. After the reaction, a fraction (11.6 g, bp 139—145 °C/10^{-2} mmHg) was obtained by distillation under reduced pressure. It was found to be identical with **3** by a comparison of the NMR and GLPC data (an 1×3 mmϕ column packed with 10% Silicone SE-30 on Uniport B, at 200 °C).

*The Reaction of Ethyl 2-Bromo-3-ethoxypropanoate (**1**) with Sodium Diethyl Phosphonate.* Stripts of sodium (2.3 g, 0.1 atm) was added, portion by portion, into diethyl phosphonate (52 g, 0.4 mol). After the disappearance of the metal, the reaction mixture was cooled with ice water, and then **1** (11.3 g, 0.05 mol) was added, drop by drop. The resulting mixture was stirred at room temperature for 5 h and then poured into 5% sulfuric acid–ice water. The reaction product was extracted with ether, and the ethereal solution was washed with water and dried over sodium sulfate. After the removal of the ether, ethyl ethoxypropanoate was obtained by distillation (bp 66—68 °C/17 mmHg†,[7] 5.3 g, 72% yield).

References

1) a) K. Sasse, "Methoden der Organischen Chemie Band XII/1, Organische Phosphorverbindungen Teil 1," ed by E. Muller, Georg Thieme Verlag. Stuttgart (1963), p. 436; b) R. G. Harvey and E. De Sombre, "Topics in Phosphorus Chemistry Vol. 1," ed by M. Grayson and E. J. Griffith, Interscience Publishers, New York (1964), p. 57.

2) W. Feely and V. Boekelheide, *Org. Synth.*, Coll. IV, 298 (1963).

3) V. S. Abramov and N. A. Il'ina, *Zh, Obsch. Khim.* **26**, 2014 (1956).

4) A. J. Kirby and S. G. Warren, "The Organic Chemistry of Phosphorus," Elsevier Publishing Co., New York (1967), p. 103.

5) R. G. Harvey, *Tetrahedron*, **22**, 2561 (1966).

6) P. Nylen, *Chem. Ber.*, **59**, 1119 (1926).

7) C. F. Koelsch, *J. Am. Chem. Soc.*, **65**, 438 (1943).

† 1 mmHg≈133.3 Pa.

Synthesis of *o*-(2-Indolyl)benzoic Acids from Indole

Toshio ITAHARA

Institute of Chemistry, College of Liberal Arts, Kagoshima University, Kagoshima 890

(Received June 13, 1980)

Synopsis. Treatment of 6*H*-isoindolo[2,1-*a*]indol-6-ones with potassium *t*-butoxide/*t*-butyl alcohol containing a small amount of water at 82° afforded *o*-(2-indolyl)benzoic acids in good yields.

Some 2-arylindoles often have potent physiological activities. However, little attention has been paid to the preparation of some 2-(*o*-substituted phenyl)indoles, such as *o*-(2-indolyl)benzoic acids (**3**), although Pailer *et al.*[1] reported that the reduction of 2-nitrodeoxybenzoin-2'-carboxylic acid afforded *o*-(2-indolyl)benzoic acid (**3a**). On the other hand, we reported the synthesis of 6*H*-isoindole[2,1-*a*]indol-6-ones (**2**) by the oxidation of 1-aroylindoles (**1**) with palladium acetate,[2] although **2** was also prepared by the irradiation of 1-(*o*-iodobenzoyl)indole[3] or of *N*-(*o*-methylphenyl)-phthalimides.[4] As a study of the synthetic application of the reaction, we were interested in the synthesis of **3** by hydrolysis of **2**. The results will provide a new route to prepare 2-arylindoles from indole (Scheme 1).

Attempted hydrolysis of 6*H*-isoindolo[2,1-*a*]indol-6-one (**2a**) in the usual conditions (HCl/MeOH+H_2O and NaOH/MeOH+H_2O) was unsuccessful. On the other hand, Gassman *et al.*[5] previously reported the *t*-BuOK-promoted hydrolysis of amides in diethyl ether containing H_2O. We attempted the hydrolysis of **2** by an application of their method. Treatment of **2a** with *t*-BuOK in *t*-BuOH containing a small amount of H_2O at 82 °C under nitrogen afforded **3a** in 75% yield. Under similar conditions the treatment of **2b** and **2c** with *t*-BuOK gave **3b** (74%) and **3c** (70%), respectively. The structure of **3** was independently confirmed by the elemental analysis, the molecular weight (mass specroscopy), and NMR and IR data. The physiological activities of **3b** and **3c** were examined. The compounds **3b** and **3c** exhibit antifungal activities at concentration of 0.1%. The results are listed in Table 1.

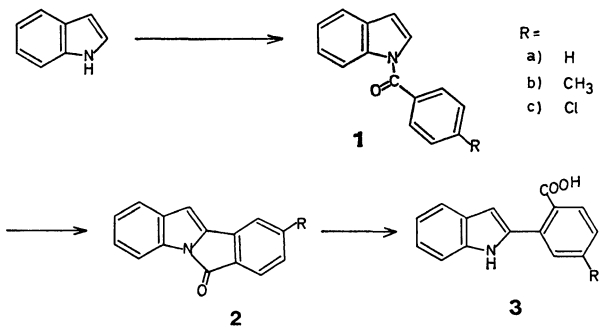

Scheme 1.

Experimental

All the melting points are uncorrected. Elemental analyses were performed by the Analytical Center of Kyoto University. Infrared spectra were recorded with a JASCO IRA-1 spectrometer. Proton magnetic resonance spectra were recorded with a JEOL JNM-60 spectrometer using TMS as the internal reference.

*Treatment of **2** with Potassium* t*-Butoxide.* The solution of **2** (1.0 mmol) in *t*-BuOH (50 ml) and H_2O (5 ml) containing *t*-BuOK (10.0 mmol) was heated at 82° under nitrogen for 12 h. The reaction mixture was evaporated, diluted with a large amount of water, carefully neutralized with diluted HCl, and extracted with ether. The ether extract was dried with sodium sulfate and evaporated to give a brown semicrystalline residue which was triturated with ether/hexane to give **3**, light brown needles from ether/hexane.

*o-(2-Indolyl)benzoic Acid (**3a**)*: Mp 155—157°, partially decomposed at 128—132° (lit.[1] 159°); IR (Nujol): 3430 (NH), 3200—2250 (COOH), 1680 (COOH) cm^{-1}; NMR ($CDCl_3$): δ 6.84 (1H, s), 7.12—8.30 (8H, m), 8.60 (1H, broad), 9.42 (1H, broad); Mass (relative intensity, %): 237 (M^+, 47), 219 (M^+-H_2O, 100). Found: C, 75.95; H, 4.62; N, 5.74%. Calcd for $C_{15}H_{11}NO_2$: C, 75.93; H, 4.67; N, 5.90%.

*2-(2-Indolyl)-4-methylbenzoic Acid (**3b**)*: Mp 143—144°, IR (Nujol): 3430 (NH), 3180—2200 (COOH), 1680 (COOH) cm^{-1}; NMR ($CDCl_3$): δ 2.46 (3H, s), 6.86 (1H, s), 7.21—8.25 (6H, m), 8.12 (1H, d, J=9.0 Hz), 8.50 (1H, broad), 9.50 (1H, broad); Mass (relative intensity, %): 251 (M^+, 42), 233 (M^+-H_2O, 100). Found: C, 76.49; H, 5.11; N, 5.40%. Calcd for $C_{16}H_{13}NO_2$: C, 76.47; H, 5.22; N, 5.57%.

*2-(2-Indolyl)-4-chlorobenzoic Acid (**3c**)*: Mp 167—168°; IR (Nujol): 3460 (NH), 3200—2400 (COOH), 1690 (COOH) cm^{-1}; NMR ($CDCl_3$): δ 6.80 (1H, s), 7.13—8.60 (8H, m), 9.30 (1H, broad); Mass (relative intensity, %): 271 (M^+, 52), 273 (M^++2, 18), 253 (M^+-H_2O, 100), 255 (M^++2$-H_2O$, 34). Found: C, 66.12; H, 3.58; N, 5.07%. Calcd for $C_{15}H_{10}NO_2Cl$: C, 66.31; H, 3.71; N, 5.16%.

The author wishes to thank Professor Tsunao Hase and Mr. Tetsuo Iwagawa of Kagoshima University (Faculty of Science) for mass spectrometric analyses and Dr. Masaaki Takami of Kuraray Co., Ltd., for biological assays.

TABLE 1. ANTIFUNGAL ACTIVITIES OF *o*-(2-INDOLYL)BENZOIC ACIDS **3b** AND **3c**

	Sphaerotheca Fuliginca (Cucumber powdery mildew) (% Inhibition)	*Collectotrichum lagenarium* (Cucumber anthraenose) (% Inhibition)	*Pyricularia oryzoe* (Rice blast) (% Inhibition)
3b	0	0	94
3c	7	66	100

References

1) M. Pailer, A. Schleppnik, and A. Meller, *Mh. Chem.*, **96**, 1695 (1965).
2) T. Itahara, *Synthesis*, **1979**, 151.
3) W. Carruthers and E. Evans, *J. Chem. Soc., Perkin Trans. 1*, **1974**, 1523.
4) Y. Kanaoka and K. Koyama, *Tetrahedron Lett.*, **1972**, 4517; Y. Kanaoka, C. Nagasawa, H. Nakai, Y. Sato, H. Ogiwara, and T. Mizoguchi, *Heterocycles*, **3**, 553 (1975); M. Terashima, K. Koyama, and Y. Kanaoka, *Chem. Pharm. Bull.*, **26**, 630 (1978).
5) P. G. Gassman, P. K. G. Hodgson, and R. J. Balchunis, *J. Am. Chem. Soc.*, **98**, 1275 (1976).

The Mechanism of the Reaction of (Aryloxy)trimethylstannane with Benzyl Bromide giving Aryl Benzyl Ether

Seizi KOZUKA,* Akihiko KIKUCHI, and Shigeru YAMAGUCHI

Department of Applied Chemistry, Faculty of Engineering, Osaka City University, Sugimotocho, Sumiyoshi, Osaka 558

(Received June 23, 1980)

Synopsis. A kinetic study has been performed for the reaction of (aryloxy)trimethylstannane with benzyl bromide giving aryl benzyl ether and bromotrimethylstannane. Bimolecular nucleophilic attack of the aryloxy-oxygen on the benzyl-carbon has been suggested for the reaction based on the substituent effect.

Recently, we have reported kinetic and stereochemical results of the reactions of (alkylthio and arylthio)trimethylstannanes with haloalkanes.[1] A bimolecular nucleophilic attack of the sulfur atom on

$$Me_3SnSR + R'X \rightarrow [Me_3SnS^{\delta+}(R)\cdots R'\cdots X^{\delta-}] \rightarrow Me_3SnX + RSR'$$

the alkyl-carbon has been suggested for the reaction. A similar reaction has been known for the alkoxy analogue of the (alkylthio)stannane *i.e.*, the reaction of alkoxystannane with haloalkane.[2]

$$Bu_3SnOMe + BuI \rightarrow Bu_3SnI + BuOMe$$

Since the nucleophilicity of oxygen atom is much weaker than that of sulfur, it is doubtful whether the mechanism suggested for the reactions of (alkylthio and arylthio)stannanes is also applicable for that of alkoxystannane. We have extended our mechanistic study to the reaction of alkoxystannane with haloalkane.

The reaction of trimethyl(phenoxy)stannane with benzyl bromide was examined in the present study and found that the reaction gave bromotrimethylstannane and benzyl phenyl ether. The bromostannane was detected by GLC analysis of the reaction solution and the ethereal product was isolated and characterized.

$$Me_3SnOPh + PhCH_2Br \xrightarrow{120\,^\circ C,\ 24\,h} Me_3SnBr + PhCH_2OPh$$

The reaction, however, was found to proceed much slower than that of the (arylthio)stannane with benzyl bromide.[1] Almost no reaction was found under the same reaction conditions used for the reaction of the (arylthio)stannane. Accordingly, the rate of the reaction was measured in a polar solvent at higher temperature with high concentration of the substrate in order to increase the observed rate. A good pseudo-first-order plot was obtained. The results are given in Table 1. Hammett plot of the rates given in Table 1 gave apparently negative ρ value [$\rho_{(\sigma)} = -0.78$] with fair linearity ($\gamma = 0.982$). This would reveal that the nucleophilicity of aryloxy-oxygen played an important role during the reaction although the magnitude of the value appeared somewhat smaller than that obtained for the analogous reaction of (arylthio)stannane.[1] A charge separated 4-center mechanism could not be ruled out by the rather small ρ value alone but is unlikely considering the lower reactivity of the (aryloxy)stannane. The relative reactivity of (aryloxy)stannane toward (arylthio)stannane is consistent with relative nucleophilicities of oxygen and sulfur atoms.[3] Furthermore, the four-center mechanism has recently been ruled out for the bimolecular reaction of this type.[4] Thus, the most plausible mechanism is the nucleophilic attack of the

$$Me_3SnOPh + PhCH_2Br \rightarrow [Me_3Sn{-}O^{\delta+}(Ph)\cdots CH_2(Ph)\cdots Br^{\delta-}] \rightarrow \text{Products}$$

oxygen atom similar to that suggested for the reactions of analogous (alkylthio and arylthio)stannanes with haloalkane.[1] The reaction of alkoxystannane with haloalkane[2] would proceed *via* the same process, that is nucleophilic attack of oxygen atom, since this mechanism has been suggested in the present study even for the less nucleophilic (aryloxy)stannane.

Table 1. Pseudo-first-order rate constants for the reaction of $Me_3SnOC_6H_4X$-*p* + $C_6H_5CH_2Br$ in PhCN at 120 °C

X	k_{obsd}/s^{-1}
OCH_3	2.70×10^{-4}
CH_3	1.63×10^{-4}
H	1.15×10^{-4}
Cl	9.05×10^{-5}
NO_2	3.47×10^{-5}

Experimental

(Aryloxy)trimethylstannane. The compounds were prepared either by the reaction of sodium aryl oxide with bromotrimethylstannane in liquid ammonia[5] or by a modified alkoxyl exchange reaction[6] of methoxytrimethylstannane with appropriate phenol. The latter mathod gave better yields with simple procedure. Substituent X of Me_3Sn-OC_6H_4X-*p*, yield, physical properties, and elemental analysis were as follows: H, 36%, 109 °C/8 mmHg (1 mmHg = 133.322 Pa), δ_{CDCl_3} 0.53 ppm (Me_3); CH_3, 21%, mp 87—88 °C (from hexane-chloroform), δ_{CDCl_3} 2.22 (*p*-Me), 0.50 ppm (Me_3). Found: C, 44.06, H, 5.68%. Calcd for $C_{10}H_{16}OSn$: C, 44.33; H, 5.95; OCH_3, 34%. Mp 65—66 °C, bp 137 °C/3 mmHg, δ_{CDCl_3} 3.70 (OCH_3), 0.49 ppm (Me_3). Found C, 41.91; H, 5.25%. Calcd for $C_{10}H_{16}O_2Sn$: C, 41.86; H, 5.62; Cl, 65% (by exchange). Bp 137 °C/3 mmHg, δ_{CDCl_3} 0.53 ppm (Me_3). Found C, 36.60; H, 4.34%. Calcd for $C_9H_{13}ClOSn$: C, 37.10; H, 4.50; NO_2, ≈100% (by exchange). Mp 83.5—84 °C (from hexane–benzene), δ_{CDCl_3} 0.67 ppm (Me_3). Found C, 36.16; H, 4.33%. Calcd for $C_9H_{13}NO_3Sn$: C, 35.81, H, 4.34%.

Product Analysis. Trimethylphenoxystannane (1.2 g, 4.5 mmol) and benzyl bromide (3.8 g, 9.0 mmol) were dissolved in benzonitrile (5 cm^3) and the solution was heated

at 120 °C for 24 h in a sealed tube. The solvent and volatile product were evapolated under reduced press. Bromotrimethylstannane was detected in the volatile components by GLC analysis and benzyl phenyl ether was isolated from the residue by recrystallization, mp 40 °C (from hexane), 68% yield.

Kinetics. In a polar solvent, both the trimethyl signals of trimethylphenoxystannane (δ 0.53 ppm) and bromotrimethylstannane (δ 0.77 ppm) are submerged into one signal due to exchange reaction and the rate could not be measured by integration of those two signals. Accordingly, (aryloxy)-trimethylstannane (1.8×10^{-3} mol) and benzyl bromide (1.8×10^{-2} mol) were dissolved in benzonitrile (total 5 cm^3) with the addition of dichloromethane (5.4×10^{-4} mol) as the internal standard. The solution was devided into ten portions and sealed in glass tubes. The tubes were dipped in a constant temperature bath (120±0.1 °C). The tubes were picked up at time intervals and the amount of benzyl phenyl ether at the time was measured by integration of the benzyl proton signal (δ 4.98 ppm) relative to the internal standard (CH_2Cl_2, δ 5.21 ppm). Rate constant was obtained by least square calculation. The reaction of the (aryloxy)-stannane with dichloromethane was found to be negligible under the reaction conditions used.

References

1) S. Kozuka and S. Ohya, *J. Organomet. Chem.*, **149**, 161 (1978); *Bull. Chem. Soc. Jpn.*, **51**, 2651 (1978).

2) J. C. Pommier and J. Valade, *C. R. Acad. Sci.*, **260**, 4549 (1965).

3) Trimethylphenoxystannane is less reactive than trimethyl(phenylthio)stannane by a factor of *ca.* 10^4 which is estimated by inspection of the present result and that reported in Ref. 1.

4) S. Kozuka and T. Higashino, *Tetrahedron Lett.*, **21**, 2067 (1980).

5) C. A. Kraus and A. M. Neal, *J. Am. Chem. Soc.*, **51**, 2403 (1929).

6) M. F. Shostakovskii, V. M. Vlasov, and R. G. Mirskov, *Zh. Obshsh. Khim.*, **34**, 1354 (1964).

Crosslinked Polyvinylpyridine Hydrochloride as a Mild Polymeric Catalyst for Acetalization of Carbonyl Compounds and Esterification of Carboxylic Acids

Jun-ichi YOSHIDA, Jiro HASHIMOTO, and Nariyoshi KAWABATA*

Department of Chemistry, Faculty of Polytechnic Science, Kyoto Institute of Technology, Matsugasaki, Sakyo-ku, Kyoto 606

(Received July 19, 1980)

Synopsis. Crosslinked poly(4-vinylpyridine) hydrochloride was found to be an effective catalyst for acetalization of carbonyl compounds and esterification of carboxylic acids. The polymeric catalyst was inert to some acid sensitive functional groups which cannot tolerate under the influence of a strong acid cation exchange resin.

One of the advantages provided by insoluble polymeric catalyst[1] is their easy recovery from the reaction system which prevents the leakage of toxic chemicals. The use of them may be valuable from environmental point of view. Although cation exchange resins[2] are historically one of the earliest examples of the polymeric catalysts, there have been few works available in the literature on milder and more selective polymeric acid catalysts. We have now found that crosslinked poly(4-vinylpyridine) hydrochloride (**1**) was a mild and effective catalyst for acetalization of carbonyl compounds and esterification of carboxylic acids.

The experimental results of the acetalization of carbonyl compounds are given in Table 1. The reaction of cyclohexanone with ethylene glycol proceeded smoothly in the presence of **1** at room temperature to give the corresponding acetal in 96% yield. The spent catalyst was easily rejuvenated by washing with small amounts of organic solvents, and was reused several times with little loss of activity. Acetalization of octanal and citronellal with ethylene glycol also proceeded smoothly in the presence of **1**.

The polymeric catalyst (**1**) was also effective for the esterification of acetic acid with 1-butanol, and the reaction at 80 °C gave butyl acetate in a quantitative yield. In the corresponding esterification of acetic acid with 2-butanol, however, yield of the ester was low. Results are given in Table 2.

Although pyridine hydrochloride has been known as a good catalyst for acetalization of carbonyl compounds,[3] it is very hygroscopic and must be protected from moisture.[4] This disadvantage can be overcome by the use of the polymeric catalyst (**1**) which is non-hygroscopic and very easy to handle in comparison with the monomeric analogue.

A strong acid cation exchange resin containing sulfonic acid group was also an efficient catalyst for the acetalization and the esterification. On the other hand, a weak acid cation exchange resin containing carboxyl group was almost inactive as a catalyst for the reactions. It should be noted, however, that the use of **1** as a catalyst has an advantage over the use of strong acid cation exchange resins, because the use of **1** allowed the application of reactions to the reactants having some acid sensitive functional groups which cannot tolerate the strong acid cation exchange resins. In order to demonstrate this advantage of the use of **1**, esterification of acetic acid with 1-butanol was carried out in the presence of a polymeric catalyst and an additive which contained some acid sensitive functional groups. Results are given in Table 3. For example, 1-phenylethanol used as an additive was recovered quantitatively in the reaction of acetic acid

Table 1. Acetalization of carbonyl compounds with ethylene glycol catalized by polymeric acid catalysts[a]

Carbonyl compound	Catalyst	Products	Yield %[b]
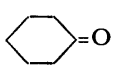	**1**	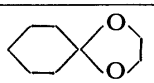	96
	1[c]		98
	IR-120B[d]		95
	IRC-50[e]		0
$C_7H_{15}CHO$	**1**	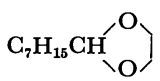	90
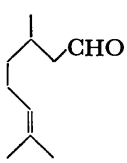	**1**	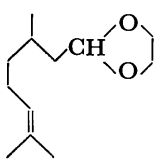	62

a) Reactions were carried out with 2.0 mmol of carbonyl compound, 10.0 mmol of ethylene glycol, and 50 mg of polymeric acid catalyst at room temperature for 1 h. b) Determined by GLC analysis of the reaction mixture, and were based on the carbonyl compound. c) Fifth use. d) A strong acid cation exchange resin in the H form. e) A weak acid cation exchange resin in the H form.

Table 2. Esterification of acetic acid with alcohols catalyzed by polymeric acid catalysts[a]

Alcohol	Catalyst	Products	Yield %[b]
n-C_4H_9OH	**1**	$CH_3COOC_4H_9$-*n*	100
	IR-120B[c]		100
	IRC-50[d]		3
s-C_4H_9OH	**1**	$CH_3COOC_4H_9$-*s*	27
	IR-120B[c]		74

a) Reactions were carried out with 5.0 mmol of acetic acid, 10.0 mmol of alcohol, and 125 mg of polymeric acid catalyst at 80 °C for 1 h. b) Determined by GLC analysis of the reaction mixture, and was based on acetic acid. c) See footnote (d) in Table 1. d) See footnote (e) in Table 1.

Table 3. Esterification of acetic acid with 1-butanol in the presence of some acid sensitive additives[a)]

Additive	Catalyst	Yield of the ester/%[b)]	Recovered additive/%[b)]
	**1**	93	100
	IR-120B[c)]	98	21[d)]
	**1**	2	20
	IR-120B[c)]	85	0
	**1**	88	100
	IR-120B[c)]	89	45

a) The reactions were carried out with 5.0 mmol of acetic acid, 10.0 mmol of 1-butanol and 2.5 mmol of additive at 80 °C for 1 h. b) Determined by GLC analysis of the reaction mixture. c) See footnote (d) in Table 1. d) Significant amounts of styrene and other unidentified products were formed.

and 1-butanol catalyzed by **1**. On the contrary, in the corresponding reaction catalyzed by the strong acid cation exchange resin, only 21% of 1-phenylethanol was recovered and significant amounts of styrene and other unidentified products were formed. Norcarane contains an acid sensitive cyclopropane ring, but was not affected under the influence of **1**. In contrast, only 45% of norcarane was recovered in the presence of the strong acid cation exchange resin. (Epoxyethyl)benzene was unable to tolerate both of the catalysts.

The results obtained here may suggest the synthetic utility of **1** as a mild and efficient polymeric acid catalyst which provides an attractive alternate to the commercially available cation exchange resins.

Experimental

General. ^{1}H NMR spectra were recorded on a Varian T-60A spectrometer in carbon tetrachloride using tetramethylsilane as internal standard. IR spectra were recorded on a Hitachi 215 grating spectrometer. GLC analyses were performed on a Shimadzu GC-4B or GC-4C gas chromatograph.

Materials. 4-Vinylpyridine provided by Koei Chem. Co. Ltd., Osaka and commercial ethanol were purified by distillation before polymerization. A commercial product of divinylbenzene (*ca.* 55%) was washed with 5% aqueous sodium hydroxide and with deionized water, dried over potassium carbonate, and distilled. Dry hydrogen chloride was prepared by dropping concentrated sulfuric acid on dry lumps of ammonium chloride, and dried by passing through concentrated sulfuric acid. Other chemicals and nitrogen were used as obtained commercially.

*Preparation of Crosslinked Poly(4-vinylpyridine) Hydrochloride (**1**).* Crosslinked poly(4-vinylpyridine) containing 75 mol% 4-vinylpyridine was prepared by a copolymerization of 4-vinylpyridine with divinylbenzene followed by grinding and sifting to 60—80 mesh as was described elsewhere.[5)] The dry copolymer (1.500 g) was placed in a glass tube (5.0 mm diam × 180 mm) and excess dry hydrogen chloride was passed through the tube. To remove excess hydrogen chloride in the resin layer, nitrogen was passed through the tube until no hydrogen chloride was detected at the other end of the tube. After drying *in vacuo*, 1.845 g of **1** was obtained. Elemental analysis of the polymer showed the content of 6.82% of N and 17.98% of Cl, suggesting that the pyridyl group in the resin was quantitatively converted to the hydrochloride form (5.1 mequiv of HCl/dry g).

Resins. For comparison, two commercial resins were used in this work. Amberlite IR-120B and Amberlite IRC-50 supplied by Rohm & Haas Co., Philadelphia, Pa., U.S.A., were used as a strong acid cation exchange resin and a weak acid cation exchange resin, respectively. They were preconditioned and transferred to the H form in usual manners, and were dried *in vacuo* before use. The ion exchange capacity of IR-120B was 4.76 mequiv/dry g, which was determined by titration with standard 0.1 mol/l aqueous NaOH using phenolphthalein as indicator in 1 mol/l aqueous NaCl. The ion exchange capacity of IRC-50 was 10.0 mequiv/dry g, which was determined by back titration with standard 0.1 mol/l aqueous HCl using phenolphthalein as indicator after treatment with a large excess of 0.1 mol/l aqueous NaOH overnight at room temperature.

Acetalization of Carbonyl Compounds. A mixture of carbonyl compound (2.0 mmol), ethylene glycol (10.0 mmol), and a polymeric catalyst (50 mg) was stirred at room temperature for 1 h. After the reaction, the mixture was analyzed by GLC. After removal of the polymeric catalyst by filtration, the products were isolated and identified by comparison of their spectral data with those of authentic materials.

Crosslinked poly(4-vinylpyridine) (**1**) can be reused several times with little loss of activity. In this case, the spent polymeric catalyst was recovered by filtration, and was washed with benzene, methanol, and ether. After dried *in vacuo*, the recovered polymeric catalyst was reused for the acetalization.

Esterification of Carboxylic Acids. A mixture of carboxylic acid (5.0 mmol), an alcohol (10.0 mmol) and a polymeric catalyst (125 mg) was stirred at 80 °C for 1 h, and the mixture was analyzed by GLC. After removal of the catalyst by filtration, the products were isolated and identified by comparison of their spectral data with those of authentic materials.

The esterification reactions of acetic acid with 1-butanol in the presence of an additive were carried out in a similar manner.

References

1) For example, D. C. Neckers, *J. Chem. Educ.*, **52**, 695 (1975).

2) a) R. Kunin, E. Meitzner, and N. Bortnick, *J. Am. Chem. Soc.*, **84**, 305 (1962); b) G. F. Vesley and V. I. Stenberg, *J. Org. Chem.*, **36**, 2548 (1971); c) V. I. Stenberg, G. F. Vesley, and D. Kubik, *ibid.*, **36**, 2550 (1971).

3) a) J. Egyed, P. Demerseman, and R. Royer, *Bull. Soc. Chim. Fr.*, **1972**, 2287; b) R. Rausser, A. M. Lyncheski, H. Harris, R. Grocela, N. Murrill, E. Bellamy, D. Ferchinger, W. Gebert, H. L. Herzog, E. B. Hershberg, and E. P. Oliveto, *J. Org. Chem.*, **31**, 26 (1966).

4) M. D. Taylor and L. R. Grant, *J. Chem. Educ.*, **32**, 39 (1955).

5) N. Kawabata and K. Ohira, *Environ. Sci. Technol.*, **13**, 1396 (1979).

The Synthesis of Thermally Stable Oils by the Benzylation of Biphenyl with Benzyl Chloride Catalyzed by Iron(III) Oxide

Makoto Hino and Kazushi Arata*,†

Hakodate Technical College, Tokura-cho, Hakodate 042

† *Hokkaido University of Education, Hachiman-cho, Hakodate, 040*

(Received June 5, 1980)

Synopsis. The benzylation of biphenyl with various amounts of benzyl chloride was performed at 80 °C or at room temperature in the presence of iron(III) oxide prepared by calcining, at 300 °C, iron(III) hydroxide which has been precipitated by hydrolyzing $FeCl_3$ with ammonia. The products with various viscosities were thermally stable up to 200—300 °C, and no chlorine was detected in the products.

Several works concerning the decomposition of PCB by methods using pyrolysis,[1] radiolysis,[2] photolysis[3] and plasma[4] have been reported. On the other hand, some workers have investigated the alkylations of biphenyl in the presence of Friedel-Crafts catalysts in order to use the products as liquid heat stabilizers.[5,6] Biphenyl is also used as a high-boiling heating medium by mixing it with diphenyl ether as a liquid at room temperature.[7] Previously, we reported that the iron(III) oxide thus prepared is an exceedingly effective catalyst for the polycondensation of benzyl chloride, and that the product is poly(*p*-phenylenemethylene) and stable up to 400 °C.[8] In this work, we wish to report that thermally stable oils with various viscosities can be synthesized with ease by the benzylation of biphenyl with benzyl chloride in the presence of the iron(III) oxide catalyst.

Experimental

The iron(III) oxide catalyst was prepared by calcining iron(III) hydroxide in a glass tube in air at 300 °C for 3 h; it was then stored in a glass ampoule until use. The iron(III) hydroxide was precipitated by hydrolyzing $FeCl_3$ with aqueous ammonia. The hydroxide was washed, dried at 100 °C, and finally powdered below 100 mesh. The benzyl chloride (guaranteed reagent of Wako Pure Chemical Co.) and biphenyl (Wako Pure Chemical Co.) were used without further purification.

Benzylation was carried out in bulk following two methods: (A): 10—60 ml of benzyl chloride were stirred, in 2-ml portion, into a mixture of 20 g of biphenyl (mp, 70 °C) and 0.1 g of the catalyst at 80 °C. Each reaction occurred immediately, with a violent evolution of HCl. Benzyl chloride was added at intervals of 10—30 s for the first 20 ml, and afterwards at 1—2 min intervals, without any additional catalyst. (B): 10—50 g of biphenyl were dissolved in 50 ml of benzyl chloride at room temperature, after which the benzylation was performed by stirring with 0.2 g of the catalyst. The reaction started immediately, with an evolution of HCl gas, and was completed within 7—10 min in every reaction. After the reactions by both methods, the reaction mixture was diluted with benzene, separated from the catalyst by filtration, washed with water several times, and dried; finally, the benzene was removed by vacuum evaporation.

Results and Discussion

Table 1 shows the yields and viscosities of the products. Brownish oils with various viscosities were obtained in high yields depending on the amount ratios of benzyl chloride and biphenyl reacted. In the cases of excess amounts of benzyl chloride (Runs 3—6), the products are considered to also contain poly(*p*-phenylenemethylene), judging from the high activity of the catalyst for the polycondensation of benzyl chloride to poly(*p*-phenylenemethylene).[8] Elemental analysis showed no chlorine in any of the products in the table. NMR spectroscopy showed a singlet peak at 3.85 ppm (CH_2) and a multiplet at 6.7—7.5 ppm (phenylene H) in the ratio 1:7 for the samples in Runs 2 and 8.

The TG analyses of the products were done in nitrogen; some of the results are shown in Fig. 1, together with that of biphenyl. The products were thermally stable up to 200—300 °C, above which decomposition occurs, and they decomposed completely at 550 °C. The weight decrease in biphenyl was 100%

Table 1. Benzylation of biphenyl with benzyl chloride

Run	Amount of benzyl chloride / ml	Amount of biphenyl / ml	Reaction temperature / °C	Yield / g	Viscosity[a] η_{rel}
1	10	20	80	25	2.76
2	20	20	80	34	3.37
3	40	20	80	47	4.74
4	60	20	80	60	5.97
5	50	10	RT[b]	43	8.95
6	50	20	RT	53	5.58
7	50	30	RT	65	3.88
8[c]	50	50	35	82	3.31

a) Relative viscosity of a 50 wt% benzene solution to benzene determined at 25 °C in a Cannon-Fenske viscosity. b) Room temperature. c) Since the biphenyl was not all soluble in benzyl chloride at room temperature, the reaction was carried out at 35 °C.

below 200 °C.

The molecular-weight distribution of the sample in Run 3 was determined by gel-permeation chromatography, as is shown in Fig. 2. The main products have a molecular weight of 220—380; this indicates that the degree of the benzylation of biphenyl is predominantly 1—3.

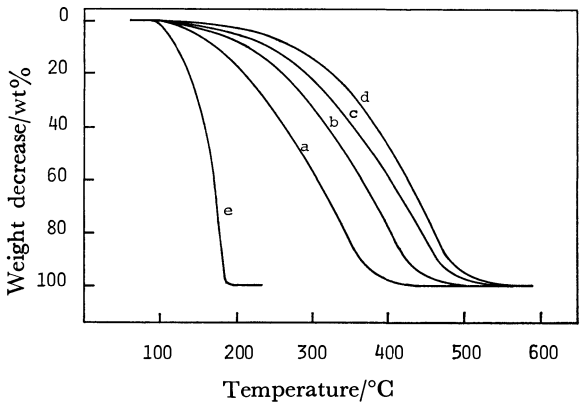

Fig. 1. TG curves of products.
a, b, c, and d refer to the products given by Runs 2, 3, 6, and 4, respectively. e: Biphenyl, heating rate: 5 °C/min.

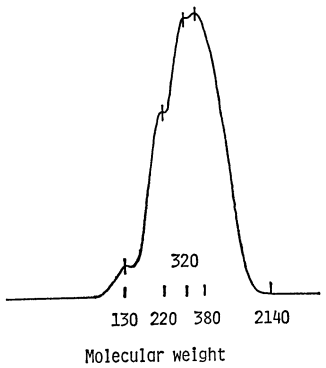

Fig. 2. GPC curve of the sample produced by Run 3. Concentration: 0.4 g in 100 ml of THF, flow rate: 1 ml/min.

The present synthesis was carried out with $AlCl_3$ and $FeCl_3$, typical Lewis acid catalysts, under the same conditions. The reaction was complete when 28 ml of benzyl chloride was added, in 2-ml portions, to a mixture of 20 g of biphenyl and 0.1 g of $AlCl_3$ at 80 °C. However, further reactions did not occur with additional benzyl chloride, in spite of another addition of the catalyst. It is considered that the oily product poisoned the acidic sites of the catalyst surface. Another run was performed at room temperature with 30 g of biphenyl dissolved in 50 ml of benzyl chloride and 0.2 g of $FeCl_3$, but the reaction was extremely slow; 1.38% chlorine was detected in the product after a reaction of 45 min.

The product obtained by the present easy method of synthesis with the conventional and active iron(III) oxide catalyst can replace PCB, whose synthesizing method is to liquidize biphenyl by chlorination. The present method could also be applicable to naphthalene as well as biphenyl, both of which are produced in great quantities in petroleum industries.

The authors are grateful to the Toyota Foundation for its finantial support of the present work.

References

1) L. Karlson and E. Rosen, *Chem. Scripta*, **1**, 61 (1971).
2) T. Tawai and Y. Shinozaki, *Chem. Lett.*, **1972**, 865.
3) T. Nishiwaki, J. Ninomiya, S. Yamanaka, and K. Ando, *Nippon Kagaku Kaishi*, **1972**, 2225.
4) K. Hiroaki, K. Mitsumori, and S. Mochizaki, *Chem. Lett.*, **1979**, 739.
5) D. B. Friddy, *I. E. C. Prod. Res. Develop.*, **8**, 239 (1969).
6) K. Ajimoto, Japan Pat. 74104890 (1974).
7) Monsanto Industrial Chemicals, *Chem. Process*, **39**, 118 (1976).
8) M. Hino and K. Arata, *Chem. Lett.*, **1979**, 1141.

The Effect of γ-Irradiation on the Biodegradability of Landfill Leachate

Takeshi SAWAI,* Teruko SAWAI, and Masao YAMAZAKI

Tokyo Metropolitan Isotope Research Center, 2-11-1, Fukazawa, Setagaya-ku, Tokyo 158

(Received June 16, 1980)

Synopsis. A preliminary examination of the enhancement of biodegradability for landfill leachate, humic acid, and fulvic acid solutions, and aqueous solutions of polyethylene glycol-6000 by irradiation by ^{60}Co γ-rays under aeration was performed. In all cases, the BOD_5/TOC and BOD_5/COD ratios increased with the dose. This suggests that the γ-irradiation modified these refractory materials to more biodegradable compounds.

The object of the treatment of landfill leachate is to remove organic substances and nitrogen contained in large amounts in the leachate. It is not easy to remove the organic substances by microbial- and physical-chemical treatment processes, because most of these substances consist of high-molecular-weight fulvic-like and humic-like materials.[1] In the determinations of the biodegradability for many kinds of waste water, Murakami *et al.* recently showed that landfill leachate was an especially refractory waste and was hardly treated by a present biological process.[2]

There has been much interest in the possible application of ionizing radiation to the treatment of waste water. The principal effects that can be turned to advantage are related to disinfection, the degradation of organic compounds, modifications in the biodegradability, and changes in the colloidal properties.[3]

The authors have examined the radiation-induced degradation of organic substances in the leachate generated from the landfill in Tokyo Bay by the irradiation of ^{60}Co γ-rays under aeration at room temperature. It was found that these substances were degradated by oxidation reaction, leading to a decrease in the chemical oxygen demand(COD) and the total organic carbon(TOC), and the conversion to lower-molecular-weight compounds, while oxygen-containing compounds, such as organic acids and carbon dioxide, were also produced.[4]

These results suggest that the irradiation is capable of enhancing the biodegradability for the leachate, since the biodegradability is dependent upon the chemical composition[5] and the molecular-weight distribution.[6] In some experiments carried out by Alexander, the irradiation produced a slight decrease in the biodegradability of the primary effluent.[7] Thus, preliminary experiments for the modification of the biodegradability of the landfill leachate by irradiation by ionizing radiation were undertaken.

Experimental

The leachate (COD, about 2000 ppm), solutions of humic acid and fulvic acid separated from the leachate, and dilute aqueous solutions of polyethylene glycol-6000** were used as the samples. These solutions were put into a glass vessel about 30 mm in diameter and irradiated under aeration with γ-rays from a 185 TBq (5 kCi) ^{60}Co source at room temperature. Almost all the irradiations were performed at the dose rate of 95 Gy·s^{-1} (0.57 Mrad·h^{-1}), as determined by means of a ferrous sulfate solution. After irradiation, the COD (permanganate method at 100 °C), TOC (Toshiba-Beckman Type Model 102 Total Organic Carbon Analyzer), and biochemical oxygen demand(BOD_5) were measured. For the determination of BOD_5, the return sludge from a sewage-treatment process was cultured with skim milk, and the filtrate was used for seeding.

**The mean molecular weight is about 6000.

Results and Discussion

There are several methods for determining the biodegradability, but a general method has not yet been established. It is known that, simply, the biodegradability can be estimated from the ratio of the BOD to the theoretical oxygen demand(ThOD) and that it becomes higher with an increase in the ratio. However, the ThOD can not be estimated for such complicated components as the leachate and the samples denatured by irradiation. In such cases, the TOC or COD can be used instead of the ThOD.[8]

The BOD_5, COD, TOC, and pH values in the leachate and in solutions of humic acid, fulvic acid, and polyethylene glycol-6000 are summarized in Table 1 as a function of the dose. As can be seen in Table 1, the COD and TOC in the leachate, humic acid, and fulvic acid decreased monotonously; on the contrary, the BOD_5 increased with an increase in the dose except for the BOD_5 in humic acid at 86 kGy (8.6 Mrad). Then, the BOD_5/COD and BOD_5/TOC ratios increased with the dose from almost zero in unirradiated solutions. The BOD_5/TOC ratios in these solutions are shown in Fig. 1 as a function of

Table 1. Changes in COD, TOC, and BOD_5 by γ-irradiation

Sample	Dose 10^4Gy(Mrad)	pH	COD	TOC	BOD_5
			ppm		
Leachate	0	8.6	375	262	~6
	1.71	8.5	292	222	81
	3.36		223	200	100
	5.34[a]	8.5	169	166	102
Humic acid	0	10.6	607	540	30
	0.86	7.2	598	516	61
	1.71	6.7	529	480	76
	3.42	4.5	390	352	104
	8.55	3.6	182	260	57
Fulvic acid	0	7.2	370	360	20
	1.80	6.0	309	318	101
	3.42	4.9	239	265	122
PEG-6000	0	5.8	403	532	~3
	0.57	3.7	400	530	97
	1.71	3.3	409	520	181
	3.42	3.2	395	528	332
	9.69		339	300	273

Dose rate: 95 Gy·s^{-1} (0.57 M rad·h^{-1})

a) 148 Gy·s^{-1} (0.89 M rad·h^{-1})

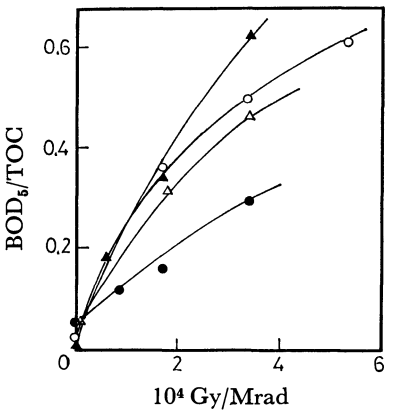

Fig. 1. Enhancement of BOD_5/TOC as a function of dose.
○: Leachate, ●: humic acid, △; fulvic acid, ▲: PEG-6000.

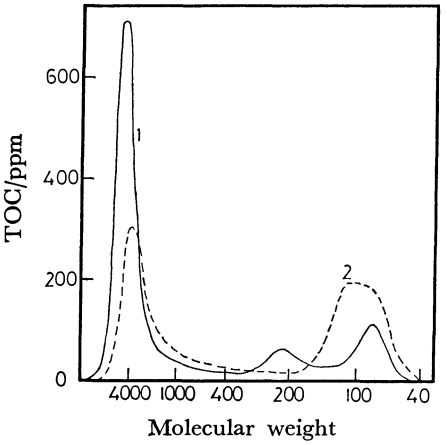

Fig. 2. Effect of irradiation on molecular weight distribution of humic acid solution.
1: Unirradiation, 2: 20 kGy (2.0 M rad).

the dose. The pH lowered with dose except in the leachate. It is because of the pH value's dependence on the buffer-capacity that there was little change in the pH of the leachate. These facts indicate that the irradiation modified the properties of those organic substances, so that they became more biodegradable compounds.

The same experiments were undertaken for the aqueous solutions of polyethylene glycol-6000, which is a refractory material for a biological-treatment process.[6] In this case, no marked change was seen in the COD and TOC up to at least 34 kGy (3.4 Mrad), while the BOD_5 increased markedly with the dose. Therefore, the ratios of BOD_5 to COD and of BOD_5 to TOC increased with the dose; moreover, these values were higher than those of the leachate (Fig. 1). The polyethylene glycol molecule seems to be easily modified to more biodegradable compounds.

The one reason for the enhancement of the biodegradability of these refractory materials by γ-irradiation may be the formation of lower-molecular-weight substances and of organic acids, such as acetic acid.[4] A typical finding regarding the molecular-weight distribution by gel-permeation chromatography of the humic acid solutions is shown in Fig. 2. From Fig. 2, one can find that the higher-molecular-weight components were degradated to lower ones by irradiation. The drops in the BOD_5/TOC and BOD_5/COD ratios of the humic acid solution at the dose of 86 kGy (8.6 Mrad) may be dependent upon the formation of less biodegradable materials by the high-dose irradiation.

These results show that the irradiation of ionizing radiation might increase the efficiency of the biological treatment process; however, more detailed experiments will be required.

The authors wish to thank Mr. Tomiji Tsuji, Tokyo Metropolitan Cleansing Laboratory, for his many helpful discussions and suggestions and Mr. Makoto Nonomura, Tokyo Metropolitan Industrial Technology Center, for the use of the TOC analyzer.

References

1) E. S. K. Chian, *Water Res.*, **11**, 225 (1977).
2) K. Murakami, H. Watanabe, and K. Komori, *Environ. Res. Jpn.*, **1**, 111 (1978).
3) F. S. Feates and D. George, "Radiation for a Clean Environment," (Proc. of Symposium, Munich, 1975), IAEA, Vienna (1975), p. 61.
4) T. Sawai, T. Shimokawa, and T. Sawai, *Radioisotopes*, **28**, 355 (1979); T. Sawai and T. Sawai, *ibid.*, **29**, 67 (1980); T. Tsuji, M. Okuzumi, T. Sawai, T. Sawai, and T. Shimokawa, *Yoshui To Haishui*, **21**, 935 (1979).
5) Z. Inoue, *Yoshui To Haishui*, **14**, 142 (1972).
6) M. M. Zuckerman and A. H. Molof, *J.W.P.C.F.*, **42**, Part 1, 437 (1970).
7) D. M. J. Compton, S. J. Black, F. L. Lieurance, and W. L. Whittemore, "Large Radiation Sources for Industrial Processes," (Proc. of Symposium, Munich, 1969), IAEA, Vienna (1969), p. 399.
8) S. Nakano, *Kagaku To Kogyo*, **48**, 336 (1974).

The Electronic Spectra of Psoralens in Their Ground and Triplet Excited States

Pill-Soon SONG,* Sang Chul SHIM,† and William W. MANTULIN
Department of Chemistry, Texas Tech University, Lubbock, TX 79409, U.S.A.
(Received December 4, 1979)

Synopsis. The first absorption band in psoralens arises from the coumarin moiety, and its location, intensity and polarization are strongly dependent on 5- and 8-substitution. The first two absorption bands in psoralen, angelicin, and methylpsoralens are polarized nearly parallel (angle between them $\Delta\theta \leq 20°$), while methoxypsoralens display wider polarization angles.

Psoralens are photobiologically reactive agents which undergo photocycloaddition to nucleic acids upon irradiation with near UV light.[1] The UV spectra of psoralen and coumarin have already been analyzed by linear dichroism and fluorescence polarization.[2,3] We now extend the spectral analysis to other psoralens.

The T-T absorption spectra of psoralens have been measured.[4,5] In this paper, we attempt to assign the broad absorption bands of psoralen in terms of MO predictions.

Experimental

Absorption spectra were recorded on a Cary 118C spectrophotometer, using a specially built adaptor for the liquid N_2 dewars. Concentrations of all compounds were kept at approximately 50 μM (1 M=1 mol/dm³). The polarized luminescence excitation spectra were recorded on a single photon counting spectrofluorometer (at a spectral resolution of ≈1 nm) by using a pair of Glan-Thompson polarizers under photoselection conditions.[6,7]

Results and Discussion

From the low temperature spectra shown in Figs. 1 and 2, it can be seen that the first absorption band (331 nm for psoralen; Ps) is the most sensitive to perturbation of the furocoumarin system by substitution. 5- and 8-Methoxy substituents exert the strongest perturbation, as the three resolved band system of Ps (Fig. 1) nearly converges into a two band system for 8-MOP and 5-MOP (Fig. 2). While other psoralens show relatively small variations in polarization degree over the first and second absorption bands, 8- and 5-MOP's display polarization differences of *ca.* 0.4 and 0.3, respectively (Fig. 2). This suggests that the angle ($\Delta\theta$) between the two transition moments for the first and second absorption bands is greater (40—50°) than that in other psoralens.

The above noted difference in polarization arises from the fact that the methoxy substitution at position 5 or 8 realigns the transition vector for the first absorption band from the C_3-C_5 axis orientation in Ps to the C_5-C_8 axis orientation in the methoxypsoralens. The polarization of the first band in iPs remains along the long molecular axis (Fig. 1), and is nearly parallel to the polarization direction of the second band, consistent with relatively small differenee in polarization values over the two bands (yielding $\Delta\theta=20°\pm10°$).**

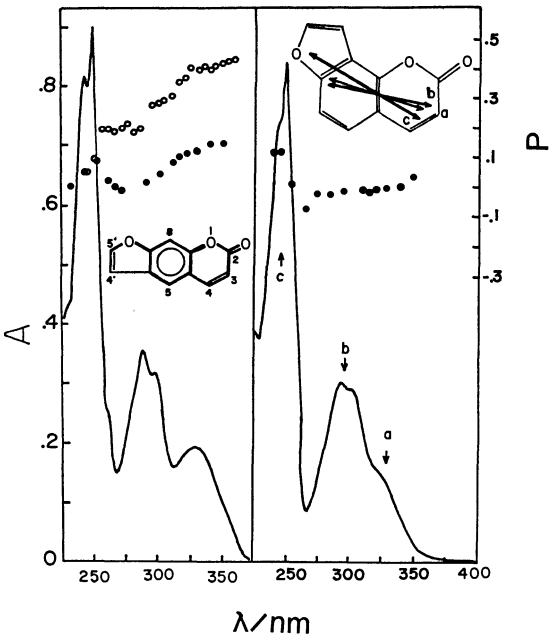

Fig. 1. The absorption spectra of psoralen (left panel) and isopsoralen (right panel) in ethanol at 77 K. Fluorescence excitation polarization (open circle) for psoralen was monitored with respect to emission at 410 nm. Phosphorescence excitation polarization (solid circle) for psoralen and angelicin monitored with respect to the 0-0 phosphorescence at 455 nm. The inset (right panel) shows transition moment directions for the three bands (a, b, c).

In coumarin, the first band is polarized along the long axis, while the second is polarized along the C_2-C_6 axis, with $\Delta\theta=10°\pm5°$.[2] MO calculations are in agreement with the nearly parallel, long axis polarization for the first two bands. For example, MO calculations predict that the first two bands of 7-hydroxycoumarin (λ calculated at 317 and 290 nm) are polarized along the long molecular axis.

Since psoralen is isoelectronic with anthracene, it is reasonable to assign the first and second bands as L_b and L_a origin. The third band in psoralens, which likely contains contribution from a fourth transition,[2] can then be assigned as B_a and/or B_b. It is clear that the first band arises from the coumarin moiety, since the hydrogenation at the pyrone 3,4-C=C bond results in a benzofuran-like spectrum (Fig. 3). The spectral genealogy of psoralens with coumarins is predictable in view of the fact that the first absorption band in both Ps and coumarin is long-axis polarized.[2] In this regard, it is significant that *o*-coumaric acid [3-(2-hydroxyphenyl)propionic acid] ($\lambda_{max}\approx336$ nm) displays an absorption spectrum closely resembling that of coumarin or Ps (Fig. 3), although the two bands

† Permanent address: Department of Chemistry, The Korea Advanced Institute of Science, Chongyangni, P. O. Box 150, Seoul, Korea.

** Fluorescence polarization data (not shown) for angelicin (iPs) are similar to those for Ps shown in Fig. 1.

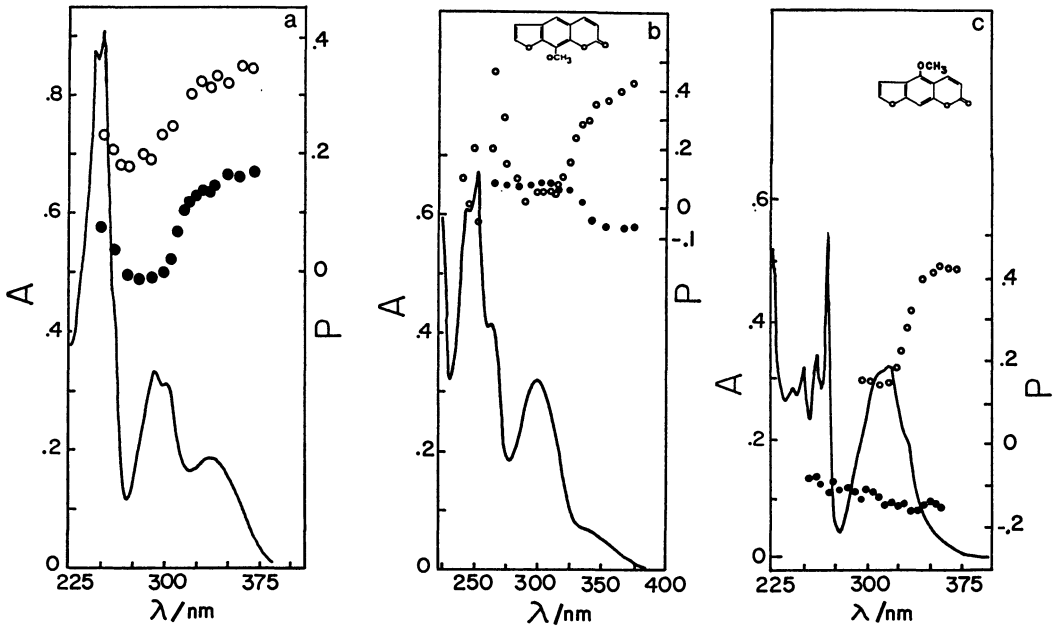

Fig. 2. The absorption spectra of (a) 4,5′,8-trimethylpsoralen, (b) 8-MOP, and (c) 5-MOP in ethanol at 77 K. Fluorescence (open circle) and phosphorescence (solid circle) excitation polarizations were monitored with respect to fluorescence at 415, 435, and 435 nm, respectively, and phosphorescence at 478, 458, and 466 nm, respectively.

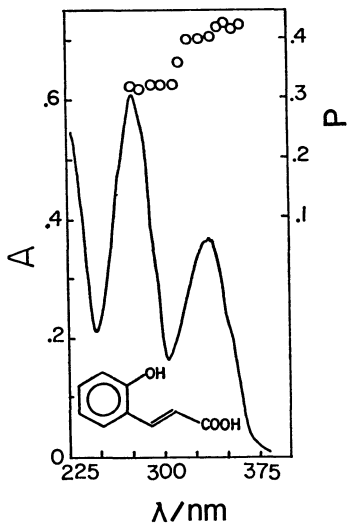

Fig. 3. The absorption spectrum of *o*-coumaric acid in ethanol at 77 K. Fluorescence excitation polarization (open circle) was monitored with respect to fluorescence at 375 nm.

collapse into one overlapping band in *p*-coumaric acid [3-(4-hydroxyphenyl)propionic acid] ($\lambda_{max}\approx318$ nm). Polarization directions for the two bands in *o*-coumaric acid are also nearly parallel, as the fluorescence polarization values differ by only *ca.* 0.1 (Fig. 3).

The phosphorescence of coumarins and psoralens is substantially out-of-plane polarized, particularly 0-0 phosphorescence.[6] This is confirmed by the polarized phosphorescence excitation spectra in Figs. 1 and 2, further suggesting that the first absorption band is largely due to an in-plane polarized $\pi\rightarrow\pi^*$ transition in psoralens and coumarins. However, the phosphorescence polarization over the first absorption band of Ps and trimethyl Ps is not negative (Fig. 1), suggesting that n, π^* perturbations (*e.g.*, vibronic and spin-orbit couplings)[6] are stronger in these molecules than in the others. This may be attributed to the close proximity of the first π, π^* and n, π states in the former.

From MO data calculated (not shown), we tentatively assign the observed T-T absorption maximum at 428 nm to either the $T_1\rightarrow T_9$ or T_8. We further predict that a strong absorption occurs in the near UV region, as suggested by the MO calculation (*i.e.*, $T_1\rightarrow T_{10}$ transition at 324 nm with $f=0.7274$). In coumarin, the intense T-T band is predicted at 283 nm with $f=0.7154$. However, the reported spectrum covers from 300—500 nm, with a broad maximum at 400—460 nm,[8,9] extending to 600 nm.[10] The most intense transitions predicted in this region from MO calculations are at 370 and 319 nm, corresponding to $T_1\rightarrow T_7$ ($f=0.0355$) and $T_1\rightarrow T_8$ ($f=0.0626$), respectively.

This work was supported by the Robert A. Welch Foundation (D-182) and the U.S.P.H.S. grant CA 13598 (to PSS) and CA 21729 (to SCS).

References

1) P. S. Song and K. J. Tapley, Jr., *Photochem. Photobiol.*, **29**, 1177 (1979).
2) T. A. Moore, M. L. Harter, and P. S. Song, *J. Mol. Spectrosc.*, **40**, 144 (1971).
3) P. S. Song and W. H. Gordon, *J. Phys. Chem.*, **74**, 4234 (1970).
4) R. V. Bensasson, E. J. Land, and C. Salet, *Photochem. Photobiol.*, **27**, 273 (1978).
5) R. W. Sloper, T. G. Truscott, and E. J. Land, *Photochem. Photobiol.*, **29**, 1025 (1979).
6) W. W. Mantulin and P. S. Song, *J. Am. Chem. Soc.*, **95**, 5122 (1973).
7) T. Azumi and S. P. McGlynn, *J. Chem. Phys.*, **37**, 2413 (1962).
8) B. R. Henry and R. V. Hunt, *J. Mol. Spectrosc.*, **30**, 466 (1971).
9) P. Crozet, *Chem. Phys. Lett.*, **25**, 114 (1974).
10) E. J. Land and T. G. Truscott, *Photochem. Photobiol.*, **29**, 861 (1979).

Uncatalyzed Chemical Oscillatory Behavior in the Oxidation of Catechol with Acidic Bromate Solution

Punnappillil K. R. NAIR,* Archana MITTAL, and Kotra SRINIVASULU
School of Studies in Chemistry, Vikram University, Ujjain, 456-010, India
(Received September 6, 1979)

Synopsis. A temporal oscillatory behavior of the redox potential in the oxidation of catechol with potassium bromate in sulfuric acid medium is reported.

Uncatalyzed temporal oscillations in bromide ion concentration and redox potential in the oxidation of phenols and anilines with acidic bromate solution have recently been reported by M. Orban and E. Koros, who claim that chemical oscillations do not take place in the oxidation of catechol.[1-3] Our observation shows that catechol is a better substrate to exhibit oscillations in their oxidation with acidic bromate at appropriate concentrations of the reactants. The effect of different catalysts on the system was also observed.

Experimental

Catechol (BDH) was purified by sublimation, $KBrO_3$ (Reidel), H_2SO_4 (BDH) and 1,10-phenanthroline iron(II) sulfate complex (ferroin, BDH) were used. All the solutions were prepared in conductivity water.

Freshly prepared catechol solution (0.25 M†) and H_2SO_4 (18 M) were mixed in a reaction cell thermostated at room temperature (30±0.5 °C) and the reaction was initiated by addition of the required amount of potassium bromate solution (0.4 M). Total volume was kept 25 ml in all cases by addition of the required amount of conductivity water. The reaction was monitored by noting the potential changes from a Systronics (India) pH meter, type 322-1 using Pt–Pt electrodes.[4] In the case of catalysed systems the catalysts were added just before the addition of bromate. Observation was made without stirring, since stirring was found to interfere with the reaction. The boundary concentrations for each reactant to exhibit oscillations were determined by altering the concentration of one of the reactants and keeping that of the rest unaltered. The results are reproducible within the limits of experimental error.

Results and Discussion

Chemical oscillation takes place over narrow ranges of concentration of the reactants, *i.e.* catechol (0.015—0.080 M), bromate (0.048—0.128 M), and acid (0.36—2.88 M). The optimum concentrations for maximum number of oscillations: catechol (0.05 M), bromate (0.096 M), and acid (1.8 M). The oscillations were observed for more than 4 h with decreasing amplitudes as the reaction proceeds (Fig. 1A). Increase in concentration of catechol, bromate or acid, within the boundary conditions, diminished the induction period. Though the reaction starts after the addition of bromate, the oscillatory behavior starts only after an induction (preoscillatory) period of *ca.* 70 min. However, a dark colored species appearing in the system after the addition of bromate vanishes quickly, with a definite potential change.

According to Orban and Koros[2,3] oxidation of catechol with acidic bromate results in the formation of a stable quinone and bromine and thus oscillations do not take place. Though a dark colored species, probably quinone, is formed in the system after bromate addition, it disappears quickly, indicated by the sudden disappearance of the dark color with simultaneous potential change, in the concentration ranges in which reactants exhibit oscillatory behavior. However, the quinone turns into a black or brown precipitate on either side of the boundary conditions of the reactants showing oscillatory behavior. Though bromine is produced in the system, it is consumed probably by brominating the substrate, as evidenced by the gradual disappearance of the brown color from the system before oscillatory behavior appears.

The oscillatory behavior is strongly inhibited by stirring of the reaction mixture; an insignificant number of oscillations could be observed even with slower stirring rate. Inhibitory role of stirring on oscillatory behavior in $BrCH(COOH)_2/BrO_3^-/H_2SO_4/Ce$ system was also reported by Sorensen.[5]

Effect of Catalysts. Belousov-Zhabotiniskii (BZ) catalysts, (Ce(IV), Mn(II), and ferroin) can catalyse the system, ferroin being found to be the most effective one. Introduction of a catalyst decreases the preoscillatory period, while the frequency, number of oscillations and total time for exhibiting oscillations (life time) increase with a slight increase in the amplitude of oscillations (Fig. 1B). Revival of oscillations take place by the introduction of catalyst (2×10^{-4} M ferroin) when the oscillations become insignificant in both uncatalyzed and catalyzed systems. However, no regeneration of oscillations of this type was observed when the catalyst was added at a later stage.

Effect of Halide Ions: Addition of Cl^-, Br^-, or I^- inhibits the reaction. Above 10^{-4} M all the ions inhibit the number and shape of the oscillatory cycles. The inhibitory effect of Cl^- is most prominent.

Effect of Silver Ion: Removal of bromide ions from the system by precipitation of AgBr with Ag^+ ($AgNO_3$) has a pronounced effect on the reaction. By partial removal of bromide ions the oscillations continue, while complete removal inhibits the reaction strongly.

Effect of Radical Scavenger: Addition of acrylonitrile after addition of bromate or in between oscillations suppresses the behavior.

Similar to BZ reaction the uncatalysed bromate oxidation of catechol is controlled by bromide ion and inhibited by chloride ion. The reaction can be explained by means of the Field, Koros and Noyes mechanism,[6] by considering the fact that catechol plays the role of substrate as well as catalyst. The reaction might consist

† 1 M=1 mol dm^{-3}.

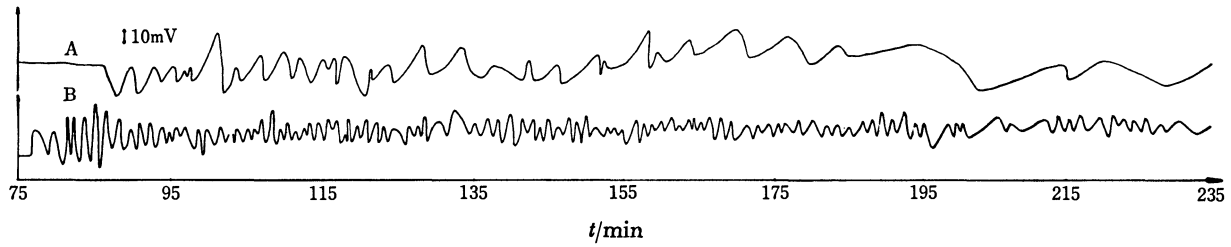

Fig. 1. Oscillatory behavior of the redox potential in the oxidation of catechol with acidic bromate solution.
A. Uncatalyzed system: catechol (0.05 M), bromate (0.096 M), and acid (1.8 M).
B. Catalyzed system: catechol (0.05 M), bromate (0.096 M), acid (1.8 M), and ferroin (2×10^{-4} M).

of two steps of kinetics, the oxidation of catechol by bromate with the subsequent reduction of the latter to bromide ions and bromination of the aromatics. The source of bromide ions for the continuance of the reaction is the brominated products of the aromatics. Brominated products of catechol, *o*-benzoquinone, and 3-bromo-*o*-benzoquinone have been separated from the butanol extract of the reaction mixture by chromatography. So far no bromine has been observed in the BZ reaction.[7,8] However, bromine has been observed in the oscillatory oxidation of catechol.

The authors, P. K. R. and A. M., are grateful to C. S. I. R. (India) for financial assistance and to Prof. M. M. Bokadia, Head of the School, for providing necessary facilities.

References

1) E. Koros and M. Orban, *Nature*, **273**, 371 (1978).
2) M. Orban and E. Koros, *J. Phy. Chem.*, **82**, 1672 (1978).
3) M. Orban and E. Koros, *React. Kinet. Catal. Lett.*, **8**, 273 (1978).
4) J. Sreekantha Babu and K. Srinivasulu, *Z. Phys. Chem.*, **259**, 1191 (1978).
5) G. Sorensen, "Kinetics of Physicochemical Oscillations," ed by U. F. Franck, Aachen (1979), Vol. I, p. 41.
6) R. J. Field, E. Koros, and R. M. Noyes, *J. Am. Chem. Soc.*, **95**, 1394 (1972).
7) A. M. Zhabotiniskii, *Biophysics*, **9**, 329 (1964).
8) H. D. Forsteling, H. Schreiber, and W. Zittlau, *Z. Naturforsch., Teil A*, **33**, 1552 (1978).

Optical Determination of Pair Correlation in π-Electron System

Sadhan Basu

Pure Chemistry Department, University College of Science, 92, Acharya Prafulla Ch. Road, Calcutta-700009, India

(Received January 18, 1980)

Synopsis. α, p, and β bands in the electronic spectra of polynuclear aromatic hydrocarbons have been found to converge to a limiting value. This has been ascribed to pair correlation effect arising from interaction of π-electrons with σ-framework and with molecular vibrations of appropriate symmetry.

Pair correlation effect plays an extremely important role in systems consisting of a large number of Fermi particles. This effect is caused by the presence of attractive force between Fermi particles and are manifested in diverse fields. Thus pair correlation in metals and degenerate semiconductors leads to the development of superconductivity. The pair correlation between nucleons in atomic nucleus explains the regularities observed in the nuclear moment of inertia. The problem of pair correlation of π-electrons in aromatic hydrocarbon has been theoretically analysed by Kresin.[1] Kresin[2] has also shown that such pair correlation is responsible for the characteristic difference in the electronic spectra of perylene and its mono- and dianions.[2] The pair correlation between π-electrons in linear polyene chains has been shown to give rise to convergence in the longest wavelength electron transition with the length of the conjugated chain, *i.e.*, number of π-electrons.[3] This means that pair correlation in π-electron systems may be demonstrated optically. The object of the present note is to analyse if pair correlation could be detected optically in polynuclear aromatic compounds. Clar[4] has prepared hundreds of polynuclear aromatic hydrocarbons where the number or π-electrons ranges from 6 to over 50. Clar has also documented the electronic spectra, which have been divided into α, p, and β regions, for most of these compounds. Since the attraction between electrons is maximum when they have opposite projection quantum numbers, we have selected molecules which have at least one symmetry axis. The frequency of spectral transition (ν) for the α, p, and β bands as well as the number of π-electrons present in the molecules (n) selected are summarised in Table 1. The plot of $\nu(\mathrm{cm}^{-1})$ *vs.* n is given in Fig. 1, where the curves have been drawn by a method of curve fitting.

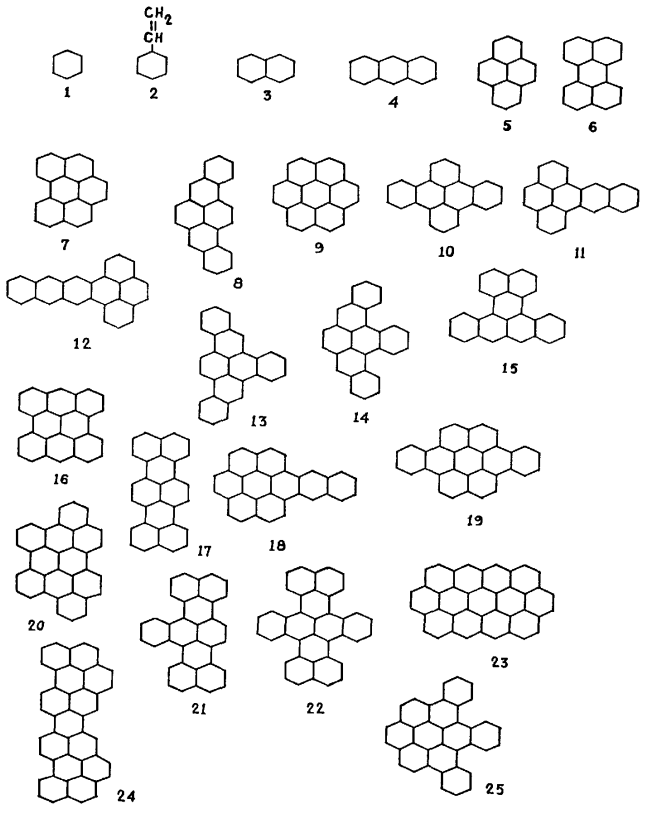

It may be observed that all the three bands α, p, and β converge to a limiting value. The convergence is faster for the β and α bands but much slower for the p band. In presence of pair correlation, the single particle excitation spectrum is given as[1]

$$E = \sqrt{\xi^2 + \Delta^2}, \quad (1)$$

Table 1. Absorption bands in polynuclear aromatic hydrocarbons

Compound	n[a]	ν/cm^{-1}		
		α band	p band	β band
1	6	38000	48050	54500
2	8	34000	38000	46500
3	10	32000	34000	45400
4	14	26400	—	39000
5	16	26900	29985	36765
6	20	29629	23045	39840
7	22	24000	25806	33003
8	24	23094	25188	33670
9	24	23364	29283	32787
10	24	26881	30487	34722
11	24	24539	28985	31153
12	28	—	22624	28169
13	28	23923	25974	33727
14	28	21691	25445	29629
15	28	23419	16474	33112
16	28	23584	15094	32051
17	30	17857	—	37037
18	32	22522	23640	—
19	32	22988	24937	30303
20	34	21459	23980	27932
21	34	25510	15540	33557
22	38	23529	13559	31250
23	40	20243	16339	25000
24	44	—	17331	29069
25	36	21551	24570	28248

a) n denotes the number of π-electrons.

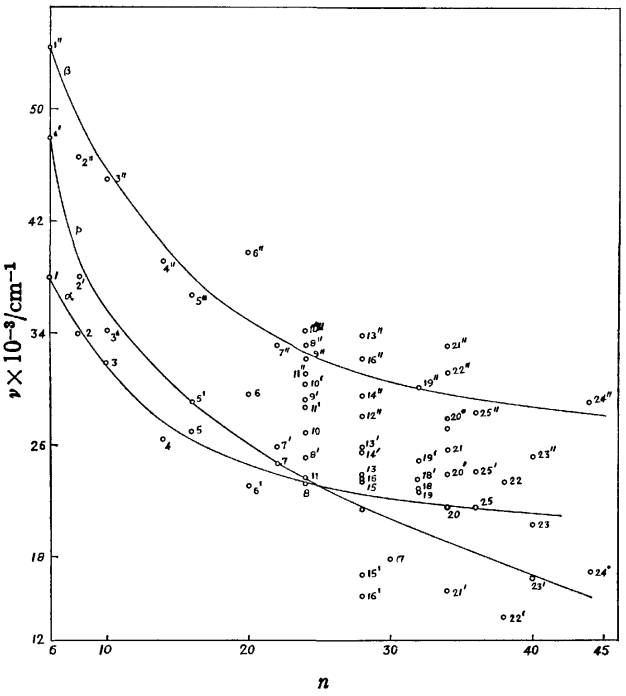

Fig. 1. Longest wavelength transition peaks of the α, p, and β bands in the absorption spectra of poly nuclear aromatic hydrocarbons. The numbers in the figure refer to the serial number in Table 1. Unprimed numbers refer to α, singly primed to p and doubly primed to β transitions.

where $\xi=\varepsilon_b-\varepsilon_a$, ε_b and ε_a being HF energy of an unoccupied and an occupied orbital respectively in absence of pair correlation and Δ is a gap parameter which gives the minimum excitation energy which separates the first excited state from the ground level and it is related to pair correlation energy between electrons having projection quantum numbers of opposite sign. As the number of electrons goes to infinity, ξ goes to zero, and the excitation energy goes to Δ, *i.e.*, Δ gives the convergence limit of the excitation spectrum. From Fig. 1 we get the convergence limit for β, α, and p transitions as 22666, 17333, and 10166 cm^{-1} respectively. The pair correlation energy is largest for a β-transition and smallest for a p-transition, with an α-transition in between. Before searching for a cause for this difference let us first analyse how pair correlation arises in π-electron system.

The major factor which determines the appearance of correlation effect and the energy gap is the presence of attractive force between π-electrons. The primary cause is the polarization of 6-framework, in the field of which the π-electrons move. Due to Coulombic interaction π-electrons cause transition of a σ-electron to a virtual orbital. On return of the σ-electron to the original orbital the energy liberated is transmitted to the π-electrons, which can surmount the repulsive force between similarly charged particles to some extent and the net result is effective attraction between π-electrons. This mechanism will be most effective for allowed π-transitions which have large oscillator strength and can polarise σ-framework. The second mechanism is the interaction of electronic energy with the molecular vibrational quanta. Virtual vibration will be excited and when the oscillator returns to the ground state, the energy transferred to the π-electron will lead to effective attraction. It is obvious that the vibrational quanta is of much lower energy than the electronic quanta, so the first effect will cause stronger correlation than the second.

The various bands observed in the hydrocarbons listed in Table 1 have not been assigned completely. Only for lower members the assignment is agreed upon. If we assume that assignment for the lower members also holds for higher members, then we may propose the following tentative explanation for pair correlation energy.

The presently accepted explanation[5] of the α-band is that they are symmetry forbidden transitions. They are made allowed by simultaneous excitation of some vibrational mode of the molecule so that the product function has proper symmetry to make the transition allowed. It may be suggested that pair correlation in the α-band arises from the interaction of electron with vibrational quanta. The β-bands are orbitally allowed transitions and have high oscillator strength. The polarization of σ-framework therefore may be responsible for pair correlation observed. The p-band is also orbitally forbidden singlet transition made allowed by combination with excited vibrational state. This band is rather diffuse. The pair correlation effect in this band also arises from the interaction of electrons with vibrational quanta, but because of the lower probability of interaction of ground electronic state with excited vibrational state, the correlation energy is low. This phenomenological analysis of the convergence in the absorption bands of various polynuclear aromatic hydrocarbons appears to indicate that a detailed theoretical analysis of the problem must be taken up to establish if the convergence is really due to pair correlation effect as suggested.

References

1) V. Z. Kresin, *Dokl. Akad. Nauk SSSR*, **177**, 1306 (1967).
2) V. Z. Kresin, *Zh. Strukt. Khim.*, **12**, 745 (1971).
3) S. Basu, *Adv. Quant. Chem.*, **11**, 33 (1978) and references cited there.
4) E. Clar, "Polycyclic Hydrocarbons," Academic Press, N. Y. (1964).
5) K. S. Pitzer, "Quantum Chemistry," Prentice Hall, Inc. (1977), p. 293, and references cited there.

Iron Catalyst Local Concentration Fluctuations Found in Dissipative Reactions by X-Ray Microanalysis

Csaba P. Keszthelyi,*,†† József Soós, András G. S. Janossy, and Kristóf Vovács†
Institute of Biophysics, Biological Research Centre, Hungarian Academy of Sciences, H-6701 Szeged, Hungary
†*Department of Silicate Chemistry, Technical University for Chemistry, H-8200 Veszprém, Hungary*
(Received January 26, 1980)

Synopsis. The present work provides the first application of the powerful X-ray microanalysis technique in the study of "Zhabotinskii-type" oscillatory reactions. The modified HNO_3: $KBrO_3$: $[Fe(phen)_3]^{2+}$: malonic acid system is quantitatively described. Systematic variation, spatially correlated with the dissipative structures, was found in the Fe concentration.

The very occurrence of concentration oscillations and temporal periodicity in initially homogeneous chemical systems was a matter of scientific controversy until recent years. His unusual insight into biological morphogenesis led Turing[1] to propose the feasibility of the formation of spatial concentration patterns in an initially uniform chemical medium as early as 1952. Such were the ramifications of the ideas raised by Turing's paper that a new area of thermodynamics, the "far from equilibrium" or "dissipative" branch was born.[2,3] Related research stands out in a unique way: while science is experiencing day to day fragmentation due to the sheer bulk of new results and new techniques, while researchers often fit into the order of things by adopting a mosaic vision, the theories on dissipative structures cut across diverse fields such as biology, chemistry, ecology, mathematics, physics, population dynamics and sociology, once again giving impetus to the quest for fundamental principles and inter-relationships.[3] The topic has claimed the interest of several major research groups, as can be gauged from some excellent review articles.[4] Particularly relevant is the conclusion of Procaccia and Ross,[5] that experimental efforts lag behind theoretical advances in this area.

The present work provides the first application of the powerful X-ray microanalysis technique in the study of "Zhabotinskii-type," dissipative oscillatory chemical reactions. Upon cursory examination, the match between the system of interest and the chosen instrumental technique appears distressing: the oscillatory reactions commonly occur in aqueous solution, whereas no water is admissible to the analytical electron microscope. In devising a suitable procedure, as a first step we found in agreement with Winfree[6] that the oscillatory reactions proceed quite well in membrane filters also. Next it is an easy matter to quench the reaction by immersing the filter bearing the characteristic bands of spatial periodicity into liquid N_2. Subsequent drying of the fixed reaction by vacuum under a temperature gradient is not feasible with the typical mixtures containing H_2SO_4 or $HClO_4$, due to non-volatility of these acids. Nitric acid was found to be an acceptable substituent for H_2SO_4 as reported by Winfree;[6] the modified system is described in conjunction with Fig. 1 as follows. The solutions used to prepare the reaction mixture: **A.** 5 g $KBrO_3$+67 ml H_2O+3 ml concd HNO_3; **B.** 10% aq KBr; **C.** 10% aq malonic acid; **D.** 25 mM aq $[Fe(phen)_3]^{2+}$. Reagent **D** needs to be prepared under rigorously chloride free conditions, in agreement with Winfree's comment. The reagents were mixed in the sequence: 3 ml **A**+0.5 ml **B**, followed by the addition of 0.5 ml **C**. At this stage bromination of the malonic acid occurs within 3—4 min at room temperature. Addition of 0.3—0.5 ml **D** initiates the characteristic temporal oscillations which can be visually followed by observing the red-blue color change of the catalyst. Spatial patterns emerge subsequently, either spontaneously or facilitated.[6]

We measured oscillation period parameters at 27 °C in the standard manner at 550 nm, using a UNICAM SP 1800 spectrophotometer with 5 mm cuvettes. Determined from the data depicted in Fig. 1 by the method of least squares, we obtained with better than 0.99 correlation coefficient:

$$\text{induction period(s)} = 394 \times 0.0227C, \quad (1)$$

$$\text{first oscillation period(s)} = 181.7 \times 2.90C, \quad (2)$$

where C is the concentration (mol/dm^3) of HNO_3.

With the modified system it was possible to produce membrane filters (Sartorius SM 11306) on which the original dissipative structures were preserved intact after drying. Working with ferroin as catalyst had the great advantage of constantly being able to see the status and quality of the samples, and correlate

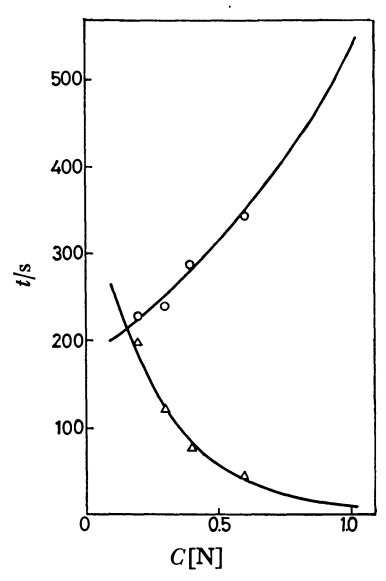

Fig. 1. Temporal oscillatory characteristics of the HNO_3: $[Fe(phen)_3]^{2+}$: $KBrO_3$: malonic acid system.

†† U. S. National Academy of Sciences–Hungarian Academy of Sciences exchange professor; permanent address: Louisiana Academy of Science, University Station # 22315, Baton Rouge, Louisiana 70893, U. S. A.

instrumental readings with visual observations.

From properly prepared filters selected portions *ca.* 3 mm wide and over 1 cm long were introduced to the analytical electron microscope, JEOL JEM 100B. Analysis was performed in the SEI mode, using 20, 40, and 80 kV nominal excitation voltage. Areas of 0.1×0.1 mm^2 were subjected to X-ray microanalysis in steps of 0.25 mm. Utilizing an EDAX 707B X-ray analyser, a typical result is shown in Fig. 2. In the energy dispersive X-ray spectrum covering the 0—10 keV range, Br L_α, K K_α, and Fe K_α peaks are readily identifiable (Cu lines are indigenous to the measuring technique). Over 100 linearly correlated points were individually subjected to microanalysis, and weight ratios were calculated with the 7. EP program of EDAX, Inc. Major fluctuations spatially correlated with the dissipative structures were found in the Fe/K and Fe/Br, but not in the Br/K ratios (Fig. 3). The fact that we did not pick up the small changes in bromide concentration superimposed on a high bromine background was anticipated. The unmistakable correlation between the dissipative structures and total Fe(ferroin+ferriin)based on Fe/K and Fe/Br, on the other hand, indicates that the catalyst participates in the oscillatory reaction dynamics in a more profound manner than commonly envisaged. Although direct measurements of this kind have not been reported, nor are there model calculations which could be called closely relevant, the results on secondary participation in dissipative processes are in qualitative agreement with some recent theoretical advances.[7,8]

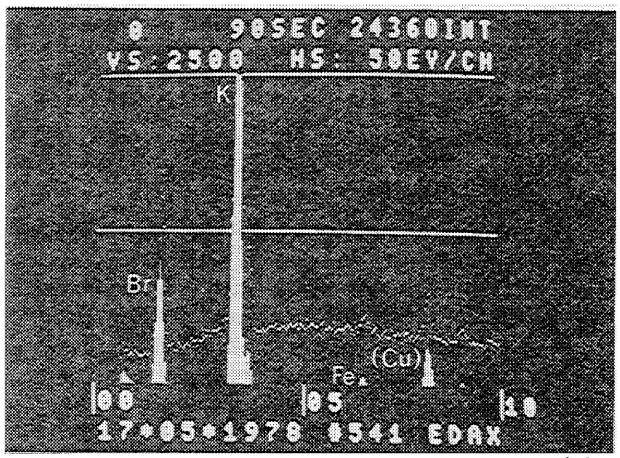

Fig. 2. Typical energy dispersive X-ray spectrum of the Zhabotinskii-type reaction described in Fig. 1. The spectrum shows Br L_α line at 1.48 keV, K K_α line at 3.30 keV, and Fe K_α line at 6.40 keV. Additional peaks at 8.04 and 8.90 keV represent the Cu K_α and K_β lines, and stem from microscope hardware outside the analyzed area excited by scattered electrons and X-rays.

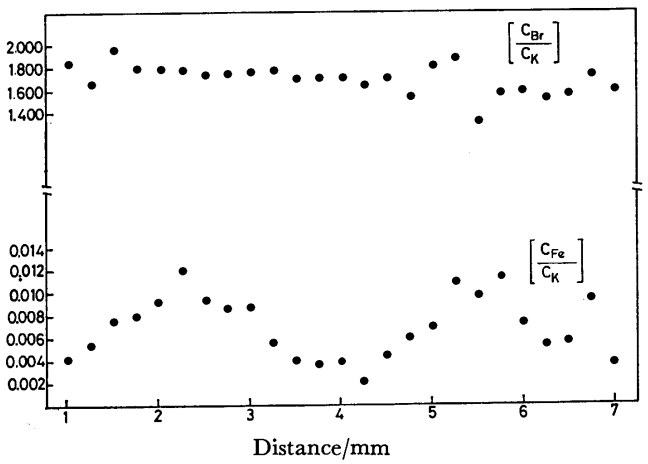

Fig. 3. Weight ratios of Fe/K show fluctuation pattern characteristic of dissipative structures if displayed as a function of distance (here in steps of 0.25 mm). For comparison, Br/K weight ratios show only random variation within limits of accuracy.

In closing we should like to make a few brief remarks about the experimental aspects, deemed so essential by Procaccia and Ross.[5] We have invariably noted, even on the satisfactory samples, a slight broadening of the dissipative structures during the drying process. Such limitation of spatio-featural resolution could be circumvented by using an electron microscope equipped with a cryogenic stage. Additional advantages to consider in this respect are: (1) the cumbersome drying procedure would be bypassed; (2) the frozen samples would be completely free of possible complications arising from different solubility of the oxidized and reduced form of the catalyst. With experimental methodology that does not depend on visual confirmation to the extent afforded by the ferroin-ferriin pair, the investigation of secondary participation effect could be extended to cerium and manganese catalysed reactions, for example, thereby allowing comparison, and promoting fuller theoretical explanation.

Presented at the First Chemical Congress of the Pacific, co-sponsored by the American Chemical Society and the Chemical Society of Japan, held in Honolulu, Hawaii, April 1—6, 1979. Financial support was received from the U. S. National Academy of Sciences/ National Science Foundation.

References

1) A. M. Turing, *Phil. Trans. R. Soc. London, B*, **237**, 37 (1952).

2) P. Glansdorff and I. Prigogine, "Thermodynamic Theory of Structure, Stability and Fluctuations," Wiley-Intersci., New York (1971).

3) G. Nicholis and I. Prigogine, "Self-Organisation in Non-Equilibrium Systems: From Dissipative Structure to Order Through Fluctuations," Wiley-Intersci., New York and London (1977).

4) U. F. Franck, *Angew. Chem. Intl. Ed. Engl.*, **17**, 1 (1978).

5) I. Procaccia and J. Ross, *Science*, **198**, 716 (1977).

6) A. T. Winfree "Faraday Symp. 9: Physical Chemistry of Oscillatory Phenomena," The Chemical Soc. Faraday Div., Paper No. 4, 1974.

7) H. Haken, "Synergetics A Workshop-Proc. Intl. Workshop on Synergetics at Schloss Elman, Bavaria, May 2—7, 1977," Springer-Verlag (1977).

8) "Kinetics of Physicochemical Oscillations," ed by U. F. Franck, Deutsche Bunsenges. Phys. Chem., Aachen (1979).

Potentiometric and Spectroscopic Investigations of the Reaction of Fluorescein Isothiocyanate with an Amine Chemically Bound on Solid Surfaces

Naoto YAMAMOTO,* Yoshikatsu NAGASAWA,** Sadanobu SHUTO, and Hiroshi TSUBOMURA
Department of Chemistry, Faculty of Engineering Science, Osaka University, Toyonaka, Osaka 560
(Received February 18, 1980)

Titanium electrode surface was chemically modified with an aminosilane. The potential of the electrode was shifted to the negative direction by a reaction of fluorescein isothiocyanate in solution with the amine on the electrode surface. The absorption and emission spectra were measured for the fluorescein isothiocyanate, fixed by the reaction with the aminosilane which was chemically bound on the surfaces of tin oxide, titanium oxide and quartz, in solutions and in air. In an alkaline solution, the absorption and emission spectra showed the band ascribable to the dianion of the fluorescein. A peak, attributable to the monoanion, was observed in both absorption and emission spectra measured for the samples kept in air. The surface coverage of the dye was estimated from the absorbances to be about 10^{-6} mol m^{-2} for both tin oxide and quartz. The bound dye fluoresced under exposure to ultraviolet light, due probably to the energy transfer from tin oxide to the dye.

Recently, immobilization techniques of organic molecules on inorganic substrates have been extensively developed by several groups in relation to electrochemical studies.[1-4]

In previous papers, we have described the electrode potential changes arising from antigen-antibody and enzyme-enzyme inhibitor reactions which take place on the electrode surface and proposed an electrical double layer model for the interpretation of these potential changes.[5-7] The applicability of such a potentiometric method to the analysis of very small quantities of biological substances in solutions has also been pointed out.

Numerous studies on surface potentials have so far been made for liquid-gas and solid-gas interfaces, but few potentiometric investigations have been made for solid-liquid interface.[8] The adsorptions of ions and molecules on the electrode surface are known to influence the electrode potential in solution. In cases where the solid surface has an active site interacting only with a particular substance, as in the case of antigen-antibody reactions mentioned above, the surface potential of the solid may change specifically by the interaction. In order to elucidate the relationship between the molecular interaction at an electrode surface and the resultant potential change, the surface reaction of an amine chemically bonded on inorganic substrates with fluorescein isothiocyanate was studied by both potentiometric and spectroscopic methods. The related physicochemical properties of solid surfaces have also been investigated.

Experimental

Materials. (3-Aminopropyl)triethoxysilane (KBE903) and methyltrimethoxysilane (KBM13) from Shinetsu Chemical Co. were used without further purification. Special grade toluene was shaken with concentrated sulfuric acid, dried over anhydrous calcium chloride for 1 d, and distilled. Fluorescein isothiocyanate (isothiocyanatofluorescein) isomer 1, abbreviated as FITC, from Sigma Chemical Co. and fluorescein from Wako Pure Chemical Industries Ltd. were used without further purification.

Preparation of Modified Titanium Electrode. The tip of a titanium wire was heated at about 1000 °C so as to produce thin oxide film on the surface. Silanization of the heat-treated tip was carried out by a method based on Murray's[9,10] as follows. The titanium wire was allowed to stand in an oven at 200 °C for 1 h, the tip was immersed into a 10% toluene solution of (3-aminopropyl)triethoxysilane and the solution was refluxed for 17 h. The tip thus aminosilanized was washed successively with toluene, acetone and distilled water, and attached to a glass tube with epoxy resin as illustrated in Fig. 1a. The electrode thus formed was heated at 80 °C for 1 h to harden the epoxy resin.

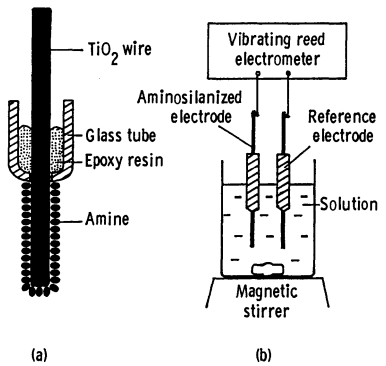

Fig. 1. Aminosilanized titanium electrode (a), and the apparatus for measuring the electrode potential (b).

The reference electrode was similarly prepared by treating the heat-treated wire with a 10% toluene solution of methyltrimethoxysilane for 17 h at 20 °C.

Silanization and FITC Modification of Tin Oxide Film, Quartz and Titanium Oxide Powder. Glass slides coated with tin oxide film were obtained from Hiraoka Glass Co. The tin oxide surface was wiped with a piece of soft cloth damped with commercially available anionic detergent. The glass was then successively washed in an ultrasonic cleaning bath with the washing agent solution for 30 min, distilled water for 10 min, isopropyl alcohol for 10 min and distilled water for 30 min, and soaked in 10 M (1 M=1 mol dm^{-3}) sodium hydroxide solution for 17 h following the method used by Kuwana *et al.*[11] Washed with distilled water in the ultrasonic bath, the glass was dried in an oven for 1 h at 150 °C. Chemi-

** Present address: Toray Research Center, Toray Industries Inc., Sonoyama, 3, Otsu 520.

cal modification of the tin oxide film was performed by the same method as that used for the preparation of titanium electrode.

In order to prepare the FITC bound tin oxide for the spectroscopic measurements, the tin oxide film modified with the aminosilane was allowed to react with 4.4×10^{-4} M FITC solution of 0.05 M carbonate–hydrogencarbonate buffer, pH 10.4, at 5 °C overnight. An ES grade quartz plate from Japan Quartz Co. was modified according to the same method as that for the tin oxide film described above.

The coupling reaction of (3-aminopropyl)triethoxysilane to titanium oxide (rutile) powder, purchased from Merck Co., was performed in the same manner. The aminosilanized powder and *ca.* 2 mg of FITC were added at once to 30 ml of a 0.05 M carbonate–hydrogencarbonate buffer solution, pH 10.4, cooled at 4 °C to prevent the degradation of FITC and allowed to stand overnight. The modified powder was then washed with distilled water in an ultrasonic bath for 10 min and spread on a piece of filter paper and dried for 4 d.

Measurement of the Electrode Potential. The electrical potential between the modified and the reference electrodes was measured in a 30 ml reaction vessel at 20 °C by using a Takedariken TR 84M vibrating reed electrometer in the same manner as described elsewhere (Fig. 1b).[5,6]

Spectroscopic Measurement. The absorption spectra of the modified tin oxide film and quartz plate in air were measured by use of a single beam UV-visible spectrophotometer equipped with a photon counting system.[12] A Shimadzu MPS-50L UV-visible spectrophotometer was used to measure the spectra of the powder and the samples in solution.

The emission spectra were measured by using two Nippon Jarrell–Ash JE 25 monochromators having a focal length of 25 cm, a Hamamatsu R136 photomultiplier and an NF LI 573 lock-in amplifier together with a PAR 125A light chopper. The samples were excited with light of 465 nm in wavelength incident at an angle of 75° with the line normal to the sample face. The emission spectra were not corrected for the response of the monitring system.

Results and Discussion

Reaction with FITC. Figure 2 shows the change of potential with time in the aminosilanized titanium electrode by reaction with FITC. When the solution was replaced with a simple buffer solution (containing no FITC) at a time designated by X in curve a in Fig. 2,

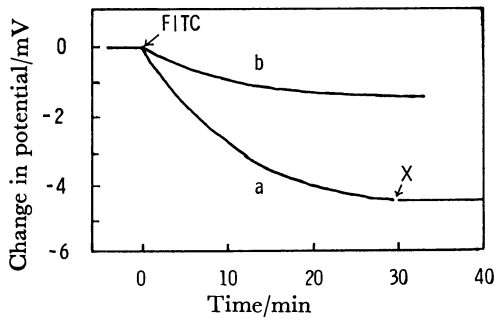

Fig. 2. The change of potential of the aminosilanized titanium electrode caused by the addition of FITC solution. The concentrations of the FITC were 2.1×10^{-4} M for curve a and 7.0×10^{-5} M for curve b. The arrow X indicates the replacement of the solution with a buffer solution.

the potential held the same value as that before the replacement. The magnitude of change in potential was roughly exponential suggesting the first order kinetics of the reaction between the electrode and FITC. This kinetic result is reasonable because the number of FITC molecules in the solution is remarkably larger than that of the amino groups on the electrode surface. The concentration of FITC in the vessel was 2.1×10^{-4} M for curve a and 7.0×10^{-5} M for curve b in Fig. 2. The rate of potential change was nearly proportional to the FITC concentration. Zanker and Peter have shown that fluorescein exists as a dianion in an alkaline solution of pH>7.[13] The negative potential change observed can be explained by the attachment of dianion on the electrode surface.

The vibrating reed electrometer used has the time response less than 0.1 s and the input impedance of 10^5 Ω or more. The observed change in potential as shown in Fig. 2 is too slow to be explained by the change in the redox level of the solution by the addition of FITC. In addition, the potential induced by the reactant is unchanged by replacement of the solution with a simple buffer solution and remained the same for a long time (Fig. 2a), indicating that the observed potential change is caused by the irreversible reaction on the surface, not by the electrochemical properties of the bulk solution. The impedance yielding the potential for the immuno-electrode was measured to be the order of 10^9 Ω,[5] suggesting an existence of highly insulating layer at the interface between electrode and solution. The potential observed is, therefore, understood by taking into account a surface potential formed by the FITC, and other ions bound on the electrode surface.

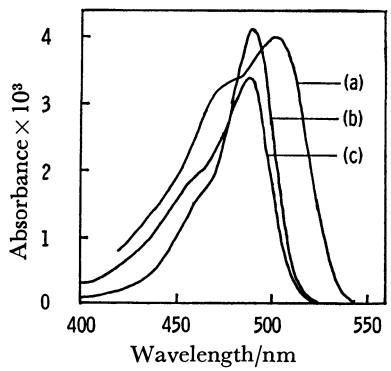

Fig. 3. The absorption spectra of FITC bound on a tin oxide film measured in air (a) and of fluorescein in aqueous solution of pH 5.7 (b) and pH 10.4 (c). The absorption intensities for (b) and (c) are in arbitrary unit.

The absorption spectrum of the aminosilanized tin oxide film that reacted with FITC was studied for a sample immersed in the FITC solution for 90 min followed by washing in the ultrasonic cleaning bath and drying (curve a of Fig. 3). Curves b and c in Fig. 3 show the absorption spectra of fluorescein in aqueous solutions of pH 5.7 and 10.4, respectively. Since the FITC bound on the surface maintains the π-electron network of fluorescein, the absorption spectrum of the

bound FITC must be similar to those of fluorescein. Fluorescein in aqueous solutions is in various protolytic equilibria as shown below:

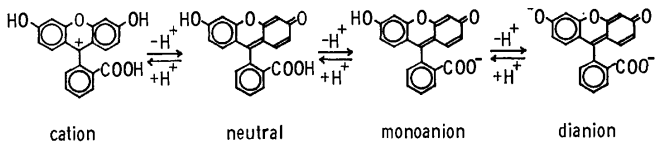

The pH dependence of the absorption and emission spectra of fluorescein in aqueous solution was studied by several investigators.[14-16] Martin and Lindqvist[16] reported that a strong absorption at 491 nm ($\varepsilon=8.8\times10^4$) in the case of an alkaline solution can be identified to the dianion of fluorescein, and that the monoanion existing in a weak acid solution has bands at 475 nm ($\varepsilon=3.1\times10^4$) and at 437 nm. From these assignments the 465 and 500 nm bands of the FITC bound on SnO_2 can be reasonably assigned to the monoanion and the dianion of the fluorescein fragment bound on the solid.

These electrical and spectroscopical results indicate that FITC has certainly reacted with the amino group on the modified solid surfaces as follows.

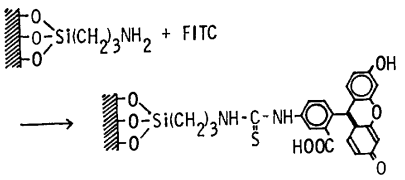

Assuming that the molar extinction coefficient of the dianion peak of bound FITC is 8.8×10^4, equal to that of fluorescein dianion in alkaline solution, and that of the monoanion of bound FITC is 3.1×10^4 at the absorption peak,[16] the surface coverage of immobilized FITC on the tin oxide and the ratio of the monoanion to dianion can be roughly evaluated from the result in Fig. 3. The resultant coverage is 9.7×10^{-7} mol m^{-2} and the ratio of monoanion to dianion is 1.2: 1, taking account of the fact that the absorbance at 465 nm is expressed by a superposition of the monoanion peak and the dianion tail. Similarly, the coverage on the quartz was estimated to be 6.7×10^{-7} mol m^{-2}, very close to the result on tin oxide. Murray *et al.*[10] estimated from ESCA measurement that organosilanes are bound on the surface to a density of 1 to 2×10^{-6} mol m^{-2} on tin oxide and titanium oxide. Our coverages obtained are in good agreement with their values.

In order to evaluate the reaction rate from absorption spectral measurements, the aminosilanized tin oxide film was immersed into a 4.4×10^{-4} M FITC solution for various periods of time, and the absorption spectrum was measured in air. The optical density at the absorption maximum, 500 nm, of the bound FITC was 1.07×10^{-3}, 4.43×10^{-3}, and 4.71×10^{-3} for the period of 30, 90, and 1440 min, respectively, indicating that the reaction is completed mostly in 90 min, in agreement with the rate of change in electrode potential observed. It was confirmed spectrophotometrically that the FITC thus attached was not removed by washing with water or acetone in the ultrasonic bath for 10 min. In contrast, the tin oxide film which was not modified with organosilane did not show any sign of the absorption spectrum of FITC, indicating that the physical adsorption of FITC onto the tin oxide surface was negligible.

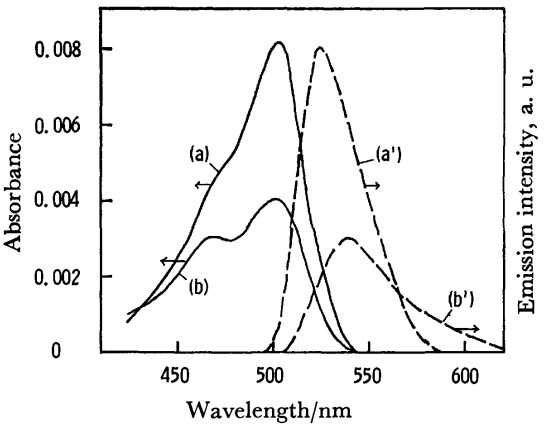

Fig. 4. Absorption and emission spectra of FITC bound on a tin oxide film mesaured in alkaline solution of pH 10.4 : (a) and (a'), and in air : (b) and (b').

Emission Spectra of the Bound Dye. Figure 4 shows the absorption and emission spectra of FITC bound on tin oxide film measured in air and in a carbonate–hydrogencarbonate buffer solution of pH 10.4. In an alkaline solution of fluorescein, both the absorption peak at 493 nm and the emission peak at 515 nm were assigned to the monomeric dianion by Leonhardt *et al.*[15] and Martin and Lindqvist.[16] The equilibrium constant, pK, between the monoanion and the dianion was reported, from absorption measurement, to be 6.7.[15,16] Therefore, the bound FITC is thought to exist mostly in the dianion form when in contact with the alkaline solution, so that the absorption and the emission bands observed in the alkaline solution (Fig. 4 curve a and a') are attributed to the dianion. As the emission band measured in air (Fig. 4, b') is considerably different from that measured in the alkaline solution, it is most reasonably assigned to the monoanion. In the case of titanium oxide powder or quartz used as the substrate, the bound TITC was found to have essentially the same absorption and emission spectra as those in the case of tinoxide film described above.

In the case of FITC bound on a tin oxide film, an emission was observed by excitation with light of 313 nm from a mercury arc lamp. The emission peak was found at 517 nm in water and at 537 nm in air, ascribable to the dye dianion and monoanion, respectively. As the absorption of the dye is very weak at around 313 nm, and the photon energy at 313 nm is much higher than the band gap, 3.2 eV, of tin oxide, the ocurrence of the emission from the bound FITC can only be explained by the excitation of the tin oxide from the valence band to the conduction band followed by the energy transfer from tin oxide to the dye. A similar energy transfer process was pointed out for the system of fluorescein adsorbed on zinc sulfide and zinc oxide crystals by Lendvay.[17]

References

1) G. B. Harper, *Anal. Chem.*, **47**, 348 (1975).
2) T. Osa and M. Fujihira, *Nature*, **264**, 349 (1976).
3) M. Fujihira, T. Osa, D. Hursh, and T. Kuwana, *J. Electroanal. Chem.*, **88**, 285 (1978).
4) L. T. Mimms, M. A. McKnight, and R. W. Murray, *Anal. Chim. Acta*, **89**, 355 (1977).
5) N. Yamamoto, Y. Nagasawa, S. Shuto, M. Sawai, T. Sudo, and H. Tsubomura, *Chem. Lett.*, **1978**, 245.
6) N. Yamamoto, Y. Nagasawa, M. Sawai, T. Sudo, and H. Tsubomura, *J. Immunological Methods*, **22**, 309 (1978).
7) N. Yamamoto, Y. Nagasawa, S. Shuto, H. Tsubomura, M. Sawai, and H. Okumura, *Clin. Chem.*, **26**, 1569 (1980).
8) See, for example, A. W. Adamson, "*Physical Chemistry of Surfaces*," John Wiley and Sons, New York (1976), Chaps. 3 and 14.
9) P. R. Moses, L. Wier, and R. W. Murray, *Anal. Chem.*, **47**, 1882 (1975).
10) D. F. Untereker, J. C. Lennox, L. M. Wier, P. R. Moses, and R. W. Murray, *J. Electroanal. Chem.*, **81**, 309 (1977).
11) A. W. C. Lin, P. Yeh, A. M. Yacynych, and T. Kuwana, *J. Electroanal. Chem.*, **84**, 411 (1977).
12) N. Yamamoto, T. Sawada, and H. Tsubomura, *Bull. Chem. Soc. Japan*, **52**, 987 (1979).
13) V. Zanker and W. Peter, *Chem. Ber.*, **91**, 572 (1958).
14) F. M. Abdel-Halim, R. M. Issa, M. S. El-Ezaby, and A. A. Hasanein, *Z. Phys. Chem.*, N. F., **73**, 59 (1970).
15) H. Leonhardt, L. Gorden, and R. Livingston, *J. Phys. Chem.*, **75**, 245 (1971).
16) M. M. Martin and L. Lindqvist, *J. Luminescence*, **10**, 381 (1975).
17) E. Lendvay, *J. Phys. Chem.*, **69**, 738 (1965).

  Bull. Chem. Soc. Jpn., 54, 327—334 (1981)

Theoretical Treatment of Solvent Effects on the Frequency Shifts of Electronic Spectra of Anions

Takehiro Abe

College of General Education, Tohoku University, Kawauchi, Sendai 980

(Received March 13, 1980)

A theoretical expression for the spectral solvent shifts of an anion has been presented by assuming the system to consist of a large anion, its counter cations, and numerous solvent molecules. In the zeroth-order all the component particles in the system do not interact with one another. The interaction energy among the particles for the ith-excited state of the system, in which only the anion is in the ith-excited state, is calculated by the second-order perturbation treatment as the sum of electrostatic interaction energies between pairs of particles. The expression derived from the difference between the interaction energies of the ground and excited states of the system contains the dipole-dipole and dipole-induced dipole interaction terms and the dispersion force terms and is somewhat different from the previous results for neutral solutes (*Bull. Chem. Soc. Jpn.*, **38**, 1314 (1965)). Effects of the counter cations are discussed. This expression is applied to the spectral shifts of an Eosin-Y^{2-} anion, a Meisenheimer complex, and Janovsky complexes.

Many theories have hitherto been proposed for spectral solvent shifts of neutral organic molecules.[1] There are, however, only a few theories relating to anions.[2,3] Miertuš and Kyselǐ[2] have calculated frequencies of some anion radicals in solvents by incorporating the solvent effects into the Hamiltonian operator for the radicals in the restricted SCF MO method. Hirano[3] has extended McRae's theory[4] for neutral molecules to organic anions by considering the effects of their counter cations. Hirano has obtained a general expression involving no dipole-dipole and dipole-induced dipole interaction terms but only the dispersion force contribution. According to his theory, the effects of the counter cations can be ignored.

In order to compare results with Hirano's expression, the author has attempted to derive an expression for the spectral solvent shifts of anions on the basis of the previous theory[5,6] for neutral molecules. The previous expressions[5,6] will be somewhat improved. Moreover, an attempt has been made to clarify the similaritities and differences between McRae's theory[4] and the author's.[5,6]

Theoretical

Model. Electronic spectra of solutions are generally measured at very low concentrations of solutes. Let us, therefore, consider a system consisting of a large anion (A^{n-}), its n counter cations (M^+), and N identical neutral solvent molecules. The anion is not an anion radical or a small anion solvated by coordination of solvent molecules. The cations are monatomic. In the zeroth-order, all the component particles in the system do not interact with one another. Let us consider the ion-pair formation between the anion and the n monovalent cations, because such formation is well-known. The solvent molecules are assumed to form no hydrogen bonds and no complexes with the anion and to have small enough dipole moments that they are not tightly oriented with respect to each other. For convenience, let the origin of the coordinates be the center of mass of the anion. In the spectral measurements of solutes in solutions, one usually chooses solvents that absorb light at much shorter wavelengths than the solutes do. The monovalent cations such as Na^+ and K^+ require transition energies considerably higher than those of the anion and the solvent molecule. One therefore assumes that the solvent molecules and the cations remain in their ground states when a transition from the ground state to the ith excited state occurs in the anion.

The Wave Functions and Energies of the System. Let us write the ith electronic state of the system in the zeroth-order as follows:

$$\Phi_i^\circ = \phi_i^A \prod_{c=1}^{n} \phi_0^c \prod_{s=1}^{N} \phi_0^s. \tag{1}$$

Here the zeroth-order wave functions of ϕ_i^A, ϕ_0^c, and ϕ_0^s denote the ith state of the anion, the ground state of the cth counter cation, and the ground state of the sth solvent molecule, respectively. In the present paper, the suffices and shoulders of A, c and s denote the anion, the cth cation, and the sth solvent molecule, respectively. The ground state of the system is obtained by replacing i by 0 in Eq. 1. Let us assume orthonormality for all the zeroth-order wave functions.

The energy of the ith state of the system in which all the particles interact with one another can be written by the second-order perturbation theory as

$$E_i = E_i^\circ + (\Phi_i^{\circ *}|H'|\Phi_i^\circ) + \sum_{m \neq i} \frac{(\Phi_m^{\circ *}|H'|\Phi_i^\circ)(\Phi_i^{\circ *}|H'|\Phi_m^\circ)}{E_i^\circ - E_m^\circ}, \tag{2}$$

where E_i° is the unperturbed energy corresponding to Φ_i°, E_m° is an unperturbed energy of the mth excited state of the system, and H' is the perturbation due to the interactions among the particles in the system. It may be sufficient to consider transitions only in the anion and the solvent molecules for the mth excited states of the system, because the cation requires much high transition energies, as mentioned above.

A General Expression for the Spectral Solvent Shift. The transition energies from the ground state to the ith excited state of the anion in the vapor and in the solution are denoted by the frequencies of $\nu_{i_0}^\circ$ and ν_{i_0}, respectively. The total interaction energy among the particles in the system of the ith state is obtained by $(E_i - E_i^\circ)$ according to Eq. 1. The difference between $(E_i - E_i^\circ)$ and $(E_0 - E_0^\circ)$ is equal to that between

stabilization energies of the ith-excited and ground states of the anion in the solution, because all the counter cations and the solvent molecules are in their ground states in both the ground and ith-excited states of the system. The spectral solvent shift $(\nu_{i0}-\nu_{i0}^{\circ})$ of the anion is due to the difference between the stabilization energies of the ith-excited and ground states of the anion. Accordingly, the spectral solvent shift is given by $(1/h)\{(E_i-E_i^{\circ})-(E_0-E_0^{\circ})\}$, where h is the Planck constant.

The Frank-Wen model[7] has been accepted for hydration in aqueous solutions. However, solvation numbers of the large picrate anion in organic solvents such as methanol, acetone, acetonitrile, and 1,2-dichloroethane are zero at 25 °C.[8] As described above, the solvent molecules are assumed not to be oriented with respect to each other. The value of $(E_i-E_i^{\circ})$ for the large anion may, therefore, be averaged over all orientations of all the solvent molecules. Thus, one obtains the following expression for the spectral solvent shift:

$$\nu_{i0}-\nu_{i0}^{\circ}=\frac{1}{h}\{<E_i-E_i^{\circ}>_{\mathrm{av}}-<E_0-E_0^{\circ}>_{\mathrm{av}}\}, \quad (3)$$

where $<\ >_{\mathrm{av}}$ denotes the average over all orientations of all the solvent molecules.

An Expression for the Perturbation of H'. According to Böttcher *et al.*,[9] the general expression for the electrostatic interaction energy W_{12} between two unpolarizable particles denoted by 1 and 2 is written as

$$W_{12}=\frac{1}{4\pi\varepsilon_0}\left\{\frac{Q_1Q_2}{R_{12}}-(Q_1\boldsymbol{p}_2-Q_2\boldsymbol{p}_1)\cdot\frac{\boldsymbol{R}_{12}}{R_{12}}-(Q_1\boldsymbol{\theta}_2-\boldsymbol{p}_1\boldsymbol{p}_2+Q_2\boldsymbol{\theta}_1):\boldsymbol{T}_{12}\right\}, \quad (4)$$

where ε_0 is the permittivity of vacuum, Q_1, $\boldsymbol{p}_1$, and $\boldsymbol{\theta}_1$ are the electric charge, permanent dipole moment, and quadrupole moment of particle 1, respectively, and R_{12} is the distance between the centers of masses of the two particles. Here $\boldsymbol{T}_{12}$ is the charge-quadrupole and dipole-dipole interaction tensor of $R_{12}^{-3}(\boldsymbol{I}-3R_{12}^{-2}\boldsymbol{R}_{12}\boldsymbol{R}_{12})$ where $\boldsymbol{I}$ is a unit tensor and $\boldsymbol{R}_{12}$, the position vector from 1 to 2. The dipole and quadrupole moments of the monatomic cation are zero.

On the assumption of the two-body interaction among the particles in the system, one can write H' as

$$H'=H'_{\mathrm{AS}}+H'_{\mathrm{AC}}+H'_{\mathrm{SS}}+H'_{\mathrm{CS}}+H'_{\mathrm{CC}}. \quad (5)$$

Here H'_{AS}, H'_{AC}, H'_{SS}, H'_{CS}, and H'_{CC} are perturbations due to the anion-solvent, anion-cation, solvent-solvent, cation-solvent, and cation-cation interactions, respectively. From Eq. 4, these perturbations can be written as follows:

$$H'_{\mathrm{AS}}=\frac{1}{4\pi\varepsilon_0}\sum_{s=1}^{N}\left\{\frac{ne}{R_s^3}\times\tilde{\boldsymbol{p}}_s\cdot\boldsymbol{R}_s+ne\tilde{\boldsymbol{\theta}}^s:\boldsymbol{T}_{\mathrm{A}s}+\tilde{\boldsymbol{p}}_{\mathrm{A}}\cdot\boldsymbol{T}_{\mathrm{A}s}\cdot\tilde{\boldsymbol{p}}^s\right\} \quad (6)$$

$$H'_{\mathrm{AC}}=\frac{1}{4\pi\varepsilon_0}\sum_{c=1}^{n}\left\{-\frac{ne^2}{R_c}+\frac{e}{R_c^3}\times\tilde{\boldsymbol{p}}_{\mathrm{A}}\cdot\boldsymbol{R}_c-e\tilde{\boldsymbol{\theta}}^{\mathrm{A}}:\boldsymbol{T}_{\mathrm{A}c}\right\} \quad (7)$$

$$H'_{\mathrm{SS}}=\frac{1}{8\pi\varepsilon_0}\sum_{s=1}^{N}\sum_{t=1}^{N}\tilde{\boldsymbol{p}}_s\cdot\boldsymbol{T}_{st}\cdot\tilde{\boldsymbol{p}}_t \quad (8)$$

$$H'_{\mathrm{CS}}=\frac{1}{4\pi\varepsilon_0}\sum_{c=1}^{n}\sum_{s=1}^{N}\left\{-\frac{e}{R_{cs}^3}\times\tilde{\boldsymbol{p}}_s\cdot\boldsymbol{R}_{cs}-e\tilde{\boldsymbol{\theta}}^s:\boldsymbol{T}_{cs}\right\} \quad (9)$$

$$H'_{\mathrm{CC}}=\frac{1}{8\pi\varepsilon_0}\sum_{c=1}^{n}\sum_{d=1}^{n}\frac{e^2}{R_{cd}}. \quad (10)$$

Here e is the elementary charge, a ripple mark denotes an operator, R_s and R_c are the distances from the anion to the sth solvent molecule and the cth cation, respectively, R_{st} is the distance from the sth solvent molecule to the tth solvent one, and R_{cd}, the distance from the cth cation to the dth cation.

Average Values of the Second and Third Terms in Eq. 2. Using Eqs. 5—10, one can calculate average values of the second and third terms on the right hand side of Eq. 2 as below. Here the suffix of double zeros, such as p_{00} and θ_{00}, denotes the moment of the ground state, and p_{ii} and θ_{ii} denote the dipole and quadrupole moments of the ith state. All the dipole moments of the solvent molecules are the same as p_{00}^{S}.

In the calculation of $<E_i-E_i^{\circ}>_{\mathrm{av}}$, one may always neglect terms containing powers higher than the sixth power of $1/R$, because contributions of these terms to the whole are probably negligible. Moreover, for convenience one writes only terms contributing to the frequency shift. The terms are restricted to those surviving through the calculation of $<E_i-E_i^{\circ}>_{\mathrm{av}}-<E_0-E_0^{\circ}>_{\mathrm{av}}$. Common terms appearing in both $<E_0-E_0^{\circ}>_{\mathrm{av}}$ and $<E_i-E_i^{\circ}>_{\mathrm{av}}$ will vanish through the calculation and may be omitted in the expression of $<E_i-E_i^{\circ}>_{\mathrm{av}}$. In the calculation of $<E_i-E_i^{\circ}>_{\mathrm{av}}$, the Boltzmann factor for the ground state of the system is applied even to the distribution of orientations of solvent molecules for the ith-excited state of the system, because the electronic transition in the anion is much faster than reorientations of the solvent molecules according to the Franck-Condon principle.

Paying attention to the assumption of orthonormality for all the zeroth-order wave functions, one obtains

$$\begin{aligned}(\Phi_i^{\circ *}|H'|\Phi_i^{\circ})&=\frac{1}{4\pi\varepsilon_0}\sum_{s=1}^{N}\left\{\frac{ne}{R_s^3}\times\boldsymbol{p}_{00}^s\cdot\boldsymbol{R}_s+ne\boldsymbol{\theta}_{00}^s:\boldsymbol{T}_{\mathrm{A}s}+\boldsymbol{p}_{ii}^{\mathrm{A}}\cdot\boldsymbol{T}_{\mathrm{A}s}\cdot\boldsymbol{p}_{00}^s\right\}\\&+\frac{1}{4\pi\varepsilon_0}\sum_{c=1}^{n}\left\{-\frac{ne^2}{R_c}+\frac{e}{R_c^3}\times\boldsymbol{p}_{ii}^{\mathrm{A}}\cdot\boldsymbol{R}_c-e\boldsymbol{\theta}_{ii}^{\mathrm{A}}:\boldsymbol{T}_{\mathrm{A}c}\right\}\\&+\frac{1}{8\pi\varepsilon_0}\sum_{s=1}^{N}\sum_{t=1}^{N}\boldsymbol{p}_{00}^s\cdot\boldsymbol{T}_{st}\cdot\boldsymbol{p}_{00}^t\\&-\frac{1}{4\pi\varepsilon_0}\sum_{c=1}^{n}\sum_{s=1}^{N}\left\{\frac{e}{R_{cs}^3}\times\boldsymbol{p}_{00}^s\cdot\boldsymbol{R}_{cs}+e\boldsymbol{\theta}_{00}^s:\boldsymbol{T}_{cs}\right\}\\&+\frac{1}{8\pi\varepsilon_0}\sum_{c=1}^{n}\sum_{d=1}^{n}\frac{e^2}{R_{cd}}. \quad (11)\end{aligned}$$

Then one obtains

$$\begin{aligned}&<(\Phi_i^{\circ *}|H'|\Phi_i^{\circ})>_{\mathrm{av}}\\&=<(\Phi_i^{\circ *}|H'_{\mathrm{AS}}|\Phi_i^{\circ})\exp\{-(\Phi_0^{\circ *}|H'|\Phi_0^{\circ})/kT\}>_{\mathrm{av}}\\&+(\Phi_i^{\circ *}|H'_{\mathrm{AC}}|\Phi_i^{\circ})\\&+<(\Phi_i^{\circ *}|H'_{\mathrm{SS}}|\Phi_i^{\circ})\exp\{-(\Phi_0^{\circ *}|H'|\Phi_0^{\circ})/kT\}>_{\mathrm{av}}\\&+<(\Phi_i^{\circ *}|H'_{\mathrm{CS}}|\Phi_i^{\circ})\exp\{-(\Phi_0^{\circ *}|H'|\Phi_0^{\circ})/kT\}>_{\mathrm{av}}\\&+(\Phi_i^{\circ *}|H'_{\mathrm{CC}}|\Phi_i^{\circ}), \quad (12)\end{aligned}$$

where k is the Boltzmann constant and T is the thermodynamic temperature. For example, calculation of the first term on the right hand side of Eq. 12 is performed first by expanding the exponential part in a Taylor series and then by averaging all the resulting terms over all orientations of the solvent molecules. Thus one obtains

$$\begin{aligned}
&\langle(\Phi_i^{\circ *}|H'|\Phi_i^\circ)\rangle_{\mathrm{av}} \\
&\approx -\frac{1}{(4\pi\varepsilon_0)^2 kT}\sum_{s=1}^{N}\langle(\boldsymbol{p}_{00}^{\mathrm{A}}\cdot\boldsymbol{T}_{\mathrm{A}s}\cdot\boldsymbol{p}_{00}^{s})(\boldsymbol{p}_{ii}^{\mathrm{A}}\cdot\boldsymbol{T}_{\mathrm{A}s}\cdot\boldsymbol{p}_{00}^{s})\rangle_{\mathrm{av}} \\
&\quad+\frac{1}{4\pi\varepsilon_0}\sum_{c=1}^{n}\left\{\frac{e}{R_c^3}\times\boldsymbol{p}_{ii}^{\mathrm{A}}\cdot\boldsymbol{R}_c-e\boldsymbol{\theta}_{ii}^{\mathrm{A}}:\boldsymbol{T}_{\mathrm{A}c}\right\} \\
&=-\frac{2(p_{00}^{\mathrm{S}})^2(\boldsymbol{p}_{00}^{\mathrm{A}}\cdot\boldsymbol{p}_{ii}^{\mathrm{A}})}{3(4\pi\varepsilon^0)^2kT}\sum_{s=1}^{N}\frac{1}{R_s^6} \\
&\quad+\frac{e}{4\pi\varepsilon_0}\sum_{c=1}^{n}\left\{\frac{\boldsymbol{p}_{ii}^{\mathrm{A}}\cdot\boldsymbol{R}_c}{R_c^3}-\boldsymbol{\theta}_{ii}^{\mathrm{A}}:\boldsymbol{T}_{\mathrm{A}c}\right\}. \qquad (13)
\end{aligned}$$

In view of the mode of transition from the ith state to the mth-excited state, the average value of $I=\langle\sum_{m\neq i}(\Phi_m^{\circ *}|H'|\Phi_i^\circ)(\Phi_i^{\circ *}|H'|\Phi_m^\circ)/(E_i^\circ-E_m^\circ)\rangle_{\mathrm{av}}$ is calculated as the sum of three values, *i.e.*, $I=I_1+I_2+I_3$. Each value results from a different mode of transition and is calculated individually in the manner described below.

The first case is a transition mode in which the anion is excited from the ith-excited state to the jth-excited state and all the other particles remain in their ground states: Let us denote the average of all values of $(E_j^{\mathrm{A}}-E_i^{\mathrm{A}})$ by ΔE_i^{A}, where E_j^{A} is the energy of the jth state (Φ_j^{A}) of the anion except for $j=i$. In this case one obtains $E_i^\circ-E_m^\circ=E_i^{\mathrm{A}}-E_j^{\mathrm{A}}$ and

$$\begin{aligned}
&(\Phi_m^{\circ *}|H'|\Phi_i^\circ) \\
&=\frac{1}{4\pi\varepsilon_0}\sum_{s=1}^{N}\boldsymbol{p}_{ij}^{\mathrm{A}}\cdot\boldsymbol{T}_{\mathrm{A}s}\cdot\boldsymbol{p}_{00}^{s}+\frac{e}{4\pi\varepsilon_0}\sum_{c=1}^{n}\left\{\frac{\boldsymbol{p}_{ij}^{\mathrm{A}}\cdot\boldsymbol{R}_c}{R_c^3}-\boldsymbol{\theta}_{ij}^{\mathrm{A}}:\boldsymbol{T}_{\mathrm{A}c}\right\}, \qquad (14)
\end{aligned}$$

where $\boldsymbol{p}_{ij}^{\mathrm{A}}=(\phi_i^{\mathrm{A}*}|\tilde{\boldsymbol{p}}^{\mathrm{A}}|\phi_j)$ and $\boldsymbol{\theta}_{ij}^{\mathrm{A}}=(\phi_i^{\mathrm{A}}|\tilde{\boldsymbol{\theta}}^{\mathrm{A}}|\phi_j^{\mathrm{A}})$. Here one denotes an isotropic electric polarizability of the anion in the ith state by $\alpha_{ii}^{\mathrm{A}}=(2/3)\sum_{j\neq i}(|\boldsymbol{p}_{ij}^{\mathrm{A}}|^2/4\pi\varepsilon_0\Delta E_i^{\mathrm{A}})$ in the units of m^3. Then one obtains

$$\begin{aligned}
I_1&=-\Big\langle\sum_{j\neq i}\frac{1}{\Delta E_i^{\mathrm{A}}}(\Phi_m^{\circ *}|H'|\Phi_i^\circ)^2\exp\{-(\Phi_0^{\circ *}|H'|\Phi_0^\circ)/kT\}\Big\rangle_{\mathrm{av}} \\
&\approx-\sum_{j\neq i}\frac{1}{(4\pi\varepsilon_0)^2\Delta E_i^{\mathrm{A}}}\Big[\sum_{s=1}^{N}\langle(\boldsymbol{p}_{ij}^{\mathrm{A}}\cdot\boldsymbol{T}_{\mathrm{A}s}\cdot\boldsymbol{p}_{00}^{s})^2\rangle_{\mathrm{av}} \\
&\quad+e^2\sum_{j\neq i}\left\{\sum_{c=1}^{n}\left(\frac{\boldsymbol{p}_{ij}^{\mathrm{A}}\cdot\boldsymbol{R}_c}{R_c^3}-\boldsymbol{\theta}_{ij}^{\mathrm{A}}:\boldsymbol{T}_{\mathrm{A}c}\right)\right\}^2\Big] \\
&=-\frac{(p_{00}^{\mathrm{S}})^2\alpha_{ii}^{\mathrm{A}}}{4\pi\varepsilon_0}\sum_{s=1}^{N}\frac{1}{R_s^6} \\
&\quad-\frac{e^2}{(4\pi\varepsilon_0)^2\Delta E_i^{\mathrm{A}}}\sum_{j\neq i}\left\{\sum_{c=1}^{n}\left(\frac{\boldsymbol{p}_{ij}^{\mathrm{A}}\cdot\boldsymbol{R}_c}{R_c^3}-\boldsymbol{\theta}_{ij}^{\mathrm{A}}:\boldsymbol{T}_{\mathrm{A}c}\right)\right\}^2. \qquad (15)
\end{aligned}$$

The second case is a transition mode in which the anion remains in the ith state and one of the N solvent molecules is excited to the lth-excited state: Let us write the average of all values of $(E_l^{\mathrm{S}}-E_0^{\mathrm{S}})$ as ΔE_0^{S}, where E_0^{S} and E_l^{S} are energies of the ground and lth-excited states, respectively, of the solvent molecule. One obtains $E_i^\circ-E_m^\circ=E_0^{\mathrm{S}}-E_l^{\mathrm{S}}$ and

$$\begin{aligned}
&(\Phi_m^{\circ *}|H'|\Phi_i^\circ) \\
&=\frac{1}{4\pi\varepsilon_0}\sum_{s=1}^{N}\left\{\frac{ne}{R_s^3}\times\boldsymbol{p}_{0l}^{s}\cdot\boldsymbol{R}_s+ne\boldsymbol{\theta}_{0l}^{s}:\boldsymbol{T}_{\mathrm{A}s}+\boldsymbol{p}_{ii}^{\mathrm{A}}\cdot\boldsymbol{T}_{\mathrm{A}s}\cdot\boldsymbol{p}_{0l}^{s}\right\} \\
&\quad+\frac{1}{8\pi\varepsilon_0}\sum_{s=1}^{N}\sum_{t=1}^{N}\boldsymbol{p}_{0l}^{s}\cdot\boldsymbol{T}_{st}\cdot\boldsymbol{p}_{00}^{t} \\
&\quad-\frac{e}{4\pi\varepsilon_0}\sum_{c=1}^{n}\sum_{s=1}^{N}\left\{\frac{\boldsymbol{p}_{0l}^{s}\cdot\boldsymbol{R}_{cs}}{R_{cs}^3}+\boldsymbol{\theta}_{0l}^{s}:\boldsymbol{T}_{cs}\right\}. \qquad (16)
\end{aligned}$$

Then one obtains

$$\begin{aligned}
I_2&\approx-\frac{1}{(4\pi\varepsilon_0)^2\Delta E_0^{\mathrm{S}}}\Big\langle\sum_{m\neq i}(\Phi_m^{\circ *}|H'|\Phi_i^\circ)^2\Big\rangle_{\mathrm{av}} \\
&=-\frac{1}{(4\pi\varepsilon_0)^2\Delta E_0^{\mathrm{S}}}\sum_{s=1}^{N}\sum_{l\neq 0}\langle(\boldsymbol{p}_{ii}^{\mathrm{A}}\cdot\boldsymbol{T}_{\mathrm{A}s}\cdot\boldsymbol{p}_{0l}^{s})^2\rangle_{\mathrm{av}} \\
&=-\frac{(p_{ii}^{\mathrm{A}})^2\alpha_{00}^{\mathrm{S}}}{4\pi\varepsilon_0}\sum_{s=1}^{N}\frac{1}{R_s^6}, \qquad (17)
\end{aligned}$$

where α_{00}^{S} is the isotropic electric polarizability of the solvent molecule in the ground state.

When any two of the N solvent molecules are simultaneously excited, no terms contributing to the frequency shift appear, because $(\Phi_m^{\circ *}|H'|\Phi_i^\circ)=(1/8\pi\varepsilon_0)\sum_{s=1}^{N}\sum_{t=1}^{N}\boldsymbol{p}_{0l}^{s}\cdot\boldsymbol{T}_{st}\cdot\boldsymbol{p}_{0l}^{t}$ in this case. When more than two of the solvent molecules are simultaneously excited, $(\Phi_m^{\circ *}|H'|\Phi_i^\circ)$ is always zero according to Eqs. 5—10.

The third case is a transition mode in which the anion in the ith state and one of the N solvent molecules in the ground states are simultaneously excited: Since $E_i^\circ-E_m^\circ=E_i^{\mathrm{A}}-E_j^{\mathrm{A}}+E_0^{\mathrm{S}}-E_l^{\mathrm{S}}$ and

$$(\Phi_m^{\circ *}|H'|\Phi_i^\circ)=\frac{1}{4\pi\varepsilon_0}\sum_{s=1}^{N}\boldsymbol{p}_{ij}^{\mathrm{A}}\cdot\boldsymbol{T}_{\mathrm{A}s}\cdot\boldsymbol{p}_{0l}^{s}, \qquad (18)$$

in this case, one obtains

$$\begin{aligned}
I_3&\approx-\frac{1}{(4\pi\varepsilon_0)^2(\Delta E_0^{\mathrm{S}}+\Delta E_i^{\mathrm{A}})} \\
&\quad\times\Big\langle\sum_{j\neq i}\sum_{l\neq 0}\Big(\sum_{s=1}^{N}\boldsymbol{p}_{ij}^{\mathrm{A}}\cdot\boldsymbol{T}_{\mathrm{A}s}\cdot\boldsymbol{p}_{0l}^{s}\Big)^2\Big\rangle_{\mathrm{av}} \\
&=-\frac{3\Delta E_0^{\mathrm{S}}\Delta E_i^{\mathrm{A}}\alpha_{00}^{\mathrm{S}}\alpha_{ii}^{\mathrm{A}}}{2(\Delta E_0^{\mathrm{S}}+\Delta E_i^{\mathrm{A}})}\sum_{s=1}^{N}\frac{1}{R_s^6}. \qquad (19)
\end{aligned}$$

Simultaneous excitations of more than two of the N solvent molecules together with the excitation of the anion lead to $(\Phi_m^{\circ *}|H'|\Phi_i^\circ)=0$.

An Expression for ν_{i0}. From Eqs. 3, 13, 15, 17, and 19, one obtains

$$\begin{aligned}
&h(\nu_{i0}-\nu_{i0}^\circ) \\
&=\frac{e}{4\pi\varepsilon_0}\sum_{c=1}^{n}\left\{\left(\frac{\boldsymbol{p}_{ii}^{\mathrm{A}}\cdot\boldsymbol{R}_c}{R_c^3}-\boldsymbol{\theta}_{ii}^{\mathrm{A}}:\boldsymbol{T}_{\mathrm{A}c}\right)-\left(\frac{\boldsymbol{p}_{00}^{\mathrm{A}}\cdot\boldsymbol{R}_c}{R_c^3}-\boldsymbol{\theta}_{00}^{\mathrm{A}}:\boldsymbol{T}_{\mathrm{A}c}\right)\right\} \\
&\quad+\frac{1}{(4\pi\varepsilon_0)^2}\times\Big[\frac{e^2}{\Delta E_0^{\mathrm{A}}}\sum_{j\neq 0}\left\{\sum_{c=1}^{n}\left(\frac{\boldsymbol{p}_{0j}^{\mathrm{A}}\cdot\boldsymbol{R}_c}{R_c^3}-\boldsymbol{\theta}_{0j}^{\mathrm{A}}:\boldsymbol{T}_{\mathrm{A}c}\right)\right\}^2 \\
&\quad-\frac{e^2}{\Delta E_i^{\mathrm{A}}}\sum_{j\neq i}\left\{\sum_{c=1}^{n}\left(\frac{\boldsymbol{p}_{ij}^{\mathrm{A}}\cdot\boldsymbol{R}_c}{R_c^3}-\boldsymbol{\theta}_{ij}^{\mathrm{A}}:\boldsymbol{T}_{\mathrm{A}c}\right)\right\}^2\Big] \\
&\quad+\frac{2(p_{00}^{\mathrm{S}})^2\{(p_{00}^{\mathrm{A}})^2-(\boldsymbol{p}_{00}^{\mathrm{A}}\cdot\boldsymbol{p}_{ii}^{\mathrm{A}})\}}{3(4\pi\varepsilon_0)^2kT}\sum_{s=1}^{N}\frac{1}{R_s^6}
\end{aligned}$$

$$+\frac{(p_{00}^{S})^2(\alpha_{00}^{A}-\alpha_{ii}^{A})}{4\pi\varepsilon_0}\sum_{s=1}^{N}\frac{1}{R_s^6}+\frac{\alpha_{00}^{S}(p_{00}^{A}-p_{ii}^{A})}{4\pi\varepsilon_0}\sum_{s=1}^{N}\frac{1}{R_s^6}$$

$$+\frac{3}{2}\times\left\{\frac{\Delta E_0^{S}\Delta E_0^{A}\alpha_{00}^{S}\alpha_{00}^{A}}{\Delta E_0^{S}+\Delta E_0^{A}}-\frac{\Delta E_0^{S}\Delta E_i^{A}\alpha_{00}^{S}\alpha_{ii}^{A}}{\Delta E_0^{S}+\Delta E_i^{A}}\right\}\sum_{s=1}^{N}\frac{1}{R_s^6}. \quad (20)$$

Both the first and second terms on the right hand side of Eq. 20 are due to the anion-cation interactions and are independent of the solvent. The second term is probably much smaller than the first, because the former contains coefficients of the sixth power of $1/R_c$, while coefficients of the latter are of the third power. The second term may therefore be ignored. The third, fourth, fifth and sixth terms are due to the anion dipole-solvent dipole interactions, the solvent dipole-anion induced dipole ones, the anion dipole-solvent induced dipole ones, and the anion-solvent dispersion forces, respectively. All these terms relating to the solvent contain coefficients of R_s^{-6}. Therefore, the solvent molecules mainly contributing to the frequency shift are attributed to those around the anion. Here one may approximately consider only the closely neighboring solvent molecules. According to the previous treatment,[5,6] this approximation leads to

$$\sum_{s=1}^{N}\frac{1}{R_s^6}\approx\frac{\pi}{(r_A+r_S)^4}\times\left(\frac{4\pi N_A}{3}\right)^{2/3}\left(\frac{d^S}{M_r^S}\right)^{2/3}, \quad (21)$$

where N_A is Avogadro's number, r_A and r_S are radii of the anion and the solvent molecule, respectively, and d^S and M_r^S, the relative density and molecular weight, respectively, of the solvent. For example, r_S is given by

$$r_S=\left(\frac{3M_r^S}{4\pi N_A d^S}\right)^{1/3}. \quad (22)$$

Thus, Eq. 20 is reduced to

$$\nu_{i0}=\nu'_{i0}+A\times\frac{(d^S/M_r^S)^{2/3}(p_{00}^S)^2}{(r_A+r_S)^4}+B\times\frac{(d^S/M_r^S)^{2/3}\alpha_{00}^S}{(r_A+r_S)^4}, \quad (23)$$

where

$$\nu'_{i0}=\nu^\circ_{i0}+\frac{1}{4\pi\varepsilon_0}\sum_{c=1}^{n}\frac{e}{R_c^3}\left\{(\boldsymbol{p}_{ii}^A-\boldsymbol{p}_{00}^A)\cdot\boldsymbol{R}_c+(\boldsymbol{\theta}_{00}^A-\boldsymbol{\theta}_{ii}^A):\left(\boldsymbol{I}-\frac{3}{R_c^2}\boldsymbol{R}_c\boldsymbol{R}_c\right)\right\} \quad (24)$$

$$A=\frac{\pi}{h}\left(\frac{4\pi N_A}{3}\right)^{2/3}\times\left[\frac{2\times\{(p_{00}^A)^2-(\boldsymbol{p}_{00}^A\cdot\boldsymbol{p}_{ii}^A)\}}{3(4\pi\varepsilon_0)^2kT}+\frac{(\alpha_{00}^A-\alpha_{ii}^A)}{4\pi\varepsilon_0}\right], \quad (25)$$

and

$$B=\frac{\pi}{h}\left(\frac{4\pi N_A}{3}\right)^{2/3}\times\left[\frac{(p_{00}^A)^2-(p_{ii}^A)^2}{4\pi\varepsilon_0}+\frac{3}{2}\times\left(\frac{\Delta E_0^A\alpha_{00}^A}{1+\Delta E_0^A/\Delta\bar{E}_0^S}-\frac{\Delta E_i^A\alpha_{ii}^A}{1+\Delta E_i^A/\Delta\bar{E}_0^S}\right)\right]. \quad (26)$$

Although ΔE_0^S varies with the solvent, ΔE_0^S is for convenience replaced by the average $\Delta\bar{E}_0^S$ of values of ΔE_0^S in Eq. 26. Then, A and B may be approximately characteristic of the anion. Equation 24 indicates that ν'_{i0} is independent of the solvent. According to Eq. 23, therefore, values of ν'_{i0}, A, and B can be estimated by the least-squares method from experimental frequencies of the anion in several solutions. From Eq. 24, effects of the ion pairings between the anion and its cations are shown by the second term in Eq. 24 and can be regarded as being involved at a constant magnitude in the experimental frequency (ν_{i0}).

Discussion

As shown by Eq. 20, the solvent shift is due to the dipole-dipole interactions, the induced dipole-dipole ones, and the dispersion forces between the anion and the solvent molecules, because the first and second terms are independent of the solvent. On the other hand, Hirano's expression for the same shift involves only the dispersion force terms.[3] The essential difference between the present treatment and Hirano's seems to arise from the different results of calculations of the first- and second-order terms of Eq. 2. Moreover, according to Hirano, the effects of the counter cations on the frequency shift can be approximately ignored, while in the present treatment the effects are included approximately at a constant magnitude in the experimental frequency. The difference may be attributed to the operation of averaging over all orientations of the counter cations. Hirano has performed this operation; it is not done in the present treatment.

Equation 23 can be applied not only to the large anions but also to neutral molecules, because the effects of charge of the anion are not involved in Eqs. 25 and 26 and ν'_{i0} is equal to ν°_{i0} in the absence of the counter cations. The previous expressions[5,6] have been derived from assuming van der Waals' equation at the beginning for interactions between the neutral solute molecule in the ith state and the solvent molecules. The present treatment is the theoretical basis of the previous theory:[5,6] If the first and second terms are omitted and $(\boldsymbol{p}_{00}^A\cdot\boldsymbol{p}_{ii}^A)$ is replaced by $(p_{ii}^A)^2$ in Eq. 20, Eq. 20 is essentially the same as the previous expressions. Accordingly, the previous expressions can be derived in the same way as in the present treatment, if the Boltzmann factor of exp $\{-(\Phi_i^{\circ *}|H'|\Phi_i^\circ)/kT\}$ is used instead of that of exp $\{-(\Phi_0^{\circ *}|H'|\Phi_0^\circ)/kT\}$ for the ith-excited state of the system. This leads to the conclusion that the Franck-Condon principle has not been considered in the previous expressions. When the principle is considered in the previous expressions,[5,6] the value of $(p_{ii}^A)^2$ appearing in the solute dipole-solvent dipole interaction terms should be replaced by $(\boldsymbol{p}_{00}^A\cdot\boldsymbol{p}_{ii}^A)$.

In McRae's theory[4] the Hamiltonian operator in Eq. 2 consists of instantaneous dipole-dipole interactions between two neutral molecules in the system. In the case of the neutral solute molecule (U), H' is written from Eq. 4 as

$$H'=\sum_{S=1}^{N}\tilde{\boldsymbol{p}}^U\cdot\boldsymbol{T}_{Us}\cdot\tilde{\boldsymbol{p}}^s. \quad (27)$$

Equation 27 is the dipole-dipole interaction operator. Accordingly, the previous treatment[5,6] is fundamentally similar to that of McRae, as also described by Amos and Burrows.[1a] An essential difference between McRae's theory[4] and that of the present author lies in the following point: In McRae's theory the second and third terms in Eq. 2 have been concretely calculated by using reaction fields of the Onsager type,[10] while

in the present treatment these terms have been consistently obtained in terms of the two-body interactions among the particles of the system. Although the value of local relative permittivity in the neighborhood of the solute differs from that of the bulk relative permittivity of the solvent, the local permittivity is not considered at all in deriving the Onsager reaction field. In order to consider the local permittivity, the Block-Walker reaction field[11] should be used instead of the Onsager one in McRae's theory for the neutral molecule. For the description of experimental results for solvent effects on several phenomena, the Block-Walker reaction field is much superior to the Onsager one.[12] In McRae's theory,[4] another problem arises due to the following assumption: A time average of a square field at the solute dipole owing to the presence of permanent dipoles of surrounding solvent molecules is arbitrarily assumed to be equal to three times the squared value of the reaction field. On the other hand, the present treatment is not accompanied by such problems, because the relative permittivity and the reaction field are not used.

Hirano[3] has extended McRae's theory for the neutral molecule to the anion, using the Onsager reaction field. Both the Onsager reaction field and the Block-Walker one are derived from the assumption that the solute molecule has no excess charge and from solving Laplace equations. These reaction fields can not be applied to the anion, because a reaction field for the anion must be derived by solving a Poisson equation. Instead of the Onsager reaction field, the Kirkwood reaction field[13,14] consisting of the Born charging energy[15] and the Onsager reaction field should be used for the anion, but this field is also derived after neglecting the local relative permittivity. Beveridge and Schnuelle[14] have theoretically treated the polarization energy of a charged solute and have presented a general expression definitely containing the local relative permittivity. One, however, finds difficulty in applying the expression, because it is hard to determine values of the local relative permittivity and thickness of a local solvent shell. These values are necessary for applying the expression. Thus, the solvent shift of the anion has been studied by the present treatment.

In the present calculation of the interaction energies between the solute and the solvent molecules, a serious problem arises from the evaluation of the "average energies" such as ΔE_0^{A}, ΔE_i^{A}, and ΔE_0^{S}. It is found that ΔE_0^{A} and ΔE_0^{S} are approximately equal to ionization potentials (I_0^{A} and I_0^{S}) of the solute and solvent molecules, respectively, in their ground states.[16] The replacement of the average energy by the ionization potential has not been justified theoretically.[1a,17] At the present stage, however, there is no approach to this problem other than the replacement. The value of ΔE_i^{A} may be replaced by $I_i^{\mathrm{A}}=I_0^{\mathrm{A}}-hc\nu_{i0}^{\circ}$ as in the previous papers,[5,6] where c is the speed of light *in vacuo* and I_i^{A}, an ionization potential of the anion in the ith state. Amos and Burrows[1a,17] have stated that approximately the same average energies should be taken for both the ground and excited states. So far as the average energy is assumed to be approximated by the ionization potential, the assumption of $I_i^{\mathrm{A}}=I_0^{\mathrm{A}}-hc\nu_{i0}^{\circ}$ is valid for a low-lying excited state: The energy of the ground state of the solute molecule is denoted by $E(^1\Psi_0)$. The energy of the ith-excited state ($^1\Psi_{i0}$) resulting from a transition of an electron from the highest occupied MO (ϕ_0) to the ith vacant MO (ϕ_i) is written as

$$E(^1\Psi_{i0}) = E(^1\Psi_0) + hc\nu_{i0}^{\circ}. \tag{28}$$

According to Roothaan,[18] a singly ionized state ($^2\Psi_0$) obtained by removing either of the two electrons occupying ϕ_0 has an energy given by

$$E(^2\Psi_0) = E(^1\Psi_0) - \varepsilon_0(\Psi_0) = E(^1\Psi_0) + I_0, \tag{29}$$

where $\varepsilon_0(\phi_0)$ is the energy of ϕ_0, and I_0 is the ionization potential of the ground state of the molecule. From Eqs. 28 and 29, one can write the ionization potential of $^1\Psi_{i0}$ as

$$I_i = E(^2\Psi_0) - E(^1\Psi_{i0}) = I_0 - hc\nu_{i0}^{\circ}. \tag{30}$$

If the anion is small and is solvated by coordination of the solvent molecules, the second and third terms in Eq. 2 must be calculated without the operation of averaging over all the orientations of all the solvent molecules. Of course, Eq. 23 can not be applied to such a small anion. In the case of a small solvated anion, one may calculate the second and third terms by considering only the solvating solvent molecules surrounding the anion.

Since a molecule generally has a dipole moment larger than its quadrupole moment, Eq. 24 may be approximated by

$$\nu'_{i0} = \nu_{i0}^{\circ} + \Delta\nu_{\mathrm{C}}, \tag{31}$$

where

$$\Delta\nu_{\mathrm{C}} = \frac{e}{4\pi\varepsilon_0}\sum_{c=1}^{n}\frac{(\boldsymbol{p}_{ii}^{\mathrm{A}}-\boldsymbol{p}_{00}^{\mathrm{A}})\cdot\boldsymbol{R}_{\mathrm{C}}}{R_c^3}. \tag{32}$$

Here $\Delta\nu_{\mathrm{C}}$ is a frequency shift due to the ion pairings between the anion and its counter cations. Equation 32 shows that $\Delta\nu_{\mathrm{C}}$ becomes smaller with increasing values of R_c, *i.e.*, with an increasing radius of the cation. As described above, $\Delta\nu_{\mathrm{C}}$ is contained in the experimental frequency (ν_{i0}). Consequently, as the radius of cation increases in the same solvent, a wavelength corresponding to ν_{i0} will shift to the red if $(\boldsymbol{p}_{ii}^{\mathrm{A}}-\boldsymbol{p}_{00}^{\mathrm{A}})\cdot\boldsymbol{R}_c>0$, because $\Delta\nu_{\mathrm{C}}$ decreases in this case. If $(\boldsymbol{p}_{ii}^{\mathrm{A}}-\boldsymbol{p}_{00}^{\mathrm{A}})\cdot\boldsymbol{R}_c<0$, the shift of the wavelength will be toward the blue, because $\Delta\nu_{\mathrm{C}}$ increases. Because of the negative charge, the dipole moment of the anion varies with the way of setting the origin of the coordinates,[19] and often takes a minus sign, as exemplified below. Accordingly, the minus sign as well as a plus one must be considered for values of $\boldsymbol{p}_{00}^{\mathrm{A}}$ and $\boldsymbol{p}_{ii}^{\mathrm{A}}$ which satisfy an inequality of $(\boldsymbol{p}_{ii}^{\mathrm{A}}-\boldsymbol{p}_{00}^{\mathrm{A}})\cdot\boldsymbol{R}_c\lesseqgtr 0$. Such red shifts seem to be seen in the cases of xanthene and thioxanthene in 2-methyltetrahydrofuran.[20] For example, xanthene shows absorption maxima at 413, 436, 470, and 482 nm owing to the ion pairings with Li^+, Na^+, K^+, and Cs^+, respectively.[20]

The ion pairings of 4,4-dimethoxy-1,3,5-trinitro-2,5-cyclohexadienide anion with $(n\text{-}C_4H_9)_4N^+$, Na^+, Ca^{2+}, and Ba^{2+} in methanol show the first bands at 480, 490, 490, and 500 nm, respectively, and the second bands at 418, 412, 404, and 405 nm, respectively.[21] The first

and second bands tend to shift to the red and to the blue, respectively, with an increasing radius of the cation. In the solution the counter cation is probably held by the four oxygen atoms of two methoxyl groups and two nitro groups on the 3,5-positions.[21] Moreover, a symmetrical structure of crystalline potassium salt of the anion has been determined by the X-ray method.[22] In view of the symmetrical structure of the ion pair between the anion and its cation, all $\boldsymbol{p}^{A}_{00}$, $\boldsymbol{p}^{A}_{ti}$, and $\boldsymbol{R}_c$ probably lie along the same axis of the C_{2v}-symmetry. In the anion, the position vector of the center of negative-charge distribution is much greater in magnitude than that of the positive-charge distribution, though the former magnitude depends on the way of setting the origin. The dipole moment of the anion may, therefore, be in the direction opposite to that of the neutral molecule. One may, therefore, assume that $\boldsymbol{p}^{A}_{00}$ and $\boldsymbol{p}^{A}_{ti}$ are in the opposite direction of $\boldsymbol{R}_c$ in this case. Consequently, one obtains inequalities of $P^{A}_{00}>P^{A}_{ti}$ and $P^{A}_{ti}>P^{A}_{00}$ from the red and blue shifts, respectively. Thus, the dipole moment of the ground state of the anion may be larger than that of the first-excited state but may be smaller than that of the second-excited state.

Equation 32 also shows that, in the case of the same solvent, the shift does not vary with the cation if $P^{A}_{00}\simeq 0$ and $P^{A}_{ti}\simeq 0$ or if $P^{A}_{00}\simeq P^{A}_{ti}$. Such behavior seems to appear in the case of the triiodide anion.[23] The first and second excited states of the triiodide anion as well as its ground state are likely to be nonpolar since their structures consist of three identical iodine atoms. For example, the triiodide anion in diethyl ether shows the first absorption bands at 366.5, 366.7, and 366.4 nm owing to the ion pairings with $(C_2H_5)_4N^+$, $(C_2H_5)_3AsI^+$, and Cs^+, respectively.[23]

In applying Eq. 23, it is convenient to use a wave number σ_{t0} instead of ν_{t0}, because the former is calculated with somewhat greater ease than the latter from the λ_{t0} wavelength observed. Then, ν'_{t0} and ν°_{t0} are replaced by σ'_{t0} and σ°_{t0}. The value of λ_{t0} measured with a spectrophotometer is not a wavelength in the solution but is approximately converted into a wavelength *in vacuo*. In Eq. 23, therefore, ν_{t0} can be replaced by $c\sigma_{t0}$. If λ_{t0} is a value in the solution, ν_{t0} should be replaced by $(c/n_S)\sigma_{t0}$, where n_S is the refractive index of the solvent.

Applications

All the dipole moments and polarizabilities of the anion and the solvent molecule in Eqs. 23—26 are values measured in vapors, because in the zeroth-order approximation all the particles in the system are assumed not to interact with one another. In applying Eq. 23, the temperature was always assumed to be 20 °C and the dipole moments (p^{S}_{00}) of the solvent molecules in vapors were taken from Refs. 24 and 25. Dipole moments of *N,N*-dimethylformamide, *N,N*-dimethylacetamide, dimethyl sulfoxide, 1,2-dimethoxyethane and diethyloxalate were values measured in benzene,[26] since their moments in vapors were not found. Values of α^{S}_{00} were calculated from sums of bond refractions. Unfortunately, few systematic experimental studies have been reported on the spectral solvent shifts of anions.

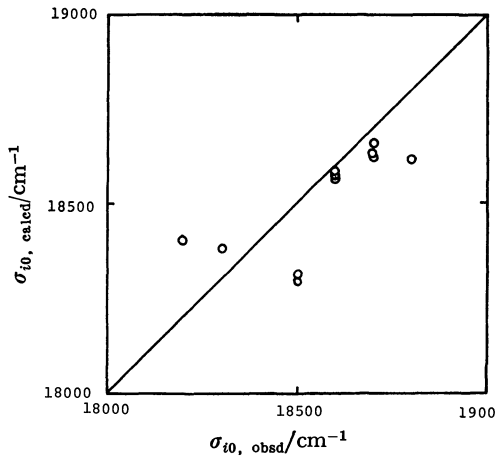

Fig. 1. Correlation of $\sigma_{t0,\ calcd}$ with $\sigma_{t0,\ obsd}$ for the first band of Eosin-Y^{2-} anion.

Eosin-Y^{2-} Anion. Values used for σ_{t0} of Eosin-Y^{2-} were those measured by Hirano.[3] He did not report the kind of counter cation used. The value of r_A was assumed to be 0.56 nm from the molecular volume (0.7—0.8 nm^3) estimated in footnote 25 in Ref. 3. These results were obtained: $\sigma'_{t0}=18990\ cm^{-1}$, $A=5.60\times10^{12}\ J^{-1}\ m^2$, and $B=-5.75\times10^{-6}\ m^2$. The frequencies ($\sigma_{t0.calcd}$) calculated by using these values are plotted in Fig. 1 against the $\sigma_{t0.obsd}$ observed. The correlation of $\sigma_{t0.calcd}$ with $\sigma_{t0.obsd}$ is as good as that in the application of Hirano.[3] The value of σ'_{t0} is smaller than that of σ°_{t0} (19300 cm^{-1}) obtained by Hirano, though σ'_{t0} is interpreted to involve a constant shift due to the ion pairings with cations.

The Meisenheimer Complex of 1,3,5-Trinitrobenzene with Cyanide Ion. An application was made to spectral solvent shifts of the first and second absorption bands of the tetrabutylammonium salt of 4-cyano-1,3,5-trinitro-2,5-cyclohexadienide (**1**).[27] The value of r_A was assumed to be 0.44 nm from crystal data[22] of the potassium salt of 4,4-dimethoxy-1,3,5-trinitro-2,5-cyclo-

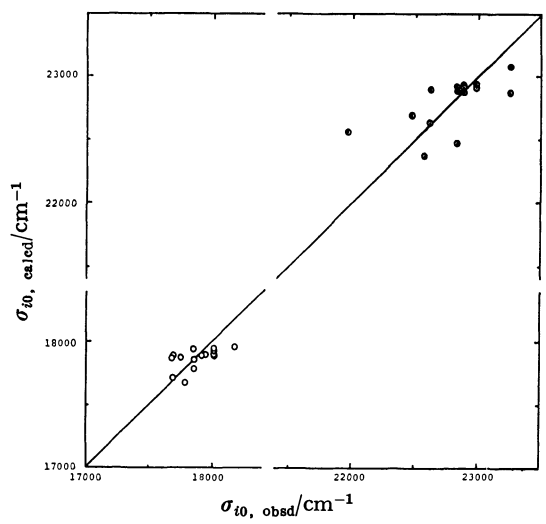

Fig. 2. Correlations of $\sigma_{t0,\ calcd}$ with $\sigma_{t0,\ obsd}$ for the first (○) and second (⊙) bands of **1**.

hexadienide. These results were obtained: $\sigma'_{i0}=18200$ cm^{-1}, $A=-9.32\times10^{11}$ J^{-1} m^2, and $B=-2.271\times10^{-6}$ m^2 for the first band, and $\sigma'_{i0}=23260$ cm^{-1}, $A=-1.153\times10^{13}$ J^{-1} m^2, and $B=-2.571\times10^{-6}$ m^2 for the second band. The frequencies calculated by using these values of σ'_{i0}, A, and B are roughly correlated with those observed, as shown in Fig. 2.

Putting the above values of A and B for the first band into Eqs. 25 and 26, respectively, one obtains the following equations:

$$\{(p^{A}_{00})^2-(\boldsymbol{p}^{A}_{00}\cdot\boldsymbol{p}^{A}_{ii})\}+6.17\times10^{-21}\,\mathrm{J}\times(\alpha^{A}_{00}-\alpha^{A}_{ii})=-0.20\times10^{-49}\,\mathrm{J\,m^3} \quad (33)$$

$$\{(p^{A}_{00})^2-(p^{A}_{ii})^2+1.5\times\left(\frac{\Delta E^{A}_{0}\alpha^{A}_{00}}{1+\Delta E^{A}_{0}/\Delta\bar{E}^{S}_{0}}-\frac{\Delta E^{A}_{i}\alpha^{A}_{ii}}{1+\Delta E^{A}_{i}/\Delta\bar{E}^{S}_{0}}\right)=-77.49\times10^{-49}\,\mathrm{J\,m^3}. \quad (34)$$

Generally, upon an electronic excitation from a ground state to an excited one, an increase in polarizability might be expected, because an orbital of the excited state is larger and more diffuse than that of the ground state. Actually, such increases in polarizabilities have been confirmed experimentally for several neutral molecules.[28] An inequality of $\alpha^{A}_{ii}>\alpha^{A}_{00}$ may also be expected for the anion under consideration. Since (1 Debye)$^2=1.000\times10^{-49}$ J m^3, -77.49×10^{-49} J m^3 in Eq. 34 is rather large. This large negative value is probably due not only to $\alpha^{A}_{ii}>\alpha^{A}_{00}$ but also to $|p^{A}_{ii}|>|p^{A}_{00}|$, because ΔE^{A}_{0} is larger than ΔE^{A}_{i}, according to Eq. 30, and the second term on the left hand side of Eq. 34 is probably not so large that the value can be attributed to it alone. On the other hand, the absolute value of -0.20×10^{-49} J m^3 in Eq. 33 is relatively very small. This small negative value should be due to cancellation between the first and second terms on the left hand side of Eq. 33. This leads to the inequality of $\{(p^{A}_{00})^2-(\boldsymbol{p}^{A}_{00}\cdot\boldsymbol{p}^{A}_{ii})\}>0$, since $\alpha^{A}_{ii}>\alpha^{A}_{00}$. Changes in dipole moments between the ground and excited states of the anion are probably due to those of the π-electron system of 1,3,5-trinitro-2,4-pentadien-1-ide. In view of the symmetric structure of the π-electron system, both p^{A}_{00} and p^{A}_{ii} are approximately in the same direction. Therefore, the inequality of $\{(p^{A}_{00})^2-(\boldsymbol{p}^{A}_{00}\cdot\boldsymbol{p}^{A}_{ii})\}>0$ comes probably from the relation of $p^{A}_{00}>0$ and $0>p^{A}_{ii}$, since $|p^{A}_{ii}|>|p^{A}_{00}|$. Thus, the positive dipole moment of the ground state of **1** is larger than the negative dipole moment of the first-excited state, while the absolute value of the latter is larger than the former. In a similar way the relative large values of both A and B for the second band lead to the opposite conclusion, that the dipole moment of the second-excited state is larger than that of the ground state.

These conclusions are supported by the results ($p^{A}_{00}>p^{A}_{ii}$ (the first-excited state) and $p^{A}_{00}<p^{A}_{ii}$ (the second-excited state)) obtained above from the red and blue shifts due to the ion pairings of 4,4-dimethoxy-1,3,5-trinitro-2,5-cyclohexadienide anion, because the changes in the dipole moments between the ground and excited states of both the anions can be attributed approximately to those of the same π-electron system of 1,3,5-trinitro-2,4-pentadien-1-ide.

The conclusions obtained above from the spectral solvent shifts of **1** are also supported by calculating the dipole moments of the π-electron system. Hosoya *et al.*[29] have reported the SCF MO's and atomic coordinates for the π-electron system of 1,3,5-trinitro-2,4-pentadien-1-ide anion. Using their MO's and coordinates, one obtains the dipole moments of -7.2, -12.2, and -0.8 Debyes for the ground, first-excited, and second-excited states, respectively, of the π-electron system in the same direction of the y axis (the axis of C_{2v} symmetry). When the values of these dipole moments are divided by $-e$, centers of negative-charge distributions may be approximately obtained, because the magnitude of the position vector of the center of the negative-charge distribution is much greater than that of the positive-charge distribution in the anion, as described above. Even if the origin is shifted by y_0, the positions of these centers of the negative-charge distributions do not change and their coordinates only change by y_0. The center of mass of **1** is apparently located above the origin set by Hosoya *et al.* at the position of 1-carbon. When their origin is shifted upward by 0.16 nm along the y axis, one obtains the dipole moments of 0.5, -4.5 and 6.9 Debyes for the ground, first-excited, and second-excited states, respectively. These dipole moments of the π-electron system can explain the conclusions obtained from the spectral solvent shifts of **1**.

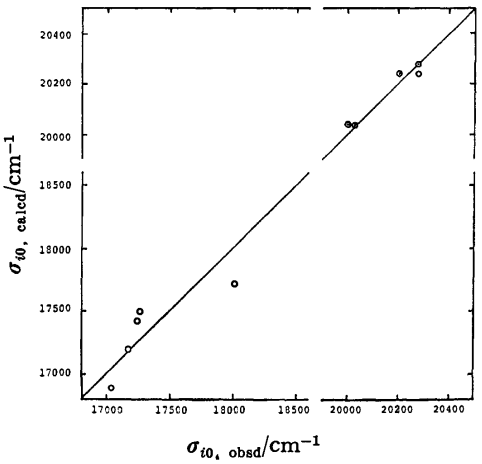

Fig. 3. Correlations of $\sigma_{i0,\,calcd}$ with $\sigma_{i0,\,obsd}$ for the first bands of **2** (○) and **3** (◉).

Janovsky Complexes. Applications were tried to the first absorption bands of the Janovsky complexes of the potassium salts of 4-acetonyl-1,3-dinitro-2,5-cyclohexadienide (**2**) and 4-acetonylidene-1,3-dinitro-2,5-cyclohexadienide (**3**). As in the case of **1**, r_A was assumed to be 0.44 nm. The values of $\sigma'_{i0}=18170$ cm^{-1}, $A=-2.434\times10^{13}$ J^{-1} m^2 and $B=-2.636\times10^{-6}$ m^2 were obtained for **2** and those of $\sigma'_{i0}=20560$ cm^{-1}, $A=6.43\times10^{11}$ J^{-1} m^2 and $B=-2.453\times10^{-6}$ m^2 were obtained for **3**. The correlation of $\sigma_{i0,calcd}$ with $\sigma_{i0,obsd}$ is fairly good, as shown in Fig. 3. The magnitudes of A for **3** and **2** correspond to those of the first and second bands of **1**, respectively. Accordingly, in a similar way as in the case of **1**, one will arrive at the conclusions that in the case of **3** the dipole moment of the ground state may be larger than that of the first-excited state, while in the case of **2** the latter is larger than the former.

References

1) For example, see the following reviews and recent paper: a) A. T. Amos and B. L. Burrows, *Adv. Quant. Chem.*, **7**, 289 (1973); b) M. F. Nicol, *Appl. Spectrosc. Rev.*, **8**, 183 (1974); c) C. N. R. Rao, S. Singh, and V. P. Senthilnathan, *Chem. Soc. Rev.*, **15**, 297 (1976); d) I. Fischer-Hjalmars, A. Henriksson-Enflo, and C. Herrmann, *Chem. Phys.*, **24**, 167 (1977).
2) S. Miertuš and O. Kysel̆, *Chem. Phys.*, **21**, 33, 47 (1977).
3) K. Hirano, *Nippon Kagaku Kaishi* **1978**, 481.
4) E. G. McRae, *J. Phys. Chem.*, **61**, 562 (1957).
5) T. Abe, *Bull. Chem. Soc. Jpn.*, **38**, 1314 (1965).
6) T. Abe, *Bull. Chem. Soc. Jpn.*, **41**, 1260 (1968).
7) H. S. Frank and W. Y. Wen, *Discuss. Faraday Soc.*, **24**, 133 (1957).
8) E. S. Amis and J. F. Hinton, "Solvent Effects on Chemical Phenomena," Academic Press, New York (1973), Vol. 1, p. 65.
9) C. J. F. Böttcher, O. C. van Belle, P. Bordewijk, and A. Rip, "Theory of Electric Polarization," Elsevier Scientific Publishing Co., Amsterdam (1973), Vol. 1, p. 113.
10) L. Onsager, *J. Am. Chem. Soc.*, **58**, 1486 (1936).
11) H. Block and S. M. Walker, *Chem. Phys. Lett.*, **19**, 363 (1973).
12) J. -L. M. Abboud and R. W. Taft, *J. Phys. Chem.*, **83**, 412 (1979).
13) J. G. Kirkwood, *J. Chem. Phys.*, **1**, 351 (1934).
14) D. L. Beveridge and G. W. Schnuelle, *J. Phys. Chem.*, **79**, 2562 (1975).
15) M. Born, *Z. Phys.*, **1**, 45 (1920).
16) For example: a) J. O. Hirschfelder, C. F. Curtiss, and R. B. Bird, "Molecular Theory of Gases and Liquids," John Wiley and Sons, New York (1967), p. 963; b) H. Margenau and N. R. Kestner, "Theory of Intermolecular Forces," 2nd ed, Pergamon Press, Oxford (1971), p. 28.
17) A. T. Amos and B. L. Burrows, *Theor. Chim. Acta*, **29**, 139 (1973).
18) C. C. J. Roothaan, *Rev. Mod. Phys.*, **23**, 69 (1951).
19) D. W. Davies, "The Theory of the Electric and Magnetic Properties of Molecules," John Wiley and Sons, London (1967), p. 77.
20) H. W. Vos, G. G. A. Rietveld, C. MacLean, and N. H. Velthorst, *J. Chem. Soc., Faraday Trans. 2*, **1976**, 1636.
21) M. R. Crampton and H. A. Khan, *J. Chem. Soc., Perkin Trans. 2*, **1973**, 1103.
22) H. Ueda, N. Sakabe, J. Tanaka, and A. Furusaki, *Bull. Chem. Soc. Jpn.*, **41**, 2866 (1968).
23) C. Detellier and P. Laszlo, *J. Phys. Chem.*, **80**, 2503 (1976).
24) "Kagaku Binran," ed by the Chemical Society of Japan, Maruzen Publishing Co., Tokyo (1975), Kisohen (Fundamental Part), II, p. 1404.
25) T. Shimozawa, "Yudenritsu no Kaishaku (Interpretation of Relative Permittivities)," Kyoritsu Publishing Co., Tokyo (1967), p. 83.
26) J. A. Riddick and W. B. Bunger, "Organic Solvents," 3rd ed, Wiley-Interscience, New York (1970).
27) A. R. Norris, *Can. J. Chem.*, **45**, 2703 (1967).
28) a) K. Seibold, H. Navangul, and H. Labhart, *Chem. Phys. Lett.*, **3**, 275 (1969); b) J. W. Barker and L. J. Noe, *J. Chem. Phys.*, **58**, 5192 (1973); c) R. Mathies and A. C. Albrecht, *J. Chem. Phys.*, **60**, 2500 (1974); d) G. C. Causley and B. R. Russell, *J. Chem. Phys.*, **68**, 3797 (1978).
29) H. Hosoya, S. Hosoya, and S. Nagakura, *Theor. Chim. Acta*, **12**, 117 (1968).
30) M. Kimura, M. Kawata, and M. Nakadate, *Chem. Ind. (London)*, **1965**, 2065.

  Bull. Chem. Soc. Jpn., 54, 335—342 (1981)

A Thermodynamic Study on Hydrolytic Reactions of Lead(II) Ions in an Aqueous Solution and Dioxane-Water Mixtures. II. A Calorimetric Study

Shin-ichi Ishiguro and Hitoshi Ohtaki*

Department of Electronic Chemistry, Tokyo Institute of Technology, Nagatsuta-cho, Midori-ku, Yokohama 227

(Received March 17, 1980)

The hydrolytic reactions of lead(II) ions were calorimetrically studied at 25 °C in an aqueous solution and dioxane-water mixtures (dioxane contents: 0.1 and 0.2 mole fractions, which correspond to 35.21 and 55.01 % w/w, respectively) both containing 3 mol dm^{-3} (Li)ClO_4 as a constant ionic medium. A fully automatic on-line system was used for the calorimetric titrations. Values of enthalpies and entropies for the formation of the $Pb_3(OH)_3^{3+}$, $Pb_4(OH)_4^{4+}$, $Pb_3(OH)_4^{2+}$ and $Pb_6(OH)_8^{4+}$ complexes in the aqueous solution, 0.1 and 0.2 mole fraction dioxane solutions were given. For the reaction $qPb^{2+}+pH_2O=Pb_q(OH)_p^{(2q-p)+}+pH^+$, the values of ΔH^*_{pq}/kJ mol^{-1} and $T\Delta S^*_{pq}$/kJ mol^{-1} were determined as follows: $Pb_3(OH)_3^{3+}$: 66.6, −20.7 (in aqueous solution); 72.1, −13.4 (in 0.1 mole fraction dioxane solution); 66.9, −17.7 (in 0.2 mole fraction dioxane solution); $Pb_4(OH)_4^{4+}$: 81.4, −29.5; 84.1, −22.1; 94.7, −14.7; $Pb_3(OH)_4^{2+}$: 61.6, −68.4; 83.4, −41.0, 99.8, −24.3; $Pb_6(OH)_8^{4+}$: 242.8, 1.3, 243.2, 10.6; 236.7, 2.0. The solvent effects on ΔH^*_{pq} were discussed in terms of a function of the formal charge per metal ion of the complex, $z'=(2q-p)/q$. The thermodynamic parameters obtained for the $Pb_6(OH)_8^{4+}$ complex were better explained by assuming the reaction, $2Pb_3(OH)_4^{2+}=Pb_6O(OH)_6^{4+}+H_2O$, than the reaction, $2Pb_3(OH)_4^{2+}=Pb_6(OH)_8^{4+}$, and thus the $Pb_6(OH)_8^{4+}$ complex formally written from the result of the potentiometric measurements will be described as $Pb_6O(OH)_6^{4+}$ which has previously been proposed by X-ray diffraction.

In a previous paper,[1] we have discussed the Gibbs energy ΔG_{pq} of the hydrolytic reaction, $qM^{z+}+pOH^- = M_q(OH)_p^{(zq-p)+}$, of divalent metal ions such as beryllium, copper, nickel, cadmium and lead in aqueous solutions and dioxane-water mixtures containing 3 mol dm^{-3} (Li)ClO_4 as an ionic medium. The Gibbs energy of transfer divided by p, $\Delta G^t_{pq}/p$ [$=\{\Delta G_{pq}(\text{mix})-\Delta G_{pq}(\text{aq})\}/p$], was found to be approximately independent of the composition of the complexes and the kind of the metal ions, and furthermore, the following relation was obtained:

$$\frac{1}{q}\Delta g^t_{pq} \approx \Delta g^t_M + k(z-z'),$$

where Δg^t_{pq} and Δg^t_M denote the partial molar Gibbs energies of transfer of $M_q(OH)_p^{(zq-p)+}$ and M^{z+}, respectively, and z' indicates the formal charge per metal ion of $M_q(OH)_p^{(zq-p)+}$ [$z'=(zq-p)/q$], k being a constant. In the preceding work, on the other hand, we found that the enthalpies and entropies of transfer of the hydroxo complexes of beryllium ion strongly depend on the composition of the complexes.[2] In order to throw more light for elucidating solvent effects on thermodynamic parameters of hydrolytic reactions of metal ions, we examined a calorimetric study on hydrolytic reactions of lead(II) ion in an aqueous solution and dioxane-water mixtures.

Experimental

The calorimetric measurements were carried out in a room thermostated at 25 °C.[2] All the cells used were Dewar vessels, which were immersed in a water bath at (25.00±0.05) °C. Fluctuation of the temperature of the bath during one course of the measurement was within ±0.007 °C. About 150 cm^3 of a test solution which contained hydrolyzed lead(II) ions was placed in a titration vessel, then it was titrated with a standard perchloric acid solution. Initial concentrations of total lead ions in the test solution were changed from 0.005

Table 1. Determination of heat evolved per addition of the titrant

t/s	$Q_{ev}(t)$/J	$C_pV\{\theta(t)-\theta_0\}$/J	$Q_L(t)$/J
10	1.533	1.532	0.002
20	3.922	3.913	0.010
30	6.279	6.254	0.025
40	8.514	8.467	0.046
50	9.013	8.942	0.072
60	9.049	8.951	0.098
70	9.045	8.922	0.123
80	9.041	8.892	0.149
90	8.987	8.813	0.174
100	9.041	8.843	0.199
110	9.037	8.813	0.224
120	8.983	8.734	0.249
130	9.038	8.764	0.274
140	9.023	8.724	0.299
150	8.999	8.675	0.324
160	8.984	8.635	0.349
170	9.019	8.645	0.374
180	8.994	8.596	0.398
190	8.979	8.556	0.423
200	9.023	8.576	0.447
210	8.998	8.527	0.472
220	8.973	8.477	0.496
230	9.017	8.497	0.520
240	9.002	8.457	0.545
250	8.987	8.418	0.569
260	9.011	8.418	0.593
270	9.015	8.398	0.617
280	8.999	8.359	0.641
290	9.003	8.339	0.665
300	8.988	8.299	0.688
$q=(9.000\pm0.015)$ J[a]			

a) q is estimated by averaging $Q_{ev}(t)$ values from 201 to 300 s (100 points).

to 0.2 mol dm^{-3}. Both the test solution and the titrant contained 3.0 mol dm^{-3} perchlorate ion as a constant ionic medium. The test solutions were prepared by mixing stock solutions of lead perchlorate and lithium hydroxide.

The cell arrangement used was essentially the same as that described in the previous paper.[2] All the procedures for the calorimetric titrations were carried out by using a fully automatic on-line system reported in the previous paper[2] with a slight modification. In the present study, the titrant was automatically added from an automatic piston buret (Dosimat E535, Metrohm, Switzerland) controlled by an electronic computer. Other devices were the same as those used previously. The titrant was added stepwise and the volume of the titrant added in one step was about 0.5—1 cm^3 with an accuracy ± 0.001 cm^3.

We previously described the method of calorimetric determinations of heat evolved.[2] However, the estimation of the heat escaping from the titration vessel was simple in the previous treatment, so that the method was applicable only to systems involving fast reactions which reached equilibria within a few minutes. In the present procedure, a more generalized treatment is adopted to evaluate the heat escaping during the measurement. The total heat which has escaped from the titration vessel until t seconds after the start of the addition of the titrant, $Q_L(t)$, is expressed by

$$Q_L(t) = C_p V \alpha \int_0^t \{\theta(\tau) - \theta_0\} d\tau, \quad (1)$$

where C_p, V, and α stand for the heat capacity per unit volume of the test solution, the total volume of the solution in the vessel and the rate of heat escaping from the titration vessel, respectively. C_p and α were obtained by the same method as that used previously.[2] θ_0 represents the temperature of the test solution at the initial stage where the solution is at the thermal equilibrium with the thermostated bath and $\theta(\tau)$ is the temperature of the test solution at time τ after

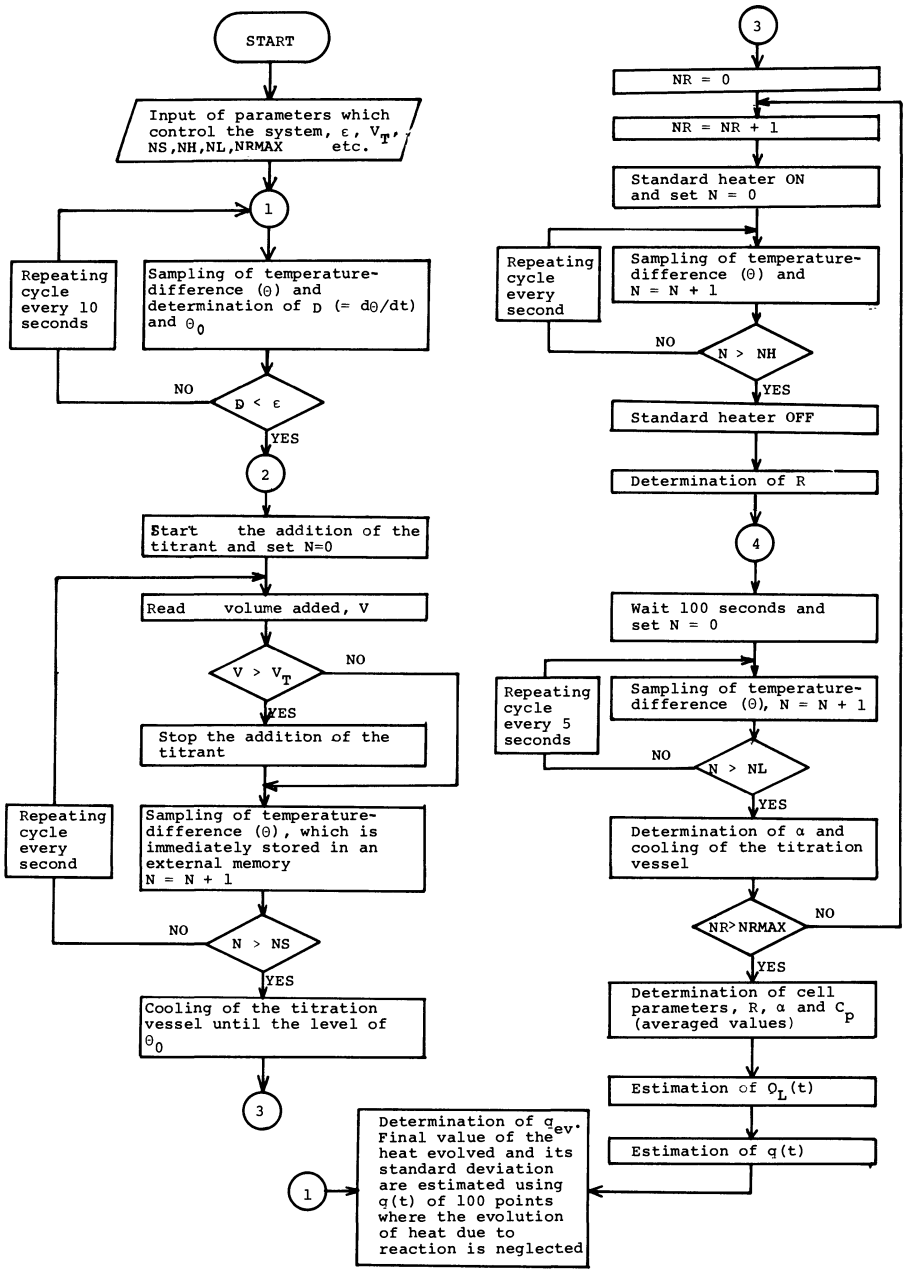

Fig. 1. The flow chart for determination of heat evolved per addition of the titrant.

the start of the addition of the titrant. The temperature change was measured at every second. Then, the heat evolved $Q_{ev}(t)$ until a time t after the start was determined by the following equation:

$$Q_{ev}(t) = k_1 C_p V\{\theta(t) - \theta_0\} + Q_L(t) + k_2, \quad (2)$$

where k_1 and k_2 denote empirical constants (k_1 is close to unity and k_2 is nearly zero joule) which had been determined by separate experiments by using a standard heater. $Q_{ev}(t)$ approaches a constant value q when the evolution of heat due to the reactions becomes negligible. A typical set of $Q_{ev}(t)$ and $Q_L(t)$ as functions of time is shown in Table 1. The heat evolved q was finally estimated by averaging $Q_{ev}(t)$ values of the last 100 points (data from 201 to 300 s in Table 1). The standard deviation was usually within ± 0.03 J.

The flow chart for determination of heat evolved per addition of the titrant is presented in Fig. 1. A least-squares method was employed for the analysis of the set of the data obtained.

Reagents. Stock solutions were prepared by similar ways described in the previous paper.[1)]

Results

The total heat evolved Q by complex formation involving several species is expressed as follows:

$$Q = \sum_j q_j = \sum_i \Delta H_i \cdot \delta n_i, \quad (3)$$

where ΔH_i and δn_i stand for the enthalpy of formation of the complex species i and the amount of the complex species decomposed by the addition of the standard acid solution at each step of titration, respectively. j represents the number of portions of the titrant added in one course of the titation.

We have previously reported that four hydroxo complexes of lead(II) ions, $Pb_3(OH)_3^{3+}$, $Pb_4(OH)_4^{4+}$, $Pb_3(OH)_4^{2+}$, and $Pb_6(OH)_8^{4+}$ are formed in both an aqueous solution and dioxane–water mixtures,[1)] and thus, the total heat evolved in the solvent systems is represented in terms of the enthalpy ΔH^*_{pq} of the reaction, $qPb^{2+} + pH_2O = Pb_q(OH)_p^{(2q-p)+} + pH^+$, as follows:

$$Q = \Delta H^*_{33} \cdot \delta n_{33} + \Delta H^*_{44} \cdot \delta n_{44} + \Delta H^*_{43} \cdot \delta n_{43} + \Delta H^*_{86} \cdot \delta n_{86}. \quad (4)$$

δn_{pq} is calculated on the basis of the formation constants previously determined.[1)] Since only $Pb_3(OH)_3^{3+}$ and $Pb_4(OH)_4^{4+}$ complexes are predominant in solutions of pH<6, the total heat evolved in the solutions is approximately written as follows:

$$Q = \Delta H^*_{33} \cdot \delta n_{33} + \Delta H^*_{44} \cdot \delta n_{44}, \quad (5)$$

and hence

$$Q/\delta n_{33} = \Delta H^*_{33} + \Delta H^*_{44}(\delta n_{44}/\delta n_{33}). \quad (6)$$

Therefore, plots of $Q/\delta n_{33}$ against $\delta n_{44}/\delta n_{33}$ should be a straight line with the slope of ΔH^*_{44} and the intercept ΔH^*_{33}. As is seen from Fig. 2, the plots are straight for all the solvent systems examined. The values of ΔH^*_{33} and ΔH^*_{44} are then inserted into Eq. 7 in order to determine the values of ΔH^*_{43} and ΔH^*_{86} by assuming that the four complexes coexist in the region of pH>6.

$$(Q - \Delta H^*_{33} \cdot \delta n_{33} - \Delta H^*_{44} \cdot \delta n_{44})/\delta n_{43} = \Delta H^*_{43} + \Delta H^*_{86}(\delta n_{86}/\delta n_{43}) \quad (7)$$

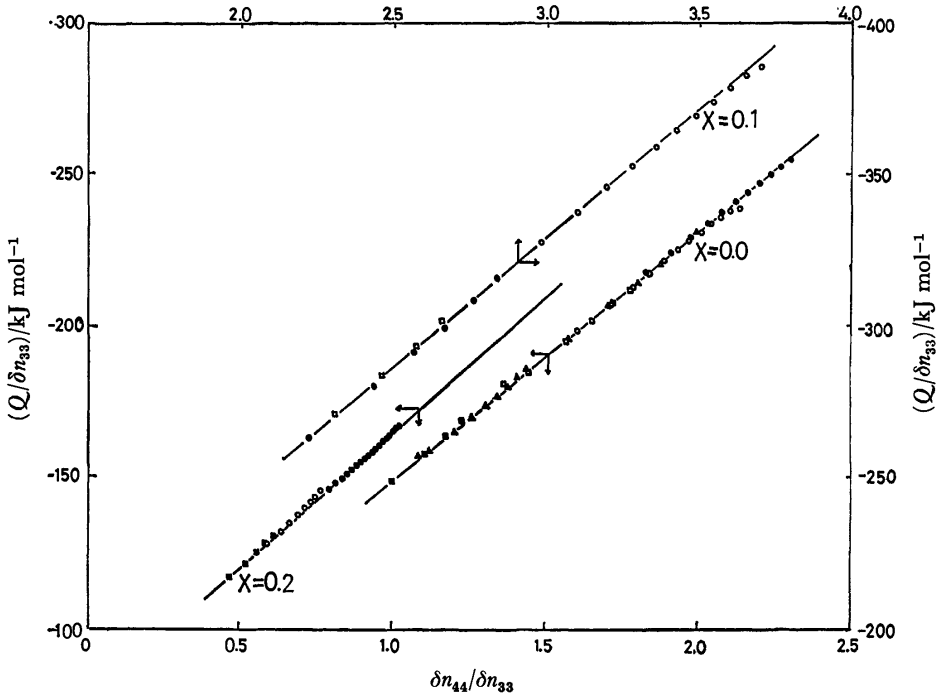

Fig. 2. Determination of the enthalpies, ΔH^*_{33} and ΔH^*_{44} for the hydrolytic reactions of lead (II) ions in the aqueous solution and dioxane–water mixtures containing 3 mol dm^{-3} (Li)ClO_4 as an ionic medium. X denotes the mole fraction of dioxane in the mixtures. Initial concentrations (mol dm^{-3}) of the total lead (II) ions are as follows: Aqueous; ● 0.2040, ○ 0.1503, △ 0.1005, □ 0.07913, ▲ 0.04149, ■ 0.02151: 0.1 mole fraction dioxane; ○ 0.07990, ● 0.05690, □ 0.03756: 0.2 mole fraction dioxane; ● 0.1585, ○ 0.07941, □ 0.04218.

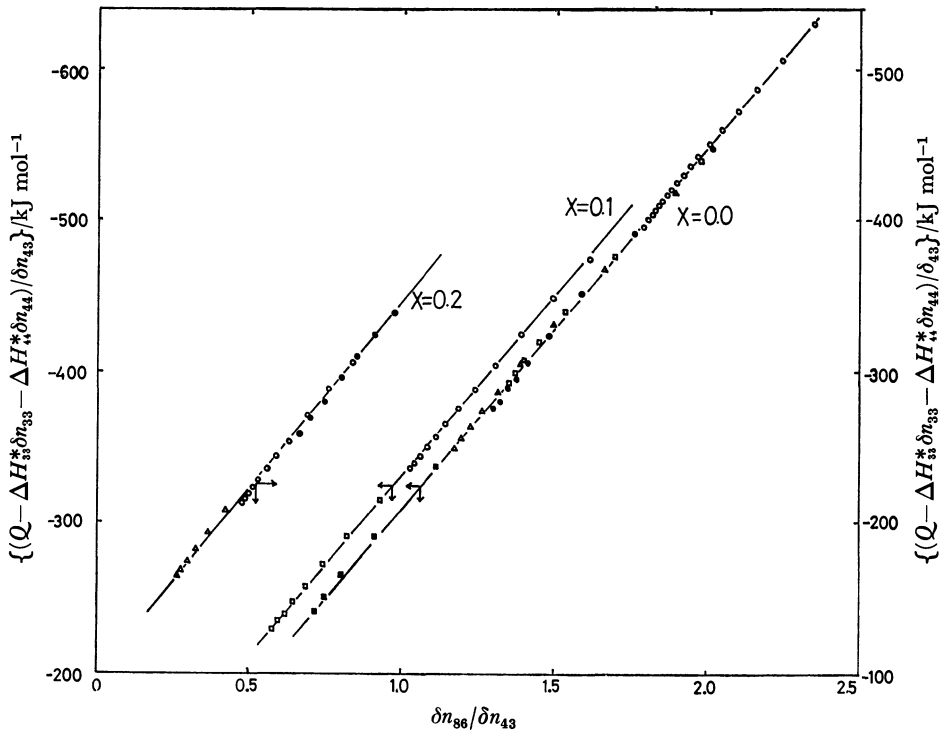

Fig. 3. Determination of the enthalpies, ΔH^*_{43} and ΔH^*_{86} for the hydrolytic reactions of lead (II) ion in the aqueous solution and dioxane-water mixtures containing 3 mol dm^{-3} (Li)ClO_4 as an ionic medium. X denotes the mole fraction of dioxane in the mixtures. Initial concentrations (mol dm^{-3}) of the total lead (II) ions are as follows: Aqueous; ○ 0.04149, △ 0.02151, □ 0.01234, ● 0.01039, □ 0.00564: 0.1 mole fraction dioxane: ○ 0.03756, □ 0.02028: 0.2 mole fraction dioxane; ● 0.04218, ○ 0.02061, △ 0.01042.

Table 2. The formation constants ($*\beta_{pq}$) and the enthalpies (ΔH^*_{pq}/kJ mol^{-1}) and entropies ($T\Delta S^*_{pq}$/kJ mol^{-1}) of the hydrolytic reactions of lead(II) ion in the aqueous solution and dioxane-water mixtures

$qPb^{2+}+pH_2O=Pb_q(OH)_p^{(2q-p)+}+pH^+$

		Mole fraction of dioxane		
		0.0	0.1	0.2
$Pb_3(OH)_3^{3+}$	$-\log *\beta_{33}$	−15.29 (0.01)[a]	−14.98 (0.01)[a]	−14.81 (0.01)[a]
	ΔH^*_{33}	66.6 (1.8)	72.1 (2.9)	66.9 (1.3)
	$T\Delta S^*_{33}$	−20.7 (1.9)	−13.4 (3.0)	−17.7 (1.4)
$Pb_4(OH)_4^{4+}$	$-\log *\beta_{44}$	−19.42 (0.01)[a]	−18.60 (0.01)[a]	−19.17 (0.01)[a]
	ΔH^*_{44}	81.4 (0.4)	84.1 (1.0)	94.7 (1.6)
	$T\Delta S^*_{44}$	−29.5 (0.5)	−22.1 (1.1)	−14.7 (1.7)
$Pb_3(OH)_4^{2+}$	$-\log *\beta_{43}$	−22.78 (0.02)[a]	−21.79 (0.02)[a]	−21.74 (0.02)[a]
	ΔH^*_{43}	61.6 (2.0)	83.4 (2.5)	99.8 (2.0)
	$T\Delta S^*_{43}$	−68.4 (2.1)	−41.0 (2.6)	−24.3 (2.1)
$Pb_6(OH)_8^{4+}$	$-\log *\beta_{86}$	−42.33 (0.01)[a]	−40.75 (0.01)[a]	−41.12 (0.01)[a]
	ΔH^*_{86}	242.8 (1.1)	243.2 (2.3)	236.7 (3.6)
	$T\Delta S^*_{86}$	1.3 (1.2)	10.6 (2.4)	2.0 (3.7)

Uncertaities are given in parentheses as the standard deviation. a) Ref. 1.

The plot of $(Q-\Delta H^*_{33}\cdot\delta n_{33}-\Delta H^*_{44}\cdot\delta n_{44})/\delta n_{43}$ against $\delta n_{86}/\delta n_{43}$ was a straight line in each solvent as shown in Fig. 3, from which the values of ΔH^*_{86} and ΔH^*_{43} were determined.

The enthalpies were finally evaluated by the least-squares method by minimizing $U=\sum(Q-Q_{calcd})^2$ over the whole points measured in a system. The results obtained are summarized in Table 2. Typical calorimetric data obtained for the hydrolytic reactions of lead(II) ion in aqueous solution and the differences between the measured heats and the calculated ones are shown in Table 3.

TABLE 3. TYPICAL HEAT DATA OBTAINED FOR THE HYDROLYTIC REACTIONS OF LEAD(II) IONS IN AN AQUEOUS SOLUTION CONTAINING 3 mol dm^{-3} (Li)ClO_4 AT 25 °C

V_{add}/cm^3	Q/J	$(Q-Q_{calcd})$/J
1) c_{Pb}=0.2040 mol dm^{-3}		
c_H=−0.06259 mol dm^{-3}		
0.801	16.45	−0.01
1.604	33.02	0.04
2.407	49.01	0.10
3.210	66.20	0.34
4.012	82.81	0.25
4.814	99.52	0.43
5.616	116.15	0.52
6.418	132.18	0.66
7.221	149.54	0.68
8.023	166.40	0.92
8.827	183.39	1.19
2) c_{Pb}=0.1502 mol dm^{-3}		
c_H=−0.04793 mol dm^{-3}		
0.604	12.31	−0.11
1.210	24.79	−0.11
1.816	37.23	−0.16
2.421	49.75	−0.11
3.025	62.18	−0.13
3.629	74.71	−0.07
4.234	87.27	−0.00
4.840	99.80	0.00
5.445	112.32	−0.05
6.050	124.89	−0.03
6.657	137.62	0.08
7.264	150.80	0.62
3) c_{Pb}=0.07912 mol dm^{-3}		
c_H=−0.07056 mol dm^{-3}		
0.817	18.78	−0.34
1.634	36.35	−0.19
2.435	53.24	−0.10
3.235	69.81	−0.11
4.036	86.34	−0.12
4.837	102.78	−0.18
5.638	119.17	−0.29
6.437	135.59	−0.36
7.239	151.98	−0.56
8.041	168.48	−0.63
8.842	184.96	−0.73
9.643	201.52	−0.79
10.444	218.24	−0.78
4) c_{Pb}=0.04148 mol dm^{-3}		
c_H=−0.04452 mol dm^{-3}		
0.164	9.00	−0.90
1.227	17.80	−1.15
1.843	26.16	−0.97
2.455	33.67	−0.65
3.067	40.36	−0.36
3.672	46.34	−0.14
4.283	51.94	−0.00
4.894	57.32	0.14
5.499	62.45	0.19
6.111	67.55	0.24
6.716	72.56	0.28
7.321	77.50	0.29
7.927	82.44	0.29
8.539	87.40	0.28
9.151	92.37	0.28
9.756	97.27	0.27
10.361	102.19	0.27
10.966	107.05	0.22
11.572	111.94	0.18
12.183	116.87	0.15
12.795	121.81	0.11
13.405	126.75	0.08
14.018	131.67	0.01
14.629	136.61	−0.03
15.234	141.55	−0.05
15.846	146.53	−0.08
16.451	151.47	−0.11
17.061	156.54	−0.08
5) c_{Pb}=0.02150 mol dm^{-3}		
c_H=−0.02224 mol dm^{-3}		
0.740	9.54	−0.14
1.345	16.22	0.08
1.951	22.04	0.30
2.563	27.37	0.44
3.175	32.45	0.44
3.784	37.42	0.42
4.395	42.37	0.40
5.006	47.27	0.33
5.610	52.09	0.34
6.221	57.04	0.19
6.830	61.90	0.08
7.440	66.80	−0.00
8.044	71.67	−0.09
8.654	75.93	−0.26
6) c_{Pb}=0.01233 mol dm^{-3}		
c_H=−0.01479 mol dm^{-3}		
0.512	7.67	−0.34
1.021	14.60	−0.30
1.534	20.53	0.00
2.044	25.46	0.27
2.558	29.47	−0.03
3.072	33.56	−0.15
3.585	37.71	−0.18
4.100	41.80	−0.27
4.614	45.87	−0.39
5.128	49.97	−0.49
5.639	54.12	−0.56

c_{Pb} denotes the total concentration of lead(II) ion in a test solution. c_{Pb} decreases by dilution by adding the titrant in the course of titration. c_H represents the concentration of analytical excess of hydrogen ion in the test solution. The negative values show that the solutions contain the corresponding excess amounts of hydroxide ions. The initial volume of the test solution is 149.83 cm^3. Concentrations of hydrogen ions in the titrant are 0.9887 mol dm^{-3} for runs 1—3 and 0.3887 mol dm^{-3} for runs 4—6. Q_{calcd} is calculated by using the enthalpies listed in Table 2. V_{add} stands for the total volume of the titrant added.

Discussion

The enthalpies and entropies for the hydrolytic reactions of lead(II) ions in the aqueous solution containing 3 mol dm^{-3} (Li)ClO_4 listed in Table 2 may be compared with those obtained by Carell and Olin[3] in an aqueous solution containing 3 mol dm^{-3} (Na)ClO_4. They have reported the enthalpies, ΔH_{44}^*, ΔH_{43}^*, and ΔH_{86}^*, which are 83.97 110.9 and 206.9 kJ mol^{-1}, respectively. Their ΔH_{44}^* value coincides well with our result, whilst their ΔH_{43}^* and ΔH_{86}^* are appreciably different from ours.

The enthalpy ΔH_D of the reaction

$$2Pb_3(OH)_4^{2+} = Pb_6(OH)_8^{4+} \quad (8)$$

was estimated as $\Delta H_D = \Delta H_{86}^* - 2\Delta H_{43}^*$, and the values in various solvents are shown in Table 4 together with the corresponding Gibbs energies and entropies. The enthalpies and entropies of the reaction were all largely positive. These results are in contrast to those obtained by Carell and Olin,[3] who reported that the enthalpy of reaction (8) was negative.

TABLE 4. THE GIBBS ENERGY (ΔG_D/kJ mol^{-1}), ENTHALPY (ΔH_D/kJ mol^{-1}) AND ENTROPY ($T\Delta S_D$/kJ mol^{-1}) OF THE REACTION, $2Pb_3(OH)_4^{2+} = Pb_6(OH)_8^{4+}$, IN THE AQUEOUS SOLUTION AND DIOXANE–WATER MIXTURES AND THE THERMODYNAMIC PARAMETERS OF TRANSFER FROM THE AQUEOUS SOLUTION TO DIOXANE–WATER MIXTURES (INDICATED BY A SUPERSCRIPT t)

Mole fraction of dioxane	ΔG_D	ΔH_D	$T\Delta S_D$	ΔG_D^t	ΔH_D^t	$T\Delta S_D^t$
0.0	−18.47	119.6	138.1	—	—	—
0.1	−16.13	76.4	92.6	2.34	−43.2	−45.5
0.2	−13.44	37.1	50.6	5.03	−82.5	−87.5

In recent years, structural information of the hydroxo complexes of lead(II) ions in aqueous solutions has been obtained by means of X-ray diffraction.[4–7] According to Olin and Söderquist,[6,7] in the $Pb_6(OH)_8^{4+}$ complex one oxygen atom is located at the center of four lead atoms which are tetrahedrally arranged and the other two lead atoms are located outside the tetrahedral unit. If the complex formally written as $Pb_6(OH)_8^{4+}$ exists in the form of $Pb_6O(OH)_6^{4+}$ in solution, the dimerization reaction given in Eq. 8 should be written as Eq. 9:

$$2Pb_3(OH)_4^{2+} = Pb_6O(OH)_6^{4+} + H_2O. \quad (9)$$

The reaction involves a heterolysis of an O–H bond which may be largely endothermic. Thus, reaction (9) can appropriately account for our result that the enthalpy is largely positive. The positive enthalpies of transfer from an aqueous solution to dioxane–water mixtures for reaction (9) can be expected as we will discuss in the following section.

The Solvent Effects on the Thermodynamic Parameters of the Hydrolytic Reactions of Lead(II) Ion. The hydrolytic reaction of lead(II) ions may be expressed as follows:

$$qPb^{2+} + pH_2O = Pb_q(OH)_p^{(2q-p)+} + pH^+, \quad (10)$$

or

$$qPb^{2+} + (p+r)H_2O = Pb_qO_r(OH)_p^{(2q-p-2r)+} + (p+2r)H^+. \quad (11)$$

Combination of the thermodynamic parameters for reaction (10) given in Table 2 with those for the reaction, $H_2O = H^+ + OH^-$,[1,2] leads to Gibbs energies, enthalpies and entropies, ΔG_{pq}, ΔH_{pq} and ΔS_{pq}, respectively, for the following reaction:

$$qPb^{2+} + pOH^- = Pb_q(OH)_p^{(2q-p)+}. \quad (12)$$

The enthalpy of transfer for reaction (12), ΔH_{pq}^t, from an aqueous solution to a dioxane–water mixture is represented as follows:

$$\Delta H_{qp}^t = \Delta H_{pq}(\text{mix}) - \Delta H_{pq}(\text{aq}) = \Delta h_{pq}^t - q\Delta h_{Pb}^t - p\Delta h_{OH}^t, \quad (13)$$

where Δh_i^t denotes the partial molar enthalpy of transfer of species i. The Gibbs energies, enthalpies and entropies of transfer for the hydrolytic reactions of lead(II) ions from an aqueous solution to dioxane–water mixtures examined are summarized in Table 5, together with those quantities divided by the number of hydroxide ions, $\Delta G_{pq}^t/p$, $\Delta H_{pq}^t/p$, and $T\Delta S_{pq}^t/p$. In this table, $Pb_6O(OH)_6^{4+}$ is formally written as $Pb_6(OH)_8^{4+}$ according to reaction (10).

A question whether a complex is a hydroxo or an oxo-hydroxo complex always arises when we discuss the composition of $M_q(OH)_p^{(2q-p)+}$ type complexes. For lead(II)-hydroxo complexes, all of the complexes found, except the $Pb_6(OH)_8^{4+}$ complex, are believed to have only hydroxide ions as the ligands. Therefore,

TABLE 5. THE THERMODYNAMIC PARAMETERS OF TRANSFER (ΔG_{pq}^t/kJ mol^{-1}, ΔH_{pq}^t/kJ mol^{-1}, AND $T\Delta S_{pq}^t$/kJ mol^{-1}) FOR THE HYDROLYTIC REACTIONS OF LEAD(II) IONS FROM THE AQUEOUS SOLUTION TO DIOXANE–WATER MIXTURES: $qPb^{2+} + pOH^- = Pb_q(OH)_p^{(2q-p)+}$

	0.1 mole fraction of dioxane			0.2 mole fraction of dioxane		
	ΔG_{pq}^t	ΔH_{pq}^t	$T\Delta S_{pq}^t$	ΔG_{pq}^t	ΔH_{pq}^t	$T\Delta S_{pq}^t$
$Pb_3(OH)_3^{3+}$	−14.40(−4.83)	1.0(0.3)	15.5(5.2)	−28.59(−9.53)	−13.5(−4.5)	15.1(5.0)
$Pb_4(OH)_4^{4+}$	−21.63(−5.41)	−3.3(−0.8)	18.3(4.6)	−35.84(−8.96)	−5.0(−1.2)	30.8(7.7)
$Pb_3(OH)_4^{2+}$	−22.60(−5.65)	15.8(4.0)	38.4(9.6)	−40.35(−10.1)	19.8(5.0)	60.2(15.0)
$Pb_6(OH)_8^{4+}$	−42.92(−5.37)	−11.6(−1.5)	31.3(3.9)	−75.85(−9.48)	−42.9(−5.4)	33.0(4.1)

Values in parentheses give thermodynamic parameters per hydroxide ion, $\frac{1}{p}\Delta G_{pq}^t$, $\frac{1}{p}\Delta H_{pq}^t$, and $\frac{T}{p}\Delta S_{pq}^t$.

the discussion about the composition of the complexes on the basis of the thermodynamic quantities will be focused on the $Pb_6(OH)_8^{4+}$ complex in the following section.

As we have already described in the previous paper,[1] the $\Delta G^t_{pq}/p$ values of various metal ions such as beryllium(II), copper(II), nickel(II), cadmium(II), and lead(II) have been found to be approximately independent of not only the composition but also the kind of metal ions of the hydroxo complexes.[1] However, the ΔH^t_{pq} values are strongly dependent on the composition of the hydroxo complexes. The solvent effects on the enthalpies of the hydrolytic reactions of beryllium ion from an aqueous solution to dioxane–water mixtures have been previously discussed in terms of the solvent structure of the bulk, the structure of the solvated ions involved in the reactions and the charge distribution within the hydroxo complexes.[2] A similar consideration can be made for interpreting the enthalpies of transfer from an aqueous solution to dioxane–water mixtures for the reactions of lead(II) ions.

As seen from Table 5, the $\Delta H_{44}/4$ value becomes more negative with the increase in the content of dioxane in the mixtures. However, the reverse is found for $\Delta H^t_{43}/4$, which is positive. Therefore, the relation $\Delta H^t_{44}/4 < \Delta H^t_{43}/4$ holds in the solvent systems examined. By using Eq. 13, the relation is rewritten in terms of the partial molar enthalpies of transfer of the relevant species involved in the reactions as follows:

$$\frac{1}{4}\Delta h^t_{44} - \Delta h^t_{Pb} < \frac{3}{4}\left(\frac{1}{3}\Delta h^t_{43} - \Delta h^t_{Pb}\right). \quad (14)$$

As seen in Table 2, the enthalpies of transfer for the reaction, $qPb^{2+} + pH_2O = Pb_q(OH)_p^{(2q-p)+} + pH^+$, are zero or positive $[\Delta H^{*t}_{pq} = \Delta H^*_{pq}(\text{mix}) - \Delta H^*_{pq}(\text{aq}) = \Delta h^t_{pq} + p\Delta h^t_H - q\Delta h^t_{Pb} - p\Delta h^t_{OH}]$. The partial molar enthalpy of transfer of a neutral water molecule will be less than those of the ions involved in reaction (10), and thus the value $q\Delta h^t_{Pb}$ will be more negative than the values Δh^t_{pq} and $p\Delta h^t_H$. Therefore, both sides of Eq. 14 will be positive, thus:

$$\frac{1}{4}\Delta h^t_{44} < \frac{1}{3}\Delta h^t_{43} < 0. \quad (15)$$

The formal charge per metal ion of the $Pb_4(OH)_4^{4+}$ and $Pb_3(OH)_4^{2+}$ complexes are +1 and +0.67, respectively. Therefore, the result obtained in Eq. 15 is consistent with what is expected from the consideration based on the formal charge per metal ion of the complexes, which has been discussed in the previous paper.[2]

Since the formal charge per metal ion z' of the $Pb_3(OH)_3^{3+}$ and $Pb_4(OH)_4^{4+}$ complexes are both +1, the relation $\Delta h^t_{33}/3 \simeq \Delta h^t_{44}/4$ will approximately hold, if we assume as the first approximation that the local charges per metal ion within the complexes are the same. The values of $\Delta H^t_{33}/3$ were +0.3 and −4.5 kJ mol^{-1} for the dioxane systems containing 0.1 and 0.2 mole fraction of dioxane, respectively. If we take into account the uncertainties in ΔH^*_{33} listed in Table 2, it appears that ΔH^t_{33} tends to monotonously decrease as the dioxane content increases (see Table 5). The same trend is also seen in ΔH^t_{44}. Although the value $\Delta H^t_{33}/3$ is more negative than that of $\Delta H^t_{44}/4$ in the 0.2 mole fraction dioxane system, the difference is not significant, and we can assume $\Delta H^t_{33}/3 \simeq \Delta H^t_{44}/4$. The values $\Delta H^t_{33}/3$ of the $Be_3(OH)_3^{3+}$ complex are −2.3 and −5.5 kJ mol^{-1} for 0.1 and 0.2 mole fraction dioxane systems, respectively,[2] which are more negative than the corresponding values of the $Pb_4(OH)_4^{4+}$ or $Pb_3(OH)_3^{3+}$ complex. This seems to be attributed to stronger solvation of beryllium(II) ions than that of lead(II) ions.

As is discussed above, at least at the first step of approach, the formal charge per metal ion of a hydroxo complex is an important factor which controls solvent effects on hydrolytic reactions of metal ions. The formal charge per metal ion of the $Pb_6(OH)_8^{4+}$ complex is +0.67, which is the same as that of the $Pb_3(OH)_4^{2+}$ complex. Therefore, if the approach so far examined for the estimation of the partial molar enthalpy of transfer of a hydroxo complex is applicable to the case of the $Pb_6(OH)_8^{4+}$ complex, the value $\Delta H^t_{86}/8$ would be similar to $\Delta H^t_{43}/4$, that is, it would be positive. In fact, the values $\Delta H^t_{86}/8$ obtained are −1.5 and −5.4 kJ mol^{-1} for the 0.1 and 0.2 mole fraction dioxane systems, respectively. Thus, the value $\Delta H^t_{86}/8$ becomes more negative with an increase in the dioxane content in the mixtures in contradiction to that of $\Delta H^t_{43}/4$. This fact can be explained by assuming the formation of the $Pb_6O(OH)_6^{4+}$ complex instead of the $Pb_6(OH)_8^{4+}$ complex.

The hydrolytic reaction of formation of the $Pb_6O(OH)_6^{4+}$ complex is represented as follows:

$$6Pb^{2+} + 7OH^- = Pb_6O(OH)_6^{4+} + H^+. \quad (16)$$

The enthalpy of transfer for the reaction (16) is written as follows:

$$\Delta H^t_{616} = \Delta h^t_{616} - 8\Delta h^t_{OH} - 6\Delta h^t_{Pb} + (\Delta h^t_H + \Delta h^t_{OH}), \quad (17)$$

which may be compared with that for the reaction, $6Pb^{2+} + 8OH^- = 2Pb_3(OH)_4^{2+}$,

$$2\Delta H^t_{43} = 2\Delta h^t_{43} - 8\Delta h^t_{OH} - 6\Delta h^t_{Pb}. \quad (18)$$

Here ΔH^t_{616} and Δh^t_{616} represent the quantities defined by Eq. 13 for the $Pb_6O(OH)_6^{4+}$ complex.

The formal charge per metal ion of the $Pb_6O(OH)_6^{4+}$ complex is +0.67, and thus, the value Δh^t_{616} will be similar to that of $2\Delta h^t_{43}$. The term $\Delta h^t_H + \Delta h^t_{OH}$ in Eq. 17 is negative.[2] Therefore, even if the value $\Delta h^t_{616} - 8\Delta h^t_{OH} - 6\Delta h^t_{Pb}$ is as largely positive as that $2\Delta H^t_{43}$, the value ΔH^t_{616} will remain negative owing to the term $\Delta h^t_H + \Delta h^t_{OH}$ which is more negative than $\Delta h^t_{616} - 8\Delta h^t_{OH} - 6\Delta h^t_{Pb}$.

The enthalpy of transfer for reaction (9), ΔH^t_D, is expressed as follows:

$$\Delta H^t_D = \Delta h^t_{616} + \Delta h^t_{H_2O} - 2\Delta h^t_{43}. \quad (19)$$

If we assume that

$$\frac{1}{6}\Delta h^t_{616} \simeq \frac{1}{3}\Delta h^t_{43}, \quad (20)$$

we obtain the following equation:

$$\Delta H^t_D \simeq \Delta h^t_{H_2O}. \quad (21)$$

The values ΔH^t_D were found to be −43.2 and −82.5 kJ mol^{-1} for the systems of the dioxane contents of 0.1 and 0.2 mole fractions, respectively (Table 4). Although

the values of $\Delta h^{t}_{H_2O}$ estimated by using Eq. 21 may be too largely negative because of the oversimplified assumption given as Eq. 20, we can conclude that the partial molar enthalpies of transfer of water $\Delta h^{t}_{H_2O}$ from an aqueous solution to dioxane–water mixtures will be negative. This result is consistent with that derived in the previous paper.[2] The hydrogen bonded structure of water in an aqueous solution is broken down by the addition of dioxane,[8,9] and thus, the value of $\Delta h^{t}_{H_2O}$ will be negative by enhancement of the intramolecular O–H bonds within water molecules in dioxane–water mixtures.

The work has been partially supported by a Grant-in-Aid for Scientific Research No. 343011 from the Ministry of Education, Science and Culture.

References

1) T. Kawai, S. Ishiguro, and H. Ohtaki, *Bull. Chem. Soc. Jpn.*, **53**, 2221 (1980).
2) S. Ishiguro and H. Ohtaki, *Bull. Chem. Soc. Jpn.*, **52**, 3198 (1979).
3) B. Carell and Å. Olin, *Acta Chem. Scand.*, **16**, 2350 (1962).
4) O. E. Esval, *Diss. Abstracts*, **24**, 3091 (1964); Thesis, Univ. North Calorina (1963).
5) G. Johansson and Å. Olin, *Acta Chem. Scand.*, **22**, 3197 (1968).
6) Å. Olin and R. Söderquist, *Acta Chem. Scand.*, **26**, 3505 (1972).
7) Å. Olin and R. Söderquist, *Trans. Royal Inst. Tech., Pure and Appl. Chem.*, **34**, 519 (1972).
8) G. Mavel, *C. R. Acad. Sci.*, **248**, 1505 (1959).
9) H. P. Bennetto and D. Feakins, "Hydrogen-bonded Solvent Systems," Taylor and Francis Ltd., London (1968), p. 235.

  Bull. Chem. Soc. Jpn., 54, 343—347 (1981)

Catalytic Activity of V-Sn Oxides for Oxidation Reactions

Takehiko Ono,* Yoshiro Nakagawa, and Yutaka Kubokawa
Department of Applied Chemistry, University of Osaka Prefecture, Sakai, Osaka 591
(Received March 28, 1980)

The rate of oxidation of C_3H_6, C_2H_4, C_3H_8, and CO has been investigated over V-Sn oxides of various compositions. The rate shows two maxima at V-Sn(V/Sn=2/1) and (1/8) oxides. Comparison between the rate of reduction of the oxides with C_3H_6 and that of the corresponding catalytic oxidation suggests that the oxygen species responsible for oxidation differs for V-Sn(2/1) and V-Sn(1/8) oxides. The amount of oxygen desorbed in the temperature range 400—530 °C varies with the composition of the V-Sn oxides, showing a maximum at V-Sn(2/1) oxide. With V-Sn(1/8) oxide, little or no oxygen desorption is observed. On the basis of these results together with those of structural studies, it is concluded that the rate maximum with V-Sn(2/1) oxide arises from formation of an amorphous material from which lattice oxygen is easily released, while the rate maximum with V-Sn(1/8) oxide is associated with the presence of V^{4+} ions dissolved in SnO_2.

It has been shown by many workers that catalytic oxidation over V_2O_5 proceeds *via* lattice oxygen,[1] its activity being promoted by addition of the second component such as MoO_3, SnO_2, *etc.* As regards the V_2O_5–SnO_2 system, several explanations have been proposed for the effect of promoters.[2-5] Sachtler *et al.*[2] reported that the promoter action of SnO_2 in V–Sn oxides is due to the lowering of ΔG for oxygen release from the oxide which arises from the dissolution of V ions in the SnO_2 lattice.

In the present work, the rate of C_3H_6, C_2H_4, C_3H_6, and CO oxidation has been measured over V–Sn oxides of various compositions. Oxygen desorption experiments as well as measurements of the rate of reduction of the oxides with C_3H_6 have been carried out. On the basis of these results together with those of structural studies such as X-ray diffraction, IR, and ESR, the nature of the promoter effect has been discussed.

Experimental

Materials. V–Sn oxide catalysts were prepared as follows. The precipitate obtained from solutions of tin(II) chloride and ammonia was added to a solution containing the required quantity of ammonium metavanadate. The resulting precipitate was washed, dried, and heated in the air at 450 °C. The atomic ratio V/Sn of the catalysts and their surface area determined by the BET method are as follows. (V/Sn=1/0), 2.1; (4/1), 12.3; (2/1), 14.7; (1/2), 26.1; (1/8), 43.2; and (0/1), 6.8 m^2/g.

Apparatus and Procedure. Catalytic oxidation and reduction of the oxides were carried out in a closed circulation system (290 cm^3). In order to obtain the initial rates, the conversions were kept below ≈5%. The reaction products such as acryladehyde, CO_2, and CO were analyzed by gas chromatography. Carbonaceous deposits formed during the course of reduction were converted into CO_2 by oxidization with oxygen at 450 °C. The amount was then determined.

X-Ray diffraction patterns of the catalysts were obtained on a Rigaku Denki D-3F X-ray diffractometer using Cu $K\alpha$ radiation with a Ni filter. IR spectra were recorded on a Hitachi G2 spectrometer, the samples being prepared by the KBr pellet technique, and ESR spectra on a JES-ME-1X spectrometer. Oxygen desorption from V–Sn oxides was investigated by means of a Töpler pump. It was confirmed by gas chromatography that desorbed gas consists entirely of oxygen.

Results

Catalytic Oxidation of C_3H_6 over V–Sn Oxides and Their Reduction with C_3H_6. The rate of C_3H_6 oxidation on various V–Sn oxides at 320 °C (Fig. 1) shows two maxima at V–Sn(2/1) and (1/8) oxides. Similar maxima are observed in low oxygen pressure experiments. Selectivity toward acrylaldehyde formation was determined for all the V–Sn oxides at similar conversion values, which were obtained by adjusting the catalyst weight as well as the reaction time (Fig. 2). The

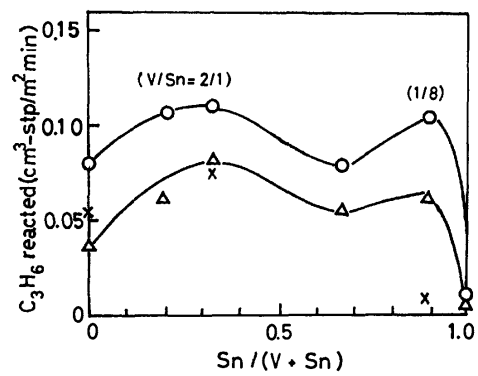

Fig. 1. Rates of C_3H_6 oxidation at 320 °C.
$P_{C_3H_6}$=35 Torr (1 Torr=133.3 Nm^{-2}); P_{O_2}; —△—, 8; —○—, 40 Torr; X, rates of reduction of the oxides with C_3H_6.

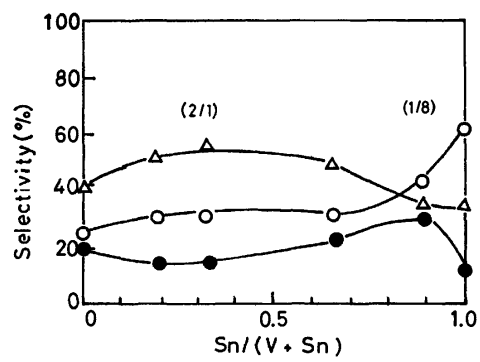

Fig. 2. Selectivities of C_3H_6 oxidation.
Experimental conditions are the same as in Fig. 1.
—●—, Acrylaldehyde; —○—, CO_2; —△—, CO.

selectivity toward acrylaldehyde formation is ≈20% for V_2O_5, ≈15% for V-Sn(2/1) oxide and ≈30% for V-Sn(1/8) oxide. As regards CO and CO_2 formation, with V_2O_5, V-Sn(4/1) and (2/1) oxides the ratio of the amount of CO to that of CO_2 in the products is *ca.* 2, being essentially the same, while with SnO_2 and V-Sn-(1/8) oxide, CO_2 formation is larger than CO formation. This indicates that the same mechanism is involved in CO and CO_2 formation for the former group of oxides.

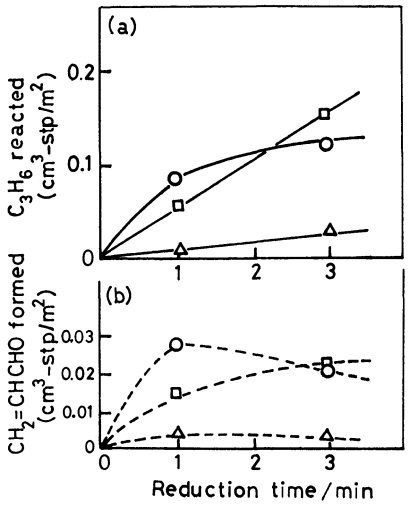

Fig. 3. Reduction of V-Sn oxides with C_3H_6 at 320 °C.
$P_{C_3H_6}$=35 Torr; —○—, V-Sn (2/1) oxide; —□—, V_2O_5; —△—, V-Sn (1/8) oxide.

Figure 3a shows the rate of reduction of various oxides with C_3H_6. The initial rates of reduction obtained from the plots are 0.06—0.05 for V_2O_5, 0.08 for V-Sn-(2/1) oxide and 0.01 cm^3/m^2 min for V-Sn(1/8) oxide. The initial rate values are also given in Fig. 1. Carbonaceous deposits were formed during the course of reduction. The amount formed for one minute was found to *ca.* 0.03 for V_2O_5, 0.05 for V-Sn(2/1) oxide and 0.04 cm^3/m^2 for V-Sn(1/8) oxide. No significant difference among the three catalysts suggests that the extent of inhibition by carbonaceous deposits is essentially the same for all the catalysts.

Comparison of catalytic oxidation at two different oxygen pressures (Fig. 1) yields the reaction order 0.3—0.5 in oxygen for all the V-Sn oxides investigated. The difference between the rate of reduction of the oxides with C_3H_6 and that of the corresponding catalytic oxidation is considerably larger for V-Sn(1/8) oxide than for V_2O_5 and V-Sn(2/1) oxides. It seems that the oxygen species responsible for oxidation differs for both groups of oxides.

In the initial stage of the reaction acrylaldehyde formation is larger over V-Sn(2/1) oxide than over V_2O_5 (Fig. 3b). In fact, the initial selectivity toward acrylaldehyde formation obtained with V-Sn(2/1) oxide is 30%, being higher than the selectivity with V_2O_5(≈20%). As regards the selectivity in the later stage, the situation is reversed. V_2O_5 is more selective than V-Sn(2/1) oxide, indicating that further oxidation of acrylaldehyde to CO and CO_2 occurs more efficiently over V-Sn(2/1) oxide.

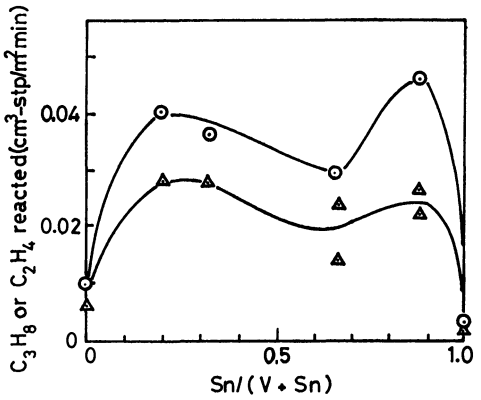

Fig. 4. Rates of oxidation of C_2H_4 and C_3H_8 at 320 °C.
$P_{C_3H_8}$=40 Torr; P_{O_2}=40 Torr; —⊙—, C_2H_4; —△—, C_3H_8.

Catalytic Oxidation of C_2H_4, C_3H_8, and CO. The rates of oxidation of C_2H_4 and C_3H_8 are shown in Fig. 4. With the V-Sn(2/1) and (1/8) oxides, two maximum rates of oxidation similar to those with C_3H_6 oxidation are observed. No partial oxidation products were formed. Rate enhancement by the addition of SnO_2 is more significant for C_2H_4 and C_3H_8 oxidation than for the C_3H_6 oxidation.

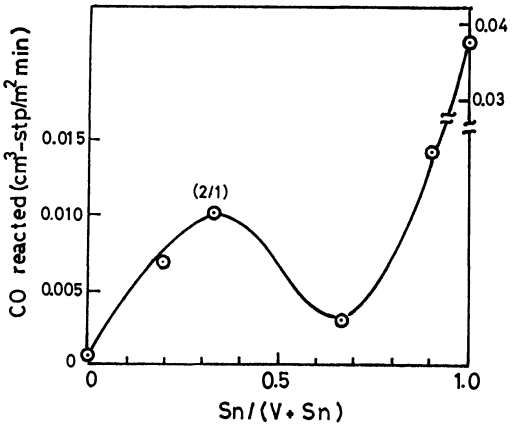

Fig. 5. Rates of CO oxidation at 320 °C.
P_{CO}=40 Torr, P_{O_2}=40 Torr.

The rate of CO oxidation over SnO_2, shown in Fig. 5, is about 140 times higher than that over V_2O_5. If the V-Sn oxide is a mixture of V_2O_5 and SnO_2, its catalytic activity would increase monotonously with increasing SnO_2 content, in disagreement with the result shown. The rate of CO oxidation passes through a maximum at V-Sn(2/1) oxide. Another maximum seems to be masked by a high rate of oxidation of CO over SnO_2. Thus, the existence of two different types of maximum rate of oxidation has been established.

Oxygen Desorption from V-Sn Oxides. Oxygen easily desorbs from V-Sn oxides at 350—500 °C.[2] It was found that the dissociation pressure of oxygen over V-Sn oxides depends upon the amount of sample, decreasing with increase in the amount of oxygen removed from the oxides.[2] Accordingly, dissociation pressure measurements appear to be inadequate for comparison of the ability to release oxygen from various oxides.

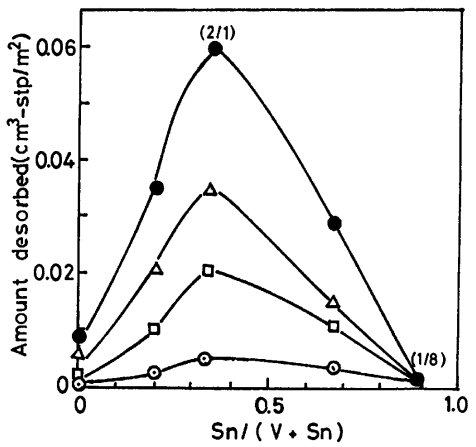

Fig. 6. Oxygen desorption from V–Sn oxides.
—○—, 450 °C; —□—, 500 °C; —△—, 530 °C; —●—, amount desorbed up to 530 °C; desorption time, 1 h at each temperature.

After the catalyst had been treated with oxygen at 400 °C followed by evacuation at 150 °C for 10 h, the temperature of the catalyst was raised stepwise up to 530 °C, the amount of oxygen desorbed being determined. During the course of experiments the pressure over the catalyst was kept below 10^{-2}Torr. As seen in Fig. 6, the amount of oxygen desorbed changes with the composition of V–Sn oxide, showing a maximum at V-Sn(2/1) oxide, in a similar manner to that observed with the rate of oxidation. With V–Sn(1/8) oxide, little or no oxygen desorption is observed. The oxygen desorption begins around 400 °C, being predominant in the temperature range 450—530 °C. This suggests that the oxygen desorbed originates from lattice oxygen and not from adsorbed oxygen. The interaction of vanadium oxide with tin oxide would lead to formation of some active part, from which oxygen release takes place easily.

Structure of V–Sn Oxides. X-Ray Diffraction: X-Ray diffraction studies of the V–Sn oxides showed only diffraction lines due to V_2O_5 and SnO_2. No lines indicating formation of a new compound between V_2O_5 and SnO_2 appeared, in agreement with the results of previous workers.[2,6] It appears that the active part described above exhibits no definite diffraction lines. As a result of the interaction of vanadium oxide and tin oxide an amorphous material might be formed. In fact, with V–Sn(4/1), (2/1), and (1/2) oxides, the intensities of the lines due to V_2O_5 were found to be much smaller than what are expected from the composition of V–Sn oxides. V–Sn(4/1) oxide showed lines due to V_2O_5 alone. With V–Sn(1/8) oxide only lines which are attributed to SnO_2 appeared, the observed lattice constants being somewhat smaller than those of the crystalline SnO_2. The sizes of V_2O_5 and SnO_2 crystals in various V–Sn oxides, determined from the broadening of the diffraction lines,[7] were >200 nm and 10—20 nm, respectively.

IR: IR spectra of V–Sn(2/1) oxide (Fig. 7a) show bands at 1020 cm^{-1} (V=O stretching vibration) and 818 cm^{-1} (V–O–V stretching vibration). Similar spectra were obtained with V–Sn(4/1) and (1/2) oxides.

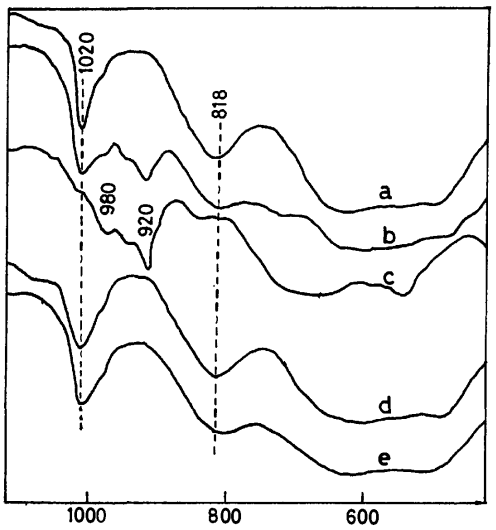

Fig. 7. IR spectra of V–Sn (2/1) oxide before and after the reduction by C_3H_6 and CO.
Before reduction (a), after reduction with C_3H_6 at 320—350 °C; 1.1 atom% (b) or 6.3% (c) of lattice oxygen was removed: After reduction with CO at 450—500 °C; 2.0% (d) or 3.8% (e). 1 wt% of V–Sn oxide in KBr (≈50 mg).

V–Sn(1/8) oxide exhibited no IR absorption due to V_2O_5. IR spectra of SnO_2 showed a broad band at ≈620 cm^{-1}. In order to examine the amorphous part in the V–Sn oxides, the intensity of the band at 1020 cm^{-1} observed with the V–Sn oxides has been determined as a function of the concentration of vanadium ions in the KBr pellets. Similar experiments have been carried out for V_2O_5 with the result that Lambert-Beer's law is applicable (Fig. 8). The intensity of the band at 1020 cm^{-1} with the V–Sn oxides is about 30% of the intensity observed with V_2O_5, suggesting that a considerable fraction of vanadium oxide in V–Sn oxides exhibits no IR absorption. Figure 7a shows that

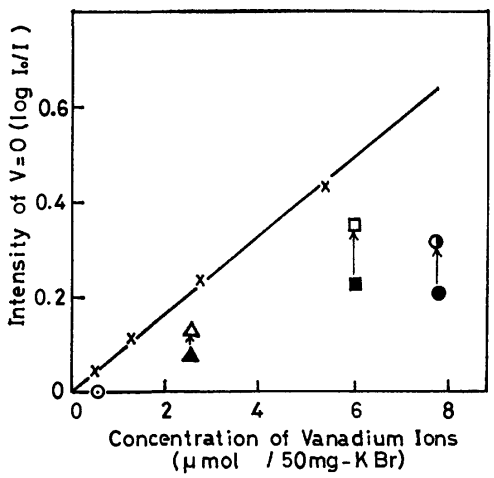

Fig. 8. Estimation of V_2O_5 concentration in V–Sn oxides.
×, V_2O_5; ○, V–Sn (1/8) oxide; ▲, (1/2); ■, (2/1); ●, (4/1); △, □, ◑, After calcination at 600 °C; 2 wt% of V–Sn oxide in KBr.

no alternative new bands appear. So far no explanation can be offered. The new bands might be masked by the bands due to V_2O_5 or SnO_2. It appears that the part which exists in the amorphous state corresponds to the part which exhibits no IR absorption.

It seems necessary to consider the effect of crystal size of the sample upon the intensity of the IR band. Since only V=O groups in the surface layer are responsible for IR absorption, the intensity of the band at 1020 cm^{-1} would increase with increase in the surface area of V_2O_5 crystals, *i.e.*, with decrease in particle size. From the extent of broadening of diffraction lines, it was concluded that the size of V_2O_5 crystals in V–Sn oxides is somewhat smaller than that in V_2O_5 specimen. The fraction of the amorphous state to the total amount of V_2O_5 in the V–Sn oxides seems to be larger than that shown in Fig. 8.

When the V–Sn oxides are calcined at 600 °C, the intensity of the band at 1020 cm^{-1} increase from ≈30% to ≈60% of those expected from the composition of the V–Sn oxides. This suggests that the amorphous part in the V–Sn oxides is decomposed to form V_2O_5 and SnO_2.

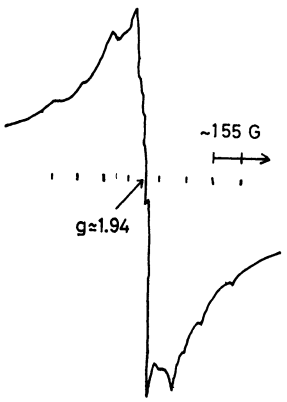

Fig. 9. ESR spectrum of V–Sn (1/8) oxide at 77 K after reduction with C_3H_6.

ESR: ESR measurements have been carried out with V–Sn(2/1) and (1/8) oxides, which exhibited the maximum oxidation activities. With V–Sn(2/1) oxide, only a broad signal appeared at $g=1.96$. After reduction with C_3H_6 there was no hyperfine structure at 77 K. On the other hand, after reduction with C_3H_6 V–Sn(1/8) oxide showed a signal having a hyperfine structure (Fig. 9) with $g=1.94$ and $A\approx155$ G at 77 K, in agreement with the results of Kasai,[8] who reported a signal with $g_z=1.942$ and $A_z=155$ G for V^{4+} ions dissolved in the SnO_2 crystalline. On the basis of these results together with a slight contraction of SnO_2 lattice in V–Sn(1/8) oxide described above, it is concluded that with V–Sn(1/8) oxide some fraction of vanadium ions are dissolved in the SnO_2 lattice as V^{4+} ions.

Discussion

Two maxima are observed at V–Sn(2/1) and (1/8) oxides for the rate of oxidation of various reactants such as C_3H_6, C_2H_4, C_3H_8, and CO, although in the case of CO one maximum is masked by a high activity of pure SnO_2. Considering the marked difference between the rate of reduction of the oxides with C_3H_6 and that of the corresponding catalytic oxidation observed with V–Sn(1/8) oxide, it is concluded that the oxygen species responsible for oxidation differs for V–Sn(2/1) and (1/8) oxides.

The rate of catalytic oxidation as well as of oxygen desorption shows a maximum at the same composition of V–Sn oxide (V/Sn=2/1). From the results together with those of structural studies such as X-ray diffraction and IR absorption, it is concluded that the maximum rate of oxidation observed with V–Sn(2/1) oxide can be attributed to formation of amorphous material from which lattice oxygen is easily released. The fraction of vanadium ions in the amorphous state is roughly constant with V–Sn(4/1), (2/1), and (1/2) oxides, being somewhat in contradiction with the maximum activity observed with V–Sn oxide (Fig. 8). When tin oxide is added to vanadium oxide, both enhancement of the activity due to formation of the amorphous part and decrease in the number of vanadium ions present in unit mass occurs simultaneously. Such a decrease in the number of vanadium ions would cause decrease in the activity of V–Sn oxides resulting from the presence of vanadium ions. Thus, the maximum activity with V=Sn(2/1) oxide is explicable.

The following results suggest that the reactivity of the amorphous material differs from that of the crystalline V_2O_5 and SnO_2. With the reduction of V–Sn(2/1) oxide by CO (Fig. 7), the intensity of the band due to V=O scarcely changes (Figs. 7d, e), while it decreases markedly in the case of the reduction by C_3H_6(b, c). New bands appear in the region 920—980 cm^{-1}. Similar spectra have been reported by Vadelievre *et al.*[9] and Inomata *et al.*[10] There is no marked difference between the amount of oxygen removed by the reduction in both cases. This suggests that the reduction by C_3H_6 proceeds on V_2O_5 crystals as well as on the part which exhibits no IR absorption, *i.e.*, the amorphous part, while the reduction by CO is limited to such an amorphous part alone, thus cofirming the above conclusion.

Another maximum, *i.e.*, the maximum rate observed with V–Sn(1/8) oxide is not associated with the oxygen release. From the results of ESR and X-ray diffraction studies, it appears that the maximum rate observed with V–Sn(1/8) is associated with the presence of V^{4+} ions in SnO_2 lattice. According to the work of Kon *et al.*,[11] Yoshida *et al.*,[12] and Takita *et al.*,[13] the presence of V^{4+} ions appear to facilitate the formation of adsorbed oxygen species which play a significant role in the oxidation reaction. A similar situation would be expected for V–Sn oxides. A marked enhancement in the rate of oxidation of C_3H_6 by the presence of gaseous oxygen observed with V–Sn(1/8) oxide might support this conclusion. However, the reactivity of adsorbed oxygen appears to be similar to that of lattice oxygen, since there is little or no difference between the product distributions for the C_3H_6 oxidation over V–Sn(2/1) and (1/8) oxides. It seems very diffcult to distinguish adsorbed oxygen from surface lattice oxygen,

i.e., adsorbed oxygen can be regarded as a special type of surface lattice oxygen.

Considering the fact that two maximum activities are observed with the V–Sn oxides, it seems unlikely that the lowering of ΔG for oxygen release from the oxide is closely associated with dissolution of V ions in the SnO_2 lattice as suggested by Sachler *et al.*[2] The maximum activity observed with V–Sn oxides containing a small amount of V ions as described above has not been found by Sachtler *et al.*[2] and other workers.[3,4] They used silica or pumice supported V–Sn oxides, in contrast to the present work which deals with unsupported V–Sn oxides. Lack of the maximum rate of oxidation of CO over V–Sn oxides reported by Tarama *et al.*[5] appears to be attributed to the preparation of their catalyst by fusion of mixture of V_2O_5 and SnO_2, where formation of the amorphous material is unexpected.

The authors wish to thank Mr. Shinji Doi for carrying out part of the experiments.

References

1) E. G. J. Mars and D. W. Van Krevelen, *Chem. Eng. Sci.*, (s. p. Suppl.), **3**, 4 (1954); S. Yoshida, *Shokubai*, **10**, 90 (1968); K. Hirota, Y. Kera, and S. Teratani, *J. Phys. Chem.*, **72**, 3133 (1968); Y. Kubokawa and T. Ono, *Bull. Chem. Soc. Jpn.*, **51**, 3435 (1978).

2) W. M. H. Sachtler, G. H. Dorgero, J. Fahrenfort, and R. J. H. Voorhoeve, Proc. 4th Int. Cong. Catal., Moscow, 1968, Vol. 1, p. 454.

3) M. Ai, *J. Catal.*, **40**, 318 (1975).

4) K. Kaneko, T. Koyama, Y. Nagashima, and S. Wada, *Nippon Kagaku Kaishi*, **1974**, 1105.

5) K. Tarama, S. Teranishi, N. Tamura, and S. Yoshida, *Shokubai*, **4**, 346 (1961).

6) L. N. Kurina and N. V. Kudrina, *Kinet. Catal.*, **16**, 1416 (1975).

7) "X-Sen Kessho-Gaku," ed by I. Nitta, Maruzen, Tokyo (1961).

8) P. H. Kasai, *Phys. Lett.*, **7**, 5 (1963).

9) M. Valdelievere, H. Baussart, R. Delobel, and J. M. Leroy, *Bull. Soc. Chim. Fr.*, **1975**, 2467.

10) M. Inomata, A. Miyamoto, and Y. Murakami, *J. Catal.*, **62**, 140 (1980).

11) Ya. M. Kon, A. M. Gritskov, V. A. Shvets, and V. B. Kazansky, *Kinet. Catal.*, **17**, 834 (1976).

12) S. Yoshida, T. Matsuzaki, T. Kashiwazaki, K. Mori, and K. Tarama, *Bull. Chem. Soc. Jpn.*, **47**, 1564 (1974).

13) Y. Takita, K. Iwanaga, N. Yamazone, and T. Seiyama, *Oxidation Communications*, **1**, No. 2 (1979); K. Nitta, Y. Takita, N. Yamazoe, and T. Seiyama, Catal. Sympo. Catal. Soc. Jpn., Prepr. No. 3H12, 1976.

carried out, were directly determined by X-ray diffraction using the methods of Wissenberg and/or precession photographs.

In order to obtain the absorption spectrum from the observed reflection spectrum, we used the dispersion analysis method (the curve-fitting method) by using Helmholtz-Kettler type dispersion functions. The details of this analysis method were described in our previous paper.[12]

Results and Discussion

(NEP)(TCNQ)$_2$. The crystal of (NEP)-(TCNQ)$_2$ is triclinic with the space group $P\bar{1}$, the lattice constants being $a=7.070$ Å, $b=14.993$ Å, $c=8.006$ Å, $\alpha=84.3°$, $\beta=111.9°$, and $\gamma=99.8°$.[14] The unit cell contains one molecular unit of (NEP)(TCNQ)$_2$. The arrangement of TCNQ molecules (or ions) in this crystal is illustrated in Fig. 1. The infinite zigzag chain of TCNQ along the a-axis can be considered to be composed of TCNQ dimers, each of which consists of a pair of crystallographically equivalent TCNQ molecules, having one excess electron delocalized over them. We will express this dimer as $(TCNQ)_2^-$. The average intermolecular separation within the dimer is 3.17 Å, which is appreciably smaller than the average intermolecular separation between the dimers, 3.46 Å.

Figure 2 shows the polarized reflection spectra meausred at room temperature on the well-developed

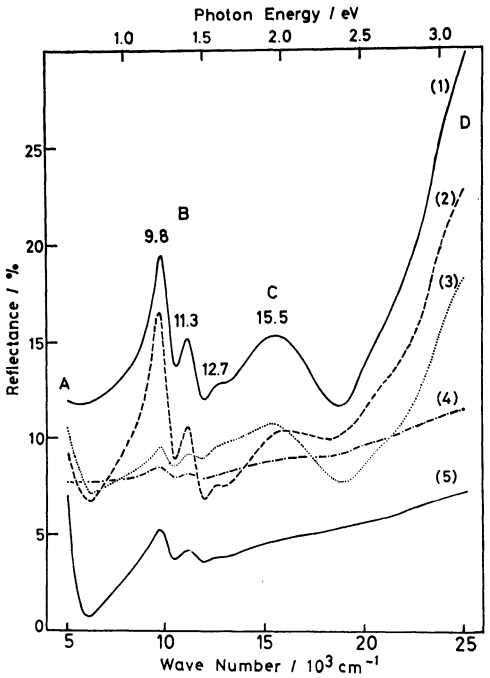

Fig. 2. Reflection spectra on the (100) and (011) crystal faces of (NEP) (TCNQ)$_2$. The number of each spectrum corresponds to that drawn in Figs. 1 (a) and 1 (b).

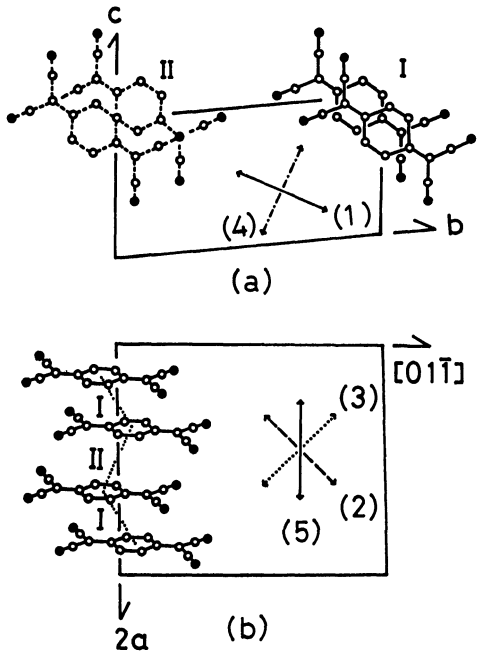

Fig. 1. (a) Projection of the TCNQ molecules onto the (100) plane in the crystal of (NEP) (TCNQ)$_2$. TCNQ molecules drawn by solid line shows the relative orientation of TCNQ molecules in the $(TCNQ)_2^-$ dimer, TCNQ molecules drawn by dashed line shows the relative orientation of TCNQ molecules between the $(TCNQ)_2^-$ dimer.
(b) Projection of the TCNQ molecules onto the (011) plane. The arrows means the directions of the polarization of incident light used to measure the reflection spectra shown in Fig. 2.

(100) and (011) crystal faces. Since $(NEP)^+$ ion has no allowed electronic transition in the observed spectral range, the dispersions observed here are entirely due to the transitions associated with the TCNQ columns. The spectra show that there exist four dispersions in the observed spectral range: The first is located below 5×10^3 cm^{-1}, the second which has a sharp structure, is at about 10×10^3 cm^{-1}, the third at about 16×10^3 cm^{-1} and the fourth above 25×10^3 cm^{-1}. These dispersions must correspond to the four absorption bands which have been reported to be characteristic of the absorption spectra of semiconductive TCNQ complex salts. Thus we will denote them as A, B, C, and D, respectively, as indicated in Fig. 2.

The polarization directions employed to measure these spectra are indicated with arrows in Fig. 1. The number given for each spectrum refers the number of the polarization direction with which the spectrum was obtained. The variation of the amplitude of a dispersion with the change of polarization direction reflects the direction of the transition moment of the electronic transition concerned. Thus one can conclude from the spectra shown in Fig. 2 that the electronic transition concerned with the dispersion A is strongly polarized in the direction of TCNQ column, while the transition concerned with the dispersion D is polarized parallel to the long molecular axis of TCNQ. According to the widely accepted interpretation of the absorption spectra of TCNQ complex salt, the dispersion A is due to the charge transfer form $(TCNQ)^-$ to $(TCNQ)^0$ which we will express as CT1(A→N), and the dispersion D is due to the lowest π-π^* transition of $(TCNQ)^0$ which we will express as LE1(N). The observed polarizations

of these two dispersions are consistent with the assignments mentioned above.

As we have mentioned before, the band B (at about 10×10^3 cm^{-1}) in the spectra of TCNQ complex salts has been assigned to the charge transfer between $(TCNQ)^-$ ions.[6] But the corresponding dispersion (the dispersion B) clearly exhibits a sharp structure in the reflection spectra observed in the present study. We note also that the dispersion B is polarized not in the direction of the TCNQ stacking axis. To know the polarization direction that gives the maximum dispersion amplitude, we observed the variation of the amplitude by rotating the polarization direction within (011) plane. We took the difference between the reflectance values at 9.8×10^3 cm^{-1} (maximum) and 10.5×10^3 cm^{-1} (minimum), R(9800)—R(10500), as the measure of the amplitude around the first peak, and the difference between the reflectance values at 11.1×10^3 cm^{-1} (maximum) and 11.9×10^3 cm^{-1} (minimum), R(11100)—R(11900), as that around the second peak. The result is shown in Fig. 3, where the observed amplitudes are plotted against the angle of polarization direction θ measured from the direction of the a-axis. We can see that the θ dependence of amplitude is exactly the same between the two peaks of the dispersion B, showing a maximum at $\theta\simeq60°$ which is the direction bisecting the angle between the direction of the long molecular axis of TCNQ and that connecting the centers of two TCNQ molecules within the dimer. The fact that the amplitudes of the two peaks exhibit the same angular dependence implies that they are associated with the same electronic transition.

The reflection spectra which were measured at 27 and 298 K on the (100) crystal face for the polarization (1), are shown in Fig. 4. The structure in the region of the dispersion B becomes markedly sharper at 27 K as compared with the spectrum at 298 K, while the

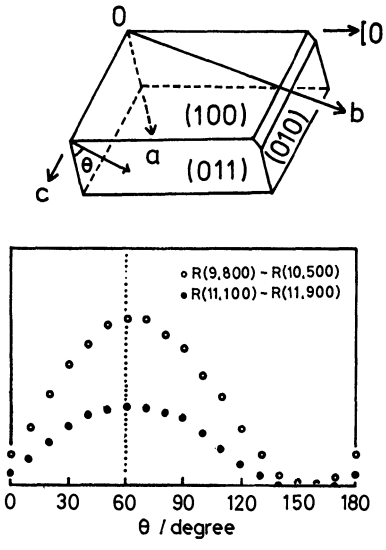

Fig. 3. The crystal shape of $(NEP)(TCNQ)_2$ single crystal used in this study and the angular dependency of the difference of the reflectivity between the crystal axis and polarization direction of incident light. R(9,800) means the reflectivity at 9.8×10^3 cm^{-1}.

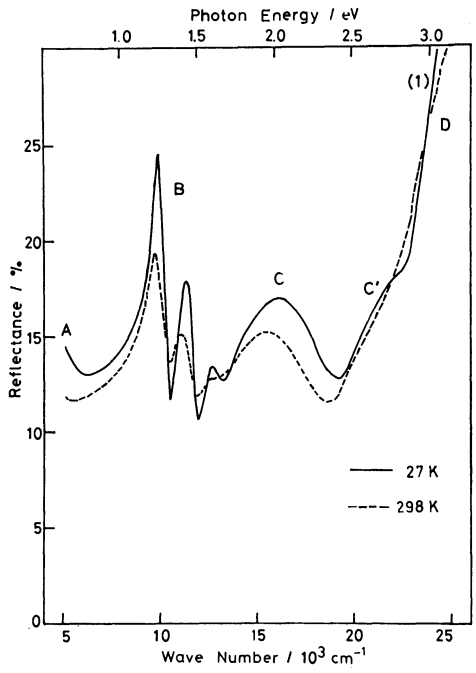

Fig. 4. Low temperature reflection spectrum polarized to the [01$\bar{1}$] direction on the (100) face of $(NEP)(TCNQ)_2$. Room temperature reflection spectrum is drawn by dashed line for the purpose of comparison.

dispersion C remains broad and structureless even at 27 K. In order to see more details of the structure of the dispersion B, we carefully measured at 27 K the reflection spectrum of the concerned region with the resolution of 40 cm^{-1}. The reflectance data thus obtained are shown by points in Fig. 5 where the solid line is the best-fitted curve obtained in the final stage of the curve fitting procedure employing seven Helmholtz-Kettler oscillator functions for the region from 5×10^3 cm^{-1} to 25×10^3 cm^{-1}, three oscillator functions being used for the region of the dispersion B.

In Fig. 6, the broken line shows the imaginary part of the complex dielectric function obtained by the curve

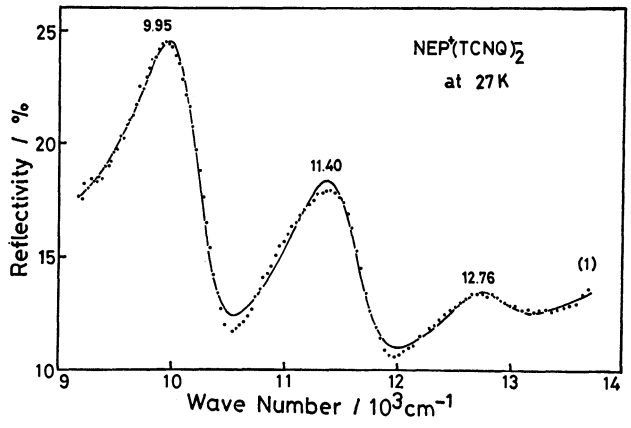

Fig. 5. The low-temperature reflection spectrum of $(NEP)(TCNQ)_2$ single crystal in the range from 9×10^3 cm^{-1} to 14×10^3 cm^{-1}. The dots means the experimental data and the solid line is the best-fitted curve obtained by the Helmholtz-Kettler model functions.

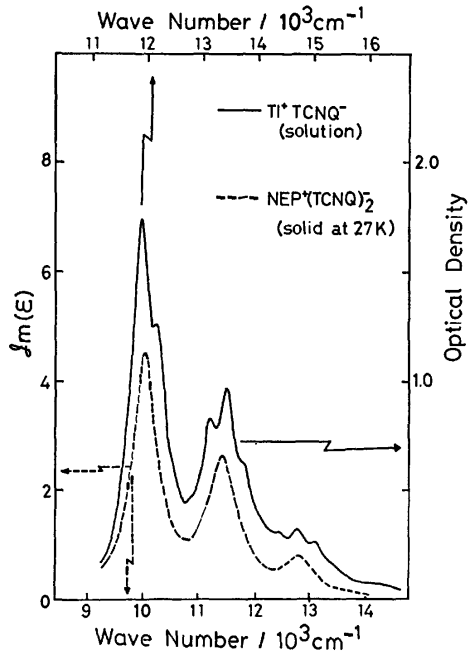

Fig. 6. Comparison between the absorption spectrum of $TCNQ^-$ in acetonitrile solution and the imaginary part of the complex dielectric function obtained by the dispersion analysis of the reflection spectrum at low temperature.

fitting mentioned above, and the solid line is the lowest π-π^* band of $(TCNQ)^-$ ion in the absorption spectrum of the acetonitrile solution of Tl(TCNQ). The both spectra agree quite well with each other. Such a good agreement can be expected only when the dispersion B is mainly due to the lowest π-π^* transition of $(TCNQ)^-$ ion. Thus we assign the dispersion B to LE1(A) not to the charge transfer between $(TCNQ)^-$ ions. Naturally, there must be a mixing with other excited configurations, in particular with CT configurations such as CT1(A→N) as it is suggested from the observed polarization direction of the dispersion B.

Other interesting aspects which we note in the low-temperature spectrum, is a blue shift of the dispersion C and the appearance of a shoulder at about 22×10^3 cm^{-1} which we have denoted as C′ in Fig. 4. The dispersion C is polarized parallel to the long molecular axis of TCNQ. As we have mentioned before, the corresponding absorption band in the absorption spectra of TCNQ complex salts has been considered to be attributable to LE1(A). We can not accept this assignment since we have already shown that it is the dispersion B that should be attributed to LE1(A). Therefore, we have to find out a new interpretation for the dispersion C.

In the ground state of $(TCNQ)^0$, sixteen π electrons are occupying up to the 8th π orbital from the lowest one, and the lowest allowed π-π^* transition which gives a strong absorption band at 24.9×10^3 cm^{-1} in the absorption spectrum of the chloroform solution of TCNQ,[15] is associated with the transition to the singlet excited state which can be mainly expressed by the configuration where an electron has been excited from the 8th MO to the 9th MO. There must be a triplet excited state corresponding to the singlet excited state mentioned above. This lowest triplet excited state of $(TCNQ)^0$ was determined to be located at 2.0 ± 0.2 eV (16×10^3 cm^{-1}) above the ground state by the electron energy loss experiment.[16] In the ground state of $(TCNQ)^-$, π electrons are doubly occupying up to the 8th MO and singly occupying the 9th MO. The lowest π-π^* transition is associated with the excitation of an electron from the 8th MO to the 9th MO.

Let us consider the situation in the dimer $(TCNQ)_2^-$, since the structural characteristics of $(NEP)(TCNQ)_2$ suggest that the intermolecular CT interaction is very muth stronger within the dimer than between the dimers, so that the essential features of the observed reflection spectrum are expected to be understandable from the considerations on the electronic states of the dimer. The lowest CT configuration of the dimer must be the one where an electron has been transfered from the 9th MO of $(TCNQ)^-$ to the 9th MO of $(TCNQ)^0$. However this is not a proper expression of the CT excited state of the dimer which is composed of a pair of strictly equivalent molecules. The ground electronic configuration of such a dimer must be expressed by the two doublet configurations which are mutually different as regards the molecular site which has one unpaired electron on its 9th MO. By taking up only the 8th and 9th MO's of the two molecules, we can schematically represent the configuration as follows;

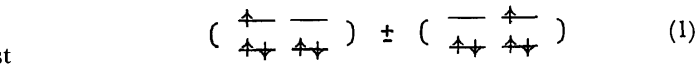
(1)

where the plus sign gives the gerade state and the minus sign gives the ungerade state. The gerade state must be energetically lower than the ungerade state, hence the former corresponds to the ground state of the dimer and the latter corresponds to the CT excited state. The lowest CT transition CT1(A→N) is to be considered as the transition between these two states. We will attribute the dispersion A of $(NEP)(TCNQ)_2$ to this CT transition.

Next we will consider the charge transfer from the 8th MO of $(TCNQ)^-$ to the 9th MO of $(TCNQ)^0$, which can be expressed as CT2(A→N). When the total spin of the dimer is considered, there will be doublet and quartet states. Since the optical transition from the ground state (doublet) is possible only to the doublet excited states, we will take up here only the doublet states. The wave function of these state can be schematically represented as follows;

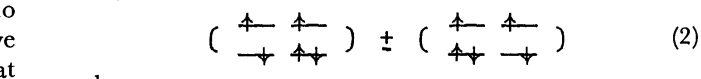
(2)

and

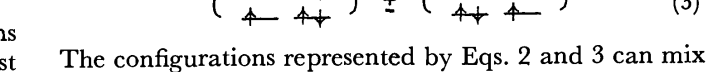
(3)

The configurations represented by Eqs. 2 and 3 can mix with each other and also with the configurations expressed by Eq. 1 since all of them are doublet states of the dimer. When we look at the electronic configurations 2 and 3 from another side, we note that they are equivalent to the expressions of the following LE configurations of the dimer: The expression given by Eq. 2 corresponds to the state where $(TCNQ)^0$ is in

the lowest singlet excited state, and $(TCNQ)^-$ is in the ground state, and the expression given by Eq. 3 correspond to the state where $(TCNQ)^0$ is in the lowest triplet excited state and $(TCNQ)^-$ is in the ground state. Thus one could denote these configurations as LE1(N, singlet) and LE1(N, triplet) states of the dimer, respectively. It should be noted that both of them are, in reality, the doublet excited states of the dimer and, therefore, they can mix with each other as we have already mensioned (Refer the appendix for the theoretical background of the explanation mentioned here).

From these considerations, we can conclude that there will be two kinds of doublet-doublet transition associated with CT2(A→N), one of which has the character of LE1(N, triplet) and the other has the character of LE1(N, singlet), and that the former transition will gain its intensity by borrowing intensity from the latter which is expected to be very strong, provided that an intermolecular CT interaction is strongly taking place in the dimer.

The doublet-doublet transition which has the character of LE1(N, triplet) is expected to appear at the wave number approximately equal to the energy of the lowest triplet state of $TCNQ^0$ (16×10^3 cm^{-1}).[16] The position of the dispersion C of $(NEP)(TCNQ)_2$ is in good agreement with this value. Thus, we attribute the dispersion C to the transition mentioned above, and will denote it as LE1(N, triplet)[CT2(A→N)]. There must by a strong dispersion associated with LE1(N, singlet)-[CT2(A→N)]. We can safely assign the dispersion D to this transition.

The low-temperature spectrum of $(NEP)(TCNQ)_2$ exhibits a shoulder at 22×10^3 cm^{-1}. This shoulder is separated by $(11—12)\times10^3$ cm^{-1} from the dispersion B which we have attributed to LE1(A) transition. This separation agrees with the separation between the first and second π-π^* transitions of $(TCNQ)^-$.[17] Thus we attribute the shoulder to the dispersion mainly associated with LE2(A).

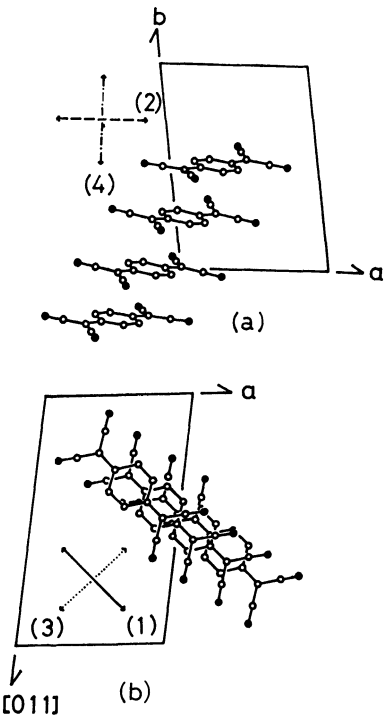

Fig. 7. Projection of the TCNQ molecules onto (a) the (001) and (b) the (01$\bar{1}$) plane in the crystal of (MTPP)$(TCNQ)_2$.

$(MTPP)(TCNQ)_2$. The crystal of $(MTPP)(TCNQ)_2$ is triclinic with the space group P$\bar{1}$, the lattice constants being $a=9.01$ Å, $b=12.89$ Å, $c=18.18$ Å, $\alpha=121.80°$, $\beta=90.58°$ and $\gamma=97.30°$.[18] The unit cell contains one molecular unit of $(MTPP)(TCNQ)_2$. In this crystal TCNQ molecules (or ions) are forming tetramers, and a zigzag TCNQ column is formed by the stacking of these tetramers along the b-axis. The molecular arrangement within a tetramer is shown in Fig. 7. This salt exhibits a phase transition at 315 K between the low-temperature (low spin) phase and the high-temperature (high-spin) phase.[19] According to the results of crystal structure analysis, the molecular arrangement within the TCNQ tetramer remains the same between the two phases, but the separation of TCNQ molecules between tetramers changes from 3.57 Å in the low-temperature phase to 3.55 Å in the high-temperature phase.[20] As compared with the intermolecular separation between tetramers, the molecular separations within a tetramer are appreciably small, which are reported to be 3.24, 3.22, and 3.26 Å. Thus the main feature of the spectrum will be determined by the intermolecular interaction wihtin the tetramer.

The absorption spectrum of the single crystal of $(MTPP)(TCNQ)_2$ was observed by Tanaka *et al.*,[5] and the reflection spectrum was observed by Oohashi and Sakata,[4] both the groups made the measurements only on the (001) crystal face at room temperature. These authors reported that $(MTPP)(TCNQ)_2$ exhibits the four absorption bands which are characteristic of the absorption spectra of TCNQ complex salts.

In the present study, we measured the reflection spectrum of this salts not only on the (001) crystal face, but also on the (01$\bar{1}$) crystal face. The polarization directions employed in those measurements are shown in Fig. 7.

Figure 8 shows the reflection spectra obtained at room temperature. From the comparison of these spectra, we can see that the dispersions denoted as B, C and D are polarized almost in the direction of the long molecular axis of TCNQ, while the dispersion A is polarized in the direction of the TCNQ column. The general features of these spectra are quite similar to the reflection spectrum of $(NEP)(TCNQ)_2$, except that the vibrational structure of the dispersion B less sharply appears in the spectra of $(MTPP)(TCNQ)_2$ than in the spectra of $(NEP)(TCNQ)_2$.

However, as we cool down $(MTPP)(TCNQ)_2$, there appears a new dispersion at about 8×10^3 cm^{-1}, while no corresponding dispersion was found in the case of $(NEP)(TCNQ)_2$. We will denote this new dispersion as A′ (see Fig. 9). It should be noted also that the dispersion B is blue shifted on lowering the temperature while such an appreciable temperature-dependent shift was not found in the case of $(NEP)(TCNQ)_2$. In other respects, the temperature dependence of the reflection

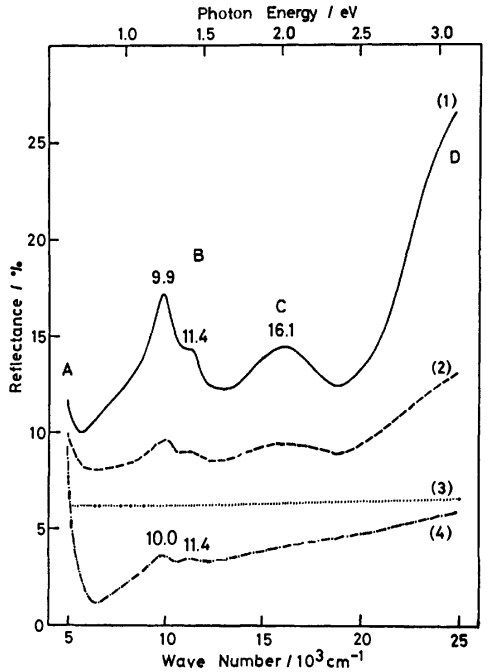

Fig. 8. Reflection spectra on the (100) and the (01$\bar{1}$) crystal faces of (MTPP) $(TCNQ)_2$. The number of each spectrum corresponds to that drawn in Figs. 7 (a) and 7(b).

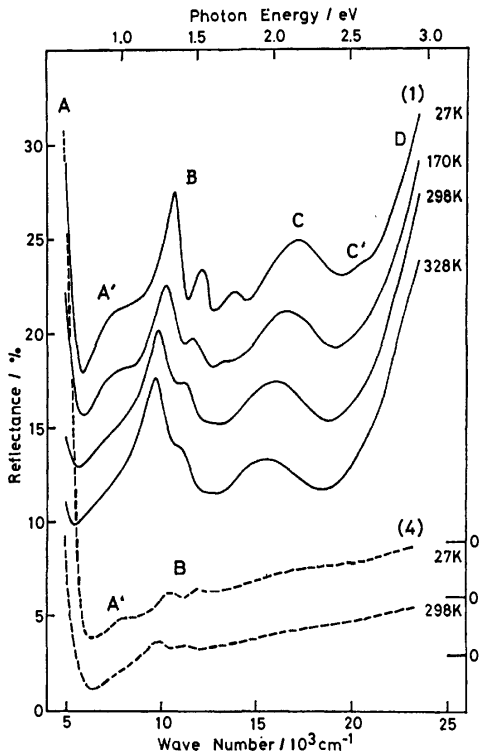

Fig. 9. Temperature dependency of the reflection spectra of (MTPP) $(TCNQ)_2$ single crystal polarized parallel to the [111] direction (solid line) and perpendicular to the a-axis (dashed line).

spectrum of (MTPP)$(TCNQ)_2$ very resembles that of (NEP)$(TCNQ)_2$.

The experimental results described above can be interpreted if we assume a model that the TCNQ tetramer in (MTPP)$(TCNQ)_2$ is essentially composed of two TCNQ dimers, between which a CT interaction can take place. According to this model, the electronic transitions of the TCNQ tetramer can be classified into those mainly associated with the electronic transitions within each dimer and those associated with the charge transfer between the dimers. Let us consider the temperature dependence of the latter transition. Since each dimer $(TCNQ)_2^-$ has one unpaired electron, there will be singlet and triplet state for the ground electronic configuration of the tetramer when the spin state is taken into account. On the other hand, the CT configuration where an electron is transfered from a singly occupied orbital of a dimer to the corresponding orbital of another dimer, is necessarily a singlet state. Consequently, the singlet ground configuration can be stabilized by the mixing with this CT configuration, but not in the case of the triplet ground configuration. The optical transition to the CT singlet state is allowed only from the singlet ground state, so that the intensity of the CT band associated with this transition should increase on lowering the temperature accompanying the increase of the population of the tetramers which are in the singlet ground state. This situation is analogous to the singlet-triplet model proposed for a radical ion dimer.

The ESR signal due to the triplet exciton in (MTPP)-$(TCNQ)_2$ was actually observed by Chesnut and Phillip.[19] The temperature dependence of the paramagnetic susceptibility of this salt was approximately

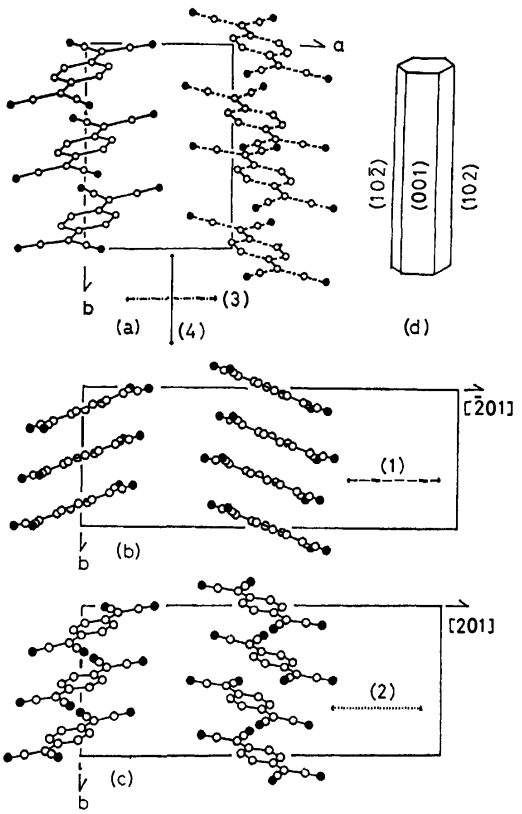

Fig. 10. Projection of the TCNQ molecules onto the crystal faces of (a) (001), (b) (102), and (c) (10$\bar{2}$). (d) Crystal morphology for Cs_2TCNQ_3 single crystal.

explained in terms of the singlet-triplet model with the energy separation of 0.065 eV.[21] This singlet-triplet separation is significantly smaller than the value (0.2—0.4 eV) usually obtained for TCNQ simple salts.[22] This is also understandable from the model described above, since the stabilization of the singlet ground state caused by the CT interaction between dimers must be much smaller than that caused by the CT interaction between closely contacting $(TCNQ)^-$ ions within a $(TCNQ)^-$ dimer.

According to the consideration mentioned above, we will attribute the dispersion A′ which exhibits a marked increase of amplitude at lower temperature, to the charge transfer between dimers, and the remaining dispersions, A, B, C, C′, and D, to the transitions within a dimer, thus attributable to the transitions which we have discussed in the cases of the corresponding dispersions of the spectrum of $(NEP)(TCNQ)_2$.

$Cs_2(TCNQ)_3$. The crystal of $Cs_2(TCNQ)_3$ is monoclinic with the space group $P2_1/c$, the lattice constants being $a=7.34$ Å, $b=10.40$ Å, $c=21.98$ Å and $\beta=97.18°$.[23] The unit cell contains two molecular units of $Cs_2(TCNQ)_3$. The observed molecular geometries of TCNQ in this crystal indicate that the charges in the TCNQ column are rather localized, so that $(TCNQ)^0$ sites and $(TCNQ)^-$ sites are regularly arranged along the column by the repetition of $(TCNQ)^-(TCNQ)^0(TCNQ)^-$ (see Fig. 10). But we should not consider that the TCNQ column is composed of discrete TCNQ trimers since the intermolecular separation is 3.22 Å between $(TCNQ)^0$ and $(TCNQ)^-$ within a trimeric repeating unit and 3.26 Å between $(TCNQ)^-$ ions of the neighboring units.

$Cs_2(TCNQ)_3$ crystallizes as a needle-like crystal, the shape of which is illustrated in Fig. 10(d). The $//b$ and $\perp b$ absorption spectra were previously observed in our laboratory on the (001) face of a single crystal at room temperature, by using a microspectrophotometer for transmission method.[2] The absorption spectra obtained by a similar measurement were reported later by Tanaka *et al.*[5] These two results showed a good agreement with each other. However, no observation of absorption spectrum has been done so far on the crystal faces other than the (001) face. This left some ambiguities as regards interpretation of the spectrum.

Figure 11 shows the reflection spectra measured on the (001), (102), and $(10\bar{2})$ faces of a single crystal of $Cs_2(TCNQ)_3$ at room temperature. The polarization directions employed to obtain these spectra are illustrated in Fig. 10 which shows the projection of the crystal structure onto each crystal face, Cs ions having been omitted in the projections shown there. The number of each spectrum corresponds to the number of the polarization direction by which it was measured.

The spectra (3) and (4) correspond quite well to the reported absorption spectra measured on the same crystal face, (001), with the $\perp b$ and $//b$ polarizations, respectively.[2,6] However, the spectra (1) and (2) reveal the features which have never been found from the measurements on the (001) face only. First, the spectrum (1) shows a strong maximum at 11.3×10^3 cm^{-1}, which is clearly different from the position of

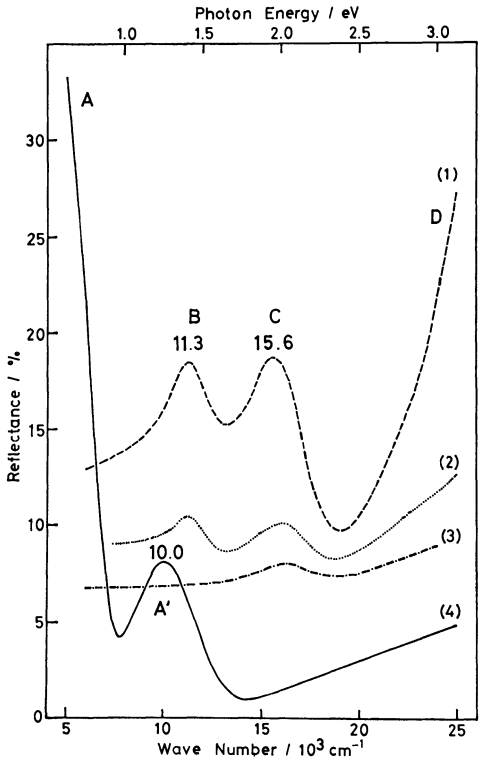

Fig. 11. Reflection spectra on the (001), the (102) and the $(10\bar{2})$ crystal faces of Cs_2TCNQ_3 single crystal. The number of each spectrum corresponds to that drawn in Figs. 10(a), 10(b), and 10(c). The $//b$ spectra measured on the (102) and $(10\bar{2})$ faces were exactly the same as the $//b$ spectrum measured on the (001) face, hence they are not shown here.

the maximum found in the spectrum (1). Second, the maximum at 15.6×10^3 cm^{-1} strongly appears in the spectrum (1) as compared with the spectra obtained with other polarizations, indicating that it is associated with the transition polarized in the direction of the long molecular axis of TCNQ.

The reflection spectra obtained at 27 K for the polarization directions (1) and (4) are shown in Fig. 12, where the broken lines are the corresponding room-temperature spectra. Note that the peak at 11.4×10^3 cm^{-1} becomes sharp and a new small peak does appear at 12.8×10^3 cm^{-1} in the spectrum (1) measured at 27 K. On the other hand, the spectrum (4) at 27 K shows a broad maximum at 10.2×10^3 cm^{-1} which is accompanied by small sharp peaks at 11.6×10^3 and 13.0×10^3 cm^{-1}. Probably the small sharp peaks observed in the spectrum (4) at 27 K are corresponding to the 11.4×10^3 and 12.8×10^3 cm^{-1} peaks of the spectrum (1). This fact implies that the broad maximum (at 10.2×10^3 cm^{-1}) of the spectrum (4) is of an origin entirely different from that of the sharp peaks which strongly appear in the spectrum (1). We note that the spectrum (1) at 27 K closely resembles the spectrum of $(NEP)(TCNQ)_2$, although the TCNQ column of $Cs_2(TCNQ)_3$ has not any discrete dimeric unit corresponding to the dimer $(TCNQ)_2^-$ which has been discussed in the case of $(NEP)(TCNQ)_2$. Seemingly the similarity between the

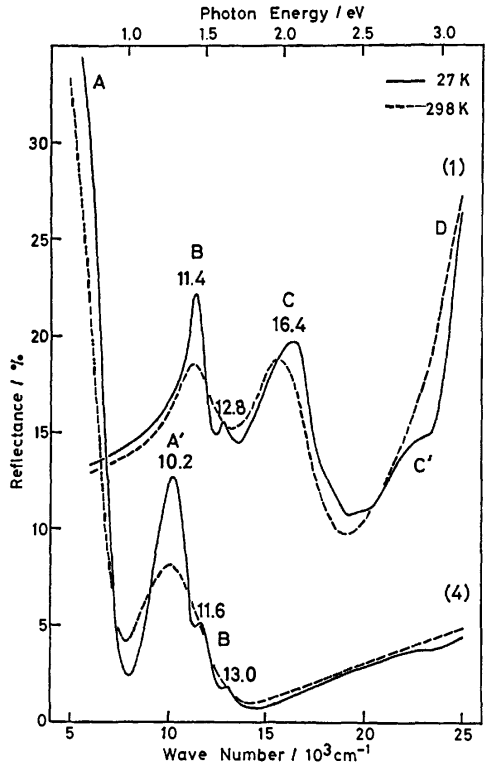

Fig. 12. Low-temperature reflection spectra of Cs_2-$TCNQ_3$ single crystal polarized parallel to the [$\bar{2}$01] and the [010] directions.

spectrum of $Cs_2(TCNQ)_3$ and that of (NEP)$(TCNQ)_2$ arises because the main feature of the former is also determined by the interaction between $(TCNQ)^0$ and $(TCNQ)^-$. Thus, from the analogy with the assignments given for the dispersions of the spectrum of (NEP)-$(TCNQ)_2$, we assign the dispersion B with a relatively sharp peaks at 11.4×10^3 and 12.8×10^3 cm^{-1} to LE1(A) and the dispersion C' which appear as a shoulder at the low-temperature spectrum (1) to LE2(A), and the dispersion C at 16.4×10^3 cm^{-1} to the transition associated with the charge transfer from the second highest occupied orbital (8th MO) of $TCNQ^-$ to the lowest unoccupied orbital (9th MO) of $TCNQ^0$, thus to CT2(A→N). This CT2(A→N) transition must have a character of LE1(N, triplet) as we have pointed out in the case of (NEP)$(TCNQ)_2$. As a matter of fact, the dispersion C is completely polarized in the direction of the long molecular axis of TCNQ. The strong dispersion D which is located above 25×10^3 cm^{-1} can be safely assigned to LE1(N, singlet)[CT2(A→N)].

The dispersion A' which appears as a maximum at 10.2×10^3 cm^{-1} in the spectrum (4), can be assigned to the charge transfer between $(TCNQ)^-$ ions, CT1-(A→A). In the case of TCNQ simple salts, there exists a strong mixing between CT1(A→A) and LE1(A). This makes the absorption band associated with LE1(A) broad and structureless, and, gives at the same time an increase of the separation between CT1(A→A) band and the band which is mainly associated with LE1(A), their separation being usually $(5—6)\times10^3$ cm^{-1} in the absorption spectra of TCNQ simple salts.

In the case of $Cs_2(TCNQ)_3$, the overlap of mutually interacting $(TCNQ)^-$ ions is of the short-axis-shifted mode where one of the ions is shifted against the other along the short molecular axis from the position of the direct overlap. With this mode of molecular overlap, the CT1(A→A) state cannot mix with the LE1(A) state. Probably this might be the reason why the separation between the dispersion A'(CT1(A→A)) and the dispersion B (LE1(A)) is small, and the latter clearly shows a vibrational structure, although there must be a strong CT interaction between $(TCNQ)^-$ ions.

Conclusion and Summary

In this study, we measured the polarized reflection spectra on the single crystals of the three different types of TCNQ complex salt, (NEP)$(TCNQ)_2$, (MTPP)-$(TCNQ)_2$, and $Cs_2(TCNQ)_3$, not only at room temperature but also at low temperatures down to 27 K. We have revealed that the dispersion B which appears at about $(10—11)\times10^3$ cm^{-1} shows a sharp structure corresponding to the vibrational structure of the lowest π-π^* band of the solution spectrum of $(TCNQ)^-$ ion, and is polarized in the direction rather close to the direction of the long molecular axis of TCNQ. We have also found that a new dispersion appears at $(7—8)\times10^3$ cm^{-1} in the low-temperature spectrum of (MTPP)$(TCNQ)_2$ and its amplitude increases on lowering the temperature. The low-temperature spectrum of $Cs_2(TCNQ)_3$ showed that there is a broad dispersion at 10.2×10^3 cm^{-1}, polarized parallel to the TCNQ column, besides a sharp dispersion at 11.4×10^3 cm^{-1} polarized in the direction of the long-molecular axis of $(TCNQ)^-$.

These new results cannot be explained by the interpretations which have been hitherto proposed for the absorption bands of the spectra of semiconductive TCNQ complex salts.

On the bases of those experimental results, we have proposed a new interpretation, particularly for the origin of the dispersion B which appears at about 10×10^3 cm^{-1} with a vibrational structure and the dispersion C which appears at about 16×10^3 cm^{-1}.

Finally we wish to point out that, as we have revealed in this study, it is extremely important to observe the reflection (or absorption) spectra on various crystal faces with different polarizations, not only at room temperature but also at low temperatures in order to know the true characteristics of the spectra of highly anisotropic organic solids such as TCNQ salts, and to establish the interpretations of the spectra.

The authors wish to thank Mr. Nobuhiro Kosugi for helpful discussion.

Appendix

We will consider the ground and excited states of the dimer $(TCNQ)_2^-$ by using a simple configuration interaction method, in order to reveal the mechanism of the mixing of the states of the doublet-singlet pair and the doublet-triplet pair. To simplify the model we take account only of the 8th and 9th

molecular orbitals of TCNQ. Let us express the wave functions of various configurations of the dimer as follows denoting the molecules in the dimer as A and B, respectively;

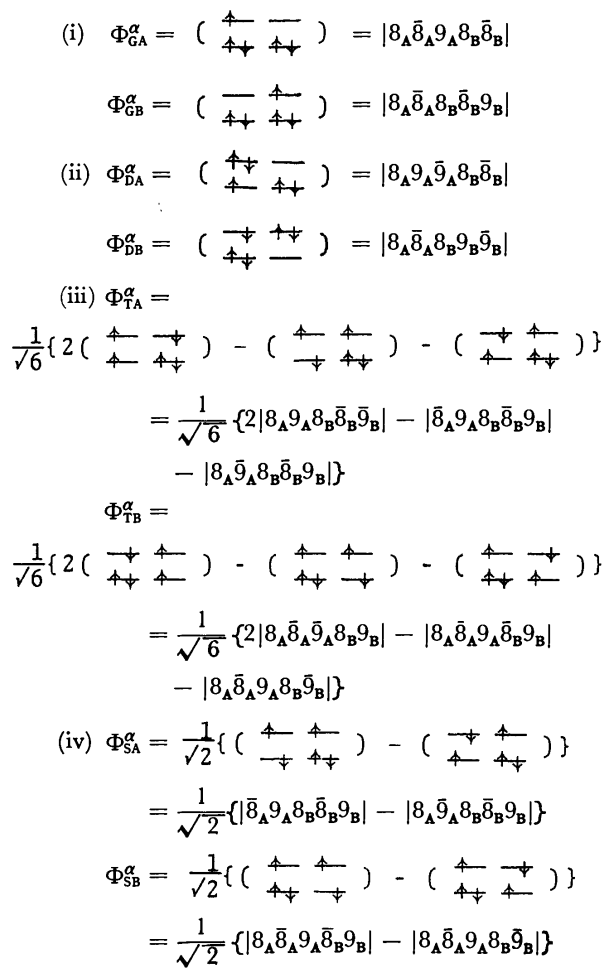

where α represents the spin state of the doublet system, 8_A and $\bar{8}_B$ mean the 8th molecular orbital of the molecule A with α spin and that of the molecule B with β spin, and $|8_A\bar{8}_A9_A8_B\bar{8}_B|$ means the Slater determinant.

When we neglect the intermolecular interaction, (i), (ii), (iii), and (iv) correspond, respectively, to the ground configuration, the LE configurations associated with the first excited state of $TCNQ^-$, the ones associated with the first triplet and singlet excited states of $TCNQ^0$. When the intermolecular interaction H_{AB} is introduced, the electronic states of the dimer can be described by the linear combination of these states. As the first approximation, we will take account of the following transfer integrals:

$$
\begin{aligned}
t_0 &= \langle\Phi^\alpha_{GA}|H|\Phi^\alpha_{GB}\rangle \simeq \langle|8_A9_A\bar{9}_A8_B\bar{8}_B|H|8_A9_A8_B\bar{9}_B\bar{8}_B|\rangle \\
&= \langle|8_A\bar{8}_A8_B9_B\bar{9}_B|H|8_A\bar{8}_A\bar{9}_A8_B9_B|\rangle \\
&\simeq -\langle|8_A9_A\bar{9}_A8_B\bar{8}_B|H|8_A\bar{9}_A8_B\bar{8}_B9_B|\rangle \\
&= -\langle|8_A\bar{8}_A8_B9_B\bar{9}_B|H|8_A\bar{8}_A9_A8_B\bar{9}_B|\rangle \\
t_1 &= -\langle|8_A\bar{8}_A9_A8_B\bar{8}_B|H|8_A9_A8_B\bar{8}_B\bar{9}_B|\rangle \\
&= -\langle|8_A\bar{8}_A8_B\bar{8}_B9_B|H|8_A\bar{8}_A\bar{9}_A8_B9_B|\rangle \\
&\simeq \langle|8_A\bar{8}_A9_A\bar{8}_B8_B|H|\bar{8}_A9_A8_B\bar{8}_B9_B|\rangle \\
&= \langle|8_A\bar{8}_A8_B\bar{8}_B9_B|H|8_A\bar{8}_A9_A\bar{8}_B9_B|\rangle \\
t_2 &= \langle|8_A9_A8_B\bar{8}_B\bar{9}_B|H|8_A\bar{8}_A9_A8_B\bar{9}_B|\rangle \\
&= \langle|8_A\bar{9}_A8_B\bar{8}_B9_B|H|8_A\bar{8}_A\bar{9}_A8_B9_B|\rangle \\
&\simeq \langle|\bar{8}_A9_A8_B\bar{8}_B9_B|H|8_A\bar{8}_A9_A\bar{8}_B9_B|\rangle,
\end{aligned}
$$

where, $H=H_0+H_{AB}$. The origin of the energy is chosen so that $\langle\Phi^\alpha_{GA}|H|\Phi^\alpha_{GA}\rangle$ is equal to zero. The matrix of the secular equation will be given by (1) for the gerade states,

$$
\begin{array}{c}
\\
\Phi_G^+ \\
\Phi_D^+ \\
\Phi_T^+ \\
\Phi_S^+
\end{array}
\begin{pmatrix}
t_0 & 0 & -\frac{3}{\sqrt{6}}t_1 & \frac{1}{\sqrt{2}}t_1 \\
 & E_D & \frac{3}{\sqrt{6}}t_0 & \frac{1}{\sqrt{2}}t_0 \\
 & & E_T-\frac{1}{2}t_2 & -\frac{\sqrt{3}}{2}t_2 \\
 & & & E_S+\frac{1}{2}t_2
\end{pmatrix} \qquad (1)
$$

and by (2) for the ungerade states,

$$
\begin{array}{c}
\\
\Phi_G^- \\
\Phi_D^- \\
\Phi_T^- \\
\Phi_S^-
\end{array}
\begin{pmatrix}
-t_0 & 0 & -\frac{3}{\sqrt{6}}t_1 & \frac{1}{\sqrt{2}}t_1 \\
 & E_D & \frac{3}{\sqrt{6}}t_0 & \frac{1}{\sqrt{2}}t_0 \\
 & & E_T+\frac{1}{2}t_2 & \frac{\sqrt{3}}{2}t_2 \\
 & & & E_S-\frac{1}{2}t_2
\end{pmatrix} \qquad (2)
$$

where,

$$
\begin{aligned}
\Phi^\pm_G &= \frac{1}{\sqrt{2}}(\Phi^\alpha_{GA} \pm \Phi^\alpha_{GB}) \\
\Phi^\pm_D &= \frac{1}{\sqrt{2}}(\Phi^\alpha_{DA} \pm \Phi^\alpha_{DB}) \\
\Phi^\pm_T &= \frac{1}{\sqrt{2}}(\Phi^\alpha_{TA} \pm \Phi^\alpha_{TB}) \\
\Phi^\pm_S &= \frac{1}{\sqrt{2}}(\Phi^\alpha_{SA} \pm \Phi^\alpha_{SB})
\end{aligned}
$$

The integrals, t_0, t_1, and t_2, have negative values because of the symmetry of the molecular orbitals[24] and the geometrical configuration of TCNQ molecules in the dimer. Therefore, the ground state of this system will be Φ_G^+, and the optical transition from this state is allowed only to Φ_G^-, Φ_D^-, Φ_T^-, and Φ_S^-. The wave function of the ground state and those of the ungerade states can be expressed as follows when they are calculated by the first order perturbation method.

$$
\begin{aligned}
\Phi_G &= \Phi_G^+ + \frac{\frac{3}{\sqrt{6}}t_1}{E_T-\frac{1}{2}t_2-t_0}\Phi_T^+ - \frac{\frac{1}{\sqrt{2}}t_1}{E_S+\frac{1}{2}t_2-t_0}\Phi_S^+ \\
\Phi_{CT} &= \Phi_G^- + \frac{\frac{3}{\sqrt{6}}t_1}{E_T+\frac{1}{2}t_2+t_0}\Phi_T^- - \frac{\frac{1}{\sqrt{2}}t_1}{E_S-\frac{1}{2}t_2+t_0}\Phi_S^- \\
\Phi_D &= \Phi_D^- - \frac{\frac{3}{\sqrt{6}}t_0}{E_T+\frac{1}{2}t_2-E_D}\Phi_T^- - \frac{\frac{\sqrt{3}}{2}t_0}{E_S-\frac{1}{2}t_2-E_D}\Phi_S^- \\
\Phi_T &= \Phi_T^- - \frac{\frac{3}{\sqrt{6}}t_1}{E_T+\frac{1}{2}t_2+E_D}\Phi_G^- + \frac{\frac{3}{\sqrt{6}}t_0}{E_T+\frac{1}{2}t_2-E_D}\Phi_D^- \\
&\quad - \frac{\frac{\sqrt{3}}{2}t_2}{E_S-t_2-E_T}\Phi_S^-
\end{aligned}
$$

$$\Phi_S = \Phi_S^- + \frac{\frac{1}{\sqrt{2}}t_1}{E_S - \frac{1}{2}t_2 + t_0}\Phi_G^- + \frac{\frac{1}{\sqrt{2}}t_0}{E_S - \frac{1}{2}t_2 - E_D}\Phi_D^- + \frac{\frac{\sqrt{3}}{2}t_2}{E_S - t_2 - E_T}\Phi_T^-$$

The transitions to Φ_{CT}, Φ_D, Φ_T, and Φ_S from Φ_G correspond to CT1(A→N), LE1(A), LE1(N, triplet) and LE1(N, singlet), respectively, and the last two transitions have, at the same time, the nature of CT2(A→N). Thus, the transition $\Phi_G \rightarrow \Phi_T$ can borrow its intensity from the very strong transition of the type $\Phi_G^+ \rightarrow \Phi_S^-$, provided that t_2 is not zero. Although the present formulation has been carried out by taking up only the 8th and 9th MO, the conclusion will not change qualitatively even if we carried out a more elaborate calculation.

References

1) Y. Iida, *Bull. Chem. Soc. Jpn.*, **42**, 637 (1969).
2) S. Hiroma, H. Kuroda, H. Akamatu, *Bull. Chem. Soc. Jpn.*, **44**, 9 (1971).
3) A. Brau, P. Bruesch, J. P. Farges, W. Hinz, and D. Kuse, *Phys. Status. Solidi B*, **62**, 615 (1974).
4) Y. Oohashi and T. Sakata, *Bull. Chem. Soc. Jpn.*, **48**, 1725 (1975).
5) J. Tanaka, M. Tanaka, T. Kawai, T. Tanabe, and O. Maki, *Bull. Chem. Soc. Jpn.*, **49**, 2358 (1976).
6) J. B. Torrance, B. A. Scott, and F. B. Kaufman, *Solid State Commun.*, **17**, 1369 (1975).
7) J. B. Torrance, Proc. Conf. on Organic Metals and Semiconductors, p. 453, Siofok, Hungary, Sept. 1976.
8) J. Hubbard; *Phys. Rev. B*, **17**, 494 (1978).
9) K. Kamaras, G. Gruner, and G. A. Sawatcky, *Solid State Commun.*, **27**, 1171 (1978).
10) L. R. Melby, R. J. Harder, W. R. Hertler, W. Mahler R. E. Benson, and W. E. Mochel, *J. Am. Chem. Soc.*, **84**, 3374 (1962).
11) K. Yakushi, T. Kusaka, and H. Kuroda, *Chem. Phys. Lett.*, **68**, 139 (1979).
12) K. Yakushi, M. Iguchi, and H. Kuroda, *Bull. Chem. Soc. Jpn.*, **52**, 3180 (1979).
13) Y. Iyechika, K. Yakushi, and H. Kuroda, *Bull. Chem. Soc. Jpn.*, **53**, 603 (1980).
14) D. Chasseau, J. Gaultier, and C. Hauw, *Acta. Crystallogr., Sect. B*, **32** 3262 (1976).
15) R. R. Pennelly and C. J. Eckhardt, *Chem. Phys.*, **12**, 89 (1976).
16) J. J. Ritsko, L. J. Brillson, and D. J. Sandman, *Solid State Commun.*, **24**, 109 (1977).
17) Y. Oohashi and T. Sakata, *Bull. Chem. Soc. Jpn.*, **46**, 3330 (1973).
18) A. T. McPhail, G. M. Semeniuk, D. B. Chesnut, and P. M. Gross, *J. Chem. Soc., A*, **1971**, 2174.
19) D. B. Chesnut and W. D. Phillips, *J. Chem. Phys.*, **35**, 1002 (1961).
20) M. Konno and Y. Saito, *Acta Crystallogr., Sect. B*, **29**, 2815 (1973).
21) R. G. Kepler, *J. Chem. Phys.*, **39**, 3528 (1963).
22) Z. Soos, "Molecular Association," ed by R. Foster, Academic Press (1975), Vol. 1, p. 1.
23) C. J. Fritchie, Jr., and P. Arthur, Jr., *Acta. Crystallogr.*, **21**, 139 (1966).
24) The symmetry of the 8th and 9th MO is b_{1u} and b_{2g}, respectively.

The Rate Constants of the Reactions of Hydrogen and Oxygen Atoms with Fluoroethylenes

Ko-ichi SUGAWARA, Kiyoshi OKAZAKI, and Shin SATO*

Department of Applied Physics, Tokyo Institute of Technology, Ookayama, Meguro-ku, Tokyo 152

(Received May 1, 1980)

The pulse-radiolysis technique combined with the atomic resonance absorption method was used for the measurement of the room-temperature rate constants of the reactions of hydrogen and oxygen atoms with fluoroethylenes. The rate constants obtained at 298±2 K are as follows, in units of 10^{-12} cm^3 molecule^{-1} s^{-1} (1 cm^3 molecule^{-1} s^{-1} = 6.022 × 10^{17} m^3 mol^{-1} s^{-1}). The standard deviation is within 10%.

Atoms	C_2H_4	C_2H_3F	CH_2CF_2	C_2HF_3	C_2F_4
H	1.1	0.52	0.36	0.090	0.082
O	1.0	0.52	0.20	0.63	0.81

The correlation between the rate constants and the reactivity index calculated by the INDO method is discussed.

The determination of the absolute rate constants for the addition of hydrogen and oxygen atoms to monoolefins in the gas phase has been the subject of a number of investigations.[1-6] Although some discrepancies still remain in the temperature dependence, the rate constants at room temperature now appear to be established.

Recently we used the pulse-radiolysis technique for the determination of these rate constants and obtained results consistent with previous measurements.[7-9]

Using the product analysis, Jennings and his collaborators determined the relative rate constants for the addition of hydrogen and oxygen atoms to many fluorinated olefins.[10,11] Moss used a similar technique to measure the relative rate constants of the reactions of oxygen atoms with all the fluoroethylenes.[12] The relative rate constants they reported have an interesting dependence on the number of the substitution of fluorine atoms. In the reactions of hydrogen atoms with fluoroethylenes, the increase in the number of substituted fluorine atoms reduces the relative rate constants, while in the case of oxygen atoms, difluoroethylenes have the lowest reactivity. These results are still open to theoretical interpretation.

We, therefore, attempted the measurement of the absolute rate constants of the reactions of hydrogen and oxygen atoms with some fluoroethylenes, and tried to explain the results theoretically by using the reactivity index calculated by the INDO method.

Experimental

The apparatus used for the measurement of the rate constants has been described previously.[9] The time resolved measurements of hydrogen and oxygen atoms are the same as those described in previous papers.[7,9]

Fluoroethylenes were the products of Daikin Co. After a few freeze-pump-thaw cycles at liquid nitrogen temperature, the middle third was retained. The gas chromatographic analysis using a 2-m Porapak N column at room temperature showed that all compounds contain no detectable impurities.

Results

For the reactions of hydrogen atoms, the H_2 pressure ranging from 180 to 900 Torr (1 Torr=133.3 Pa) was used. No H_2-pressure dependence of the rate constant could be observed. All the decay curves obtained on the oscillograms were of the first-order. Figure 1 summarizes the decay rates obtained as functions of the initial pressure of four kinds of fluoroethylenes. For comparison, the decay rates previously obtained with ethylene are plotted.[7]

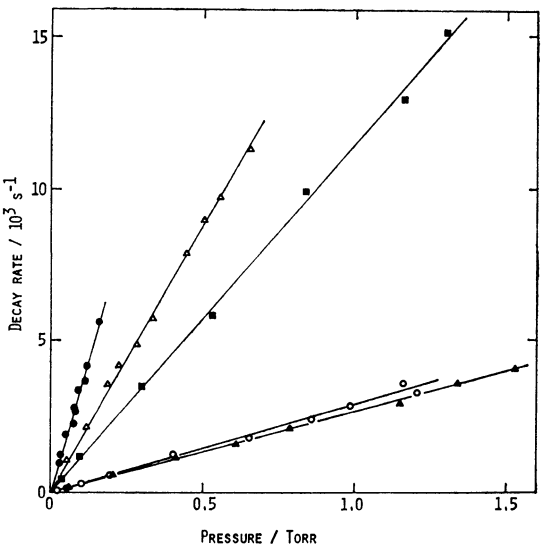

Fig. 1. Plots of the decay rates of hydrogen atoms against reactant pressures.
●: C_2H_4, △: C_2H_3F, ■: CH_2CF_2, ○: C_2HF_3, ▲: C_2F_4.

As the source of oxygen atoms, the mixtures of O_2 (4—10 Torr) and He (100—900 Torr) were used. All the decay curves obtained on the oscillograms were of the first-order. The procedure for the determination of the rate constants of the reactions of oxygen atoms with olefins is the same as that described in the previous paper.[9] Figure 2 summarizes the decay rates obtained as functions of the initial pressure of fluoroethylenes. For comparison, the decay rates previously obtained with ethylene are also plotted.

From the linear plots shown in Figs. 1 and 2, we can calculate the rate constants of the reactions of hydrogen and oxygen atoms with fluoroethylenes. The results are summarized in Fig. 3 as functions of the number of

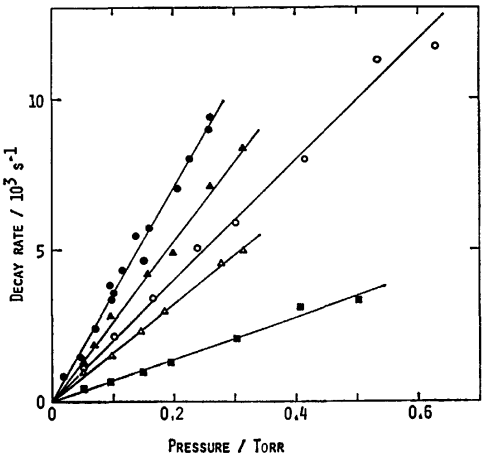

Fig. 2. Plots of the decay rates of oxygen atoms against reactant pressure.
●: C_2H_4, △: C_2H_3F, ■: CH_2CF_2, ○: C_2HF_3, ▲: C_2F_4.

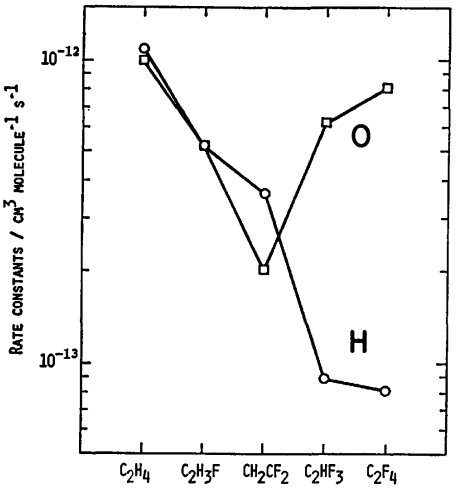

Fig. 3. Comparison of the rate constants of the reactions of H and O atoms with fluoroethylenes.

substituted fluorine atoms.

INDO Calculation

The calculation by the approximate MO theory on fluoroethylenes has already been made by Pople and his colleagues, and the interesting effects of the substitution of fluorine atoms on the charge distribution in the molecules have been discussed.[13] The electron density of the σ-part in the C=C double bond is reduced by the inductive effect of fluorine atoms, while the π-electron density is increased by the so-called mesomeric effect. By performing the INDO calculation, we carefully studied these effects to find if any correlations exist between these electron densities and the rate constants we obtained above, but no clear correlations could be found. The calculation without considering attacking atoms seems to be useless for the discussion on the rate constants. We, therefore, performed the calculation on a model which included the attacking atoms.

According to the recent *ab initio* calculations, when an H atom adds to ethylene, the atom approaches the C atom attached to the double bond from the direction perpendicular to the plane of the ethylene molecule.[14] A similar reaction path has been derived for the addition reaction of O(^{3}P) atom to ethylene,[15,16] although this mechanism seems to be somewhat contradictory to that proposed by Cvetanović.[17] In the present treatment, we assumed that no deformation of the geometry of fluoroethylene molecule occurs during the approach of the attacking atom, and calculated the total energy change as a function of the distance between the attacking atom and the ethylene molecule. The geometry of the calculated model is shown in Fig. 4.

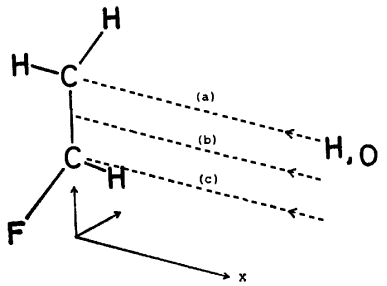

Fig. 4. The geometry used for the INDO calculation.

Among the three calculated reaction paths, the one leading the attacking atom to the C atom which is less substituted by fluorine atoms was found to be the lowest energy path, irrespective of the kind of the attacking atoms. This is consistent with the observations that hydrogen atoms add almost exclusively to the CH_2 group in CH_2CHF and CH_2CF_2,[18] and that oxygen atoms add mainly to the CH_2 group in CH_2CHF.[19] The calculated energy differences, δE, between the total energy change of fluoroethylene, ΔE(fluoroethylene), and that of ethylene, ΔE(ethylene) as functions of the distance, x, between attacking atom and ethylene are shown in Fig. 5. The smaller the value of δE, the more easily can the attacking atoms approach

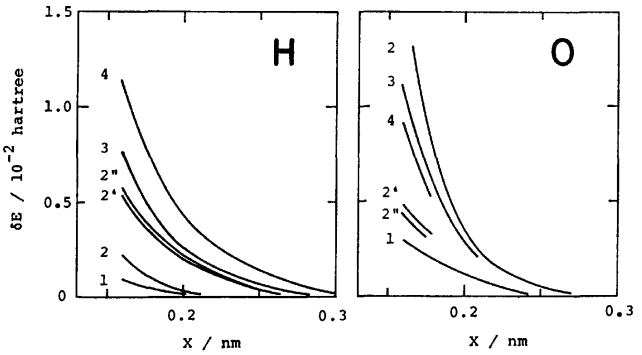

Fig. 5. The energy differences, δE, between the total energy change of fluoroethylene, ΔE(fluoroethylene), and that of ethylene, ΔE(ethylene) in units of hartree (1 hartree=627.51 kcal/mol) as functions of the distance, x, between attacking atom and fluoroethylene, $\Delta E = E(\text{at } x) - E(x \to \infty)$.[27]
1: C_2H_3F, 2: CH_2CF_2, 2′: *trans*-CHFCHF, 2″: *cis*-CHFCHF, 3: C_2HF_3, 4: C_2F_4.

the fluoroethylene. This property may be called approachability. As Fig. 5 shows, the approachability obtained with H atoms decreases with the increase in the number of substituted fluorine atoms, while that obtained with O atoms has a minimum with CH_2CF_2 molecule.

We can find some correlations between the calculated approachabilities and the rate constants obtained in the previous section. The other obtained with H atoms is in agreement with that of the rate constants. In the case of O atoms, the approachability calculated for C_2H_3F seems to be too large. In spite of the discrepancy, the general trend of the order of the rate constants may be said to be explicable by the calculated approachability.

Discussion

Comparison with Other Investigations. In Table 1, the relative rate constants of the reactions of hydrogen atoms with fluoroethylenes obtained by previous investigations are compared with those calculated from the present data. The results obtained by Kilcoyne and Jennings are in good agreement with our data, although our data are not complete because of the difficulty of obtaining *trans*- and *cis*-1,2-difluoroethylenes. The results of Penzhorn and Sandoval are quite different from those of the others.[20] Since possible reasons for this discrepancy have already been discussed by Kilcoyne and Jennings, it is unnecessary to restate them.

Table 2 compares the absolute rate constants of the reactions of oxygen atoms obtained by Huie *et al.*[21] and Gilbert *et al.*[19] with ours and the relative rate constants reported by Moss.[12] Serious disagreement is observed in the case of C_2F_4. For the reaction of $O+C_2H_3F$, Atkinson and Pitts reported 0.27 ± 0.03 in units of 10^{-12} cm^3 molecule^{-1} s^{-1}.[23] Our result seems to be too large. More extensive investigations on this reaction are now in progress. Recently, Koda discussed the absolute rate constant of the reaction of $O+C_2F_4$.[24] The rate constants he estimated are 0.83 and 1.30 in units of 10^{-12} cm^3 molecule^{-1} s^{-1}. Our result agrees with the smaller value. Further investigations are obviously desirable.

Reactivity Index. When Sato and Cvetanović carried out the simple Hückel MO calculation on a series of monoolefins,[25] they anticipated that the calculated parameters such as charge density, bond-order, free valence, or atom localization energy might correlate with the relative rate constants of the reactions of various active species with monoolefins. Actually, the relative rate constants of the reactions of oxygen atoms with monoolefins were found to be well correlated with the excitation energies and bond-orders calculated. When Jennings and Cvetanović determined the relative rate constants of the reactions of hydrogen atoms with a series of monoolefins, they found that these relative rate constants are well correlated with the atom localization energies of the monoolefins.[26] However, when Jennings and his colleagues applied these correlations to the relative rate constants obtained with fluoroethylenes, they failed to find clear correlations.[11] The substitution of fluorine atoms seems to induce an exceptional effect on the molecule.

In the above treatment, the parameters were calculated only on the olefins, one component of the reactants, and the attacking atoms were not included. So, we tried to include the attacking atoms in the calculation, and found some success. We believe that this success is somewhat fortuitous; more extensive investigations are necessary before definite conclusions are drawn from such calculations.

Table 1. Comparison of the relative rate constants of the reactions of H atoms with fluoroethylenes

Compound	PS[a]	KJ[b]	This work
CH_2=CH_2	1.00	1.00	1.00
CH_2=CHF	0.79	0.44	0.47
CH_2=CF_2	1.45	0.36	0.33
trans-CHF=CHF	1.15	0.09	
cis-CHF=CHF	0.70	0.06	
CHF=CF_2	1.65	0.05	0.082
CF_2=CF_2	1.70	0.08	0.075

a) PS: Penzhorn and Sandoval, Ref. 20. b) KJ: Kilcoyne and Jennings, Ref. 11.

Table 2. Comparison of the rate constants of the reactions of O atoms with fluoroethylenes (in units of 10^{-12} cm^3 molecule^{-1} s^{-1})

Compound	HHD	SGG	This work	Moss (Relative)
CH_2=CH_2			1.0	(1.00)[b]
CH_2=CHF	0.436	0.41	0.52	(0.38)
CH_2=CF_2		0.31	0.20	(0.22)
trans-CHF=CHF	0.448[a]	0.58		(0.54)
cis-CHF=CHF		0.37		(0.32)
CHF=CF_2	0.363	0.83	0.63	(0.57)
CF_2=CF_2			0.81	(1.60)

HHD: Huie, Herron, and Davis, Ref. 21; SGG: Slagle, Gutman, and Gilbert, Refs. 19 and 22. a) Mixture of *trans* and *cis*. b) Ref. 12.

The authors wish to express their thanks to Professor Nobuo Ishikawa of this Institute for the supply of fluoroethylenes, and also to Dr. Kazuo Shimokoshi of this Institute for allowing the use of the program for INDO calculation.

References

1) J. H. Lee, J. V. Michael, W. A. Payne, and L. J. Stief, *J. Chem. Phys.*, **68**, 1817 (1978).
2) K. Oka and R. J. Cvetanović, *Can. J. Chem.*, **57**, 777 (1979).
3) R. Atkinson and R. J. Cvetanović, *J. Chem. Phys.*, **56**, 432 (1972).
4) D. L. Singleton and R. J. Cvetanović, *J. Am. Chem. Soc.*, **98**, 6812 (1976).
5) R. Atkinson and J. N. Pitts, Jr., *J. Chem. Phys.*, **67**, 38 (1977).
6) R. Atkinson and J. N. Pitts, Jr., *J. Chem. Phys.*, **67**, 2492 (1977).
7) Y. Ishikawa, M. Yamabe, A. Noda, and S. Sato, *Bull.*

Chem. Soc. Jpn., **51**, 2488 (1978).
8) Y. Ishikawa and S. Sato, *Bull. Chem. Soc. Jpn.*, **52**, 984 (1979).
9) K. Sugawara, Y. Ishikawa, and S. Sato, *Bull. Chem. Soc. Jpn.*, **53**, 1344 (1980).
10) S. J. Moss and K.R. Jennings, *Trans. Faraday Soc.*, **65**, 415 (1969).
11) J. P. Kilcoyne and K. R. Jennings, *J. Chem. Soc., Faraday I*, **70**, 379 (1974).
12) S. J. Moss, *Trans. Faraday Soc.*, **67**, 3503 (1971).
13) J. A. Pople and D. L. Beveridge, "Approximate Molecular Orbital Theory," McGraw-Hill Book Co., New York (1970).
14) S. Nagase, T. Fueno, and K. Morokuma, *J. Am. Chem. Soc.*, **101**, 5849 (1979).
15) R. F. W. Bader, M. E. Stephens, and R. A. Gangi, *Can. J. Chem.*, **55**, 2755 (1977).
16) K. Yamaguchi, S. Yabushita, T. Fueno, S. Kato, and K. Morokuma, *Chem. Phys. Lett.*, **70**, 27 (1980).
17) R. J. Cvetanović, *Adv. Photochem.*, **1**, 115 (1963).
18) P. M. Scott and K. R. Jennings, *J. Phys. Chem.*, **73**, 1521 (1969).
19) J. R. Gilbert, I. R. Slagle, R. E. Graham, and D. Gutman, *J. Phys. Chem.*, **80**, 14 (1976).
20) R. D. Penzhorn and H. L. Sandoval, *J. Phys. Chem.*, **74**, 2065 (1970).
21) R. E. Huie, J. T. Herron, and D. D. Davis, *Int. J. Chem. Kinet.*, **6**, 521 (1972).
22) I. R. Slagle, D. Gutman, and J. R. Gilbert, 15th Int. Symp. Combust., Tokyo, Japan, 1974, p. 785.
23) R. Atkinson and J. N. Pitts, Jr., *Int. J. Chem. Kinet.*, **8**, 475 (1976).
24) S. Koda, *J. Phys. Chem.*, **83**, 2065 (1979).
25) S. Sato and R. J. Cvetanović, *J. Am. Chem. Soc.*, **81**, 3223 (1959).
26) K. R. Jennings and R. J. Cvetanović, *J. Chem. Phys.*, **35**, 1233 (1961).
27) The total energies calculated for the systems of O+C_2F_4, O+*trans*-CHFCHF, and O+*cis*-CHFCHF did not converge when x was larger than 0.18 nm. The order of these three compounds, therefore, was determined at $x=0.17$ nm.

The Precursors of Phenols Produced in the γ-Radiolysis of Aromatic Hydrocarbons in Liquid Carbon Dioxide

Hidetoshi KARASAWA, Rei YUGETA, Akira YAMAGUCHI, and Shin SATO*

Department of Applied Physics, Tokyo Institute of Technology, Ookayama, Meguro-ku, Tokyo 152

(Received July 17, 1980)

The γ-ray-induced oxidation of toluene in liquid carbon dioxide has been reinvestigated. In order to discuss the precursors of the main products: three kinds of cresols and benzyl alcohol, 1-butene was used as the scavenger of oxygen atoms. The formation of cresols and benzyl alcohol was well explained by the participation of two precursors: one is oxygen atoms and the other is ionic species, O^- or/and CO_3^- ions. The ratio of the *G*-value of oxygen atoms to that of the sum of O^- and CO_3^- ions initially formed was estimated to be 4 : 1 for pure liquid carbon dioxide. The spur model previously proposed was applied to explain the formation of O^- and CO_3^- ions.

The γ-ray induced oxidation of hydrocarbons in liquid carbon dioxide has been extensively investigated by two research groups. Sakurai and his collaborators used a stainless steel autoclave for γ-irradiation. In this a small amount of hydrocarbon was packed with a large amount of carbon dioxide, with a mole fraction larger than 0.9.[1-6] Using a series of methyl-substituted benzene as the substrate, they estimated the relative rate constants for the formation of the corresponding phenols and benzyl alcohols.[3] On the basis of these relative rate constants, they concluded that the precursors of these products are oxygen atoms.

On the other hand, our group used a small glass tube for γ-irradiation at low temperatures, usually −18 °C.[7-10] The mixing ratio of carbon dioxide to hydrocarbon was changed from 0 to 1, and the *G*-values of noncondensable products, mainly carbon monoxide, were measured, as well as those of condensable ones. In a previous paper,[10] we used a series of monoolefins as the substrate and measured the relative rate constants of the reactions of oxygen atoms with seven monoolefins. This estimate was made by measuring the *G*-values of the reaction products: epoxides, aldehydes, and ketones. In these experiments, the formation of several alcohols was also observed. We tentatively assigned these alcohols as the products in the reaction of ionic species with hydrocarbons.

Five years ago, we reported the formation of cresols and benzyl alcohol in the γ-radiolysis of toluene in liquid carbon dioxide, and suggested that the precursors of these products are O^- or/and CO_3^- ions, because the formation of these products was considerably suppressed by the addition of a small amount of sulfur hexafluoride, a well-known electron scavenger.[8] This suggestion is obviously contradictory to the conclusion reached by Sakurai *et al.* This paper will discuss this discrepancy and will estimate what percentage of the oxygen-containing products are formed from oxygen atoms and what percentage from ionic species.

In a previous paper,[11] we reported the γ-ray-induced oxidation of aromatic hydrocarbons in liquid dinitrogen oxide, and showed that the corresponding phenols and benzyl alcohols are produced through two processes: one is the reactions of oxygen atoms and the other is the reactions of ionic species, probably N_2O^- ions, followed by the neutralization reactions with aromatic hydrocarbon cations. A similar technique may be applied to discriminate the precursors in the reactions in carbon dioxide.

Carbon dioxide is known to be an electron scavenger, although the efficiency is much less than that of dinitrogen oxide;[12] however, CO_2^- ions cannot be the precursor for cresols. When this compound is used as the electron scavenger in the γ-radiolysis of cyclohexane, the formation of hydrogen is effectively suppressed, but the formation of carbon monoxide is not balanced by the decrease in the hydrogen yield, suggesting that the neutralization reaction between CO_2^- ions and hydrocarbon cations does not produce carbon monoxide and oxygen atom-added products.

Experimental

The experimental procedures were the same as those described in previous papers.[10,11]

Results

The *G*-values of carbon monoxide from the CO_2–toluene system are shown in Fig. 1 as a function of the electron fraction of CO_2; the values of oxygen-containing products are given in Fig. 2. The fractional yields of three kinds of cresols and of benzyl alcohol are plotted

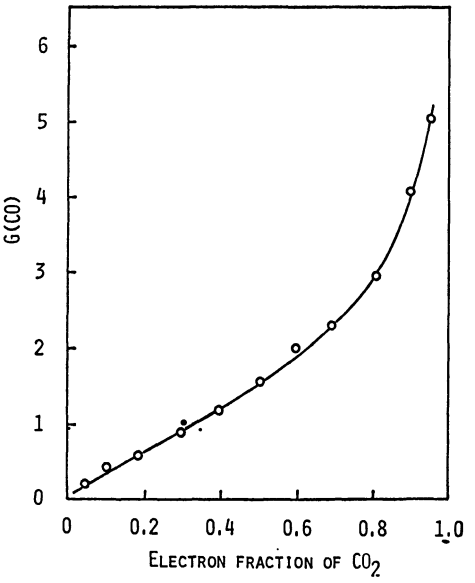

Fig. 1. The *G*-values of carbon monoxide from the toluene–CO_2 system.

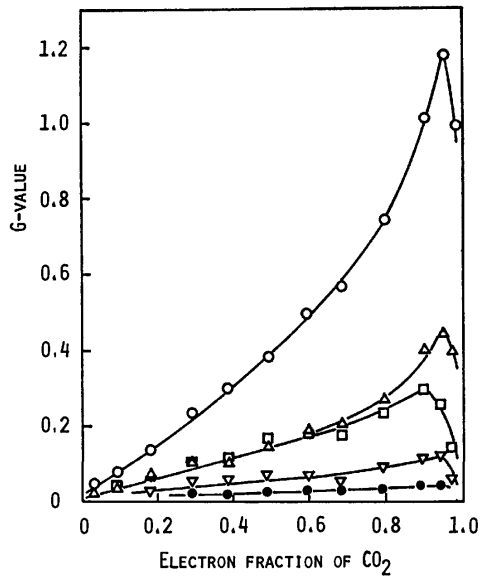

Fig. 2. The *G*-values of *o*-cresol (○), *p*-cresol (△), *m*-cresol (□), benzyl alcohol (▽), and phenol (●) from the toluene–CO_2 system.

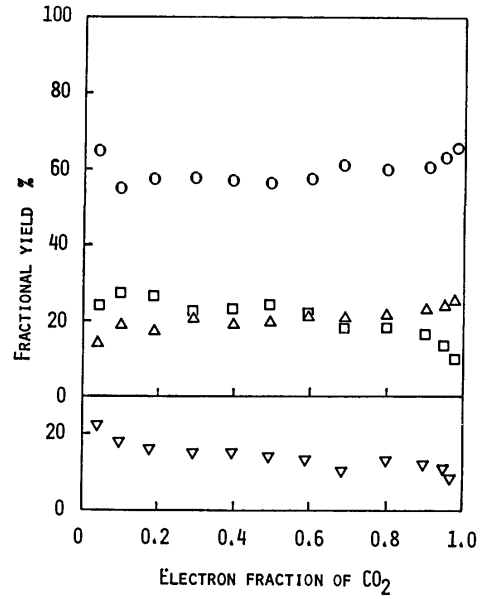

Fig. 3. The fractional yields of *o*-cresol (○), *p*-cresol (△), *m*-cresol (□), and benzyl alcohol (▽) against the sum of three cresols.

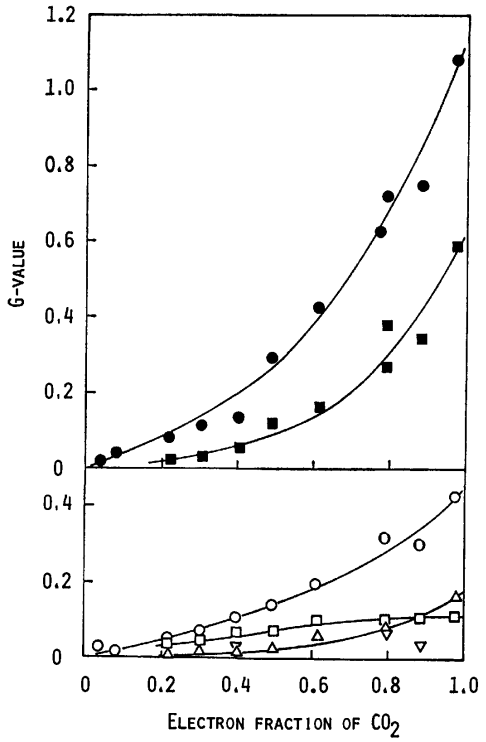

Fig. 4. The *G*-values of 1,2-epoxybutane (●), butanal (■), *o*-cresol (○), *p*-cresol (△), *m*-cresol (□), and benzyl alcohol (▽) from the toluene (0.9)–1-butene (0.1)–CO_2 system. The numbers in parentheses are the mole fractions of each hydrocarbon in the mixture.

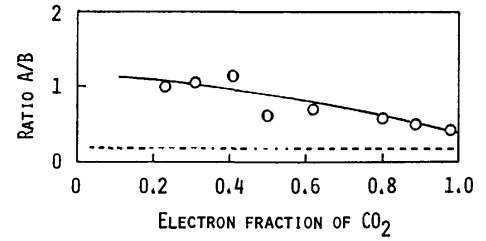

Fig. 5. The ratio of A/B as a function of the electron fraction of CO_2. A is the sum of the *G*-values of three cresols and benzyl alcohol, and B, the sum of the *G*-values of 1,2-epoxybutane and butanal. The dotted line shows 0.18. For this value, see the Text.

Table 1. The effect of sulfur hexafluoride on the γ-radiolysis of the toluene–CO_2 system
The electron fraction of CO_2 is 0.48.

Sulfur hexafluoride	*G*-value						
mol%	CO	H_2	*o*-Cresol	*p*-Cresol	*m*-Cresol	Benzyl alcohol	Bibenzyl
0	1.20	0.13	0.38	0.14	0.14	0.06	0.14
0.71	1.07	0.12					
2.29			0.08	0.02	0.06	0.06	0.36
3.99			0.06	0.02	0.06	0.07	0.40
4.46	0.79	0.12					
8.17	0.68	0.11					
9.10			0.03	0.01	0.03	0.07	0.50

$$CO_2 \rightsquigarrow CO + O \quad (1)$$
$$\rightsquigarrow CO_2^+ + e^- \quad (2)$$
$$[e^- + CO_2] \rightarrow CO_2^- \quad (4)$$
$$[CO_2^+ + CO_2^-] \rightarrow CO + O + CO_2 \quad (5)$$
$$[O + CO_2^-] \rightarrow CO_3^-. \quad (13)$$

The O and CO_3^- thus produced react with aromatic hydrocarbons to produce phenol.

In isolated spurs, the ratio of the amount of oxygen atoms, [O], initially produced, to that of ionic oxidizing species, $[O^-]+[CO_3^-]$, must be independent of the electron fraction of carbon dioxide since no reactions between active species are expected to occur; but in condensed spurs, this ratio should increase with the increase in the electron fraction, since Reaction 5 becomes important for the formation of oxygen atoms.

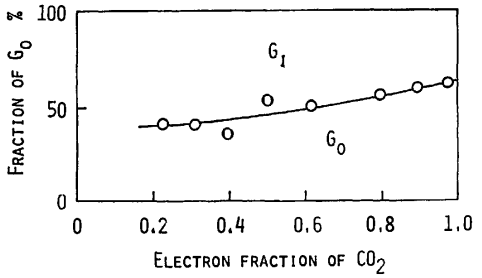

Fig. 6. The fractions of G_0 as a function of the electron fraction of CO_2. G_0 is the fraction of oxygen-containing products produced through the reactions of oxygen atoms with toluene, and G_1, the fraction of oxygen-containing products produced through ionic reactions.

Estimate of the Ratio of the G-value of Oxygen Atoms to That of the Sum of O^- and CO_3^- Ions. As has been discussed in a previous paper,[11] the fraction of 1,2-epoxybutane to the total consumption of oxygen atoms in the reaction with 1-butene is 0.42, while the fraction of oxygen-containing products to the total consumption of oxygen atoms in the reaction with toluene is 0.36. Moreover, we know that the ratio of k(O+1-butene)/k(O+toluene) is about 50, and that 1,2-epoxybutane is produced only in the reaction of oxygen atoms with 1-butene. From this knowledge, we can estimate the G-value of cresols (G_0) produced in the reaction of oxygen atoms with toluene in the CO_2–toluene system. Figure 6 shows the fraction of G_0 in the total G-value of oxygen-containing products observed, as a function of the electron fraction of carbon dioxide. This result suggests that more than 40% of cresols are produced by the ionic process in the entire range of the electron fraction of carbon dioxide.

On the other hand, the rate constant ratio of $k(N_2O^-+1\text{-butene})/k(N_2O^-+\text{toluene})$ was estimated to be 2.5,[11] and the fraction of oxygen-containing products in the total consumption of N_2O^- ions in the reaction with toluene was estimated to be 0.74. These values may be applicable to the reactions of O^- and CO_3^- ions in the present system. Then, we can calculate the ratio of the G-value of oxygen atoms to that of the sum of O^- and CO_3^- ions initially produced, by using the data shown in Fig. 4. The results are shown in Fig. 7; *i.e.*,

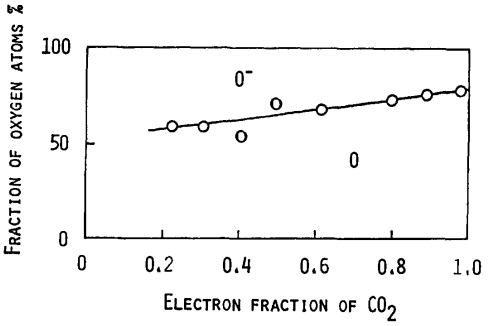

Fig. 7. The fractions of oxygen atoms in the total oxidizing species, O, O^-, and CO_3^-, initially produced in the γ-radiolysis of the toluene–CO_2 system.

$G(O) : G(O^-+CO_3^-)=4 : 1$ for the pure liquid carbon dioxide. With the decrease in the electron fraction of carbon dioxide, this ratio decreases and approaches 3 : 2 at the lower limit of the electron fraction of carbon dioxide.

Effect of Sulfur Hexafluoride. As Table 1 shows, the formation of cresols was considerably suppressed by the addition of a small amount of sulfur hexafluoride, which is known to be an effective electron scavenger. According to Fig. 6, even if all ionic processes should be inhibited, about 50% of cresols should remain as the product; however, this is not the case. We have no proper interpretation for this discrepancy, but we feel that sulfur hexafluoride is not simply an electron scavenger in the systems studied.

In the previous paper,[8] we suggested that cresols are formed only from the reactions of ionic species with toluene. This seems to be the result of a simplified interpretation of the electron scavenging effect of sulfur hexafluoride.

With the increase in the mole fraction of sulfur hexafluoride, the formation of bibenzyl became important. This increase may be due to the reactions of F atoms, which come from the electron scavenging of sulfur hexafluoride, with toluene to produce benzyl radicals.

The formation of bibenzyl is always observed in the radiolysis of toluene; however, the quantitative measurement for this product has not been made in the present experiments since no significant dependence of the G-value on the electron fraction of carbon dioxide has been observed in the absence of sulfur hexafluoride.

References

1) H. Sakurai, K. Akimoto, S. Toki, and S. Takamuku, *Chem. Lett.*, **1975**, 469.
2) A. Hori, S. Takamuku, and H. Sakurai, *J. Chem. Soc., Chem. Commun.*, **1976**, 686.
3) A. Hori, S. Takamuku, and H. Sakurai, *J. Org. Chem.*, **42**, 2318 (1977).
4) A. Hori, H. Matsumoto, S. Takamuku, and H. Sakurai, *J. Chem. Soc., Chem. Commun.*, **1978**, 16.
5) A. Hori, H. Matsumoto, S. Takamuku, and H. Sakurai, *Chem. Lett.*, **1978**, 467.
6) S. Goto, A. Hori, S. Takamuku, and H. Sakurai, *Bull. Chem. Soc. Jpn.*, **51**, 1569 (1978).
7) S. Sato, K. Hosoya, S. Shishido, and S. Hirokami, *Bull.*

Chem. Soc. Jpn., **45**, 2308 (1972).
8) K. Ishizaki and S. Sato, *Chem. Lett.*, **1975**, 123.
9) L. Wojnarovits, S. Hirokami, and S. Sato, *Bull. Chem. Soc. Jpn.*, **49**, 2956 (1976).
10) H. Karasawa, T. Sasamoto, R. Yugeta, and S. Sato, *Bull. Chem. Soc. Jpn.*, **52**, 902 (1979).
11) H. Karasawa, R. Yugeta, and S. Sato, *Bull. Chem. Soc. Jpn.*, **53**, 1479 (1980).
12) S. Sato, T. Terao, M. Kono, and S. Shida, *Bull. Chem. Soc. Jpn.*, **40**, 1818 (1967).
13) R. Atkinson and J. N. Pitts, Jr., *J. Phys. Chem.*, **79**, 295 (1975).
14) R. Atkinson and J. N. Pitts, Jr., *J. Chem. Phys.*, **67**, 38 (1977).
15) A. Mozumder and J. L. Magee, *Radiat. Res.*, **28**, 203 (1966).
16) K. Kowari and S. Sato, *Bull. Chem. Soc. Jpn.*, **51**, 741 (1978).
17) T. Saito and S. Sato, *Bull. Chem. Soc. Jpn.*, **42**, 2228 (1969).

An Analysis of the CF_2 Emission Spectrum in a CF_2Cl_2 Plus Metastable He System

Takahiko ISHIGURO,** Yoshiaki HAMADA, and Masamichi TSUBOI*
Faculty of Pharmaceutical Sciences, The University of Tokyo, Hongo, Bunkyo-ku, Tokyo 113
(Received May 23, 1980)

Ultraviolet chemiluminescence caused by a reaction of metastable He and CF_2Cl_2 was observed. Laser-excited single-vibronic-level fluorescence of the CF_2 radical thus produced was also examined. The main feature in the 250—400 nm region was explained as the CF_2 $\tilde{A}^1B_1$-$\tilde{X}^1A_1$ transition. The observed vibrational-level population of CF_2 ($\tilde{A}^1B_1$) resulting from this reaction exhibits a maximum near $v_2'=5$. This fact implies that the product has a FCF angle of about 104°, which is nearly equal to the FCF angle (105.4°) of the reactant (CF_2Cl_2) molecule, rather than to the equilibrium FCF angle (122°) of the CF_2 ($\tilde{A}^1B_1$) itself.

The difluorocarbene radical, CF_2, an important transient intermediate in fluorocarbon reactions, has been examined by a great number of reseachers.[2] In 1950 Venkateswarlu first observed an emission spectrum between 239.9 and 342.9 nm which was attributed to the CF_2 radical.[3] Its absorption spectrum in the 260 nm region was measured with high dispersion by Mathews in 1967.[4] According to his rotational analysis, the upper and lower electronic states corresponding to this band system are $^1B_1$ and $^1A_1$ respectively, and the molecule is bent with $r_0(CF)=1.32$ Å and $\angle FCF=122.3°$ in the ($^1B_1$) excited state and with $r_0(CF)=1.300$ Å and $\angle FCF=104.94°$ in the ground state. The absorption and emission spectra gave vibrational frequencies $\nu_2'=496$ cm^{-1} and $\nu_2''=668$ cm^{-1}.

Since then, a debate arose as to the location of the CF_2 triplet state, $\tilde{a}^3B_1$. Recently, Quach-Tat-Trung *et al.*[5] noted that an emission band system, 340—450 nm, found in the microwave discharge of CF_2X_2 (X=Cl, Br), probably belonged to the CF_2 $\tilde{a}^3B_1$-$\tilde{X}^1A_1$ transition. Shortly thereafter, however, Koda[6] observed a structured emission spectrum in the region 470—720 nm resulting from the reaction with $O(^3P)$ and CF_2=CF_2, and tentatively assigned this emission to the CF_2 $\tilde{a}^3B_1$-$\tilde{X}^1A_1$ phosphorescence transition. Unfortunately, their discussions are based upon a lower dispersion spectra, and the subject does not yet seem to be fully fixed.

We have observed, with a higher dispersion, an ultraviolet emission spectrum resulting from a reaction of a metastable helium atom and dichlorodifluoromethane CF_2Cl_2 ("freon 12") in a discharge flow system. A laser excited single-vibronic-level fluorescence of the CF_2 radical thus produced was also examined. From the results, a number of new pieces of information have been obtained on the reaction as well as on the CF_2 molecule itself. These will be reported below.

Our special attention has been focused on the FCF angle of the $CF_2(\tilde{A}^1B_1)$ molecule in the initial stage of the reaction, because its equilibrium FCF angle (122.3°) is dramatically different from the FCF angle (105.4°) of the reactant CF_2Cl_2 molecule.[21] A discussion on this point will be given, in the present paper, in more detail than those on other points.

Experimental

The arrangement of the experimental apparatus is shown in Fig. 1. Active species of helium were produced by microwave discharge with a magnetron (2450 MHz, 500 W). The discharge portion was made of a 15 mm i.d. (inside diameter) quartz tube, and the product was admitted into a reaction chamber made of a 40 mm i. d. pyrex tube. The reactant gas, that is CF_2Cl_2, was injected into the reaction chamber through a 0.5 mm i. d. pyrex tube at 15 cm downstream from the discharge portion. The reaction chamber was evacuated with a 500-liter/min mechanical pump.

The pressure in the reaction chamber was measured with a Pirani gauge. The pressure of CF_2Cl_2 was about 0.4 Torr (1 Torr=133 Pa), and the total pressure in the reaction chamber was about 1.0 torr. The helium gas was purified by

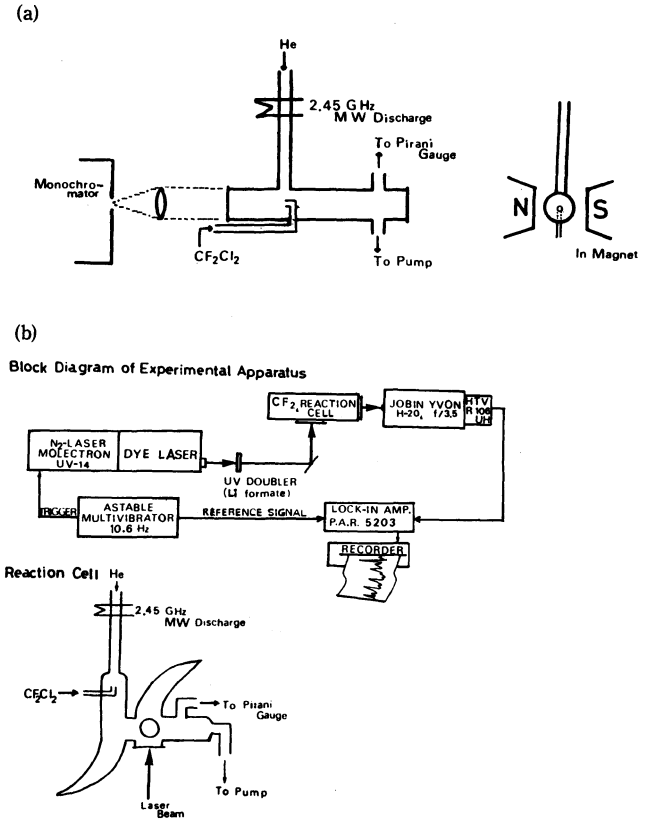

Fig. 1. Experimental set-up (a) for the observation of the CF_2Cl_2+He* chemiluminescence and (b) for the single-vibronic-level fluorescence measurement of CF_2.

** Present address: Todd Wehr Chemistry Building, Marquette University, Milwaukee, Wisconsin 53233, U.S.A.

passing it through a trap at 77 K before it was introduced into the discharge portion. The CF_2Cl_2 gas was purified by the trap to trap distillation method before use.

Emission spectra were observed through a quartz window by a 3.4 m (f) Jarrell-Ash spectrograph. The emission were photographically recorded with exposure times ranging from 8h to 15h on Kodak SA-1 film. The measurements of the spectra were also made by means of a photomultiplier (HTV R106 UH) with the aid of a lock-in amplifier (Princeton Applied Research Model-5203). In case of using the 1st-order diffraction of a 590 grooves/mm (300 nm blaze) grating, the reciprocal dispersion was 0.52 nm/mm. The higher dispersion spectra were also examined with the 2nd and 3rd order diffractions of other gratings.

In Fig. 1, the arrangement of the apparatus for a laser-excited single-vibronic-level (SVL) fluorescence is also shown. The flow of the $He^*+CF_2Cl_2$ reaction products was irradiated downstream from the mixing portion with a pulse laser beam, which was generated by a Molectron UV-14 dye laser system with a Li-formate frequency doubler. The SVL fluorescence was observed through a Jobin-Yvon H-20 monochromator with a HTV R106UH photomultiplier. By detecting the signal synchronized to the laser pulses, only the emission due to the laser excitation was selectively detected.

Results and Discussion

1. General Feature of the Chemiluminescence. The observed spectrum is shown in Fig. 2. Here vibrational bands are arranged in a long progression with the spacing 150 cm^{-1}. As will be detailed below, these bands are assignable to the $A^1B_1 \rightarrow \tilde{X}^1A_1$ transition of the CF_2 molecule. Besides these, the 0-0 transition of the CF $\tilde{A}^2\Sigma^+ \rightarrow \tilde{X}^2\Pi$ system[7] was observed in the vicinity of 247.6 nm (see also Fig. 3). The $\Delta v=0$ and $\Delta v=1$ transitions of the C_2 Deslandres-d'Azambuja system[8] were also observed near 385.2 and 360.7 nm, respectively (Fig. 4). The strong atomic line at 388.9 nm (Fig. 4) was attributable to the He $^3P \rightarrow {}^3S$ transi-

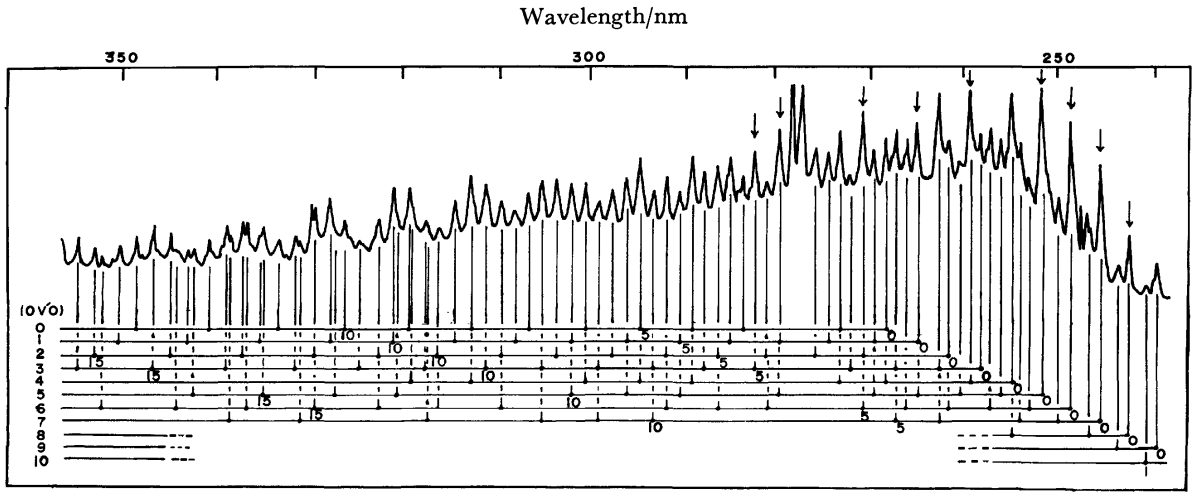

Fig. 2. Chemiluminescence spectrum of the $CF_2Cl_2+He^*$ system. Photo-trace of a spectrogram with a dispersion 0.52 nm/mm (the lst order diffraction from a 300 nm blaze 590 grooves/mm grating), with a slitwidth 20 μm, and with 8 h exposure. The arrows indicate bands for which K-subband structure were observed.

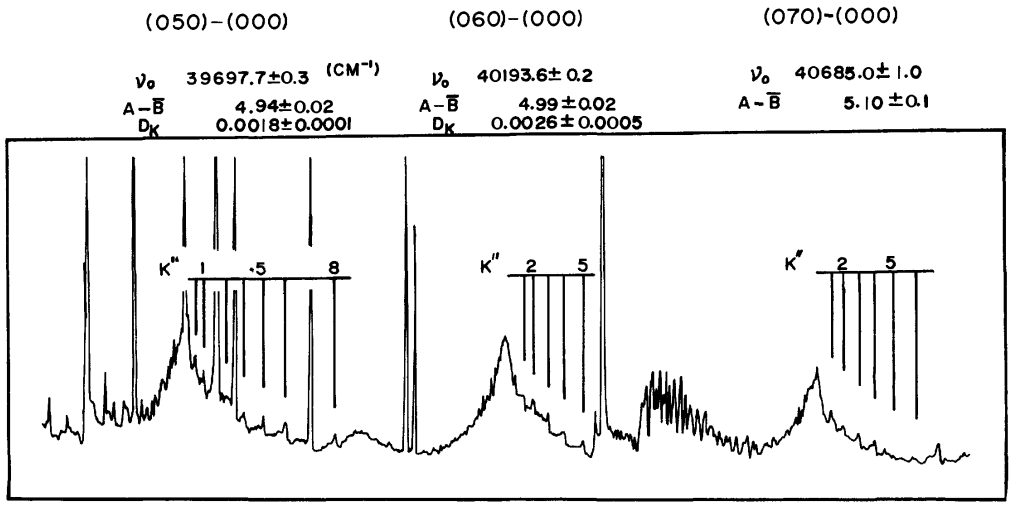

Fig. 3. Chemiluminescence spectrum of the $CF_2Cl_2+He^*$ system. Photo-trace of a spectrogram with a dispersion 0.17 nm/mm (the 3rd order diffraction from a 1000 nm blaze 590 grooves/mm grating) and slitwidth 100 μm.

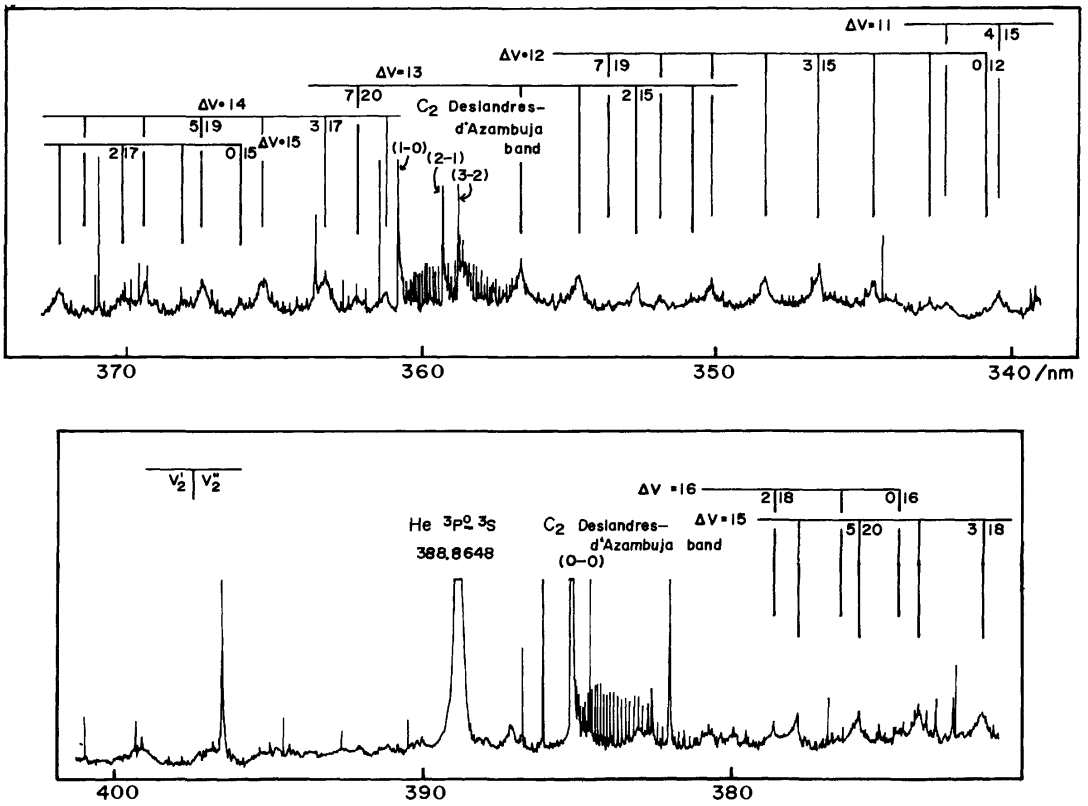

Fig. 4. Chemiluminescence spectrum of the CF_2Cl_2+He* system. Photo-trace of a spectrogram with a dispersion 0.24 nm/mm (the 2nd order diffraction from a 750 nm blaze 590 grooves/mm grating), with a slitwidth 20 μm, and with 13 h exposure.

tion.[9] It is certain that there is the metastable ^3S species involved in the reaction, which has by 19.8 eV higher energy than its ground state, and whose lifetime is a few second at 1 Torr.

2. Rotational Structures of the 2_0^5, 2_0^6, and 2_0^7 Bands. On the basis of a comparison with the absorption spectrum $\tilde{A}^1B_1 \leftarrow \tilde{X}^1A_1$ of CF_2 reported by Mathews,[4] the vibrational bands in the spectral region 240—270 nm, are all assignable to CF_2. In a higher dispersion (0.17 nm/mm) spectrogram (Fig. 3), a K-subband structure for $\Delta K=+1$ was found in each of the 2_0^5, 2_0^6, 2_0^7, and 2_0^8 bands. Here 2 means the ν_2 (bending) vibration and the super- and subscripts mean the vibrational quantum numbers of the upper and lower electronic states, respectively, in the transition. The peak positions ν_0^{sub} are fitted with the equation for a perpendicular-type transitions,

$$\nu_0^{sub} = \nu_0 + (A'-\bar{B}') + 2(A'-\bar{B}')K + [(A'-\bar{B}') - (A''-\bar{B}'')]K^2 - D_k'(K+1)^4 + D_k''K^4, \quad (1)$$

and the band center ν_0, the rotational constant $A'-\bar{B}'$, and the centrifugal distortion constant D_k' of the upper state have been determined as given in the upper part of Fig. 3. The $A''-\bar{B}''$ value for $v_2''=0$ was fixed at what Mathews determined[4] (2.5564 cm^{-1}). The $A'-\bar{B}'$ value (4.94±0.04 cm^{-1}) thus determined for $v_2'=5$ is in agreement with what was given by Mathews[4] (4.879±0.003 cm^{-1}) within our experimental error. The $A'-\bar{B}'$ values for $v_2'=6$ and 7 are now newly obtained. It has been found that $A'-\bar{B}'$ becomes greater with v_2'.

3. Vibrational Structure in the 270—360 nm Region. The vibrational bands in this spectral region are all explained as progression of the bending mode (ν_2) belonging to the same electronic transition $\tilde{A}^1B_1$-$\tilde{X}^1A_1$. The assignments are given in Fig. 2. By assuming that observed frequencies (ν) are given as

$$\nu = \nu_{00} + \nu' v_2' - \nu' x' v_2'^2 - \nu'' v_2'' + \nu'' x'' v_2''^2, \quad (2)$$

and by the use of the observed 81 transitions, the values of parameters, ν' (bending frequency in $\tilde{A}$), $\nu' x'$ (anharmonicity constant in $\tilde{A}$), ν'' (bending frequency in $\tilde{X}$), and $\nu'' x''$ (anharmonicity constant in $\tilde{X}$) were determined. The results are given in Table 1, where the deviations of the frequencies calculated on these parameters from the observed ones are also shown. These values explain the total of 135 vibrational transitions with quantum numbers $v_2'=0$—10, $v_2''=0$—17 in a whole region we observed.

4. Vibrational Structure in the 360—400 nm Region. The spectrum observed with a higher dispersion in this spectral region is illustrated in Fig. 4. The structure appears at first sight to be of different type from that in the 270—360 nm region. Actually, however, all the bands are explained by taking the ν_2 vibration in the $\tilde{A}^1B_1$ state of CF_2 into account; the observed frequencies here also fit with Eq. 2, as those in the 270—360 nm region. The apparent difference is found to be caused by the fact that the spectral region 360—400 nm involves greater Δv(=11—16) transitions whereas the 270—360

Table 1. Vibrational bands in the 270—360 nm region of the chemiluminescence

Observed frequency ν/cm^{-1}	v'	v''	Obsd—Calcd[a)]	v'	v''	Obsd—calcd[a)]	Observed frequency ν/cm^{-1}	v'	v''	Obsd—Calcd[a)]	v'	v''	Obsd—Calcd[a)]
41680.4	9	0	18.4				33078.2	1	7	6.4	5	10	−7.8
41500.6	10	1	−0.1				32908.6	2	8	−0.5	6	11	−21.9
41168.1	8	0	6.4				32752.1	3	9	3.6	7	12	−25.0
41002.5	9	1	3.1				32587.6	0	7	7.8	4	10	−2.3
40674.2	7	0	11.7				32422.2	1	8	6.1	5	11	−11.2
40451.2	8	1	−47.9				32250.6	2	9	−3.9	6	12	−28.3
40174.6	6	0	10.3				32103.7	3	10	8.9	7	13	−22.8
39950.5	7	1	−49.4				31911.7	0	8	−12.5	4	11	−25.6
39676.8	5	0	9.6				31816.2	1	9	54.7	5	12	−34.4
39473.3	6	1	−28.4					9	15	−11.5			
39323.1	7	2	−15.2				31591.0	6	13	−37.3			
39177.9	4	0	6.8	8	3	1.0	31566.8	2	10	−34.0			
39011.2	5	1	6.7	9	4	−6.3	31451.6	7	14	−25.2			
38844.1	3	2	4.0				31427.9	3	11	−14.3			
38690.9	3	0	20.9	7	3	13.3	31293.6	4	12	7.9			
38522.0	4	1	13.6	8	4	4.7	31264.8	0	9	−4.8			
38319.7	5	2	−23.2				31147.6	5	13	16.5			
38178.0	2	0	−4.0	6	3	−1.5	31100.8	1	10	−7.1			
38019.4	3	1	6.0	7	4	1.4	30953.5	2	11	5.3	6	14	−25.2
37680.4	1	0	−8.6				30745.3	3	12	−45.3			
37526.9	2	1	7.5	6	4	7.1	30657.0	8	16	−22.8			
37357.7	3	2	5.9	7	5	−1.7	30617.0	0	10	1.1			
37189.2	4	3	3.0	0	0	−7.9	30509.1	5	14	27.6			
37010.4	1	1	−16.0	5	4	−12.3	30460.4	1	11	5.2			
36892.1	2	2	34.3	10	8	1.7	30311.9	2	12	15.3	6	15	−18.1
36528.2	0	1	−6.3	4	4	1.6	30160.6	7	16	−20.0	3	13	20.6
36673.5	3	3	−17.7				30118.3	3	13	−21.7			
36362.4	1	2	−2.4	5	5	−1.7	29960.4	0	11	−3.9	4	14	−25.0
36204.8	2	3	7.7	6	6	1.2	29806.9	5	15	−26.0	1	12	3.3
35696.8	1	3	−7.4	5	6	−9.7	29789.8	1	12	−13.8	10	19	45.2
35539.2	6	7	−7.8				29659.9	6	16	−22.5			
35509.6	2	4	−27.9	6	7	−37.4	29626.8	2	13	−19.2			
35369.6	3	5	−3.3	7	8	−20.0	29514.8	7	17	−19.2			
35205.5	0	3	−6.8	8	9		29471.4	3	14	−19.0			
35040.3	1	4	−4.3				29317.6	0	12	5.9			
34878.9	2	5	0.0	6	8	−12.5	29177.9	5	16	−7.4			
34719.2	3	6	3.9				29131.7	1	13	−21.3			
34547.7	0	4	−4.9	4	7	−6.1	28999.4	6	17	−35.4			
34384.1	1	5	−1.8	5	8	−10.1	28972.8	2	14	−23.5			
34220.0	2	6	−1.3	6	9	−16.8	28823.1	3	15	−18.6			
34062.8	3	7	4.1	7	10	−18.5	28670.7	0	13	9.6			
33886.6	0	5	−7.4	4	8	−11.5	28531.1	1	14	27.7			
33719.9	1	6	−8.4	5	9	−19.7	28389.9	6	18	−0.3			
33558.7	2	7	−6.0	6	10	24.4	28328.1	2	15	−19.6			
33397.4	3	8	−5.7	7	11	−31.3	28175.2	3	16	−18.9			
33243.2	0	6	6.8	4	9	−0.3	28022.7	0	14	11.2	4	17	−19.8

a) Deviations of the frequencies calculated on Eq. 2, with $\nu_{00}=37197.1(\pm3.8)$ cm^{-1}, $\nu'=491.4(\pm1.4)$ cm^{-1}, $\nu'x'=-0.52(\pm0.16)$ cm^{-1}, $\nu''=663.1(\pm0.9)$ cm^{-1}, and $\nu''x''=0.50(\pm0.06)$ cm^{-1}.

nm region only smaller $\Delta v(\leqq 11)$ transitions. The observed frequencies are given in Table 2, with those calculated on the same set of parameters as what was used for the 270—360 nm region.

5. SVL Fluorescence of CF_2. This experiment was attempted to confirm the assignments so far made to the vibrational bands in the chemiluminescence spectrum. The $He^*+CF_2Cl_2$ reaction system was irradiated with a laser beam of 255.10 nm or 251.92 nm. The 255.10 nm beam is now known to correspond to the 2_0^4 transition of CF_2, and therefore should repopulate the $v_2'=4$ level of the $\tilde{A}^1B_1$ state of CF_2. Because the radiative lifetime of this level is 61 ± 3 ns,[10] which is much shorter than the vibrational relaxation time (at 1 Torr), a fluorescence only from this level (SVL fluorescence) should now be observed.

Table 2. Vibrational bands in the 340—380 nm region of the chemiluminescence (CF_2)

Observed frequency, ν/cm^{-1}	Assignment v'	Assignment v''	Obsd−Calcd[a] cm^{-1}
29303.7	4	15	−33.1
29164.6	5	16	−20.7
29120.8	1	13	−32.3
28972.9	2	14	−23.5
28830.1	3	15	−11.6
28687.3	4	16	−1.8
28553.4	5	17	14.8
28499.5	1	14	−3.9
28416.5	6	18	26.3
28296.0	2	15	−51.7
28224.1	7	19	−19.7
28159.2	3	16	−34.9
28008.9	4	17	−33.7
27680.2	2	16	−20.0
27611.7	7	20	11.6
27537.0	3	17	−10.5
27385.4	4	18	−11.5
27334.7	0	15	−28.1
27244.6	5	19	−3.8
27203.7	1	16	−3.4
27089.3	6	20	−12.6
27036.4	2	17	−17.1
26953.5	7	21	−4.0
26891.5	3	18	−10.3
26745.6	4	19	−6.7
26702.6	0	16	−12.6
26609.5	5	20	4.7
26569.6	1	17	9.1
26477.7	6	21	18.4
26421.4	2	18	13.6

a) Deviations of the frequencies calculated on Eq. 2, with the same values of the parameters: ν_{00}, ν', $\nu'x'$, ν'', and $\nu''x''$; as those used for the 270—360 nm region (Table 1).

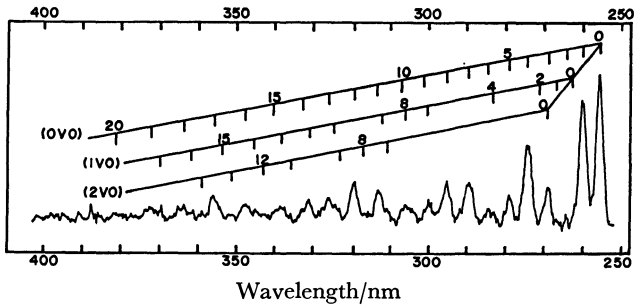

Fig. 5. A single-vibronic-level (SVL) fluorescence spectrum of CF_2, produced by the CF_2Cl_2+He* reaction. The ground state CF_2 molecule was excited to the $v_2'=4$ level of the electronic $\tilde{A}^1B_1$ state by a 255.10 nm laser beam, and the fluorescence spectrum was observed.

This is shown in Fig. 5. As is seen here, a long progression assignable to $2^4_{v''}$ (where $v''=0$, 1, 2, ···, 20) is found to cover the 240—400 nm region. Likewise, a long progression $2^5_{v''}$ was found on the 251.92 nm irradiation, which corresponds to the 2^5_0 excitation of this electronic system. These results support the idea that the He*+CF_2Cl_2 chemiluminescence is solely caused by the $\tilde{A}^1B_1$-$\tilde{X}^1A_1$ transition, not only in the 240—360 nm region but also in the 360—400 nm region.

After we have completed this SVL fluorescence experiment, a similar SVL work on CF_2 independently made by King *et al.*[10] was published. They prepared CF_2 in a different method from ours, but their SVL fluorescence spectra are in agreement with ours.

6. Effect of Magnetic Field. If there is any triplet-state contribution of CF_2 involved in the chemiluminescence spectrum, this would be detected by examining it in a magnetic field. With this expectation in mind, we have observed the chemiluminescence from the He*+CF_2Cl_2 system placed in a 5.3 kG magnetic field (see upper-right corner of Fig. 1). In the vibronic and ro-vibronic bands of CF_2, so far mentioned, however, detectable broadening or intensity shift, as was seen in the case of SO_2 and CS_2,[22] was not observed with our optical resolution of about 0.5 cm^{-1}. Thus, the assignments of these bands to the singlet-singlet transition ($\tilde{A}^1B_1$-$\tilde{X}^1A_1$) of CF_2 are again supported here. An appreciable effect has been found, on the other hand, in the relative amounts of the reaction products. In the magnetic field, all of the $\Delta v=1$ (1-0, 2-1, 3-2, and 4-3) C_2 systems appear as very strong series of lines, while in the spectrum without magnetic field many of these lines are buried in the CF_2 bands. As is shown in Fig. 6, the 247.6 nm band of CF becomes much stronger in the magnet; the intensity ratio of the CF(0-2) over CF_2(6-0) is doubled by the 5.3 kG field.

7. Intensity Distribution among the Vibrational Bands. Having established the assignments of practically all of the vibrational bands in the chemiluminescence

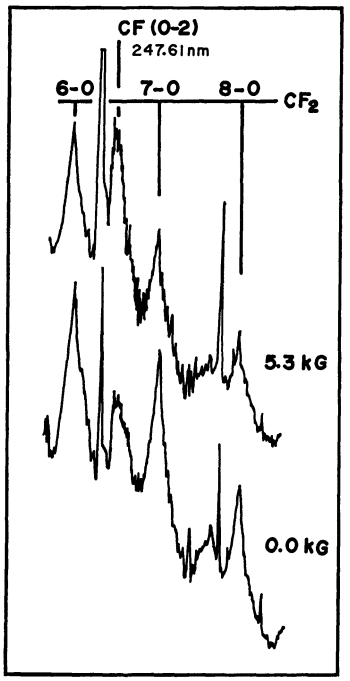

Fig. 6. Chemiluminescence spectrum of the CF_2Cl_2+He* system, with (5.3 kG) and without a magnetic field. Photo-trace of spectrograms with a dispersion 0.52 nm/mm and with a slitwidth 20 μm.

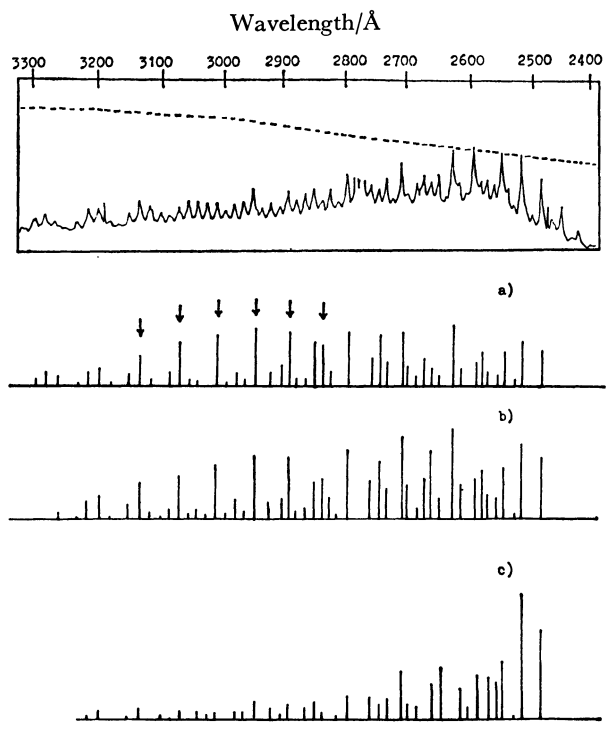

Fig. 7. Observed and calculated intensity distributions among the vibrational bands in the chemiluminescence spectrum of the CF_2Cl_2+He* system. Top: observed with a 3.4 m Jarrel-Ash spectrometer, a 300 nm blaze 590 grooves/mm grating (lst order), 100 μm (entrance) and 150 μm (exit) slitwidths, an HTV R106 UH photomultiplier, and a PAR 5203 lock-in amplifier. The broken line indicates the relative spectral sensitivity of the monochromator and photomultiplier system used in the measurement. Lower three: calculated on the assumptions that the population of the CF_2* molecules in each vibrational level in the excited electronic state $\tilde{A}^1B_1$ is given by a) the Boltzmann distribution at 2100 K, b) the Boltzmann distribution at 3000 K, and c) the distribution shown by the white circles in Fig. 8, which was reached by the least squares fit (that is detailed in the text). The arrows indicate the vibrational bands $2^0_{v''}$ ($v''=3$, 4, 5, 6, 7, and 8), whose intensities are too great on the assumption a) or b).

spectrum, we now proceed to an examination of their intensities. The relative intensities were determined by the use of photoelectronic detection system described above, and the results are shown in Fig. 7 (top). Theoretically, on the other hand, the intensity $I(v_2', v_2'')$ of the band corresponding to the $\tilde{A}^1B_1$, $v_2' \rightarrow \tilde{X}^1A_1$, v_2'' transition is given as

$$I(v_2', v_2'') \propto S(\nu)N(v_2')\nu^4|\langle v_2'|v_2''\rangle|^2, \qquad (3)$$

where $S(\nu)$ is the spectral response of the monochromator and detector system, $N(v_2')$ is the population in the vibrational $(0v_2'0)$ level of the electronic $\tilde{A}^1B_1$ state of CF_2, ν is the transition frequency, and $\langle v_2'|v_2''\rangle$ is the Franck-Condon overlap integral.

For $S(\nu)$, the efficiency-wavelength curve of the grating and spectral response of the photomultiplier (given by the manufacturer) were taken into account. The ultimate $S(\nu)$ value assumed here is given in Fig. 7, (top) with broken line. The $\langle v_2'|v_2''\rangle$ values were obtained primarily from the SVL fluorescence experiments of ourselves (Section 6) as well as of King *et al.*[10] Where the experimental values are not available ($v' \geqq 7$), however, the Franck-Condon overlap integrals were estimated by a calculation on the basis of the geometry and vibrational frequencies of the CF_2 molecule both in $\tilde{A}^1B_1$ and $\tilde{X}^1A_1$ states.[4] In the calculation, the effect of anharmonicity (detectable in the observed frequencies) was first taken into account. The effect, however, has been found to be very small on the Franck-Condon integrals; each perturbed eigenfunction was found to be practically equal to the corresponding unperturbed eigenfunction, the amount of contribution from other unperturbed eigenfunctions being less than 0.1%. Therefore, the effect has finally been ignored. The calculation was made in the two-dimensional space involving the symmetric stretching as well as the bending modes, in order to take a probable Duschinsky effect into acount.[11,12] The calculation was made by the method of Sharp and Rosenstock.[13] A computer program prepared by Professor A. J. Merer (University of British Columbia) was used after some modifications. To reach a proper set of vibrational modes we need a proper set of force constants. In the ground state $\tilde{X}$, this can be fixed by the use of the centrifugal distortion constants obtained by a microwave spectral study.[14] For the excited state $\tilde{A}$, the values of inertial defects[4] in the (000) and (010) states, $\Delta(000)=0.138$ amu·Å^2, and $\Delta(010)=0.314$ amu·Å^2, were used to fix the force constants, in combination with Oka-Morino equation[15] and Meal-Polo equation.[16]

Only the $N(v_2')$ values are now left unknown in Eq. 3. As a first trial, a Boltzmann distribution was assumed for $N(v_2')$. As may be seen in Figs. 7(a) and (b), however, this causes a serious disagreement between the observed intensity distribution and what is calculated on Eq. 3. The observed chemiluminescence spectrum indicates that relative value of $N(v_2'=0)$ is greatly lower than what is expected from a Boltzmann distribution.

8. Population Distribution $N(v_2')$ *among Vibrational Levels of a Nascent* CF_2*.* The relative values of $N(v_2')$ were next determined so as to reach the best fit between the observed intensity distribution among the vibrational bands (Fig. 7, top) and what is calculated on Eq. 3. What are obtained by a least squares method are shown in Fig. 8 with white circles. In this procedure, the values of $N(5)$, $N(6)$, $N(7)$, $N(8)$ are well fixed, because $2^{v'}_0$ bands with $v_2'=5$, 6, 7, and 8 are all well isolated from other bands. While, the uncertainties for the values of $N(0)$, $N(1)$, $N(2)$, and $N(4)$ are great (see the error bars in Fig. 8), because every $2^{v'}_{v''}$ band overlaps with $2^{v''+4}_{v''+3}$ band in the 280—323 nm region. Especially, the fixing of the $N(3)$ value was not found to be practical, because every $2^3_{v''}$ band overlaps with $2^7_{v''+3}$ band; here no experimental values are available of the Franck-Condon overlap integrals $\langle 7|v''+3\rangle$, and very reliable calculations for the Franck-Condon overlap integrals with higher v' and v'' are not practical.

In spite of such an ambiguity, however, it is now quite certain that the initial-state ($\tilde{A}^1B_1$) population $N(v')$ in the chemiluminescence, now in question, is

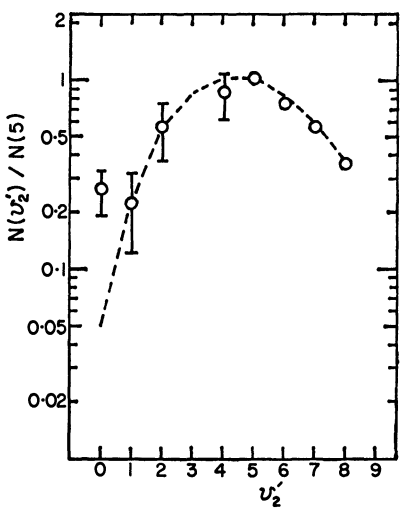

Fig. 8. The population of the CF_2^* molecules, produced by the CF_2Cl_2+He* reaction, in each vibrational level (v_2'=0, 1, ..., or 8) in the excited electronic state $\tilde{A}^1B_1$. White circle: determined by a least squares fit with the observed intensities of the vibrational bands in the 240—330 nm region of the CF_2Cl_2+He* chemiluminescence spectrum. Broken line: calculated on an assumption that the change from the CF_2 moiety of CF_2Cl_2 into CF_2^* (caused by a collision with He* and by throwing Cl_2 away) takes place according to the Franck-Codon priniciple, *i.e.*, vertically upward in the potential energy diagram with the FCF angle along the abscissa.

distributed among the vibrational levels with a great deviation from a Boltzmann distribution. Instead, it shows a maximum at v_2'=5. Since the radiative lifetime of the vibronic levels of the $\tilde{A}^1B_1$ state of CF_2 is 61±3 ns,[10] and since this is much shorter than the vibrational relaxation time ≈(5 μs) at 1 Torr, the population distribution $N(v')$ just found is considered to be exactly what is produced by the CF_2Cl_2+He* reaction.

9. On the CF_2Cl_2+He Reaction Mechanism.* The observed $N(v')$ *versus* v' relation (Fig. 7) is concerned with the mechanism of the CF_2^* production. The result suggests that the scission of the CF_2Cl_2 molecule into CF_2*+Cl_2* (caused by a collision with the metastable He*) takes place so rapidly that no vibration of the CF_2 moiety occurs during this process. The FCF angle of the ground-state CF_2Cl_2 molecule is 105.4±1.0° determined by microwave study[21] and this would tend to be retained in the product when the reaction is sufficiently rapid. This means that the product tends to have a greater population in a higher level of the bending vibration, because the equilibrium FCF angle of the product CF_2*(122°) is greatly different from 105.4°. Let us tentatively assume that the $CF_2Cl_2 \rightarrow CF_2$* change takes place according to the Franck-Condon principle.[17] By assuming that the CF_2 bending is a harmonic oscillation both in the reactant (ground state CF_2Cl_2 molecule) and the product (excited $\tilde{A}^1B_1$ CF_2 radical), and that their frequencies are 458[18] and 491 cm^{-1} (our value), respectively, one-dimensional Franck-Condon overlap (reactant-product) integrals were calculated. The squares of these integrals are to be compared with the observed populations $N(v')$. What were calculated (given in Fig. 8 by broken line) agree with the observed populations, if ΔQ_2 is assumed to be 0.88 Å $amu^{1/2}$. Here ΔQ_2 is the shift of the potential minimum in the bending normal coordinate Q_2 in the reactant (CF_2Cl_2) from that in the product (CF_2*). This ΔQ_2 value corresponds to a shift of about 18° in the FCF angle (*i.e.*, ∠FCF=122−18=104°); this is fairly close to what is expected in the simple model (the CF_2* and CF_2Cl_2 difference in ∠FCF is 122.3°−105.4°=16.9°).

Lastly, let us take a look at the energy balance in the reaction. On the basis of a thermochemical data,[19] approximately 8.8 eV is considered to be required to dissociate the CF_2Cl_2 molecule into CF_2 and Cl_2 and then to excite CF_2 up to CF_2*($\tilde{A}^1B_1$). Because He*($^3S_0$) has 19.8 eV, an excess energy of 2.6 eV is available, even if the Cl_2 molecule takes 8.4 eV to excite itself to $\tilde{D}^3\Pi_{1g}$.[20] The excess energy would be converted into the translational energy of the products (CF_2*+Cl_2*+He), so that Cl_2* would be rapidly removed from the CF_2* moiety after the reaction.

We wish to express our sincere thanks to Professor Saburo Nagakura, the University of Tokyo, for his kindness extended in our use of Jarrel-Ash spectrograph as well as for his valuable discussions. Our thanks are also due to Professor A.J. Merer, the University of British Columbia, for the computer program used in our calculation of two-dimensional Franck-Condon overlap integrals. This work was supported partly by a Grant-in-Aid for Scientific Research No. 354153 from the Ministry of Education, Science and Culture.

References

1) The present ariticle is a part of T. Ishiguro's Doctor Thesis, The University of Tokyo, Japan, 1980.
2) D. S. Y. Hsu, M. E. Umstead, and M. C. Lin, Fluorine Containing Free Radicals, Kinetics, and Dynamics of Reactions, A. C. S. Symposium Series (No. 66), American Chem. Soc., Washington (1978).
3) P. Venkateswarlu, *Phys. Rev.*, **77**, 676 (1950).
4) C. W. Mathews, *Can. J. Phys.*, **45**, 2355 (1967).
5) Quach-Tat-Trung, G. Durocher, P. Sauvageau, and C. Sandorfy, *Chem. Phys. Lett.*, **47**, 404 (1977).
6) S. Koda, *Chem. Phys. Lett.*, **55**, 353 (1978).
7) T. L. Porter, D. E. Mann, and N. Acquista, *J. Mol. Spectrosc.*, **16**, 228 (1965).
8) H. Kopfermann and H. Schweitzer, *Z. Phys.*, **61**, 87 (1930).
9) A. R. Striganov, N. S. Sventitskii, Tables of Spectral Lines of Neutral and Ionized Atoms, IFI/Plenum, New York (1968).
10) D. S. King, P. K. Schenck, and J. C. Stephenson, *J. Mol. Spectrosc.*, **78**, 1 (1979).
11) F. Duschinsky, *Acta Physicochim. URSS*, **1**, 551 (1937).
12) G. J. Small, *J. Chem. Phys.*, **54**, 3300 (1971).
13) T. E. Sharp and H. M. Rosenstock, *J. Chem. Phys.*, **41**, 3453 (1964).
14) W. H. Kirchhoff, D. R. Lide, Jr., and F. X. Powell, *J. Mol. Spectrosc.*, **47**, 491 (1973).
15) T. Oka and Y. Morino, *J. Mol. Spectrosc.*, **8**, 9 (1962).
16) J. H. Meal and S. R. Polo, *J. Chem. Phys.*, **24**, 1126 (1956).

17) J. F. Prince, C. B. Collins, and W. W. Robertson, *J. Chem. Phys.*, **40**, 2619 (1964).
18) T. Shimanouchi, Tables of Molecular Frequencies, Consolidated Vol. II, *J. Phys. Chem.*, Reference Data, **6**, (3) (1977).
19) E. N. Okafo and E. Whittle, *J. Chem. Soc., Faraday Trans. 1*, **70**, 1366 (1974).
20) G. Herzberg, "Spectra of Diatomic Molecules," Van Nostrand Company, Princeton, N. J. (1950), p. 519.
21) C. F. Su and E. L. Beeson, Jr., *J. Chem. Phys.*, **66**, 330 (1977).
22) A. E. Douglas, *Can. J. Phys.*, **36**, 147 (1958).

  Bull. Chem. Soc. Jpn., 54, 375—377 (1981)

Binding of Sodium Decyl Sulfate to a Cationic Polymer

Keishiro SHIRAHAMA,* Hidefumi YUASA, and Shinji SUGIMOTO

Department of Chemistry, Faculty of Science and Engineering, Saga University, Saga 840

(Received May 26, 1980)

Interaction between sodium decyl sulfate and a cationic copolymer of dimethyldiallylammonium chloride and sulfur dioxide was studied by a potentiometric method utilizing a surfactant-selective electrode. Binding occurs suddenly and is completed in a very narrow range of equilibrium concentration, indicating the strongly cooperative nature of the binding process. The characteristic concentration at which binding starts is about two orders of magnitude smaller than the critical micelle concentration. The cooperativeness parameters as estimated by a nearest neighbor interaction model remains almost constant on increasing sodium chloride concentration, affinity for an isolated binding site decreasing.

Surfactants are bound not only to two-dimentional interfaces, but also to linear polymers, *viz.*, synthetic nonelectrolytes such as poly(*N*-vinylpyrrolidone),[1] and poly(ethylene oxide),[2,3] and biological polyelectrolytes such as polypeptides,[4,5] and nucleic acid.[6] The binding process is characterized on a binding isotherm by remarkable cooperativeness: sudden occurrence and completion of binding in a very narrow range of equilibrium concentration.

The present study deals with the binding of an anionic surfactant, sodium decyl sulfate (SDeS), to a synthetic polycation as measured by potentiometry. The polyelectrolyte used is a copolymer of dimethyldiallylammonium chloride and sulfur dioxide with the following structure.[7] The polymer has proportionate hydrophobic character in addition to positive charge, being very stable around neutral pH. This polycation is considered to be a good model compound for examining the effect of electric charge and hydrophobicity in surfactant-polymer interactions. A surfactant-selective electrode was used for potentiometry.[5,8,9]

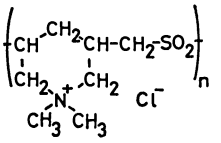

The results obtained were analyzed in the framework of one-dimentional nearest neighbor interaction model.[4,10]

Experimental

Materials. The polycation (Nittō Bōseki Co., Ltd., PAS-250, degree of polymerization≒800) was purified by dialysis against water for 3 days, the concentration being determined by colloid titration using poly(vinyl potassium sulfate) as a titrant and Toluidine Blue as an indicator.[11] Sodium decyl sulfate was synthesized by esterification of fractionally distilled 1-decanol with concentrated sulfuric acid followed by neutralization with sodium hydroxide. The crude surfactant was recrystallized once from acetone and twice from ethanol. The recrystallized sample was extracted with diethyl ether in a Soxhlet extractor for 40 h in order to remove trace of residual decanol. The critical micelle concentration (cmc) determined by an electric conductivity method was 32 mol m^{-3} in water at 25 °C.[12]

Potentiometry. The carrier used in the surfactant-selective electrode was prepared by suspending equivalent amounts of SDeS and dioctadecyldimethylammonium chloride (Kaō Soap Co., Ltd.,) in water. The resulting white precipitate (dioctadecyldimethylammonium decyl sulfate) was collected by centrifugation (3000 rpm for 30 min) and resuspended in distilled water. Decantation was repeated three times followed by recrystallization from acetone. A mixture of poly (vinyl chloride) (0.6 g) and tritolyl phosphate (2.4 g) was added to a tetrahydrofuran solution (15 cm^3) containing an appropriate amount of the carrier (0.25 mmol kg^{-1} membrane). The resulting mixture was heated (80 °C) to give a clear viscous solution which was then cast on a flat glass plate. The solvent was gradually evaporated in a desiccator for 2 d. The poly(vinyl chloride) gel membrane, *ca.* 0.3 mm thick, was put on one end of a poly(vinyl chloride) tube (i.d. 9 mm, length 11 cm), tetrahydrofuran being found to be a good adhesive. The electrode was annealed in a vacuum at 40 °C for 2 d. The electrode forms a concentration cell,

$$\text{Calomel} \left| \begin{matrix} 1\ \text{mol dm}^{-3} \\ NH_4NO_3 \end{matrix} \right| \begin{matrix} 0.5\ \text{mol m}^{-3}\ \text{SDeS} \\ 20\ \text{mol m}^{-3}\ \text{NaCl} \end{matrix} \left| \begin{matrix} \text{PVC gel} \\ \text{membrane} \end{matrix} \right|$$

$$\left| \begin{matrix} C_s\ \text{SDeS} \\ C_a\ \text{NaCl} \end{matrix} \right| 1\text{mol dm}^{-3}\ NH_4NO_3 \left| \text{Calomel} \right.$$

The electrode was treated in 1 mol m^{-3} SDeS solution for *ca.* 30 min before each run. Potentiometric titration was carried out in a small cocylindrical cell (25 cm^3) thermostated at 25 °C. The electromotive force was measured with an electrometer (Takeda Riken TR-8651) equipped with a paper recorder.

Results and Discussion

The surfactant-selective electrode shows the Nernstian response above 0.2 mol m^{-3} SDeS, slightly deviating from it at lower concentration. The reproducibility is so good that an emf *vs.* log C_s (C_s: SDeS concentration) plot can be used as a calibration curve. A potentiometric curve deviates from the calibration curve when the polymer exists in a solution (Fig. 1) where ΔC is the amount of SDeS bound to the polymer, C_f the corresponding equilibrium concentration. The binding isotherms thus constructed in three NaCl concentrations at 25 °C are shown in Fig. 2, where X (number of bound SDeS/number of cationic groups on polymer) is the degree of binding. The tendency that X becomes unity with increase in equilibrium concentration indicates that binding sites are primarily the cationic groups. Binding occurs all of sudden and concludes within a narrow range of C_f indicating cooperative effect. The isotherm shifts to a higher C_f with increase in the added

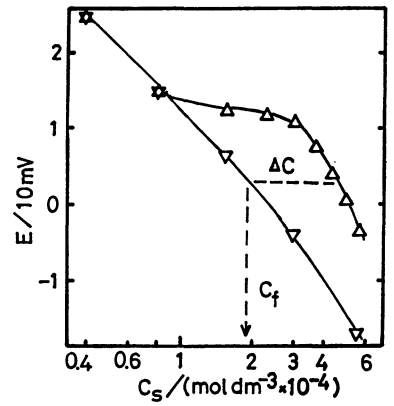

Fig. 1. Emf. *vs.* SDeS concentration plot.
NaCl concentration: 20 mmol dm^{-3}, the polymer concentration: 0.3 mmol dm^{-3} as cationic groups, temperature: 25 °C.

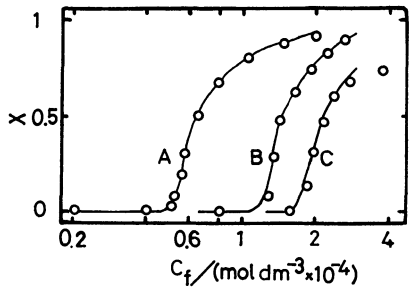

Fig. 2. Binding isotherms of SDeS–PAS systems at 25 °C.
X: degree of binding, C_f: free SDeS concentration, NaCl concentration: A; 20, B; 50, C; 100 mmol dm^{-3}.

electrolyte, C_a, the surfactant becomes less affinitive. This can be analyzed in terms of the Ising model with the nearest neighbor interaction.[4,10]

Let us consider a system where a polymer molecule binding surfactant molecules is in equilibrium with the surfactant whose equilibrium concentration is C_f. The partition function Z, for the system is

$$Z = (1,1)\begin{pmatrix} 1 & 1 \\ s/u & s \end{pmatrix}^n \begin{pmatrix} 1 \\ 0 \end{pmatrix}, \quad (1)$$

where s ($=KuC_f$) is a sort of binding "*pressure*," K being a binding constant of a surfactant molecule bound to an isolated binding site on a polymer molecule, u a parameter of interaction between adjacently bound surfactants, or a cooperativeness parameter, and n the number of binding sites on a polymer molecule.[10] Equation 1 furnishes various useful quantities such as[4]

$$K = 1/[uC_f(0.5)], \quad (2)$$

and

$$(\mathrm{d}X/\mathrm{d}\ln C_f)_{X=0.5} = \sqrt{u}/4. \quad (3)$$

In Eq. 2, $C_f(0.5)$ is an equilibrium concentration at X=0.5. The parameters derived from Eqs. 2 and 3 are given in Table 1.

Table 1. Binding parameters

C_a/mol dm^{-3}	0.02	0.05	0.10
u	25.6	26.3	26.1
K/mol^{-1} dm^3	601	271	180
K'/mol^{-2} dm$^6\times10^3$	30.1	5.42	1.80

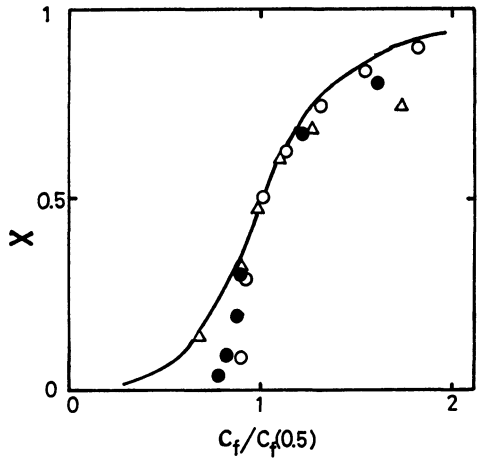

Fig. 3. X *vs.* C_f/C_f (0.5) plot.
NaCl concentration: ○ 20, ● 50, △ 100 mmol dm^{-3}, u=26.

We see how the parameters fit the experimental data in Fig. 3, where X is plotted against $C_f/C_f(0.5)$ (*cf.* Eq. 15 in Ref. 4). The value of K decreases with increase in sodium chloride concentration, u remaining nearly constant. The decrease in the binding affinity should be even steeper, since contribution from the counterions should be taken into account in the binding process of an electrolyte. Ionic product C_fC_a in place of C_f in $s=KuC_f$ and therefore in Eq. 2 should be used. A new equilibrium constant is defined by $K'=K/C_a$ (Table 1). The steeper decrease in K' than K reflects a substantial shielding effect of electrostatic potential of the polymer which overwhelms the effect by the increase in sodium chloride concentration. It is enlightening to compare the characteristic concentration, C_t, at which binding starts, of a nonelectrolytic polymer, poly(ethylene oxide)-SDeS system with that of the present system. C_t was deduced to be about 13 mol m^{-3} for the former[3] and 0.16 mol m^{-3} for the latter, both in 0.1 mol dm^{-3} NaCl. By consideration of free energy we find that the polycation binds SDeS more strongly than poly(ethylene oxide) does by $\Delta G_e=-kT\ln(13/0.16)=-4.4\,kT$. If the free energy is entirely ascribed to an electrostatic term, we have $\Delta G_e=ze\phi$ with ϕ=133 mV. This potential difference might be high, but not unrealistic for ordinary polyelectrolytes.[13] Hydrophobic interaction should be included since the hydrophobicity of the polycation is larger than that of poly(ethylene oxide).

The parameter u changes little in contrast with the drastic change in K'. Once bound onto the polycation, surfactants are scarcely influenced by electrostatic potential, and interact one another through short-range interaction. The parameter u is defined by

$$u = (11)(00)/(01)(01), \quad (4)$$

where (01) denotes the number of bound surfactants on isolated binding sites, (11) that of surfactants bound side by side, and (00) the number of unoccupied sites (*cf.* Eq. 10 in Ref. 4). u is an equilibrium constant for an aggregation process of surfactants on the polymer. The corresponding free energy is

$$\Delta G^\circ = -kT\ln(u) = -3.3\,kT. \quad (5)$$

ΔG° is divided by the free energy of transfer of a methylene group ($1.32\,kT$),[14] to give $m=3.3/1.32=2.5$. It is presumed that the strong cooperativeness is brought about by mutual contact of certain 2—3 methylene groups of adjacently bound surfactants. Takagishi *et al.* reported that anionic dye, Methyl Orange and its homologs are bound to the same polycation in such a way as to give Klotz plots which are quite straight.[15] This indicates that there is no interaction amoung bound dye molecules. Shorter and stiff molecular structures of these dyes are not susceptible to mutual contact on the polycation, longer and flexible decyl chain being ready to interact.

In conclusion, electrostatic force enhances binding and surfactans are anckored on charged groups on the polycation with subsequent interaction between alkyl chains giving rise to marked cooperativeness.

The samples were kindly supplied by Nittō Bōseki Co. Ltd., and Kaō Soap Co., Ltd.

References

1) H. Arai, M. Murata, and K. Shinoda, *J. Colloid Interface Sci.*, **37**, 223 (1971).
2) K. Shirahama, *Kolloid Z. Z. Polym.*, **252**, 978 (1974).
3) K. Shirahama and N. Ide, *J. Colloid Interface Sci.*, **54**, 450 (1976).
4) I. Satake and J. T. Yang, *Biopolymers*, **15**, 2263 (1976).
5) I. Satake, T. Gondo, and H. Kimizuka, *Bull. Chem. Soc. Jpn.*, **52**, 361 (1979).
6) R. Chatterjee and D. K. Chattoraj, *Biopolymers*, **18**, 147 (1979).
7) S. Harada and M. Katayama, *Makromol. Chem.*, **90**, 177 (1966).
8) S. G. Cutler, P. Mears, and D. G. Hall, *J. Electroanal. Chem.*, **85**, 145 (1977).
9) S. G. Cutler, P. Mears, and D. G. Hall, *J. Chem. Soc. Faraday Trans. 1*, **74**, 1758 (1978).
10) G. Schwarz, *Eur. J. Biochem.*, **12**, 442 (1970).
11) R. Senju, "Koroido Tekiteihō," Nankōdō, Tokyo (1969).
12) P. Mukerjee and K. J. Mysels, "Critical Micelle Concentrations of Aqueous Surfactant Solutions," U. S. Government Printing Office, Washington, D. C. (1971).
13) C. Tanford, "Physical Chemistry of Macromolecules," John Wiley Inc. (1961), p. 457.
14) Taken from the difference in free energy of transfer for a methylene group from water to hydrocarbon between hexanol and pentanol, *cf.* R. Aveyard and R. W. Mitchell, *Trans. Faraday Soc.*, **65**, 2645 (1969).
15) T. Takagishi, Y. Nakata, and N. Kuroki, *J. Polym. Sci., Polym. Chem. Ed.*, **12**, 807 (1974).

Electronic Structures and Spectra of the Enol Form of Some β-Diketones

Hiroshi MORITA* and Hiroshi NAKANISHI†

The Institute for Solid State Physics, The University of Tokyo, Roppongi, Minato-ku, Tokyo 106

(Received May 29, 1980)

Near and vacuum UV absorption spectra have been measured with benzoylacetone (BA), dibenzoylmethane (DBM), and 3-phenyl-2,4-pentanedione (PPD) in heptane, in acetonitrile, and in ethanol at room temperature. Theoretical analysis of the spectra with the aid of the composite molecule method clearly shows that the π-electron interaction between the enol ring and the benzene ring is rather strong in BA and DBM, but is weak in PPD. The charge-transfer (CT) bands from the benzene ring to the enol ring are observed at 44000 cm^{-1} in BA, at 40000 and 44000 cm^{-1} in DBM, and at 41500 and 43800 cm^{-1} in PPD. The electronic structure of the enol form of malonaldehyde has been elucidated by a modified CNDO-CI method; the result indicates the first and second σ-σ^* excited states predicted at 8.76 and 9.35 eV being the CT band pertinent to the intramolecular hydrogen-bonding.

Keto-enol tautomerism of β-diketones (1,3-propanediones)[1,2] has been studied by IR[3-9] and NMR[10-12] spectroscopies, special attention being paid to solvent and substituent effects on intramolecular hydrogen-bonding (H-bonding) and on chelating ability to a transition-metal atom in forming coordination compounds.[12-15] From the IR and NMR studies[6,10,12] benzoylacetone (BA), dibenzoylmethane (DBM), 3-phenyl-2,4-pentanedione (PPD), and malonaldehyde (MA) (Fig. 1) are shown to exist predominantly (90—100%) as *cis*-enol form (which has strong intramolecular H-bonding) in pure liquid and in nonpolar solvents.

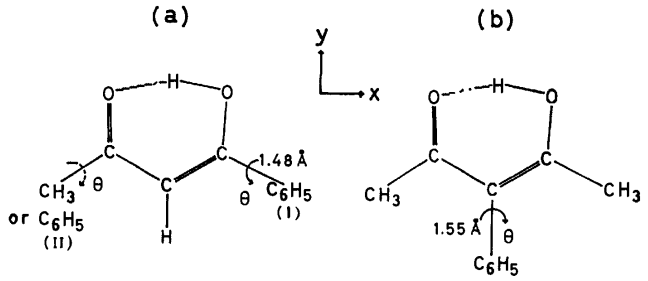

Fig. 1. Molecular structure and parameters for (a) BA and DBM, and (b) PPD. The structure of the enol ring is taken to be the same to the one of MA.

Although the electronic absorption spectra of β-diketones[16-20] and of their chelate compounds[13,17,19,21] have been measured extensively in the visible and near UV regions, the interpretation of the absorption spectra is rather qualitative. As for the simplest β-diketone, *i.e.*, MA, many theoretical calculations[22-25] have been done to investigate molecular geometry and electronic structure in the ground state, special attention being paid to the strong intramolecular H-bonding. Combined with the experimental value of $R(O\cdots O)=2.55$ Å determined by microwave spectroscopy,[26] theoretical results support the molecular geometry of C_s symmetry (asymmetrical H-bond) rather than of C_{2v} symmetry (symmetrical H-bond) in the ground state. Theoretical and experimental investigations of excited states of MA are few.[27,28] Excited states of MA are of particular interest in respect to charge-transfer (CT) character pertinent to H-bond as in the case of acetylacetone (acac) and its fluoro derivatives.[29,30] The elucidation of the CT character in the excited states is the first purpose of the present paper.

Phenyl-substituted β-diketones such as BA, DBM, and PPD are expected to have π-electron interaction between the enol ring and the benzene ring.[6,11,18] To interprete electronic structure of such large molecules, near and vacuum UV absorption spectra have been measured, and π-electron structure has been investigated by the method of composite molecule.[31,32]

Experimental

BA, DBM, and PPD (Tokyo Kasei G. R. grade) were purified by repeated recrystallizations from ethanol and finally by vacuum sublimation. Acetonitrile and heptane (Dotite spectrograde), and ethanol (Wako S. S. grade) were used as solvents without further purification.

Near UV absorption spectra were measured with a Cary recording spectrophotometer model 14, and with a Hitachi recording spectrophotometer model 556, a cell of 1.05 mm light path length being used. Vacuum UV absorption spectra were measured with a spectrophotometer constructed in our laboratory,[30,33] a cell of 0.134 mm light path length being used.

Theoretical

The electronic structure of MA was calculated by a modified CNDO-CI method.[34] The semiempirical parameters of H, C, and O atoms were taken to be the same as reported previously.[30,34] The electronic structures of the π-electron systems for the enol form of BA, DBM, and PPD were calculated by the method of composite molecule[31,32] by considering the configuration interaction (CI) among the ground, locally excited (LE), and CT configurations constructed from π-MO's of benzene[32] and MA (corresponding to the enol ring) calculated above. The four LE configurations ($^1B_{2u}$, $^1B_{1u}$, and $^1E_{1u}$) of the benzene ring and the lower two LE configurations (denoted as ϕ_1 and ϕ_2) of the enol ring were taken into account. The energies of the LE configurations were evaluated from the observed transition energies of benzene (4.86 and 6.08 eV in heptane,[35] 6.98 eV in the vapor phase[32]), of acac (4.56 and 7.04 eV in perfluorohexane[29]), and of MA (5.08 eV in ethanol,[28] 7.87 eV calculated in the present

† Present address: Toshiba Research and Development Center, 1, Toshiba-cho, Komukai, Saiwai-ku, Kawasaki 210.

paper (Table 4)) combined with the electrostatic interaction energies between excited configuration of the benzene ring and the ground configuration of the enol ring.

Concerning the combination of each of the benzene rings with the enol ring, four CT (from benzene to the enol ring) and four back CT (from the enol ring to benzene) (BCT) configurations were considered. Their energies were evaluated by the usual formula;[31,32] $I-A-Q$, where I is the ionization potential of electron donor, A, the electron affinity of electron acceptor, and Q, the electrostatic energy between electron donating and electron accepting MO's including electrostatic interaction energy between the ground configuration of the enol ring and the vacant MO's of the benzene ring. Ionization potentials were taken from the study by photoelectron spectroscopy of benzene,[36] acac,[37,38] and MA.[38] The electron affinity was taken to be −1.0 eV for the benzene ring,[32] and assumed for the lower two vacant π-orbitals of the enol ring to be 0 eV and −2.4 eV in both BA and DBM, and to be 0.5 eV and −1.9 eV in PPD. Two-center Coulomb repulsion integrals necessary for the evaluation of Q were calculated by the use of Klopman's equation.[34,39]

The resonance integral, β, in the off-diagonal matrix elements[31,40] of the total electronic Hamiltonian was considered only to the C–C bond between the benzene ring and the enol ring by the formula, $\beta=9.73\times S$, where S is the overlap integral between the 2pπ AO's of bonded C atoms.

The full matrices (15×15 for BA and PPD, 27×27 for DBM) of the total electronic Hamiltonian were solved to obtain energy levels and wave functions of the whole molecules. Oscillator strength for each absorption band was calculated by taking transition dipole moments between all pairs of the configurations into account. Each transition moment was evaluated including all the terms up to the first order in overlap, S.

The bond lengths and bond angles of MA were taken from the *ab initio* calculations by Karlström, *et al.*[24] and by Del Bene and Kochenour,[25] respectively. The O···O distance was taken to be 2.55 Å from the analysis of microwave spectrum,[26] and the position of the hydrogen-bonded hydrogen atom, from the X-ray crystal analysis of DBM.[41]

In BA, DBM, and PPD, the benzene ring(s)[41] with r(C–C) = 1.389 Å is(are) bonded to the enol ring through the C–C bond(s) of 1.48 Å in BA and DBM,[41] and of 1.55 Å in PPD. The angle, θ, between the planes of the enol ring and the benzene ring was treated as a variable in the actual calculations. As is shown in Fig. 1, BA is enolized toward the phenyl group.[6]

Results and Discussion

Near and Vacuum UV Absorption Spectra of BA, DBM, and PPD. Near and vacuum UV absorption spectra observed with the heptane solutions of BA, DBM, and PPD are shown in Fig. 2. The spectra measured in ethanol and acetonitrile show only a slight shift of the bands, and are essentially the same as the spectra of the corresponding molecules in heptane. The observed band positions and intensities are tabulated in Tables 1—3. As pointed out by the NMR[10,12] and IR[6] spectroscopic studies, the β-diketones under considerations predominantly exist as the *cis*-enol form at room temperature. The spectra shown in Fig. 2 and Tables 1—3 are due to the enol form. Compared to the spectrum of acetylacetone reported previously,[29] the first allowed band at ≈300 nm shifts to longer wavelengths with increasing intensity in the order of acac ≲PPD<BA<DBM.

Electronic Structure of MA. Preliminary calculations of MA have been done on the basis of different

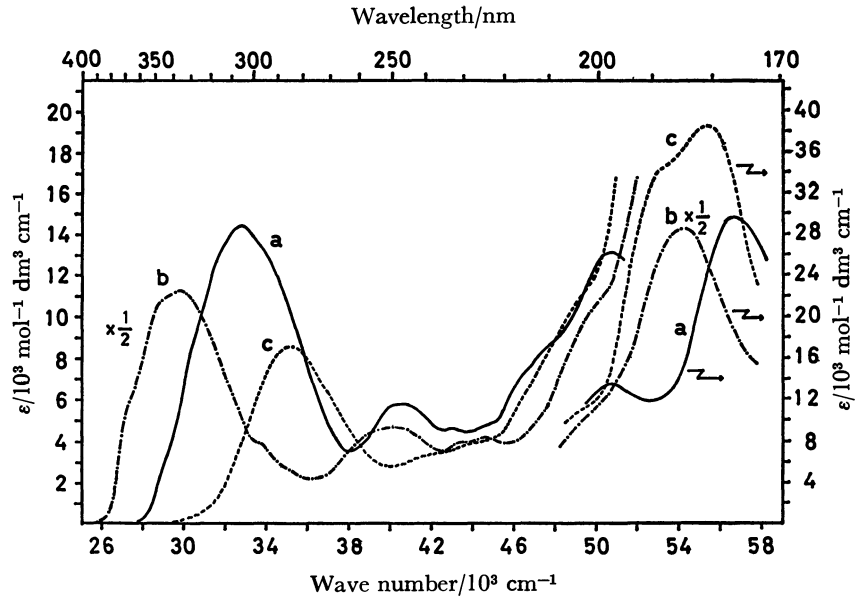

Fig. 2. Near and vacuum UV absorption spectra measured with the heptane solution of (a) BA, (b) DBM, and (c) PPD at room temperature. Absorption intensity of DBM is plotted as one half of the observed one.

TABLE 1. TRANSITION ENERGIES ($^1\Delta E$ (eV or cm^{-1})) AND OSCILLATOR STRENGTHS (f) OBSERVED AND CALCULATED FOR BENZOYLACETONE (BA)

In heptane			In acetonitrile	In ethanol	Calcd			Assignment
$^1\Delta E$ / cm^{-1}	$^1\Delta E$ / eV	f[a]	$^1\Delta E$ / eV	$^1\Delta E$ / eV	$^1\Delta E$ / eV	f	Main config.[b]	
32700	4.06	0.38	4.04	4.03	4.52	0.877	ϕ_1	LE
					4.80	0.017	B_{2u}	LE
40500	5.02	0.10	5.04	5.01	5.60	0.094	15←2+ϕ_1+B_{1u}	LE+CT
43000	5.33	0.06	5.37	5.37	6.02	0.152	15←3	CT
44500	5.52		5.56	5.56				
46100[c]	5.71	0.11	5.71	5.71	6.60	0.242	B_{1u}	LE
47400[c]	5.88				7.00	0.080	14→5+ϕ_2	LE(+BCT)
50800	6.29	0.24	6.28	6.23	7.18	0.233	14→4	BCT
					7.55	0.536	E_{1u}+E'_{1u}	LE
56500	7.00	0.63			7.60	0.495	E'_{1u}+E_{1u}	LE
					8.00	0.626	ϕ_2	LE

a) Oscillator strength was estimated by resolving the spectrum into overlapped bands tentatively. b) Main configurations of respective excited states are shown. In the $i-j$ CT or BCT configuration, i denotes the vacant (*i.e.*, 15th and 16th) or occupied (14th) π-MO's of MA (corresponding to the enol ring), respectively, and j denotes the occupied (2nd and 3rd) or vacant (4th and 5th) π-MO's of the benzene ring, respectively. c) Shoulder.

TABLE 2. TRANSITION ENERGIES ($^1\Delta E$ (eV or cm^{-1})) AND OSCILLATOR STRENGTHS (f) OBSERVED AND CALCULATED FOR DIBENZOYLMETHANE (DBM)

In heptane			In acetonitrile	In ethanol	Calcd			Assignment[c]
$^1\Delta E$ / cm^{-1}	$^1\Delta E$ / eV	f[a]	$^1\Delta E$ / eV	$^1\Delta E$ / eV	$^1\Delta E$ / eV	f	Main config.[b]	
29800	3.69	0.51	3.64	3.63	4.88	1.193	ϕ_1	LE
33800[d]	4.19	0.05	4.17	4.19	5.09	0.026	B_{2u}	LE_I
(35200)[d]	(4.36)				5.15	0.012	B_{2u}	LE_{II}
40000	4.96	0.23	4.96	4.93	5.66	0.300	15←2+B_{1u}	CT_{II}
					5.92	0.152	15←2+ϕ_1+B_{1u}	LE_I+CT_I
43300	5.37	0.08	5.37	5.37	6.31	0.152	15←3	CT_I
44600	5.53		5.51	5.52	6.38	0.151	15←3	CT_{II}
46500[d]	5.76	0.06	6.14	6.05	6.85	0.248	B_{1u}	LE_{II}+LE_I
49000[d]	6.08	0.23			6.94	0.172	B_{1u}	LE_I+LE_{II}
					7.17	0.253	14→5+ϕ_2	BCT_{II}+BCT_I
					7.58	0.958	E'_{1u}+E_{1u}+14−4	LE_I+LE_{II}
					7.62	0.462	E_{1u}+E'_{1u}	LE_{II}
54100	6.71	1.38	6.65		7.70	0.689	E'_{1u}	LE_{II}
					7.84	0.589	E_{1u}	LE_I
					8.04	0.420	14→4	BCT_I
					8.11	0.004	14→4	BCT_{II}

a) See footnote (a) in Table 1. b) See footnote (b) in Table 1. c) LE, CT, or BCT configuration I and II are related to the benzene ring I and II, respectively. d) Shoulder.

molecular geometries predicted by several investigations;[24-26,41,42] the results showed that the electronic structure of MA is sensitive to the change of molecular geometry, especially to the position of intramolecularly H-bonded O and H atoms. From the comparison with the observed spectra[28] and by referring to the experimental results of microwave spectrum[26] and of X-ray crystal analysis of DBM,[41] we have chosen the nonlinear asymmetrical H-bond with $R(O\cdots O)=2.55$ Å and $r(O-H)=1.18$ Å as one of the plausible structure of MA.

The electronic structure of MA calculated by the modified CNDO-CI method is tabulated in Table 4, together with the observed values.[28] The agreement between the theoretical and observed values is satisfactory for the lower excited states. It is noteworthy that the first and the second σ-σ^* bands predicted at 8.76 and 9.35 eV, respectively, is the CT band pertinent to the H-bond in the sense that the CT configurations, 13—17 and 13—18 in the H-bond (corresponding to the transition from O-H···O structure to O···H-O structure in the valence-bond scheme[29]) mainly contribute

Table 3. Transition energies ($^1\Delta E$ (eV or cm^{-1})) and oscillator strengths (f) observed and calculated for 3-phenyl-2,4-pentanedione (PPD)

In heptane			In acetonitrile	In ethanol	Calcd			Assignment
$^1\Delta E$ / cm^{-1}	$^1\Delta E$ / eV	f[a]	$^1\Delta E$ / eV	$^1\Delta E$ / eV	$^1\Delta E$ / eV	f	Main config.[b]	
35200	4.37	0.19	4.34	4.33	4.48	0.314	ϕ_1	LE
					4.86	0	B_{2u}	LE
41500	5.14	0.04	5.12	5.12	5.29	0.040	15←2	CT
43800	5.43	0.04	5.39	5.39	5.45	0.002	15←3	CT
46900[c]	5.82	0.06			5.91	0.196	B_{1u}+14→5	LE
49000[c]	6.08	0.10	6.05	6.05	6.31	0.280	B_{1u}+14→5	LE
52500	6.51	0.39	6.63		6.54	0.143	14→4	BCT
					6.68	0.643	ϕ_2+E_{1u}+14→5	LE
55400	6.87	0.70			7.06	0.996	E'_{1u}	LE
					7.37	0.203	16←2+E_{1u}	CT+LE
					7.55	0.043	ϕ_2+16←2	LE

a) See footnote (a) in Table 1. b) See footnote (b) in Table 1. c) Shoulder.

Table 4. Singlet and triplet transition energies ($^1\Delta E$ and $^3\Delta E$ (eV)) and oscillator strengths (f) observed and calculated for malonaldehyde (MA)

Assignment	Obsd[a]		Calcd			Main config.[c]
	$^1\Delta E$	f	$^1\Delta E$	$^3\Delta E$	f[b]	
n-π*	3.51			3.33	0.000 (z)	13—15
π-π*	4.71 (5.08)[d]	0.3	5.18	3.92	0.114 (x)	14—15
n-π*				6.29	0.000_3(z)	13—16
π-σ*				7.44	0.008 (z)	14—17
σ-π*				7.51	0.003 (z)	12—15
π-π*	>6.3	>0.2	7.87	5.85	0.239 (y)	14—16
π-σ*				8.18	0.019 (z)	14—18
σ-π*				8.72	0.015 (z)	12—16, 9—15
σ(n)-σ*			8.76	8.40	0.012 (x$\bar{y}$)[e]	13—18, 13—17, 13—19
π-σ*				9.15	0.026 (z)	14—19
σ(n)-σ*			9.35	7.35	0.372 (x)	13—17, 13—18
σ-σ*			9.46	9.25	0.014 (x$\bar{y}$)[e]	13—19, 13—18
π-π*			9.81	8.44	0.203 (x$\bar{y}$)[e]	11—15
π-σ*				9.83	0.019 (z)	14—20
σ-π*				10.40	0.000_3(z)	10—15
π-σ*				11.03	0.003 (z)	14—21, 14—22, 11—19
σ-σ*			11.03	10.74	0.058 (x)	13—20
σ-π*				11.04	0.002 (z)	7—15

a) Observed value in the vapor phase taken from Ref. 28. b) Oscillator strength is calculated for the singlet manifold. The direction of transition moment is shown in parentheses, x-, y-, and z-axes being taken as in Fig. 1. c) Singly excited configuration, $i-j$, denotes one-electron excitation from the i-th occupied MO to the j-th vacant MO. The 14th MO is the highest occupied one. d) Observed value in ethanol. e) x- and y-components of transition moment contribute equally with opposite signs.

to the first (55.8%) and to the second (53.5%) σ-σ* excited states. The CT configurations also contribute considerably (11.6%) to the first π-π* excited state of MA as in the case of the corresponding band of the enol form of acac and its fluoro derivatives.[29,30]

Electronic Structures of BA, DBM, and PPD. The electronic structures of the π-electron systems of BA, DBM, and PPD were calculated by the method of composite molecule[31,32] in which the β-diketone is divided into the enol ring and the benzene ring(s). The rotating angle, θ, between the enol ring and the benzene ring (Fig. 1) was treated as a variable. Figure 3 shows the θ-dependence of energy levels calculated for BA, DBM, and PPD.[43] By referring to the absorption spectra in Fig. 2, and also by referring to the observed θ-value of DBM (16.9°)[41] and tetraacetylethane (89°)[42] in crystalline state, theoretical results with θ=20° are taken to BA and DBM, and the result with θ=70°, to PPD, as tabulated in Tables 1—3. The theoretical energy diagrams of BA and DBM are illustrated in Fig. 4 and the one of PPD, in Fig. 5.

As is shown in Table 1 and in Fig. 4, the first allowed

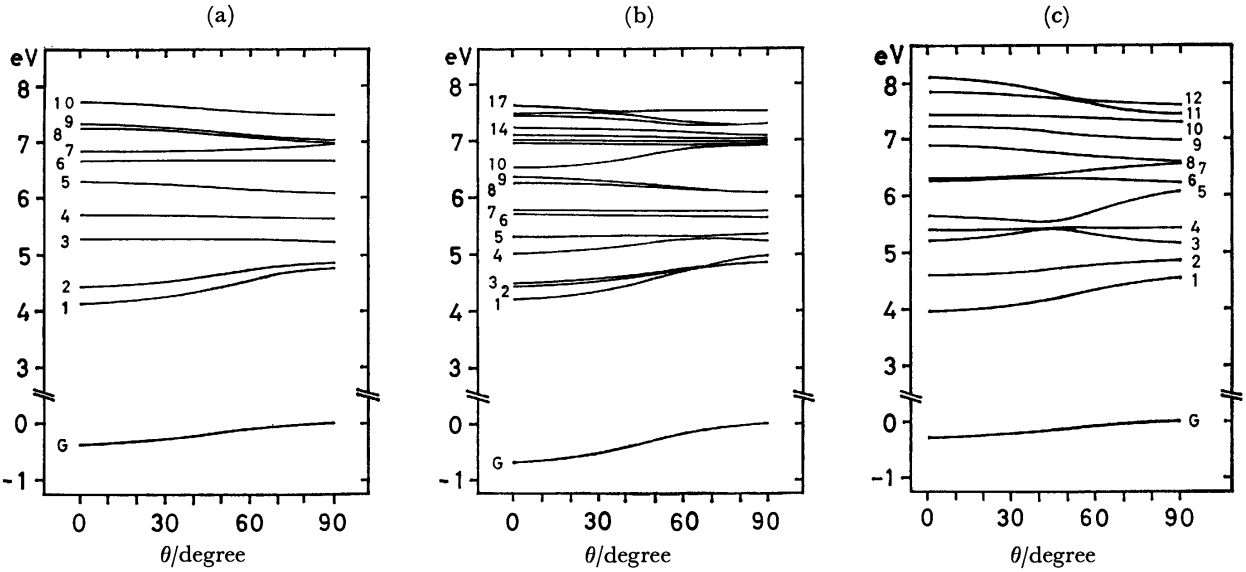

Fig. 3. θ-dependence of energy levels calculated for (a) BA, (b) DBM, and (c) PPD.

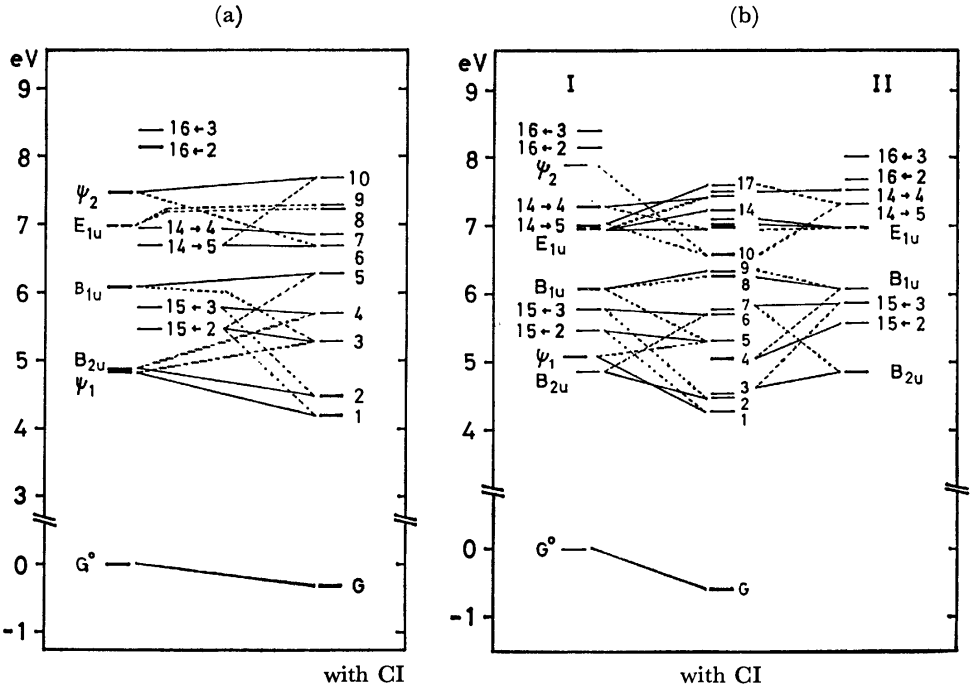

Fig. 4. Energy levels calculated with and without CI treatment for (a) BA and (b) DBM. In DBM, the configurations related to the benzene ring I and the LE configurations of the enol ring are shown on the left column and the configurations related to the benzene ring II, on the right column. For the CT or BCT configuration, i—j, see the footnote (b) in Table 1.

band of BA observed at 32700 cm^{-1} in heptane can safely be assigned to the LE state of the enol ring, ϕ_1 (60.3%) mixed with the CT (from the benzene ring to the enol ring) (18.5%) and BCT (from the enol ring to the benzene ring) (9.6%) configurations. The second excited state of BA which is mainly (73.2%) composed of B_{2u} state of the benzene ring and the absorption intensity of which is predicted to be weak may be covered with the first π-π^* band. The assignment may be supported from the fact that the corresponding band of DBM is observed near 33800 cm^{-1} as a shoulder. The 40500 cm^{-1} band of BA can be assigned to the third excited state which is mainly composed of the 15←2 CT (42.4%), and ϕ_1 (26.7%) and B_{1u} (19.6%) LE configurations. The 44000 cm^{-1} band has two peaks at 43000 and 44500 cm^{-1} in heptane and can be assigned to the fourth excited state which is mainly composed of the 15←3 CT (55.8%) and B_{2u} LE (22.7%) configurations. The 44000 cm^{-1} band is the CT band between the benzene and enol rings.

From the comparison with the theoretical result, we can expect three bands in the 45000—53000 cm^{-1} region. The shoulder at $\approx$46100 cm^{-1} is assigned to the fifth excited state which is mainly composed of the B_{1u} LE (61.8%) and 15←2 CT (20.1%) configurations. To the 6th and 7th excited states, BCT configurations contribute significantly. The 6th excited state is mainly composed of the 14→5 BCT (41.9%), and ϕ_2 (24.1%), ϕ_1 (9.4%), E_{1u} (11.1%), and B_{1u} (9.2%) LE configurations, and is tentatively assigned to the weak shoulder near 47400 cm^{-1}. The 7th excited state which is safely assigned to the 50800 cm^{-1} band is the BCT band to which the 14→4 BCT (64.8%) and E'_{1u} LE (19.4%) configurations mainly contribute.

The very strong 56500 cm^{-1} band is predicted to be composed of three bands, *i.e.*, 8th—10th excited states. The 8th and 9th excited states are mainly composed of the E_{1u} and E'_{1u} LE configurations (47.4% and 18.6%, respectively, for the 8th, and 26.2% and 31.6%, respectively, for the 9th excited state) mixed with BCT and CT configurations. The 10th excited state is mainly composed of the ϕ_2 LE (51.9%) and 14→5 BCT (20.8%) configurations.

The electronic structure of DBM is illustrated in Fig. 4, compared with the one of BA. Because two benzene rings, I and II interact with the enol ring, the 2nd and 3rd, 4th and 5th, 6th and 7th, and 8th and 9th excited states of DBM appear in pairs with the corresponding character related to each benzene ring. As is shown in Table 2, the observed bands at 29800, 33800, 40000, and 44000 cm^{-1} in heptane can be assigned to the first, 2nd and 3rd, 4th and 5th, and 6th and 7th excited states, respectively. The character of the bands is semiquantitatively the same to the corresponding first four bands of BA. The 44000 cm^{-1} band has two peaks at 43300 and 44600 cm^{-1} as in the case of BA. In the 46000—50500 cm^{-1} region, three bands, *i.e.*, 8th—10th excited states are predicted to overlap. The character of the pair (*i.e.*, the 8th and 9th) and the 10th excited states corresponds to the one of the 5th and 6th excited states of BA, respectively. In the very strong 54100 cm^{-1} region, six bands corresponding to the 11th—16th excited states are expected to locate. The 11th—14th states are mainly composed of the E_{1u} and E'_{1u} LE configurations of two benzene rings, and the 15th and 16th excited states, of the 14→4 BCT configuration from the enol ring to each benzene ring.

In conclusion, theoretical investigation of the spectra clearly shows strong π-electron interaction between the enol and benzene rings in BA and DBM.

Contrary to BA and DBM, the spectrum of PPD is well reproduced when θ value around 70° is employed, indicating that π-electron interaction between the enol and benzene rings is weak. The theoretical result of PPD with $\theta=70°$ is shown in Table 3 and in Fig. 5. Because the PPD molecule is of approximate C_2 symmetry and because the π-electron interaction between the rings is rather weak, configuration interaction in PPD is more limited than in BA. As is shown in Table 3, qualitative assignment for each band is similar to the one of BA. The 35200 cm^{-1} band assigned to the first excited state is the LE state, ϕ_1 (87.3%), and the

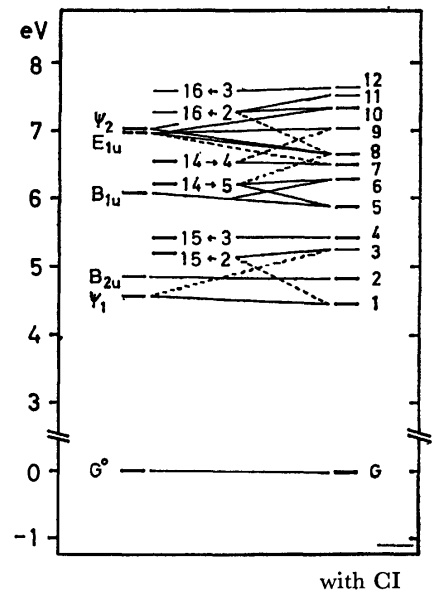

Fig. 5. Energy levels calculated with and without CI treatment for PPD. For the CT or BCT configuration, *i*—*j*, see the footnote (b) in Table 1.

second excited state is B_{2u} state of the benzene ring (97.4%). The latter band is again too weak to be observed. The 41500 cm^{-1} band assigned to the third excited state is the 15←2 CT state (86.3%), and the 43800 cm^{-1} band assigned to the 4th excited state is the 15←3 CT state (97.8%).

The B_{1u} LE and 14→5 BCT configurations contribute predominantly to the 5th (50.9% and 34.7%, respectively) and to the 6th (47.1% and 39.3%, respectively) excited states, which are tentatively assigned to the shoulders at 46900 cm^{-1} and 49000 cm^{-1}, respectively. To the strong 52500 cm^{-1} region, the 7th (14→4 BCT (85.8%)) and the 8th (ϕ_2 (32.4%)+E_{1u} (32.1%)+14→5 BCT (24.7%)) excited states can be assigned. To the very strong 55400 cm^{-1} region, the strong 9th (E'_{1u} (82.6%)) and 10th (E_{1u} (39.4%)+16←2 CT (51.3%)) excited states mainly contribute.

Theoretical oscillator strength of the first band predicts well the increase of the observed transition intensity in the order of PPD<BA<DBM. Table 5 shows coefficients of several main configurations in the ground and the first excited states. The wave functions clearly show that the increase of the interaction of the 15←2 CT configuration with the ground and ϕ_1 LE configurations is mainly responsible for the increase of the transition intensity.

UV Absorption Spectra in KOH Aqueous Solution. Near UV absorption spectra measured with the KOH aqueous solutions of BA, DBM, PPD, and acac are shown in Fig. 6. The strong bands at 320.5 nm of BA, at 347 nm of DBM, and at 304.5 nm of PPD can be assigned to the first π-π* band of the anion with planar chelate ring as in the case of the 292.5 nm band of the acac anion.[29] As is shown in Fig. 6, the spectra of the KOH aqueous solutions were found to change with time, and the strong bands at 300—350 nm finally disappear. In Fig. 7, time dependence of the absorbance, $\Delta A(=A(t)-A(t=\infty))$, for the 320.5 nm band of the

Table 5. Wave functions (coefficients of main configurations) of the ground and the first π-π^* excited states of BA, DBM, and PPD

Configuration[a]	BA		DBM		PPD	
	Ground state	1st π-π^* state	Ground state	1st π-π^* state	Ground state	1st π-π^* state
G^0	0.9728	−0.0835	−0.9554	0.0620	0.9973	0.0062
ϕ_1 LE	0.0051	0.7767	−0.0039	−0.7202	−0.0003	0.9341
B_{1u} LE I	−0.0177	−0.2151	0.0159	0.2331	0.0006	0.0488
E_{1u} LE I	0.0157	0.2228	−0.0139	−0.2333	−0.0005	−0.0705
II			−0.0130	0.1115		
15←2 CT I	−0.1909	−0.4134	0.1779	0.4667	0.0241	−0.3370
II			−0.1475	0.1389		
16←2 CT I	0.1044	0.1194	−0.0983	−0.1362	−0.0385	0.0391
II			−0.1244	0.0600		
14→5 BCT I	−0.0696	0.3104	0.0631	−0.2589	−0.0571	−0.0629
II			0.0004	0.1292		
f calcd		0.877		1.193		0.314
f obsd		0.38		0.51		0.19

a) Configuration I or II is related to the benzene ring I or II, respectively.

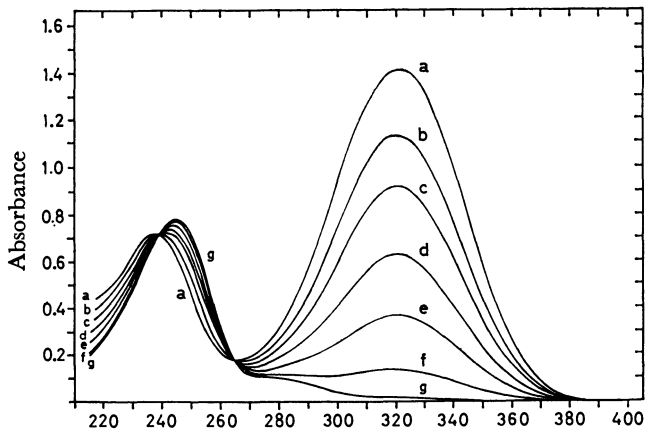

Fig. 6A. Near UV absorption spectra measured with the KOH aqueous solution of BA at (a) t=0.8 h, (b) t=8.7 h, (c) t=15.5 h, (d) t=27.0 h, (e) t=43.4 h, (f) t=75.9 h, and (g) t=163.8 h.

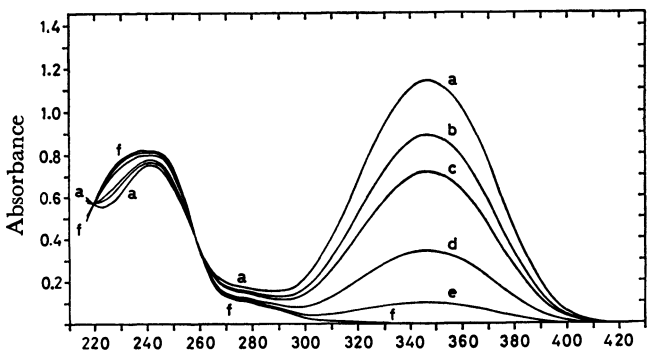

Fig. 6B. Near UV absorption spectra measured with the KOH aqueous solution of DBM at (a) t=1.0 h, (b) t=6.1 h, (c) t=10.1 h, (d) t=25.0 h, (e) t=50.8 h, and (f) t=151.4 h.

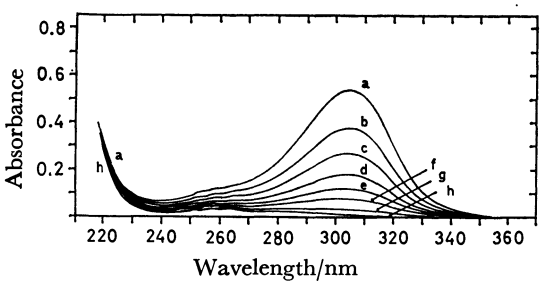

Fig. 6C. Near UV absorption spectra measured with the KOH aqueous solution of PPD at (a) t=24 min, (b) t=29 min, (c) t=35 min, (d) t=42 min, (e) t=49 min, (f) t=57 min, (g) t=76 min, and (h) t=194 min.

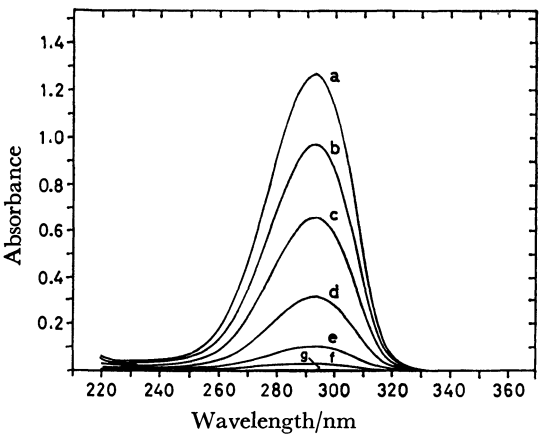

Fig. 6D. Near UV absorption spectra measured with the KOH aqueous solution of acac at (a) t=0.8 h, (b) t=9.1 h, (c) t=22.3 h, (d) t=49.6 h, (e) t=94.6 h, (f) t=145.0 h, and (g) t=239.2 h.

BA anion is shown as an example; the absorbance (ΔA) decreases exponentially with time. The exponential decay of the absorbance was also observed for the first π-π^* bands of the DBM, PPD, and acac

Table 6. Rate constant ($k(s^{-1})$), initial absorbance (ΔA_0), and initial molar extinction coefficient[a] (ε_0) for the first band of the KOH aqueous solution of BA, DBM, PPD, and acac

	BA		DBM		PPD			acac	
[β-diketone]×10⁴/M	8.53	7.78	6.21	5.76	19.55	12.03	14.50	4.2	5.76
[KOH]×10/M	9.52	0.894	9.52	0.894	0.248	0.119	0.0594	9.52	0.991
$k\times10^5/s^{-1}$	10.2	0.904	14.3	1.39	116	102	113	13.8	0.846
ΔA_0	1.67	1.49	1.35	1.20	3.65	2.23	2.70	1.01	1.29
ε_0	18700	18300	20700	19800	17800	17700	17700	23000	21300
Average	18500		20300		17700			22200	

a) Estimated at the band maximum.

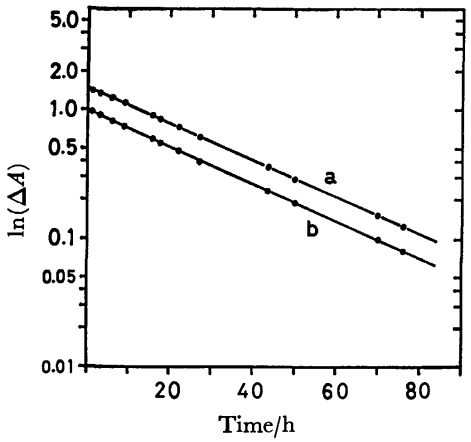

Fig. 7. Time dependence of the absorption intensity (ΔA) measured with the first π-π^* band of the BA anion at (a) 320.5 nm and (b) 340 nm.

anions, indicating that the spectral change is due to the unimolecular reaction, A→A′, of the anions. The rate constants (k) under several experimental conditions are listed in Table 6. In the BA, DBM, and acac anions, the rate constant is roughly proportional to the concentration of KOH, strongly suggesting that the planar structure of the chelate ring is broken by the action of the KOH molecules. Under the fixed concentration of KOH, the rate constant increases in the order of the BA<acac<DBM≪PPD anions. The true absorption intensity of the 300—350 nm band of the anion can be evaluated from the extrapolated absorbance at $t=0$ (ΔA_0) with the correction of the final absorbance ($A(t=\infty)$). The results are tabulated in Table 6. The absorption intensities are rather equal for the PPD, BA, and DBM anions in contrast to the ones of the corresponding bands in neutral species.

The authors wish to express their sincere thanks to Professor Saburo Nagakura, the University of Tokyo, for valuable discussions and for reading manuscript carefully.

References

1) O. Dimroth, *Ann.*, **399**, 91 (1913).
2) E. M. Kosower, *J. Am. Chem. Soc.*, **80**, 3267 (1958).
3) R. S. Rasmussen, D. D. Tunnicliff, and R. R. Brattain, *J. Am. Chem. Soc.*, **71**, 1068 (1949).
4) S. Bratož, D. Hadži, and G. Rossmy, *Trans. Faraday Soc.*, **52**, 464 (1956).
5) K. L. Wierzchowski and D. Shugar, *Spectrochim. Acta*, **21**, 943 (1965).
6) J. U. Lowe, Jr., and L. N. Ferguson, *J. Org. Chem.*, **30**, 3000 (1965).
7) H. Ogoshi and K. Nakamoto, *J. Chem. Phys.*, **45**, 3113 (1966).
8) H. Ogoshi and Z. Yoshida, *Spectrochim. Acta, Part A*, **27**, 165 (1971).
9) E. Grens, A. Grinvalde, and J. Stradiņš, *Spectrochim. Acta, Part A*, **31**, 555 (1975).
10) J. L. Burdett and M. T. Rogers, *J. Am. Chem. Soc.*, **86**, 2105 (1964); M. T. Rogers and J. L. Burdett, *Can. J. Chem.*, **43**, 1516 (1965).
11) R. L. Lintvedt and H. F. Holtzclaw, Jr., *J. Am. Chem. Soc.*, **88**, 2713 (1966); *Inorg. Chem.*, **5**, 239 (1966).
12) M. Tanaka, T. Shono, and K. Shinra, *Bull. Chem. Soc. Jpn.*, **42**, 3190 (1969).
13) R. H. Holm and F. A. Cotton, *J. Am. Chem. Soc.*, **80**, 5658 (1958).
14) M. Mikami, I. Nakagawa, and T. Shimanouchi, *Spectrochim. Acta, Part A*, **23**, 1037 (1967).
15) G. T. Behnke and K. Nakamoto, *Inorg. Chem.*, **6**, 433, 440 (1967).
16) R. A. Morton, A. Hassan, and T. C. Calloway, *J. Chem. Soc.*, **1934**, 883.
17) L. Sacconi and G. Giannoni, *J. Chem. Soc.*, **1954**, 2751.
18) G. S. Hammond, W. G. Borduin, and G. A. Guter, *J. Am. Chem. Soc.*, **81**, 4682 (1959).
19) Y. Murakami and K. Nakamura, *Bull. Chem. Soc. Jpn.*, **39**, 901 (1966).
20) P. Gacoin, *J. Chem. Phys.*, **57**, 1418 (1972).
21) D. W. Barnum, *J. Inorg. Nucl. Chem.*, **21**, 221 (1961); **22**, 183 (1961).
22) P. Schuster, *Chem. Phys. Lett.*, **3**, 433 (1969).
23) A. D. Issacson and K. Morokuma, *J. Am. Chem. Soc.*, **97**, 4453 (1975).
24) G. Karlström, B. Jönsson, B. Roos, and H. Wennerström, *J. Am. Chem. Soc.*, **98**, 6851 (1976).
25) J. E. Del Bene and W. L. Kochenour, *J. Am. Chem. Soc.*, **98**, 2041 (1976).
26) W. F. Rowe, Jr., R. W. Duerst, and E. B. Wilson, *J. Am. Chem. Soc.*, **98**, 4021 (1976).
27) J. E. Del Bene, *Chem. Phys. Lett.*, **44**, 512 (1976).
28) C. J. Seliskar and R. E. Hoffman, *Chem. Phys. Lett.*, **43**, 481 (1976); *J. Am. Chem. Soc.*, **99**, 7072 (1977).
29) H. Nakanishi, H. Morita, and S. Nagakura, *Bull. Chem. Soc. Jpn.*, **50**, 2255 (1977).
30) H. Nakanishi, H. Morita, and S. Nagakura, *Bull. Chem. Soc. Jpn.*, **51**, 1723 (1978).
31) H. C. Longuet-Higgins and J. N. Murrell, *Proc. Phys.*

Soc. (*London*), **A68**, 601 (1955); J. N. Murrell, *ibid.*, **A68**, 969 (1955).
32) K. Kimura and S. Nagakura, *Mol. Phys.*, **9**, 117 (1965).
33) K. Kaya and S. Nagakura, *J. Mol. Spectrosc.*, **44**, 279 (1972).
34) H. Morita, K. Fuke, and S. Nagakura, *Bull. Chem. Soc. Jpn.*, **50**, 645 (1977).
35) Re-measured in the present study.
36) D. W. Turner, C. Baker, A. D. Baker, and C. R. Brundle, "Molecular Photoelectron Spectroscopy," John Wiley, London (1970).
37) S. Evans, A. Hamnett, A. F. Orchard, and D. R. Lloyd, *Faraday Discuss. Chem. Soc.*, **54**, 227 (1972).
38) C. Nishijima, H. Nakayama, T. Kobayashi, and K. Yokota, *Chem. Lett.*, **1975**, 5.
39) G. Klopman, *J. Am. Chem. Soc.*, **86**, 4550 (1964); **87**, 3300 (1965).
40) J. A. Pople, *Proc. Phys. Soc.*, **A68**, 81 (1955).
41) D. E. Williams, *Acta Crystallogr.*, **21**, 340 (1966).
42) J. P. Schaefer and P. J. Wheatley, *J. Chem. Soc.*, *A*, **1966**, 528.
43) When $\theta \neq 0°$, the CT configurations can interact with low-lying n-π^* LE configurations in the enol ring through the resonance integral, $\beta_{n\pi}$, between the n-orbital in the enol ring and the occupied π-MO in the benzene ring. Because the $\beta_{n\pi}$ value is very small even when θ is large, the influence of the n-π^* LE configurations on the π-electronic structure is negligibly small.

  Bull. Chem. Soc. Jpn., 54, 387—390 (1981)

The Photoelectrochemical Reaction of the Chlorophyll-Irisquinone Electrode

Fujio Takahashi,* Katsura Seki, Ryohei Kaneko, Kenji Sato, and Yasushi Kusumoto

Faculty of Engineering, Utsunomiya University, Utsunomiya 321

(Received May 30, 1980)

The role of irisquinone (IQ) in the chlorophyll-IQ electrode was studied by measuring the photoresponse under illumination and the photocurrent at the controlled potential. It was concluded that the hydrophobic property of IQ was necessary for the photoresponse to occur at the chlorophyll electrode, and that the photoexcited chlorophyll was likely to eject electrons to a counter electrode *via* an outer circuit and to pull electrons from the reduced IQ, which had been produced by the oxidation of a reducing compound in the electrolyte on the chlorophyll-IQ electrode.

Recently many photoelectrochemical studies of chlorophyll lined on the electrode have been reported.[1,2] We have already contributed to this field: We found that the potential shifts to a less noble value under illumination on the platinum electrode coated with a mixture of chlorophyll and quinone, such as 1,4-naphthoquinone or chloranil.[3] The conductive adhesive was used as the binder of quinone with an electrode to prevent the quinone spread on the chlorophyll layer from dissolving into the electrolyte. However, the existence of the conductive adhesive made it difficult to speculate on the role of quinone in producing a photocurrent from the electrode in the light. It was, therefore, thought to be necessary to investigate the photoelectrochemical reaction on the chlorophyll quinone electrode without the conductive adhesive.

Two of the present authors isolated a new quinone from the seed oil of *Iris pseudacorus* L.[4] The structure of the quinone has been identified as 2-(*cis*-10-heptadecenyl)-6-methoxy-*p*-benzoquinone,** which is insoluble in water, miscible with chlorophyll, and adhesive to the electrode. These properties were thought to be suitable for the study of the chlorophyll-quinone electrode.

This paper will present the results of photoelectrochemical studies of the chlorophyll-IQ electrode undertaken in order to clarify the role of quinone.

Experimental

Materials. The chlorophyll was purchased from Nihon Chlorophyll Kogyo Co., Ltd., and was purified to separate it from an oily material by elution through the talc column with 80% acetone. The chlorophyll used was a mixture of chlorophyll a and b. The chlorophyll was determined by the spectrophotometric method.[5] The IQ used was isolated by the method described in a previous paper.[4] All the other chemicals were of a reagent grade or were the best commercially available.

Electrodes and Electrolytes. A chlorophyll or IQ solution in hexane or acetone and a cholesteryl oleate solution in hexane were prepared. The requisite amounts of the chlorophyll solution or the mixture of these stock solutions were spread onto the platinum electrode (1 × 1 cm) and then dried to produce a homogeneous chlorophyll layer. The chlorophyll-coated electrode was then immersed in a M/40 phosphate-buffer (pH 6.9) or carbonate-buffer electrolyte adjusted at each pH; various redox compounds had been dissolved in the electrolytes. All the experiments were carried out at 35 °C by using 50-ml dual beaker containing the electrolyte, with nitrogen gas being passed through.

Equipment. The potential was measured by means of a Kikusui Denshi volt-ammeter model 116 connected to the recorder, with a calomel electrode as the reference electrode. A Hokuto Denko potentiostat HA101 and a linear scanner were used for the measurement of the photocurrent at each controlled potential. A platinum plate was used as a counter electrode. The potential-current curves were obtained by using a Yokogawa Denki Type 3036 X-Y recorder, with the scanning set at a rate of 100 mV/s. The projector lamp (100 V, 150 W) was used as the source of light. The light of wavelengths shorter than 460 nm was cut off by a color filter (V-Y46) to avoid the complication arising from the simultaneous photochemical reaction of IQ, which exhibited its λ_{max} at 363 nm.[4]

Results and Discussion

Photoresponse of the Chlorophyll-IQ Electrode. To investigate the effect of IQ on the electrode with respect to the photoresponse, the electrode was prepared by covering 0.01 μmol/cm² of a layer containing chlorophyll and IQ mixed in various molar ratios. Same typical results of the potential-time curve are shown in Fig. 1. In Fig. 2 the values of photovoltage (the potential under illumination subtracted that in the dark) of all the electrodes are plotted against the molar ratio of IQ to the total amount of chlorophyll and IQ. The photovoltage of the chlorophyll electrode was found to shift to a positive value under illumination. On the other hand, the photovoltage turned into a

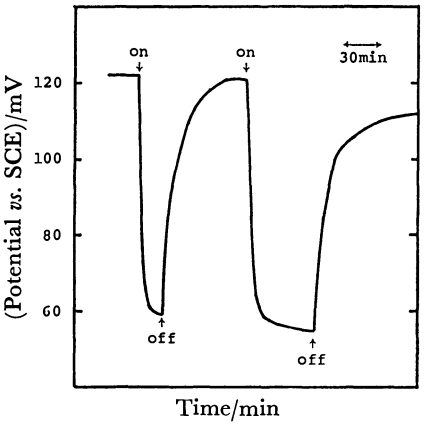

Fig. 1. Photoresponse of chlorophyll-IQ electrode. pH 6.9, 35 °C, 6 × 10⁴ lx, [Chl]+[IQ]=0.01 μmol/cm², [Chl] : [IQ]=1 : 3.

** Abbreviated to IQ, because we named it Irisquinone.

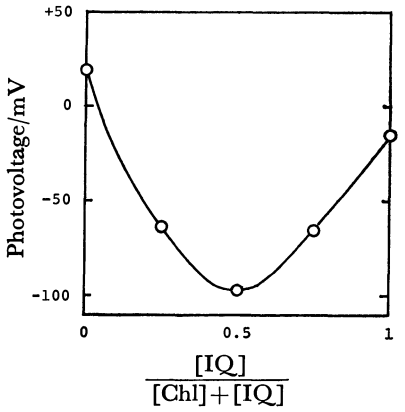

Fig. 2. Influence of the molar ratio to the photovoltage of chlorophyll-IQ electrode.
pH 6.9, 35 °C, 6×10^4 lx, [Chl]+[IQ]=0.01 μmol/cm².

negative value as the IQ content in the layer of the electrode increased. The maximum photoresponse was obtained at the molar ratio of IQ to chlorophyll of 1 : 1. The magnitude of the photovoltage became smaller at higher molar ratios of IQ, caused by the decrease in the amount of chlorophyll, which exhibited a photoconductive property. The values of the photovoltage were measured at various thicknesses of the chlorophyll-IQ layer (with the molar ratio of 1 : 1). The results are shown in Fig. 3a. The photovoltage was nearly constant at layer thicknesses thicker than 0.01 μmol/cm².

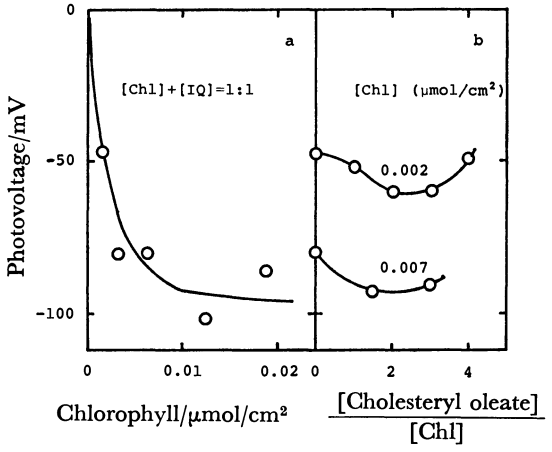

Fig. 3. Influence of the thickness of chlorophyll layer and the ratio of cholesteryl oleate to chlorophyll to the photovoltage.
pH 6.9, 35 °C, 6×10^4 lx.

It is very plausible that chlorophyll molecules are located in the hydrophobic region as a result of the existence of excess IQ, which is hydrophobic itself, and that, in turn, the chlorophyll-IQ electrode generates the photovoltage due to the photoexcitation of chlorophyll in the hydrophobic region. The chlorophyll-IQ-cholestery oleate electrode was prepared and illuminated in order to verify the influence of hydrophobicity on the photovoltage. Cholesteryl oleate is hydrophobic, miscible to chlorophyll and IQ, and exhibits the property of a liquid crystal. It is known that not only the molecules of a liquid crystal, but also guest molecules will be oriented in the electric field.[6] It was expected that the photovoltage might increase by the orientation of the photo-conductive chlorophyll molecules in the layer. The results of the photovoltage of the chlorophyll-IQ-cholesteryl oleate electrode are shown in Fig. 3b. The molar ratio of chlorophyll and IQ is 1 : 1, and the total amounts of chlorophyll and IQ in the layer were kept constant when the amount of cholesteryl, oleate was varied. The photovoltage was found to increase up to the molar ratio of chlorophyll, IQ, and cholesteryl oleate of 1 : 1 : 2, and then decrease as more cholesteryl oleate was added. It is said that the following reaction may occur in the hydrophobic region:[7]

$$\mathrm{Chl}^* + \mathrm{Q} \longrightarrow \mathrm{Chl}^+ + \mathrm{Q}^-, \qquad (1)$$

where Chl*, Chl^+, and Q^- are a photoexcited chlorophyll, a cation of chlorophyll, and an anion of quinone, respectively. In a nonaqueous solvent, one-electron-reduced ubiquinone is known to be stable and to exhibit a remarkably negative (less noble) reduction potential.[8] Judging from the fact that the photoresponse of the chlorophyll-IQ electrode was observed in a negative direction, like an n-type semiconductor, an anion of IQ seems to exist inside the chlorophyll-IQ layer, apart from the interface of the electrode and the electrolyte.

The Redox Compounds in the Electrolyte. The electrolyte should contain an equi-molar concentration of the oxidized and reduced forms of the redox compound in order to keep the composition of the electrolyte constant during the photoelectrochemical reaction, so that the oxidized form of the redox compound might be reduced at the cathode and the reduced form might be oxidized at the anode. Therefore, the redox compounds were surveyed for a photocell producing as

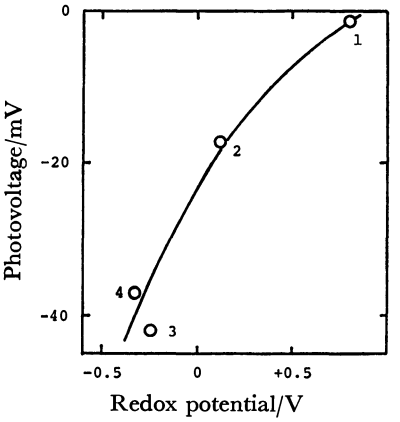

Fig. 4. Relation between the redox potential and the photovoltage. Total concentration of redox compound 2 mM. Molar ratio of oxidized and reduced form=1 : 1.
1: Quinone hydroquinone (+0.80V), 2: Fe^{3+}EDTA/Fe^{2+}EDTA (+0.12 V), 3: 1/2 GSSG/GSH (−0.24 V), 4: NAD^+/NADH (−0.32 V), pH 6.9, 35 °C, 5×10^4 lx, chlorophyll-IQ electrode: [Chl] : [IQ]=1 : 5, thickness of chlorophyll: 0.02 μmol/cm².

high a photovoltage and photocurrent as possible. The photovoltage was measured on the system of a chlorophyll-IQ (the molar ratio: 1 : 5) electrode immersed into an electrolyte containing a different redox compound. The concentrations of the oxidized and reduced forms of the redox compound were 1 mM each. The results are shown in Fig. 4. The photovoltage was found to shift to a more negative value as the oxidation-reduction potential of the redox compound became less noble. The highest photovoltage was obtained when the mixture of glutathione-oxidized (GSSG) and -reduced (GSH) was used. The photovoltage in the system of the chlorophyll-IQ electrode connected with GSSG or GSH alone in the electrolyte was −58 or −45 mV, while that in the system of the chlorophyll electrode connected with GSSG or GSH alone was +53 or +39 mV respectively.

The Photocurrent at the Controlled Potential. In order to clarify the role of IQ on the chlorophyll-IQ electrode, the photocurrent was measured at the controlled potential on the various electrodes immersed into the electrolyte. The molar ratio of chlorophyll to IQ or

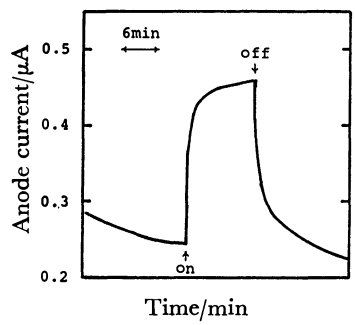

Fig. 5. Photocurrent at controlled potential.
pH 6.9, 35 °C, 5×10^4 lx, chlorophyll-IQ electrode: [Chl] : [IQ]=1 : 5, thickness of chlorophyll: 0.02 μmol/cm², electrolyte : 1 mM GSH, controlled potential at +0.22 V *vs.* SCE.

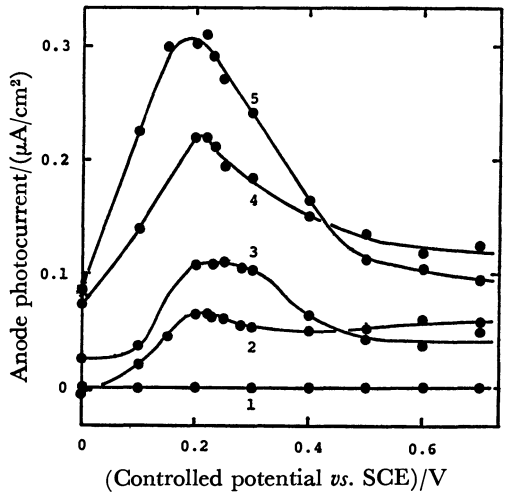

Fig. 6. Anode photocurrent at controlled potential.
pH 6.9, 35 °C, 5×10^4 lx, 0.02 μmol/cm² chlorophyll, molar ration of Chl : IQ=1 : 5, 1: E(none)/buffer, 2: E(Chl)/buffer, 3: E(Chl, IQ)/buffer, 4: E(Chl, IQ)/1 mM GSH, 5: E(Chl, IQH_2)/buffer.

that of chlorophyll to reduced IQ (IQH_2) in the layer of the electrode was 1 : 5. A typical anodic photocurrent-time curve is shown in Fig. 5, while the curves of the photocurrent at various controlled potentials are shown in Fig. 6. The maximum photocurrent was obtained around +0.2 V *vs.* SCE in every case. The same reaction may occur by the photoexcitation of chlorophyll in all cases. It is known that the half-wave oxidation potential of the chlorophyll a appears at +0.52 V (SCE) in acetonitril.[9] This is not a photoelectrochemical reaction. Judging from these facts, the photocurrent may be produced by the following reaction:

$$Chl + h\nu \longrightarrow Chl^* \longrightarrow Chl^+ + e. \quad (2)$$

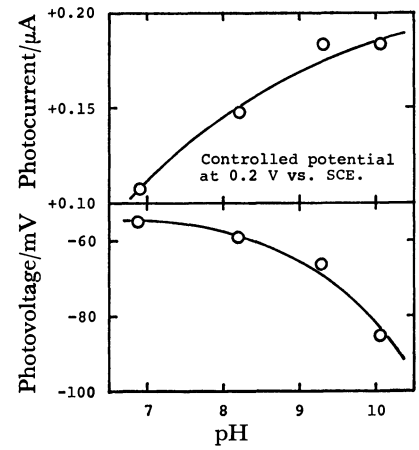

Fig. 7. Influence of pH to photovoltage and photocurrent. 35 °C, 5×10^4 lx, 0.02 μmol/cm² chlorophyll, molar ratio of Chl : IQ=1 : 5.

The anodic photocurrent at +0.2 V on the chlorophyll-IQ electrode was found to increase at higher pH values, in other words, at higher concentrations of OH^-, as is shown in Fig. 7. OH^- is as the only anode-active substance in the electrolyte. It may, therefore, be assumed that the IQ on the electrode is reduced in the process of the anodic reaction of OH^- and, in turn, that reduced IQ reacts with Chl^+ to reproduce IQ and chlorophyll. The assumptions can be expressed as follows:

$$IQ \xrightarrow{OH^-} IQH_2 \quad (3)$$

$$2\,Chl^+ + IQH_2 \longrightarrow 2\,Chl + IQ + 2\,H^+. \quad (4)$$

This is plausible, because the photocurrent in the case of the chlorophyll-IQ electrode is larger than that in the case of the chlorophyll electrode, and because the photocurrent produced by the chlorophyll-IQH_2 electrode is 2.8 times as large as that of the chlorophyll-IQ electrode, as is shown in Fig. 6.

The photocurrent and the dark current of the system of the GSH-containing electrolyte were twice and 1.4 times as large as these of the system omitting GSH. It is very possible that the IQ on the electrode is reduced to form IQH_2 in the dark as follows:

$$IQ + 2GSH \longrightarrow IQH_2 + GSSG. \quad (5)$$

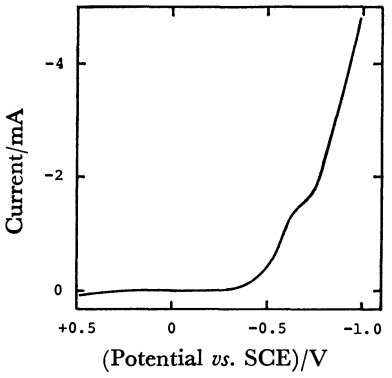

Fig. 8. Potential-current curve of IQ on Pt electrode.
pH 6.9, 35 °C, 0.05 μmol of IQ on Pt (1×1 cm^2), The potential was scanned at a rate of 100 mV/s.

Then, the photocurrent can be obtained in the same way as with the chlorophyll-IQH_2 electrode.

The IQ layer was spread onto the platinum electrode to determine the reduction potential, because the redox potential of IQ was not yet known. The reduction wave of IQ appeared around −0.5 V (SCE), as is shown in Fig. 8. This fact suggests that IQ^- tends to release electrons. The electrons could transfer from IQ^- to platinum at +0.2 V. Then, the chlorophyll-IQ electrode produced the anodic photocurrent by means of Eqs. 1 and 2 at +0.2 V. No matter ho w Eq. 1 might participate, the maximum photocurrent was produced at the same potential in every system in Fig. 6. Therefore, the reaction of Eq. 2 appears to occur predominantly rather than the reaction of Eq. 1. It is concluded that the IQ on the electrode plays a role in the accelaration of the anodic reaction.

References

1) F. K. Fong and N. Winograd, *J. Am. Chem. Soc.*, **98**, 2287 (1976); T. Miyasaka, T. Watanabe, A. Fujishima, and K. Honda, *ibid.*, **100**, 6657 (1978).

2) A. F. Janzen and J. R. Bolton, *J. Am. Chem. Soc.*, **101**, 6342 (1979); C. W. Tang and A. C. Albrecht, *J. Chem. Phys.*, **62**, 2139 (1975); **63**, 953 (1975).

3) F. Takahashi and R. Kikuchi, *Biochim. Biophys. Acta*, **430**, 490 (1976); *Bull. Chem. Soc. Jpn.*, **49**, 3394 (1976); F. Takahashi, M. Aizawa, R. Kikuchi, and S. Suzuki, *Electrochim. Acta*, **22**, 289 (1977).

4) K. Seki and R. Kaneko, *Chem. Ind.*, **1975**, 349.

5) L. P. Vernon, *Anal. Chem.*, **32**, 1144 (1960).

6) M. Aizawa, N. Suzuki, F. Takahashi, and S. Suzuki, *J. Solid-phase Biochem.*, **2**, 111 (1977); R. Journeaux and R. Viovy, *Photochem. Photobiol.*, **28**, 243 (1978).

7) B. J. Hales and J. R. Bolton, *J. Am. Chem. Soc.*, **94**, 3314 (1972).

8) "Progress in Bioorganic Chemistry," ed by E. T. Kaiser and F. J. Kézdy, John Wiley and Sons (1976), Vol. 4, p. 157.

9) L. P. Vernon and G. R. Seely, "The Chlorophylls," Academic Press (1966), p. 523.

  Bull. Chem. Soc. Jpn., 54, 391—393 (1981)

^{14}N Nuclear Quadrupole Resonance of the Molecular Complexes of Urea

Hisao Negita,* Tsuneo Kubo, and Hitoshi Kato

Department of Chemistry, Faculty of Science, Hiroshima University, Hiroshima 730

(Received June 21, 1980)

The ^{14}N nuclear quadrupole resonance (NQR) was studied in four kinds of molecular complexes of urea, such as urea-nitric acid, urea-phosphoric acid, urea-oxalic acid, and urea-ammonium chloride. The ^{14}N quadrupole coupling constants and asymmetry parameters at liquid nitrogen temperature are as follows: $|e^2Qq/h|=3.157$ MHz and $\eta=0.475$ for the HNO_3 complex; $|e^2Qq/h|=3.277$ MHz and $\eta=0.414$ for the H_3PO_4 complex; $|e^2Qq/h|=3.456$ MHz and $\eta=0.363$ for the $(COOH)_2$ complex; and $|e^2Qq/h|=3.544$ MHz and $\eta=0.298$ for the NH_4Cl complex. From the temperature dependence of the resonance lines in these complexes, the strength of hydrogen bonds are discussed. The differences of the electron densities at the nitrogen atoms between urea and its complexes were derived from the corresponding NQR parameters, and the bond characters in these complexes are discussed.

It is well known that urea forms molecular complexes with a number of compounds, being held together by hydrogen bonding. These hydrogen bonds have been investigated by various spectroscopic methods.[1,2] It is interesting to study the hydrogen bonds in these complexes by means of the nuclear quadrupole resonance (NQR) of nitrogen-14. The molecular complexes of urea examined are urea–nitric acid (1 : 1) (HNO_3 complex), urea–phosphoric acid (1 : 1) (H_3PO_4 complex), urea–oxalic acid (2 : 1) ($(COOH)_2$ complex), and urea–ammonium chloride (1 : 1) (NH_4Cl complex). On the basis of the ^{14}N NQR results, the strength of the hydrogen bonds and the charge distributions at nitrogen atoms were compared with those in urea itself.

Experimental

^{14}N NQR measurements were carried out using a pulse spectrometer described previously.[3] The resonance lines were observed by the spin-echo signals using a 90—180° pulse sequence series. The pulse width of a 90° pulse was about 50 μs. The spin-echo signal was averaged in a Nicolet Instrument Model 527 signal averager. The temperature was controlled by the method of Abe.[4] The temperature was measured by the use of a copper-constantan thermocouple and stabilized within ±0.1 K. The frequency was checked by means of a frequency counter, TR-5104, from Takeda Riken Co.

The sample of the HNO_3 complex was prepared by crystallization at 0 °C from an aqueous solution containing an equimolar amount of urea and nitric acid, and was purified by recrystallization from methanol.[5] Found: C, 9.95; H, 4.13; N, 34.42%. Calcd for $CH_5N_3O_4$: C, 9.76; H, 4.10; N, 34.14%. The sample of the H_3PO_4 complex was obtained by slowly evaporating an equimolar solution of urea and phosphoric acid.[6] Found: C, 7.60; H, 4.54; N, 17.63%. Calcd for $CH_7N_2O_5P$: C, 7.60; H, 4.46; N, 17.72%. The sample of the $(COOH)_2$ complex was obtained from an aqueous solution of urea and oxalic acid in the stoichiometric ratio.[7] Found: C, 22.91; H, 4.84; N, 26.51%. Calcd for $C_3H_6N_2O_5$: C, 22.86; H, 4.80; N, 26.66%. The sample of the NH_4Cl complex was prepared by slowly evaporating a solution containing urea and ammonium chloride in a molar ratio of 1 : 1.[8] Found: C, 10.69; H, 7.17; N, 36.78; Cl, 30.8%. Calcd for CH_8ClN_3O: C, 10.58; H, 7.10; N, 37.01; Cl, 31.2%. All the samples were ground into powder after drying, and about 20 g of the samples were used for the measurements.

Results and Discussion

For the case of nitrogen-14 one observes in general a spectrum consisting of two NQR absorption lines ν_- and ν_+:

$$\nu_\pm = \frac{|e^2Qq|}{4h}(3\pm\eta), \qquad (1)$$

where $|e^2Qq/h|$ and η are the quadrupole coupling constant and asymmetry parameter, respectively. In the cases of the HNO_3 complex, the H_3PO_4 complex, and the $(COOH)_2$ complex, two pairs of resonance lines were observed at liquid nitrogen temperature. On the other hand, three closely spaced pairs of resonance lines were observed in the NH_4Cl complex. These lines could not be paired because the third possible resonance line $\nu_d=\nu_+-\nu_-$ could not be observed on account of its very low frequency. Accordingly, the quadrupole coupling constants and the asymmetry parameters in these complexes were derived from the average values of ν_- and ν_+; they are listed in Table 1.

The average temperature coefficient $\langle\alpha\rangle$ was calculated by the following equation:

$$\langle\alpha\rangle = 2(\nu_1-\nu_2)/[(\nu_1+\nu_2)(T_1-T_2)], \qquad (2)$$

where ν_1 and ν_2 are the resonance frequencies of the ν_+ lines at liquid nitrogen temperature (T_1) and about 275 K (T_2), respectively. These coefficients in the complexes are calculated as listed in Table 1, and decrease in the order of the $(COOH)_2$ complex, the HNO_3 complex, and the H_3PO_4 complex. Every coefficient is smaller than the value in urea, which is calculated from the reference[9] to be 13.43×10^{-5} deg^{-1}. This fact suggests that the vibrations of the nitrogen atoms in the urea molecules are suppressed in the order of urea, the $(COOH)_2$ complex, the HNO_3 complex, and the H_3PO_4 complex, that is, the strength of the hydrogen bonds, N–H···O, increases in this order. On the other hand, in the NH_4Cl complex, the temperature dependence of three ν_+ lines was nearly equal, and the resonance line ($\nu=2.9318$ MHz), the intensity of which was largest among in these lines, could be observed at about 200 K, whereas the other two lines were able to be observed at about 190 K. Therefore, the average temperature coefficient was calculated between liquid nitrogen temperature and about 200 K for the line ($\nu=2.9318$ MHz); the value

TABLE 1. NQR PARAMETERS AND THE AVERAGE TEMPERATURE COEFFICIENTS IN UREA COMPLEXES

Complex	ν_- / MHz	ν_+ / MHz	$\lvert e^2Qq/h\rvert$ / MHz	η	$\langle\alpha\rangle$ / deg^{-1}
$OC(NH_2)_2 \cdot HNO_3$	2.0505 1.9347	2.7828 2.7015	3.157	0.475	8.37×10^{-5}
$OC(NH_2)_2 \cdot H_3PO_4$	2.1476 2.0901	2.8159 2.7783	3.277	0.414	4.95×10^{-5}
$OC(NH_2)_2 \cdot (COOH)_2$	2.3701 2.1863	2.9634 2.8484	3.456	0.363	11.24×10^{-5}
$OC(NH_2)_2 \cdot NH_4Cl$	2.4335 2.4006 2.3473	2.9488 2.9318 2.8853	3.544	0.298	14.97×10^{-5}

is listed in Table 1. The temperature coefficient in the NH_4Cl complex is larger than that in urea. This suggests that the hydrogen bond in this complex, N–H···Cl, is weaker than the bond in urea, N–H···O. This may be explained by the difference of the electronegativities between a chlorine atom and an oxygen atom.

According to the results of the neutral diffraction study of the HNO_3 complex[5] and the X-ray diffraction studies of the H_3PO_4 complex and the $(COOH)_2$ complex,[6,7] the geometry of the NH_2 groups in these complexes is nearly equal to that in urea; we thus assumed the nitrogen σ-bond orbitals to be sp^2-hybrids. In the case of the NH_4Cl complex, there are three crystallographically nonequivalent nitrogen atoms, and each nitrogen atom forms two weak hydrogen bonds with a chlorine ion of ammonium chloride, the length of which is in the range from 3.14 to 3.40 Å.[8] Therefore, the electronic state of nitrogen atom in the NH_2 group may be considered not to be largely different from that in urea; we thus assumed that the nitrogen σ-bond orbitals are sp^2-hybrids.

The electron densities at the nitrogen atoms in these complexes can be calculated by means of the following equations:[10]

$$\alpha = |e^2Qq/e^2Qq_p| = n - (2/3)\sigma_{NH} - (1/3)\sigma_{NC}, \qquad \alpha\eta = \sigma_{NH} - \sigma_{NC}, \tag{3}$$

where n is the electron density in the lone-pair orbital; σ_{NH} and σ_{NC} are the σ-electron densities in the N–H and N–C bonds, respectively; and $|e^2Qq_p/h|$ is the quadrupole coupling constant due to one 2p-electron of a nitrogen atom. The α and $\alpha\eta$ values in urea and its complexes are denoted by α^u, $(\alpha\eta)^u$, α^c, and $(\alpha\eta)^c$. Defining the differences in the α and $\alpha\eta$ values between urea and its complexes by $\Delta\alpha=\alpha^u-\alpha^c$ and $\Delta(\alpha\eta)=(\alpha\eta)^u-(\alpha\eta)^c$,

$$\Delta\alpha = (n^u-n^c) - (2/3)(\sigma^u_{NH}-\sigma^c_{NH}) - (1/3)(\sigma^u_{NC}-\sigma^c_{NC}), \qquad \Delta(\alpha\eta) = (\sigma^u_{NH}-\sigma^c_{NH}) - (\sigma^u_{NC}-\sigma^c_{NC}) \tag{4}$$

are obtained. Letting

$$\Delta n = n^u - n^c, \ \Delta\sigma_{NH} = \sigma^u_{NH} - \sigma^c_{NH}, \text{ and } \Delta\sigma_{NC} = \sigma^u_{NC} - \sigma^c_{NC} \tag{5}$$

then

$$\Delta\alpha = \Delta n - (2/3)\Delta\sigma_{NH} - (1/3)\Delta\sigma_{NC}, \qquad \Delta(\alpha\eta) = \Delta\sigma_{NH} - \Delta\sigma_{NC}. \tag{6}$$

Assuming that in these complexes $\Delta\sigma_{NC}=0$ and $|e^2Qq_p/h|=9$ MHz, the $\Delta\sigma_{NH}$ and Δn values can be calculated from Eq. 6; the values are listed in Table 2.

TABLE 2. THE $\Delta\sigma_{NH}$ AND Δn VALUES IN THE MOLECULAR COMPLEXES OF UREA

Complex	$\Delta\sigma_{NH}$	Δn
$OC(NH_2)_2 \cdot HNO_3$	−0.04	−0.01
$OC(NH_2)_2 \cdot H_3PO_4$	−0.03	−0.01
$OC(NH_2)_2 \cdot (COOH)_2$	−0.01	0
$OC(NH_2)_2 \cdot NH_4Cl$	+0.01	0

The $\Delta\sigma_{NH}$ values in the HNO_3 complex, the H_3PO_4 complex, and the $(COOH)_2$ complex are negative. This indicates that the hydrogen bonds in these complex are stronger than that in urea. On the contrary, in the case of the NH_4Cl complex, the $\Delta\sigma_{NH}$ value is positive so that the hydrogen bond in this complex is weaker than the bond in urea.

On the other hand, the Δn values in the HNO_3 complex and the H_3PO_4 complex are positive, that is, the electron populations in the lone-pair orbitals of the nitrogen atoms in the urea molecules are smaller in these complexes than in urea. This may be explained by the decrease of the lone-pair electron population due to the formation of the hydrogen bond such as N···H–N, in which the lone-pair orbital of a nitrogen atom is used, or to the increase of the contribution of the following resonance structures II and III. However,

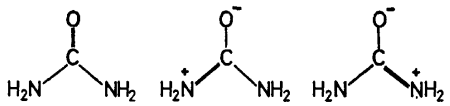

I II III

the hydrogen bond such as N···H–N is absent in these complexes[5,6] and urea.[10] Therefore, the decrease of the lone-pair electron is attributed to the latter reason. The resonance structures bring about the increase of the double-bond character in the N–C bond in the urea molecule, resulting in the shortening of this bond. The average N–C bond lengths are 1.314 Å in the HNO_3 complex and 1.322 Å in the H_3PO_4 complex, whereas the value in urea is 1.352 Å.[11] Furthermore, it is considered that the negative charge on the oxygen atom of the urea molecule increases and the C–O bond becomes longer because of the contribution of the structures II and III in these complexes. From these combined effects, the strong hydrogen bond, O···H–O, is formed. In fact, the C–O distances in urea, the HNO_3 complex, and the H_3PO_4 complex, are 1.260, 1.298, and 1.281 Å, respectively. The O···H–O dis-

tances in the HNO_3 complex and the H_3PO_4 complex are 2.596 and 2.424 Å respectively, and the acidic protons are attached to the carbonyl oxygen atom of urea.

References

1) K. Aida, *J. Inorg. Nucl. Chem.*, **25**, 165 (1963).
2) H. Negita, T. Kubo, and M. Maekawa, *Bull. Chem. Soc. Jpn.*, **50**, 2215 (1977).
3) H. Negita, T. Kubo, M. Maekawa, A. Ueda, and T. Okuda, *Bull. Chem. Soc. Jpn.*, **52**, 1881 (1979).
4) Y. Abe, *J. Phys. Soc. Jpn.*, **18**, 1804 (1963).
5) J. E. Worsham, Jr., and W. R. Busing, *Acta Crystallogr., Sect. B*, **25**, 572 (1969).
6) E. C. Konstansek and W. R. Busing, *Acta Crystallogr., Sect. B*, **28**, 2454 (1972); D. Mootz and K. R. Albrand, *ibid.*, **28**, 2459 (1972).
7) S. Harkema, J. W. Bats, A. M. Weyenberg, and D. Feil, *Acta Crystallogr.*, **28**, 1646 (1972).
8) A. Rimsky, *Bull. Soc. Fr. Mineral Crist.*, **83**, 187 (1960).
9) T. Chiba, M. Toyama, and Y. Morino, *J. Phys. Soc. Jpn.*, **14**, 379 (1959).
10) E. A. C. Lucken, "Nuclear Quadrupole Coupling Constants," Academic Press, London and New York (1969), p. 225; T. Oja, *J. Chem. Phys.*, **59**, 2668 (1973).
11) P. Vaughan and J. Donohue, *Acta Crystallogr.*, **5**, 530 (1952).
12) A. W. Pryor and P. L. Sanger, *Acta Crystallogr., Sect. A*, **26**, 543 (1970).

Electron Spin Resonance Study on the Difference of Structure in Diastereomeric Nitroxyl Radicals

Yashige KOTAKE* and Keiji KUWATA

Department of Chemistry, Faculty of Science, Osaka University, Toyonaka, Osaka 560

(Received July 5, 1980)

Electron spin resonance spectra of nitroxyl radicals bearing two asymmetric carbons were observed. The radicals were produced by the abstraction of a hydrogen atom from ethers and amines by photoexcited benzophenone, followed by spin trapping with phenyl-*N*-*t*-butylnitrone. The spectra showed the presence of two radical species assignable to diastereomers in most cases. The presence of isomers was seen more clearly in ESR spectra of radicals produced from ethers than those from amines. The origin of the different ESR parameters of the isomer was discussed in detail and it was concluded that the functional group on β-carbon acts as a group of proximity to nitroxyl function. The difference of the electronegativity of the atom in each functional group causes the difference of the extent of the separation of isomers. The effects of proximity groups on observed ESR parameters are concluded to be the same as the solvent effect.

Diastereomers have chemically different properties. Different spectroscopic properties are also found, which are caused by the difference in the interaction of substituents.

As for free radicals having two chiral centers, it is possible to identify each diastereomer by ESR spectroscopy. Jonkman *et al.* detected the difference of hyperfine structure (hfs) in nitroxyl radicals having two asymmetric carbons on both sides of the nitroxyl function.[1] Also, Laroff *et al.* observed the difference of hfs in anion radicals from both ascorbic and araboascorbic acid.[2] However, the difference has not been discussed in relation to the structure of the radical because of the difficulty in systematic production of radicals.

Recently, it was pointed out that the spin trapping reaction using phenyl-*N*-*t*-butylnitrone (PBN, *N*-benzylidene-*t*-butylamine *N*-oxide) is an effective way of producing nitroxyl radicals having two asymmetric carbons on one side of the nitroxyl function.[3] In the case of spin adducts produced from alcohol, a clear separation of hfs of the isomer was detected in an aprotic solvent; this was attributed to the formation of an intramolecular hydrogen bond. In the present study the difference of ESR parameters was also observed in open chain diastereomeric nitroxyls.

The condition which should be fulfilled for the detection of the difference in ESR parameters in an open chain diastereomeric nitroxyl radical is that the substituents attached to the asymmetric carbons should be bulky. The nitroxyl radicals produced by the addition of the radical formed by the abstraction of a hydrogen atom from an etherial compound have an alkoxyl group on β-carbon. Also, those from amines have amino or alkylamino group on β-carbon. In these radicals most of the substituents on β-carbon are bulky. In addition, there is no functional group to form tight hydrogen bonding.

The notable experimental result shown in this report is that the separations of isomers in spin adducts from ethers were much larger than those from amines. Moreover, the reproduction of the spectrum by the spectrum simulation showed that the difference of the g-value and hfs of $^{14}N(A_N)$ play a dominant role in giving the characteristic overlapped spectrum pattern. The hfs of β-H ($A_{\beta H}$) depends on the magnitude of the dihedral angle, which is directly derived from the steric conformation. The g-value and A_N depend on the electronic and steric structure of nitroxyl group. Thus, the result was interpreted by the difference of the dipole moment of CO bond and CN bond when they act as a group of proximity to the nitroxyl group. This leads to the conclusion that the difference of g- and A_N-value in stereoisomer of spin adducts from ether is based on the difference in the distance between oxygen atom and nitroxyl group. The effect of a proximity group is shown to be the same as the solvent effect on nitroxyl radicals.

Experimental

Approximately 10^{-4} mol PBN and 10^{-4} mol benzophenone was dissolved in 1 cm^3 ether and amine. The solution was packed into a pyrex ampoule having an ESR sample tube as a side arm and was degassed by the freeze-pump-thaw method. Radicals are produced by the irradiation of UV light from an 1 kW mercury arc.[3,4] The period of irradiation was 5 to 10 min, depending on the yield of radicals.

The PBN used was purified by the sublimation technique. Benzophenone was recrystallized twice from a petroleum ether solution. Guaranteed grade ethers were treated with potassium hydroxide to remove peroxy derivatives and were dried over Na–K alloy. Amines were distilled and stored over potassium hydroxide. The ampoule were charged with ether or amine by vacuum distillation.

The solvent effect on the spectral pattern was examined in some cases with the use of same technique as described elsewhere.[3]

The hfs and g-value were determined by use of aqueous solution of potassium peroxylamine disulfonate buffered with 0.2 M K_2CO_3 solution. The solution was packed in a capillary tube and attached on the sample tube, ESR spectra being recorded simultaneously. The g-value and ^{14}N hfs have been reported to be 2.005560 ± 0.000004[5] and 13.091 ± 0.004,[6] respectively. Computer spectrum simulation was applied to analyze the overlapped spectra.

Results and Discussion

Ether. It is well known that photoexcited benzophenone abstracts hydrogen on the carbon adjacent to the etherial oxygen.[4–10] When one applies the spin trapping reaction with PBN, the assignment

of the resulting radical is sometimes ambiguous because of the absence of the hfs from the trapped group. However there have been some examples in which the hfs from the trapped group appears.[11] Also, the ENDOR study of spin adducts has clearly shown the presence of the hfs from trapped groups.[12] In the present experiment, the spin adducts from anisole showed the hfs of methylene proton in phenoxymethyl group. Therefore, it is reasonable to assign the nitroxyl radicals as spin adducts of a radical hydrogen abstracted from the carbon adjacent to the etherial oxygen.

The ethers chosen as radical sources are symmetric to avoid a system which would produce two different radicals to be trapped. The reaction scheme for the production of the nitroxyl radical is as follows:

$$(RCH_2)_2O \longrightarrow R\dot{C}HOCH_2R$$

$$R\dot{C}HOCH_2R + \text{Ph-CH=N}(\text{O})\text{-}C(CH_3)_3 \longrightarrow \text{Ph-}\overset{*}{C}H(\text{R-}\overset{*}{C}H\text{-OCH}_2R)\text{-N}(\dot{O})\text{-}C(CH_3)_3 \quad (1)$$

The formed radical should have an open chain structure because there is no donative hydrogen which is capable of forming an appreciable intramolecular hydrogen bond. The fact that the hfs of β-hydrogen was very insensitive to the change of solvent from aprotic to protic shows the absence of intramolecular hydrogen bonds.

Figure 1A shows a typical ESR spectra observed in the etherial system. In tetrahydrofuran, the spectrum shows an asymmetric pattern due to the presence of two radical species. These are reproducible by means of spectrum simulation by overlapping two ESR spectra which have four different parameters, namely $A_{\beta H}$, A_N, g-value, and linewidth. The stick spectrum in Fig. 1A shows the position of the ESR lines from each radical. Almost all ethers tried in this experiment gave ESR spectra which showed the presence of two radical species which have different hfs and g-value. The result of the analysis for several etherial spin adducts are listed in Table 1.

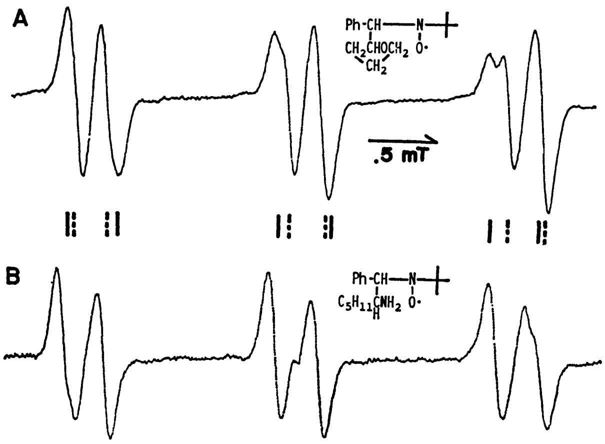

Fig. 1. ESR spectra of nitroxyl radicals produced by spin trapping with PBN.
A: From tetrahydrofuran, B: from *n*-hexylamine. Stick spectrum shows the line position of spectrum A.

In order to confirm that the overlapped spectrum is due to two asymmetric carbons, some radical sources which cannot produce the spin adducts with two asymmetric carbons by reaction (1) were examined. Diisopropylether, anisole (Fig. 2A), and 1,3,5-trioxane were chosen for this purpose. All of the resulting spin adducts showed a symmetric line shape and can be assignable to single radical species.

Table 1 shows that the radical with larger $A_{\beta H}$ has smaller A_N and larger g-value. Therefore the resolution

Table 1. Hyperfine splitting constants of nitroxyls produced from ethers

Parent ether	R[a)]	R′[b)]	R″[c)]	$A_{\beta H}$ / 10^{-4} T	A_N / 10^{-4} T	Δg[d)] / 10^{-4} T	ΔH_{msl}[e)] / 10^{-4} T
Ethyl ether	H	CH_3	C_2H_5	2.5 1.7	14.6 15.0	0.2	1.1 1.0
Propyl ether	H	C_2H_5	C_3H_7	2.4 1.7	14.2 14.6	0.2	1.3 1.0
Butyl ether	H	C_3H_7	C_4H_9	2.6 1.8	14.5 15.0	0.2	1.0 0.8
Tetrahydrofuran	H	CH_2–	CH_2–	2.5 1.7	14.3 14.7	0.2	1.0 0.8
Tetrahydopyran	H	CH_2–	CH_2–	2.5 1.7	14.3 14.8	0.2	1.3 1.0
Dioxane	H	CH_2–	CH_2O–	2.4 1.6	14.6 15.0	0.2	1.3 1.0
Phenylethyl ether	H	CH_3	Ph	2.4 1.5	14.2 14.5	0.2	1.3 1.0
Isopropyl ether	CH_3	CH_3	$CH(CH_3)_2$	2.3	14.5		
Trioxane	H	CH_2O	CH_2O	2.1	14.7		
Anisole	H	H	Ph	2.5[f)]	14.7		

a), b), c) Substituents in the structure shown as $\text{Ph-CH(R-C(R')-OR'')-N}(\dot{O})\text{-}C(CH_3)_3$. d) First set minus second set. 10^{-4} T corresponds to the g difference of 0.0007 at the observed external field. e) Maximum slope line width of Gaussian line shape used for spectrum simulation. f) $A_{\gamma H}=0.4\times10^{-4}$ T (2H).

of lines from each radical is the best for the high field doublet, as is noticed in the spectra of Fig. 1A. It is also noted that the ESR parameters do not largely depend on the difference of R′ and R″.

Amine. Photoexcited benzophenone also abstracts hydrogen on the carbon adjacent to each amino group.[13-15] To avoid the formation of spin adducts of different substituents from a single amine source, chosen secondary and tertiary amines have a symmetric structure in which alkyl groups are the same. The reaction scheme of the formation of the radical in a primary amine is as follows:

$$RCH_2NH_2 \longrightarrow R\dot{C}HNH_2$$

$$R\dot{C}HNH_2 + Ph\text{-}CH{=}N^{+}(O^{-}) \longrightarrow Ph\text{-}\overset{*}{C}H\text{-}N^{+}(O\cdot)\text{-}\overset{*}{C}(H)(R)\text{-}NH_2 \quad (2)$$

Figure 1B shows the typical recorder trace for the adduct from hexylamine. The difference in the ESR spectral pattern in diastereomer is small compared to the radical from ether. The results of the analysis using spectrum simulation are listed in Table 2. The difference of the ESR parameters of isomers is mainly characterized by the magnitude of $A_{\beta H}$. However, the difference within an isomer is very small when R and R′ are small substituents. Isopropylamine was chosen as a source of radical which cannot produce diastereomers. The ESR spectrum shows the presence of a single radical (Fig. 2B).

The solvent effect on the spectral pattern was also very poor in both protic and aprotic solvents, which showed that the structure of the alkylamino adduct is open chain.

Interpretation of the Difference of ESR Parameters in Isomer. By the inspection of the ESR parameters summarized in Tables 1 and 2, one can find some

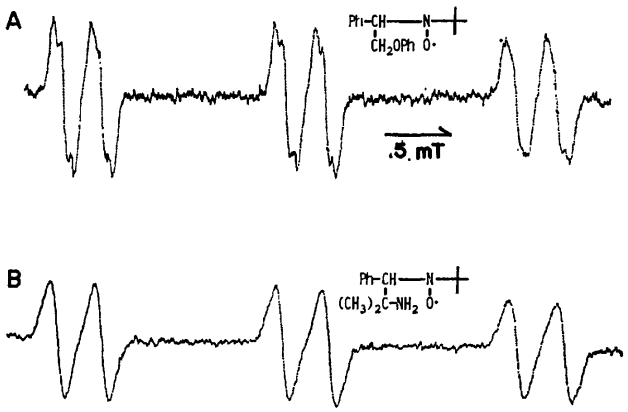

Fig. 2. ESR spectra of nitroxyl radicals produced by spin trapping with PBN.
A: From anisole, B: from isopropylamine.

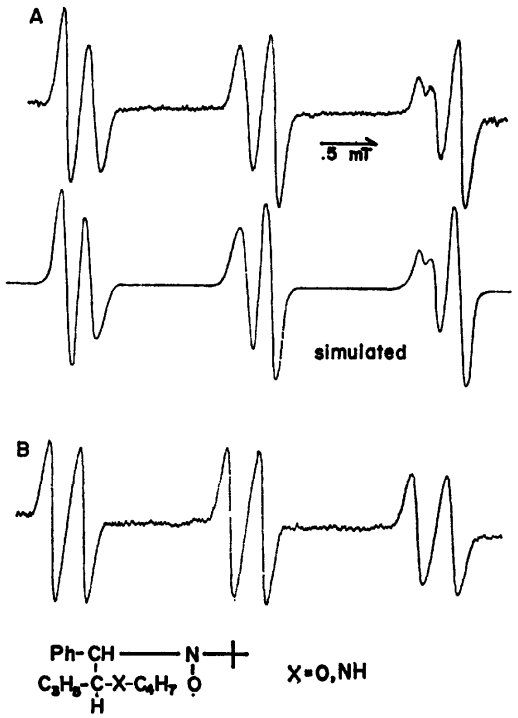

Fig. 3. ESR spectra of nitroxyl radicals produced by spin trapping with PBN.
A: From butyl ether, B: from dibutylamine.

TABLE 2. HYPERFINE SPLITTING CONSTANTS OF NITROXYLS PRODUCED FROM AMINES

Parent amine	R[a]	R′[b]	R″[c]	$\frac{A_{\beta H}}{10^{-4}\,T}$	$\frac{A_N}{10^{-4}\,T}$	$\frac{\Delta g^{d}}{10^{-4}\,T}$
Propylamine	H	C_2H_5	NH_2	2.8	15.1	
Butylamine	H	C_3H_7	NH_2	2.7	14.7	
Hexylamine	H	C_5H_{11}	NH_2	2.7 3.0	14.8 15.0	0
Diethylamine	H	CH_3	NHC_2H_5	2.9	14.8	
Dibutylamine	H	C_3H_7	NHC_4H_9	2.6	14.8	
Triethylamine	H	CH_3	$N(C_2H_5)_2$	1.9 2.3	15.1 15.3	0.1
Phenethylamine	CH_3	Ph	NH_2	2.5 2.9	14.6 14.8	0
Isopropylamine	CH_3	CH_3	NH_2	2.8	14.7	

a), b), c) Substituents in the structure shown as Ph–CH(R′)(R″)–N(O·)–+. d) First set minus second set. 10^{-4} T corresponds to the g difference of 0.0007 at the observed external field.

contrast due to the difference of radical sources. The difference within each diastereomer is larger for the spin adducts from ether than those from amines. This is illustrated in Fig. 3 as the comparison of the ESR spectra of the adducts produced from dibutyl ether and dibutylamine. In spite of the similarity of the structure of the radical, the extent of the separation of the isomer in ESR spectra is very different. In particular, the difference of A_N and g-value can be noted from Table 1. It is also noted that the dependence of ESR parameters on the bulkiness of R, R′, and R″ is poor. The origin of the difference is discussed in connection with the steric structure of radicals.

Conformation of Radical: Though the radical has an open chain structure, the most probable conformation of the molecule can be specified because of the bulkiness of the substituents. Based on the fact that the magnitude of the $A_{\beta H}$ is 0.2 to 0.3 mT, the dihedral angle between C–H_β and the unpaired electron orbital is estimated to be around 70° to 80° by McConnell's $\cos^2\theta$ rule.[16,17]

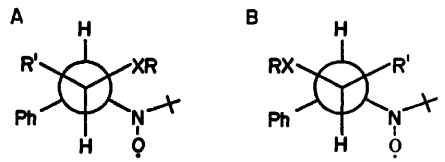

Fig. 4. Steric conformation of diastereomeric nitroxyls. Note the distance between X and N.

The most probable conformation around C_α and C_β is *trans* with respect to two hydrogens considering the smallest possible interaction between substituents.[18] Then the difference of the configuration in diastereomer produces the difference of the conformational structure, as illustrated in Fig. 4. It is noted that in one stereoisomer (Fig. 4A) the distance between XR and NO is closer than in the other. In the structure shown in Fig. 4, the dominant steric interactions between substituents are (R′-Ph) and (XR-NO) for Fig. 4A and (R′-NO) and (XR-Ph) for Fig. 4B. The repulsive interactions among (XR-Ph) and (R′-Ph) are effective for the determination of the equilibrium conformations which cause the characteristic $A_{\beta H}$ for each radical. In contrast, the interactions shows (XR-NO) and (R′-NO) should be effective not only in determining the conformation but in changing the electronic structure of the nitroxyl group. The change of the electronic state of nitroxyl group reflected on the g-value and A_N.

By taking into account the fact that the bond angles of C–O–C and C–N–C are around 110°, the total structures of the spin adducts from dialkyl ether and dialkylamine are very similar. In spite of such similarities of the structure, the extents of the separation of the ESR parameters are very different.

It is now almost clear that the difference is caused by the presence of oxygen and nitrogen atoms in the side chain of each radical. The difference of the magnitude of the perturbation from oxygen and nitrogen decides the difference of the spectral pattern.

Proximity Effect on Nitroxyl Group: As has been discussed by many investigators, the solvent effects on the ESR parameters of nitroxyl radicals can be explained qualitatively by the amount of contribution from each resonance structure shown below:

$$\underset{\text{I}}{\text{N-O}\cdot} \rightleftharpoons \underset{\text{II}}{\dot{\text{N}}^{+}\text{-O}^{-}}.$$

The effect of increasing the dipole moment of the solvent results in the increase of the contribution from structure II. This also explains the result of the present experiment: If one replaces the dipole moment of the solvent by the bond moment[19] of the proximity group, the larger bond moment of C–O bond explains that the separation of the isomer in the spin adducts from ether is larger than in those from amines which are perturbed by the bond moment of C–N.

The present experimental result of the solvent effect on A_N and g-value also supports the interpretation. The shifts of A_N and g-value are almost the same for the isomer in various solvents. Also, $A_{\beta H}$ did not change appreciably by the solvent. As a result the manner of the overlap of the two spectra of isomer did not change. This shows that the interaction which determines the spectral pattern is an intramolecular one which acts in a way additive to the solvent effect.

The solvent effect on the ESR parameters of the nitroxyl radicals has been analyzed on a molecular orbital basis. Kawamura *et al.* thoroughly described the solvent effect on g-value and A_N of di-*t*-butyl nitroxyl radical on the basis of a molecular orbital treatment.[20] As regards the A_N of the present system the effect of the neighboring group on each nitroxyl function can be explained by a simple MO scheme. The inspection of Dreiding model tells us that the hetero atom (X) in Fig. 4B is very close to the p orbital of nitrogen atom. The simplest MO feature of nitroxyl group is that the three electrons are in orbitals derived from linear combinations of the nitrogen and oxygen 2p orbitals. The bonding orbital is occupied by two electrons and the antibonding orbital is occupied by the unpaired electron. The effect of the nearby electronegative group on the 2p atomic orbital of the nitrogen atom is identical to the decrease of the absolute value of the Coulomb integral of the nitrogen. Consequently, the nitrogen character of π^* orbital increased, resulting in the increase of the A_N. The extent of the increase depends on the electronegativity of the hetero atom in the neighboring group. Therefore, the larger separations of the isomer in the adducts from ether than in those from amines can be explained.

Moreover the discussion above makes the assignment of the isomer possible. The isomer which has larger A_N value is assignable to the structure shown in Fig. 4B.

In alkylamino adduct the presence of diastereomer was detected clearly when the higher alkylamine was chosen as the radical source. The inspection of Table 2 tells us that the difference of g-value was small and the spectrum pattern was characterized mainly by the difference of β-hydrogen hfs. It is concluded that steric hindrance is the main cause of the separation in alkylamino adduct.

References

1) J. Jonkman, H. Muller, and J. Kommandeur, *J. Am. Chem. Soc.*, **93**, 5833 (1971).
2) G. P. Laroff, R. W. Fessenden, and R. H. Schuler, *J. Am. Chem. Soc.*, **94**, 9062 (1972).
3) Y. Kotake, K. Kuwata, and E. G. Janzen, *J. Phys. Chem.*, **83**, 3024 (1979).
4) E. G. Janzen and J. I. -P. Liu, *J. Magn. Reson.*, **9**, 510 (1973).
5) M. T. Jones, R. Ahmed, R. Kastrup, and V. Rapini, *J. Phys. Chem.*, **83**, 1327 (1979).
6) R. J. Faber and G. K. Fraenkel, *J. Chem. Phys.*, **47**, 2462 (1967).
7) S. G. Cohen and S. Aktipis, *J. Am. Chem. Soc.*, **88**, 3587 (1966).
8) E. Bergmann and J. Fujise, *Ann.*, **483**, 65 (1930).
9) G. Ciamician and P. Silber, *Ber.*, **44**, 1554 (1911).
10) I. H. Leaver and G. C. Ramsay, *Tetrahedron*, **25**, 5669 (1969).
11) E. G. Janzen, Y. Y. Wang, and R. V. Shetty, *J. Am. Chem. Soc.*, **100**, 2923 (1978).
12) Y. Kotake, M. Okazaki, and K. Kuwata, *J. Am. Chem. Soc.*, **99**, 5198 (1977).
13) R. S. Davidson, *Chem. Commun.*, **1966**, 575.
14) S. G. Cohen and R. J. Baumgarten, *J. Am. Chem. Soc.*, **89**, 3471 (1967).
15) S. G. Cohen and H. M. Chao, *J. Am. Chem. Soc.*, **90**, 165 (1968).
16) C. Heller and H. M. McConnell, *J. Chem. Phys.*, **32**, 1525 (1960).
17) E. G. Janzen, *Topics Stereochem.*, **6**, 177 (1971).
18) E. L. Eliel, "Stereochemistry of Carbon Compounds," McGraw-Hill, New York, N. Y. (1962).
19) C. P. Smyth, "Dielectric Behavior and Structure," McGraw-Hill, New York (1955), p. 244.
20) T. Kawamura, S. Matsunami, and T. Yonezawa, *Bull. Chem. Soc. Jpn.*, **38**, 1935 (1965).

  Bull. Chem. Soc. Jpn., 54, 399—403 (1981)

Liposomal Membranes. IX. Fluorescence Depolarization Studies on *N*-Dansylhexadecylamine in Liposomal Bilayers

Kiyoshi Iwamoto and Junzo Sunamoto*

Department of Industrial Chemistry, Faculty of Engineering, Nagasaki University, Nagasaki 852

(Received August 9, 1980)

A fluorescent probe, *N*-dansylhexadecylamine (DSHA), was found to aggregate in aqueous media by monitoring the emission maximum, relative intensity, and polarization of fluorescence as functions of solvent polarity and probe concentration. In aqueous methanol, the *critical solvent polarity* for DSHA at a given concentration to form self-aggregates corresponded to 57% (v/v) aqueous methanol, while the *critical aggregate concentration* for the probe was 2.3×10^{-6} M in 50% aqueous methanol. In liposomal bilayers, the dansyl moiety seemed to be localized in a polar region close to the surface of membranes. Fluorescence characteristics of DSHA in liposomes as a function of incubation temperature revealed the phase transition of liposomal bilayers, which was almost consistent with those previously estimated by other methods. As the salt concentration was increased up to about 1.5 M, DSHA in liposomes underwent the phase separation and formed self-aggregates even in liposomal bilayers.

In recent years fluorescence techniques have been extensively applied to study on the dynamic and static nature of biological membranes,[1] liposomes,[2] and aqueous[3] or reversed micelles.[4] Since the rotation rate of fluorescent probes closely relates to the resistance offered by the microenvironment against the mobility of the probes,[5] fluorescence depolarization provides useful information about the apparent "microviscosity" in terms of the environmental resistance. Shinitzky and Barenholz have recently studied on the fluidity and phase transition characteristics of single-walled and multilamellar liposomes of synthetic phospholipids using 1,6-diphenyl-1,3,5-hexatriene (DPH) as a probe to know the nature of hydrophobic domain of liposomal bilayers.[6,7] On the other hand, to obtain the information about the surface of membranes 8-anilino-1-naphthalenesulfonate (ANS) has been employed.[8] Romero *et al.* adopted *N*-dansyloctadecylamine(DSOA) to obtain a knowledge about the less polar region of phospholipid bilayers,[9] since the fluorophore is localized in the vicinity of the phospholipid ester moiety.[10] The present studies have been undertaken using *N*-dansylhexadecylamine (DSHA) to measure the fluidity and microenvironment of the region close to the hydrophilic surface of bilayers as a function of incubation temperature or ionic strength. Besides these problems, in conjunction with Nagaraj and Balaram's postulate that the dansylated hydrophobic peptides aggregate in water,[11] we have studied also on the self-aggregation of DSHA by measuring fluorescence spectra and depolarization at very low concentrations in aqueous media and in bilayers as well.

Experimental

Materials. Egg yolk lecithin (egg L) was isolated and purified from fresh egg yolk as described before.[12,13] Dipalmitoyl-DL-α-phosphatidylcholine (DPPC) was purchased from Sigma Chemical Co., St. Louis, Mo. Phospholipids employed were found to be pure on TLC (a precoated silica gel plate, Spotfilm, Tokyo Kasei, Tokyo) as developed with chloroform/methanol/water (65 : 25 : 4, by vol).[12,13] *N*-Dansylhexadecylamine was prepared according to the method described in literature[9,14] with minor modification. A mixture of hexadecylamine (482 mg, 2.0 mmol) and dansyl chloride (593 mg, 2.1 mmol) was refluxed for 14 h in 20 ml of chloroform containing 3.0 ml of triethylamine. The resulting reaction mixture was washed six times with 50 ml of 10% aqueous citric acid and then twice with 50 ml of water, and the chloroform layer was dried over anhydrous magnesium sulfate. Removing off the solvent *in vacuo* gave a pale yellow crystalline mass, which was recrystallized from ether; yield, 540 mg (57%); mp 59—61 °C. Found: C, 70.16; H, 9.88; N, 5.77%. Calcd for $C_{28}H_{46}N_2O_2S$: C, 70.85; H, 9.77; N, 5.90%. IR (KBr): ν_{NH}, 3290; ν_{C-H}, 2930, 2860, 1592; ν_{S-O}, 1320 and 1150 cm^{-1}. Other organic and inorganic reagents were commercially available as analytical grade and used without further purification.

Preparation of Liposomes. Single-walled liposomes of egg L and DPPC were formed and isolated by the same method as that described previously.[12,15] Gel-filtration was carried out on a Sepharose 4B column (1.8×38 cm) equilibrated in water containing a given amount of sodium chloride. The concentration of liposomal suspension was determined as inorganic phosphate according to Allen's procedure.[16] The molar ratio of phospholipid to DSHA was in a range of 250—300.

Fluorescence and Depolarized Fluorescence Measurements. Fluorescence spectra and depolarization were measured by the essentially same procedures as those described before.[17,18] All the spectral measurements were run on a Hitachi 650-10S fluorospectrophotometer equipped with a thermoregulated cell compartment connecting to a Toyo Thermo Electric TE-104S.

The fluorescence polarization p is calculated by Eq. 1:

$$p = \frac{I_{VV} - C_f I_{VH}}{I_{VV} + C_f I_{VH}}, \quad (1)$$

where I is the fluorescence intensity and subscripts V and H refer to the vertical and horizontal orientations of the excitation (first) and analyzer (second) polarizers, respectively. C_f ($=I_{HV}/I_{HH}$) is the grating correction factor.[19] Depolarization measurements were run on a Union Giken fluorescence polarization spectrophotometer FS-501S using a sharp cut-filter Y-46 (Hoya Glass Works, Tokyo), of which cell compartment was connected to a Komatsu-Yamato Coolnics Model CTR-120. A Sord Microcomputer M 200 Mark II system was adopted to control the measurement conditions and to collect all the data.

Results and Discussion

Fluorescence Characteristics of DSHA in Homogeneous System. Both the emission maximum and intensity of DSHA were highly sensitive to solvents adopted as

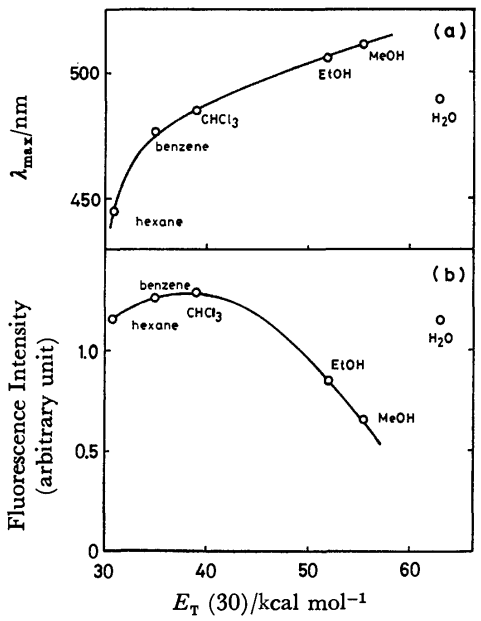

Fig. 1. Emission maximum (a) and relative intensity (b) of fluorescence from DSHA (8.6×10^{-6} M (1M=1 mol dm^{-3})) as a function of solvent polarity at 25.0 °C.

shown in Fig. 1. In apolar solvents, increasing the solvent polarity brings about a red shift of the maximum and a hypsochromic effect on the intensity. Interestingly, on the other hand, in polar protic solvents such as alcohols and water further increasing the solvent polarity causes a decrease in the intensity. In any event, the fluorescence characteristics of DSHA in water is rather different from those in organic solvents (Fig. 1).[9]

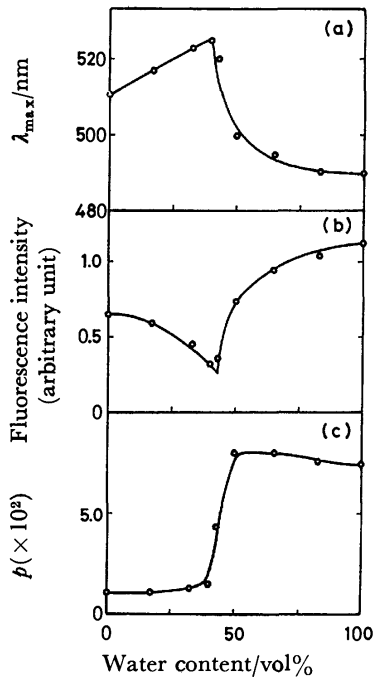

Fig. 2. Emission maximum (a), relative intensity (b), and polarization (c) of fluorescence from DSHA (8.6×10^{-6} M) in methanol as a function of water content at 25.0 °C.

When DSHA is excited at 340 nm in water, it emits the fluorescence at 487 nm. At first glance, this suggests that the microenvironment around the dansyl moiety of DSHA is close to that with the polarity of chloroform (Fig. 1). This is very interesting but unlikely. Figure 2 shows the maxima of fluorescence from DSHA in methanol as a function of water content. Up to 40% of water, the emission maximum first shifts toward a longer wavelength with an increase in the solvent polarity and further increasing the water content drastically shifts the maximum toward a shorter wavelength. Above 80% of water, it becomes almost constant (Fig. 2). The blue shift of the maximum means the translocation of the dansyl fluorophore from a polar environment to a less polar one, which means that DSHA may entangle by itself or form aggregates in aqueous media. On the basis of an evidence that a fluorophore-labeled peptide shows a blue shift of the emission maxima in an aqueous solution, Nagarj and Balaram have previously postulated an idea that peptides form micelles in water.[11] In order to confirm the self-aggregation of DSHA in aqueous media, hence, the fluorescence polarization p in methanol as a function of water content was measured (Fig. 3-c). The change of the p-value as a function of water content in methanol closely correlates with that of the emission maximum (Fig. 2-a). This suggests that DSHA molecules start to aggregate in methanol containing 43% (v/v) of water, giving rise to a decrease in the mobility. This point may be called the *critical solvent polarity* for the self-aggregation of DSHA at a given concentration. The relative intensity of fluorescence emission as a function of water content also reveals evidence for the aggregate formation of DSHA (Fig. 2-b). The self-aggregation is effected also by the DSHA concentration itself: for example, in 50% aqueous methanol the *critical aggregate concentration* for DSHA was found to be about 2.3×10^{-6} M by measuring the fluorescence spectra and depolarization. The *critical aggregate concentration* in methanol decreases with an increase in the water content.

Microenvironment around DSHA in Liposomal Bilayers. Various techniques such as NMR,[20,21] ESR,[22] and fluorescence spectroscopies[1,23] have been utilized so far to obtain information about the dynamic nature of lipid membranes. On the basis of the above results in homogeneous system where DSHA is sensitive enough to know the microscopic polarity and viscosity around the probe, in this work the fluorescence characteristics of DSHA in the liposomal bilayers were investigated. The emission maximum of DSHA in single-walled liposomes of egg L was 518 nm, while that in DPPC liposomes was 512 nm at 25.0 °C as seen in Fig. 3. The slight difference between the two liposomes must come from the difference in the state of bilayers at the temperature adopted; that is, single-walled liposomes of egg L are in a liquid-crystalline state,[24] while DPPC liposomes are in a gel state at 25.0 °C. In any event, using the ruler established for the microenvironmental polarity (Fig. 1), for both liposomes the fluorescent moiety of DSHA seems to be located in an environment with a polarity close to that of methanol. This means that the

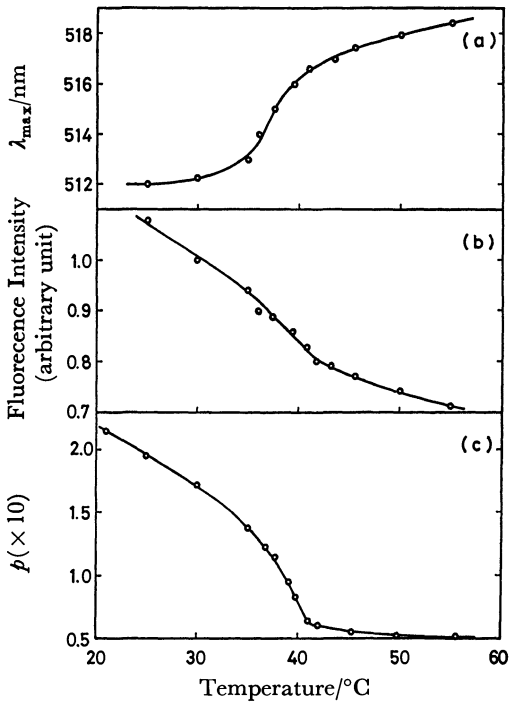

Fig. 3. Emission maximum (a), relative intensity (b), and polarization (c) of fluorescence from DSHA (4.0×10^{-6} M) as a function of incubation temperature in DPPC single-walled liposomes (8.0×10^{-4} M) dispersed in 0.1 M aqueous sodium chloride solution.

dansyl moiety is in a region close to the surface of liposomal bilayers.[9] At 55.0 °C the emission maximum of DSHA in DPPC single-walled liposomes shifts to 518.5 nm. At the temperature, DPPC liposomes are in a liquid crystalline state.[25]

Figures 3-a and -b show the maximum and relative intensity of fluorescence from DSHA in DPPC single-walled liposomes as a function of incubation temperature. Raising the incubation temperature of liposome suspension causes a red shift of the emission maximum and a simultaneous decrease in the quantum yield. Especially at temperatures between 35 and 45 °C, an abrupt change in the fluorescence characteristics was observed. The temperature-emission maximum profile reveals the phase transition between the gel and liquid crystalline states of bilayers (Fig. 3-a). Table 1 gives the phase transition temperatures determined by different techniques for DPPC liposomes, which indicates

Table 1. Phase transition temperature of DPPC single-walled liposome estimated by various techniques

Method	Phase transition temp/°C	Reference
(1) DSHA fluorescence polarization	38.4±0.5	this work
(2) DSHA fluorescence spectrum	39.0±0.5	this work
(3) Dilatometry	39	26
(4) DPH fluorescence polarization	36.4±0.5	7
(5) DPDL excimer formation	36.7±0.5	17
(6) Differential scanning calorimetry	36.9±0.9	25

that the phase transition temperature estimated in this work is in good agreement with those by other methods. As expected,[32] although the fluorescent moiety of the probe is located in the vicinity of the membrane surface, it is considerably sensitive to the phase transition of the hydrophobic domain. Table 1 also reveals that there may exist a temperature lag in the phase transition between hydrophilic and hydrophobic parts of bilayers: Methods 1—3 may reflect mostly the phase transition at the surface of bilayers, while Methods 4—6 at the deep hydrophobic domain. The most acceptable model for the conformation of phospholipid headgroups is that the headgroups lie parallel to the surface of bilayers and engage to the intermolecular electrostatic interaction with neighboring phospholipids.[27] It is well known that the motion and conformation of lecithin headgroup also change with the phase transition.[28,29] Above the phase transition temperature, the inter-headgroup interaction of lecithins is weakened and the distance between phosphorous atom and choline methyl group is far apart,[30,31] resulting in an increase in the hydration of the membrane surface.[27,32] Therefore, the red shift of emission maximum of DSHA is interpreted in terms of the increase in the polarity of the microenvironment around the probe. The correlation between the incubation temperature and the relative intensity of fluorescence was consistent with that between the temperature and the emission maximum (Fig. 3-b).

In order to monitor the mobility of the probe in egg L and DPPC single-walled liposomes, the fluorescence polarization p was measured (Figs. 3-c and 4). The increase in the fluidity of lipid membrane with raising the incubation temperature is reflected on the increase in the mobility of DSHA in bilayers. The fluorescence polarization-temperature profile also revealed the exsistence of a phase transition in the DPPC liposomes (Table 1 and Fig. 3-c). For the egg L liposomes, on the other hand, no abrupt change in the profile is observed (Fig. 4), since the egg L liposomes are in a liquid crystalline state over the temperature range adopted.[24]

The effect of ionic strength in the bulk aqueous phase on the fluorescence characteristics of DSHA in liposomal bilayers is of much interest. Above and below 1.5 M

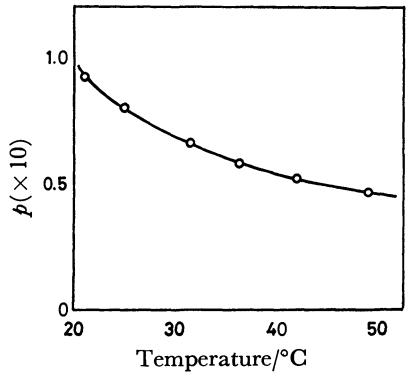

Fig. 4. Fluorescence polarization of DSHA (3.5×10^{-6} M) in egg L single-walled liposomes (8.0×10^{-4} M) dispersed in 0.1 M aqueous sodium chloride solution as a function of incubation temperature.

26) M. P. Sheetz and S. E. Chan, *Biochemistry*, **11**, 4573 (1972).
27) P. L. Yeagle, *Acc. Chem. Res.*, **11**, 321 (1978).
28) Y. K. Levine, N. J. M. Birdsall, A. G. Lee, and J. C. Metculfe, *Biochemistry*, **11**, 1416 (1972).
29) S. J. Kohler and M. P. Klein, *Biochemistry*, **16**, 519 (1977).
30) V. Viti and M. Minetti, private communication.
31) D. Lichtenberg, S. Amselem, and I. Tamir, *Biochemistry*, **18**, 4169 (1979).
32) P. L. Yeagle, W. C. Hutton, C.-H. Huang, and R. B. Martin, *Biochemistry*, **16**, 4344 (1977).
33) H. Träuble and H. Eibl, *Proc. Natl. Acad. Sci. U.S.A.*, **71**, 214 (1974).
34) G. Lindblom, N. Persson, B. Lindman, and G. Arvidson, *Ber. Bunsenges. Phys. Chem.*, **78**, 955 (1974).

Photoelectrochemical Properties of $CdSnO_3$ and $LaRhO_3$ Electrodes in Aqueous Solutions

Hiroshi YONEYAMA,* Toshikazu OHKUBO, and Hideo TAMURA

Department of Applied Chemistry, Faculty of Engineering, Osaka University, Yamadakami, Suita, Osaka 565

(Received August 21, 1980)

$CdSnO_3$ sinter electrodes work as n-type photoanodes with a high electrochemical stability in alkaline solutions. A thin film $LaRhO_3$ electrode prepared on a substrate platinum plate shows p-type photoresponse in aqueous solutions, giving rise to the hydrogen evolution with a fair stability. The threshold wavelength beyond which no photoresponse appears is *ca.* 700 nm for the former and 950 nm for the latter electrode.

The photovoltaic effect that appears on illumination of semiconductor electrodes immersed in electrolytes can be utilized to convert solar energy into either electricity or chemical substances, or the both in photoelectrochemical cells or heterogeneous chemical reaction systems.[1-8] The stability of semiconductors is essential in these applications, but most of semiconductor materials are unstable in aqueous solutions, suffering either anodic decomposition or the cathodic decomposition or the both.[9] Although a principle for stabilizing unstable semiconductor electrodes has been proposed,[10,11] semiconductors of high electrochemical stability are still desirable for elimination of any corrosion problem of photoelectrodes.

Until now several n-type semiconducting oxides have been found to possess high stabilities under anodic bias,[3,4] but searches for another stable materials are still important in the following two respects. (1) Through such investigations, a material of high electrochemical stability and negative flat-band potentials, which are essential for photoanodes in water photolysis cell,[1] may be found. (2) Besides photoelectrodes in photoelectrochemical cells, semiconductors are useful as photocatalysts. Studies in this area are steadily growing. In order to find an efficient heterogeneous reaction system using photocatalysts, investigations on the activity of photocatalysts for an objective reaction are desirable to be done for as many photocatalysts as possible, because the prediction of the activity of photocatalysts is impossible to be done in the present status. The kind of stable semiconductors is quite limited and not much enough to satisfy such requirements. By these reasons, we have been investigating photoelectrochemical properties of a variety of oxides. This paper describes our findings obtained by the investigations with such purposes.

We have found that $CdSnO_3$ having the n-type conductivity shows a high electrochemical stability with a large photoresponse which is comparable to α-Fe_2O_3, although a result showing the photoresponse has recently been reported.[12] Besides this material, we have observed that a $LaRhO_3$ thin film prepared on a substrate platinum plate shows a fairly stable p-type photoresponse in aqueous solutions. It has already been reported from studies in solid states that both $CdSnO_3$[13] and $LaRhO_3$[14] possess semiconductivity, but no conductivity type has been reported. As for the former material, however, the n-type conductivity is suggested from the finding[12] that it shows the photoresponse under anodic bias. To our knowledges, no optical properties of $CdSnO_3$ and $LaRhO_3$ have been investigated to date.

Electrochemical stabilities of these materials cannot be predicted in advance. In order to do this, we need knowledges on flat-band potentials and energy gaps of these materials.[10,11] The flat-band potentials can in principle be estimated by combining the energy gap value and the bulk electronegativity of the material[15,16] which is calculated by employing the Nethercot's hypothesis.[17] The lack of knowledge on the energy gap of $CdSnO_3$ and $LaRhO_3$, however, makes it impossible to take such an approach. In the present study, therefore, basic properties has been obtained.

Experimental

The preparation of $CdSnO_3$ was made in a manner similar to that reported by Smith.[18] Reagent grade CdO and SnO_2 powders in a molar ratio 1 : 1 were mixed in an agate mortar, and pressed into 13 mm diameter and 1 mm thickness. The pressed disc was then fired at 1000 °C for 6 h in air. According to X-ray diffraction patterns of the prepared oxide, it consisted of a $CdSnO_3$ single phase. The prepared oxide sinter was then subjected to water proofing in the following manner. The sinter was immersed in 1% polystyrene in benzene, and evacuation was made until no gas bubble was evolved from the sinter surface, followed by heating up to 100 °C to evaporate benzene. After repeating such water-proofing procedures several times, the surface of the sinter was gently polished with #2000 emery papers to remove off surface-covered polystyrene. Indium was then evaporated onto the one end face and an electrical lead wire was attached there. Finally, the sinter was mounted in a glass tube with epoxy resin to serve as an electrode.

$LaRhO_3$ was prepared on a substrate Pt plate. The Pt plate was polished with #1500 emery papers, followed by immersion in aqua regia. After boiling in a mixed solution of NaOH and Na_2CO_3 as a defatting procedure, it was washed with de-ionized water. 0.1 mol·dm^{-3} solutions of $LaCl_3 \cdot 7H_2O$ and $RhCl_3 \cdot 3H_2O$ were mixed with the same volume, and the mixed solution was applied to one side of the Pt plate in five successive coatings to give 1.2×10^{-5} mol of metal/cm^2. After each coating, the solution was dried at *ca.* 100 °C in a drying oven. The sample was then pre-heated at 480 °C for 1 h to decompose the chlorides, followed by firing at 1100 °C for 34 h in air. X-Ray diffraction peaks of the prepared sample were composed of reported diffraction peaks of Pt and $LaRhO_3$.[19] The back face and edge portions of the substrate Pt were coated with silicone adhesive(Silicone Sealant, Shinetsu Chemicals) to serve as an electrode.

Polarization measurements were carried out by using a Nikko Keisoku model DPGS-1 potentiogalvanostat. A 500 W super high pressure mercury arc lamp was used as a light

source except where measurements of action spectra of photocurrents were carried out. The action spectra were obtained with monochromatic light which was obtained by using a 500 W xenon lamp as a light source and a grating monochrometer (JASCO, model CT-25), and were not corrected for the intensity variation of the lamp-monochrometer output. Electrode capacitance *vs.* potential relations were obtained by using the bridge method as described previously.[20]

Results and Discussion

Photoelectrochemical Properties of $CdSnO_3$ Electrodes. The resistivity of the prepared samples was in a range between 1 and 10 Ω cm, as determined by the four probe method. Figure 1 shows steady state current-potential curves of the prepared electrode in 1 mol·dm^{-3} NaOH and 0.5 mol·dm^{-3} H_2SO_4. Also given in this figure are current-potential curves obtained with illumination of chopped light at 2 Hz in a mixed solution of 0.5 mol·dm^{-3} acetic acid and 0.5 mol·dm^{-3} sodium acetate. It is seen in this figure that the onset potential of the anodic photocurrents shifts towards the negative direction with a decrease in acidity, as usually observed at other oxide semiconductor electrodes.

Shottky-Mott plots of electrode capacitance *vs.* potential relations are given in Fig. 2. Although a large frequency dispersion is observed in the plots, the potentials which are obtained by extrapolating $1/C^2$ to the potential axis are in good agreements with each other between 1 and 5 kHz. Therefore, the flat-band potential determined by such plots, which is *ca.* 0.3 V *vs.* SCE in 0.5 mol·dm^{-3} H_2SO_4 and *ca.* −0.4 V *vs.* SCE in 1 mol·dm^{-3} NaOH, is of significance. The onset potential of the anodic photocurrents, given in Fig. 1, is in rough accord with the determined flat-band potentials.

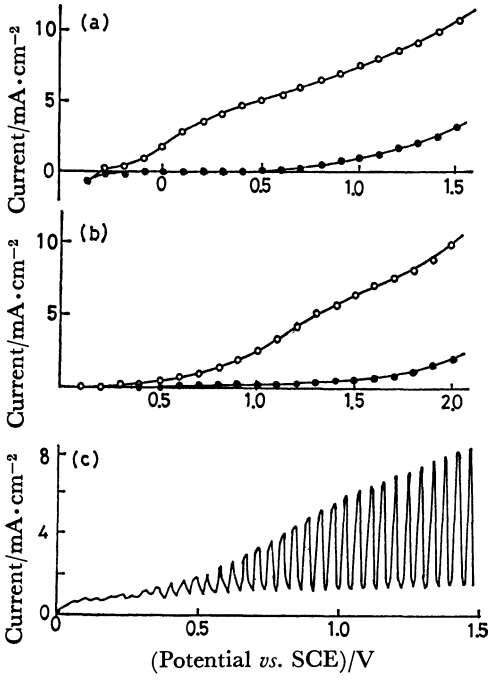

Fig. 1. Current-potential curves of $CdSnO_3$ electrode in (a) 1 mol·dm^{-3} NaOH and (b) 0.5 mol·dm^{-3} H_2SO_4 under steady state conditions, and (c) 0.5 mol·dm^{-3} acetic acid+0.5 mol·dm^{-3} sodium acetate with illumination of chopped light at 2 Hz.
○: Under illumination, ●: in the dark.

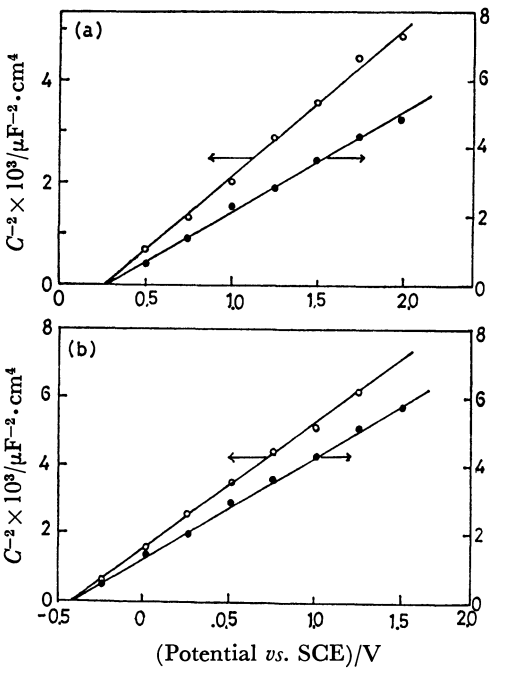

Fig. 2. Schottky–Mott plots of electrode capacitance *vs.* potential relations in (a) 0.5 mol·dm^{-3} H_2SO_4 and (b) 1 mol·dm^{-3} NaOH.
Frequency chosen; ○: 1 kHz, ●: 5 kHz.

By anodic polarization in 0.5 mol·dm^{-3} H_2SO_4, the electrode surface was gradually changed from yellow to white, suggesting that the electrode is unstable in acidic solutions. X-Ray diffraction patterns of the color-changed surface showed the existence of SnO_2. Similar observations have recently been reported for Cd_2SnO_4 electrodes.[21,22] In alkaline solutions, however,

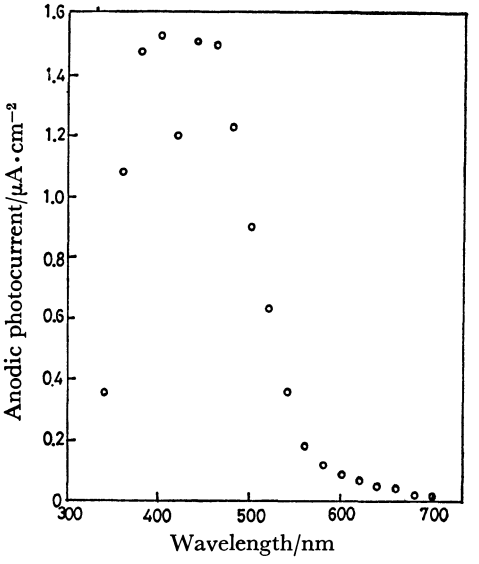

Fig. 3. Action spectrum of anodic photocurrents at $CdSnO_3$ electrode at 0.5 V *vs.* SCE in 1 mol·dm^{-3} NaOH.

the electrode was found to be fairly stable. The anodic polarization to give the total charge of 9.86 C in 0.2 mol·dm^{-3} NaOH caused anodic dissolution of the electrode less than 0.1% of the current efficiency, as determined by atomic absorption analysis of dissolved cadmium. The rest of the charge was believed to be consumed in the evolution of oxygen.

An anodic photocurrent spectrum obtained in 1 mol·dm^{-3} NaOH at 0.5 V *vs.* SCE is shown in Fig. 3, from which the response to light of wavelengths shorter than 700 nm is appreciable. A hollow in the action spectrum, observed in wavelengths between 400 and 440 nm, is believed to be due to the intensity variation in monochromatic light which is characteristics of the xenon lamp. If the assumption is made that the photoresponse is due to band-band transitions, the bandgap of $CdSnO_3$ is then obtained to be 1.77 eV.

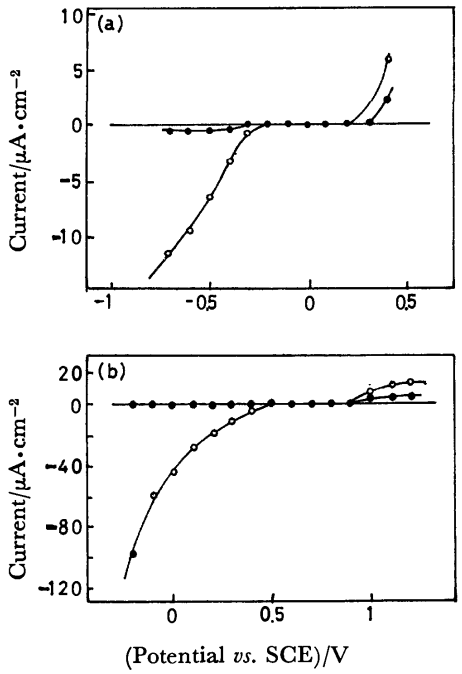

Fig. 4. Steady state current-potential curves of $LaRhO_3$ electrode in (a) 1 mol·dm^{-3} NaOH and (b) 0.5 mol·dm^{-3} H_2SO_4.
●: In the dark, ○: Under illumination.

Photoelectrochemical Properties of $LaRhO_3$ Prepared on the Substrate Pt Plate. Figure 4 shows current-potential curves of the prepared electrode in 1 mol·dm^{-3} NaOH and 0.5 mol·dm^{-3} H_2SO_4. As this figure shows, noticeable photoresponses appear in the cathodic branch. A result obtained for a stability test is given in Fig. 5. As shown in this figure, the photocurrent usually showed a spike at the instant of the on- and off-time of illumination. The appearance of the spike seems to be due to charging currents in capacitive components of the electrode which is not well known at present. It is seen in Fig. 5 that the cathodic photocurrent is so stable as to give almost the constant photocurrent with polarization for as long as 30 min.

Among a variety of oxides, Cu_2O is known to show p-type photoresponse.[10,23] However, this material is

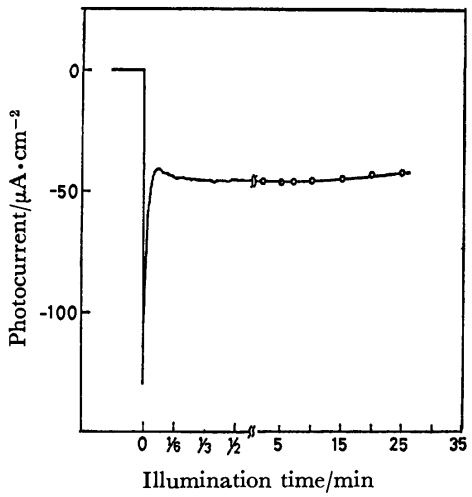

Fig. 5. Stability test of cathodic photocurrent at $LaRhO_3$ electrode at 0 V *vs.* SCE in 0.5 mol·dm^{-3} H_2SO_4.

quite easily decomposed by both anodic and cathodic polarizations. Compared to this material, $LaRhO_3$ showed no such a serious instability. Judging from the stability of photocurrents shown in Fig. 5, a large part of the cathodic charge consumed during the electrolysis for 30 min must concerned with the evolution of hydrogen. There will be of no doubt, however, that the hydrogen evolution on oxide surfaces must be accompanied with their reduction more or less. A slight decrease in the photocurrent in Fig. 5, observed after the electrolysis for 15 min, may be connected to such an electrode reduction, but still $LaRhO_3$ will be useful as a photocathode at least in aqueous solutions containing another electroactive species besides proton and water if the redox potential of the species is more positive than the hydrogen electrode potential.

An action spectrum of the cathodic photocurrent is shown in Fig. 6. Effects of the intensity variation of monochromatic light are again reflected in the action spectrum in the wavelengths between 400 and 440 nm and between 800 and 950 nm. If the threshold wavelength of the electrode, 950 nm, is assumed to be

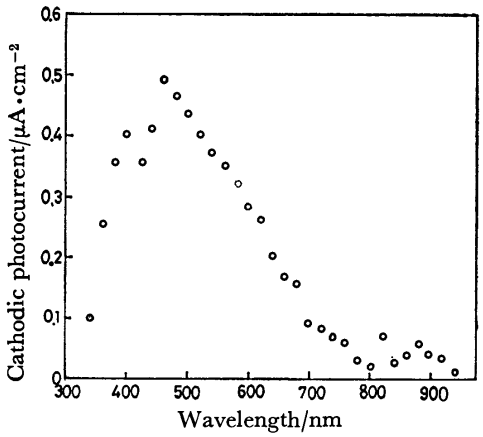

Fig. 6. Action spectrum of cathodic photocurrent at $LaRhO_3$ electrode at 0 V *vs.* SCE in 0.5 mol·dm^{-3} H_2SO_4.

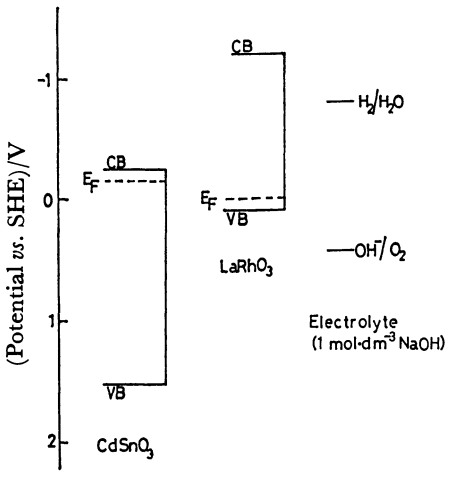

Fig. 7. Energetic correlation between electrodes and 1 mol·dm^{-3} NaOH.
CB, VB, and E_F denote the conduction band, the valence band and the Fermi level of the electrode.

determined by the bandgap of the material, it will then be 1.35 eV.

Energetic Correlation of the Electrode and Electrolytes. Figure 7 shows energetic correlations of $CdSnO_3$ and $LaRhO_3$ electrodes to the hydrogen and oxygen electrodes in 1 mol·dm^{-3} NaOH (pH=13.8). For illustration of this figure, the followings are assumed. (1) The Fermi level of the electrodes locates at 0.1 eV below the conduction band edge for $CdSnO_3$ and above the valence band edge for $LaRhO_3$. (2) The flat-band potential of $LaRhO_3$ electrodes is equal to the onset potential of the cathodic photocurrents.

As shown in this figure, these materials do not efficiently work as photoelectrodes in water photolysis cells, because the efficient photoelectrodes must have both of the energy levels of the hydrogen and oxygen evolution reactions within their bandgaps.[1] In this respect, photoelectrochemical properties of these materials are unsatisfactory. However, these semiconductors may find application fields as photocatalysts in aqueous solutions. An important point lies in that these are superior to other stable semiconductor materials in the point of spectral response to solar energy.

The present work was supported by Grant-in-Aid for Scientific Research No. 543021 from the Ministry of Education, Science and Culture.

References

1) H. Gerischer, "Solar Power and Fuels," ed by J. M. Bolton, Academic Press, New York N. Y. (1977), p. 77.
2) A. J. Bard, *J. Photochem.*, **10**, 59 (1979); *Science*, **207**, 139 (1980).
3) M. S. Wrighton, *Acc. Chem. Res.*, **12**, 303 (1979).
4) A. J. Nozik, *Ann. Rev. Phys. Chem.*, **29**, 189 (1978).
5) K. Rajeshwar, P. Singh, and J. Dubow, *Electrochim. Acta*, **23**, 11 (1978).
6) M. A. Butler and D. S. Ginley, *J. Mat. Sci.*, **15**, 1 (1980).
7) A. Heller and B. Miller, *Electrochim. Acta*, **25**, 29 (1980).
8) R. Memming, *Electrochim. Acta*, **25**, 77 (1980).
9) H. Gerischer, *Electrochim. Acta*, **13**, 1329 (1968).
10) H. Gerischer, *J. Electroanal. Chem.*, **82**, 133 (1977); *J. Vac. Sci. Technol.*, **15**, 1442 (1978).
11) A. J. Bard and M. S. Wrighton, *J. Electrochem. Soc.*, **124**, 1706 (1977).
12) K. J. D. Mackenzie, W. A. Gerrard, and F. Golestni-Fard, *Silicate Ind.*, **44**, 97 (1979).
13) R. D. Shannon, J. L. Gillson, and R. J. Bouchard, *J. Phys. Chem. Solids*, **38**, 877 (1977).
14) R. J. Bouchard and J. F. Weiher, *J. Solid State Chem.*, **4**, 80 (1972).
15) M. A. Butler and D. S. Ginley, *Chem. Phys. Lett.*, **47**, 319 (1977).
16) M. A. Butler and D. S. Ginley, *J. Electrochem. Soc.*, **125**, 228 (1978).
17) A. H. Nethercot, Jr., *Phys. Rev. Lett.*, **33**, 1088 (1974).
18) A. J. Smith, *Acta Crystallogr.*, **13**, 749 (1960).
19) A. Wold, B. Post, and E. Banks, *J. Am. Chem. Soc.*, **79**, 6365 (1956).
20) H. Yoneyama and H. Tamura, *Bull. Chem. Soc. Jpn.*, **45**, 3048 (1972).
21) D. Hall, *J. Electrochem. Soc.*, **124**, 805 (1977).
22) D. Hall, *J. Electrochem. Soc.*, **127**, 308 (1980).
23) H. R. Scöppel and H. Gerischer, *Ber. Bunsenges. Phys. Chem.*, **75**, 1237 (1971).

Vacuum UV Photoelectron Intensity of Gaseous Compounds. II. Experimental Processes of Determination of Differential and Partial Photoionization Cross Sections

Yohji ACHIBA,*,† Tomoko YAMAZAKI, and Katsumi KIMURA†

Institute of Applied Electricity, Hokkaido University, Sapporo 060

†*Institute for Molecular Science, Okazaki 444*

(Received September 11, 1980)

Experimental processes recently developed to determine differential and partial photoionization cross sections of molecules are described in detail, based on photoelectron intensity measurements using a gaseous binary mixture of a sample with a standard gas. The quantities obtained here in these processes are 1) relative photoelectron peak heights, 2) normalized photoelectron spectra, 3) relative photoelectron band areas, and 4) differential and partial photoionization cross sections. Corrections are made for electron collecting efficiency. In connection with the photoelectron intensity determination, we propose here a method of obtaining the mole ratio of the components of a binary mixture entered into the ionization chamber of a photoelectron spectrometer. Satisfactory results on partial photoionization cross sections have been obtained for several testing samples.

In molecular photoelectron spectroscopy, much attention has been devoted to studies of ionization energies rather than photoelectron intensities, so that its quantitative character is still very poor. It seems quite important to study relative photoelectron intensities from molecule to molecule not only analytical points of view but also theoretical points of view. If intensity-normalized spectra for a number of molecules are obtained with respect to a certain peak of a standard molecule, photoelectron spectroscopy will strengthen its ability as an analytical tool. On the other hand, the band intensity for each photoelectron band is closely associated with the partial photoionization cross section or the branching ratio which is the probability of producing a specific ionic state, so that experimental intensity data are important for testing theoretical models of photoionization processes.

Previously we have reported an essence of our photoelectron intensity determination, together with some preliminary results of its application to simple molecules.[1] Since then we have been developing the system using a mini-computer based data-processing system.

The purpose of the present paper is to describe our detailed processes of intensity determination which were not reported in our previous paper.

Most of photoelectron intensity works published so far have been limited to relative band intensities within molecule for various molecules.[2-4] Concerning relative band intensities among different compounds, only several works have been published in which rare gas atoms and several simple molecules are treated.[5-9] This may be partly due to serious requirement for the knowledge of various instrumental parameters in comparing photoelectron intensities among different molecules.

Partial photoionization cross section of a molecule can be determined by combining the total photoionization cross section and branching ratios. The total photoionization cross section has traditionally been obtained from optical absorption measurements,[10,11] while the branching ratio can be obtained from photoelectron intensity measurements. Combining optical absorption data with photoelectron intensity data, Blake and Carver[12,13] earlier obtained partial photoionization cross sections (as a function of the incident photon energy) for several simple compounds. Samson[10] has proposed a method of using a double ionization chamber to obtain total photoionization cross sections, and they have determined partial photoionization cross sections for several simple molecules at various photon energies. This is probably the most orthodox method of determining the partial photoionization cross section.

Kemeny *et al.*[8,9] have first shown the use of photoelectron intensities of binary mixtures to determine partial photoionization cross sections of the rare gas atoms (Ar, Kr, and Xe), using a relation of the inverse square root of mass to determine mole fractions of the binary mixture. However, such correction may not be always valid for molecules, especially for large molecules. It seems to be important to determine experimentally the real mole fractions of each binary mixture entered into the ionization chamber of a spectrometer.

In order to obtain partial photoionization cross sections for various molecules, we have recently developed our own experimental system applicable to a wide range of molecules, which is somewhat similar to that of Kemeny.[8,9] In the present work we have established an experimental procedure of determining mole fractions of a binary mixture entered into the ionization chamber.

Principle of the Method

The differential photoionization cross section $I_j(\theta) = d\sigma_j/d\Omega$ for producing the jth ionic state in the solid angle $d\Omega$ at the angle θ for unpolarized light is related to the corresponding partial photoionization cross section σ_j by[10]

$$I_j(\theta) = (\sigma_j/4\pi)\{1-(\beta_j/4)(3\cos^2\theta-1)\}, \quad (1)$$

where θ is the angle between the incident photon, beam and the direction of photoelectron detection and β_j is the asymmetry parameter.

When photoelectron measurements are carried out with a pulse counting technique under conditions that the gas pressure is kept constant in the ionization chamber and electron scattering by the gas is not

significant, the number of counts per unit time at the jth photoelectron band may be expressed by

$$N_j \propto I_0 n S I_j(\theta) C(E_j), \quad (2)$$

where I_0 is the incident photon flux, n is the density of molecules in the effective ionization volume, S is the sample factor, and $C(E_j)$ is the spectrometer collecting efficiency for electrons with kinetic energy E. The relation (2) is the same as represented by Gardner and Samson[14] except for S which should be taken into account since sensitivity of a channeltron depends more or less on gaseous samples.

For a binary mixture of A (standard) and B (sample), the following formula can be obtained from the relation

$$\frac{N_j^B}{N_1^A} = \frac{n^B I_j(\theta)^B C(E_j)^B}{n^A I_1(\theta)^A C(E_1)^A} \quad (3)$$

(2) under the same apparatus conditions. Using this relationship we can obtain the relative intensity of the jth band of B with respect to the first band of A. The advantage of this method is that the both instrumental factors I_0 and S are excluded in Eq. 3. If the mole fraction of the binary mixture and the electron collecting efficiencies are known, then differential photoionization cross sections I_j^B can be obtained relatively with respect to I_1^A. Furthermore, partial photoionization cross sections may also be evaluated relatively with respect to σ_1^A, if assymmetry parameter β_j^B are known. Therefore, differential and partial photoionization cross sections of molecules may be determined in absolute values on the basis of those of the standard molecule.

Experimental

Apparatus. A block diagram of the whole experimental apparatus is shown in Fig. 1. All of the gas inlet system, the data-processing system, and data-recording system have been constructed for the present purposes. A HeI photoelectron spectrometer with a hemispherical electrostatic analyzer is essentially the same as used previously.[15]

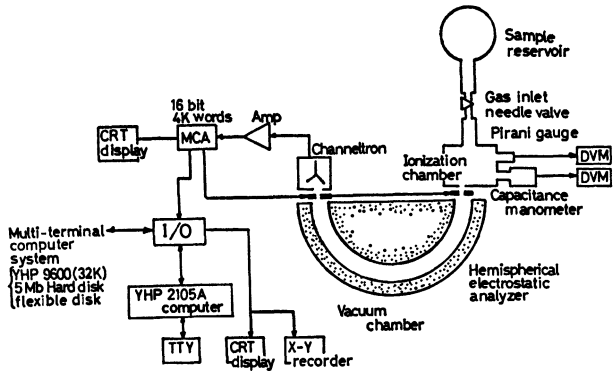

Fig. 1. A block diagram of the photoelectron spectrometer and the data-processing system.

The sample reservoir system is attached to the ionization chamber across a variable leak valve, consisting of three 2-l glass bulbs in which binary gaseous mixtures of the sample and the standard (mainly, N_2) were filled with different mole ratios at total pressures of about 50 Torr. The ionization chamber (20 × 20 × 30 mm) has a rectangular slit (0.4 mm × 10 mm) through which photoelectrons are emitted. The sample gas introduced into the ionization chamber is evacuated also through this slit. The sample pressure in the ionization chamber was monitored with two kinds of different pressure gauges, one of which is an MKS Baratron pressure gauge (Model 220) and the other is an Edwards Pirani gauge (Model 11). Outputs of the two pressure gauges were fed into the data processing system.

Photoelectron measurements were carried out by varying accelerating/retarding voltages on the analyzer entrance slit in synchronization with the channel-advance clock of the multichannel analyzer. Pulse signals detected by a channeltron electron multiplier were preamplified and shaped, and then counted by a multichannel analyzer with 16 bit-4K words. Intensity data stored in the multichannel analyzer were then transferred to a minicomputer (Model YHP 2105A) through input-output interfaces (I/O) for further data processing. Numerical data of normalized photoelectron spectra were stored in a floppy disk through an online-multiterminal computer system (Model YHP 9600) of the Institute of Applied Electricity, Hokkaido University.[16] In this computer system, the programming is allowed in only FORTRAN language by using some PROMs for code conversions.

Determination of Mole Fraction. In the present gas inlet and outlet systems, it is considered that the mole fraction of the binary mixture in the ionization area differs from that in the gas reservoir. This is probably true for commonly used photoelectron spectrometers. (In such a gas flowing system there may be some deviation in the mole fraction from the law of the inverse square root of the mass.)

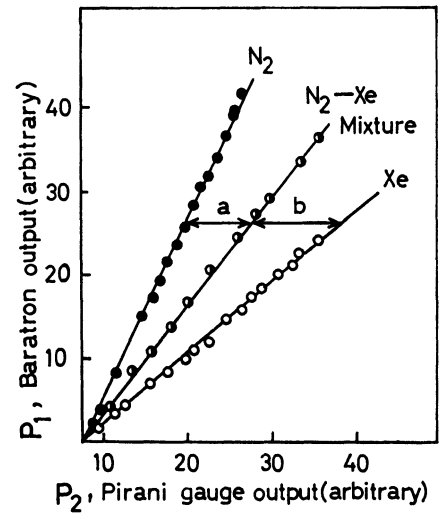

Fig. 2. Plots of the Baratron and Pirani outputs measured for Xe, N_2, and Xe–N_2 mixture, indicating that the mole ratio in the ionization chamber is given by $a:b$. (The initial mole ratio of Xe to N_2 in the mixture in the gas reservoir was 1 : 3 in the present case.)

An example of the mole fraction determination is illustrated in Fig. 2, in which various output data of the Baratron gauge are plotted against those of the Pirani gauge in the case of a binary mixture of N_2 and Xe. The three kinds of plots in Fig. 2 show approximately linear lines with different slopes in the pressure range studied. The partial prassures of Xe and N_2 should be proportional to a and b in Fig. 2, respectively.

Electron Collecting Efficiency Curve. Since the electron collecting efficiency $C(E)$ depends on the photoelectron energy, it is necessary to construct a curve of $C(E)$ as a function of E

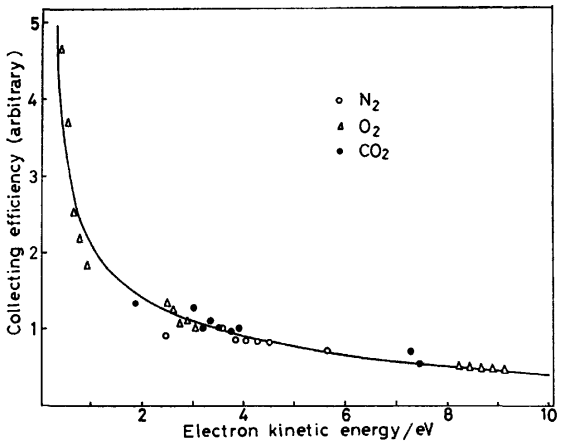

Fig. 3. The electron collecting efficiency curve of the photoelectron spectrometer used here. The solid curve was obtained by a least squares fitting.

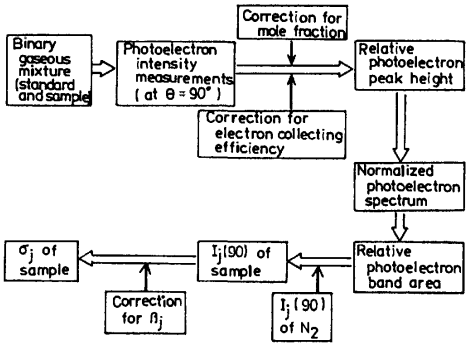

Fig. 4. A flowchart for the determination of differential and partial photoionization cross sections.

in order to obtain real photoelectron intensities. In the present work a curve of $C(E)$ was constructed by correlating our photoelectron peak intensities of N_2, O_2, and CO_2 with the corresponding data of Gardner and Samson.[17] Many typical data thus obtained for electron collecting efficiency are plotted in Fig. 3, the solid curve being obtained by a least-squares fitting with a fifth-order polynominal. The standard error involved is about 4% below 19 eV, while it is 15% above 19 eV.

Data Processing. All the processes included in the determination of differential and partial photoionization cross sections are shown by a flowchart in Fig. 4. Experimental data obtained from HeI spectrum in this scheme are : 1) relative peak heights with respect to the nitrogen first peak, 2) normalized spectra, 3) relative band areas with respect to the nitrogen first band, 4) differential photoionization cross sections, and 5) partial photoionization cross sections. During these processes, corrections are made for 1) the mole fraction of the binary mixture in the ionization area, 2) the electron collecting efficiency of the spectrometer, and 3) the photoelectron angular distribution. In the evaluation of differential and partial photoionization cross sections of molecules, a value of $I_1(90)=0.78\pm0.05$ Mb of the nitrogen first band was used as a reference, that is derived from Eq. 1 with $\sigma_1=8.4\pm0.3$ Mb and $\beta_1=0.68\pm0.05$ reported by Samson *et al.*[18]

Normalized Photoelectron Spectra. HeI 'normalized' photoelectron spectra were obtained with respect to the first photoelectron peak of N_2. Some examples of the normalized spectra are shown in Fig. 5. Photoelectron intensity measurements were carried out several times repeatedly for each photoelectron band with a reproducibility within 3%. Background

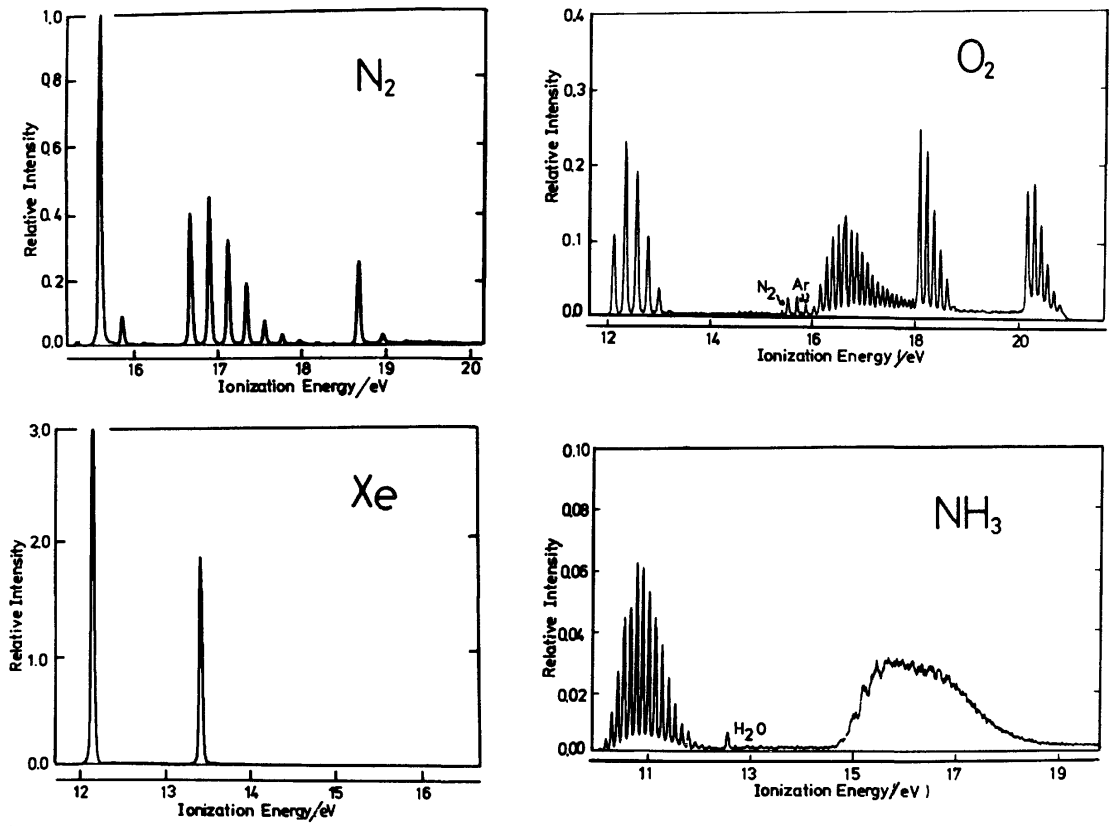

Fig. 5. HeI normalized photoelectron spectra obtained here for N_2, Xe, O_2, and NH_3. The first peak of N_2 is taken as unity. (The spectra were obtained at 90° with respect to the unpolarized light.)

signals were subtracted prior to the normalization process of HeI spectra.

Results and Discussion

Separation factors obtained here for several binary mixtures with an original mole ratio of 1 : 1 are summarized in Table 1, compared with those estimated from the law of the inverse square root of the mass. It is seen from Table 1 that there is a large discrepancy only in the case of benzene, while good agreements are obtained in the other cases, even in rather extreme cases of H_2 and Xe which largely differ from N_2 in the masses. For large molecules such as benzene, such mole fraction determinations are especially important. Probably a more or less similar situation occurs for other conventional spectrometers. It is desirable to construct a new apparatus with a molecular-beam gas inlet system for photoelectron intensity measurements, since the mole fraction separation of binary mixture completely obeys the law of the inverse square root of the mass of its component.

Table 1. Ratios of partial pressures of binary mixtures in the ionization chamber (the initial mole ratio in the gas reservoir is 1 : 1)

Mixture (A+B)	(p_B/p_A)[a)]	$(\sqrt{m_B/m_A})$[b)]
N_2+Ar	1.2	1.2
N_2+Kr	1.6	1.7
N_2+Xe	2.1	2.2
N_2+H_2	0.27	0.27
N_2+CH_4	0.81	0.76
N_2+NH_3	0.78	0.78
N_2+benzene	1.0	1.6

a) p_A and p_B are the partial pressures of A (N_2) and B (sample), respectively, in the ionization chamber. b) m_A and m_B are the masses of A (N_2) and B (sample), respectively.

Table 2. Partial photoionization cross sections (σ_j/Mb) of the rare gas atoms (Ar, Kr, and Xe) at 58.4 nm

Atom	This work	Samson and Cairns[19)]	West and Marr[20)]	Kemeny *et al.*[8,9)]
Ar	37.1	36.4	36.5	36.4
Kr	39.2	36.5	35.7	42.6
Xe	32.0	29.5		33.3

It should be mentioned that there are some gases such as CO which is very similar in the Baratron-Pirani curve to N_2. In such cases another gas instead of N_2 should be selected as a standard.

Partial photoionization cross sections obtained here at 58.4 nm are summarized in Table 2, together with available data.[8,19,20)] The purpose of studying the rare gas atoms in the present work is only to test the validity of the whole procedure proposed here. As can be seen from Table 2, satisfactory results have been obtained.

Only the HeI resonance line has been used in the present work. The purpose of this was to establish the whole system at first. Samson *et al.*[18)] have recently studied energy dependence of partial photoionization cross sections for several simple compounds by a combination of photoelectron spectroscopy and ion current measurements, using a variety of resonance lines through a monochromator. Brion *et al.*[21)] have also studied the energy dependence for several simple molecules, using an electron impact ionization technique. Synchrotron radiation is of course a very useful source to carry out such studies in wide energy range. The present method proposed here may be applicable to any light sources, and its future application to various molecules with synchrotron radiation seems to be very interesting.

The advantage of the present method is that the partial photoionization cross sections of molecules can be obtained from only photoelectron intensity measurements with a conventional photoelectron spectrometer. It is also desirable to carry out photoelectron measurements at the magic angle rather than at right angle as already pointed out by Samson.[10)]

The authors wish to thank Mr. Y. Shindo of Hokkaido University for his expert advice on the construction of the whole data processing system. They also wish to thank Dr. S. Katsumata for many useful discussion and Mr. S. Mitani and Mr. M. Morishita for their contributions to the initial stages of the photoelectron intensity measurements.

References

1) K. Kimura, Y. Achiba, M. Horishita, and T. Yamazaki, *J. Electron Spectrosc.*, **15**, 269 (1979).
2) A. Schweig and W. Thiel, *J. Electron Spectrosc.*, **3**, 27 (1974).
3) J. W. Rabalais, T. P. Debies, J. L. Berkosky, J. T. J. Huang, and F. O. Ellison, *J. Chem. Phys.*, **61**, 516 (1974).
4) D. A. Allison and R. G. Cavell, *J. Chem. Phys.*, **68**, 593 (1978).
5) D. Betteridge, M. A. Williams, and G. G. Chandler, *J. Electron Spectrosc.*, **6**, 327 (1975).
6) D. Betteridge, S. K. Hasanuddin, and D. I. Rees, *Anal. Chem.*, **48**, 1078 (1976).
7) S. Suzer, P. R. Hilton, N. S. Hush, and S. Nordholm, *J. Electron Spectrosc.*, **12**, 357 (1977).
8) P. C. Kemeny, R. T. Poole, J. G. Jenkin, J. Liesegang, and R. C. G. Leckey, *Phys. Rev. A*, **10**, 190 (1974).
9) P. C. Kemeny, R. C. G. Leckey, J. G. Jenkin, and J. Liesegang, *J. Electron Spectrosc.*, **5**, 881 (1974).
10) J. A. R. Samson, *Phys. Rep.*, **28**, 303 (1976).
11) G. V. Marr, "Photoionization Processes in Gases," Academic Press, New York (1976), p. 59.
12) A. J. Blake and J. H. Carver, *J. Chem. Phys.*, **47**, 1038 (1967).
13) J. L. Bahr, A. J. Blake, J. H. Carver, J. L. Gardner, and Vijay Kumar, *J. Quant. Spectrosc. Radiat. Transfer*, **12**, 59 (1972).
14) J. L. Gardner and J. A. R. Samson, *J. Electron Spectrosc.*, **2**, 267 (1973).
15) K. Kimura, S. Katsumata, T. Yamazaki, and H. Wakabayashi, *J. Electron Spectrosc.*, **6**, 41 (1975).

16) H. Mishina, Y. Shindo, T. Kado, and T. Nakamura, *Bull. Res. Inst. Applied Electricity*, **29**, 95 (1977).
17) J. L. Gardner and J. A. R. Samson, *J. Electron Spectrosc.*, **8**, 469 (1976).
18) J. A. R. Samson, G. N. Haddad, and J. L. Gardner, *J. Phys. B*, **10**, 1749 (1977).
19) J. A. R. Samson and R. B. Cairns, *Phys. Rev.*, **173**, 80 (1968).
20) J. B. West and G. V. Marr, *Proc. R. Soc. London, Ser. A*, **349**, 397 (1976).
21) C. E. Brion, A. Hamnett, G. R. Wight, and M. J. van der Wiel, *J. Electron Spectrosc.*, **12**, 323 (1977).
22) E. W. Plummer, T. Gustafsson, W. Gudat, and D. E. Eastman, *Phys. Rev. A*, **15**, 2339 (1977).
23) T. Gustafsson, E. W. Plummer, D. E. Eastman, and W. Gudat, *Phys. Rev. A*, **17**, 175 (1978).

  Bull. Chem. Soc. Jpn., 54, 413—419 (1981)

Redox Reaction of the Central Metal Ions Coordinated to Tetra-(*p*-sulfophenyl)porphine(TPPS). I. Photoreduction of Co(III)TPPS by Methanol and 2-Propanol

Keiichiro HATANO,* Kiyoko USUI, and Yoshitaka ISHIDA

Department of Pharmaceutical Sciences, Nagoya City University, Mizuho-ku, Nagoya 467

(Received March 19, 1980)

Trivalent cobalt ion coordinated to 5,10,15,20-tetra(*p*-sulfophenyl)porphine (TPPS) in deaerated solution was reduced to the divalent ion on illumination of light with simultaneous oxidation of alcohols. The resulting divalent ion in the porphyrin was reoxidized by admission of dioxygen or air into the solution. It was found that the metalloporphyrin played a photocatalytic role in the autoxidation of alcohols. The kinetic study on the photoreduction revealed that the reduction rate of Co(III) followed the pseudo-first-order rate expression at 20 °C and pH 6.5 to 11.5 in the presence of excess methanol or 2-propanol. The observed rate constants were dependent on [alcohol] and/or pH. Possible mechanism for the photoreduction of Co(III)TPPS in the aqueous solution was discussed in terms of preequilibrium reactions of the axial ligation of substrates to the metalloporphyrin.

Very few papers have been published on the photoreduction reactions involving changes only in oxidation state of the central metal of metalloporphyrins,[1] although a number of papers have dealt with photohydrogenation of the peripheral porphyrin ring.[2] This paper describes a light-induced redox reaction of cobalt ion coordinated to 5,10,15,20-tetra(*p*-sulfophenyl)porphine (abbreviated as TPPS[3]) with the concomitant catalytic oxidation of alcohols, *i.e.*, photoreduction of Co(III)TPPS by alcohols and the subsequent oxidation of Co(II)TPPS by O_2 without the degradation of the porphyrin ring. A closely related "respiratory" reaction of manganese phthalocyanine and etioporphyrin was reported by Engelsma *et al.*[4] in relation to the photosynthesis reactions. Moreover, clarifying the oxidation state of metal ions, axial ligands, and reducing reagents involved in the photochemical reactions of metalloporphyrins in view of recent advances in the spectral and structural characterization of metalloporphyrins[5] seemed appropriate.

The present work was initiated with the aim of understanding the function-structure relationship of metalloporphyrin enzymes. When we observed the spectral changes induced by light in stock solutions of metalloporphyrins, we were intersted in the photocatalytic activity of them and the possibility of interconversion of photonic energy into chemical energy. Since metalloporphyrins, beside being the analogy of chlorophylls, have intense absorption bands in the visible and near ultraviolet region, they are expected to be good photosensitizers. Furthermore, the redox reaction of metalloporphyrins is of interest with respect to understanding the function of the biologically important hemeproteins such as electron transfer reactions in the photosynthesis. Metal-TPPS, which are easily soluble in water, appear to offer more information with respect to quantitative kinetic studies of the photochemical reactions.

In this paper we show that the cobalt ion in CoTPPS is a photo-catalytic active center in the autoxidation of alcohols. The kinetic results suggest that the manner of the axial coordination of alcohols is crucial to the photoreaction leading to the exclusive metal ion reduction.

Experimental

Materials. Sodium salt of TPPS ($TPPSNa_4$) was prepared as described by Fleischer *et al.*[6] Since Co(II)TPPS is oxidized slowly in aerobic aqueous solution, all the synthetic processes were carried out in nitrogen stream. TPPS was metallized in water using reagent grade $Co(CH_3COO)_2 \cdot 4H_2O$, and the water was removed by rotary evaporation from the reaction mixtures. The resulting solid was extracted with methanol. Co(II)TPPS was purified as a sodium salt by treatment of crude product in methanol with sodium methoxide several times.

Found: C, 43.28; H, 3.61; N, 4.25; S, 11.07%. Calcd for $CoTPPSNa_4 \cdot 8H_2O$, $C_{44}H_{40}N_4S_4O_{20}CoNa_4$: C, 43.18; H, 3.29; N, 4.58; S, 10.48%. UV-Visible spectra in pH 5.0 phosphate buffer; λ_{max}, nm(ε, $M^{-1}\,cm^{-1}$):[7a] 526 (1.2×10^4), 413 (2.1×10^5).

Co(III)TPPS formed in aqueous solution by autoxidation was found to be diamagnetic by electron paramagnetic resonance (EPR) at 77 K, but was not isolated. Spectral data of Co(III)TPPS; λ_{max} (ε), 538 (1.3×10^4), 424 nm ($2.7\times10^5\ M^{-1}\,cm^{-1}$) were observed in pH 5.0 phosphate buffer. The molar extinction coefficient at 424 nm diminished to $2.4\times10^5\ M^{-1}\,cm^{-1}$ in the pH 8.0 to 10.0.

Water was deionized through ion exchange resins and doubly distilled. 2-Propanol (spectroscopic grade, Katayama Chem. Co.) was used. Methanol of reagent grade was doubly distilled. Phosphate–borate (pH 6.0 to 9.2), borate-carbonate (pH 9.2 to 11.0), and borate-Hydroxide ($\geq$pH 11.0) buffers were prepared according to the reported methods[7b] with the ionic strength maintained at $\mu=0.1$. pH was adjusted with a pH meter (TOA, HM-7B model).

Instrumentation. Light irradiation was carried out with light source of (a) tungsten projection lamp (either unfiltered or filtered by Toshiba glass filters), or (b) four 700 W medium-pressure mercury lamps equipped with a plant growing apparatus 'phytotron'.

UV-visible absorption spectra and EPR spectra were recorded on a Shimadzu Model 200S spectrophotometer and a JEOL-PElX X-band spectrometer with 100 kHz field modulation, respectively.

Procedures. A solution of Co(III)TPPS in an appropriate buffer was degassed by three cycles of freeze-pump-thaw in a pyrex tube (i.d. 19 mm) with two side arms: a quartz cell (10 mm light pass) for spectral measurements and a container with a deaerated buffer solution of alcohols. The

alcohol solution was poured into the pyrex tube in the dark *in vacuo*, then irradiated by light. The irradiation was carried out at 20 °C in a water bath or an air bath of the phytotron. The intensity of the incident light in the phytotron measured by means of the trioxalatoferrate (III) actinometer[8] using the quantum yield 1.10 in the region 430—300 nm corresponding to the major absorption of the metalloporphyrin, was of the order of 7×10^{16} quanta/ml min. The quantum yield for the present reactions was obtained by one of two methods; (a) spectrometric method using the ratio of absorbed quanta to the incident light intensity (derived by comparison of the actinometer irradiated by the light passed through a dilute Co(III)TPPS solution with that through water using a coaxial photolysis cell[9]), (b) measurement of the quantity of formaldehyde produced in the methanolic solution of about 10^{-2} M CoTPPS which was considered to absorb the full incident light.

Formaldehyde was detected by the chromotropic acid method[10] on a sample condensed from the photolyzed solution by vacuodistillation. Acetone was tested qualitatively by the nitroprusside method.

The kinetic studies on the photoreduction and oxidation reactions were carried out by monitoring the changes in the absorption spectra during the light illumination and after O_2 introduction.

Results and Discussion

Photoreduction of Co(III) TPPS. In aqueous solution, the electronic absorption spectra of Co(III)TPPS change slightly with the pH variation and addition of alcohols. However, the fact that the Lambert-Beer law holds for the solution over wide range of concentration (10^{-6} to 10^{-3} M) eliminates the possibility of the participation of oligomeric species in a dilute Co(III)-TPPS solution.[11] Although it is probable that there are several equilibrating reactions involving five- and six-coordination of various solvents and solutes to Co(III)TPPS, the magnitude of the spectral changes is too small and complicated to determine these species definitely.

The typical spectral changes during photolysis of the deaerated Co(III)TPPS solution in the presence of 0.67 M methanol (Fig. 1(a)) have distinct isosbestic points at 360, 419, 454, 534, and 615 nm. The new spectrum appearing on prolonged irradiation is identical with that of Co(II)TPPS prepared and measured in the absence of air.

In order to obtain more information on the nature of species in this photo-reaction, the process was followed by EPR. No signals were detected in the original solution of CoTPPS at 77 K (Fig. 2(a)). As the photolysis proceeds, a new spectrum, having approximate parameters of $g_\perp=2.4$, $g_{//}=2.02$, $A_\perp=55\times10^{-4}$ cm^{-1}, and $A_{//}=105\times10^{-4}$ cm^{-1}, increases its intensity (Fig. 2(b)). By the addition of imidazole to the solution, the spectrum altered into a prototype spectrum of the five-coordinate Co(II)porphyrins with a nitrogen base at the fifth position[12] (Fig. 2(c)). The results show that the photoreduction of CoTPPS occurs at the metal ion of the metalloporphyrin and that the original solution contains the diamagnetic Co(III)species[13] and no paramagnetic species such as Co–O_2. The product can be assigned to a five-coordinate Co(II)TPPS in

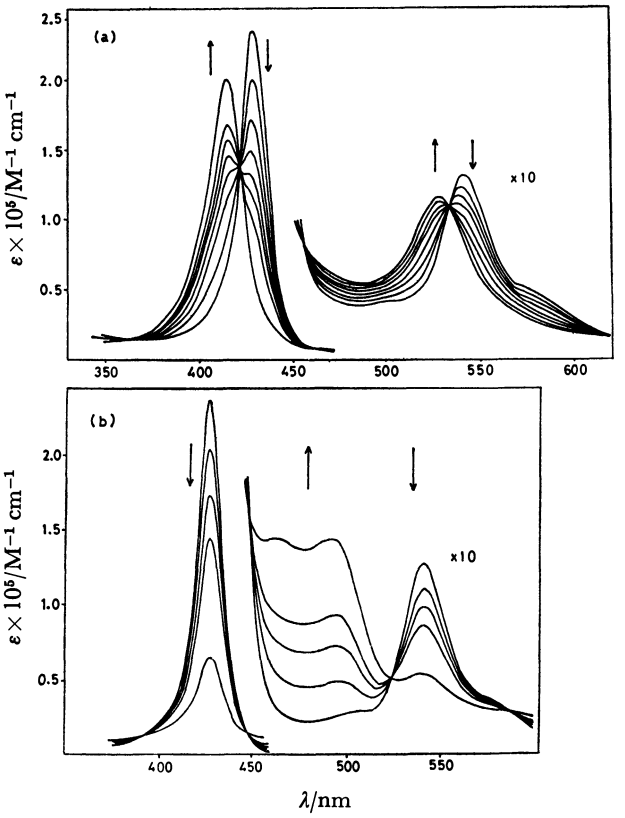

Fif. 1. Spectral changes of Co(III)TPPS during photolysis as a function of reaction times in the order shown by arrows; (a) 0, 20, 40, 60, 80, 100, 120, and 180 min in the 0.67 M methanol solution; (b) 0, 20, 40, 60, and 120 min in the 0.54 M 2-propanol solution. Both runs were carried out at pH 8.7 and 20 °C.

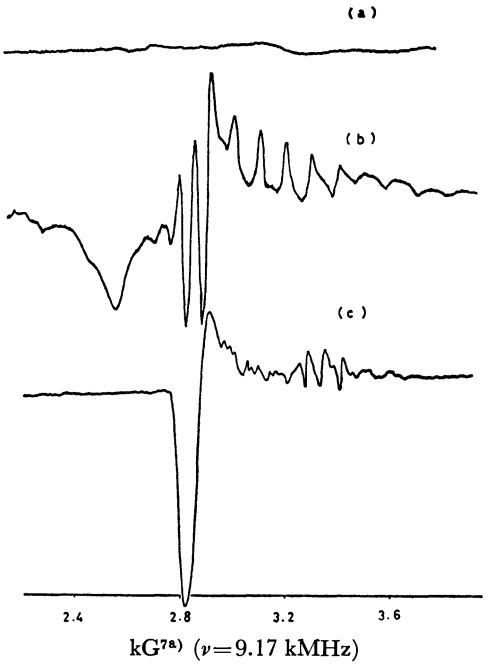

Fig. 2. The EPR spectra of CoTPPS species appearing in the photolysed solution (see text and note).

which the fifth position is occupied weakly by water (or methanol) consistent with the spectra reported by Walker.[14] Our EPR parameters of the product most resemble those of CoTTP(or CoTAP)–acridine system in her paper. The steric constraint of acridine (hindered base) is considered to prevent the metal ion from strong bonding to the base. Thus the EPR parameters should be similar to weakly bonded complexes.

The dependence of the photoreduction on the wavelength of the incident light was examined by setting glass filters in the light path from the projection lamp. The reaction rate resulting from light of 430 nm$>\lambda>$330 nm was compared with that of $\lambda>450$ nm and it was suggested that the light absorbed in the Soret region was more effective in driving the reaction than light in the visible region. However, an accurate determination of the quantum yields in the two regions has not been achieved.

The apparent quantum yield of the formaldehyde formation in degassed solution of *ca.* 10^{-2} M CoTPPS and 0.67 M methanol at pH 8.7 by 30 h irradiation was 0.9×10^{-3}. No gaseous products were detected manometrically in that run. The quantum yield of Co(II)TPPS determined by the spectrometric procedure was 2.2×10^{-3} in solutions of 10^{-6}—5×10^{-5} M CoTPPS and 0.67 M methanol at pH 8.7. The results are consistent with the following stoichiometric reaction within experimental errors. The lack of the evolution

$$2\,\text{Co(III)TPPS} + \text{CH}_3\text{OH} \xrightarrow{h\nu} 2\,\text{Co(II)TPPS} + \text{H}_2\text{CO} + 2\text{H}^+ \quad (1)$$

of molecular hydrogen also supports one electron photoreduction of Co(III) in this equation.

The primary and secondary alcohols, *e.g.*, methanol, ethanol, and 2-propanol, were found to be effective reducing reagents. However, t-butyl alcohol did not bring about the photoreduction. This suggests that the photooxidation of alcohols occurs with a proton elimination at α-carbon position.

Autoxidation of Co(II) TPPS. With O_2 or air introduction into the solution photolyzed, the spectrum of Co(II)TPPS returns to the initial Co(III)TPPS spectrum *via* the exact reverse course of the spectral changes in the photoreduction. The ultimate spectrum of Co(III) TPPS is restored with more than 95% of its initial intensity. The reaction must be the following autoxidation of Co(II)TPPS:[15]

$$2\,\text{Co(II)TPPS} + 1/2\text{O}_2 + 2\text{H}^+ \longrightarrow 2\,\text{Co(III)TPPS} + \text{H}_2\text{O}. \quad (2)$$

Therefore, the overall photochemical reaction is found to be the autoxidation of alcohols catalyzed by CoTPPS:

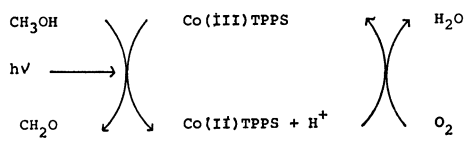

The kinetic study of the oxidation of Co(II)TPPS by O_2 reveals the following rate expression which is substantially identical to the analogous study reported by Stynes *et al.*[16]

$$-\text{d[Co(II)TPPS]}/\text{d}t = k'\text{[Co(II)TPPS][O}_2\text{]},$$

where k' is the observed rate constant. A value of 1.8×10^{-4} min^{-1} Torr^{-1} for k' was obtained in the aqueous 2-propanol (1.0×10^{-2} M) solution at 25 °C without buffer. This is comparable with 4.2×10^{-4} min^{-1} Torr^{-1} which is extrapolated from the reported result of the oxidation of CoTTP in toluene with 0.002 M imidazole at 23 °C.[16] It is surprising to obtain such apparently consistent data despite the vastly different properties of the solution and substances.

Other Photochemical Reactions of CoTPPS. In the absence of alcohols and/or organic amines such as piperidine, Co(III)TPPS in aqueous solution is considerably stable against light irradiation. In the case of methanol or ethanol as reducing agent, the photoreduction of Co(III) ion of the metalloporphyrin is predominant over wide range of pH and alcohol concentration [A]. The recovery of Co(III)TPPS, even after several cycles of the photoreduction-autoxidation, usually exceeds 70% of the initial amount. A drastic change in spectral aspects for the photoreaction is observed in solution containing relatively high concentrations of 2-propanol (10^{-1} M). The spectral changes shown in Fig. 1(b) also have some isosbestic points. However, the spectrum of the product shows no recovery to the spectrum of Co(III)TPPS by the admission of air into the cell. The monotonic decrease of the Soret band may be related to the degradation of peripheral porphyrin ring of CoTPPS; although the chemical characterization of the product has not yet been done. Meanwhile the Co(II)TPPS generated by photoreduction in the presence of 2-propanol was found to be stable against long irradiation of light. This rules out the stepwise photodegradation reaction *via* the formation of Co(II)TPPS. The degradation reaction seems to occur *via* a direct process from a Co(III) species formed in the high [2-propanol] solution. The formation of such a species in methanolic or ethanolic solution may be restricted by its stability constant.

Formaldehyde, acetaldehyde, and acetone in water did not function as the reducing reagents for the reaction.

Kinetic Experiments of the Photoreduction of Co(III) TPPS. The reaction rates of the photoreduction at 20 °C were determined by monitoring changes in the optical density at 424 nm (decrease) and 413 nm (increase) with complementary measurements in the visible region for high [Co(III)TPPS]. The different original intensity at 424 nm depending on the nature of solution did not affect the present kinetic treatment, since, during most kinetic runs, satisfactory isosbestic points were obtained. This is expected for a fixed distribution of various coordination states of Co(III)TPPS being reduced to one five coordinate Co(II) species. Two different kinds of photoreaction took place in certain ranges of [2-propanol]. The determination of the photoreduction rate in such cases has been done at the initial stage of the reaction where the conversion of Co(III)TPPS was less than 40% and the recovery by the autoxidation exceeded 85% of the initial intensity.

Plots of $\ln([\text{Co(III)TPPS}]_t/[\text{Co(III)TPPS}]_0)$ *vs.* time,

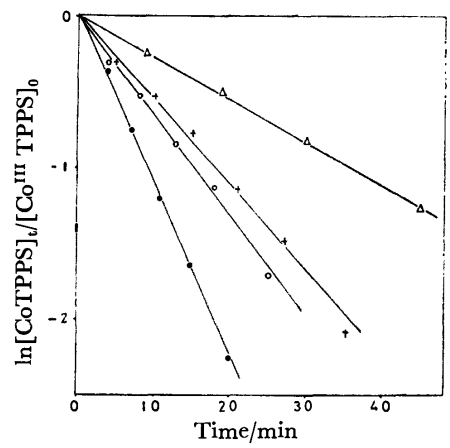

Fig. 3. The first-order rate dependence on Co(III)-TPPS for various methanol concentrations; (△) 1.67 M, (+) 3.21 M, (○) 4.29 M, (●) 6.25 M; in the solution of $[Co(III)TPPS]_0=6.6\times10^{-6}$ M and pH 9.7.

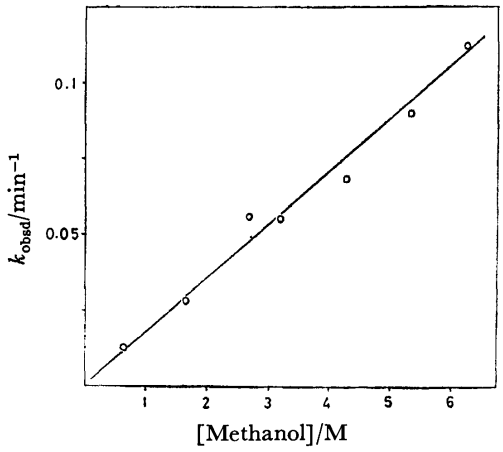

Fig. 4. The k_{obsd} *vs.* [methanol] plots. Conditions are the same as Fig. 3.

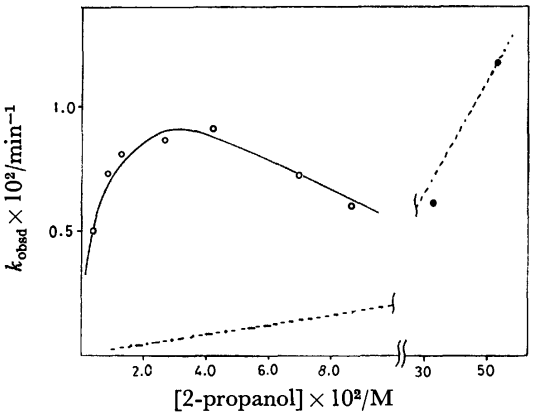

Fig. 5. The k_{obsd} *vs.* [2-propanol] plots, $[Co(III)-TPPS]_0=3.3\times10^{-6}$ M, pH 8.7. The (●) and dashed line denote experimental and estimated rate constants, respectively, for the degradation reaction.

where the subscripts denote time t and zero, are shown in Fig. 3. The linear relationship indicates a first-order rate dependence on Co(III)TPPS. Pseudo-first-order rate constants, k_{obsd}, were obtained from the slope of the plots, and found to be dependent on the concentration of alcohols and/or pH. The profile of k_{obsd} to [methanol] (Fig. 4) shows a first-order relationship to the methanol concentration. However, the dependence of k_{obsd} on [2-propanol] is unusual (Fig. 5). At low [2-propanol] (2×10^{-2} M), the dependence seems to be of first-order, decreasing toward zero to minus with increasing concentration. There is an obvious maximum in the k_{obsd} *vs.* [2-propanol] curve *ca.* $3—4\times10^{-2}$ M 2-propanol at pH 8.7. The photo-degradation reaction is appreciable at higher [2-propanol] than that corresponding to the maximum. However, the increase of the degradation rate (estimated from the data at high [2-propanol] by assuming the first-order dependence on the alcohol concentration) is not responsible for the decrease of photoreduction rate. The anomaly in the curve demonstrates that there are at least two coordination states formed by stepwise attachment of 2-propanol to Co(III)TPPS.

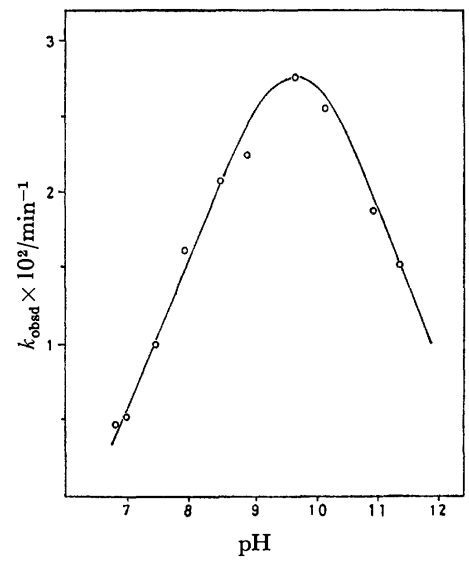

Fig. 6. The pH profile of k_{obsd}, $[Co(III)TPPS]_0=6.6\times10^{-6}$ M, [methanol]=1.67 M, ionic strength=0.1.

The k_{obsd} are also dependent on pH (Fig. 6). The profile of k_{obsd} is volcano-shaped in the solution of constant [methanol], having a peak around pH 9.5 to 10.0. Studies of the rate dependence on pH in 2-propanol solution were not carried out since the rates are very slow at low [2-propanol] where the first-order rate on the alcohol can be expected.

The kinetic studies imply that various coordination states of Co(III)TPPS presented in the aqueous solution behave differently toward light irradiation.

Preequilibrium Reactions in the Aqueous Solution. Both water and alcohol molecules are known to associate with some metalloporphyrins by the definitive X-ray structure determination.[17] However, the stability constants are seldom clear for such weakly bonded molecules owing to the difficulty of spectroscopic characterization of the complexes in solution. Let us assume that Co(III)TPPS has two axial sites to bind ligands, solvents and solutes. Participation of

dimeric metalloporphyrin species such as CoTPPS–O_2–CoTPPS[13] can be ruled out in dilute solution, since the first-order rate laws in cobalt metal are confirmed in both photoreduction and autoxidation processes in conjunction with the EPR evidence of Co(II)TPPS monomer. The observed rate dependence of the photoreduction on pH and [A] can be interpreted by a mechanism in which competitive ligation of alcohols, water, and hydroxide ion to the two axial sites occurs prior to the photoreaction. Accounting for these, we can classify coordination states of Co(III)TPPS in aqueous solution into at least four groups: (i) light-insensitive species formed predominantly in acidic solution and/or in the absence of alcohol, (ii) species to be photoreduced at the central metal ion, (iii) species to be degradated by light, which is appreciable at high [A], especially, [2-propanol], (iv) species which appear at high pH region and depress photoreactions.

Since a limited number of structural determinations[18] and reliable stability constants for Co(III)porphyrins ligated by weakly bonded molecules are available, we can only speculate about the coordination states of each species and the mechanism involving them. The key species for the photoreduction belongs to group (ii) and can be assigned to Co(III)TPPS(A) (OH) where A denotes a general alcohol. The substance is formed by coordination (or substitution) of alcohol and/or hydroxide ion to species (i) which are represented by Co(III)TPPS(H_2O)$_2$ and Co(III)TPPS(H_2O)(OH). Co(III)TPPS(A)$_2$ and Co(III)TPPS(OH)$_2$ may represent species (iii) and (iv), respectively. Beside the four representative species, there may be many other states and reactions in the actual solution, so that it seems neither feasible nor significant to analyse the kinetic data quantitatively. The following scheme may help elucidate the parts of kinetic data, *i.e.*, the presence of maxima (Figs. 5 and 6). The photoreduction is

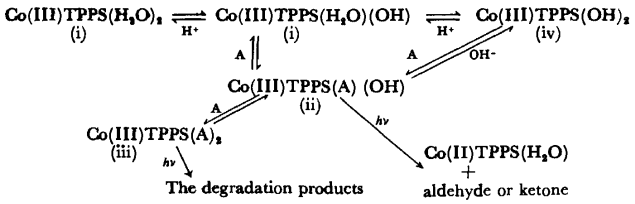

considered to occur *via* formation of Co(III)TPPS(A)-(OH) located in the middle of the scheme. The rate constants, k_{obsd}, are dependent solely on the concentration of this particular species as a function of [A] and pH inasmuch as a constant quantum efficiency is imposed on the photoreduction of the species. Thus, the efficient photoreduction requires optimal control of pH and [A]. In methanolic solution, the equilibrium constant for the second step of methanol coordination is very small as compared with that of 2-propanol. This is rationalized by the photo-degradation reaction which occur *via* formation of bis-alcohol species. The degradation of CoTPPS in methanolic solution was almost negligible under the usual experimental conditions.

It is intriguing to note that the proposed mechanism involving two binding sites for substrates in the catalyst provides similar kinetic aspects to those of certain enzymatic reactions, *e.g.*, fumarase reaction although its active site is not metal ion[19a] and nitric oxide reductase reaction with NO.[19b]

The relative broad curve observed in the k_{obsd} *vs.* pH plot (Fig. 6) suggests that the mono-hydroxy attachment to Co(III)porphyrins is favorable in the pH region 8—11 which corresponds to hydroxide concentration 10^{-6}—10^{-3} M. Isolation of such a species may be possible in analogous system. The occupation of two OH ions on the axial sites is possible, since two CN anion ligands have been confirmed in the X-ray structure of FeTPP(CN)$_2$ anion.[20]

Mechanistic Consideration of the Photoreduction. The observed maximum value of the quantum yield of Co(II) is *ca.* 0.025 under the conditions [methanol]= 6.25 M at pH 9.7. The quantum efficiency[21] could be enhanced by increasing methanol concentration and we could predict the best efficiency to reach the order of 10^{-1} if the solubility of CoTPPS and other solutes allowed the conditions. The relatively high quantum yield observed or predicted suggests that the photoreduction conjugates with the most efficient deactivation of the metalloporphyrin *via* an allowed electronic transition state induced by light absorption in the Soret region. However, very low yield and short life, if any, of the luminescent excited state of Co(III)-porphyrins are known even in rigid media at low temperatures.[22] Consequently, the primary photochemical process of Co(III)TPPS can be attributed to the radiationless and direct chemical reaction from the excited Franck-Condon state of the coordinated complexes. An immediate assignment to this process is attained by the photodissociation of a proton at the α-carbon position of the coordinated alcohol molecule. However, such a dissociation reaction is considered to proceed fast with a fast reverse reaction. Thus the primary process can be treated as an additional preequilibrium reaction induced by light irradiation. In order to adjust the additional reaction and keeping consistency with kinetic data, especially, pH dependence, we could rewrite the process as an innersphere proton transfer of Co(III)TPPS(A)(OH).

The determining step of the quantum yield, which we assign to an intramolecular electron transfer from ligand to metal ion of the metalloporphyrin, can be placed after the primary processes. The speculations are summarized by formulation in the case of methanol as follows:

$$\text{Co(III)TPPS(CH}_3\text{OH)(OH)} \overset{h\nu}{\rightleftharpoons} \text{Co(III)TPPS(CH}_2\text{OH}^-\text{)(H}_2\text{O)}$$

$$\text{Co(III)TPPS(CH}_2\text{OH}^-\text{)(H}_2\text{O)} \longrightarrow \text{Co(II)TPPS(}\dot{\text{C}}\text{H}_2\text{OH) + H}_2\text{O.}$$

A following fast reaction is required to complete the stoichiometry of the photoreduction.

$$\text{Co(II)TPPS(}\dot{\text{C}}\text{H}_2\text{OH) + Co(III)TPPS(H}_2\text{O)(OH)} \longrightarrow 2\,\text{Co(II)TPPS(H}_2\text{O) + CH}_2\text{O}$$

(or any Co(III)TPPS)

To estimate the difference of free energies in the

photoreduction processes is of interest in relation to the possibility of photonic energy utilization. The free energy difference of overall reaction, *i.e.*, autoxidation of methanol to formaldehyde, is exothermic. The value is obtained from the thermodynamic standard data by ignoring solvation energy and estimating coordination energy of methanol as 10 kJ/mol. Based

$$CH_3OH + 1/2\,O_2 \rightleftharpoons CH_2O + H_2O$$
$$\Delta G = -150\ \text{kJ/mol}$$

on the standardization, $\Delta G=0$ for $H_2=2H^+ + 2e^-$ on a platinum electrode (SHE), the energy level of a hypothetical system, $CH_2O+2H^+ + 2e^-$ or CH_2O+H_2, can be put at 237 kJ/mol above the product level or 87 kJ/mol above the reactants level (Fig. 7). Since the electrochemical redox properties of CoTPPS have not yet been determined, the free energy difference in the Eq. 1 is estimated by the voltametric data of analogous complexes. The reported value of 0.32 V *vs.* the saturated calomel electrode (SCE) (0.59 V *vs.* SHE was presumed) for the anodic half-wave potential of CoTPP in butyronitrile was used.[23] Therefore, the energy level of the right-hand term of Eq. 1 is calculated as the difference between the hypothetical level by assuming 0.59 V for Co(III)TPPS$+e^-$=Co(II)TPPS and using the relationship, $\Delta G=-nFU=(-2)(96500)(0.59)=-114$ kJ/mol. Thus we have the free energy diagram shown in Fig. 7. The free energy difference of Eq. 1 is *ca.* −27 kJ/mol.

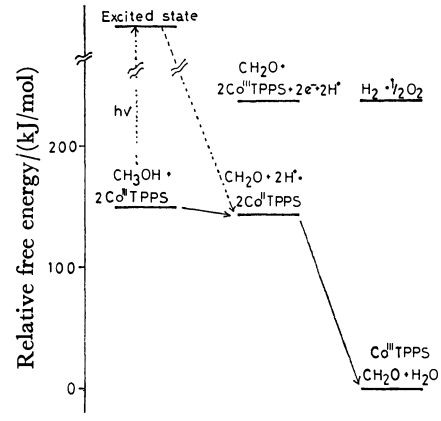

Fig. 7. Energy level diagram for photoreduction of Co(III)TPPS by methanol.

The semi-quantitative treatment leads to the conclusion that the present photoreduction of Co(III)TPPS may not acquire photonic energy in chemical forms, but merely the activation energy by light absorption. However, if there are other metal-TPPSes whose redox potentials are comparable to SHE, it may be possible to interconvert photonic energy into chemical one. We have observed that iron and manganese TPPS undergo similar photoreduction-oxidation reactions in alcoholic solution.

We thank Drs. A. Hanaki, H. Yamamoto, and T. Ozawa for EPR measurements and Prof. W. R. Scheidt for reviewing this manuscript before publication. This work was supported in part by a Grant-in-Aid from the Ministry of Educations, Science and Culture.

References

1) a) D. Mauzerall, "The Porphyrins," ed by D. Dolphin, Academic Press, N. Y. (1978), Vol. V; b) F. R. Hopf and D. G. Whitten, "Porphyrins and Metalloporphyrins," ed by K. M. Smith, Elsevier, Amsterdam (1975), Chap. 16.

2) a) Y. Harel and J. Manassen, *J. Am. Chem. Soc.*, **99**, 5817 (1977); b) D. G. Whitten, J. C. Yau, and F. A. Carroll, *ibid.*, **93**, 2291 (1971); c) J. H. Fuhrhop and T. Lumbantobing, *Tetrahedron Lett.*, **1970**, 2815.

3) TPPS can also be ionized at sulfonyl positions in aqueous solution. We use this abbreviation similarly to TPP for the dianion of 5,10, 15, 20-tetraphenylporphine, *i.e.*, the possible ionization of sulfonyl is ignored for clarity of expression. Other abbreviations: TTP, the dianion of 5,10,15,20-tetra(*p*-methylphenyl)porphine. TAP, the dianion of 5,10,15,20-tetra(*p*-methoxyphenyl)porphine.

4) G. Engelsma, A. Yamamoto, E. Markham, and M. Calvin, *J. Phys. Chem.*, **66**, 2517 (1962).

5) W. R. Scheidt, *Acc. Chem. Res.*, **10**, 339 (1977).

6) E. B. Fleischer, J. M. Palmar, T. S. Srivastava, and A. Chatterjee, *J. Am. Chem. Soc.*, **93**, 3162 (1971).

7) a) Following definitions are required in this text to conform SI units, 1 M=1 mol dm^{-3}, 1 Torr=133.322 Pa, 1 G=10^{-4} T; b) "Kagakubenran, Kisohen II (Handbook for Chemists, Fundamental Section II)," ed by the Chem. Soc. Jpn., Maruzen, Tokyo (1975).

8) G. G. Hatchard and C. A. Parker, *Proc. R. Soc. London, Ser. A*, **235**, 518 (1956).

9) We thought this method for absorbed quantum measurement in a dilute substrate solution to be more reliable than the calculation method using a spectrum and average light path, but the difference was found to be trivial.

10) R. L. Whistler and M. L. Wolfrom, *Methods Carbohydr. Chem.*, **1**, 441 (1962).

11) a) M. Krishnamurthy, J. R. Sutter, and P. Hambright, *J. Chem. Soc., Chem. Commun.*, **1975**, 13; b) K. R. Ashley, M. Berggren, and M. Cheng, *J. Am. Chem. Soc.*, **97**, 1422 (1975); c) R. F. Pasternack and M. A. Cobb, *J. Inorg. Nucl. Chem.*, **34**, 4327 (1973).

12) a) The EPR parameters for the principal signal in Fig. 2 (c): $g_\perp=2.99$, $g_{//}=2.003$, $A_{//}=90\times10^{-4}$ cm^{-1}, $A_N=17\times10^{-4}$ cm^{-1}; b) The small triplet signal appearing at $g=2.00$ with about 6×10^{-3} cm^{-1} separation in Fig. 2 (c) is due to impurity formed by the addition of imidazole.

13) K. Yamamoto and T. Kwan, *J. Catal.*, **18**, 354 (1970).

14) F. A. Walker, *J. Magn. Reson.*, **15**, 201 (1974).

15) It was recently claimed that hydrogen peroxide is generated as reduced oxygen products in autoxidation of a Co(II) complex (J. J. Pignatello and F. R. Jensen, *J. Am. Chem. Soc.*, **101**, 5929 (1979)). However, this was found not to be the case, since a preliminary spot test utilizing the iodostarch reaction was not positive for the formation of H_2O_2.

16) D. V. Stynes, H. C. Stynes, J. A. Ibers, and B. R. James, *J. Am. Chem. Soc.*, **95**, 1142 (1973).

17) a) W. R. Scheidt, I. A. Cohen, and M. E. Kastner, *Biochemistry*, **18**, 3546 (1979); b) F. W. B. Einstein and A. C. Willis, *Inorg. Chem.*, **17**, 3040 (1978).

18) a) T. Sakurai, K. Yamamoto, N. Seino, and M. Katsuta, *Bull. Chem. Soc. Jpn.*, **49**, 3042 (1976); b) M. E. Kastner and W. R. Scheidt, *J. Organomet. Chem.*, **157**, 109 (1978).

19) a) S. Rajender and R. J. McColloch, *Arch. Biochem. Biophys.*, **118**, 279 (1967); b) M. Miyata, T. Matsubara, and T. Mori, *J. Biochem.*, **66**, 759 (1969).

20) W. R. Scheidt, K. J. Haller, and K. Hatano, *J. Am. Chem. Soc.*, **102**, 3017 (1980).

21) For general comparison, the following data may be useful; 90% level conversion of Co(III)TPPS into Co(II)-TPPS in 10^{-5} to 10^{-6} M solution is reached within 10 min by the direct sunlight of a midsummer day at north 35° latitude.

22) M. Gouterman, "The porphyrins," ed by D. Dolphin, Academic Press (1978), Vol. III.

23) a) A. Stanienda, *Z. Phys. Chem.*, **229**, 256 (1964); b) Recently 0.2 V for CoTTP in dimethyl sulfoxide has been reported; K. M. Kadish, L. A. Bottomley, and D. Beroiz, *Inorg. Chem.*, **17**, 1124 (1978).

Studies on Mixed Chelates. XI. Syntheses and Comparative Study of a New Series of Mixed Nickel(II) Chelates with Halide and Pseudohalide Ligands[1)]

Naomi Hoshino, Yutaka Fukuda, and Kozo Sone*

Department of Chemistry, Faculty of Science, Ochanomizu University, Otsuka, Bunkyo-ku, Tokyo 112

(Received May 12, 1980)

A new series of mixed chelates of nickel(II), Ni(diam)(β-dik)X·nH$_2$O (X=halide or pseudohalide anion, n=0—2), was prepared, and their structures in solid state and in various organic solvents were studied. Most of the chelates were octahedral, many of them being obtained as mono- or dihydrates. When the solid chelates were heated at reduced pressure, the main reactions were dimerization (X=pseudohalide), dehydration (X=I), and disproportionation (X=Br or Cl). On the other hand, the chelates showed complicated structural changes in organic solvents, some of which were not observed in solids, depending upon the nature of X and the polar characteristics of the solvent.

We previously reported that the mixed nickel(II) chelate, Ni(tmen)(acac)NCS·nH$_2$O(n=0 or 1)† shows interesting structural changes in various organic solutions.[2)] In a solvent of poor coordination ability(1,2-dichloroethane=DCE), it exists as a square pyramidal 5-coordinate complex [Ni(tmen)(acac)NCS] in a very dilute solution. However, with increase in concentration it forms a 6-coordinate species, probably a dimer formulated as [(tmen)(acac)Ni$\overset{NCS}{\underset{SCN}{<\!\!>}}$Ni(tmen)(acac)]. In nitromethane, (=NM), ionic dissociation of these species leads to the formation of a small amount of square planar species [Ni(tmen)(acac)]$^+$. In more polar solvents, 6-coordinate solvated complexes such as [Ni(tmen)(acac)(Solv.)$_2$]$^+$ or [Ni(tmen)(acac)NCS(Solv.)] predominate.

A report was given on two related chelates, Ni(tmen)(acac)X·2H$_2$O(X=Br$^-$ or I$^-$).[1)] In this same study, we found that the bromide is thermally unstable, easily undergoing disproportionation by slight heating into [Ni(tmen)Br$_2$] and [Ni(tmen)(acac)$_2$], *i.e.* a tetrahedral 4-coordinate complex and an octahedral one. With the iodide, however, such disproportionation occurs only slightly, its main part being converted into [Ni(tmen)(acac)]I with the square planar cation by heating. When dissolved in DCE, both the bromide and iodide undergo disproportionation remarkably even at room temperature,†† but here again the ionization into [Ni(tmen)(acac)]$^+$ and X is favored in nitromethane.

We also prepared related complexes with other halide (Cl$^-$) and pseudohalide (NCO$^-$, NCSe$^-$, and N$_3^-$) ions. A comparative study of all these complexes is given in this paper.

† Abbreviations: diam=*N*-alkylated ethylenediamine such as *N*,*N*,*N*′,*N*′-tetramethylethylenediamine(tmen) or *N*,*N*-*N*,*N*′-triethylethylenediamine(Et$_3$en); β-dik=β-diketonate ion such as acetylacetonate(acac), benzoylacetonate(bza), or dipivaloylmethanate (dpm); X=halide or pseudohalide ions such as Cl$^-$, Br$^-$, I$^-$, NCS$^-$, NCSe$^-$, NCO$^-$, or N$_3^-$.

†† This view is different from that reported;[1)] for detail, see text.

Experimental

Preparation of the New Complexes. The general method of preparation adopted is shown in Scheme 1.

i) NCS-complexes: In addition to the complex Ni(tmen)(acac)NCS·nH$_2$O(n=0 or 1) reported,[2)] three new complexes Ni(tmen)(bza)NCS·H$_2$O, Ni(tmen)(dpm)NCS, and Ni(Et$_3$en)(acac)NCS·H$_2$O were prepared. In the course of preparation, crystals of [Ni(diam)(β-dik)$_2$] and [Ni(tmen)(NCS)$_2$] sometimes appeared first, obstructing isolation of the desired product. In general, the best yield could be obtained when the solution was concentrated at a relatively high temperature and quickly filtered after being cooled down to room temperature.

ii) NCSe-complex: Only Ni(tmen)(acac)NCSe·H$_2$O could be obtained. All operations had to be carried out under cooling: even at 25 °C, NCSe$^-$ ion tends to decompose, separating out red selenium. The decomposition also occurs when the isolated complex is heated gently in solid state or in solution, so that it must be kept in a freezer.

iii) NCO- and N_3-complexes: These complexes, both with tmen and acac, were hard to obtain in pure state; the products obtained by the general method were always impure, containing much ClO$_4^-$. Very small amounts of reasonably pure complexes were obtained when the filtrates of these trials were kept in a refrigerator for several months.

iv) Halide Complexes: In addition to the complexes Ni(tmen)(acac)X·2H$_2$O(X=Br$^-$ or I$^-$),[1)] Ni(tmen)(acac)Cl·H$_2$O, Ni(tmen)(bza) I·nH$_2$O(n=1 or 2), and Ni(tmen)(dpm)I·2H$_2$O were obtained. The two hydrates of the bza complex were obtained depending on the solvent for recrystallization, *i.e.* the dihydrate from methanol and monohydrate from an acetone-DCE mixture. The dpm complex loses its water easily in a desiccator or in dry open air, yielding a reddish orange, diamagnetic anhydrous chelate.

Chemicals. "Extra Pure" reagents and solvents were used. Nitromethane, DCE, acetone, and DMSO were distilled after being dried with Wako synthetic zeolite A-3.

Physical Measurements. Electronic spectra of solutions were obtained with Shimadzu MP-5000 and Hitachi 340 spectrophotometers, using quartz cells of 5 mm to 5 cm. Solid reflectance spectra were recorded with the latter instrument with a visible and near IR integrating sphere attachment, using BaSO$_4$ as a reference. Other instruments used in IR spectral, magnetic, and conductmetric studies were the same as those reported.[2)]

10 mM of [Ni(diam)(β-dik)$(OH_2)_n$]ClO_4 (n=0 or 2)[3]

in acetone (50 cm³)	in methanol (30 cm³)
↓ 10 mM of KX (in acetone)	↓ 10 mM of KX (as solid)
filtration (to remove $KClO_4$)	filtration (to remove $KClO_4$)
↓	↓
evaporation to dryness (under reduced pressure)	allowing to stand in open air
↓	↓
dissolving into DCE	crude crystals
↓	↓
evaporation at low temperature	recrystallization from methanol
↓	(B) Halide complexes[b]
crude crystals	
↓	
recrystallization from DCE[a]	
(A) Pseudohalide complexes	

Scheme 1. Preparation of the complexes, Ni(diam) (β-dik)X·nH_2O (n=0, 1, or 2)

a) When X=NCS^- and diam=Et_3en, acetone or methanol should be used instead of DCE, and the solution must be kept in a refrigerator. b) When X=Cl^-, this method was found to be inadequate, so that the complex was obtained by direct reaction of $NiCl_2 \cdot 6H_2O$, tmen and acac in methanol.

Results and Discussion

The analytical data of the new mixed complexes together with those reported are summarized in Table 1, and their magnetic moments and $\tilde{\nu}_{max}$ values of their reflectance spectra in Table 2. All the complexes are blue to green and in high spin state (μ_{eff}: 3.0—3.2 BM) except XII which is reddish orange and diamagnetic (*cf.* Experimental). These results and the spectral evidence given below lead to the formulation of the complexes as shown in Table 2.

Table 1. Analytical data of complexes[a]

No.-n[b]	Complex	C/%	H/%	N/%
I-1	Ni(tmen)(acac)(NCS)(H_2O)	40.48 (41.16)	7.06 (7.21)	12.11 (12.00)
II-1	Ni(tmen)(acac)(NCSe)(H_2O)	36.25 (36.30)	6.31 (6.35)	10.64 (10.58)
III	Ni(tmen)(acac)(NCO)	44.91 (45 61)	7.24 (7 34)	13.01 (13 30)
IV	Ni(tmen)(acac)(N_3)	41.05 (41.81)	7.23 (7.34)	22.11 (22.16)
V-1	Ni(tmen)(bza)(NCS)(H_2O)	48.95 (49.54)	6.54 (6.60)	10.09 (10.19)
VI	Ni(tmen)(dpm)(NCS)	51.23 (51.94)	8.42 (8.47)	10 08 (10.09)
VII-1	Ni(Et_3en)(acac)(NCS)(H_2O)	45.29 (44.47)	7.74 (7.73)	11.43 (11.11)
VIII-2	Ni(tmen)(acac)(I)$(H_2O)_2$	30.24 (30.24)	6.20 (6.23)	6.48 (6.41)
IX-2	Ni(tmen)(acac)(Br)$(H_2O)_2$	33.92 (33.88)	6.90 (6.98)	7.16 (7.18)
X-1	Ni(tmen)(acac)(Cl)(H_2O)	39.94 (40.34)	7.61 (7.69)	8.55 (8.56)
XI-2	Ni(tmen)(bza)(I)$(H_2O)_2$	38.50 (38.51)	5.95 (5.86)	5.57 (5.61)
XI-1	Ni(tmen)(bza)(I)(H_2O)	39.82 (39.95)	5.66 (5.66)	5.88 (5.82)
XII-2	Ni(tmen)(dpm)(I)$(H_2O)_2$	40.77 (39.18)	7.84 (7.54)	5.22 (5.38)
XII	Ni(tmen)(dpm)(I)	41.03 (42 09)	7.16 (7 22)	5.73 (5.77)

a) Calculated values are in parentheses. b) Number of water molecules. 0 is omitted for n=0.

(A) Pseudohalide Complexes.

(i) Solid Structures: All the pseudohalide complexes (Table 2, I-1 to VII-1) show two d-d bands in their reflectance spectra which can be ascribed to $\tilde{\nu}_1(^3T_{2g} \leftarrow {}^3A_{2g})$ and $\tilde{\nu}_2(^3T_{1g} \leftarrow {}^3A_{2g})$ of octahedral complexes of Ni(II).

As in the case of I-1 formulated formerly as [Ni(tmen)-(acac)(H_2O)NCS], the complexes II-1, V-1, and VII-1 can be formulated as [Ni(tmen)(β-dik)(H_2O)NCX]; the IR data (Table 3) which indicate the N-coordination of NCS^- or $NCSe^-$ in the complexes also support these formulas. The water molecules are only loosely held, and driven off by slight heating or mere dissolution in

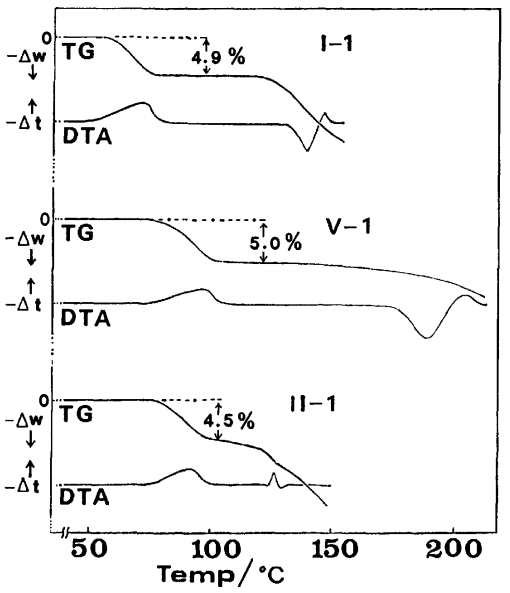

Fig. 1. TG and DTA data of three monohydrated complexes; I-1, V-1, and II-1. Numbers (%) on TG curves show the observed mass losses; the theoretical values are 5.1%, 4.4%, and 4.5%, respectively.

Table 2. Magnetic moments and reflectance spectra of solid complexes

No.-*n*	Complex	μ_{eff}/BM	$\bar{\nu}_{max}/10^3$ cm^{-1}	
I-1	[Ni(tmen)(acac)(H_2O)(NCS)]	3.16(19 °C)	9.64	15.80
I	[Ni(tmen)(acac)(NCS)]$_2$	3.14(18 °C)	9.15	16.05
II-1	[Ni(tmen)(acac)(H_2O)(NCSe)]	3.20(18 °C)	9.70	15.85
III	[Ni(tmen)(acac)(NCO)]$_2$	3.20(18 °C)	—	—
IV	[Ni(tmen)(acac)(N_3)]$_2$	3.02(18 °C)	—	—
V-1	[Ni(tmen)(bza)(H_2O)(NCS)]	3.21(21 °C)	9.42	16.18
VI	[Ni(tmen)(dpm)(NCS)]$_2$	3.09(17 °C)	8.77	16.05
VII-1	[Ni(Et_3en)(acac)(H_2O)(NCS)]	3.14(17 °C)	9.63	16.00
VIII-2	[Ni(tmen)(acac)(H_2O)$_2$]I	3.21(23 °C)	9.30	15.87
IX-2	[Ni(tmen)(acac)(H_2O)$_2$]Br	3.21(22 °C)	9.27	15.92
X-1	[Ni(tmen)(acac)(H_2O)Cl]	3.29(18 °C)	8.90	15.40
XI-2	[Ni(tmen)(bza)(H_2O)$_2$]I	3.18(18 °C)	9.60	16.03
XI-1	[Ni(tmen)(bza)(H_2O)I]	3.18(18 °C)	8.45	15.55
XII-2	[Ni(tmen)(dpm)(H_2O)$_2$]I	3.08(19 °C)	9.53	15.85
XII	[Ni(tmen)(dpm)]I	diamagnetic	20.50	

Table 3. IR spectra of complexes (ν, δ/cm^{-1})

No.-*n*	Complex	ν(O–H)	δ(OH)	ν(CN)[a]	ν(CS)[b]	ν(C=C)	ν(C=O)
I-1	[Ni(tmen)(acac)(H_2O)(NCS)]	3475—3200	1655	2100[c]	772	1595	1523
I	[Ni(tmen)(acac)(NCS)]$_2$	—	—	2150	760	1600	1518
II-1	[Ni(tmen)(acac)(H_2O)(NCSe)]	3475—3200	1652	2105	625	1593	1520
III	[Ni(tmen)(acac)(NCO)]$_2$	—	—	2230 2200	1305	1610	1515
IV	[Ni(tmen)(acac)(N_3)]$_2$	—	—	2120	1292	1605	1518
V-1	[Ni(tmen)(bza)(H_2O)(NCS)]	3140	1660	2090	760	—[d]	—[d]
VI	[Ni(tmen)(dpm)(NCS)]$_2$	—	—	2140	—[d]	—[d]	—[d]
VII-1	[Ni(Et_3en)(acac)(H_2O)(NCS)]	3390—3240	1660	2100	760	1595	1513
VIII-2	[Ni(tmen)(acac)(H_2O)$_2$]I	3370	1665	—	—	1595	1518
IX-2	[Ni(tmen)(acac)(H_2O)$_2$]Br	3350	1670	—	—	1593	1518
X-1	[Ni(tmen)(acac)(H_2O)Cl]	3401, 3225	1680	—	—	1600	1515
XI-2	[Ni(tmen)(bza)(H_2O)$_2$]I	3240	1650	—	—	—[d]	—[d]
XI-1	[Ni(tmen)(bza)(H_2O)I]	3240	1650	—	—	—[d]	—[d]
XII-2	[Ni(tmen)(dpm)(H_2O)$_2$]I	3260	—[d]	—	—	—[d]	—[d]

a) ν_a(NCO) and ν_a(NNN) for III and IV. b) ν_s(NCO) and ν_s(NNN) for III and IV. c) The value in the former report (2170 cm^{-1})[2] was a misprint. d) This band could not be assigned clearly.

nonpolar solvents; TG measurements in static air (heating rate: 1°/min) show that I-1, II-1, and V-1 lose their water quantitatively at 58—76, 78—100, and 75—100 °C, respectively (Fig. 1). The anhydrous complexes of I and V could be easily prepared in this way, but decomposition of $NCSe^-$ ion hindered the preparation of anhydrous II. On the other hand, no monohydrate could be obtained in the system tmen–dpm–NCS, only the anhydrous complex VI being isolated. Since the anhydrous complexes V and VI are also of high spin and show octahedral spectra (Table 2, VI), they are probably dimeric chelates with bridging pseudohalide ions, such as [(tmen)(acac)-Ni$\begin{smallmatrix}\diagup\text{NCS}\diagdown\\ \diagdown\text{SCN}\diagup\end{smallmatrix}$Ni(tmen)(acac)].[2] Similar dimeric structures can be tentatively assigned to the complexes of NCO^- and N_3^- (III and IV) which are also anhydrous, of high spin and similar in color, although other types of bridging and polymerization can not be ruled out.[5,6]

A few interesting trends may be pointed out as to the ease of dehydration of these complexes. In the series [Ni(tmen)(β-dik)(H_2O)NCS], the water beoomes more tightly held in the order:

$$\text{dpm (no hydrate isolated)} \ll \text{acac} < \text{bza}$$

and in the series [Ni(tmen)(acac)(H_2O)X]:

$$NCO^- \approx N_3^- \text{ (no hydrate isolated)} \ll NCS^- < NCSe^-$$

The order seems to indicate that the bonding of water is strengthened by the weakening of the ligand field strength (l.f.s.) produced by other ligands.[3,7]

Another interesting complex prepared was [Ni(Et_3en)(acac)(H_2O)NCS] (VII-1), containing a diamine with very bulky alkyl groups. The spectral feature is essentially similar to that of (I-1), showing that H_2O can still be coordinated in this complex. No corresponding complex with Et_4en(teen),[8] [Ni(teen)(acac)(H_2O)-NCS], could be isolated, but the formation of a 5-coordinate complex (probably [Ni(teen)(acac)NCS]) in

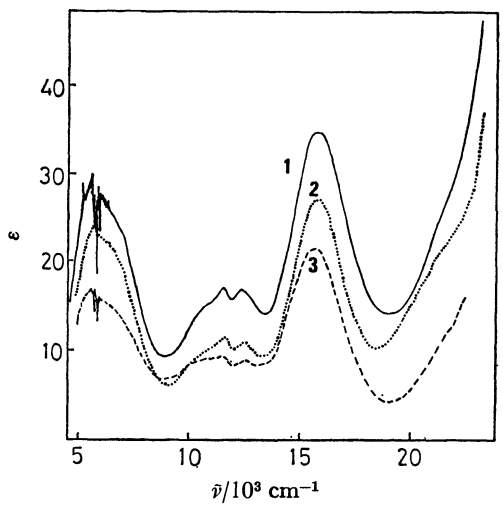

Fig. 2. Electronic spectra of VII-1 in various organic solvents (1=DCE; 2=NM; 3=acetone). Strong noises observed at *ca.* 6×10^3 cm^{-1} in the spectra of 1 and 3 were due to the absorption bands of the solvents.

an acetone solution of its components could be confirmed by its electronic spectrum. Coordination of solvent molecule is thus strongly hindered by the increase of the number of ethyl groups in the diamine (see below).

(ii) Structures in Organic Solutions: The structural changes of the complexes I-1 and I in various organic solvents were described in detail.[2] The spectral curves of VII-1 (Fig. 2) are most interesting in this connection; the curve in DCE is typically square pyramidal,[9] showing four bands assigned as follows:

$^3E(F) \leftarrow {}^3B_1(F)$, 5750 cm^{-1}; $^3A_2(F) \leftarrow {}^3B_1(F)$, 11550 cm^{-1}; $^3B_2(F) \leftarrow {}^3B_1(F)$, 12470 cm^{-1}; $^3E(F) \leftarrow {}^3B_1(F)$, 15900 cm^{-1}.

Two other spin allowed bands ($^3A_2(P)\leftarrow{}^3B_1(F)$ and $^3E(P)\leftarrow{}^3B_1(F)$) are probably under the strong CT band observed in the ultraviolet. Thus the water molecule escapes easily on dissolution, causing a structural change from 6- to 5-coordination. The 5-coordinate structure is also retained fairly well in more polar solvents (nitromethane or acetone), but the decrease in band intensity suggests that it is partially converted into other forms, such as planar $[Ni(Et_3en)(acac)]^+$ (in nitromethane) or $[Ni(Et_3en)(acac)(solv.)NCS]$ (in acetone), as in the case of I. However, it can be seen that the dimerization observed with I in DCE or nitromethane is hindered by the bulky substituents in Et_3en, and the 5-coordinate structure is notably stabilized in comparison with the case of I.

The case of VI (Fig. 3) is in strong contrast with that of VII-1. Here the spectrum depends much more (and seemingly more than I) on the solvent, and the 5-coordinate species in DCE (which coexists with some $[Ni(tmen)(dpm)]^+$, as indicated by a notable hump at about 20000 cm^{-1}) is converted easily into $[Ni(tmen)(dpm)]^+$ in nitromethane, and solvated 6-coordinate species (probably $[Ni(tmen)(dpm)(Solv.)NCS]$) in acetone. The bulky substituents in dpm are somewhat apart from the central metal ion, so that the 5th and 6th coordination sites around it are not so sterically

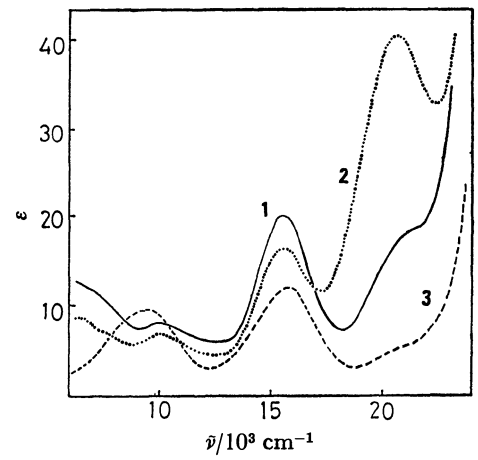

Fig. 3. Electronic spectra of VI in various solvents. For the numbering of curves, *cf.* Fig. 2.

hindered as in the case of VII-1. The NCS^- can be dissociated away in nitromethane of relatively high dielectric constant (35.9), while a polar solvent molecule can enter into the coordination sphere. The effect of dimerization on the spectra is not so apparent as with I, probably owing to the stronger ligand field of dpm and larger interligand repulsion in the dimer.

As regards the complex with $NCSe^-$ (II-1), its spectrum in DCE is generally similar to spectra of I-1 and V-1, indicating an equilibrium between 5- and 6-coordinate species. Not much could be done with this complex, however, owing to its thermal instability.

The complexes with NCO^- (IV) and N_3^- (VI) could not be studied in sufficient detail owing to their poor yield, but they show typically octahedral spectra in DCE. This fact, and the non-conductivity of their solutions, indicate that their 6-coordinate dimeric (or polymeric) structure is retained also in solution, probably owing to the higher coordination and bridge formation ability of the NCO^- and N_3^- ions than NCS^- and $NCSe^-$ ions.[5,6] The $\bar{\nu}_{max}$ and ε_{max} values of the solution spectra are summarized in Table 4.

(B) Halide Complexes. (i) Solid Structures: Unlike the pseudohalide complexes, almost all the complexes obtained (Table 1) are dihydrates. Their appearance and solid spectra are very similar to those of $[Ni(tmen)(acac)(H_2O)_2]ClO_4$,[3] suggesting their formulation as $[Ni(diam)(\beta\text{-dik})(H_2O)_2]X$.

When β-dik=bza and X=I^-, both the mono- and dihydrate can be obtained, the latter being partially transformed into the former in a desiccator (*cf.* Experimental). Careful observation of the dehydration process of IX-2 by heating also shows that it is first converted into a yellowish green mass, apparently very similar to the complex $[Ni(tmen)(bza)(H_2O)I]$. Thus the number (n) in the hydrates $Ni(tmen)(\beta\text{-dik})X\cdot nH_2O$ varies as follows:

a) β-dik=acac

X=	I	Br	Cl
n=	2	2	—
	—	(1)	1

b) X=I

β-dik=	dpm	acac	bza
n=	2	2	2
	—	—	1

Table 4. Spectral data of solutions of pseudohalide complexes, $\bar{\nu}_{max}/10^3$ cm^{-1} (ε_{max} in parenthesis)

I-1	[Ni(tmen)(acac)(H_2O)(NCS)]					
	1,2-dichloroethane		6.0—9.5 (8.4—11.0)	15.67 (16.9)		c*
	nitromethane		6.0—9.5 (7.3—8.5)	15.60 (15.5)	20.92 (16.7)	c*
	acetonitrile		9.76 (11.3)	16.21 (10.4)		c*
	acetone		9.35 (11.0)	15.80 (11.7)		c*
	DMSO		9.48 (10.0)	15.77 (7.6)		c*
I	[Ni(tmen)(acac)(NCS)]$_2$					
	1,2-dichloroethane	6.67 (12.5)	9.80 (9.3sh)	15.46 (20.4)		c*
	nitromethane	6.67 (10.1)	9.76 (9.8sh)	15.55 (18.6)	20.83 (20.7)	c*
	acetonitrile		9.73 (11.1)	16.21 (10.8)		c*
	acetone		9.22 (10.8)	15.75 (13.0)		c*
	DMSO		9.43 (9.9)	15.70 (7.6)		c*
II-1	[Ni(tmen)(acac)(H_2O)(NCSe)]					
	1,2-dichloroethane		6.0—9.5 (9.3—7.6)	15.87 (16.6)		c
III	[Ni(tmen)(acac)(NCO)]$_2$					
	1,2-dichloroethane		9.20 (9.2)	15.15 (8.3)		b
IV	[Ni(tmen)(acac)(N_3)]$_2$					
	1,2-dichloroethane		9.28 (13.8)	15.27 (12.2)		b
V-1	[Ni(tmen)(bza)(H_2O)(NCS)]					
	1,2-dichloroethane		6.0—9.5 (8.7—11.0)	15.63 (20.2)		b
VI	[Ni(tmen)(dpm)(NCS)]$_2$					
	1,2-dichloroethane	6.17 (12.8)	10.20 (8.0)	15.63 (20.2)	20.6 (17sh)	b
	nitromethane	6.17 (9.0)	10.05 (6.8)	15.60 (16.5)	20.70 (40.8)	d
	acetone		9.47 (9.6)	15.80 (12.2)	20.6 (5.2sh)	b
VII-1	[Ni(Et$_3$en)(acac)(H_2O)(NCS)]					
	1,2-dichloroethane	5.75 (30)	10.4 (14sh)	11.55 (17.0)	12.47 (17.0) 15.90 (34.8)	b
	nitromethane	5.80 (24)	10.4 (9.2sh)	11.60 (11.7)	12.50 (11.0) 15.85 (27.1)	a
	acetone	5.60 (16.8)	10.4 (9.0)	11.50 (9.4)	12.50 (8.8) 15.80 (21.6)	b

Concentration: a *ca.* 1.0×10^{-2} M, b *ca.* 2.0—2.9×10^{-2} M, c *ca.* 5.1×10^{-2} M, d *ca.* 5.0×10^{-3} M (1 M=1 mol dm^{-3}). Temperature: *=25 °C; otherwise, room temperature (17—21 °C). sh=shoulder.

Table 5. Spectral data of solutions of halide complexes, $\bar{\nu}_{max}/10^3$ cm^{-1} (ε_{max} in parenthesis, sh=shoulder)

VIII-2	[Ni(tmen)(acac)(H_2O)$_2$]I					
	1,2-dichloroethane	9.43 (16.6)	14.49 (21.2)	17.80 (51.2)	21.72 (342)	b
	nitromethane	20.60 (154)				b
	acetone	9.45 (16.2)	14.50 (12.5)	17.82 (40.1)	21.96 (264)	b
	methanol	9.52 (8.1)	15.90 (6.4)			e
	DMSO	9.44 (8.7)	15.73 (6.4)			e
IX-2	[Ni(tmen)(acac)(H_2O)$_2$]Br					
	1,2-dichloroethane	9.80 (22.5)	14.60 (17.8)	19.05 (50.1)	24.75 (86.8)	b
	nitromethane	9.90 (11.1)	14.70 (8.0)	20.10 (91.6)		d
	acetone	9.85 (29.4)	15.74 (13.6)	19.05 (65.7)	24.2 (46.7sh)	d
	methanol	9.55 (7.5)	15.95 (5.8)			d
X-1	[Ni(tmen)(acac)(H_2O)Cl]					
	1,2-dichloroethane	9.80 (10.4)	14.40 (12.0)	19.87 (12.9)	24.6 (54sh)	d
	nitromethane	10.00 (11.6)	14.60 (11.0)	19.90 (24.4)	24.6 (52sh)	d
	acetone	10.00 (18.9)	14.15 (8sh)	16.13 (9.0)	18.18 (18sh)	d
		19.74 (32.1)	24.6 (35sh)			
XI-1	[Ni(tmen)(bza)(H_2O)I]					
	1,2-dichloroethane	9.52 (21.1)	14.60 (26.6)	17.80 (58.4)	21.85 (418)	b
XII	[Ni(tmen)(dpm)]I					
	1,2-dichloroethane	14.40 (9.7)	20.83 (133)			b
IX′	[Ni(tmen)Br$_2$][a]					
	1,2-dichloroethane	9.85 (65.0)	15.6 (26sh)	19.00 (108)	24.2 (29sh)	c
XIII	[Ni(tmen)(acac)$_2$][a]					
	1,2-dichloroethane	9.43 (10.3)	16.23 (8.3)			c

Concentration: b *ca.* 5.0—5.9×10^{-3} M, c *ca.* 2.5×10^{-3} M, d *ca.* 1.0×10^{-2} M, e *ca.* 2.7×10^{-2} M. Temperature: room temperature (13—20 °C). a) The data on these complexes[3,4] are given for comparison.

We see that there is a competition between the water molecules and halide ions in the coordination sphere, and the nature of the β-diketonate (probably its steric requirement) also affects this competition. The water molecules are combined only weakly,[3] and easily lost on dissolution in relatively nonpolar solvents.

[Ni(tmen)(dpm)]I, a reddish orange diamagnetic solid with a typically square planar reflectance spectrum (a band at 20500 cm^{-1}), is obtained easily from the hydrate (*cf.* Experimental). On the other hand, the complexes VIII-2 and XI-1 dehydrate with more difficulty, losing their water at 80—120 and 100—145 °C, respectively, under the same conditions as in the case of pseudohalide complexes.††† Their anhydrous complexes are both reddish orange but slightly paramagnetic ($\chi_g = 3.4 \times 10^{-6}$ and 4.3×10^{-7}, respectively) and show weak bands (9300, 11000(sh), and 12150 cm^{-1} in XI, and 9550 cm^{-1} in VIII) together with a strong square planar band (20500—21000 cm^{-1}). VIII is remarkably hygroscopic; its paramagnetism may be due to the formation of its hydrate during storage. However, XI is apparently not very hygroscopic and a very small amount of blue crystals were observed to deposit at the top of the vessel during the course of dehydration in a vacuum (50—60 °C, 2 d). Thus the paramagnetism of XI, and at least a part of that of VIII, seem to be due to the product of decomposition which, to a small extent, accompanies their dehydration.

The nature of decomposition is understandable, if we compare the results with those of IX-2 and X-1.[1] With IX-2, the water is lost between 70 and 100 °C, but the weight decreases steadily on further heating, and when it is heated at under 60 °C for 17 d, it separates into a violet powder and a pale blue sublimate. The analysis of the latter (Found: C, 51.49; H, 8.08; N, 7.61%. Calcd: C, 51.50; H, 8.10; N, 7.51%) confirms its formulation as [Ni(tmen)$(acac)_2$], while that of the former indicates that it is chiefly composed of [Ni(tmen)-Br_2] (Found: C, 23.29; H, 4.82; N, 7.77%. Calcd for: C, 21.53; H, 4.82; N, 8.37%). The deviations from the calculated values can be ascribed to a small amount of red crystals contained in the former (probably [Ni(tmen)(acac)]Br) which can be discerned by careful observation. Thus the decomposition of this complex can be formulated as:

$$[Ni(tmen)(acac)(H_2O)_2]Br \longrightarrow \begin{cases} [Ni(tmen)Br_2] + [Ni(tmen)(acac)_2] \cdots\cdots (A) \\ \qquad\qquad\qquad\qquad \text{Disproportionation}\dagger\dagger\dagger\dagger \\ [Ni(tmen)(acac)]Br \cdots\cdots (B) \quad \text{Dehydration.} \end{cases}$$

(A) is the main reaction. With X-1, this reaction seems to occur nearly exclusively; after being heated at 90 °C for 7 d it decomposed perfectly into [Ni(tmen)$(acac)_2$] (subliming away from the vessel) and green [Ni(tmen)-Cl_2] with no trace of red complex.

Thus we can summarize the thermal decompositions of XII-2, VIII-2, XI-1, IX-2 (or IX-1), and X-1 as follows:

$$\text{XII-2} \rightarrow \text{(B) (no(A))} \qquad \left.\begin{matrix}\text{VIII-2}\\ \text{XI-1}\end{matrix}\right\} \nearrow \text{(B)} \; \searrow \text{(A)}$$

$$\text{IX-2} \nearrow \text{(B)} \; \searrow \text{(A)} \qquad \text{X-1} \rightarrow \text{(A) (no (B))}$$

if we assume that the reaction (A) occurs to a small extent with VIII-2 and XI-1, producing the blue sublimate observed with VIII-2, and paramagnetic impurity (presumably [Ni(tmen)I_2]) in the dehydration products.

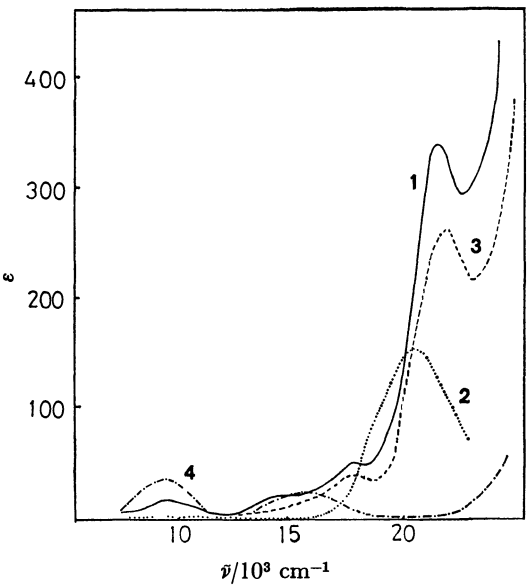

Fig. 4. Electronic spectra of VIII-2 in various solvents (1=DCE; 2=NM; 3=acetone; 4=DMSO ($\varepsilon \times 5$ as ordinate)).

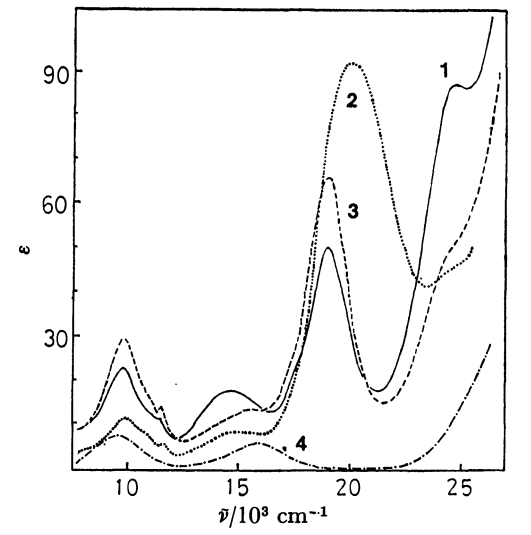

Fig. 5. Electronic spectra of IX-2 in various solvents. For the numbering of curves, *cf.* Fig. 4.

††† The ease of dehydration is in the order dpm ≫acac> bza, *i.e.* the same as in the case of pseudohalide complexes. XI-1 and XI-2 both melt between 98 and 104 °C, seemingly leading to the same product.

†††† This reaction can be reversed, *i.e.*, when we mix the violet powder and blue sublimate in a 1 : 1 molar ratio in DCE, concentrate, and add some acetone, the crystals of [Ni-(tmen)(acac)$(H_2O)_2$]Br appear again.

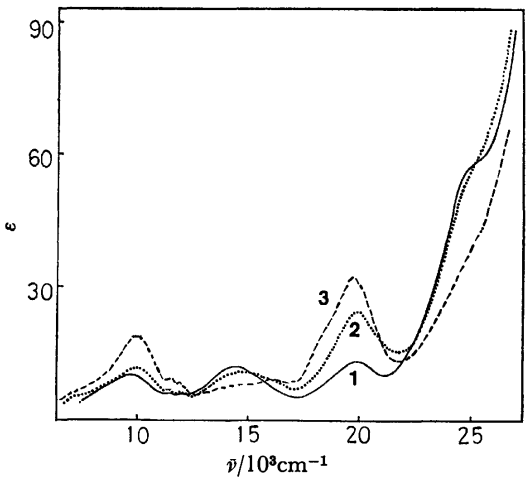

Fig. 6. Electronic spectra of X-1 in various solvents. For the numbering of curves, *cf.* Fig 2.

(ii) Structures in Organic Solutions. Figures 4, 5, and 6 show the spectra of VIII-2, IX-2, and X-1 in various organic solvents. Their $\tilde{\nu}_{max}$ and ε_{max} values are summarized in Table 5.

In general, in highly polar and coordinating solvents like DMSO or methanol, the spectra show that the complexes tend to form 6-coordinate species ([Ni(tmen)(acac)(Solv.)$_2$]$^+$ or [Ni(tmen)(acac)(Solv.)X]), as in the case of the pseudohalide complexes. However, the situation is quite different in solvents of low polarity and/or coordination ability (DCE, nitromethane, or acetone).

As to IX-2 (Fig. 5), the curve in DCE indicates the occurrence of reaction (A),[1] since it is very similar to that of 1 : 1 mixture of the products, [Ni(tmen)Br$_2$] and [Ni(tmen)(acac)$_2$]. The similarity is still more pronounced in acetone, and the band at 14600 cm^{-1}, which should be ascribed to some unidentified by-product formed in DCE, apparently disappears. Thus it is clear that reaction (A) occurs quite easily by mere dissolution of this complex in these solvents.

In nitromethane, however, a strong band at *ca.* 20000 cm^{-1} appears, showing a remarkable dissociation into [Ni(tmen)(acac)]$^+$ and Br$^-$ (*ca.* 60%, if the true ε_{max} of this band is assumed to be *ca.* 150).[3] On the other hand, the bands of products of reaction (A) are correspondingly weakened. This indicates that the higher polarity of nitromethane as an ionizing medium as compared with those of DCE and acetone (*cf.* their dielectric constants and E_T values,[11] and note that the latter decreases as nitromethane$\gg$DCE$\approx$acetone) favors the formation of charged species (*i.e.* ionization) in comparison with that of non-charged species (*i.e.* reaction (A)).

The data on X-1 (Fig. 6) can be understood on the same basis. Here the curve for acetone is similar to that of IX-2, indicating that reaction (A) occurs remarkably. The curves in nitromethane and DCE are essentially similar to that in acetone, although a band of some unidentified byproduct appears again at 14400—14600 cm^{-1}, and the band at *ca.* 10000 cm^{-1} and 19900 cm^{-1} are weakened. The band at 19900 cm^{-1} in nitromethane is much higher than that in DCE; this is probably due to the partial ionization (*ca.* 10%) into [Ni(tmen)(acac)]$^+$ and Cl$^-$ which takes place in nitromethane (Table 6), and the overlap of the band of [Ni(tmen)(acac)]$^+$ on that of [Ni(tmen)Cl$_2$] which is in the same region.

Table 6. Conductivity of DCE and NM solutions (1.0×10^{-3} M, 25 °C; Λ_M/Ω^{-1} cm^2 mol^{-1})[a]

		DCE	NM
I-1	[Ni(tmen)(acac)(H$_2$O)(NCS)]	$\approx$0	16.6
I	[Ni(tmen)(acac)(NCS)]$_2$	$\approx$0	18.8
III	[Ni(tmen)(acac)(NCO)]$_2$	1.1	—
VI	[Ni(tmen)(dpm)(NCS)]$_2$	2.5	—
VIII-2	[Ni(tmen)(acac)(H$_2$O)$_2$]I	19.0[b]	85.0
IX-2	[Ni(tmen)(acac)(H$_2$O)$_2$]Br	2.1	67.1
X-1	[Ni(tmen)(acac)(H$_2$O)Cl]	0.7	21.0
XII	[Ni(tmen)(dpm)]I	24.3	—
Standard 1 : 1 electrolytes		10—24	75—95

a) Care must be taken in comparing these data with the spectral ones, since the latter were mostly obtained with much more concentrated solutions. b) At 5×10^{-3} M, Λ_M drops to 12 Ω^{-1} cm^2 mol^{-1}.

The data on VIII-2 (Fig. 4) are more complicated. However, it is clear that, in nitromethane, there is almost perfect ionization into [Ni(tmen)(acac)]$^+$ and I$^-$, since the spectrum is very similar to those of [Ni(tmen)(acac)]X(X=ClO$_4^-$ or B(C$_6$H$_5$)$_4^-$) in highly non-coordinating media.[3] Comparing the data of the three complexes in nitromethane, we can conclude that: (i) the coordinated water is easily lost on dissolution, (ii) the complex then either ionizes into [Ni(tmen)(acac)]$^+$ and X, or undergoes disproportionation into [Ni(tmen)X$_2$] and [Ni(tmen)(acac)$_2$]. The ionization is nearly complete when X=I$^-$, and occurs strongly when X=Br$^-$, but only weakly when X=Cl$^-$. The anions tend to remain coordinated in the order I$^-$<Br$^-$<Cl$^-$, as can be expected from their l.f.s.

The spectra of VIII-2 in DCE and acetone present some questions. Since their general appearance is similar to the spectrum of the trigonal bipyramidal [Ni(tren-Me)Cl]Cl reported by Ciampolini *et al.*,[10] we mistakenly ascribed the curves to the complex [Ni(tmen)(acac)I].[1] We have found, however, that they are very similar to the spectrum of [Ni(tmen)I$_2$][4] in DCE. The bands in the former spectra are much weaker, and it can be estimated that only 10—15% of VIII-2 dissolved in DCE are converted into [Ni(tmen)I$_2$], *i.e.* 20—30% undergo disproportionation into [Ni(tmen)I$_2$] and [Ni(tmen)(acac)$_2$] (the bands of [Ni(tmen)(acac)$_2$] are much weaker than those of [Ni(tmen)I$_2$], and will be completely covered by them, if the two species coexist in equimolar amounts).

On the other hand, the Λ_M values (Table 6) show that a large part of VIII-2 (50% or more in a 5×10^{-2} M solution) is converted into ionic species in DCE. A similar situation is also expected in acetone. There is no spectral indication for these ionic species, but this may be due to the fact that the bands of the expected ionic species ([Ni(tmen)(acac)]$^+$, [Ni(tmen)(acac)(acetone)$_2$]$^+$, and possibly [Ni(tmen)(H$_2$O)$_4$]$^{2+}$ produced

by the hydrolysis of [Ni(tmen)I_2]) are considerably weaker than those of [Ni(tmen)I_2]. They would thus be nearly buried under the strong bands of [Ni(tmen)I_2], even if a considerable amount of the ionic species is present in solution.

Comparing the data in DCE and acetone, we see that reaction (A) takes place with IX-2 or X-1 but VIII-2 mainly ionizes, showing that I^- is held more weakly to the metal ion than Br^- and Cl^-.

Spectral data were also obtained in DCE with complexes XI-1 and XII, containing bza and dpm instead of acac. XI-1 shows nearly the same spectrum as VIII-2; the curve of XII, however, is similar to that of VIII in nitromethane, and together with the high Λ_M value of its solution (Table 6), shows that most of it is dissociated into [Ni(tmen)(dpm)]$^+$ and I^- in DCE, although a weak band at 14400 cm^{-1} might indicate a slight occurrence of reaction (A). This is evidently due to the bulkiness and strong l.f.s. of dpm, which stabilizes the square planar cation.

Concluding Remarks. Although only limited information could be obtained with complexes containing NCO^-, $NCSe^-$, and N_3^-, there are clear-cut differences between the behavior of the pseudohalide complexes and that of the halide complexes. The most characteristic feature of the latter is the peculiar disproportionation reaction (A), which occurs both in solid state and in non-polar solvents, with ease which increases with the l.f.s. of the halide anion. The behavior of all these complexes in solution is governed not only by the donor number of the solvent, but also by other polarity parameters, such as dielectric constant and E_T value, especially when the polarity is relatively low.

Some of these solutions are notably thermochromic; for example, when an acetone solution of IX-2 was frozen in liquid nitrogen, and the spectral change of its melt with the rise of temperature was followed up to room temperature, the band *ca.* 19000 cm^{-1} was found to increase several times, indicating strong shift of the disproportionation equilibrium.

Cordial thanks are due to Dr. Kenzo Nagase, Tohoku University, who kindly carried out the TG-DTA measurements of the new complexes. This work was supported in part by a Grant-in-Aid for Scientific Research No. 347033 from the Ministry of Education, Science and Culture.

References

1) Part X: N. Hoshino, Y. Fukuda and K. Sone, *Chem. Lett.*, **1979**, 437.
2) N. Hoshino, Y. Fukuda and K. Sone, *Transition Met. Chem.*, **4**, 183 (1979).
3) Y. Fukuda and K. Sone, *J. Inorg. Nucl. Chem.*, **34**, 2315 (1972).
4) L. Sacconi, I. Bertini, and F. Mani, *Inorg. Chem.*, **6**, 262 (1967).
5) U. Müller, "Structure and Bonding," ed by J. D. Dunitz *et al.*, Springer, Berlin (1973), p. 141.
6) J. Kohout, M. Hvastijova, and J. Gazo, *Coord. Chem. Rev.*, **27**, 141 (1978).
7) Y. Fukuda, N. Sato, N. Hoshino, and K. Sone, *Bull. Chem. Soc. Jpn.*, **54**, 428 (1981).
8) Y. Fukuda, R. Morishita, and K. Sone, *Bull. Chem. Soc. Jpn.*, **49**, 1017 (1976).
9) L. Sacconi, P. Nannelli, N. Nardi, and U. Campigli, *Inorg. Chem.*, **4**, 943 (1965); M. Ciampolini, *Inorg. Chem.*, **5**, 35 (1966).
10) M. Ciampolini, N. Nardi, and G. P. Speroni, *Coord. Chem. Rev.*, **1**, 222 (1966).
11) E. M. Kosower, "An Introduction to Physical Organic Chemistry," Wiley, New York (1968); J. Burgess, "Metal Ions in Solution," Ellis Horwood, Chichester, Sussex (1978).
12) W. J. Geary, *Coord. Chem. Rev.*, **7**, 81 (1971).

Studies on Mixed Chelates. XII. Formation and Electronic Spectra of 5-Coordinated Mixed Copper(II) Chelates Containing *N*-Alkylated Ethylenediamine, Acetylacetonate, and Pseudohalide Anions[1]

Yutaka FUKUDA,* Noriko SATO, Naomi HOSHINO, and Kozo SONE
Department of Chemistry, Faculty of Science, Ochanomizu University, Bunkyo-ku, Tokyo 112
(Received June 5, 1980)

The visible absorption spectra of three new mixed chelates of copper(II), Cu(tmen)(acac)X (tmen=*N,N,N',N'*-tetramethylethylenediamine, acac=acetylacetonate ion, X=NCS, N_3, or NCO) were studied in various organic solvents. It was found that the $\tilde{\nu}_{max}$ values of their d-d bands depend strongly on the nature of the solvent, and shift in the opposite direction as compared with the case of $[Cu(tmen)(acac)]ClO_4$ studied before, where $\tilde{\nu}_{max}$ shifted to red with the increase of the donor number (DN) of the solvent. Here the magnitude of the red shift is affected not only by the DN, but also by other parameters of the solvent polarity, such as Kosower's Z or Reichardt's E_T. The obtained data can reasonably be explained, if an equilibrium

$$\underset{\text{(5-coordinated)}}{[Cu(tmen)(acac)X]} \rightleftharpoons \underset{\text{(4-coordinated)}\\\text{(with axial solvation)}}{[Cu(tmen)(acac)]^+} + X^-$$

is assumed to exist in such solutions.

It was pointed out by Fukuda *et al.*[2] that the visible absorption spectra of the mixed copper(II) chelates [Cu(tmen)(acac)]X (X=ClO_4, or NO_3) in organic solvents are strongly influenced by the nature of the solvent used. In general, it was observed that the d-d band is shifted to the red with the increase of the donor number (Gutmann's DN) of the solvent. The effect was explained as the result of the strengthening of the axial solvation, which decreases the apparent ligand field strength observed as $\tilde{\nu}_{max}$.

Recently we prepared three new complexes with the general formula Cu(tmen)(acac)X (X=NCS, N_3, or NCO), and studied their spectra in organic solvents. A number of fundamentally different behaviors were found out, as compared with the case of perchlorate or nitrate chelate. These results and their probable explanations will be presented in this paper.

Experimental

Preparation of the New Complexes. *i) Cu(tmen)(acac)(NCS)*: A large excess of KNCS(*ca.* 50 mmol) was added to a solution of $[Cu(tmen)(acac)]ClO_4$[2] in 1,2-dichloroethane (=DCE, 10 mmol in *ca.* 50 cm^3). A few drops of methanol were added to the mixture, and it was heated at *ca.* 40 °C for several hours under constant stirring. The color of the solution changed from reddish violet to indigo, and then finally to deep green. Stirring was continued for a while after completion of this color change, and then the solution was cooled thoroughly by keeping it in a freezer for several hours. After filtering off the white precipitate formed ($KNCS+KClO_4$), the filtrate was evaporated to dryness, and further dried in vacuum. Since the green product obtained was seemingly quite raw, it was dissolved in DCE, and the solution was filtered and concentrated until it became noticeably viscous, and kept in the freezer again. The crystalline product obtained was further recrystallized from DCE. Deep green prismatic crystals were thus obtained.

ii) Cu(tmen)(acac)NCO: This complex could be obtained in the same way as i), using KNCO instead of KNCS. Deep green prismatic crystals were obtained.

iii) Cu(tmen)(acac)N_3: This complex could not be obtained in the same way as *i*). For its preparation, an excess of NaN_3 (15 mmol) was added to a solution of $[Cu(tmen)(acac)]NO_3$ in methanol(MeOH) (10 mmol in *ca.* 50 cm^3), and the mixture was stirred for some time. The color of the solution changed gradually from indigo to olive green; this solution was filtered to remove the white precipitate formed (NaN_3+NaNO_3), and transferred into a flask (A), which was connected with an inverted U-tube with another flask (B). The content of A was frozen with liquid nitrogen, and the whole system was evacuated and closed. The liquid N_2 around A was then removed, and B was cooled with it instead. Nearly all of the solvent in A was thus distilled into B, leaving the raw complex which crystallized out. The complex was separated from the mother liquor by filtration, dissolved in dichloromethane and filtered again. Similar procedures (*i.e.* dissolution in dichloromethane, filtration, and distillation of the solvent at low temperature) were repeated until a product of sufficient analytical purity was obtained. It was a bluish green powder, which had to be kept in a vacuum in a refrigerator, since spontaneous decomposition seemed to take place.

iv) Cu(tmen)(acac)NCSe: Deep green crystals which were very similar in appearance to Cu(tmen)(acac)NCS were obtained by the method i), using KNCSe instead of KNCS, but they were very unstable and decomposed in the course of recrystallization. Their identification with Cu(tmen)(acac)(NCSe) was, however, also supported by the close resemblance of its IR spectrum to that of the NCS-complex.

Physical Measurements. The electronic spectra of the solutions (350—850 nm) were measured with a Hitachi 340 Recording Spectrophotometer at room temperature (20—25 °C), using 10 mm quartz cells. The reflection spectra of the solid samples (300—800 nm) were measured with the same instrument, using $BaSO_4$ as the reference. IR spectra (600—5000 cm^{-1}) were measured in nujol mulls with a JASCO IR-A3 Grating IR Spectrophotometer. Magnetic susceptibility measurements were performed with a Shimadzu Tortion Magnetometer MB-100 (NCS- and NCO-complexes at 31 °C, N_3-complex at 17 °C). Electric conductivities of the solutions were measured with a Yanagimoto Conductivity Outfit Model MY-7 at 25 °C.

Results and Discussion

Properties of the Solid Chelates. Table 1 summarizes the analytical data, colors and magnetic moments of the

Table 1. Elementary analyses, colors, and magnetic moments of the chelates obtained

Formula	C(%)[a]	H(%)[a]	N(%)[a]	Color	μ_{eff}/BM
Cu(tmen)(acac)NCS	42.62(42.78)	7.71(6.88)	12.52(12.47)	bluish green	1.89
Cu(tmen)(acac)N_3	40.62(41.17)	7.13(7.23)	20.89(21.83)	bluish green	1.85
Cu(tmen)(acac)NCO	44.98(44.92)	8.01(7.23)	13.05(13.10)	green	1.92

a) Calculated values are in parentheses.

Table 2. Assignment of IR bands of the pseudohalide ions(X) in the complexes, Cu(tmen)(acac)X (cm^{-1})

X=NCS⁻		X=N_3⁻			X=NCO⁻		
ν_{CN}	ν_{CS}	$\nu_{a(NNN)}$	$\nu_{s(NNN)}$	$\delta_{(NNN)}$	$\nu_{a(NCO)}$	$\nu_{s(NCO)}$	$\delta_{(NCO)}$
2070	770	2060	1330	640	2200	1305	620
		2030	1305				

three new chelates. All of them show normal magnetic moments expected for monomeric copper(II) chelates, but their colors are notably different from that of [Cu(tmen)(acac)]ClO_4 (reddish violet). The IR spectra of these chelates show sharp bands of the pseudohalide ions, and their positions shown in Table 2 indicate that all of these ions are coordinated to Cu(II) with their N atoms.[4]

Electronic Spectra of the Chelates. As expected from the colors, the visible reflection spectra of these solid chelates are all quite different from that of [Cu(tmen)(acac)]ClO_4. These chelates are all readily soluble in various organic solvents, but the visible absorption spectra observed in them are also remarkably different from those of [Cu(tmen)(acac)]ClO_4 in the same solvents. As an example, the spectra of Cu(tmen)(acac)NCS in four solvents are given in Fig. 1. The observed values of $\bar{\nu}_{max}$ and ε_{max} for all three chelates are summarized in Table 3 and the shifts of $\bar{\nu}_{max}$ of each chelate are shown in Fig. 2, in comparison with the data of [Cu(tmen)(acac)]ClO_4.[2]

As stated in the introduction, the $\bar{\nu}_{max}$ value of the perchlorate shifts to the red approximately in the order of the donor number of the solvent. However, the data shown above clearly show that the $\bar{\nu}_{max}$ of the

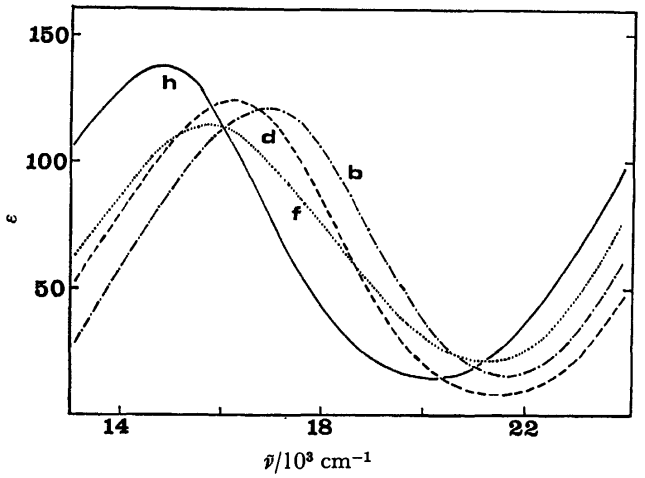

Fig. 1. Absorption spectra of [Cu(tmen)(acac)NCS] in various organic solvents. As to the symbols on the curves, *cf.* Fig. 2. Concentration: 5.5×10^{-3} M.

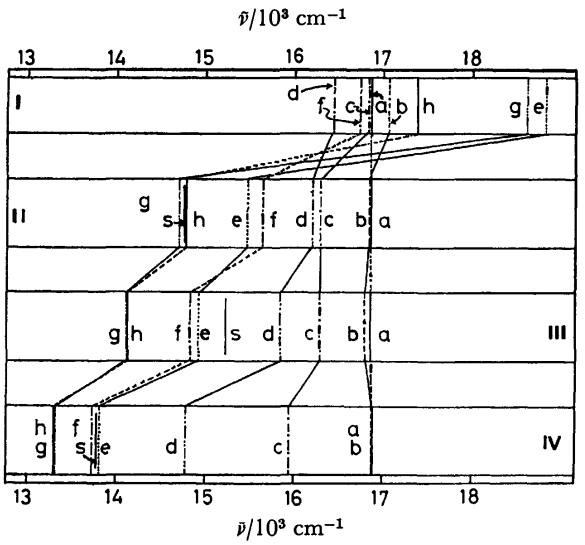

Fig. 2. Diagrammatic representation of the $\bar{\nu}_{max}$ values of [Cu(tmen)(acac)]ClO_4 (I), [Cu(tmen)(acac)NCS](II), [Cu(tmen)(acac)NCO](III) and [Cu(tmen)(acac)N_3]-(IV) in various organic solvents. The symbols a to h correspond to the following solvents: a=H_2O b=MeOH, c=EtOH, d=DMSO, e=NM, f=AN, g=DCE, h=acetone. The $\bar{\nu}_{max}$ of the solid reflection spectra are shown by S.

Table 3. $\bar{\nu}_{max}$ and ε_{max} values of Cu(tmen)(acac)X in solid state and in various solvents[a,b]

	X=NCS	X=N_3	X=NCO
Solid	14.79	15.24	13.77
H_2O	16.86(99)	16.86(111)	16.89(105)
CH_3OH(MeOH)	16.84(121)	16.78(113)	16.89(118)
C_2H_5OH(EtOH)	16.29(123)	16.29(126)	15.92(108)
$(CH_3)_2SO$(DMSO)	16.21(125)	15.85(136)	14.79(101)
$(CH_3)_2NCHO$(DMF)	16.21(111)	15.34(137)	13.97(98)
CH_3NO_2(NM)	15.48(118)	14.93(136)	13.81(111)
CH_3CN(AN)	15.67(115)	14.84(138)	13.74(109)
$C_2H_4Cl_2$(DCE)	14.71(153)	14.12(159)	13.32(118)
$(CH_3)_2CO$	14.79(138)	14.12(157)	13.30(107)

a) $\bar{\nu}_{max}$ in 10^3 cm^{-1}, ε_{max} in parentheses. b) Concentrations: 5.18—5.28×10^{-3} M in organic solutions of the NCS⁻ complex, and 5.92×10^{-3} M in its aqueous solution; 5.06—5.51×10^{-3} M in solutions of the N_3⁻ complex, and 7.23—7.50×10^{-3} M in those of the NCO⁻ complex, respectively (1 M=1 mol dm^{-3}).

pseudohalide complexes shift to the red with the decrease of solvent polarity, *i.e.* in apparently opposite direction as compared with the case of the perchlorate. The order of $\bar{\nu}_{max}$ in various solvents is, nearly in all three cases, expressed as:

$$H_2O > MeOH > EtOH > DMSO > DMF > NM > AN > DCE \approx Acetone. \quad (i)$$

Now it can be noted that this order (i) is not the order of DN of the solvents, but can better be correlated with the order of Kosower's Z values,[5] or Reichardt's E_T values,[6] which are other parameters of solvent polarity. Table 4 shows these correlations.

TABLE 4. DN, Z, AND E_T VALUES OF THE SOLVENTS[a]

Solvent	DN	Z	E_T
H_2O	18.0	94.6	63.1
MeOH	23.5	83.6	55.5
EtOH	30.0	79.6	51.9
DMSO	29.8	71.1	45.0
DMF	26.6	68.5	43.8
NM	2.7	—	46.3
AN	14.1	71.3	46.0
DCE	0.0	—	41.9
$(CH_3)_2CO$	17.0	65.7	42.2

a) See Refs. 5—7. The DN values of MeOH and EtOH are those of DeWitte and Popov,[13] and may not be strictly comparable with those of the other solvents proposed by Gutmann.

Thus we can understand that the order (i) is the order of the increase of Z or E_T, except a few small discrepancies. Since Z and E_T are linear functions of each other,[5] and more E_T values are available for the present study, we shall use E_T in our following discussions.

Before going further, it may be of interest to compare the meanings of these polarity parameters. The DN is a measure of the donor ability of the solvent or its Lewis basicity, *i.e.* its tendency to donate an electron pair to a positive solute particle. On the other hand, E_T is a measure of the polar influence of the solvent on the interactions between charged particles (or between charged parts inside of a large molecule) dissolved in it.

Now the pseudohalide ions (NCS^-, N_3^-, and NCO^-) are all good ligands, and their coordination ability is generally expected to be much higher than that of common organic solvents. Therefore, it will be possible to explain our spectral results of the NCS-complex in the following way:

(i) In a highly polar solvent like H_2O or MeOH, where the E_T values are highest among the solvents tried, the Cu–NCS bond is remarkably weakened, and remarkable dissociation of the complex into $[Cu(tmen)(acac)]^+$ and NCS^- takes place. The $[Cu(tmen)(acac)]^+$ planar cation formed has vacant coordination sites above and below it, and they are immediately occupied (*i.e.* solvated) by the solvent molecules. This is the reason why the $\bar{\nu}_{max}$ of the complex in these solvents are nearly the same as those of the perchlorate in the same solvents, where similar nearly complete dissociation of the anion is expected to occur.

It is interesting to note that the very important step involved in these changes is the dissociation of the strongly coordinated NCS^- ion from the complex, since the surrounding solvent molecules will spontaneously occupy the coordination sites which are open to them. In other words, the effect of E_T (polar influence of the solvent to weaken the polar bond (Cu–NCS) in the solute) is seemingly more important than that of DN (the ease of coordination of the solvent molecules to the vacant coordination sites produced around Cu^{2+}) in these changes. Further supports of this view will be found in the following examples.

(ii) In a highly non-polar solvent like DCE, where both the E_T and DN values are the lowest, the solvent can neither drive out the NCS^- ion from the complex, nor occupy its coordination site. Thus the complex is dissolved in the form of the 5-coordinated molecule, [Cu(tmen)(acac)(NCS)], which shows a d-d band of much lower $\bar{\nu}_{max}$ and somewhat higher ε_{max} than those of the solvated tetragonal ions formed in highly polar solvents.

(iii) In a solvent of intermediate polarity such as EtOH, DMSO, DMF, NM, or AN, the situations are more complicated. In the first three solvents, the DN values are even much higher than those of H_2O and MeOH, but the E_T values are noticeably lower. So it is more difficult to drive off the NCS^- ion in these solvents. In NM and AN, on the other hand, the DN values are much lower, but the E_T values are comparable to those of DMSO or DMF. These solvents will be able to drive out NCS^- ions from the complex to some extent, *i.e.* more or less like DMSO and DMF, but will not be able to occupy the vacant sites produced so readily. At any rate, in these solvents, there will be incomplete dissociation of NCS^- from the complex, leading to an equilibrium

$$\underset{\text{(5-coordinated)}}{[Cu(tmen)(acac)(NCS)]} \rightleftarrows \underset{\text{(4-coordinated) (with axial solvation)}}{[Cu(tmen)(acac)]^+} + NCS^- \quad (1)$$

which shifts to the right hand side with the increase of DN and E_T. As the d-d bands of the complexes on both sides of (1) are broad and of comparable intensity, they will mutually overlap, and lead to the formation of an apparent spectral maximum, which will shift to the red with the increase of [Cu(tmen)(acac)(NCS)] in the equilibrium mixture, *i.e.* with the decrease of DN and E_T. The fact that the observed shift is more closely related to E_T than to DN indicates that the main driving force of the forward reaction of (1) is the weakening of Cu–NCS bond, and not the strength of solvation. The most striking evidence for this view is the case of acetone, which has a DN much higher than those of NM or AN, but a E_T which is very low and comparable with that of DCE. The observed $\bar{\nu}_{max}$ in acetone is in the vicinity of that in DCE, showing that no coordination of the solvent can occur unless it can drive out the NCS^- by its polar influence.

The results of the N_3- and NCO-complexes can be explained in the same way, but the comparison of the three pseudohalide complexes shows that the ease of 5-coordinate complex formation increases in the order:

$$NCS^- < N_3^- < NCO^-. \quad (ii)$$

This can most clearly be seen by comparing the data of the NCS-complex with those of the NCO-

complex. In the latter case, all the $\tilde{\nu}_{max}$ values shift to the red, and flock together at the left end of Fig. 2, leaving only the values in very polar solvents (H_2O and MeOH) which remain nearly unchanged from those of the perchlorate. This means that NCO^- is bound strongly to Cu(II), so that even solvents like DMSO or EtOH can ionize it only partially. It is also clear that N_3^- comes just between NCS^- and NCO^- in its coordination power.

This order of the coordination ability of pseudohalide ions may be related to the values of their "optical electronegativities," proposed by Jørgensen.[8] The values for the σ- and π-optical electronegativities of halide and pseudohalide ions are:

Ligand	σ	π	Ligand	σ	π
Cl^-	3.4	3.0	NCO^-	—	3.0
Br^-	3.3	2.8	NNN^-	—	2.8
I^-	3.0	2.5	NCS^-	—	2.6

Although the σ-values for the pseudohalide ions are lacking, we can see that the π-values of Cl^-, Br^-, and I^- are comparable to those of NCO^-, N_3^-, and NCS^-, respectively. It is well known that the coordination tendencies of the halide ions toward 3d transition metal cations are, in general, in the order $Cl^- > Br^- > I^-$, so we can suppose that the order of the pseudohalide ions should be $NCO^- > N_3^- > NCS^-$, as is observed in Fig. 2. One can also imagine that the "hardness" of these ions increases just in the order (ii), *i.e.* from NCS^- with the soft S to N_3^- with highly delocalized π-system and then to NCO^- with much more rigid electronic structure, and that the coordination of an anion onto $[Cu(tmen)(acac)]^+$ is favored when it is hard, since the interaction may be weak and chiefly electrostatic in nature.

Table 5. Molar conductivities of the chelates (Ω^{-1} cm^2 mol^{-1}, 25 °C) and approximate degrees of dissociation (%, in parentheses)[b]

X-	DCE	NM	DMSO
NCS^-	1.1(6)	56.6(65)	39.8(100)
N_3^-	1.0(5)	27.0(32)	32.0(92)
NCO^-	0.5(3)	21.7(26)	14.8(42)

a) Concentration of the solutions: $\approx 10^{-3}$ M.
b) Calculated on the assumption that the Λ_M values of a typical 1 : 1 electrolyte in these three solvents are 20, 85, and 35 Ω^{-1} cm^2 mol^{-1}, respectively (see Ref. 9).

To confirm all these points of view, further spectral and conductometric measurements were carried out. Some data of them are shown in Table 5; it can clearly be seen that all the three chelates are nearly non-electrolytes in DCE, and the NCS- and N_3-chelates are nearly 1 : 1 electrolytes in DMSO, while in all other cases there is an ionization equilibrium, and the degree of ionization increases, in every case, in the order of DCE<NM<DMSO and $NCS^- < N_3^- < NCO^-$ just as expected from the above discussions.

As to the spectral measurements, a number of observations were made with the NCS-chelate which is the easiest to prepare. It was found first that the spectrum

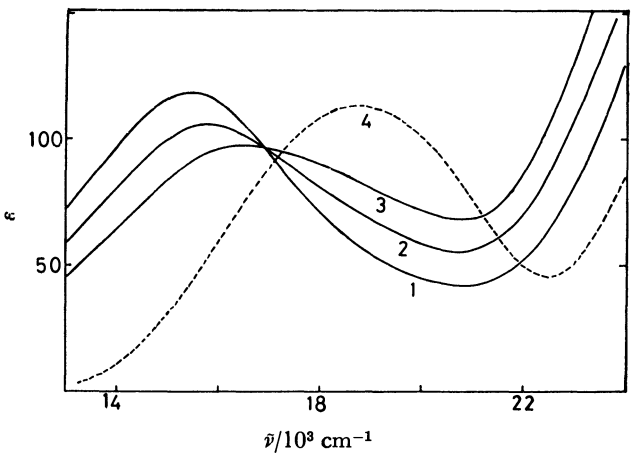

Fig. 3. Concentration dependence of the absorption spectra of [Cu(tmen)(acac)NCS] in NM, curves 1, 2, and 3 are those for 5.24×10^{-3}, 2.52×10^{-3} and 1.27×10^{-3} M solutions, respectively. Curve 4 is that of $[Cu(tmen)(acac)]ClO_4$ in the same solvent.

of this chelate in NM is remarkably dependent on concentration (*cf.* Fig. 3); its $\tilde{\nu}_{max}$ shifts to the red with increasing concentration and its ε_{max} increases, just as observed with the decrease of solvent polarity. Furthermore, the addition of KNCS to such a solution causes similar spectral changes, while the substitution of a part of NCS^- with ClO_4^- (this can conveniently be done by mixing the nitromethane solutions of $[Cu(tmen)(acac)]ClO_4$ and [Cu(tmen)(acac)(NCS)]) shifts the band in the opposite way. In all cases, a clear-cut isosbestic point appears on the curves, showing the existence of an equilibrium between two distinct species (*cf.* Fig. 4).** All these evidences indicate the existence of the equilibrium of the type (1) in these solutions. Very similar spectral changes were also observed in AN. The spectra of the same complex in H_2O or DCE are, on the other hand, not remarkably dependent on concentration, showing that they are either perfectly ionized or unionized, and that in acetone (which is very much like that in DCE) is affected only slightly by the addition of KNCS. All these facts are in line with the viewpoints proposed above. It may be added that the curve 6 of Fig. 4, *i.e.*, that of a NM solution of $[Cu(tmen)(acac)]^+$ with a large excess of NCS ($\tilde{\nu}_{max}$: 15.15×10^3 cm^{-1}, ε_{max}: 126), is very similar to those of the complex [Cu(tmen)(acac)-NCS] in DCE or acetone, indicating again the formation of the 5-coordinated species in NM, and also the fact that its spectrum is influenced only little by the solvent, *i.e.*, the 5-coordinated complex is only weakly solvated

** Strangely, the curve of $[Cu(tmen)(acac)]ClO_4$ itself slightly deviates from the isosbestic point, and its UV absorption is remarkably weaker than that of all other systems in Figs. 3 and 4. The reason for such deviations is not clear as yet, but may be due to the effect of ion-pair formation,[10] or the coexistence of a small amount of another species with strong ultraviolet absorption in the NCS^--containing solutions. These and other problems (e.g. solubility relationship) are hindering the estimation of K values of (1) from these data at present.

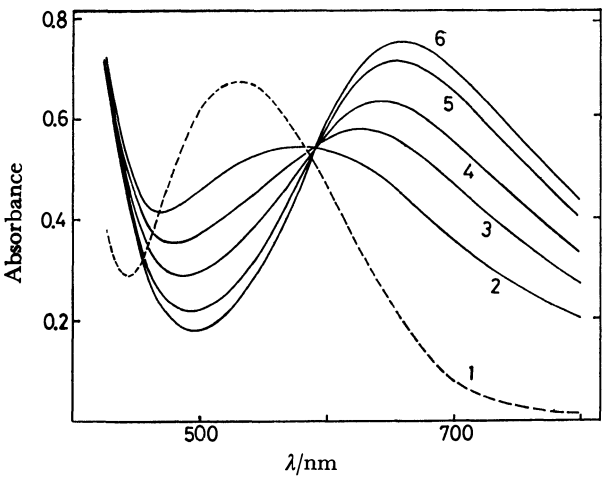

Fig. 4. The effect of NCS^- ions on the spectrum of $[Cu(tmen)(acac)]^+$(concentration: 6×10^{-3} M) in NM. The curve 1 is that of $[Cu(tmen)(acac)]ClO_4$ and curves 2 to 6 correspond to solutions in which the ratios $[Cu(tmen)(acac)]^+$: NCS^- are 1 : 0, 1 : 0.5, 1 : 0.75, 1 : 1, 1 : 1.5, and 1 : 2 respectively.

in solution.†

Finally, mention may be made of the structure of these three chelates in solid state. The comparison of the $\tilde{\nu}_{max}$ values of the solids (*cf.* Table 3) with those of the solutions indicates that the NCS-complex is typically 5-coordinate in its solid and to be formulated as [Cu(tmen)(acac)X]. The same can probably be said as to the NCO-complex. In the case of N_3-complex, the $\tilde{\nu}_{max}$ value is noticeably higher to be purely 5-coordinate: here the N_3-ions may be forming bridges between the $[Cu(tmen)(acac)]^+$ cations, making the Cu^{2+} in it to some extent 6-coordinate.[11] Some such bridge formation may also be present in the NCO-complex, in which the $\tilde{\nu}_{max}$ is slightly higher than that in DCE and comparable with those in NM or AN.[12]

Thus it is evident that these three new chelates are interesting examples of the stereochemistry of copper(II), with which one can easily observe the competition of pseudohalide ions and solvents for the coordination sites above or below the chelate plane with the aid of their visible spectra.

The present work was partially supported by a Grant-in-Aid for Scientific Research No. 347033 from the Ministry of Education, Science and Culture.

† The viewpoints stated here are supported further by the comparison of these data with those of the corresponding halide complexes,[14] which will be reported in another paper.

References

1) Part XI: N. Hoshino, Y. Fukuda, and K. Sone, *Bull. Chem. Soc. Jpn.*, **54**, 420 (1981).
2) Y. Fukuda and K. Sone, *Bull. Chem. Soc. Jpn.*, **45**, 465 (1972); Y. Fukuda, A. Shimura, M. Mukaida, E. Fujita and K. Sone, *J. Inorg. Nucl. Chem.*, **36**, 1265 (1974).
3) V. Gutmann, "Coordination Chemistry in Non-Aqueous Solutions," Springer, Wien (1968).
4) K. Nakamoto, "Infrared and Raman Spectra of Inorganic and Coordination Compounds," 3d ed, John-Wiley, New York (1978).
5) E. M. Kosower, "An Introduction to Physical Organic Chemistry," Wiley Internat. Ed., Toppan, Tokyo (1968).
6) K. Dimroth, C. Reichardt, T. Spiepmann, and F. Bohlmann, *Ann.*, **661**, 1 (1963).
7) J. Burgess, "Metal ions in Solutions," Ellis Horwood, Chichester (1978).
8) C. K. Jørgensen, "Oxidation Numbers and Oxidation States," Springer, Berlin (1969).
9) W. J. Geary, *Coord. Chem. Rev.*, **7**, 81 (1971).
10) H. Yoneda, *Bull. Chem. Soc. Jpn.*, **29**, 68 (1956).
11) U. Müller, "Structure and Bonding," ed by J. D. Dunitz *et al.*, Springer, Berlin (1973).
12) J. Kohout, M. Hvastijova, and J. Gazo, *Coord. Chem. Rev.*, **27**, 141 1978).
13) W. J. DeWitte and A. I. Popov, *J. Solution Chem.*, **5**, 231 (1976).
14) H. Kimura, Y. Fukuda, and K. Sone, unpublished data (1979).

Bridges in Polynuclear Complexes. II.† An X-Ray Investigation of the Coordination of Silver Ion to the μ-Peroxo Bridge of a Dinuclear Cobalt(III) Complex

Takashi SHIBAHARA,*,** Masayasu MORI, Keiji MATSUMOTO, and Shun'ichiro OOI

Department of Chemistry, Faculty of Science, Osaka City University, Sugimoto-cho, Sumiyoshi-ku, Osaka 558

(Received May 15, 1980)

The crystal structure of $[(en)_2Co(NH_2)(O_2)Co(en)_2](NO_3)_3 \cdot 15/8(AgNO_3) \cdot H_2O$ has been determined from X-ray diffraction data collected by the counter method. The crystal is monoclinic with the space group C2/c and with $a=8.710(3)$, $b=16.413(5)$, $c=20.024(8)$ Å, $\beta=90.30(4)°$, and $Z=4$. The structure was refined by the block-diagonal least-squares method to $R=0.107$ for 2157 independent reflections. It has been elucidated that the Ag atom is bound to each of the two peroxo oxygen atoms with the Ag–O bond length of 2.27(1) Å. Each Ag atom is also surrounded by two more oxygen atoms belonging to the nitrate anions and these Ag–O bond lengths are 2.45(2) and 2.50(2) Å. The central five-membered ring has a symmetric envelope conformation, with the peroxo O atom deviating from the Co, N, Co plane, by 0.38 Å. The crystals contain an equal amounts of the enantiomeric forms $(^{\delta}_{\delta}\Lambda\delta\Lambda^{\delta}_{\delta})$ and $(^{\lambda}_{\lambda}\Delta\lambda\Delta^{\lambda}_{\lambda})$. The formation constant of Ag^+ and $[(en)_2Co(NH_2)(O_2)Co(en)_2]^{3+}$ in aqueous solution was found to be less than 0.5.

The peroxo moiety of μ-amido-μ-peroxo dicobalt complex can be regarded as a Lewis base. The protonation to the peroxo moiety of the μ-amido-μ-peroxo dicobalt complex and subsequent isomerization was suggested by Mori and Weil from the analysis of kinetic data[1] and was confirmed by Thewalt by the X-ray structure analysis.[2]

Werner[3] reported the preparation of an addition compound, $[(en)_2Co(NH_2)(O_2)Co(en)_2](NO_3)_3 \cdot 5/3(AgNO_3)$. As the peroxo bridge of the complex is a Lewis base and the silver ion a Lewis acid, it seemed of interest to know whether a coordinate bond between the silver ion and the peroxo moiety is realized in this compound, and, if so, to determine the mode of coordination of the peroxo bridge to the cobalt atoms in connection with the isomerization scheme stated previously.

In the course of the study to elucidate this kind of problem, the addition compound obtained after Werner's description was shown by elemental analysis to have the composition $[(en)_2Co(NH_2)(O_2)Co(en)_2](NO_3)_3 \cdot 15/8(AgNO_3) \cdot H_2O$. The present paper reports the result of the X-ray structure analysis of this addition compound.

Experimental

Preparation of the Complex $[(en)_2Co(NH_2)(O_2)Co(en)_2](NO_3)_3 \cdot 15/8(AgNO_3) \cdot H_2O$. The addition compound of the above formula was prepared by Werner's method.[3] Recrystallization from water containing a large excess of silver nitrate gave deep red crystals suitable for the X-ray structure analysis.

Found: C, 10.38; H, 3.92; N, 21.27; NO_3^-, 32.58; Co, 12.53; Ag, 21.47; loss in wt over P_2O_5, in a vacuum, 1.71%. Calcd for $[Co_2C_8H_{34}N_9O_2](NO_3)_3 \cdot 15/8(AgNO_3) \cdot H_2O$: C, 10.34; H, 3.91; N, 20.92; NO_3^-, 32.54; Co, 12.69; Ag, 21.77; H_2O, 1.94%. The above composition appears to be maintained even when the amount of the silver nitrate was varied to some extent.

For comparison, the calculated values for two other different formulae are given. Calculated for $[Co_2C_8H_{34}N_9O_2](NO_3)_3 \cdot 2(AgNO_3)$: C, 10.31; H, 3.68; N, 21.04; Co, 12.65; Ag, 23.15; NO_3^-, 33.06%. Calcd for $[Co_2C_8H_{34}N_9O_2](NO_3)_3 \cdot 5/3(AgNO_3)$ (Werner's formula); C, 10.89; H, 3.91; N, 21.87; Co, 13.46; Ag, 20.54; NO_3^-, 33.06%.

X-Ray Data Collection. The specimen employed for data collection had a shape of an approximate sphere and its diameter was 0.23 mm. The Laue symmetry, space group, and approximate unit-cell dimensions were determined from oscillation and Weissenberg photographs taken with Cu Kα radiation. Crystal Data: $[Co_2C_8H_{34}N_9O_2](NO_3)_3 \cdot 15/8(AgNO_3) \cdot H_2O$, $M=929.12$, monoclinic, $a=8.710(3)$, $b=16.413(5)$, $c=20.024(8)$ Å, $\beta=90.30(4)°$, $V=2862.6(15)$ Å^3, $Z=4$, $D_m=2.15$, $D_c=2.16$ g·cm^{-3}, space group C2/c, λ(Mo Kα)=0.7101 Å, μ(Mo Kα)=25.2 cm^{-1}. Both the structure refinement and piezoelectric test suggest that the centrosymmetric space group C2/c is the correct choice. The unit-cell dimensions were refined by the least-squares analysis of the 36θ values measured on a Philips PW1100 automated diffractometer. The intensity data with $2\theta \leqq 55°$ were collected at room temperature by the use of graphite-monochromated Mo Kα radiation. The ω-2θ scan technique was employed. The scan range was $(0.9+0.2\tan\theta)°$, and the scan speed, 1°/min in ω: the background was counted for half of the scan time at each end of the scan. The three standard reflections, 200, 080, and 006, monitored every 180 min, showed no appreciable decay. A total of 2159 intensities with $F^2 \geqq 3\sigma(F^2)$ were observed and used for the structure analysis. A spherical absorption correction was applied.[4]

Structure Determination and Refinement. The structure was solved by the heavy-atom technique. The parameters were refined by the block-diagonal least-squares method using isotropic temperature factor for each atom. The R factor was 0.16. Further refinement, based on the anisotropic temperature factores for the Co and Ag atoms, resulted in $R=0.107$ and the refinement was terminated at this point. When the anisotropic temperature factors were applied to all non-hydrogen atoms, the R-factor decreased to 0.085. There is some doubt, however, as to the meaning of this value, since all the nitrate anions and water of crystallization were found to be disordered. The minimized function was $\sum w(F_o - |F_c|)^2$ and weighting scheme, $w=(24.7/F_o)^2$ for $F_o > 24.7$, $w=1$ for $24.7 \geqq F_o \geqq 16.5$, $w=0.9$ for $F_o < 16.5$ was used.

† Part I: S. Kubo, T. Shibahara, and M. Mori, *Bull. Chem. Soc. Jpn.*, **52**, 101 (1979).

** Present address: Department of Chemistry, Okayama University of Science, 1-1 Ridai-cho, Okayama 700.

Full occupation of the general position in the C2/c system suggests the formula $[(en)_2Co(NH_2)(O_2)Co(en)_2](NO_3)_3 \cdot 2AgNO_3 \cdot H_2O$, but the actual composition was $[(en)_2Co(NH_2)(O_2)(Co(en)_2](NO_3)_3 \cdot 15/8(AgNO_3) \cdot H_2O$. In order to accomodate this descrepancy, the occupation factor of 0.938 (15/16) was used for the Ag ions. For the nitrate ions, the occupation factor of 0.975 based on an equal partition of the nitrate shortage (0.125) over all the five nitrate positions was adopted, because it has been difficult to determine the extent of lattice defect to each nitrate position. Application of the occupation factors different from unity as above, however, did not produce any significant difference of structural parameters. In the final cycle of the refinement, all the parameter shifts were less than their standard deviations. The large peaks in the final difference synthesis were 3.5 and 2.2 $eÅ^{-3}$ in the vicinity of the Ag atom and H_2O molecules, respectively. No attempt was made to locate the hydrogen atoms. The atomic scattering factors of the Ag, Co, O, N, and C atoms were taken from Ref. 5. The real part of the anormalous dispersion correction were applied for the Co and Ag atoms.[5] A complete list of the F_o and F_c tables is preserved by the Chemical Society of Japan (Document No. 8112). All the computation were carried out by the FACOM 230-60 computer at Osaka City University. The programs used included a local version of the UNICS.[6]

Measurement of Ag^+ activity in the Aqueous Solution. The activity of Ag^+ in the presence of Co complexes was measured by using a Horiba CN^- ion electrode 8001 and a Horiba ion meter N-7 ⟨ION⟩.

Results and Discussion

Figure 1 gives two projections of the complex ion which show the coordination mode of the Ag atom to the peroxo oxygen atom. Figure 2 shows the crystal structure viewed down the a axis. The nearest neighbor to the Ag atom is the oxygen atom of the peroxo moiety of the complex ion (Fig. 2). The Ag–O(1) bond distance of 2.27(1) Å, indicating the presence of a coordinate bond between the Ag and O(1)$(1/2-x, -1/2+y, 1/2-z)$ atoms, is somewhat longer than the strongest Ag–O bond length (2.17 Å) in $Ag_2C_2O_4$.[7] The OA(2) and OA(4) atoms of the nitrate anions lies at a slightly greater distance than that between Ag and O(1). The Ag–OA(2) and Ag–OA(4) bond distances are 2.47(2)

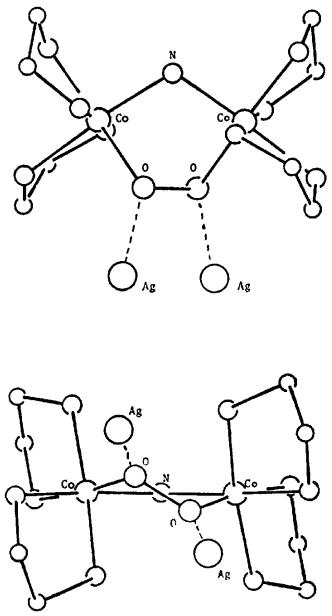

Fig. 1. Perspective drawing of complex ion.

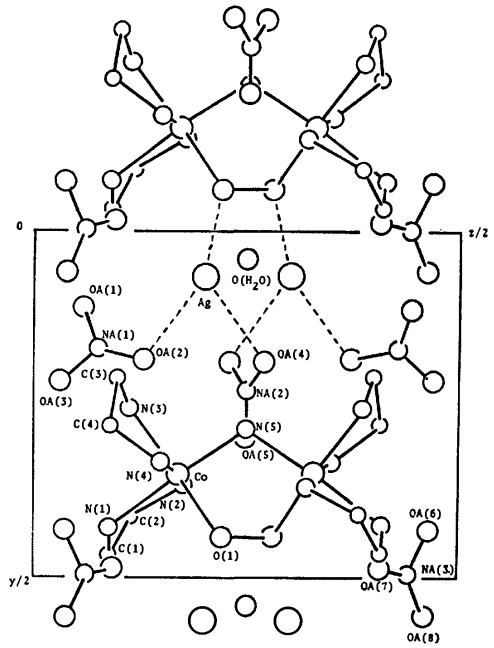

Fig. 2. The crystal structure viewed down the a axis. The dotted lines indicate possible Silver–Oxygen bonds.

Table 1. Positional and thermal parameters

Atom	$10^3 \times x$	$10^3 \times y$	$10^3 \times z$	$10 \times B$
Co	498.6(0.2)	351.3(0.1)	167.9(0.1)	a)
Ag	152.1(0.2)	67.0(0.1)	201.4(0.1)	a)
N(1)	482(2)	426(1)	90(0.5)	31(2)
N(2)	275(2)	369(1)	177(0.5)	32(2)
N(3)	470(2)	252(1)	112(0.5)	34(2)
N(4)	719(2)	337(1)	151(0.5)	32(2)
N(5)	500(0)	287(1)	250(0)	26(2)
C(1)	334(2)	471(1)	95(1)	49(3)
C(2)	212(2)	412(1)	117(1)	50(3)
C(3)	626(2)	210(1)	100(1)	45(3)
C(4)	742(2)	281(1)	92(1)	43(3)
O(1)	544(1)	444(0.5)	220(0.5)	25(1)
NA(1)	106(1)	171(1)	74(0.5)	34(2)
NA(2)	0(0)	231(1)	250(0)	32(3)
NA(3)	139(4)	493(2)	441(2)	113(8)
OA(1)	35(2)	113(1)	57(1)	76(4)
OA(2)	152(2)	188(1)	128(1)	64(3)
OA(3)	100(3)	217(2)	31(1)	119(7)
OA(4)	120(2)	193(1)	269(1)	59(3)
OA(5)	0(0)	301(1)	250(0)	44(3)
OA(6)	127(6)	432(3)	462(3)	230(19)
OA(7)	179(4)	481(2)	409(2)	136(9)
OA(8)	43(4)	552(2)	460(2)	148(10)
$O(H_2O)$	500(0)	46(2)	250(0)	70(5)

a) Anisotropic temperature factores ($\times 10^5$) in the forms

$$\exp[-(B_{11}h^2+B_{22}k^2+B_{33}l^2+B_{12}hk+B_{13}hl+B_{23}kl)]$$

Atom	B_{11}	B_{22}	B_{33}	B_{12}	B_{13}	B_{23}
Co	671(17)	248(6)	98(3)	−2(16)	−16(11)	9(9)
Ag	1896(25)	267(5)	496(6)	−251(16)	47(20)	60(8)

The Character of Acid Sites on the Gypsum Surface

Susumu OKAZAKI* and Mituo YAMAZAKI

Department of Industrial Chemistry, Faculty of Engineering, Ibaraki University, Hitachi, Ibaraki 316

(Received January 21, 1980)

The maximum value in the number of acid sites per unit of surface area of the gypsum formed in the reaction between $Ca(NO_3)_2$ and H_2SO_4 was observed at the heat-treatment temperature of 200 °C, corresponding to the dehydration temperature for the change from its hemihydrate form to soluble anhydrite. The IR-absorption spectra of the gypsum showed no bands assignable to isolated OH groups or Ca–OH species. The IR spectra of the pyridine adsorbed on the gypsum showed only the bands due to Lewis-acid sites. The gypsum heat-treated at temperatures lower than 500 °C showed catalytic activities for the double-bond isomerization of 1-butene. The *cis-/trans-* ratio of 2-butene was 2—2.5, showing that the catalytic activity was due to Lewis acid, not to Brönsted acid. The isomerization of cyclopropane to propene was scarcely promoted by the gypsum at 250 °C. This fact is another indication of the absence of Brönsted acid sites on the heat-treated gypsum. Most of the weak Lewis acid sites ($H_0 \leqq +4.8$) were ascribable to exposed Ca^{2+} ions surrounded by monodentate sulfate ions on the surface of metastable anhydrite III-$CaSO_4$.

In recent years, gypsum has been obtained in great quantities as a by-product in the SO_2-recovery process from exhaust gases. Accordingly, the development of a new method of utilizing the recovered gypsum is desirable. Use as a filler or a reinforcement agent in composite materials seems to be promising. Because of the polar nature of the gypsum surface, however, surface modification or an increase of lipophilicity is necessary for the two uses mentioned above. As has been shown in the previous study[1] dealing with the increase in lipophilicity of the gypsum surface upon interaction with butylamine, acid sites on the surface may be used for the surface modification.

The presence of acid sites on the calcium-sulfate surface was first reported about thirty years ago.[2] The surface acidity of gypsum has been investigated by subsequent workers.[3–6] Although the acid sites have been assumed to be the Lewis type,[7] the Lewis acidity has not beed substantiated. The absence of Brönsted sites has not yet been examined. Furthermore, the relation between the surface acidity and the catalytic activities for the acid-catalyzed reaction has scarcely been investigated.

In the present work, the character of acid sites on the surface of precipitated gypsum was investigated mainly by means of IR-spectroscopic measurements and by the determination of catalytic activities for the isomerization of 1-butene and the conversion of cyclopropane to propene.

Experimental

Materials. The precipitated gypsum used was prepared by the addition of concentrated sulfuric acid to an aqueous solution of $Ca(NO_3)_2$, followed by aging and completely washing with deionized water. The nitrate ions remaining in the precipitate could be removed with ease by the heat-treatment of the product, as evidenced by the trace amounts of NO_2 gas evolved during the heat-treatment. The carbonate content was determined to be 0.09 wt% by the gas-chromatographic analysis of the gas evolved during the heat-treatment of the sample up to 900 °C.

IR Spectra. Except for the study relating to the coordinations of SO_4^{2-} ions, which was carried out by using KBr pellets, the IR spectra were measured using a self-supporting disc in an *in situ* cell. The samples were compressed into thin discs and were evacuated at different temperatures.

X-Ray Diffraction and Surface Area. The X-ray powder diffraction patterns were recorded using Cu $K\alpha$ as the radiation source. The specific surface area was determined by applying the BET method to the adsorption of N_2 at −196 °C.

Acid Properties. The acid properties of samples were examined by titrating with butylamine in benzene according to Johnson's method.[8] The Brönsted and Lewis acidities were determined by observing the IR spectra of pyridine adsorbed on the samples.

1-Butene Isomerization. The 1-butene isomerization was carried out in a closed gas-circulation reactor having a volume of 0.43 l. Above 0.7 g of the sample was placed in the reactor and degassed for 2 h at various temperatures. After the sample has then been cooled to room temperature, 1-butene of 110 Torr was introduced and circulated for 0.5 h at 200 °C. The products were analyzed by gas chromatography using a 7-m column packed with VZ-7.

The catalytic activity was expressed by the mole percentage of the product per unit of weight of the catalyst (g^{-1}) per unit of time (min^{-1}) determined at the reaction time of 30 min. As an indication of the acid character, the mole ratio of *cis*-2-butene to *trans*-2-butene (abbreviated as *cis-/trans-*) at zero conversion in the isomerization was determined by extrapolation.

Conversion of Cyclopropane to Propene. The conversion was carried out in a glass reactor containing 0.05 g of gypsum which had been heat-treated at various temperatures. Pulses of cyclopropane were injected into the helium-carrier stream from a calibrated, 1.09-ml doser and were passed through the gypsum at a total pressure of 1 atm. The product gas was analyzed by gas chromatography using a 3-m column packed with Porapack N. The conversion of cyclopropane to propene in the first pulse was taken as a measure of the catalytic activity.

Results and Discussion

Changes in Structures and Surface Areas of Gypsum with Increase in Treatment Temperature. As is shown in Table 1, the results of the X-ray diffraction analysis for the sample show that the monoclinic structure of the dihydrate changed into the hexagonal structure of the hemihydrated gypsum (β-$CaSO_4$l/$2H_2O$) or soluble anhydrite (III-$CaSO_4$) at about 100 °C, and then into the orthorhombic structure of the insoluble anhydrite (II-$CaSO_4$) at about 400 °C. The changes in the

Table 1. Crystal structure and specific surface area of gypsum heat-treated at different temperatures

Treatment temp °C	Crystal structure	Specific surface area/$m^2\ g^{-1}$
Room temperature	$CaSO_4 2H_2O$	3.3
100	$CaSO_4 1/2H_2O$ or III-$CaSO_4$	13.5
200	$CaSO_4 1/2H_2O$ or III-$CaSO_4$	7.3
300	$CaSO_4 1/2H_2O$ or III-$CaSO_4$	21.8
400	II-$CaSO_4$	26.8
500	II-$CaSO_4$	26.7
600	—	21.3
700	—	4.3

crystal structure of the sample with the increase in the temperature almost coincided with that reported for gypsum ($CaSO_4 2H_2O$).[9] However, the change of β-$CaSO_4 1/2H_2O$ into III-$CaSO_4$ at 190—210 °C[9] could not be observed, since these two forms are very similar or the almost isomorphous with each other.[10,11]

Table 1 also shows the effect on the surface area of heating up to 700 °C. The specific surface area of the sample depends largely on the heat-treatment temperature. Two maxima are observed at about 100 °C and 400—500 °C. These temperatures are nearly equal to the transition points of the dihydrate to the hemihydrate, and of the soluble anhydrite to the insoluble anhydrite, respectively. These facts suggest that the change in crystal structure may increase the surface area. Because of the similarity in crystal form, the transformation of β-$CaSO_4 1/2H_2O$ to III-$CaSO_4$ may not cause the increase in the surface area.

Surface Acidity Determined by Amine Titration. Figure 1 shows the surface acidities of the sample heat-treated at different temperatures. The sample has no acid sites stronger than those corresponding to an H_0 value (indicator, pK_a) of 3.0, but it does display some weak acidity in the range of H_0 from 4.8 to 3.0. The acid amount per unit of weight showed a maximum value at a heat-treatment temperature of 300 °C.

To discuss the acid-site concentration on the surface, the acid amounts per unit of surface were calculated, as is shown by the dotted line in Fig. 1. A maximum in the acid-site concentration is shown at about 200 °C. From a structural point of view, the temperature at which the maximum acid concentration was obtained (200 °C) corresponds to the transition temperature of the hemihydrated gypsum to the soluble anhydrite form.[9] The soluble anhydrite has a crystal structure almost isomorphous with that of hemihydrated gypsum and has an active cleavage plane, on which Ca^{2+} and SO_4^{2-} ions are unevenly distributed.[7] It is well known that the soluble anhydrite is metastable and tends to be converted to the hemihydrated gypsum with the absorption of water. It is probable that the acid sites are formed on the metastable, or soluble, anhydrite.

Infrared Spectroscopy. The Ca^{2+} ions on the plane of the hemihydrated gypsum may be the sites of Lewis acidity (in a general sense). However, it is also possible that the ions may polarize adjacent OH groups or the O–H bonds in H_2O molecules adsorbed on the surface and produce Brönsted acid sites. Hence, the elucidation of the characteristics and behavior of OH groups and H_2O molecules on/in gypsum was attempted by means of IR spectroscopy.

Previously, the presence of a small amount of water in the so-called soluble anhydrite gypsum has been detected in the IR studies using the KBr[12] or Nujol[13] method. However, since the anhydrous form is very hygroscopic, these methods are inadequate for the confirmation of the presence and behavior of H_2O and related OH groups in the course of heat-treatment. Accordingly, the IR absorption analysis was carried out using a self-supporting disc in an *in situ* cell. As is shown in Fig. 2, the broad bands due to OH stretching

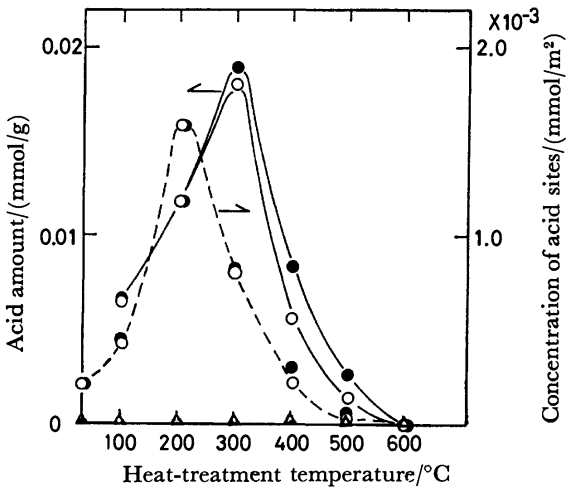

Fig. 1. Effect of treatment temperature on acid amount and acid site concentration.
△: $H_0 \leqq 3.0$, ○: $H_0 \leqq 4.8$, ●: $H_0 \leqq 6.8$.

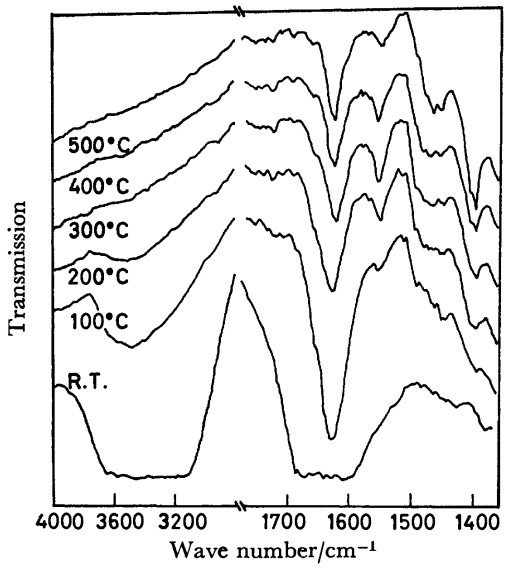

Fig. 2. Infrared spectra for precipitated gypsum evacuated at various temperatures.

and H_2O bending were observed at 3200—3600 cm^{-1} and 1600—1700 cm^{-1} respectively for the evacuation at room temperature. The band at 1600—1700 cm^{-1} was converted into a sharp 1627 cm^{-1} band at 100 °C, and this band still remained at higher temperatures such as 500 °C. Even though this band is ascribable to H_2O bending vibrations, the band assignable to OH stretching disappeared above 300 °C, as is shown in Fig. 2. Therefore, the absorption band which survived above 300 °C may be assigned not to H_2O but to bidentate carbonate, which gives the absorption at 1630 cm^{-1}.[14] Thus, the band at about 1620 cm^{-1} in the spectra observed for the gypsum heat-treated below 300 °C is probably due to both H_2O and carbonate. The bands at 1396 and 1405 cm^{-1} might be due to the asymmetric stretching vibration of the N–O bond belonging to the NO_3^- ion,[15] which could not be completely removed during the preparation. Other bands at 1430—1500 cm^{-1} might be assigned to carbonate or hydrogen carbonate ions.[16]

In general, the bands at 3600—3700 cm^{-1} due to isolated OH groups are observed for many heat-treated metal oxides. As has been shown in the discussion with respect to the surface acidities of Al_2O_3 and SiO_2–Al_2O_3,[17] the isolated OH groups may be acidic, for they are surrounded by three metal atoms, and so would be affected by the greatest induction due to metal atoms. In the case of gypsum, there are no distinct bands due to isolated OH groups in the region of 3600—3700 cm^{-1}. Thus, the existence of Brönsted acid sites due to the isolated OH groups on the gypsum surface seems impossible.

Infrared Spectra of Pyridine on the Surface of Gypsum. Infrared spectroseopic studies of pyridine adsorbed on a solid surface have made it possible to distinguish between Brönsted and Lewis acids.[18] The IR spectra of pyridine on gypsum evacuated at different temperatures were measured in order to elucidate the character of the acid sites. As is shown in Fig. 3, a strong absorption band at 1445 cm^{-1} was observed in the case of gypsum which had been dried in the air at 200 °C for 2 h and then evacuated in a cell at 200 °C for 2 h. As the evacuation temperature was raised, the band at 1445 cm^{-1} became weaker. This band is attributable to hydrogen-bonded (at 1440—1447 cm^{-1} [19]). The band at about 1445 cm^{-1} is not so sharp, as is shown in Fig. 3, the bands due to hydrogen bonding and to coordinative bonding are close to each other. Therefore, it is difficult to determine the character of the active sites merely by the inspection of the IR spectrum of pyridine on the surface. However, the shoulder at 1605 cm^{-1} is more readily attributable to the coordinatively bonded pyridine (at 1600—1663 cm^{-1} [19]) than to the hydrogen-bonded pyridine (at 1580—1600 cm^{-1} [19]). The finding that the absorption band at 1445 cm^{-1} remained after evacuation at 200 °C also supports the presence of Lewis acid sites rather than that of hydrogen-bonding sites, which may be weak with respect to retaining the pyridine molecules.

The absorption bands at 1540 cm^{-1} and about 1640 cm^{-1} are characteristic of pyridinium ions and are generally used for finding of Brönsted-acid sites.[19] The band at about 1540 cm^{-1} is indistinguishable from the bands of gypsum (as shown in the spectrum (B. G.) in Fig. 3). However, the absence of the band at 1640 cm^{-1} suggests that there are no Brönsted-acid sites on gypsum.

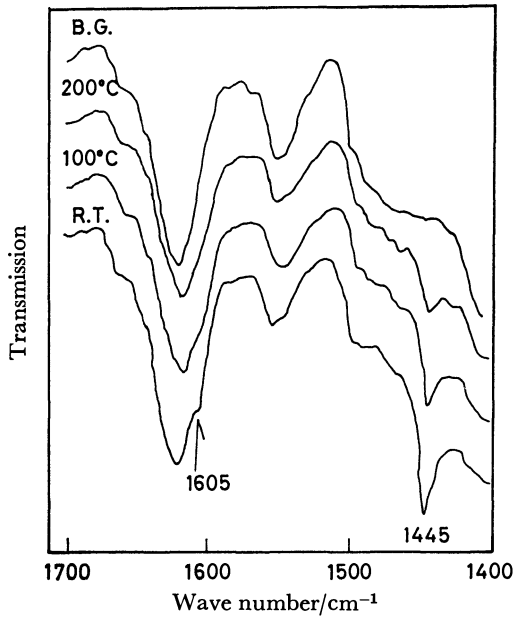

Fig. 3. Infrared spectra for pyridine adsorbed on precipitated gypsum.
B.G.: Background; Precipitated gypsum treated in the air at 200 °C for 3 h and evacuated for 2 h. R.T., 100 and 200 denote the evacuation temperature of samples treated with 10 Torr of pyridine for 10 min.

Table 2. Conversion of cyclopropane to propene[a]

Catalyst	Heat-treatment temperature[b] °C	Conversion %
Gypsum	300	0.7
	400	0.8
	500	0.3
	600	0.4
SiO_2–Al_2O_3	500	100
TiO_2	500	100
None		0.4

a) The reaction condition were as follows; temperature: 250 °C, catalyst weight: 50 mg, carrier and its velocity: He, 10 ml/min. b) All the catalysts had been heat-treated for 3 h.

Catalytic Activities for Conversion of Cyclopropane and for the Double-bond Isomerization of 1-Butene. The catalytic activity of heat-treated gypsum in the conversion of cyclopropane was examined at 250 °C. As is shown in Table 2, the conversion of cyclopropane to propene, which should be catalyzed by Brönsted acids,[20] were all less than 1%, irrespective of the heat-treatment temperature, and were close to those obtained in the absence of the gypsum. The conversion of the reaction catalyzed by the commercial SiO_2–Al_2O_3 catalyst, named N 631 (Nikki Chem. Co.), which is a typical Brönsted-acid catalyst, was 65% at such a low

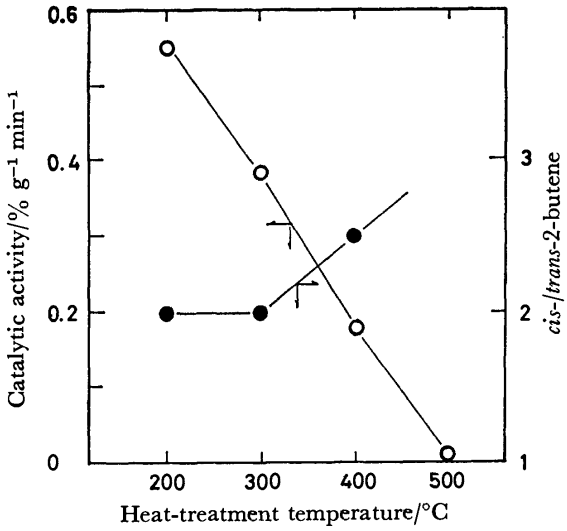

Fig. 4. Catalytic activity and selectivity *vs.* treatment temperature.
Reaction temperature : 200 °C, Pressure of 1-butene : 110 Torr.
Evacuation was carried out for 2 h at each tretment temperature.

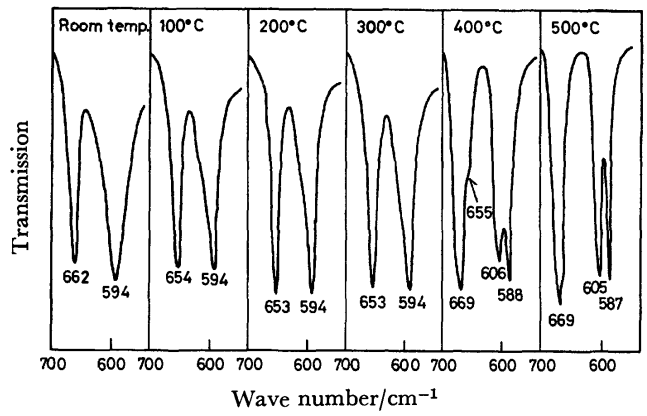

Fig. 5. Infrared spectra for sulfate ions on precipitated gypsum heat-treated at different temperatures

temperature as 150 °C for the same contact time. In addition, the conversion of the reaction at 250 °C catalyzed by TiO_2, which had been prepared from $TiOSO_4$ and which had a considerable quantity of Brönsted-acid sites,[21] was nearly 100%. These contrasted results indicate that there are no Brönsted-acid sites on the gypsum surface.

In order to further investigate the acid character of the gypsum, the isomerization of 1-butene was carried out at 200 °C in the presence of the heat-treated gypsum. The catalytic activity and *cis-/trans-* ratio at zero conversion are plotted as functions of the evacuation temperature in Fig. 4. When the gypsum was evacuated at 200 °C, its catalytic activity was relatively high. The activity decreased with an increase in the evacuation temperature, and almost disappeared when the gypsum was treated at 500 °C under evacuation. For lower evacuation temperatures, such as 200 °C and 300 °C, the initial *cis-/trans-* ratio was 2; this was elevated to 2.5 as the evacuation temperature was raised to 400 °C. It is already known that the *cis-/trans-* ratio in the products of the reaction of 2-butenes is determined by the nature of the active site; that is, if the active site is the Brönsted type, the ratio should be about 1, while if the active site is the Lewis type, the ratio should be about 2.[22] Since the value in Fig. 4 is 2—2.5 throughout the evacuation-temperature range, the acid must be the Lewis type.

Coordination of Sulfate Ions to Calcium Ions. In order to discuss the coordinations of SO_4^{2-} ions to Ca^{2+} ions, the IR spectra due to SO_4^{2-} ions were observed in the wave-number region of about 400 to 1400 cm^{-1}. The IR spectra showed the absorption band (ν_3) due to the stretching vibration of S–O, S=O at 1100—1200 cm^{-1} and that (ν_4) due to the bending vibration of –O–S–O– in the region of 580—680 cm^{-1}. In a previous report,[12] the splitting of ν_3 and ν_4 has already been observed for gypsum heat-treated at 337—390 °C and 358—375 °C respectively; it was there ascribed to the transition from III-$CaSO_4$ to II-$CaSO_4$.

The splitting of ν_3 could also be found in this study. However, the details of the splitting could not be made clear, because the bands are essentially broad. Therefore, the splitting of the sharp band due to –O–S–O– bending was examined. Fig. 5 shows the IR absorption spectra of gypsum heat-treated at different temperatures in the 550—700 region. As is shown in this figure, the spectra gave bands at 594 cm^{-1} and near 653 cm^{-1} which were specific to the monodentate SO_4^{2-} ions.[23] With increases in the heat-treatment temperature, these bands gradually disappeared, while bands appeared at 588, 606, and 669 cm^{-1} when the sample was heat-treated at a temperature higher than 300 °C. According to the study of Nakamoto *et al.*, these bands are ascribable to bidentate SO_4^{2-} ions.[23] Since the X-ray diffraction analysis (shown in Table 1) of the sample showed that soluble anhydrite (III-$CaSO_4$) was transformed into insoluble anhydrite (II-$CaSO_4$) between 300 °C and 400 °C, the monodentate and bidentate ions are considered to be present in soluble and insoluble anhydrite respectively.

Thus, when gypsum was heat-treated at temperatures higher than 300 °C, the metastable anhydrite (III-$CaSO_4$) was converted into stable anhydrous form (II- or I-$CaSO_4$) and Ca^{2+} ions on the surface became closely surrounded by bidentate sulfate ions. In such a configuration, the Ca^{2+} ions on the surface cannot interact with other molecules as electron acceptors. This is possibly the reason why the Ca^{2+} ions on the insoluble, or stable, anhydrite do not function as Lewis-acid sites. On the other hand, the Ca^{2+} ions on the soluble anhydrite, which are less closely surrounded by monodentate sulfate ions, are able to accept electron pairs of other molecules. Thus, the Lewis-acid center may be formed by an empty orbital of the Ca^{2+} ions on the surface of III-$CaSO_4$. A similar phenomenon has also been observed in the dehydration of $NiSO_4xH_2O$, in which strong acid sites ($H_0 \leqq -3.0$) have been found.[24] However, the electronegativity of the Ca^{2+} ion is smaller than that of the Ni^{2+} ion;[25] hence, the Lewis acidity due to the Ca^{2+} ion should not be so

strong. In fact, the acid function (H_0) was determined to be mostly 3.0—4.8, as has been described previously.

The maximum acid-site concentration of heat-treated gypsum (shown in Fig. 1) is about twice that reported for alumina, which is a typical Lewis acid, heat-treated at 500 °C (0.0008 mmol/m^2 at $H_0 \leqq +1.5$).[26] However, the amount is considerably less than that for heat-treated nickel sulfate (0.011 mmol/m^2 at $H_0 \leqq +4.8$ and 0.005 mmol/m^2 at $H_0 \leqq -3.0$).[24] The concentration of Ca^{2+} ions on the surface is much more than that of acid sites. For example, the former concentration on the (001) plane is calculated to be 0.0034 mmol/m^2 on the basis of the lattice constant ($a,b=6.99$ Å, $c=6.34$ Å).[11] As suggested by the comparison between the concentration of the acid sites and Ca^{2+} ions, not all the Ca^{2+} ions on the III-$CaSO_4$ surface can be Lewis-acid sites. The details of the active-site formation must be studied further.

Even if a small amount of water should be occluded in the III-$CaSO_4$ formed at temperatures lower than 300 °C, as has been shown in previous studies,[12,13] the polarization of the surface OH groups and/or H_2O molecules by Ca^{2+} ions must be impossible because Ca^{2+} ions have only a low electrostatic potential (ion valency/radius). Therefore, the weak solid acidity should be of the Lewis type ascribable to the Ca^{2+} ions on the unstable crystal surface.

The authors wish to thank Mr. Akito Kurosaki and Mr. Haruo Ogino of our laboratory for their great assistance. The present work was partially supported by a Grant-in-Aid for Scientific Research from the Ministry of Education, Science and Culture.

References

1) H. Ogino and S. Okazaki, *Nippon Kagaku Kaishi*, **1980**, 4.
2) C. Walling, *J. Am. Chem. Soc.*, **72**, 1164 (1950).
3) a) K. Tanabe and K. Katayama, *J. Res. Inst. Catal., Hokkaido Univ.*, **7**, 106 (1959); b) K. Tanabe, *Shokubai*, **5**, 129 (1963).
4) Y. Arai, T. Yasue, and S. Kikuchi, *Nippon Kagaku Kaishi*, **1973**, 1425.
5) T. Yasue, K. Miyamoto, and Y. Arai, *Gypsum and Lime*, **151**, 261 (1977).
6) T. Kawakami and Y. Ogino, *Shokubai*, **10**, 136 (1968).
7) S. Iwabuchi, *Funtai To Kogyo*, **1972**, 61.
8) O. A. Johnson, *J. Phys. Chem.*, **59**, 827 (1955).
9) I. Terada, *J. Jpn. Petrol. Inst.*, **20**, 600 (1977).
10) J. Bensted and S. Prakash, *Nature*, **219**, 60 (1968).
11) M. Sekiya, "Sekko," Kasai Shuppan, Tokyo (1964), p. 84.
12) N. Tsuyuki, T. Saitoh, T. Miyakawa, and J. Kasai, *Kogyo Kagaku Zasshi*, **74**, 2242 (1971).
13) K. Takemoto and Y. Saiki, *Gypsum Lime*, **61**, 277 (1962).
14) M. L. Hair, "Infrared Spectroscopy in Surface Chemistry," Marcel Dekker, New York (1967), p. 208.
15) K. Nakamoto, "Infrared Spectra of Inorganic and Coordination Compounds," John Wiley, New York (1953), p. 325.
17) M. L. Hair, "Infrared Spectroscopy in Surface Chemistry," Marcel Dekker, New York (1953), p. 168.
18) E. P. Parry, *J. Catal.*, **2**, 371 (1963).
19) K. Tanabe, "Solid Acids and Bases," Kodansha, Tokyo (1970), p. 27.
20) a) J. W. Hightower and W. K. Hall, *J. Am. Chem. Soc.*, **90**, 851, (1968); b) J. W. Hightower and W. K. Hall, *J. Phys. Chem.*, **72**, 4555 (1968); c) J. G. Larson, H. R. Gaberich, and W. K. Hall, *J. Am. Chem. Soc.*, **87**, 1880 (1965).
21) T. Kantoh and S. Okazaki, Ann. Meeting Tohoku District. Chem. Soc. Japan (Kagakukei Rokugakukyokai Rengo Tohoku Chiho Taikai), Morioka, Abstr. Paper (1976), p. 69.
22) K. Tanabe, "Shokubai no Hataraki," Kagaku Dojin, Kyoto (1974), p. 20.
23) K. Nakamoto, J. Fujita, S. Tanaka, and M. Kobayashi, *J. Am. Chem. Soc.*, **79**, 4904 (1957).
24) a) T. Takeshita, R. Ohnishi, T. Matsui, and K. Tanabe, *J. Phys. Chem.* **69**, 4077 (1965); b) K. Tanabe, "Solid Acids and Bases," Kodansha, Tokyo (1970), p. 27.
25) K. Tanaka and A. Ozaki, *J. Catal.*, **8**, 1 (1967).
26) T. Shiba, M. Satoh, H. Hattori, and K. Yoshida, *Shokubai*, **6**, 80 (1964).

  Bull. Chem. Soc. Jpn., 54, 441—444 (1981)

The Aluminium(III) Ion-assisted Aquation of the Pentaammine-fluorochromium(III) Ion

Masayasu IIDA* and Hideo YAMATERA**

Department of Chemistry, Faculty of Science, Nara Women's University, Nara 630
***Department of Chemistry, Faculty of Science, Nagoya University, Chikusa-ku, Nagoya 464*

(Received February 12, 1980)

The aquation of the pentaamminefluorochromium(III) complex was found to be assisted by the aluminium ion. The observed pseudo-first-order rate constant, k_{obsd}, can be written approximately as: $k_{obsd}=k_{Al}[Al^{3+}]$ ($k_{Al}=7.5\times10^{-4}$ dm^3 mol^{-1} s^{-1} at 35 °C, pH 3.0, $I=2.0$ mol dm^{-3}). The rate constant decreased with an increase in the hydrogen-ion concentration, and this hydrogen-ion dependence was explained by assuming that the attack of aluminium ions on $CrF(NH_3)_5^{2+}$ was blocked by the protonation of the fluoro ligand. The analysis of the experimental results gave 3.0 ± 0.1 for the logarithm of the protonation constant. The effects of ClO_4^- and $Co(CN)_6^{3-}$ on the reaction rate were explained by considering the formation of ion-pairs between the anions and the reacting cations.

Among the reactions of transition-metal complexes, metal ion-induced aquation, or metal ion-assisted aquation, is particularly interesting as a model ionic reaction. In order to understand this kind of reaction in more detail, it is significant to extend the study to the reactions of types that have not yet been studied. The greater part of the studies of the metal ion-assisted aquation have been concerned with the reactions of chloro, bromo, and iodo complexes with soft acids, such as Ag^+, Hg^{2+}, and Tl^{3+}. There have been no detailed studies of the aquation of fluoro complexes induced by hard metal ions.[1,2]

The present paper is concerned with a rarely studied type of reaction, *i.e.*, the dissociation of hard basic anions induced by hard metal ions. The investigation of such a type of reaction is expected to disclose some characteristic behavior which has not appeared in the aquations assisted by soft metal ions. Another purpose of this study is to see how the reaction is influenced by the hexacyanocobaltate(III) ion. This ion tends to form a precipitate with soft metal ions; therefore, its effect on the metal ion-assisted aquations cannot be investigated when the metal ion is soft, as is usually the case; however, it can be examined in the present study where a hard metal ion is used to induce the aquation.

Experimental

Materials. Pentaamminefluorochromium(III) perchlorate was prepared from pentaammineaquachromium(III) ammonium nitrate by the method of Zinato *et al.*[3] The purity of the crystals was confirmed spectrophotometrically and by means of SP-sephadex ion-exchange chromatography; the complex was sorbed on the top of the column and was eluted with a 0.1 mol dm^{-3} sodium sulfate solution. The appearance of a well-formed single band indicated the absence of impurities.

Aluminium perchlorate was prepared by dissolving $AlCl_3\cdot6H_2O$ in an aqueous solution containing perchloric acid in excess. The salt was then precipitated in a rotating evaporator and recrystallized twice from water. The crystals were dissolved in an aqueous solution of perchloric acid for the preparation of a stock solution. The aluminium-ion concentration was determined to be Al_2O_3 by precipitating aluminium hydroxide and igniting it at about 1100 °C.

Sodium hexacyanocobaltate(III) dihydrate was prepared by the conventional method,[4] in which potassium cyanide was replaced by sodium cyanide. Anhydrous sodium perchlorate was prepared from a saturated sodium hydroxide solution and perchloric acid. Heavy-metal impurities in the sodium perchlorate solution were precipitated at pH 9. After the evaporation of the solution, crystals of sodium perchlorate were obtained by cooling (above 60 °C).

The other reagents used were of a guaranteed reagent grade from Wako Pure Chemicals Industries, Ltd.

Kinetic Procedure. The kinetic measurements were made with a Hitachi 200-10 spectrophotometer. The concentration of $[CrF(NH_3)_5](ClO_4)_2$ was controlled at 5.0×10^{-3} mol dm^{-3} in all the experiments unless otherwise stated. The change in the absorbance was followed at 510 nm. As the rates were of first-order in the presence of excess aluminium ions (more than five times the amount of the chromium(III) complexes), they were determined by plotting $\ln(D_t-D_\infty)$ against the time, where D_t and D_∞ are the absorbances at the time t and at an infinite time respectively. The pseudo-first-order rate constant, k_{obsd}, was thus obtained as the slope of this plot.

pH *Measurements.* The pH value of the sample solution containing a 0.1 mol dm^{-3} portion of $Al(ClO_4)_3$ was controlled by the addition of Na_2CO_3 crystals. The solution was used one day after the preparation.[5] The $(pH)_{obsd}$ values of the sample solutions were determined by means of a Beckman Century SS-1 pH meter, using a Beckman 39301 glass electrode and a 39402 calomel reference electrode. As the internal solution of the reference electrode, a saturated NaCl solution was used to avoid the precipitation of $KClO_4$. The pH meter was calibrated in terms of the H^+ concentration; *i.e.*, the pH was defined as $-\log[H^+]$ instead of $(pH)_{obsd}$.[6] As the pH dependency of the reaction rate was studied in a 0.1 mol dm^{-3} $Al(ClO_4)_3$ solution, the calibration of $-\log[H^+]$

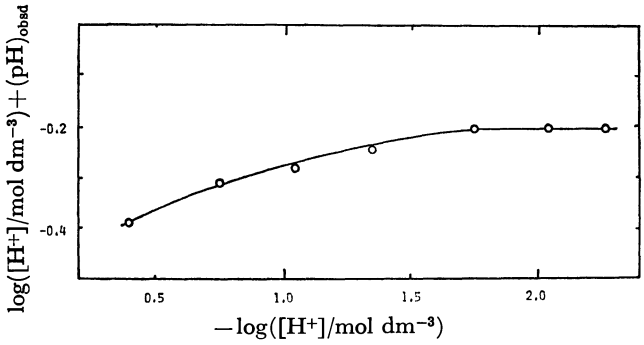

Fig. 1. Deviations of $(pH)_{obsd}$ from $-\log[H^+]$ in a 0.10 mol dm^{-3} $Al(ClO_4)_3$ aqueous solution.

vs. $(pH)_{obsd}$ was carried out for this solution in the pH range where the hydrolysis of aluminium ions could be neglected ($-\log[H^+]<3.2$). The results are shown in Fig. 1. The liquid-junction error is independent of the pH above $-\log[H^+]=1.7$; below that it increases with a decrease in the pH. Therefore, this equation:

$$(pH)_{obsd} + \log[H^+] = -0.21$$

is used above pH 1.7.

Results and Discussion

Spontaneous Aquation. Spontaneous and proton-catalyzed aquations of the pentaammine fluorochromium(III) ion were studied polarographically by Jones and Phillips.[7]

$$CrF(NH_3)_5^{2+} + H_2O \xrightarrow{k_0} Cr(OH_2)(NH_3)_5^{3+} + F^-$$

$$CrF(NH_3)_5^{2+} + H_3O^+ \xrightarrow{k_H} Cr(OH_2)(NH_3)_5^{3+} + HF$$

These reactions were found to be very slow, and the rate constants obtained were $k_0=1.4\times10^{-5}$ s^{-1} (pH range, 1—10.5) and $k_H=3.5\times10^{-5}$ mol^{-1} s^{-1} dm^3 (pH <1) at 65 °C. (The ionic strength was maintained at 1.0 by the addition of sodium perchlorate.) In fact, the mechanism of aquation is complex.[7,8] Fluoro, aqua, and ammine mixed-ligand complexes were formed as the by-products, indicating that the aquation was accompanied by the dissociation of the ammine ligands. To confirm the stoichiometry, we carried out spontaneous aquation at 35 °C in the dark. The $CrF(NH_3)_5^{2+}$ and H^+ concentrations were both controlled to 10^{-2} mol dm^{-3}. The reaction was followed for 10 d with a fluoride-ion electrode and by means of the SP-sephadex chromatographic technique. The former detects the fluoride ion released from the complex, and the latter, the complexes produced by the reaction with the aid of spectrophotometric measurements. Although the analysis hardly led to a quantitative conclusion, the following facts were proved: 1) In the early stage of the reaction, *cis*-$[CrF(OH_2)(NH_3)_4]^{2+}$ ($\lambda_{max}=512$ and 375 nm[9]) is formed. 2) No $[Cr(OH_2)(NH_3)_5]^{3+}$ can be detected throughout the measurement. 3) The release of fluoride ion is much slower than that of ammonia, and less than 5% of the fluoride ions in the complex are released in about 10 d. These results are similar to those obtained by Linhard and Weigel[8] and to those described by Wong and Kirk for the photoaquation of this complex,[10] but they are different from those reported by Jones and Phillips.[7]

No further investigation of the spontaneous aquation has been made, as it is not our present purpose.

Aluminium(III)-assisted Aquation. The hard aquation, $CrF(NH_3)_5^{2+}\rightarrow Cr(OH_2)(NH_3)_5^{3+}$, easily proceeds in the presence of aluminium ions. The spectrum of the complex changes with isosbestic points at 382, 415, and 480 nm, which shows the absence of by-products. In 0.1 mol dm^{-3} of $Al(ClO_4)_3$, the reaction proceeds to completion after about 1 d (pH 3.3, 35 °C). The pseudo-first-order rate constants, k_{obsd}, obtained depend on the concentration of the aluminium ion. The results summarized in Table 1 show that k_{obsd}

Table 1. Dependence of the rate constant on the concentration of the aluminium ion (35 °C)

$[Al^{3+}]$/mol dm^{-3}	k_{obsd}/s^{-1}
$((pH)_{obsd}=2.0, I=3.0$ mol dm$^{-3})$	
0.50	1.5×10^{-4}
0.20	6.4×10^{-5}
0.10	3.5×10^{-5}
$((pH)_{obsd}=2.8, I=2.0$ mol dm$^{-3})$	
0.30	2.1×10^{-4}
0.20	1.4×10^{-4}
0.12	9.5×10^{-5}
0.10	8.2×10^{-5}

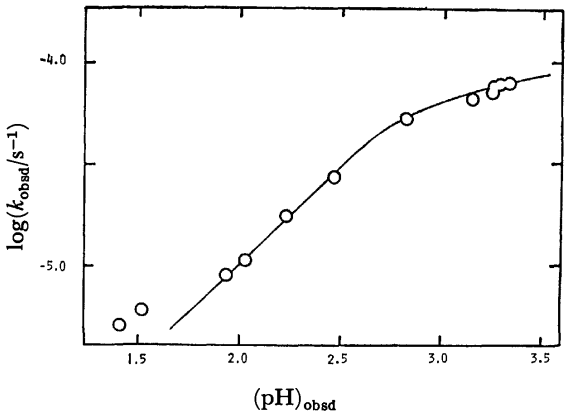

Fig. 2. pH dependence of the pseudo-first-order rate constant (0.10 mol dm^{-3} $Al(ClO_4)_3$ at 35 °C).

can be expressed approximately as $k_{Al}[Al^{3+}]$ if pH is kept constant. An additional term, k_0, for the spontaneous aquation can be neglected under our present experimental conditions.

Figure 2 shows the pH dependency of the reaction rate in the presence of 0.1 mol dm^{-3} of $Al(ClO_4)_3$. The observed rate constant increases with an increase in the pH value and becomes approximately constant at a $(pH)_{obsd}$ value of about 3.2. This pH dependency of the reaction rate has not been observed for the metal ion-assisted aquations hitherto studied. As the reaction proceeds between $CrF(NH_3)_5^{2+}$ and Al^{3+}, the pH dependency is attributed to the pH-dependent properties of the reactants. One of these properties is the hydrolysis of Al^{3+}, which is known to begin around pH($-\log[H^+]$) 3. Gradual hydrolysis proceeds up to a pH of about 3.5, where an abrupt change takes place.[11-13] Only $AlOH^{2+}$ is formed in the experimental pH range, and so polynuclear cationic species need not be considered. Figure 2 shows only a slight change in the rate in the pH range where a marked hydrolysis of Al^{3+} occurs. Therefore, the hydrolysis product, $AlOH^{2+}$, appears to have no appreciable effect on the reaction.

Another possibility is that the pH dependence of the rate is due to the protonation of the fluoro ligand of $CrF(NH_3)_5^{2+}$. Such protonation will block the attack of aluminium ions upon the fluoro ligand. Including the protonated complex, the reaction scheme can be formulated as follows:

$$CrF(NH_3)_5^{2+} + Al^{3+} \xrightarrow{k_1} Cr(OH_2)(NH_3)_5^{3+} + AlF^{2+}$$
$$K_H \uparrow\downarrow$$
$$CrFH(NH_3)_5^{3+} + Al^{3+} \xrightarrow{k_2} Cr(OH_2)(NH_3)_5^{3+} + AlF^{2+} + H^+.$$

In this scheme, k_2 can be assumed to be negligibly small in comparison with k_1. Then, the pseudo-first-order rate constant, k_{obsd}, can be rewritten as:

$$k_{obsd} = (1 + K_H[H^+])^{-1}k_1[Al^{3+}],$$

where K_H is the concentration equilibrium constant for the protonation of pentaammine fluorochromium(III) ions. Beginning with this equation, we can carry out a curve fitting such as is shown in Fig. 2 and obtain $\log(k_1[Al^{3+}]) = -4.00 \pm 0.05$ and $\log K_H = 3.0 \pm 0.1$. The failure of fitting in the lowest pH region may be attributed to such side reactions as the dissociation of the ammine ligands, which may not be ignored at such low k_{obsd} values. The value of $\log K_H$ seems to be too large considering the equilibrium constant for $H^+ + F^- \rightleftharpoons HF$ ($\log K = 3.2 \pm 0.2$ at 35 °C.[14]), because the logarithms of the protonation constants of oxoanions are lowered by 2—3 units by their coordination to the pentaamminecobalt(III) cations.[15] This suggests that the Cr–F bond is considerably ionic and that the F ligand is more easily protonated than expected.

Table 2. First-order rate constants at varying temperatures
($(pH)_{obsd} = 3.2$, $[Al(ClO_4)_3] = 0.10$ mol dm^{-3})

	k_{obsd}/s^{-1}
25 °C	3.2×10^{-5}
30 °C	6.5×10^{-5}
35 °C	8.3×10^{-5}
40 °C	1.6×10^{-4}
45 °C	2.7×10^{-4}

From the rate constants measured at various temperatures (Table 2), the activation enthalpy, ΔH^*, and the activation entropy, ΔS^*, can be estimated: $\Delta H^* = 83 \pm 5$ kJ mol^{-1} and $\Delta S^* = -62 \pm 17$ J K^{-1} mol^{-1}. The activation entropy for a Cr^{2+}-assisted reduction of this complex (-126 J K^{-1} mol^{-1})[16] is about 60 J K^{-1} mol^{-1} smaller than that for this reaction; this relationship holds also between the $CrCl(NH_3)_5^{2+}$–Hg^{2+} system and the $CrCl(NH_3)_5^{2+}$–Cr^{2+} system.[17,18] The minus sign of the activation entropies reflects the formation of halide-bridged binuclear complexes in the transition states. If the electron transfer proceeds adiabatically in the reduction process, the change in the entropy will be nearly zero in this step and the activation entropy can mostly be ascribed to the formation of the bridged complex. In view of this, the difference in the activation entropy between the reduction and the aquation can be said to be due mainly to the difference in the structure of the activated complex.[19] A more stringent geometrical condition may have to be satisfied in the reduction.

Effects of Anions. Table 3 summarizes the effects of the anions. As five-coordinated intermediates are formed in the metal ion-assisted aquation,[20] such anions as SO_4^{2-} and $H_2P_2O_7^{2-}$ may react with the intermediate to form inner-sphere complexes. The instability of the oxoanionopentaamminechromium(III) complexes makes the reactions complicated, however.[21]

Table 3. Effect of anions on the reaction

Anions	
ClO_4^-	Small accelerating effect.
SO_4^{2-}(pH 3)	Formation of sulfato complex, followed by the dissociation of ammine ligands.
$H_2P_2O_7^{2-}$(pH 2)	Formation of some polynuclear complex.[a]
$Co(CN)_6^{3-}$	Large accelerating effect.

a) After the absorbance change had almost terminated (for 0.1 mol dm^{-3} $Na_2H_2P_2O_7$ at 35 °C, one day after the reaction had started), the reaction solution was poured onto a column of SP-sephadex. Then, most of the complex was adsorbed at the top of the column. Elution with one molar sodium sulfate solution did not develop the band. The complex formed is likely to be a highly-charged cation.

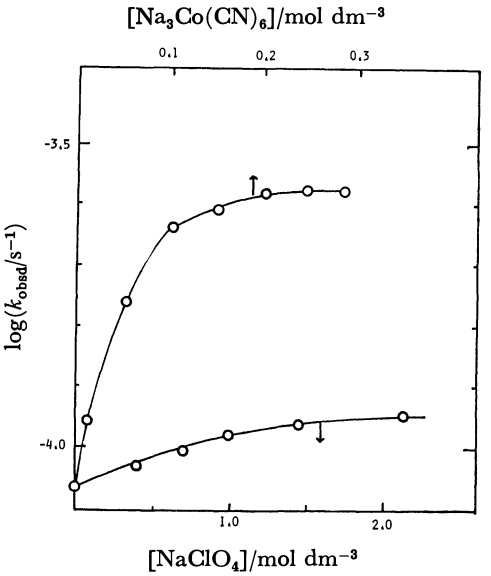

Fig. 3. Effects of anions on the reaction rate ($[Al^{3+}] = 0.10$ mol dm^{-3}, $(pH)_{obsd} = 3.1 \pm 0.1$).

The role of anions such as ClO_4^- and $Co(CN)_6^{3-}$, which are reluctant to coordinate, is to assist the reactant cations in their approaching each other and to increase the chances of the reaction between them. Figure 3 shows the effects of perchlorate and hexacyanocobaltate(III) ions in accelerating the aluminium ion-assisted aquation. The reactions were carried out in the presence of the respective anions at $(pH)_{obsd} = 3.1 \pm 0.1$, where the reacting species can be considered to be $CrF(NH_3)_5^{2+}$ and Al^{3+}. A rough analysis was carried out for the relative magnitudes of the effects of $Co(CN)_6^{3-}$ and ClO_4^- with the following assumptions. Firstly, the effects of anions on the reaction rate are assumed to be mainly determined by the charge and the radius of the anion. Secondly, the effect of added neutral salts is considered to be the formation of ion-pairs between the reacting cations and the mediating anions. The formation of the ion-pairs with Na^+ is neglected,

however. The third is that the activity coefficients of ion-pairs change according to the Davies equation:

$$\log y_i = -0.521\, z_i^{*2}\left(\frac{\sqrt{I}}{1+\sqrt{I}} - 0.3\,I\right), \quad (1)$$

where z_i^* is the effective charge number of the ion-pairs, and I, the ionic strength. On the basis of the above assumptions, we can express the rate constant of the reaction between A and B ions at saturation as follows:

$$k_{AB} = k_{AB}^0 \frac{K_{AB}}{K_{AB}^0} = k_0^0 \frac{K_{AB}}{K_{AB}^0} \exp\left(-\frac{z_A^* z_B^* e^2}{kT\varepsilon a}\right), \quad (2)$$

where the superscript 0 indicates the value at an infinite dilution and where the symbols have the following meanings:

K_{AB}: Equilibrium constant between the activated complex and the reactants.
k_0^0 : Hypothetical rate constant for uncharged ions.
z_A^*e, z_B^*e : Effective charges of A and B ions respectively, decreased by the approach of ions of the opposite sign.
k : Boltzmann constant.
T : Absolute temperature.
ε : Dielectric constant of the solvent.
a : Closest distance of the approach of the A and B ions.

For the present system containing sodium perchlorate, the rate constant at the saturation is:

$$k_{12} = k_0^0 \frac{K_{12}}{K_{12}^0} \exp\left(-\frac{2e^2}{kT\varepsilon a}\right) = k_0^0 \frac{y_1 y_2}{y_{12}} \exp\left(-\frac{2e^2}{kT\varepsilon a}\right), \quad (3)$$

where the subscript 12 indicates $z_A^*=1$ and $z_B^*=2$. Using Eq. 1, Eq. 3 is transformed to:

$$\log k_{12} = \log k_0^0 - 0.521\,(1+4-9)\left(\frac{\sqrt{I}}{1+\sqrt{I}} - 0.3\,I\right) - 0.86,$$

where $T=308$ K and $a=0.7$ nm are used.

The ionic strength at the saturation (Fig. 3) is 1.1 ± 0.2,[22] which is substituted to give this result:

$$\log k_{12}\,(I = 1.1 \pm 0.2) = \log k_0^0 - (0.47 \pm 0.08).$$

On the other hand, ion-pair formation between the reactants and $[Co(CN)_6]^{3-}$ makes $z_A^*=-1$ and $z_B^*=0$; therefore, the pseudo-first-order rate constant, k_{10}, at saturation with $[Co(CN)_6]^{3-}$ will not depend appreciably on the ionic strength. Thus, one obtains this approximate equality:

$$\log k_{10} \approx \log k_{10}^0 \approx \log k_0^0.$$

From the above argument, the saturation rate constant for the Al^{3+}-assisted aquation of $[CrF(NH_3)_5]^{2+}$ can be expected to be greater in the sodium hexacyanocobaltate(III) solution than in the sodium perchlorate solution:

$$\log k_{10} = \log k_{12}\,(I = 1.1 \pm 0.2) + (0.47 \pm 0.08).$$

This calculated difference in the saturation rate constant is in good agreement with the experimental results (Fig. 3):

$$\log k_{10}\,(\text{exp.}) = \log k_{12}\,(\text{exp.}) + (0.39 \pm 0.02).$$

References

1) A. A. Vlček, *Nature*, **197**, 786 (1963).
2) I. V. Kozhevnikov and E. S. Rudakov, *Zh. Neorg. Khim.*, **18**, 3344 (1973).
3) E. Zinato, R. Lindholn, and A. W. Adamson, *J. Inorg. Nucl. Chem.*, **31**, 449 (1969).
4) J. H. Bigelow, *Inorg. Synth.*, Vol. II, 225 (1946).
5) As the hydrolysis of aluminium ions is known to proceed very slowly at a higher pH, sample solutions of $(pH)_{obsd}=3.3$ were left for a long time; the pH did not change even after three months, however.
6) R. G. Bates, "Determination of pH, "2nd ed, John Wiley and Sons, New York (1973), p. 261.
7) T. P. Jones and J. K. Phillips, *J. Chem. Soc., A*, **1968**, 674.
8) M. Linhard and M. Weigel, *Z. Anorg. Allg. Chem.*, **278**, 24 (1955).
9) H. N. Po. Y-H. Chung and S. R. Davis, *J. Inorg. Nucl. Chem.*, **35**, 2849 (1973).
10) C. F. C. Wong and A. D. Kirk, *Inorg. Chem.*, **16**, 3148 (1977).
11) J. Aveston, *J. Chem. Soc.*, **1965**. 4438.
12) H. Ohtaki, *Bull. Chem. Soc. Jpn.*, **43**, 2463 (1970).
13) R. C. Turner, *Can. J. Chem.*, **53**, 2811 (1975),.
14) L. G. Sillén and A. E. Martell, "Stability Constants of Metal-Ion Complexes," The Chemical Society, London (1964), p. 256.
15) T. A. Beech, N. C. Lawrence, and S. F. Lincoln, *Aust. J. Chem.*, **26**, 1877 (1973).
16) A. E. Ogard and H. Taube, *J. Am. Chem. Soc.*, **80**, 1084 (1958).
17) J. H. Espenson and S. R. Hubbard, *Inorg. Chem.*, **5**, 686 (1966).
18) H. Taube, "Electron Transfer Reactions of Complex Ions in Solution," Academic Press, New York (1970), p. 60.
19) Reference 16 and H. Taube, *Advan. Inorg. Nucl. Chem.*, **1**, 1 (1959).
20) R. G. Wilkins, "The Study of Kinetics and Mechanism of Reactions of Transition Metal Complexes," Allyn and Bacon, Boston (1974), p. 78.
21) T. Ramasami, R. K. Wharton, and A. G. Sykes, *Inorg. Chem.*, **14**, 359 (1975).
22) In calculating an ionic strength at saturation we took the conditions of $[NaClO_4]=0.8\pm0.2$ mol dm^{-3} and $[Al(ClO_4)_3]=0.1$ mol dm^{-3}, where Al^{3+} is considered to be completely associated with ClO_4^- to form $[Al\cdot ClO_4]^{2+}$ and where the contribution of the chromium complex to the ionic strength can be neglected.

  Bull. Chem. Soc. Jpn., 54, 445—447 (1981)

Kinetics of the Formation of Alkoxy-derived Barium Metasilicate

Osamu YAMAGUCHI,* Kazuhiro TOMINAGA, and Kiyoshi SHIMIZU*

Department of Applied Chemistry, Faculty of Engineering, Doshisha University, Karasuma Imadegawa, Kamigyo-ku, Kyoto 602

(Received May 28, 1980)

Amorphous $BaSiO_3$ or a mixture of this and $BaSiO_3 \cdot H_2O$ was formed by the simultaneous hydrolysis of barium and silicon alkoxides. The temperature of hydrolysis and the time of aging influence the crystallization of amorphous $BaSiO_3$ into $BaSiO_3 \cdot H_2O$. The decomposition of $BaSiO_3 \cdot H_2O$ into crystalline $BaSiO_3$ was analyzed by isothermal thermogravimetry. Decomposition isotherms were constructed by the equation $-\ln(1-\alpha)=kt$ and the activation energy was determined as 143.5 kJ/mol. The kinetics of crystallization of amorphous into crystalline $BaSiO_3$ was interpreted by the equation $1-(1-\alpha)^{1/3}=kt$. Activation energies were 276 kJ/mol and 204 kJ/mol for the initial and final stages, respectively.

Barium metasilicate ($BaSiO_3$) can be prepared by two methods: (a) solid state reaction of an equimolar mixture of barium carbonate and silica;[1-4] (b) decomposition of barium metasilicate hydrates. Barium metasilicate hydrates, such as $BaSiO_3 \cdot H_2O$, $BaSiO_3 \cdot 1.5H_2O$, and $BaSiO_3 \cdot 6H_2O$, are formed by the reaction of sodium silicate solutions and either barium chloride or barium hydroxide solutions.[5,6] Krüger and Wieker[6] reported that amorphous barium silicates are precipitated by addition of barium chloride solutions to sodium silicate solutions, and their crystallization into various barium silicate hydrates is dependent on the Na : Si ratio, the concentration of sodium silicate solutions, the Ba : Si ratio and the temperature during precipitation. The hydrothermal reaction using barium silicate hydrates of various compositions was studied.[5] However, no kinetic study on the formation of crystalline $BaSiO_3$ from amorphous $BaSiO_3$ and barium metasilicate hydrates has been carried out.

In the present study, it was found that amorphous $BaSiO_3$ or mixtures of this amorphous compound and $BaSiO_3 \cdot H_2O$ are formed by the simultaneous hydrolysis of barium and silicon alkoxides. Conditions for the crystallization of amorphous $BaSiO_3$ into $BaSiO_3 \cdot H_2O$ during hydrolysis were examined, and kinetic studies made on the decomposition of $BaSiO_3 \cdot H_2O$ and the crystallization of amorphous into crystalline $BaSiO_3$. The kinetic data were analyzed with use of available solid state models.

Experimental

Materials and Procedure. Silicon ethoxide of guaranteed purity was used. Barium isopropoxide was synthesized by heating barium metal (purity 99.9%) in an excess amount of dehydrated 2-propanol at 82 °C for 5 h in a nitrogen atmosphere. An alcoholic solution containing 12 wt% mixed alkoxides prepared in the mole ratio, Ba^{2+}/Si^{4+} 1 : 1, was refluxed under the same conditions. Hydrolysis was carried out as follows. A five-necked flask equipped with a refluxed condenser, a dropping funnel, a strirring rod, a thermometer and a thermo-controller was used. 400 ml of water was introduced into the flask, and then heated to the desired temperature. 100 ml of the mixed alkoxide solution was added dropwise from the dropping funnel to the stirred water in the flask. The resulting suspension was stirred. The product was separated from the suspension by filtration and dried at 60 °C under reduced pressure.

Measurement. Differential thermal analysis (DTA) was performed in the air at a 10 °C/min rate. Alpha-alumina of high purity was used as a reference substance. The products and the heated specimens were identified by means of DTA data and X-ray diffraction using nickel filtered copper K_α. The weight change was recorded as function of time with a thermobalance.

Results and Discussion

Hydrolysis Product. Results obtained under various conditions are given in Table 1. The products at 30 °C were amorphous. Barium silicates other than $BaSiO_3$ and free species were not observed during the course of heating. Thus, the products might be considered to be a compound corresponding to amorphous $BaSiO_3$. The peaks of $BaSiO_3 \cdot H_2O$[7] were recognized when subjected to hydrolysis at 45 °C for 30 min. Their intensity increased gradually with increase in hydrolysis temperature and time. Judging from this and the amount of crystalline $BaSiO_3$ formed by the decomposition of $BaSiO_3 \cdot H_2O$, the temperatures of hydrolysis and the aging time were found to be impor-

TABLE 1. HYDROLYSIS PRODUCT AND THE AMOUNT OF $BaSiO_3$ FORMED BY THE DECOMPOSITION OF $BaSiO_3 \cdot H_2O$ AND BY THE CRYSTALIZATION OF AMORPHOUS $BaSiO_3$

Run	Temp °C	Time min	Identified phase	Fraction/% A[a]	Fraction/% B[b]
1	30	15	Amorphous	0	100
2	30	30	Amorphous	0	100
3	30	60	Amorphous	0	100
4	45	15	Amorphous	0	100
5	45	30	$BaSiO_3 \cdot H_2O$	5.6	94.4
6	45	60	$BaSiO_3 \cdot H_2O$	7.2	92.8
7	60	15	$BaSiO_3 \cdot H_2O$	18.7	81.3
8	60	30	$BaSiO_3 \cdot H_2O$	21.6	78.4
9	60	60	$BaSiO_3 \cdot H_2O$	23.5	76.5
10	70	15	$BaSiO_3 \cdot H_2O$	26.5	73.5
11	70	30	$BaSiO_3 \cdot H_2O$	28.8	71.2
12	70	60	$BaSiO_3 \cdot H_2O$	30.2	69.8
13	80	15	$BaSiO_3 \cdot H_2O$	36.3	63.7
14	80	30	$BaSiO_3 \cdot H_2O$	38.8	61.2
15	80	60	$BaSiO_3 \cdot H_2O$	40.4	59.6

a) Amount of $BaSiO_3$ formed by decomposition of $BaSiO_3 \cdot H_2O$. b) Amount of $BaSiO_3$ formed by crystallization of amorphous $BaSiO_3$.

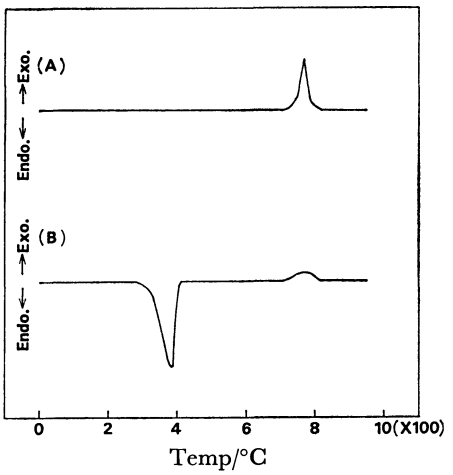

Fig. 1. DTA curves of the products hydrolyzed for 15 min at 30 °C (A) and for 1 h at 80 °C (B).
Sample weight: 60 mg.

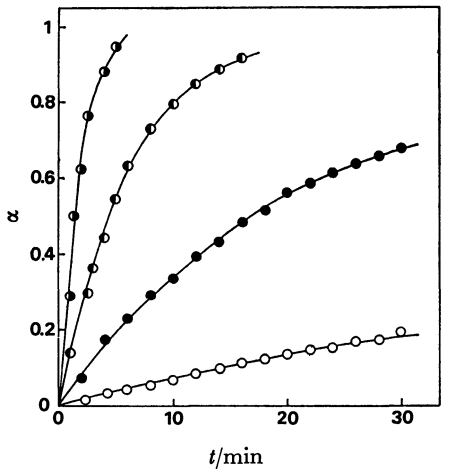

Fig. 2. Decomposition of $BaSiO_3 \cdot H_2O$ as a function of time at different temperatures.
○: 290 °C, ●: 320 °C, ◐: 250 °C, ◑: 380 °C.

tant factors for the crystallization of amorphous $BaSiO_3$ into $BaSiO_3 \cdot H_2O$.

Formation Process of Crystalline $BaSiO_3$. The DTA curves of the products (Table 1, runs 1 and 15) are shown in Fig. 1. An exothermic reaction (run 1) was observed at 700—820 °C. X-Ray diffraction analysis confirmed that the reaction is due to the crystallization of amorphous $BaSiO_3$. On the other hand, a large endothermic peak (run 15) corresponding to the decomposition of $BaSiO_3 \cdot H_2O$ was observed at 280—410 °C. The compound $BaSiO_3 \cdot H_2O$ turned into crystalline $BaSiO_3$ after the completion of decomposition. The small exothermic peak (700—820 °C) is due to the crystallization of amorphous $BaSiO_3$ as in the case of run 1. This suggests that $BaSiO_3$ is formed *via* two stages: (a) decomposition of $BaSiO_3 \cdot H_2O$, (b) crystallization of amorphous $BaSiO_3$.

All the products were heated at 450 °C and 900 °C for 1 h, respectively, and the amount of crystalline $BaSiO_3$ formed at each stage was determined from the height of the peak of d=3.43 Å which is the strongest of the $BaSiO_3$ spectrum.[8] The fractions of crystalline $BaSiO_3$ formed by the decomposition of $BaSiO_3 \cdot H_2O$ and the crystallization of amorphous $BaSiO_3$ are dependent on the starting products which is strongly affected by hydrolysis temperature (Table 1).

Kinetics of the Decomposition of $BaSiO_3 \cdot H_2O$. The decomposition of $BaSiO_3 \cdot H_2O$ (run 15) was analyzed by isothermal thermogravimetric measurement. The product (average particle size *ca.* 800 Å) was heated at 200 °C for 30 min. Figure 2 shows α-t curves obtained at various temperatures, where α is the fractional decomposition and t time. Attempts were made to fit the results to kinetic laws. As shown in Fig. 3, decomposition isotherms are represented by the following equation over the whole range of fraction:

$$-\ln(1-\alpha) = kt. \quad (1)$$

The rate constants were determined from the slopes of the straight lines. The activation energy calculated from the Arrhenius plot is 143.5 kJ/mol. This might represent the activation energy consumed for establishing

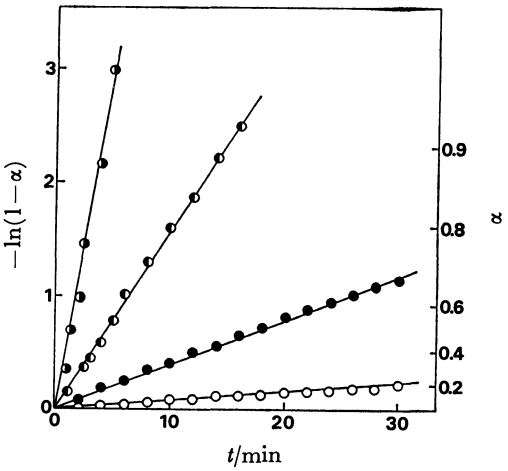

Fig. 3. Plots of $-\ln(1-\alpha)$ *vs.* time t of the data shown in Fig. 2.
○: 290 °C, ●: 320 °C, ◐: 350 °C, ◑: 380 °C.

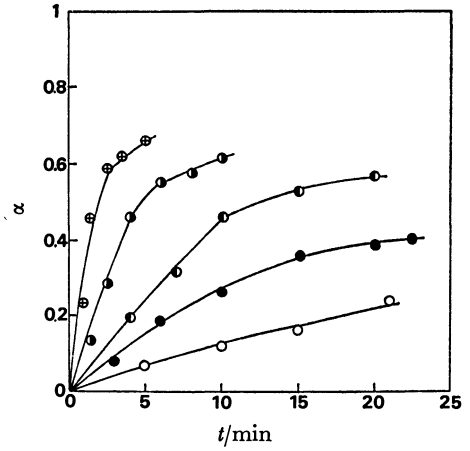

Fig. 4. Crystallization of amorphous $BaSiO_3$ as a function of time at different temperatures.
○: 680 °C, ●: 700 °C, ◐: 720 °C, ◑: 750 °C, ⊕: 780 °C.

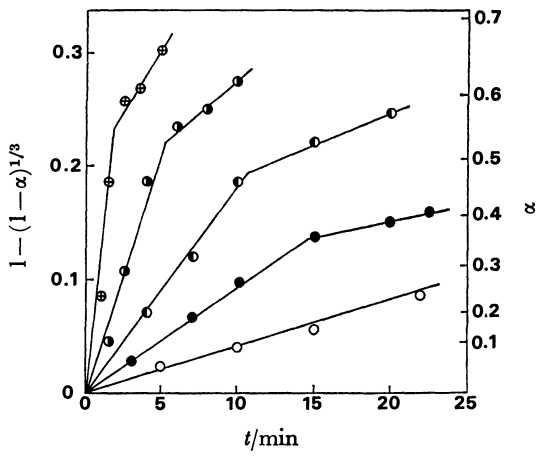

Fig. 5. Plots of $1-(1-\alpha)^{1/3}$ *vs.* time t of the data shown in Fig. 4.
○: 680 °C, ●: 700 °C, ◐: 720 °C, ◑: 750 °C, ⊕: 780 °C.

active nucleation centers.[9]

Kinetics of the Crystallization of Amorphous $BaSiO_3$. Figure 4 shows the fraction of the crystallized $BaSiO_3$ at different temperatures. The product of run 1 was heated at 550 °C for 1 h. The fractional crystallization of each specimen was determined from the height of the main characteristic peak (d=3.43 Å). A well-crystallized specimen was obtained by heating the starting product at 900 °C for 1 h. Magnesium oxide was used as an internal standard. The data can be interpreted by means of the equation

$$1-(1-\alpha)^{1/3}=kt, \quad (2)$$

where α is the fractional crystallization and t time (Fig. 5).[10] This indicates that crystallization is controlled by the rate of advance of the reaction interface. Two different linear portions, except at 680 °C, can be recognized in each of the plots. The rate constants were determined from the slopes of the straight lines. Activation energies were 276 kJ/mol and 204 kJ/mol for the initial and final stages, respectively.

References

1) W. Jander, *Z. Anorg. Allg. Chem.*, **163**, 1 (1927); **174**, 11 (1928).
2) V. B. Glushkova and E. K. Keler, *Russian J. Inorg. Chem.*, **5**, 424 (1960).
3) W. Trezebiatowski, *Rocz. Chim.*, **36**, 1427 (1962).
4) T. Yamaguchi, K. Matumura, and H. Kuno, *Nippon Kagaku Kaishi*, **1974**, 17.
5) H. Funk, *Z. Anorg. Allg. Chem.*, **296**, 46 (1958).
6) G. Kruger and W. Wieker, *Z. Anorg. Allg. Chem.*, **340**, 277 (1965).
7) X-Ray powder diffraction data file (ASTM card 18-179).
8) X-Ray powder diffraction data file (ASTM card 6-0247).
9) For example, R. W. Grimshaw, J. Hargreaves, and A. L. Roberts, *Trans. Brit. Ceram. Soc.*, **55**. 36 (1956).
10) For example, D. Dollimore and D. Tinsely, *J. Chem. Soc., A*, 1971, 3043.

Metal Complexes of Amino Acids. XIII.[1] The Relationships between the ^{13}C Chemical Shifts and Ligand Field in the *trans(O)*-$[Co(O)_2(N)_4]$ Type Complexes

Tomoharu AMA,* Hiroshi KAWAGUCHI, and Takaji YASUI
Department of Chemistry, Faculty of Science, Kochi University, Akebono-cho, Kochi 780
(Received July 10, 1980)

The relationship between the ligand field of the carboxyl groups and the chemical shift of carboxyl carbon or α-carbon has been investigated on the basis of the absorption and ^{13}C-NMR spectral data of the *trans(O)*-$[Co(OCO-R)_2(en)_2]X_n$ type complexes (OCO–R denotes amino acid or fatty acid coordinating unidentately with the carboxyl group to cobalt(III)). The linear correlations were observed between the $\bar{\nu}_{max}$ (^1E_g component of the first absorption band) and the chemical shifts of carboxyl- and α-carbons.

A number of reports containing an application of ^{13}C-NMR to metal complexes have been published, and the technique has proved to be a very powerful tool for the structural investigation of the complexes. For the metal complexes, the ^{13}C-NMR studies have been concentrated on the cobalt(III) complexes, because most of the cobalt(III) complexes are inert and diamagnetic.[2-24]

Only few papers have been reported on the relation between the d-d absorption spectra and ^{13}C chemical shifts of the metal complexes.[23-25] However, it can be expected that some interesting informations concerning the ligand field will be obtained from the ^{13}C chemical shift data, because both the ligand field and ^{13}C chemical shift are related to the electron density on the ligand.[26-29]

Previously, we reported the ^{13}C-NMR of the *trans(O)*-$[Co(OCO-R)_2(en)_2]^{n+}$ type complexes,[30] where OCO–R denotes amino acid or fatty acid which coordinates to cobalt(III) as a unidentate ligand through its carboxyl group. It has been clarified by the report that such unidentate coordinations of the carboxylic acids to cobalt(III) ($R-C_\alpha-C_{oxy}-OOH \rightarrow R-C_\alpha-C_{oxy}-COOCo$) show the different chemical shift changes, $\Delta_{uni}(C_{oxy})$ ($\delta_{uni}(C_{oxy})-\delta(C_{oxy})$) and $\Delta_{uni}(C_\alpha)$ ($\delta_{uni}(C_\alpha)-\delta(C_\alpha)$), and these shift changes can be also correlated to the chemical shifts of the free acids, $\delta(C_{oxy})$ and $\delta(C_\alpha)$, where $\delta_{uni}(C_{oxy})$ and $\delta_{uni}(C_\alpha)$ represent the chemical shifts of C_{oxy} and C_α of the unidentate ligands in the *trans(O)*-$[Co(OCO-R)_2(en)_2]^{n+}$ type complexes, and $\delta(C_{oxy})$ and $\delta(C_\alpha)$ represent those of the free acids in acidic D_2O solutions. The *trans(O)*-$[Co(OCO-R)_2(en)_2]^{n+}$ type complexes are very suitable for the study of the ligand field of the coordinated carboxylic acids, because the ^1E_g component in the first absorption band of the complex is well apart from another component.[31] In the present paper we will describe the relation between the chemical shifts and the first absorption bands of the *trans(O)*-$[Co(OCO-R)_2(en)_2]^{n+}$ type complexes.

Experimental

Preparation of Complexes. trans*(O)-Bis(*N*-propylglycine)-bis(ethylenediamine)cobalt(III) Perchlorate(*trans*(O)-[Co(Hpgly)$_2$(en)$_2$](ClO$_4$)$_3$)*: To an aqueous solution containing 5 g of $[Co(OH_2)_2(en)_2](ClO_4)_3$ in 50 cm^3 of water, 2.5 g of *N*-propylglycine (Hpgly) was added. The mixture was then evaporated almost to dryness on a water bath at about 80 °C. After cooling, the crude product obtained was dissolved in a small amount of hot water. A few drops of 60% perchloric acid were added to the solution and then cooled in an ice bath. The violet-red crystals obtained were washed with cold water and dried in air. Found: C, 23.55; H, 5.44; N, 11.90%. Calcd for $[Co(Hpgly)_2(en)_2](ClO_4)_3 \cdot H_2O$: C, 23.49; H, 5.35; N, 11.74%.

trans*(O)-Bis(*N*-ethylglycine)bis(ethylenediamine)cobalt(III) Perchlorate (*trans*(O)-[Co(Hegly)$_2$(en)$_2$](ClO$_4$)$_3$)*: *N*-Ethylglycine hydrochloride (Hegly·HCl, 3 g) was dissolved in 10 cm^3 of water and the pH of the solution was adjusted to *ca.* 7 by adding 1 M NaOH aqueous solution. The neutralized solution was evaporated to dryness using a vacuum evaporator, and the Hegly in the residue was extracted with 30 cm^3 of methanol. The methanolic solution of Hegly was evaporated to dryness. The resulted residue was dissolved in 10 cm^3 of water, and then the solution was added to a solution containing 5 g of $[Co(OH_2)_2(en)_2](ClO_4)_3$ in 10 cm^3 of water. The mixed solution was evaporated to a few milliliters on a water bath at about 80 °C. After cooling, the complex deposited was filtered. The crude product was recrystallized from hot water. Found: C, 20.34; H, 5.19; N, 11.96%. Calcd for $[Co(Hegly)_2(en)_2](ClO_4)_3$: C, 20.54; H, 5.17; N, 11.98%.

trans*(O)-(Acetato)(glycine)bis(ethylenediamine)cobalt(III) Perchlorate (*trans*(O)-[Co(ac)(Hgly)(en)$_2$](ClO$_4$)$_2$)*: To an aqueous solution containing 3 g of *trans(O)*-$[Co(ac)_2(en)_2](ClO_4)$ (ac=acetate anion) in 30 cm^3 of water was added 1 g of glycine (Hgly). The mixture was then evaporated to a few milliliters on a steam bath. The residual solution was diluted to about 500 cm^3 and then poured into a SP–Sephadex column (C-25, Na^+ form, 4.5 cm × 50 cm). The adsorbed band was separated into three bands by developing with 0.2 M aqueous solution of sodium perchlorate. The solution of the second eluted band was concentrared to a few milliliters in a vacuum evaporator at 30—40 °C. Ethanol was added to the concentrated solution in order to deposit crude complex. The complex was recrystallized from aqueous solution by adding ethanol. Found: C, 18.32; H, 4.99; N, 13.12%. Calcd for $[Co(ac)(Hgly)(en)_2](ClO_4)_2 \cdot H_2O$: C, 18.12; H, 4.94; N, 13.21%.

trans*(O)-(Acetato)(β-alanine)bis(ethylenediamine)cobalt(III) Perchlorate (*trans*(O)-[Co(ac)(β-Hala)(en)$_2$](ClO$_4$)$_2$)*: The mixed ligand complex with acetate and β-alanine (β-Hala) was prepared by a procedure similar to that described for the *trans(O)*-$[Co(ac)(Hgly)(en)_2](ClO_4)_2$. Found: C, 20.51; H, 5.07; N, 13.22%. Calcd for $[Co(ac)(\beta\text{-Hala})(en)_2](ClO_4)_2$: C, 20.54; H, 4.98; N, 13.31%.

Other complexes, *trans(O)*-$[Co(Haa)_2(en)_2]^{3+}$ (Haa=L-alanine, β-alanine, γ-aminobutyric acid, hydroxyl-L-proline, glycine, L-leucine, L-proline, and L-serine)[32] and *trans(O)*-

[Co(a)$_2$(en)$_2$]$^+$ (a=acetate, propionate, and butyrate anions),[30] examined in this study, were prepared by the methods described in the references.

Measurements. The electronic absorption spectra of the complexes were measured with Hitachi 557 spectrophotometer in aqueous solution. The ^{13}C-NMR spectra were measured on a JEOL Model MFT-100 spectrometer in pulsed Fourier transform/proton noise decoupled mode at 25.15 MHz in deuterium oxide solution. The ^{13}C chemical shifts were measured relative to benzene (capillary) and converted into chemical shifts from TMS by the relation

$\delta_{TMS}=\delta_{benzene}-128.5$ (ppm).[26]

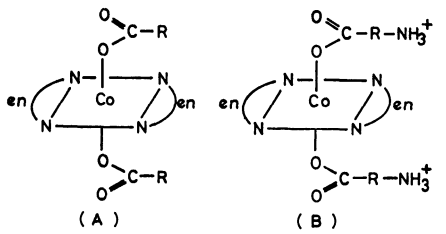

Fig. 1. Structures of the *trans*(*O*)-[Co(O)$_2$(N)$_4$] type complexes.
(A): *trans*(*O*)-[Co(OCO-R)$_2$(en)$_2$]$^+$ (OCO-R= fatty acid), (B): *trans*(*O*)-[Co(OCO-R-NH$_3^+$)$_2$(en)$_2$]$^{3+}$ (OCO-R-NH$_3^+$=amino acid).

Results and Discussion

At least three factors are important in determining carbon chemical shifts. These are the diamagnetic term (σ_d), the paramagnetic term (σ_p), and the anisotropy of neiboring atoms (σ_{others}).[29] Of these terms, σ_p makes major contribution to carbon chemical shifts.[26] The σ_p was related to the charge density, bond order of the carbon, and other factors (the averaged excitation energy (ΔE), the mean inverse cube radius for the carbon 2p orbitals ($\langle r^{-3}\rangle_{2p}$), and so on) by Karplus *et al.*[26] The ^{13}C chemical shifts are mainly influenced by the electron density of the carbons in a series of related compounds, if the differences in the σ_d, σ_{others}, and ΔE among the carbons under consideration are small. This was experimentally demonstrated by Horsley *et al.*[27] and Miyajima *et al.*[28] who plotted the ^{13}C chemical shifts against the charge density changes of the carbons in the substituted compounds relative to the parent compound.

The change of the substituent at α-carbon of carboxylic acid is attended with the change in the electron density at the carboxyl group, which is one of the reasons of the chemical shift change of the carboxyl carbon in the acid. It is expected that the change in the electron density at the carboxyl group also brings about the band shift in the first absorption band region of the cobalt(III) complex. The complex of the type *trans*(*O*)-[Co(OCO-R)$_2$(en)$_2$]$^{n+}$ is suitable to study this effect, because the ^1E_g component in the first absorption band is sufficiently apart from another component[30,31] ($^1A_{2g}$) in the same band (Fig. 2).

The plots of $\bar{\nu}_{max}$ (^1E_g component of the first absorption band) *vs.* $\delta_{uni}(C_{oxy})$ and $\bar{\nu}_{max}$ *vs.* $\delta_{uni}(C_\alpha)$ are shown in Fig. 3. The data provided here reveal that

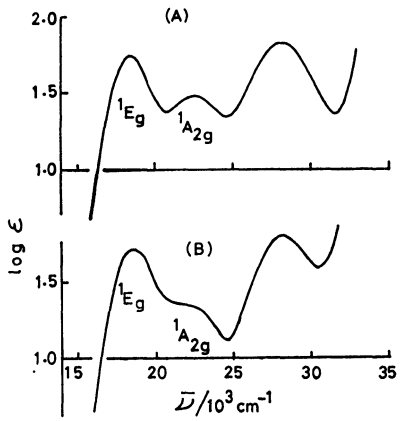

Fig. 2. Absorption spectra of the *trans*(*O*)-[Co(O)$_2$(N)$_4$] type complexes.
(A): *trans*(*O*)-[Co(Hgly)$_2$(en)$_2$]$^{3+}$, (B): *trans*(*O*)-[Co(bu)$_2$(en)$_2$]$^+$ (bu=butyrate anion).

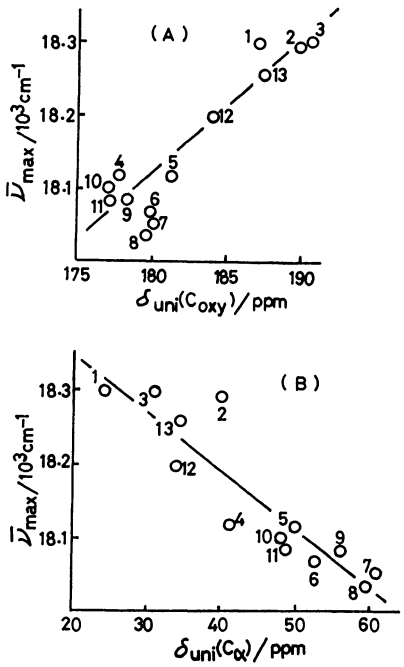

Fig. 3. Plots of first absorption maxima (^1E_g) of *trans*(*O*)-[Co(O)$_2$(N)$_4$] type complexes *vs.* ^{13}C chemical shifts.
(A): For carboxyl carbon (C_{oxy}), (B): for α-carbon (C_α).
1: Acetic acid, 2: butyric acid, 3: propionic acid, 4: glycine, 5: L-alanine, 6: L-leucine, 7: L-proline, 8: hydroxy-L-proline, 9: L-serine, 10: *N*-ethylglycine, 11: *N*-propylglycine, 12: β-alanine, 13: γ-aminobutyric acid.

the linear correlations are present between $\bar{\nu}_{max}$ and $\delta_{uni}(C_{oxy})$ and between $\bar{\nu}_{max}$ and $\delta_{uni}(C_\alpha)$. That is to say, both the $\delta_{uni}(C_{oxy})$ and $\delta_{uni}(C_\alpha)$ values are closely related to the ligand field of the carboxylic acid. The sign of the slope of Fig. 3(A) is opposite to that of the slope of Fig. 3(B). If we assume that the chemical shift of the carbon is related to the electron density as mentioned above, the following consideration is possible. The substituent at α-carbon which causes a decrease of the electron density on the α-carbon will cause an increase of the π-electron density on the carboxyl carbon

neighboring to the α-carbon and cause a decrease of the electron density on the oxygen atom of the carboxyl group. These processes are shown in the following scheme. A decrease of the electron density on the

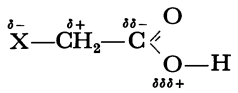

(as compared with CH_3COOH)

coordinated oxygen atom weakens the ligand field of the carboxylic acid, and increases of the electron densities on the α- and carboxyl carbon cause the shift changes of their ^{13}C-NMR to higher field side. Accordingly, the $\bar{\nu}_{max}$ value becomes larger as the $\delta_{uni}(C_{oxy})$ value becomes larger (to lower field) and the $\delta_{uni}(C_\alpha)$ becomes smaller (to higher field).

The consideration mentioned above is based on the effect from the substituent at α-carbon. Another effect to be taken into account is that from the cobalt(III) chromophore. Making a rough estimation, the substituent effect at α-carbon nearly equals in both *trans*(*O*)-$[Co(OCO\text{–}R)_2(en)_2]^{n+}$ and free carboxylic acid. Therefore, the effect from the substituent at α-carbon may be cancelled for the $\Delta_{uni}(C_\alpha)$. The $\Delta_{uni}(C_\alpha)$ value should be related rather to the residual effect which will originate from the cobalt(III). Accordingly, the relation between $\Delta_{uni}(C_\alpha)$ and $\bar{\nu}_{max}$ may be more intimate than that between $\delta_{uni}(C_\alpha)$ and $\bar{\nu}_{max}$. Similarly, the relation between $\Delta_{uni}(C_{oxy})$ and $\bar{\nu}_{max}$ may be more intimate than that between $\delta_{uni}(C_{oxy})$ and $\bar{\nu}_{max}$. Figure 4 shows the plots of $\Delta_{uni}(C_{oxy})$ *vs.* $\bar{\nu}_{max}$ and $\Delta_{uni}(C_\alpha)$ *vs.* $\bar{\nu}_{max}$. There are linear relations between them. These relations can be represented by the following equations. Where r and N are correlation

$$\Delta_{uni}(C_{oxy})/ppm = 12.37\,\bar{\nu}_{max}/10^3\,cm^{-1} - 216.62 \quad (r = 0.96,\ N = 13)$$

$$\Delta_{uni}(C_\alpha)/ppm = 13.79\,\bar{\nu}_{max}/10^3\,cm^{-1} - 248.22 \quad (r = 0.95,\ N = 13)$$

coefficient and number of measurements, respectively. The slopes for the two equations are nearly equal to each other with the same sign. Though one might think that the Δ_{uni} value results from the magnetic anisotropy arising from the cobalt(III) chromophore,[33] the calculated chemical shift changes based on the anisotropy are much smaller than the observed ones.

In the present study, we prepared the mixed ligand complexes of the type *trans*(*O*)-$[Co(OCO\text{–}R)(OCO\text{–}R')(en)_2]^{n+}$. The $\bar{\nu}_{max}$ values of the mixed type complexes are nearly equal to the mean value of the two $\bar{\nu}_{max}$ of *trans*(*O*)-$[Co(OCO\text{–}R)_2(en)_2]^{n+}$ and -$[Co(OCO\text{–}R')_2(en)_2]^{n+}$. That is, the $\bar{\nu}_{max}$ of *trans*(*O*)-$[Co(ac)(Hgly)(en)_2]^{2+}$ ($18.21\times10^3\,cm^{-1}$) is nearly equal to the mean value ($18.21\times10^3\,cm^{-1}$) of the two $\bar{\nu}_{max}$ of *trans*(*O*)-$[Co(ac)_2(en)_2]^+$ ($18.30\times10^3\,cm^{-1}$) and *trans*-(*O*)-$[Co(Hgly)_2(en)_2]^{3+}$ ($18.12\times10^3\,cm^{-1}$). Similar relation was observed for *trans*(*O*)-$[Co(ac)(\beta\text{-Hala})(en)_2]^{2+}$, -$[Co(ac)_2(en)_2]^+$, and -$[Co(\beta\text{-Hala})_2(en)_2]^{3+}$ (Table 1). These results suggest that the ^1E_g component of the mixed type complex can be expressed by the two ligand fields of *trans*-position. On the other hand, the $\Delta_{uni}(C_{oxy})$ and $\Delta_{uni}(C_\alpha)$ values of the mixed

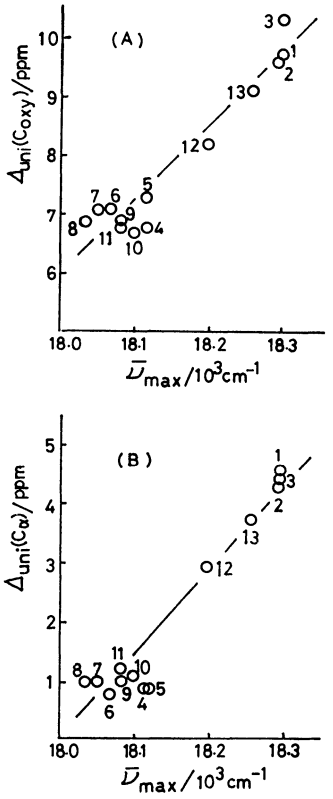

Fig. 4. Plots of ^{13}C chemical shift changes *vs.* first absorption maxima of the *trans*(*O*)-$[Co(O)_2(N)_4]$ type complexes.
(A): For carboxyl carbon (C_{oxy}), (B): for α-carbon (C_α). Numbers making the data plots correspond to the ordinal numbers of the complexes in Fig. 3.

Table 1. Absorption maxima of the *trans*(*O*)-$[Co(OCO\text{–}R)_2(en)_2]^{n+}$ type complexes

trans(*O*) type complexes	$\bar{\nu}_{max}/10^3\,cm^{-1}$
$[Co(Hgly)_2(en)_2]^{3+}$	18.12
$[Co(\beta\text{-Hala})_2(en)_2]^{3+}$	18.20
$[Co(ac)_2(en)_2]^+$	18.30
$[Co(ac)(Hgly)(en)_2]^{2+}$	18.21
$[Co(ac)(\beta\text{-Hala})(en)_2]^{2+}$	18.26

Table 2. Chemical shift changes of the *trans*(*O*)-$[Co(OCO\text{–}R)_2(en)_2]^{n+}$ type complexes

Carboxylic acid[a]	*trans*(*O*) type complexes	$\Delta_{uni}(C_{oxy})$ ppm	$\Delta_{uni}(C_\alpha)$ ppm
ac	$[Co(ac)_2(en)_2]^+$	+9.7	+4.5
Hgly	$[Co(Hgly)_2(en)_2]^{3+}$	+6.8	+0.9
β-Hala	$[Co(\beta\text{-Hala})_2(en)_2]^{3+}$	+8.2	+2.9
ac	$[Co(ac)(Hgly)(en)_2]^{2+}$	+9.7	+4.5
Hgly		+6.7	+1.0
ac	$[Co(ac)(\beta\text{-Hala})(en)_2]^{2+}$	+9.9	+3.8
β-Hala		+8.2	+2.4

a) ac=CH_3COO^-, Hgly=$CH_2(NH_3^+)COO^-$, and β-Hala=$CH_2(NH_3^+)CH_2COO^-$.

type complex are nearly equal to those of the corresponding ligands in the *trans*(*O*)-[Co(OCO–R)$_2$(en)$_2$]$^{n+}$ and -[Co(OCO–R')$_2$(en)$_2$]$^{n+}$ complexes but not to the mean value (Table 2).

Ćelap *et al.*[23,24] and Stewrat *et al.*[11] pointed out that the ^{13}C chemical shift of a ligand is affected by another ligand at *trans*-position to it. However, no distinctive difference of the *trans*-effect was observable for the complexes examined in the present study. That is to say, the ^{13}C resonance peaks of a carboxylate ligand in the mixed complex appears independently of another carboxylate ligand at *trans*-position. These results suggest that the *trans*-effect is not necessarily to be connected directly with the linearities in Figs. 4(A) and 4(B). Therefore, one should consider the effects (the through-space and through-bond effects of cobalt(III) ion, *etc.*) other than the *trans*-effect, which is responsible for the difference of the Δ_{uni} values, relating to the electron density. What effect is most responsible to the Δ_{uni} values is very interesting problem. However, there are some uncertain points remaining at present stage, although some of them were clarified by this study.

It has been clarified by this study that the chemical shifts of the coordinated carboxylic acids are closely related to the ligand fields of the acids and demonstrated that the ^{13}C chemical shifts are useful to estimate the ligand fields of the carboxylic acids.

The authers wish to thank Professor Yoichi Simura of Osaka University for his valuable suggestion and discussion.

References

1) Part XII of this series; T. Ama, H. Kawaguchi, M. Kanekiyo, and T. Yasui, *Bull. Chem. Soc. Jpn.*, **53**, 956 (1980).
2) J. Hammel and J. A. S. Smith, *J. Chem. Soc., A*, **1969**, 2883.
3) G. L. Blackmer and T. M. Vickrey, *J. Coord. Chem.*, **3**, 225 (1973).
4) a) T. Ama and T. Yasui, *Chem. Lett.*, **1974**, 1295; b) T. Ama and T. Yasui, *Bull. Chem. Soc. Jpn.*, **52**, 79 (1979); *ibid.*, **48**, 3171 (1975).
5) K. Ohba and J. Fujita, *Chem. Lett.*, **1978**, 595.
6) K. D. Gailey, K. Igi, and B. E. Douglas, *Inorg. Chem.*, **14**, 2956 (1975); *J. Coord. Chem.*, **5**, 171 (1976).
7) K. D. Gailey and B. E. Douglas, *J. Coord. Chem.*, **5**, 23 (1975).
8) a) C. A. Chang and B. E. Douglas, *J. Coord. Chem.*, **9**, 93 (1979); b) G. G. Hawn, C. A. Chang, and B. E. Douglas, *Inorg. Chem.*, **18**, 1266 (1979).
9) K. D. Gailey, D. J. Radanović, M. Djuran, and B. E. Douglas, *J. Coord. Chem.*, **8**, 161 (1978).
10) W. C. Trogler, R. C. Stewart, L. A. Epps, and L. G. Marzilli, *Inorg. Chem.*, **13**, 1564 (1974).
11) R. C. Stewart and L. G. Marzilli, *Inorg. Chem.*, **16**, 424 (1977).
12) M. Kojima and J. Fujita, *Chem. Lett.*, **1976**, 429.
13) H. Toftlund and T. Laier, *Acta Chem. Scand., A*, **31**, 651 (1977).
14) G. H. Searle, F. R. Keene, and S. F. Lincoln, *Inorg. Chem.*, **17**, 2362 (1978).
15) S. Bagger and O. Barg, *Acta Chem. Scand., A*, **30**, 765 (1976).
16) G. H. Searle, S. F. Lincoln, F. R. Keene, S. G. Teague, and D. G. Rowe, *Aust. J. Chem.*, **30**, 1221 (1977).
17) Y. Yoshikawa, *Chem. Lett.*, **1978**, 109.
18) M. Kojima and K. Yamasaki, *Bull. Chem. Soc. Jpn.*, **48**, 1093 (1975).
19) W. Hay, B. Jeragh, S. F. Lincoln, and H. Searle, *Inorg. Nucl. Chem. Lett.*, **14**, 435 (1978).
20) Y. Hung, L. Y. Martin, S. F. Jackels, A. M. Tail, and D. H. Busch, *J. Am. Chem. Soc.*, **99**, 4029 (1977).
21) H. Gerlach and K. Müller, *Helv. Chim. Acta*, **57**, 2234 (1974).
22) M. Fujita, Y. Yoshikawa, and H. Yamatera, *Bull. Chem. Soc. Jpn.*, **50**, 3209 (1977).
23) N. Juranić, M. B. Ćelap, D. Vučelić, M. J. Malinar, and P. N. Radivojša, *Inorg. Chim. Acta*, **25**, 229 (1977).
24) N. Juranić, M. B. Ćelap, D. Vučelić, M. J. Malinar, and P. N. Radivojša, *Inorg. Chem.*, **19**, 802 (1980).
25) O. W. Howarth, P. Moore, and N. Winterton, *J. Chem. Soc., Dalton Trans.*, **1974**, 2271.
26) a) J. A. Pople and M. Gordon, *J. Am. Chem. Soc.*, **89**, 4253 (1967); b) M. Karplus and J. A. Pople, *J. Chem. Phys.*, **38**, 2803 (1963); c) J. B. Stothers, "Carbon-13 NMR Spectroscopy," Academic Press, New York (1972).
27) W. Horsley and H. Sternlicht, *J. Am. Chem. Soc.*, **90**, 3738 (1968).
28) G. Miyajima and K. Nishimoto, *Org. Magn. Reson.*, **6**, 313 (1974).
29) D. E. Leyden and R. H. Cox, "Analytical Application of NMR," John Wiley & sons, Inc, New York (1977).
30) T. Ama and T. Yasui, *Bull. Chem. Soc. Jpn.*, **49**, 472 (1976).
31) H. Yamatera, *Bull. Chem. Soc. Jpn.*, **31**, 95 (1958).
32) a) T. Yasui, J. Hidaka, and Y. Shimura, *Bull. Chem. Soc. Jpn.*, **39**, 2417 (1966); b) T. Yasui, T. Ama, H. Morio, M. Okabayashi, and Y. Shimura, *Bull. Chem. Soc. Jpn.*, **47**, 2801 (1974).
33) H. Yoneda, U. Sakaguchi, and Y. Nakashima, *Bull. Chem. Soc. Jpn.*, **48**, 209 (1975).

Transition-metal Complexes of Pyrrole Pigments. XIX. Electrochemical and Coordination Behaviors of (5,10,15,20-Tetraphenylporphinato)niobium(V) Complexes†

Yoshihisa MATSUDA, Sunao YAMADA, Takashi GOTO, and Yukito MURAKAMI*

Department of Organic Synthesis, Faculty of Engineering, Kyushu University, Hakozaki, Higashi-ku, Fukuoka 812

(Received July 11, 1980)

The redox chemistry of acetato(5,10,15,20-tetraphenylporphinato)oxoniobium(V) (**1**) was investigated in dichloromethane by means of cyclic voltammetry and controlled potential electrolysis. One-electron reduction potentials were observed at −0.89, −1.05, and −1.41 V *vs.* SCE for the range from 0 to −2.0 V; the reduction of niobium(V) to niobium(III) occurred prior to ligand-reduction. The potential separation between first and second metal-reductions ($\Delta E_{1/2}$) for **1** is 0.16 V, while $\Delta E_{1/2}$ between reductions of the Mo^{VI} and Mo^{V} species for the corresponding molybdenum complex is 1.24 V. In order to elucidate the origin of such potential difference between the niobium and molybdenum complexes, the change of coordination structures which takes place in the course of redox reactions was examined. The coordination reaction of **1** with pyridine was also studied.

As a step toward preparation of one-dimensional electric conductors by stacking planar complexes with the formation of metal–metal bonds, molybdenum and niobium complexes of macrocyclic tetrapyrroles are plausible ones for this purpose since the metal ions have a strong tendency to form metal to metal bonds in their low oxidation states. The redox behaviors of these metal complexes needs to be investigated in order to establish chemical conditions for the formation of complexes involving low valency metals. We have previously studied the redox properties of several molybdenum(V) complexes of macrocyclic tetrapyrroles.[1] Acetato(5,10,15,20-tetraphenylporphinato)oxoniobium(V) [Nb^{V}(O)(TPP)(AcO), **1**][2] and tri-μ-oxo-bis[(5,10,15,20-tetraphenylporphinato)niobium(V)] [$Nb^{V}_2(O)_3(TPP)_2$, **2**][3,4] have been prepared and their crystallographic structures determined. However, the redox chemistry of these niobium complexes has not been examined so far.

We have investigated in the present work the redox properties of Nb^{V}(O)(TPP)(AcO) by cyclic voltammetry and controlled potential electrolysis in reference to the behavior of the corresponding molybdenum(V) complex, Mo^{V}(O)(TPP)(AcO), and the niobium(III) species was produced electrochemically for the first time. Since Nb^{V}(O)(TPP)(AcO) and $Nb^{V}_2(O)_3(TPP)_2$ assume a unique hepta-coordination geometry around the niobium(V) atom, the coordination interactions of both complexes with pyridine as well as the interaction of the latter complex with acetic acid have also been studied.

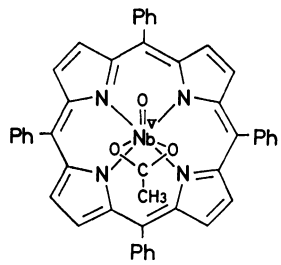

Nb(O)(TPP)(AcO)

† Contribution No. 596 from this Department.

Experimental

Materials. Acetato(5,10,15,20-tetraphenylporphinato)-oxoniobium(V) [Nb^{V}(O)(TPP)(AcO), **1**] and tri-μ-oxo-bis[(5,10,15,20-tetraphenylporphinato)niobium(V)] [$Nb^{V}_2(O)_3(TPP)_2$, **2**] were prepared by the methods of Lecomte and Protas.[2] Dichloromethane was treated with concentrated sulfuric acid, neutralized with aqueous sodium hydroxide, washed with distilled water, and refluxed over anhydrous calcium chloride for 2 d. After being fractionally distilled, dichloromethane thus purified and dried was stored over molecular sieve (3A, 1/16; Ishizu Pharmaceutical Co.). Pyridine was refluxed over potassium hydroxide and fractionally distilled. Tetrabutylammonium perchlorate (TBAP) of polarographic grade (Nakarai Chemicals) was used without further purification.

Spectroscopic Measurements. A Bruker WH-90 FT and a Hitachi R-24B spectrometer were used to obtain ^{1}H NMR spectra in chloroform-*d* (>99.5%; E. Merck, Darmstadt) at room temperature. Chemical shifts are given in ppm from internal TMS and calibrated with a chloroform signal as the secondary external reference. ESR spectra were recorded on a JEOL JES-ME-3 X-band spectrometer equipped with a 100 kHz field modulation unit; a standard MgO/Mn(II) sample calibrated with a NMR magnetometer was employed for calibration of the magnetic field. Electronic spectra were taken on a Union Giken SM-401 high sensitive spectrophotometer at 25 °C.

Electrochemical Measurements. Cyclic voltammetry was carried out on a YANACO P-8 polarograph equipped with platinum wire of 0.5 mm diameter as working and auxiliary electrodes; the surface area of the former electrode being about 30 times smaller than that of the latter. A saturated calomel electrode (SCE) was served as a reference which was separated from a bulk electrolyte solution by a salt bridge prepared with benzyliden-D-glucitols[5] and a dichloromethane solution of TBAP. A dichloromethane solution containing a niobium complex (5.0×10^{-4} mol dm^{-3}) and TBAP (5.0×10^{-2} mol dm^{-3}) was deaerated prior to each measurement and the inside of the cell was maintained under argon atmosphere throughout each measurement. All the measurements were carried out at 25±2 °C. The scan rate was varied in a range from 5 to 500 mV s^{-1}. Half-wave potentials ($E_{1/2}$) and anodic (i_{pa}) and cathodic (i_{pc}) currents were evaluated by referring to the literature methods.[6]

Controlled potential electrolysis was carried out in a three-electrode cell, modified for ESR and electronic spectral

measurements, with platinum wire of 0.5 mm diameter as working and auxiliary electrodes. The reference electrode was the same as used for cyclic voltammetry. An applied potential between the working and auxiliary electrodes was maintained constant with a conventional potentiostat and monitored with a Takeda Riken TR-6656 digital multimeter.

Results

Coordination Behavior of Nb(O)(TPP)(AcO). In order to examine the further coordination ability of **1**, the interaction between **1** and pyridine was investigated by electronic and NMR spectroscopy. The electronic spectrum of **1** was measured by changing the concentration of pyridine in a range of 0 to 3.09 mol dm^{-3} while the concentration of **1** was maintained constant (3.7×10^{-6} mol dm^{-3}). The results are shown in Fig. 1, where

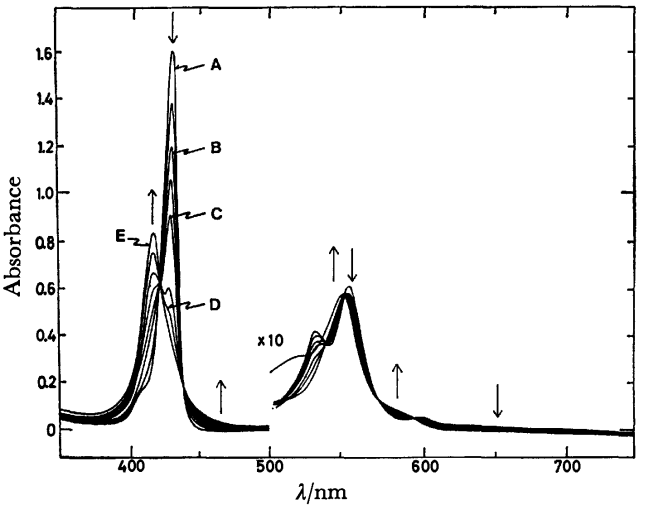

Fig. 1. Electronic spectra of Nb(O)(TPP)(AcO) (3.7×10^{-6} mol dm^{-3}) at 25.2 °C in the presence of pyridine at various concentrations (0—3.09 mol dm^{-3}): A, 0; B, 3.09×10^{-2}; C, 1.55×10^{-1}; D, 6.18×10^{-1}; E, 3.09 mol dm^{-3}. Trends of spectral change with increase in pyridine concentration are shown by arrows (↑ and ↓).

isosbestic points are observed at 420, 437, ≈510, 538, 550, 575, and 593 nm. The spectral behavior shows the formation of a single pyridine adduct of **1**. The NMR spectra clearly indicate the coordination of pyridine to **1**. A methyl signal of the coordinated acetate for **1** was observed at 1.27 ppm as shown in Fig. 2; appeared in a upper field range relative to the signal of acetic acid (2.20 ppm). This is attributed to a magnetic anisotropy effect provided by the macrocyclic ligand on the coordinated acetate group. This signal was, however, drastically shifted to a lower field range (5.28 ppm) in chloroform–pyridine (7 : 3 v/v) as shown in Fig. 2. This indicates that the methyl protons are displaced from a shielding to a deshielding zone of the porphyrin skeleton. Furthermore, signals due to the coordinated pyridine were observed in a range of 6 to 7 ppm, which are separated from those of the coordination-free pyridine appeared in the lower field range. By referring to the signal intensity of methyl protons

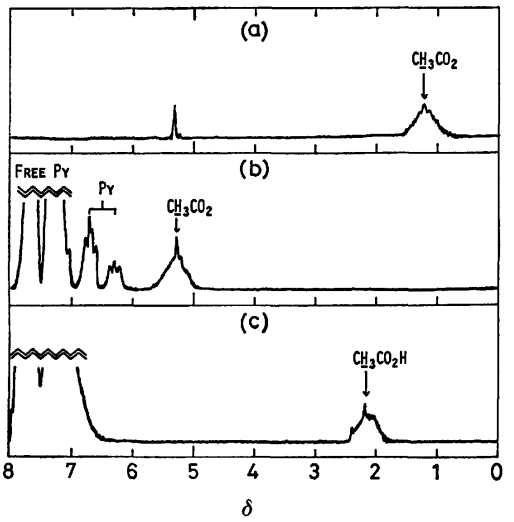

Fig. 2. NMR spectra of Nb(O)(TPP)(AcO) and acetic acid at room temperature: (a), Nb(O)(TPP)(AcO) in chloroform-*d* (a signal due to dichloromethane used as solvent for recrystallization appeared at 5.31 ppm); (b), Nb(O)(TPP)(AcO) in pyridine–chloroform-*d* (3 : 7 v/v); (c), acetic acid in pyridine–chloroform-*d* (3 : 7 v/v).

of the coordinated acetate, a number of pyridine molecules coordinated to **1** was evaluated to be one. Other signals observed in a low-field region below 7 ppm are: 7.78 (12H, m, *m*- and *p*-phenyl H's), 8.22 (8H, m, *o*-phenyl H's), and 9.04 (8H, s, pyrrole H's). The effect of pyridine coordination on the electronic and NMR spectra is consistent with the following solution equilibrium, where Py stands for pyridine.

$$\text{Nb(O)(TPP)(AcO)} + \text{Py} \overset{K}{\rightleftharpoons} \text{Nb(O)(TPP)(AcO)(Py)} \quad (1)$$

The equilibrium constant (K) was obtained from the intensity change at 427 nm by the aid of Benesi-Hildebrand equation[7] (Eq. 2), where $[Nb]_T$ and $[Py]_T$ stand for the total concentrations of **1** and pyridine, respectively; $\Delta\varepsilon$ is for the difference in molar absorption coefficient between **1** and its pyridine adduct, and ΔA represents the extent of absorbance change upon

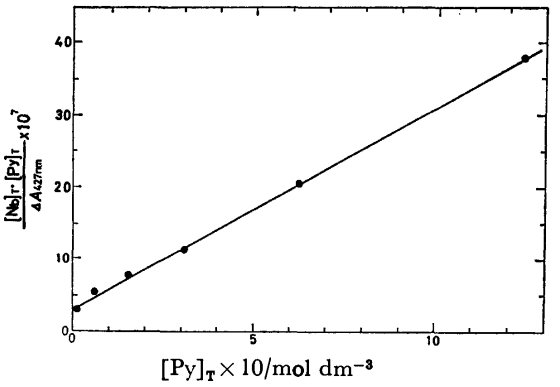

Fig. 3. Benesi-Hildebrand plot for the complex-forming equilibrium between Nb(O)(TPP)(AcO) and pyridine.

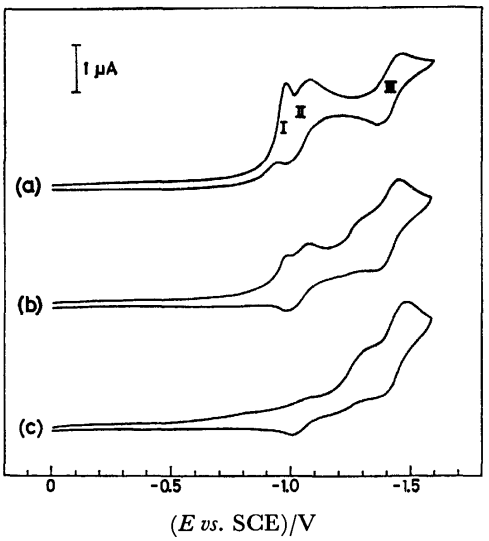

Fig. 4. Cyclic voltammograms of Nb(O)(TPP)(AcO) (5.0×10^{-4} mol dm^{-3}) in dichloromethane containing TBAP (5.0×10^{-2} mol dm^{-3}) at 25.2 °C in the presence of pyridine at various concentrations: (a), 0; (b), 0.8; (c), 3.5 mol dm^{-3}; scan rate 50 mV s^{-1}.

addition of pyridine. A good linear correlation based

$$\frac{[\mathrm{Nb}]_\mathrm{T}[\mathrm{Py}]_\mathrm{T}}{\Delta A}=\frac{1}{\Delta\varepsilon\cdot K}+\frac{[\mathrm{Py}]_\mathrm{T}}{\Delta\varepsilon} \qquad (2)$$

on Eq. 2 is observed as shown in Fig. 3: $K=9.6$ mol^{-1} dm^3; and $\Delta\varepsilon=3.48\times10^5$. The $\Delta\varepsilon$-value is in good agreement with that observed in the presence of a large excess of pyridine (3.44×10^5). The coordination of pyridine to **1** was also confirmed by cyclic voltammetry as shown in Fig. 4. Addition of pyridine to **1** resulted in marked cathodic shifts of reduction peaks I and II, from *ca.* −1 to −1.3 V *vs.* SCE, and the corresponding oxidation peaks appeared at −1.2 and −1.0 V *vs.* SCE. Redox peaks III, however, remained almost unchanged even in the presence of a large excess of pyridine.

Interaction of $Nb_2(O)_3(TPP)_2$ with Acetic Acid. The cyclic voltammogram of **2** for the range of 0 to −2.0 V *vs.* SCE in dichloromethane is shown in Fig. 5. The distinct cathodic peaks at −1.30, −1.56, and −1.80 V are coupled with anodic peaks at −1.23, −1.44, and −1.66 V, respectively, each being referred to one-electron transfer process. Redox peaks due to **1** appeared upon addition of acetic acid to a solution of **2**, and the cyclic voltammogram was completely converted to that of **1** in the presence of a 2-fold excess amount of acetic acid as shown in Fig. 5. Such conversion of **2** into **1** through reaction with acetic acid was also confirmed by electronic spectroscopy. The spectral change upon addition of acetic acid to **2** is shown in Fig. 6, where isosbestic points are observed at 421, 441, ≈500, 540, and 551 nm. Since the reaction was accelerated under anaerobic conditions, oxygen must participate in the reverse reaction as shown by Eq. 3.

$$\mathrm{Nb_2(O)_3(TPP)_2}+2\mathrm{AcOH}\underset{\mathrm{O_2}}{\rightleftharpoons}2\,\mathrm{Nb(O)(TPP)(AcO)}+\mathrm{H_2O} \qquad (3)$$

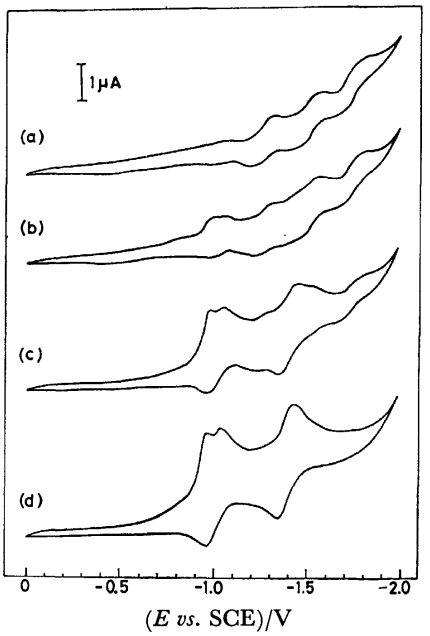

Fig. 5. Cylic voltammograms of $Nb_2(O)_3(TPP)_2$ (2.4×10^{-4} mol dm^{-3}) in dichloromethane containing TBAP (5.0×10^{-2} mol dm^{-3}) at 24 °C in the presence of acetic acid at various concentrations: (a), 0; (b), 1.24×10^{-4}; (c), 4.7×10^{-4}; (d), 9.7×10^{-4} mol dm^{-3}; scan rate 100 mV s^{-1}.

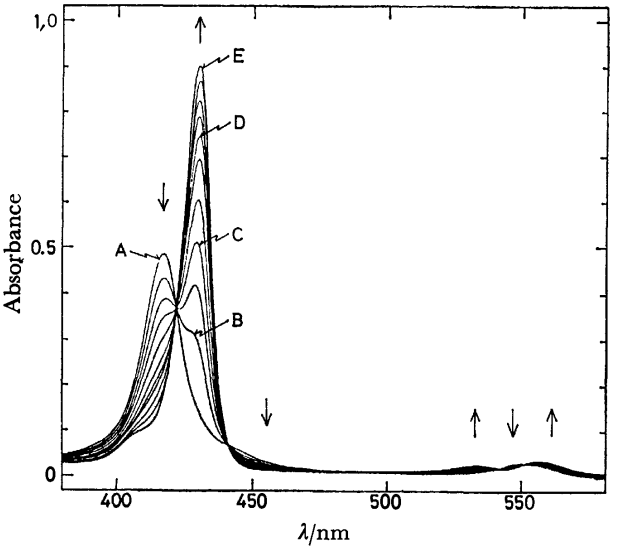

Fig. 6. Electronic spectral change during the reaction of $Nb_2(O)_3(TPP)_2$ (2.3×10^{-6} mol dm^{-3}) with acetic acid (7.1×10^{-5} mol dm^{-3}) in dichloromethane at 25 °C: A, 0; B, 0.5; C, 1.5; D, 3.0; E, 7.5 h. Trends of spectral change with time are shown by arrows (↑ and ↓).

Electrochemical Behavior of Nb(O)(TPP)(AcO). A typical cyclic voltammogram of **1** for the range of 0 to −1.6 V *vs.* SCE in dichloromethane is shown in Fig. 4. No other peak was observed in a cathodic range up to −2.0 V at any scan rate in a range from 10 to 200 mV s^{-1}. Two distinct cathodic peaks at −1.09 and −1.47 V are coupled with anodic peaks at −0.98 and −1.36 V, respectively. Although the anodic wave

coupled with the first cathodic peak at −0.97 V *vs.* SCE was obscure for faster scan rates, it became apparent by reducing the rate below 20 mV s^{-1}. We, therefore, evaluated three half-wave potentials for one-electron reduction steps, indicated by I, II, and III in Fig. 4(a), as −0.89, −1.05, and −1.41 V *vs.* SCE (within an accuracy of ±0.02 V), respectively. It has been generally realized that redox potentials of the central metal atom, incorporated into planar complexes formed with macrocyclic ligands, are quite sensitive to the nature of axial ligands, while those of the macrocyclic ligands are hardly affected by the variation of such ligands.[8] In the light of the coordination effect provided by pyridine on redox potentials, as described in a foregoing section, peaks I and II in Fig. 4(a) are attributed to the reductions of niobium, Nb^{V}/Nb^{IV} and Nb^{IV}/Nb^{III}, respectively, and peak III is due to that of the porphyrin ligand.

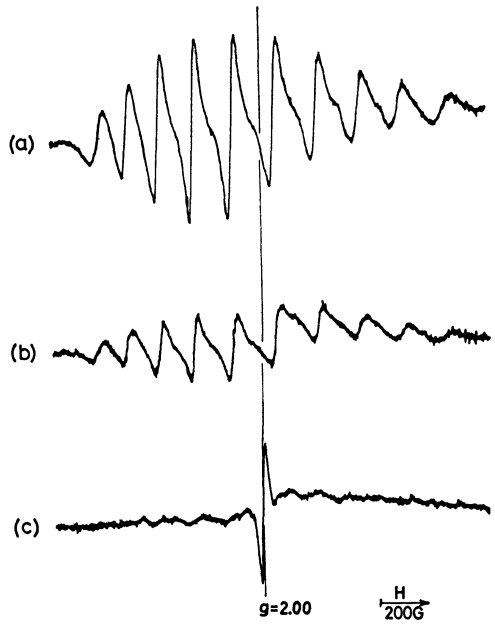

Fig. 7. ESR spectral change during the electrochemical reduction of Nb(O)(TPP)(AcO) at room temperature in dichloromethane containing TBAP (0.30 mol dm^{-3}) at potentials: (a), −0.92; (b), −1.1; (c), −1.46 V *vs.* SCE

We carried out the controlled potential reduction of **1** at −0.92, −1.1, and −1.46 V *vs.* SCE in dichloromethane in the presence of TBAP; potentials sufficient for respective one-electron reductions of **1** as confirmed by voltammetric measurements. The parent complex is diamagnetic itself, so that no ESR signal was observed. When **1** was reduced at −0.92 V *vs.* SCE, ten intense lines caused through interaction with ^{93}Nb (I=9/2) nucleus were observed over a wide range of magnetic field as shown in Fig. 7(a); this indicates the formation of a paramagnetic niobium(IV) species. These lines, however, decreased their intensities to a large extent upon electrolysis at −1.1 V *vs.* SCE as shown in Fig. 7(b). This implies that the two-electron reduced species is either a diamagnetic niobium(III) complex or a paramagnetic spin-triplet species involving unpaired electrons in both metal and ligand sites, such as π-cation radical of copper(II)–porphyrin.[9] A considerable cathodic shift of peak II upon addition of pyridine to **1** as demonstrated by cyclic voltammetry as well as the ESR pattern for a species obtained by the following electrolysis at peak III range excludes the latter possibility. The controlled potential reduction at −1.46 V *vs.* SCE provided a new signal due to a radical species with concomitant disappearance of the lines due to ^{93}Nb nucleus as shown in Fig. 7(c). The third reduction step undoubtedly corresponds to reduction of the porphyrin ligand. Reversible oxidation reactions were observed after ceasing the respective electrolytic reductions. As a result, complete redox behavior of **1** is illustrated as in Scheme 1.

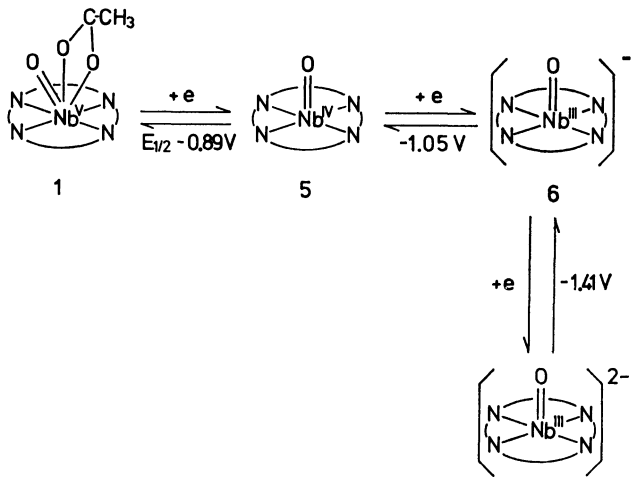

Scheme 1.

Discussion

The tri-μ-oxo dimer (**2**) does not undergo coordination interaction with pyridine as confirmed by cyclic voltammetry. An overall feature as well as cathodic and anodic peak potentials of the voltammogram was not influenced by the presence of pyridine for its concentration range from 0 to 3.5 mol dm^{-3} under otherwise identical conditions as stated in Fig. 5. According to the X-ray crystallographic analysis of **2**,[3,4] each niobium atom is hepta-coordinate and displaced from the mean ligand plane toward the tri-μ-oxo group by 1.01 Å as shown in **3**. Thus, an additional ligand can not attack at the axial site *trans* to the tri-μ-oxo group due to geometrical reasons, and must approach from the site sandwiched in between the two porphyrin ligands. As a result, pyridine fails to interact with niobium(V) likely due to steric hindrance while acetic acid undergoes substitution reaction with **2** to yield **1**. The coordination geometry around niobium(V) for **1** bears a close

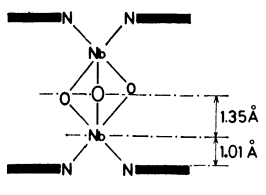

3

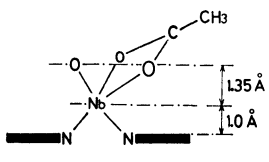

4

TABLE 1. REDUCTION AND OXIDATION POTENTIALS FOR H_2TPP AND ITS NIOBIUM AND MOLYBDENUM COMPLEXES IN DICHLOROMETHANE AT 25 °C IN THE PRESENCE OF TBAP (5.0×10^{-2} mol dm^{-3})[a]

Compound	Metal			Ligand		Reference
	$E^{ox}_{1/2}$	$E^{red}_{1/2}(1)$	$E^{red}_{1/2}(2)$	$E^{red}_{1/2}(1)$	$E^{red}_{1/2}(2)$	
H_2TPP				−1.23	−1.56	1
				−1.21		13
Nb(O)(TPP)(AcO)		−0.89	−1.05	−1.41	[c]	This work
Mo(O)(TPP)(AcO)[b]	1.2	−0.04		−1.11	−1.51	1

a) $E_{1/2}$ values are given in V *vs.* SCE; within an accuracy of ±0.02 V. b) Acetic acid (1.0 mol dm^{-3}) added. c) No peak was detected in a cathodic range up to −2.0 V.

TABLE 2. PHYSICAL PARAMETERS FOR NIOBIUM(IV) AND MOLYBDENUM(V) COMPLEXES

Complex	$\nu_{M=O}$/cm^{-1} [a]	Spin Hamiltonian parameters[b]			$\lvert\mu_I\rvert$[c]	$\rho\times10^4$ [d]
		g	$A_{metal}\times10^4$/cm^{-1}	$A_N\times10^4$/cm^{-1}		
Nb^{IV}(O)(TPP)[e]	(905)[f]	1.96	175	—	6.17	127.8
Mo^{V}(O)(TPP)(AcO)[g]	942, 919	1.961	48.5	2.4	0.92	131.8

a) Nujol mull. b) Measured in dichloromethane. c) μ_I, nuclear magnetic moment; cited from Ref. 14. d) $\rho=A_{metal}/(\mu_I/I)$. e) One-electron reduced species of the Nb^V complex (**1**). f) Measured with **1**. g) ESR parameters cited from Ref. 1.

resemblance to that for **2** as depicted in **4** by referring to the X-ray crystallographic analysis of **1**.[2] On the basis of the same reasoning as mentioned for **2**, pyridine undergoes coordination with **1** at the same site that the oxo and acetato groups are placed even though the site becomes further sterically crowded. Such a profound effect and a strong affinity of niobium(V) for oxygen in part seem to be responsible for a weak coordination tendency of **1** toward pyridine, compared with other metalloporphyrins.[10]

Reduction and oxidation potentials for H_2TPP, **1**, and the corresponding molybdenum(V) complex, Mo(O)(TPP)(AcO) (**7**), are listed in Table 1. Table 2 summarizes the M=O stretching frequency for **1** and **7**, and spin Hamiltonian parameters for **7** and the one-electron reduced species of **1**. The one-electron reduced species of **1** shows ten intense lines over a wide range of magnetic field (1500—2000 G) due to hyperfine interaction with niobium nucleus (I=9/2). However, the superhyperfine structure due to four nitrogen nuclei was not detected for the present complex. Since both **7** and the one-electron reduced species of **1** provide ESR signals with remarkable intensity at room temperature, there is no excited d-orbital level placed close to the d-orbital of lowest energy for both species. Consequently, the second electron donated to the central metal atoms during the reductions, $Nb^{IV}\rightarrow Nb^{III}$ and $Mo^{V}\rightarrow Mo^{IV}$, must also be placed in the ground state orbital, which is then occupied with two electrons. The potential separation between first and second metal-reductions ($\Delta E_{1/2}$) for **1** is 0.16 V, while $\Delta E_{1/2}$ for **7** is 1.24 V since the corresponding processes for **7** are reductions of the Mo^{VI} and Mo^{V} species with reference to the number of d-electrons.

The acetato group seems to be released from the niobium(III) and molybdenum(IV) sites, as shown by structures **6** (Scheme 1) and **9** (Scheme 2) due to the reasons stated later, and both complexes may assume

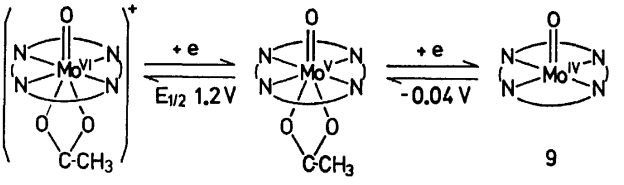

8 7

Scheme 2.

a similar coordination geometry consequently. On this basis, Racah's interelectronic repulsion parameters (B) for d^2 configuration[11] are cited for comparison; 682 and 602 cm^{-1} for Mo^{IV} and Nb^{III}, respectively. Such a small difference in Racah parameter, however, does not explain the large difference in $\Delta E_{1/2}$ stated above. The odd electron density at the metal nucleus is strictly reflected on hyperfine splitting constant A_{metal} for the same metal species. A ρ-value, which is proportional in general to the odd electron density at a metal nucleus, is given by $A_{metal}/(\mu_I/I)$ where μ_I and I stand for nuclear magnetic moment and nuclear spin, respectively. ρ-Values for the molybdenum(V) and niobium(IV) complexes of d^1 configuration listed in Table 2 are comparable to each other, and again do not explain the large difference in $\Delta E_{1/2}$.

In order to elucidate the origin of such potential difference, the change of coordination structures in the course of redox reactions needs to be taken into consideration as shown in Schemes 1 and 2. We reported previously the plausible structures at various metal oxidation states for **7**; **7**, **8**, and **9** in Scheme 2 for the Mo^V, Mo^{VI}, and Mo^{IV} species, respectively.[1] The molybdenum species in d^0 and d^1 configurations retain the acetato group while it seems liberated in d^2 configuration. The marked structural change assigned to **9** is reflected in its redox reaction rate. When the Mo^{IV}

species was electrolytically re-oxidized at 0 V *vs.* SCE under anaerobic conditions, it took about 12 h to return to the Mo^{V} state. On the other hand, when the Nb^{III} species in d^2 configuration was re-oxidized under anaerobic conditions, the ESR signal due to the Nb^{IV} species appeared in 1—2 min. However, even the Nb^{IV} species underwent electrolytic re-oxidation to the Nb^{V} state at 0 V *vs.* SCE under anaerobic conditions, the ESR signal due to the Nb^{IV} species still remained even after *ca.* 12 h of oxidation. On the basis of these kinetic results, structures **5** and **6** are reasonably assigned to the Nb^{IV} and Nb^{III} complexes, respectively.

By referring to equilibrium data for substitution reaction of Mo(O)(TPP)(MeO) with acetate and chloride ions[1] as well as the X-ray crystallographic analysis of Mo(O)(TPP)Cl,[12] the acetato group involved in **7** is coordinated to the molybdenum atom with some ionic character. Such an ionic character of the axial bond tends to stabilize the lowest d-orbital due to the effective positive charge localized on the molybdenum atom. An additional energy is required to cleave the axial bond in reduction process from **7** to **9**. Such a bond-cleavage effect is more pronounced for the reduction of Mo(O)(TPP)(MeO). Since the Mo–OMe bond has a significant covalent character as reported previously,[1] the lowest d-orbital would not be so much stabilized as in the case of **7**. Nevertheless, the reduction potential for Mo^{V}/Mo^{IV} was shifted toward cathodic direction by 0.7 V relative to the same potential for **7**.[1] Consequently, the axial bond cleavage seems predominantly to control the reduction potential for Mo^{V}/Mo^{IV}. A large $\Delta E_{1/2}$ value (1.24 V) for **7** is presumably due to such a bond cleavage effect, while a small $\Delta E_{1/2}$ value (0.16 V) confirms the **5**→**6** process which does not require the axial bond cleavage.

Both H_2TPP and **7** have comparable values of first and second potentials for the ligand reduction, the separation between the potentials being 0.33—0.4 V. This is consistent with the situation that the lowest d-orbital of **7** undergoes little interaction with ligand orbitals. On the other hand, not only the first ligand reduction potential for **1** is a little shifted toward cathodic direction, but also the separation between first and second reduction potentials is much larger than those for H_2TPP and the molybdenum complex. We conclude, therefore, that a considerable cathodic shift of the second ligand reduction potential in particular is attributed to an increase in π-electron density provided by delocalization of added two electrons in the ground state d-orbital of niobium through d-π interactions.

This work provides the first example for the two-electron reduction of the central metal atom to occur prior to the two-electron reduction of the macrocyclic ligand among metalloporphyrins involving second and third transition metals. Now, we are at the gate of research toward developments of stacked complex polymers by using a novel niobium(III) complex obtained in this work.

This work was supported in part by the Asahi Glass Foundation for Industrial Technology.

References

1) Y. Matsuda, S. Yamada, and Y. Murakami, *Inorg. Chem.*, in press.
2) C. Lecomte and J. Protas, *J. Chem. Soc., Chem. Commun.*, **1976**, 434.
3) J. F. Johnson and W. R. Scheidt, *J. Am. Chem. Soc.*, **99**, 294 (1977).
4) J. F. Johnson and W. R. Scheidt, *Inorg. Chem.*, **17**, 1280 (1978).
5) F. Endo, *Yakugaku Zasshi*, **79**, 595 (1959).
6) R. N. Adams, "Electrochemistry at Solid Electrodes," Marcel Dekker, New York, N. Y. (1969), pp. 143—162.
7) H. A. Benesi and J. H. Hildebrand, *J. Am. Chem. Soc.*, **71**, 2703 (1949).
8) K. M. Kadish, L. A. Bottomley, and J. S. Cheng, *J. Am. Chem. Soc.*, **100**, 2731 (1978).
9) J.-H. Fuhrhop and D. Mauzerall, *J. Am. Chem. Soc.*, **91**, 4174 (1969).
10) For example, see: F. A. Walker, *J. Am. Chem. Soc.*, **95**, 1150 (1973).
11) Racah's *B* parameters were evaluated from the energy separation between ^3F and ^3P states for free ions, Nb^{III} and Mo^{IV}. Term energies were cited from: C. E. Moore, "Atomic Energy Levels," Circular of the National Bureau of Standards 467, Washington, D. C. (1952, 1958), Vols. II and III.
12) H. Ledon and B. Mentzen, *Inorg. Chim. Acta*, **31**, L393 (1978).
13) A. Giraudeau, H. J. Callot, and M. Gross, *Inorg. Chem.*, **18**, 201 (1979).
14) Proceedings of the International Conference on Nuclear Moments and Nuclear Structure (1972); *Suppl. J. Phys. Soc. Jpn.*, **34** (1973).

New Application of Crown Ether. V.[1] The Effect of Crown Ethers on the Acid-Base Interaction between 2,4,4′,6-Tetranitrodiphenylamine and Primary Amines in Benzene

Fumio WADA,* Yoshiko WADA, Kiyoshi KIKUKAWA, and Tsutomu MATSUDA

Department of Organic Synthesis, Faculty of Engineering, Kyushu University, Hakozaki, Higashi-ku, Fukuoka 812

(Received April 22, 1980)

The effect of crown ethers on the acid-base interaction of 2,4,4′,6-tetranitrodiphenylamine (HA, λ_{max} 380 nm, $pK_a=8.88$ in water) with primary amines (RNH_2) in benzene was investigated spectrophotometrically. Crown ethers assisted strongly the formation of association complexes, $R\overset{+}{N}H_3\cdot$crown ether$\cdot A^-$, which existed as a single chemical species (λ_{max} 478 nm) assignable to "crown ether-separated ion pair." The effect of the steric factors of various primary amines on the equilibrium to form the association complex was discussed on the basis of the equilibrium constants and thermodynamic parameters of the systems involving 18-crown-6 and benzo-18-crown-6.

Macrocyclic polyethers (crown ethers) form stable complexes with mono-alkylammonium salts as well as alkali and alkaline earth metal salts. Structural effect of crown ethers on the ion-association extraction of an alkylammonium salt as crown ether complexes was investigated in detail by Cram and his collaborators[2] for t-$Bu\overset{+}{N}H_3\cdot\overset{-}{SCN}$, but structural effect of alkylamine moiety has not yet been studied. It is known that the formation of the crown ether complexes is dependent not only on the structure of crown ether itself, but also on the nature of the anion involved in the association complexes extracted in a non-polar solvent. In the case of the alkylammonium complexes, steric interactions between the substituent on the alkylamines and the crown ethers are presumed to be an important factor to affect the extent of the formation of the association complexes.

We recently showed that alkylamine–water–crown ether systems could be used as an effective hydroxide ion source in the reduction of unsaturated carbonyl compounds by hydridocarbonylferrate in a two-phase system (benzene–water).[3] The efficiency of the reduction was dependent not only on the nature of the crown ether added but also on the structure of the alkylamines.

The circumstances prompted us to study the association equilibrium between a weak acid and primary amines in a non-polar solvent (benzene) in the presence of crown ethers. Variation of the extent of the equilibrium (Eq. 1) with the structure of the amines and crown ethers (18-crown-6 and benzo-18-crown-6) is discussed in a quantitative manner in this paper.

$$\underset{\mathbf{1}}{HA} + RNH_2 + CR \overset{K}{\rightleftharpoons} \underset{\mathbf{2}}{R\overset{+}{N}H_3\cdot CR\cdot A^-} \qquad (1)$$

CR: crown ether

HA: 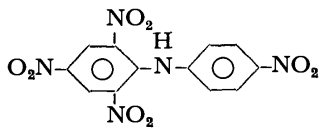

Results and Discussion

Structure of the Association Complexes. Among several weak acids examined, 2,4,4′,6-tetranitrodiphenylamine (**1**; $pK_a=8.88$, $\lambda_{max}(Na^+\cdot A^-)$ 465 nm, ε_{max} 23800 in water[4]) was proved to be a suitable probe for spectroscopic study of the equilibrium. The acid (**1**) showed a strong absorption maximum at 380 nm in benzene. The reaction of **1** with RNH_2 to form $R\overset{+}{N}H_3\cdot A^-$ lies so far to the starting materials in a non-polar solvent such as benzene. Thus, the absorption spectra did not change even in the presence of excess amount of n-$BuNH_2$ (n-$BuNH_2$/**1**=10—500). When 18-crown-6 (18C6) was added to the benzene solution of **1** and n-$BuNH_2$ a strong bathochromic shift of the absorption maximum from 380 to 478 nm was observed (Fig. 1). The presence of an isosbestic point at 412.5 nm indicated that a single chemical species was formed by the addition of the crown ether. The increase in the intensity of the band at 478 nm ceased when the ratio of the crown ether to **1** reached around 1500 at 26.6 °C (150 at 6 °C) as shown in Fig. 1. Addition of an equimolar amount of DBU (1,8-diazabicyclo[5.4.0]undec-7-ene, a strong organic base) to a benzene solution of **1** produced a bathochromic shift of the absorption (380 nm) to 455

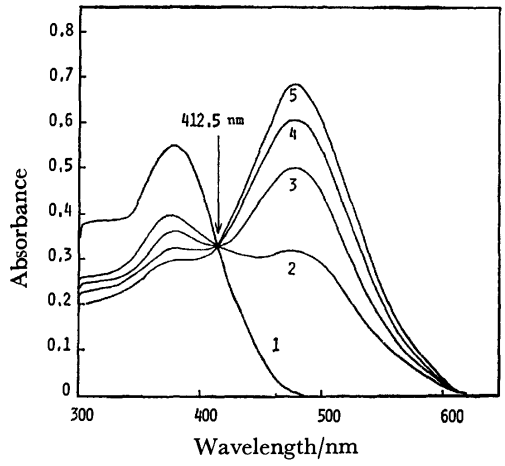

Fig. 1. UV spectra of $BuNH_2$–HA–18C6 system.

		A⁻(mol %)
1	HA : 18C6=1 : 0	0
2	HA : 18C6=1 : 6.5	28
3	HA : 18C6=1 : 13	44
4	HA : 18C6=1 : 19	53
5	HA : 18C6=1 : 26	61

HA=3.3×10^{-5} mol/dm³, $BuNH_2$=8.25×10^{-4} mol/dm³, temp 26.6 °C.

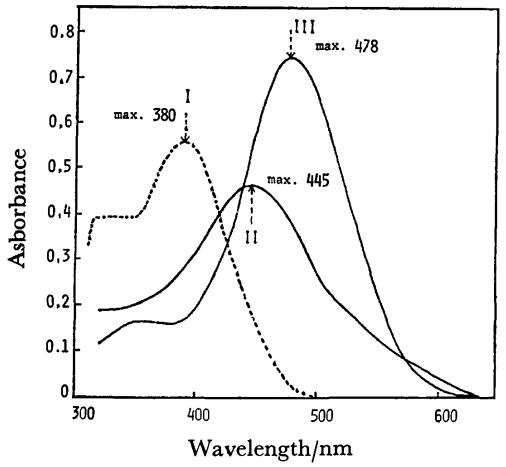

Fig. 2. UV spectra of crown ether complexes.
I: HA, II: Na^+A^- -B15C5, III: $\overset{+}{R}NH_3$–A^-–18C6.

Table 1. Efficiency of crown ethers for the formation of the ammonium ion complexes

Crown ether[b]	Crown ether/HA[a]		
	n-$BuNH_2$	*s*-$BuNH_2$	*t*-$BuNH_2$
18C6	4	13	18
DC18C6 (*cis-syn-cis*)	15	105	450
DC18C6 (*cis-anti-cis*)	105	635	1400
B15C5	4800[c]	10000[c]	14000[c]
B18C6	170	306	194

a) The amount of crown ether (in molar ratio to HA) necessary to reach equal concentration of HA (380 nm) and A^- (478 nm). HA=1.09×10^{-4} mol/dm^3, RNH_2=5.5×10^{-3} mol/dm^3, Temp 27.3 °C.
b) C: crown, DC: perhydrodibenzo, B: benzo.
c) Those to reach [A]/[HA]=1/9.

nm in the absence of the crown ether, and the absorption maximum moved up to 478 nm by further addition of DBU (≈100 fold excess). The latter bathochromic shift can be accounted for on the basis of the change in the structure of the resulting acid–base association complex, *i.e.* the change from a contact ion pair to a solvent-separated ion pair. It is to be noted that in *n*-$BuNH_2$–**1**–18C6 system, the position of the absorption maximum did not materially change with the variation of amine/**1** ratio from 10 to 500. The behavior of the crown ether complex of the alkylamine as well as that of the DBU-complex are noticeably compared with the observation that the absorption of $Na^+\cdot A^-$–benzo-15-crown-5 complex in benzene at 445 nm (Fig. 2) showed very little shift on further addition of B15C5 (≈50 fold excess). From these observations, it could be reasonably concluded that the ionic species with the absorption at 445 nm (and 455 nm for the DBU–**1** system) and the one absorbing at 478 nm are assigned to the contact ion pair and the crown ether-separated ion pair (or solvent-separated ion pair), respectively. Other crown ethers included in Table 1 as well as a bis(benzocrown ether), 1,7-bis[3,4-(1,4,7,10,13-pentaoxatridecane-1,13-diyl)phenyl]-1,4,7-trioxaheptane,[5] showed the behavior same as 18C6 forming complexes with an absorption maximum at 478 nm. It is to be added incidentally that in the absence of a crown ether the addition of a large amount of alkylamine (RNH_2/**1**≈1000) to the benzene solution of **1** caused a slow displacement of *p*-nitroanilino group in **1** by the amine giving *N*-alkylpicrylamine, which was characterized by the appearance of new absorptions at 338 and 417 nm.

Effect of the Structures of Alkylamines and Crown Ethers. Table 1 shows a qualitative comparison of the extent of the formation of the butylammonium ion complexes (**2**), where the values represent the amounts of a crown ether (molar basis) being necessary to reach to [**2**]/[**1**]=1 (for B15C5 see footnote in the Table). In line with the previous results,[2] 18C6 entered into the formation of the association complexes to a large extent, and B15C5 was much less efficient. With most of the crown ethers the increase in steric bulk of the alkyl group of

Table 2. Equilibrium constants in RNH_2–HA–crown ether system in benzene

Temp °C	RNH_2 R–	*K* ($mol^{-2}\,dm^6$)		
		18C6	B18C6	AB18C6[a]
6.0	*n*-Bu	$(5.66\pm0.09)\times10^7$	$(2.28\pm0.09)\times10^6$	
	s-Bu	$(1.50\pm0.02)\times10^7$	$(1.28\pm0.01)\times10^6$	
	t-Bu	$(9.47\pm0.10)\times10^6$	$(1.92\pm0.02)\times10^6$	
26.6	*n*-Pr	$(2.29\pm0.07)\times10^6$	$(1.22\pm0.01)\times10^5$	
	i-Pr	$(1.64\pm0.05)\times10^6$	$(1.44\pm0.03)\times10^5$	
	n-Bu	$(2.31\pm0.10)\times10^6$	$(1.52\pm0.03)\times10^5$	$(6.16\pm0.20)\times10^4$
	s-Bu	$(7.01\pm0.13)\times10^5$	$(7.56\pm0.14)\times10^4$	$(3.56\pm0.07)\times10^4$
	t-Bu	$(4.59\pm0.14)\times10^5$	$(9.99\pm0.30)\times10^4$	$(4.74\pm0.25)\times10^4$
	Pentyl	$(2.30\pm0.06)\times10^6$	$(1.75\pm0.01)\times10^5$	
	1-Methylbutyl	$(8.09\pm0.19)\times10^5$	$(8.36\pm0.22)\times10^4$	
	1-Ethylpropyl	$(8.44\pm0.07)\times10^4$	$(9.65\pm0.60)\times10^3$	
	t-Pentyl	$(2.22\pm0.20)\times10^5$	$(4.54\pm0.61)\times10^4$	
35.0	*n*-Bu	$(9.76\pm0.08)\times10^5$	$(5.98\pm0.22)\times10^4$	
	s-Bu	$(3.06\pm0.04)\times10^5$	$(3.13\pm0.01)\times10^4$	
	t-Bu	$(1.99\pm0.04)\times10^5$	$(4.18\pm0.05)\times10^4$	

a) 4′-Acetylbenzo-18-crown-6.

TABLE 3. COMPARISON OF EQUILIBRIUM CONSTANTS (K/K_0) ON THE BASIS OF FRAMEWORK OF AMINES

Amine R–	K/K_0[a] 18C6	K/K_0[a] B18C6
C–C–C–	0.99_1	0.052_8
C–C–C–C–	1.00	0.065_8
C–C–C–C–C–	0.99_6	0.075_8
C–C–C–	0.99_1	0.052_8
C–C–C– (C)	0.30_3	0.032_7
C–C–C– (C)	0.096_1	0.019_7
C–C–C– (C)	0.036_5	0.004_2
C–C–C–	0.99_1	0.052_8
C–C– (C)	0.71_0	0.062_3
C–C– (C)	0.19_9	0.043_2

a) K_0 is the equilibrium constant of 18C6– *n*-$BuNH_2$ system at 26.6 °C.

the amines depressed the formation of the complex, but benzo-18-crown-6 (B18C6) showed an irregular order of the efficacy as *n*-$BuNH_2$>*t*-$BuNH_2$>*s*-$BuNH_2$. In order to inquire the factors which are related to the discrepancy, equilibrium constants for Eq. 1 were determined for various alkylamines with the use of 18C6 and B18C6, and the results are summarized in Table 2. Table 3 shows the relative ratios of the equilibrium constants at 26.6 °C which are derived by taking the 18C6–*n*-$BuNH_2$ system as a reference. The values for normal alkylamine–18C6 system were almost invariant with the chain length of the amines, while those in the B18C6 system showed some increase with the increase of the alkyl chain. A noticeable difference between the two systems was observed in the effect of α-alkyl substitution of the amines. The decrease of the ratio by the introduction of methyl group(s) was clearly smaller in the B18C6 system than in that of 18C6 as seen in the set involving *n*-$PrNH_2$, *i*-$PrNH_2$, and *t*-$BuNH_2$. The presence of α-ethyl group, however, caused larger steric effect in both systems, as is observed in the case of 3-aminopentane.

Thermodynamic parameters of the equilibrium in 18C6– and B18C6–*n*-$BuNH_2$ systems in benzene at 26.6 °C are shown in Table 4. The entropy change in the 18C6 system are almost constant ($\Delta S = -2.12$—-2.16×10^2 J/K mol), and the enthalpy term seems to mainly determine the extent of the complex formation decreasing in the order : *n*-$BuNH_2$>*s*-$BuNH_2$>*t*-$BuNH_2$. In the system of B18C6, however, the change of the two terms occurs in an opposite manner with the increase of the steric bulk of the amines to yield the orders, *t*-$BuNH_2$>*s*-$BuNH_2$>*n*-$BuNH_2$ for the enthalpy term and *n*-$BuNH_2$>*s*-$BuNH_2$>*t*-$BuNH_2$ for the entropy term, respectively. Thus, a subtle balance of the two terms would lead to the unexpected order of the stability among the alkylammonium complexes of B18C6 and also of 4′-acetylbenzo-18-crown-6, though the origin for the specificity of the B18C6 systems is not clear at present.

TABLE 4. THERMODYNAMIC PROPERTIES OF BUTYLAMINE–HA–CROWN SYSTEM[a]

Crown	$BuNH_2$	$-\Delta G$ kJ/mol	$-\Delta H$ kJ/mol	$-\Delta S$ kJ/mol
18C6	*n*-	36.5	102	216
	s-	33.5	97.5	213
	t-	32.5	96.7	212
B18C6	*n*-	29.7	90.2	201
	s-	28.0	92.4	213
	t-	28.7	95.6	222

a) ΔG, ΔH, and ΔS at 26.6 °C.

Thermodynamic parameters for the complex-forming equilibria between crown ethers and various metal or ammonium salts have been reported mainly in a protic or a dipolar medium such as DMF. The entropy terms obtained[6] vary widely depending on the nature of the salts and crown ethers as well as the medium, but scarcely exceed −20 e.u. for the systems utilizing the crown ethers bearing 15- or 18-ring. The large loss of entropy (around -2.1×10^2 J/K mol or −50 e.u.) in the present equilibrium system suggests that several molecules of the medium, excess alkylamine (and/or benzene), are interacting with the alkylammonium complexes, in view of the result[7] that in the equilibrium of Eq. 2 in chloroform the entropy term much decreases from −23 to −40 e.u. by replacement of the crown ether with diglyme.

$$HBr + Br_2 + \text{di-Br-DBC} \rightleftharpoons H^+\cdot(\text{di-Br-DBC})\cdot Br_3^- \quad (2)$$

di-Br-DBC: 4,4′-dibromodibenzo-18-crown-6

Experimental

Materials. All crown ethers used were prepared according to the conventional methods;[8] 18C6: mp 39.9—40.2 °C, B18C6: mp 44.1—44.5 °C, 4′-acetylbenzo-18-crown-6: mp 77.9—78.2 °C,[5] and B15C5: mp 80.8—81.7 °C.

2,4,4′,6-Tetranitrodiphenylamine (HA, **1**) was prepared by the reaction of picryl chloride and *p*-nitroaniline in ethanol in the presence of sodium carbonate, and then recrystallized from ethanol (three times); yellow needles, mp 222.8—224.2 °C (uncorrected) (lit, 219 °C,[9] 220—220.6 °C[10]), Found: C, 41.20; H, 2.03; N, 19.98%. Calcd for $C_{12}H_7N_5O_8$: C, 41.27; H, 2.02; N, 20.06%. 1-Methylbutylamine and 1-ethylpropylamine were prepared by the methods described in the literature,[11] and other alkylamines (RNH_2) were of reagent grade. These amines were distilled over KOH and stored under nitrogen atmosphere prior to use. Benzene was dried over sodium metal and distilled under nitrogen atmosphere before use.

The complex of B15C5 with $Na^+\cdot A^-$ was prepared by the addition of a methanol solution of the crown ether to $Na^+\cdot A^-$ in methanol.

Absorption Spectra. The electronic spectra of the solutions were recorded on a Shimadzu UV-200 spectrophotometer over a temperature range from 6.0 to 35.0 °C (±0.1 °C).

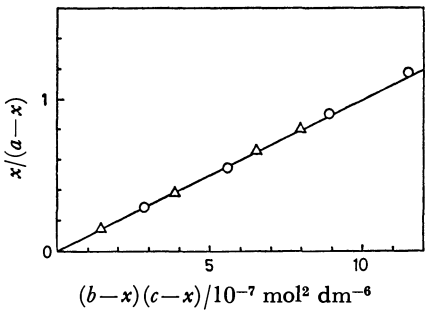

Fig. 3. Determination of formation constant according to Eq. 4.
○: [*n*-BuNH$_2$]/[HA]=25, [HA]=3×10^{-5} M (M=mol·dm^{-3}), [18C6]/[HA]=11—75 at 35.0 °C.
△: [18C6]/[HA]=1.8, [HA]=5×10^{-5} M, [*n*-BuNH$_2$]/[HA]=33—266 at 35.0 °C.
Both systems gave the same formation constant (K=(0.976±0.08)×10^4 M^{-2}) within the experimental error.

A quartz cell with a silicone rubber stopper was used in all determinations. A constant temperature of ±0.1 °C was maintained by circulating water from a thermostated bath. The temperature inside the cell compartment was monitored with a thermocouple. In benzene solution, the absorption maxima and absorption coefficients of **1** and Na$^+$·A$^-$–B15C5 were 380 nm (ε_{max}: 1.64×10^4) and 445 nm (ε_{max}: 1.72×10^4), respectively. The absorption maxima and absorption coefficient of crown separated ion pair, $\overset{+}{R}NH_3\cdot CR\cdot A^-$, in benzene were obtained from the RNH$_2$–**1**–18C6 system containing such amount of the crown ether that the absorbance of the system did not increase by its further addition. Concentration change of **1** was corrected. The resulting absorption coefficient for *n*-BuNH$_2$– and *n*-pentylamine–**1**–18C6 (and B18C6) systems was the same value (λ_{max}: 478 nm, ε_{max}: 3.41×10^4). The conductance of these solutions was negligible.

Calculations. The formation constants of the complexes were calculated from the measured concentration of $\overset{+}{R}NH_3\cdot CR\cdot A^-$ by considering the following equilibrium.

$$\underset{(a-x)}{HA} + \underset{(b-x)}{CR} + \underset{(c-x)}{RNH_2} \overset{K}{\rightleftharpoons} \underset{x}{\overset{+}{R}NH_3\cdot CR\cdot A^-} \qquad (3)$$

CR : A crown ether
a, b, and c : Initial concentrations of **1**, CR, and RNH$_2$, respectively.
K : Formation constant

The constant K may be represented by

$$K = x/(a-x)(b-x)(c-x) = \frac{d-d_{HA}}{d_A-d} \times \frac{1}{\left(b-\frac{d-d_{HA}}{\varepsilon_A-\varepsilon_{HA}}\right)\left(c-\frac{d-d_{HA}}{\varepsilon_A-\varepsilon_{HA}}\right)}, \qquad (4)$$

where the symbols have the following significance, x: the fraction of ionized HA, ε_{HA}, and ε_A: the absorption coefficients of HA and $\overset{+}{R}NH_3\cdot CR\cdot A^-$ at 478 nm, respectively; $d_{HA}=a\cdot\varepsilon_{HA}$ and $d_A=a\cdot\varepsilon_A$. On the basis of the absorbance at 478 nm ($=d$) concentrations of HA and $\overset{+}{R}NH_3\cdot CR\cdot A^-$ are given by $x=(d-d_{HA})(\varepsilon_A-\varepsilon_{HA})^{-1}$ and $(a-x)=(d-d_A)(\varepsilon_{HA}-\varepsilon_A)^{-1}$. Substitution of the values of x and $(a-x)$ into Eq. 4 leads to Eq. 5.

$$\frac{d-d_{HA}}{d_A-d} = K\cdot\left(b-\frac{d-d_{HA}}{\varepsilon_A-\varepsilon_{HA}}\right)\cdot\left(c-\frac{d-d_{HA}}{\varepsilon_A-\varepsilon_{HA}}\right) \qquad (5)$$

A plot of $(d-d_{HA})(d_A-d)^{-1}$ *vs.* $[b-(d-d_{HA})(\varepsilon_A-\varepsilon_{HA})^{-1}]\times[c-(d-d_{HA})\times(\varepsilon_A-\varepsilon_{HA})^{-1}]$ gives a straight line, and hence K can be obtained from its slope. Figure 3 shows the validity of this method. Initial concentrations of HA and RNH$_2$ used were 3×10^{-5} and 7.5×10^{-4} mol/dm^3, respectively.

References

1) Part IV: K. Kikukawa, S. Takamura, H. Hirayama, H. Namiki, F. Wada, and T. Matsuda, *Chem. Lett.*, **1980**, 511.
2) a) D. J. Cram and J. M. Cram, *Science*, **183**, 803 (1974). b) D. J. Cram, R. C. Helgeson, L. R. Sousa, J. M. Timko, N. Newcomb, P. Moreau, F. Dejong, G. W. Gokel, L. A. Domeir, S. O. Peacock, M. Madan, and I. Kaplan, *Pure Appl. Chem.*, **43**, 327 (1975).
3) F. Wada, R. Ishihara, Y. Kamohara, and T. Matsuda, *Bull. Chem. Soc. Jpn.*, **52**, 2959 (1979).
4) R. Stewart and J. P. O'Donnell, *J. Am. Chem. Soc.*, **84**, 493 (1962).
5) F. Wada, R. Arata, T. Goto, K. Kikukawa, and T. Matsuda, *Bull. Chem. Soc. Jpn.* **53**, 2061 (1980).
6) M. Hiraoka, "Kuraun Kagōbutsu," Kōdan-sha, Tokyo (1978), Chap. 3, pp. 121—125.
7) E. Shchori and J. Jagur-Grodzinski, *J. Am. Chem. Soc.*, **94**, 7957 (1972).
8) C. J. Pedersen, *J. Am. Chem. Soc.*, **89**, 2495 (1967).
9) E. Hertel and M. Schinzel, *Ztschr. Elektrochem.*, **45**, 51 (1939).
10) T. L. Davis and A. A. Ashdown, *J. Am. Chem. Soc.*, **46**, 1051 (1924).
11) N. L. Drake, R. A. Hayes, J. A. Garman, R. B. Johnson, G. W. Kelley, S. Melamed, and R. M. Peck, *J. Am. Chem. Soc.*, **71**, 455 (1949).

Photoinduced Intramolecular Aromatic Nucleophilic Substitution (the Photo-Smiles Rearrangement) in Amino Ethers[1]

Kiyoshi MUTAI* and Keiji KOBAYASHI

Department of Chemistry, College of General Education, The University of Tokyo, Komaba, Meguro-ku, Tokyo 153

(Received May 20, 1980)

Intramolecular rearrangement was induced by light as well as base in a homologous series of 1-(*p*-nitrophenoxy)-ω-anilinoalkanes, p-$O_2NC_6H_4O(CH_2)_nNHPh$(n=2—5), yielding *N*-(*p*-nitrophenyl)-ω-anilino-1-alkanols, p-$O_2NC_6H_4N(Ph)(CH_2)_nOH$. The reaction rate in acetonitrile showed abnormal order, $n=4>5>3>2$, which was reversed by the addition of triethylamine. The mechanism of this photorearrangement through a radical ion pair and a spiro type Meisenheimer complex was proposed. The anomaly in the reaction rate order was discussed on the basis of this mechanism.

The intramolecular nucleophilic aromatic substitution is generally called the Smiles rearrangement,[2] which is in most cases induced by base. The reaction of the same type induced by light may be called the photo-Smiles rearrangement. A homologous series of 1-(*p*-nitrophenoxy)-ω-anilinoalkane (**1**) gave *N*-(*p*-nitrophenyl)-ω-anilino-1-alkanol (**2**) on irradiation of light (>300 nm). The product **2** was also obtained by the reaction with strong base such as sodium hydride or sodium ethoxide, undoubtedly through nucleophilic attack of the corresponding anilide type anion at the ring carbon atom attached to the ether oxygen, followed by formation of a Meisenheimer type complex. Thus the photorearrangement of **1** to **2** is a photo-Smiles rearrangement.

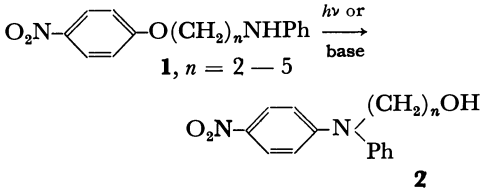

There is only one precedent[3] for this type of photorearrangement so far as we know. We report here the effects of the chain length in **1** on reaction kinetics and some mechanistic aspects of this photoreaction.

Results and Discussion

Photorearrangement. Solutions of a homologous series of **1** are almost colorless, but become yellow when irradiated with a high-pressure Hg lamp. As an example, the change of the ultraviolet-visible region of the spectrum of p-$ON_2C_6H_4O(CH_2)_4NHPh$ (**1**, n=4) in acetonitrile is shown in Fig. 1. The spectral maximum at *ca.* 305 nm, characteristic of *p*-nitrophenoxyl group, disappears with time and a new peak appears at *ca.* 395 nm. This photoreaction was observed in polar solvents such as acetonitrile, alcohols, and tetrahydrofuran, but not in cyclohexane or hexane.

The structure of the products (**2**) was confirmed by spectral and elemental analysis. Their spectral features agreed well with those of the rearranged products obtained by base-induced reaction.[4] One of the most striking characteristics is the absorption peak at *ca.* 395 nm suggesting the presence of nitroaniline type chromophore. As seen in Fig. 1, the increase of the

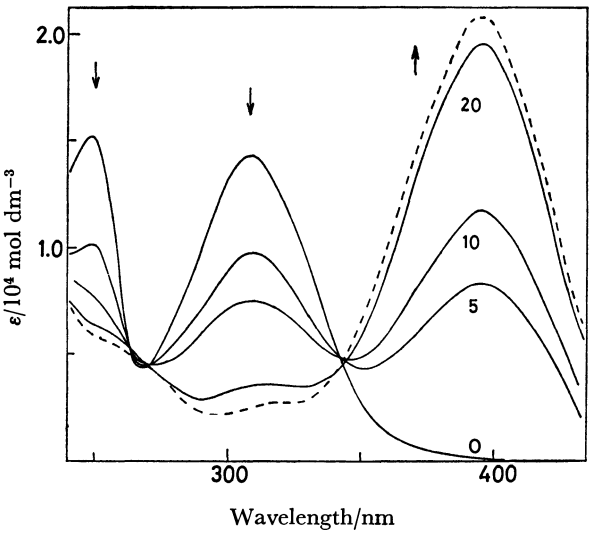

Fig. 1. Absorption spectra of p-$O_2NC_6H_4O(CH_2)_4NHPh$ in acetonitrile (0.8×10^{-4} mol/dm^3), irradiated with a high-pressure Hg lamp. Numerals attached to the curves denote time of irradiation in min. The curve in broken line is the absorption spectrum of the product.

product (**2**, n=4) can be easily followed with ultraviolet spectroscopy. It also shows isosbestic points, suggesting one-to-one correspondent conversion of **1** to **2**. Since the starting materials showed no appreciable absorption at visible region, the reaction rate was determined simply by the measurement of the time dependence of the intensity at *ca.* 395 nm. Close examination of the Fig. 1 shows that the absorption curves irradiated for a long time deviate slightly from the isosbestic points. This phenomenon is due to the formation of polymeric substances probably produced by the photodecomposition of **2**.

In order to avoid the further reaction of **2** which absorbs mainly at longer wavelength region (>330 nm), a filter of an aqueous $NiSO_4$ solution as well as Pyrex was used as the standard conditions for the determination of the rate constants.[5] Employing acetonitrile as representing aprotic solvent, the photoreaction rates were determined and the relative rate constants (first order reaction) are summarized in Table 1. These are relative values because they are variable with photolysis conditions such as concentration of the solution, intensity of the light, form of the reaction vessel, *etc.*

Table 1. Relative initial rate constants (k_{rel}) for the photorearrangement of **1** in CH_3CN

	n=2	3	4	5
k^0_{rel} a)	1.0	2.0	420	120
k^{TEA}_{rel} a,b)	710	400	110	8.6
k^{TEA}_{rel}/k^0_{rel}	710	200	0.25	0.072

a) $k^0_{rel}(n=2)=1.0$. b) Values in the presence of triethylamine (2.84×10^{-2} mol/dm^3).

A notable fact in Table 1 is low reactivity of the lower homologs (n=2 and 3) in comparison with the higher ones. It is generally accepted that lower homologs are favored (*i.e.*, react faster or give products in higher yields) in intramolecular reaction. In fact, the Smiles rearrangement of **1** in the presence of sodium hydride in DMF showed the rate order, $n=2\gg3>4>5$.[4] The anomaly in the photoreaction is closely connected with the reaction mechanism and will be discussed in the later part of this paper.

Addition of triethylamine or pyridine to the solution accelerated the reaction remarkably. The amines are weak bases unable to catalyze the rearrangement of **1** in the dark. The results for triethylamine are summarized in Table 1. The resulting reactivity order with regard to n is the same as that observed in the base-catalyzed reaction. In the third row of Table 1, the ratios of the rate constants in the presence *vs.* in the absence of the amine are shown. The rate increase in the lower homologs is in the order of 10^2, but the higher homologs showed a slight decrease. This rather unexpected behavior of the higher homologs is a result of a concomitant photoreaction of **1** with the added amine. The electronic spectrum of the solution containing triethylamine showed a new peak at *ca.* 290 nm in addition to those of **2** on irradiation. This side reaction, which apparently retarded the rate, was also observed in the lower homologs but to a far less extent. Since irradiation under the same conditions of an acetonitrile solution of *p*-nitrophenetole containing the amine induced a similar spectroscopic behavior, the side reaction observed in **1** is probably due to a reaction between *p*-nitrophenoxyl moiety and triethylamine whose photoreductive capability is well known.[6]

In order to see the effect of protic solvent, the rate constants in methanol were determined and summarized in Table 2.

Table 2. Relative initial rate constants (k_{rel}) for the photorearrangement of **1** in CH_3OH

	n=2	3	4
k_{rel} a)	1.0	0.5	1.0
k^{TEA}_{rel} a,b)	75	30	4.0
k^{TEA}_{rel}/k_{rel}	75	60	4.0

a) $k_{rel}(n=2)=1.0$. b) Values in the presence of triethylamine (2.84×10^{-2} mol/dm^3).

It is interesting that there is little difference in the rate of three homologs studied, though considering the distance of the two reacting centers, the rate of n=4 should be regarded still as unusually large. Comparison of the absolute values of k^0 in methanol with those in acetonitrile shows acceleration by a factor of 10 and 2 in methanol for n=2 and 3, respectively, and reduction by 0.02 for n=4. The observed rate acceleration may be due to the destruction of intramolecular N-H···O hydrogen bond which is present in these lower homologs[7] and arranges the molecule in conformation with two π-electron systems far apart, unfavorable situation for exciplex formation (**3**). Different solvating

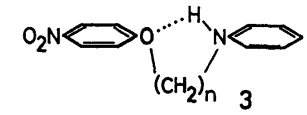

3

manner of methanol from acetonitrile for **1** in the ground and excited states and for reaction intermediates is also an important factor, though the details are yet unknown.

In the presence of triethylamine, the absolute k^{TEA}'s of the n=2 homolog in these two solvents are nearly the same, implying the upper limit of the reaction rate of this homolog. The smaller accelerating effect of the base in n=3 (one order less than in acetonitrile) may be due to lower activity of triethylamine in this protic solvent. It is notable that a small but definite rate acceleration by the amine is observed for the n=4 homolog. In contrast to the reaction in acetonitrile, no reaction of **1** with the amine was observed in methanol.

Some Mechanistic Aspects. The effect of the amine suggests ionic character of the photoreaction. The most probable ionic process is abstraction of the N-H proton by the amine, thus producing an anilide type anion, *p*-$O_2NC_6H_4O(CH_2)_n\overset{\ominus}{N}Ph$, which then takes the same course as in the Smiles rearrangement. The same reactivity order with regard to n in both cases supports this possibility. The key step in this mechanism is the increase of the acidity of the N-H group on absorption of ultraviolet light. There are two possibilities: (i) The acidity of the anilino moiety increases on excitation[1] as is the case in naphthylamine[8] and phenols;[9] (ii) Intramolecular exciplex or excited state of intramolecular charge-transfer interaction may facilitate proton release from the N-H group. Of these, the mechanism (ii) has been proved to be valid by Yokoyama *et al.*[10] They confirmed the presence of a radical ion pair (**4**)

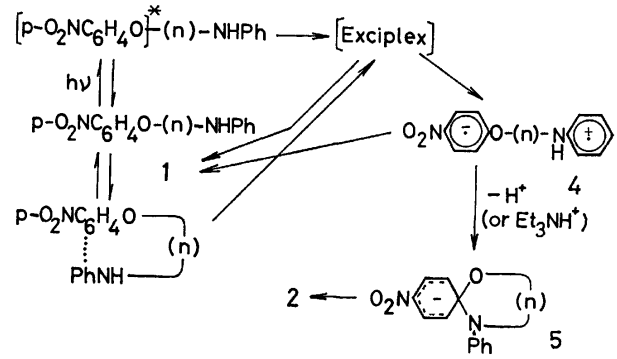

Fig. 2. Photolysis mechanism of **1**, where (n) denotes $(CH_2)_n$ group.

and a spiro type Meisenheimer complex (**5**) by means of time dependent transient absorption spectral measurement of solutions irradiated with N_2-laser pulse. Therefore a probable photorearrangement mechanism is as depicted in Fig. 2.

One of the possible processes which lead to the ion pair may start with the excitation of the *p*-nitrophenoxyl chromophore absorbing at *ca.* 305 nm, followed by formation of an intramolecular exciplex. Another one leading to a similar exciplex may be the excitation of the molecule in the state of intramolecular charge-transfer interaction.[11] Since the charge-transfer interaction in the ground state is very weak, the ionic character of the exciplex is large and the electron transfer to form the radical ion-pair (**4**) is probably a smooth process. In the step following the exciplex formation, an electron from the anilino group in **1** is transferred to the nitrophenoxyl group, and the resulting radical cation moiety has an N–H group with sufficiently strong acidity to release its proton. Here, the role of triethylamine is evident, because the basicity of the amine is far stronger than acetonitrile. The failure of the photo-Smiles rearrangement in cyclohexane or hexane is also apparent, as these solvents are poor acceptors of proton and have meager solvating power for ions. In fact, the formation of the ion pair (**4**) has not been detected in these solvents.[10]

There remains a question why the reactivity of the lower homologs in acetonitrile is abnormally low in the absence of bases. The anomaly is in the lower homologs (n=2 and 3), and not in the higher ones (n=4 and 5). Since the process subsequent to the release of the N–H proton should be the same as the Smiles rearrangement, the step where the reaction rates in question are mainly determined is after the excitation of **1** and before the proton release. Therefore, the factors governing the reactivity may be concerned with the fate of excited chromophores and/or of the radical ion pair.

It should be mentioned here that the lifetimes of the ion pair, **4**, for n=2, 3, and 4 are 65, 73, and 98 ns, respectively.[10] Similar effect of chain length on the process of intramolecular fluorescence quenching has been reported.[12] Since the electron return process and conformational change to form a sandwich type form is far faster than proton transfer,[13] the reason of the low reactivity in the absence of the amine is probably due to the presence of effective quenching routes for the ion pairs of the homologs with short chain length.

Experimental

Reaction Kinetics of Photolysis. A 200-cm^3 solution was irradiated with a 100 W high-pressure Hg lamp equipped with a Pyrex cooling jacket, through which a solution of nickel sulfate (500 g $NiSO_4$/dm^3 aqueous solution) was passed. The lamp was immersed in a vessel containing the solution of $0.8—0.9\times10^{-4}$ mol/dm^3. For the determination of the reaction rate, the solution was circulated through a flow-cell set in a Hitachi 100-50 spectrophotometer. Time dependence of the increase of the characteristic absorbance of the product at *ca.* 395 nm was recorded and the initial rate constant calculated, assuming first-order reaction.

Solvents. Acetonitrile (Wako, G. R. grade) was distilled from the mixture with phosphorus pentaoxide (5 g/dm^3 CH_3CN). Methanol (Wako, G. R. grade) was used after distillation.

Preparation of 2. General Procedure: A 250-cm^3 acetonitrile solution containing *ca.* 50 mg of **1**[10] is irradiated with a 100 W high-pressure Hg lamp through Pyrex and aqueous $NiSO_4$ filters. For the solutions of n=2 and 3 homologs of **1**, 2 cm^3 of triethylamine was added. After removing the solvent, the residue was dissolved in dichloromethane, and the solution was passed through a column packed with silica gel using benzene–dichloromethane (1 : 1) and dichloromethane as eluents.

N-*(p-Nitrophenyl)-2-anilinoethanol (2, n=2)*: This compound was obtained in 87% isolated yield as dark red liquid; 3,5-dinitrobenzoate, mp 172—173 °C; UV_{max} (95% EtOH), 392 nm (ε 19200); NMR ($CDCl_3$) δ=2.72 (1H s, OH), 3.8 (4H, m, CH_2CH_2), 6.57 and 7.82 (4H, two d, J=9 Hz, *p*-$O_2NC_6H_4$), and 7.2 (5H, m, C_6H_5); MS (70 eV), *m/e* 258 (M^+), 227 ($O_2NC_6H_4(Ph)NCH_2^+$), and 181 (227−NO_2).

Found: C, 64.97; H, 5.43; N, 10.68%. Calcd for $C_{14}H_{14}N_2O_3$: C, 65.10; H, 5.46; N, 10.85%.

N-*(p-Nitrophenyl)-3-anilino-1-propanol (2, n=3)*: This compound was obtained in 74% isolated yield as red liquid, 3,5-dinitrobenzoate, mp 124—125 °C; UV_{max} (95% EtOH), 391 nm (ε 18900); NMR ($CDCl_3$)δ=1.94 (2H, m, C-CH_2-C), 2.91 (1H, s, OH), 3.71 and 3.88 (4H, two t, NCH_2 and OCH_2), 6.57 and 7.87 (4H, two d, J=9 Hz, *p*-$O_2NC_6H_4$), and 7.2 (5H, m, C_6H_5); MS (70 eV), *m/e*, 272 (M^+), 227, and 181.

Found: C, 66.27; H, 5.84; N, 10.37%. Calcd for $C_{15}H_{16}N_2O_3$: C, 66.15; H, 5.92; N, 10.29%.

N-*(p-Nitrophenyl)-4-anilino-1-butanol (2, n=4)*: This compound was obtained in 82% isolated yield as yellow needles: mp 75—76 °C; UV_{max} (95% EtOH), 391 nm (ε 19400); NMR ($CDCl_3$) δ=1.7 (5H, m, C-CH_2-CH_2-C and OH), 3.7 (4H, m, NCH_2 and OCH_2), 6.50 and 7.87 (4H, two d, J=9 Hz, *p*-$O_2NC_6H_4$), and 7.2 (5H, m, C_6H_5); MS (70 eV), *m/e*, 286 (M^+), 227, and 181.

Found: C, 67.27; H, 6.43; N, 9.59%. Calcd for $C_{16}H_{18}N_2O_3$: C, 67.11; H, 6.34; N, 9.78%.

N-*(p-Nitrophenyl)-5-anilino-1-pentanol (2, n=5)*: This compound was obtained in 61% isolated yield as dark red liquid; UV_{max} (95% EtOH), 389 nm (ε 19400); NMR ($CDCl_3$) δ= 1.55 (7H, m, C-CH_2-CH_2-CH_2-C and OH), 3.8 (4H, m, NCH_2 and OCH_2), 6.79 and 8.28 (4H, two d, J=10 Hz, *p*-$O_2NC_6H_4$), and 7.5 (5H, m, C_6H_5); MS (70 eV), *m/e*, 300 (M^+), 227, and 181.

Found: C, 67.74; H, 6.93; N, 9.42%. Calcd for $C_{17}H_{20}N_2O_3$: C, 67.98; H, 6.71; N, 9.33%.

The authors wish to express their thanks to Dr. Kenji Yokoyama of Institute of Physical and Chemical Research for helpful discussion. The present work was partially supported by a Grant-in-Aid for Scientific Research No. 254153 from the Ministry of Education, Science and Culture.

References

1) Preliminary communication: K. Mutai, S. Kanno, and K. Kobayashi, *Tetrahedron Lett.*, **1978**, 1273.

2) a) W. E. Truce, E. M. Kreider, and W. W. Brand, *Org. React.*, **18**, 99 (1970); b) H. J. Shine, "Aromatic Rearrangements," Elsevier, New York, N. Y. (1967), p. 307; c) M. S. Newman, *Acc. Chem. Res.*, **5**, 354 (1972).

3) K. Matsui, N. Maeno, S. Suzuki, H. Shizuka, and T. Morita, *Tetrahedron Lett.*, **1970**, 1467.

4) K. Mutai and K. Kobayashi, unpublished work. The

lowest homolog studied (**2**, $n=2$) has been reported by Kleb as the double Smiles rearrangement product of *N*-(2-hydroxyethyl)-*p*-nitrobenzenesulfonamide; K. G. Kleb, *Angew. Chem. Int. Ed. Engl.*, **7**, 291 (1968). See also, A. C. Knipe, N. Sridhar, and J. Lound-Keast, *Tetrahedron Lett.*, **1979**, 2541.

5) Though the term, rate constant, is generally used for an elementary reaction in photochemistry, the words used here are for the velocity of the formation of the product, as employed in organic reactions.

6) a) M. Ohashi, *Kagaku No Ryoiki*, **32**, 56 (1978); b) D. Döpp, D. Müller, and K.-H. Sailer, *Tetrahedron Lett.*, **1974**, 2137.

7) M. Ōki and K. Mutai, *Spectrochim. Acta, Part A*, **25**, 1941 (1969).

8) a) Th. Förster, *Z. Elektrochem.*, **54**, 42 and 531 (1950); b) G. Jackson and G. Porter, *Proc. R. Soc. London, Ser. A*, **260**, 13 (1961).

9) a) Ref. 8a; b) A. Weller, *Discuss. Faraday Soc.*, **27**, 28 (1959); c) N. Mataga and Y. Kaifu, *Mol. Phys.*, **7**, 137 (1964); d) H. Beens, K. H. Greelmann, M. Gurr, and A. H. Weller, *Discuss. Faraday Soc.*, **39**, 183 (1965).

10) K. Yokoyama, R. Nakagaki, J. Nakamura, K. Mutai, and S. Nagakura, *Bull. Chem. Soc. Jpn.*, **53**, 2472 (1980).

11) K. Mutai, *Tetrahedron Lett.*, **1971**, 1125.

12) Y. Hatano, M. Yamamoto, and Y. Nishijima, *J. Phys. Chem.*, **82**, 367 (1978).

13) a) J. Hinatsu, H. Masuhara, N. Mataga, Y. Sakata, and S. Misumi, *Bull. Chem. Soc. Jpn.*, **51**, 1032 (1978); b) M. Migita, M. Kawai, N. Mataga, Y. Sakata, and S. Misumi, *Chem. Phys. Lett.*, **53**, 67 (1978).

Hydration of Aza-aromatic Aldehydes. II. Solvent Effect on the Equilibrium Constants of the Hydration

Kazuhisa ABE, Hiroko ENDO, and Minoru HIROTA*

Department of Applied Chemistry, Faculty of Engineering, Yokohama National University, Hodogaya-ku, Yokohama 240

(Received May 24, 1980)

The equilibrium constants for the hydration reaction of 4-pyridinecarbaldehyde were determined in several solvents by ^{1}H-NMR spectroscopic measurements. The hydration reactions were sensitive to the nature of the solvents. In strong donor solvents such as hexamethylphosphoric triamide, pyridine, and dimethyl sulfoxide, formation of the hydrate is far more favorable than in water or other poor donor solvents. Thus the stabilization of the product by hydrogen bond formation is assumed to favor the reaction. Polarity of the solvent alone does not explain the solvent effect, even if it is supposed to affect the equilibria secondarily.

The hydration reaction to form geminal diols is known on several aliphatic aldehydes carrying electronegative groups.[1-5] The present authors have reported in a previous paper[6] that the corresponding geminal diols were produced when the six-membered aza-aromatic aldehydes carrying a formyl group at 2 or 4-position were submitted to the reaction with water. The enthalpies of hydration were determined from the temperature dependence of their ^{1}H-NMR spectra. In this report, equilibrium constants (K) of the hydration of 4-pyridinecarbaldehyde (given by Eq. 1) were determined in several organic solvents by means of ^{1}H-NMR spectroscopy.[7] The advantage of NMR

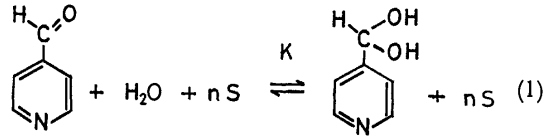

(1)

spectroscopy in the determination of free and hydrated species of aldehydes in mixtures has been described by several authors.[8-12] In the case of 4-pyridinecarbaldehyde, it is possible to observe two sets of resonance lines assigned to the hydrated and the free species in its ^{1}H-NMR spectrum.[6] The methine proton signal of the hydrated species appears at *ca.* 4 ppm upfield relative to the formyl proton signal of the unhydrated species. Similarly, ring proton signals of the hydrated species shift *ca.* 0.5 ppm upfield relative to those of the unhydrated species.

The hydration of aza-aromatic aldehydes is an addition reaction initiated by the nucleophilic attack of water molecule on the positively-charged carbonyl carbon atom. In an aldehyde–water–solvent ternary system, the hydration reaction is supposed to be affected considerably by the nature of solvent because of the difference in polarity and in hydrogen-acceptability, or electron-donability, in hydrogen bond formation. Thus the equilibrium constants were determined in various solvents and with various proportions of reactant system in order to study the specific interaction between the solvent and the solute molecules, and to elucidate how the solvent participates in the reaction mechanism.

Experimental

Preparation of Materials. 4-Pyridinecarbaldehyde was distilled prior to use. Deuterium oxide was used as the nucleophilic reagent in place of H_2O in most runs. No remarkable difference in equilibrium constant was observed in comparison with the results using H_2O.[13] Deuterated solvents were used without further purification. Other solvents were purified by the usual procedures.

Measurement of ^{1}H-NMR Spectra. ^{1}H-NMR experiments were performed with a JEOL JNM C-60H NMR spectrometer. In cases of very dilute solutions, the spectra were measured with a JEOL JNM FX-60 or an FX-100 NMR spectrometer, accumulations carried out hereby in order to get a high signal-to-noise ratios. Equilibrium constants of the hydration in various solvents were determined from the ratios of integrated intensities of the free and the hydrated species of the aldehyde. The relative integrated intensity was obtained as a mean of the observed values by several (at least 3) times of scans in the integration mode. Chemical shifts are given in terms of part per million (ppm) downfield from TMS. The probe temperature was kept at 34.5 °C in all measurements except otherwise stated.

Table 1. The enthalpy of hydrogen bond formation between 4-(hydroxymethyl)pyridine and dimethyl sulfoxide

$C=4.42\times10^{-3}$ mol/l $H=21.1$ KJ/mol

T/K	ε_f/l mol^{-1} cm^{-1}	ε_h/l mol^{-1} cm^{-1}
292.5	39.5	58.5
297.7	40.6	52.7
303.7	42.5	46.5
309.3	44.8	41.4
316.2	46.1	35.1

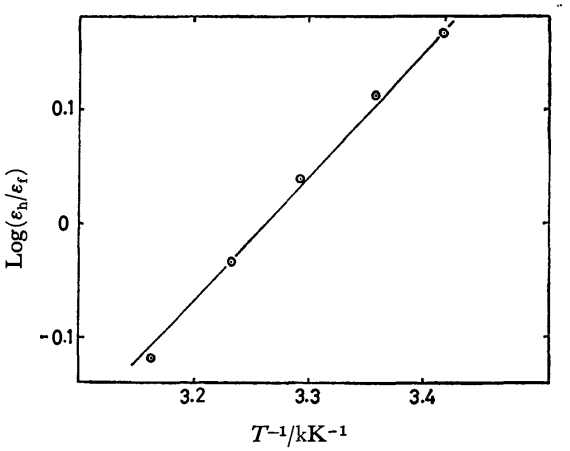

Fig. 1. The log ($\varepsilon_h/\varepsilon_f$) *vs.* $1/T$ of 4-(hydroxymethyl)-pyridine–dimethyl sulfoxide hydrogen bond system.

Determination of $\Delta\nu_{OD}$ and the Enthalpy of Hydrogen Bond Formation by Infrared Spectroscopic Measurements. Infrared O–D stretching absorptions of methanol-*d* were measured with a Hitachi Model 225 grating infrared spectrometer. The reference O–D absorption in benzene was also measured under the same conditions.

The enthalpy of hydrogen bond formation of 4-(hydroxymethyl)pyridine was obtained by measuring the O–H absorption intensities of free and hydrogen-bonded species (ε_f and ε_h, respectively) at several temperatures. The slope and the abscissa of the ($\varepsilon_h/\varepsilon_f$) *vs.* $1/T$ plot gave the enthalpy and the entropy, respectively. The results are given in Table 1 and Fig. 1.

Results and Discussion

Formation Constants of the Hydrate in Several Organic Solvents. Equilibrium constants of the hydration in various solvents are given together with some indices for the solvent polarity and the hydrogen acceptability in Table 2. The $\Delta\nu_D$ value is defined as the solvent induced shift (in cm^{-1}) of the O–D stretching band of methanol-*d* (CH_3OD) in a solvent with reference to that in benzene (2688 cm^{-1}) and used as a measure for the electron donating power of solvent. Most $\Delta\nu_D$ values were cited from reference,[14] some of them being determined in the present investigation. From the above definition, the $\Delta\nu_D$ value increases with the increasing order of the electron donating power in the hydrogen bond formation. The log K *vs.* $\Delta\nu_D$ plot gives a straight line with $r=0.982$ representing a very good linear relation. A good correlation is also observed between ln K and the donor number (Dn) defined by Gutaman ($r=0.984$).[15] From the results, it is supposed that strong donor solvents facilitate hydrogen bond formation of the produced geminal diol with water, playing an important role in the hydration reaction.

In the reactant system (consisting of the aldehyde, water, and solvent), water molecules form hydrogen bonds with solvent molecules preferably when the solvent is a stronger donor than water. This is estimated from the hydrogen bond energies obtained by NMR and infrared spectroscopic measurements.[16,17] Thus the energy of formation of water–dimethyl sulfoxide hydrogen bond (4.6 kcal/mol) is shown to be larger than that for the self-association of water (4.4 kcal/mol). The water–solvent hydrogen bond stabilizes the aldehyde, disfavoring the formation of geminal diol in the equilibrium. The strong hydrogen bond between the solvent and water molecules tends to destroy the cluster structure of liquid water by breaking the O–H···O hydrogen bond constructing the structure. The destruction of the cluster is especially remarkable in the range of larger mole fractions of the strongly donable solvents, being proved by the measurement of neutron inelastic scattering and X-ray diffraction studies.[18] Hydrogen bond formation between the carbonyl oxygen atom and water is also possible in the reactant system. However the hydrogen bond of this type is supposed to be a little weaker than the O–H···O hydrogen bond in water-donable solvent and the O–H···N hydrogen bond in water–aza-aromatic aldehyde pairs, the difference in the enthaplies of hydrogen bond formations being very small in these two cases. Hence this interaction might affect less remarkably the equilibrium of the hydration reaction.

Similar stabilization may occur in the product system consisting of the geminal diol, water, and the solvent. Contrary to the case of reactant system, the stabilization by forming hydrogen bonds will favor the hydration reaction. As the geminal diol has two O–H functions, it can attain considerably large stabilization in strong donor solvents. In order to estimate the energies of hydrogen bond formation in the product system, 4-(hydroxymethyl)pyridine was used as a model compound and the enthalpy of association with dimethyl sulfoxide was determined by the infrared spectroscopic method. Ternary 4-(hydroxymethyl)pyridine–dimethyl sulfoxide–carbon tetrachloride system shows two O–H absorptions at 3637 and 3380 cm^{-1}, which are assigned to the free and the hydrogen-bonded species, respectively. Then the temperature dependence measurement of their intensities gives the enthalpy of hydrogen bond formation to be 5.03 kcal/mol. As 4-(hydroxymethyl)-pyridine has a similar structure to the geminal diol and the additional α-hydroxyl group is expected to favor the hydrogen bond by its electronic effect, the hydrogen bond in the geminal diol is assumed to be stronger than that in the reactant. The geminal diol can exist as the two types of associated species given by (A) and (B).

Table 2. Thermodynamic quantities for the hydration of 4-pyridinecarbaldehyde in several organic solvents

Solvent	K(34.5 °C)	δ:ppm (formyl proton) aldehyde	*gem*-diol	ΔH / K J mol^{-1}	ΔS / J mol^{-1} K^{-1}	ε	$\Delta\nu_D$ / cm^{-1}	D_n
HMPA	4.26×10^{-2}	10.25	5.98	−23.1	−102	30.0	177	38.8
Pyridine-d_5	3.76×10^{-2}	10.21	6.41	−24.3	−107	12.1	168	33.1
DMSO-d_6	3.16×10^{-2}	10.18	6.03	−21.7	−99	45.0	141	29.8
DMF	2.27×10^{-2}	10.21	6.03	−22.6	−104	36.1	107	26.6
Dioxane	2.04×10^{-2}	10.22	5.95			2.2	77	
Acetone-d_6	1.75×10^{-2}	10.08	6.05	−14.7	−82	20.7	64	17.0
D_2O	1.62×10^{-2}			−25.8	−118	81.0		18.0
Acetonitrile-d_3	1.32×10^{-2}	10.20	5.96	−10.2	−69	38.0	49	14.1

HMPA: Hexamethylphosphoric triamide, DMSO: Dimethyl sulfoxide, DMF: *N*,*N*-Dimethylformamide.

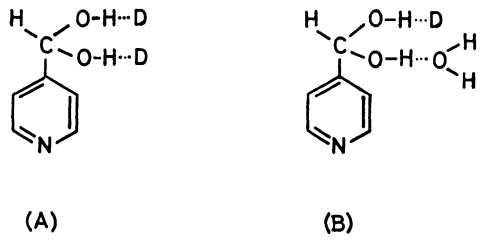

(A) (B)

The second hydrogen bonds in these species might be a little weaker. Thus, the stabilization caused by the hydrogen bond in the 1 : 2 associated species, (A) or (B), is expected to overcome that in the reactant system.

The solvent polarity can be another factor which controls the hydration reaction. If a polar molecule (dipole moment μ, radius r) is transferred from the vaccum ($\varepsilon=1$) to a medium of which dielectric constant is ε, the energy change ($\Delta\Delta G$) is given by the Kirkwood Eq. 2.

$$\Delta\Delta G = -\frac{\mu^2}{r^3}\frac{\varepsilon-1}{2\varepsilon+1} \qquad (2)$$

Therefore, the contribution of the solvent polarity to $\Delta G°$(hydration) should be proportional to $(\varepsilon-1)/(2\varepsilon+1)$. In practice, no definite correlation is observed between log K and $(\varepsilon-1)/(2\varepsilon+1)$, implying that the polar effect of solvent is not a predominant factor to affect the equilibrium of hydration. However, by comparison of the results in deuterium oxide with those in acetonitrile-d_3 and acetone-d_6 it is probable that the polarity of solvent favors the hydration secondarily. Since acetone and acetonitrile are less donable than water, effect of the polarity which is masked by the effect of hydrogen bonding in cases of more strongly donable solvents becomes apparent in cases of acetone and acetonitrile solutions.

Influence of the Composition of Reaction Medium on the Equilibrium Constant. In the experiments discussed above, the mole fractions (x) of the solvents were kept approximately 0.30, which is the most convenient concentration to observe NMR signals of the hydrated and the unhydrated species accurately. However, the eqilibrium constant (K) is dependent upon the composition of the reaction medium, *i.e.* the mole fractions of the components. Thus the equilibrium constants were determined as a function of the mole fraction of solvent in the ternary aldehyde–water–solvent mixture. Results are given in Table 3 and Fig. 2. The solvents can be classified into two groups from the shape of their concentration *vs.* log K plots. The first group consists of strongly donable solvents such as hexamethylphosphoric triamide, pyridine, and dimethyl sulfoxide. The other consists of less donable solvents such as acetone and acetonitrile. In a solvent more donable than water, K increases almost linearly with the mole fraction of solvent in the region of $x \lesssim ca.$ 0.5. This phenomenon is explained by the formation of stronger hydrogen

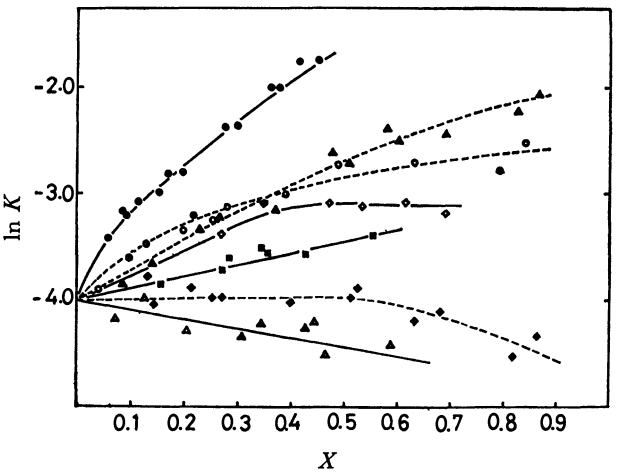

Fig. 2. The dependence of equilibrium constant K values on the mole fraction (X) of solvent molecule.
—●—: Hexamethylphosphoric triamide, —▲—: pyridine-d_5, —○—: dimethyl-d_6 sulfoxide, —◇—: *N,N*-dimethylformamide, —■—: dioxane, —◆—: acetone-d_6, —△—: acetonitrile-d_3.

Table 3. Equilibrium constants (K) in several solvents with various mole fractions (X) of solvents

HMPA		Pyridine		DMSO		DMF		Dioxane		Acetone		Acetonitrile	
X	ln$K$	X	ln$K$	X	ln$K$	X	ln$K$	X	ln$K$	X	ln$K$	X	ln$K$
0.060	−3.420	0.084	−3.860	0.038	−3.869	0.131	−3.785	0.213	−3.893	0.141	−4.045	0.074	−4.195
0.085	−3.170	0.137	−3.637	0.097	−3.592	0.274	−3.378	0.272	−3.719	0.255	−3.976	0.127	−3.983
0.090	−3.212	0.229	−3.431	0.126	−3.439	0.354	−3.069	0.284	−3.598	0.270	−3.913	0.202	−4.310
0.115	−3.080	0.262	−3.232	0.204	−3.329	0.474	−3.080	0.347	−3.516	0.402	−4.049	0.294	−4.442
0.155	−2.946	0.374	−3.150	0.217	−3.201	0.534	−3.120	0.357	−3.562	0.512	−3.904	0.309	−4.343
0.172	−2.821	0.477	−2.623	0.257	−3.272	0.618	−3.074	0.427	−3.560	0.521	−3.987	0.343	−4.236
0.199	−2.811	0.508	−2.727	0.279	−3.104	0.625	−3.434	0.553	−3.383	0.525	−3.806	0.427	−4.294
0.278	−2.373	0.581	−2.376	0.388	−3.023	0.634	−3.322			0.632	−4.195	0.443	−4.204
0.299	−2.360	0.600	−2.498	0.413	−3.170	0.694	−3.187			0.681	−4.094	0.463	−4.566
0.358	−2.276	0.641	−2.567	0.489	−2.690					0.819	−4.553	0.591	−4.422
0.365	−1.993	0.691	−2.431	0.632	−2.701					0.865	−4.334		
0.378	−1.999	0.829	−2.238	0.794	−2.778								
0.416	−1.725	0.869	−2.056	0.848	−2.492								
0.452	−1.721												

Cf. in D_2O, ln $K=-3.984$.

bond between geminal diol and solvent in the product system than those in the reactant system. As the hydrogen bonded species of the geminal diol is supposed to increase in proportion to x, K becomes larger than that in water. The increase in log K becomes gradually less when the mole fraction of donable solvent is larger than 0.5. In some instances, the log K *vs.* x plots become flat or turn to decrease in a higher mole fraction range of the solvent. In this range of mole fraction, polarity of the medium seems to be decreased in comparison with that of water, since all solvents employed in the experiments have dielectric constants lower than water (Table 2). Therefore the equilibrium of the hydration reaction is not so favorable as expected from the solvent donicity alone.

Another factor suspected to affect the equilibrium constants is the decrease of the number of the O–H···N hydrogen bonds between water and 4-pyridinecarbaldehyde molecules during the process of hydration, since one molecule of water is consumed in this process. The produced geminal diol molecule can form two hydrogen bonds alternatively. If the solvent is a stronger donor than pyridine, the effect is less predominant because O–H···D (where D refers to a donable solvent molecule) hydrogen bond might be more favorable than O–H···N hydrogen bond both in the reactant and the product systems. In case when the solvent is less donable than pyridine, the O–H(in water)···N hydrogen bond in the reactant is replaced by the O–H(in the geminal diol) ···D hydrogen bond during the hydration, disfavoring the equilibrium to a certain extent. Another O–H···N hydrogen bond can be formed by the self-association of the aza-aromatic geminal diol. However, the concentration of the aldehyde is kept to be relatively low, preventing the produced geminal diol from self-associating to a measurable extent. The former case is the reaction in hexamethylphosphoric triamide, the typical examples of the latter case being those in dimethyl sulfoxide and in *N*,*N*-dimethylformamide.

In contrast to the results in strongly donable solvents, the dependence of the equilibrium constants on x was not remarkable in several less donable solvents which does not perturb the hydrogen-bonded structure of water considerably. As shown in Fig. 2, the equilibrium constants in acetone and acetonitrile tend to decrease monotonously in the wide range of X. The lowering of K values in these solvents are due to the decrease in polarity of the solvent, because the molecules of such solvents are unable to interact strongly with water and geminal diol molecules. It is deduced from the results in these less donable solvents that the effect of polarity which is masked by the effect of hydrogen bonding in cases of strongly donable solvents will also contribute to the hydration reaction apparently.

The authors are grateful to Prof. M. Ōki, the University of Tokyo, for his generously allowing us to use the FT-NMR spectrometer. They are also grateful to Mr. M. Ohuchi, Japan Electron Optics Laboratories Ltd., for his technical assistance in the measurement of NMR spectra with a JNM-FX 100 spectrometer. This research was partly supported by a Grant-in-Aid for Special Project Research from the Ministry of Education, Science and Culture.

References

1) E. S. Stern and C. J. Timmons, "Electronic Absorption Spectroscopy in Organic Chemistry," 3rd ed, Edward Arnold Ltd., London (1970), p, 221.
2) E. Laviron and J. Tirouflet, *C. R. Acad. Sci.*, **248**, 826 (1959).
3) P. Greenzaid, Z. Luzand, and D. Samvel, *J. Am. Chem. Soc.*, **89**, 756 (1967).
4) Y. Fujiwara and S. Fujiwara, *Bull Chem. Soc. Jpn.*, **36**, 574, 1106 (1963).
5) M. L. Ahrons and H. Strehlow, *Discuss. Faraday Soc.*, **39**, 112 (1965).
6) K. Abe, M. Hirota, I. Takeuchi, and Y. Hamada, *Bull. Chem. Soc. Jpn.*, **50**, 2028 (1977).
7) S refers to a solvent molecule in Eq. 1. Hereafter, the members of the left side in Eq. 1 are called reactant system and those of the right side product system.
8) E. Lombardi and P. G. Sogo, *J. Chem. Phys.*, **32**, 635 (1960).
9) P. G. Evans, G. R. Miller, and M. M. Kreevoy, *J. Phys. Chem.*, **69**, 4325 (1965).
10) J. Hine, J. G. Houstor, and J. H. Jensen, *J. Org. Chem.*, **30**, 1184 (1965).
11) V. Gold, G. Socrates, and M. R. Crampton, *J. Chem. Soc.*, **1964**, 5888.
12) K. Moedritzer and J. R. Van Wazer, *J. Phys. Chem.*, **70**, 2025 (1966).
13) 4-Pyridinecarbaldehyde+D_2O in acetone-d_6 $K=1.75\times10^{-3}$ mol^{-1} l. 4-Pyridinecarbaldehyde+H_2O in acetone-d_6 $K=1.65\times10^{-3}$ mol^{-1} l.
14) T. Kagiya and Y. Sumida, *Bull Chem. Soc. Jpn.*, **41**, 769 (1968).
15) Viktor Gutmann, *Angew. Chem. Int. Ed. Engl.*, **9**, 843 (1970).
16) J. R. Holmes, D. Kivelson, and W. C. Drinkard, *J. Am. Chem. Soc.*, **84**, 4677 (1962).
17) G. H. Haggis, J. B. Hasted, and T. J. Buchanan, *J. Chem. Phys.*, **20**, 1452 (1952).
18) G. J. Safford, F. C. Schaffer, P. S. Leurg, G. F. Doebbler, George W. Brady, and E. F. X. Lyden, *J. Chem. Phys.*, **50**, 2140 (1969).

Synthesis of Four Stereoisomers of γ-Hydroxyarginine *via* the Corresponding Isomers of γ-Hydroxyornithine

Koichi MIZUSAKI and Satoru MAKISUMI*

Department of Chemistry, Faculty of Science, Kyushu University 33, Hakozaki, Higashi-ku, Fukuoka 812

(Received May 29, 1980)

Diastereomeric γ-hydroxy-L- and D-ornithines were prepared by reduction of the corresponding γ-oxoornithines synthesized from L- and D-histidines with sodium borohydride. The isomeric composition of the product obtained from L-histidine was estimated to be 68% *erythro* and 32% *threo* isomers and that of the product from D-histidine 65% *erythro* and 35% *threo* isomers by automatic amino acid analysis after conversion of the basic amino acids into neutral N^{δ}-acetyl derivatives. The diastereoisomers of each γ-hydroxyornithine were separated by chromatography on a Dowex 50 column, four optically active isomers being isolated as their hydrochlorides in crystalline state. Guanidination of these isomers with 1-amidino-3,5-dimethylpyrazole nitrate (ADPN) gave the corresponding optically active isomers of γ-hydroxyarginine which were isolated as crystalline hydrochlorides. *Erythro*-γ-hydroxy-L-arginine hydrochloride shows a specific rotation which agrees very closely with that of natural product of γ-hydroxyarginine.

γ-Hydroxyarginine was first isolated from the sea cucumber *Polycheira rufescens* by Fujita[1] and subsequently from the sea anemone *Anthopleura japonica* Verrill by Makisumi.[2] In plants, this amino acid has been detected in the seeds of many species of *Vicia*[3] and isolated as its lactone from the seeds of *Vicia sativa* by Bell and Tirimanna.[4] Although little is known concerning the significance of the presence of this amino acid in animals and plants, the compound is known to participate in several enzymatic reactions.[1,2,5-7] An assumption that this amino acid exists as an intermediate in the metabolic pathway of L-arginine to 2-nitroimidazole in *Streptomyces eurocidicus* has been proposed by Nakane *et al.*[8]

γ-Hydroxyarginine contains two asymmetric carbon atoms (α and γ) and should thus exist theoretically in four stereoisomeric forms. The whole configuration of the natural γ-hydroxyarginine was confirmed to be *erythro*-γ-hydroxy-L-arginine by Fujita.[9] Synthetic attempts leading to an epimeric mixture of γ-hydroxyarginine have been reported.[1,10] However, none of the optically active isomers, other than the natural product, has hitherto been isolated and characterized.

In the present study the four stereoisomers of γ-hydroxyarginine were prepared by guanidination of the corresponding isomers of γ-hydroxyornithine synthesized from optically active histidines (Scheme 1).

Results and Discussion

γ-Oxoornithine (**5**) was synthesized from optically active histidine by the method of Heath *et al.*[12] Histidine (**1**) was first converted into the methyl ester (**2**) dihydrochloride by the conventional method and then transformed into methyl 2,4,5-tribenzamido-4-pentenoate (**3**) by Bamberger cleavage.[13] α,δ-Dibenzoyl-γ-oxoornithine methyl ester (**4**) was formed on heating the tribenzoyl compound (**3**) in methanolic hydrogen chloride. Acid hydrolysis of the ester **4** with 20% hydrochloric acid afforded the keto amino acid (**5**) dihydrochloride as oily residues. Owing to the instability of the acid hydrochloride, the oily product was used for further reduction without crystallization. Treatment of the aqueous solution of **5** dihydrochloride with sodium

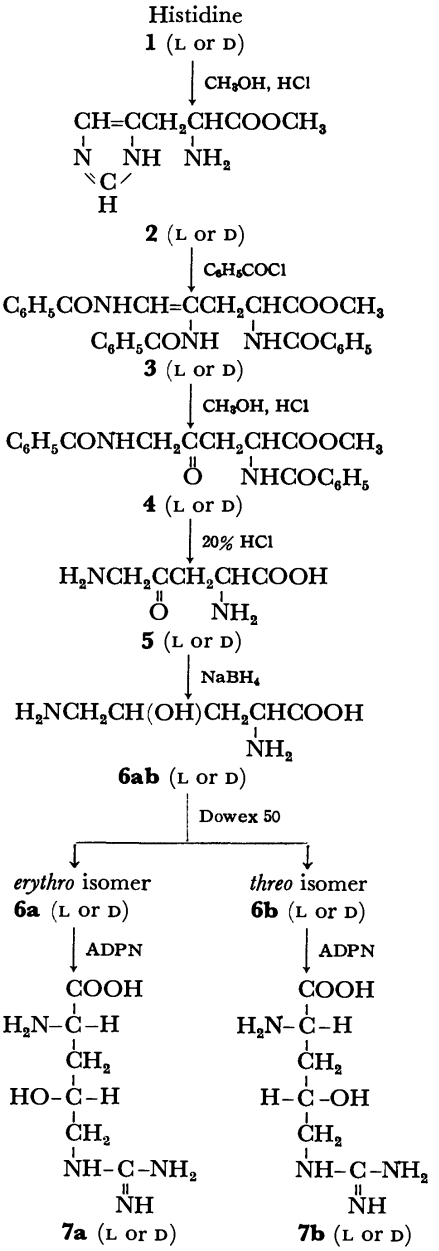

Scheme 1. Synthesis of stereoisomers of γ-hydroxyornithine (**6**) and γ-hydroxyarginine (**7**).

borohydride gave diastereoisomeric γ-hydroxyornithine (**6ab**), which was isolated as a crystalline hydrochloride. The diastereoisomeric composition of **6ab** thus obtained was estimated by amino acid analysis of its N^{δ}-acetylated derivative.[11] The amino acid L-**6ab** was composed of 68% *erythro* and 32% *threo*, the D-enantiomorph (D-**6ab**) of 65% *erythro* and 35% *threo* isomers.

Witkop and Beiler[14] pointed out the significance of their failure to esterify or reduce with sodium borohydride γ-oxo-L-ornithine and its derivatives. However, the keto amino acid **5** was hydrogenated smoothly to the hydroxy amino acid **6ab** with the same reducing agent in the present study. With regard to the racemization of α-carbon atom of **5**, no racemization took place during the course of synthesis of mercaptohistidine *via* L-**5** from L-histidine.[12,15,16] The optical purity of L-**5** obtained in this study was ascertained by the conversion of γ-hydroxy-L-ornithine (L-**6ab**) prepared from the compound L-**5** into γ-hydroxy-L-arginine and the digestion of the resulting arginine derivative with the L-directed arginase. The approach described abov seems to be useful for the synthesis of γ-hydroxyornithine which retains the configuration of α-carbon atom, starting from readily available histidine through simple and relatively high-yield operations.

Diastereoisomeric γ-hydroxyornithines (L-**6ab** and D-**6ab**) were separated into the two diastereoisomers by chromatography using a column (3.8×275 cm) of Dowex 50 (Na^+ form).[11] The separated diastereoisomers of γ-hydroxyornithine were isolated as their crystalline hydrochlorides, their stereochemical purities being ascertained by assay using an amino acid analyzer.[11] The specific rotations of natural γ-hydroxyornithine obtained enzymatically from natural γ-hydroxyarginine and the four stereoisomers obtained are given in Table 1. The value for *erythro* L-isomer attained by synthesis is close to that of natural γ-hydroxyornithine. This suggests that surprisingly little racemization or epimerization occurred during the series of reactions and, consequently, the synthetic isomers of γ-hydroxy-L-ornithine were almost optically pure.

The four stereoisomers of γ-hydroxyornithine were separately guanidinated with 1-amidino-3,5-dimethylpyrazole nitrate (ADPN) and the products, the corresponding γ-hydroxyarginines, were isolated as their hydrochlorides.[11] The data of specific rotation for natural and synthetic preparation of γ-hydroxyarginine measured in alkaline medium are given in Table 1. The value for *erythro* L-isomer agrees very closely with that for natural γ-hydroxyarginine. The specific rotations of D-antipodes are expected to be equal but opposite to those of L-antipodes. The value for *erythro* D-isomer is also in good agreement with the value expected. It is evident that the synthetic *erythro* L- and D-isomers are optically pure. On the other hand, *threo* isomers seem to be optically pure.

Table 1. Specific rotations of γ-hydroxyornithine and γ-hydroxyarginine hydrochlorides

Isomer	γ-Hdyroxyornithine hydrochloride $[\alpha]_D^{20}$ (*c* 2, H_2O)	γ-Hydroxyarginine hydrochloride $[\alpha]_D^{20}$ (*c* 1, 0.5 M NaOH)
Natural		
erythro L	+10.5°[a]	− 8.5°
Synthetic		
erythro L	+ 9.4°[b]	− 8.4°
D	− 9.8°	+ 8.5°
threo L	− 6.3°[c]	+11.0°
D	+ 6.4°	−11.0°

a) Ref. 9, $[\alpha]_D^{20}$ +10.6° (*c* 5, H_2O). b) Ref. 11, $[\alpha]_D^{20}$ +10.5° (*c* 2, H_2O). c) Ref. 11, $[\alpha]_D^{20}$ −7.0° (*c* 2, H_2O).

Two different values measured in 5 M (1 M=1 mol dm^{-3}) hydrochloric acid were reported with regard to the specific rotation of natural preparations of γ-hydroxyarginine. We also measured the specific rotation of natural γ-hydroxyarginine in 5 M hydrochloric acid, but obtained no such values as reported.[1,2] We found that the solution had at first $[\alpha]_D$ +17.6° which dropped to +7.5° in 10 min, to −5.6° in 3 h, and then remained constant. Partial transformation of γ-hydroxyarginine into a compound more basic than the original amino acid was ascertained by paper electrophoresis. The mutarotation may be ascribed to the formation of the lactone[4] of γ-hydroxyarginine. The above-cited authors[1,2] overlooked this mutarotative nature of γ-hydroxyarginine.

Experimental

All melting points are uncorrected. Amino acid analyses were carried out using a JEOL-6AS amino acid analyzer. The optical rotations were measured with a Union high sensitivity polarimeter PM-71. Paper chromatography was carried out by the ascending technique on Toyo Roshi No. 52 paper with 1-butanol–acetic acid–pyridine–water(4 : 1 : 1 : 2,v/v). Paper electrophoresis was carried out at 300 V for 2.5 h on Toyo Roshi No. 52 paper in a buffer solution of pyridine–acetic acid–water (20 : 10 : 970, v/v). Spots were made visible with ninhydrin and Sakaguchi reagents.

Methyl 2,4,5-Tribenzamido-4-pentenoate (3). Compound **3** was prepared from the ester **2**·2HCl by Bamberger cleavage[13] according to the procedure of Heath *et al.*[12] The product was recrystallized from Methyl Cellosolve. The yield of L-**3** from L-**2**·2HCl (24.1 g, 0.1 mol) was 34.3 g (73%); mp 215—216 °C.

Compound D-**3** was obtained from D-**2**·2HCl (14.5 g, 60 mmol); yield, 21.8 g (77%); mp 214—215 °C.

Found (L-**3**): C, 68.59; H, 5.33; N, 9.00%. Found (D-**3**): C, 68.54; H, 5.28; N, 8.70%. Calcd for $C_{27}H_{25}O_5N_3$: C, 68.73; H, 5.34; N, 8.91%.

α,δ-Dibenzoyl-γ-oxoornithine Methyl Ester (4). Compound **4** was obtained from the parent tribenzoyl compound **3** by boiling for 30 min with 10% methanolic hydrogen chloride.[12] Recrystallization of the crude product was performed from hot ethanol. The yield of L-**4** from L-**3** (22 g, 47 mmol) was 7.1 g (42%); mp 168—170 °C.

The yield of D-**4** from D-**3** (21.2 g, 45 mmol) was 6.5 g (40%); mp 168—170 °C.

Found (L-**4**): C, 65.01; H, 5.45; N, 7.55%. Found (D-**4**): C, 65.11; H, 5.43; N, 7.50%. Calcd for $C_{20}H_{20}O_5N_2$: C, 65.20; H, 5.47; N, 7.61%.

γ-Oxoornithine (5) Dihydrochloride. Compound **5**·2HCl was prepared from the dibenzoyl ester **4** (5.5 g, 15 mmol) by

refluxing with 20% hydrochloric acid (54 ml) for 7 h. The oily product could not be crystallized by treatment with ethanol. Paper electrophoretic analysis showed that it was almost pure. Owing to the instability of the acid dihydrochloride the oily product was used directly.

*Diastereoisomeric γ-Hydroxyornithine (**6ab**) Hydrochloride.* γ-Oxoornithine (**5**) dihydrochloride obtained as above was dissolved in water (30 ml) and cooled in an ice-water bath. To the solution was added 2 equivalents of sodium borohydride (0.57 g, 15 mmol) in small portions with continuous stirring over a period of 30 min. The cold mixture was stirred for 2 h and neutralized with 2 M hydrochloric acid. The progress of the reaction was checked by paper electrophoresis. The solution containing γ-hydroxyornithine was applied to a column (3.6×9 cm) of Dowex 50 (H^+ form). After the column had been washed with water and 2.5 M pyridine (300 ml), the amino acid was eluted with 2 M aqueous ammonia (350 ml) and the pooled eluate was evaporated to dryness *in vacuo*. The residue, taken up in water, was adjusted to pH 5 with 1 M hydrochloric acid, decolorized with charcoal and concentrated to a syrup *in vacuo*. The syrup was dissolved in a small amount of 50% ethanol, γ-hydroxyornithine being crystallized as its hydrochloride with the addition of absolute ethanol. Yield of L-**6ab**·HCl, 2.5 g (90%); mp 167—168 °C (dec). Yield of D-**6ab**·HCl, 2.4 g (88%); mp 169 °C (dec).

Found (L-**6ab**·HCl): C, 32.21; H, 7.01; N, 14.83%. Found (D-**6ab**·HCl): C, 31.92; H, 7.16; 14.93%. Calcd for $C_5H_{12}O_3N_2$·HCl: C, 32.53; H, 7.10; N, 15.17%.

*Separation of the Diastereoisomers of γ-Hydroxyornithine (**6ab**).* A diastereoisomeric compound **6ab**·HCl (600 mg) was separated into its two diastereoisomers by chromatography using a column (3.8×275 cm) of Dowex 50 (Na^+ form).[11] Two ninhydrin positive peaks were obtained. The component of the forepeak was confirmed to be *threo* isomer and that of the afterpeak *erythro* isomer by the assay using an amino acid analyzer.

erythro-*γ-Hydroxy*-L-*ornithine* (L-*6a*) *Hydrochloride.* The diastereoisomers of γ-hydroxy-L-ornithine were separated chromatographically as described above. The combined eluate containing *erythro* L-isomer was treated as described for L-**6ab**. The *erythro* isomer was obtained as its hydrochloride. It was recrystallized from water–ethanol; yield, 272 mg (67%); mp 176—177 °C (dec); $[\alpha]_D^{20}$ +9.4° (*c* 2, H_2O). [lit,[9] $[\alpha]_D^{20}$ +10.6° (*c* 5, H_2O), lit,[11] $[\alpha]_D^{20}$ +10.5° (*c* 2, H_2O)].

threo-*γ-Hydroxy*-L-*ornithine* (L-*6b*) *Hydrochloride.* From the pooled forepeak fractions of the eluate, the *threo* isomer was obtained as its hydrochloride. It was recrystallized from water–ethanol; yield, 146 mg (76%); mp 193—194 °C (dec); $[\alpha]_D^{20}$ −6.3° (*c* 2, H_2O). [lit,[11] $[\alpha]_D^{20}$ −7.0° (*c* 2, H_2O)].

erythro-*γ-Hydroxy*-D-*ornithine* (D-*6a*) *Hydrochloride.* The diastereoisomers of γ-hydroxy-D-ornithine were separated as described above. From the combined afterpeak fractions of the eluate, the *erythro* isomer was obtained as its hydrochloride. It was recrystallized from water–ethanol; yield, 260 mg (67%); mp 174—175 °C (dec); $[\alpha]_D^{20}$ −9.8° (*c* 2, H_2O).

threo-*γ-Hydroxy*-D-*ornithine* (D-*6b*) *Hydrochloride.* From the pooled forepeak fractions of the eluate, the *threo* isomer was obtained as its hydrochloride. It was recrystallized from water–ethanol; yield, 132 mg (63%); mp 189—190 °C (dec); $[\alpha]_D^{20}$ +6.4° (*c* 2, H_2O).

Found (L-**6a**·HCl): C, 32.05; H, 7.12; N, 14.81%. Found (L-**6b**·HCl): C, 32.44; H, 7.12; N, 14.91%. Found (D-**6a**·HCl): C, 31.97; H, 7.11; N, 14.87%. Found (D-**6b**·HCl): C, 32.32; H, 7.10; N, 14.71%. Calcd for $C_5H_{12}O_3N_2$·HCl: C, 32.53; H, 7.10; N, 15.17%.

Guanidination of Four Stereoisomers of γ-Hydroxyornithine. Each isomer of γ-hydroxyornithine (184.5 mg) was converted into the corresponding γ-hydroxyarginine by treatment with 1-amidino-3,5-dimethylpyrazole nitrate (ADPN), the unchanged material and the product being separated by chromatography using a column (1.6×16 cm) of Dowex 50 (pyridinium form).[11]

erythro-*γ-Hydroxy*-L-*arginine* (L-*7a*) *Hydrochloride.* Compound L-**6a**·HCl was guanidinated with ADPN and the reaction mixture subjected to column chromatography, as described above. From the pooled afterpeak fractions of the eluate, *erythro* L-isomer (L-**7a**) was crystallized as its hydrochloride. It was recrystallized from water–ethanol; yield, 95 mg (42%); mp 188—189 °C (dec); $[\alpha]_D^{20}$ −8.4° (*c* 1, 0.5 M NaOH).

erythro-*γ-Hydroxy*-D-*arginine* (D-*7a*) *Hydrochloride.* Compound D-**7a**·HCl was obtained from D-**6a**·HCl in the same manner as described above. It was recrystallized from water–ethanol; yield, 115 mg (51%); mp 188—189 °C (dec); $[\alpha]_D^{20}$ +8.5° (*c* 1, 0.5 M NaOH).

threo-*γ-Hydroxy*-L-*arginine* (L-*7b*) *Hydrochloride.* Compound L-**6b**·HCl was treated in the same manner as above. *threo* L-Isomer L-**7b** was obtained as a hygroscopic crystalline hydrochloride; yield, 90 mg (40%); $[\alpha]_D^{20}$ +11.0° (*c* 1, 0.5 M NaOH).

threo-*γ-Hydroxy*-D-*arginine* (D-*7b*) *Hydrochloride.* Compound D-**7b**·HCl was obtained from D-**6b**·HCl in the same manner as described above. It was obtained as a hygroscopic crystalline hydrochloride; yield, 105 mg (46%); $[\alpha]_D^{20}$ −11.0° (*c* 1, 0.5 M NaOH).

Found (L-**7a**·HCl): C, 31.76; H, 6.75; N, 24.65%. Found (D-**7a**·HCl): C, 31.86; H. 6.69; N, 24.77%. Found (L-**7b**·HCl): C, 31.70; H, 6.72; N, 24.20%. Found (D-**7b**·HCl): C, 31.39; H, 6.85; N, 24.40%. Calcd for $C_6H_{14}O_3N_4$·HCl: C, 31.79; H, 6.67; N, 24.72%.

References

1) Y. Fujita, *Bull. Chem. Soc. Jpn.*, **32**, 439 (1959).
2) S. Makisumi, *J. Biochem.* (*Tokyo*), **49**, 284 (1961).
3) E. A. Bell and A. S. L. Tirimanna, *Nature* (*London*), **197**, 901 (1963).
4) E. A. Bell and A. S. L. Tirimanna, *Biochem. J.*, **91**, 356 (1964).
5) S. Makisumi, *J. Biochem.* (*Tokyo*), **49**, 292 (1961).
6) Y. Fujita, *J. Biochem.* (*Tokyo*), **49**, 468 (1961).
7) S. Makisumi, *Mem. Fac. Sci. Kyushu Univ. Ser. C. Chem.*, **5**, 107 (1964).
8) A. Nakane, T. Nakamura, and Y. Eguchi, *J. Biol. Chem.*, **252**, 5267 (1977).
9) Y. Fujita, *Bull. Chem. Soc. Jpn.*, **33**, 1379 (1960).
10) B. A. Santa Rossa and T. Viswanatha, *Can. J. Biochem.*, **46**, 725 (1968).
11) K. Mizusaki, H. Yamamoto, and S. Makisumi, *Bull Chem. Soc. Jpn.*, **53**, 2605 (1980).
12) H. Heath, A. Lawson, and C. Rimington, *J. Chem. Soc.* **1951**, 2215.
13) E. Bamberger and B. Berlé, *Justus Liebigs Ann. Chem.*, **273**, 342 (1893).
14) B. Witkop and T. Beiler, *J. Am. Chem. Soc.*, **78**, 2882 (1956).
15) J. N. Ashley and C. R. Harington, *J. Chem. Soc.*, **1930**, 2586.
16) C. Tesar and D. Rittenberg, *J. Biol. Chem.*, **170**, 35 (1947).

Restricted Rotation Involving the Tetrahedral Carbon. XXXV.[1] Stereodynamics of 9-(3,5-Dimethylbenzyl)triptycene Derivatives

Gaku YAMAMOTO and Michinori ŌKI*

Department of Chemistry, Faculty of Science, The University of Tokyo, Hongo, Bunkyo-ku, Tokyo 113

(Received May 31, 1980)

Stereodynamics of a variety of 9-(3,5-dimethylbenzyl)triptycene derivatives was studied. Atropisomerism about the bridgehead-to-methylene bond was realized in a triply *peri*-substituted derivative, 8,13-dichloro-1,4-dimethyl-9-(3,5-dimethylbenzyl)triptycene: the activation enthalpy for the *ap*→±*sc* conversion was 26.4 kcal/mol. Barriers to rotation about the bridgehead-to-methylene bond in a variety of triply, doubly, and singly *peri*-substituted derivatives were obtained by DNMR method. DNMR behavior of the diastereotopic *m*-methyl groups in the benzyl moiety revealed the dual mechanisms of the methyl exchange process: rotation about the methylene-to-aryl bond by 180° without rotation about the bridgehead-to-methylene bond ("isolated rotation (IR)") and rotation about the methylene-to-aryl bond by 180° synchronous with rotation about the bridgehead-to-methylene bond by 120° ("gear motion (GM)"). The GM process predominates in *peri*-unsubstituted derivatives, while the IR process predominates in triply *peri*-substituted ones.

Ample examples of restricted rotation about the bridgehead-to-substituent bond in 9-substituted triptycene derivatives have been reported.[2] Among them, 9-benzyltriptycenes have drawn much attention because of several interesting aspects in their conformational behavior. One is the apparently anomalous conformational preference for the ±*sc* rotamers on the basis of the steric consideration, especially when the *peri*-substituent X is a methoxyl (Scheme 1).[3,4] This

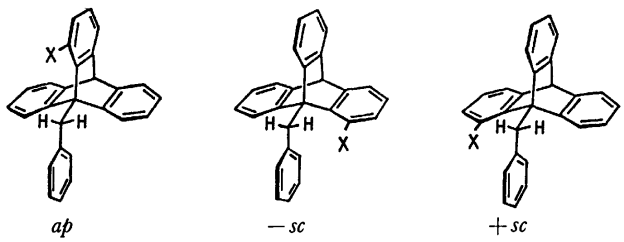

ap −*sc* +*sc*

Scheme 1.

phenomenon suggests the existence of some kind of attractive interaction between the methoxyl and the phenyl groups.[3] Another interesting aspect is about the energy barriers to the conformational interconversion among these rotamers. In case of singly *peri*-substituted derivatives, the barrier to interconversion between *ap* and ±*sc* rotamers is dependent on the nature of the *peri*-substituent X. Interconversion between the +*sc* and −*sc* rotamers may occur either directly by passing of the aryl group over the *peri*-substituent or stepwise by way of the *ap* rotamer. DNMR studies on this aspect have been made revealing that the stepwise process is energetically more favored.[4] In addition, the rotational barriers are highly dependent on the number of *peri*-substituents. For instance, the $\Delta G^{\ddagger}$ for the *ap*→±*sc* process in compound **1** with one *peri*-substituent was 11.9 kcal/mol at −15 °C,[5] while that for the +*sc*⇌−*sc* interconversion in **2** with two *peri*-substituents rose up to 18.1 kcal/mol at 100 °C.[3c] These data make one expect that the triply *peri*-substituted derivatives might have an even higher barrier, which is possibly so high that atropisomerism can be realized. We found this was actually the case in one of the derivatives and the detail is described in this paper.[6] Third aspect of interest is the conformational behavior of the benzylic phenyl group. Several lines of evidence suggest that the stable conformation with respect to the phenyl group is the one in which the benzene ring is coplanar with the bridgehead-to-methylene bond as shown in Scheme 1.[3] Molecular model consideration indicated that the rotation of the phenyl group might be considerably hindered, but hithertofore NMR studies have given no definite information on this point because the benzylic aromatic signals are overshadowed by the triptycyl aromatic signals. We therefore planned to introduce two *m*-methyl groups into the benzylic benzene ring as an NMR probe in order to have a deeper insight into the conformational behavior of the aryl group.

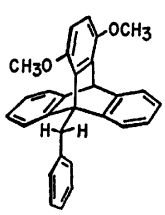

1

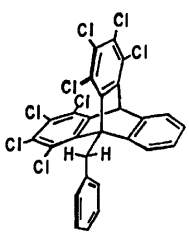

2

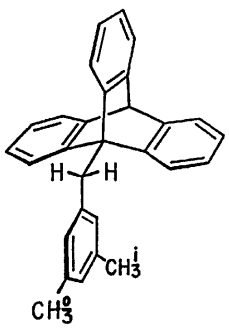

3

If conformation **3** has a sufficiently long lifetime on the NMR time scale, two methyl groups should be diastereotopic and anisochronous. Two processes that exchange the magnetic environments of the two methyl groups can be *a priori* deduced. One is a simple rotation

of the aryl group by 180°, without rotation about the bridgehead-to-methylene bond, by way of the transition state shown by **4**. We call this process "isolated rotation (IR)." Another process is a correlated rotation of the aryl and the triptycyl groups in which rotation about the methylene-to-aryl bond by 180° occurs synchronously with rotation about the bridgehead-to-methylene bond by 120° by way of the transition state shown by **5**.

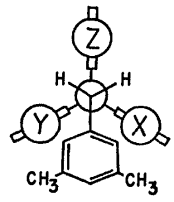

4

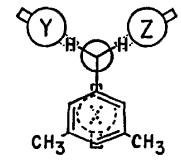

5

We refer to this process as "gear motion (GM)." Strictly speaking, exchange of the methyl groups by this process occurs only when the rotamers before and after the process are homomeric or enantiomeric to each other, namely X=Y=Z or at least Y=Z. We report here the stereodynamics of the aryl groups as revealed by DNMR behavior of the *m*-methyl groups in some detail.[7]

Results and Discussion

Atropisomerism. In order to investigate the possibility of atropisomerism, several triply *peri*-substituted 9-(3,5-dimethylbenzyl)triptycenes (**6**—**9**) were synthesized.

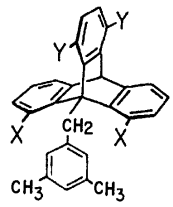

6: X=Cl, Y=CH_3
7: X=Cl, Y=OCH_3
8: X=F, Y=CH_3
9: X=F, Y=OCH_3

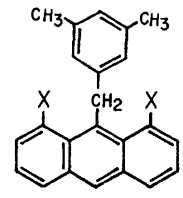

10a: X=Cl
10b: X=F

Reactions of 3,6-dimethylbenzyne, generated *in situ* from the corresponding anthranilic acid, with **10a** and with **10b** gave the triptycene skeletons of **6** and **8**, while Diels-Alder reactions of *p*-benzoquinone with **10a** and with **10b** followed by treatment with dimethyl sulfate and potassium hydroxide gave the skeletons of **7** and **9**. Among the compounds obtained only **6** afforded atropisomers.

Anthracene **10a** reacted with 3,6-dimethylbenzyne to give a mixture of *ap* and ±*sc* rotamers of the triptycene **6**. NMR spectral investigation of the mixture revealed that the interconversion between the rotamers was considerably slow at room temperature in the classical sense, and that the formation ratio of the two rotamers was dependent on the reaction temperature. The reaction in boiling dichloromethane at *ca.* 40 °C gave the highest *ap*/±*sc* ratio of *ca.* 9 and the higher reaction

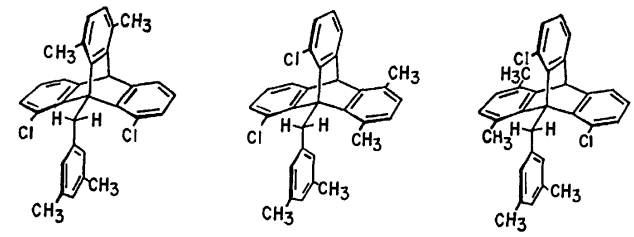

ap −*sc* +*sc*

temperature caused the decrease of the rotamer ratio because of the probable decrease in the stereoselectivity and the partial isomerization of the *ap* to the ±*sc* rotamer at the reaction temperature. The high stereoselectivity shown in the reaction is consistent with our previous finding that the Diels-Alder addition of a dienophile to a 9-substituted anthracene preferentially gives an atropisomer in which the bulkiest α-group in the 9-substituent ocuppies the antiperiplanar position to the entering dienophile.[8,9]

Recrystallization from chloroform–ethanol of the rotamer mixture thus obtained gave the pure *ap*-**6**. ±*sc*-**6** was isolated in a pure state by column chromatography of the equilibrated mixture of the two rotamers (*vide infra*) followed by recrystallization from chloroform–ethanol. Rotamer assignment was clearly made from the ^{1}H NMR spectral pattern of the methylene protons: a singlet for the *ap* and an AB-quartet for the ±*sc* rotamer. Although these rotamers are quite stable at room temperature both in solution and in the crystalline state, elevation of the temperature caused the isomerization of the rotamers in solution. Detailed kinetic study was made by following the change of the relative intensities of the 1-methyl signals in ^{1}H NMR spectra at 48—69 °C with chloroform-*d* solution. The data agreed with the rate law for a first order reversible reaction, and the first order rate constants were obtained at four temperatures, and the activation parameters were calculated as shown in Table 1. The equilibrium constant ±*sc*/*ap* for **6** was 2.0 throughout the temperature range examined and this value may reflect the same degree of interaction of the methyl and the chloro groups as exerted to the flanking aryl group.

DNMR Study on Rotation about the Bridgehead-to-Methylene Bond. The other triply *peri*-substituted derivatives **7**—**9** carrying the smaller *peri*-groups than those of **6** were shown to be too labile to give rise to atropisomers and their stereodynamics was studied by DNMR.

TABLE 1. KINETIC DATA OF THE *ap*$\rightleftharpoons$±*sc* INTERCONVERSION OF **6** IN $CDCl_3$

ap-**6** $\underset{k_{-1}}{\overset{2k_1}{\rightleftharpoons}}$ ±*sc*-**6** $\quad K=2k_1/k_{-1}$

Temperature °C	k_1 10^{-5} s^{-1}	$\Delta G^{\ddagger}$ kcal/mol	K
69	55.5	$25.2_1\pm0.05$	2.0 ± 0.1
61	21.2	$25.2_4\pm0.05$	2.0 ± 0.1
54	8.55	$25.2_9\pm0.05$	2.0 ± 0.1
48	4.17	$25.2_7\pm0.05$	2.0 ± 0.1

$\Delta H^{\ddagger}=26.4\pm0.7$ kcal/mol, $\Delta S^{\ddagger}=3.5\pm2.1$ eu.

Table 2. Rotational barriers around the bridgehead-to-methylene bond in 9-(3,5-dimethylbenzyl)triptycenes[a)]

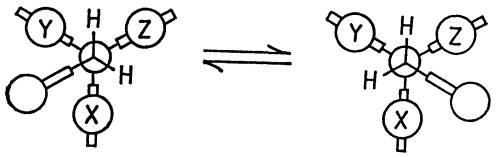

Compound	X	Y	Z	Solvent	$\pm sc/ap$	Obsd process	Obsd protons	T_c °C	k_c[c)] s^{-1}	$\Delta G_c^{\ddagger}$[d)] kcal/mol
6[b)]	Cl	Cl	CH_3	$CDCl_3$	2.0	$ap \rightleftarrows \pm sc$				25.2
7	OCH_3	Cl	Cl	C_4Cl_6	∞	$+sc \rightleftarrows -sc$	CH_2	167	102	22.1
8	F	F	CH_3	C_6H_5Cl	0.5	$ap \rightleftarrows \pm sc$	4-CH_3	100	2.7	21.3 ($ap \rightarrow \pm sc$)
									10.9	20.2 ($\pm sc \rightarrow ap$)
9	F	F	OCH_3	C_6H_5Cl	3.0	$ap \rightleftarrows \pm sc$	1-OCH_3	92	47	18.7 ($ap \rightarrow \pm sc$)
									31	19.0 ($\pm sc \rightarrow ap$)
11	H	Cl	Cl	$CDCl_3$	∞	$+sc \rightleftarrows -sc$	CH_2	51	184	15.7
12	H	H	OCH_3	$CDCl_3$	3.3	$ap \rightleftarrows \pm sc$	1-OCH_3	−28	45	12.4 ($ap \rightarrow \pm sc$)
									28	12.6 ($\pm sc \rightarrow ap$)
14	H	H	H	CS_2	1.3	$ap \rightleftarrows \pm sc$	2-OCH_3	−64	14	11.0 ($ap \rightarrow \pm sc$)
									21	10.8 ($\pm sc \rightarrow ap$)

a) Obtained by DNMR method except for **6**. b) Obtained by classical kinetics. See Table 1. c) See Experimental. d) With errors of ±0.1 kcal/mol due mainly to the errors in T_c of ±2 °C.

^{1}H NMR spectrum of the thermodynamically equilibrated sample of **7** showed the sole existence of the $\pm sc$ rotamer at room temperature, as indicated by an AB-quartet signal for the methylene protons and only one pair of the methoxyl signals. Smaller bulkiness of the methoxyl group compared with that of the chloro group should be responsible for this phenomenon, as the oxygen atom with the van der Waals radius of 1.40 Å mainly interacts with the aryl group. Attractive interaction between the aryl and the methoxyl groups may contribute to the rotamer equilibrium.[3)] The AB-quartet signal due to the methylene protons coalesced into a singlet on elevation of the temperature and this DNMR behavior gave the $+sc \rightleftarrows -sc$ interconversion barrier shown in Table 2. In fluorinated compounds **8** and **9**, both the *ap* and the $\pm sc$ rotamers were present at equilibrium. DNMR of the 4-methyl signals of **8** and the 1-methoxyl signals of **9** afforded the $ap \rightleftarrows \pm sc$ interconversion barrier as shown in Table 2. Interesting is the large rotamer ratio ($\pm sc/ap$) of 3.0 shown by **9**. As the fluoro group is thought to be smaller than the methoxyl group, the ratio smaller than the statistical value of 2.0 would be expected on the steric ground. This result suggests that the methoxyl group exerts some attractive interaction with the aryl group as suggested before,[3)] while the fluoro group does not exert such an interaction.

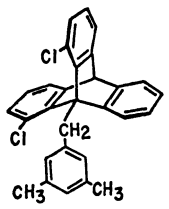

11

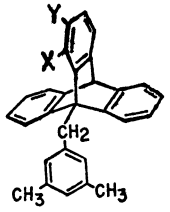

12: X=OCH_3, Y=H
13: X=Y=H
14: X=H, Y=OCH_3

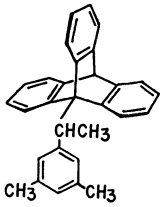

15

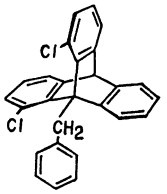

16

Although stereodynamics of some doubly and singly *peri*-substituted 9-benzyltriptycenes has been studied,[3-5)] several additional compounds **11**—**15** carrying two *m*-methyl groups in the benzyl moiety were now synthesized and their DNMR behaviors were examined. Energy barriers to the $+sc \rightleftarrows -sc$ process for **11** and to the $ap \rightleftarrows \pm sc$ processes for **12** and **14** were obtained as shown in Table 2

Table 2 indicates the significant dependence of the barrier upon the number and the size of the *peri*-substituents. The transition state for these processes must be best represented by **5**, and the nature of the *peri*-group X over which the aryl group passes should have the largest effect on the barrier, but the *peri*-groups Y and Z which eclipse the benzylic hydrogens also exert a large effect (**8** *vs.* **9** and **11** *vs.* **12**).

1,8-Dichloro-9-benzyltriptycene (**16**) was synthesized in order to check the effect of the *m*-methyl groups on the energy barrier by comparing the DNMR data with those of **11**. Compound **16** existed solely in the $\pm sc$ rotamer and the AB-quartet signal due to the methylene protons coalesced into a singlet at 60 °C corresponding to the $+sc \rightleftarrows -sc$ barrier of 16.1 kcal/mol. This barrier has a small but significant difference from that in **11**. The difference might be attributed to the buttressing

effect of the *m*-methyl groups against the ortho protons, which operates to destabilize the ground state resulting in the decrease of the barrier.

Stereodynamics of the Aryl Group. Low temperature ^{1}H NMR spectra of the above mentioned compounds **6**—**9** and **11**—**15** showed equally intense singlets for the *m*-methyl groups, indicating the freezing of the conformation **3** on the NMR time scale. The higher field singlet may be assigned to the inner methyl group (CH_3^i) and the lower field one to the outer methyl (CH_3^o), if one considers the ring current effect of the triptycyl benzene rings. Similarly, the signal ascribed to the proton at the inner ortho position appeared at the higher field of the aromatic region (δ 6.0—6.4), while the outer *o*-proton appeared around δ 7.2 although it could not be definitely assigned as it was overshadowed by the other aromatic signals.

Two *m*-methyl singlets coalesced into a singlet at higher temperatures to indicate the presence of rate process(es) exchanging the magnetic environments of the two methyl groups. The rate constants for the methyl exchange process at the coalescence temperatures were calculated and are shown in Table 3 together with the free energies of activation therefrom.

As for $\pm sc$-**6**, the DNMR study was made on the equilibrium mixture of *ap*- and $\pm sc$-**6**, because the isomerization of the $\pm sc$ rotamer to the *ap* occurred with considerable rates at around the coalescence temperature of the methyl signals of $\pm sc$-**6**. In compounds **8** and **9** which existed as a mixture of *ap* and $\pm sc$ rotamers, low temperature chemical shifts of the *m*-methyl groups of the two rotamers coincided, but the coalescence temperatures could be separately determined for each rotamer; the overlap of the signals somewhat decreased the accuracy of $\Delta\delta$ and T_c determination affording the errors of *ca.* $\pm$0.2 kcal/mol for ΔG^* values. In **12** and **14**, the coalescence temperatures could not be separately determined for each rotamer; this would cause rather large errors in ΔG^* values.

As discussed in the introductory section, magnetic exchange of the two *m*-methyl groups can occur by two processes: IR and GM. Rotation about the bridgehead-to-methylene bond can be naturally assumed to occur exclusively by the GM process, and therefore the barrier data in Table 2 correspond to the GM barriers of these compounds. Thus we can discuss on the contribution of these two mechanisms on the methyl exchange process for each compound.

Judging from the observation that the GM barrier sharply dropped as the number of *peri*-substituents decreased, while the methyl exchange barrier was not so sensitive to the *peri*-groups, we expect that the GM process can be a main contributor to the methyl exchange in *peri*-unsubstituted derivatives. The IR barrier in the *peri*-unsubstituted derivatives was estimated as follows. Compound **15** with a methyl group in the benzyl methylene position showed broadening of the signals in the aromatic region at 80—100 °C reflecting that the rotation about the bridgehead-to-methylene bond became fast on the NMR time scale at this temperature region. The barrier to rotation was roughly estimated to be about 18—20 kcal/mol, which may be reasonable if one takes it into account that 2,4-dimethyl-9-isopropyltriptycene has the $ap \rightleftharpoons \pm sc$ barrier of 19.9 kcal/mol.[10] DNMR behavior of the *m*-methyl groups in this compound suggests that the methyl exchange with ΔG_c^* of 13.3 kcal/mol occurs by the IR process. It can be assumed that the introduction of a methyl group into the benzylic position does not significantly affect the IR barrier, and therefore compounds **13** and **14** which do not carry *peri*-groups have similar IR barrier to **15**. One may argue that the presence of a methyl group in the benzylic position considerably modifies the potential curve of the IR process. But the methyl group cannot significantly affect the rate determining transition state (**4**) in which

Table 3. DNMR data for the methyl exchange

Compound and rotamer	Solvent	$\delta^i_{CH_3}$ [a]	$\delta^o_{CH_3}$ [a]	$\Delta\delta$ [b] / Hz	T_c [d] / °C	ΔG_c^* [f] / kcal/mol
$\pm sc$-**6**	$CDCl_3$	1.84	2.39	33	58	16.6
ap-**6**	$CDCl_3$	1.87	2.38	31	35	15.5
7	$CDCl_3$	1.88	2.39	31	38	15.6
8 *ap*	$CDCl_3$	1.92[c]	2.39[c]	29	−3	13.5[g]
$\pm sc$					80	17.9[g]
9 *ap*	$CDCl_3$	1.93[c]	2.38[c]	27	18	14.5[g]
$\pm sc$					43	16.0[g]
11	$CDCl_3$	1.89	2.41	31	30	15.2
12 *ap*	CS_2	1.80	2.37[c]	34	−20[e]	12.6[h]
$\pm sc$		1.91		28		
13	CS_2	1.93	2.40	28	−67	10.2
14 *ap*	CS_2	1.93[c]	2.41[c]	29	−71[e]	10.0[h]
$\pm sc$						
15	$CDCl_3$	1.98	2.49	29	−8	13.3

a) Obtained at the lowest temperature examined (*ca.* −35 °C for **6**—**9**, **11**, and **15**, and *ca.* −90 °C for **12**—**14**). b) Independent of the temperature within the experimental errors. c) Coincident between the *ap* and $\pm sc$ rotamers. d) With errors of $\pm$2 °C unless otherwise stated. e) With uncertainty of *ca.* $\pm$5 °C because of the impossibility of determining T_c's separately for each rotamer. f) With errors of $\pm$0.1 kcal/mol unless otherwise stated. g) With uncertainty of $\pm$0.2 kcal/mol. h) With uncertainty of *ca.* $\pm$0.5 kcal/mol.

the largest steric interaction occurs between the *o*-hydrogens of the aryl group and the *peri*-substituents, as is suggested by inspection of molecular models. Nor can the methyl group significantly affect the ground state (**3**) of the molecule. Therefore we believe that the assumption is reasonable. Then it is the GM process that showed the barrier of *ca.* 10 kcal/mol for the methyl exchange. The GM barrier obtained from the DNMR of 2-methoxyl signals in **14**, 11.0 kcal/mol, agrees well, if one takes the probable large error into account. Thus, the GM barrier is lower than that of the IR in *peri*-unsubstituted compounds and the exchange of the *m*-methyl groups is concluded to occur preferentially by the GM process.

In the ^{1}H NMR spectrum at −90 °C of compound **12**, the signal assigned to the inner *m*-methyl group appeared as two slightly shifted singlets of the relative intensity of 3.3 : 1 corresponding to the ±*sc* and the *ap* rotamers, respectively, while only one singlet was observed for the outer methyl group. These peaks coalesced into a singlet at −20 °C and the analysis using the approximate method for coalescing two equally intense peaks gave a rough estimate of the methyl exchange barrier of 12.6 kcal/mol. The GM barrier obtained from the DNMR of the 1-methoxyl peaks was 12.4 kcal/mol for the *ap*→±*sc* conversion at −28 °C (Table 2). The IR barrier in the *ap* rotamer of this compound should also be similar to that in **15**, around 13 kcal/mol. It can therefore be deduced that both the IR and the GM processes contribute to the methyl exchange in this singly *peri*-substituted derivative.

Compound **11**, a sole doubly *peri*-substituted derivative examined, showed the barrier of 15.7 kcal/mol for the GM process and 15.2 kcal/mol for the methyl exchange process. The IR barrier in this compound should not exceed 15.6 kcal/mol, the IR barrier in **7**, because the latter compound has a chloro and a methyl groups as the *peri*-substituents flanking the aryl group while the former has a hydrogen and a chloro groups. Thus the IR and the GM processes in this compound should have almost the same barrier and comparably contribute to the methyl exchange.

From the above discussion it has been demonstrated that the actual mechanism of the methyl exchange detected by DNMR vary on successive substitution in the *peri*-positions, from the GM process in *peri*-unsubstituted compounds to the IR process in the triply *peri*-substituted ones. This must come from the fact that the GM barrier sharply increased on substitution in the *peri*-positions, from 11.0 kcal/mol of *peri*-unsubstituted compound **14** to 25.2 kcal/mol of the triply *peri*-substituted one **6**, while the change in the IR barrier was relatively small, from 13.3 kcal/mol in **15** to 17.9 kcal/mol in ±*sc*-**8**.

Table 4 lists the energy barriers definitely assigned to the IR process. The IR barrier increases with the increasing size of the *sc*-substituents X and Y if the *ap*-substituent Z is the same (±*sc*-**8** *vs.* ±*sc*-**9**, ±*sc*-**6** *vs.* ±*sc*-**7**, and *ap*-**6** *vs.* *ap*-**8**), indicating the destabilization of the transition state **4** to a greater extent than the ground state **3**. Interesting is the effect of the *ap*-substituent Z; the larger the *ap*-group is, the lower the IR barrier becomes if the *sc*-substituents are unaltered (*ap*-**8** *vs.* *ap*-**9**). This clearly suggests that the buttressing effect of the *ap*-substituent causes the destabilization of the ground state rather than the transition state of the IR process. Similar barriers of *ap*-**8** and **15** can be ascribed to the compensating effects of the *ap*- and the *sc*-substituents: destabilization of the transition state by the *sc*-fluoro groups and that of the ground state by the *ap*-methyl group of *ap*-**8** relative to the hydrogens of **15**. Another similarity in the IR barriers of *ap*-**6** and ±*sc*-**7** may be ascribed to the effect of the *sc*-substituents, the transition-state-destabilizing chloro group in *ap*-**6** and the ground-state-stabilizing methoxyl group in ±*sc*-**7**, if one takes the similar size of the *ap*-groups into account.

Table 4. Energy barriers to the IR process[a)]

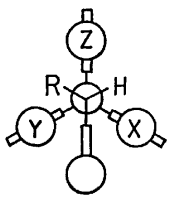

Compound and rotamer	R	X	Y	Z	T_c / °C	$\Delta\delta$ / Hz	ΔG_c^* / kcal/mol
±*sc*-**8**	H	CH_3	F	F	80	29	17.9
±*sc*-**6**	H	CH_3	Cl	Cl	58	33	16.6
±*sc*-**9**	H	OCH_3	F	F	43	27	16.0
±*sc*-**7**	H	OCH_3	Cl	Cl	38	31	15.6
ap-**6**	H	Cl	Cl	CH_3	35	31	15.5
ap-**9**	H	F	F	OCH_3	18	27	14.5
ap-**8**	H	F	F	CH_3	−3	29	13.5
15	CH_3	H	H	H	−8	29	13.3

a) Extracted from Table 3.

Experimental

Melting points are not corrected. ^{1}H NMR spectra at ambient temperature (*ca.* 35 °C) were recorded on either a Hitachi R-20B (60 MHz) or a Varian EM-390 (90 MHz) spectrometer with tetramethylsilane as an internal standard. ^{19}F NMR spectra were obtained on a Varian EM-390 spectrometer operating at 84.67 MHz with *ca.* 10% (w/v) solutions in $CDCl_3$ containing 2% of hexafluorobenzene. Chemical shifts were read with a Hewlett-Packard 5381A frequency counter relative to C_6F_6 as an internal lock signal and expressed in ppm downfield from it.

DNMR Studies. Sample solutions were prepared by dissolving *ca.* 10% (w/v) of the compounds in appropriate solvents containing 0.5% of tetramethylsilane (in case of $CDCl_3$ and CS_2) or hexamethyldisiloxane (in case of hexachloro-1,3-butadiene and chlorobenzene) as an internal standard. Variable temperature ^{1}H NMR spectra were obtained on a Hitachi R-20B spectrometer at 60 MHz and the temperatures were calibrated using methanol or ethylene glycol.[11] Because the unreliability of the enthalpies and entropies of activation obtained from DNMR analysis of relatively simple patterns ($AB \rightleftharpoons A_2$ with or without mutual coupling) is often questioned in detailed discussions, we have not attempted the computer-assisted total lineshape analysis: only the first order rate constants at the coalescence temperatures and the free energies of activation therefrom were calculated and used in discussion. Rate constants at T_c were obtained from Eq. 1 in case of two singlets of equal intensity and Eq. 2 in case of an AB-quartet,[12] and the graphical method by Shanan-Atidi and Bar-Eli in case of two singlets of unequal intensity.[13] Validity of the use of Eqs. 1 and 2 was discussed by Kost *et al.*[14]

$$k_c = \frac{\pi}{\sqrt{2}} \Delta\delta \quad (1)$$

$$k_c = \frac{\pi}{\sqrt{2}} \sqrt{(\Delta\delta)^2 + 6J^2} \quad (2)$$

1,8-Difluoroanthraquinone. A mixture of 10 g of thoroughly dried 1,8-dichloroanthraquinone and 20 g of completely anhydrous caesium fluoride in 50 mL of anhydrous dimethyl sulfoxide was heated with efficient stirring at 130—135 °C for 8 h. The mixture was cooled and poured into 300 mL of water. The solid mass was collected by filtration, dried in air, and submitted to column chromatography on alumina with hexane–dichloromethane (4 : 1) as an eluent. 1,8-Dichloro-, 1-chloro-8-fluoro-, and 1,8-difluoroanthraquinones were eluted successively in this order. 1,8-Difluoroanthraquinone was recrystallized from tetrahydrofuran–ethanol to give 3.0 g (34%) of yellow crystals, mp 227—228 °C. Found: C, 69.07; H, 2.19%. Calcd for $C_{14}H_6F_2O_2$: C, 68.86; H, 2.48%. ^{19}F NMR ($CDCl_3$): 50.5 ppm.

1,8-Difluoroanthrone. To a solution of 3.47 g (14.2 mmol) of 1,8-difluoroanthraquinone in 35 mL of concentrated sulfuric acid was added portionwise 1.0 g of aluminium powder and the mixture was stirred for 15 h at room temperature. The reaction mixture was poured onto ice. The solid formed was filtered, washed with water and dried in air. ^{19}F NMR of the crude reaction products revealed the presence of *ca.* 10% of 4,5-difluoroanthrone (44.3 ppm) as well as the desired 1,8-difluoroanthrone (49.1 ppm), which was purely isolated upon recrystallization of the mixture from benzene–hexane in the yield of 2.06 g (63%), mp 167—168 °C (dec). Found: C, 73.34; H, 3.24%. Calcd for $C_{14}H_8F_2O$: C, 73.04; H, 3.50%. ^{1}H NMR ($CDCl_3$, δ): 4.27 (2H, s), 6.8—7.7 (6H, m). ^{19}F NMR ($CDCl_3$): 49.1 ppm.

4-Methoxyanthrone. Simple and high-yield synthesis of the compound was developed. A mixture of 24.3 g (0.1 mol) of 1-chloroanthraquinone in 500 mL of sodium methoxide solution prepared from 6.0 g of sodium metal was heated under reflux for 40 h. The mixture was evaporated and diluted with water. The residual solid was filtered, washed with water, dried in air and recrystallized from tetrahydrofuran–hexane to give 20.5 g (86%) of 1-methoxyanthraquinone, mp 164—165 °C (lit,[15] 169.5 °C). The mixture of 7.14 g (30 mmol) of 1-methoxyanthraquinone and 18 g of sodium dithionite in 200 mL of 1 mol/L aqueous sodium hydroxide was heated under reflux for 3 h. The solid formed was filtered, washed with water, dried in air, and recrystallized from tetrahydrofuran–hexane to give 5.54 g (82%) of 4-methoxyanthrone, mp 134—135 °C (lit,[16] 142—143 °C).

General Procedure for the Synthesis of Anthracene Derivatives by Grignard Reaction. To an ethereal solution of two-fold excess of a Grignard reagent prepared from benzyl chloride, 3,5-dimethylbenzyl chloride,[17] or 1-(3,5-dimethylphenyl)ethyl chloride, which was prepared from the corresponding alcohol[18] and thionyl chloride, was added portionwise an appropriate anthrone in a powdery form and the mixture was stirred at room temperature for 1 h and then heated under reflux for 1 h. The reaction mixture was decomposed with aqueous ammonium chloride to give a 9-benzyl-9,10-dihydro-9-anthrol derivative, which, without further purification, was dissolved in benzene and treated with thionyl chloride and pyridine at 50 °C for 1 h. Column chromatography on alumina of the reaction products followed by recrystallization from tetrahydrofuran–hexane gave the desired anthracene.

9-(3,5-Dimethylbenzyl)anthracene, mp 134—135 °C, was prepared from 3,5-dimethylbenzyl magnesium chloride and anthrone in 97% yield. Found: C, 93.43; H, 6.58%. Calcd for $C_{23}H_{20}$: C, 93.20; H, 6.80%. ^{1}H NMR ($CDCl_3$, δ): 2.14 (6H, s), 4.91 (2H, s), 6.73 (3H, s), 7.1—7.6 (4H, m), 7.8—8.4 (4H, m), 8.39 (1H, s).

1,8-Dichloro-9-(3,5-dimethylbenzyl)anthracene, mp 196—197 °C, was prepared from 3,5-dimethylbenzylmagnesium chloride and 1,8-dichloroanthrone[19] in 88% yield. Found: C, 75.55; H, 4.88; Cl, 19.40%. Calcd for $C_{23}H_{18}Cl_2$: C, 75.62; H, 4.97; Cl, 19.41%. ^{1}H NMR ($CDCl_3$, δ): 2.08 (6H, s), 5.61 (2H, s), 6.23 (2H, s), 6.63 (1H, s), 7.1—8.0 (6H, m), 8.33 (1H, s).

1,8-Difluoro-9-(3,5-dimethylbenzyl)anthracene, mp 189—190 °C, was prepared from 3,5-dimethylbenzylmagnesium chloride and 1,8-difluroanthrone in 53% yield. Found: C, 83.24; H, 5.36%. Calcd for $C_{23}H_{18}F_2$: C, 83.11; H, 5.46%. ^{1}H NMR ($CDCl_3$, δ): 2.18 (6H, s), 5.13 (2H, br s), 6.70 (3H, s), 6.8—7.9 (6H, m), 8.32 (1H, br t, J_{HF}=1.8 Hz). ^{19}F NMR ($CDCl_3$): 54.2 ppm.

2-Methoxy-9-(3,5-dimethylbenzyl)anthracene, mp 87—89 °C, was prepared from 3,5-dimethylbenzylmagnesium chloride and 2-methoxyanthrone[20] in 59% yield. Found: C, 88.53; H, 6.60%. Calcd for $C_{24}H_{22}O$: C, 88.31; H, 6.79%. ^{1}H NMR ($CDCl_3$, δ): 2.03 (6H, s), 3.64 (3H, s), 4.68 (2H, s), 6.72 (3H, s), 6.9—8.2 (5H, m), 8.10 (1H, s).

9-[1-(3,5-Dimethylphenyl)ethyl]anthracene, mp 153—155 °C, was prepared from 1-(3,5-dimethylphenyl)ethylmagnesium chloride and anthrone in 34% yield. Found: C, 93.07; H, 6.99%. Calcd for $C_{24}H_{22}$: C, 92.86; H, 7.14%. ^{1}H NMR ($CDCl_3$, δ): 1.96 (3H, d, J=7.2 Hz), 2.20 (6H, s), 5.70 (1H, q, J=7.2 Hz), 6.81 (1H, s), 6.89 (2H, s), 7.2—7.6 (4H, m), 7.8—8.4 (4H, m), 8.38 (1H, s).

4-Methoxy-10-(3,5-dimethylbenzyl)anthrone. To a mixture of 1.7 mL (*ca.* 11 mmol) of 3,5-dimethylbenzyl chloride

and 2.24 g (10 mmol) of 4-methoxyanthrone in 60 mL of methanol was added dropwise under nitrogen a solution of 0.6 g of potassium hydroxide in 15 mL of methanol in the course of 1 h. The mixture was stirred at room temperature for 2 h, evaporated, diluted with water and extracted with benzene. The benzene solution was washed with water, dried over magnesium sulfate, and evaporated. The residue was recrystallized from benzene–hexane to give 4-methoxy-10-(3,5-dimethylbenzyl)anthrone in the yield of 1.72 g (50%), mp 108—109 °C. Found: C, 83.97; H, 6.29%. Calcd for $C_{24}H_{22}O_2$: C, 84.17; H, 6.47%. ^{1}H NMR ($CDCl_3$, δ): 2.05 (6H, s), 2.87 (1H, dd, J=12.7 and 6.4 Hz), 3.13 (1H, dd, J=12.7 and 4.4 Hz), 3.97 (3H, s), 4.78 (1H, dd, J=6.4 and 4.4 Hz), 5.99 (2H, s), 6.72 (1H, s), 7.0—7.6 (5H, m), 7.78 (1H, dd), 8.13 (1H, s).

1-Methoxy-9-(3,5-dimethylbenzyl)anthracene. To a boiling solution of 685 mg (2.0 mmol) of 4-methoxy-10-(3,5-dimethylbenzyl)anthrone in 20 mL of ethanol was added dropwise a solution of 756 mg (20 mmol) of sodium borohydride in 20 mL of 10% aqueous ethanol. The mixture was heated under reflux for 1 h, evaporated, poured into water, and extracted with chloroform. Evaporation of the solvent gave 4-methoxy-9,10-dihydro-10-(3,5-dimethylbenzyl)-9-anthrol as a pale yellow solid, which was shown to be of a single isomer by ^{1}H NMR. The alcohol was immediately treated with 10 g of phosphorus pentaoxide in 50 mL of carbon tetrachloride under reflux for 2 h. Removal of the solid and evaporation of the solvent gave 506 mg of a yellow oil, which was shown to be a 5 : 1 mixture of the desired anthracene and a by-product which was spectrally assigned to a homotriptycene derivative **17** [^{1}H NMR (CCl_4, δ): 2.00 (3H, s), 2.54 (3H, s), 3.08 (2H, d, J= 4 Hz), 3.72 (3H, s), 4.63 (1H, t, J=4 Hz), 5.17 (1H, s).] Recrystallization of the mixture from hexane gave a pure sample of the anthracene, mp 112—113 °C. Found: C, 88.38; H, 6.79%. Calcd for $C_{24}H_{22}O$: C, 88.31; H, 6.79%. ^{1}H NMR ($CDCl_3$, δ): 2.17 (6H, s), 3.72 (3H, s), 5.20 (2H, s), 6.65 (1H, m), 6.72 (3H, s), 7.1—8.3 (6H, m), 8.30 (1H, s).

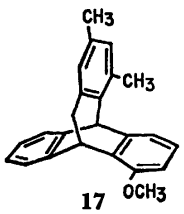

17

1,8-Dichloro-9-benzylanthracene, mp 110—112 °C, was prepared from 1,8-dichloroanthrone and benzylmagnesium chloride in 67% yield. Found: C, 74.92; H, 3.91; Cl, 21.35%. Calcd for $C_{21}H_{14}Cl_2$: C, 74.79; H, 4.18; Cl, 21.03%. ^{1}H NMR ($CDCl_3$, δ): 5.63 (2H, s), 6.4—7.9 (11H, m), 8.28 (1H, s).

General Procedure for the Synthesis of Triptycenes by Benzyne Reaction. To a boiling solution of 1 mmol of an anthracene and 1 mL of isopentyl nitrite in 30 mL of dichloromethane was added a solution of 2—3 mmol of an anthranilic acid in 10 mL of tetrahydrofuran in the course of 1 h and the mixture was heated under reflux for further 1 h. The desired triptycene was obtained after evaporation of the solvent, column chromatography of the residue on alumina with dichloromethane–hexane as an eluent, and recrystallization of the elute from dichloromethane–hexane.

ap-*8,13-Dichloro-1,4-dimethyl-9-(3,5-dimethylbenzyl)triptycene* (ap-**6**). Reaction of 578 mg (1.58 mmol) of 1,8-dichloro-9-(3,5-dimethylbenzyl)anthracene with the benzyne from 3,6-dimethylanthranilic acid[21] gave 355 mg (48%) of a rotameric mixture of the triptycene ($ap/\pm sc$=9) upon column chromatography on alumina. Recrystallization from chloroform–ethanol gave 242 mg (33%) of the pure *ap* rotamer: mp 305—307 °C. Found: C, 79.30; H, 5.42; Cl ,15.02%. Calcd for $C_{31}H_{26}Cl_2$: C, 79.31; H, 5.58; Cl, 15.11%. ^{1}H NMR ($CDCl_3$, δ): 1.6—2.5 (6H, br d), 2.40 (3H, s), 2.84 (3H, s), 5.44 (2H, s), 5.58 (1H, s), 6.68 (2H, s), 6.7—7.5 (9H, m).

$\pm$sc-*8,13-Dichloro-1,4-dimethyl-9-(3,5-dimethylbenzyl)triptycene* ($\pm$sc-**6**). The equilibrated mixture of *ap*- and $\pm sc$-**6** was chromatographed through an alumina column with benzene–hexane (15 : 85) as an eluent. The $\pm sc$ rotamer eluted slightly faster than the *ap*. Fractions consisting of more than 85% of the $\pm sc$ rotamer were collected and recrystallized from chloroform–ethanol to give the pure $\pm sc$-**6**, mp 305—306 °C. Found: C, 79.10; H, 5.30%. Calcd for $C_{31}H_{26}Cl_2$: C, 79.31; H 5.58%. ^{1}H NMR ($CDCl_3$, δ): 1.82 (3H, br s), 2.16 (3H, s), 2.37 (3H, br s), 2.56 (3H, s), 5.20 and 5.67 (2H, AB-q, J=18 Hz), 5.56 (1H, s), 6.04 (1H, br s), 6.4—7.5 (10H, m).

8,13-Difluoro-1,4-dimethyl-9-(3,5-dimethylbenzyl)triptycene (**8**), mp 252—253 °C, was prepared from 1,8-difluoro-9-(3,5-dimethylbenzyl)anthracene and 3,6-dimethylanthranilic acid in 70% yield. Found: C, 85.58; H, 6.05%. Calcd for $C_{31}H_{26}F_2$: C, 85.29; H, 6.00%. NMR spectra showed that the compound existed as a 7 : 3 mixture of the *ap* and $\pm sc$ rotamers. ^{1}H NMR ($CDCl_3$, δ): 1.90 and 2.37 (br s, $\pm sc$), 2.13 (br s, *ap*), *ca.* 2.1 (s, $\pm sc$), 2.42 (s, *ap*), 2.53 (s, $\pm sc$), 2.79 (s, *ap*), 4.88 (br s, $ap/\pm sc$), 5.66 (t, J_{HF}=2.0 Hz, $ap/\pm sc$), 6.3—7.4 (m, $ap/\pm sc$). ^{19}F NMR ($CDCl_3$): 44.8 and 54.2 ppm ($\pm sc$), and 50.9 ppm (*ap*).

1,8-Dichloro-9-(3,5-dimethylbenzyl)triptycene (**11**), mp 270—271 °C, was prepared from 1,8-dichloro-9-(3,5-dimethylbenzyl)anthracene and anthranilic acid in 47% yield. Found: C, 78.96; H, 4.90; Cl, 16.09%. Calcd for $C_{29}H_{22}Cl_2$: C, 78.91; H, 5.02; Cl, 16.06%. ^{1}H NMR ($CDCl_3$, δ): 1.7—2.6 (6H, br s), 4.75 and 5.90 (2H, AB-q, J=18 Hz), 5.35 (1H, s), 6.7—7.6 (13H, m).

1-Methoxy-9-(3,5-dimethylbenzyl)triptycene (**12**), mp 239—240 °C, was prepared from 1-methoxy-9-(3,5-dimethylbenzyl)-anthracene and anthranilic acid in 29% yield. Found: C, 89.60; H, 6.49%. Calcd for $C_{30}H_{26}O$: C, 89.51; H, 6.51%. ^{1}H NMR ($CDCl_3$, δ): 2.18 (6H, s), 3.27 (3H, s), 4.62 (2H, s), 5.38 (1H, s), 6.4—7.6 (14H, m).

9-(3,5-Dimethylbenzyl)triptycene (**13**), mp 215—217 °C, was prepared from 9-(3,5-dimethylbenzyl)anthracene and anthranilic acid in 46% yield. Found: C, 93.81; H, 6.37%. Calcd for $C_{29}H_{24}$: C, 93.51; H, 6.49%. ^{1}H NMR ($CDCl_3$, δ): 2.19 (6H, s), 4.41 (2H, s), 5.42 (1H, s), 6.7—7.6 (15H, m).

2-Methoxy-9-(3,5-dimethylbenzyl)triptycene (**14**), mp 196—197 °C, was prepared from 2-methoxy-9-(3,5-dimethylbenzyl)-anthracene and anthranilic acid in 19% yield. Found: C, 89.59; H, 6.39%. Calcd for $C_{30}H_{26}O$: C, 89.52; H, 6.51%. ^{1}H NMR ($CDCl_3$ δ): 2.19 (6H, s), 3.56 (3H, s), 4.37 (2H, s), 5.34 (1H, s), 6.48 (1H, dd, J=8 and 3 Hz), 6.7—7.5 (13H, m).

9-[1-(3,5-Dimethylphenyl)ethyl]triptycene (**15**), mp 179—180 °C, was prepared from 9-[1-(3,5-dimethylphenyl)ethyl]-anthracene and anthranilic acid in 62% yield. Found: C, 93.00; H, 6.81%. Calcd for $C_{30}H_{26}$: C, 93.22; H, 6.78%. ^{1}H NMR ($CDCl_3$, δ): 2.07 (3H, d, J=7.2 Hz), 2.19 (6H, s), 4.71 (1H, q, J=7.2 Hz), 5.37 (1H, s), 6.5—7.9 (15H, m).

1,8-Dichloro-9-benzyltriptycene (**16**), mp 239—241 °C, was prepared from 1,8-dichloro-9-benzylanthracene and anthranilic acid in 52% yield. Found: C, 78.42; H, 4.18; Cl, 17.07%. Calcd for $C_{27}H_{18}Cl_2$: C, 78.46; H, 4.39; Cl, 17.15%. ^{1}H NMR ($CDCl_3$, δ): 4.80 and 5.98 (2H, AB-q, J=18 Hz), 5.33 (1H, s), 6.5—7.6 (15H, m).

General Procedure for the Synthesis of Triptycenes by p-*Benzoquinone Addition.* A mixture of 2 mmol of an anthracene and 10 mmol of *p*-benzoquinone in 30 mL of acetonitrile was heated under reflux for 40 h. After evaporation of the solvent and removal of most of the unreacted *p*-benzoquinone by sublimation, the residue was dissolved in 20 mL of 1,4-dioxane and stirred with an aqueous solution of 0.5 g of potassium hydroxide and 1 mL of dimethyl sulfate overnight at room temperature and then at 90 °C for 1 h. The reaction mixture was extracted with diethyl ether, and the ether layer was washed with water and dried over magnesium sulfate. Evaporation and column chromatography on alumina followed by recrystallization from dichloromethane–hexane gave the desired triptycene.

8,13-Dichloro-1,4-dimethoxy-9-(3,5-dimethylbenzyl)triptycene(7), mp 277—278 °C, was prepared from 1,8-dichloro-9-(3,5-dimethylbenzyl)anthracene in 52% yield. Found: C, 74.38; H, 5.11; Cl, 14.02%. Calcd for $C_{31}H_{26}Cl_2O_2$: C, 74.25; H, 5.23; Cl, 14.14%. ^{1}H NMR ($CDCl_3$, δ): 1.5—2.5 (6H, br d), 2.89 (3H, s), 3.85 (3H, s), 5.29 and 5.54 (2H, AB-q, J=18 Hz), 6.38 and 6.62 (2H, AB-q, J=9 Hz), 6.6—7.5 (9H, m).

8,13-Difluoro-1,4-dimethoxy-9-(3,5-dimethylbenzyl)triptycene (9), mp 265—266 °C, was prepared from 1,8-difluoro-9-(3,5-dimethylbenzyl)anthracene in 25% yield. Found: C, 79.36; H, 5.54%. Calcd for $C_{31}H_{26}F_2O_2$: C, 79.47; H, 5.59%. NMR spectra showed the existence of the *ap* and $\pm sc$ rotamers in the ratio of 1 : 3. ^{1}H NMR ($CDCl_3$, δ): 1.93 and 2.34 (br s, $\pm sc$), 2.13 (br s, *ap*), 2.90 (s, $\pm sc$), 3.75 (s, *ap*), 3.78 (s, *ap*), 3.82 (s, $\pm sc$), 4.6—5.1 (br m, *ap*/$\pm sc$), 5.91 (t, J_{HF}= 2 Hz, *ap*/$\pm sc$), 6.2—7.4 (m, *ap*/$\pm sc$). ^{19}F NMR ($CDCl_3$): 45.7 and 52.6 ppm ($\pm sc$), and 51.4 ppm (*ap*).

Kinetics of Isomerization of ap-**6**. A solution of *ap*-**6** in $CDCl_3$ (*ca.* 10%(w/v)) in an NMR sample tube was inserted to the NMR probe heated at constant temperature which was calibrated using ethylene glycol, and the change in the relative intensity of the singlets at δ 2.84 (*ap*) and 2.54 ($\pm sc$) was followed. The rate law for a first order reversible reaction is given by Eq. 3,

$$\log\left[1-\left(1+\frac{1}{K}\right)\frac{x}{a}\right]=-\frac{2k_1}{2.303}\left(1+\frac{1}{K}\right)t, \qquad (3)$$

where a is the initial quantity of the *ap*-**6**, x the quantity of $\pm sc$-**6** at time t and K the equilibrium constant $[\pm sc]/[ap]$. The left side of the Equation was obtained from the NMR measurement and plotted against t to afford a good straight line, the slope of which gave the rate constant k_1, from which $\Delta G^{\ddagger}$ was calculated. Determination of the rate constants was made at four temperatures between 48 and 69 °C and the Eyring plot gave $\Delta H^{\ddagger}$ and $\Delta S^{\ddagger}$ values.

References

1) Preceding paper: M. Nakamura and M. Ōki, *Bull. Chem. Soc. Jpn.*, **53**, 3248 (1980).
2) M. Ōki, *Angew. Chem. Int. Ed. Engl.*, **15**, 87 (1976).
3) a) F. Suzuki and M. Ōki, *Tetrahedron Lett.*, **1974**, 2845; b) F. Suzuki and M. Ōki, *Bull. Chem. Soc. Jpn.*, **48**, 596 (1975); c) F. Suzuki, Ph. D. Thesis, The University of Tokyo (1975).
4) M. Kono, H. Kihara, N. Nakamura, F. Suzuki, and M. Ōki, *Bull. Chem. Soc. Jpn.*, **52**, 1682 (1979).
5) M. Ōki, M. Kono, H. Kihara, and N. Nakamura, *Bull. Chem. Soc. Jpn.*, **52**, 1686 (1979).
6) Preliminary results have been reported previously: G. Yamamoto and M. Ōki, *Angew. Chem. Int. Ed. Engl.*, **17**, 518 (1978).
7) Preliminary results have been reported previously: G. Yamamoto and M. Ōki, *Chem. Lett.*, **1979**, 1271.
8) G. Yamamoto, M. Nakamura, and M. Ōki, *Bull. Chem. Soc. Jpn.*, **48**, 2592 (1975).
9) G. Yamamoto and M. Ōki, *Bull. Chem. Soc. Jpn.*, **48**, 3686 (1975).
10) F. Suzuki, M. Ōki, and H. Nakanishi, *Bull. Chem. Soc. Jpn.*, **47**, 3114 (1974).
11) A. L. Van Geet, *Anal. Chem.*, **40**, 2227 (1968).
12) M. Ōki, H. Iwamura, and N. Hayakawa, *Bull. Chem. Soc. Jpn.*, **37**, 1865 (1964).
13) H. Shanan-Atidi and K. H. Bar-Eli, *J. Phys. Chem.*, **74**, 961 (1970).
14) D. Kost, E. H. Carlson, and M. Raban, *J. Chem. Soc., Chem. Commun.*, **1971**, 656.
15) K. Zahn and H. Koch, *Ber.*, **71**, 172 (1938).
16) C. Graebe and H. Bernhard, *Liebigs Ann.*, **349**, 222 (1906).
17) P. Canonne and L. C. Leitch, *Can. J. Chem.*, **45**, 1761 (1967).
18) C. S. Marvel, J. H. Saunders, and C. G. Overberger, *J. Am. Chem. Soc.*, **68**, 1085 (1946).
19) E. de B. Barnett and M. A. Matthews, *J. Chem. Soc.*, **123**, 2549 (1923).
20) E. de B. Barnett, N. F. Goodway, and L. H. W. Savage, *Ber.*, **64**, 2185 (1931).
21) S. Gronowitz and G. Hansen, *Arkiv Kemi*, **27**, 145 (1967).

Restricted Rotation Involving the Tetrahedral Carbon. XXXVI.[1] Stereodynamics of 9-(2-Methylbenzyl)triptycene Derivatives

Gaku YAMAMOTO and Michinori ŌKI*

Department of Chemistry, Faculty of Science, The University of Tokyo, Hongo, Bunkyo-ku, Tokyo 113

(Received July 19, 1980)

DNMR study of a series of singly *peri*-substituted 9-(2-methylbenzyl)triptycene derivatives showed that the interconversion among the *ap* and $\pm sc$ rotamers with the *o*-methyl group pointing outside the triptycyl skeleton occurs by two consecutive gear motion steps by way of the unstable rotamers with the *o*-methyl group pointing inside. The $+sc \rightleftharpoons -sc$ interconversion barriers (13.2—14.1 kcal/mol) are lower than the $ap \rightleftharpoons \pm sc$ ones (17.7—20.8 kcal/mol). The aryl group passes over a *peri*-hydrogen at the transition state of the former process and over the *peri*-substituent in the latter.

Our recent DNMR study on 9-(3,5-dimethylbenzyl)-triptycene derivatives[2] has revealed the freezing of the conformation **1** at low temperatures rendering the two *m*-methyl groups in the benzyl moiety diastereotopic and anisochronous. The coalescence of the two *m*-methyl

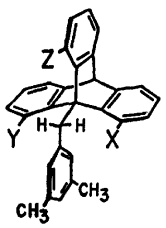

1

groups caused by the temperature rise indicates the occurence of rate processes which exchange the magnetic environments of the two methyl groups. In order to understand the stereodynamic behavior, two degrees of freedom of internal rotation should be considered: rotation about the bridgehead-to-methylene bond and that about the methylene-to-aryl bond. Rotation about the bridgehead-to-methylene bond by 120° is assumed to occur by way of the transition state shown by **2**, being always accompanied by the rotation about the methylene-to-aryl bond by 180°, thus exchanging the magnetic environments of the two methyl groups if the conformations before and after the process are homomeric (X=Y=Z) or enantiomeric (Y=Z) to each other. We refer to this process as "gear motion (GM)." Exchange of the methyl groups can occur not only by GM but also by a process in which the methylene-to-aryl bond rotates by 180° without rotating the bridgehead-to-methylene bond, by way of the transition state **3**. We refer to this process as "isolated rotation (IR)." It was shown[2] that the two processes actually participate in the methyl exchange in compounds **1** as detected by DNMR and the relative contribution of the processes is dependent on the number and size of the *peri*-substituents; IR is the main process in triply *peri*-substituted derivatives, GM predominating in the *peri*-unsubstituted ones. This comes from the fact that the GM barrier sharply drops with decrease in the number of the *peri*-substituents while the IR barrier is less sensitive to the *peri*-substitution.

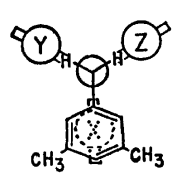

2

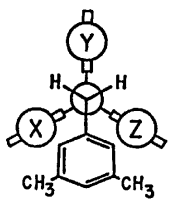

3

The structural modification which raises the IR barrier is expected to make GM the sole process rendering the rotations about the bridgehead-to-methylene and the methylene-to-aryl bonds completely correlated. In order to attain this situation we planned to introduce a methyl group in one of the ortho positions of the benzylic phenyl group. We have synthesized a series of singly *peri*-substituted 9-(2-methylbenzyl)triptycene derivatives (**4**—**8**) and examined their DNMR behavior to find that the observed process can best be explained in terms of correlated motion of the bonds under consideration.[3]

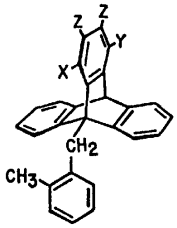

4: X=OCH_3, Y=Z=H
5: X=Y=CH_3, Z=H
6: X=CH_3, Y=Z=H
7: X=Cl, Y=Z=H
8: X=Y=Z=Cl

Ample examples have been reported on correlated rotation of two or more sp^3-sp^2 or sp^2-sp^2 bonds in triarylmethanes,[4] tetraarylethanes,[5] triarylboranes,[4] and triarylamines[6] and other systems. The present results constitute the first example of correlated rotation of an sp^3-sp^2 and an sp^3-sp^3 bonds.

Results and Discussion

Syntheses. Triptycenes **4**—**8** were synthesized by the reaction of 9-(2-methylbenzyl)anthracene derivatives **9a**—**d** with benzynes **10a**—**c** generated *in situ* from the corresponding anthranilic acids (**9c**+**10a**→**4**, **9a**+**10b**→**5**, **9d**+**10a**→**6**, **9b**+**10a**→**7**, and **9a**+**10c**→**8**). Anthracenes **9a** and **9b** were prepared by the Grignard reaction of 2-methylbenzyl chloride with 1-substituted anthrones **11**, followed by dehydration with thionyl chloride–pyridine. Synthesis of anthracene **9c**

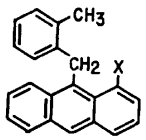

9a: X=H
9b: X=Cl
9c: X=OCH_3
9d: X=CH_3

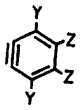

10a: Y=Z=H
10b: Y=CH_3, Z=H
10c: Y=Z=Cl

by the Grignard reaction of 1-methoxyanthrone (**11**: X=OCH_3) was abandoned because preliminary examination of the anthrone suggested that it existed not as a keto form but as an enol form. 4-Methoxyanthrone (**13a**) was condensed with 2-methylbenzyl chloride to give 4-methoxy-10-(2-methylbenzyl)anthrone (**14a**). Reduction with sodium borohydride followed by dehydration with either phosphorus pentaoxide or thionyl chloride–pyridine gave **9c**. Anthracene **9d** was also prepared by 2-methylbenzylation of 4-methylanthrone (**13b**) followed by reduction and dehydration because of the easier availability of the anthrone **13b** as compared with 1-methylanthrone (**11**: X=CH_3).

Rotamer Equilibrium. ^{1}H NMR data at low temperatures (*ca.* −30 °C) are given in Tables 1 and 2. Both of the *ap* and ±*sc* rotamers with respect to the bridgehead-to-methylene bond were present in each compound. Methylene protons of the *ap* rotamer appeared as a singlet, while those of the ±*sc* rotamer did as an AB-quartet. *o*-Methyl protons appeared as two singlets of the relative intensity corresponding to the *ap*/±*sc* ratio with the exception of **4** in $CDCl_3$

TABLE 1. LOW TEMPERATURE CHEMICAL SHIFTS IN $CDCl_3$[a]

Compound	Temp °C	±*sc*/*ap*	Rotamer	CH_2	*o*-CH_3	1-X	10-H
4	−32	2.9	*ap*	4.73		3.82	
					2.66[b]		5.50[b]
			±*sc*	4.00d, 4.65d (*J*=17 Hz)		2.92	
5	−33	1.0	*ap*	4.57	2.47[c]	2.81	5.76[b]
			±*sc*	4.14d, 4.54d (*J*=18.5 Hz)	2.58 2.63 2.67	1.98	
6	−22	1.0	*ap*	4.53	2.60[d]	2.80	5.41[b]
			±*sc*	4.09d, 4.47d (*J*=18.5 Hz)	2.63	1.97	
7	−25	0.6$_7$	*ap*	4.79	2.68	—	5.48[b]
			±*sc*	4.08d, 4.85d (*J*=18 Hz)	2.62	—	
8	−35	0.6$_7$	*ap*	4.79	2.70	—	6.18
			±*sc*	4.08d, 4.91d (*J*=18 Hz)	2.64	—	6.13

a) Chemical shifts are shown in δ relative to internal tetramethylsilane. Singlet unless otherwise stated. Aromatic protons are omitted. b) Coincident between the rotamers. c) Definite rotamer and position assignment could not be made. d) Definite rotamer assignment could not be made.

TABLE 2. LOW TEMPERATURE CHEMICAL SHIFT DATA[a]

Compound	Temp °C	Solvent	±*sc*/*ap*	Rotamer	CH_2	*o*-CH_3	1-X	10-H[b]
4	−32	C_7D_8	2.9	*ap*	4.73	2.51	2.98	5.08
				±*sc*	3.85d, 4.60d (*J*=17.5 Hz)	2.31	2.43	
5	−20	C_7D_8	1.0	*ap*	4.34	2.26[c]	2.37	5.48
				±*sc*	3.95d, 4.35d (*J*=18.5 Hz)	2.24[c]	1.85	
6	−22	C_6H_5Cl	1.0	*ap*	4.40	2.39	2.47	5.23
				±*sc*	3.97d, 4.35d (*J*=18.5 Hz)	2.30	1.80	
7	−25	C_6H_5Cl	0.6$_7$	*ap*	4.78	2.52	—	5.23
				±*sc*	3.96d, 4.80d (*J*=18 Hz)	2.37	—	
8	−25	C_6H_5Cl	0.6$_7$	*ap*	4.67	2.54	—	5.92
				±*sc*	3.91d, 4.77d (*J*=18 Hz)	2.37	—	

a) Chemical shifts are relative to internal hexamethyldisiloxane. Singlet unless otherwise stated. Aromatic protons are omitted. b) Coincident between the rotamers. c) Assignment is tentative. Two other peaks due to 4-methyl appeared at δ 2.12 and 2.17.

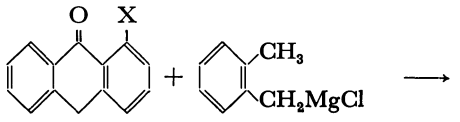

11a: X=H
11b: X=Cl

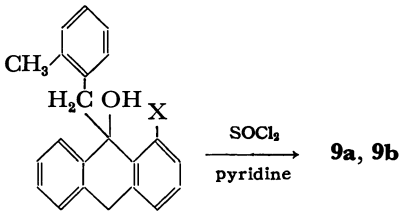

12a: X=H
12b: X=Cl

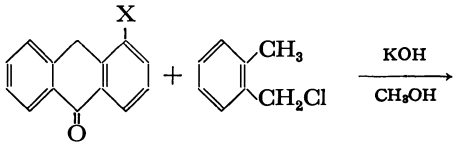

13a: X=OCH_3
13b: X=CH_3

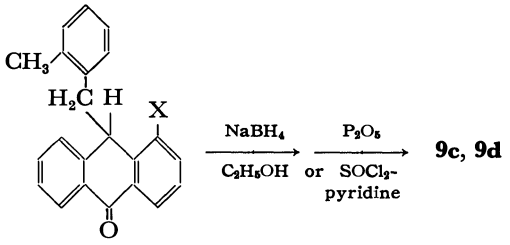

14a: X=OCH_3
14b: X=CH_3

where coincidence of the chemical shifts occurred. 1-Methoxyl protons in **4**, 1- and 4-methyls in **5**, and 1-methyl in **6** also appeared as two singlets reflecting the presence of two rotamers.

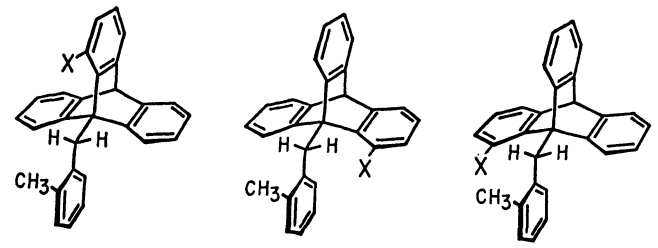

ap *−sc* *+sc*

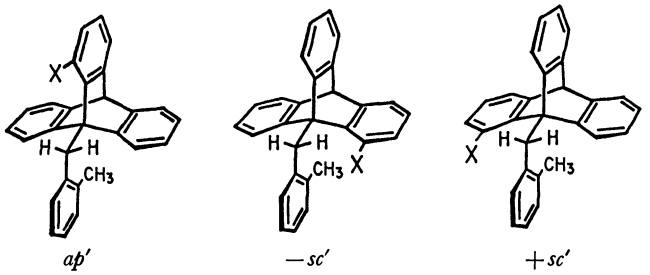

ap′ *−sc′* *+sc′*

Scheme 1.

It is assumed that the benzylic moiety adopts a conformation in which the benzene ring is coplanar with the bridgehead-to-methylene bond as decuced for 9-benzyl-[7] and 9-(3,5-dimethylbenzyl)triptycenes,[2] and that the *o*-methyl group points toward outside the triptycyl skeleton as shown in Scheme 1. This is supported by ^{1}H NMR spectra. The *o*-methyl signal resonated at δ 2.6—2.7 (Table 1), considerably lower field than the methyl signal of toluene (δ 2.32) or *o*-xylene (δ 2.25),[8] suggesting that the methyl group is located in the deshielding region of the ring current effect of the triptycyl benzene rings in line with the conformations. A multiplet signal assigned to the 6-proton of the 2-methylbenzyl group appeared at higher field of the aromatic region of δ 6.2—6.4 which is also consistent with the suggested conformations. Molecular model consideration indicates that the conformers with the *o*-methyl group pointing inside (*ap′* and $\pm sc'$ in Scheme 1) would be highly unstable because of the severe steric interaction between the methyl group and the triptycyl moiety. If these rotamers could exist in a detectable amount, the *o*-methyl group would show a definite signal at a considerably higher field, since the rotamers should have lifetimes long enough for detection on the NMR time scale at these low temperatures. No such signals were detected at δ 0—2 region, and these rotamers were concluded to be at least 2.0 kcal/mol (1 kcal/mol=4.18 kJ/mol) less stable than the rotamers with *o*-methyl group outside.

No significant temperature dependence of the equilibrium constants ($\pm sc/ap$) was detected except for **5** and **6**, which showed a slight increase of the $\pm sc$ rotamers at higher temperatures. The equilibrium constants of **4**—**8** were similar to those of the corresponding 9-benzyltriptycenes,[7,9] suggesting that the interaction between the aryl and the triptycyl moieties do not largely differ in these two systems.

DNMR Behavior. Upon gradual elevation of the temperature the AB-quartet signal due to the methylene protons of the $\pm sc$ rotamer broadened and then coalesced into a singlet in the range of −1 to 17 °C depending on the compound, while the other part of the spectrum except for the aromatic region showed no noticiable change. This indicates that the interconversion between the $+sc$ and $-sc$ rotamers becomes fast on the NMR time scale in the temperature range. The rate constants and the free energies of activation at the coalescence temperatures for the $+sc \rightleftharpoons -sc$ interconversion were calculated; the results are given in Table 3.

The $\pm sc$-methylene signal sharpened on further elevation of temperature until the half-width of the signal became *ca.* 2.5 Hz, almost the same as that of

Table 3. DNMR data for $+sc \rightleftharpoons -sc$ interconversion

Compound	Solvent	$\Delta\delta$ Hz	J_{AB} Hz	T_c °C	k_c s^{-1}	$\Delta G_c^{\ddagger}$ kcal/mol
4	C_7D_8	45	17.5	−1	138	13.2
5	C_7D_8	24	18.5	14	114	14.1
6	C_6H_5Cl	23	18.5	10	113	13.9
7	C_6H_5Cl	51	18.0	7	150	13.6
8	C_6H_5Cl	52	18.0	17	151	14.1

TABLE 4. DNMR DATA FOR $ap \rightleftharpoons \pm sc$ INTERCONVERSION

$$ap \underset{k_{-1}}{\overset{2k_1}{\rightleftharpoons}} \pm sc \qquad : \quad K=\frac{2k_1}{k_{-1}}=\frac{[\pm sc]}{[ap]}$$

Compound	Solvent	Obsd protons	$\Delta\delta$ Hz	T_c °C	$ap \rightarrow \pm sc$ k_{1c} s^{-1}	$ap \rightarrow \pm sc$ $\Delta G_c^{\ddagger}$ kcal/mol	$\pm sc \rightarrow ap$ k_{-1c} s^{-1}	$\pm sc \rightarrow ap$ $\Delta G_c^{\ddagger}$ kcal/mol	K[a]
4	C_7D_8	CH_2	26	66	27	17.7	18	18.0	2.9
		1-OCH_3	41	72	42	17.7	29	18.0	
5	C_7D_8	CH_2	13	98	12	20.0	20	19.7	1.2
6	C_6H_5Cl	CH_2	13	90	12	19.6	20	19.3	1.2
		1-CH_3	42	111	42	19.8	71	19.4	
		o-CH_3	3.1	71	2.4	19.6	3.9	19.3	
7	C_6H_5Cl	CH_2	22	98	14	19.9	40	19.1	0.6_7
		o-CH_3	6.4	79	3.8	19.8	$11._3$	19.0	
8	C_6H_5Cl	CH_2	20	112	13	20.8	38	20.0	0.6_7
		o-CH_3	5.2	94	3.1	20.8	8.9	20.0	

a) Extrapolated to T_c.

the *ap*-methylene singlet, and then began to broaden together with the *ap*-methylene signal. Finally these two signals coalesced into a singlet in the temperature region 66—112 °C.

These coalescence phenomena of the singlets of unequal intensity were analyzed according to the method of Jaeschke *et al.*,[10] affording the rate data for the $ap \rightleftharpoons \pm sc$ interconversion. The rate constants thus obtained and the free energies of activation at the coalescence temperatures are given in Table 4.

The other pairs of signals due to the two rotamers, *i.e.*, *o*-methyls of **4**—**8**, 1-methoxyl of **4**, 1-methyls of **5** and **6**, and 4-methyl of **5** also showed similar coalescence phenomena. DNMR data from some of these signals are also included in Table 4. Free energies of activation obtained from the analysis of different signals agree with each other to support the validity of the approximation in deriving these values if we consider that the entropies of activation would be small for internal rotation.

The observation that, while the signals due to the *ap* rotamer remained completely intact, the coalescence of the AB-quartet signal due to the $\pm sc$-methylene protons occurred suggests that the $+sc \rightleftharpoons -sc$ interconversion takes place without intervention of the *ap* rotamer. An explanation for this is that the interconversion occurs by two consecutive gear motion steps by way of the unstable *ap'* rotamer with the *o*-methyl group pointing inside. The two transition states lying between the *ap'* and $\pm sc$ rotamers, where the aryl group passes over a *peri*-hydrogen, are enantiomeric to each other. The energy barriers to this process can be compared with those to the $ap \rightleftharpoons \pm sc$ process of the corresponding non-*o*-methylated analogs since the two processes have similar transition states. Thus the free energies of activation for the $\pm sc \rightarrow ap$ process of **16a** to **16c** are 12.2,[9a] 13.6,[7b] and 13.5 kcal/mol,[9b] respectively, calculated for 0 °C from the available data. They are 0.6—1.1 kcal/mol lower than those of the corresponding *o*-methylated analogs. This is understandable if we consider that the presence of the *o*-methyl group should raise the transition state to some extent.

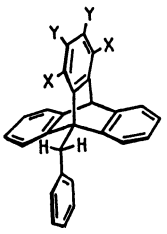

16a: X=OCH_3, Y=H
16b: X=CH_4, Y=H
16c: X=Y=Cl

The IR process of $ap' \rightleftharpoons ap$ should have a higher barrier than the $ap' \rightleftharpoons \pm sc$ step, otherwise the coalescence of the *ap*-methylene signal with those of the $\pm sc$-methylene should have occurred at the same time as the coalescence of the AB-quartet signal of the $\pm sc$-methylene.

Interconversion between the *ap* and $\pm sc$ rotamers can occur by two types of pathways. One consisting of two consecutive gear motion steps ($ap \rightleftharpoons \mp sc' \rightleftharpoons \pm sc$) and the other consisting of a gear motion (GM) step and an isolated rotation (IR) step ($ap \rightleftharpoons \pm sc' \rightleftharpoons \pm sc$ with IR in the $\pm sc$ sites or $ap \rightleftharpoons ap' \rightleftharpoons \pm sc$ with IR in the *ap* site). Of these two possible pathways, the former (2GM) seems more reasonable than the latter (GM-IR) as a process actually occurring. The feasibility is discussed from the *peri*-substituent effects on the barrier in the following sections.

If the $ap \rightleftharpoons \pm sc$ interconversion takes place by the GM-IR pathways, the rate determining step should be IR since the barrier to the GM steps should be *ca.* 14 kcal/mol as was actually observed for the $\pm sc \rightleftharpoons ap'$ step (Table 3), while the barriers observed for the process in question are much higher (Table 4). Studies on 9-(3,5-dimethylbenzyl)triptycenes revealed that the bulkier *peri*-substituent flanking the aryl group raises the IR barrier as a result of destabilization of the transition state to a greater extent than the ground state.[2] Considering that the presence of the *o*-methyl group in the present case would increase the dependence of the IR barrier on the flanking *peri*-groups, we can reasonably assume that the $\pm sc \rightleftharpoons \pm sc'$ barrier should be larger than the $ap \rightleftharpoons ap'$ barrier. Even though we may have to take the difference of the *ap*-substituent into account (*vide infra*), the effect of the *ap*-substituent

is not large enough to revert the circumstance. The GM-IR process should occur by the $ap \rightleftharpoons ap' \rightleftharpoons \pm sc$ pathway rather than the $ap \rightleftharpoons \pm sc' \rightleftharpoons \pm sc$ pathway, if at all.

The energy barrier to the IR process in 9-(3,5-dimethylbenzyl)triptycene derivatives was found to decrease with a larger *peri*-substituent at the *ap*-position to the aryl group,[2] *e.g.*, the IR barrier in the *ap* rotamer of compound **17a** (13.5 kcal/mol) is lower by 1.0 kcal/

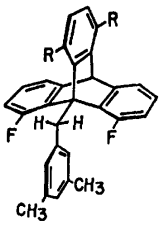

17a: R=CH_3
17b: R=OCH_3

mol than that in the *ap* rotamer of compound **17b** (14.5 kcal/mol). This was explained by assuming that the ground state was destabilized due to the buttressing effect of a bulky *ap*-substituent pushing the aryl moiety into the triptycyl skeleton, while the transition state for the IR was not appreciably affected. In 9-(2-methylbenzyl)triptycenes, the steric situation of the ground state is similar to that of 9-(3,5-dimethylbenzyl)-triptycenes, destabilization of the ground state by the bulkier *ap*-substituent being expected. Although it is difficult to estimate the effect of the *ap*-substituent on the transition state of the IR process, molecular model consideration suggests that the effects should be small if any. Thus replacement of the *ap*-substituent with a bulkier one is expected to lower the $ap \rightleftharpoons ap'$ IR barrier to a small extent, and to lower the $ap \rightleftharpoons \pm sc$ barrier observed by DNMR.

As Table 4 shows, the contrary to the above discussion is true: the $ap \rightleftharpoons \pm sc$ barrier increases with the increasing bulkiness of the *peri*-substituent. Thus the GM-IR process is not the lowest energy pathway of the $ap \rightleftharpoons \pm sc$ interconversion.

In the 2GM process, the $\pm sc \rightleftharpoons \mp sc'$ step should be rate-determining because the aryl group passes over the *peri*-substituent. The energy barrier to this process is naturally expected to increase with the bulkier *peri*-substituent, this being actually observed (Table 4). It is thus reasonable to consider that the $ap \rightleftharpoons \pm sc$ interconversion occurs by the 2GM process.

The process with two consecutive gear motion steps is concluded to be responsible not only for the $+sc \rightleftharpoons -sc$ interconversion but also for the $ap \rightleftharpoons \pm sc$ interconversion in this 9-(2-methylbenzyl)triptycene system (Scheme 2).

The energy diagram for rotation about the bridgehead-to-methylene bond can be drawn as in Fig. 1. Rotation by 720° about the bridgehead-to-methylene bond is required to complete the rotational circuit. Neither the depth of the wells corresponding to the unstable *ap'* and $\pm sc'$ rotamers is known, nor the height of the enantiomeric saddle points between the *ap* and $\pm sc'$ rotamers, which are presumably of almost the same relative height from the nearest minima as those between the *ap'* and $\pm sc$ rotamers.

Total line shape analysis of the DNMR spectra of

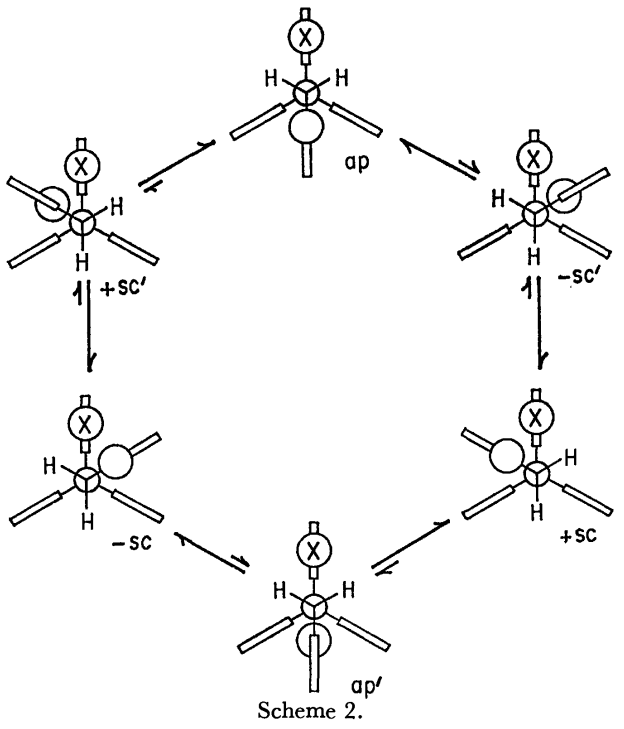

Scheme 2.

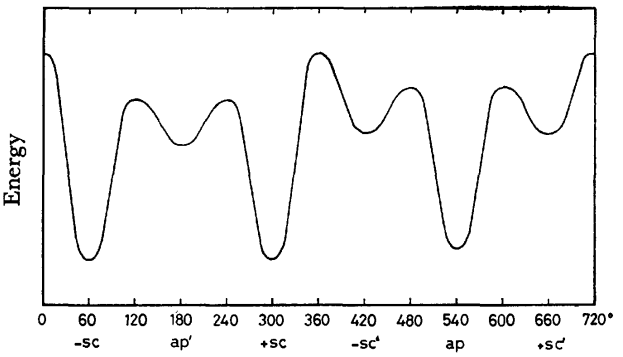

Fig. 1. Energy diagram for rotation about the bridgehead-to-methylene bond.

1,4-dimethoxy-9-(4-chlorobenzyl)triptycene (**18**) suggests that the $+sc \rightleftharpoons -sc$ process in which the aryl group passes over the *peri*-methoxyl group has an energy barrier *ca.* 1 kcal/mol higher than that to the $ap \rightleftharpoons \pm sc$ process in which the aryl group passes over a *peri*-hydrogen.[9a] The energy barrier difference between the $\pm sc \rightleftharpoons ap'$ and $\pm sc \rightleftharpoons \mp sc'$ steps in compound **4** is 4.8 kcal/mol from Tables 3 and 4, which is considerably larger than that of the above case. The reason for the

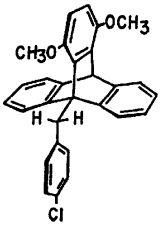

18

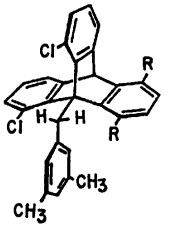

19a: R=H
19b: R=OCH_3

difference is unknown at the moment although the *o*-methyl group must affect the transition states of these two steps.

Energy barriers to the $+sc \rightleftharpoons -sc$ interconversion in compounds **19a** and **19b** were determined to be 15.7 and 22.1 kcal/mol, respectively.[2] The difference of 6.4 kcal/mol can be compared with the data for **4**. The buttressing effect of the *peri*-chloro groups in the transition state may be responsible for the larger difference for compounds **19**, if we neglect the energy difference in the ground states.

Experimental

Melting points are not corrected. ^{1}H NMR spectra at ambient temperature (*ca.* 35 °C) were recorded on either a Hitachi R-20B (60 MHz) or a Varian EM-390 (90 MHz) spectrometer with tetramethylsilane as an internal standard.

DNMR Spectra. Sample solutions were prepared by dissolving the compounds in an appropriate solvent containing 0.5% of tetramethylsilane (in case of $CDCl_3$) or hexamethyldisiloxane (in case of toluene-d_8 and chlorobenzene). The concentration was *ca.* 10% (w/v) for compounds **4**—**6** and *ca.* 6% for **7** and **8** because of the poor solubility. Variable temperature ^{1}H NMR spectra were obtained on a Hitachi R-20B spectrometer. Temperature was calibrated with ethylene glycol or methanol.[11] Rate constants at the coalescence temperatures from coalescing AB-quartet signals were calculated by[12]

$$k_c = \frac{\pi}{\sqrt{2}}\sqrt{(\Delta\delta)^2 + 6J_{AB}{}^2}.$$

Rate constants from two coalescing singlets of unequal intensity were obtained by the graphical method of Jaeschke *et al.*[10] which takes the line widths of the signals without exchange into account. Graphical method of Shanan-Atidi and Bar-Eli[13] which neglects the line widths gave similar results only when the chemical shift differences of the two singlets were sufficiently large (>20 Hz), the inconsistency between the two methods becoming large when the chemical shift differences were small.

*9-(2-Methylbenzyl)anthracene (**9a**).* To the Grignard reagent in 60 mL of diethyl ether prepared from 5.62 g (40 mmol) of 2-methylbenzyl chloride[14] was added portionwise 3.38 g (20 mmol) of anthrone powder. The mixture was stirred at room temperature for 2 h and decomposed with saturated aqueous ammonium chloride. After evaporation of the solvent, the crude 9-(2-methylbenzyl)-9,10-dihydro-9-anthrol (^{1}H NMR (CCl_4, δ): 1.40 (3H, s), 2.25 (1H, s), 2.88 (2H, s), 2.91 and 3.41 (2H, AB-q, J=19 Hz), 6.1—7.8 (12H, m) was dissolved in 50 mL of benzene and treated with 3 mL of thionyl chloride and 6 mL of pyridine at 50 °C for 1 h. The reaction mixture was cooled, washed with water and dried over sodium sulfate. The crude product was recrystallized from tetrahydrofuran–hexane to give 4.02 g (71%) of yellow granules, mp 165—167 °C. Found: C, 93.61; H, 6.22%. Calcd for $C_{22}H_{18}$: C, 93.57; H, 6.43%. ^{1}H NMR ($CDCl_3$, δ): 2.62 (3H, s), 4.81 (2H, s), 6.2—8.2 (12H, m), 8.42 (1H, s).

*1-Chloro-9-(2-methylbenzyl)anthracene (**9b**).* To the Grignard reagent in 50 mL of diethyl ether prepared from 2.11 g (15 mmol) of 2-methylbenzyl chloride[14] was added portionwise 2.29 g (10 mmol) of 1-chloroanthrone[15] and the mixture was stirred at room temperature for 2 h and decomposed with saturated aqueous ammonium chloride. Evaporation of the solvent gave 2.55 g of the crude 1-chloro-9-(2-methylbenzyl)-9,10-dihydro-9-anthrol; ^{1}H NMR ($CDCl_3$, δ): 1.47 (3H, s), 2.65 and 3.45 (2H, AB-q, J=20 Hz), 3.16 and 3.51 (2H, AB-q, J=12.6 Hz), 3.75 (1H, s), 6.17 (1H, d, J=7 Hz), 6.5—7.9 (10H, m). Treatment of the alcohol with 2 mL of thionyl chloride and 4 mL of pyridine at 50 °C for 1 h followed by column chromatography on alumina with benzene–hexane (1 : 4) as an eluent gave 1.86 g (59%) of **9b**, mp 134—135 °C (from tetrahydrofuran–hexane). Found: C, 83.62; H, 5.23; Cl, 11.15%. Calcd for $C_{22}H_{17}Cl$: C, 83.40; H, 5.41; Cl, 11.19%. ^{1}H NMR ($CDCl_3$, δ): 2.53 (3H, s), 5.13 (2H, s), 6.5—8.1 (11H, m), 8.40 (1H, s).

*1-Methoxyanthrone (**11**: $X=OCH_3$).* A mixture of 715 mg (3 mmol) of 1-methoxyanthraquinone[2] and 0.8 g of copper powder in 10 mL of concentrated sulfuric acid was stirred at 40—45 °C for 3 h, poured onto ice–water, and extracted with benzene. The benzene layer was washed with aqueous sodium hydrogencarbonate and then with water, dried over magnesium sulfate, and evaporated to give 265 mg (39%) of orange crystals upon recrystallization from dichloromethane–hexane, mp 86—88 °C. The compound was too unstable to give satisfactory elemental analysis. Spectral data were consistent with the enol form, 1-methoxy-9-anthrol; ^{1}H NMR ($CDCl_3$, δ): 3.96 (3H, s), 6.52 (1H, dd), 7.0—7.6 (4H, m), 7.76 (1H, s), 7.85 (1H, m), 8.40 (1H, m), 10.12 (1H, s). IR (Nujol): 3340 cm^{-1}, no carbonyl stretching.

*4-Methoxy-10-(2-methylbenzyl)anthrone (**14a**).* To a mixture of 1.12 g (5 mmol) of 4-methoxyanthrone (**13a**)[2] and 0.75 mL of 2-methylbenzyl chloride[14] in 40 mL of methanol under nitrogen atmosphere was added dropwise 0.4 g of potassium hydroxide in 15 mL of methanol in the course of 2 h and the mixture was stirred at room temperature for further 2h. Yellow solid formed was collected by filtration, washed with methanol and recrystallized from tetrahydrofuran–methanol to give 1.38 g (84%) of **14a**: mp 151—152 °C. Found: C, 84.26; H, 5.97%. Calcd for $C_{23}H_{20}O_2$: C, 84.12; H, 6.14%. ^{1}H NMR ($CDCl_3$, δ): 1.84 (3H, s), 2.67 (1H, *A*BX-dd, J=13.0 and 8.7 Hz), 3.25 (1H, A*B*X-dd, J=13.0 and 4.7 Hz), 3.91 (3H, s), 4.70 (1H, AB*X*-dd, J=8.7 and 4.7 Hz), 6.4—8.3 (11H, m).

*1-Methoxy-9-(2-methylbenzyl)anthracene (**9c**).* To a boiling solution of 1.68 g (5.12 mmol) of 4-methoxy-10-(2-methylbenzyl)anthrone (**14a**) in 50 mL of ethanol was added dropwise a solution of 1.5 g of sodium borohydride in 20 mL of 90% aqueous ethanol and the mixture was heated under reflux for 2 h. After evaporation of the solvent, the mixture was poured into water and extracted with chloroform. The chloroform solution was washed with water, dried over magnesium sulfate, and evaporated to give crude 4-methoxy-10-(2-methylbenzyl)-9,10-dihydro-9-anthrol (single isomer of undecided stereochemistry; ^{1}H NMR ($CDCl_3$, δ): 1.88 (3H, s), 2.18 (1H, d, J=11 Hz), 2.79 (1H, *A*BX-dd, J=12.8 and 7.5 Hz), 2.95 (1H, A*B*X-dd, J=12.8 and 5.7 Hz), 3.76 (3H, s), 4.65 (1H, AB*X*-dd, J=7.5 and 5.7 Hz), 5.19 (1H, d, J=11 Hz), 6.3—7.9 (11H, m)). The alcohol was dissolved in 50 mL of carbon tetrachloride and heated under reflux with 20 g of phosphorus pentaoxide for 1.5 h. The solid mass was filtered off and washed with carbon tetrachloride. The combined organic solution was evaporated affording 0.87 g (54%) of **9c** upon recrystallization from benzene–hexane (1 : 9): mp 145—146 °C. Found: C, 88.66; H, 6.37%. Calcd for $C_{23}H_{20}O$: C, 88.42; H, 6.45%. ^{1}H NMR ($CDCl_3$, δ): 2.57 (3H, s), 3.57 (3H, s), 5.08 (2H, s), 6.3—8.2 (11H, m), 8.33 (1H, s).

*4-Methyl-10-(2-methylbenzyl)anthrone (**14b**).* To a stirred mixture of 2.08 g (10 mmol) of 4-methylanthrone[16] and 1.4 mL of 2-methylbenzyl chloride[14] in 80 mL of methanol was added dropwise a solution of 0.6 g of potassium hydroxide in 30 mL of methanol in the course of 2 h under nitrogen atmos-

phere and the mixture was stirred at room temperature for further 2 h. After evaporation of the solvent, the residue was extracted with diethyl ether. The ether layer was washed with water, dried over sodium sulfate and evaporated to afford 1.67 g (53%) of **14b** after recrystallization from dichloromethane–hexane: mp 135—136 °C. Found: C, 88.50; H, 6.15%. Calcd for $C_{23}H_{20}O$: C, 88.42; H, 6.45%. ^1H NMR ($CDCl_3$, δ): 1.60 (3H, s), 2.52 (3H, s), 2.78 (1H, *A*BX-dd, J=13.8 and 8.1 Hz), 3.10 (1H, A*B*X-dd, J=13.8 and 5.4 Hz), 4.54 (1H, AB*X*-dd, J=8.1 and 5.4 Hz), 6.5—7.6 (9H, m), 8.0—8.3 (2H, m).

1-Methyl-9-(2-methylbenzyl)anthracene (9d). To a boiling solution of 1.26 g (4.0 mmol) of 4-methyl-10-(2-methylbenzyl)-anthrone (**14b**) in 50 mL of ethanol was added a solution of 1.3 g of sodium borohydride in 20 mL of 90% aqueous ethanol and the mixture was heated under reflux for 2 h. Evaporation of the solvent and extraction with diethyl ether gave 1.09 g (87%) of 4-methyl-10-(2-methylbenzyl)-9,10-dihydro-9-anthrol (single isomer of undecided stereochemistry); ^1H NMR ($CDCl_3$, δ): 1.74 (3H, s), 2.24 (3H, s), 2.50 (1H, d, J= 10 Hz), 2.79 (2H, d, J=6.9 Hz), 4.33 (1H, t, J=6.9 Hz), 5.27 (1H, d, J=10 Hz), 6.5—7.9 (11H, m). The alcohol in 50 mL of benzene was treated with 1 mL of thionyl chloride and 2 mL of pyridine at 70 °C for 5 h to give **9d** in 76% yield: mp 150—151 °C. Found: C, 93.19; H, 6.68%. Calcd for $C_{23}H_{20}$: C, 93.20; H, 6.80%. ^1H NMR ($CDCl_3$ δ): 2.56 (3H s), 2.75 (3H, s), 4.94 (2H, s), 6.5—7.6 (8H, m), 7.8—8.2 (3H, m), 8.48 (1H, s).

General Procedure of Benzyne Addition to Anthracenes. A solution of 2.0—3.0 mmol of an anthranilic acid in 20 mL of tetrahydrofuran was added dropwise to a boiling solution of 1.5 mmol of an anthracene and 1 mL of isopentyl nitrite in 30 mL of dichloromethane in the course of 1 h and the mixture was heated under reflux for further 1 h. After evaporation of the solvent, the residue was chromatographed through an alumina column using benzene–hexane mixture as an eluent. Recrystallization from tetrahydrofuran–ethanol gave a triptycene derivative as colorless crystals.

1-Methoxy-9-(2-methylbenzyl)triptycene (4), mp 258—259 °C, was prepared from 1-methoxy-9-(2-methylbenzyl)anthracene (**9c**) and anthranilic acid in 69% yield. Found: C, 89.77; H, 6.46%. Calcd for $C_{29}H_{24}O$: C, 89.65; H, 6.23%. ^1H NMR ($CDCl_3$, δ) showed the presence of the *ap* and $\pm sc$ rotamers in the ratio of 1 : 3.6 : 2.64 (s, *ap*/$\pm sc$), 2.94 (s, $\pm sc$), 3.83 (s, *ap*), 4.34 (br s, $\pm sc$), 4.74 (br s, *ap*), 5.40 (s, *ap*/$\pm sc$), 6.3—7.6 (m, *ap*/$\pm sc$).

1,4-Dimethyl-9-(2-methylbenzyl)triptycene (5), mp 208—209 °C, was prepared from 9-(2-methylbenzyl)anthracene (**9a**) and 3,6-dimethylanthranilic acid[17] in 76% yield. Found: C, 93.23; H, 6.79%. Calcd for $C_{30}H_{26}$: C, 93.22; H, 6.78%. ^1H NMR ($CDCl_3$, δ) showed the presence of the *ap* and $\pm sc$ rotamers in the ratio of 1 : 1: 1.97 (s, $\pm sc$), 2.44 (s), 2.54 (s), 2.61 (s), 2.64 (s), 2.78 (s, *ap*), 4.33 (br s, $\pm sc$), 4.57 (s, *ap*), 5.72 (s, *ap*/$\pm sc$), 6.3—7.6 (m, *ap*/$\pm sc$).

1-Methyl-9-(2-methylbenzyl)triptycene (6), mp 235—237 °C, was prepared from 1-methyl-9-(2-methylbenzyl)anthracene (**9d**) and anthranilic acid in 28% yield. Found: C, 93.60; H, 6.24%. Calcd for $C_{29}H_{24}$: C, 93.51; H, 6.49%. ^1H NMR ($CDCl_3$, δ) showed the presence of the *ap* and $\pm sc$ rotamers in the ratio of 1 : 1: 1.97 (s, $\pm sc$), 2.59 (s), 2.63 (s), 2.78 (s, *ap*), 4.29 (br s, $\pm sc$), 4.53 (s, *ap*), 5.33 (s, *ap*/$\pm sc$), 6.3—7.6 (m, *ap*/$\pm sc$).

1-Chloro-9-(2-methylbenzyl)triptycene (7), mp 265—266 °C, was prepared from 1-chloro-9-(2-methylbenzyl)anthracene (**9b**) and anthranilic acid in 51% yield. Found: C, 85.64; H, 5.53; Cl, 9.04%. Calcd for $C_{28}H_{21}Cl$: C, 85.59; H, 5.39; Cl, 9.02%. ^1H NMR ($CDCl_3$, δ) showed the presence of the *ap* and $\pm sc$ rotamers in the ratio of 3 : 2: 2.61 (s, $\pm sc$), 2.67 (s, *ap*), 4.46 (br s, $\pm sc$), 4.79 (s, *ap*), 5.40 (s, *ap*/$\pm sc$), 6.2—7.6 (m, *ap*/$\pm sc$).

1,2,3,4-Tetrachloro-9-(2-methylbenzyl)triptycene (8), mp 286—288 °C, was prepared from 9-(2-methylbenzyl)anthracene (**9a**) and tetrachloroanthranilic acid[18] in 22% yield. Found: C, 67.82; H, 3.96; Cl, 28.07%. Calcd for $C_{28}H_{18}Cl_4$: C, 67.77; H, 3.66; Cl, 28.57%. ^1H NMR ($CDCl_3$, δ) showed the presence of the *ap* and $\pm sc$ rotamers in the ratio of 3 : 2: 2.63 (s, $\pm sc$), 2.68 (s, *ap*), *ca.* 4.5 (br, $\pm sc$), 4.81 (s, *ap*), 6.12 (s, $\pm sc$), 6.16 (s, *ap*), 6.1—7.7 (m, *ap*/$\pm sc$).

References

1) Preceding paper: Ref. 2.

2) G. Yamamoto and M. Ōki, *Bull. Chem. Soc. Jpn.*, **54**, 473 (1981).

3) Preliminary results have been reported: G. Yamamoto and M. Ōki, *Chem. Lett.*, **1979**, 1255.

4) K. Mislow, *Acc. Chem. Res.*, **9**, 26 (1976).

5) P. Finnochiaro, W. D. Hounshell, and K. Mislow, *J. Am. Chem. Soc.*, **98**, 4952 (1976).

6) R. Glaser, J. F. Blount, and K. Mislow, *J. Am. Chem. Soc.*, **102**, 2777 (1980).

7) a) F. Suzuki and M. Ōki, *Bull. Chem. Soc. Jpn.*, **48**, 596 (1975); b) F. Suzuki, Ph. D. Thesis, The University of Tokyo (1975).

8) "NMR Spectra Catalog," Varian Associates (1962).

9) a) M. Kono, H. Kihara, N. Nakamura, F. Suzuki, and M. Ōki, *Bull. Chem. Soc. Jpn.*, **52**, 1682 (1979); b) M. Ōki, M. Kono, H. Kihara, and N. Nakamura, *Bull. Chem. Soc. Jpn.*, **52**, 1686 (1979).

10) A. Jaeschke, G. Munsch, H. G. Schmid, H. Friebolin, and A. Mannschreck, *J. Mol. Spectrosc.*, **31**, 14 (1969).

11) A. L. Van Geet, *Anal. Chem.*, **40**, 2227 (1968).

12) M. Ōki, H. Iwamura, and N. Hayakawa, *Bull. Chem. Soc. Jpn.*, **37**, 1865 (1964).

13) H. Shanan-Atidi and K. H. Bar-Eli, *J. Phys. Chem.*, **74**, 961 (1970).

14) W. H. C. Rueggeberg, A. Ginsburg, and R. K. Frantz, *J. Am. Chem. Soc.*, **67**, 2154 (1945).

15) E. de B. Barnett and M. A. Matthews, *J. Chem. Soc.*, **123**, 2549 (1923).

16) L. F. Fieser and H. Heymann, *J. Am. Chem. Soc.*, **64**, 376 (1942).

17) S. Gronowitz and G. Hansen, *Arkiv Kemi*, **27**, 145 (1967).

18) V. Villiger and L. Blangey, *Ber.*, **42**, 3549 (1909).

Chiral and Stereoselective Total Synthesis of (−)-Deoxoprosopinine and (−)-Deoxoprosophylline. Intramolecular Aminomercuration of an ε,ζ-Unsaturated Amine[1,2]

Yutaka SAITOH, Yoshihiko MORIYAMA,† Hiroshi HIROTA, Takeyoshi TAKAHASHI,* and Qui KHUONG-HUU††

Department of Chemistry, Faculty of Science, The University of Tokyo, Hongo, Bunkyo-ku, Tokyo 113
†Institute of Chemistry, Kyoto Prefectural University of Medicine, Taishogun, Kita-ku, Kyoto 603
††Institut de Chimie des Substances Naturelles, Centre National de la Recherche Scientifique, 91190-Gif-sur-Yvette, France

(Received June 11, 1980)

L-Serine was transformed in 8 steps into (4*R*,5*S*)-2,2-dimethyl-4-[(*Z*)-3-pentadecenyl]-1,3-dioxan-5-amine. This chiral ε,ζ-unsaturated amine was subjected to intramolecular aminomercuration and then acid hydrolysis to give (−)-deoxoprosopinine and (−)-deoxoprosophylline.

Seven piperidine alkaloids have been isolated from *Prosopis africana* TAUB. and their structures have been determined, (+)-(2*R*,3*S*,6*R*)-prosopinine (**1**) and (±)-prosophylline (**2**) being two representatives of these Prosopis alkaloids.[3] Although some approaches to the synthesis of Prosopis alkaloids have been reported,[4] no chiral synthesis has yet been accomplished. Recently, an intramolecular aminomercuration[5] was successfully applied to the synthesis of (±)-solenopsin A and (±)-isosolenopsin A, piperidine derivatives related to fire ant venom.[6] This paper deals with a chiral and stereoselective total synthesis of (−)-deoxoprosopinine (**3**) [an enantiomer of (+)-deoxoprosopinine derived from natural **1**] and (−)-deoxoprosophylline (**4**) starting from L-serine (**5**) by a route involving the intramolecular aminomercuration of an ε,ζ-unsaturated amine (**6**).

(2*S*)-3-Acetoxy-2-phthalimidopropanal (**7**) was prepared from L-serine (**5**) *via* (2*S*)-3-acetoxy-2-phthalimidopropanoic acid (**8**) by the known procedure.[7] The carbon chain of the aldehyde (**7**) was elongated by C_{15}-unit by the Grignard reaction. A C_{15}-bromide (**9**) was prepared as follows. Hydrogenation of 3-pentadecyn-1-ol[8] in ethanol in the presence of a palladium–barium sulfate catalyst deactivated with quinoline[9] gave (*Z*)-3-pentadecen-1-ol (**10**) in a quantitative yield. The alcohol (**10**) was brominated with dibromotriphenylphosphine in dichloromethane to afford (*Z*)-3-pentadecenyl bromide (**9**) in 89% yield.

The chiral aldehyde (**7**) in a mixture of tetrahydrofuran and ether was treated with the Grignard reagent prepared from **9** at −70 °C and then at −45 °C to give a mixture of diol monoacetates (**11** and **12**), the separation of which by column and thin-layer chromatographies was unsuccessful. Acid hydrolysis of this mixture afforded, after separation by silica gel column chromatography, (2*S*,3*R*,6*Z*)-2-phthalimido-6-octadecene-1,3-diol (**13**) and (2*S*,3*S*,6*Z*)-2-phthalimido-6-octadecene-1,3-diol (**14**) in 16.5 and 2.4% yields from **8**, respectively. On treatment with 2,2-dimethoxypropane in the presence of *p*-toluenesulfonic acid, the diols **13** and **14** gave their acetonides **15** and **16** in 97% and 70% yields, respectively. The coupling constant between a C-4 proton and a C-5 proton was determined by ^{1}H-NMR measurements to be 10 and 5 Hz for **15** and **16**, respectively; this led to the *erythro* and *threo* configurations for **13** and **14**, respectively. The formation of **13** and **14** from **7** in a *ca.* 7 : 1 ratio showed that a stereoselective attack[7] of the Grignard reagent to the aldehyde (**7**) was effected preferentially from the less hindered side of **7** to give predominantly the desired *erythro* derivative (**11**).

Hydrazinolysis of the *N*-protective phthaloyl group of **15** gave (4*R*,5*S*)-2,2-dimethyl-4-[(*Z*)-3-pentadecenyl]-1,3-dioxan-5-amine (**6**) in a quantitative yield. The ε,ζ-unsaturated amine (**6**) was subjected to aminomercuration with mercury(II) acetate in methanol at room temperature and then demercuration with sodium borohydride to afford two piperidine acetonides, (1*R*,6*S*,8*S*)-8-dodecyl-3,3-dimethyl-2,4-dioxa-7-azabicyclo[4.4.0]decane (**17**) and its (1*R*,6*S*,8*R*)-diastereomer (**18**), in 3.3 and 76% yields, respectively; this shows that the reaction proceeded stereoselectively. The 8*S* and 8*R* stereochemistry was shown for **17** and **18** by their conversion into **3** and **4**, respectively, as described below. In the ^{1}H-NMR spectrum (270 MHz) of **17** in deuteriochloroform the proton on C-8 resonated at δ 2.99 as a broad signal with a half-band width ($W_{1/2}$) 21 Hz, while in the spectrum of **18** in deuteriobenzene the C-8 proton signal appeared at δ 2.33 as a broad signal with $W_{1/2}$=25 Hz. These $W_{1/2}$ values are in line with those ($W_{1/2}$=18 Hz[3b] and $W_{1/2}$=24 Hz[3c]) observed for the corresponding proton signals of *O*,*O*′-benzylidene

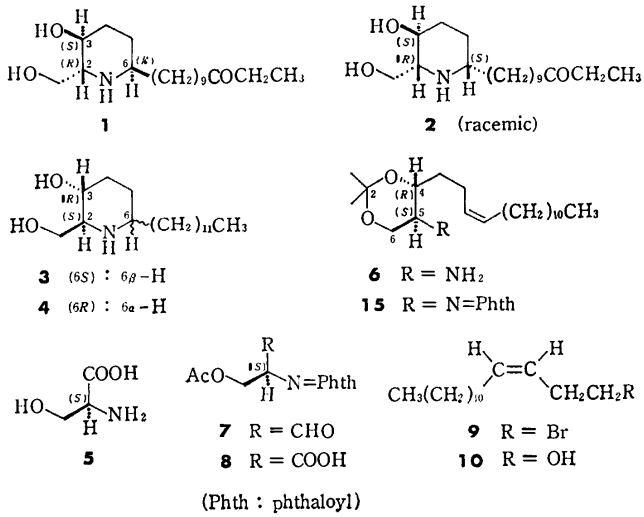

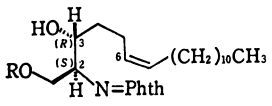

11 R = Ac
13 R = H

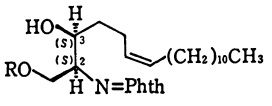

12 R = Ac
14 R = H

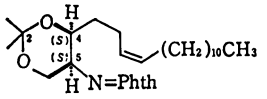

16

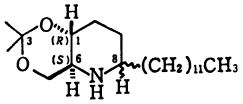

17 (8S) : 8β-H
18 (8R) : 8α-H

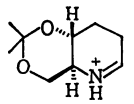

19

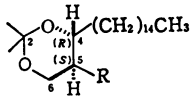

20 R = NH_2
21 R = N=Phth

derivatives of deoxoprosopinine[3b] and deoxoprosophylline,[3c] respectively. A peak at *m/e* 170 (**19**) due to a loss of the side chain was observed as a base peak in the mass spectra of both **17** and **18**.

Finally, the acetonides **17** and **18** were hydrolyzed to afford (−)-deoxoprosopinine (**3**) and (−)-deoxoprosophylline (**4**) in 58 and 86% yields, respectively. The two synthetic piperidines **3** and **4** were found to be identical, except for optical property, with authentic (+)-deoxoprosopinine[3a,b] and (±)-deoxoprosophylline[3c] derived from natural (+)-prosopinine (**1**)[3a,b] and (±)-prosophylline (**2**),[3c] respectively. Since the absolute value of optical rotation ($[\alpha]_D$ −14.7°) of the synthetic deoxoprosopinine (**3**) is almost the same as that ($[\alpha]_D$ +12°) of deoxoprosopinine derived from natural **1**, no racemization occurred during the course of synthesis.

Thus, (−)-deoxoprosopinine (**3**) and (−)-deoxoprosophylline (**4**) were synthesized from L-serine (**5**) in overall yields of 0.12 and 4.3%, respectively. This constitutes the first example of stereoselective total synthesis of optically active Prosopis alkaloids, presenting a useful synthetic route applicable to the other piperidine alkaloids.

Experimental

Melting points were measured on a Mel-temp capillary melting point apparatus (Laboratory Devices) and are uncorrected. IR spectra were measured with a Hitachi EPI-G2, a Hitachi 260-30, or a JEOL JIR-03F (FT) spectrometer, ^{1}H-NMR spectra with a Hitachi R-20B (60 MHz), a Varian EM-390 (90 MHz), a JEOL PS-100 (100 MHz), or a Brucker WH 270 (270 MHz, FT) spectrometer in deuteriochloroform solution containing tetramethylsilane as an internal standard, low resolution mass spectra with a Hitachi RMU-6-Tokugata mass spectrometer with a direct inlet system operating at 70 eV, high resolution mass spectra and chemical ionization mass spectra (CI-MS) with a JEOL JMS-D300 mass spectrometer. Measurenents of optical rotation were carried out with JASCO DIP-SL and DIP-4 polarimeters. Vaper-phase chromatographic (VPC) analyses were performed on Shimadzu gas chromatographs GC-4A PF and GC-6A PF. Thin-layer chromatography (TLC) was carried out on Kieselgel GF_{254} (E. Merck, Darmstadt) and Alumina B-10F (Wako Pure Chemical Industries) in 0.25 mm thickness for analytical use and in 1 mm thickness for preparative use. Wakogel C-200 and Aluminiumoxid Woelm (neutral; M. Woelm, Eschwege) were used for column chromatography.

*(Z)-3-Pentadecen-1-ol (**10**).* 3-Pentadecyn-1-ol[8] (20 g) in methanol (150 ml) was hydrogenated in the presence of a 5% palladium–barium sulfate catalyst (400 mg) deactivated with quinoline[9] at room temperature for 3 h. The reaction was monitored by VPC examination. After filtration of the catalyst, the solvent was removed to give a residue, which was dissolved in hexane (200 ml). The hexane solution was washed with 1.5 M (1 M=1 mol dm^{-3}) hydrochloric acid, saturated aqueous sodium hydrogencarbonate solution, and brine, dried, and evaporated. The residue was chromatographed on a column of silica gel (150 g; elution with benzene) to give **10** (20.4 g) in a quantitative yield. (*Z*)-3-Pentadecen-1-ol (**10**): mp 12—13 °C, bp 105 °C/0.1 kPa; IR (neat) 3350, 3000, 2950, 2850, 1660, 1470, 1380, 1050, 1020, and 720 cm^{-1}; absence of absorption around 965 cm^{-1}; ^{1}H-NMR ($CDCl_3$) δ 0.89 (3H, t, J=5 Hz, $-CH_2C\underline{H}_3$), 1.27 (18H, s, 9×CH_2), 2.00 (3H, m, $-C\underline{H}_2CH$=CH– and OH), 2.38 (2H, m, –CH=CH–$C\underline{H}_2$–CH_2OH), 3.62 (2H, t, J=6.5 Hz, $-C\underline{H}_2OH$), and 5.45 (2H, m, $-CH_2-C\underline{H}$=$C\underline{H}-CH_2$–); MS *m/e* 208 [relative intensity (%): 15; $(M-18)^+$], 186 (100), and 141 (95). Found: C, 79.32; H, 13.41%. Calcd for $C_{15}H_{30}O$: C, 79.57; H, 13.36%. On VPC examination (DEGS; 2 m; 205 °C; N_2 50 ml/min), the retention time (R_t) of **10** was found to be 8.8 min; a peak (R_t=7.2 min) due to pentadecan-1-ol was absent.

*(Z)-3-Pentadecenyl Bromide (**9**).* A solution of (*Z*)-3-pentadecen-1-ol (**10**; 14.4 g) in dichloromethane (50 ml) was added to a solution of dibromotriphenylphosphine in dichloromethane (380 ml) prepared from triphenylphosphine (52 g) and bromine (26.15 g), and the mixture was stirred at room temperature for 1.5 h. The organic solution was washed with water and brine, and concentrated to 100 ml. Hexane (700 ml) was added to this concentrated solution with vigorous stirring to produce a precipitated mass of triphenylphosphine oxide, which was separated by filtration and washed with hexane (total 200 ml). The filtrate and the washings were combined, and the solvents were removed to give a residue, which was subjected to dry column chromatography (silica gel, 150 g; elution with hexane) and then distillation under reduced pressure, giving **9** (16.3 g) in 89% yield. (*Z*)-3-Pentadecenyl bromide (**9**): a colorless oil, bp 156—156.5 °C/0.4 kPa; IR (neat) 3000, 2950, 2900, 2860, 1660, 1460, 1380, 1310, 1280, 1210, 720, 675, and 640 cm^{-1}; absence of absorption around 965 cm^{-1}; ^{1}H-NMR ($CDCl_3$) δ 0.89 (3H, t, J=6 Hz, $-CH_2-C\underline{H}_3$), 1.27 (18H, s, 9×CH_2), 2.03 (2H, m, $-C\underline{H}_2CH$=CH–), 2.67 (2H, m, –CH=CH–$C\underline{H}_2$–CH_2Br), 3.35 (2H, t, J=6.5 Hz, $-CH_2Br$), and 5.44 (2H, m, $-CH_2-C\underline{H}$=$C\underline{H}$–CH_2–; a coupling constant between the two olefinic protons was determined to be 10.5 Hz by decoupling experiments, indicating a (*Z*)-olefin stereochemistry); MS *m/e* 290 and 288 (each 6.5; M^+), 186 (88), and 149 (100). Found: C, 62.09; H, 10.07%. Calcd for $C_{15}H_{29}Br$: C, 62.28; H, 10.10%.

When a part of **9** was left at room temperature for 6 months, **9** isomerized into (*E*)-3-pentadecenyl bromide: a colorless oil; IR (neat) 3000, 2950, 2920, 2850, 1660, 1460, 1380, 1260, 1200, 1070, 965, 800, 720, 665, and 640 cm^{-1}; ^{1}H-NMR ($CDCl_3$) δ 0.90 (3H, t-like, $-CH_2C\underline{H}_3$), 1.27 (18H, s, 9×CH_2), 2.00 (2H, m, $-C\underline{H}_2CH$=CH–), 2.59 (2H, m, –CH=CH–$C\underline{H}_2$–CH_2Br), 3.37 (2H, t, J=7 Hz, $-CH_2Br$), and 5.44 (2H, m, $-CH_2C\underline{H}$=$C\underline{H}-CH_2$–; decoupling experiments showed a

coupling constant between the two olefinic protons to be 15 Hz, indicating an (*E*)-olefin structure).

(2S)-3-Acetoxy-2-phthalimidopropanal (7). According to the procedure described by Newman,[7] L-serine (**5**) was converted into (2*S*)-3-acetoxy-2-phthalimidopropanoic acid (**8**) in 41% yield, which was then transformed into the aldehyde (**7**) in 95% yield. Because of an unstability of the aldehyde (**7**), **7** was used immediately for the following Grignard reaction.

Grignard Reaction of (2S)-3-Acetoxy-2-phthalimidopropanal (7) with (Z)-3-Pentadecenylmagnesium Bromide. A solution of (*Z*)-3-pentadecenylmagnesium bromide (4.96 mmol) in ether (62 ml) [prepared from the bromide (**9**) and magnesium in ether by the usual procedure] was added dropwise to a solution of the aldehyde (**7**; 1.298 g; 4.97 mmol) in a mixture of tetrahydrofuran (10 ml) and ether (5 ml) with stirring under an argon atmosphere at a temperature between −72 and −70 °C. After the mixture had been stirred at this temperature for 1 h and then at −45 °C for 1 h, a saturated aqueous solution (50 ml) of ammonium chloride was added at −45 °C. The reaction mixture was treated in the usual way to give a residue (2.75 g) which was chromatographed on a column of silica gel (100 g). Elution with hexane–ethyl acetate (17 : 3) gave a mixture (760 mg; 32% yield from **7**; 30% yield from **8**) of diol monoacetate (**11** and **12**). However, separation of each of two diastereomers (**11** and **12**) by column and thin-layer chromatographies was unsuccessful. Mixture of **11** and **12**: an oil; IR (neat) 3450, 2900, 1770, 1740, 1705, 1380, 1230, 1040, 720, and 675 cm^{-1}; ^1H-NMR ($CDCl_3$) δ 0.89 (3H, t-like, $-CH_2C\underline{H}_3$), 1.24 (18H, broad s, $9\times CH_2$), 1.60 (2H, m, $-\underline{C}H(OH)-C\underline{H}_2CH_2-$), 1.95 (3H, s, CH_3CO-), 2.10 (4H, broad m, allylic H's), *ca.* 3.5 (1H, broad signal, OH), 4.15 (1H, m, HO–$C\underline{H}$–), 4.55 (3H, m, AcO–$C\underline{H}_2-\underline{C}H-N-$), 5.36 (2H, m, $-CH_2-C\underline{H}=C\underline{H}-CH_2-$), and 7.83 (4H, m, aromatic H's).

Acid Hydrolysis of the Mixture of Diol Monoacetates (11 and 12). The mixture of diol monoacetates (**11** and **12**; 838 mg) was added to a solution (20 ml) prepared from 1 M hydrochloric acid and methanol (1 : 9 v/v), and the whole mixture was refluxed for 4 h. After the solvent had been removed under reduced pressure, the mixture was extracted with ether. The ethereal solution was washed with saturated aqueous sodium hydrogencarbonate solution and brine, dried (Na_2SO_4), and evaporated to give an oil, which was chromatographed on a column of silica gel (15 g). Elution with hexane–ethyl acetate (7 : 3) gave a mixture of **13** and **14**, and then pure **13** (306 mg). This mixture was subjected to separation by TLC to afford **13** (116 mg) and **14** (59 mg; 2.6% yield from **7**; 2.4% yield from **8**). The *erythro*-diol (**13**; total 422 mg) was obtained in 17.6% yield from **7** (16.5% yield from **8**). (2*S*, 3*R*, 6*Z*)-*erythro*-2-Phthalimido-6-octadecene-1,3-diol (**13**): mp 32.5—34.5 °C [purified by molecular distillation: 110—130 °C (bath temperature)/13 Pa], $[\alpha]_D^{19}$ −15° (*c* 0.20; $CHCl_3$); IR (Nujol) 3450, 1780, and 1705 cm^{-1}; absence of absorption around 965 cm^{-1}; ^1H-NMR ($CDCl_3$) δ 0.89 (3H, t-like, $-CH_2C\underline{H}_3$), 1.26 (18H, broad s, $9\times CH_2$), 1.55 (2H, m, HO–$\underline{C}H-C\underline{H}_2CH_2-$), 2.10 (4H, broad m, allylic H's), *ca.* 3.1—3.8 (2H, broad signals, $2\times OH$), 4.17 [4H, m, HO–$C\underline{H}_2-C\underline{H}$(NPhth)–$C\underline{H}$(OH)–], 5.35 (2H, m, $-CH_2-C\underline{H}=C\underline{H}-CH_2-$), and 7.82 (4H, m, aromatic H's). Found: C, 72.74; H, 9.17; N, 3.45%. Calcd for $C_{26}H_{39}NO_4$: C, 72.69; H, 9.15; N, 3.26%. (2*S*, 3*S*, 6*Z*)-*threo*-2-Phthalimido-6-octadecene-1,3-diol (**14**): an oil [purified by molecular distillation: 110—130 °C (bath temperature)/13 Pa], $[\alpha]_D^{19}$ +5° (*c* 0.23; $CHCl_3$); IR (Nujol) 3450, 1770, and 1700 cm^{-1}; absence of absorption around 965 cm^{-1}; ^1H-NMR ($CDCl_3$) δ 0.89 (3H, t-like, $-CH_2C\underline{H}_3$), 1.27 (18H, broad s, $9\times CH_2$), 1.50 (2H, m, HO–$\underline{C}H-C\underline{H}_2-CH_2-$), 2.05 (4H, broad m, allylic H's), *ca.* 3.2—3.8 (2H, broad signals, $2\times OH$; disappeared on addition of D_2O), 4.16 (3H, m, HO–$C\underline{H}_2-\underline{C}H-\underline{N}-$ and HO–$\underline{C}H-$), 4.40 (1H, t-like, J=*ca.* 6 Hz, HO–$CH_2-\underline{C}H-N-$), 5.37 (2H, m, $-CH_2-C\underline{H}=C\underline{H}-CH_2-$), and 7.88 (4H, m, aromatic H's). Found: *m/e* 429.2883. Calcd for $C_{26}H_{39}NO_4$: M, 429.2878.

Acetalization of the erythro*-Diol (13).* The *erythro*-diol (**13**; 176 mg) was dissolved in 2,2-dimethoxypropane (10 ml) containing a trace of *p*-toluenesulfonic acid, and the solution was stirred at room temperature for 12 h. The reaction mixture was treated in the usual way to give a residue, which was purified by chromatography on a column of silica gel [3 g; elution with hexane–ethyl acetate (19 : 1)] giving an acetonide (**15**; 119 mg) in 62% yield. When the reaction was carried out for 10 d, **15** was obtained in 97% yield. (4*R*, 5*S*)-2,2-Dimethyl-4-[(*Z*)-3-pentadecenyl]-5-phthalimido-1,3-dioxane (**15**): mp 47—48 °C (crystallized from ethanol), $[\alpha]_D^{19}$ −6° (*c* 0.23, $CHCl_3$); IR (Nujol) 1780, 1720, 1705, 1110, and 1070 cm^{-1}; absence of absorption around 965 cm^{-1}; ^1H-NMR ($CDCl_3$) δ 0.88 (3H, t-like, $-CH_2C\underline{H}_3$), 1.24 (18H, broad s, $9\times CH_2$), 1.45 and 1.64 [each 3H, s, $(CH_3)_2\underline{C}-$], 1.48 (2H, m, –O–$\underline{C}H-C\underline{H}_2-CH_2-$), 2.00 (4H, broad m, allylic H's), 3.70 (1H, dd, J=10 and J=5 Hz, $C_{(6\alpha)}$–H), 4.20 (1H, td, J=10 and J=5 Hz, $C_{(5\alpha)}$–H), 4.51 (1H, t, J=10 Hz, $C_{(6\beta)}$–H), 4.65 (1H, m, $C_{(4\beta)}$–H), 5.26 (2H, m, $-CH_2-C\underline{H}=C\underline{H}-CH_2-$), and 7.80 (4H, m, aromatic H's). Found: C, 74.37; H, 9.20; N, 3.23%. Calcd for $C_{29}H_{43}NO_4$: C, 74.16; H, 9.23; N, 2.98%.

Acetalization of the threo*-Diol (14).* A soltuion of the *threo*-diol (**14**; 34 mg) in 2,2-dimethoxypropane (1 ml) containing a trace of *p*-toluenesulfonic acid was stirred at room temperature for 10 d. The reaction mixture was treated in the usual way to give a residue, which was chromatographed on a column of silica gel [elution with hexane–ethyl acetate (2 : 1)] giving the corresponding acetonide (**16**; 26.2 mg) in 70% yield, besides unchanged **14** (8.5 mg). (4*S*, 5*S*)-2,2-Dimethyl-4-[(*Z*)-3-pentadecenyl]-5-phthalimido-1,3-dioxane (**16**): mp 56—56.5 °C, $[\alpha]_D^{19}$ +2° (*c* 0.43; $CHCl_3$); IR (Nujol) 1775, 1720, 1705, 1260, 1110, and 1060 cm^{-1}; absence of absorption around 965 cm^{-1}; ^1H-NMR ($CDCl_3$) δ 0.89 (3H, t-like, $-CH_2C\underline{H}_3$), 1.26 (18H, broad s, $9\times CH_2$), 1.44 and 1.61 [each 3H, s, $(CH_3)_2\underline{C}-$], 1.46 (2H, m, –O–$\underline{C}H-C\underline{H}_2-CH_2-$), 2.05 (4H, broad m, allylic H's), 3.95 (1H, dd, J=11 and J=7 Hz, $C_{(6)}$–H), 4.15 (1H, dt, J=9 and J=5 Hz, $C_{(4\alpha)}$–H), 4.38 (1H, dd, J=11 and J=7 Hz, $C_{(6)}$–H), 4.67 (1H, td, J=7 and J=5 Hz, $C_{(5\alpha)}$–H), 5.26 (2H, m, $-CH_2-C\underline{H}=C\underline{H}-CH_2-$), and 7.81 (4H, m, aromatic H's). Found: *m/e* 469.3205. Calcd for $C_{29}H_{43}NO_4$: M, 469.3192.

Hydrazinolysis of the Acetonide (15) Derived from erythro*-Diol Phthalimide (13).* Hydrazine hydrate (100%; 40.9 mg; 0.82 mmol; *ca.* 3 equivalent moles) was added to a solution of the acetonide (**15**; 132 mg; 0.28 mmol) in ethanol (5 ml), and the mixture was refluxed under an argon atmosphere for 2.5 h. The reaction mixture was extracted with dichloromethane (total 30 ml) after addition of water (3 ml) and potassium hydroxide (*ca.* 0.2 g). The organic layer was treated in the usual way to give an *erythro*-amine (**6**; 99 mg; 0.29 mmol) in a quantitative yield. (4*R*, 5*S*)-2,2-Dimethyl-4-[(*Z*)-3-pentadecenyl]-1,3-dioxan-5-amine (**6**): an oil; IR (neat) 3350, 2930, 1660, 1460, 1380, 1270, 1200, 1160, 1070, 860, 720, and 660 cm^{-1}; absence of absorption around 965 cm^{-1}; ^1H-NMR ($CDCl_3$) δ 0.88 (3H, t-like, $-CH_2C\underline{H}_3$), 1.27

(18H, broad s, 9×CH_2), 1.38 and 1.40 [each 3H, s, $(CH_3)_2\underline{C}$–], 1.70 (2H, m, –O–$\underline{CH}$–$C\underline{H}_2$–CH_2–), 2.00 (4H, m, allylic H's), 2.60 (1H, m, $C_{(5\alpha)}$–H), *ca.* 3.0—3.9 (3H, m, $C_{(4\beta)}$–H, $C_{(6\beta)}$–H, and $C_{(6\alpha)}$–H), and 5.34 (2H, m, –CH_2–$C\underline{H}$=$C\underline{H}$–CH_2–); MS *m/e* 339 (27; M^+), 324 (81), 281 (38), 267 (40), 264 (32), 250 (34), 170 (98), 101 (100), and 100 (92); peaks at *m/e* 341 and 326 due to its dihydro derivative (**20**) were not observed (*vide infra*). Found: *m/e* 339.3134. Calcd for $C_{21}H_{41}NO_2$: M, 339.3135.

When the hydrazinolysis of **15** was carried out with 8 equivalent moles of hydrazine hydrate under reflux for 2 h, a mixture of **6** and its dihydro derivative (**20**) was obtained. Although separation of these products by means of various techniques including VPC was unsuccessful, the mass spectrum showed that the mixture consisted of **6** [*m/e* 339 (M^+) and 324 ($M-15)^+$] and **20** [*m/e* 341 (M^+) and 326 ($M-15)^+$] in a ratio of *ca.* 7 : 6. The formation of **20** could be explained by reduction of **6** with diimide, which may be produced from hydrazine by oxidation with oxygen present in the system, even when the reaction was carried out under an argon atmosphere.

Aminomercuration of the ε,ζ-Unsaturated Amine (6). A solution of mercury(II) acetate (486 mg) in methanol (20 ml) was added to a solution of the ε,ζ-unsaturated amine (**6**; 266 mg) in methanol (15 ml), the whole solution being stirred at room temperature for 2 weeks. After addition of a solution of sodium borohydride (72 mg) in 2 M aqueous sodium hydroxide solution (5 ml), the aqueous methanol solution was separated from a white precipitate of mercury by decantation. This aqueous methanol solution was evaporated under reduced pressure, and extracted with dichloromethane (total 30 ml) after addition of water (10 ml). The organic layer was washed with brine, dried ($MgSO_4$), and evaporated, giving an oil, which was chromatographed on a column of alumina (5 g). Elution with hexane–ether (6 : 1) afforded an (8*R*)-acetonide (**18**; 202 mg) in 76% yield. Successive elution with ether gave an (8*S*)-acetonide (**17**; 8.9 mg) in 3.3% yield. (1*R*, 6*S*, 8*S*)-8-Dodecyl-3,3-dimethyl-2,4-dioxa-7-azabicyclo[4.4.0]decane (**17**): an oil, $[\alpha]_D^{19}$ +2° (*c* 0.10; $CHCl_3$); IR (neat) 3300, 2920, 1460, 1380, 1270, 1200, 1160, 1095, 1060, 960, and 855 cm^{-1}; ^{1}H-NMR (270 MHz; $CDCl_3$) δ 0.89 (3H, t, *J*=7 Hz, –$CH_2C\underline{H}_3$), 1.42 and 1.51 [each 3H, s, $(CH_3)_2\underline{C}$–], 2.80 (1H, m, $C_{(6\alpha)}$–H), 2.99 (1H, broad signal, $W_{1/2}$=21 Hz, $C_{(8\beta)}$–H), 3.58 (1H, td, *J*=10 and *J*=4 Hz, $C_{(1\beta)}$–H), 3.68 (1H, dd, *J*=12.6 and *J*=10 Hz, $C_{(5)}$–H), and 3.70 (1H, dd, *J*=10 and *J*=2.5 Hz, $C_{(5)}$–H); MS *m/e* 339 (0.3; M^+), 324 (6), 264 (8), 224 (23), and 170 (100). Found: *m/e* 339.3090. Calcd for $C_{21}H_{41}NO_2$: M, 339.3135. The fragment ion peak due to **19** was observed at *m/e* 170.1200. Calcd for $C_9H_{16}NO_2$: $M-C_{12}H_{25}$, 170.1180. (1*R*, 6*S*, 8*R*)-8-Dodecyl-3,3-dimethyl-2,4-dioxa-7-azabicyclo-[4.4.0]decane (**18**): mp 45—47.5 °C (crystallized from hexane–ether), $[\alpha]_D^{23}$ +9° (*c* 0.27; $CHCl_3$); IR (Nujol) 3550, 3300, 1270, 1200, 1090, 1060, 855, and 760 cm^{-1}; ^{1}H-NMR (270 MHz; C_6D_6) δ 0.92 (3H, t, *J*=6.5 Hz, –$CH_2C\underline{H}_3$), 1.40 and 1.56 [each 3H, s, $(CH_3)_2\underline{C}$–], 2.33 (1H, broad signal, $W_{1/2}$=25 Hz, $C_{(8\alpha)}$–H); 2.56 (1H, td, *J*=10 and *J*=4.9 Hz, $C_{(6\alpha)}$–H), 3.47 (1H, ddd, *J*=10.5. *J*=10, and *J*=4 Hz, $C_{(1\beta)}$–H), 3.59 (1H, dd, *J*=10.7 and *J*=10 Hz, $C_{(5\beta)}$–H), and 3.64 (1H, dd, *J*=10.7 and *J*=4.9 Hz, $C_{(5\alpha)}$–H); MS *m/e* 339 (8; M^+), 324 (35), 224 (49), and 170 (100). Found: *m/e* 339.3114. Calcd for $C_{21}H_{41}NO_2$: M, 339.3135. The fragment ion peak due to **19** was observed at *m/e* 170.1193. Calcd for $C_9H_{16}NO_2$: $M-C_{12}H_{25}$, 170.1180.

When a mixture (*ca.* 7 : 6) of **6** and **20** (*vide supra*) was subjected to aminomercuration and then separation by column chromatography as described above, **17**, **18**, and unchanged **20** [elution with ether–methanol (9 : 1)] were obtained in 2, 41, and 46% yields, respectively. The saturated amine (**20**) was found to be identical with an authentic specimen (**20**) described below.

Preparation of the Saturated Amine (20) from its Phthalimide Derivative (21). The known (4*R*, 5*S*)-2,2-dimethyl-4-pentadecyl-5-phthalimido-1,3-dioxane[10] (**21**; *N*-phthaloyldihydrosphingosine acetonide; 25.8 mg) was added to a solution (0.4 ml) prepared from hydrazine hydrate (80%) and ethanol (1 : 7 v/v), and the mixture was refluxed under an argon atmosphere for 1.5 h. The reaction mixture was treated as described for the hydrazinolysis of **15**, giving the saturated amine (**20**; 16.8 mg) in 87% yield. (4*R*, 5*S*)-2,2-Dimethyl-4-pentadecyl-1,3-dioxan-5-amine (**20**): an oil; IR (neat) 3350, 2920, 1265, 1200, 1165, 1090, 860, and 660 cm^{-1}; ^{1}H-NMR ($CDCl_3$) δ 0.88 (3H, t-like, –$CH_2C\underline{H}_3$), 1.27 (s, methylene protons in the side chain), 1.38 and 1.43 [each 3H, s, $(CH_3)_2\underline{C}$–], *ca.* 2.4 (1H, m, $C_{(5\alpha)}$–H), 3.44 (2H, m, $C_{(6\beta)}$–H and $C_{(4\beta)}$–H), and 3.85 (1H, dd-like, $C_{(6\alpha)}$–H); MS *m/e* 341 (7; M^+), 326 (100), and 266 (89). Found: *m/e* 341.3282. Calcd for $C_{21}H_{43}NO_2$: M, 341.3292.

Acid Hydrolysis of the (8S)-Acetonide (17). The (8*S*)-acetonide (**17**; 5.1 mg) was added to a solution (2 ml) prepared from 8 M hydrochloric acid and methanol (1 : 9 v/v), and the mixture was refluxed for 2 h. The reaction mixture was treated in the usual way to give a residue, which crystallized from acetone to afford pure **3**. The mother liquor was evaporated, giving a residue which was subjected to purification by preparative TLC to afford additional **3**. The diol (**3**; total 2.6 mg) was obtained in 58% yield. (−)-Deoxoprosopinine (**3**): mp 89.5 °C, $[\alpha]_D^{20}$ −14.7° (*c* 0.30; $CHCl_3$); MS *m/e* 299 (0.2; M^+), 268 (100), and 250 (55). Found: *m/e* 299.2780. Calcd for $C_{18}H_{37}NO_2$: M, 299.2822. The IR (FT-IR; Nujol) and the ^{1}H-NMR (270 MHz; $CDCl_3$) spectra of **3** were found to be identical with those of (+)-deoxoprosopinine[3b] [an enantiomer of **3**; mp 90.7—91 °C (lit,[3b] 85.5 °C); $[\alpha]_D^{18}$ +13° (*c* 0.31; $CHCl_3$) (lit,[3b] +12°); IR (FT-IR; Nujol) 3370, 3310, 3120, 1153, 1095, 1076, 1061, 1053, 1032, 953, and 864 cm^{-1}; ^{1}H-NMR (270 MHz; $CDCl_3$) δ 0.88 (3H, t, *J*=6 Hz, –$CH_2C\underline{H}_3$), 1.27 (24H, s, 12×CH_2), *ca.* 1.6 (2H, m, $C_{(4\alpha)}$–H and $C_{(4\beta)}$–H), 2.55 (2H, broad signal, 2×OH), 2.77 (1H, broad signal, $C_{(6\alpha)}$–H), 2.85 (1H, m, $C_{(2\beta)}$–H), 3.53 (1H, td, *J*=6.5 and *J*=4 Hz, $C_{(3\alpha)}$–H), 3.62 (1H, dd, *J*=10.6 and *J*=4.8 Hz; A part of ABX-system: HO–$C\underline{H}_2$–$\underline{C}$H–), and 3.66 (1H, dd, *J*=10.6 and *J*=8 Hz; B part of ABX-system: HO–$C\underline{H}_2$–$\underline{C}$H–)], prepared from natural (+)-prosopinine (**1**).[3b]

Acid Hydrolysis of the (8R)-Acetonide (18). The same acid hydrolysis of the (8*R*)-acetonide (**18**; 31 mg) gave a product which crystallized from acetone, affording a diol (**4**; 23.5 mg) in 86% yield. (−)-Deoxoprosophylline (**4**): mp 90.5 °C, $[\alpha]_D^{23}$ −14° (*c* 0.24; $CHCl_3$); IR (Nujol) 3400, 3200, 1260, 1120, 1100, 1070, 1060, 1020, 1000, 935, 910, 890, 865, and 830 cm^{-1}; ^{1}H-NMR (270 MHz; $CDCl_3$) δ 0.88 (3H, t, *J*=6 Hz, –$CH_2C\underline{H}_3$), 1.26 (24H, s, 12×CH_2), 1.75 and 2.05 (each 1H, m, $C_{(4\alpha)}$–H and $C_{(4\beta)}$–H), *ca.* 2.3 (2H, broad signal, 2×OH), 2.50 (1H, broad signal, $C_{(6\alpha)}$–H), 2.56 (1H, m, $C_{(2\alpha)}$–H), 3.44 (1H, td, *J*=6.5 and *J*=4 Hz, $C_{(3\beta)}$–H), 3.71 (1H, dd, *J*=10.8 and *J*=5.3 Hz; A part of ABX-system: HO–$C\underline{H}_2$–$\underline{C}$H–), and 3.83 (1H, dd, *J*=10.8 and *J*=4.6 Hz; B part of ABX-system: HO–$C\underline{H}_2$–$\underline{C}$H–); VPC: R_t=13.0 min (SP-1000; 1.5 m; 175 °C; N_2 37 ml/min), R_t=12.7 min (OV-1; 1 m; 175 °C; N_2 38 ml/min), and R_t=14.8 min (OV-17; 1.5

m; 220 °C; N_2 32 ml/min); MS *m/e* 299 (4; M^+), 250 (90), and 130 (100). Found: *m/e* 299.2800. Calcd for $C_{18}H_{37}NO_2$: M, 299.2822. The ^{1}H-NMR (270 MHz; $CDCl_3$) spectrum and retention times (under the three conditions described above) observed for **4** were found to be identical with those for (±)-deoxoprosophylline[3c] [(±)-**4**; mp 83—83.5 °C (lit,[3c] 83 °C)] derived from natural (±)-prosophylline[3c] [(±)-**2**].

The authors wish to thank Prof. Tatsuo Miyazawa, The University of Tokyo, for the measurements of ^{1}H-NMR spectra at 270 MHz, and Dr. Maki Kawai and Miss Setsuko Kagami, The University of Tokyo, for the FT-IR measurements.

References

1) Part VI of "Piperidine Alkaloids (Alcaloïdes Pipéridiniques)" by Q. Khuong-Huu; Part V: Ref. 2.

2) Preliminary account of this report: Y. Saitoh, Y. Moriyama, T. Takahashi, and Q. Khuong-Huu, *Tetrahedron Lett.*, **21**, 75 (1980).

3) a) G. Ratle, X. Monseur, B. C. Das, J. Yassi, Q. Khuong-Huu, and R. Goutarel, *Bull. Soc. Chim. Fr.*, **1966**, 2945; b) Q. Khuong-Huu, G. Ratle, X. Monseur, and R. Goutarel, *Bull. Soc. Chim. Belges*, **81**, 425 (1972); *Chem. Abstr.*, **77**, 101950e (1972); c) Q. Khuong-Huu, G. Ratle, X. Monseur, and R. Goutarel, *Bull. Soc. Chim. Belges*, **81**, 443 (1972); *Chem. Abstr.*, **77**, 101954j (1972).

4) G. Fodor, J. -P. Fumeaux, and V. Sankaran, *Synthesis*, **1972**, 464; A. J. G. Baxter and A. B. Holmes, *J. Chem. Soc. Perkin Trans. 1*, **1977**, 2343, and references cited therein.

5) J. J. Périé, J. P. Laval, J. Roussel, and A. Lattes, *Tetrahredon*, **28**, 675 (1972), and references cited therein.

6) Y. Moriyama, H. -D. Doan, C. Monneret, and Q. Khuong-Huu, *Tetrahedron Lett.*, **1977**, 825.

7) H. Newman, *J. Am. Chem. Soc.*, **95**, 4098 (1973), and references cited therein.

8) D. E. Ames, A. N. Covell, and T. G. Goodburn, *J. Chem. Soc.*, **1965**, 894.

9) D. J. Cram and N. L. Allinger, *J. Am. Chem. Soc.*, **78**, 2518 (1956).

10) Y. Saitoh, Y. Moriyama, H. Hirota, and T. Takahashi, *Bull. Chem. Soc. Jpn.*, **53**, 1783 (1980).

  Bull. Chem. Soc. Jpn., 54, 493—495 (1981)

Effect of Cationic Micelles on the pK_a Values of Disulfones

Yumihiko YANO,* Shuji KAWADA, and Waichiro TAGAKI*,†

Department of Chemistry, Faculty of Engineering, Gunma University, Kiryu, Gunma 376
†*Department of Applied Chemistry, Faculty of Engineering, Osaka City University, Sugimoto-cho, Sumiyoshi-ku, Osaka 558*

(Received June 30, 1980)

The acid dissociation constants of carbon acids activated by two sulfonyl groups were determined spectrophotometrically in aqueous solution with and without CTAB micelles. The results indicate that a cationic micelle causes larger pK_a decrease for more hydrophobic disulfones. Hydrophobic properties of cyclic and acyclic disulfones are discussed.

Cationic micelles stabilize carbanions,[1] this becoming more pronounced for more delocalized carbanions. In the H-D exchange reaction of micelle-forming sulfonium salts, micellar rate enhancement for the allyl-methylene group is much larger than that for the methyl group.[2] Similar phenomena were observed in the micellar effects on the acid dissociation constants of α-substituted *p*-nitrophenylacetonitrile,[3] the mechanism of hydrolysis of some activated carboxylic acid esters,[4] and the transition state of E2 elimination reaction of phenethyl bromide.[5] The carbanions are delocalized through conjugation with carbon-carbon or carbon-oxygen double bond. It is of interest to alter the behavior of carbanions by attaching other conjugative groups such as sulfonyl group.

We have examined the micellar effect on pK_a values of cyclic and acyclic disulfones, **1**—**3** and **4**—**7**, respectively, and also of β-diketone, **8**. The compounds were chosen because (a) their carbanions except for those of **4**, are stable, (b) the carbanions show suitable absorption for pK_a determination in UV region, and (c) possible variation of micellar effects with respect to cyclic and acyclic structures can be examined.

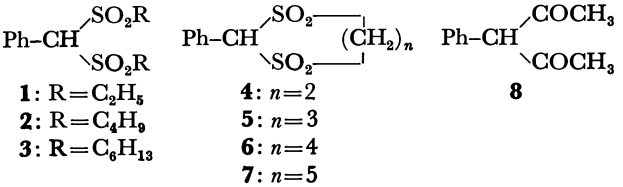

1: R=C_2H_5 **2**: R=C_4H_9 **3**: R=C_6H_{13} **4**: n=2 **5**: n=3 **6**: n=4 **7**: n=5 **8**

Results and Discussion

Stability of Carbanions. The carbanions of all the compounds except **4** were confirmed to be stable in alkaline solution (2 M NaOH) under a nitrogen atmosphere. While the five-membered disulfone (**4**) decomposes in an alkaline solution,[6] the spectra of sulfonyl carbanions (λ_{max} 270—286 nm) can be reproduced quantitatively by neutralization followed by addition of excess alkali. In a 0.01 M NaOH solution, **4** shows absorption at λ_{max} 253 nm (ε=6000 M^{-1} cm^{-1}), unchanged by acidification, the original spectrum of undissociated disulfone (λ_{max} 265 nm, ε=510 M^{-1} cm^{-1}) not being restored (1 M=1 mol dm^{-3}).

Determination of Acid Dissociation Constants (pK_a). Acid dissociation constants were determined spectrophotometrically by means of the following equations.[7]

$$pK_a = pH + \log \frac{OD_{S^-} - OD_{obsd}}{OD_{obsd} - OD_{SH}} \quad (1)$$

$$\varepsilon_{app} = \varepsilon_{S^-} - \frac{K_w \varepsilon_{app}}{K_a[OH^-]} \quad (2)$$

$$OD^- \quad \varepsilon_{app} = \varepsilon_{S^-} - \frac{1}{K_a}(h_- \varepsilon_{app}), \quad (3)$$

where OD_{S^-}, OD_{SH}, and OD_{obsd} denote optical densities of carbanion, undissociated disulfone and observed optical density, respectively, ε_{app} and ε_S- apparent extinction coefficient and extinction coefficient of a carbanion, respectively, and h_- denotes acidity function in concentrated NaOH solutions. Equation 1 is applicable when the carbanion is generated in buffer solutions, at a given pH and a λ_{max}. Equation 2 is applicable when the carbanion is generated in a solution of concentration below 0.1 M NaOH. It is necessary to use h_- instead of [OH^-] (Eq. 3) when the concentration of NaOH is 0.1—4 M.[8]

Optical densities at 290 nm except for **8** (310 nm) were recorded at various alkaline concentrations. The spectra of **2** and the plots of ε_{app} *vs.* $\varepsilon_{app}/[OH^-]$ are shown in Figs. 1 and 2, respectively. The K_a values were then calculated from the slopes by the least squares method.

Effect of a Cationic Micelle. The concentrations of hexadecyltrimethylammonium bromide (CTAB) were

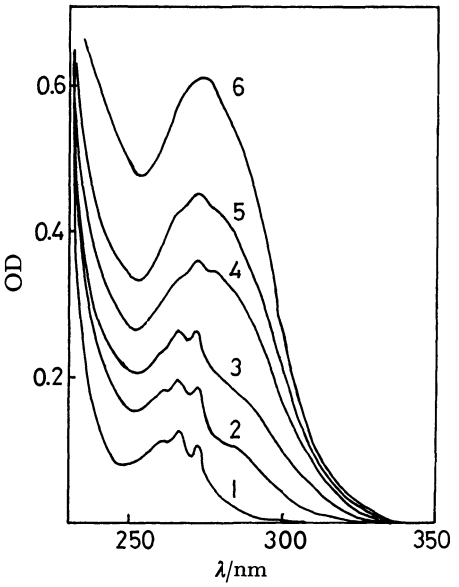

Fig. 1. Change of UV spectra of **2** as the function of base concentration.
1: ([NaOH]=0), 2: (0.005), 3: (0.01), 4: (0.025), 5: (0.05), 6: (0.1).

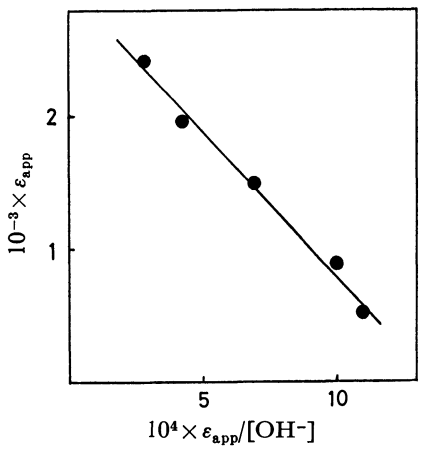

Fig. 2. Plots of ε_{app} *vs.* $\varepsilon_{app}/[OH^-]$ for **2** (see Eq. 2 and Fig. 1): $K_w/K_a=2.11\times10^{-2}$, $K_a=4.74\times10^{-13}$, $pK_a=12.33$.

TABLE 1. EFFECT OF CTAB CONCENTRATION ON pK_a

$10^3\times$[CTAB]/M	pK_a		
	1	**2**	**8**[a]
0	12.09[b]	12.33[b]	9.08
0.4	—	11.90[b]	9.08
0.6	11.86[b]	—	—
1.0	11.26[c]	10.63[d]	—
2.0	11.11[c]	10.47[d]	8.94
4.0	11.06[c]	10.41[d]	8.61
8.0	11.12[c]	10.57[d]	8.62
12.0	—	—	8.61
20.0	—	—	8.61

a) Eq. 1 used (pH 6.62—10.2, 8 or 9 points). b) Eq. 2 used (0.004—0.1 M NaOH, 6 points). c) Eq. 1 used (pH 10.00—11.92, 7 points). d) Eq. 1 used (pH 10.00—11.60, 8 points).

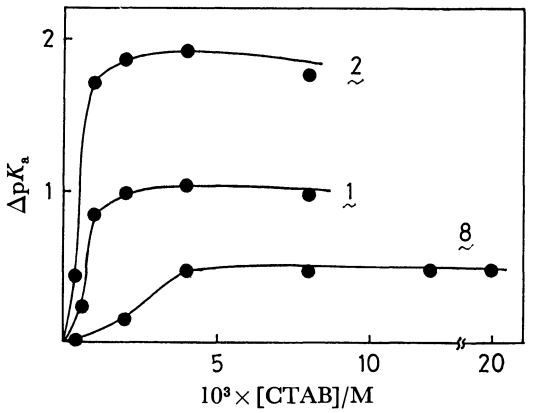

Fig. 3. Plots of ΔpK_a $[pK_a(H_2O)-pK_a(CTAB)]$ *vs.* CTAB concentration (see Table 1).

varied as usual for **1**, **2**, and **8**. The results are given in Table 1. The plots of $\Delta pK_a[pK_a(H_2O)-pK_a(CTAB)]$ against CTAB concentration gave saturation curves (Fig. 3), indicating the incorporation of substrates into the micelle. Larger ΔpK_a values were observed for more hydrophobic substrates (**2**>**1**>**8**).

The pK_a and λ_{max} of carbanions in the micellar phase and in the absence of CTAB are summarized in Table 2. The absorption spectra (λ_{max}) of the carbanions of disulfones shift to longer wave length ($\Delta\lambda$=9—12 nm) in the presence of CTAB (8×10^{-3} M), the λ_{max} of diketone (**8**) remaining unchanged irrespective of the presence of CTAB. The ΔpK_a of **8** is also small. In the case of disulfone, both equilibrium (ΔpK_a) and delocalization ($\Delta\lambda_{max}$) of carbanion are favored to a greater extent in a cationic micellar phase than in aqueous phase. In the case of diketone, the carbanion might assume the enolate form preferentially which is stablized by hydration. No change in λ_{max} and the small ΔpK_a value in **8** suggest that such hydration is little affected by incorporation into a cationic micelle.

TABLE 2. pK_a AND λ_{max} OF CARBANIONS WITH AND WITHOUT CTAB (8×10^{-3} M)

Compd	pK_a (λ_{max}/nm)		ΔpK_a	$\Delta\lambda$/nm
	CTAB=0	CTAB=8×10^{-3} M		
1	12.09[a] (274)	11.12 (284)	0.97	10
2	12.33 (274)	10.48 (286)	1.85	12
3	12.37[b] (274)	10.14[c] (286)	2.23	12
5	14.24[d] (270)	13.35[d] (280)	0.89	10
6	14.24[d] (274)	11.17[c] (283)	1.12	9
7	12.24[b] (274)	10.69[c] (284)	1.55	10
8	9.08 (305)	8.61 (305)	0.47	0

a) Reported value 12.12. b) Eq. 2 used for NaOH in the range 0.004—0.1 M. c) Eq. 1 used in the pH range 10.36—11.61. d) Eq. 3 used for NaOH in the range 0.1—2 M.

Hydrophobic Nature of Carbanion. A certain relation holds between pK_a and the hydrophobic nature of substrates. The plots of ΔpK_a against the number of methylene group of the disulfones are shown in Fig. 4. If a single least squares line is drawn for the six points, the slope gives 200 cal/mol as the standard free energy change associated with pK_a decrease per methylene group. However, if two lines are drawn separately for the acyclic and cyclic derivatives, they give 210 and 450 cal/mol, respectively. The choice of

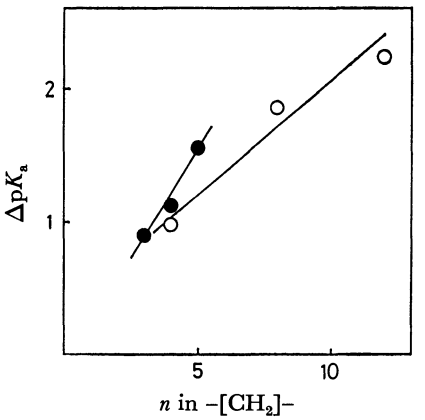

Fig. 4. Plots of ΔpK_a *vs.* methylene number of alkyl chains:
○: Acylic disulfones, ●: cyclic disulfones (see Table 2).

value is difficult due to insufficiency of data. The value of 450 cal/mol for cyclic disulfones seems to be normal as compared to the values (350—900 cal/mol) suggested for hydrophobic interactions.[9] A micellar effect associated with the change of methylene number might be larger for more rigid molecules than for flexible ones, since conformational changes such as curling up of long alkyl chain in aqueous phase are much more easy for acyclic than for cyclic compounds which reduce the free energy change (micellar effect) between aqueous and micellar phase.

The unusually high pK_a of six membered disulfone **5**, is puzzling although ΔpK_a is normal.

Experimental

Melting points are uncorrected. NMR spectra were recorded on a Varian A-60 spectrometer, the chemical shifts being given downfield from tetramethylsilane, and UV spectra on a Shimadzu UV 200 spectrophotometer. pH was measured with a Hitachi-Horiba F-7DE pH meter. Water used for pK_a measurement was purified by distillation of deionized water.

Materials. Commercial 3-phenyl-2,4-pentanedione (**8**) was used after recrystallization from benzene–hexane, mp 57—58 °C (lit,[10] 58—60 °C).

Disulfones were prepared by oxidation of the corresponding thioacetals with 30% hydrogen peroxide in acetic acid containing acetic anhydride.[11],.

1: Yield 56%, mp 133 °C (EtOH–H_2O) (lit,[11] mp 133—134 °C). NMR (DMSO-d_6): δ 1.22 (6H, t), 3.31 (4H, q), 6.56 (1H, s), 7.37—7.84 (5H, m).

2: Yield 56%, mp 90—91 °C (EtOH–H_2O) (lit,[12] mp 86 °C). Found: C, 54.36; H, 7.10; S, 19.5%. Calcd for $C_{15}H_{24}O_4S_2$: C, 54.18; H, 7.29; S, 19.28%.

3: Yield 47%. 78.5—80.5 °C (MeOH). NMR (DMSO-d_6): δ 0.84 (6H, t), 1.10—1.40 (16H, br. s), 3.25 (4H, t), 6.53 (1H, s), 7.35—7.75 (5H, m). Found: C, 59.00; H, 8.34; S 17.0%. Calcd for $C_{19}H_{32}O_4S_2$: C, 58.72; H, 8.32; S, 16.50%.

4: Yield 43%, mp 243—245 °C (benzene). NMR (DMSO-d_6): δ 4.20 (4H, s), 6.27 (1H, s), 7.50—7.70 (5H, m). Found: C, 43.90; H, 4.13; S, 26.2%. Calcd for $C_9H_{10}O_4S_2$: C, 43.88, H, 4.10; S, 26.03%.

5: Yield 49%, mp 259—262 °C (EtOH) (lit,[13] 264—265 °C). NMR (DNSO-d_6): δ 2.30—2.60 (2H, m), 3.45—3.77 (4H, m), 6.53 (1H, s), 7.45—7.75 (5H, m). Found: C, 46.13; H, 4.51; S, 24.1%. Calcd for $C_{10}H_{12}O_4S_2$: C, 46.13; H, 4.66; S, 24.63%.

6: Yield 55%, mp 249—251 °C (EtOH). NMR (DMSO-d_6): δ 2.00—2.33 (6H, m), 3.60—3.97 (4H, m), 6.63 (1H, s), 7.45—7.62 (5H, m). Found: C, 48.47; H, 5.23; S, 23.4%. Calcd for $C_{11}H_{14}O_4S_2$: C, 48.16; H, 5.14; S, 23.37%.

7: Yield 40%, mp 258—260 °C (EtOH). NMR (DMSO-d_6); δ 1.42—2.08 (6H, m), 3.14—3.62 (4H, m), 6.35 (1H, s) 7.38—7.78 (5H, m). Found: C, 49.89; H, 5.51; S, 22.3%. Calcd for $C_{12}H_{16}O_4S_2$: C, 50.00; H, 5.59; S, 22.20%.

pK_a Measurement. The pK_a values were determined by the spectrophotometric method.[7] The stock solutions (4×10^{-2} M) were prepared in EtOH for **1**, **2**, **3**, and **8**, and in CH_3CN for **4**, **5**, **6**, and **7**. Aqueous alkaline solution in a septum-rubber capped volumetric flask (5 ml) was bubbled with nitrogen for 15 min. The CTAB solution was added with a microsyringe, the solution being equilibrated at 25 °C. The substrate solution (25 μl) was added with a microsyringe, *ca.* 3 ml of the solution being put into the rubber-capped UV cell with a syringe. Optical densities at 290 nm except for **8** (310 nm) were recorded at various alkaline concentrations with a Shimadzu 200 UV instrument. Typical spectra are shown in Fig. 1. The pK_a of **3** in water (CTAB=0) could not be determined because of solubility. Thus, pK_a in H_2O was estimated from the pK_a values in 40, 60, and 80% EtOH. The pK_a values in these solvents (12.29, 12.14, and 11.81) were plotted against reciprocal of H_2O %, giving a straight line and allowing extrapolation to give $pK_a=12.37$ (Table 2).

References

1) a) J. H. Fendler and E. J. Fendler, "Catalysis in Micellar and Macromolecular Systems," Academic Press, New York (1975); b) C. A. Bunton, "Application of Biochemical Systems in Organic Chemistry," ed by J. B. Jones, C. J. Sih, and D. Perlman, Wiley-Interscience, New York, Part II, Chap. IV.

2) a) Y. Yano, T. Okonogi, and W. Tagaki, *J. Org. Chem.*, **38**, 392 (1972); b) T. Okonogi, T. Umezawa, and W. Tagaki, *J. Chem. Soc., Chem. Commun.*, **1974**, 363.

3) M. J. Minch, M Giaccio, and R. Wolff, *J. Am. Chem. Soc.*, **97**, 3766 (1975).

4) W. Tagaki, S. Kobayashi, K. Kurihara, A. Kurashima, Y. Yoshida, and Y. Yano, *J. Chem. Soc. Chem. Commun.*, **1976**, 843.

5) Y. Yano, Y. Yoshida, A. Kurashima, Y. Tamura, and W. Tagaki, *J. Chem. Soc., Prekin Trans. 2*, **1979**, 1128.

6) R. Kuhn and F. A. Neugebauer, *Chem. Ber.*, **94**, 29 (1961).

7) a) R. P. Bell and B. G. Cox, *J. Chem. Soc., B*, **1971**, 652; b) F. Hibbert, *J. Chem. Soc., Perkin Trans. 2*, **1973**, 1289.

8) K. Bowden, *Chem. Rev.*, **66**, 119 (1966).

9) G. Nemethy and H. A. Scheraga, *J. Phys. Chem.*, **66**, 1773 (1962).

10) G. T. Morgan, H. D. K. Drew, and C. R. Porter, *Ber.*, **58**, 333 (1925).

11) K. W. Wilson, J. D. Roberts, and W. G. Young, *J. Am. Chem. Soc.*, **72**, 215 (1950).

12) T. C. Whitner, Jr., and E. E. Reid, *J. Am. Chem. Soc.*, **43**, 638 (1921).

13) W. Autenrieth and K. Wolff, *Ber.*, **32**, 1375 (1899).

Branched-chain Sugars. XXI. Synthesis of New Branched-chain Cyclitols Having *neo*-, *myo*-, and *chiro*-Configurations from 3-*O*-Benzyl-5,6-dideoxy-5-*C*-(1,3-dithian-2-yl)-6-nitro-D-galactofuranose and -L-altrofuranose[1]

Masaharu IWAKAWA,* Juji YOSHIMURA, and Masuo FUNABASHI†

Laboratory of Chemistry for Natural Products, Faculty of Science, Tokyo Institute of Technology, Nagatsuta, Midori-ku, Yokohama 227

(Received July 17, 1980)

The Michael addition of 2-lithio-1,3-dithiane to 3-*O*-benzyl-5,6-dideoxy-1,2-*O*-isopropylidene-6-nitro-β-L-*arabino*-hex-5-enofuranose afforded a 1 : 1.8 mixture of 3-*O*-benzyl-5,6-dideoxy-5-*C*-(1,3-dithian-2-yl)-1,2-*O*-isopropylidene-6-nitro-α-D-galactofuranose and -β-L-altrofuranose. Removal of the isopropylidene group and intramolecular cyclization under weakly basic conditions afforded a mixture of branched-chain cyclitols having *neo*-, *myo*-, and *chiro*-configuration. A similar cyclization of the *O*-deisopropylidenated product of 3-*O*-benzyl-5,6-dideoxy-1,2-*O*-isopropylidene-6-nitro-5-*C*-(nitromethyl)-β-L-*arabino*-hexofuranose also afforded a mixture of cyclitols having *neo*-, *myo*-, and *chiro*-configuration. The results confirm the importance of two bulky groups such as benzyloxy at C-3 and 1,3-dithiane residue at C-5 in determining the stereodirection of cyclization.

In previous papers[2-4] it was reported that the intramolecular cyclization of 3-*O*-benzyl-5,6-dideoxy-5-*C*-(1,3-dithian-2-yl)-6-nitrohexoses gives stereoselectively a few nitro cyclitols in which bulky substituents at C-5 and C-6 exclusively occupy *trans*-orientation and the newly formed hydroxyl group substantially occupies equatorial orientation when 3-*O*-benzyl group takes an axial orientation. Thus, the corresponding D-*gluco* derivatives[2,4] gave *muco*-nitro cyclitols exclusively, and L-*ido* derivative[2] *scyllo*- and *myo*-nitroinositols in a 1 : 1 ratio. The validity of this hypothesis was confirmed by the fact that the corresponding L-*talo* derivative gave only *myo*-nitroinositol, and the D-*allo* derivative gave *epi*- and *allo*-nitroinositols in a 1 : 1 ratio.[3] We have examined our hypothesis by the intramolecular cyclization of D-*galacto*- and L-*altro*-derivatives (**4a** and **4b**).

Results and Discussion

3-*O*-Benzyl-5,6-dideoxy-5-*C*-(1,3-dithian-2-yl)-6-nitro-D-galactofuranose (**4a**) and -L-altrofuranose (**4b**) were prepared in the same manner as reported.[2-4] 3-*O*-Benzyl-1,2-*O*-isopropylidene-α-D-galactofuranose (**1**)[5] was at first oxidized with sodium periodate in aqueous methanol, and the resulting aldehyde was treated with nitromethane in methanol in the presence of sodium methoxide to give C-5 epimeric nitro alcohols (**2**)[6] in a good yield. Direct dehydration of the compound **2** with acetic anhydride–sodium acetate[7] afforded 3-*O*-benzyl-5,6-dideoxy-1,2-*O*-isopropylidene-6-nitro-β-L-*arabino*-hex-5-enofuranose (**3**) in 95% yield. Addition of 2-lithio-1,3-dithiane to **3** in dry tetrahydrofuran at −45 to −50 °C gave a syrupy mixture of **4a** and **4b** in 50% yield after being subjected to silica gel column chromatography. The ratio of **4a** to **4b** was estimated to be 1 : 1.8 by comparison of intensities of H-1 protons. Addition of nitromethane to **3** also gave 3-*O*-benzyl-5,6-dideoxy-1,2-*O*-isopropylidene-6-nitro-5-*C*-nitromethyl-β L-*arabino*-hexofuranose (**5**) in 65% yield.

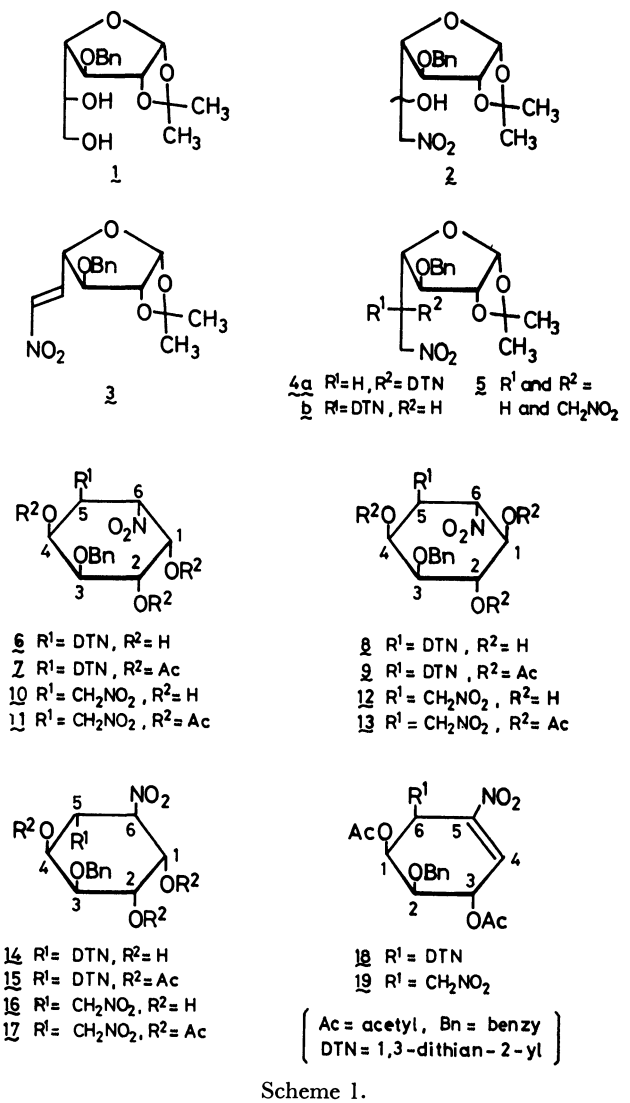

Scheme 1.

From a theoretical point of view, D-*galacto* isomer **4a** should give branched-chain *chiro*- and/or *muco*-inositol derivatives, whereas L-*altro* isomer **4b** should give *myo*- and *neo*-inositol derivatives. However, stereo-

† Present address: Chiba University, College of Arts and Sciences, Yayoicho, Chiba 260.

Table 1. NMR parameters of branched-chain nitro cyclitols[a)]

	H_1 ($J_{1,2}$)	H_2 ($J_{2,3}$)	H_3 ($J_{3,4}$)	H_4 ($J_{4,5}$)	H_5 ($J_{5,6}$)	H_6 ($J_{6,1}$)	$H_{1'}$ ($J_{5,1'}$)	Acetyl
7	5.98t	5.16dd	3.78dd	6.02t	3.14oct	5.28dd	4.24d	2.00
(*neo*)	(3.5)	(10.0)	(3.0)	(3.0)	(12.0)	(3.0)	(5.0)	2.06
								2.16
9	5.53t	5.30t	3.56dd	5.95t	2.8m	5.24dd	4.12d	1.97
(*myo*)	(9.5)	(9.5)	(3.0)	(3.0)	(11.0)	(9.5)	(4.0)	2.03
								2.10
11	6.06t	5.17dd	3.88dd	5.83t	3.53m	4.98dd	4.50d	2.00
(*neo*)	(3.7)	(10.5)	(3.5)	(2.5)	(11.5)	(3.5)	(6.0)	2.07
								2.10
13	5.59t	5.25t	3.70dd	5.73t	3.21m	4.84dd	4.32dd 4.48dd,	1.98
(*myo*)	(10.0)	(9.5)	(2.5)	(2.5)	(12.0)	(10.0)	(5.0) (8.0)	2.02
								2.20
15	5.81dd	5.55dd	3.84dd	5.24dd	3.30dt	5.16t	4.08d	2.00
(*chiro*)	(3.0)	(5.0)	(3.5)	(11.0)	(10.5)	(10.0)	(2.5)	2.06
								2.12
17	5.79dd	5.59t	3.97dd	5.08dd	3.44tt	5.08dd	4.52d	1.96
(*chiro*)	(3.0)	(4.0)	(3.0)	(12.0)	(12.0)	(11.0)	(3.5)	2.00
								2.15

a) d=doublet, m=multiplet, oct=octet, t=triplet, dd=double doublet, dt=double triplet, tt=triple triplet.
b) $J_{1'a,1'b}=14.0$.

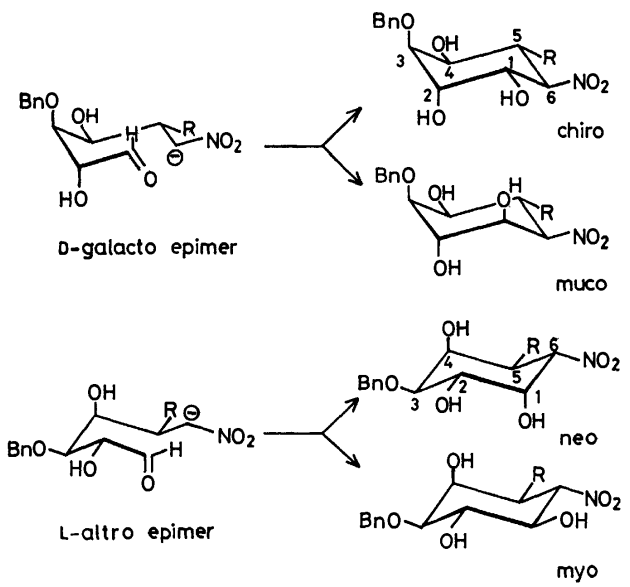

Scheme 2.

direction of the cyclization is rather limited,[2,3)] since it depends on whether or not the benzyloxy group at C-3 can occupy an axial orientation. The failure to form a *muco*-isomer would be anticipated since it would generate a 1,3-diaxial non-bonded interaction. This would destabilize the system.

Since the separation of **4a** and **4b** was unsuccessful, the mixture was refluxed in 75% acetic acid for 2 h to remove the 1,2-*O*-isopropylidene group. The free sugars obtained were treated with 2 equivalent sodium hydrogen-carbonate in aqueous methanol for 20 h to give a mixture of cyclitols, showing two main spots having R_f values of 0.43 and 0.32 on TLC (solvent C). The two components were separated by preparative TLC. From the less polar component *neo*-inositol derivative (**6**) was obtained in 27% yield as white needles. Acetylation of **6** with acetic anhydride in the presence of *p*-toluenesulfonic acid gave a crystalline triacetate (**7**) in 88% yield. Its configuration was demonstrated by NMR spectrum data (Table 1). However, recrystallization (from ethanol-hexane) or purification with preparative TLC caused a partial degradation of **7** to the corresponding nitro olefin (**18**). Such a transformation is usually observed in the cases of similar nitro cyclitols in which the nitro group and the newly formed, vicinal hydroxyl group occupy the *cis*-orientation.[2)]

A mixture of other inositol derivatives (other than *neo*-configuration) was obtained from a more polar component in 54% yield as a syrup, from which *chiro*-isomer (**14**) crystallized out as prisms in 20% yield. The structure of **14** is supported by the NMR spectrum of its triacetate (**15**). The mother liquor of **14** was evaporated and the residue was treated with acetone in the presence of anhydrous copper(II) sulfate and a few drops of concentrated sulfuric acid to remove trace of **14** from the mixture.

After separation of **14** by means of preparative TLC, compound (**8**) (*myo*-configuration) was isolated, its structure being confirmed by means of the NMR parameters of its crystalline tri-*O*-acetate (**9**).

Similar cyclization of **5** was achieved by treating **5** with 70% acetic acid and sodium hydrogencarbonate in aqueous methanol successively, three isomers of nitro cyclitols having *neo*- (**10**), *myo*- (**13**), and *chiro*- (**16**) configuration being isolated in 18, 10, and 10% yields, respectively. Each structure was confirmed by the analysis of NMR spectra of their acetates. *O*-acetyl derivatives of these nitro cyclitols were also very labile and could not be obtained in the pure state except for *myo*-isomer. In the case of *neo*-isomer **10**, its tri-*O*-acetate **11** was readily transformed into the correspond-

ing nitro olefin (**19**) during the course of recrystallization. The formation of three isomeric nitro cyclitols is of interest as compared with the results in which only two out of four possible isomers were formed in the case of 3-*O*-benzyl-5,6-dideoxy-1,2-*O*-isopropylidene-5-*C*-(nitromethyl)-6-nitro-α-D-*ribo*-hexofuranose.[3]

Such bulky groups as benzyloxy group, 1,3-dithian-2-yl group and nitromethyl group have decisive influence on the stereodirection of the intramolecular cyclization of **4** and **5** to afford branched-chain nitro cyclitols.

Experimental

Melting points were determined with a YANACO micro melting-point apparatus and are uncorrected. IR spectra were recorded on a Hitachi 260-10 spectrophotometer. Proton magnetic resonance (100 MHz) were recorded on a JNM-PS-100 spectrometer in chloroform-*d* with tetramethylsilane as an internal standard. Chemical shifts and coupling constants were recorded in δ and Hz units, respectively, and IR frequencies in cm^{-1}. Optical rotations were determined on a JASCO DIP-4 digital polarimeter or a Karl Zeiss LEP Al polarimeter. TLC and preparative TLC were performed with silica gel (E. Merck type 60) as an adsorbent in the following solvent systems (v/v): A, hexane–ethyl acetate, 3 : 1; B, 2 : 1; C, 1 : 1, D, 1 : 2. Solvents were evaporated under reduced pressure below 40 °C.

A Mixture (2) of 3-O-Benzyl-6-deoxy-1,2-O-isopropylidene-6-nitro-α-D-galactofuranose and -β-L-altrofuranose. Sodium periodate (1.90 g, 8.9 mmol) was added to an ice-cooled solution of 3-*O*-benzyl-1,2-*O*-isopropylidene-α-D-galactofuranose (**1**)[5] (2.54 g, 8.2 mmol) in aqueous methanol (methanol: water=70 : 35 v/v). The reaction mixture was stirred at the same temperature for 30 min, and then at room temperature for 1.5 h. The mixture was filtered and the solid washed with methanol. The filtrate and washings were combined, concentrated to remove as much methanol as possible, and extracted several times with dichloromethane (*ca.* 150 ml). The organic layer was washed with brine, dried over anhydrous magnesium sulfate, and concentrated to afford aldehyde as a clear syrup.

To an ice-cooled solution of the aldehyde obtained above and nitromethane (35 ml) in absolute methanol (70 ml) was added 1 M sodium methoxide in methanol (8.2 ml), and the mixture was kept at room temperature for 15 h. Acetic acid (1.5 ml) was added to the light brown solution thus obtained, the solvent being removed by evaporation. The residue was partitioned between dichloromethane (100 ml) and water (50 ml), and the water layer further extracted with dichloromethane (20 ml×2). Combined dichloromethane layer was washed with brine, dried over anhydrous magnesium sulfate, and concentrated to dryness to afford an epimeric mixture of nitro aclohols as a thick syrup. One of the epimers crystallized from ethanol–hexane (1.38 g, 50%): mp 94°; $[\alpha]_D^{17.5}$ −8.7° (*c* 0.74, CH_2Cl_2). Purification of the mother liquor on a silica gel column (solvent A) afforded a mixture of epimers as a syrup (1.35 g, 37%): IR 3450 (OH), 1550, 1575 ($-NO_2$); NMR (after the addition of D_2O), 1.31, 1.51 (s, 3H each), 3.95—4.48 (m, 7H), 4.66 (d, H-2), 5.92 (d, 1H, $J_{1,2}$=4.0, H-1), 7.33 (s, 5H, Ph). Found: C, 56.59; H, 7.25; N, 4.28%. Calcd for $C_{16}H_{21}NO_7$: C, 56.63; H, 6.24; N, 4.13%.

3-O-Benzyl-5,6-dideoxy-1,2-O-isopropylidene-6-nitro-β-L-arabino-hex-5-enofuranose (3). A mixture of **2** (1.23 g, 3.63 mmol) and anhydrous sodium acetate (2.20 g) in acetic anhydride (7.1 ml) was stirred at room temperature for 48 h and poured into aqueous sodium hydrogencarbonate (50 ml). The oil precipitated was extracted with dichloromethane (50 ml×3), washed with aqueous sodium hydrogencarbonate and brine and dried with anhydrous sodium sulfate. The solvent was evaporated to afford **3** as a light yellow syrup (1.12 g, 95%), sufficiently pure for further preparation; purification on a silica gel column and/or preparative TLC was not successful: IR 1530, 1350 (C=C–NO_2).

3-O-Benzyl-5,6-dideoxy-5-C-(1,3-dithian-2-yl)-1,2-O-isopropylidene-6-nitro-β-L-altrofuranose and -α-D-galactofuranose (4). To a cooled (−45——50 °C) solution of **3** (2.22 g, 6.9 mmol) in dry tetrahydrofuran (THF, 10 ml) was added all at once a solution of 2-lithio-1,3-dithiane prepared at −45 °C from 1,3-dithiane (1.22 g, 10.2 mmol) and butyllithium (15% hexane solution, 6.2 ml, 9.68 mmol) in dry THF (14 ml). The reaction mixture was stirred at the same temperature for 45 min, then at room temperature for 30 min, and acidified with acetic acid (1 ml). The light brown solution was concentrated to a residue which was partitioned between water (50 ml) and dichloromethane (50 ml). The water layer was extracted with dichloromethane (25 ml×2). The dichloromethane layers were combined, washed with brine, dried ($MgSO_4$), and concentrated to a syrup (3.32 g); TLC (solvent A) revealed the presence of a major component having the R_f value 0.40. Isolation of the major component by means of silica gel column chromatography afforded a mixture of 5-*C*-epimers **4** as a syrup (1.51 g, 50%). In a NMR spectrum of **4** taken in benzene-d_6 in the presence of tris(1,1,1,2,2,3,3-heptafluoro-7,7-dimethyl-4,6-octanedionato)-praseodymium were observed two anomeric protons with a coupling constant of 3.75 at 5.36 and 5.48. Since *neo*-(**6**) and *myo*-nitro cyclitol (**9**) were isolated to a greater extent (the sum of 44%) than *chiro*-isomer (**14**) (20%), the peak at 5.36 was assigned to H_1 of D-*galacto*-isomer (**4a**) and the one at 5.48 to H-1 of L-*altro*-isomer (**4b**). The ratio D-*galacto*: L-*altro* was estimeted to be 1 : 1.8. Found: C, 54.70; H, 6.08; N, 2.91; S, 14.43%. Calcd for $C_{20}H_{27}NO_6S_2$: C, 54.40; H, 6.16; N, 3.17; S, 14.52%.

3-O-Benzyl-5,6-dideoxy-1,2-O-isopropylidene-6-nitro-5-C-nitromethyl-β-L-arabino-hexofuranose (5). A solution of nitro olefin **3** (642 mg, 2 mmol) in methanol (6 ml) was added to an ice-cooled solution of nitromethane (3 ml, 55 mmol) in dry methanol (15 ml) containing 1.6 ml of 1 M sodium methoxide in absolute methanol. The reaction mixture was kept at room temperature for 1 h, acidified with acetic acid (1 ml), and concentrated to dryness. The residue was partitioned between dichloromethane (70 ml) and water (20 ml). The dichloromethane layer was washed with brine, dried ($MgSO_4$), and concentrated to a syrup. TLC (solvent A) showed a presence of a major component having the R_f value 0.45. Isolation of the major component by means of preparative TLC afforded **5** as a syrup (501 mg, 66%): $[\alpha]_D^{26}$ −34.4° (*c* 0.72 chloroform); IR 1560, 1380 ($-NO_2$); NMR 1.36, 1.52 (3Hs each, C–CH_3), 3.26 (m, 1H, $J_{5,6}$=5.9, $J_{5,6'}$=4.3, H-5), 3.94 (d, 1H, $J_{3,4}$=3.8, H-3), 4.06 (dd, 1H, $J_{4,5}$=9.7, H-4), 4.4—4.8 (6H, $-CH_2NO_2\times2$, $-CH_2$–Ph), 4.68 (d, 1H, $J_{1,2}$=3.75, H-2), 5.86 (d, 1H, H-1), 7.36 (s, 5H, Ph), Found: C, 53.82; H, 5.65; N, 7.10%. Calcd for $C_{17}H_{22}N_2O_8$: C, 53.40; H, 5.80; N, 7.33%.

Hydrolysis of 4 and Intramolecular Cyclization. A solution of **4** (0.6815 g) in 75% acetic acid (35 ml) was heated to reflux for 2 h. The light brown solution was concentrated to dryness. A trace of acetic acid was codistilled with toluene. The residue was then dissolved in methanol (30 ml) and treated with sodium hydrogencarbonate (260 mg) in water (15 ml) at room temperature for 20 h. The solution was neutralized by the addition of ion exchange resin (Dowex

50 W×8, H^+ form, 4 ml). Evaporation of the solvent afforded a crude mixture of nitrocyclitols as light brown foam (567 mg, 94.2%). TLC (solvent C) indicated the presence of two components having the R_f values 0.43 and 0.32, respectively. Preparative TLC (solvent C) afforded a less polar component having the R_f value 0.43 (168.5 mg, 27%), and a more polar component having the R_f value 0.32 (334.4 mg, 54%).

1D-(1,2,6/3,4,5)-3-O-Benzyl-5-(1,3-dithian-2-yl)-6-nitro-1,2,3,4-cyclohexanetetrol (6).[8] Recrystallization of the component having the R_f value 0.43 from ethanol afforded **6** as needles: mp 166—169 °C; $[\alpha]_D^{18}$ −5.7° (*c* 2.1, methanol); IR 3420 (OH), 1545, 1370 (-NO_2). Found: C, 50.80; H, 6.10; N, 3.13%. Calcd for $C_{17}H_{23}O_6NS_2$: C, 50.86; H, 5.77; N, 3.49%.

1D-(1,2,6/3)-1,3-Di-O-acetyl-2-O-benzyl-6-(1,3-dithian-2-yl)-5-nitrocyclohex-4-ene-1,2,3-triol (18). Acetylation of **6** in acetic anhydride in the presence of catalytic amount of *p*-toluenesulfonic acid gave crude tri-*O*-acetate **7**, in 88% yield, which gradually decomposed into nitro olefin (**18**) which was isolated with preparative TLC as yellow syrup: $[\alpha]_D^{27}$ +129.7° (*c* 3.38, methanol–dichloromethane: 1 : 3 v/v); NMR 2.07, 2.10 (s, 3H each, OAC), 2.91 (m, 4H), 3.79 (m, 1H, H-6), 4.15 (dd, 1H, $J_{2,3}$=8.0, $J_{1,2}$=2.5, H-2), 4.36 (d, 1H, $J_{1',6}$=7.5, H-1'), 4.56 and 4.72 (ABq, 2H, J_{AB}=12.0, -CH_2-), 5.65 (ddd, 1H, $J_{3,6}$=1.5, $J_{3,4}$=3.5, H-3), 6.03 (t, 1H, $J_{1,6}$=2.5), 7.10 (d, 1H, H-4), 7.35 (m, 5H, Ph). Found: C, 54.56; H, 5.64; N, 2.82%. Calcd for $C_{21}H_{25}O_7NS_2$: C, 53.95; H, 5.39; N, 3.00%.

1D-(1,2,5/3,4,6)-3-O-Benzyl-5-(1,3-dithian-2-yl)-6-nitro-1,2,3,4-cyclohexanetetrol (14). The more polar component obtained above was tritulated and recrystallized from ethanol–hexane to afford **14** as prisms (20%): mp 191.5—193.5° (dec); $[\alpha]_D^{26.5}$ +5.7° (*c* 1.06, methanol); IR 3550, 3400, 3330 (OH), 1550 (-NO_2). Found: C, 50.59; H, 5.71; N, 3.31%. Calcd for $C_{17}H_{23}NO_6S_2$: C, 50.86; H, 5.77; N, 3.49%. Tri-*O*-acetate **15** was prepared by treatment **14** with acetic anhydride-*p*-toluenesulfonic acid.

1L-(1,3,4,5/2,6)-1,2,4-Tri-O-acetyl-3-O-benzyl-5-(1,3-dithian-2-yl)-6-nitro-1,2,3,4-cyclohexanetetrol (9). The mother liquor left from the isolation of **14** was concentrated to dryness and treated with acetone and anhydrous copper(II) sulfate in the presence of a catalytic amount of sulfuric acid for one week. The reaction mixture was then passed through a short column of silica gel and concentrated to dryness.

TLC of the mixture (solvent C) indicated the presence of two components, which were separated by means of preparative TLC.

The more polar component was treated with acetic anhydride in the presence of *p*-toluenesulfonic acid to afford crystalline **9** in 17% yield (from **4**): mp 215—217°; $[\alpha]_D^{18}$ +48.6° (*c* 0.5, dichloromethane); IR 1755 (-$OCCH_3$), 1560, 1370 (-NO_2). Found: C, 52.58; H, 5.72; N, 2.62%. Calcd for $C_{23}H_{29}NO_9S_2$: C, 52.36; H, 5.54; N, 2.65%.

The less polar component was treated with boiling 75% acetic acid for 2 h and acetylated with acetic anhydride-*p*-toluenesulfonic acid to give **15**.

Hydrolysis of 5 and Intramolecular Cyclization. A solution of **5** (1.15 g) in 70% acetic acid (50 ml) was heated to reflux for 2 h. The dark brown solution was concentrated to dryness and a trace of acetic acid was removed by codistillation with toluene. The residue was dissolved in methanol (50 ml) and treated with sodium hydrogencarbonate (427 mg) in water (25 ml) at room temperature for 16 h. The light brown solution was neutralized with Dowex 50 W×8 (H^+) (5 ml) and concentrated to dryness to afford a half crystalline residue (0.9825 g, 95%). TLC indicated the presence of two major components having R_f values 0.29 and 0.22 (solvent C).

1D-(1,2,6/3,4,5)-3-O-Benzyl-6-nitro-5-nitromethyl-1,2,3,4-cyclohexanetetrol (10). To the residue obtained above (983 mg) was added ethanol (*ca.* 20 ml) and the mixture was kept in a refrigerator overnight. Crystals precipitated were collected (194 mg, 18.8% from **5**) and recrystallized from ethanol to afford **10** as prisms: mp 225—228° (dec); R_f 0.29 (solvent C); $[\alpha]_D^{27.5}$ −46.1° (*c* 0.77, acetone); IR 3540, 3350, 3300 (OH), 1555, 1570, 1340, 1380 (-NO_2). Found: C, 48.89; H, 5.21; N, 8.19%. Calcd for $C_{14}H_{18}N_2O_8$: C, 49.12; H, 5.30; N, 8.18%.

1D-(1,2,6/3)-1,3-Di-O-acetyl-2-O-benzyl-5-nitro-6-nitromethylcyclohex-4-ene-1,2,3-triol (19). A solution of **10** (26.2 mg) in acetic anhydride containing a catalytic amount of *p*-toluenesulfonic acid was kept overnight at room temperature. The solution was poured into ice water, extracted with dichloromethane, washed with water, dried (Na_2SO_4), and concentrated to afford crude tri-*O*-acetate **11** (29.6 mg, 82.5%) sufficiently pure for NMR analysis. Purification of crude tri-*O*-acetate **11** was performed on preparative TLC (solvent system A). The major fraction was isolated and recrystallized from ethanol–hexane to afford cyclohexene derivative **19** as prisms (20.1 mg, 78% from **11**): mp 138—139°; $[\alpha]_D^{27}$ +57.9° (*c* 0.88, methanol: dichloromethane=5 : 1 v/v); IR 1755, 1740 (esters), 1575, 1370 (aliph-NO_2), 1535, 1340 (vinyl-NO_2); NMR 1.96, 2.10 (s, 3H each -OAc), 3.83 (dt, 1H, $J_{2,4}$=1.0, $J_{1,2}$=$J_{2,3}$=2.5, H-2), 4.34 (m, 1H, H-6), 4.46 (dd, 1H, $J_{1',1''}$=14.0, $J_{1',6}$=3.0, H-1'), 4.66 and 4.73 (ABq, 2H, J=12.5, -CH_2-), 5.22 (dd, 1H, $J_{1'',6}$=7.0, H-1''), 5.32 (dd, 1H, $J_{1,6}$=6.5, H-1), 5.62 (dd, 1H, $J_{3,6}$=1.0, $J_{3,4}$=4.0, H-3), 7.30 (dd, 1H, H-4), 7.37 (m, 5H, Ph). Found: C, 52.43; H, 4.98; N, 6.91%. Calcd for $C_{18}H_{20}N_2O_9$: C, 52.94; H, 4.94; N, 6.86%.

1L-(1,3,4,5/2,6)-1,2,4-Tri-O-acetyl-3-O-benzyl-6-nitro-5-nitromethyl-1,2,3,4-cyclohexanetetrol (13). To a suspension of an intramolecular cyclization mixture of **5** (315 mg) in dry acetone (3 ml) and 2,2-dimethoxypropane (6 ml) was added a catalytic amount *p*-toluenesulfonic acid monohydrate, and the clear solution obtained immediately was kept at room temperature overnight. The mixture was then diluted with dichloromethane (100 ml) and washed twice with aqueous sodium hydrogenecarbonate (10 ml). The water layer was extracted with dichloromethane (20 ml). Dichloromethane layers were combined, washed with brine, and dried (anhydrous sodium sulfate). Evaporation of the solvent afforded a syrupy mixture. TLC indicated the presence of two major components having R_f values 0.73 and 0.63 (solvent C).

The component having the R_f value 0.73 was isolated by preparative TLC as syrup (76.0 mg, 22%) dissolved in 80% acetic acid and heated to reflux 1.5 h. The reaction mixture was concentrated to a solid residue. The residue was acetylated with acetic anhydride (1 ml) containing a catalytic amount of *p*-toluenesulfonic acid, and the usual work-up of the acetylation mixture afforded a solid mass which recrystallized from ethanol to give **13** as prisms (44.7 mg, 10.3% from **5**): mp 141—143°; $[\alpha]_D^{30}$ +111.2° (*c* 1.0, dichloromethane); IR 1750 (ester), 1575, 1560, and 1375 (aliph-NO_2). Found: C, 51.20; H, 5.30; N, 6.14%. Calcd for $C_{20}H_{24}N_2O_{11}$: C, 51.28; H, 5.16; N, 5.98%.

1D-(1,2,5/3,4,6-)-3-O-Benzyl-6-nitro-5-nitromethyl-1,2,3,4-cyclohexanetetrol (16). The component having the R_f value 0.63 was isolated with preparative TLC as a syrup (62.4 mg, 18%), dissolved in 80% acetic acid (10 ml) and heated to reflux for 1.5 h. The reaction mixture was concentrated to a solid mass, and recrystallized from ethanol–

hexane to afford **16** as needles (38.9 mg, 10.2% from **5**): mp 187—189°; $[\alpha]_D^{27}$ −36.8° (*c* 1.0, methanol); IR 3500, 3400 (OH), 1560, 1550, 1380, 1360 (NO_2). Found: C, 49.10; H, 5.26; N, 8.17%. Calcd for $C_{14}H_{18}N_2O_8$: C, 49.12; H, 5.30; N, 8.18%.

1,2,4-Tri-*O*-acetyl derivative **7** was prepared by the treatment of **16** with acetic anhydride and *p*-toluenesulfonic acid.

References

1) Part XX; K. Sato, K. Koga, H. Hashimoto, and J. Yoshimura, *Bull. Chem. Soc. Jpn.*, **53**, 2639 (1980).

2) M. Funabashi and J. Yoshimura, *J. Chem. Soc., Perkin Trans. 1*, **1979**, 1425.

3) M. Funabashi, K. Kobayashi, and J. Yoshimura, *J. Org. Chem.*, **44**, 1618 (1979).

4) M. Funabashi, H. Wakai, K. Sato, and J. Yoshimura, *J. Chem. Soc., Perkin Trans. 1*, **1980**, 14.

5) R. C. Anderson and B. Fraser-Reid, *Tetrahedron Lett.*, **1977**, 2865.

6) NMR spectrum of **2** indicated that one of the epimers was formed predominantly (more than 90%).

7) R. L. Whistler and P. E. Pyler, *Carbohydr. Res.*, **12**, 201 (1970).

8) Nomenclature follows the IUPAC-IUB 1973 Recommendations for Cyclitols: *Eur. J. Biochem.*, **57**, 1 (1975).

  Bull. Chem. Soc. Jpn., 54, 501—504 (1981)

Polarographic Studies on Ninhydrin in DMF and Dehydration from *gem*-Diol Structure

Mitsuaki OHMORI** and Masanosuke TAKAGI*

Laboratory of Food Chemistry, College of Agriculture, University of Osaka Prefecture, Sakai 591
***Osaka City Institute of Public Health and Environmental Sciences, Tennoji-ku, Osaka 543*

(Received July 24, 1980)

The d.c.-polarogram of ninhydrin (I) in DMF containing 0.1 M TEAP shows three cathodic waves whose $E_{1/2}$ are −0.38, −0.65, and −1.23 V (*vs.* SCE), respectively. The first wave with a large maximum is attributed to one-electron reduction of 1,2,3-indantrione (II), the hydrated form of I, the second to one-electron reduction of I, and the third to one-electron reduction of the preceding electrochemical product from both I and II. CV Curves of I show three cathodic peaks, pc_1, pc_2, and pc_3, and two anodic peaks, pa_1, and pa_2, showing reversible character of pc_1 and pc_3 but not of pc_2. Different equilibria seem to take place between I and II in the bulk of the solution and at electrode surface. Hydration of II and dehydration of I in DMF were observed at 550 nm spectroscopically. A scheme is proposed for the electrolytic reduction of I in DMF.

The electrochemical behavior of carbonyl compounds is of interest as regards the electron transfer in biological systems. Aldehydes,[1,2] ketones,[3] α-keto acids,[4,5] di- and tricarbonyl compounds[6,7] and many other carbonyl compounds have been studied. However, ambiguities with origins mostly attributed to the hydration of carbonyl groups in aqueous systems remain and studies in nonaqueous systems are expected to clarify them.

Ninhydrin (I) is available as a stable monohydrated form of the corresponding tricarbonyl compound 1,2,3-indantrione (II). Its polarographic behavior in aqueous[8–12] and nonaqueous[13] solutions was reported. The effect of hydration and dehydration in nonaqueous solvents should be examined more in detail for the clarification of its electrochemical characteristics. We are interested in this study in relation to its partial structural similarity to dehydro-L-ascorbic acid[14,15] of biological importance.

Experimental

Chemicals. Ninhydrin (I) (analytical grade, Ishizu Pharmaceutical Co., Ltd., Osaka) was used without further purification. 1,2,3-Indantrione (II) was prepared as a purple powder by heating I under reduced pressure at 125—130 °C.[13]

Tetraethylammonium perchlorate (TEAP) (prepared for polarography, Nakarai Chemical Co., Ltd., Kyoto) was used after cautious drying under reduced pressure with appropriate heating.

Nonaqueous Solvent. *N,N*-Dimethylformamide (DMF) (analytical grade, Wako Pure Chemical Co., Ltd., Osaka) was dried as described by Mann.[16] For polarographic measurements, DMF containing 0.1 M (1 M=1 mol dm^{-3}) TEAP was deoxygenated by bubbling nitrogen gas dried with silica gel and phosphorus pentaoxide.

Apparatus. Polarographic measurements were carried out with a Yanagimoto Voltammetric Analyzer Type P-1000, characteristics of the capillary being $m=1.52$ mg/s, $t=4.00$ s^{-1} in DMF containing 0.1 M TEAP, when Hg level was 51.5 cm and −1.0 V was applied. Cyclic voltammetry was carried out with the Analyzer Type P-1000 with a function generator (NF Circuit Design Block Co., Ltd., Osaka). The working electrode was a hanging mercury electrode or a Pt electrode, a saturated calomel electrode (SCE), with a salt bridge[5] constructed of three gel layers, and an Ag/AgCl electrode being used as reference electrodes.

Results and Discussion

Polarographic Behavior of Ninhydrin (I). Polarograms of I were examined in dried and deoxygenated DMF, containing 0.1 M TEAP. A polarogram recorded immediately after direct dissolution of a necessary amount of crystalline I in the electrolyte solution (Fig. 1-a) showed an anomalous first wave with a large maximum and two other successive waves. The height of the first wave decreased with time, polarogram (a) changing into d *via* b and c. At the state of d, the first wave became stable, the shape of the wave not being anomalous. The half-wave potentials ($E_{1/2}$) of the three reduction waves were −0.38, −0.65, and −1.23V, respectively. At a very early period, the sum of the first and the second wave heights was a little higher than the height of the third wave, but decreased gradually with time and finally became equal to it. The slopes of logarithmic analysis for the three waves $dE/d \log [i_d/(i_d-i)]$ are 61, 38, and 85 mV, respectively.

When a very small amount of water (below 0.25%) was added to the electrolyte solution after recording

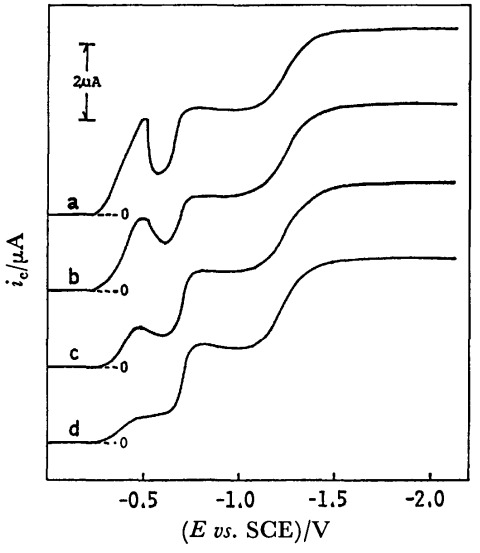

Fig. 1. Polarograms of ninhydrin.
Concn: 1×10^{-3} M, temp: 22 °C, a: Immediately after dissolving ninhydrin, b: 30 min, c: 60 min, d: 90 min.

(Fig. 1-a), a similar polarogram to d was obtained much more quickly than without addition of water.

The decrease in the first wave height seems to be related to the water content in the system. However, it is difficult to attribute the maximum observed in a to the water content. An equilibrium between the dehydrated form (II) and the hydrated form (I) in DMF should be considered, not only in the bulk of the solution but also at the electrode surface.

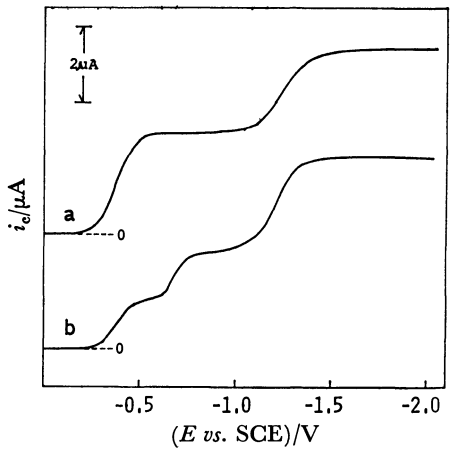

Fig. 2. Polarograms of 1,2,3-indantrione.
Concn: 1×10^{-3} M, temp: 19 °C, H_2O: a-0%, b-0.11%.

A polarogram of 1,2,3-indantrione (II), a dehydrated form of I, was also examined (Fig. 2-a). It showed two successive waves ($E_{1/2} = -0.38$ and -1.23 V). Kalinowski and Lasia reported that they observed two successive waves of II in absolute DMF containing 0.2 M $NaNO_3$ ($E_{1/2} = -0.39$ and -0.86 V *vs.* SCE),[13] each of which was ascribed by the authors to one-electron reduction.

When a small amount of water (0.11%) was added to the electrolyte solution after recording the polarogram (Fig. 2-a), a new wave ($E_{1/2} = -0.67$ V) appeared between the two waves at the expense of the first wave, *i.e.* in total, three waves were observed (Fig. 2-b). The first wave showed no maximum during the course of current decrease, the three waves corresponding to the three in Fig. 1-d, respectively. The newly appearing wave in Fig. 2-b may thus be attributed to I which is the hydration product of II in Eq. 1.

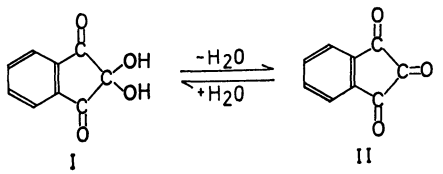

I II (1)

It is suggested that the first wave in Fig. 1 is attributed to II, since it has the same $E_{1/2}$ value as that of the first wave in Fig. 2. Polarogram a in Fig. 3 was observed when the necessary amount of I was added in dried DMF containing TEAP which had been exposed to atmosphere in crystalline form, the exposure time not exceeding 1 h. Polarograms b and c showed a very small but more positive wave with time (Fig. 3).

The results can be interpreted as follows. The chemically bound H_2O in I, *i.e.* in *gem*-diol structure, can be slowly removed even in an electrolyte solution dried insufficiently; equilibrium between I and II in

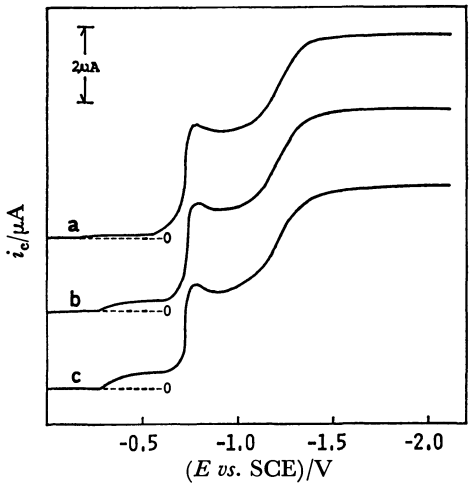

Fig. 3. Polarograms of ninhydrin taken with TEAP exposed to the atmosphere for about 1 h.
Concn: 1.1×10^{-3} M, temp: 22 °C, a: immediately after dissolving ninhydrin, b: 20 min, c: 60 min.

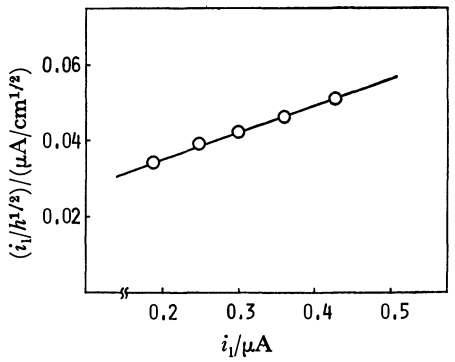

Fig. 4. Relation between i_l and $i_l/h^{1/2}$.
Concn: 1.1×10^{-3} M, h: 30—70 cm.

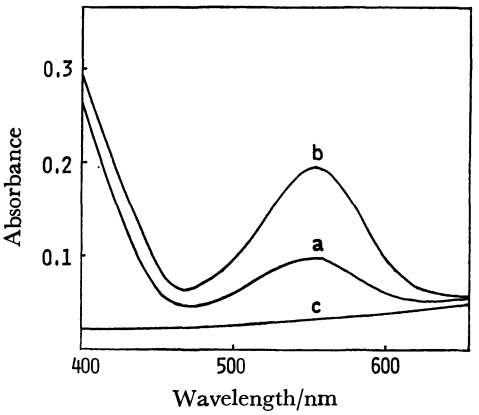

Fig. 5. Absorption spectra of ninhydrin and 1,2,3-indantrione in DMF.
a: Ninhydrin 1×10^{-2} M, b: 1,2,3-indantrione 1×10^{-2} M, c: DMF only.
Spectra were taken immediately after dissolving the specimen.

DMF can be attained with time.

However, as shown in Fig. 4, the plot of i_l of the first wave in Fig. 1-d against $i_l/h^{1/2}$ (i_l: limiting current, h: the level of the Hg reservoir) exhibited no kinetic character, suggesting a diffusion accompanied with adsorption of the electroactive chemical species for the corresponding electrode reaction.[17] It is difficult to demonstrate the direct participation of the dehydration reaction at the electrode.

On the other hand, the absorption spectra taken with I and II (Fig. 5), qualitatively supported an equilibrium between the two species in DMF. A relatively small absorption peak at 550 nm was obtained with I and a larger one with II. Prevention of the intrusion of atmospheric moisture into DMF medium was not satisfactory as compared with polarographic conditions, and the observed purple color due to the absorption at 550 nm faded with time for both I and II.

Table 1. ^{13}C-NMR chemical shifts for ninhydrin in DMF-d_7

Compound	Carbon	δ ^{13}C[ppm]
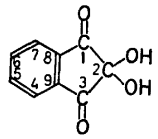	1,3	197.6
	2	139.5
	8,9	137.7
	4,7	124.4
	5,6	88.4

(Reference: TMS)

The predominance of the hydrated form (I) in DMF was also observed by ^{13}C-NMR spectroscopy (Table 1), where no signal due to C-2 carbonyl group of II was detected, when each signal was assigned to the possible structure.

Let us discuss the first wave of reduction current with a large maximum in the polarogram (Fig. 1;. It is evidently due to the reduction of dehydrated form (II) at the electrode. If the current is due to species II in equilibrium, it would be difficult to interpret the presence of the maximum.

We might assume a different equilibrium between I and II, accompanied by adsorption at the electrode or a relatively fast dehydration from I to II, the equilibrium or rate of which may be largely dependent on the applied potential in a limited range. It is interesting to consider this characteristic phenomenon of ninhydrin in nonaqueous solution, in comparison with the observation made by Holleck and Lehman[10] that ninhydrin in aqueous buffer solutions also shows the reduction wave due to II, whose shape is very similar to the present one in DMF, though intensity and potential, *etc.* largely differ from each other.

The electrocapillary curve of the present system was also studied, an abnormal change of drop time being observed with applied potential corresponding to the maximum of curve a in Fig. 1. However, the drop time gave fairly scattered values for repeated measurements at the potential. This may suggest possible adsorption of I or II at the electrode.

Cyclic Voltammetry of Ninhydrin. Cyclic voltammetry of I was studied with use of the hanging mercury

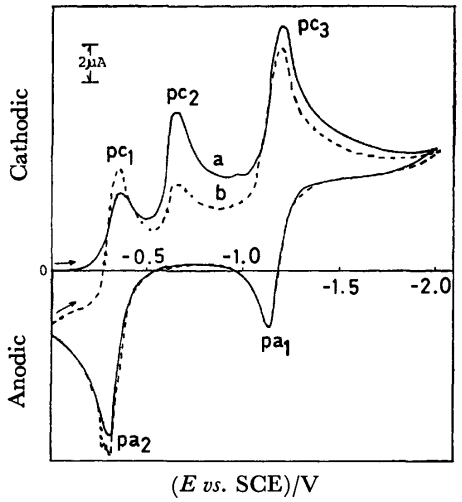

Fig. 6. Cyclic voltammograms of ninhydrin in DMF. Concn: 2.1×10^{-3} M, temp: 26 °C, sweep: 50 mV/s, electrode: HME, a: single sweep, b: multiple sweep.

electrode (HME). The cyclic voltammogram (CV) is shown in Fig. 6, curve (a) being recorded by a single sweep and curve (b) by a multiple sweep. In both cases three cathodic peaks (pc_1, pc_2, and pc_3), corresponding to the polarographic three waves, respectively, and two anodic peaks (pa_1 and pa_2) corresponding to pc_3 and pc_1, respectively, were observed. Peak potential differences, $|E_{pc_1}-E_{pa_2}|$ and $|E_{pc_3}-E_{pa_1}|$, were found to be 60 mV for both cases, suggesting one-electron reversible redox system.[18]

In b, the peak current of pc_2 was smaller, while that of pc_1 became larger as compared with those in a. Irregularity of pa_2 in b was observed, suggesting an abrupt change in surface conditions.

A similar CV was observed with use of the Pt electrode, $|E_{pc_3}-E_{pa_1}|$ being approximately 70 mV. These cyclic voltammograms are similar to those of II observed by Kalinowski and Lasia[13] except for peak height of pc_2.

Mechanism of the Electrode Reaction. From the results of d.c.-polarography, CV and the proposed mechanism[13] of DME reaction of II, the electrode reaction mechanism of I in DMF can be discussed. Kalinowski and Lasia simplified the problem of ninhydrin (I) only in its dehydrated form (II), as proposed in Eq. 2.[13] However, the equilibrium between I and II in the bulk of the solution and also at the electrode

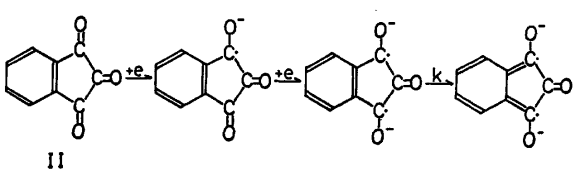

II (2)

surface should be taken into consideration. The reversibility of the electrode reaction for three steps of reduction is more clearly visualized by CV than by d.c.-polarography. The first and third waves in d.c.-polarography can be described each as reversible one-electron transfer on the basis of logarithmic analysis

and the peak potential differences $|E_{pc_1}-E_{pa_2}|$ and $|E_{pc_3}-E_{pa_1}|$. The second wave is typically irreversible, since peak pc_2 does not exhibit its corresponding anodic peak.

The following scheme is proposed for the principal process of electrolytic reduction of ninhydrin in DMF.

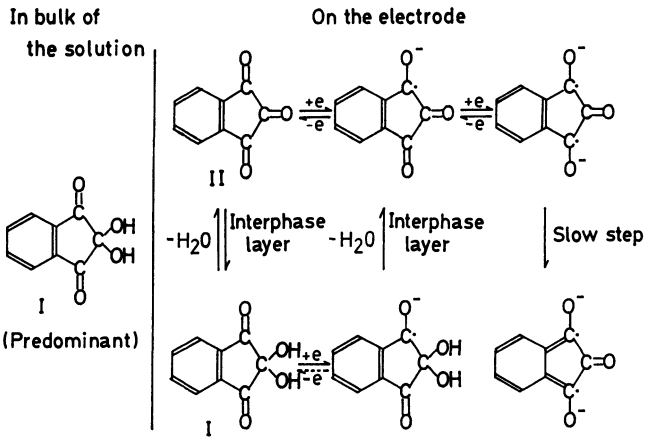

Scheme 1.

The hydrated form can be reduced at the electrode as the second wave, but the reduction product easily liberates H_2O and is converted into the dehydrated form identical with the direct reduction product from II. In nonaqueous solvents the dehydration is understood as an irreversible process.

References

1) K. Veselý and R. Brdička, *Collect. Czech. Chem. Commun.*, **12**, 313 (1947).
2) P. Zuman and H. Zinner, *Chem. Ber.*, **95**, 2089 (1962).
3) G. A. Russell and S. A. Weiner, *J. Am. Chem. Soc.*, **89**, 6623 (1967).
4) S. Ono, M. Takagi, and T. Wasa, *Collect. Czech. Chem. Commun.*, **26**, 141 (1961).
5) M. Ohmori and M. Takagi, *Bull. Chem. Soc. Jpn.*, **50**, 773 (1977).
6) M. B. Fleury and G. Molle, *Electrochimica Acta.*, **20**, 951 (1975).
7) S. Ono, M. Takagi, and T. Wasa, *Bull. Chem. Soc. Jpn.*, **31**, 364 (1958).
8) G. A. Melkonian and L. Holleck, *Z. Elektrochem.*, **64**, 1210 (1960).
9) L. Holleck and O. Lehman, *Monatsh. Chem.*, **92**, 499 (1961).
10) L. Holleck and O. Lehman, *Ber. Bunsenges. Phys. Chem.*, **67**, 609 (1963).
11) L. Holleck and O. Lehman, *Collect. Czech. Chem. Commun.*, **30**, 4024 (1965).
12) J. C. Dufresne, *Electrochimica Acta.*, **20**, 965 (1975).
13) M. K. Kalinowski and A. Lasia, *Ann. Soc. Chim.Polonorum.*, **43**, 1265 (1969).
14) S. Ono, M. Takagi, and T. Wasa, *J. Am. Chem. Soc.*, **75**, 4369 (1953).
15) S. Ono, M. Takagi, and T. Wasa, *Bull. Chem. Soc. Jpn.*, **31**, 356 (1958).
16) C. K. Mann, *Electroanal. Chem.*, **3**, 57 (1969).
17) As a convenient method for diagnosis of electrode reaction characteristics, for example, see monograph by P. Zumann "Organic Polarographic Analysis," Pergamon Press, Oxford (1964), p. 23.
18) P. Delahay "New Instrumental Methods in Electrochemistry," Interscience Publishers, Inc., New York (1954), p. 137.

Jasmonoid Synthesis from *cis*-4-Heptenoic Acid

Toshio SATO, Tatsuo KAWARA, Kazumi SAKATA, and Tamotsu FUJISAWA*

Chemistry Department of Resources, Mie University, Tsu, Mie 514

(Received August 25, 1980)

Jasmonoids with *cis*-2-pentenyl side chain such as *cis*-jasmone, methyl jasmonate, and jasmolone were easily synthesized from *cis*-4-heptenoic acid obtained by the ring opening reaction of β-propiolactone with di-*cis*-butenylcuprate.

Recently there have been a large amount of researches developing synthetic routes to 2-(*cis*-2-alkenyl)-2-cyclopentenones.[1a] This has been due in large part to interest in several biologically active natural products which have this moiety as a major structural feature. In the synthesis of these compounds, stereoselective introduction of *cis*-2-alkenyl side chain has been one of the major subjects. For example, as for the synthesis of jasmonoids,[1b] the *cis*-2-pentenyl group has been formed by elaborate routes, *e.g.*, the partial hydrogenation of carbon-carbon triple bond with the Lindlar catalyst,[2,3] the Wittig reaction of a formylmethyl group with propylidenetriphenylphosphorane under salt free conditions,[4] and the reductive desulfurization of 5,6-dihydro-2*H*-thiopyran derivative.[5] Recently *cis*-4-alkenoic acids were found to be synthesized in one-pot operation from dialkylcuprates, acetylene, and β-propiolactone.[6] Among them, *cis*-4-heptenoic acid would be a useful precursor of these jasmonoids, because it has a structure corresponding to a skeleton from the side chain to the carbonyl carbon of the cyclopentenone in the jasmonoids with *cis*-2-pentenyl moiety such as *cis*-jasmone, methyl jasmonate and jasmolone. Thus, the synthetic route to the jasmonoids from *cis*-4-heptenoic acid as a key intermediate was investigated *via* well documented cyclization of 1,4-diketones.

cis-4-Heptenoic acid (**1**) was easily synthesized in a high yield by utilizing two reactions, *i.e.*, the *syn* addition of dialkylcuprates to acetylene for the formation of di-*cis*-1-alkenylcuprates[7] and the regioselective ring opening reaction of β-propiolactone with diorganocuprates.[8] Thus, acetylene was introduced at −78 °C into bromomagnesium diethylcuprate, which was prepared from copper(I) iodide and ethylmagnesium bromide in THF–Me_2S (9 : 1) at −30 °C. After the reaction mixture was allowed rapidly to warm to −30 °C and stirred for 30 min, the reaction of β-propiolactone with the cuprate was performed at −30 °C for 2 h. By quenching the reaction with 3 M (1 M=1 mol dm^{-3}) HCl solution, the desired acid **1** was isolated by distillation in a yield of 81%.

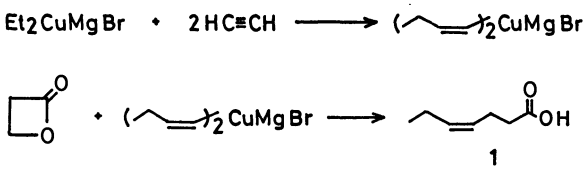

Scheme 1.

The precursor of *cis*-jasmone, *cis*-8-undecene-2,5-dione (**5**) was easily derived from *cis*-4-heptenoic acid and 3-oxo-butyl equivalent. As a latter compound, 3,3-ethylenedioxybutyl group was chosen. Treatment of **1** with thionyl chloride and pyridine in ether gave *cis*-4-heptenoyl chloride (**2**) in a yield of 74%. Condensation of **2** with the Grignard reagent **3**[9] prepared from magnesium metal and 3,3-ethylenedioxybutyl bromide, which was derived from methyl vinyl ketone, ethylene glycol, and hydrogen bromide, in THF at −78 °C and then warming to room temperature, afforded *cis*-2,2-ethylenedioxy-8-undecen-5-one (**4**) quantitatively. Deacetalization of the keto acetal **4** with dilute hydrochloric acid solution afforded the dione **5**, which was then cyclized with dilute aqueous base in the usual manner[10] to give *cis*-jasmone (**6**) in 68% yield from **3**.

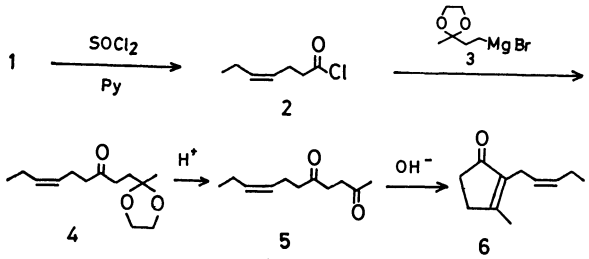

Scheme 2.

Methyl jasmonate (**11**) can also be synthesized from *cis*-4-heptenoic acid *via* 2-(*cis*-2-pentenyl)-2-cyclopentenone (**10**). In this case, 3,3-trimethylenedioxypropyl group was chosen for the stability of the Grignard reagent as functional group for the three carbon elongation. Condensation of **2** with the Grignard reagent **7**[11] of 3,3-trimethylenedioxypropyl bromide, prepared from acrylaldehyde, hydrogen bromide, and 1,3-propanediol, furnished *cis*-1,1-trimethylenedioxy-7-decen-4-one (**8**). Deacetalization of **8** with aqueous oxalic acid gave *cis*-4-oxo-7-undecenal (**9**) in 68% yield from **2**. Cyclization of aldehyde **9** with 1% sodium

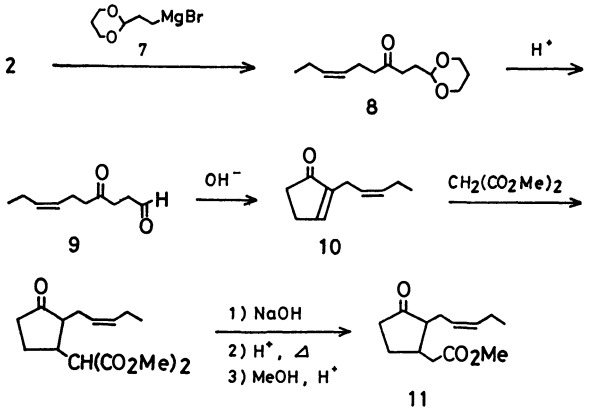

Scheme 3.

hydroxide in water–dioxane (1 : 1) afforded the cyclopentenone **10** in 69% yield. According to the standard procedure[2,12] **10** was converted into methyl jasmonate (**11**), *i.e.*, the Michael addition of dimethyl malonate to **10**, followed by hydrolysis, decarboxylation, and esterification furnished **11** in a yield of 66%.

Jasmolone, an ester component of jasmoline, was also prepared from *cis*-4-heptenoic acid *via* cyclization of 1,4-diketone. The dianion **12**[13] of ethyl hydrogen malonate reacted with **2** in THF at −65 °C for 1 h to afford ethyl *cis*-3-oxo-6-nonenoate (**13**) in a yield of 76%. Then, according to the procedure by LaForge *et al.*,[14] **13** was hydrolyzed with dilute potassium hydroxide solution, followed by condensation with methylglyoxal and successive decarboxylation to give *cis*-3-hydroxy-8-undecene-2,5-dione (**14**), which was cyclized by the treatment with 2% sodium hydroxide aqueous solution to give jasmolone (**15**) in 23% yield from **13**.

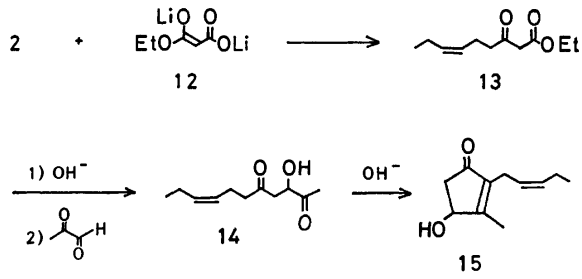

Scheme 4.

As mentioned above, *cis*-4-heptenoic acid, easily prepared from β-propiolactone and di-*cis*-1-butenylcuprate, was proved to be a very useful precursor for the synthesis of the jasmonoids with *cis*-pentenyl moiety. Further, by the use of various *cis*-alkenylcuprates, the regioselective ring opening of β-propiolactone should provide a promising method for the synthesis of a wide variety of natural products possessing *cis* carbon-carbon double bond.

Experimental

The IR spectra were recorded on a Hitachi EPI-G2 spectrometer. The NMR spectra were taken with a Varian A-60 spectrometer using TMS as an internal standard. Grignard reagents and butyllithium were titrated by Eastham's method.[15] All boiling points are uncorrected.

cis-4-Heptenoic Acid (1). To a solution of copper(I) iodide (5.713 g, 30 mmol) in THF (90 ml) and dimethyl sulfide (10 ml) was added an ethereal solution of ethylmagnesium bromide (1.85 M, 32.5 ml, 60 mmol) at −30 °C. Then, acetylene (2160 ml, 90 mmol) was introduced using a gas buret through a drying tube ($CaCl_2$) into a suspension of the cuprate at −78 °C at an approximate rate of 20 ml/min. After introduction of acetylene, the temperature was allowed to warm rapidly to −30 °C and the mixture was stirred for 30 min. β-Propiolactone (1.081 g, 15 mmol) in THF (2 ml) was added dropwise and stirring was continued at −30 °C for additional 2 h. The reaction was quenched with 3 M hydrochloric acid solution (20 ml) and extracted with ether. The separated organic layer was extracted with 3 M sodium hydroxide solution. The alkaline solution was washed with ether, acidified with 6 M hydrochloric acid solution, and then extracted with ether. The ether extracts were washed with brine (10 ml) and dried over anhydrous $MgSO_4$. Distillation gave **1** (1.56 g, 81%): bp 97—99 °C/5 mmHg (lit,[16] bp 97—99 °C/4 mmHg); IR (neat) 1710 (C=O) and 720 cm^{-1} (*cis*-CH=CH); NMR (CCl_4) δ 0.95 (3H, t, J=7 Hz), 1.90—2.40 (6H, m), 5.10—5.60 (2H, m), and 11.90 (1H, s).

cis-4-Heptenoyl Chloride (2). A mixture of **1** (4.35 g, 34.0 mmol) and pyridine (3.06 g, 40.8 mmol) in ether (20 ml) was added to a solution of thionyl chloride (4.45 g, 37.4 mmol) in ether (50 ml) at −15 °C. The reaction mixture was stirred at room temperature for 2 h. The precipitate formed was filtered off. Distillation of the filtrate gave **2** (3.66 g, 74%): bp 63—64 °C/13 mmHg (lit,[17] bp 72—76 °C/35 mmHg); IR (neat) 1800 (C=O) and 720 cm^{-1} (*cis*-CH=CH); NMR (CCl_4) δ 0.98 (3H, t, J=7 Hz), 1.72—2.63 (4H, m), 2.63—3.07 (2H, m), 4.83—5.61 (2H, m).

3,3-Ethylenedioxybutyl Bromide. To a solution of hydrogen bromide (12.0 g, 133 mmol) in ethylene glycol (20.0 g, 327 mmol) was added dropwise methyl vinyl ketone (7.00 g, 100 mmol) at 0 °C. The reaction mixture was stirred at room temperature for 1 h and extracted with hexane. The extracts were washed with 5% sodium hydrogencarbonate solution and dried over anhydrous $MgSO_4$. Distillation gave 3,3-ethylenedioxybutyl bromide (9.26 g, 48%): bp 88—94 °C/27 mmHg; (lit,[18] bp 58—60 °C/12 mmHg); IR (neat) 1120 (C=O) and 540 cm^{-1} (CBr); NMR (CCl_4) δ 1.31 (3H, s), 2.20 (2H, t, J=9 Hz), 3.45 (2H, t, J=9 Hz), and 3.95 (4H, s).

cis-2,2-Ethylenedioxy-8-undecen-5-one (4). To a solution of **2** (0.784 g, 5.28 mmol) in THF (5 ml) was added the Grignard reagent **3** (0.61 M, 7.87 ml, 4.80 mmol), prepared from 3,3-ethylenedioxybutyl bromide and magnesium in THF at room temperature,[9] at −78 °C. The mixture was allowed to warm to room temperature for 1.5 h. It was poured into a saturated sodium hydrogencarbonate solution (10 ml), extracted with ether, and dried over anhydrous $MgSO_4$. The crude product was purified by TLC on silica gel (R_f 0.6, benzene) to afford **4** quantitatively (1.087 g): IR (neat) 1710 (C=O), 1150, 1050 (C–O), and 720 cm^{-1} (*cis*-CH=CH); NMR (CCl_4) δ 0.95 (3H, t, J=7 Hz), 1.30 (3H, s), 1.66—2.67 (10H, m), 4.01 (4H, s), and 5.23—5.67 (2H, m).

cis-8-Undecene-2,5-dione (5). A solution of **4** (0.279 g, 1.23 mmol) and two drops of 3 M hydrochloric acid solution in acetone (5 ml) and water (5 ml) was refluxed for 4 h. After evaporation of the acetone, the residue was extracted with ether. The ether extracts were washed with brine and dried over anhydrous $MgSO_4$. Removal of the solvent gave **5** (0.187 g, 84%): IR (neat) 1720 (C=O), and 720 cm^{-1} (*cis*-CH=CH); NMR (CCl_4) δ 0.97 (3H, t, J=7 Hz), 2.00—2.57 (9H, m), 2.67 (4H, s), and 5.20—5.59 (2H, m). The spectral data of **5** were in agreement with the literature.[10]

cis-Jasmone (6). According to the procedure of Büchi *et al.*,[10] a solution of the diketone **5** in 0.5 M sodium hydroxide solution and ethanol was refluxed for 6 h to give **6** (82%): IR (neat) 1720 (C=O) and 720 cm^{-1} (*cis*-CH=CH); NMR (CCl_4) δ 1.00 (3H, t, J=7 Hz), 2.00—3.00 (11H, m), and 5.20—5.70 (2H, m). The spectral data of **6** were in agreement with the literature.[10]

3,3-Trimethylenedioxypropyl Bromide. To a solution of hydrogen bromide (21.6 g, 0.27 mol) in 1,3-propanediol (43.6 g, 0.57 mol) was slowly added acrylaldehyde (11.0 g, 0.18 mol, 90% purity) at room temperature. The reaction mixture was stirred at room temperature for 1 h and extracted with hexane. The extracts were washed with 5% sodium hydrogencarbonate solution and dried over anhydrous $MgSO_4$. Distillation gave 3,3-trimethylenedioxypropyl bromide (25.3 g,

† 1 mmHg=133.322 Pa.

74%): bp 89—91 °C/10 mmHg† (lit,[11] bp 67—70 °C/2.8 mmHg); NMR (CCl_4) δ 1.00—1.50 (1H, m), 1.50—2.47 (3H, m), 3.36 (2H, t, J=8 Hz), 3.75—4.25 (4H, m), and 4.57 (1H, t, J=5 Hz).

cis-*1,1-Trimethylenedioxy-7-decen-4-one (8).* To a solution of *cis*-4-heptenoyl chloride (**2**) (3.64 g, 24.8 mmol) in THF (20 ml) was added dropwise the Grignard reagent **7** (0.72 M, 31.3 ml, 22.5 mmol), prepared from 3,3-trimethylenedioxypropyl bromide and magnesium in THF,[11] at −78 °C. The mixture was allowed to warm to room temperature for 2 h and the THF was removed. The residue was extracted with ether and the organic layer was washed with water, and then dilute sodium carbonate solution, dried over anhydrous K_2CO_3. Removal of the solvent afforded **8** (5.77 g), which was used in the next reaction without purification. IR (neat) 1720 (C=O), 1150, 1050 (C–O), and 720 cm^{-1} (*cis*-CH=CH); NMR (CCl_4) δ 0.97 (3H, t, J=7 Hz), 1.25—2.67 (13H, m), 3.32—4.25 (4H, m), 4.40 (1H, t, J=5 Hz), and 5.10—5.43 (2H, m).

cis-*4-Oxo-7-undecenal (9).* A mixture of crude **8** (2.53 g), oxalic acid (1 g), and water (20 ml) was refluxed for 3 h, during which time the product was continuously steam-distilled into a Dean Stark trap. The distillate was extracted with ether. The ether extracts were dried over anhydrous Na_2SO_4. Distillation under reduced pressure gave **9** (1.26 g, 68% from **7**): bp 104—105 °C/1.7 mmHg; IR (neat) 1725 (C=O), 1715 (CHO), and 730 cm^{-1} (*cis*-CH=CH); NMR (CCl_4) δ 0.95 (3H, t, J=7 Hz), 1.77—2.50 (6H, m), 2.62 (4H, s), 5.20—5.63 (2H, m), and 9.60 (1H, s). The spectral data of **9** were in agreement with the literature.[12]

*2-(*cis*-2-Pentenyl)-2-cyclopentenone (10).* To a refluxing solution of water (45 ml), dioxane (45 ml) and 10% sodium hydroxide solution (10 ml) was added dropwise a dioxane solution of **9** (0.922 g, 5.49 mmol) for 1.5 h. The mixture was refluxed for 10 min. After neutralization with 1 M hydrochloric acid solution, it was extracted with chloroform. The extracts were dried over anhydrous Na_2SO_4. Distillation afforded **10** (0.565 g, 69%): bp 90 °C (bath)/0.6 mmHg (lit,[2] bp 70 °C/0.05 mmHg); IR (neat) 1700 (C=O), 1625 (CH=CH, ring), and 730 cm^{-1} (*cis*-CH=CH); NMR (CCl_4) δ 0.97 (3H, t, J=7 Hz), 1.60—3.08 (8H, m), 5.16—5.70 (2H, m), and 7.25 (1H, m). The spectral data of **10** were in agreement with the literature.[2]

Methyl Jasmonate (11). Sodium hydride (0.02 g, 0.46 mmol, 55% in mineral oil) was washed with dry hexane, and dry methanol (0.7 ml) was added. To the mixture was added dropwise dimethyl malonate (0.258 g, 1.95 mmol) and then cyclopentenone (**10**) (0.187 g, 1.25 mmol) in dry methanol (1 ml) at −5 °C for 40 min. The resulting mixture was stirred at −10—−5 °C for 3 h. After the reaction was quenched with acetic acid (2 ml), the methanol was evaporated. The residue was dissolved in ether, washed with water and dried over anhydrous Na_2SO_4. Distillation gave 3-[bis(methoxycarbonyl)methyl]-2-(*cis*-2-pentenyl) cyclopentenone (0.325 g, 92%): bp 200 °C (bath)/2 mmHg; IR (neat) 1740 ($COOCH_3$), 1700 (C=O), and 735 cm^{-1} (*cis*-CH=CH); NMR (CCl_4) δ 0.95 (3H, t, J=7 Hz), 1.75—2.50 (10H, m), 3.47 (1H, s), 3.70 (6H, s), and 5.00—5.50 (2H, m).

To 0.269 g (1.05 mmol) of the cyclopentenone was added dropwise 10% sodium hydroxide aqueous solution (0.9 ml) for 4 h and the mixture was allowed to stand overnight. Then 3% sulfuric acid solution (0.35 ml) was added and the resulting mixture was refluxed for 5 h. The cooled reaction mixture was extracted with ether and washed with water. The ether extract were then extracted with 3 M sodium hydroxide solution. The alkaline solution was washed with ether, acidified with 6 M hydrochloric acid solution, and then extracted with ether. The extracts were dried over anhydrous Na_2SO_4 and evaporated to afford jasmonic acid (0.172 g, 78%): IR (neat) 3150 (OH), 1740 (C=O), 1750 (COOH) and 720 cm^{-1} (*cis*-CH=CH); NMR (CCl_4) δ 0.97 (3H, t, J=7 Hz), 1.65—3.08 (12H, m), 5.15—5.67 (2H, m), and 11.0 (1H, s).

A solution of jasmonic acid (0.142 g, 0.68 mmol) in methanol (5 ml) was stirred at 40 °C for 3 h with a catalytic amount of concd H_2SO_4. The reaction mixture was cooled, and a small amount of $NaHCO_3$ and water (5 ml) was added. The mixture was extracted with ether and the extracts were dried over anhydrous Na_2SO_4. Removal of the solvent gave **11** (0.138 g, 92%): IR (neat) 1740 (C=O), 720 cm^{-1} (*cis*-CH=CH); NMR (CCl_4) δ 0.95 (3H, t, J=7 Hz), 1.55—3.05 (12H, m), 3.65 (3H, s), and 4.82—5.55 (2H, m). The spectral data of **11** were identical with the literature.[2]

Ethyl cis-*3-Oxo-6-nonenoate (13).* To a solution of ethyl hydrogen malonate (0.231 g, 1.75 mmol) and 2,2′-bipyridyl (3 mg) in THF (4 ml) was added a hexane solution of butyllithium (1.52 M, 2.30 ml, 3.5 mmol) at −70 °C, during which time the temperature was raised from −70 to −5 °C.[13] To a solution of the dianion **12** was added **2** (0.147 g, 1.00 mmol) in THF (1 ml) at −65 °C. After 1 h ether (7 ml) and 1 M hydrochloric acid solution (3 ml) were added. The organic layer was washed with saturated sodium hydrogencarbonate solution and then water, and dried over anhydrous Na_2SO_4. Removal of the ether gave the crude product, which was purified by TLC on silica gel (R_f 0.5, hexane : ether=2 : 1) to give **13** (0.151 g, 76%): IR (neat) 1750 (COO), 1730 (C=O), and 730 cm^{-1} (*cis*-CH=CH); NMR (CCl_4) δ 0.95 (3H, t, J=7 Hz), 1.20 (3H, t, J=7 Hz), 1.70—2.60 (6H, m), 3.22 (3H, s), 4.12 (2H, q, J=7 Hz), and 4.85—5.55 (2H, m).

cis-*3-Hydroxy-8-undecene-2,5-dione (14).* To **13** (0.135 g, 0.70 mmol) was added dropwise 10% potassium hydroxide solution (0.46 ml) and the mixture was allowed to stand at −3—−2 °C for 3 d. After washed with ether, the reaction mixture was acidified with 0.5 M hydrochloric acid solution to pH 3—4, extracted with ether, and dried over anhydrous Na_2SO_4. Evaporation of the solvent gave *cis*-3-oxo-6-nonenoic acid (0.086 g, 73%): IR (KBr) 3150 (OH), 1710 (C=O), and 720 cm^{-1} (*cis*-CH=CH); NMR (CCl_4) δ 1.00 (3H, t), 1.78—2.80 (6H, m), 4.80—5.50 (2H, m), and 10.88 (1H, s).

cis-3-Oxo-6-nonenoic acid (0.816 g, 1.86 mmol) in water (1 ml) was neutralized with 10% sodium hydroxide solution using phenolphthalein as an indicator at 0 °C. To the solution was added methylglyoxal (0.156 g, 2.20 mmol, 40% aqueous soln) and then 10% sodium hydroxide solution to make the mixture basic (pH 8). The resulting mixture was allowed to stand at room temperature for 2.5 d and extracted with ether. The extracts were dried over anhydrous Na_2SO_4, and evaporated. Purification by TLC on silica gel (R_f 0.4, ether : hexane=2 : 1) gave **14** (0.220 g, 60%): IR (neat) 3450 (OH), 1720 (C=O), and 720 cm^{-1} (*cis*-CH=CH); NMR (CCl_4) δ 0.95 (3H, t, J=7 Hz), 1.80—2.90 (11H, m), 4.00—4.40 (2H, m), and 4.80—5.50 (2H, m). The spectral data of **14** were in agreement with the literature.[19]

Jasmolone (15). To **14** (0.148 g, 0.75 mmol) was added dropwise 2% potassium hydroxide solution (0.6 ml) and the mixture was allowed to stand at room temperature for overnight. The reaction mixture was extracted with ether, washed with brine, and dried over anhydrous Na_2SO_4. Purification by TLC on silica gel (R_f 0.4, ether : hexane=3 : 1, developed twice) gave **15** (0.069 g, 52%): IR (neat) 3400 (OH), 1710 (C=O), 710 cm^{-1} (*cis*-CH=CH); NMR (CCl_4) δ 0.95 (3H, t, J=7 Hz), 1.60—3.00 (9H, m), 4.10 (1H, broad), 4.45 (1H, m), and 4.80—5.50 (2H, m). The spectral

data were in agreement with the literature.[19]

The present work was partially supported by a Grant-in-Aid for Scientic Research No. 554144 from the Ministry of Education, Science and Culture.

References

1) a) R. A. Ellison, *Synthesis*, **1973**, 397; b) T.-L. Ho, *Synth. Commun.*, **4**, 265 (1974); S. Torii and H. Tanaka, *Koryo*, **1976**, 41.

2) G. Büchi and B. Egger, *J. Org. Chem.*, **36**, 2021 (1971).

3) J. E. McMurry and J. Melton, *J. Am. Chem. Soc.*, **93**, 5309 (1971); J. L. Herrmann, J. E. Richman, and R. H. Schlessinger, *Tetrahedron Lett.*, **1973**, 3275; A. E. Greene and P. Crabbe, *ibid.*, **1976**, 4867; H. J. Monteiro, *J. Org. Chem.*, **42**, 2324 (1977); S. Torii, H. Tanaka, and Y. Kobayasi, *ibid.*, **42**, 3474 (1977); K. Kondo, Y. Takahatake, K. Sugimoto, and D. Tunemoto, *Tetrahedron Lett.*, **1978**, 907.

4) H. Tanaka and S. Torii, *J. Org. Chem.*, **40**, 462 (1975); P. Bakuzis and M. L. F. Bakuzis, *ibid.*, **42**, 2362 (1977).

5) S. Torii, H. Tanaka, and Y. Tomotaki, *Bull. Chem. Soc. Jpn.*, **50**, 537 (1977).

6) T. Fujisawa, T. Sato, T. Kawara, and K. Naruse, *Chem. Lett.*, **1980**, 1123.

7) H. Westmijze, J. Meijer, H. J. T. Bos, and P. Vermeer, *Recl. Trav. Chim. Pays-Bas*, **95**, 304 (1976); A. Alexakis, G. Cahiez, and J. F. Normant, *Synthesis*, **1979**, 826.

8) T. Fujisawa, T. Sato, T. Kawara, M. Kawashima, H. Shimizu, and Y. Ito, *Tetrahedron Lett.*, **21**, 2181 (1980).

9) A. A. Ponaras, *Tetrahedron Lett.*, **1976**, 3105.

10) G. Büchi and H. Wüest, *J. Org. Chem.*, **31**, 977 (1966).

11) J. C. Stowell, *J. Org. Chem.*, **41**, 560 (1976).

12) P. Dubs and R. Stüssi, *Helv. Chim. Acta*, **61**, 990 (1978).

13) W. Wierenga and H. I. Skulnick, *J. Org. Chem.*, **44**, 310 (1979).

14) M. S. Schechter, N. Green, and F. B. LaForge, *J. Am. Chem. Soc.*, **71**, 3165 (1949).

15) S. C. Watson and J. F. Eastham. *J. Organomet. Chem.*, **9**, 165 (1967).

16) K. Furukawa and M. Iwakiri, *Yuki Gosei Kagaku Kyokai Shi*, **33**, 496 (1975).

17) L. Crombie, S. H. Harper, R. E. Stedman, and D. Thompson, *J. Chem. Soc.*, **1951**, 2445.

18) C. Feugeas, *Bull. Soc. Chim. Fr.*, **1963**, 2568.

19) L. Crombie, P. Hemesley, and G. Pattenden, *J. Chem. Soc., C*, **1969**, 1016.

The Determination of the "Flat-band" Potential of Nitrogen-stabilized n-TiO_2 Photoanode

Taketsugu HIRAI,* Isao TARI, and Tsutomu OHZUKU
Department of Synthetic Chemistry, Faculty of Engineering, Okayama University, Tsushima, Okayama 700
(Received March 28, 1980)

The differential capacitance (C) and the photocurrent onset voltage (E_p) of nitrogen-stabilized n-TiO_2 semiconductor electrodes were measured in buffered Na_3PO_4 solutions. The C^{-2} *vs.* E plots did not show the Mott-Schottky (MS) behavior. In order to explain the nonlinearity in MS plots, the distribution in donor density (N_d) at the solid side and the contribution of the electrical double layer at the solution side to the total capacitance were considered. The characterized flat-band potential (E_{fb}) and the zero-charge potential (E_{zc}) were defined from the derived equations. The roles of the defined E_{fb} and E_{zc} in the photocurrent onset voltage (E_p) were also considered, and the reason why E_p differed from E_{fb} was explained using the "Gate" model.

In semiconductor electrochemistry, the determinations of both the flat-band potential and the charge carrier density are important, for they are the basic parameters of semiconductor electrodes. These quantities can be determined by the Mott-Schottky relationship from the measurement of the differential capacitance. However, the experimental results which have been reported for single and polycrystalline semiconductor electrodes usually show some deviations from ideality.[1-6] The possible sources of such deviation from ideality have been discussed by several authors.[1,4,7-9] One of these treatments, that by De Gryse *et al.*,[7] is a quantitative one. They derived another expression by considering the effect of the Helmholtz layer at the semiconductor/electrolyte interface. However, the C^{-2} *vs.* E plots do not allow the E_{fb} values to be determined unless the Helmholtz layer capacitance is known, even when the experimental C^{-2} *vs.* E plot is a straight line.

Our differential capacitance data for nitrogen-stabilized n-TiO_2 semiconductor electrodes, to be reported here, do not show the Mott-Schottky behavior. The objective of this report is to understand the capacitance data, together with the photoelectrochemical property, and to discuss the uncertainty in the determination of the flat-band potential.

Experimental

The nitrogen-stabilized n-type semiconductor ($TiN_{0.07}O_{1.93}$) electrode, which had been proved to be highly resistive to photocorrosions, was the same as that described in a previous paper.[12]

The cell impedance between the $TiN_{0.07}O_{1.93}$ electrode and a far larger platinum electrode was measured by means of an impedance bridge, type DRZ-1 (Ando Electric Corp.), with an audio oscillator, type 4200-A (Yokogawa-Hewlett-Packard), and a tuned null detector, type 4403-A (Yokogawa-Hewlett-Packard). The absolute values of the impedance $|z|$ and the phase angle, θ, as functions of the bias voltage (*vs.* SCE) were measured at 0.3—10 kHz. The electrolytes used were 0.1 M Na_3PO_4 aqueous solutions, adjusted their pHs with a concd NaOH or H_3PO_4 solution.

The anodic photocurrent was measured in the usual manner under full illumination by a 500-W xenon arc lamp at room temperature.

Results

Differential Capacitance Measurements. Figure 1 shows the differential capacitance at 500 Hz as a function of the electrode potential for the $TiN_{0.07}O_{1.93}$ electrode in several buffered Na_3PO_4 solutions. All the C *vs.* E curves showed their peaks in the cathodic region. Although the capacitance values varied somewhat, thus showing the frequency dispersion, a similar trend was usually observed in the frequency range of 0.3—10 kHz.

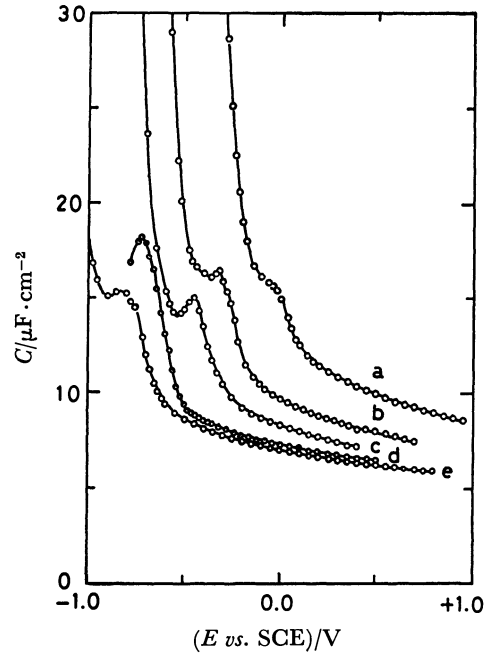

Fig. 1. C *vs.* E curves for $TiN_{0.07}O_{1.93}$ electrode in 0.1 M Na_3PO_4 solutions.
pH; (a): 1.0, (b): 5.0, (c): 7.0, (d): 10.0, (e): 12.0.

In order to determine the basic parameters for this electrode, the C^{-2} *vs.* E plots were applied. According to the Mott-Schottky relationship, the C^{-2} *vs.* E plots should give a straight line over a wide range of potentials. However, the experimental results in Fig. 2 do not show an ideal MS-behavior, so the E_{fb} and N_d values could not be determined.

Photocurrent Onset Voltage. The anodic photo-

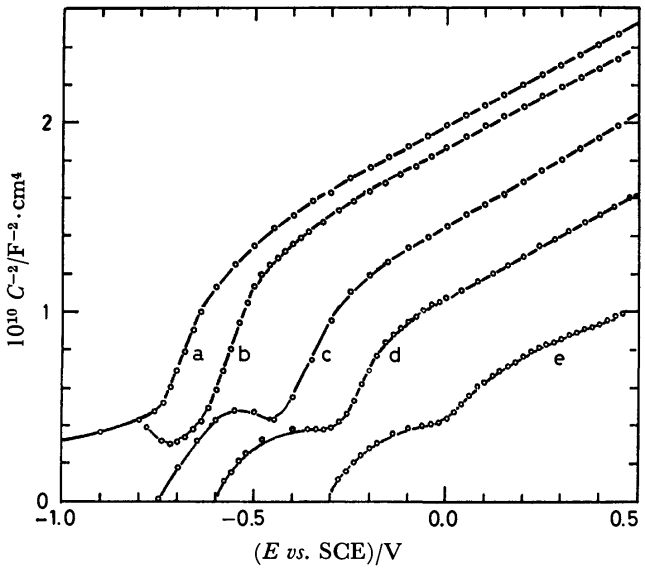

Fig. 2. C^{-2} *vs.* E plots of $TiN_{0.07}O_{1.93}$ electrode in 0.1 M Na_3PO_4 buffered solutions.
pH; (a): 12.0, (b): 10.0, (c): 7.0, (d): 5.0, (e): 1.0.

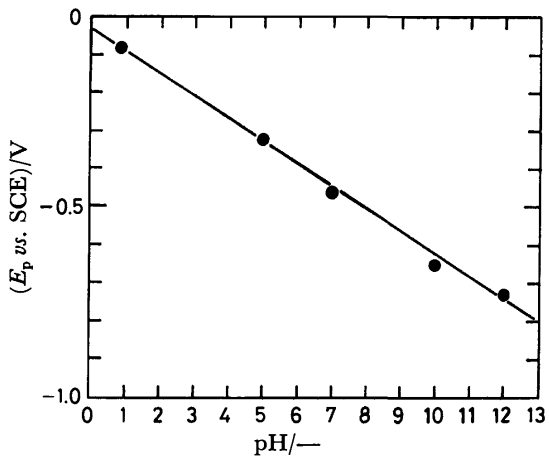

Fig. 3. The pH dependence of the anodic photocurrent onset voltage E_p.

current onset voltage (E_p) against the solution pH is plotted in Fig. 3. The anodic photocurrent onset voltage showed a linear dependence on pH, which can be represented by:

$$E_p = -0.04 - 0.06\ \text{pH}\ (vs.\ \text{SCE}).$$

Discussion

Differential Capacitance at the Semiconductor/Electrolyte Interface. In order to elucidate the nonlinearity in C^{-2} *vs.* E plots, we considered the possible sources of effects on the total capacitance. The whole differential capacity (C) across the semiconductor/electrolyte interface is represented by:

$$1/C = 1/C_{sc} + 1/C_d + 1/C_c, \quad (1)$$

where C_{sc}, C_d, and C_c indicate the capacitance of the space charge layer, the diffused double layer, and the compact double layer respectively. Some investigators omit the $1/C_d$ and/or $1/C_c$ terms in Eq. 1 when the ionic strength is fairly large. The $1/C_d+1/C_c$ term, however, cannot be omitted, especially when the potential drop across the space charge layer is nearly equal to zero, because the condition of $1/C_{sc} \gg 1/C_d + 1/C_c$ does not hold.

The C_{sc} as a function of the potential is usually represented by MS's equation. However, the practical experimental conditions seem to be far from the given conditions of MS assumptions. Among them, the assumptions concerning donor density, which is independent of the distance from the semiconductor surface and the absence of an interfacial layer, such as an insulating layer, are not fulfilled in many real cases for semiconductors exposed to an electrolyte. The semiconductor surface in contact with an electrolyte has, more or less, interfacial layers, which may be formed by a chemical reoxidation or an ion-exchange reaction, because one is a solid electric conductor, and another is a liquid ionic conductor. Therefore, the donor density at the semiconductor surface must be zero, and the distribution in the donor density is developed in the direction perpendicular to the surface. Such situations seem to be readily formed in the case of heavily doped semiconductors,[1,2] as in our case, and the ideal linearity in C^{-2} *vs.* E plots is not to be expected.

As has been stated above, we presume the distribution in donor density, N_d, to be:

$$N_d = ax, \quad (2)$$

where a is a distribution coefficient in cm^{-4} and where x is a distance in cm.

The corresponding boundary conditions are:

$$\phi = \Delta\phi_{sc} - \frac{kT}{e} \text{ at } x = 0, \quad (3)$$

$$\frac{d\phi}{dx} = 0,\ \phi = 0 \text{ at } x = d, \quad (4)$$

in which kT/e indicates the volts of the equivalent thermal energy. By solving Poisson's equation under the given boundary conditions, we obtain:

$$C_{sc}^{-2} = \left(\frac{3}{\varepsilon^2\varepsilon_0^2 ea}\right)\left(\Delta\phi_{sc} - \frac{kT}{e}\right), \quad (5)$$

where ε and ε_0 are the dielectric constants of the semiconductor and the vacuum respectively and where e is an electron charge. The $\Delta\phi_{sc}$ is related to an electrode potential by:

$$\Delta\phi_{sc} = E - E_{fb}. \quad (6)$$

E_{fb} is the flat-band potential at which the electric field is reversed in the depletion layer.

From Eq. 1, we define the capacity, C_e, as:

$$1/C_e = 1/C_d + 1/C_c. \quad (7)$$

The dependence of C_e on the potential is represented by:

$$C_e = C_0 + b(E - E_{zc})^2. \quad (8)$$

C_0 is a minimum capacity, and E_{zc} is the zero-charge potential where the charge in the diffused double layer is reduced to zero. Equation 8 is a phenomelogical equation analogous to the electrical double-layer theory for mercury electrodes.[10]

Equations 5, 7, and 8 give the whole representation

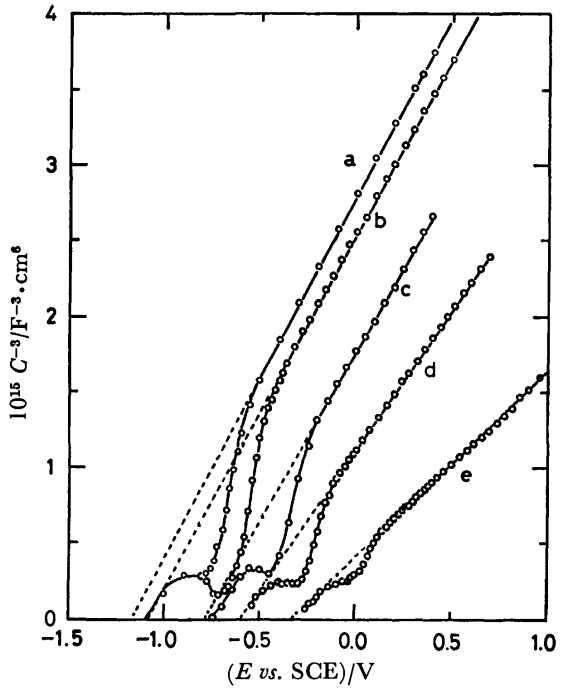

Fig. 4. C^{-3} *vs.* E plots of $TiN_{0.07}O_{1.93}$electrode in 0.1 M Na_3PO_4 buffered solutions.
pH; (a) 12.0 (b) 10.0 (c) 7.0 (d) 5.0 (e) 1.0.

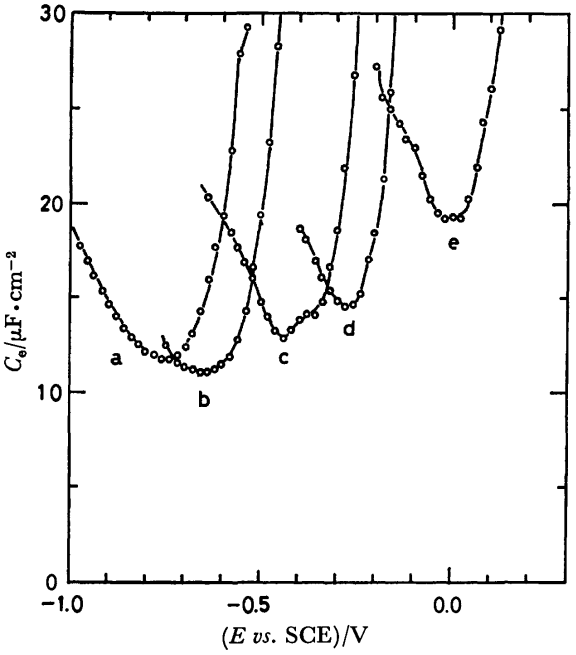

Fig. 5. C_e *vs.* E plots of $TiN_{0.07}O_{1.93}$ electrode in 0.1 M Na_3PO_4 buffered solutions.
pH; (a): 12.0, (b): 10.0, (c) 7.0, (d): 5.0, (e): 1.0.

of the differential capacity across the semiconductor/electrolyte interface as function of the electrode potential.

In order to check the validity of the above treatment, the original experimental results in Fig. 1 are replotted as Fig. 4. As predicted by Eq. 5, straight lines over adequate range of applied potentials are obtained in the C^{-3} *vs.* E plots when $C_e \gg C_{sc}$. In the region of $C_e < C_{sc}$, a distinct deviation from the straight line is observed. From Eq. 1, such a deviation can be said to be caused by the C_e component. The C_e values calculated from Eq. 1 are shown in Fig. 5. The C_e *vs.* E plots obey the parabolic relationship of Eq. 8. Consequentry, the presumptions of Eqs. 2 and 8 are valid in this case.

From the above considerations, we can determine the E_{fb}, E_{zc}, and a values in Eq. 5 as basic parameters of the semiconductor electrode in contact with an electrolyte.

Photocurrent Onset Voltage. It is said that the anodic photocurrent begins to flow at the "flat-band" potential in the case of an n-type semiconductor system.[11] This is the reason why the "flat-band" potential can be determined by measuring the E_p values, even when the capacitance measurement is not attainable. However, it is questionable whether the true E_{fb} values are thus obtained. In order to illustrate this, we compared the characterized E_{fb} and E_{zc} values with the E_p values in Table 1. E_{fb}, as defined by Eq. 5, is obtained by extrapolating to $C^{-3}=0$ in Fig. 4, while E_{zc}, as defined by Eq. 8, is obtained from the minimum of the C *vs.* E plots in Fig. 5.

Table 1. Comparison of E_{fb}, E_{zc}, and E_p values for several pH's of solutions

pH	E_{fb} *vs.* SCE / V	E_{zc} *vs.* SCE / V	E_p *vs.* SCE / V
1.0	−0.41±0.02	−0.02±0.03	−0.08±0.02
5.0	−0.57	−0.28	−0.32
7.0	−0.76	−0.44	−0.46
10.0	−1.07	−0.65	−0.65
12.0	−1.14	−0.75	−0.73

As is shown in Table 1, the E_{fb} values do not agree with the E_p values, which are usually more anodic than the E_{fb} values. However, the E_p values agree with the E_{zc} values within the limits of experimental error. This indicates that the anodic photocurrent begins to flow not at the flat-band potential, but at the zero-charge potential. In order to understand how the anodic photocurrent is allowed to pass across the semiconductor/electrolyte interface, and to find the reason why the photocurrent onset voltage differs from the flat-band potential, the following "Gate" model is proposed.

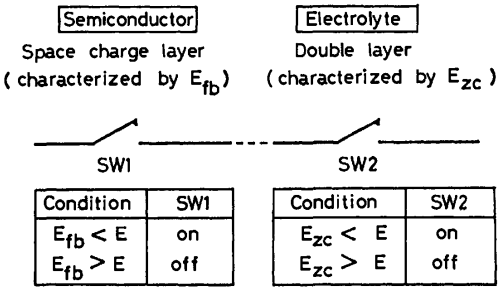

Fig. 6. "Gate" model for an explanation of the photocurrent onset voltage related to E_{fb} and E_{zc} in the case of N-type semiconductor electrode in contact with an electrolyte solution.

SW1 and SW2 in Fig. 6 behave like "Gate" because of its field effect, connected with holes and related ions for an n-type semiconductor electrode in contact with an electrolyte solution. If the condition of $E_{fb}<E_{zc}$ holds, the E_p value should be equal to the E_{zc} value. This is because the hole is permited to migrate to the semiconductor surface, *i.e.*, SW1 is closed, in the potential range of $E_{fb}<E$, but the mass transfer of the related ions is forbidden until E is more positive than E_{zc}, *i.e.*, SW2 is opened. Conversely, the E_p value should be equal to the E_{fb} value when $E_{fb}>E_{zc}$. By considering the "Gate" model, we could explain why the E_p value differed from the E_{fb} value.

We feel that all the semiconductors in contact with an electrolyte solution have the basic parameters of E_{fb} and E_{zc}. Such behavior was also observed for the reduced rutile single crystal and the CVD-TiO_2 semiconductor electrode. Recently, the existence of the surface state has been reported.[13-17] However, the argument of the surface state is not dealt with in this study. We think its capacitance probably contains the measured C_e value. From the above considerations, it can be emphasized that the determination of E_{fb} by E_p measurements has the possibility of being misleading as to the E_{fb} value.

Conclusion

We could give an explanation of the possible sources of deviation from the Mott-Schottky behavior of the nitrogen-stabilized TiO_2 semiconducting electrode, and point out some problems in the determination of the "flat-band" potential. The distribution of the donor density, N_d, in the direction perpendicular to the semiconductor surface and the contribution of the double layer to the total capacity caused the non-linearity in C^{-2} *vs.* E plots. When the distributed donor density is represented by $N_d=ax$, the C^{-3} *vs.* E plots are linear instead of the C^{-2} *vs.* E plots. The remaining capacitive component, C_e, in C^{-3} *vs.* E is proved to be an effect of the double-layer capacity by showing the C_e *vs.* E plots, which are characterized by their E_{zc} values.

In order to understand the roles of E_{fb} and E_{zc} in photoelectrochemical effect, the "Gate" model was proposed. By using the "Gate" model, which was characterized by both the E_{fb} and E_{zc} values for an n-type semiconductor electrode in contact with an electrolyte solution, we explained why the photocurrent onset, E_p, differed from E_{fb}. Moreover, a warning on the determination of the flat-band potential from the photocurrent onset voltage measurement was given.

Although the essential problems concerned with the semiconductor/electrolyte interface remain, we could partly elucidate the complicated behavior of a semiconductor electrode in contact with an electrolyte solution.

The present work was supported by a Grant-in-Aid for Energy Research No. 505035 from the Ministry of Education, Science and Culture.

References

1) D. M. Tench and E. Yeager, *J. Electrochem. Soc.*, **120**, 164 (1973).
2) R. H. Wilson, L. A. Harris, and M. E. Gerstner, *J. Electrochem. Soc.*, **126**, 844, 850 (1979).
3) A. Fujishima, A. Sakamoto, and K. Honda, *Seisan Kenkyu*, **21**, 450 (1969).
4) J. H. Kennedy and K. W. Frese, Jr., *J. Electrochem. Soc.*, **125**, 723 (1978).
5) J. S. Curran and W. Gissler, *J. Electrochem. Soc.*, **126**, 56 (1979).
6) R. A. Fredlein and A. J. Bard, *J. Electrochem. Soc.*, **126**, 1892 (1979).
7) R. De Gryse, W. P. Gomes, F. Cordon, and J. Vennik, *J. Electrochem. Soc.*, **122**, 711 (1975).
8) M. Tomkiewicz, *J. Electrochem. Soc.*, **126**, 1505 (1979).
9) F. Cordon and W. P. Gomes, *J. Phys. D.*, **11**, L63 (1978).
10) P. Delahay, in "Double-layer and Electrode Kinetics," John Wiley & Sons, New York (1965), Chaps. 3 and 5.
11) H. H. Kung, H. S. Jarrett, A. W. Sleight, and A. Ferretti, *J. Appl. Phys.*, **48**, 2463 (1977).
12) T. Hirai, I. Tari, and J. Yamura, *Bull. Chem. Soc. Jpn.*, **51**, 3057 (1978).
13) V. E. Henrich, G. Dresselhaus, and H. J. Zeiger, *Phys. Rev. Lett.*, **36**, 1335 (1976).
14) V. E. Henrich, G. Dresselhaus, and H. J. Zeiger, *Solid State Commun.*, **24**, 623 (1977).
15) W. J. Lo, Y. W. Chung, and G. A. Somorjai, *Surf. Sci.*, **71** 199 (1978).
16) W. J. Lo and G. A. Somorjai, *Phys. Rev. B*, **17**, 4942 (1978).
17) V. E. Henrich, G. Dresselhaus, and H. J. Zeiger, *Phys. Rev. B*, **17**, 4908 (1978).

  Bull. Chem. Soc. Jpn., 54, 513—519 (1981)

Induced Circular Dichroism of β-Cyclodextrin Complexes with *o*-, *m*-, and *p*-Disubstituted Benzenes

Hiroshi SHIMIZU, Akira Kaito,† and Masahiro HATANO*

Chemical Research Institute of Non-aqueous Solutions, Tohoku University, Katahira, Sendai 980

(Received April 23, 1980)

The induced circular dichroism (ICD) spectra of β-cyclodextrin (β-CD_x) complexes with *o*-, *m*-, and *p*-disubstituted benzenes were observed. The comparison of the observed rotational strengths with the ones calculated by using the Kirkwood-Tinoco expression is examined; the possible orientations of the guest molecules which are included in the cavity of β-CD_x are presented. These results suggest that the orientation of the guest molecule is confined about the axis of the β-CD_x torus.

The cyclodextrins (CD_x's) are α-1,4 linked oligomers of D-glucose formed during the degradation of starch by an amylase of *Bacillus macerans*, and have 6, 7, or 8 glucose residues per molecule.[1] It is known that CD_x can include aromatic compounds, alkyl halides, and gases, as guest molecules in its cavity, resulting in the formation of inclusion complexes.[2] This characteristic has led to their utilization as enzyme models.[3-6] In recent years, many extensive investigations on the suitability of modified CD_x or capped CD_x as a enzyme model have been carried out.[7-9]

The orientation of the guest molecule which is included in the cavity of CD_x plays an important role in the inclusion phenomenon. More information on the structure of the CD_x complex with mono- or di-substituted benzene will be very significant, since substituted benzenes are sometimes used as substrates of the reactions catalyzed by CD_x's.

The circular dichroism (CD) study is one of the most useful physico-chemical methods for elucidating the orientation of the guest molecule included by CD_x in solution. That is to say, the CD is expected to be induced at the absorption bands of the achiral guest molecules which are included in the cavity of the chiral CD_x host molecule, since CD_x is composed of chiral glucose units.

Harata and Uedaira[10] have recently measured the ICD spectra of β-CD_x complexes with naphthalene derivatives and determined the structure of the β-CD_x complexes on the basis of the calculation of the rotational strengths by the Kirkwood-Tinoco equation.[11] Yamaguchi *et al.* have studied the ICD spectra of β-CD_x complexes with 2-hydroxytropone[12] and azulene,[13] and have discussed the direction of the electronic transition moment of the guest molecules.

In the previous paper,[14] we have reported the ICD spectra of β-CD_x inclusion complexes with mono-substituted and para-disubstituted benzenes in aqueous solution, and have shown that these β-CD_x complexes favor the axial inclusion in which the long axis of the substituted benzenes is parallel to the axis of the β-CD_x cavity. We can estimate the orientation of the guest molecule from the comparison between the observed and calculated rotational strengths, when the direction of the electric transition dipole moment is known.

In the present article we report the ICD spectra of the β-CD_x complexes with *o*-, *m*-, and *p*-disubstituted benzenes in aqueous solution, and predict the orientation direction of the guest molecules in these inclusion complexes by the comparison between the observed rotational strengths of each ICD band and the values calculated by using the Kirkwood-Tinoco equation. In the manner of inclusion, β-CD_x complexes with *o*- and *m*-disubstituted benzenes cannot be classified into either the so-called axial or the equatorial inclusion, since the long- and/or short-axis of these molecules cannot be defined unequivocally.

Experimental

β-CD_x and homo- and hetero-disubstituted benzenes were obtained commercially. β-CD_x, *o*-nitroaniline, and *o*-, *p*-phenylenediamines were purified by the recrystallization from aqueous solutions. Pyrocatechol and hydroquinone were recrystallized from benzene. *m*-Nitroaniline, *p*-nitroaniline, resorcinol, and *m*-phenylenediamine were recrystallized from ethanol, methanol, chloroform, and ether, respectively.

An inclusion complex was prepared by mixing β-CD_x and the corresponding disubstituted benzene using the following solvents: an aqueous solution for nitroanilines, 0.1 M†† aqueous HCl for benzenediols, 1.0×10^{-3} M or 1.0×10^{-5} M aqueous KOH for phenylenediamines.

The circular dichroism and absorption spectra were measured at room temperature using a JASCO J-500 circular dichrograph with a J-DP 500 data-processor and a Hitachi EPS-3T recording spectrophotometer, respectively.

In particular, an appropriate amount of nitrogen was bubbled through each solution of the β-CD_x–phenylenediamine systems before the measurements, since phenylenediamines were easily oxidized by dissolved oxygen.

The experimental values of the dipole strengths, D, and the rotational strengths, R, of disubstituted benzenes were estimated in the same way as was used in the previous work.[14]

In the present paper, molar ellipticity was normalized by the concentration of the guest molecule.

Theoretical

The theoretical rotational strength of the transition from the ground state 0 to the excited state a in benzene derivative (i), R_{i0a}, was calculated by the following expression developed by Kirkwood and Tinoco:

$$R_{i0a} = \pi\tilde{\nu}_{a1}\mu^2_{i0a}\sum_j \frac{\tilde{\nu}^2_{bj}(\alpha_{33}-\alpha_{11})_j(GF)_{1j}}{\tilde{\nu}^2_{bj}-\tilde{\nu}^2_{a1}}, \quad (1)$$

† Present address: Research Institute for Polymers and Textiles, 1-1-4, Yatabe-Higashi, Tsukuba, Ibaraki 305.

†† 1 M=1 mol/dm³.

$$(GF)_{ij} = \frac{1}{r_{ij}^3}\left[\hat{e}_i \cdot \hat{e}_j - \frac{3(\hat{e}_i \cdot \vec{r}_{ij})(\hat{e}_j \cdot {}_i\vec{r}_j)}{r_{ij}^2}\right]\hat{e}_i \times \hat{e}_j\vec{r}_{ij}. \quad (2)$$

Here e_j is the unit vector in the direction of the symmetry axis of the bond (j) in β-CD_x; e_i is the unit vector in the direction of the electric transition dipole moment, μ_{ioa}, of the transition from the ground state 0 to the excited state a in the disubstituted benzene, and $\tilde{\nu}_{ai}$ is its wave number; α_{33} and α_{11} are bond polarizabilities at zero frequency parallel and perpendicular, respectively, to the symmetry axis of the bond in β-CD_x; $\vec{r}_{ij}$ is the vector pointing from the center of benzene derivatives to each bond in β-CD_x; and $\tilde{\nu}_{bj}$ is the averaged wave number of the electronic transitions of the bond in β-CD_x.

In this calculation, $\tilde{\nu}_{bj}$ is approximated by a wave number midway between the first absorption band in the bond of β-CD_x and its ionization potential. We

TABLE 1. OBSERVED AND CALCULATED ENERGY AND DIPOLE STRENGTH (D) OF THE ELECTRONIC TRANSITIONS OF DISUBSTITUTED BENZENES

Disubstituted benzenes	Experiment $\bar{\nu}\times10^{-3}$ / cm^{-1}	Experiment D / Debye^2	Calculation $\bar{\nu}\times10^{-3}$ / cm^{-1}	Calculation D / Debye^2	Assignment and Φ	
		a)				
Pyrocatechol	36.3	1.84			A_1	
	46.5	6.39			B_2	
		a)				
Resorcinol	36.6	1.34		f)	B_2	
	46.5		45.2	1.75	A_1	
		a)				
Hydroquinone	34.6	2.35			B_{2u}	
	45.3	4.35			B_{1u}	
		b)				
o-Phenylenediamine	34.6	3.35			A_1	
	43.1	8.53			B_2	
		b)				
m-Phenylenediamine	34.6	2.04			B_2	
	42.0	7.53[e]			A_1	
		c)				
p-Phenylenediamine	32.8	2.59			B_{2u}	
	41.5	13.61			B_{1u}	
		d)		f)		
o-Nitroaniline	24.3	9.48	27.6	19.15	A′	(−38.9°)
	35.3	7.64	38.5	5.83	A′	(−3.6°)
			42.5	8.27	A′	(20.8°)
	44.7	27.09	44.6	28.69	A′	(29.3°)
		d)		f)		
m-Nitroaniline	27.9	3.34[e]	27.7	8.29	A′	(48.0°)
	35.7	4.44[e]	38.1	6.64	A′	(36.6°)
	40.2[e]	6.95[e]	41.4	30.82	A′	(−19.3°)
	44.3	19.66[e]	44.8	22.10	A′	(−44.1°)
		d)		f)		
p-Nitroaniline	26.3	27.51	32.6	18.90	A_1 (CT)	
			34.7	0.24	B_2	
	44.1	14.52	43.1	4.10	B_2 (CT)	
			48.7	0.15	A_1	

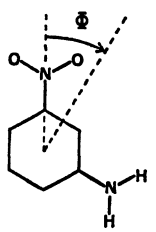

a) In 0.1 M aqueous HCl. b) In 1.0×10^{-5} M aqueous KOH. c) In 1.0×10^{-3} M aqueous KOH. d) In aqueous solution. e) Obtained by a curve fitting method. f) Obtained by the PPP SCF-MO calculation. A. Kaito, A. Tajiri, and M. Hatano, *Bull. Chem. Soc. Jpn.*, **49**, 2207 (1976).

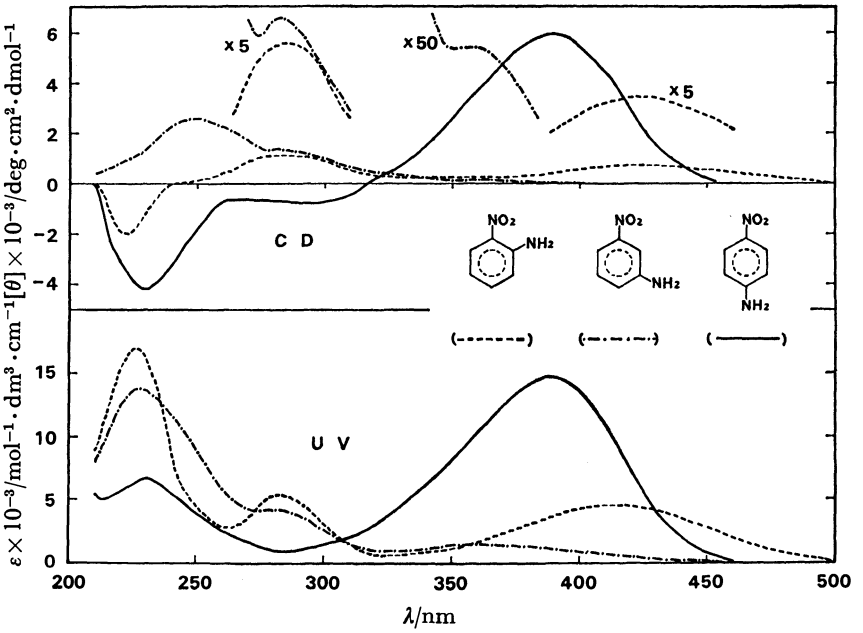

Fig. 1. CD (upper) and UV absorption (lower) spectra of the β-CD$_x$ complexes with *o*-, *m*-, and *p*-nitroanilines in aqueous solution at room temperature.
Broken line: β-CD$_x$ (1.11×10^{-2} M) +*o*-nitroaniline (3.24×10^{-4} M), dotted broken line: β-CD$_x$ (1.29×10^{-2} M)+*m*-nitroaniline (1.12×10^{-3} M), solid line: β-CD$_x$ (1.47×10^{-2} M)+*p*-nitroaniline (8.41×10^{-5} M).

used the values of $(\alpha_{33}-\alpha_{11})$ and $\tilde{\nu}_{bj}$ for each bond as listed in our previous paper.[14]

Table 1 shows the observed and calculated wave number, $\tilde{\nu}$, and the dipole strength, D, of the electronic transitions of disubstituted benzenes, along with the assignment of each electronic transition.[15] The calculated values in this table were obtained by the Pariser-Parr-Pople (PPP) SCF-MO method. The directions of the electric transition moment in homo-disubstituted benzenes were available easily from the results of the perturbation theory formulas by Petruska.[16] The experimental values in Table 1 were used for the calculation of rotational strength except in the case of the $^1A_1\leftarrow{}^1A_1$ transition of resorcinol, the third $\pi^*\leftarrow\pi$ transition of *o*-nitroaniline, and the $^1B_2\leftarrow{}^1A_1$ and $^1A_1\leftarrow{}^1A_1$ transitions of *p*-nitroaniline.

In the present calculation, the determination of the coordinates of β-CD$_x$ was carried out in the manner used in our previous paper.[14]

Results and Discussion

Figures 1—3 show the CD (upper) and UV (lower) spectra of the β-CD$_x$ complexes with *o*-, *m*-, and *p*-disubstituted benzenes. ICD bands were observed at absorption frequencies of achiral benzene derivatives.

As shown in Fig. 1, the β-CD$_x$ complex with *o*-nitroaniline showed two positive and one negative ICD bands at 427, 286, and 222 nm, respectively. These ICD bands were assigned to the first $\pi^*\leftarrow\pi$, the second $\pi^*\leftarrow\pi$, and the fourth $\pi^*\leftarrow\pi$ transitions, respectively, on the basis of the results calculated by the PPP SCF-MO method in Table 1.

The β-CD$_x$-*m*-nitroaniline complex exhibited positive

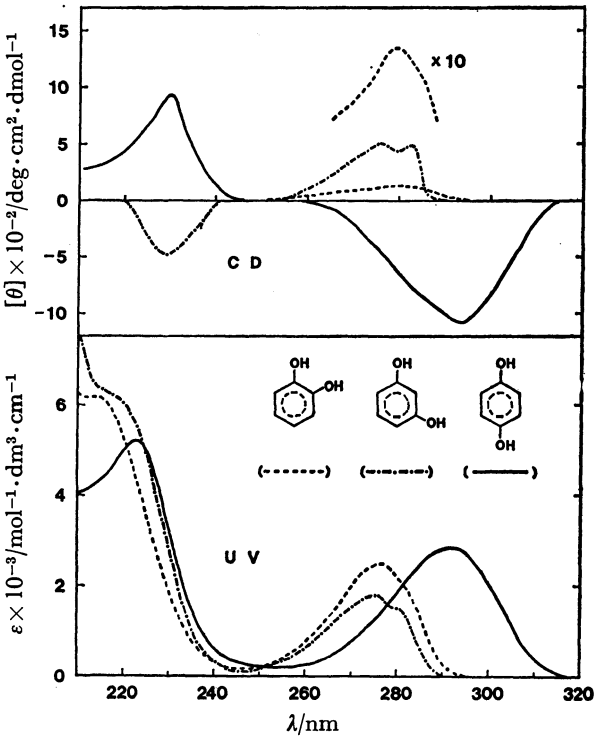

Fig. 2. CD (upper) and UV absorption (lower) spectra of the β-CD$_x$ complexes with *o*-, *m*-, and *p*-benzenediols in 0.1 M aqueous HCl at room temperature.
Broken line: β-CD$_x$ (1.17×10^{-2} M)+pyrocatechol (5.10×10^{-4} M), dotted broken line: β-CD$_x$ (1.43×10^{-2} M)+resorcinol (5.90×10^{-4} M), solid line: β-CD$_x$ (1.11×10^{-2} M)+hydroquinone (2.77×10^{-4} M).

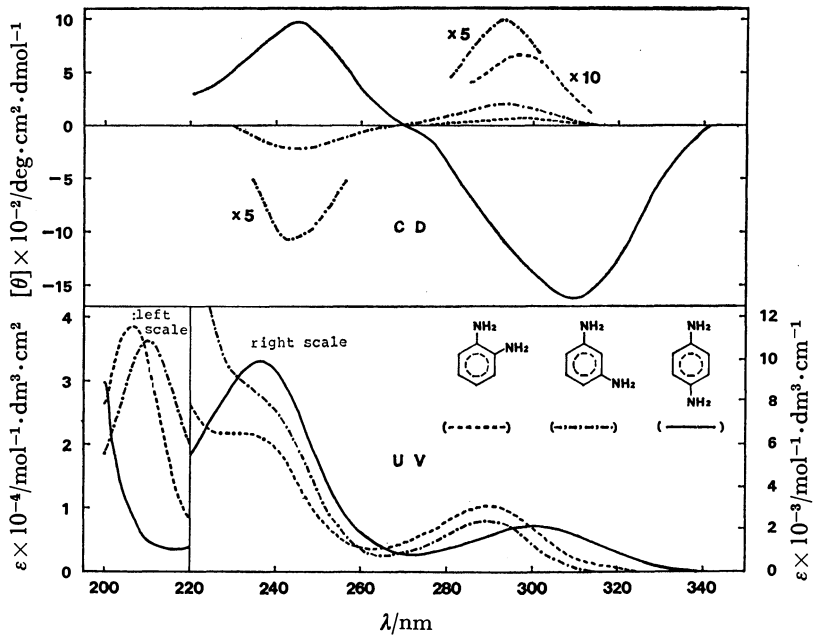

Fig. 3. CD (upper) and UV absorption (lower) spectra of the β-CD_x complexes with *o*-, *m*-, and *p*-phenylenediamines in aqueous KOH at room temperature. Broken line: β-CD_x (1.44×10^{-2} M)+*o*-phenylenediamine (1.83×10^{-4} M) (pH 7.5), dotted broken line; β-CD_x (1.43×10^{-2} M)+*m*-phenylenediamine (1.44×10^{-4} M) (pH 7.2), solid line; β-CD_x (1.45×10^{-2} M)+*p*-phenylenediamine (6.23×10^{-4} M) (pH 11.0).

ICD bands at 358, 281, and 249 nm, which are attributed to the first $\pi^*\leftarrow\pi$, the second $\pi^*\leftarrow\pi$, and the third $\pi^*\leftarrow\pi$ transitions, respectively. The lowest positive ICD band of the β-CD_x–*p*-nitroaniline complex observed at 390 nm was assigned to the $^1A_1\leftarrow{}^1A_1$ transition, and the two negative ICD bands found at 296 and 230 nm were attributed to the $^1B_2\leftarrow{}^1A_1$ transitions.

On the other hand, as seen in Fig. 2, the β-CD_x complex with pyrocatechol showed only a positive ICD band at 279 nm, originating from the $^1A_1\leftarrow{}^1A_1$ transition. But the ICD band derived from the $^1B_2\leftarrow{}^1A_1$ transition was not observed in the shorter wavelength region. The β-CD_x–resorcinol complex exhibited positive and negative ICD bands at 276 and 229 nm. These ICD bands were assigned to the $^1B_2\leftarrow{}^1A_1$ and $^1A_1\leftarrow{}^1A_1$ transitions, respectively. The β-CD_x–hydroquinone complex showed a negative ICD band attributed to the $^1B_{2u}\leftarrow{}^1A_g$ at 294 nm and exhibited a positive ICD band derived from the $^1B_{1u}\leftarrow{}^1A_g$ transition at 230 nm.

As shown in Fig. 3, each sign of the ICD spectra of the β-CD_x complexes with *o*-, *m*-, and *p*-phenylenediamines is in agreement with that of the β-CD_x complexes with *o*-, *m*-, and *p*-benzenediols (Fig. 2).

In our previous work,[14] we discussed the orientation of the guest molecule which is included in the cavity of the β-CD_x by the comparison of observed and calculated rotational strengths. One might conclude from the results of the investigation that the favorable orientation of the guest molecule about the axis of β-CD_x cavity (the Z-axis) can be estimated when the direction of the electric transition dipole moment is known. It was shown that the calculated rotational strengths were

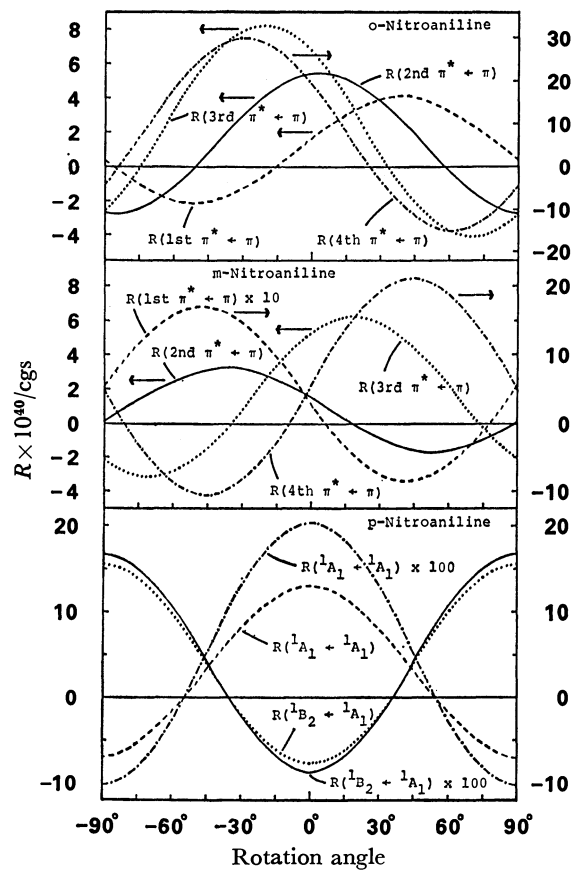

Fig. 4. The dependence of the calculated rotational strengths of the β-CD_x–nitroanilines complexes on the rotation angle in the X-Z plane.

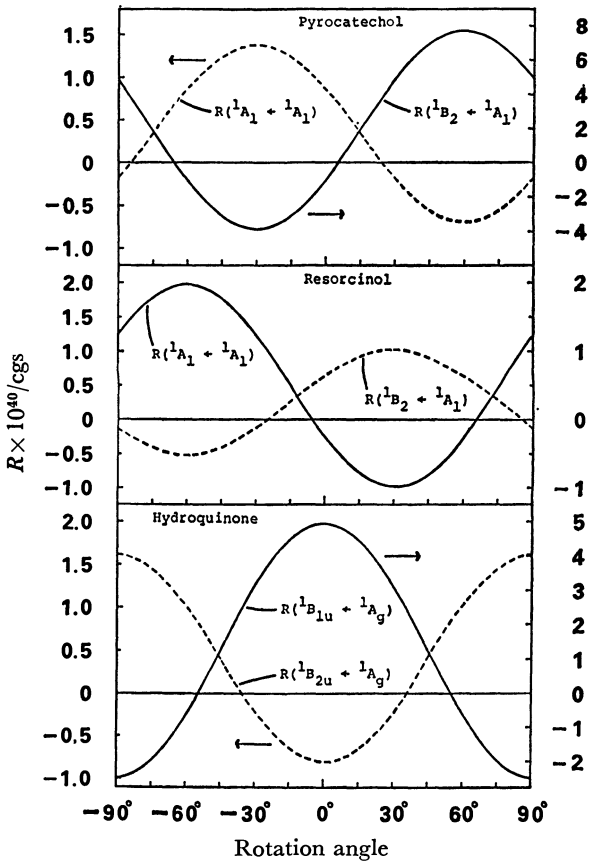

Fig. 5. The dependence of the calculated rotational strengths of β-CD$_x$–benzenediols complexes on the rotation angle in the X-Z plane.

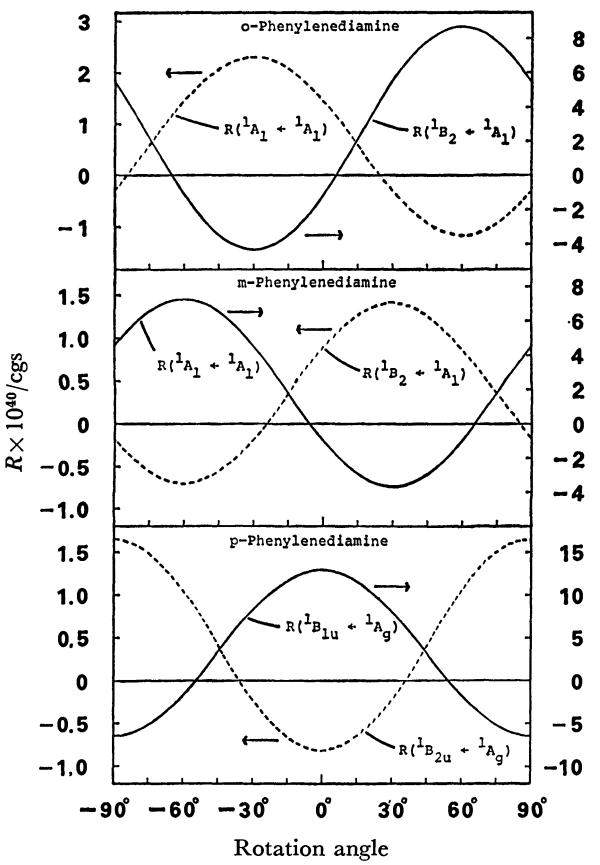

Fig. 6. The dependence of the calculated rotational strengths of β-CD$_x$–phenylenediamines complexes on the rotation angle in the X-Z plane.

very sensitive to the electric transition moment of the guest molecule and the orientation of the guest molecule in the β-CD$_x$ cavity. So, in the present work, we studied how to fit the calculated rotational strengths with the observed values obtained from ICD spectra by changing the direction of the guest molecule in the X-Z plane.

Figures 4—6 show the dependence of the calculated rotational strengths of the β-CD$_x$ complexes with disubstituted benzenes on the orientation of the guest molecule in the X-Z plane. In Fig. 4 the rotation angle on the abscissa indicates the inclined angle of the vector pointing from the center of nitroanilines to the nitro group with respect to the Z-axis (the axis of β-CD$_x$ torus). Similarly, in Figs. 5 and 6 the abscissa represents the inclined angle of the vector pointing from the center of homo-disubstituted benzenes to one of the substituents with respect to the Z-axis.

The comparison of the observed rotational strengths obtained from ICD spectra with the values calculated for the favorable orientation is listed in Table 2.

As shown at the top of Fig. 4, the calculated rotational strengths of the β-CD$_x$–*o*-nitroaniline complex in which the nitro group of *o*-nitroaniline inclines to the Z-axis by about 32° to 33° are in good agreement with the experimental values. On the other hand, in the case of *m*-nitroaniline the calculated values with an inclined angle of about −10° to −11° are compatible with the observed values. The calculated values of the β-CD$_x$–*p*-nitroaniline complex agree well with the experimental data when the nitro group of *p*-nitroaniline has an inclination with respect to the Z-axis in the range of about 0° to ±20° (bottom of Fig. 4). The experimental rotational strengths of the β-CD$_x$ complex with pyrocatechol are well reproduced by the calculation when the rotation angle is about 5° (top of Fig. 5). The calculated results of the β-CD$_x$–resorcinol complex are in accord with the observed values in the range of rotation angle from 0° to 30° (middle of Fig. 5). In this case, the orientation with roration angle 0° is equivalent to that with rotation angle 60°. The theoretical values of the β-CD$_x$–hydroquinone complex in which one of hydroxyl groups is inclined in the range of about 0° to ±20° with respect to the Z-axis are consistent with the experimental data (bottom of Fig. 5).

The same rotation angle for the β-CD$_x$ complexes with *o*-, *m*-, and *p*-phenylenediamines as that for the corresponding complexes with *o*-, *m*-, and *p*-benzenediols, respectively, gives the theoretical results in agreement with the experimental data, as demonstrated in Fig. 6 and/or in Table 2. This suggests that *o*-, *m*-, and *p*-phenylenediamines are included in the β-CD$_x$ cavity in a same way that *o*-, *m*-, and *p*-benzenediols, respectively, are included.

The results discussed above are summarized in Figs. 7 and 8. These figures illustrate the orientation directions of disubstituted benzenes included as guest molecules

TABLE 2. COMPARISON OF THE OBSERVED AND CALCULATED ROTATIONAL STRENGTH (R_{10a}) OF THE β-CD_x COMPLEXES WITH *o*-, *m*-, AND *p*-DISUBSTITUTED BENZENES

Benzene derivative	λ_{max} / nm		$R_{10a} \times 10^{40}$/cgs Experiment	Calculation	
				(32°)	
o-Nitroaniline	427	A′	1.00	3.98	
	286	A′	1.25	3.62	
	[235][a]	A′	—	0.40	
	222	A′	−1.01	−4.60	
				(−11°)	
m-Nitroaniline	358	A′	0.23[c]	0.78	
	281	A′	0.56[c]	2.33	
	249	A′	3.42[c]	3.83	
	(226)[b]	A′	—	0.19	
				(0°)	(20°)
p-Nitroaniline	390	A_1	9.14	13.05	10.75
	[296][a]	B_2	−0.52	−0.08	−0.06
	230	B_2	−5.37	−7.78	−5.05
	[205][a]	A_1	—	0.20	0.17
				(5°)	
Pyrocatechol	279	A_1	0.08	0.70	
	(215)[b]	B_2	—	−0.05	
				(0°)	(30°)
Resorcinol	276	B_2	0.25	0.64	1.02
	229	A_1	−0.18	−0.25	−0.99
				(0°)	(20°)
Hydroquinone	294	B_{2u}	−0.72	−0.82	−0.53
	230	B_{1u}	0.52	4.94	1.72
				(5°)	
o-Phenylenediamine	297	A_1	0.04	1.18	
	(232)[b]	B_2	—	−0.06	
				(0°)	(30°)
m-Phenylenediamine	293	B_2	0.12	0.89	1.42
	243	A_1	−0.14	−0.91	−3.65
				(0°)	(20°)
p-Phenylenediamine	313.5	B_{2u}	−1.46	−0.83	−0.54
	245	B_{1u}	0.86	12.89	10.63

a) Value calculated by the PPP SCF-MO method. b) UV absorption peak in the presence of β-CD_x.
c) Obtained by a curve fitting method.

in the cavity of β-CD_x. The β-CD_x cavity, in both figures, was represented schematically by a pair of rectangles with oblique lines. Each dotted line in Fig. 7 indicates the direction of the transition dipole moment obtained from the PPP SCF-MO calculation, and the numbers, 1, 2, 3, and 4 designate the first $\pi^* \leftarrow \pi$, the second $\pi^* \leftarrow \pi$, the third $\pi^* \leftarrow \pi$, and the fourth $\pi^* \leftarrow \pi$ transitions of *o*- and *m*-nitroanilines, respectively. Similarly, each dotted line in Fig. 8 indicates the directions of the electric transition moments of homo-disubstituted benzenes derived from the perturbation theory formulas by Petruska.[16] In addition, the symbols (+) and (−) give the signs of the CD spectra induced by the electronic transitions of the corresponding disubstituted benzenes.

We could make no reference to the discrimination of the top side from the bottom side of β-CD_x, because the coulombic interaction between CD_x and the guest molecule was approximated by the interaction between the distributed bond dipole of CD_x and the point dipole of the guest molecule in the present calculation.

On the other hand, it seems likely from Figs. 7 and 8 that some of the substituents of the guest molecules are linked by the hydrogen bond to the hydroxyl group of β-CD_x, or are in van der Waals contact with the interior of the β-CD_x torus. However, it appears that the conformational change in one or two of the C(5)–O(6) bonds is required for the guest-host linkage by a hydrogen bond with the primary hydroxyl group.[17]

In conclusion, the orientation of the guest molecule which is included in the β-CD_x cavity seems to be confined about the axis of the β-CD_x torus.

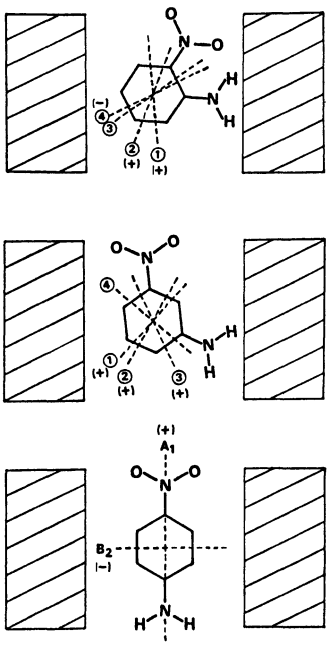

Fig. 7. The schematic drawing of the orientation of *o*-, *m*-, and *p*-nitroanilines included in the cavity of β-CD_x.

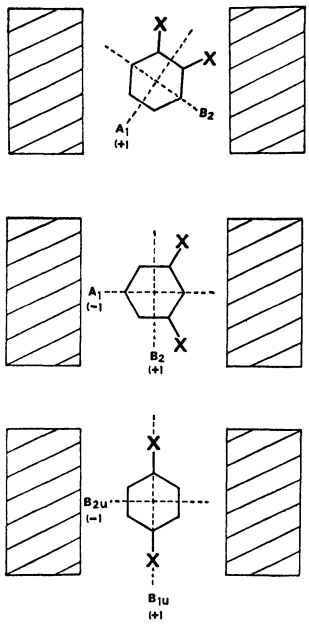

X = OH , NH_2

Fig. 8. The schematic drawing of the orientation of *o*-, *m*-, and *p*-homodisubstituted benzenes included in the cavity β-CD_x.

References

1) F. Schardinger, *Zentr. Bakt. Parasitenk., II*, **29**, 188 (1911).

2) M. L. Bender and M. Komiyama, "Cyclodextrin Chemistry," Springer-Verlag, Berlin (1978).

3) F. Cramer and W. Kampe, *J. Am. Chem. Soc.*, **87**, 1115 (1965).

4) M. L. Bender, R. L. VanEtten, G. A. Clowes, and J. F. Sebastian, *J. Am. Chem. Soc.*, **88**, 2318, 2319 (1966); R. L. VanEtten, J. F. Sebastian, G. A. Clowes, and M. L. Bender, *ibid.*, **89**, 3242, 3253 (1967).

5) R. Breslow and P. Campbell, *J. Am. Chem. Soc.*, **91**, 3085 (1969).

6) I. Tabushi, K. Yamamura, K. Fujita, and H. Kawakubo, *J. Am. Chem. Soc.*, **101**, 1019 (1979).

7) R. Breslow, J. B. Doherty, G. Guillot, and C. Lipsey, *J. Am. Chem. Soc.*, **100**, 3227 (1978); R. Breslow, M. F. Czarniecki, J. Emert, and H. Hamaguchi, *ibid.*, **102**, 762 (1980).

8) A. Ueno, H. Yoshimura, R. Saka, and T. Osa, *J. Am. Chem. Soc.*, **101**, 2779 (1979).

9) I. Tabushi, Y. Kuroda, and K. Shimokawa, *J. Am. Chem. Soc.*, **101**, 4759 (1979); I. Tabushi, Y. Kuroda, and A. Mochizuki, *ibid.*, **102**, 1152 (1980).

10) K. Harata and H. Uedaira, *Bull. Chem. Soc. Jpn.*, **48**, 375 (1975).

11) I. Tinoco, Jr., *Adv. Chem. Phys.*, **4**, 113 (1962).

12) H. Yamaguchi, N. Ikeda, F. Hirayama, and K. Uekama, *Chem. Phys. Lett.*, **55**, 75 (1978).

13) N. Ikeda and H. Yamaguchi, *Chem. Phys. Lett.*, **56**, 167 (1978).

14) H. Shimizu, A. Kaito, and M. Hatano, *Bull. Chem. Soc. Jpn.*, **52**, 2678 (1979).

15) A. Kaito, A. Tajiri, and M. Hatano, *Bull. Chem. Soc. Jpn.*, **49**, 2207 (1976).

16) J. Petruska, *J. Chem. Phys.*, **34**, 1111 (1961).

17) W. Saenger, R. K. McMullan, J. Fayos, and D. Mootz, *Acta Crystallogr., Sect. B*, **30**, 2019 (1974).

Mechanochemical Reactions at High Pressures. I. The Design and Construction of the Apparatus and Preliminary Experiments

Yoshiaki Ogo,* Noboru Nishiguchi,** and Yasuhiro Okuri

Department of Applied Chemistry, Faculty of Engineering, Osaka City University, Sugimoto-cho, Sumiyoshi-ku, Osaka 558

(Received May 23, 1980)

An apparatus for investigating mechanochemical reactions at high pressures of up to 50 kbar and preliminary experiments on acrylamide are described. The essentials of the apparatus are a rotating platen inserted in a Bridgman-type opposed-anvil press. The central platen is rotated by the force of an electric motor or by manual strokes under high pressure. The pressure distribution on the anvil surface was evaluated from the changes in the electric resistances of CdSe and CdTe as calibrants. The pressure observed at the center was 4.5 times the nominal load pressure. The phase-transition pressure of naphthalene was identified as about 25 kbar from the measurement of the pressure effect on the shearing strength. The mechanochemical behavior of acrylamide was investigated at room temperature and at static pressures of up to 15 kbar. The determinations of the IR spectrum, the ESR signal, the X-ray diffraction pattern, and the molecular weight confirmed that the reaction products were amorphous polyacrylamides and that the mechanical shear stress on the conversion of acrylamide to a polymer was exceedingly effective in comparison with static pressure.

The terms "mechanochemistry" and "mechanochemical reaction" have recently been used to designate chemical behavior caused by mechanical energy. Although mechanochemistry is an ambiguous research field at present, the knowledge of mechanochemistry has been widely extended and rapidly advanced in connection with the structure, chemical properties, and reactivity of a solid, *etc.* Thus, the interest in mechanochemistry extends over a wide range of scientific and technical disciplines.

Mechanochemical reactions at high pressures are significant in two important ways.

First, we consider that a strong mechanochemical force on substances, especially on organic materials, can be easily applied at high pressures. Mechanochemical reactions are generally not so appreciable as thermochemical or photochemical reactions. Therefore, a very sensitive detector is required to follow the reaction. The application of pressures makes detection by usual instruments possible.

Second, some shear stress is unavoidable when solid materials are compressed. In other words, solid-phase reactions under high pressures are somewhat or mostly mechanochemical changes.

These experiments were initiated to study the mechanochemical reactions of organic compounds from the above two points of view by means of a self-made high-pressure apparatus which is capable of loading the mechanical force simultaneously.

This unique technique was discovered by Bridgman. However, previous investigations by using this technique have dealt almost exclusively with phase-transitions, except for the group in communist countries. Recently investigations of the organic reaction under high pressures with mechanochemical shear force have been mainly done by Russian scientists, and it seems likely that they each belong to one of two groups. The first is Enikolopyan's group in the Chemical Physics Institute of Academy Sciences USSR. The mechanochemical behavior of many organic compounds has been investigated under high pressure by his group.[1-10] The second, Gonikberg-Zhulin's group in the Zelinskii Organic Chemistry Institute of Academy Sciences USSR, was also studied the organic reactions[11-18] from the same standpoint.

Our series of studies was initiated in order to synthesize new materials by means of solid-phase organic reactions under extreme conditions and in order to investigate the mechanochemical effect, which is unavoidable in solid-phase reactions under high pressures. The present paper will describe the design and the technique of the apparatus for the mechanochemical reactions and will present some preliminary experimental results on the reaction of acrylamide.

Design and Construction of the Apparatus

Despite the great interest in high-pressure studies, very little fundamental work has been reported on the design of high-pressure units (anvils). The development of this apparatus has, therefore, been based mainly on empirical experience gained through use. In the selection of an optimum design for the apparatus, questions regarding the ratio of the diameter of the sample face to that of the body of the anvil, or of the angle of the cone, could not be answered by recourse to the results of systematic studies. It should be emphasized, however, that economical considerations are among the most important factors. The diameter of the anvil surface of 12-mm determined the minimum sample quantity (≈10-mg) required to follow the mechanochemical reaction. (A 5-mm anvil was used in a special case).

The essentials of the apparatus are a flat metal plate (central platen), inserted between Bridgman-type opposed-anvils for pressuring and shearing, and a copper jacket for controlling the temperature. Enlarged views of the anvils, central platen, and sample assemblies are shown in Fig. 1. Two powdered or crystal samples, 1, between the mating surface of three cobalt-cemented

** Present address: Daido Chemicals Co. Ltd., 28-4-4, Takeshima, Nishiyodogawa-ku, Osaka 555.

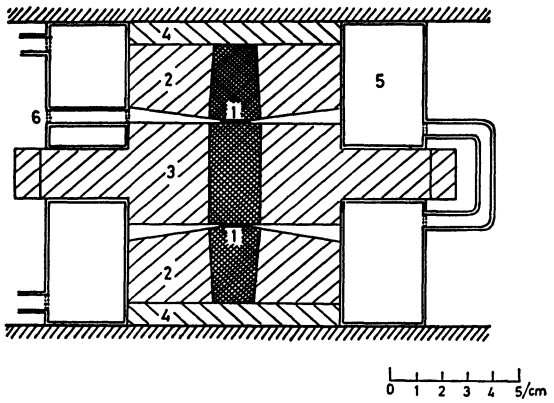

Fig. 1. Schematic diagram of anvil assembly.

tungsten carbides are compressed up to the desired pressure. The tungsten carbide conical cylinders of the opposed-anvils are 20-mm and 17-mm in diameter by 30-mm long and are supported by steel jacket shrunk around them. Both anvils, 2, are ground as truncated cones with 12-mm-diameter flats and a cone half-angle of 85°. The central platen, 3, is pinned into the hub of a 165-mm diameter spur gear. Two flat disks, 4, are attached to the top and bottom of the opposed-anvils. All the parts are surrounded by a pair of copper jackets, 5, through which thermostated water is circulated to keep the temperature constant throughout the experimental period. In order to fit a thermometer for the measurement of the temperature, a narrow hole, 6, is made in the copper jacket. A surface-type thermister thermometer is used to measure the temperature of the anvil surface near the sample region.

The load is applied to these anvils by means of a 50-t hydraulic-ram as the load unit. A pressure of up to 50 kbar (1 kbar$=10^8$ Pa) can be generated between them. During the compression, some of the sample extrudes from between the anvil faces until an equilibrium thickness is attained. Torque was applied to the gear holding the central platen by means of a mechanical drive forcing it to rotate about the common axis at various speeds with respect to the opposed-anvils. A torque can be generated by two different methods. One is the use of a continuous slow rotation in one direction of the central platen against the other by using an electric motor and various gear combinations. In our apparatus, shearing stresses are applied to the sample by rotating the central platen about its vertical axis through a maximum of 2.5° in 60 s. The other method is the use of a manual stroke. Mechanical driving is also given by the movement of the rack connected with the spur gear by means of another 10-t hydraulic-ram, serving as the shear unit instead of an electric motor. In this case, we can calculate the shear stress, τ, by the use of the following equations by assuming a constant value of shear stress across the radius, r:

$$M = \int_0^{r'} \tau r 2\pi r \cdot \mathrm{d}_r \text{ or } \tau = 3M/2\pi(r')^3 = 3PSR/2\pi(r')^3, \quad (1)$$

where M represents the torque; r', the effective radius of the anvils; P, the pressure produced in the 10-t hydraulic-ram to rotate the central platen; S, the surface area of the piston in the hydraulic-ram used as the shear unit, and R, the radius of the spur gear.

Under the conditions of our experiments, heating due to friction is negligible.

Pressure Distribution

Since the pressure at the center of the sample area in the opposed-anvil press is not equal to the applied pressure or to some predictable function of the applied pressure, it is necessary to use various internal standards (fixed points) for determining the actual pressure. We tried to measure the internal (true) pressure on the anvil surface without mechanical shear force by using acrylamide tablet as a model organic sample and cadmium selenide (CdSe) and cadmium telluride (CdTe) as the pressure-standard substances. CdSe and CdTe sharply change in their electrical resistances at 25 and 33 kbar respectively.[19]

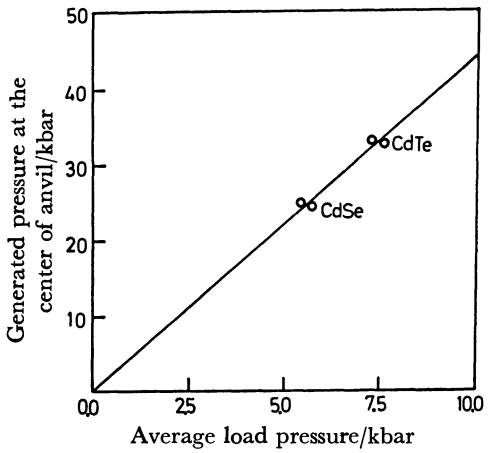

Fig. 2. Generated pressure at the center of anvil by measuring phase transitions of CdSe and CdTe.

Figure 2 shows the pressure at the center of the sample at various load pressures, which are detected by means of the changes in the electrical resistances of CdSe and CdTe. The internal pressure at the center is about 4.5 times larger than the average load pressure, and the two pressures are correlated by a single straight line through the original point. It has been concluded that the "pressure-multiplication effect" is independent of the press force in our pressure range.

Figure 3 shows the pressure distribution on the anvil surface. In this experiment, the semi-conducting materials used were placed in a certain position in the acrylamide tablet.

It can be readily shown that the press force on the anvil surface is expressed by the following formulas:

The force on the sample side, F_{ss}, is:

$$F_{ss} = \int 2\pi r \cdot P(r) \cdot \mathrm{d}r. \quad (2)$$

The force on the hydraulic-ram side, F_{rs} is:

$$F_{rs} = S_2 P_{obsd}, \quad (3)$$

where r represents the radius of the anvil surface on the sample side; $S_1(=\pi r^2)$, S_2, the surface areas of the

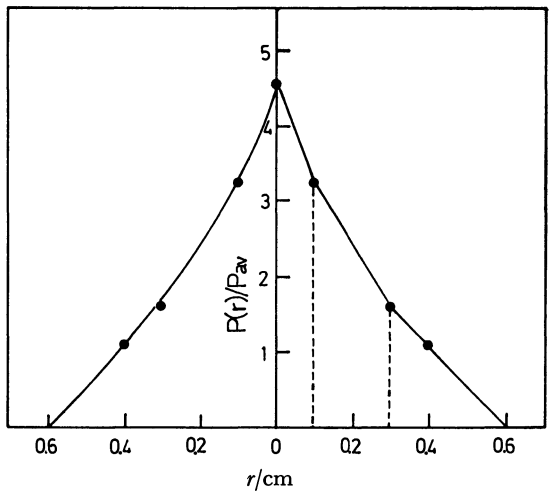

Fig. 3. Pressure distribution on anvil face.

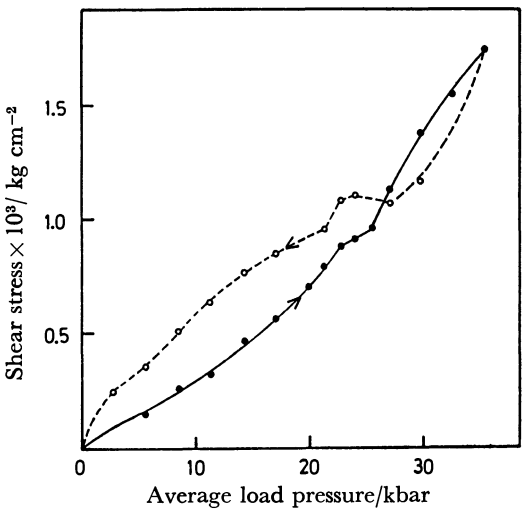

Fig. 4. Shearing curve for naphthalene by using anvil of 5 mm diameter.

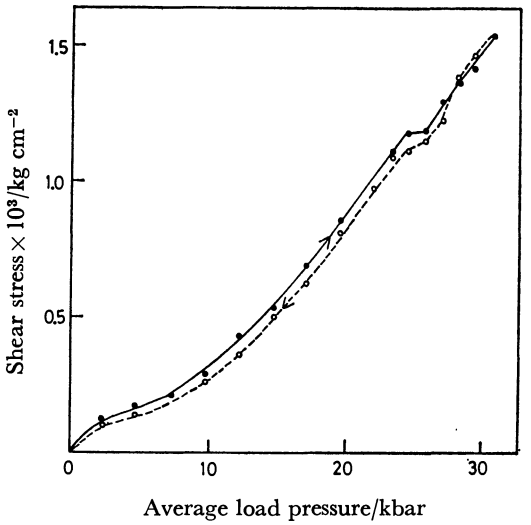

Fig. 5. Shearing curve for naphthalene by using anvil of 12 mm diameter.

anvils on the sample side and the hydraulic-ram side respectively; and P_{obsd}, the pressure as measured by means of a pressure gauge installed at the hydraulic-ram as the load unit. Moreover, one function, $P(r)$, is the pressure distribution on the anvil surface.

Theoretically

$$F_{ss} = F_{rs} = \int 2\pi r \cdot P(r) \cdot dr = S_2 P_{obsd}. \quad (4)$$

Instead of P_{obs}, the average load pressure on the anvil surface, P_{av}, as defined by Eq. 4, we obtain:

$$P_{av} = P_{obsd}(S_2/S_1) \quad (5)$$

$$\int 2\pi r \cdot P(r) \cdot dr/P_{av}S_1 = 1. \quad (6)$$

Since $S_2/S_1=62.7$ and $r=6$-mm in our apparatus, the calculation of Eq. 6 gives $1.294/1.131=1.14\fallingdotseq 1$, where it has been assumed that the pressure distribution, $P(r)$, is a linear function in the three divided regions, as is shown on the right-hand side of Eq. 3. Therefore, the value of P_{av} defined by Eq. 5 has been used as a pressure parameter in the foregoing discussion unless otherwise stated.

The distribution of pressure in the compressed material is evidently complicated when the mechanical shearing stress is loaded (that is, the central platen is rotated). At present, it is impossible to measure directly the distribution of pressure in that case. Although there is, therefore, no definite evidence, it seems reasonable to assume from the following considerations that the pressure distribution becomes uniform as a result of the plastic flow.

In general, the mechanical strengths of the organic substances are dependent on their modifications, which, of course, have different crystal structures; therefore, the curve of the shearing strength should change on passing from one modification to the other.

We have also tried to investigate the effect of the pressure on the shearing strength of naphthalene; some typical shearing curves are shown in Figs. 4 and 5. In this experiment we undertook to squeeze a purified single crystal of naphthalene in the direction of the c-axis and to rotate the central platen by 1 rad/h (1°/min) at room temperature by means of a manual stroke. The shear stress applied to the sample was calculated from Eq. 1 by assuming $r'=r$.

The curves exhibited a characteristic variation at

Table 1. Transition pressure and shear force of naphthalene

	Anvil diameter / mm	Pressure / kbar	Shear force / kg cm^{-2}
Experimental values	12	25[a)]	1.1—1.2×10^3
	12	30	1.5×10^3
	5	23—27[a)]	0.9—1.1×10^3
	5	30	1.35×10^3
Literature values			
Bridgman[20]	5	25—30[a)]	
	5	50	4.2×10^3
Gonikberg[10]	4.8	25—27[a)]	2.0—2.3×10^3
Enikolopyan[4]	4, 5, 10	30	1.3×10^3

a) Transition pressure.

about 25 kbar, which corresponds to the phase-transition of naphthalene. The results of such measurements are summarized in Table 1, together with the literature values.

Under ideal conditions such a transition should be accompanied by a sharp discontinuity in the shearing force itself, but because the pressure is not perfectly uniform over the anvil surface, the transition is spread over the interval of the mean pressure. With simultaneous mechanical deformation, the pressure distribution on the anvil surface would not be so sharp as in Fig. 3. It can be seen that the mechanical shear force induces a flattening of the distribution curve and that the distribution approaches a uniform state by its plastic flow if the rotation of the central platen is appropriate. Considering that our finding agree with the literature value, regardless of the anvil size, it seems reasonable to conclude that the pressure distribution in the organic sample on the anvil surface is almost uniform when mechanical shear force is applied. Therefore, nominal load pressures, as evaluated from Eq. 5, are defined as the operative and the effective pressures.

The above discussions are based on the results for acrylamide and naphthalene. However, it is probable that many organic compounds show the same behavior.

Reaction of Acrylamide

Experimental. Acrylamides were allowed to react at a high pressure (HP) combined with simultaneous shear deformation (SSD). The apparatus described in the preceding chapter will be abbreviated below as HP+SSD. In this experiment, the reactions proceeded at the constant shearing velocity (the rotation speed of the central platen) of 2.51 rad/h (2.4°/min) at room temperature unless otherwise stated. Therefore, 1 h of reaction time corresponds to a rotation angle of the central platen of 300°.

A commercial sample of acrylamide was purified by repeated crystallizations from a benzene solution and was finally vacuum-dried at room temperature for over 24 h. The purity of this acrylamide was proved by its melting point to be 84.5—85.0 °C.

A sample tablet was obtained from the purified acrylamide powder by preforming in a N_2 stream. The preforming pressure was about 5 kbar. The sample tablet was placed into the HP+SSD apparatus, and the experiment was carried out at the desired pressure.

The ESR data were obtained by rapidly inserting the sample into the ESR cavity immediately after the HP+SSD experiment. The concentrations of free-radicals were determined by integrations of the spectra and by subsequent comparison with those of 1,3,5-triphenylverdazyl as references.

A sample sheared at a high pressure was extracted from a large amount of methanol for separating into soluble and insoluble fractions. The insoluble fraction was dried *in vacuo* at room temperature to a constant weight, and the conversion was determined. The identification of the product took place by means of measurements of the melting point, the IR spectrum, the X-ray diffraction pattern, and the intrinsic viscosity.

The molecular weight of the product (polyacrylamide, as will be described below) was determined, by means of the following relations, from the viscosity data obtained from the Ubbelohde viscometer at 25 °C:[21]

$$[\eta]_{25}^{H_2O} = 3.73 \times 10^{-4} M_v^{0.66}$$

$$[\eta]_{25}^{H_2O} = 4.65 \times 10^{-4} M_n^{0.64}.$$

Results and Discussion. Judging from the following experimental evidence, acrylamide was clearly polymerized under conditions of HP+SSD. First of all, the product did not show a definite melting point. Secondly, the IR spectra of the product were the same as those of commercial polyacrylamide, while the IR spectra of the dissolved fraction in methanol were identical with those of the acrylamide monomer. Thirdly, when the X-ray diffraction patterns of the acrylamide monomer were compared with those of the product, the product was shown to be in an amorphous state. Therefore, we concluded that the product of this reaction was amorphous polyacrylamide.

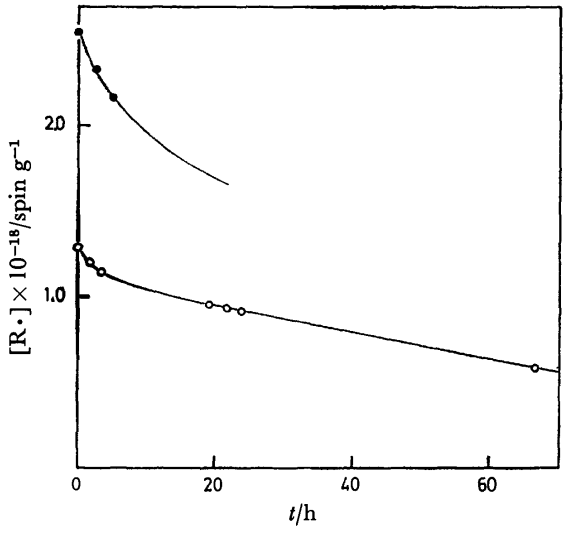

Fig. 6. Time dependence of radical concentrations at room temperature.
● 5 kbar, 4.54 rad; ○ 10 kbar, 2.27 rad.

The curve of the ESR signal yields a resolved three-peak system, about 64 G wide, with the central peak twice the height of the outer ones. No other signals could be identified under our experimental conditions. Such a signal corresponded well to that of the growing polyacrylamide radical reported by Alder and his collaborators.[22] Evidently, therefore, the reaction of acrylamide under the conditions of HP+SSD is a free-radical polymerization or depolymerization; in other words, the mechanochemical reaction of acrylamide proceeds *via* a free-radical mechanism. Figure 6 shows its time-dependence at room temperature. The resulting radicals are fairly stable for a long period. Morawetz and Fadner[23] have reported that the radical concentration obtained by γ-ray irradiation in the solid state was reduced to 67% after 60 h at 25 °C. We concluded, from our similar results shown in Fig. 6,

that the strain in the sheared sample disappears for periods up to several hours after the mechanical stress or static pressure is removed.

It is instructive to compare the experimental data with the time-dependence of the expected radical decay. If bimolecular radical termination is assumed,

$$-d[R\cdot]/dt = k_2[R\cdot]^2. \quad (7)$$

This leads to a radical decay of the form:

$$k_2t = 1/[R\cdot] - 1/[R\cdot]_0, \quad (8)$$

and if unimolecular spontaneous termination is assumed,

$$-d[R\cdot]/dt = k_1[R\cdot]. \quad (9)$$

This leads to a radical decay of the other form:

$$k_1t = \ln[R\cdot]_0/[R\cdot]. \quad (10)$$

The experimental data obtained are plotted in Figs. 7 and 8 as suggested by Eqs. 8 and 10. The initial parts of the time-dependence curves were satisfactorily expressed by Eq. 8, and the rate constants, k_2, were evaluated from the slopes of the straight line as 2.97×10^{-20} g spin^{-1} h^{-1} for the radicals generated at 10 kbar and as 1.47×10^{-20} g spin^{-1} h^{-1} for those generated at 5 kbar.

However, the hypothesis of chain termination by mutual recombination can be ruled out over the whole experimental range. Equation 10 is apparently verified in the range, as is shown in Fig. 8. Therefore, the hypothesis of a first-order termination of the chains,

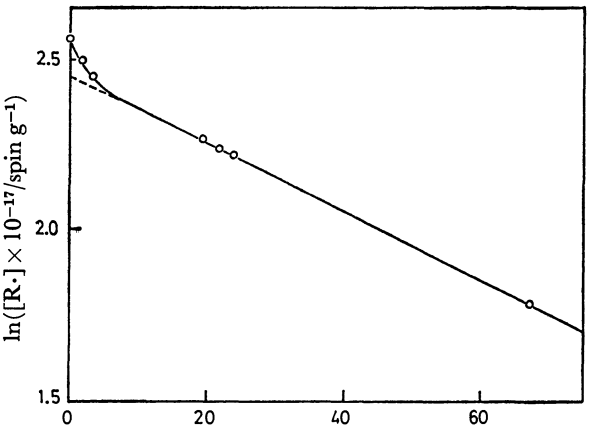

Fig. 8. Logarithm of free radical concentration as a function of time.
(Generated at 10 kbar and 2.27 rad)

deactivated by steric hindrance or by the fact that the free-radical site is "bogged down" in the mass of the polymer formed, is generally applicable.

The conversion of acrylamide to polymer was negligible without the application of mechanical shear force.

Figure 9 shows the relation between the conversion and the shearing degree at 5, 10, and 15 kbar pressures. The relation between the shearing degree and the

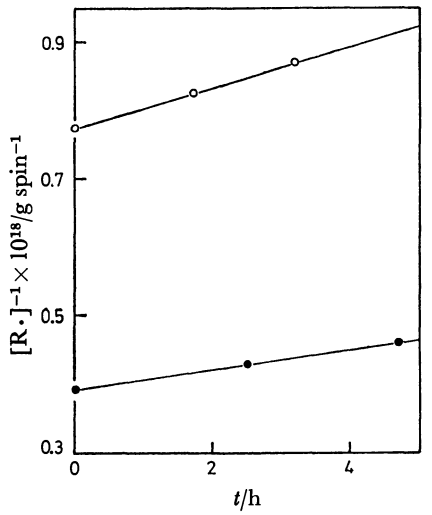

Fig. 7. Reciprocal of free radical concentration as a function of time.
● 5 kbar, 4.54 rad; ○ 10 kbar, 2.27 rad.

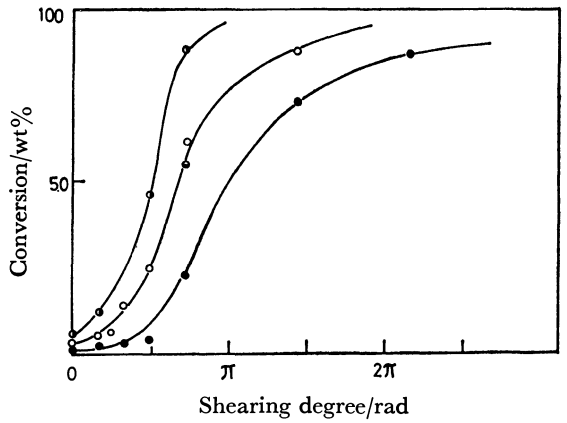

Fig. 9. Relation between conversion and shearing degree at various static pressures.
● 5 kbar; ○ kbar; ◑ 15 kbar; ◒ at different (twice) shearing speed.

Table 2. Molecular weight of the product polymer and the number of polymer molecules and free radicals in a gram of the sheared sample

Pressure / kbar	Shearing / rad	Degree / °	M_v viscosity-average	M_n number-average	Polyacrylamine / molecule g^{-1}	Free radical / spin g^{-1}
5	2.27	130	175000	180000	7.62×10^{17}	2.66×10^{17}
5	4.54	260	59000	59000	7.64×10^{18}	2.56×10^{18}
5	6.81	390	61000	61000		
10	2.27	130	132000	135000	2.77×10^{18}	1.29×10^{18}
10	4.54	260	68000	68000	7.50×10^{18}	4.25×10^{18}
15	2.27	130	67000	62000		

conversion showed a *S*-type curve and was somewhat analogous to a typical solid-phase reaction. Furthermore, the shearing velocities were independent of the conversion in our experimental region.

Table 2 shows the molecular weight of polyacrylamide as obtained by HP+SSD, together with the concentrations of the polymer and of the radical in sample layer, as evaluated from the M_n and ESR data. The molecular weight of the polymer obtained by HP+SSD was considerably lower than those of the polyacrylamides obtained commercially and by radiation-induced solid-phase polymerization.[21] The order of concentration of the polymer was, however, the same as that of the radicals in the sample layer. These facts suggest that the radicals identified by ESR are almost all reacting polymer radicals, as in the preceding discussions. This table also suggests that polyacrylamide degrades at a later stage of the HP+SSD reaction, judging from the facts that the molecular weight becomes much lower with the increase in the shearing degree. It can be roughly concluded from this table that the mechanochemical degradation of polyacrylamide affects this type of reaction in the range of large shear deformations.

The authors wish to thank Dr. Akifumi Onodera of Osaka University for helpful advice on the measurement of the pressure distribution and Dr. Yozo Miura of Osaka City University for the ESR studies.

References

1) V. M. Kapustyan, A. A. Zharov, and N. S. Enikolopyan *Dokl. Akad. Nauk SSSR*, **179**, 627 (1968).
2) A. G. Kazakevich, A. A. Zharov, P. A. Yampol'skii, N. S. Enikolopyan, and V. I. Gol'danskii, *Dokl. Akad. Nauk SSSR*, **186**, 1348 (1969).
3) N. P. Chistina, A. A. Zharov, Yu. V. Kissin, and N. S. Enikolopyan, *Dokl. Akad. Nauk SSSR*, **191**, 632 (1970).
4) V. G. Dzamukashvili, A. A. Zharov, N. P. Chistina, Yu. V. Kissin, and N. S. Enikolopyan, *Dokl. Akad. Nauk SSSR*, **215**, 127 (1974).
5) V. A. Zhorin, A. A. Zharov, Yu. V. Kissin, and N. S. Enikolopyan, *Dokl. Akad. Nauk SSSR*, **219**, 647 (1974).
6) N. S. Enikolopyan, A. A. Zharov, and A. G. Kazakevich, *Dokl. Akad. Nauk SSSR*, **230**, 354 (1976).
7) V. A. Zhorin, Yu. V. Kissin, N. M. Fridman, and N. S. Enikolopyan, *Dokl. Akad. Nauk SSSR*, **232**, 118 (1977).
8) A. B. Solov'eva, V. A. Zhorin, L. A. Krinitskava, Yu. V. Kissin, and N. S. Enikolopyan, *Izv. Akad. Nauk SSSR, Ser. Khim.*, **3**, 717 (1977).
9) A. B. Solov'eva, V. A. Zhorin, L. A. Krinitskava, Yu. V. Kissin, and N. S. Enikolopyan, *Izv. Akad. Nauk SSSR, Ser. Khim.*, **5**, 1161 (1977).
10) V. A. Zhorin, A. Yu. Shaulov, and N. S. Enikolopyan, *Vysokomol. Soedin., Ser. B*, **9**, 11, 841 (1977).
11) M. G. Gonikberg, G. P. Shakhikhovskii, and A. A. Petrov, *Zh. Fiz. Khim.*, **15**, 2510 (1966).
12) A. A. Petrov, M. G. Gonikberg, and Dzh. N. Aneli, *Vysokomol. Soedin., Ser. A*, **10**, 875 (1968).
13) M. G. Gonikberg, A. A. Petrov, Dzh. N. Aneli, G. P. Shakhovskii, and I. P. Yakovlev, *Izv. Akad. Nauk SSSR, Ser. Khim.*, **3**, 486 (1968).
14) A. A. Petrov, M. G. Gonikberg, S. N. Salazkin, Dzh. N. Aneli, and Ya. S. Vygodsky, *Izv. Akad. Nauk SSSR, Ser. Khim.*, **3**, 279, (1968).
15) M. G. Gonikberg., V. M. Zhulin, I. E. Pakhomova, and I. P. Yakovlev, *Dokl. Akad. Nauk SSSR*, **185**, 832 (1969).
16) I. E. Pakhomova, V. M. Zhulin, M. G. Gonikberg, and V. P. Ivanov, *Izv. Akad. Nauk SSSR, Ser. Khim.*, **4**, 857 (1972).
17) I. E. Pakhomova, V. M. Zhulin, M. G. Gonikberg, I. P. Yakovlev, V. I. Suskina, E. G. Rozantsev, and A. B. Shapiro, *Vysokomol. Soedin., Ser. A*, **12**, 1849 (1970).
18) V. M. Zhulin, I. P. Yakovlev, Z. G. Makarova, A. B. Shapiro, E. S. Rozant, M. I. Loktev, and G. P. Shakhovskoi, *Vysokomol. Soedin., Ser. A*, **9**, 12 2708 (1977).
19) A. Onodera, *Rev. Phys. Chem. Jpn.*, **39**, 65 (1969).
20) P. W. Bridgman, *Proc. Acad. Arts Sci.*, **72**, 227 (1938).
21) Y. Tabata and T. Suzuki, *Makromol. Chem.*, **81**, 223 (1965).
22) G. Adler, D. Ballantine, and B. Baysal, *J. Polym. Sci.*, **48**, 195 (1960).
23) H. Morwetz and T. A. Fadner, *Makromol. Chem.*, **34**, 162 (1959).

Synergistic Solvent Extraction of Alkali Metal Picrates by Crown Ethers

Yasuyuki TAKEDA

Department of Chemistry, Faculty of Science, Chiba University, Yayoi-chō, Chiba 260

(Received June 17, 1980)

The solvent extraction of rubidium and caesium picrates has been studied between benzene and water at 25 °C in the presence of tributyl phosphate (B), 12-crown-4 (12C4), 15-crown-5 (15C5), or both B and 15C5, and the complex-formation constants for the synergistic reactions in the benzene solution have been calculated. For both rubidium and caesium, the sequences of the complex-formation constants for these ligands are B<12C4<15C5, indicating that the complex-formation constant increases with an increase in the number of the donor oxygen atoms of the ligand. The complex-formation constant of rubidium is greater than that of caesium in every system.

For the rigid crown ethers such as 12-crown-4 (12C4), 15-crown-5 (15C5), and 18-crown-6, in a crown ether complex with a metal ion whose size is larger than the cavity size of the crown ether, the metal ion is located partly outside the plane of the crown ether ring. Thus, the exposed part of the metal ion can interact strongly with another crown ether or a neutral donor solvent in a solution; *e.g.*, benzo-15-crown-5 and dibenzo-18-crown-6 (DB18C6) form 2 : 1 complexes with rubidium and caesium ions.[1]

The solvent extraction of alkali and alkaline earth metal ions with crown ethers has been widely investigated in terms of thermodynamics[1c,2] and analytical chemistry.[3] However, few synergistic effects for alkali and alkaline earth metal ions in the crown ether-neutral donor extractant system have been reported.

In the present study, the solvent extraction of rubidium and caesium picrates has been studied between benzene and water in the presence of 12C4, 15C5, or both tributyl phosphate (B) and 15C5, and the complex-formation constants for the synergistic reactions in the benzene solution have been calculated in order to compare the synergistic effects due to the crown ethers with those due to B.

Experimental

Materials. 12C4 and analytical-grade B were obtained from Wako-Pure Chemicals, Ltd., and 15C5 from Nisso Co., Ltd. They were used without further purification. The concentrations of the alkali metal hydroxides and picric acid solutions were determined by means of acid and basic titrations respectively. Benzene (analytical-grade) was washed twice with distilled water.

Apparatus and Procedure. An aqueous phase contained the alkali metal hydroxide (4.4×10^{-3}—2.0×10^{-2} M; 1 M= 1 mol dm^{-3}) and the picric acid (2.0×10^{-3}—1.0×10^{-2} M). An organic phase contained one of the extractants (B: 9.4×10^{-2}—9.9×10^{-1} M, crown ether: 4.9×10^{-2}—7.5×10^{-1} M), or both B (6.8×10^{-2}—8.0×10^{-1} M) and the crown ether (4.8×10^{-3}—5.8×10^{-2} M). The two phases in stoppered glass tubes (30 ml) were shaken in a thermostated water bath for approx. 30 min at 25±0.2 °C and then centrifuged. The initial volume of each phase was 10 ml in all cases. A portion of the aqueous phase (8 ml) was transferred into a 10-ml beaker, and the hydrogen ion concentration was determined by a Hitachi-Horiba F-5 pH meter. The extractions were conducted at pH 8.2—11.8. The picrate in the organic phase was back-extracted into 8 ml of a 0.01 M NaOH aqueous solution, and the picrate concentration was determined at 356 nm by means of a Shimadzu UV-200 spectrophotometer ($\varepsilon=1.45\times10^4$ cm^{-1} M^{-1}).

Results

When equilibrium occurs between an aqueous solution of a univalent metal ion (M^+) and a picrate ion (A^-), and a benzene solution of B, a crown ether (L), or both B and L, the equilibrium constants may be defined by the following equations:

$$K_{ex}(MB_3A) = [MB_3A]_o[H^+]/[M^+][B]_o^3[HA]_o \quad (1)$$

$$K_{ex}(ML_2A) = [ML_2A]_o[H^+]/[M^+][L]_o^2[HA]_o \quad (2)$$

$$K_{ex}(MLBA) = [MLBA]_o[H^+]/[M^+][L]_o[B]_o[HA]_o \quad (3)$$

$$K_{D,L} = [L]_o/[L] \quad (4)$$

$$K_{ML} = [ML^+]/[M^+][L] \quad (5)$$

$$K_{ex}(HA) = [HA]_o/[H^+][A^-], \quad (6)$$

where the subscript "o" means organic and the lack of a subscript refers to the aqueous phase. The value of $K_{ex}(HA)$ was spectrophotometrically determined to be 247. For the B system the distribution ratio of the metal may be represented by

$$D = [MB_3A]_o/[M^+]. \quad (7)$$

The substitution of Eqs. 1 and 6 into Eq. 7 gives

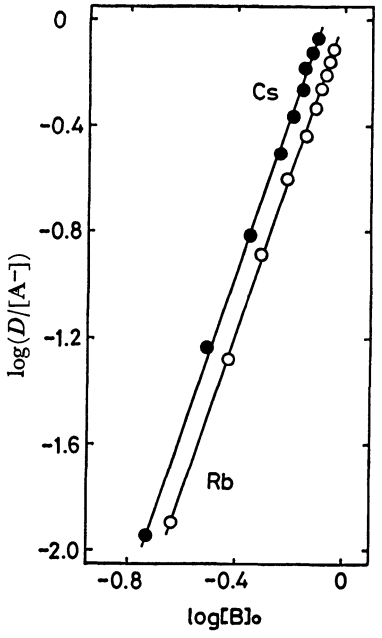

Fig. 1. Plots of $\log(D/[A^-])$ *vs.* $\log[B]_o$ for the B system.

$$D = K_{ex}(MB_3A)K_{ex}(HA)[B]_o^3[A^-]. \quad (8)$$

The log $(D/[A^-])$ *vs.* log $[B]_o$ plot in Fig. 1 shows a straight line with a slope of 3 in each case, indicating that the $K_{ex}(MB_3A)$ in the present study can be described by Eq. 1. The value of $[B]_o$ in Eq. 8 was considered to be approximately equal to that of $[B]_t$ under the present experimental conditions and that of $[A^-]$ calculated from Eq. 9:

$$[A^-] = [HA]_t - [MB_3A]_o, \quad (9)$$

where the subscript "t" denotes the total concentration.

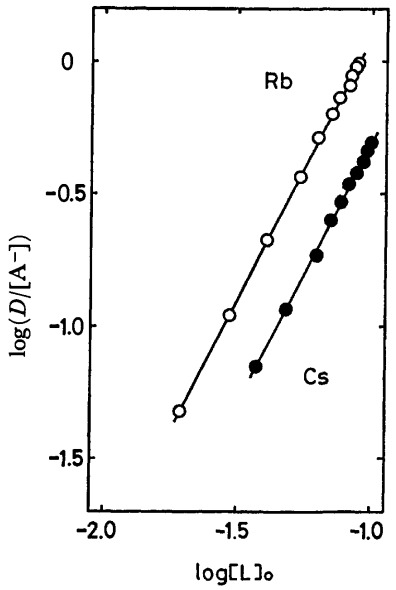

Fig. 2. Plots of $\log(D/[A^-])$ *vs.* $\log[L]_o$ for the 12C4 system.

For the 12C4 system D may be represented by

$$D = [ML_2A]_o/([M^+] + [ML^+] + [ML_2^+]). \quad (10)$$

In the case of $[M^+] \gg [ML^+] + [ML_2^+]$, Eq. 10 becomes

$$D = K_{ex}(ML_2A)K_{ex}(HA)[L]_o^2[A^-]. \quad (11)$$

The log $(D/[A^-])$ *vs.* log $[L]_o$ plot in Fig. 2 shows a linear relationship with a slope of 2 in each case, indicating that 12C4 forms a 2 : 1 complex with the monovalent metal ion. The values of $[L]_o$ and $[A^-]$ in Eq. 11 were calculated from Eqs. 12 and 13 respectively:

$$[L]_o = ([L]_t - 2[ML_2A]_o)/(1 + K_{D,L}^{-1}) \quad (12)$$

($K_{D,L} = 0.15$ for 12C4[4])

$$[A^-] = [HA]_t - [ML_2A]_o. \quad (13)$$

For the 15C5 system D may be described by Eq. 10. In the case of $[M^+] + [ML^+] \gg [ML_2^+]$, Eq. 10 becomes

$$D = K_{ex}(ML_2A)K_{ex}(HA)[L]_o^2[A^-]/(1 + K_{ML}K_{D,L}^{-1}[L]_o). \quad (14)$$

The log $\{D(1+K_{ML}K_{D,L}^{-1}[L]_o)/[A^-]\}$ *vs.* log $[L]_o$ plots of both Rb and Cs in Fig. 3 fall on the straight lines with a 2 slope. Thus, the extraction equilibrium can be represented by Eq. 2. The values of $[L]_o$ and $[A^-]$ in Eq. 14 were calculated from Eqs. 15 and 16 respectively:

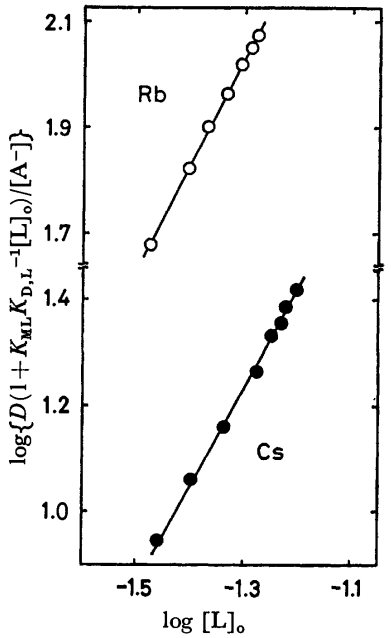

Fig. 3. Plots of $\log\{D(1+K_{ML}K_{D,L}^{-1}[L]_o)/[A^-]\}$ *vs.* $\log[L]_o$ for the 15C5 system.

$$[L]_o = ([L]_t - 2[ML_2A]_o)/(1 + K_{D,L}^{-1} + K_{ML}K_{D,L}^{-1}[M^+]), \quad (15)$$

($K_{D,L}=0.15_6$ for 15C5;[2b] $K_{ML}=4.2$ and 6.3 for Rb and Cs respectively[5])

$$[A^-] = ([HA]_t - [ML_2A]_o)/\{1 + (K_{HA} + K_{ex}(HA))[H^+]\}, \quad (16)$$

where K_{HA} is the association constant of picric acid ($K_{HA}=1.9_5$[6]).

When both 15C5 and B exist in the extraction system, D may be represented by

$$D = [MLBA]_o/([M^+]+[ML^+]). \quad (17)$$

The substitution of Eqs. 3, 4, 5, and 6 into Eq. 17 gives

$$D = K_{ex}(MLBA)K_{ex}(HA)[L]_o[B]_o[A^-]/(1 + K_{ML}K_{D,L}^{-1}[L]_o). \quad (18)$$

The log $\{D(1+K_{ML}K_{D,L}^{-1}[L]_o)/[A^-]\}$ *vs.* log $[L]_o$ and log $[B]_o$ plots are illustrated in Figs. 4 and 5 respectively.

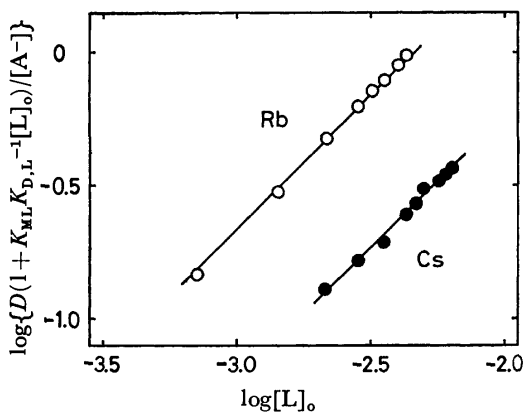

Fig. 4. Plots of $\log\{D(1+K_{ML}K_{D,L}^{-1}[L]_o)/[A^-]\}$ *vs.* $\log[L]_o$ for the 15C5–B system.

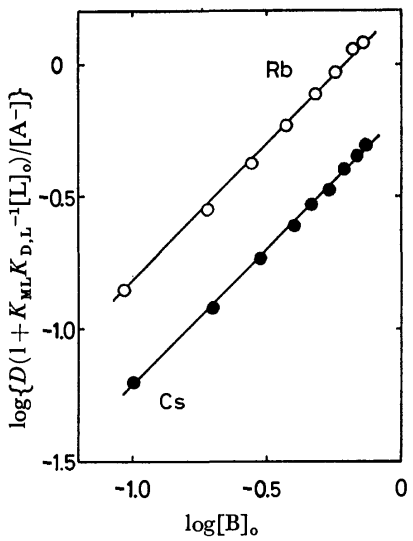

Fig. 5. Plots of $\log\{D(1+K_{ML}K_{D,L}^{-1}[L]_o)/[A^-]\}$ *vs.* $\log[B]_o$ for the 15C5–B system.

It may be noted from Figs. 4 and 5 that, in each case, the plots of both Rb and Cs have a slope of 1. Thus, the K_{ex}(MLBA) in the present study can be described by Eq. 3. The value of $[B]_o$ in Eq. 18 was considered to be nearly equal to that of $[B]_t$ under these experimental conditions, and those of $[L]_o$ and $[A^-]$ were calculated from Eqs. 19 and 20 respectively:

$$[L]_o = ([L]_t - [MLBA]_o)/(1+K_{D,L}^{-1}+K_{ML}K_{D,L}^{-1}[M^+]), \quad (19)$$

$$[A^-] = [HA]_t - [MLBA]_o. \quad (20)$$

The extraction equilibrium constants obtained from these data are summarized in Table 1, together with those from the literature.

TABLE 1. EXTRACTION EQUILIBRIUM CONSTANTS AT 25 °C

		Rb^+	Cs^+
$\log K_{ex}(MB_3A)$		−2.26	−2.14
$\log K_{ex}(MLBA)$	15C5	0.56	0.19
$\log K_{ex}(ML_2A)$	12C4	−0.29	−0.64
	15C5	2.15	1.48
	DB18C6[1c]	4.11	3.21
$\log K_{ex}(MLA)$	12C4[4]	−2.10	−2.18
	15C5[2c]	−0.25	−0.49
	DB18C6[1c]	1.36	0.68

Discussion

As can be seen from Table 1, the $\log K_{ex}(MB_3A)$ value of Rb^+, which is more strongly hydrated than Cs^+, is smaller than that of Cs^+. On the contrary, for the MLA, MLBA, and ML_2A systems, Rb^+ is more extractable than Cs^+. In the cases of 12C4 and DB18C6, the extractabilities and the difference in the extractabilities of Rb^+ and Cs^+ are enhanced in going from the MLA system to the ML_2A one, and, in the case of 15C5, those increase in the system order MLA< MLBA<ML_2A.

When MLA forms MLBA and ML_2A with B and L in the organic phase, the equilibria can be written as Eqs. 21 and 22 respectively:

$$MLA_o + B_o \rightleftarrows MLBA_o$$

$$K_{MLBA,o} = K_{ex}(MLBA)/K_{ex}(MLA) = [MLBA]_o/[MLA]_o[B]_o \quad (21)$$

$$MLA_o + L_o \rightleftarrows ML_2A_o$$

$$K_{ML_2A,o} = K_{ex}(ML_2A)/K_{ex}(MLA) = [ML_2A]_o/[MLA]_o[L]_o, \quad (22)$$

where $K_{MLBA,o}$ and $K_{ML_2A,o}$ are the formation constants for the MLBA and the ML_2A complexes in a benzene solution respectively; they are given in Table 2.

TABLE 2. COMPLEX-FORMATION CONSTANTS FOR SYNERGISTIC REACTIONS IN A BENZENE SOLUTION AT 25 °C

		Rb^+	Cs^+
$\log K_{MLBA,o}$	15C5	0.81	0.68
$\log K_{ML_2A,o}$	12C4	1.81	1.54
	15C5	2.40	1.97
	DB18C6[1c]	2.7	2.5

It has been reported that in the benzene-water system at 20±2 °C the extraction of Cs^+ is enhanced by a factor of 60 with a mixture of 2-thenoyltrifluoroacetone (HTTA) and B compared with that by HTTA alone, and that the formula for the extracted species is $Cs(TTA)B_2$;[7] in the present study, the extraction is enhanced by a factor of only 4.8 with a mixture of 15C5 and B compared with that by 15C5 alone (Table 2). The large difference in the synergistic effects of the HTTA and the 15C5 systems may chiefly depend on the fact that the HTTA complex has more B than the 15C5 complex. There were no appreciable synergistic effects for the Na^+ and the K^+–15C5–B systems. Since a cation whose size exceeds the cavity size of the crown ether cannot get into the plane of the oxygen atoms of the crown ether, for the 15C5 complex, Rb^+ (crystal ionic radius: 1.48 Å[8]) and Cs^+ (crystal ionic radius: 1.69 Å[8]) may protrude from the plane of 15C5 (cavity radius: 0.85—1.1 Å[9]) much more than Na^+ (crystal ionic radius: 0.95 Å[8]) and K^+ (crystal ionic radius: 1.33 Å[8]). Consequently, the 15C5 complexes with RbA and CsA may easily accept a B molecule, while, it may be very difficult for those with NaA and KA.

It may be noted from Table 2 that the complex-formation constant of Rb^+ is greater than that of Cs^+ in every system. For the MLBA system, this may be attributed to the higher charge density of Rb^+ compared with that of Cs^+. For the ML_2A system, this may be due to the fact that Rb^+ has higher charge density than Cs^+, and moreover that Rb^+ has a more optimum size for each of the cavities of these crown ethers (cavity radius: 12C4 (0.5—0.65 Å[9]), 18C6 (1.3—1.6 Å[9])) than Cs^+.

The sequences of the number of the donor oxygen atoms for these ligands are B<12C4<15C5<DB18C6. The small number of the donor oxygen atoms of B may be the reason why, in each case of Rb^+ and Cs^+, the complex-formation constant value of MLBA is the

smallest of all the complexes (Table 2). For the crown ethers, in each case of Rb^+ and Cs^+, the accommodation of the metal ion into the crown ether cavity and the complex-formation constant value increase in the crown ether order 12C4<15C5<DB18C6 (Table 2). These results indicate that, for the same alkali metal ion, the larger the number of the donor oxygen atoms of the crown ether and the more closely the metal ion fits into the crown ether cavity, the greater is the complex-formation constant value.

The author thanks Mr. Yasumasa Hirasawa of this laboratory for his experimental assistance.

References

1) a) H. K. Frensdorff, *J. Am. Chem. Soc.*, **93**, 600 (1971); b) K. H. Wong, M. Bourgoin, and J. Smid, *J. Chem. Soc., Chem. Commun.*, **1974**, 715; c) A. Sadakane, T. Iwachido, and K. Tōei, *Bull. Chem. Soc. Jpn.*, **48**, 60 (1975).

2) a) H. K. Frensdorff, *J. Am. Chem. Soc.*, **93**, 4684 (1971); b) Y. Takeda and H. Katō, *Bull. Chem. Soc. Jpn.*, **52**, 1027 (1979); c) Y. Takeda and H. Gotō, *ibid.*, **52**, 1920 (1979); d) Y. Takeda, *ibid.*, **52**, 2501 (1979).

3) a) T. Kimura, K. Iwashima, T. Ishimori, and H. Hamaguchi, *Chem. Lett.*, **1977**, 563; b) Y. Takeda, S. Suzuki, and Y. Ohyagi, *ibid.*, **1978**, 1377; c) Y. Takeda, K. Oshio, and Y. Segawa, *ibid.*, **1979**, 601; d) H.Nakamura, M. Takagi, and K. Ueno, *Talanta*, **26**, 921 (1979).

4) Y. Takeda, *Bull. Chem. Soc. Jpn.*, **53**, 2393 (1980).

5) R. M. Izatt, R. E. Terry, B. L. Haymore, L. D. Hansen, N. K. Dalley, A. G. Avondet, and J. J. Christensen, *J. Am. Chem. Soc.*, **98**, 7620 (1976).

6) "Dissociation Constants of Organic Acids in Aqueous Solution," ed by G. Kortün, W. Vogel, and K. Andrussov, Butterworths, London (1961).

7) T. V. Healy, *J. Inorg. Nucl. Chem.*, **30**, 1025 (1968).

8) L. Pauling, "The Nature of the Chemical Bond," 3rd ed, Cornell Univ. Press (1960).

9) C. J. Pedersen and H. K. Frensdorff, *Angew. Chem. Int. Ed.*, **11**, 16 (1972).

Shock Tube Studies of the Acetylene and Ethylene Pyrolysis by UV Absorption

Tohru KOIKE* and Kihei MORINAGA

Department of Chemistry, National Defense Academy, Hashirimizu, Yokosuka 239

(Received July 22, 1980)

Absorption measurements at 216 and 230 nm of shock heated C_2H_2, $C_2H_2+H_2$, and C_2H_4 diluted in Ar were made over the temperature range 1800 K to 2600 K at half of atmospheric pressure. Absorptivities were evaluated for C_4H_2, which is the main product of C_2H_2 pyrolysis, as well as for C_2H_2 and C_2H_4. The relative value of C_4H_2 absorption was confirmed to decrease with the presence of H_2 in accordance with a computer modeling result using a 25-reaction mechanism. The time profile of C_4H_2 absorption could be modeled well with $k=10^{12.4}$ cm^3 mol^{-1} s^{-1} for the reaction $H_2+C_2H=C_2H_2+H$.

The pyrolysis of C_2H_2 in shock waves has been studied by many workers and has become explainable through computer modeling with a rather definite reaction mechanism.

Recently, two groups studied the C_2H_2 pyrolysis using real-time kinetic absorption spectroscopy and the laser schlieren method. Frank and Just[1] measured the [H] profile in the C_2H_2 pyrolysis by atomic resonance absorption spectroscopy (ARAS) in mixtures of C_2H_2 highly diluted in Ar to ppm order and evaluated the initiation reaction rate constant in the low pressure region. Tanzawa and Gardiner[2] did laser schlieren experiments on the C_2H_2 pyrolysis. They proposed a reaction mechanism, in which the experimental results obtained by TOF mass spectroscopy[3,4] and single pulse shock tube[5] as well as their laser schlieren results were analyzed by computer modeling studies. Their later efforts[6] led them to a final mechanism which accords with almost all of the experimental results from 625 to 3400 K.

The new mechanism of the C_2H_2 pyrolysis so derived is expected to improve the C_2H_4 pyrolysis mechanism, because C_2H_4 decomposes to C_2H_2 and H_2 by a molecular reaction very rapidly in the high temperature region.[7]

Cundall *et al.*[8] studied the C_2H_2 and C_2H_4 pyrolysis in shock waves by absorption spectroscopies with Xe-lamp and He–Ne laser. The reaction mechanism used by them was rather primitive and the values of heat of formation for C_2H and polyacetylene radicals are subject to correction,[1,2,9] though they could obtain qualitative information about soot formation.

The present paper is concerned with the C_2H_2 and C_2H_4 pyrolysis behind incident shock waves. The reaction features were examined by UV absorption at 216 and 230 nm and were interpreted more quantitatively by the computer modeling with a refined mechanism.[6]

Experimental

The shock tube used in this study has been described in detail already.[10]

The light from a D_2-lamp (Hamamatsu-TV, L544) or Xe-lamp (Ushio, UXL500D), made parallel with a quartz lens, was measured using a photomultiplier (Hamamatsu-TV, R208) with a monochrometer (Jarrell-Ash, JE25) after passing through two shock tube windows. The output from the photomultiplier was displayed on an oscilloscope (Tektronix, 7603).

The signal from piezo-gauges mounted on the shock tube every 10 cm was detected by a universal counter (Takeda-Riken, TR5002). Shock temperature was calculated from the measured shock velocity assuming full relaxation and no chemical reaction.

Gases used were 99.7% pure C_2H_2 and 99.6% pure C_2H_4 purchased from Takachiho and 99.999% pure Ar from Nippon Sanso. All gases were used without further purification. The test gas was prepared in a 20 l glass bulb manometrically and used after more than 48 h mixing time. The test gas compositions are shown in Table 1.

Table 1. Measured A and modeled $[C_4H_2]$ and $[C_6H_2]$ at 2000 K in each test gas mixture (cm and mol units)

No.	Gas composition in Ar	A	$[C_4H_2]/10^{-9}$	$[C_6H_2]/10^{-10}$
1	3.2% C_2H_2	1.11	15	11
2	2.0% C_2H_2/2.3% H_2	0.26	4.3	1.1
3	4.0% C_2H_4	0.94	10	2.0

The test section of the shock tube was evacuated to less than 10^{-4} Torr before each run. Neither emission from C_2H_2 or C_2H_4 in Ar mixtures nor absorption by Ar was observed under the present experimental conditions. (1 Torr=133.322 Pa)

Computer modeling was done using the program mentioned previously.[10] The flow model used for reflected shock waves was modified and a constant density calculation was adopted.[11] Thermochemical properties of the species which appear in the reaction mechanism were taken from the JANAF thermochemical table [12] or other available sources.[9,13,14]

Results and Discussion

A sample oscillogram of the UV absorption (216 nm, 3.2% C_2H_2 in Ar, and P_2=0.35 atm) is shown in Fig. 1. We evaluated absorptivities of C_2H_2 and C_2H_4 from the absorption at the shock front for two wavelengths, 216 and 230 nm, by using the following definition:

$$a = \ln(I_0/I)/[C]_0/d,$$

where I_0=incident light intensity, I=transmitted intensity at the shock front, $[C]_0=C_2H_2$ or C_2H_4 concentration at the shock front, and d=optical path length (7.2 cm). The obtained a values of C_2H_2 and C_2H_4 are shown in Figs. 2a and 2b.

Acetylene shows an absorption due to the electronic transition X→A in the wavelength region 210—237

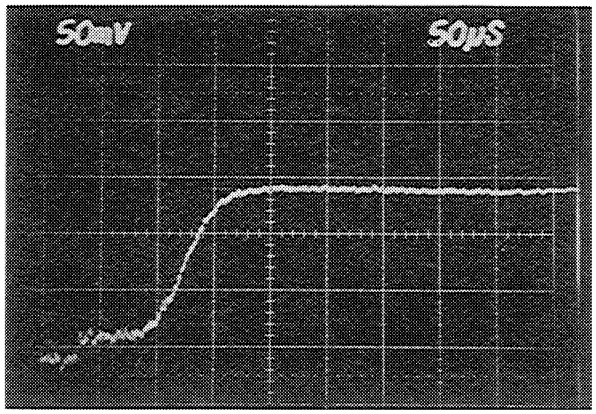

Fig. 1. A representative profile of transmitted D_2-lamp intensity for 3.2% C_2H_2 in Ar mixture, $T_2=2084$ K, and $P_2=0.35$ atm.

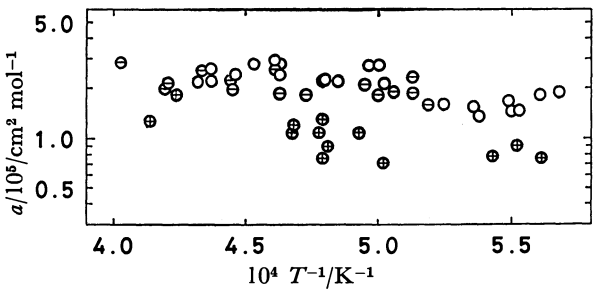

Fig. 2a. Temperature dependence of C_2H_2 absorptivity at 216 and 230 nm with D_2-lamp. The symbols are as follows.
○: for 3.2/96.8=C_2H_2/Ar at 216 nm, ⊖: for 2.0/2.2/95.8=C_2H_2/H_2/Ar at 216 nm, ⊕: for 3.2/96.8=C_2H_2/Ar at 230 nm.

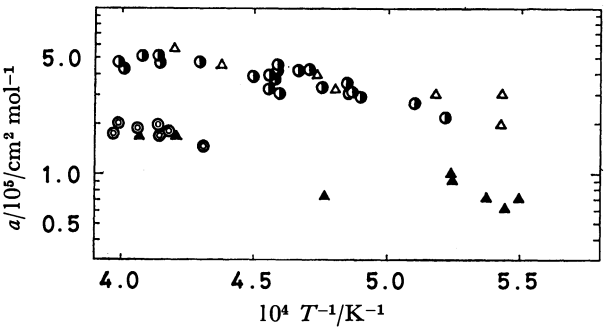

Fig. 2b. Temperature dependence of C_2H_4 absorptivity at 216 and 230 nm. The symbols are as follows.
◑: for 4.0% C_2H_4 in Ar with D_2-lamp at 216 nm, ◎: for 4.0% C_2H_4 in Ar with D_2-lamp at 230 nm, △: for 4.5% C_2H_4 in Ar with Xe-lamp at 216 nm, ▲: for 4.5% C_2H_4 in Ar with Xe-lamp at 230 nm. Data taken with Xe-lamp were corrected for higher-order wavelengths.

nm.[15] In comparison with C_2H_2, C_2H_4 has greater absorptivity in this region, though no absorption which can be attributed to an electronic transition is reported for C_2H_4.[15] Figures 2a and 2b show that the absorptivities of C_2H_2 and C_2H_4 at 216 nm are larger than those at 230 nm in the temperature range measured. This may imply that the absorption of C_2H_4 at 216 nm is attributed to an extended transition of X→A. Since the wavelength 230 nm is too far from the wavelength region of the X→A transition, the absorption at 230 nm may not be the extended transition. No clear explanations of the C_2H_4 absorption at 230 nm at these high temperatures can be given only on the basis of the present experimental results.

The a values of C_2H_2 and C_2H_4 increase slightly with increasing temperature, in contrast with the reported a values of CH_3 which have the opposite behavior.[16,17] Similar observations are reported recently for 3.39 μm He–Ne laser absorption of small hydrocarbons, *i.e.*, the infrared a values of C_2H_2 and C_2H_4 increase with increasing temperature, while those of the alkanes decrease with increasing temperature.[18,19]

The absorption measurement at 216 nm was employed to study ethane decomposition and CH_3 recombination in shock waves.[16,17] The results shown above imply that the absorption at 216 nm is not only due to CH_3 but also to C_2H_2 and C_2H_4. For alkane pyrolysis measured at high temperatures, CH_3 is usually formed at an early stage of the reaction and C_2H_2 and C_2H_4 gradually accumulate afterwards. The absorption at 216 nm at the early stage of alkane pyrolysis represents the features of CH_3 alone; the later absorption begins to show aggregate features of CH_3, C_2H_2, and C_2H_4. Our trial runs for the C_2H_6 pyrolysis measured by 230 nm absorption, on the other hand, showed neglibible absorptivity for CH_3 at the 1st stage of the pyrolysis. This result and the above may explain why we selected 216 and 230 nm absorptions to study the C_2H_2 and C_2H_4 pyrolysis. The computer program, which incorporates these absorptivities for C_2H_2 and C_2H_4 at 216 and 230 nm and the absorptivity for CH_3 at 216 nm, may solve the alkane pyrolysis measured at the two wavelengths by a procedure similar to that adopted in the C_2H_6 and C_3H_8 pyrolysis studies monitored by a 3.39 μm He–Ne laser.[14,20]

The oscillogram of Fig. 1 shows that the absorption increases almost linearly after the absorption at the shock front and finally reaches a high plateau value. The plateau absorption A was defined by $A=\ln(I_0/I_f)$, where I_f is the transmitted light intensity at the plateau and I_0 the incident light intensity. In Fig. 3, the relative A value or the value of A divided by the shock front concentration of $[C_2H_2]_0$ or $[C_2H_4]_0$ are shown *vs.* $10^4/T$.

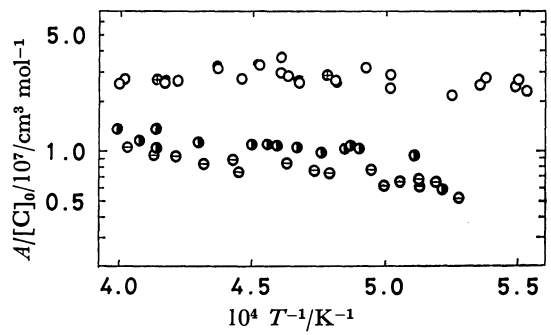

Fig. 3. Temperature dependence of relative steady absorption at 216 and 230 nm. The symbols are as in Figs. 2a and 2b.

In this case, the relative values are free from the choice between the two wavelengths, 216 and 230 nm, but the values show distinct mixture dependence, splitting into two groups as shown in Fig. 3. Searches for the chemical species which are responsible for the plateau absorption were made by the computer modeling, adopting the reaction mechanism shown in Table 2.

TABLE 2. REACTION MECHANISM AND RATE CONSTANTS $k=A\exp(-E/RT)$ (mol, cm, s, and kcal units)

Reaction	log A	E	Ref. No.
1) $C_2H_4+M=C_2H_2+H_2+M$	17.4	79.3	7
2) $C_2H_4+M=C_2H_3+H+M$	17.6	98.2	7
3) $C_2H_4+C_2H_4=C_2H_3+C_2H_5$	14.8	64.0	24
4) $C_2H_4+H=C_2H_3+H_2$	15.7	22.9	7
5) $C_2H_3+C_2H_4=C_4H_6+H$	12.0	7.3	25
6) $C_2H_3+H=C_2H_2+H_2$	13.0	0.	14
7) $C_2H_5+M=C_2H_4+H+M$	15.3	30.1	14
8) $C_2H_2+M=C_2H+H+M$	16.6	106.5	1
9) $C_2H_2+C_2H_2=C_4H_3+H$	12.3	45.0	6
10) $C_2H_3+M=C_2H_2+H+M$	14.9	31.0	25
11) $C_2H_2+C_2H_3=C_4H_4+H$	13.2	25.0	6
12) $C_4H_4+C_2H=C_4H_3+C_2H_2$	13.6	0.	6
13) $C_2H+H_2=C_2H_2+H$	12.4	0.	This work
14) $C_2H_2+C_2H=C_4H_2+H$	13.6	0.	2
15) $C_4H_3+M=C_4H_2+H+M$	16.0	60.0	2
16) $C_4H_2+M=C_4H+H+M$	17.5	80.0	2
17) $C_6H_2+M=C_6H+H+M$	16.7	80.0	2
18) $C_8H_2+M=C_8H+H+M$	16.7	80.0	2
19) $H_2+M=2H+M$	12.4	92.6	26
	$+0.5\log T$		
20) $C_4H_3+H+M=C_4H_4+M$	15.0	0.	2
21) $C_2H_2+C_4H=C_6H_2+H$	13.6	0.	2
22) $C_4H_2+C_2H=C_6H_2+H$	13.6	0.	2
23) $C_2H_2+C_6H=C_8H_2+H$	12.0	0.	2
24) $C_6H_2+C_2H=C_8H_2+H$	12.0	0.	2
25) $C_4H_2+C_4H=C_8H_2+H$	12.0	0.	2

Acetylene radical and polyacetylene radicals can not be the absorbers; if they were, they must have large, temperature-dependent absorptivities. For example, the steady concentration of C_2H at 2500 K is about 20 times larger than that at 2000 K in 3.2% C_2H_2 in Ar mixtures. This means that the absorptivity of C_2H decreases by a similar factor between the two temperatures, because the A values are almost constant over the temperature range measured. We are unaware of any species having such large, temperature-dependent absorptivity.

Table 1 shows the A values, obtained by a least squares fitting for the $A/[C]_0$ and $10^4/T$ relation shown in Fig. 3, and the steady $[C_4H_2]$ and $[C_6H_2]$, obtained by the computer modeling, at 2000 K in different three mixtures. The ratios of the A values, A_m/A_n, are not in accord with the $[C']_m/[C']_n$ values, where subscripts m and n denote the mixture number shown in Table 1 and C' is C_4H_2 or C_6H_2. Although these modeled $[C_4H_2]$ and $[C_6H_2]$ are subject to the values of heat of formation adopted, no clear-cut explanation with appropriate thermochemical data could be given.

There is an electronic transition designated as X→B over the wavelength range 200 to 265 nm for C_4H_2.[15] The reported C_4H_2 profiles in the C_2H_2 pyrolysis measured by TOF mass spectroscopy[4] are similar to the absorption profile of Fig. 1. These results strongly support the conjecture that the steady absorption is mainly due to C_4H_2. The absorptivity of C_4H_2 was evaluated as: $a(\mathrm{cm^2\ mol^{-1}})=(1.1\pm0.3)\times10^7$ at 2000 K and $(1.4\pm0.2)\times10^7$ at 2500 K.

The plateau absorption shown in Fig. 1 indicates that the overall reaction of the C_2H_2 and C_2H_4 pyrolysis reaches an equilibrium under the present experimental conditions; this was confirmed also by the computer modeling. The primary reactions of the C_2H_2 pyrolysis in these temperature ranges are:[6]

$$H + C_2H_2 = H_2 + C_2H \qquad (-13)$$

$$C_2H + C_2H_2 = C_4H_2 + H. \qquad (14)$$

Ethynyl, C_2H, and H play roles as chain carriers in the reactions. An equilibrium between these species leads to an equilibrium for $[C_4H_2]$:

$$[C_4H_2] = K_{-13}K_{14}[C_2H_2]^2/[H_2],$$

where K_{-13} and K_{14} are the equilibrium constants of the reactions, (−13) and (14). The above equation is in accordance with the result shown in Fig. 3 that the presence of H_2 inhibits the formation of C_4H_2, which is one of the precursors to soot.[8] Relative A values in the C_2H_4/Ar mixture are smaller than those in the C_2H_2/Ar mixture. This result also can be explained in the same way. Ethylene decomposes by a molecular reaction fairly rapidly in this temperature range[7] and forms C_2H_2 and H_2 in equal amounts. Therefore, in the C_2H_4/Ar mixture, C_4H_2 is produced by the pyrolysis of C_2H_2 so formed in the presence of H_2. The fact that the measured relative A values in the C_2H_4/Ar and C_2H_2/H_2/Ar mixtures are similar to each other may support the above explanation.

Figure 1 provides us with time parameters whose value can be used as a measure to estimate the overall rate of the C_2H_2 and C_2H_4 pyrolysis. In the conventional manner, the induction time can be defined as: the time between the shock arrival and the foot of the linear absorption rise. If the absorptivity of C_4H_2 is exactly known, the threshold value of $[C_4H_2]$ at the foot can be estimated and compared with the modeled $[C_4H_2]$. But there are still uncertainties in the C_4H_2 absorptivity obtained above. Instead, we defined a parameter, t_m: time between the shock arrival and the crossing point where the linear absorption rise and the steady absorption are extrapolated to each other. The parameter, t_m, so defined is independent of the C_4H_2 absorptivity. The modeled t_m was evaluated from the C_4H_2 profile. First of all, we compared the measured t_m with the modeled one using the mechanism and the rate constants in Table 2 except for the k_{13} value in the C_2H_2/Ar mixture. As for the k_{13} value, $10^{13.54}$ in Ref. 6 was used. Figure 4 shows the relation between $t_m[C_2H_2]_0$ or $t_m[C_2H_4]_0$ and $10^4/T$ for the measured and modeled results. As is shown by the broken line, the modeled t_m was found to be smaller than that measured by a similar factor over the temperature range measured. To confirm the correctness of the interpretations for the

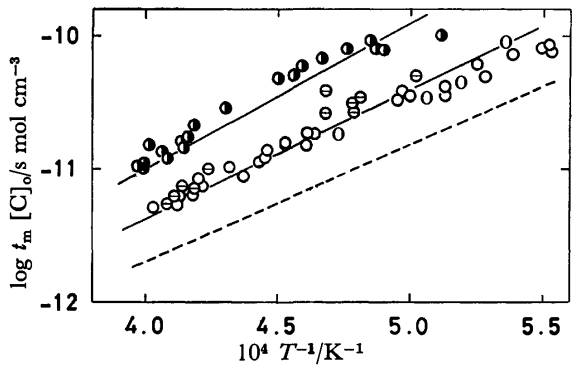

Fig. 4. $t_m[C_2H_2]_o$ or $t_m[C_2H_4]_o$ *vs.* $10^4/T$. The symbols are the same as in Figs. 2a and 2b. The solid lines show modeled value using Table 2 mechanism and rate constants. The upper one is for C_2H_4/Ar mixture and the lower one is for both of C_2H_2/Ar and C_2H_2/H_2/Ar mixtures. The broken line shows modeled value for 3.2% C_2H_2 in Ar mixture using Table 2 mechanism and rate constants except for the k_{13} value: $k_{13}=10^{13.53}$ was used.[6]

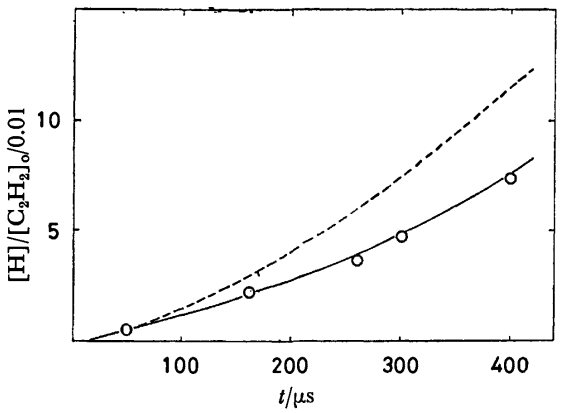

Fig. 5. Comparison measured [H] profile[1] with modeled ones. The circles are data points of measured [H] profile in reflected shock wave for 20 ppm in Ar mixture at $T_5=2450$ K and $[Ar]_5=8.2\times10^{-6}$. The solid and broken lines are modeled values as are in Fig. 4.

present experiment and modeling, another C_2H_2 pyrolysis result was adopted for the modeling.

Gas sampling problems due to boundary layer growth are present in the results obtained by the single pulse shock tube technique.[21] Since TOF mass spectroscopy may also have the same problems, we selected the results obtained by ARAS[1] for the modeling. Figure 5 shows both the measured and the modeled [H] profiles. It is clear that the modeled [H] increasing rate shown by the broken line is larger than the measured one, which is in accordance with the result obtained from Fig. 4, *i.e.*, the modeled overall reaction rate is faster than the measured one.

The first mechanism proposed by Tanzawa and Gardiner,[2] which was derived to explain the high temperature pyrolysis of C_2H_2 in shock waves, could model the results of TOF mass spectroscopy[3,4] and single pulse shock tube[5] fairly well, whereas the new mechanism in Ref. 6 gave rather poor modeling results. The new mechanism in Ref. 6 seems to have an improper

Table 3. Sensitivity spectrum with PS values[a]

Reaction	t_m[b]	$[H]_{100\,\mu s}$[c]	$[H]_{400\,\mu s}$[c]
$C_2H_2+M=C_2H+H+M$	−8/−5[d]	87/97	54/87
$C_2H_2+C_2H_2=C_4H_3+H$	−8/−5	—	—
$C_2H+H_2=C_2H_2+H$	−29/−42	30/47	29/57
$C_2H_2+C_2H=C_4H_2+H$	−3/−18	11/3	25/15
$C_4H_2+M=C_4H+H+M$	−21/−27	—	—

a) PS=log (parameter′/parameter)/log (multiplier)×100. Details are shown in Ref. 22. b) For 3.2% C_2H_2 in Ar mixture, $P_2=0.37$ atm, and $T_2=2200$ K. c) For 50 ppm C_2H_2 in Ar mixture, $P_5=1.77$ atm, and $T_5=2420$ K. d) The first entry is obtained by multiplying each rate constant by 5; the second entry, by 0.2.

value for some rate constant. To find which reaction is responsible to the disageement shown in Figs. 4 and 5, a sensitivity calculation with PS values[22] was tried for our experiment and for the ARAS measurement.[1]

Table 3 shows the reactions having large PS values and the obtained PS values for the parameters. The reaction which has the largest PS values is different in our experiment and in the ARAS experiment. The effect of secondary reactions on the [H] profile is surpressed in the latter case, in which highly diluted test gas mixtures were used, and the measured and modeled [H] profiles reflect the initiation reaction, $C_2H_2+M=C_2H+H+M$, especially at the early stages of the reaction. The PS values of reaction 14 becomes large as the reaction proceeds, in contrast to those of the initiation reaction, while reaction 13 has an almost constant PS values. The time dependent variations of PS values imply that the chain carrier concentrations such as H and C_2H increase and the chain reactions dominate. These effects of the chain reactions on the parameters adopted are very distinct in our experiment.

Reaction 16, $C_4H_2+M=C_4H+H+M$, has the second largest PS values for t_m in our experiment. Frank and Just[1] measured the k_{16} value in the high pressure limit directly by monitoring the [H] profile produced by the C_4H_2 pyrolysis using the ARAS. Although it is possible to derive the k_{16} value suitable for the modeling of our experiment from the reported k_{16} value by making a reduced fall-off curve,[23] we left the k_{16} value used in this study at the value determined indirectly by Tanzawa and Gardiner,[2] through the computer modeling for the laser schlieren experiment because the experimental conditions selected by them are similar to the present ones except for the temperature range.

Since the C_2H_2 pyrolysis is almost equilibrated at the reaction time when the parameter t_m is measured, it is to be expected that reaction 13 has the largest PS values. So only the k_{13} value was changed so as to fit the modeled t_m to the measured over the temperature range measured. An excellent agreement between the experiment and the modeling for the [H] profiles, as well as for the t_m values, was obtained by adopting the following k_{13} value:

$$k_{13} = 10^{12.4}(\mathrm{cm^3\ mol^{-1}\ s^{-1}}).$$

This is shown in Figs. 4 and 5. In our computer

program,[10] reverse rate constant of a given elementary reaction is calculated using an equilibrium constant; an assembly of first order differential equations of both forward and reverse reactions is numerically integrated. Then, when either k_{13} or k_{-13}, where $K_{-13}=k_{-13}/k_{13}$, is incorporated into the reaction mechanism with reasonable thermochemical data, the same modeling results can be obtained. Tanzawa and Gardiner[2] proposed a non-Arrhenius temperature-dependent k_{-13} value in the first mechanism. The k_{13} value so evaluated from the k_{-13} value was found to have exactly the same value at 2200 K as the present k_{13} value. Then, it is not surprising that the k_{13} value obtained in this study is about 10 times smaller than that in Ref. 6.

We note that the modeling result of the C_2H_2 and C_2H_4 pyrolysis is affected by the ΔH°_{f0} value adopted for acetylene and polyacetylene radicals. Two recent papers about the C_2H_2 pyrolysis study[1,2] demonstrated the correctness of the new ΔH°_{f0} for C_2H.[9] As has been shown already, this new value of ΔH°_{f0} for C_2H will be a help to improve the ΔH°_{f0} values for polyacetylene radicals using the additivity rule.[27] The ΔH°_{f0} value for C_4H so derived is 180 kcal†/mol,[1] which is 26 kcal/mol larger than the old value.[13] If the old value for C_4H is adopted, unusual profiles of C_4H_2 and C_4H can be obtained, *e.g.*, steady $[C_4H]$ is larger than steady $[C_4H_2]$.

We have little to say about the C_2H_4 pyrolysis during the early reaction period on the basis of the present experimental results. The computer modeling for the C_2H_4/Ar mixture showed that almost all of C_2H_4 is pyrolyzed to C_2H_2 and H_2 already at the reaction time when the linear absorption starts.

References

1) P. Frank and Th. Just, *Ber. Bunsenges. Phys. Chem.*, **81**, 1119 (1977).

2) T. Tanzawa and W. C. Gardiner, Jr., "17th Int. Symp. Combust.," The Combustion Institute, Pittsburgh (1979), p. 563.

3) J. N. Bradley and G. B. Kistiakowsky, *J. Chem. Phys.*, **35**, 264 (1961).

4) I. G. Gay, G. B. Kistiakowsky, J. V. Michael, and H. Niki, *J. Chem. Phys.*, **43**, 1720 (1965).

5) G. B. Skinner and E. M. Sokoloski, *J. Phys. Chem.*, **64**, 1952 (1960).

6) T. Tanzawa and W. C. Gardiner, Jr., *J. Phys. Chem.*, **84**, 236 (1980).

7) Th. Just, P. Roth, and R. Damm, "16th Int. Symp. Combust.," The Combustion Institute, Pittsburgh (1977), p. 961.

8) R. B. Cundall, D. E. Fussey, A. J. Harrison, and D. Lampard, "Proc. 11th Shock Tube Symp.," Univ. Washington Press, Seattle (1977), p. 375.

9) H. Okabe and V. H. Dibeler, *J. Chem. Phys.*, **59**, 2430 (1973).

10) T. Koike and K. Morinaga, *Bull. Chem. Soc. Jpn.*, **49**, 1457 (1976).

11) W. C. Gardiner, Jr., B. F. Walker, and C. B. Wakefield, "Shock Waves in Chemistry," ed by A. Lifshitz, Dekker, New York (1980), Chap. 1.

12) D. R. Stull and H. Prophet, "JANAF Thermochemical Tables," 2nd ed, NSRDS-NBS 37 (1971).

13) R. S. Duff and S. H. Bauer, *J. Chem. Phys.*, **36**, 1754 (1962).

14) D. B. Olson, T. Tanzawa, and W. C. Gardiner, Jr., *Int. J. Chem. Kinet.*, **11**, 23 (1979).

15) G. Hertzberg, "Molecular Spectra and Molecular Structure," D. Van Nostrand, N. J. (1966), Vol. 3.

16) K. Glänzer, M. Quack, and J. Troe, "16th Int, Symp, Combust.," The Combustion Institute, Pittsburgh (1977). p. 949.

17) T. Tsuboi, *Jpn. J. Appl. Phys.*, **17**, 709 (1978).

18) D. B. Olson, W. G. Mallard, and W. C. Gardiner, Jr., *Appl. Spectrosc.*, **32**, 48 (1978).

19) T. Koike and W. C. Gardiner, Jr., *Appl. Spectrosc.*, **34**, 81 (1980).

20) T. Koike and W. C. Gardiner, Jr., *J. Phys. Chem.*, in press.

21) G. B. Skinner, *Int. J. Chem. Kinet.*, **9**, 863 (1977).

22) W. C. Gardiner, Jr., *J. Phys. Chem.*, **81**, 2367 (1977).

23) J. Troe, *J. Phys. Chem.*, **83**, 114 (1979).

24) M. L. Boyd, T. M. Mu, and M. H. Back, *Can. J. Chem.*, **46**, 2415 (1968).

25) S. W. Benson and G. R. Haugen, *J. Phys. Chem.*, **71**, 1735 (1967).

26) A. L. Myerson and W. S. Watt, *J. Chem. Phys.*, **49**, 425 (1968).

27) S. W. Benson, "Thermochemical Kinetics," 2nd ed, Wiley, New York (1976).

† 1 kcal=4.184 kJ.

  Bull. Chem. Soc. Jpn., 54, 535—539 (1981)

Adsorption of D-, L-, and DL-Phenylalanines at the Mercury-Aqueous Solution Interface

Takashi KAKIUCHI and Mitsugi SENDA*

Department of Agricultural Chemistry, Faculty of Agriculture, Kyoto University, Sakyo-ku, Kyoto 606

(Received July 25, 1980)

The adsorption of D-, L-, and DL-phenylalanines at the mercury-aqueous sodium fluoride solution interface has been studied by measuring differential capacities, potentials of zero charge, pzc, and surface tensions at the pzc. The racemate of phenylalanine showed higher surface activity than the enantiomers. This difference has been interpreted in terms of the intermolecular interactions, orientation and re-orientation of adsorbed molecules at the interface.

In a previous paper[1] we described the adsorption properties of a series of aliphatic α-amino acids at the mercury-aqueous solution interface with reference to two factors, *i.e.*, the contribution of the zwitterion group and that of the hydrocarbon group. This paper reports adsorption behavior of D-, L-, and DL-phenylalanines at the mercury-aqueous solution interface. Our major interest in this study is to investigate a possible difference in the adsorption properties between either of the enantiomers and the racemate. Although in liquid state and in solution a racemate is usually considered to have very similar physicochemical properties to those of the pure enantiomers,[2] the difference between them may become appreciable in the processes involving interfacial phenomena, since the contribution of molecular interaction between chiral adsorbate molecules at the interface is generally much more significant owing to higher concentration and the preferential orientation of adsorbed molecules.

Inesi *et al.*[3] reported on the difference between two adsorption properties of the racemate and the enantiomer at the mercury-aqueous solution interface. They found that DL-dibenzoyltartaric acid is more surface active than the enantiomers. They interpreted this difference by the analogy of surface sate to crystal state. In this paper we describe the difference between the adsorption properties of DL-phenylalanine and D-, or L-phenylalanine at the mercury-aqueous solution interface, interpretation being given in terms of the intermolecular interaction, orientation and re-orientation of adsorbed molecules.

Experimental

The differential capacities of the interface were measured as functions of the phenylalanine concentration and electrode potential with the a.c. bridge method.[1] The bridge was adjusted to balance at the moment when a mercury drop spontaneously fell from the dropping mercury electrode. The drop time was measured as follows. The sudden unbalanced signal from the bridge due to the detachment of the drop from the capillary tip was transformed by a lock-in amplifier into an electric pulse, which was then fed to an electronic counter for pulse interval measurement. Drop times of the capillary used were between 13 and 15 s at the potential of zero charge, pzc, in 0.5 mol l^{-1} sodium fluoride. The a.c. signal superimposed to the electrode was of 1 kHz and 5 mV peak to peak.

The potentials of zero charge were determined by a streaming mercury method.[4] The surface tensions at the pzc were measured by the drop time method. Glass tubes, outer diam 4 mm and inner diam 0.1 mm, were drawn to get fine capillaries having *ca.* 0.5 mm and 0.025 mm outer and inner diameters, respectively. The capillaries were dewetted with a silicone coating reagent (Fuji Systems, Japan) and cut to expose clean orifice and give a suitable drop time. Typical characteristics of the capillaries thus prepared were $t=14$ s and $m=0.3$ mg s^{-1} when the height of mercury was 110 cm and at the pzc in 0.5 mol l^{-1} sodium fluoride. The drop times recorded 30 times for each solution were reproducible within $\pm 0.05\%$ as relative standard deviation. The drop times tended to become shorter over several sets of measurements probably due to deterioration of the capillary glass wall by chemical attack of sodium fluoride solution.[5] Thus, it was necessary to calibrate the capillary before and after each measurement. For the calibration we used 0.05 mol l^{-1} sodium sulfate for which the surface tension of mercury is 426.2 mN m^{-1} at the pzc.[6] For conversion of drop time into surface tension we used the approximate relation $\ln(\gamma/\gamma_r)=K\ln(t/t_r)$, where γ and γ_r are surface tensions for the test and a reference solutions, respectively, proposed by Verdier *et al.*[7] Parameter K is a function of the height of mercury, inner diameter of the capillary and surface tension. However, it can be taken as a constant over a fairly wide range of surface tension when the height of mercury is sufficiently large.[7] For a particular capillary of inner diameter 0.002 cm, the value of K was calculated to be 0.976 over a 390—427 mN m^{-1} range of surface tension when the height of mercury was 110 cm. The average standard deviation of the surface tensions we obtained was 0.15 mN m^{-1}.

A test solution was deaerated by bubbling nitrogen gas through the solution for 30 min before measurement and was kept under nitrogen atmosphere during the course of measurement. The electrode potentials were measured with respect to a saturated calomel electrode, SCE. All the measurements were at 25 ± 0.2 °C.

Reagent grade D-, L-, and DL-phenylalanines(Nakarai Chem. Co., Japan) were recrystallized twice from triple distilled water. Recrystallized D-, and L-phenylalanines showed 95 and 93% optical purity, respectively, in optical rotation measurements. Sodium fluoride, a standard reagent for quantitative analysis of 99.95% purity (Hashimoto Chem. Co., Japan), was used without further purification. An ultra pure grade sodium sulfate (E. Merk, Germany) was used for a standard solution in surface tension measurements.

Results

The potentials of zero charge and the surface tensions at the pzc for seventeen concentrations of L-phenylalanine (0.003—0.120 mol l^{-1}), twelve concentrations of D-phenylalanine (0.010—0.120 mol l^{-1}), and twelve

TABLE 1. POTENTIALS OF ZERO CHARGE, E_{pzc}, AND SURFACE TENSIONS OF MERCURY AT THE PZC, γ_{pzc}, IN CONTACT WITH 0.5 mol l^{-1} AQUEOUS SODIUM FLUORIDE SOLUTION CONTAINING D-, L-, OR DL-PHENYLALANINE AT 25 °C

c/mol l^{-1}	$(-E_{pzc}$ *vs.* SCE)/V			γ_{pzc}/mN m^{-1}		
	D	L	DL	D	L	DL
0.003	—	0.458	—	—	419.1	—
0.004	—	0.460	—	—	417.7	—
0.005	—	0.462	0.459	—	417.0	419.6
0.006	—	0.464	0.463	—	416.2	416.3
0.008	—	0.464	0.466	—	414.8	414.7
0.010	0.469	0.467	0.465	413.7	413.7	413.7
0.012	0.467	0.466	0.467	412.5	412.6	412.7
0.015	0.469	0.467	0.464	411.3	411.6	411.5
0.020	0.467	0.467	0.463	409.8	409.8	410.0
0.025	0.467	0.467	0.464	408.5	408.6	408.7
0.030	0.466	0.465	0.463	407.3	407.7	407.5
0.040	0.462	0.462	0.460	405.7	405.8	405.4
0.050	0.459	0.457	0.456	404.1	404.1	403.8
0.060	0.454	0.452	0.453	402.9	402.8	402.5
0.080	0.447	0.444	—	400.7	400.9	—
0.100	0.441	0.437	—	399.2	399.2	—
0.120	0.432	0.432	—	397.6	397.7	—

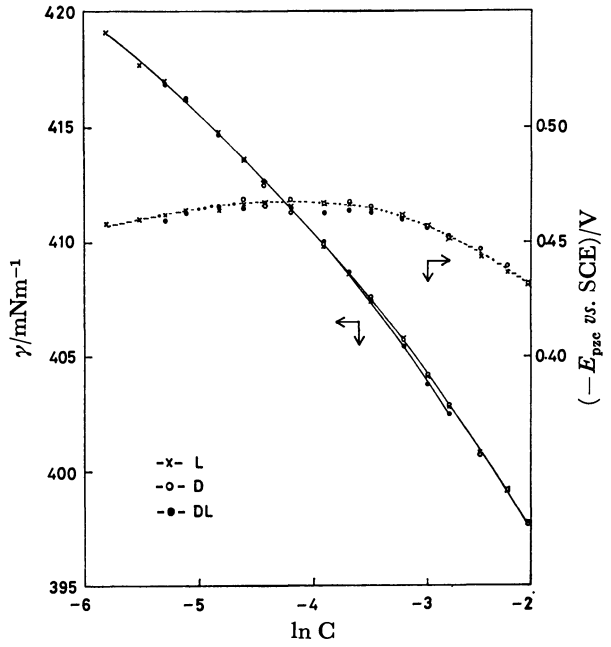

Fig. 1. Potentials of zero charge and surface tensions at the pzc for L-(×), D-(○), and DL-(●) phenylalanines as a function of the logarithm of the phenylalanine concentration in the adsorption on mercury from aqueous 0.5 mol l^{-1} sodium fluoride solutions.

concentrations of DL-phenylalanine (0.005—0.060 mol l^{-1}) in 0.500 mol l^{-1} sodium fluoride are given in Table 1. Due to the limited solubility no data were available beyond 0.06 mol l^{-1} for DL-phenylalanine. Surface tension is plotted in Fig. 1 as a function of the logarithm of phenylalanine concentration. The curves for D-, and L-phenylalanines show excellent agreement over the whole concentration range. At concentration lower than 0.030 mol l^{-1} the curve for DL-phenylalanine is indistinguishable from the curve for both enantiomers. However, with increasing concentration of phenylalanine, it starts to split away from the curve for the enantiomers and lies below them in higher concentration region. This indicates that the racemate is more surface active than the enantiomers.

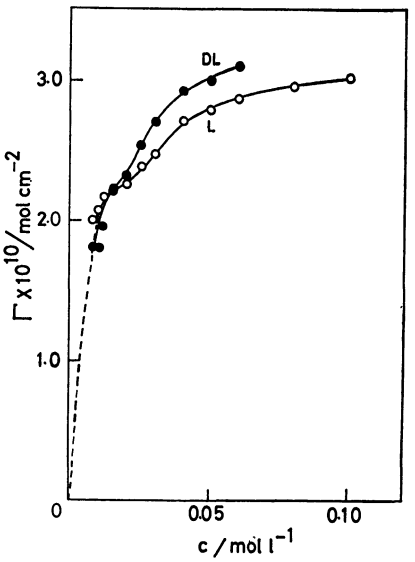

Fig. 2. Adsorption isotherms for L-(○) and DL-(●) phenylalanines at the potential of zero charge.

The surface excesses of L- and DL-phenylalanines, which may be regarded as the actual amount of adsorbed phenylalanines under the present experimental conditions,[8] are plotted in Fig. 2 as a function of the molarity of phenylalanines. As expected, the surface excesses of the racemate are greater than those of the enantiomer. Both these isomers have a kink around 0.02 mol l^{-1} which is characteristic of the change of orientation of adsorbed species at the interface.[9] We have calculated these relative surface excesses from the curves in Fig. 1 using the electrocapillary equation for ideally polarized interfaces.[10] A moving second order least square method[11] with five data points as one set was employed in the numerical differentiation of the curves. Constancy of the activity coefficients of phenylalanines was assumed over the experimental concentration range. The activity of sodium fluoride was also assumed to remain unchanged when the concentration of phenylalanine was varied, though no information is available for the present ternary system to confirm these assumptions. The possible error due to these assumptions[12] is of minor importance in our case since our primary concern here is the difference in the surface excesses between D- or L-phenylalanine and DL-phenylalanine rather than their absolute magnitude.

No significant difference was detected in the potentials of zero charge between the enantiomer and the racemate (Table 1). The potentials of zero charge are plotted against the logarithm of the phenylalanine molarity

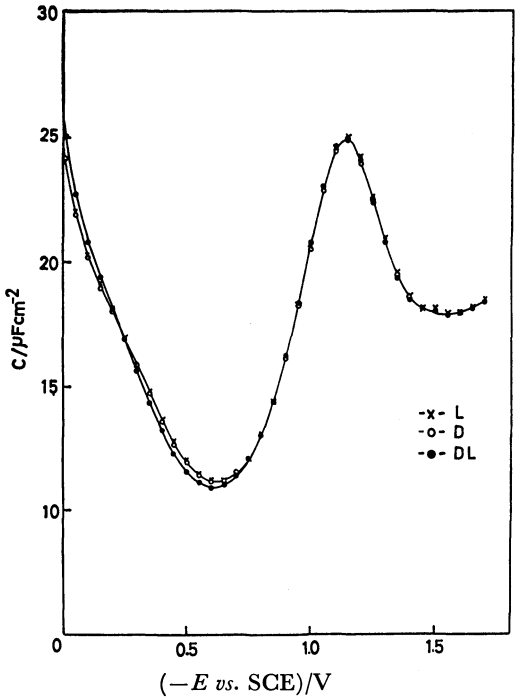

Fig. 3 Comparison of the differential capacity curves for L-(×), D-(○), and DL-(●) phenylalanines in aqueous solution of 0.5 mol l^{-1} sodium fluoride containing 0.05 mol l^{-1} phenylalanine at 25 °C.

in Fig. 1, in which the slopes of the curves change sign with increase in phenylalanine concentration. This suggests the re-orientation of adsorbed phenylalanine molecules with the increase of the surface coverage, as has often been observed in the adsorption of aromatic compounds at electrified interfaces.[13,14]

Differential capacities were measured as functions of the electrode potential and the phenylalanine concentration covering the same range as the surface tension measurements. Comparison is made of the differential capacity curves obtained for D-, L-, and DL-phenylalanines at 0.05 mol l^{-1} in Fig. 3. The curves for D- and L-phenylalanines agree with each other throughout the potential range studied. On the other hand, the curve for the racemate shows appreciable deviation from those curves and lies below them around the pzc. This also indicates the stronger adsorption of the racemate around the pzc than the enantiomers.

In order to estimate the surface excess of phenylalanines at different electrical states of the interface other than the pzc, the differential capacity curves for L- and DL-phenylalanines were twice integrated numerically with respect to the electrode potential. The potentials of zero charge and surface tensitions at the pzc (Table 1) were used as the two independent integration constants. From the electrocapillary curves thus obtained the surface excesses of phenylalanines were calculated as a function of the electrode potential at each phenylalanine concentration. The surface excess *vs.* electrode potential curves for L- and DL-phenylalanines are compared in Fig. 4 at 0.04 mol l^{-1}. The difference between the surface excesses of the racemate and the enantiomer exists not only at the pzc

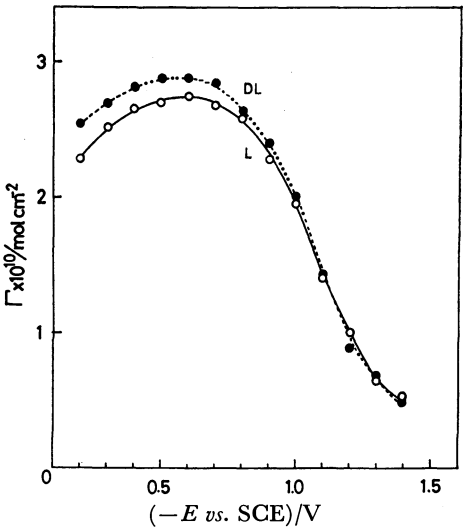

Fig. 4. Comparison of surface excesses of L-phenylalanine with those of DL-phenylalanine at 0.04 mol l^{-1} at various electrode potentials.

but throughout the positive branch, whereas it vanishes at the negative extreme of the potential.

Discussion

Figures 2 and 4 indicate that the racemate of phenylalanine has the higher surface activity than its enantiomers at the mercury-aqueous solution interface in the sense that DL-phenylalanine gives greater surface excess than L- or D-phenylalanine at a given bulk concentration and electrode potential except the cathodic extreme. In Fig. 2 the two isotherms significantly deviate from each other at increased bulk concentrations of phenylalanine, while they merge together with increasing concentration of phenylalanine giving the same limiting slope of the adsorption isotherms at infinite dilution. Similar behavior of adsorption isotherms has been reported by Inesi *et al.*[3] for the adsorption of DL- and D-(and L-)dibenzoyltartaric acids from aqueous solution onto the mercury electrode.

The difference in surface activity should be interpreted in terms of the difference between the adsorption free energy of the racemate and the enantiomers. If we choose the infinite dilution as a reference state of the chemical potentials of phenylalanines in both the adsorption phase and solution phase, the standard adsorption free energy of the racemate should be the same as that of the enantiomers. The difference in surface activity is then ascribed to the difference in the non-ideality due to the intermolecular interactions between the adsorbed phenylalanine molecules. The difference in the interaction energy in the solution phase between racemates and the corresponding enantiomers has been studied theoretically[2,15] and experimentally.[16–18] These works show that the difference in solution phase is negligible in dilute solutions as in our case. Therefore, the observed difference in the adsorbability of phenylalanines should arise from the different molecular interaction in the adsorption phase where the surface concentration of phenylalanine is much

higher than in the solution phase. For example, the surface excess of 3×10^{-10} mol cm^{-2} corresponds to the surface coverage of 0.71 if the maximum surface concentration is assumed to be 4.2×10^{-10} mol cm^{-2}, a value based on CPK model[19] of phenylalanine adsorbed with its aromatic ring plane oriented perpendicular to the mercury surface.

At the lower surface coverage and at the potential around the pzc phenylalanine probably adsorbs with its aromatic ring plane parallel to the electrode surface, as commonly observed in the adsorption of simple aromatic compounds on mercury.[13] This orientation brings the pzc to more negative potential (see Fig. 1) due to the partial charge transfer of π-electron of the aromatic ring to the electrode,[20] while the zwitterion group of phenylalanine may be oriented with its dipole axis parallel to the electrode surface. With increasing surface coverage phenylalanine molecules adsorb with their aromatic ring plane oriented perpendicular to the electrode surface, so that the closer packing of the adsorbed molecules is attained. Since the vertical orientation is unfavorable to the interaction between the π-electron and the electrode, the pzc then shifts to the positive direction[20] with increasing surface excess at the higher surface coverage (Fig. 1).

As an isotherm in which the re-orientation is taken into account, Parry and Parsons[13] and Damaskin[21] have proposed a couple of isotherms assuming that the adsorbate can take two different orientations at the interface;

$$B_1c = \frac{\theta_1}{n_1(1-\theta_1-\theta_2)^{n_1}}\exp(-2n_1a_{11}\theta_1 - 2n_1a_{12}\theta_2)$$

$$B_2c = \frac{\theta_2}{n_2(1-\theta_1-\theta_2)^{n_2}}\exp(-2n_2a_{22}\theta_2 - 2n_2a_{21}\theta_1),$$

where B_i is the adsorption coefficient, θ_i the surface coverage, n_i the ratio of the area occupied by an adsorbate molecule to that of a water molecule and a_{ij} the parameter of intermolecular interactions between adsorbed molecules; indices 1 and 2 are referred to the verical and flat orientations of adsorbed molecules. These isotherms have seven adjustable parameters apart from two maximum surface concentrations, $\Gamma_{m(1)}$ for vertically oriented species and $\Gamma_{m(2)}$ for flatly oriented one and it seems impractical in our case to determine these parameters by fitting experimental data to the theoretical isotherms. Instead, we shall show by invoking these isotherms that the basic features of the experimental adsorption isotherms can be reproduced by choosing probable values for the parameters. Because of the specific interaction between the aromatic π-electron and the mercury surface, the adsorption coefficient of the flatly oriented phenylalanine should be larger than that of the vertically oriented one.[20] We chose the values $B_1=20$ and $B_2=50$ l mol^{-1} and estimated that $n_2/n_1=1.4$ ($\Gamma_{m(1)}=4.3\times10^{-10}$ and $\Gamma_{m(2)}=3.1\times10^{-10}$ mol cm^{-2}) on the basis of the CPK model. The intermolecular interaction would be stronger for the vertical position than the flat position because of the hydrophobic interaction between the adjacent aromatic rings.[20] Hence, we assumed $a_{22}=0.2$ and calculated the isotherms with $a_{11}=1.5$, 1.3, and 1.1 for curves 1, 2, 3 in Fig. 5, in which we further assumed that $n_1=1$ and $a_{12}=a_{21}=0$. The relative surface excesses are plotted against concentration in Fig. 5, from which it is seen that the features of the isotherms are very sensitive to the choice of the interaction parameters. A comparison of Fig. 5 with the experimental isotherms in Fig. 2 suggests that the attractive interaction between the adsorbed phenylalanine molecules is larger for the racemate than for the enantiomers.

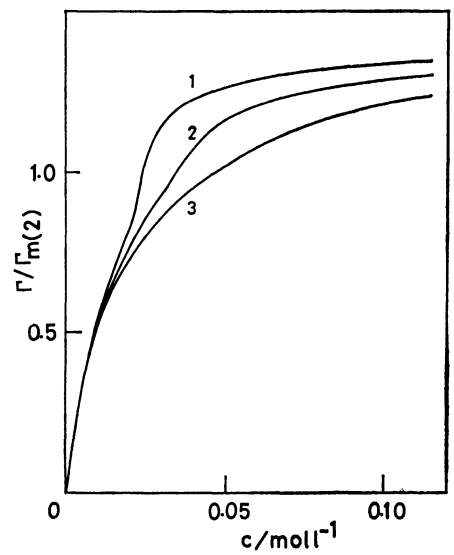

Fig. 5. Calculated curves for reduced adsorption isotherms according to equations in the text with $a_{22}=0.2$, $a_{12}=a_{21}=0$, $n_1=1.0$, $n_2=1.4$, $B_1=20$, $B_2=50$, for $a_{11}=$ 1.5 (1), 1.3 (2), and 1.1 (3).

There are two possible modes in the vertical orientation; one with the axis of the zwitterion group oriented parallel to the electrode and the other with its dipole axis oriented vertical. The former orientation mode should be predominant around the pzc, whereas the latter with the positive end of the dipole facing toward the electrode surface should prevail in the extremely negative branch. In this orientation the dipole would exert repulsive interaction between adsorbed molecules, leading to a smaller value of a_{11} parameter which would give rise to monotonic, Langmuir-type isotherms without kink (curve 3, in Fig. 5). This actually corresponds to the fact that the difference between the surface excess of DL- and D-(or L-) phenylalanines disappears in the cathodic branch away from the pzc (Fig. 4) and also the fact[22] that the adsorption isotherms for L-phenylalanine in the negative extreme have no kink and are well described by Langmuir isotherms which lack the interaction parameter.

References

1) T. Kakiuchi and M. Senda, *J. Electroanal. Chem. Interfacial Electrochem.*, **88**, 219 (1978).
2) H. Mauser. *Chem. Ber.*, **90**, 299, 307 (1957).
3) A. Inesi, F. Rallo, and L. Rampazzo, *Trans. Faraday Soc.*, **64**, 3340 (1968).
4) D. C. Grahame, R. P. Larsen, and M. A. Poth, *J. Am. Chem. Soc.*, **71**, 2978 (1948).
5) A. De Battisti, A. Amadelli, and S. Trasatti, *J. Colloid*

Interface Sci., **63**, 61 (1978).
6) C. A. Smolders and E. M. Duyvis, *Recl. Trav. Chim. Pays-Bas*, **80**, 635 (1961).
7) E. Verdier, R. Grand, and P. Vanel, *J. Chim. Phys.*, **66**, 376 (1969).
8) B. B. Damaskin, O. A. Petrii, and V. V. Batrakov, "Adsorption of Organic Compound on Electrodes," Plenum Press, New York (1971), Chap. 1.
9) B. B. Damaskin, *Eletrokhimiya*, **13**, 816 (1977).
10) D. M. Mohilner, "Electroanalytical Chemistry," ed by A. Bard, Marcel Dekker, New York (1966), Vol. 1, p. 241.
11) P. R. Mohilner and D. M. Mohilner, "Computers in Chemistry and Instrumentation," ed by J. S. Mattson, H. B. Mark, Jr., and H. C. MacDonald, Jr., Marcel Dekker, New York (1972), Vol. 2, p. 3.
12) D. M. Mohilner and H. Nakadomari, *J. Electroanal. Chem. Interfacial Electrochem.*, **65**, 843 (1975).
13) J. M. Parry and R. Parsons, *J. Electrochem. Soc.*, **113**, 992 (1966).
14) K. G. Baikerikar and R. S. Hansen, *J. Colloid Interface Sci.*, **61**, 239 (1977).
15) K. Amaya, *Bull. Chem. Soc. Jpn.*, **34**, 1689 (1961).
16) C. J. McGinn, *J. Phys. Chem.*, **65**, 1896 (1961).
17) S. Takagi, R. Fujishiro, and K. Amaya, *J. Chem. Soc., Chem. Commun.*, **1968**, 480.
18) A. Horeau, *Tetrahedron Lett.*, **1969**, 3121.
19) R. A. Harie, "Molecules in Three Dimensions," Am. Soc. of Biol. Chem., Bethesda, Maryland.
20) Ref. 7, Chap. 3.
21) B. B. Damaskin, *Electrokhimiya*, **5**, 346 (1969).
22) T. Kakiuchi, Thesis, Kyoto University, (1978).

Interaction between Aromatics and Zinc Chloride. III. The Dissociation of Triphenylmethane and 9,10-Dihydroanthracene into Ions

Mikio MORITA,* Kunio HIROSAWA, Toshio SATO, and Koji OUCHI†

Government Industrial Development Laboratory, Hokkaido, Tsukisamu-higashi, Toyohira-ku, Sapporo 061-01

†*Department of Applied Chemistry, Faculty of Engineering, Hokkaido University, Sapporo 060*

(Received January 5. 1980)

Triphenylmethane and 9,10-dihydroanthracene were found to produce colored complexes when placed in contact with molten zinc chloride or with solid zinc chloride pulverized or supported on porous Vycor glass. The triphenylmethane complex gave the same electronic absorption spectrum as that of the triphenylmethyl cation generated by contact with silica–alumina and BF_3 on silica. The 9,10-dihydroanthracene complex exhibited the same electronic absorption band as that of the 9-anthracenium ion produced by the reaction of anthracene with concd H_2SO_4. The reaction of the triphenylmethane complex with deuterium gas provided HD gas and $(C_6H_5)_3CD$. Similarly, the 9,10-dihydroanthracene complex and deuterium gas produced HD gas and 9,10-dihydroanthracene-9-*d*. Furthermore, their colored complexes on the supported zinc chloride gave a very weak IR absorption band at about 1720 cm^{-1}, which is interpreted as corresponding to the formation of a Zn–H bond. These observations led us to conclude that triphenylmethane and 9,10-dihydroanthracene dissociate into ions upon contact with zinc chloride:

$$(C_6H_5)_3CH + n ZnCl_2 \rightleftharpoons (C_6H_5)_3C^+(ZnCl_2)_n^-H$$

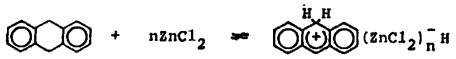

As has previously been reported,[1,2] zinc chloride reacts with aromatic hydrocarbons to form (Ar^+)-$(ZnCl_2)_n^-$ electron-donor acceptor-complexes(Ar: aromatics). It has been suggested that these (Ar^+)-$(ZnCl_2)_n^-$ EDA-complexes act as reaction intermediates in the hydrogenation and hydrocracking of aromatic hydrocarbons over a zinc chloride catalyst; their conversions are correlated positively to the ionization potentials of the corresponding aromatic hydrocarbons.[3]

As a part of a systematic study to elucidate the behavior of the zinc chloride catalyst in the hydrocracking of aromatic hydrocarbons, which would be helpful for this reaction,[4,5] the mechanism of the ionization of triphenylmethane and 9,10-dihydroanthracene was investigated by measurements of the electronic and IR absorption spectra of the colored complexes formed in molten zinc chloride or on solid zinc chloride, which was powdered or supported on porous Vycor glass, by means of exchange reactions with deuterium gas and by the analyses of their reaction products.

Experimental

Materials. Triphenylmethane and 9,10-dihydroanthracene of a G. R. grade were used without further purification. Porous Vycor glass plate and powder were used as supports of the zinc chloride for measuring the IR and electronic absorption spectra. The other chemicals were the same as those mentioned in our previous work.[2]

Apparatus and Procedure. Anhydrous zinc chloride was prepared and attached onto a porous Vycor glass support as described in the previous paper.[2] Triphenylmethane or 9,10-dihydroanthracene was allowed to react with zinc chloride under various conditions, and changes in the transmittance or in the reflectance of visible light by the colored complexes were measured with a Hitachi 624 spectrophotometer equipped with an integrating sphere.

For the measurements of the IR absorption spectra, a cell device designed by Angel *et al.*[6] and Hino[7] was used. A rod of porous Vycor glass was sliced into a plate with 0.3 mm thick, and then it was cut to fit the cell windows. After zinc chloride and a plate purified by the method described previously[2] has been introduced into the cell device, the device was evacuated to below 10^{-4} Torr at about 500 °C until 10—20 wt % of the zinc chloride had evaporated onto the plate. The cell was then cooled to room temperature, and a hydrocarbon was introduced from the top of the cell under a vacuum and brought to full contact with the supported zinc chloride at the reaction temperature until colored products formed on the catalyst. The IR absorption spectra were measured with a JASCO IRA-2 spectrophotometer.

For the D_2-exchange reaction, a glass vessel 17 ml in size was used as a reactor. About 3 g of dehydrated zinc chloride or 500 mg of supported zinc chloride and about 5 mg of a reactant were charged into the vessel under a vacuum, and then deuterium gas was introduced at 600 Torr. The vessel was heated at a given temperature for a given time.

Analysis. After the measurements of the electronic absorption spectra of the colored products, water was introduced into the quartz cell and the mixture was extracted with a large amount of tetrahydrofuran and dichloromethane. The extracts were analyzed by gas chromatography. The details were described in a previous paper.[8]

The D_2-exchanged products were identified by the use of a Finnigan 3000 mass spectrometer. The formation of HD gas was confirmed by the method reported by Sato *et al.*[9]

Results and Discussion

Electronic Absorption Spectra. Triphenylmethane produced a colored complex upon contact with dehydrated solid zinc chloride, anhydrous zinc chloride supported on porous Vycor glass, and porous Vycor glass alone pretreated at 550 °C. The complex exhibited a characteristic double-peaked absorption band in the 415—450 nm region of the spectrum, as is shown in Figs. 1(a)—(d). The (a) spectrum was obtained by measuring the reflectance of the triphenylmethane

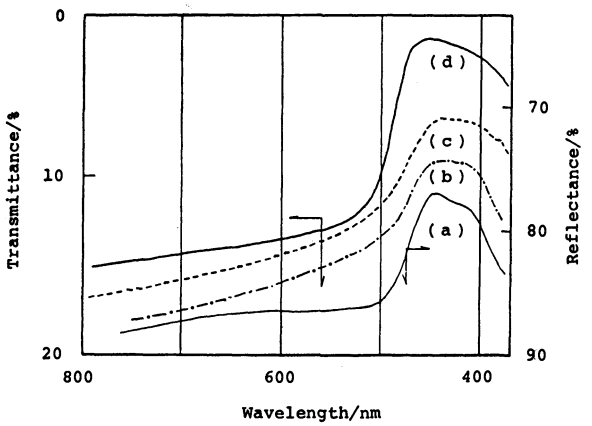

Fig. 1. Electronic spectra of triphenylmethane on zinc chloride, supported zinc chloride, and a support.
(a): On solid zinc chloride which was dehydrated by melting under a vacuum, at room temperature for 7d, (b): on powdered zinc chloride which was dehydrated at 250 °C for 3 h under a vacuum, at 220 °C for 10 min, (c): on porous Vycor glass pretreated at 550°C, at 70°C for 180 min, (d): on anhydrous zinc chloride supported on porous Vycor glass, at room temperature for 20 h.

yellow intermediate formed on the solid zinc chloride dehydrated by melting under a vacuum in a quartz cell. The spectra from (b) to (d) were measured for the transmittance of the yellow complex developed on the powdered zinc chloride, the pulverized porous Vycor glass, and the supported zinc chloride. This double-peaked absorption band disappeared when the complex was treated with water vapor.

9,10-Dihydroanthracene also gave a yellow intermediate upon contact with anhydrous zinc chloride supported on porous Vycor glass or with molten zinc chloride. It exhibited a strong absorption band at 420 nm and a weak absorption band at about 725 nm, as is shown in Fig. 2(a) and in Fig. 3(a), when reacted with supported zinc chloride at 60 °C for 10 min and with molten zinc chloride at about 300 °C for 5 min. The further reaction over supported zinc chloride at temperatures higher than 60 °C decreased the reflectance of the samples and altered the spectrum from that shown in Fig. 2(a) to that of Fig. 2(c). It is noteworthy in these spectra that the band at 420 nm was common, but the weak band at 725 nm disappeared with the progress of the reaction.

The treatment of porous Vycor glass alone, pretreated at 550 °C, with 9,10-dihydroanthracene at temperatures higher than 200 °C also gave a colored product. Its absorption spectrum is shown in Fig. 3(b).

The common band at 420 nm (Fig. 2(a) to (b) and Fig. 3(a)) disappeared when the products were decomposed with water. However, when the colored products obtained at higher temperatures, whose electronic absorption spectra are shown in Fig. 2(c) and Fig. 3(b), were decomposed with water, other, new colored products were recovered. The electronic absorption spectrum of the products in dichloromethane solution is shown in Fig. 3(c).

IR Absorption Spectra. Figures 4(a) and (b) are the IR absorption spectra of colored complexes of

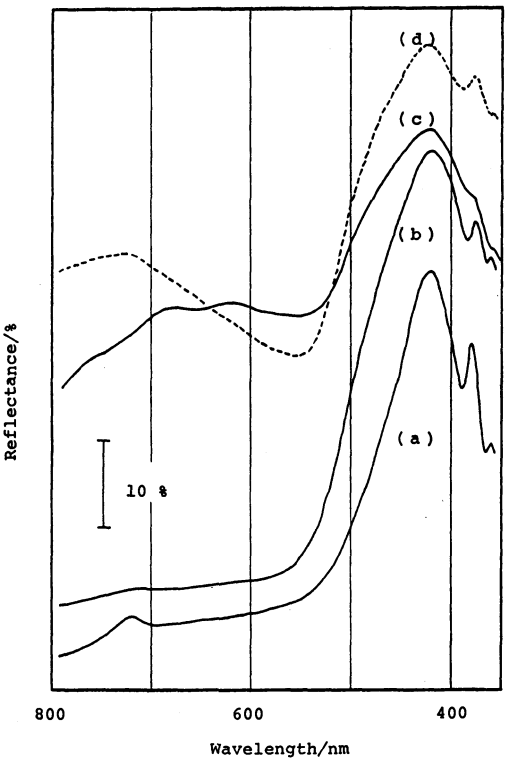

Fig. 2. Change in electronic spectra of colored products of 9,10-dihydroanthracene and anthracene on supported zinc chloride.
9,10-Dihydroanthracene; (a) at 60 °C for 10 min, (b) at 80 °C for 20 min, (c) at 100 °C for 30 min, anthracene; (d) at 60 °C for 10 min.

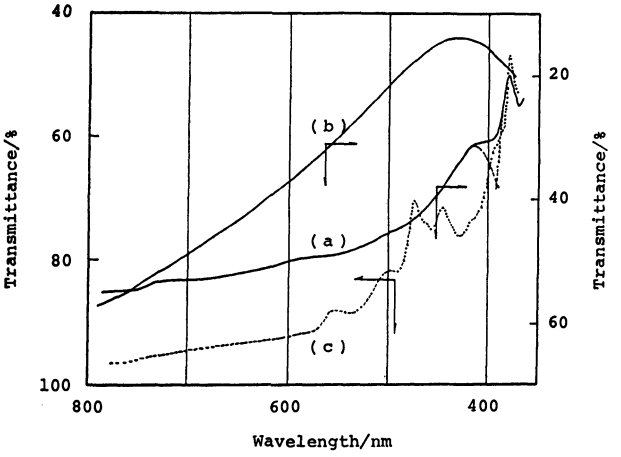

Fig. 3. Electronic spectra of 9,10-dihydroanthracene in molten zinc chloride (a) and on porous Vycor glass (b), and of polycondensed products of 9,10-dihydroanthracene formed on the supported zinc chloride and on the support (c) (in dichloromethane solution).

triphenylmethane and 9,10-dihydroanthracene absorbed on zinc chloride supported on porous Vycor glass platelets.

In these spectra, the intensity of the stretching vibration band of the aliphatic C–H relative to that of the aromatic C–H of the colored complexes seemed to be slightly smaller than that of the original molecule

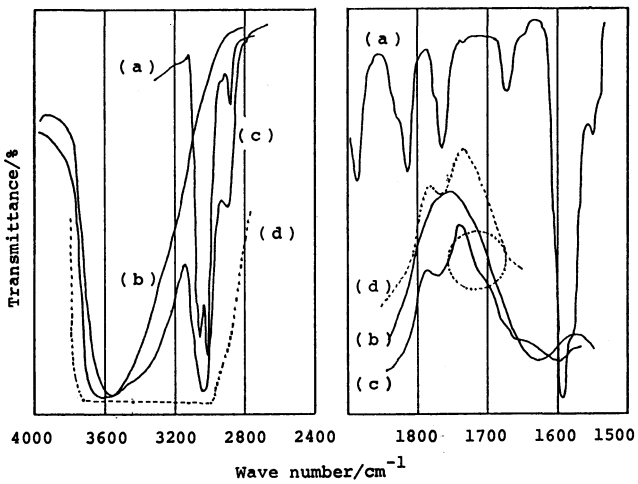

Fig. 4(a). Change in IR spectra of colored products of triphenylmethane on supported zinc chloride.
(a) Triphenylmethane on KBr, (b): zinc chloride on porous Vycor glass, (c): colored products on the catalyst after the reaction, (d) after decomposition of the colored products with water vapor.

on KBr, and the intensity of the OH groups on the silica surface increased more than that of the original. Furthermore, a very weak new absorption band appeared at about 1720 cm^{-1} for each complex. This band disappeared when the intermediates came in contact with water vapor, whereas none of the other bands, except those at 3600 cm^{-1} and 1620 cm^{-1}, changed (these two bands increased upon this water-contact).

Reaction Products. Triphenylmethane was the only identifiable product from the decomposition of its colored intermediate with water. This observation indicates that no reaction other than colored-complex formation took place on the catalyst under the present conditions.

Table 1 summarizes the analyses of the products obtained after the decomposition of 9,10-dihydroanthracene–zinc chloride colored complexes with water; these complexes had been produced by the reaction of 5 mg of the compound with 500 mg of the supported zinc chloride at various reaction temperatures for varying periods.

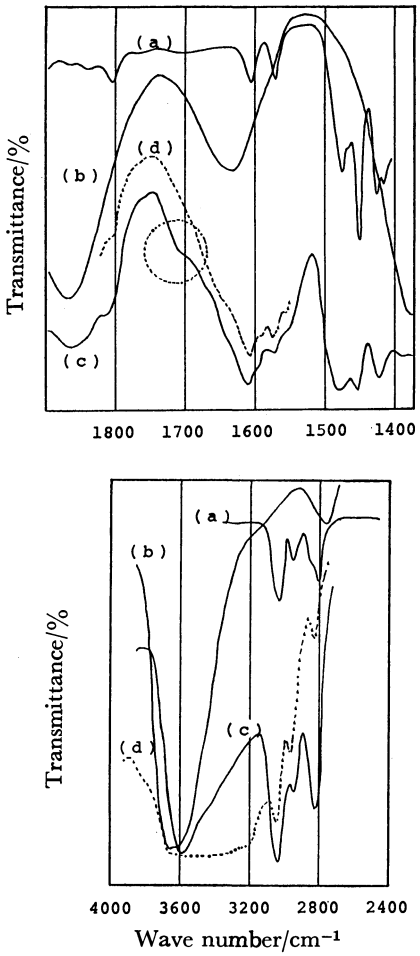

Fig. 4(b). Change in IR spectra of colored products of 9,10-dihydroanthracene on supported zinc chloride.
(a): 9,10-dihydroanthracene on KBr, (b): zinc chloride supported on porous Vycor glass, (c): colored products on the catalyst after the reaction, (d): after decomposition of the colored products with water vapor.

The electronic absorption spectra of the 9,10-dihydroanthracene-zinc chloride complexes were similar to those shown in Fig. 2(a) to (c). The products obtained below 100 °C were identified as anthracene and 1,2,3,4-tetrahydroanthracene, in nearly a 1 : 1 mol ratio. This observation indicates that the main reaction at

Table 1. Results of the decomposition of 9,10-dihydroanthracene over zinc chloride supported on porous Vycor glass

Reaction conditions: Sample/Catalyst=5mg/500 mg, Pressure 10^{-4} Torr.

Catalyst	Temp °C	Time min	9,10-Dihydroanthracene	Product distribution (wt%) 1,2,3,4-Tetrahydroanthracene +1,2,3,4-Tetrahydrophenanthrene	Anthracene
Zinc chloride on Vycor glass	150	10	39.1	34.4	26.5
	100	30	59.5	19.9	20.6
	80	90	65.9	16.2	17.9
	60	90	86.7	6.2	7.1
Vycor glass	200	5	39.6	2.9	57.5

(Hydrogen gas and condensed compounds of 9,10-dihydroanthracene or of anthracene were confirmed as the other products at reaction temperatures higher than 100 °C. Although the analytical results fluctuate somewhat, they are enough to suggest the formation of some active species of 9,10-dihydroanthracene in the course of the reaction.)

temperatures lower than 100 °C is the disproportionation of 9,10-dihydroanthracene. When this substrate was treated at temperatures higher than 100 °C, hydrogen gas, anthracene dimers, and other polycondensed products, including anthracene and 1,2,3,4-tetrahydroanthracene (together with an unnegligible amount of 1,2,3,4-tetrahydrophenanthrene), were identified by gas and liquid chromatography, and by mass spectrometry. That is, at higher temperatures, the dehydrogenation of 9,10-dihydroanthracene and the condensation of 9,10-dihydroanthracene and anthracene occurred in addition to the disproportionation. The electronic spectrum of Fig. 3(c) can be attributed to some condensed polymers of 9,10-dihydroanthracene or anthracene.

The electronic-absorption spectrum of 9,10-dihydroanthracene in molten zinc chloride is reproduced in Fig. 3(a). This complex gave hydrogen gas and anthracene as the major products, in addition to 1,2,3,4-tetrahydroanthracene as a minor product. In this instance, the main reaction is the dehydrogenation of 9,10-dihydroanthracene.

9,10-Dihydroanthracene over porous Vycor glass alone pretreated at 550 °C was converted mainly to hydrogen gas and anthracene (Table 1). The main reaction is dehydrogenation.

D_2-exchanged Products. About 5 mg of triphenylmethane was treated with 600 Torr of deuterium gas at 280 °C for 3 h in the presence of 3 g of dehydrated zinc chloride. The products were $(C_6H_5)_3CD$ (15%) and HD. Similarly, 9,10-dihydroanthracene gave 13% of 9,10-dihydroanthracene-9-*d*, 8% of 1,2,3,4-tetrahydroanthracene (including deuterated derivatives), and 57% of anthracene (including deuterated derivatives). HD was also formed.

The treatment of 9,10-dihydroanthracene with 600 Torr of deuterium gas at 120 °C for 3 h over the supported zinc chloride also produced about 8% of 9,10-dihydroanthracene-9-*d*, 43% of 1,2,3,4-tetrahydroanthracene (including deuterated derivatives), 21% of anthracene (including deuterated derivatives), HD, and polycondensed products.

A glass wall or porous Vycor glass alone did not promote this D_2-exchange reaction under the same conditions.

Dissociation into Ions. The double-peaked absorption band at about 450 nm of a colored product from triphenylmethane is also present in the spectrum of the triphenylmethyl cation produced by the reaction of triphenylmethane with silica–alumina and BF_3 on silica.[10] We confirmed that HD and triphenylmethane-1-*d* were the products in the reaction of triphenylmethane with D_2 gas on the zinc chloride. These results lead us to the conclusion that the triphenylmethane absorbed on zinc chloride dissociates into ions as follows:

$$(C_6H_5)_3CH \rightleftarrows (C_6H_5)_3C^+ + H^-.$$

Portions of the hydride ions formed by this reaction may be supposed to be chemisorbed on the Lewis-acid centers of the zinc chloride catalyst, judging from a new, weak absorption band at 1720 cm^{-1} which is interpreted as arising from the Zn–H bond (Fig. 4(a)).[11] It was also found that the IR spectrum of triphenylmethane absorbed on zinc chloride/porous Vycor glass showed a marked absorption at about 3600 cm^{-1} of the OH groups on the silica surface; this is known to be depend on hydrogen bonding between the surface hydroxyl groups and the adsorbate,[12] but H^- ions might contribute to the formation of the OH groups on the silica surface. This should further be investigated. However, triphenylmethane on zinc chloride, even if it is not supported on porous Vycor glass, substantially dissociates into ions. Therefore, the ionization of triphenylmethane on zinc chloride can be represented as follows:

$$(C_6H_5)_3CH + n ZnCl_2 \rightleftarrows (C_6H_5)_3C^+(ZnCl_2)_n^-H.$$

9,10-Dihydroanthracene absorbs strongly at 420 nm and weakly at about 725 nm on the supported zinc chloride upon their first contact (Fig. 2(a)). Similarly, it gives the same absorption bands in molten zinc chloride (Fig. 3(a)).

Anthracene–zinc chloride complexes may be supposed to be formed, for anthracene was confirmed as an impurity of the sample and a reaction product. Therefore, the present band at 725 nm corresponds to that of the anthracene cation radical, for the anthracene–zinc chloride complexes absorb at 430 nm and at 730 nm (Fig. 2(d)), the absorption bands of which are assigned to the anthracene–zinc chloride EDA-complex and the anthracene cation radical respectively.[2] However, the band at 725 nm disappeared with increases in the contact time and the temperature, whereas the position of the band at 420 nm almost did not change. On the other hand, anthracene in concd H_2SO_4 impregnated with porous Vycor glass gave electronic absorption bands at 420 nm and at 725 nm, as is shown in Fig. 5. They are assigned to the 9-anthracenium ion and the anthracene cation radical respectively.[13,14] We may note here that the absorption band at 420 nm of the present complex is strikingly similar to that of the 9-anthracenium ion. Moreover, this band is distinctly different from the characteristic absorption band of the anthracene–zinc chloride EDA complex with regard to the strength of the absorption and the position of the peak. As has been mentioned above, it was found

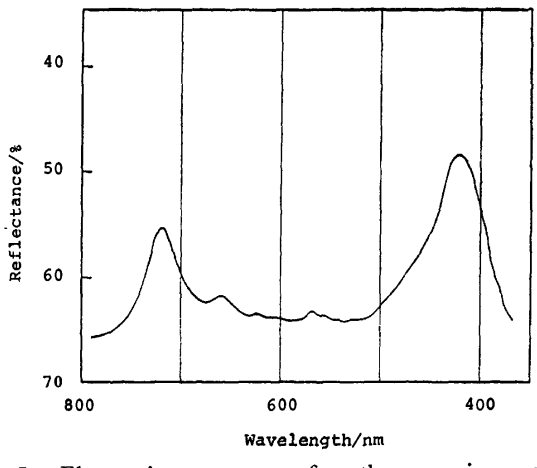

Fig. 5. Electronic spectrum of anthracene in concd H_2SO_4 impregnated with porous Vycor glass.

that aliphatic hydrogen of 9,10-dihydroanthracene is so mobile on zinc chloride that it can be exchanged with D_2 gas, that 9,10-dihydroanthracene decomposes into anthracene and 1,2,3,4-tetrahydroanthracene, and that zinc chloride abstracts the hydride ion from 9,10-dihydroanthracene. A colored 9,10-dihydroanthracene–zinc chloride complex formed on porous Vycor glass platelets also gave a weak absorption band at 1720 cm^{-1}. This can also be interpreted as an H^- ion from 9,10-dihydroanthracene being chemisorbed on Lewis acid centers of zinc chloride.

The results presented above lead us to the conclusion that 9,10-dihydroanthracene dissociates on zinc chloride as follows:

The disappearance of the anthracene cation radical at the early stage of the reaction can be explained if one assumes the following reaction:

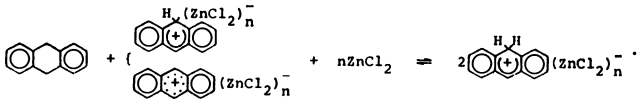

The yellow complexes of triphenylmethane and 9,10-dihydroanthracene, which were formed at higher temperatures on porous Vycor glass pretreated at 550°C under a vacuum, are also supposed to be triphenylmethyl cations and 9-anthracenium ions respectively, but further investigation should be carried out before an assignment can be made certainly.

References

1) M. Morita, K. Hirosawa, and T. Sato, *Bull. Chem. Soc. Jpn.*, **50**, 1256 (1977).
2) M. Morita, K. Hirosawa, T. Sato, and K, Ouchi, *Bull. Chem. Soc. Jpn.*, **53**, 3013 (1980).
3) M. Morita and K. Hirosawa, *Nippon Kagaku Kaishi*, **1975**, 1555.
4) C. W. Zielke, R. T. Struck, J. M. Evans, C. P. Costanza, and E. T. Gorin, *Ind. Eng. Chem., Process Des. Dev.*, **5**, 151 (1966).
5) M. Morita and K. Hirosawa, *Nenryo Kyokai Shi*, **54**, 675 (1975).
6) C. L. Angell and P. C. Schaffer, *J. Phys. Chem.*, **67**, 1621 (1965).
7) M. Hino, *Bull. Chem. Soc. Jpn.*, **50**, 574 (1977).
8) M. Morita and K. Hirosawa, *Nippon Kagaku Kaishi*, **1976**, 1259.
9) T. Sato, S. Okoshi, and T. Takahashi, *J. Chromatogr.*, **65**, 413 (1972).
10) H. P. Leftin and M. C. Hobson, *Adv. Catal.* **14**, 115 (1963).
11) R. P. Eischens, M. A. Pliskin, and M. J. D. Low, *J. Catal.*, **1**, 180 (1962).
12) M. R. Basila, *J. Chem. Phys.*, **35**, 1151 (1961).
13) V. Gold, B. W. V. Hawes, and F. L. Tye, *J. Chem. Soc.*, **1952**, 2172.
14) W. K. Hall, *J. Catal.*, **1**, 53 (1962).

  Bull. Chem. Soc. Jpn., 54, 545—548 (1981)

The Solubility Curves of Water in Normal Alkane Derivatives with a Polar Group

Nobuo NISHINO* and Masao NAKAMURA

Department of Chemistry, Faculty of Science, Tokai University, 1117 Kitakaname, Hiratsuka 259-12

(Received May 15, 1980)

Measurements were made of the solubility *vs.* temperature curves of water in normal alkane derivatives: alkanols, alkylamines, and alkanoic acids. The solubility of water increases monotonically with an increase in the temperature in alkanols and alkanoic acids, while it decreases in alkylamines. The solubility is so great that it often exceeds 1/2 in the mole fraction scale. Phase diagrams were constructed by combining such solubility curves with the solubility curves of these substances in water. The heat of solution at an infinite dilution *vs.* the temperature for 1-butanol in water is obtained by taking account of the activity coefficient of 1-butanol in its own phase.

When an organic substance containing a hydrophobic group, such as an alkyl group, is introduced to water, the water is considered to change in structure and to form an iceberg around the molecule, which breaks down gradually with a rise in the temperature.[1] As a result, such an aqueous solution shows various complicated phenomena.[2] The present authors have found that a minimum commonly exists on the solubility *vs.* temperature curve for normal alkane derivatives in water, such as alkanols, alkylamines, and alkanoic acids.[3] The heat of solution at an infinite dilution, which is the difference between the partial molar enthalpy of a solute at an infinite dilution and the molar enthalpy in its pure state, serves to elucidate the dissolution state of the solute molecule energetically.[4] The heat of solution at an infinite dilution should be obtained thermodynamically from the phase diagram of the solute and solvent if both phases at equilibrium are ideal. In order to construct the phase diagram for the binary system of water and an organic substance, it is necessary to know the mutual solubility *vs.* temperature curves, *i.e.*, the solubility curves, of the organic compound in water as well as of water in the organic phase. Measurements have not been made of the solubility of water in most normal alkane derivatives, whose solubility curves in water have been measured in a previous paper.[3]

Experimental

The materials used were the same as those described in a previous paper.[3] Twenty to thirty glass ampoules containing various compositions around the solubility of water at room temperature were immersed in a water thermostat. The distinction between clear and turbid ampoules was made after a time long enough for equilibrium to be established, say, *ca.* 2 h, at each temperature.

The behavior of the binary system of 1-pentanol and water is presented as an example in Fig. 1; here an open circle shows the most water-rich composition among the clear ampoules at each temperature and a solid one, the most 1-pentanol-rich among the turbid ones. The solubility curve is drawn smoothly between open and solid circles. The solubility curves for other compounds are similarly precise.

Results and Discussion

The solubility curves of water in the organic phases measured are expressed as the mole fraction of water,

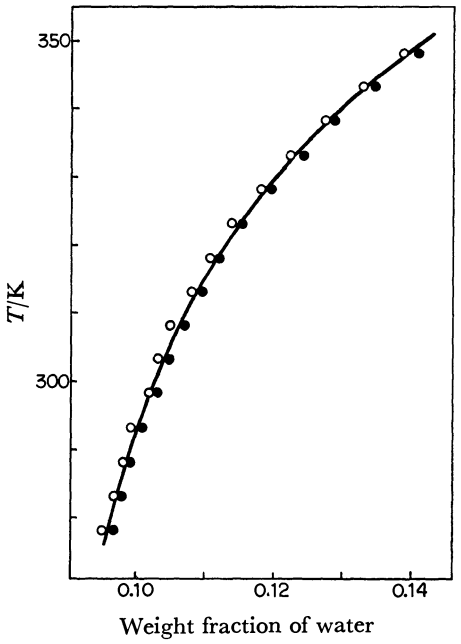

Fig. 1. Solubility behavior of water in 1-pentanol.
○: The most water-rich composition in clear ampoules,
●: the most 1-pentanol-rich composition in turbid ampoules.

x_1^{or}, *vs.* the temperature, T, in Figs. 2 and 3. The solubility of water in either hexylamine or heptylamine could not be determined below 293 or 307 K, because these mixtures were in jelly-like states at the lower temperatures. A large amount of water dissolves in each organic phase, and x_1^{or} exceeds often 1/2; this is natural, as it has been expected that the solubility of water in an organic liquid is more than that of the organic compound in water, because the molar volume of water is generally less than that of an organic liquid.[5] Particularly, hexylamine can decrease to as low as 0.10 in the mole-fraction scale in its own phase at 300 K. As expected, the greater solubility of water is seen in the compound with the smaller number of carbon atoms in a homologous series at a given temperature.

The solubility of water increases monotonically with a rise in the temperature in alkanols and alkanoic acids, while it decreases in alkylamines. The increase is steeper in alkanoic acids than in alkanols. Such behavior is significantly different from that of these substances in water.[3] When ln x_1^{or} is plotted against T^{-1}, the curve

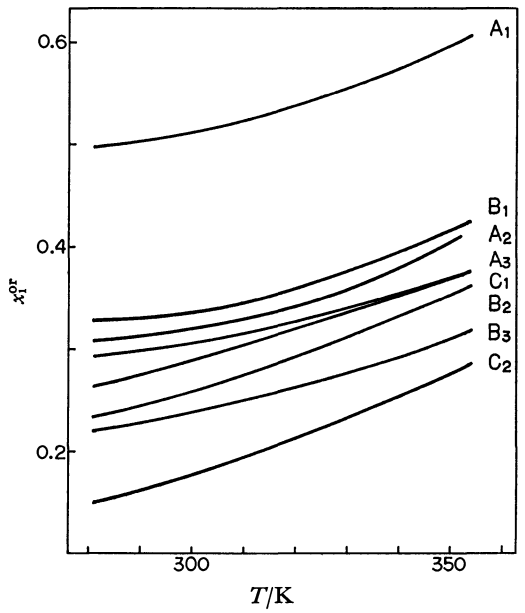

Fig. 2. Solubility curve of water in alkanols.
A_1: 1-Butanol, A_2: 1-pentanol, A_3: 1-hexanol, B_1: 2-pentanol, B_2: 2-hexanol, B_3: 2-heptanol, C_1: 3-pentanol, C_2: 3-hexanol.

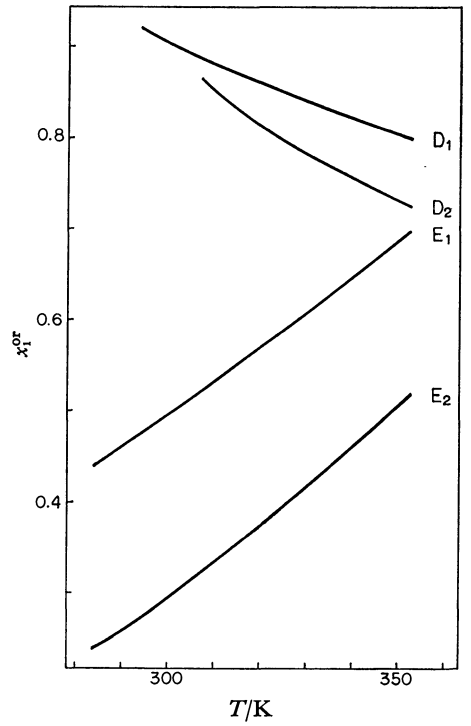

Fig. 3. Solubility curve of water in alkylamines and alkanoic acids.
D_1: Hexylamine, D_2: heptylamine, E_1: pentanoic acid, E_2: hexanoic acid.

does not deviate very much from a straight line for any compound. This fact reveals that the structure in an organic phase does not change with the temperature so remarkably as in an aqueous phase.

The phase diagrams of the binary systems of water and one of these substances are shown in Figs. 4, 5,

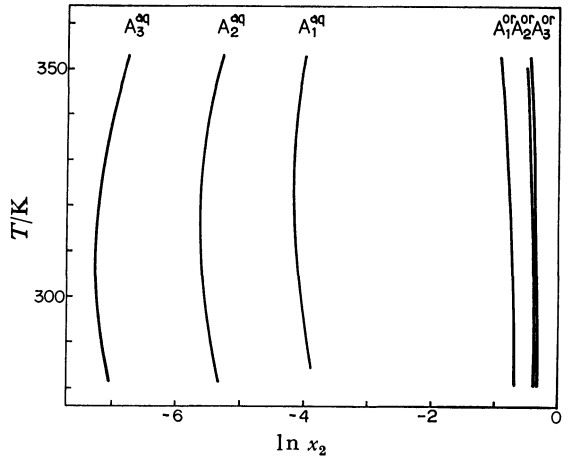

Fig. 4. Phase diagram of the binary system of water and 1-alkanol expressed as temperature *vs.* the natural logarithm of mole fraction of organic substance.
Superscripts aq and or denote aqueous and organic phases, respectively.

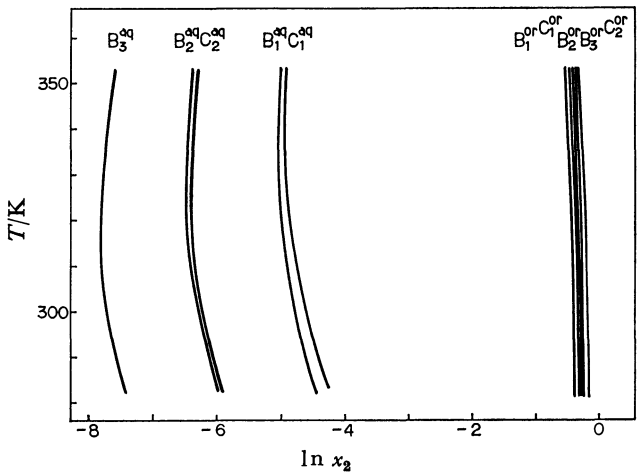

Fig. 5. Phase diagram of the binary system of water and 2- or 3-alkanol expressed as temperature *vs.* the natural logarithm of mole fraction of organic substance.

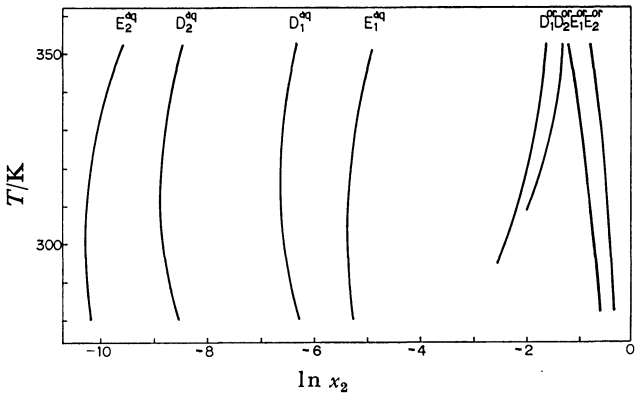

Fig. 6. Phase diagram of the binary system of water and alkylamine or alkanoic acid expressed as temperature *vs.* the natural logarithm of mole fraction of organic substance.

and 6, which were constructed by combining the solubility curves of water in Figs. 2 and 3 with the solubility curves of the substances in water reported in a previous paper.[3] The abscissa expresses the natural logarithm of the mole fraction of an organic compound. The region between two solubility curves corresponds to the turbid two-phase region; outside of this region there are clear one-phase regions.

In order to know the states of an organic substance in water, it is useful to estimate the heat of solution at an infinite dilution of the organic substance in water, $\Delta_s h_2^\ominus$.[4] If the system consists of water and an organic substance, the chemical potential of the organic substance, either in the aqueous phase, μ_2^{aq}, or in the organic one, μ_2^{or}, may be generally expressed by:[6]

$$\mu_2^{aq} = \mu_2^{\ominus aq}(T,p) + RT \ln x_2^{aq}\gamma_2^{aq}$$

and:

$$\mu_2^{or} = \mu_2^{\circ}(T,p) + RT \ln x_2^{or}\gamma_2^{or}.$$

When both phases are mutually saturated ($\mu_2^{aq}=\mu_2^{or}$), $\Delta_s h_2^\ominus$ can be expressed generally as:

$$\Delta_s h_2^\ominus = h_2^{\ominus aq} - h_2^{\circ} = \left[\frac{\partial\{\mu_2^{\ominus aq}(T,p) - \mu_2^{\circ}(T,p)\}T^{-1}}{\partial T^{-1}}\right]_p$$

$$= R\left[\frac{\partial \ln(x_2^{or}\gamma_2^{or}/x_2^{aq}\gamma_2^{aq})}{\partial T^{-1}}\right]_{p,sat.}, \quad (1)$$

where $\mu_2^{\ominus aq}(T,p)$ and $h_2^{\ominus aq}$ are the chemical potential and the partial molar enthalpy of the organic substance in the aqueous phase at an infinite dilution at a certain temperature, T, and pressure, p, where $\mu_2^{\circ}(T,p)$ and h_2° are the molar Gibbs free energy and enthalpy in its pure state, where x_2^{aq} and x_2^{or} ($=1-x_1^{or}$) are the mole fractions of the organic substance in aqueous and organic phases at mutual saturation, where γ_2^{aq} and γ_2^{or} are the activity coefficients of the substance in aqueous and organic phases, with reference to the infinite dilution and to the pure state respectively, and where R is the gas constant. When the aqueous phase is dilute enough to be an ideal solution ($\gamma_2^{aq}=1$), Eq. 1 is reduced to:

$$\Delta_s h_2^\ominus = R\left[\frac{\partial \ln(x_2^{or}\gamma_2^{or}/x_2^{aq})}{\partial T^{-1}}\right]_{p,sat.}. \quad (2)$$

When the organic phase is also ideal ($\gamma_2^{or}=1$), Eq. 2 gives:

$$\Delta_s h_2^\ominus = R\left[\frac{\partial \ln(x_2^{or}/x_2^{aq})}{\partial T^{-1}}\right]_{p,sat.}. \quad (3)$$

If, further, the amount of water in the organic phase in equilibrium with the aqueous phase is either zero or independent of the temperature, Eq. 3 is reduced to:

$$\Delta_s h_2^\ominus = -R\left[\frac{\partial \ln x_2^{aq}}{\partial T^{-1}}\right]_{p,sat.}. \quad (4)$$

Equation 4 has frequently been used to obtain the heat of solution from the solubility curve of a solid substance.[7] Such a value is almost entirely correct, because the solvent is rarely dissolved in a solid substance and $\ln x_2^{or}$ may be regarded as zero. On the other hand, $\Delta_s h_2^\ominus$ has been evaluated from the solubility curve in water for several substances which are in the liquid state under the conditions measured.[8-11] Such a solubility curve corresponds to the curve with the superscript aq on the left-hand side in Figs. 4, 5, and 6. The conditions for Eq. 4, however, would fail for most liquid organic substances, since the solubilities of water in them must exceed their solubilities in water.[5] Equation 4 cannot be used, of course, for the substances studied here, because neither $\ln x_1^{or}$ nor its derivative with respect to T is zero, as is shown by the right-hand side curves with the superscript or in Figs. 4, 5, and 6. If the mutual solubility is small and both aqueous and organic phases are ideal, $\Delta_s h_2^\ominus$ can be obtained by means of Eq. 3 from the phase diagrams shown in Figs. 4, 5, and 6. In the present cases, however, the organic phases cannot be assumed to be ideal, because the solubilities of water x_1^{or} are as high as between 0.15 and 0.90 as is shown in Figs. 2 and 3, while the aqueous phases are dilute enough to be assumed to be ideal.[3] Unfortunately, $\Delta_s h_2^\ominus$ cannot be evaluated from the phase diagram only, but it can with the use of Eq. 2. The activity coefficient, γ_2^{or}, however, is not available from the literature for most of the substances investigated in the present paper. For 1-butanol, though, the values of γ_2^{or} at 298 K have been found over a wide range of compositions.[12] If γ_2^{or} is assumed to be independent of the temperature at an equal composition,[13] $\Delta_s h_2^\ominus$ for 1-butanol can be estimated from the phase diagram in Fig. 4 by applying Eq. 2. Thus, the difference in $\Delta_s h_2^\ominus$ according to the respective assumption can be checked here for the 1-butanol–water system. The relation between the $\Delta_s h_2^\ominus$ estimated from Eq. 2 and the T for 1-butanol is shown as Curve 2 in Fig. 7. It is expected that the value for $\Delta_s h_2^\ominus$ obtained by Eq. 1 is not so very different from that on Curve 2, since the solubilities of the organic substances are small enough to be ideal. The most likely values of $\Delta_s h_2^\ominus$ shown by Curve 2 increase with an increase in the temperature. The increment of Curve 2 corresponds to the increase in the partial molar enthalpy of 1-butanol in water at an infinite dilution with the rise in the temperature, because the heat of evaporation is almost independent of the temperature.[3] The values for $\Delta_s h_2^\ominus$ which are

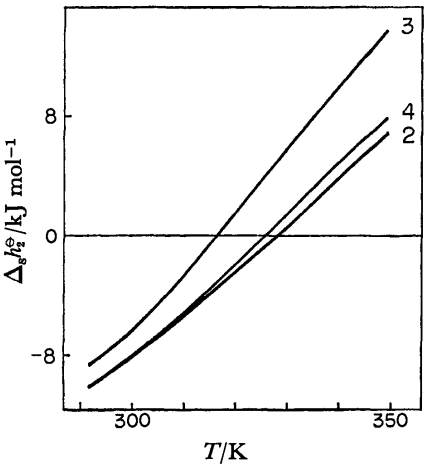

Fig. 7. Heat of solution at infinite dilution *vs.* temperature curves for 1-butanol in water estimated by three different methods.
2: Eq. 2, 3: Eq. 3, 4: Eq. 4.

obtained by the use of Eqs. 3 and 4 are also shown as Curves 3 and 4 respectively in Fig. 7 for the purposes of comparison. It is very impressive that Curve 3 is distant from Curve 2 as a result of our neglecting the deviation of γ_2^{or} from unity and that Curve 4 again approaches Curve 2 as a result of our further neglecting the solubility of water in the organic phase. This suggests that the $\Delta_s h_2^o$ value obtained by the simplest method using Eq. 4 may be close to the real value because of the compensation of the two effects of x_2^{or} and γ_2^{or}.

References

1) H. S. Frank and M. W. Evans, *J. Chem. Phys.*, **13**, 507 (1945).
2) W. -Y. Wen, "Water and Aqueous Solutions: Structure, Thermodynamics, and Transport Processes," ed by R. A. Horne, Wiley-Interscience, New York (1972), p. 613.
3) N. Nishino and M. Nakamura, *Bull. Chem. Soc. Jpn.*, **51**, 1617 (1978).
4) T. Miura and M. Nakamura, *Bull. Chem. Soc. Jpn.*, **50**, 2528 (1977).
5) J. H. Hildebrand and R. L. Scott, "Regular Solutions," Prentice-Hall, Englewood Cliffs, New Jersey (1962), p. 143.
6) I. Prigogine, R. Defay, and D. H. Everett, "Chemical Thermodynamics," Longmans, Green, London and New York (1952), p. 311.
7) W. J. Moore, "Physical Chemistry," 2nd ed, Longmans, Green, London and New York (1956), p. 128.
8) K. Shinoda, *J. Phys. Chem.*, **81**, 1300 (1977).
9) R. L. Bohon and W. F. Claussen, *J. Am. Chem. Soc.*, **73**, 1571 (1951).
10) F. Franks, M. Gent, and H. H. Johnson, *J. Chem. Soc.*, **1963**, 2716.
11) S. J. Gill, N. F. Nichols, and I. Wadsö, *J. Chem.. Thermodyn.*, **8**, 445 (1976).
12) J. A. V. Butler, D. W. Thomson, and W. H. Maclennan, *J. Chem. Soc.*, **1933**, 674.
13) M. Wrewsky, *Z. Phys. Chem.*, **81**, 1 (1912).

The Optical Absorption Spectra of Ferrocene and Biferrocene Anions Produced in the γ-Ray Irradiation by the Matrix-protection Method

Shigeru IKUTA,* Akira KIRA,† Masashi IMAMURA,† Izumi MOTOYAMA, and Hirotoshi SANO

Department of Chemistry, Faculty of Science, Tokyo Metropolitan University, Fukasawa, Setagaya-ku, Tokyo 158
†*The Institute of Physical and Chemical Research, Wako, Saitama 351*

(Received May 19, 1980)

The absorption spectra of the transient species produced through the one-electron reduction of ferrocene and biferrocene were determined by applying a radiation-chemical method in frozen glass matrices. The spectral shapes were assigned to ferrocene- and biferrocene-anionic species on the basis of the experimental results. In the biferrocene anion, the "intervalence transfer" band was observed at about 2050 nm.

Oxidized ferrocene and biferrocene have been extensively studied by the measurement of their optical-absorption, EPR, and Mössbauer spectra, and much information about their physical and chemical properties has been accumulated.[1-8] On the contrary, nothing is known about the reduced forms of ferrocene and biferrocene, because their syntheses have not yet been completed. The failure of efforts thus far undertaken for the syntheses suggests that the reduced forms are too unstable to be isolated by the usual chemical processes. In the present work, we wish to report on the optical-absorption spectra of the transient species which are observed after a one-electron reduction of ferrocene and biferrocene by applying radiation-chemical reactions to frozen glass solution. The spectra were assigned to the ferrocene and biferrocene anions.

Experimental

All the chemicals used were of the purest grade commercially available. The biferrocene was synthesized by the ordinary method.[9] The 2-methyltetrahydrofuran (MTHF) was purified by distillation over metallic sodium. The distillate was stored in vacuo over a sodium–potassium alloy. The ferrocene was recrystallized before use.

Each ferrocene solution (15 mM) and biferrocene solution (9 mM) in MTHF was sealed in an optical cell with an optical path of 1.5 mm or in an EPR sample tube, and irradiated at 77 K with γ-rays from ^{60}Co; the total doses for the ferrocene and biferrocene MTHF-glass matrix were 215 krad and 420 krad, respectively, for H_2O.

The absorption spectra were measured on a Cary 14 RI, while the EPR measurement was carried out by using a JEOL PF 3AX at 77 K.

Radiation-chemical Method for Preparation of Ion Radicals

Although there seems to be an inveterate prejudice that says radiation-chemical processes are too complicated, it has been demonstrated that the irradiation of a frozen solution in a selected solvent with ionizing rays provides us with an excellent method for the selective preparation of solute cation or anion species.[10,11] The scheme has also been well examined as will be briefly illustrated below.

For the selective preparation of solute anion species in an alcoholic or ethereal glass solution, the processes may be described as follows:

$$e^- + S \longrightarrow S^- \quad (1)$$

$$RH^+ + RH \longrightarrow RH_2^+ + R\cdot, \quad (2)$$

where S and RH denote the solute and a solvent species; e^- and RH^+, the electrons and holes induced by ionizing radiations and S^- and RH_2^+, the solute anion species and protonated holes, respectively. The protonated holes are stable species such as hydronium ions produced in the irradiated water. The reaction of RH^+ with the surrounding solvent molecules (Reaction 2) proceeds so fast that solutes added in a small amount cannot scavenge the holes. The absorption bands of the trapped electrons, which are observed in γ-irradiated glass solutions in the absence of solutes, are replaced by the bands of solute anions when a sufficient amount of solute is added to the glass solution. No absorption band is observed for RH_2^+ and R· in the visible and near-infrared regions.

The selective production of solute cations is also proved by the use of organic halides, RX, such as Freons as solvents:

$$RX^+ + S \longrightarrow S^+ \quad (3)$$

$$e^- + RX \longrightarrow R\cdot + X^-. \quad (4)$$

In Reaction 4, RX works to prevent the solute species from forming a solute-anion species, removing electrons in the system. Those methods described above, which will hereafter be referred to as "matrix protection method," have been successfully applied to the study of radical ions of many organic compounds[10-13] and to the study of the one-electron reduction of several organometallic compounds.[14,15] We have also carefully applied this method to ferrocene and biferrocene in order to prepare their anions.

Results and Discussion

Prior to applying the method for the one-electron reduction of ferrocene and biferrocene, the absorption spectra of the cationic species produced in γ-ray irradiated frozen solutions of ferrocene and biferrocene in a freon mixture ($CFCl_3$ 1: CF_2BrCF_2Br 1) were determined. Figures 1-a and 1-b show the spectra taken after irradiating frozen freon mixture glass solutions contain-

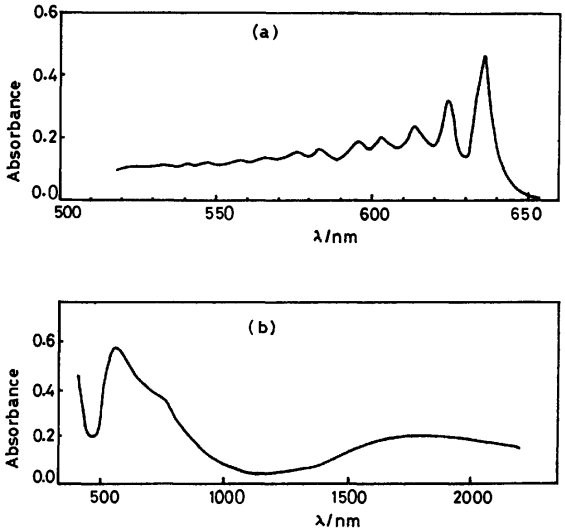

Fig. 1. Absorption spectra of ferrocenium (a) and biferrocene (b) cation obtained by a radiation-chemical method; the total dose for ferrocence (50 mM) and biferrocene (2 mM) Freon-mixture glass solution was 430 krad and 215 krad for H_2O, respectively.

ing ferrocene and biferrocene respectively. The spectral shapes agree well with those of the ferrocenium ions and biferrocene mono-cations prepared by chemical methods.[3,7,8] The dark blue precipitates obtained by warming the solutions to room temperature were determined to be cationic salts.

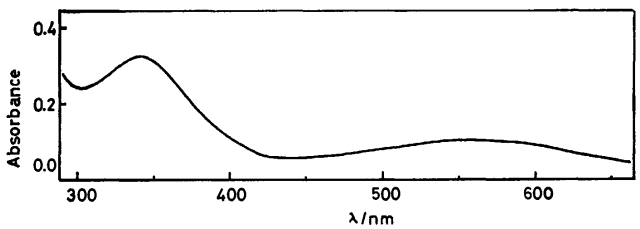

Fig. 2. Absorption spectrum of ferrocene anion taken after photobleaching of residual trapped electrons.

The spectrum taken after the photobleaching of the residual trapped electrons with a filtered light (λ>520 nm) for the γ-ray irradiated MTHF glass solution containing ferrocene is shown in Fig. 2. The two characteristic bands with peaks at 340 and 550 nm in the spectrum can not be found when the solution includes biphenyl (30 mM) as an additional solute before the irradiation, while the bands of biphenyl anions appear clearly. This suggests that the 340- and 500-nm bands are associated with a species resulting from a reaction which competes with the biphenyl-anion formation; *i.e.*, a kind of one-electron reduction process. The results also suggest that the electron affinity of ferrocene should be lower than that of biphenyl previously reported by us.[16] Another experimental result obtained in methanol glass containing ferrocene showed that trapped electrons are not scavenged by ferrocene. In the process of Reaction 1, it is obvious that solutes, S, which a lower electron affinity than the solvent cannot be reduced.

The possibility of the protonation of the anions may be excluded, because the spectrum shown in Fig. 2 is not in accordance with that of the cyclopentadiene anions observed by Shida,[17] although cyclopentadiene anions, $C_5H_6^-$, would be formed if protonation occurred. A dissociative electron attachment, like Reaction 4, was observed for solutes of certain organic halides.[10] Recent studies have revealed that cobalt(III) coordination compounds can undergo a one-electron reduction in the γ-ray irradiation of a MTHF glass solution at 77 K to form their anions, which they decompose on warming.[14,15] EPR studies of γ-ray irradiated tetraphenylporphyrinatocobalt(III) chloride in MTHF at 77 K indicate that the cobalt ions and chloride ions remain at a distance close enough to interact with each other in a transient species.[15] This suggests that MTHF glass is very effective for protecting the dissociation of any fragments at 77 K. In conclusion, therefore, the spectrum shown in Fig. 2 may be safely assigned to ferrocene anions. The disappearance of the spectra on warming the glass solution indicates that ferrocene anions are too unstable to be isolated at higher temperatures. The assignment is also verified by the resemblance of the observed spectrum of cobaltocene,[18] an isoelectronic analogue to the ferrocene anion. The band around 550 nm is attributable to the transition of an electron from a doubly occupied e_{2g} or a_{1g} orbital to the half-occupied e_{1g} orbital, by analogy to cobaltocene. EPR measurements taken for the same species with the absorption bands at 340 and 550 nm showed the g-values, g_x and g_z, to be 1.52 and 1.66 respectively. These values are close to those ($1.65<g_x<1.85$ and $g_z=1.685$) reported for cobaltocene doped in ferrocene at 4.2 K.[18]

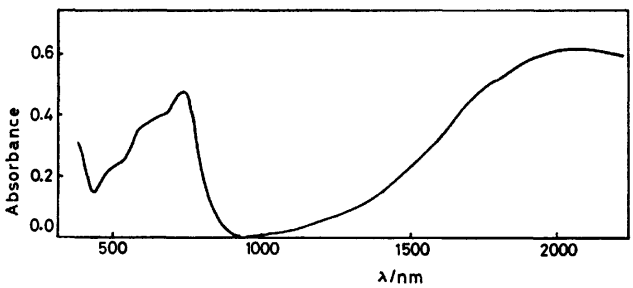

Fig. 3. Absorption spectrum of biferrocene anion taken after photobleaching of residual trapped electrons.

Figure 3 demonstrates the spectrum of a γ-ray-irradiated MTHF glass solution containing biferrocene, measured after photobleaching the residual trapped electrons with a filtered light (λ>520 nm). The spectrum consists of the visible bands (500—800 nm) and a near-infrared band with a peak at *ca.* 2050 nm. All those bands decay when the solution is warmed, and may be attributed to a single species. The spectrum can be assigned to biferrocene mono-anions, on the basis of the radiation-chemical studies described in the consideration of the ferrocene anions.

The visible bands are attributable to the ferrocene-

anion moiety in the biferrocene mono-anion because of its similarity to the 550-nm broad band in Fig. 2. (No transition occurs above 550 nm for ferrocene and biferrocene.[3,8]) The near-infrared band at 2050 nm that was not observed in the ferrocene anion is quite similar to the 1900-nm band of the biferrocene mono-cation found in Fig. 1-b, which has been known as the "intervalence transfer" band.[7,8] It seems, therefore, reasonable to ascribe the 2050-nm band to the "intervalence transfer" between $[Fc(I)Fc(II)]^- \rightarrow [Fc(II)Fc(I)]^-$, where Fc(I) and Fc(II) denote the ferrocene anion and the ferrocene moiety respectively. The near-infrared band has a shoulder at about 1700 nm, as is found in Fig. 3.

The results of the work on the ferrocene and biferrocene anions show that the reduced organometallic compounds can be prepared by applying the matrix-protection method in a MTHF glass solution. The observation of the absorption spectra on the reduced species will provide us with valuable information about the physical and chemical properties of the species too unstable to be isolated, such as the intriguing character of mixed-valence species.

References

1) R. Prins, *Mol. Phys.*, **19**, 603 (1970).
2) J. H. Ammeter, N. Oswald, and R. Bucher, *Helv. Chim. Acta*, **58**, 671 (1975).
3) Y. S. Sohn, D. N. Hendrickson, and H. B. Gray, *J. Am. Chem. Soc.*, **93**, 3603 (1971).
4) G. K. Wertheim and R. H. Herber, *J. Chem. Phys.*, **38**, 2106 (1963).
5) L. M. Epstein, *J. Chem. Phys.*, **36**, 2731 (1962).
6) U. Zahn, P. Kienle, and H. Eicher, *Z. Phys.*, **166**, 220 (1962).
7) W. H. Morrison, Jr., and D. N. Hendrickson, *Inorg. Chem.*, **10**, 2331 (1975).
8) D. O. Cowan, C. LeVanda, J. Park, and F. Kaufman, *Acc. Chem. Res.*, **6**, 1 (1973).
9) M. D. Rausch, *J. Org. Chem.*, **26**, 1802 (1961).
10) W. H. Hamill, "Radical Ions," ed by E. T. Kaiser and L. Kevan, Interscience, New York (1968), Chap. 9.
11) T. Shida and S. Iwata, *J. Am. Chem. Soc.*, **95**, 3473 (1973).
12) T. Shida, N. Nosaka, and T. Kato, *J. Phys. Chem.*, **82**, 695 (1978).
13) T. Shida, "Report of the Physical and Chemical Properties Data, Chemical Kinetics Data," Promotion Bureau, Science and Technology Agency (1975—1978), Vols. 1—4.
14) H. Seki, T. Shida, and M. Imamura, *Biochim. Biophys. Acta*, **372**, 100 (1974).
15) S. Konishi, M. Hoshino, K. Yamamoto, and M. Imamura, *Chem. Phys. Lett.*, in press.
16) A. Kira and M. Imamura, *J. Phys. Chem.*, **82**, 1966 (1978).
17) The peak maxima of $C_5H_6^-$ (410 and 605) were first observed by T. Shida (private communication, 1980).
18) J. H. Ammeter and J. D. Swalen, *J. Chem. Phys.*, **57**, 678 (1972).

The Stability of Spherical Micelles of Dodecyltrimethylammonium Chloride in Aqueous NaCl Solutions

Sumio Ozeki and Shoichi Ikeda*

Department of Chemistry, Faculty of Science, Nagoya University, Chikusa-ku, Nagoya 464

(Received June 2, 1980)

Light scattering from solutions of dodecyltrimethylammonium chloride in water and 4.00 M (1 M=1 mol dm^{-3}) NaCl has been measured at 25 °C, and the critical micelle concentrations and the micellar molecular weights have been determined. The critical micelle concentration, when combined with the previous data, follows the linear Corrin-Harkins equation over the whole range of NaCl concentrations. The micellar molecular weight remains low, *i.e.*, about 20000 even in the presence of 4.00 M NaCl, and the double-logarithmic relation between the micellar molecular weight and the ionic strength is represented by a straight line over the whole range of NaCl concentrations, when plotted together with the previous data. These results indicate that only spherical micelles are formed by dodecyltrimethylammonium chloride in the presence of added NaCl. The stability of the spherical micelle is attributed to the low degree of binding of Cl^- on the cationic micelles.

In a recent work on light scattering[1] we have shown that the micelle of dodecyldimethylammonium chloride is subject to a transition of its shape from spheres to rods when the concentration of added NaCl is increased across 0.80 M (1 M=1 mol dm^{-3}) and when the surfactant concentration considerably exceeds the critical micelle concentration (c.m.c.). By measurements of the viscosity of the micellar solutions,[2] we have confirmed such a transition of micelle shape induced by the change in ionic strength.

In another work[3] we have also demonstrated that even sodium dodecyl sulfate can form rodlike micelles in concentrated NaCl solutions beyond 0.45 M. The formation of large micelles of sodium dodecyl sulfate in 0.6 M NaCl was observed by Mazer and his coworkers[4,5] and by Corti and Degiorgio,[6,7] using both quasi-elastic and elastic light scattering, although the latter workers reserved to draw a conclusion for the formation of rodlike micelles and considered other possibilities as well.

Kushner and his co-workers[8] measured both the light scattering and intrinsic viscosity of micellar solutions of dodecylammonium chloride in different concentrations of added NaCl. Their data on micellar molecular weight can be interpreted as indicating the formation of rodlike micelles in NaCl solutions more concentrated than 0.07 M.[1] The observed intrinsic viscosity of the micellar solutions also suggests the formation of rodlike micelles.[2,9]

In the previous paper[1] we have pointed out that the NaCl concentration or the ionic strength where the sphere-rod transition of an ionic micelle occurs is closely related to the preference of a surfactant molecule to a spherical micelle over a rodlike micelle. This preference is determined by the geometrical ease of packing of surfactant ions in a micelle and by the magnitude of repulsion among polar head groups on a micelle surface. From the geometry of a surfactant molecule we can see that dodecylammonium chloride is more adequately incorporated into a rodlike micelle than dodecyldimethylammonium chloride, and thus, dodecyltrimethylammonium chloride remains to form spherical micelles even in the presence of 0.5 mol kg^{-1} NaCl.[10]

In order to investigate the nature of the sphere-rod transition of ionic micelles, it is worth observing the light scattering of dodecyltrimethylammonium chloride micelles in more concentrated NaCl solutions and determining the micellar molecular weight as well as the micelle shape. This cationic surfactant has already been studied by Kushner and his co-workers[8] and by Emerson and Holtzer,[10] using the light-scattering method; they found it to associate into spherical micelles in the presence of NaCl less concentrated than 0.5 mol kg^{-1}.

Experimental

The sample of dodecyltrimethylammonium chloride was purchased from the Tokyo Kasei Kogyo Co., Inc., and was recrystallized from acetone three times. Thermal-decomposition gas chromatography was applied to this sample at the injection temperature of 300 °C and with the column temperature of 240 °C; the results showed that the sample contained 88.2% C_{12}, 9.5% C_{14}, 0.90% C_{10}, 0.86% C_{16}, and 0.55% C_8. The contaminating higher alkyl homologs would not influence the conclusion derived in this work.

NaCl was a special-grade reagent and was used after having been roasted. Water was redistilled from alkaline $KMnO_4$ in a glass still.

The light scattering and the refractive index increment were measured on Shimadzu apparatuses, PG-21 and DR-3, using the unpolarized light of 436 nm of mercury lamps. A cylindrical cell for light scattering was put in a thermostat jacket. The temperature for measurements was kept at 25±0.05 °C by circulating water of a constant temperature through the cell jackets. The procedure for the optical cleaning of the solutions and the methods of measurement and calibration were described previously.[1,3]

Measurements were carried out on solutions of dodecyltrimethylammonium chloride in water and in 4.00 M NaCl. The reduced intensity of light scattered in the 90° direction, R_{90}, was recorded, and the angular dissymmetry in the 45° direction, z_{45}, was examined. The value of dissymmetry was less than 1.02 above the c.m.c., but it was sometimes higher at lower concentrations. Data showing dissymmetries higher than 1.03 were discarded.

Results

Figure 1 shows the reduced intensity, R_{90}, of the surfactant solutions as a function of the concentration, c (g cm^{-3}). The reduced intensity increases with an

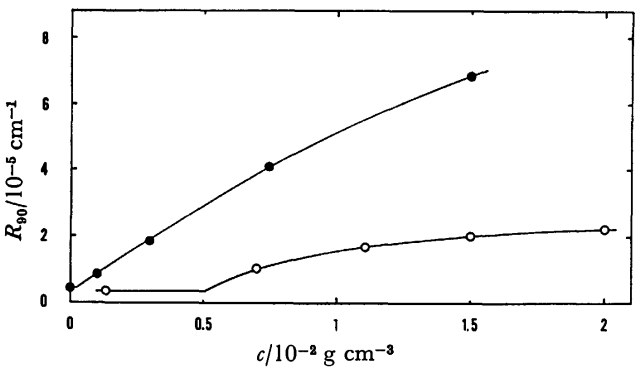

Fig. 1. Reduced intensity of scattered light plotted against surfactant concentration at 25 °C.
○: In water, ●: in 4.00 M NaCl.

Table 1. Refractive index increment and light scattering

C_s / M	$(\partial\tilde{n}/\partial c)_{C_s}$ / cm^3 g^{-1}	C_0 / 10^{-3} M	c_0 / 10^{-2} g cm^{-3}	R_{90}^0 / 10^{-6} cm^{-1}
0	0.158	19.3	0.51	3.34
4 00	0.123	0.68±0.07	0.018±0.002	4.18

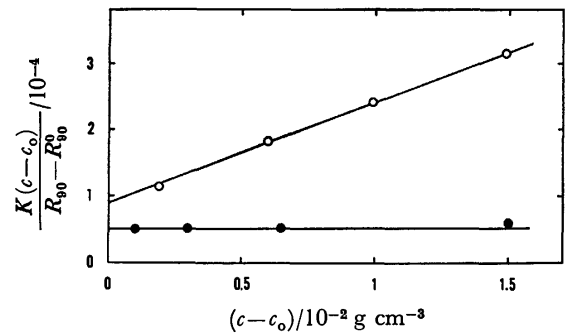

Fig. 2. The Debye plots for dodecyltrimethylammonium chloride micelles at 25 °C.
○: In water, ●: in 4.00 M NaCl.

increase in the concentration above the c.m.c. The values of c.m.c., c_0 (g cm^{-3}) or C_0 (M), and of the reduced intensity there, R_{90}^0, are given in Table 1, together with the refractive index increment, $(\partial\tilde{n}/\partial c)_{C_s}$, where C_s is the molar concentration of added NaCl.

Figure 2 shows that the Debye plots both in water and in 4.00 M NaCl are straight lines expressed by

$$\frac{K(c-c_0)}{R_{90}-R_{90}^0} = \frac{1}{M} + 2B(c-c_0), \quad (1)$$

where M is the micellar molecular weight and B is the second virial coefficient. The optical constant is

$$K = 2\pi^2\tilde{n}_0^2(\partial\tilde{n}/\partial c)^2_{C_s}/N_A\lambda^4, \quad (2)$$

where $\tilde{n}_0$ is the refractive index of the solvent; λ the wavelength of light, and N_A the Avogadro number.

Table 2. Characteristics of the spherical micelles

C_s / M	M	m'	B / 10^{-3} cm^3 g^{-1}	M_m	m	p/m
0	11 500±500	43.6	7.50	13 900	52.8	0.18
4.00	20 000±1 500	75.8	0.05	21 500	81.4	0.2

Table 2 lists the values of the micellar molecular weight, the micellar aggregation number, $m'=M/264$, and the second virial coefficient. The value of the aggregation number indicates that the micelle of dodecyltrimethylammonium chloride is spherical even in 4.00 M NaCl solutions. The positive value of the second virial coefficient also supports the formation of spherical micelles alone, because it has been previously established that rodlike micelles are formed only when the surfactant concentration exceeds the c.m.c.[1,3,6] We have also observed a negative second virial coefficient for a rodlike micelle of *N,N*-dimethyldodecylamine oxide half-neutralized by HCl in 0.2 M NaCl.[11] Debye and Anacker[12] reported positive second virial coefficients for the rodlike micelles of hexadecyltrimethylammonium bromide in 0.178 and 0.233 M KBr, but it proves that even for these solutions negative coefficients can be assigned at low micelle concentrations if lower values of c.m.c. are chosen.

To confirm the formation of spherical micelles only and the absence of rodlike micelles for dodecyltrimethylammonium chloride over the whole range of NaCl concentrations, we have performed an experiment to observe the light scattering from a solution of the cationic surfactant in saturated NaCl. To a 0.75×10^{-2} g cm^{-3} solution of the cationic in 4.00 M NaCl, solid NaCl was added in such a way as to give a 5.9 M NaCl solution if it dissolved completely. The supernatant was sufficiently clean to permit reliable light-scattering measurements and gave a value of reduced intensity slightly lower than that for the 4.00 M NaCl solution.

Discussion

The Double-logarithmic Relations of the c.m.c. and the Micellar Molecular Weight to the Ionic Strength. Figure 3 shows the Corrin-Harkins plot for dodecyltrimethylammonium chloride in the presence of NaCl. The data of previous workers[8,10] are also plotted. It is seen that the Corrin-Harkins equation

$$\log C_0 = -0.631\log(C_0+C_s) - 2.794 \quad (3)$$

proposed by Emerson and Holtzer[10] can be extended up to 4.00 M NaCl. In previous papers[1,13] we have

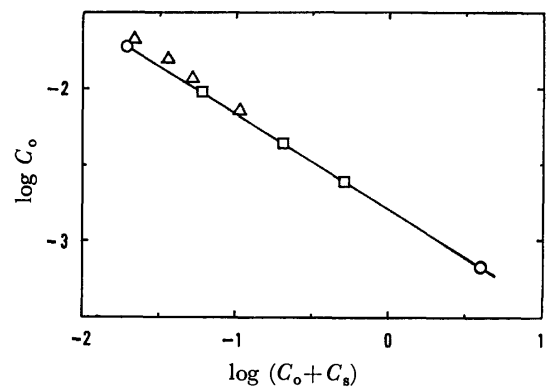

Fig. 3. The Corrin-Harkins plot for the micelles in NaCl solutions.
○: Present results, △: Kushner and his coworkers,[8]
□: Emerson and Holtzer.[10]

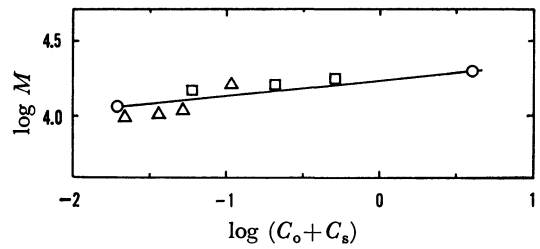

Fig. 4. The double-logarithmic relation of micellar molecular weight with ionic strength in NaCl solutions.
○: Present results, △: Kushner and his coworkers,[8]
□: Emerson and Holtzer.[10]

pointed out that the linear Corrin-Harkins relation holds only when spherical micelles are formed; now we have confirmed that proposition. For the stabilization of spherical micelles, the added salt simply serves to shield the electrostatic effect of a charged micelle.

Figure 4 shows the double-logarithmic relation of the micellar molecular weight to the ionic strength. Together with the data of other workers,[8,10] it is represented by a linear relation:

$$\log M = 0.105 \log(C_0 + C_s) + 4.26. \quad (4)$$

The low value of the coefficient of Eq. 4 is consistent with the spherical micelles.

The scatter of the points in Fig. 4 could be partly attributed to different values of the refractive index increment: *e.g.*, the value of Kushner and his coworkers[8] is 0.155 in water, but the value of Emerson and Holtzer,[10] obtained by an extrapolation, is 0.160 in water; while our value is 0.158. But the deviation seems to occur mostly in the opposite direction.

The Factors Determining the Sphere-rod Transition. In the previous paper[1] we proposed a postulate that the salt-induced transition of the micelle shape is controlled by the ratio of the size of the polar head group to the hydrocarbon part of a surfactant molecule and by the degree of counterion binding on the micelle surface. The first factor is related to the geometrical packing of surfactant molecules in a micelle. The ionic strength where the transition occurs should be higher when the head group is more bulky; this was confirmed for the head-group homologs of dodecylammonium chloride in NaCl solutions. That is, the transition occurs at 0.07 M NaCl for dodecylammonium chloride and at 0.80 M NaCl for dodecyldimethylammonium chloride. We can now add an example of dodecyltrimethylammonium chloride, for which the transition NaCl concentration is higher than the saturated NaCl concentration.

The second factor is related to the electrostatic repulsion among polar head groups. The counterion binding on the micelle surface may be examined by changing either the counterion species or the concentration of added salt. The effect of counterion species on the size of dodecyltrimethylammonium micelles in water was investigated by means of light scattering; it was found that only spherical micelles are formed, as suggested by the observed low aggregation numbers.[14-17] The effect of the concentration of added KBr or NaBr on the micelle size of dodecyltrimethylammonium bromide was also investigated by light scattering; it was demonstrated that only spherical micelles are formed in the presence of salt less than 0.5 mol kg^{-1}.[10,15,17]

Anacker and Ghose[18] measured the micellar molecular weight of dodecyltrimethylammonium bromide in 0.500 mol kg^{-1} sodium salt solutions and found that a large micelle with an aggregation number as high as 10 000 is formed in 0.500 mol kg^{-1} NaSCN. The large micelle must be rodlike, and its formation may be attributed to the reduced electrostatic repulsion among surfactant ions caused by the high degree of binding of SCN^- on the cationic. That is, only a strongly hydrophobic ion, SCN^-, can bind with the cationic micelle to an amount large enough to stabilize a rodlike micelle.

Consequently, we may conclude that the sphere-rod transition of dodecyltrimethylammonium micelles cannot be induced by the addition of NaCl, because Cl^- does not bind with the surfactant micelle sufficiently.

It is known that the Prins-Hermans-Princen-Mysels theory[19,20] can derive the apparent degree of ionization, p/m, of an ionic micelle, together with its "true" molecular weight, M_m, and its "true" aggregation number, m, based on the assumption of an ideal polyelectrolyte solution. Table 2 also includes these values of the micelles. The low degree of binding of Cl^- would be revealed in the rather large values of the apparent degree of ionization of the micelle, as given in Table 2.

If the hydrocarbon part of alkyltrimethylammonium is longer, the cationic is adapted to a rodlike micelle better than to a spherical micelle. Thus, hexadecyltrimethylammonium bromide can form the rodlike micelles in 0.178 and 0.233 M KBr,[12] while it forms spherical micelles in water and in 0.0130 M KBr.[14,15]

Small-angle X-ray scattering measurements demonstrated that the radius of gyration of an ionic micelle in water suddenly increases with an increase in the surfactant concentration beyond a certain value, and this change was attributed to the transition of the micelle shape from a sphere to a rod.[21,22] We can interpret such a transition as also being caused by the increase in ionic strength given by the surfactant itself.

In this concentration-induced transition of micelle shape, we can still see evidence for the counterion binding. Reiss-Husson and Luzzati[21] determined the surfactant concentration for the sphere-rod transition and tabulated its approximate values as 40×10^{-2} g cm^{-3} for hexadecyltrimethylammonium chloride and as 5×10^{-2} g cm^{-3} for hexadecyltrimethylammonium bromide. This difference in concentration for the transition could be considered to stand for the stronger binding of Br^- than Cl^- to the cationic micelle.

The authors are deeply indebted to Mrs. Keiko Kotani of the Aichi-ken Kogyo Shido-sho for her skilful gas-chromatographic analysis.

References

1) S. Ikeda, S. Ozeki, and M. Tsunoda, *J. Colloid Interface Sci.*, **73**, 27 (1980).
2) S. Ozeki and S. Ikeda, *J. Colloid Interface Sci.*, **77**, 219 (1980).
3) S. Hayashi and S. Ikeda, *J. Phys. Chem.*, **84**, 744 (1980).

4) N. A. Mazer, G. Benedek, and M. C. Carey, *J. Phys. Chem.*, **80**, 1075 (1976).
5) C. Y. Young, P. Missel, N. A. Mazer, G. B. Benedek, and M. C. Carey, *J. Phys. Chem.*, **82**. 1375 (1978).
6) M. Corti and V. Degiorgio. *Ann. Phys.*, **3**, 303 (1978).
7) M. Corti and V. Degiorgio, "Solution Chemistry of Surfactants," ed by K. L. Mittal, Plenum Press, New York (1979), Vol. I, p. 377.
8) L. M. Kushner, W. D. Hubbard, and R. A. Parker, *J. Res. Nat. Bur. Stad.*, **59**, 113 (1957).
9) D. Stigter, *J. Phys. Chem.*, **70**, 1323 (1966).
10) M. F. Emerson and A. Holtzer, *J. Phys. Chem.*, **71**, 1898 (1967).
11) S. Ikeda, M. Tsunoda, and H. Maeda, *J. Colloid Interface Sci.*, **70**, 448 (1979).
12) P. Debye and E. W. Anacker, *J. Phys. Colloid. Chem.*, **55**, 644 (1951).
13) S. Ozeki and S. Ikeda, *Bull. Chem. Soc. Jpn.*, **53**, 1832 (1980).
14) P. Debye, *J. Phys. Colloid. Chem.*, **53**, 1 (1949).
15) P. Debye, *Ann. N. Y. Acad. Sci.*, **51**, 575 (1949).
16) H. J. L. Trap and J. J. Hermans, *Proc. Koninkl. Neder. Akad. Wetenschap.*, **B58**, 97 (1955).
17) H. V. Tartar and A. L. Lelong, *J. Phys. Chem.*, **59**, 1185 (1956).
18) E. W. Anacker and H. M. Ghose, *J. Phys. Chem.*, **67**, 1713 (1963).
19) W. Prins and J. J. Hermans, *Proc. Koninkl. Neder. Akad. Wetenschap.*, **B59**, 162 (1956).
20) L. H. Princen and K. J. Mysels, *J. Colloid Sci.*, **12**, 594 (1957).
21) F. Reiss-Husson and V. Luzzati, *J. Phys. Chem.*, **68**, 3504 (1964).
22) F. Reiss-Husson and V. Luzzati, *J. Colloid Interface Sci.*, **21**, 534 (1966).

Structure of Mercury Layer Deposited on Platinum and Hydrogen-evolution Reaction at the Mercury-coated Platinum Electrode

Zenko YOSHIDA

Chemistry Division, Japan Atomic Energy Research Institute, Tokai, Ibaraki 319-11

(Received May 6, 1980)

The thermal evaporation of mercury is investigated in order to ascertain the structure of mercury electrodeposited on platinum. At first, Pt_2Hg is formed on platinum, and a hydrogen(H)-overpotential at the surface is identical with that at the mercury-free platinum. With the increase in the amount of mercury to more than the amount corresponding to PtHg, the H-overpotential increases. When a large amount of mercury is deposited, the layer is composed of three mercury compounds (Pt_2Hg, Pt_2Hg_2, and $PtHg_4$), metallic mercury, and adatom mercury. Even when a sufficiently large amount of mercury is deposited, *e.g.*, several thousand atomic layers, the H-overpotential is much less than that at a hanging mercury drop electrode (HMDE). From the general relationship between the hydrogen evolution at a metal electrode and the work function of the metal, the change in the H-overpotential with the increase in the amount of mercury is attributable to the work-function change.

In spite of the importance of hydrogen-evolution reaction at the surface of thin metal film deposited on a foreign metal from the viewpoints of corrosion and electrocatalytic reactions[1,2] at the surface and the utility of thin film electrodes, there have been only a few quantitative investigations of hydrogen evolution at thin metal film. Furuya *et al.* investigated hydrogen-evolution reaction at platinum[3] or palladium[4] deposited on gold and copper,[5] gold,[3] or arsenic[6] deposited on platinum. Through these studies they concluded that, when a monolayer metal was deposited, the hydrogen evolution at the surface was identical with that at the bulk metal to be deposited. On the other hand, at the surface of thin mercury film deposited on platinum[7] or silver,[8] the hydrogen evolution was far from that at pure mercury itself, even when the amount of mercury was sufficiently large. This phenomenon has been well known, because platinum- or silver-based thin mercury film electrodes (TMFE) have been widely used[7-14] as indicator electrodes in electroanalytical chemistry. Like mercury, silver on platinum[15] also behaved similarly. Many authors have empirically discussed the preparation and stability of the TMFE with regard to hydrogen evolution. Bruckenstein *et al.*[16] investigated the adsorption behavior of the hydrogen atom at less than a monolayer amount of mercury-coated platinum surface with regard to the structure of deposited mercury. In general, hydrogen-evolution reaction at a metal surface can be correlated to the work function of the electrode as well as the potential of zero charge and the strength of hydrogen adsorption.[17-22]

In this report, hydrogen-evolution reactions at the mercury layer, from less than a monolayer to several thousand atomic layers, deposited on platinum are described with regard to the structure of mercury. The structure of the deposited mercury was investigated by means of the thermal evaporation of the mercury, followed by the determination of the mercury atoms using flameless atomic absorption spectrophotometry (AAS).[23,24] Using this procedure, the quantitative determination of a trace amount of mercury as well as the characterization of the deposited mercury layer from the evaporation temperature are possible.

Experimental

The electrolysis and the determination of the mercury were carried out with the same electrolytic cell, potentiostat, and flameless AAS mercury analyzer as those reported previously.[23,24] A Hokuto Denko Co., Model HB-107A, wave-function generator was used for the linear-potential sweep.

The mercuric perchlorate solution was prepared by dissolving mercuric oxide in 2.5×10^{-1} M (1 M=1 mol dm^{-3}) perchloric acid, and the concentration of mercury (II) was determined by EDTA titration. Triple-recrystallized potassium perchlorate was used as the electrolyte, and the other chemicals used were of a reagent grade. The water used was distilled over 3% potassium permanganate in the presence of 0.1 M sulfuric acid, and then distilled twice. Argon (99.99% or more) was purified by passing it through a titanium sponge (700 °C). All the electrolytic measurements were carried out at 25±0.2 °C, and the potentials were referred to a saturated calomel electrode (SCE). The electrode surface area was 1.13 cm^2.

Pretreatment of Platinum.[25] The platinum plate (15×20×0.3t in mm) used as an electrode had a purity above 99.99%. It was electropolished anodically at 4—4.5 V *vs.* the platinum cathode for 10 s in a mixture of potassium chloride and sodium chloride (1+1) fused at 650 °C. Then it was kept in (1+1) perchloric acid for a few min and washed with water.

Deposition of Mercury. Mercury was deposited on the platinum by means of controlled-potential electrolysis at +0.55 V (underpotential region) or +0.20 V (more negative than the reversible potential for mercury (II)/(0)), unless otherwise mentioned. Electrolysis was carried out for 15 min in a deaerated electrolyte solution (1×10^{-1} M in potassium perchlorate and 1×10^{-3} M in perchloric acid) containing 10^{-6}—10^{-4} M of mercury (II).

Investigation of Hydrogen-evolution Reaction. Cylic Voltammetry: After the deposition of mercury, the solution containing mercury (II) was drained off and the cell was washed with an electrolyte solution (1×10^{-1} M potassium perchlorate and 1×10^{-3} M perchloric acid) five times. A voltammogram was run cathodically and then anodically at a rate of 2 mV s^{-1} in 10 ml of an electrolyte deaerated for 15 min by passing argon through.

Tafel Plot: The relation between the electrode potential and the current density (10^{-7}—10^{-3} A cm^{-2}) was galvanostatically investigated in 1×10^{-1} M of potassium perchlorate and 1×10^{-1} M of perchloric acid.

Thermal Evaporation. Immediately after the completion of the electrolysis, the mercury-coated platinum was washed with water and then ethanol; it was thereafter heated in a quartz tube while the temperature was raised at a rate of 20 °C min^{-1}. The evaporated mercury was introduced into the mercury analyzer by means of an argon stream (2 l min^{-1}). The absorption intensity of mercury was recorded against the temperature (*T*-Hg curve).[23]

Results

Structure of Mercury Layer Deposited on Platinum. The *T*-Hg curves of mercury (0.12—4.1 μg cm^{-2}) deposited on platinum are illustrated in Fig. 1. With the increase in the amount of mercury deposited, one to five peaks are observed. The development of each peak with the increase in the total mercury deposited is shown in Fig. 2. With a small amount of mercury (less than 0.29 μg cm^{-2}), only Peak I at 300 °C is observed (Region A in Fig. 2). After the saturation of Peak I at 0.29 μg cm^{-2}, Peak II at 160 °C and Peak III at 110 °C start to be observed (Region B). Peak II is also saturated; the saturated amount under Peak II is 0.29 μg cm^{-2}. With more mercury, Peak III develops, and Peak IV at around 20 °C and Peak V at 190 °C appear (Regions C and C'). While the ratio of the amount of mercury under Peak III to that under Peak V

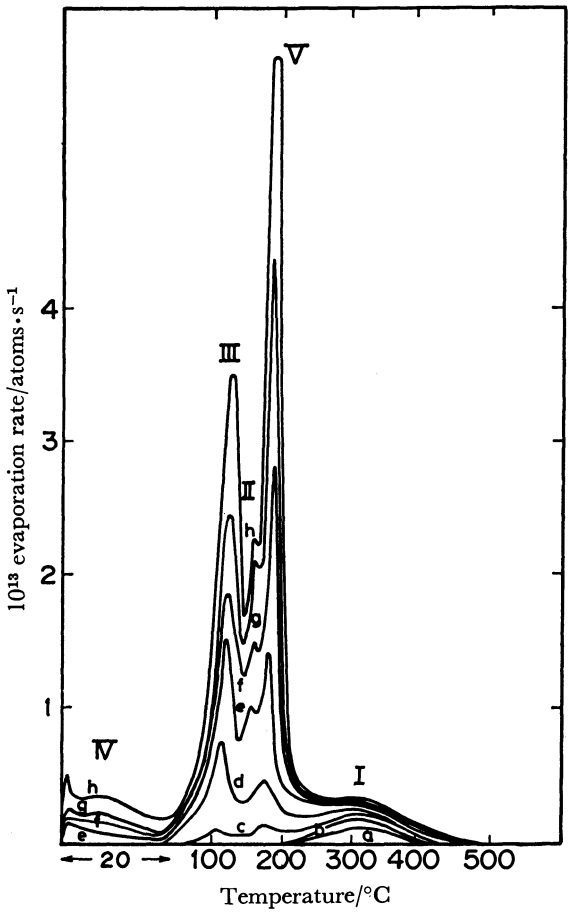

Fig. 1. *T*-Hg curves of mercury deposited on platinum. Amounts of mercury deposited (μg cm^{-2}): (a) 0.12, (b) 0.20, (c) 0.35, (d) 0.87, (e) 1.7, (f) 2.4, (g) 3.2, (h) 4.1.

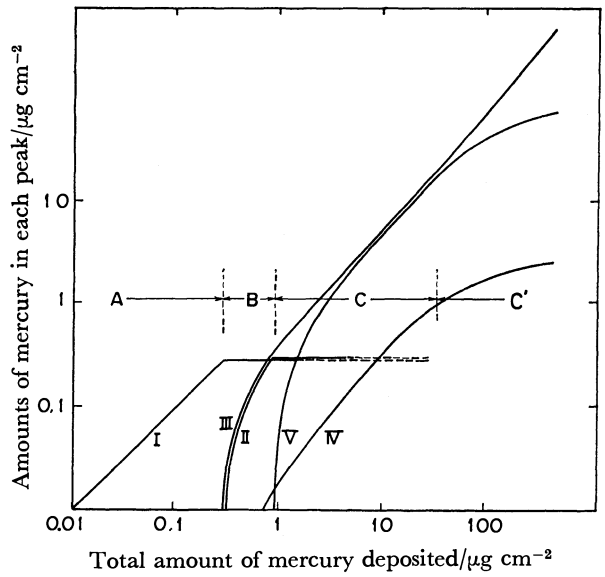

Fig. 2. Developments of various peaks in *T*-Hg curve with the increase of the amount of mercury deposited.

nearly equals unity in Region C, the ratio increases with the increase of mercury in Region C'.

The character of each peak is as follows;

Peak I. When mercury is deposited at +0.55 V (underpotential region), even in a rather concentrated mercury (II) solution (10^{-4} M), the amount of mercury under this peak, I, is also saturated at 0.29 μg cm^{-2}. Similarly to the determination of the underpotential shift, ΔU, for mercury deposition on gold,[23] the ΔU value for mercury deposition on platinum was determined to be 0.45 V from the relation between the electrode potential of controlled-potential electrolysis and the amount of mercury deposited (*E*-Hg plot). Moreover, the first wave in the *E*-Hg plot is saturated at 0.29 μg cm^{-2} of mercury, which agrees well with the saturation of Peak I in the *T*-Hg curve. In this connection, the relation between the amount of mercury deposited and the amount of hydrogen adsorbed at the platinum surface, Q_H-Hg, was investigated according to the procedure proposed by Bruckenstein *et al.*[16] The quantity of adsorbed hydrogen, Q_H, decreases linearly with the increase of mercury, and with 0.29 μg cm^{-2} of mercury Q_H comes to be zero. This indicates that the deposition of the first mercury layer proceeds *via* a site mechanism[16] showing a combination of two platinum surface atoms with one mercury atom deposited. According to the results obtained by the *E*-Hg and Q_H-Hg measurements, it is evident that Peak I in the *T*-Hg curve corresponds to the evaporation of mercury from the stable mercury layer, Pt_2Hg, which is deposited at the underpotential. Actually, the saturated value, 0.29 μg cm^{-2}, is about one-half of the amount of mercury calculated by assuming that each platinum surface atom is associated with one mercury atom and that a roughness factor of the electrode is unity.

Peak II. Because Peak II is saturated with the same amount of mercury as Peak I (0.29 μg cm^{-2}), this peak corresponds to the evaporation of one mercury

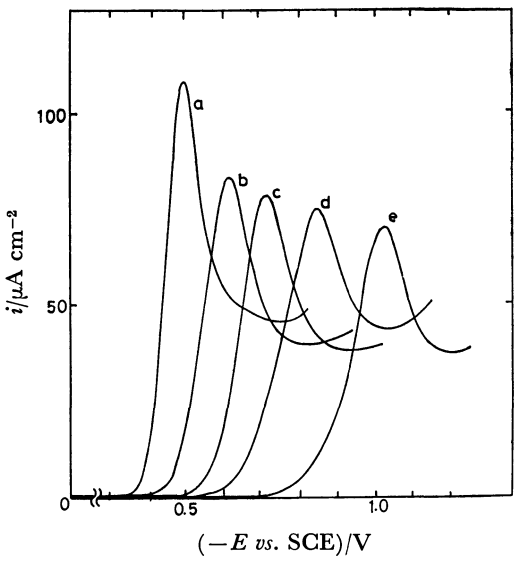

Fig. 3. Voltammograms for hydrogen evolution at platinum electrode with and without mercury.
Electrolyte: 1×10^{-1} M potassium perchlorate and 1×10^{-3} M perchloric acid. Rate of potential scanning: 2 mV s^{-1}. Amounts of mercury deposited ($\mu g\ cm^{-2}$): (a) 0—0.29, (b) 8, (c) 22, (d) 60, (e) more than 200.

atom from Pt_2Hg_2 (or 2PtHg), thus forming Pt_2Hg.

Peaks III and IV. Peaks III and IV were previously reported to be due to the evaporation of metallic mercury and adatom mercury, respectively.[23,24]

Peak V. Peak V is identical with that of the evaporation of mercury from the $PtHg_4$ alloy produced by the procedure reported by Barlow *et al.*[26] and identified by X-ray diffraction.

Hydrogen-evolution Reaction at the Mercury-coated Platinum Electrode. Voltammograms for hydrogen-evolution reaction at the platinum electrode with and without mercury are illustrated in Fig. 3. Although the reduction potential of the hydrogen ion should be determined using a constant and small current density, the hydrogen-reduction peak potential, E_p, in the voltammogram is employed for convenience for the study of the H-overpotential in the present study. The peak potential, E_p, in the second cathodic potential scan is adopted because E_p in the second scan is more negative than that in the first scan as a result of the structural change of mercury film during the first cathodic polarization.[7] E_p at the mercury-free platinum electrode is -0.50 V. The relation between E_p at the mercury-coated platinum electrode and the amount of mercury deposited is shown by Curve (a) in Fig. 4. With less than 0.29 $\mu g\ cm^{-2}$ of mercury, E_p is identical with that at platinum. With more than 0.29 $\mu g\ cm^{-2}$, E_p shifts to a negative value with the increase in the amount of mercury. With more than 200 $\mu g\ cm^{-2}$, E_p is constant at -1.05 V, E_p^1. Even when 20 mg cm^{-2} of mercury is deposited, E_p halts at E_p^1.

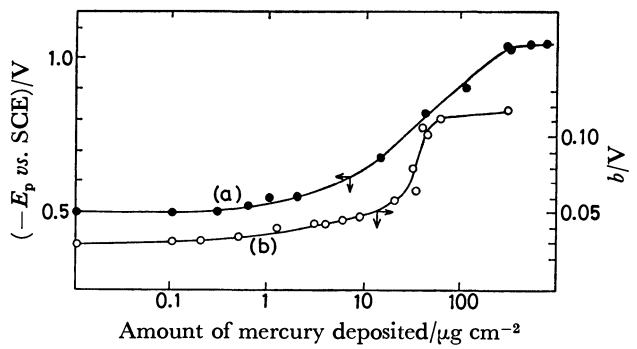

Fig. 4. Hydrogen evolution reaction at mercury-coated platinum electrode with various amount of mercury.
(a): Peak potential in cyclic voltammogram, E_p, (b): Tafel slope b.

As may be seen in Fig. 3, the slope of the voltammogram in the range of low current density decreases when an electrode with a larger amount of mercury is used. To study the polarization characteristics more quantitatively, a galvanostatical investigation of the Tafel plot was carried out. The b slope in the Tafel equation, $\eta=a+b\log i$, where a and b are constants and η is the overpotential, for a hydrogen-evolution reaction is changed with the amount of mercury deposited, as is illustrated by Curve (b) in Fig. 4. With less than 1 $\mu g\ cm^{-2}$ of mercury, b is about 0.030 V, which is identical with the value observed at mercury-free platinum. With the mercury is between 1 and 40 $\mu g\ cm^{-2}$, the slope changes from 0.030 to 0.085 V, and with more than 40 $\mu g\ cm^{-2}$ of mercury, the slope is from 0.085 to 0.120. The b slope, 0.120 V, is identical with that at a hanging mercury drop electrode (HMDE). The amount of mercury, 40 $\mu g\ cm^{-2}$, corresponds to the boundary amount of mercury between C and C′ in Fig. 2.

Stability of Mercury Layer Deposited on Platinum. The stability of the mercury layer was investigated by measuring the T-Hg and the hydrogen-evolution reaction after lefting it stand at 25 °C in a deaerated supporting electrolyte for a definite period of time. The relation between the amount of mercury and E_p, or the b value obtained at the electrode on which mercury had been deposited for 15 min in 10^{-4}—10^{-6} M mercury (II) and which was left standing for 30 min (Fig. 4), was identical with that obtained at the electrode on which mercury had been deposited for 30 s in 10^{-3}—10^{-5} M mercury (II) and which left standing for 2—5 min. Therefore, it is concluded that a standing time within 30 min exerts no significant effect on hydrogen evolution at the surface, regardless of the amount of mercury deposited. When the amount of mercury deposited was less than 10 $\mu g\ cm^{-2}$, no discrepancy was found in T-Hg and hydrogen evolution between those obtained after standing for 30 h and those obtained after only 30 min. When platinum coated with more than 10 $\mu g\ cm^{-2}$ of mercury was allowed to stand for more than 3 h, the T-Hg curve changed from that obtained after 30 min standing; *i.e.*, Peak III decreased and Peak V increased. Also, after more than 20 h's standing, T-Hg showed only Peak V. Hydrogen evolution also changed with the standing time, much as with the T-Hg curve. After 2 h's standing, E_p began to shift to a more positive value; after 3, 5, and 12 h's standings, E_p were -0.95, -0.82, and -0.65 V, respectively.

Table 1. Structure of mercury deposited on platinum and hydrogen-evolution reaction at the surface

Region	Amount of mercury deposited / $\mu g\ cm^{-2}$	Structure of mercury layer	E_p *vs.* SCE / V	b / V
A	0—0.29	Pt_2Hg	−0.50	0.030
B	0.29—1	Pt_2Hg_2+Hg	−0.50→−0.53	0.030→0.035
C	1—40	$Pt_2Hg_2+Hg+PtHg_4+Hg_{adatom}$	−0.53→−0.80	0.035→0.085
C′	More than 40	As region C but $Hg>PtHg_4$	−0.80→−1.05	0.085→0.118

With more than 20 h's standing, E_p reached −0.60 V, which was only 100 mV more negative than that at platinum.

The platinum contents in a mercury layer at various standing times were determined colorimetrically by means of a modified tin(II) chloride method[27] after dissolving the deposited mercury layer in nitric acid (60 °C) and treating it with aqua regia. The platinum content increased with the standing time; after standing for 3, 5, 12, and more than 20 h, the platinum contents were 10.5, 12.8, 16.0, and 19.2 at. %. The final platinum content, 19.2%, agrees well with the finding that Peak V in the *T*-Hg curve is $PtHg_4$.

Discussion

The structure of the mercury layer deposited on platinum and the hydrogen-evolution reaction at the surface are summarized in Table I as a function of the amount of mercury deposited. Although many platinum–mercury alloys, such as $PtHg_4$, $PtHg_2$, PtHg, Pt_2Hg, and Pt_3Hg, have been identified,[28] $PtHg_4$, PtHg, and Pt_2Hg are the main components in the mercury layer deposited on platinum. Particularly in the underpotential region, Pt_2Hg is preferentially formed (Region A in Fig. 2).

Bruckenstein *et al.*,[16] on the basis of the results of Q_H-Hg measurement, suggested the formation of Pt_2Hg in the initial step of the deposition. They deposited mercury at a more negative potential than the reversible potential for mercury (II)/(0) and reported that Q_H was not equal to be zero even when the platinum surface was covered with mercury in an amount large enough to saturate the Pt_2Hg layer. In the present study, if mercury is deposited on platinum in the underpotential region, Q_H comes to be zero at the electrode with mercury corresponding to the completion of the Pt_2Hg layer; this indicates that Pt_2Hg is preferentially formed at the underpotential. The reoxidation current peak, from which Pt_2Hg can be identified, was not observed in the anodic stripping voltammograms reported by Bruckenstein *et al.* Two evaporation peaks, Peak I and Peak II in the *T*-Hg curve in Region B, of mercury from Pt_2Hg_2 (or 2PtHg) indicates that the evaporation of one mercury atom from Pt_2Hg_2 requires less energy than that required for the evaporation of mercury from Pt_2Hg. This evaporation behavior obviously supports the preferential formation of Pt_2Hg at the initial step of the deposition. Bruckenstein *et al.* also described the development of $PtHg_4$. The anodic stripping peak of mercury from $PtHg_4$, however, was too broad to be distinguished from such other layers as Pt_2Hg. A well-defined peak, V, which corresponds to the evaporation of mercury from $PtHg_4$, is observed in the *T*-Hg curve in the present work. Although Bruckenstein *et al.* reported that $PtHg_2$ was formed on PtHg, $PtHg_2$ was not observed in the *T*-Hg curve.

The rate-determining step of the hydrogen-evolution reaction has been widely recognized[1] to be one of the following three reaction steps: (*i*) the discharge of the hydrogen ion, (*ii*) the chemical desorption of the hydrogen molecule, or (*iii*) electrochemical desorption. Because the Tafel slopes, b, for hydrogen evolution at Pt_2Hg and mercury-free platinum are 0.030 V, it is considered that the rate-determining step at their surfaces is (*ii*).[29] In the C′ region, the b value is 0.110—0.120 V, which is identical with that at the HMDE. The rate-determining step at their surfaces is (*i*),[30] which agrees with the dominant formation of metallic mercury in the C′ region, Peak III in the *T*-Hg curve. Although Peak III is observed in the *T*-Hg curves whenever more than 0.29 $\mu g\ cm^{-2}$ of mercury is deposited (Regions B, C, and C′), the electrode property of the surface is far from that of mercury in Regions B and C. In the C and C′ regions, E_p is shifted in the negative direction with the increase in mercury. The relation between E_p and the amount of mercury, given as Curve (a) in Fig. 4, can be expressed empirically by the following equation:

$$E_p = E_p^{Pt} + \alpha W(E_p^{l} - E_p^{Pt})/(1 + \alpha W), \qquad (1)$$

where E_p^{Pt} and W are E_p at mercury-free platinum and the amount of mercury in $\mu g\ cm^{-2}$, respectively. Comparing the experimental results illustrated as Curve (a) in Fig. 4 with Eq. 1, the constant, α, is determined to be 0.026.

Even at a freshly prepared electrode with a large amount of mercury, the hydrogen-evolution peak was at −1.05 V, far positive than that at the HMDE. The platinum content in the mercury layer on such an electrode was confirmed by chemical analysis to be less than 0.01 wt%. Butler *et al.*[31] discovered, by using a dropping mercury electrode, that the presence of 0.027 wt% platinum did not affect the hydrogen-evolution reaction. The present study also confirmed the absence of any effect when a hanging mercury drop containing 0—0.35 wt% platinum was used. Therefore, the lower H-overpotential at the mercury-coated

platinum with a large amount of mercury is not attributed to the trace amount of platinum dissolved in the mercury layer.

Furuya *et al.*[15] reported that the exchange-current density for hydrogen evolution at twenty atomic layers of silver deposited on platinum was far from that at pure silver metal. On the other hand, in such systems as copper on platinum,[5] gold on platinum,[3] platinum on gold,[3] and palladium on gold,[4] with the deposition of a monolayer metal, hydrogen evolution changed from that at the base metal to that at the deposited metal. Considering the hydrogen-evolution reaction at the deposited thin metal film, the combinations of deposited metal and base metal can be classified into two groups as follows: (*i*) Deposited metal forms stable intermetallic compounds with the base metal. The chemical interaction is too strong, and the property of the surface of the deposited metal is affected by an underlying layer, such as the base metal itself and/or a stable-compound layer formed. This group includes Pt/Hg and Pt/Ag, which show intermetallic compounds, PtHg, $PtHg_2$, and $PtHg_4$, and Pt_3Ag, PtAg, and $PtAg_3$, in the phase diagrams.[28] (*ii*) Deposited metal forms a solid solution with the base metal at any ratio instead of the formation of the stable intermetallic compounds. The property of the deposited metal atom is rather independent of the property of the base metal, and the electrochemical property of the deposited metal surface is hardly affected by the base metal when the base metal surface is completely covered with the deposited metal film. This group includes Pt/Cu, Pt/Au, and Pd/Au.

The remarkable standing-time effect on mercury-coated platinum is explained by the growth of stable intermetallic compounds because of the large interaction between mercury and platinum. In addition, it is also considered that the diffusion coefficient of base-metal atoms in metallic (liquid) mercury is much larger than that in other solid metals. In connection with the work function of the thin metal film surface, it has been reported that metal monolayers deposited on foreign substrates, such as alkali metals deposited on nickel or tungsten,[32-34] show the same work-function value as that of bulk alkali metal. In these systems, no intermetallic compounds have been reported, and the diffusion coefficient of nickel or tungsten in an alkali solid metal is smaller than that in liquid metal.

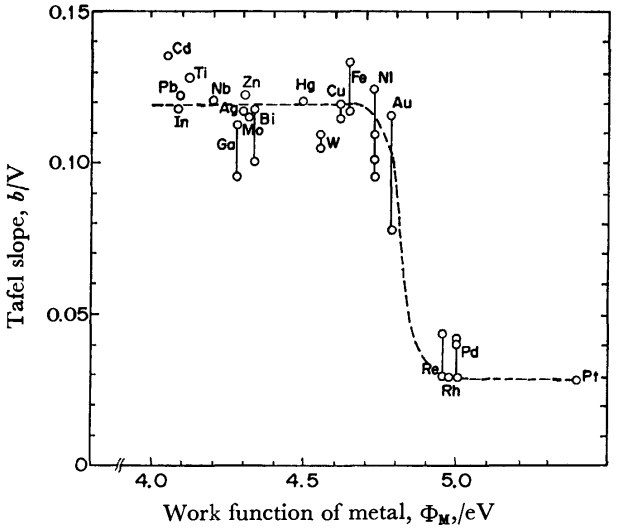

Fig. 5. Relation between Tafel slope *b* and work function of metal.
Tafel slopes *b* are cited from Ref. 35. Work function of metals are cited from Refs. 17 and 18.

Generally, hydrogen evolution at the metal surface is related to the work function of the metal.[19,20] Trasatti suggested a linear relationship between the H-overpotential at a metal surface and the work function of the metal (see Fig. 1 in Ref. 19). The relation between the Tafel slope, *b*, previously reported and the work function of the metal is shown in Fig. 5. It is evident that the *b* slopes are constant at 0.030 and 0.120 V, when the work-function values are more than 4.9 eV and less than 4.7 eV, respectively. When the work function of the metal is between 4.7 and 4.9 eV, the *b* slope shows an intermediate value of 0.030—0.120 V.

Because E_p and the *b* slope at the surface of monolayer mercury deposited on platinum is identical with those at the platinum surface, the work function of monolayer mercury film can be said to be close to that of platinum, but not to that of mercury. It is also estimated, from the difference between E_p^1 and E_p at the HMDE, that the work function at the electrode surface with a large amount of mercury deposited is still different from that of pure mercury. The experimental relation (Curve(b) in Fig. 4) shows a remarkable change in the *b* slope when 40 $\mu g\ cm^{-2}$ of mercury is deposited. Therefore, it is considered that the work function of the surface is around 4.8 eV. This is supported by the facts that the E_p values observed at gold, nickel, and copper, the work-function values of which are 4.78, 4.73, and 4.70 eV, are −0.74, −0.68, and −0.84 V, respectively, and that the E_p value at the mercury-coated platinum with 40 $\mu g\ cm^{-2}$ of mercury is −0.8 V.

Through the present study it is clear that the hydrogen-evolution reaction at the mercury-coated platinum is characterized by the structure of the mercury layer, which affects the work function of the electrode surface.

Because the platinum-based TMFE is found to be troublesome with respect to the stability, the property of thin mercury film deposited on various metals will be discussed in a subsequent paper in preparation for developing an ideal TMFE.

The author would like to thank Dr. Sorin Kihara, professor Taichiro Fujinaga and his coworkers, and Dr. Kenji Motojima for their helpful discussions and useful suggestions.

References

1) J. O'M. Bockris and A. K. N. Reddy, "Modern Electrochemistry," Plenum Press, New York (1970), Vol. 2.
2) D. M. Kolb, "Advances in Electrochemistry and Electrochemical Engineering," Wiley-Interscience, New York (1978), Vol. 11, p. 125.
3) N. Furuya and S. Motoo, *J. Electroanal. Chem.*, **88**, 151 (1978).

4) N. Furuya and S. Motoo, *Denki, Kagaku*, **41**, 364 (1973).
5) N. Furuya and S. Motoo, *J. Electroanal. Chem.*, **72**, 165 (1976).
6) N. Furuya and S. Motoo, *J. Electroanal. Chem.*, **78**, 243 (1977).
7) A. M. Hartly, A. G. Hiebert, and J. A. Cox, *J. Electroanal. Chem.*, **17**, 81 (1968).
8) Z. Stojek and Z. Kublik, *J. Electroanal. Chem.*, **60**, 349 (1975).
9) Z. Stojek and Z. Kublik, *J. Electroanal. Chem.*, **77**, 205 (1977).
10) W. R. Matson, D. K. Roe, and D. E. Carrit, *Anal. Chem.*, **37**, 1594 (1965).
11) T. M. Florence, *J. Electroanal. Chem.*, **27**, 273 (1970).
12) G. E. Bartley and T. M. Florence, *J. Electroanal. Chem.*, **55**, 23 (1974).
13) R. Neeb, *Z. Anal. Chem.*, **180**, 161 (1961).
14) G. D. Robbins and C. G. Enke, *J. Electroanal. Chem.*, **23**, 343 (1969).
15) N. Furuya and S. Motoo, *Denki Kagaku*, **41**, 307 (1973).
16) M. Z. Hassan, D. F. Untereker, and S. Bruckenstein, *J. Electroanal. Chem.*, **42**, 161 (1973).
17) S. Trasatti, *J. Electroanal. Chem.*, **33**, 351 (1971).
18) S. Trasatti, *J. Chem. Soc. Faraday Trans. 1*, **68**, 229 (1972).
19) S. Trasatti, *J. Electroanal. Chem.*, **39**, 163 (1972).
20) A. T. Kuhn, C. J. Mortimer, G. C. Bond, and J. Lindley, *J. Electroanal. Chem.*, **34**, 1 (1972).
21) L. Y. Firsiva and V. N. Gramm-Osipova, *Z. Fiz. Khim.*, **52**, 3166 (1978).
22) E. W. Brooman and A. T. Kuhn, *J. Electroanal. Chem.*, **49**, 325 (1974).
23) Z. Yoshida and S. Kihara, *J. Electroanal. Chem.*, **86**, 167 (1978).
24) Z. Yoshida and S. Kihara, *J. Electroanal. Chem.*, **95**, 159 (1979).
25) P. B. Hirsch, A. Howie, P. B. Nicholson, D. M. Pashley, and M. J. Whelan, "Electron Microscopy of Thin Crystals," Butterworths, London (1965), p. 455.
26) M. Barlow and P. J. Planting, *Z. Metallkde*, **60**, 292 (1969).
27) F. E. Beamish and J. C. Van Loon, "Recent Advances in the Analytical Chemistry of the Noble Metals," Pergamon Press, Oxford (1972), p. 306.
28) M. Hansen and K. Anderko, "Constitution of Binary Alloys," McGraw-Hill, New York (1958).
29) A. N. Frumkin, "Advances in Electrochemistry and Electrochemical Engineering," Interscience Pub., New York (1963), Vol. 3, p. 307.
30) A. N. Frumkin, "Advances in Electrochemistry and Electrochemical Engineering," Interscience Pub., New York (1961), Vol. 1, p. 65.
31) J. N. Butler and A. C. Makrides, *Trans. Farad. Soc.*, **60**, 938 (1964).
32) L. D. Schmidt and R. Gomer, *J. Chem. Phys.*, **42**, 3573 (1965).
33) L. D. Schmidt and R. Gomer, *J. Chem. Phys.*, **45**, 1605 (1966).
34) R. L. Gerlach and T. N. Rhodin, *Surface Sci.*, **19**, 403 (1970).
35) H. Kita, *J. Electrochem. Soc.*, **133**, 1095 (1966).

Preparation of an Ideal Thin Mercury Film Electrode and Its Electrochemical Property

Zenko Yoshida

Chemistry Division, Japan Atomic Energy Research Institute, Tokai, Ibaraki 319-11

(Received May 6, 1980)

In order to get an ideal thin mercury film electrode, the structure of mercury film electrodeposited on foreign metals was investigated with the aid of the thermal-evaporation behavior of mercury and correlated to the electrode properties of the mercury-deposited surfaces. A mercury layer deposited on gold, copper, nickel, or platinum consists of stable mercury compounds with the base metal at their interface and a uniform metallic mercury layer on them. The hydrogen(H)-overpotential at the mercury-coated surface increases with the increase in the amount of mercury deposited. Mercury on molybdenum or stainless steel forms island-like metallic mercury droplets by electrodeposition. The H-overpotential at the surface is identical with that at molybdenum or stainless steel without mercury. Mercury deposited on lead or zinc easily forms a stable amalgam with the base metal, and no metallic mercury is present. The H-overpotential at the surface is slightly less than that at a base metal without mercury. A nickel-based thin mercury film electrode is recommended for such electroanalytical uses as anodic stripping voltammetry.

Thin mercury film electrodes (TMFE) are widely used[1-6] in such electroanalytical fields as stripping analysis. Platinum and silver are usually used as base metals of such TMFE. It has been well known[1,4] that the hydrogen(H)-overpotential at the TMFE is less than that at pure mercury, even when a fairly large amount of mercury is deposited, and that the H-overpotential decreases with the standing time. These disadvantages of the TMFE restrict the electrochemical and analytical use of the TMFE. Generally, the reason for the lowering of the H-overpotential has been empirically understood[1,4] as the diffusion of base metal atoms into the mercury layer or the droplet formation of deposited mercury. However, few reports have discussed the H-overpotential at the mercury-coated electrode theoretically and systematically.

Regarding with the hydrogen-evolution reaction or other electrode properties at thin metal film electrodes, combinations of deposited metals and base metals are divided into two groups.[7] In one group, the monolayer metal deposited shows an electrode property identical with that at the pure metal to be deposited,[8-10] while in the other the electrode property at the thin metal film electrode is different from that at the pure metal, even when the amount of metal deposited is fairly large.[7,11] As a typical example of the latter, the mercury-coated platinum electrode was investigated in the preceding report.[7] The cause of the gradual change in electrode properties with the increase in the amount of mercury was explained by the development of the stable platinum-mercury intermetallic compounds, which affect the electrode property of the surface of mercury deposited. Moreover the decrease in the H-overpotential with the standing time was attributed to the formation of $PtHg_4$.

From the analytical point of view, a stable indicator electrode with a large H-overpotential is required. Mercury is indispensable because of its large H-overpotential. On the other hand, a suitable base metal for the TMFE should make the stable mercury layer both mechanically and chemically and should not lower the H-overpotential of mercury.

In the present report, the structure of the mercury layer deposited and the hydrogen-evolution reaction at the deposited mercury surface are studied employing gold, copper, nickel, molybdenum, lead, zinc, and stainless steel as base metals. On the basis of these results, a criterion for selecting the most preferable metal as the base metal of the TMFE is suggested.

Experimental

The metals used were of purities more than 99.9%. Mercury (II) and supporting electrolyte solutions were prepared using specially purified water as has been reported previously.[7] The electrolytic measurement and determination of mercury vapor by flameless atomic absorption spectrophotometry (AAS) were carried out by means of the apparatus described in the previous paper.[7] The electrolytic measurements were carried out at 25 ± 0.5 °C, and the potentials were referred to a saturated calomel electrode (SCE) unless otherwise mentioned. The surface area of the electrode was 1.13 cm^2.

Pretreatments of the Metals.[12] The gold, copper, nickel, molybdenum, lead, zinc, and stainless steel used as base metals were electropolished anodically by using a stainless steel cathode at applied potentials of 6 V in a cyanide bath,[13] at 5 V in 60% phosphoric acid in water, at 5 V in 60% sulfuric acid in water, at 5 V in 12.5% sulfuric acid in methanol, at 6 V in 60% nitric acid in methanol, at 2.5 V in 20% nitric acid in methanol, and at 8 V in 64% phosphoric acid + 15% sulfuric acid in water, respectively. Then the polished metals were washed with water.

Deposition of Mercury. Mercury was electrodeposited on metals, except on copper, by controlled-potential electrolysis for 15 min in a deaerated electrolyte solution which contained various concentrations of mercury (II), 1×10^{-1} M (1 M= 1 mol dm^{-3}) in potassium perchlorate, and 1×10^{-3} M in perchloric acid. The electrodeposition potentials of mercury on gold, nickel, molybdenum, lead, zinc, and stainless steel were at +0.20, −0.45, −0.10, −0.50, −1.30, and 0.0 V, respectively. Mercury was deposited on copper spontaneously when the copper plate was dipped in a solution containing mercury (II).

H-overpotential Measurements. The hydrogen-reduction peak potential, E_p, in a cyclic voltammogram which was obtained in 1×10^{-1} M potassium perchlorate and 1×10^{-3} M perchloric acid at a potential scanning rate of 2 mV s^{-1} was employed for convenience in studying the H-overpotential.[7] The cathodic potential scan was started at potentials about

50 mV more negative than the dissolution potential of the electrode. The galvanostatic measurements were carried out by the procedures described previously.[7]

Thermal Evaporation of Mercury (T-Hg curve). In order to ascertain the structure of the mercury layer deposited, the thermal-evaporation behavior of mercury was investigated by means of the procedure and apparatus reported previously.[7,13]

Results

Mercury-coated Gold, Copper, or Nickel. Structure of Mercury Deposited: A mercury-coated electrode was heated in an argon stream (2 l min^{-1}) at a raising rate of temperature of 20 °C min^{-1}, and the evaporated mercury was detected by means of flameless AAS (*T*-Hg curve).[13] With the increase in the amount of mercury, one to four peaks were observed.

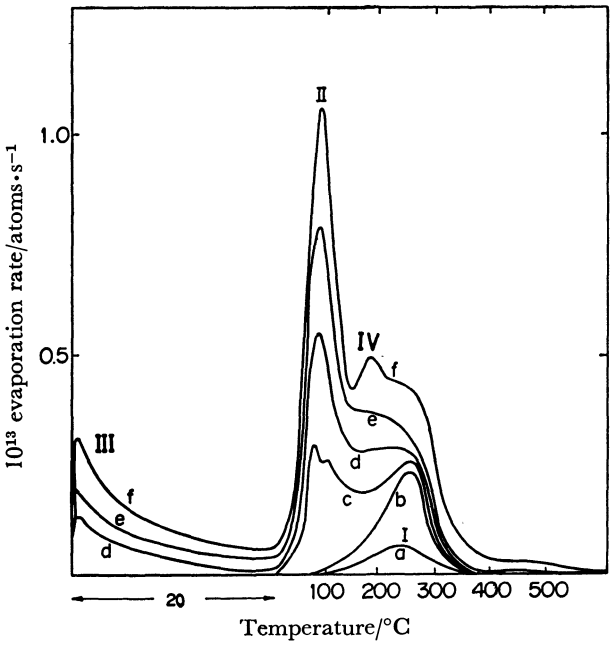

Fig. 1. *T*-Hg curves of mercury deposited on gold.
Amounts of mercury deposited (μg cm^{-2}): (a) 0.07, (b) 0.20, (c) 0.50, (d) 0.97, (e) 1.28, (f) 2.32.

The *T*-Hg curves of mercury, 0.07—2.3 μg cm^{-2}, deposited on gold are illustrated in Fig. 1. Peaks I, II, III, and IV are observed at 243, 100, 20, and 160 °C, respectively. These *T*-Hg curves are analogous to those of mercury deposited on platinum.[7] By comparing them with the results of the detailed investigations of mercury on platinum[7] or gold[13] in the previous papers, Peaks I, II, III, and IV in Fig. 1 are identified as the mercury evaporations from a stable first mercury layer, metallic mercury, adatom mercury, and alloy between gold and mercury, respectively. With a small amount of mercury (less than 0.20 μg cm^{-2}), only Peak I is observed, and this peak is saturated at 0.20 μg cm^{-2}. In the previous study,[7] the structure of the first mercury layer on platinum was confirmed to be Pt_2Hg. Assuming that each mercury atom deposited is combined with one platinum or gold atom of the electrode surface, with a roughness factor of unity, the amount of mercury which makes the complete monolayer should be about 0.5 μg cm^{-2}, because the lattice constants of platinum or gold are nearly equal to 4 Å. In view of the saturated amount of the first mercury layer on gold (0.20 μg cm^{-2}), and the generally accepted structure of stable mercury-gold intermetallic compounds,[14] the first mercury layer on gold is considered to be Au_xHg, where x is 2 or 3.

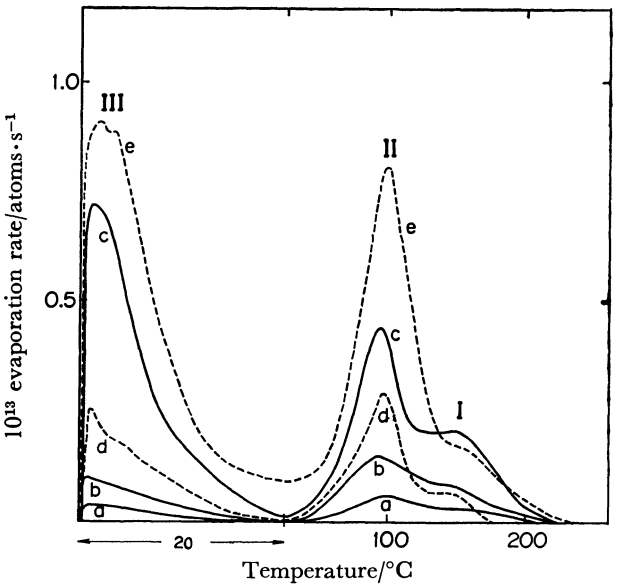

Fig. 2. *T*-Hg curves of mercury deposited on copper and nickel.
Amounts of mercury deposited (μg cm^{-2}): (a) 0.06, (b) 0.16, (c) 0.64, (d) 0.25, (e) 0.95. Based metal: (a)—(c) copper, (d), (e) nickel.

The mercury layer deposited on copper or nickel shows a different *T*-Hg behavior from those on platinum and gold, as is shown in Fig. 2. Even when less than 0.20 μg cm^{-2} of mercury is deposited, three peaks are observed in the *T*-Hg curves, *i.e.*, Peak I at about 160 °C, Peak II at 100 °C, and Peak III at about 20 °C. With the increase in mercury, these peaks develop and Peak I is not saturated. The mercury evaporates from the stable layer at a lower temperature (Peak I at 160 °C) than that of mercury on platinum or gold, indicating that the interaction between mercury and copper or nickel is less than that between mercury and platinum or gold. The idea of a small interaction is also supported by the large adatom layer on copper or nickel, shown in Fig. 2, because a large amount of the adatom layer was formed on the glassy carbon (GC) electrode,[15] which has very weak interaction with mercury. The absence of any preferential saturation of the stable mercury layer on copper or nickel can also be explained by the small interaction with mercury.

The large amount of mercury (100—250 μg cm^{-2}) deposited on gold, copper, or nickel shows the *T*-Hg curves shown in Fig. 3. The *T*-Hg curves of mercury deposited on platinum[7] or GC[15] previously investigated are also illustrated in this figure. The mercury deposited on GC is purely metallic and is unstable from the mechanical point of view, for no stable mercury layer

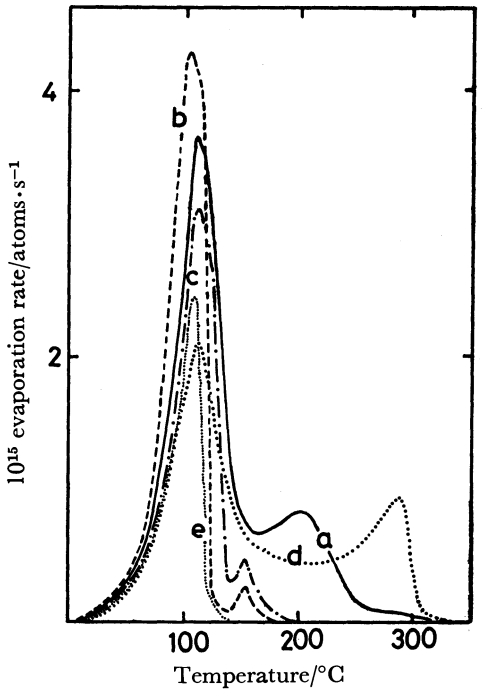

Fig. 3. *T*-Hg curves of mercury deposited on gold, copper, nickel, platinum, and glassy carbon.
Amounts of mercury deposited (μg cm^{-2}): (a) 230, (b) 172, (c) 138, (d) 190, (e) 97. Based metal: (a) gold, (b) copper, (c) nickel, (d) platinum, (e) glassy carbon.

is formed at the GC-mercury interface. The mercury layer deposited on platinum or gold consists of the stable mercury and metallic mercury layer, and the stable mercury occupies quite a large portion of the total deposited mercury, while a small amount of the stable mercury is formed in the mercury layer deposited on copper or nickel. The mercury layer on copper or nickel is mechanically stable because of the interaction between mercury and the base-metal surfaces, though the interaction is rather small.

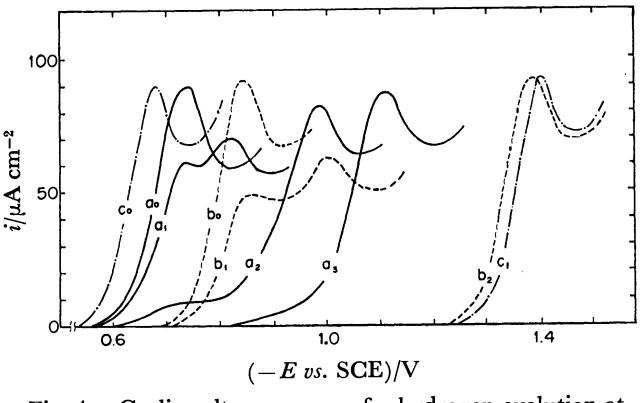

Fig. 4. Cyclic voltammograms for hydrogen evolution at gold, copper, and nickel electrodes with and without mercury.
Electrolyte: 1×10^{-1} M potassium perchlorate and 1×10^{-3} M perchloric acid. Rate of potential scanning: 2 mV s^{-1}. Based metal: (a) gold, (b) copper, (c) nickel. Amounts of mercury deposited (μg cm^{-2}): (a_0) 0, (a_1) 0.40, (a_2) 0.85, (a_3) more than 1.0, (b_0) 0, (b_1) 1.1, (b_2) more than 80, (c_0) 0, (c_1) more than 100.

Hydrogen-evolution Reaction at Mercury-coated Gold, Copper, or Nickel. The cathodic parts of cyclic voltammograms for hydrogen evolution in an electrolyte solution containing 1×10^{-1} M in potassium perchlorate and 1×10^{-3} M in perchloric acid, obtained at the gold, copper, or nickel electrode with and without mercury, are shown in Fig. 4. The cyclic voltammograms in the second potential scan are adopted in order to determine the H-overpotential at mercury-coated metals for the same reason as in the previous paper.[7] Two waves are frequently observed in voltammograms when the amount of mercury is small. The first peak corresponds to the hydrogen evolution at the base-metal surface which is not covered with mercury. The peak potential of this wave is identical with that at a base metal without mercury, and the peak current of this wave decreases with the increase in mercury. The second peak potential is employed as the H-overpotential at a mercury-coated electrode.

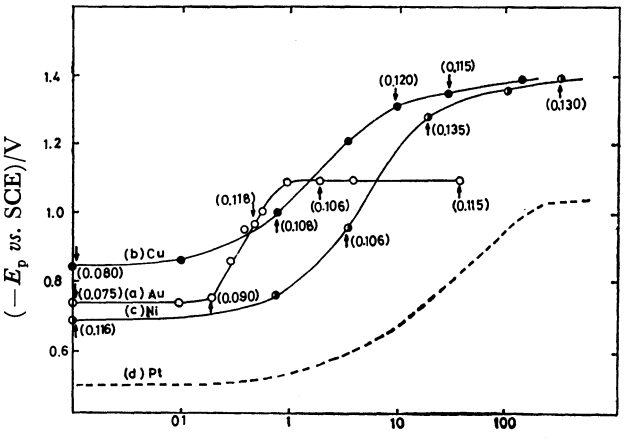

Fig. 5. Hydrogen overpotential, E_p, and Tafel slope, b, at mercury-coated gold, copper, and nickel with various amounts of mercury.
Based metal: (a) gold, (b) copper, (c) nickel, and (d) platinum (------).

The relation between the amount of mercury deposited and the second peak potential, E_p, observed is illustrated in Fig. 5. The value in parentheses indicates the Tafel slope, b[7] (in V), for the hydrogen-evolution reaction at the electrode which corresponds to the plot indicated with an arrow. When two waves are observed in a cyclic voltammogram, the Tafel slope for the second wave is employed. The dashed curve (d) shows the relation for mercury deposited on platinum, which was reported in the previous paper.[7] With the increase in the amount of mercury deposited, the b slope increases and E_p shifts to a more negative value. As has been described in the preceding section, the coverage of the surface of a gold or platinum electrode is complete with the deposition of a monolayer amount of mercury because of the large interaction between gold or platinum and mercury. E_p does not change from that at mercury-free gold or platinum when less than a monolayer amount

of mercury is deposited. With a larger amount of mercury than the monolayer, the coverage with the mercury deposited is considered not to be uniform because of the small interaction between the first mercury layer and the subsequent mercury layer to be deposited. Moreover, it is obvious from the *T*-Hg curve that compounds are formed between a base metal and mercury. On the other hand, the preferential monolayer formation is not observed when mercury is deposited on copper or nickel, because the interaction between these base metals and mercury is small. Also, the coverage of the surface increases slowly with the increase in the amount of mercury. Therefore, the gradual change in E_p with the increase in the amount of mercury, as shown in Fig. 5, is attributable both to the change in the coverage of the electrode surface and to the formation of the stable compounds.

When more than 1, 80, and 100 μg cm^{-2} of mercury are deposited on gold, copper, and nickel, the E_p values show limiting values, E_p^l, at −1.10, −1.38, and −1.40 V, respectively. These E_p^l values are more positive than that at the HMDE.

Stability of Mercury Layer Deposited on Gold, Copper, or Nickel. When the mercury (200 μg cm^{-2})-coated copper was allowed to stand at 25 °C for 70 h in a deaerated supporting-electrolyte solution, Peak II at 110 °C in the *T*-Hg curve (b) in Fig. 3 decreased to one-half of the initial peak height; instead, a peak at 164 °C and an additional peak at 175 °C develop. With the same standing time (70 h), E_p for hydrogen evolution shifted from −1.38 to −1.10 V. In view of the results of the previous study of the mercury-coated platinum,[7] the effect of the standing time on the *T*-Hg curve and H-overpotential may be attributed to the structural change in the deposited mercury layer due to the alloy formation of mercury with copper which has diffused into the mercury layer. In this connection, the peak height at 110 °C in the *T*-Hg curve for the mercury (200 μg cm^{-2})-coated platinum decreased to one-half within the standing time of only 3 h, as has been reported previously,[7] and E_p shifted from −1.05 to −0.95 V during the standing.

The mercury (200 μg cm^{-2})-coated gold and nickel are chemically stable, and no change in the *T*-Hg curve or H-overpotential is observed with a standing time of up to 70 h.

Mercury-coated Molybdenum or Stainless Steel. Only the peak at 110 °C was observed in the *T*-Hg curves for mercury (0—500 μg cm^{-2}) deposited on these metals. No peak at a higher temperature in the *T*-Hg curve was observed, even when the amount of mercury was increased up to 2—3 mg cm^{-2} and when the mercury-coated electrode was allowed to stand for 70 h. By considering the analogous *T*-Hg curve of mercury deposited on the GC electrode,[15] it is clear that the chemical interaction between mercury and molybdenum or stainless steel is negligibly small. In addition, the amount of mercury deposited on these metals decreased with the standing time.

Cyclic voltammograms at mercury (0—500 μg cm^{-2})-coated molybdenum or stainless steel were identical with those at mercury-free molybdenum or stainless steel; *i.e.*, the E_p values were −0.78 or −0.81 V, respectively.

These results indicate that mercury deposited on these metals forms an island-like deposit instead of a stable mercury layer and that the coverage of the surface of these metals by mercury is incomplete.

Mercury-coated Lead or Zinc. Mercury deposited on lead or zinc formed stable compounds with the base metal and no metallic mercury layer existed at the electrode surface, even when the amount of mercury was 1 mg cm^{-2}; this is apparent in the *T*-Hg curves in Fig. 6.

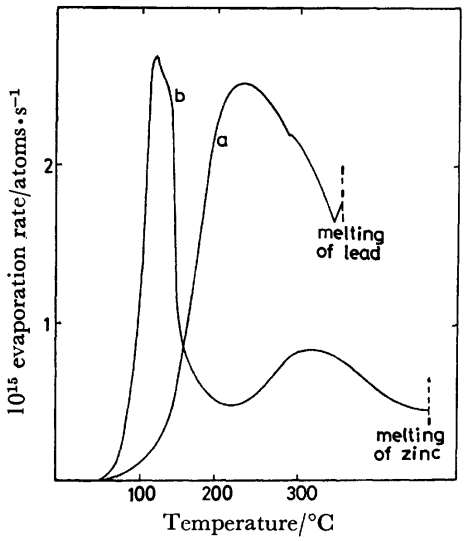

Fig. 6. *T*-Hg curves of mercury deposited on lead and zinc.
Amounts of mercury deposited: more than 1 mg cm^{-2}.
Based metal: (a) lead, (b) zinc.

The hydrogen-evolution potentials, E_p, at a large amount of mercury (about 1 mg cm^{-2})-coated lead or zinc were at −1.43 or −1.32 V, about 100 mV more positive than those at mercury-free lead (at −1.50 V) or zinc (at −1.43 V).

Discussion

Considering the structure of the mercury layer deposited on metals and the hydrogen-evolution reactions at their surfaces described in the Results, base metals can be classified into three groups.

The metals in Group I have fairly large interactions with mercury, and stable mercury layers are formed at the mercury-base metal interfaces. With more than 0.3 μg cm^{-2} of mercury, a metallic mercury surface appears. The H-overpotentials at mercury-coated surfaces increase with the increase in mercury until the limiting potentials, E_p^l, are reached.

The metals in Group II have negligibly small interactions with mercury, and the mercury deposited on these metals forms island-like metallic mercury deposits. The mercury is mechanically unstable. The H-overpotentials at the surfaces on which mercury is deposited are identical with those at mercury-free surfaces.

The metals in Group III form very stable amalgams with mercury, and metallic mercury does not coexist, even when 1 mg cm^{-2} of mercury is deposited. The H-overpotentials at their surfaces are slightly less than those at mercury-free surfaces.

Gold, copper, nickel, and platinum belong to Group I, molybdenum and stainless steel, (and GC) to Group II, and lead and zinc, to Group III.

An ideal thin mercury film electrode (TMFE) should be stable both mechanically and chemically, and it should have a large H-overpotential. In view of these requirements for the TMFE, the metals in Group I are most suitable as the base metals.

The strength of the interaction between mercury and the base metal determines the mechanical stability of mercury film; this strength is semi-quantitatively given by the peak-temperature difference between the evaporation of mercury from the stable mercury layer and the metallic mercury layer, ΔT, in the T-Hg curve. A large ΔT value certifies a stable mercury layer. On the other hand, too large ΔT value reduces the chemical stability and decreases the H-overpotential because of the structural change in the mercury layer during standing (alloy formation). For example, the H-overpotential at the mercury-coated platinum, the ΔT value of which was 190 °C, was remarkably changed with standing.[7] Among the metals studied in the present work, the best base metal for the TMFE was nickel, the ΔT value of which was about 50 °C.

Although ΔT was conventionally used to ascertain the qualitative evaporation behavior of mercury, the activation free energy of thermal evaporation, ΔG^*, was also investigated for a more quantitative treatment. The activation free energy was determined using a procedure similar to that described previously.[13] The differences between the ΔG^* value for the evaporation of the stable mercury and that for metallic mercury, $\Delta(\Delta G^*)$, here obtained were 0.98, 0.42, 0.16, and 0.16 eV for mercury deposited on platinum, gold, copper, and nickel, respectively.

The interaction between the deposited metal and the base metal has been electrochemically recognized as an underpotential[16] for the metal deposition. Kolb *et al.*[17] expressed the underpotential shift, ΔU, correlating to the work function difference between the deposited metal and the base metal, $\Delta\phi$, by using an empirical equation (1):

$$\Delta U = 0.5\,\Delta\phi/e, \tag{1}$$

where ΔU was the difference in peak potentials between the anodic oxidation of the stable layer and the bulk layer, as determined from an anodic stripping voltammogram (ASV). Employing the work function values of 5.40 and 4.50 eV for platinum and mercury reported in Ref. 19, ΔU is calculated to be 0.45 V for mercury deposition on platinum by using Eq. 1. On the other hand, if the rate-determining step in both the thermal evaporation and anodic oxidation reactions is assumed to be the same and is a breaking of the metal bond, producing an atom to be evaporated or oxidized, ΔU can be expressed by using ΔG^*, as in Eq. 2:

$$\Delta U = \Delta(\Delta G^*)/ne, \tag{2}$$

where n is the number of electrons involved in the anodic oxidation reaction. By using the experimentally obtained value as $\Delta(\Delta G^*)$, 0.98 eV for mercury on platinum, and Eq. 2, ΔU is found to be 0.49 V. The underpotential, ΔU, for mercury deposition on platinum has been reported as 0.47 V by Bruckenstein *et al.*[18] and Kolb *et al.*[17] using the ASV curve. In the previous report,[7] ΔU was determined to be 0.45 V from the relation between the electrolysis potential and the amount of mercury deposited (E-Hg plot). For mercury deposition on gold, ΔU was determined as 0.20 V using the E-Hg plot, as has been reported previously.[13] ΔU is calculated as 0.14 V using Eq. 1 or as 0.21 V using Eq. 2. Here, as a work-function value of gold, the value of 4.78 eV which was recommended by Trasatti[19] is employed, although the reported values are distributed from 4.78 to 5.32 eV.[20] The good agreement between the ΔU values calculated from both Eqs. 1 and 2 and the experimental values indicates that ΔU can be correlated to $\Delta(\Delta G^*)$ and $\Delta\phi$, and that the relation between $\Delta\phi$ and $\Delta(\Delta G^*)$ can be expressed by Eq. 3:

$$\Delta(\Delta G^*) = 0.5\,n\,\Delta\phi. \tag{3}$$

Although ΔU cannot be experimentally determined for mercury deposition on copper or nickel using the electrochemical method because of the anodic dissolution of the electrode, ΔU can be predicted from the T-Hg curve by using Eq. 2 to be 0.08 V for the mercury deposition on these metals. The ΔU values are also calculated using Eq. 1 to be 0.03—0.10 and 0.12 V by using the work-function values of copper, 4.55—4.70,[19,21] and nickel, 4.73 eV,[19] respectively.

Because interaction between deposited and base metals is a function of $\Delta\phi$, as has been mentioned above, the general criterion for selecting a suitable TMFE and other metal-film electrodes can be expressed using the work function, which is a general physicochemical parameter and which has been determined for a number of metals. For the ideal TMFE, $\Delta\phi$ should be large enough to form a stable mercury layer with respect to the mechanical stability and should be small with respect to the chemical stability and E_p^1. The reason has not yet been explained, but E_p^1 is more negative with a small value of $\Delta\phi$. $\Delta\phi$ and E_p^1 for the mercury-coated platinum, gold, copper, and nickel are 0.90, 0.28, 0.05—0.20, and 0.23 eV, and −1.05, −1.10, −1.38, and −1.40 V, respectively. By considering that the nickel-based TMFE is the best, a $\Delta\phi$ value of about 0.2 eV is considered to be most suitable for an ideal TMFE. In this connection, the cobalt-based TMFE (the work function of cobalt equals 4.7 eV,[19] $\Delta\phi$=0.2 eV) was stable and showed a large H-overpotential; *i.e.*, E_p^1 was −1.38 V at the mercury (120 μg cm^{-2})-coated cobalt electrode, and E_p^1 did not change upon standing for 70 h.

In the present work, the hydrogen-evolution reaction at the electrode surface was employed in order to investigate the electrode property because of its simplicity and reproducibility of the measurements, though other electrochemical measurements such as pzc, which may be closely correlated to the work function of the electrode surface, can be employed for this purpose.

The *T*-Hg curve is considered to be most available and the simplest for studying the structure of the deposited mercury film directly.

Application of Nickel-based TMFE

The nickel-based TMFE recommended in this work was applied to the anodicstripping voltammetric (ASV) determinations of copper(II), bismuth(III), lead(II), thallium(I), and cadmium(II) in an electrolyte which consisted of 0.5 M of ammonium acetate and 0.1 M of tartaric acid, and the results were compared with the results obtained using the platinum-based TMFE and the HMDE. The mercury layer of the TMFE was 200 μg cm^{-2} (*ca.* 0.15 μm thick). After electrolysis at −0.90 V for 2 min in a stirred solution containing 1×10^{-7} M of metal ions, the voltammogram was recorded anodically from −0.90 to 0 V at a rate of 50 mV s^{-1}.

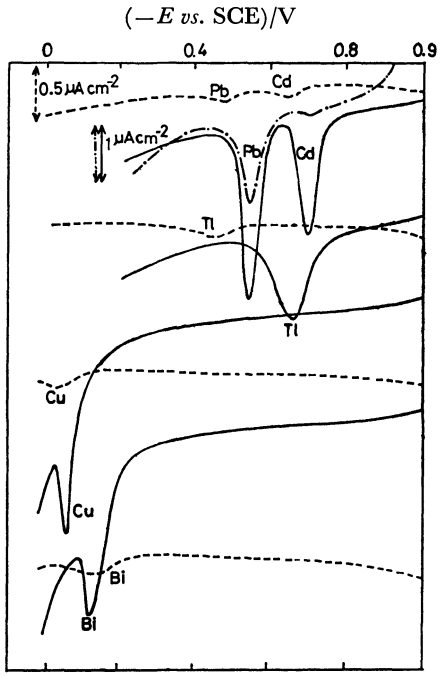

Fig. 7. ASV curves of copper (II), bismuth (III), lead (II), thallium (I), and cadmium (II) using nickel-or platinum-based TMFE and HMDE.
Electrodes; ——mercury (200 μg cm^{-2})-coated nickel, —·— mercury (200 μg cm^{-2})-coated platinum, ------ HMDE. Electrolyte solution; 0.5 M ammonium acetate and 0.1 M tartaric acid containing 1×10^{-7} M of metal ions. Pre-electrolysis; at −0.9 V for 2 min with stirring. ASV; from −0.9 to 0 V at a rate of 50 mV s^{-1}.

As is shown in Fig. 7, the ASV curves obtained by the use of the nickel-based TMFE are more quantitative than those obtained using the HMDE.

When lead and cadmium were simultaneously determined using the nickel-based TMFE, the peak heights in ASV were nearly proportional to the concentrations of the metal ions of 5×10^{-9}—2×10^{-7} M. The standard deviations for the determinations of 5×10^{-9} M of lead and cadmium obtained from five repeated runs were within 5%. The TMFE which had been left standing for 5 d after preparation gave reproducible ASV curves.

When the platinum-based TMFE was used instead of the nickel-based TMFE, the peak height in ASV for lead was proportional to the concentration of lead(II) of 2×10^{-8}—2×10^{-7} M, and 2×10^{-8} M of lead(II) was determined with a standard deviation of about 10%. No ASV peak of cadmium was obtained when the concentration was less than 1×10^{-7} M. The platinum-based TMFE was unstable and could not be used in the ASV determination of cadmium, because hydrogen evolution at the electrode started at about −0.65 V and E_p was at −0.8 V when the electrode had been left standing for 5 h after preparation.

Thus, the nickel-based TMFE is superior to the HMDE and the platinum-based TMFE which have usually been used for the determination of trace metal ions by ASV.

The author would like to thank Dr. Sorin Kihara, Professor Taichiro Fujinaga and his coworkers, and Dr. Kenji Motoiima for their helpful discussions and useful suggestions.

References

1) A. M. Hartley, A. G. Hiebert, and J. A. Cox *J. Electroanal. Chem.*, **17**, 81 (1968).
2) K. Z. Brainina, *Talanta*, **18**, 513 (1971).
3) G. E. Bartley and T. M. Florence, *J. Electroanal. Chem.*, **55**, 23 (1974).
4) Z. Stojek and Z. Kublik, *J. Electroanal. Chem.*, **60**, 349 (1975).
5) T. M. Florence and G. E. Bartley, *J. Electroanal. Chem.*, **75**, 791 (1977).
6) L. Sipos, S. Kozar, I. Kontusic, and M. Branica, *J. Electroanal. Chem.*, **87**, 347 (1978).
7) Z. Yoshida, *Bull. Chem. Soc. Jpn.*, **54**, 556 (1981).
8) N. Furuya and S. Motoo, *J. Electroanal. Chem.*, **88**, 151 (1978).
9) N. Furuya and S. Motoo, *Denki Kagaku*, **41**, 364 (1973).
10) N. Furuya and S. Motoo, *J. Electroanal. Chem.*, **72**, 165 (1976).
11) N. Furuya and S. Motoo, *Denki Kagaku*, **41**. 307 (1973).
12) P. B. Hirsch A. Howie, P. B. Nicholson, D. M. Pashley, and M. J. Whelan, "Electron Microscopy of Thin Crystals," Butterworths, London (1965), p. 455.
13) Z. Yoshida and S. Kihara, *J. Electroanal. Chem.*, **86**, 167 (1978).
14) M. Hansen and K. Anderko, "Constitution of Binary Alloys," McGraw-Hill, New York (1958).
15) Z. Yoshida and S. Kihara, *J. Electroanal. Chem.*, **95**, 159 (1979).
16) D. M. Kolb, "Advances in Electrochemistry and Electrochemical Engineering," Wiley-Interscience, New York (1978), Vol. 11, p. 125.
17) D. M. Kolb, M. Przasnyski, and H. Gerischer, *J. Electroanal. Chem.*, **54**, 25 (1974).
18) M. Z. Hassan, D. F. Untereker, and S. Bruckenstein, *J. Electroanal. Chem.*, **42**, 161 (1973).
19) S. Trasatti, *J. Electroanal. Chem.*, **33**, 351 (1971).
20) S. Trasatti, *J. Electroanal. Chem.*, **54**, 19 (1974).
21) S. Trasatti, *J. Electroanal. Chem.*, **39**, 163 (1972).

Metal-semiconductor Transition with Anomalous Thermal Hysteresis Observed in Hexagonal $(Ni_{1-x}Fe_x)_{1-y}S$, $(0 \leq x \leq 0.30,\ 0 \leq y \leq 0.035)$

Tsukio OHTANI,*,† Koji KOSUGE, and Sukeji KACHI

Department of Chemistry, Faculty of Science, Kyoto University, Sakyo-ku, Kyoto 606

(Received July 7, 1980)

The phase relation of $(Ni_{1-x}Fe_x)_{1-y}S$ system was determined by the X-ray powder diffraction method. $Fe_{1-y}S$ can be dissolved in $Ni_{1-y}S$ in *ca.* 30 at.%. Transition temperature (T_t) was measured mainly by the DSC method. T_t increases with increase in Fe contents. T_t in the forward direction, however, shows a significant increase as high as 50 degrees, when specimens are aged at a temperature below T_t. The reverse transformation is not affected by thermal hystory at all. This is explained by the relaxation process in which the strain energy stored in the low temperature phase is relieved by aging.

NiS (NiAs structure) can be obtained by quenching from high temperature (above 600 K).[1] The first detailed investigations of NiS were performed by Sparks and Komoto[2-4] who found that NiS shows a first-order phase transition at T_t=265 K, the high temperature phase (H-phase) being a Pauli paramagnetic metal and the low temperature phase (L-phase) an antiferromagnetic semiconductor. They also found that the cell volume expands by *ca.* 2.0% through T_t with fall in temperature.[3] Trahan *et al.* performed powder X-ray diffraction measurements and found a crystal symmetry change at T_t.[5] On the other hand MacWhan *et al.* found no crystal symmetry change by X-ray study of single crystals.[6] Various electrical measurements revealed that the H-phase is a normal metal with n-type conduction and the L-phase a p-type semiconductor.[7-12] One of us (T. O.) found that the L-phase is a degenerate semiconductor in which carriers are substantially produced from Ni vacancies.[9] On the basis of magnetic measurements, the H-phase is considered to be a weakly-correlated Pauli paramagnet and the L-phase an antiferromagnet with the itinerant nature.[13,14] T_t is lowered by the deviation from stoichiometry[4] and by external pressure.[15,16] T_t is also sensitive to the impurity ions.[17-20] Thermal hysteresis at T_t was reported by many authors. The hysteresis width is several degrees.[9,21] Trahan and Goodrich, however, reported that an extremely long time is required for the equilibrium near the transition, the thermal hysteresis width being about ten degrees.[22]

There are less complete data and discussions on the origin of the transition. It was found that the enthalpy change at T_t is about 5.0 J mol^{-1} deg^{-1} for stoichiometric NiS.[21,22] Some authors assumed that the large part of entropy change at the transition is due to lattice contribution, suggesting the importance of electron-lattice interaction.[9,23] Strong electron-correlation effect would also play an important role in this transition, as in the case of some transition metal oxides such as V_2O_3 and related vanadium oxides.[24] White and Mott first discussed this transition on the basis of correlation effects.[25] So far, we have few data on NiS which suggest the effect.

The pseudo-binary NiS–FeS system was investigated by Misra and Fleet.[26] They found that the solubility of $Fe_{1-y}S$ into $Ni_{1-y}S$** increases with increasing y (metal deficiency). Continuous solid solution of this system was found to be in metal-poor region above 500 °C. T_t of NiS, Ni being substituted by Fe, has been observed.[17,19,20] We reported that T_t is raised by substitution of Fe ions (T_t increases by about 20 K for 2.0% of Fe substitution), suggesting that the increase in T_t is significantly related to the increase of cell volume.[17] Recently Coey *et al.*[23] and Barthelemy *et al.*[19] investigated the system $(Ni_{1-x}Fe_x)_{1-y}S$. The former proposed the phase diagram in the region with $x<0.10$, $y \simeq 0.04$, which is classified into three distinct regions according to their magnetic behavior. The latter observed two phases: the region with $0 \leq x \leq 0.05$ and that with $0.10 \leq x \leq 0.20$ where c-parameter is greater than that in the first region. So far, no systematic investigation on this system seems to have been performed. No detailed report has appeared on the thermal hysteresis of this transition. We have investigated $(Ni_{1-x}Fe_x)_{1-y}S$ solid solution and the effects of Fe substitution on the phase transition of NiS in the wide composition range and the anomalous thermal hysteresis of the transition.[27] In this paper, we will report the results of investigations.

Experimental

Starting samples of $Ni_{1-y}S$ and $Fe_{1-y}S$ were prepared separately from the pure elements. The method is the same as that reported.[9] $Ni_{1-y}S$ and $Fe_{1-y}S$ obtained were mixed in an appropriate ratio and heated at 1000 °C in evacuated silica tubes for a week, and then quenched into cold water after being annealed at 800 °C for 3 d. Reground samples were heated at 1000 °C and then annealed at temperatures 150—800 °C for a month. Annealed samples were quenched into cold water. Several kinds of measurements were performed for powder and ingot specimens. X-Ray powder diffraction measurements were made on annealed samples. The temperature dependence of the lattice constants was measured in the temperature range 270—360 K for $(Ni_{0.8}Fe_{0.2})_{0.965}S$. DSC measurements were carried out with a Rigaku Thermoflex DSC at 110—373 K using Al_2O_3 as a reference, measurements being made on polycrystals ground in an agate motor. Aging effects on T_t were measured by the DSC method. Electrical resistivity measurements were performed by an oridnary four

† Present address: Okayama University of Science, Laboratory for Solid State Chemistry, 1-1 Ridaicho, Okayama 700.

** Suffix, $1-y$, means that nonstoichiometric specimens contain only the defficient metals.

probes method on ingot samples, and aging effects on resistivity were examined at 290 K. Magnetic susceptibility was measured with a Faraday type torsion balance from liquid N_2 temperature to 373 K. Mössbauer effect measurements were carried out on $(Ni_{0.8}Fe_{0.2})_{0.985}S$ with a conventional spectrometer in a transmission setting at liquid N_2 temperature and at 373 K for samples of both immediately after quenching and after aging for 20 days.

Results

Phase Identification. Phase determination of the pseudo-binary $Ni_{1-y}S$-$Fe_{1-y}S$ system was made on the identification of X-ray powder pattern for quenched samples. Figure 1(a) shows the phase relation of $Ni_{1-y}S$-$Fe_{1-y}S$ system at 800 °C. The closed square indicates hexagonal NiAs phase and the open square two-phase region consisting of NiAs phase and cubic pentlandite phase, $(Fe,Ni)_9S_8$. Stoichiometric NiS takes only less than 30 at. % FeS into solid solution. A continuous solid solution was found to exist in the metal-poor region ($y \leq 0.035$). No extra line due to superstructure development as reported by Misra and Fleet was observed in all samples within experimental errors. At lower temperatures, the two phase region spreads out towards metal-poor compositions; for example at 150 °C the two phase region on NiS–FeS line extends from 20 to 80% of FeS concentration, while on a $Ni_{0.955}S$–$Fe_{0.955}S$ line only up to 20% of $Fe_{0.955}S$ can be dissolved into $Ni_{0.955}S$. Figure 1(b) shows the lattice spacings of the continuous solid solution of $(Ni,Fe)_{0.965}S$ at 800 °C. The a-parameter curve as a function of composition has a minimum at 50 at. % of Fe, while c-parameter changes smoothly with Fe contents.

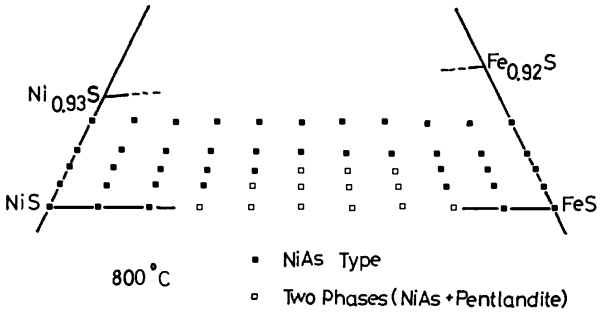

Fig. 1(a). Phase relations of pseudo-binary $Ni_{1-y}S$–$Fe_{1-y}S$ system obtained by quenching from 800 °C. The closed square indicates the hexagonal solid solution (NiAs-type), and the open square the two phase region consisting of hexagonal NiAs and cubic pentlandite phase.

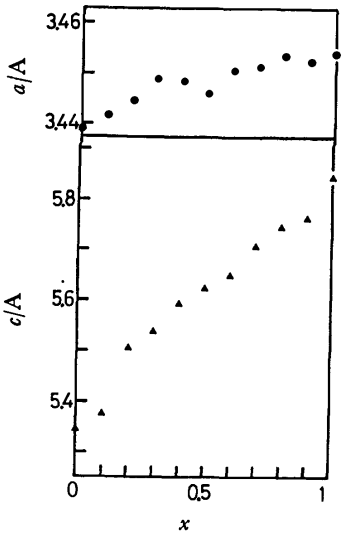

Fig. 1 (b). Lattice spacings measured at room temperature of $(Ni_{1-x}Fe_x)_{0.965}S$ quenched from 800 °C. a-axis is shown by circles and c-axis triangles. Fe contents is taken as abscissa.

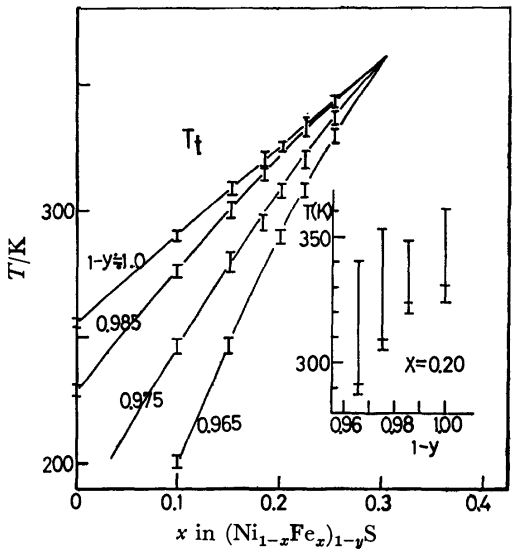

Fig. 2. Transition temperatures (T_t) of $(Ni_{1-x}Fe_x)_{1-y}S$ obtained by DSC measurements. Measurements were carried out on specimens immediately after quenching. x in $(Ni_{1-x}Fe_x)_{1-y}S$ is taken as abscissa and T_t as ordinate. The short vertical lines indicate the width of thermal hysteresis. The upper end of vertical lines corresponds to T_t in heating run, and the lower end T_t in cooling run. The inset shows the aging effects on T_t(F) (T_t in the forward direction) for $(Ni_{0.8}Fe_{0.2})_{1-y}S$. The vertical lines indicate the increase of T_t(F) for various "$1-y$" compositions. Aging temperature is 290 K. Detail is described in the text.

Phase Transition. Transition temperatures were determined mainly by the DSC method. The method of determination of T_t is shown in Fig. 3(b). T_t is very sensitive to thermal history. Results of unaged specimens are as follows. Variation of T_t with Fe contents is given in Fig. 2, where x in $(Ni_{1-x}Fe_x)_{1-y}S$ is taken as abscissa and T_t as ordinate. T_t was measured on heating-cooling cycles on specimens immediately after quenching from 800 °C. Endothermic and exothermic peaks were observed for heating and cooling, respectively. The value of T_t remained unchanged with heating-cooling rate. When "$1-y$" is fixed, T_t increases smoothly with increasing x. All curves of constant "$1-y$" seem to cross at $x=0.30$ (*ca.* 360 K). At $x=0.30$, DSC peaks are somewhat broadened after the first heating run, and for $x>0.30$, no DSC peaks could be detected in any "$1-y$" composi-

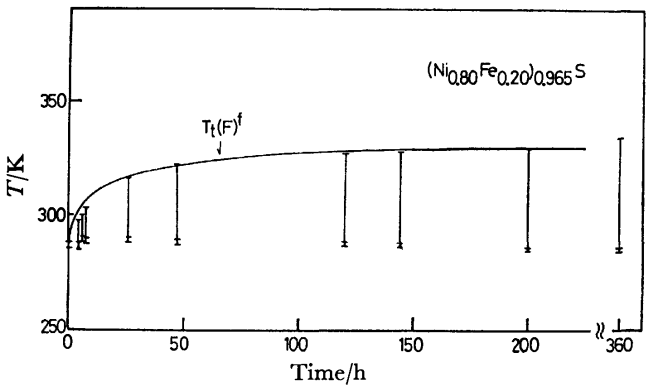

Fig. 3(a). T_t as a function of aging time for $(Ni_{0.8}Fe_{0.2})_{0.965}S$. Aging temperature is 290 K. The time elapsed from immediately after quenching is taken as abscissa. The upper end of vertical lines corresponds to T_t in the forward direction in the first heating run. Two horizontal lines in the lower end of vertical lines show the hysteresis width in the subsequent heating-cooling runs.

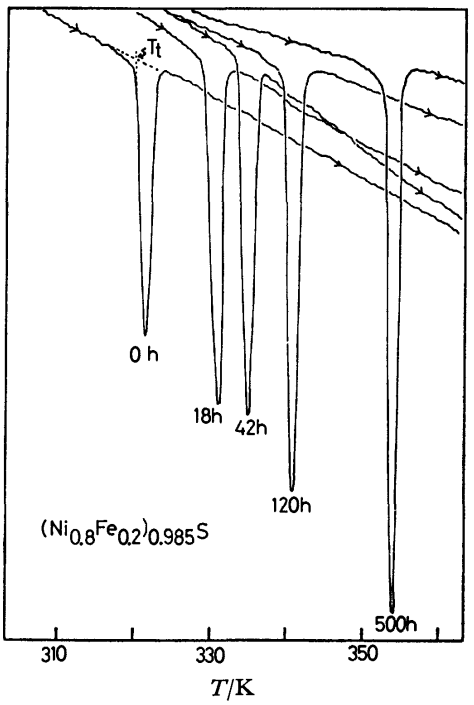

Fig. 3(b). The variation of DSC curves in the first heating runs with time elapsed for $(Ni_{0.8}Fe_{0.2})_{0.985}S$. Aging temperature is 290 K. Transition is endothermic.

tion. The short vertical lines in Fig. 2 indicate the width of thermal hysteresis observed in heating-cooling runs. The width of thermal hysteresis is within several degrees, and seems to be independent of composition. Hereafter, T_t in the heating run (forward direction) is referred to as $T_t(F)$, and T_t in the cooling run (reverse direction) $T_t(R)$.

The results on aged specimens are as follows. The forward transformation shows an anomalous thermal hysteresis in aged specimens. When samples are aged at temperatures below $T_t(R)$, $T_t(F)$ gradually increases with the lapse of time and after sufficiently long time (about 20 days), reaches the final $T_t(F)$ (the final $T_t(F)$ is referred to as $T_t(F)^f$), which is about 50 degrees higher than the initial $T_t(F)$ (the initial $T_t(F)$ is referred to as $T_t(F)^i$). T_t as a function of the time elapsed in the case of $(Ni_{0.8}Fe_{0.2})_{0.965}S$ aged at 290 K is shown in Fig. 3(a). The vertical lines show the width of increase of $T_t(F)$. Endothermic DSC peaks of $(Ni_{0.8}Fe_{0.2})_{0.985}S$ in the first heating run are shown for various aging times, the aging temperature being 290 K (Fig. 3(b)). No evidence of extra peaks can be detected throughout aging. The shape of DSC peaks is very sharp at all aging times, the height of peaks increasing with increasing $T_t(F)$. The inset in Fig. 2 illustrates the "$1-y$" dependence of the width of increase of $T_t(F)$ for $x=0.20$. The upper end of the vertical line corresponds to $T_t(F)^f$. The width of increase of $T_t(F)$ seems to decrease with increasing "$1-y$". The tendency, however, is somewhat ambiguous since the width of increase of $T_t(F)$ is sensitive to experimental conditions. x dependence of $T_t(F)$ is shown in Fig. 4 for

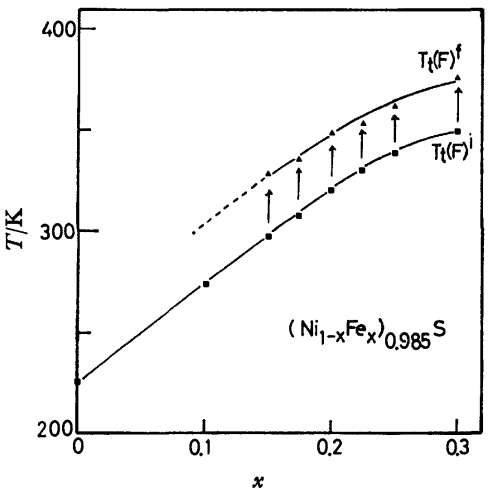

Fig. 4. x dependence of $T_t(F)$ (T_t in the forward direction) for $(Ni_{1-x}Fe_x)_{0.985}S$. Aging temperature is 290 K. Arrows show the increase of $T_t(F)$ by aging. The closed triangles show the final $T_t(F)$ ($T_t(F)^f$). The closed squares show the initial T_t (F) ($T_t(F)^i$).

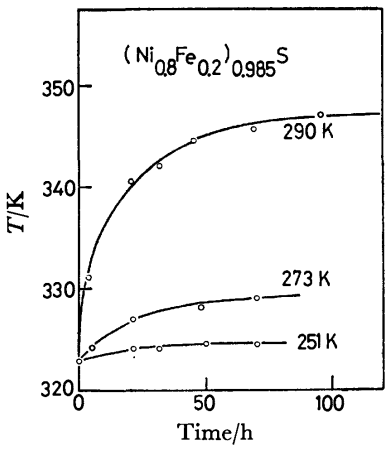

Fig. 5. Aging time dependence of transition temperatures in the first heating run of $(Ni_{0.8}Fe_{0.2})_{0.985}S$ for various aging temperatures (290, 273, and 251 K).

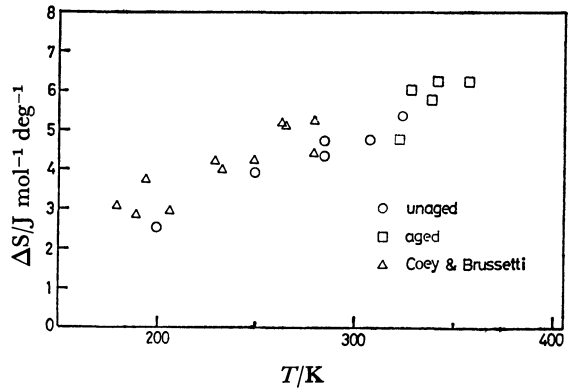

Fig. 6. Entropy change at T_t (ΔS) as a function of T_t for $(Ni_{1-x}Fe_x)_{1-y}S$ system. Open circles show ΔS for unaged specimens. Open square is ΔS for sufficiently aged specimens. Open triangles are those obtained by Coey and Brussetti.[21]

$(Ni_{1-x}Fe_x)_{0.985}S$ which was aged at 290 K. The lower curve shows the x dependence of $T_t(F)^i$ and the upper curve that of $T_t(F)^f$. The width of increase of $T_t(F)$ seems to be independent of x. In specimens of $x \leq 0.10$, the increase could not be observed since $T_t(R)$ is lower than 290 K. Figure 5 shows the variation of $T_t(F)$ with aging temperature for $(Ni_{0.8}Fe_{0.2})_{0.985}S$. Samples were aged at 290 K, 273 K (in ice water) and 251 K (in a mixture of ice, water, and NaCl). Increase in rate is more rapid at the higher aging temperatures. We tried to carry out aging at temperature immediately below $T_t(F)^f$ after aging for a sufficiently long time at 290 K. We could observe no more increase of $T_t(F)$. Increase of $T_t(F)$, however, was also observed in the case of aging at slightly higher temperatures (less than 5 degrees higher) than $T_t(F)^i$. Figure 6 shows the variation of entropy change (ΔS) at the transition with T_t. ΔS was determined from the endothermic peaks. Open circles show the entropy changes of unaged specimens, and open squares those of specimens aged for a sufficiently long time. We see that entropy change at the transition increases almost linearly with increasing T_t. We can recognize no significant difference of entropy change between unaged and aged specimens. For example, ΔS of $(Ni_{0.8}Fe_{0.2})^0{}_{.985}S$ is 4.26 and 6.01 J mol^{-1} deg^{-1} for unaged and aged speciments, respectively: both values fit the curve in Fig. 6. Our results are almost the same as those of Coey and Brussetti[21] shown by open triangles.

The increase of $T_t(F)$ was observed only in the first heating run. When aged samples are once passed through $T_t(F)$ ($>T_t(F)^i$), transition temperatures in the subsequent cooling and heating runs return to the initial $T_t(R)$ and $T_t(F)$ (Fig. 7(a)). When the samples are again aged at temperatures below $T_t(R)$, $T_t(F)$ increases asymptotically approaching $T_t(F)^f$, as in the previous aging process.

Aging effects on other physical properties were examined. X-ray powder diffraction measurements were performed on specimens aged for a sufficiently long time. No extra diffraction peak or shift of diffraction peaks was found. The temperature dependence of lattice spacings of $(Ni_{0.8}Fe_{0.2})_{0.965}S$ aged at 290 K

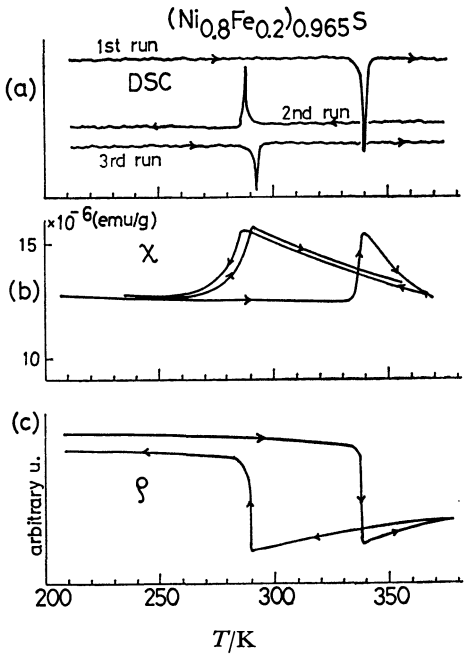

Fig. 7. Typical behaviors of the transition in the first heating run and subsequent cooling-heating runs for $(Ni_{0.8}Fe_{0.2})_{0.965}S$ aged for a long time at 290 K.
(a): DSC curves, (b): magnetic susceptibility, (c): electrical resistivity.

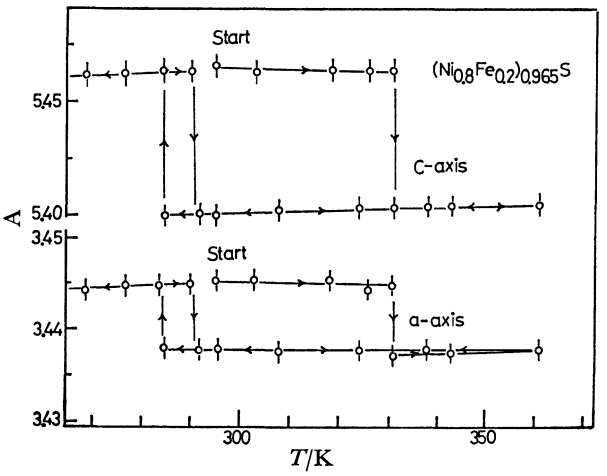

Fig. 8. Lattice spacings of $(Ni_{0.8}Fe_{0.2})_{0.965}S$ as a function of temperature. X-Ray measurements were done firstly on heating run for a sufficiently long time aged specimens, and subsequently on cooling run. Procedure of measurements is shown by arrows.

for sufficiently long time is shown in Fig. 8. The order of X-ray diffraction measurements is indicated by arrows. Both a- and c-parameters decrease slightly with temperature in the first heating run. Abrupt shrinkage was observed at $T_t(F)^f$, and abrupt expansion at $T_t(R)$ in the cooling run. In the second heating run, the transition was observed at $T_t(F)^i$. The results are in line with those of DSC measurements. Typical electrical resistivity (ρ) as a function of temperature is shown in Fig. 7(c) for $(Ni_{0.8}Fe_{0.2})_{0.965}S$ aged for a long time. In Fig. 9, the electrical resistivity (ρ)

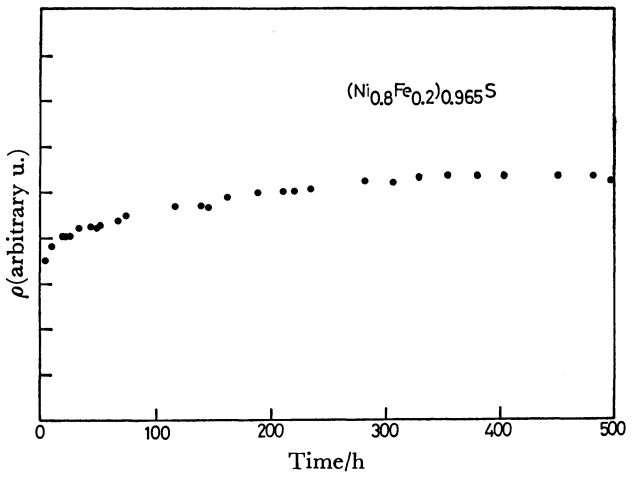

Fig. 9. Aging time dependence of electrical resistivity of $(Ni_{0.8}Fe_{0.2})_{0.965}S$. Aging temperature is 290 K.

at 290 K is plotted against the lapse of time for $(Ni_{0.8}Fe_{0.2})_{0.965}S$ which was quenched from 800 °C. Since $T_t(F)^i$ is slightly above 290 K, $T_t(F)$ increases with time elapsed. Resistivity increases with time elapsed and seems to be saturated after aging for *ca.* 400 h. Magnetic susceptibility (χ) of $(Ni_{1-x}Fe_x)_{0.085}S$ ($x \lesssim 0.30$) aged for sufficiently long time is given in Fig. 10 as a function of temperature. Heating and cooling rate is 10 °C/min. Heating and cooling cycles are shown by arrows. Typical behavior of χ is shown in Fig. 7(b) for $(Ni_{0.8}Fe_{0.2})_{0.965}S$ aged for a long time. The kinks in χ curves correspond to the transition. The difference of χ between aged and unaged samples is very small except for near transition. There is a broad maximum in χ curves in samples of $x \geq 0.250$ at about 140 K, while χ of the other samples is almost constant with temperature. The results of Mössbauer measurements are shown in Fig. 11. Measurements were carried out for both aged (for 20 d) and unaged specimens of $(Ni_{0.8}Fe_{0.2})_{0.985}S$. An absorption spectrum with quadrupole splitting was observed at 373 K

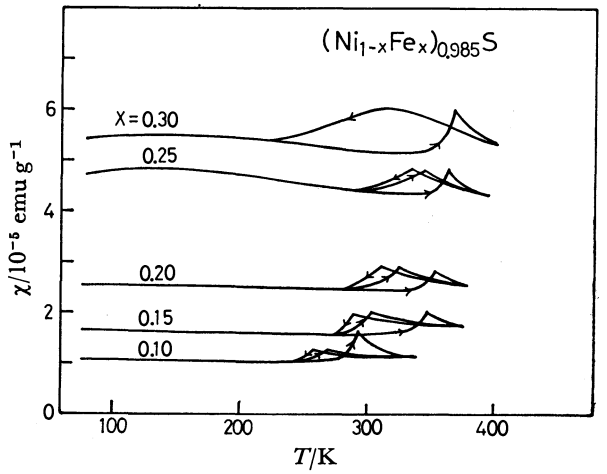

Fig. 10. Magnetic susceptibility of sufficiently long time aged $(Ni_{1-x}Fe_x)_{0.965}S$ ($x \lesssim 0.30$) as a function of temperature. Heating-cooling cycles are shown by arrows.

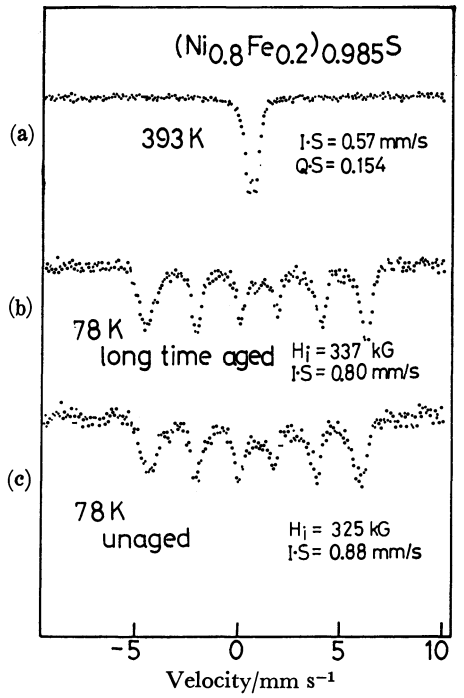

Fig. 11. Mössbauer spectra for $(Ni_{0.8}Fe_{0.2})_{0.985}S$. (a): Spectra at 393 K (above $T_t(F)^f$), (b): spectra at 78 K for a long time aged specimen, (c) spectra at 78 K for unaged specimen.

(Fig. 11(a)), the isomer shift and quadrupole splitting being 0.57 and 0.154 mm/s, respectively. Magnetic sextets were observed at 78 K. Figures 11(b) and (c) show the results obtained at 78 K for $(Ni_{0.8}Fe_{0.2})_{0.985}S$ aged for a long time and unaged, respectively. Internal magnetic field is 2.68×10^7 and 2.59×10^7 A m^{-1} for aged and unaged specimen, respectively. Isomer shift is 0.80 and 0.88 mm/s for aged and unaged specimen, respectively.

The results of anomalous thermal hysteresis are summarized as follows.

a) $T_t(F)$ increases with time, when the specimens are aged at temperature below $T_t(R)$. $T_t(F)^f$ is *ca.* 50 degrees higher than $T_t(F)^i$. $T_t(F)$ is unchanged when specimens are aged at temperatures above $T_t(F)$. $T_t(R)$ is not affected by heat treatment.

b) When aged specimens are once passed through $T_t(F)$ ($> T_t(F)^i$), $T_t(F)$ in the subsequent heating runs return to $T_t(F)^i$. When samples are again aged at temperatures below $T_t(R)$, the same aging effects are also observed.

c) Two phase mixture of the initial and the final state is not observed in the course of aging in both DSC curves and X-ray powder diffraction patterns. No new phase was observed during the course of aging.

d) Increase in the rate of $T_t(F)$ increases with rise in aging temperature.

e) The width of increase of $T_t(F)$ seems to be almost independent of x composition.

f) The nature of phase transition, *i.e.* metal-semiconductor transition accompanied by magnetic change, is essentially unchanged by aging treatment. Physical properties of both aged and unaged specimens are

compared as follows.

1) No crystallographycal difference is found in X-ray diffraction patterns.

2) Electrical resistivity of aged specimens is higher than that of unaged one.

3) Difference of magnetic susceptibility is very small.

4) Internal magnetic field of aged specimen is higher than that of aged one.

Discussion

In the course of studies on the phase transition of $(Ni_{1-x}Fe_x)_{1-y}S$ system, we found anomalous aging effects on the transition temperature. First let us consider the phase relation of this system. Misra and Fleet[26] have reported the monosulfide solid solution in the temperature range 230—600 °C. They found extra peaks such as super lines in powder patterns of all of monosulfide-bearing products. However, we found no extra peak in X-ray diffraction patterns, confirming the distinct region of solid solution of this system. Solid solution was also confirmed by DSC measurements which show smooth increase of the transition temperature with Fe contents up to 30 at. %. Barthelemy *et al.*[19] found two phases in $Ni_{1-x}Fe_xS$ with small amount of Fe at 550 °C, one with $0 \leq x \leq 0.05$, the other with $0.10 \leq x \leq 0.20$ and a mixture of two phases with $0.05 < x < 0.10$. c-parameter of the second phase is greater than that of the first one. This can be explained by our results of aging effects. T_t in the composition range of $0.05 < x < 0.10$ lies near room temperature. Thus, in the range $0 \leq x \leq 0.05$, X-ray diffraction patterns at room temperature show a pattern of the H-phase; in the range $0.10 \leq x \leq 0.20$ they show one of the L-phase which has a greater c-parameter than the H-phase. Two phase mixture in the region $0.05 < x < 0.10$ can be explained by the following results. In specimens which have T_t slightly below room temperature, T_t gradually increases with the lapse of time at room temperature. X-Ray diffraction patterns at room temperature show the two phase mixture of the H- and L-phases, both phases having the NiAs type structure while lattice spacings differ from each other. Two phase mixture has been observed for 48 h in X-ray charts; this feature is remarkable especially in (102) reflection. No lattice modification was found in the $(Ni_{1-x}Fe_x)_{1-y}S$ system.

The phase transition of this system is accompanied by the drastic changes of electrical and magnetic properties, this being metal-semiconductor transition similar to that of pure NiS. $(Ni_{1-x}Fe_x)_{1-y}S$ with Ni-rich composition has substantially the same characteristics of phase transition as that of pure NiS.

Let us consider the aging effects on the phase transition. It is important to examine whether this is characteristic of only Fe substituted $Ni_{1-y}S$. Trahan and Goodrich[22] found in their calorimetric measurements that it takes a long time for stoichiometric NiS to attain equilibrium near the transition, exhibiting a considera ble- hysteresis. T_t was observed to be 276 K in heating run, and 269 K in cooling run, while in cooling run the samples supercooled approximately by 2.5 K. All previous publications except that of Trahan and Goodrich reported that T_t of NiS lies in the neighbourhood of 265 K. The anomalous high transition temperature in heating runs of Trahan and Goodrich is presumably due to the aging effects. For the sake of confirmation we performed DSC measurements for undoped NiS. We observed the increase of T_t(F) : T_t(F) increases by about 1 degree by annealing at 250 K for 24 h, in line with the data of Fig. 5. Thus the increase of T_t(F) by aging is considered to be characteristic phenomenon in NiS as well as in $(Ni_{1-x}Fe_x)_{1-y}S$.

The phenomenon can be regarded as thermal hysteresis, a common feature of the first order transition. In the reversible transformation of the first order, the hysteresis width is closely related to the volume change at the transition, ΔV.[28,29] For example, for the transition of NH_4Cl ($P_{m3m} \rightarrow F_{m3m}$) the width of hysteresis is 35 K, and $\Delta V + 7.14$ cm^3/mol; for CsCl ($P_{m3m} \rightarrow F_{m3m}$) hysteresis width is 33 K, $\Delta V + 10.28$ cm^3/mol. In the case of $(Ni_{1-x}Fe_x)_{1-y}S$, the reversible thermal hysteresis is observed in unaged specimens, where the hysteresis width is several degrees. This seems to be reasonable since ΔV is relatively small, *ca.* -0.3 cm^3/mol. The increase of T_t(F) by aging, as high as 50 degrees, seems to be enormously large.

Gradual increase of T_t(F) with aging indicates that the initial unaged state is in thermally non-equilibrium, passing gradually into equilibrium. This has been reported, *e.g.* anatase-rutile or brookite-rutile in TiO_2[30] or hexagonal-tetragonal transformation in GeO_2.[31] The transformation is a function of time and temperature. In the transient state from metastable to stable one, two phases usually coexist. Transformation kinetics has been investigated by using the Avrami equation. The present case differs a great deal from above cases. DSC measurements show continuous shift of T_t(F), but X-ray diffraction measurements show no two phase mixture. Thus, the present case can not

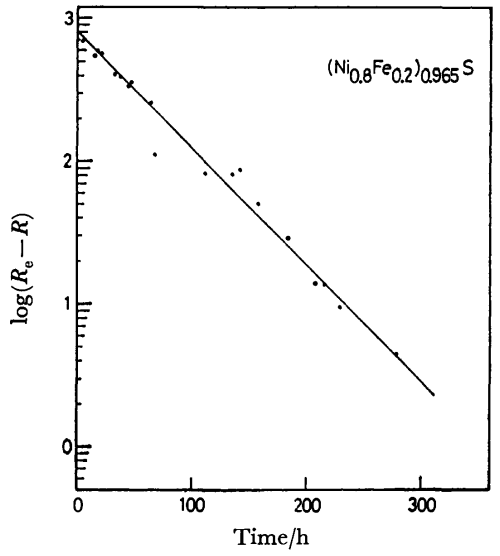

Fig. 12. The logarithm of $(R_e - R)$ as a function of elapsed time. $(R_e - R)$ is the difference between the resistivity at $t = \infty$ and time t.

be interpreted in a similar manner to the above substance.

As shown in Fig. 9, the electrical resistivity (ρ) increases very gradually with elapsed time if samples are aged at 290 K (below T_t(R)). After a sufficiently long time, ρ attained the value of thermal equilibrium state, R_e. In Fig. 12, the logarithm of the difference between the resistivity at time $t=\infty$ and time t, (R_e-R) is plotted against t (data are the same as in Fig. 9). For an exponential change the graph should be a straight line, and this is the case. Thus, it is presumed that the time dependence of ρ has the form

$$R_e - R = Ae^{-t/\tau},$$

where A is a constant and τ the relaxation time. From the slope, we estimated τ to be 118 h. A similar treatment was performed by Trahan and Goodrich,[22] who measured the electrical resistivity near the transition temperature of stoichiometric NiS, and estimated τ to be 48 h. They did not, however, specify the aging temperature. From analogy with the present case, we suppose their measurements were taken at temperature below T_t(R). Thus, we can conclude that the aging effect is the relaxation process from thermally non-equilibrium state to equilibrium one.

Generally, phase transition is described in terms of nucleation and growth. At the start of transition, the nuclei of a new phase are first formed in the parent phase, followed by development of the new phase. If specific volumes differ from each other, the product phase in the parent phase produces strain. If the parent phase is not sufficiently soft, the elastic strain energy might be stored in the crystal. The interfacial energy formed between the product and the parent phase should also be considered. Ubbelohde[32] suggested that extra terms for the strain energy and the interfacial energy should be added to the usual independent variables that determine the free-energy; the strain energy is a main factor controlling thermal hysteresis.

We should consider the following characteristics of the transition. The transition is accompanied by drastic volume expansion with fall in temperature (about 2.0%). The material becomes brittle below T_t; *i.e.* specimens cracked through transition with lowering temperature. The mechanism of phase transition differs for the case of the forward and reverse directions. In the forward direction (a), the relatively soft phase grows in the brittle phase associated with volume contraction, while in the reverse direction (b) a brittle phase grows in soft matrix associated with volume expansion. In (a) the product phase is strained under tension, and in (b) it is strained under compression. The large difference in the sensitivity of the transition temperature between (a) and (b) may be due to such different transition mechanism. Since the L-phase is brittle, it has a larger contribution to the strain energy than the H-phase. Thus, (a) would be more sensitive to the thermal treatments than (b).

Considering the L-phase which is in a state immediately after reverse transition (non-equilibrium state), excess energy such as strain energy would be expected to be stored in the crystal. Such a state would

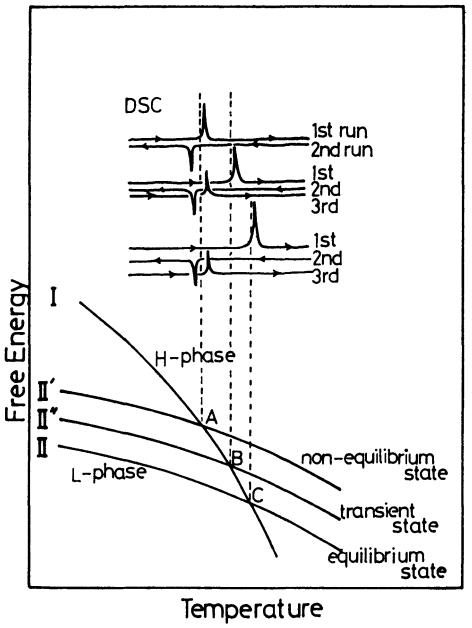

Fig. 13. Tentative Gibbs free-energy diagram for $(Ni_{1-x}Fe_x)_{1-y}S$ system. Curve I, II, II′, and II″ are Gibbs free-energy curves of the H-phase, equilibrium state of L-phase, non-equilbrium state of L-phase and the transient state from non-equilibrium to equilibrium state of L-phase, respectively. Free-energy curve of nonequilibrium state is in a higher energy state than the equilibrium state due to the stored strain energy in the L-phase. Curve I is assumed to be invariant to thermal treatments. The upper side of the figure indicates DSC curves corresponding to each state.

be in a higher energy state than the equilibrium state stabilized by aging for long time below T_t(R). Thus, free energy-temperature curve for the non-equilibrium state is expected to lie slightly above that of the equilibrium one. Such a relation is schematically illustrated in Fig. 13, where curves I, II, II′, and II″ are Gibbs free-energy curves, corresponding to the H-phase, the equilibrium state of L-phase, the nonequilibrium state of L-phase and the transient state from non-equilibrium to equilibrium state of L-phase, respectively. Curve I is assumed to be independent of thermal history of the specimens. Curve II′, II″, and II intersect with curve I at points A, B, and C, respectively. DSC curves are shown for each state. Relaxation phenomenon would be considered to be the process where the stored strain energy is relieved by aging, corresponding to the lowering in free energy curve from II′ to II, accompanied by the increase of transition temperature.

The relaxation phenomenon would be also considered as an order-disorder process, where non-equilibrium disordered state is transformed to the equilibrium ordered state with aging. The disordered state would be expected to have higher energy than the ordered one. In Fig. 13, the disordered state corresponds to curve II′, and the ordered state curve II. The order-disorder transition is considered to occur at the same temperature as T_t(F). If this is not the case, aging effect should be observed also in the H-phase. This mechanism,

however, does not seem to be applicable to the present case. If the ordering is due to metal vacancies, superlines due to ordering should be observed in X-ray charts. This could not be confirmed. If the ordering process occurred between Ni and Fe atoms, no aging effects should be observed in pure NiS. According to Trahan and Goodrich,[22] and our present measurements, aging effects were observed also in NiS. The difference of entropy change at T_t between aged and unaged state could not be detected by DSC measurements.

So far, aging effects similar to the present case have been observed in a few materials. Murray and Allison[33] observed the aging effects in ZrO_2, where the tetragonal to monoclinic phase transition (reverse transition) is slightly affected by heat treatments; *i.e.* the transition temperature of the reverse direction is drastically raised by either heating-cooling cycles through the transition or aging at tetragonal phase (above the transition temperature). They interpreted this phenomenon as the ordering process in the tetragonal phase. On the other hand, Maiti *et al.*[34] attributed this to the superplastic nature of the tetragonal phase. Another example was reported by Murakami *et al.*,[35] who found a very similar phenomenon to the present case in Au-Cu-Zn alloys. Martensite reverse transition temperature of $Au_{26}Cu_{30}Zn_{44}$ alloy increases by about 20 K, when it is aged at 290 K (below the transition temperature). They assumed that the aging effect is due to the stabilization and pinning of the martensite plate boundaries, which give rise to an increase in the driving force for the transition.

In conclusion, we have observed a new type of thermal hysteresis in $(Ni_{1-x}Fe_x)_{1-y}S$ system. It is considered to be a relaxation process where the strain energy stored in the L-phase is relieved by aging.

The author wish to express their sincere thanks to Prof. T. Takada and Dr. T. Shinjo for enabling them to carry out the Mössbauer measurements.

References

1) M. Laffitte, *Bull. Soc. Chim. Fr.*, **1959**, 1211.
2) J. T. Sparks and T. Komoto, *J. Appl. Phys.*, **34**, 1191 (1963).
3) J. T. Sparks and T. Komoto, *Phys. Lett. A*, **25**, 398 (1968).
4) J. T. Sparks and T. Komoto, *Rev. Mod. Phys.*, **40**, 752 (1968).
5) J. Trahan, R. G. Goodrich, and S. F. Watkins, *Phys. Rev. B*, **2**, 2859 (1970).
6) D. B. McWhan, M. Marezio, J. P. Remeika, and P. D. Dernier, *Phys. Rev. B*, **5**, 2552 (1972).
7) T. Ohtani, K. Kosuge, and S. Kachi, *J. Phys. Soc. Jpn.*, **28**, 1558 (1970).
8) T. Ohtani, K. Kosuge, and S. Kachi, *J. Phys. Soc. Jpn.*, **29**, 521 (1970).
9) T. Ohtani, *J. Phys. Soc. Jpn.*, **37**, 701 (1974).
10) M. G. Townsend, R. Tremblay, J. L. Horwood, and L. B. Ripley, *J. Phys. C*, **4**, 598 (1971).
11) J. L. Horwood, L. G. Ripley, M. G. Townsend, and R. J. Tremblay, *J. Appl. Phys.*, **42**, 1476 (1971).
12) E. Barthelemy, O. Gorochov, and M. McKinzie, *Mat. Res. Bull.*, **8**, 1401 (1973).
13) J. M. D. Coey, R. Brussetti, A. Kallel, J. Schweizer, and H. Fuess, *Phys. Rev. Lett.*, **32**, 1257 (1974).
14) R. Brussetti, Thesis, Grenoble University, 1978.
15) S. Anzai and K. Ozawa, *J. Phys. Soc. Jpn.*, **24**, 271 (1968).
16) S. Anzai and K. Ozawa, *J. Appl. Phys.*, **48**, 2139 (1977).
17) T. Ohtani, K. Kosuge, and S. Kachi, *Phys. Status Solidi B*, **66**, 765 (1974).
18) T. Sawa and S. Anzai, *J. Appl. Phys.*, **49**, 5612 (1978).
19) E. Barthelemy, C. Chavant, G. Collin, and O. Gorochov *J. Phys. (Paris), Colloq.*, **37**, C4-17 (1976).
20) R. F. Koehler, Jr., R. S. Feigelson, H. W. Swarts, and R. L. White, *J. Appl. Phys.*, **43**, 3127 (1972).
21) J. M. D. Coey and R. Brussetti, *Phys. Rev. B*, **11**, 671 (1975).
22) J. Trahan and R. G. Goodrich, *Phys. Rev. B*, **6**, 199 (1972).
23) J. M. D. Coey, H. Roux-Buisson, and R. Brussetti, *J. Phys. (Paris), Colloq.*, **37**, C4-1 (1976).
24) S. Kachi, K. Kosuge, and H. Okinaka, *J. Solid State Chem.*, **6**, 258 (1973).
25) R. M. White and N. F. Mott, *Philos. Mag.*, **24**, 845 (1972).
26) K. C. Misra and M. E. Fleet, *Mat. Res. Bull.*, **8**, 669 (1973).
27) T. Ohtani, K. Kosuge, and S. Kachi, *Phys. Status Solidi B*, **96**, K69 (1979).
28) D. C. Thomas and L. A. K. Staveley, *J. Chem. Soc.*, **1420**, 2572 (1951).
29) K. J. Rao and C. N. R. Rao, *J. Mater. Sci.*, **1**, 238 (1966).
30) A. W. Czanderna, C. N. R. Rao, and J. M. Honig, *Trans. Faraday Soc.*, **54**, 1069 (1958).
31) Y. Kotera and M. Yonemura, *Trans. Faraday Soc.*, **59**, 147 (1963).
32) A. R. Ubbelohde, *Quart. Rev. Chem. Soc. (London)*, **11**, 246 (1957).
33) P. Murray and E. B. Allison, *Trans. Brit. Ceram. Soc.*, **53**, 335 (1954).
34) H. S. Maiti, K. V. G. K. Gokhale, and E. C. Subbarao, *J. Am. Ceram. Soc.*, **55**, 317 (1972).
35) Y. Murakami, S. C. Singh, and L. Delaey, *Scripta Met.*, **12**, 1095 (1978).

The Stereoselective Deacylation of Long-chain Amino Acid Esters by Comicelles of *N*-Acyl-L-histidine and Various Cationic Surfactants

Katsutoshi OHKUBO,* Kiyoshi SUGAHARA, Hidefumi OHTA, Katsuro TOKUDA,† and Ryuichi UEOKA†

Department of Synthetic Chemistry, Faculty of Engineering, Kumamoto University, Kumamoto 860
†*Department of Industrial Chemistry, Kumamoto Institute of Technology, Kumamoto 860*

(Received February 18, 1980)

The stereoselective deacylation of H–$(CH_2)_{\overline{n-1}}$CONHCH(R)CO_2–$C_6H_4NO_2$-*p* (R = CH_3, $CH(CH_3)_2$, $CH_2CH(CH_3)_2$, and $C_6H_5CH_2$; *n*=2—16) with *N*-acyl-L-histidine (acyl=octanoyl, dodecanoyl, and hexadecanoyl) and cationic surfactants ($C_mH_{2m+1}\overset{+}{N}(CH_3)_2R$ X; (R,X,m)=(CH_3,Br,16), (C_2H_5,Br,16), ($C_6H_5CH_2$,Cl,16), and ($\overset{*}{C}H(CH_3)C_6H_5$,Br, 14—18) was examined with particular reference to the structural effects of surfactants, nucleophiles, and substrates on both the deacylation rates and the stereoselectivity. The cationic surfactant, R-(+)-$C_{16}H_{33}\overset{+}{N}(CH_3)_2\overset{*}{C}H(CH_3)C_6H_5$ Br, which possesses the hydrophobic and chiral groups near the polar head, formed the stereoselectively most effective comicelles with *N*-dodecanoyl-L-histidine. The order of stereoselectivity observed in the deacylation of the amino acid esters including the identical acyl chain length (n), phenylalanine>leucine>alanine~valine, suggested steric effects of the substituent bound to the asymmetric carbon atom of the substrate on the stereoselectivity. The highest stereoselectivity (enantiomer rate ratio=4.4 at 25 °C under pH 7.61) was observed in the deacylation of the *N*-decanoylphenylalanine *p*-nitrophenyl ester, involving an appropriately long acyl chain.

The stereoselective micelle-catalyzed deacylation of amino acid esters has recently received considerable attention in the field of enzyme model reactions, and the deacylation of *N*-protected amino acid esters including *N*-CH_3CO, *N*-CH_3OCO, or *N*-$C_6H_5CH_2OCO$ by the amino acid-functionalized surfactants[1-5] or by the mixed micelles of *N*-acyl-L(or D)-histidine (acyl=CH_3CO, C_6H_5CO, $C_7H_{15}CO$, $C_{11}H_{23}CO$, or $C_{17}H_{35}CO$) and hexadecyltrimethylammonium bromide(CTAB)[6-8] has hitherto been documented at enantiomer rate ratios below or around 3.0. However, the stereoselective catalysis of mixed micelles composed of structurally different nucleophiles and surfactants in the deacylation of amino acid esters including long *N*-acyl chains has not yet been investigated systematically. Therefore, we have examined the stereoselective deacylation of amino acid esters possessing a series of *N*-acyl chain lengths by chiral micelles of *N*-acyl-L-histidine and various cationic surfactants at 25 °C (pH 7.61).

In this paper, we wish to report the structural effects of surfactants, nucleophiles, and substrates on the deacylation rate and stereoselectivity when the following compounds were used:

Substrate

H–$(CH_2)_{\overline{n-1}}$CONHCHCO$_2$C$_6$H$_4$NO$_2$-*p*
(R on the CH)

Phe–S_n (R=$CH_2C_6H_5$; *n*=2,6,10,12,14, and 16)
Ala–S_n (R=CH_3; *n*=10)
Val–S_n (R=$CH(CH_3)_2$; *n*=10)
Leu–S_n (R=$CH_2CH(CH_3)_2$; *n*=10)

Nucleophile

RCONH$\overset{*}{C}$H(CO$_2$H)CH$_2$–(imidazole)

OctHis (R=C_7H_{15})
LauHis (R=$C_{11}H_{23}$)
PalHis (R=$C_{15}H_{31}$)

Surfactant

$C_mH_{2m+1}\overset{+}{N}(CH_3)_2R$ X

CTAB (R=CH_3; X=Br; *m*=16)
CEAB (R=C_2H_5; X=Br; *m*=16)
CBzAC (R=$CH_2C_6H_5$; X=Cl; *m*=16)
R-(+)-SUR$_{14}$ (R = $C_6H_5\overset{*}{C}H(CH_3)$; X = Br; *m* = 14)
R-(+)-SUR$_{16}$ (R = $C_6H_5\overset{*}{C}H(CH_3)$; X = Br; *m* = 16)
R-(+)-SUR$_{18}$ (R = $C_6H_5\overset{*}{C}H(CH_3)$; X = Br; *m* = 18)

Experimental

N-Acylphenylalanine p-Nitrophenyl Esters (Phe-S_n). Phe–S_n (*n*=2—16) esters were prepared from *N*-benzyloxycarbonyl-D(or L)-phenylalanine by the esterification of the CO_2H group, the hydrobromination of the NH_2 group, and then the acylation of the NH_2HBr group in a way similar to the previous method.[9] Satisfactory results of elemental analyses were obtained for Phe–S_n (*n*=2—16). L-Phe–S_2: mp 137.5—138 °C (lit,[9] mp 140.0—140.5 °C). $[\alpha]_D^{25}$ −17.57° (*c* 2, $CHCl_3$) (lit,[9] $[\alpha]_D^{20}$ −18.6° (*c* 2, $CHCl_3$)). Found: C, 61.96; H, 5.00; N, 8.66%. Calcd for $C_{17}H_{16}N_2O_5$: C, 62.19; H, 4.91; N, 8.53%. D-Phe–S_2: mp 133.5—134.0 °C (lit,[9] 135—137 °C). $[\alpha]_D^{25}$ +18.15° (*c* 2, $CHCl_3$) (lit,[9] $[\alpha]_D^{20}$ +17.4° (*c* 2, $CHCl_3$)). Found: C, 62.06; H, 4.84; N, 8.66%. Calcd for $C_{17}H_{16}N_2O_5$: C, 62.19; H, 4.91; N, 8.53%. L-Phe–S_6: mp 113.7—114.5 °C. $[\alpha]_D^{25}$ −14.71° (*c* 2, $CHCl_3$). Found: C, 65.98; H, 6.28: N, 7.35%. Calcd for $C_{21}H_{24}O_5N_2$: C, 65.61; H, 6.29; N, 7.29%. D-Phe–S_6: mp 113.5—114.0 °C. $[\alpha]_D^{25}$ +15.02° (*c* 2, $CHCl_3$). Found: C, 65.83; H, 6.24; N, 7.25%. Calcd for $C_{21}H_{24}N_2O_5$: C, 65.61; H, 6.29; N, 7.29%. L-Phe–S_{10}: mp 100.0—100.5 °C $[\alpha]_D^{25}$ −13.01° (*c* 2, $CHCl_3$). Found: C, 68.29; H, 7.42; N, 6.23%. Calcd for $C_{25}H_{32}N_2O_5$: C, 68.16; H, 7.32; N, 6.36%. D-Phe–S_{10}: mp 99.5—100.0 °C, $[\alpha]_D^{25}$ +12.28° (*c* 2, $CHCl_3$). Found: C, 68.36; H, 7.50; N, 6.18%. Calcd for $C_{25}H_{32}N_2O_5$: C, 68.16; H, 7.32; N, 6.36%. L-Phe–S_{12}: mp 107.0—107.5

°C. $[\alpha]_D^{25}$ −11.44° (*c* 2, $CHCl_3$). Found: C, 69.17; H, 7.74; N, 6.01%. Calcd for $C_{27}H_{36}N_2O_5$: C, 69.21; H, 7.74; N, 5.98%. D-Phe-S_{12}: mp 107.5—108.0 °C. $[\alpha]_D^{25}$ +11.91° (*c* 2, $CHCl_3$). Found: C, 69.27; H, 7.85; N, 5.89%. Calcd for $C_{27}H_{36}N_2O_5$: C, 69.21; H, 7.74; N, 5.98%. L-Phe-S_{14}: mp 100.5—101.0 °C. $[\alpha]_D^{25}$ −11.23° (*c* 2, $CHCl_3$). Found: C, 70.18; H, 8.28; N, 5.66%. Calcd for $C_{29}H_{40}N_2O_5$: C, 70.13; H, 8.12; N, 5.64%. D-Phe-S_{14}: mp 100.5—101.0 °C. $[\alpha]_D^{25}$ +10.95° (*c* 2, $CHCl_3$). Found: C, 69.81; H, 8.29; N, 5.36%. Calcd for $C_{29}H_{40}N_2O_5$: C, 70.13; H, 8.12; N, 5.64%. L-Phe-S_{16}: mp 101.0—101.5 °C. $[\alpha]_D^{25}$ −9.97° (*c* 2, $CHCl_3$). Found: C, 70.83; H, 8.47; N, 5.37%. Calcd for $C_{31}H_{44}N_2O_5$: C, 70.96; H, 8.45; N, 5.34%. D-Phe-S_{16}: mp 100.5—101.0 °C. $[\alpha]_D^{25}$ +11.62° (*c* 2, $CHCl_3$). Found: C, 70.36; H, 8.41; N, 5.23%. Calcd for $C_{31}H_{44}N_2O_5$: C, 70.96; H, 8.45; N, 5.34%.

N-Decanoylamino Acid p-Nitrophenyl Esters (Ala-S_{10}, Val-S_{10}, and Leu-S_{10}). These substrates were prepared by the method used for the Phe-S_n formation. L-Ala-S_{10}: mp 100.5—101.0 °C. Found: C, 62.57; H, 7.73; N, 7.57%. Calcd for $C_{19}H_{28}N_2O_5$: C, 62.62; H, 7.74; N, 7.69%. D-Ala-S_{10}: mp 101.5—102.0 °C. Found: C, 63.07; H, 7.26; N, 7.66%. Calcd for $C_{19}H_{28}N_2O_5$: C, 62.62; H, 7.74; N, 7.69%. L-Val-S_{10}: mp 70.5—71.0 °C. Found: C, 63.99; H, 8.46; N, 6.69%. Calcd for $C_{21}H_{32}N_2O_5$: C, 64.26; H, 8.22; N, 7.14%. D-Val-S_{10}: mp 71.0—71.5 °C. Found: C, 64.04; H, 8.15; N, 7.09%. Calcd for $C_{21}H_{32}N_2O_5$: C, 64.26; H, 8.22; N, 7.14%. L-Leu-S_{10}: mp 67.5—68.0 °C. Found: C, 65.10; H, 8.41; N, 6.91%. Calcd for $C_{22}H_{34}N_2O_5$: C, 65.00; H, 8.43; N, 6.89%. D-Leu-S_{10}: mp 68.0—68.5 °C. Found: C, 65.01; H, 8.54; N, 6.90%. Calcd for $C_{22}H_{34}N_2O_5$: C, 65.00; H, 8.43; N, 6.89%.

N-Acyl-L-histidine (OctHis, LauHis, and PalHis). These nucleophiles were prepared by the reaction of L-histidine and the corresponding acid chlorides.[10] Satisfactory results of elemental analyses were also obtained for these compounds. OctHis: mp 179—181 °C. Found: C, 52.97; H, 7.36; N, 13.29%. Calcd for $C_{14}H_{23}N_3O_3 \cdot HCl$: C, 52.90; H, 7.61; N, 13.22%. LauHis: mp 161—162 °C (lit,[11] 160—161 °C). Found: C, 64.03; H, 9.27; N, 12.11%. Calcd for $C_{18}H_{31}N_3O_3$: C, 64.06; H, 9.27; N, 12.45%. PalHis: mp 153—155 °C. Found: C, 67.13; H, 10.18; N, 10.37%. Calcd for $C_{22}H_{39}N_3O_3$: C, 67.14; H, 9.99; N, 10.68%.

Surfactants (CTAB, CEAB, CBzAC, R-(+)-SUR$_m$ (m=14, 16, and 18)). Commercially available CTAB, CEAB, and CBzAC were used after recrystallization with absolute ethanol and diethyl ether. The chiral surfactants were prepared by the reaction of R-(+)-*N,N,α*-trimethylbenzylamine and the corresponding alkyl bromide in accordance with the previous method.[12] R-(+)-SUR_{14}: mp 109.0—110.0 °C. Found: C, 68.02; H, 10.55; N, 3.30%. Calcd for $C_{24}H_{44}NBr$: C, 67.57; H, 10.42; N, 3.28%. R-(+)-SUR_{16}: mp 110.5—112.5 °C (lit,[12] 111.5—113.0 °C). $[\alpha]_D^{18}$ +20.44° (*c* 4, CH_3OH) (lit,[12] $[\alpha]_D^{21}$ +19.82° (*c* 45, CH_3OH)). Found: C, 67.38; H, 10.87; N, 2.98%. Calcd for $C_{26}H_{48}NBr$: C, 68.70; H, 10.64; N, 3.22%. R-(+)-SUR_{18}; mp 112.0°—113.5 °C. Found: C, 68.76; H, 10.99; N, 2.84%. Calcd for $C_{28}H_{52}NBr$: C, 69.67; H, 10.88; N, 2.90%.

Deacylation. The stereoselective micelle-promoted deacylation of L or D-substrates (5×10^{-5} mol dm^{-3}) with and without the nucleophile (9×10^{-5} mol dm^{-3}) in the presence of the cationic surfactant ($(4.5—55)\times10^{-4}$ mol dm^{-3}) was carried out at 25 °C (pH 7.61) in a Tris buffer (0.083 mol dm^{-3}) containing KCl (0.083 mol dm^{-3}) in 10% (v/v) CH_3CN–H_2O. The above concentrations of the surfactants were higher than their critical micelle concentrations (CMC); for example, the CMC values of CTAB, CBzAC, and R-(+)-SUR_{16} are 1×10^{-3},[13] 2.7×10^{-4},[12] and 2.08×10^{-4} mol dm^{-3} [12] respectively. The deacylation rate was followed by the spectrophotometric determination of *p*-nitrophenolate (400 nm). In the present experiments, the substrate deacylation by the nucleophile was not performed in the absence of the cationic surfactant because the precipitation of the substrates during the reaction was observed in the absence of the surfactant under the present conditions.

Determination of Rate Constants. The rate constants for the present reaction with and without the nucleophile (k_ψ and $k_{surfact}$ respectively) were obtained from good pseudo-first-order deacylation rates, while the apparent catalytic rate constant (k_{cat}) was evaluated in the usual way ($k_{cat}=(k_\psi - k_{surfact})/[\text{nucleophile}]$).

Results and Discussion

Structural Effects of Surfactants and Nucleophiles. The structural effects of the polar head groups of the cationic surfactants (CTAB, CEAB, CBzAC, and R-(+)-SUR_{16}) involving the same alkyl chain length on both the deacylation rate and the stereoselectivity were first examined in the deacylation of Phe-S_n (n= 2, 10, and 16) with LauHis; the results of a series of experiments are shown in Table 1. In the deacylation

Table 1. Structural effects of surfactants on deacylation rate and stereoselectivity[a]

Surfactant	Phe-S_n	k_{cat}/mol^{-1} dm^3 s^{-1}		k_{cat}^L/k_{cat}^D
		L	D	
CTAB	n=2	57	35	1.6
	=10	304	108	2.8
	=16	50	31	1.6
CEAB	n=2	73	40	1.8
	=10	302	100	3.0
	=16	54	33	1.6
CBzAC	n=2	64	37	1.7
	=10	281	97	2.9
	=16	326	152	2.1
R-(+)-SUR_{16}	n=2	86	47	1.8
	=10	380	86	4.4
	=16	362	114	3.2

a) Tris buffer (0.083 mol dm^{-3}) containing KCl (0.083 mol dm^{-3}) at 25 °C, pH 7.61, in 10% (v/v) CH_3CN–H_2O; [LauHis]$=9\times10^{-5}$ mol dm^{-3}, [Phe-S_n]$=5\times10^{-5}$ mol dm^{-3}, and [Surfactant]$=2.5\times10^{-3}$ mol dm^{-3}.

of the short-chain substrate (Phe-S_2), neither the deacylation rate nor the stereoselectivity (defined by k_{cat}^L/k_{cat}^D) was affected remarkably by the surfactant structure. The increase in the acyl chain length of Phe-S_n from n=2 to n=10, however, increased both the rate and the selectivity in all the cases by intensifying the stereoselective micellar catalysis through the substrate incorporation by the comicelles of LauHis and the surfactant. The rate increase was about 4—5 fold for the L-enantiomer, while it was about 2—3 fold for the D-enantiomer. Therefore, the nucleophilic attack of the imidazolyl group of LauHis on the susceptible carbonyl group of the substrate incorporated into the comicelles occurred more favorably in the L-Phe-S_{10}

Table 2. Concentration effects of surfactants on deacylation rate and stereoselectivity[a)]

10^4[Surfactant]	LauHis+R-(+)-SUR_{14}			LauHis+R-(+)-SUR_{16}			LauHis+R-(+)-SUR_{18}		
	k_{cat}/mol^{-1} dm^3 s^{-1}		k^L_{cat}/k^D_{cat}	k_{cat}/mol^{-1} dm^3 s^{-1}		k^L_{cat}/k^D_{cat}	k_{cat}/mol^{-1} dm^3 s^{-1}		k^L_{cat}/k^D_{cat}
	L	D		L	D		L	D	
4.5				1227	561	2.2	1095	375	2.9
8.3	520	253	2.1						
9.0				890	303	2.9	788	261	3.0
15	509	170	3.0	596	189	3.2	548	177	3.1
18				500	161	3.1	461	144	3.2
25	351	113	3.1	380	86	4.4	355	128	2.8
35	271	86	3.2	300	80	3.8	300	108	2.8
45	223	62	3.6	267	73	3.7	228	77	3.0
55	179	52	3.4						

a) The reaction conditions are the same as in Table 1 except for the surfactant concentration. Substrate=Phe-S_{10}.

deacylation than in the D-Phe-S_{10} deacylation. In this respect, the comicelles of LauHis and R-(+)-SUR_{16} resulted in the highest deacylation rate of L-Phe-S_{10} (and a slightly lower rate of D-Phe-S_{10}) as compared with the other comicellar systems. Since the stereoselective efficiency of R-(+)-SUR_{16} *per se* was negligibly small ($k^L_{surfact}/k^D_{surfact}$=1.00—1.08), the hydrophobic and chiral α-methylbenzyl group at the polar head of R-(+)-SUR_{16} might facilitate the interaction of LauHis with L-Phe-S_{10}. In the deacylation of Phe-S_{16}, the structural effects of CTAB and CEAB on the deacylation rate and the stereoselectivity were appreciably different from those of CBzAC and R-(+)-SUR_{16}; that is, CTAB and CEAB decreased both the rate and the stereoselectivity of Phe-S_{16} remarkably as compared with those of Phe-S_{10}, while CBzAC and R-(+)-SUR_{16} did not reduce the rate of L-Phe-S_{16}, but increased the rate of D-Phe-S_{16} considerably. The rates of L and D-Phe-S_{16} in the LauHis+CBzAC (or R-(+)-SUR_{16}) system were about 6—7 fold and about 3.5—5 fold with respect to those in the LauHis+CTAB (and +CEAB) systems respectively. Therefore, the hydrophobicity of the benzyl (or α-methylbenzyl) group of CBzAC (or R-(+)-SUR_{16}) contributes to the rate enhancement of the long-chain substrates (Phe-S_{10} and Phe-S_{16}). It is noteworthy, with respect to the stereoselectivity, that the enantiomer-rate ratio of 4.4 for Phe-S_{10} (or that of 3.2 for Phe-S_{16}) in the case of the LauHis+R-(+)-SUR_{16} system is 1.5 times as high as the rate ratio of 2.9 for Phe-S_{10} (or that of 2.1 for Phe-S_{16}) in the case of the LauHis+CBzAC system. This might be due not to the hydrophobicity difference in the polar-head groups of the surfactants, but to the chirality of the hydrophobic α-methylbenzyl group of R-(+)-SUR_{16}. It is deduced, therefore, that the comicelles consisting of chiral nucleophiles and chiral surfactants tend to enhance the stereoselectivity of the long-chain substrates, especially such substrates as Phe-S_{10} which possess an appropriately long acyl chain.

The concentration effects of surfactants on the stereoselective comicellar catalysis were, then, examined in the deacylation of Phe-S_{10} with LauHis and R-(+)-SUR_m (m=14, 16, and 18); the experimental results are shown in Table 2. In all the comicellar systems of LauHis+R-(+)-SUR_m (m=14—18), the increase in the surfactant concentration in the range of 4.5×10^{-4}—5.5×10^{-3} mol dm^{-3} with respect to 9×10^{-5} mol dm^{-3} of LauHis decreased the deacylation rate of Phe-S_{10} monotonously. The stereoselectivity in the deacylation of Phe-S_{10} (5×10^{-5} mol dm^{-3}) with LauHis (9×10^{-5} mol dm^{-3}) and R-(+)-SUR_m (m=14—18) was also affected by the surfactant concentration; the highest enantiomer-rate ratios (k^L_{cat}/k^D_{cat}=3.6, 4.4, and 3.2) were obtained under the conditions of [R-(+)-SUR_{14}]=4.5×10^{-3} mol dm^{-3}, [R-(+)-SUR_{16}]=2.5×10^{-3} mol dm^{-3}, and [R-(+)-SUR_{18}]=1.8×10^{-3} mol dm^{-3}

Table 3. Structural effects of nucleophiles on deacylation rate and stereoselectivity[a)]

System	Phe-S_2			Phe-S_{10}			Phe-S_{16}		
	k_{cat}/mol^{-1} dm^3 s^{-1}		k^L_{cat}/k^D_{cat}	k_{cat}/mol^{-1} dm^3 s^{-1}		k^L_{cat}/k^D_{cat}	k_{cat}/mol^{-1} dm^3 s^{-1}		k^L_{cat}/k^D_{cat}
	L	D		L	D		L	D	
OctHis+R-(+)-SUR_{16}	17	14	1.2	41	38	1.1	59	59	1.0
LauHis+R-(+)-SUR_{16}	86	47	1.8	380	86	4.4	362	114	3.2
LauHis+R-(+)-SUR_{18}	93	59	1.6	461	144	3.2	429	129	3.3
PalHis+R-(+)-SUR_{14}	66	44	1.5	253	72	3.5	304	98	3.1
PalHis+R-(+)-SUR_{16}	111	69	1.6	469	116	4.0	511	169	3.0
PalHis+R-(+)-SUR_{18}	111	60	1.9	636	174	3.7	483	181	2.7

a) Tris buffer (0.083 mol dm^{-3}) containing KCl (0.083 mol dm^{-3}) at 25 °C, pH 7.61, in 10% (v/v) CH_3CN–H_2O; [OctHis]=[LauHis]=[PalHis]=9×10^{-5} mol dm^{-3}, [Substrate]=5×10^{-5} mol dm^{-3}, [R-(+)-SUR_{14}]=4.5×10^{-3} mol dm^{-3}, [R-(+)-SUR_{16}]=2.5×10^{-3} mol dm^{-3}, and [R-(+)-SUR_{18}]=1.8×10^{-3} mol dm^{-3}.

respectively. Therefore, the stereoselective efficiency of the comicelles of the Phe-S_{10} deacylation followed the order of LauHis+R-(+)-SUR_{16}>LauHis+R-(+)-SUR_{14}>LauHis+R-(+)-SUR_{18}. This fact might imply that the hydrophobic chain length of the nucleophile requires an appropriately long (not too short and not too long) hydrophobic chain length of the surfactant for the formation of stereoselectively effective comicelles. The effects of the hydrophobic chain length of the surfactant on the stereoselective comicellar catalysis were also recognized in the deacylation of Phe-S_n (n=2, 10, and 16) with PalHis and R-(+)-SUR_m (m=14, 16, and 18) (see Table 3); the comicellar system of PalHis+R-(+)-SUR_{16} was rather more efficient for the stereoselective deacylation of the long-chain substrate (Phe-S_{10}) than that of PalHis+R-(+)-SUR_m (m=14 and 18).

The experimental results shown in Table 3 also indicate the effects of the hydrophobic chain length of nucleophiles on the stereoselective comicellar catalysis. In the deacylation of Phe-S_n (n=2, 10, and 16) with the nucleophile (OctHis, LauHis, or PalHis) and R-(+)-SUR_{16}, the lengthening of the alkyl chain of the nucleophile increased the deacylation rate of Phe-S_n (n=2—16) monotonously, and the enantiomer-rate ratios in the deacylation of the identical substrate followed the order of LauHis+R-(+)-SUR_{16}>PalHis+R-(+)-SUR_{16}≫OctHis+R-(+)-SUR_{16}. At any rate, among the present comicellar systems, the LauHis+R-(+)-SUR_{16} system was found to contain the most efficient comicelles for the stereoselective deacylation of Phe-S_n (n=2—16). Therefore, stereoselectively efficient comicellar systems do not require too long hydrophobic chains for the nucleophile or the surfactant. Table 3 also indicates that the comicelles of LauHis+R-(+)-SUR_m (m=16 and 18) or PalHis+R-(+)-SUR_m (m=14,16, and 18) resulted in a high stereoselectivity (k^L_{cat}/k^D_{cat}=3.2—4.4) in the deacylation of Phe-S_{10} rather than in the deacylation of Phe-S_{16} or Phe-S_2.

Structural Effects of Substrates. Although the effects of the *N*-acyl chain length of the amino acid esters on the stereoselectivity have already been briefly discussed, a more detailed explanation of the structural effects of the substrates will be developed in this section. With regard to the dependence of the rates and stereoselectivity on the *N*-acyl chain length of a substrate in the deacylation of Phe-S_n (n=2—16) by the LauHis+R-(+)-SUR_{16} system (Fig. 1), the rate increases upon a change in the chain length (n) from n=2 to n=6 were 2.7 and 2.3 fold for the L and D-enantiomer respectively, while the stereoselectivity enhancement was very slight. However, the rate increase upon a change in the chain length from n=2 to n=10—16 was remarkable for the L-enantiomer (4.2—4.4 fold), but slight for the D-enantiomer (1.8—2.4 fold). Therefore, the stereoselectivity enhancement became larger with the increase in the chain length from n=6 to n=10—16, and the highest stereoselectivity was found in the Phe-S_{10} deacylation; that is, Phe-S_{10} incorporated into the comicelles (LauHis+R-(+)-SUR_{16}) might be exposed to the asymmetric environment of the comicelles more directly than with the other Phe-S_n substrates.

Table 4. Structural effects of substrates on deacylation rate and stereoselectivity[a)]

Substrate	k_{cat}/mol^{-1} dm^3 s^{-1}		k^L_{cat}/k^D_{cat}
	L	D	
Ala-S_{10}	89	73	1.1
Val-S_{10}	19	16	1.2
Leu-S_{10}	221	70	3.2
Phe-S_{10}	380	86	4.4

a) The deacylation reactions were carried out by the use of the comicelles of LauHis and R-(+)-SUR_{16} under the same conditions as are shown in Table 1.

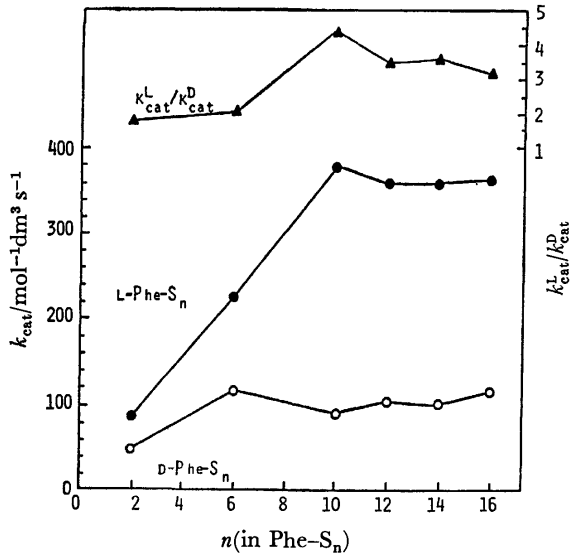

Fig. 1. Dependence of deacylation rate and stereoselectivity on the acyl chain length of Phe-S_n (The deacylation was carried out with LauHis and R-(+)-SUR_{16} under the same conditions as shown in Table 1).

The structural effects of amino-acid esters on the stereoselectivity were also observed in the deacylation of Ala-S_{10}, Val-S_{10}, Leu-S_{10}, and Phe-S_{10} by the comicelles of LauHis+R-(+)-SUR_{16} (Table 4). The deacylation rates followed the order of L-Phe-S_{10}>L-Leu-S_{10}≫L-Ala-S_{10}≫L-Val-S_{10} for the L-enantiomers or of D-Phe-S_{10}>D-Leu-S_{10}~D-Ala-S_{10}≫D-Val-S_{10} for the D-enantiomers. The very low rates of L- and D-Val-S_{10} might be due to the steric hindrance of the isopropyl group, which is adjacent to the susceptible carbonyl group in the substrate, toward the nucleophilic attack of LauHis. In this regard, the very low rate of the *N*-benzyloxycarbonylvaline *p*-nitrophenyl ester was observed in the deacylation of *N*-(benzyloxycarbonyl)-amino acid esters by the L (or D)-LauHis+CTAB system.[8)] Such a steric hindrance might be reduced in the other substrates, $RCH_2CH(NHCO(CH_2)_8CH_3)$-$CO_2C_6H_4NO_2$-*p* (R=H, $(CH_3)_2CH$, and C_6H_5); the deacylation rate increases with the increase in the bulkiness (and/or hydrophobicity) of the R group in the substrate. Table 4 also indicates that the order of the stereoselectivity. Phe-S_{10}>Leu-S_{10}>Val-S_{10}~

Ala–S_{10}, is parallel with the bulkiness (and/or hydrophobicity) of the substituent in the ester. Presumably, the bulkiness (and/or hydrophobicity) of the substrate plays an important role in the increase in the energy difference between the interaction of L-S_{10}–LauHis and D-S_{10}–LauHis in the transition state of the present deacylation.

References

1) J. M. Brown and C. A. Bunton, *J. Chem. Soc., Chem. Commun.*, **1974**, 969.
2) J. M. Brown, C. A. Bunton, and S. Diaz, *J. Chem. Soc., Chem. Commun.*, **1974**, 971.
3) R. A. Moss, T. J. Lukas, and R. C. Nahas, *Tetrahedron Lett.*, **1977**, 3851.
4) R. A. Moss, R. C. Nahas, and T. J. Lucas, *Tetrahedron Lett.*, **1978**, 507.
5) R. A. Moss, Y.-S. Lee, and T. J. Lukas, *J. Am. Chem. Soc.*, **101**, 2499 (1979).
6) Y. Ihara, *J. Chem. Soc., Chem. Commun.*, **1978**, 984.
7) K. Yamada, H. Shosenji, and H. Ihara, *Chem. Lett.*, **1979**, 491.
8) K. Yamada, H. Shosenji, H. Ihara, and Y. Otsubo, *Tetrahedron Lett.*, **1979**, 2529.
9) D. W. Ingles and J. R. Knowles, *Biochem. J.*, **104**, 369 (1967).
10) C. Gitler and A. Ochoa-Solano, *J. Am. Chem. Soc.*, **90**, 5004 (1968).
11) T. Inoue, K. Nakamura, and H. Kimizuka, *Bull. Chem. Soc. Jpn.*, **49**, 719 (1976).
12) R. A. Moss and W. L. Sunshine, *J. Org. Chem.*, **39**, 1083 (1974).
13) R. Ueoka, H. Matsuura, S. Nakahata, and K. Ohkubo, *Bull. Chem. Soc. Jpn.*, **53**, 347 (1980).

Synthesis of (+)-Hinokiol, (+)-Hinokione, (+)-Salviol, and (+)-2-Oxoferruginol

Takashi MATSUMOTO,* Shuji USUI, Hiroyuki KAWASHIMA, and Masanori MITSUKI

Department of Chemistry, Faculty of Science, Hiroshima University, Higashisenda-machi, Naka-ku, Hiroshima 730

(Received August 11, 1980)

Reduction of abieta-5,8,11,13-tetraen-3-one with lithium aluminium hydride afforded the corresponding alcohol, which was submitted to catalytic hydrogenation to yield abieta-8,11,13-trien-3β-ol (**7**) together with its 5βH-isomer. Acetylation of **7**, followed by the Friedel-Crafts acylation, afforded 3β-acetoxy-12-acetylabieta-8,11,13-triene. This compound was converted into 3β,12-diacetoxyabieta-8,11,13-triene (**11**) by the Baeyer-Villiger oxidation. Treatment of **11** with lithium aluminium hydride yielded hinokiol, which was oxidized to hinokione. Subsequently, hinokiol was methylated and the resulting 12-methyl ether was dehydrated to afford 12-methoxyabieta-2,8,11,13-tetraene. The tetraene was then submitted to hydroboration-oxidation to give 12-methoxyabieta-8,11,13-trien-2α-ol (**15**) which, on demethylation with ethanethiol and anhydrous aluminium chloride, afforded salviol. Oxidation of **15** with pyridinium chlorochromate, followed by demethylation, gave 2-oxoferruginol.

Hinokiol (**1**) and hinokione (**2**) have been isolated from the heartwood of *Chamaecyparis obtusa*, Sieb. et. Zucc.,[1] *Cupressus torulosa* Don,[2] and *Tetraclinis articulata* (Vahl) Masters,[3] and from the leaf of *Torreya nucifera* Sieb. et. Zucc.[4] The similar diterpenes, salviol (**3**) and 2-oxoferruginol (**4**), have also been isolated from the roots of *Salvia miltiorrhiza* Bunge[5] and from the bark of *Podocarpus ferrugineus* D. Don,[6] respectively. All these natural diterpenes possess the oxygen functions in both the rings A and C of the abietane skeleton. As a part of our synthetic studies on the naturally-occurring terpenes, we have attempted the syntheses of these tricyclic diterpenes. This paper will describe the syntheses of (+)-hinokiol (**1**), (+)-hinokione (**2**),[7] (+)-salviol (**3**), and (+)-2-oxoferruginol (**4**), starting from the optically active abieta-5,8,11,13-tetraen-3-one (**5**) which was prepared from (+)-dehydroabietic acid by the known procedure.[8]

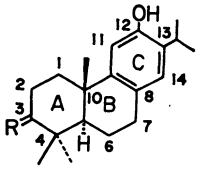

1 R=α-H, β-OH
2 R=O

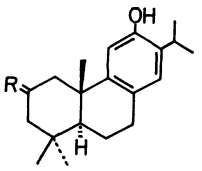

3 R=α-OH, β-H
4 R=O

Reduction of **5** with lithium aluminium hydride in ether afforded abieta-5,8,11,13-tetraen-3β-ol (**6**). The β-configuration of the hydroxyl group at the C-3 position was supported by its NMR spectrum, which showed a triplet at δ 2.80 ppm with a half-height width of 16 Hz, suggesting the presence of an axial α hydrogen. Catalytic hydrogenation of **6** in methanol over Pd–C, followed by chromatographic purification, gave abieta-8,11,13-trien-3β-ol (**7**) as a major product and its 5βH-isomer (**8**) as a minor one. The NMR spectrum of **7** showed signals at δ 0.89 and 1.06 ppm due to the *gem*-dimethyl groups at the C-4 position, while that of **8** showed the corresponding signals at δ 0.39 and 0.99 ppm. The *cis*-configuration of the A/B ring junction in **8** was supported by the appearance of the signal due to one of the *gem*-dimethyl groups in very high field (δ 0.39 ppm),[9] owing to the shielding effect of the C ring The *trans*-isomer (**7**) was acetylated with acetic anhydride in pyridine to give 3β-acetoxyabieta-8,11,13-triene (**9**). The Friedel-Crafts acylation of **9** with acetyl chloride in dichloromethane in the presence of anhydrous aluminium chloride afforded 3β-acetoxy-12-acetylabieta-8,11,13-triene (**10**), whose IR spectrum showed carbonyl bands at 1725 and 1675 cm^{-1}. The NMR spectrum of **10** showed two singlets at δ 6.98 and 7.32 ppm due to the two aromatic protons. These spectral data of **10** supported the presence of an acetyl group at the C-12 position. The Baeyer-Villiger oxidation of **10** with *m*-chloroperbenzoic acid in dichloromethane afforded 3β,12-diacetoxyabieta-8,11,13-triene (hinokiol diacetate) (**11**).[1,4] Treatment of **11** with lithium aluminium hydride in ether yielded abieta-8,11,13-triene-3β,12-diol (hinokiol) (**1**)[1-4] which, on methylation with methyl iodide and anhydrous potassium carbonate in refluxing ethyl methyl ketone, afforded 12-methoxyabieta-8,11,13-trien-3β-ol (hinokiol 12-methyl ether) (**12**).[1] The synthetic **1** was then oxidized with Jones reagent to give 12-hydroxyabieta-8,11,13-trien-3-one (hinokione) (**2**).[1-3]

Our next effort was directed toward the syntheses of salviol (**3**) and 2-oxoferruginol (**4**). The methyl ether (**12**) was dehydrated with phosphoryl chloride in refluxing pyridine to yield 12-methoxyabieta-2,8,11,-13-tetraene (**13**). Hydroboration of **13**, followed by oxidation with alkaline hydrogen peroxide, afforded a mixture of alcohols. This was separated by column chromatography on silica gel to give 12-methoxyabieta-8,11,13-trien-3α-ol (**14**), **12**, and 12-methoxyabieta-8,11,13-trien-2α-ol (**15**). Oxidation of **14** with pyridinium chlorochromate[10] in dichloromethane afforded 12-methoxyabieta-8,11,13-trien-3-one(hinokione methyl ether) (**16**).[1,11] The alcohol (**14**) was also converted into **13** by dehydration with phosphoryl chloride in refluxing pyridine. The stereochemistry of the hydroxyl group at the C-2 position in **15** was assigned to be α-configuration by its NMR spectrum, which showed a signal due to the C-2 proton at δ 4.08 ppm with a half-height width of 22 Hz, suggesting the presence of an axial β hydrogen. Demethylation of **15** with anhydrous aluminium chloride and ethanethiol[12] in dichloro-

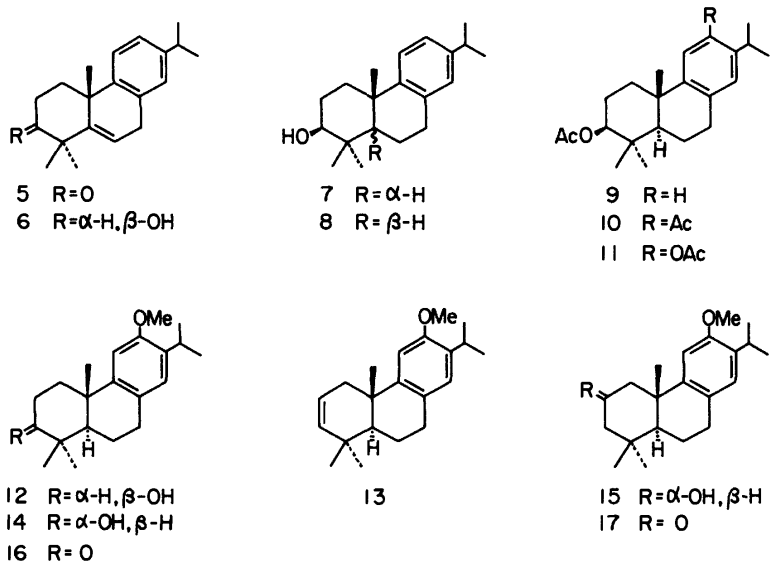

5 R=O
6 R=α-H,β-OH
7 R=α-H
8 R=β-H
9 R=H
10 R=Ac
11 R=OAc
12 R=α-H,β-OH
14 R=α-OH,β-H
16 R=O
13
15 R=α-OH,β-H
17 R=O

methane afforded abieta-8,11,13-triene-2α,12-diol (salviol) (**3**).[5] Subsequently, the alcohol (**15**) was oxidized with pyridinium chlorochromate in dichloromethane to give 12-methoxyabieta-8,11,13-trien-2-one (**17**) which, on demethylation with boron tribromide in dichloromethane, afforded 12-hydroxyabieta-8,11,13-trien-2-one (2-oxoferruginol) (**4**).[6]

Experimental

All melting points are uncorrected. The IR spectra and optical rotations were measured in chloroform, and the NMR spectra in carbon tetrachloride at 60 MHz, with tetramethylsilane as an internal standard, unless otherwise stated. The chemical shifts are presented in terms of δ values; s: singlet, bs: broad singlet, d: doublet, bd: broad doublet, t: triplet, m: multiplet. Column chromatography was performed using Merck silica gel (0.063 mm).

Abieta-5,8,11,13-tetraen-3-one (5). According to the known procedure,[8] (+)-dehydroabietic acid was converted into **5**, $[\alpha]_D$ +32.9°, IR: 1705 cm^{-1}, NMR: 1.17, 1.23, and 1.32 (each 3H and s, $-\dot{C}(CH_3)_2$ and C_{10}-CH_3), 1.22 (6H, d, J=7 Hz, $-CH(C\underline{H}_3)_2$), 3.37 (2H, d, J=4 Hz, $=CH-C\underline{H}_2-$), 5.90 (1H, t, J=4 Hz, C_6-H). Found: C, 84.76; H, 9.38%. Calcd for $C_{20}H_{26}O$: C, 85.05; H, 9.28%.

Abieta-5,8,11,13-tetraen-3β-ol (6). A mixture of **5** (1.159 g) and lithium aluminium hydride (156 mg) in dry ether (25 ml) was stirred at room temperature for 90 min. The mixture was poured into ice-dilute hydrochloric acid and extracted with ether. The ether extract was washed with brine, dried over sodium sulfate, and evaporated. The residue was purified by column chromatography on silica gel (30 g), using ether–benzene (2 : 98) as the eluent, to give **6** (1.107 g: 94.8%), $[\alpha]_D$ −69.7°; IR: 3615, 3450 cm^{-1}; NMR: 1.15, 1.20, and 1.27 (each 3H and s, $-\dot{C}(CH_3)_2$ and C_{10}-CH_3), 1.21 (6H, d, J=6.5 Hz, $-CH(C\underline{H}_3)_2$), 2.80 (1H, t, J=7 Hz, $W_{1/2}$= 16 Hz, C_3-H), 3.31 (2H, bd, J=4 Hz, $=CH-C\underline{H}_2-$), 5.95 (1H, t, J=4 Hz, C_6-H). Found: C, 84.36; H, 10.04%. Calcd for $C_{20}H_{28}O$: C, 84.45; H, 9.92%.

Catalytic Hydrogenation of 6. A mixture of **6** (1.007 g) and 5% Pd-C (500 mg) in methanol (15 ml) was subjected to catalytic hydrogenation at room temperature for *ca.* 20 h. After the usual work-up, the crude product was purified by column chromatography on silica gel (60 g), using ether-benzene (0.5 : 99.5) as the eluent, to give 5βH-abieta-8,11,13-trien-3β-ol (**8**) (104 mg: 10.3%), $[\alpha]_D$ +22.4°; IR: 3628, 3463 cm^{-1}; NMR: 0.39, 0.99, and 1.18 (each 3H and s, $-\dot{C}(CH_3)_2$ and C_{10}-CH_3), 1.22 (6H, d, J=6.5 Hz, $-CH(C\underline{H}_3)_2$), 1.87 (1H, s, -OH), 3.25 (1H, m, $W_{1/2}$=7 Hz, C_3-H). Found: C, 83.76; H, 10.73%. Calcd for $C_{20}H_{30}O$: C, 83.86; H, 10.56%.

Further elution with ether-benzene (5 : 95) afforded abieta-8,11,13-trien-3β-ol (**7**) (683 mg: 67.3%), which was recrystallized from hexane; mp 136.5—138 °C; $[\alpha]_D$ +50.4°; IR: 3617, 3453 cm^{-1}; NMR ($CDCl_3$): 0.89, 1.06, and 1.18 (each 3H and s, $-\dot{C}(CH_3)_2$ and C_{10}-CH_3), 1.22 (6H, d, J=6.5 Hz, $-CH(C\underline{H}_3)_2$), 1.68 (1H, s, -OH), 3.30 (1H, m, $W_{1/2}$=17 Hz, C_3-H). Found: C, 84.03; H, 10.75%. Calcd for $C_{20}H_{30}O$: C, 83.86; H, 10.56%.

3β-Acetoxyabieta-8,11,13-triene (9). A solution of **7** (679 mg) and acetic anhydride (2.5 ml) in pyridine (7.0 ml) was heated at 74—77 °C for 1.5 h. After the usual work-up, the crude product was purified by column chromatography on silica gel (30 g), using hexane–benzene (35 : 65) as the eluent, to give **9** (750 mg: 96.3%), which was recrystallized from hexane; mp 112—114 °C; $[\alpha]_D$ +58.9°; IR: 1720 cm^{-1}; NMR: 0.94 (6H, s, $-\dot{C}(CH_3)_2$), 1.19 (3H, s, C_{10}-CH_3), 1.20 (6H, d, J=7 Hz, $-CH(C\underline{H}_3)_2$), 2.00 (3H, s, $-OCOCH_3$), 4.5 (1H, m, C_3-H), 6.79 (bs), 6.87 (bd, J=8 Hz), and 7.07 (bd, J=8 Hz) (each 1H, aromatic protons). Found: C, 80.71; H, 9.99%. Calcd for $C_{22}H_{32}O_2$: C,80.44; H, 9.83%.

3β-Acetoxy-12-acetylabieta-8,11,13-triene (10). Anhydrous aluminium chloride (850 mg) was added at 0—5 °C to a stirred solution of **9** (696 mg) and acetyl chloride (500 mg) in dichloromethane (10 ml). The mixture was stirred at this temperature for 30 min and then at room temperature for 24 h, poured into ice-dilute hydrochloric acid, and extracted with ether. The ether extract was washed successively with water, aqueous sodium hydrogencarbonate, and water. The dried extract was evaporated *in vacuo* to give a crude product, which was purified by column chromatography on silica gel (15 g), using ether–benzene (1 : 99) as the eluent, to afford **10** (748 mg: 95.3%). This was recrystallized from a mixture of acetone and hexane; mp 163.5—165.5 °C; $[\alpha]_D$ +62.6°; IR: 1725, 1675 cm^{-1}; NMR: 0.95 (6H, s, $-\dot{C}(C\underline{H}_3)_2$), 1.16 and 1.20 (each 3H, d, and J=7 Hz, $-CH(C\underline{H}_3)_2$), 1.21 (3H, s, C_{10}-CH_3), 2.00 (3H, s, $-OCOCH_3$), 2.46 (3H, s, $-COCH_3$), 3.46 (1H, m, $-C\underline{H}(CH_3)_2$), 4.45 (1H, m, C_3-H), 6.98 (1H, s, C_{14}-H), 7.32 (1H, s, C_{11}-H). Found: C, 77.85; H, 9.48%. Calcd for $C_{24}H_{34}O_3$: C, 77.80; H, 9.25%.

3β,12-Diacetoxyabieta-8,11,13-triene (Hinokiol Diacetate) (11). A mixture of **10** (739 mg), *m*-chloroperbenzoic acid (85%: 610 mg), and *p*-toluenesulfonic acid (40 mg) in 1,2-dichloroethane (10 ml) was refluxed for 3.5 h. The mixture was then cooled, diluted with ether, and washed successively with aqueous potassium iodide, aqueous sodium thiosulfate, aqueous sodium hydrogencarbonate, and water. The dried ether solution was evaporated *in vacuo* and the residue was purified by column chromatography on silica gel (25 g), using ether–benzene (1 : 99) as the eluent, to give **11** (647 mg: 83.9%), which was recrystallized from ethanol; mp 145—146 °C; $[\alpha]_D$ +69.8° (EtOH) (lit,[1] mp 143 °C, $[\alpha]_D$ +70.39° (EtOH)); IR: 1750, 1725 cm^{-1}; NMR: 0.94 (6H, s, $-\dot{C}(CH_3)_2$), 1.16 (6H, d, J=6.5 Hz, $-CH(C\underline{H}_3)_2$), 1.22 (3H, s, $C_{10}-CH_3$), 2.00 (3H, s, $C_3-OCOCH_3$), 2.22 (3H, s, $C_{12}-OCOCH_3$), 4.48 (1H, m, C_3–H), 6.76 and 6.89 (each 1H and s, C_{11}–H and C_{14}–H). Found: C, 74.27; H, 8.92%. Calcd for $C_{24}H_{34}O_4$: C, 74.57; H, 8.87%.

Further elution gave the recovered **10** (58 mg: 7.9%).

Abieta-8,11,13-triene-3β,12-diol (Hinokiol) (1). A mixture of **11** (575 mg) and lithium aluminium hydride (140 mg) in dry ether (10 ml) was stirred at 0—5 °C for 45 min and then at room temperature for 30 min. The mixture was poured into ice-dilute hydrochloric acid and extracted with ether. The ether extract was washed with brine, dried over sodium sulfate, and evaporated. The residue was purified by column chromatography on silica gel (30 g), using acetone–benzene (3 : 7) as the eluent, to give hinokiol (**1**) (401 mg: 89.1%), which was recrystallized from ethanol; mp 240—242 °C; $[\alpha]_D$ +66.2° (EtOH) (lit, mp 240—242 °C,[3] $[\alpha]_D$ +67.3° (EtOH)[4]); IR (KBr): 3540, 3280 cm^{-1}; NMR (pyridine-d_5): 1.09, 1.23, and 1.25 (each 3H and s, $-\dot{C}(CH_3)_2$ and $C_{10}-CH_3$), 1.39 (6H, d, J=7 Hz, $-CH(C\underline{H}_3)_2$), 7.15 and 7.18 (each 1H and s, C_{11}–H and C_{14}–H). Found: C, 79.19; H, 10.11%. Calcd for $C_{20}H_{30}O_2$: C, 79.42; H, 10.00%. The identity of the synthetic **1** with natural hinokiol provided by Professor T. Hirose was confirmed by mixed melting point determination and by IR spectral comparison.

12-Hydroxyabieta-8,11,13-trien-3-one (Hinokione) (2). A solution of **1** (69 mg) in acetone (6.0 ml) was oxidized with Jones reagent (1 M†: 0.2 ml) at 5 °C for 3 min. The mixture was diluted with ether, washed with water, and dried over sodium sulfate. The ether solution was evaporated and the residue was purified by column chromatography on silica gel (10 g), using ether–benzene (3 : 97) as the eluent, to give **2** (49.2 mg: 71.8%), which was recrystallized from a mixture of ether and hexane; mp 192—193 °C; $[\alpha]_D$ +115.6° (EtOH) (lit,[3] mp 191—192 °C, $[\alpha]_D$ +111.9° (EtOH)); IR: 3605, 3380, 1696 cm^{-1}; NMR ($CDCl_3$): 1.14, 1.18, and 1.30 (each 3H and s, $-\dot{C}(CH_3)_2$ and $C_{10}-CH_3$), 1.22 (6H, d, J=7 Hz, $-CH(C\underline{H}_3)_2$), 6.66 and 6.89 (each 1H and s, C_{11}–H and C_{14}–H). Found: C, 79.71; H, 9.53%. Calcd for $C_{20}H_{28}O_2$: C, 79.95; H, 9.39%.

12-Methoxyabieta-8,11,13-trien-3β-ol (12). A mixture of **1** (99 mg), methyl iodide (0.5 ml), anhydrous potassium carbonate (1.0 g), and ethyl methyl ketone (5.0 ml) was stirred and refluxed for 8 h. The mixture was cooled, diluted with ether, and water was added. The organic layer was separated, washed first with aqueous sodium thiosulfate and then with water, and then dried over sodium sulfate. After the solvent had been evaporated *in vacuo*, the residue was purified by column chromatography on silica gel (10 g), using ether–benzene (1 : 99) as the eluent, to give **12** (75.8 mg: 72.8%), which was recrystallized from hexane; mp 105.5—107.5 °C (softened at *ca.* 94 °C); $[\alpha]_D$ +61.0° (EtOH) (lit,[1] mp 95—96 °C, $[\alpha]_D$ +59.46° (EtOH)); IR: 3625, 3455 cm^{-1}; NMR: 0.86, 1.04, and 1.19 (each 3H and s, $-\dot{C}(CH_3)_2$ and $C_{10}-CH_3$), 1.15 (6H, d, J=7 Hz, $-CH(C\underline{H}_3)_2$), 1.61 (1H, s, –OH), 3.75 (3H, s, $-OCH_3$), 6.58 and 6.72 (each 1H and s, C_{11}–H and C_{14}–H). Found: C, 79.46; H, 10.35%. Calcd for $C_{21}H_{32}O_2$: C, 79.70; H, 10.19%.

12-Methoxyabieta-2,8,11,13-tetraene (13). a): A mixture of **12** (938 mg), phosphoryl chloride (1.4 ml), and pyridine (10 ml) was refluxed for 1 h, cooled, and then poured into ice-dilute hydrochloric acid. The mixture was extracted with ether. The ether extract was washed with brine, dried over sodium sulfate, and evaporated *in vacuo*. The crude product was purified by column chromatography on silica gel (40 g), using hexane–benzene (7 : 3) as the eluent, to give **13** as an oil (764 mg: 86.3%); $[\alpha]_D$ +163°; IR: 1655 cm^{-1}; NMR: 0.98, 1.03, and 1.23 (each 3H and s, $-\dot{C}(CH_3)_2$ and $C_{10}-CH_3$), 1.17 (6H, d, J=7 Hz, $-CH(C\underline{H}_3)_2$), 3.21 (1H, m, $-C\underline{H}(CH_3)_2$), 3.75 (3H, s, $-OCH_3$), 5.49 (2H, s, C_2–H and C_3–H), 6.58 and 6.71 (each 1H and s, C_{11}–H and C_{14}–H). Found: C, 84.49; H, 10.32%. Calcd for $C_{21}H_{30}O$: C, 84.51; H, 10.13%.

b): A mixture of 12-methoxyabieta-8,11,13-trien-3α-ol (**14**) (56.4 mg), phosphoryl chloride (0.09 ml), and pyridine (2.0 ml) was refluxed for 1 h. After the work-up described in *a*), the crude product was chromatographed on silica gel (5 g) to give the tetraene derivative (46.2 mg: 86.9%), whose IR and NMR spectra were identical with those of **13**.

Hydroboration-oxidation of 13. Boron trifluoride etherate (1.16 ml) was added dropwise at 0—5 °C to a stirred mixture of **13** (759 mg) and sodium borohydride (260 mg) in dry tetrahydrofuran (12 ml) in a stream of nitrogen. After the mixture had been stirred at this temperature for 2 h, there was added successively aqueous tetrahydrofuran (50%: 1.0 ml), aqueous sodium hydroxide (12%: 3.0 ml), and hydrogen peroxide (30%: 3.0 ml) at −5—0 °C. The mixture was stirred at −5—0 °C for 30 min and then at room temperature for 1 h, poured into dilute hydrochloric acid, and extracted with ether. The ether extract was washed with brine, dried over sodium sulfate, and evaporated *in vacuo*. The crude product was purified by column chromatography on silica gel (70 g), using ether–benzene (2 : 98) as the eluent, to give 12-methoxyabieta-8,11,13-trien-3α-ol (**14**) (305 mg: 37.9%), which was recrystallized from hexane; mp 114—114.5 °C; $[\alpha]_D$ +49.1° (EtOH) (lit,[1] mp 117—118 °C, $[\alpha]_D$ +45.25° (EtOH)); IR: 3630, 3455 cm^{-1}; NMR: 0.90, 0.96, and 1.16 (each 3H and s, $-\dot{C}(CH_3)_2$ and $C_{10}-CH_3$), 1.15 (6H, d, J=7 Hz, $-CH(C\underline{H}_3)_2$), 1.72 (1H, s, –OH), 3.20 (1H, m, $-C\underline{H}(CH_3)_2$), 3.36 (1H, m, $W_{1/2}$=7 Hz, C_3–H), 3.75 (3H, s, $-OCH_3$), 6.59 and 6.71 (each 1H and s, C_{11}–H and C_{14}–H). Found: C, 79.70; H, 10.48%. Calcd for $C_{21}H_{32}O_2$: C, 79.70; H, 10.19%.

Further elution gave **12** (102 mg: 12.7%). Elution with ether–benzene (5 : 95) gave 12-methoxyabieta-8,11,13-trien-2α-ol (**15**) (141 mg: 17%), which was recrystallized from hexane; mp 130—131.5 °C; $[\alpha]_D$ +64.3°; IR 3611, 3430 cm^{-1}; NMR ($CDCl_3$): 0.98, 1.01, and 1.24 (each 3H and s, $-\dot{C}(CH_3)_2$ and $C_{10}-CH_3$), 1.19 (6H, d, J=7 Hz, $-CH(C\underline{H}_3)_2$), 3.25 (1H, m, $-C\underline{H}(CH_3)_2$), 3.80 (3H, s, $-OCH_3$), 4.08 (1H, m, $W_{1/2}$= 22 Hz, C_2–H), 6.76 and 6.88 (each 1H and s, C_{11}–H and C_{14}–H). Found: C, 79.99; H, 10.40%. Calcd for $C_{21}H_{32}O_2$: C, 79.70; H, 10.19%.

12-Methoxyabieta-8,11,13-trien-3-one (16). Pyridinium chlorochromate (220 mg) was added at 0—5 °C to a stirred solution of **14** (193 mg) in dichloromethane (4.5 ml). The mixture was stirred at room temperature for an additional 1.5 h and then diluted with ether. After the addition of

† 1M = 1 mol dm^{-3}.

water, the mixture was extracted with ether. The ether extract was washed with brine, dried over sodium sulfate, and evaporated *in vacuo*. The residue was purified by column chromatography on silica gel (10 g), using ether–benzene (1 : 99) as the eluent, to give **16** (132 mg: 68.4%), which was recrystallized from ethanol; mp 123.5—124.5 °C; $[\alpha]_D$ +132° (EtOH) (lit,[1] mp 126 °C, $[\alpha]_D$ +122.2° (EtOH)); IR: 1700 cm^{-1}; NMR: 1.10 (6H, s, $-\dot{C}(CH_3)_2$), 1.16 (6H, d, J=7 Hz, $-CH(C\underline{H}_3)_2$), 1.28 (3H, s, $C_{10}-CH_3$), 3.20 (1H, m, $-C\underline{H}-(CH_3)_2$), 3.77 (3H, s, $-OCH_3$), 6.58 and 6.75 (each 1H and s, C_{11}–H and C_{14}–H). Found: C, 80.03; H, 9.86%. Calcd for $C_{21}H_{30}O_2$: C, 80.21; H, 9.62%.

Abieta-8,11,13-triene-2α,12-diol (Salviol) (3). A mixture of **15** (51.5 mg), ethanethiol (0.5 ml), anhydrous aluminium chloride (150 mg), and dichloromethane (1.5 ml) was stirred at room temperature for 1 h, poured into ice-dilute hydrochloric acid, and extracted with ether. The ether extract was washed with brine, dried over sodium sulfate, and then evaporated *in vacuo*. The crude product was purified by column chromatography on silica gel (5 g), using ether–benzene (4 : 6) as the eluent, to give salviol (**3**) (47.3 mg: 96.1%), which was recrystallized from benzene; mp 106—107 °C (softened at *ca.* 103 °C); $[\alpha]_D$ +55.7° (EtOH) (lit,[5] mp 108 °C); IR (KBr): 3395 cm^{-1}; NMR ($CDCl_3$, 90 MHz): 0.96, 1.00, and 1.23 (each 3H and s, $-\dot{C}(CH_3)_2$ and $C_{10}-CH_3$), 1.23 (6H, d, J=7 Hz, $-CH(C\underline{H}_3)_2$). 3.15 (1H, m, $-C\underline{H}(CH_3)_2$) 4.09 (1H, m, $W_{1/2}$=22 Hz, C_2–H), 6.06 (1H, s, $=\dot{C}-OH$), 6.68 and 6.83 (each 1H and s, C_{11}–H and C_{14}–H). Found: C, 79.15; H, 10.13%. Calcd for $C_{20}H_{30}O_2$: C, 79.42; H, 10.00%. The IR and NMR spectra of the synthetic **3** were identical with those of natural salviol provided by Professor H. Kakisawa.

12-Methoxyabieta-8,11,13-trien-2-one (17). Pyridinium chlorochromate (148 mg) was added at 0—5 °C to a stirred solution of **15** (140 mg) in dichloromethane (2.5 ml) and the mixture was stirred at room temperature for 1.5 h. After the work-up described for the preparation of **16**, the crude product was purified by column chromatography on silica gel (10 g), using ether–benzene (3 : 97) as the eluent, to give **17** (109 mg: 78.1%). This was recrystallized from ethanol; mp 152.5—153.5 °C; $[\alpha]_D$ +48.6°; IR: 1703 cm^{-1}; NMR: 0.98, 1.13, and 1.21 (each 3H and s, $-\dot{C}(CH_3)_2$ and $C_{10}-CH_3$), 1.15 (6H, d, J=7 Hz, $-CH(C\underline{H}_3)_2$), 3.20 (1H, m, $-C\underline{H}-(CH_3)_2$), 3.77 (3H, s, $-OCH_3$), 6.51 and 6.76 (each 1H and s, C_{11}–H and C_{14}–H). Found: C, 79.93; H, 9.83%. Calcd for $C_{21}H_{30}O_2$: C, 80.21; H, 9.62%.

12-Hydroxyabieta-8,11,13-trien-2-one (2-Oxoferruginol) (4). A mixture of **17** (76.9 mg) and boron tribromide (0.07 ml) in dichloromethane (1.5 ml) was stirred at 0—5 °C for 30 min. The reaction mixture was poured into ice–water and extracted with ether. The ether extract was washed successively with aqueous sodium thiosulfate and brine, dried over sodium sulfate, and then evaporated *in vacuo*. The crude product was purified by column chromatography on silica gel (7 g) using chloroform as the eluent, to give 2-oxoferruginol (**4**) (61.8 mg: 84.1%), which was recrystallized from methanol; mp 237—239 °C; $[\alpha]_D$ +48.3° (MeOH) (lit,[6] mp 232—234 °C, $[\alpha]_D$ +50° (MeOH)); IR (KBr): 3450, 1706 cm^{-1}; NMR ($CDCl_3$, 90 MHz): 0.99, 1.15, and 1.21 (each 3H and s, $-\dot{C}-(CH_3)_2$ and $C_{10}-CH_3$), 1.23 (6H, d, J=7 Hz, $-CH(C\underline{H}_3)_2$), 3.14 (1H, m, $-C\underline{H}(CH_3)_2$), 5.48 (1H, s, –OH), 6.55 and 6.85 (each 1H and s, C_{11}–H and C_{14}–H). Found: C, 80.08; H, 9.56%. Calcd for $C_{20}H_{28}O_2$: C, 79.95; H, 9.39%.

The authors are grateful to Arakawa Chemical Co. Ltd. for a generous gift of rosin. Thanks are also due to Professor H. Kakisawa, Tsukuba University, and to Professor T. Hirose, Science University of Tokyo, for kindly supplying the spectral data and natural hinokiol.

References

1) Y. Yoshiki and T. Ishiguro, *Yakugaku Zasshi*, **53**, 73 (1933); G. Fukui and T. Chikamori, *ibid.*, **59**, 116 (1939).
2) H. S. Barreto and C. Enzell, *Acta Chem. Scand.*, **15**, 1313 (1961).
3) Y.-L. Chow and H. Erdtman, *Acta Chem. Scand.*, **16**, 1291 (1962).
4) I. Fukushima, Y. Sayama, K. Kyogoku, and H. Murayama, *Agric. Biol. Chem.*, **32**, 1103 (1968).
5) T. Hayashi, T. Handa, M. Ohashi, and H. Kakisawa, *J. Chem. Soc., Chem. Commun.*, **1971**, 541.
6) E. Wenkert, J. P. Campello, J. D. McChesney, and D. J. Watts, *Phytochemistry*, **13**, 2545 (1974).
7) The racemic hinokione was recently synthesized by Watt *et al.* D. L. Snitman, R. J. Himmelsbach, and D. S. Watt, *J. Org. Chem.*, **43**, 4758 (1978).
8) H. H. Zeiss, *J. Am. Chem. Soc.*, **69**, 302 (1947); T. Wirthlin, H. Wehrli, and O. Jeger, *Helv. Chim. Acta*, **57**, 351 (1974); H. Koike and T. Tokoroyama, *Chem. Lett.*, **1979**, 333; R. C. Cambie and R. A. Franich, *Aust. J. Chem.*, **23**, 93 (1970).
9) T. Matsumoto, T. Ohmura, and S. Usui, *Bull. Chem. Soc. Jpn.*, **52**, 1957 (1979).
10) E. J. Corey and J. W. Suggs, *Tetrahedron Lett.*, **1975**, 2647.
11) R. C. Cambie and T. J. Fullerton, *Aust. J. Chem.*, **24**, 2611 (1971).
12) M. Node, K. Nishide, M. Sai, K. Ichikawa, K. Fuji, and E. Fujita, *Chem. Lett.*, **1979**, 97.

  Bull. Chem. Soc. Jpn., 54, 585—590 (1981)

Studies on the Uptake of Some Complex Cations of Copper by Molecular Sieves 4A and 5A

S. S. Thantry, K. Veeramoni Iyer, and P. S. Ramanathan*

Analytical Chemistry Division, Bhabha Atomic Research Centre, Trombay, Bombay-400 085, India

(Received September 22, 1979)

Studies on the uptake of Cu^{2+} and a few of its complex cations (*i.e.*, $[Cu(NH_3)_4]^{2+}$, $[Cu(en)]^{2+}$, $[Cu(en)_2]^{2+}$, $[Cu(pn)]^{2+}$, $[Cu(pn)_2]^{2+}$, and $[Cu(tea)]^{2+}$, where en, pn, and tea represent ethylenediamine, propylenediamine, and triethanolamine respectively) by molecular sieves 4A and 5A were undertaken using batch equilibration procedure. $[Cu(pn)]^{2+}$, $[Cu(en)_2]^{2+}$, $[Cu(pn)_2]^{2+}$, and $[Cu(tea)]^{2+}$ showed very little affinity for the zeolite phases, while the uptake of Cu^{2+} and $[Cu(en)]^{2+}$ was comparatively higher. $[Cu(NH_3)_4]^{2+}$ occupied a position in between these two sets. During the equilibration of $[Cu(en)]^{2+}$ and $[Cu(pn)]^{2+}$ some side reactions could be observed leading to the conclusion that the 1:1 complex species underwent disproportionation, generating Cu^{2+} and an equivalent amount of $[Cu(en)_2]^{2+}$ or $[Cu(pn)_2]^{2+}$. These conclusions drawn from the batch equilibration studies were confirmed by appropriate column experiments.

Ion exchange studies using zeolite exchangers of various types have been reviewed from time to time by different workers.[1-9] Scores of publications have appeared in the literature dealing with the studies on the uptake of simple cations by molecular sieves 4A(MS4). Similar studies on molecular sieves 5A-(MS5) are comparatively fewer in number. Recently Schoonheydt and coworkers[10] prepared complexes of ammonia and ethylenediamine with Cu^{2+} on zeolite A and conducted EPR and reflectance spectral studies of the various complexes. The existing literature does not appear to contain any other information on the uptake of complex cations by MS4 and MS5. It was, therefore, decided to undertake a systematic study of the uptake of a few complex cations** of Cu^{2+} (*i.e.*, $[Cu(NH_3)_4]^{2+}$, $[Cu(en)]^{2+}$, $[Cu(pn)]^{2+}$, $[Cu(en)_2]^{2+}$, $[Cu(tea)]^{2+}$, and $[Cu(pn)_2]^{2+}$) by MS4 and MS5. Studies were also carried out with Cu^{2+} for comparison.

Experimental

Chemical analyses of Anasorb MS4 and MS5 samples (40—60 mesh, supplied by Analabs Inc., U.S.A.) were carried out, following procedures given in standard books. Loading studies were carried out by the batch equilibration procedure. All reagents/chemicals used were of Analytical reagent or C.P. grade.

For studying the uptake as a function of time, 20 ml of solutions of Cu^{2+} (0.1 M), $[Cu(en)]^{2+}$ (0.05 M), $[Cu(en)_2]^{2+}$ (0.1 M), $[Cu(pn)]^{2+}$ (0.01 M), $[Cu(pn)_2]^{2+}$ (0.05 M), $[Cu(tea)]^{2+}$ (0.1 M), and $[Cu(NH_3)_4]^{2+}$ (0.1 M) were equilibrated with 0.5 g of the sieve at 30 °C for the prescribed period. The ligand to metal ratio maintained in the last 6 cases were 1, 2, 1, 2, 6, and 60 respectively. The pH values of the solutions of the first six cations used for equilibration were 2.0, 5.0, 7.0, 5.5, 7.0, and 8.0 in that order.

The quantitative and exclusive formation of the complex cation of interest, under the conditions specified above, was confirmed by comparing the spectra of their solutions with those reported in the literature.

To arrive at the 'K' values (mmol of M^{n+} per g of the sieve/mmol of M^{n+} per ml of the solution, at any contact time 't'), the concentrations of the cation of interest in the original solution and in the external solution left out after equilibration were estimated spectrophotometrically. Cu^{2+} was estimated after converting it to $[Cu(NH_3)_4]^{2+}$ by adding aqueous ammonia in excess (6 M) and measuring the absorbance(E) at 600 nm(λ_{max}). In the case of the other complex cationic species (*i.e.*, $[Cu(en)]^{2+}$, $[Cu(pn)]^{2+}$ *etc.*) the 'E' values were measured at the corresponding λ_{max} (after appropriate dilution to bring the concentration within the range of the corresponding calibration graph). The concentrations were then computed. In a few cases the amount of Na^+(or Ca^{2+}) displaced from the molecular sieve was also estimated to understand the extent of uptake by ion exchange. These estimations were carried out after removing the copper from the solutions by electrolysis in the Fischer Electroanalyser.

Equilibration studies were also carried out to understand the influence of concentration on the uptake. In these cases, solutions containing different concentrations of the cation of interest were equilibrated for 24 h. The 'K' values were then calculated as described in the earlier paragraph.

Results and Discussion

Chemical Analysis of the MS4 and MS5 Specimens. The number of AlO_2, Na, and H_2O species per unit cell of the MS4(computed from the results of chemical analysis, on the assumption that the SiO_2 content corresponds exactly to 12 SiO_2 groups) worked out to 11.60, 11.00, and 20.80 respectively. The corresponding figures for MS5 were 12.82, 1.66, and 21.52. In this case, the number for Ca was 4.34.

The results of chemical analysis speak against the possible presence of occluded $NaAlO_2$ in the MS4. The Na, H_2O, and AlO_2 figures are all smaller than those expected from the generally accepted unit cell formula ($Na_{12}(AlO_2)_{12}(SiO_2)_{12}\cdot 27H_2O$). In the MS5 specimen, there is (i) a marginal decrease in the number of Ca atoms and (ii) a significant decrease and increase in the Na and AlO_2 contents respectively(in comparison to the unit cell formula of MS4 in which 75% Na^+ has been replaced by Ca^{2+}). The results provide a measure of free Al_2O_3 and SiO_2 in the zeolite samples.

Equilibration Studies. The pH of the equilibrated Cu^{2+} solution increased from 2.0 to around 4.0 during equilibration.*** The uptake of Cu^{2+} was so slow

** In the subsequent sections, the symbols 'en', 'pn', and 'tea' will be used to represent ethylenediamine, propylenediamine, and triethanolamine respectively.

*** In this case, an undesirable but unavoidable side-effect of the comparatively higher acidity maintained (to keep the Cu^{2+} in solution) is the structural breakdown of a small fraction of the zeolite matrix.

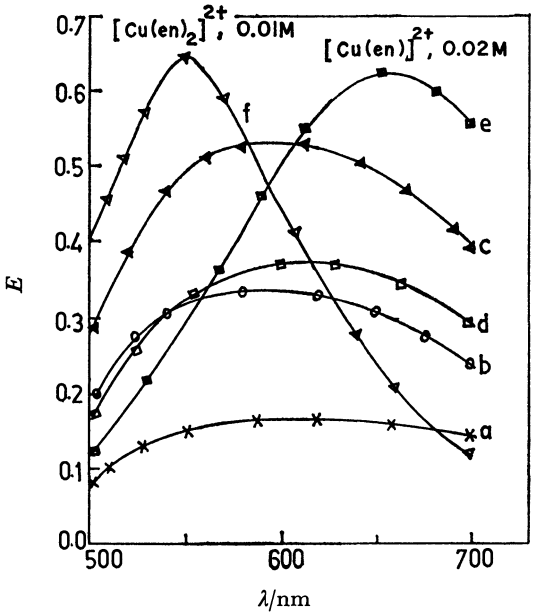

Fig. 1. Spectra of $[Cu(en)]^{2+}$, $[Cu(en)_2]^{2+}$, and the equilibrated solutions of $[Cu(en)]^{2+}$—MS4.
Concentration of $[Cu(en)]^{2+}$ before equilibration= 0.02, 0.03, 0.04, and 0.05 M for a—d.
Dilution: 2 times for d.

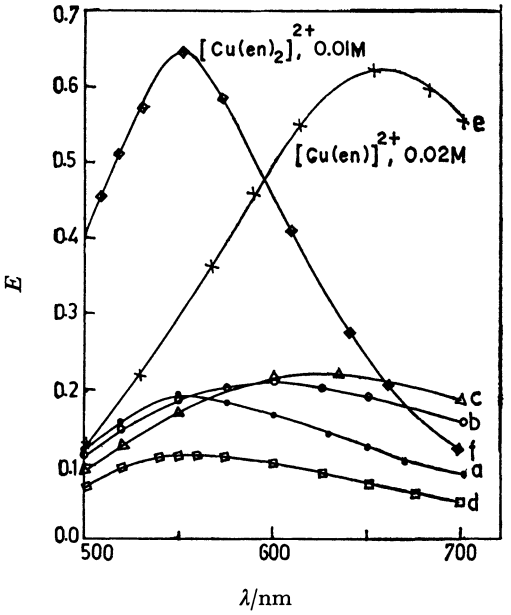

Fig. 2. Spectra of i) Equilibrated solutions, ii) $[Cu(en)]^{2+}$, and iii) $[Cu(en)_2]^{2+}$—MS5.
a=0.01 M, b=0.03 M, c=0.05 M, d=effluent from column experiment.
Dilution b: 3, c: 5, d: 10.

that final equilibrium was attained only after about 48 h. The 'K' values observed in the case of MS4 and MS5, after this time interval, were 42 and 27 respectively(when the initial concentration of Cu^{2+} solution employed was 0.1 M).

Analysis of Na^+ released during equilibration revealed that the uptake of Cu^{2+} by MS4 was predominantly by ion exchange. In the case of MS5, however, the Ca^{2+} released was only around 30% of the amount equivalent to the total Cu^{2+} taken up.

When 20 ml of water at pH 2.0 were equilibrated with 0.5 g of the sieves, the Na^+ and Ca^{2+} released were found to be 4 mg and 0.8 mg respectively in the two cases.

Spectral studies of Cu^{2+}-aqueous ammonia mixtures revealed that the formation of $[Cu(NH_3)_4]^{2+}$ was complete only when $C_{NH_3}/C_{Cu} \geq 40$(when C_{Cu}=0.1 M). 'K' values for this cation were lower ($\approx$5 for a solution of concentration of 0.1 M) than those found for Cu^{2+}. Only marginal increases in 'K' were observed beyond 2 h. The much faster kinetics suggest that the uptake is probably restricted to the external surfaces which are in direct contact with the solution.

Increase in the concentration of aqueous ammonia (to 60 and 80 times the concentration of Cu^{2+}) produced only a marginal change in the uptake of $[Cu(NH_3)_4]^{2+}$ species. The uptake of NH_4^+ by ion exchange was then investigated in each case by equilibrating aqueous ammonia solution of the same concentration, but in the absence of Cu^{2+}. While 8 M aqueous ammonia released about 15 mg of Na^+ from MS4, the release of Ca^{2+} from MS5 was insignificant($\approx$0.2%).

The 'K' values found for $[Cu(en)_2]^{2+}$, $[Cu(pn)_2]^{2+}$, and $[Cu(tea)]^{2+}$ were extremely small($\approx$1). The uptake was also very quick, suggesting thereby, that the process involved was probably pure physical adsorption. It appears that the sizes of these ions are unfavourable for entry into the pores of the zeolites. On this basis it can be qualitatively concluded that the size of each of these three complex cations (in the hydrated form) may be greater than 5Å, the pore dimension of MS5.

The pH of $[Cu(en)]^{2+}$ solution used for equilibration was adjusted to 5.0 as the complex forms quantitatively when the reactants are mixed in stoichiometric amounts at this acidity. The pH of the external solution rose to around 6.0 after equilibration. In this case the exchange was slow(as in the case of Cu^{2+}). 0.01 M solution, when equilibrated with MS4 for 24 h became practically colourless, indicating a nearly quantitative uptake in this concentration range. The uptake was, however, not quantitative when more concentrated solutions($\approx$0.02 M and above) were employed for equilibration. Moreover, the post-equilibration spectra of these concentrated solutions were not superimposable on that of the 1:1 complex. The λ_{max} shifted from 650 nm(expected for the 1:1 complex) to a lower value. The extent of shift depended on the time of equilibration as well as the concentration of the solution used. Some typical spectra are shown in Fig. 1. The results obtained with MS5 were of the same nature except for the fact that the uptake was not quantitative at low concentrations(*i.e.*, $\approx$0.01 M). Some typical spectra obtained in the case of MS5 are shown in Fig. 2.

A careful scrutiny of the spectra of the external solutions indicated the possibility of the presence of varying amounts of the higher complex(1:2, with λ_{max} at 550 nm) in them. As both 1:1 and 1:2 complexes are known to be very stable under the experimental conditions employed, and Cu^{2+} cannot remain in/solution in the weakly acidic conditions

TABLE 1. CONCENTRATIONS OF CATIONS IN THE ADSORBENT AND EXTERNAL SOLUTION

Solution used for equilibration: 20 ml of $[Cu(en)]^{2+}$ at pH 5.0

λ values chosen for spectrophotometric analyses of binary mixtures: 550 and 650 nm

$(\varepsilon_1)_{550}=16$; $(\varepsilon_2)_{550}=64$; $(\varepsilon_1)_{650}=32$; $(\varepsilon_2)_{650}=24$

S. No.	Concentration of $[Cu(en)]^{2+}$ used for equilibration $\times 10^3$/M	Concentration in the external solution at equilibrium $\times 10^3$/M		Millimoles of cation taken up by 0.5 g of the sieve $\times 10^2$	
		$[Cu(en)]^{2+}$	$[Cu(en)_2]^{2+}$	Cu^{2+}	$[Cu(en)]^{2+}$
A. MS4					
1	10.0	N.D.[a]	N.D.[a]	N.D.[a]	20.0
2	20.0	4.25	1.4	2.8	25.9
3	30.0	7.1	3.3	6.6	32.6
4	40.0	11.7	4.9	9.8	37.0
5	50.0	17.7	5.9	11.8	41.0
B. MS5					
6	10.0	2.1	2.45	4.9	6.0
7	20.0	8.0	3.55	7.1	9.8
8	30.0	13.8	5.2	10.4	11.6
9	40.0	21.7	5.65	11.3	14.0
10	50.0	29.1	6.0	12.0	18.0

a) N.D. means not detectable.

maintained, the possibility of the presence of free Cu^{2+} in the external solutions was ruled out. Taking the external solutions (equilibrated for 24 h) as mixtures of 1:1 and 1:2 complexes, the individual concentrations(C_1 and C_2)/of the two complexes were calculated by solving simultaneous equations. The results obtained are given in Table 1.

The above-mentioned observations may be interpreted as shown below: It appears that the MS4 phase induces the dissociation of $[Cu(en)]^{2+}$ and takes up the Cu^{2+} generated *in situ*(along with $[Cu(en)]^{2+}$, for which also MS4, shows comparable affinity). The 'en' generated by the above process combines with $[Cu(en)]^{2+}$ present in the external solution, giving rise to an equivalent amount of $[Cu(en)_2]^{2+}$. When dilute solutions($\approx$0.01 M) are employed, the uptake of all the three cationic species occurs practically quantitatively, making the external solution practically colourless. However, with increase in concentration of the external solution, a comparatively larger concentration of the 1:2 complex is formed. As it is a strong complex and it has very little affinity for the zeolite phase, the post-equilibration solution phase gradually becomes a mixture of $[Cu(en)]^{2+}$ and $[Cu(en)_2]^{2+}$. The side equilibria represented by Eqs. 1—3 summarise the above-mentioned points.

$$[Cu(en)]^{2+} \rightleftharpoons Cu^{2+} + en \quad (1)$$

$$Cu^{2+} + 2NaZ \rightleftharpoons CuZ_2 + 2Na^+ \quad (2)$$

$$[Cu(en)]^{2+} + en \longrightarrow [Cu(en)_2]^{2+} \quad (3)$$

In Eq. 2, Z stands for the zeolite anion.

In the case of MS5, the results(Table 1) were qualitatively of the same type(*i.e.*, as described above in the case of MS4). The notable differences were: (i) The uptake was not quantitative in low concentrations. (ii) The quantity of $[Cu(en)]^{2+}$ taken up was smaller and the uptake of Cu^{2+} was greater than those found in the case of MS4. (iii) The total uptake (as Cu^{2+} and $[Cu(en)]^{2+}$) was, however, much lower. Equation 2 takes the following form in this case, while (1) and (3) continue to remain applicable.

$$0.5Cu^{2+} + Ca_{0.5}Z \rightleftharpoons Cu_{0.5}Z + 0.5Ca^{2+} \quad (4)$$

In this context it is worth mentioning that a significant part(>60%) of Cu^{2+} and $[Cu(en)]^{2+}$ going to the MS5 phase is by physical adsorption. Irrespective of whether the uptake is by ion exchange or by physical adsorption, the arguments presented earlier concerning the apparent disproportionation of $[Cu(en)]^{2+}$ (giving Cu^{2+} and an equivalent amount of $[Cu(en)_2]^{2+}$) will hold good.

To understand the nature of the results obtained in a column experiment, a MS4 column(5 g packed in a column of i.d. 1.2 cm) was fed with 100 ml of $[Cu(en)]^{2+}$ solution of concentration 0.05 M(pH= 5.0). The flow rate was 0.5 ml per min. The effluent solution was colourless. When 50 ml of 0.05 M $[Cu(en)]^{2+}$ solution were passed through a column containing 2 g of MS4, the effluent contained about 5% of the total copper as the 1:2 complex, while the effluent was colourless when 25 ml of 0.01 M solution were passed through the same column. All these observations point out that the disproportionation reaction does take place in the column experiment as well. When dilute solutions are employed, copper is not found in the effluent as $[Cu(en)]^{2+}$, as well as the small amount of Cu^{2+} and $[Cu(en)_2]^{2+}$, formed by the disproportionation reaction, are all retained by the column. On increasing the concentration, a small amount of the 1:2 complex leaks out as its affinity for the adsorbent is low.

In the case of MS5, the effluent contained around 50% of the copper as a mixture of 1:1 and 1:2 complexes(in approximately equal concentrations) when 20 ml of 0.05 M $[Cu(en)]^{2+}$ solution at pH 5.0 were passed through a column containing 2 g of the sieve. The higher extent of disproportionation and the comparatively lower affinities for the cations seem

TABLE 2. CONCENTRATIONS OF CATIONS IN THE ADSORBENT AND EXTERNAL SOLUTION

Solution used for equilibration: 20 ml of $[Cu(pn)]^{2+}$ at pH 5.5
λ values chosen for spectrophotometric analyses of binary mixtures: 550 and 650 nm
$(\varepsilon_1)_{550}=16$; $(\varepsilon_2)_{550}=66$; $(\varepsilon_1)_{650}=33$; $(\varepsilon_2)_{650}=28$

S. No.	Concentration of $[Cu(pn)]^{2+}$ used for equilibration $\times 10^3$/M	Concentration in the external solution at equilibrium $\times 10^3$/M		Millimoles of Cu^{2+} taken up by 0.5 g of the sieve $\times 10^2$
		$[Cu(pn)]^{2+}$	$[Cu(pn)_2]^{2+}$	
A. MS4				
1	5.0	N.D.[a]	1.95	3.90
2	10.0	0.66	4.25	8.50
3	15.0	1.55	6.37	12.74
4	20.0	3.17	8.02	16.04
B. MS5				
5	5.0	0.4	2.3	4.6
6	10.0	1.3	4.3	8.6
7	15.0	2.8	6.0	12.0
8	20.0	6.5	6.7	13.4

a) N.D. means not detectable. The calculations reveal that 0.022, 0.017, 0.014, and 0.016 millimoles of Cu-pn complex species go to the MS4 phase in the four cases respectively. The uptake is negligible in the case of MS5.

to be responsible for this situation.

In view of the above-mentioned side reactions, 'K' values, as defined earlier, cannot be given for $[Cu(en)]^{2+}$ uptake by MS4 and MS5. One can, however, arrive at 'K_{av}' and 'K^*' values, defined as shown below:

$$K_{av}=\frac{\text{mmol of } Cu^{2+} \text{ in all forms per g of sieve}}{\text{mmol of } Cu^{2+} \text{ in all forms per ml of the solution}}$$

$$K^*=\frac{\text{mmol of } [Cu(en)]^{2+} \text{ per g of sieve}}{\text{mmol of } [Cu(en)]^{2+} \text{ per ml of the solution}}.$$

These values are tabulated in Table 3.

From the earlier sections it becomes obvious that Cu^{2+} and $[Cu(en)]^{2+}$ exhibit good affinity for the zeolite phase. Uptake of these preferred cationic species, with the consequential breakdown of the less favoured $[Cu(en)_2]^{2+}$, is not observed because of the very high stability of the 1:2 complex.

In this context it is worth pointing out that Schoonheydt *et al.*[10] recently reported the preparation of the following complexes (by gas phase adsorption) on the A type zeolite surface:

(i) $[Cu(NH_3)_4]^{2+}$ and a small amount of tetrahedrally coordinated Cu^{2+} ions by adsorption of NH_3 on a dehydrated CuA zeolite,

(ii) $[Cu(en)]^{2+}$ by the adsorption of 'en' on a dehydrated CuA zeolite and

(iii) $[Cu(en)_2]^{2+}$ and $[Cu(en)_3]^{2+}$ by adsorption of 'en' on CuA in the presence of water.

They also found that $[Cu(en)]^{2+}$ could be loaded on NaA by ion exchange from aqueous solution, but the bis-complex could not be loaded in this way. The impossibility of loading the bis-complex has been attributed by them to the fact that its dimensions (0.47×0.77 nm) exceed the free diameter of the 8-membered windows ($\approx$0.44 nm). Another factor was the instability of the bis-complex in the supercage of zeolite A. They found that the bis-complex could be synthesised *in situ* by equilibrating either the Cu^{2+} or the mono-complex loaded zeolite with excess of 'en'. They also observed the uptake of both Cu^{2+} and $[Cu(en)]^{2+}$ by the zeolite when the solution of the latter was equilibrated with NaA at pH 6. The above-mentioned conclusions were drawn by them from EPR and reflectance spectral studies of the various complex loaded zeolites. Our findings reported in the earlier paragraphs have been obtained by the spectrophotometric investigations of the solutions prior to and after equilibration with the zeolite. They are thus complementary to those reported by Schoonheydt *et al.*[10]

Results of equilibration studies using $[Cu(pn)]^{2+}$ were somewhat similar to those described in the case of $[Cu(en)]^{2+}$. In this case also computations were made to arrive at the distribution of the different cationic species between the aqueous and zeolite phases. The results are tabulated in Table 2. As discussed in the case of $[Cu(en)]^{2+}$ the affinity of Cu^{2+} for the zeolite phase stimulates the dissociation of $[Cu(pn)]^{2+}$ also. Essentially, the zeolite phase gets loaded with Cu^{2+}, leaving behind a mixture of $[Cu(pn)]^{2+}$ and $[Cu(pn)_2]^{2+}$ (formed by the combination of $[Cu(pn)]^{2+}$ and free 'pn' released during the migration of Cu^{2+} to the zeolite phase) in the external solution. In other words, the side equilibria of the type represented by Eqs. 1—4 apply for the case of $[Cu(pn)]^{2+}$ as well. The low uptake of $[Cu(pn)]^{2+}$ compared to $[Cu(en)]^{2+}$ is to be attributed to the larger size of the former (>0.5 nm). Moreover, even this small uptake may be due to physical adsorption.

The conclusions concerning the disproportionation reaction were confirmed further by carrying out column experiments. The spectrum of the effluent was that of the 1:2 complex. The copper content was found to be slightly less than 50% of that present in the initial solution. These results indicate that the disproportionation reaction is practically complete in this case (*i.e.*, 1 mol of the 1:1 complex gives 0.5 mol

TABLE 3. VARIATION OF 'K', 'K_{av}', AND K^* AS A FUNCTION OF CONCENTRATION

S. No.	Concentration $\times A$/M	Cu^{2+}		$[Cu(NH_3)_4]^{2+}$		$[Cu(en)]^{2+}$				$[Cu(pn)]^{2+}$	
						K_{av}		K^*		K_{av}	
		I	II	I	II	I	II	I	II	I	II
1	0.03	—	80	—	—	—	—	—	—	—	—
2	0.05	103	45	—	—	—	—	—	—	40	34
3	0.10	38	19	—	—	a)	48	a)	57	35	31
4	0.15	—	—	—	—	—	—	—	—	32	27
5	0.20	—	10	—	—	102	29	120	25	29	20
6	0.25	—	—	69	—	—	—	—	—	—	—
7	0.30	10	6	—	31	75	23	92	17	—	—
8	0.40	6	—	—	—	56	19	63	13	—	—
9	0.50	5	—	24	16	45	17	46	12	—	—
10	1.00	—	—	5	6	—	—	—	—	—	—

A=1.0 for Cu^{2+}; 10.0 for all other cations. a) The values are very high (as the solution left out after equilibration was practically colourless and did not show any measurable E value at 550 and 650 nm). I and II are data for MS4 and MS5 respectively.

of Cu^{2+} and 0.5 mol of the 1:2 complex). As a small amount of the 1:2 complex is retained on the sieves, besides Cu^{2+}, the concentration of copper in the effluent turns out to be slightly less than 50% of the total amount taken.

Because of the above-mentioned disproportionation reactions, 'K' values for $[Cu(pn)]^{2+}$ also cannot be calculated. In view of the low uptake of $[Cu(pn)]^{2+}$ by the sieves, K^* values were not computed. The 'K_{av}' values were, therefore, the only set computed in this case. These are included in Table 3. These 'K_{av}' values can be considered as an indirect measure of the influence of 'pn' on the uptake of Cu^{2+}.

Interestingly enough, 20 ml of a solution of 'pn' (0.22 M), when equilibrated for 3 h with 0.5 g of 75% Cu^{2+} substituted MS4, eluted about two thirds of Cu^{2+} as $[Cu(pn)_2]^{2+}$. The MS4 phase ceased to have the green colour characteristic of Cu^{2+} form, but attained the blue colour characteristic of $[Cu(pn)]^{2+}$. From this experiment it was qualitatively concluded that 'pn', taken up by the MS4 phase, complexed Cu_2^+ present there (to give 1:1 complex *in situ*), even though $[Cu(pn)]^{2+}$ itself was not taken up (inside the pores) by MS4 because of its larger size.

It would be quite fruitful to refer here once again to the earlier work of Schoonheydt *et al.*[10] According to them $[Cu(en)_2]^{2+}$ is unstable in the supercage of zeolite A. The bis-complex can be synthesized in aqueous suspensions by first exchanging Cu^{2+} or the monocomplex and then adding large excess of 'en' to the suspensions (pH≥11). The instability of the bis-complex was further substantiated by the observation of Schoonheydt and others that Cu^{2+} moved out of the zeolite phase into the 'en' solution upon standing overnight.

From considerations of electroneutrality, reactions of the type discussed above (in which about two-thirds of Cu^{2+} is eluted out by the amine) cannot be classified as regular ion exchange processes. As the loss of Cu^{2+} from the solid phase occurs without the uptake of an equivalent amount of another cation, a change in the nature of the solid phase becomes an inevitable consequence. It would then be logical to conclude that structural alterations may have to occur to satisfy electroneutrality conditions in the solid phase left out after equilibration.

Table 3 includes the following parameters obtained as a function of concentration: (i) 'K' values of Cu^{2+} and $[Cu(NH_3)_4]^{2+}$, (ii) 'K_{av}' values of $[Cu(en)]^{2+}$ and $[Cu(pn)]^{2+}$ and (iii) K^* values of $[Cu(en)]^{2+}$. The data for the other cations are not being included as they are too small to deserve any consideration.

A scrutiny of the data included in Table 3 reveals that the 'K', K^*, and 'K_{av}' values decrease with increase in concentration of the cation equilibrated. This is to be attributed to the fact that the uptake tends to reach a saturation value with increase in concentration of the equilibrated solution.

From a comparison of the data given in Table 3 one can understand the relative affinities of the different cationic species for the two sieves. The 'K', K^*, or 'K_{av}' (as the case may be) for the same ion on MS4 and MS5 reveal that the uptake on the latter sieve is considerably less in the case of all the cations included in the Table. One possible reason for this may be the fact that the Ca^{2+} ions preferentially occupy a more stable site in the A type zeolites. (The difficulty encountered in displacing the Ca^{2+} is further illustrated by equilibration experiments with water at pH 2.0 and 8 M aqueous ammonia discussed earlier). In addition to this, the influence of cation valency on the ion exchange process cannot be ignored. The cation to be displaced in the case of MS5 has the same charge (+2) as the displacing (simple or complex) one, while the displacement of a univalent ion (Na^+) by bivalent ones is involved in the case of MS4. Though the larger pore dimension of MS5 is a favourable factor for migration of ions into the zeolite phase, the occupation of preferential sites by Ca^{2+} and its higher charge turn out to be unfavourable factors (from the point of view of ion exchange).

As already stated, dilute solutions of $[Cu(en)]^{2+}$ give colourless effluents when passed through a MS4

column. Solutions of $[Cu(pn)]^{2+}$, however, give around 50% of the total copper in the effluent (as the 1:2 complex). These differences can be fruitfully used to estimate (with some limitations) the amounts of 'en' and 'pn' in their mixture. In principle, this type of estimation can be extended further to cover mixtures of 'en' and other higher homologues of 'pn' as well. Experimental data substantiating this expectation have been obtained by the authors.

The authors are grateful to Dr. M. Sankar Das, Head, Analytical Chemistry Division and Dr. Ch. Venkateswarlu for their constructive suggestions.

References

1) S. P. Zdhanov, *Neorg. Ionoobmen. Mater.*, **1**, 124 (1974).
2) L. V. C. Rees, *Ann. Rep. Progr. Chem., Sect. A.*, **67**, 191 (1970).
3) F. S. Stone, *Acta Cient Venez.*, Suppl., **24**, 32 (1973).
4) H. S. Sherry, Phy. Chem. Sci. Res. Rep. 1975, 1 (Nat. Sea Water, Rep. Dahlem Workshop, 1975), 523.
5) K. Wacks, *Fette, Seifen., Anstrichm.*, **77**, 366 (1975).
6) V. Grba, Z. Soljic, and I. Dican, *Nafta(Zagreb)*, **26**, 520 (1975).
7) J. H. Lunsford, A. C. S. Symp. Ser, **40** (Mole. Sieves—2, Int. Conf., 4th), (1977) 473.
8) A. Cremers, A. C. S. Symp. Ser., **40** (Mole. Sieves—2, Int. Conf., 4th), (1977) 179.
9) K. Seff, *Acc. Chem. Res.*, **9**, 121 (1976).
10) R. A. Schoonheydt, P. Peigneur, and J. B. Uytterhoeven, *J. Chem. Soc., Faraday Trans. I*, **74**, 2550 (1978).

Exchange Kinetics of Rubidium and Caesium Ions on Pyridinium Tungstoarsenate Exchanger

Ajay K. Jain,* Raj P. Singh, and Sushma Agrawal
Chemistry Department, University of Roorkee, Roorkee-247672, India
(Received February 12, 1980)

The Kinetics of exchange of Rb^+ and Cs^+ has been investigated on pyridinium tungstoarsenate ion exchanger using limited bath technique. The exchange rate was studied as a function of concentration, temperature and particle size of exchanger to determine the slowest step. It was found that Rb^+ exchange is particle diffusion controlled whereas Cs^+ exchange shows dual behaviour at low concentration level. However, at higher concentrations, particle diffusion controls Cs^+ exchange but the rate is concentration dependent. This anomalous behaviour has been explained by assuming that Cs^+ exchange approaches closely to a chemical reaction. Thermodynamic parameters of exchange such as effective diffusion coefficient (D), activation energy (E_a) and entropy of activation (ΔS^*) were calculated. The D and E_a values were found in the same order as that of ionic size, ΔS^* value being positive for Cs^+ exchange and negative for Rb^+ exchange. A negative ΔS^* value is usual but a positive value for Cs^+ exchange might be due to dehydration of the cation while passing through the channels of the exchanger. This explanation is in line with that of interaction energy for the exchange of Cs^+ on pyridinium tungstoarsenate.

The study of the kinetics of ion exchange process is important since it provides information on the mechanism of the rate controlling process, reactions accompanying the ion exchange, as well as internal physical structure of the exchanger and the extent of hydration of exchanging ion.

Systematic kinetic studies on ion exchangers were started by Nachod and Wood,[1,2] the earliest theory being developed by Boyd *et al.*[3] The kinetics of cation exchange in organic resins[4-6] and synthetic zeolites[7-9] has been studied in length. However, little information is available on other inorganic ion exchangers. Of synthetic inorganic ion exchangers, kinetic studies on hydrated oxides of thorium,[10] titanium[11] and zirconium,[12] zirconium phosphate,[13] hydrated alumina,[14] tantalum arsenate[15] and zirconium antimonate[16] have been reported.

Heteropolyacid salts form well defined crystalline inorganic ion exchangers.[17] They show high affinity for Tl^+, Cs^+, and Rb^+ and are used for ^{137}Cs separation in nuclear waste. However, no kinetic studies, necessary for ion exchange mechanism, seem to have been carried out on these exchangers.

Malik and coworkers[18] reported on the ion exchange properties of pyridinium tungstoarsenate, a new heteropolyacid salt, showing its selectivity for Rb^+ and Cs^+ amongst alkali metal ions. In order to explain their results they assumed the dehydration of Cs^+ during the course of exchange. In the present communication, we report on the kinetic studies of exchange of Rb^+ and Cs^+ on pyridinium tungstoarsenate (PWA). Effective diffusion coefficient, activation energy, and entropy of activation have been calculated, the results confirming the assumption that Cs^+ becomes dehydrated before undergoing exchange.

Experimental

Reagents and Materials. All the reagents used were of AR grade. The exchanger, pyridinium tungstoarsenate ($(C_5H_5NH)_3W_{12}AsO_{40}$) was prepared by the method reported.[18]

Apparatus. A unicam SP 500 spectrophotometer was used for the estimation of pyridine. A Leitz Wetzler microscope, Germany, model 12.5 X was used for the determination of the particle size of exchanger.

Kinetic Measurements. Limited bath technique[19] was used to study the exchange rate. PWA was ground and sieved to the desired mesh size (−50 to +100, −100 to +200). Solutions of Rb^+ and Cs^+ were thermostated at the required temperature in stoppered pyrex boiling tubes containing pyridinium nitrate and nitric acid,[18] the total volume in each tube being made 10 cm^3. The final concentrations of pyridinium nitrate and nitric acid were 0.001 mol dm^{-3} and 0.01 mol dm^{-3}, respectively, while that of the cation were varied from 0.05—0.2 mol dm^{-3} (for Rb^+) and 0.05—0.3 mol dm^{-3} (for Cs^+).

A weighed amount (0.1 g) of the exchanger of desired mesh size was added to these tubes which were thoroughly shaken, mechanically. After appropriate intervals of time the contents of the tubes were filtered with Whatman No. 1 filter paper, the extent of exchange being measured by determining pyridinium cations released spectrophotometrically at 256 nm. The exchange between Rb^+/Cs^+ and pyridinium cation is stoichiometric.[18] Experiments were conducted at 300.5, 305.5, 310.5, 315.5, and 320.5±0.1 K.

Particle Size. The average particle radius of each sieved fraction was determined by measuring the diameter of about 100 beads on a micrometer microscope. Measurements were carried out on dry particles as well as on particles which had been immersed for 24 hours in an appropriate electrolyte solution (concentration 0.1 mol dm^{-3}). There was no significant difference between the size of dry and immersed particles.

Results and Discussion

According to the theory developed by Boyd *et al.*,[3] the following equation holds in particle diffusion controlled exchange:

$$F = 1 - \frac{6}{\pi^2}\sum_{n=1}^{\infty}\frac{\exp(-n^2Bt)}{n^2},$$

where F is the extent of exchange at time t, $B=\pi^2D/r^2$, r is the average radius of the exchanger particle and D the effective diffusion coefficient. Thus the rate of particle diffusion controlled exchange should be dependent on r but independent of the concentration of exchanging ion; a plot of Bt *vs.* t (Reichenberg's test[20]) should be a straight line passing through origin.

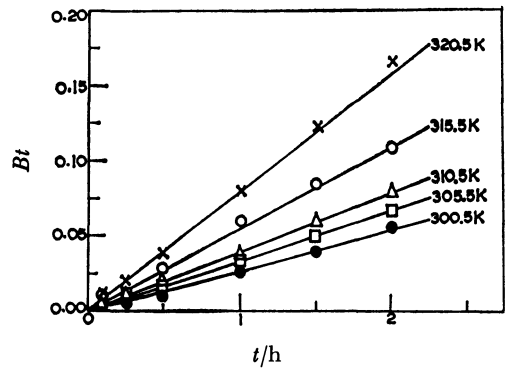

Fig. 1. Plots of *Bt vs. t* for Rb^+ exchange at different temperatures (r=0.0160 cm, concentration=0.1 mol dm^{-3}).

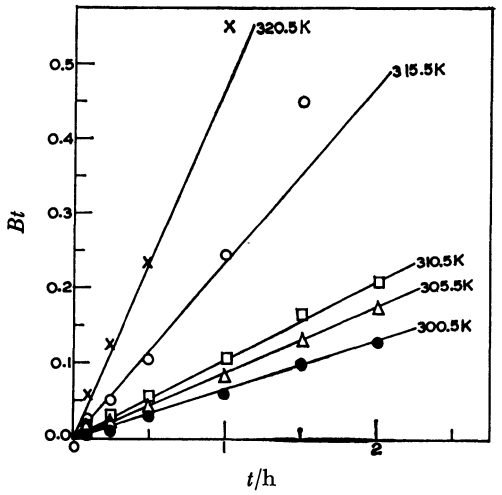

Fig. 2. Plots of *Bt vs. t* for Cs^+ exchange at different temperatures (r=0.0160 cm, concentration=0.1 mol dm^{-3}).

The kinetics of exchange of Rb^+ and Cs^+ on PWA was studied in the light of these considerations.

Figures 1 and 2 show the plots, *Bt vs. t*, for the exchange of Rb^+ and Cs^+ at different temperatures. These plots are linear, passing through origin, showing that the exchange is particle diffusion controlled. The plots of $-\log(1-F)$ *vs. t* (Mc Kay plots[21]) are nonlinear, supporting the above result. The effect of particle size of the exchanger shows that in both cases rate increases with decrease in particle radius. The rate of exchange of Rb^+ was found to be independent of concentration (Fig. 3), but not for Cs^+ exchange. Figure 4 shows *Bt vs. t* plots for Cs^+ exchange at four different concentrations. At concentration 0.05 mol dm^{-3}, the nonlinear behavior and fast uptake of Cs^+ shows that film diffusion also contributes to exchange.[3,22] At concentrations 0.1, 0.2, and 0.3 mol dm^{-3}, though the plots are linear (for 0.2 and 0.3 mol dm^{-3}, only initially) the rate is concentration dependent. Such an anomalous behavior was also reported.[23-25] Helfferich[26] showed theoretically that particle diffusion controlled exchange accompanied by ionic reactions (association, neutralization or complex formation) would exhibit such a behavior.

In the present case, it seems that the Cs^+ is dehydrated[18] during the course of exchange, getting chemically associated to tungstoarsenate ion. The resulting compound forms a shell around the exchanger particle which prevents further entry of Cs^+ into the core. This would eliminate Donnan exclusion of the co-ions. If a sufficient number of counter ions pass through the shell, they should carry with them co-ions so as not to disturb electroneutrality.[26] The invasion of counter and co-ions should be concentration dependent. This may also be the reason why the *Bt vs. t* plots (Fig. 4) are a bit nonlinear towards the end. The assumption of Cs^+ becoming dehydrated while exchanging with pyridinium cation is further supported by the entropy data.

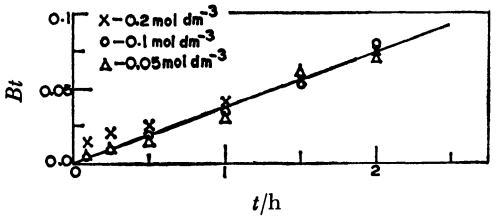

Fig. 3. Plots of *Bt vs. t* for Rb^+ exchange at different concentrations (r=0.0160 cm, T=310.5 K).

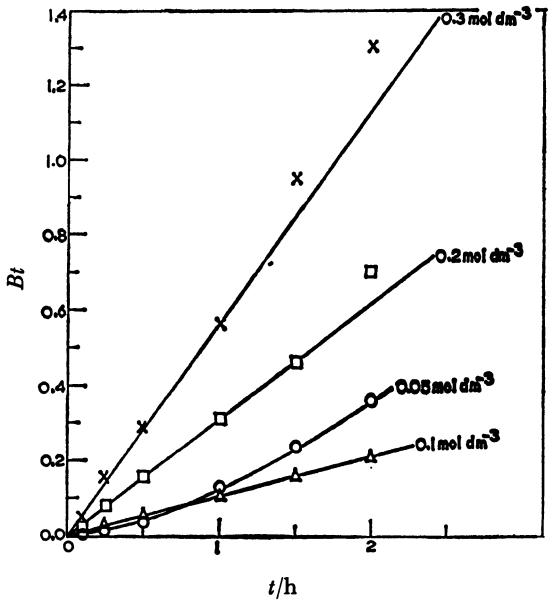

Fig. 4. Plots of *Bt vs. t* for Cs^+ exchange at different concentrations (r=0.0160 cm, T=310.5 K).

The exchange data at different temperatures (Figs. 1 and 2) have been used to calculate the values of effective diffusion coefficient (D), activation energy (E_a) and entropy of activation (ΔS^*). The D values computed from the B values are given in Table 1. They are in the order $Cs^+ > Rb^+$, in line with the order reported for alkali metal ions exchange on other exchangers.[12,27] The values are much lower than those reported on organic resins.[27,28] Nancollas and Paterson[10] inferred that crystallinity of the exchanger affects the D values such that more crystalline the exchanger, the lower the values. For PWA, a crystalline heteropolyacid salt, the D values of Rb^+ and Cs^+ exchange on it are very low.

Table 1. B values and effective diffusion coefficient D as a function of temperature (average particle radius of the exchanger = 0.0160 cm, concentration of Rb^+ and Cs^+ = 0.1 mol dm^{-3})

S. No.	Temp/K	Rb^+-exchange		Cs^+-exchange	
		B/s^{-1}	$D/m^2\ s^{-1}$	B/s^{-1}	$D/m^2\ s^{-1}$
1	300.5	0.75×10^{-5}	1.95×10^{-14}	1.81×10^{-5}	4.68×10^{-14}
2	305·5	0.97×10^{-5}	2.52×10^{-14}	2.64×10^{-5}	6.85×10^{-14}
3	310.5	1.11×10^{-5}	2.88×10^{-14}	2.92×10^{-5}	1.07×10^{-13}
4	315.5	1.53×10^{-5}	3.96×10^{-14}	6.67×10^{-5}	1.73×10^{-13}
5	320.5	2.22×10^{-5}	5.76×10^{-14}	13.19×10^{-5}	3.42×10^{-13}

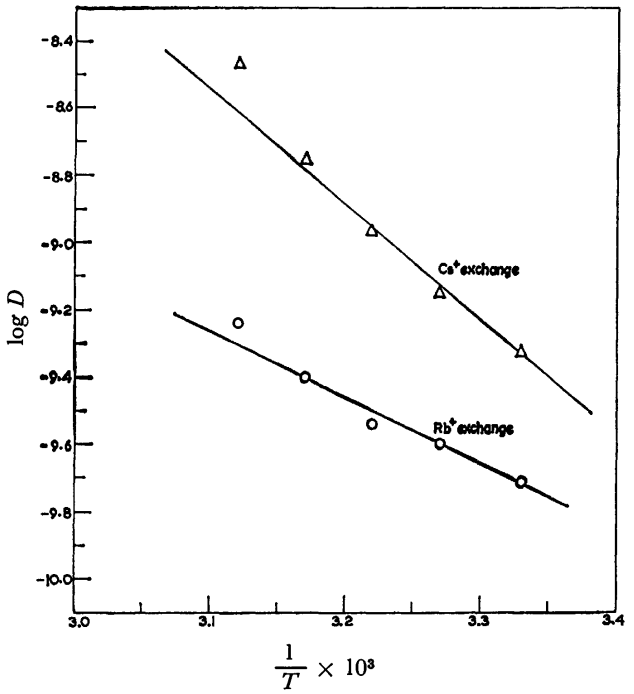

Fig. 5. Plots of $\log D$ *vs.* $1/T$.

The linearity of $\log D$ *vs.* $1/T$ plots (Fig. 5) indicates the validity of the Arrhenius equation

$$D = D_0 \exp(-E_a/RT),$$

which is used to calculate E_a values. The activation energy of a cation diffusion process reflects the ease with which cations can pass through exchanger particles. Freeman and Stamirs[29] observed an increase in E_a with increase in ion size of the alkaline earth metal ions. The increase is explained in terms of an increase in the strength of bonding to two crystallographically separated sites for the large, more polarizable cations. Similar findings were also observed for monovalent cations on analcite[30] and for alkaline earth metal ions on tantalum arsenate.[15] Our results (Table 2) which show that E_a for Cs^+ exchange is higher as compared to that of Rb^+ are in agreement with the increasing ion size.[15,29,30] In the present case the E_a values are higher as compared to the values 20—40 kJ mol^{-1} obtained for the exchange of hydrogen by monovalent ions on strong cation exchangers.[4,5] This may be due to low swelling of the exchanger. Similar findings were obtained by Heitner-Wirguin and Markovits.[19]

Table 2. D_0 values and thermodynamic parameters for Rb^+/Py^+ and Cs^+/Py^+ exchange on PWA exchanger

S. No.	System	$D_0/m^2\ s^{-1}$	E_a/kJ mol^{-1}	ΔS^*/J $mol^{-1}\ K^{-1}$
1	Rb^+/py^+	3.1×10^{-8}	35.7	−40.2
2	Cs^+/Py^+	3.4×10^{-2}	68.4	+75.7

Py^+ = pyridinium ion

The Arrhenius equation was also used to calculate D_0 which in turn is used to obtain ΔS^* by means of the following equation proposed by Barrer *et al.*[31]

$$D_0 = 2.72\, d^2k\, T/h \exp(\Delta S^*/R)$$

where k is Boltzmann constant, h Planck constant, d the distance between adjacent exchanging sites in the exchanger, and T is 273 K. For the calculation of ΔS^*, the value of d has usually been assumed to be equal to 5×10^{-8} cm.[15,16,32] We have also used the same value for ΔS^* calculation (Table 2). The entropy change normally depends on the extent of hydration of the exchangeable and exchanging ions along with any change in water structure around ions that may occur when they pass through the channels of exchanger particles. In general, negative values of ΔS^* have been reported.[15,16,29] ΔS^* for Rb^+ exchange in our case is negative whereas a positive value is obtained for Cs^+ exchange.

The positive value for Cs^+ exchange is unusual but not exceptional, being accounted for on the basis of disordering of water structure[32] around exchanging cations or their dehydration[33] during exchange. In our case, it appears that hydrated Cs^+ cation becomes dehydrated before exchanging with pyridinium ions of the exchanger. The explanation is in line with the one given by Malik, Srivastava and Satish[18] to explain higher interaction energy value for Cs^+ exchange on PWA which we utilized to explain the dependence of Cs^+ exchange rate on concentration.

Two of the authors (RPS and SA) are grateful for financial assistance from the Council from Scientific and Industrial Research (New Delhi).

References

1) F. C. Nachod and W. Wood, *J. Am. Chem. Soc.*, **66**, 1380 (1944).

2) F. C. Nachod and W. Wood, *J. Am. Chem. Soc.*, **67**, 629 (1945).

3) G. E. Boyd, A. W. Adamson, and L. S. Myers, *J. Am. Chem. Soc.*, **69**, 2836 (1947).
4) D. E. Conway, J. H. S. Green, and D. Reichenberg, *Trans. Faraday Soc.*, **50**, 511 (1954).
5) T. R. E. Kressman and J. A. Kitchener, *Discus. Faraday Soc.*, **4**, 90 (1949).
6) K. A. Karaus and H. O. Phillip, Proc. of the Second Int. Conf. of Peaceful Uses of Atomic Energy, Geneva (1958) Vol. 28.
7) F. Wolf and H. Haedicke, *Tonind. Ztg. Keram, Rundschau*, **91**, 41 (1967).
8) L. L. Ames, *Am. Min.*, **50**, 465 (1965).
9) E. Hoinkis and H. W. Levi, *Z. Naturforsch., Teil A*, **22**, 226 (1967).
10) G. H. Nancollas and R. Paterson, *J. Inorg. Nucl. Chem.*, **22**, 259 (1961).
11) C. Heitner-Wirguin and A. Albu-Yaron, *J. Appl. Chem.*, **15**, 445 (1965).
12) E. Hallaba, N. Z. Mizak, and H. N. Salama, *Indian J. Chem.*, **11**, 580 (1973).
13) C. B. Amphlett, L. A. McDonald, and M. J. Redman, *J. Inorg. Nucl. Chem.*, **6**, 220 (1958).
14) S. C. Churms, *J. S. African Chem. Inst.*, **19**, 108 (1966).
15) J. P. Rawat and P. S. Thind, *J. Phys. Chem.*, **80**, 1384 (1976).
16) J. Mathew and S. N. Tandon, *Can. J. Chem.*, **55**, 3857 (1977).
17) V. Vesely and V. Pekarek, *Talanta*, **19**, 219, 1245 (1972).
18) W. U. Malik, S. K. Srivastava, and Satish Kumar, *Talanta*, **23**, 323 (1976).
19) C. Heitner-Wirguin and G. Markovits, *J. Phys. Chem.*, **67**, 2263 (1963).
20) D. Reichenberg, *J. Am. Chem. Soc.*, **75**, 589 (1953).
21) H. Mckay, *Nature (London)*, **142**, 977 (1938).
22) F. Helfferich, "Ion Exchange," McGraw Hill, N. Y. (1962), pp. 254—255.
23) M. K. Rahman and J. Barrett, *J. Inorg. Nucl. Chem.*, **36**, 1899 (1974).
24) M. B. Hanley, S. C. Churms, and E. C. Leisengang, *Chem. Commun.*, **1967**, 78.
25) A. Varon and W. Rieman, III, *J. Phys. Chem.*, **68**, 2716 (1964).
26) F. Helfferich, *J. Phys. Chem.*, **69**, 1178 (1965).
27) V. I. Gorshkov, G. M. Panchenkov, and T. V. Ivanova, *Zh. Fiz. Khim.*, **36**, 1690 (1962).
28) G. E. Boyd and B. A. Soldano, *J. Am. Chem. Soc.*, **75**, 6091, 6105 (1953).
29) D. C. Freeman and D. N. Stamirs, *J. Chem. Phys.*, **35**, 799 (1961).
30) R. M. Barrer and L. V. C. Rees, *Nature (London)*, **187**, 768 (1960).
31) R. M. Barrer, R. F. Bartholomew, and L. V. C. Rees, *J. Phys. Chem. Solids*, **21**, 12 (1961).
32) A. Dyer and J. M. Fawcett, *J. Inorg. Nucl. Chem.*, **28**, 615 (1966).
33) D. Britz and G. H. Nancollas, *J. Inorg. Nucl. Chem.*, **31**, 3861 (1969).

Photopolymerization of Methyl Methacrylate Using *N,N*-Dimethylformamide–Sulfur Dioxide Complex as the Photoinitiator

Premamoy Ghosh,* Samir Biswas, and Subhankar Jana

Plastics and Rubber Technology Division, Department of Applied Chemistry, Calcutta University, 92, A. P. C. Road, Calcutta-700 009, India

(Received August 8, 1980)

Photopolymerization of MMA in visible light was studied at 40 °C using DMF–SO_2 complex as the photoinitiator. Initiator exponent was found to be 0.41 and monomer exponent varied between 1.12 to 1.50 depending on the nature of the solvent. Analysis of data revealed that the photopolymerization was induced by a free radical mechanism. Nonideality of the kinetics was explained on the basis of (a) monomer-dependent chain initiation and (b) initiator-dependent chain termination *via* degradative initiator transfer.

In recent years the role of SO_2 in catalytic concentrations in vinyl polymerization has been studied in detail. It is now well established that SO_2 can act both as an initiator and as a comonomer in vinyl polymerization.[1] SO_2, being a good acceptor, also forms charge transfer complexes with many donor compounds. SO_2 complexes of pyridine and quinoline are reported[2-4] to effectively induce polymerization of methyl methacrylate (MMA). In the polymerization of MMA initiated by pyridine–SO_2 complex, it was found that the presence of such additives as *N,N*-dimethylformamide (DMF) greatly accelerated the rate of polymerization[5] probably through participation of DMF in the initiation step. This idea led us to the preparation of the C.T. complex of SO_2 with DMF with the objective of examining its suitability as an independent initiator of vinyl polymerization using MMA as the monomer. Related results and the kinetics of polymerization under photoactivation are reported in the present paper.

Experimental

Materials. Methyl methacrylate (MMA) monomer was purified by usual procedures.[6] *N,N*-Dimethylformamide (DMF) obtained from E. Merck and stored over KOH pellets, was purified by distillation. All solvents used were of reagent grade and were distilled once before use in polymerization reaction.

Preparation of N,N-*dimethylformamide-sulfur dioxide Complex.* DMF (5 ml) was taken in a test tube which was then cooled to about −5 °C in crushed ice/salt mixture. Pruified sulfur dioxide gas was bubbled through the cold DMF. SO_2 gas generated by heating fresh copper turnings with reagent grade concentrated sulfuric acid was passed through a scrubber of concentrated sulfuric acid before its final passage in DMF. Bubbling was stopped when the liquid appeared supersaturated with SO_2. Excess SO_2 was allowed to bubble out at room temperature, occasionally aided by slow stirring with a glass rod. The theoretical SO_2-content of 1:1 DMF–SO_2 complex is 46.7%. Analysis by iodimetry showed that the SO_2 content of the prepared complex was 46.92%.

UV absorption spectra of dilute solutions of SO_2 (0.002 mol l^{-1}) and of DMF–SO_2 complex (0.002 mol l^{-1}) in CCl_4 are given in Fig. 1, A, curves 1 and 4 respectively. λ_{max} for each spectrum is 290 nm. DMF itself has no absorption in the wavelength range studied. For a fixed SO_2-content (0.002 mol l^{-1}) in CCl_4, the absorbance at λ_{max} increased progressively with increasing proportion of DMF till the latter was used in equimolar proportion (0.002 mol l^{-1}), Fig. 1, A, and with further increase in DMF content, no further change in the absorbance of the mixture was visible.

The absorbance values at λ_{max} (290 nm) for solutions of SO_2 and of DMF–SO_2 complex in CCl_4 at several concentrations were measured and the data were plotted as in Fig. 1, B. In each case the plot, passing through the origin, is linear, DMF–SO_2 plot giving a higher slope than the SO_2 plot. The overall absorbance at λ_{max} (290 nm) for each of the various mixtures of DMF and SO_2, Fig. 1, A, is equal to the summation of the absorbance corresponding to the calculated amount of 1:1 DMF–SO_2 complex formed *in situ* in the system and that of SO_2 present in excess of DMF.

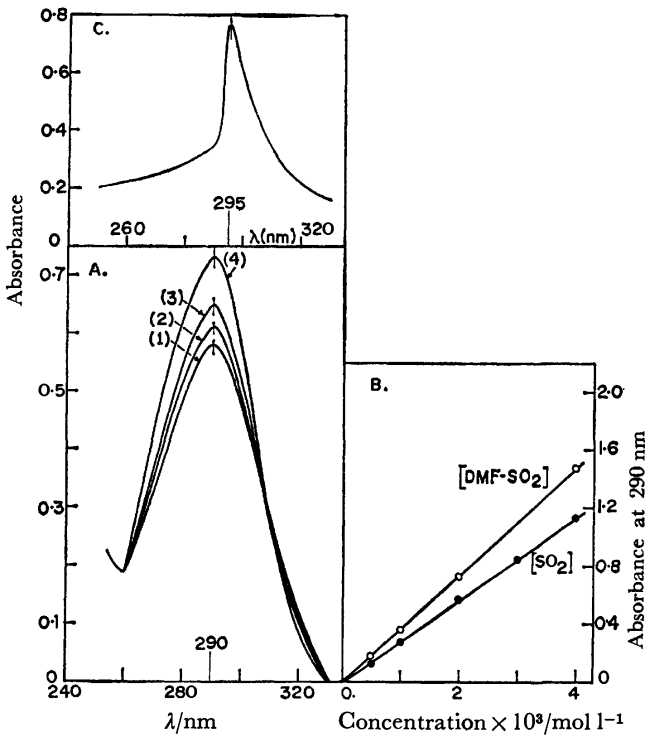

Fig. 1. A) UV absorption spectra of SO_2, (DMF–SO_2), complex and different mixtures of SO_2 and DMF in CCl_4 solution using CCl_4 in the reference cell in each case:
1) SO_2=0.002 mol l^{-1}; 2) SO_2=0.002 mol l^{-1} and DMF=0.0005 mol l^{-1}; 3) SO_2=0.002 mol l^{-1} and DMF=0.001 mol l^{-1}; 4) SO_2=0.002 mol l^{-1} and DMF=0.002 mol l^{-1}, 0.003 mol l^{-1}, 0.005 mol l^{-1}; and DMF–SO_2 complex=0.002 mol l^{-1}.
B) Plot of absorbance at 290 nm *vs.* concentration for SO_2 and DMF–SO_2 complex, each in CCl_4 solution (CCl_4 in the reference cell).
C) UV absorption spectra of DMF–SO_2 complex, 0.002 mol l^{-1}, in MMA (MMA in the reference cell).

Table 1. Photopolymerization of MMA at 40 °C using DMF-SO_2 complex as the photoinitiator

$[DMF\text{-}SO_2]\times10^4$ / mol l^{-1}	$R_p\times10^5$ / mol l^{-1} s^{-1}	$R_p/[M]^2\times10^7$ / l mol^{-1}	$[\eta]$ / dl g^{-1}	$1/\bar{P}_n\times10^4$	Initiator exponent	$(k_p^2/k_t)\times10^2$ / l mol^{-1} s^{-1}
2.051	5.400	6.379	2.900	1.120		
2.56	6.010	7.097	2.690	1.230		
4.85	7.515	8.875	2.300	1.460		
5.82	8.350	9.861	2.22	1.590	0.41	1.42
7.25	8.810	10.400	2.125	1.680		
9.70	9.6025	11.340	1.880	1.980		
12.16	10.850	12.810	1.500	2.66		
20.00	9.6129	—	—	—		

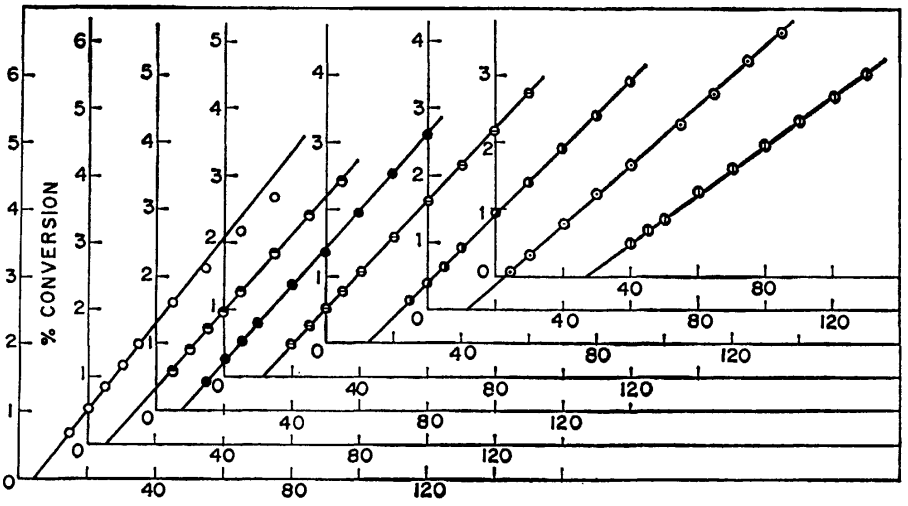

Fig. 2. Photopolymerization of MMA using DMF-SO_2 complex as initiator at 40 °C, for each curve $[DMF\text{-}SO_2]$ in mol l^{-1} is,
◓: 20.00×10^{-4} mol l^{-1} $[DMF\text{-}SO_2]$, ◑: 5.82×10^{-4} mol l^{-1} $[DMF\text{-}SO_2]$,
○: 12.16×10^{-4} mol l^{-1} $[DMF\text{-}SO_2]$, ⊙: 4.85×10^{-4} mol l^{-1} $[DMF\text{-}SO_2]$,
●: 9.70×10^{-4} mol l^{-1} $[DMF\text{-}SO_2]$, ⓘ: 2.56×10^{-4} mol l^{-1} $[EMF\text{-}SO_2]$,
⊖: 7.25×10^{-4} mol l^{-1} $[DMF\text{-}SO_2]$.

Excess DMF wherever present has little influence on the overall absorbance. It is, thus, clearly indicated that complexation between DMF and SO_2 takes place almost instantaneously and that the complex is of the 1:1 kind.

When taken in MMA solution, the peak absorption of DMF-SO_2 complex shifts slightly to higher wave length (λ_{max}=295 nm, MMA in reference cell), Fig. 1, C, indicating further complexation of DMF-SO_2 complex with MMA.

Polymerization. The polymerization of MMA in bulk or in solution was studied dilatometrically in visible light at 40±0.05 °C using DMF-SO_2 complex initiator following usual procedures.[7-9] Polymers formed at low conversions (<10%) in the dilatometers were removed and isolated by precipitation with petroleum ether and drying at 50 °C under vacuum.

Intrinsic Viscosity. Intrinsic viscosity, $[\eta]$ in dl/g of polymers taken in benzene solution were obtained from measurements of solution viscosity at 30±0.05 °C using a Ubbelohde viscometer. Molecular weights ($\bar{M}_n$) of poly(methyl methacrylate) (PMMA) were calculated from the viscosity data using the following equation:[10]

$$[\eta] = 8.69\times10^{-5}\,\bar{M}_n^{0.76}. \quad (1)$$

Results and Discussion

In presence of DMF-SO_2 complex, no polymerization of MMA was observed within 2 h at 40 °C in the dark. Polymerization was, however, readily induced in presence of light after inhibition periods (IP) of the order of 5—30 min, lower $[DMF\text{-}SO_2]$ giving higher IP in general. IP is considered to arise due to adventitious impurities (such as, last traces of oxygen) in the polymerization system.

Initiator Exponent. Data on bulk photopolymerization of MMA at 40 °C using different $[DMF\text{-}SO_2]$ (0.000256—0.002 mol l^{-1}) are presented in Table 1. Rates of polymerization, R_p, were calculated from the initial linear zones of % conversion *vs.* time plots, Fig. 2. Initiator exponent determined from the slope of the plot of log R_p *vs.* log $[DMF\text{-}SO_2]$, is 0.41, Fig. 3. Photopolymerization in open dilatometers (in contact with air) produced slightly enhanced inhibition but in presence of dissolved hydroquinone (0.001 mol l^{-1}) there was much pronounced inhibition of polymerization. The polymers gave positive response to

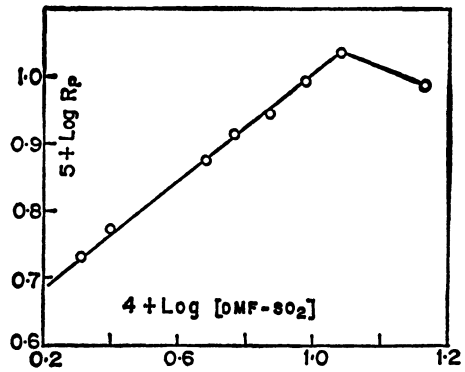

Fig. 3. Photopolymerization of MMA (bulk) using DMF-SO_2 complex as initiator at 40 °C.

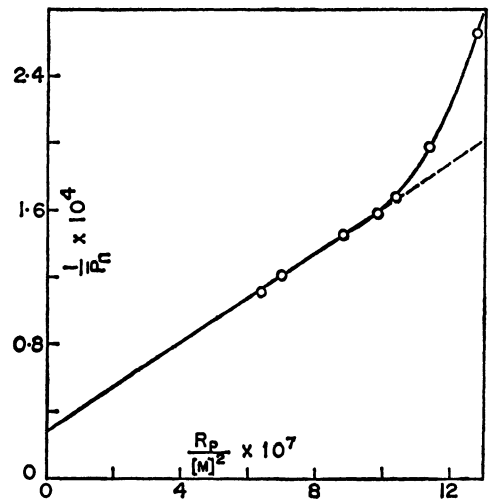

Fig. 4. Photopolymerization of MMA (bulk) using DMF-SO_2 complex as initiator.

dye partition test[11] for (anionic) sulfoxy end groups.

k_p^2/k_t Value. The kinetic parameter k_p^2/k_t at 40 °C was evaluated from the slope of the plot of $1/\overline{P}_n$ *vs.* $R_p/[M]^2$, Fig. 4 (Table 1), in accordance with the Mayo equation:

$$1/\overline{P}_n = 1.85\frac{k_t}{k_p^2} \cdot \frac{R_p}{[M]^2} + \Sigma\frac{R_{tr}}{R_p}, \quad (2)$$

where the last term in the right hand side was included to account for chain transfer effects, assuming this would not affect the slope of the plot over low range of initiator concentration. The apparent k_p^2/k_t value, calculated from the slope of the initial linear zone of the plot, is 1.42×10^{-2} l mol^{-1}; it was assumed in the calculation that any perturbation of the termination process from the usual bimolecular mechanism (85% disproportionation, 15% combination)[10,12] will not measurably affect the initial slope of the plot in Fig. 4.

Monomer Exponent. With a fixed [DMF-SO_2], (0.000205 mol l^{-1}), photopolymerization of MMA was further studied in presence of different concentrations of several solvents such as benzene, toluene, DMF, carbon tetrachloride, pyridine, and tetrahydrofuran (THF). Monomer exponents calculated from the slope

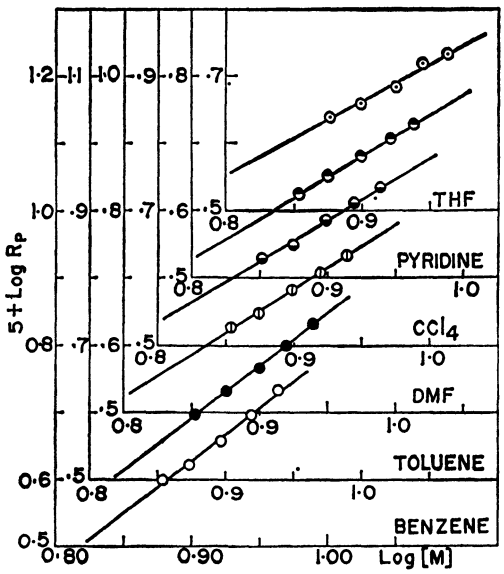

Fig. 5. Photopolymerization of MMA (solution) using DMF-SO_2 complex as initiator.
[DMF-SO_2] = 2.05×10^{-4} mol l^{-1} (fixed); data given for each curve are, solvent and slope (monomer exponent).
○: Benzene, 1.50, ●: toluene, 1.50, ⊙: THF, 1.12, ◒: CCl_4, 1.20, ◓: pyridine, 1.20, ⓓ: DMF, 1.30.

of the respective plots of log R_p *vs.* log [M], Fig. 5, range between 1.12—1.50, depending on the nature of the solvent used.

Mechanism. Kinetic data, the inhibitory effect of hydroquinone and the results of end group analysis indicate a radical mechanism. The radical generation process may be considered to follow an initial complexation reaction between monomer and initiator molecules:

$$\text{DMF-SO}_2 + \text{M} \overset{K}{\rightleftharpoons} \underset{\text{Initiating Complex (I)}}{\text{DMF-SO}_2\cdots\text{M}} \quad (3)$$

$$\text{I} \xrightarrow{h\nu} \text{Pair of radicals (R}\cdot\text{)}. \quad (4)$$

Initial concentration of the initiating complex (I) is then equal to K[DMF-SO_2][M], where K is the equilibrium constant of the initiator monomer complexation reaction envisaged.

Initiator Transfer. Equation 2 may be used in the following form to determine the initiator transfer parameter (C_IK), where C_I is the initiator transfer constant, in the photopolymerization of MMA in bulk:

$$\frac{1}{\overline{P}_n} - 1.85\frac{k_t}{k_p^2} \cdot \frac{R_p}{[M]^2} = C_M + C_IK\,[\text{DMF-SO}_2]. \quad (5)$$

Here, [DMF-SO_2] is the initial concentration of *N,N*-dimethylformamide-sulfur dioxide complex and C_M is the monomer transfer constant. A plot of left hand side of Eq. 5 *vs.* [DMF-SO_2] is given in Fig. 6, and initial slope of the plot, giving the value of C_IK, is 8×10^{-3} l mol^{-1}. A deviation from linearity of this plot, prominent at high [DMF-SO_2], indicates that the transfer process apparently of the normal kind at low [DMF-SO_2], becomes largely degradative in

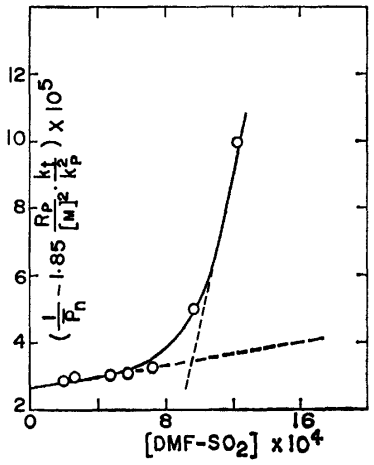

Fig. 6. Photopolymerization of MMA using DMF-SO_2 complex as initiator.

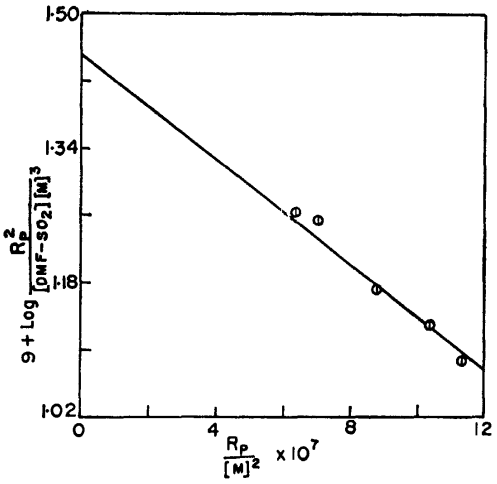

Fig. 7. Photopolymerization of MMA using DMF-SO_2 complex as initiator. Analysis of primary radical termination effect.

nature at high [DMF-SO_2].

Termination. The observed initiator exponent of 0.41 indicates that some initiator dependent termination process is significant along with the usual bimolecular termination.

The initiator dependent termination process may be of two different kinds:

1) Primary radical termination

$$M^{\cdot} + R^{\cdot} \xrightarrow{k_{prt}} \text{Polymer product}$$

and

2) Termination *via* degradative initiator transfer, which may be considered to proceed by two distinctive mechanisms:

a) With reinitiation effect, such as:

$$M^{\cdot} + I \xrightarrow{k_{trI}} \text{Polymer product} + I^{\cdot} \quad \text{(Initiator transfer)}$$

$$I^{\cdot} + M^{\cdot} \xrightarrow{k_{rtI}} \text{Polymer product} \quad \text{(Chain termination)}$$

$$I^{\cdot} + M \xrightarrow{k_{1I}} M^{\cdot} \quad \text{(reinitiation)}$$

or,

b) With little reinitiation effect, such as:

$$M^{\cdot} + I \xrightarrow{k_t'} \text{Polymer product (Chain termination giving non radical or inactive radical by product).}$$

1) *Analysis of Primary Radical Termination Effect.*

The equation of Deb and Meyerhoff[13] which would assume the following form for present polymerization, may be used to evaluate primary radical termination effect (in absence of degradative initiator transfer process)

$$\log \frac{R_p^2}{[\text{DMF-SO}_2][M]^3} = \log \frac{Kfk_dk_p^2}{k_t} - 0.8686 \cdot \frac{k_{prt}}{k_1k_p} \cdot \frac{R_p}{[M]^2}. \quad (6)$$

Negative slope for the plot of left hand side of Eq. 6 *vs.* $R_p/[M]^2$, Fig. 7, indicating measurable primary radical termination effect, was obtained for photopolymerization of MMA in bulk at 40 °C. The value of k_{prt}/k_1k_p calculated from the slope of this plot is 3.135×10^5 mol s l^{-1}.

2) *Analysis of Degradative Chain (Initiator) Transfer Effect.* *a) Degradative Initiator Transfer with reinitiation Effect*: An equation derived by Deb[14] to analyse degradative chain (initiator) transfer with reinitiation effect was simplified by Ghosh *et al.*[15] to the following form:

$$\ln \frac{R_p^2}{[I][M]^2} = \ln \frac{fk_dk_p^2}{k_t} - \frac{k_p^2}{k_t} \cdot \frac{k_{rtI}}{k_{1I}k_p} \cdot C_I \cdot \frac{[I]}{[M]}.$$

In the present case $[I]=K$ [DMF-SO_2][M] and hence we have

$$\log \frac{R_p^2}{[\text{DMF-SO}_2][M]^3} = \log Kfk_d\frac{k_p^2}{k_t} - 0.434\frac{k_p^2}{k_t} \cdot \frac{k_{rtI}}{k_{1I}k_p} \cdot C_IK[\text{DMF-SO}_2]. \quad (7)$$

Here, C_I is the initiator transfer constant. A plot of left hand side of Eq. 7 *vs.* [DMF-SO_2], is shown in Fig. 8. The plot gives a straight line with a negative slope, thereby clearly indicating the existence of degradative initiator transfer process. The value of $k_{rtI}/(k_{1I}k_p)$ obtained from the slope of the plot is 5.486×10^6 mol s l^{-1}.

b) Degradative Initiator Transfer with Little Reinitiation Effect: This aspect may be analysed according to the following approach:

Under steady state condition, we have

$$\frac{R_I}{R_p} = \frac{R_t}{R_p} = \frac{2k_t[M^{\cdot}]^2 + k_t'[I][M]}{R_p} = \frac{2k_t[M^{\cdot}]^2 + k_t'K[\text{DMF-SO}_2][M][M^{\cdot}]}{R_p}$$

or,

$$R_I = \frac{2k_t}{k_p^2} \cdot \frac{R_p^2}{[M]^2} + \frac{k_t'K}{k_p} \cdot R_p[\text{DMF-SO}_2] = 2\phi\varepsilon I_0K[\text{DMF-SO}_2][M]$$

or,

$$2\frac{k_t}{k_p^2} \cdot \frac{R_p^2}{[M]^3[\text{DMF-SO}_2]} = 2\phi\varepsilon I_0K - \frac{k_t'K}{k_p} \cdot \frac{R_p}{[M]}. \quad (8)$$

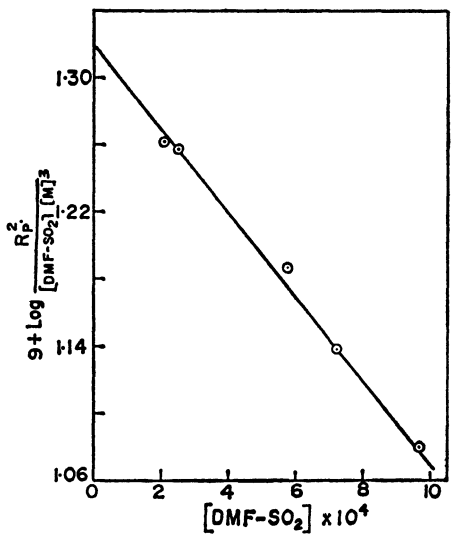

Fig. 8. Photopolymerization of MMA using DMF-SO_2 as initiator. Analysis of degradative initiator transfer (with reinitiation effect).

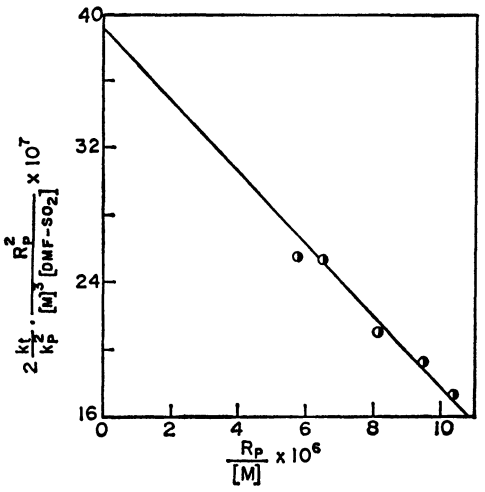

Fig. 9. Photopolymerization of MMA using DMF-SO_2 complex as initiator. Analysis of degradative initiator transfer (no reinitiation effect).

The left hand side of Eq. 8 is plotted *vs.* $R_p/[M]$, Fig. 9. The plot gives a straight line with a negative slope indicating that degradative initiator transfer with no reinitiation effect is significant. The value of $k_t'K/k_p$ obtained from the slope of the plot is 0.23 l mol^{-1}.

It is interesting to note that this value is reasonably close to the value of the final slope of the plot in Fig. 6, corresponding to high [DMF-SO_2], indicating degradative nature of the initiator transfer process at high initiator concentration. Thus, the degradative effect is detectable from analysis of both $\bar{P}_n$ and R_p data and from each analysis degradative effects of comparable order are more or less indicated, particularly for high [DMF-SO_2]. The value of Kfk_d, equivalent to $K\phi\varepsilon I_0$ for photopolymerization (where ϕ is the quantum yield for chain initiation, ε is the molar absorptivity for the active radiation and I_0 is the incident light intensity) obtained from the three plots, Figs. 7—9, are in reasonably close agreement, the mean value being 1.80×10^{-6} l mol^{-1} s^{-1}.

Although, primary radical termination may be considered as a possible cause for non-ideality, consideration of dependence of R_p on [M] predicts it to be of much less consequence. If the present photopolymerization followed the normal kinetics (bimolecular termination) one would expect a value of 1.5 for monomer exponent on the basis of initiation mechanism envisaged; for significant primary radical termination, the expected monomer exponent would be >1.5, the limiting value being 2.0 and for some kind of significant degradative initiator transfer, the expected value of monomer exponent would be <1.5, the limiting value being 1.0. With observed monomer exponent in the range of 1.12—1.50 the non-ideality in the present polymerization appears to be largely due to degradative initiator transfer effect.

Thanks are due to the Council of Scientific and Industrial Research and University Grants Commission, India for supporting this research through Fellowship Grants to S. J. and S. B. respectively.

References

1) *P. Ghosh and S. Chakraborty, Eur. Polym. J.*, **15**, 137 (1979).
2) M. Matsuda, Y. Ishioroshi, and T. Hirayama, *J. Polym. Sic.*, **B-4**, 815 (1966).
3) Y. Ishioroshi and M. Matsuda, Presented at the 19th Symposium on Polymer Chemistry, Kyoto 1970, Preprint p. 315.
4) P. Ghosh, S. Chakraborty, and S. Biswas, *Makromol. Chem.*, **181**, 1331 (1980).
5) Y. Ishioroshi, T. Hirayama, and M. Matsuda, *Kobunshi Ronbunshu*, **34**, 347 (1977).
6) P. Ghosh, P. S. Mitra, and A. N. Banerjee, *J. Polym. Sci., Polym. Chem. Ed.*, **11**, 2021 (1973).
7) P. Ghosh and A. N. Banerjee, *J. Polym. Sci., Polym. Chem. Ed.*, **12**, 375 (1974).
8) P. Ghosh and P. S. Mitra, *J. Polym. Sci., Polym. Chem. Ed.*, **13**, 921 (1973).
9) P. Ghosh and S. Chakraborty, *J. Polym. Sci., Polym. Chem. Ed.*, **13**, 1531 (1975).
10) T. G. Fox, J. B. Kinsinger, H. F. Mason, and E. M. Shuele, *Polymer*, **3**, 71 (1962).
11) P. Ghosh, S. C. Chandha, A. R. Mukherjee, and S. R. Palit, *Indian J. Polym. Sci.*, **A-2**, 4433 (1964).
12) J. C. Bevington, H. W. Melville, and R. P. Taylor, *J. Polym. Sci.*, **14**, 463 (1954).
13) P. C. Deb and G. Meyerhoff, *Eur. Polym. J.*, **10**, 709 (1974).
14) P. C. Deb, *Eur. Polym. J.*, **11**, 31 (1975).
15) P. Ghosh and P. S. Mitra, *J. Polym. Sci., Polym. Chem. Ed.*, **15**, 1743 (1977).

Liquid-Liquid Extraction and Separation of Lanthanum (III)

A. D. Langade and V. M. Shinde*

Analytical Laboratory, Department of Chemistry, Shivaji University, Kolhapur 416 004, India

(Received May 19, 1980)

Separation of lanthanum(III) from iron(III), molybdenum(VI), vanadium(V), chromium(VI), titanium (IV), bismuth(III), zirconium(IV), scandium(III), uranium(VI), and beryllium is achieved by solvent extraction with mesityl oxide from sodium salicylate solution (0.1 M adjusted to pH 7). Lanthanum from the organic phase is stripped with water and determined photometrically as its arsenazo complex at 570 nm. The extracted species is trisolvated *i.e.* $La(HOC_6H_4COO)_3 \cdot 3MeO$. The results of separation are reported.

Mesityl oxide has been used in this laboratory for the solvent extraction of uranium from salicylate media.[1] In this communication we propose a simple and rapid method for the selective extraction of lanthanum from 0.1 M sodium salicylate solution (adjusted to pH 7) into mesityl oxide. The lanthanum (III) from the organic phase is stripped with water and determined photometrically with arsenazo[2] at 570 nm. The method affords separation of lanthanum from iron (III), molybdenum(VI), vanadium(V), chromium(VI), titanium(IV), bismuth(III), zirconium (IV), scandium(III), uranium(VI), and beryllium.

Extraction of lanthanum with various chelating agents have been reviewed by Stary in his monograph.[3] The extraction of lanthanum from nitric acid, perchloric acid or thiocyanate media with oxygen containing solvents, organophosphorus acids, esters and oxides have been earlier reported.[4-17] Extraction with high molecular weight amines and carboxylic acids have also been reported,[18-20] but systematic separation studies of lanthanum is lacking. This communication describes a simple and rapid method for the solvent extraction of lanthanum(III) from sodium salicylate solution (pH 7) using mesityl oxide as an extractant. The method permits selective separation of lanthanum from metal ions such as iron, molybdenum, vanadium, chromium, titanium, zirconium, bismuth, scandium, uranium, and beryllium.

Experimental

Apparatus and Reagents. Absorbances were measured with a Zeiss Spectrophotometer (Jena) employing 1 cm quartz cells and pH values were measured with Philips pH meter (Precision type).

The stock solution of lanthanum was prepared by dissolving 0.587 g of lanthanum(III) oxide (BDH, England) in 4 ml of concentrated hydrochloric acid and diluting to 100 ml with distilled water. The solution was standardized by known method[21] and further diluted as required for working solutions.

Mesityl oxide, bp 125—128 °C (BDH) was used after double distillation.

Arsenazo I, 0.05% aqueous solution was used.

All other chemicals used in this work were of guaranteed grade.

General Extraction Procedure. Take an aliquot solution containing 40 μg of lanthanum, add sodium salicylate (0.4 g) to give the final concentration of 0.1 M in a total volume of 25 ml. Adjust the pH of the solution to 7 by diluted NaOH/HCl solutions and transfer into a 100 ml separatory funnel. Equilibrate the mixture for 30 s with 10 ml of neat mesityl oxide. Allow the layers to settle and strip lanthanum from organic phase with two 10 ml portions of water (containing a few drops of HCl to avoid emulsion) and determine it photometrically with arsenazo I at 570 nm.

Results and Discussion

Effect of pH, Salicylate Concentration and Mesityl Oxide Concentration. The extraction of lanthanum was studied at various pH. The extraction commences at pH 3, becomes quantitative at pH 7 and then decreases (Fig. 1). The pH was adjusted with diluted NaOH/HCl solutions. The optimum pH for quantitative extraction of lanthanum is 7. The concentration of mesityl oxide was varied from 35 to 100% with benzene as diluent and the sodium salicylate concentration was varied from 0.01 to 0.1 M. The results show that lanthanum extracts quantitatively from 0.1 M sodium salicylate solution with neat mesityl oxide. The percentage extraction of the metal ions was computed by stripping the metal ion from the organic phase and subsequent photometric determination with arsenazo I. The distribution ratio was calculated by using relationship.

$$\%E = \frac{100D}{D(V_w/V_o)}$$

where V_w and V_o are the volumes of aqueous and organic phase respectively. A log-log plot of distribution ratio *vs.* mesityl oxide concentration at fixed

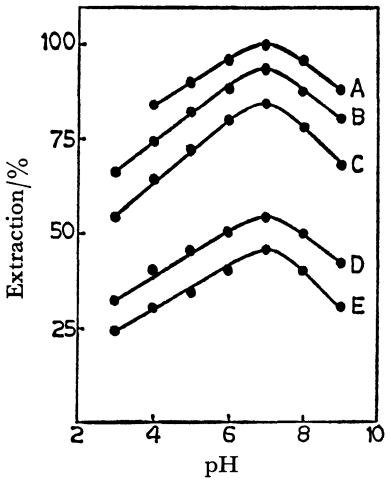

Fig. 1. Extraction behaviour of lanthanum-salicylate into mesityl oxide as function of pH and sodium salicylate concentration.
A=0.1 M; B=0.075 M; C=0.05 M; D=0.025 M; E=0.01 M sodium salicylate.

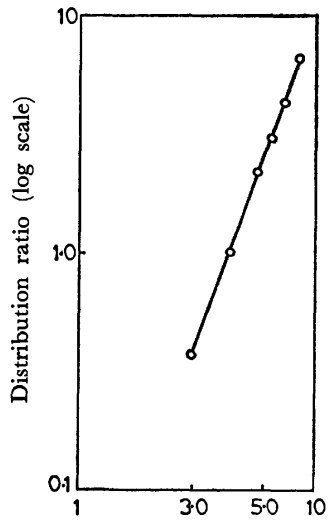

Fig. 2. Distribution ratio of lanthanum as a function of mesityl oxide concentration at 0.05 M sodium salicylate concentration and pH 7.

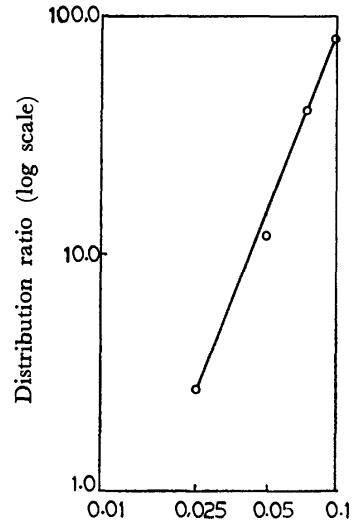

Fig. 3. Distribution ratio of lanthanum as a function of sodium salicylate concentration at pH 6.5

pH (7.0) and salicylate concentration (0.05 M) gave a slope of 2.7 (Fig. 2) indicating the presence of three solvent molecules in the extracted species. Similarly the log-log plot (Fig. 3) of distribution ratio *vs.* salicylate concentration at fixed pH (6.5) and mesityl oxide concentration gave a slope of 2.6 indicating a molar ratio of 1:3 for the reaction of lanthanum and salicylate ion. The extraction equilibria for lanthanum (III) extraction (from salicylate media) into mesityl oxide could be written as:

$$La^{3+} + 3(HOC_6H_4COO)^- \rightleftharpoons La(HOC_6H_4COO)_3 \quad (1)$$

$$La(HOC_6H_4COO)_3 \cdot 3\,H_2O + 3\,MeO \rightleftharpoons La(HOC_6H_4COO)_3 \cdot 3\,MeO + 3\,H_2O. \quad (2)$$

MeO stands for mesityl oxide.

The extractable species is thus trisolvated.

Distribution of Salicylic Acid and Sodium Salicylate.

Table 1. Distribution ratio of salicylic acid (A) and sodium salicylate (B) between mesityl oxide and aqueous solution

$\mu = 0.1$ M sodium perchlorate

	pH[a]	D_{Sal} (Exptl)	$D_{Sal}\left(1+\frac{K_1}{[H^+]}\right)$	D_{Sal} (Calcd)
(A)	4.5	2.86	115.7	2.03
	5.5	2.33	177.4	0.30
	6.5	2.16	768.1	0.13
(B)	5	0.31	129.5	0.72
	6	0.19	311.4	0.17
	7	0.11	2122.0	0.12

a) Before extraction.

The distribution of salicylic acid and sodium salicylate between mesityl oxide and aqueous solution of different pH values (adjusted with diluted perchloric acid and sodium hydroxide solution) at constant ionic strength (0.1 M sodium perchlorate) was studied by equilibrating known concentration of salicylic acid or sodium salicylate for more than 16 hours at room temperature. The volume of aqueous phase and organic phase was kept equal (10 ml). After equilibration the layers were allowed to settle and separate and concentration of unextracted salicylic acid or salicylate ions in the aqueous phase is determined colorimetrically. The experimental distribution ratio and the calculated one are obtained by equations given by Irwing and Sinha[22] and reported in Table 1. Both salicylic acid and sodium salicylate show extraction into mesityl oxide but the probability of dimerization of salicylic acid in mesityl oxide which is a ketone is negligible.

The period of equilibration was varied and for quantitative extraction of lanthanum, single extraction for 30 s with neat mesityl oxide is adequate. Prolonged shaking has no adverse effect on the extraction.

An interference study showed that for the extraction of 40 μg of lanthanum by the recommended procedure, 2500 μg each of Ag, Ca, Ba, Zn, Hg, Ni, Bi, As(III), Au(III), Ti(IV), Zr(IV), Ga(III), Mo(VI), tartrate, ascorbate, nitrate, thiocyanate, sulfate, thiourea, phosphate and carbonate do not interfere. Similarly no interference is observed for 2000 μg each of Co, Mn, Fe(III); 1000 μg each of Pd, Cd, Pb, V(V), Cr(VI), fluoride; 500 μg each of Sn(II), Al, Rh, Ru, W(VI), and 100 μg of Cr(III). However, cerium (III and IV) and Nd(III) interfere severely.

Separation of Lanthanum(III) from Iron(III), Molybdenum(VI), Vanadium(V), Chromium(VI), Titanium(IV), and Beryllium. Ions such as iron, molybdenum, vanadium(V), chromium(VI), beryllium, and titanium(IV) do not extract into mesityl oxide. Hence their separation (from binary mixtures) is achieved by extraction of lanthanum by the recommended procedure. Lanthanum from the organic phase is stripped and determined as described above and the added ions, are estimated in the aqueous phase by standard procedure. The recovery of lanthanum and added

TABLE 2. ANALYSIS OF SYNTHETIC MIXTURES

Sample No.	Composition of synthetic mixture and amount taken in mg	Recovery of Lanthanum from duplicate analysis %	Relative error %	Recovery of added ion %	Relative error %	Estimation procedure for added ions and references
1	La, 0.04; Fe, 1.0	99.8	0.2	99.6	0.4	Colorimetry with thiocyanate (23)
2	La, 0.04; Mo, 2.5	99.8	0.2	99.6	0.4	Colorimetry with thiocyanate (23)
3	La, 0.04; V, 0.5	99.6	0.4	99.2	0.8	Colorimetry with PAR (24)
4	La, 0.04; Cr, 1.5	99.4	0.6	99.4	0.6	Colorimetry with diphenylcarbazide (23)
5	La, 0.04; Ti, 1.0	99.6	0.4	99.0	1.0	Colorimetry with H_2O_2 (23)
6	La, 0.04; Zr, 2.5	99.2	0.8	99.0	1.0	Complexometry with EDTA (25)
7	La, 0.04; Bi, 1.0	99.4	0.6	99.2	0.8	Colorimetry with thiourea (23)
8	La, 0.04; Sc, 0.025	99.0	1.0	99.0	1.0	Colorimetry with arsenazo I (26)
9	La, 0.04; U, 0.5	99.2	0.8	99.2	0.8	Colorimetry with PAR (27)
10	La, 0.04; Be, 1.0	99.2	0.8	99.0	1.0	Colorimetry with aluminon (28)

Note: (1) Lanthanum is estimated photometrically with arsenazo I. (2) Aqueous solution containing titanium, scandium, or beryllium is evaporated to dryness, treated with HNO_3 and $HClO_4$ to decompose salicylate and residue is dissolved in water and then used for titanium or scandium or beryllium estimation.

ions is >99.0%. The results of the analysis of synthetic mixtures are reported in Table 2.

Separation of Lanthanum from Zirconium(IV) and Bismuth(III) Both zirconium and bismuth show co-extraction with lanthanum, but do not back extract with water. Separation of lanthanum from binary mixture is achieved by first stripping lanthanum with water and subsequent scrubbing of zirconium with two 10 ml portions of 1 M HCl solution and bismuth with two 10 ml portions of 1 M NaOH solution. The results of the separation are reported in Table 2.

Separation of Lanthanum(III) from Scandium(III) and Uranium(VI). Lanthanum (from 0.1 M sodium salicylate solution adjusted to pH 7) also extracts into 4-methyl-2-pentanol but scandium and uranium do not. This facilitates separation of lanthanum from scandium and uranium. Binary mixture containing lanthanum–scandium or lanthanum–uranium in 0.1 M sodium salicylate solution adjusted to pH 7, is extracted for 30 sec with 10 ml of undiluted 4-methyl-2-pentanol. Lanthanum transfers into organic phase keeping scandium and uranium in the aqueous phase. Lanthanum is stripped with two 10 ml portions of water containing few drops of HCl and then determined as described above. Scandium and uranium in the aqueous extract are estimated by known methods. Separation results are reported in Table 2.

The reproducibility of results was satisfactory and results were found to be accurate within ±0.5% with the standard deviation of ±0.8%. The total operation requires only 15 min. The wide applicability of the method is shown by the satisfactory analysis of a variety of samples.

Thanks are due to Council of Scientific and Industrial Research, New Delhi, for awarding fellowship to one of us (ADL) and University grants commission, New Delhi for financing the project.

References

1) A. D. Langade and V. M. Shinde, *Mikrochim Acta* (in press).
2) S. Shibata, F. Takeuchi, and T. Matsumae, *Anal. Chim. Acta*, **21**, 177 (1959).
3) J. Stary, "The Solvent Extraction of Metal Chelates," Pergamon Press, Lodon (1964).
4) E. B. Panasenko, V. I. Belokoskov, and T. M. Ivanova, *Khim. Tekhnol.*, **1966**, 76 and 70.
5) R. A. Edge, *Anal. Chim. Acta*, **27**, 396 (1962).
6) A. V. Nikolaev, *Dokl. Akad. Nauk. USSR*, **163**, 897 (1968).
7) I. N. Popkov, I. N. Tselik, L. P. Chernge, T. A. Pentkovskaga, T. I. Bwrova, and B. N. Laskoria, *Dokl. Akad. Nauk. USSR*, **173**, 1351 (1967).
8) V. Jagodic, M. J. Herak, and R. Radosevic, *J. Less Common Metals*, **15**, 371 (1968).
9) E. B. Mikhlin and G. V. Korpusov, *Zh. Neorg. Khim.*, **10**, 2787 (1965).
10) A. M. Golub, M. M. Olevinkis, F. P. Gorlanko, and E. O. Kuchkina, *Anal. Khim. Ekstr. Protessy*, **1970**, 19.
11) A. M. Golub, M. I. Olevinskii, and E. F. Lutsenko, *Ukr. Khim. Zh.*, **31**, 12 (1968).
12) T. Sekine, Y. Koike, and Y. Hasegawa, *Bull. Chem. Soc. Jpn.*, **42**, 432 (1969).
13) K. P. Lunichkina and E. V. Renard, *Radiokhimiya*, **15**, 30 (1973).
14) S. G. K. Nair and M. Smutz, *J. Inorg. Nucl. Chem.*, **29**, 1787 (1967).
15) F. E. Kosinski and H. Bostian, *J. Inorg. Nucl. Chem.*, **31**, 3623 (1969).
16) A. Aziz and S. J. Lyle, *J. Inorg. Nucl. Chem.*, **32**, 1925

(1970).
17) H. Suisho, *Nippon Kagaku Zasshi*, **34**, 859 (1961).
18) H. Watanabe, *Bull. Chem. Soc. Jpn.*, **43**, 100 (1970).
19) A. K. De, *J. Indian. Chem. Soc.*, **51**, 195 (1974).
20) B. Hock, *Bernstroem, Sunsk Kem. Tidskr.*, **68**, 34 (1956).
21) F. Welcher, "The Analytical Uses of EDTA," D. Van Nostrand, New York (1958), p. 50.
22) H. M. N. H. Irving and S. P. Sinha, *Anal. Chim. Acta*, **49**, 449 (1970).
23) E. B. Sandell, "Colorimetric Determination of Traces of Metals," 3rd ed, Interscience, New York, pp. 338, 397, 534, 649, 874.
24) E. Gagliardi and B. Ilmair, *Mikrochim. Acta I*, **1967**, 180.
25) J. S. Fritz and Johnson, *Anal. Chem.*, **27**, 1653 (1955).
26) T. Shimizo, *Anal. Chim. Acta*, **37**, 75 (1967).
27) A. I. Busev and V. M. Ivanov, *Ser. Khim.*, **3**, 52 (1960).
28) G. E. Kosel and W. F. Neuman, *Anal. Chem.*, **22**, 936 (1950).

Reaction between Azibenzil and Diarylmethanimine

Kailash Nath MEHROTRA* and Girija PRASAD
Department of Chemistry, Banaras Hindu University, Varanasi-221005, India
(Received March 24, 1980)

The thermal reaction of azibenzil with diarylmethanimine (**1**) leads to *N*-(diarylmethylene)diphenylacetamide (**2**) which from methanol or ethanol yields *N*-(α-alkoxydiarylmethyl)diphenylacetamide (**4**). The reduction of **2** with sodium borohydride gives *N*-(diarylmethyl)diphenylacetamide. The photochemical reaction of azibenzil and **1** results in the formation of cyano ethers besides the amido ethers **4**. A mechanism of formation of products is discussed.

Azibenzil (2-diazo-1,2-diphenylethanone) has been known to form 1,3-oxathiole[1] in the reaction with thiobenzophenone and oxazoles[2] with benzonitrile. It has been observed that ketocarbenes undergo cycloaddition with olefins leading to cyclopropanes.[3] The benzoylphenylcarbene, formed from the thermal or photochemical decomposition of azibenzil, may add on carbon-nitrogen double bond of diarylmethanimine (**1**) giving rise to substituted aziridines. The interest in the attempted synthesis of aziridines[4] prompted us to carry out the above reaction. We now report the formation of *N*-(diarylmethylene)diphenylacetamide (**2**) on treatment of a benzene solution of 2-diazo-1,2-diphenylethanone with diarylmethanimine (**1**) at refluxing temperature. The products **2** lead to amido ethers (**4**) with alcohols. On irradiation of the reaction mixture with UV light, cyano ethers (**5**) are obtained besides the amido ethers (**4**).

Results and Discussion

The product mixture, obtained by refluxing 2-diazo-1,2-diphenylethanone and diphenylmethanimine (**1a**, Ar=Ar′=C_6H_5) in benzene, was crystallized from 2-propanol; it gave *N*-(diphenylmethylene)diphenylacetamide (**2a**, 90%). The structure was assigned on the basis of analytical and spectral data (Table 1). The product **2a** resulting from an intermediate **A** presumably can be formed as an adduct of diphenylketene, generated from the decomposition of 2-diazo-1,2-diphenylethanone,[5] and diphenylmethanimine (**1a**) (Scheme 1). A similar zwitterionic intermediate has been proposed[6] in the formation of 2-azetidinones from the reaction of *N*-benzylideneaniline with diphenylketene. The migration of hydrogen appears to be more feasible than the cyclization of the intermediate **A** to the β-lactam **B** due to steric factors (presence of four bulky aryl groups on the terminal carbon atoms in **A**). The reaction of **2a** with sodium borohydride in 2-propanol at room temperature yields the reduction product **3a** (Table 1).

The crystallization of the above reaction products obtained from 2-diazo-1,2-diphenylethanone and **1a** from methanol afforded *N*-(α-methoxydiphenylmethyl)-diphenylacetamide (**4a**). Crystallization of **2a** from

TABLE 1. ANALYTICAL AND SPECTRAL DATA OF **2a**, **2b**, **2c**, **3a**, **3b**, AND **3c**

Compound	Ar	Ar′	Yield %	Mp °C	ν_{max}^{Nujol}/cm^{-1}	NMR[a] (δ)	Molecular formula	Found (%)	Calcd (%)
2a	C_6H_5	C_6H_5	90	110—111	1685 (C=O) 1640 (C=N)	$CDCl_3$: 7.28 (m, 20H, arom.), 4.88 (s, 1H, CH, benzhydrylic)	$C_{27}H_{21}NO$	C: 86.51 H: 5.68 N: 3.80	86.40 5.60 3.73
2b	C_6H_5	*p*-$CH_3 \cdot C_6H_4$	86	118—119	1685 (C=O) 1635 (C=N)	CCl_4: 7.25 (m, 19H, arom.), 4.80 (s, 1H, CH, benzhydrylic), 2.35 (s, 3H, Me)	$C_{28}H_{23}NO$	C: 86.28 H: 6.12 N: 3.56	86.37 5.91 3.60
2c	*p*-$CH_3 \cdot C_6H_4$	*p*-$CH_3 \cdot C_6H_4$	89	108—109	1680 (C=O) 1635 (C=N)	CCl_4: 7.21 (m, 18H, arom.), 4.80 (s, 1H, CH, benzhydrylic), 2.40 (s, 6H, 2Me)	$C_{29}H_{25}NO$	C: 86.42 H: 6.25 N: 3.51	86.35 6.20 3.47
3a	C_6H_5	C_6H_5	87	201—202	3260 (N-H) 1650 (C=O)	$CDCl_3$: 7.28 (m, 20H, arom.), 6.25—6.45 (bs, 2H, NH, CHArAr′), 5.05 (s, 1H, CH benzhydrylic)	$C_{27}H_{23}NO$	C: 86.01 H: 6.15 N: 3.90	85.94 6.10 3.71
3b	C_6H_5	*p*-$CH_3 \cdot C_6H_4$	82	185—187	3260 (N-H) 1645 (C=O)	$CDCl_3$: 7.24 (m, 19H, arom.), 6.10—6.27 (bs, 2H, NH, CHArAr′), 5.05 (s, 1H, CH benzhydrylic), 2.35 (s, 3H, Me)	$C_{28}H_{25}NO$	C: 86.17 H: 6.45 N: 3.48	85.93 6.39 3.58
3c	*p*-$CH_3 \cdot C_6H_4$	*p*-$CH_3 \cdot C_6H_4$	96	206—207	3270 (N-H) 1650 (C=O)	$CDCl_3$: 7.25 (m, 18H, arom.), 6.20—6.35 (bs, 2H, NH, CHArAr′), 5.05 (s, 1H, CH benzhydrylic) 2.35 (s, 6H, 2Me)	$C_{29}H_{27}NO$	C: 86.07 H: 6.72 N: 3.41	85.98 6.67 3.45

a) Signals are abbreviated as: s=singlet; m=multiplet; bs=broad singlet.

Table 2. Analytical and spectral data of amido ethers **4a**, **4b**, **4c**, and **4d**

Compound	Ar	Ar′	R	Yield %	Mp °C	ν_{max}^{Nujol}/cm^{-1}	NMR[a] (δ, $CDCl_3$)	Molecular formula	Found (Calcd) (%)
4a	C_6H_5	C_6H_5	CH_3	89	199—201	3300 (N–H) 1660 (C=O) 1080 (C–O–C)	7.33 (m, 20H, arom.), 6.71 (b, 1H, NH), 5.10 (s, 1H, CH benzhydrylic), 3.18 (s, 3H, OMe)	$C_{28}H_{25}NO_2$	C: 82.85 (82.54) H: 6.03 (6.14) N: 3.40 (3.44)
4b	C_6H_5	C_6H_5	C_2H_5	82	166—167	3320 (N–H) 1675 (C=O) 1080 (C–O–C)	7.25 (m, 20H, arom.), 6.68 (b, 1H, NH), 5.08 (s, 1H, CH benzhydrylic), 3.28 (q, 2H, OCH_2, J=7 Hz), 1.20 (t, 3H, Me, J=7 Hz)	$C_{29}H_{27}NO_2$	C: 82.52 (82.66) H: 6.39 (6.41) N: 3.29 (3.33)
4c	C_6H_5	*p*-CH_3·C_6H_4	CH_3	83	177—178	3300 (N–H) 1665 (C=O) 1080 (C–O–C)	7.31 (m, 19H, arom.), 6.75 (b, 1H, NH), 5.08 (s, 1H, CH benzhydrylic), 3.17 (s, 3H, OMe), 2.26 (s, 3H, Me)	$C_{29}H_{27}NO_2$	C: 82.43 (82.66) H: 6.38 (6.41) N: 3.30 (3.33)
4d	*p*-CH_3·C_6H_4	*p*-CH_3·C_6H_4	CH_3	82	179—180	3330 (NH) 1668 (C=O) 1080 (C–O–C)	7.32 (m, 18H, arom.), 6.75 (b, 1H, NH), 5.10 (s, 1H, CH benzhydrylic), 3.17 (s, 3H, OMe), 2.25 (s, 6H, 2Me)	$C_{30}H_{29}NO_2$	C: 82.51 (82.76) H: 6.72 (6.67) N: 3.10 (3.22)

a) Signals are abbreviated as: s=singlet; b=broad; m=multiplet; q=quartet; t=triplet.

methanol also gave **4a**. The structure assignment of product **4a** has been made on the basis of analytical and spectral data (Table 2). On treatment with 0.1 mol dm^{-3} HCl the amido ethers (**4**) gave diphenylacetamide, mp 166—167 °C and the IR spectrum shows bands at 3400 (ν_{NH_2}) and 1660 cm^{-1} ($\nu_{C=O}$). The amido ether **4a** on heating at 225 °C for 15 min gave **2a** presumably with the loss of alcohol. The formation of products can be explained as shown in Scheme 1.

Similar treatment of imines **1b—c** gave the *N*-acylimines **2b—c** and amido ethers **4b—d**. The reduction of **2b—c** in 2-propanol gave **3b—c**. These products (**2a—c** and **4a—d**) were also obtained in the reaction of diphenylketene with diarylmethanimines (**1a—c**).

Irradiation of a solution of 2-diazo-1,2-diphenylethanone and diphenylmethanimine (**1a**) in dry benzene with UV light gave α-(diphenylmethoxy)diphenylacetonitrile (**5a**) and amido ether (**4a**). The cyano ether (**5a**)

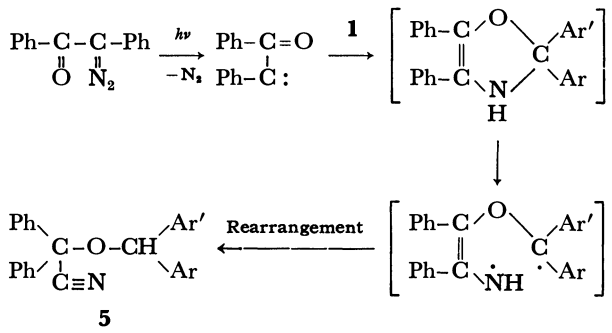

Scheme 2.

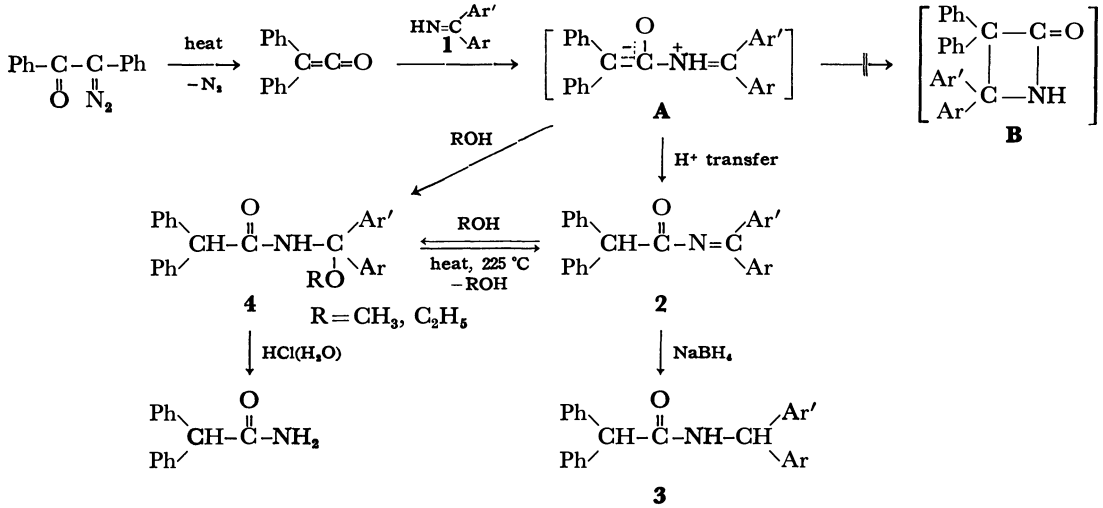

Scheme 1.

Table 3. Analytical and spectral data of cyano ethers **5a**, **5b**, and **5c**

Compound	Ar	Ar′	Yield %	Mp °C	$\nu_{max}^{CHCl_3}$/cm^{-1}	λ_{max}^{EtOH}/nm	NMR (δ, $CDCl_3$)	Molecular formula	Found (%)	Calcd (%)
5a	C_6H_5	C_6H_5	37	178—179	2270 (C≡N) 1080 (C–O–C)	264	7.11 (m, 20H, arom.), 5.10 (s, 1H, CH benzhydrylic)	$C_{27}H_{21}NO$	C: 86.51 H: 5.82 N: 3.42	86.40 5.60 3.73
5b	C_6H_5	p-$CH_3 \cdot C_6H_4$	34	141—142	2275 (C≡N) 1090 (C–O–C)	264	7.18 (m, 19H, arom.), 5.10 (s, 1H, CHArAr′), 2.25 (s, 3H, Me)	$C_{28}H_{23}NO$	C: 86.59 H: 6.16 N: 3.67	85.38 5.91 3.60
5c	p-$CH_3 \cdot C_6H_4$	p-$CH_3 \cdot C_6H_4$	38	157—158	2270 (C≡N) 1090 (C–O–C)	268	7.15 (m, 18H, arom.), 5.16 (s, 1H, CHArAr′), 2.25 (s, 6H, 2Me)	$C_{29}H_{25}NO$	C: 86.67 H: 6.10 N: 3.32	86.35 6.20 3.47

did not lead to amido ether (**4a**) on treatment with methanol. The probable reaction sequence is shown in Scheme 2.

The loss of nitrogen from 2-diazo-1,2-diphenylethanone would lead to ketocarbene, which would condense with diphenylmethanimine (**1a**) *in situ* to form 1,3-oxazole in an analogous manner as observed in the case of the reaction of 2-diazo-1,2-diphenylethanone and thiobenzophenone.[1] The oxazole may further rearrange to cyano ether (**5a**) (Scheme 2) as observed in the ring opening of 2-thiazolines.[7]

Similar irradiation of imines **1b—c** gave cyano ethers (**5b—c**) besides amido ethers (**4b—d**). The amido ethers (**4b—d**) are presumably formed from diphenylketene and **1** through zwitterionic intermediate **A** as shown in Scheme 1.

Experimental

Melting points have been determined in capillaries on Büchi apparatus and are uncorrected. The NMR spectra were recorded with a Varian A-60 D spectrometer, with tetramethylsilane as an internal standard. The IR spectra were measured on a Perkin-Elmer 720 spectrophotometer and the UV spectra on a Beckman DB-G spectrophotometer.

Preparation of N-*(Diarylmethylene) diphenylacetamide (2) and Amido Ethers (4). General Procedure From 2-Diazo-1,2-diphenylethanone*: A solution containing 3.0 g (13.5 mmol) of 2-diazo-1,2-diphenylethanone[8] (freshly prepared by the oxidation of benzil monohydrazone with yellow mercury(II) oxide) and diarylmethanimine (**1**)[9] (14.0 mmol) in 60 ml of dry benzene was heated under reflux for 6 h and kept overnight at room temperature. The solvent was removed under reduced pressure and the residue on recrystallization from 2-propanol afforded *N*-(diarylmethylene)diphenylacetamide (**2**). The analytical and spectral data are shown in Table 1.

Crystallization of the products from methanol or ethanol yielded the amido ethers (**4**). The analytical and spectral data are given in Table 2.

From Diphenylketene: A solution containing 1.94 g (10 mmol) of diphenylketene[10] in 5 ml of dry benzene and 10 mmol of diarylmethanimine (**1**) in 5 ml of dry benzene were mixed at room temperature. The vessel became hot at once and the contents were kept overnight at room temperature. Crystallization of the reaction mixture from alcohol afforded the same amido ethers (**4a—d**) as obtained from 2-diazo-1,2-diphenylethanone.

Preparation of Cyano Ethers 5. General Procedure: A solution containing 4.9 g (22.0 mmol) of 2-diazo-1,2-diphenylethanone and 24.0 mmol of diarylmethanimine (**1**) in 330 ml of dry benzene was irradiated by UV light from a 200 W Hanovia mercury arc lamp under a continuous slow stream of nitrogen for 6 h and kept overnight at room temperature. The solvent was removed under reduced pressure and the residual material was fractionally crystallized from benzene–methanol mixture to afford the cyano ethers (**5**, 34—38%) (Table 3) and amido ethers (**4**, 45—50%) (Table 2).

Conversion of 4a to 2a: 1.0 g of the amido ether (**4a**) was allowed to melt at 225 °C in an oil bath and was kept for 15 min at 225 °C. The flask was cooled and the residual material was recrystallized from 2-propanol to give 0.9 g (90%) of **2a**. Similarly **4b** and **4c** were converted to **2b** and **2c**, respectively.

Reduction of 2a to 3a: To a solution of 1.0 g of **2a** in 20 ml of 2-propanol was added 30 mg of sodium borohydride and was allowed to stand at room temperature (40 °C) for 30 min. The solvent was evaporated and the residual matter recrystallized from ethanol to give 0.87 g (87%) of **3a**. Similar reduction of **2b** and **2c** gave **3b** and **3c**, respectively (Table 1).

References

1) S. Mataka, S. Ishii, and M. Tashiro, *Chem. Lett.*, **1977**, 955.

2) K. Kitatani, T. Hiyama, and H. Nozaki, *Tetrahedron Lett.*, **1974**, 1531.

3) M. Jones and W. Ando, *J. Am. Chem. Soc.*, **90**, 2200 (1968); R. J. Mohrbacker and N. H. Cromwell, *ibid.*, **79**, 401 (1957).

4) K. N. Mehrotra and T. V. Singh, *Tetrahedron Lett.*, **1972**, 4949; K. N. Mehrotra and G. Prasad, *Indian J. Chem.*, **16B**, 77 (1978); *Tetrahedron Lett.*, **1978**, 4179.

5) G. Frater and O. P. Strausz, *J. Am. Chem. Soc.*, **92**, 6654 (1970).

6) H. B. Kagan and J. L. Luche, *Tetrahedron Lett.*, **1968**, 3093; G. Wittig and A. Hesse, *Ann. Chem.*, **1976**, 500.

7) T. Matsuura and Y. Ito, *J. Chem. Soc., Chem. Commun.*, **1972**, 896.

8) C. D. Nenitzescu and E. Solomonica, *Org. Synth.*, Coll. Vol. II, 496 (1943).

9) P. L. Pickard and T. L. Tolbert, *J. Org. Chem.*, **26**, 4886 (1961).

10) W. Reid and P. Junker, *Angew. Chem. Int. Ed. Engl.*, **6**, 631 (1967).

Chemistry at Hydrocarbon-Water Phase Boundaries. Biphase Hydrolysis of Organic Halides[1]

Noritaka OHTANI,[2] Jacques J. BESSE, and Steven L. REGEN*

Contribution from the Department of Chemistry, Marquette University, Milwaukee, Wisconsin 53233, U.S.A.

(Received August 7, 1980)

The kinetics of the biphase hydrolysis of 1-bromoadamantane and 1-phenylethyl chloride in toluene–water and decane–water systems have been investigated. Evidence has been obtained for the first examples of rate-limiting S_N1 reactions occurring at a hydrocarbon–water phase boundary, based on (1) the influence of temperature, mild stirring, interfacial area, reaction volume, and pH on the observed first-order rate constants, (2) comparison of absolute rates and activation energies with analogous homogeneous hydrolysis reactions, (3) the temperature dependence of the initial rate of diffusion of tritiated 1-methoxyadamantane from toluene into water, and (4) the initial rate of diffusion of ^3H_2O into toluene.

Hydrocarbon–water interfaces are found in many important bioorganic and synthetic organic systems.[3-6] Despite this fact, their precise structure and overall chemical significance have not been well characterized.[7-9] Several years ago, Menger reported a detailed study of the biphase hydrolysis of *p*-nitrophenyl laurate catalyzed by imidazole in a heptane–water system.[3-10] Compelling evidence was presented which supported an interfacial reaction. Based on a very low apparent activation energy, it was also concluded that mass transport of the reactants to the interface makes a significant contribution to the observed kinetics. Remarkably few studies have since appeared which consider organic reactions at liquid–liquid interfaces.[11,12]

In the present paper we report the results of a kinetic study of the biphase hydrolysis of 1-bromoadamantane and 1-phenylethyl chloride carried out in toluene–water and decane–water systems.[13] Our data provide strong evidence for what we believe are the first examples of rate-limiting S_N1 reactions at a hydrocarbon–water liquid–liquid phase boundary. As such, they represent the simplest interfacial organic reactions investigated to date.

Results

Kinetics of the Hydrolysis. Biphase hydrolysis of 1-bromoadamantane and 1-phenylethyl chloride were carried out using culture tubes as reaction vessels. Rates were monitored by following the disappearance of the organic halide from the organic phase. For 1-bromoadamantane, hydrolysis rates were identical to those determined by following the appearance of 1-hydroxyadamantane in the organic phase (material balance was >95%). Partitioning of 1-phenylethyl alcohol into water was too high to permit the simultaneous analysis of reactant and product. In all cases, clean first-order kinetics was maintained over at least three half-lives. A typical first-order plot is shown in Fig. 1.

Table 1 shows the influence of mild stirring on observed first-order rate constants, k_{obsd}. For both organic halides, stirred reactions were similar in rate to unstirred processes. 1-Phenylethyl chloride hydrolized more than one order of magnitude faster than 1-bromoadamantane, and was carried out under mild stirring conditions in all subsequent experiments.

In order to evaluate the dependence of k_{obsd} on the hydrocarbon–water interfacial area, S, as well as the volumes of the aqueous (V_{aq}) and organic (V_{org}) phases used, biphase hydrolyses were carried out in culture tubes of varying dimensions. Results for 1-phenylethyl chloride, reported in Table 2, show that a normalized rate constant, k_0 (where $k_0=k_{obsd}\ V_{org}/S$), is constant over a wide range of experimental

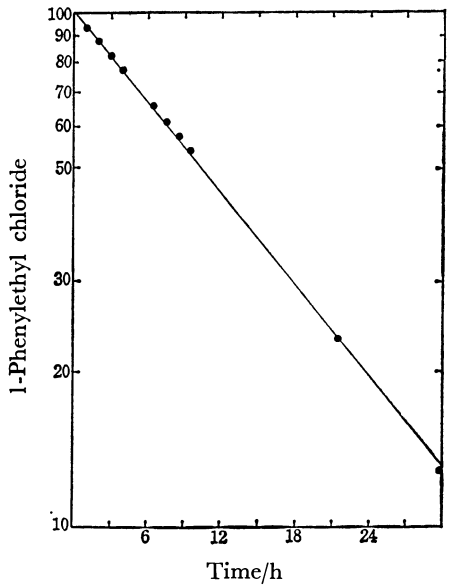

Fig. 1. Plot of percent of 1-phenylethyl chloride in the organic phase as a function of time for reaction of 4 ml of 0.01 M 1-phenylethyl chloride in toluene with 10 ml of 0.1 M aqueous sodium hydroxide at 90 °C, carried out as a mildly stirred process ($S\approx4.16$ cm^2).

TABLE 1. EFFECT OF STIRRING ON K_{obsd}[a]

Organic halides	Stirring speed / rpm	Interfacial area / cm^2	$10^5\,k_{obsd}$ / s^{-1}
1-Phenylethyl chloride	0	4.16	1.50
	70	≈4.16	1.90
1-Bromoadamantane	0	4.16	0.10
	70	≈4.16	0.16

a) Reaction of 4.0 ml of 0.01 M organic halide in toluene with 10 ml of 0.1 M aqueous sodium hydroxide in a 50 ml culture tube at 90 °C.

conditions and is independent of the volume of the aqueous phase.[14] Exactly analogous results have been obtained for 1-bromoadamantane.[13]

Data presented in Table 3 show the influence of temperature, hydroxide ion concentration, added sodium bromide and the nature of the hydrocarbon solvent on the biphase hydrolysis of 1-bromoadamantane. The apparent activation energy E_a for toluene–water and decane–water systems was 23.1 and 19.2 kcal mol^{-1} respectively. These values lie in the range found for comparable homogeneous hydrolysis (Table 4).[15] Values of k_0 at 100 °C using pure water, 0.1 M NaOH, or 1.0 M NaBr as the aqueous phase were very similar. When decane was used as the organic solvent in place of toluene, higher rates were observed. Similar results have been obtained for 1-phenylethyl chloride (Tables 4 and 5).

Diffusion of ^3H_2O into Toluene. The initial rate of diffusion of tritiated water from 0.1 M aqueous sodium hydroxide into dry toluene was measured at 70 °C and found to be 1.3×10^{-6} M s^{-1}; V_{org} and S used in this experiment were 4 ml and 1.26 cm^2, respectively.

Table 2. Influence of V_{org}, V_{aq}, and S on k_0 for 1-phenylethyl chloride[a]

V_{org} / cm^3	V_{aq} / cm^3	S / cm^2	$10^3 k_0$ / min^{-1} cm
1	2	1.26	1.1
2	5	2.83	1.2
4[b]	10	4.16	1.1
10	40	9.08	1.2

a) Reaction of 0.05 M 1-phenylethyl chloride in toluene with 0.1 M aqueous sodium hydroxide at 90°C, using mild stirring; $k_0=k_{obsd}V_{org}/S$. b) Organic halide concentration used was 0.01 M.

Discussion

Two fundamental questions which are central to this investigation are (1) what is the rate-controlling process and (2) where does reaction occur. In principle the rate-limiting step could be (a) diffusion of the organic halide through the bulk organic phase or through the aqueous–organic phase boundary, (b) diffusion of water into the bulk organic phase, (c) chemical reaction, or (d) a combination of (a)—(c). Based on the hydrolysis data, several lines of evidence point to chemical reaction as being the rate-determining step. First, the apparent activation energy observed for both organic halides is high and is similar to that measured for comparable homogeneous reactions. These values contrast sharply with activation energies found for diffusion in most liquids (3—5 kcal mol^{-1}).[16] Furthermore, the rate of diffusion of tritiated 1-methoxyadamantane from toluene into 0.1 M aqueous sodium hydroxide has previously been shown to be only slightly sensitive to temperature ($E_a\leq3.5$ kcal mol^{-1}).[13] This shows that the diffusional resistance for organic substrates, similar to those investigated in the present work, through the interface is low, as expected. Second, mild stirring has a relatively small effect on the biphase hydrolysis rates. This result further argues against diffusion as being an important contributor to the observed kinetics. Third, if water transport were rate limiting, the observed hydrolyses should obey zero order kinetics; also the rate for both organic halides would be equal to the diffusion rate of water into toluene. Experimentally, however, clean first-order kinetics are followed and the initial diffusion rate of water into toluene (70 °C) and the initial reaction velocity for 1-phenylethyl chloride (70 °C) and 1-bromoadamantane

Table 3. Biphase hydrolysis of 1-bromoadamantane

Organic solvent	Aqueous solution	V_{org} / cm^3	V_{aq} / cm^3	S / cm^2	Temp / °C	$10^7 k_0$[b] / s^{-1} cm	E_a / kcal mol^{-1}
Toluene	0.1 M NaOH	1	1	1.26	75	2.03	23.07
		1	1	1.26	80	3.08	
		1	1	1.26	85	6.42	
		1	2	1.26	90	8.25	
		1	1	1.26	95	9.76	
		1	2	1.26	100	22.78	
		1	1	1.26	105	26.98	
		1	1	1.26	110	36.75	
		1	2	1.26	120	106.03	
Toluene	pure water	1	2	1.26	100	21.27	
Toluene	1.0 M NaBr	1	2	1.26	100	18.89	
Decane	0.1 M NaOH	1	10	4.16	70	4.18[c]	19.24
		1	10	4.16	80	9.09[c]	
		1	10	4.16	90	18.12[c]	
		1	1	1.26	100	42.06	
		1	1	1.26	110	77.06	
		1	1	1.26	120	144.70	

a) When the volume of the aqueous phase was >1 ml, material balance was >95%. b) $k_0=k_{obsd}V_{org}/S$. c) Mild stirring was used.

Table 4. Rate constants and activation energy for hydrolysis of organic halides in aqueous dioxane

Organic halide	Solvent, Dioxane in water(V/V)	Temp °C	$10^5 k_{obsd}$ s^{-1}	E_a kcal mol^{-1}
1-Phenylethyl[a] chloride	90	70	0.31	19.94
		80	0.81	
		90	1.54	
	80	70	4.57	25.32
		75	7.72	
		80	13.00	
	70	65	20.44	22.94
		75	55.47	
		80	86.05	
1-Bromo-adamantane	92[b]	100	0.128	23.39
		110	0.292	
		120	0.635	
	88[b]	100	0.96	22.72
		110	2.24	
		120	4.54	
	80[c]	25	0.007	21.28
		75	1.22	
		100	9.75	

a) Reactions were carried out in 8-ml culture tubes using 4 ml of 0.01 M 1-phenylethyl chloride in aqueous dioxane. b) Taken from Ref. 13. c) Taken from D. J. Raber, R. C. Bingham, J. L. Fry, and P. v. R. Schleyer, *J. Am. Chem. Soc.*, **92**, 5977 (1970).

Table 5. Biphase hydrolysis of 1-phenylethyl chloride[a]

Organic solvent	Aqueous solution	Temp °C	$10^5 k_{obsd}$ s^{-1}	E_a kcal mol^{-1}
Toluene	pure water	70	1.39	17.60
		80	2.74	
		90	5.74	
	0.1 M NaOH	70	1.56	17.26
		80	3.43	
		90	6.26	
	0.5 M NaOH	70	1.24	17.20
		80	2.40	
		90	4.96	
Decane	0.1 M NaOH	70	6.83	13.33
		80	12.78	
		90	19.94	

a) Reaction of 1.0 ml of 0.01 M 1-phenylethyl chloride with 10 ml of 0.1 M aqueous sodium hydroxide using mild stirring ($S \approx 4.16$ cm^2).

(75 °C) are 1.3×10^{-6}, 1.6×10^{-7}, and 6.9×10^{-9} M s^{-1}, respectively ($S=4.16$ cm^2; $V_{org}=1$ ml; [organic halide]=0.01 M). Taken together, these data provide very strong evidence that diffusion plays a minor role in the apparent kinetics and that chemical reaction dominates.

For a rate-limiting chemical reaction, the constancy of k_0 over a wide range of V_{org}, V_{aq}, and S can be rationalized only in terms of an interfacial process. If reaction were occurring in the bulk water phase, the rate should increase with increasing V_{aq}, due to an increase in the molar amount of water soluble organic halide. Experimentally, the observed rate was independent of V_{aq}. That reaction is not occurring in the bulk organic phase is further demonstrated by a comparison of observed first-order rate constants for hydrolysis in toluene–water (two phase) *vs.* dioxane–water (one phase) systems. At 100 °C, k_{obsd} found for reaction of 1 ml of 0.01 M 1-bromoadamantane with 2 ml of 0.1 M aqueous sodium hydroxide ($S=1.26$ cm^2) was 2.87×10^{-6} s^{-1}. In contrast, k_{obsd} for the hydrolysis of 2.0 ml of 0.01 M 1-bromoadamantane in homogeneous 92% (v/v) dioxane–water was 1.28×10^{-6} s^{-1}. Similarly, at 90 °C, k_{obsd} for the biphase hydrolysis of 1.0 ml of 0.01 M 1-phenylethyl chloride with 10 ml of 0.1 M aqueous sodium hydroxide ($S=4.16$ cm^2) was 6.26×10^{-5} s^{-1}. The k_{obsd} for homogeneous hydrolysis of 4 ml of 0.01 M 1-phenylethyl chloride in 90% (v/v) dioxane–water was 1.54×10^{-5} s^{-1}. Thus, the observed first-order rate constants for homogeneous reactions which contained substantial amounts of water were *lower* than those found for comparable biphase reactions. Finally, the higher biphase hydrolysis rates observed with decane–water *vs.* toluene–water, while difficult to rationalize in terms of chemical reaction occurring in the organic phase (water is more soluble in toluene than in decane), is easily accounted for as an interfacial process; *i.e.*, partitioning of the relatively polar organic halide into the phase boundary should be greater when a less polar solvent (decane) is used.

The results presented in this paper provide strong evidence that chemistry at hydrocarbon–water phase boundaries can play an important role in liquid–liquid biphase ractions.[3,11,12] Further studies aimed at establishing the generality and chemical significance of interfacial organic chemistry are in progress.

Experimental

General Methods. 1-Bromo- and 1-hydroxyadamantane (Aldrich Chem. Co.) were purified by sublimation at 90 °C (1 mm), and 120 °C (1 mm) respectively. 1-Phenylethyl chloride was prepared from 1-phenylethyl alcohol using established procedures. Toluene and decane (Aldrich Chem. Co., spectrophotometric grade) were used as obtained. Deionized water was purified by distillation from $KMnO_4/Ba(OH)_2$. The temperature of the oil bath used for the kinetic experiments was controlled (±0.5 °C) with the aid of a "Therm-O-Watch" electronic controller Model L6-1000 (I^2R Co., Cheltenhan, Pa), attached to a thermometer. All kinetic experiments were conducted in culture tubes equipped with a Teflon-lined screw cap. Reaction mixtures were analyzed by GLC on a Hewlett-Packard Model 5830A flame ionization instrument (2 ft.×0.125 in UCW-982 on Chromosorb W column). Culture tubes (interfacial area) used were the following: Corning No. 9826, 13×100 mm (1.26 cm^2); Corning No. 9825, 20×125 mm (2.83 cm^2); Corning No. 9825, 25×150 mm (4.16 cm^2); Kimax No. 45066, 38×200 mm (9.08 cm^2). Radioactivity was measured using a Packard Tri-Carb Model 3330 scintillation spectrometer.

Kinetic Methods. All biphase hydrolysis reactions were studied between 70 and 120 °C. In a typical experiment, 1 ml of a solution of 1-phenylethyl chloride (0.01 M) in toluene containing a known quantity of undecane (internal standard) and 10 ml of (0.1 M) sodium hydroxide were introduced *via* pipet into a 50-ml culture tube (Corning No. 9826, 25×150 mm) containing a Teflon-coated magnetic stirring bar (1/2×5/16 in octagonal bar with pivot ring).

The tube was sealed with a Teflon-lined screw cap and was placed in an oil bath maintained at the desired temperature. The reaction was followed by withdrawing 1-μl samples of the organic phase at different times (no less than 30 min intervals) and monitoring the disappearance of the reactant by GLC. For sampling, the tube was removed from the oil bath, quickly cooled to nearly room temperature, opened, resealed, and returned to the bath (the overall process took less than 1 min). In all cases, clean first-order kinetics was observed over at least 3 half-lives. First-order rate constants were calculated with a least-squares program. The reproducibility of the observed rate constants was good (±10%). For biphase hydrolysis of 1-bromoadamantane, reactions were conducted in 8-ml culture tubes as unstirred processes using procedures previously described.[13] Apparent activation energies were derived from Arrhenius plots made by plotting k_0 as a function of $1/T$.

Diffusion of ^3H_2O into Toluene. An 8-ml culture tube was charged with 4.0 ml of dry toluene (distilled from sodium benzophenone ketyl) and sealed with a Teflon-lined screw cap. The tube was placed in an oil bath maintained at 70 °C. After thermal equilibration (15 min), 0.5 ml of 0.1 M NaOH in ^3H_2O (preequilibrated at 70 °C) was injected into the bottom of the toluene phase. The appearance of tritium in the organic layer was then monitored as a function of time by withdrawing 10 μl aliquots. The aliquots were blended with 2 ml of a scintillation liquid (dioxane solution of Omnifluor (New England Nuclear)) and the concentration of ^3H_2O in toluene computed using a standard curve.

References

1) Supported by the donors of the Petroleum Research Fund, administered by the American Chemical Society and the Division of Basic Energy Sciences of the Department of Energy (Contract EG-77-S-02-4446).

2) On leave from Akita University, Akita, Japan.

3) F. M. Menger, *J. Am. Chem. Soc.*, **92**, 5965 (1970).

4) F. M. Menger, *Acc. Chem. Res.*, **12**, 111 (1979); E. H. Cordes, "Reaction Kinetics in Micelles," Plenum Press, New York (1973); J. H. Fendler, *Acc. Chem. Res.*, **9**, 153 (1976). C. A. Bunton, *Progr. Solid State Chem.*, **8**, 239, (1973).

5) C. M. Starks, *J. Am. Chem. Soc.*, **93**, 195 (1971); C. M. Starks and C. Liotta, "Phase-Transfer Catalysis," Academic Press, New York (1978); W. P. Weber and G. W. Gokel, "Phase-Transfer Catalysis in Organic Synthesis," Springer-Verlag, New York (1977); E. V. Dehmlow, *Angew. Chem. Int. Ed. Engl.*, **16**, 493 (1977); A. Brandstrom, *Adv. Phys. Org. Chem.*, **15**, 267 (1977).

6) S. L. Regen, *Angew. Chem. Int. Ed. Engl.*, **18**, 421 (1979); M. Cinquini, S. Colonna, H. Molinari, F. Montanari, and P. Tundo, *J. Chem. Soc., Chem. Commun.*, **1976**, 394; J. M. Brown and J. A. Jenkins, *ibid.*, **1976**, 458.

7) We consider here only liquid-liquid hydrocarbon-water interfaces. Our discussion does not include well defined monolayer films.[8]

8) G. L. Gaines, Jr., "Insoluble Monolayers at Liquid-Gas Interfaces," Interscience, New York, N. Y. (1966); S. J. Valenty, *J. Am. Chem. Soc.*, **101**, 1 (1979); B. E. Horsey and D. G. Whitten, *J. Am. Chem. Soc.*, **100**, 1293 (1978).

9) S. Ross, "Chemistry and Physics of Interfaces," Am. Chem. Soc., Washington, D. C. (1965), p. 44; J. T. Davies and E. K. Rideal, "Interfacial Phenomena," Academic Press, New York, N. Y. (1961).

10) Prior to Menger's study, Bell reported the biphase permanganate oxidation of *N*-benzoyl-*o*-toluidine in water–benzene, and concluded that the reaction was interfacial in nature: R. P. Bell, *J. Phys. Chem.*, **32**, 882 (1928).

11) M. Makosza and E. Bialecka, *Tetrahedron Lett.*, **1977**, 183; Y. Sasson, A. Zoran, and J. Blum, *J. Mol. Catal.* **6**, 289 (1979).

12) Tomita *et al.* have reported hydrolysis studies of certain esters carried out as aqueous-organic biphase reactions. Although diffusion was shown to be important, the location of the reaction was not established: A. Tomita, N. Ebina, and Y. Tamai, *J. Am. Chem. Soc.*, **99**, 5725 (1977).

13) This work has appeared in preliminary form: S. L. Regen and J. J. Besse, *J. Am. Chem. Soc.*, **100**, 7117 (1978).

14) First-order rate constants were determined by following the decrease in concentration of the organic halide. For an interfacial reaction, as the volume of organic phase/surface area increases, the observed rate constant must decrease proportionally.

15) In our preliminary report, ΔH^*, ΔS^*, and ΔG^* were computed from observed first-order rate constants and compared with analogous homogeneous reactions. Unfortunately, since hydrocarbon-water liquid-liquid interfaces have not been unequivocally defined (three dimensional *vs.* two dimensional), absolute values of rate constants and corresponding ΔS^* and ΔG^* values cannot be meaningfully compared with homogeneous systems.

16) S. Glasstone, K. J. Laidler, and H. Eyring, "Theory of Rate Processes," McGraw-Hill, New York (1941), p. 522; S. Benson, "The Foundations of Chemical Kinetics," McGraw-Hill, New York (1960), p. 499; D. Shooter, "Comprehensive Chemical Kinetics," ed by C. H. Bamford and C. F. H. Tipper, Elsevier, Amsterdam (1969), Vol. 1, p. 253.

The Crystal Structure of Bis(acetylacetonato)platinum(II) Benzene Solvate

Mitsunori KATOH, Kunio MIKI, Yasushi KAI, Nobuo TANAKA, and Nobutami KASAI*

Department of Applied Chemistry, Faculty of Engineering, Osaka University, Yamadakami, Suita, Osaka 565

(Received July 7, 1980)

Synopsis. The crystal structure of bis(acetylacetonato)platinum(II) benzene solvate has been determined by means of X-ray diffraction. The geometry around the platinum atom is square-planar. Acetylacetonato ligands are bonded to the Pt atom by the *O,O'*-chelation, the Pt–O bond lengths being 2.008 (15) and 1.979 (14) Å.

The transition metal complexes containing acetylacetonato (abbreviated as acac hereafter) ligands have been widely studied, and some of their structures have been reported hitherto. In the case of group VIII transition metal complexes, especially the nickel group transition metal complexes, molecular structures of $[Ni(acac)_2]$,[1,2] $[Ni(acac)_2]_3$,[3] and $[Pd(acac)_2]$[4,5] have been determined by means of diffraction methods. This paper will deal with the crystal structure analysis of bis(acetylacetonato)platinum(II) benzene solvate.

The yellow, prismatic crystals were obtained by recrystallization from a benzene solution. A well-shaped crystal with approximate dimensions of $0.40\times0.43\times0.25$ mm was sealed in a glass capillary tube with a small amount of benzene in order to prevent its decomposition.

Crystal Data. $C_{10}H_{14}O_4Pt\cdot C_6H_6$, F.W.=471.4, $F(000)=452$, monoclinic, space group $P2_1/c$, $a=7.165(2)$, $b=12.836(2)$, $c=9.240(1)$ Å, $\beta=92.17(2)°$, $V=849.1(2)$ Å^3, $D_m=1.84$ g cm^{-3} (by flotation in $ZnBr_2$ aqueous solution), $D_c=1.85$ g cm^{-3} for $Z=2$, μ(Mo $K\alpha$)=87.0 cm^{-1}.

Intensity data were collected on a Rigaku automated four-circle diffractometer with graphite monochromatized Mo $K\alpha$ radiation employing the θ-2θ scan technique. The scan rate was 4° min^{-1}. A total of 1959 reflections were obtained, of which 1460 reflections were $F_o>3\sigma(F_o)$. Lorentz and polarization corrections were made, but no absorption nor extinction correction was applied, which might limit the accuracy of the present structure determination.

TABLE 1. ATOMIC COORDINATES

Atom	x	y	z
Pt	0.	0.	0.
O(1)	0.2460(17)	−0.0703(11)	−0.0305(16)
O(2)	−0.0879(17)	−0.1072(11)	0.1349(15)
C(1)	0.290(3)	−0.1558(16)	0.027(3)
C(2)	0.188(3)	−0.2141(17)	0.118(3)
C(3)	0.006(3)	−0.1897(17)	0.167(3)
C(4)	0.478(4)	−0.195(3)	−0.018(4)
C(5)	−0.095(4)	−0.260(3)	0.266(4)
C(B1)	0.373(11)	−0.007(3)	0.392(7)
C(B2)	0.540(10)	−0.010(4)	0.361(6)
C(B3)	0.675(9)	−0.005(3)	0.451(10)

† Complete F_o-F_c data and Tables of anisotropic thermal parameters are kept at the Chemical Society of Japan, Document No. 8113.

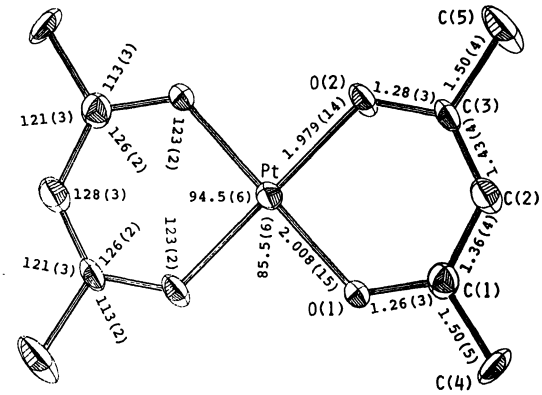

Fig. 1. An *ORTEP* drawing[9] of a $[Pt(acac)_2]$ molecule together with the atomic numbering system and selected bond lengths (l/Å) and angles (φ/°). The thermal ellipsoids correspond to 20% probability level.

The structure was solved by the heavy atom method, and refined anisotropically by the block-diagonal least-squares procedure using *HBLS*-V program.[6] The weighting scheme of Hughes,[7] $w=(50.0/|F_o|)^{-2}$ for $|F_o|>50.0$ and $w=1$ for $|F_o|\leq50.0$, was employed. Atomic scattering factors used were taken from International Tables for X-Ray Crystallography.[8] The final R value is 0.086 for 1460 reflections.† Atomic coordinates are listed in Table 1.

Figure 1 represents an *ORTEP* drawing[9] of the $[Pt(acac)_2]$ molecule together with the atomic numbering system and selected bond lengths and bond angles.

Similar to $[Pd(acac)_2]$,[4,5] the $[Pt(acac)_2]$ molecule is centrosymmetric. The Pt atom is located on a crystallographic center of symmetry, and surrounded by four oxygen atoms of acac ligands. The geometry around the Pt atom is square-planar. Two Pt–O bond lengths are 2.008(15) and 1.979(14) Å, which are approximately

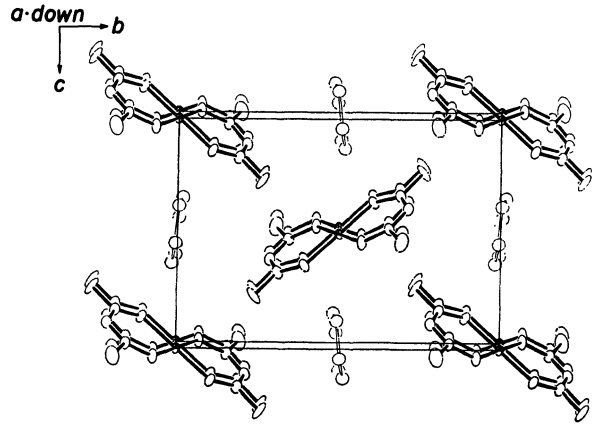

Fig. 2. Crystal structure(*ORTEP*[9]) projected along the c axis. Atoms in $[Pt(acac)_2]$ complex are drawn as thermal ellipsoids with 20% probability ,while those in benzene molecule as spheres with $B=5.0$ Å^2.

equal to the sum of the single bond radius of O atom (0.74 Å)[10] and the covalent bond radius of Pt(1.295 Å).[11]

The acac ligand is planar, the maximum atomic deviation from the least-squares plane being 0.02 Å. The dihedral angle between the acac plane and the plane defined by the Pt, O(1), and O(2) atom is 176.9°. Bond lengths and bond angles in the acac ligand are nearly equal to the values found for $[Pd(acac)_2]$.[5]

Very recently, Onuma *et al.* reported the crystal structure analysis of the triclinic crystal of $[Pt(acac)_2]$ which contains no crystalline benzene molecule.[12] The molecular structure of $[Pt(acac)_2]$ in the present crystal is essentially identical with that obtained by Onuma *et al.*

Figure 2 shows an *ORTEP* drawing[9] of the crystal structure. The $[Pt(acac)_2]$ molecules are piled up to form columns along the a axis. The crystalline benzene molecules lie, approximately parallel to the ac plane, in channels formed by piles of $[Pt(acac)_2]$ molecules and are linked loosely with adjacent $[Pt(acac)_2]$ and benzene molecules, which may explain the instability of the crystal.

All computations were carried out on an ACOS 700 computer at Crystallographic Research Center, Institute for Protein Research, Osaka University.

The authors wish to express their thanks to Professor Seichi Okeya, Wakayama University for crystals.

References

1) M. Ota and S. Shibata, 41st National Meeting of the Chemical Society of Japan, Osaka, April 1980, Abstr. I, p. 432 (3L29).
2) S. Shibata, *Bull. Chem. Soc. Jpn.*, **30**, 753 (1975).
3) G. J. Bullen, R. Mason, and P. Pauling, *Inorg. Chem.*, **4**, 456 (1965).
4) A. N. Knyazeva, E. A. Shugam, and L. M. Shkol'nikova, *Zh. Strukt. Khim.*, **11**, 938 (1970).
5) M. Sato, K. Miki, Y. Kai, N. Yasuoka, and N. Kasai, 38th National Meeting of the Chemical Society of Japan, Nagoya, October 1978, Abstr. III, p. 1039 (3F09).
6) T. Ashida, "The Universal Crystallographic Computing System-Osaka," The Computation Center, Osaka University (1979), p. 53.
7) E. W. Hughes, *J. Am. Chem. Soc.*, **63**, 1737 (1941).
8) "International Tables for X-Ray Crystallography," Kynoch Press, Birmingham (1974), Vol. IV, p. 71.
9) C. K. Johnson, *ORTEP*-II, Report ORNL-5138. Oak Ridge National Laboratory, Tennessee (1976).
10) V. Schomaker and D. P. Stevenson, *J. Am. Chem. Soc.*, **63**, 37 (1941).
11) L. Pauling, "The Nature of the Chemical Bond," 3rd ed, Cornell University Press, Ithaca, New York (1960).
12) S. Onuma, K. Horioka, H. Inoue, and S. Shibata, *Bull. Chem. Soc. Jpn.*, **53**, 2679 (1980).

X-Ray Photoelectron Spectra of Adsorbed Methyl Acetoacetate and Coordinated Tartaric Acid, Aspartic Acid and Alanine on the Nickel Surface

Yasunobu INOUE,* Kiyomi OKABE, and Iwao YASUMORI
Department of Chemistry, Tokyo Institute of Technology, Ookayama, Meguro-ku, Tokyo 152
(Received June 18, 1980)

Synopsis. The adsorption of methyl acetoacetate and the coordination of tartaric acid, aspartic acid, and alanine on the nickel surface were studied by means of X-ray photoelectron spectroscopy. The adsorbed methyl acetoacetate was partly in the enol-form, and the amino acids were coordinated with the surface through COO^- and NH_2 groups in a manner similar to the corresponding nickel chelate complexes, whereas the interaction of OH groups of tartaric acid with the surface was rather weak.

In the study of asymmetric hydrogenation catalyzed by metals modified with optically active molecules, it is of particular importance to ascertain not only the surface conditions of metals, but also the adsorbed states of the modifiers and reacting molecules. Few attempts have so far been made to analyze the surfaces from a physicochemical point of view. By using X-ray photoelectron spectroscopy (XPS), we previously studied nickel metals coordinated with tartaric acid and characterized the surface states of nickel responsible for the enantioface-differentiating hydrogenation.[1] In this work, we extended the XPS study to reveal the structures of the tartaric acid, aspartic acid, and alanine modifiers adsorbed on the Ni surface and to investigate the effect upon their stability of heat treatments in a hydrogen atmosphere. The adsorbed state of the reactant, methyl acetoacetate, was also studied.

Experimental

The X-ray photoelectron spectra were recorded at room temperature on a Hewlett-Packard 5950A ESCA spectrometer using monochromatized Al *Kα* exciting radiation. The nickel powder catalyst was prepared by decomposing nickel formate of an extra pure grade *in vacuo* and by then reducing with H_2 at 573 K. The modifications of the catalysts with (2*R*,3*R*)-tartaric acid, (*S*)-aspartic acid or (*S*)-alanine were performed in a manner analogous to those used in the previous studies.[1,2] The unmodified Ni catalyst used as a reference was also prepared similarly except for the absence of these optically-active modifiers. The catalysts were subjected to the *in situ* treatment in the preparation chamber of the spectrometer. The C 1s peak due to contaminant carbons, 285.0 eV, was taken as standard. For the experiments on the adsorption of methyl acetoacetate, a nickel foil of a 99.99% purity, obtained from the Material Research Co., was employed after being cleaned by an argon-ion bombardment following oxidation-reduction treatments.

Results and Discussion

Figure 1(a) compares the C 1s photoelectron spectrum of tartaric acid adsorbed on Ni with the spectra of nickel tartrate, sodium tartrate, and tartaric acid. Two peaks with almost the same intensity appeared apart from Peak I due to contaminant carbons; Peak II at

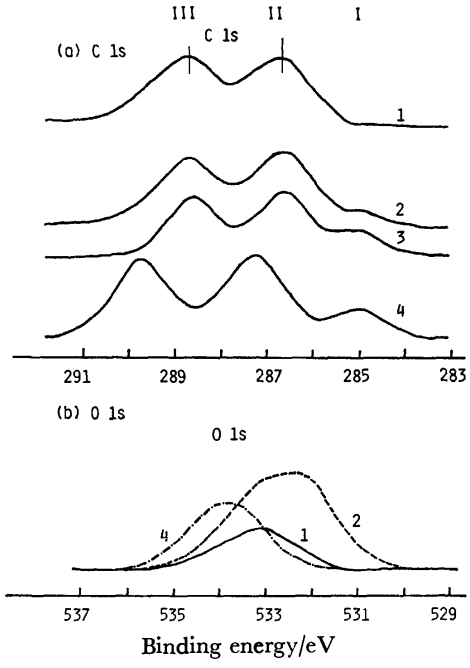

Fig. 1. X-Ray photoelectron spectra in the C 1s (a) and O 1s (b) regions.
1: Difference spectrum between unmodified nickel and tartaric acid-modified nickel (pH=5), 2: nickel tartrate, 3: sodium tartrate, 4: tartaric acid.

286.8 eV is assigned to the carbon atom combining with a hydroxyl group, whereas Peak III, 288.8 eV, is assigned to the carbon atom in the carboxyl group. These binding energy values were closer to those from nickel tartrate (286.7 and 288.7 eV) and sodium tartrate (286.6 and 288.6 eV) than to those for tartaric acid (287.3 and 289.7 eV). Figure 1(b) shows the O 1s spectra. The peak of the adsorbed tartaric acid appeared at the higher binding-energy side of a broad peak of nickel tartrate and was lower by 0.6 eV than that of tartaric acid. The broad O 1s peak of nickel tartrate is due to the characteristic structure of the complex; oxygen atoms in the carboxyl and hydroxyl groups undergo strong interactions with central nickel ions.[3] The close similarity on the C 1s level, while there is a difference in the O 1s level between the complex and the adsorbate, suggests that the adsorbed tartaric acid is linked to a surface Ni atom through a carboxyl group by dissociating hydrogen atoms, whereas the hydroxyl groups have little interaction with the surface atoms. Such a description of the adsorbed structure agreed substantially with the model proposed previously.[1]

The doublet peaks in the C 1s region, due to the adsorbed tartaric acid, remained almost unchanged with heat treatments in a H_2-atmosphere up to 353 K,

indicating that the adsorbed modifier retains its original structure. By a treatment at 383 K, the peak intensity was considerably attenuated but the doublet structure still existed. Further heating at 603 K changed the doublets to a single peak appearing at 284.4 eV, indicating that the adsorbed tartaric acid underwent decomposition to produce a carbonaceous deposit by this treatment, corresponding to a complete loss of the enantioselective capacity of this surface. The O 1s and Ni $2p_{3/2}$ spectra showed that the modification of Ni catalysts in air, as an ordinary procedure, gave rise to the oxygen peaks associated with NiO and Ni_2O_3 oxides, but the subsequent H_2-treatment at 353 K resulted in an almost complete removal of both oxides. The corresponding oxygen species with binding energies of 529.3 and 531.5 eV were reproduced by exposing to a O_2-atmosphere at room temperature and were then again reacted off with H_2 at 353 K. Such high reactivity suggests that the catalyst surfaces, even though they were modified in air, were readily changed to be oxide-free under the conditions of hydrogenation at 323—373 K.

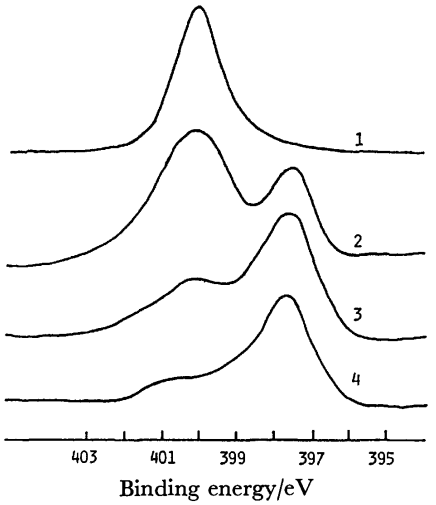

Fig. 2. Nitrogen 1s photoelectron spectra of adsorbed amino acids.
1: Aspartic acid, evacuated at room temperature, 2: aspartic acid, exposed to 6 Torr of H_2 at 363 K, 3: alanine, exposed to 10 Torr of H_2 at 373 K, 4: aspartic acid, exposed to 6 Torr of H_2 at 553 K.

Figure 2 shows the N 1s spectra of the adsorbed amino-acids. A single peak appeared at 400.1 eV by the coordination of aspartic acid; the binding-energy value was lower by 0.8 eV than that of aspartic acid (which is in the form of a zwitter ion, NH_3^+ and COO^-) and was close to that of the nickel ammine complex, *e.g.*, 400.0 eV for N atom in $[Ni(NH_3)_6]Cl_2$. The C 1s peak in the carboxyl group, 288.7 eV, was virtually identical with Peak III for the adsorbed tartaric acid. A similar correspondence was observed between the adsorbed alanine and the nickel–alanine complex. These spectral coincidences confirm a model[4] in which the amino acid is linked to a surface Ni atom through both amino and carboxyl groups. The heat treatment at 373 K gave rise to an additional N 1s peak at 397.5 eV (Spectra 2 and 3). Since such a low binding energy is characteristic of a nitride-like species,[5] it is evident that a part of the adsorbed amino acids was decomposed to produce nitrogen atoms.

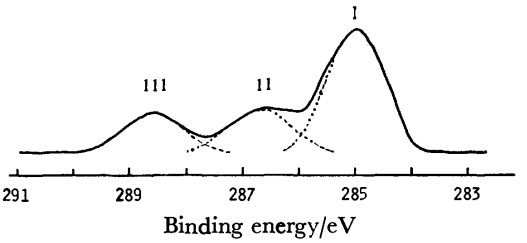

Fig. 3. Carbon 1s photoelectron spectrum of methyl acetoacetate adsorbed at room temperature on nickel surface.

As is shown in Fig. 3, the adsorption of methyl acetoacetate on a clean Ni surface provided three peaks in the C 1s region; they appeared at 285.0 (Peak I), 286.6 (Peak II) and 288.6 (Peak III) with an intensity ratio of 2.7 : 1 : 1. Peak III can apparently be assigned to C atoms in the carbonyl groups, whereas Peak I is associated with C atoms of hydrocarbons. Peak II is due to the carbon atom in the methoxy group, and its binding energy is close to that of a carbon atom combining with a hydroxyl group.[6] The appreciably higher intensity of Peak I, relative to the other two peaks, is partly due to contaminant carbons accumulated during prolonged evacuation following the adsorption. As for Peaks II and III, the original keto-form of methyl acetoacetate should provide the intensity ratio of 1 : 2, and it is to be noted that the observed equal intensity is derived on the basis of the assumption that about a half of the adsorbed species is in the enol-form. This finding is in line with the conclusion obtained from the tracer and IR spectroscopic studies.[1]

The authors are indebted to Professor Yoshiharu Izumi, Associate Professor Akira Thai and Dr. Tadao Harada of the Institute for Protein Research, Osaka University, for their helpful discussions. The present work was supported by a Grant-in-Aid for Scientific Research No. 464139 from the Ministry of Education, Science and Culture.

References

1) I. Yasumori, Y. Inoue, and K. Okabe, "Catalysis, Heterogeneous and Homogeneous," ed by B. Delmon and G. Jannes, Elsevier, Amsterdam (1975), pp. 41—50; I. Yasumori, *Pure Appl. Chem.*, **50**, 971 (1978).
2) Y. Izumi, *Angew. Chem.*, **23**, 956 (1971).
3) J. Bolard, *J. Chim. Phys.*, **62**, 900 (1965).
4) J. A. Groenewegen and W. M. H. Sachtler, *J. Catal.*, **33**, 176 (1974); A. Hatta, Y. Moriya, and W. Suetaka, *Bull. Chem. Soc. Jpn.*, **48**, 3441 (1975).
5) C. R. Brundle, *J. Vac. Sci. Technol.*, **13**, 301 (1976); K. Kishi and S. Ikeda, *Bull. Chem. Soc. Jpn.*, **47**, 2532 (1974).
6) U. Gelius, P. F. Hedman, B. J. Lindberg, R. Manne, R. Nordberg, C. Noldling, and K. Siegbahn, *Phys. Scripta*, **2**, 70 (1970).

Characterization of Intramolecular Charge-transfer Transitions. 1-Aryl-1,2,2-tricyanoethylenes and 7-Aryl-7,8,8-tricyanoquinodimethanes

Jun-ichi AIHARA,* Kotaro ARAYA, and Yoshio MATSUNAGA

Department of Chemistry, Faculty of Science, Hokkaido University, Sapporo 060

(Received May 8, 1980)

Synopsis. For the title compounds, the energy of the first electronic transition is linearly related to the vertical ionization potential of the aromatic nucleus (*e.g.*, benzene in the case of 1-phenyl-1,2,2-tricyanoethylene). This relationship gives a definite experimental support to the charge-transfer character of the electronic transitions concerned.

An intramolecular charge-transfer (CT) compound is an organic compound in which an electron-attracting group is attached to an electron-donor molecule, forming a single conjugated system as one whole.[1] In previous papers,[2-5] we have identified various types of compounds as such species by analyzing electronic spectra of the solutions and the condensed phases carefully. We found that, for a series of 2-(arylmethylene)-1,3-indandiones (A), the first intramclecular CT transition energy, $h\nu_{ICT}$, can be expressed in the form:[4]

$$h\nu_{ICT} = aI_p - b, \quad (1)$$

where a and b are constants which are substantially characteristic of the acceptor part (*i.e.*, 2-methylene-1,3-indandione), and where I_p is the vertical ionization potential of the donor part (*e.g.*, anthracene in the case of 2-(9-anthrylmethylene)-1,3-indandione). The same relationship was found to hold for the first absorption bands of 1-aryl-2,2-dicyanoethylenes (B).[5]

In this connection, we can fully anticipate the existence of such a linear relationship for the first absorption bands of 1-aryl-1,2,2-tricyanoethylenes (C) and for those of 7-aryl-7,8,8-tricyanoquinodimethanes (D) alike, because both tricyanoethylene and 7,8,8-tricyanoquinodimethane are supposedly good electron acceptors. If so, it would constitute the most conclusive evidence for a CT character of the electronic transitions concerned.[6]

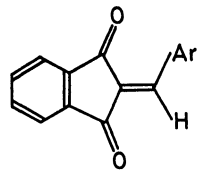

A

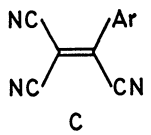

C

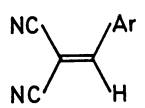

B

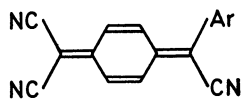

D

In order to see this, the spectroscopic data available on 1-aryl-1,2,2-tricyanoethylenes were first collected in Table 1.[7-13] The first absorption maxima of the seven 1-aryl-1,2,2-tricyanoethylenes in chloroform were then found to correlate well with the ionization potentials of the donor parts. As has been anticipated, a linear relationship between the two quantities was deduced thereform with a correlation coefficient of 0.989. By the least-squares analysis, we obtain

$$(h\nu_{ICT}/\text{eV}) = 0.614\,(I_p/\text{eV}) - 2.14. \quad (2)$$

It is now quite natural to attribute the first absorption band of every compound in Table 1 to the intramolecular CT transition from the highest occupied molecular orbital (HOMO), localized largely in the aryl group, to the lowest unoccupied molecular orbital (LUMO), localized largely in the tricyanoethylene part.

Next, Bespalov *et al.* prepared many 7-aryl-7,8,8-tricyanoquinodimethanes, and measured their electronic absorption spectra in acetonitrile.[14] They suggested that the first electronic transition might be of the CT type. This is exactly true from the present viewpoint. By the least-squares analysis, we again see with certainty the existence of a linear relationship between the first absorption maxima of these compounds[15] and the best vertical ionization potentials of the donor parts, namely,

$$(h\nu_{ICT}/\text{eV}) = 0.619\,(I_p/\text{eV}) - 2.78. \quad (3)$$

The correlation coefficient is 0.969. We can, hence, attribute the first absorption band of every such compound to the intramolecular CT transition from the HOMO, localized largely in the aryl group, to the LUMO, localized largely in the tricyanoquinodimethane part.

TABLE 1. INTRAMOLECULAR CT ABSORPTION BANDS OF 1-ARYL-1,2,2-TRICYANOETHYLENES (C) IN CHLOROFORM

Ar	$h\nu_{ICT}$ / 10^3 cm^{-1}	ε[a] / mol^{-1} dm^3 cm^{-1}	I_p/eV
Phenyl	29.15[b]	16600[b]	9.24[f]
2-Furyl	26.11[b]	25200[b]	8.89[g]
p-Methoxyphenyl	24.57[b]	25400[b]	8.54[f]
2-Pyrrolyl	23.74[c]	24300[c]	8.20[h]
3-Indolyl	21.86[c]	20700[b,e]	7.79[i]
p-Dimethylaminophenyl	19.46[c]	53100[c]	7.51[f]
3-Indolizinyl	18.76[d]	33200[d]	7.24[j]

a) Molar absorptivity. b) Ref. 7. c) Present work. d) Ref. 8. e) Value measured in acetone solvent. f) Ref. 9. g) Ref. 10. h) Ref. 11. i) Ref. 12. j) Ref. 13.

Here, it is noteworthy that, as in the case of 2-(arylmethylene)-1,3-indandiones[4] and 1-aryl-2,2-dicyanoethylenes,[5] the a value is relatively small for both 1-aryl-1,2,2-tricyanoethylenes and 7-aryl-7,8,8-tricyanoquinodimethanes. Considering that the a value for binary CT complexes usually lies in the 0.82—0.97 range,[16] the a=0.614 value for 1-aryl-1,2,2-tricyano-

Table 2. The relationship $h\nu_{ICT}=aI_p-b$ for intramolecular CT transitions

Type of compounds	Solvent	a	b/eV
A[a]	Chloroform	0.592	1.84
B[b]	Chloroform	0.675	2.23
C[c]	Chloroform	0.614	2.14
D[c]	Acetonitrile	0.619	2.78

a) Ref. 4. b) Ref. 5. c) Present work.

ethylenes and the $a=0.619$ value for 7-aryl-7,8,8-tricyanoquinodimethanes are obviously small. The a values determined for the four types of intramolecular CT bands are summarized in Table 2. It has now been established that the a value is close to 0.6 in the case of typical intramolecular CT bands measured in solution. According to Flurry's molecular orbital description of CT transitions,[17] the $a\approx0.6$ value indicates that about 1.6 of the two frontier electrons, on the average, reside in the donor ring in the ground state. Therefore, all these intramolecular CT compounds can assuredly be regarded as undissociable CT complexes.

On the other hand, the b value reflects the acceptor electron affinity and some other effects including structural factors, so it is quite difficult to analyze the b value in detail. However, the smallest b value for 2-(arylmethylene)-1,3-indandiones may be an indication of the smallest electron affinity of the common acceptor part (*i.e.*, 2-methylene-1,3-indandione).

In 1953, the study of intramolecular CT spectra was initiated with monosubstituted benzenes, such as aniline and benzaldehyde.[1] We have now a number of colorful intramolecular CT compounds, which are quite similar in many respects to binary CT complexes.[4] Most of them indeed show CT absorption bands isolated in the visible region. These compounds can, hence, be viewed as model compounds of binary CT complexes, each with a fairly fixed molecular geometry. As suggested in previous papers,[4,5] they will be of great help in obtaining insight into various electronic processes related to the CT transition in binary CT complexes.

One of us (J.A.) is grateful to the Ministry of Education, Science and Culture, Japan, for a Scientific Research Grant-in-Aid (No. 164116).

References

1) S. Nagakura and J. Tanaka, *J. Chem. Phys.*, **22**, 236 (1954); S. Nagakura, *Pure Appl. Chem.*, **7**, 79 (1963).
2) J. Aihara, G. Kushibiki, and Y. Matsunaga, *Bull. Chem. Soc. Jpn.*, **46**, 3584 (1973); J. Aihara, *ibid.*, **47**, 2063 (1974); K. Araya and J. Aihara, *ibid.*, **52**, 935 (1979).
3) A. Sasaki, J. Aihara, and Y. Matsunaga, *Bull. Chem. Soc. Jpn.*, **47**, 2926 (1974).
4) K. Chiba, J. Aihara, K. Araya, and Y. Matsunaga, *Bull. Chem. Soc. Jpn.*, **53**, 1703 (1980).
5) J. Aihara, K. Araya, K. Chiba, and Y. Matsunaga, *Adv. Mol. Relaxation Interaction Processes*, **18**, 199 (1980).
6) H. McConnell, J. S. Ham, and J. R. Platt, *J. Chem. Phys.*, **21**, 66 (1953).
7) G. N. Sausen, V. A. Engelhardt, and W. J. Middleton, *J. Am. Chem. Soc.*, **80**, 2815 (1958).
8) O. Ceder and B. Hall, *J. Heterocycl. Chem.*, **15**, 1471 (1978).
9) A. D. Baker, D. P. May, and D. W. Turner, *J. Chem. Soc., B*, **1968**, 22.
10) D. W. Turner, C. Baker, A. D. Baker, and C. R. Brundle, "Molecular Photoelectron Spectroscopy," Wiley, London (1970).
11) K. Watanabe, T. Nakayama, and J. Mottl, *J. Quant. Spectrosc. Radiat. Transfer*, **2**, 369 (1962).
12) M. H. Palmer and S. M. F. Kennedy, *J. Chem. Soc., Perkin Trans.* **2**, **1974**, 1893.
13) M. H. Palmer, D. Leaver, J. D. Nisbet, and R. W. Millar, *J. Mol. Struct.*, **42**, 85 (1977).
14) B. P. Bespalov, E. V. Getmanova, V. V. Titov, and A. A. Pankratov, *Zh. Org. Khim.*, **14**, 351 (1978); B. P. Bespalov and V. V. Titov, *Tetrahedron Lett.*, **1979**, 357.
15) In order to obtain Eq. 3, we used the absorption maxima of the compounds where aryl groups are phenyl, *p*-chlorophenyl, *p*-tolyl, *p*-hydroxyphenyl, *p*-methoxyphenyl, *p*-aminophenyl, 3-indolyl, *p*-dimethylaminophenyl, and 1-azulenyl.[14]
16) See. *e.g.* G. Briegreb, "Elektronen-Donator-Acceptor-Komplexe," Springer-Verlag, Berlin (1961); R. Foster, "Organic Charge-Transfer Complexes," Academic Press, London (1969).
17) R. L. Flurry, Jr., *J. Phys. Chem.*, **69**, 1927 (1965); **73**, 2111 (1969).

Effect of Halogen Substituents of Anion Radicals on the Electronic States of Crystalline Anion Radical Salts; K^+ *p*-Chloranil$^{\cdot-}$, K^+ 2,5-Dibromo-3,6-dichloro-*p*-benzoquinone$^{\cdot-}$, and K^+ *p*-Bromanil$^{\cdot-}$

Yôichi IIDA

Department of Chemistry, Faculty of Science, Hokkaido University, Sapporo 060

(Received July 23, 1980)

Synopsis. The intermolecular interactions in crystalline anion radical salts of K^+ *p*-Chloranil$^{\cdot-}$, K^+ 2,5-Dibromo-3,6-dichloro-*p*-benzoquinone$^{\cdot-}$, and K^+ *p*-Bromanil$^{\cdot-}$ were examined in terms of one-dimensional half-occupied Hubbard model. Effect of substituents of the anion radicals on the crystal electronic states was discussed with the parameter values estimated by the Hubbard model.

Many papers have been written on the prominent magnetic, electrical and optical properties of a number of crystalline ion radical salts.[1-4] In such ion radical salts, the planar ion radical molecules are known to form, in themselves, a segregated stacking into one-dimensional columns so as to make a large overlap between their half-occupied molecular orbitals. In this case, since any individual radical molecule interacts through charge transfer most strongly with two adjacent radicals, the electronic and magnetic properties of the solid salt differ distinctly from those of the ion radical monomer.[1] In a previous paper,[3] we examined crystalline anion radical salts derived from halogen-substituted *p*-benzoquinones, and explained their optical and magnetic properties by applying half-occupied Hubbard model to the segregated stacks of those *p*-benzoquinone anion radicals. In the present paper, we take K^+ *p*-Chloranil$^{\cdot-}$, K^+ 2,5-Dibromo-3,6-dichloro-*p*-benzoquinone$^{\cdot-}$, and K^+ *p*-Bromanil$^{\cdot-}$, and compare the magnitudes of the Hubard-model parameters together with the ground-state stabilization energies of those anion radical salts.[5] Since the counter K^+ cation is common, we shall discuss the effect of halogen substituents of the anion radicals on the electronic states of those anion radical salts.

First, we consider the electronic state of solid K^+ *p*-Chloranil$^{\cdot-}$ salt. At room temperature, although there are several polymorphs, in the structure of the orthorhombic α-form, the *p*-chloranil anion radicals are stacked in themselves with equal intervals, forming non-alternant one-dimensional columns parallel to the c-axis, the interplanar spacing being 3.47 Å.[6] The K^+ ion lies at a center of a rectangle formed by four oxygen atoms of the *p*-chloranil anion radicals related by the c translation. In order to understand the optical and magnetic properties of this salt, we applied non-alternant one-dimensional half-occupied Hubbard model to the segregated stack of the *p*-chloranil anion radicals.[3] This model is a simplification of the real crystal and is described by two parameters, I and T.[7] Here, T is the transfer matrix element of an unpaired electron which describes hopping between adjacent molecular sites, while I is the Coulomb repulsion between two electrons with up and down spins on the same site. Then, T favors electron delocalization through band formation, whereas I favors localization due to electron-electron repulsions. On the basis of this model, we can well understand the reasons why the intermolecular charge-transfer absorption appears in the solid-state spectrum of K^+ *p*-Chloranil$^{\cdot-}$ at 11800 cm^{-1} and why the antiferromagnetic spin exchange interaction, $J=113$ cm^{-1}, acts between adjacent *p*-chloranil anion radicals.[2-4] The values of $I=11800$ cm^{-1} and $T=-820$ cm^{-1} explain well those observed optical and magnetic data of K^+ *p*-Chloranil$^{\cdot-}$. Once the I and T values are obtained experimentally, it is easy to determine the magnitude of ground-state energy stabilization, E, due to charge-transfer interaction between ion radicals in non-alternant one-dimensional system of the ion radicals. In previous papers,[4] we obtained in a limit of $I/|T|=\infty$ the expression of $E=-(4NT^2/I)$ ln 2, where N is the number of ion radicals. In the case of the one-dimensional system of *p*-chloranil anion radicals, where $I=11800$ cm^{-1} and $T=-820$ cm^{-1}, the magnitude of $I/|T|=14.39\cdots$ is found to be much larger than unity. Therefore, the condition of $I/|T|=\infty$ is approximately fulfilled in our case, and the value of E is estimated to be -1.87 kJ mol^{-1}.

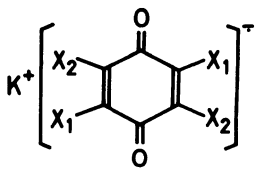

(a); $X_1 = X_2 = Cl$
(b); $X_1 = X_2 = Br$
(c); $X_1 = Br$, $X_2 = Cl$

Fig. 1. Halogen-substituted *p*-benzoquinone anion radical salts with potassium cation; (a) *p*-chloranil anion radical salt, (b) *p*-bromanil anion radical salt, and (c) 2,5-dibromo-3,6-dichloro-*p*-benzoquinone (*p*-QBr_2Cl_2) anion radical salt.

In a similar way, the electronic state of solid K^+ *p*-Bromanil$^{\cdot-}$ salt was analyzed in terms of a segregated stack of *p*-bromanil anion radicals. The non-alternant one-dimensional half-occupied Hubbard model was then applied to this segregated stack, and the values of $I=10900$ cm^{-1} and $T=-730$ cm^{-1} were obtained.[3] Since the magnitude of $I/|T|=14.93\cdots$ is also much larger than unity, the ground-state stabilization energy, E, in the one-dimensional system of *p*-bromanil anion radicals is calculated, in a way similar to the case of *p*-chloranil anion radicals, to be -1.61 kJ mol^{-1}.

As for the electronic state of solid K^+ *p*-$QBr_2Cl_2^{\cdot-}$ salt,

two models were previously proposed to explain its optical and magnetic properties; one is a dimer model of p-QBr_2Cl_2 anion radicals and the other, non-alternant one-dimensional model of p-QBr_2Cl_2 anion radicals.[3] However, because of the reason given in Ref. 8, the latter model is more probable in K^+ p-$QBr_2Cl_2^{\cdot}$ than the former model, and our approach of non-alternant one-dimensional half-occupied Hubbard model is still applicable to that system. The values of $I=11500$ cm^{-1} and $T=-750$ cm^{-1} were thus estimated for the one-dimensional system of p-QBr_2Cl_2 anion radicals. When we note that $I/|T|=15.33\cdots$ is also much greater than unity, the ground-state stabilization energy, E, of this system is calculated to be -1.61 kJ mol^{-1} by using the estimated I and T values.

In the following, we compare the magnitudes of the parameters in the Hubbard model, that is, on-site Coulomb repulsion (I), transfer matrix element (T) and ground-state stabilization energy (E) estimated for K^+ p-Chloranil$^{\cdot}$, K^+ p-$QBr_2Cl_2^{\cdot}$, and K^+ p-Bromanil$^{\cdot}$ salts. Since the counter K^+ cation is common to these salts, and since all the anion radicals are closely related chloro- and bromo-substituted p-benzoquinone anion radicals, the difference in the values of those physical parameters should come from the difference in the substituents of the anion radicals. As for the on-site Coulomb repulsion, I, the order of its magnitude is found to be 11800 cm^{-1} (p-Chloranil$^{\cdot}$)$>$11500 cm^{-1} (p-$QBr_2Cl_2^{\cdot}$)$>$10900 cm^{-1} (p-Bromanil$^{\cdot}$). The magnitude of Coulomb repulsion between two electrons with up and down spins on the same site will be decreased if the molecular size of ion radical is extended and if polarizable substituents are introduced into ion radical. In this respect, we can understand the successive decrease of on-site Coulomb repulsion in going from p-chloranil anion radical to p-QBr_2Cl_2 and p-bromanil anion radicals, because the replacement of chloro-substituents of the anion radical by bromo-substituents leads to the expansion of the size of the molecule and also to the introduction of more polarizable substituents into the anion radical.

The transfer matrix element, T, between adjacent anion radical molecules is closely related to the overlap integral between the half-occupied molecular orbitals of the anion radicals. The absolute values of $|T|$ are found to range as 820 cm^{-1} (p-Chloranil$^{\cdot}$)$>$750 cm^{-1} (p-$QBr_2Cl_2^{\cdot}$)$>$730 cm^{-1} (p-Bromanil$^{\cdot}$). This result is also reasonable, because the replacement of the chloro-substituents in the anion radical by the bulky bromo-substituents increases the intermolecular spacing between adjacent anion radicals, and thus, decreases definitely the overlap between their half-occupied molecular orbitals.

As for the ground-state stabilization energy due to charge-transfer interaction between anion radicals, E, the absolute value of 1.87 kJ mol^{-1} of p-chloranil anion radical salt is greatest. The value of 1.61 kJ mol^{-1} of p-QBr_2Cl_2 anion radical salt coincides with that of 1.61 kJ mol^{-1} of p-bromanil anion radical salt, and these two values are smaller than the 1.87 kJ mol^{-1} value of p-chloranil anion radical salt. As has been mentioned, the ground-state stabilization energy, E, is given by $-(4NT^2/I)\ln 2$, and both I and $|T|$ values decrease progressively in going from p-chloranil anion radical salt to p-QBr_2Cl_2 and p-bromanil anion radical salts. However, the value of T^2/I is found to be greatest in p-chloranil anion radical salt. For p-QBr_2Cl_2 and p-bromanil anion radical salts, although both I and $|T|$ values of the former salt are larger than those of the latter salt, the quantities of T^2/I are of the same magnitudes.

References

1) See, for example, Z. G. Soos and D. J. Klein, "Molecular Association," ed by R. Foster, Academic Press, London, New York, San Francisco (1975), Vol. 1, Chap. 1, and the references cited therein.

2) Y. Iida, *Bull. Chem. Soc. Jpn.*, **50**, 1445, 2481 (1977); **51**, 434, 631, 1549, 3637 (1978); **52**, 689, 1523, 2791 (1979).

3) Y. Iida, *Bull. Chem. Soc. Jpn.*, **51**, 2523 (1978).

4) Y. Iida, *Bull. Chem. Soc. Jpn.*, **52**, 3447 (1979); **53**, 1447 (1980).

5) Hereafter, 2,5-dibromo-3,6-dichloro-p-benzoquinone is abbreviated as p-QBr_2Cl_2, and its anion radical salt with potassium cation, as K^+ p-$QBr_2Cl_2^{\cdot}$.

6) M. Konno, H. Kobayashi, F. Marumo, and Y. Saito, *Bull. Chem. Soc. Jpn.*, **46**, 1987 (1973).

7) J. Hubbard, *Proc. R. Soc. London, Ser. A*, **276**, 238 (1963); **281**, 401 (1964).

8) According to Ref. 3, if dimer Hubbard model is applied to p-QBr_2Cl_2 anion radicals in solid K^+ p-$QBr_2Cl_2^{\cdot}$ salt, the values of I and T have been reported to be 11300 cm^{-1} and -710 cm^{-1}, respectively. Then, the ground-state stabilization energy due to charge-transfer interaction between p-QBr_2Cl_2 anion radicals in a dimer is given by $I/2-\sqrt{(I/2)^2+(2T)^2}=-153$ cm^{-1} per dimer or -0.92 kJ mol^{-1}. On the other hand, if non-alternant one-dimensional model is applied to the anion radicals, the ground-state stabilization energy is estimated to be -1.61 kJ mol^{-1} (see text). Unfortunately, at the present time, no data on the crystal Madelung energy, which is a major source of cohesive energy, are available for K^+ p-$QBr_2Cl_2^{\cdot}$ salt. However, if the Madelung energy of the crystal lattice of the dimer model is almost the same as that of the one-dimensional model, the ground-state stabilization energy due to the charge-transfer interaction becomes important for the cohesive energy. In this respect, the ground state of the non-alternant one-dimensional model seems to be more stable in K^+ p-$QBr_2Cl_2^{\cdot}$ salt than that of the dimer model.

Equilibria of Aluminium(III) Complexes with 3,3′-Bis[*N*,*N*′-bis-(carboxymethyl)aminomethyl]-*o*-cresolsulfonphthalein

Sadaaki MURAKAMI* and Takashi YOSHINO

Department of Industrial Chemistry, Faculty of Engineering, Yamaguchi University, Tokiwadai, Ube 755

(Received February 23, 1980)

Synopsis. A potentiometric and spectrophotometric study of aluminium(III) complexes with 3,3′-bis[*N*,*N*′-bis-(carboxymethyl)aminomethyl]-*o*-cresolsulfonphthalein has been performed. Evidence was found for the formations of 1 : 1 and 2 : 1 (metal : ligand) complexes and it was assumed that protonated and hydroxo complexes are formed in addition to the simple complexes. The formation constants for these complexes were determined and suggestions are made concerning the probable structures of the complexes.

Xylenol Orange (abbreviated as XO or H_6xo) has been widely used as an indicator in chelatometric and spectrophotometric determinations of numerous metal ions.[1,2] These are also many findings concerning the solution chemistry of its metal complexes. However, most of these reports have treated bivalent metal ions,[3-6] but not trivalent ones. In a previous work,[7] the Fe(III) complexes of XO were investigated and it was found that hydroxo complexes are formed in neutral and alkaline media. With regard to Al(III), Otomo[8] pointed out that its complex formation equilibria are complicated, when he studied the spectrophotometric determination of aluminium with XO. The complexes for the Al(III) system are expected to be similar to those found in the Fe(III). This paper reports the results of a potentiometric and spectrophotometric study on the Al(III) complexes with XO.

Experimental

XO was synthesized and purified as described in reference 9. The other reagents and procedures were the same as described previously.[10,11] All the measurements were performed at 25±0.1 °C; the ionic strength of the solutions was maintained at 0.1 with sodium perchlorate.

The formation constants of the complexes were calculated in the manner described previously.[10,11] The acid formation constants of XO used in the calculations were those determined previously[9] (log k_i: 12.23, 10.56, 6.74, 2.85, 2.32, and 1.5 for $i=1$ to 6, respectively).

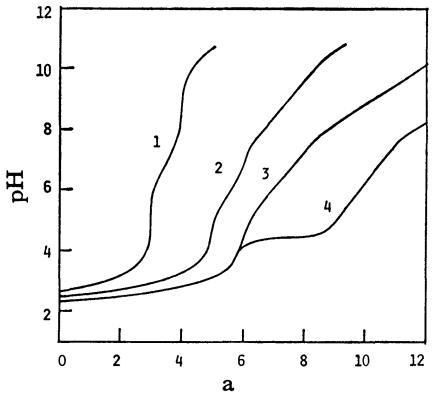

Fig. 1. Potentimetric titration curves of Al(III) and XO solutions. a=number of moles of base added per mole of XO.
1-XO, 2, 3 and 4-1/1, 2/1 and 3/1 solutions, respectively. [XO]=about 1×10^{-3} mol/1, and [Al(III)] is varied.

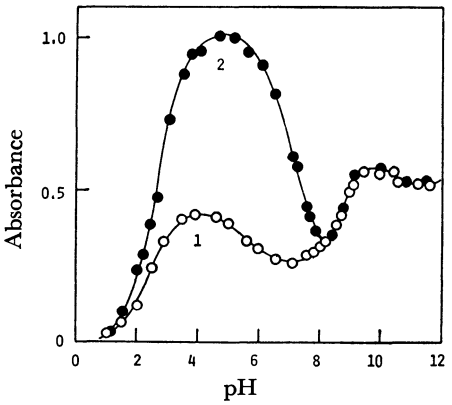

Fig. 2. Variations in the absorbances of Al(III) and XO solutions at a given wavelength as a function of pH. 1-1/1 and 2-2/1 solutions, respectively. Wavelength: 1-554 and 2-555 nm.

Results

Potentiometric titrations of XO solutions containing 1 : 1, 2 : 1, and 3 : 1 molar ratios of Al(III) to XO were performed (the molar ratios of Al(III) to XO, hereinafter, are referred to as "1/1", "2/1", and "3/1"). The results are shown in Fig. 1. The visible absorption spectra of the 1/1 and 2/1 solutions at various pH

TABLE 1. FORMATION CONSTANTS, WAVELENGTHS, AND ABSORPTIVITIES OF Al (III) COMPLEXES WITH XO AT 25 °C AND μ=0.1 ($NaClO_4$)

Reaction	log K	λ_{max} / nm	$\varepsilon\times10^{-4}$ / $cm^{-1}\,mol^{-1}\,l$
$Al^{3+}+Hxo^{5-} \rightleftharpoons {}^*AlHxo^{2-}$	16.3	554	3.67
$2Al^{3+}+xo^{6-} \rightleftharpoons {}^*Al_2xo$	27.0	555	8.29
$H^+ + {}^*Al(OH)Hxo^{3-} \rightleftharpoons AlHxo^{2-}+H_2O$	5.8 5.6[a]	502	3.51
$2H^+ + {}^*[Al(OH)]_2xo^{2-} \rightleftharpoons Al_2xo+2H_2O$	13.4 13.1[a]	510	3.45

*The complexes corresponding to the λ_{max} and ε values. a) Determined spectrophotometrically (the others potentiometrically).

values (pH 1—13) were measured between 350 and 700 nm. Figure 2 shows the variations in the absorbances at a given wavelength as a function of pH. The formation constant, absorptivity, and wavelength of each complex species are listed in Table 1.

Discussion

Complex Formation Equilibria. Both 1/1 and 2/1 titration curves have two inflections: at $a=5$ and 6, and at $a=6$ and 8, respectively. The 3/1 titration curve is quite the same as the 2/1 curve up to $a=6$, but beyond this a value up to 9 there is another buffer region in which aluminium(III) hydroxide was precipitated. The extent of this buffer region over three units of a indicates that there exists one mole of free Al(III) ion per mole of XO, and that not more than two Al(III) ions can combine with one XO molecule.[11] One proton in a XO molecule remains undissociated at $a=5$ for the 1/1 solution, and all available protons dissociate at $a=6$ for the 2/1 solution, indicating the formations of the complexes, $AlHxo^{2-}$ and Al_2xo, at the respective a values. The extent of the buffer region from $a=6$ to 8 for the 2/1 solution is just double that from $a=5$ to 6 for the 1/1 solution. These facts suggest that each Al(III) ion in the 1 : 1 and 2 : 1 complexes is hydrolyzed to liberate one proton from a water molecule in its inner coordination sphere.[12] Thus, the hydroxo complexes, $Al(OH)Hxo^{3-}$ and $[Al(OH)]_2xo^{2-}$, are assumed to be formed as found in the Fe(III) and XO system.[7]

Both 1/1 and 2/1 titration curves show a long buffer region beyond $a=6$ and $a=8$, respectively. The change in the absorbance is observed in Fig. 2 between pH 7 and 10 for the 1/1 solution and between pH 8 and 10 for the 2/1 solution. With increase in pH from 7 and from 8, each spectrum shifted to longer wavelengths (502 to 578 nm for the 1/1 solution and 510 to 578 nm for the 2/1 solution). Both 1/1 and 2/1 spectra above pH 10 were exactly the same as those of the free XO solutions. These facts suggest that the complexes, $Al(OH)Hxo^{3-}$ and $[Al(OH)]_2xo^{2-}$, are further hydrolyzed to dissociate into $Al(OH)_4^-$ and XO in such alkaline media. In acidic media, the 1/1 and 2/1 titration curves have a long buffer region. The change in the absorbance is observed in Fig. 2 from pH 4 down to 1 for the 1/1 solution and from pH 5 to 1 for the 2/1 solution. With decrease in pH from 4 and from 5, the 1/1 and 2/1 spectrum bands at 554 and at 555 nm respectively disappeared and a new band appeared at 435 nm for both 1/1 and 2/1 solutions. Both 1/1 and 2/1 spectra around pH 1 were just the same as those of the free XO solutions. These facts suggest that the complexes, $AlHxo^{2-}$ and Al_2xo, dissociate into Al(III) aquo ion and XO in such acidic media.

Summarizing the foregoing discussion, the equilibria of complex formations for the Al(III) and XO system are as indicated in the following scheme.

The 1/1 solution:

$$\underset{}{\overset{pH<1}{Al^{3+} + H_6xo}} \rightleftharpoons \underset{}{\overset{pH\ 4}{AlHxo^{2-}}} \rightleftharpoons \underset{}{\overset{pH\ 7}{Al(OH)Hxo^{3-}}} \rightleftharpoons \underset{}{\overset{pH>10}{Al(OH)_4^- + H_2xo^{2-}}}.$$

The 2/1 solution:

$$\underset{}{\overset{pH<1}{2Al^{3+} + H_6xo}} \rightleftharpoons \underset{}{\overset{pH\ 5}{Al_2xo}} \rightleftharpoons \underset{}{\overset{pH\ 8}{[Al(OH)]_2xo^{2-}}} \rightleftharpoons \underset{}{\overset{pH>10}{2Al(OH)_4^- + H_2xo^{4-}}},$$

where each pH value indicates that the corresponding species is predominant in the solution around this pH value.

Complex Structures. The XO molecule has two chelating groups on each side of its large sulfonphthalein nucleus; each chelating group reacts with metal ion independently of each other.[2] Thus, the proton of the 1 : 1 complexes, $AlHxo^{2-}$ and $Al(OH)Hxo^{3-}$, may be the one which attaches to the amino nitrogen of another bis(carboxymethyl)aminomethyl group which is not coordinating to an Al(III) ion, because the amino nitrogen may dissociate the proton in more alkaline media.[9]

With regard to the 1 : 1 hydroxo complex, $Al(OH)Hxo^{3-}$, there is some possibility of a dimerized structure with hydroxo bridges, $[Hxo\cdot Al\langle^{OH}_{OH}\rangle Al\cdot Hxo]^{6-}$, as discussed for $Al(OH)sxo^{2-}$[12] and $Fe(OH)Hxo^{3-}$.[7] A polynuclear complex[13,14] is possible for the 2 : 1 hydroxo complex, $[Al(OH)]_2xo^{2-}$, as a result of hydrolysis of two Al(III) ions attached to either side of the sulfonphthalein nucleus, $[_{HO}\rangle Al\cdot XO\cdot Al\langle^{OH}\ ]_n^{2n-}$ ($n\geqslant 2$), as discussed for $[Fe(OH)]_2xo^{2-}$.[7] However, a complete discussion of the structures for these hydroxo complexes must await further investigation.

References

1) K. Ueno, "Kireito Tekiteiho," Nankodo, Tokyo (1960).
2) M. Otomo, *Bunseki Kagaku*, **21**, 436 (1972).
3) T. Yoshino, H. Okazaki, S. Murakami, and M. Kagawa, *Talanta*, **21**, 676 (1974).
4) M. Yamada, *Bull. Chem. Soc. Jpn.*, **49**, 1023 (1976).
5) M. Yamada, *Bull. Chem. Soc. Jpn.*, **49**, 1861 (1976).
6) S. Murakami, T. Yoshino, and K. Ogura, *Bull. Chem. Soc. Jpn.*, **53**, 2228 (1980).
7) T. Yoshino, S. Murakami, and K. Ogura, *J. Inorg. Nucl. Chem.*, **41**, 1011 (1979).
8) M. Otomo, *Bull. Chem. Soc. Jpn.*, **36**, 806 (1963).
9) M. Murakami, T. Yoshino, and S. Harasawa, *Talanta*, **14**, 1293 (1967).
10) T. Yoshino, S. Murakami, M. Kagawa, and T. Araragi, *Talanta*, **21**, 79 (1974)
11) T. Yoshino, H. Imada, S. Murakami, and M. Kagawa, *Talanta*, **21**, 211 (1974).
12) S. Murakami, *J. Inorg. Nucl. Chem.*, **41**, 209 (1979).
13) A. E. Martell, Ed., "Coordination Chemistry," Van Nostrand Reinhold, New York (1971), Vol. 1, Chap. 9.
14) C. F. Bates, Jr., and R. E. Mesmer, "The Hydrolysis of Cations," Wiley, New York (1976), p. 117.

Synthesis and Activity of Antitumor Agents, Methyl [*N'*-(2-Chloroethyl)-*N'*-nitrosoureido]deoxygentiobiosides

Yoshimasa FUKUDA and Tetsuo SUAMI*

Department of Applied Chemistry, Faculty of Engineering, Keio University, Hiyoshi, Kohoku-ku, Yokohama 223

(Received January 24, 1980)

Synopsis. Chlorozotocin[1-4] and GANU[5-7] are nitrosoureido derivatives of D-glucose, exhibiting remarkable antitumor activities against leukemia L1210 in mice. We wish to report a synthesis of the derivatives of gentiobioside.

Tritylation of methyl 2-(benzyloxycarbonylamino)-2-deoxy-α-D-glucopyranoside,[8] followed by acetylation, afforded methyl 3,4-di-*O*-acetyl-2-(benzyloxycarbonylamino)-2-deoxy-6-*O*-trityl-α-D-glucopyranoside. Detritylation of the compound gave methyl 3,4-di-*O*-acetyl-2-(benzyloxycarbonylamino)-2-deoxy-α-D-glucopyranoside. Condensation of the compound with 2,3,4,6-tetra-*O*-acetyl-α-D-glucopyranosyl bromide[9] yielded methyl hexa-*O*-acetyl-2-(benzyloxycarbonylamino)-2-deoxy-α-gentiobioside, which was further converted into methyl 2-(benzyloxycarbonylamino)-2-deoxy-α-gentiobioside (**1**). Catalytic hydrogenolysis of **1**, followed by addition with 2-chloroethyl isocyanate, gave the 2-[*N'*-(2-chloroethyl)ureido] compound (**2**). Nitrosation of **2** with N_2O_3 gave the *N'*-nitroso compound (**3**).

Starting from methyl hexa-*O*-acetyl-2'-(benzyloxycarbonylamino)-2'-deoxy-α-gentiobioside (**4**), methyl 2'-[*N'*-(2-chloroethyl)-*N'*-nitrosoureido]-2'-deoxy-α-gentiobioside (**7**) was obtained by analogous reactions. The position of the nitroso group was demonstrated by ammonia-induced degradation[10] of **3** and **7**.

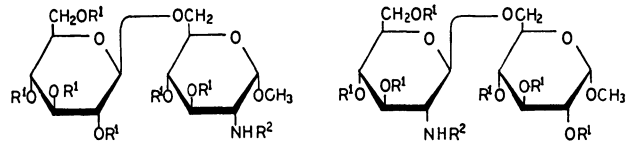

1, R¹= H , R²= Cbz
2, R¹= H , R²= CONHCH₂CH₂Cl
3, R¹= H , R²= CON(NO)CH₂CH₂Cl
4, R¹= Ac , R²= Cbz
5, R¹= H , R²= Cbz
6, R¹= H , R²= CONHCH₂CH₂Cl
7, R¹= H , R²= CON(NO)CH₂CH₂Cl

Scheme 1.

TABLE 1. ANTITUMOR EFFECT OF **3** AND **7** ON LEUKEMIA L1210[a]

Dose mg/kg	Compound **3** ILS[b] (%)	Compound **3** 60-d survivors	Compound **7** ILS[b] (%)	Compound **7** 60-d survivors
56	25.7	0/5	28.2	0/5
48	42.9	0/5	30.8	0/5
40	226.3	1/5	202.6	1/5
32	118.4	0/5	466.7	3/5
16	84.2	0/5	241.7	1/5
8	39.5	0/5	94.4	0/5
4	28.9	0/5	61.1	0/5

a) Male BDF_1 hybrid mice were inoculated intraperitoneally with 10^6 cells of lymphoid leukemia L1210. Intraperitoneal injection of a compound was begun 24 h after the inoculation and performed once a day for 3 d. b) Percentage increase in life span of treated animals compared with control tumor bearers [100(T/C-1)].

Compounds **3** and **7** were subjected to determination of antitumor activity against leukemia L1210 in mice by the established protocol[11] (Table 1). Both compounds are highly active, **7** seeming to be more effective than **3**.

Experimental

Methyl 3,4-Di-O-acetyl-2-(benzyloxycarbonylamino)-2-deoxy-6-O-trityl-α-D-glucopyranoside. Trityl chloride (20.0 g) was added to a stirred solution of methyl 2-(benzyloxycarbonylamino)-2-deoxy-α-D-glucopyranoside[8] (10.0 g) in pyridine (120 ml), acetic anhydride (50 ml) being added after 24 h. After 16 h, the mixture was poured into ice cold water. The product precipitated was collected and recrystallized from ethanol, giving 8.7 g (44%) of the product, mp 90—91 °C, $[\alpha]_D^{20}$ +85° (*c* 1.2, chloroform).

Found: C, 69.67; H, 6.18; N, 2.30%. Calcd for $C_{38}H_{39}NO_9$: C, 69.82; H, 6.01; N, 2.14%.

Methyl 3,4-Di-O-acetyl-2-(benzyloxycarbonylamino)-2-deoxy-α-D-glucopyranoside. Acetic acid (0.3 ml) containing HBr was added under ice cooling with agitation to a solution of the trityl derivative (1.0 g) in glacial acetic acid (4 ml). After 1 min, the mixture was quenched in ice cold water and extracted with $CHCl_3$. The organic layer was washed with $NaHCO_3$ solution and water, and concentrated. Recrystallization of the residue from ether–petroleum ether gave 294 mg (37%) of the product, mp 112—113 °C, $[\alpha]_D^{20}$ +110° (*c* 0.8, chloroform). ^1H NMR (60 MHz, $CDCl_3$): δ 1.88 (s, 3, OAc), 2.03 (s, 3, OAc), 3.37 (s, 3, OCH_3), 4.76 (d, 1, J=4 Hz, H-1).

Found: C, 55.59; H, 6.14; N, 3.62%. Calcd for $C_{19}H_{25}NO_9$; C, 55.47; H, 6.13; N, 3.41%.

Methyl 2-(Benzyloxycarbonylamino)-2-deoxy-α-gentiobioside (1). A solution of the 3,4-di-*O*-acetyl derivative (995 mg) and 2,3,4,6-tetra-*O*-acetyl-α-D-glucopyranosyl bromide[9] (2.0 g) in benzene (40 ml) was heated under reflux in the presence of $Hg(CN)_2$ (1.6 g) and Drierite (2.0 g) for 20 h. The mixture was diluted with $CHCl_3$ (60 ml) and filtered. The filtrate was washed with brine and water, and concentrated. The residue was purified on a silica gel column using 2 : 5 (v/v) acetone–benzene. Fractions (R_f 0.56 on TLC) were concentrated. The residue was deacetylated in methanolic ammonia and recrystallized from methanol to give 303 mg (42%) of **1**, mp 235—236 °C, $[\alpha]_D^{20}$ +50.9° (*c* 1.0, water).

Found: C, 51.78; H, 6.41; N, 2.75%. Calcd for $C_{21}H_{31}NO_{12}$: C, 51.53; H, 6.38; N, 2.86%.

Methyl 2-[N'-(2-Chloroethyl)ureido]-2-deoxy-α-gentiobioside (2). Compound **1** (850 mg) was hydrogenated in methanol (25 ml) with Pd black under H_2 (2.7 kg/cm²) for 2.5 h. The product was treated with 2-chloroethyl isocyanate (0.2 ml) in methanol (15 ml) overnight and the mixture was concetnrated. The residue was triturated in ethanol-ethyl acetate to give 620 mg (72%) of **2**, mp 151—152 °C (dec), $[\alpha]_D^{20}$ +54.2° (*c* 1.0, water).

Found: C, 41.74; H, 6.21; N, 5.88; Cl, 7.49%. Calcd for

$C_{16}H_{29}N_2ClO_{11}$: C, 41.70; H, 6.34; N, 6.08; Cl, 7.69%.

Methyl 2-[N'-(2-Chloroethyl)-N'-nitrosoureid]-2-deoxy-α-gentiobioside (3). N_2O_3 was bubbled into a suspension of **2** (200 mg) in acetone (5 ml) at 0 °C for 3 min. The solution was concentrated and the residue was washed with hexane-diisopropyl ether to give 153 mg (73%) of **3**, mp 67—68 °C (dec), $[\alpha]_D^{22}$ +39.4° (*c* 1.0, water).

Found: C, 39.21; H, 5.99; N, 8.58; Cl, 7.24%. Calcd for $C_{16}H_{28}N_3ClO_{12}$: C, 38.97; H, 5.77; N, 8.92; Cl, 6.92%.

Degradation of **3** in methanolic ammonia gave methyl 2-deoxy-2-ureido-α-gentiobioside, which was identified by TLC and by comparison of its IR spectrum [(KBr) 1650, 1610, 1565 cm^{-1}] with that of an authentic sample prepared by a definite route.

Methyl 2,3,3',4,4',6'-Hexa-O-acetyl-2'-(benzyloxycarbonylamino)-2'-deoxy-α-gentiobioside (4). A mixture of methyl 2,3,4-tri-*O*-acetyl-α-D-glucopyranoside[12] (1.7 g) and 3,4,6-tri-*O*-acetyl-2-(benzyloxycarbonylamino)-2-deoxy-α-D-glucopyranosyl bromide[13] (2.9 g) in benzene (35 ml) was heated under reflux for 2 h in the presence of $Hg(CN)_2$ (2.7 g) and Drierite (3.5 g). The mixture was diluted with $CHCl_3$ and filtered. The filtrate was washed with brine and water, and concentrated. Recrystallization of the residue from ethanol gave 943 mg (26%) of **4**, mp 162—163 °C, $[\alpha]_D^{25}$ +68.7° (*c* 1.0, chloroform).

Found: C, 53.29; H, 5.96; N, 1.99%. Calcd for $C_{33}H_{43}NO_{18}$: C, 53.43; H, 5.84; N, 1.89%.

Methyl 2'-(Benzyloxycarbonylamino)-2'-deoxy-α-gentiobioside (5) A solution of **4** (195 mg) in methanolic ammonia was settled overnight and concentrated. Recrystallization of the residue from methanol afforded 91 mg (72%) of **5**, mp 212—214 °C, $[\alpha]_D^{20}$ +37.6° (*c* 1.0, water)

Found: C, 51.32; H, 6.30; N, 2.83%. Calcd for $C_{21}H_{31}NO_{12}$: C, 51.53; H, 6.38; N, 2.86%.

Methyl 2'-[N'-(2-Chloroethyl)ureido]-2'-deoxy-α-gentiobioside (6). Compound **5** (393 mg) was hydrogenated in a similar way to that described above, and the product was treated with 2-chloroethyl isocyanate to give 172 mg (47%) of **6**, mp 189—190 °C (dec), $[\alpha]_D^{20}$ +29.9° (*c* 0.6, water).

Found: C, 41.74; H, 6.21; N, 5.88, Cl, 7.49%. Calcd for $C_{16}H_{29}N_2ClO_{11}$: C, 41.70; H, 6.34; N, 6.08; Cl, 7.69%.

Methyl 2'-[N'-(2-Chloroethyl)-N'-nitrosoureido]-2'-deoxy-α-gentiobioside (7). Compound **6** (200 mg) was nitrosated in a similar way to that described above to give 198 mg (97%) of **7**, mp 116 °C (dec), $[\alpha]_D^{20}$ +27.1° (*c* 1.0, water).

Found: C, 39.53; H, 5.99; N, 8.24; Cl, 7.28%. Calcd for $C_{16}H_{28}N_3ClO_{12}$: C, 39.21; H, 5.76; N, 8.58; Cl, 7.24%.

Degradation of **7** in methanolic ammonia gave the 2'-ureido derivative as described above.

References

1) T. P. Johnston, G. S. McCaleb, and J. A. Montgomery, *J. Med. Chem.*, **18**, 104 (1975).
2) T. Anderson, M. G. McMenamin, and P. S. Schein, *Cancer Res.*, **35**, 761 (1975).
3) P. A. Fox, L. C. Panasci, and P. S. Schein, *Cancer Res.*, **37**, 783 (1977).
4) L. C. Panasci, D. Green, R. Nagourney, P. A. Fox, and P. S. Schein, *Cancer Res.*, **37**, 2915 (1977).
5) T. Machinami, S. Nishiyama, K. Kikuchi, and T. Suami, *Bull. Chem. Soc. Jpn.*, **48**, 3763 (1975),
6) T. Hisamatsu and S. Uchida, *Gann*, **68**, 819 (1977).
7) M. Aoshima and Y. Sakurai, *Gann*, **68**, 247 (1977).
8) A. Neuberger and R. P. Rivers, *J. Chem. Soc.*, **1939**, 122.
9) E. Fischer, *Ber.*, **44**, 1898 (1911).
10) S. M. Hecht and J. W. Kozarich, *J. Org. Chem.*, **38**, 1821 (1973).
11) R. I. Geran, N. H. Greenberg, M. M. MacDonald, A. M. Schumacher, and B. J. Abbott, *Cancer Chemother. Rep. (Part 3)*, **3** (2), 7 (1972).
12) D. Horton and J. H. Lauterback, *J. Org. Chem.*, **34**, 86 (1969).
13) E. L. May and E. Mosettig, *J. Org. Chem.*, **15**, 890 (1950); L. Zervas and S. Konstas, *Chem. Ber.*, **93**, 435 (1960).

Enolate Anions. IV. The ^{13}C NMR Spectra of Sodium Enolates of Ethyl Phenylacetates in DMSO[1)]

Syun-ichi KIYOOKA* and Kojiro SUZUKI

Department of Chemistry, Faculty of Science, Kochi University, Akebono-cho, Kochi 780

(Received April 7, 1980)

Synopsis. The ^{13}C NMR spectra of the sodium enolates of ethyl (*p*-substituted phenyl)acetates are presented. The polar interactions between the substituents and the anionic moiety in the sodium enolates are estimated by means of their ^{13}C chemical shifts.

In previous papers,[1)] the ^{13}C NMR data of sodium enolate from diethyl malonates were reported and the substituent effects on the structures of the enolate anions from ethyl phenylacetates and diethyl malonates in DMSO were investigated by means of their UV-visible, IR, and ^1H NMR spectra. The ^1H chemical shifts of the residual methine protons of the sodium enolates from ethyl phenylacetates were correlated to the σ^- constant as well as the carbonyl-stretching vibrations of the enolates. The substituent effects seem mainly to depend on the variation in the electron density of the delocalized-anion moiety. The studies of the IR and ^1H NMR spectra of sodium enolates prepared from ethyl phenylacetates found the existence of extremely different ρ values for meta-line and para-line against σ and σ^-, and suggested two different modes of explanation of the substituent-transmission mechanism. Many workers have reported on the correlations between the ^{13}C substituent chemical shifts (^{13}C SCS) and the relative electron densities on the carbon atoms of interest.[2)]

Table 1 shows the ^{13}C chemical shifts of the parent ester (A) and their sodium enolates (B) and the chemical-shift differences ($\Delta\delta$), which are given by $\delta_A-\delta_B$. These ^{13}C chemical shifts were assigned according to the additivity rule.[3)] In the case of the NO derivative, all benzene-ring ^{13}C signals of the enolate were distinguished because of the fixation of the partial double bond between the benzene ring and the enolate-anion moiety on the NMR time scale, as supported by ^1H NMR.[1b)] The nonequivalence of the two signals of C-m and C-m′ in the enolates with the CN and MeCO substituents is also supported by such a partial double-bond character.

The $\Delta\delta$ values at C-α and C-p were observed as downfield shifts, while those at C-γ and C-ipso were observed as upfield shifts, despite the kinds of substituents. The $\Delta\delta$ values at C-m and C-o are very small. The signs of the $\Delta\delta$ values at C-β are plus (downfield shifts) with electron-releasing substituents and minus (upfield shifts) with electron-attracting substituents. An analogous trend has also been found in

TABLE 1. THE ^{13}C NMR CHEMICAL SHIFTS (δ FROM TMS) OF ETHYL (*p*-SUBSTITUTED PHENYL)-ACETATES AND THEIR SODIUM ENOLATES IN DMSO-d_6

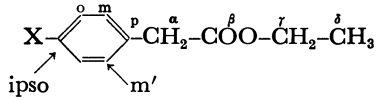

X		C-δ	C-γ	C-β	C-α	C-p	C-m	C-m′	C-o	C-ipso	X-part		
NO_2	A)[a)]	14.5	60.7	172.8	40.9	144.6	132.8		125.3	149.0			
	B)	16.0	57.5	168.4	88.4	152.1	{117.4	b)	121.1}	117.3			
	C)	+1.5	−3.2	−4.4	+47.5	+7.5	{125.6		126.4}	−31.7			
CN	A)	14.5	61.6	172.9	41.1	142.4	132.6		134.2	111.6	120.6		
	B)	16.6	56.3	167.8	74.9	152.3	133.2	124.5	131.7	89.9	103.6		
	C)	+2.1	−5.3	−5.1	+33.8	+9.9	+0.6	−8.1	−2.5	−21.7	−17.0		
MeCO	A)	14.5	61.5	173.1	41.1	142.1	131.6		130.2	137.7	200.3	27.2	
	B)	16.5	56.3	167.9	76.6	153.3	130.5	128.8	130.0	121.9	192.7	26.1	
	C)	+2.1	−5.2	−5.2	+35.5	+11.2	+1.1	−2.8	−0.2	−15.8	−7.6	−1.1	
COOEt	A)	14.4	61.6	172.9	41.2	141.9	{131.5	b)	131.1}	130.8	168.0	61.6	14.4
	B)	16.6	56.1	167.6	74.7	153.2	{130.1		130.2}	111.7	167.4	59.4	16.5
	C)	+2.2	−5.5	−5.3	+33.5	+11.3				−19.1	−0.6	−2.2	+2.1
Cl	A)	14.8	61.7	173.4	41.0	135.8	133.3		130.6	134.3			
	B)	19.5	56.9	178.2	45.8	139.6	132.1		128.5	127.7			
	C)	+4.7	−4.8	+4.8	+4.8	+3.8	−1.2		−2.1	−6.6			
H	A)	14.3	61.4	173.6	41.3	136.6	131.3		130.3	128.7			
	B)	19.5	56.9	176.4	46.9	140.7	130.2		128.6	126.0			
	C)	+5.2	−4.5	+2.8	+5.6	+4.1	−1.1		−1.7	−2.7			
Me	A)	14.5	61.2	173.7	41.1	133.6	130.1		130.1	138.1	21.1		
	B)	19.1	57.3	179.4	46.0	138.8	131.1		129.8	136.0	21.3		
	C)	+4.6	−3.9	+5.7	+4.9	+5.2	+0.1		−1.2	−2.1	+0.2		
MeO	A)	14.4	61.2	173.7	40.5	128.4	115.5		132.2	160.8	55.9		
	B)	19.3	57.4	180.0	46.0	133.9	115.3		132.5	160.0	56.2		
	C)	+4.9	−3.8	+6.3	+5.5	+5.5	−0.2		+0.3	−0.8	+0.3		

a) A; Ethyl phenylacetates. B; Enolate anions. C; $\Delta\delta=\delta_A-\delta_B$. A plus sign denotes a downfield shift.
b) These chemical shifts could not be assigned to any carbons in the benzene ring.

the $\Delta\delta$ values of the residual methine protons.[1b] The $\Delta\delta$ values at C-γ and C-δ are affected by the negative moiety of the enolate anions in the same pattern as those of the malonate system.[1a]

In the case of benzyl methyl ketone, the $\Delta\delta$ value at benzyl carbon has been reported to be +42.5 ppm (a downfield shift), and the chemical-shift difference of the sodium enolate from the enol acetate, to be −23.2 ppm (an upfield shift).[4] By anion formation, the hybridization of the benzyl carbon changes from sp^3 to sp^2, accompanied by a large downfield shift of the ^{13}C chemical shift; *e.g.*, ethylene carbon resonates at a point downfield by more 117 ppm than that of ethane carbon; simultaneously, the increase in the pi-electron density on the carbon atom is forced to shift the chemical shift upfield.[5] These two opposing effects seem to cancel each other out and to give an apparent $\Delta\delta$ value to such an anionic carbon. The $\Delta\delta$ value at C-α of ethyl phenylacetate was +5.6 ppm. This small value appears to be attributable to the above-mentioned cancelling. Consequently, the small downfield shift at C-α seems to be associated with the increase in the electron density on the carbon rather than with the decrease based on sp^2 hybridization. The sign of the $\Delta\delta$ value at C-β in ethyl phenylacetate shows a downfield shift, while those at C-p and C-ipso show downfield and upfield shifts respectively. The $\Delta\delta$ values indicate the existence of pi-interaction between the benzene ring and the anion moiety (C=C=O$^-$), even in a nonsubstituted case.[6]

Several studies of ^{13}C SCS have been reported.[7] The purpose of this ^{13}C SCS study is to clarify the direction of the ^{13}C SCS on the carbons in the enolates against σ^- and σ. Such an anion system attached directly to a benzene ring is very rare in ^{13}C SCS studies.[8]

In Fig. 1, the ^{13}C chemical shifts at C-α, C-β, C-p, and C-ipso of sodium enolates are plotted against σ^-; those at the other carbons are scarcely affected at all by any substituents. The effect by the electron-attracting groups is quite different from that by the electron-releasing groups, as has been suggested by other physical data.[1] The electron-releasing groups act much like an H substituent, without any strong interaction between the substituents and the anion moiety, while the electron-attracting groups conjugate strongly with the anionic moiety through the benzene ring.

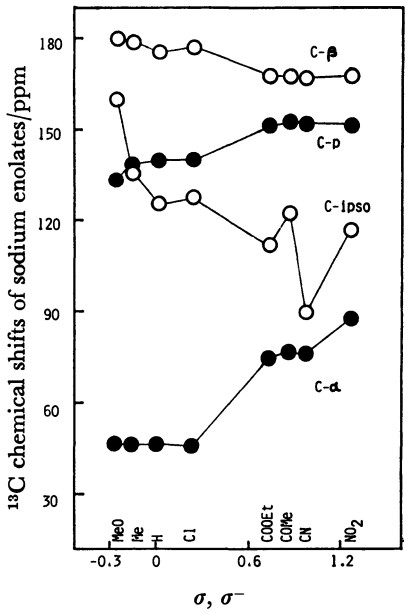

Fig. 1. Plots of the ^{13}C chemical shifts at C-α, C-β, C-p, and C-ipso of the sodium enolates derived from ethyl phenylacetates in DMSO-d_6 against σ^- and σ constants.

In the case of the electron-attracting groups, large downfield shifts were observed at C-α: the electron densities on the carbons decrease, while large upfield shifts were observed at C-ipso that is, the electron densities on the carbons increase. The ^{13}C SCS at C-ipso show a little irregularity which is directly affected by the inductive effect of the attached substituents. Small downfield shifts at C-p by electron-attracting groups are observed. At the β-carbonyl carbon atoms, the electron-attracting groups in the enolate cause small, but definite, upfield shifts. The above explanations for the ^{13}C SCS must be verified using the perturbation molecular-orbital theory.

Experimental

The proton-decoupled ^{13}C FT NMR spectra were measured at 25.15 MHz on a JEOL MH-100/PFT-100 spectrometer (pulse width, 31 μs; spectral width, 6250 Hz; data points, 4096; aquisition time, 327.8 ms). The spectra were observed on 0.5 M solutions in DMSO-d_6 in 5-mm tubes at 35—45 °C. The chemical shifts were obtained using the signal of DMSO in a 99% d-enriched solvent as the internal standard (δ 40.5 ppm), and were then converted to the TMS scale.

The sodium enolates of ethyl (p-substituted phenyl)acetates were prepared in a manner similar to that described in a previous report.[1b]

References

1) a) S. Kiyooka and K. Suzuki, *Chem. Lett.*, **1975**, 793; b) S. Kiyooka, Y. Ueda, and K. Suzuki, *Bull. Chem. Soc. Jpn.*, **53**, 1656 (1980); c) S. Kiyooka, T. Kodani, and K. Suzuki, *ibid.*, **53**, 2318 (1980).

2) a) G. L. Nelson, G. C. Levy, and J. D. Cargioli, *J. Am. Chem. Soc.*, **94**, 3089 (1972); b) A. Saika and C. P. Slichter, *J. Chem. Phys.*, **22**, 26 (1954); c) M. Karplus and J. A. Pople, *ibid.*, **38**, 2803 (1963).

3) J. B. Stothers, "Carbon-13 NMR Spectroscopy," Academic Press, New York (1972).

4) H. O. House, A. V. Prabhu, and W. V. Phillips, *J. Org. Chem.*, **40**, 1209 (1976).

5) a) G. C. Levy and G. L. Nelson, "Carbon-13 Nuclear Magnetic Resonance for Organic Chemists," Wiley-Interscience (1972), p. 142; b) R. Waak, M. A. Doran, E. B. Baker, and G. A. Olah, *J. Am. Chem. Soc.*, **88**, 1272 (1966).

6) a) O. Kajimoto and T. Fueno, *Tetrahedron Lett.*, **1972**, 3329; b) R. T. C. Brownlee, G. Butt, M. P. Chan, and R. D. Topsom, *J. Chem. Soc., Perkin Trans.* **2**, 1486 (1976); c) N. Inamoto, S. Masuda, W. Nakanishi, and Y. Ikeda, *Chem. Lett.*, **1977**, 759; d) W. F. Reynolds and G. K. Hamer, *J. Am. Chem. Soc.*, **98**, 7296 (1976).

7) a) Spiesecke and W. G. Schneider, *J. Chem. Phys.*, **35**, 731 (1961); b) J. Bromilow, R. T. C. Brownlee, R. D. Topsom, and R. W. Taft, *J. Am. Chem. Soc.*, **98**, 2020 (1976); c) M. Mishima, M. Fujio, R. Takeda, and Y. Tsuno, *Memoir. Fac. Sci., Kyushu Univ., Ser. C*, **11**, 97 (1978); d) N. Inamoto, S. Masuda, K. Tokumaru, K. Tori, M. Yoshida, and Y. Yoshimura, *Tetrahedron Lett.*, **1976**, 3711.

8) S. Bradamante, F. Gianni, and G. A. Pagani, *J. Chem. Soc., Chem. Commun.*, **1976**, 478.

Oxidation of Steroidal π-Allyl Palladium Chloride Complexes Using Chromium(VI) Oxide in *N,N*-Dimethylformamide†

J. Yasuo SATOH and C. Akira HORIUCHI*

Department of Chemistry, Rikkyo (St. Paul's) University, Nishi-Ikebukuro, Toshima-ku, Tokyo 171

(Received June 7, 1980)

Synopsis. The oxidation of steroidal π-allyl palladium chloride complexes with the mild oxidizing agent composed of chromium(VI) oxide in *N,N*-dimethylformamide containing ether to dissolve the complex and a trace of sulfuric acid, afforded efficiently the corresponding α,β-unsaturated ketones.

It has been reported[1] that the oxidation of π-allyl palladium complexes in the presence of palladium(II) chloride and sodium acetate in aqueous acetic acid gave unsaturated aldehyde or ketone. However, the more heavily substituted π-allyl complexes such as the π-allyl complex of 3-methyl-2-pentene did not react with palladium(II) chloride. The oxidation of π-allyl complexes of the chain compounds[1] and complexes of 1-*p*-menthene[2] with, respectively, sodium dichromate containing sulfuric acid in ether and manganese dioxide containing sulfuric acid in 25% aqueous acetic acid has also been investigated. However, the yields of the α,β-unsaturated ketones were quite low. We have previously reported[3] that the reaction of the cholestene derivatives with palladium(II) chloride in the presence of potassium acetate in acetic acid afforded the corresponding steroidal palladium complexes. Hence, we attempted the oxidation of steroidal π-allyl complexes according to the procedures described by R. Hüttel and H. Christ,[1] G. A. Gray *et al.*,[2] and Jones reagent;[4] but we found that they gave the corresponding α,β-unsaturated ketone and considerable quantities of by-products, namely, carboxylic acids. In the present paper, we would like to report that the oxidation of the steroidal complexes with the mild oxidizing agent[5] composed of chromium(VI) oxide in *N,N*-dimethylformamide containing ether to dissolve the complex and a trace of sulfuric acid, gave the corresponding α,β-unsaturated ketones.

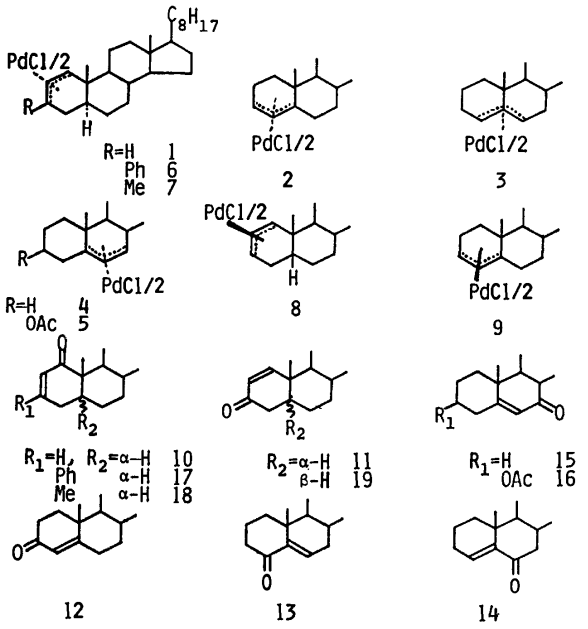

Results and Discussion

The oxidation of the steroidal π-allyl palladium complexes with chromium(VI) oxide in *N,N*-dimethylformamide and ether, containing a trace of sulfuric acid yielded in all cases the α,β-unsaturated ketones. These ketones were isolated by preparative TLC on silica gel, and identified by comparison with the IR and UV spectral data, and with the melting points of authentic samples. The reaction of di-μ-chloro-bis-[(1-3η-alkyl-5α-cholesten-2α-yl)palladium(II)] (**6**, **7**) gave the 3-alkyl-α,β-unsaturated ketone (**17**, **18**), which showed IR absorptions at 1660 and 1615 cm^{-1} (for R=phenyl); 1673 and 1644 cm^{-1} (for R=methyl). This α,β-unsaturated ketone was determined to be 3-alkyl-5α-cholest-2-en-1-one by means of its NMR spectrum, which showed a singlet at δ 6.10 ppm (CCl_4) (for R=phenyl) and at δ 5.63 ppm ($CDCl_3$) (for R=methyl) due to the olefinic proton.

The results of the oxidation of the steroidal π-allyl complexes are given in Table 1. On the basis of these results, it can be concluded that the mild oxidizing agent

Table 1. Products and isolated yields (%) in oxidation of steroidal π-allyl palladium complexes (**1**—**9**)

Materials	Time / h	Products	Isolated yield/%	Mp / °C
1	5	**10**	28	55—56[6]
		11	38	83—85[7]
2	5	**12**	54	78—81[8]
3	5	**13**	6	108—110[9]
		14	14	100—102[9]
4	5	**15**	62	129—131[10]
5	5	**16**	96	139—145[11]
6	20	**17**[a]	52	213—215
7	20	**18**[b]	64	114—117
8	5	**12**	31	79—81
		19	25	96—99[12]
9	5	**12**	83	78—81

a) IR(KBr): 1660 and 1615 cm^{-1}; λ_{max}^{EtOH} (nm): 219 (ε 8,500) and 281 (ε 15,900); NMR (CCl_4): δ 6.10 ppm (s, 1H) and *ca.* δ 7.2—7.6 ppm (m, 5H). Found: C, 85.94; H, 10.42%. Calcd for $C_{33}H_{48}O$: C, 86.03; H, 10.50%. b) IR (KBr): 1673 and 1644 cm^{-1}; λ_{max}^{EtOH} (nm): 234 (ε 11,400), NMR ($CDCl_3$): δ 5.63 ppm (s, 1H). Found: *m/e* 398.3516. Calcd for $C_{28}H_{46}O$: M, 398.3553.

† A preliminary report of this work was presented at the 38th National Meeting of the Chemical Society of Japan, Yokohama, April 1978.

used in this work is efficient in comparison to the various methods reported in the literature for the oxidation of the steroidal π-allyl complexes. In the case of the α-1-3η-type complex of 5α-cholestene, an oxo group was introduced in the direction of the C_1 and C_3 positions. In the case of the β-1-3η-type complex of 5β-cholestene, the oxidation occurred in the direction of the less hindered C_3 position rather than in the direction of the C_1 position, and formed Δ^1- and Δ^4-3-oxo derivative. In the reaction of the α-1-3η-type complex with a functional group at the C_3 position, the product was Δ^2-1-oxo derivative, and the oxidation occurred more slowly than in the case of a complex possessing no functional group. The α- and β-3-5η-type complex yielded cholest-4-en-3-one, and the α-5-7η-type complex gave the Δ^5-7-oxo derivative, quantitatively.

Experimental

All the melting points are uncorrected. The IR, UV, and NMR spectra were measured using a Hitachi model 215 grating infrared spectrometer, a Hitachi recording spectrophotometer model 323, and a nuclear magnetic resonance spectrometer, Hitachi-Perkin Elmer R-20A, in carbon tetrachloride and in deuteriochloroform with TMS as the internal standard.

General Procedure. A mixture of steroidal π-allyl palladium complex (6.0×10^{-1} mmol), chromium(VI) oxide (3.96 mmol), and *N*,*N*-dimethylformamide–ether (1 : 1) (50 ml) containing a trace of sulfuric acid was stirred at 25 °C for 5—20 h. After the usual work-up, the resultant oil was purified by preparative TLC coated with silica gel (2 mm thick) (E. Merck). Elution with benzene–ether (10 : 1) gave the α,β-unsaturated ketone from ethanol.

Materials. The steroidal π-allyl palladium complexes were synthesized by the methods described in the previous paper.[3]

The authors are indebted to Mr. Takayuki Sugiyama for his collaboration in the experimental work. This research was supported in part by a Matsunaga Research Grant from the Matsunaga Science Foundation.

References

1) R. Hüttel and H. Christ, *Chem. Ber.*, **97**, 1439 (1964).
2) G. A. Gray, W. R. Jackson, and J. J. Rooney, *J. Chem. Soc.*, **1970**, 1788.
3) J. Y. Satoh and C. A. Horiuchi, *Bull. Chem. Soc. Jpn.*, **52**, 2653 (1979).
4) K. Bowden, I. M. Heilbron, E. R. H. Jones, and B. C. L. Weedon. *J. Chem. Soc.* **1946**, 39; A. Bower, T. G. Halsall, E. R. H. Jones, and A. J. Lemin, *ibid.*, **1953**, 2548.
5) G. Snatzke, *Chem. Ber.*, **94**, 729 (1961).
6) C. Djerassi, D. H. Williams, and B. Berkoz, *J. Org. Chem.*, **27**, 2205 (1962).
7) C. Djerassi and C. R. Scholz, *J. Am. Chem. Soc.*, **69**, 2404 (1947).
8) N. Rabjohn, *Org. Synth.*, Coll. Vol. **4**, 192 (1963).
9) D. N. Jones, J. R. Lewis, C. W. Shoppee, and G. H. R. Summers, *J. Chem. Soc.*, **1955**, 2876.
10) C. W. Shoppee and R. Lack, *J. Chem. Soc.*, **1960**, 4864.
11) A. Windaus, H. Lettré, and Fr. Schenck, *Ann.*, **520**, 98 (1935).
12) J. Y. Satoh, K. Misawa, T. T. Takahashi, M. Hirose, C. A. Horiuchi, S. Tsuji, and A. Hagitani, *Bull. Chem. Soc. Jpn.*, **46**, 3155 (1973).

The Selective Preparation of *N*-Acylindigo

Yoshimori OMOTE,* Kiyoko FUJIKI,† Hiroshi AWANO, Ikuo KUBOTA, Takehiko NISHIO, and Hiromu AOYAMA

Department of Chemistry, The University of Tsukuba, Sakuramura, Niihari, Ibaraki 305
†*Department of Agricultural Chemistry, Faculty of Agriculture, Meiji University, Ikuta, Tama-ku, Kawasaki 214*

(Received July 5, 1980)

Synopsis. The hitherto unknown *N*-acylindigo has been selectively prepared by heating the corresponding known *N,N'*-diacylindigo in aqueous pyridine. The data of *N*-acetyl, *N*-benzoyl, *N*-(*p*-toluoyl), *N*-(*p*-chlorobenzoyl), *N*-(*p*-nitrobenzoyl), and *N*-(3,5-dinitrobenzoyl)indigo are summarized.

Indigo is a *trans* compound; it is stable and cannot be converted to the *cis*-isomer, not even by irradiation, while *N,N'*-diacetyl[1] and *N,N'*-dimethyl[2] derivatives have been known to show phototropic behavior. Recently we reported the *cis*-to-*trans* isomerization of *N,N'*-diacylindigo (**1**).[3] Therefore, it is of interest to see if *N*-acylindigo (**2**) can isomerize photochemically just like *N,N'*-diacylindigo.

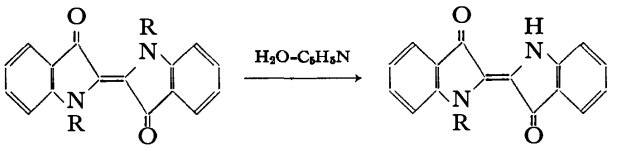

1 R **2**

a: CH_3CO, **b**: C_6H_5CO, **c**: *p*-$CH_3C_6H_4CO$, **d**: *p*-ClC_6H_4CO, **e**: *p*-$NO_2C_6H_4CO$, **f**: 3,5-$(NO_2)_2C_6H_3CO$.

To our surprise, we cannot find any *N*-acylindigo in the literature, although several *N,N'*-diacylindigo have been known. In order to obtain *N*-acylindigo, we attempted to modify the partial acylation of indigo as well as the partial hydrolysis of *N,N'*-diacylindigo, and finally found a facile method of selectively preparing **2** from **1**.

The first trial at the acylation of indigo was as follows. Indigo and an equivalent amount of acetyl chloride were heated in acetic anhydride under reflux. The conditions were similar to those in the preparation of *N,N'*-diacetylindigo (**1a**)[4] except that excess molar acetyl chloride was used in the latter method. The products were found to be indigo and **1a**. The partial hydrolysis of **1a** was then examined. When **1a** was partially hydrolyzed by potassium hydroxide, the products were found to be indigo and **1a**. In neither case could we obtain an economical amount of **1a**. In the next trial, indigo was treated with sodium hydride in hexamethylphosphoric triamide, and then an excess amount of acetyl chloride was added. The product was a mixture of **2a** and **1a**; however, it seemed difficult to regulate the reaction, in which the formation of **2a** was predominant.

Finally, the partial hydrolysis of **1a** which had been heated in aqueous pyridine was found to be successful in giving **2a**. The reaction products were analyzed at time intervals by liquid chromatography and by means of the visible-absorption spectrum. The suitable conditions for the formation of **2a** were established to be as will be shown in the Experimental section.

TABLE 1. PROPERTIES OF N-ACYLINDIGO (**2**)

R	Mp °C	$\nu_{C=O}$ cm^{-1}	ν_{N-H} cm^{-1}	$\lambda^{C_6H_6}_{max}$ nm	ε
CH_3CO	185—186	1700 1650	3320	568	12000
C_6H_5CO	268	1690 1655	3300	575	14000
p-$CH_3C_6H_4CO$	276—277	1690 1645	3310	575	15000
p-ClC_6H_4CO	290—291	1690 1660	3310	574	13000
p-$NO_2C_6H_4CO$	> 290	1700 1650	3320	574	12000
3,5-$(NO_2)_2$-C_6H_3CO	> 290	1690 1655	3350	572	9000

The infrared and visible spectra of *N*-acylindigo are summarized in Table 1. The data support the structure of monoacylindigo. Furthermore, the preliminary experiment shows that these examples of *N*-acylindigo do not show any phototropic behavior.

Experimental

N-Acetylindigo (2a). *a)*: Sodium hydride (227 mg) was washed with petroleum ether and dispersed in HMPA (15 ml); indigo (500 mg) was then added, and the solution was stirred for 4 h at 0 °C under an argon atmosphere. Then acetyl chloride (725 mg) was added, and the solution was stirred for 15 h. The products were extracted with dichloromethane, dried over anhydrous magnesium sulfate, and chromatographed over silica gel with chloroform–acetone (60 : 1) to give reddish-purple needles (89 mg). Mp 185—186 °C. Found: C, 71.41; H, 4.04; N, 8.91%. Calcd for $C_{18}H_{12}N_2O_3$: C, 71.04; H, 3.97; N, 9.20%.

b): A solution of **1a** (20 mg) in a pyridine–water mixture (80 : 20 v/v, 100 ml) was heated at 88 °C for 120 min. After the pyridine had been removed under reduced pressure, the product was recrystallized from ethyl acetate–hexane. The yield was 37%. Mp 185—186 °C (dec).

N-Benzoylindigo (2b). A solution of **1b** (273 mg) in a pyridine–water mixture (60 : 40 v/v, 100 ml) was heated at 88 °C for 80 min. After the pyridine had been evaporated the product was precipitated and recrystallized from chloroform–hexane and then acetone–hexane to give purple needles. Mp 268 °C (dec). 85%. Found: C, 75.35; H, 3.77; N, 7.48%. Calcd for $C_{23}H_{14}N_2O_3$: C, 75.40; H, 3.85; N, 7.64%.

N-(p-Toluoyl)indigo (2c). *N,N'*-Bis(*p*-toluoyl)indigo (4.0 mg) (**1c**) was dissolved in aqueous pyridine (50 : 50 v/v, 10 ml), and the solution was heated at 70 °C for 4 h. After having been treated with 6 M hydrochloric acid, the reaction mixture was extracted with chloroform, washed with water, and dried over magnesium sulfate. The product was purified by silica gel chromatography using ethyl acetate–benzene. The residue was recrystallized from acetone–hexane, as purple needles. Found: C, 75.42; H, 4.06; N, 7.15%. Calcd for

$C_{24}H_{16}N_2O_3$: C, 75.77; H, 4.23; N, 7.36%.

N-(p-*Chlorobenzoyl)indigo (**2d**)*. Fine purple needles. Found: C, 68.78; H, 3.20; N, 6.83%. Calcd for $C_{23}H_{13}N_2O_3Cl$: C, 68.92; H, 3.26; N, 6.98%.

N-*(p-Nitrobenzoyl)indigo (**2e**)*. Fine purple needles. Found: C, 66.94; H, 3.10; N, 9.86%. Calcd for $C_{23}H_{13}N_3O_5$: C, 67.15; H, 3.18; N, 10.21%.

N-*(3,5-Dinitrobenzoyl)indigo (**2f**)*. A solution of **1f** (377 mg) in a pyridine–water mixture (90 : 10 v/v, 100 ml) was heated at 60 °C for 80 min. After the pyridine had been evaporated under reduced pressure, the residue was added to boiling water. The precipitates were collected, dried, and recrystallized from ethyl acetate–hexane and then benzene, as purple plates. Found: C, 60.01; H, 2.68; N, 11.96%. Calcd for $C_{23}H_{12}N_4O_7$: C, 60.53; H, 2.65; N, 12.27%.

References

1) a) W. R. Brode, E. G. Pearson, and G. M. Wyman, *J. Am. Chem. Soc.*, **76**, 1034 (1954); b) G. M. Wyman and A. F. Zenhäusern, *J. Org. Chem.*, **30**, 2348 (1956).

2) a) J. Weinstein and G. M. Wyman, *J. Am. Chem. Soc.*, **78**, 4007 (1956); b) C. R. Giuliano, L. D. Hess, and J. D. Margerum, *J. Am. Chem. Soc.*, **90**, 587 (1968); c) H.-D. Scharf, J. Fleischauer, H. Leismann, I. Ressler, W. Schleker, and R. Weitz, *Angew. Chem. Int. Ed. Engl.*, **18**, 652 (1979).

3) Y. Omote, S. Imada, R. Matsuzaki, K. Fujiki, T. Nishio, and C. Kashima, *Bull. Chem. Soc. Jpn.*, **52**, 3397 (1979).

4) a) J. Blanc and D. L. Ross, *J. Phys. Chem.*, **72**, 2818 (1968); b) T. Posner, *Chem. Ber.*, **59B**, 1977 (1926).

Reaction of Allyl Diphenyl Phosphates with Soft Bases

Shuki ARAKI, Kazuhiro MINAMI, and Yasuo BUTSUGAN*

Department of Synthetic Chemistry, Nagoya Institute of Technology, Gokiso-cho, Showa-ku, Nagoya 466

(Received July 21, 1980)

Synopsis. The title phosphates were found to react with a variety of soft bases to give nucleophilic substitution products in high yields. The reaction proceeded regiospecifically under mild reaction conditions with preservation of the double bond geometry.

It was first reported in 1958 that soft nucleophiles attack the alkyl group of trialkyl phosphates while hard bases attack the hard phosphorus atom.[1] However, the reaction of allylic phosphates with various nucleophiles has received relatively little attention. In 1968, Miller and Wood synthesized a series of allyl diphenyl phosphates (**1**) and examined their reactions with phenols[2] and β-diketones[3] as a model for the biosynthesis of phenolic isoprenoids. Kitagawa *et al.* reported the regio- and stereospecific substitution of allylic phosphates using organoaluminum reagents.[4] In the present paper, we describe the reaction of **1** with a variety of soft nucleophiles which involves the regio- and stereospecific substitutions of the diphenoxyphosphinyloxy group leading to good yields of allylic products (**2**).

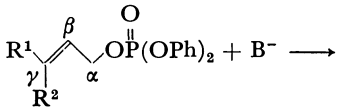

1A: $R^1 = R^2 = H$
B: $R^1 = Me_2C{=}CH(CH_2)_2$, $R^2 = Me$
C: $R^1 = Me$, $R^2 = Me_2C{=}CH(CH_2)_2$

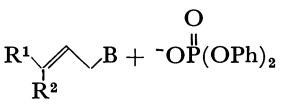

2

The reactions were carried out as follows. The phosphates **1** were stirred with a slight excess (1.0—1.5 eq) of nucleophiles in *N,N*-dimethylformamide at room temperature for 3 h. The reaction mixtures were poured into water, and the products were extracted with ether or collected by filtration. Analytically pure materials were obtained after distillation, column chromatography on silica gel, or recrystallization. Products were identified by their analytical and spectral properties and, in the case of known materials, by comparison of these physical constants with those of the reported ones.[5] Treatment of **1** with soft bases such as iodide, cyanide, benzenethiolate and sulfide anions resulted in smooth displacement of the diphenoxyphosphinyloxy group to yield the corresponding allylated products in high yields. The results are given in Table 1. The phosphates **1B** and **1C** reacted with thiourea to give *S*-geranyl- and *S*-nerylisothiuronium salts (**2f** and **2j**), respectively, as colorless crystals. The reaction of **1B** with sodium thiocyanate gave an equilibrium mixture (**2g**) of linalyl isothiocyanate and geranyl thiocyanate. The ratio (81/19) estimated by ^{1}H-NMR analysis (in CCl_4 at 31.5 °C) is in good agreement with the reported one[6] (80.56/19.44, in CCl_4 at 36 °C). The reaction of **1** with carbanionic reagents such as Grignard reagents and organolithium reagents is of special interest in view of a carbon-carbon bond formation.[7] In fact, it has been demonstrated that the treatment of allyl diphenyl phosphates **1** with aryl Grignard reagents gives allylbenzenes in high yields.[8] In contrast, we have found that excess (5 eq) phenyllithium, a carbanion harder than aryl Grignard reagents, attacked the phosphorus atom of **1B** to produce triphenylphosphine oxide (80% yield) together with geraniol (92%) and phenol (86%). The reaction of **1B** with sodium ethoxide, a representative of hard bases, in ethanol at room temperature gave a complex product mixture.

It has been shown that the reaction of **1** with soft

Table 1. Reaction of allyl diphenyl phosphates (**1A**—**1C**) with soft nucleophiles

Entry	Phosphate (**1**)	Nucleophile (B^-)[a]	Products (**2**)[b]	Isolated yield/%
a	**1A**	I^-	Allyl-I (**2a**)	47
b	**1A**	PhS^-	Allyl-SPh (**2b**)	78
c	**1B**	$N{\equiv}C^-$	Geranyl-C≡N (**2c**)	85
d	**1B**	PhS^-	Geranyl-SPh (**2d**)	83
e	**1B**	S^{2-}	$(Geranyl)_2S$ (**2e**)	74
f	**1B**	$(H_2N)_2C{=}S$	Geranyl-$SC^+(NH_2)_2 \cdot O^-P(O)(OPh)_2$ (**2f**)	56
g	**1B**	$N{\equiv}CS^-$	Linalyl-N=C=S ⇋ Geranyl-SC≡N (**2g**)	82
h	**1C**	$N{\equiv}C^-$	Neryl-C≡N (**2h**)	84
i	**1C**	PhS^-	Neryl-SPh (**2i**)	94
j	**1C**	$(H_2N)_2C{=}S$	Neryl-$SC^+(NH_2)_2 \cdot O^-P(O)(OPh)_2$ (**2j**)	63

a) Counter cation: Na^+. b) Allyl: Geranyl: Neryl: 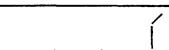 Linalyl: 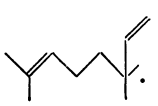

bases proceeds with complete preservation of the double bond geometry as evidenced by the fact that geranyl diphenyl phosphate **1B** gave geranyl derivatives (**2c**—**2f**) and the corresponding *cis*-isomer **1C** yielded neryl ones (**2h**—**2j**). All the reactions (except entry g) are regiospecific, exclusively leading to the α-substituted products. No evidence for the allylic rearrangement (γ-substitution) was detected.

Experimental

Melting points are uncorrected. The elemental analyses were performed at the Elemental Analysis Center of Kyoto University. IR spectra were measured with a JASCO IRA-1 spectrometer. ^{1}H- and ^{13}C-NMR were obtained on a Hitachi R-24A spectrometer and a JEOL JNM-FX100 spectrometer, respectively, in deuteriochloroform using tetramethylsilane as an internal standard. Phosphates **1A**—**1C** were prepared according to the method of Miller and Wood.[2] The following preparation of **2f** is representative of the reactions between **1** and soft nucleophiles.

Reaction of Geranyl Diphenyl Phosphate (1B) with Thiourea. A mixture of **1B** (386 mg, 1 mmol) and thiourea (76 mg, 1 mmol) in 2 ml of *N,N*-dimethylformamide was stirred at room temperature for 3 h. The reaction mixture was poured into water and the resulting white precipitate was collected by filtration, and washed with water. The crude product was recrystallized from ethanol to afford colorless needles of *S*-geranylisothiuronium diphenyl phosphate (**2f**) (253 mg, 56% yield), mp 134.5—135.5 °C. IR (KBr): 3280, 3068, 1676, 1500, 1240, 1218, 1094, and 922 cm^{-1}. ^{1}H-NMR: δ 9.81 (2H, br, NH), 8.03 (2H, br, NH), 7.04 (10H, m, Ph), 4.90 (2H, m, olefin), 3.37 (2H, d, J=7 Hz, SCH_2), 1.91 (4H, m, CH_2), 1.61, 1.52, 1.46 (each 3H, s, CH_3). ^{13}C-NMR: 171.7 ($SC^+(NH_2)_2$), 153.3 (P–O–C), 144.9 (=C–), 132.7 (=C–), 129.9 (=CH–), 124.2 (=CH–), 121.1 (=CH–), 120.9 (=CH–), 115.5 (=CH–), 40.1 (CH_2), 30.1 (CH_2), 26.9 (CH_2), 26.4 (CH_3), 18.4 (CH_3), 17.0 (CH_3). Found: C, 59.75; H, 6.87%. Calcd for $C_{23}H_{31}N_2O_4PS$: C, 59.73; H, 6.76%.

In a similar way, *S*-nerylisothiuronium diphenyl phosphate (**2j**) was obtained in 63% yield, mp 128.5—130.0 °C. IR (KBr): 3250, 3000, 1678, 1500, 1240, 1218, 1096, and 926 cm^{-1}. ^{1}H-NMR: δ 9.90 (2H, br, NH), 8.00 (2H, br, NH), 7.10 (10H, m, Ph), 4.96 (2H, m, olefin), 3.42 (2H, d, J=7 Hz, SCH_2), 1.92 (4H, m, CH_2), 1.62 (6H, m, CH_3), 1.50 (3H, s, CH_3). ^{13}C-NMR: 171.4 ($SC^+(NH_2)_2$), 153.3 (P–O–C), 144.5 (=C–), 132.8 (=C–), 129.8 (=CH–), 124.1 (=CH–), 121.0 (=CH–), 120.8 (=CH–), 116.5 (=CH–), 32.5 (CH_2), 29.8 (CH_2), 27.0 (CH_2), 26.3 (CH_3), 24.0 (CH_3), 18.3 (CH_3). Found: C, 59.21; H, 6.72%. Calcd for $C_{23}H_{31}N_2O_4PS$: C, 59.73; H, 6.76%.

We wish to thank the Instrument Center, the Institute for Molecular Science, for assistance in obtaining the ^{13}C-NMR spectra.

References

1) D. C. Harper and R. F. Hudson, *J. Chem. Soc.*, **1958**, 1356.

2) J. A. Miller and H. C. S. Wood, *J. Chem. Soc., C*, **1968**, 1837.

3) J. Carnduff, J. A. Miller, B. R. Stockdale, J. Larkin, D. C. Nonhebel, and H. C. S. Wood, *J. Chem. Soc., Perkin Trans. 1*, **1972**, 692.

4) Y. Kitagawa, S. Hashimoto, S. Iemura, H. Yamamoto, and H. Nozaki, *J. Am. Chem. Soc.*, **98**, 5030 (1976), see also S. Ozawa, A. Itoh, K. Oshima, and H. Nozaki, *Tetrahedron Lett.*, **1979**, 2909.

5) **2b**: C. D. Hurd and H. Greengard, *J. Am. Chem. Soc.*, **52**, 3356, (1930); **2c**: M. Matsui and G. Yabuta, *Agric. Biol. Chem.*, **32**, 1044 (1968); **2d** and **2i**: J. F. Biellmann and J. B. Ducep, *Tetrahedron*, **27**, 5861 (1971); **2e**: J. E. Baldwin and D. P. Kelly, *J. Chem. Soc., Chem. Commun.*, **1968**, 899; **2g**: see Ref. 6.

6) G. Pala, A. Antonio, and G. Coppi, *J. Med. Chem.*, **12**, 725 (1969).

7) Alkylation of **1B** and **1C** with trialkylaluminum, see Ref. 4.

8) R. C. Haley, J. A. Miller, and H. C. S. Wood, *J. Chem. Soc., C*, **1969**, 264.

Polymer-bound "Dimethylaminopyridine" as a Catalyst for Facile Ester Synthesis

Seiji SHINKAI,* Hifumi TSUJI, Yōichiro HARA, and Osamu MANABE
Department of Industrial Chemistry, Faculty of Engineering, Nagasaki University, Nagasaki 852
(Received July 21, 1980)

Synopsis. Polystyrene beads which covalently link a dimethylaminopyridine unit act as a catalyst for ester synthesis by the DCC method. The polystyrene beads are reusable and the synthetic method is very simplified.

The dicyclohexylcarbodiimide (DCC) method has been widely adopted for the synthesis of some sugar and amino acid derivatives. Recently, it was communicated that the method is applicable to the esterification of carboxylic acids in the presence of catalytic amounts of 4-dimethylaminopyridine (DMAP).[1,2] Klotz *et al.*[3] reported that the catalytic activity is due to both the increased electron-donating ability of the ring nitrogen and the augmented stability of the *N*-acylpyridinium species. Although this is an excellent, mild one-pot esterification method, there are two defects: (i) in the conventional DCC method in the amide synthesis the product is directly recovered by filtration owing to the precipitating nature of *N,N'*-dicyclohexylurea, whereas in the presence of DMAP one has to isolate the product ester from DMAP, and (ii) DMAP is relatively expensive. It occurred to us that two defects would be improved by immobilizing the DMAP unit in polymer beads. Here, we wish to report the method of the immobilization and the catalytic activity of the immobilized DMAP unit.

p-Chlormethylated polystyrene (**1**) (4% crosslinked, 4.0 mequiv Cl/g) was kindly supplied from Mitsubishi Kasei Co. Ltd. The polystyrene beads were treated according to the following reaction sequence. **1**→**2** : **1** was swelled in *N,N*-dimethylformamide and dry methylamine gas was introduced into the solution. The reaction was continued for 12 h at 60—70 °C. **2**→**3** : **2** was swelled in an ampule containing water and ethanol (3 : 1 in vol), and 4-chloropyridine and triethylamine (excess) were added. After sealing the ampule, the reaction mixture was heated at 150 °C for 4 d. **3**→**4** : **3** in dichloromethane was treated with acetic anhydride (excess). The reaction was continued for 3 h at room temperature. All the reactions were performed under efficient stirring. We also prepared the catalytic beads which have a spacer between the polymer surface and the DMAP unit. **5** was prepared according to the method of Molinari *et al.*[4] The reaction methods from **5** to **8** were similar to those from **1** to **4**. The DMAP contents determined by acid-base titration were: 1.6 mequiv DMAP/g for **4** and 0.60 mequiv DMAP/g for **8**.

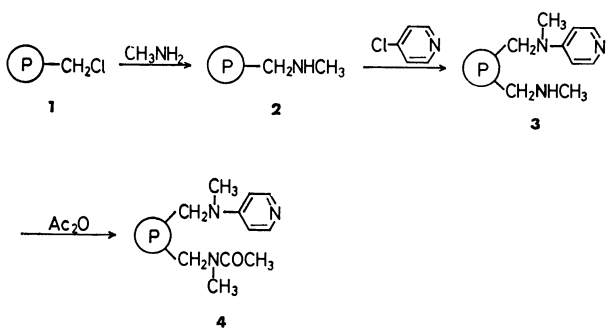

1 2 3 4

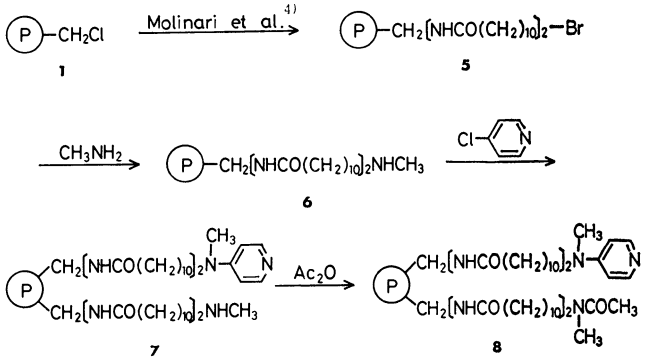

1 5 6 7 8

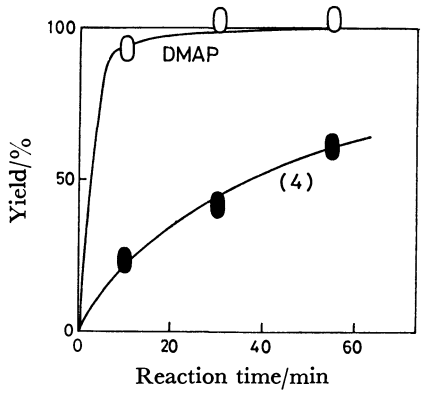

Fig. 1. Yield of methyl benzoate *vs.* reaction time. The yield was determined by GLC method (interanal standard, anisole). 20 °C, 10 ml of dichloromethane, 10 mmol of benzoic acid, 100 mmol of methanol, 12 mol of DCC, and 1.0 mmol of DMAP or DMAP unit in **4**.

Figure 1 shows the plots of the yield of methyl benzoate *versus* reaction time. The reaction conditions are recorded in the caption for Fig. 1. The homogeneous reaction catalyzed by DMAP was completed within 10 min, and the conversion was almost quantitative.[5] On the other hand, the reaction catalyzed by **4** was relatively slow, the half-life being about 30 min. After one day, the precipitate (*N,N'*-dicyclohexylurea) and **4** were removed by filtration and the filtrate was analyzed by GLC. The dichloromethane solution contained only methyl benzoate and methanol, so that the concentration *in vacuo* readily gave "pure" methyl benzoate. The yield of methyl benzoate was 65%, but unreacted benzoic acid was not detected in the filtrate. The loss may be caused by the adsorption to the polystyrene

Table 1. Yield of esters[a)]

Catalyst	Acid	Alcohol	Yield (%) after 1 h	3 h	1 d
DMAP	$C_6H_5CO_2H$	MeOH	100[d)]		
4	$C_6H_5CO_2H$	MeOH	61	59	65
4 reused	$C_6H_5CO_2H$	MeOH		65	
4[b)]	$C_6H_5CO_2H$	MeOH		51[e)]	
8	$C_6H_5CO_2H$	MeOH		41	53
4	$C_6H_5CO_2H$	*t*-BuOH		0	0
4	$CH_2(CO_2H)_2$	MeOH		84	98
4	$CH_5CH=CHCO_2H$	MeOH		61	
4[c)]	CH_3CO_2H	$C_6H_5CH_2OH$		40	47

a) The reaction solution (10 ml of dichloromethane) contains 1.0 mmol of catalyst, 10 mmol of acid, 100 mmol of alcohol, and 12 mmol of DCC. The yields were calculated on the basis of acid. b) 20 mmol of DCC were added. c) The reaction solution (10 ml of dichloromethane) contains 1.0 mmol of catalyst, 20 mmol of acetic acid, 10 mmol of benzyl alcohol, and 20 mmol of DCC. The yield was calculated on the basis of benzyl alcohol. d) 30 min. e) 4 h.

beads. The same reaction was carried out with **8**, but the yield was not improved significantly (yield 53%). After washing the recovered **4** by hot *N*,*N*-dimethylformamide, it was reused for the synthesis of methyl benzoate. The yield after 3 h was 53%. The result indicates that **4** is reusable without losing the catalytic activity.

The yields of other esters are summarized in Table 1. As mentioned above, starting carboxylic acids were not found in the filtrate. Table 1 shows that the yields in the present two phase system are somewhat lower than those in the homogeneous system.[2)] In particular, the yield of *t*-butyl benzoate was extremely low. Also in the homogeneous system catalyzed by DMAP,[2)] the low yield (40%) resulted for this ester due to the steric hindrance. The steric term may be further amplified in the solid catalyst system. On the contrary, dimethyl malonate was produced quantitatively. We cannot explain readily the difference in the yield between methyl benzoate and dimethyl malonate. One possible explanation is that benzoic acid which is more apolar than malonic acid is adsorbed to the resin surface in a non-productive manner in preference to malonic acid.

In conclusion, the catalytic activity of the DMAP unit bound to polystyrene beads is somewhat lower than that of DMAP in the homogeneous system. However, there are two merits in the immobilized DMAP catalysis: (i) the product esters are directly recovered by filtration, and (ii) the catalytic resin is reusable by simply washing with *N*,*N*-dimethylformamide.

References

1) A. Hassner and V. Alexanian, *Tetrahedron Lett.*, **1978**, 4475.

2) B. Neises and W. Steglich, *Angew. Chem. Int. Ed. Engl.*, **17**, 522 (1978).

3) M. A. Hierl, E. P. Gamson, and I. M. Klotz, *J. Am. Chem. Soc.*, **101**, 6020 (1979).

4) H. Molinari, F. Montanari, S. Quici, and P. Tundo, *J. Am. Chem. Soc.*, **101**, 3920 (1979).

5) The homogeneous system in the absence of DMAP gave methyl benzoate in 1.1% yield (after 1 d).

The Copyrolysis of 1,2,3-Trichloropropane and Methanol on Activated Alumina

Kiyonori SHINODA* and Kensei YASUDA
Toyama Technical College, Hongo, Toyama 930-11
(Received July 21, 1980)

Synopsis. The copyrolysis of 1,2,3-trichloropropane and methanol gave 1,2-dichloro-3-methoxypropane as well as dichloropropenes and their derivatives. The formation of 1,2-dichloro-3-methoxypropane is also described.

Significant amounts of methoxy compounds are obtained by the copyrolyses of such allylic compounds as 3,4-dichloro-1-butene and 1,4-dichloro-2-butenes with methanol on activated alumina.[1,2] Allylic halides have been reported to undergo bimolecular nucleophilic replacement reactions in solutions.[3-5] On the other hand, the reaction of 1,2,3-trichloropropane (TCP) with methanolic sodium hydroxide affords only 2,3-dichloropropene (2,3-DCP), and scarcely no formation of 1,2-dichloro-3-methoxypropane (DCM) is observed.[6] The formation of DCM, which is formed by substituting a methoxyl group for a α-chlorine of TCP, characterizes the copyrolysis of TCP and methanol on activated almina. It is a great difference in comparison with the previous works that TCP is substituted by a methoxyl group at the α-position. The copyrolysis of TCP and methanol on activated alumina was carried out under various conditions in order to understand the formation of DCM.

Results and Discussion

Time Factor(W/F). The time factor was varied by adjusting the feed rate of TCP (F : g-mol/h), the weight of catalyst (W : g) being kept at 20 g. The TCP was mixed with methanol at the mole ratio of 1.00 : 12.7. The product distributions in the copyrolysis with various time factors at 250 °C are shown in Table 1. 2,3-Dichloropropene and 1,3-dichloropropene are abbreviated as 2,3-DCP and 1,3-DCP respectively. As the time factor increased, the conversion of TCP and the formation of such methoxy compounds as DCM were conclusively increased.

Mole Ratio(MeOH/TCP). A 20 g portion of the catalyst was placed in the middle of the reactor, the reaction temperature being kept at 300 °C. Mixtures of TCP and methanol were prepared at various mole ratios, while the time factor was kept constant at 416.3 (g of catalyst/g-mol of TCP/h). Figure 1 shows the effect of the mole ratio on the product composition.

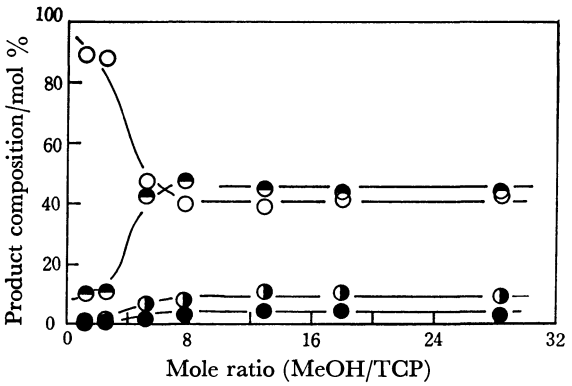

Fig. 1. The effect of the mole ratio on the product composition.
Reaction temperature: 300 °C, W/F=416.3 (g·h/g-mol). ○: TCP, ◓: $CH_2=CClCH_2Cl+CH_2=CCl-CH_2OMe$, ◑: $CHCl=CHCH_2Cl+CHCl=CHCH_2-OMe$, ●: DCM.

With a mole ratio of more than 7.0, the conversion of TCP remained constant, regardless of the mole ratio.

Reaction Temperature. TCP was mixed with methanol at the mole ratio of 1.0 : 12.7. The mixture was fed in over 20 g of activated alumina at a constant temperature with various feed rates. As the reaction temperature increased, the conversion of TCP increased. The effect of the reaction temperature on the conversion of TCP into DCM is shown in Fig. 2. Because of the decomposition of DCM on the alumina surface at higher temperatures, the yield of DCM showed a maximum value at 270 °C. DCM might catalytically dehydrochlorinate to the chloro(methoxy)propenes.

The methoxide anion generated on the basic sites of alumina[7] might play an important role, much as in the copyrolyses of allylic chlorides and chloroethanes with methanol.[1,2,8] However, it has been suggested that a β-chlorine of TCP was abstracted on the acidic sites of alumina, while a carbonium ion was formed and converted into 1,3-DCP (E1). E2 and S_N2 reactions were predominant in the copyrolysis of TCP and methanol on activated alumina, as is shown in Fig. 1. 2,3-DCP and 1,3-DCP were substituted for a chlorine in the allyl position with methanol to form chloro-

Table 1. Product distribution (mol %) in the copyrolysis of TCP and methanol on activated alumina at 250 °C

Products	W/F (g·h/g-mol)					
	208.1	312.5	416.2	614.3	832.4	1248.6
$CH_2=CClCH_2OCH_3$	0.87	1.22	2.19	2.79	5.41	8.92
cis-$CHCl=CHCH_2OCH_3$	1.07	1.46	1.49	2.37	3.19	4.95
2,3-DCP	2.71	4.72	3.06	2.51	5.14	5.05
cis-1,3-DCP	0.17	0.15	0.12	0.10	0.17	0.14
trans-1,3-DCP	0.05	0.04	0.22	0.21	0.04	0.03
DCM	3.35	3.11	3.91	4.92	5.63	6.02
TCP	91.78	89.30	89.01	87.10	80.42	74.89

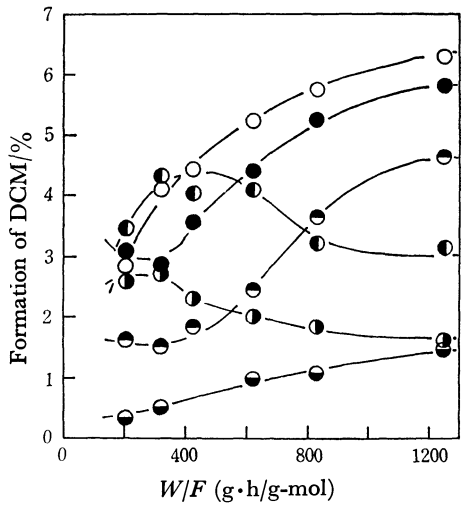

Fig. 2. The effect of the reaction temperature on the formation of DCM.
Mole ratio (MeOH/TCP): 12.7, reaction temperature (°C); ◓: 200, ◒: 230, ●: 250, ○: 270, ◐: 300, ◑: 330.

(methoxy)propenes, according to the reaction mechanisms described in a previous paper.[2]

Therefore, the reaction scheme can be given by the following equations:

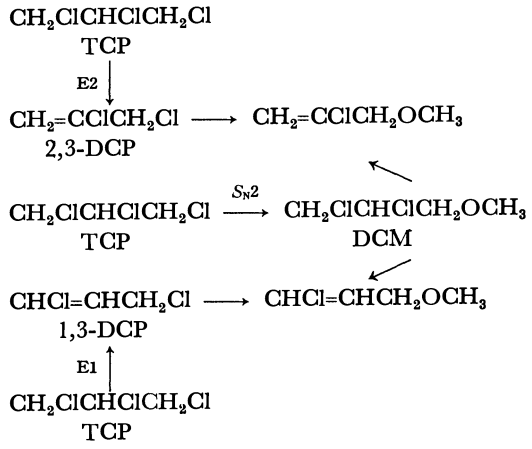

Experimental

Catalyst. The activated alumina (KHO-24) was obtained from the Sumitomo Chemical Co.; the particle diameter was in the range of 2—4 mm.

Reagents. The methanol was purchased from the Nakarai Chemicals as guaranteed-reagent-grade. TCP of a guaranteed-reagent-grade was obtained from the Tokyo Kasei Co. 2,3-DCP, *cis*- and *trans*-1,3-DCP were purchased from the Tokyo Kasei Co. as extra-pure-grade. These reagents were used without further purification.

Equipment and Procedure. The experiments were conducted a continuous-flow type reactor, the details of which were reported in a previous paper.[8]

Analytical Methods. The IR, NMR, and mass spectra were recorded on a Hitachi 125 spectrophotometer, a JMN-MH 100 spectrometer using TMS as the internal standard, and a Hitachi RMU-6MG spectrometer respectively. Gas-chromatographic analyses were performed on a Shimadzu GC-5A apparatus using a 2 m×3 mm column with 10% PEG 6000 operating at 100 °C with a helium flow.

Syntheses of Authentic Samples. *DCM*: Allyl methyl ether, generated by the action of allyl chloride with sodium hydroxide in methanol, was chlorinated in carbon tetrachloride. The DCM thus obtained was distilled at atmospheric pressure; bp 169.5 °C.

Chloro(methoxy)propenes: Chloro(methoxy)propenes were prepared from 2,3-DCP and 1,3-DCP by modifying the method of Henne and Haeckl.[6]

Identification of Products. The crude solution obtained by the copyrolysis was poured into water. The organic layer was taken up and washed with water, dried ($CaCl_2$), and distilled. Each component of the products was separated by means of VPC. The identification was carried out by a comparison of their IR, NMR, and MS spectra with those of authentic samples. The spectroscopic data are as follows:

2-Chloro-3-methoxypropene. IR (cm^{-1}): 720 (C-Cl), 900 (C=C(H)H), 1110 (C-O-C), 2830 (-OMe), 2940 ($-CH_2-$), NMR (CCl_4) δ (ppm): 3.17 (3H, s) [$-OCH_3$], 3.75 (2H, s, t) [$-CH_2OMe$], 5.09 (H, s, m)[H(Cl)C=C], 5.17 (H, s. m) [H(C=C)CH_2OMe], MS (*m/e*) (%): P+2=108 (2.5), P+1= 107 (5.0), P=106 (6.0), P−1=105 (5.4), 71 (100), 45 (81), 41 (100).

cis-*1-Chloro-3-methoxypropene.* IR (cm^{-1}): 750 (C-Cl), 1110 (C-O-C), 1630 (H(H)C=C), 2820 (-OMe), 2920 ($-CH_2-$)NMR (CCl_4) δ (ppm): 3.16 (3H, s) [$-OCH_3$], 3.91 (2H, d, d) [$-CH_2OMe$], 5.63 (H, d, t) [=C(CH_2OMe)H], 5.83 (H, d, t) [=C(Cl)H], MS (*m/e*) (%): P+2=108 (3.2), P+1= 107 (12.4), P=106 (3.6), P−1=105 (20.6), 75 (100), 71 (100), 45 (100), 41 (100).

trans-*1-Chloro-3-methoxypropene.* IR (cm^{-1}): 800 (C-Cl), 930 (H(H)C=C), 1110 (C-O-C), 2820 (-OMe), 2920 ($-CH_2-$), NMR (CCl_4) δ (ppm): 3.15 (3H, s) [$-OCH_3$], 3.70 (2H, d, d) [$-CH_2OMe$], 5.70 (H, d, t) [=C(CH_2OMe)H], 5.84 (H, d, t) [=C(H)Cl], MS (*m/e*) (%): P+2=108 (0.3), P+1= 107 (3.4), P=106 (2.4), P−1=105 (6.4), 71 (100), 41 (59).

DCM. IR (cm^{-1}): 740 (C-Cl), 1130 (C-O-C), 2830 (-OMe), 2940 ($-CH_2-$), NMR (CCl_4) δ (ppm): 3.40 (3H, s) [$-OCH_3$], 3.62 (2H, q) [$-CH_2OMe$], 3.72 (2H, q) [$-CH_2Cl$], 4.00 (H, m) [-CHCl-], MS (*m/e*) (%): P+4=146 (1.4), P+2= 144 (5.6), P=142 (7.6), 45 (100).

References

1) K. Shinoda, *Nippon Kagaku Kaishi*, **1977**, 1785.
2) K. Shinoda, *Nippon Kagaku Kaishi*, **1977**, 1789.
3) W. G. Young and L. J. Andrews, *J. Am. Chem. Soc.*, **66**, 421 (1944).
4) L. J. Andrews and R. E. Kepner, *J. Am. Chem. Soc.*, **70**, 3456 (1948).
5) L. F. Hatch and S. G. Ballin, *J. Am. Chem. Soc.*, **71**, 1039 (1949).
6) A. L. Henne and F. W. Haeckl, *J. Am. Chem. Soc.*, **63**, 2692 (1941).
7) J. R. Jain and C. N. Pallai, *J. Catal.*, **9**, 322 (1967).
8) K. Shinoda, *Bull. Chem. Soc. Jpn.*, **47**, 2406 (1974).

The Reduction of 2-Benzylidene-3(2*H*)-benzofuranones with Lithium Aluminium Hydride–Aluminium Chloride

Kazu KUROSAWA* and Yasuhiro MORITA

Department of Chemistry, Faculty of Science, Kumamoto University, 2-39-1, Kurokami, Kumamoto 860

(Received July 30, 1980)

Synopsis. The reduction of various 2-benzylidene-3(2*H*)-benzofuranones with lithium aluminium hydride–aluminium chloride in ether gave the corresponding 2-benzylbenzofurans in moderate yields. The reduction of 6-methoxy-2-(4-methoxybenzoyl)benzofuran also yielded 6-methoxy-2-(4-methoxybenzyl)benzofuran.

Although the syntheses of 2-benzylidene-3(2*H*)-benzofuranones (**1**) (aurones) were investigated in detail,[1] the synthesis of 2-benzylbenzofurans (**2**) which have the same carbon skeleton has not been reported. Our interest in the preparation of new C_6–C_3–C_6 type compounds[2,3] led us to examine the reduction of **1** with lithium aluminium hydride–aluminium chloride. It has often been observed that the reduction of α,β-unsaturated carbonyl compounds with lithium aluminium hydride–aluminium chloride proceeds with a double bond migration.[4-10] Therefore, it could be expected that the reduction of **1** with these reagents gives stable 2-benzylbenzofuran (**2**) rather than 2-benzylidene-2,3-dihydrobenzofuran (**3**) (Fig. 1).

2-Benzylidene-3(2*H*)-benzofuranones (**1a—h**) were prepared from 2′-hydroxychalcones by the procedures reported by Donnelly *et al.*[11] and by one of the authors.[12] When 6-methoxy-2-(4-methoxybenzylidene)-3(2*H*)-benzofuranone (**1d**) was treated with lithium aluminium hydride in ether, followed by the addition of aluminium chloride, a single product was obtained. Its NMR showed the presence of two methoxyl groups [δ=3.72 (3H, s) and δ=3.75 (3H, s)], a methylene group [δ=3.93 (2H, s)], a vinylic proton [δ=6.11 (1H, broad s)], and aromatic protons [δ=6.5—6.9 (4H, m) and δ=6.95—7.3 (3H, m)]. The IR spectrum showed absorptions at 1625, 1615, and 1590 cm^{-1}. The reduction of 6-methoxy-2-(4-methoxybenzoyl)benzofuran[13] (**4**) with lithium aluminium hydride–aluminium chloride yielded identical **2d**. These results indicate that the product is not 6-methoxy-2-(4-methoxybenzylidene)-2,3-dihydrobenzofuran (**3**, R=OCH_3), but 6-methoxy-2-(4-methoxybenzyl)benzofuran (**2d**). The oxidation of **2d** with manganese(IV) oxide gave **4**.

Seven other 2-benzylidene-3(2*H*)-benzofuranones (**1a—c** and **1e—h**) were also subjected to the reduction, which gave the corresponding 2-benzylbenzofurans (**2a—c** and **2e—h**) in moderate yields. The results are shown in Table 1. The reduction of **1b** with lithium aluminium hydride without the addition of aluminium chloride gave an intractable mixture of products. This may be due to the instability of the allylic alcohol formed by the reduction of **1b**. In the reduction of **1a**, 3-(2-hydroxyphenyl)-1-phenyl-1-propene (**5**) was obtained together with 2-benzylbenzofuran (**2a**), which was the major product. There were a number of minor products which could not be purified.

Thus it can be concluded that the reduction of 2-benzylidene-3(2*H*)-benzofuranones (**1**) with lithium aluminium hydride–aluminium chloride can be used for a preparation of 2-benzylbenzofuran derivatives (**2**).

TABLE 1. THE REDUCTION OF 2-BENZYLIDENE-3(2*H*)-BENZOFURANONES (**1a—h**) WITH LITHIUM ALUMINIUM HYDRIDE–ALUMINIUM CHLORIDE IN ETHER AT ROOM TEMPERATURE

Entry	Substrate	Reaction conditions: Molar ratio of substrate: $LiAlH_4$: $AlCl_3$	Time/min A[a]	Time/min B[b]	2-Benzylbenzofuran(**2**) (yield/%)[c]
1	**1a**[14]	1 : 2 : 2	60	60	36[d]
2	**1b**[12]	1 : 2 : 2	60	105	78
3	**1c**[15]	1 : 2 : 2	60	90	57
4	**1d**[12]	1 : 2 : 2	60	120	59
5	**1e**[12]	1 : 2 : 2	60	90	41
6	**1f**[12]	1 : 2 : 2	60	60	64
7	**1g**[12]	1 : 4 : 4	240	90	48[e]
8	**1h**[12]	1 : 2 : 2	60	60	40

a) Time before addition of $AlCl_3$. b) Time after addition of $AlCl_3$. c) The yields are based on the amount of the substrate used. d) **5** was obtained as a minor product in a 16% yield. e) **1g** (4%) was recovered.

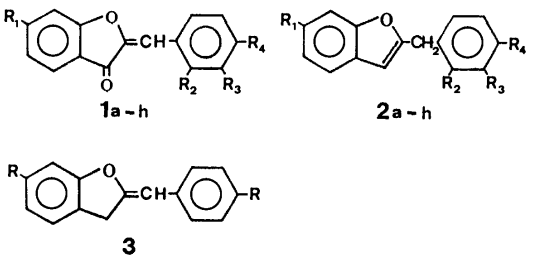

3

a: R_1=R_2=R_3=R_4=H b: R_1=R_2=R_3=H, R_4=OCH_3
c: R_2=R_3=R_4=H, R_1=OCH_3 d: R_2=R_3=H, R_1=R_4=OCH_3
e: R_1=R_3=H, R_2=R_4=OCH_3 f: R_3=H, R_1=R_2=R_4=OCH_3
g: R_2=H, R_1=R_3=R_4=OCH_3 h: R_1=R_2=R_3=R_4=OCH_3

Fig. 1.

Experimental

All the ^1H NMR spectra were recorded for the carbon tetrachloride solution with a Hitachi-Perkin-Elmer R-24 spectrometer, with tetramethylsilane as the internal standard. The IR spectra were taken for the chloroform solution on a JASCO grating spectrometer, while the UV spectra were recorded for the methanol solution, unless otherwise stated, with a Hitachi EPS-3T spectrophotometer. The high-resolution mass spectra were recorded on JMS-OlSG-2 instrument with direct inlet at 75 eV. The melting points were determined with a Yanagimoto micro-melting point apparatus and were not corrected.

2-Benzylidene-3(2H)-benzofuranones (***1a—h***). **1a—e** and **1g** were prepared by the procedure described by Donnelly *et al.*,[11] and **1f** and **1h** were obtained by the oxidation[12] of the

corresponding 2'-hydroxychalcones with manganese(III) acetate.

*Reduction of 2-Benzylidene-3(2H)-benzofuranones (**1a**—**h**) with Lithium Aluminium Hydride–Aluminium Chloride.* The general procedure for the reduction of **1** was as follows. To a stirred solution of lithium aluminium hydride (2 mmol) in anhydrous ether (30 ml), a 2-benzylidene-3(2*H*)-benzofuranone (**1**) (1 mmol) was added and the reaction mixture was stirred at room temperature for the time shown in Table 1. Then aluminium chloride (2 mmol) was added and the mixture was again stirred for the time shown in Table 1. The reaction mixture was passed through a silica gel column, eluting with ether, and the ether was evaporated. The crude product was chromatographed on TLC and crystalline products were recrystallized from ethanol. In the case of **1a**, the reaction mixture was treated with 1 M sulfuric acid (30 ml) and extracted with ether. The ethereal solution was washed with a saturated sodium chloride solution and then evaporated. The resulting liquid was chromatographed on TLC with benzene as the developing solvent.

*2-Benzylbenzofuran (**2a**)*: Colorless liquid (lit,[16] bp_{15} 180—185 °C); IR 1600 and 1618 cm^{-1}; UV λ_{max} (ε) 251 (17000), 280 (4770), and 287 nm (4690); NMR δ=3.97 (2H, s, $-CH_2-$), 6.17 (1H, s, =CH–), and 6.9—7.5 (9H, m, aromatic).

*3-(2-Hydroxyphenyl)-1-phenyl-1-propene (**5**)*: Colorless liquid (lit,[4] mp 67—68 °C); IR 975, 3340, and 3600 cm^{-1}; UV (EtOH)[4] λ_{max} (ε) 254 (18100), 277_{sh} (6260), 284_{sh} (4950), 293_{sh} (2180), and 304 nm (1240); NMR δ=3.58 (2H, m, $-CH_2-$), 5.0 (1H, broad s, OH), 6.32 (2H, m, –CH=CH–), and 6.5—7.4 (9H, m, aromatic). When the methylene group at δ=3.58 was irradiated, the vinyl protons became singlet.

*2-(4-Methoxybenzyl)benzofuran (**2b**)*: MP 60—62 °C; IR 1590 and 1615 cm^{-1}; UV λ_{max} (ε) 253 (17000), 280 (6310), and 287 nm (6170); NMR δ=3.73 (3H, s, OCH_3), 4.00 (2H, s, $-CH_2-$), 6.28 (1H, broad s, =CH–), 6.6—7.4 (8H, m, aromatic) (Found: C, 80.78; H, 5.61%. Calcd for $C_{16}H_{14}O_2$: C, 80.64; H, 5.92%).

*2-Benzyl-6-methoxybenzofuran (**2c**)*: Colorless liquid; IR 1580 and 1625 cm^{-1}; UV λ_{max} (ε) 252 (17000) and 292 nm (6780); NMR δ=3.69 (3H, s, OCH_3), 3.97 (2H, s, $-CH_2-$), 6.11 (1H, broad s, =CH–), 6.5—6.85 (2H, m, $H_{(5)}$ and $H_{(7)}$), 7.11 (1H, d, J=8.5 Hz, $H_{(4)}$), and 7.13 (5H, s, Ph); MS *m/e* 238.0989 (100%, M^+) (Calcd for $C_{16}H_{14}O_2$, MW 238.0994), 223 (49%, M^+-15), and 161 (26%, $C_{10}H_9O_2$).

*6-Methoxy-2-(4-methoxybenzyl)benzofuran (**2d**)*: Mp 90—91 °C; UV λ_{max} (ε) 255 (18600) and 291 nm (8320) (Found: C, 76.44; H, 5.81%. Calcd for $C_{17}H_{16}O_3$: C, 76.10; H, 6.01%).

*2-(2,4-Dimethoxybenzyl)benzofuran (**2e**)*: Colorless liquid; IR 1585 and 1610 cm^{-1}; UV λ_{max} (ε) 251 (16200), 280 (7550), and 287 nm (7650); NMR δ=3.62 (3H, s, OCH_3), 3.64 (3H, s, OCH_3), 3.90 (2H, s, $-CH_2-$), 6.10 (1H, broad s, =CH–), 6.0—6.4 (2H, m, aromatic), and 6.9—7.4 (5H, m, aromatic); MS *m/e* 268.1144 (100%, M^+) (Calcd for $C_{17}H_{16}O_3$, MW 268.1099) 253 (78%, M^+-15), 237 (62%, M^+-31), and 131 (90%, C_9H_7O).

*2-(2,4-Dimethoxybenzyl)-6-methxybenzofuran (**2f**)*: Colorless liquid; IR 1585 and 1615 cm^{-1}; UV λ_{max} (ε) 253 (19400) and 289 nm (8780); NMR δ=3.69 (3H, s, OCH_3), 3.71 (3H, s, OCH_3), 3.72 (3H, s, OCH_3), 3.90 (2H, s, $-CH_2-$), 6.03 (1H, broad s, =CH–), 6.2—7.3 (6H, m, aromatic); MS *m/e* 298.1161 (43.8%, M^+) (Calcd for $C_{18}H_{18}O_4$, MW 298.1205), 283 (16%, M^+-15), 267 (14%, M^+-31), and 161 (13%, $C_{10}H_9O_2$).

*2-(3,4-Dimethoxybenzyl)-6-methoxybenzofuran (**2g**)*: Mp 63—64 °C; IR 1595 and 1625 cm^{-1}; UV λ_{max} (ε) 253 (20000) and 290 nm (10100); NMR δ=3.68 (9H, s, $3\times OCH_3$), 3.87 (2H, s, $-CH_2-$), 6.09 (1H, broad, s, =CH–), 6.55—7.3 (6H, m, aromatic) (Found: C, 72.41; H, 6.22%. Calcd for $C_{18}H_{18}O_4$: C, 72.46; H, 6.08%).

*6-Methoxy-2-(2,3,4-trimethoxybenzyl)benzofuran (**2h**)*: Colorless liquid; IR 1580, 1590, and 1620 cm^{-1}; UV λ_{max} (ε) 253 (17300) and 292 nm (6900); NMR δ=3.71 (3H, s, OCH_3), 3.75 (3H, s, OCH_3), 3.78 (6H, s, $2\times OCH_3$), 3.93 (2H, s, $-CH_2-$), 6.11 (1H, broad s, =CH–), 6.45 (1H, d, J=9.0 Hz, $H_{(5')}$), 6.5—6.9 (3H, m, $H_{(5)}$, $H_{(6')}$, and $H_{(7)}$), and 7.19 (1H, m, $H_{(4)}$); MS *m/e* 328.1316 (100%, M^+) (Calcd for $C_{19}H_{20}O_5$, MW 328.1311), 313 (55%, M^+-15), 297 (25%, M^+-31), and 161 (49%, $C_{10}H_9O_2$).

*Reduction of 6-Methoxy-2-(4-methoxybenzoyl)benzofuran (**4**).* To a stirred solution of lithium aluminium hydride (43.4 mg) in anhydrous ether (20 ml), **4** (140.8 mg) was added at room temperature and the reaction mixture was stirred for 50 min. Aluminium chloride (141.7 mg) was added and the reaction mixture was further stirred for 96 min. After working-up in a manner similar to the above experiments, **2d**, mp 90—91 °C (111 mg, 83%), was obtained.

*Oxidation of 6-Methoxy-2-(4-methoxybenzyl)benzofuran (**2d**).* A mixture of **2d** (134 mg), freshly prepared manganese(IV) oxide (1 g), and anhydrous ether (30 ml) was heated under reflux for 8 h. After manganese (IV) oxide was removed by filtration, the ether was distilled off and the resulting solid was recrystallized from ethanol to give **4** (93.4 mg, 66%), mp 149 °C (lit,[13] mp 149 °C).

The authors wish to thank Professor Hitoshi Takeshita and Assistant Professor Akira Mori of Research Institute of Industrial Science, Kyushu University, for their kind arrangements for the mass spectra measurements.

References

1) E. Ochiai and S. Fujise, "Jikken Kagaku Koza," ed by M. Kotake, Maruzen, Tokyo (1958), Vol. 21, Part 2, p. 65.
2) K. Kurosawa, A. Hashiba, and H. Takahashi, *Bull. Chem. Soc. Jpn.*, **51**, 3612 (1978).
3) K. Kurosawa and F. Araki, *Bull. Chem. Soc. Jpn.*, **52**, 529 (1979).
4) T. Hase, *Acta Chem. Scand.*, **22**, 2845 (1967).
5) B. L. Verma, P. N. Verma, and M. M. Bokadia, *Indian J. Chem.*, **2**, 565 (1965).
6) B. R. Brown, *J. Chem. Soc.*, **1952**, 2756.
7) A. J. Birch and M. Slaytor, *Chem. Ind. (London)*. **1956**, 1524.
8) O. H. Wheeler and J. L. Mateos, *Chem. Ind. (London)*, **1957**, 395.
9) R. Albrecht and C. Tamm, *Helv. Chim. Acta*, **40**, 2216 (1957).
10) J. Broome, B. R. Brown, A. Roberts, and A. M. S. White, *J. Chem. Soc.*, **1960**, 1406.
11) J. A. Donnelly, M. J. Fox, and T. C. Sharma, *Tetrahedron*, **35**, 875 (1979).
12) K. Kurosawa and J. Higuchi, *Bull. Chem. Soc. Jpn.*, **45**, 1132 (1972).
13) K. Kurosawa, K. Yamaguchi, H. Ohki, and Y. Nagata, *Bull. Chem. Soc. Jpn.*, **53**, 1769 (1980).
14) P. Friedländer and J. Neudörfer, *Ber.*, **30**, 1077 (1897).
15) J. Brüll and P. Friedländer, *Ber.*, **30**, 297 (1897).
16) R. Stoemer, C. W. Chydenius, and E. Schinn, *Ber.*, **57**, 72 (1924).

Palladium Catalyzed Cyanocarbonylation of Organic Iodides

Masato TANAKA

National Chemical Laboratory for Industry, Yatabe, Tsukuba, Ibaraki 305

(Received August 14, 1980)

Synopsis. Palladium complex catalyzed carbonylation of aromatic and heteroaromatic iodides in the presence of potassium cyanide gave aroyl cyanides in fair to excellent yields, offering the first example of cyanocarbonylation.

Palladium complex catalyzed carbonylation of organic halides has been successfully performed, but limited to synthesis of carboxylic acids and their derivatives such as esters, aldehydes, and amides.[1] We have recently found that ketones are formed in excellent yield when the reaction was run with organotin compounds.[2] In the catalytic cycle of this reaction, an electrophilic attack of an acyl-palladium intermediate on an organotin compound is postulated. As a continuation of halide carbonylation with carbon nucleophiles, we tried the reaction with potassium cyanide. This paper describes the results of this entirely new carbonylation, namely, cyanocarbonylation of halides.

$$R\text{-}X + CO + KCN \longrightarrow R\text{-}CO\text{-}CN + KX$$

The cyanocarbonylation was effected using a palladium complex, $C_6H_5PdI[P(C_6H_5)_3]_2$, as a catalyst precursor. This complex is believed to be an intermediate in other carbonylation reactions of organic halides by palladium complex catalysts.[3] Aromatic and heteroaromatic iodides were smoothly carbonylated in the presence of potassium cyanide to give aroyl cyanide in fair to excellent yields. Nitriles were generally formed as by-products, but the amount was negligible except the iodothiophene reaction. The catalysis of this reaction was quite sensitive to the ratio of potassium cyanide to the palladium complex. At a much higher ratio than that specified in Table 1 for each halide, the reaction did not work well. This may be connected with poisoning effect of cyanide ion[4] which makes the palladium catalyst inactive. The extent of poisoning seemed to be very dependent on the structure of halides. Thus, the yield of aroyl or acyl cyanide from ethyl *p*-iodobenzoate, *p*-dibromobenzene, *p*-bromoacetophenone, *β*-bromostyrene, and benzyl chloride was some 10% at best or even below under the analogous reaction conditions. This may be because of diminishing catalytic activity due to poisoning which eventually led to the cease of catalysis.[5] Hopefully, the poisoning problem will be solved by a slow addition of potassium cyanide to the reaction system as Cassar and co-workers did for nickel-catalyzed cyanation of aromatic halides.[6]

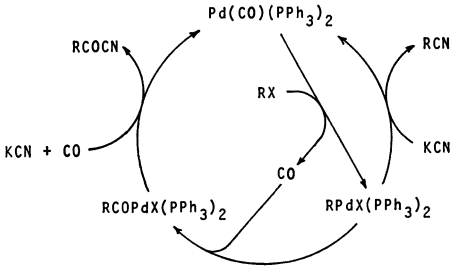

Scheme 1.

The cyanocarbonylation can be accounted for by the mechanism outlined in scheme 1.[3] Oxidative addition of an iodide to the palladium(0) complex affords an aryl-palladium intermediate which is then transformed into an aroyl-palladium species through CO insertion. Electrophilic attack of potassium cyanide on the aroyl moiety of the latter species would give aroyl cyanide, regenerating the palladium(0) species. Another possibility would be displacement of iodide from the aroyl-palladium-iodide complex by cyanide. The aroyl-palladium-cyanide complex thus formed would undergo reductive elimination to give aroyl cyanide and the palladium(0) catalyst.

In summary, a novel aroyl cyanide synthesis occurs by carbonylation of aryl iodides with potassium cyanide. This paper offers another useful variation of halide carbonylation.

Experimental

Melting points were determined using a Yanagimoto hot-stage apparatus and are uncorrected. PMR and IR spectra were recorded on a Hitachi R-40 and JASCO A-302 spectrometers, respectively. Tetrahydrofuran was dried and purified by the standard techniques. Iodophenylbis(triphenylphosphine)palladium[8] and 2-iodothiophene[9] were prepared by the published methods. Other halides were purchased and purified before use.

Carbonylation of Iodobenzene. General Procedures: A 27 ml stainless steel autoclave was charged with iodophenylbis(triphenylphosphine)palladium (20.9 mg, 2.5×10^{-2} mmol),

Table 1. Cyanocarbonylation of organic halides[a]

RX / mmol	KCN / mmol	Amount of solvent/ml	P_{CO} / atm	Time / h	RCOCN[b] (%)	RCN[b] (%)
C_6H_5I (7.5)	3.75	1.5	20	20	91 (83)	1.4
C_6H_5I (3.75)	3.98	1.5	20	19	48	1.7
p-$CH_3OC_6H_4I$ (7.5)	3.75	1.5	20	15	92 (88)	1.1
p-$CH_3C_6H_4I$ (5.63)	1.88	0.75	8	18	69 (64)	2.5
2-C_4H_3SI (2.82)	0.94	0.5	8	24	45	22.0

a) 100 °C, $PhPdI(PPh_3)_2=2.5\times10^{-2}$ mmol, tetrahydrofuran solvent. b) Estimated by GLC analysis using internal standard. Yields for isolated samples are shown in parentheses. c) 2-Thienyl iodide.

dry potassium cyanide powder (245 mg, 3.75 mmol), iodobenzene (0.84 ml, 7.5 mmol), and 1.5 ml of tetrahydrofuran. Carbon monoxide was introduced at 20 atm. The mixture was stirred at 100 °C overnight, diluted with ether, and was filtered. The solvent was evaporated. The residue was subjected to chromatography through a short silica gel column, iodobenzene being first eluted by hexane followed by benzoyl cyanide eluted by benzene, 410 mg, 83.2%. A short-path distillation gave an analytical sample, mp 33.0—34.0 °C. PMR ($CDCl_3$) δ 7.45—8.30 (aromatic). IR (melt) 2220 (ν_{CN}) and 1677 cm^{-1} (ν_{CO}). Found: C, 73.24; H, 3.91%. Calcd for C_8H_5NO: C, 73.27; H, 3.91%.

Melting points, spectral, and analytical data for other aroyl cyanides were as follows.

p-*Methoxybenzoyl Cyanide*: Mp 58.1—59.0 °C. PMR ($CDCl_3$) δ 3.99 (3H, s, CH_3), 7.10 (2H, d, J=9 Hz, meta protons), and 8.16 (2H, d, ortho protons). IR (nujol) 2220 (ν_{CN}) and 1675 cm^{-1} (ν_{CO}). Found: C, 67.06; H, 4.37%. Calcd for $C_9H_7NO_2$: C, 67.08; H, 4.38%.

p-*Methylbenzoyl Cyanide*: Mp 49.5—50.0 °C. PMR ($CDCl_3$) δ 2.53 (3H, s, CH_3), 7.45 (2H, d, J=8 Hz, meta protons), and 8.11 (2H, d, ortho protons). IR (melt) 2225 (ν_{CN}) and 1670 cm^{-1} (ν_{CO}). Found: C, 74.31; H, 4.84%. Calcd for C_9H_7NO: C, 74.47; H, 4.86%.

2-Thenoyl Cyanide: Mp 53.1—54.6 °C. PMR ($CDCl_3$) δ 7.25—7.43 (1H, m, 4-position) and 7.93—8.22 (2H, m, 3- and 5-positions). IR (melt) 2220 (ν_{CN}) and 1648 cm^{-1} (ν_{CO}). Found: C, 52.55; H, 2.31%. Calcd for C_6H_3NOS: C, 52.54; H, 2.20%.

The author is grateful to Dr. Ikuei Ogata for a fruitful discussion.

References

1) A. Schoenberg and R. F. Heck, *J. Am. Chem. Soc.*, **96**, 7761 (1974); A. Schoenberg, I. Bartoletti, and R. F. Heck, *J. Org. Chem.*, **39**, 3318 (1974); A. Schoenberg and R. F. Heck, *ibid.*, **39**, 3327 (1974); J. K. Stille and P. K. Wong, *ibid.*, **40**, 532 (1975); M. Hidai, T. Hikita, Y. Wada, Y. Fujikura, and Y. Uchida, *Bull. Chem. Soc. Jpn.*, **48**, 2075 (1975); L. Cassar, M. Foà, and A. Gardano, *J. Organometal. Chem.*, **121**, C55 (1976).

2) M. Tanaka, *Tetrahedron Lett.*, **1979**, 2601.

3) For the mechanism of halide carbonylation reactions in the presence of palladium complex catalysts, see P. E. Garrou and R. F. Heck, *J. Am. Chem. Soc.*, **98**, 4115 (1976).

4) A similar effect of cyanide ion on the nickel or palladium complex catalyzed cyanation of aromatic halides has been reported. See the Refs. 6 and 7.

5) From a β-bromostyrene reaction where the catalytic activity had completely lost at the early stage, a palladium complex which exhibited a ν_{CN} band at 2140 cm^{-1} could be recovered. Its structure has not been studied in detail.

6) L. Cassar, S. Ferrara, and M. Foà, *Adv. Chem. Ser.*, **132**, 252 (1974).

7) K. Takagi, T. Okamoto, Y. Sakakibara, A. Ohno, S. Oka, and N. Hayama, *Bull. Chem. Soc. Jpn.*, **49**, 3177 (1976).

8) P. Fitton and E. A. Rick, *J. Organometal. Chem.*, **28**, 287 (1971).

9) *Org. Synth.*, Coll. Vol. II, 357 (1943).

A Method for Independent Determination of Equilibrium Constant and Molar Absorptivity of Molecular Complexes from Spectrophotometric Data†

Bejoy Kumar SEAL,* Harideb SIL, Manas BANERJEE, and Dulal Chandra MUKHERJEE**,***

Department of Chemistry, Burdwan University, W. Bengal, India

** *Department of Chemistry, University of Calcutta, 92, Acharya Prafulla Chandra Road, Calcutta-700009, India*

(Received May 30, 1980)

Synopsis. Two separate equations, one cubic in K and the other quadratic in ε, have been developed for calculating K and ε of molecular complexes independently of each other. The equations on testing with various spectrophotometric data yielded values of K and ε which agree with those obtained by others using well known procedures.

After the important observation of Benesi and Hildebrand[1] and subsequently the interpretation of the phenomenon by Mulliken,[2] several equations[1,3-6] have been derived and tested for the evaluation of equilibrium constants of molecular complexes. The applicability of these equations are, for some obvious reasons,[7] specific. The reported values of K and ε while showing fair constancy among the values obtained by different investigators for strong complexes deviate widely for weak complexes. Various explanations have been suggested[8-19] to account for the observed discrepancies. However, Person[8] has mentioned about some criteria for the reliable determination of equilibrium constant in the case of weak molecular complexes. But this requires a previous knowledge of an approximate value of the equilibrium constant and, due to solubility restriction of the components, it is difficult to fulfil the criteria in all cases. Briegleb[20] and Person[8] indicated that one difficulty in obtaining reliable values of K and ε for weak molecular complexes may be due to the difficulty in the independent determination of K and ε using spectral method, although it is easy to determine the product $K\varepsilon$.

In the present communication we have developed single parameter equations for independent evaluation of K and ε from spectral data, and these equations have been tested for different systems, including strong and weak CT complexes, using the experimental data of various workers from literature.

Principle and Derivation of the Equations

Equation for K Independent of ε. Considering the following equilibrium

$$A + D \rightleftharpoons AD \qquad (1)$$

the equilibrium concentration, C_c, in terms of the equilibrium constant K, is given by

$$C_c = \frac{1+K(C_A^0+C_D^0)-[\{K(C_D^0-C_A^0)\}^2+2K(C_A^0+C_D^0)+1]^{1/2}}{2K} \qquad (2)$$

where C_A^0 and C_D^0 denote the initial concentrations of the acceptor and donor respectively. Substituting $C_c=d/\varepsilon l$ in Eq. 2, we obtain

$$d = \frac{1+Kx-(yK^2+2xK+1)^{1/2}}{2K}\varepsilon l \qquad (3)$$

where $d=d_{obsd}-d_A^0-d_D^0$, $\varepsilon=\varepsilon_C-\varepsilon_A-\varepsilon_D$, l is the optical path length, d's are the optical densities and ε's the molar absorptivities and $x=C_A^0+C_D^0$ and $y=(C_D^0-C_A^0)^2$.

Now, the ratio of the optical densities of the ith and jth solution

$$\frac{d_i}{d_j} = \frac{1+x_iK-(y_iK^2+2x_iK+1)^{1/2}}{1+x_jK-(y_jK^2+2x_jK+1)^{1/2}} \qquad (4)$$

which on rearrangement gives

$$z+(d_ix_j-d_jx_i)K = d_i(y_jK^2+2x_jK+1)^{1/2} - d_j(y_iK^2+2x_iK+1)^{1/2} \qquad (5)$$

where $z=d_i-d_j$. Equation 5, on squaring and rearrangement, yields

$$pK^2+qK+r = r\{(y_jK^2+2x_jK+1)(y_iK^2+2x_iK+1)\}^{1/2} \qquad (6)$$

where

$$p = (d_ix_j-d_jx_i)^2 - d_i^2y_j - d_j^2x_i$$
$$q = 2\{(d_ix_j-d_jx_i)Z - d_i^2x_j - d_j^2x_i\}$$

and

$$r = -2d_id_j = z^2 - d_i^2 - d_j^2.$$

Equation 6 on squaring, rearranging and using the following substitutions

$$a = p^2 - r^2y_iy_j,\ b=2(pq-r^2x_iy_j-r^2y_ix_j),$$
$$g = q^2 + 2pr - r^2y_i - r^2y_j - 4r^2x_ix_j,$$

and $h = 2(qr-r^2x_i-r^2x_j)$,

yields

$$aK^4 + bK^3 + gK^2 + hK = 0$$

or,

$$aK^3 + bK^2 + gK + h = 0 \qquad (7)$$

Since $K \neq 0$

This cubic equation in K is independent of ε. Equation 7 has been solved numerically by a general method of root determination for real polynomials. The Burroughs system program Library subroutine RLPOLY has been employed for this part, which uses a three-stage variable-shift iteration method developed by Jenkins and Traub.[21] Equation 7 is more general than that developed and used by Nagakura[7] in connection with his studies on amine–iodine systems.

Equation for ε Independent of K. Considering a pair, ith and jth of solutions, we get from the equation

$$K/C_c = \frac{1}{(C_A^0-C_C)(C_D^0-C_c)}$$

an equation

$$\frac{d_j}{d_i} = \frac{S_j\varepsilon^2l^2+d_j^2-d_jx_j\varepsilon l}{S_i\varepsilon^2l^2+d_i^2-d_ix_i\varepsilon l} \qquad (8)$$

where $S=C_A^0C_D^0$. Equation 8, after suitable rearrangement and substitution yields

$$m\varepsilon^2l^2 - n\varepsilon l + f = 0 \qquad (9)$$

† An abstract of this work was presented at the 14th European Congress on Molecular Spectroscopy held in Frankfurt in September (3—7), 1979.

*** Present address: Eye Research Institute of Retina Foundation, 20 Staniford St., Boston, MA 02114, U.S.A.

where

$m = d_jS_i - d_iS_j$, $n = d_id_j(x_i - x_j)$, and $f = d_id_j(d_i - d_j)$.

Equation 9 is quadratic in εl and yields

$$\varepsilon = [n \pm (n^2 - 4mf)^{1/2}]/2\,ml \qquad (10)$$

which is independent of K. Only one value of ε is accepted, neglecting the physically inadmissible one.

Results and Discussion

Equations 7 and 10 have been solved by Burroughs 6700 systems using our program for calculating the values of K and ε, independent of one another, of a large number of wide variety of molecular complexes, using the experimental data of different investigators from existing literature. These include the data on strong and weak complexes, wavelength dependence of K and ε and also the effects of solvents. Some representative results are shown in Table 1. The noted differences in many cases may be due to the different approach of the two types of methods. While our procedure evaluates K and ε independent of each other, the reported ones require the separation of K and ε, through the intercept and slope of linear plots, from the product $K\varepsilon$ occurring in the derived equations.

The accuracy of the proposed method like any pairwise evaluation procedure depends on the precision of the experimental data. With precise data our equations yield values of K and ε whose standard deviations lie within 1 to 12%.

Sincere thanks are due to Prof. S. K. Siddhanta, Head of the Department of Chemistry, Burdwan University for constant encouragement received during progress of the work.

Table 1.

System	K/mol l^{-1}		ε/l mol^{-1} cm^{-1}	
	Our method	Reported	Our method	Reported
TCPA[a]-Phenanthrene[22]	7.5	7.3	712	714
TCPA-Biphenyl[22]	2.6	2.9	552	500
TCPA-Quinoline[23]	30.75	26	130	132
TCPA-2-Methylquinoline[23]	14.6	15	228	226
TBPA[a]-Phenanthrene ($CHCl_3$)[24]	0.8	0.9	612	513
TBPA-Phenanthrene (C_6H_6)[24]	3.49	3.41	470	455
TBPA-Acenaphthene ($CHCl_3$)[24]	2.97	2.8	878	909
TBPA-Acenaphthene (C_6H_6)[24]	1.29	1.46	1084	769
DDQ[a]-Toluene[25]	0.94	0.92	2214	2332
DDQ-Biphenyl[25]	0.95	0.96	1212	1366
DDQ-Phenanthrene[25]	14.15	14.54	2041	2000
DDQ-Fluorene[25]	15.22	14.60	1612	1666
Chloranil-Indole[26]	2.83	2.86	1557	1510
1,3,5-Tricyanobenzene-TMPD[27] [a]	4.07	4.0	369	354
1,3,5-Trinitrobenzene-Diphenylamine[28]	0.5	0.4	1410	1390
ICl-Dioxane (335 nm)[29]	22.94	23.86	814	830
ICl-Dioxane (345 nm)	21.97	23.12	1123	1146
ICl-Dioxane (355 nm)	22.47	23.07	1338	1391
ICl-Dioxane (365 nm)	22.77	23.03	1357	1509
Br_2-Naphthalene[21]	0.235	0.23	5608	5660
I_2-DMA[a] (CH_2Cl_2)[30]	1.32	1.4	661	624
I_2-Naphthalene[31]	0.25	0.26	7479	7250
I_2-Pyrene[32,34] [b]	40	43	143	161
I_2-α-Picoline[33]	50.52	50	1032	1000
I_2-Isoquinoline[33]	40.1	39.4	1607	1538
I_2-Pyridine[33]	47.29	43.74	947	952

a) TCPA: tetrachlorophthalic anhydride, TBPA: tetrabromophthalic anhydride, DDQ: 2,3-dichloro-5,6-dicyano-*p*-benzoquinone, TMPD: *N,N,N',N'*-tetramethyl-*p*-phenylenediamine, DMA: dimethyl acetamide. b) For Pyrene-iodine system the iterative value of K obtained by processing the data in Ref. 32 is 43 mol l^{-1}. The recalculated value of molar absorptivity is 140 l mol^{-1} cm^{-1}.

References

1) H. Benesi and J. H. Hildebrand, *J. Am. Chem. Soc.*, **70**, 2832 (1948); **71**, 2703 (1949).
2) R. S. Mulliken, *J. Am. Chem. Soc.*, **74**, 811 (1952).
3) J. A. A. Ketelaar, C. Vande Stolpe, A. Goudsmit, and W. Dzcubas, *Rec. Trav. Chim.*, **71**, 1104 (1952).
4) R. L. Scott, *Rec. Trav. Chim.*, **75**, 787 (1956).
5) R. Foster, *J. Chem. Soc.*, **1957**, 5098.
6) N. J. Rose and R. S. Drago, *J. Am. Chem. Soc.*, **81**, 6138 (1959).
7) J. Rose, "Molecular Complexes," Oxford (1967), pp. 37—39.
8) W. B. Person, *J. Am. Chem. Soc.*, **87**, 167 (1965).
9) P. H. Emslie, R. Foster, C. A. Fyfe, and I. Horman, *Tetrahedron*, **21**, 2843 (1965).
10) S. Carter, *J. Chem. Soc., A*, **1968**, 404.
11) S. D. Ross and M. M. Labes, *J. Am. Chem. Soc.*, **79**, 76 (1957).
12) G. D. Johnson and R. E. Bowen, *J. Am. Chem. Soc.*, **87**, 1655 (1965).
13) S. Carter, J. N. Murrel, and E. J. Rosch, *J. Chem. Soc.*, **1965**, 2048.
14) D. W. Tanner and T. C. Bruice, *J. Phys. Chem.*, **70**, 3816 (1966).
15) J. D. Childs, S. D. Christian, and J. Glundness, *J. Am. Chem. Soc.*, **94**, 5657 (1972).
16) R. Foster, "Organic Charge-transfer Complexes," Academic Press, London and New York (1969), pp. 160—165 and 171—173.
17) S. D. Christian and E. E. Jucker, *J. Phys. Chem.*, **74**, 214 (1970).
18) R. S. Mulliken and W. B. Person, "Molecular complexes," Wiley-Interscience, New York, N. Y. (1969), pp. 92—100.
19) G. Briegleb, "Elektronen-Donator-Acceptor-Komplexe," Springer-verlag, Berlin (1961).
20) G. Briegleb, "Elektronen-Donator-Acceptor-Komplexes," Springer-verlag, Berlin (1961), p. 203.
21) M. A. Jenkins and J. F. Traub, Tech. Report No. CS 138 (1969), Computer Science Dept., Stanford University, California.
22) M. Chowdhury and S. Basu, *Trans. Faraday Soc.*, **56**, 335 (1960).
23) M. Chowdhury, *J. Phys. Chem.*, **65**, 1899 (1961).
24) R. D. Srivastava and P. D. Gupta, *Spectrochim. Acta, Part A*, **24**, 373 (1968).
25) R. D. Srivastava and G. Prasad, *Spectrochim. Acta, Part A*, **22**, 825, 1869 (1966).
26) R. Foster and P. Hanson, *Trans. Faraday Soc.*, **60**, 2189 (1964).
27) R. Foster and J. J. Thompson, *Trans. Faraday Soc.*, **59**, 2287 (1963).
28) R. Foster, D. Hammick, and A. A. Wardley, *J. Chem. Soc.*, **1953**, 3817.
29) A. I. Popov, C. C. Bisi, and W. B. Person, *J. Phys. Chem.*, **64**, 691 (1960).
30) R. S. Drago, T. F. Bells, and R. J. Niedzielski, *J. Am. Chem. Soc.*, **88**, 2717 (1966).
31) N. W. Blake, H. Winston, and J. A. Patterson, *J. Am. Chem. Soc.*, **73**, 4437 (1951).
32) R. Bhattacharya and S. Basu, *Trans. Faraday Soc.*, **54**, 1286 (1958).
33) J. Nagchaudhuri and S. Basu, *Trans. Faraday Soc.*, **55**, 898 (1959).
34) B. K. Seal, A. K. Mukherjee, and D. C. Mukherjee, *Bull. Chem. Soc. Jpn.*, **52**, 2088 (1979).

Mass Spectral Dehydration and Decarboxylation in Cyclic α-Hydroxy Acids, Alcohols, and Carboxylic Acids

Khalid H. Akkari, Michael S. Matta, and Timothy B. Patrick*
Department of Chemistry, Southern Illinois University, Edwardsville, Illinois 62026, U.S.A.
(Received June 30, 1980)

Synopsis. The relative ease of mass spectral decarboxylation is greater than the ease of mass spectral dehydration as determined from a comparison of the alcohols **1a—4a** with acids **1b—4b**. However, the relative ease is reversed in α-hydroxy acids **2c—4c**; and dehydration predominates over decarboxylation.

The dehydration of alcohols and the decarboxylation of acids are both well known mass spectrometric processes.[1] Alcohol dehydration in the mass spectrometer usually occurs by a 1,4 or 1,3 elimination pathway as opposed to the 1,2 elimination found in solution chemistry. Mass spectrometric decarboxylation of aliphatic acids often occurs by simple α-fragmentation similar to reactions observed in solution. α-Hydroxy acids, although little studied, prefer a fragmentation pathway that favors decarboxylation over dehydration.[2]

A problem of considerable importance is the analysis of hydroxy and carboxy metabolites occurring in natural processes.[3,4] In connection with this problem we have conducted a study designed to determine the preferred mass spectrometric fragmentation pathway, decarboxylation or dehydration, in a series of acyclic and cyclic alcohols, acids, and α-hydroxy acids. The substances studied, shown below, also permit an evaluation of ring size effects on the fragmentation process.

Results and Discussion

The results are summarized in Tables 1 and 2. Dehydration in alcohols **1a—4a** occurs with less facility than does decarboxylation in acids **1b—4b**. Only 2-hydroxytetralin (**3a**) can dehydrate by a favorable 1,3 elimination pathway whereas a 1,2 elimination is required in **1a** and **2a**. Decarboxylation appears as a very favorable process in the cyclic acids

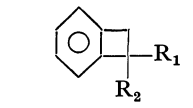

	R_1	R_2
1a	OH	H
1b	COOH	H

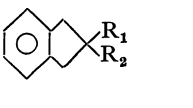

	R_1	R_2
2a	OH	H
2b	COOH	H
2c	OH	COOH

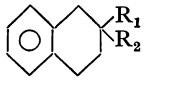

	R_1	R_2
3a	OH	H
3b	COOH	H
3c	OH	COOH

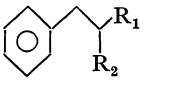

	R_1	R_2
4a	OH	H
4b	COOH	H
4c	OH	COOH

Fig. 1.

Table 1. Relative ion intensities for the loss of H_2O and COOH in **1a—4c**[a]

Compd	$[M-H_2O]^{+\cdot}$ [b]	$[M-CO_2H]^+$	Base peak[c]
1a	0	—	$[T]^+$
2a	23	—	$[CH_3T]^+$
3a	100	—	$[M-H_2O]^{+\cdot}$
4a	4	—	$[T]^+$
1b	—	67	$[M]^{+\cdot}$
2b	—	100	$[M-COOH]^+$
3b	—	100	$[M-COOH]^+$
4b	—	18	$[T]^+$
2c	68	26	$[M-CO_2H, H_2O]^+$
3c	46	26	$[M-CO_2H, H_2O]^+$
4c	11	0	$[T]^+$

a) Intensities are related to the base peak (100%) in each spectrum. b) $[T]^+$ means tropylium ion. c) M means molecular ion.

1b, **2b**, and **3b**, and is responsible for formation of the base peak in **2b** and **3b**. Decarboxylation can occur by either a thermal reaction or α-fission process. The high abundance of the M—COOH peak is moderately independent of ring size. Both acyclic analogies **4a** and **4b** prefer fragmentation to form the tropylium ion, but the trend of decarboxylation favored over dehydration is still evident in these compounds.

Interestingly fragmentation of α-hydroxy acids **2c—4c** shows that dehydration is preferred over decarboxylation in contrast to the monosubstituted analogues previously discussed. This phenomenon can be explained by using either a 1,2 thermal elimination process which produces a conjugated acid or a 1,3 elimination which produces a saturated carboxy cation radical as shown below.[5]

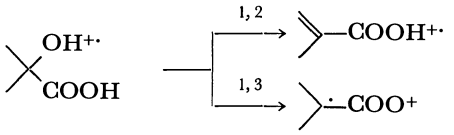

The base peak in the cyclic hydroxy acids **2c** and **3c** arises through loss of both COOH and H_2O. The acyclic hydroxy acid shows preference for α-fission to form the tropylium ion, similar to the acyclic compounds **4a** and **4b**.

In conclusion, decarboxylation is preferred over dehydration in the monosubstituted compounds, but the trend reverses in α-hydroxy acids with dehydration preferred over decarboxylation. Furthermore, dehydration and decarboxylation occur in the hydroxy acids, perhaps synergystically, to produce the base peak.

TABLE 2. MASS SPECTRA (80 eV) OF COMPOUNDS **1a—4c**[a]

1a	120 (62, $[M]^{+\cdot}$), 119 (88, $[M-H]^{+}$), 106 (4, $[M-CH_2]^{+\cdot}$), 91 (100, [tropylium]$^{+}$), 77 (4, $[M-C_2H_3O]^{+}$), 65 (25), 51 (8), 39 (16).
2a	134 (35, $[M^{+\cdot}]$), 116 (23, $[M-H_2O]^{+\cdot}$), 117 (28, $[M-H_3O]^{+}$), 105 (100, [CH_3−tropylium]$^{+}$), 91 (28, [tropylium]$^{+}$), 79 (39), 77 (40), 65 (19), 63 (25), 51 (40).
3a	148 (8, $[M]^{+\cdot}$), 130 (100, $[M-H_2O]^{+\cdot}$), 115 (32), 104 (75, $[M-CH_3CHO]^{+\cdot}$), 91 (20, [tropylium]$^{+}$), 79 (25), 51 (15).
4a	122 (22, $[M]^{+\cdot}$), 104 (4, $[M-H_2O]^{+\cdot}$), 92 (62, $[M-CH_2O]^{+\cdot}$), 91 (100, [tropylium]$^{+}$), 77 (7, $[M-C_2H_5O]^{+}$), 65 (29), 51 (4), 39 (16).
1b	148 (100, $[M]^{+\cdot}$), 147 (50, $[M-H]^{+}$), 131 (49, $[M-OH]^{+}$), 120 (60, $[M-CO]^{+\cdot}$), 103 (67, $[M-COOH]^{+}$), 91 (51, [tropylium]$^{+}$), 77 (51), 51 (32).
2b	162 (76, $[M]^{+\cdot}$), 118 (81, $[M-CO_2]^{+\cdot}$), 119 (100, $[M-COOH]^{+}$), 116 (61, $[M-COOH_2]^{+\cdot}$).
3b	176 (1, $[M]^{+\cdot}$), 159 (30, $[M-OH]^{+}$), 148 (18, $[M-CO]^{+\cdot}$), 131 (100, $[M-CO_2H]^{+}$), 104 (10, $[M-CH_2{=}CHCOOH]^{+\cdot}$), 91 (25, [tropylium]$^{+}$), 77 (8).
4b	150 (56, $[M]^{+\cdot}$), 132 (15, $[M-H_2O]^{+\cdot}$), 106 (11, $[M-CO_2]^{+\cdot}$), 105 (18, $[M-COOH]^{+}$), 91 (100, [tropylium]$^{+}$), 77 (15), 65 (10), 51 (14).
2c	178 (7, $[M]^{+\cdot}$), 160 (68, $[M-H_2O]^{+\cdot}$), 134 (22, $[M-CO_2]^{+\cdot}$), 135 (26, $[M-CO_2H]^{+}$), 116 (98, $[M-CO_2, H_2O]^{+\cdot}$), 115 (100, $[M-CO_2H, H_2O]^{+}$), 105 (58, $[M-HOCCO_2]^{+}$), 104 (60, $[M-HOCCOOH]^{+\cdot}$), 91 (13, [tropylium]$^{+}$), 77 (50), 65 (30).
3c	192 (3, $[M]^{+\cdot}$), 174 (46, $[M-H_2O]^{+\cdot}$), 148 (12, $[M-CO_2]^{+\cdot}$), 147 (26, $[M-CO_2H]^{+}$), 129 (100, $[M-H_2O, CO_2H]^{+\cdot}$), 105 (10, $[M-HOCCO_2]^{+}$), 104 (54, $[M-HOCCO_2H]^{+\cdot}$), 77 (12).
4c	166 (12, $[M]^{+\cdot}$), 148 (11, $[M-H_2O]^{+\cdot}$), 91 (100, [tropylium]$^{+}$), 77 (12), 65 (19), 51 (11).

a) *m/e* (relative abundance [probable genesis]). The genesis is based on standard mass spectrometric fragmentations.

Experimental

The compounds used in this study have been previously described.[6,7] Mass spectra were recorded on a low-resolution Varian MAT-111 magnetic sector instrument at 80 eV. All samples were introduced into the ionization chamber by the use of a direct probe at ambient temperature. The mass spectra are reported in Table 2.

This research was supported by the African-American Institute, through the Republic of Sierra Leone, in the form of a fellowship to K.H.A., and by the National Institutes of Health Grant GM 18652 (M.S.M).

References

1) F. W. McLafferty, "Interpretation of Mass Spectra," 2nd ed, W. A. Benjamin, Reading, Mass. (1973), Chap. 6; H. Budziekiewicz, C. Djerassi, and D. H. Williams, "Interpretation of Mass Spectra of Organic Compounds, Holden-Day, San Francisco (1964).

2) H. C. Hill, "Introduction to Mass Spectrometry," Heyden and Son, London (1966).

3) H. Budziekiewicz, C. Djerassi, and D. H. Williams, "Structure Elucidation of Natural Products by Mass Spectrometry. Steroids, Triterpenes, and Related Classes," Holden-Day, San Francisco (1964), Vol. 2.

4) "Biochemical Applications of Mass Spectrometry," ed by G. R. Waller, Wiley-Interscience, New York, N. Y. (1972), Section III.

5) A referee has suggested the elimination of OH from COOH in the H_2O loss as an alternative to the 1,3 elimination. A test of this interesting possibility requires labeling experiments which have not yet been performed.

6) M. S. Matta and M. F. Rhode, *J. Am. Chem. Soc.*, **94**, 8573 (1972).

7) T. B. Patrick and P. H. Patrick, *J. Am. Chem. Soc.*, **95**, 5192 (1973).

  Bull. Chem. Soc. Jpn., 54, 643—647 (1981)

The Concentration Dependence of the Apparent Molal Adiabatic Compressibility of Electrolytes in Water

Masao SAKURAI,* Tsuyoshi KOMATSU, and Tsurutaro NAKAGAWA

Department of Polymer Science, Faculty of Science, Hokkaido University, Sapporo 060

(Received April 8, 1980)

The apparent molal adiabatic compressibilities of NaCl, KCl, NaBr, and KBr in water have been measured in the concentration range from 0.01 to 1 mol kg^{-1} at 5, 25, and 45 °C. The results have been fitted to a Redlich-type equation: $\phi_{Ks}=\phi_{Ks}^{\circ}+S_{Ks}c^{1/2}+B_{Ks}c$. The limiting slope, S_{Ks}, was found experimentally as 5.6×10^{-4} at an ordinary temperature. Convenient equations for the conversion of adiabatic to isothermal compressibilities have been derived; the limiting slope for isothermal compressibility, S_{KT}, should be larger than S_{Ks} at all the temperatures studied. The value of S_{Ks} determined experimentally has been compared with that predicted from the S_{KT} values calculated by Mathieson and Conway, by Millero, and by Bradley and Pitzer.

In earlier papers,[1] we have shown that the effects of polar groups on the hydrophobic hydration play an important role in the volumetric behavior of aqueous organic electrolyte solutions. Compressibility study is of great use in obtaining further information concerning the structural effects. For dilute nonelectrolyte solutions, the limiting partial molal adiabatic compressibility, $\bar{K}_s^{\circ}(=\phi_{Ks}^{\circ})$, can readily be determined from a linear plot of the apparent molal adiabatic compressibility, ϕ_{Ks}, against the molal concentration;[2] on the contrary, the reliable estimation of $\bar{K}_s^{\circ}$ of electrolytes may be difficult for reasons to be described below.

In dilute solutions, the apparent molal quantities of electrolytes are usually fitted to a Redlich-type equation in terms of molarity, c:

$$\phi_X = \phi_X^{\circ} + S_X c^{1/2} + B_X c, \quad (1)$$

where ϕ_X° is the limiting apparent (partial) molal quantity, S_X is the theoretical slope given by the limiting Debye-Hückel law, and B_X is a deviation constant. The values of ϕ_X° and B_X can be determined from a linear plot of $(\phi_X-S_Xc^{1/2})$ against c. For the apparent molal adiabatic compressibility, unfortunately such a linear plot cannot be obtained because the limiting slope, S_{Ks}, has not yet been calculated. Mathieson and Conway[3] measured the ϕ_{Ks} values of various electrolytes in a very low concentration range and represented its concentration dependence by this simple limiting-law equation:

$$\phi_{Ks} = \phi_{Ks}^{\circ} + S_{Ks}m^{1/2}. \quad (2)$$

This extrapolation procedure, however, may be disadvantageous, since Eq. 2 holds only in highly dilute solutions (where the $B_{Ks}c$ term in Eq. 1 should be negligible) and the error in ϕ_{Ks} is progressively increased with a decrease in the concentration.

In our opinion, a more reliable evaluation of ϕ_{Ks}° would be based on Eq. 1; therefore, it is necessary to estimate the limiting slope, S_{Ks}. In a preliminary study,[4] we derived a simple relation for the conversion of the limiting slope for isothermal compressibility, S_{KT}, to S_{Ks} and showed that S_{KT} is larger by about 10% than S_{Ks} at 25 °C. In the present paper, we wish to report on our measurements of the adiabatic compressibility of NaCl, KCl, NaBr, and KBr solutions at 5, 25, and 45 °C and compare the experimental with the theoretical S_{Ks} values in order to obtain a reasonable value of the limiting slope.

Experimental

All the salts used were of a "Merck Ultra Pure" grade and were dried at 50 °C *in vacuo*. All the solutions were prepared in molalities with doubly distilled water.

The ultrasonic velocities, v cm s^{-1}, in solutions were measured at 5, 25, and 45 °C using a "sing-around" velocimeter which is capable of a precision of 1 cm s^{-1}. The details of the apparatus and procedure have been reported elsewhere.[2] The densities, d g ml^{-1}, of the solutions were determined at 5 and 45 °C with a float densimeter described previously.[5,6]

The adiabatic compressibility, β_s bar^{-1}, and the apparent molal adiabatic compressibility, ϕ_{Ks} ml mol^{-1} bar^{-1}, are given by:

$$\beta_s = 10^6/v^2d, \quad (3)$$

$$\phi_{Ks} = 10^3(\beta_s-\beta_{s0})/c + \beta_{s0}\phi_V, \quad (4)$$

where ϕ_V ml mol^{-1} is the apparent molal volume related to the solution density and the solute molecular weight, M_2, by

$$\phi_V = 10^3(d_0-d)/d_0c + M_2/d_0. \quad (5)$$

Here, the subscript zero refers to pure water. The density and sound-velocity data for water were taken from Kell[7] and from Del Grosso and Mader[8] respectively.

Results and Discussion

The sound velocities in aqueous NaCl, KCl, NaBr, and KBr solutions were measured relative to pure water at 5, 25, and 45 °C from 0.01 to 1 mol kg^{-1}. The results are given in Table 1,[9] along with the calculated ϕ_{Ks} values.

In dilute solutions, the concentration dependence of ϕ_V is represented by the Redlich-type equation 1:[10]

$$\phi_V = \phi_V^{\circ} + S_V c^{1/2} + B_V c. \quad (6)$$

The values of ϕ_V° and B_V obtained at 5 and 45 °C are summarized in Table 2, along with the values derived by Desnoyers *et al.*[11] at 25 °C. The ϕ_V° values obtained here were in good agreement with the literature values, and the accuracy of the data was confirmed by the additivity principle.[10] The additivity was within ±0.05 ml mol^{-1} units. On the other hand, the agreement between the B_V values obtained here and the literature values was less satisfactory, especially at 45 °C.

TABLE 2. LIMITING APPARENT MOLAL VOLUMES AND DEVIATION CONSTANTS OF ALKALI HALIDES IN WATER AT 5, 25, AND 45 °C

	ϕ_V°/ml mol^{-1}			B_V/l ml mol^{-2}		
	5 °C	25 °C[a]	45 °C	5 °C	25 °C[a]	45 °C
NaCl	14.09	16.62	17.64	0.76	−0.03	−0.74
KCl	24.67	26.87	27.59	0.82	0.10	−0.61
NaBr	20.58	23.48	24.83	0.64	−0.26	−1.64
KBr	31.07	33.73	34.72	0.74	−0.16	−1.34

a) Ref. 11.

Error in ϕ_{Ks}. The accuracy of ϕ_{Ks} depends on the precision of the determination of the density, the sound velocity, and the concentration. In this study, the apparent molal volume, and hence the density, of each solution used for the sound-velocity measurement were evaluated from Eqs. 5 and 6, where a succesive approximation method was applied to the conversion of the molality to molarity. In view of the accuracies of the ϕ_V° and B_V data mentioned above, it seems that the uncertainty in d or ϕ_V may be small, but it *increases* as the concentration is *increased.*

Now, neglecting the density errors and differentiating Eqs. 3 and 4, the uncertainty in ϕ_{Ks} caused by uncertainties in the sound velocity and concentration, δv and δc, is given by:

$$\delta\phi_{Ks} = \frac{2\times10^3\beta_s}{c}\left(\frac{\delta v}{v}\right) + \frac{10^3(\beta_{s0}-\beta_s)}{c}\left(\frac{\delta c}{c}\right). \quad (7)$$

The absolute error in determining the sound velocity is $\delta v = \pm 1$ cm s^{-1}; hence, the relative error is $(\delta v/v) = \pm 6.6\times10^{-6}$. The uncertainty due to the sound-velocity error rapidly decreases with an increase in the concentration, whereas the uncertainty due to the concentration error is approximately constant. The scatter of ϕ_{Ks} values at higher concentrations observed in Fig. 1 is, therefore, mainly due to the concentration error. We estimated the uncertainty in the concentration determination to be within 0.1%, *i.e.*, $(\delta c/c) = 10^{-3}$. Thus, the total error in ϕ_{Ks} is:

$$\delta\phi_{Ks} = \frac{1}{c}\{1.33\times10^{-2}\beta_s + (\beta_{s0}-\beta_s)\}. \quad (8)$$

Experimental Estimation of S_{Ks}. A typical example of the plot of ϕ_{Ks} against $c^{1/2}$ is shown in Fig. 1, from which it is apparent that the simple limiting-law equation 2 does not hold in the concentration range studied. Alternatively, our ϕ_{Ks} data should be represented by Eq. 1. Thus,

$$\phi_{Ks} = \phi_{Ks}^\circ + S_{Ks}c^{1/2} + B_{Ks}c. \quad (9)$$

Taking into account the large error in ϕ_{Ks} at lower concentrations, the estimation of three parameters was based on the relationship between β_s and c instead of on the ϕ_{Ks} *vs.* $c^{1/2}$ plot. The combination of Eqs. 4, 6, and 9 leads to an expression with this form:

$$10^3(\beta_s-\beta_{s0}) = (\phi_{Ks}^\circ - \beta_{s0}\phi_V^\circ)c + (S_{Ks}-\beta_{s0}S_V)c^{3/2} + (B_{Ks}-\beta_{s0}B_V)c^2. \quad (10)$$

The parameters, ϕ_{Ks}°, S_{Ks}, and B_{Ks}, were calculated by the least-squares method and are given in Table 3. Since S_{Ks} corresponds to the limiting Debye-Hückel slope for adiabatic compressibility, it depends only on the temperature and solvent properties for electrolytes of a fixed valency. As is shown in Table 3, however, we could not obtain a constant S_{Ks} value for four alkali halides; furthermore, we found no simple relationship between S_{Ks} and the temperature. These empirical S_{Ks} values for various salts and temperatures ranged between 4.2×10^{-4} and 6.7×10^{-4}, with the mean value being $(5.6\pm0.7)\times10^{-4}$ ml mol$^{-3/2}$ l$^{1/2}$ bar^{-1}. This mean value is in fair agreement with that

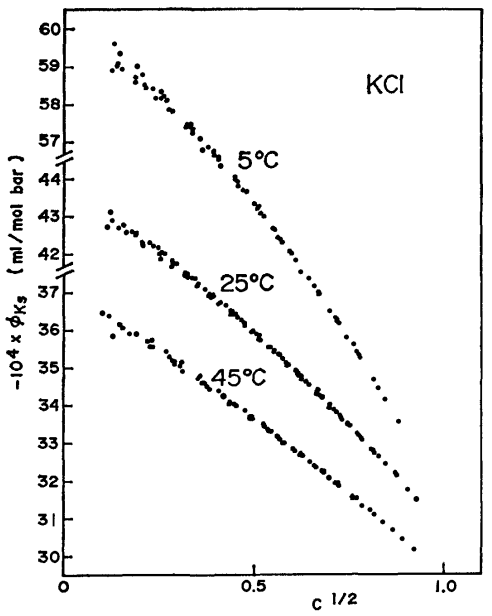

Fig. 1. ϕ_{Ks} as a function of $c^{1/2}$ for KCl in water at 5, 25, and 45 °C.

TABLE 3. PARAMETERS OF Eq. 9 DETERMINED BY USING Eq. 10 FOR SALT CONCENTRATIONS LESS THAN 0.5 mol dm^{-3}

	$-10^4\phi_{Ks}^\circ$	10^4S_{Ks}	10^4B_{Ks}
		5 °C	
NaCl	67.67 (67.91)[a]	5.12 (6.10)[a]	6.28 (5.33)[a]
KCl	60.25 (60.45)	6.72 (7.66)	6.34 (5.34)
NaBr	59.00 (59.24)	4.15 (5.05)	4.78 (3.99)
KBr	51.30 (51.36)	5.75 (6.01)	4.73 (4.49)
av.		5.43 (6.20)	
		25 °C	
NaCl	50.63 (50.59)	5.75 (5.53)	2.50 (2.77)
KCl	43.74 (43.82)	6.16 (6.50)	3.00 (2.64)
NaBr	42.91 (42.81)	4.96 (4.54)	1.65 (2.06)
KBr	35.87 (35.79)	5.85 (5.53)	1.52 (1.85)
av.		5.68 (5.52)	
		45 °C	
NaCl	42.71 (42.74)	5.16 (5.29)	1.67 (1.54)
KCl	37.10 (37.14)	6.30 (6.50)	1.31 (1.11)
NaBr	35.53 (35.46)	5.08 (4.78)	0.01 (0.29)
KBr	29.63 (29.52)	6.11 (5.61)	−0.20 (0.28)
av.		5.66 (5.54)	

a) The values in parentheses are those calculated by using Eq. 10 over the entire concentration range.

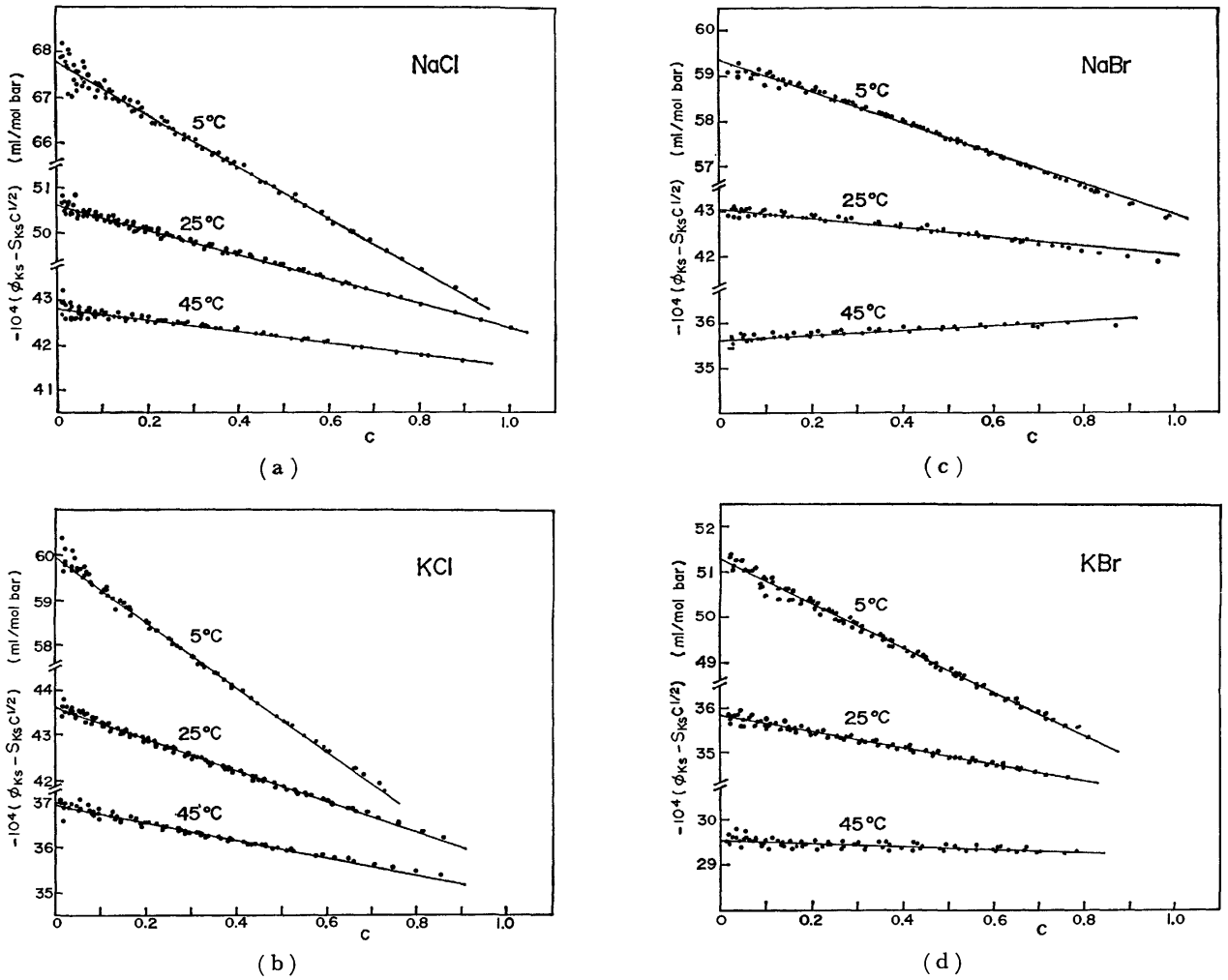

Fig. 2. $\phi_{Ks}-S_{Ks}c^{1/2}$ as a function of c for NaCl, KCl, NaBr, and KBr in water at 5, 25, and 45 °C, where S_{Ks} was taken as 5.6×10^{-4} ml mol$^{-3/2}$ l$^{1/2}$ bar^{-1}.

estimated by Mathieson and Conway[3] using Eq. 2 at very low concentrations for most 1:1 electrolytes at 25 °C.

Gucker and his co-workers[12] studied the concentration dependence of ϕ_{Ks} for some alkali halides at 25 °C. They also calculated the empirical S_{Ks} value by using Eq. 10; their mean S_{Ks} value is $(10.5\pm1.6)\times10^{-4}$, which is considerably higher than that estimated in this study. This disagreement seems to be ascribable to the fact that their work was performed at higher concentrations (up to 2—6 mol kg^{-1}) than those used here. Millero and his coworkers[13] have recently reported on their sound-velocity measurements of 28 electrolyte solutions at 25 °C and fitted the ϕ_{Ks} data to Eq. 9. The S_{Ks} values thus determined ranged between 1.74×10^{-4} and 7.79×10^{-4}. They have regarded S_{Ks} as an adjustable parameter for the purpose of the estimation of the ϕ°_{Ks} values. However, we believe that the S_{Ks} should be the limiting slope, which is independent of the electrolyte species except for the valency.

Figure 2 shows the plot of $(\phi_{Ks}-S_{Ks}c^{1/2})$ *vs.* c, where S_{Ks} was taken as 5.6×10^{-4}, irrespective of the temperature. As may be anticipated from Table 3, good linearities were obtained over the concentration range studied, except for KCl and NaBr solutions at higher concentrations. The values of ϕ°_{Ks} and B_{Ks}, estimated graphically from Fig. 2, are given in Table 4. The ϕ°_{Ks} values at 25 °C agree very well with those obtained from Eq. 2 by Mathieson and Conway.[3] This means that the absolute values of B_{Ks} are small for alkali halides at 25 °C (see Table 4) and that the

Table 4. Limiting apparent molal adiabatic compressibilities and deviation constants of alkali halides determined using $S_{Ks}=5.6\times10^{-4}$ ml mol$^{-3/2}$ l$^{1/2}$ bar^{-1}

	$-10^4\phi^{\circ}_{Ks}$ / ml mol^{-1} bar^{-1}			10^4B_{Ks} / ml mol^{-2} l bar^{-1}		
	5 °C	25 °C	45 °C	5 °C	25 °C	45 °C
NaCl	67.8	50.6	42.8	5.9	2.7	1.3
KCl	59.9	43.6	36.9	7.2	3.5	1.9
NaBr	59.3	43.0	35.6	3.4	1.0	−0.6
KBr	51.3	35.8	29.6	4.9	1.8	0.3

Literature values of $-10^4\phi^{\circ}_{Ks}$ at 25 °C: NaCl 50.5,[3] 52.88,[12] 50.5,[13] 52.79,[21] 50.8[22]; KCl 43.5,[3] 46.34,[12] 44.1,[13] 45.58,[21] 42.6[22]; NaBr 42.8,[3] 46.47,[12] 41.8[13]; KBr 36.0,[3] 35.0.[13]

Table 5. Limiting apparent molal adiabatic compressibilities of electrolytes obtained from the original sound velocity and density data of Millero *et al.*[13] Using $S_{Ks}=5.6\times10^{-4}$ at 25 °C

	$-10^4\,\phi^\circ_{Ks}$/ml mol^{-1} bar^{-1}					
	F	Cl	*Δ*	Br	I	NO_3
Na	74.8 (75.4)[a]	50.5 (50.5)	7.7	42.8 (41.8)	32.5 (31.9)	40.4 (39.9)
Δ	10.9	7.1		7.2	7.2	7.4
K	63.9 (64.5)	43.4 (44.1)	7.8	35.6 (35.0)	25.3 (23.9)	33.0 (33.0)
NH_4		20.6 (21.2)	7.6	13.0 (13.7)		

a) The values in parentheses are the results of Millero *et al.*[13]

accuracy of their ϕ_{Ks} determination is very excellent in spite of the measurements having been done at very low concentrations. The self-consistency of our data can be confirmed by the additivity principle; the differences in ϕ°_{Ks} between chlorides and bromides, or between sodium and potassium salts, show that the ϕ°_{Ks} values are additive to a precision of 0.2 ml mol^{-1} bar^{-1} at all the temperatures studied.

It is evident from Fig. 1 and Table 4 that the deviation constant, B_{Ks}, is increased with a decrease in the temperature and varies with the electrolytes. Particularly large deviations are anticipated for organic salts or polyvalent electrolytes considering that the ϕ_v data show large deviations from the limiting law for these salts.[10] These facts suggest that the extrapolation procedure based on Eq. 2 is, even in a very low concentration range, not convincingly applicable to solutions of any electolyte or at any temperature. Furthermore, as has been described in the previous section, the error in the measurement of ϕ_{Ks} becomes significantly larger as the concentration is decreased. Therefore, despite the limitations in the experimental determination of S_{Ks}, the linear extrapolation method based on Eq. 9, as shown in Fig. 2, appears to be more reliable than that based on Eq. 2 for the evaluation of ϕ°_{Ks}. Based on our linear extrapolation method, we recalculated the ϕ°_{Ks} values of several 1:1 electrolytes from the sound velocity and density data recently reported by Millero and his co-workers.[13] The results are summarized in Table 5, which gives the differences in the ϕ°_{Ks} of the cations (K^+–Na^+) and anions (Br^-–Cl^-). Compared with the results of Millero and his co-workers,[13] given in parentheses, the recalculated ϕ°_{Ks} values agree more closely with our results and the results reported by Mathieson and Conway.[3] Furthermore, it may be pointed out that the accuracy of the recalculated values was checked from the additivity of the ϕ°_{Ks}, except in the case of fluorides: $\phi^\circ_{Ks}(K^+)-\phi^\circ_{Ks}(Na^+)=(7.2\pm0.1)\times10^{-4}$ and $\phi^\circ_{Ks}(Br^-)-\phi^\circ_{Ks}(Cl^-)=(7.7\pm0.1)\times10^{-4}$. These results are in fair agreement with our results (Table 4).

Relation between S_{Ks} and S_{KT}. The difference between ϕ_{Ks} and the apparent molal isothermal compressibility, ϕ_{KT}, is also given by Eq. 1 as a function of the concentration. Thus,

$$\phi_{KT}-\phi_{Ks}=(\phi^\circ_{KT}-\phi^\circ_{Ks})+(S_{KT}-S_{Ks})c^{1/2}+(B_{KT}-B_{Ks})c. \quad (11)$$

The difference, $\phi_{KT}-\phi_{Ks}$, is related to the volume, the expansivity, and the heat capacity by:

$$\phi_{KT}-\phi_{Ks}=10^3(\delta-\delta_0)/c+\delta_0\phi_V, \quad (12)$$

$$\delta=\beta_T-\beta_s=\alpha^2T/10\sigma, \quad (13)$$

where α is the thermal expansivity and σ is the volumetric specific heat.[14] Here, α and σ can be converted to the apparent molal expansibility, ϕ_E, and heat capacity, ϕ_C, using these relations:

$$\phi_E=10^3(\alpha-\alpha_0)/c+\alpha_0\phi_V, \quad (14)$$

$$\phi_C=10^3(\sigma-\sigma_0)/c+\sigma_0\phi_V. \quad (15)$$

The combination of these equations with Eqs. 12 and 13 leads to:

$$\phi_{KT}-\phi_{Ks}=\frac{10^3\delta_0\sigma_0\{10^{-3}(\phi_E-\alpha_0\phi_V)c+\alpha_0\}^2}{\alpha_0^2c\{10^{-3}(\phi_C-\sigma_0\phi_V)c+\sigma_0\}}+\delta_0\left(\phi_V-\frac{10^3}{c}\right). \quad (16)$$

Since, as in the case of ϕ_V, the concentration dependence of ϕ_E or ϕ_C is also given by Eq. 1, Eq. 16 can be expressed in terms of ϕ°_X, S_X, and B_X (X=V, E, and C). Now, expanding this equation with respect to $c^{1/2}$, and neglecting the terms higher than $c^{3/2}$, we may rewrite it in the same form as in Eq. 11. Thus, we obtain the following simple relations:[4]

$$\phi^\circ_{KT}-\phi^\circ_{Ks}=\delta_0(2\phi^\circ_E/\alpha_0-\phi^\circ_C/\sigma_0), \quad (17)$$

$$S_{KT}-S_{Ks}=\delta_0(2S_E/\alpha_0-S_C/\sigma_0), \quad (18)$$

$$B_{KT}-B_{Ks}=\delta_0\{2B_E/\alpha_0-B_C/\sigma_0+10^{-3}(\phi^\circ_E/\alpha_0-\phi^\circ_C/\sigma_0)^2\}. \quad (19)$$

Equation 17 is the same as that derived by Desnoyers and Philip.[15] We note that, for the conversion of ϕ_{Ks} to ϕ_{KT}, Harned and Owen[14] have derived alternative formulas, which can be reduced to much simpler expressions, 17 and 18.

Since the expansivity[7] and heat capactity[16] of pure water are known, and since the limiting slopes, S_E,[17] S_C,[18] and S_{KT},[3,19,20] have been calculated, we can estimate the value of S_{Ks} from Eq. 18. The results at 5, 25, and 45 °C are given in Table 6. Unfortunately, the S_{KT} values reported in the references are inconsistent with one another; nevertheless, the calculated S_{Ks} (even S_{KT}) values are, in any event, smaller than the experimental S_{Ks} value obtained in the previous section. Mathieson and Conway[3] have stated that S_{Ks} appears experimentally to be about twice the isothermal S_{KT} value at 25 °C. The difference ($S_{KT}-S_{Ks}$) in Table 6, however, clearly shows

Table 6. Theoretical estimation of S_{Ks} from S_{KT} for 1:1 electrolytes in water at 5, 25, and 45 °C[a]

	5 °C		25 °C			45 °C	
$10^2 S_E$[b]	1.674		1.717			1.892	
S_C[c]	22.52		28.99			35.74	
$10^4\alpha_0$[d]	0.1598		2.5705			4.2260	
σ_0[e]	4.2017		4.1669			4.1383	
$10^7\delta_0$	0.0169		4.728			13.73	
$10^4(S_{KT}-S_{Ks})$	0.035		0.599			1.142	
$10^4 S_{KT}$	0.776[f]	1.9[g]	2.550[f]	3.8[g]	3.25[h]	3.913[f]	5.3[g]
$10^4 S_{Ks}$	0.741	1.9	1.951	3.2	2.65	2.771	4.2

a) Units: S_E, ml mol$^{-3/2}$ l$^{1/2}$ deg^{-1}; S_C, J mol$^{-3/2}$ l$^{1/2}$ deg^{-1}; S_{KT} and S_{Ks}, ml mol$^{-3/2}$ l$^{1/2}$ bar^{-1}; α_0, deg^{-1}; σ_0, J deg^{-1} cm^{-3}; δ_0, bar^{-1}. b) Ref. 17; c) Ref. 18; d) Ref. 7; e) Ref. 16; f) Ref. 3; g) Ref. 19; h) Ref. 20.

that the isothermal S_{KT} value should be *larger* than the adiabatic S_{Ks} value at all the temperatures studied. It seems to us that the S_{KT} values in Table 6 are too small; this may originate from difficulties in the estimation of the second derivatives of the dielectric constant and the density of water with respect to the pressure *at one atmosphere* used for the calculation of S_{KT}. It appears that a reliable S_{KT} or S_{Ks} value cannot yet be definitely determined theoretically, although S_{KT} values over a wide range of temperatures and pressures have very recently been tabulated by Bradley and Pitzer.[20] Attempts to linearize the plot of $\phi_{Ks}-S_{Ks}c^{1/2}$ against c by using $S_{Ks}=2.65\times10^{-4}$ at 25 °C were unsuccessful, even in a very low concentration range.

In conclusion, it seems to us at present that the concentration dependence of ϕ_{Ks} of the 1:1 electrolytes in dilute aqueous solutions is reasonably represented by Eq. 9, with $S_{Ks}=5.6\times10^{-4}$ ml mol$^{-3/2}$ l$^{1/2}$ bar^{-1} at an ordinary temperature, although there still remains some uncertainty as to the absolute accuracy of the S_{Ks} value.

The authors would like to thank Dr. Hatsuho Uedaira and Mr. Toshio Nakajima for their helpful discussions. The financial support of this work by a Grant-in-Aid for Scientific Research No. 174134 from the Ministry of Education, Science and Culture is gratefully acknowledged.

References

1) M. Sakurai, T. Komatsu, and T. Nakagawa, *J. Solution Chem.*, **4**, 511 (1975); *Bull. Chem. Soc. Jpn.*, **48**, 3491 (1975).
2) T. Nakajima, T. Komatsu, and T. Nakagawa, *Bull. Chem. Soc. Jpn.*, **48**, 788 (1975).
3) J. G. Mathieson and B. E. Conway, *J. Solution Chem.*, **3**, 455 (1974); *J. Chem. Soc. Faraday Trans. 1*, **70**, 752 (1974).
4) M. Sakurai, T. Nakajima, T. Komatsu, and T. Nakagawa, *Chem. Lett.*, **1975**, 971.
5) M. Sakurai, *Bull. Chem. Soc. Jpn.*, **46**, 1596 (1973).
6) T. Nakajima, T. Komatsu, and T. Nakagawa, *Bull. Chem. Soc. Jpn.*, **48**, 783 (1975).
7) G. S. Kell, *J. Chem. Eng. Data*, **12**, 66 (1967).
8) V. A. Del Grosso and C. W. Mader, *J. Acoust. Soc. Am.*, **52**, 1442 (1972).
9) Table 1 has been deposited with the Chemical Society of Japan (Document No. 8101).
10) F. J. Millero, "Water and Aqueous Solutions," ed by R. A. Horne, Wiley-Interscience, New York (1972), Chap. 13 and Appendix.
11) J. E. Desnoyers, M. Arel, G. Perron, and C. Jolicoeur, *J. Phys. Chem.*, **73**, 3346 (1969).
12) F. T. Gucker, D. Stubley, and D. J. Hill, *J. Chem. Thermodyn.*, **7**, 865 (1975).
13) F. J. Millero, G. K. Ward, and P. V. Chetirkin, *J. Acoust. Soc. Am.*, **61**, 1492 (1977).
14) H. S. Harned and B. B. Owen, "The Physical Chemistry of Electrolyte Solutions," 3rd ed, Reinhold, New York (1958), Chap. 8.
15) J. E. Desnoyers and P. R. Philip, *Can. J. Chem.*, **50**, 1094 (1972).
16) H. F. Stimson, *Am. J. Phys.*, **23**, 614 (1955).
17) F. J. Millero, *J. Phys. Chem.*, **74**, 356 (1970).
18) P. A. Leduc, J. L. Fortier, and J. E. Desnoyers, *J. Phys. Chem.*, **78**, 1217 (1974).
19) F. J. Millero, *J. Solution Chem.*, **2**, 1 (1973); F. J. Millero, G. K. Ward, F. K. Lepple, and E. V. Hoff, *J. Phys. Chem.*, **78**, 1636 (1974).
20) D. J. Bradley and K. S. Pitzer, *J. Phys. Chem.*, **83**, 1599 (1979).
21) F. T. Gucker, C. L. Chernick, and P. Roy-Chowdhury, *Proc. Natl. Acad. Sci. U.S.A.*, **55**, 12 (1966).
22) R. Garnsey and R. J. Boe, *J. Chem. Phys.*, **50**, 5222 (1969).

A Solid-state Electrochemical Study on the Phenothiazine–Iodine and Related Complexes

Toshiyuki MATSUMOTO and Yoshio MATSUNAGA*

Department of Chemistry, Faculty of Science, Hokkaido University, Sapporo 060

(Received May 30, 1980)

The electromotive force (emf) of a solid-state galvanic cell, Ag|AgI|PT–I_n, where PT–I_n is the phenothiazine–iodine complex, was examined as functions of the composition, n, and also of the temperature. Below n=2.5, a value of 616 mV was obtained at 25 °C. The emf increases stepwise to 620 mV at n=2.5 in conformity with the formation of a complex cation radical pentaiodide, as established by our earlier work. A continuous increase up to 649 mV was found before n=3, indicating the appearance of a nonstoichiometric phase covering the range from n=2.8 to 3. The upper limit of the existence region exactly corresponds with the minimum in the resistivity-composition isotherm. Similar studies with benzo[*a*]- and benzo[*c*]phenothiazines revealed the formation of three or four distinct nonstoichiometric complexes in each system. The Gibbs energy, enthalpy, and entropy of cell reactions and complex formation reactions are presented. The stability of the iodine complexes was found in the following order: benzo[*a*]phenothiazine>benzo[*c*]phenothiazine>phenothiazine.

The phenothiazine–iodine complex (PT–I_n) has been known as a semiconducting material with a relatively low electrical resistivity.[1] The vibrational spectrum of the complex at n=3, where the minimum resistivity is obtainable, has been shown to be distinctly different from that of the parent organic compound but nearly identical with that of the cation radical bromide prepared by the method of Kehrmann and Diserens.[2] Our subsequent studies have distinguished two vibrational patterns for the bromide samples,[3] and established the existence of both the simple and complex bromides.[4] The spectrum of the iodine complex is in accordance with that of the complex bromide where the two thiazine molecules share a unit positive charge and are equivalent in the time scale of infrared spectroscopy. This conclusion is in conflict with the fact that six atoms of iodine per $(phenothiazine)_2^+$ ion do not fit to the composition of any polyiodide. We have also examined the electrical properties as a function of the composition.[5] Such a study has showed that the resistivity-composition isotherm measured with polycrystalline compactions consists of three portions of smooth curves. A sharp edge is located at n= 2.5, the value at room temperature being about 800 Ω cm. At the same composition, a decrease in the activation energy for semiconduction by a factor of a half and a change in the sign of the Seebeck coefficient from negative to positive have been noted. These results clearly indicate the formation of a complex cation radical salt, $(phenothiazine)_2^+I_5^-$, and resolve, at least in part, the above-mentioned conflict. By further addition of iodine, the resistivity reaches a minimum of about 20 Ω cm at n=3 and then increases rapidly. The drastic decrease between n=2.5 and 3 was attributed to the charge carriers generated by the incorporation of extra iodine into the complex cation radical pentaiodide. However, the exact form of the incorporated iodine remains to be clarified.

Undoubtedly the careful examination of the electrical properties as functions of the composition could have served as a powerful tool available for elucidating the constitution of semiconducting phenothiazine–iodine complex. Nevertheless, we are not certain that the observed edge is indicative of the formation of a stoichiometric complex or of the ideal composition of a nonstoichiometric one. As to the resistivity minimum, it may represent the composition of a stoichiometric complex or the limit of the deviation from n=2.5 or some other stoichiometry. Moreover, the formation of other complexes which do not show significant anomalies in the isotherm cannot be ruled out. Consequently, it seemed desirable to examine the other physical quantity which depends on the composition quite differently from the electronic properties studied before. Of particular interest for this purpose are experiments on solid-state galvanic cells, as two-phase mixtures should be identified by constant electromotive force (emf), a stoichiometric complex by a discontinuous increase and a nonstoichiometric single-phase region by a continuous increase in emf with n.

Gutmann *et al.* were the first to explore solid-state galvanic cells using the electronically-conducting iodine complexes as cathodes.[6] The development of similar cells consisting of AgI-based solid electrolyte and the perylene–iodine complex has been described by Louzos *et al.*[7] Furthermore, Pampallona *et al.* have shown that iodine electrodes based on phenothiazine and its *N*-methyl derivative offer excellent prospects as practical cathodes.[8] Aside from such applied research results, attempts to determine the thermodynamic formation values for some solid iodine complexes have been made by measuring the emf of solid-state cells by Aronson *et al.* and also by McKechnie *et al.*[9,10] The complexes studied by the latter group include the phenothiazine–iodine (n=3).

Experimental

Materials. The phenothiazine was commercially obtained and purified by recrystallization and then by sublimation in a vacuum. The benzo[*a*]- and benzo[*c*]phenothiazines were prepared by the reaction of sulfur on *N*-phenyl-1- and -2-naphthylamines respectively, using a small amount of iodine as the catalyst.[11] The former thiazine was purified by recrystallization from ligroine, mp 135—136 °C. The melting point of the latter after recrystallization was found to be 177 °C, in agreement with the value reported by Knoevenagel, 176 °C;[11] however, this value was raised to 185 °C by sublimation in a vacuum. The complexes were obtained by careful grinding of the weighed

thiazine and iodine in an agate mortar in the presence of a small amount of benzene. The samples thus prepared were heated to 80 °C in a short time to complete the reaction and also to remove all traces of the solvent. The iodine contents were determined by microanalysis.

Measurements. The galvanic cell, Ag|AgI|thiazine-iodine complex (T-I_n), was assembled in the following way. A cylindrical block of Teflon with a 1-cm-diameter hole was placed on a piece of platinum plate fixed on a brass block. Silver powder and then silver iodide powder were pressed inside the Teflon cylinder. An 8-mm-diameter compaction of the iodine complex was made and was placed on the flat surface of the silver iodide. The upper surface of the compaction accommodated in the Teflon cylinder was covered with another piece of platinum plate fixed on a 1-cm-diameter brass rod with a rim, which was fitted into the hole of the second cylindrical block of Teflon. The cell placed between the two platinum electrodes was tightened employing three pairs of bolts and nuts applied to the brass block and the second block of Teflon, so that the iodine complex compaction made good contact with the silver iodide layer. Platinum leads provided electrical contact to the electrodes. The whole assembly, with a diameter of 3 cm and a height of less than 4 cm, was placed in a glass tube and dipped into an oil-bath. The temperature was regulated between room temperature and 80 °C with an accuracy better than ±0.25 °C. The emf was measured by means of a high-impedance ($\approx 10^{10}\,\Omega$) universal digital meter, Yokogawa 2502. For the readings of emf, the cell was kept at each temperature for about one hour. The measurements were made only while the temperature was increased and were repeated until steady, reproducible emf data could be attained. The emf was a linear function of the temperature in most of the examined temperature range. When the emf near room temperature deviated from the expected linear relationship, the value at 25 °C was estimated by the extrapolation of the high-temperature data.

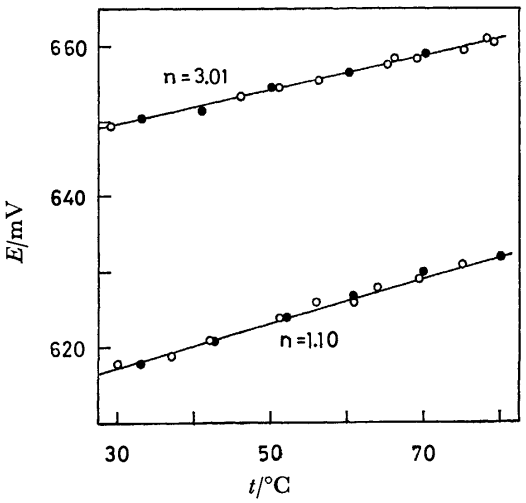

Fig. 1. Electromotive force of the solid-state cells, Ag|AgI|phenothiazine-iodine (PT-I_n).

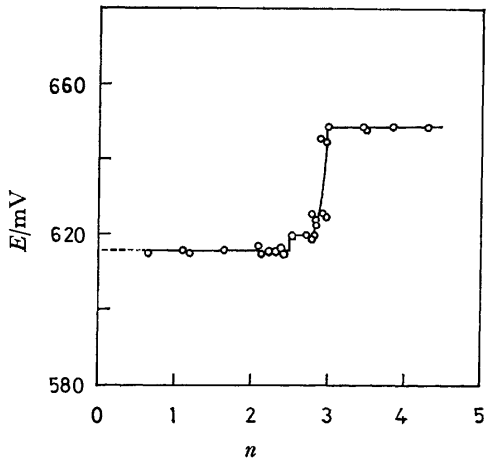

Fig. 2. Electromotive force of the solid-state cell, Ag|AgI|phenothiazine-iodine (PT-I_n) *versus* n at 25 °C.

Results and Discussion

Phenothiazine–Iodine. The emf increases linearly by raising the temperature. For example, the data at $n=1.10$ and 3.01 are presented in Fig. 1. The open and shaded circles indicate the values measured by different runs on the same cell. They are expressed by $E/\mathrm{mV}=616+0.300(t-25)$, and by $E/\mathrm{mV}=649+0.230(t-25)$ respectively.

The compositional variation of the emf at 25 °C is shown in Fig. 2. Below $n=2.5$, the cell maintains an emf of 616 mV. Attempts to obtain steady, reproducible emf with the complexes below $n=0.5$ were unsuccessful, probably because of the high electrical resistivity of the complex.[5] As the vibrational spectrum of a sample at $n=0.65$ clearly shows the coexistence of free phenothiazine, the samples below $n=2.5$ may be mixtures of the parent organic compound and its iodine complex ($n=2.5$). In our previous work, we tried to prepare "monoiodide" by the reaction of hydroiodic acid with an equimolar mixture of phenothiazine and its *S*-oxide and obtained a product which is approximately expressed by PT-$I_{1.35}$.[5] It now seems probable that the "monoiodide" does not exist in this system.

The emf increases stepwise at $n=2.5$, indicating that the complex is stoichiometric. This composition corresponds exactly to the edge appearing in the resistivity-composition isotherm. The two solid phases are involved in the composition range from $n=2.5$ to 2.8. Then, a continuous increase observed between $n=2.8$ and 3.0 implies that the complex is homogeneous over this range. In other words, a nonstoichiometric complex is formed. Although the lower limit of the region of existence was not detected by the resistivity-composition isotherm, the upper limit is in accordance with the composition of a deep minimum. Pampallona *et al.* have reported an emf of 630 mV for the cell Ag, $RbAg_4I_5$|$RbAg_4I_5$|PT-I_3,[8] and also McKechnie *et al.* have obtained 646 mV with the cell, Ag|AgI|PT-I_3.[10] These values are lower than ours at $n=3$; however, small deviations of n from 3 may easily give rise the observed differences. Both the reported values fit into the emf range of the nonstoichiometric complex.

A plateau indicative of a two-phase region appears above $n=3$, giving an emf of 649 mV. As this value is markedly lower than 688.3 mV reported by McKechnie *et al.* for the cell reaction, $\mathrm{Ag(s)}+1/2\mathrm{I_2(s)}\rightarrow \mathrm{AgI(s)}$, another complex with $n>4.3$ must exist in

the present system. We noted before that the vibrational spectrum of phenothiazine mixed with a large amount of iodine is different from that of the complex at $n=3$, but essentially identical with that of the simple cation radical bromide;[5] therefore, the expected complex may be some kind of simple polyiodide. No attempt was made to determine its composition by the present technique, because of the high vapor pressure of iodine and also of the high electrical resistivity.

Since only silver ions migrate in AgI, the emf values observed in the two-phase regions below $n=2.5$ and between $n=2.5$ and 2.8 are determined by the following virtual cell reactions:

$$Ag + 1/2.5\ PT\text{-}I_{2.5} \longrightarrow AgI + 1/2.5\ PT$$

and

$$Ag + 1/0.3\ PT\text{-}I_{2.8} \longrightarrow AgI + 1/0.3\ PT\text{-}I_{2.5}.$$

If the Gibbs energies are calculated in terms of the reactions,

$$2.5\ Ag + PT\text{-}I_{2.5} \longrightarrow 2.5\ AgI + PT \quad (1)$$

and

$$0.3\ Ag + PT\text{-}I_{2.8} \longrightarrow 0.3\ AgI + PT\text{-}I_{2.5}, \quad (2)$$

they are -148.5 and -17.9 kJ mol^{-1} (of the complex). These values represent the area under the emf composition curve between the upper and lower limits of n defined in each cell reaction.[12] Consequently, the Gibbs energy for the cell reaction to which the nonstoichiometric complexes with $n=2.8$ and 3 par-

$$0.2\ Ag + PT\text{-}I_3 \longrightarrow 0.2\ AgI + PT\text{-}I_{2.8} \quad (3)$$

ticipate, may be estimated by a graphic method to be -12.3 kJ mol^{-1} (of the complex). Combining with $\Delta G_f^\circ(AgI) = -66.4$ kJ mol^{-1},[10] the Gibbs energies in terms of the complex formation reactions,

$$PT + 2.5/2\ I_2 \longrightarrow PT\text{-}I_{2.5},$$

$$PT + 2.8/2\ I_2 \longrightarrow PT\text{-}I_{2.8},$$

and

$$PT + 3/2\ I_2 \longrightarrow PT\text{-}I_3$$

are determined to be -17.5, -19.5, and -20.5 kJ mol^{-1} respectively. McKechnie *et al.* have assumed that the reaction occurring in their cell is

$$Ag + 1/3\ PT\text{-}I_3 \longrightarrow AgI + 1/3\ PT,$$

and computed the ΔG value of -62.3 kJ mol^{-1} (of Ag). As the assumed reaction is not correct, their Gibbs energy of the complex formation, -12.3 kJ mol^{-1} (of the complex), is appreciable smaller than ours.

The slope of the emf *versus* the temperature graph shows considerable scatter and differs up to 15% from the mean value; this is shown in Fig. 3. The entropy changes for the cell reactions (1), (2), and (3) are estimated to be 73.5 ± 1.3, 8.8 ± 0.2, and 4.4 ± 0.1 J K^{-1} mol^{-1}. The application of Gibbs-Helmholtz equation yields enthalpies of -126.6 ± 0.4, -15.3 ± 0.04, and -11.0 ± 0.03 kJ mol^{-1} for these cell reactions. With the aid of $\Delta S_f^\circ(AgI) = 13.4\pm0.1$ J K^{-1} mol^{-1},[10] the entropy changes in terms of the complex formation reactions can be computed to be -40.0 ± 1.5, -44.8 ± 1.7, and -46.5 ± 1.8 J K^{-1} mol^{-1}, and

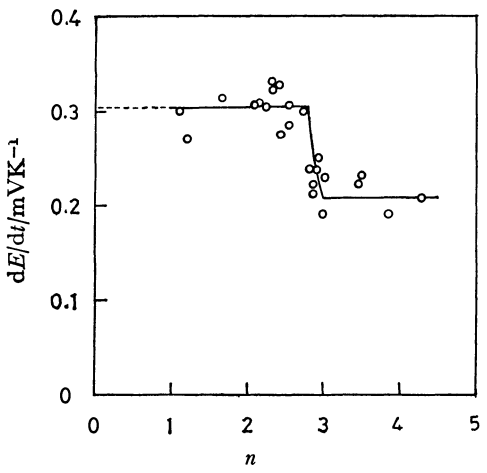

Fig. 3. Temperature coefficient of electromotive force of the solid-state cell, Ag|AgI|phenothiazine-iodine ($PT\text{-}I_n$) versus n.

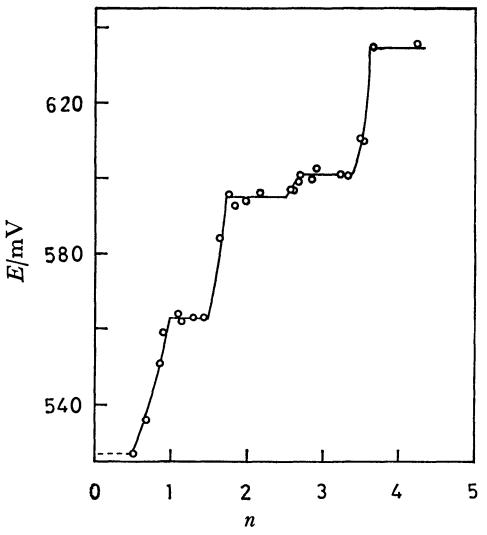

Fig. 4. Electromotive force of the solid-state cell, Ag|AgI|benzo[*a*]phenothiazine-iodine ($B[a]PT\text{-}I_n$) *versus* n at 25 °C.

with $\Delta H_f^\circ(AgI) = -62.4$ kJ mol^{-1}, the enthalpy changes are found to be -29.4 ± 0.5, -32.8 ± 0.5, and -34.3 ± 0.5 kJ mol^{-1}. It must be added that the temperature coefficient of the emf at and above $n=3$ is twice as large as that reported by McKechnie *et al.*, 0.114 mV K^{-1}, for unknown reasons. Since their coefficient is less than that for the cell reaction, Ag(s)+1/2 I_2(s)→AgI(s), the entropy change for the complex formation reported by them is positive and the magnitude is smaller by a factor of one-tenth.

Benzo[a]*phenothiazine–Iodine.* The results presented in Fig. 4 clearly indicate the formation of four distinct complexes, $B[a]PT\text{-}I_n$, in the examined composition range. The interesting feature of this system is the nonstoichiometry in all the phases. The first phase appears at and below $n=1$, the second, between $n=1.5$ and 1.7, the third, between $n=2.5$ and 2.7, and the fourth, between $n=3.4$ and 3.6. The two-phase region appearing between $n=1$ and 1.5 exhibits an emf of 563 mV; the region between

Table 1. Thermodynamic data for the cell reaction, Δn Ag+T-I_n⟶Δn AgI+T-$I_{n-\Delta n}$

Eq.	n	Δn	E/mV	ΔG/kJ mol^{-1}	ΔH/kJ mol^{-1}	ΔS/J K^{-1} mol^{-1}
			Phenothiazine–Iodine complexes			
1	2.5	2.5	616	−148.5	−126.6±0.4	73.5±1.3
2	2.8	0.3	620	−17.9	−15.3±0.04	8.8±0.2
3	3.0	0.2	a)	−12.3	−11.0±0.03	4.4±0.1
			Benzo[*a*]phenothiazine–Iodine complexes			
4	0.5	0.5	527	−25.4	−13.9±0.7	38.6±2.4
5	1.0	0.5	a)	−26.2	−18.3±0.7	26.5±2.4
6	1.5	0.5	563	−27.2	−22.6±0.3	15.4±1.0
7	1.7	0.2	a)	−11.2	−9.4±0.2	6.2±0.4
8	2.5	0.8	595	−45.9	−38.5±0.4	24.7±1.6
9	2.7	0.2	a)	−11.6	−10.0±0.04	5.3±0.2
10	3.4	0.7	601	−40.6	−35.9±0.1	15.8±0.2
11	3.6	0.2	a)	−12.0	—	—
			Benzo[*c*]phenothiazine–Iodine complexes			
12	0.5	0.5	550	−26.5	−23.3±0.2	10.6±0.5
13	1.0	0.5	a)	−27.0	−23.8±0.2	10.6±0.5
14	2.3	1.3	614	−77.0	−68.8±0.4	27.6±1.3
15	2.5	0.2	a)	−11.9	−10.6±0.1	4.2±0.2
16	3.0	0.5	616	−29.7	−26.5±0.2	10.6±0.5
17	3.5	0.5	a)	−30.4	—	—

a) One-phase region.

n=1.7 and 2.5, 595 mV; the region between n=2.7 and 3.4, 601 mV; and the region above n=3.6, 635 mV. Earlier, one of the present authors attempted the preparation of "monoiodide" and succeeded in isolating a product whose composition almost agrees with the ideal one.[13] Now it is certain that the monoiodide is formed in this system at the higher extreme of the existence region of a nonstoichiometric complex. On the other hand, the existence of the complex with n=3 studied earlier is not supported by the present work.[14] The resistivity-composition isotherm exhibits a sharp maximum at n=2.5 and broad minima which may be located anywhere near n=2 and 3. The composition at the resistivity maximum is the lower extreme of the third phase, possibly representing the ideal composition. The resistivity minimum located below n=2.5 is now identified as the upper limit of the existence region of the second phase (n=1.7) and that located above n=2.5 must be the lower limit of the existence region of the fourth phase (n=3.4). The complex at the former minimum may be regarded as (B[*a*]PT)$_2$$^+$$I_3^-$ containing an excess of iodine, and the complex at the latter as (B[*a*]PT)$_2$$^+$$I_7^-$ containing an excess of the thiazine.

The Gibbs energies are to be determined for the following eight cell reactions:

$$0.5\,Ag + B[a]PT\text{-}I_{0.5} \longrightarrow 0.5\,AgI + B[a]PT \quad (4)$$

$$0.5\,Ag + B[a]PT\text{-}I \longrightarrow 0.5\,AgI + B[a]PT\text{-}I_{0.5} \quad (5)$$

$$0.5\,Ag + B[a]PT\text{-}I_{1.5} \longrightarrow 0.5\,AgI + B[a]PT\text{-}I \quad (6)$$

$$0.2\,Ag + B[a]PT\text{-}I_{1.7} \longrightarrow 0.2\,AgI + B[a]PT\text{-}I_{1.5} \quad (7)$$

$$0.8\,Ag + B[a]PT\text{-}I_{2.5} \longrightarrow 0.8\,AgI + B[a]PT\text{-}I_{1.7} \quad (8)$$

$$0.2\,Ag + B[a]PT\text{-}I_{2.7} \longrightarrow 0.2\,AgI + B[a]PT\text{-}I_{2.5} \quad (9)$$

$$0.7\,Ag + B[a]PT\text{-}I_{3.4} \longrightarrow 0.7\,AgI + B[a]PT\text{-}I_{2.7} \quad (10)$$

$$0.2\,Ag + B[a]PT\text{-}I_{3.6} \longrightarrow 0.2\,AgI + B[a]PT\text{-}I_{3.4}. \quad (11)$$

We failed to obtain steady reproducible emf values for the cell reaction (4). As none of the known existence regions of the nonstoichiometric complexes is wider than 0.5 in the present system, we tentatively assumed the appearance of a two-phase region below n=0.5 where one of the phases is the parent organic compound. The computed Gibbs energies are summarized in Table 1. The Gibbs energy of complex formation and the value per iodine atom are given in Table 2. The latter value becomes less negative as more iodine is combined with benzo[*a*]phenothiazine. It must be emphasized that the benzo[*a*]phenothiazine complexes are far more stable than the phenothiazine complexes are. For example, the Gibbs energy divided by the number of iodine atoms at n=2.5 is −12.0 kJ mol^{-1} for the former complex, while the corresponding value is −7.0 kJ mol^{-1} for the latter.

As there are so many phases in this system, our data are insufficient to assign a temperature coefficient to each one. The coefficient decreases from about 0.8 mV K^{-1} at n=0.5 to 0.3 mV K^{-1} at n=1, and then maintains roughly the latter value (0.32±0.02 mV K^{-1}) up to n=2.5. Between n=2.7 and 3.4, the cells show a steady value of 0.234±0.005 mV K^{-1}. Because of the lack of data for the cell reaction (4) and also the inaccurate data for the other reactions, the probable errors of ΔH and ΔS values of the complex formation reactions are, much larger than those for the phenothiazine–iodine complexes (see Table 2).

Benzo[c]*phenothiazine–Iodine.* The emf *versus* the composition graph indicates the formation of three nonstoichiometric complexes, B[*c*]PT-I_n, in the studied range (see Fig. 5). The first complex covers the range from n=0.5 to 1, the second, n=2.3 to 2.5, and the third, n=3.0 to 3.5. The emf is 614 mV in the two-phase region between n=1 and 2.3, 616 mV be-

TABLE 2. THERMODYNAMIC DATA FOR THE COMPLEX FORMATION REACTION, $T+n/2\ I_2 \longrightarrow T\text{-}I_n$

n	ΔG/kJ mol^{-1}	ΔH/kJ mol^{-1}	ΔS/J K^{-1} mol^{-1}	$\Delta G \div n$/kJ mol^{-1}
		Phenothiazine–Iodine complexes		
2.5	−17.5	−29.4±0.5	−40.0±1.5	−7.0
2.8	−19.2	−32.8±0.5	−44.8±1.7	−6.9
3.0	−20.5	−34.3±0.5	−46.5±1.8	−6.8
		Benzo[*a*]phenothiazine–Iodine complexes		
0.5	−7.8	−17.3±0.7	−31.9±2.4	−15.6
1.0	−14.8	−25.8±1.4	−51.7±4.8	−14.8
1.5	−20.8	−34.4±1.7	−60.4±5.8	−13.9
1.7	−22.9	−37.5±1.9	−63.9±6.2	−13.5
2.5	−30.1	−48.9±2.3	−77.9±7.8	−12.0
2.7	−31.8	−51.4±2.3	−80.5±8.0	−11.8
3.4	−37.7	−59.2±2.4	−86.9±8.2	−11.1
3.6	−38.9	—	—	−10.8
		Benzo[*c*]phenothiazine–Iodine complexes		
0.5	−6.7	−7.9±0.2	−3.9±0.5	−13.4
1.0	−12.9	−15.3±0.3	−7.8±1.0	−12.9
2.3	−22.2	−27.6±0.7	−18.0±2.3	−9.7
2.5	−23.6	−29.5±0.8	−19.5±2.5	−9.4
3.0	−27.1	−34.2±1.0	−23.4±3.0	−9.0
3.5	−29.9	—	—	−8.5

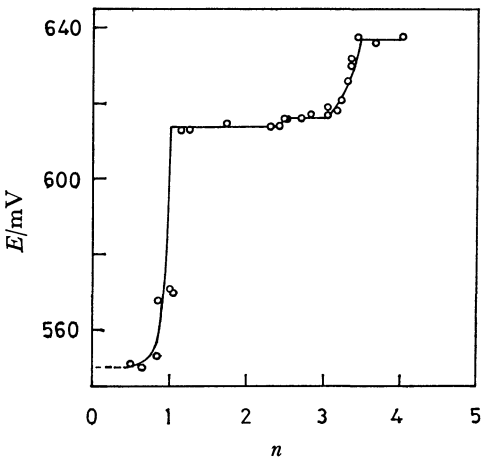

Fig. 5. Electromotive force of the solid-state cell, Ag|AgI|benzo[*c*]phenothiazine-iodine (B[*c*]PT-I_n) *versus* n at 25 °C.

tween n=2.5 and 3.0, and 637 mV above n=3. The "monoiodide" isolated in our previous work does exist in this system at the upper limit of a single phase region. Furthermore, the existence of the complex with n=3 is also firmly established by the emf data. The resistivity-composition isotherm shows an edge at n=2.5 and a broad minimum around n=2. The emf data strongly suggest that the minimum is located at n=2.3. The complex at this composition is the lower limit of a nonstoichiometric complex, the ideal composition of which is $(B[c]PT)_2{}^+I_5{}^-$.

The following six cell reactions are conceivable:

$$0.5\,Ag + B[c]PT\text{-}I_{0.5} \longrightarrow 0.5\,AgI + B[c]PT \quad (12)$$

$$0.5\,Ag + B[c]PT\text{-}I \longrightarrow 0.5\,AgI + B[c]PT\text{-}I_{0.5} \quad (13)$$

$$1.3\,Ag + B[c]PT\text{-}I_{2.3} \longrightarrow 1.3\,AgI + B[c]PT\text{-}I \quad (14)$$

$$0.2\,Ag + B[c]PT\text{-}I_{2.5} \longrightarrow 0.2\,AgI + B[c]PT\text{-}I_{2.3} \quad (15)$$

$$0.5\,Ag + B[c]PT\text{-}I_3 \longrightarrow 0.5\,AgI + B[c]PT\text{-}I_{2.5} \quad (16)$$

$$0.5\,Ag + B[c]PT\text{-}I_{3.5} \longrightarrow 0.5\,AgI + B[c]PT\text{-}I_3. \quad (17)$$

In this system too, we assumed that the samples with $n<0.5$ contain the free parent organic compound. The Gibbs energies computed for the cell reactions and the complex formation reactions are presented in Tables 1 and 2 respectively. The stabilities of these complexes are intermediate between those of the respective benzo[*a*]phenothiazine and phenothiazine complexes, the Gibbs energy divided by the number of iodine atoms at n=2.5 being −9.4 kJ mol^{-1}.

The temperature coefficients of the emf for Eqs. 12—16 are not distinguishable from each other; therefore, the average value of 0.22±0.01 mV K^{-1} was employed in the whole composition range below n=3. Above this limit, the coefficient decreases by a factor of a half by n=3.5. It must be noted that the ΔS values of the complex formation reactions for these three thiazines are so different that the value at n=2.5 in the benzo[*c*]phenothiazine complex is about a half of that in the phenothiazine complex, which in turn is about a half of that in the benzo[*a*]phenothiazine complex. As mentioned above, the ΔG values of the complex formation reactions for benzo[*c*]phenothiazine are considerably larger than those for phenothiazine; nevertheless, the ΔH values for these two thiazines are almost identical. In conclusion, the solid-state electrochemical study on these thiazine–iodine complexes has been able to determine clearly a number of phases which are often nonstoichiometric. We believe that the present technique deserves more attention in the investigation of electronically-conducting iodine complexes.

This work was partly supported by two Grants-in-Aid for Scientific Research Nos. 234028 and 434023 from the Ministry of Education, Science and Culture.

References

1) Y. Matsunaga, *Helv. Phys. Acta*, **36**, 800 (1963).
2) F. Kehrmann and L. Diserens, *Ber.*, **48**, 318 (1915).
3) Y. Matsunaga and K. Shono, *Bull. Chem. Soc. Jpn.*, **43**, 2007 (1970).
4) S. Doi and Y. Matsunaga, *Bull. Chem. Soc. Jpn.*, **48**, 3747 (1975).
5) S. Doi, T. Inabe, and Y. Matsunaga, *Bull. Chem. Soc. Jpn.*, **50**, 837 (1977).
6) F. Gutmann, A. M. Hermann, and A. Rembaum, *J. Electrochem. Soc.*, **114**, 323 (1967).
7) D. V. Louzos, W. G. Darland, and G. W. Mellors, *J. Electrochem. Soc.*, **120**, 1151 (1973).
8) M. Pampallona, A. Ricci, B. Scrosati, and C. A. Vincent, *J. Appl. Electrochem.*, **6**, 269 (1976).
9) S. Aronson, G. Sinensky, Y. Langsam, and M. Binder, *J. Inorg. Nucl. Chem.*, **38**, 407 (1976).
10) J. S. McKechnie, L. D. S. Turner, and C. A. Vincent, *J. Chem. Thermodyn.*, **1979**, 1189.
11) E. Knoevenagel, *J. Prakt. Chem.*, **89**, 1 (1914).
12) A. S. Nagelberg and W. L. Worrell, *J. Solid State Chem.*, **29**, 345 (1979).
13) Y. Matsunaga and Y. Suzuki, *Bull. Chem. Soc. Jpn.*, **46**, 719 (1973).
14) Y. Matsunaga and Y. Suzuki, *Bull. Chem. Soc. Jpn.*, **45**, 3375 (1972).

The Activities of Sodium Salts of 1-Amino-4-alkylaminoanthraquinone-2-sulfonic Acid in Aqueous Solutions

Masaru MITSUISHI* and Yuzoh YAMAGUCHI
Faculty of Textile Science and Technology, Shinshu University, Tokida, Ueda 386

(Received May 30, 1980)

The mean activity coefficients of sodium salts of 1-amino-4-alkylaminoanthraquinone-2-sulfonic acid (alk= Me(MAS), Et, *n*-Pr, or *n*-Bu (*n*-BAS)) in aqueous solutions ranging in concentration from 10^{-3} to 10^{-2} mol kg^{-1} have been determined by means of isopiestic measurements at 50 and 60 °C respectively. It has been found that the mean activity coefficients of these dyes are much smaller than unity, the coefficients of MAS being the largest, and those of *n*-BAS, the smallest. The coefficients have been found to decrease with an increase in the dye concentration. An examination of the results obtained by Milicéivic treatment suggests that the MAS exists as dimer or trimers, and the other dyes, as tetramers, at 60 °C.

In a previous paper,[1] we have reported on the mean activity coefficients of such azo-acid dyes as Methyl Orange and its homologs in aqueous solutions, and on the effects of the hydrophobic groups on the activity coefficients. The derivatives of sodium salts of 1-aminoanthraquinone-2-sulfonic acid also belong to the acid dye class. The behavior of aminoanthraquinone acid dyes in aqueous solutions is known to be different from that of azo-acid dyes; *e.g.*, the aqueous solutions of sodium salts of 1-amino-4-alkylaminoanthraquinone-2-sulfonic acid (alk=Me, Et, *n*-Pr, or *n*-Bu) have been found to have their critical concentration for dimer formation at from 1 to 4×10^{-3} mol kg^{-1}, and the critical concentrations have been found to decrease with an increase in the alkyl groups in the dye molecules.[2] The mean activities of these dyes are supposed to be influenced strongly by dimerization; however, there have been few reports on the mean activities of sodium salts of 1-amino-4-alkylaminoanthraquinone-2-sulfonic acid. Therefore, it would seem valuable to examine the mean activities of these dyes.

In this paper, the mean activity coefficients of sodium salts of 1-amino-4-alkylaminoanthraquinone-2-sulfonic acid (alk=Me, Et, *n*-Pr, or *n*-Bu) in aqueous solutions will be determined by means of isopiestic measurements, and the results will be examined by means of a Milicéivic treatment in order to obtain information on the association of these dyes.

Experimental

Materials. The sodium salts of 1-amino-4-alkylaminoanthraquinone-2-sulfonic acid (AAS) used in this experiment were as follows;

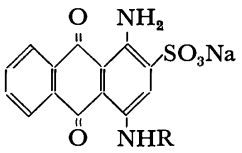

R: CH_3 (MAS)
R: C_2H_5 (EAS)
R: n-C_3H_7 (*n*-PAS)
R: n-C_4H_9 (*n*-BAS)

These dyes were prepared as follows. 1-Amino-4-bromoanthraquinone-2-sulfonic acid (50 g) was refluxed with the corresponding alkylamine (10 g) for 8 h in the presence of copper(II) sulfate and sodium carbonate. The product was isolated by column chromatography on activated alumina, and then purified by recrystallization from ethanol.

Vapor-pressure Osmotic Measurements. The vapor-pressure osmotic measurements were carried out by the procedures described in the previous paper[1] at 50 and 60 °C. The measured resistance difference, ΔR, is dependent upon the osmotic concentration of the dye solution according to Eq. 1:[3]

$$\Delta R\,k = -\ln(p/p_0) = \nu\phi m_2/m_1, \quad (1)$$

where k is the constant[4] dependent on the temperature of the solution and the instrumental characteristics; p and p_0 are the partial pressures of the solvent over the solution and over the solvent; ν is the number of the particles into which the dye dissociates; ϕ is the osmotic coefficients, and m_2 and m_1 are the solute and solvent molalities respectively.

The evaluation of the mean activity coefficients ($\gamma_\pm$) of the dye from the ϕ values can be made by means of Eq. 2:

$$\ln\gamma_\pm = (\phi-1) + \int_0^m (\phi-1)d\ln m_2. \quad (2)$$

The integration can be carried out graphically from the plot of $(1-\phi)\,m_2^{-1}$ *vs.* m_2.

Results and Discussion

Measured Resistance Differences. The measured resistance differences, ΔR, of MAS, EAS, *n*-PAS, and *n*-BAS solutions at 50 and 60 °C are plotted against m_2 in Figs. 1 and 2 respectively. From Figs. 1 and 2, it may be seen that the plots of urea solutions are almost linear, while the plots of the dye solutions display slight downward curvatures. It is noteworthy that the ΔR values of MAS solutions are the largest, while those of *n*-BAS are the smallest. All of the ΔR values of the dye solutions are smaller than twice the ΔR values of urea solutions.

Osmotic Coefficients. The osmotic coefficients, ϕ, of MAS, EAS, *n*-PAS, and *n*-BAS solutions ragning in concentration from 10^{-3} to 10^{-2} mol kg^{-1} were obtained from ΔR values in Figs. 1 and 2 by means of Eq. 1; they are given in Table 1. The ϕ values of all four kinds of dyes may be seen to be much smaller than unity. The ϕ values of the MAS solutions are the largest, while those of the *n*-BAS solutions are the smallest. In Fig. 3, the ϕ values of the MAS and *n*-BAS solutions at 50 °C are plotted against m_2. Since the ϕ values of these dye solutions were found to decrease monotonically with an increase in m_2, no evidence for the presence of Iyer's critical concentrations of the dimerization of these dyes was found. The ϕ values given in Table 1 strongly suggest that the aqueous solutions of the AAS deviate from the ideal.

Table 1. Osmotic coefficients of sodium salts of 1-amino-4-alkylaminoanthraquinone-2-sulfonic acid at 50 and 60 °C

$10^3\ m_2$ / mol kg^{-1}	MAS		EAS		PAS		BAS	
	50° C	60 °C	50 °C	60 °C	50 °C	60 °C	50 °C	60 °C
1.0	0.818	0.941	0.798	0.833	0.833	0.833	0.719	0.877
2.0	0.748	0.820	0.709	0.739	0.729	0.739	0.659	0.766
3.0	0.705	0.779	0.679	0.717	0.672	0.717	0.632	0.735
4.0	0.684	0.746	0.659	0.692	0.654	0.692	0.619	0.699
5.0	0.671	0.736	0.643	0.693	0.639	0.688	0.611	0.688
6.0	0.662	0.717	0.635	0.681	0.629	0.685	0.605	0.681
7.0	0.653	0.710	0.630	0.672	0.622	0.672	0.602	0.668
8.0	0.649	0.705	0.624	0.669	0.616	0.672	0.592	0.662
9.0	0.643	0.696	0.621	0.663	0.612	0.666	0.594	0.654

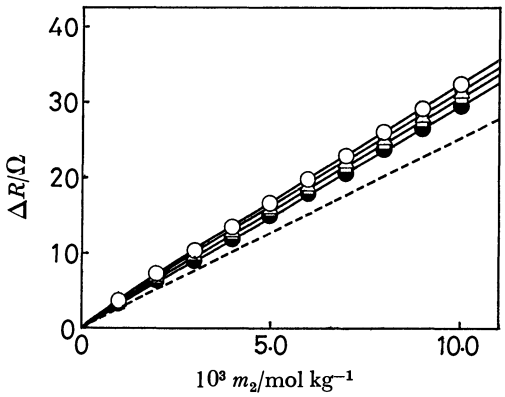

Fig. 1. Measured resistance differences of solutions of sodium salts of 1-amino-4-alkylaminoanthraquinone-2-sulfonic acid at 50 °C.
○: MAS, △: EAS, □: *n*-PAS, ●: *n*-BAS, ——: urea.

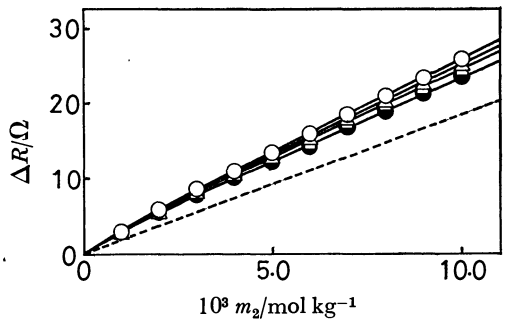

Fig. 2. Measured resistance differences of solutions of sodium salts of 1-amino-4-alkylaminoanthraquinone-2-sulfonic acid at 60 °C.
○: MAS, △: EAS, □: *n*-PAS, ●: *n*-BAS, ---: urea.

Determinations of Mean Activity Coefficients. The determinations of the mean activity coeeficients, $\gamma_{\pm}$, was done as follows. The $(1-\phi)m_2^{-1}$ value at 50 °C was plotted against m_2, as shown in Fig. 4. After the plots had been extrapolated to zero concentration, the area under the curve was measured and the $\gamma_{\pm}$ values were calculated according to Eq. 2. The $\gamma_{\pm}$ values of MAS, EAS, *n*-PAS, and *n*-BAS at 50 and 60 °C are shown in Table 2. In Table 2 it can be seen that the $\gamma_{\pm}$ values are much smaller than unity and that they decrease with an increase in the chain length of the alkyl groups in the dye molecules.

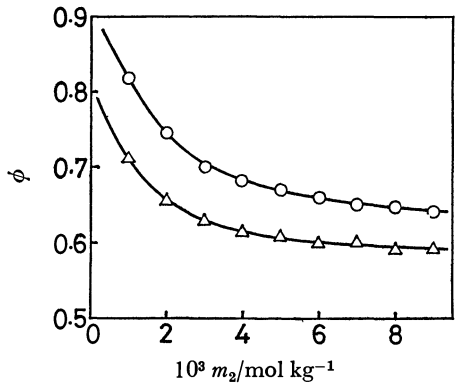

Fig. 3. Osmotic coefficients of solutions of MAS and *n*-BAS at 50 °C.
○: MAS, △: *n*-BAS.

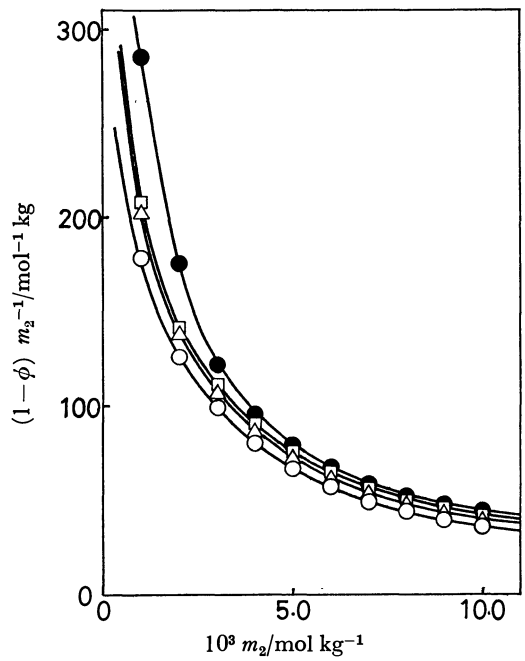

Fig. 4. Plots of $(1-\phi)\ m_2^{-1}$ against m_2.
○: MAS, △: EAS, □: *n*-PAS, ●: *n*-BAS.

Generally, the $\gamma_{\pm}$ values of the AAS dyes seem to be less than those of Methyl Orange and its homologs reported in the previous paper.[1] These $\gamma_{\pm}$ values

Table 2. Mean activity coefficients of sodium salts of 1-amino-4-alkylaminoanthraquinone-2-sulfonic acid at 50 and 60 °C

$10^3\ m_2$ / mol kg^{-1}	MAS		EAS		PAS		BAS	
	50 °C	60 °C	50 °C	60 °C	50 °C	60 °C	50 °C	60 °C
1.0	0.676	0.839	0.647	0.703	0.646	0.703	0.540	0.760
2.0	0.593	0.677	0.532	0.551	0.550	0.551	0.459	0.598
3.0	0.508	0.607	0.477	0.525	0.470	0.525	0.422	0.532
4.0	0.478	0.553	0.452	0.477	0.447	0.480	0.406	0.494
5.0	0.462	0.542	0.429	0.488	0.427	0.473	0.395	0.473
6.0	0.451	0.526	0.418	0.472	0.414	0.481	0.387	0.476
7.0	0.434	0.502	0.420	0.453	0.405	0.449	0.386	0.454
8.0	0.433	0.523	0.403	0.454	0.397	0.458	0.375	0.449
9.0	0.416	0.484	0.372	0.448	0.349	0.445	0.369	0.436

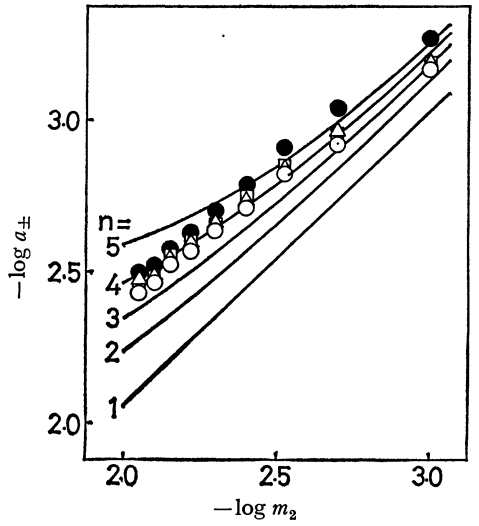

Fig. 5. Mean activities of sodium salts of 1-amino-4-alkylaminoanthraquinone-2-sulfonic acid at 50 °C.
○: MAS, △: EAS, □: *n*-PAS, ●: *n*-BAS.

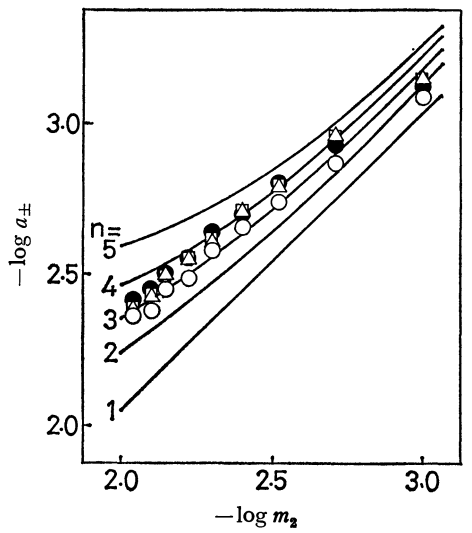

Fig. 6. Mean activities of sodium salts of 1-amino-4-alkylaminoanthraquinone-2-sulfonic acid at 60 °C.
○: MAS, △: EAS, □: *n*-PAS, ●: *n*-BAS.

strongly suggest that the $\gamma_\pm$ values of the AAS dyes are also dependent on the hydrophobic parts of the dye molecules; *i.e.*, the differences in the $\gamma_\pm$ values among these dyes are due to the association of the dye anions.

Examination of Results Obtained by Milicéivic Treatment. Since these dyes are known to dissociate completely, and since the ionic strengths of these solutions are small, the Debye-Hückel limiting law can also hold.

The relation between the mean activity, $a_\pm$, and the mean association number of the dye anions, n, was given by Milicéivic as:[5]

$$\log a_\pm = \log m_2 - \frac{1}{n+1}\log n - A\,n\,m_2\sqrt{\frac{1+n}{2}}, \qquad (3)$$

where A is the constant and where the numerical values at 50 and 60 °C are 0.5320 and 0.5425 respectively.

The mean activities of MAS, EAS, *n*-PAS, and *n*-BAS at 50 and 60 °C are plotted against $\log m_2$ in Figs. 5 and 6 respectively. The solid lines in Figs. 5 and 6 are Milicéivic lines drawn according to Eq. 3.

In Fig. 5 the plots of MAS, EAS, and *n*-PAS are seen to be close to the trimer (n=3) and tetramer (n=4) curves. The plots of *n*-BAS are close to the pentamer (n=5) curves. The results suggest that MAS, EAS, *n*-PAS dye anions are present as trimers or tetramers, and n-BAS dye anions, as tetramers, on the average usually, at 50 °C. From Fig. 6, MAS dye anions are seen to exist as dimers or trimers, and EAS, *n*-PAS, and *n*-BAS, as tetramers, at 60 °C. These results also suggest that there is no evidence for the presence of Iyer's critical concentration of the dimerization of these dyes. The quantities of the dye association become larger with an increase in the number of alkyl groups in the dye molecules.

References

1) M. Mitsuishi and Y. Yamaguchi, *Bull. Chem. Soc. Jpn.*, **52**, 3496 (1979).
2) S. R. Sivaraja Iyer and G. S. Singh, *J. Soc. Dyers Colour.*, **89**, 128 (1973).
3) I. Porigoric and I. J. Gal, *Trans. Faraday Soc.*, **68**, 1093 (1972).
4) Urea was used in order to determine the numerical values of k,[3] and the k values at 50 and 60 °C are 71.8×10^{-6} and $9.67\times10^{-6}\ \Omega^{-1}$ respectively.[1]
5) M. Milicéivic and G. Eigen, *Helv. Chim. Acta.*, **44**, 1039 (1964).

  Bull. Chem. Soc. Jpn., 54, 657—660 (1981)

The Crystal and Molecular Structure of Grayanotoxin XVIII. A New Minor Diterpene from *Leucothoe Grayana Max.*

Akio Furusaki,* Shinsei Gasa, Ryūzō Ikeda, Takeshi Matsumoto, Noritake Yasuoka,† and Yoshiki Matsuura†

Department of Chemistry, Faculty of Science, Hokkaido University, Sapporo 060

† *Institute for Protein Research, Osaka University, Suita, Osaka 565*

(Received July 9, 1980)

The molecular structure of grayanotoxin XVIII $C_{20}H_{28}O_4$, has been determined by means of X-ray crystal analysis. The crystals are monoclinic, with two molecules in a unit cell with dimensions of $a=9.592$, $b=11.414$, $c=8.180$ Å, and $\beta=93.21°$; the space group is $P2_1$. 1484 unique intensity data were collected on a four-circle diffractometer with Ni-filtered Cu $K\alpha$ radiation. The structure was solved by the Monte Carlo direct method, using the 20 strongest reflections as the starting set; the 25th random-phase set led to the correct solution. The R value reached 4.6% by block-diagonal least-squares refinements. The structure thus obtained corresponds to 3-dehydrograyanotoxin VII. The C-ring takes a boat conformation. The force-field calculations suggest that this energy loss is probably compensated for by the stabilization of the B-ring conformation. The crystal consists of hydrogen-bonded molecular layers parallel to the (100) plane.

A number of grayanane diterpenoids have been isolated from *Leucothoe grayana Max.*, *Pieris japonica* D. Don, *Rhododendron japonicum* Suringer, *etc.*, and their structures have been extensively investigated.[1-4] In this paper, we wish to report on the X-ray structure determination and molecular geometry of grayanotoxin (hereafter G) XVIII, a new constituent from *Leucothoe grayana Max.*

Experimental

Isolation of G XVIII. Grayathol A[5] was crystallized and removed from a diethyl ether solution of the unknown-compound-containing fraction (81 mg)[6] obtained from the crude extract of *Leucothoe grayana Max.* The chromatography of the filtrate on silica gel (1 g) afforded G XVIII (15 mg) in a 4×10^{-7}% yield from dried leaves; mp 204—210 °C (recrystallized from methanol), $[\alpha]_D$ −102° (c 1, MeOH); IR (Nujiol) 3400, 1725, 1655, 1628 cm^{-1}; ^{1}H-NMR (C_5D_5N) 1.35, 1.58 (each 3H, s), 1.70 (3H, d, $J=2$ Hz), 3.37 (1H, q, $J_{AX+BX}=6+10$ Hz), 4.70 (1H, s), 5.04, 5.11 (each 1H, s), 5.25 (1H, bs); MS m/e 332 (M^+). Found: C, 72.58; H, 8.98%. Calcd for $C_{20}H_{28}O_4$: C, 72.26; H, 8.49%. The PMR spectrum was recorded on a Hitachi R-20B spectrometer by the use of TMS as the internal reference. The chemical shifts are given on the δ scale (s=singlet, d=doublet, q=quartet, bs=broad singlet). The IR spectrum was obtained on a JASCO Model IR-S spectrophotometer.

X-Ray Measurement. A colorless single crystal with dimensions of about $0.4\times0.5\times0.6$ mm^3 was used. The crystal data are summarized in Table 1. The cell dimensions and reflection intensities were measured on a Rigaku four-circle diffractometer using Ni-filtered Cu $K\alpha$ radiation (40 kV, 60 mA, $\lambda=1.5418$ Å). The θ-2θ continuous-scan technique was applied at a θ scan rate of 8° min^{-1}; the background was measured for 5 s at each end of the scan range. Three standard reflections, measured at intervals of every 60 reflections, showed no significant decrease in intensity during the course of data collection. The intensities were corrected for the Lorentz and polarization factors, but not for the absorption or the extinction effect. In the range of 2θ values up to 125°, 1484 unique structure-factor magnitudes above the $\sigma(F)$ level were selected for the structure determination.

Table 1. The crystal data

Molecular formula	$C_{20}H_{28}O_4$
Molecular weight	332.4
Crystal system	Monoclinic
Space group	$P2_1$
Cell dimensions	$a=9.592(1)$ Å
	$b=11.414(1)$ Å
	$c=8.180(1)$ Å
	$\beta=93.21(1)°$
V	894.2 Å^3
Z	2
D_x	1.235 g cm^{-3}
μ(Cu $K\alpha$)	6.43 cm^{-1}

Structure Determination

The structure was solved by the Monte Carlo direct method.[7] The 20 strongest reflections were chosen as the starting set. Tentative phase values for the starting reflections were derived from successively-generated random numbers. In order to extend this tentative phase set, 10 cycles of the tangent procedure were performed using 300 $|E|$ values above 1.30. Since the 25th phase set showed a low R_K value of 26.6% ($R_K=\Sigma||E_o|-k|E_c||/\Sigma|E_o|$), 6 additional cycles of the tangent procedure were carried out using 386 $|E|$ values above 1.20; the R_K value thereupon dropped to 22.2%. An E-map calculated with 375 phases clearly revealed the locations of all the 24 non-hydrogen atoms.

The structure thus obtained was refined by the block-diagonal-matrix least-squares method, first with isotropic and then with anisotropic temperature factors. After all the 28 hydrogen atoms had been located in a difference Fourier map, further least-squares refinement was repeated including these hydrogen atoms with isotropic temperature factors. For this refinement, the following weighting scheme was used:

$$W = 1/\{\sigma(F)^2 \exp(AX^2+BY^2+CXY+DX+EY)\},$$

where $X=|F_o|$ and $Y=\sin\theta/\lambda$. The A, B, C, D, and E coefficients are constants which were determined from the $(\Delta F)^2$ values. The final value of $R=\Sigma|$

Table 2. The final atomic parameters and estimated standard deviations

The coordinates of the non-hydrogen and hydrogen atoms are multiplied by 10^4 and 10^3 respectively.

(1) The non-hydrogen atoms

Atom	x	y	z	B_{eq}[a]/Å^2	Atom	x	y	z	B_{eq}[a]/Å^2
O(1)	6455(3)	1476(4)	−2110(3)	4.95	C(9)	1512(3)	2168(3)	2308(4)	2.22
O(2)	4746(2)	120(2)	1490(3)	2.50	C(10)	2292(3)	1578(3)	969(3)	2.12
O(3)	6055(2)	1108(2)	4342(3)	2.77	C(11)	961(3)	3370(3)	1679(4)	2.90
O(4)	3681(2)	3619(2)	5731(3)	2.92	C(12)	471(4)	4237(4)	2975(4)	3.14
C(1)	3737(3)	2012(3)	655(3)	2.12	C(13)	1293(4)	4092(3)	4638(4)	2.83
C(2)	4186(4)	1878(4)	−1116(4)	3.22	C(14)	2725(3)	3570(3)	4335(4)	2.25
C(3)	5726(4)	1645(4)	−975(4)	3.00	C(15)	1233(4)	2120(3)	5287(4)	2.87
C(4)	6269(3)	1662(3)	828(4)	2.47	C(16)	648(4)	3129(4)	5630(4)	3.26
C(5)	4915(3)	1358(3)	1700(3)	1.95	C(17)	−523(5)	3365(6)	6715(6)	5.97
C(6)	4900(3)	1703(3)	3508(3)	1.99	C(18)	7485(4)	828(4)	1129(5)	3.76
C(7)	3548(3)	1408(3)	4307(3)	2.17	C(19)	6768(4)	2917(4)	1194(5)	3.49
C(8)	2329(3)	2272(3)	4021(3)	2.03	C(20)	1664(4)	714(4)	102(4)	3.29

a) $B_{eq}=8\pi^2(u_1^2+u_2^2+u_3^2)/3$, where u_i is the root-mean-square deviation in the ith principal axis of the thermal ellipsoid.

(2) The hydrogen atoms

Atom[a]	x	y	z	B/Å^2	Atom[a]	x	y	z	B/Å^2
H(1)	383(3)	284(4)	98(4)	2.6(7)	H(17a)	−60(5)	261(5)	716(6)	6.5(13)
H(2a)	390(3)	257(3)	−190(4)	2.6(7)	H(17b)	−132(5)	358(5)	611(6)	7.2(13)
H(2b)	370(4)	117(4)	−175(5)	4.3(9)	H(17c)	−31(6)	415(6)	763(7)	8.9(16)
H(6)	496(3)	259(3)	353(4)	2.8(7)	H(18a)	799(4)	108(4)	230(5)	4.5(9)
H(7a)	386(3)	137(3)	546(3)	1.0(5)	H(18b)	822(4)	100(4)	41(5)	5.0(10)
H(7b)	326(3)	60(3)	401(4)	2.6(7)	H(18c)	722(6)	15(6)	98(7)	8.6(16)
H(9)	67(3)	173(3)	251(4)	2.3(7)	H(19a)	740(4)	324(4)	57(5)	5.1(10)
H(11a)	169(4)	369(3)	119(4)	3.2(8)	H(19b)	708(4)	299(4)	234(5)	4.9(10)
H(11b)	28(4)	326(4)	93(4)	3.2(8)	H(19c)	611(5)	347(5)	91(5)	6.1(12)
H(12a)	59(3)	504(3)	258(4)	2.8(7)	H(20a)	80(3)	46(3)	35(4)	2.5(7)
H(12b)	−52(4)	411(3)	316(4)	2.7(7)	H(20b)	201(4)	29(4)	−74(5)	4.4(9)
H(13)	139(4)	496(4)	516(4)	4.0(9)	H(O2)	408(4)	−4(5)	182(5)	5.4(10)
H(14)	307(3)	394(3)	339(4)	1.7(6)	H(O3)	606(3)	132(3)	525(4)	2.5(7)
H(15)	101(4)	139(4)	574(5)	4.4(9)	H(O4)	377(4)	416(4)	597(5)	4.0(9)

a) The hydrogen atoms are denoted by the number of the carbon atom to which they are attached, suffixed by a, b, or c where necessary.

$|F_o|-k|F_c||/\Sigma|F_o|$ was 4.6%. The atomic parameters are listed in Table 2. The tables of the anisotropic thermal parameters and of the observed and calculated structure factors are kept at the Chemical Society of Japan (Document No. 8102).

The calculations were performed on an ACOS 700 computer at the Institute for Protein Research, Osaka University, and on a FACOM 230-75 computer at the Hokkaido University Computing Center. The atomic scattering factors were taken from the International Tables.[8]

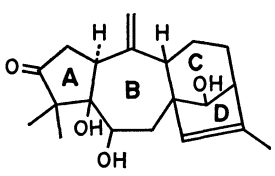

1

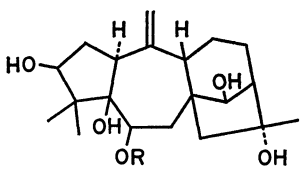

2: R = H 3: R = Ac

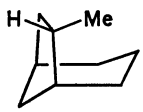

4

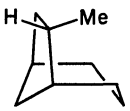

5

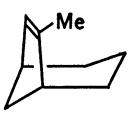

6

7

Results and Discussion

Molecular Structure. The molecular structure of G XVIII is illustrated in Fig. 1, where each atom is represented as a thermal ellipsoid enclosing a 50% probability. As can be seen in Fig. 1, the molecular framework obtained corresponds to **1**. The bond distances and angles are listed in Table 3; all these

Table 3. The bond distances (l/Å) and angles (ϕ/°), with their standard deviations
The standard deviations given in parentheses refer to the last decimal position.

C(1)-C(2)	1.542(4)	C(15)-C(16)	1.318(5)	C(7)-C(8)-C(9)	115.1(2)
C(1)-C(5)	1.567(4)	C(16)-C(17)	1.494(6)	C(7)-C(8)-C(14)	114.3(2)
C(1)-C(10)	1.508(4)	C(2)-C(1)-C(5)	103.6(2)	C(7)-C(8)-C(15)	111.8(3)
C(1)-C(3)	1.499(5)	C(2)-C(1)-C(10)	115.8(2)	C(9)-C(8)-C(14)	109.1(2)
C(3)-C(4)	1.536(4)	C(5)-C(1)-C(10)	113.1(3)	C(9)-C(8)-C(15)	105.6(2)
C(3)-O(1)	1.209(4)	C(1)-C(2)-C(3)	105.7(2)	C(14)-C(8)-C(15)	99.7(3)
C(4)-C(5)	1.556(4)	C(2)-C(3)-C(4)	110.6(3)	C(8)-C(9)-C(10)	115.8(2)
C(4)-C(18)	1.515(5)	C(2)-C(3)-O(1)	125.4(3)	C(8)-C(9)-C(11)	111.9(3)
C(4)-C(19)	1.535(5)	C(4)-C(3)-O(1)	124.0(3)	C(10)-C(9)-C(11)	109.0(3)
C(5)-C(6)	1.531(4)	C(3)-C(4)-C(5)	101.0(2)	C(1)-C(10)-C(9)	118.2(3)
C(5)-O(2)	1.432(4)	C(3)-C(4)-C(18)	111.4(3)	C(1)-C(10)-C(20)	122.9(3)
C(6)-C(7)	1.522(4)	C(3)-C(4)-C(19)	106.5(3)	C(9)-C(10)-C(20)	118.9(3)
C(6)-O(3)	1.438(4)	C(5)-C(4)-C(18)	116.1(3)	C(9)-C(11)-C(12)	116.9(3)
C(7)-C(8)	1.538(4)	C(5)-C(4)-C(19)	112.2(3)	C(11)-C(12)-C(13)	112.2(3)
C(8)-C(9)	1.572(4)	C(18)-C(4)-C(19)	109.0(3)	C(12)-C(13)-C(14)	108.5(3)
C(8)-C(14)	1.548(4)	C(1)-C(5)-C(4)	103.8(2)	C(12)-C(13)-C(16)	110.2(3)
C(8)-C(15)	1.526(4)	C(1)-C(5)-C(6)	111.0(2)	C(14)-C(13)-C(16)	101.6(3)
C(9)-C(10)	1.519(4)	C(1)-C(5)-O(2)	109.4(2)	C(8)-C(14)-C(13)	100.7(3)
C(9)-C(11)	1.548(5)	C(4)-C(5)-C(6)	116.1(2)	C(8)-C(14)-O(4)	108.1(2)
C(10)-C(20)	1.338(5)	C(4)-C(5)-O(2)	104.9(2)	C(13)-C(14)-O(4)	113.4(3)
C(11)-C(12)	1.543(5)	C(6)-C(5)-O(2)	111.2(2)	C(8)-C(15)-C(16)	111.3(3)
C(12)-C(13)	1.543(5)	C(5)-C(6)-C(7)	114.4(2)	C(13)-C(16)-C(15)	109.1(3)
C(13)-C(14)	1.530(5)	C(5)-C(6)-O(3)	106.7(2)	C(13)-C(16)-C(17)	122.0(4)
C(13)-C(16)	1.518(5)	C(7)-C(6)-O(3)	110.1(2)	C(15)-C(16)-C(17)	128.8(4)
C(14)-O(4)	1.425(4)	C(6)-C(7)-C(8)	116.8(3)		

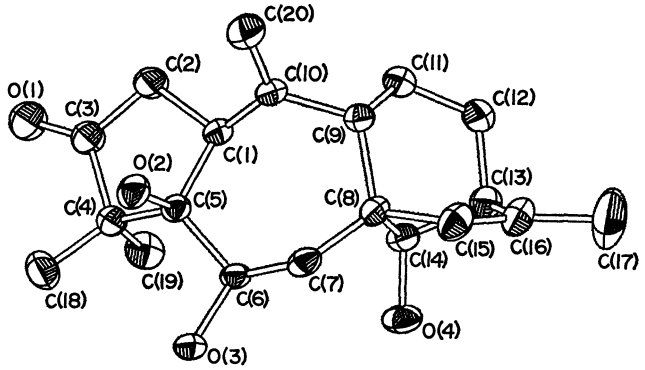

Fig. 1. A perspective view of the G XVIII molecule.

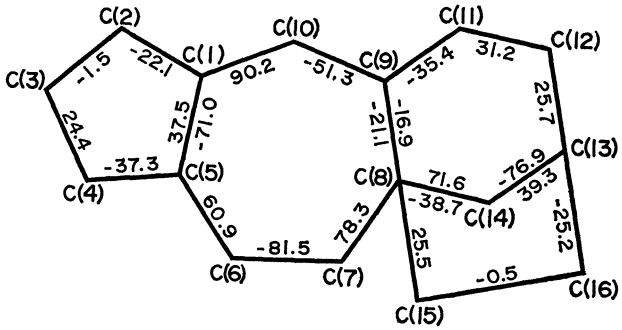

Fig. 2. The torsion angles (ϕ/°) of the A-, B-, C-, and D-rings. Only the torsion angles relevant to atoms which form the same ring are given in the ring.

values are normal. The torsion angles for the tetracyclic system are given in Fig. 2.

The five-membered A-ring takes an envelope form different from those of the A-rings in G II (**2**)[9] and G XVI (**3**):[10] In the former an approximate mirror plane runs through the C(5) atom, while in the latter two it goes through the C(4) atom. The conformation of the latter type is probably unfavorable to the present A-ring, because it makes the O(1) carbonyl oxygen atom almost eclipse the C(18)H_3 methyl group around the C(3)–C(4) bond.

The C(5)–C(4)–C(18) and C(5)–C(4)–C(19) bond angles, 116.1 and 112.2°, are somewhat larger than the C(3)–C(4)–C(18) and C(3)–C(4)–C(19) angles, 111.4 and 106.5°, respectively. This distortion of the C(4)–C(18) and C(4)–C(19) bonds may be caused by the steric repulsions between the C(18)H_3 and O(2)H groups and between the C(19)H_3 and C(6)H groups; C(18)···O(2), 2.780(4) Å; C(19)···C(6), 3.016(5) Å. As is found also in **2** and **3**, these steric repulsions further result in a small lengthening of the C(4)–C(5) bond.

The conformation adopted by the seven-membered B-ring is intermediate between the chair form with the mirror plane through the C(5) atom and the twist-chair form with the two-fold rotation axis through the C(9) atom. In this conformation, the severe 3a-3'a or 2a-3'a repulsion characteristic of the chair and twist-chair cycloheptane rings[11] is much relieved, since the exocyclic methylene group, C(20)H_2, occupies exactly the 3a or 2a position. This suggests that the present B-ring conformation may contain less strain than the twist-chair form in **2** and the twist-chair and chair forms** in **3**. This tentative conclusion is supported by a comparison of the values of

**The G XVI hemihydrate crystal contains two conformers with regard to the B-ring conformation: (a) the twist-chair form and (b) the chair form.

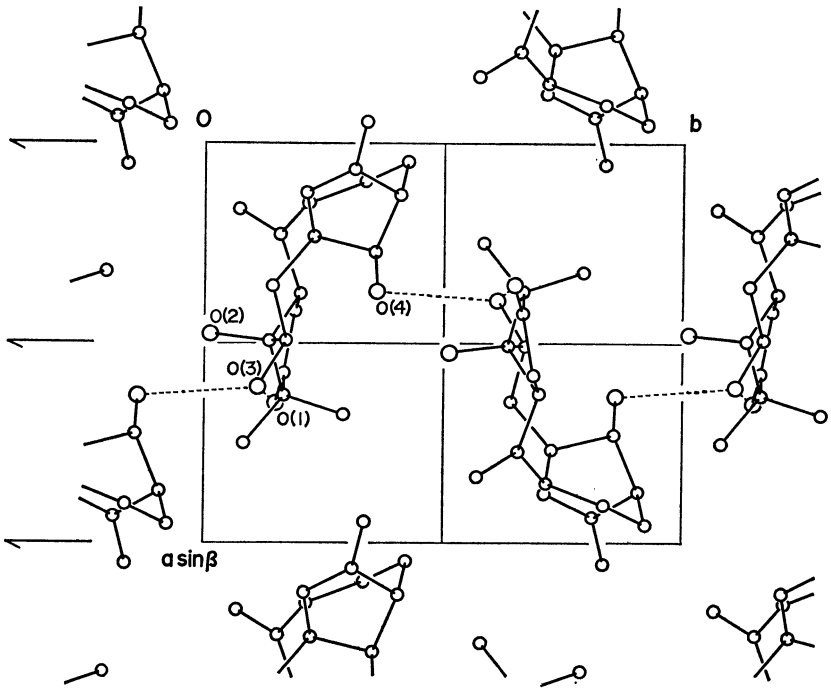

Fig. 3. The crystal structure viewed along the c axis.

$EB=(\theta_i-\theta^0_i)^2$, where the θ_i's ($i=1, 2, \cdots, 7$) are the observed bond angles in the B-ring and where the θ^0_i's are 109.5 and 116.6° for the sp^3 and sp^2 bond angles respectively. The calculated values of *EB* are as follows: G II, 438; G XVI (a), 345; G XVI (b), 288; G XVIII, 166 (°)[2].

The possibility exists that the O(2)H hydroxyl group may form an intramolecular hydrogen bond of the O–H···π type:[12] O(2)···C(10), 2.895(4) Å; H(O2)···C(10), 2.59(5) Å; H(O2)···C(20), 2.78(4) Å. This weak interaction may also contribute to the stability of the present B-ring conformation.

It should be noted that the six-membered C-ring adopts the unstable boat conformation, while it takes the chair conformation in both **2** and **3**. In order to clarify the cause of this boat conformation, we performed force-field calculations for **4**—**7**, using the MMI program.[13] The calculated heats of formation are as follows: **4**, −28.8; **5**, −22.4; **6**, −4.7; **7**, −0.1 kcal/mol. These results show that the transformation of the C(15)–C(16) single bond into the double bond reduces the chair-boat enthalpy difference of the C-ring from 6.4 to 4.6 kcal/mol. Therefore, if one assumes that the present B-ring conformation is more stable than those in **2** and **3** by more than 4.6 kcal/mol and by less than 6.4 kcal/mol, the conformational behavior of the C-ring can be easily understood.

Crystal Structure. The crystal structure viewed along the c axis is shown in Fig. 3. There are two kinds of intermolecular hydrogen bonds, O(3)–H···O(1′) and O(4)–H···O(3″); their O···O distances are 2.937(3) and 2.854(4) Å respectively. Through these hydrogen bonds, the molecules form a molecular layer parallel to the (100) plane. These molecular layers are further held together mainly by the van der Waals interactions.

We wish to thank Dr. Eiji Ōsawa of Hokkaido University for allowing the free use of the MMI program. We are also grateful to Dr. Hiroshi Yoshioka of Kwansei Gakuin University for his valuable discussion of hydrogen bonds.

References

1) S. Miyajima and S. Takei, *J. Agric. Chem. Jpn.*, **10**, 1093 (1934); H. Kakisawa, M. Kurono, S. Takahashi, and Y. Hirata, *ibid.*, **1961**, 59; J. Iwasa and Y. Nakamura, *Tetrahedron Lett.*, **1969**, 3937; H. Hikino, M. Ogura, T. Ohta, and T. Takemoto, *Chem. Pharm. Bull.*, **18**, 1072 (1970).

2) T. Okuno, N. Hamanaka, H. Miyakoshi, and T. Matsumoto, *Tetrahedron*, **26**, 4765 (1970); N. Hamanaka, H. Miyakoshi, A. Furusaki, and T. Matsumoto, *Chem. Lett.*, **1972**, 779.

3) M. Yasue, Y. Kato, T. Kishida, and H. Ohta, *Chem. Pharm. Bull.*, **9**, 171 (1961); H. Hikino, K. Ito, and T. Takemoto, *ibid.*, **17**, 854 (1969); H. Hikino, M. Ogura, T. Ohta, and T. Takemoto, *ibid.*, **18**, 1071 (1970).

4) S. Gasa, R. Ikeda, N. Hamanaka, and T. Matsumoto, *Bull. Chem. Soc. Jpn.*, **49**, 835 (1976).

5) A. Furusaki, S. Gasa, N. Hamanaka, R. Ikeda, and T. Matsumoto, *Chem. Lett.*, **1979**, 665.

6) The fraction consisting of "unknown compounds" described in the experimental section of Ref. 4).

7) A. Furusaki, *Acta Crystallogr., Sect. A*, **35**, 220 (1979).

8) "International Tables for X-Ray Crystallography," The Kynoch Press, Birmingham (1974), Vol. IV.

9) A. Furusaki, N. Hamanaka, and T. Matsumoto, *Bull. Chem. Soc. Jpn.*, **53**, 1956 (1980).

10) A. Furusaki, S. Gasa, R. Ikeda, and T. Matsumoto, unpublished.

11) J. B. Hendrickson, *J. Am. Chem. Soc.*, **83**, 4537 (1961).

12) A. T. McPhail, G. A. Sim, A. J. Frey, and H. Ott, *J. Chem. Soc., B*, **1966**, 377; A. D. U. Hardy and D. D. MacNicol, *J. Chem. Soc., Perkin Trans. 2*, **1976**, 1140.

13) QCPE 318; N. L. Allinger, J. T. Sprague, and J. Liljefors, *J. Am. Chem. Soc.*, **96**, 5100 (1974); D. H. Wertz and N. L. Allinger, *Tetrahedron*, **30**, 1579 (1974).

  Bull. Chem. Soc. Jpn., 54, 661—668 (1981)

Electrode Kinetics of Eu(III) Ion in the Presence of 1,4-Benzenedimethanol

Osamu IKEDA,* Katsuhiko TSUURA, and Hideo TAMURA

Department of Applied Chemistry, Faculty of Engineering, Osaka University, Yamadakami, Suita, Osaka 565

(Received July 23, 1980)

In order to know the role of aromatic ring on the electrode kinetics, d. c. polarogram of Eu(III) ion was measured in the presence of 1,4-benzenedimethanol (1,4-BDM). The effect of the adsorption has been discussed by correlating the kinetic data to the adsorption behaviors of 1,4-BDM estimated from the electrocapillary curves. At the standard potential of Eu(III)/Eu(II) (−0.600 V *vs.* SCE), 1.4-BDM on the electrode changed its orientation from horizontal to vertical with an increase in the coverage. Both orientations showed an inhibition effect for the electroreduction of Eu(III) ion. When the coverage due to the horizontal orientation is less than 0.8, the inhibition was interpreted by an additional energy to deform the surface layer. On the other hand, the inhibition at full coverage due to both the horizontal and the vertical orientations was interpreted by the tunneling probability through the adsorbed layer differed in the thickness.

Electroinactive organic compounds adsorbed on the electrode influence the reduction rate of metal cations. It has been proposed that various factors influence the reduction rate, for example blocking effect,[1-6] interaction between the activated complex and the adsorbed ions or molecules,[7] additional energy to bring the discharging ion to the pre-electrode state,[8] electrostatic potential[9] and dipole,[10] and so on. The above factors have been reviewed by Lipkowski and Galus,[11] and Damaskin and Afanas'ev.[12]

Organic compounds adsorbed on the electrode usually inhibit the reduction rate of metal cations. However, Loshkarev *et al.*[13] observed that 1-naphthol inhibited the reduction rate of Bi(III) when its aromatic ring was vertical to the electrode surface, but it did not prevent the electron transfer to the discharging ion when the ring was horizontal. They explained these results on the basis of the idea proposed by Dyatkina and Damaskin[14] that aromatic compounds, adsorbed horizontally on the electrode, extend the metal surface toward the solution. Dutkiewicz and Paucz[15] have also discussed the electrode reaction of Cd(II) ion in the presence of benzenesulfonate ion on the same explanation as Loshkarev *et al.*[13] However, such an effect of aromatic compounds is observed only for the electroreduction of deposition type such as Bi(III)/Bi(0) and Cd(II)/Cd(0). It is of interest to study their effect on the electroreduction of simple charge transfer type, namely Eu(III)/Eu(II).

In this study, 1,4-benzenedimethanol (1,4-BDM) was chosen as the aromatic compound, because it has a good solubility in water and it is a neutral compound which does not form a complex with Eu(III) ion. The initial study was the adsorption behaviors of 1,4-BDM at the mercury/water interface, and then the effect of the adsorption on the electrode kinetics of Eu(III)/Eu(II).

Experimental

All chemicals were analytical grade materials. 1,4-Benzenedimethanol (1,4-BDM) was recrystallized twice from distilled water. Aqueous 1 M $NaClO_4$† prepared from triply distilled water was used as the supporting electrolyte, and was treated with purified active charcoal before use. Mercury was purified by treatment with dilute nitric acid, then distilled triply in a vacuum. Nitrogen gas, after passing through a purification line, was used for deaeration.

Adsorption behaviors of 1,4-BDM were estimated from the analysis of the electrocapillary curves, which were measured with the maximum bubble pressure method.[16,17] Twelve different concentrations of 1,4-BDM solutions were prepared to cover between 0.2 mA and 15 mA. The interfacial tension was measured at 50 mV intervals, except for positive and negative extremes where 25 mV intervals were chosen. The error of the measurement was ±0.1 mN m^{-1} near the electrocapillary maximum, and ±0.3 mN m^{-1} at positive and negative extremes. Most of the parameters essential to adsorption were derived by analyzing the electrocapillary curves with a computer programme. At the analysis, no corrections were taken into consideration for the medium effect on the activity coefficient of the supporting electrolyte,[18,19] and the activity coefficient of the adsorbate.[20]

Differential capacity was measured with a cell and a bridge similar to those described by Hills and Payne.[21] The measurement was carried out at a frequency of 850 Hz with an amplitude of 5 mV, and at 7.0 s after the birth of a mercury drop whose total life was about 12 s in 1.0 M $NaClO_4$.

The capillaries used in the above two measurements were siliconed on the internal wall by passing a vapor of dimethyldichlorosilane for several seconds.

Polarographic measurement, in which an instantaneous current at the end of the drop life was recorded, were carried out with a three-electrode system consisting of a Yanagimoto Voltammetric Analyzer (Model P-1000). The drop time was adjusted to 3.5 s, and the flow rate of mercury was determined by weighing mercury recovered during a given time, and it was 1.781 mg s^{-1} at a mercury height of 60 cm. The concentration of Eu(III) ion was 0.98 mM. Currents were corrected for the residual current which was measured independently. The true standard rate constant was obtained following the method due to Asada *et al.*[22] The apparent heat of activation of the electrode reaction at the standard potential was determined from the dependence of the apparent standard rate constant on temperature.

All the measurements except for the apparent heat of activation were carried out in a water bath thermostated at 25±0.1 °C, and potentials were measured against a saturated calomel electrode (SCE).

Results and Discussion

Electrocapillary and Differential Capacity-potential Curves.

† 1 M = 1 mol dm^{-3}.

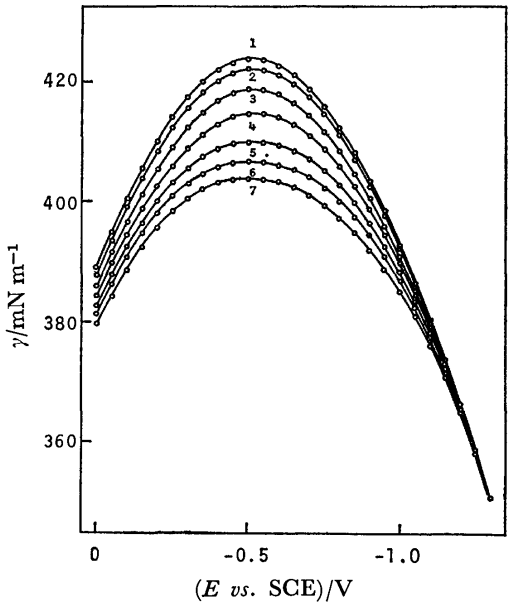

Fig. 1. Electrocapillary curves for aqueous 1.0 M $NaClO_4$ solutions containing 1,4-benzenedimethanol in various concentrations at 25 °C.
The concentrations (mM): (1) 0 (base solution, 1.0 M $NaClO_4$), (2) 0.5, (3) 2.0, (4) 4.0, (5) 7.0, (6) 10.0, and (7) 15.0.

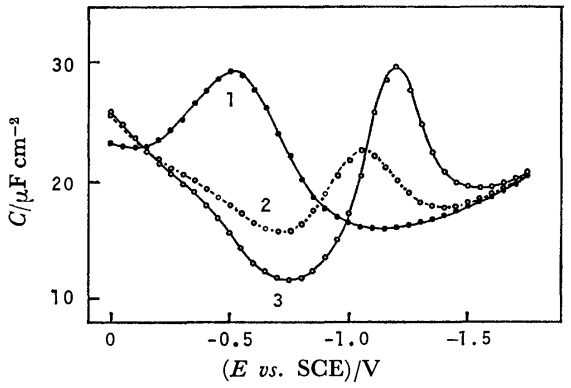

Fig. 2. Typical differential capacity-potential curves of the mercury electrode in aqueous 1.0 M $NaClO_4$ solutions with and without 1,4-benzenedimethanol at 25 °C.
The concentrations of 1,4-benzenedimethanol (mM): 0 (base solution, 1.0 M $NaClO_4$), (2) 3.0, and (3) 15.0.

Figure 1 shows the electrocapillary curves obtained for the 1.0 M $NaClO_4$ containing 1,4-BDM in various concentrations. The drop in the interfacial tension, γ, due to an increase in the concentration is most remarkable at -0.5 V, which approximately corresponds to the electrocapillary maximum, E_{ecm}. This suggests that 1,4-BDM adsorbed on the electrode does not take an orientation with a large dipole moment in the direction normal to the electrode surface.

Figure 2 shows the typical differential capacity-potential curves obtained for the 1.0 M $NaClO_4$ containing 1,4-BDM. The adsorption-desorption peak at more positive potentials was not observed clearly, in contrast to that at more negative potential. This indicates that π-electrons in 1,4-BDM interact with the positive charge on the electrode, as have been

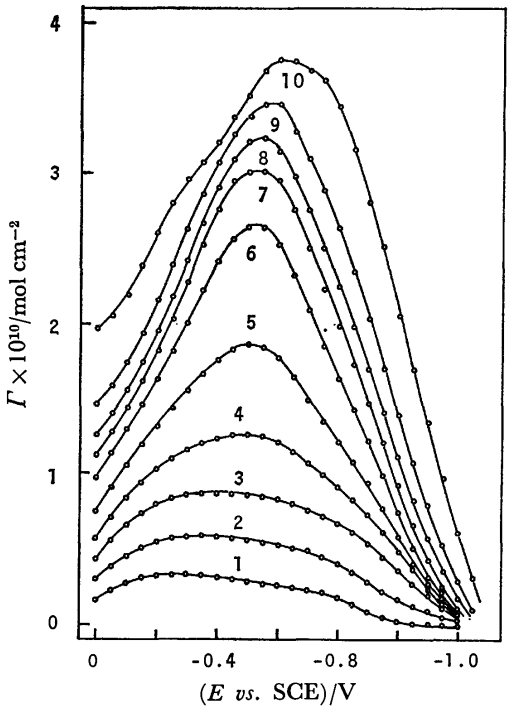

Fig. 3. Surface excess of 1,4-benzenedimethanol as a function of potential.
The concentrations of 1,4-benzenedimethanol (mM): (1) 0.2, (2) 0.5, (3) 1.0, (4) 1.4, (5) 2.0, (6) 3.0, (7) 4.0, (8) 5.0, (9) 7.0, and (10) 15.0.

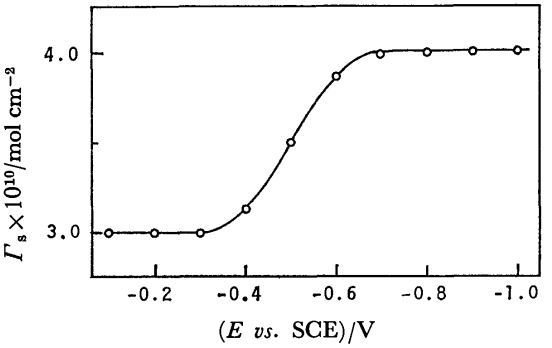

Fig. 4. Variation of surface excess at saturation, Γ_s, with the electrode potential.

accounted for in organic compounds with π-electrons.[23–25]

The curve for the base 1.0 M $NaClO_4$ showed a large peak due to specific adsorption of perchlorate anion.[26] However, the peak was diminished with an increase in the concentration of 1,4-BDM, and completely disappeared at more concentrated solutions than 1.0 mM. It was thought that the specific adsorption of perchlorate anion becomes unimportant at higher concentrations of 1,4-BDM.

Adsorption Behaviors. Surface excess, Γ, of 1,4-BDM was obtained using Eq. 1,

$$(\partial\gamma/\partial \ln C_{org})_{E,P,T} = -RT\Gamma, \quad (1)$$

where C_{org} is the concentration of 1,4-BDM, and the others have usual meaning. The surface excess at various concentrations is shown in Fig. 3 as a function of potential. Figure 4 shows a relation between the

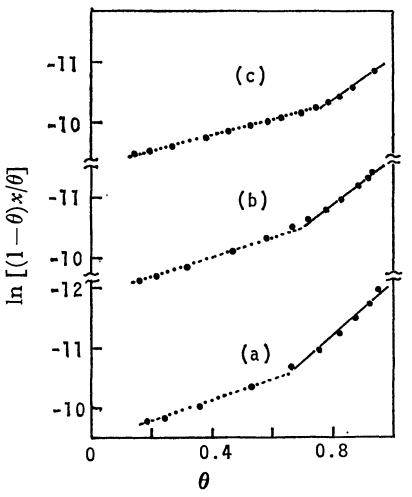

Fig. 5. Test of the Frumkin isotherm at different potentials. Potential and Γ_s used for the estimation of coverage: (a) −0.5 V and 3.5×10^{-10} mol cm^{-2}, (b) −0.6 V and 3.9×10^{-10} mol cm^{-2}, and (c) −0.7 V and 4.0×10^{-10} mol cm^{-2}.

potential and the surface excess at saturation, Γ_s, which are obtained by extrapolating the plots of $1/\Gamma$ *vs.* $1/C_{org}$ at a given potential to $1/C_{org}=0$. The value of Γ_s obtained in this way reflects the orientation at higher surface excess from the nature of the plots. Two limiting values of Γ_s were observed depending on the potential. One was 3.0×10^{-10} mol cm^{-2} and the other was 4.0×10^{-10} mol cm^{-2}. Since the center of the change in Γ_s was −0.5 V which nearly corresponded to E_{ecm}, this change was thought to result from an interaction between π-electrons in the adsorbed 1,4-BDM molecules and the surface charge on the electrode. Then, it was considered that the lower value of Γ_s corresponds to a horizontal orientation and the higher one to a vertical orientation with a smaller projected area.

As the adsorption behavior of 1,4-BDM was expected to be complicated, it was somewhat closely examined by fitting to a Frumkin isotherm with two parameters, Γ_s and the interaction parameter. Equation 2 shows the Frumkin isotherm,

$$\beta x = \theta/(1-\theta)\exp(-2a\theta), \quad (2)$$

where β is the adsorption coefficient being a function of the standard free energy of adsorption, x and θ are the molar fraction and the coverage defined as Γ/Γ_s, respectively, and $2a$ is the interaction parameter whose positive (negative) value means that an attractive (repulsive) force acts among adsorbed molecules. The Frumkin isotherm plot at various potentials is shown in Fig. 5. The value of θ necessary for this plot was evaluated using the value of Γ_s corresponding to each potential in Fig. 4. In this treatment, it is assumed that the orientation of 1,4-BDM around E_{ecm} is intermediate between the horizontal and the vertical orientation, regardless of coverage. However, a linear relation over the whole coverage, which was actually observed for −0.2 and −0.9 V far from E_{ecm}, was not obtained for the potentials around E_{ecm}. A change in the orientation owing to coverage seems to be the cause, because the plots

Table 1. Interaction parameter at various potentials

(Potential *vs.* SCE)/V	−0.4	−0.5	−0.6	−0.7	−0.8
$2a$	1.5	1.9	2.0	1.5	1.0

in Fig. 5 change the slope at higher coverage. It has already been described that aromatic compounds have a tendency to change the orientation with the surface charge on the electrode, namely a horizontal orientation at positive charge owing to attractive interaction with π-electrons and a vertical orientation at negative charge owing to repulsive interaction with π-electrons. Except for this electrostatic effect, at potentials around E_{ecm} where the surface charge density is low, the hydrophobic interaction between the adsorbate and the electrode with a structured water, and the need for an increased packing seem to control the orientation. From this point of view, 1,4-BDM around E_{ecm} was considered to take a horizontal orientation with higher hydrophobicity at lower surface excess and a vertical one with a smaller projected area at higher surface excess. Then, the Frumkin isotherm in Fig. 5 was replotted using $\Gamma_s=3.0\times10^{-10}$ mol cm^{-2} for $\theta\leq0.7$. In this case, the plot showed an inflection at $\theta\simeq0.8$—0.9. The values of $2a$ obtained from the above treatment are summarized in Table 1. They were positive, and it was found that the attractive interaction acts among the adsorbed 1,4-BDM molecules in the horizontal orientation. It was also observed that the interaction parameter changes with potential. Although the cause is not clear, a change in the configuration of the hydroxyl groups due to the electric field seems to be a cause.

There remains a problem how to interpret the intermediate values of Γ_s around E_{ecm}. It can be interpreted in connection with the consideration of the orientation state of 1,4-BDM at higher surface excess. Thus, 1,4-BDM begins to take the vertical orientation, as the coverage evaluated with respect to the horizontal orientation exceeds 0.8—0.9. Then, the electrode surface is thought to be completely covered with 1,4-BDM molecules which consist of the two orientations. The fraction of the vertical orientation in the mixed two orientations increases with an increase in the surface excess, but the maximum fraction which is associated with the value of Γ_s changes with the potential or the surface charge on the electrode. Above consideration seems to be more natural than that of the intermediate orientation corresponding to each Γ_s, and was actually verified in the following discussion with respect to adsorption effect of 1,4-BDM on the electrode kinetics of Eu(III).

Orientation Model. Figure 6 shows the variation of E_{ecm} with the surface excess. E_{ecm} showed a slight cathodic shift with an increase in the surface excess, but at higher surface excess it showed a slight anodic shift oppsitely. This result was thought to be another proof for the change in the orientation due to coverage. When 1,4-BDM is adsorbed without net dipole moment, one can expect a positive shift of E_{ecm} by 30 mV[27] or 70 mV,[28] which has been

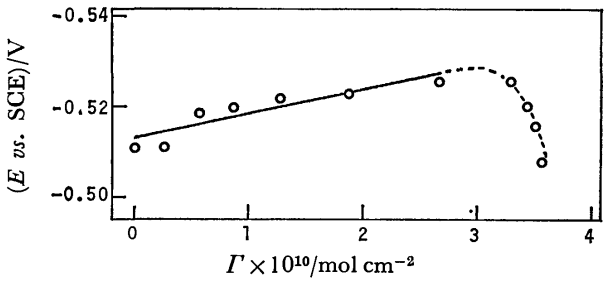

Fig. 6. Variation of the electrocapillary maximum, E_{ecm}, due to adsorption of 1,4-benzenedimethanol.

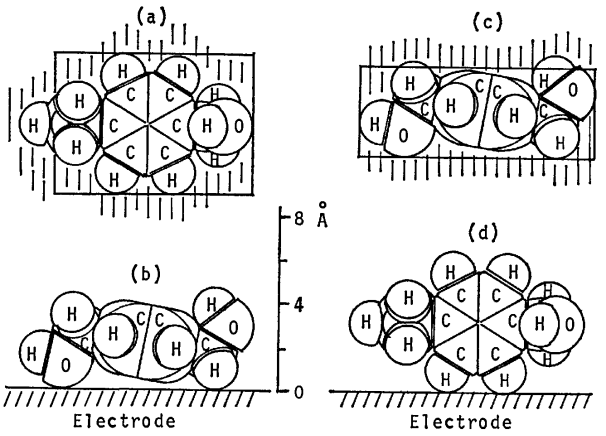

Fig. 7. Scale drawings of a 1,4-benzenedimethanol molecule adsorbed on the electrode through the horizontal orientation (a) and (b), and the vertical orientation (c) and (d). (a) and (c) show the top view, and (b) and (d) the side view. At the determination of the molecular configuration, the CPK precision molecular model was used.

estimated for the potential drop due to water dipoles at E_{ecm}. Therefore, the result in Fig. 6 can be interpreted as follows: the horizontal orientation at lower surface excess has a small dipole moment and at the interface the negative end of the dipole directs to the electrode, but the normal component of this dipole becomes unimportant with the change in the orientation from horizontal to vertical.

On the basis of the above consideration and the two different values of Γ_s, such orientation models as shown in Fig. 7 were considered for the horizontal and the vertical orientations at the potentials around E_{ecm}. The area of the rectangles enclosing the molecule in Figs. 7-a and 7-c are 55.3 Å^2 or 3.0×10^{-10} mol cm^{-2} and 41.5 Å^2 or 4.0×10^{-10} mol cm^{-2}, respectively. Moreover, the height of the molecule estimated from Figs. 7-b and 7-d were about 4.2 Å and 6.3 Å, respectively. When these molecules form a monolayer on the electrode, the difference in the thickness of the layer can be expected to be about 2.1 Å.

Kinetic Data for the Reduction of Eu(III) in the Presence of 1,4-BDM. In order to know the effect of π-electrons in 1,4-BDM on the reduction rate of Eu(III) ion, d.c. polarogram was measured with the aqueous 1.0 M $NaClO_4$ solution containing 0.98 mM Eu(III) ion and 1,4-BDM in various concentrations. Figure 8 shows the polarograms. It is obvious that

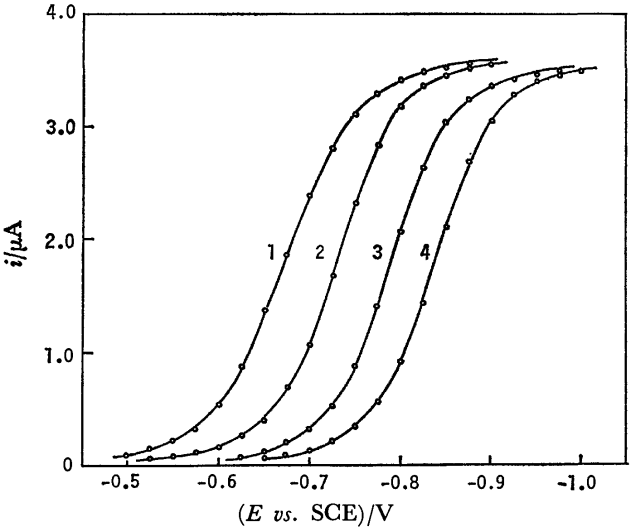

Fig. 8. D.c. polarograms of 0.98 mM Eu(III) ion in aqueous 1.0 M $NaClO_4$ solutions containing 1,4-benzenedimethanol at 25 °C.
The concentrations of 1,4-benzenedimethanol (mM): (1) 0 (base solution, 1.0 M $NaClO_4$), (2) 1.0, (3) 4.0, and (4) 15.0.

the presence of 1,4-BDM in the solution inhibits the reduction of Eu(III) ion.

The true standard rate constant was determined from the analysis of the *i-E* curve at the foot of the wave ($i\leq0.05\ i_d$). Equation 3 represents the current for the reduction of Eu(III) to Eu(II),

$$i_\theta = FAk_s^\theta C^\circ_{Eu(III)}\exp\{(\alpha-z)F\phi_2/RT\}\exp(-\alpha F\eta/RT), \quad (3)$$

where A is the electrode area, $C^\circ_{Eu(III)}$ is the bulk concentration of Eu(III) ion, α is the true transfer coefficient, z is the ionic valence of Eu(III) ion, ϕ_2 is the inner potential at the outer Helmholtz plane which was determined using the Gouy-Chapman theory,[29] η is the overpotential, k_s^θ is the true standard rate constant, and the others have usual meaning. As a first approximation, Eu(III) ion was assumed to take an electron at the outer Helmholtz plane with its hydration shell.[30] Various kinetic data are summarized in Table 2 with the adsorption data of 1,4-BDM at the standard potential of Eu(III)/Eu(II) (−0.600 V *vs.* SCE[31]). For lower surface excess, the coverage θ was evaluated as Γ/Γ_s, where $\Gamma_s=3.0\times10^{-10}$ mol cm^{-2}. However, for surface excess higher than 3.0×10^{-10} mol cm^{-2}, the fraction of the vertical orientation in the mixture which consists of the vertical and the horizontal orientations, θ_V was estimated on the basis of the previous consideration of the full coverage. The diffusion constant of Eu(III), D, was constant throughout the solutions in an experimental error. On the other hand, the apparent heat of activation at the standard potential, ΔH_s^*, was increased with an increase in the coverage, but it came to constant near and at full coverage.

Inhibition Effect at Intermediate Coverage. The rate constant in the presence of organic adsorbates is generally a function of coverage, and it has been expressed in theoretical equations by considering various factors.

Table 2. Adsorption and kinetic data

Concn of 1,4-BDM / mM	$\Gamma \times 10^{10}$ a) / mol cm^{-2}	θ b)	θ_v c)	$E_{1/2}$ *vs.* SCE / V	$k_s^\theta \times 10^6$ / cm s^{-1}	α	$D \times 10^6$ / cm^2 s^{-1}	ΔH_s^* / kJ mol^{-1}
0 (base soln.)	—	—		−0.672	—	—	8.1	
0.5	0.48	0.16		−0.709	25.8	0.39	8.2	
0.7	0.62	0.21		−0.717	19.3	0.39	8.2	79.1
1.0	0.83	0.28		−0.734	13.0	0.40	8.1	
1.4	1.22	0.41		−0.743	9.24	0.39	8.0	89.9
2.0	1.78	0.59		−0.757	6.61	0.36	8.2	
2.5	2.20	0.73		−0.767	5.44	0.38	8.2	95.4
3.0	2.53	0.84		−0.773	4.59	0.40	8.3	
4.0	2.96	0.99		−0.791	3.50	0.39	8.2	
5.0	3.20	1.00	0.20	−0.799	2.65	0.44	8.2	94.1
7.0	3.50	1.00	0.50	−0.812	1.64	0.50	8.1	
10.0	3.66	1.00	0.66	−0.824	1.15	0.56	8.2	
15.0	3.79	1.00	0.79	−0.837	0.797	0.55	8.1	
20.0	—	(1.00) d)	(0.90) d)	−0.848	0.773	0.59	8.1	95.8

a) The values at the standard potential of Eu(III)/Eu(II), −0.600 V *vs.* SCE. b) For the solutions up to 4 mM, the coverage θ was evaluated with the horizontal orientation, but in the solutions beyond 4 mM, the electrode surface was considered to be completely covered with a mixture consisting of the horizontal and the vertical orientations. c) The θ_v is the fraction of the vertical orientation in the mixture. d) Speculated values.

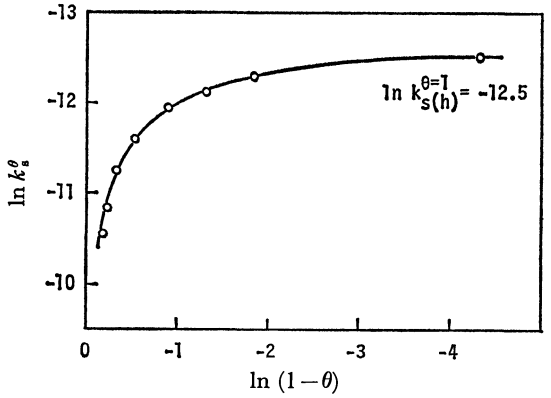

Fig. 9. Plot of $\ln k_s^\theta$ against $\ln(1-\theta)$.

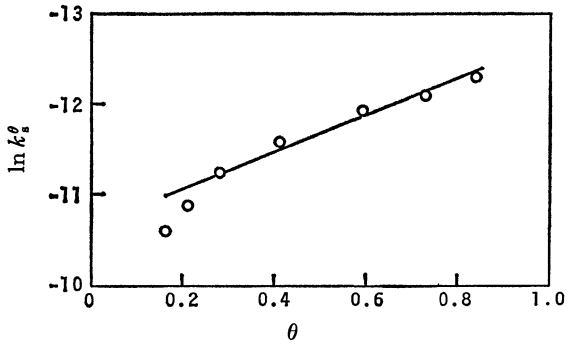

Fig. 10. Plot of $\ln k_s^\theta$ against θ.

The most simple form is the following equation,[1-3]

$$k_s^\theta = k_s^{\theta=0}(1-\theta) + k_s^{\theta=1}, \quad (4)$$

where $k_s^{\theta=0}$ and $k_s^{\theta=1}$ are the standard rate constants at zero and full coverage, respectively. Equation 4 is the sole equation that predicts a linear relation between k_s^θ and θ. When $k_s^{\theta=0} \gg k_s^{\theta=1}$, it changes to Eq. 5,

$$k_s^\theta = k_s^{\theta=0}(1-\theta), \quad (5)$$

which describes a simple blocking effect. However, Lipkowski and Galus[32] have recently pointed out that the interpretation of Eq. 5 is different depending on the thermodynamics of the interface.

Figure 9 shows the plot of $\ln k_s^\theta$ against $\ln(1-\theta)$. In contrast to the prediction of Eq. 5, this plot showed a curvature. Further the plot based on Eq. 4 also showed a curvature, thus it was concluded that the electroreduction of Eu(III) ion in the presence of 1,4-BDM could not be described by Eqs. 4 and 5.

Afanas'ev and Ternovskoi[8] have presented the next equation which is one of the equations predicting a non-linear relation between k_s^θ and θ,

$$k_s^\theta = k_s^{\theta=0}\exp(-2ar\theta), \quad (6)$$

where $2a$ is the interaction parameter of the Frumkin isotherm for adsorbate in the absence of discharging ion, r is a coefficient taking into consideration the decrease in the attractive interaction between the adsorbed molecules when the discharging ion is transferred into the adsorbed layer. This equation is based on the consideration that the concentration of the discharging ion in the surface layer is determined by the additional energy ($2ar\theta RT$) required to transfer the discharging ions from the bulk of the solution into the structured surface layer consisting of water and the adsorbed molecules.

Figure 10 shows the plot based on Eq. 6 in the region of $\theta \leq 0.8$. A linear relation was observed in the region of $0.2 \leq \theta \leq 0.8$. The deviation of the plot from the linear relation in $\theta < 0.2$ seems to result from a specific adsorption of perchlorate anion which acts as an accelerator. The slope was 2.0 and it agreed well with the value of $2ar$ at $r=1$, 2.0 which was estimated from the fit to the Frumkin isotherm.

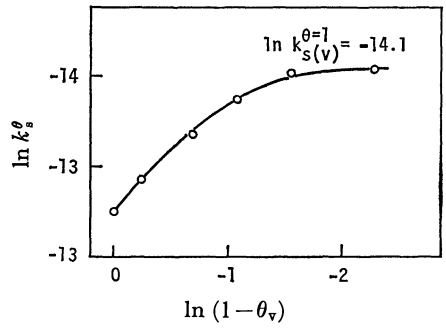

Fig. 11. Plot of $\ln k_s^\theta$ against $\ln(1-\theta_v)$.

It was pointed out in Ref. 8 that Eq. 6 is set up when the transfer of the discharging ion into the surface layer is reversible, while the electrode reaction rate is limited by the electron transfer step. Such a surface layer also does not influence the diffusion limiting current.[32] The constancy of D in Table 2 satisfies the requirement. Further, the increase in ΔH_s^* due to adsorption of 1,4-BDM is thought to support the above inhibition effect, although the change is somewhat larger than that expected from the additional energy.

Inhibition Effect at Full Coverage. Figure 11 shows the plot of $\ln k_s^\theta$ against $\ln(1-\theta_v)$. The standard rate constant was diminished with an increase in θ_v, and showed a limiting value of -14.1. A similar limiting value of -12.5 has also been observed in Fig. 9. Taking into consideration the adsorption behavior of 1,4-BDM, the former can be assigned to the rate constant relating to the vertical orientation $\ln k_{s(v)}^{\theta=1}$, indeed the vertical orientation at this time is not so perfect as in $E \leq -0.7$ V, and the latter to that relating to the horizontal one $\ln k_{s(h)}^{\theta=1}$. The difference between above two values was 1.6, and the inhibition effect due to the vertical orientation was larger than that due to the horizontal one.

It is also considerable for this result that the deformation of the structured surface layer is a factor for the inhibition of the electroreduction of Eu(III) ion at full coverage.

However, the process that Eu(III) ion penetrates into the adsorbed monolayer by surmounting only the deformation energy seems to be improbable at full coverage, because the penetration at full coverage needs another additional energy due to the displacement of 1,4-BDM adsorbed on the electrode, which is larger than the deformation energy and nearly the same as the adsorption energy, about 23 kJ mol^{-1}. As can be seen from Table 2, the values of ΔH_s^* near and at full coverage were approximately constant, regardless of the structure of the adsorbed monolayer. This result can not be explained by the penetration process based on the deformation or the displacement. As the another factor for the inhibition effect at full coverage, the electron tunneling process through the adsorbed monolayer was considered. This process explains the constancy of ΔH_s^*. Thus, the reactant which accepts an electron at the tunneling transition is not Eu(III) ion at the ground state, but the ion at the activated state. Eu(III) ion is thought to be

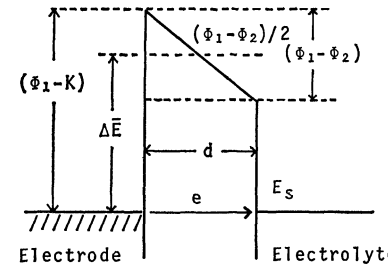

Fig. 12. Idealized rectangular barrier model for the electron tunneling from the mercury electrode to Eu(III) ion through the adsorbed 1,4-benzenedimethanol monolayer. Here, Φ_1 and Φ_2 are the electronic energy of the electrode and the electrolyte, respectively, K and $\Delta\bar{E}$ are the electron affinity of the monolayer and the mean height of the barrier, respectively, E_s is the standard potential of Eu(III)/Eu(II) in the absolute potential scale, and d is the thickness of the monolayer.

activated through the thermal and the electrostatic interactions of the ion with the sorrounding water molecules, the so-called solvent rearrangement,[33] and the energy necessary for such an activation can be expected to be independent of the surface layer structure, if a specific interaction between the reactant and the adsorbed molecules is not present.

Furthermore, appearance of the limiting value of $\ln k_s^\theta$ as shown in Fig. 9 has been attributed to a possibility of the electron tunneling through the adsorbed organic layer.[34] Therefore, such a possibility was examined using the theory of elastic tunneling. Application of such a tunneling theory to the electrode kinetics has been carried out by Gurney[35] and Gerisher,[36] and has been verified by the experiment at the oxide covered electrodes.[37-40] The electron tunneling through organic monolayer between metals has also been verified with respect to various fatty acid salts.[41,42]

If the current at the electroreduction of Eu(III) ion is governed by the electron tunneling through the adsorbed organic monolayer, it is represented by Eq. 7,

$$i_{\theta=1} = e_0 \int_{-\infty}^{+\infty} \upsilon(E) N_b(E) D_{ox}(E) dE, \quad (7)$$

where e_0 is the charge of an electron, $N_b(E)$ and $D_{ox}(E)$ are the density of occupied electron states in the electrode and that of unoccupied states in the electrolyte, respectively, and $\upsilon(E)$ is the electronic frequency factor involving the tunneling probability. This tunneling probability is a function of the thickness of the adsorbed layer, d, and the mean height of the potential barrier, $\Delta\bar{E}$. On the basis of the idealized rectangular barrier model shown in Fig. 12, $\upsilon(E)$ is represented by the following equation,

$$\upsilon(E) \propto \exp\{-(4\pi d/h)\sqrt{2m_e\Delta\bar{E}}\}, \quad (8)$$

where h and m_e are Planck's constant and the mass of an electron, respectively. The frequency factor can be assumed to be independent of the energy, E. Further, assuming that $\Delta\bar{E}$ does not change with the

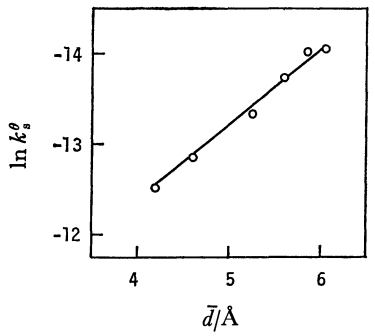

Fig. 13. Plot of $\ln k_s^\theta$ against $\bar{d}$.

orientation of 1,4-BDM, one obtains the next relation for the ratio of the true standard rate constant at full coverage with the horizontal and the vertical orientations,

$$\ln\{k_{s(v)}^{\theta=1}/k_{s(h)}^{\theta=1}\} = -(4\pi\Delta d/h)\sqrt{2m_e\Delta\bar{E}}, \quad (9)$$

where Δd is the difference in the thickness of the adsorbed organic layer. The possibility of the electron tunneling process can be proved by using Eq. 9.

In general, $\Delta\bar{E}=(\Phi_1+\Phi_2)/2-K$, where Φ_1 and Φ_2 are the electronic energy of the mercury used as the electrode and of the electrolyte, respectively, and K is the electron affinity of the adsorbed organic monolayer. One can use the work function of mercury and the standard potential of Eu(III)/Eu(II) in the absolute potential scale as Φ_1 and Φ_2, respectively. One obtains 4.5 eV[43] for Φ_1, and 4.1 eV for Φ_2 using the value of 4.43 V[44] as the absolute potential of the standard hydrogen electrode. Further, K is defined as (I_p-E_g), where I_p and E_g are the ionization potential and the band gap of the adsorbed 1,4-BDM monolayer, respectively. These values must be actually for the monolayer, but those for the molecule were used. The value of E_g was evaluated from the ultraviolet spectrum measured in the 1.0 M $NaClO_4$ solution dissolved 1,4-BDM, and it was 5.69 eV for $\lambda_{max}=218$ nm. Since the value of I_p was not found in the literature, instead, that of benzenemethanol 9.14 eV[45] was used.

Finally, one obtains 1.7 Å for Δd by introducing $\ln\{k_{s(v)}^{\theta=1}/k_{s(h)}^{\theta=1}\}=-1.6$ and the others into Eq. 9. Taking into consideration the imperfection of the adsorbed monolayer and rough approximations used, this calculated value of 1.7 Å seems to agree well with 1.9 Å, which was estimated by applying the arithmetic mean to Γ_s of 3.9×10^{-10} mol cm^{-2} at -0.600 V on the basis of the consideration of the mixed orientation and the orientation model in Fig. 7.

Figure 13 shows the plot of $\ln k_s^\theta$ against the arithmetic mean thickness of the adsorbed layer saturated with the two orientations, $\bar{d}$. A linear relation observed in this Figure is considered to support the previous consideration of the full coverage at higher surface excess, and also the electron tunneling process through the adsorbed organic monolayer.

Concluding Remarks. In the results and the discussions so far mentioned, it was clarified that the horizontal orientation of the benzene ring inhibited the electroreduction rate of Eu(III) ion, which is known as the reaction of simple charge transfer type. This result was distinct from that obtained by Loshkarev *et al.*[13] with respect to the reaction of deposition type. In considering that Eu(III) ion takes an electron with its hydration shell, the reduction intermediates of Bi(III) and Cd(II), which seem to be partially dehydrated, may have such an interaction with π-electrons that does not lead to the inhibition of charge transfer rate. However, the idea[14] that aromatic compounds adsorbed horizontally extend the electrode surface toward the solution side through the aromatic rings was not applicable to the system in this study.

References

1) J. Weber, J. Koutecký, and J. Koryta, *Z. Elektrochemie*, **63**, 583 (1959).
2) J. Kuta and I. Smoler, *Z. Elektrochemie*, **64**, 285 (1960).
3) W. Miller and W. Lorenz, *Z. Phys. Chem. (Frankfurt)*, **27**, 23 (1961).
4) K. K. Niki and N. Hackerman, *J. Electroanal. Chem.*, **32**, 257 (1971).
5) F. Scheller, R. Landsberg, and H. Wolf, *Z. Phys. Chem. (Leipzig)*, **244**, 273 (1970).
6) J. Lipkowski and Z. Galus, *J. Electroanal. Chem.*, **39**, 333 (1972).
7) R. Parsons, *J. Electroanal. Chem.*, **21**, 35 (1969).
8) B. N. Afanas'ev and L. A. Ternovskoi, *Elektrokhimiya*, **10**, 901 (1974).
9) R. Parsons, *Adv. Electrochem. Electrochem. Eng.*, **1**, 1 (1961).
10) S. Sathyanarayana, *J. Electroanal. Chem.*, **50**, 195 (1974).
11) J. Lipkowski and Z. Galus, *J. Electroanal. Chem.*, **61**, 11 (1975).
12) B. B. Damaskin and B. N. Afanas'ev, *Elektrokhimiya*, **13**, 1099 (1977).
13) Yu. M. Loshkarev, V. V. Trofinenko, and A. A. Kuznetsov, *Elektrokhimiya*, **11**, 1724 (1975).
14) S. L. Dyatkina and B. B. Damaskin, *Elektrokhimiya*, **2**, 1340 (1966).
15) E. Dutkiewicz and A. Paucz, *J. Electroanal. Chem.*, **100**, 947 (1979).
16) D. J. Schiffrin, *J. Electroanal. Chem.*, **23**, 168 (1969).
17) O. Ikeda, Y. Matsuda, H. Yoneyama, and H. Tamura, *Electrochim. Acta*, **21**, 519 (1976).
18) A. De. Battisti and S. Trasatti, *J. Electroanal. Chem.*, **54**, 1 (1974).
19) D. M. Mohilner and H. Nakadomari, *J. Phys. Chem.*, **77**, 1594 (1973).
20) D. M. Mohilner, L. W. Browman, S. J. Freeland, and H. Nakadomari, *J. Electrochem. Soc.*, **120**, 1658 (1973).
21) G. J. Hills and R. Payne, *Trans. Faraday Soc.*, **61**, 316 (1965).
22) K. Asada, P. Delahay, and A. K. Sundaram, *J. Am. Chem. Soc.*, **83**, 3396 (1961).
23) M. A. Gerovich and G. F. Rybalchenko, *Zh. Fiz. Khim.*, **32**, 109 (1958).
24) E. Blomgren and J. O'M. Bockris, *J. Phys. Chem.*, **63**, 1475 (1959).
25) B. E. Conway and R. G. Barradas, *Electrochim. Acta*, **5**, 319 (1961).
26) R. Payne, *J. Phys. Chem.*, **70**, 204 (1966).
27) J. O'M. Bockris and M. A. Habib, *Electrochim. Acta*,

22, 41 (1977).
28) S. Trasatti, *J. Electroanal. Chem.*, **91**, 293 (1978).
29) D. C. Grahame, *Chem. Rev.*, **41**, 441 (1947).
30) C. W. De. Kreuk, M. Sluyters-Rehbach, and J. H. Sluyters, *J. Electroanal. Chem.*, **28**, 391 (1970).
31) L. Gierst and P. Cornelissen, *Collect. Czech. Chem. Commun.*, **25**, 3004 (1960).
32) J. Lipkowski and Z. Galus, *J. Electroanal. Chem.*, **98**, 91 (1979).
33) D. B. Matthews and J. O'M. Bockris, "Modern Aspects of Electrochemistry," ed by J. O'M. Bockris and B. E. Conway, Butterworth, London (1971), Vol. 6, p. 242.
34) J. Lipkowski, E. Kosińska, M. Goledzinowski, J. Nieniewska, and Z. Galus, *J. Electroanal. Chem.*, **59**, 344 (1975).
35) R. W. Gurney, *Proc. R. Soc. London, Ser. A*, **134**, 137 (1932).
36) H. Gerisher, *Z. Phys. Chem. N. F.*, **26**, 223, 325 (1960).
37) J. W. Schultze and K. J. Vetter, *Electrochim. Acta*, **18**, 889 (1973).
38) J. W. Schultze and U. Stimming, *Z. Phys. Chem. N.F.*, **98**, 285 (1975).
39) K. E. Heusler and M. Schultze, *Electrochim. Acta*, **20**, 237 (1975).
40) W. Schmickler and J. Ulstrup, *Chem. Phys.*, **19**, 217 (1977).
41) B. Mann and H. Kuhn, *J. Appl. Phys.*, **42**, 4398 (1971).
42) E. E. Polymeropoulos, *J. Appl. Phys.*, **48**, 2404 (1977).
43) S. Trasatti, *Adv. Electrochem. Electrochem. Eng.*, **10**, 213 (1977).
44) A. Henglein, *Ber. Bunsenges. Phys. Chem.*, **78**, 1078 (1974).
45) S. Pignataro, A. Foffani, G. Innorta, and G. Distefano, *Z. Phys. Chem. N.F.*, **49**, 291 (1966).

On Behaviors of a New Chemical Reaction Model Showing Hard Oscillations

Kazutoshi IWAMOTO and Manabu SENŌ*

Institute of Industrial Science, The University of Tokyo, 7-22, Roppongi, Minato-ku, Tokyo 106

(Received August 1, 1980)

The behavior of a new chemical reaction model was studied and the existence of hard oscillations was confirmed. This chemical reaction model is useful because it is easy to apply to investigations of the behavior of a chemically oscillating system surrounded by membranes or in a well-stirred continuous flow reactor. The latter was discussed relating to the chaotic oscillations due to the Belousov-Zhabotinskii reaction in a well-stirred continuous flow reactor reported by Schmitz *et al.*

Until now many papers about behaviors of chemical systems far from equilibrium states have been presented.[1-20] A system far from an equilibrium state occasionally shows a characteristic phenomenon like chemical oscillations.[1-6] The representative exemplified phenomenon is observed on the Belousov-Zhabotinskii reaction.[1] This chemical system has been investigated by many investigators and especially Noyes *et al.* of Oregon University studied in detail[11] and proposed a well-known chemical reaction model called "Oregonator."[4] The fundamental theory of nonequilibrium thermodynamics has been developed mainly by Prigogine and his school.[2] According to them, the steady state of the system far from an equilibrium state is not always stable and transits to formation of a new type of structures when the system changes beyond a critical point of instability. These structures, which are occasionally heterogeneous and oscillatory states, are called the dissipative structures. It is quite remarkable that some of the most spectacular aspect of biological activities, such as control of cellular division, cellular differentiation and morphogenesis, can be modeled in terms of dissipative structures.[2,12]

We have studied a model chemical system having multiple steady states in order to investigate the chemically oscillatory phenomena,[13] and these studies were applied to the problem of absolutely asymmetric synthesis.[14] In this paper, a new chemical reaction model, which is derived from our model of chemical oscillations,[13] is proposed and studied in detail. This chemical system shows stable oscillations around a stable steady state and pulse generations around the sustained oscillatory state with a small amplitude.

The present chemical reaction model can be applied to investigate the behavior of a chemical oscillatory system which is enclosed by a membrane or in a well-stirred continuous flow reactor. It seems that the application to the latter system is useful for interpreting the chaotic oscillations of the Belousov-Zhabotinskii reaction in a well-stirred continuous flow reactor observed by Schmitz *et al.*[15]

Behaviors of Chemical Reaction Model

Chemical Reaction Model. We consider the following reaction system;

$$P \xrightarrow{k_1} E, \tag{R-1}$$

$$E + X \xrightarrow{k_2} X + R, \tag{R-2}$$

$$A + 2X + E \underset{k_4}{\overset{k_3}{\rightleftharpoons}} 3X + E, \tag{R-3}$$

$$B + X \underset{k_6}{\overset{k_5}{\rightleftharpoons}} C, \tag{R-4}$$

$$E \xrightarrow{k_7} S, \tag{R-5}$$

$$X \xrightarrow{k_8} T. \tag{R-6}$$

These reaction steps proceed homogeneously at constant temperature and pressure. The concentrations of P, A, B, and C are kept constant by means of an external control in order to sustain the system far from equilibrium. E and X are the reaction intermediates and the rates of changes in the concentrations of E and X are expressed respectively by

$$\frac{dE}{dt} = k_1P - k_2EX - k_7E, \tag{1}$$

$$\frac{dX}{dt} = k_3AEX^2 - k_4EX^3 - k_5BX + k_6C - k_8X. \tag{2}$$

In order to study the behavior of this chemical system at the steady state, the conditions $dE/dt=0$ and $dX/dt=0$ are applied to Eqs. 1 and 2 to obtain

$$k_1P - k_2EX - k_7E = 0, \tag{3}$$

$$k_3AEX^2 - k_4EX^3 - k_5BX + k_6C - k_8X = 0. \tag{4}$$

We put $k_7=k_8=\alpha$ hereafter for simplicity. The steady state values of X and E were obtained by solving these equations and plotted in Fig. 1 as a function of α for various values of P. The solid and dotted portions indicate stable and unstable steady states, respectively. Parameter values used are as follows;

$A=1.332$, $B=5.02$, $C=5.35$, $k_1=0.1$, $k_2=0.476$,

$k_3=100.0$, $k_4=48.64$, $k_5=10.0$, $k_6=1.0$,

$P=1.50$(a), 2.0(b), 2.5(c), 2.9(d), and 3.2(e).

These parameter values were also used for study of a chemical oscillation model in the preceding paper.[13] In the case (e), the steady state is stable in a range of adequately small α values and changes into unstable when α increases beyond a critical point near $\alpha=0.014$ and again returns stable in a range beyond a critical point near $\alpha=0.224$; that is, it is expected that a sustained oscillatory state is realized in the dotted line region. To confirm this expectation, Eqs. 1 and 2 were solved for $P=3.2$ by the Runge-Kutta method with a digital computer. Three of calculated results are shown in Fig. 2. In the case (a), the amplitude of oscillations is small, but in the cases (b) and (c), the amplitudes are equally large. In Fig.

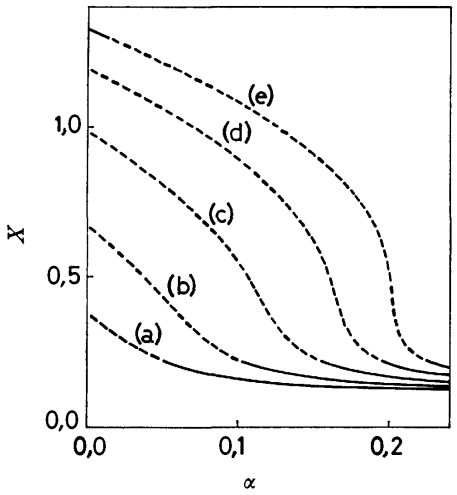

Fig. 1. Plots of steady state concentration of X obtained from Eqs. 3 and 4 against α. Solid lines represent stable steady states and dotted lines represent unstable ones. Parameter values used are; $A=1.332$, $B=5.02$, $C=5.35$, $k_1=0.1$, $k_2=0.476$, $k_3=100.0$, $k_4=48.64$, $k_5=10.0$, $k_6=1.0$, (a) $P=1.50$, (b) $P=2.0$, (c) $P=2.5$, (d) $P=2.9$, and (e) $P=3.2$.

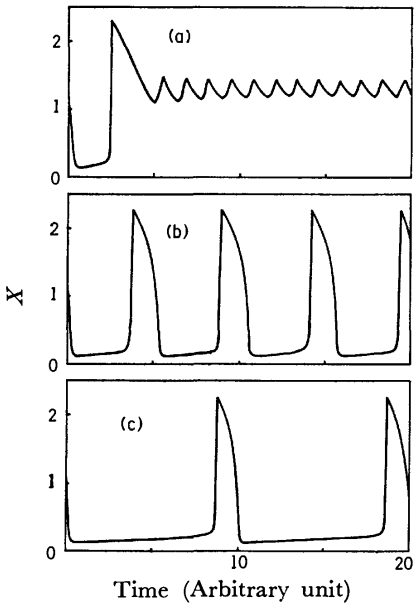

Fig. 2. Results of numerical solution of Eqs. 1 and 2 for $P=3.2$, (a) $\alpha=0.015$, (b) $\alpha=0.14$, and (c) $\alpha=0.222$. Other paremeter values used are the same with those of Fig. 1. The steady states are unstable for these parameter values and oscillations occur.

3, the amplitude of oscillation is plotted against α. The upper and lower thin dotted lines show the width of oscillations. The thick solid and dotted line indicates stable and unstable steady state, respectively. The amplitude of oscillation decreases drastically at the critical point of $\alpha=0.2238$, and this suggests coexistence of stable oscillatory and stable non-oscillatory states, where the oscillatory states are not self-induced but are initiated by a finite perturbation at the stable non-oscillatory states. This phenomenon is called hard oscillations.[16] Actually, it was confirmed from cal-

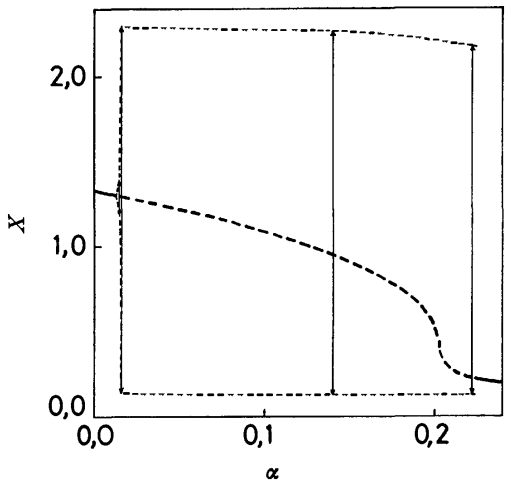

Fig. 3. Plot of amplitude of oscillations against α value determined from Eqs. 1 and 2. All the parameter values are the same with those of Fig. 1. Two types of transition points are shown. At the transition point near $\alpha=0.014$, the amplitude increases continuously with an increasing value of α, while a hard oscillation occurs at the transition point near about $\alpha=0.2238$. See Fig. 5.

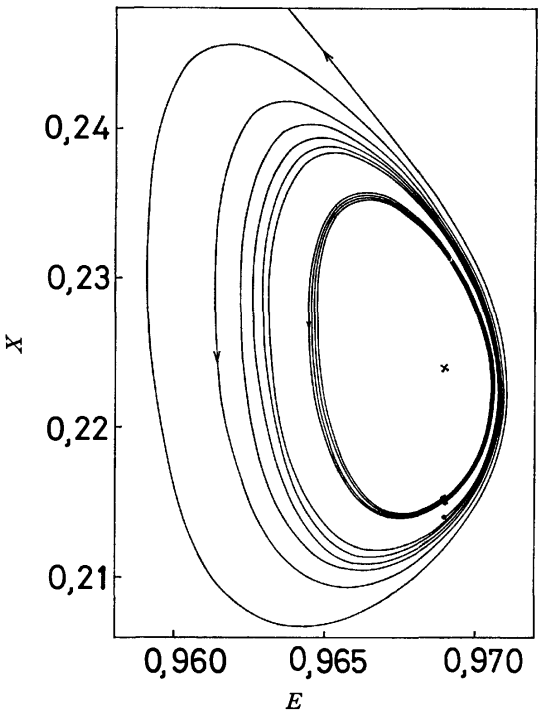

Fig. 4. Behaviors of the chemical system around the stable steady state. × indicates the stable steady state. When a calculation is started from the initial state of $X=0.215$ and $E=0.969$, the chemical system falls into the stable steady state and it is started from the initial state of $X=0.214$ and $E=0.969$, the system falls into the stable oscillatory state. $\alpha=0.2237$. × ($X=0.224$, $E=0.9689$).

culations of Eqs. 1 and 2 at $\alpha=0.2237$ that a sustained oscillatory state encloses a stable steady state. The enlarged picture of a region around the stable steady state is shown in Fig. 4. When a calculation is started

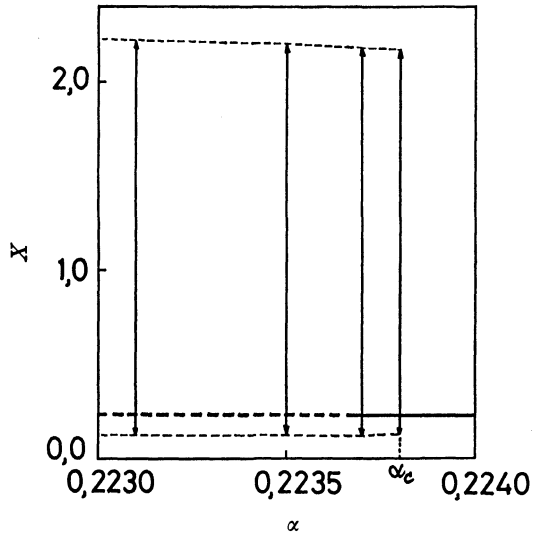

Fig. 5. Amplitude behavior of oscillations at the transition point. $\alpha_c=0.2238$.

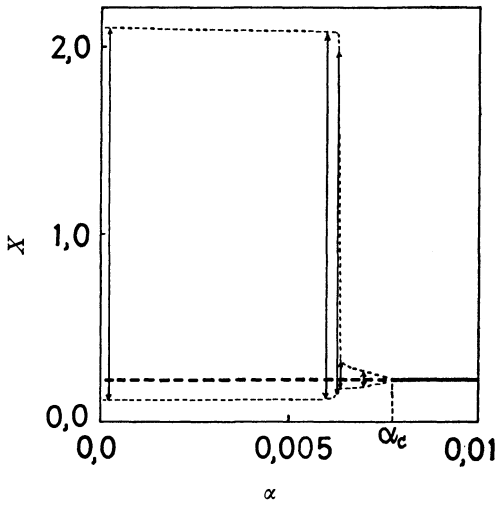

Fig. 6. Amplitude behavior of oscillations near $\alpha=0.0077$ for $k_1=0.5$, $k_2=2.38$, and $P=1.05$. Other parameter values are the same with those of Fig. 1. $\alpha_c=0.0077$.

from the initial state of $X=0.215$ and $E=0.969$, the chemical system falls into the stable steady state and when it is started from the initial state of $X=0.214$ and $E=0.969$, the system falls into the stable oscillatory state. In this case, both the oscillatory and non-oscillatory states coexist, and the transition from (or to) sustained oscillatory state to (or from) non-oscillatory state has a threshold.[16]

The diagram relating the amplitude of hard oscillations to α is depicted in Fig. 5. Hysteresis behavior would be observed for the transition between the sustained oscillatory state and the stable steady state. When α decreases from 0.224 to lower values, the steady non-oscillatory state would result until α becomes to 0.22366; at this point the transition from the non-oscillatory to the oscillatory states would occur. When α is lower than 0.22366, only the oscillatory state appears. Reversely, the oscillations would persist until α increases beyond 0.2238. This situation

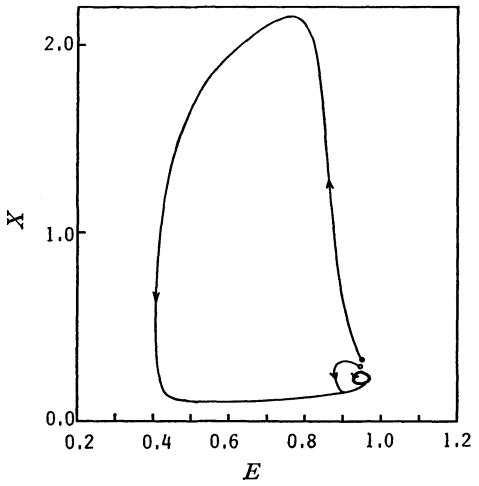

Fig. 7. Behaviors of the chemical system starting from two different initial states. When it starts from ($X=0.33$, $E=0.95$), the chemical system goes on a long excursion before falling into the stable oscillatory state displayed with a thick closed line. While, when it start from ($X=0.30$, $E=0.95$), it falls into the stable oscillatory state accompanying damped oscillations. $\alpha=0.0072$.

results in a hysteresis phenomenon.

Excitation Around a Sustained Oscillatory State. The solution of Eqs. 1 and 2 are shown in Fig. 6 for $k_1=0.5$, $k_2=2.38$, and $P=1.05$. The amplitude of oscillation changes drastically at about $\alpha=0.0064$, and the amplitude decreases gradually with increasing α and eventually disappears when the stability of steady state becomes stable. When $\alpha=0.0072$, this chemical system has an oscillatory state with a small amplitude. This oscillatory state is shown with a closed cycle drawn by thick line in Fig. 7. The chemical system falls into this stable oscillatory state from any initial states, although the routes to the oscillatory state depend greatly on the initial states. When it starts from the state ($X=0.33$, $E=0.95$), the chemical system goes on a long excursion before falling into the sustained oscillatory state, and when it starts from the state ($X=0.30$, $E=0.95$), it falls into the stable oscillatory state accompanying a damped oscillatory behavior. Only pulse generation is observed when the system is brought by a certain distance from the oscillatory state. This system shows therefore the phenomenon of pulse generation with a threshold.[5,13,17,18]

Application to a Membrane-chemical System

Now let us consider a membrane-chemical system which consists of the chemically oscillatory model (R-1)—(R-4) surrounded by a membrane. This model was used in our preceding paper[13] to investigate the chemically oscillatory behaviors. In this system, the concentrations of A, B, C, and P inside the membrane are kept constant by means of an external control, and the concentrations of E and X outside the membrane are maintained to be zero. All of the chemical species are homogeneously distributed inside the mem-

brane. Then, the rates of permeation of E and X through the membrane are expressed as;

$$J_E = h_E E, \tag{5}$$

$$J_X = h_X X, \tag{6}$$

where h_E and h_X are the permeation coefficients of E and X, respectively. Then, the rate equations of E and X inside the membrane are written as;

$$\frac{dE}{dt} = k_1 P - k_2 EX - h_E ES/V, \tag{7}$$

$$\frac{dX}{dt} = k_3 AEX^2 - k_4 EX^3 - k_5 BX + k_6 C - h_X XS/V, \tag{8}$$

where S and V are the surface area and the volume of the reaction region surrounded by the membrane, respectively. If we put $h_E S/V = h_X S/V = \alpha$, Eqs. 7 and 8 become the same type equations with Eqs. 1 and 2, respectively. Therefore, we can discuss the behaviors of the chemical system surrounded by a membrane with the completely same method described in the preceding section.

Every living system is constructed of cells and every cell is surrounded by a lipid bilayer membrane which transports substances necessary for living process, and, therefore, it is important to explain behaviors of the chemically oscillatory system surrounded by membrane.[3,6,10]

Behaviors of the Chemically Oscillatory Model in a Well-stirred Continuous Flow Reactor

In this section, let us study behaviors of the chemically oscillatory model (R-1)—(R-4) in a well-stirred continuous flow reactor. Schmitz *et al.* studied the behaviors of the Belousov-Zhabotinskii reaction in a well-stirred continuous flow reactor and observed chaotic oscillations in a certain region of flow rate.[15] They explained this behavior based on the idea of Rösseler;[19] that is, a phase point moves on a folded surface with an unstable steady state in a phase space of three variables, and hysteresis transition across a fold generates chaotic behaviors.

Noyes *et al.*[20] reported that chaotic oscillations of the Oregonator can be explained by some modifications of their chemical model. They used a model containing seven intermediates and analyzed the stability of steady states by introducing a new variable P, which represents the concentration of the intermediate HOBr. There exists a certain value of P where the stability of steady state reverses, and the linkage of P with other chemical species results in random oscillations of large and small amplitudes under suitable conditions.

The present investigation shows that the chaotic behaviors can be explained without any modification of the reaction steps of the original model and, therefore, the chaotic oscillations of the Oregonator observed by Schmitz *et al.*[15] can be also explained by the present method, which is quite different from the method by Noyes *et al.*[20]

Now let us consider a well-stirred continuous flow reactor, in which a series of reactions (R-1)—(R-4) is taking place with a constant feed of a fresh raw solution and a continuous removal of a reacted solution. The feed solution is composed of chemical species A, B, C, and P and the reacted solution is composed of A, B, C, E, P, R, and X. The total flow rate of the solution into the reactor is J and the volume of the flow reactor is V. We put J/V as β for abbreviation.

The material balance of these chemical species in the reactor is expressed as

$$\frac{dP}{dt} = \beta(P_0 - P) - k_1' P, \tag{9}$$

$$\frac{dA}{dt} = \beta(A_0 - A) - k_3' AEX^2 + k_4' EX^3, \tag{10}$$

$$\frac{dB}{dt} = \beta(B_0 - B) - k_5' BX + k_6' C, \tag{11}$$

$$\frac{dC}{dt} = \beta(C_0 - C) + k_5' BX - k_6' C, \tag{12}$$

$$\frac{dE}{dt} = k_1' P - k_2' EX - \beta E, \tag{13}$$

$$\frac{dX}{dt} = k_3' AEX^2 - k_4' EX^3 - k_5' BX + k_6' C - \beta X. \tag{14}$$

Here A_0, B_0, C_0, and P_0 are concentrations in the feed solution and A, B, C, and P are uniform concentrations in the reactor. The terms including β represent flow terms.

Equation 9 is solved to give the solution

$$P = \frac{\beta P_0}{\beta + k_1'} + \left(P' - \frac{\beta P_0}{\beta + k_1'}\right) e^{-(\beta + k_1')t}, \tag{15}$$

where P' is an initial value of P. When t is adequately large, P becomes to $\beta P_0/(\beta + k_1')$, independently of P' value. Here we adopt the following values; $k_1' = 0.5 \times 10^{-5}$, $k_2' = 2.38$, $k_3' = 1.0 \times 10^{-3}$, $k_4' = 48.64$, $k_5' = 1.0 \times 10^{-4}$, and $k_6' = 1.0 \times 10^{-5}$. Then, P is nearly equal to P_0 when β is sufficiently larger than k_1'. The values of A, B, and C are similarly discussed and it was shown that their final concentrations are nearly equal to A_0, B_0, and C_0, respectively.[21] When we put $P_0 = 1.05 \times 10^5$, $A_0 = 1.332 \times 10^5$, $B_0 = 5.02 \times 10^5$, and $C_0 = 5.35 \times 10^5$, the values of $k_1' P_0$, $k_3' A_0$, $k_5' B_0$, and $k_6' C_0$ are equal to those of $k_1 P$, $k_3 A$, $k_5 B$, and $k_6 C$, which were used in the preceding sections. Then, we can discuss the behaviors of the chemical system (R-1)—(R-4) in a well-stirred continuous flow reactor by the aid of the results shown in Figs. 6 and 7, where α is exactly equivalent to β. In this situation there is an abrupt change in amplitude at about $\beta = 0.0064$ and a small deviation causes pulse generation around the sustained oscillatory state, as shown already. Therefore, small random deviations of flow rate cause randomly large or small amplitude oscillations. Moreover, any actual system is under influences of fluctuation. Then, we have to use the rate equations including fluctuation terms in order to investigate the behaviors of the chemical system at a critical point.[13]

$$\frac{dE}{dt} = k_1' P_0 - k_2' EX - [\beta + \beta' F(t)]E + \gamma G(t), \tag{16}$$

$$\frac{dX}{dt} = k_3'A_0EX^2 - k_4'EX^3 - k_5'B_0X + k_6'C_0 - [\beta+\beta'F(t)]X + \delta H(t), \quad (17)$$

where $F(t)$, $G(t)$, and $H(t)$ are the fluctuation terms of Gaussian type.[13] The average values $\langle F(t)\rangle$, $\langle G(t)\rangle$, and $\langle H(t)\rangle$ are zero and the standard deviations are set to be 0.1. The coefficients β', γ, and δ represent the strengths of fluctuations, and $\beta'F(t)$ corresponds to the fluctuation of flow rate and $\gamma G(t)$ and $\delta H(t)$ correspond to the concentration fluctuations of E and X, respectively. Figure 8 illustrates behaviors of the chemical reaction model in a well-stirred continuous flow reactor for various values of β. At lower values of flow rate J, only large amplitude oscillations appear and in some range of flow rate, shown by (c) and (d), both large and small amplitude oscillations appear randomly. When the flow rate increases much more, only small amplitude oscillations occur and fade out, as shown by the cases of (e) and (f). These results agree essentially well with that of Schmitz *et al.*[15]

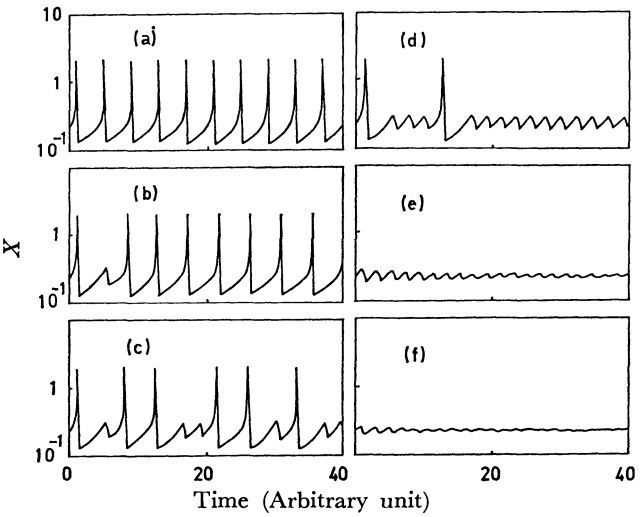

Fig. 8. Oscillatory behaviors under influences of fluctuations. $\beta=J/V$. $\beta'=0.001$, $\gamma=0.001$, $\delta=0.001$, (a) $\beta=0.001$, (b) $\beta=0.006$, (c) $\beta=0.0065$, (d) $\beta=0.007$, (e) $\beta=0.008$, and (f) $\beta=0.01$. $A_0=1.332\times10^5$, $B_0=5.02\times10^5$, $C_0=5.35\times10^5$, $P_0=1.05\times10^5$, $k_1'=0.5\times10^{-5}$, $k_2'=2.38$, $k_3'=1.0\times10^{-3}$, $k_4'=48.64$, $k_5'=1.0\times10^{-4}$, and $k_6'=1.0\times10^{-5}$.

References

1) A. M. Zhabotinskii, *Dokl. Akad. Nauk SSSR*, **157**, 392 (1964).
2) P. Glansdorff and I. Prigogine, "Thermodynamic Theory of Structure, Stability, and Fluctuations," Wiley, New York (1971).
3) H. S. Hahn, P. Ortoleva, and J. Ross, *J. Theor. Biol.*, **41**, 503 (1973).
4) R. J. Field and R. M. Noyes, *J. Chem. Phys.*, **60**, 1877 (1974).
5) H. S. Hahn, A. Nitzan, P. Ortoleva, and J. Ross, *Proc. Nat. Acad. Sci. U. S. A.*, **71**, 4067 (1974).
6) M. Senō, K. Iwamoto, and K. Sawada, *J. Theor. Biol.*, **72**, 577 (1978).
7) B. B. Edelstein, *J. Theor. Biol.*, **29**, 57 (1970).
8) F. Schlögl, *Z. Phys.*, **253**, 147 (1972).
9) M. H. Kaufman and G. Nicolis, *J. Chem. Phys.*, **56**, 1890 (1972).
10) M. P. Hanson, *J. Chem. Phys.*, **60**, 3210 (1974).
11) R. J. Field, E. Körös, and R. M. Noyes, *J. Am. Chem. Soc.*, **94**, 8649 (1972).
12) G. Nicolis and I. Prigogine, "Self-organization in Nonequilibrium Systems," Wiley, New York (1977).
13) K. Iwamoto and M. Senō, *J. Chem. Phys.*, **70**, 5851 (1979).
14) K. Iwamoto and M. Senō, *J. Chem. Phys.*, **70**, 5858 (1979).
15) R. A. Schmitz, K. R. Graziani, and J. L. Hudson, *J. Chem. Phys.*, **67**, 3040 (1977).
16) A. Uppal, W. H. Ray, and A. B. Poore, *Chem. Eng. Sci.*, **29**, 967 (1974).
17) R. J. Field, *J. Chem. Phys.*, **63**, 2289 (1975).
18) J. J. Tyson, *J. Chem. Phys.*, **66**, 905 (1977).
19) O. E. Rössler, *Z. Naturforsch., Teil A*, **31**, 259 (1976).
20) K. Showalter, R. M. Noyes, and K. Bar-Eli, *J. Chem. Phys.*, **69**, 2514 (1978).
21) This was confirmed by solving Eqs. 9—14 with a digital computer. The calculated results will appear elsewhere soon.

A Study of the Calcium Oxide–Water Vapor System by Means of the Transpiration Method

Kazutoshi MATSUMOTO* and Toshiyuki SATA
Research Laboratory of Engineering Materials, Tokyo Institute of Technology, Nagatsuta, Midori-ku, Yokohama 227

(Received August 7, 1980)

The system of calcium oxide and water vapor was studied using the transpiration method. Under the conditions of a temperature range from 1678 to 2016 K and P_{H_2O} values from 1.2×10^{-2} to 4.7×10^{-1} atm, the predominant reaction in this system was found to be $CaO(s)+H_2O(g)=Ca(OH)_2(g)$. The standard Gibbs free energy of the reaction is given by this equation: $\Delta G_r^\circ=(61300\pm820)-(12.8\pm0.48)T$ (cal/mol) in the present temperature range. From the thermochemical cycle, the dissociation energy, $D_0^\circ(Ca\text{-}(OH)_2)$, was estimated to be 206.4 kcal/mol.

The volatility of alkaline-earth oxides is greatly increased by the presence of water vapor as a result of the formation of volatile hydroxide vapors by the following reactions:

$$MO(s) + H_2O(g) = M(OH)_2(g), \quad (1)$$

and:

$$MO(s) + \frac{1}{2}H_2O(g) = MOH(g) + \frac{1}{4}O_2, \quad (2)$$

where M is a Group IIa element. This has been shown to be true for BeO,[1-3] MgO,[4,5] and BaO.[6,7]

Although calcium oxide is one of the most important components in the ceramic industry, no systematic investigation of its vaporization behavior under various atmospheres had been made. Only a few investgators[8-11] have measured the dissociation energy, D_0°, for the $Ca(OH)_2(g)=Ca(g)+2OH(g)$ reaction using flamespectral measurements.

In the present study, the reaction of water vapor with solid calcium oxide was investigated by means of the transpiration method as part of a series of studies[5,7] of the effects of water vapor upon the vaporization of alkaline earth oxides. The vapor pressures of the gaseous $Ca(OH)_2$ formed according to Reaction 1 and the related thermodynamic properties were evaluated.

Experimental

Transpiration Apparatus. Figure 1 shows a schematic drawing of the reaction zone in the apparatus used in this study. The sample was placed in a reaction chamber, N (12 mm i.d.×30 mm long), made of Pt/20% Rh alloy. The reaction chamber had a capillary, L (1 mm i.d.×10 mm long), to prevent the vapor species formed in the chamber from back-diffusing and had a bottom with holes below which a Pt/Rh 20—40 themocouple, calibrated at the melting points of Pd and Pt (IPTS-68) and placed in a protective alumina tube was located.

The vaporized species were collected in a condenser, J, made of Pt/20% Rh alloy (3.4 mm i.d.×300 mm long). The capillary, L, had a thorium oxide sleeve, M, in order to minimize the leakage of vapor species through the space between the condenser and the capillary and to prevent sticking with the condenser at high temperatures. The temperature of the reaction chamber was raised by the use of 6 rods of a $LaCrO_3$ heater up to 2016 K and then regulated with ±3 °C.

A wet gas mixture, O_2–H_2O–Ar, was obtained by bubbling a dry O_2–Ar gas in water controlled about 10 degrees higher than desired temperature; it was then passed through a scerwed glass coil around which precisely thermostatted water was passed continuously to condense the oversaturated water vapor in the wet gas. This method has already been described in a preceding paper.[5] The partial pressure of the water vapor was determined from the weight increase in the P_2O_5 powder placed in a stream of the wet gas. The vapor pressure thus determined agreed with the saturated water vapor pressure at the temperature of the coil within ±2%. The water vapor pressure in the range from 1.2×10^{-2} to 4.7×10^{-1} atm was used in the experiments.

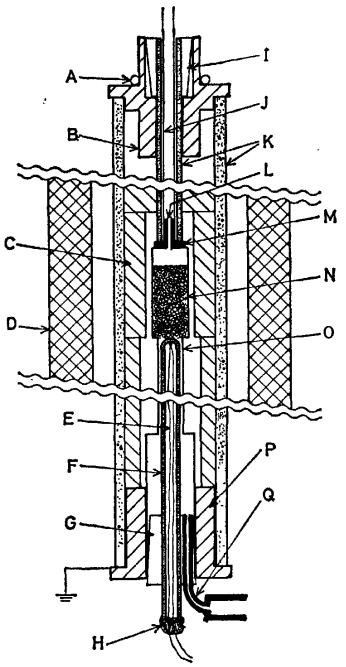

Fig. 1. Cross section of reaction zone in transpiration apparatus. A: cooling water, B: brass, C: alumina insulator, D: $LaCrO_3$ heater, E: Pt/Rh 20—40 thermocouple, F: alumina protective tube, G: Viton stopper, H: silicone seal, I: silicone stopper, J: condenser(Pt/20%Rh), K: alumina tube, L: capillary, M: thoria sleeve, N: reaction chamber and charge, O: reaction tube (Pt/20%Rh), P: brass, and Q: stainless steel.

Sample. Powder of CaO from $CaCO_3$ with a 99.9% purity (supplied by Merck), fired at 1200 °C, was pressed and sintered at 2400 °C by means of H_2/O_2 flames and then crushed to particles of 15—30 mesh. The particles of CaO were used to fill about 80% of the reaction chamber, and

Table 1. Impurity content of CaO used in this experiment

Element	Content ppm	Element	Content ppm
Na	9	V	<1
Mg	116	Cr	144
Al	25	Fe	11
Si	38	Mn	<1
P	<1	Co	<1
S	23	Cu	1
K	5	Zn	2
Ti	<1		

These values were measured by means of a spark-source mass spectrograph.

a rid with the capillary was welded.

The impurities in the CaO specimens were analyzed by means of spark-ion-source mass spectrometry; the results are given in Table 1.

Procedure. The wet carrier gas, with a constant partial pressure of water vapor, was allowed to flow in a pipe leading the reaction tube. The pipe was heated to about 100 °C by means of a ribbon heater around it in order to keep the water vapor from condensing. The water vapor reacted with CaO in the reaction chamber at a constant temperature to form Ca-bearing hydroxide vapors. The carrier gas was saturated with vapors formed at an appropriate flow rate, and the vapors were transported into the condenser. The condenser was washed with a hot nitric-acid solution, and calcium in the solution was analyzed quantitatively using an atomic-absorption spectrophotometer.

The partial pressure of the volatile calcium hydroxide has been calculated from the amount of collected calcium. Assuming that each molecule of the volatile species contains one atom of calcium, and that the vapor is approximated to an ideal gas, the partial pressure at equilibrium is given by:

$$p(\mathrm{Ca(OH)_{2x}}) = n_v P/(n_c + n_v), \quad (3)$$

where n_c is the number of moles for the carrier gas; n_v, that for the sample vapor, and P, the total pressure, assumed here to be 1 atm.

Results and Discussion

Effect of Flow Rate on Vapor Pressure. Figure 2 shows the apparent vapor pressure of the assumed molecule, $Ca(OH)_{2x}$, as a function of the flow rate at 1926 K and $p(H_2O)$ of 1.52×10^{-1} atm. A "plateau region" is seen in the range from 1.0 to 2.0 cm^3/s. The decrease in the vapor pressure at the flow rate< 1.0 cm^3/s is thought to be due to vapor escaping from the space between the condenser and the capillary.

The "plateau region" for other temperatures and $p(H_2O)$ were obtained in a similar flow-rate region.

The output gas from the condenser was passed into a nitric solution, and the solution was subjected to the atomic-absorption analysis. Since no calcium was detected in the solution, the amount of Ca uncondensed in the condenser was considered negligible under the present experimental conditions.

Water-vapor Dependence. In addition to Eqs. 1 and 2, the following reactions must be considered

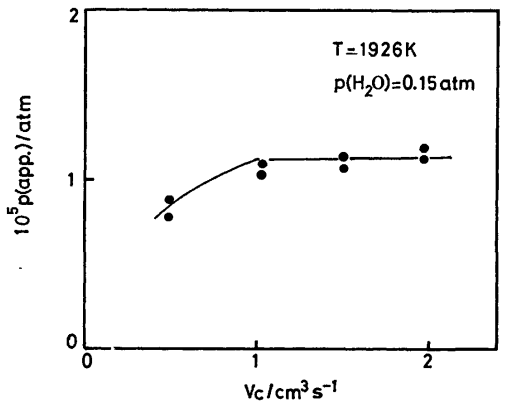

Fig. 2. Apparent vapor pressure, p(app.), *vs.* flow rate of carrier gas at $T=1926$ K and $p(H_2O)=0.15$ atm.

under these conditions:

$$\mathrm{CaO(s) = Ca(g) + \frac{1}{2}O_2}, \quad (4)$$

$$\mathrm{CaO(s) = CaO(g)}. \quad (5)$$

Using the JANAF data,[12,14,15] the partial pressures of Ca(g) and CaO(g) at $p(O_2)$ of 0.5 atm are 2.8×10^{-16} and 4.8×10^{-14} atm at 1600 K, and 4.1×10^{-11} and 9.2×10^{-10} atm at 2000 K, respectively. On the other hand, the apparent vapor pressure is 1.1×10^{-5} atm at 1926 K, judging from Fig. 2. Hence, no correction was made for Reactions 4 and 5.

A logarithmic plot of the equilibrium pressure of the volatile complex as a function of the partial pressure of water at a constant temperature and partial pressure of oxygen will indicate whether Reaction 1 or 2 occures.

Combining Reaction 1 with 2 yields the following equation for the CaO–H_2O–O_2 system:

$$\mathrm{CaO(s) + xH_2O(g) = Ca(OH)_{2x}(g) + \frac{1-x}{2}O_2}. \quad (6)$$

The equilibrium constant, k_p for the above reaction is written as:

$$k_p = \frac{p(\mathrm{Ca(OH)_{2x}})\,p(\mathrm{O_2})^{(1-x)/2}}{a(\mathrm{CaO})\,p(\mathrm{H_2O})^x}. \quad (7)$$

Assuming $a(CaO)=1$, and taking the logarithms of both sides, we obtain:

$$\log p(\mathrm{Ca(OH)_{2x}}) = x\log p(\mathrm{H_2O}) - \frac{(1-x)}{2}\log p(\mathrm{O_2}) + \log k_p. \quad (8)$$

The value of x in Eq. 8 can be determined to ascertain the contribution of Reaction 1 or 2.

A series of measurements were made at 1678 to 2016 K and $p(O_2)=0.5$ atm with a varied water vapor pressure at atmospheric pressure; the results are shown in Fig. 3. The values of x were obtained from the slopes of a log $p(Ca(OH)_{2x})$ versus log $p(H_2O)$ plot. The average value of x was 1.04 ± 0.04, which was very close to unity. Considering the experimental errors, the value of x has been determined as unity. Therefore, the predominant reaction of water vapor with calcium oxide under these experimental conditions is:

$$\mathrm{CaO(s) + H_2O(g) = Ca(OH)_2(g)}. \quad (9)$$

TABLE 2. EQUILIBRIUM CONSTANT, k_p, FOR THE $CaO(s)+H_2O(g)=Ca(OH)_2(g)$ REACTION

$\frac{T}{K}$	No. of points	Time / h	Flow rate / $cm^3\ s^{-1}$(STP)	$p(H_2O)$ / atm	k_p	$-\Delta fef$ / cal $mol^{-1}\ K^{-1}$	$\Delta H^\circ_r(298\ K)$ / kcal mol^{-1}
2016	7	1.00—12.5	1.50—1.62	5.87×10^{-2}—4.33×10^{-1}	$(1.39\pm0.10)\times10^{-4}$	13.549	62.90±0.30
1976	7	2.00—13.0	1.49—1.63	5.83×10^{-2}—4.00×10^{-1}	$(1.05\pm0.07)\times10^{-4}$	13.566	62.78±0.26
1926	11	2.00—37.8	1.03—1.97	5.64×10^{-2}—4.07×10^{-1}	$(6.87\pm0.85)\times10^{-5}$	13.587	62.88±0.46
1829	8	3.00—45.3	1.51—1.57	2.59×10^{-2}—3.65×10^{-1}	$(3.21\pm0.23)\times10^{-5}$	13.627	62.53±0.27
1762	8	3.00—44.7	1.46—1.61	2.66×10^{-2}—4.03×10^{-1}	$(1.58\pm0.12)\times10^{-5}$	13.653	62.77±0.28
1678	6	5.00—89.2	1.46—1.61	2.66×10^{-2}—3.90×10^{-1}	$(6.50\pm0.90)\times10^{-6}$	13.687	62.94±0.32
	47						Av. 62.79±0.37

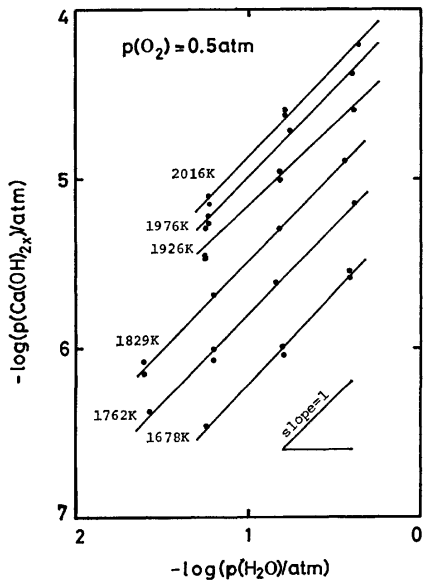

Fig. 3. Variation of log (vapor pressure of calcium bearing species) *vs.* log (partial pressure of water).

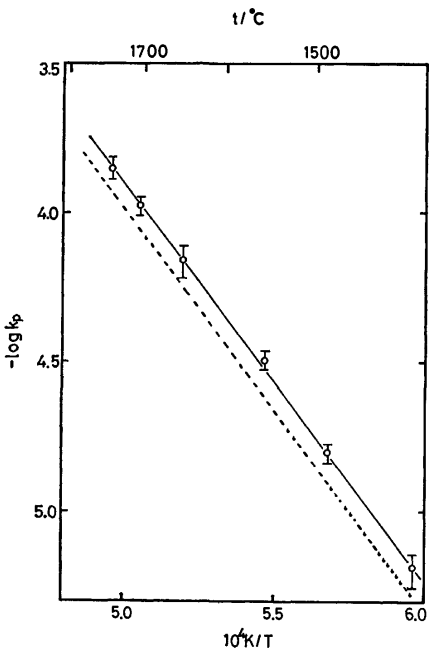

Fig. 4. Plot of equilibrium constant k_p for the reaction $CaO(s)+H_2O(g)=Ca(OH)_2(g)$ *vs.* reciprocal temperature.
——: This work, ----: JANAF data.

The high partial pressure of oxygen in the carrier gas would suppress the formation of gaseous CaOH and lead to a value of x close to unity.

Vapor Pressure of $Ca(OH)_2(g)$ and Related Thermodynamic Values. The vapor pressures of gaseous $Ca(OH)_2$ and the equilibrium constant, k_p, have been calculated from the amount of calcium collected; the results are given in Table 2 and illustrated graphically in Fig. 4. The values of k_p for Reaction 9, obtained from the JANAF data[12–15] are also shown in Fig. 4. The results of this work differ from those of the JANAF data by 20%.

The solid line in Fig. 4, obtained from a least-square treatment for the data of 47 points, corresponds to the expression:

$$\log k_p = (2.80\pm0.10) - (13400\pm180)/T\ (1678-2016\ K). \quad (10)$$

Hence, the standard Gibbs energy for Reaction 9 is given by:

$$\Delta G^\circ_r = (61300\pm820) - (12.8\pm0.48)T. \quad (11)$$

This gives:

$$\Delta H^\circ_r(1850\ K) = 61.3\pm0.8\ kcal/mol, \quad (12)$$

and:

$$\Delta S^\circ_r(1850\ K) = 12.8\pm0.5\ cal/mol\ K, \quad (13)$$

Using the changes of heat capacity, ΔC_p, for Reaction 9 obtained from the JANAF data, Eqs. 12 and 13 lead to:

$$\Delta H^\circ_r(298\ K) = 62.6\pm0.8\ kcal/mol, \quad (14)$$

and:

$$\Delta S^\circ_r(298\ K) = 13.9\pm0.5\ cal/mol\ K. \quad (15)$$

This entropy change at 298 K coincides with the value, 14.0±2.0 cal/mol K, obtained from the JANAF data.

From the free-energy functions, *fef*, of CaO(s),[14] $H_2O(g)$,[12] and $Ca(OH)_2(g)$[15] and the following rela-

tionship:

$$\Delta H_r^\circ(298\,\mathrm{K}) = -RT\ln k_p - T\Delta fef, \quad (16)$$

the ΔH_r° (298 K) was calculated for each k_p; the results are given in the last column of Table 2. The average value of the ΔH_r° (298 K) values obtained by a third-law treatment, 62.8±0.4 kcal/mol, agrees well with the second-law treated value (Eq. 14); this indicates the high reliability of this work.

Using the JANAF data, the ΔH_r° (298 K) obtained by the 3rd-law treatment leads to:

$$\Delta H_r^\circ(0\,\mathrm{K}) = 63.1\pm0.4\ \mathrm{kcal/mol}. \quad (17)$$

Dissociation Energy of $Ca(OH)_2(g)$. The dissociation energy of $Ca(OH)_2(g)$ into 2OH(g) and Ca(g), $D_0^\circ(Ca\text{–}(OH)_2)$, has been estimated using the following thermochemical cycle:

$$\begin{array}{ccc} Ca(OH)_2(g) & \xrightarrow{D^\circ} & Ca(g) + 2OH(g) \\ \uparrow \Delta H_r^\circ & & \uparrow \Delta H_s^\circ \quad \uparrow \Delta H_f^\circ \\ CaO(s) + H_2O(g) & \xleftarrow{\Delta H_r^\circ} & Ca(s) + \frac{1}{2}O_2 + H_2O(g) \end{array} \quad (18)$$

whereby:

$$D_0^\circ(Ca\text{–}(OH)_2) = -\Delta H_{r,0}^\circ(Ca(OH)_2) - \Delta H_{f,0}^\circ(CaO) + \Delta H_{s,0}^\circ(Ca) + 2\Delta H_{f,0}^\circ(OH), \quad (19)$$

where $\Delta H_{r,0}^\circ(Ca(OH)_2)$ represents the heat of reaction for Reaction 9; $\Delta H_{f,0}^\circ(CaO)$, the heat of formation for CaO(s); $\Delta H_{s,0}^\circ(Ca)$, the heat of sublimation for Ca(s), and $\Delta H_{f,0}^\circ(OH)$, the heat of formation for OH(g) from $H_2O(g)$ and O_2. The values required were 63.12±0.4 (Eq. 17), −150.99±0.21,[14] 42.74±0.3,[12] and 37.90±0.04[12] kcal/mol at 0 K, respectively. The substitution of these values into Eq. 19 gives the value of $D_0^\circ(Ca\text{–}(OH)_2)$. This result is shown in Table 3, along with the literature values.[8–11]

This value is in very good agreement with the JANAF table's recommended value (No. 1 in Table 3). From the D_0° thus obtained, we calculated $\Delta H_{f,0}^\circ(Ca(OH)_2, g) = -145.0\pm1.0$ kcal/mol.

Table 3. Dissociation energy of $Ca(OH)_2(g)$

No.	Method	$D_0^\circ(Ca\text{–}(OH)_2)$ / kcal mol^{-1}	Ref.
1	Flame photometry	205.6[a),b),c)]	8
2	Flame photometry	207.6[a),b)]	9
3	Flame photometry	210.4[b)]	10
4	Flame photometry	207.8	11
5	Transpiration	206.4	This work

a) Recalculated from Refs. 8 and 9 by Cotton and Jenkins. b) Treated with current JANAF data. c) JANAF table's recommended value.

References

1) L. I. Grossweiner and F. L. Seifer, *J. Am. Chem. Soc.*, **74**, 2701 (1952).
2) W. A. Young, *J. Phys. Chem.*, **64**, 1003 (1960).
3) T. B. Douglas, *J. Res. Natl. Bur. Stdn.*, **76A**, 511 (1972).
4) C. A. Alexander, J. S. Ogden, and A. Levy, *J. Chem. Phys.*, **39**, 3057 (1963).
5) E. Maeda, T. Sasamoto, and T. Sata, *Yogyo Kyokai Shi*, **86**, 461 (1978).
6) F. E. Stafford and J. Berkowitz, *J. Chem. Phys.*, **40**, 2963 (1964).
7) T. Sasamoto, K. Mizushima, and T. Sata, *Bull. Chem. Soc. Jpn.*, **52**, 2127 (1979).
8) V. G. Ryabova and V. L. Gurvich, *Teplofiz. Vys. Temp.*, **3**, 318 (1965).
9) K. Schofield and T. M. Sugden, *Trans. Faraday Soc.*, **62**, 566 (1966).
10) D. H. Cotton and D. R. Jenkins, *Trans. Faraday Soc.*, **64**, 2988 (1968).
11) E. M. Starovoitov, V. G. Ryaboba, L. V. Gurvich, A. N. Khitrov, I. I. Nazarenko, and A. V. Belyaev, *Teplofiz. Vys. Temp.*, **15**, 909 (1977).
12) D. R. Stull and H. Prophet, "JANAF Thermochemical Tables," Dow Chemical Co. (1970).
13) M. W. Chase, J. L. Curnutt, A. T. Hu, H. Prophet, A. N. Syverud, and L. C. Walker, *J. Phys, Chem. Ref. Data*, **3**, 443 (1974).
14) M. W. Chase, J. L. Curnutt, H. Prophet, R. A. McDonald, and A. N. Syverud, *J. Phys. Chem. Ref. Data*, **4**, 62 (1975).
15) M. W. Chase, Jr., J. L. Curnutt, R. A. McDonald, and A. N. Syverud, *J. Phys. Chem. Ref. Data*, **7**, 882, 883 (1978).

Reaction of Metastable Ar Atoms with Propylene in Flow System

Akiko SIBATA, Makoto TAKAHASI,*,** Shinichi OHNO,† and Hitoshi MIKUNI

Department of Pure and Applied Sciences, College of General Education, The University of Tokyo, Komaba, Meguro-ku, Tokyo 153

† *Japan Atomic Energy Research Institute, Tokai Research Establishment, Tokai-mura, Naka, Ibaraki 319-11*

(Received August 30, 1980)

The reaction of metastable Ar atoms with propylene was studied in a discharge flow system. The major product is ethylene, although ethane, propane and butadiene are also identified as minor products. Within a limited range of propylene concentration the yield of ethylene is proportional to the concentration of propylene. Competitive quenching methods using mixtures of propylene and N_2O or CO_2 provided a rate constant of $(8.4\pm 0.3)\times 10^{-10}$ cm^3 molecule^{-1} s^{-1} for the reaction of metastable Ar atom with propylene to yield ethylene. The assumption of a radical mechanism for the main reaction is consistent with the results of competitive quenching, radical scavenger and spin trapping experiments. Measurements of ion current in the reaction mixtures allow an estimation that ionic species contribute less than 2% to the reaction path leading to the formation of ethylene. The metastable Ar atom reaction was also compared to the direct and mercury-sensitized photolysis of propylene.

Reactions of metastable rare gas atoms have been studied by many workers interested in both the physical and chemical aspects of the reaction.[1-5] Various types of ionizations (Penning, associative and dissociative) and the chemiluminescence of atoms and molecules on collision with metastable rare gas atoms have been studied.[6-8] Quenching rate constants of the metastables by various atoms and molecules also have been determined in discharge flow systems or pulsed radiolysis systems. However, in contrast to the many studies on mercury-sensitized photolysis of inorganic and organic compounds, studies on the reaction mechanism of excited rare gas atoms by product analysis are quite few in number apart from several papers on the rare gas sensitized photolysis of simple alkanes.[9,10] In the rare gas sensitized photolysis, the wavelength for the exciting light is in the far ultraviolet region, and it is usually difficult to differentiate the direct photolysis and the sensitized photolysis, unless the reactant is transparent or has only a weak absorption at the wavelength corresponding to the atomic resonance line of the rare gas atom.

The comparison between direct photolysis, rare gas sensitized photolysis and the metastable rare gas atom reaction would be interesting in order to help to elucidate the reaction modes of molecules electronically excited to high energy states near or above their ionization levels. Here we will report on the reaction of metastable Ar atoms with propylene. Electron impact methods including discharge and radiolysis are required for the generation of metastable rare gas atoms. The discharge flow method may be preferable to the radiolysis method for the product analysis, since the metastable atom source can be separated from the reaction region, and the metastables can be brought together with the reactant downstream from the source of the metastable atom. One difficulty in working with flow methods, in particular if the reactants are volatile compounds, is how to achieve quantitative recovery of the volatile products in the flow system. We succeeded in carrying out the quantitative determination of the product yield by working at a conveniently selected flow rate.

** Present address: International Christian University, 10-2, 3-Chome, Osawa, Mitaka, Tokyo 181.

Experimental

Apparatus and Procedures. A schematic diagram of the apparatus is shown in Fig. 1. Metastable Ar atoms are produced by cold discharge in a hollow cathode. A mixture of $Ar(^3P_2)$ and $Ar(^3P_0)$ is produced by the discharge, but their differentiation is not possible in the system, and hereafter we will describe the mixture as Ar*. In order to avoid exposing the reactant to UV light from discharge source, the discharge tube is equipped with a rightangle bend and a light trap between the reaction zone and the discharge region. The flow rate is monitored by a rotar meter (Ueshima Brooks tube). Since the rotar meter was calibrated with Ar at 1 atm of pressure, the flow rate at reduced pressure was determined by measuring the decrease in the amount of Ar in a container, keeping the flow conditions same as in the actual discharge experiment. Discharge current was kept at 10—11 mA. Reactant propylene and quenching materials (N_2O, CO_2, and NO) were introduced through a sintered glass disk into the Ar flow. The reaction part of the tube is 20 mm in diameter and 300 mm in length. Pressure in the tube was measured by an oil manometer. Two pairs of electrodes (P_1 and P_2) are furnished in the reaction tube upstream and downstream from the reactant mixing position.

Condensable amounts of product and propylene were collected in a helical trap, D, cooled by liquid nitrogen. Quantitative recovery of products of high vapor pressure in the flow system was carefully checked by measuring the

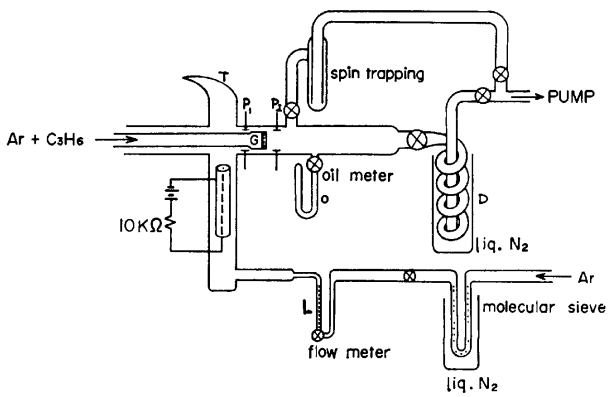

Fig. 1. The schematic diagram of the apparatus.

amounts of ethylene, ethane and propane contained in the original propylene at three different flow rates from 4.5 to 20.8 μmol s^{-1} of Ar. The quantitative recovery of the impurity hydrocarbons was achieved when the flow rate of Ar was 4.5 μmol s^{-1} (0.2 Torr (1 Torr≈133.3 Pa) and 1.3 m s^{-1} linear flow velocity). With larger flow rates, the recovery of the impurity hydrocarbons was not sufficient. We could not determine the recovery efficiency for the propylene reactant because of its large amount, but we may assume that it is nearly quantitative, considering its low vapor pressure compared with those of ethylene and ethane. All experimental runs described hereafter were carried out with a flow rate of 4.5 μmol s^{-1} at 0.2 Torr.

Product identification and yield determination were performed by GC with a TCD and a FID in train with He carrier. For ethylene, ethane and propane analysis, an activated alumina TR column of 3.75 m was used. The retention times of these compounds at 90 °C are 3 min 30 s for ethane, 6 min 50 s for ethylene, 9 min for propane and 20 min 42 s for propylene. A 3 m long activated charcoal column was used for the analysis of acetylene, propyne, and allene. The retention times for authentic compounds at 190 °C are 3 min 30 s for acetylene, 19 min 20 s for allene, 19 min 40 s for propyne and 27 min 50 s for propylene.

Before each reaction run, the system was cleaned by passing Ar for 30 to 60 min with discharge. Several minutes after the propylene was introduced, the helical trap D was cooled with liquid nitrogen. We assumed that the starting time of the reaction corresponds to the time when the trap was first cooled. The run time for each reaction was usually 10 min. No appreciable change in flow rate was noticed when the trap was cooled with liquid nitrogen. The collected condensates were transferred to a gas sampler and analyzed by GC.

The formation of Ar* in the system was confirmed by observing the well known emission of N_2 ($C^3\Pi_u \rightarrow B^3\Pi_g$) at 337 nm, introducing N_2 into the Ar flow. Since the linear flow velocity was small (1.3 m s^{-1}), the intensity of the emission was very weak, and a photon counting technique was necessary to take the spectrum. A determination of the Ar* concentration was not attempted. When a mixture of N_2 and propylene was introduced into the Ar flow, the emission disappeared.

Materials. Ar was obtained from a cylinder with a stated purity of 99.999% and was used after passage through a molecular sieve column cooled with liquid nitrogen. Propylene, N_2O, CO_2, and NO were obtained from Takachiho Co. The propylene contained 2.1×10^{-3}% ethane, 2.2×10^{-3}% propane, and 2.3×10^{-4}% ethylene, but these amounts were much smaller than those produced by the reaction, so the propylene was used without further purification. For the competitive experiments with propylene and other quenchers, mixtures of propylene and N_2O or CO_2 of three different concentration ratios were prepared, and their exact concentration ratios were determined by GC.

Results and Discussion

Product Identification, and the Relationship between Product Yields and Propylene Concentration. The major product was ethylene, with ethane and propane as minor products. Although usually H_2 and CH_4 were not collected in the present sampling method using a liquid nitrogen trap, occasionally some amount of CH_4 was detected. Butadiene was identified by a MS analysis of the products, but a quantitative determination of its amount was not attempted. Acetylene, propyne, and allene were carefully searched for, but not found in the product. Figure 2 shows the relationship between the yields of ethylene, ethane and propane and the propylene concentration. The concentration of the products is defined as the final concentration at the end of the reaction path, and it is calculated from the yield of the product per unit time and the linear flow velocity (1.3 m s^{-1}). It is the yield of the product integrated over a given residence time (0.3 s) in the flow system (see Eqs. 12 and 13). Over a limited range the yield of ethylene is proportional to the concentration of propylene; however, the yield decreases at higher concentrations of propylene. The yields of ethane and propane also appear to increase with an increase of propylene concentration, but their proportionalities are not conclusive due to their low yields. The plot of ethylene yield *vs.* propylene concentration appears not to pass through origin, but we consider this to be due to the experimental error. Although we could not determine the initial concentration of Ar*, the yield of ethylene, *ca.* 3×10^{10} molecule cm^{-3}, may indicate a lower limit for the Ar* con-

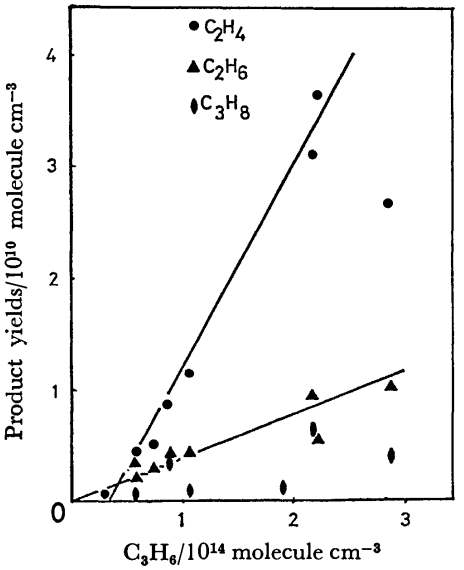

Fig. 2. Product yields *vs.* propylene concentration.

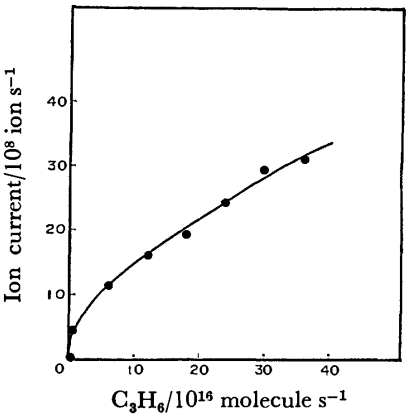

Fig. 3. Dependence of ion current on propylene concentration.

TABLE 1. RATIO OF ION YIELD TO ETHYLENE YIELD

Flow rate of propylene molecule s^{-1}	Ion yield per unit time ion s^{-1}	Ethylene yield per unit time molecule s^{-1}	Ratio of ion yield to ethylene yield
1.2×10^{17}	1.6×10^{11}	8.5×10^{12}	1.9×10^{-2}
2.5×10^{17}	2.5×10^{11}	1.3×10^{13}	1.9×10^{-2}

centration, if we assume one atom of Ar* produces one molecule of ethylene.

Ion Current Measurement. Ion current was measured at electrodes P_1 and P_2. Ion current upstream from the reactant inlet position is less than 1.0×10^{-11} A (6×10^7 ion s^{-1}), indicating that the participation of charged particles (possibly Ar^+) as reactants is negligible compared with Ar* ($\approx3\times10^{10}$ atom s^{-1}). In Fig. 3 the relationship between ion current at P_2 and propylene concentration is shown. The ion current increases with increasing propylene concentration, but not exactly linear. Since the measured ion current corresponds approximately to the amount of ions produced in the volume defined by the two electrodes P_2, we would need parallel electrodes 300 mm long in order to know the total ion yield in the flow system. Here we calculated an upper limit of the yield in the total volume of the reaction region by multiplying the measured ion current a factor of 100 (the ratio of the total volume of the reaction region to the volume defined by the two electrodes). Table 1 gives the ion yield (calculated upper limit), ethylene yield under the same conditions, and ratio of ion yield to ethylene yield. From these results we may conclude that the formation of ionic species is less than 2% of the ethylene yield.

In the present experimental setup the identification of ionic products was not possible, but we may assume that the measured ions are propylene parent ions or associated ions[11] (possibly $Ar(C_3H_6)^+$) and not fragment ions. Since the ionization potential of propylene is 9.73 eV, and the energy of Ar* is 11.5 eV for $Ar(^3P_2)$ and 11.7 eV for $Ar(^3P_0)$, the formation of propylene parent ion is possible. However, the formation of fragment ions is less likely, since the appearance potentials for allyl and vinyl ions from propylene are 12.1 eV and 13.8 eV respectively.[12]

The competitive quenching method for determining the rate constant for the Ar+propylene reaction.* If we assume ethylene is formed through the propylene quenching of Ar*, the following two processes compete when a mixture of propylene and another quencher is mixed with Ar*:

$$Ar^* + C_3H_6 \xrightarrow{k_1} Ar + C_3H_6^* \longrightarrow \text{ethylene and other product(s)}, \quad (1)$$

$$Ar^* + Q\,(\text{another quencher}) \xrightarrow{k_q} Ar + Q^*(\text{or product(s) from } Q^*). \quad (2)$$

According to the conventional treatment of competitive reactions, we may obtain the following equation:

$$[C_2H_4]_0/[C_2H_4]_q = 1 + (k_q[Q]/k_1[C_3H_6]), \quad (3)$$

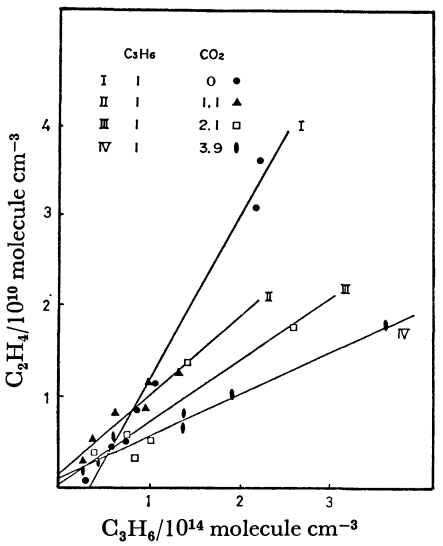

Fig. 4. Ethylene yields *vs.* propylene concentration in the absence and in the presence of CO_2.

where $[C_2H_4]_0$ and $[C_2H_4]_q$ are the yields of ethylene in the absence and in the presence of another quencher Q but with the same concentration of propylene. In the present flow system we need a more detailed consideration to derive Eq. 3 which is different from the case of batch photolysis. This will be given later. If Eq. 3 holds, we may expect that a plot of ($[C_2H_4]_0/[C_2H_4]_q$) *vs.* concentration ratio of Q to propylene should give an intercept of unity and a slope of k_q/k_1.

This seems to be the case for this system as is shown in Fig. 4, which presents ethylene yield as a function of propylene to CO_2 ratio for three different concentration ratios. It is seen that the slope decreases with an increase in the $[CO_2]/[C_3H_6]$ ratio, indicating the decrease of ethylene yield with increase of CO_2 concentration. In order to see if Eq. 3 holds or not, we plot the value of $[C_2H_4]_0/[C_2H_4]_q$ against $[CO_2]/[C_3H_6]$ and $[N_2O]/[C_3H_6]$ at a normalized propylene concentration as Fig. 5 shows. The intercepts of the plots for CO_2 and N_2O are both 1.1 ± 0.1, and the slope is 0.67 ± 0.04 for CO_2 and 0.51 ± 0.03 for N_2O. Combining these values with the quenching rate constants determined by Setser et al.[12] for $Ar(^3P_2)$ (5.3×10^{-10} cm^3 $molecule^{-1}$ s^{-1} for k_{CO_2} and 4.4×10^{-10} cm^3 $molecule^{-1}$ s^{-1} for k_{N_2O}) we obtain $(7.9\pm0.5)\times10^{-10}$ cm^3 $molecule^{-1}$ s^{-1} from the CO_2 experiment and $(8.6\pm0.5)\times10^{-10}$ cm^3 $molecule^{-1}$ s^{-1} from the N_2O experiment for the value of k_1. We consider these two values of k_1 determined from two different series of experiments to be identical within the range of experimental error. Unfortunately the rate constant for propylene quenching of Ar* as determined by

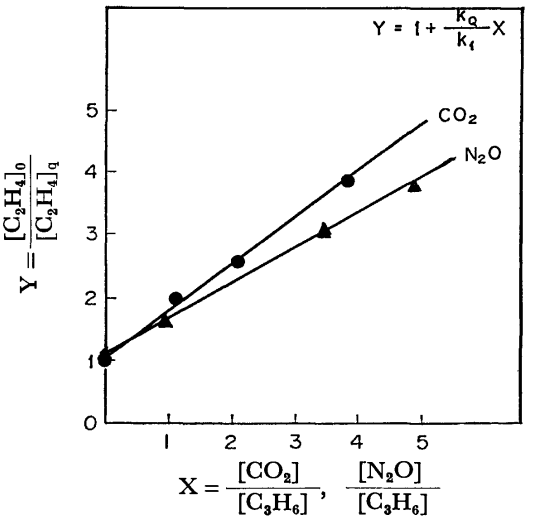

Fig. 5. Plots of $[C_2H_4]_0/[C_2H_4]_Q$ *vs.* $[CO_2]/[C_3H_6]$ and $[N_2O]/[C_3H_6]$

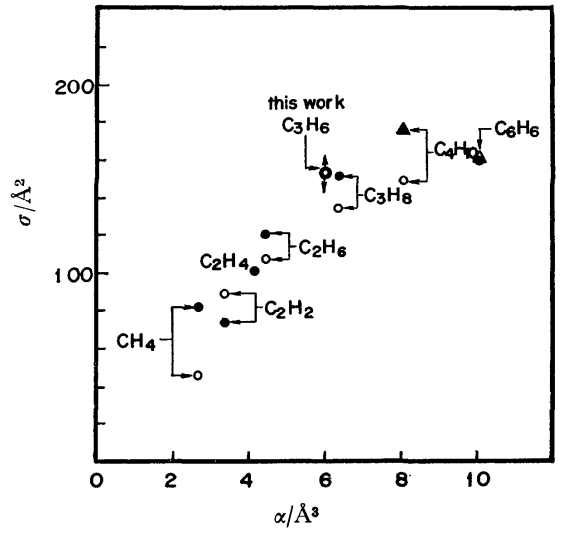

Fig. 6. Ar* quenching cross section by propylene and its polarizability in Bourène's plot.

the atomic absorption method has not been reported yet, and we cannot compare our value with what may be called a physical quenching rate constant or the total quenching rate constant including all quenching processes of Ar*.

Several authors have claimed a good correlation between the quenching cross sections of Ar* and several physical parameters such as polarizability,[13] van der Waals dispersion parameter,[14] and molecular diameter.[15] We would not judge which parameter is the best, but we tentatively plot our value for propylene against polarizability according to Bourène and Le Calvé in Fig. 6. It is seen that our value fits Bourène's plot.

When we used a mixture of propylene and NO for the reaction with Ar*, we observed a more remarkable decrease of ethylene yield than would be expected from a simple competing quenching of Ar* by NO which has an observed quenching rate constant for $Ar(^3P_2)$ of 2.2×10^{-10} cm^3 molecule^{-1} s^{-1}.[12] This

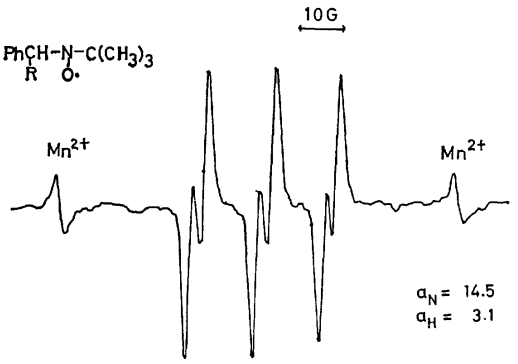

Fig. 7. ESR spectrum of a spin adduct of BPN produced in the reaction of Ar* with propylene.

decrease may be ascribed to NO scavenging of the intermediate vinyl radical.

Spin Trapping Experiment. Presuming that the reaction proceeds through a radical mechanism, we applied spin trapping technique to the present system to identify the intermediate radical(s), (vinyl, methyl, allyl radicals, and H atom might be considered possible). *N-t*-Butyl-α-phenylnitrone (*N*-benzylidene-*t*-butylamine *N*-oxide, BPN),[16] 2-methyl-2-nitrosopropane and nitrosobenzene were tested as spin trapping materials. BPN was used by sprinkling powder BPN over glass fibers and placing it in a straight trap instead of the helical trap D. After passing the reaction mixture for several hours with discharge under reaction conditions similar to those in the usual experiment, the powder was dissolved in cyclohexane. The ESR spectrum of the deaerated cyclohexane solution (JRS-PF-3X ESR spectrometer) is shown in Fig. 7. The coupling constants of the spin adduct are 14.5 G (1 G= 10^{-4} T) for a_N and 3.1 G for a_H. On comparing the spin coupling constants with the reported values of several spin adducts,[17] this spectrum is interpreted as that of an alkyl radical. Since the coupling constant of the BPN spin adducts is not very sensitive to the structure of the alkyl radical, we are not able to identify its structure uniquely, but methyl radical adduct may be the most probable.

We could not find any evidence of a vinyl radical adduct in the spectrum. Although the values of the spin coupling constants of vinyl radical adduct have not been reported in the literature, we would expect the value of a_H for vinyl radical adduct to be much smaller than those of an alkyl radical, considering that the a_H value of phenyl radical adduct is 2.08—2.14 G. It is, however, to be noted that the absence of ESR signals from a vinyl radical adduct in the spectrum does not necessarily mean that vinyl radical is not formed as a reaction intermediate, since the lifetime of some spin adducts is too short to be detected. Generally spin adducts of 2-methyl-2-nitrosopropane and nitrosobenzene show ESR spectra more sensitive to the radical structure. Although we obtained spin adduct ESR spectra with 2-methyl-2-nitrosopropane as the spin trap, we could not obtain an ESR spectrum of the adduct, when nitrosobenzene was used as the spin trap. The 2-methyl-2-nitrosopropane was too volatile to use as a powder, so the

Ar and propylene mixture was bubbled through a dibutyl phthalate solution of the trapping compound. Although the spin adduct spectrum could be observed, the adduct concentration was so low, and we could determine only a_N (14.5 G) but not a_H.

Reaction Mechanism and Rate Equations. The experimental results may be summarized as follows:
(1) Ethylene is the major product, with ethane, propane and butadiene identified as minor products. Hydrogen and methane may be products also, but they could not be confirmed due to sampling difficulties. Acetylene, propyne, and allene were not found in the product.
(2) Within a limited range of propylene concentration, the ethylene yield is proportional to the concentration of propylene.
(3) The remarkable decrease of ethylene yield from a mixture of propylene and NO suggests that ethylene is formed through a radical mechanism.
(4) The spin trapping experiments indicate the formation of an alkyl radical as an intermediate.
(5) The competitive quenching experiments with CO_2 and N_2O show that ethylene formation is directly related to the quenching of Ar* by propylene, and allow the determination of a reasonable rate constant for the propylene quenching of Ar*.
(6) The yield of ionic species as primary product is estimated to be less than 2% of the ethylene yield.

In consideration of these results, the following reaction mechanism is proposed:

$$Ar^* \longrightarrow Ar \text{ (including quenching by wall collision, two and three body collisions with Ar)} \quad (4)$$

$$Ar^* + C_3H_6 \xrightarrow{k_1} Ar + C_3H_6^* \quad (1)$$

$$Ar^* + Q \xrightarrow{k_q} Ar + Q^* \text{ (or products from Q*)} \quad (2)$$

$$C_3H_6^* \xrightarrow{k_5} C_2H_3 \text{ (vinyl radical)} + CH_3 \quad (5)$$

$$C_3H_6^* + C_3H_6 \xrightarrow{k_6} 2C_3H_6 \quad (6)$$

$$C_2H_3 + C_3H_6 \xrightarrow{k_7} C_2H_4 + C_3H_5 \text{ (allyl radical)} \quad (7)$$

$$2C_2H_3 \xrightarrow{k_8} C_4H_6 \text{ (butadiene)} \quad (8)$$

$$2C_2H_3 \xrightarrow{k_9} C_2H_4 + C_2H_2. \quad (9)$$

In order to assess accurately the contribution of these elementary processes, we would need a more complete product analysis and determination of intermediate radical. Here, however, we concentrate our concern on the mechanism of ethylene formation. We consider Reaction 1, 2, and 7 as essentially important in the ethylene formation, but we will briefly discuss the contribution of Reactions 6 and 9. Deactivation of Ar* by wall collision, two and three body quenching with Ar have been studied and discussed by several workers. Wall collision is in the diffusion regime, and the values for two body and three body quenching rate constants are not consistent but depending on the authors. Here in order to estimate the magnitude of these quenching processes under the present conditions, we calculated the sum of the rates of these three terms at 0.2 Torr of Ar (expressed as K),

$$K = (D/\Lambda^2 P) + k'[Ar] + k''[Ar]^2 = 1.5\times10^3\ s^{-1}, \quad (10)$$

where D is the diffusion rate of Ar at 1 Torr of Ar (54 Torr cm^2 s^{-1}), P is the pressure of Ar in Torr, Λ is the characteristic diffusion length given as $1/\Lambda^2=(\pi/l)^2+(2.4/R)^2$ (l: length of the reaction tube, R: radius of the reaction tube, both in mm).[18] For the values of k' and k'', we used the large ones from the reported values, that is, 6×10^{-15} cm^3 molecule^{-1} s^{-1} for k'[19] and 8.6×10^{-31} cm^6 molecule^{-2} s^{-1} for k''.[20] The concentration of Ar* decreases exponentially with travel time or travel length along the reaction tube:

$$[Ar^*] = [Ar^*]_0\exp(-(K+k_1[C_3H_6]+k_q[Q])t), \quad (11)$$

where $[Ar^*]_0$ is the concentration of [Ar*] at $t=0$.

Ionization processes of propylene and molecular formation of ethylene from propylene are disregarded. The reaction of propylene with Ar excimer is also neglected considering the excimer concentration is supposed to be much smaller than the Ar* concentration. Although the electronic state of the C_3H_6* formed through excitation transfer is not known, it may be a superexcited state locating above the first ionization level of propylene. The excited propylene may decompose either through a direct process or through a vibrationally excited ground state. Since the concentration of propylene is low, the rate of the deactivation process 6 may be slower than Reaction 5 and can be neglected. The disproportionation Reaction 9 is also neglected in consideration of the small magnitude of k_9 (5×10^{-12} cm^3 molecule^{-1} s^{-1}) at room temperature.[21] Our experimental finding that acetylene is not found as a product is consistent with this assumption.

According to the proposed reaction mechanism the derivation of the rate equations for C_3H_6*, C_2H_3, and C_2H_4 are straight-forward, assuming the local steady states for the concentrations of the intermediates. In order to solve the rate equations, the additional approximation of discarding the term $k_8[C_2H_3]^2$ is also introduced for mathematical convenience. Although k_8 must be larger than k_9, we believe that neglecting this term does not lead to any serious change in the present analysis of the kinetics.

In the flow system we need an expression for the integrated yield of ethylene as a function of residence time ($\tau=l/v$) which can be expressed as follows:

$$[C_2H_4]_q = \int_0^\tau k_7[C_2H_3][C_3H_6]dt$$

$$= \frac{k_1[Ar^*]_0[C_3H_6]}{(k_1[C_3H_6]+k_q[Q]+K)}(1-\exp(-k_7[C_3H_6]\tau)). \quad (12)$$

When we take a value of τ as 0.3 s, $[C_3H_6]$ as 10^{14} molecule cm^{-3}, and 10^{-14} cm^3 molecule^{-1} s^{-1} for the tentative value of k_7, the following approximation is possible:

$$[C_2H_4]_q \fallingdotseq \frac{k_1[Ar^*]_0[C_3H_6]}{(k_1[C_3H_6]+k_q[Q]+K)}k_7[C_3H_6]\tau. \quad (13)$$

This is consistent with our finding that the ethylene yield is nearly proportional to the propylene concentration in a limited low concentration range.

Bearing in mind that $K(\approx10^3\ s^{-1})$ is much smaller

TABLE 2. PRODUCT DISTRIBUTION IN THE REACTION OF Ar* WITH PROPYLENE, THE DIRECT PHOTOLYSIS, AND THE MERCURY-SENSITIZED PHOTOLYSIS OF PROPYLENE

Products	Present work	Direct photolysis			Hg-sensitized photolysis
	$Ar(^3P_2)$ + $Ar(^3P_0)$ (11.5 eV) (11.7 eV)	123.6 nm[a] (10.0 eV)	147.0 nm[b] (8.4 eV)	184.9 nm[c] (6.7 eV)	$Hg(^3P_1)$[d] (4.9 eV)
Hydrogen	not det.	0.8	0.6	0.8	66.5
Methane	not det.	0.2	0.3	0.7	3.4
Acetylene	not found	1.9	3.1	1.1	9.2
Ethylene	(1.0)	(1.0)	(1.0)	(1.0)	(1.0)
Ethane	0.3	0.2	0.6	0.6	1.1
Propyne + allene	not found	0.4	1.2	0.6	54.8
Propane	0.1		0.6	1.1	2.1
Butadiene	found		0.3		0.3
Butenes	not found	0.5	1.0	1.4	5.2
Isobutane	not found	0.5	1.0	0.8	0.4

a) Ref. 22, b) Ref. 22, c) Ref. 24, d) Ref. 27.

than $k_1[C_3H_6]+k_q[Q]$, when we take the ratio $[C_2H_4]_0/[C_2H_4]_q$ for a given propylene concentration, we obtain Eq. 3 as presented before.

Finally we have to admit that the proposed reaction mechanism does not cover all the reaction products. Ethane may be formed through the recombination of two methyl radicals, but the mechanism for propane formation is not certain. In the proposed mechanism the formation of allyl radical is assumed to take place by the abstraction of H atom from propylene, but we do not know the final destiny of the allyl radical. Further, we discarded the addition reaction of vinyl radical to propylene, although usually radical addition is faster than abstraction. In order to elucidate answers to these still unresolved problems we will need a more thorough product analysis in the future.

Reaction of Ar with Propylene in Comparison with the Direct and Mercury-sensitized Photolysis.* The comparison between the reaction of Ar* with propylene and the direct photolysis[22-25] and mercury-sensitized photolysis[26-28] would be interesting in order to see how the exciting energy and the exciting mode affect the reaction behavior of the excited molecule. In order to compare the reactions in detail we would need to know the electronic state of the excited molecule and the quantum yields of the primary processes or branching ratios. Our experimental results for the product analysis itself is incomplete, and most works on the far ultraviolet photolysis of propylene lack any estimation of the quantum yields of the primary processes. Furthermore, the results reported by the authors in two laboratories are not completely consistent. Bearing these points in mind, we give in Table 2 the relative yields of the final products normalizing the yields to ethylene yield, and discuss the reaction characteristics qualitatively. In the mercury-sensitized photolysis the yield of allene is distinct. Allene is probably formed through H atom abstraction by a $Hg(^3P_0)$ atom. The photolysis of propylene with 184.9 nm radiation was reported by Arai *et al.*[24] Acetylene, propane, allene, propyne and various C_4- and C_5- hydrocarbons are identified in addition to ethylene. Borrel *et al.*[25] also investigated the same photolysis. Their results are not completely consistent with the previous results, and they estimated the quantum yields of the primary processes as follows:

$$C_3H_6^* + h\nu \longrightarrow CH_2{=}CHCH_2 + H \qquad \phi = 0.41$$
$$\longrightarrow C_2H_3 + CH_3 \qquad \phi = 0.36.$$

They found that the quantum yields of the products decrease with the addition of an inert gases and ascribed this pressure effect to the participation of a Rydberg state as well as the valence bond excited state.

Becker *et al.*[22] studied the photolysis of propylene with 147.0 nm and 123.6 nm radiations and determined the relative yields of the products. Tsuikow-Roux[23] reinvestigated the photolysis at 147.0 nm and compared his results with the previous ones. In all these photolysis the formation of acetylene is confirmed, and with 147.0 and 123.6 nm radiations its yields exceed those of ethylene. Some portions of acetylene may be formed through a disproportionation reaction between two vinyl radicals. However, in order to explain acetylene yields that are twice or three times larger than ethylene yield in the direct photolysis at 147.0 and 123.6 nm, we must call for the direct formation of acetylene from excited propylene or of the decomposition of vibrationally excited ethylene as is assumed in the various reaction systems.[29] In view of the high excitation energy available in Ar*, it is rather unexpected that acetylene is not found in the products of Ar* reaction.

As a whole, the complete reaction system of Ar* with propylene appears to be simpler than that in the direct photolysis in spite of the comparable amounts of energy. One possible explanation for this simple reaction features may be due to the flow technique used in these experiments and the suppression of successive radical reactions by the rapid cooling of the reactant mixture to liquid nitrogen temperature. However, we would like to suggest that in the energy transfer reaction between metastable atoms and acceptor molecules only electron in the outer valence orbital may be subject to excitation,[30] while in the direct photolysis electrons both in outer and inner shells may be excited resulting in more violent or complicated

reaction pathways even if the amounts of the excitation energies are comparable. However, at present this suggestion remains speculative one and requires theoretical and experimental evidence.

The authors would like to express sincere thanks to Prof. Soji Tsuchiya and Dr. Seiichiro Koda of The University of Tokyo for their valuable discussions, and to Dr. Shiegeo Tsujimura for his kindness to give facilities for one of the authors (A.S.) to carry out a part of this study at Japan Atomic Energy Research Institute. The authors are also indebted to Prof. Yasuo Itoh and Prof. Rei Hirasawa of The University of Tokyo in the measurement and interpretation of the spin trapping ESR spectra, and to Prof. R. A. Loeliger of International Christian University for careful reading and revision of the manuscript.

References

1) P. H. Stedman and D. W. Setser, "Progress in Reaction Kinetics," ed by K. R. Jennings and R. B. Cundall, Pergamon Press, Oxford (1972), Vol. 6, p. 193.
2) J. E. Velazco, J. H. Kolts, and D. W. Setser, *J. Chem. Phys.*, **69**, 4357 (1978).
3) J. H. Kolts, and D. W. Setser, "Reactive Intermediates in the Gas Phase," ed by D. W. Setser, Academic Press, New York (1979), p. 152.
4) M. F. Gold, "Gas Kinetics and Energy Transfer," The Chemical Soc., London (1977), Vol. 2, p. 123.
5) T. Ueno and Y. Hatano, *Ohyo Butsuri*, **47**, 1006 (1978).
6) A. Fontijn, "Progress in Reaction Kinetics," ed by K. R. Jennings and R. B. Cundall, Pergamon Press, Oxford (1972), Vol. 6, p. 99.
7) E. Muschlits, *Ber. Bunsenges. Phys. Chem.*, **77**, 628 (1973).
8) A. Niehaus, *Ber. Bunsenges. Phys. Chem.*, **77**, 632 (1973).
9) L. W. Siek, *J. Chem. Phys.*, **50**, 1748 (1969).
10) G. vonBünau and R. N. Schindler, *J. Chem. Phys.*, **44**, 420 (1966).
11) N. T. Holcombe and F. W. Lampe, *J. Chem. Phys.*, **56**, 1127 (1972).
12) F. H. Field and J. L. Franklin, "Electron Impact Phenomena," Academic Press, New York (1970), pp. 280 and 281.
13) M. Bourène and J. LeCalvé, *J. Chem. Phys.*, **58**, 1452 (1973).
14) L. G. Piper, J. E. Velazco, and D. W. Setser, *J. Chem. Phys.*, **59**, 3323 (1973).
15) K. Matsubara, Y. Oono, S. Kai, and Y. Nishimura, *Bull. Chem. Soc. Jpn.*, **52**, 1583 (1979).
16) We are indebted to Dr. K. Koyano for her kindness of donation of this compound.
17) E. G. Janzen and B. J. Blackburn, *J. Chem. Soc.*, **91**, 4481 (1969).
18) E. Ellis and N. D. Twiddy, *J. Phys., B*, **2**, 1366 (1969).
19) O. J. Dunn and R. A. Yong, *J. Chem. Phys.*, **62**, 1996 (1975).
20) A. V. Phelps and J. P. Molnar, *Phys. Rev.*, **89**, 1202 (1953).
21) K. O. McFadden and C. L. Currie, *J. Chem. Phys.*, **58**, 1213 (1973).
22) D. A. Becker, H. Okabe, and J. R. McNesby, *J. Phys. Chem.*, **69**, 538 (1965).
23) E. Tsuikow-Roux, *J. Phys. Chem.*, **71**, 2355 (1967).
24) S. Arai, S. Shida, and T. Nishikawa, *Bull. Chem. Soc. Jpn.*, **39**, 2548 (1966).
25) P. Borrel, A. Cervenka, and J. W. Turner, *J. Chem. Soc., Perkin Trans. 1*, **1971**, 2293.
26) F. P. Lossing, D. G. H. Marsden, and J. B. Farmer, *Can. J. Chem.*, **34**, 701 (1956).
27) M. Avrahami and P. Kebarle, *J. Phys. Chem.*, **67**, 354 (1963).
28) C. A. Heller and A. S. Gordon, *J. Chem. Phys.*, **42**, 1262 (1965).
29) K. Honda, H. Mikuni, M. Takahasi, and Y. Morii, *J. Photochem.*, **3**, 199 (1974); and references cited therein.
30) T. Munakata, K. Kuchitsu, and Y. Harada, *Chem. Phys. Lett.*, **64**, 409 (1979).

  Bull. Chem. Soc. Jpn., 54, 685—686 (1981)

Photodissociation Reaction from Higher Excited Triplet States of [2.2]Paracyclophane

Shun-ichi Ishikawa, Junko Nakamura,† and Saburo Nagakura*

The Institute for Solid State Physics, The University of Tokyo, Roppongi, Minato-ku, Tokyo 106

† *The Institute of Physical and Chemical Research, Wako, Saitama 351*

(Received September 3, 1980)

The mechanism of photodissociation of [2.2]paracyclophane in glassy solvent at 77 K was studied. It is concluded that the dissociation of the CH_2–CH_2 bridge occurs from higher triplet states (T_n) *via* the lowest triplet state as an intermediate. The efficiency of the reaction depends on the characters of T_n states; high from the locally excited state, and low from the charge-transfer state.

The electronic structure of [2.2]paracyclophane (PC) has been studied both experimentally and theoretically.[1] The most predominant character of the molecule is the transannular interaction. In PC, there exist two different kinds of excited states, the locally excited (LE) state within the constituent moieties, the benzene rings of PC, and the charge-transfer (CT) state. The LE and CT bands were observed in the $S_n \leftarrow S_0$ and $T_n \leftarrow T_1$ absorption spectra.[1] When PC is excited to different kinds of electronic states, photoreactions characteristic of respective states are expected to occur.

Helgeson and Cram studied photochemistry of PC in the alcoholic solution at room temperature.[2] From the analysis of photoproducts at various exciting wavelengths, they proposed an interpretation that the excitation to different singlet electronic states of PC produces different reaction intermediates.[2] In a previous paper,[3] we found that photodissociation occurred on the CH_2–CH_2 bridge of PC in glassy solvents at 77 K, and that a species with two benzyl radicals linked together ($H_2\dot{C}$– 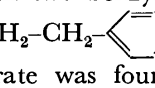 –CH_2–CH_2– 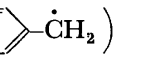 –$\dot{C}H_2$) was produced. The reaction rate was found to be proportional to the square of the exciting light intensity.

In this paper, the relation between the reactivity and the nature of excited states of PC was investigated.

Experimental

PC and the solvents, 2-methylpentane (2-MP) and 2-methyltetrahydrofuran (MTHF), were purified by the same methods as described previously.[3] The samples with the concentration of 10^{-3} mol dm^{-3} in each solvent were degassed by freeze-pump-thaw cycles.

For photolysis of PC, the following exciting sources were used; a 1 kW super high-pressure mercury lamp (Pyrex and $NiSO_4$ solution filters for 313 nm light, and Toshiba UV-D33 S and UV 35 filters for 365 nm), a 500 W super high-pressure mercury lamp with a Jarrell-Ash 1/4 m monochromator, and a nitrogen laser (Molectron UV 24) pumped dye laser (DL 14). Dyes used are 2-(4-biphenylyl)-5-phenyl-1,3,4-oxadiazole (365—380 nm), 4,4‴-bis(2-butyloctyloxy)-*p*-quarterphenyl (380—395 nm), 2-(4-biphenylyl)-6-phenylbenzoxazole (395—405 nm), 4,4′-diphenylstilbene (405—415 nm), 1,4-bis(2-methylstyryl)benzene (415—425 nm), coumarin 120 (425—445 nm), and 7-diethylamino-4-methylcoumarin (445—450 nm). The intensity of the dye laser was monitored by the use of a power meter (Laser Precision RKP 312).

The optical alignment used for pursuing radical production from PC is of the parallel beam type[1b] (Fig. 1). An

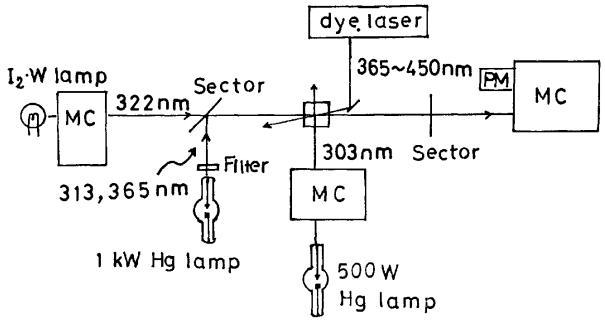

Fig. 1. Optical alignment used for the measurement of the reaction rate of PC.

exciting light (1 kW mercury lamp or dye laser) and a monitoring light were set to pass the same part of a sample. The wavelength of the monitoring light is 322 nm which corresponds to the absorption peak of the radical produced from PC.[3]

Results and Discussion

In the present study, experiments were made by using two different exciting light beams; a weak monochromatic light beam at 303 nm from a 500 W mercury lamp (first beam) and a strong light beam at 365 nm from a 1 kW mercury lamp (second beam). The second beam alone caused no reaction because PC has no absorption at 365 nm. With the use of the first beam only, the reaction occurs very slowly. With the simultaneous use of both beams, the reaction proceeds faster by an order of magnitude than with the use of the first beam alone. The reaction product is known to be $H_2\dot{C}$– 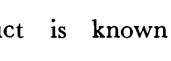 –CH_2–CH_2– 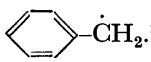 –$\dot{C}H_2$.[3] Since the produced radical is stable at 77 K, the relative reaction rate, R, can be defined by the absorbance change, ΔA, at an appropriate wavelength. Actually we measured ΔA at 322 nm corresponding to one of the peak wavelengths of the product. The reaction rate is proportional to the intensity of the second beam. This experimental result confirms that the reaction proceeds through an intermediate state.

In rigid media at 77 K, the most appropriate state for this intermediate is the lowest triplet state, T_1, which has a sufficiently long lifetime (a few seconds).

This is supported by the facts that the reaction occurs by the irradiations of the first and second beams with intervals of several seconds as well as by their

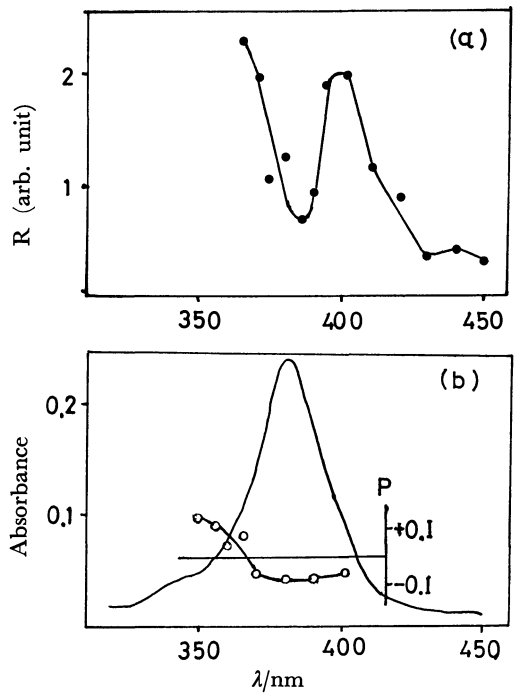

Fig. 2. (a) Dependence of reaction rate, R (ΔA (322 nm) s^{-1}), upon the wavelength of second exciting light. (b) $T_n \leftarrow T_1$ absorption spectrum of PC along with its polarization, P.

simultaneous irradiations and also that the reaction does not occur at room temperature at which the lifetime of T_1 is very short. From this veiw, the higher triplet states which are populated by $T_n \leftarrow T_1$ absorption are considered to be the reactive state of PC.

Several reactions show the biphotonic nature in the rigid media at low temperature; photoionization,[4] decomposition of solvent sensitized by solute,[4b] photoisomerization,[5] β-bond fission of substituted aromatics[6] and hydrogen abstraction from solvent.[7] The intermediate states of these reactions were found to be T_1.

In the next experiment, a weak 313 nm light (first beam) by which the reaction occurs to a negligibly small extent and a dye laser (second beam) were used for excitation. The dye laser beam is suitable for the present experiment since it is highly monochromatic (line-width is less than 0.01 nm) and the intensity per unit wavelength is high. Figure 2(a) shows the relative reaction rate (normalized to the second beam intensity) with 365—450 nm light as the second beam. The $T_n \leftarrow T_1$ absorption spectrum of PC and its polarization are also shown in Fig. 2(b).

In the present case where the first beam is weak, the concentration of the molecules populated in the T_1 state is small. Under these conditions, the reaction rate, R, is proportional to the second beam intensity, $I(\lambda)$, the molar extinction coefficient of $T_n \leftarrow T_1$ absorption, $\varepsilon(\lambda)$, and the reaction efficiency of the T_n state, $\phi_n(\lambda)$. Here λ is the wavelength of the second beam.

$$R \propto I(\lambda)\varepsilon(\lambda)\phi_n(\lambda).^{8)}$$

A plot of R *versus* λ in Fig. 2(a) shows the λ dependence of $\varepsilon(\lambda)\phi_n(\lambda)$, since the R values are normalized to the second beam intensity. We can see from this figure that the rate of radical production around 380 nm which corresponds to the maximum of the $T_n \leftarrow T_1$ absorption is smaller compared with the rate at the shorter and longer wavelengths. This means that ϕ is much smaller for the upper triplet state of the 380 nm band than for the neighboring triplet states.

The $T_n \leftarrow T_1$ absorption spectrum of PC was analyzed previously.[1b] According to the analysis, the upper state of the 380 nm band is the CT state and the LE states exist at the higher and lower energy sides. Therefore, it is reasonable to consider that the radical production occurs effectively from the LE state but ineffectively from the CT state. This indicates that the photoreactivity is sensitive to the electronic structure of the excited state from which the reaction occurs.

References

1) a) S. Iwata, K. Fuke, M. Sasaki, S. Nagakura, T. Otsubo, and S. Misumi, *J. Mol. Spectrosc.*, **46**, 1 (1973). b) S. Ishikawa, J. Nakamura, S. Iwata, M. Sumitani, S. Nagakura, Y. Sakata, and S. Misumi, *Bull. Chem. Soc. Jpn.*, **52**, 1346 (1979); and the references cited therein.

2) R. C. Helgeson and D. J. Cram, *J. Am. Chem. Soc.*, **88**, 509 (1966).

3) S. Ishikawa, J. Nakamura, and S. Nagakura, *Bull. Chem. Soc. Jpn.*, **53**, 2476 (1980).

4) a) R. Lesclaux and J. Joussot-Dubien, "Organic Molecular Photophysics," ed by J. B. Birks, Wiley, New York, N. Y. (1973), Vol. 1, p. 457. b) Kh. S. Bagdasaryan, Yu. I. Kirjkhin, and Z. A. Sinitsina, *Chem. Phys. Lett.*, **57**, 417 (1978).

5) A. Castellan, J. Kolc, and J. Michl, *J. Am. Chem. Soc.*, **100**, 6687 (1978).

6) H. Yamada, N. Nakashima, and H. Tsubomura, *J. Phys. Chem.*, **74**, 2897 (1970).

7) H. Murai and K. Obi, *J. Phys. Chem.*, **79**, 2246 (1975).

8) K. D. Cadogan and A. C. Albrecht, *J. Phys. Chem.*, **72**, 929 (1968).

  Bull. Chem. Soc. Jpn., 54, 687—691 (1981)

Pressure-induced Phase Transition and Compressive Behavior of Substituted Adamantanes

Kimihiko HARA,* Yoshikazu KATOU, and Jiro OSUGI

Department of Chemistry, Faculty of Science, Kyoto University, Sakyo-ku, Kyoto 606

(Received September 11, 1980)

The compressive behavior of adamantane and its secondary monosubstituted derivatives; adamantanone, 2-methyladamantane, and 2-bromoadamantane was measured at various temperatures in a piston-cylinder apparatus. A first-order solid-solid phase transition was found under pressure in each system. The transition pressures, the equilibrium pressures, the volume changes, and the entropy changes for the transition were determined. The compression data for the low pressure phases were fitted to an equation of the form $-\Delta V/V_0=a_0+a_1P+a_2P^2$. The effects of substituent groups on the entropy changes of the transitions of these molecular crystals were discussed.

The first-order phase transitions undergone by crystals containing globular (or cage-like) molecules that form plastic crystals have been studied from various viewpoints. Adamantane is one of the few compounds whose phase transition is fully characterized at atmospheric pressure. This compound is known to undergo a phase transition under pressure from a disordered face-centered cubic (fcc) structure to an ordered body centered tetragonal structure,[1] which is the same as the temperature-induced transition at 208.62 K.[2,3] The transition pressure was determined as 4.8 kbar at 20 °C by X-ray measurement. The volume change for the transition ΔV is reported to be -1.8 cm^3 mol^{-1} at 4.1 kbar and 20 °C by Pistorius and Resing[4] and $-\Delta V/V_0$ is 1.4% at 4.1 kbar and 25 °C by Breitling, Jones, and Boyd.[5] For adamantanone and 2-methyladamantane, as reported in our previous papers,[6-8] the analogous phase transitions from fcc to tetragonal structure were found at high pressures. For 2-bromoadamantane the high pressure phase was not determined, although the atmospheric phase was fcc.

Such a simple crystal structure in the low pressure phase is not only due to the high symmetrical globular, cage-like molecular structure, but also due to the disordered phase, where the molecules are able to rotate rather freely[9] or to assume different and hence random orientation on the lattice sites. By the application of pressure the transition from the disordered phase to the ordered phase is expected.

We report here the pressure-induced phase transitions of adamantane, or tricyclo[3.3.1.1^{3,7}]decane (**1**) and its secondary monosubstituted derivatives, *i.e.* adamantanone (**2**), 2-methyladamantane (**3**), and 2-bromoadamantane (**4**).

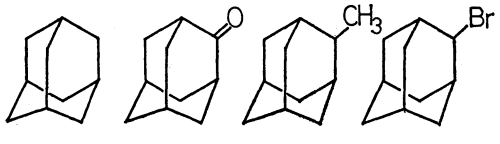

1 **2** **3** **4**

Precise measurements were made of the pressures of the transitions and the volume changes of the transitions at various temperatures. The entropy changes were calculated. Such thermodynamic data characterize phase transitions and are particularly useful in interpreting solid-solid transformations in which order-disorder effects are predominant.

Experimental

Materials. Guaranteed-grade adamantane (**1**) (Nakarai Chem. Co.) was repeatedly recrystallized from light petroleum and dried *in vacuo*. Adamantanone (**2**) (Aldrich Chem. Co.) and 2-bromoadamantane (**4**) (Aldrich Chem. Co.) were recrystallized from ethanol. 2-Methyladamantane (**3**) was prepared from adamantanone by published procedures[10] and purified by recrystallization from ethanol. No impurity was detectable in gas-chromatographic analysis of the purified samples.

Measurements. The phase transitions and compression data were obtained in a piston-cylinder device, using a tungsten carbide piston and a 12 mm i.d., 50 mm o.d. cylinder of hardened maraging steel supported by Ni–Cr–Mo steel. The pressure was generated by a 60 t hydraulic press. Extrusion was prevented by the gasket rings which are made from hardened maraging steel. The oil pressure in the press was measured to about 0.1 bar by a 250 bar Heise bourdon gauge. A thin coat of Moly-Kote which was lubricated on the piston and inside of the cylinder as friction reducer has little effect on the transition pressures. The same sample length with a mass of about 1.54 g was used throughout. The transition pressure was affected by the sample length within *ca.* 9% for (**2**).

Each sample was precompressed to the maximum pressure before each run. The displacement of piston was measured by a dial micrometer accurate to $\pm$0.001 mm. It should

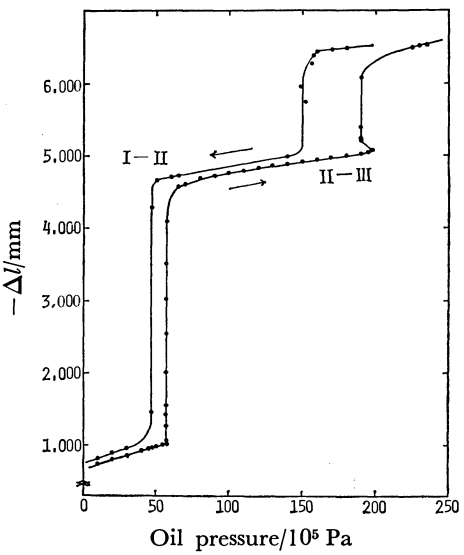

Fig. 1. Piston displacement against pressure for NH_4F used as the fixed points of pressure calibration.

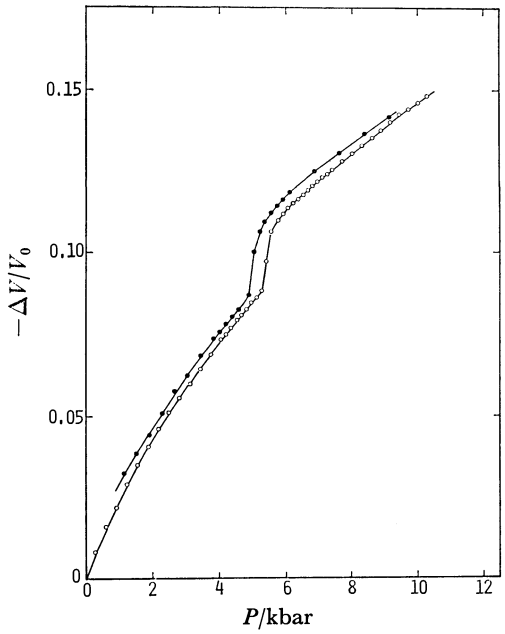

Fig. 2. (a) Compressive behavior of **1** at 22.4 °C.
○: Compression cycle, ●: decompression cycle.

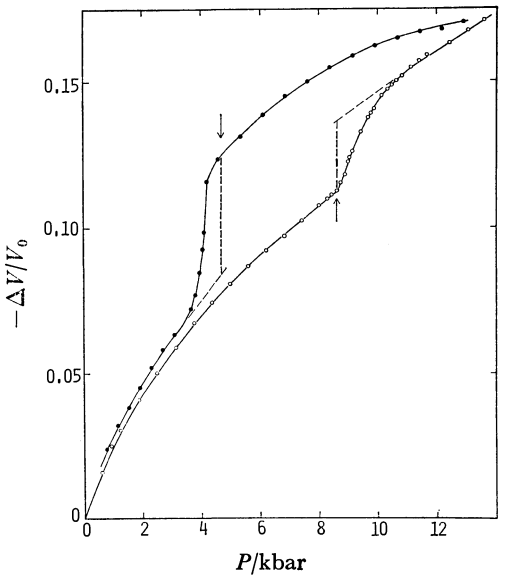

Fig. 2. (b) Compressive behavior of **2** at 21.5 °C.
○: Compression cycle, ●: decompression cycle.

be mentioned that the correction was made for the compression of piston as a function of pressure. The effective area was taken as that of cylinder. The effect of elastic distortion of the cylinder on the volume is less than 0.7% at 10 kbar. The internal pressure was calibrated with I-II and II-III transitions of NH_4F, which is shown in Fig. 1. The transition pressures at 25 °C are 3.605 kbar and 11.531 kbar,† respectively.[11] The friction of this apparatus was symmetrical between compression and decompression cycles.

The sample temperature could be maintained to within better than ±0.1 °C by circulating the water of constant temperature into the outer jacket of the cylinder. The temperature was measured with a calibrated chromel-alumel thermocouple inserted in the cylinder.

† 1 bar=10^5 Pa.

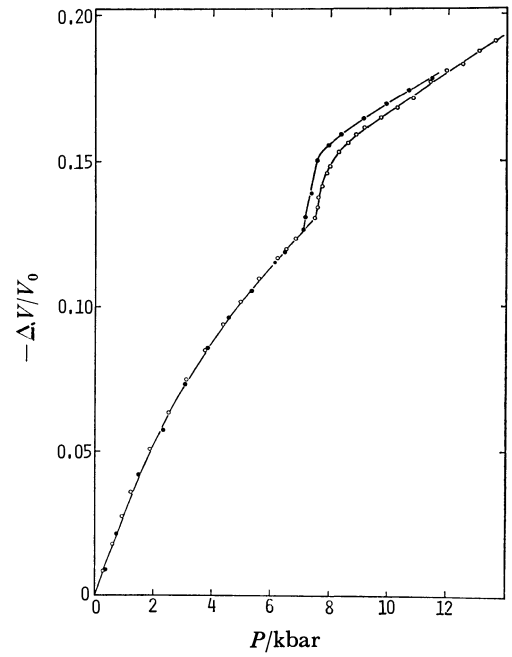

Fig. 2. (c) Compressive behavior of **3** at 20.5 °C.
○: Compression cycle, ●: decompression cycle.

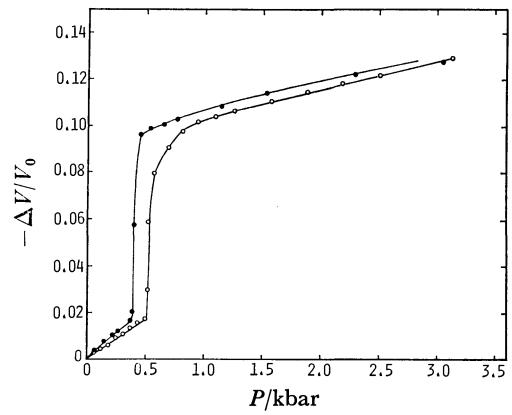

Fig. 2 (d). Compressive behavior of **4** at 20.0 °C.
○: Compression cycle, ●: decompression cycle.

Results

Every compound exhibits a discontinuous volume change at high pressure below 20 kbar, which indicates a first-order phase transition. The relative volume change $-\Delta V/V_0$ against pressure are shown in Fig. 2 (a), (b), (c), and (d) for (**1**), (**2**), (**3**), and (**4**), respectively. They are the results after correcting the friction of apparatus. The curves represent the best fit passing through the experimental points. The inflection point was used to characterize the transition pressure P_t, and the equilibrium pressure P for transition was taken as the average between the transition pressures for the compression and decompression cycles. The volume change at the transition ΔV_t was obtained by extrapolating the compression curve to the inflection pressure and measuring the difference of displacement. The volume change for the transition ΔV was determined as the average

TABLE 1. TRANSITION PARAMETERS FOR PRESSURE-INDUCED TRANSITIONS OF SUBSTITUTED ADAMANTANES

Compound	T °C	P_t kbar	P kbar	ΔP kbar	$-\Delta V$ cm³ mol⁻¹	$-\Delta V/V_0$ %	$-\Delta S$ J K⁻¹ mol⁻¹	$-\Delta H$ kJ mol⁻¹
1	0.0	4.00	3.80		2.2_9	1.78	14.2	3.9
	22.4	5.35	5.28		2.2_7	1.73	14.1	4.2
	32.2	5.85	5.75	0.2	2.1_9	1.70	13.6	4.2
	41.5	6.45	6.30		2.1_9	1.70	13.6	4.3
	54.5	7.30	7.23		2.1_2	1.65	13.1	4.3
2	0.0	6.80	4.93		4.6_4	3.5	33.7	9.2
	21.5	8.65	6.68		4.3_7	3.3	31.7	9.4
	32.5	9.30	7.30	4.0	3.9_7	3.0	28.8	9.1
	44.5	10.30	8.18		3.9_7	3.0	28.8	9.5
	55.5	11.10	9.00		—	—	—	—
3	0.0	6.00	6.00		2.9_0	2.00	19.4	5.3
	20.5	7.45	7.45		2.8_0	1.93	18.7	5.5
	32.5	8.30	8.30	≈0	2.4_4	1.68	16.3	5.0
	42.3	8.80	8.80		2.3_2	1.60	15.5	4.9
	51.5	9.40	9.40		2.1_5	1.48	14.4	4.7
4	14.0		(1 bar) a)					
	20.0	0.55	0.49		11.7_6	7.82	51.3	15.0
	40.0	1.35	1.29	0.10—0.13	10.6_0	7.05	46.2	14.5
	59.0	2.14	2.10		9.9_0	6.58	43.2	14.3
	78.8	3.05	3.00		9.5_5	6.35	41.6	14.6

a) DSC data at atmospheric pressure.

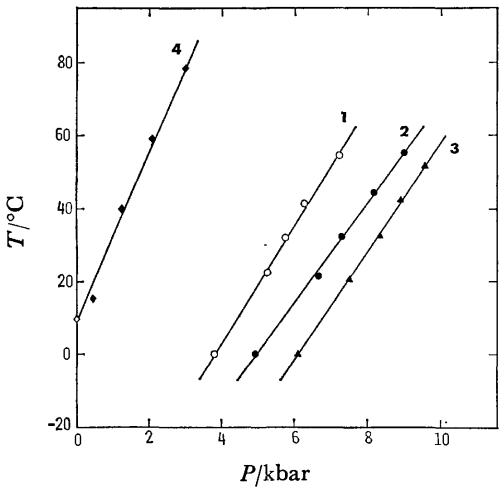

Fig. 3. Phase diagrams of **1**, **2**, **3**, and **4**.

between the volume changes at the transition pressure in compression cycle P_t and that in decompression cycle P_t', *i.e.* $1/2(\Delta V_t+\Delta V_t')$, which is shown in Fig. 2 (b). The volume changes of the transition were determined to an accuracy of 0.2 cm³ mol⁻¹. The transition pressures, the equilibrium pressures, and the volume changes for the transitions at various temperatures are summarized in Table 1. The transition pressure for (**1**), which has been determined previously from X-ray measurements as 4.8 kbar at 20 °C,[1] is in reasonable agreement with the present equilibrium pressure of 5.1 kbar at 20 °C. But the values of the transition pressure and the volume change reported by Pistorius *et al.*[4] and by Breitling *et al.*[5] are a little lower than those of the present work. Hysteresis, the reproducible difference in the transition pressure between compression and decompression cycles, ΔP is quite large for (**2**), as compared with other compounds. Its temperature dependence was not beyond the experimental errors.

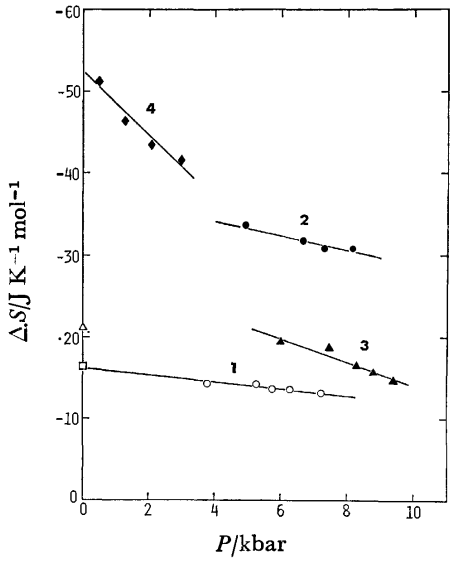

Fig. 4. Entropies of transitions against pressure.

The obtained phase diagrams are shown in Fig. 3. The slopes (dP/dT) of the equilibrium lines were obtained by means of least square fit. They were used in conjunction with ΔV to determine the entropies and enthalpies of transitions by the Clausius-Clapeyron equation.

The transition temperature of 14.0 °C for (**4**) at atmospheric pressure was determined by the differential scanning calorimetry (dsc).

The entropy changes ΔS and enthalpy changes ΔH of the transitions are listed in Table 1. The values of ΔS are plotted against the pressure in Fig. 4. The value of ΔS for (**1**) obtained from the dsc at atmospheric pressure by Chang *et al.* (16.2 J K⁻¹ mol⁻¹)[12] is just on the extrapolated line of the present data. As for (**3**) the value from the dsc by Clark *et al.*[13] is smaller than the extrapolated value.

Discussion

It is interesting to note that by the application of pressure all of the secondary monosubstituted adamantanes examined here, which have disordered fcc structure at atmospheric pressure, undergo the phase transitions to ordered body centered tetragonal structure. The structural results were reported previously.[7,8] We found that (**4**) underwent the corresponding phase transition at atmospheric pressure and that the phase diagram could be determined to atmospheric pressure. Presumably, for both (**2**) and (**3**) the temperature-induced transition with the same structural change will appear at low temperature on the extrapolated line of the phase diagram just in the similar way as (**4**).

Figure 4 indicates that ΔS increases with pressure, *i.e.*

$$\frac{\partial \Delta S}{\partial P} = \frac{\partial S(\mathrm{h})}{\partial P} - \frac{\partial S(\mathrm{l})}{\partial P} > 0,$$

where $S(\mathrm{h})$ and $S(\mathrm{l})$ refer to the entropy of high pressure phase and that of low pressure phase, respectively. This means a normal phenomenon that the pressure dependence of entropy is higher in the low pressure phase than in the high pressure phase, since $(\partial S/\partial P)<0$ for the most substances. On the other hand, we can see in Table 1 that the temperature dependence of ΔH, which indicates ΔC_p, is too small to find a comprehensive trend.

Compressibility and Crystal Density of Low Pressure Phase. The compression data of the low pressure phases at around 20 °C shown in Fig. 2 were fitted to the following equation by using the method of least squares.

$$\mathbf{1}: \quad -\frac{\Delta V}{V_0} = 1.94\times10^{-3} + 2.26\times10^{-5}P - 1.22\times10^{-9}P^2,$$

$$\mathbf{2}: \quad -\frac{\Delta V}{V_0} = 5.80\times10^{-3} + 1.93\times10^{-5}P - 0.83\times10^{-9}P^2,$$

$$\mathbf{3}: \quad -\frac{\Delta V}{V_0} = 1.85\times10^{-3} + 2.80\times10^{-5}P - 1.51\times10^{-9}P^2,$$

where V_0 is the volume of the crystal under atmospheric pressure and the unit of P is bar. For (**4**) the transition pressure was too low to get the reliable compression data of low pressure phase. The initial compressibility β_0, which is given by

$$\beta_0 = -\frac{1}{V_0}\left(\frac{\mathrm{d}V}{\mathrm{d}P}\right)_{P=0},$$

and the crystal density that was obtained from the measurement of the sample size are listed in Table 2. The size of the unit cell and the crystal desity calculated from X-ray data are also included in Table 2. The agreement between both data of the crystal density is satisfactory. We can find a correlation that the higher compressibility corresponds to the structure with the larger unit cell parameter, or the loose structure. This correlation may confirm an evidence that in molecular crystals hydrostatic compression causes the contraction of intermolecular free volume in the crystal especially in an early stage of compression and that the contraction of molecules themselves (or electron clouds) is negligible in the first approximation.

Table 2. Initial compressibility and crystal density

Compound	Initial compressibility β_0 / 10^{-6} bar^{-1}	Crystal density ρ / g cm^{-3}	
		A [a]	B [b]
1	22.7	1.06	1.08
2	19.3	1.13	1.14
3	28.0	1.03	0.99
4	—	1.43	1.40

a) Determined in the present work. b) Calculated from the X-ray data.

Entropy of Transition. Much information has been obtained about the disordered phases of molecular crystals from the entropies of transition.[14] There has been an attempt to interpret the entropy of transition of caged hydrocarbon crystals in terms of the Guthrie-McCullough method[15] which is treated for simple tetrahedral molecules and is based on sets of equivalent, distinguishable molecular orientations obtained by combining the symmetry elements of the crystal lattice with the symmetry elements of the molecule. In this method the orientational disorder is assumed to account for the entropy of transition entirely, all other effect being negligible. This treatment, however, includes some oversimplifications and is invariance with various experimental results except for some typical examples. Clark *et al.*,[13,16] on the other hand, proposed that the lattice slackening and other effects contribute a significant proportion of the entropy of transition and separated this contribution as excess entropy $\Delta S_{\mathrm{excess}}$ from the orientational entropy.

$$\Delta S = R \ln (N_{\mathrm{I}}/N_{\mathrm{II}}) + \Delta S_{\mathrm{excess}},$$

where N_{I} is the number of molecular orientational states statistically occupied in the low pressure disordered phase, N_{II} is the corresponding number in the high pressure ordered phase which is usually unity, and R is the gas constant.

Adamantane is a simple polycyclic saturated hydrocarbon with carbon atoms arranged in a cage-like skelton and has tetrahedral symmetry. Its orientational entropy change based on the Guthrie-McCullough method is $R \ln 2 = 5.8\ \mathrm{J\ K^{-1}\ mol^{-1}}$, since two distinguishable orientations are allowed in the disordered phase. By comparing with the observed entropy of transition (14.1 J K^{-1} mol^{-1} at 22.4 °C), 8.3 J K^{-1} mol^{-1} is the excess entropy of transition.

By the analogous application of this method, the orientational entropy change of adamantanone should be $R \ln 12 = 20.7\ \mathrm{J\ K^{-1}\ mol^{-1}}$, since there are six orientations in each one of adamantane. Thus, the excess entropy of 11 J K^{-1} mol^{-1} is obtained by comparing with the observed entropy of transition (31.7 J K^{-1} mol^{-1} at 21.5 °C). This is in accord with the result of Clark *et al.*[16] that the excess entropy is 10—

15 J K^{-1} mol^{-1}. Namely, the most part of the difference between the transition entropies of adamantane and adamantanone is originated from the difference in the orientational entropy change.

In the case of (**3**) and (**4**), on the other hand, there are two further distinguishable orientations in each one of (**2**), so that the orientational entropy change should be R ln 24=26.4 J K^{-1} mol^{-1}. If we compare the orientational entropy of (**4**) with the observed entropy of transition (51.3 J K^{-1} mol^{-1} at 20.0 °C), the excess entropy becomes 25 J K^{-1} mol^{-1}. This value is beyond the range proposed by Clark *et al.*, although the larger value is expected for the compounds having the larger substituents. By the application of the semiempirical equation of Clark *et al.*, since the temperature range for the orientational disordered phase, $T_m - T = 129$ °C is obtained at atmospheric pressure, we get a little lower excess entropy of 16.6 J K^{-1} mol^{-1}. As for (**3**), the value of the observed entropy is much lower than that would be expected. This abnormality may come from the fact that has been pointed out by Clark et al. Thus, the obtained order of ΔS_{excess} is (**4**)<(**1**)<(**2**)<(**3**).

The values of ΔS_{excess} can be explained if we take the effects of intermolecular ordering and intermolecular forces into account. The value of ΔS_{excess} of (**2**) is greater than that of (**1**), although they have almost the same molecular size, and hence must have similar intermolecular ordering. The same is the case for the larger value in (**4**), as compared with (**3**). Thus, we can propose that the dipolar interactions in the ordered crystal are considerably more favorable than those in the disordered phase, increasing ΔS_{excess}. The intermolecular ordering effect is another striking effect that must be considered. Large substituent groups loosen the ordered crystal lattice. This would be the reason why the values of ΔS_{excess} of (**1**) and (**3**) are smaller than (**2**) and (**4**), respectively. We can say conclusively that the molecules with the more sphericity and the higher dipole moment can give more stable ordered crystal.

We wish to thank Dr. Yoshihiro Taniguchi of Ritsumeikan University for measuring dsc of (**4**) and Mr. Fujitsugu Amita of this university for his technical assistance.

References

1) T. Ito, *Acta Crystallogr., Sect. B*, **29**, 364 (1973).
2) C. E. Nordman and D. L. Schmitkons, *Acta Crystallogr.*, **18**, 764 (1965).
3) P. Wu, L. Hsu, and D. Dows, *J. Chem. Phys.*, **54**, 2714 (1971).
4) C. W. F. T. Pistorius and H. A. Resing, *Mol. Cryst. Liq. Cryst.*, **5**, 353 (1969).
5) S. M. Breitling, A. D. Jones, and R. H. Boyd, *J. Chem. Phys.*, **54**, 3959 (1971).
6) K. Hara, G. B. Schuster, and H. G. Drickamer, *Chem. Phys. Lett.*, **47**, 462 (1977).
7) K. Hara, J. Osugi, Y. Taniguchi, and K. Suzuki, *High Temp.-High Pressures*, **12**, 221 (1980).
8) K. Hara, Y. Katou, J. Osugi, Y. Taniguchi, and K. Suzuki, *Chem. Lett.*, **1980**, 803.
9) D. W. McCall and D. C. Douglass, *J. Chem. Phys.*, **33**, 777 (1960).
10) P. R. Schleyer and R. D. Nicholas, *J. Am. Chem. Soc.*, **83**, 182 (1961).
11) R. Kaneda, S. Yamamoto, and K. Nishibata, "Accurate Characterization of the High Pressure Environment," Nat. Bur. Stand. (U.S.), Spec. Publ. 326, 257 (1971).
12) S. S. Chang and E. F. Westrum, Jr., *J. Phys. Chem.*, **64**, 1546 (1960).
13) T. Clark, T. Mc. O. Knox, H. Mackle, and M. A. McKervey, *J. Chem. Soc., Faraday Trans. 1*, **72**, 1224 (1976).
14) E. F. Westrum, Jr., and J. P. McCullough, "Physics and Chemistry of the Organic Solid State," ed by D. Fox, M. M. Labes, and A. Weissberger, Interscience Publishers Inc., New York (1963), Vol. 1.
15) J. B. Guthrie and J. P. McCullough, *J. Phys. Chem. Solids*, **18**, 53 (1961).
16) T. Clark, M. A. McKervey, H. Mackle, and J. J. Rooney, *J. Chem. Soc., Faraday Trans. 1*, **70**, 1279 (1974).

Influence of Chemisorption of 2-Propanethiol on the Electrical Properties of Silver Oxide Compaction

Naoto YAMAMOTO,* Shoichiro TONOMURA, Tsugufumi MATSUOKA, Takashi AMAMIYA, and Hiroshi TSUBOMURA

Department of Chemistry, Faculty of Engineering Science, Osaka University, Toyonaka, Osaka 560

(Received September 18, 1980)

The work function of silver oxide (Ag_2O) decreased by as much as 0.8 eV on exposure to 2-propanethiol [$(CH_3)_2CHSH$]. The change in work function was irreversible at room temperature, and proportional to the amount of thiol in case where the partial pressure is low, but reversible at 200 °C. The conductivity of the Ag_2O disk showed no substantial change by exposure to thiol. From the infrared absorption spectral studies, it was found that the thiol reacted with the silver oxide forming a $(CH_3)_2CH$–S–Ag group on the surface. The relationship between the work function and the chemical processes occurirng at the solid surface is discussed.

Recently, the employment of semiconductors for specific detection of gases taking advantage of the change in electric conductivity has been attempted by many authors.[1–5] Concerning the mechanism in such systems, it is essentially important to clarify how the electrical properties of the semiconductors are correlated with chemical processes occurring at the solid-gas interface. From this point of view, we have studied the influence of gases on the surface potentials and other electrical properties of metals and metal-semiconductor assemblies.[6] The surface potentials have also been studied for electrodes chemically modified with antibodies or enzymes. The change in electrode potentials by specific reactions between biological substances at the electrode-solution interface[7,8] has been found to be capable of serving as a sensitive device for analysis of these substances.

In this work, the effect of thiol gas on the electrical properties of silver oxide in the form of compaction (compressed powder) or thin film has been investigated. It has been found that the conductivity is insensitive, but the surface potential is very sensitive to the gas. The results are discussed in relation with informations obtained on the chemical processes on the solid surface from infrared absorption measurements.

Experimental

Materials. Copper plate, 99.9% pure, 1 mm thick, was used as the reference electrode, or the substrate for evaporated metal films. The purities of Ag, Fe, Ni, Pd, and Al used were higher than 99.9%. 2-Propanethiol gas used was evolved from the liquid 98% pure 2-propanethiol, obtained from Tokyo Kasei Kogyo Co. The silver oxide powder 99.9% pure, having the grain size of about 0.5 μm, was obtained from Kishida Chemical Co.

Procedure. The contact potential of the silver oxide samples against copper was measured by use of a vibrating capacitor method.[9] The experimental setup is schematically shown in Fig. 1. The metal to be studied, Ag, Fe, Ni, Pd, or Al, was evaporated on a Cu plate at 2×10^{-5} Torr (1 Torr=133.322 Pa). Silver oxide powder, 1.0 g in weight, was compressed at 150 kg/cm² into a disk form and the disk was attached onto a Cu plate with silver paste.

The reference electrode, a semicircular Cu plate 15 mm in radius, was rotated with a speed of 30 Hz by use of a synchronous motor. The space between both electrodes was adjusted with a micrometer to *ca.* 0.2 mm. The ac current arising from the capacity change between the electrodes was measured by use of a Teledyne Philbrick 1702 parametric amplifier and an NF LI-573 lock-in-amplifier. The contact potential between these electrodes was determined by employing the null current method with the aid of a potentiometer. The electrodes were kept in a box, 7 l in capacity. For electric conductivity measurements, gold was vacuum-evaporated onto the silver oxide disk as shown in Fig. 2.

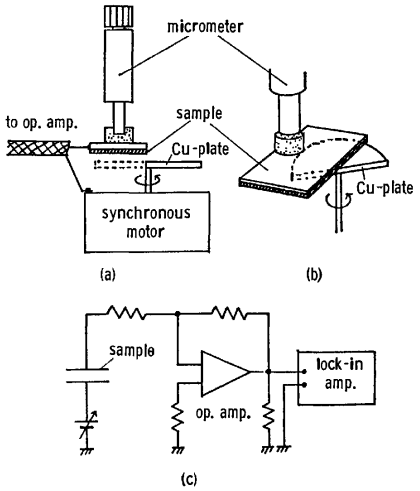

Fig. 1. Schematic representation of the experimental setup for contact potential measurements: (a) a front view and (b) a bird's-eye view. (c) The electric circuit.

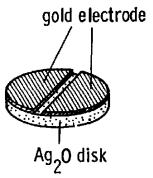

Fig. 2. The Ag_2O disk used for measuring its electric conductivity.

Infrared spectra were measured by use of a JEOL JIR 10 Fourier transform infrared spectrometer. Silver film to be measured was prepared by vacuum-deposition onto a NaCl disk, the transmittance of the film being 40% at 600 nm.

Results and Discussion

Surface Potential of Ag_2O. The average contact potential difference between an Ag_2O disk and a

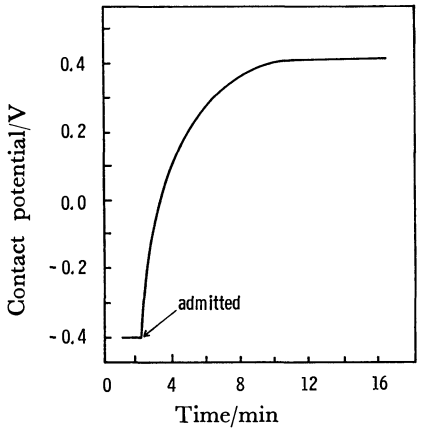

Fig. 3. The response in the contact potential of the Ag_2O disk to 2-propanethiol at room temperature.

copper reference electrode was found to be −0.40 V, when measured in air, indicating that the work function of Ag_2O is 0.40 eV larger than that of the copper electrode. The copper electrode is presumably covered with a thin copper oxide film in air and the absolute value of its work function cannot be determined directly by the capacitor method.

Figure 3 shows the change in the contact potential caused by admission of 5.0×10^{17} molecules of 2-propanethiol, into the box. The potential increased from −0.40 V to +0.40 V and became constant after about 10 min. No change in potential was observed by dissipating the gas into open air. When a disk previously exposed to thiol was heated at 200 °C in air, the potential decreased and returned to the value of unexposed Ag_2O, −0.40 V. These changes in potential are obviously due to chemisorption of the thiol on the Ag_2O surface.

It was confirmed from the following experiment that the work function of the copper reference did not change by the introduction of 2-propanethiol: First, the thiol gas was introduced into the box. The contact potential of the Ag_2O disk against the copper electrode changed as shown above. After that, the gas was removed from the box and only the Ag_2O disk was replaced by a new Ag_2O disk. The contact potential between the new disk and the copper electrode exposed to the gas showed the same value as that obtained between fresh Ag_2O and Cu electrodes in air. On replacement of the disk by a new copper plate, the contact potential was almost zero between the new and the gas exposed copper electrode. These experimental results indicate that the change in surface potential of Cu plate by exposure to thiol is negligible.

The induced potential is plotted against the amount of 2-propanethiol admitted into the box (Fig. 4). In the low partial pressure region, it is proportional to the amount of thiol introduced, but gradually saturated at higher pressure region.

The work function, ϕ, of Ag_2O, corresponding to the energy required to transfer an electron from its Fermi level to vacuum, is determined from our experiment in air as 5.6 eV, taking the work function of copper to be 5.2 eV that was obtained in the presence of oxygen.[10,11] Before chemisorption, the po-

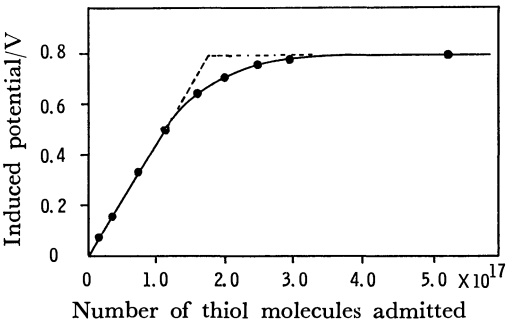

Fig. 4. The induced change of potential of the Ag_2O disk against the amount of 2-propanethiol introduced.

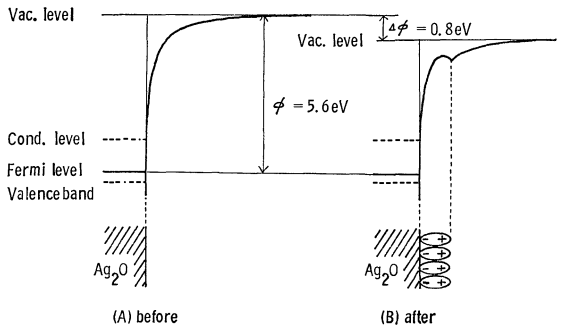

Fig. 5. Schematic energy diagrams of the Ag_2O disk near the surface before and after the introduction of 2-propanethiol gas.

tential for an electron near the disk surface may be described as shown in Fig. 5(A)[12] by taking account of the image force. The chemisorbed thiol will form an electric dipole on the Ag_2O surface (Fig. 5(B)). The potential can, then, be expressed by the superposition of the image force and electric double layer potentials as illustrated, lowering the vacuum level outside the Ag_2O surface by $\Delta\phi=0.8$ eV at its maximum.

The electrical behavior of a silver film against the gas introduction was almost similar to that of Ag_2O disk. The contact potential difference of the evaporated silver film was −0.25 eV against a copper reference electrode in air. The magnitude of surface potential change was 0.45 eV by admission of 5.0×10^{17} molecules of 2-propanethiol. The surface of the Ag film is presumably covered with a thin film of the oxide in air, and therefore the chemisorption mechanism on the film is essentially the same as on the Ag_2O disk.

As described earlier the changes in surface potential resulting from the reaction of 2-propanethiol can be explained by taking account of the induced dipole moment, $\Delta\mu$, by the chemisorption. The electrical potential, $\Delta\phi$, owing to the double layer formation is expressed by the following equation.

$$\Delta\phi = -\Delta\mu\cdot N/\varepsilon_0 \qquad (1)$$

Where N is surface density of the chemisorbed thiol and ε_0 is permittivity of vacuum. An 2-propanethiol molecule has a cross section of about 26 Å^2. Then, taking $\Delta\phi=0.8$ V, the highest value obtained, and $N=3.7\times10^{18}$ m^{-2}, calculated from the closest array

TABLE 1. THE ASSIGNMENT OF IR ABSORPTION BANDS (in cm^{-1}) OBTAINED FOR 2-PROPANETHIOL ADSORBED ON THE Ag FILM AND THE Ag_2O DISK

$(CH_3)_2CHSH$		$(CH_3)_2CHSAg$	$(CH_3)_2CHSH$ Vapor[a)]	Assignment
Ads. on Ag_2O	Ads. on Ag			
1037	1041	1045	1063	CH_3 rock
1145	1146	1150	1161	CH_3 rock
1226 1240	1236	1232	1244 1266	CH wag
	1377	1380	1389	CH_3 bend(sym)
	1456	1440 1456	1448	CH_3 bend(unsym)
			2572	SH stretch
	2850	2860	2867	CH_3 stretch(sym)
	2923	2920	2909 2927	CH stretch
	2952	2050	2967	CH_3 stretch(unsym)

a) Taken from Ref. 14.

of thiol molecular layer on the surface, $\Delta\mu$ is calculated to be 0.57 D, which seems to be a reasonable value in view of the dipole moment of 2-propanethiol molecule, 1.64 D, in liquid state.[13)]

Crystalline Ag_2O has a body centered cubic structure, where four silver atoms exist in a unit cell and its lattice constant is 4.72 Å. If the unit cells are assumed to align regularly at the surface, the cross-sectional area of 2-propanethiol is comparable to that of a unit cell of Ag_2O, so that approximately one of the four silver atoms in the cell can react with the thiol.

As up to *ca.* 4.0×10^{17} molecules of 2-propanethiol is capable of changing the disk surface potential, the actual area of the disk surface is estimated to be 0.1 m^2 under the assumption of monomolecular chemisorption. The radius of the grain of Ag_2O powder is *ca.* 0.25 μm, so that the total surface area of the powder of 1 g is calculated to be *ca.* 1.7 m^2 before making the disk. Such a decrease in the surface area seems reasonable as a result of compression in the process of disk formation.

The Pd electrode shows very high response to hydrogen gas as described in a previous paper.[6)] The Ag_2O electrode was, however, insensitive to hydrogen or carbon monoxide, but showed a small response to water and carbon dioxide. The electrode of Ni or Al had no response to the thiol up to the concentration of 2.5 ppm. The potential of the electrode of Fe changed by 23 mV with 0.3 ppm thiol.

Electrical Resistance of Ag_2O. The electrical resistance of an Ag_2O disk in a 1.0 mm gap between gold electrodes (Fig. 2) was *ca.* 6.5 MΩ in air at room temperature. No change in electrical resistance was observed as 1.0×10^{18} molecules of 2-propanethiol was introduced into the box. This fact indicates that the conductivity is mostly through the bulk of Ag_2O disk, and is not affected by the chemical processes occurring at the solid surface.

Infrared Spectra of 2-Propanethiol Adsorbed on Ag and Ag_2O. Infrared absorption spectrum was measured for the thiol adsorbed on an Ag_2O disk, 0.1 mm thick, and the band positions observed are shown in column 1 of Table 1. The IR spectrum measured for thiol adsorbed on a silver film evaporated on a sodium chloride disk (Fig. 6) gives more clear bands than on the Ag_2O disk. The spectrum was taken from fifty sweeps of transmittance measurements at room temperature. The negative absorption at around 2349 cm^{-1} is due to carbon dioxide present in air. Even after allowing to stand for 8 d in contact with air, the film showed almost the same spectrum as that in Fig. 6. The absorption peak positions are also listed in column 2 of Table 1. These assignments given in the last column in Table 1 were based on the spectral data obtained for gaseous 2-propanethiol by Smith and Devlin.[14)]

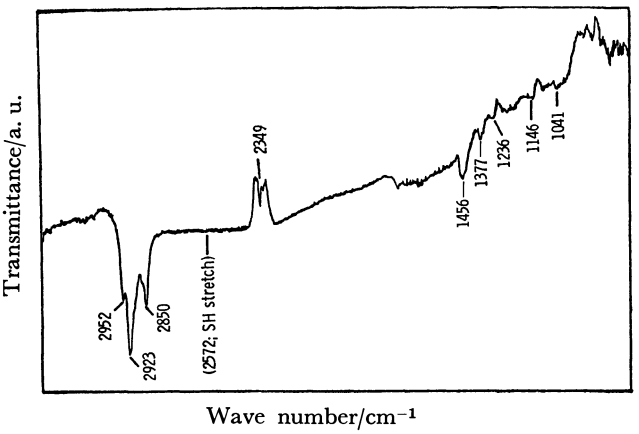

Fig. 6. Infrared absorption spectrum of Ag film exposed to the thiol gas.

The adsorbed thiol on the silver film shows several bands ascribable to CH_3 symmetric and unsymmetric stretchings at 2850 and 2952 cm^{-1}, CH wagging at 1236 cm^{-1} and CH stretching at 2923 cm^{-1}, but does not show any absorption at 2572 cm^{-1} where gaseous 2-propanethiol shows a band assigned to the S–H stretching. It was also confirmed that the infrared spectrum of silver 2-propanethiolate powders synthesized by the reaction of 2-propanethiol and $AgNO_3$ in solution is essentially the same as that shown in Fig. 6 (column 3 of Table 1). These results indicate

that most of the chemisorbed molecules are dissociatively adsorbed as follows,

$$RSH \longrightarrow RS\cdots\overset{|}{\underset{|}{Ag}} + (H).$$

It can thus be concluded that the potentiometric response of the silver oxide disk arises predominantly from the surface potential change due to the chemisorption, and that the electric property of bulk is little affected by the change of the surface structure.

References

1) T. Seiyama and S. Kagawa, *Anal. Chem.*, **38**, 1069 (1966).
2) H. A. Himpler, S. F. Brand, and M. J. D. Brand, *Anal. Chem.*, **50**, 1623 (1978).
3) P. J. Shaver, *Appl. Phys. Lett.*, **11**, 255 (1967).
4) H. Obayashi, Y. Sakurai, and T. Gejo, *J. Solid State Chem.*, **17**, 299 (1976).
5) H. Windischmann and P. Mark, *J. Electrochem. Soc.*, **126**, 627 (1979).
6) N. Yamamoto, S. Tonomura, T. Matsuoka, and H. Tsubomura, *Surf. Sci.*, **92**, 400 (1980).
7) N. Yamamoto, Y. Nagasawa, S. Shuto, M. Sawai, T. Sudo, and H. Tsubomura, *Chem. Lett.*, **1978**, 245; N. Yamamoto, Y. Nagasawa, M. Sawai, T. Sudo, and H. Tsubomura, *J. Immunol. Methods*, **22**, 309 (1978).
8) N. Yamamoto, T. Nagasawa, S. Shuto, and H. Tsubomura, *Clin. Chem.*, **26**, 1569 (1980).
9) J. C. Riviere, "Solid State Surface Science," ed by M. Green, Marcel Dekker, New York, N. Y. (1969), Vol. 1, Chap. 4.
10) W. F. Krolikowski and W. E. Spicer, *Phys. Rev.*, **185**, 882 (1969); S. Trasatti, "Advances in Electrochemistry and Electrochemical Engineering," ed by C. W. Tobias and H. Gerischer, John Wiley & Sons, Inc., New York, N. Y. (1977), Vol. 10, p. 213.
11) F. C. Tompkins, "The Solid-Gas Interface," ed by E. A. Flood, Marcel Dekker, Inc., New York, N. Y. (1967), Chap. 25.
12) The energy gap between the conduction band and the valence band of Ag_2O is reported to be 1.1 to 1.5 eV [See E. Fortin and F. L. Weichman, *Phys. Status Solidi*, **5**, 515 (1964)], although the detailed nature of the compound as a semiconductor has not been clarified.
13) S. Mathias and E. de Carvalho Filho, *J. Phys. Chem.*, **62**, 1427 (1958).
14) D. Smith, J. P. Devlin, and D. W. Scott, *J. Mol. Spectrosc.*, **25**, 174 (1968).

The Extraction of the Vanadium(V)-Pyrocatechol Violet Complex with Tridodecylethylammonium Bromide

Yoshio Shijo,* Tokuo Shimizu, and Kaoru Sakai
Department of Environmental Chemistry, Faculty of Engineering, University of Utsunomiya, Ishii-machi, Utsunomiya 321
(Received May 9, 1980)

Vanadium(V) can be quantitatively extracted from an aqueous solution into carbon tetrachloride as the ion-association system formed between its Pyrocatechol Violet complex anion and tridodecylethylammonium salt. The optimum pH range for the extraction is around 5. The ternary complex has an absorption maximum at 570 nm in the organic layer. The distribution ratio and the molar absorptivity are 1.78×10^2 and 4.0×10^4 l mol^{-1} cm^{-1} respectively. Omitting the other adducts which may be combined with vanadium, the composition of the ternary complex is estimated to be $V(PV)_2(R_3R'N)_2$. The extraction constant is given by log K_{ex}= 12.58. The interference of foreign ions is discussed, too.

The extraction of the ionic associates formed between metal-complex anions with bulky organic cations offers bright prospects of the separation of many metals, because the extraction of the ionic associates usually proceeds rapidly and the miscellaneous metal-complex anions are widely extracted under various conditions. Vanadium can be extracted with 8-hydroxy-5-quinolinesulfonic acid–zephiramine,[1] tiron–diphenylguanidine,[2] *o*-mercaptobenzoic acid–pyridine,[3] Bromopyrogallol red–diphenylguanidine,[4] 3-methylcatechol–dodecyltrimethylammonium,[5] 4-(2-thiazolylazo)resorcinol–trioctylamine,[6] 4-(2-pyridylazo)resorcinol(PAR)–nitron,[7] ascorbic acid–methyltrioctylammonium,[8] thiocyanate–pyridine,[9] ferron–tribenzylamine,[10] Pyrocatechol Violet(PV)–1,10-phenanthroline,[11] PV–diphenylguanidine,[12] pyrocatechol–aniline,[13] thiocyanate-diantipyrylmethane,[14] thiocyanate–N^2-hydroxy-N',N'-diarylbenzamidines,[15] and PAR–zephiramine[16] systems. In the process of investigating the extraction of the metal–PV complex anions with tridodecylethylammonium bromide (TDEABr), we ourselves previously reported on the extraction systems for copper,[17] tin,[18] aluminium,[19] zirconium,[20] niobium,[21] and iron.[22] The vanadium(V)–PV complex also can be extracted with TDEABr in carbon tetrachloride around pH 5. In this paper, the extraction equilibrium and the fundamental conditions will be discussed for extracting the vanadium(V)–PV complex with TDEABr.

Experimental

Reagent. A 2.5×10^{-3} mol/l vanadium(V) solution was prepared by dissolving a definite amount of ammonium vanadate(V) in a 0.25 mol/l surfuric acid solution. The solution was then diluted as required. A 5×10^{-4} mol/l PV solution was prepared by dissolving the Dotite PV in de-ionized water without further purification. TDEABr was prepared by the method described in a previous work.[22] A 5×10^{-3} mol/l TDEABr solution was prepared by dissolving TDEABr in purified carbon tetrachloride. A 2 mol/l sodium acetate solution was used as the buffer solution. All the other chemicals used were of a guaranteed reagent quality.

Apparatus. A Hitachi 101 spectrophotometer, a Hitachi 200-20 UV-VIS recording spectrophotometer, and a Hitachi Horiba F-7 pH meter were employed.

Standard Procedure. Up to 5 μg of vanadium(V), a definite amount of 1 mol/l sulfuric acid, and 3 ml of a 5×10^{-4} mol/l PV solution were mixed in a 100-ml polypropylene beaker. The pH of the solution was adjusted to 5 by the addition of 2 ml of a 2 mol/l sodium acetate solution, and then the solution was diluted to 20 ml with de-ionized water. The solution was transferred into a 35-ml test tube, and 5 ml of 5×10^{-3} mol/l TDEABr in carbon tetrachloride was added. The extraction was carried out for 5 min by turning the test tube upside down twice every 5 s. After the phase separation, the organic layer was taken out and centrifuged for 2 min at 3000 rpm. The extract was then transferred into an absorption cell, and the absorbance at 570 nm was measured against the reagent blank obtained in the same way.

Results and Discussion

Absorption Spectra. Figure 1 shows the absorption spectra of the ternary complex extracted into carbon tetrachloride, of the vanadium(V)–PV complex anion in an aqueous solution, and also of the respective blank solutions. As is evident from Fig. 1, the ternary complex and the vanadium(V)–PV complex anion have their absorption maxima at 570

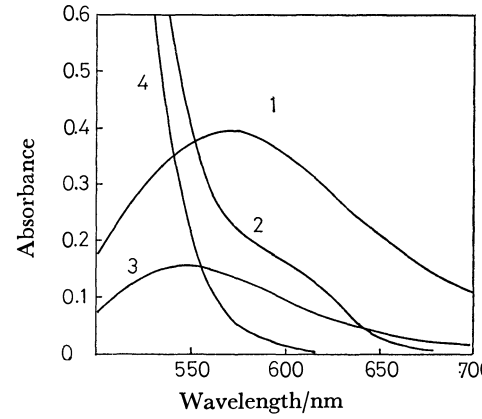

Fig. 1. Absorption spectra of the V–PV–TDEA in carbon tetrachloride and the V–PV complexes in aqueous solution.
pH=5.0, $[TDEABr]_o=5\times10^{-3}$ mol/l, $V_{aq}=20$ ml, $V_o=5$ ml.
1: V–PV–TDEA in carbon tetrachloride $[V]=2.5\times10^{-6}$ mol/l, 2: V–PV in aq soln $[V]=1\times10^{-5}$ mol/l, 3: PV–TDEA in carbon tetrachloride $[PV]=7.5\times10^{-5}$ mol/l, 4: PV in aq soln $[PV]=3\times10^{-4}$ mol/l.

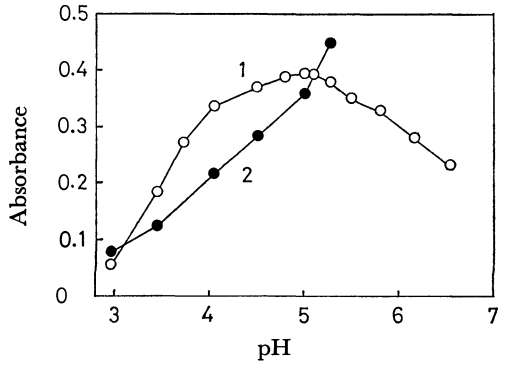

Fig. 2. Effect of pH on the extraction of the V–PV–TDEA complex.
$[V]=2.5\times10^{-6}$ mol/l, $[PV]=7.5\times10^{-5}$ mol/l, $[TDEABr]_o=5\times10^{-3}$ mol/l, 570 nm.
1: V–PV–TDEA, 2: PV–TDEA.

nm and 550 nm respectively. As compared with the corresponding absorption maximum of the complex anion, that of the ternary complex is shifted toward wavelengths longer by 20 nm. The increase in the absorbance at the absorption maximum in the case of the ternary complex over the absorbance of the binary complex is considerable. PV itself is readily extracted from an aqueous solution by TDEABr in carbon tetrachloride.

Effect of pH. Figure 2 shows that the extraction of the ternary complex starts about pH 3, reaches a maximum around pH 5, and thereafter decreases gradually. The extract is stable for at least 30 min.

Organic Solvents. Of the solvents examined, carbon tetrachloride, butyl acetate, chloroform, and benzene are suitable for the quantitative extraction of the ternary complex. The absorbance of the extract is maximal when the carbon tetrachloride is used.

Effect of the Reagent Concentration. The variation in the absorbance was investigated as a function of the PV concentration in an aqueous solution and as a function of the TDEABr concentration in carbon tetrachloride for extracting the ternary complex. The optimum concentration range or PV is from 6×10^{-5} mol/l to 1.25×10^{-4} mol/l. Besides, the concentration range of TDEABr for the quantitative extraction is from 4×10^{-4} mol/l to 5×10^{-3} mol/l.

Extractability and Molar Absorptivity. An aqueous solution of 20 ml containing 6.37 μg of vanadium(V) and 3 ml of 5×10^{-4} mol/l PV was shaken with 5 ml of 5×10^{-3} mol/l TDEABr in carbon tetrachloride under optimum conditions. Extraction was repeated for the remaining aqueous phase after the separation of the extract. The extractability of vanadium(V) was calculated from the absorbances of the extracts. It was found that 97.8% of the vanadium(V) was extracted by one extraction. The distribution ratio and the molar absorptivity were 1.78×10^2 and 4.0×10^4 l mol^{-1} cm^{-1} respectively. A calibration curve for the determination of vanadium(V) was made under optimum conditions. A good linear relationship is obtained over the concentration range from 0.25 μg to 5 μg of vanadium(V) per 5 ml of carbon tetrachloride. The coefficient of variation of ten measurements was 3.9%.

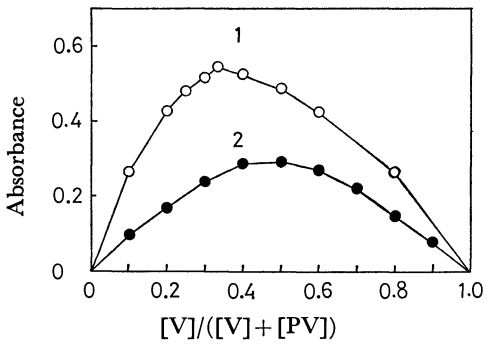

Fig. 3. Continuous variation method applied to the V–PV–TDEA and the V–PV complexes (V:PV).
1: V–PV–TDEA; $[V]+[PV]=1\times10^{-4}$ mol/l, $[TDEABr]_o=5\times10^{-3}$ mol/l pH=5.0, 570 nm. 2: V–PV; $[V]+[PV]=1\times10^{-4}$ mol/l, pH=5.0, 550 nm.

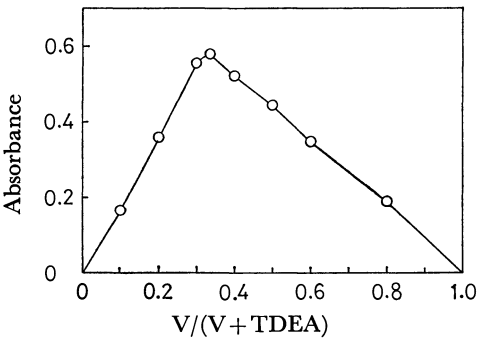

Fig. 4. Continuous variation method applied to the V–PV–TDEA complex (V:TDEA).
$V\text{–}PV+TDEA=1.5\times10^{-6}$ mol, pH=5.0, 570 nm.

The Composition of the Ternary Complex. The estimate of the composition of the complexes was attempted by means of the continious-variation method. Figure 3 shows that the mole ratios of vanadium(V): PV in the ternary complex and in the vanadium(V)–PV complex anion were found to be 1:2 and 1:1 respectivery. Figure 4 shows the mole ratio of vanadium(V): TDEA to be 1:2. Thus, the composition of the ternary complex is estimated to be $V(PV)_2(R_3R'N)_2$.

Extraction Constant. When the ionic associate of the vanadium(V)–PV complex anion with the TDEA cation is extracted in the organic layer, the extraction equilibrium may be expressed by the following equation:

$$V(PV)_2^{2-} + 2R_3R'N^+ = V(PV)_2(R_3R'N)_{2(o)}, \quad (1)$$

where we omit the other adducts which may be combined with vanadium. The extraction constant, K_{ex}, is given by:

$$K_{ex} = \frac{[V(PV)_2(R_3R'N)_2]_o}{[V(PV)_2^{2-}][R_3R'N^+]^2}, \quad (2)$$

where the subscript o denotes the organic layer. An attempted direct determination of each concentration of the components in Eq. 1 was unsuccessful, for the pure ternary complex can not be prepared easily. The equilibrium in Eq. 1 can be represented by the following two steps:

$$V(PV)_2^{2-} + 2R_3R'N\cdot NS_{(o)} = V(PV)_2(R_3R'N)_{2(o)} + 2NS^- \quad (3)$$

$$K = \frac{[V(PV)_2(R_3R'N)_2]_o[NS^-]^2}{[V(PV)_2^{2-}][R_3R'N\cdot NS]_o^2}, \quad (4)$$

where NS denotes 2-naphthalenesulfonic acid.

$$NS^- + R_3R'N^+ = R_3R'N\cdot NS_{(o)} \quad (5)$$

$$K'_{ex} = \frac{[R_3R'N\cdot NS]_o}{[NS^-][R_3R'N^+]}, \quad (6)$$

Thus, K_{ex} is given by

$$K_{ex} = K \times (K'_{ex})^2. \quad (7)$$

The concentration of the $V(PV)_2(R_3R'N)_{2(o)}$ species in Eq. 3 was determined spectrophotometrically as a function of $[NS^-]$, and the value of K was calculated from Eq. 4. The extraction constant, K'_{ex}, of $R_3R'N\cdot NS$ in Eq. 6 was also determined from the extraction equilibrium between $R_3R'N\cdot NS$ in CCl_4 and the PV anion. Table 1 shows the value of log K_{ex} as calculated from Eq. 7. It is given by log $K_{ex}=12.58$.

Effect of Foreign Ions. The effect of foreign ions on the determination of 2.55 μg vanadium(V) was examined under optimum conditions. Cadmium, cobalt, chromium, lanthanum, lead, magnesium, manganese, mercury, nickel, and zinc do not interfere when present separately 0.1-mg amounts, but aluminium, beryllium, bismuth, iron, molybdenum, tin, thorium, uranium, and tungsten interfere seriously. Of the anions tested, 10 mg of iodide, thiocyanate, and perchlorate interfere seriously, giving a negative error. Chelating agents such as EDTA and citrate also interfere. Table 2 shows the main interfering ions.

Table 1. Equilibrium extraction data for $V(PV)_2^{2-}$ with $R_3R'N^+$ in carbon tetrachloride at 25 °C ($I=0.005$ in NaOAc and Na_2SO_4 solutions) pH=5.0 in an acetate buffer solution (2×10^{-3} mol/l), $[V]=2.5\times10^{-6}$ mol/l, $[PV]=7.5\times10^{-5}$ mol/l, $[TDEABr]_o=5\times10^{-3}$ mol/l, $V_{aq}=20$ ml, $V_o=5$ ml

10^3 $[NS^-]$/mol l^{-1}	log K_{ex}
0.5	12.54
1.0	12.56
1.5	12.62
2.0	12.58
2.5	12.59
	log $K_{ex}=12.58$

All the concentrations in Table 1 show the initial concentrations.

Table 2. Effects of diverse ions on the determination of vanadium(V)

Ions	Amount added / mg	Vanadium(V) found/μg	Error / %
—	—	2.55	0
Al^{3+}	0.1	1.51[a)]	−41
Be^{2+}	0.1	3.03[a)]	+19
Bi^{3+}	0.1	2.27[a)]	−11
Fe^{3+}	0.1	2.86[a)]	+12
Mo(VI)	0.1	3.74[a)]	+46
Sn^{4+}	0.1	10.4[a)]	+309
Th^{4+}	0.1	1.47[a)]	−42
U(VI)	0.1	2.83[a)]	+11
W(VI)	0.1	4.20[a)]	+65
I^-	10	0.59	−77
SCN^-	10	0.40	−84
ClO_4^-	10	0.07	−97
Citrate	10	1.57	−38
EDTA	10	0.09	−96

a) KH_2PO_4 and $Na_2S_2O_3$ solutions were added as masking agents.

References

1) T. Kambara and M. Sugawara, *Bull. Chem. Soc. Jpn.*, **46**, 500 (1973).
2) Y. Wakamatsu and M. Otomo, *Bull. Chem. Soc. Jpn.*, **47**, 761 (1974).
3) R. S. Ramakrishna and S. Pathmanaban, *J. Inorg. Nucl. Chem.*, **36**, 741 (1974).
4) M. N. Gordeeva, A. M. Ryndina, and L. A. Khait, *Vestn. Leningr. Univ. Fiz. Khim.*, **1974**, 149.
5) A. M. Nardillo and J. A. Catoggio, *Anal. Chim. Acta*, **74**, 85 (1975).
6) E. Grzegrzolka, *Chem. Anal.* (Warsawa), **20**, 347 (1975).
7) R. M. Pogranichnaya, B. E. Reznik, V. V. Nerubashchenko, A. G. Zezyanova, and A. V. Tsevina, *Zh. Anal. Khim.*, **30**, 180 (1975).
8) J. Adam and R. Pribil, *Talanta*, **22**, 905 (1975).
9) V. Yatirajam and S. P. Arya, *Talanta*, **22**, 861 (1975).
10) V. Yatirajam and S. P. Arya, *Anal. Chim. Acta*, **86**, 209 (1976).
11) L. I. Ganago and L. N. Bukhteeva, *Zh. Anal. Khim.*, **32**, 1537 (1977).
12) M. N. Gordeeva, S. S. Konopleva, and A. M. Ryndian, *Vestn. Leningr. Univ. Fiz. Khim.*, **1978**, 115.
13) T. D. Ali-Zade, G. A. Gamidzade, and O. M. Agamirova, *Azerb. Khim. Zh.*, **1977**, 127.
14) A. S. Lozovik, M. I. Ovrutskii, S. V. Freger, and N. B. Tovbis, *Zavod. Lab.* **44**, 1340 (1978).
15) K. S. Patel and R. K. Mishra, *Bull. Chem. Soc. Jpn.*, **52**, 592 (1979).
16) M. Tajika, H. Hoshino, T. Yotsuyanagi, and K. Aomura, *Nippon Kagaku Kaishi*, **1979**, 85.
17) Y. Shijo, *Bull. Chem. Soc. Jpn.*, **47**, 1642, (1974).
18) Y. Shijo, *Nippon Kagaku Kaishi*, **1974**, 1658.
19) Y. Shijo, *Nippon Kagaku Kaishi*, **1974**, 1912.
20) Y. Shijo, *Bull. Chem. Soc. Jpn.*, **49**, 3029 (1976).
21) Y. Shijo, *Bull. Chem. Soc. Jpn.*, **50**, 1011 (1977).
22) Y. Shijo, *Bull. Chem. Soc. Jpn.*, **50**, 1013 (1977).

Negative Ions Formed by Vacuum Spark Discharge. II.[1] Relative Sensitivity Coefficients for Negative Ions of the Elements Contained in Compressed Aluminium Powder Electrodes for Spark Source Mass Spectroscopy

Hiroshi KISHI*

Department of Chemistry, Faculty of Science, Kyoto University, Kitashirakawa, Sakyo-ku, Kyoto 606

(Received May 13, 1980)

The relative sensitivity coefficients for negative ions of 15 elements contained in compressed aluminium powder electrodes were measured by spark source mass spectroscopy. The relative sensitivity coefficients for the halogens and group VIB elements were found to be the largest, the difference of relative sensitivity coefficients between the elements being larger than in the case of positive ion relative sensitivity coefficients. The logarithm of the relative sensitivity coefficients of negative ions are linearly correlated to the electron affinities of the elements.

A study on negative ion spark source mass spectroscopy has been carried out with a Mattauch-Herzog type double focusing mass spectrograph. The formation of atomic negative ions of 48 elements was reported.[1] Formation of negative ions with a spark discharge type ion source is more difficult than that of positive ions. No negative ion formation took place in rare gas elements, alkaline earth elements, Zn, Cd, Hg, Mn, Re, and rare earth elements. On the other hand, negative ion formation is easy for halogen elements and the group VIB elements. Qualitative investigation was made on the relation between the formation of atomic negative ions by spark discharge and the polarity of the electron affinities of the elements.[1] In the present study, the relative intensities of the negative ions formed by the spark discharge ion source were measured and the results compared with the reported electron affinities of the elements.

The relative sensitivity coefficients of positive ions in spark source mass spectroscopy reported by various authors[2-5] are correlated to the square root of the ionization potentials of the elements and to the heats of sublimation and dissociation energies of the compounds contained in the electrodes. Various empirical formulas[6,7] have been applied to the chemical analysis of solids.[8-10] However, except for the work of Schuy *et al.*,[11] Hintenberger *et al.*,[12] Kishi *et al.*,[13] and Kodera *et al.*,[14] few mass spectroscopic studies have been made on negative ions formed by a spark discharge ion source. The relative sensitivity coefficients of negative ions seem to have hardly been examined at all. This might be due to the difficult formation of negative ions by spark discharge as compared with positive ions.[15]

The results of this study can be applied to the chemical analysis of solids. The relative sensitivity coefficients for negative ions are necessary for applying spark source nagative ion mass spectroscopy to chemical analysis. The present study deals with the relative sensitivity coefficients of negative ions formed by the spark discharge of the elements contained in compressed aluminium powder electrodes, the results being correlated to the electron affinities of the elements.

* Present address: Oyama Technical College, Nakakuki, Oyama, Tochigi 323.

Experimental

Apparatus. A Mattauch-Herzog type double focusing mass spectrograph equipped with an r. f. spark discharge ion source was used. Details of the instrument were reported.[16-18] Operational conditions: spark voltage 20 kV; pulse width, 200 μs; repetition rate 100 s^{-1}; ion accelerating potential, 15 kV for both positive and negative ions.

Materials. Powdered samples containing an equal weight (1.28% for each element) of 49 common elements (SPEX MIX 1000; SPEX MIX INDUSTRIES INC.), and powdered samples containing 10 noble metal elements (SPEX MIX 1041) were used. Various metal alloy samples were also used (Table 6). Compounds and gravity factors for SPEX MIX 1000 are given in Table 1. SPEX MIX 1041 contains 9.32% Au, Ga, Hf, In, Ir, Pd, Pt, Re, Rh, and Ru by weight, some of them being solutions and the others salts or powdered metals. The powdered samples were ground down to 325 mesh with a ball-mill for a few hours. In order to compress them, the samples were mixed thoroughly with pure aluminium powder in 1:1 ratio by weight (Mitsuwa-Kagaku Co. Ltd., purity 99.999%; impurities Cu, As, B (each 1 ppm), Mg, Si (each 0.5 ppm)). In negative ion spark source mass spectra, background peaks of hydrocarbon ions are usually very intense. Thus graphite powder is not suitable as compressing material, since C_n^-, C_nH^-, and $C_nH_2^-$ ion peaks are very intense in the spark discharge of a graphite electrode, the peaks interfering with the mass spectral peaks of the sample elements. The powders were compressed[19] into pellets, 12 mm × 3 mm × 1 mm with an 8 t/cm^2 press. Aluminium powder only was also compressed in order to measure background peak spectra.

Procedure for Calculating RSC. Positive ion mass spectra and negative ion mass spectra were both recorded on an Ilford Q2, 30 × 150 mm^2 photographic plate. Characteristic curves of the emulsions were constructed from positive ion spectra using the isotope peaks of Pt^+ and Zn^+ ions from the spectra obtained by the spark discharges of different exposure times. In a characteristic curve, the abscissa represents the logarithm of (monitor ion current) × (isotopic abundance ratio), and the ordinate the values $D=\log(I_0/I)$ or $\Delta=\log((I_0-I)/I)$. In order to estimate weak line intensity, Δ(Seidel function[20]) in which the curve is linear in the region of low ion intensity, was used. A characteristic curve obtained by means of positive ion mass spectra was used to calculate negative ion peak intensity. It was assumed that the response of the photographic emulsion is the same for positive and negative ions.

Table 1. Compounds and gravity factors for SPEX MIX 1000

Element	Compound	Grav. factor	Element	Compound	Grav. factor
Aluminium	Al_2O_3	1.89	Manganese	$MnCO_3$	2.09
Antimony	Sb_2O	1.26	Mercury	HgO	1.08
Arsenic	As_2O_3	1.32	Molybdenum	MoO_3	1.50
Barium	$BaCO_3$	1.44	Nickel	NiO	1.27
Beryllium	BeO	2.77	Niobium	Nb_2O_5	1.43
Bismuth	Bi_2O_3	1.11	Phosphorus	$(NH_4)_2HPO_4$	4.26
Boron	H_3BO_3	5.72	Potassium	K_2CO_3	1.77
Bromine	NH_4Br	1.23	Rubidium	RbCl	1.41
Cadmium	CdO	1.14	Selenium	SeO_2	1.41
Calcium	CaF_2	1.95	Silicon	Si	1.00
Cerium	CeO_2	1.23	Silver	Ag_2O	1.07
Cesium	$CsNO_3$	1.47	Sodium	Na_2CO_3	2.30
Chlorine	NH_4Cl	1.51	Strontium	$SrCO_3$	1.68
Chromium	Cr_2O_3	1.46	Tantalum	Ta_2O_5	1.22
Cobalt	CoO_2	1.41	Tellurium	TeO_2	1.25
Copper	CuO	1.25	Thallium	Tl_2O_3	1.12
Fluorine	CaF_2	2.05	Thorium	ThO_2	1.14
Gallium	Ga_2O_3	1.34	Tin	SnO_2	1.27
Germanium	GeO_2	1.44	Titanium	TiO_2	1.67
Iodine	NH_4I	1.14	Tungsten	WO_3	1.26
Indium	In_2O_3	1.21	Uranium	UO_2	1.18
Iron	Fe_2O_3	1.43	Vanadium	V_2O_5	1.79
Lead	PbO	1.08	Zinc	ZnO	1.24
Lithium	Li_2CO_3	5.32	Zirconium	ZrO_2	1.35
Magnesium	MgO	1.66			

In order to compare the results with those reported and to confirm the method, the relative sensitivity coefficients of positive ions were first measured and then those of negative ions. The procedure for calculation is essentially the same for positive and negative ion mass spectra. In the latter, however, the background hydrocarbon peaks are very intense and seem to originate from the diffusion pump oil. For the purpose of reducing the background peak intensity, the cryopumping system[21] was considered, but the discharge between the cryopumping plate (earth potential) and the ion accelerating plate (−15 kV from earth) prevented this attempt. It was thus necessary to make background subtraction in the spectra. In the negative ion spark spectra, the mass spectral peaks were broadened by discharge between the accelerating electrode and the earth (defining) electrode. Line width correction was also necessary.

The procedure for calculating the relative sensitivity coefficients is as follows. (1) The relative ion intensities of the isotope peaks are obtained from the characteristic curve, and correction for isotopic abundance ratio is made. (2) The data are further corrected for peak width at half maximum, and the emulsion sensitivity is corrected by means of the $(m)^{-1/2}$ law.[22] (3) Background subtraction is made. For the positive ion mass spectra, multicharged peak intensity is subtracted by estimation from the non-integral isotopic ion intensities. Background peak intensities, *e.g.*, hydrocarbon ions and Al_n^+ ions, are subtracted from the Al/Al blank spark spectra by means of the monitor ion current.

In the negative ion mass spectra, no multicharged negative ion peaks were detected,[1] but background hydrocarbon peaks were very intense. Because of the electron current, the monitor ion current was unreliable and could not be used to estimate the background ion peak intensity. In the negative ion spectra, the m/z 34 peak was not a sample ion peak but a background ion peak. The background peak intensities of the mass spectra of the Al/Al spark spectra were normalized (m/z 34 peak intensity = 1), and subtracted from those of the sample/sample spark spectra, in which peak intensities were also normalized (m/z 34 peak intensity = 1). When the background peak intensity exceeded 50% of the sample peak intensity, no peak intensity was estimated. In A/B spark spectra, A and B indicate the substances in the vacuum spark discharge electrodes.

Results and Discussion

Positive Ion Relative Sensitivity Coefficients. The relative sensitivity coefficients of positive ions for 49 common elements are given in Table 2, and those of 10 noble metal elements in Table 3.

The relative sensitivity values are larger than those reported,[6] except for those for the elements Fe, Co, Si, V, and Cu. The difference between the two values for alkali metal elements is very large. For the halogen elements, the relative sensitivity values are larger than the reported values, the discrepancy between the two values being larger than that for the other elements. The alkali metal elements and halogen elements are present as carbonate and ammonium salt, respectively, and are probably more easily volatilized than other compounds in the spark discharge. The discrepancy in the relative sensitivity coefficients can thus be explained by the assumption that the spark discharge condition in this experiment is more discriminative for volatilization of the compounds contained in the spark electrodes. Aluminium

Table 2. Relative sensitivity coefficients for positive ions of 49 common elements (Li, Be, B, Al, and Hg not included)

Element	RSC[a]	Run	σ[b]	Ref. 6[c]	Element	RSC[a]	Run	σ[b]	Ref. 6[c]
Na	22.1	2	0.70	3.5	Cl	2.1	3	1.1	0.45
Rb	17.6	4	5.3	3.4	Ag	2.0	4	0.44	1.3
Cs	17.3	4	5.2	5.0	Ce	1.9	4	0.67	1.1
K	13.6	4	5.0	3.8	Sn	1.6	4	0.29	1.2
Tl	7.5	4	2.4	2.4	U	1.4	2	0.41	0.73
Ba	4.8	4	3.3	1.7	Mn	1.4	4	0.066	1.2
Bi	4.1	3	0.92	1.2	As	1.2	4	0.22	0.99
Pb	3.9	3	0.69	1.6	P	1.2	4	0.47	0.83
I	3.7	4	0.94	0.78	Cr	1.1	4	0.43	1.0
Te	3.6	4	0.90	0.75	Ge	1.1	4	0.18	0.85
Br	3.2	4	1.3	0.45	Ti	1.1	4	0.32	0.85
In	3.2	4	0.79	1.8	Fe	1.0	4	—	1.0
Zn	2.9	4	0.68	0.98	Co	0.86	4	0.11	1.0
Ta	2.8	2	1.9	0.56	Zr	0.84	3	0.24	0.51
Mg	2.7	4	0.61	2.0	Nb	0.80	4	0.30	0.65
Sr	2.6	4	0.56	1.5	Si	0.79	1	—	0.98
Se	2.5	4	0.73	0.64	V	0.79	4	0.24	0.80
Ga	2.5	4	0.43	1.8	Cu	0.77	3	0.19	0.79
Cd	2.3	4	0.81	0.81	Ni	0.73	4	0.22	0.63
Sb	2.2	4	0.40	0.89	F	0.69	4	0.22	0.18
Ca	2.2	3	0.40	1.8	W	0.67	1	—	0.55
Th	2.1	1	—	0.53	Mo	0.66	4	0.33	0.75

a) Mean of each run. b) Standard deviation of each value. c) SPEX MIX 1000, compressing material graphite.

Table 3. Relative sensitivity coefficients for positive ions of 10 noble metal elements

Element	RSC[a]	Run	σ[b]	Element	RSC[a]	Run	σ[b]
In	1.41	4	0.18	Rh	0.335	4	0.048
Ga	1.00	4	—	Pt	0.320	4	0.10
Hf	0.577	4	0.11	Pd	0.320	4	0.057
Au	0.361	4	0.11	Ru	0.305	4	0.043
Re	0.352	4	0.064	Ir	0.305	4	0.083

a) Mean of each run. b) Standard deviation of each value.

powder was used as compressing material, and the spark voltage was 20 kV; Konishi used graphite, the spark voltage being 40 kV.[6]

The standard deviation σ is large for the elements Ba, Ta, and Cl, but less than 40% for the other elements (Table 2). This value is usually given[23] on spark source mass spectroscopy.

Indium and Ga have the largest relative sensitivity values, and Ru and Ir the smallest values (Table 3). The standard deviation of each relative sensitivity value is less than 30%. This might be due to the fact that the relative sensitivity values do not differ a great deal between these elements as in the case of 49 common elements (SPEX MIX 1000). Nearly the same parts and the linear portion of the emulsion characteristic curve could be used for estimating the peak intensity.

Both SPEX MIX 1000 and SPEX MIX 1041 contain Ga. The relative sensitivity values of the noble metal elements can be normalized to Fe=1 by multiplying all values by 2.47. These relative sensitivity values of 54 elements are plotted against the $(\text{I.P.})^2$ in Fig. 1. We see that the relative sensitivity coefficients are inversely correlated with the $(\text{I.P.})^2$, by a gradient of *ca.* -1.0. The result is in line with other results reported.[6,7] Na, Te, Zn, and the halogen elements deviate upward, and the transition metal elements and the noble metal elements deviate downward from the straight line. This might be due to the fact that the heats of evaporation of the transition metal elements are large as compared with those of the other typical elements.[6]

Negative Ion Relative Sensitivity Coefficients. The relative sensitivity coefficient values for negative ions were obtained for 15 of the 49 common elements, and for 8 of the 10 noble metal elements. No relative sensitivity coefficients were obtained for the other elements, since no negative ion peaks for these elements were detected or the peak intensities were too low to estimate the relative sensitivity coefficients. The results are given in Table 4 for the 15 common elements, and in Table 5 for the 8 noble metal elements, with the published values of electron affinities.[24-34] N and σ indicate run number and standard deviation as in Tables 2 and 3.

In Table 4, a large standard deviation is observed

TABLE 4. RELATIVE SENSITIVITY COEFFICIENTS FOR NEGATIVE IONS OF 15 COMMON ELEMENTS

Element	RSC[a)]	Run	σ[b)]	E.A./eV	Element	RSC[a)]	Run	σ[b)]	E.A./eV
Cl	1.5	2	0.16	3.628	As	4.9×10^{-3}	4	3.7×10^{-3}	1.1
I	1.00	4	—	3.076	Ni	4.6×10^{-3}	3	1.8×10^{-3}	1.28
Br	9.2×10^{-1}	3	4.4×10^{-2}	3.363	P	4.2×10^{-3}	3	4.4×10^{-4}	0.78
Te	2.0×10^{-1}	4	6.7×10^{-2}	1.96	Ge	3.6×10^{-3}	3	3.0×10^{-3}	1.4
Se	1.3×10^{-1}	4	3.4×10^{-2}	2.1	Si	2.8×10^{-3}	4	2.0×10^{-3}	1.39
Ag	2.0×10^{-2}	3	1.0×10^{-2}	1.303	Cr	1.2×10^{-3}	2	7.2×10^{-4}	0.98
Sb	9.8×10^{-3}	3	5.0×10^{-3}	0.94	Na	9.0×10^{-4}	4	2.5×10^{-4}	0.41
Cu	5.3×10^{-3}	2	1.3×10^{-3}	1.226					

a) Mean of each run. b) Standard deviation of each value.

TABLE 5. RELATIVE SENSITIVITY COEFFIENTS FOR NEGATIVE IONS OF 8 NOBLE METAL ELEMENTS

Element	RSC[a)]	Run	σ[b)]	E.A./eV	Element	RSC[a)]	Run	σ[b)]	E.A./eV
Au	1.00	2	—	2.128	Ru	1.4×10^{-1}	2	1.6×10^{-2}	1.49
Pt	3.0×10^{-1}	4	6.4×10^{-2}	2.3086	Rh	1.4×10^{-1}	2	5.0×10^{-3}	1.68
Ga	2.9×10^{-1}	2	6.4×10^{-2}	0.3	Ir	1.4×10^{-1}	2	3.0×10^{-2}	1.97
Pd	1.6×10^{-1}	4	2.8×10^{-2}	1.03	In	7.0×10^{-2}	2	3.5×10^{-3}	0.2

a) Mean of each run. b) Standard deviation of each value.

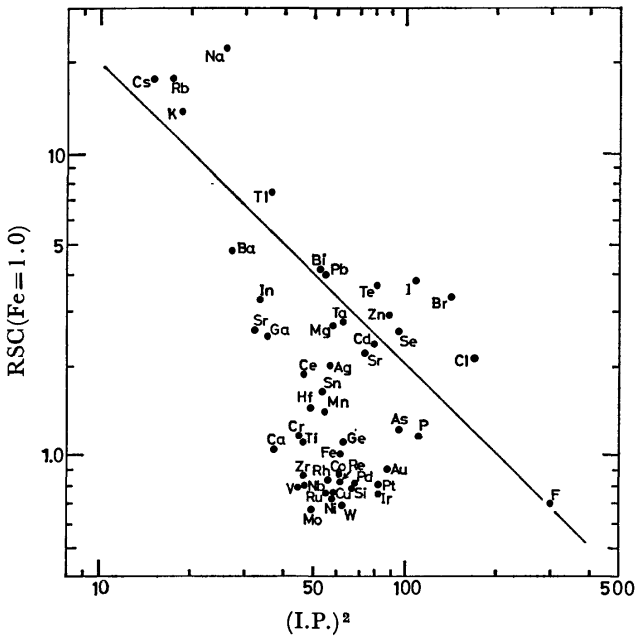

Fig. 1. Relation between the relative sensitivity coefficients for positive ions *versus* $(I.P.)^2$.

for the elements of low relative sensitivity coefficient values except Cu and Na. For the elements of high relative sensitivity coefficient values, such as Cl, I, and Br, the standard deviation is small. There are two possible reasons: (1) In the calculation of the relative sensitivity coefficients of negative ions, a background subtraction procedure is involved, the background peak intensity becoming relatively larger for a negative ion peak of weak intensity than for one of strong intensity. (2) The absolute values of the relative sensitivity coefficients for negative ions are diverse covering the range $1—10^{-3}$. It is necessary to use the non-linear portion of the emulsion characteristic curve for estimating the peak intensity.

On the other hand, for the noble metal elements (Table 5), the standard deviation for each relative sensitivity coefficient value is smaller than 20%. This might be due to the fact that the relative sensitivity coefficient values for the negative ions of these elements do not diverge so widely as in the common elements. The values cover the range only $1—10^{-1}$. Thus the linear portion of the emulsion characteristic curve can be used for estimating the peak intensity. Of noble metal elements, no Hf^- and Re^- ions were detected. Au^- and Pt^- were the most intense, and Ir^- and In^- were the least intense.

It is desirable to estimate the relative sensitivity coefficients of negative ions with use of samples which contain elements with near values of the relative sensitivity coefficients. Various metal alloy samples were also examined (Table 6). In these samples, the concentration of each element was not certain. The positive ion intensity ratio of the elements was measured first, the ratio being considered to be the concentration ratio of the elements in samples. The negative ion intensity ratio was then estimated, and the ratio was divided by the positive ion intensity ratio. This quotient was considered to be the relative sensitivity coefficient for the negative ions of these elements. The results are given with the published values of the electron affinity of the elements (Table 6). The run number is 1 for all the elements, no standard deviation being given.

From the results of the experiment with the Pt–Au–Ag–Pd–Cu–Zn alloy we see that the relative sensitivity coefficients of the elements Pt and Au are 1:0.4 (0.3:1 in the results from SPEX MIX 1041). The discrepancy might be due to the difference in the state of the compounds contained in samples. For the other elements, the values of the relative sensitivity coefficients are in the same order between the two samples, though the absolute values hardly change. For example, Ni^-:Cu^- is 1:1.3 for Ni–Cu alloy, and 1:1.2 for the SPEX MIX 1000. Ni^-:Cr^- is 1:0.20 for the Ni–Cr alloy, and 1:0.26 for the SPEX MIX

Table 6. Relative sensitivity coefficients for negative ions of the elements contained in various metal alloys

Element	Positive ion intensity ratio	Negative ion intensity ratio	RSC	E.A./eV
(1) Nichrom-1				
Fe	1.0	1.0	1.0	0.58
Ni	1.13	10.1	9.7	1.28
(2) Nichrom-2				
Ni	1.0	1.0	1.0	1.28
Cr	0.42	0.087	0.20	0.98
(3) Meteorite				
Fe	1.0	1.0	1.0	0.58
Ni	0.081	0.76	9.5	1.28
(4) Ni–Cu Alloy				
Ni	1.0	1.0	1.0	1.28
Cu	0.12	0.17	1.3	1.226
(5) Ni–Co Alloy				
Ni	1.0	1.0	1.0	1.28
Co	0.091	0.080	0.88	0.94
(6) Pt–Rh Alloy				
Pt	1.0	1.0	1.0	2.3086
Rh	1.17	0.28	0.24	1.68
(7) Pt–Au–Ag–Pd–Cu–Zn Alloy				
Pt	1.0	1.0	1.0	2.3086
Au	1.00	0.41	0.4	2.128
Ag	54.4	2.5	0.050	1.303
Pd	34.0	1.3	0.040	1.03
Cu	25.8	2.3	0.10	1.226
Zn	4.4	—	—	−0.67

1000. Pt^-: Rh^- is 1:0.24 for the Pt–Rh alloy, and 1:0.48 for the SPEX MIX 1041.

We see that the relative sensitivity coefficient values for the elements of large electron affinity values are large, and small for the elements of small electron affinity values (Tables 4, 5, and 6). The logarithm of the relative sensitivity coefficients of negative ions versus the published values of the electron affinities of the elements are plotted. The results are given for the samples of SPEX MIX 1000 and SPEX MIX 1041, respectively (Figs. 2 and 3). The logarithms of the relative sensitivity coefficients has a rough linear correlation to the electron affinities of the elements. Se and Te deviate upward from the linear line, but the reported values of the electron affinities of Se and Te diverge from 2.2 eV[23] to 3.7 eV,[35] and from 2.1 eV[36,37] to 3.6 eV,[35] respectively (Fig. 2). Correlation seems to exist between the logarithm of the relative sensitivity coefficient and the electron affinity of the element. Ga having low melting point shows upward deviation.

The author would like to express his hearty thanks to Dr. K. Kodera and Dr. T. Makita, Kyoto University, for their encouragement and helpful suggestions throughout this work, and to Dr. F. Konishi, the Central Research Laboratory of Matsushita Electric Co. Ltd., for his technical help in preparing the compressed aluminium powder electrodes.

A part of this study was reported at the International Conference on Mass Spectroscopy held in Kyoto.[38,39]

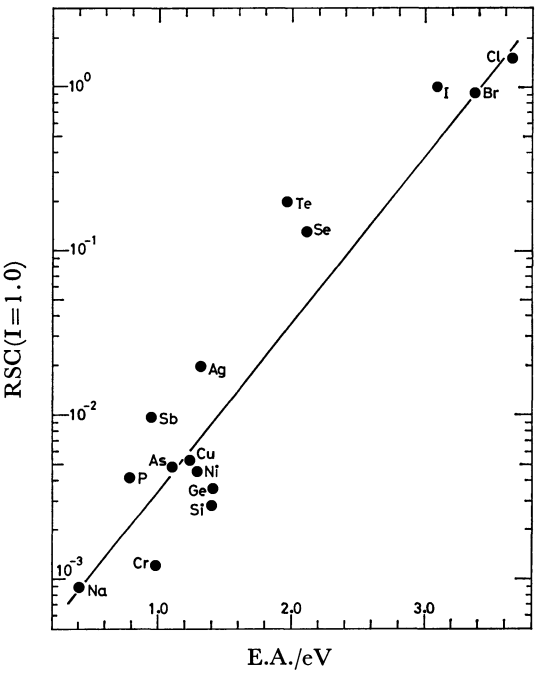

Fig. 2. Relation between the logarithm of the relative sensitivity coefficients for negative ions of 15 common elements *versus* the electron affinities of the elements.

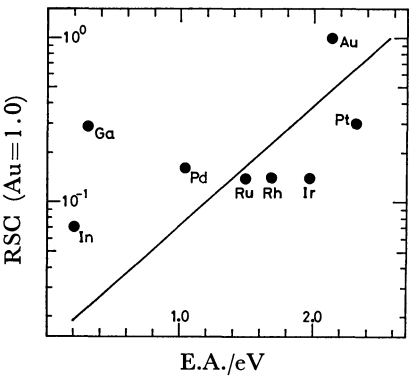

Fig. 3. Relation between the logarithm of the relative sensitivity coefficients for negative ions of 8 noble metal elements *versus* the electron affinities of the elements.

References

1) Part I: T. Makita, H. Kishi, and K. Kodera, *Mass Spectroscopy (Japan)*, **21**, 293 (1973).
2) R. D. Craig, G. A. Errock, and J. D. Waldron, "Advances in Mass Spectroscopy," ed by J. D. Waldron, Pergamon Press, London (1959), pp. 136—156.
3) E. B. Owens and N. A. Giardino, *Anal. Chem.*, **35**, 1172 (1960).
4) H. Kawano, *Bull. Chem. Soc. Jpn.*, **37**, 697 (1964).
5) J. Kai and M. Miki, *Mass Spectroscopy (Japan)*, **12**, 81 (1964).
6) F. Konishi, *Mass Spectroscopy (Japan)*, **18**, 878 (1970).

7) T. Sasamoto, T. Hara, and T. Sato, *Mass Spectroscopy (Japan)*, **24**, 121 (1976).
8) A. J. Ahearn, "Mass Spectrometric Analysis of Solid," Elsevier Pub. Co. (1966).
9) G. H. Morrison and K. Skogerboe, "Trace Analysis," Interscience Pub. Co. (1965).
10) T. Makita, J. Kai, and S. Ohshima, "Jikken Kagaku Koza —Zoku," ed by R. Goto, Maruzen Pub. Co., Tokyo (1966), Vol. 14, pp. 129—205.
11) K. D. Schuy, J. Franzen, and H. Hintenberger, *Z. Naturforsch., Teil A*, **19**, 153 (1964).
12) H. Hintenberger, J. Franzen, and K. D. Schuy, *Z. Naturforsch., Teil A*, **18**, 1236 (1963).
13) H. Kishi, S. Sakamoto, T. Makita, and K. Kodera, Report at Annual Meeting on Mass Spectroscopy, 14-th (1966).
14) K. Kodera, T. Makita, and H. Kishi, Report at Annual Meeting on Mass Spectroscopy, 15-th (1967).
15) C. E. Melton, "Mass Spectrometry of Organic Ions," ed by F. W. McLafferty, Academic Press (1963), p. 163.
16) N. Sasaki and J. Kai, *Mass Spectroscopy (Japan)*, **7**, 64 (1959).
17) M. Gotoh and M. Kai, *Mitsubishi Denki Lab. Report*, **1**, 51 (1960).
18) T. Makita and K. Kodera, *Mass Spectroscopy (Japan)*, **12**, 1, (1964).
19) F. Konishi, *Mass Spectroscopy (Japan)*, **16**, 251 (1968).
20) A. S. T. M. E-2 Committee: Method for Emission Spectrochemical Analysis (1957), p. 13.
21) W. L. Harrington, R. K. Skogerboe, and G. H. Harrison, *Anal. Chem.*, **37**, 1480 (1965).
22) E. Burlefinger and H. Ewald, *Z. Naturforsch., Teil A*, **16**, 430 (1961).
23) F. Konoshi, K. Kusao, and N. Nakamura, *Mass Spectroscopy (Japan)*, **14**, 275 (1966).
24) G. Glockler, *Phys. Rev.*, **46**, 111 (1934).
25) A. P. Ginsberg and J. M. Miller, *J. Inorg. Chem.*, **7**, 351 (1958).
26) B. Edlén, *J. Chem. Phys.*, **50**, 4251 (1969).
27) E. Clementi, *Phys. Rev. A*, **135**, 980 (1964).
28) S. J. Smith and L. M. Burch, *Phys. Rev.*, **99**, 1657 (1955).
29) L. M. Branscomb, S. J. Smith, and G. Tisone, *J. Chem. Phys.*, **43**, 2906 (1965).
30) L. M. Seman and L. M. Branscomb, *Phys. Rev.*, **125**, 1602 (1962).
31) L. M. Branscomb and S. J. Smith, *J. Chem. Phys.*, **25**, 598 (1956).
32) B. Steiner, M. L. Seman, and L. M. Branscomb, *J. Chem. Phys.*, **37**, 1200 (1962).
33) H. Hotop, R. A. Bennett, and W. C. Lineberger, *J. Chem. Phys.*, **58**, 2373 (1973).
34) H. Hotop and W. C. Lineberger, *J. Chem. Phys.*, **58**, 2379 (1973).
35) Von Klaus Doerffel, *Z. Anorg. Allg. Chem.*, **281**, 212 (1955).
36) A. O. Pritchard, *Chem. Rev.*, **52**, 529 (1953).
37) G. Glockler, *J. Chem. Phys.*, **32**, 708 (1960).
38) International Conference on Mass Spectroscopy, Preprints, September 8—12, 1969, Kyoto.
39) "Recent Developments in Mass Spectroscopy," ed by K. Ogata and T. Hayakawa, Univ. of Tokyo Press, pp. 329—333 (1970).

An X-Ray Photoelectron Spectroscopic Study of Several Hydroxy Azo Metal Complexes

Tooru YOSHIDA

Osaka Prefectural Industrial Research Institute, 2-1-53, Enokojima, Nishi-ku, Osaka 550

(Received June 3, 1980)

The X-ray photoelectron spectra of the copper(II) and nickel(II) complexes of five *o*-hydroxy azo compounds were measured. The N(1s) electron spectra of the complexes of 1-phenylazo- and 1-(1-naphthylazo)-2-naphthols showed the presence of only one kind of nitrogen atom, suggesting an equalization in the electron densities on the two nitrogen atoms of an azo group. Such equalization was observed also in the complexes of 1-(8-quinolylazo)-2-naphthol. The N(1s) spectra of the complexes of 1-(2-pyridylazo)- and 1-(2-thiazolylazo)-2-naphthols, on the other hand, showed the presence of three kinds of nitrogen atoms, suggesting the non-equalization of the two nitrogen atoms of an azo group. These results were explained mainly on the basis of the mode of ligand coordination and the resonance structure of the sodium salt of the ligand. Furthermore, the relation between the structures of the complexes and the O(1s) chemical shifts was discussed.

o-Hydroxy azo dyes are very important in analytical chemistry, particularly in the spectrophotomeric and titrimetric determination of metal ions.[1] Furthermore, it is interesting to know whether the azo group is coordinated to the metal ion as a whole or through one of the component nitrogen atoms, since the N=N system is isoelectronic with the CH=CH group, which is capable of coordinating through the π-systems to transition metals, as in Zeise's salt.[2] Therefore, there have been several studies of the structures of their metal complexes by means of some physicochemical techniques.[3] It has been found by X-ray structural analysis that, in the complexes of *o*-hydroxy azo compounds with transition metal ions, one of the component nitrogen atoms of an azo group is coordinated to a metal ion.[3c-3g]

X-Ray photoelectron spectroscopy (XPS), which is sensitive to the charge distribution,[4] is suitable for the examination of the mode of ligand coordination in coordination compounds. The examination is based primarily upon the concept that the coordination of a ligand to a metal ion causes a decrease in the electron density on the coordination atom, giving rise to an increase in the core-electron binding energy of the atom. The XPS study of several hydroxy azo compounds has been reported.[5] The purpose of the present study is to examine the chemical structures of the copper(II) and nickel(II) complexes of several *o*-hydroxy azo compounds by means of XPS.

Experimental

The X-ray photoelectron spectra were measured on an AEI ES200 spectrometer. Al $K\alpha$ (1486.6 eV) X-ray radiation was used as the excitation source. The samples were ground to a powder and dusted onto double-backed adhesive tape. The measurements were conducted at room temperature under a vacuum of about 10^{-7} Torr. The binding energy of the C(1 s) electron peak was used as the energy standard throughout the present work; it has been taken to be 285.0 eV. The reproducibilities of the values thus obtained were within ± 0.1 eV. No appreciable X-ray damage was observed throughout the experiments. All the compounds used and their binding energies measured are given in Table 1. 1-Phenylazo-, 1-(1-naphthylazo)-, 1-(2-pyridylazo)-, 1-(2-thiazolylazo)-, and 1-(8-quinolylazo)-2-naphthols (abbreviated as L_AH, L_BH, L_CH, L_DH, and L_EH respectively) were used as ligands. 1,1′-Azonaphthalene (abbreviated as L) was used as the reference compound. 1-(2-Thiazolylazo)-2-naphthol was obtained commercially and was used after recrystallization from an ethanol-water mixture. The sodium salt of 1-(2-pyridylazo)-2-naphthol (abbreviated as L_CNa) was obtained by treating the naphthol with NaOH in a mixture of ethanol and water. This salt was fairly stable compared with the sodium salt of 1-phenylazo-2-naphthol (abbreviated as L_ANa), which was subject to hydrolysis by water.[5] Attempts to prepare the sodium salts of L_BH and L_EH were unsuccessful. The other free azo compounds in Table 1 were obtained in the way indicated in the literature.[5] All the complexes were prepared based upon the literature.[3a] However, in the preparation of the complexes in a 1:1 ratio of an azo ligand to a metal ion, the chlorides were used instead of the acetates as metal salts. Furthermore, in the preparation of the complexes of L_BH and L_EH, an *N,N*-dimethylformamide–ethanol mixture was used as the solvent because of the insuffcient solubility of L_BH and L_EH in ethanol only. When we attempted to prepare $Ni(L_C)Cl$ and $Ni(L_D)Cl$, these complexes were not obtained at all, but $Ni(L_C)_2$ and $Ni(L_D)_2$ were obtained. All the compounds used were dried in an air oven at 95 °C and were checked by elemental analysis.

Results

The N(1s) electron spectra of L_AH, L_CH, and their sodium salts are shown in Figs. 1 and 2. Eb in the figures indicates the binding energy. The peaks indicated by the broken lines in the spectra, as well as those in the other N(1s) spectra, were obtained by graphical resolution on the basis of the symmetrical peak with almost the same full-width at half-maximum height (FWHM) as that (1.6 eV) of L containing one type of nitrogen atom. The spectrum of L_AH as well as that of L_BH showed a single peak with an FWHM value of about 1.6 eV, while the spectrum of L_ANa showed two comparable peaks. The spectrum of L_CH as well as those of L_DH and L_EH showed two peaks with an intensity ratio of approximately 2:1, while the one of L_CNa showed peaks with a ratio of 1:2.

The N(1s) spectra of $Cu(L_A)_2$, $Cu(L_C)_2$, and $Cu(L_E)_2$ are shown in Fig. 3. The spectrum of $Cu(L_A)_2$, like those of $Ni(L_A)_2$, $Cu(L_B)_2$, and $Ni(L_B)_2$, was almost the same as that of L_AH in shape. The spectrum of $Cu(L_C)_2$, like those of $Ni(L_C)_2$, $Cu(L_D)_2$, $Ni(L_D)_2$, $Cu(L_C)Cl$, and $Cu(L_D)Cl$, showed a broad

Table 1. Measured binding energies

Compound[a]	Binding energy/eV			
	N(1s)	O(1s)	S($2p_{3/2}$)	Metal($2p_{3/2}$)
$Cu(L_A)_2$	400.1	531.5		934.5
$Ni(L_A)_2$	400.2	531.6		855.2
$Cu(L_B)_2$	400.1	531.6		934.6
$Ni(L_B)_2$	400.2	531.8		855.3
$Cu(L_C)_2$	400.6; 399.7; 399.0	531.0		934.2
$Ni(L_C)_2$	400.6; 399.7; 399.0	531.0		855.6
$Cu(L_D)_2$	400.6; 399.6; 398.9	531.1	164.8	934.3
$Ni(L_D)_2$	400.5; 399.6; 399.0	531.0	164.8	855.7
$Cu(L_E)_2$	400.0; 399.1	530.9		934.2
$Ni(L_E)_2$	400.0; 399.2	531.0		855.4
$Cu(L_C)Cl$	400.8; 399.8; 399.1	531.3		934.6
$Cu(L_D)Cl$	400.7; 399.8; 399.1	531.4	164.8	934.7
$Cu(L_E)Cl$	400.2; 399.4	531.5		934.4
$Ni(L_E)Cl$	400.1; 399.4	531.7		855.4
L_AH	400.5	533.1; 531.1		
L_BH	400.5	533.0; 531.0		
L_CH	400.5; 399.0	533.0; 530.9		
L_DH	400.5; 399.0	533.1; 531.1	164.8	
L_EH	400.3; 398.9	533.0; 530.8		
L_ANa	400.5; 399.0	531.0		
L_CNa	400.4; 399.1	530.9		
L	400.2			

a) L, L_AH, L_BH, L_CH, L_DH, and L_EH indicate 1, 1'-azonaphthalene, 1-phenylazo-, 1-(1-naphthylazo)-, 1-(2-pyridylazo)-, 1-(2-thiazolylazo)-, and 1-(8-quinolylazo)-2-naphthols respectively. L_ANa and L_CNa indicate the sodium salts of L_AH and L_CH.

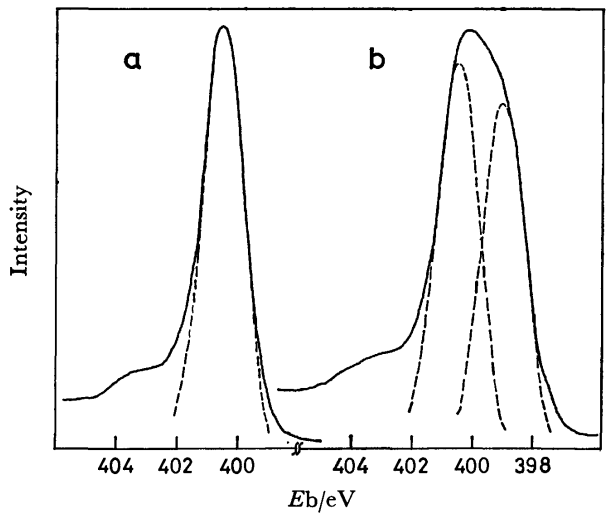

Fig. 1. N(1s) electron spectra of a: L_AH and b: L_ANa.

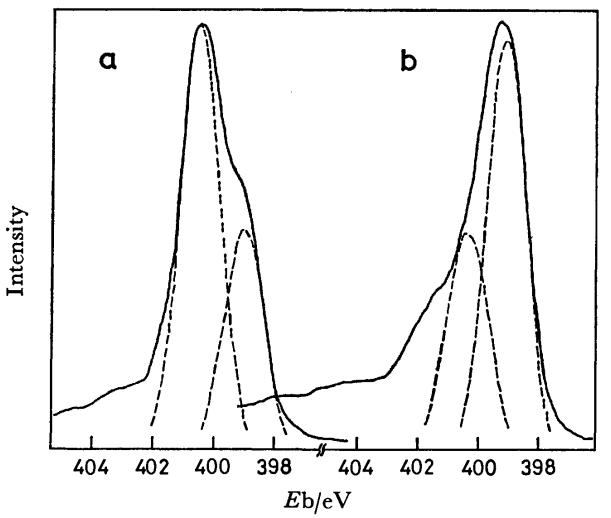

Fig. 2. N(1s) electron spectra of a: L_CH and b: L_CNa.

peak with an FWHM value of about 2.4 eV comprising three peaks with similar intensities. The spectrum of $Cu(L_E)_2$, like those of $Ni(L_E)_2$, $Cu(L_E)Cl$, and $Ni(L_E)Cl$, showed two peaks with an intensity ratio of approximately 2:1.

Satellite signals on the higher-energy side of the primary peak, as are seen in Figs. 1—3, were observed in the N(1s) spectra of all the compounds in Table 1.

The O(1s) spectra of L_AH and $Cu(L_A)_2$ are shown in Fig. 4. The spectrum of L_AH as well as those of L_BH, L_CH, L_DH, and L_EH showed two peaks with comparable intensities, while the spectrum of $Cu(L_A)_2$ as well as those of the other complexes showed one primary peak.

Discussion

All the N(1s) spectra of five free ligands indicated that the electron densities on the two nitrogen atoms of an azo group are almost the same. Here, the peak with the lower binding energy in Fig. 2a was easily

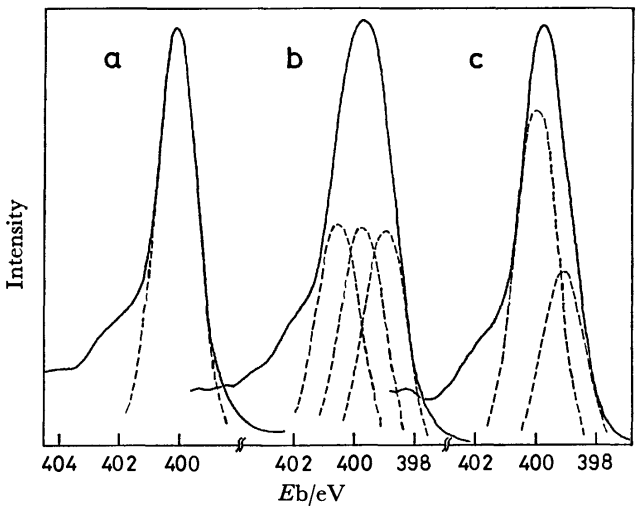

Fig. 3. N(1s) electron spectra of a: $Cu(L_A)_2$, b: $Cu(L_C)_2$, and c: $Cu(L_E)_2$.

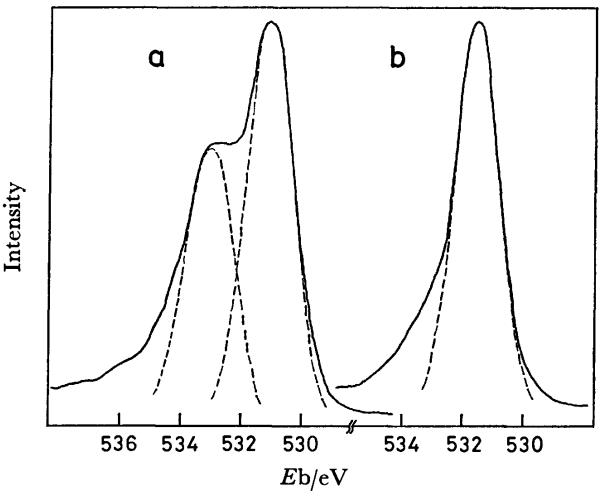

Fig. 4. O(1s) electron spectra of a: L_AH and b: $Cu(L_A)_2$.

assigned to the nitrogen atom of a hetero ring by comparing with Fig. 1a.

The presence of two kinds of peaks in Fig. 1b was due to the following resonance structures:[5]

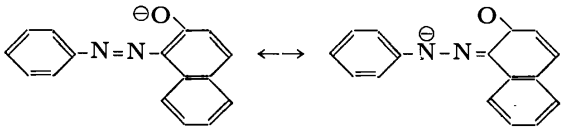

This resonance suggests that the electron density on the nitrogen atom of an azo group farthest from a naphthalene ring is higher than that on the other nitrogen. Therefore, the peak with the lower binding energy in Fig. 1b can be assigned to the former nitrogen atom, and the other peak to the latter nitrogen.

The peak with the higher energy in Fig. 2b may be assigned to the nitrogen atom of an azo group nearest to a naphthalene ring, and the lower-energy peak, to the other nitrogen of the azo group in addition to the nitrogen of a pyridine ring, by considering the resonance structure of L_CNa to be similar to that of L_ANa. Such resonance structures as those in L_ANa may be expected also in the sodium salts of the other *o*-hydroxy azo compounds in this study.

The spectra of the complexes may be explained in the following way, based upon the structure of the sodium salt estimated above.

In the complexes of L_AH, the hydroxyl group and the nitrogen atom of an azo group farthest from a naphthalene ring are involved in chelate formation.[3c,3d] Therefore, such complex formation may be considered to act to equalize the electron densities on the two nitrogen atoms of an azo group due to the electron transfer from a coordinating atom to a metal ion.

The N(1s) binding energies of an azo group (400.1—400.2 eV) of the complexes of L_AH were slightly lower than the value (400.5 eV) of the nitrogen atom nearest to a naphthalene ring in L_ANa, which does not participate in bond formation. This may be due to the delocalization of π-electrons in the chelate ring suggested by the IR study of the metal complexes of 2-hydroxyazobenzene.[3a] Such delocalization may be supported also by the results of X-ray structural analysis that the N–N distances in $Cu(L_A)_2$ and $Ni(L_A)_2$ are 1.32 Å[3c] and 1.28 Å,[3d] while that of azobenzene is 1.23—1.24 Å.[6] That is, the distances for the complexes are slightly longer than that for azobenzene.

The mode of ligand coordination in the complexes of L_BH is considered to be almost the same as that in the complexes of L_AH, because the N(1s) spectra of the former complexes are very close to those of the latter.

In the complexes of L_CH and L_DH, each of the ligands acts as a terdentate ligand, the hydroxyl group, the nitrogen atom of an azo group nearest to a naphthalene ring, and the heterocyclic nitrogen atom, to give two five-membered chelate rings.[3e–3g] The nitrogen atom farthest from a naphthalene ring, which is expected to be rich in electron density, cannot be coordinated to a metal atom because of steric hindrance. This suggests that the electron densities on the two nitrogen atoms of an azo group cannot become equal on complex formation, unlike in the case of the complexes of L_AH and L_BH.

Therefore, it seems reasonable to assign the three peaks in the N(1s) spectra of the complexes of L_CH and L_DH to the nitrogen atom of an azo group nearest to a naphthalene ring, the nitrogen of a hetero ring, and the remaining nitrogen of the azo group, successively from the higher-energy side.

The N(1s) chemical shifts (0.6—0.8 eV) of the nitrogen atom of a hetero ring of the complexes of L_CH and L_DH, *i.e.* the difference between the N(1s) binding energies of the complex and the free ligand, were comparable with those (0.5—0.9 eV) of the copper and nickel complexes of 8-quinolinol and 2-pyridinecarboxylic acid.[7] This may support the above assignment of the three peaks in the N(1s) spectra. The N(1s) chemical shifts (<0.3 eV) of the nitrogen atom of an azo group which participates in bond formation were smaller than those of the nitrogen of a hetero ring. This seems to be associated with the coordination ability of the donor atoms.

In the complexes of L_EH, it is not known which

nitrogen atom of an azo group is coordinated to a metal ion because of the absence of the data of the X-ray structural analysis. In this study, it may be easily expected from the following facts that the nitrogen atom farthest from a naphthalene ring participates in the bond formation, as in the complexes of L_AH and L_BH.

The spectra of the complexes of L_EH showed the presence of two kinds of nitrogen atoms in the proportion of 2:1, unlike the spectra of the complexes of L_CH and L_DH, which show three kinds of peaks. Furthermore, the binding energy (400.0—400.2 eV) of the peak with the larger intensity was very close to those (400.1—400.2 eV) of the nitrogen atoms of an azo group of the complexes of L_AH and L_BH. Therefore, it seems reasonable to assign the peak with the larger intensity to the two nitrogen atoms of an azo group, and the other peak, to that of a quinoline ring. Here, the equalization in the electron densities on the two nitrogen atoms of an azo group can be explained much as in the case of the complexes of L_AH and L_BH.

The N(1s) chemical shifts (0.2—0.5 eV) of a hetero ring in the complexes of L_EH were slightly smaller than those in the complexes of L_CH and L_DH. This may be due to the difference of the mode of the coordination of an azo group in the two groups of complexes.

In hydroxy azo compounds, two kinds of oxygen atoms, keto and enol forms, usually coexist as a result of tautomerism. The peak with the higher binding energy in the O(1s) spectra of L_AH, L_BH, L_CH, L_DH, and L_EH corresponds to the protonated oxygen atom, and the other to the deprotonated oxygen.[5]

The O(1s) binding energies of $Cu(L_A)_2$, $Ni(L_A)_2$, $Cu(L_B)_2$, $Ni(L_B)_2$, $Cu(L_C)Cl$, $Cu(L_D)Cl$, $Cu(L_E)Cl$, and $Ni(L_E)Cl$, all of which are four coordinate species, were 0.3—0.9 eV higher than those of the deprotonated oxygen atom of the corresponding free ligands, while in the other complexes, which are all six-coordinate species, there were no appreciable chemical shifts of the O(1s) binding energies. Such a result suggests that the interaction between the metal and the oxygen atoms in the complexes of the former group is stronger than that of the latter group. This is consistent with the fact that the nickel–oxygen distance (1.85 Å)[3d] in $Ni(L_A)_2$, one of the complexes of the former group, is slightly shorter than that (1.98 Å)[3f] in $Ni(L_D)_2$, one of the complexes of the latter.

The differences of the metal($2p_{3/2}$) binding energies of the complexes were small throughout the present experiment; the values for all the copper complexes were 934.2—934.7 eV, and those for all the nickel complexes were 855.2—855.7 eV. Therefore, no notable information concerning the structures of the complexes could be obtained from the metal binding energies.

In the complexes of L_DH, the thiazole sulfer atom was not considered to participate in the chelate-ring formation, because there was no appreciable chemical shift in the S($2p_{3/2}$) binding energy. This agrees with the results of X-ray analysis.[3f,3g]

The satellites at $\approx$4 eV on the higher-binding energy side of the primary peak in the N(1s) spectra in this study may be partly assigned to the shake-up satellite, which is mainly due to the co-excitations of valence electrons, n-π^*, π-π^*, on the ejection of the inner electrons, on the basis of the following facts. These satellites are observed in the spectra of both free ligands and their metal complexes. Such satellites have previously been observed in the N(1s) spectra only of compounds containing the unsaturated bonds with a hetero-atom.[8] Furthermore, the electron spectra of the aromatic azo compounds generally show the absorption bands due to n-π^*, π-π^* transitions in a region of about $(17—40)\times10^3$ cm^{-1}, which approximately corresponds to 2—5 eV.[1a,9]

The author wishes to thank Drs. Kiyoshi Yamasaki and Shigemasa Sawada for their helpful discussions and suggestions during this work, Dr. Masakazu Miyagi for his help in performing this experiment, and Mr. Taichiro Hirohara for the elemental analysis.

References

1) a) B. F. Pease and M. B. Williams, *Anal. Chem.*, **31**, 1044 (1959); b) A. Corsini, I. M. Yih, Q. Fernand, and H. Freiser, *ibid.*, **34**, 1090 (1962); c) D. Betteridge and D. John, *Analyst*, **98**, 377, 390 (1973); d) D. Betteridge, D. John, and F. Snape, *ibid.*, **98**, 512, 520 (1973).

2) a) J. A. Wunderlich and D. D. Mellor, *Acta Crystallogr.*, **7**, 130 (1954); b) J. Chatt and L. A. Duncanson, *J. Chem. Soc.*, **1953**, 2939.

3) a) K. Ueno, *J. Am. Chem. Soc.*, **79**, 3066 (1957); b) R. H. Prince and R. C. Spencer, *Inorg. Chim. Acta*, **1969**, 54; c) J. A. J. Jarvis, *Acta Crystallogr.*, **14**, 961 (1961); d) N. W. Alcock, R. C. Spencer, R. H. Prince, and O. Kennard, *J. Chem. Soc., A*, **1968**, 2383; e) S. Ooi, D. Carter, and Q. Fernando, *Chem. Commun.*, **1967**, 1301; f) M. Kurahashi, *Bull. Chem. Soc. Jpn.*, **47**, 2045, 2067 (1974); g) M. Kurahashi and A. Kawase, *ibid.*, **49**, 127, 1419 (1976).

4) a) K. Siegbahn *et al.*, "ESCA Atomic, Molecular and Solid State Structure Studied by Means of Electron Spectroscopy," Almqvist and Wiksells AB, Uppsala (1967); b) K. Siegbahn *et al.*, "ESCA Applied to Free Molecules," North-Holland Publ. Co., Amsterdam (1969).

5) T. Yoshida, *Bull. Chem. Soc. Jpn.*, **53**, 498 (1980).

6) G. C. Hampson and J. M. Robertson, *J. Chem. Soc.*, **1941**, 409.

7) T. Yoshida, *Bull. Chem. Soc. Jpn.*, **53**, 1327 (1980).

8) T. Yoshida, *Bull. Chem. Soc. Jpn.*, **51**, 3257 (1978).

9) a) J. N. Ospenson, *Acta Chem. Scand.*, **4**, 1351 (1950); b) H. M. Haendler and G. M. Smith, *J. Am. Chem. Soc.*, **62**, 1669 (1940); c) Jaffe and Orchin, "Theory and Applications of Ultraviolet Spectroscopy," John Wiley & Sons, New York (1964).

  Bull. Chem. Soc. Jpn., 54, 713—718 (1981)

Nuclear Magnetic Resonance and Circular Dichroism Spectra of 2-(Aminomethyl)cyclohexylamine Platinum(II) Complexes

Koji Okamoto,* Masahide Noji, and Yoshinori Kidani

Faculty of Pharmaceutical Sciences, Nagoya City University, Tanabe-dori, Mizuho-ku, Nagoya 467

(Received June 30, 1980)

Six-membered platinum(II) complexes of 2-(aminomethyl)cyclohexylamine (=amcha), whose four isomers are (1*R*,2*R*)-, (1*S*,2*S*)-, (1*R*,2*S*)-, and (1*S*,2*R*)-amcha, were synthesized. The conformations of [Pt(en)(1*S*,2*R*-amcha)]Cl_2, [Pt(NH_3)$_2$(1*S*,2*R*-amcha)]Cl_2, [Pt(en)(1*R*,2*R*-amcha)]Cl_2, and [Pt(NH_3)$_2$(1*R*,2*R*-amcha)]Cl_2 were determined by ^{1}H-NMR, ^{13}C-NMR, and CD spectra. It is proposed that [Pt(en)(1*S*,2*R*-amcha)]Cl_2 and [Pt(NH_3)$_2$(1*S*,2*R*-amcha)]Cl_2 take a fixed chair form with a dihedral angle (Pt–N–C(1)–C(6)) of 180°, while [Pt(en)(1*R*,2*R*-amcha)]Cl_2 and [Pt(NH_3)$_2$(1*R*,2*R*-amcha)]Cl_2 are interconverting between two chair forms.

2-(Aminomethyl)cyclohexylamine (=amcha) has four isomers, which are represented as 1*R*,2*S* (*trans-l*), 1*S*,2*R* (*trans-d*), 1*R*,2*R* (*cis-l*) and 1*S*,2*S* (*cis-d*) isomers (Fig. 1). Various platinum(II) complexes containing these amcha isomers were synthesized and their antitumor activities were tested against leukemia P388.[1] Some differences were found among their activities. Therefore, it would be meaningful to study the conformations of six-membered platinum(II) complexes of amcha isomers.

In general, a six-membered chelate ring is more flexible than a five-membered one and the possible conformations of the former are chair, skew, or boat forms. The chair conformation has been considered to be the most stable form, and ^{1}H-NMR and ^{13}C-NMR spectral data supporting this view have been reported by Hall[2] and Yano *et al.*[3] But few CD spectral studies of platinum(II) complexes containing optically active diamine forming six-membered chelate have been done. In order to determine the conformations of amcha we prepared the following types of complexes for the first time: [Pt(en)(amcha)]Cl_2 and [Pt(NH_3)$_2$(amcha)]Cl_2 (amcha=(1*S*,2*R*)- and (1*R*, 2*R*)-2-(aminomethyl)cyclohexylamine). In the present paper, we will discuss the conformations of these platinum(II) complexes from NMR and CD spectral data.

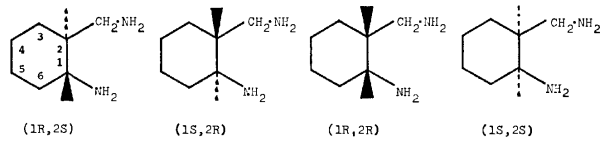

Fig. 1. Absolute configurations of 2-(aminomethyl)-cyclohexylamine.

Experimental

Ligands. *1) Synthesis of* cis- *and* trans-*2-(Aminomethyl)-cyclohexylamine*: They were prepared from the corresponding *cis-* and *trans-*1,2-cyclohexanedicarboxylic acid according to the method reported by Armarego *et al.*[4]

2) Resolution of trans-*2-(Aminomethyl)cyclohexylamine*: A hot filtered solution of (2*R*,3*R*)-di-*O*-benzoyltartaric acid monohydrate (46.7 g) in ethanol (307 cm^3) was added to a solution of freshly distilled *trans-dl*-amcha (15.9 g) in water (307 cm^3). After the solution was kept standing overnight at 0 °C, fibrous crystals and a few plate crystals were deposited. When the solution was kept standing for several hours at room temperature, only the plate crystals were dissolved again. The fibrous crystals were collected by filtration and were recrystallized from an aqueous ethanol (1:1 V/V) solution, giving 6.9 g of (1*R*,2*S*)-amcha (2*R*,3*R*)-di-*O*-benzoyltartrate with $[\alpha]_D=-106°$ (1% H_2O:EtOH= 1:1 V/V). Found: C, 59.50; H, 6.30; N, 5.55%. Calcd for $C_{25}H_{30}N_2O_8\cdot H_2O$: C, 59.50; H, 6.41; N, 5.55%.

The filtrate of (1*R*,2*S*)-amcha (2*R*,3*R*)-di-*O*-benzoyltartrate was evaporated to dryness and the residue was recrystallized from an aqueous ethanol (1:1 V/V) solution. The plate crystals of (1*S*,2*R*)-amcha (2*R*,3*R*)-di-*O*-benzoyltartrate obtained showed $[\alpha]_D=-75°$ (1% H_2O: EtOH=1:1 V/V).

The free amine from the (2*R*,3*R*)-di-*O*-benzoyltartrate was regenerated by the method of Bosnich.[5] The free (1*R*,2*S*)-amcha (1.5 g) and (1*S*,2*R*)-amcha (2.5 g) gave specific rotations of $[\alpha]_D=-39°$ and +40° (1% EtOH), respectively.

3) Resolution of cis-*2-(Aminomethyl)cyclohexylamine*: A hot solution of (2*R*,3*R*)-di-*O*-benzoyltartaric acid monohydrate (44 g) in ethanol (395 cm^3) was added to a solution of freshly distilled *cis-dl*-amcha (15 g) in water (80 cm^3). When the resultant solution was kept standing overnight at 0 °C, prism crystals were deposited. They were collected by filtration, washed with ethanol, and dried in air, yielding 26 g of (1*R*, 2*R*)-amcha (2*R*,3*R*)-di-*O*-benzoyltartrate with a specific rotation of $[\alpha]_D=-87°$ (1% H_2O: EtOH=1:1 V/V). According to the method of Bosnich,[5] 3.6 g of free (1*R*,2*R*)-amcha were obtained with a specific rotation of $[\alpha]_D=-15°$ (1% EtOH).

The filtrate was allowed to stand overnight at 0 °C to precipitate fibrous crystals. Alkalization and extraction[5] with ether gave 0.2 g of free (1*S*,2*S*)-amcha with a specific rotation of $[\alpha]_D=+14°$ (1% EtOH).

Among the four resolved optical isomers, (1*S*,2*R*)- and (1*R*,2*R*)-amcha were used as the ligands in this work because of their better specific rotations.

Preparation of 2-(Aminomethyl)cyclohexylamine Platinum(II) Complexes. [Pt(en)(1*S*,2*R*-amcha)]Cl_2, [Pt(NH_3)$_2$(1*S*,2*R*-amcha)]Cl_2, [Pt(en)(1*R*,2*R*-amcha)]Cl_2, and [Pt(NH_3)$_2$(1*R*, 2*R*-amcha)]Cl_2 were synthesized according to the method reported by Appleton and Hall,[6] and their analytical data are tabulated in Table 1.

Measurements. ^{1}H-NMR spectra were recorded at 100 MHz (JEOL JNM-MH-100). DSS was used as an internal reference.

FT ^{13}C-NMR spectra were obtained at 25 MHz with broad-band proton decoupling on a JEOL JNM-FX-100 spectrometer employing the solvent deuterium signal as an internal lock. A total of 1000—21200 FID's (8192 points) was averaged to provide the desired signal to noise ratio in the 2.5-kHz frequency spectra. Pulse angles of 45° were employed with no pulse delay. The ambient temperature was room temperature. TMS sealed in a capillary was used as an external reference. All NMR spectra were measured in D_2O solutions.

Table 1. Analytical data of the amcha Pt(II) complexes

Complexes	C%		H%		N%	
	Found	Calcd	Found	Calcd	Found	Calcd
$[Pt(en)(1S,2R\text{-amcha})]Cl_2$	23.71	23.79	5.18	5.33	12.61	12.33
$[Pt(NH_3)_2(1S,2R\text{-amcha})]Cl_2 \cdot 1/2H_2O$	19.21	19.22	5.07	5.31	12.06	12.81
$[Pt(en)(1R,2R\text{-amcha})]Cl_2$	23.55	23.79	5.32	5.33	12.49	12.33
$[Pt(NH_3)_2(1R,2R\text{-amcha})]Cl_2 \cdot 3/2H_2O$	18.70	18.46	5.27	5.55	11.65	12.31

Absorption spectra were obtained in H_2O with a Shimadzu UV 200 Recording Spectrometer.

CD spectra were measured in H_2O with a JASCO J-40 Spectropolarimeter. All measurements were performed at room temperature.

Results and Discussion

^{1}H-NHR Spectra. As shown in Fig. 2, two multiplet peaks around 1.20 and 1.78 ppm can be assigned to the axial and equatorial methylene protons in the cyclohexane ring of (1*S*,2*R*)-amcha. From the integrated intensities, a peak of the methine proton (>CH–C) in the cyclohexane ring seems to be overlapping with these equatorial methylene protons. Two multiplet peaks around 2.48 and 2.88 ppm are attributable to the resonance of aminomethyl protons ($-CH_2-N$) and the methine proton (>CH–N). For (1*S*,2*R*)-amcha, two chair forms with diequatorial or diaxial orientation of amino and aminomethyl groups can be expected. But the behavior of the methylene protons in the cyclohexane ring indicates a fixed chair form with preferential diequatorial orientation.

The multiplet peak around 1.50 ppm (Fig. 2(b)) can be assigned to eight methylene protons and a methine proton (>CH–C) in the cyclohexane ring of (1*R*,2*R*)-amcha. Two multiplet peaks around 2.56 and 3.08 ppm can be assigned to aminomethyl protons ($-CH_2-N$) and a methine proton (>CH–N) by the integrated intensities. For (1*R*,2*R*)-amcha, two chair forms with axial and equatorial orientations of the amino and aminomethyl groups are possible, but the multiplet peak of the methylene protons in the cyclohexane ring indicates an averaging of axial and equatorial protons by rapid interconversion between two chair forms on the NMR time scale.

Figure 3 shows ^{1}H-NMR spectra of $[Pt(en)(amcha)]Cl_2$ and $[Pt(NH_3)_2(amcha)]Cl_2$ (amcha=(1*S*,2*R*)- and (1*R*,2*R*)-amcha) in D_2O. In the spectrum of $[Pt(en)(1S,2R\text{-amcha})]Cl_2$, multiplets due to axial and equatorial methylene protons in the cyclohexane ring were observed at 1.26 and 1.70 ppm, respectively. This behavior of the methylene protons suggests that the cyclohexane ring takes a fixed chair form preferentially. In the spectrum of $[Pt(en)(1R,2R\text{-amcha})]Cl_2$, a multiplet due to methylene protons in the cyclohexane ring was observed at 1.30 ppm, suggesting the averaging of axial and equatorial protons by rapid interconversion between two chair forms. ^{1}H-NMR spectra of $[Pt(NH_3)_2(1S,2R\text{-amcha})]Cl_2$ and $[Pt(NH_3)_2(1R,2R\text{-amcha})]Cl_2$ are almost similar to those of $[Pt(en)(1S,2R\text{-amcha})]Cl_2$ and $[Pt(en)(1R,2R\text{-amcha})]Cl_2$, respectively, except for peaks of ethylenediamine.

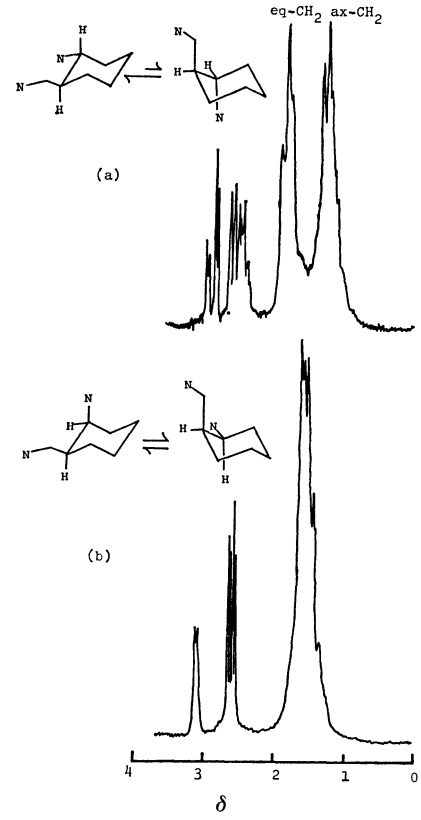

Fig. 2. ^{1}H-NMR spectra of (a) (1*S*,2*R*)-amcha and (b) (1*R*,2*R*)-amcha.

Recent studies[2,7] suggest that the dihedral angle dependence of the vicinal coupling constant $^3J_{Pt-H}$ in Pt–N–C–H fragments would parallel the Karplus equation for the $^3J_{H-H}$ in H–C–C–H fragments. The $^3J_{Pt-H}$ value has offered very important information for determining the conformation of 1,2-diamine and 1,3-diamine platinum(II) complexes. $[Pt(en)(1S,2R\text{-amcha})]Cl_2$ and $[Pt(en)(1R,2R\text{-amcha})]Cl_2$ gave a single sharp peak, together with satellite peaks due to the coupling with ^{195}Pt (I=1/2, 34% abundance) at 2.73 ppm. The single sharp peak and the satellite peaks are overlapping with the aminomethyl protons ($-CH_2-N$) and the methine proton (>CH–N), but by comparing $[Pt(en)(1S,2R\text{-amcha})]Cl_2$ and $[Pt(en)(1R,2R\text{-amcha})]Cl_2$ with $[Pt(NH_3)_2(1S,2R\text{-amcha})]Cl_2$ and $[Pt(NH_3)_2(1R,2R\text{-amcha})]Cl_2$, the single sharp peak can be assigned to methylene protons of ethylenediamine. The observed $^3J_{Pt-H}$ values of $[Pt(en)(1S,2R\text{-amcha})]Cl_2$ and $[Pt(en)(1R,2R\text{-amcha})]Cl_2$ were 41.0 Hz. This $^3J_{Pt-H}$ value is in good harmony with $^3J_{Pt-H}$ values previously reported for $[Pt(en)_2]Cl_2$ (41.0 Hz) and

Table 2. ^{13}C-NMR chemical shifts[a] and coupling constants[b]

Complexes	C(1)	C(2)	C(3)	C(4)	C(5)	C(6)	N-CH_2
[Pt(en)(1*S*,2*R*-amcha)]Cl_2	57.75	41.40	29.73	25.02	24.24	33.53	48.97
	(23.8)	(17.7)				(43.3)	(28.7)
[Pt(NH_3)$_2$(1*S*,2*R*-amcha)Cl_2	57.94	41.44	29.92	25.17	24.41	33.65	49.22
	(22.6)	(18.9)				(43.9)	(26.9)
[Pt(en)(1*R*,2*R*-amcha)]Cl_2	53.53	37.13	27.51	22.88	21.03	28.75	44.03
	(26.3)	(21.4)				(20.2)	(28.1)
[Pt(NH_3)$_2$(1*R*,2*R*-amcha)]Cl_2	53.63	37.23	27.48	22.90	21.37	28.97	44.42
	(25.0)	(22.0)				(22.0)	(27.5)

a) ^{13}C shifts in ppm from external TMS. b) The values in parentheses are the coupling constants (^{195}Pt–^{13}C).

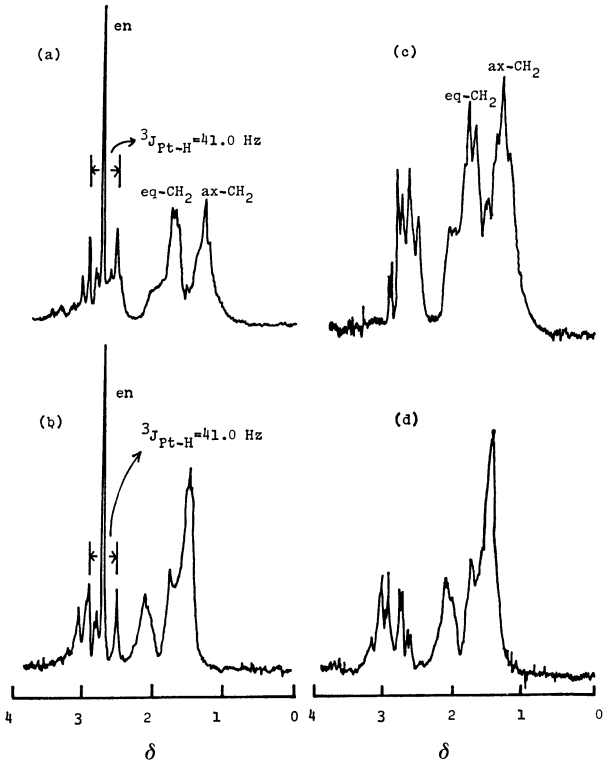

Fig. 3. ^{1}H-NMR spectra of (a) [Pt(en)(1*S*,2*R*-amcha)]-Cl_2, (b) [Pt(en)(1*R*,2*R*-amcha)]Cl_2, (c) [Pt(NH_3)$_2$-(1*S*,2*R*-amcha)]Cl_2, and (d) [Pt(NH_3)$_2$(1*R*,2*R*-amcha)]Cl_2.

[Pt(en)(NH_3)$_2$]Cl_2 (41.5 Hz),[2] indicating that the chelate ring of ethylenediamine shows a rapid conformational interconversion.

Unfortunately, other satellite peaks could not be assigned, and information on six-membered chelate ring could not be obtained from the $^3J_{Pt-H}$ value.

^{13}C-NMR Spectra. Figure 4 shows ^{13}C-NMR spectra of [Pt(en)(1*S*,2*R*-amcha)]Cl_2 and [Pt(en)(1*R*,2*R*-amcha)]Cl_2 in D_2O. In both complexes, assignments of C(1), C(2), C(6), aminomethyl carbons, and methylene carbons of ethylenediamine were facilitated on the basis of the spectrum with off-resonance proton decoupling. Three peaks on the upfield side are attributable to the resonance of C(3), C(4), and C(5) carbons, but assignments of these three peaks may be difficult because of complicated steric factors.

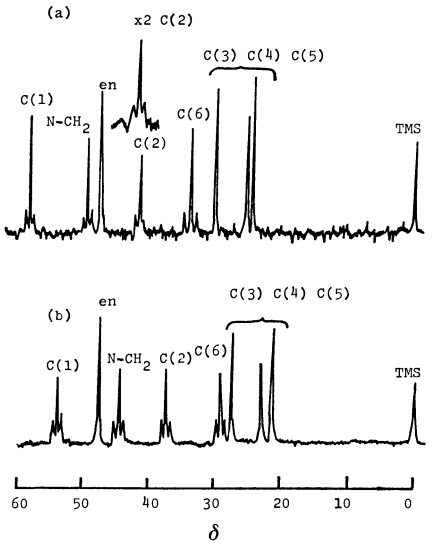

Fig. 4. ^{13}C-NMR spectra of (a) [Pt(en)(1*S*,2*R*-amcha)]-Cl_2 and (b) [Pt(en)(1*R*,2*R*-amcha)]Cl_2.

Table 2 shows chemical shifts and coupling constants (^{195}Pt–^{13}C) of these platinum(II) complexes. By comparing the coupling constants of these complexes, a significant difference in $^3J_{Pt-C(6)}$ values was detected. [Pt(en)(1*S*,2*R*-amcha)]Cl_2 and [Pt(NH_3)$_2$(1*S*,2*R*-amcha)]Cl_2 gave 43.3 and 43.9 Hz, respectively, while [Pt(en)(1*R*,2*R*-amcha)]Cl_2 and [Pt(NH_3)$_2$(1*R*,2*R*-amcha)]Cl_2 gave 20.2 and 22.0 Hz. Recently, Bagger[8] and Erickson *et al.*[9] have demonstrated that in five-membered platinum(II) complexes the coupling constant $^3J_{Pt-N-C-C}$ shows a Karplus-type angle dependence on the dihedral angle between the planes Pt–N–C and N–C–C. It turns out that the significant difference in $^3J_{Pt-C}$ found would be explained if the relationship $^3J_{Pt-N-C-C}=a\cos^2\phi$ is also valid in six-membered platinum(II) complexes, ϕ being the dihedral angle between the planes Pt–N–C and N–C–C, and a being a constant. The molecular models suggest that [Pt(en)(1*S*,2*R*-amcha)]Cl_2 and [Pt(NH_3)$_2$ (1*S*,2*R*-amcha)]Cl_2 may take either a chair form or a δ-skew form. Whichever form these platinum(II) complexes take, the dihedral angle of Pt–N–C(1)–C(6) is about 180° (Fig. 5). The $^3J_{Pt-C(6)}$ values for [Pt(en)(1*S*,2*R*-amcha)]Cl_2 and [Pt(NH_3)$_2$(1*S*,2*R*-amcha)]Cl_2 were 43.3 and 43.9 Hz, respectively. A

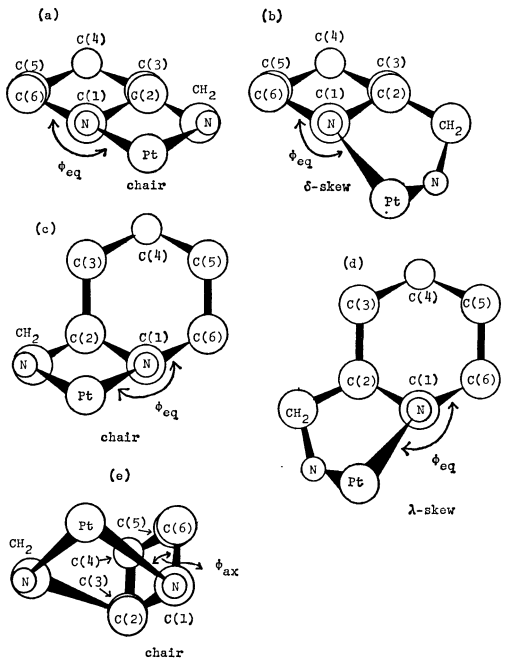

Fig. 5. The chelate ring viewed down an N–C bond. (a) and (b) for $[PtX(1S,2R\text{-amcha})]Cl_2$; (c), (d), and (e) for $[PtX(1R,2R\text{-amcha})]Cl_2$ (X=en, $(NH_3)_2$).

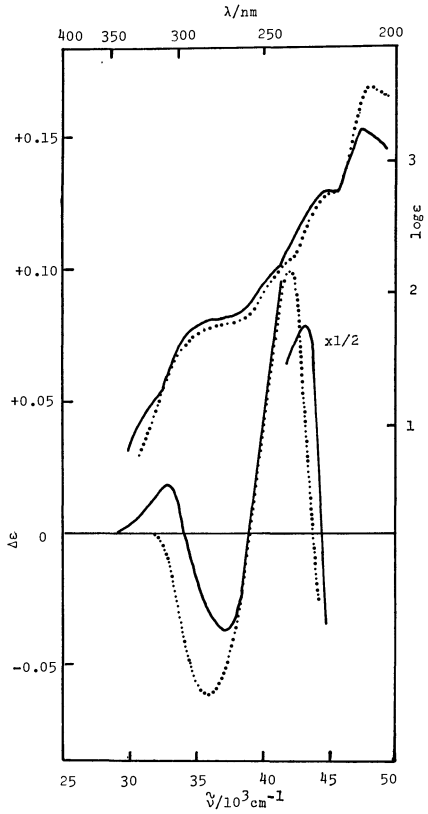

Fig. 6. Absorption and CD spectra of ——: $[Pt(en)(1S,2R\text{-amcha})]Cl_2$ and ·····: $[Pt(NH_3)_2(1S,2R\text{-amcha})]Cl_2$.

similar value has been reported for (*R,S*)-1,3-diphenyl-1,3-propanediamine platinum(II) complexes in which both phenyl groups are equatorial.[10] The *a* values in the equation $^3J_{Pt-N-C-C}=a\cos^2\phi$ seem to be 43—44 Hz. $[Pt(en)(1R,2R\text{-amcha})]Cl_2$ and $[Pt(NH_3)_2(1R,2R\text{-amcha})]Cl_2$ may take two chair forms or a λ-skew form, but may not take a δ-skew form because of the steric hindrance. As shown in Fig. 5, an angle of 180° may be expected for one chair form or the λ-skew form and about 60° for the other chair form. The ^{1}H-NMR data show that the cyclohexane ring of (1*R*,2*R*)-amcha platinum(II) complexes is interconverting between two chair forms, and hence that the chelate ring will interconvert. When two chair forms interconvert with each other rapidly on a NMR time scale, the averaged coupling constant due to a rapid ring interconversion would be $^3J_{Pt-C(6)}=1/2$ $(a\cos^2180°+a\cos^260°)$ $(a=43—44$ Hz), that is $^3J_{Pt-C(6)}=$ 27.0—27.5 Hz. If the population of a λ-skew intermediate which appears in interconverting between two chair forms cannot be neglected, the $^3J_{Pt-C(6)}$ value is expected to be larger than 27.0—27.5 Hz. According to the conformational analysis of the planar $ML_2(tn)$ type complex (L=a monodentate ligand, tn=1,3-propanediamine), the interconversion occurred *via* a skew intermediate,[3,11] but the population of the intermediate conformer was small at room temperature.[3,11] Experimental values of $^3J_{Pt-C(6)}$ for $[Pt(en)(1R,2R\text{-amcha})]Cl_2$ and $[Pt(NH_3)_2(1R,2R\text{-amcha})]Cl_2$ were 20.2 and 22.0 Hz, respectively. Thus the λ-skew may be neglected because the experimental values are smaller than the values calculated from the 1:1 abundance ratio of the two chair forms. Assuming the equatorial and axial C–C(6) chair form exactly take the angles of 180° and 60°, respectively, the population of the former conformer may be smaller than the latter.

Absorption and CD Spectra. In aqueous solution, $[Pt(en)(1S,2R\text{-amcha})]Cl_2$ exhibited five absorption bands in the ultraviolet region, as shown in Fig. 6. The band at 37000 cm^{-1}, on the basis of D_{4h} symmetry, can be assigned to $^1A_{1g}$-^3E_g (band II), and those at 41700 (shoulder), 44400, and 47000 cm^{-1} to $^1A_{1g}$-$^1A_{2g}$ (band III), $^1A_{1g}$-^1E_g (band IV), and charge transfer transitions, respectively. The shoulder at 31300 cm^{-1} may be assigned to the $^1A_{1g}$-$^3A_{2g}$ (band I) transition.[12] Similarly, $[Pt(NH_3)_2(1S,2R\text{-amcha})]Cl_2$ exhibited four bands. The band at 35700 cm^{-1} can be assigned to band II and the bands at 41700 (shoulder), 44400, and 48100 cm^{-1} to band III, band IV, and charge transfer transitions, respectively. As shown in Fig. 7, $[Pt(en)(1R,2R\text{-amcha})]Cl_2$ and $[Pt(NH_3)_2(1R,2R\text{-amcha})]Cl_2$ exhibited four absorption bands. The bands at 35700, 41700 (shoulder), 44400, and 48100 cm^{-1} may be assigned to band II, band III, band IV, and charge transfer transitions, respectively.[12]

Figure 6 also shows the CD spectra of $[Pt(en)(1S,2R\text{-amcha})]Cl_2$ and $[Pt(NH_3)_2(1S,2R\text{-amcha})]Cl_2$ in water. $[Pt(en)(1S,2R\text{-amcha})]Cl_2$ exhibited three CD bands at 32700, 37000, and 42600 cm^{-1} with signs of positive, negative, and positive, respectively. These CD bands correspond to bands I, II ,and III in the absorption spectrum. $[Pt(NH_3)_2(1S,2R\text{-amcha})]Cl_2$ exhibited two CD bands, corresponding to bands II

and III in the absorption spectrum. Although the peak of band IV in both complexes could not be detected in the CD spectra, its sign can be estimated to be negative, as shown in Fig. 6. The CD spectral data of the platinum(II) complexes are presented in Table 3. The absolute CD strength ($=|\Delta\varepsilon|$) of [Pt(en)(1*S*,2*R*-amcha)]Cl_2 and [$Pt(NH_3)_2$(1*S*,2*R*-amcha)]Cl_2 is lower than that of the five-membered platinum(II) complexes containing (*R*)-1,2-propanediamine and (*R*,*R*)-1,2-cyclohexanediamine.[12] The optical activity due to the chelate ring of amcha may be expected to arise from (i) the conformational effect of the chelate ring and (ii) the vicinal effect of the asymmetric carbon. However, only the vicinal effect of the asymmetric carbon seems to contribute to the $|\Delta\varepsilon|$ values of [Pt(en)(1*S*,2*R*-amcha)]Cl_2 and [$Pt(NH_3)_2$(1*S*,2*R*-amcha)]Cl_2. Namely, the observed low $|\Delta\varepsilon|$ values of these complexes can be explained by considering as preferential the chair form which does not make any conformational contribution to the CD spectra. The chair and the λ-skew form could not be distinguished by ^{13}C-NMR analyses, but the CD spectral data indicate a fixed chair form with a dihedral angle of 180° (Fig. 8). As shown in Fig. 7, the CD spectra of [Pt(en)(1*R*,2*R*-amcha)]Cl_2 and

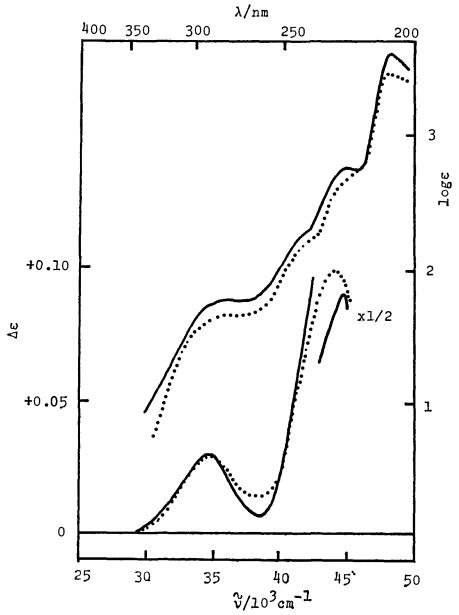

Fig. 7. Absorption and CD spectra of ——: [Pt(en)(1*R*,2*R*-amcha)]Cl_2 and ·····: [$Pt(NH_3)_2$(1*R*,2*R*-amcha)]Cl_2.

Table 3. Absorption and CD spectral data

Complexes	Absorption $\tilde{\nu}/10^3$ cm^{-1} (log ε)	CD $\tilde{\nu}/10^3$ cm^{-1} ($\Delta\varepsilon$)
[Pt(en)(1*S*,2*R*-amcha)]Cl_2	31.3(1.15)	32.7(+0.019)
	37.0(1.82)	37.0(−0.036)
	41.7 sh	42.6(+0.160)
	44.4(2.78)	
	47.0(3.23)	
[$Pt(NH_3)_2$(1*S*,2*R*-amcha)]Cl_2	35.7(1.75)	35.7(−0.061)
	41.7 sh	41.7(+0.099)
	44.4(2.74)	
	48.1(3.57)	
[Pt(en)(1*R*,2*R*-amcha)]Cl_2	35.7(1.77)	34.5(+0.060)
	41.7 sh	
	44.4(2.75)	44.4(+0.358)
	48.1(3.63)	
[$Pt(NH_3)_2$(1*R*,2*R*-amcha)]Cl_2	35.7(1.66)	34.5(+0.060)
	41.7 sh	
	44.4(2.66)	43.7(+0.203)
	48.1(3.47)	

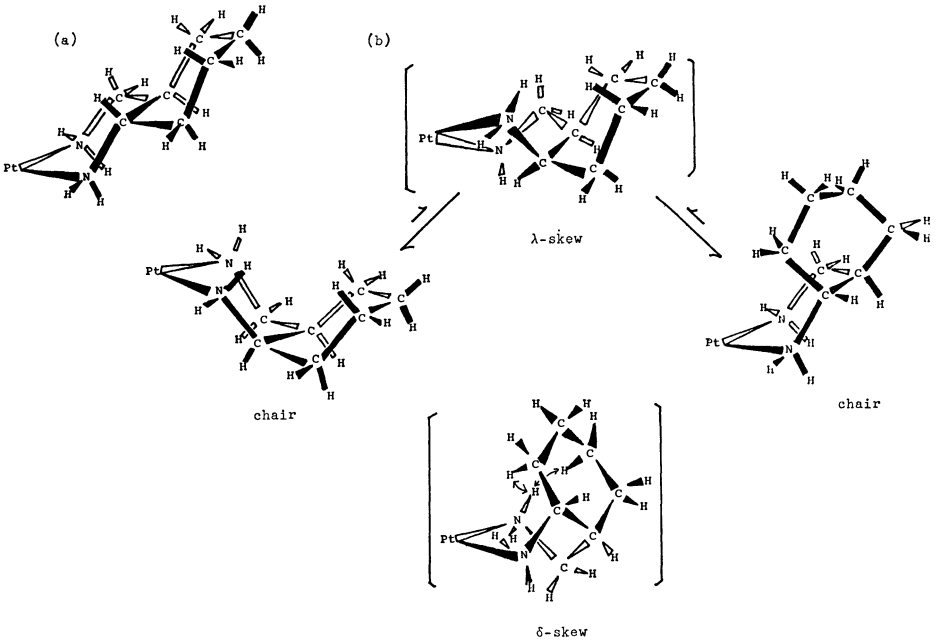

Fig. 8. Proposed conformations of (a) [PtX(1*S*,2*R*-amcha)]Cl_2 and (b) [PtX(1*R*,2*R*-amcha)]Cl_2 (X=en, $(NH_3)_2$).

$[Pt(NH_3)_2(1R,2R\text{-amcha})]Cl_2$ showed positive bands at 34500 and *ca.* 44000 cm^{-1}, corresponding to bands II and IV in their absorption spectra. As shown in Table 3, the $|\Delta\varepsilon|$ values of $[Pt(en)(1R,2R\text{-amcha})]Cl_2$ and $[Pt(NH_3)_2(1R,2R\text{-amcha})]Cl_2$ indicate that these complexes take a chair form, which has no conformational effect. Although two chair forms may be interconverting with each other *via* a λ-skew intermediate, the population of the λ-skew form can be neglected, according to the ^{13}C-NMR and CD spectral data. It is concluded that $[Pt(en)(1R,2R\text{-amcha})]Cl_2$ and $[Pt(NH_3)_2(1R,2R\text{-amcha})]Cl_2$ are apparently interconverting between two chair forms (Fig. 8).

The authors are sincerely grateful to Dr. John C. Bailar, Jr., University of Illiois, for his helpful advice and suggestions in reviewing this paper. This work was supported in part by a Grant-in-Aid for Scientific Research from the Ministry of Education, Science and Culture of Japan.

References

1) Y. Kidani, K. Okamoto, M. Noji, and T. Tashiro, *Gann*, **69**, 863 (1978).
2) T. G. Appleton and J. R. Hall, *Inorg. Chem.*, **9**, 1807 (1970).
3) S. Yano, I. Toshimitsu, M. Matsumoto, M. Yamaguchi, and S. Yoshikawa, Proceeding of the 28th Symposium of Coordination Chemistry (1978), p. 241.
4) W. L. F. Armarego and T. Kobayashi, *J. Chem. Soc.*, **1970**, 1597.
5) B. Bosnich and J. MacB. Harrowfield, *J. Am. Chem. Soc.*, **94**, 3426 (1972).
6) T. G. Appleton and J. R. Hall, *Inorg. Chem.*, **9**, 1800 (1970).
7) T. G. Appleton and J. R. Hall, *Inorg. Chem.*, **10**, 1717 (1971).
8) S. Bagger, *Acta Chem. Scand.*, **28**, 467 (1974).
9) L. E. Erickson, J. E. Sarenski, and C. N. Reilley, *Inorg. Chem.*, **14**, 3007 (1975).
10) M. Noji, K. Okamoto, and Y. Kidani, *Chem. Lett.*, **1979**, 741.
11) J. R. Gollogly and C. J. Hawkins, *Inorg. Chem.*, **11**, 156 (1972); C. J. Hawkins, R. M. Peachey, and C. L. Szoredi, *Aust. J. Chem.*, **31**, 973 (1978).
12) H. Ito, J. Fujita, and K. Saito, *Bull. Chem. Soc. Jpn.*, **40**, 2584 (1967).

  Bull. Chem. Soc. Jpn., 54, 719—721 (1981)

A Kinetic Study of the Base Hydrolysis of (2-Aminoethanol)bis-(ethylenediamine)halogenocobalt(III) Complexes

Kazuko Ogino* and Hitoshi Seki**

College of Medical Sciences, Tohoku University, Seiryo-machi, Sendai 980

(Received July 1, 1980)

The base hydrolysis of *cis*-$[CoX(etaH)(en)_2]^{2+}$(X=Cl or Br, etaH=2-aminoethanol, en=ethylenediamine) has been studied. The hydrolysis results in the formation of $[Co(eta)(en)_2]^{2+}$ (≈35%) and $[Co(OH)(etaH)(en)_2]^{2+}$ (≈65%) at I=1.0 (KNO_3), 25 °C, the product ratio being independent of the pH. The base hydrolysis has also been studied in the presence of sodium azide.

The base hydrolysis of *cis*-$[CoX(etaH)(en)_2]^{2+}$ has been studied by several workers. Chan and Leh,[1] Hay and Cropp[2] and Udovenko *et al.*[3] reported that the hydrolysis product of the chloro complex was the hydroxo complex $[Co(OH)(etaH)(en)_2]^{2+}$ in which the etaH is unidentate. On the other hand, the synthesis of $[Co(etaH)(en)_2]^{3+}$ complexes containing the chelated etaH *via* the base hydrolysis of *cis*-$[CoBr(etaH)(en)_2]^{2+}$ was reported by Buckingham *et al.*[4] Similarly, several complexes of the $[Co(amOH)(diamine)_2]^{3+}$ type (amOH=2-amino-1-alkanol) were synthesized through the base hydrolysis of $[CoX(amOH)(diamine)_2]^{2+}$.[5,6] The present investigation has been undertaken in order to clarify the products of the hydrolysis of *cis*-$[CoX(etaH)(en)_2]^{2+}$ and to elucidate the mechanism of the reaction.

Experimental

Materials. The *cis*-$[CoX(amine)(en)_2]X_2$(amine=$C_2H_5NH_2$ or etaH) and $[Co(etaH)(en)_2]Br_3$ were prepared according to the literature method.[4,7] All the other reagents were of a reagent grade.

Kinetic Measurements. The base hydrolysis of *cis*-$[CoX(amine)(en)_2]^{2+}$ was followed by the pH stat method using a Metrohm Combi 6-1 titrator under a nitrogen atmosphere at 25 °C and I=1.0 (KNO_3). Product analyses were performed pH-metrically. The titrant was 0.05 M NaOH (1 M=1 mol dm^{-3}).

Results and Discussion

Equivalent amounts of the base are consumed during the course of base hydrolyses of $[CoX(amine)(en)_2]^{2+}$.[8] The rate of hydrolysis was measured by the pH stat method at pH 9—10. The data fit the rate law of $k_{obsd}=k[OH^-]$, the values of k being 51 and 31 M^{-1} s^{-1} for *cis*-$[CoBr(etaH)(en)_2]^{2+}$ and *cis*-$[CoBr(C_2H_5NH_2)(en)_2]^{2+}$ respectively at I=1.0(KNO_3) and 25 °C. The values for the former is somewhat smaller than that at I=0.1 reported by Buckingham *et al.*[4]

After the base hydrolyses had been completed, the solutions were acidified with appropriate amounts of 0.1 M HCl and were then titrated with 0.05 M NaOH. The titration curve remained unchanged after the solution had been left standing at pH 10 at 25 °C for 1 h. The base hydrolysis of *cis*-$[CoBr(C_2H_5NH_2)(en)_2]^{2+}$ resulted in the formation of a product with a pK_a value of 6.25 at I=1.0(KNO_3) and 25 °C; this indicates that the product should be $[Co(H_2O)(C_2H_5NH_2)(en)_2]^{3+}$. The titration curve of the hydrolysis products of *cis*-$[CoBr(etaH)(en)_2]^{2+}$ shows two inflection points, as is shown in Fig. 1, indicating that two species, **1** and **2**, are produced during the base hydrolysis of $[CoBr(etaH)(en)_2]^{2+}$. The abundance ratio and pK_a values of these two species were determined by analyzing the titration curves in the manner described in the Appendix. The results are given in Table 1. Species **1** with a pK_a value of 6.2, is considered to be $[Co(H_2O)(etaH)(en)_2]^{3+}$ by a comparison of the pK_a value with those of several cobalt(III) complexes with a coordinated water.[9] Species **2** with a pK_a value of 4.0, is considered to be $[Co(etaH)(en)_2]^{3+}$, because the titration of the solution of $[Co(etaH)(en)_2]Br_3$ showed its pK_a to be 4.0 at I=1.0, 25 °C. These values are somewhat larger than those at lower ionic strengths reported in previous papers.[4,5]

The conjugate-base mechanism has been established for the base hydrolyses of cobalt(III) aniono amine complexes. According to the S_N1 CB mechanism, the base hydrolysis of $[CoX(etaH)(en)_2]^{2+}$ can be expressed by the following scheme.

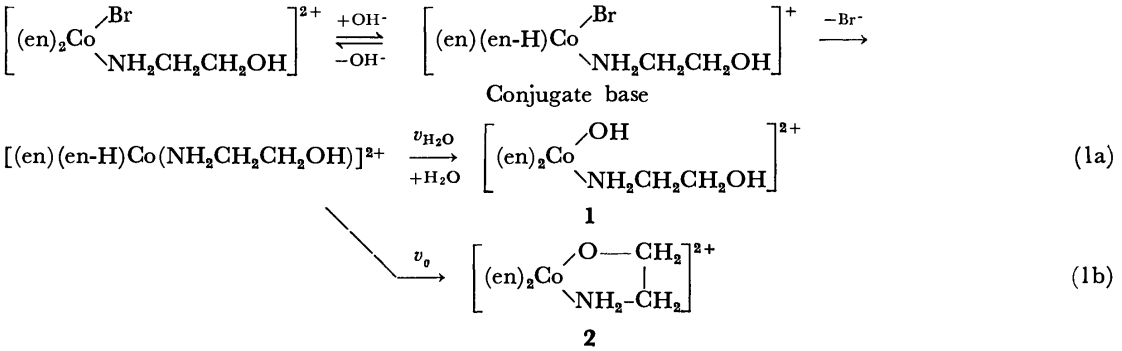

** Present address: Osaka Research Laboratory, Rasa Industries, Ltd., 9-134, 1-Chome, Takami, Konohana-ku, Osaka 554.

Table 1. Products of the base hydrolysis of *cis*-$[CoX(etaH)(en)_2]^{2+}$ as determined by the analysis of the titration curves. $I=1.0(KNO_3)$, 25 °C

X	pH[a]	Complex-hydrolyzed / mmol[b]	Species **1** / mmol[c]	pK_1	[1] / [Complex-hydrolyzed]
Br	9.3	0.0229	0.0142	6.22	0.62
Br[d]	10.0	0.0304	0.0190	6.16	0.63
Br	10.6	0.0241	0.0151	6.27	0.62
Cl	10.0	0.0354	0.0232	6.22	0.65

a) The pH at which base hydrolysis was performed. b) The volume of the solution was 4 cm³. c) The deviation is ±0.005 mmol. d) In this run, the amount of Species **2** formed and the pK_2 were obtained as 0.0109 mmol and 3.98 respectively.

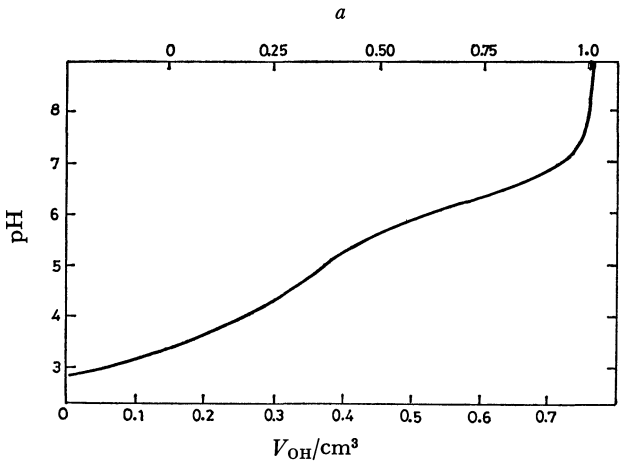

Fig. 1. Titration curve of products formed by the base hydrolysis of 0.0304 mmol *cis*-$[CoBr(etaH)(en)_2]Br_2$ at pH 10.0, followed by the addition of 0.038 mmol of HCl. $I=1.0$ (KNO_3), 25 °C. The abscissa V_{OH} is the volume of 0.05 M NaOH added during the titration and a is the ratio: [Moles of NaOH consumed for the dissociation of the complex]/[Moles of total complex].

The results in Table 1 show that the product ratio [Species **1**]/[Total amount of complex-hydrolyzed] is independent of the pH within the limit of experimental error. This means that both v_{H_2O} and v_0 are independent of the pH. Table 1 shows also that Species **2**, which contains an amino alcohol chelate ring, is the minor product of the base hydrolysis. The reaction paths by which Species **1** is converted into Species **2** will be described elsewhere.

Buckingham *et al.*[10-12] disclosed that the base hydrolyses of complexes of the *cis*-$[CoBr(\widehat{NO})(en)_2]^{m+}$ type ($\widehat{NO}$=$NH_2CH_2COO^-$, $NH_2CH_2COOC_3H_7$, $NH_2CH_2CONH_2$, *etc.*; the underlining denotes the coordinating atom) result in the formation of two types of products, $[Co(OH)(\widehat{NO})(en)_2]^{m+}$ and $[Co(\widehat{NO})(en)_2]^{m+}$. The relative amounts of these two products were also reported; the formation ratio of the chelated species is 35—45% for various $\widehat{NO}$ ligands.[10-12] The similarity of the product ratios, including ours given in Table 1, indicates that the lifetime of the five-coordinate intermediate is not long enough to be able to distinguish various entering moieties, $-CH_2COO^-$, $-CONH_2$, $-CH_2OH$, *etc.*, with differing nucleophilicities.

The product ratio study was also performed in the presence of sodium azide. In this case, the procedure described in the Appendix could not be used because of the interference due to the HN_3–N_3^- equilibrium ($pK_a \approx 4.7$). In the presence of azide, the base hydrolysis is assumed to proceed by Path 1c in addition to Paths 1a and 1b, by analogy with the base hydrolyses of various pentaaminehalogenocobalt(III) complexes.[12-15]

$$[(en)(en\text{-}H)Co(NH_2CH_2CH_2OH)]^{2+} \xrightarrow[+N_3^-,\ +H^+]{v_{N_3^-}} \left[(en)_2Co\begin{matrix}N_3\\ NH_2CH_2CH_2OH\end{matrix}\right]^{2+} \quad (1c)$$

3

The formation of the azido complex was confirmed spectrophotometrically by the appearence of an intense absorption at 516 nm. Since the azido complex is formed from the bromo complex without consuming the base, the amount of base consumed during the base hydrolysis should correspond to the amount of Species **1** and **2** formed:[8]

$$\alpha \equiv \frac{\text{Moles of base consumed}}{\text{Moles of complex hydrolyzed}} = \frac{[1]+[2]}{[1]+[2]+[3]}. \quad (2)$$

According to the S_N1 CB mechanism, the product ratio should be related to the relative magnitudes of the rates of Paths 1a—1c:

$$\alpha = \frac{v_0+v_{H_2O}}{v_0+v_{H_2O}+v_{N_3^-}}. \quad (3)$$

Equation 3 can be transformed to:

$$\frac{1-\alpha}{\alpha} = \frac{v_{N_3^-}}{v_0+v_{H_2O}}. \quad (4)$$

The plots of the left-hand side of Eq. 4 against the azide concentration are given in Fig. 2 for $[CoBr(etaH)(en)_2]^{2+}$ and $[CoBr(NH_2C_2H_5)(en)_2]^{2+}$. They are almost straight lines, implying that $v_{N_3^-}$ is proportional to $[N_3^-]$ within the limits of experimental error. Such first-order dependence of product ratios has been reported and discussed for the base hydrolyses of several anionopentaaminecobalt(III) complexes.[13,14] At the same azide concentration (1 M), the ratio of the amount of the azido complex in the products is 10% for $[CoBr(NH_3)_5]^{2+}$,[13,14] 20% for $[CoBr(NH_2CH_2COO)(en)_2]^+$,[12] 24% for $[CoBr(NH_3)(en)_2]^{2+}$,[13] 30% for $[CoBr(etaH)(en)_2]^{2+}$, and 40% for $[CoBr(NH_2C_2H_5)$-

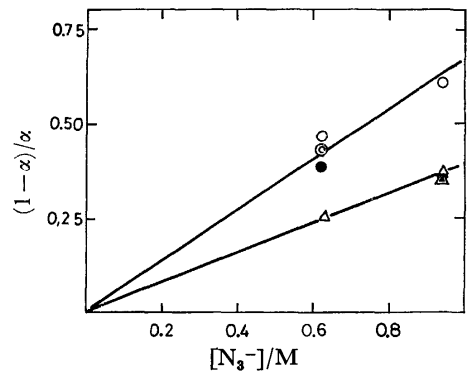

Fig. 2. The dependence of the product ratio of base hydrolysis on azide concentration, I=1.0 (KNO_3), 25 °C.
$[CoBr(NH_2C_2H_5)(en)_2]^{2+}$: pH 9.0 (○), pH 9.3 (◎), pH 9.6 (●) $[CoBr(etaH)(en)_2]^{2+}$: pH 9.3 (△), pH 9.6 (▲), pH 10.6 (◬).

$(en)_2]^{2+}$. The rather large variation in these competition ratios is in contrast with the similarity of the $[Co(\widehat{NO})(en)_2]$/[Total amount of complex hydrolyzed] ratio. It may at least partly be attributed to the ion-pair effect between the cobalt(III) complex and azide ions; the $[CoBr(NH_2CH_2COO)(en)_2]^+$ ions show a smaller value than the $NH_2C_2H_5$ or the etaH complex with a +2 charge. The importance of the ion-pair effect in the product ratio has been pointed out by Buckingham *et al.*[12,16] The smaller value for the etaH complex than that for the $NH_2C_2H_5$ complex may be partly due to the presence of Path 1b in the hydrolysis of the former.

Appendix

The titration curves of mixtures of $[Co(H_2O)(etaH)(en)_2]^{3+}$ (abbreviated as AH) and $[Co(etaH)(en)_2]^{3+}$ (BH) are analyzed in the following manner in order to determine the ratio of the amounts of these species as well as their pK_a values. The abbreviations given by Eqs. 5—8 are used:

$$[A]_T = [AH] + [A^-] = [AH](1+K_1/[H^+]), \quad (5)$$

$$[B]_T = [BH] + [B^-] = [BH](1+K_2/[H^+]), \quad (6)$$

where K_1 and K_2 are the acid-dissociation constants of AH and BH respectively;

$$[Co]_T = [A]_T + [B]_T, \quad (7)$$

$$[Cl^-] = (\text{Moles of HCl added after base hydrolysis})/V, \quad (8)^{8)}$$

where V is the volume of the solution under titration. When the balance of the positive and negative charges is taken into account, the following equation is obtained:

$$[AH] + [BH] + [H^+] = [Cl^-] - \frac{N_{OH}V_{OH}}{V}, \quad (9)$$

where N_{OH} is the concentration of sodium hydroxide used for the titration and V_{OH} is the volume of the hydroxide solution added during the titration. The substitution of Eqs. 5—8 into Eq. 9 gives:

$$\frac{[B]_T(K_2-K_1)}{[H^+]+K_2} = [H^+] + [Co]_T - [Cl^-] + \frac{N_{OH}V_{OH}}{V} - \frac{K_1}{[H^+]}\left([Cl^-] - \frac{N_{OH}V_{OH}}{V} - [H^+]\right), \quad (10)$$

$$\frac{[A]_T(K_2-K_1)}{[H^+]+K_1} = [Cl^-] - [H^+] - [Co]_T - \frac{N_{OH}V_{OH}}{V} + \frac{K_2}{[H^+]}\left([Cl^-] - \frac{N_{OH}V_{OH}}{V} - [H^+]\right). \quad (11)$$

When $K_2 \gg K_1$ and $[H^+] \ll K_2$, Eq. 11 can be simplified as:

$$\left([Cl^-] - \frac{N_{OH}V_{OH}}{V}\right)^{-1} = \left(1+\frac{K_1}{[H^+]}\right)\frac{1}{[A]_T}. \quad (12)$$

Plotting the left-hand side of Eq. 12 against $[H^+]^{-1}$, one should obtain a straight line; from its slope and intercept, the values of K_1 and $[A]_T$ can be calculated. The $[B]_T$ value can be obtained by the use of Eq. 7 if $[A]_T$ is known.

The right-hand side of Eq. 10 can be calculated provided the K_1 value is known. The condition $K_2 \gg K_1$ being assumed, the following equation is obtained:

$$(\text{The right-hand side of Eq. 10})^{-1} = \left(1+\frac{[H^+]}{K_2}\right)\frac{1}{[B]_T}. \quad (13)$$

The plot of the left-hand side of Eq. 13 against $[H^+]$ gives a straight line; from its slope and intercept, the values of K_2 and $[B]_T$ can be calculated.

We wish to acknowledge a Grant-in-Aid for Scientific Research No. 25419 from the Ministry of Education, Science and Culture.

References

1) S. C. Chan and F. Leh, *J. Chem. Soc., A*, **1967**, 1730.
2) R. W. Hay and P. L. Cropp, *J. Chem. Soc., A*, **1969**, 42.
3) V. V. Udovenko, L. G. Reiter, and E. P. Shkurman, *Zh. Neorg. Khim.*, **15**, 3108 (1970); V. V. Udovenko, L. G. Reiter, and T. V. Batyushkina, *ibid.*, **18**, 234 (1973).
4) D. A. Buckingham, C. E. Davis, and A. M. Sargeson, *J. Am. Chem. Soc.*, **92**, 6159 (1970).
5) K. Ogino, T. Uchida, T. Nishide, J. Fujita, and K. Saito, *Chem. Lett.*, **1973**, 679.
6) T. Nishide, K. Ogino, J. Fujita, and K. Saito, *Bull. Chem. Soc. Jpn.*, **47**, 3057 (1974).
7) J. C. Bailar, Jr., and L. B. Clapp, *J. Am. Chem. Soc.*, **67**, 171 (1945).
8) Strictly speaking, the amount of base required is in a slight excess (≈0.001 mmol) over the amount of complex hydrolyzed. The excess base is required to bring the pH of the solution to the pH at which the base hydrolysis is performed. This amount was evaluated by titrating the solution containing an appropriate amount of KNO_3 (and/or NaN_3), but no complex. The amount of base in Eq. 2 and those of hydrochloric acid in Eq. 8 and Fig. 1 are the values corrected for the excess base.
9) "Stability Constants of Metal-Ion Complexes," ed by L. G. Sillén and A. E. Martell, The Chemical Society, London (1964); Supplement No. 1 (1971).
10) D. A. Buckingham, D. M. Foster, and A. M. Sargeson, *J. Am. Chem. Soc.*, **91**, 4102 (1969).
11) C. J. Boreham, D. A. Buckingham, and F. R. Keene, *Inorg. Chem.*, **18**, 28 (1979).
12) C. J. Boreham, D. A. Buckingham, and C. R. Clark, *Inorg. Chem.*, **18**, 1990 (1979).
13) D. A. Buckingham, I. I. Olsen, and A. M. Sargeson, *J. Am. Chem. Soc.*, **88**, 5443 (1966).
14) W. L. Reynolds and S. Hafezi, *Inorg. Chem.*, **17**, 1819 (1978).
15) D. A. Buckingham, I. I. Olsen, and A. M. Sargeson, *J. Am. Chem. Soc.*, **90**, 6654 (1968).
16) D. A. Buckingham, C. R. Clark, and T. W. Lewis, *Inorg. Chem.*, **18**, 1985 (1979).

The Polarized Spectra and Thermal Diffusivity of Brown Tourmaline as Studied by Photoacoustic Spectroscopy

Yoshinori SUGITANI* and Masahisa FUJINAMI
Institute of Chemistry, The University of Tsukuba, Sakura-mura, Ibaraki 305
(Received August 21, 1980)

The strong pleochroic band of brown tourmaline at around 24000 cm^{-1} in the E⊥c photoacoustic spectra was assigned to d-d($^6A_1 \rightarrow {}^4A_1$, ^4E) transition of Fe and to charge transfer of Ti, that in the E//c spectra being entirely assigned to charge transfer of Ti. The analysis of the photoacoustic signal intensity *vs.* chopping frequency gave the thermal diffusivity constant of tourmaline as $\alpha = 0.15$ cm^2/s.

Tourmaline is a complex solid-solution mineral represented by $Na(Mg,Fe)_3Al_6(BO_3)_3(Si_6O_{18})(OH)_4$.[1,2] The color is usually black but varies a great deal with composition, being brown, blue, green, colorless (iron-free varieties) and pink (lithium-bearing varieties). Some varieties with intermediate coloration of brown or bluish green show strong pleochroism. The origin of the colors and the pleochroism of silicate minerals including tourmaline have been extensively studied mainly by means of polarized absorption spectra. Many of the bands or peaks observed are explained in terms of the d-d transitions and/or charge transfer electron hopping within transition metal ions contained.[3] However, the strong pleochroic band of brown tourmaline observed around 22000—24000 cm^{-1}, has not yet been clarified. Two contradicting explanations have been given,[4,5] ascribing the band to (a) the d-d transition of Fe and (b) the electron hopping (charge transfer) of $Ti^{3+} \rightarrow Ti^{4+}$ type.

Polarized photoacoustic spectra of a brown tourmaline we observed in both the in-phase and out-of-phase modes will help clarify the nature of the relaxed thermal energy and make assignment of the band. The dependence of the photoacoustic intensity on the chopping frequency of the irradiating light gives information on the thermal diffusivity of the sample.

Experimental

Sample. A single crystal of brown tourmaline was used (locality unknown). ICP analysis gave the metal contents of Mg: 0.64 wt%, Ti: 0.32%, Mn: 0.28%, Fe: 5.74%, and Li: 0.54%, showing that the sample has the intermediate composition of typical endmembers of dravite $NaMg_3Al_6B_3Si_6O_{27}(OH,F)_4$, schorl $Na(Fe,Mn)_3Al_6B_3Si_6O_{27}(OH,F)_4$, and elbaite $Na(Li,Al)_3Al_6B_3Si_6O_{27}(OH,F)_4$.[1]

The structure of dravite has been determined by Donnay and Buerger.[6] Each magnesium ion is surrounded by four oxygen and two OH ions forming a fairly regular octahedron. Three of these octahedra are combined in an arrangement similar to the "trigonal brucite units", where each octahedron shares two of its octahedral edges with its neighbors in the 001 plane. Aluminium ion is centered in distorted (O,OH) octahedra. Each shares two of its edges with another two Al-octahedra diagonally above and below the 001 plane, resulting in spiral chains of Al-octahedra parallel to the c-axis. The ratios $Fe^{2+}:Fe^{3+}$ and $Ti^{3+}:Ti^{4+}$ are not known. However, small amounts of Fe^{3+} and Ti^{4+} are considered to occupy the Al sites.

Apparatus. The apparatus for measuring photoacoustic spectra consists of a 300 W xenon lamp, mechanical light chopper, spectrometer (25 cm, CT-25N, JASCO), photoacoustic cell with a microphone, lock-in amplifier (NF Circuit Design Block, LI-574) and a recorder. The block diagram and a brief account of the setup was reported.[7,8] In order to normalize the power spectrum of the xenon lamp, a part of the incident light was reflected by a mirror and led to another photoacoustic cell with a carbon black reference, the output of which was also lock-in amplified and compared with the signal from the main cell at the dividing unit (Rika-Denki, XB-20).

For the measurement of polarized spectra, the spectra of the tourmaline and the carbon black sample were recorded in separate runs, the comparison (division) of the results being manually conducted. This is because the intensity of the exciting light gets down to 1/4—1/5 of that just before the polarizer, resulting in an unstable work of the dividing unit. Separate measurement is also appropriate for avoiding the polarizing characteristics of the reflecting mirror.

Results and Discussion

Figure 1 shows the photoacoustic spectra of the tourmaline crystal for the case of E⊥c, *i.e.*, when the electric vector is vibrating in the plane perpendicular to the c-axis, and for the case of E//c. The solid lines indicate the in-phase spectra and the dashed lines the out-of-phase spectra which show the 90° phase-delayed signal (slow heat) with respect to the in-phase signal. The in-phase spectral patterns are very similar to those of the optical absorption spectra

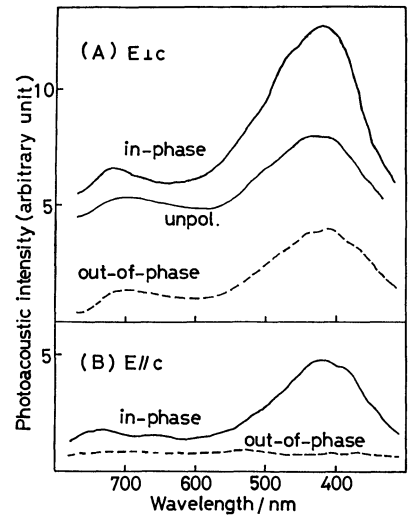

Fig. 1. In-phase and out-of-phase photoacoustic spectra of brown tourmaline at 80 Hz for polarized irradiation of E⊥c (A), and E//c (B). Unpolarized spectrum is also shown in (A).

of a Brazilian dravite[4] or a Gouverneur dravite,[5] suggesting that the origin of the color and the strong pleochroism is attributed to a similar mechanism in these tourmalines. The pleochroism is considered to arise from the band at 24000 cm^{-1}, which is larger in the E⊥c spectrum than in the E//c spectrum. The 14500 cm^{-1} band has little influence on the color of the crystal, since the spectrum is strongly dominated by the pleochroic band at 24000 cm^{-1}.

Wilkins *et al.*[4] assigned the 24000 cm^{-1} band to the d-d transition of Fe^{3+} ($^6A_1 \rightarrow {}^4A_1$, ^4E) which might be present in the aluminium position of dravite from Brazil containing 1.38% total Fe. On the other hand, Manning[5] assigned the band to the charge transfer of titanium ions located at Mg and Al site in a dravite sample containing Ti 1.15% and Fe 1.01% (the ratio Ti^{3+}:Ti^{4+} not known). According to his discussion lobes of t_{2g} orbitals of a cation located in the trigonal units are directed towards neighboring cations in the same trigonal units and in the spiral chains, making t_{2g}-t_{2g} orbital overlap in the 001 plane. Thus the charge transfer is most likely to occur in the trigonal cation plane, as represented by the E⊥c spectra. A small fraction of the Ti^{3+} is located in the spiral chains which run parallel to the c-axis. Metal-metal orbital overlap also takes place. The transition t_{2g}-e_g would have appreciable intensity in E//c spectra.

The key to the assignment of the 24000 cm^{-1} band should be found in the out-of-phase spectra, where an appreciable band intensity is observed in the E⊥c spectra and none in the E//c spectra. This shows that the band at 24000 cm^{-1} in the in-phase E⊥c spectra consists of thermally delayed signal (slow heat) with a certain contribution from fast heat component, while that in the in-phase E//c spectra entirely consists of the fast heat component. Assuming that the transition occurs only between the two energy levels concerned, a rough estimation of the characteristic lifetime of the slow heat is made by means of the relation

$$\tan\theta = 2\pi\nu\tau,$$

where θ is the phase delay angle and ν the chopping frequency. With the data of ν=80 Hz and θ=10.0°, lifetime τ is obtained as slow as $3\text{—}4\times10^{-4}$ s. This suggests that the transition responsible for the slow heat is due to the forbidden d-d type transition. The fast heat should be attributed to the allowed charge transfer type transition and order of magnitude greater than the d-d transition. Consequently the 24000 cm^{-1} band in the in-phase E⊥c spectra should be assigned to the d-d ($^6A_1$—$^4A_1$, ^4E) transition of Fe^{3+} as proposed by Wilkins *et al.*, as well as to the charge transfer of $Ti^{3+}\rightarrow Ti^{4+}$ as proposed by Manning. The band in the in-phase E//c spectra should be assigned entirely to the charge transfer of Ti located in the spiral chains of Al-centered octahedra as explained by Manning. Although the ratio of the contributions from the d-d transition of Fe and the charge transfer of Ti is not known in the in-phase E⊥c spectra, the latter contribution should not be completely neglected, since the tourmaline sample contains 0.32% Ti which exceeds the detectable amount for the charge transfer band as in the in-phase E//c spectra.

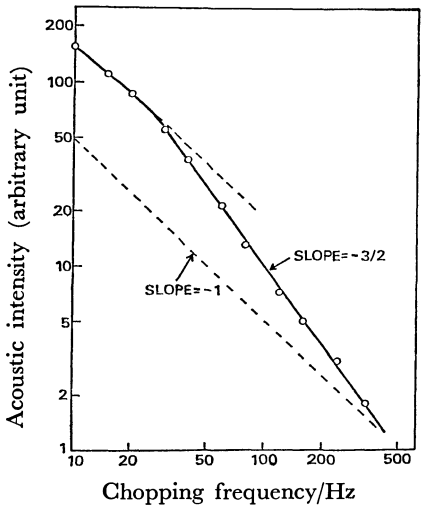

Fig. 2. A log-log plot of the photoacoustic intensity *versus* chopping frequency for brown tourmaline at 588 nm.

Thermal Diffusivity of Tourmaline. By photoacoustic study we can measure the thermal diffusivity of materials, since the intensity of photoacoustic signal depends on the thermal characteristics of the specimen as well as on the extent of the optical absorption. Adams and Kirkbright[9] estimated the thermal diffusivity of macromolecular film by measurement of phase delay as a function of the chopping frequency. An alternative way of measuring the thermal diffusivity of materials is presented here by way of the analysis of the photoacoustic signal intensity as a function of the chopping frequency.

Rosencwaig and Gersho[10] solved a heat flow equation for the treatment of the photoacoustic effect, and showed six cases depending on the relative magnitude of the optical absorption length μ_β and the thermal diffusion length μ_s with respect to the thickness l of the material. The μ_β is defined as an inverse of the optical absorption coefficient β, μ_s being defined by $\mu_s=\sqrt{2\alpha/\omega}$, where α is thermal diffusivity of the material. The photoacoustic signal would show ω^{-1} dependence for the case $\mu_s>l$ corresponding to the cases 1a and 1b, and $\omega^{-3/2}$ dependence for the case $\mu_s<l$ corresponding to the case 1c.[10,11]

The experiment on the tourmaline sample with thickness of l=0.044 cm belongs to the $\mu_\beta>l$ case (case 1), since the μ_β value is obtained as 0.08 cm at the wavelength 588 nm.

Figure 2 shows the plots of the photoacoustic intensity of the toumaline sample as a function of the chopping frequency. With the increase of ω it moves at around $\omega/2\pi$=25 Hz from a region where the dependence is primarily ω^{-1} to another region where it is $\omega^{-3/2}$. The moving point corresponds to the state of $\mu_s=l$, giving the thermal diffusivity α as

$$\mu_s = l = 0.044 = \sqrt{\frac{\alpha}{\pi\times25}}$$

$$\alpha \approx 0.15\ \mathrm{cm^2\ s^{-1}}.$$

A similar procedure was applied to a synthetic ruby sample with l=0.025 cm, giving the value of α=0.12 cm^2 s^{-1}, very close to that of tourmaline.

The authors wish to express their thanks to Prof. Kozo Nagashima, The University of Tsukuba, for his valuable advice. The work was partially supported by a Grant-in-Aid for Scientific Research No. 484032 from the Ministry of Education, Science and Culture.

References

1) J. D. Dana and E. S. Dana, "The System of Mineralogy," 7th ed, ed by C, Palache, H. Berman, and C. Frondel, John Wiley and Sons, Inc., London (1952).
2) H. Strunz, "Mineralogische Tabellen," 7th ed, Akad. Verlag., Leipzig (1978), p. 407.
3) R. G. Burns, "Mineralogical Applications of Crystal Field Theory," Cambridge University Press (1970).
4) R. W. T. Wilkins, E. F. Farrell, and C. S. Naiman, *J. Phys. Chem. Solids*, **30**, 43 (1969).
5) R. G. Manning, *Can. Miner.*, **9**, 678 (1969).
6) G. Donnay and M. J. Buerger, *Acta Crystallogr.*, **3**, 379 (1950).
7) Y. Sugitani and K. Kato, *Bull. Chem. Soc. Jpn.*, **52**, 3499 (1979).
8) K. Kato and Y. Sugitani, *Bull. Chem. Soc. Jpn.*, **52**, 3733 (1979).
9) M. J. Adams and G. F. Kirkbright, *Analyst*, **102**, 281, 678 (1977).
10) A. Rosencwaig and A. Gersho, *J. Appl. Phys.*, **47**, 64 (1976).
11) A. Rosencwaig, *Rev. Sci. Instrum.* **48**, 1133 (1977).

Absorption, Circular Dichroism, and Nuclear Magnetic Resonance Studies of Bis(acetylacetonato)cobalt(III) Complexes Containing 2-Aminoalkylphosphine Chelates with Phosphorus and Nitrogen Donor Atoms

Kazuo KASHIWABARA, Isamu KINOSHITA,† Tasuku ITO,†† and Junnosuke FUJITA*

Department of Chemistry, Faculty of Science, Nagoya University, Chikusa-ku, Nagoya 464

††*Institute for Molecular Science, Myodaiji, Okazaki 444*

(Received October 6, 1980)

Bis(acetylacetonato)cobalt(III) complexes containing a variety of 2-aminoalkylphosphines, $NH_2CH_2CH_2P(C_6H_5)_2$, $(CH_3)_2NCH_2CH_2P(C_6H_5)_2$, (*S*)-$NH_2CH(CH_3)CH_2P(C_6H_5)_2$, *rac*-$NH_2CH_2CH_2P(CH_3)(C_6H_5)$, (*R*)-$NH_2CH_2CH_2P(C_4H_9)(C_6H_5)$, and $NH_2CH_2CH_2P(CH_3)_2$, and a diphosphine, $(C_6H_5)_2PCH_2CH_2P(C_6H_5)_2$ were prepared and resolved (or separated) into optical isomers by SP-Sephadex column chromatography. Absorption, circular dichroism, and ^1H and ^{13}C NMR spectra of the new complexes were measured and the results compared with those of the related complexes. Positions of the 2-aminoalkylphosphine and the related ligands in the spectrochemical series were as follows; $CN^- > NH_2CH_2CH_2P(CH_3)_2 > (C_6H_5)_2PCH_2CH_2P(C_6H_5)_2 > NH_2CH_2CH_2P(CH_3)(C_6H_5) \geqq NH_2CH_2CH_2P(C_4H_9)(C_6H_5) > NH_2CH(CH_3)CH_2P(C_6H_5)_2 \geqq NH_2CH_2CH_2P(C_6H_5)_2 \geqq NH_2CH_2CH_2NH_2 > (CH_3)_2NCH_2CH_2P(C_6H_5)_2$. For the ^{13}C NMR spectra, all the signals including those due to two diastereotopic phenyl groups on a phosphorus atom were assigned, and the chemical shifts and the coupling constants were determined. The methyl and carbonyl carbons which are *trans* to a phosphorus atom give a doublet signal due to four-bond (^4J(C,P)=6—7 Hz) and three-bond (^3J(C,P)=2—3 Hz) couplings, respectively, through a cobalt(III) ion.

A 2-aminoalkylphosphine can act as a bidentate ligand with phosphorus and nitrogen donor atoms, forming a five-membered chelate ring. Issleib and his coworkers prepared 2-aminoethyldiphenylphosphine[1] and its derivatives including those with a chiral phosphorus atom.[2] However, little metal complexes with such ligands have been prepared[3] and no cobalt(III) complex seems to be reported. A cobalt(III) ion which belongs to a hard acid would prefer a hard base such as a nitrogen or oxygen donor atom rather than a phosphorus donor atom which belongs to a soft base,[4] and a few cobalt(III)–phosphine complexes have been known.[5] Since 2-aminoalkylphosphines have an amino group which can strongly coordinate to a cobalt(III) ion, they might form stable chelate complexes facilitating the bond-formation between cobalt(III) and phosphorus. In this paper, we have prepared bis(acetylacetonato)cobalt(III) complexes of various 2-aminoalkylphosphines, resolved or separated them into optically active forms, and characterized the complexes by absorption, circular dichroism (CD), and ^1H and ^{13}C NMR spectroscopy. The results would be useful for studying detailed stereochemistry of other chiral metal phosphine complexes which recently attract much attention as complex catalysts in asymmetric hydrogenation of some organic compounds.[6]

Experimental

Free aminophosphines were handled under nitrogen atmosphere until they formed air-stable cobalt(III) complexes. Solvents were dried in the usual way and degassed by distillation in a stream of pure nitrogen. Absorption, CD, and ^1H and ^{13}C NMR spectra were recorded on a Hitachi 323 spectrophotometer, a JASCO J-40 spectropolarimeter, and JEOL JNM-PMX 60 and JNM-FX 100 spectrometers, respectively. Low-temperature absorption and CD measurements were made using a Union Giken SM 404 spectrophotometer and a JASCO J-40 spectropolarimeter, respectively, equipped with a Oxford Cryostat CF 204 and a DTC-2-CLOl controller.

Preparation of Aminophosphines. 2-Aminoethyldiphenylphosphine: The method of Issleib and Haferburg[1] was modified. Small pieces of lithium metal (1.7 g, 240 mmol) were added to a refluxing tetrahydrofuran (THF) solution (300 cm^3) of triphenylphosphine (32.5 g, 120 mmol). The mixture was refluxed for 6 h with stirring to give a deep red solution. *t*-Butyl chloride (11.5 g, 114 mmol) was added dropwise to the solution with stirring under cooling in an ice–salt bath. After 1 h, aziridine (7.0 g, 160 mmol) was added dropwise to the solution at 60 °C, which was then refluxed for 8 h and filtered. To the filtrate was added water (5 cm^3) dropwise and then anhydrous magnesium sulfate (*ca.* 10 g) to remove excess water. The mixture was stirred for 5 h and permitted to stand for a while. The desicant was filtered and the residue was washed with diethyl ether. The filtrate and washings were combined and the solvents were evaporated under reduced pressure. The residue was distilled to give viscous liquid at *ca.* 150 °C and *ca.* 60 Pa. Yield: 6.5 g (60%).

(S)-2-Aminopropyldiphenylphosphine: Hydrogen chloride gas was bubbled into a chloroform solution (50 cm^3) of (*S*)-2-amino-1-propanol[7] (5 g, 65 mmol), yielding a red oily product. $SOCl_2$ (7 cm^3, 100 mmol) was added to the solution dropwise with stirring. The resulting solution was gradually warmed, refluxed for 4 h, and allowed to stand overnight at room temperature. Needle crystals of (*S*)-1-chloro-2-aminopropane hydrochloride (3.3 g) thus formed were filtered. They were then added to sodium diphenylphosphide which was prepared from 1.8 g of sodium metal and 5.6 g of chlorodiphenylphosphine in liquid ammonia (70 cm^3). The solution was stirred for 3 h and mixed with THF (100 cm^3). Liquid ammonia was evaporated at room temperature, and the solution was filtered. The filtrate was concentrated under reduced pressure and an oily product remained was distilled to give colorless liquid at *ca.* 130 °C and *ca.* 10 Pa. Yield: 1.5 g.

2-Aminoethylmethylphenylphosphine: This was prepared from lithium methylphenylphosphide[8] and aziridine by a method similar to that for 2-aminoethyldiphenylphosphine. The

† Present address: Department of Chemistry, Faculty of Science, Osaka City University, Sumiyoshi-ku, Osaka 558,

TABLE 1. ANALYTICAL DATA OF THE NEW COMPLEXES

Complex		C% Found(Calcd)	H% Found(Calcd)	N% Found(Calcd)
$[Co(acac)_2\{NH_2CH_2CH_2P(C_6H_5)_2\}]PF_6$	**1**	45.50(45.65)	4.84(4.79)	2.17(2.22)
$[Co(acac)_2\{(CH_3)_2NCH_2CH_2P(C_6H_5)_2\}]PF_6$	**2**	47.35(47.36)	5.04(5.20)	2.20(2.12)
$[Co(acac)_2\{NH_2CH(CH_3)CH_2P(C_6H_5)_2\}]PF_6\cdot H_2O$(F-I)	**3a**	45.32(45.25)	5.02(5.17)	2.25(2.11)
$[Co(acac)_2\{NH_2CH(CH_3)CH_2P(C_6H_5)_2\}]PF_6\cdot H_2O$(F-II)	**3b**	45.11(45.25)	5.31(5.17)	2.25(2.11)
$[Co(acac)_2\{NH_2CH_2CH_2P(CH_3)(C_6H_5)\}]B(C_6H_5)_4$(F-I)	**4a**	69.05(69.46)	6.37(6.51)	1.67(1.88)
$[Co(acac)_2\{NH_2CH_2CH_2P(CH_3)(C_6H_5)\}]B(C_6H_5)_4$(F-II)	**4b**	69.99(69.46)	6.56(6.51)	2.33(1.88)
$[Co(acac)_2\{NH_2CH_2CH_2P(CH_3)(C_6H_5)\}]PF_6\cdot 1/2H_2O$(F-II)	**4c**	39.99(39.73)	4.88(4.38)	2.40(2.40)
$[Co(acac)_2\{NH_2CH_2CH_2P(C_4H_9)(C_6H_5)\}]B(C_6H_5)_4$(F-I)	**5a**	70.28(70.32)	7.10(6.93)	2.06(1.78)
$[Co(acac)_2\{NH_2CH_2CH_2P(C_4H_9)(C_6H_5)\}]B(C_6H_5)_4$(F-II)	**5b**	70.27(70.32)	7.20(6.93)	2.10(1.78)
$[Co(acac)_2\{NH_2CH_2CH_2P(CH_3)_2\}]Br\cdot H_2O$	**6**	36.27(36.54)	6.06(6.13)	3.04(3.04)
$[Co(acac)_2\{(C_6H_5)_2PCH_2CH_2P(C_6H_5)_2\}]PF_6$	**7**	54.10(54.01)	4.91(4.78)	——

acac=$C_5H_7O_2^-$

optical resolution was unsuccessful with $(+)_{589}$-di-μ-chloro-bis[(*S*)-*N*,*N*-dimethyl-α-methylbenzylamine-2*C*,*N*]dipalladium(II).[9] Yield: 25%.

Other 2-aminoalkylphosphines: (*R*)-2-Aminoethylbutylphenylphosphine,[10] 2-(dimethylamino)ethyldiphenylphosphine,[11] and 2-aminoethyldimethylphosphine[12] were prepared according to the methods reported.

Preparation of $[Co(acac)_2(L)]^+$ *Complexes. L=achiral phosphines*; $NH_2CH_2CH_2P(C_6H_5)_2$, $(CH_3)_2NCH_2CH_2P(C_6H_5)_2$, *and* $NH_2CH_2CH_2P(CH_3)_2$: A methanol solution containing $[Co(acac)_3]$ and an achiral phosphine (1:1) was stirred with active charcoal overnight at room temperature. The resulting dark red solution was filtered, adjusted the pH to *ca.* 7 with hydrochloric acid, and diluted ten times with water. This was passed through a column ($\phi 3\times 120$ cm) of an SP-Sephadex C-25 ion exchanger. The product adsorbed was eluted with a 0.02 mol/dm^3 aqueous solution of Na_2SO_4. A main red violet eluate was saturated with NaCl and the complex was extracted with chloroform except for the case of 2-aminoethyldimethylphosphine complex. The chloroform was removed under reduced pressure and the residue was dissolved in water. The complex was precipitated by the addition of excess $NaPF_6$. The 2-aminoethyldimethylphosphine complex was isolated as tetraphenylborate by the addition of $NaB(C_6H_5)_4$ to the main red violet eluate which had been concentrated under reduced pressure. The tetraphenylborate was converted to bromide with a Dowex 1×8 ion exchanger in methanol.

L=chiral phosphines; (S)-$NH_2CH(CH_3)CH_2P(C_6H_5)_2$, *rac*-$NH_2CH_2CH_2P(CH_3)(C_6H_5)$, *and* (R)-$NH_2CH_2CH_2P(C_4H_9)$-$(C_6H_5)$: The complexes were prepared by a method similar to that for 1). By elution with a 0.02 mol/dm^3 aqueous sodium $(+)_{589}$-tartratoantimonate(III) solution, two red violet bands, F-I and F-II were obtained, F-I being eluted faster than F-II. From the eluates, a pair of diastereomers, $\Lambda(S)$ (F-I) and $\Delta(S)$ (F-II) for the optically active aminophosphines,[13] and $\Delta(R)$-$\Lambda(S)$ (F-I) and $\Lambda(S)$-$\Delta(R)$ (F-II) for the racemic aminophosphine, were isolated as hexafluorophosphate or tetraphenylborate by a method similar to that described for 1) (Table 1). Δ and Λ represent the absolute configuration of a cobalt(III) ion, and *R* and *S* that of a phosphorus and carbon atom.

Bis(acetylacetonato)[1,2-bis(diphenylphosphino)ethane]cobalt(III) hexafluorophosphate: This was prepared from $[Co(acac)_3]$ and 1,2-bis(diphenylphosphino)ethane (Strem. Chem. Inc.) by a method similar to that for the aminophosphine complexes.

Optical Resolution: Resolutions of the $NH_2CH_2CH_2P$-$(C_6H_5)_2$ and $(C_6H_5)_2PCH_2CH_2P(C_6H_5)_2$ complexes were attempted by SP-Sephadex column chromatography using a 0.02 mol/dm^3 aqueous sodium $(+)_{589}$-tartratoantimonate(III) solution as an eluent. However, the bands of enantiomers were separated incompletely, so that the chromatography was repeated until no further increase in $\Delta\varepsilon/\varepsilon$ values for the first and the last fractions was observed. From the eluates, the optical isomers were isolated by a method similar to that for the racemates. Resolutions of the methylphenyl- and dimethyl-phosphine complexes were poor in similar SP-Sephadex column chromatography.

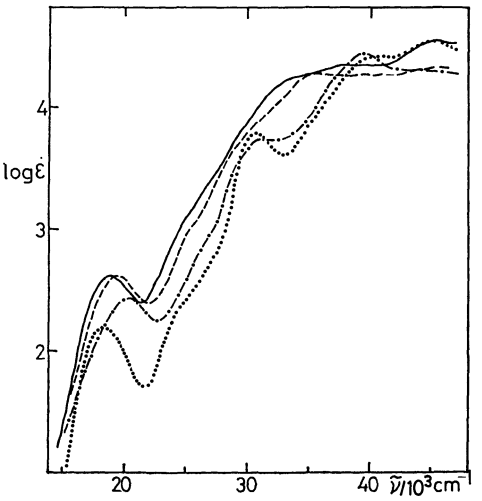

Fig. 1. Absorption spectra of complexes, **1**(———), **4c**(------), **6**(—·—·—·—), and $[Co(acac)_2(en)]ClO_4$ (·····) in ethanol.

Analytical data of the new complexes are given in Table 1.

Results and Discussion

Absorption Spectra. Reports have been given on the spectrochemical series of various unidentate[14,15] and bidentate[16] phosphine ligands, although there are some discordances among the reports. The bis(acetylacetonato)aminophosphine–cobalt(III) complexes prepared in this study show the first absorption bands around 20000 cm^{-1} with fairly strong intensity. Figure 1 shows absorption spectra of the NH_2CH_2-$CH_2P(CH_3)_n(C_6H_5)_{2-n}$ (n=0,1,2) complexes along

Table 2. Absorption (AB) and CD spectral data in the region of the first absorption band

Complex	$\nu^{AB}/10^3$ cm^{-1}(log ε)	$\nu^{CD}/10^3$ cm^{-1}($\Delta\varepsilon$)
1	18.83(2.67)	16.56(−1.83)
		18.18(+1.74)
		20.24(−7.05)
2	18.05(2.56)	
3a	18.92(2.62)	16.64(+2.26)
		18.35(−2.14)
		20.37(+6.97)
3b	18.97(2.61)	16.75(−2.46)
		18.25(+1.31)
		20.28(−8.54)
4a	19.65(2.40)	
4b, 4c	19.51(2.62)	
5a	19.51(2.51)	16.65(+3.25)
		18.59(−3.68)
		20.66(+5.17)
5b	19.49(2.63)	16.58(−1.82)
		18.43(+2.99)
		20.58(−8.00)
6	20.35(2.43)	
7	20.16(2.99)	16.26(−1.22)
		18.38(+8.76)
		20.70(−16.8)
8[a]	18.58(2.20)	16.67(−1.11)
		19.70(−4.46)
9[b]	19.0 (1.97)	
	ca. 23.3 (2.45)	

a) **8**: $[Co(acac)_2(NH_2CH_2CH_2NH_2)]ClO_4$, R. D. Archer and B. P. Cotsoradis, *Inorg. Chem.*, **4**, 1584 (1965). b) **9**: $K[Co(CN)_2(acac)_2]$.[18]

with that of the corresponding ethylenediamine complex for comparison. Spectral data of all the aminophosphine and the related complexes are summarized in Table 2. When a phenyl group on a phosphorus atom is replaced by a methyl group, the absorption peaks shift to higher energy. The spectrochemical series of the ligands is determined as $CN^- > NH_2CH_2CH_2P(CH_3)_2 > (C_6H_5)_2PCH_2CH_2P(C_6H_5)_2 > NH_2CH_2CH_2P(CH_3)(C_6H_5) \geqq NH_2CH_2CH_2P(C_4H_9)(C_6H_5) > NH_2CH(CH_3)CH_2P(C_6H_5)_2 \geqq NH_2CH_2CH_2P(C_6H_5)_2 \geqq NH_2CH_2CH_2NH_2 > (CH_3)_2NCH_2CH_2P(C_6H_5)_2$, and that of the donor groups as $CN^- > -P(CH_3)_2 > -P(CH_3)(C_6H_5) \geqq -P(C_4H_9)(C_6H_5) > -P(C_6H_5)_2 \geqq -NH_2 > -N(CH_3)_2$. Since a phosphorus donor group occupies a fairly higher position than an acetylacetonate ion in the spectrochemical series, it is expected that the first absorption band of a bis(acetylacetonato)phosphine–cobalt(III) complex splits into two components[17] as observed for analogous complexes, *cis*-$[Co(CN)_2(acac)_2]^-$ (19000 and *ca.* 23300 cm^{-1})[18] and *cis*-$[Co(CN)_2(C_2O_4)_2]^{3-}$ (18000 and 23400 cm^{-1}).[19] The 1,2-bis(diphenylphosphino)ethane complex (**7**) gives only a single broad band at 20160 cm^{-1} at 304 K. However, the band clearly exhibits two components at *ca.* 19400 and 20600 cm^{-1} at 173 K (Fig. 2). The 2-aminoethyldiphenylphosphine complex (**1**) shows no indication of such a splitting even at 173 K.

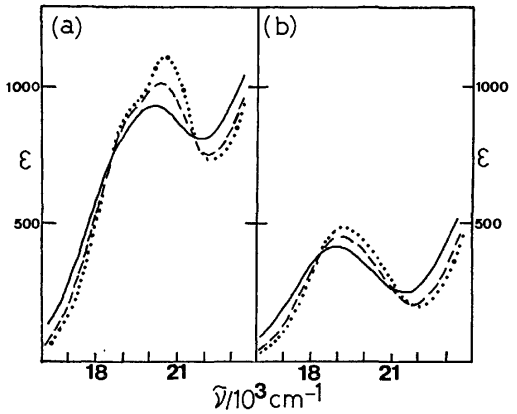

Fig. 2. Absorption spectra of complexes, **7**(a) and **1**(b) at 304 K (———), 223 K(------), and 173 K (·····) in ethanol.

The intensities of the first absorption bands increase with an increase in the number of phenyl groups on a phosphorus atom. Two diastereomers **4a** and **4b** show fairly different intensities from each other (ε(**4b**)/ε(**4a**)=1.7). However, the average intensity (2.51) of these isomers is nearly the same as that (2.55) of the diphenylphosphine (**1**) and the dimethylphosphine (**6**) complexes. The difference in intensity between diastereomers **4a** and **4b** might be related with the relative location of a phenyl group to an acetylacetonate ring, since the intensities of **4a** and **4b** are similar to those of the dimethylphosphine (**6**) and the diphenylphosphine (**1**) complexes, respectively. Complexes **4a** and **6**, and **4b** and **1** have a methyl and a phenyl group, respectively, over one acetylacetonate ring (*vide post*, Fig. 7). A similar difference in intensity is seen between diastereomers of the butylphenylphosphine complex, **5a** and **5b**.

The second absorption bands of the present complexes are hidden by intense absorptions due to charge transfer transitions between the ligands and the cobalt(III) ion or internal transitions of the ligands. The absorptions around 30500 and 33000 cm^{-1} could be assigned to those due to the acetylacetonate and phenylphosphine moieties, respectively.

Circular Dichroism Spectra. Absorption and CD spectra of complexes **1**, **7**, and $[Co(acac)_2(NH_2CH_2CH_2NH_2)]^+$ (**8**) are shown in Fig. 3, and the spectral data in Table 2 with those of the related complexes. In the region of the first absorption band, the CD intensities increase remarkably with an increase in absorption intensity. The phosphine complexes **1** and **7** show three CD bands with minus, plus, and minus signs from the low energy side, while the ethylenediamine complex (**8**) two negative CD bands. However, the CD spectrum of complex **8** shows remarkable temperature dependence in the region of the first absorption band and exhibits three

CD bands at 168 K (Fig. 4), the spectral pattern being very similar to those of complexes **1** and **7**. The phosphine complexes also show temperature dependence in the CD, but the spectral patterns remain unchanged (Fig. 4). The enantiomer of the ethylenediamine complex with the negative main CD band has been assigned to Λ configuration.[20] Thus both phosphine complexes in Fig. 3 can be assigned to the same Λ configuration. These enantiomers are those moving more slowly on columns of SP-Sephadex (Experimental).

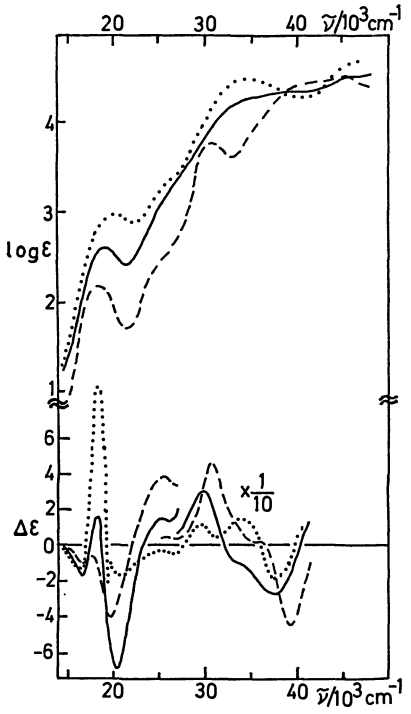

Fig. 3. Absorption and CD spectra of complexes, **1** (———), **7**(·····), and Λ-$[Co(acac)_2(en)]^+$ [20] (------) in ethanol.

A pair of diastereomers, $\Lambda(S)$ and $\Lambda(S)$ of the (S)-$NH_2CH(CH_3)CH_2P(C_6H_5)_2$ complex show CD spectra nearly enantiomeric to each other as observed for the corresponding diastereomers of the (S)-$NH_2CH_2CH_2P(C_4H_9)(C_6H_5)$ complex[21] (Fig. 5). The results indicate that the vicinal effects of the chiral ligands to CD are small compared with the configurational effect in these complexes. The vicinal and configurational effect curves were calculated in the usual way[21] (Fig. 6). The configurational effect CD curves of the (S)-$NH_2CH(CH_3)CH_2P(C_6H_5)_2$ and (S)-$NH_2CH_2CH_2P(C_4H_9)(C_6H_5)$ complexes are nearly the same as the CD spectrum of the $NH_2CH_2CH_2P(C_6H_5)_2$ complex, although the curve of the (S)-$NH_2CH_2CH_2P(C_4H_9)(C_6H_5)$ complex in the ultraviolet region deviates a little from the other curves probably because of the substituent variation on the donating phosphorus atom. Thus the additivity rule[22] for the configurational and vicinal effects can be applied to the CD spectra of cobalt(III) phosphine complexes. The vicinal effect CD curve of the (S)-$NH_2CH(CH_3)CH_2P(C_6H_5)_2$ chelate ligand should be caused by the chiral conformation and the chiral carbon atom. In general, the effect of a chiral conformation is much stronger than that of a non-ligating chiral atom,[23] and the effect of a δ-gauche chelate ring gives negative CD in the region of the first absorption band.[24] The vicinal effect CD curve of the (S)-$NH_2CH(CH_3)CH_2P(C_6H_5)_2$ ligand shows a negative main CD band in this region, indicating the δ-gauche conformation. When the ligand is in the δ-gauche form, the methyl group is disposed equatorially. The vicinal effect CD curve of the (S)-$NH_2CH_2CH_2P(C_4H_9)(C_6H_5)$ ligand shows two CD bands with different signs in the region of the first absorption band, the higher energy negative band being stronger than the lower energy positive one (Fig. 6). The chelate conformation of this ligand might not be fixed in a particular chirality, δ or λ,

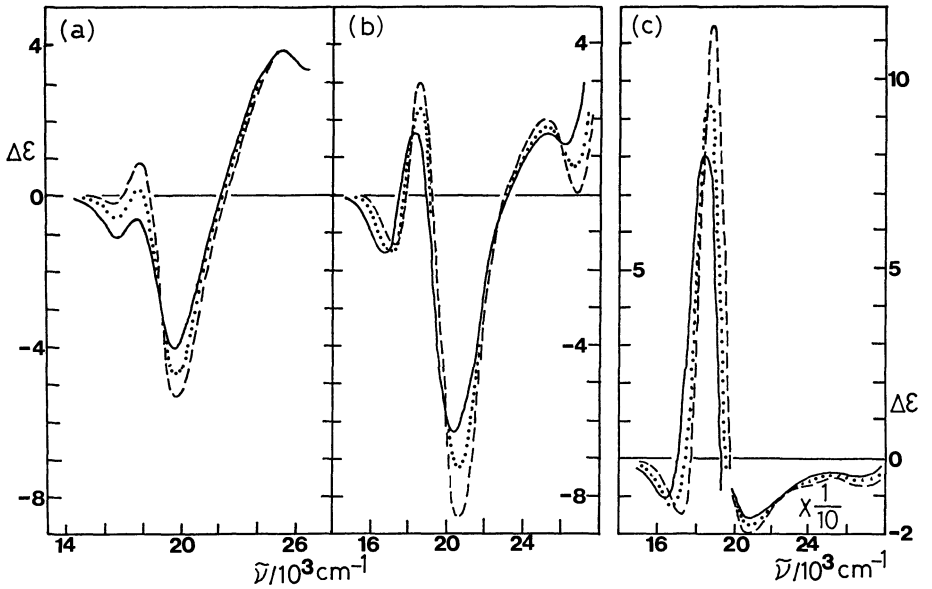

Fig. 4. CD spectra of complexes, Λ-$[Co(acac)_2(en)]ClO_4$(a), **1**(b), and **7**(c) at 298 K(———), 223 K(·····), and 168 K(------) in ethanol.

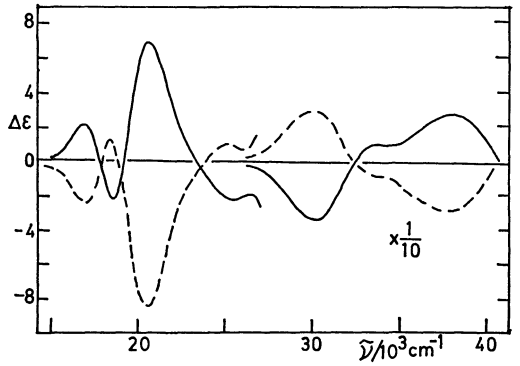

Fig. 5. CD spectra of complexes, **3a**(———) and **3b** (------) in ethanol.

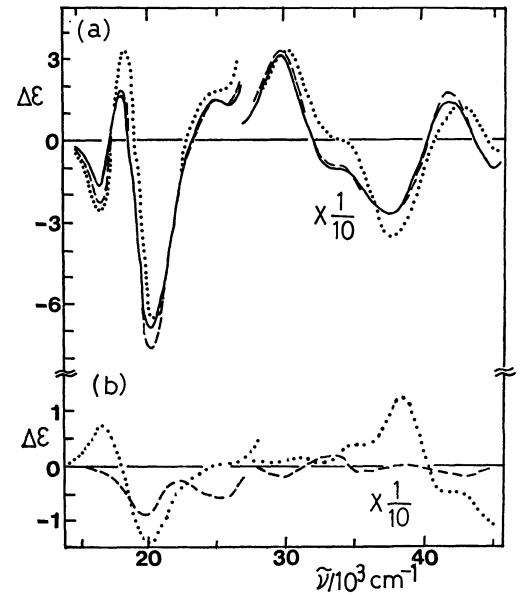

Fig. 6. (a) Calculated configurational CD curves of bis(acetylacetonato)cobalt(III) complexes of (*S*)-$NH_2CH(CH_3)CH_2P(C_6H_5)_2$ (--------) and (*R*)-$NH_2CH_2CH_2P(C_4H_9)(C_6H_5)$ (·····) and the CD spectrum of Δ-$[Co(acac)_2\{NH_2CH_2CH_2P(C_6H_5)_2\}]^+$ (———). (b) Calculated vicinal CD curves of bis(acetylacetonato)cobalt(III) complexes of (*S*)-$NH_2CH(CH_3)CH_2P(C_6H_5)_2$ (--------) and (*R*)-$NH_2CH_2CH_2P(C_4H_9)(C_6H_5)$ (·····).

since X-ray analysis on *trans*-$[CoCl_2\{(S)\text{-}NH_2CH_2CH_2P(C_4H_9)(C_6H_5)\}_2]ClO_4$ reveals that one chelate ring forms a δ-gauche conformation and the other λ-gauche one.[25] Hence, the vicinal effect of the (*S*)-$NH_2CH_2CH_2P(C_4H_9)(C_6H_5)$ ligand should arise primarily from the chiral phosphorus atom. The vicinal effect of such a chiral phosphorus donor atom seems to be as strong as that of a chiral nitrogen donor atom.[26] The relation between the CD sign and the absolute configuration remains unknown.

^1H NMR Spectra. ^1H NMR spectral data of the acetylacetonate group and the methyl group of phosphines in the aminophosphine and the related complexes are given in Table 3. The methine and methyl groups of acetylacetonate ligands give two or one, and four or two peaks, respectively, depending on the symmetry of the complexes. The methine signals

Table 3. ^1H NMR spectral data for the acac ligands[a]

Complex	δ(CH)/ppm		δ(CH_3)/ppm	
1	4.93	5.57	1.61	1.78
			1.96	2.29
2	4.97	5.69	1.62	1.77
			1.91	2.33
3a	4.94	5.55	1.51	1.80
			1.96	2.28
3b	4.81	5.56	1.74	1.77
			1.87	2.28
4a		5.44	1.82	1.97
		5.50	2.04	2.31
4b	4.78	5.58	1.54	1.86
			2.10	2.31
5a		5.47	1.55	2.05[d]
		5.52	2.29	
5b	4.87	5.57	1.46	1.91
			2.01	2.29
6		5.34	1.95[d]	2.00
		5.51	2.32	
7	4.93		1.64	1.88
8[b]		5.64	2.13	2.14
9[c]		5.55	1.94	2.21

a) Solvent: $CDCl_3$, internal reference: $Si(CH_3)_4$. b) **8**: $[Co(acac)_2(NH_2CH_2CH_2NH_2)]ClO_4$ in CD_3OD, R. J. York, W. D. Bonds Jr., B. P. Cotsoradis, and R. D. Archer, *Inorg. Chem.*, **8**, 789 (1969). c) **9**: $K[Co(acac)_2(CN)_2]$ in CD_3OD.[18] d) Peak intensity is twice those of others by accidental degeneracy.

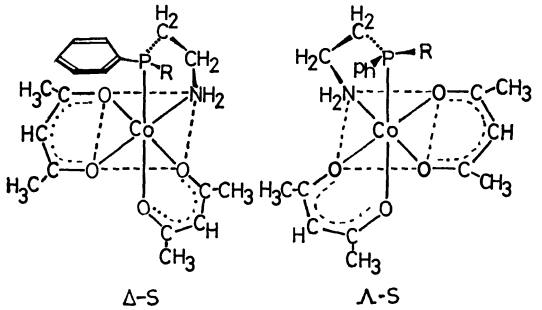

Fig. 7. Schematic structures of a pair of diastereomers of $[Co(acac)_2\{(S)\text{-}NH_2CH_2CH_2P(R)(C_6H_5)\}]^+$.

resonate in two fairly different regions, 4.78—4.99 and 5.34—5.69 ppm. In a pair of diastereomers of the (*S*)-$NH_2CH_2CH_2P(C_4H_9)(C_6H_5)$ complex, (**5a**, F-I, $\Delta(S)$) isomer gives two methine signals in the low field region, whereas (**5b**, F-II, $\Delta(S)$) isomer one methine signal in the low field and the other in the high field region. The phenyl group on the phosphorus atom in the $\Delta(S)$ isomer is disposed over one acetylacetonate ring and its methine proton is shielded by this phenyl ring to cause the high field shift.[21] On the other hand, the phenyl group of the $\Delta(S)$

Table 4. ^{13}C NMR spectral data for the phosphine ligands in δ/ppm[a)]

Complex	P-CH_3	P-CH_2-	N-CH_3	N-CH_2-	P-C_1	*o*-C	*m*-C	*p*-C
1		27.7		42.0	123.5	131.8	128.8	131.5
					127.0	133.5	128.9	132.2
2		24.5	48.8	62.5	123.9	131.8	129.1	131.7
			49.4		127.0	133.4	129.2	132.1
4a[b)]	7.6	29.5		41.5	126.3	132.3	129.0	131.1
4c	5.7	28.4		42.1	127.6	131.2	129.2	132.0
6	7.1	30.7		41.6				
	8.2							
7		23.5			122.8	131.9	128.5	131.2
					127.0	133.8	128.8	132.2
Free ligand[c)]								
I		32.5		39.0	138.4	132.7	128.5	128.7
II	10.7	34.5		38.2	139.3	130.5	127.5	127.6
III		23.8			138.2	132.8	128.5	128.7

a) Solvent: $CDCl_3$, internal reference: $Si(CH_3)_4$. b) The tetraphenylborate was converted to bromide by an ion exchanger. c) I=$NH_2CH_2CH_2P(C_6H_5)_2$, II=$NH_2CH_2CH_2P(CH_3)(C_6H_5)$, III=$(C_6H_5)_2PCH_2CH_2P(C_6H_5)_2$.

Table 5. ^{31}P-^{13}C coupling constants for the phosphine ligands in ^nJ/Hz

Complex	P-CH_3	P-CH_2-	N-CH_2-	P-C_1	*o*-C	*m*-C	*p*-C
1		27.3		48.3	9.0	10.3	4.5
				47.0	7.3	11.0	2.3
2		26.9	2.5	50.0	8.6	9.8	3.7
				47.7	6.1	11.5	2.5
4a[a)]	25.6	28.1		50.0	7.3	10.9	<3
4c	29.3	28.1		47.6	8.5	11.0	3.7
6	29.3	26.9					
	26.9						
7[b)]		42.0		43.5	8.0	10.3	
				45.5	7.3	8.8	
Free ligand[c)]							
I		12.2	20.8	12.2	18.3	7.3	
II	13.4	12.2	17.1	13.5	18.3	6.1	
III		0		13.6	18.5	7.8	

a) The tetraphenylborate was converted to bromide by an ion exchanger. b) All signals are a triplet, the values being $|J_{AX}+J_{Bx}|$ of an ABX pattern (X=^{13}C). c) I, II, and III; see Table 4.

isomer is disposed far from two acetylacetonate rings to give their methine signals at similar frequencies in the low field region (Fig. 7). A pair of diastereomers, (**4a**, F-I) and (**4b**, F-II) of the $NH_2CH_2CH_2P(CH_3)(C_6H_5)$ complex give very similar spectra to those of complexes **5a** and **5b**, respectively, and can be assigned to the $\Lambda(S)$-$\Lambda(R)$ and $\Lambda(S)$-$\Lambda(R)$ racemic pairs, respectively. From the strength of such well separated methine signals, the formation ratio of F-II/F-I for the (*S*)-$NH_2CH_2CH_2P(C_4H_9)(C_6H_5)$ complex was determined to be *ca.* 2.7. The same shielding effect of a phenyl group to methine protons of the acetylacetonate ligands is observed for all the other phenylphosphine complexes. The diphosphine complex **7** gives a sharp singlet in the high field region by this effect. No assignment for the methyl group was made because of complexity.

^{13}C NMR Spectra. ^{13}C NMR spectral data of the phosphine complexes and the free ligands measured in this study were summarized in Tables 4, 5, and 6. The assignments were made on the basis of the chemical shifts, the magnitudes of coupling constants, the intensities, and the off-resonance spectra. A representative spectrum (complex **4c**) is shown in Fig. 8.

Spectral Assignments for Diastereotopic Phenyl Carbons: The diphenylphosphine complexes, **1**, **2**, and **7** give complicated spectra in the phenyl region (Fig. 9), since the two phenyl groups in each complex are diastereotopic to each other. Such complicated spectra were successfully assigned by comparing with spec-

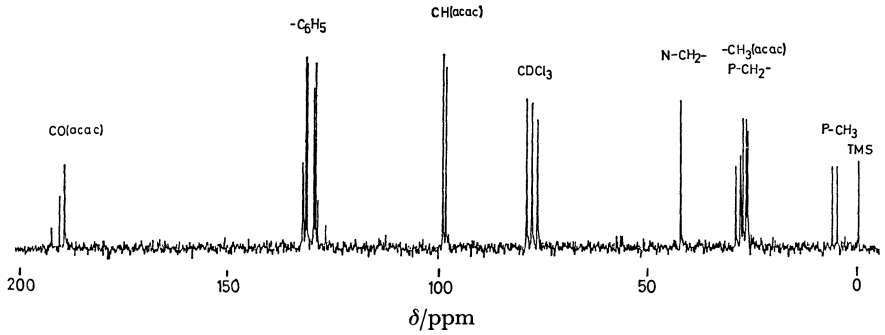

Fig. 8. The ^{13}C NMR spectrum of complex **4c**.

Table 6. ^{13}C NMR spectral data for the acac ligands in δ/ppm (^{n}J(C,P)/Hz)[a)]

Complex	CH_3	CH	CO
1	26.1	98.2	187.7
	26.2		188.8
	26.4		189.5
	27.5(7.3)		191.3(2.3)
2	26.0	98.5	187.7
	26.2	98.8	189.0
	26.5		189.9
	27.6(7.3)		191.4(2.5)
4a	26.6	98.6	188.8
	26.8		189.2
	27.1		190.9
	27.8(6.1)		191.0(3.7)
4c	26.2	98.1	188.5
	26.6	98.9	188.6
	27.3		189.7
	27.9(6.1)		191.5(3.8)
6	26.5	98.8	188.3
	26.8		189.1
	27.5		190.9
	28.1(6.1)		191.6(3.7)
7	26.3	98.2	186.8
	27.4		189.5
$[Co(acac)_3]$	27.5	97.6	189.2

a) Solvent: $CDCl_3$, internal reference: $Si(CH_3)_4$.

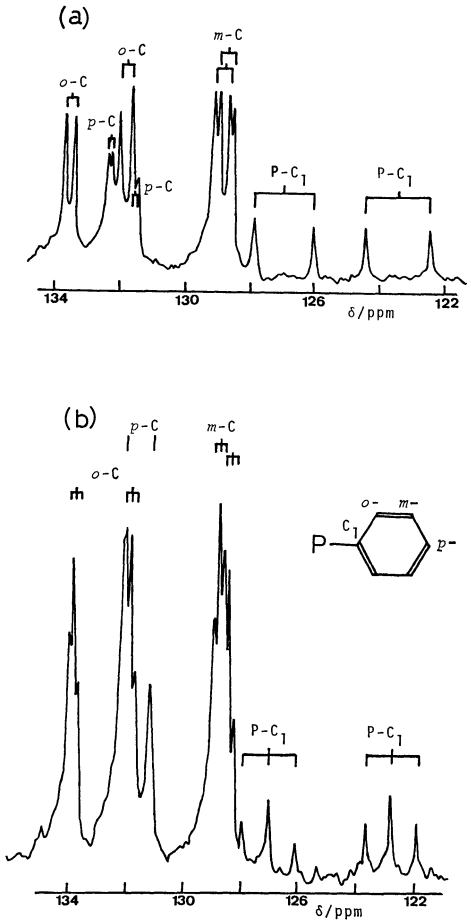

Fig. 9. ^{13}C NMR spectra of complexes, **1**(a) and **7**(b) in the phenyl region.

tra of the methylphenylphosphine complexes, **4a** and **4c**. These complexes are a pair of diastereomers formed with the ligand having a single phenyl group and thereby give a simple spectrum in the phenyl region (Fig. 10). The spectrum of **4c** isomer in Fig. 10 consists of four kinds of doublets. The carbon bonded to the phosphorus atom ($P-C_1$) and the *p*-carbon were assigned on the bases of the off-resonance and the intensities. The *o*- and *m*-carbons can be assigned from their chemical shifts. It is known that the chemical shift of *m*-carbon of a monosubstituted benzene remains almost unchanged from that of benzene, 128.7 ppm.[27] Thus the doublet at 129.2 ppm is assigned to the *m*-carbon and the remaining doublet at 131.2 ppm to the *o*-carbon. Table 5 gives the coupling constants, ^{n}J(C,P) observed from the spectra.

The spectrum in the phenyl region of another isomer, **4a** was similarly assigned, although the doublet of the *p*-carbon is overlapped by one of the doublet signals of the *o*-carbon. With the aid of the chemical shifts and the coupling constants for these isomers, the complicated phenyl signals of the diphenylphosphine complexes, **1**, **2**, and **7** were assigned (Fig. 9 and Tables 4 and 5).

Carbon-Phosphorus Couplings through a Cobalt(III) Ion: Four methyl and four carbonyl carbons of two acetylacetonate ligands in the aminophosphine complexes exhibit fairly different chemical shifts in the region of each kind of carbons (Fig. 11 and Table 6). Furthermore, each one of the methyl and carbonyl carbons

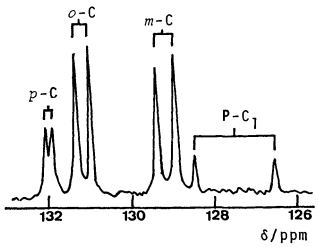

Fig. 10. The ^{13}C NMR spectrum of complex **4c** in the phenyl region.

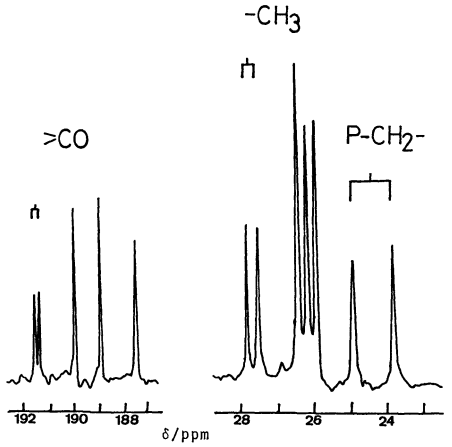

Fig. 11. ^{13}C NMR spectra of complex **2** in the methyl and carbonyl regions.

gives a doublet due to coupling with a phosphorus atom *trans* to the carbon, ^4J(C,P) and ^3J(C,P), respectively. Both doublet are observed at the lowest field among each kind of carbons and the values of ^4J(C,P) for the methyl and ^3J(C,P) for the carbonyl carbons are 6—7 and 2—4 Hz, respectively. Such long-range couplings through a cobalt(III) ion would be useful for assigning structures of cobalt(III)–phosphine complexes. No coupling between carbon and phosphorus in the *cis* positions is observed.

Spectral Parameters in Free and Complexed Aminoalkylphosphines: Spectral data of the free and complexed aminoalkylphosphines are given in Tables 4 and 5. The effects of coordination of the ligands on spectral parameters are summarized as follows.

1) Carbons bonded to a phosphorus atom shift to an upfield upon coordination, and the coupling constants, ^1J(C,P) become much larger.

2) Methylene carbons bonded to a nitrogen atom shift slightly to a downfield upon coordination, and no coupling with a phosphorus atom is observed.

3) Chemical shifts of P–C_1 and *o*-carbon atoms depend largely on the kind of compounds, but those of *m*- and *p*-carbon atoms do not. Such trends are similar to those for monosubstituted benzenes.

These features will provide useful information not only for assigning ^{13}C NMR spectra of cobalt(III) phosphine complexes, but also for elucidating bonding properties between a phosphorus atom and a cobalt(III) ion.

This work was partially supported by a Grant-in-Aid for Scientific Research No. 454194 from the Ministry of Education, Science and Culture and The Kurata Research Grant of the Kurata Foundation, and by the Joint Studies Program (1980—1981) of the Institute for Molecular Science.

References

1) K. Issleib and D. Haferburg, *Z, Natureforsch., Teil B*, **20**, 916 (1965).
2) K. Issleib and H. Oehme, *Chem. Ber.*, **100**, 2685 (1967).
3) K. Issleib, A. Kipke, and V. Hahnfeld, *Z. Anorg. Allg. Chem.*, **444**, 5 (1978); K. Issleib and A. Kipke, *ibid.*, **464**, 176 (1980).
4) R. G. Pearson, *J. Am. Chem. Soc.*, **85**, 3533 (1963); *J. Chem. Educ.*, **45**, 581, 643 (1968).
5) C. A. McAuliffe and W. Levason, "Phosphine, Arsine, and Stibine Complexes of the Transition Elements," Elsevier, Amsterdam (1979).
6) J. M. Brown and P. A. Chaloner, *J. Am. Chem. Soc.*, **102**, 3040 (1980); K. Kashiwabara, K. Hanaki, and J. Fujita, *Bull. Chem. Soc. Jpn.*, **53**, 2275 (1980).
7) P. Karrer, P. Portmann, and M. Suter, *Helv. Chim. Acta*, **31**, 1617 (1948).
8) N. K. Roberts and S. B. Wild, *J. Am. Chem. Soc.*, **101**, 6254 (1979).
9) K. Tani, L. D. Brown, J. Ahmed, J. A. Ibers, M. Yokota, A. Nakamura, and S. Otsuka, *J. Am. Chem. Soc.*, **99**, 7876 (1977).
10) I. Kinoshita, K. Kashiwabara, and J. Fujita, *Bull. Chem. Soc. Jpn.*, **53**, 3715 (1980).
11) D. W. Meek, P. E. Nicpon, and V. I. Meek, *J. Am. Chem. Soc.*, **92**, 5351 (1970).
12) I. Kinoshita, K. Kashiwabara, J. Fujita, K. Matsumoto, and S. Ooi, *Chem. Lett.*, **1980**, 95.
13) The configuration of the *R* phosphorus atom in the free ligand becomes *S* upon coordination by the sequence rule. R. S. Cahn, C. K. Ingold, and V. Prelog, *Angew. Chem. Int. Ed. Engl.* **5**, 385 (1966).
14) M. A. Bennet, R. J. H. Clark, and A. D. J. Goodwin, *Inorg. Chem.*, **6**, 1625 (1967).
15) G. Thomas, *Z. Anorg. Allg. Chem.*, **362**, 191 (1968).
16) W. Levason and C. A. McAuliffe, *J. Chem. Soc., Dalton Trans.*, **1974**, 2238; *Inorg. Chim. Acta*, **11**, 33 (1974); **14**, 127 (1975).
17) H. Yamatera, *Bull. Chem. Soc. Jpn.*, **31**, 95 (1958).
18) H. Nishikawa, K. Konya, and M. Shibata, *Bull. Chem. Soc. Jpn.*, **41**, 1492 (1968).
19) S. Fujinami and M. Shibata, *Bull. Chem. Soc. Jpn.*, **46**, 3443 (1973).
20) K. Kashiwabara, K. Igi, and B. E. Douglas, *Bull. Chem. Soc. Jpn.*, **49**, 1573 (1976).
21) K. Kashiwabara, I. Kinoshita, and J. Fujita, *Chem. Lett.*, **1978**, 673.
22) C. T. Liu and B. E. Douglas, *Inorg. Chem.*, **3**, 1356 (1964).
23) M. Kojima and J. Fujita, *Bull. Chem. Soc. Jpn.*, **50**, 3237 (1977).
24) K. Ogino, K. Murano, and J. Fujita, *Inorg. Nucl. Chem. Lett.*, **4**, 35 (1968).
25) Y. Yokota, I. Kinoshita, K. Matsumoto, S. Ooi, K. Kashiwabara, and J. Fujita, Abstr. No. 3L07, 41th National Meeting of the Chemical Society of Japan, Osaka, April 1980.
26) B. Halpern, A. M. Sargeson, and K. R. Turnbull, *J. Am. Chem. Soc.*, **88**, 4630 (1966); K. Okamoto, J. Hidaka, and Y. Shimura, *Bull. Chem. Soc. Jpn.*, **44**, 1601 (1971).
27) J. B. Stothers, "Carbon-13 NMR Spectroscopy," Academic Press, New York (1972), p. 196.

  Bull. Chem. Soc. Jpn., 54, 733—737 (1981)

Recovery of Heavy Metals with Calcium Silicon. I. Its Stability in Water and Reducing Effect on Metal Ions

Shuzo Tokunaga,* Kitoshi Uematsu, and Yoshinobu Nagawa
National Chemical Laboratory for Industry, Yatabe, Ibaraki 305
(Received April 17, 1980)

The stability of calcium silicon in aqueous solutions was studied by determining dissolution rates of Ca and Si at a constant pH. Calcium silicon was found to be fairly stable in solutions of pH 3.0—8.0, at most less than 2.8%of Ca and 0.5% of Si being dissolved after 24 h. In a strong acid solution of pH 2.5 or less the dissolution rates of Ca and Si considerably increased. Ca dissolution reached a plateau and the whole amount of Ca did not dissolve even in a 3.0-mol dm^{-3} HCl solution, while Si dissolution continued to increase. Calcium silicon apparently reduces metal ions to the elemental state for metal ions having higher standard electrode potentials than Cd(II) ions except Ni(II) and Co(II) ions. For Ag(I) ions, nitrate ions interfere with the reduction, but chloride ions favor it. Reduction of Cr(VI) and Fe(III) ions terminated at the stage of Cr(III) and Fe(II). Pb-(II), Cu(II), and Hg(II) ions were reduced to the metals, the acidity of the solution and the metal ion concentration not affecting the reduction. Calcium silicon is effective also for low-solubility compounds of these elements in suspension.

The amount of heavy metals discharged into water has increased with development of industrial activities, causing serious environmental pollution. On the other hand the heavy metals are valuable resources and it is important to develop techniques for their recovery. The method utilizing reducing agents is effective for recovering metals. Base metals such as iron, aluminum, or zinc in the form of powder or scrap have been used for recovering metals of higher standard electrode potentials, such as Cu and Hg.[1-5] However, such processes are generally low in efficiency, requiring time and post-treatment of the reductant brought into solution.

McKaveney *et al.*[6] proposed an alloy process in which silicon alloys including Ca, Al, Ba, Fe, or Mg are used as reductants to remove heavy metals from waste water and brine solution in the pH range of 2—12. Both batch and continuous flow operations can be applied, As, Cd, Cu, Cr, Fe, Hg, Pb, and Zn being removed successfully. By using Ca or Mg silicon alloy, no post-treatment of the exchanged metal ions is necessary. Case[7] studied the silicon alloy process using magnesium ferrosilicon and calcium silicon granules. Both alloys afforded a high rate removal of Cu(II), Zn(II), Cr(III), and Cr(VI) ions, but a difference in percentage removal and pH variation was observed among the methods of contact between the alloy and metal-bearing solution (magnetic stirring, tumbling and continuous flow methods were examined). Calcium silicon was found to be very effective for removing Hg(II) ions, which were removed as insoluble Hg(I) compound and Hg(0); as much as *ca.* 40 matom (*ca.* 8 g) of Hg(II) ions were removed per unit mass of calcium silicon.[8]

Calcium silicon has long been used in the steel manufacturing industry as a deoxidizing agent, and was rarely used in water until the time McKaveney *et al.* carried out their study. In this report discussions are given on the behavior of calcium silicon in aqueous solutions and its use for the recovery of various metal ions.

Experimental

Calcium Silicon. Calcium silicon (Shin-Etsu Chemical Industry Co., Ltd.) was pulverized with a crusher. Particulates passed through a 200-mesh sieve (0.074 mm) were used. The composition was 31.3% Ca, 60.4% Si, and 0.40% C.

Reagents. Chlorides were used for the runs of Mn(II), Zn(II), Cr(III), Cd(II), Co(II), Ni(II), Sn(II), Pb(II), Cu(II), Fe(III), and Hg(II) ions. $FeSO_4$, K_2CrO_4, and $AgNO_3$ were used. All of these were of reagent grade and used by dissolving in distilled water.

Analysis. Concentration of metals in solution was determined with a Model 503 Atomic Absorption Spectrophotometer (The Perkin-Elmer Corporation). Mn, Zn, Fe, Cr, Cd, Ni, Sn, Pb, and Cu were determined by flame atomic absorption spectrophotometry, and Ca, Co, and Ag by flame emission spectrophotometry. Hg was determined by flameless atomic absorption spectrophotometry with a MV-253 Mercury Vapor Meter (Beckman-Toshiba, Ltd.). Cr(VI) and Fe(II) were determined by colorimetry[9] with diphenylcalbazide and 1,10-phenanthroline, respectively. Silicate was determined by the Molybdenum Blue method.[10] Solid products were analyzed for chemical species by means of X-ray diffraction with a Model 2100 Diffractometer (Rigaku Corporation) with Ni-filtered Cu $K\alpha$ radiation.

Stability of Calcium Silicon in Aqueous Solutions. Three grams of calcium silicon was added to 2.0 dm^3 of aqueous solution, which was placed in a 25 °C thermostat and agitated with a magnetic stirrer. The pH of the solution was maintained constant in the course of the run by using a Model HSM-10A pH Stat (Toa Electronics Ltd.) with 0.1-mol dm^{-3} HCl for a run of pH 8.0, 0.25-mol dm^{-3} HCl for runs of pH 6.0, 4.0, and 3.0, and with 1.0-mol dm^{-3} HCl for runs of pH 2.5 and 2.0. Calcium silicon was added to a 1.0-mol dm^{-3} HCl solution, the acidity not being controlled. At intervals an aliquot was taken and filtered through a glass fiber filter paper (Whatman GF/A), analysis being made on the filtrate for Ca and Si.

Recovering Metals with Calcium Silicon. In a 100-cm^3 glass-stoppered Erlenmeyer flask, 100 cm^3 of *ca.* 18- or 0.2-matom dm^{-3} metal ion solution was prepared, the acidity being adjusted to pH 1∼4, 0.1 mol dm^{-3}, and 1.0 mol dm^{-3} with HCl. With addition of 0.3 g of calcium silicon, the solution was shaken intermittently at room temperature. After 24 h it was filtered through a glass fiber filter paper, and the filtrate was analyzed for the metal, Ca, and Si. The residue was dried at *ca.* 60 °C under reduced pressure and its X-ray diffraction pattern was obtained.

Results and Discussion

Stability of Calcium Silicon in Aqueous Solutions. In reducing metal ions in an aqueous solution with a reductant, its stability in water is an important factor especially in acid solutions, since too strong a reductant decomposes water, evolving hydrogen gases in solutions of high acidity. Calcium silicon is composed of elemental calcium and silicon, both strong reducing agents; the former reacts with water violently while the latter is stable in water due to the irreversibility of the oxidation-reduction reaction and to passivation by a film of silica in acid solution.[11] The reactivity of elemental calcium and silicon with water has been studied but not that of calcium silicon.

When calcium silicon is added to water, the pH tends to increase with dissolution of Ca moiety ($Ca+2H_2O=Ca(OH)_2+H_2$), the dissolution rate decreasing when the solution turns alkaline. In order to find the relation between pH and the stability of calcium silicon, the dissolution rates of Ca and Si were determined in solutions of constant pH maintained with a pH stat. The concentrations of dissolved Ca and Si were found to be lower than their respective solubilities, and thus they exist in the soluble form. The results are given in Figs. 1 and 2. The amounts of Ca and Si dissolved in solution are given in terms of percentage to the respective initial amounts contained in the calcium silicon added.

The dissolution of Ca was very small at pH 3.0 or higher; only 1.2, 1.8, 1.9, and 2.8% of Ca dissolved after 24 h at pH 8.0, 6.0, 4.0, and 3.0, respectively. When pH was not maintained constant, the dissolution decreased to less than 1% in a solution of an initial pH of 3.9 (final pH 9.1). At pH below 2.5 the dissolution became significant but did not increase continuously with lapse of time, plateaus being observed according to the acidity. At pH 2.5 and 2.0, a steady state was reached after *ca.* 8 and 3 h with dissolution of 21.4 and 62.8% of Ca, respectively. In the 1.0-mol dm^{-3} HCl solution, the plateau was reached within 5 min with dissolution of 74.3% of Ca. In the 2.0- and 3.0-mol dm^{-3} HCl solutions, 83.7 and 84.1% of Ca dissolved, respectively. The Ca moiety would not entirely dissolve even in a strong acid solution, possibly due to the formation of silica film on the surface of calcium silicon which prevents the dissolution.

Percentages of dissolved Si were fairly low in comparison to those of Ca. The stability of calcium silicon in an aqueous solution is mainly affected by that of Ca moiety. Dissolution of Si was insignificant at pH 3.0 or higher, less than 0.5% of Si being dissolved. This was also the case even in the alkaline solution of pH 8.0. In strong acid solutions of pH 2.5 or less, the dissolution of Si as well as of Ca increased significantly, spontaneously combustible silicon hydride, SiH_4, being produced in a 1.0-mol dm^{-3} HCl solution at the first stage of the reaction. On the other hand, elemental silicon dissolves in a hot alkaline solution but not in an acid solution.[11] Significant increase in Ca dissolution in a solution of low pH might promote Si dissolution, *i.e.*, degradation of alloy particulates

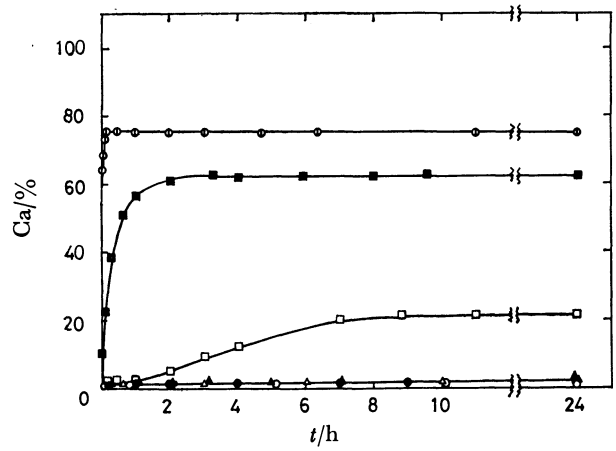

Fig. 1. Dissolution rates of calcium at various acidities. Acidity; ○: pH 8.0, ●: pH 6.0, △: pH 4.0, ▲: pH 3.0, □: pH 2.5, ■: pH 2.0, ⓘ: 1.0 mol dm^{-3} HCl.

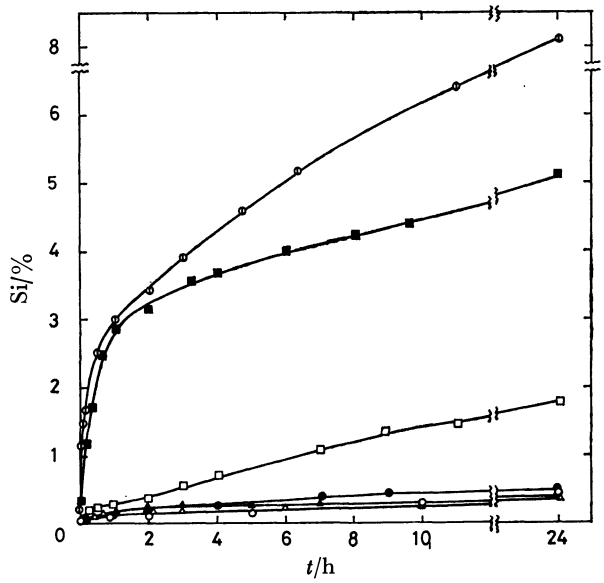

Fig. 2. Dissolution rates of silicon at various acidites. Acidity; ○: pH 8.0, ●: pH 6.0, △: pH 4.0, ▲: pH 3.0, □: pH 2.5, ■: pH 2.0, ⓘ: 1.0 mol dm^{-3} HCl.

caused by dissolution of Ca moiety may favor Si dissolution. Since the amount of Si dissolved is much lower than the solubility of silicate, the dissolution of Si increases continuously without reaching a plateau.

The explosive reactivity of elemental Ca with water is thus reduced considerably by making an alloy containing silicon. The Si moiety is very stable against water. Calcium silicon is sufficiently stable as a solid reducing agent in aqueous solutions of pH higher than 3.0.

Recovering Metals with Calcium Silicon. The reduction-oxidation reaction of a metal in an aqueous solution can be discussed in terms of the standard electrode potential. For practical use in acid solutions, the standard electrode potential of a reductant should be higher than *ca.* −0.7 V to avoid decomposition of water, and somewhat lower than that of a metal

Table 1. Recovery of metal ions with calcium silicon

Metal ion	ε° [a] V	Initial concn matom dm^{-3}	Removal %	Acidity[b] Initial	Acidity[b] Final	Dissolution Ca matom dm^{-3}	Dissolution Si matom dm^{-3}
Mn(II)	−1.180	18.0	0	pH 3.5	pH 7.8	0.3	0.10
		18.3	1	0.1	pH 1.8	16.0	3.56
		18.3	1	1.0	—	16.8	3.06
Zn(II)	−0.763	18.0	4(−1)	pH 3.5	pH 6.1	0.5	0.09
		18.4	−1	0.1	pH 1.7	16.0	3.64
		18.4	3	1.0	—	16.8	3.17
Fe(II)	−0.4402	18.0	−2	pH 2.8	pH 4.0	0.1	0.08
		18.0	−3	0.1	pH 1.8	3.1	2.35
		18.0	−2	1.0	—	3.2	2.35
Cr(III)	−0.408[3]	18.0	20	pH 2.9	pH 3.3	7.8	1.69
		18.0	7	0.1	pH 1.7	13.3	3.44
		18.0	8	1.0	—	14.5	2.91
		0.2	50(10)	pH 3.1	pH 4.8	0.5	0.14
Cd(II)	−0.4029	18.0	6(0)	pH 3.1	pH 6.6	0.5	0.09
		18.0	32	0.1	pH 1.7	16.8	3.92
		18.0	5	1.0	—	17.0	2.96
		0.2	10(0)	pH 3.1	pH 6.4	0.4	0.15
		0.2	2	0.1	pH 1.7	17.2	4.71
Co(II)	−0.277	17.9	0	pH 3.6	pH 5.7	0.4	0.09
		17.9	1	0.1	pH 1.7	15.1	4.09
		17.9	1	1.0	—	16.4	3.35
Ni(II)	−0.250	18.0	7(0)	pH 3.5	pH 7.4	0.6	0.30
		18.1	3	0.1	pH 1.8	16.8	3.27
		18.1	3	1.0	—	17.2	2.96
Sn(II)	−0.136	16.8	69	0.1	pH 1.6	11.9	2.80
Pb(II)	−0.126	18.0	82(81)	pH 3.5	pH 4.8	15.2	2.98
		18.0	83	0.1	pH 1.7	16.5	3.47
		18.0	79	1.0	—	16.8	3.39
		0.2	100(5)	pH 3.5	pH 8.5	0.4	0.17
		0.2	40	0.1	pH 1.5	18.1	2.97
Cu(II)	0.337	18.1	98	pH 3.4	pH 2.5	16.3	3.77
		18.1	99	0.1	pH 1.6	16.9	4.69
		18.1	93	1.0	—	16.8	3.78
		0.2	96(96)	pH 3.5	pH 6.2	0.5	0.07
Fe(III)	0.771[d]	18.0	8(3)	pH 2.0	pH 4.1	12.6	1.48
		18.1	7	0.1	pH 1.7	16.8	2.47
		18.1	5	1.0	—	16.6	2.15
Ag(I)	0.799	18.5	12	pH 3.9	pH 3.2	0.6	0.03
		18.5	100	0.1	pH 1.7	13.2	3.64
		18.5	100	1.0	—	15.3	3.03
		0.2	61	0.1	pH 1.7	14.3	4.59
Hg(II)	0.920[e]	18.0	99	pH 3.9	pH 2.3	11.1	2.53
	0.788[f]	18.0	99	0.1	pH 1.7	15.8	5.14
		18.0	99	1.0	—	16.8	2.66
Cr(VI)		18.0	8	pH 3.2	pH 5.4	0.1	0.48
		18.0	50	0.1	pH 2.7	16.1	4.73
		18.0	2	1.0	—	15.9	2.36
		0.2	0	pH 3.5	pH 10.1	0.5	0.54
		0.2	0	0.1	pH 1.4	18.7	2.84

a) Standard electrode potential for an electrode reaction $M^{z+}+ze=M$ (unless otherwise noted); the value being quoted from "Kagaku Binran Kiso-hen II," Maruzen, Tokyo (1977), pp. 1203—1206. b) Adjusted with HCl, and the values are in mol dm^{-3} unless ohterwise noted. c) For the reaction $Cr^{3+}+e=Cr^{2+}$. d) For the reaction $Fe^{3+}+e=Fe^{2+}$. e) For the reaction $2Hg^{2+}+2e=Hg_2^{2+}$. f) For the reaction $Hg_2^{2+}+2e=2Hg$.

to be reduced for accomplishing the reduction-oxidation reaction. Since the standard electrode potential of calcium silicon is unknown, we estimated its strength as a reductant by reactions with various metal ions whose potentials are known. We employed finer particulates of calcium silicon and higher concentrations of metal ions than those used in the previous studies in order to analyze the solid products by means of X-ray diffraction. Since metal-ion reducing reactions proceed efficiently in acid solutions, reactions were carried out in solutions of various acidities in order to suppress hydrolysis of metal ions and examine the effects of acidity.

The results of metal ion recovery are given in Table 1. When occurrence of hydrolysis of metal ions was expected from the final pH, an aliquot of the sample solution was filtered after being maintained at near the initial pH for 5 min to dissolve the hydroxide. The metal ion removal thus attained is indicated in parentheses. Discussions are given on 0.2-matom dm^{-3} solutions of metal ions which proved to be reduced by calcium silicon.

Practically no reducing effects were observed for Mn(II), Zn(II), and Fe(II) ions which show very low standard electrode potentials. In the study of McKaveney *et al.*,[6] more than 99% removal was attained for Zn(II) ions in the column contact operation by using a parent solution of 0.15 Zn matom dm^{-3} and pH 5.6. More than 98% removal was attained at final pH of 9.95—7.95 in the batch operations by using a parent solution of 0.66 Zn matom dm^{-3} and pH 2.05.[7] At final pH of 5.05, the extent of removal significantly decreased down to 9%. Thus, it can be concluded that Zn(II) ions do not undergo reduction with calcium silicon but are removed only by hydrolysis which becomes significant from above pH *ca.* 6.5. The dissolution of Ca was much lower for Fe(II) ions than that for other cases, which seems to be due to presence of sulfate ions.

For Cr(III) ions, 20% removal was achieved in the run of initial pH of 2.9. The amounts of Ca and Si dissolved were much higher than those obtained in the above-mentioned metal-free solution of nearly the same pH (*ca.* 0.3 and 0.1 matom dm^{-3} for Ca and Si, respectively). This indicates the reduction of Cr(III) ions, the reaction $Cr^{3+}+e=Cr^{2+}$ being most likely to occur according to its standard electrode potential. However, no Cr(II) was detected since it is extremely unstable in aqueous solution and readily oxidized to Cr(III). Formation of Cr(0) is very unlikely to occur, since the standard electrode potentials for the reactions $Cr^{3+}+3e=Cr$ and $Cr^{2+}+2e=Cr$ are -0.774 and -0.913 V,[12] respectively. Although no pattern of chromium compounds was obtained by means of X-ray diffraction, the chromium removed was entirely recovered from the solid phase as Cr(III) ions by alkali digestion of the product. The removal of Cr(III) ions seems to be due to the formation of chromium(III) hydroxide.

For Cd(II) ions, removal higher than for the above-mentioned metal ions was achieved in the 18.0-matom dm^{-3}, 0.1-mol dm^{-3} HCl solution, formation of Cd(0) being recognized by X-ray diffraction of the solid product obtained. The removal deteriorated in the solutions of both lower and higher acidities as well as of lower cadmium concentration. Optimum conditions of acidity and cadmium concentration should be established in order to attain high efficiency of the reduction.

Although Co and Ni show higher standard electrode potentials than Cd does, the ions were not removed in acid solution. The cause of the ineffectiveness of calcium silicon on these ions is unknown. Thus, the reduction of metal ions with calcium silicon can not always be interpreted only in terms of standard electrode potential.

The high removal of Sn(II) ions in the 0.1-mol dm^{-3} HCl solution and the presence of Sn(0) confirmed by means of X-ray diffraction indicate that Sn(II) ions were removed by reduction to the metal.

For 18.0 Pb matom dm^{-3} solution, removal was attained regardless of the acidity and formation of Pb(0) was recognized in every case. In the run of initial pH of 3.5, removal of Pb(II) ions would not decrease significantly even by adjusting the final pH. This indicates that the removal of Pb(II) ions is due to the reduction of the ions to the metal. In the run of 0.2 matom dm^{-3}, initial pH of 3.5, the increase in pH interfered with the reduction of Pb(II) ions. The 40% removal for the run of 0.2 matom dm^{-3}, 0.1 mol dm^{-3} HCl, shows that the reduction of Pb(II) ions would not proceed so efficiently at such low concentration.

Considerably high removal was attained for Cu(II) ions in every solution irrespective of the acidity and Cu(II) concentration, indicating that Cu(II) ions can be reduced efficiently. The solid product was found to consist of Cu(0) and a trace amount of Cu_2O. The reaction was complete in 30 min after addition of calcium silicon.

Removal of Fe(III) ions was very low. However, the colorimetric determination of Fe(II) ions in the solution showed that Fe(III) ions are almost entirely reduced to Fe(II) ions. Reduction to Fe(0) is unlikely to occur according to the standard electrode potential.

Since no effect was observed with $AgNO_3$ solutions whose acidity was adjusted with HNO_3, the effect of calcium silicon on Ag(I) ions was examined with a suspension of AgCl precipitate prepared by addition of HCl to a $AgNO_3$ solution followed by addition of calcium silicon after 10 min. Thus the solid phase might contain AgCl precipitate, and the removal values given in Table 1 do not necessarily indicate that the removal was due to reduction of Ag(I) ions. Determination of Ag and AgCl in the solid product was made by means of X-ray diffraction. The areas of the diffraction peaks corresponding to d=2.359 and 2.774 Å for Ag and AgCl, respectively, were obtained by the integral mode, and their ratio was compared with a calibration curve similarly prepared by using mixtures of standard Ag and AgCl of various compositions. The silver compositions of the solid products were *ca.* 100, 100, and 43% for the runs at initial pH 3.9, 0.1-mol dm^{-3}, and 1.0-mol dm^{-3} HCl, respectively. The low Ag content for the 1.0-mol dm^{-3} HCl run can be attributed to flocculation of AgCl

precipitate which interfered with the contact with calcium silicon. Chloride ions favored the reduction of Ag(I) ions while nitrate ions disturbed it. When calcium silicon was added 1 h after the formation of AgCl, the silver compositions of the solid phase were *ca.* 100 and 55% Ag for the runs at initial pH 3.3 and 0.1 mol dm^{-3}, respectively, a trace amount of Ag being contained in the solid phase of the 1.0-mol dm^{-3} run. Aging of AgCl precipitate adversely affected the reduction reaction.

Reduction of Hg(II) ions proceeded efficiently in all solutions, the recovered solid products consisting of Hg(0) and Hg_2Cl_2.[8]

For Cr(VI) ions, 50% removal was attained in the 18.0-matom dm^{-3}, 0.1-mol dm^{-3} HCl solution. Of the chromium ions remaining in the solution, Cr(III) ions accounted for 72.5% and Cr(VI) ions the remainder, indicating that the reduciton of Cr(VI) to Cr(III) occurred. According to Pourbaix,[12] both Cr(VI) and Cr(III) ions would not hydrolyze at the pH we employed. We carried out analysis of the solid phase obtained in order to find the cause for the removal of Cr(VI) ions. The solid product dried at 60 °C under reduced pressure was poorly soluble in HCl solution and completely soluble in NaOH solution, which showed a chromium composition of 89.7% Cr(III) and the remainder Cr(VI). Cr(VI) ions were reduced to Cr(III) ions which partly remained in the solution and partly precipitated into the solid phase. The solid product was further analyzed by X-ray diffraction to identify the chromium compounds. Although the product dried at 60 °C gave no evidence for the existence of any chromium compound on its X-ray diffraction pattern, the one heated at *ca.* 700 °C for 6 h gave patterns corresponding to chromium(III) oxide, Cr_2O_3 (ASTM File No. 6-0504), and calcium chromate, $CaCrO_4$ (ASTM File No. 8-458). We might attribute the formation of Cr_2O_3 and $CaCrO_4$ to the dehydration of their hydrous forms which were amorphous to X-rays but determined by the alkali digestion. Therefore, the reduction reaction $Cr_2O_7^{2-} + 8H^+ + 6e = Cr_2O_3(\text{hydrated}) + 4H_2O(\varepsilon^\circ = 1.242 - 0.0788pH$[12]) is most likely to occur, supporting the increase in pH from *ca.* 1 to 2.7. The reduction of Cr(VI) ions did not proceed efficiently at both higher and lower acidities than pH *ca.* 1, where bulk of the Cr(VI) ions remained not reduced to Cr(III). No reduction of Cr(VI) ions took place in dilute solutions.

Since calcium silicon exhibited reducing action on the suspension of AgCl precipitate, we examined the effectiveness on low-solubility compounds of Cd(II), Ag(I), Cu(I), Cu(II), Hg(II), and Pb(II). The effectiveness was judged on the X-ray diffraction pattern of the solid product obtained. Great reducing effect was observed on Cu_2Cl_2, in which formation of Cu(0) and a trace amount of Cu_2O was recognized. Partial reducing effect was observed on Ag_2O, Ag_2SO_4, $Cu(OH)_2$, CuS, PbO, HgO, and $HgSO_4$, in which metallic species were recognized as well as the starting material. It seems that the reduction of these low-solubility compounds is due to that of the metal ions dissolving in trace amount into the metal, which consequently causes dissociation of the molecular species.

Appreciable reducing effect to the metal is recognized on metal ions that show standard electrode potentials equal to or higher than that of Cd, except Ni(II) and Co(II) ions. The reduction reaction of Cr(VI) and Fe(III) ions terminates at the stage of formation of Cr(III) and Fe(II) ions, neither Cr(0) nor Fe(0) being produced. Dissolution of calcium silicon in aqueous solution increases pH, favoring the removal of metal ions through hydrolysis. The acidity of a solution would not affect the reducing effect for Pb(II), Cu(II), and Hg(II) ions that show high standard electrode potentials. Calcium silicon is effective also for low-solubility compounds of these metals.

References

1) T. Yajima and Y. Eguchi, *Rodo Eisei*, **2**, 30 (1961).
2) R. Sei, *Mizu Shori Gijutsu*, **3** (8), 19 (1962).
3) K. Irukayama, *Soda To Enso*, **21**, 216 (1970).
4) J. G. Dean, F. L. Bosqui, and K. H. Lanouette, *Environ. Sci. Technol.* **6**, 518 (1972).
5) T. Katsura and A. Tanaka, *Mizu Shori Gijutsu*, **20**, 351 (1979).
6) J. P. McKaveney, W. P. Fassinger, and D. A. Stivers, *Environ. Sci. Technol.*, **6**, 1109 (1972).
7) O. P. Case, PB Report 233 143, U.S. Department of Commerce, Springfield Va., Jan. 1974.
8) S. Tokunaga and K. Uematsu, *Nippon Kagaku Kaishi*, **1978**, 619.
9) JIS-K-0102, "Testing Methods for Industrial Waste Water," Japanese Stadards Association, Tokyo (1974).
10) JIS-K-0101, "Testing Method for Industrial Water," Japanese Standards Association, Tokyo (1966).
11) M. Pourbaix, "Atlas of Electrochemical Equilibria in Aqueous Solutions," Pergamon Press, Oxford (1966), p. 462.
12) M. Pourbaix, "Atlas of Electrochemical Equilibria in Aqueous Solutions," Pergamon Press, Oxford (1966), pp. 256—271.

The Mechanism of the Hydrolysis of Polyphosphates. V.[1] The Effect of Cations on the Hydrolysis of Pyro- and Triphosphates

Makoto WATANABE,* Makoto MATSUURA, and Tamotsu YAMADA
Department of Industrial Chemistry, Chubu Institute of Technology, Matsumoto-cho, Kasugai, Aichi 487

(Received May 15, 1980)

The effect of cations on the rate of hydrolysis of pyro- and triphosphates was studied by adding metal chloride to aqueous solutions of the phosphates. The concentrations of the phosphates and metal chlorides were 0.025 and 0.1 mol dm^{-3} respectively. Alkali metal, alkaline earth metal, aluminium, and some transition-metal (Mn(II), Co(II), Ni(II), Cu(II), and Zn(II)) cations retarded the hydrolysis of the phosphates in acidic media. The following sequence of efficiency resulted:

trivalent > bivalent > univalent.

The efficiency of elements within one group of the periodic table decreased from top to bottom. On the other hand, in alkaline solutions, alkali metal cations accelerated the hydrolysis of the phosphates and the catalytic effectiveness decreased with an increase in the ionic radius.

Though many papers have been reported about the hydrolysis of polyphosphates, there have been few studies concerning the effect of cations except for hydrogen and oxonium ions. Many workers have discussed the rate order, the pH dependence, and the reaction process of the hydrolysis of polyphosphates, but no explanation of the reaction mechanism from the point of view of the interaction between a water molecule and a phosphate ion has ever been made. One of the present authors (M. W.) discussed the reaction mechanism of the hydrolysis of polyphosphates from this point of view by using aqueous organic solvents; he pointed out that the rate of the hydrolysis of chain and small-ring phosphates is seriously affected by the nucleophilicity of water molecules and that the hydrolysis is of an S_N2 type.[1-4] Thilo and Wieker reported the catalytic efficiencies of cations on the hydrolysis of high polyphosphates at pH 8 and obtained the following sequence of efficiency:

$Al^{3+} > Mg^{2+} > Ca^{2+} > Sr^{2+} > Ba^{2+} > H^+ > Li^+ > Na^+ > K^+$.[5-7]

In this paper, the effects of alkali metal, alkaline earth metal, aluminium, and some transition metal cations of the hydrolysis of pyro- and triphosphates will be discussed.

Experimental

Materials and Procedure. The materials used other than triphosphate were of a commercial grade. The sodium triphosphate was made by the method described in Ref. 8. The concentration of sodium pyro- or triphosphate was controlled to be 0.025 mol dm^{-3} because that concentration was suitable for analysis. Metal chloride was added to the phosphate solution to make it 0.1 mol dm^{-3}. The metal chlorides used were LiCl, NaCl, KCl, $MgCl_2$, $CaCl_2$, $AlCl_3$, $MnCl_2$, $CoCl_2$, $NiCl_2$, $CuCl_2$, and $ZnCl_2$. The pH of the solution was controlled with hydrochloric acid and/or aqueous tetramethylammonium hydroxide, with the aid of a Hitachi-Horiba pH meter, F-7, at a given reaction temperature. The separation and determination of the phosphate species in the sample solution were carried out by the method described in our previous paper.[2] The phosphates in the solution containing aluminium ions were not separated well by one-dimensional paper chromatography, so only the measurement of the hydrolysis of pyrophosphate to orthophosphate was done by means of the molybdenum-blue method. When any precipitate was formed during the experiment, no further treatment was made. Pyro- and triphosphate solutions free from sodium ions were prepared by passing the phosphate solutions mentioned above through cation-exchange resin in the H^+ form. The same treatment as in the case of sodium pyro- and triphosphate solutions was done for the phosphate solutions thus prepared in order to test the effect of coexisting sodium ions; the effect of alkali metal cations on the rate of the hydrolysis of triphosphate in basic media was also studied by using the triphosphate solution, but the effect of cations on the hydrolysis of pyrophosphate could not be studied because the rate of the hydrolysis of pyrophosphate was too slow to measure in basic media.

Results and Discussion

The Effect of Cations. The rate of the hydrolysis of pyro- and triphosphates obeyed first-order kinetics with respect to the concentration of the respective phosphates under all the conditions studied. As Tables 1 and 2 show, in every reaction system the rate of the hydrolysis of either phosphate decreased with an increase in the pH value of the solutions. These results agree well with those of previous studies.[1,2,9] The hydrolysis of pyro- and triphosphates was retarded by the addition of the alkali metal ions in the pH ranges smaller than 7.0 and by the addition of other metal ions in the pH ranges smaller than 3.0. The rate of the hydrolysis of pyrophosphate in the system containing aluminium ions, measured at pH 0.9, was smaller than those of other systems measured at pH 1.0. As has been mentioned above, the hydrolysis of pyrophosphate is an acid-catalyzed reaction. Therefore, the retardation efficiency of aluminium ions is the largest among the cations tested here. According to the results, the following order of the retardation efficiency of metal ions on the rate of hydrolysis of short-chain polyphosphates resulted at pH 1.0:

$$\underbrace{Mg^{2+} > Ca^{2+}}_{\text{typical element}}$$

$$\underbrace{Al^{3+} > Mn^{2+} > Cu^{2+} > Zn^{2+} > Co^{2+} > Ni^{2+} > Li^+ > Na^+ > K^+}_{\text{transition element}}.$$

(trivalent) (bivalent) (univalent)

Similar retardation effects were observed for alkali metal, alkaline earth metal, manganese(II), cobalt(II), and nickel(II) ions at pH 2.0 or at higher pH regions than that. However, the order of efficiency of man-

Table 1. Rate constants/min^{-1} of the hydrolysis of pyrophosphate

Phosphate	Added cation	pH	Reaction temp/°C 35	50	70
$Na_4P_2O_7$	—	1.0	$1.44\ 10^{-4}$	$7.40\ 10^{-4}$	$4.73\ 10^{-3}$
		2.0	$1.52\ 10^{-5}$	$1.30\ 10^{-4}$	$1.55\ 10^{-3}$
		3.0	$6.40\ 10^{-6}$	$4.92\ 10^{-5}$	$6.95\ 10^{-4}$
		5.0	$5.32\ 10^{-6}$	$4.64\ 10^{-5}$	$6.03\ 10^{-4}$
	Li^+	1.0	$1.18\ 10^{-4}$	$6.78\ 10^{-4}$	$4.31\ 10^{-3}$
		2.0	$1.28\ 10^{-5}$	$1.02\ 10^{-4}$	$1.35\ 10^{-3}$
		3.0	$5.86\ 10^{-6}$	$4.43\ 10^{-5}$	$6.40\ 10^{-4}$
		5.0	$4.29\ 10^{-6}$	$3.52\ 10^{-5}$	$4.93\ 10^{-4}$
	Na^+	1.0	$1.25\ 10^{-4}$	$6.91\ 10^{-4}$	$4.53\ 10^{-3}$
		2.0	$1.40\ 10^{-5}$	$1.19\ 10^{-4}$	$1.49\ 10^{-3}$
		3.0	$6.38\ 10^{-6}$	$4.75\ 10^{-5}$	$7.03\ 10^{-4}$
		5.0	$4.93\ 10^{-6}$	$4.04\ 10^{-5}$	$5.49\ 10^{-4}$
	K^+	1.0	$1.40\ 10^{-4}$	$7.47\ 10^{-4}$	$4.58\ 10^{-3}$
		2.0	$1.48\ 10^{-5}$	$1.24\ 10^{-4}$	$1.51\ 10^{-3}$
		3.0	$6.86\ 10^{-6}$	$4.89\ 10^{-5}$	$7.18\ 10^{-4}$
		5.0	$5.04\ 10^{-6}$	$4.16\ 10^{-5}$	$5.86\ 10^{-4}$
	Mg^{2+}	1.0	$7.32\ 10^{-5}$	$3.48\ 10^{-4}$	$3.27\ 10^{-3}$
		2.0	$6.67\ 10^{-6}$	$5.31\ 10^{-5}$	$6.33\ 10^{-4}$
	Ca^{2+}	1.0	$7.46\ 10^{-5}$	$3.62\ 10^{-4}$	$3.54\ 10^{-3}$
		2.0	$9.70\ 10^{-6}$	$8.21\ 10^{-5}$	$1.12\ 10^{-3}$
	Mn^{2+}	1.0	$4.50\ 10^{-5}$	$2.41\ 10^{-4}$	$2.09\ 10^{-3}$
	Co^{2+}	1.0	$7.33\ 10^{-5}$	$3.53\ 10^{-4}$	$2.89\ 10^{-3}$
	Ni^{2+}	1.0	$7.73\ 10^{-5}$	$3.78\ 10^{-4}$	$3.31\ 10^{-3}$
		2.0	$8.34\ 10^{-6}$	$6.03\ 10^{-5}$	$8.30\ 10^{-4}$
	Zn^{2+}	1.0	$6.47\ 10^{-5}$	$3.06\ 10^{-4}$	$2.72\ 10^{-3}$
	Al^{3+}	0.9	$3.02\ 10^{-5}$	$1.92\ 10^{-4}$	$1.36\ 10^{-3}$
$H_4P_2O_7$	—	1.0	$1.61\ 10^{-4}$	$8.39\ 10^{-4}$	$5.01\ 10^{-3}$
		2.0	$1.91\ 10^{-5}$	$1.50\ 10^{-4}$	$1.61\ 10^{-3}$
		3.0	$7.79\ 10^{-6}$	$5.56\ 10^{-5}$	$7.88\ 10^{-4}$
		5.0	$5.83\ 10^{-6}$	$4.87\ 10^{-5}$	$6.44\ 10^{-4}$
		7.0		$8.22\ 10^{-6}$	$1.05\ 10^{-4}$
	Li^+	3.0		$4.95\ 10^{-5}$	$7.21\ 10^{-4}$
		5.0		$3.83\ 10^{-5}$	$4.96\ 10^{-4}$
		7.0		$5.97\ 10^{-6}$	$8.03\ 10^{-5}$

Table 2. Rate constants/min^{-1} of the hydrolysis of triphosphate

Phosphate	Added cation	pH	Reaction temp/°C 35	50	70
$Na_5P_3O_{10}$	—	1.0	$1.06\ 10^{-3}$	$5.38\ 10^{-3}$	$2.94\ 10^{-2}$
		2.0	$1.36\ 10^{-4}$	$8.29\ 10^{-4}$	$6.10\ 10^{-3}$
		3.0	$2.51\ 10^{-5}$	$1.73\ 10^{-4}$	$1.87\ 10^{-3}$
	Li^+	1.0	$8.43\ 10^{-4}$	$3.02\ 10^{-3}$	$2.78\ 10^{-2}$
		2.0	$8.04\ 10^{-5}$	$6.91\ 10^{-4}$	$5.28\ 10^{-3}$
		3.0	$2.22\ 10^{-5}$	$1.48\ 10^{-4}$	$1.68\ 10^{-3}$
	Na^+	1.0	$9.76\ 10^{-4}$	$3.49\ 10^{-3}$	$2.80\ 10^{-2}$
		2.0	$8.90\ 10^{-5}$	$7.12\ 10^{-4}$	$5.61\ 10^{-3}$
		3.0	$2.30\ 10^{-5}$	$1.68\ 10^{-4}$	$1.85\ 10^{-3}$
	K^+	1.0	$1.05\ 10^{-3}$	$3.52\ 10^{-3}$	$2.93\ 10^{-2}$
		2.0	$9.59\ 10^{-5}$	$7.33\ 10^{-4}$	$5.79\ 10^{-3}$
		3.0	$2.44\ 10^{-5}$	$1.80\ 10^{-4}$	$1.96\ 10^{-3}$
	Mg^{2+}	1.0	$3.23\ 10^{-4}$	$1.32\ 10^{-3}$	$9.16\ 10^{-3}$
		2.0	$2.66\ 10^{-5}$	$1.70\ 10^{-4}$	$1.66\ 10^{-3}$
		3.0	$1.16\ 10^{-5}$	$8.01\ 10^{-5}$	$9.06\ 10^{-4}$
	Ca^{2+}	1.0	$3.49\ 10^{-4}$	$1.54\ 10^{-3}$	$1.04\ 10^{-2}$
		2.0	$5.11\ 10^{-5}$	$4.07\ 10^{-4}$	$3.91\ 10^{-3}$
	Mn^{2+}	1.0	$1.64\ 10^{-4}$	$6.28\ 10^{-4}$	$5.95\ 10^{-3}$
		2.0	$2.36\ 10^{-5}$	$1.72\ 10^{-4}$	$1.82\ 10^{-3}$
	Co^{2+}	1.0	$2.70\ 10^{-4}$	$9.80\ 10^{-4}$	$7.65\ 10^{-3}$
		2.0	$2.35\ 10^{-5}$	$1.59\ 10^{-4}$	$1.56\ 10^{-3}$
	Ni^{2+}	1.0	$3.04\ 10^{-4}$	$1.36\ 10^{-3}$	$9.05\ 10^{-3}$
		2.0	$2.86\ 10^{-5}$	$1.75\ 10^{-4}$	$1.63\ 10^{-3}$
		3.0	$1.27\ 10^{-5}$	$9.88\ 10^{-5}$	$1.10\ 10^{-3}$
	Cu^{2+}	1.0	$2.40\ 10^{-4}$	$9.25\ 10^{-4}$	$7.38\ 10^{-3}$
	Zn^{2+}	1.0	$2.46\ 10^{-4}$	$9.72\ 10^{-4}$	$7.40\ 10^{-3}$
$H_5P_3O_{10}$	—	1.0	$1.29\ 10^{-3}$	$6.34\ 10^{-3}$	$3.57\ 10^{-2}$
		2.0	$1.95\ 10^{-4}$	$9.47\ 10^{-4}$	$8.03\ 10^{-3}$
		3.0	$2.80\ 10^{-5}$	$1.93\ 10^{-4}$	$2.08\ 10^{-3}$
		5.0		$9.53\ 10^{-5}$	$1.03\ 10^{-3}$
		7.0		$1.39\ 10^{-5}$	$2.30\ 10^{-4}$
		10.0		$6.33\ 10^{-7}$	
		11.5		$5.42\ 10^{-7}$	
	Li^+	3.0		$1.51\ 10^{-4}$	$1.74\ 10^{-3}$
		5.0		$8.20\ 10^{-5}$	$9.15\ 10^{-4}$
		7.0		$1.13\ 10^{-5}$	$1.72\ 10^{-4}$
		10.0		$5.17\ 10^{-6}$	
		11.5		$4.69\ 10^{-6}$	
	Na^+	3.0		$1.87\ 10^{-4}$	$1.54\ 10^{-3}$
		5.0		$1.02\ 10^{-4}$	$1.21\ 10^{-3}$
		7.0		$1.57\ 10^{-5}$	$2.31\ 10^{-4}$
		10.0		$1.71\ 10^{-6}$	
		11.5		$1.61\ 10^{-6}$	
	K^+	3.0		$2.06\ 10^{-4}$	$1.83\ 10^{-3}$
		5.0		$1.07\ 10^{-4}$	$1.25\ 10^{-3}$
		7.0		$1.82\ 10^{-5}$	$2.32\ 10^{-4}$
		10.0		$1.19\ 10^{-6}$	
		11.5		$1.13\ 10^{-6}$	

ganese(II) ions for the hydrolysis of triphosphate at pH 2.0 is not the same as that at pH 1.0. As is also shown in Tables 1 and 2, the rate of the hydrolysis of pyro- and triphosphates is larger than that of the respective sodium phosphates, and a similar retardation effect of lithium ions is observed in the pH regions smaller than 7.0. On the other hand, the rate of the hydrolysis of triphosphate was remarkably accelerated by the addition of alkali metal ions at pH 10.0 and 11.5. The order of the acceleration efficiency of alkali metal ions is as follows:

$$Li^+ > Na^+ > K^+.$$

Reaction Mechanism. The activation parameters for the hydrolysis of pyro- and triphosphates were calculated by means of the Arrhenius plot; they are listed in Tables 3 and 4 respectively. In any reaction system, the activation energy and the frequency factor increase with an increase in the pH value. This indicates that the catalytic action of H^+ affects exclusively the energy term of the hydrolysis of short-chain polyphosphates. In our previous papers,[2,4] we proposed the following hydrolysis mechanism for pyro- and triphosphates and concluded that Reaction (2) is the rate-determining step:

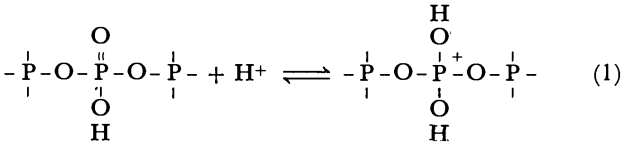

(1)

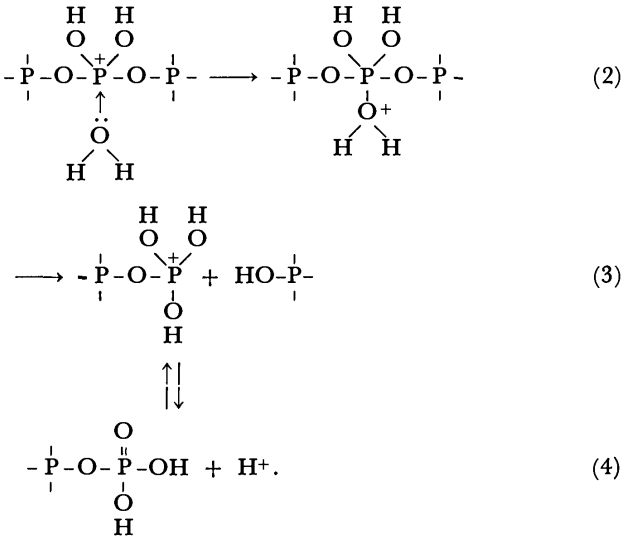

The present kinetic measurements have shown that the retardation efficiency within one group of the periodic table decreases from top to bottom, that is, with an increase in the ionic radius, and increases with an increase in the charge of the cation. Since the reaction rate is retarded and the activation energy increases upon the addition of a metal cation in any reaction system, it could be considered that the elementary reactions (1) and (2) are affected by metal ions. Therefore, the retardation of the degradation reaction by metal ions in acidic solutions may be explained by the exchange of protons by the catalytically less effective metal ions. The ion-exchange efficiency of a cation increases with an increase in the charge. This fact well explains the order of the retardation efficiency of metal cations for the hydrolysis of pyro- and triphosphates. In one group of the periodic system, the ion-exchange efficiency of a cation decreases with a decrease in the ionic radius because of strong hydration. This tendency does not agree with the results obtained in this work. However, Strauss and Ross indicated that the binding constant of alkali metal and alkaline earth metal cations with phosphate ions decreases in the order of an increase in the ionic radius of the cations.[10] This result well explains the order of the retardation efficiency of alkali metal and alkaline earth metal cations obtained here. Accordingly, the retardation of the degradation may be caused by the following exchange reaction:

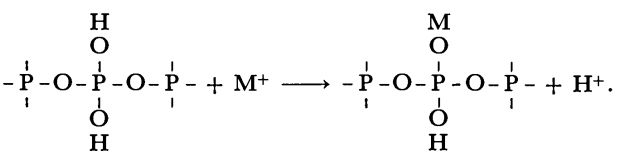

In the case of transition metal-ions, the order of ionic radius is as follows:

$$Mn^{2+} > Zn^{2+} > Co^{2+} > Ni^{2+},$$

and the order of the retardation efficiency at pH 1.0 is the same as that of the ionic radius. Therefore, the binding force of these transition metal ions with the phosphate ions may increase with an increase in the ionic radius in strongly acidic media. The catalytic effect of alkali metal ions for the degradation of triphosphate ions in alkaline solutions may be explained by the formation of the complex as follows:

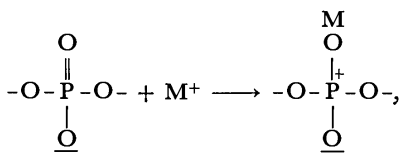

because the phosphate ion on the right-hand side is considered to be more susceptible to the nucleophilic attack of a water molecule than that on the left-hand side.

Table 3. Activation parameters for the hydrolysis of pyrophosphate

Phosphate	Added cation	pH=1.0		pH=2.0		pH=3.0	
		I[a]	II[b]	I	II	I	II
$H_4P_2O_7$	—	86.0	10.8	111.0	14.1	115.8	14.5
$Na_4P_2O_7$	—	87.4	11.0	115.8	14.8	117.5	14.7
	Li^+	89.9	11.3	116.7	14.9	117.7	14.7
	Na^+	89.8	11.3	116.9	15.0	118.0	14.8
	K^+	87.2	10.9	115.8	14.8	116.7	14.6
	Mg^{2+}	95.4	12.0	114.0	14.2		
	Ca^{2+}	96.9	12.3	119.0	15.2		
	Mn^{2+}	96.2	12.0				
	Co^{2+}	92.2	11.5				
	Ni^{2+}	94.3	11.9				
	Zn^{2+}	93.8	11.7				
	(Al^{3+})[c]	95.2	11.6				

a) I stands for the activation energy/kJ mol^{-1}. b) II stands for the log(frequency factor/min^{-1}). c) The values obtained at pH 0.9.

Table 4. Activation parameters for the hydrolysis of triphosphate

Phosphate	Added cation	pH=1.0		pH=2.0		pH=3.0	
		I[a]	II[b]	I	II	I	II
$H_5P_3O_{10}$	—	83.0	11.2	93.3	12.1	107.9	13.7
$Na_5P_3O_{10}$	—	83.0	11.1	95.1	12.3	108.0	13.7
	Li^+	88.0	11.8	104.4	13.7	108.5	13.7
	Na^+	84.4	11.3	103.5	13.5	110.0	14.0
	K^+	83.8	11.2	102.4	13.4	109.8	14.0
	Mg^{2+}	83.9	10.7	103.6	13.0	109.2	13.6
	Ca^{2+}	85.1	11.0	108.5	14.1		
	Mn^{2+}	90.4	11.5	108.8	13.8		
	Co^{2+}	84.1	10.7	105.1	13.2		
	Ni^{2+}	85.1	10.9	101.3	12.6	111.7	14.0
	Cu^{2+}	86.1	10.9				
	Zn^{2+}	85.5	10.9				

a) I stands for the activation energy/kJ mol^{-1}. b) II stands for log(frequency factor/min^{-1}).

References

1) Part IV; M. Watanabe, S. Sato, and H. Saito, *Bull. Chem. Soc. Jpn.*, **49**, 2474 (1976).
2) M. Watanabe, *Bull. Chem. Soc. Jpn.*, **47**, 2048 (1974).
3) M. Watanabe, S. Sato, and H. Saito, *Bull. Chem. Soc. Jpn.*, **48**, 896 (1975).

4) M. Watanabe, S. Sato, and H. Saito, *Bull. Chem. Soc. Jpn.*, **48**, 3593 (1975).
5) W. Wieker and E. Thilo, *Z. Anorg. Allg. Chem.*, **306**, 48 (1960).
6) E. Thilo and W. Wieker, *J. Polym. Sci.*, **53**, 55 (1961).
7) W. Wieker and E. Thilo, *Z. Anorg. Allg. Chem.*, **313**, 296 (1961).
8) L. F. Audrith, "Inorganic Syntheses," McGraw-Hill, New York (1950), Vol. III, p. 101.
9) J. R. Van Wazer, "Phosphorus and Its Compounds," Interscience Publishers, New York (1958), p. 452; and the references cited there.
10) U. P. Strauss and P. D. Ross, *J. Am. Chem. Soc.*, **81**, 5295 (1959).

Kinetics of the Catalytic Decomposition of Hydrogen Iodide in the Magnesium-Iodine Thermochemical Cycle

Yoshinao Oosawa,* Toshiya Kumagai, Susumu Mizuta, Wakichi Kondo, Yoshio Takemori, and Kinjiro Fujii

National Chemical Laboratory for Industry, Higashi, Yatabe-cho, Tsukuba-gun, Ibaraki 305

(Received July 11, 1980)

The decomposition of hydrogen iodide serves as the hydrogen-evolution step in several thermochemical water-splitting cycles, including the Magnesium–Iodine cycle. A kinetic analysis of the catalytic decomposition of hydrogen iodide has been carried out by the use of a flow method at 500—700 K. The platinum-supported active carbon catalyst (1 wt%) and the active carbon catalyst which have been found effective in the research reported previously, are used as the catalysts. The contact time-conversion relationships for both the catalysts are simulated successfully on the basis of an assumed reaction scheme. The influence of water vapor on the rate and the equilibrium of the decomposition of hydrogen iodide is negligibly small. The inhibition effect of iodine on the rate of the decomposition of hydrogen iodide over the platinum-supported active carbon catalyst is remarkable below 550 K.

The decomposition of hydrogen iodide serves as the hydrogen-evolution step in several thermochemical water-splitting cycles,[1–4] including the Magnesium–Iodine cycle[5] previously proposed by the present authors. It is favorable for the reaction to be carried out around or below 700 K from the standpoint of the construction of the present cycle. However, since the rate of the reaction in the form of a homogeneous gas-phase reaction is low in the temperature range below 700 K, the present authors attempted to carry out the reaction catalytically.

In the first step of the study of the catalytic decomposition of hydrogen iodide, a screening test of various catalysts prepared by an impregnation method from the compounds of all the members of the first transition-metal series, from the compounds of the members of the platinum-group metals, and so on, and from various catalyst supports were carried out. In the research, a platinum-supported active carbon catalyst (abbreviated as the Pt/C catalyst) and an active carbon catalyst were found to reveal favorable catalytic activities.[6]

For the second step of the research, a kinetic analysis of the reaction, a quantitative investigation of the influence of iodine and water vapor that may coexist with the hydrogen iodide to be decomposed on the rate and the equilibrium of the reaction, and a life test of the catalysts were necessary.

There have been very few reports on the kinetic studies of the decomposition of hydrogen iodide. Hinshelwood and Burk,[7] however, reported that the reaction over platinum wire under the conditions of a continuous removal of the iodine formed proceeded according to the following rate equation:

$$-\frac{dP_{HI}}{dt} = k,$$

where P_{HI} is the partial pressure of hydrogen iodide and where k is the rate constant. Iida[8] reported recently that the reaction over platinum supported on Teflon under the conditions of a continous removal of the iodine formed proceeded according to the following rate equation:

$$-\frac{dP_{HI}}{dt} = \frac{P_{HI}}{14.76P_{H_2} + 7.49P_{HI} + 208},$$

where P_{HI} is the partial pressure of hydrogen iodide, and so on. In both the researches, the reaction systems were simplified by the continuous removal of the iodine formed. The results of both the researches gave only insufficient information, however, on the unresolved questions related to thermochemical water splitting.

Therefore, the present authors have investigated the influence of the contact time and the partial pressure of hydrogen iodide, iodine, and water vapor on the reaction rate over the Pt/C catalyst and the active carbon catalyst, and analyzed the results on the basis of an assumed reaction scheme. They have also examined the lifetime of both the catalysts and the water-gas reaction of the carbon used as a catalyst or a support. On the basis of the results, it was confirmed that both the catalysts can be used for the decomposition of hydrogen iodide in the presence of water vapor at 550—700 K.

Experimental

The Pt/C catalyst (1.05 wt%) was prepared from the active carbon (Shirasagi-C granular, Takeda) and $H_2PtCl_6 \cdot 6H_2O$ by an impregnation-calcination method (Ar stream, 1000 K, 6 h), and was ground to a diameter of less than 0.30 mm (0.30—0.15 mm, 47 wt%; 0.15—0.03 mm, 42 wt% <0.03 mm, 11 wt%) before use. The active carbon catalyst was prepared by a calcination-grinding treatment of the active carbon similar to that used for the Pt/C catalyst. The experiments were carried out by the use of a tubular reactor with the aid of argon carrier gas. The apparatus was similar to that depicted in the preceding paper.[6] Hydrogen iodide was fed in the form of hydriodic acid (7.5 mol l^{-1}, Wako, Sp. Gr.) to obtain reaction conditions similar to those in the decomposition of hydrogen iodide included in the present thermochemical cycle, in which a certain amount of water vapor might coexist with hydrogen iodide. The reactant and the carrier gas were fed in at the following rates: HIaq, 32.3 ml/h; Ar, 9.0 l/h (P_{HI}=0.125 atm, P_{H_2O}=0.682, P_{Ar}= 0.193), unless otherwise stated. In all cases, the reactions were carried out under a total pressure equal to 1 atm. The contact time was varied by varying the catalyst amount at a fixed feed rate of the reactants and the carrier gas. The catalyst amount of 1.71 g (for both the Pt/C catalyst and the active carbon catalyst) corresponded to the contact time of 2.86×10^{-1} s (S.V.=1.26×10^4 h^{-1}). All the exhaust components except for hydrogen and argon were condensed out in the scrubber. The hydrogen concentration of the

exhaust gas was determined by the use of gas chromatography (YANACO, G180) with a molecular sieve 13 X column, while the flow rate of the exhaust gas (H_2+Ar) was measured with a soap-film flowmeter. The conversions of hydrogen iodide at each temperature were monitored by measuring the hydrogen concentration of the exhaust gas for about 1 h. After the concentration had become constant, the conversions were determined in each run in the directions of both the decreasing and increasing temperatures by taking the flow rate of the exhaust gas into account. The steady state of the reaction was confirmed by the close agreement of both conversions at each temperature. As the conversion in the blank experimentation was low (5.3×10^{-5} (600 K), 4.5×10^{-4} (650 K), 1.6×10^{-3} (700 K), it was clear that both the thermal decomposition in the gas phase and the catalytic decomposition on the surface of the glass wall of apparatus were negligible. The relative error in the conversion measurement was, in general, less than 4%.

Results and Discussion

Water-gas Reaction and Life Test. Active carbon is consumed through the reaction with water vapor, yielding hydrogen and carbon monoxide at high temperatures.

$$C + H_2O \longrightarrow H_2 + CO;\ \text{water-gas reaction}$$

It was assumed that the life of both catalysts for the decomposition of hydrogen iodide in the presence of water vapor was mainly dependent on the rate of the water-gas reaction. The rate of the hydrogen evolution through the reaction of both the catalysts with water vapor was measured. The results are presented in Table 1. The rate over the Pt/C catalyst was higher than that over the active carbon catalyst over the whole range of temperatures studied. It would be desirable to use the former catalyst below 700 K or the latter below 800 K to avoid a catalyst loss through the water-gas reaction. The conversion of hydrogen iodide over the Pt/C catalyst (0.171 g, 650 K) or the active carbon catalyst (0.570 g, 700 K) was confirmed to remain almost unchanged after 100 h of operation under the following feed rates: HIaq, 36.2 ml/h; Ar, 4.5 l/h.

Effect of Mass Transfer on the Reaction Rate.[9-11] When 0.171 g of the Pt/C catalyst was used, the ratio of the length of the catalyst layer to the average diameter of the catalyst particle was about 15. As it is accepted that the back-mixing effect is negligible when the ratio is about 20 or more, the back-mixing effect was almost negligible in the present experiment.

Both the feed rate and the catalyst amount were varied at a fixed contact time (2.86×10^{-2} s) over the Pt/C catalyst that shows a higher catalytic activity of the two kinds of catalysts: HIaq 32.3 ml/h, Ar 9.0 l/h, Pt/C 0.171 g and HIaq 21.5 ml/h, Ar 6.0 l/h, Pt/C 0.114 g. As the conversions were almost the same for each feed rate at 500—700 K, the external film diffusion did not seem to influence the reaction rate in this range of feed rates.

Table 1. Hydrogen evolution rate through water-gas reaction

T/K	Pt/C ml(STP)/h	Active carbon ml(STP)/h
500	0	0
600	0.2	0
700	2.2	0.1
800	9.5	0.4

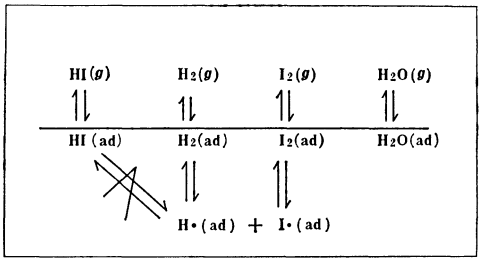

Fig. 1. Assumed reaction scheme for the catalytic decomposition of hydrogen iodide over the Pt/C catalyst or the active carbon catalyst in the presence of water vapor.

The conversion by the use of the Pt/C catalyst with a particle diameter of less than 0.15 mm differed little from that over the Pt/C catalyst with a diameter of less than 0.30 mm at a contact time of 1.43×10^{-2} s at 500—700 K. Therefore, the effect of internal diffusion in the micro pore of the catalyst on the reaction rate was considered to be insignificant.

Reaction Scheme. As the basis of the kinetic analysis of the catalytic decomposition of hydrogen iodide over the Pt/C catalyst or the active carbon catalyst, an appropriate reaction scheme was assumed. In the preceding paragraph, the effect of mass transfer on the reaction rate was shown to be negligibly small under the present experimental conditions. Therefore, the present authors assumed, on the basis of the results obtained by Hinshelwood and Burk[7] and Iida[8] that: (i) the reaction proceeds according to the reaction scheme depicted in Fig. 1 and (ii) the reaction kinetics can be analyzed according to a Langmuir-Hinshelwood type of mechanism.

Under the above assumption, the rate equation of the decomposition of hydrogen iodide, V_f, is written as follows, where k_f is the rate constant of the first-order surface reaction and θ_{HI} is the surface coverage by hydrogen iodide:

$$V_f = -\frac{dP_{HI}}{dt} = k_f\theta_{HI}. \quad (1)$$

θ_{HI} is written as follows, where K_{HI} is the adsorption coefficient of hydrogen iodide, p_{HI} is the partial pressure of hydrogen iodide, K_H is the adsorption coefficient of dissociated hydrogen, and so on:

$$\theta_{HI} = \frac{K_{HI}P_{HI}}{1+K_{HI}P_{HI}+K_{H_2}P_{H_2}+\sqrt{K_HP_{H_2}}+K_{I_2}P_{I_2}+\sqrt{K_IP_{I_2}}+K_{H_2O}P_{H_2O}}. \quad (2)$$

As has been mentioned above, Iida found that the rate equation of the catalytic decomposition of hydrogen iodide over the Pt/Teflon was expressed as follows under his experimental conditions:

$$-\frac{dP_{HI}}{dt} = \frac{P_{HI}}{14.76P_{H_2}+7.49P_{HI}+208}. \quad (3)$$

In Eq. 3, no term corresponding to the dissociated chemical species is included. Therefore, the present authors eliminate $\sqrt{K_H P_{H_2}}$ and $\sqrt{K_H P_{I_2}}$ from Eq. 2 as negligible and thus obtain the following equation:

$$\theta_{HI} = \frac{K_{HI}P_{HI}}{1+K_{HI}P_{HI}+K_{H_2}P_{H_2}+K_{I_2}P_{I_2}+K_{H_2O}P_{H_2O}}. \quad (4)$$

P_{HI}, P_{H_2}, and P_{I_2} are expressed as follows under the conditions that no condensed phase is present, where P is the initial partial pressure of hydrogen iodide and where x is the conversion of hydrogen iodide:

$$\left.\begin{aligned} P_{HI} &= P(1-x) \\ P_{H_2} &= Px/2 \\ P_{I_2} &= Px/2 \end{aligned}\right\}. \quad (5)$$

Substituting Eq. 5 in Eq. 4, Eq. 6 is obtained:

$$\theta_{HI} = \frac{PK_{HI}(1-x)}{1+K_{H_2O}P_{H_2O}+K_{HI}P+(K_{H_2}/2+K_{I_2}/2-K_{HI})Px}. \quad (6)$$

With Eq. 1 and Eq. 5, Eq. 7 is obtained:

$$-\frac{dP_{HI}}{dt} = -\frac{d(P(1-x))}{dt} = \frac{Pdx}{dt} = k_f\theta_{HI}. \quad (7)$$

Substituting Eq. 6 in Eq. 7, the following equation is given:

$$\frac{Pdx}{dt} = \frac{k_fPK_{HI}(1-x)}{1+K_{H_2O}P_{H_2O}+K_{HI}P+(K_{H_2}/2+K_{I_2}/2-K_{HI})Px} = \frac{\dfrac{k_fPK_{HI}(1-x)}{1+K_{H_2O}P_{H_2O}+K_{HI}P}}{1+\dfrac{(K_{H_2}/2+K_{I_2}/2-K_{HI})Px}{1+K_{H_2O}P_{H_2O}+K_{HI}P}}. \quad (8)$$

Consequently, the rate equation for the catalytic decomposition of hydrogen iodide is expressed by Eq. 9:

$$\frac{dx}{dt} = \frac{k(1-x)}{1+ax}, \quad (9)$$

where:

$$a = \frac{(K_{H_2}/2+K_{I_2}/2-K_{HI})P}{1+K_{H_2O}P_{H_2O}+K_{HI}P} \quad (10)$$

$$k = \frac{k_fK_{HI}}{1+K_{H_2O}P_{H_2O}+K_{HI}P}. \quad (11)$$

As the reaction rate of the formation of hydrogen iodide from hydrogen and iodine, V_b is proportional to the product of the surface coverage by the dissociated hydrogen and that by the dissociated iodine, according to the reaction scheme assumed in Fig. 1, V_b is expressed as follows, where k_b is the rate constant of the formation of hydrogen iodide:

$$V_b = \frac{dP_{HI}}{dt} = k_b\theta_H\theta_I. \quad (12)$$

θ_H and θ_I are expressed as follows by a treatment similar to that for Eq. 4;

$$\theta_H = \frac{\sqrt{K_HP_{H_2}}}{1+K_{HI}P_{HI}+K_{H_2}P_{H_2}+K_{I_2}P_{I_2}+K_{H_2O}P_{H_2O}} \quad (13)$$

$$\theta_I = \frac{\sqrt{K_IP_{I_2}}}{1+K_{HI}P_{HI}+K_{H_2}P_{H_2}+K_{I_2}P_{I_2}+K_{H_2O}P_{H_2O}}. \quad (14)$$

Equation 15 is obtained by substituting Eqs. 5, 13, and 14 into Eq. 12:

$$-\frac{Pdx}{dt} = \frac{k_bPx\sqrt{K_HK_I}}{2(1+K_{H_2O}P_{H_2O}+K_{HI}P)^2\left(1+\dfrac{(1+K_{H_2}/2+K_{I_2}/2-K_{HI})Px}{1+K_{H_2O}P_{H_2O}+K_{HI}P}\right)^2}. \quad (15)$$

Equations 15 is transformed to give Eqs. 16 and 17:

$$-\frac{dx}{dt} = \frac{k'x}{(1+ax)^2}, \quad (16)$$

where:

$$k' = \frac{k_b\sqrt{K_HK_I}}{2(1+K_{H_2O}P_{H_2O}+K_{HI}P)^2} \quad (17)$$

and where P is the initial partial pressure of hydrogen iodide.

Consequently, combining Eq. 9 with Eq. 16 gives the rate equation of the catalytic decomposition of hydrogen iodide, including the backward reaction:

$$\frac{dx}{dt} = \frac{k(1-x)}{1+ax} - \frac{k'x}{(1+ax)^2}. \quad (18)$$

Integrating Eq. 18 under the initial conditions (when t equals zero, x equals zero) and the equilibrium conditions (when x equals x_e, the equilibrium conversions of hydrogen iodide, dx/dt equals zero) yields the following expression:

$$-kt = ax + \frac{(ax_e^2+2x_e-1)}{x_e}\ln\left(\frac{x_e-x}{x_e}\right) + \frac{(x_e-1)^2}{x_e(ax_e^2+1)}\ln\frac{(x_e-x)}{x_e(ax_ex-1)}, \quad (19)$$

where k and a are expressed as in Eqs. 10 and 11 respectively.

Thus, the contact time-conversion relationship of the catalytic decomposition of hydrogen iodide is expressed by the Rate Equation 19, which has two constants independent of the contact time: k, mainly concerned with the reaction rate, and a, mainly concerned with the adsorption.

Contact Time-Conversion Relationship. The experimental results obtained over the Pt/C catalyst and the active cabon catalyst are depicted as the points in Figs. 2 and 3. The error in the measurement of the conversion of hydrogen iodide caused by the water-gas reaction, significant only in the case of the Pt/C catalyst at 700 K, was corrected by assuming that the rate of hydrogen evolution by the water-gas reaction was proportional to both the feed rate of water vapor and the amount of the catalyst. The results were simulated on the basis of Eq. 19. By considering the form of the equation, the simulation of the experimental results was performed by first determining the value of a which gave the least coefficient of variation of k, $(((k_i-\bar{k})^2/n)^{1/2}/\bar{k})$, then, the value of k as the average of k corresponding to the respective data in each run by employing the value of the a. The values

Table 2. Values of k, a, and x_e(equilibrium conversion) for Eq. 20

T/K	Pt/C		Active carbon		x_e
	k/s	a	k/s	a	
500	4.45×10^{-1}	3.75×10	1.78×10^{-1}	1.92×10^{2}	0.151
550	1.47	1.47×10	7.46×10^{-1}	9.66×10	0.166
600	3.64	2.76	1.06	2.21×10	0.182
650	8.47[a]	1.20[a]	1.44	2.90	0.195
700	1.71×10[a]	5.10×10^{-1} [a]	2.25	5.74×10^{-1}	0.210

a) As the number of the effective data for the calculation is small, both k and a are obtained by extrapolation assuming the linearity of the $\ln k$ *vs.* $1/T$ plot and the $\ln a$ *vs.* $1/T$ plot, respectively.

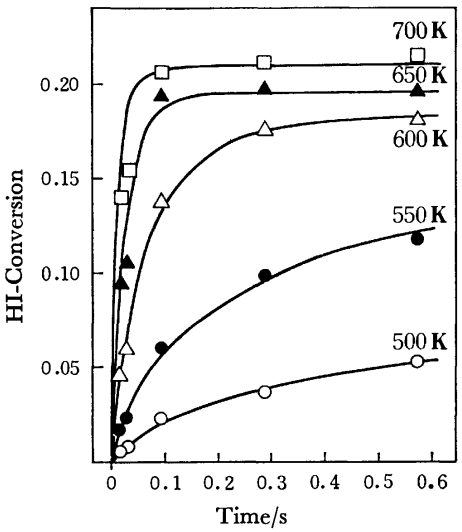

Fig. 2. Contact time-conversion relationship of hydrogen iodide over the Pt/C catalyst.

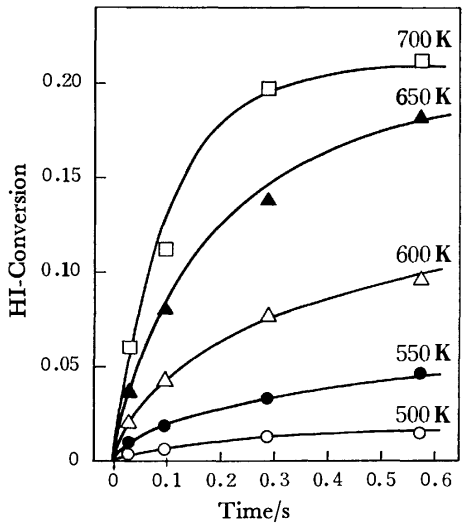

Fig. 3. Contact time-conversion relationship of hydrogen iodide over the active carbon catalyst.

of k and a are presented in Table 2. The continuous curves in Figs. 2 and 3 are obtained by employing Eq. 19 along with the k and a in Table 2. Because the equilibrium conversions of hydrogen iodide at temperatures of 600 K, 650 K, or 700 K in the presence of water vapor differed little from the values calculated by employing the free-energy changes cited from the JANAF Thermochemical Tables,[12] as will be explained in the section on the "Influence of the Partial Pressure of Water Vapor," the authors adopted the latter for x_e at each temperature from 500 K to 700 K for simulation by the use of Eq. 19. The continuous curves in Figs. 2 and 3 simulate the experimental data fairly well, supporting the conclusion that the assumed reaction scheme is comparatively appropriate.

Influence of the Partial Pressure of Hydrogen Iodide. For the rate equation at the initial stage, Eq. 20 is obtained by substituting zero for x in Eq. 8:

$$v = \frac{P\mathrm{d}x}{\mathrm{d}t} = \frac{k_f K_{HI} P}{1+K_{H_2O}P_{H_2O}+K_{HI}P}. \quad (20)$$

Equation 20 is transformed to Eq. 21:

$$\frac{v}{P} = \frac{\mathrm{d}x}{\mathrm{d}t} = \frac{k_f K_{HI}}{1+K_{H_2O}P_{H_2O}+K_{HI}P}. \quad (21)$$

It is reasonable to regard the data at 500 K, 550 K, and 600 K at a contact time of 1.43×10^{-2} s in Fig. 2 as those for the initial stage of the reaction. The conversion obtained when P, P_{H_2O}, and P_{Ar} were equal to 0.0761 atm, 0.415 atm, and 0.509 atm respectively at a contact time of 1.43×10^{-2} s were 0.00521 (500 K), 0.0159 (550 K), and 0.0444 (600 K). These values differ little from those shown in Fig. 2, for which the following partial pressures were used: P (0.125 atm), P_{H_2O} (0.682 atm), and P_{Ar} (0.193 atm). From these results, it is concluded that both $K_{H_2O}P_{H_2O}$ and $K_{HI}P$ are negligibly small compared to 1 in this range of their partial pressure by considering the form of Eq. 21, as $k_f K_{HI}$ remains constant.

Influence of the Partial Pressure of Water Vapor. The polarity of hydrogen iodide is strong. However, the polarities of hydrogen and iodine, the decomposition products of hydrogen iodide are weak. Therefore, there is the possibility that only hydrogen iodide is stabilyzed by the interaction with water vapor and that the conversion of hydrogen iodide decreases in the presence of water. The influence of the coexistence of water vapor on the equilibrium conversion of hydrogen iodide is small, as is shown by a comparison of the experimental conversions corresponding to that at the long contact time at 600—700 K in Fig. 2 with the calculated equilibrium conversions presented in Table 2.

When water vapor is added to the vapor of hydriodic acid, the rate equation at the initial stage is expressed as follows, on the basis of Eq. 20, where P_{H_2O} is the partial pressure of the water vapor including the added

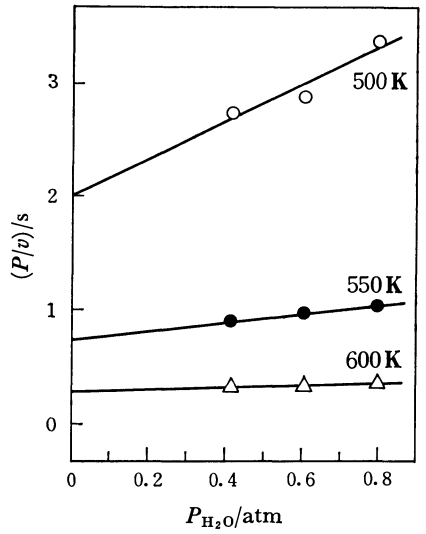

Fig. 4. Effect of water vapor addition on the initial rate of the decomposition of hydrogen iodide over the Pt/C catalyst (0.086 g): $P=0.0761$ atm, $P_{H_2O}=0.415$, 0.605, and 0.795 atm, P_{Ar}=balance.

water vapor:

$$v=\frac{P\mathrm{d}x}{\mathrm{d}t}=\frac{k_fK_{HI}P}{1+K_{H_2O}P_{H_2O}+K_{HI}P}. \quad (22)$$

The transformation of Eq. 22 yields Eq. 23:

$$\frac{P}{v}=\frac{1}{\frac{\mathrm{d}x}{\mathrm{d}t}}=\frac{1+K_{HI}P}{k_fK_{HI}}+\frac{K_{H_2O}P_{H_2O}}{k_fK_{HI}}. \quad (23)$$

It is shown in Eq. 23 that the plot of $1/(\mathrm{d}x/\mathrm{d}t)$ against the partial pressure of water vapor gives a straight line and that the intercept of the extrapolated line at the partial pressure zero is the reciprocal of $(\mathrm{d}x/\mathrm{d}t)$ in the absence of water vapor. The experimental results are depicted in Fig. 4. If the extrapolation of the straight line is significant even in the range where the partial pressure of water vapor is small or near zero, it can be said that the reaction rate of the decomposition of hydrogen iodide in the presence of water vapor does not differ so much from that in its absence.

Influence of the Partial Pressure of Iodine. Figure 5 shows the calculated values of the equilibrium conversion of hydrogen iodide in the presence of iodine in the gas phase added in advance of the decomposition. Calculation was carried out according to the following equation, where K is the equilibrium constant for the decomposition of hydrogen iodide, m is the ratio of the pressure of iodine added in advance of the decomposition to that of hydrogen iodide, and x is the conversion of hydrogen iodide:

$$K=\frac{\sqrt{x(x+2m)}}{2(1-x)}.$$

It can be seen from Fig. 5 that the coexistence of iodine in the gas phase lowers the equilibrium conversion of hydrogen iodide remarkably.

When iodine is added to hydriodic acid, the rate equation at the initial stage of the reaction is expressed as follows on the basis of Eq. 20, where $P^\circ_{I_2}$ is the

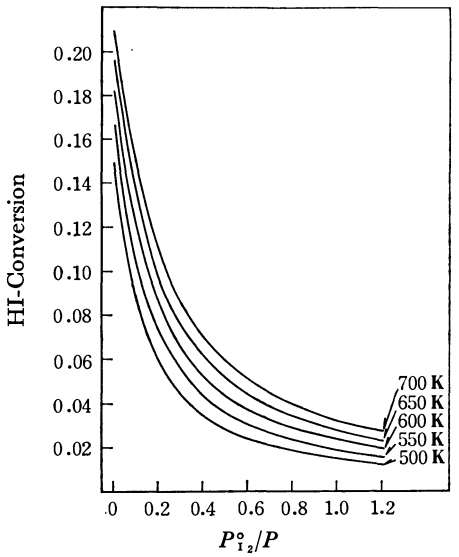

Fig. 5. Dependence of the equilibrium conversion of hydrogen iodide on the ratio of the pressure of iodine present in advance of the reaction ($P^\circ_{I_2}$) to the initial pressure of hydrogen iodide (P).

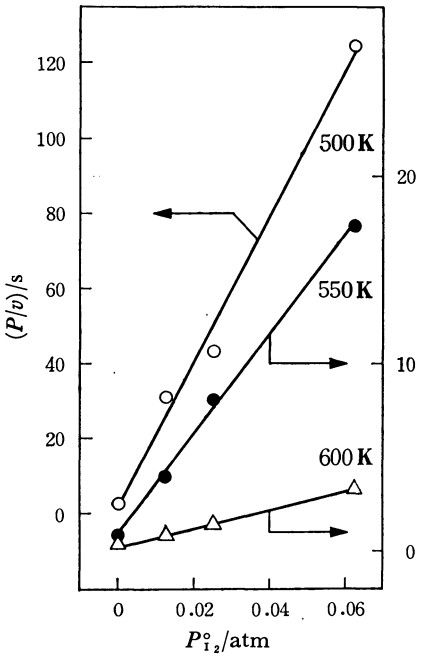

Fig. 6. Effect of iodine addition on the initial rate of the decomposition of hydrogen iodide over the Pt/C catalyst (0.086 g): $P=0.125$ atm, $P_{H_2O}=0.682$ atm, $P^\circ_{I_2}=0$, 0.0125, 0.0250, and 0.0625 atm, P_{Ar}=balance.

partial pressure of the added iodine:

$$v=\frac{P\mathrm{d}x}{\mathrm{d}t}=\frac{k_fK_{HI}P}{1+K_{H_2O}P_{H_2O}+K_{HI}P+K_{I_2}P^\circ_{I_2}}. \quad (25)$$

The transformation of Eq. 25 yields Eq. 26:

$$\frac{P}{v}=\frac{\mathrm{d}t}{\mathrm{d}x}=\frac{1+K_{H_2O}P_{H_2O}+K_{HI}P}{k_fK_{HI}}+\frac{K_{I_2}P^\circ_{I_2}}{k_fK_{HI}}. \quad (26)$$

Therefore, the plot of $1/(\mathrm{d}x/\mathrm{d}t)$ against the partial pressure of iodine gives a straight line, and the intercept at the zero pressure, the reciprocal of $(\mathrm{d}x/\mathrm{d}t)$ in the absence of iodine. The experimental results

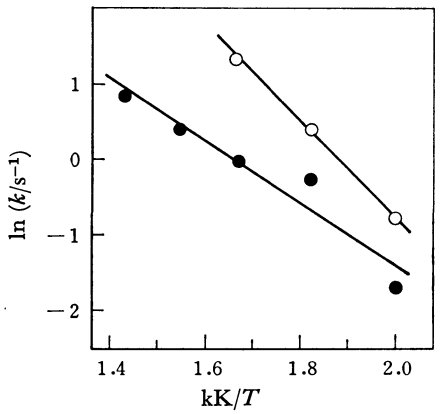

Fif. 7. Arrhenius plots for the decomposition of hydrogen iodide over the Pt/C catalyst and active carbon catalyst.
○: Pt/C catalyst, ●: active carbon catalyst.

are shown in Fig. 6. It is notable that the reaction rate at the initial stage decreased remarkably with the addition of iodine in the low-temperature range. For example, the reaction rate at the initial stage in the presence of 0.0625 atm ($P_{HI}/P^{\circ}_{I_2}=2$) of iodine was about a fiftieth of that in the absence of iodine at 500 K.

Activation Energy and Heat of Adsorption. As has been described above, k and a are expressed as follows:

$$k = \frac{k_f K_{HI}}{1+K_{H_2O}P_{H_2O}+K_{HI}P} \tag{10}$$

$$a = \frac{(K_{H_2}/2+K_{I_2}/2-K_{HI})P}{1+K_{H_2O}P_{H_2O}+K_{HI}P}. \tag{11}$$

As has been mentioned above, $K_{H_2O}P_{H_2O}$ and $K_{HI}P$ are negligible compared to 1 under the present experimental conditions. Therefore, Eqs. 10 and 11 are transformed to give the following equations:

$$k \approx k_f K_{HI} \tag{27}$$

$$a \approx (k_{H_2}/2+K_{I_2}/2-K_{HI})P. \tag{28}$$

Equation 27 shows that k is nearly equal to the apparent rate constant of the decomposition reaction of hydrogen iodide on the catalyst surface. Figure 7 shows the plot of ln k *vs.* $1/T$; the straight line in the figure was obtained by the treatment of least-squares fitting. From Fig. 7, the apparent activation energy of the decomposition of hydrogen iodide was given as 12.7 kcal/mol over the Pt/C catalyst and as 8.21 kcal/mol over the active carbon catalyst. The value obtained over the Pt/C catalyst is near to that obtained over the Pt wire by Hinshelwood and Burk[7] (14 kcal/mol).

K_{H_2}, K_{I_2}, and K_{HI} in Eq. 28 are expressed as follows by the use of the heats of adsorption of the corresponding chemical species:

$$K_{H_2} = \exp(-\Delta G^{\circ}_{H_2}/RT) = \exp(\Delta S^{\circ}_{H_2}/R)\cdot\exp(-\Delta H^{\circ}_{H_2}/RT)$$
$$= c_1\cdot\exp(q(H_2)/RT)$$
$$K_{I_2} = c_2\cdot\exp(q(I_2)/RT)$$
$$K_{HI} = c_3\cdot\exp(q(HI)/RT), \tag{29}$$

where $\Delta G^{\circ}_{H_2}$, $\Delta S^{\circ}_{H_2}$, $\Delta H^{\circ}_{H_2}$, and $q(H_2)$ are the standard Gibbs free energy change, the standard entropy change, the standard enthalpy change of adsorption of hydrogen, and the heat of adsorption of hydrogen, respectively. The other symbols are defined as above. By substituting Eq. 29 in Eq. 28, Eq. 30 is obtained:

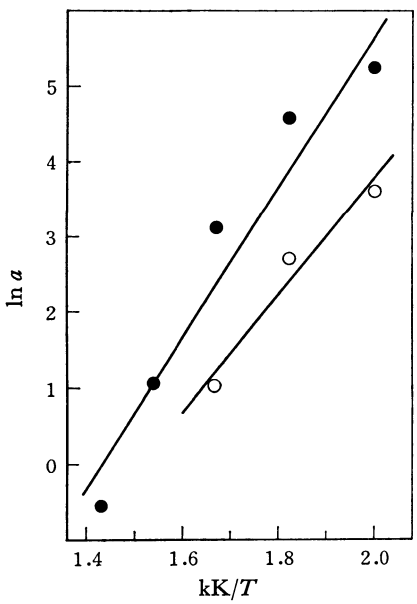

Fig. 8. Relations between the reciprocal of T and ln a.
○: Pt/C catalyst, ●: active carbon catalyst.

$$a = (c_1\cdot\exp(q(H_2)/RT)/2 + c_2\cdot\exp(q(I_2)/RT)/2$$
$$- c_3\cdot\exp(q(HI)/RT))P. \tag{30}$$

The values of $q(H_2)$ and $q(HI)$ on the active carbon have been reported in the literature: $q(H_2)$ is 2.5 kcal/mol[13] and $q(HI)$ is 21—23[14] kcal/mol. As is shown in Table 2, the values of a on the active carbon are positive, and when ln a is plotted against $1/T$ on a straight line by the least-squares fitting, the slope of the line is positive and big as is shown in Fig. 8. Therefore, none of the terms except for $c_2\cdot\exp(q(I_2)/RT)/2$ are considered to be dominant in Eq. 30. On the basis of this discussion, the following equation is obtained:

$$\ln a \approx q(I_2)/RT + \ln(c_2\cdot P/2). \tag{31}$$

Equation 31 means that, when ln a is plotted against $1/T$ on a straight line, the slope of the line gives $q(I_2)/R$. The value of $q(I_2)$ on the active carbon has not yet been reported. However, it may be estimated as follows:

$$q(I_2) = 2q(C_2H_5I) - q(n\text{-}C_4H_{10}),$$

where $q(C_2H_5I)$ and $q(n\text{-}C_4H_{10})$ are the heat of adsorption of ethyl iodide and butane on an active carbon, as reported in Ref. 13. The value of $q(I_2)$, 16.4 kcal/mol, is obtained by the use of the values of $q(C_2H_5I)$, 14.0 kcal/mol, and $q(n\text{-}C_4H_{10})$, 11.6 kcal/mol. The estimated value of $q(I_2)$ on the active carbon is comparable to that obtained from the slope of the ln a *vs.* $1/T$ plot of the active carbon catalyst (20.7 kcal/mol). This fact also supports the validity of the kinetic analysis employed in the present research.

The results obtained in the present research may be summarized as follows: 1) The contact time-

conversion relationship of the catalytic decomposition of hydrogen iodide over the Pt/C catalyst and the active carbon catalyst was simulated successfully by the use of a rate equation derived from an assumed reaction scheme. 2) The influence of water vapor on the rate and equilibrium of the decomposition of hydrogen iodide was small. 3) The Pt/C catalyst and the active carbon catalyst were consumed through the water-gas reaction in the high-temperature range (above 700 K for the former catalyst and above 800 K for the latter). 4) The presence of iodine in the gas phase in advance of the decomposition of hydrogen iodide lowers its equilibrium conversion remarkably, as judged on the basis of a thermodynamic calculation. 5) The inhibition effect of iodine on the rate of the catalytic decomposition of hydrogen iodide over the Pt/C catalyst was remarkable below 550 K.

On the basis of these results, the present authors have concluded that the Pt/C catalyst and the active carbon catalyst should be used in the temperature range of 550—700 K, where the water-gas reaction is almost negligible and where the inhibition effect of iodine is small. For the catalytic decomposition of hydrogen iodide in the lower temperature range, the development of a catalyst which suffers little inhibition effect from iodine is required, or the decomposition should be carried out in combination with a separation method that can continuously remove the iodine formed in the gas phase, even in the presence of water.

The authors wish to thank Drs. Naoyuki Todo, Kenzo Fukuda, and Etsuo Akiba for their valuable discussions. We also would like to thank Mr. Eiji Miyazawa for his cooperation in the experiment and Mr. Atsushi Kinase for his cooperation in several calculations.

References

1) J. H. Norman, K. J. Mysels, D. R. O'Keefe, S. A. Stowell, and D. G. Williamson, Proceedings of the 2nd World Hydrogen Energy Conference (WHEC), Zürich, 513 (1978).
2) M. Dokiya, K. Fukuda, T. Kameyama, Y. Kotera, and S. Asakura, *Denki Kagaku*, **45**, 139 (1977).
3) G. De Beni, G. Pierini, G. Spelta, D. van Velzen, and H. Langenkamp, Proceedings of the 2nd WHEC, Zürich 617 (1978).
4) T. Ohta, N. Kamiya, and M. Yamaguchi, *Int. J. Hydrogen Energy*, **3**, 203 (1978).
5) W. Kondo, S. Mizuta, T. Kumagai, Y. Oosawa, Y. Takemori, and K. Fujii, Proceedings of the 2nd WHEC, Zürich, 909 (1978).
6) Y. Oosawa, Y. Takemori, and K. Fujii, *Nippon Kagaku Kaishi*, **1980**, 1081.
7) C. N. Hinshelwood and R. E. Burk, *J. Chem. Soc.*, **127**, 2896 (1925).
8) I. Iida, *Z. Phys. Chem. Neue Folge*, **109**, 221 (1978).
9) O. Levenspiel, "Chemical Reaction Engineering," John Wiley & Sons, New York (1962), Chap. 6.
10) O. Levenspiel and K. B. Bishoff, *Ind. Eng. Chem.*, **53**, 313 (1961).
11) "Shokubai Chosei Oyobi Shikenho," ed by Y. Ogino, Chijin Shokan, Tokyo (1965), p. 293.
12) "JANAF Thermochemical Tables," Dow Chemical Company, Midland (1977).
13) "Landolt Börnstein Tabellen," 6 Aufl., II Band, 4 Teil, "Kalorische Zustandsgrössen," Springer Verlag, Berlin (1961).
14) C. L. Mantell, "Industrial Carbon," D. van Nostrand Company, New York (1946).

Alkali Metal Ion Exchange on Crystalline Zirconium Titanium Phosphate

Isao Tomita,* Kenkichi Iwase,** Kazuhiko Saito,** Yoshiyuki Sugiyama**

Tokyo University of Fisheries, Minato-ku, Tokyo 108

***Department of Chemistry, The University of Tsukuba, Ibaraki 305*

(Received July 21, 1980)

Ion-exchange studies of crystalline zirconium titanium phosphate with variable zirconium-to-titanium mole ratios have been extended to sodium-ion exchange on the exchangers with Zr-to-Ti mole ratios of 0.37 and 0.61, and to lithium and potassium ion exchange on the exchanger with a Zr-to-Ti mole ratio close to unity. In the sodium-ion exchange, a mono-sodium phase formed up to about a half of the exchange; then a disodium phase with a different amount of water of crystallization formed. In the lithium-ion exchange, the reaction proceeded with the formation of fully exchanged phases whose water content varied depending upon the environment in which the exchanger was placed during or after the reaction. The exchange amount of potassium ions was much less than that of sodium or lithium ions, and the ion exchange proceeded in parallel with an extensive hydrolysis of the exchanger. The half-exchanged phase could not be confirmed in this case. For the three alkali metal ions studied, the selectivity series was found as a function of loading, *i.e.*, within the range of the load from 0 to 1.3 meq/g, the selectivity is in the order of $Na^+>K^+>Li^+$, between 1.3 and 4.5 meq/g, it is $Na^+>Li^+>K^+$, and above 4.5 meq/g loading, it turns out to be $Li^+>Na^+>K^+$.

The sodium-ion-exchange behavior on crystalline zirconium titanium phosphate (ZTP) with three different Zr-to-Ti mole ratios has been reported in some detail, and it was revealed[1] that, in the titanium-rich exchanger, a disodium phase was formed without the formation of the intermediate monosodium phase, as was the case in H^+–Li^+ or H^+–Na^+ exchange on α-titanium phosphate(α-TP). The investigation has now been extended to sodium-ion exchange on ZTP with some other Zr/Ti mole ratios, and further to lithium and potassium-ion exchange on ZTP with the Zr/Ti mole ratio close to unity. A comparison of the exchange behavior of these alkali metal ions with each other is of interest from the viewpoint of ion selectivity as well as the ion-sieve effect.

Experimental

ZTP Exchangers. The ZTP exchangers used in this experiment were prepared as has been described earlier[1] with the refluxing time of 200 h. The Zr/Ti mole ratio in the starting solutions was varied between the sodium-ion experiment and the lithium- and potassium-ion experiment.

Analysis of the Exchangers. The sum of Zr and Ti was determined gravimetrically by means of precipitation with cupferron.[1] In a separate experiment, the exchanger (300 mg) was dissolved in hot concd H_2SO_4 (40 cm^3). After cooling, 10% H_2O_2 (10 cm^3) was added to the solution. The mixture was heated, and the resulting clear solution was diluted to 150 cm^3. Then the solution was transferred into a reduction vessel containing a liquid zinc amalgam, carbon dioxide gas was introduced to repalce the air, and the vessel was shaken vigorously for 10 min under slight warming. Titanium(IV) was thus quantitatively reduced to a trivalnet state. Then the aqueous phase was titrated with a standard $NH_4Fe(SO_4)_2$ solution in the presence of a saturated KSCN solution (10 cm^3), the Zr-to-Ti mole ratio being calculated from the results.[2]

Ion Exchange. The experiment was conducted by means of the batch method in the way described previosuly. Mixed solutions of MCl (0.1 mol dm^{-3}) and MOH (0.1 mol dm^{-3}), where M is Li, Na, or K, were prepared in variable mixing ratios. The sodium experiment was carried out at 25 °C, whereas the lithium and potassium experiments were made at 25, 45, and 60 °C. After equilibration with the exchanger in interest, the solution was centrifuged, and then the pH of the supernatant liquid was measured. Analyses for Na, Li, and K was performed by flame photometry with a Hitachi atomic absorption/flame spectrophotometer, while P was analyzed colorimetrically by the phosphomolybdic acid method. X-Ray powder diffractometry was made on exchangers obtained at various stages of ion exchange by using a Rigaku Geigerflex X-ray diffractometer.

Results and Discussion

Synthesized Exchangers. Three kinds of ZTP exchangers have been prepared, as is shown in Table 1. ZTP(Zr/Ti=0.37) and ZTP(0.61) were used for the Na^+-ion exchange, and ZTP(1.02), for the Li^+- and K^+-ion exchange.

The interlayer distance (d_{002}), as estimated from the X-ray powder patterns, was approximately 7.6 Å in all three cases. As has been reported,[1] the exchangers are considered as solid solutions of zirconium and titanium phosphate and as isomorphous with α-zirconium phosphate(α-ZP) and α-TP.

Sodium-ion Exchange. Figure 1 illustrates the pH-titration curves for Na^+-ion exchange and the corresponding phosphate-release curves. The titration

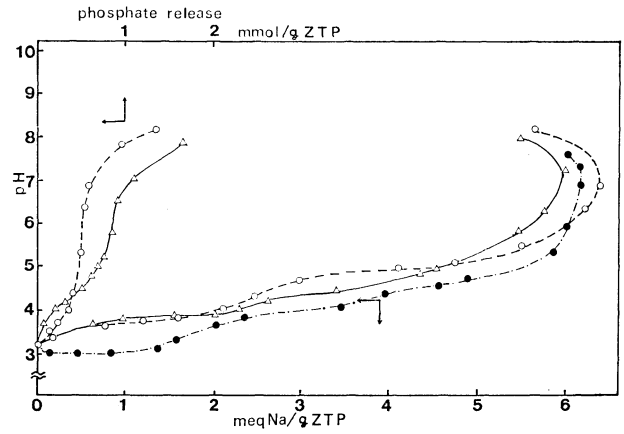

Fig. 1. The pH-titration curves for sodium ion exchange and the phosphate release curves.
—○—: ZTP (0.61), —△—: ZTP (0.37), —·●·—: α-TP.

Table 1. Composition of synthesized ion exchanger, $Zr_xTi_{1-x}(HPO_4)_2 \cdot H_2O$

Notation	Mixing mole ratio (Zr/Ti) of starting materials	Mole ratio (Zr/Ti) of products	x	Estimated exchange capacity (meq/g)
ZTP(0.37)	0.50	0.37	0.27	7.41
ZTP(0.61)	0.67	0.61	0.37	7.30
ZTP(1.02)	1.0	1.02	0.51	7.15

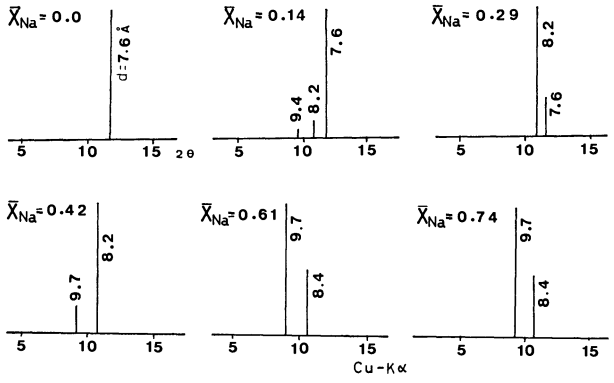

Fig. 2. The lowest angle regions of the X-ray powder diffraction patterns of ZTP(0.37) at several stages of exchange. $\bar{X}_{Na}$ denotes the ionic fraction of sodium ion in the exchanger.

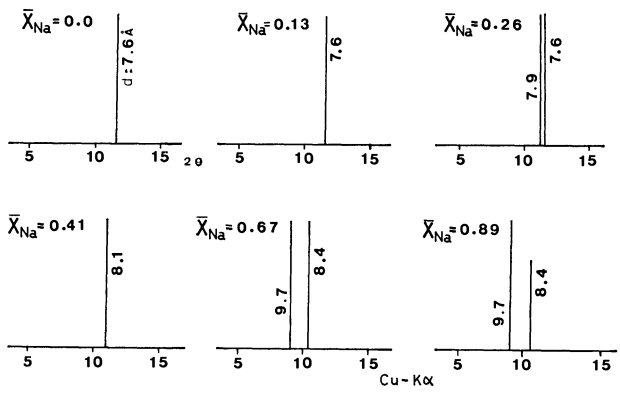

Fig. 3. The lowest angle regions of the X-ray powder diffraction patterns of ZTP(0.61) at several stages of exchange.

curve for ZTP(0.37) has a small point of inflection at approximately 2.3 meq Na^+/g ZTP. The curve for ZTP(0.61) also has an inflection at approximately 2.4 meq Na^+/g ZTP. The titration curve for Na^+-ion exchange on α-TP given by Takaguchi[3] is included in the figure, where an inflection exists at approximately 2 meq Na^+/g TP. The titration curve for Na^+-ion exchange on α-TP is similar to those given by previous investigations, but the existence of any inflection was not very clear[4,5] previously, except for the recent study by Clearfield and Frianeza.[6] The shift of the inflection toward a lower sodium loading with a decrease in the Zr content has been observed in the experiment[1] for ZTP(3.25) [3.5 meq/g], ZTP (0.93) [3 meq/g], and ZTP(0.25) [2.2 meq/g]. The data given in the present study again confirms the trend.

The X-ray powder patterns for ZTP(0.37) and ZTP (0.61) at several stages of exchange were measured; their lowest angle regions are shown in Figs. 2 and 3. The reflection peak at the lowest angle corresponds to the interlayer distance (d_{002}). The ionic fraction of sodium in the exchanger phase is denoted by $\bar{X}_{Na}$. As is shown in Fig. 2, in ZTP(0.37), the intensity of the peak at 7.6 Å representing the unexchanged phase decreased with an increase in sodium loading, and a peak appeared at 8.2 Å. This peak seems to correspond to the monohydrate of monosodium salt (d= 7.9 Å), with some excess of water obtained in the dehydration process of pentahydrate (d=11.9 Å). Beyond a 50% exchange, the unexchanged phase was no longer present and the peaks at 8.4 and 9.7 Å arose. These peaks indicate disodium phases with different amounts of water of crystallization.[1] These patterns suggest that ZTP(0.37) still behaves toward the Na^+ ion like α-ZP in that the monosodium phase exists as an intermediate.

In ZTP(0.61), the interlayer distance remained almost constant until $\bar{X}_{Na}$=0.26, where the peak at 7.9 Å appeared at the expense of the peak at 7.6 Å (Fig. 3). Thus, it shows the formation of the solid solution of ZTP with the Na^+ ion up to about 25% exchange. At $\bar{X}_{Na}$=0.41, the 7.6 Å peak disappeared, leaving only the peak at 8.1 Å. The d-values for the monosodium form seem to vary between 7.9 and 8.2 Å depending upon the drying condition of the samples used for X-ray examination. If the sample was dried in a silica-gel desiccator, d-values of around 7.9 Å were obtained, whereas the samples only air-dried gave somewhat higher values.

In conclusion, for the Na^+-ion exchange process, the monosodium phase is present in ZTP(0.37) and ZTP(0.61), as was the case for α-ZP, ZTP(3.25), and ZTP(0.93).

Lithium-ion Exchange. The ion-exchange experiment was conducted by using ZTP(1.02), its formula being $Zr_{0.505}Ti_{0.495}(HPO_4)_2 \cdot H_2O$. The pH-titration curves and the phosphate-release curves measured at 25, 45, and 60 °C are given in Fig. 4. At any temperature examined, the titration curve reached a plateau at a pH close to about 5 soon after the exchange started. In the case of the experiment at 25 °C, the plateau continued until the exchange proceeded up to 80% of the theoretical exchange capacity. Thereafter, the curve steeply rose to the pH of 7.5 and recorded the maximum exchange of 88.5%. At a higher pH value, the exchange amount of the Na^+ ion decreased as a result of the hydrolysis of the exchanger. The absence of any pH jump at a half-exchange reminds one of the lithium-ion exchange on α-TP.[7] As the temperature rose, the hydrolytic decomposition of the exchanger proceeded further, resulting in a decrease in the maximum exchange

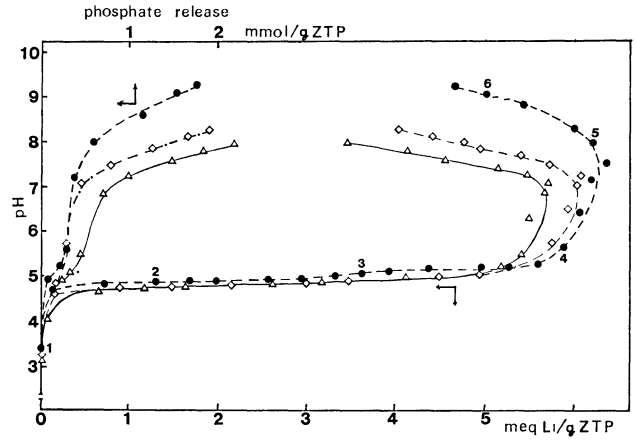

Fig. 4. The pH-titration curves for lithium ion exchange and the phosphate release curves.
—●—: 25 °C, —·◇·—: 45 °C, —△—: 60 °C.
The exchanger is ZTP(1.02) in all the cases.

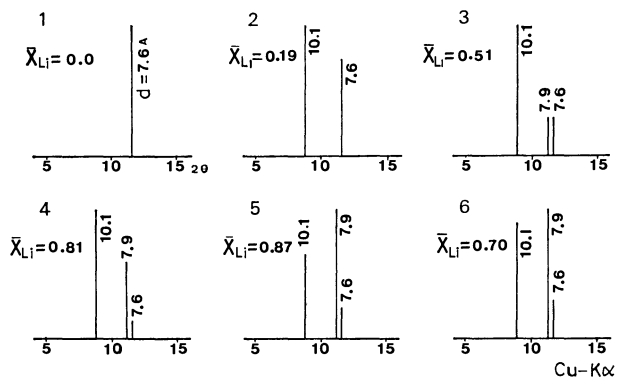

Fig. 5. The lowest angle regions of the X-ray powder diffraction patterns of ZTP(1.02) at several stages of lithium exchange at 25 °C. The numbers 1 to 6 indicate the extent of reaction shown in the titration curve in Fig. 4. $\bar{X}_{Li}$ denotes the ionic fraction of lithium ion in the exchanger.

amount of the Li^+ ion, which was 84% at 45 °C and 79% at 60 °C compared to the theoretical value. As far as the ion-exchange behavior is concerned, however, the temperature dependence is very little, as is clearly observed in the fact that there is almost the same pH value in the plateau region. In other words, the exchange equilibrium is attained within 4 d even at 25 °C, but hydrolysis tends to proceed even further if the exchanger is in contact with alkaline solutions for a longer period.

The lowest-angle regions of the X-ray powder patterns of the exchanger at several stages of Li^+-ion exchange are reproduced in Fig. 5. Numbers 1 to 6 indicate the extent of exchange shown in the titration curve (Fig. 4). Unlike the Na^+-ion exchange on ZTP (0.61), a hardly no formation of the solid solution was observed in the present case; that is, as soon as the exchange started, the reflection peak at 10.1 Å appeared, followed by the peak at 7.9 Å. These two peaks retained considerable intensities up to the maximum exchange, namely, to the end of the reaction. At the same time, the peak at 7.6 Å representing the unexchanged phase also survived with much smaller intensity. It is considered that the increasing steric hindrance occurred as the hydrated Li^+ ions replaced protons, and that this resulted in incomplete substitution. The peaks at 10.1 and 7.9 Å correspond to the tetra- and mono-hydrate of dilithium salt, (Zr, Ti)$(LiPO_4)_2 \cdot 4H_2O$ and (Zr, Ti)$(LiPO_4)_2 \cdot H_2O$, as assumed from the lithium-exchanged phases formed in α-ZP.[8] In fact, if the exchanged solid was heated at 100 °C for 30 min, the peak at 10.1 Å completely disappeared and the peak at 7.9 Å remained.

From the shape of the titration curves and the X-ray evidence, it may be concluded that, in the Li^+-ion exchange on ZTP(1.02), the reaction proceeds with the formation of fully exchanged phases whose water content varies depending upon the environment during or after the exchange process.

It is interesting to compare the Li^+-ion exchange behavior on ZTP with that on α-ZP and α-TP. In α-ZP, two exchangeable protons are said to have differing acidities, and a half-exchanged phase is often observed for the reaction with many counter ions. This exchanger also allows variations in the water content at various stages of ion exchange, and it leads to a change in the interlayer spacing. In α-TP, on the other hand, the formation of a half-exchanged phase is difficult to confirm.† Especially for the Li^+-ion exchange, the water content is rather unchanged throughout the reaction and the interlayer spacing is also kept constant. The case of ZTP(1.02) is just intermediate inbetween α-ZP and α-TP. It resembles α-TP in that a monolithium phase is absent, but it resembles α-ZP in that the water content varies during exchange, resulting in a change in the interlayer distance. However, taking the exchange behavior of Na^+ ion into consideration, the existence or absence of a half-exchanged form is not always simply related to the difference in the acidity of the two exchangeable protons of ZTP. To elucidate the mechanism of the direct formation of the fully exchanged phase, further investigation, including that of the diffusion kinetics of cations in the exchanger solid, are needed.

Potassium-ion Exchange. The same exchanger as used for the Li^+-ion exchange, ZTP(1.02), was utilized. The potassium-uptake curves and the phosphate-release curves obtained at 25, 45, and 60 °C are shown in Fig. 6. It is clear that potassium uptake on ZTP(1.02) is not so easy compared to the sodium and lithium uptake. Thus, up to pH 7 about 2 meq K^+ ions per g of exchanger were taken up. This value falls to between the corresponding potassium uptakes on α-TP and α-ZP, about 1 meq/g[3] and 3 meq/g[9] respectively. These values are much less than the exchange amount of alkali metal ions with smaller ionic radii for this pH. The equilibrium pH reached a plateau at about 7.1, where the K^+-ion exchange proceeded in parallel with the hydrolysis of the exchanger. No step-by-step exchange such as has been observed in the K^+-ion exchange on α-ZP[9] was found in the case of ZTP(1.02).

† Clearfield and Frianeza reported the formation of two sodium-ion-exchanged phases.[6]

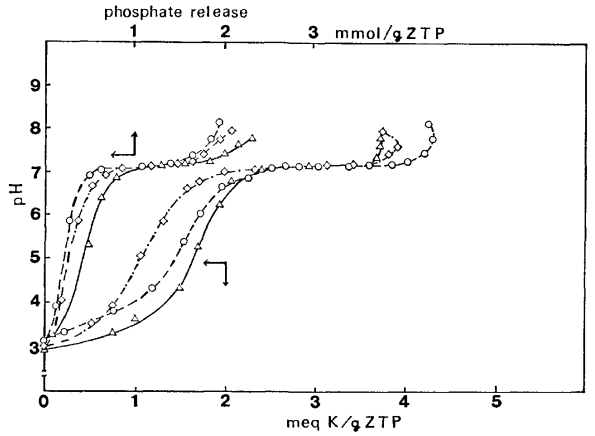

Fig. 6. The pH-titration curves for potassium ion exchange and the phosphate release curves.
—○—: 25 °C, —·◇·—: 45 °C, —△—: 60 °C.
The exchanger is ZTP(1.02) in all the cases.

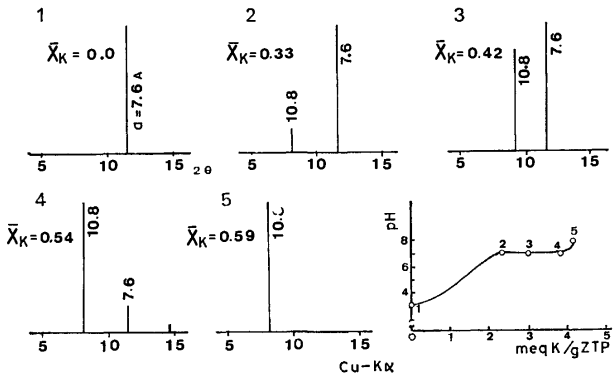

Fig. 7. The lowest angle regions of the X-ray powder diffraction patterns of ZTP(1.02) at several stages of potassium exchange at 25 °C. The numbers 1 to 5 indicate the extent of reaction shown in the titration curve given at the bottom right. $\bar{X}_K$ denotes the ionic fraction of potassium ion in the exchanger.

The maximum exchange was about 60% of the theoretical capacity at 25 °C and even less at higher temperatures. The phosphate release in alkaline solutions was much more extensive in the K^+ uptake than in the Li^+ and Na^+ ion exchange, reflecting the large ionic radius of the K^+ ion, which encounters cavity openings of comparable size.

In Fig. 7, the lowest angle region of the X-ray powder diffractograms of various exchanged solids for the 25 °C experiment are given schematically. Up to an exchange of about 33%, where the equilibrium pH is still below 7, no new solid phase can be observed, indicating the formation of a solid solution; *i.e.*, the K^+ ions are incorporated with ZTP without changing its structure. Above this point, the reflection corresponding to d_{002}=10.8 Å appeared, while the peak at 7.6 Å diminished. It should be noted that the exchanger decomposes to such an extent that, at $\bar{X}_K$= 0.59, no reflection from the unexchanged phase was observed any longer. The X-ray powder patterns obtained in the 45 and 60 °C experiments were similar to those described above, except that the degree of crystallinity became poorer in the exchange at a higher pH.

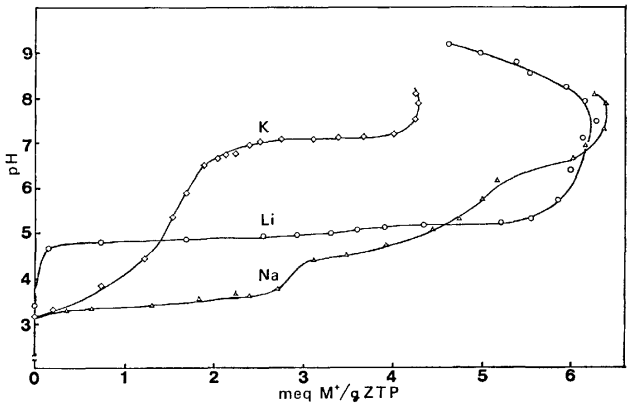

Fig. 8. The alkali metal ion uptake curves at 25 °C. For sodium ion uptake, ZTP(0.93) exchanger was used. For other two ions, ZTP(1.02) was employed.

In the K^+-ion exchange on α-ZP, monopotassium salt, $Zr(KPO_4)(HPO_4)\cdot H_2O$, with an interlayer distance of 7.95 Å, and dipotassium salt, $Zr(KPO_4)_2\cdot 3H_2O$, with an interlayer distance of 10.8 Å, were produced during the exchange process.[9] In the present study, the new solid phase confirmed has the interlayer distance of 10.8 Å, which most probably corresponds to a trihydrate of dipotassium salt, $(Zr, Ti)(KPO_4)_2\cdot 3H_2O$. This means that the half-exchanged phase could not be confirmed in this case either.

Ion-selectivity Series. Comparison is now possible between the ion-exchange behavior of three alkali metal ions on this particular inorganic exchanger. Titration curves measured under quite similar conditions are reproduced in Fig. 8. The selectivity series depends on the load of exchanger. Thus, within the range of loads from 0 to 1.3 meq/g, the selectivity is in the order: $Na^+>K^+>Li^+$, while between 1.3 and 4.5 meq/g, it is $Na^+>Li^+>K^+$. Above 4.5 meq/g loading, it turns out to be $Li^+>Na^+>K^+$, and practically no potassium ions are taken up at all.

It is noticeable that the lithium-ion selectivity increases relative to other ions as the load of the exchanger increases. However, this is a result of the rather constant equilibrium pH for lithium exchange compared to the case of sodium or potassium. In lithium exchange, essentially a single exchanged crystal form seems to exist. Thus, the tetrahydrate of dilithium salt is the most probable form on the exchange site. On the other hand, in the case of sodium exchange, the shape of the titration curve seems to be related to two exchanged forms, mono- and disodium salts. Further, in potassium exchange, the initial formation of a solid solution, followed by the formation of a potassium salt phase, may be responsible for the unique shape of its titration curve.

References

1) Y. Yazawa, T. Eguchi, K. Takaguchi, and I. Tomita, *Bull. Chem. Soc. Jpn.*, **52**, 2923 (1979).

2) JIS-M-8311(1961). (Japanese Industrial Standard).
3) K. Takaguchi, M. Sc. Thesis, Tokyo Kyoiku University, Tokyo (1977).
4) G. Alberti, P. Cardini-Gallti, U. Costantino, and E. Torracca, *J. Inorg. Nucl. Chem.*, **29**, 571 (1967).
5) E. Kobayashi, *Bull. Chem. Soc. Jpn.*, **48**, 3114 (1975).
6) A. Clearfield and T. N. Frianeza, *J. Inorg. Nucl. Chem.*, **40**, 1925 (1978).
7) K. Takaguchi and I. Tomita, *J. Chromatogr.*, **118**, 263 (1976).
8) A. Clearfield and J. Troup, *J. Phys. Chem.*, **74**, 314 (1970).
9) A. Clearfield, W. L. Duax, J. M. Garces, and A. S. Medina, *J. Inorg. Nucl. Chem.*, **34**, 329 (1972).

Phase Relations in the System PbO–$PbSiO_3$

Kazushi HIROTA* and Yasutoshi T. HASEGAWA

National Institute for Research in Inorganic Materials, Namiki, Sakura-mura, Niihari-gun, Ibaraki 305

(Received July 24, 1980)

Phase relations in the system PbO–$PbSiO_3$ were determined at temperatures above 650 °C. Two new lead silicate phases, Pb_5SiO_7 and $Pb_{11}Si_3O_{17}$ were found to be stable. The former melts incongruently at 733±1 °C to solid PbO plus liquid, and decomposes below 702±1 °C. The latter melts congruently at 728±1 °C. The compound Pb_4SiO_6, which has been accepted as stable, could not be confirmed.

Considerable work has been done by various investigators[1-11] on the system PbO–SiO_2. These workers agree about the temperature region of liquidus and solidus lines of the PbO–SiO_2 system, and the phase diagram given by Geller *et al.*[6] has long been accepted as definitive by many investigators.[7-11] Beyond this, however, there is little agreement. Compounds with the PbO:SiO_2 molar ratios of 4:1, 3:1, 2:1, 3:2, 1:1, 5:8, and 1:2 have been reported. Billhardt,[7] Ott and McLaren,[8] and Smart and Glasser[9] have studied subsolidus reactions and compound formation in this system, with the result that there are 3 quite different sets of conclusions regarding the identity, polymorphism, and thermodynamic stability of the lead silicates.

In the present study, we re-examined the phase equilibrium relations of the system PbO–$PbSiO_3$ in the region above 650 °C, of which the phase diagram has been given by Geller *et al.*[6] Two new lead silicate phases, 5:1 and 11:3, were found to be stable.

Experimental

The reaction products quenched in the equilibration runs were examined by X-ray diffraction of powdered specimens, by electron probe microanalysis, and by microscopy. The approach to equilibrium was studied as a function of run durations. Starting from a mixture of PbO and SiO_2, a complex mixture of more than three phases was obtained when the run duration was too short to attain an equilibrium state. A quenched specimen was judged to be at equilibrium when two phases or a single phase only was found. The starting mixtures were enclosed by welding them in platinum capsules 6 mm in diameter and 35 mm long. Otherwise, sublimation of components during the run durations was not negligible.

A fine powder of SiO_2 used as the starting material was prepared from a commercial $SiCl_4$ (Shin-Etsu Chemical Co. Ltd.) prepared for semiconductor use. The $SiCl_4$ was added to water in a platinum dish. The product was dried on a sand bath. Then the product silica was crushed into a powder and heated at 1300 °C to eliminate the volatile impurities. The PbO used as starting material was prepared from a commercial basic lead carbonate (Nakarai Chemicals, Ltd., CP grade). About 10 ppm of Al and Ni were detected in the PbO by means of spectroscopic analysis. Further details of the experimental procedures are the same as those given in our previous report on the PbO–$PbGeO_3$ system.[12]

Results

Observed equilibrium phase relations are summarized in Fig. 1. In the PbO–$PbSiO_3$ system, three intermediate compounds, Pb_5SiO_7, $Pb_{11}Si_3O_{17}$, and Pb_2SiO_4, appear above 650 °C. The last one, Pb_2SiO_4 has been already reported by Krakau *et al.*,[5] but the former two phases have not yet been reported.

In the present investigation, electron probe microanalysis was used successfully for identification of phases in quenched samples. Results of analysis for equilibration runs are shown in Table 1. Each starting mixture was sealed by welding it inside a plutinum

Table 1. Analytical results of the products kept at 718 °C for 820 h[a]

Starting materials Composition		Products							
		Phase 1		Phase 2		Phase 3		Phase 4	
SiO_2/wt%	PbO/wt%	SiO_2/wt%	PbO/wt%	SiO_2/wt%	PbO/wt%	SiO_2/wt%	PbO/wt%	SiO_2/wt%	PbO/wt%
3.0	97.0	0.0_5	$100._1$	5.1_2	$94._2$				
		0.0_2	$100._2$	5.3_2	$94._2$				
		0.0_0	$99._8$	5.2_4	$94._5$				
6.0	94.0			5.1_0	$94._9$	6.8_2	$92._9$		
				5.1_9	$94._5$	6.8_3	$93._7$		
				5.2_0	$94._5$	6.9_5	$93._9$		
9.0	91.0					6.7_4	$94._0$	11.6_9	$88._7$
						6.7_6	$92._7$	11.7_5	$88._7$
						6.9_4	$94._4$	11.9_4	$88._6$
Average		0.0_2	$100._0$	5.2_0	$94._5$	6.8_7	$93._3$	11.7_9	$88._7$
Formula		PbO		Pb_5SiO_7		$Pb_{11}Si_2O_{17}$		Pb_2SiO_4	
Calculated		0.00	100.0	5.10	94.90	6.83	93.17	11.85	88.15

a) Computational method was taken from Bence and Albee.[13] Under experimental conditions of 20 kV accelerating potential and 40° take-off angle, the correction factors α were: $\alpha^{Pb}_{SiO_2}=1.60$ and $\alpha^{Si}_{PbO}=1.04$.

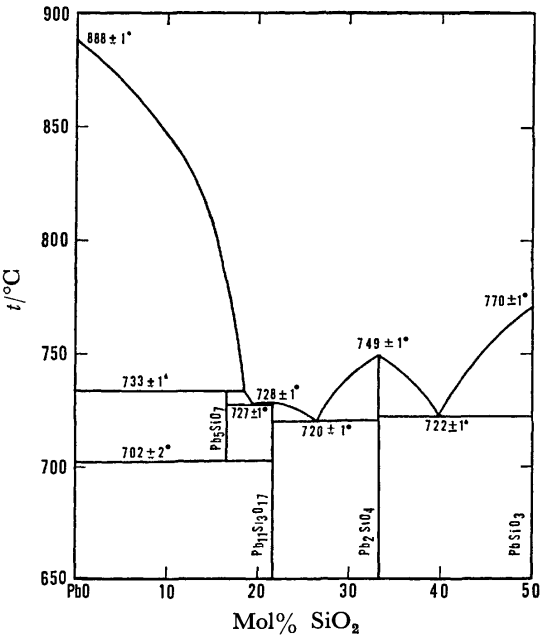

Fig. 1. Phase relations in the system PbO-$PbSiO_3$.

capsule. This was kept at 718 °C for 820 h and then quenched to room temperature. Only two phases were found in each capsule. Crystals in the quenched samples thus obtained were several tens of microns or more in size, and were large enough to allow the analysis. The standard deviation σ for SiO_2 concentration in the $Pb_{11}Si_3O_{17}$ phase was determined to be 0.08 wt% SiO_2; this was sufficient to determine the chemical composition of this phase.

Pb_5SiO_7. The Pb_5SiO_7 phase was determined to be stable only between 733±1 °C and 702±2 °C. By spontaneous crystallization of a melt of composition $5PbO \cdot SiO_2$, brown plates of Pb_5SiO_7, together with PbO and fine crystals of $Pb_{11}Si_3O_{17}$, were obtained. Well developed crystals of Pb_5SiO_7 were obtained by keeping a mixture of PbO and $Pb_{11}Si_3O_{17}$ for a week at 725 °C. The Pb_5SiO_7 decomposes slowly into PbO and $Pb_{11}Si_3O_{17}$ at temperatures below 702 °C. Runs of several weeks duration were necessary to attain an equilibrium state.

$Pb_{11}Si_3O_{17}$. The phase $Pb_{11}Si_3O_{17}$ melts congruently at 728±1 °C. The composition of this phase was determined, at the first stage of investigation, by means of electron probe microanalysis. The results of this analysis were scattered in a range from 78.4_3 to 78.9_6 mol% PbO. The average value was 78.6_5 mol% PbO. The atomic ratio Pb/Si=11/3 (78.57 mol% PbO) is the simplest integral ratio for these analytical results. To confirm this conclusion, a mixture of the composition $11PbO \cdot 3SiO_3$ was enclosed in a platinum capsule by welding. Keeping the mixture at a temperature only slightly lower than that required for melting, and grinding repeatedly, it was possible to prepare a microscopically single-phase product of $Pb_{11}Si_3O_{17}$. A rapid and reversible structural inversion at 145±5 °C was detected by X-ray powder diffraction measurement of this phase.

Discussion

In the early investigations,[1-5] the workers agree on the existence of the compounds Pb_2SiO_4 and $PbSiO_3$. The phase "Pb_4SiO_6" has been reported by Geller *et al.*[6] In their investigations, they came to the conclusion that "Pb_4SiO_6" has three crystal modifications: alpha form stable above 720 °C and melting incongruently at 725 °C to PbO and liquid, beta form stable between 720° and about 140 °C, and gamma form stable below 140 °C. The phase "Pb_4SiO_6" has been accepted by Billhaldt,[7] by Ott and McLaren[8] and by Smart and Glasser,[9] who studied subsolidus phase equilibria in the system PbO–SiO_2. In their investigations, a single phase "Pb_4SiO_6" was obtained both when the constituent oxides were sintered and when the glass was devitrified. X-Ray powder data for the alpha form and the gamma form were given by McMurdie and Bunting,[10] by Billhardt,[7] and by Argyle and Hummel.[11] Their data coincide with each other satisfactorily within their experimental errors.

But, as regards the alpha-beta inversion of "Pb_4SiO_6," some ambiguities have been pointed out. Geller *et al.*[6] reported that the results of heating curves obtained by a DTA method, as well as of the quenching tests, were not entirely satisfactory as regards the establishment of the alpha-beta inversion, but these results were believed to indicate that the tetralead silicate, on heating, undergoes an inversion at 720±2 °C. Billhaldt[7] has reported that the questions whether the chemical formula given for the phase α-Pb_4SiO_6 is the right one and wherther the composition of this phase is Pb_3SiO_5 could not be solved. He also reported that a crystallized single phase sample is necessary to determine the chemical composition of this phase.

The synthesis of "α-Pb_4SiO_6" was readily repeated by Smart and Glasser.[9] But they reported that the available data are insufficient to prove that the composition ratio of this phase is 4:1. Irrespective of the bulk composition of the mixture or the time and temperature used in the experiment, a single-phase product was never obtained in either isothermal or dynamic runs. They also reported that the α-phase was sometimes obtained free of other crystalline phases, but these preparations always contained glass, and, more often, the α-phase occurred with β-Pb_4SiO_6, PbO, or both. They added that the narrow range of temperatures essential to formation of this phase makes more detailed investigation difficult.

It is possible to suspect that the "α-Pb_4SiO_6" is the Pb_5SiO_7 obtained in the present investigation. Certainly, X-ray powder data for this phase given by McMurdie and Bunting,[10] and Billhaldt[7] coincide with that for the Pb_5SiO_7 phase found in the present investigation. Practically all reflections in their X-ray powder data of "α-Pb_4SiO_6" are found also in that of Pb_5SiO_7 phase; these are shown in Table 2.

Similarly, the phases "β-Pb_4SiO_6" and "γ-Pb_4SiO_6" correspond with the compound $Pb_{11}Si_3O_{17}$ in the present investigation. X-Ray powder data for "γ-

TABLE 2. X-RAY DIFFRACTION DATA OF POWDERED SAMPLES

Spacing d/Å	Relative intensity	Spacing d/Å	Relative intensity	Spacing d/Å	Relative intensity
Pb_5SiO_7					
6.63	3	3.241	9	2.511	2
5.90	4	3.127	6	2.370	4
5.68	6	3.110	15	2.318	9
5.50	4	3.087	13	2.248	4
4.289	2	3.038	100	2.225	3
4.210	2	2.944	29	2.181	6
4.024	5	2.855	28	2.124	2
3.679	13	2.833	40	2.009	8
3.489	3	2.794	21	1.890	13
3.431	2	2.751	12	1.851	4
3.362	4	2.710	12	1.838	4
3.312	12	2.682	4	1.817	9
$Pb_{11}Si_3O_{17}$					
7.249	12	3.006	37	2.316	16
5.441	7	2.974	5	2.181	5
4.608	3	2.939	8	2.101	5
3.663	4	2.914	30	2.032	4
3.636	5	2.853	8	2.025	5
3.494	5	2.823	8	2.009	11
3.460	7	2.792	20	1.959	6
3.236	13	2.738	15	1.897	24
3.203	4	2.717	26	1.859	14
3.147	13	2.656	11	1.848	9
3.115	100	2.543	9	1.826	24
3.034	43	2.486	12		

Pb_4SiO_6" given by McMurdie and Bunting,[10] and X-ray powder data for "T-Pb_4SiO_6" given by Billhaldt[7] coincide with that of $Pb_{11}Si_3O_{17}$ at room temperature in the present investigation. The difference in composition between "Pb_4SiO_6" and $Pb_{11}Si_3O_{17}$ is only 0.534 wt% SiO_2. The experimental techniques used in the previous investigations may not have been sufficient to distinguish such a small difference in chemical compositions.

The authers are greately indebted to Professor Takashi Katsura of Tokyo Institute of Technology for his encouragement and helpful discussions.

References

1) H. C. Cooper, L. I. Shaw, and N. E. Loomis, *Am. Chem. J.*, **42**, 461 (1909).
2) S. Hilpert and P. Weiler, *Ber. Deut. Keram. Gesell.*, **42**, 2969 (1909).
3) S. Hilpert and R. Nacken., *Ber. Deut. Keram. Gesell.*, **43**, 2565 (1910).
4) H. C. Cooper, E. H. Krause, and A. A. Klein, *Am. Chem. J.*, **47**, 273 (1912).
5) K. A. Krakau and N. A. Vachrameev, *Keramica Steklo*, **8**, 42 (1932).
6) R. F. Geller, A. S. Creamer, and E. N. Bunting, *J. Res. Nat. Bur. Stand.*, **13**, 237 (1934).
7) H. W. Billhardt, *Glastech. Ber.*, **42**, 498 (1969).
8) W. R. Ott and M. G. McLaren, *J. Am. Ceram. Soc.*, **53**, 374 (1970).
9) R. M. Smart and F. P. Glasser, *J. Am. Ceram. Soc.*, **57**, 378 (1974).
10) H. F. McMurdie and E. N. Bunting, *J. Res. Nat. Bur. Stand.*, **23**, 543 (1939).
11) J. F. Argyle and G. A. Hummel, *J. Am. Ceram. Soc.*, **43**, 452 (1960).
12) K. Hirota and T. Sekine, *Bull. Chem. Soc. Jpn.*, **52**, 1368 (1979).
13) A. E. Bence and A. L. Albee, *J. Geology*, **76**, 382 (1968).

  Bull. Chem. Soc. Jpn., 54, 757—760 (1981)

Effect of the Buffering Capacity of a Supporting Solution on Paper Electrophoretic Migrations of Adenine, Adenosine, and Adenosine Nucleotides

Yoshinori KITAOKA

Research Reactor Institute, Kyoto University, Kumatori-cho, Sennan-gun, Osaka 590-04

(Received September 1, 1980)

Paper electrophoretic migrations of adenine, adenosine, and adenosine nucleotides as a function of pH-values of various supporting solutions have been studied. The buffering capacity of the supporting solution played an important role in the migration and is discussed along with the electroosmosis. The R_f-values of adenines in the supporting solutions are also presented.

In the previous paper,[1] we reported the electrophoretic behavior of adenine, adenosine, and adenosine nucleotides as a function of the pH and of the concentration of inorganic acids. In the case of a supporting solution of lower buffering capacity, the deprotonation of protonated adenine or the dissociation of the secondary hydrogen of the phosphate moiety in the nucleotides did not take place at the pH-value expected from other chemical analyses. In order to elucidate the cause of this behavior, we carried out more paper electrophoresis in supporting solutions having different buffering capacities in a range of pH=2—13. Electroosmotic flows and the R_f-values of samples in solutions to be used for the electrophoresis are also shown.

Experimental

Materials. Adenine and adenosine were purchased from Wako (Osaka, Japan), and the sodium salts of the nucleotides from Sigma (St. Louis, Mo., U.S.A). Guaranteed grades of chemicals were used for preparation of supporting solutions without further purification.

Paper Electrophoresis. The procedures and apparatus[1] used were similar to those described previoulsy. Supporting solutions (ionic strength $\mu=0.1$) of NaOH in various concentrations were prepared by diluting 0.1 M NaOH solution with 0.1 M NaCl solution (1 M=1 mol dm^{-3}). The supporting solution of pH=13 was a 0.1 M NaOH solution containing no NaCl. Sørensen's buffer solutions[2] were prepared in the following way. A 0.1 M sodium citrate solution was prepared by dissolving 21 g (0.1 M) of $C_6H_8O_7\cdot H_2O$ and 8.0 g (0.2 M) of NaOH in one liter of distilled water. The citrate solution was mixed with 0.1 N HCl or 0.1 N NaOH solution to obtain citrate buffer solutions of different pH values. Glycine buffer solutions were prepared by mixing 0.1 M glycine +0.1 M NaCl solution with 0.1 M NaOH, and phosphate buffers by mixing 0.2 M Na_2HPO_4 and 0.2 M NaH_2PO_4. The buffering capacity (β) of the supporting solution was calculated by this equation:[3]

$$\beta = 2.303\{[C]\cdot[H^+]\cdot K_a/([H^+]+K_a)^2+[H^+]+10^{-14}/[H^+]\},$$

where C is the concentration of the solute, K_a the dissociation constant of the solute, and $[H^+]$ the concentration of hydrogen ions. The calculated buffering capacities of the solutions are listed in Table 1.

Adenosine and adenosine nucleotides were dissolved in distilled water and adenine was dissolved in 0.1 M sodium acetate. A 5 μl volume of sample solution (5×10^{-2} M) was spotted at the center of a filter paper (Toyo Roshi No. 51A, 1×40 cm) wetted with a supporting solution. The filter paper was dipped in hexane in the migration chamber and a voltage gradient (1000 V/30 cm) was applied it for 30 min at *ca.* 20 °C. Adenines after migration on the filter paper were detected using the absorption band at 253 nm.

Table 1. Buffering capacities(β) of supporting solutions

Component	pH	β
HCl+0.1 M NaCl	2.0	2.3×10^{-2}
	3.0	2.3×10^{-3}
	4.0	2.3×10^{-4}
	5.0	2.3×10^{-5}
	6.0	2.5×10^{-6}
0.1 M NaCl	7.0	4.6×10^{-7}
NaOH+0.1 M NaCl	8.0	2.5×10^{-6}
	9.0	2.3×10^{-5}
	10.0	2.3×10^{-4}
	11.0	2.3×10^{-3}
	12.0	2.3×10^{-2}
	13.0	2.3×10^{-1}
Citric acid buffer	2.0	3.3×10^{-2}
	3.0	2.5×10^{-2}
	4.0	2.2×10^{-2}
	5.0	5.6×10^{-2}
	6.0	3.0×10^{-2}
	6.7	2.6×10^{-2}
Phosphoric acid buffer	7.0	2.8×10^{-2}
	8.0	6.6×10^{-3}
Glycine+NaOH buffer	8.9	2.5×10^{-2}
	10.1	2.9×10^{-2}
	11.0	7.8×10^{-3}
	12.0	2.4×10^{-2}
	12.9	1.8×10^{-1}

The electroosmotic flows were estimated from the movement of glucose (5×10^{-2} M), which migrated along with the sample solution. The results are shown in Fig. 1. The different migrations of glucose among spotting positions are due to a capillary action, which is towards the center of a filter paper and almost disappears in 1 h.[4] The contribution of the capillary action to the movement of glucose is minimum at the center and usually zero within experimental errors. That is why the samples are spotted at the center of a filter paper. Since electroosmotic flows[5] should vary with the charge and porosity of filter paper, different batches of the same type of filter paper may give different results. The different electroosmotic flow for Toyo Roshi No. 51A filter papers were within 0.5 cm at 1000 V per 30 cm at 20 °C for 30 min. Glucose on a filter paper was detected by spraying *o*-aminophenol solution.[6]

Paper Chromatography. No ideal method to evaluate the adsorption effects of migrants on a filter paper has been proposed.[7] The measurement of R_f-value may be one convenient method, since it is useful for the estimation of

the interaction between a filter paper and the migrants in a given solvent. Samples were developed in solvents used for the paper electrophoresis for 3.5—4 h at 15 °C

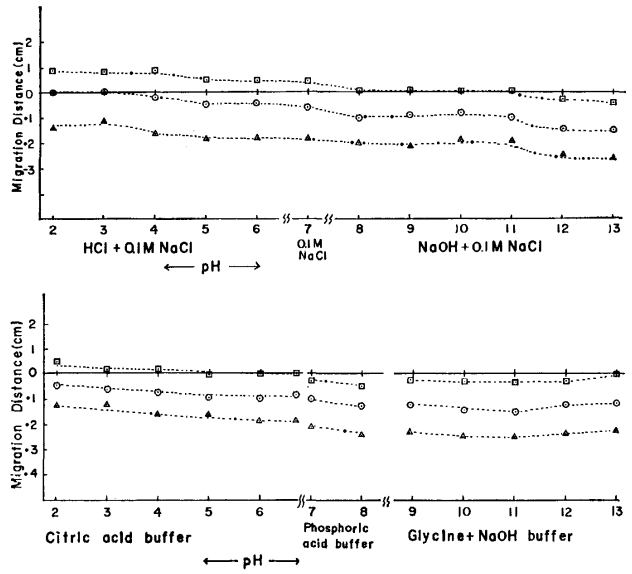

Fig. 1. The movement of glucose.
Conditions: voltage gradient, 1000 V per 30 cm; migration time, 30 min; migration temperature, *ca.* 20 °C; supporting solutions are referred to Experimental. Spotting positions: ⊡, 5 cm to the cathodic side from the center of the filter paper; ⊙, the center; ▲, 5 cm to the anodic side from the center. Positive movement is towards the anode, negative movement towards the cathode.

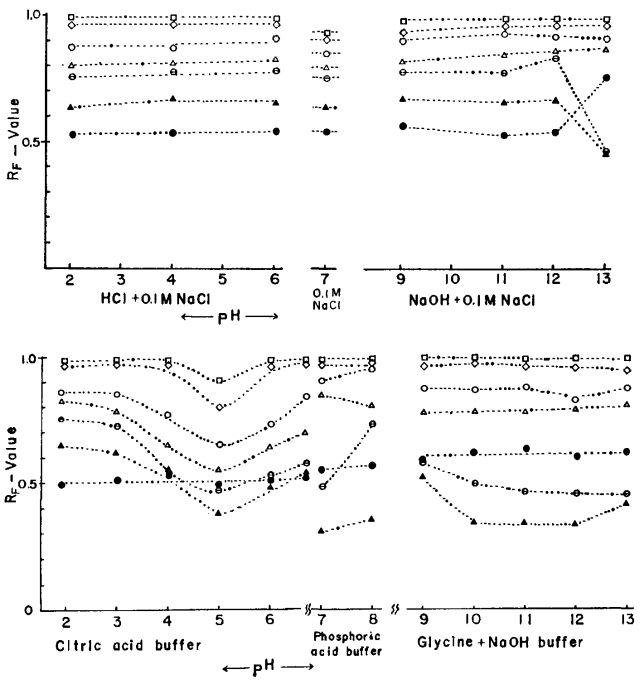

Fig. 2. R_f-values of paper chromatography in various solvents.
Conditions: developing time, 3.5—4.0 h; temperature, *ca.* 15 °C; ascending method. Developing solvents are referred to Experimental. ○: AMP, △: c-AMP, ◇: ADP, □: ATP, ▲: adenine, ⊖: adenosine, ●: picric acid.

on Toyo Roshi No. 51A (2×40 cm) filter paper by an ascending method. The results are shown in Fig. 2. Adenosine nucleotides showed larger R_f-values than adenosine and adenine; ATP moved nearly the same distances in all solvents as the solvent moved. The lower R_f-values of adenine and adenosine in phosphoric acid and glycine buffers suggest the presence of specific weak interactions in these solutions. The R_f-values of picric acid were almost constant in all solvents (R_f=0.5—0.6). The R_f-values decreased in the order: ATP>ADP>AMP>c-AMP>adenosine>adenine.

Results and Discussion

Under ideal conditions, the relationship between the electrophoretic migration distance and the pH value of the supporting solution could be expressed by a sigmoid curve having an inflection point at the pH value equal to pK_a of the migrant.[8] The pK_a-values of the adenine, adenosine, and adenosine nucleotides which are studied in this experiment are shown in Table 2.[9] The values are determined by the

Table 2. pK_a-Values
The ionic strength in each instance was 0.1 at 25 °C.

Compound	pK_a (base)	pK_a (secondary phosphate)	pK_a (>N_9H)
Adenine	4.2	—	9.7
Adenosine	3.6	—	—
5′-AMP	3.8	6.2	—
5′-ADP	3.9	6.4	—
5′-ATP	4.1	6.5	—

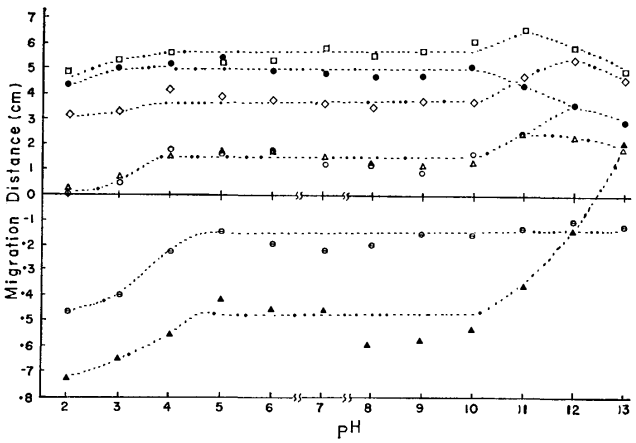

Fig. 3. Migration distances of adenine, adenosine and adenosine nucleotides in supporting solutions of low buffering capacity. Conditions: voltage gradient, 1000 V per 30 cm; migration time, 30 min, migration temperature, *ca.* 20 °C. Supporting solution, HCl+0.1 M NaCl (pH=2—6); 0.1 M NaCl (pH=7.0); NaOH+0.1 M NaCl (pH=8—13). Positive movement is towards the anode, negative movement towards the cathode. Symbols as in Fig. 2. Buffering capacity of each solution is referred to Table 1.

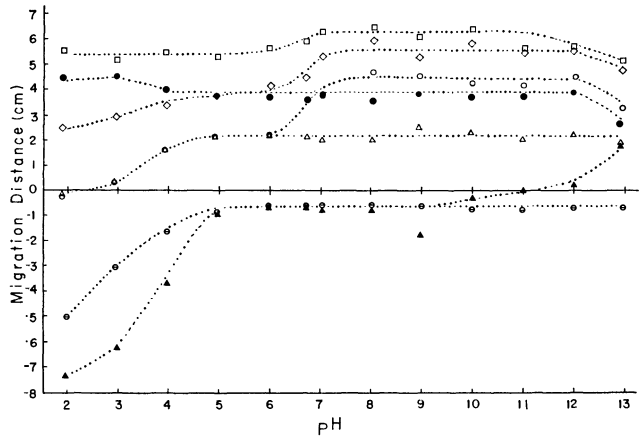

Fig. 4. Migration distances of adenine, adenosine, and adenosine nucleotides in supporting solutions of high buffering capacity. Electrophoresis conditions and symbols as in Fig. 3. Supporting solutions, citric acid buffer (pH=1.9—6.7); phosphoric acid buffer (pH=7—8); glycine+NaOH buffer (pH=8.9—12.9). Buffering capacity is referred to Table 1.

usual chemical methods, such as pH titration and spectrophotometry, rather than by electrophoresis.

The dependence of the observed migration distances of adenine, adenosine and adenosine nucleotides on the pH values of the supporting solutions are shown in Fig. 3. The migration distances in acidic region (HCl) in the previous experiment[1] and those in basic regions(NaOH) in this experiment are plotted against the pH values of the supporting solutions. Both adenine and adenosine moved to the cathode and showed an inflection point near pH=4. For pH values higher than pH=5, considerable migration was observed, showing that the deprotonation of protonated adenine or adenosine is incomplete. In the range of pH=11—13, the rapid decrease in the negative movement (the movement towards the cathode) of adenine and the increase in the positive movement with increasing pH values seem to be due to a dissociation of the imino hydrogen atom ($>N_9H$) of the purine ring, resulting in anions of adenine. Although the primary-hydrogen dissociation in the phosphate moiety of nucleotides took place near pH=1.0, AMP and c-AMP (adenosine cyclic 3′,5′-monophosphate) almost did not move in the range of pH=2—3 because adenine moiety of the nucleotide was protonated. ADP and ATP, which have two and three dissociable primary-hydrogen atoms respectively, moved to the anode. The migration distances of AMP, c-AMP, ADP and ATP increased in the range of pH=3—4. The nucleotides showed almost constant migration distances in the range of pH=5—10 and no inflection point near pH=7.

The graphs in Fig. 4 show the results obtained in the usual supporting solutions of rather high buffering capacity over a range of pH=2—13. Citric acid has three dissociable hydrogen atoms (pK_a=3.1, 4.8, and 6.4 at 25 °C[10]) and is a good supporting solution, having high buffering capacity, in the range of pH=2—7. Adenine and adenosine showed an inflection point near pH=3.5. The small negative migrations of adenine and adenosine (*ca.* −0.6 cm) at more than pH=5 are due to an electroosmotic flow (see Experimental). The electrophoretic behavior of adenine and adenosine in the strong basic region are similar to those in Fig. 3. The migration curves of the nucleotides in Fig. 4 show two inflection points, around pH=4 and 7.

Comparing the graphs in Fig. 3 with those in Fig. 4, we will find the differences of electrophoretic behavior to be larger in the range of pH=5—10. Assuming that an electroosmotic flow would coincide with the movement of glucose, we tried to correct the observed migrations for the flow. Although we subtracted the migration distance of glucose from that of a sample in a given solution (in the case of anions, we added the migration distances of glucose to that of a sample), graphs in Fig. 3 did not agree with those in Fig. 4, because the differences of the electroosmotic flow among graphs in Fig. 1 are within 0.5 cm. The considerable migrations of adenine and adenosine in Fig. 3 are unreasonable because the protonated adenine or adenosine should dissociate a proton in basic region and result in a neutral molecule, and because the contribution of the electroosmotic flow to the migration was within 1.0 cm, as seen in Fig. 1. The most probable explanation for the discrepancy between Figs. 3 and 4 would be made on the basis of the buffering capacity of the supporting solution. When the buffering capacity of a supporting solution is not large enough to neutralize the acid groups present as contaminants in a filter paper(probably -COOH), the pH value of the solution in the filter paper during electrophoresis will be shifted to be more acidic than the pH value initially prepared. The considerable negative migration distances of adenine and adenosine in pH=5—10 in Fig. 3, and the absence of dissociation of the secondary-hydrogen atom of the phosphate moiety (no inflection point of the curve near pH=7) are considered to reflect the effects of acid groups of the filter paper. The strength of the effect depends on the physicochemical nature of the filter paper as a supporting material. In the migration of a strong acid or base in a paper electrophoresis, we may not need to take so much a care about the buffering capacity. However, in the migration of a weak acid or base, its dissociation is often not observed at the expected pH value in a supporting solution of lower buffering capacity, as seen in Fig. 3; it is therefore necessary to consider the buffering capacity of the supporting solution. Further, to get good reproducibility and to lessen the chemical effects of the supporting material, a supporting solution of high buffering capacity is desirable. In our experimental conditions, a buffering capacity of more than β=0.023 is desirable to keep the pH value of the supporting solution constant during migration. These results remind us that the buffering capacity of the supporting solution should be paid attention to in paper electrophoresis in addition to its pH value.

References

1) Y. Kitaoka, *J. Chromatogr.*, **168**, 241 (1979).
2) S. P. L. Sørensen, *Erg. Physiol.*, **12**, 393 (1912).

3) R. G. Bate, "Electrometric pH Determination," John Wiley & Sons, New York (1954).
4) Y. Kitaoka, *Annu. Rep. Res. Reactor Inst. Kyoto Univ.*, **10**, 15 (1977).
5) J. R. Whitaker, "Paper Chromatography and Electrophoresis," Academic Press, New York (1967), Vol. 1, p. 11.
6) V. B. Kupressova, *Izv. Sibirk. Otd. Akad. Nauk SSSR, Ser. Biol. Med. Nauk*, **141** (1965).
7) H. Waldmann-Meyer, *Chromatogr., Rev.* **5**, 1 (1963).
8) Y. Kiso, M. Kobayashi, Y. Kitaoka, K. Kawamoto, and J. Takada, *J. Chromatogr.*, **36**, 215 (1968).
9) R. M. Izatt, J. J. Christensen, and J. H. Rytting, *Chem. Rev.*, **71**, 439 (1971).
10) R. A. Robinson and R. S. Stokes, "Electrolyte Solution," Butterworths Scientific Publ., London (1955).

The Crystal and Molecular Structure of [*trans*-1,2-Bis(diphenylphosphinamino)cyclohexane](1,5-cyclooctadiene)rhodium(I) Perchlorate Dichloromethane Solvate

Ken-ichi ONUMA* and Asao NAKAMURA

Central Research Laboratories, Ajinomoto Co., Inc. 1-1, Suzuki-cho, Kawasaki-ku, Kawasaki 210

(Received March 28, 1980)

The molecular structure of the title compound has been determined from three-dimensional X-ray diffraction data. The crystal belongs to the triclinic system: $P\bar{1}$, $a=11.488(2)$, $b=18.163(2)$, $c=10.998(2)$Å, $\alpha=101.70(2)$, $\beta=118.29(1)$, $\gamma=85.32(3)°$, $Z=2$. The structure has been refined by block-diagonal least-squares techniques using 3749 non-zero reflections to the final R value of 0.067. The rhodium atom is coordinated in a slightly distorted square-planar geometry by the bisphosphine and the diene ligand, with average Rh–P and Rh–C distances of 2.301(2) and 2.26(1)Å, respectively. The seven-membered chelate ring takes a distorted boat conformation, and the two phenyl groups of diphenylphosphine are arranged in a face-edge manner and those of the other diphenylphosphine are in a helical arrangement like a propeller, viewed from cyclooctadiene.

The stereoselectivity in the asymmetric hydrogenation of α-acylaminocinnamic acid by the rhodium complex with (1*R*,2*R*)-1,2-bis(diphenylphosphinamino)-cyclohexane has been reported to be inverted by *N*-methylation of the ligand.[1] We have been interested in such a chiral inversion of the stereoselectivity. In order to elucidate the stereochemistry of those complexes, the crystal structure of the title compound has been determined.

Experimental and Structure Determination

Preliminary Weissenberg photographs showed that crystals of [(1*S*,2*S*)-1,2-bis(diphenylphosphinamino)cyclohexane](1,5-cyclooctadiene)rhodium(I) perchlorate were unsuitable for X-ray analysis. Therefore, we determined the crystal structure of the racemic complex of [*trans*-1,2-bis(diphenylphosphinamino)cyclohexane](1,5-cyclooctadiene)rhodium(I) perchlorate.

Crystal and Intensity Data. Wine-red rhombohedral crystals were obtained from dichloromethane solution. Preliminary Weissenberg photographs suggested that the crystals were triclinic, and the space group was confirmed to be $P\bar{1}$ by the following structure analysis. The crystal chosen for data collection had approximate dimensions of $0.1\times0.3\times0.3$ mm. Accurate unit-cell parameters were obtained by least-squares refinement of 18 high angle reflections. The crystal data are summarized in Table 1. Intensity data were collected on a Phillips PW-1100 computer-controlled diffractometer using a θ-2θ scan technique with monochromated Cu $K\alpha$ radiation in the range of $2\theta\leqq100°$. A total of 3749 non-zero independent reflections was collected at room temperature. Standard reflections monitored during the course of data collection showed that no significant decomposition and no mispositioning had occurred. No absorption correction was applied.

Structure Solution and Refinement. The positional parameters of the Rh atom were determined from a three-dimensional Patterson synthesis. All the non-hydrogen atoms were found from subsequent Fourier and difference electron density maps. The electron densities of all the oxygen atoms were broad, and particularly the O(1) atom showed only a half of the densities of the other oxygen atoms. The positional and thermal parameters were refined by block-diagonal least-squares techniques; seven cycles for isotropic and four cycles for anisotropic parameters of non-hydrogen atoms. Three types of weight factors were assigned, depending on the value of F_o: $w=0.5$ ($F_o\leqq5.0$), $w=1$ ($5.0<F_o\leqq20.0$), $w=20.0/F_o$ ($20.0<F_o$). The electron density map at this stage showed that the perchlorate anion was disordered, so that another oxygen atom O(1)′ occupied the opposite position across the Cl atom from O(1). The perchlorate anion was further refined by assuming a half occupancy for O(1) and O(1)′ atoms. The final R value was 0.067 for non-zero reflections. The positional and thermal parameters are given in Tables 2 and 3,[2] respectively. The observed and calculated structure factors are listed in Table 4.[2] Atomic scattering factors of the rhodium cation and the other neutral atoms were taken from International Tables for X-Ray Crystallography.[3]

Results and Discussion

A perspective view of the molecule is given in Fig. 1, together with the numbering system of the atoms. A stereographic drawing of the molecule is shown in Fig. 2. A stereographic drawing of the packing of the molecules in a unit cell is shown in Fig. 3, excluding the O(1)′ atom.

Bond distances and bond angles are listed in Table 5. The bond distances show that C(51)–C(58) and C(54)–C(55) are the double bonds in cyclooctadiene. The rhodium atom is coordinated in a slightly distorted square-planar geometry to the bisphosphine and the two double bonds in the diene ligand. The dihedral angle between the plane defined by P(1)–Rh–P(2) and the plane containing Rh and mid-points of the two double bonds is 20.0°. Bond distances of Rh–P(1) and Rh–P(2) are 2.286(2) and 2.315(2)

Table 1. Crystal data

$C_{39}H_{46}N_2O_4Cl_3P_2Rh$	$F.W.=878.01$
Triclinic	Space group $P\bar{1}$
$a=11.488(2)$ Å	$\alpha=101.70(2)°$
$b=18.163(2)$ Å	$\beta=118.29(1)°$
$c=10.998(2)$ Å	$\gamma=85.32(3)°$
$U=1978.5(4)$ Å^3	$F(000)=452$
$D_m=1.47$ g cm^{-3} (by flotation)	
$D_c=1.474$ g cm^{-3}	$Z=2$
μ(Cu $K\alpha$) $=47.9$ cm^{-1}	

Table 2. The atomic parameters and their estimated standard deviations
* Perchlorate ** Dichloromethane

Atom	x	y	z	Atom	x	y	z
Rh	0.09201(5)	0.21625(3)	0.43523(6)	C(24)	0.3242(10)	0.4516 (6)	0.9105(10)
P(1)	0.0651 (2)	0.3432 (1)	0.4475 (2)	C(25)	0.1934(10)	0.4732 (5)	0.8421(10)
P(2)	0.9723 (2)	0.2162 (1)	0.5554 (2)	C(26)	0.1141 (8)	0.4412 (5)	0.7012 (9)
*Cl	0.7225 (3)	0.3170 (2)	0.8379 (3)	C(31)	0.8469 (8)	0.1407 (5)	0.4788 (9)
*O(1)′	0.6566(49)	0.3859(19)	0.7967(63)	C(32)	0.7947 (9)	0.1073 (5)	0.3364(10)
*O(1)	0.8306(24)	0.2601(14)	0.8511(36)	C(33)	0.6841(10)	0.0601 (6)	0.2690(11)
*O(2)	0.6212(13)	0.2684 (7)	0.7378(10)	C(34)	0.6263(10)	0.0444 (6)	0.3477(14)
*O(3)	0.8123(16)	0.3394 (9)	0.8172(14)	C(35)	0.6780(10)	0.0774 (5)	0.4933(12)
*O(4)	0.7295(13)	0.3304(11)	0.9642(12)	C(36)	0.7889 (9)	0.1262 (5)	0.5583(11)
N(1)	0.9126 (6)	0.3763 (4)	0.3910 (7)	C(41)	0.0771 (8)	0.2002 (5)	0.7345 (9)
N(2)	0.8950 (6)	0.2946 (3)	0.5869 (7)	C(42)	0.1036 (9)	0.1265 (5)	0.7584(10)
C(1)	0.7943 (8)	0.3342 (5)	0.3541 (9)	C(43)	0.1908(11)	0.1156 (6)	0.8966(11)
C(2)	0.7777 (8)	0.3277 (5)	0.4804 (8)	C(44)	0.2481(10)	0.1780 (6)	0.0073(10)
C(3)	0.6492 (8)	0.2894 (6)	0.4351(10)	C(45)	0.2173 (9)	0.2485 (6)	−0.0207(10)
C(4)	0.5313 (9)	0.3304 (6)	0.3411(11)	C(46)	0.1341 (8)	0.2617 (5)	0.8443 (9)
C(5)	0.5443(10)	0.3371 (7)	0.2092(11)	C(51)	0.2295 (9)	0.1252 (5)	0.5273(11)
C(6)	0.6747 (8)	0.3727 (5)	0.2526 (9)	C(52)	0.3614(11)	0.1396 (7)	0.5355(14)
C(11)	0.1231 (8)	0.3903 (4)	0.3551 (9)	C(53)	0.3508(10)	0.1675 (6)	0.4095(13)
C(12)	0.2427 (9)	0.4358 (5)	0.4246(11)	C(54)	0.2344(10)	0.2188 (5)	0.3464(11)
C(13)	0.2781(11)	0.4699 (5)	0.3470(12)	C(55)	0.1076 (9)	0.1914 (5)	0.2381 (9)
C(14)	0.2036(13)	0.4612 (6)	0.2020(13)	C(56)	0.0695(13)	0.1114 (6)	0.1735(12)
C(15)	0.0864(12)	0.4171 (6)	0.1315(12)	C(57)	0.1051(13)	0.0558 (6)	0.2698(12)
C(16)	0.0490 (9)	0.3830 (5)	0.2110(11)	C(58)	0.1192(11)	0.0882 (5)	0.4161(11)
C(21)	0.1658 (8)	0.3856 (4)	0.6316 (8)	**Cl(1)	0.7068 (4)	0.0572 (3)	0.9014 (5)
C(22)	0.2926 (9)	0.3623 (5)	0.7011(10)	**Cl(2)	0.4982 (5)	0.1442 (5)	0.9261 (5)
C(23)	0.3763(10)	0.3965 (6)	0.8454(10)	**C(0)	0.6492(14)	0.1455 (8)	0.9328(18)

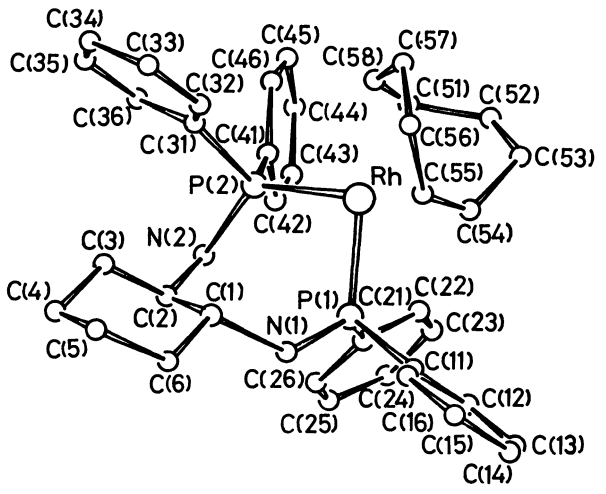

Fig. 1. Perspective view of the molecule with the numbering system of atoms.

Å, respectively, and the bond angle of P(1)–Rh–P(2) is 89.91(8)°.

A seven-membered chelate ring can take three types of conformations, boat, chair, and twist-chair forms, in which four atoms lie on a plane.[4] In the present complex, the seven-membered chelate ring consists of Rh, P(1), P(2), N(1), N(2), C(1), and C(2) atoms, and its conformation is a boat form, in which the nitrogen atom N(2) lies nearly on the plane of P(1)–Rh–P(2); the deviation of the N(2) atom from the plane is 0.21 Å. This conformation is, however, a little distorted and has no mirror symmetry, because the bond distance of N(2)–P(2) is not equal to that of Rh–P(1).

The chair conformation of seven-membered chelate ring has been observed in several complexes: *e.g.* in (1,5-cyclooctadiene)[(2*S*,4*S*)-*N*-pivaloyl-4-diphenylphosphino-2-(diphenylphosphinomethyl)pyrrolidine]-rhodium(I),[5] (1,5-cyclooctadiene)[(2*S*,4*S*)-4-diphenylphosphino-2-(diphenylphosphinomethyl)pyrrolidine]-rhodium(I),[6] chloro(1,5-cyclooctadiene)[(+)-2,3-*O*-isopropylidene-2,3-dihydroxy-1,4-bis(diphenylphosphino)butane]iridium(I),[7] and dichloro[(−)-2,3-*O*-isopropylidene-2,3-dihydroxy-1,4-bis(diphenylphosphino)butane]nickel(II).[8] Thus the boat conformation of the present complex seems to be unusual. The intramolecular distance of Rh–C(1) is found to be 3.71(1) Å. Although the distance is not so short to make a bond,[9] it might be close enough to have some interaction.[10] The coordinates of the hydrogen atom bonded to C(1) are estimated to be (−0.1967, 0.2774, 0.3062) by assuming that the C(1) is sp^3 and that the C–H distance is 1.08 Å. A projection of this hydrogen atom on the P(1)–Rh–P(2) plane is shown in Fig. 4. As seen in this figure, the hydrogen projects toward the rhodium atom. The Rh–H distance thus calculated is 3.13 Å. Therefore, the boat conformation may be caused by the intramolecular interaction between rhodium and hydrogen.

The configuration of a product in the asymmetric

TABLE 5. BOND DISTANCES AND BOND ANGLES WITH THEIR ESTIMATED STANDARD DEVIATION IN PARENTHESES

Bond distances [l/Å]

Rh-P(1)	2.286 (2)	C(11)-C(12)	1.445(15)	C(43)-C(44)	1.415(17)
Rh-P(2)	2.315 (2)	C(12)-C(13)	1.364(18)	C(44)-C(45)	1.358(16)
Rh-C(51)	2.235(12)	C(13)-C(14)	1.388(20)	C(45)-C(46)	1.392(15)
Rh-C(54)	2.275(12)	C(14)-C(15)	1.411(20)	C(46)-C(41)	1.399(14)
Rh-C(55)	2.212(11)	C(15)-C(16)	1.397(18)	C(51)-C(52)	1.516(19)
Rh-C(58)	2.301(13)	C(16)-C(11)	1.382(15)	C(52)-C(53)	1.517(20)
P(1)-N(1)	1.663 (8)	C(21)-C(22)	1.364(14)	C(53)-C(54)	1.522(18)
P(1)-C(11)	1.816(10)	C(22)-C(23)	1.442(16)	C(54)-C(55)	1.422(16)
P(1)-C(21)	1.823 (9)	C(23)-C(24)	1.375(16)	C(55)-C(56)	1.483(18)
P(2)-N(2)	1.679 (8)	C(24)-C(25)	1.389(16)	C(56)-C(57)	1.504(21)
P(2)-C(31)	1.835(10)	C(25)-C(26)	1.397(15)	C(57)-C(58)	1.532(20)
P(2)-C(41)	1.829(10)	C(26)-C(21)	1.407(13)	C(58)-C(51)	1.374(17)
N(1)-C(1)	1.456(13)	C(31)-C(32)	1.402(15)	Cl-O(1)	1.52 (4)
N(2)-C(2)	1.486(12)	C(32)-C(33)	1.388(17)	Cl-O(1)′	1.45 (7)
C(1)-C(2)	1.516(14)	C(33)-C(34)	1.394(20)	Cl-O(2)	1.38 (2)
C(2)-C(3)	1.398(14)	C(34)-C(35)	1.430(20)	Cl-O(3)	1.27 (2)
C(3)-C(4)	1.574(16)	C(35)-C(36)	1.407(18)	Cl-O(4)	1.33 (2)
C(4)-C(5)	1.556(17)	C(36)-C(31)	1.398(15)	Cl(1)-C(0)	1.72 (2)
C(5)-C(6)	1.498(16)	C(41)-C(42)	1.397(15)	Cl(2)-C(0)	1.70 (2)
C(6)-C(1)	1.526(14)	C(42)-C(43)	1.415(17)		

Bond angles [ϕ/°]

P(1)-Rh-P(2)	89.91(8)	C(23)-C(24)-C(25)	121.7(11)
Rh-P(1)-N(1)	118.2 (3)	C(24)-C(25)-C(26)	119.5(10)
Rh-P(1)-C(11)	118.7 (3)	C(25)-C(26)-C(21)	119.8 (9)
Rh-P(1)-C(21)	106.0 (3)	P(2)-C(31)-C(32)	120.5 (8)
N(1)-P(1)-C(11)	100.0 (4)	P(2)-C(31)-C(36)	118.4 (8)
N(1)-P(1)-C(21)	109.3 (4)	C(36)-C(31)-C(32)	120.0(10)
C(11)-P(1)-C(21)	103.6 (4)	C(31)-C(32)-C(33)	122.0(11)
Rh-P(2)-N(2)	119.6 (3)	C(32)-C(33)-C(34)	118.4(12)
Rh-P(2)-C(31)	114.2 (3)	C(33)-C(34)-C(35)	120.8(13)
Rh-P(2)-C(41)	112.1 (3)	C(34)-C(35)-C(36)	119.7(12)
N(2)-P(2)-C(31)	105.3 (4)	C(35)-C(36)-C(31)	119.0(11)
N(2)-P(2)-C(41)	100.4 (4)	P(2)-C(41)-C(42)	119.3 (8)
C(31)-P(2)-C(41)	103.3 (4)	P(2)-C(41)-C(46)	119.5 (7)
P(1)-N(1)-C(1)	126.3 (7)	C(46)-C(41)-C(42)	121.1 (9)
P(2)-N(2)-C(2)	126.1 (6)	C(41)-C(42)-C(43)	118.2(10)
N(1)-C(1)-C(2)	113.3 (8)	C(42)-C(43)-C(44)	120.4(11)
N(1)-C(1)-C(6)	108.2 (8)	C(43)-C(44)-C(45)	119.1(11)
C(2)-C(1)-C(6)	110.0 (8)	C(44)-C(45)-C(46)	122.2(10)
N(2)-C(2)-C(1)	112.3 (8)	C(45)-C(46)-C(41)	118.9 (9)
N(2)-C(2)-C(3)	113.6 (8)	C(58)-C(51)-C(52)	128.9(11)
C(1)-C(2)-C(3)	109.5 (8)	C(51)-C(52)-C(53)	114.3(12)
C(2)-C(3)-C(4)	114.5 (9)	C(52)-C(53)-C(54)	114.2(11)
C(3)-C(4)-C(5)	105.9 (9)	C(53)-C(54)-C(55)	122.9(11)
C(4)-C(5)-C(6)	110.3(10)	C(54)-C(55)-C(56)	125.9(11)
C(5)-C(6)-C(1)	114.4 (9)	C(55)-C(56)-C(57)	118.0(12)
P(1)-C(11)-C(12)	123.4 (8)	C(56)-C(57)-C(58)	115.5(12)
P(1)-C(11)-C(16)	118.6 (8)	C(57)-C(58)-C(51)	125.2(12)
C(16)-C(11)-C(12)	118.0(10)	O(1)-Cl-O(2)	94.4(16)
C(11)-C(12)-C(13)	119.5(11)	O(1)-Cl-O(3)	66.0(17)
C(12)-C(13)-C(14)	121.9(13)	O(1)-Cl-O(4)	103.5(17)
C(13)-C(14)-C(15)	119.8(13)	O(2)-Cl-O(3)	123.2(11)
C(14)-C(15)-C(16)	118.4(12)	O(2)-Cl-O(4)	114.4(11)
C(15)-C(16)-C(11)	122.5(11)	O(3)-Cl-O(4)	121.8(12)
P(1)-C(21)-C(22)	118.8 (8)	O(1)-Cl-O(1)′	150.8(31)
P(1)-C(21)-C(26)	120.8 (7)	O(2)-Cl-O(1)′	96.8(28)
C(26)-C(21)-C(22)	120.4 (9)	O(3)-Cl-O(1)′	85.4(29)
C(21)-C(22)-C(23)	120.2(10)	O(4)-Cl-O(1)′	96.2(29)
C(22)-C(23)-C(24)	118.4(10)	Cl(1)-C(0)-Cl(2)	113.0(12)

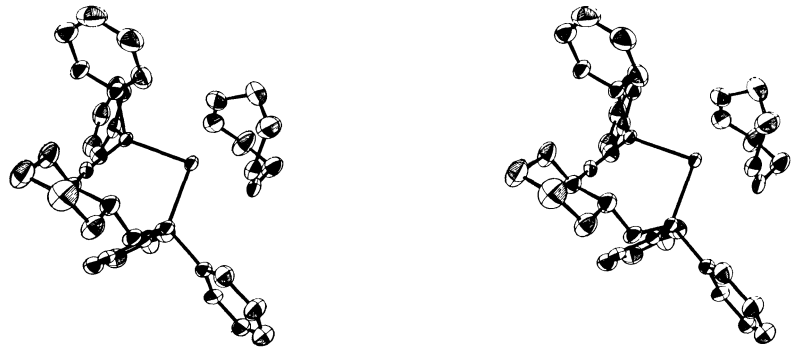

Fig. 2. Stereographic drawing of the molecule. Non-hydrogen atoms are represented by thermal ellipsoids of 50% probability.

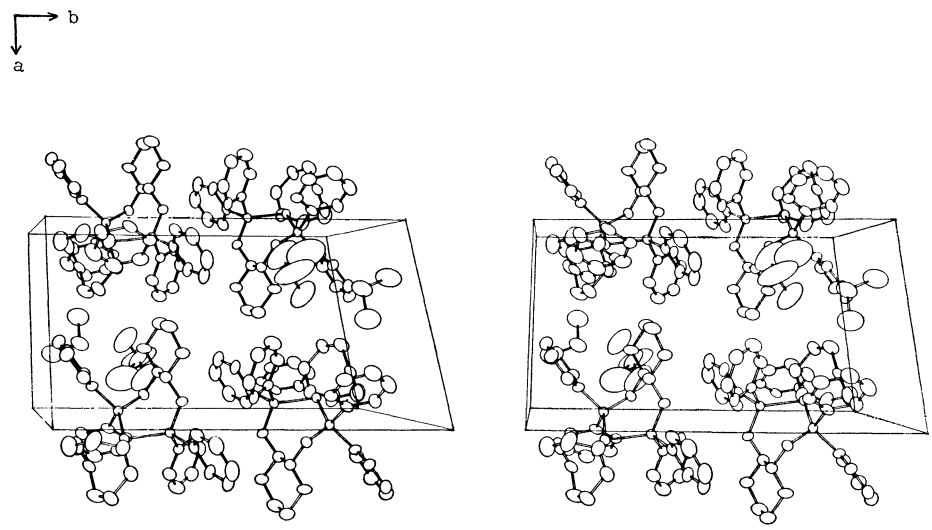

Fig. 3. Stereographic drawing of the packing of the molecules along the c axis.

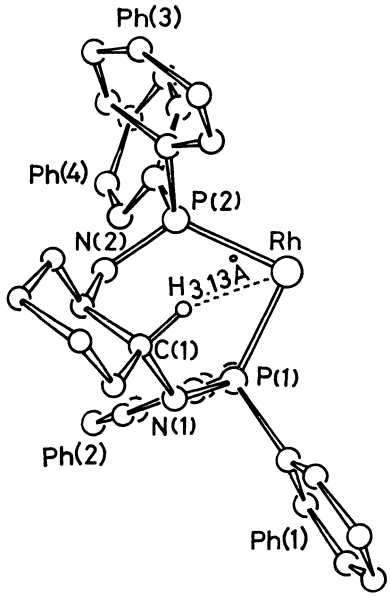

Fig. 4. Projection of the selected atoms on the P(1)–Rh–P(2) plane. Ph(1) is composed of C(11)–C(16), Ph(2) is composed of C(21)–C(26), Ph(3) is composed of C(31)–C(36), and Ph(4) is composed of C(41)–C(46).

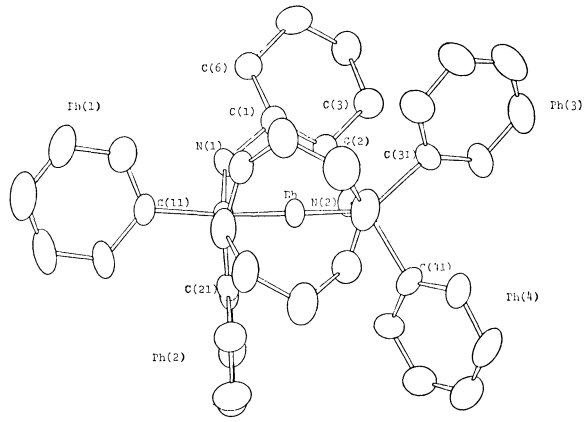

Fig. 5. The arrangement of the four phenyl groups.

hydrogenation may be derived from a chiral arrangement of the four phenyl groups which differentiate an enantiomeric face of a substrate. The arrangement of the phenyl groups, looked at from the side of cyclooctadiene, is shown in Fig. 5. As can be seen there, Ph(1) and Ph(2) are arrayed in a face-edge manner and, Ph(3) and Ph(4) are twisted like a propeller. Ph(2) and Ph(4) stretch out below the coordination lane so that there is a vacancy between Ph(1) and

Ph(3). If this structure is maintained in solution, the substrate may approach from the space between Ph(1) and Ph(3).

The positions of hydrogen atoms on N(1) and N(2) are estimated by assuming that the nitrogen atoms are sp^3 and that the N–H distance is 1.03 Å. The coordinates for N(1) are (H-1: −0.1073, 0.3964, 0.3021) or (H-2: −0.0814, 0.4209, 0.4684), and those for N(2) are (H-3: −0.0334, 0.3364, 0.6349) or (H-4: −0.1331, 0.2849, 0.6585). The shortest distances between each of the hydrogen atoms and their adjacent atoms are 2.4 Å for H-1···C(6), H-1···C(11), and H-1···C(16); 2.5 Å for H-2···C(2) and H-2···C(26); 2.4 Å for H-3···C(26); 2.5 Å for H-4···C(3). These distances are almost the same. Therefore, the hydrogen atoms on the nitrogens may actually occupy either of the two positions.

To examine the *N*-methylation effect, a hypothetical structure was given for the *N,N'*-dimethyl derivative on the basis of the present structure, and by assuming the N–C distance to be 1.45 Å. The coordinates of the methyl carbon on N(1) are (CH_3-1: −0.1154, 0.4045, 0.2658) or (CH_3-2: −0.0789, 0.4391, 0.5000), and those on N(2) are (CH_3-3: −0.0041, 0.3535, 0.6544) or (CH_3-4: −0.1446, 0.2810, 0.6877). The shortest distances between the methyl carbons and their adjacent atoms are 2.2 Å for CH_3-1···C(16); 2.3 Å for CH_3-2···C(26); 2.0 Å for CH_3-3···C(26); 2.7 Å for CH_3-4···C(3) and CH_3-4···C(41). Considering that the sum of the van der Waals radii of the methyl group and the carbon atom is 3.7 Å, there are no sufficient space for the methyl groups in the present structure. The complex with the *N,N'*-dimethylated ligand, therefore, seems to take another conformation.

References

1) a) K. Onuma, T. Ito, and A. Nakamura, *Tetrahedron Lett.*, **1979**, 3163; *Chem. Lett.*, **1979**, 905; *Bull. Chem. Soc. Jpn.*, **53**, 2016 (1980); b) K. Hanaki, K. Kashiwabara, and J. Fujita, *Chem. Lett.*, **1978**, 489; K. Kashiwabara, K. Hanaki, and J. Fujita, *Bull. Chem. Soc. Jpn.*, **53**, 2275 (1980); c) M. Fiorini and G. M. Giongo, *J. Mol. Catal.*, **5**, 303 (1979).

2) Tables 3 and 4 are kept at the Office of the Editor of the Bulletin of the Chemical Society of Japan, Kanda, Surugadai, Chiyoda-ku, Tokyo (Document No. 8110).

3) "International Tables for X-Ray Crystallography," Kynoch Press, Birmingham (1974), Vol. IV, pp. 72—83.

4) M. Hanack, "Conformation Theory," Academic Press, New York (1965), pp. 158—162.

5) Y. Ohga, Y. Iitaka, K. Achiwa, T. Kogure, and I. Ojima, 25th Symposium on Organometallic Chemistry, Japan (Osaka), 1978, Abstracts 3A15.

6) Y. Ohga, Y. Iitaka, and K. Achiwa, 26th Symposium on Organometallic Chemistry, Japan (Kyoto), 1979, Abstracts B203.

7) S. Brune, J. Mazan, N. Langlois, and H. B. Kagan, *J. Organometal. Chem.*, **114**, 225 (1976).

8) V. Gramlich and C. H. Salomon, *J. Organometal. Chem.*, **73**, c61 (1974).

9) a) T. Yoshida, T. Okano, D. L. Thorn, T. Tulip, S. Otsuka, and J. A. Ibers, *J. Organometal. Chem.*, **181**, 183 (1979). Rh–H is 1.62 Å; b) From Ref. 6: Rh···N is 2.147 Å and Rh–H is 1.43 Å.

10) B. D. Vineyard, W. S. Knowles, M. J. Sabacky, G. L. Bachman, and D. J. Weinkauff, *J. Am. Chem. Soc.*, **99**, 5946 (1977). The Rh···O distance (3.7 Å) is considered to be close enough to assume some interaction.

Nonbenzenoid Aromatic Compounds Containing an *anti*-Aromatic Four-membered Ring. Synthesis and Some Properties of 7-Hydroxy-6*H*-benzo[3,4]cyclobuta[1,2]cyclohepten-6-one (Benzo[3,4]cyclobuta[1,2-*e*]tropolone)

Masaru Sato, Seiji Ebine,* Kazumi Nishijima, and Josuke Tsunetsugu
Department of Chemistry, Saitama University, Urawa, Saitama 338

(Received May 6, 1980)

Biphenylene-2,3-quinone reacts with diazomethane in the presence of boron trifluoride etherate to give 7-hydroxy-6*H*-benzo[3,4]cyclobuta[1,2]cyclohepten-6-one (**5**) and its boron difluoride chelate. The latter is convertible quantitatively into the former. Compound **5** has a reduced troponoid character due to fusion of the benzocyclobutadiene ring. Tautomerism of the tropolone ring in **5** seems to be imposed exclusively to one of the tautomers. Protonation of **5** gives a tropylium ion whose positive charge is partially localized. Bromination, nitration, and azo-coupling of **5** give only 7-substituted products. The reaction of **5** with maleic anhydride gives the Diels-Alder adduct in good yield.

Much information has been obtained on the fused polycyclic aromatic compounds containing both $4n\pi$- and $(4n+2)\pi$-electron ring systems. Of these compounds, tropone and tropolone analogs of biphenylene are of particular interest, since their tropone and tropolone nuclei would have relatively small resonance energy because of perturbation caused by the fused anti-aromatic four-membered ring. The chloro derivative of 6*H*-benzo[3,4]cyclobuta[1,2]cyclohepten-6-one (**1a**) was found to have more bond-alternated tropone nucleus.[1,2] The parent compound (**1b**) further confirmed the above indication.[3] The formation of 7*H*-benzo[3,4]cyclobuta[1,2]cyclohepten-7-one (**2**) was also confirmed by trapping it as the adduct with cyclopentadiene.[7] 5*H*-Cyclobutacyclohepten-5-one (**3**), a lower homolog of **1**, was isolated as the $Fe(CO)_3$ complex.[5]

The first tropolone analog (**4**) of biphenylene was prepared by the ring-enlargement of 1,2-dimethoxybiphenylene with dichlorocarbene, and the tautomerism of **4**, unlike that of monocyclic tropolones,[6] was found to be extremely inclined to one tautomer. We report the synthesis and some reactions of the parent 7-hydroxy-6*H*-benzo[3,4]cyclobuta[1,2]cyclohepten-6-one (**5**).[7]

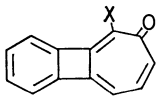

(1a) X=Cl
(1b) X=H

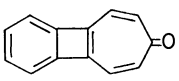

(2)

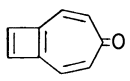

(3)

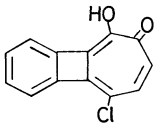

(4)

A convenient route to tropolone derivatives is the ring-enlargement of quinone with diazomethane.[8] Biphenylene-2,3-quinone was treated with diazomethane in the presence of boron trifluoride etherate to give the desired tropolone **5** in 45% yield and its boron difluoride chelate (**6**) in 26% yield. A catalytic amount of boron trifluoride is indispensable for the formation of **5** and **6**. Their spectral data agree with the assigned structure. In the mass spectrum, **5** has the ion peaks at *m/e* 196 (M^+ 100%), 168 (M^+—CO, 62%), and 139 (M^+—CO—CHO, 45%), and **6** at *m/e* 244 (M^+, 100%) and 216 (M^+—CO, 51%). The IR spectrum of **5** showed a strong absorption at 1570 cm^{-1} characteristic of tropolones and **6** a broad absorption at 1200—1000 cm^{-1} characteristic of chelate compounds. The ^{1}H-NMR spectrum of **5** ($CDCl_3$, 100 MHz) showed two doublets (J=9.0 Hz) at δ 6.32 (H-9) and 6.64 (H-8), a singlet at δ 6.70 (H-6), a multiplet at δ 7.11 (benzenoid), and a broad singlet at 8.27 (OH). The ^{1}H-NMR spectrum of **6** (DMSO-d_6, 100 MHz) showed a multiplet at δ 7.06 (H-9 and benzenoid), a doublet (J=9.1 Hz) at δ 7.34 (H-8), and a singlet at δ 7.54 (H-5). The chelate **6** was hydrolyzed in acidic aqueous ethanol to **5** quantitatively, which returned to **6** quantitatively on treatment with boron trifluoride etherate.

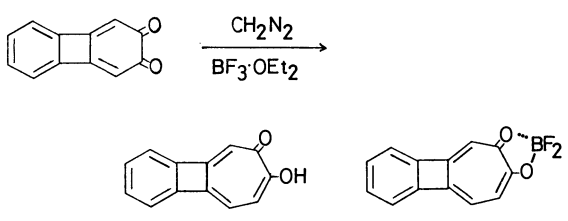

(5) (6)

The tropolone **5** showed some chemical features characteristic of monocyclic tropolones:[9] it gave red coloration in the chloroform layer with aqueous iron(III) chloride, reacted with aqueous sodium carbonate forming a red precipitate of the sodium salt, but not with aqueous sodium hydrogencarbonate, and dissolved in concentrated sulfuric acid or trifluoroacetic acid forming a red solution of the corresponding proto-

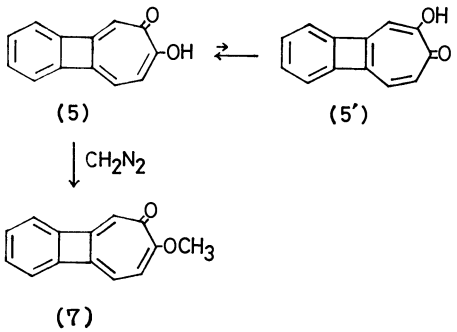

(5) (5′) (7)

Table 1. Vicinal coupling constants of the ^{1}H-NMR of tropolone and its methyl ether

Compound	J_{vic}/Hz		J_{vic}/Hz
	Tropolone	Its methyl ether	
Tropolone	10.9[a]	10.1[a]	0.8
9	9.8[a]	9.3	0.5
5	9.0	9.1	0.1

a) Ref. 11.

nated species (*vide infra*). In contrast to 6-hydroxy-5*H*-benzocyclohepten-5-one (3,4-benzotropolone) (**9**), it gave the methyl ether (**7**) in 59% yield on treatment with ethereal diazomethane for 9 d, no alternate methyl ether of (**5'**) being detected. The structure of **7** was assigned by the following ^{1}H-NMR spectrum: δ 3.78 (s, 3H, methoxyl protons), 6.11 (d, 1H, J=9.1 Hz, H-8), 6.58 (s, 1H, H-5), and 7.13 (m, 4H, aromatic protons). The results suggest that the troponoid character of **5** decreases with fusion of the benzocyclobutadiene ring but the extent of the decrease seems to be smaller than that of tropolone character caused by fusion of benzene in 3,4-benzotropolone (**9**), since **9** gives no methyl ether on treatment with diazomethane.[10]

The potentially expectable tautomerism **5**⇄**5'**, unlike that of monocyclic tropolones, seems to be imposed to one tautomer **5**. The shape of the electronic spectrum of **5** is closely similar to those of the methyl ether **7** and 7-chloro-6*H*-benzo[3,4]cyclobuta[1,2]cyclohepten-6-one (**8**),[2] except for the bathochromic shift in the long-wavelength region. This indicates that these compounds have a similar conjugate system. The ^{1}H-NMR spectral coupling constants of the vicinal protons intervening a single bond in the seven-membered ring in **5** and the related compounds are summarized in Table 1. The coupling constant J_{vic}=9.0 Hz of the seven-membered ring in **5** is the same as J_{vic}=9.1 Hz in **7**, and is smaller than the corresponding $J_{vic}(J_{7,8})$=9.8 Hz in 3,4-benzotropolone **9** and J_{vic}= 10.1 Hz in tropolone methyl ether, where the latter two compounds have a nearly planar structure but no tautomerism.[11] Moreover, the difference in the vicinal coupling constant (ΔJ_{vic}=0.1 Hz) between benzocyclobutatropolone **5** and its methyl ether is smaller than not only that (ΔJ_{vic}=0.8 Hz) between monocyclic tropolone and its methyl ether, but also that (ΔJ_{vic}=0.5 Hz) between 3,4-benzotropolone **9** and its methyl ether. This suggests that the seven-membered ring in **5** has larger bond alternation and deviation from planarity than tropolone and benzotropolone. The fact that only one methyl ether **7** was obtained on methylation of **5** might support the exclusive inclination to the one tautomer **5** in the tautomerism **5**⇄**5'**. The ^{13}C-NMR spectrum of **5** has thirteen signals containing only one carbon resonance at 182.3 ppm. The lack of the tautomerism in **5** would be due to the fusion of the benzocyclobutadiene ring. However, it is questionable whether the effect is caused only by the anti-aromaticity of the benzocyclobutadiene ring, since a similar tautomerism con-

Table 2. Difference in ^{1}H-NMR spectral chemical shifts and coupling constants of the ring protons between the neutral and protonated species of troponoids

Compound	$\Delta\delta$				$\Delta J_{8,9}$/Hz
	H_5	H_8	H_9	Aromatic	
5	0.5	0.80	0.50	0.08	0.6
7	0.58	1.19	0.90	0.08	0.6
8	0.44	0.56	0.43	0.08	0.6

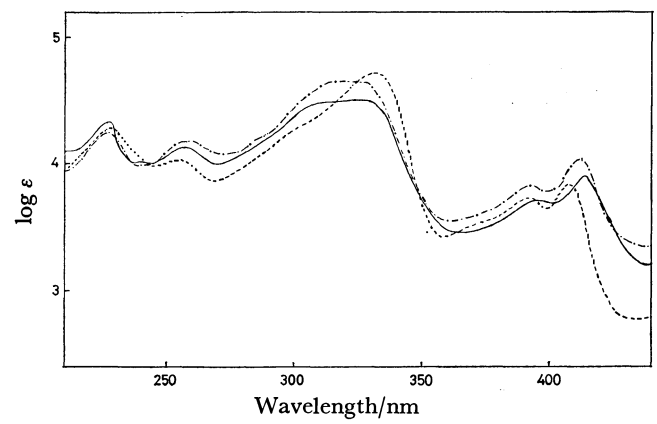

Fig. 1. The electronic spectra of 7-hydroxy-6*H*-benzo[3,4]cyclobuta[1,2]cyclohepten-6-one (**5**) (——), its derivatives (**7**) (—·—·), and (**8**) (——) in concd sulfuric acid.

siderably inclined to one tautomer was also observed in 1,2-dihydrocyclobuta[*e*]tropolone.[12]

The protonation of monocyclic tropolones affords the corresponding dihydroxytropylium ion, in which the positive charge is delocalized in all the ring carbon atoms. The electronic spectrum of the protonated 7-hydroxy-6*H*-benzo[3,4]cyclobuta[1,2]cyclohepten-6-one **5** is shown in Fig. 1, along with the spectra of the protonated 7-chloro- (**8**) and 7-methoxy-6*H*-benzo[3,4]cyclobuta[1,2]cyclohepten-6-one (**7**). The shape of their spectra is similar. The λ_{max} peaks of these cations are nearly in line with those of benzo[3,4]cyclobuta[1,2]tropylium ion having a partially localized positive charge.[13] The ^{1}H-NMR spectrum of **5** in trifluoroacetic acid showed two doublets (J=9.6 Hz) at δ 6.82 (H_9) and δ 7.44 (H_8) and a multiplet at δ 7.1—7.2 (H_5 and benzenoid). Protonation of **5** resulted in a significant low-field shift ($\Delta\delta_8$=0.80 and $\Delta\delta_9$=0.50 ppm) of the seven-membered ring protons, while the benzenoid protons remained naerly unchanged (Table 2). The low-field shifts ($\Delta\delta_8$ and $\Delta\delta_9$) of the seven-membered ring protons of the protonated **5** is nearly similar to those ($\Delta\delta_8$ and $\Delta\delta_9$) of the protonated **8**, but much smaller than the corresponding shifts ($\Delta\delta_9$=1.12 and $\Delta\delta_8$=0.96 ppm) of the protonated 7*H*-benzocyclohepten-7-one (4,5-benzotropolone). The large low-field shift in **7** seems to be due to protonation on the methoxyl group, because the signal of the methoxyl group shifted to low field by 0.39 ppm on protonation. The difference ($\Delta J_{8,9}$) in the coupling constants between **5** and protonated **5** is similar

to the corresponding values ($\Delta J_{8,9}$) of other 6*H*-benzo[3,4]cyclobuta[1,2]cyclohepten-6-one derivatives **7** and **8** (Table 2). The spectral data indicate that the positive charge in the protonated 6*H*-benzocyclobutacyclohepten-6-one system is insufficiently delocalized in the seven-membered ring and considerably localized on the carbonyl oxygen, that is, the protonated **5** is derived more from the canonical form **A** than **B**.

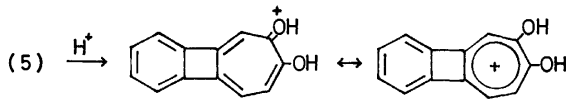

(A) (B)

On protonation of **5**, the low-field shift of the benzenoid protons is very small, suggesting no perpheral 12π-conjugation. This is in contrast to the fact that, on protonation of 4,5-benzotropolone, the positive charge delocalized to the benzene ring completing the 10π-electron conjugation, as indicated by the large low-field shift (*ca.* 0.5 ppm). The insufficient positive charge delocalization and the absence of the peripheral conjugation of the protonated **5** might be caused by the requirement that the central four-membered ring of **5** does not take *anti*-aromatic cyclobutadiene structure, while the strained 1,2-dihydrocyclobuta[*e*]tropolone, like monocyclic tropolones, showed a positive charge delocalization on protonation.[12]

One of the characteristics of tropolonoid compounds is that they react with various electrophilic reagents to afford the substitution products. The tropolone **5** underwent the following electrophilic substitutions, reacting with bromine to give 8-bromo-7-hydroxy-6*H*-benzo[3,4]cyclobuta[1,2]cyclohepten-6-one (**10**) in 47% yield. Similarly, **5** underwent nitration and azo-coupling reactions to give 8-nitro (**11**) and 8-tolylazo derivatives (**12**), in 30 and 89% yields, respectively.

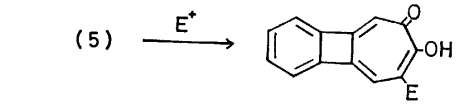

(10) E=Br
(11) E=NO_2
(12) E=$N_2C_6H_4CH_3$-p

The results indicate that **5** has a character similar to that of monocyclic tropolones. Its extremely inclined tautomerism is suggested also by the fact that **5** undergoes electrophilic substitution only at the 8-position excluding 5-position. This is in line with the behavior of 6-hydroxy-7*H*-benzocyclohepten-7-one (4,5-benzotropolone) which has no tautomerism and is attacked by electrophiles only at the 5-position.[13,14] However, the chemical behavior of **5** differs somewhat from that of 6-hydroxy-5*H*-benzocyclohepten-5-one **9** which is attacked by electrophiles at 7-position as well as 9-position,[10,15,16] undergoing also ring contraction.[17]

Tropolone **5** reacted with maleic anhydride to give 1:1 Diels-Alder adduct (**13**) in a good yield. The structure of **13** was assigned mainly by its ^{1}H-NMR spectrum: two aliphatic doublets (δ 3.61 and 3.85, J=9.0 Hz), two olefinic doublets (δ 6.22 and 6.62, J=9.0 Hz) and an olefinic singlet (δ 6.16). The Diels-Alder adduct (**13**) was obtained by refluxing both

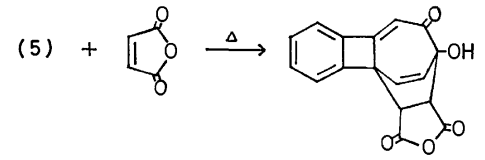

(13)

in xylene and in benzene, no isomerization of the adduct being observed.[18] Monocyclic tropolones undergo no Diels-Alder reaction in refluxing benzene[19] but they do in refluxing xylene with maleic anhydride.[20] Thus, **5** seems to have considerable bond localization, becoming susceptive of the cyclo-addition owing to the fusion of benzocyclobutadiene. Tropolone **5** and its methyl ether were subjected to Diels-Alder reaction with 1,3-diphenylisobenzofuran and condensation with guanidine, respectively, no definite product being obtained.

Experimental

Reaction of Biphenylene-2,3-quinone with Diazomethane in the Presence of Boron Trifluoride. Boron trifluoride etherate (0.9 ml of 47% solution, 3 mmol) was added to a solution of biphenylene-2,3-quinone (455 mg, 2.5 mmol) in dichloromethane (20 ml) on an ice-water bath under an atmosphere of nitrogen. A yellow precipitate appeared. After 10 min, to the mixture was added a solution of diazomethane in ether (45 ml) prepared from *N*-nitroso-*N*-methylurea (2.06 g, 20 mmol) and alkali. The mixture turned to a red-violet solution. After being stirred for 30 min, the solution was poured into water. The mixture was extracted with dichloromethane. The extract was washed with water and dried over anhydrous sodium sulfate. After evaporation, the residue was chromatographed on silica gel to give the following products in turn. Boron difluoride chelate (**6**) of 7-hydroxy-6*H*-benzo[3,4]cyclobuta[1,2]cyclohepten-6-one (156 mg, 25.6%), red-violet needles (from acetonitrile), mp 237.2—237.9 °C. Found: C, 63.75; H, 2.76%. Calcd for $C_{13}H_7O_2BF_2$: C, 63.99, H, 2.89%. IR(KBr): 1524, 1409, 1310, 1150—1040, 849, and 748 cm^{-1}. NMR (DMSO-d_6, 100 MHz): δ 7.34 (d, 1H, J=9.1 Hz, H_8), 7.45 (s, 1H, H_5), 7.06—7.27 (m, 5H, aromatic and H_9). MS(75 eV): *m/e* 244 (M^+, 100%) and 216 (M^+-CO, 51%). UV (CH_3CN): 231 (log ε 4.33), 262 (4.32), 308 (4.74), 393 (3.85), and 416 nm (4.00). 7-Hydroxy-6*H*-benzo[3,4]cyclobuta[1,2]cyclohepten-6-one (**5**), 219 mg (44.7%), yellow needles (from ethanol), mp 166—167 °C. Found: C, 79.53; H, 4.22%. Calcd for $C_{13}H_8O_2$: C, 79.58; H, 4.11%. IR (KBr): 3250, 1580, 1450, 1430, 1241, 1206, 903, 757, and 680 cm^{-1}. NMR($CDCl_3$, 100 MHz): δ 6.32 (d, J=9.0 Hz, H_9), 6.64 (d, 1H, J=9.0 Hz, H_8), 6.70 (s, 1H, H_5), 7.11 (m, 4H, aromatic), and 8.27 (s, 1H, OH). NMR (CF_3COOH): δ 6.82 (d, 1H, J=9.5 Hz), 6.82—7.19 (m, 5H), and 7.44 (d, 1H, J=9.5 Hz). ^{13}C-NMR($CDCl_3$): 113.7, 117.9, 118.4, 119.0, 120.7, 130.0, 132.4, 146.6, 147.1, 149.9, 157.3, 160.8, and 182.3 ppm. MS (75 eV): *m/e* 196 (M^+, 100%), 168 (M^+-CO, 28%), and 139 ($M^+-CO-CHO$, 45%). UV(EtOH): 228 (log ε 4.09), 249 (4.13), 290 (4.52), 372 (3.77), 390 (3.83), and 422 nm (3.71). UV(H_2SO_4): 227 (log ε 4.34), 257 (4.14), 308sh (4.48), 325 (4.51), 394 (3.70), and 413.5 nm (3.90). At last, the

unreacted starting material (7 mg, 1.5% recovery) was eluted out.

Hydrolysis of the Chelate **6**. A mixture of the chelate **6** (50 mg, 0.21 mmol), hydrochloric acid (2 mol dm^{-3}, 3 ml), water (1 ml) and acetone (15 ml) was refluxed for 2 h. The mixture was poured into water. The aqueous mixture was extracted with dichloromethane. The extract was washed with water and dried over anhydrous sodium sulfate. After evaporation, the residue was sublimed under reduced pressure (≈125 °C/2 mmHg). Tropolone **5** (38 mg, 92%) was obtained.

Reaction of Tropolone **5** *with Boron Trifluoride Etherate.* Boron trifluoride etherate (47% solution, 0.03 ml, 0.1 mmol) was added to a mixture of tropolone **5** (20 mg, 0.1 mmol) in anhydrous ether (10 ml). The mixture was stirred for 1 h and the solvent evaporated. The residue was chromatographed on silica gel with elution of dichloromethane. Chelate **6** (24 mg, 96%) was obtained.

Tropolone Methyl Ether **7**. Tropolone **5** (49 mg, 0.25 mmol) was dissolved in a solution of diazomethane, prepared from *N*-nitroso-*N*-methylurea (0.93 g, 0.9 mmol) and alkali, in ether (20 ml). The solution was kept in refrigerator for 9 d. After evaporation, the residue was chromatographed on silica gel with elution of dichloromethane. Tropolone methyl ether **7** (yellow needles, mp 191—193 °C) (30 mg, 59%) was obtained, the starting material (17 mg, 35%) being recovered. Found: C, 80.16; H, 5.05%. Calcd for $C_{14}H_{10}O_2$: C, 79.98; H, 4.79%. IR(KBr): 1608, 1541, 1330, 1234, 1078, 1010, 842, and 764 cm^{-1}. NMR($CDCl_3$): δ 3.79 (s, 3H, methyl), 6.13 (d, 1H, J=9.4 Hz, H_9), 6.31 (d, 1H, J=9.4 Hz, H_8), 6.60 (s, 1H, H_5), and 7.13 (m, 4H, aromatic). NMR(CF_3COOH): δ 4.18 (s, 3H, methyl), 7.03 (d, 1H, J=10.0 Hz, H_9), 7.18 (s, 1H, H_5), 7.48 (d, 1H, J=10.0 Hz, H_8), and 7.23 (s, 4H, aromatic). UV (EtOH): 227 (log ε 4.12), 244 (4.15), 288 (4.63), 320 (3.79), 361 (3.98), and 376 nm (3.95). UV(H_2SO_4): 227 (log ε 4.25), 258 (4.18), 315 (4.65), 328 (4.64), 393 (3.82), and 412 nm (4.03).

8-Bromo-7-hydroxy-6H-benzo[3,4]cyclobuta[1,2]cyclohepten-6-one (**10**). To a solution of **5** (0.1 g, 0.5 mmol) in acetic acid (5 ml) was added a solution of bromine (90 mg, 0.56 mmol) in acetic acid (1 ml) over a period of 5 min. After being stirred for 30 min, the solvent was evaporated under reduced pressure. The residue was dissolved in dichloromethane. The solution was washed with water and dried over anhydrous sodium sulfate. After evaporation, the crystalline residue was recrystallized from ethanol to give the title compound (67 mg, 47%) as yellow-orange needles, mp 166—168 °C. Found: C, 57.23; H, 2.37%. Calcd for $C_{13}H_7O_2Br$: C, 56.76; H, 2.56%. IR(KBr): 3300, 1580, 1340, and 1230 cm^{-1}. NMR($CDCl_3$): δ 6.61 (s, 1H, H_9), 6.70 (s, 1H, H_5), 7.13 (m, 4H, aromatic), and 8.88 (broad s, 1H, OH). UV(EtOH): 234 (log ε 4.13), 291 (4.54), 370 sh, 388 (3.75), and 425 sh nm.

8-Nitro-7-hydroxy-6H-benzo[3,4]cyclobuta[1,2]cyclohepten-6-one (**11**). To a solution of **5** (0.1 g, 0.5 mmol) in acetic acid (5 ml) was added a solution of concentrated nitric acid (60—62%, 64 mg, 6 mmol) in acetic acid (0.1 ml) at 0 °C over a period of 5 min. After being stirred for 30 min, the solution was diluted with water (40 ml). The resulting yellow crystals were collected by filtration and washed with water. After drying, the crystals were recrystallized from ethanol to give pure title compound **11** (36 mg, 29%), yellow-orange needles, mp 174—175 °C. Found: C, 64.38; H, 2.72; N, 5.48%. Calcd for $C_{13}H_7O_4N$: C, 64.73; H, 2.92; N, 5.81%. IR(KBr): 3200, 1600, 1580, 1530, 1320, and 1220 cm^{-1}. NMR($CDCl_3$): δ 6.55 (s, 1H, H_9), 6.76 (s, 1H, H_5), and 7.27 (m, 4H, aromatic). UV (EtOH): 233 (log ε 4.28), 254 (4.25), 305 (4.49), 382 (4.12), and 537 nm (3.63).

8-Tolylazo-7-hydroxy-6H-benzo[3,4]cyclobuta[1,2]cyclohepten-6-one (**12**). To a solution of **5** (0.1 g, 5 mmol) and sodium acetate (3 g) in water (4 ml) and acetic acid (24 ml) was added a solution of the diazonium salt, prepared from *p*-toluidine (70 mg, 0.56 mmol), hydrochloric acid (2 mol dm^{-3}, 0.5 ml) and sodium nitrite (43 mg, 0.62 mmol), at 0—2 °C over a period of 15 min. After being stirred for 20 min, the solution was kept in a refrigerator overnight. The solvent was then evaporated. The dark violet residue was diluted with water. The aqueous solution was controlled at pH 3 and the resulting crystals (0.142 g, 88%) were collected by filtration. Recrystallization from acetonitrile gave the pure title compound **12** as blue-violet needles (mp 213—214 °C). Found: C, 76.37; H, 4.39; N, 8.89%. Calcd for $C_{20}H_{14}O_2N_2$: C, 76.42; H, 4.49; N, 8.91%. IR (KBr): 3300, 1630, 1480, and 1300 cm^{-1}. NMR($CDCl_3$): δ 2.38 (s, 3H, CH_3), 6.53 (s, 1H, H_9), 6.70 (s, 1H, H_5), and 7.30 (m, 8H, aromatic). UV(EtOH): 252 (log ε 4.55), 340 (4.67), and 564 nm (4.32).

Diels-Alder Reaction of **5**. A solution of **5** (0.1 g, 0.5 mmol) and maleic anhydride (0.15 g, 1.5 mmol) in anhydrous xylene (2.5 ml) was refluxed for 5.5 h. The solvent was evaporated. The resulting pale yellow residue was recrystallized from benzene–dichloromethane to give the adduct **13** (0.103 g, 68.8%) as colorless prisms (mp 194—196 °C). Found: C, 69.50; H, 3.41%. Calcd for $C_{17}H_{10}O_5$: C, 69.39; H, 3.43%. IR(KBr): 1855, 1760, and 1650 cm^{-1}. NMR ($CDCl_3$): δ 3.61 (d, 1H, J=9.0 Hz, methine), 3.85 (d, 1H, J=9.0 Hz, methine), 5.2 (broad s, 1H, OH), 6.16 (s, 1H, H_5), 6.22 (d, 1H, J=9.0 Hz, H_8), 6.62 (d, 1H, J=9.0 Hz, H_9), and 7.3—7.9 (m, 4H, aromatic). UV(EtOH): 223 sh, 287 (log ε 4.21), and 310 nm (4.15).

The authors wish to thank Dr. K. Takahashi and Prof. K. Takase, Tohoku University, for measurement of 100 MHz ^{1}H-NMR and ^{13}C-NMR spectra.

References

1) M. Sato, S. Ebine, and J. Tsunetsugu, *J. Chem. Soc., Chem. Commun.*, **1974**, 846.
2) M. Sato, S. Ebine, and J. Tsunetsugu, *J. Chem. Soc., Perkin Trans. 1*, **1977**, 1282.
3) L. Lombardo and D. Wege, *Tetrahedron Lett.*, **1975**, 115.
4) R. K. McCulloch and D. Wege, *Tetrahedron Lett.*, **1976**, 3213.
5) F. A. Kaplan and B. W. Roberts, *J. Am. Chem. Soc.*, **99**, 513 (1977); M. B. Stringer and D. Wege, *Tetrahedron Lett.*, **1977**, 65.
6) M. Sato, S. Ebine, and J. Tsunetsugu, *Tetrahedron Lett.*, **1977**, 855.
7) A preliminary report: M. Sato, H. Fujino, S. Ebine, and J. Tsunetsugu, *Tetrahedron Lett.*, **1978**, 143.
8) M. Sato, J. Tsunetsugu, and S. Ebine, *Bull. Chem. Soc. Jpn.*, **45**, 638 (1972).
9) T. Nozoe, *Proc. Jpn. Acad.*, **26**, 30 (1950).
10) J. W. Cook, A. R. M. Gibb, R. A. Raphael, and A. R. Somerville, *J. Chem. Soc.*, **1952**, 603.
11) D. J. Bertelli, T. G. Andrews, Jr., and P. O. Crews, *J. Am. Chem. Soc.*, **91**, 5286 (1969).
12) M. Sato, S. Ebine, and J. Tsunetsugu, *J. Chem. Soc., Chem. Commun.*, **1978**, 215.
13) D. S. Tarbell and J. C. Bill, *J. Am. Chem. Soc.*, **74**,

1234 (1952).
14) H. Fernholz, E. Hartwig, and J. C. Salfeld, *Ann.*, **576**, 131 (1952).
15) S. Ebine, *Bull. Chem. Soc. Jpn.*, **35**, 122 (1962); **38**, 2029 (1965).
16) T. Nozoe, Y. Kitahara, and T. Ando, *Proc. Jpn. Acad.*, **27**, 107 (1951).
17) S. Ebine, *Chem. Ind. (London)*, **1961**, 513.
18) S. Ito, H. Takeshita, Y. Shoji, Y. Toyooka, and T. Nozoe, *Tetrahedron Lett.*, **1968**, 3215.
19) J. W. Cook, A. R. Gibb, R. A. Raphael, and A. R. Sommerville, *J. Chem. Soc.*, **1951**, 503.
20) T. Nozoe, S. Seto, and T. Ikemi, *Proc. Jpn. Acad.*, **27**, 655 (1951).

  Bull. Chem. Soc. Jpn., 54, 771—775 (1981)

Products from the Nitration of 2,5-Dimethylthiophene and Its 3,4-Dibromo Derivative. Two Modes of the Formation of Dithienylmethanes[1]

Hitomi Suzuki,* Ichiro Hidaka, Akemi Iwasa,** Tadashi Mishina,** and Atsuhiro Osuka

Department of Chemistry, Faculty of Science, Ehime University, Bunkyo-cho, Matsuyama 790
***Department of Chemistry, Faculty of Science, Hiroshima University, Higashi-sendamachi, Naka-ku, Hiroshima 730*

(Received June 7, 1980)

The reaction of 2,5-dimethylthiophene with copper(II) nitrate in acetic anhydride gave 3-nitro-2,5-dimethylthiophene and 2,5-dimethyl-3-(5-methyl-2-thenyl)thiophene as major isolable products. The treatment of 3,4-dibromo-2,5-dimethylthiophene with nitric acid ($d=1.5$) in dichloromethane in the presence of a catalytic amount of sulfuric acid afforded 3,4-dibromo-5-methyl-2-(nitrooxymethyl)thiophene, which, on thin-layer chromatography over silica gel using hexane as the eluant, underwent a partial novel coupling reaction through the loss of one methylene carbon atom, thus giving 3,3′,4,4′-tetrabromo-5,5′-dimethyldi-2-thienylmethane along with the expected 3,4-dibromo-2-hydroxymethyl-5-methylthiophene and bis(3,4-dibromo-5-methyl-2-thenyl) ether.

When treated with nitric acid in dichloromethane at a low temperature, polymethylbenzenes and their derivatives often undergo the nitrooxylation of the alkyl group to give benzyl nitrates.[2] Under similar conditions, polymethylnaphthalenes and polymethylanthracenes yield naphthylnitromethanes and anthrylnitromethanes respectively.[3] For these side-chain reactions of arenes, we have previously proposed an ionic S_Ni' mechanism involving a methylenecyclohexadiene intermediate (**1**); the heterolytic fission of the C–N bond in **1** to form a benzyl cation/nitrite anion pair (**2**) and the subsequent recombination of these ions at the benzylic carbon atom, either *via* a C–N bond or *via* a C–O bond, the ratio of the C–N/C–O bond formation being mainly determined by the electronic requirements of the *exo*-cyclic sp^2 carbon atom (Scheme 1).[3,4] Thus, the marked change in the modes of reaction toward nitrating agents observed on going from the benzenes to naphthalenes and anthracenes has been related to the change in the development of the carbonium ion character on the methylene carbon atom of the intermediate ion pair, **2**. In order to test the validity of our proposal further, we have now investigated the effect of the fused benzene ring on the side-chain reactions of heteroaromatic systems.

There has, to our knowledge, been only one report in the literature pertaining to the side-chain nitration of heteroaromatics; Bordwell and Cutshall treated 2,3-dimethylbenzo[*b*]thiophene (**3**) with nitric acid in acetic anhydride and obtained 3-methyl-2-(nitromethyl)-benzo[*b*]thiophene (**4**) and 3-methylbenzo[*b*]thiophene-2-carboaldehyde (**6**) (Scheme 2). The carbonyl compound presumably arose from the initially formed nitrate (**5**). Preferential substitution occurred at an alkyl group attached to the heterocycle.[5] If the S_Ni' mechanism shown in Scheme 1 works in that case, we may reasonably expect that the removal of a fused benzene ring from the benzo[*b*]thiophene system would lead to a change in the mode of the side-chain reaction of the thiophene nucleus from nitration to nitrooxylation. Thus, we have prepared several polymethylthiophenes and their derivatives and treated them with nitrating agents under a variety of conditions.

Trimethylthiophenes and tetramethylthiophene were extremely reactive toward a nitrating agent and failed to give any isolable products. A significant part of the substrate suffered the destruction of the thiophene nucleus. Even with such a mild nitrating agent as copper(II) nitrate in acetic anhydride, these reactive thiophenes were converted into a complicated mixture of products which were difficult to separate. We therefore turned our interest to the nitration of 2,5-dimethylthiophene (**7**) and its dibromo derivative (**8**).

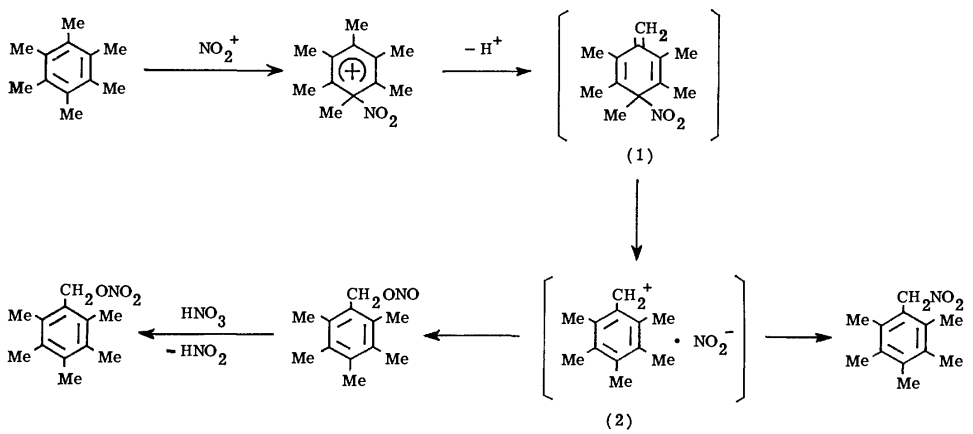

Scheme 1.

The reaction of **7** with copper(II) nitrate proceeded smoothly in acetic anhydride at a low temperature; the two major products thus obtained were identified as 3-nitro-2,5-dimethylthiophene (**11**) and 2,5-dimethyl-3-(5-methyl-2-thenyl)thiophene (**14**) respectively on the basis of IR, ^{1}H NMR and mass spectroscopy as well as elemental analysis. Although the crude product mixture was shown by its IR and NMR spectra to contain small amounts of a nitrate supposed to be **13**, it could not be isolated as such. However, the significant formation of dithienylmethane, **14**, strongly suggests the initial formation of a nitrite, **12**, or a nitrate, **13**, and the subsequent acid-catalyzed condensation of these with **7** to yield **14** (Scheme 3).

In order to avoid complications arising from a further reaction of the reactive nitrate, **13**, we then filled the unoccupied positions in **7** with bromine atoms and treated the dibromo derivative, **8**, thus obtained with nitric acid. Compound **8** was quite slow to react with nitric acid alone in dichloromethane at a low temperature. However, in the presence of a catalytic amount of sulfuric acid, it underwent a facile side-chain substitution to afford a pasty substance, from which 3,4-dibromo-5-methyl-2-(nitrooxymethyl)-thiophene (**15**) was isolated as a major product. Thus, the removal of a benzene ring from the benzo[*b*]-thiophene system led to a change in the mode of the side-chain reaction of the thiophene nucleus from nitration to nitrooxylation. This remarkable effect of the fused benzene ring parallels that observed in the reactions of benzenes and higher polybenzenoid hydrocarbons and may be taken to indicate that the side-chain reaction of the thiophenes also proceeds through a heterolytic mechanism similar to that depicted in Scheme 1.

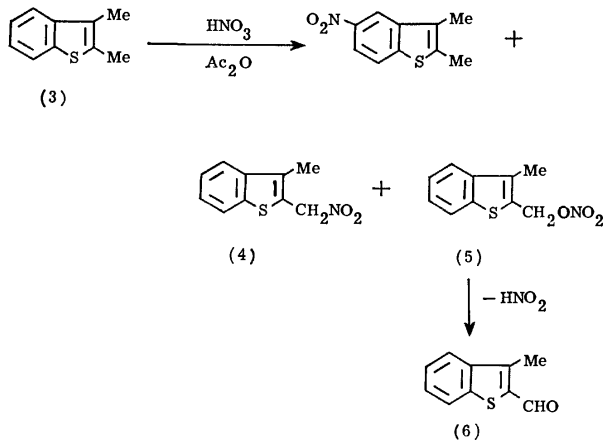

Scheme 2.

When an attempt was made to purify crude **15** by thin-layer chromatography over silica gel (Merck Kieselguhr 60 GF_{254}), using hexane as the eluant, we obtained a small amount of a crystalline compound, **17** (mp 149—150 °C), in addition to the expected 3,4-dibromo-2-hydroxymethyl-5-methylthiophene (**18**) and bis(3,4-dibromo-5-methyl-2-thenyl) ether (**19**) (Scheme 4). The elemental analysis and molecular weight of **17** were consistent with a formula of $C_{11}H_8Br_4S_2$. Its infrared spectrum ($CDCl_3$) showed prominent bands at ν_{max} 1540, 1420, 1300, 1120, and 835 cm^{-1}, and its ^{1}H NMR spectrum ($CDCl_3$) contained peaks at δ 2.40 and 4.22 ppm, with a relative intensity ratio of 3:1. Its mass spectrum exhibited peaks at *m/e* 524 (M^+), 445 (M^+—Br), 364 (M^+—2 Br), and 269 ($M^+-C_5H_3Br_2S$). These data are consistent with the structure of 3,3′,4,4′-tetrabromo-5,5′-dimethyldi-2-thienylmethane (**17**). This structural assignment was confirmed by an unequivocal synthesis of an authentic sample of **17**; 2-methylthiophene was condensed with formaldehyde in the presence of an acid catalyst to give 5,5′-dimethyldi-2-thienylmethane (**16**), which was

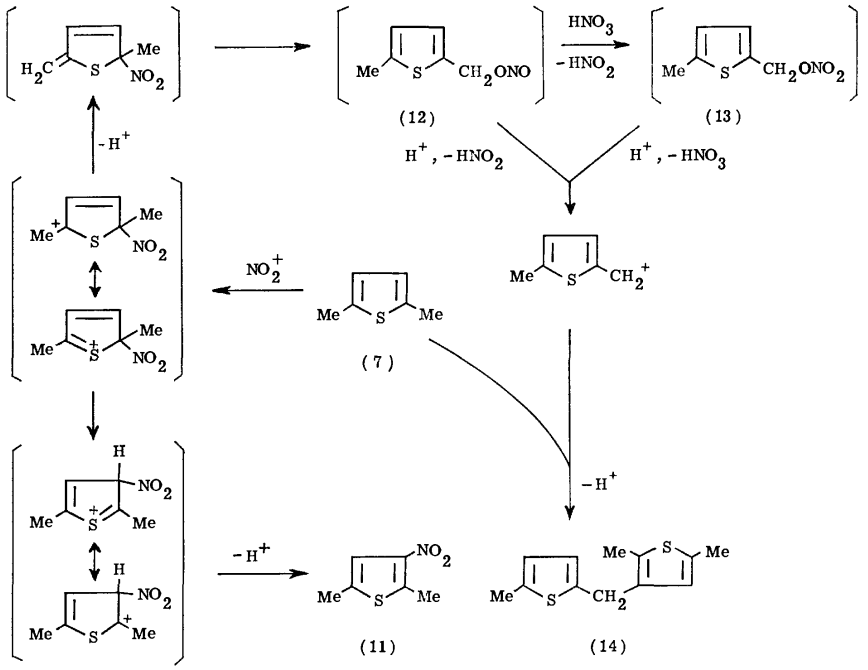

Scheme 3.

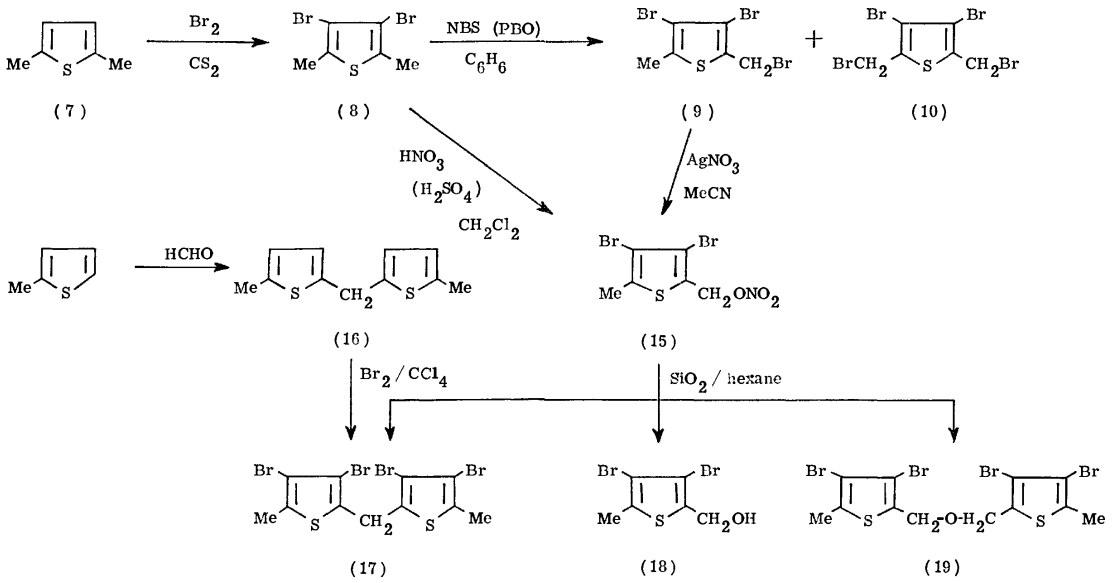

Scheme 4.

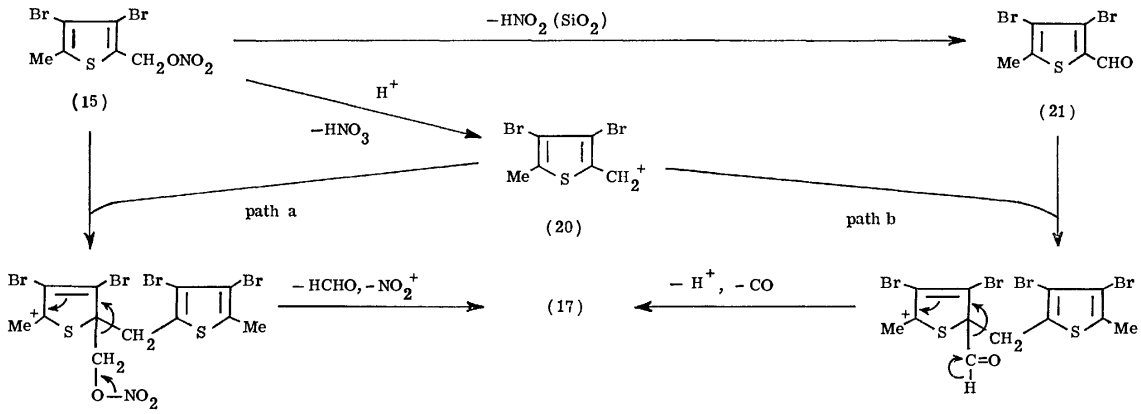

Scheme 5.

then brominated in the dark to give **17** (mp 150—151 °C), identical in all respects with a sample obtained from **15**. That compound **17** had been formed during chromatography over silica gel was confirmed by an experiment in which **15** and silica gel were stirred together in hexane overnight at room temperature to yield an appreciable amount of **17**, along with other products. The previous literature contains no references to the formation of diarylmethanes during the chromatography of arylalkyl nitrates. The unexpected formation of **17** from **15** lacks a convincing explanation at present; so, too, does the fate of the missing carbon atom. However, we suggest two possible reaction pathways, as outlined in Scheme 5. According to this scheme, nitrate **15** undergoes the acid-induced C–O bond cleavage on the silica gel surface to form a carbonium-ion intermediate, **20**, which may subsequently replace the nitrooxymethyl group in **15** (Path a) or expel the formyl group from aldehyde **21** (Path b). Activated primary nitrates are known to undergo acid-catalyzed decomposition to give aldehydes.[6]

It is interesting to compare this coupling reaction with that reported by King and Brown, where diethyl 4,4′-dimethyl-5,5′-methylenedi-2-pyrrolecarboxylate is obtained in the nitration of ethyl 4,5-dimethyl-2-pyrrolecarboxylate.[7] Although they suggested the implication of a nitromethyl function in the unexpected pyrromethane formation, the present result seems to favor the role of a nitrooxymethyl function. The scope and possible utility of this novel coupling reaction is currently being investigated.

Experimental

The melting points were determined on a hot-stage apparatus and are uncorrected. The infrared spectra were run as Nujol mulls on a Hitachi 215 spectrophotometer. The ^{1}H NMR spectra were determined in deuteriochloroform on a Varian T-60 spectrometer, using TMS as the internal standard, unless otherwise stated. The mass spectra were obtained on a Hitachi RMS-4 mass spectrometer with an ionizing current of 70 eV, and bromine-containing peaks have been reported for ^{79}Br. Thin-layer chromatographic separations were carried out on Merck Kieselguhr 60 GF_{254} plates. 2,5-Dimethylthiophene (**7**) was prepared from 2,4-pentanedione as has previously been reported.[8] 2,3,5-

Trimethylthiophene and tetramethylthiophene were obtained by treating an appropriate polymethylthiophene with *N*-methylformanilide and phosphoryl chloride and by then reducing the resulting aldehyde by the Wolff-Kishner method.[9,10]

3,4-Dibromo-2-(bromomethyl)-5-methylthiophene (9). A solution of 3,4-dibromo-2,5-dimethylthiophene (**8**; mp 45—46 °C; 0.9 g; 3.3 mmol) and benzoyl peroxide (BPO; 10 mg; 0.04 mmol) in dry benzene (5 ml) was brought to reflux; a mixture of *N*-bromosuccinimide (0.6 g; 3.4 mmol) and BPO (10 mg; 0.04 mmol) was then added, portion by portion over a period of 10 min. The mixture was kept under reflux for another 10 min and then allowed to cool. A white precipitate was removed by filtration, and the filtrate evaporated under reduced pressure. The solid residue (1.20 g) crystallized out from hexane in two different forms, which were separated by hand-picking.

Large cubes were recrystallized from hexane and identified as **9**. Mp 68—69 °C. Yield, 0.54 g (46%). ^{1}H NMR (CCl_4): δ 2.40 (s, 3H) and 4.60 ppm (s, 2H); IR ν_{max} 1425, 1300, 1205, 1190, 1160, 1100, and 900 cm^{-1}. Found: C, 20.79; H, 1.46%. Calcd for $C_6H_5Br_3S$: C, 20.65; H, 1.44%.

Needles were recrystallized from hexane and identified as *3,4-dibromo-2,5-bis(bromomethyl)thiophene (10).* Mp 117—118 °C. Yield, 0.20 g (14%). ^{1}H NMR (CCl_4): δ 4.61 ppm (s, 4H); IR ν_{max} 1420, 1305, 1220, 1200, 1115, and 905 cm^{-1}. Found: C, 17.11; H, 0.97%. Calcd for $C_6H_4Br_4S$: C, 16.84; H, 0.94%.

3,4-Dibromo-5-methyl-2-(nitrooxymethyl)thiophene (15). Silver nitrate (0.09 g; 0.53 mmol) was added to a solution of **9** (0.175 g; 0.50 mmol) in acetonitrile (5 ml), after which the mixture was stirred at room temperature for 1 h. The silver bromide was removed by filtration, and the filtrate was evaporated to give a solid residue, which was subsequently recrystallized from pentane; white needles; mp 50—51 °C. Yield, 0.09 g (54%). ^{1}H NMR (CCl_4): δ 2.47 (s, 3H) and 5.53 ppm (s, 2H); IR: ν_{max} 1620, 1295, 950, and 880 cm^{-1}. Found: C, 22.06; H, 1.57%; N, 3.97%. Calcd for $C_6H_5NO_2Br_2S$: C, 21.77; H, 1.52; N, 4.23%.

5,5'-Dimethyldi-2-thienylmethane (16). A mixture of 2-methylthiophene (3.63 g; 37 mmol), zinc chloride (3.40 g; 25 mmol), and concentrated hydrochloric acid (2.55 ml; 43 mmol) was stirred at −7—0 °C, after which an aqueous solution of formaldehyde (2.35 g; 29 mmol) was added, drop by drop, over a period of 1.5 h. After the addition was complete, stirring was continued for 1 h, and then the mixture was diluted with water. A white precipitate was collected by filtration, the aqueous phase was extracted with ether, and the solvent was evaporated. The solid products were combined and recrystallized from methanol to give **16** as white needles (0.956 g; 25%); mp 32—34 °C. ^{1}H NMR: δ 2.42 (s, 6H), 4.10 (s, 2H), and 6.53 ppm (s, 4H). Found: C, 63.29; H, 5.86%. Calcd for $C_{11}H_{12}S_2$: C, 63.41; H, 5.81%.

3,3',4,4'-Tetrabromo-5,5'-dimethyldi-2-thienylmethane (17). Into a solution of the above dithienylmethane, **16** (0.1 g; 48 mmol), in carbon disulfide (5 ml) cooled to −10 °C, bromine (0.308 g; 198 mmol) in the same solvent (5 ml) was stirred, drop by drop, over a period of 4 h. The mixture was kept for 5 h at this temperature and then worked up as usual, giving a crude bromo derivative (0.22 g). This was chromatographed on a thick-layer silica gel plate, using hexane as the eluant, to afford **17** as fine needles (0.089 g; 35%); mp 148—149 °C. ^{1}H NMR: δ 2.43 (s, 6H) and 4.23 ppm (s, 2H); IR: ν_{max} 1290 and 940 cm^{-1}.

Reaction of 2,5-Dimethylthiophene with Copper(II) Nitrate in Acetic Anhydride. To a solution of copper(II) nitrate trihydrate (1.2 g; 5 mmol) in acetic anhydride (15 ml), cooled to −10—−15 °C, **7** (1.1 g; 9.8 mmol) in the same solvent (15 ml) was added, drop by drop, over a period of 30 min; the mixture was then stirred at this temperature for an additional 30 min. A change in color from blue to deep green was observed. Water (20 ml) and then ether (20 ml) were added, and the acetic anhydride was allowed to hydrolyze at room temperature. The organic phase was separated, and the aqueous phase was extracted with hexane. The combined organic solutions were washed with water until neutral, and then evaporated. An oily residue (0.937 g) was chromatographed over silica gel, using hexane as the eluant, to give *2,5-dimethyl-3-(5-methyl-2-thenyl)thiophene* (**14**; 0.253 g; 23%) and *3-nitro-2,5-dimethylthiophene* (**11**; 0.263 g; 17%) as major products.

11: yellow needles; mp 29—30 °C; ^{1}H NMR (CCl_4): δ 2.42 (s, 3H), 2.70 (s, 3H), and 7.12 ppm (s, H); IR (neat): ν_{max} 1530, 1485, 1360, 1315, 1260, 1195, 790, and 750 cm^{-1}. MS: *m/e* 157 (M^+), 140, 127, 112, 110, 85, 72, 67, and 59. Found: C, 46.06; H, 4.76; N, 9.16%. Calcd for $C_6H_7O_2NS$: C, 45.85; H, 4.49; N, 8.91%.

14: liquid; ^{1}H NMR (CCl_4): δ 2.28 (s, 3H), 2.33 (s, 3H), 2.38 (s, 3H), 3.77 (s, 2H), 6.30 (s, H), 6.33 (s, H), and 6.38 ppm (s, H); IR (neat): ν_{max} 1035, 1145, and 1215 cm^{-1}; MS: *m/e* 222 (M^+), 207, 124, and 111. Found: C, 64.52; H, 6.55%. Calcd for $C_{12}H_{14}S_2$: C, 64.81; H, 6.35%.

Reaction of 3,4-Dibromo-2,5-dimethylthiophene with Nitric Acid. To a stirred solution of **8** (1.0 g; 3.7 mmol) in dichloromethane (20 ml), nitric acid (1.17 g; d=1.5) in the same solvent (10 ml) was added, drop by drop. The reaction mixture gradually changed from pale violet to red purple. Then a drop of concentrated sulfuric acid was added, and the mixture was heated gently for 1 h. During this period, nitrogen dioxide was slowly evolved. The reaction mixture was then diluted with water, and the organic phase was separated, washed thoroughly with water, and evaporated *in vacuo* to give an oily residue (1.15 g), which solidified to a crystalline mass on standing in a refrigerator. This solid product was extracted with pentane to give **15** as white crystals; mp 47—48 °C. Yield, 0.614 g (50%). Mixed melting point determination with an authentic sample showed no depression (47—49 °C).

When the crude nitrate was subjected to thin-layer chromatography over silica gel, using hexane as an eluant, **17** was obtained along with **18** and **19**. Product **17** was recrystallized from hexane to give fine needles (0.020 g; 4.2%) (mp 150—151 °C), identical in all respects with an authentic sample prepared by the other route.

Found: C, 25.26; H, 1.54%. Calcd for $C_{11}H_8Br_4S_2$: C, 25.04; H, 1.66%.

Coupling of 3,4-Dibromo-5-methyl-2-(nitrooxymethyl)thiophene in the Presence of Silica Gel. Silica gel (1 g) was added to a solution of **15** (70 mg) in hexane (6 ml), after which the mixture was stirred overnight at room temperature. The supernatant liquid was then decanted and evaporated to give a solid residue (53 mg), which was chromatographed on a thin-layer silica gel plate, using hexane as the eluant. From the main band, **17** (7.6 mg; 14%) was obtained and identified by means of its melting point and spectral characteristics.

We are grateful to the Ministry of Education and the Saneyoshi Scientific Foundation for financial support of this work.

References

1) The reaction of polysubstituted aromatics. Part LVII. Part LVI; H. Suzuki, K. Miyoshi, and M. Shinoda, *Bull. Chem. Soc. Jpn.*, **53**, 1765 (1980).
2) For a review, see H. Suzuki, *Synthesis*, **1977**, 217.
3) H. Suzuki, H. Yoneda, and T. Hanafusa, *Bull. Chem. Soc. Jpn.*, **47**, 3106 (1974); *ibid.*, **48**, 2116 (1975); and the references cited therein.
4) H. Suzuki, T. Mishina, and T. Hanafusa, *Bull. Chem. Soc. Jpn.*, **52**, 191 (1979).
5) F. G. Bordwell and T. W. Cutshall, *J. Org. Chem.*, **29**, 2020 (1964).
6) K. Maruyama, K. Nakamura, and H. Suzuki, *Nippon Kagaku Zasshi*, **89**, 78 (1968); S. D. Rose, E. R. Coburn, and M. Finkelstein *J. Org. Chem.*, **33**, 585 (1968).
7) M. M. King and R. H. Brown, *Tetrahedron Lett.*, **1975**, 3995.
8) G. N. Jean and F. F. Nord, *J. Org. Chem.*, **20**, 1363 (1955).
9) N. P. Buu-Hoï, Ng Hoán, and D. Lavit, *J. Chem. Soc.*, **1950**, 2130.
10) W. J. King and F. F. Nord, *J. Org. Chem.*, **14**, 638 (1949).

Reaction of Acetals with Grignard Reagents

Hiroshi Ishikawa,* Teruaki Mukaiyama,** and Shigeru Ikeda***

Laboratories of Medicinal Chemistry, Otsuka Pharmaceutical Co., Ltd., Kagasuno, Kawauchi-cho, Tokushima 771-01

***Department of Chemistry, Faculty of Science, The University of Tokyo, Hongo, Bunkyo-ku, Tokyo 113*

****Department of Chemistry, Science University of Tokyo, 1-3, Kagurazaka, Shinjuku-ku, Tokyo 162*

(Received June 10, 1980)

The reaction of dialkyl acetals derived from α,β-unsaturated aldehydes with Grignard reagents using $TiCl_4$ in THF afforded the cross coupling products, allyl ethers, in high yields. The $TiCl_4$-promoted reaction of alkyl 2,4-dichlorophenyl acetals, synthesized from 3,4-dihydro-2*H*-pyran or ethyl vinyl ether and 2,4-dichlorophenol, with Grignard reagents in THF at low temperature afforded the corresponding unsymmetrical ethers in high yields. When alkyl 2,4-dichlorophenyl acetals, synthesized from aromatic aldehyde or vinyl ethers and 2,4-dichlorophenol, were treated with Grignard reagents in benzene or toluene at room temperature in the absence of $TiCl_4$, the cross coupling reaction took place and the corresponding ethers were isolated in good yields.

We briefly reported in two previous papers[1-2] that the reaction of dialkyl acetals derived from α,β-unsaturated aldehydes with Grignard reagents using $TiCl_4$ and the reaction of alkyl 2,4-dichlorophenyl acetals, synthesized from 3,4-dihydro-2*H*-pyran or vinyl ether and 2,4-dichlorophenol, with Grignard reagents in benzene or toluene afforded the corresponding allyl ethers and ethers. In this report, the reactions are explained in detail and additional results are presented.

In general, acetals, the most commonly encountered protective group for aldehydes and ketones, are stable to most alkaline reagents and known to be inert toward various nucleophiles such as Grignard reagents and organolithium compounds except for cyclic acetals, steroidal cyclic acetals and cyclic acetals of halogenated saturated ketone.[3-7] No similar reactions have hitherto been know for dialkyl and mixed acetals derived from various aldehydes and ketones.

We have studied various synthetic reactions using $TiCl_4$ and have reported in the previous paper[8] that the reduction of dialkyl acetals derived from aromatic aldehydes and ketones with $TiCl_4$–$LiAlH_4$ in THF or diethyl ether at room temperature afforded the coupling products, pinacol ethers or olefins, in high yields. We also reported that various olefins were prepared in good yields by the treatment of allyl methyl ethers with $TiCl_4$–$LiAlH_4$ in THF or diethyl ether.[9]

In the present work, the reaction of various acetals with Grignard reagents in the presence and absence of $TiCl_4$ was tried; it was found that the various ethers were given in good yields. The $TiCl_4$-promoted reaction of dimethyl acetals derived from α,β-unsaturated aldehydes with Grignard reagents was examined in THF at −78 °C. For example, 1.5 molar amount of phenethylmagnesium bromide (**2**) was added to a mixture of an equimolar amount of cinnamaldehyde dimethyl acetal (**1**) and $TiCl_4$ in THF at −78 °C under argon atmosphere. After stirring at −78 °C for 6 h, the mixture was quenched with aqueous potassium carbonate. Purification by column chromatography (silica gel) gave 3-methoxy-1,5-diphenyl-1-pentene (**3**) in 81% yield.

$$\underset{\mathbf{1}}{C_6H_5CH{=}CH\text{-}CH(OCH_3)(OCH_3)} + \underset{\mathbf{2}}{C_6H_5CH_2CH_2MgBr}$$

$$\xrightarrow[-78\,^\circ C]{TiCl_4} \xrightarrow{H_2O} C_6H_5CH{=}CHCH(OCH_3)CH_2CH_2C_6H_5$$

6 h

3 81%

In a similar manner, the reactions of various acetals derived from α,β-unsaturated aldehydes in the presence of $TiCl_4$ were tried in THF at −78 °C, and the corresponding allyl ethers were obtained in high yields, as shown in the following equation:

$$\underset{\mathbf{1}}{C_6H_5CH{=}CHCH(OCH_3)(OCH_3)} + \underset{\mathbf{4}}{CH_3CH_2MgBr}$$

$$\xrightarrow{TiCl_4} \xrightarrow{H_2O} \underset{\mathbf{5}}{C_6H_5CH{=}CHCH(OCH_3)CH_2CH_3} \quad 83\% \qquad (1)$$

$$\underset{\mathbf{1}}{C_6H_5CH{=}CHCH(OCH_3)(OCH_3)} + \underset{\mathbf{6}}{CH_2{=}CHCH_2MgBr}$$

$$\xrightarrow{TiCl_4} \xrightarrow{H_2O} \underset{\mathbf{7}}{C_6H_5CH{=}CHCH(OCH_3)CH_2CH{=}CH_2} \quad 71\% \qquad (2)$$

$$\underset{\mathbf{8}}{CH_3CH{=}CHCH(OCH_3)(OCH_3)} + \underset{\mathbf{2}}{C_6H_5CH_2CH_2MgBr}$$

$$\xrightarrow{TiCl_4} \xrightarrow{H_2O} \underset{\mathbf{9}}{CH_3CH{=}CHCH(OCH_3)CH_2CH_2C_6H_5} \quad 79\% \qquad (3)$$

$$\underset{\mathbf{10}}{CH_2{=}CHCH(OCH_2CH_3)(OCH_2CH_3)} + \underset{\mathbf{2}}{C_6H_5CH_2CH_2MgBr}$$

$$\xrightarrow{TiCl_4} \xrightarrow{H_2O} \underset{\mathbf{11}}{CH_2{=}CHCH(OCH_2CH_3)CH_2CH_2C_6H_5} \quad 70\% \qquad (4)$$

It was found that γ-arylation took place to afford vinyl ethers when phenylmagnesium bromide (**12**) was employed in the above reactions. For example, 1-methoxy-3-phenyl-1-butene (**13**) was obtained in 42% yield by the reaction of crotonaldehyde dimethyl acetal (**8**) and phenylmagnesium bromide (**12**) in the presence

TABLE 1. $TiCl_4$-PROMOTED REACTION OF ALKYL ARYL ACETALS WITH GRIGNARD REAGENTS IN THF

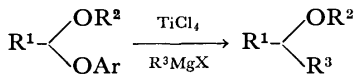

Acetal R¹	Acetal R²	Acetal Ar	Grignard reagent R³	Ether yield[a]/%	Bp (°C/mmHg)[b),c)]	
-$(CH_2)_4$-		C_6H_5	$C_6H_5CH_2CH_2$	65	69—70/0.5	(**15**)
		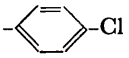		76		(**15**)
				38		(**15**)
14		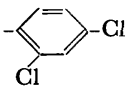		98		(**15**)
			C_6H_5	80	96—100/22	(**16**)
			n-C_8H_{17}	75	95—96/3	(**17**)
CH_3	C_2H_5	C_6H_5	$C_6H_5CH_2$	51	75—78/10	(**20**)
18		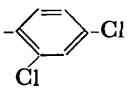	$C_6H_5CH_2CH_2$	87	106—110/12	(**19**)
			C_6H_5	82	65—68/22	(**21**)
			n-C_8H_{17}	71	76—78/15	(**22**)
			$C_6H_5CH_2$	77		(**20**)

a) Isolated by silica gel chromatography. b) All boiling points were uncorrected. c) 1 mmHg = 133.322 Pa.

TABLE 2. REACTION OF ALKYL 2,4-DICHLOROPHENYL ACETALS WITH GRIGNARD REAGENTS IN BENZENE

Acetal R¹	Acetal R²	Grignard reagent R³	Ether yield[a]/%	Bp (°C/mmHg)	
-$(CH_2)_4$-		$C_6H_5CH_2CH_2$	88[e)]		(**15**)
(**14**)		C_6H_5	84		(**16**)
		n-C_3H_7	67[b)]	78—79/30	(**23**)
		n-C_8H_{17}	85		(**17**)
			60	104—109/21	(**24**)
		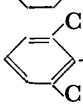	79	82—84/2	(**25**)
	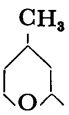	$CH_2=C(CH_3)CH_3$	86[b),d)]	86—88/2	(**27**)
	(**26**)	$CH_2CH(CH_3)CH_3$	79[b),d)]	63—64/10	(**28**)
CH_3	C_2H_5	*n*-C_5H_{17}	87		(**22**)
	(**18**)		49[b)]	61—62/18	(**29**)
		C_6H_5	83		(**21**)
		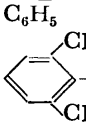	76	104—106/20	(**30**)
		$C_6H_5CH_2CH_2$	88		(**19**)
C_6H_5	CH_3	$C_6H_5CH_2CH_2$	83	131—133/2	(**32**)
	(**31**)	C_6H_5	76	145—148/20	(**33**)
		n-C_6H_{13}	81	143—146/31	(**34**)

a) Isolated by silica gel chromatography. b) Isolated by distillation. c) The unsymmetrical ether was obtained in 82% yield when the reaction was carried out in toluene. d) The composition of the product as determined by GLPC analysis, comparing with the authentic sample, was 32% *cis* and 68% *trans* isomer. e) The composition of the product was 19% *cis* and 81% *trans* isomer.

of $TiCl_4$, and 1-methoxy-1-phenyl-2-butene could not be detected.

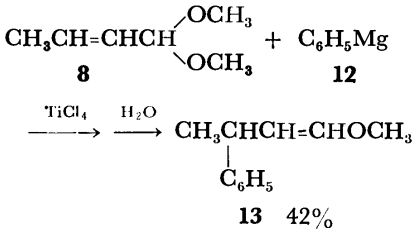

8 **12** **13** 42%

Contrary to such results, dialkyl acetals derived from aromatic and aliphatic aldehydes, such as benzaldehyde dimethyl acetal and β-phenylpropionaldehyde dimethyl acetal, were not alkylated by the coupled use of $TiCl_4$ and Grignard reagents, considerable amounts of the starting materials were recovered. But it was established that the $TiCl_4$-promoted reaction of some mixed acetals, alkyl aryl acetals synthesized from 3,4-dihydro-2*H*-pyran or ethyl vinyl ether, and phenol with Grignard reagents gave various unsymmetrical ethers by the replacing the aryloxyl group with an alkyl group (Table 1).

As shown in Table 1, when various mixed acetals synthesized from 3,4-dihydro-2*H*-pyran and phenol were treated with Grignard reagent in the presence of $TiCl_4$ in THF at −78 °C, it was found that the reaction of 2-(2,4-dichlorophenoxy)tetrahydropyran with Grignard reagent afforded the cross coupling product in higher yield than that obtained for mixed acetals. The generality of $TiCl_4$-promoted reaction was examined by the use of various alkyl 2,4-dichlorophenyl acetals, and in all cases the corresponding ethers were obtained in good yields (see Table 1).

Further, the reaction of 2-(2,4-dichlorophenoxy)-tetrahydropyran with a Grignard reagent such as phenethylmagnesium bromide in the absence of $TiCl_4$ took place in benzene or toluene at room temperature and the corresponding unsymmetrical ether was isolated in 88% yield. Even when the same reaction

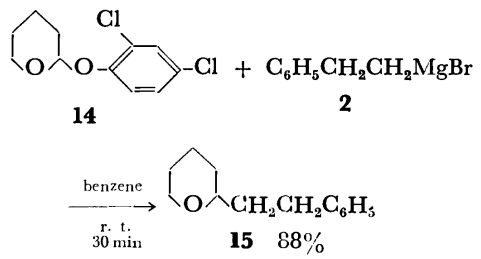

14 **2** **15** 88%

was carried out in tetrahydrofuran under refluxing, the yield of the unsymmetrical ether was below 60%. In a similar manner, various unsymmetrical ethers were obtained in good yields, as shown in Table 2.

The mechanism of the $TiCl_4$-promoted reaction of α,β-unsaturated acetals and alkyl aryl acetals with Grignard reagents may be explained as follows; the acetal forms a coordinated compound (I) with $TiCl_4$, which subsequently reacts smoothly with the Grignard reagent, probably through a six-membered cyclic intermediate (II), to afford the corresponding ethers, as sketched below:

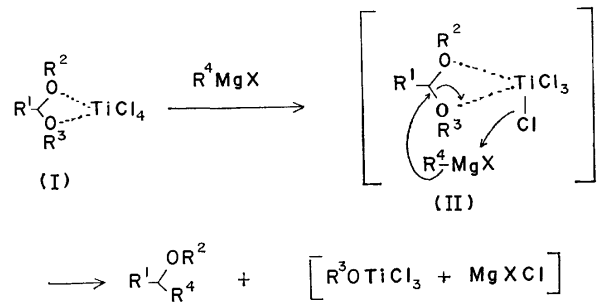

(I) (II)

The 2,4-dichlorophenoxyl group of alkyl 2,4-dichlorophenyl acetals can leave easily; thus the mechanism of the reaction of alkyl 2,4-dichlorophenyl acetals with Grignar dreagents in bezene or toluene may be a magnesium-promoted replacement reaction of 2,4-dichlorophenoxyl group with alkyl group, as shown below.

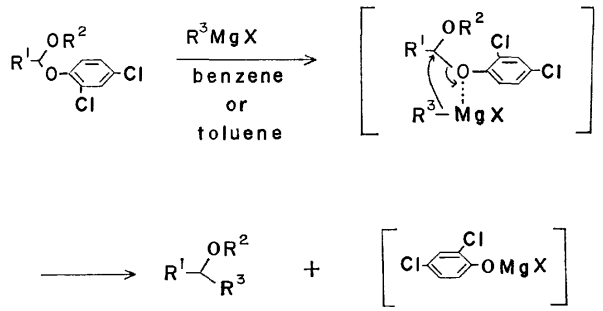

In conclusion, it has been shown that the reaction of dialkyl acetals derived from α,β-unsaturated aldehydes and mixed acetals synthesized from 3,4-dihydro-2*H*-pyran or ethyl vinyl ether and phenols with Grignard reagents, using $TiCl_4$ in THF at low temperature, afforded the cross-couling products, various ethers, in high yields. Further, when the mixed acetals synthesized from aromatic aldehydes or vinyl ethers and 2,4-dichlorophenol were treated with Grignard reagents in an aromatic hydrocarbon such as benzene or toluene at room temperature, various ethers are obtained in good yields.

Experimental

Spectra. The proton NMR spectra were recorded using a Hitachi R-24 spectrometer and a Varian EM 360 spectrometer. Chemical shifts are reported on δ scale relative to tetramethylsilane as an internal standard. Infrared spectra were taken using a Hitachi 215 grating infrared spectrophotometer. Products were identified by NMR and IR spectra and elemental analyses.

Material. Commercially available $TiCl_4$ was distilled under argon atmosphere before use. All solvents used here were distilled according to the usual methods and were stored over sodium metal as a drying agent. Various α,β-unsaturated acetals were readily prepared from α,β-unsaturated aldehyde and orthoformic esters in alcoholic solution in the presence of a catalyst such as anhydrous hydrogen chloride. Alkyl 2,4-dichlorophenyl acetals were easily prepared by the addition of 2,4-dichlorophenol to vinyl ether derivatives and by the replacement reaction of sodium 2,4-dichlorophenoxide to α-methoxybenzyl chloride.[10]

Descriptions in this experimental section are typical examples; other products are shown in the table.

Reaction of Cinnamaldehyde Dimethyl Acetal (1) with Phenethyl-

Table 3. Physical properties and analytical data of the products

Products	IR (cm^{-1})[a]	NMR (δ)[b]	Found (%) (Calcd) C	H
3[d]	2900 1105 740 695	1.6—2.1(m, 2H), 2.71(t, 2H, J=7 Hz), 3.25(s, 3H), 3.4—3.8(m, 1H), 5.94(dd, 1H, J=16, 7 Hz), 6.45(d, 1H, J=16 Hz), 7.0—7.4(m, 10H)	85.54 (85.67)	7.91 (7.99)
5[e]	2910 1100 970 700	0.92(t, 3H, J=7 Hz), 1.2—1.9(m, 2H), 3.24(s, 3H), 3.3—3.6(m, 1H), 5.93(dd, 1H, J=16, 7 Hz), 6.45(d, 1H, J=16 Hz), 7.20(br s, 5H)	81.90 (81.77)	9.21 (9.15)
7[f]	2940 1110 995	2.35(t, 2H, J=6 Hz), 3.26(s, 3H), 3.4—3.8(m, 1H), 4.8—5.2(m, 2H), 5.4—6.0(m, 1H), 5.94(dd, 1H, J=16, 7 Hz), 6.48(d, 1H, J=16 Hz), 7.26(br s, 5H)	82.76 (82.93)	8.45 (8.57)
9[g]	2900 1100 700	1.73(d, 3H, J=6 Hz), 1.5—2.0(m, 2H), 2.70(t, 2H, J=7 Hz), 3.27(s, 3H), 3.3—3.6(m, 1H), 5.0—5.8(m, 2H), 7.29(s, 5H)	81.85 (82.06)	9.38 (9.54)
11[h]	2900 1115 745 695	1.17(t, 3H, J=7 Hz), 1.5—2.0(m, 2H), 2.68(t, 2H, J=7 Hz), 3.0—3.7(m, 3H), 4.9—5.3(m, 2H), 5.4—6.0(m, 1H), 7.17(s, 5H)	81.83 (82.06)	9.36 (9.54)
13[i]	2960 1115 750 695	1.26(d, 3H, J=6 Hz), 3.24(s, 3H), 3.6—4.0(m, 1H), 5.96(dd, 1H, J=16, 7 Hz), 6.51(d, 1H, J=16 Hz), 7.27(s, 5H)	81.32 (81.44)	8.81 (8.70)
15	2930 1090 700	1.1—1.9(m, 8H), 2.5—2.9(m, 2H), 2.9—3.5(m, 2H), 3.7—4.0(m, 1H), 7.12(s, 5H)	81.88 (82.06)	9.39 (9.54)
16	2930 1090 695	1.2—2.1(m, 6H), 3.2—3.7(m, 1H), 3.9—4.4(m, 2H), 7.22(s, 5H)	81.61 (81.44)	8.84 (8.70)
17	2930 1090	0.7—1.1(m, 3H), 1.2—2.0(m, 20H), 2.9—3.5(m, 2H), 3.7—4.0(m, 1H)	78.48 (78.72)	13.09 (13.21)
19	2950 1110 700	1.08(t, 3H, J=7 Hz), 1.20(d, 3H, J=7 Hz), 2.7—2.9(m, 2H), 3.2—3.9(m, 4H), 4.5—4.8(m, 1H), 7.19(s, 5H)	80.66 (80.85)	10.01 (10.18)
20	2920 1110 700	1.05(d, 3H, J=7 Hz), 1.10(t, 3H, J=7 Hz), 2.3—3.0(m, 2H), 3.1—3.7(m, 3H), 7.15(s, 5H)	80.12 (80.44)	9.95 (9.83)
21	2970 1110 700	1.13(t, 3H, J=7 Hz), 1.35(d, 3H, J=7 Hz), 3.28(q, 2H, J=7 Hz), 4.28(q, 1H, J=7 Hz), 7.23(s, 5H)	79.78 (79.95)	9.31 (9.39)
22	2930 1110	0.8—1.5(m, 23H), 3.1—3.6(m, 3H)	77.50 (77.35)	14.22 (14.07)
23	2930 1095	0.88(t, 3H, J=7 Hz), 1.1—1.9(m, 10H), 2.9—3.6(m, 2H), 3.7—4.0(m, 1H)	74.78 (79.94)	12.40 (12.58)
24	2930 1095	0.8—2.1(m, 17H), 2.7—3.4(m, 2H), 3.7—4.3(m, 1H)	78.32 (78.51)	11.89 (11.98)
25	2940 1090 770	1.2—2.1(m, 6H), 2.36(s, 6H) 3.2—3.6(m, 1H), 3.5—4.2(m, 1H), 4.4—4.7(m, 1H), 6.83(s, 3H)	81.85 (82.06)	9.30 (9.54)
27	2930 1090	c) 1.02(dd, 3H, J=6 Hz), 1.2—2.2(m, 5H), 1.67(s, 3H), 1.70(s, 3H), 3.3—4.5(m, 3H), 5.1—5.4(m, 1H)	77.98 (77.86)	11.84 (11.76)

Table 3. Continued

Products	IR (cm^{-1})[a]	NMR(δ)[b]	Found (%) (Calcd) C	H
28	2930	c) 0.8—2.0(m, 17H),	76.70	12.78
	1100	3.1—4.1(m, 3H)	(76.86)	(12.90)
29	2390	1.01(d, 3H, J=7 Hz), 1.13(t, 3H, J=7 Hz),	76.90	12.98
		1.0—2.0(m, 11 Hz), 2.8—3.2(m, 1H), 3.43(q, 2H, J=7 Hz)	(76.86)	(12.90)
30	2930	1.15(t, 3H, J=7 Hz), 1.43(d, 3H, J=7 Hz),	80.65	10.11
	1100	2.36(s, 6H), 3.22(q, 2H, J=7 Hz),	(80.85)	(10.18)
	770	4.76(q, 1H, J=7 Hz), 6.83(s, 3H)		
32	2950	1.9—2.3(m, 2H), 2.5—2.8(m, 2H),	85.05	7.88
	1100	3.13(s, 3H), 3.94(t, 1H, J=7 Hz),	(84.91)	(8.02)
	700	7.00(s, 5H), 7.11(s, 5H)		
33	2940	3.30(s, 3H), 5.05(s, 1H),	84.60	7.07
	1098	7.28(s, 10H)	(84.81)	(7.12)
	740			
	695			
34	2930	0.7—1.8(m, 13H), 3.12(s, 3H),	81.35	10.67
	1100	3.93(t, 1H, J=7 Hz),	(81.50)	(10.75)
	755	7.11(s, 5H)		
	700			

a) Neat. b) In CCl_4. c) In $CDCl_3$. d) Bd 123—126 °C/0.5 mmHg. e) Bp 120—123 °C/20 mmHg. f) Bp 102—104 °C/3 mmHg. g) Bp 127—129 °C/16 mmHg. h) Bp 120—123 °C/16 mmHg. i) Bp 110—113 °C/18 mmHg.

magnesium Bromide (2) in the Presence of $TiCl_4$. To a mixture of cinnamaldehyde dimethyl acetal (0.89 g, 5 mmol) and $TiCl_4$ (0.95 g, 5 mmol) in 20 ml of dry THF was added a THF solution of 7.5 mmol of phenethylmagnesium bromide, prepared from phenethyl bromide (1.29 g, 7.5 mmol) and magnesium metal (0.19 g, 7.5 mmol), at −78 °C under an argon atmosphere. The reaction mixture was stirred for 6 h at −78 °C. The reaction was quenched by the addition of 20 ml of 10% aqueous potassium carbonate. The white precipitate which appeared was filtered off. The filtrate was extracted with diethyl ether. The ether extract was washed with saturated sodium chloride solution and dried over sodium sulfate. After removal of the solvent under reduced pressure, 3-methoxy-1,5-diphenyl-1-pentene (**3**) was isolated by column chromatography (silica gel), using benzene–dichloromethane (1:2) as an eluent, in 81% (1.02 g) yield.

Reaction of Crotonaldehyde Dimethyl Acetal (8) with Phenylmagnesium Bromide (12) in the presence of $TiCl_4$. To a mixture of crotonaldehyde dimethyl acetal (0.58 g, 5 mmol) and $TiCl_4$ (0.95 g, 5 mmol) in 20 ml of dry THF was added a THF solution of 7.5 mmol of phenylmagnesium bromide at −78 °C under an argon atmosphere. The reaction mixture was stirred for 6 h at −78 °C. The reaction mixture was worked up as mentioned in the previous case. After removal of the solvent and purification by column chromatography (silica gel), 1-methoxy-3-phenyl-1-butene (**13**) was isolated in 42% (0.34 g) yield.

Reaction of 2-(2,4-Dichlorophenoxy)tetrahydropyran (14) with Phenethylmagnesium Bromide (2). To a benzene solution[11] (4 ml) of phenethylmagnesium bromide (4 mmol) was added a benzene solution (2 ml) of 2-(2,4-dichlorophenoxy)tetrahydropyran (0.50 g, 2 mmol) under an argon atmosphere at room temperature. The reaction mixture was stirred for 30 min. After quenching with water, the product was extracted with ether. The ether extract was washed with 10% aqueous sodium hydroxide and dried over sodium sulfate. After removal of the solvent under reduced pressure, 2-phenethyltetrahydropyran (**15**) was isolated by column chromatography (silica gel) using hexane–dichlorometane (1:1) as an eluent in 88% (0.35 g) yield. The NMR and IR spectra of the product (**15**) are shown in Table 3.

Reaction of α-Methoxy-α-(2,4-dichlorophenoxy)toluene (31) with Phenethylmagnesium Bromide (2). To a benzene solution (5 ml) of phenethylmagnesium bromide (10 mmol) was added a benzene solution (5 ml) of α-methoxy-α-(2,4-dichlorophenoxy)toluene (1.42 g, 5 mmol) under an argon atmosphere at room temperature. The reaction mixture was stirred for 30 min and then worked up as mentioned in the previous case. After removal of the solvent, purification by column chromatography (silica gel) using hexane-dichloromethane (1:1) gave 1.06 g (94%) of 1,3-diphenyl-1-methoxypropane (**32**).

References

1) H. Ishikawa and T. Mukaiyama, *Chem. Lett.*, **1974**, 1077.
2) H. Ishikawa, S. Ikeda, and T. Mukaiyama, *Chem. Lett.*, **1975**, 1051.
3) R. A. Mallory, S. Rovinsky, and I. Scheer, *Proc. Chem. Soc.*, **1964**, 416.
4) A. Feugeas, *Bull. Soc. Chim. Fr.*, **1963**, 2568.
5) R. Zepter, *J. Prakt. Chem.*, **1964**, 74.
6) R. H. Bible, Jr., U. S. Patent 3081315 (1963); Chem. Abstr., **59**, 10180b (1963).
7) C. Blomberg, A. O. Vreugdenhil, and T. Homsma, *Recl. Trav. Chim., Pays-Bas*, **72**, 335 (1963).
8) H. Ishikawa and T. Mukaiyama, *Bull. Chem. Soc. Jpn.*, **51**, 2059 (1978).
9) H. Ishikawa and T. Mukaiyama, *Chem. Lett.*, **1976**, 737.
10) F. Straus and H. Heinze, *Ann.*, **493**, 191 (1932).
11) A benzene solution of various Grignard reagents was prepared by replacing the ether used in the formation of Grignard reagents.

Transformation of Dihydrostreptomycin into 3″-Deoxydihydrostreptomycin

Takayuki Usui, Tsutomu Tsuchiya,* Hamao Umezawa, and Sumio Umezawa
Institute of Bioorganic Chemistry, 1614, Ida, Nakahara-ku, Kawasaki 211

(Received June 20, 1980)

3″-Deoxydihydrostreptomycin active against resistant bacteria was prepared from dihydrostreptomycin (DHSM). The key intermediate in this synthesis is a protected derivative of DHSM in which all hydroxyl groups except the 3″-hydroxyl group are protected, namely, 2″-*N*-(benzyloxycarbonyl)-2,5,6-tris(*O*-tetrahydropyran-2-yl)-3′,3$_a$′:4″,6″-bis(*O*-*p*-methylbenzylidene)-1,3-di-N^G-tosyldihydrostreptomycin. 3″-Deoxygenation was successfully performed by 3″-*O*-imidazolylthiocarbonylation followed by treatment with tributylstannane. The $\Delta[M]_{TACu}$ value of the synthetic 3″-deoxydihydrostreptomycin supports the structure.

3″-Deoxydihydrostreptomycin (3″-DDHSM) (**14**) prepared by a total synthesis[1] exhibits remarkable activity against resistant as well as sensitive bacteria except *Pseudomonas aeruginosa*. The present paper describes another synthesis of the 3″-DDHSM by regiospecific deoxygenation of dihydrostreptomycin (DHSM).

Results and Discussion

The 2″-methylamino group of DHSM was protected by the phenoxycarbonyl group in order to obtain a 2″,3″-cyclic carbamate in a later step, since the phenoxycarbonyl derivative gives a better yield of the cyclic carbamate (**3**) than benzyloxycarbonyl derivative.[2] The *N*-phenoxycarbonyl DHSM (**1**) was isolated as its *p*-toluenesulfonic acid salt. The *p*-toluenesulfonic acid salts of **1** and other guanidino derivatives (**2**—**4**) showed much higher solubility in usual organic solvents than the corresponding hydrochlorides, acetates or carbonates.

Selective acetalation of **1** with *p*-tolualdehyde dimethyl acetal was achieved by a controlled procedure to give 3′,3$_a$′:4″,6″-bis(*O*-*p*-methylbenzylidene) derivative (**2**) in high yield. The purity of the *p*-methylbenzylidene derivatives (**2**—**10**) was easily estimated by the signals of the *p*-methylbenzylidene methyls in their NMR spectra.

The positions of the two cyclic acetals in **2** were presumed from the fact that the 3′,3$_a$′-positions of the dihydrostreptose portion of DHSM were acetalated in preference to the 4″,6″-positions[3] which are generally acetalated more readily than *trans*-diequatorial 5,6-positions. Attempts were also made to prepare 1-*N*, 2-*O*-(or 2-*O*, 3-*N*)-(*p*-methylbenzylidene)-5,6:3′,3$_a$′:4″,6″-tris(*O*-*p*-methylbenzylidene) derivative,[4] in which only the 3″-hydroxyl group is not protected. However, the compound could not be separated from another product suggested to be 5,6:3′,3$_a$′:4″,6″-tris(*O*-*p*-methylbenzylidene) derivative judging from its R_f value on TLC and NMR spectrum.

Treatment of the bis(*O*-*p*-methylbenzylidene) derivative (**2**) with potassium *t*-butoxide in *N*,*N*-dimethylformamide gave the cyclic carbamate (**3**). This reagent was found to give better yield than sodium hydride usually used.[2] In the NMR spectra of **2** and **3**, each peak attributable to 5′-methyl, 2″-*N*-methyl and one of the methyl groups of the *p*-methylbenzylidene groups appeared as two peaks in the ratio of approximately 6:4, indicating the mixtures of two diastereomers originating from the new-born chirality at the methine carbon of the 3′,3$_a$′-*O*-(*p*-methylbenzylidene) portion.

Tetrahydropyranyl protection of **3** by the conventional procedure gave a mixture of pertetrahydropyranyl derivatives. The mixture was negative for diacetyl-coloration test for guanidine and found to have more than five tetrahydropyranyl groups (mainly seven, judging from the NMR spectrum), indicating that the tetrahydropyranyl groups are introduced into the guanidine nitrogens as well as the hydroxyl groups. However, treatment of the mixture with ethanolic ammonia gave tris(tetrahydropyranyl) derivative (**4**) which was diacetyl-positive. This shows that the tetrahydropyranyl groups intoduced into guanidine are unusually sensitive to base.

Benzyloxycarbonylation of the guanidino groups of **4** was unsuccessful, yielding no definite product. However, tosylation was successful to give the di-N^G-tosyl derivative (**5**) in pure state and good yield. Use of excess sodium hydride and tosyl chloride resulted in ditosylation at each guanidino group, the yield of the tetra-N^G-tosyl derivative[5] being 50% at most. From a comparison of the IR spectra of **1**—**4** with those of **5**—**7**, we could determine the absorption peaks assignable to the *N*-tosylguanidine of DHSM derivatives to be 1540 and 1260 cm^{-1}.

In the derivative (**5**), the cyclic carbamate group is the only function sensitive to alkaline treatment. Cleavage of the cyclic carbamate (**5**) by alkaline hydrolysis followed by 2″-*N*-benzyloxycarbonylation gave the desired product (**6**) having a free function only at C-3″. The structure of **6** was confirmed by absence of the absorption peak at 1770 cm^{-1} (cyclic carbamate).[6]

Since deoxygenation at C-3″ of **6** through S_N2 process was presumed to be difficult[7] on account of the 1,3-diaxial interaction between the axial substituent at C-1″ and the approaching nucleophile at C-3″, several radical-type deoxygenation reactions were attempted. Among the preliminary experiments tested, 3″-*O*-dimethylsulfamoylation[7] followed by treatment of the product with sodium in liquid ammonia, and another method reported by Barton and McCombie[8] involving thiocarbonylation followed by reduction with tributylstannane gave 3″-DDHSM (**14**). The latter was found to be superior to the former in the ease of purification and yield. Treatment of **6** with 1,1′-thiocarbonyldiimidazole in boiling 1,2-dichloroethane gave the 3″-*O*-imidazolylthiocarbonyl derivative (**7**) in good yield. This procedure was found to be superior to other methods of thiocarbonylation without use of sodium

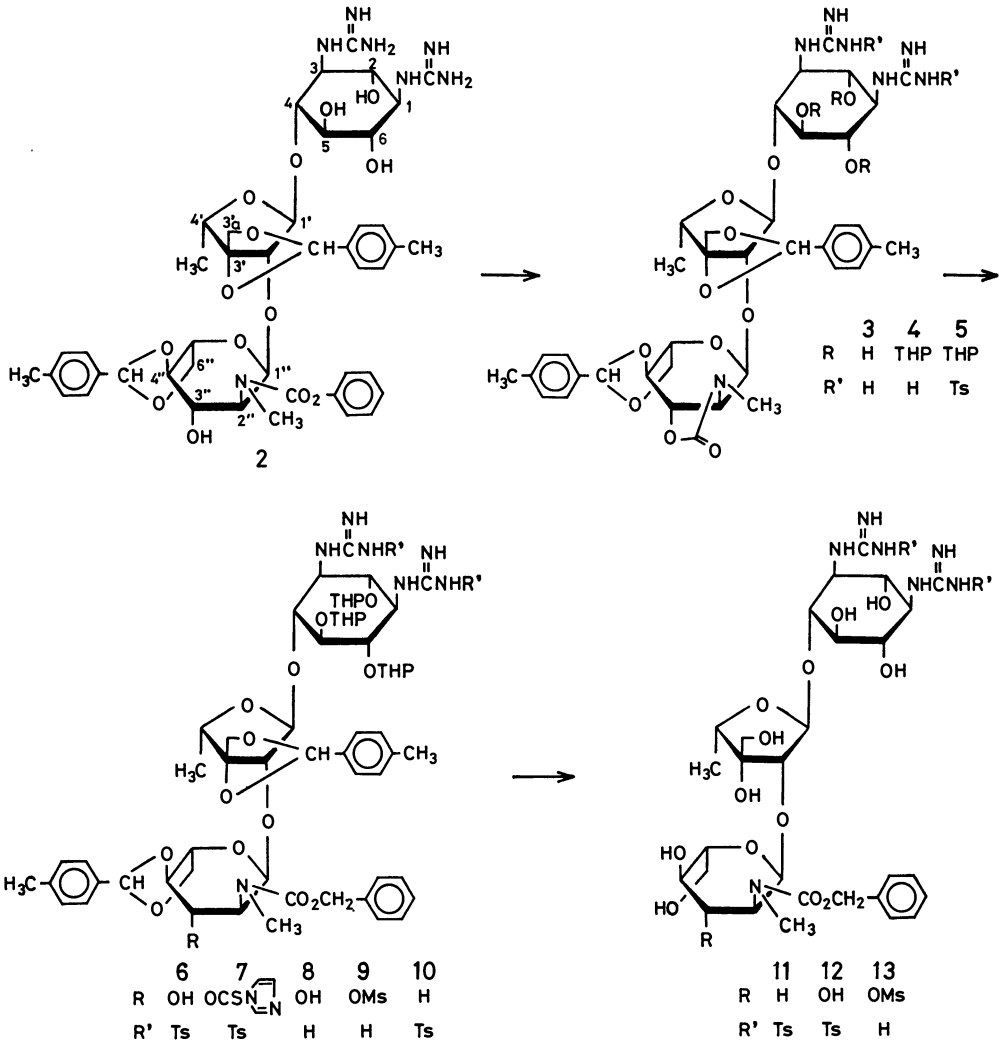

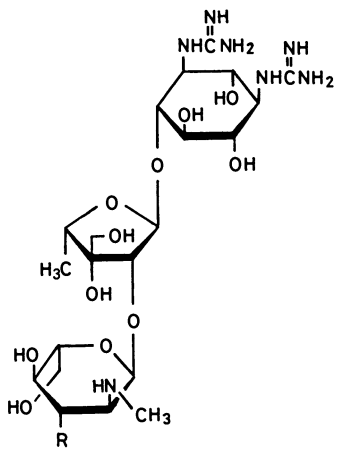

hydride.[8] Most of the other methods require sodium hydride which causes thiocarbonylation at the guanidino groups as well as at the 3″-hydroxyl.

Treatment of **7** with tributylstannane in boiling toluene gave a mixture of 3″-deoxy (**10**) and 3″-hydroxy (**6**) derivatives in a ≈5:1 ratio which was determined by the yield ratio of deprotected products, 3″-DDHSM (**14**) and DHSM. Since isomers **10** and **6** have the same mobility in column chromatography, they could not be separated. Treatment of a mixture of **10** and **6** with aqueous acetic acid to remove the acid-labile protecting groups gave a mixture of 2″-*N*-(benzyloxycarbonyl)-3″-deoxy-di-N^G-tosyl-DHSM (**11**), its 3″-hydroxy derivative (**12**) and a slight amount of 1,3-di-*N*-tosylstreptidine, which were separated by column chromatography. Formation of the last product showed that the glycoside linkage between streptidine and dihydrostreptose is notably unstable to acid.

Finally, **11** was treated with sodium in liquid ammonia to give 3″-DDHSM (**14**), the absence of the 3″-hydroxyl group being shown by its NMR spectrum. The 3″-deoxy structure was confirmed by its small value (−50°) of $\Delta[M]_{TACu}$; DHSM has a large value +1020.[9] The 3″-DDHSM (**14**) showed antibacterial activity against resistant bacteria producing 3″-adenylyltransferase and 3″-phosphotransferase, the antibacterial spectrum being the same as that of 3″-DDHSM prepared by a total synthesis.[1]

It may be worthwhile to describe another attempted route from **4** involving intermediates having unprotected guanidino groups. The cyclic carbamate (**4**) was treated with benzyl alcohol in the presence of sodium hydride to give 2″-*N*-benzyloxycarbonyl-3″-hydroxy derivative (**8**) which was mesylated to give

9. Removal of the *p*-methylbenzylidene and tetrahydropyranyl groups from **9** gave the 3″-*O*-mesyl derivative (**13**) having free guanidino groups, the yield not being high. The absence of the mesyl group on the guanidine portion of **13** was shown by the result of the acidic hydrolysis (2 M HCl in 80% methanol 55 °C, 2 h) of **13**; streptidine was produced quantitatively, indicating that the mesyl group was introduced to C-3″. However, when the 3″-hydroxy compound (**8**) was treated with dimethylsulfamoyl chloride in the presence of sodium hydride by the procedure as described above[7] or with 1,1′-thiocarbonyldiimidazole[8,10] in boiling tetrahydrofuran, no definite product was obtained.

Experimental

^{1}H-NMR spectra were recorded at 90 MHz with a Varian EM-390 spectrometer except for **14**, the spectra of which being recorded at 100 MHz with a Varian XL-100A Spectrometer. Thin-layer chromatography (TLC) was performed on Kieselgel H (Type 60) using a sulfuric acid spray for detection. Silica gel (Kieselgel 60, 230—400 mesh, E Merck Darmstadt, W. Germany) was used for separation of products by column chromatography.

2″-N-(Phenoxycarbonyl)dihydrostreptomycin (1). Anhydrous sodium carbonate (225 mg) and phenyl chloroformate (0.26 ml) were added to an ice-cold solution of DHSM trihydrochloride hydrate (990 mg) in aqueous acetone (2:1, 30 ml), and the mixture was vigorously stirred for 5 min. Ether (20 ml) was added and, after stirring, the aqueous solution was separated and washed with ether twice more. The aqueous solution was neutralized (pH 7) with hydrochloric acid and concentrated to 1 ml. Addition of ethanol (10 ml) gave a precipitate, which was removed by filtration. Concentration of the organic solution gave a solid (Solid A, 1.18 g). The solid, after being well dried, was dissolved in dry DMF (10 ml), filtered, and the solution was concentrated to give a solid. An aqueous ethanol (1:1) solution of the solid was passed through a Dowex 1×2 column (TsO$^-$ form, 200 ml, 200—400 mesh, pretreated with aqueous ethanol (1:1)) with the same solvent mixture. Concentration of the diacetyl-positive fractions gave a solid[11] of bis(*p*-toluenesulfonate) of **1**, 1.31 g (88%), $[\alpha]_D^{25}$ −48° (*c* 1, methanol); IR(KBr): 1670 cm^{-1}.

^{1}H-NMR (D_2O at 25 °C): δ 1.22 (3H d, J=6.5 Hz, CCH_3), 2.37 (6H s, CH_3 of TsOH), 3.10 and 3.21 (each ≈1.5 H s, NCH_3); at 80 °C: δ 1.32 (3H d), 2.47 (6H s), 3.25 (3H s, NCH_3).

Found: C, 47.36; H, 5.98; N, 8.64; S, 6.47%. Calcd for $C_{28}H_{45}N_7O_{14}\cdot 2C_7H_8O_3S\cdot H_2O$: C, 47.32; H, 5.96; N, 9.20; S, 6.01%.

2″-N-(Phenoxycarbonyl)-3′,3′$_a$:4″,6″-bis(O-p-methylbenzylidene)dihydrostreptomycin (2). Anhydrous *p*-toluenesulfonic acid (95 mg) and *p*-tolualdehyde dimethyl acetal (1.85 ml, ≈10 mol eq for **1**) were added to a solution of well dried crude **1** (Solid A, 874 mg) in dry DMF (9 ml, dried over molecular sieves 4A), and the solution was kept at room temperature for 1 h. On TLC with benzene–pyridine–ethanol–water–acetic acid (6:3:3:1:0.5) the solution showed a strong spot at R_f 0.47 with a slight spot at R_f 0.2 (mono(*p*-methylbenzylidene) products) (*cf* **1**, R_f 0.1). Triethylamine (0.08 ml) was added and the solution was concentrated *in vacuo* to give a syrup. The chloroform solution of the syrup was washed with saturated aqueous sodium hydrogencarbonate (10 ml) and saturated aqueous sodium chloride and dried over sodium sulfate. Concentration gave a residue, which was dissolved in acetone (10 ml). After filtration, the acetone solution was treated with ether and the precipitate was thoroughly washed with ether. The solid (980 mg) was passed through a Dowex 1×2 column (TsO$^-$ form, 50 ml) with aqueous ethanol (1:3) as a developer. The fractions containing **2** were collected and concentrated to give a solid, which was extracted with chloroform (*cf.* hydrochloride of **2** did not dissolve in chloroform). The chloroform solution was washed with water which dissolved the mono(*p*-methylbenzylidene) products. After being dried over sodium sulfate, the chloroform solution was concentrated to give a solid. The solid, after being dried well *in vacuo*, was suspended in hot water (0.5 ml) and stirred vigorously. After cooling, the suspension was filtered and the solid was again treated similarly and dried to give **2** as the bis(*p*-toluenesulfonate). Slight occlusion of chloroform was removed by this procedure. Yield, 980 mg (75%, based on DHSM·3HCl·H_2O), $[\alpha]_D^{25}$ −52° (*c* 1, chloroform); IR(KBr): 1670 cm^{-1}.

^{1}H-NMR (CD_3OD): δ 1.28 and 1.40 (≈6:4 in strength, 3H in total, each d, J=6.5 Hz, CCH_3), 2.24 and 2.31 (each s, 4:6 in strength, 3H in total, *p-methyl*benzylidene), 2.39 (9H s, CH_3 of Ts and *p-methyl*benzylidene). The peak of NCH_3 could not be discerned by overlapping with other signals.

Found: C, 54.85; H, 6.22; N, 7.76; S, 5.15%. Calcd for $C_{44}H_{57}N_7O_{14}\cdot 2C_7H_8O_3S\cdot H_2O$: C, 54.84; H, 5.95; N, 7.72; S, 5.05%.

In pyridine-d_5–D_2O (5:1 at 70 °C): δ 1.43 and 1.54 (≈6:4 in strength, CCH_3); 2.20 (≈7.2H s, CH_3 of Ts and a part of *p-methyl*benzylidene), 2.32 (≈4.8H s, *p-methyl*benzylidene); 3.43 and 3.58 (each s, in the ratio of 4:6, 3H in total, NCH_3).

An aqueous ethanol (1:3) solution of the above toluenesulfonic acid salt of **2** (190 mg) was passed through a Dowex 1×2 column (Cl$^-$ form, 5 ml) with the same aqueous ethanol to give dihydrochloride of **2**, 143 mg (96%), R_f 0.37 on TLC with benzene–ethanol–pyridine–water–acetic acid 6:3:3:1:0.5 (*cf.* bis(*p*-toluenesulfonate) of **2**: 0.47) $[\alpha]_D^{25}$ −55° (*c* 1, methanol).

^{1}H-NMR (pyridine-d_5–D_2O 5:1 at 70 °C): δ 1.41 and 1.50 (≈6:4, CCH_3); 2.18 (≈1.2H s) and 2.28 (≈4.8H s) (*p-methyl*benzylidene); 3.43 and 3.60 (each s, 4:6 in strength, 3H in total, NCH_3).

Found: C, 52.43; H, 5.96; N, 9.33 Cl, 7.77%. Calcd for $C_{44}H_{57}N_7O_{14}\cdot 2HCl\cdot H_2O$: C, 52.90; H, 6.15; N, 9.82; Cl, 7.10%.

2″-N:3″-O-Carbonyl-3′,3′$_a$:4″,6″-bis(O-p-methylbenzylidene)-dihydrostreptomycin (3). Fresh potassium *t*-butoxide (110 mg, ≈3.3 mol eq for **2**) was added under nitrogen atmosphere to an ice-cold solution of bis(*p*-toluenesulfonate) of **2**, (380 mg) in dry DMF (3.8 ml), and the solution was kept in the cold for 20 min. *p*-Toluenesulfonic acid monohydrate (190 mg) in ethanol (1 ml) was added and the solution was concentrated *in vacuo*. The chloroform (20 ml) solution of the residue was washed successively with saturated aqueous sodium hydrogencarbonate, water, 40% aqueous sodium *p*-toluenesulfonate and water, dried over sodium sulfate and concentrated. Ether was added to the chloroform (3 ml) solution of the residue, and the resulting precipitate was washed thoroughly with ether to give a solid of bis(*p*-toluenesulfonate), which was further washed with water thoroughly as described for **2** and dried. Yield, 311 mg (88%), $[\alpha]_D^{25}$ −63° (*c* 1, chloroform); IR(KBr): 1770 (cyclic carbamate), 1680 cm^{-1}.

^{1}H-NMR (pyridine-d_5–D_2O 5:1 at 70 °C): δ 1.3—1.6 (two kinds of d, 3H in total, J=6.5 Hz, CCH_3); 2.22 (6H

s, CH_3 of Ts), 2.27 and 2.30 (6H in total, *p-methyl*benzylidene); 2.78 and 3.11 (each s, 4:6 in strength, 3H in total, NCH_3).

Found: C, 52.83; H, 5.88; N, 8.02; S, 5.34%. Calcd for $C_{38}H_{51}N_7O_{13}\cdot 2C_7H_8O_3S\cdot H_2O$: C, 53.10; H, 5.91; N, 8.34; S, 5.45%.

Dihydrochloride of **3** was prepared by passing the aqueous methanol (1:9) solution of bis(*p*-toluenesulfonate) (181 mg) of **3** with a column of Dowex 1×2 (Cl^- form, 5 ml, 200—400 mesh). Yield, 136 mg (97%).

^{1}H-NMR (pyridine-d_5–D_2O 5:1): δ 1.47 (3H, CCH_3); 2.28 and 2.30 (6H, each s, *p-methyl*benzylidene); 2.90 and 3.20 (each s, 4:6 in strength, 3H in total, NCH_3).

Found: C, 50.41; S, 5.96; N, 10.58; Cl, 7.95%. Calcd for $C_{38}H_{51}N_7O_{13}\cdot 2HCl\cdot H_2O$: C, 50.44; H, 6.13; N, 10.84; Cl, 7.84%.

*2″-N:3″-O-Carbonyl-2,5,6-tris(*O*-tetrahydropyran-2-yl)-3′,3′ₐ:4″,6″-bis(*O*-p-methylbenzylidene)dihydrostreptomycin (**4**).* Fuse-dried anhydrons *p*-toluenesulfonic acid (12 mg) and freshly distilled 3,4-dihydro-2*H*-pyrane (0.8 ml) were added to a solution of bis(*p*-toluenesulfonate) of **3** (235 mg, dried at 60° *in vacuo*) in 1,2-dichloroethane (4 ml, after distillation the solvent was dried over molecular sieves 4A activated at 350 °C under a stream of nitrogen). The solution was kept at room temperature for 10 min. Triethylamine (0.02 ml) was added and the solution was poured into saturated aqueous sodium hydrogencarbonate (3 ml) with vigorous stirring. The lower layer separated was washed with 40% aqueous sodium *p*-toluenesulfonate and water, dried over sodium sulfate and concentrated. The syrup was triturated with cyclohexane to give a solid, which was thoroughly washed with cyclohexane. On TLC with chloroform–methanol–pyridine (5:1:0.2), the solid showed one spot (R_f 0.68) which was negative for diacetyl-coloration. The solid was dissolved in 1.5 M ethanolic ammonia (8 ml), heated at 70 °C for 1.5 h and concentrated. On TLC with the same solvent mixture as described above, the residue showed a diacetyl-positive spot at R_f 0.27. The chloroform solution of the residue was washed with 40% aqueous sodium *p*-toluenesulfonate, water, dried over sodium sulfate and concentrated. The residue was successively treated with chloroform, ether and water as described for **3** to give a solid of bis(*p*-toluenesulfonate), 240 mg (84%), $[\alpha]_D^{25}$ −42° (*c* 1, chloroform); IR(KBr): 1770, 1670 cm^{-1}.

^{1}H-NMR (CD_3OD): δ 1.1—2.0 (21H, CCH_3 and H-3,4,5 of THP).

Found: C, 56.38; H, 6.38; N, 6.88; S, 4.29%. Calcd for $C_{53}H_{75}N_7O_{16}\cdot 2C_7H_8O_3S\cdot H_2O$: C, 56.33; H, 6.56; N, 6.86; S, 4.49%.

*2″-N:3″-O-Carbonyl-2,5,6-tris(*O*-tetrahydropyran-2-yl)-3′,3′ₐ:4″,6″-bis(*O*-p-methylbenzylidene)-1,3-di-*N*^{G}-tosyldihydrostreptomycin (**5**).* Dry toluene (1 ml) was added to a solution of bis(*p*-toluenesulfonate) (144 mg) of **4** in dry DMF (4.5 ml), and the mixture was concentrated *in vacuo* to a volume of ≈4 ml. After ice-cooling, 50% oily sodium hydride (net 12 mg) was added and the mixture was stirred under an atmosphere of nitrogen for 1 h in the cold. *p*-Toluenesulfonyl chloride (42 mg) was added, stirring being continued for 1 h. The mixture was poured into phosphate buffer (pH 7, 10 ml) and the whole mixture was extracted with chloroform. The organic solution was washed with saturated aqueous sodium hydrogencarbonate and water, dried over sodium sulfate and concentrated to give a solid. The solid was chromatographed on silica gel with chloroform–ethanol–pyridine (15:1:0.3). The fractions containing **5** were concentrated to give a solid, which was thoroughly washed with water to give diacetyl-negative product, 99 mg (71%), $[\alpha]_D^{25}$ −46° (*c* 0.5, chloroform); IR(KBr) (the figures in parenthesis are for **4**): 1770(1770), (1670), 1620(1630), 1540(1440), 1380(1380), 1260, (1180), 1130(1120), 1070 (1070), 1030(1030), 810(810) cm^{-1}.

Found: C, 57.50; H, 6.39; N, 6.88; S, 4.49%. Calcd for $C_{67}H_{87}N_7O_{20}S_2\cdot H_2O$: C, 57.78; H, 6.44; N, 7.04; S, 4.60%.

*2″-N-(Benzyloxycarbonyl)-2,5,6-tris(*O*-tetrahydropyran-2-yl)-3′,3′ₐ:4″,6″-bis(*O*-p-methylbenzylidene)-1,3-di-*N*^{G}-tosyldihydrostreptomycin (**6**).* A solution of **5** (278 mg) in a mixture of dioxane (18 ml) and 0.2 M aqueous sodium hydroxide (10 ml) was heated at 80 °C for 5 h. After being cooled to room temperature, benzyloxycarbonyl chloride (0.17 ml) was added and the mixture was stirred vigorously for 5 min. After 1 M aqueous ammonium hydroxide (2 ml) had been added (to decompose the reagent chloride) with subsequent stirring for 3 h, the mixture was concentrated and the residue was extracted with chloroform. The chloroform-soluble portion was chromatographed on silica gel (8.5 g) at first with chloroform–pyridine (50:1, 40 ml), then with chloroform–ethanol–pyridine (15:1:0.3) to give a solid, which was thoroughly washed with water and dried, 270 mg(90 %), $[\alpha]_D^{25}$ −50° (*c* 1, chloroform); IR(KBr): 1690, 1625, 1540, 1440, 1380, 1270, 1130, 1075, 1020, 810 cm^{-1}.

Found: C, 59.25; H, 6.47; N, 6.29; S, 4.12%. Calcd for $C_{74}H_{95}N_7O_{21}S_2\cdot H_2O$: C, 59.22; H, 6.51; N, 6.53; S, 4.27%.

*2″-N-(Benzyloxycarbonyl)-3″-O-(imidazolylthiocarbonyl)-2,5,6-tris(*O*-tetrahydropyran-2-yl)-3′,3′ₐ:4″,6″-bis(*O*-p-methylbenzylidene)-1,3-di-*N*^{G}-tosyldihydrostreptomycin (**7**).* To a solution of **6** (300 mg) in 1,2-dichloroethane (10 ml) were added 1,1′-thiocarbonyldiimidazole (270 mg) and imidazole (30 mg) and the solution was gently refluxed for 6 h under nitrogen atmosphere. Concentration by addition of dioxane gave a residue, which was suspended in water, agitated for 3 h (yellow color disappeared), and then filtered. The solid collected was dried and chromatographed on silica gel (6 g) with chloroform–ethanol–pyridine (15:1:0.3) to give a solid, which was dissolved in benzene. The solution was washed with water, dried over sodium sulfate, and after concentration to a small volume, cyclohexane was added to cause precipitation, 273 mg (86%), $[\alpha]_D^{25}$ −43° (*c* 1, chloroform); on TLC with chloroform–ethanol (15:1) it gave the same R_f value (0.5) with that of **6**; IR(KBr): 1700, 1625, 1540, 1440, 1390, 1320, 1280, 1225, 1130, 1080, 1030, 990, 810 cm^{-1}.

^{1}H-NMR (acetone-d_6–D_2O 8:1): δ 8.4—8.5 (1H, H-2 of imidazolyl group).

Found: C, 58.53; H, 6.06; N, 7.74; S, 5.80%. Calcd for $C_{78}H_{97}N_9O_{21}S_3$: C, 58.81; H, 6.14; N, 7.91; S, 6.04%.

*2″-N-(Benzyloxycarbonyl)-2,5,6-tris(*O*-tetrahydropyran-2-yl)-3′,3′ₐ:4″,6″-bis(*O*-p-methylbenzylidene)dihydrostreptomycin (**8**).* Benzyl alcohol (0.1 ml) and 50% oily sodium hydride (net 55 mg) were added to a solution of bis(*p*-toluenesulfonate) (285 mg) of **4** in dry dioxane (3 ml), and the mixture was stirred under nitrogen atmosphere at room temperature for 30 min. The solution was poured into cold water (4 ml) containing *p*-toluenesulfonic acid monohydrate (450 mg) and the mixture was extracted with chloroform. The chloroform solution was washed with aqueous 40% sodium *p*-toluenesulfonate solution (5 ml) and then with water, dried over sodium sulfate and concentrated. The residue was chromatographed on a silica gel (6 g) column firstly with chloroform (15 ml) and then with chloroform–ethanol (3:1). The diacetyl-positive fractions were concentrated and the chloroform solution of the residue was washed with aqueous 40% sodium *p*-toluenesulfonate, then with water, dried over sodium sulfate and concentrated. Addition of cyclohexane

to the concentrate gave a solid, which was thoroughly washed with water and dried well to give bis(*p*-toluenesulfonate) of **8**, 251 mg (82%), $[\alpha]_D^{25}$ −31° (*c* 1, chloroform).

Found: C, 57.84; H, 6.51; N, 6.19; S, 3.91%. Calcd for $C_{60}H_{83}N_7O_{17}\cdot 2C_7H_8O_3S\cdot H_2O$: C, 57.83; H, 6.62; N, 6.38; S, 4.17%.

*2″-N-(Benzyloxycarbonyl)-3″-O-mesyldihydrostreptomycin (**13**).* Methanesulfonyl chloride (0.072 ml, 8 mol equiv for **8**) was added to an ice-cold solution of bis(*p*-toluenesulfonate) (180 mg) of **8** in dry pyridine (1.8 ml), and the solution was kept at the temperature for 1 h, and then at room temperature for 1 h. After addition of water (0.03 ml) followed by standing for 1 h at room temperature, the solution was concentrated. Addition of water to the concentrate gave a thick syrup which was collected by centrifugation. Chloroform solution of the syrup was washed successively with water, saturated aqueous sodium hydrogencarbonate, 10% aqueous potassium hydrogensulfate, water, 40% aqueous sodium *p*-toluenesulfonate and water, centrifuged to remove accompanying water, and concentrated to give bis(*p*-toluenesulfonate) of 3″-*O*-mesylate (**9**), 197 mg. The solid (195 mg) was dissolved in 90% aqueous acetic acid (6 ml) heated at 55 °C for 3 h and the solution was concentrated with occasional addition of toluene to give a syrup. Addition of ether gave a crude solid of **13**, 135 mg, which showed, on TLC (benzene–pyridine–ethanol–water–acetic acid 6:3:3:1:0.5), spots at 0.4, 0.37, 0.18 (slight), 0.1 and 0.05 (very slight, 2″-*N*-(benzyloxycarbonyl)dihydrostreptomycin[3]). Since the appearance of multiple spots on TLC was suspected to be caused by the formation of salts of **13** with anions (possibly by *p*-toluenesulfonate and acetate anions), the crude **13** was transformed into acetic acid salt. The crude solid (134 mg) was passed through a column of Dowex 1×2 (AcO^- form, 4 ml, 200—400 mesh) with aqueous methanol (3:1). Concentration of the eluate gave a solid (104 mg) which on being subjected to TLC, showed spots at R_f 0.22 (slight), 0.18(minor), 0.1(major) and 0.05(very slight), the spots at R_f 0.4 and 0.37 (possibly caused by the *p*-toluenesulfonic acid salts) disappearing. The solid (103 mg) was then chromatographed (6 g silica gel) with chloroform–methanol–pyridine–25% aqueous acetic acid (6:3:4:1) and the fractions (38—53 ml) containing the major component (R_f 0.1) were collected and concentrated. The resulting residue was thoroughly washed with ether to give a solid, 48 mg, which was chromatographically pure and contained no *p*-toluenesulfonic acid as proved by the NMR spectrum. The solid (47 mg) was passed through a column of Dowex 1×2 (Cl^- form, 9 ml) with water. Concentration of the eluate (4—5.5 ml) gave the solid of dihydrochloride of **13**, 39 mg (38% based on **8**), $[\alpha]_D^{25}$ −69° (*c* 0.6, water). The solid showed the same R_f value (0.1) with that of acetic acid salt described above.

^{1}H-NMR (D_2O): δ 1.24 (3H d, *J*=6.5 Hz, CCH_3) [2″-*N*-(benzyloxycarbonyl)dihydrostreptomycin dihydrochloride (D_2O): 1.22], 3.10 (3H s, NCH_3) [3.06], 3.20 (3H s, SO_2CH_3), 5.38 (1H d, *J*=3 Hz, H-1″) [5.26]; on heating to 60 °C, all the above peaks of **13** became sharpened.

Found: C, 40.73; H, 5.91; N, 10.81%. Calcd for $C_{30}H_{49}N_7O_{16}S\cdot 2HCl\cdot H_2O$: C, 40.63; H, 6.02; N, 11.06%.

*2″-N-(Benzyloxycarbonyl)-3″-deoxy-1,3-di-N^G-tosyldihydrostreptomycin (**11**).* Tributylstannane (0.4 ml) was added to a solution of **7** (280 mg) in dry toluene (7 ml), and the solution was gently refluxed under nitrogen atmosphere for 2 h. Concentration gave a syrup which was thoroughly washed with cyclohexane. The resulting solid was dissolved in benzene, washed with water, dried over sodium sulfate and concentrated to give a solid, which gave, on TLC with chloroform–ethanol (15:1), the same R_f value (=0.5) as that of **6** or **7**. In the NMR spectrum no peak near δ 8.4—8.5 (see the description of **7**) was observed. The solid was chromatographed on silica gel (5.5 g) first with chloroform–pyridine (50:1, 20 ml) (to remove an impurity) and then with chloroform–ethanol–pyridine (15:1:0.3) to give crude **10**, 210 mg.

A solution of the crude **10** (180 mg) in aqueous acetic acid (1:9, 18 ml) was heated at 55 °C for 4 h, and then concentrated with addition of toluene to give a residue. The residue, on TLC with chloroform–methanol (3:1), gave spots at R_f 0.54(minor), 0.46(slight), 0.34(major, **11**), 0.16 (minor **12**) and 0.11 (minor, 1,3-di-*N*-tosylstreptidine). The mixture was chromatographed on silica gel (15 g) with chloroform–methanol (3:1) to give **11**, **12**, and 1,3-di-*N*-tosylstreptidine in amounts of 65, 13, and 10 mg, respectively. Ether was added to **11** dissolved in methanol to cause precipitation, 62 mg (40% based on **7**), $[\alpha]_D^{25}$ −35° (*c* 0.6, methanol); IR(KBr): 1680, 1625, 1580, 1540, 1440, 1400, 1260, 1130, 1075, 1030, 1010, 830, 810 cm^{-1}.

^{1}H-NMR (CD_3OD at 50 °C): δ 1.23 (3H d, *J*=6.5 Hz, CCH_3), 2.40 (6H s, CH_3 of Ts), 3.01 (3H s, NCH_3), 4.90 (1H d, *J*=3.5 Hz, H-1″), 5.17 (2H s, CO_2CH_2Ph), 5.23 (1H d, *J*=2 Hz, H-1′).

Found: C, 50.43; H, 5.88; N, 9.22; S, 6.31%. Calcd for $C_{43}H_{59}N_7O_{17}S_2\cdot H_2O$: C, 50.23; H, 5.98; N, 9.53; S, 6.24%.

*3″-Deoxydihydrostreptomycin (**14**).* A solution of **11** (28 mg) in methanol was passed through a column (0.5 ml) of Sephadex LH-20 with the aid of methanol and the eluate was concentrated to give a solid, which was thoroughly dried *in vacuo* at 50 °C. Ammonia (≈1.5 ml as the liquid) was introduced to a solution of the solid in THF (0.5 ml, freshly distilled over LAH) cooled at −50 °C, sodium metal (≈30 mg) being added to the solution. The resulting deep-blue solution was kept at the same temperature for 1 h. Methanol was added until the color disappeared and the solution was gradually warmed with gradual decrease in pressure. The methanol solution of the residue was filtered and the filtrate was concentrated. The strongly alkaline aqueous solution of the resulting syrup was charged on a column of Amberlite CG50 (NH_4^+ form 2.5 ml) and the column was washed with water (25 ml). The column was then washed with 0.5% aqueous ammonium carbonate until the eluate gave no flame reaction for sodium. The eluting solution was then replaced by 6% aqueous ammonium carbonate, when a diacetyl-positive product was eluted. The eluate was concentrated *in vacuo* with addition of water and dried to give a constant weight (≈11 mg). An aqueous solution of the solid almost free from ammonium carbonate was passed through a Dowex 1×2 column (OH^- form, 1 ml) with water, and the strongly alkaline, diacetyl-positive fractions were concentrated, after bubbling carbon dioxide for a while, to give a solid, 10 mg (53%), $[\alpha]_D^{25}$ −67° (*c* 1, water) (lit,[1] −85° as carbonate); $\Delta[M]_{TACu}$ −50° (*cf.* DHSM +970°, lit,[9] +1020°).

^{1}H-NMR (20% ND_3 in D_2O): δ 1.20 (3H d, *J*=6.5 Hz, CCH_3), 1.55 (1H q, *J* ≈12 Hz, H_{ax}-3″), 2.15 (1H double t, *J* ≈4.5, ≈4.5, 12 Hz, H_{eq}-3″), 2.31 (3H s, NCH_3), 2.71 (1H incomplete double t, *J* ≈4, ≈4, 12 Hz, H-2″), 5.05 (1H d, *J*=3.5 Hz, H-1″), 5.31 (1H d, *J*=1.5 Hz, H-1′).

Irradiation of H-1″ caused the signals of H-2″ to become double doublets (*J* ≈4.5 and 12 Hz). Irradiation of H_{ax}-3″ caused the signals of H-2″ and H_{eq}-3″ to become a narrow triplet, respectively.

Found: C, 40.15; H, 6.66; N, 13.87%. Calcd for $C_{21}H_{41}N_7O_{11}\cdot 2H_2CO_3$: C, 39.94; H, 6.56; N, 14.17%.

References

1) H. Sano, T. Tsuchiya, S. Kobayashi, M. Hamada, S. Umezawa, and H. Umezawa, *J. Antibiot.*, **29**, 978 (1976).
2) D. Ikeda, T. Tsuchiya, and S. Umezawa, *J. Antibiot.*, **25**, 741 (1972).
3) S. Umezawa, Y. Takahashi, T. Usui, and T. Tsuchiya, *J. Antibiot.*, **27**, 997 (1974).
4) Y. Takagi, O. Kawashima, T. Tsuchiya, H. Sano, and S. Umezawa, *Bull. Chem. Soc. Jpn.*, **49**, 3108 (1976).
5) S. Umezawa, Abstr. of Papers, Symp. on Aminocyclitol Antibiotics, ACS/CSJ Chemical Congress, Honolulu, Hawaii, CARB 1 (1979); ACS Symposium Series 125, pp. 15—41 (1980).
6) S. Umezawa, Y. Takagi, and T. Tsuchiya, *Bull. Chem. Soc. Jpn.*, **44**, 1411 (1971).
7) T. Tsuchiya, I. Watanabe, M. Yoshida, F. Nakamura, T. Usui, M. Kitamura, and S. Umezawa, *Tetrahedron Lett.*, **1978**, 3365.
8) D. H. R. Barton and S. W. McCombie, *J. Chem. Soc., Perkin Trans. 1*, **1975**, 1574.
9) C. B. Barlow and L. Anderson, *J. Antibiot.*, **25**, 281 (1972).
10) T. Kishi, T. Tsuchiya, and S. Umezawa, *Bull. Chem. Soc. Jpn.*, **52**, 3015 (1979).
11) This product contained a small amount of sodium *p*-toluenesulfonate which was difficult to remove completely. This was confirmed by the flame reaction.

The Oligomerization and Co-oligomerization of Active Methylene Compounds and Isocyanides Catalyzed by Octaisocyanidedicobalt[1)]

Yasuhiro YAMAMOTO* and Hiroshi YAMAZAKI

The Institute of Physical and Chemical Research, Wako, Saitama 351

(Received June 30, 1980)

The reactions of RNC with $CH_2R^1R^2$ (R=2,6-$Me_2C_6H_3$; R^1, R^2=COOMe, COOEt, CN) in the presence of $Co_2(RNC)_8$ or $Co_2(CO)_8$ gave cyclic compounds in a 4:1 molar ratio. $Co_2(RNC)_8$ also catalyzed $CH_2(CN)_2$ to give a pyridine derivative.

Octacarbonyldicobalt has been widely used as a precursor of the catalyst of the hydroformylation of olefins and the carbonylation of various unsaturated organic compounds.[2)] Recently we have reported the synthesis and characterization of $Co_2(RNC)_8$, by analogy with $Co_2(CO)_8$.[3)] From the versatile reactivities of $Co_2(CO)_8$, one can expect catalytic actions similar to those of the corresponding isocyanide complexes. In fact, we established the hydrogenation of acetylene and the co-oligomerization of acetylene or azobenzene with isocyanide, catalyzed by $Co_2(RNC)_8$.[4,5)]

The compounds with an active methylene group, such as the malonic ester, malononitrile, and the cyanoacetic ester, have become keystones for syntheses of a heterocyclic system.[6)] Saegusa *et al.* reported that the reactions of *t*-butyl isocyanide with active methylene compounds gave three substituted olefins in the presence of Cu_2O (Eq. 1).[7)]

$$CH_2XY + t\text{-BuNC} \longrightarrow XYC{=}CHNHBu\text{-}t \quad (1)$$

Sawai and Takizawa have described producing a 2:1 cyclic adduct consisting of RNC and CH_2XY by the reactions of isocyanide–mercury(II) chloride complex with active methylene compounds in the presence of Et_3N (Eq. 2).[8)]

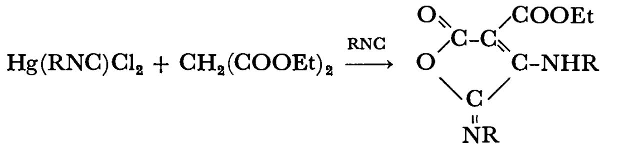

(2)

We wish here to report on cyclo-cooligomerization reactions between CH_2XY and RNC and on the oligomerization of an active methylene compound in the presence of a catalytic amount of $Co_2(RNC)_8$.

Results and Discussion

A mixture of $CH_2(COOMe)_2$, 2,6-$Me_2C_6H_3NC$, and $Co_2(2,6\text{-}Me_2C_6H_3NC)_8$ was heated in toluene at 120—125 °C.[9)] The subsequent chromatography of the mixture on alumina gave two compounds: a reddish brown compound **1a**, formulated as $(C_9H_9N)_4(C_4H_4O_3)$ from the mass spectrum, M^+ 624 (624.75), and brown crystals, **2**, with the empirical formula of $(C_6H_6N)_6$. Compound **2** was identical with the compound obtained from the oligomerization of 2,6-xylyl isocyanide with $HgCl_2$ by Sawai and Takizawa.[10)] The infrared spectrum of **1a** showed an absorption at 3403 cm^{-1} due to a NH group, two bands at 1712 and 1688 cm^{-1} due to the carbonyl groups, and two broad bands at 1616 and 1593 cm^{-1} due to the C=N groups. The ^1H NMR spectrum showed four singlets, at δ 1.90, 2.03, 2.19, and 2.39, due to the *o*-methyl groups, a singlet at δ 3.21 due to a methoxycarbonyl group, and a broad signal at δ 4.91 due to a NH group. These spectral characteristics suggest a cyclic imino derivative. The other derivatives **1b** and **1c** were also prepared from the reaction of $CH_2(COOEt)_2$ with 2,6-xylyl isocyanide, or from that of $CH_2(COOMe)_2$ with *o*-tolyl isocyanide in the presence of $Co_2(CO)_8$, respectively. However, a similar reaction with *t*-butyl isocyanide led to the recovery of the starting material without undergoing a cyclic cooligomerization.

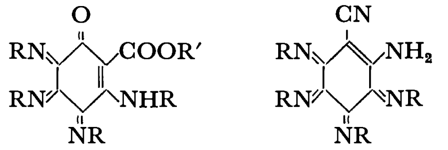

1 **3**

a R=2,6-$Me_2C_6H_3$, R′=Me
b R=2,6-$Me_2C_6H_3$, R′=Et
c R=4-MeC_6H_4 R′=Me

When malononitrile was treated with 2,6-xylyl isocyanide at 120—125 °C in the presence of $Co_2(2,6\text{-}Me_2C_6H_3NC)_8$ or $Co_2(CO)_8$, two compounds, **3** and **4**, were isolated as brown and pale yellow crystals respectively. Compound **3** was formulated as a 1:4 adduct of malononitrile and 2,6-xylyl isocyanide. The infrared spectrum showed the presence of the C≡N, C=N, and NH groups. The ^1H NMR spectrum showed four bands, at δ 1.90, 2.01, 2.23, and 2.44, due to the ortho-methyl groups and a broad singlet at δ 4.67 due to the NH group. Compound **4** was a trimer of malononitrile and was identified as 4-cyanomethyl-2,6-diamino-3,5-dicyanopyridine by a comparison of its infrared and UV spectra with those of an authentic sample.[6)] When the reactions were carried out in the absence of isocyanide, a trimerization of malononitrile occurred to give **4**. The results are listed in Table 1. The reaction of 2,6-xylyl isocyanide with methyl cyanoacetate in the presence of $Co_2(2,6\text{-}Me_2C_6H_3NC)_8$ gave a yellow compound consisting with the formula of $(C_9H_9N)_4(NCCH_2COOCH_3)$, **5**. The infrared spec-

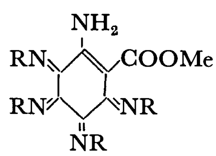

5

R=2,6-$Me_2C_6H_3$

trum showed the presence of the NH and methoxy-

TABLE 1. TRIMERIZATION OF MALONONITRILE

Catalyst[a)]	Temp/°C	Time/h	Yield/%
$Co_2(2,6\text{-}Me_2C_6H_3NC)_8$	r.t.	15	0
$Co_2(2,6\text{-}Me_2C_6H_3NC)_8$	80	2	51
$Co_2(t\text{-}BuNC)_5Co(CO)_4$[b)]	80	2	56
$Co_2(2,6\text{-}Me_2C_6H_3NC)_8$	120	1	65
$Co_2(2,6\text{-}Me_2C_6H_3NC)_8$[c)]	120	1.5	73

a) Catalyst: 0.15 mmol. $CH_2(CN)_2$; *ca.* 13 mmol. b) *t*-BuNC (0.3 mmol) was added. c) 2,6-$Me_2C_6H_3NC$ (0.2 mmol) was added.

carbonyl groups, but the absence of the C≡N group. The ^1H NMR spectrum showed four bands, at δ 2.01 (bs, 2-CH_3), 2.12 (s, CH_3), and 2.23 (s, CH_3) due to the ortho-methyl groups, a singlet at δ 3.83 due to the methoxycarbonyl group, and a broad signal at δ 3.55(2H) due to the NH groups. The treatment of methyl cyanoacetate with $Co_2(2,6\text{-}Me_2C_6H_3NC)_8$ in the absence of 2,6-xylyl isocyanide gave a dimer, **6**, and a trimer, **7**, of methyl cyanoacetate in low yields. The dimer, **6**, was identified as a tetrasubstituted olefin; it is obtained from methyl cyanoacetate and bases. The trimer, **7**, was tentatively identified as a pyridine derivative by a comparison of its UV spectrum with that of **4**.

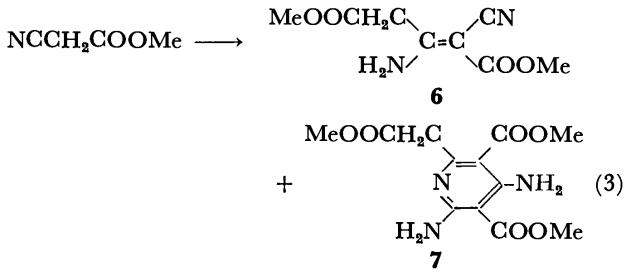

6

7

(3)

The initial step of the co-oligomerization is probably the formation of $HCo(RNC)_4$ and $R^1R^2HCCo(RNC)_4$ by a cleavage of the metal-metal bond, followed by a successive insertion of isocyanide molecules into a carbon-metal bond. The step-by-step insertion of isocyanide has been explored in various alkyl metal complexes.[11)] The intermediates, **10** and **11**, are generated by a nucleophilic attack of a tertiary carbon on the cobalt atom, accompanied by ring closure through an elimination of ROH or a transfer of hydrogen onto the cyano group. The resulting tetraimino cyclic intermediates are reduced with the $HCo(RNC)_4$ formed in the initial step. Thus, the reactions are achieved by a transfer of hydrogen to an imino nitrogen. The $Co_2(RNC)_8$ reformed in these reactions again undergoes a cleavage of a metal-metal bond, and the catalytic cycle is complete. Pyridine derivatives are probably formed by a transformation similar to that of the base-promoted reaction of active methylene compounds.[6)]

Experimental

The reactions were carried out under an atmosphere of nitrogen. The melting points are uncorrected. The IR spectra were recorded with a Shimadzu IR-27G spectrometer. The NMR spectra were measured with a JEOL C-60HL

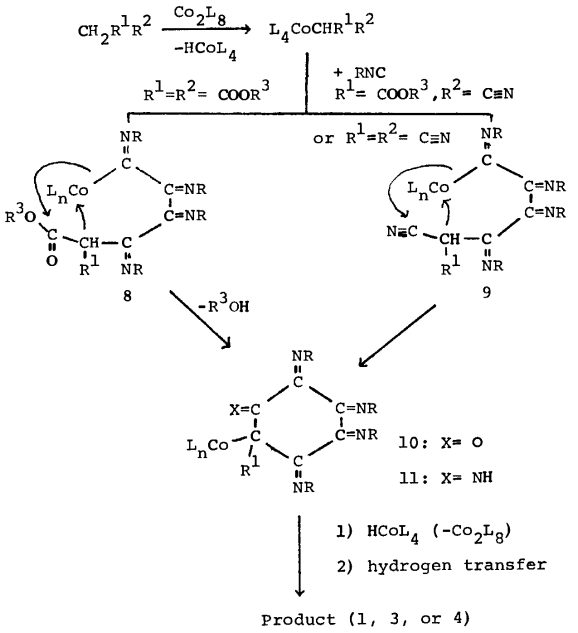

Scheme 1. Possible path for the formation of tetraiminocyclic compounds.

apparatus. The mass spectra were measured on a JEOL Type JPS-1S mass spectrometer with a directinlet system. The isocyanides were prepared according to the literature.[12)] The $Co_2(CO)_8$[13)] and $Co_2(RNC)_8$[3)] were prepared by procedures described in the ilterature.

Reactions of Isocyanides with Active Methylene Compounds. Some representative examples will be described below.

Reaction of 2,6-Xylyl Isocyanide with Dimethyl Malonate. A mixture of 2,6-$Me_2C_6H_3NC$ (0.21 g, 1.6 mmol), $CH_2(COOMe)_2$ (1.3 g, 10 mmol), and $Co_2(2,6\text{-}Me_2C_6H_3NC)_8$ (0.16 g, 0.10 mmol) in toluene (10 ml) was heated at 120—125 °C for 4 h. The solvent was then removed *in vacuo*, and the residue was chromatographed on alumina. Compounds **1a** (0.12 g, 48%) and **2** (0.07 g, 7%) were isolated by using benzene or benzene–CH_2Cl_2 (10:1) respectively as the eluents. **1a** (mp 244—246 °C). Found: C, 76.35; H, 6.43; N, 8.95%. Calcd for $C_{40}H_{40}N_4O_3$: C, 76.89; H, 6.45; N, 8.87%. By using an analogous procedure except for the use of $Co_2(CO)_8$ instead of $Co_2(RNC)_8$, the following compounds were prepared.

1b (51%, mp 247—248 °C). NMR ($CDCl_3$): δ 1.20 (t, 3.5 Hz, Me), 1.87, 2.02, 2.19, 2.38 (s, *o*-Me), 3.71 (q, 3.5 Hz, CH_2), 4.89 (b, NH), and 6.5—7.3 (c, aromatic protons). IR (KBr): 3398 (NH), 1713, 1689, 1676, 1615, and 1591 (C=O and C=N) cm^{-1}. Mass: 638 (668.78). Found: C, 77.04; H, 6.63; N, 8.77%. Calcd for $C_{41}H_{42}N_4O_3$: C, 77.09; H, 6.63; N, 8.77%. **1c** (43%, mp 186—188 °C). IR (KBr): 3498 (NH), 1740, 1693, 1625, and 1598 (C=O and C=N) cm^{-1}. Mass: 568 (568.65). Found: C, 76.32; H, 5.76; N, 9.98%. Calcd for $C_{36}H_{32}N_4O_3$: C, 76.03; H, 5.67; N, 9.85%.

Reaction of 2,6-Xylyl Isocyanide with Malononitrile. A mixture of $Co_2(CO)_8$ (0.035 g, 0.1 mmol) and 2,6-xylyl isocyanide (0.21 g, 1.6 mmol) was stirred in toluene (10 ml) at reflux. After 0.5 h, $CH_2(CN)_2$ (0.7 g, 10.6 mmol) was added to the solution. After the reaction was over (2 h), the resulting solids, **4** (0.03 g, 13%), identified as 4-cyanomethyl-2,6-diamino-3,5-dicyanopyridine, were removed by filtration. The orange-brown solution was chromatographed on alumina, CH_2Cl_2 being used as the eluent. The subsequent removal of the solvent and crystallization

of the residue from benzene–hexane gave **3** (0.1 g, (42%), mp 265 °C) as brown crystals. NMR ($CDCl_3$): δ 1.90, 2.01, 2.23, 2.44 (s, *o*-CH_3), 4.67 (b, NH_2), and 6.5—7.4 (c, aromatic protons). IR (KBr): 3310 (NH), 2195 (C≡N), 1625, 1610, and 1590 (C=N) cm^{-1}. Mass: 590 (590.78). Found: C, 79.27; H, 6.46; N, 14.43%. Calcd for $C_{39}H_{38}N_6$: C, 79.26; H, 6.48; N, 14.23%.

5 (45%, mp 203—204 °C) was obtained from 2,6-Me_2-C_6H_3NC (0.22 g), methyl cyanoacetate (0.5 g), and $Co_2(CO)_8$ (0.04 g). IR (KBr): 3350 (NH), 1755, 1740, 1623, and 1595 (C=O and C=N) cm^{-1}. Mass: 623 (623.77). Found: C, 76.80; H, 6.65; N, 11.09%. Calcd for $C_{40}H_{41}N_5O_2$: C, 77.02; H, 6.46;, N, 10.95%.

Oligomerization of Methyl Cyanoacetate. A mixture of $CH_2(CH)$ (COOMe) (0.5 g, 5.0 mmol) and Co_2[2,6-$Me_2C_6H_3NC]_8$ (0.2 g, 0.17 mmol) in toluene was stirred in toluene (10 ml) at reflux for 2 h. The solvent and the unreacted ester were then removed *in vacuo*. The residue was chromatographed on alumina, CH_2Cl_2–benzene and CH_2Cl_2 being used as the eluents. The dimer, **6** (0.03 g, 12%), from the first band was isolated. The product, **7**, from the second band was a trimer (0.01 g, (6%), mp 114—119 °C). IR (KBr): 3510, 3430 (NH), 1735, 1683, 1632, 1586, and 1538 (C=O and C=N) cm^{-1}. Mass: 297 (297.26). UV (CH_3OH): λ_{max} 244 (ε 8400), 260 (ε 7300), and 324 (ε 2800). Found: C, 48.15; H, 5.03; N, 13.78%. Calcd for $C_{12}H_{15}N_3O_6$: C, 48.48; H, 5.09; N, 14.14%.

Support of this research by Scientific Research Grant No. 264162, from the Ministry of Education is gratefully acknowledged (Y. Y.).

References

1) This paper is Part IV in the series "Organic Synthesis by Low-valent Isocyanide Complexes." Part I; Y. Yamamoto and N. Hagihara, *Bull. Chem. Soc. Jpn.*, **42**, 2077 (1969). Part II; Y. Yamamoto and H. Yamazaki, *Synthesis*, **1976**, 750. Part III; Y. Yamamoto and H. Yamazaki, *J. Org. Chem.*, **42**, 4136 (1977).

2) For example: J. Falbe, "Carbon Monoxide in Organic Synthesis," Springer Verlag, West Berlin (1970).

3) Y. Yamamoto and H. Yamazaki, *Inorg. Chem.*, **17**, 3111 (1978).

4) Y. Yamamoto and H. Yamazaki, *J. Organomet. Chem.*, **137**, C31 (1977).

5) Y. Yamamoto and H. Yamazaki, *J. Org. Chem.*, **42**, 4136 (1977).

6) A. J. Fatiadi, *Synthesis*, **1978**, 165 and 241.

7) T. Saegusa and Y. Itoh, *Synthesis*, **1975**, 298.

8) H. Sawai and T. Takizawa, *Chem. Pharm. Bull.*, **23**, 2842 (1975).

9) $Co_2(CO)_8$, instead of $Co_2(RNC)_8$, can be employed as a catalyst because it readily affords $Co_2(RNC)_8$ under these reaction conditions.[3]

10) H. Sawai and T. Takizawa, *Bull. Chem. Soc. Jpn.*, **49**, 1906 (1976).

11) Y. Yamamoto and H. Yamazaki, *Coord. Chem. Rev.*, **8**, 225 (1972).

12) H. M. Walborsky and G. E. Niznik, *J. Org. Chem.*, **37**, 187 (1972).

13) R. B. King, "Organometallic Syntheses," Academic Press, New York, N. Y. (1965), Vol. 1, p. 98.

The Addition of (Thioacyloxy)silanes to Carbonyl Compounds

Toyokazu Horii,* Shunichi Kawamura, Takeshige Nakabayashi, and Yasuo Abe
Radiation Center of Osaka Prefecture, Shinke-cho, Sakai, Osaka 593
(Received July 7, 1980)

The reactions of (thioacyloxy)silane (*O*-trimethylsilyl thioacetate and thiobenzoate) with some aldehydes (propionaldehyde, butylaldehyde, and benzaldehyde) gave *S*-(1-substituted alkyl) thioacetates (*S*-[1-(trimethylsilyloxy)propyl, and -butyl] thioacetates, and *S*-[α-(trimethylsilyloxy)benzyl] thioacetate), and the three corresponding thiobenzoates respectively. The reactions were catalyzed by 1,8-diazabicyclo[5.4.0]undec-7-ene(DBU), and also by its salt with thiobenzoic acid.

Trimethylsilylated thiols were recently disclosed to undergo a carbonyl-insertion reaction at their Si–S bonds under mild conditions and to be useful as protecting reagents of the carbonyl group.[1] Although the products formed by the trimethylsilylation of thio-

$$RCHO + R'S\text{-}Si(CH_3)_3 \longrightarrow RCH\begin{matrix}\diagup OSi(CH_3)_3\\ \diagdown SR'\end{matrix}$$

carboxylic acids have been reported to be (thioacyloxy)-silanes[2,3] with a Si–O bond, there have been only a few reports[2,4] concerning the reactions of these compounds. It is interesting to examine whether or

$$RCSH + (CH_3)_3SiX \xrightarrow[-XH]{} RCOSi(CH_3)_3$$
$$\quad\ \ \|\qquad\qquad\qquad\quad\ \ \|$$
$$\quad\ \ O\qquad\qquad\qquad\quad\ \ S$$

not carbonyl insertion at the Si–O bond of the (thioacyloxy)silane occurs.

In this paper, we wish to describe the reaction of (thioacyloxy)silanes(**1** and **2**) with aldehydes(**3a**—**c**), and the isolations, identification, and physical properties of the resulting adducts (**4a**—**c** and **5a**—**c**).

Results and Discussion

Thiocarboxylic acids are known[5] to react with aldehydes to produce the corresponding adducts, which are so stable as to be isolated even at room temperature. On the other hand, thioacetic acid–ketone adducts have been reported[6] to be present only at low temperatures, while over *ca.* −60 °C they are in fast equilibrium with the reactants:

$$RCHO + CH_3COSH \longrightarrow RCH\text{-}S\text{-}CCH_3$$
$$\qquad\qquad\qquad\qquad\quad\ \ |\quad\ \ \|$$
$$\qquad\qquad\qquad\qquad\quad OH\quad O$$

$$\text{Ketone} + CH_3COSH \xrightarrow{\text{at r.t.}} \text{No reaction.}$$

Trimethylsilylated compounds of these adducts are expected to be produced by the reaction of (thioacyloxy)silanes with carbonyl compounds.

Our preliminary studies indicated that (thioacyloxy)-silanes (**1** and **2**) react slowly at room temperature with several aldehydes to afford the corresponding

$$R\text{-}\underset{\|}{C}\text{-}OSi(CH_3)_3 + R'CHO \longrightarrow R\text{-}\underset{\|}{C}\text{-}S\text{-}\underset{|}{C}HR'$$
$$\quad\ \ S\qquad\qquad\qquad\qquad\quad\ \ O\quad\ OSi(CH_3)_3$$

1: R=CH_3 **3a—c** **4a—c**: R=CH_3
2: R=C_6H_5 **5a—c**: R=C_6H_5
a: R′=CH_3CH_2
b: R′=$CH_3CH_2CH_2$
c: R′=C_6H_5

adducts. In order to search for more appropriate conditions, *O*-trimethylsilyl thioacetate(**1**) and benzaldehyde(**3c**) were chosen as representative substances and were allowed to react in an NMR tube under several conditions; the progress was observed by monitoring the decrease in the ^1H NMR trimethylsilyl signal of the starting material(**1**) and the increase in that of the product(**4c**). The heating of equimolar amounts of **1** and **3c** at 115 °C for 6.5 h in an NMR tube resulted in the formation of the adduct(**4c**) (see Table 1). However, the reaction in the presence of a small amount (0.03 equiv) of DBU was completed within 15 min at room temperature. Also, by the addition of triethylamine, the reaction was accelarated to afford the adduct in an 82% yield after 4 h. These results show that catalytic amounts of the amines accelerate the present reaction.

Thus, a series of thiocarboxylates(**4a**—**c** and **5a**—**c**) were synthesized by the addition of a small amount (*ca.* 0.03 equiv) of DBU to an equimolar mixture of **1** or **2** and **3** at room temperature without a solvent. The yields and the properties of the products are

Table 1. Monitoring of the production of **4c** and **5b** in an NMR tube

Compd	Solvent	Catalyst	Temp °C	Time h	Yield[a] %
4c	No	No	r.t.	20	58
4c	No	No	115	6.5	46
4c	No	Et_3N[b]	r.t.	1	59
4c	No	Et_3N[b]	r.t.	4	82
4c	No	DBU[c]	r.t.	15 min	100[f]
5b	$CDCl_3$[d]	No	r.t.	20	No
5b	$CDCl_3$[d]	DBU·PhCOSH[e]	r.t.	1	100[g]

a) Indicating 100[**4c**/(**4c**+**1**)]% or 100[**5b**/(**5b**+**2**)]%, based on the peak heights[7] of the trimethylsilyl signals. b) 0.09 equiv. c) 0.03 equiv. d) Containing 0.5 mmol of **2** and 0.6 mmol of **3b** in 0.935 g of $CDCl_3$. e) 0.09 equiv. f), g) Disappearance of the **1** or **2** reactant respectively.

TABLE 2. YIELDS AND PHYSICAL AND ANALYTICAL DATA OF **4a—c** AND **5a—b**

Compd	Yield[a] %	Molecular distillation °C (mmHg)	Formula	Analysis (%)		NMR in CCl_4 δ/ppm	IR in CCl_4 ν/cm^{-1}
				Calcd	Found		
4a	60	40 (0.05)	$C_8H_{18}O_2SSi$	C, 46.56 H, 8.79 S, 15.54	46.26 8.97 15.32	0.12(s, $(CH_3)_3Si$, 9H) 0.97(t, J=7 Hz, CH_3, 3H), 1.77(qd, J=7 and 6 Hz, CH_2, 2H), 2.27(s, CH_3CO, 3H), 5.49(t, J=6 Hz, CH, 1H)	1665 1245
4b	65	40 (0.04)	$C_9H_{20}O_2SSi$	C, 49.05 H, 9.15 S, 14.55	48.83 9.33 14.10	0.11(s, $(CH_3)_3Si$, 9H), 0.95(t, J=6 Hz, CH_3, 3H), 1.1—1.8(m, CH_2CH_2, 4H), 2.25(s, CH_3, 3H), 5.54(t, J=6 Hz, CH, 1H)	1690 1252 847 740
4c	78	90 (0.1)	$C_{12}H_{18}O_2SSi$	C, 56.65 H, 7.13 S, 12.60	56.30 7.17 12.52	0.14(s, $(CH_3)_3Si$, 9H), 2.28(s, CH_3CO, 3H), 6.58(s, CH, 1H), 7.12—7.44(m, aromatic, 5H)	1685 1245
5a	70	120 (0.1)	$C_{13}H_{20}O_2SSi$	C, 58.16 H, 7.51 S, 11.94	57.80 7.58 11.76	0.15(s, $(CH_3)_3Si$, 9H), 1.03(t, J=7 Hz, CH_3, 3H), 1.89(qd, J=7 and 6 Hz, CH_2, 2H), 5.71(t, J=6 Hz, CH, 1H), 7.28—8.00(m, aromatic, 5H)	1655 1245
5b	79	120 (0.04)	$C_{14}H_{22}O_2SSi$	C, 59.53 H, 7.85 S, 11.35	59.71 7.99 11.06	0.14(s, $(CH_3)_3Si$, 9H), 0.97(t, J=7 Hz, CH_3, 3H), 1.3—2.0(m, CH_2CH_2, 4H), 5.78(t, J=6 Hz, CH, 1H), 7.28—8.00(m, aromatic, 5H)	1663 1253 848 740
5c	74	150 (0.04)	$C_{17}H_{20}O_2SSi$	C, 64.52 H, 6.37 S, 10.13	64.80 6.44 10.17	0.19(s, $(CH_3)_3Si$, 9H), 6.83(s, CH, 1H), 7.16—8.04(m, aromatic, 10H)	1665 1245

a) The values are isolated yields based on the aldehydes (**3a—c**) used.

summarized in Table 2.

The IR spectra of the products (**4a—c** and **5a—c**) showed strong absorption bands in the region of 1655—1690 cm^{-1} which were considered to be a characteristic of the carbonyl stretching mode. The results indicate that these products were not the thiocarboxylic *O*-ester (**9**), but the *S*-esters (**4** and **5**).

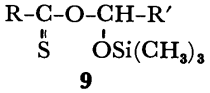

9

The present reaction was found to be catalyzed also by the salt (**10**). For example, the reaction of **2** with **3b** in chloroform-*d*, which did not proceed at room temperature even after 20 h in the absence of the catalyst, was completed within 1 h by the addition of traces of **10** prepared separately (see Table 1). Consequently, in the acceleration by DBU, the first step seems to involve the formation of the salt of DBU with thiocarboxylic acid, which may be present in traces as a hydrolysis-product of (thioacyloxy)-silane (**1** or **2**). As is shown in Scheme 1, the possible reaction mechanism of the catalytic behavior of DBU or the salt (**10**) involves the carbonyl addition of $RCOS^-$, affording the resulting **11** in equilibrium concentrations; **11** is converted to the adduct (**4** or **5**) by the subsequent bimolecular silicon transfer. Similar schemes have been presented by Evans *et al.*[1] concerning the anion-catalyzed addition reactions of a variety of silicon derivatives to aldehydes and ketones, in which cases the catalysts were the potassium cyanide–crown ether complex, tetrabutylammonium cyanide, and tetrabutylammonium fluoride.

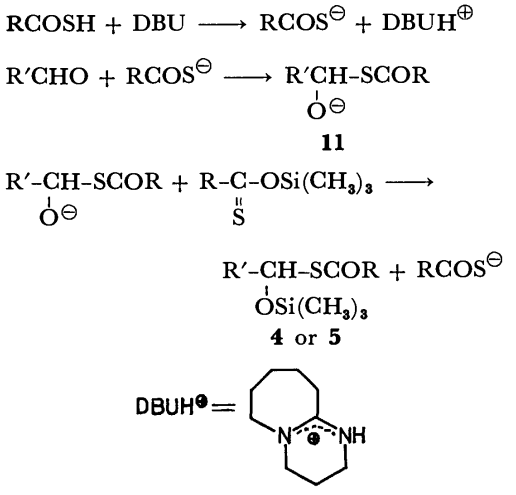

Scheme 1.

The additions of **1** or **2** to ketones, *i.e.*, acetophenone, acetone, or cyclohexanone, did not occur at high temperatures (70—115 °C) nor in the presence of a catalytic amount of DBU. However, in the presence of an equimolar amount of DBU, acetophenone reacted with **1** in benzene at room temperature to produce the corresponding *O*-silylated enolate in a 38% yield:

$$C_6H_5\overset{\overset{O}{\|}}{C}CH_3 + CH_3\overset{\overset{S}{\|}}{C}OSi(CH_3)_3 + DBU \longrightarrow C_6H_5\overset{\overset{OSi(CH_3)_3}{|}}{C}=CH_2 + DBUH^{\oplus}\ {}^{\ominus}S\overset{\overset{O}{\|}}{C}CH_3.$$

The lack of any production of the adducts of ketones seems to reflect the character of the adducts of thiocarboxylic acids to ketones.

Experimental

The NMR spectra were taken on a JEOL MH-100 spectrometer, using carbon tetrachloride as the solvent and tetramethylsilane as the internal standard, unless otherwise stated. The abbreviations in the NMR spectra are as follows: s, singlet; d, doublet; qd, quartet of doublets; m, multiplet. The infrared spectra were recorded on a JASCO IR-S or JASCO 701G spectrometer. The mass spectra were measured on a Shimadzu-LKB 9000 spectrometer. Alumina (M. Woelm, activity I) was used for the column chromatography.

Materials. The *O*-trimethylsilyl thioacetate (**1**) and thiobenzoate (**2**) were prepared by the method in the literature.[2] The DBU and aldehydes (**3a—c**) were commercially available, and the latter were used after distillation.

*General Procedure for the Preparations of **4a—c** and **5a—c**.* To a stirred mixture of 4.2 mmol of (thioacyloxy)silane (**1** or **2**) and 4 mmol of aldehyde (**3a—c**) we added one drop (0.1—0.15 mmol) of DBU. After about 15 min at room temperature, the mixture was dissolved in hexane and filtered through a short alumina column to remove any minor impurities. The subsequent removal of the solvent under a vacuum gave a colorless liquid, which was found to be pure **4a—c** or **5a—c** by NMR analyses. The samples obtained by molecular distillation were subjected to elemental analyses and spectral measurements (see Table 2).

*Preparation of DBU·PhCOSH Salt (**10**).* DBU (3.0 g, 20 mmol) was added dropwise to stirred solution of thiobenzoic acid (2.76 g, 20 mmol) in ether at room temperature. Stirring was then continued for an additional 1 h. The precipitate was collected by filtration and recrystallized from chloroform-ether to give the title compound (4.5 g) in a 75.5% yield; mp 116.5—117.5 °C; MS *m/e* 152 (DBU^+). 137 ($PhCOS^+$). Found: C, 66.26; H, 7.77; N, 9.55; S, 10.98%. Calcd for $C_{16}H_{22}N_2OS$: C, 66.17; H, 7.64; N, 9.65; S, 11.04%.

References

1) D. A. Evans, L. K. Truesdale, K. G. Grimm, and S. L. Nesbitt, *J. Am. Chem. Soc.*, **99**, 5009 (1977).

2) G. A. Gornowicz and J. W. Ryan, *J. Org. Chem.*, **31**, 3439 (1966).

3) S. Kato, W. Akada, M. Mizuta, and Y. Ishii, *Bull. Chem. Soc. Jpn.*, **46**, 244 (1973).

4) M. Mikolajczyk, P. Kielbasiński, and H. M. Schiebel, *J. Chem. Soc., Perkin Trans. 1*, **1976**, 564.

5) H. Böhme, H. Bezzenberg, M. Clement, A. Dick, E. Nurrnberg, and W. Schlephack, *Ann.*, **623**, 92 (1959).

6) T. Horii, S. Kawamura, and J. Tsurugi, *Bull. Chem. Soc. Jpn.*, **45**, 2200 (1972).

7) The intensities of sharp spectra which lie close together can be obtained more accurately by the measurement of the peak heights than by integration; "Jikken-kagaku Koza Zoku," ed by the Chemical Society of Japan, Tokyo (1967), Vol. 12, p. 552.

Mechanism of the Reaction of Nitriles with Alkaline Hydrogen Peroxide. Reactivity of Peroxycarboximidic Acid and Application to Superoxide Ion Reaction[1]

Yasuhiko SAWAKI and Yoshiro OGATA*

Department of Applied Chemistry, Faculty of Engineering, Nagoya University, Chikusa-ku, Nagoya 464

(Received July 14, 1980)

Formation of peroxycarboximidic acid (**1**) is not rate-determining in the reaction of nitrile with alkaline hydrogen peroxide to form amide and oxygen; the yield of amide based on H_2O_2 varies from 20 to 60%. When dimethyl sulfoxide (DMSO), a reactive substrate, is added, the rate is independent of [DMSO] and governed in turn by a rate-determining addition of HOO^- to nitrile. This reaction gives a reliable α-value of k_{HOO^-}/k_{HO^-}, which is 10000 for benzonitrile. A facile conversion of nitrile to amide may be achieved by the reaction in the presence of DMSO, unaccompanied by side reactions such as the epoxyamide formation from α,β-unsaturated nitrile. Kinetics and product analysis suggest that a predominant reaction is not a non-radical oxidation of H_2O_2 with **1** but a radical decomposition of H_2O_2 which is induced by the homolysis of anion of **1** (**1A**). No singlet oxygen could be trapped chemically. The reaction of superoxide ion, $O_2^{\cdot-}$, with acetonitrile is shown to be analogous to that of HOO^-; the decomposition of $O_2^{\cdot-}$ is fast in the presence of MeCN and DMSO in benzene, affording acetamide and dimethyl sulfone.

The reaction of nitrile with alkaline hydrogen peroxide is well documented[2,3] and the intermediate peroxycarboximidic acid (**1**) has been utilized as a convenient epoxidizing agent.[4,5] Because the reaction can be run under weakly basic conditions, the oxidant is useful for the epoxidation of olefins leading to acid-sensitive epoxides[4] or olefinic ketones susceptible to the Baeyer-Villiger reaction,[6] and also applicable to imines.[7] The reactivity of **1** is interesting in connection with these oxidations and with chemiluminescence from nitriles.[8,9]

$$RC{\equiv}N + H_2O_2 \xrightarrow{\text{base}} \underset{\displaystyle OOH}{\overset{\displaystyle |}{RC{=}NH}} \qquad (1)$$

1

The reaction has also been studied kinetically in relation to an α-effect of HOO^- nucleophile,[2,10,11] where a rate-determining step was assumed to be the addition of HOO^- to nitrile. By contrast, our previous study on the epoxidation of olefins with a mixture of nitrile and alkaline H_2O_2 showed that the epoxidation with **1** is rate-determining.[3] Here, we wish to report our mechanistic study on the formation and reaction of **1**, revealing that the formation of **1** becomes rate-determining in the presence of DMSO and that the oxidation of H_2O_2 with **1** is not important, no singlet oxygen being generated. The reaction of superoxide ion, $O_2^{\cdot-}$, with nitrile is also shown to be analogous to the case of HOO^-.

Results and Discussion

Stoichiometry. The stoichiometry for the reaction of nitrile with alkaline hydrogen peroxide was sometimes written as[2]

$$RCN + 2\,H_2O_2 \xrightarrow{HO^-} RCONH_2 + O_2 + H_2O. \qquad (2)$$

Table 1. Rates and product from the reaction of nitriles and alkaline hydrogen peroxide[a]

RCN	Solvent % MeOH	Base	% HOO^- [b]	Additive[c]	Rate/$M^{-1}\,s^{-1}$ [d]		Yield/%[e]	
					$10^2 k_{obsd}$	$10^2 k_{HOO^-}$	$RCONH_2$	Me_2SO_2
PhCN	75%	5 mM Na_3PO_4	10%		0.0031	(0.031)[d]	58	—
	75%	0.1 M NaOH	11%	f)	0.92	(8.4)	30	f)
	50%	0.01 M NaOH	23%		0.73	(3.2)	33	—
	50%	0.1 M NaOH	75%		8.6	(11.5)	25	g)
	75%	5 mM Na_3PO_4	10%	DMSO[h]	1.52[h]	15.2	88	86
	50%	0.01 M NaOH	23%	DMSO	2.40	10.4	64	65
	50%	0.1 M NaOH	75%	DMSO	9.0	12.0	35	24
$PhCH_2CN$	75%	5 mM Na_3PO_4	10%		0.125	(1.25)	58	—
	50%	0.01 M NaOH	23%		1.15	(5.0)	43	i)
	75%	5 mM Na_3PO_4	10%	DMSO	0.603	6.03	100	100
	50%	0.01 M NaOH	23%	DMSO	1.10	4.8	96	84

a) Reaction with 0.1 M RCN and 0.017 M H_2O_2 at 25 °C. b) % Dissociation of H_2O_2 into HOO^- as determined by UV absorbance at 280 nm (±3%). c) 0.1 M of DMSO. d) The rates were determined by iodometric titration of the remaining H_2O_2. The k_{HOO^-} value was calculated according to Eq. 5; the values in parentheses are shown to exemplify no constancy of the k_{HOO^-} value in the absence of DMSO. e) Yields were determinined by GLC and based on H_2O_2 consumed. f) When 0.04 M cumene was added, 3—6% of 2-phenyl-2-propanol was obtained. g) Oxygen was evolved in 60% yield. h) The k_{obsd} value was practically same (*i.e.*, 1.46 and 1.55) with 0.05 and 0.5 M DMSO. i) Benzaldehyde (1%) and benzyl alcohol (8%) were also detected by GLC.

However, the reaction is not so simple; the yields of amides based on H_2O_2 consumed vary in the range of 20—60% depending on the conditions and substrates (Table 1). A lower yield of amide was obtained at higher pH, perhaps suggesting a radical decomposition of H_2O_2 as discussed later.

On the other hand, the reaction in the presence of olefins was shown to have a simple stoichiometry affording a nearly quantitative yield of amide and epoxide by an ionic mechanism:[3]

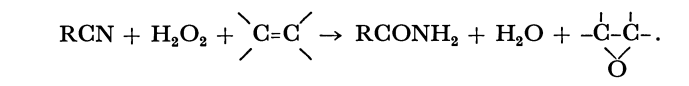

(3)

The same is true for the oxidation of dimethyl sulfoxide (DMSO) to sulfone in phosphate buffer, which shows the stoichiometry of reactant, RCN:H_2O_2:substrate= 1:1:1. The yields of amide and sulfone decrease at high alkanity, again suggesting an intervention of a radical decomposition of H_2O_2. The oxidation of sulfoxide to sulfone with alkaline H_2O_2 alone is ineffective in these protic solvents as reported previously.[12]

Kinetics. The reaction of nitrile with alkaline hydrogen peroxide has mostly been explained by a rate-determining addition of HOO^- to nitrile, the intermediary perimidic acid (**1**) being a potent oxidant capable of oxidizing H_2O_2 itself rapidly.[2,10,11] This explanation, however, contrasts with our previous observation[3] that the epoxidation of olefins with nitrile and alkaline H_2O_2 obeyed third-order kinetics:

$$v = k_4[\mathrm{RCN}][\mathrm{H_2O}][\mathrm{C{=}C}]. \quad (4)$$

Here, k_4 value was practically independent of $[HO^-]$ or $[HOO^-]$ at pH 10—12 in 75% MeOH; moreover, the consumption of H_2O_2 in the absence of olefin was very small (*i.e.*, mostly<2%). These results suggest that the rate-determining step is not the formation of **1** but the epoxidation with it.

To clarify this discrepancy, we reinvestigated the reaction of nitrile with alkaline H_2O_2 kinetically by following H_2O_2 iodometrically. As shown in Table 1, the reaction of nitrile with H_2O_2 changes with the kind and concentration of base; the resulting k_{HOO^-} value, calculated according to a rate equation 5, is far from constant.

$$v = k_{\mathrm{obsd}}[\mathrm{RCN}][\mathrm{H_2O_2}] = k_{\mathrm{HOO^-}}[\mathrm{RCN}][\mathrm{HOO^-}] \quad (5)$$

No constancy of k_{HOO^-} value indicates that the addition of HOO^- to nitrile is not rate-limiting in the reaction of nitrile and alkaline H_2O_2 alone.

When DMSO is added to the reaction mixture, the reaction is significantly accelerated under weakly alkaline conditions, the maximum being over one hundred times. In contrast to the case of olefin epoxidation (Eq. 4), the oxidation of DMSO to sulfone is independent of substrate concentration (see footnote h in Table 1) but dependent on $[HO^-]$ or $[HOO^-]$. Similar results were obtained for the case of acetonitrile, the $10^3 k_{\mathrm{obsd}}$ value being constant at $1.21 \pm 0.07\ M^{-1}\ s^{-1}$ with varying concentration of DMSO from 0.05 to 0.7 M MeCN in 75% MeOH containing 5 mM Na_3PO_4. The constancy of the k_{HOO^-} value in the presence of DMSO (Table 1) seems to be adequate in view of the accuracy in estimating $[HOO^-]$. Thus, the rate expression in the presence of DMSO is Eq. 5 where no term of [DMSO] is involved.

All of the above results may be well understood by the following scheme.

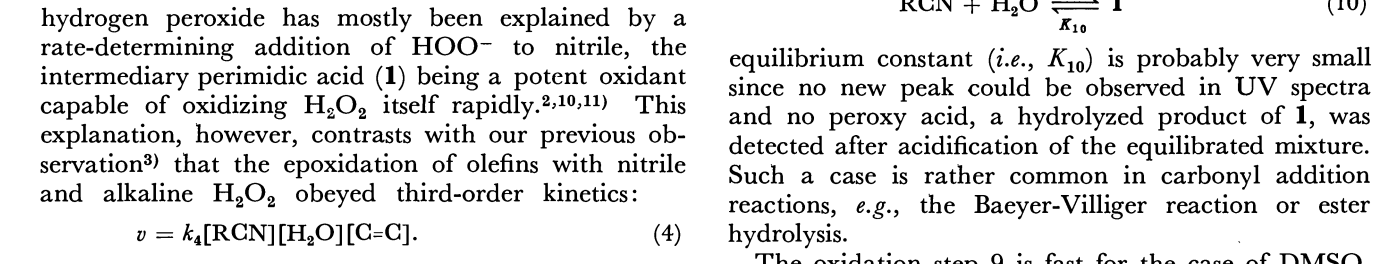

Here, k_7 equals k_{HOO^-} in Eq. 5. For olefin epoxidation, step 9 is rate-determining and preequilibrium reactions 6—8 are attained; the three equilibria could be simply written as Eq. 10, leading to the observed rate equation (Eq. 4) independent of pH. The magnitude of the

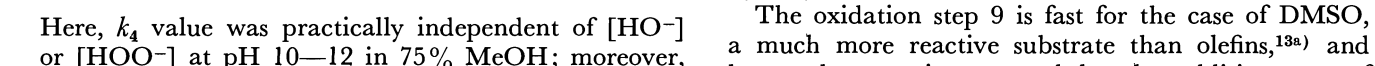

equilibrium constant (*i.e.*, K_{10}) is probably very small since no new peak could be observed in UV spectra and no peroxy acid, a hydrolyzed product of **1**, was detected after acidification of the equilibrated mixture. Such a case is rather common in carbonyl addition reactions, *e.g.*, the Baeyer-Villiger reaction or ester hydrolysis.

The oxidation step 9 is fast for the case of DMSO, a much more reactive substrate than olefins,[13a] and hence the rate is governed by the addition step of HOO^- to C≡N (step 7), thus being independent of [DMSO] as is observed. The apparent large solvent effect in k_{obsd} is due to the change in $[HOO^-]$ owing to the change in K_6 value. The constancy in k_{HOO^-} values was observed only for the DMSO oxidation, indicating the rate-determining addition of HOO^- to C≡N.

As for the reaction of nitrile with H_2O_2 alone, previous kinetics[2,10] were carried out at pH<10 and explained by assuming a rate-limiting addition of HOO^- to C≡N. This assumption is not substantiated by the fact that the k_{HOO^-} values are not constant and the reaction in the presence of olefin or sulfoxide is much faster under these weakly alkaline conditions. Thus, the preequilibrium 10 must be attained in the absence of added substrate. Then there might be a case where the oxidation of H_2O_2 with **1** occurs and determine the overall rate, requiring a rate expression: $v=k[\mathrm{RCN}][\mathrm{H_2O_2}]^2$ which was obtained by substituting $[H_2O_2]$ for [C=C] in Eq. 4. However, this case is not probable in view of the fact that the observed order in $[H_2O_2]$ is not second-order.[2,3,10] We ascertained this again; for example, the reaction of 0.05 M benzonitrile with 0.01 and 0.03 M H_2O_2 afforded $10^5 k_{\mathrm{obsd}}$ value of 0.36 and 0.34 $M^{-1}\ s^{-1}$, respectively, in the presence of 5 mM Na_2HPO_4 in 50% MeOH (1 M=1 mol dm^{-3}).

At high alkanity, *e.g.*, 0.1 M NaOH, the consump-

tion of H_2O_2 becomes independent of the presence of DMSO and the yields of amide and/or sulfone are low (*i.e.*, 20—30% based on H_2O_2 consumed). Moreover, the effect of EDTA is rather small at these higher alkaline concentrations. These facts suggest a radical decomposition of H_2O_2 induced by the homolysis of peroxyimidate ion **1A**.[13b]

$$\underset{\underset{\text{OOH}}{|}}{\text{RC=N}} \longrightarrow \text{R-C}\overset{\text{N}}{\underset{\text{O}}{\vdots}} + \text{HO}\cdot \qquad (11)$$

1A

$$\text{R'O}\cdot + \text{H}_2\text{O}_2 \longrightarrow \text{R'OH} + \text{HOO}\cdot \text{ (or } \text{H}^+ + \text{O}_2^{-}\text{)} \qquad (12a)$$

$$\text{HOO}\cdot + \text{O}_2^{-} \longrightarrow \text{HOO}^- + \text{O}_2 \qquad (12b)$$

$$\text{R'O}\cdot + \text{O}_2^{-} \longrightarrow \text{R'O}^- + \text{O}_2 \qquad (12c)$$

Here, R'O· is **2** or HO·. It is well known that the base-catalyzed decomposition of hydrogen peroxide is complex and sensitive to contaminating metal ions.[14a] Although many steps are involved in the radical decomposition of H_2O_2,[14b-d] a major step to produce oxygen is probably the reaction 12b or 12c; the pK_a value of HOO· being 4.85 in water.[14e]

Four lines of evidence were obtained for the intervention of radical decomposition of H_2O_2. First, the yield of amide or sulfone was sometimes as low as 20—30% on the basis of H_2O_2 consumed. Second, 2-phenyl-2-propanol (3—6%) was obtained when cumene was added (footnote f in Table 1), suggesting an initiation of radical autoxidation of added cumene. Third, the oxidation of 1,2-dimethylcyclohexene yielded, in addition to epoxide, products from its autoxidation as discussed later (Table 4). The fourth line of evidence for the homolysis of **1A** is the formation of benzyl alcohol and benzaldehyde from benzyl cyanide (footnote i in Table 1) (Eq. 13).

$$\text{PhCH}_2\text{CN} \xrightarrow{\text{HOO}^-} \underset{\underset{\text{OOH}}{|}}{\text{PhCH}_2\text{C=N}^-} \xrightarrow{-\text{HO}\cdot} \underset{\underset{\text{O}\cdot}{|}}{\text{PhCH}_2\text{C=N}^-}$$

3

$$\xrightarrow{-\text{OCN}^-} \text{PhCH}_2\cdot \xrightarrow{\text{O}_2} \longrightarrow \text{PhCH}_2\text{OH} + \text{PhCHO} \qquad (13)$$

Facile β-scission of benzyl radical is known.[15] Formation of benzaldehyde might be explained by a scheme *via* α-hydroperoxy nitrile;[9] but the base-catalyzed autoxidation of benzyl cyanide does not occur appreciably under these conditions. Thus, the evidence for the radical decomposition of H_2O_2 induced by the homolysis of **1A** seems to be convincing. A similar homolysis such as Eq. 11 was proposed in the reaction of nitriles with alkaline *t*-butyl hydroperoxide.[16]

On the basis of ^{18}O-tracer study yielding 81% of unscrambled oxygen, the reaction of **1** with HOO^- was proposed as a predominant pathway.[10a]

$$\text{RCN} + \text{HOO}^- \longrightarrow \mathbf{1} \xrightarrow{+\text{HOO}^-} \underset{\underset{\text{OOH}}{|}}{\overset{\overset{\text{NH}^-}{|}}{\text{R-C-OOH}}}$$

$$\longrightarrow \text{RCONH}_2 + \text{O}_2 + \text{HO}^- \qquad (14)$$

But this pathway can not be predominant since our kinetic data show that the formation of **1** is not rate-determining and, moreover, the overall rate is not governed by the reaction of **1** with HOO^- as discussed above. One possible route to the observed unscrambled oxygen, which was conducted at pH 10 in water, is a homolytic one such as Eqs. 12a—c. This seems to be not unreasonable in view of the fact that the reported k_{HOO^-} value of *ca.* 2×10^{-2} M^{-1} s^{-1} (for *p*-cyanobenzoate in water)[10a] is much higher than the present value of 3×10^{-4} M^{-1} s^{-1} in phosphate buffer (entry 1 in Table 1). The large value of the former seems to reflect an intervention of radical decomposition of H_2O_2 to yield oxygen. Since the base-catalyzed decomposition of H_2O_2 is complex[14] and peroxyl radicals yield scrambled oxygen,[17] it is not easy to clarify or explain the ^{18}O-tracer study (*i.e.*, 81% unscrambled and hence 19% scrambled).

α-Effect. The rate of addition of HOO^- to nitrile could be determined in the presence of DMSO (Table 2). The k_{HOO^-} value changes with nitriles, ranging from 10^{-3} to 3. Aliphatic nitriles are about ten times less reactive than aromatic ones. The substituent effect on benzonitrile affords a ρ-value of 1.54 (σ, r=0.991), suggesting a nucleophilic attack of HOO^- on C≡N.

Much attention has been concentrated on the origin of α-effect.[11] Although several explanations have been noted,[18] it seems to be that there is no single factor govering the α-effect. A typical example of α-effect is the addition of HOO^- to C≡N. The original value (k_{HOO^-}/k_{HO^-}) of 2×10^4 to 7×10^4 for benzonitriles[2] was often cited, but later it was corrected to be 900—1200.[10] As discussed above, a rate-determining step under these conditions is not the attack of HOO^- to C≡N but the decomposition of **1**. The obscurity may be overcome by the addition of DMSO; the results listed in Table 3 show that the α-effect is certainly large, the value of k_{HOO^-}/k_{HO^-} being in the range of 3×10^3 to 10^4.

Reactivity of Peroxyimidic Acid. Peroxyimidic acid (**1**) is a convenient epoxidizing agent.[4-6,19] The electrophilic character of **1** was shown for substituted styrenes ($\rho=-0.48$),[3] although the substituent effect was somewhat smaller compared to the epoxidation with peroxy acid ($\rho=-1.30$).[20] The epoxidation of aliphatic olefins with **1** was also shown to be less selective and possesses a greater steric demand than the case of RCO_3H.[21] Stereochemistry is retained in the present epoxidation as is the case with RCO_3H; that is, GLC analysis demonstrates that *trans*- and *cis*-β-methylstyrenes give the corresponding *trans*- and *cis*-epoxides, respectively, in the reaction with MeCN, H_2O_2, and Na_3PO_4 in 75% MeOH.

Intramolecular epoxidation was shown to occur effectively for α,β-unsaturated nitriles.[22] However, this epoxy amide formation is not so facile; for example, cinnamonitrile gave the amide: epoxy amide ratio of 90:10 (see Table 2). Similarly, a relatively low yield of epoxy amide was also obtained (*i.e.*, **5**:**6**=4:1) from β,γ-unsaturated nitrile (**4**) (Eq. 15).

The addition of DMSO to the system dramatically accelerated the conversion of nitriles to amides un-

Table 2. Substituent and DMSO effect on the reaction of nitriles with alkaline hydrogen peroxide in 75% MeOH

Nitriles	Additive	Rate constants/M^{-1} s^{-1} a)		Product yields b)	
		$10^2 k_{obsd}$	$10^2 k_{HOO^-}$	Amide	Epoxy amide
A) Benzonitriles c)					
C_6H_5CN	DMSO	1.52	15.2	84	
p-MeOPhCN	DMSO	0.969	9.69	d)	
p-MePhCN	DMSO	1.11	11.1	93	
m-MePhCN	DMSO	1.31	13.1	d)	
o-MePhCN	DMSO	0.056	0.56	83	
o-MePhCN		(<0.0001)		5	
p-ClPhCN	DMSO	e)	46.5	d)	
p-O_2NPhCN	DMSO	e)	324	d)	
B) Other nitriles					
MeCN	DMSO	0.121	1.21	d)	
i-PrCN	DMSO	0.119	1.19	d)	
$PhCH_2CN$	DMSO	0.703	7.03	92	
trans-PhCH=CHCN	DMSO	1.01	10.1	100	0
trans-PhCH=CHCN		(0.017)		55 f)	7 f)
4	DMSO	0.102	1.02	76 g)	0
4		(0.025)		16 f)	4 f)

a) Reaction with 0.1 M RCN, 0.015 M H_2O_2, 0.05 M DMSO, and 0.01 M Na_3PO_4 at 25 °C. See footnotes in Table 1. The value in parentheses is from the reaction without DMSO. b) % Yields isolated, if not noted otherwise, from the reaction with 10 mmol RCN, 15 mmol H_2O_2, 12 mmol DMSO, and 0.2 mmol NaOH in 25 ml of 80% MeOH at 50 °C for 1 h. See experimental section. c) Ph=C_6H_4. d) Not determined. e) Reaction with 0.011 M RCN and H_2O_2. f) % Yield determined by NMR. g) NMR yield is 95%.

Table 3. α-Effect on the addition of nitriles a)

Nitrile	Nucleophile	Solvent	k/M^{-1} s^{-1}	k_{HOO^-}/k_{HO^-}
PhCN	HOO^-	25% Dioxane	2.02×10^{-1}	1.02×10^4
	HO^-	25% Dioxane	1.97×10^{-5}	
MeCN	HOO^-	25% Dioxane	2.53×10^{-2}	4.0×10^3
	HO^-	25% Dioxane	0.63×10^{-5}	
MeCN	HOO^-	Water	1.40×10^{-2}	3.0×10^3
	HO^-	Water	0.47×10^{-5}	

a) Reaction at 25 °C with hydrogen peroxide: 0.1 M RCN, 0.02 M H_2O_2, 0.1 M DMSO, and 0.1 M Na_2CO_3; the k_{HOO^-} values were calculated accoding to Eq. 5 (20.1% dissociation of H_2O_2 into HOO^- by UV). The alkaline hydrolysis: 0.1—0.4 M NaOH, 1—2.5 M MeCN or 0.1 M PhCN.

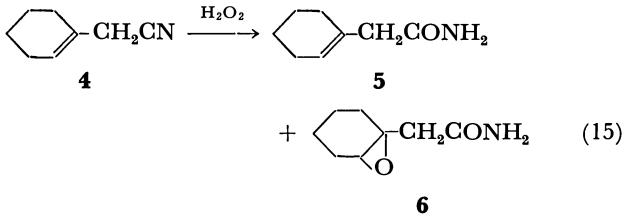

(15)

contaminated with epoxy amide (Table 2). The accelerating effect was large especially for the case of hindered nitriles such as *o*-tolunitrile or cinnamonitrile (*i.e.*, *ca.* thousand-fold increase in rate). The reaction at 50 °C for 1 h gave a high yield of pure amide even with 1 mmol scale, which may be useful as a convenient identification of nitriles. In any case, it is

Table 4. Oxidation of 1,2-dimethylcyclohexene (**7**) with nitrile and alkaline hydrogen peroxide

Condition a)	Solvent	Yields b)			
		8	**9**	**10**	**11**
Singlet oxygen (O_2/RB/hν)	MeOH	2	1	85	12
Autoxidn. (O_2/AIBN/60 °C) c)	MeCN	34	22	14	30
PhCN-H_2O_2 (0.02 M NaOH)	90% MeOH	59	21	8	11
PhCN-H_2O_2 (0.02 M NaOH) d)	90% MeOH	47	28	10	16
PhCN-H_2O_2 (5 mM Na_3PO_4) e)	85% MeOH	60	21	7	12

a) Reaction time of 30—60 min at room temperature if not noted otherwise. Reaction with 0.1 M olefin and, for the nitrile-H_2O_2 reaction, 0.2 M each of PhCN and H_2O_2. b) Product distribution (%) determined by GLC after the reduction with $NaBH_4$. c) Reaction time 4 h. d) In the presence of 1 mM EDTA. e) Reaction time 24 h.

apparent that the intramolecular epoxidation in the peroxyimidic acid intermediate is not so fast and the acid may be completely reduced by DMSO affording pure olefinic amide.

On the basis of approximate stoichiometry of RCN: H_2O_2=1:2, peroxyimidic acid **1** was noted as a potent oxidant capable of oxidizing H_2O_2 to O_2.[2] In analogy to the oxidation with RCO_3H,[8,23] hydrogen peroxide may be oxidized by **1** to oxygen (Eq. 16). However, the kinetics at lower pH (*e.g.*, pH<12 in 75% MeOH)

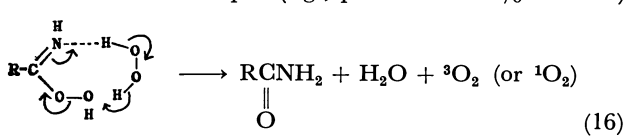

(16)

Table 5. Reaction of superoxide ion in benzene[a)]

Reagent	Decomposed KO_2/%[b)]	Products/%[c)]		
		$MeCONH_2$	Me_2SO_2	Others
KO_2	<5	—	—	
KO_2-MeCN	44	1.9	—	
KO_2-MeCN-DMSO	60	16	40	
KO_2-DMSO	18	—	3	
KO_2-DMSO-H_2O[d)]	62	—	4	
KO_2-MeCN-Olefin[e)]	80	1.3	—	None[f)]
KO_2-MeCN-**7**	78	1.5	—	Yes[g)]
KO_2-**7**	<10	—	—	Yes[h)]

a) Reaction with 0.5 mmol KO_2 (suspension) and 0.1 mmol 18-crown-6 in benzene (4 ml) at 25 °C for 2 h. Acetonitrile was added in a large excess as a co-solvent, *i.e.*, 25 vol% in benzene. DMSO was 0.3 M and olefins were of 0.1 M concentration. b) Approximate value of decomposed KO_2 by titration. c) Yields were determined by GLC and based on the charged KO_2. d) Water (0.25 mmol) was added. e) α-Methylstyrene. f) Epoxide or acetophenone was not detected. g) Yields of **8**, **9**, **10**, and **11** were 1.4, 0.3, 0.3, and 2.4%, respectively. h) Yields of **8**, **9**, **10**, and **11** were 0.7, 0.1, 0.2, and 1.0%, respectively.

is not in accordance with this scheme; if the reaction 16 were operative as a major rate-determining pathway, the overall rate should be second-order in $[H_2O_2]$ and the yield of amide based on H_2O_2 should not exceed 50% (in the absence of DMSO or olefin), both of which were not the case. At high alkalinity, **1** should shift to **1A**[13b)] which easily decomposes homolytically inducing radical decomposition of H_2O_2. This leads to the lower yield of amide or sulfone as is observed. Thus, it may be concluded that the oxidation of H_2O_2 by **1** or **1A** like Eq. 16 is not operating as a predominant reaction.

In order to examine a possible formation of singlet oxygen even as a minor reaction, 1,2-dimethylcyclohexene (**7**), a useful $^1O_2$ trapper,[24a)] was oxidized with nitrile and alkaline H_2O_2. The results in Table

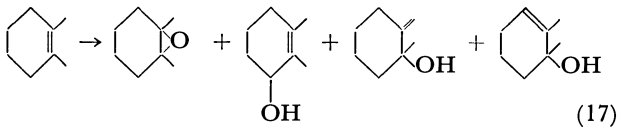

(17)

7 **8** **9** **10** **11**

4 shows that the product distributions are different from singlet oxygen reaction, but are similar to that of the radical autoxidation. A relatively high yield of epoxide was obtained by the radical autoxidation of **7** as observed for other tetrasubstituted aliphatic olefins.[25)] The oxidation of α,β,β-trimethylstyrene, which is also a $^1O_2$ trapper[24a)] but resistant to radical autoxidation at 60 °C, gave a high yield of epoxide (95% yield) together with minor products, where allyl alcohols produced by the $^1O_2$ reaction could not be detected by GLC (*i.e.*, within 1%, if any). Thus, singlet oxygen is not formed in the RCN–H_2O_2 reaction. This results are in contrast to the reported efficient formation of $^1O_2$ from H_2O_2 and cyanates ROCN under anhydrous neutral conditions.[24b)]

Finally, a comment should be added on the reported chemiluminescence from nitriles and H_2O_2.[8a)] Contrary to the report that the luminescence is visible, blue or red, we could not see or detect it as described below. We tested acetonitrile, isobutyronitrile, benzonitrile, benzyl cyanide, and acrylonitrile under the conditions of 0.01—0.1 M each of nitrile, H_2O_2, and KOH in MeOH or EtOH. The addition of dibromo- or diphenylanthracene was of no effect. Our results show that the quantum yield of the reported luminescence is much less than 10^{-9}, if any. To our knowledge, the reported chemiluminescence might be *via* α-hydroperoxy nitrile formed by the base-catalyzed autoxidation of nitriles.[9)] The reported luminescence

$$RCH_2CN \xrightarrow{base/O_2} \underset{\underset{OOH}{|}}{RCHC{\equiv}N} \longrightarrow \underset{\underset{O-O}{|\ \ |}}{RCH\text{-}C{=}NH} \longrightarrow \text{Luminescence} \qquad (18)$$

intensity of $CH_2{=}CHCN > PhCH_2CN \gg PhCN$ may be understood on the basis of Eq. 18, where an α-proton is necessary for the base-catalyzed autoxidation. Although the authors[8a)] suggested singlet oxygen formation by reaction 16, this is not in accordance with the fact that singlet oxygen could not be trapped chemically.

Reaction of Superoxide Ion with Nitrile. Much interest has been concentrated on the reactivity of superoxide ion.[26)] Acetonitrile is sometimes used as an aprotic solvent,[27)] but it is noted that the reactivity of $O_2^{\cdot-}$ in MeCN is different from that in other solvents,[16b,28)] typically the lifetime of $O_2^{\cdot-}$ is ten times shorter in the nitrile.[28a)]

As shown in Table 5, superoxide ion $O_2^{\cdot-}$ reacts with acetonitrile just as hydroperoxide ion HOO^- does. All the experiments were carried out in the presence of 18-crown-6 in benzene to dissolve some fraction of KO_2. Suspended potassium superoxide was stable in benzene but decomposed in acetonitrile–benzene. Interestingly, considerable yields of acetamide were obtained by the reaction of KO_2–MeCN–DMSO. Since it is known that sulfoxides are oxidized to sulfones by alkyl hydroperoxide ion in aprotic solvents,[29)] the sulfone might be produced by the reaction of HOO^- produced by the disproportionation of $O_2^{\cdot-}$. However, the yield of sulfone was much lower when water was added as a proton source to produce

HOO^-. These facts suggest the following scheme.

$$RC{\equiv}N + O_2^{\cdot-} \longrightarrow \underset{\underset{OO\cdot}{|}}{RC{=}N^-} \xrightarrow{O_2^{\cdot-}} \underset{\underset{OO^-}{|}}{RC{=}N^-}$$

12 **13**

$$\xrightarrow{Me_2SO} RCONH_2 + Me_2SO_2 \qquad (19)$$

The reduction of radical **12** with $O_2^{\cdot-}$ to form **13** and O_2 is similar to a known process.[26c,30] Since α-methylstyrene was not epoxidized by KO_2–MeCN (Table 5), the intermediary oxidant for the sulfoxide is probably **13** as a nucleophilic oxidant. It is known that sulfoxides are efficiently oxidized by nucleophilic oxidants.[12,29] In the absence of DMSO, **13** decomposes homolytically just as the case of RCN–HOO^- reaction at high alkalinity (*cf.* Eq. 11). The product distribution from **7** seems to be in this line, suggesting a radical autoxidation (Table 5). Thus, it may be concluded that the chemistry is essentially same for the reaction of nitrile with $O_2^{\cdot-}$ or with HOO^-.

Experimental

Melting points were measured by a Yanagimoto micro melting point apparatus and are corrected. ^1H NMR spectra were recorded with a Hitachi R-24B spectrometer. GLC analyses were performed with a Yanagimoto G180 gas chromatograph using two different columns: PEG 20 M, 10% on Chromosorb W; Silicone OV-17, 5% on Shimalite W. Chemiluminescence was monitored by a Hitachi MPF-2A fluorescence spectrophotometer.

Materials. Methanol and water were purified by redistillations. Substituted benzonitriles were described in our previous paper.[3] *trans*-Cinnamonitrile,[31] bp 124—125 °C/8 Torr (lit,[32] bp 137 °C/16 Torr), and 1-cyclohexenylacetonitrile (**4**),[33] bp 105—107 °C/21 Torr (lit,[33] 110—112 °C/25 Torr), were obtained by the literature method. 2-Methyl-3-phenyl-2-butene, bp 91—92 °C/25 Torr (lit,[34] 191—192 °C), was prepared by dehydration[35] of 2-methyl-3-phenyl-2-butanol in 40% yield. 1,2-Dimethylcyclohexene (**7**) was obtained by dehydration of 1,2-dimethylcyclohexanol (50% sulfuric acid, 100 °C, 1 h) and fractionated three times with a 30 cm Vigreux column, bp 135—136 °C (lit,[36] bp 136.2 °C). Purification *via* dibromide formation[37] was unsatisfactory. 18-Crown-6 was synthesized from triethylene glycol[38] and KO_2 from xanthone-catalyzed autoxidation of potassium in THF.[39]

Rates and Products Determination. Rates were followed iodometrically and a typical procedure was noted in the previous paper.[3] The decomposition of alkaline H_2O_2 alone was negligibly small. The reaction of nitrile with alkaline H_2O_2 was not affected by the addition of 10^{-4} M EDTA, which indicates that there was no contamination by metallic ions.

The hydrolysis rate of benzonitrile was determined by following the decrease of the nitrile by GLC analysis. The reaction of acetonitrile was followed by titrating the produced acetic acid after flashing out ammonia by passing N_2 gas for 5 min. The results are shown in Table 3.

Products were determined by GLC and/or NMR, directly or after extraction with CH_2Cl_2, in comparison to an authentic sample. Authentic samples of epoxides or epoxy amide were obtained by RCO_3H or alkaline H_2O_2 oxidation.

Facile Conversion of Nitriles to Amides. *o*-Tolunitrile (1.17 g, 10 mmol) and DMSO (0.85 ml, 12 mmol) were dissolved in MeOH (20 ml), followed by addition of 11% H_2O_2 (4.85 ml, 15 mmol) and 0.2 M NaOH (1 ml, 0.2 mmol). The reaction mixture was stirred at 50 °C for 1 h, and about half of the solvent MeOH was distilled off (*ca.* 15 min). Standing at room temperature (*ca.* 30 min) afforded pure crystals of *o*-toluamide in 83% yield, mp 142—142.5 °C (lit,[40] 141—141.5 °C).

According to this convenient procedure (total working time; 2 h) the following amides were isolated in pure form (see Table 2 for the yields): *p*-toluamide, mp 161—162 °C; phenylacetamide, mp 159—160.5 °C; benzamide, mp 129—130 °C; cyclohexenylacetamide, mp 153—154 °C; *trans*-cinnamamide, mp 148.5—149.5 °C; diphenylacetamide, mp 172—174 °C. The latter two amides were isolated without evaporation of methanol. An alternative procedure for the isolation is the addition of water (20 ml), which gave a slightly lower yield of amide. The reaction in the absence of DMSO was very slow and incomplete.

Oxidation of 1,2-Dimethylcyclohexene (7). The reaction was started by adding 1 M NaOH (0.1 ml) to the mixture of 1 mmol each of **7**, benzonitrile, and H_2O_2 in 90% MeOH (5 ml). After 1 or 19 h, 0.1 g of $NaBH_4$ was added and analyzed by GLC.

For comparison, azobisisobutyronitrile (AIBN)-initiated autoxidation of the olefin was performed under O_2 in MeCN at 60 °C for 4 h; the reaction mixture was reduced by $NaBH_4$ and MeOH, and analyzed by GLC. The results are shown in Table 4.

Reaction of KO_2 with Acetonitrile. In a dry 20 ml flask were placed benzene (2 ml), MeCN (1 ml), 0.1 M 18-crown-6 (1 ml), and DMSO (0.085 ml). The reaction was started by addition of powdered KO_2 (0.5 mmol) and stirred for 2 h at 25 °C. Products were analyzed by GLC (PEG 20 M) directly or after the reduction with $NaBH_4$ and MeOH. The remaining KO_2 was determined iodometrically after pouring the reaction mixture into AcOH–MeOH–H_2O (1:1:2). Since oxygen was evolved in each run, the recovered KO_2 is mostly unchanged. The results are listed in Table 5.

We are grateful to Professor Isao Kamiya and Dr. Keizo Aoki for their aid in the measurement of chemiluminescence.

References

1) Contribution No. 269.
2) a) K. B. Wiberg, *J. Am. Chem. Soc.*, **75**, 3961 (1953); b) K. B. Wiberg, *ibid.*, **77**, 2519 (1953).
3) Y. Ogata and Y. Sawaki, *Bull. Chem. Soc. Jpn.*, **38**, 194 (1965).
4) H. O. House, "Modern Synthetic Reactions," 2nd ed, by W. A. Benjamin, Menlo Park, Calif. (1972), p. 310.
5) a) L. F. Fieser and M. Fieser, "Reagents for Organic Synthesis," Wiley, New York, N. Y. (1967), p. 469; b) D. Swern, "Organic Peroxides," ed by D. Swern, Wiley, New York, N. Y. (1971), Vol. 2, p. 413.
6) G. B. Payne, *Tetrahedron*, **18**, 763 (1962).
7) J. P. Shirmann and F. Weiss, *Tetrahedron Lett.*, **1972**, 633.
8) a) E. McKeown and W. A. Waters, *Nature*, **203**, 1063 (1964); b) E. McKeown and W. A. Waters, *J. Chem. Soc., B*, **1966**, 1040.
9) Y. Sawaki and Y. Ogata, *J. Am. Chem. Soc.*, **99**, 6313 (1977).
10) a) J. E. McIsaac, Jr., R. E. Ball, and E. J. Behrman, *J. Org. Chem.*, **36**, 3048 (1971); b) J. E. McIsaac, Jr., L. R. Subbaraman, J. Subbaraman, H. A. Mulhausen, and

E. J. Behrman, *ibid.*, **37**, 1037 (1972).
11) a) N. J. Fina and J. O. Edwards, *Int. J. Chem. Kinet.*, **5**, 1 (1973); b) A. P. Grekov and V. Ya. Veselov, *Russ. Chem. Rev.*, **47**, 661 (1978).
12) R. Curci, A. Giovine, and G. Modena, *Tetrahedron*, **22**, 1235 (1966).
13) a) The peracid oxidation of DMSO is *ca.* 1000-fold faster than that of styrenes; Y. Sawaki, unpublished results; b) In the presence of 0.1 M NaOH, the equilibrium 8 must be shift to the left (*i.e.*, **1**→**1A**) because of the shift of Eq. 6 (*i.e.*, $H_2O_2 \rightarrow HOO^-$).
14) a) E. Koubeck, M. L. Haggett, C. J. Battaglia, K. M. Ibne-Rasa, H. Y. Pyun, and J. O. Edwards, *J. Am. Chem. Soc.*, **85**, 2263 (1963); b) J. Wilshire and D. T. Sawyer, *Acc. Chem. Res.*, **12**, 105 (1979); c) C. Walling, *ibid.*, **8**, 125 (1973); d) J. Weinstein and B. H. J. Bielski, *J. Am. Chem. Soc.*, **101**, 58 (1979); e) E. Hayon and M. Simic, *Acc. Chem. Res.*, **7**, 114 (1974).
15) a) C. Walling and R. T. Clark, *J. Am. Chem. Soc.*, **96**, 4530 (1974); b) Y. Sawaki and Y. Ogata, *J. Org. Chem.*, **41**, 2340 (1976).
16) a) D. B. Denney and J. D. Rosen, *Tetrahedron*, **20**, 271 (1964); b) M. J. Gibian and T. Ungermann, *J. Am. Chem. Soc.*, **101**, 1291 (1979).
17) a) P. D. Bartlett and T. G. Traylor, *J. Am. Chem. Soc.*, **85**, 2407 (1963); b) N. A. Clinton, R. A. Kenley, and T. G. Traylor, *ibid.*, **97**, 3757 (1975); c) R. A. Kenley and T. G. Traylor, *ibid.*, **97**, 4700 (1975).
18) For example, a) J. O. Edwards and R. G. Pearson, *J. Am. Chem. Soc.*, **84**, 16 (1962); b) J. Gerstein and W. P. Jencks, *ibid.*, **86**, 4655 (1964); c) J. E. Dixon and T. C. Bruice, *ibid.*, **93**, 6592 (1971); d) S. Oae, Y. Kadoma, and Y. Yano, *Bull. Chem. Soc. Jpn.*, **42**, 1110 (1969); e) J. L. Kice and L. F. Mullan, *J. Am. Chem. Soc.*, **98**, 4259 (1976).
19) Y. Ogata and Y. Sawaki, *Tetrahedron*, **20**, 2065 (1964).
20) Y. Ishii and Y. Inamoto, *Kogyo Kagaku Zasshi*, **63**, 765 (1960).
21) R. G. Carlson and N. S. Behn, *J. Org. Chem.*, **32**, 1363 (1967); **36**, 3832 (1971).
22) a) G. B. Payne and P. H. Williams, *J. Org. Chem.*, **26**, 651 (1961); b) G. B. Payne, *ibid.*, **26**, 663 (1961).
23) K. Akiba and O. Simamura, *Tetrahedron*, **26**, 2519, 2527 (1970).
24) a) C. S. Foote, *Acc. Chem. Res.*, **1**, 104 (1968); b) J. Rebeck, S. Wolf, and A. Mossman, *J. Org. Chem.*, **43**, 180 (1978); **44**, 1485 (1979).
25) a) D. E. Van Sickle, F. R. Mayo, E. S. Gould, and R. M. Arluck, *J. Am. Chem. Soc.*, **89**, 977 (1967); b) F. R. Mayo, *Acc. Chem. Res.*, **1**, 193 (1968).
26) a) E. Lee-Ruff, *Chem. Soc., Rev.*, **6**, 195 (1975); b) I. Fridovich, *Acc. Chem. Res.*, **5**, 321 (1972); c) W. C. Danen, J. Warner, and R. L. Arudi, "Organic Free Radicals," ed by W. A. Pryor, Am. Chem. Soc., Washigton D. C. (1978), p. 244.
27) For example, a) M. E. Peover and B. S. White, *Electrochim. Acta*, **11**, 1061 (1966); b) J. W. Peter and C. S. Foote, *J. Am. Chem. Soc.*, **98**, 875 (1976); c) Y. Moro-oka and C. S. Foote, *ibid.*, **98**, 1510 (1976).
28) a) M. Tezuka, H. Hamada, Y. Ohkatsu, and T. Osa, *Denki Kagaku*, **44**, 17 (1976); b) D. T. Sawyer, M. J. Gibian, M. M. Morrison, and E. T. Seo, *J. Am. Chem. Soc.*, **100**, 627 (1978).
29) Y. Ogata and S. Suyama, *Chem. Ind.*, **1971**, 707; *J. Chem. Soc., Perkin Trans. 2*, **1973**, 755.
30) M. J. Gibian and T. Ugermann, *J. Org. Chem.*, **41**, 2500 (1976).
31) T. Posner, *Justus. Liebigs Ann. Chem.*, **387**, 117 (1912).
32) D. T. Mowry and R. R. Morner, *J. Am. Chem. Soc.*, **69**, 1831 (1947).
33) A. C. Cope, A. A. D'Addieco, D. E. Weyte, and S. A. Glickmann, *Org. Synth.*, Coll. Vol. 4, 234 (1963).
34) G. P. Newsoroff and S. Sternhell, *Aust. J. Chem.*, **19**, 1667 (1966).
35) E. W. Garbish, Jr., *J. Org. Chem.*, **26**, 4165 (1961).
36) T. D. Nevitt and G. S. Hammond, *J. Am. Chem. Soc.*, **76**, 4121 (1954).
37) E. H. Farmer and D. A. Sutton, *J. Chem. Soc.*, **1946**, 10.
38) G. W. Gokel, D. J. Cram, C. L. Liotta, H. P. Harris, and F. L. Cook, *J. Org. Chem.*, **39**, 2445 (1974).
39) N. A. Sokolov and G. A. Matsulevich, *Neorg. Perckisnye Soedenenii Doklady Vses. Soveshch.*, 95 (1973); *Chem. Abstr.*, **83**, 212027 (1975).
40) C. R. Noller, *Org. Synth.*, Coll. Vol. 2 586 (1943).

Cyclic Carbene–Palladium(II) Complexes Derived from the Reactions of Isocyanide–Palladium(II) Complexes with Nitrilimines and Nitrilylides

Yoshio FUCHITA,* Kazuhisa HIDAKA, Shigeki MORINAGA, and Katsuma HIRAKI*

Department of Industrial Chemistry, Faculty of Engineering, Nagasaki University, Bunkyo-machi, Nagasaki 852

(Received July 16, 1980)

cis-[$PdCl_2(PPh_2R^1)(CN-C_6H_4-CH_3-p)$] ($R^1$=Ph or Et) reacts with nitrilimines or nitrilylides, derived from the reactions of either *N*-phenylarenecarbohydrazonoyl chlorides or *N*-(*p*-nitrobenzyl)arenecarboximidoyl chlorides with triethylamine, to afford novel cyclic carbene–palladium(II) complexes, *viz.* 1,2,4-triazol-5(4*H*)-ylidene- or 2-imidazolin-5-ylidenepalladium(II) ones, respectively. Halogen exchange reactions of the carbene complexes with lithium bromide or sodium iodide give the corresponding dibromo- or diiodocarbene complexes, respectively. *trans*-[$PdI_2(PPh_2-C_6H_4-CH_3-p)(CN-C_6H_4-NO_2-p)$] also reacts with the nitrilimine or the nitrilylide to produce cyclic carbene–palladium(II) complexes. All the complexes prepared in this study are characterized by elemental analysis, IR and ^{1}H-NMR.

It has been reported that coordinated isocyanide molecules undergo nucleophilic attack by alcohols and amines to yield alkoxyamino- and diamino-carbene complexes, respectively.[1-3] Recently, these carbene complexes have received considerable interest due to their important role in the catalytic formations of formimidates,[4] formamidines,[4] and heterocyclic compounds.[5] It is well known in organic chemistry that 1,3-dipolar compounds such as nitrilimines, nitrilylides, and azides react with dipolarophiles to produce various heterocycles.[6] However, hardly any work has been reported concerning the reactions between metal complexes and the 1,3-dipolar compounds except for diazo compounds.[7-9] It has been reported that tetrakis(*t*-butyl isocyanide)nickel(0) reacts with dicyanodiazomethane to afford bis(*t*-butyl isocyanide)(*N*-*t*-butyldicyanoketenimine)nickel(0),[8] and that (*t*-butyl isocyanide)nickel(0) and -palladium(0) complexes react with diazofluorene to give *N*,*N*′-coordinate complexes.[9]

It is interesting to investigate the reactions of the 1,3-dipolar compounds with isocyanide ligands coordinated to transition metals, as an extension of the 1,3-dipolar cycloaddition reaction. It has been reported from our laboratory that both the nitrilimines[10] and the nitrilylides[11] react with *cis*-dichloro(tertiary phosphine)(*p*-tolyl isocyanide)palladium(II) complexes to afford novel cyclic carbene–palladium(II) complexes. This paper deals both with the details of the reactions mentioned above and with the reactions of the nitrilimine and the nitrilylide with a palladium(II) complex containing *p*-nitrophenyl isocyanide, which increases the electrophilicity of the carbon atom linked to palladium.

Experimental

General. All the experiments were carried out in an atmosphere of dry nitrogen. IR and ^{1}H-NMR spectra, conductivities and melting points were measured according to the previous paper.[12] *N*-Phenylbenzohydrazonoyl chloride **1**,[13] *N*-(*p*-nitrobenzyl)benzimidoyl chloride **2**,[14] diphenyl-*p*-tolylphosphine,[15] and *p*-nitrophenyl isocyanide[16] were prepared according to the published methods. *N*-Phenyl-*p*-toluohydrazonoyl chloride **3** and *N*-(*p*-nitrobenzyl)-*p*-toluimidoyl chloride **4** were synthesized in the analogous way to **1** and **2**, starting from the reactions of *p*-toluoyl chloride with phenylhydrazine and *p*-nitrobenzylamine, respectively.

cis-Dichloro(triphenylphosphine)(*p*-tolyl isocyanide)palladium(II) **5**[3] and new complexes, *cis*-dichloro(ethyldiphenylphosphine)(*p*-tolyl isocyanide)palladium(II) **6**[3] and di-μ-iodo-diiodobis(diphenyl-*p*-tolylphosphine)dipalladium(II)[17] were synthesized according to the reported procedure with slight modification.

Preparation of trans-*Diiodo(diphenyl*-p-*tolylphosphine)(*p-*nitrophenyl Isocyanide)palladium(II)* **7**. *p*-Nitrophenyl isocyanide (0.78 mmol) was added to di-μ-iodo-diiodobis(diphenyl-*p*-tolylphosphine)dipalladium(II) (0.39 mmol) in dichloromethane (20 ml) and the mixture was stirred for 20 h at room temperature. After the reaction mixture had been evaporated to dryness, the residue was recrystallized twice from dichloromethane and diethyl ether to give reddish orange crystals **7**.

Yields and some properties of the new compounds, **3**, **4**, **6**, and **7** are summarized in Table 1.

Reactions of **5** *or* **6** *with* **1** *or* **3**. A benzene solution (10 ml) of triethylamine (6.5 mmol) was added to a benzene suspension (10 ml) containing **5** (0.67 mmol) and **1** (0.81 mmol). After stirring for 24 h at room temperature, the reaction mixture was filtered and the filter cake was washed with water. Recrystallization from dichloromethane and pentane gave white crystals **8a**. Yield 23%, mp 293—295 °C(dec). Complex **8b** or **8d** was also prepared in this manner from the reactions between **5** and **3**, or **6** and **3**, respectively. **8b**; yield 28%, mp 295 °C(dec): **8d**; yield 25%, mp 273 °C(dec).

Halogen-exchange Reactions of **8a** *and* **8b** *with Lithium Bromide or Sodium Iodide.* A methanol suspension containing **8a**(or **8b**) and five equivalents of lithium bromide was heated under reflux for 8 h. The resulting white solid was separated and washed with methanol to yield **9a**(or **9b**). **9a**; yield 65%, mp>300 °C: **9b**; yield 60%, mp>300 °C. The reaction between **8a** and sodium iodide was carried out in acetone in the same way as described above, and **10a** was produced: yield 70%, mp 275—280 °C(dec).

Reaction of **5** *with* **4**. To a benzene suspension (10 ml) containing **5** (1.14 mmol) and **4** (1.42 mmol) was added triethylamine (14.2 mmol) in 5 ml of benzene, and the reaction mixture was stirred for 4 d at ambient temperature. Addition of diethyl ether and pentane yielded an orange-yellow powder, which was washed with water and purified by passing through a silica gel column (200 mesh, 12ϕ×150 mm). The eluent was initially benzene/hexane (1/1) and finally acetone. Yellow eluate thus obtained was evaporated to dryness, and the residue was recrystallized from dichloromethane and diethyl ether to produce **11b**: yield 33%, mp 203—204 °C(dec).

Reactions of **6** *with* **2** *or* **4**. This reaction was carried out in the same way as described for **11b** except for omitting the chromatography technique, and **11c** or **11d** was obtained

Table 1. Yields and properties of the new compounds

Compound	Yield %	Color	Mp °C	Found(Calcd) (%) C	H	N	^{1}H-NMR(δ/ppm)[a] CH_3	Others
3	44[b]	Cream	136—137	68.63 (68.71	5.37 5.44	10.94 11.45)	2.34 s	—
4	83[c]	Greenish yellow	89	62.40 (62.68	4.54 4.59	9.70 9.72)	2.37 s	4.93 s(CH_2)
6	60[d]	Pale yellow	200—201 (dec)	51.54 (51.94	4.24 4.36	2.67 2.75)	2.40 s	1.38 dt($PCH_2C\underline{H}_3$)[e] 2.86 dq($PC\underline{H}_2CH_3$)[f]
7	76[g]	Reddish orange	176—182 (dec)	39.61 (39.80	2.70 2.70	3.42 3.57)	2.22 s	—

a) In $CDCl_3$ except for **6** (CD_2Cl_2). b) Based on β-toluoyl phenylhydrazine. c) Based on *N*-[(*p*-nitrophenyl)-methyl]benzamide. d) Based on *cis*-[$PdCl_2$(CN-C_6H_4-CH_3-*p*)$_2$]. e) $^3J_{PH}$=20 Hz. f) $^2J_{PH}$=12 Hz, $^3J_{HH}$=8 Hz. g) Based on [{PdI_2(PPh_2-C_6H_4-CH_3-*p*)}$_2$].

from the reactions between **6** and **2**, or **6** and **4**, respectively. **11c**; yield 35%, mp 187—189 °C(dec): **11d**; yield 33%, mp 189—191 °C(dec).

*Halogen-exchange Reactions of **11c** and **11d** with Lithium Bromide.* These reactions were carried out in acetone in the analogous way as described for **9a**, and yellow crystals, **12c** and **12d** were produced. **12c**; yield 43%, mp 185—190 °C(dec): **12d**; yield 45%, mp 195—198 °C(dec).

*Reaction of **7** with **3** or **4**.* Triethylamine (5.38 mmol) in 10 ml of benzene was added to a benzene solution (10 ml) of **7** (0.45 mmol) and **3**(or **4**) (0.54 mmol), and the reaction mixture was stirred for 3 d at room temperature. After the solvent had been removed under a reduced pressure, the residue was washed with water and recrystallized twice from benzene and hexane to give yellow brown powders **13**(or **14**). **13**; yield 13%, mp 270—275 °C (dec): **14**; yield 7%, mp 208—218 °C(dec).

Results and Discussion

The 1,3-dipolar compounds, *N*-phenylarylnitrilimines and nitrilylides can be generated under an inert atmosphere by the reactions of triethylamine with the corresponding *N*-phenylarenecarbohydrazonoyl chlorides (Eq. 1) and *N*-(*p*-nitrobenzyl)arenecarboximidoyl chlorides (Eq. 2), respectively.[6]

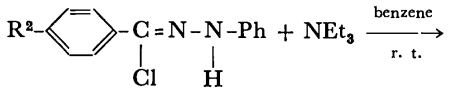

1: R^2=H
3: R^2=CH_3

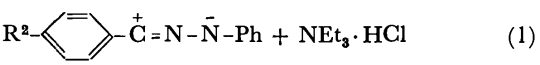

(1)

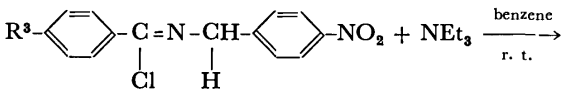

2: R^3=H
4: R^3=CH_3

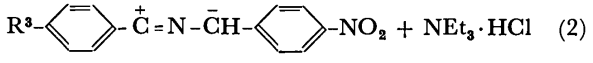

(2)

Reactions of (*p*-tolyl isocyanide)palladium(II) complexes (**5** and **6**) with the nitrilimines and the nitrilylides in benzene at room temperature gave the white complexes **8a—d**[18] and the yellow complexes **11b—d**,[18] respectively (Scheme 1). These complexes are very stable in both air and water, and remain unchanged after more than a half year under an inert atmosphere. Elemental analysis, ^{1}H-NMR and IR spectra together with some properties of the new complexes prepared in this work are summarized in Tables 2 and 3.

The IR spectra of **8a—d** lacked the ν(C≡N) frequency observed in the starting complexes (**5**, 2200 cm^{-1}; **6**, 2190 cm^{-1} in KBr disk), and a new band appeared at 1610 cm^{-1}. This band was assigned to a ν(C=N) frequency of the 1,2,4-triazol-5(4*H*)-ylidene group, which was formed by the cycloaddition reaction of the coordinated isocyanide with nitrilimines. The presence of two ν(Pd–Cl) frequencies in **8a—d** (Table 3) is consistent with the *cis* isomer, indicating that during the addition reaction the initial configuration is retained.

As for the ^{1}H-NMR spectrum of **8d** in CD_2Cl_2, the methyl proton resonance of the phosphine moiety appeared at δ 1.01 as a double triplet due to coupling with the ^{31}P nucleus ($^3J_{PH}$=21.3 Hz, $^3J_{HH}$=8.2 Hz). On the other hand, methylene proton signal of the phosphine ligand could not be distiguished clearly owing to overlapping with the two methyl resonances at δ 2.40 and 2.56, which were derived from the isocyanide group and the nitrilimine. A lower field doublet at δ 8.88 (2H, $^3J_{HH}$=*ca.* 8 Hz) was ascribed to the *o*-protons of the *p*-tolyl group derived from the isocyanide. Possible explanations for such a low field shift can be given by an electron transfer from the *p*-tolyl group to the electron-deficient carbene carbon and/or by a close interaction of the *p*-tolyl group with the central palladium metal. Similar signals were also observed in other triazolinylidene complexes **8a** and **8b** at δ 8.60 and 8.58 ($^3J_{HH}$=*ca.* 8 Hz), respectively. As for the ^{13}C-NMR spectrum of **8b**, the carbene signal of the 1,2,4-triazol-5(4*H*)-ylidene moiety was so weak and unresolved that it could not be detected clearly.

Metathetical reactions of **8a** and **8b** with lithium bromide or sodium iodide were performed in refluxing methanol or acetone to produce corresponding dibromo derivatives **9a**, **9b**, or diiodo one **10a**. In contrast to

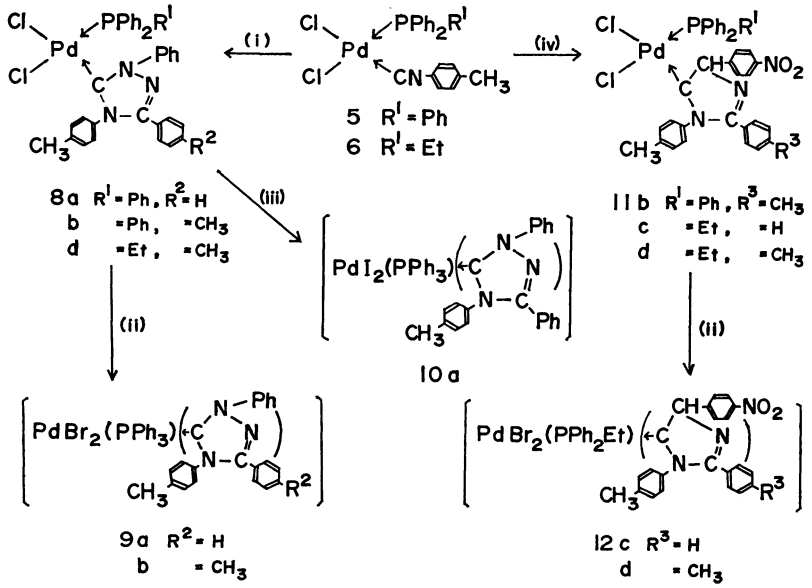

Scheme 1. Reactions of **5** and **6** with nitrilimines or nitrilylides. (i) p-R^2-C_6H_4-$\overset{+}{C}$=N-$\overset{-}{N}$-Ph (R^2=H or CH_3) (ii) $LiBr \cdot H_2O$ (iii) NaI. (iv) p-R^3-C_6H_4-$\overset{+}{C}$=N-$\overset{-}{C}$H-C_6H_4-NO_2-p (R^3=H or CH_3).

Table 2. Elemental analyses and ^{1}H-NMR spectra of the new complexes

Complex	Found(Calcd) (%)			^{1}H-NMR(δ value from TMS)[a]			
	C	H	N	CH_3		P-CH_2-	PCH_2CH_3
8a	61.84	4.38	5.43	2.48 s[b]		—	
	(62.38	4.29	5.60)				
8b	62.48	4.42	5.28	2.46 s[b]	2.32 s[c]	—	
	(62.80	4.48	5.28)				
8d	59.83	4.75	5.63	2.56 s[b]	2.40 s[c]	*ca.* 2.5[d]	1.01 dt[d]
	(60.31	4.78	5.86)				
9a	55.80	3.95	4.85	—[e]		—[e]	
	(55.77	3.84	5.00)				
9b	56.24	4.05	4.91	—[e]		—[e]	
	(56.26	4.01	4.92)				
10a	49.83	3.36	4.19	—[e]		—[e]	
	(50.16	3.45	4.50)				
11b	59.81	4.15	5.00	2.56 br s[f],	2.36 br s[b]	—	
	(60.87	4.24	5.19)				
11c	58.34	4.65	5.87	2.30 br s[b]		3.16 q	1.34 t
	(57.89	4.32	5.63)				
11d	58.45	4.70	5.64	2.42 br s[f],	2.33 br s[b]	3.18 q	1.34 t
	(58.40	4.50	5.52)				
12c	51.71	4.08	5.01	2.33 br s[b]		2.5 br	0.9 br
	(51.73	3.86	5.03)				
12d	51.82	4.19	4.88	2.28 br s[f],	2.33 br s[b]	2.5 br	0.9 br
	(52.29	4.03	4.94)				
13	50.98	4.18	5.18	2.42 br s[d]		—	
	(51.59	3.67	5.23)				
14	50.98	3.64	4.83	2.42 br s,	2.56 br s[d]	—	
	(50.63	3.53	5.02)				

a) In $CDCl_3$ for **8a**, **8b**, **13**, and **14**, or in CD_2Cl_2 for **8d**, **11b**—**11d**, **12c**, and **12d**. Aromatic protons are omitted. b) Derived from isocyanide. c) Derived from nitrilimine. d) See the text. e) Not recorded. f) Derived from nitrilylide.

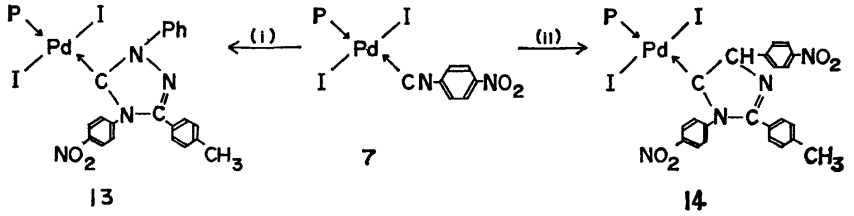

Scheme 2. Reactions of **7** with a nitrilimine and a nitrilylide.
(i) *p*-CH_3–C_6H_4–$\overset{+}{C}$=N–$\overset{-}{N}$–Ph. (ii) *p*-CH_3–C_6H_4–$\overset{+}{C}$=N–$\overset{-}{C}$H–C_6H_4–NO_2-*p*.

Table 3. IR spectra[a] and molar conductivities of the new complexes

Complex	$\nu(NO_2)$ / cm^{-1}	ν(Pd-Cl) / cm^{-1}	Λ_M[b] / Ω^{-1} cm^2 mol^{-1}
6	—	336 s, 284 vs	—
8a	—	322 s, 279 vs	—
8b	—	317 s, 277 vs	—
8d	—	318 s, 274 vs	—
11b	1505, 1330 vs	272 br s	19.9[c]
11c	1510, 1330 vs	269 br s	11.5[c], 0.63[d]
11d	1510, 1330 vs	261 br s	10.5[c]

a) Values in KBr disk. b) Molar conductivity in 10^{-3} mol dm^{-3} solution at 25 °C. c) In acetone. d) In dichloromethane. $\Lambda_M = 91.3\ \Omega^{-1}\ cm^2\ mol^{-1}$ in 0.24×10^{-3} mol dm^{-3} methanol solution.

the moderate solubility of **8a—d** in dichloromethane, these dibromo or diiodo complexes have very low solubility in this solvent, and so ^{1}H-NMR spectra could not be obtained.

On the basis of these results and the elemental analyses, **8a—d**, **9a—b**, and **10a** are assigned to new cyclic carbene–palladium(II) complexes, which are formed by the 1,3-dipolar cycloaddition reactions of nitrilimines onto the C≡N triple bond of the coordinated isocyanide ligand.

Complexes **11b—d** were also ascribed to novel cyclic carbene–palladium(II) complexes containing a 2-imidazolin-5-ylidene group, which was formed by the reaction of nitrilylides with the ligating isocyanide in the analogous way as described for **8a—d** (Scheme 1). In the IR spectra of **11b—d**, both the ν(C=N) band at 1590 cm^{-1}, associated with the 2-imidazolin-5-ylidene group, and the $\nu(NO_2)$ band of the nitrilylide moiety were observed (Table 3). The far-IR spectra of **11b—d** showed only one broad band due to ν(Pd–Cl) frequency ranging from 261 to 272 cm^{-1}, in contrast to two bands in **8a—d**. It is known that ν(Pd–Cl) frequencies in *trans*-$[PdCl_2L_2]$ fall in the range of 357—5 cm^{-1} [19] and is almost insensitive of the ligand L. This suggests that **11b—d** have a *cis* configuration rather than a *trans* one, and broadening of the band probably comes from the partial overlapping of two bands.

As for the ^{1}H-NMR spectra of **11c** and **11d**, the ethyl resonances of the phosphine moiety were observed at rather low field in comparison with those of **8d**. This suggests that a relatively stronger electron transfer from the phosphine ligand to the carbene moiety is present in **11b—d**, Complex **11b**, whic has a weaker σ-donor ability ligand, triphenylphosphine, instead of ethyldiphenylphosphine, always contains some amounts of triethylamine, unless a column chromatography purification is performed. This triethylamine probably interacts with the electron-deficient carbene carbon and forms a weak ylidic bond. This fact also supports the deshielded ethyl resonance of the phosphine ligand. The methine proton resonance of the 2-imidazolin-5-ylidene moiety could not be distinguished because of its overlapping with phenyl signals.

Molar conductivity of **11b—d** (Table 3) exhibited rather high values in acetone and methanol attributable to the dissociation equilibria as shown in Eq. 3. However, **11c** behaved as a nonelectrolyte in dichloromethane showing a very low molar conductivity value. These facts indicate that the solvent which has coordinating ability, displaces the chloro ligand linked to palladium to afford ionic species.

$$[PdCl_2(\text{Phosphine})(\text{Carbene})] + \text{Solv.} \rightleftharpoons [PdCl(\text{Phosphine})(\text{Carbene})(\text{Solv})]^+ + Cl^- \quad (3)$$

Complexes **11c** and **11d** reacted with lithium bromide in the analogous way as described for **9** to afford dibromo derivatives **12c** and **12d**, respectively. In the ^{1}H-NMR spectra of these two complexes, the splitting of the ethyl signals was not observed clearly owing to their fairly low solubility in CD_2Cl_2 or $CDCl_3$. It is not obvious whether *trans-cis* isomerization took place during the metathetical reaction or not.

A new (*p*-nitrophenyl isocyanide)palladium(II) complex **7** was synthesized from the reaction of di-μ-iododiiodobis(diphenyl-*p*-tolylphosphine)dipalladium(II) with *p*-nitrophenyl isocyanide in dichloromethane at room temperature, and reacted with the nitrilimine or the nitrilylide to produce **13** or **14**, respectively, similar to the cases of **5** and **6**. Complexes **13** and **14** contain one molecule of benzene as a solvent of crystallization (δ 7.38 in their ^{1}H-NMR).

The IR spectra of these two complexes lacked the C≡N stretching frequency at 2180 cm^{-1}, which was observed in the original complex **7**. The $\nu(NO_2)$ bands were also observed at 1490, 1320 (for **13**), and 1510, 1240 cm^{-1} (for **14**), but ν(C=N) bands were obscured owing to overlapping with the absorptions of benzene at 1590 cm^{-1}. The ^{1}H-NMR spectrum of **13** showed only one broad methyl resonance, which possibly arises from an accidental coincidence of the two methyl resonances in both the nitrilimine and the phosphine moieties. On the other hand, **14** showed two methyl resonances derived from the nitrilylide

and the phosphine ligand, but the assignment of these resonances could not be performed.

A stepwise mechanism was proposed for the reactions of ligating isocyanides with the 1,3-dipolar compounds resulting in the formation of cyclic carbene–palladium(II) complexes, analogous to the mechanism for nucleophilic attack of amine on the ligating isocyanide.[2] It may involve a nucleophilic attack of the anion of the 1,3-dipolar compound upon the isocyanide carbon to result in the formation of an amide anion. Subsequently, the ring closure took place between the amide anion and a carbonium ion of the 1,3-dipolar compound to yield the cyclic carbene complex (Eq. 4).

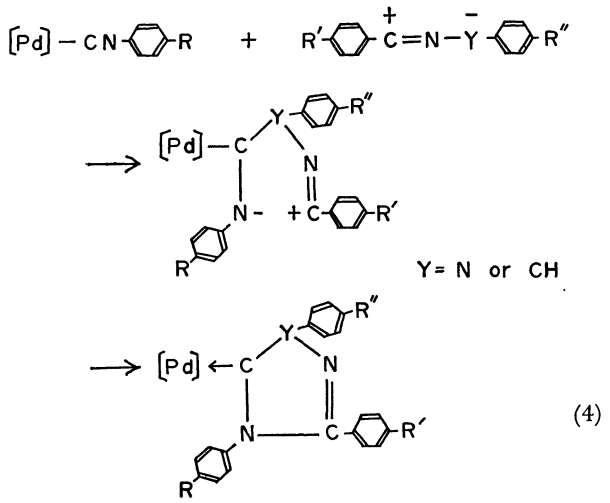

(4)

Another 1,3-dipolar compound, *p*-tolyl azide, reacted with **7** in refluxing benzene, but gave no isolable product. In the case of the reaction with **5**, only the starting materials were recovered.

We wish to express our gratitude to Professor Keinosuke Hamada and Mr. Hirofumi Morishita of Nagasaki University for far-IR measurements, and also to Mrs. Hisako Mazume and Miss Yumi Kojima of Nagasaki University for their technical assistance.

References

1) E. M. Badley, J. Chatt, R. L. Richards, and G. A. Sim, *J. Chem. Soc., Chem. Commun.*, **1969**, 1322.
2) E. Rotondo, M. Cusumano, B. Crociani, P. Uguagliati, and U. Belluco, *J. Organomet. Chem.*, **134**, 249 (1977).
3) B. Crociani, T. Boschi, M. Nicolini, and U. Belluco, *Inorg. Chem.*, **11**, 1292 (1972).
4) T. Saegusa and Y. Ito, *Synthesis*, **5**, 291 (1975).
5) Y. Ito, Y. Inubushi, M. Zenbayashi, S. Tomita, and T. Saegusa, *J. Am. Chem. Soc.*, **95**, 4447 (1973).
6) R. Huisgen, *Proc. Chem. Soc.*, **1961**, 357.
7) W. A. Herrmann, *Angew. Chem. Int. Ed. Engl.*, **17**, 800 (1978).
8) a) S. Otsuka, A. Nakamura, T. Koyama, and Y. Tatsuno, *J. Chem. Soc., Chem. Commun.*, **1972**, 1105. b) D. J. Yarrow, J. A. Ibers, Y. Tatsuno, and S. Otsuka, *J. Am. Chem. Soc.*, **95**, 8590 (1973).
9) a) S. Otsuka, A. Nakamura, T. Koyama, and Y. Tatsuno, *Justus Liebigs Ann. Chem.*, **1975**, 626; b) A. Nakanura, T. Yoshida, M. Cowie, S. Otsuka, and J. A. Ibers, *J. Am. Chem. Soc.*, **99**, 2108 (1977).
10) K. Hiraki, Y. Fuchita, and S. Morinaga, *Chem. Lett.*, **1978**, 1.
11) K. Hiraki and Y. Fuchita, *Chem. Lett.*, **1978**, 841.
12) K. Hiraki, M. Onishi, K. Sewaki, and K. Sugino, *Bull. Chem. Soc. Jpn.*, **51**, 2548 (1978).
13) R. Huisgen, M. Seidel, G. Wallbillich, and H. Knupfer, *Tetrahedron*, **17**, 3 (1962).
14) R. Huisgen, H. Stangle, H. J. Strum, R. Raab, und K. Bunge, *Chem. Ber.*, **105**, 1258 (1972).
15) J. J. Monagle, J. V. Mangenhauser, and D. A. Jones, Jr., *J. Org. Chem.*, **32**, 2477 (1967).
16) I. Ugi and R. Meyr, *Chem. Ber.*, **93**, 239 (1960).
17) J. Chatt and L. M. Venanzi, *J. Chem. Soc.*, **1957**, 2351.
18) Suffix **a** or **b** represents the products which contain both PPh_3 and the cyclic carbene moiety derived from the *C*-phenyl- or *C*-*p*-tolyl-typed 1,3-dipolar component, respectively. Similarly, suffix **c** or **d** does the products which involve both PPh_2Et and the cyclic carbene moiety derived from the *C*-phenyl- or *C*-*p*-tolyl-typed 1,3-dipolar component, respectively.
19) F. R. Hartley, "The Chemistry of Platinum and Palladium," Applied Science Publishers Ltd., London (1973), p. 240.

  Bull. Chem. Soc. Jpn., 54, 805—808 (1981)

Silylation of Relatively Acidic Compounds with Alkyl Trimethylsilylacetates[1)]

Eiichi NAKAMURA, Koichi HASHIMOTO, and Isao KUWAJIMA*

Department of Chemistry, Tokyo Institute of Technology, Ookayama, Meguro-ku, Tokyo 152

(Recieved July 26, 1980)

Silylation of ketones, alcohols, alkanethiols, phenols, and carboxylic acids with alkyl trimethylsilylacetates has been described from synthetic and mechanistic points of view.

In a previous paper we described the reaction of silylated esters with carbonyl compounds.[2,3)] In the presence of tetrabutylammonium fluoride, rather surprisingly, silyl esters underwent desilylation to effect the transfer of the silyl group onto ketones (R-H)[4)] as in Eq. 1. Subsequent studies have shown this

$$RH + Me_3SiCH_2COOR' \xrightarrow{F^-} RSiMe_3 + CH_3COOR' \quad (1)$$

silyl transfer reaction even more versatile; a wide variety of relatively acidic compounds[5)] could also be silylated by this new reaction. The purpose of this paper is to describe the scope of the reaction from synthetic and mechanistic points of view.

The use of trialkylsilyl groups, especially trimethylsilyl group, for protection or activation of some functional groups has become one of the standard tools in organic chemistry,[6)] and a number of silylation methods (replacement of acidic protons with silyl groups) have been reported.[7)] Nonetheless, the number of the basic principles has been rather small. A large body of reactions are based on the equilibrium between a substrate and a silylating reagent with a weak Si–X bond, *e.g.* silylamine or silylamide, as shown in Eq. 2.

$$RH + MeSiX \rightleftharpoons RSiMe_3 + HX \quad (2)$$

Though this methology allows the use of mild conditions, thermodynamic factors control the selectivities of the reaction.[8)] Further the silylation reactions usually result in the production of nonvolatile by-products such as tertiary amine hydrochloride, amide, *etc.*

Quenching preformed anions with a trialkylchlorosilane constitutes another important methodology, and has a distinctive advantage in enolate chemistry;[9)] this usually allows us to trap the kinetically preffered isomer of enolate anions as its stable silyl derivatives. Rather strong reaction conditions and somewhat laborious procedures, however, generally render this method to be the second choice. As described below, the reaction of an alkyl trimethylsilylacetate, with its characteristic mechanistic pathway and applicability, has proved to provide another useful methodology for silylation of various acidic compounds.

Results and Discussion

The silylation reaction was performed in a very simple manner. Treatment of a mixture of a substrate and ethyl trimethylsilylacetate (ETSA; slight excess) with 2—5 mol% tetrabutylammonium fluoride trihydrate (TBAF) either in a dry aprotic solvent such as tetrahydrofuran (THF) or without a solvent produced the silylated product and ethyl acetate in high yields. Commercially available TBAF was the catalyst of choice because of the ease of handling and the high solubility in organic solvents. Though ETSA was used generally, the methyl ester or its higher homologues could also serve the purpose nicely. The reaction proceeded at room temperature and the product was isolated either after aqueous workup or direct distillation of the reaction mixture. The silylating ability of ETSA–TBAF system is quite high. The reaction with sterically hindered tertiary alcohols and thiols[10)] proceeded exothermically at room temperature. Even such a less acidic substrate as phenylacetylene was silylated in high yield, whereas triphenylmethane remained unchanged after prolonged reaction period. Table 1 shows the examples.

TABLE 1. SILYLATION OF RELATIVELY ACIDIC COMPOUNDS

Compound	% yield	Compound	% yield
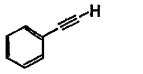	88		83
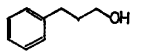	92	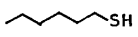	91
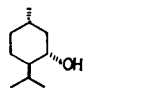	92	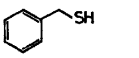	87
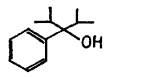	92		82
		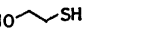	83[a)]

a) Bis-silylated product.

Interestingly, simple aliphatic ketones were silylated faster than more acidic compounds like phenols. This aroused our interests to examine the reaction in some detail. Thus, brief studies about the reaction rate with representative substrates were carried out. An equimolar mixture of methyl trimethylsilylacetate (MTSA) and the substrate was treated at 35 °C with a catalytic amount (1.5—3 mol%) of TBAF in an NMR sample tube, and the reaction was monitored mainly by observing the change of the relative intensities of the trimethylsilyl groups; the trimethylsilyl group of MTSA appeared consistently at a slightly higher field than that of the product. Measurements were done for 1-hexanethiol, phenylmethanethiol, *p*-cresol, propionic acid, and benzenethiol, and the results are shown in Fig. 1, where the product yields are plotted against the reaction time. Under these conditions aliphatic ketones and primary alcohols were silylated instantaneously, while triphenylmethane and benzenethiol were not silylated even after 10 d. While 100% conversion of MTSA was observed in

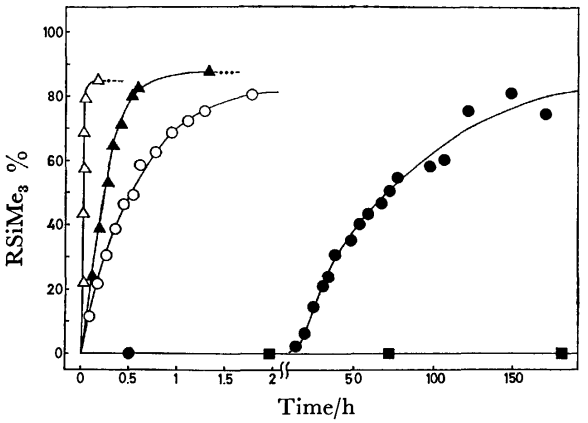

Fig. 1. Silylation of various substrates at 35 °C. △: 1-Hexanethiol (1.9 mol% TBAF), ▲: phenylmethanethiol (2.2), ○: *p*-cresol (2.6), ●: propionic acid (2.3), ■: benzenethiol (1.5).

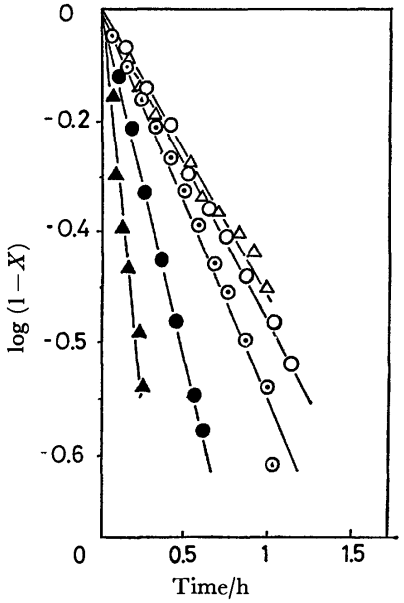

Fig. 2. Silylation of phenylmethanethiol at 35 °C. X=% yield/100, ○: 1.4 mol% TBAF, ⊙: 1.6 mol% TBAF, ●: 2.2 mol% TBAF, ▲: 3 mol% KCN-18-crown-6, △: 2.4 mol% KOMe-18-crown-6.

all runs in Fig. 1 except the case of benzenethiol, 10—15% of the substrate remained unchanged. The content of water in the system, *e.g.* in the catalyst, seems to account for the imcomplete conversion of the substrate. In fact, the substrate underwent 100% conversion when 20—30% excess MTSA was used.

Some efforts to rationalize the reaction rate revealed that the reactions fall into two types. The reaction of cresol followed a first order rate expression, whereas those of thiols and propionic acid (after an induction period) followed second order ones. However, this point was not pursued further because of the experimental difficulties due to the highly sensitive nature of the reaction.[11] Though a specific role of fluoride anion was previously suggested for the present silylation reaction (Scheme 1), the present studies implied another mechanism, namely, an autocatalytic

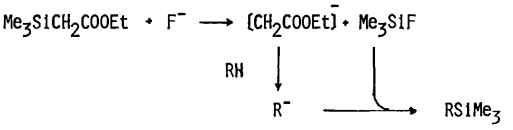

Scheme 1.

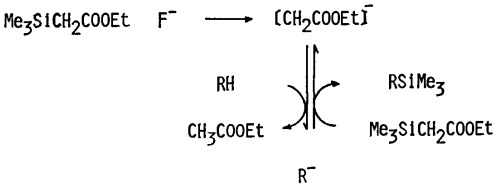

Scheme 2.

one (Scheme 2).

That fluoride is not the only effective catalyst (unlike other similar reactions[3]) was one of those implications. Treatment of a mixture of ETSA and acetophenone with a catalytic amount of KCN/18-crown-6, $KOCH_3$/18-crown-6, or Triton B effected smooth conversion of the ketone into the corresponding enol silyl ether at 0 °C. Silylation of 1-hexanethiol could also be done with those catalysts. The equal efficacy of these catalysts was further proved, in a somewhat quantitative manner, by NMR experiments in which an equimolar mixture of MTSA and phenylmethanethiol was treated with the catalysts (KCN/crown ether, $KOCH_3$/crown ether, or Triton B) as described above (Fig. 2).

In addition to this semiquantitative evidence, a qualitative but direct evidence of the autocatalytic pathway (Scheme 2) was also obtained. Thus, when a mixture of acetophenone and ETSA was treated with 10 mol% of preformed potassium enolate of this ketone solvated by 18-crown-6, quantitative silylation of the ketone occurred within 1 min at 0 °C. Similarly, 10 mol% of potassium 1-hexanethiolate and 18-crown-6 initiated the smooth reaction of 1-hexanethiol with ETSA.

In contrast to the catalytic ability of a potassium enolate/crown ether in the silylation of a ketone, this anion itself could not be silylated by MTSA or ETSA in a stoichiometric reaction. Treatment of the potassium enolate of acetophenone with one equivalent of perhydrodibenzo-18-crown-6 followed by ETSA did not yield any detectable amount of the enol silyl ether, and gave back the starting ketone in high yield. These results fit well with the proposed mechanism, since Eq. 3 involved in the overall reaction pathway does not favor the formation of the enol silyl ether unless the ester enolate on the right side is irreversibly protonated by the neutral ketone to regenerate the ketone enolate.

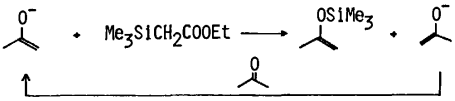

(3)

The reaction mechanism and the rate profiles described above suggest a certain perspective over the synthetic utility of ETSA as a silylating reagent. One apparent factor that limits the application is the acidity

Table 2. Silylation with ETSA-TBAF[a]

Substrate g (mmol)		ETSA g (mmol)	TBAF mg	Reaction period, h	Yield g (%)	Bp °C/mmHg[b]
3-Phenyl-1-propanol	1.36(10.0)	1.92(12.0)	50	2	1.91(92)	87/4[c]
2,4-Dimethyl-3-phenyl-3-pentanol	1.94(10.2)	1.93(12.1)	63	2.5	2.44(92)	110/7
p-Cresol	1.08(10.0)	1.61(11.0)[d]	83[e]	7	1.49(83)	77/12[f]
1-Hexanethiol	1.77(15.0)	2.40(15.0)	74	5	2.60(91)	62/5[g]
Phenylmethanethiol	3.16(25.5)	4.74(28.0)	228	22	4.42(88)	130/32[h]
2-Mercaptoethanol	0.78(10.0)	3.36(21.0)	87	3	1.85(83)[i]	51/4

a) Reactions were performed by a procedure similar to Method A. b) 1 mmHg = 133.322 Pa. c) *Cf.* Ref. 18. d) MTSA was used in place of ETSA. e) BTAF was used in place of TBAF. f) *Cf.* Ref. 19. g) *Cf.* Refs. 16 and 20. h) *Cf.* Ref. 21. i) The product was obtained as a bis-silylated form.

of the substrate relative to that of the alkyl acetate. This, however, does not appear significant for relatively acidic substrates reported here. Among these substrates, on the other hand, the nucleophilicity (toward silicon atom) of the conjugate base of the substrate (R^- in Scheme 1) appears to be important. Prominent decrease of the reaction rate on passing from alcohol to phenol and to acid, or from 1-hexanethiol, phenylmethanethiol, and finally to benzenethiol[12] is in accord with the decrease of the reactivity of their conjugate base. Striking difference of the rate between phenol and benzenethiol is in keeping with the known difference of the affinities of oxygen and sulfur toward silicon.

Thermodynamically controlled silylation reactions are performed under very mild conditions using silylating reagents such as silylamide,[7] whereas kinetically controlled ones have usually been conducted by using strongly basic reagents such as LDA or NaH. In the present reaction, being catalytic with the reactive species, the bulk of the reaction medium remains almost neutral, while the deprotonation takes place in an irreversible manner.

Finally, we draw attention to the absence of any nonvolatile side-products in this reaction, which may allow the use of the unpurified silylation product for further elaboration. Therefore, the present reaction will prove to be complementary to the various existing methodologies of the silylation reactions.

Experimental

All reactions were performed under either argon or nitrogen with magnetic stirring. Tetrahydrofuran (THF) was purified shortly before use by distillation over sodium-benzophenone. TBAF (Fluka AG) was used after overnight evacuation (0.5 mmHg,[13] room temperature) and kept under an inert atmosphere. BTAF was prepared from Triton B methanolic solution (Tokyo Kasei Co.) by the reported method.[3a] Alkyl trimethylsilylacetates were prepared as reported.[14] NMR spectra were taken on a Varian T-60 spectrometer, and chemical shifts are recorded in parts per million downfield from internal tetramethylsilane. IR spectra were taken on a Hitachi EPI G-3 or 260-10 spectrometer, and mass spectra on a Hitachi RMU-7M at 70 eV ionizing irradiation. Gas liquid chromatography (GLC) was performed on a Hitachi 163 instrument equipped with a 0.25 mm × 20 m glass capillary tube coated with OV-101. All boiling points are uncorrected.

Silylation of 2-Methyl-2-propanethiol (Method A). To a stirred mixture of 2-methyl-2-propanethiol (1.58 g, 17.6 mmol) and TBAF (992 mg, 0.35 mmol) at room temperature was added ETSA (2.96 g, 18.5 mmol) over a period of 2 min. The reaction was slightly exothermic. After stirring for 2 h, the orange colored reaction mixture was transferred to a distillation apparatus with exclusion of moisture, and distilled under a reduced pressure to give 2.33 g (82%) of (*t*-butylthio)trimethylsilane[15,16] as a colorless oil. Bp 92 °C/88 mmHg[13]; IR(neat): 1364, 1250, 1157, 842, and 754 cm^{-1}; NMR(neat): δ 0.30 (s, 9H) and 1.43 (s, 9H); MS: *m/e* (%) 162 (M^+, 15), 147 (5), 107 (33), 91 (85), 75 (8), 73 (61), 57 (100).

Silylation of l-Menthol (Method B). The reaction was carried out as described above by using *l*-menthol (4.43 g, 28.4 mmol) in 15 ml of THF, TBAF (72 mg, 0.3 mmol), and ETSA (4.77 g, 29.8 mmol). After the reaction was over, the reaction mixture was diluted with 100 ml of hexane, and poured into water. The organic layer was separated and washed once with aq NaCl. Drying over anhydrous $MgSO_4$ and concentration followed by distillation afforded *l*-menthyl trimethylsilyl ether (5.85 g, 92%), which was identical with the authentic sample by NMR and GLC. Bp 135 °C/68 mmHg;[13,17] MS: *m/e* (%) 228 (M^+, 3), 213 (8), 171 (5), 157 (5), 143 (100), 138 (14), 123 (6), 95 (11), 81 (20), 75 (57), 73 (40).

Trimethyl(phenylethynyl)silane. Phenylacetylene (100 mg, 1.0 mmol) and ETSA (192 mg, 1.2 mmol) were added to TBAF (13 mg, 0.05 mmol) in 2 ml of THF. After 26 h, the reaction mixture was diluted with hexane, filtered, and concentrated. Purification of the crude product on preparative TLC gave 151 mg (88%) of the title compound which was identical with the authentic sample by NMR, IR, and GLC.

3-Phenyl-1-(trimethylsiloxy)propane. The product obtained by the present method was identical with the authentic sample[18] by NMR and GLC. MS: *m/e* (%) 208 (M^+, 10), 193 (23), 175 (11), 165 (12), 147 (14), 135 (14), 118 (100), 107 (14), 91 (38), 89 (40), 75 (30), 73 (38).

2,4-Dimethyl-3-phenyl-3-(trimethylsiloxy)pentane. IR (neat): 850, 758, and 705 cm^{-1}; NMR(CCl_4): δ 0.28 (s, 9H), 0.75 (d, J=7 Hz, 3H), 0.80 (d, J=7 Hz, 3H), 1.9—2.7 (m, 2H), 7.17 (s, 5H); MS: *m/e* (%) 249 ($M^+ - 15$, 5), 221 (100), 131 (12), 75 (26), 73 (96).

1-Methyl-4-(trimethylsiloxy)benzene. The product obtained by the present method was identical with the authentic sample[19] by NMR and IR analyses.

(Hexylthio)trimethylsilane.[16,20] IR(neat): 1463, 1253, 1183, 1057, 845, 758 cm^{-1}; NMR(neat): δ 0.25 (s, 9H), 0.7—1.8 (m, 11H), 2.1—2.7 (m, 2H); MS: *m/e* 190 (M^+), 175, 91, 73; Exact mass: 190.1188. Calcd for $C_9H_{22}SSi$: 190.1212.

(Benzylthio)trimethylsilane.[21] Mass spectrum was identical with the reported one.[21] IR(neat): 1250, 840, 755, 700 cm^{-1}; NMR(neat): δ 0.17 (s, 9H), 3.54 (s, 2H), 6.95—7.45 (m, 5H); Exact mass: 196.0731. Calcd for $C_{10}H_{16}SSi$: 196.0742.

[2-(Trimethylsiloxy)ethylthio]trimethylsilane. IR(neat): 1253, 1090, 840 cm^{-1}; NMR(neat): δ 0.07 (s, 9H), 0.26 (s, 9H), 2.48 (t, J=7 Hz, 2H), 3.55 (t, J=7 Hz, 2H); MS: *m/e* (%) 222 (M^+, 1), 207 (19), 149 (100), 119 (35), 103 (31), 75 (40), 73 (47).

Trimethylsilyl Propionate. To a clear solution of BTAF (335 mg, 1.4 mmol) in propionic acid (1.48 g, 20 mmol) was added ETSA (3.84 g, 24 mmol), and the resulting mixture was kept at room temperature for 10 d while crystalline material separated. NMR and IR analyses of the crude reaction mixture indicated nearly complete conversion of the reactants (especially no hydroxylic absorption on IR spectrum). Distillation of the reaction mixture gave 3.08 g of forerun as a 1:1 mixture of ethyl acetate and the title compound, and 1.37 g of the title ester as a fraction boiling at 105—115 °C (lit,[22] bp 122 °C). NMR and GLC analyses of the main fraction indicated the presence of ethyl acetate (11%) and hexamethyldisiloxane (5%) as impurities. The NMR spectrum was identical with the authentic sample except for the impurities, and coinjection on GLC also supported the assignment. Typical retention times of GLC (90 °C) were 3.0, 3.4, and 5.5 min for ethyl acetate, hexamethyldisiloxane, and the title ester, respectively.

Measurement of the Reaction Rates. To preweighed TBAF in an NMR tube under argon kept at −78 °C was added an equimolar mixture of MTSA and the substrate. The tube was sealed and brought to 35 °C and inserted to NMR probe (35 °C). The progress of the reaction was monitored mainly by observing trimethylsilyl groups.

Silylation of Acetophenone in the Presence of Various Catalysts. *a) KCN/18-crown-6 Catalysis*: To a mixture of the title ketone (120 mg, 1.0 mmol) and KCN/perhydrodibenzo-18-crown-6[23] (22 mg, 0.05 mmol) in 2 ml of THF under nitrogen was added ETSA (177 mg, 1.1 mmol) at 0 °C. TLC of the reaction mixture after 10 min showed virtually 100% conversion of the ketone to the corresponding silyl ether. Workup according to Method B gave the crude enol silyl ether (200 mg, 100%) whose NMR spectrum was identical with the authentic one.

b) $KOCH_3$/18-crown-6 Catalysis: The same procedure as described in a) except for the catalyst ($KOCH_3$/perhydrodibenzo-18-crown-6, 22 mg) gave the expected silyl ether in 98% yield (NMR).

c) Triton B Catalysis: To a mixture of acetophenone (2.40 g, 20 mmol) and ETSA (3.84 g, 24 mmol) under nitrogen was added 2 drops of Triton B (40% in methanol) at room temperature. Exothermic reaction occurred, and TLC after 30 min showed complete conversion of the ketone to the enol silyl ether. The crude reaction mixture obtained according to Method B consisted of the enol silyl ether (99%) and the starting ketone (1%).

d) Enolate Catalysis: To a suspension of oil-free KH (1 mmol) and perhydrodibenzo-18-crown-6 (372 mg, 1.0 mmol) in 10 ml of THF was added acetophenone (128 mg, 1.0 mmol) at 20 °C.[24] A Mixture of acetophenone (1.20 g, 10 mmol) and ETSA (1.60 g, 10 mmol) in 2 ml of THF was added to the enolate solution at 0 °C. TLC after 1 min indicated high yield formation of the silyl ether. Workup by Method B gave a mixture of the enol silyl ether (8.1 mmol) and the starting ketone (1.5 mmol) as judged by NMR analysis using 1,1,2,2-tetrachloroethane as an internal standard.

Autocatalytic Silylation of 1-Hexanethiol. 1-Hexanethiol (118 mg, 1.0 mmol) was added to a mixture of oil-free KH (1 mmol) and perhydrodibenzo-18-crown-6 (372 mg, 1.0 mmol) in 8 ml of THF. To the resulting white solution was added a mixture of 1-hexanethiol (1.18 g, 10 mmol) and ETSA (1.60 g, 10 mmol) at −3 °C, and the mixture was stirred for 1 h at 0 °C. NMR of the reaction mixture indicated the formation of the expected silyl sulfide. Workup of the reaction mixture by Method A gave the silyl sulfide in 68% yield (1.30 g) on distillation.

References

1) Presented partly at the Meeting of the Chemical Society of Japan, Osaka, April 1976.
2) E. Nakamura, M. Shimizu, and I. Kuwajima, *Tetrahedron Lett.*, **1976**, 1699.
3) For the related reactions; a) I. Kuwajima and E. Nakamura, *J. Am. Chem. Soc.*, **97**, 3257 (1975); b) R. Noyori, K. Yokoyama, J. Sakata, I. Kuwajima, E. Nakamura, and M. Shimizu, *ibid.*, **99**, 1265 (1977).
4) E. Nakamura, T. Murofushi, M. Shimizu, and I. Kuwajima, *J. Am. Chem. Soc.*, **98**, 2346 (1976); E. Nakamura, K. Hashimoto, and I. Kuwajima, *Tetrahedron Lett.*, **1978**, 2079.
5) Full details about the silylation of carbonyl compounds will be published in a due course.
6) For a recent review; E. W. Colvin, *Chem. Soc. Rev.*, **7**, 15 (1978).
7) A. E. Pierce, "Silylation of Organic Compounds," Pierce Chemical, Rockford, I11., 1968.
8) For example, see; J. F. Klebe, *Acc. Chem. Res.*, **3**, 299 (1970).
9) G. Stork and P. F. Hudrlik, *J. Am. Chem. Soc.*, **90**, 4462, 4464 (1968); H. O. House, L. J. Czuba, M. Gall, and H. D. Olmstead, *J. Org. Chem.*, **34**, 2324 (1969).
10) See, for example; R. S. Glass, *J. Organometal. Chem.*, **61**, 83 (1973).
11) In our hand, tetraalkylammonium fluoride could not be purified to an anhydrous state, and the catalytic cycle of the reaction was extremely sensitive to minor impurities. The error of the reaction rate measured by the present studies was often as large as ±20%.
12) Neither fluoride anion nor potassium benzenethiolate could initiate the reaction.
13) 1 mmHg=133.322 Pa.
14) R. J. Fessenden and J. S. Fessenden, *J. Org. Chem.*, **32**, 3535 (1967).
15) E. W. Abel, *J. Chem. Soc.*, **1960**, 4406.
16) I. Kuwajima and T. Abe, *Bull. Chem. Soc. Jpn.*, **51**, 2181 (1978).
17) S.-L. Liu and B.-H. Rei, *J. Chinese Chem. Soc. (Taiwan)*, **8**, 237 (1971); cited in Ref. 7.
18) W. Gerrad and K. E. Kilburn, *J. Chem. Soc.*, **1956**, 1536.
19) F. A. Genglein and J. Kramer, *Chem. Ber.*, **92**, 2585 (1959).
20) J. D. Citron, *J. Organometal. Chem.*, **30**, 21 (1971).
21) J. Diekman, J. B. Thompson, and C. Djerassi, *J. Org. Chem.*, **32**, 3904 (1967).
22) E. W. Abel, *J. Chem. Soc.*, **1961**, 4933.
23) D. A. Evans, J. M. Hoffman, and L. K. Truesdale, *J. Am. Chem. Soc.*, **95**, 5822 (1973).
24) C. A. Brown, *J. Org. Chem.*, **39**, 1324 (1974).

Formation and Molecular Dynamics of Cycloamylose Inclusion Complexes with Phenylalanine

Yoshio INOUE* and Yoshiaki MIYATA

Department of Polymer Chemistry, Tokyo Institute of Technology, O-okayama 2-12-1, Meguro-ku, Tokyo 152

(Received August 4, 1980)

The molecular dynamics of the inclusion complexes of cycloamyloses with phenylalanine in aqueous solution at different pD have been studied by means of carbon-13 NMR spectroscopy. As host cycloamyloses we have chosen cyclohexaamylose, cycloheptaamylose, and cyclooctaamylose. The influences of the cavity size of cycloamyloses and of medium pD values on the molecular dynamics of inclusion complexes were studied by using the $NT_1\eta$ values, where T_1 is the carbon-13 spin-lattice relaxation time, N is the number of directly bonded proton to a given carbon, and η is the viscosity of solution. Upon complexation, the $NT_1\eta$ values of phenyl carbons of guest phenylalanine show larger decreases than those of other carbons, indicating that the guest forms the inclusion complexes with the host by the insertion of its phenyl ring into the host cavity even in the case of cyclooctaamylose. It was found that the strength of the dynamic coupling between host and guest depends on the cavity size and pD values of medium. The strongest coupling was observed for the cycloheptaamylose–phenylalanine system at pD 11.3, where the phenyl ring is deeply and tightly included into the cavity. The inclusion of phenyl ring is shallow and loose in the case of cyclohexaamylose and deep and loose in the case of cyclooctaamylose.

The cycloamyloses, well known as cyclodextrins, are a series of cyclic oligosaccharides containing six and more α-1,4-linked D-glucopyranose units. Cycloamylose has the shape of a hollow truncated cone with primary and secondary hydroxyl groups crowning opposite ends of its torus. The CH groups of carbon 3 and 5 of each glucose unit compose the inside of the hollow torus. Thus the inside and the outside of the cycloamylose cavity should be relatively hydrophobic and hydrophilic, respectively. One of the most interesting properties of cycloamyloses are their ability to make a inclusion complex with a variety of guest molecules in their hydrophobic cavity in solution as well as in the solid state, and in some cases they catalyze the reaction of the guest molecule.[1] Because of this property, the cycloamyloses are attractive for many investigators as enzyme recognition and active site models. In particular, cycloamyloses are adequate models for hydrolytic enzyme such as esterase and protease in which the hydroxyl group of a catalytic serine residue attacks the acyl group of a bound substrate.[1,2] It is well known that a typical serine protease chymotrypsin selectively cleaves peptide bonds on the carboxyl side of residues with aromatic side chains and of bulky hydrophobic residues. In these enzymatic reaction, aromatic and bulky nonpolar side chains of substrates are considered to be fitted neatly into a nonpolar pocket on chymotrypsin chain.

It is of great interest to investigate the molecular dynamics of inclusion complexes between cycloamylose and aromatic amino acids as models for enzyme-substrate specific binding. Determination of the geometry of the cycloamylose–substrate complexes as well as the tightness of complexation is essential for a right understanding of the mechanism of enzymatic catalysis of the cycloamylose.

Because of the symmetry of the cycloamyloses and the simplicities of amino acid structures, their carbon-13 nuclear magnetic resonance (^{13}C-NMR) spectra are very simple to analyze. The measurements of carbon-13 spin-lattice relaxation times (T_1) are particularly useful for the investigation of molecular dynamics of cycloamylose inclusion complexes in detail. In a preceding paper,[3] the molecular motions of both host and guest molecules in the inclusion complexes of cyclohexaamylose (α-cyclodextrin, α-CD) with L-phenylalanine (Phe), L-tyrosine, L-tryptophan, glycyl-L-phenylalanine, and L-phenylalanyl-L-lysine in acidic solution have been studied by means of carbon-13 spin-lattice relaxation. It was confirmed there that the complexation of the guest amino acids with the host α-CD are induced by an insertion of aromatic side chain into a cavity of α-CD. The overall correlation times of the substrates are about one third to one seventh shorter than those of the host molecule. It suggests the binding force between the host and the guest is relatively weak and the aromatic ring is shallowly trapped into the cavity. The shallowness of the insertion is also suggested by building a space-filling model in which the diameter of α-CD's cavity is too small for a deep insertion of phenyl ring. Thus the shape matching between the host cavity and the substrate is one of the important factors determining the strong dynamic coupling between host and substrate.

In this paper, we will study the influences of cavity size of the cycloamylose and of pH value of medium on the molecular dynamics of cycloamylose inclusion complexes with L-phenylalanine. As host cycloamyloses we will choose cyclohexaamylose (α-CD), cycloheptaamylose (β-CD), and cyclooctaamylose (γ-CD). Their internal diameters are *ca.* 4.5, 7.0, and 8.5×10^{-10} m, respectively.[1] Molecular model suggests that β-CD makes the most stable and the dynamically strongest inclusion complex with the guest phenylalanine among these cycloamyloses because of its best fitting geometry. The diameter of phenyl ring including the van der Waals radii of proton is about 6.8×10^{-10} m. The cavity sizes of α- and γ-CD may be slightly smaller and larger, respectively, for the fitted complexation with the guest phenylalanine. Since the cycloamylose has the ionizable secondary hydroxyl groups (pK= 12.1[4,5]) on the entrance region for the guest insertion, it is interesting to study the pH dependence of the molecular dynamics of the inclusion complexes between the cycloamyloses and the substrates with ionic

groups such as amino acids. In this paper, carbon-13 spin-lattice relaxation times will be measured in acidic (pD=2), phosphate buffer (pD=11), and highly alkaline (1 mol dm^{-3} NaOD) solutions.

Experimental

Materials. Cyclohexa-, cyclohepta-, and cycloocta-amyloses, D-glucose, and L-phenylalanine were purchased from Nakarai Chemicals, Ltd., Kyoto. The values of specific rotation $[\alpha]_D^{25}$ of α-, β-, and γ-CD's were +149.9, +161.9, and +177.2, respectively, which agreed well with previously reported values (*i.e.*, +150.5±0.5, +162.5±0.5, and +177.4±0.5).[1,6] D_2O (isotopic purity 99.7 atom%), 38% DCl solution in D_2O, 40% NaOD solution in D_2O, and 85% D_3PO_4 solution in D_2O were purchased from Merck Sharp and Dohme Canada Ltd..

Methods. ^{13}C-NMR spectra were measured on a JEOL JNM PS-100 spectrometer (25 MHz) equipped with a PFT-100 Fourier transform system and proton noise decoupler. Data were accumulated in a JEOL JEC-6 computer and JEOL CM-219 IC core memory (8 K) using 4000 Hz sweep widths in 4096 points. ^{13}C spin-lattice relaxation times (^{13}C-T_1) were measured by the inversion-recovery method using a 180°-t-90° pulse sequence, where t is time in seconds between the 180° and 90° pulses. The 90° pulse recycle times were chosen to be at least five times longer than the longest ^{13}C-T_1 to be measured. The estimated error in T_1 was less than ±10%. Unless otherwise specified, the molar concentrations of cycloamyloses were 1.2 times larger than those of phenylalanine to measure the relaxation times of phenylalanine and *vice versa* to measure the relaxation times of cycloamyloses.

The buffer solutions were made up with 85% D_3PO_4, 40% NaOD, and solute phenylalanine in D_2O and the final pD value was 11.3±0.1 and the ionic strength was about 0.5. The acidic solutions were prepared with 38% DCl in D_2O and they were adjusted to be pD 2.0. The 1 mol dm^{-3} NaOD solutions were prepared with 40% NaOD. The pH values were read on a pH-meter Toko Model TP-101 with a micro combination electrode CE103, which enabled the measurement of pH value of solution contained in a NMR sample tube. The pD value was obtained by adding 0.4 to the pH-meter reading for the correction of isotope effect.[7]

The macroscopic viscosities of the solutions used in the ^{13}C relaxation experiments were measured using a Cannon-Finske viscometer. The values of viscosity η were calculated from the formula $\eta=B t\rho$, where B is the calibration constant for viscometer, t is the efflux time between the two predetermined marks, and ρ is the density of the solution. The constant B was determined by using extremely pure water and the η value of water reported in literature.[8]

Ultraviolet absorption (UV) spectra were measured on a Beckman-25 spectrometer.

The temperature was kept at 34±1 °C for all experiments.

Results

Carbon-13 Chemical Shifts. All peaks appeared in the ^{13}C-NMR spectra of both cycloamyloses and phenylalanine have been assigned previously.[3] Among three cycloamyloses, any conspicuous differences in spectral pattern were not observed. As found previously, the spectra of each cycloamylose–phenylalanine system consists of only one set of peaks, indicating that only one type of complexation occurs and/or the chemical exchange of Eq. 1 is rapid process compared with the ^{13}C-NMR time scale,

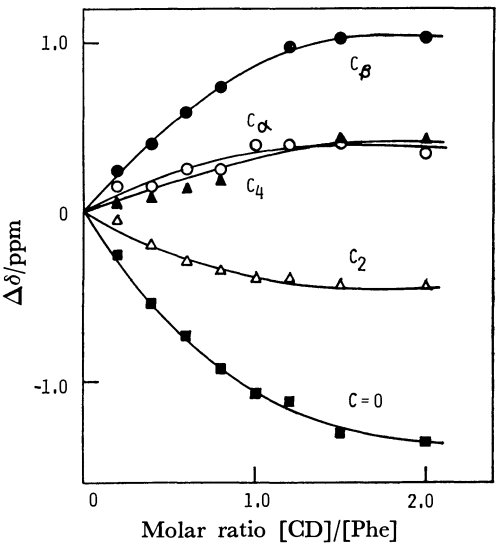

Fig. 1. ^{13}C chemical shifts displacements $\Delta\delta$ of phenylalanine carbons upon addition of β-CD in 1 mol dm^{-3} NaOD solutions as a function of molar ratio [β-CD]/[Phe].

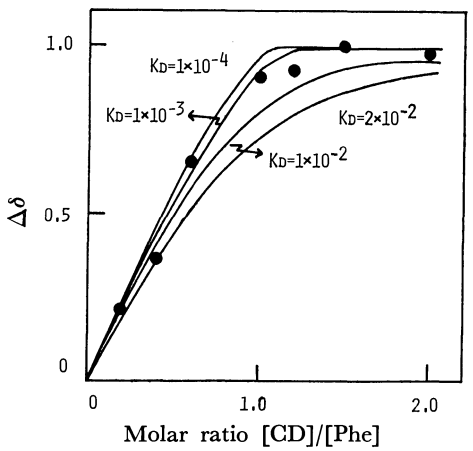

Fig. 2. Theoretically calculated binding curves for a simple CD+Phe⇄[CD,Phe] equilibrium with different dissociation constants K_d. Observed ^{13}C chemical shifts displacements shown in Fig. 1 are normalized and plotted (●).

$$CD + S \rightleftharpoons [CD, S], \quad (1)$$

where CD, S, and [CD, S] are host cycloamylose, guest (substrate) phenylalanine, and cycloamylose–phenylalanine complex, respectively.

Complexation induced small ^{13}C chemical shifts of cycloamyloses and phenylalanine because ^{13}C-NMR is not so much sensitive to perturbation through space as ^{1}H-NMR. By an addition of β-CD in alkaline solution, the resonances of phenylalanine showed exceptionally large shifts, although it is not easy to interpret the magnitudes and the directions of the shifts. Figure 1 shows the chemical shift displacements of phenylalanine carbons upon addition of β-CD in 1 mol dm^{-3} NaOD solutions. No substantial changes in

TABLE 1. VALUES OF ^{13}C NT_1[a] FOR FREE CYCLOHEXA-, CYCLOHEPTA-, AND CYCLOOCTA-AMYLOSES (α-, β-, AND γ-CD), PHENYLALANINE, AND MOLECULAR INCLUSION COMPLEXES BETWEEN THEM AT 34 °C

Compd[b]	Solvent[c]	Concn(M)	^{13}C NT_1(s)±10% Cycloamyloses						
			1	2	3	4	5	6	$\langle T_1\rangle_{1-5}$[d]
[α-CD]	1 mol dm^{-3} NaOD	0.20	0.094	0.086	0.085	0.085	0.094	0.116	0.089
[α-CD, Phe]	1 mol dm^{-3} NaOD	0.20, 0.24	0.074	0.061	0.063	0.067	0.061	0.094	0.065
[β-CD]	1 mol dm^{-3} NaOD	0.20	0.066	0.068	0.071	0.070	0.068	0.096	0.069
[β-CD, Phe]	1 mol dm^{-3} NaOD	0.20, 0.24	0.064	0.054	0.061	0.057	0.054	0.072	0.058
[γ-CD]	1 mol dm^{-3} NaOD	0.20	0.058	0.059	0.059	0.059	0.059	0.080	0.059
[γ-CD, Phe]	1 mol dm^{-3} NaOD	0.20, 0.24	0.057	0.053	0.053	0.055	0.053	0.084	0.054
[α-CD]	buffer	0.10	0.110	0.107	0.112	0.104	0.098	0.132	0.106
[α-CD, Phe]	buffer	0.10, 0.12	0.099	0.093	0.101	0.113	0.090	0.126	0.099
[β-CD]	buffer	0.02, 0.024	0.102	0.083	0.088	0.097	0.083	0.102	0.091
[β-CD, Phe]	buffer	0.025, 0.030	0.110	0.111	0.097	0.103	0.111	0.094	0.106
[γ-CD]	buffer	0.08, 0.096	0.078	0.077	0.084	0.082	0.073	0.118	0.079
[γ-CD, Phe]	buffer	0.08, 0.096	0.082	0.080	0.082	0.094	0.082	0.104	0.084

			Phenylalanine				
			α	β	δ	ε	ζ
[Phe]	1 mol dm^{-3} NaOD	0.20	1.41	1.48	1.91	1.87	1.38
[α-CD, Phe]	1 mol dm^{-3} NaOD	0.24, 0.20	0.56	0.70	0.61	0.60	0.39
[β-CD, Phe]	1 mol dm^{-3} NaOD	0.24, 0.20	0.20	0.24	0.29	0.26	0.17
[γ-CD, Phe]	1 mol dm^{-3} NaOD	0.24, 0.20	0.36	0.42	0.39	0.38	0.25
[Phe]	buffer	0.12, 0.10	1.42	1.82	1.82	1.89	1.20
[α-CD, Phe]	buffer	0.12, 0.10	0.45	0.68	0.62	0.61	0.40
[β-CD, Phe]	buffer	0.036, 0.03	0.32	0.52	0.47	0.41	0.28
[γ-CD, Phe]	buffer	0.12, 0.10	0.40	0.42	0.52	0.54	0.37
[Phe][e]	DCl (pD 2)	0.10	1.34	1.60	1.44	1.44	1.08
[α-CD, Phe][e]	DCl (pD 2)	0.10, 0.10	1.06	1.18	0.91	0.91	0.82

a) Here, T_1 is the spin-lattice relaxation time and N is the number of protons attached to the carbon. The measured NT_1 values correspond to the underlined species. b) Assignments of carbon atoms are as follows.

Cycloamylose (CD)

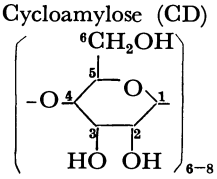

Phenylalanine (Phe)

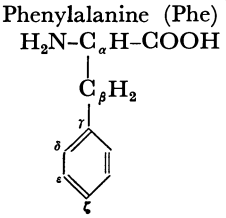

c) Solvent "buffer" is made up with D_3PO_4 and NaOD and the final pD value is 11.3. d) The mean values of T_1 for C_{1-5}. e) The data were reported by Inoue, *et al.*[3]

chemical shifts occur above molar ratio R=[CD]/[Phe] larger than unity, indicating a formation of a 1:1 complex. From this figure, it is possible to determine the value of dissociation constant K_d (reciprocal of the association constant K_a) for cycloamylose–phenylalanine complex by assuming the 1:1 complexation and by using a modified Hildebrand-Benesi equations.[9,10]

Figure 2 shows theoretically calculated binding curves for a simple CD+S⇄[CD,S] equilibrium with different dissociation constants. They realized by the plot of normalized ^{13}C chemical shift changes $\Delta\delta$ against molar ratios [CD]/[Phe]. In Fig. 2 the experimental $\Delta\delta$ corresponding to cycloheptaamylose–phenylalanine system in 1 mol dm^{-3} NaOD solutions were also included. The dissociation constant K_d for this system was estimated to be approximately 10^{-3} M ($K_a=10^3$ M^{-1}:1 M=1 mol dm^{-3}), which was comparable with K_d values of about 3×10^{-3} M for phenylalanine–cyclohexaamylose[3] and –cyclooctaamylose complexes in acidic solutions at pD 2 measured using UV spectral changes.[3,11]

Carbon-13 Spin-Lattice Relaxation Times. In Table 1 are given the values of ^{13}C spin-lattice relaxation times measured for free cycloamyloses, free phenylalanine, and cycloamylose–phenylalanine complexes.

In the limit of rapid exchange process of Eq. 1, one measures an average relaxation rate $(1/T_1)$[12]

$$1/T_1 = P_f\frac{1}{T_{1f}} + P_c\frac{1}{T_{1c}}, \qquad (2)$$

where T_{1f} and T_{1c} are intramolecular spin-lattice

Table 2. Values of ^{13}C NT_1 of phenylalanine(0.4 M) in 1 mol dm^{-3} NaOD solutions in which various amounts of D-glucose was contained at 34 °C

Concentration of D-glucose(M)		^{13}C NT_1(s)±10%				
		α	β	δ	ε	ζ
0.0		1.301	1.284	1.542	1.518	0.977
0.6		1.080	0.934	1.142	1.151	0.721
1.5		0.742	0.670	0.713	0.675	0.456
2.5		—a)	—a)	0.467	0.451	—a)
Concentration of D-glucose(M)	Viscosity(η) of solution(cp)	$NT_1\times\eta$				
0.0	1.51	1.96	1.94	2.33	2.29	1.48
0.6	2.06	2.22	1.92	2.35	2.37	1.48
1.5	3.24	2.40	2.18	2.31	2.19	1.48
2.5	4.91	—a)	—a)	2.29	2.21	—a)

a) Not measured accurately.

relaxation times for a ^{13}C spin at the free and complexed states, and P_f and P_c ($P_f+P_c=1$) are the probabilities that cycloamyloses or the substrates are found in the free and complexed states, respectively. For the reaction (1), the values P_c and P_f can be determined from the association constant.[3] For example, if K_a is 2×10^2 M^{-1} and molar ratio [CD]/[S] is 1.2, the substrate of about 99% exists in the complexed state. In our experimental condition, the values of K_a were larger than 10^2 M^{-1} and the molar concentrations of the cycloamyloses were 1.2 times larger than those of phenylalanine to measure the relaxation times of phenylalanine and *vice versa* to measure the relaxation times of cycloamyloses. Thus we can conclude that the T_1 values observed in the cycloamylose–phenylalanine mixtures are exclusively those of the complexed states. From the T_1 values in Table 1 we shall analyze the molecular motions and discuss the dynamical properties of cycloamylose–phenylalanine complexes.

The Models of Molecular Motion to Describe the Observed T_1 Values. For rapidly rotating molecules with medium size, the ^{13}C relaxation mechanism of the protonated carbon nucleus seems to be governed by ^{13}C-^1H dipole-dipole interaction.[12] In this case, ^{13}C-T_1 for the isotropically reorienting molecule is given by

$$1/NT_1 = \hbar^2\gamma_C^2\gamma_H^2 r_{CH}^{-6}\tau_{eff}, \quad (3)$$

where τ_{eff} is the effective correlation time for overall molecular reorientation, r_{CH} is the carbon-hydrogen bond length, γ_H and γ_C are the gyromagnetic ratios of ^1H and ^{13}C nuclei, and N is the number of directly bonded proton.

According to the Brownian diffusion model,[13] τ_{eff} can be related to the isotropic rotational diffusion constant D by the manner of

$$\tau_{eff} = 1/6D = \frac{8\pi\eta f_r r_o^3}{6kT} = \frac{V_m\eta f_r}{kT}, \quad (4)$$

where k is Boltzmann's constant, T is the absolute temperature, η is the viscosity of the solution in poise (1P=0.1 Pas), r_o is the radius of spherical solute molecule, V_m is the molecular volume $V_m=4/3\pi r_o^3$, and f_r is a microviscosity factor.

For anisotropic molecular motion two or more correlation times must be introduced to interpret the observed T_1 value and τ_{eff} represents a weight average of various correlation times. In general, lengthy procedure is required to construct a model of anisotropic molecular motion. In the case of a rigid ellipsoidal molecule, molecular motions are characterized by two rotational diffusion constants,[13,14] *i.e.*, the diffusion constant for rotation about the symmetry axis, D_a, and that for rotation about any axis perpendicular to the symmetry axis, D_b. For a rigid ellipsoidal molecule in which the C–H internuclear vector makes an angle θ with the symmetry axis, τ_{eff} is defined as a function of angle θ, viscosity η, diffusion constants D_a and D_b, and the lengths of the ellipse semiaxes.[14]

For the group undergoing an additional internal motion as well as isotropic overall molecular reorientation such as phenyl group of phenylalanine,[3] the NT_1 value of a protonated carbon with N directly bonded hydrogens is given by[12,15]

$$\frac{1}{NT_1} = \frac{\hbar^2\gamma_C^2\gamma_H^2}{r_{CH}^6}\tau_{eff}\left[A+B\frac{6\tau_G}{6\tau_G+\tau_{eff}}+C\frac{3\tau_G}{3\tau_G+2\tau_{eff}}\right], \quad (5)$$

where τ_G is the correlation time for internal motion and $A=1/4\ (3\cos^2\theta-1)^2$, $B=3\sin^2\theta\cos^2\theta$, $C=3/4\sin^4\theta$, and θ is the angle between the C–H vector and the axis of internal rotation.

From these discussions, it is clear that the NT_1 value depends on the viscosity of solution, molecular shape and size of rotor, and that the greater the NT_1 value, the more mobile is the ^{13}C moiety and the additional internal rotation faster than the overall one makes the NT_1 value lengthen.

Here we examine the viscosity dependences of ^{13}C-T_1 values. According to model predictions, $NT_1\eta$ values for a specified ^{13}C nuclei must be constant. As seen from Table 2, the expected constancy of $NT_1\eta$ values were certainly observed for phenylalanine in 1 M NaOD aqueous solutions, where the solution viscosities were controlled by adding various amounts of D-glucose. Thus the macroscopic viscosities (macroviscosities[16]) of these solutions, in which there are no specific interaction among solute phenylalanine,

TABLE 3. VALUES OF $NT_1\eta$[a] FOR FREE CYCLOHEXA-, CYCLOHEPTA-, AND CYCLOOCTA-AMYLOSES(α-, β-, AND γ-CD), FREE PHENYLALANINE, AND MOLECULAR INCLUSION COMPLEXES BETWEEN THEM AT 34 °C

Compd	Solvent	Viscosity(cp)	$NT_1\eta$ Cycloamylose						
			1	2	3	4	5	6	$\langle T_1\eta\rangle_{1-5}$[b]
[α-CD]	1 mol dm^{-3} NaOD	2.18	0.205	0.187	0.185	0.185	0.205	0.252	0.19
[α-CD, Phe]	1 mol dm^{-3} NaOD	2.24	0.166	0.137	0.141	0.150	0.137	0.210	0.15
[β-CD]	1 mol dm^{-3} NaOD	2.77	0.183	0.188	0.197	0.194	0.188	0.266	0.19
[β-CD, Phe]	1 mol dm^{-3} NaOD	2.67	0.177	0.144	0.163	0.152	0.144	0.192	0.16
[γ-CD]	1 mol dm^{-3} NaOD	2.98	0.173	0.176	0.176	0.176	0.176	0.238	0.18
[γ-CD, Phe]	1 mol dm^{-3} NaOD	3.28	0.187	0.174	0.174	0.180	0.174	0.276	0.18
[α-CD]	buffer	1.57	0.172	0.168	0.176	0.163	0.154	0.208	0.17
[α-CD, Phe]	buffer	1.30	0.129	0.121	0.131	0.147	0.117	0.164	0.13
[β-CD]	buffer	1.28	0.131	0.106	0.113	0.124	0.106	0.130	0.12
[β-CD, Phe]	buffer	1.06	0.117	0.118	0.103	0.109	0.118	0.100	0.11
[γ-CD]	buffer	1.51	0.118	0.116	0.127	0.124	0.110	0.178	0.12
[γ-CD, Phe]	buffer	1.40	0.115	0.112	0.115	0.132	0.115	0.146	0.12
			Phenylalanine						
			α	β	δ	ε	ζ		
[Phe]	1 mol dm^{-3} NaOD	1.35	1.90	2.00	2.58	2.52	1.86		
[α-CD, Phe]	1 mol dm^{-3} NaOD	2.48	1.39	1.74	1.51	1.49	0.97		
[β-CD, Phe]	1 mol dm^{-3} NaOD	3.13	0.63	0.76	0.91	0.81	0.53		
[γ-CD, Phe]	1 mol dm^{-3} NaOD	3.78	1.36	1.58	1.47	1.44	0.95		
[Phe]	buffer	0.97	1.38	1.76	1.77	1.83	1.16		
[α-CD, Phe]	buffer	1.29	0.58	0.88	0.80	0.79	0.52		
[β-CD, Phe]	buffer	1.04	0.33	0.54	0.49	0.43	0.29		
[γ-CD, Phe]	buffer	1.63	0.65	0.68	0.85	0.88	0.60		
[Phe]	DCl (pD 2)	0.94	1.26	1.50	1.35	1.35	1.02		
[α-CD, Phe]	DCl (pD 2)	1.20	1.27	1.42	1.09	1.09	0.98		

a) Here, T_1 is the spin-lattice relaxation time, N is the number of protons attached to the carbon, and η is the solution viscosity. The $NT_1\eta$ values correspond to the underlined species. The corresponding NT_1 values are given in Table 1. See the footnotes of Table 1, also. b) The mean values of $T_1\eta$ for C_{1-5}.

glucose, and solvent water, could be related to the observed T_1 behavior. We have shown in the previous paper[3] that the isotropic diffusion model expressed by Eqs. 3 and 4 was applicable to analyses of the overall molecular reorientation of both free α-CD and aromatic amino acids in acidic aqueous solutions.

In this paper we shall adopt the value of $NT_1\eta$ to investigate the complexation effect on the molecular motions. The $NT_1\eta$ values were tabulated in Table 3 with the viscosities. As shown in Table 1, for cycloamyloses in the free and the complexed states, the T_1 values for the pyranose ring carbons C_{1-5} are equal within experimental error in each system, indicating the absence of specific fast internal motion. Thus the mean value $\langle NT_1\eta\rangle_{1-5}$ could be used to discuss the overall motion of cycloamyloses. It is noticeable that α-, β-, and γ-CD in the free states have nearly the same $\langle NT_1\eta\rangle_{1-5}$ values. These results contradict to the model prediction of Eqs. 3 and 4, which stand for the inverse dependence of ^{13}C-T_1 value on molecular volume V_m. The lack of inverse correlation between ^{13}C-T_1 and V_m have been found for several molecules with higher molecular weight in which the various local motions such as segmental motions (localized motion along a backbone of a chain molecule) play a predominant role in ^{13}C relaxation.[17,18] The $\langle NT_1\eta\rangle_{1-5}$ values of cycloamyloses may be looked upon as standing for the measures of segmental motions.

In the case of phenylalanine, the axis of rotation of the phenyl ring about C_β–C_γ bond is identical with the C_ζ–H bond. Therefore, the rotation about C_β–C_γ bond cannot affect the T_1 values of C_ζ, since $\theta=0°$ and Eq. 5 is reduced to Eq. 3. Thus we can estimate the contribution of phenyl ring rotation to the T_1 values of ring carbons by comparing the T_1 values of $C_{\delta,\varepsilon}$ and C_ζ.[19,20] The $NT_1\eta$ values show the existence of rapid internal rotation of the primary alcohol group of cycloamyloses and the phenyl group of phenylalanine even in the complexed states. The $NT_1\eta$ values of free phenylalanine are not constant but increase greatly with pD values of solutions. According to model prediction, these pD dependences reflect the changes in apparent molecular volume of phenylalanine probably due to the pD depending changes in solvation states of charged groups. If the dynamic coupling between solute and solvent is strong, it is necessary to increase to molecular volume of the solute with that of strongly bound solvent molecules in order for it to fit the theoretical prediction.

We will discuss the complexation effect on the molecular motion of phenylalanine at different pD by comparing $NT_1\eta$ ratios between free and complexed states at same pD.

Discussion

Effect of Complexation on the Molecular Motion of Cycloamyloses and Phenylalanine. As can be seen in Table 3, all the $NT_1\eta$ values for phenylalanine greatly decrease by complexation with cycloamyloses, while those for cycloamyloses decrease slightly or remain unchanged. The reductions of the $NT_1\eta$ values are explainable with a term of the increase in apparent molecular volume by complexation as expected from Eqs. 3 and 4. Since the molecular volumes of cycloamyloses are six to nine times larger than that of phenylalanine, the change in molecular dimension induced by complexation is relatively small for cycloamyloses and relatively large for phenylalanine, namely the reductions in $NT_1\eta$ values of the former are smaller than the latter.

For the substrate phenylalanine, the greater the dynamic coupling with the host cycloamyloses, the greater is the increase in apparent molecular volume of phenylalanine. Thus the degree of $NT_1\eta$ reduction may be used as the measure of the strength of dynamic coupling of phenylalanine with cycloamyloses. In Table 4, it is shown the ratios of $NT_1\eta$ values of the complexed to the free states of phenylalanine. It is noticeable that the $NT_1\eta$ values of phenyl carbons show larger changes by complexation than those of other carbons indicating the larger slowing down of the internal rotation of the phenyl ring than that of the overall reorientation. These results are clearly showing the formation of the inclusion complexes of the guest phenylalanine with the host cycloamyloses by an insertion of the phenyl ring into the cavity of cycloamylose even in the case of γ-CD. The results that the NT_1 values of C_δ and C_ε in phenyl ring agree well with each other and they are always larger than those of C_ζ indicate that cycloamyloses favor the axial inclusion in which the internal rotation axis C_γ–C_ζ of the phenyl ring is parrallel to the axis of the cycloamylose cavity.

TABLE 4. VALUES OF $NT_1\eta$[a] RATIOS OF THE COMPLEXED STATES TO FREE STATES OF PHENYLALANINE

Compound	Solvent	$(NT_1\eta)_{complex}/(NT_1\eta)_{free}$			
		α	β	$\langle\delta, \varepsilon\rangle$[b]	ζ
[α-CD, Phe]	1 mol dm^{-3} NaOD	0.73	0.87	0.59	0.52
[β-CD, Phe]	1 mol dm^{-3} NaOD	0.33	0.38	0.34	0.29
[γ-CD, Phe]	1 mol dm^{-3} NaOD	0.72	0.79	0.57	0.51
[α-CD, Phe]	buffer (pD 11.3)	0.42	0.50	0.44	0.45
[β-CD, Phe]	buffer (pD 11.3)	0.24	0.31	0.26	0.25
[γ-CD, Phe]	buffer (pD 11.3)	0.47	0.39	0.48	0.52
[α-CD, Phe]	DCl (pD 2)	1.00	0.95	0.80	0.96

a) Here, T_1 is the spin-lattice relaxation time, N is the number of protons attached to the carbon, and η is the solution viscosity. The corresponding $NT_1\eta$ values are given in Table 3. See the footnotes of Table 1, also. b) The mean values of $NT_1\eta$ for C_δ and C_ε were used.

Effects of Cavity Size of Cycloamyloses and Medium pD on Complexation. As can be seen in Table 4, the phenyl $NT_1\eta$ values of phenylalanine suffer the largest reduction by complexation with β-CD. In these systems, the C_α- and C_β-$T_1\eta$ values also suffer the largest reductions. On the other hand, the phenyl $NT_1\eta$ values show the comparable reductions by complexation with α-CD and with γ-CD. These findings are observed in spite of the medium pD values, and can be explained with a term of the cavity size effect on complexation. According to the space-filling models, β-CD has the best fitting cavity size for the complete and tight inclusion of phenyl ring. The molecular model also suggests that the complete inclusion of the phenyl ring of phenylalanine into the α-CD cavity is sterically unfavorable and the extent of inclusion is shallow. On the contrary, γ-CD has enough cavity size for deep and loose inclusion of phenyl ring. As the results, the substrate phenylalanine is more strongly fixed in β-CD cavity and rather loosely in α- and γ-CD cavities. The shallow and deep inclusions of the phenyl ring into the cavities of α-CD and γ-CD, respectively, are also suggested by the reductions of $NT_1\eta$ values of C_β (Table 4), *i.e.*, those in [γ-CD, Phe] systems are larger than those in [α-CD, Phe] systems. The deep insertion of the phenyl ring obstructs a rotational motion of C_β around the C_α–C_β and C_β–C_γ bonds due to an increase in steric hindrance.

Several mechanisms have been proposed for the formation of cycloamylose inclusion complexes,[21-24] but the forces leading the complexation are still unclear and a matter of speculation.[1,23] Among the proposed mechanisms, hydrophobic interaction seems to be the most probable as the driving force for cycloamylose–phenylalanine complexation investigated here. In this case, the presence of additional interactions will be alter the strength of dynamic coupling between cycloamylose and phenylalanine. The pD dependences of $NT_1\eta$ values of phenylalanine must be analysed by taking into account of at least three additional factors, *i.e.*, hydrogen bonding, electrostatic interactions between host cycloamylose and guest phenylalanine, and solvation of charged groups.[25]

Since the complexation geometry which disturbs a solvation of the protonated amino group (pK 1.8) or the carboxylate anion (pK 9.24) of phenylalanine is energetically unpreferable, the inclusions of these groups into the cavity of cycloamylose are excluded. It is noticeable that the $NT_1\eta$ values of phenylalanine show the largest complexation-induced reductions at pD 11.3. Especially the reductions of C_α-$NT_1\eta$ values in three phenylalanine–cycloamylose systems at pD 11.3 are pronounced as compared with those at other pD values. These results suggest the existence of the hydrogen bond between the peripheral secondary hydroxyl groups and the amino and carboxyl (carboxylate) groups of phenylalanine. The reduction of C_α motion of phenylalanine may be due to the anchoring effect of the hydrogen bond at the chain end.[25,26]

In 1 mol dm^{-3} NaOD solutions, secondary hydroxyl groups of cycloamyloses (pK 12.0) are dissociated and

they interact repulsively with carboxylate anion of phenylalanine. These interactions reduce the strength of complexation and are explaining the reason why the reductions of $NT_1\eta$ values in 1 mol dm^{-3} NaOD solution are smaller than those in buffer solution. It is not clear at present that the $NT_1\eta$ values of phenylalanine show the smallest reductions at pD 2. More informations, especially about the solvation states, are required for the definitive explanation.

Conclusion

The cycloamylose inclusion complexes with phenylalanine show some characteristics like general peculiarities of enzyme–substrate complex. The host cycloamyloses have the hydrophobic cavity leading to specific binding of guest. The hydrophobic interaction seems to be the most probable as the driving force for the complexation of cycloamylose with phenylalanine. For these systems, the shape matching between the host cavity and the guest inserting group is one of the factors determining the strong coupling between them. It was found that the strength of the dynamic coupling depends on the cavity size of cycloamylose and pD value of solution. The strongest coupling was observed for the β-CD–phenylalanine system in phosphate buffer solution at pD 11.3, where the phenyl ring of guest is deeply and tightly included into the cavity. The inclusion of phenyl ring into the cavity is shallow and loose in the case of α-CD and is deep and loose in the case of γ-CD. The dynamic coupling is strengthened by the hydrogen bonding between the secondary hydroxyl groups of cycloamylose and the amino and carboxyl groups of phenylalanine, and is weakened by the repulsive interaction between alkoxyl anion of cycloamylose and carboxylate anion of phenylalanine. It is noteworthy that, even in the tightly coupled [β-CD, Phe] system in phosphate buffer, the $NT_1\eta$ values of phenylalanine are about four times larger than the $<NT_1\eta>_{1-5}$ values of cycloamylose and phenyl ring rotate rapidly in the cavity. Thus the dynamic coupling of phenylalanine and cycloamylose is weak and they have extensive independency of molecular motions. The characterizations of cycloamylose complexation by molecular dynamics as well as thermodynamics should offer useful informations for an application of cycloamyloses in various fields.

Finally we should refer to the validity of assignment η appeared in Eq. 4 to the solution macroviscosity. It is known that in some cases the macroviscosities of solutions are not related to the observed ^{13}C-T_1 behavior.[16] For these cases the microviscosities as defined by the various local molecular motions and local molecular interactions should be used as the values of viscosity η. Thus the alternative explanations are possible for the causes of the changes in $NT_1\eta$ values of phenylalanine carbons induced by complexation; in the first one the macroviscosity is used as the η value and the changes in $NT_1\eta$ values are attributed to those in apparent molecular volume; in another the molecular volume is looked upon as constant and the changes are attributed to those in microviscosities. In this paper we discussed the changes in $NT_1\eta$ values based on the first one, because we have no mean to measure the microviscosity. Since the NT_1 values of phenylalanine in the free states at constant pD value were inversely proportional to the macroviscosity as expected from the diffusion model, we can safely discuss the complexation effects on the molecular motions based on the first explanation.

The present work was partially supported by a Grant-in-Aid for Scientific Research from the Minister of Education, Science and Culture (1979, 1980). The authors thank Professor R. Chûjô of Tokyo Institute of Technology for stimulating discussions during this work.

References

1) a) R. J. Bergeron, *J. Chem. Educ.*, **54**, 204 (1977); b) M. L. Bender and M. Komiyama, "Reactivity and Structure Concepts in Organic Chemistry, Vol. 6, Cyclodextrin Chemistry," Springer-Verlag, New York (1978), and references cited therein.

2) R. Breslow, M. F. Czarniecki, J. Emert, and H. Hamaguchi, *J. Am. Chem. Soc.*, **102**, 762 (1980).

3) Y. Inoue, Y. Katôno, and R. Chûjô, *Bull. Chem. Soc. Jpn.*, **52**, 1692 (1979).

4) R. L. VanEtten, G. A. Clowes, J. F. Sebastian, and M. L. Bender, *J. Am. Chem. Soc.*, **89**, 3253 (1967).

5) T. -F. Chin, P. -H. Chung, and J. L. Lach, *J. Pharm. Sci.*, **57**, 44 (1968).

6) D. French, M. L. Levine, J. H. Pazur, and E. Norberg, *J. Am. Chem. Soc.*, **71**, 353 (1949).

7) P. K. Glasoe and F. A. Long, *J. Phys. Chem.*, **64**, 188 (1960).

8) "Lange's Handbook of Chemistry," 11th ed, ed by J. A. Dean, McGraw-Hill Book Co., New York (1973), p. 10—288.

9) D. J. Wood, F. F. Hruska, and W. Saenger, *J. Am. Chem. Soc.*, **99**, 1735 (1977).

10) R. J. Bergeron, M. A. Channing, G. J. Gibeily, and D. M. Pillor, *J. Am. Chem. Soc.*, **99**, 5146 (1977).

11) The solubility of cycloheptaamylose in acidic D_2O is too small to observe the UV spectra. The dissociation constants in alkaline solutions also could not be determined accurately by UV spectra due to an overlapping of large peak of alkoxide anion.

12) A. Allerhand, D. Doddrell, and R. Komoroski, *J. Chem. Phys.*, **55**, 189 (1971).

13) J. H. Noggle and R. E. Schirmer, "The Nuclear Overhauser Effect," Academic Press, New York, N. Y. (1971).

14) R. Deslauries, A. C. M. Paiva, K. Schaumburg, and I. C. P. Smith, *Biochemistry*, **14**, 878 (1975).

15) D. Doddrell, V. Glushko, and A. Allerhand, *J. Chem. Phys.*, **56**, 3683 (1972).

16) J. R. Lyerla and G. C. Levy, "Topics in ^{13}C NMR Spectroscopy," ed by G. C. Levy, (1974), Vol. 1, Chap. 3.

17) A. Allerhand and R. K. Hailstone, *J. Chem. Phys.*, **56**, 3718 (1972).

18) Y. Inoue, A. Nishioka, and R. Chûjô, *J. Polym. Sci. Polym. Phys. Ed.*, **11**, 2237 (1973).

19) G. C. Levy, J. D. Cargioli, and F. A. L. Anet, *J. Am. Chem. Soc.*, **95**, 1527 (1973).

20) a) Y. Inoue and T. Konno, *Polymer J.*, **8**, 457 (1976); b) Y. Inoue, T. Konno, and K. Nakajima, *ibid.*, **9**, 127

(1977).
21) F. Cramer and H. Hettler, *Naturwissenschaften*, **54**, 625 (1967).
22) F. Cramer, W. Saenger, and H. -Ch. Spatz, *J. Am. Chem. Soc.*, **89**, 14 (1967).
23) W. Saenger, M. Noltemeyer, P. C. Manor, B. Hingerty, and B. Klar, *Bioorg. Chem.*, **5**, 187 (1976).
24) I. Tabushi, Y. Kiyosuke, T. Sugimoto, and K. Yamamura, *J. Am. Chem. Soc.*, **100**, 916 (1978).
25) The p*K* values of amino and carboxyl groups of phenylalanine and secondary hydroxyl groups of cycloamylose are about 1.8, 9.24, and 12.0, respectively.
26) D. Doddrell and A. Allerhand, *J. Am. Chem. Soc.*, **93**, 1558 (1971).
27) U. Edlund, C. Holloway, and G. C. Levy, *J. Am. Chem. Soc.*, **98**, 5069 (1976).

  Bull. Chem. Soc. Jpn., 54, 817—821 (1981)

New Synthetic Route for the Preparation of 4-Phenylthio-4-butanolide Derivatives by the Use of the Pummerer Rearrangement

Mikio WATANABE, Seijin NAKAMORI, Hatsue HASEGAWA,
Kozo SHIRAI, and Takanobu KUMAMOTO*

Department of Chemistry, Faculty of Science, Tokai University, Kitakaname, Hiratsuka, Kanagawa 259-12

(Received August 6, 1980)

The Pummerer rearrangement reaction of 2- or 3-substituted 4-(phenylsulfinyl)butyric acids in the presence of an excess amount of acetic anhydride and a catalytic amount of *p*-toluenesulfonic acid in refluxing toluene for 1 h afforded 2- or 3-substituted 4-phenylthio-4-butanolide (**17a—f**). Thermolysis in pyridine of 4-phenylsulfinyl 4-butanolides, which were prepared by oxidation of **17a—f**, afforded 2- or 3-substituted 2- or 3-buten-4-olides.

The Pummerer rearrangement reaction is an important reaction in the sulfoxide chemistry because of its wide applicability to the synthesis of many types of organic compounds. However, only few instances have been reported of applications of this rearrangement to a cyclization reaction. Numata and Oae reported that *o*-carboxyphenyl alkyl sulfoxide was cyclized easily by the pummerer reaction to give 3,1-benzoxathiin-4-one.[1] In our earlier studies, we showed that 2- or 3-phenylthio-4-butanolide derivatives could be used for the synthesis of 3- or 2-substituted 2-buten-4-olides.[2,3] In this paper, we wish to report a new synthetic route to 2- or 3-substituted 4-phenylthio-4-butanolides (**17a—f**) from 2- or 3-substituted 4-(phenylsulfinyl)butyric acids (**9a—f**); this route involves the Pummerer rearrangement in the cyclization step. We also investigated the dehydrosulfenylation reaction of **17a—f** to form 2- or 3-buten-4-olides.

Results and Discussion

Synthesis of 4-(Phenylsulfinyl)butyric Acid (4) and Cyclization Reaction of 4 to Form 4-Phenylthio-4-butanolide (6). Preparation of 4-(phenylsulfinyl)butyric acid was carried out by the usual oxidation of 4-(phenylthio)-butyric acid, which had been synthesized by the method of Lamdan and Albarracin[4] (see Scheme 1).

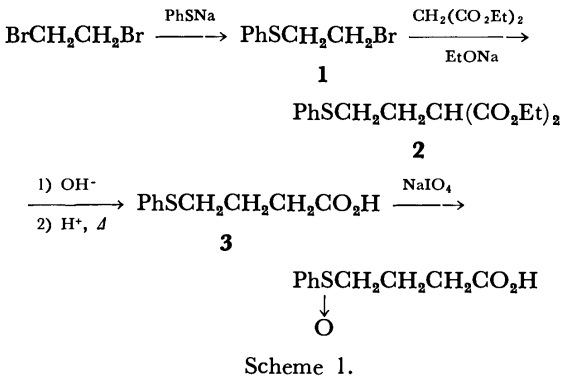

Scheme 1.

It was found that when **4** was allowed to react with acetic anhydride in the presence of *p*-toluenesulfonic acid in refluxing toluene for 1 h, 4-phenylthio-4-butanolide (**6**) was obtained in 75% yield. This reaction involves an intramolecular ester exchange reaction of intermediate (**5**) which was formed by the Pummerer rearrangement of **4**.

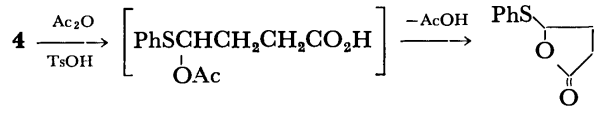

5 **6**

When the reaction was carried out in the absence of *p*-toluenesulfonic acid, starting material **4** was recovered completely. The investigation of other acid catalysts, such as phosphoric acid and chloroacetic acid, did not give good results. In this reaction, benzene and xylene were also examined as solvents, but **6** was obtained only in lower yields (see Table 1).

Preparation of 2- or 3-Substituted 4-Phenylthio-4-butanolides. The reaction sequence for the preparation of 2- or 3-substituted 4-phenylthio-4-butanolides (**17a—f**) is shown in Scheme 2.

The alkylation of **2** by alkyl halides such as methyl iodide, butyl bromide or allyl bromide were carried out in the usual way to give diethyl 2-alkyl-2-(2-phenylthioethyl)malonates (**7a—c, 7g**) in 66—89% yields (see Table 2). However, for the synthesis of **7a—c** and **7g**, when the reaction of alkyl halide with diethyl malonate was carried out as the first step and the resulting alkylated diethyl malonate was allowed to react with **1**, the yields of **7a—c** and **7g** became very low because of the formation of phenyl vinyl sulfide.

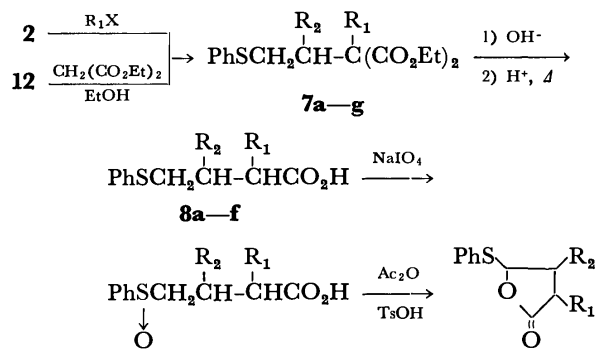

a: R_1=Me, R_2=H
b: R_1=*n*-Bu, R_2=H
c: R_1=$PhCH_2$, R_2=H
d: R_1=H, R_2=Me
e: R_1=H, R_2=Ph
f: R_1=H, R_2=Et
g: R_1=CH_2=CH-CH_2-, R_2=H

Scheme 2.

TABLE 1. THE CYCLIZATION REACTION OF **4** TO FORM **6**

Entry	Catalyst	Reaction conditions Solvent	Reflux time	Yield/%
1	—	Benzene	10 h	—
2	TsOH	Benzene	3 h	56
3	$ClCH_2CO_2H$	Benzene	14 h	10
4	H_3PO_4	Benzene	6 h	15
5	TsOH	Toluene	1 h	75
6	TsOH	Xylene	0.5 h	50
7	TsOH	$CHCl_3$	2 h	40
8	TsOH	THF	3 h	20

Further steps to form 2-substituted 4-(phenylsulfinyl)butyric acids (**9a**—**c**) were conducted as in the preparation of **4**. Yields and spectral data of **8a**—**c** are summarized in Table 3. **9a**—**c** could be used for the next cyclization step without further purification. In the case of the hydrolysis and decrboxylation of **7g**, it was found that the resulting carboxylic acid derivative was converted spontaneously to 4-methyl-2-(2-phenylthioethyl)-4-butanolide (**16**) in 55% yield by the intramolecular addition of a carboxyl group to the double bond.

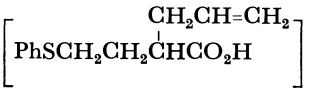

7g —(1) OH^-, (2) H^+, Δ→ [$PhSCH_2CH_2\underset{|}{C}HCO_2H$, $CH_2CH{=}CH_2$]

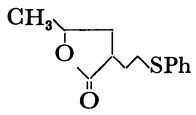

16

For the preparation of 3- or 4-substituted 4-(phenylsulfinyl)butyric acid, bromides **12** and **15** were required, and α-phenylthio ketones and α-phenylthio esters were employed as the starting materials. Reduction of α-(phenylthio)acetone (**10a**) or α-(phenylthio)-acetophenone (**10b**) with sodium borohydride in methanol at 0 °C gave the corresponding alcohols (**11a**, **b**) in high yields. These alcohols were allowed to react with phosphorus tribromide in refluxing carbon tetrachloride to give 2-bromopropyl phenyl sulfide (**12a**) and 2-bromo-2-phenylethyl phenyl sulfide (**12b**).

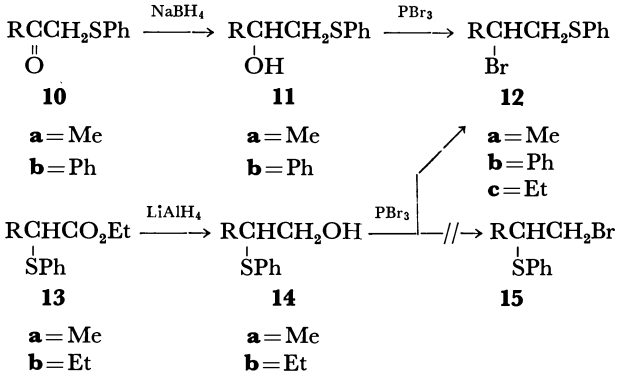

In a similar way, α-phenylthio esters such as ethyl 2-(phenylthio)propionate (**13a**) or ethyl 2-(phenylthio)butyrate (**13b**) were reduced with lithium aluminium hydride in THF at 0 °C to form corresponding alcohols (**14a**, **b**) in good yields. However, bromination of **14a** and **14b** by phosphorus tribromide gave the unexpected result of yielding **12a** and **12c** because of migration of the phenylthio group. Formation of **8d**—**f** to **9d**—**f** as performed in the usual way, as mentioned above.

The yield and spectral data of **7a**—**g** and **8a**—**f** are summarized in Table 2 and Table 3 respectively.

The reaction of **9a**—**f** thus obtained with acetic anhydride in the presence of *p*-toluenesulfonic acid in refluxing toluene for 1 h resulted in the formation of 4-phenylthio-4-butanolide derivatives (**17a**—**f**) in 27—73% yields. These results are summarized in Table 4.

*Elimination of Phenylthio Group from **17a**—**f** to Buten-4-olides.* It is well known that 2-phenylsulfinyl or 2-alkylsulfinyl-4-butanolide derivatives were converted smoothly to 2-buten-4-olides by thermal decomposition.[6-8] Further, in our previous paper, we described how 3-phenylsulfinyl-4-butanolides were also decom-

TABLE 2. YIELDS AND SPECTRAL DATA OF **7a**—**f**

Compd	Yield %	IR $\nu_{C=O}$ cm^{-1}	MS M$^+$(*m*/*e*)	^{1}H NMR ($CDCl_3$) δ
7a	81	1710	310	1.22 (6H, t), 1.44 (3H, s), 1.90—2.50 (2H, m) 2.94—3.10 (2H, m), 4.71 (4H, q), 7.02—7.48 (5H, m)
7b	66	1710	352	0.88 (3H, t), 1.21 (6H, t), 1.72—3.10 (10H, m), 4.71 (4H, q), 7.04—7.44 (5H, m)
7c	88	1720	384	1.17 (6H, t), 1.90—2.30 (2H, m), 2.40—3.06 (2H, m), 3.18 (2H, s), 4.08 (4H, q), 6.74—7.36 (10H, m)
7d	61	1730	310	1.15 (3H, d), 1.25 (6H, t), 2·12—3.80 (4H, m), 4.18 (4H, q), 7.10—7.54 (5H, m)
7e	39[a]	1730	372	0.94 (4H, t), 1.24 (3H, t), 2.74—4.04 (4H, m), 4.20 (4H, q), 7.00—7.38 (10H, m)
7f	65	1740	324	0.78—3.20 (14H, m), 3.67—4.43 (5H, m), 7.37—7.60 (5H, m)
7g	89	1730	336	1.20 (6H, t), 2.00—3.10 (6H, m), 4.18 (4H, q), 4.89—5.94 (3H, m), 7.10—7.54 (5H, m)

a) This yield is from alcohol **11b**.

Table 3. Yields and spectral data of **8a—f**

Compd	Yield %	IR $\nu_{C=O}$ cm^{-1}	MS M$^+$(*m/e*)	^{1}H NMR ($CDCl_3$) δ
8a	57	1700	210	1.20 (3H, d), 1·41—2.32 (3H, m), 2.58 (2H, q), 2.96 (2H, t), 7.14—7.54 (5H, m), 11.75 (1H, s)
8b	82	1700	252	0.90 (3H, t), 1.11—3.40 (11H, m), 7.05—7.41 (5H, m), 10.98 (1H, s)
8c	57	1720	286	1.00—1.36 (2H, m), 2.42—3.36 (4H, m), 3.84—4.30 (1H, m), 7.02—7.30 (10H, m), 10.77 (1H, s)
8d	50	1710	210	1.09, 1.07 (3H, dd), 1.64—3.40 (5H, m), 6.98—7.44 (5H, m), 10.38 (1H, s)
8e	48	1710	272	2.32—3.40 (5H, m), 6.94—7.38 (10H, m), 9.76 (1H, bs)
8f	60	1720	224	1.03 (3H, t), 1.30—2.17 (3H, m), 2.43—3.17 (4H, m), 7.03—7.53 (5H, m), 10.73 (1H, bs)

Table 4. Yields and spectral data of **17a—f**

Compd	Yield %	IR $\nu_{C=O}$ cm^{-1}	MS M$^+$(*m/e*)	^{1}H NMR ($CDCl_3$) δ
17a	51	1780	208	1.27 (3H, d), 1.68—3.10 (3H, m), 5.58—5.90 (1H, m), 7.14—7.62 (5H, m)
17b	68	1780	250	0.92 (3H, t), 1.10—3.05 (9H, m), 5.55, 5.97 (1H, m), 7.27—7.85 (5H, m)
17c	63	1770	283	1.36—3.50 (5H, m), 5.50, 5.80 (1H, m), 7.00—7.58 (10H, m)
17d	52	1780	208	1.35—1.47 (3H, m), 1.97—2.87 (3H, m), 5.18—5.37 (1H, m), 7.10—7.63 (5H, m)
17e	56	1790	270	2.59—2.93 (2H, m), 3.30—4.10 (1H, m), 5.53 (1H, d), 7.03—7.53 (10H, m)
17f	22	1790	222	0.93 (3H, t), 1.16—2.68 (5H, m), 5.30—6.40 (1H, m), 7.13—7.50 (5H, m)

posed to 2-buten-4-olides by refluxing THF in the presence of triethylamine.

Oxidation of **17a—f** with *m*-chloroperbenzoic acid (MCPBA) in dichloromethane at 0 °C gave 4-phenylsulfinyl-4-butanolide derivatives (**18a—f**). When the elimination reaction of **18a—f** carried out in refluxing pyridine for 3 h, the double bond of some products isomerized to 2-position from 3-position of buten-4-olide.[9] In the cases of **18d** and **18f**, the double bond

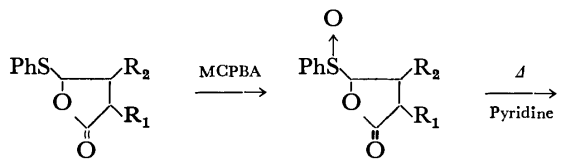

17a—f **18a—f**

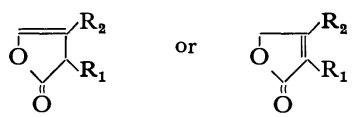

19d, f **20a—c, e**

d: R_1=H, R_2=Me
f: R_1=H, R_2=Et
a: R_1=Me, R_2=H
b: R_1=*n*-Bu, R_2=H
c: R_1=$PhCH_2$, R_2=H
e: R_1=H, R_2=Ph

Table 5. Formation of 2- or 3-buten-4-olides

Compd	IR $\nu_{C=O}$ cm^{-1}	Yield %
19d	1800	73
19e	1800	57
20a	1750	27
20b	1750	70
20c	1750	64
20e	1740	48

remained at 3-position; the other cases, however, gave only products in which the double bond was isomerized to 2-position.

The structures of these compounds were determined by IR and NMR spectra. In particular, the IR spectrum of **20a—c** and **20e** showed the carbonyl absorption at 1750 cm^{-1} and **19d** and **19f** showed the carbonyl absorption at 1800 cm^{-1}.

Experimental

Preparation of 4-Phenylthio-4-butanolide (6). A mixture of 4-(phenylsulfinyl)butyric acid (**4**, 0.69 g, 3 mmol), 1.53 g (15 mmol) of acetic anhydride, and a catalytic amount of

p-toluenesulfonic acid in 20 ml of toluene was heated under reflux for 1 h. The solvent and excess acetic anhydride were removed under reduced pressure. The residue was chromatographed on silica gel using benzene, and gave 0.44 g (75%) of **6**. IR (NaCl): 1780 cm^{-1} (C=O). NMR ($CDCl_3$) δ=1.88—2.52 (4H, m), 5.44 (1H, t), 6.75—7.22 (5H, m). MS: *m/e* 194 (M^+). Found: C, 61.73; H, 5.21%. Cacld for $C_{10}H_{10}O_2S$: C, 61.85; H, 5.19%.

Preparation of Diethyl 2-Methyl-2-(2-phenylthioethyl)malonate (7a). To a solution of sodium ethoxide, prepared from sodium (0.42 g, 18 mmol) and 25 ml of ethanol, was added a solution of **2** (4.50 g, 18 mmol) in ethanol (5 ml). The mixture was refluxed for 15 min. After the reaction mixture was cooled to room temperature, methyl iodide (2.59 g, 18 mmol) was added into the reaction mixture, which was then refluxed for 4 h. The resulted precipitate was filtered and the solvent was evaporated under reduced pressure. 10% Hydrochloric acid (20 ml) was added into the residue and the mixture was extracted with ether and dried. After removal of the solvent, the residue was chromatographed on silica gel using benzene to give **7a** (3.81 g, 81%). Spectral data are summarized in Table 2.

In a similar manner, **7b**, **c**, **d** were prepared from **2** with butyl bromide, benzyl bromide, or allyl bromide. These results are also summarized in Table 2.

Preparation of 1-Phenylthio-2-propanol (11a) and 1-Phenyl-2-(phenylthio)ethanol (11b). Sodium borohydride (1.96 g, 52 mmol) was added slowly to a 50 ml methanol solution of α-(phenylthio)acetophenone (6.64 g, 40 mmol) at 0 °C. The reaction mixture was stirred for 3 h at 0 °C and then quenched with 10 ml of acetic acid. After removal of the solvent, 50 ml of water was added to the mixture and the mixture was extracted with ether and dried. Removal of ether and distillation of residual oil under reduced pressure gave **11a** (5.29 g, 79%). Bp 115 °C/9 mmHg.

In a similar manner, **11b** was obtained in quantitative yield. In this case, product **11b** was isolated by column chromatography on silica gel by using benzene.

Bromination of 11a, b. A carbon tetrachloride (10 ml) solution of **11a** (10.00 g, 60 mmol) was added dropwise to phosphorus tribromide (16.13 g, 60 mmol) in 50 ml of carbon tetrachloride by refluxing gently. The reaction mixture was poured into ice-cold water, extracted with carbon tetrachloride, and dried. Removal of the solvent and distillation under reduced pressure gave 2-bromo-1-(phenylthio)-propane (**12a**) in 80% yield. Bp 115—122 °C/10 mmHg.

In the case of **11b**, the bromination reaction was conducted in a similar manner bromide **12b** was used for the next reaction without further purification because it was hydrolized easily to **11b**.

Preparation of Diethyl (1-Substituted 2-Phenylthioethyl)malonate (7d—f). To an abs ethanol solution of sodium salt of diethyl malonate, which was prepared from diethyl malonate (2.98 g, 19 mmol) and sodium (0.43 g, 19 mmol) in 50 ml of abs ethanol, was added a ethanol solution of bromide **12a** (3.58 g, 15 mmol). The reaction mixture was refluxed for 4 h. After removal of the resulting sodium bromide by filtration, the filtrate was evaporated under reduced pressure. 10% Hydrochloric acid (20 ml) was added to this residue. The mixture was extracted with ether and dried. After removal of the solvent, the excess amount of diethyl malonate was distilled away under reduced pressure. The residue was chromatographed on silica gel by using benzene–petroleum ether (1:1) and gave **7d** (2.95 g, 61%).

In a similar manner, **7e** and **7f** were obtained. The yields and spectral data are summarized in Table 2.

Preparation of 2- or 3-Substituted 4-(Phenylthio)butyric Acid (8a—f). A solution of **7a** (8.97 g, 29 mmol) and 50 ml of 20% sodium hydroxide in 50 ml of ethanol was refluxed for 6 h. After removal of ethanol, 80 ml 10% hydrochloric acid was added to this residue. The mixture was extracted with ether and then the etheral layer was evaporated under reduced pressure. To this residue was added 50 ml of 3 mol dm^{-3}-sulfuric acid. The reaction mixture was heated under reflux for 10 h and then cooled to room temperature. The reaction mixture was extracted with ether and dried. After removal of the solvent, the residue was chromatographed on silica gel using benzene–ether (10:1) to give 2-methyl-4-(phenylthio)butyric acid (**8a**, 3.03 g, 50%).

In a similar manner, **8b**—**f** were also obtained the yields and spectral data of **8a**—**d** are given in Table 3.

Elemental analyses of **8a**—**f** are as follows:

2-Methyl-4-(phenylthio)butyric Acid (8a). Found: C, 62.75; H, 7.09%. Calcd for $C_{11}H_{14}O_2S$: C, 62.84; H, 6.71%.

2-Butyl-4-(phenylthio)butyric Acid (8b). Found: C, 66.44; H, 7.94%. Calcd for $C_{14}H_{20}O_2S$: C, 66.64; H, 7.79%.

2-Benzyl-4-(phenylthio)butyric Acid (8c). Found: C, 66.49; H, 6.28%. Calcd for $C_{17}H_{18}O_2S$: C, 66.65; H, 5.82%.

3-Methyl-4-(phenylthio)butyric Acid (8d). Found: C, 61.26; H, 6.44%. Calcd for $C_{11}H_{14}O_2S$: C, 61.21; H, 6.19%.

3-Phenyl-4-(phenylthio)butyric Acid (8e). Found: C, 69.77; H, 5.61%. Calcd for $C_{16}H_{16}O_2S$: C, 69.75; H, 5.46%.

3-Ethyl-4-(phenylthio)butyric Acid (8f). Found: C, 63.83; H, 7.10%. Calcd for $C_{12}H_{16}O_2S$: C, 64.25; H, 7.19%.

Oxidation of 8a—f. To a solution of sodium metaperiodate (4.00 g, 19 mmol) in water (50 ml) was added a 50 ml of ethanol solution of **8a** (3.03 g, 14 mmol) with stirring at 0 °C. The reaction mixture was stirred for 12 h at 0 °C and was then filtered. The precipitate of sodium iodate was washed with chloroform. The filtrate was extracted with chloroform and dried. After removal of the solvent, the residue was chromatographed on silica gel using benzene–ether (1:1) to give (3.10 g, 99%) of **9a**.

Preparation of 2- or 3-Substituted 4-Phenylthio-4-butanolide (17a—f). The Pummerer reaction of **9a**—**f** was conducted as in the preparation of **6**. These results are summarized in Table 4. Elemental analyses of **17a**—**f** are as follows;

2-Methyl-4-phenylthio-4-butanolide (17a). Found: C, 63.20; H, 5.67%. Calcd for $C_{11}H_{12}O_2S$: C, 63.45; H, 5.81%.

2-Butyl-4-phenylthio-4-butanolide (17b). Found: C, 67.47; H, 7.12%. Calcd for $C_{14}H_{18}O_2S$: C, 67.16; H, 7.25%.

2-Benzyl-4-phenylthio-4-butanolide (17c). Found: C, 71.65%; H, 5.47%. Calcd for $C_{17}H_{16}O_2S$: C, 71.82; H, 5.64%.

3-Methyl-4-phenylthio-4-butanolide (17d). Found: C, 63.51; H, 5.16%. Calcd for $C_{11}H_{12}O_2S$: C, 63.43; H, 5.81%.

3-Phenyl-4-phenylthio-4-butanolide (17e). Found: C, 70.56; H, 4.95%. Calcd for $C_{16}H_{14}O_2S$: C, 71.08; H, 5.22%.

3-Ethyl-4-phenylthio-4-butanolide (17f). Found: C, 64.98; H, 6.57%. Calcd for $C_{12}H_{14}O_2S$: C, 64.83; H, 6.35%.

General Procedure for Oxidation of 17a—f. To a solution of 4-phenylthio-4-butanolide derivative in dichloromethane (15 ml, for 1 g of the lactone) was added 1.2 equiv of *m*-chloroperbenzoic acid at 0 °C. The reaction mixture was stirred for 1 h at 0 °C, washed with 10% aqueous sodium

hydrogencarbonate, and dried. Evaporation of the solvent under reduced pressure gave 4-phenylsulfinyl-4-butanolide derivative (**18a—f**). **18a—f** were used for subsequent thermolysis without further purification.

*General Procedure for Thermolysis of **18a—f**.* A solution of 4-(phenylsulfinyl)lactone derivative in pyridine (20 ml for 1 g of the lactone) was refluxed for 3 h. After removal of pyridine under reduced pressure, the residue was chromatographed on silica gel by using benzene–ether (3:1) as an eluent to give 2- or 3-buten-4-olide. Yields are given in Table 5.

References

1) T. Numata and S. Oae, *Tetrahedron*, **30**, 2641 (1974).
2) M. Watanabe, K. Shirai, and T. Kumamoto, *Chem. Lett.*, **1975**, 855.
3) M. Watanabe, K. Shirai, and T. Kumamoto, *Bull. Chem. Soc. Jpn.*, **52**, 3318 (1979).
4) a) S. Lamdan and D. Albarracin, *Safybi*, **1**, 41 (1959); *Chem. Abstr.*, **54**, 14234f (1960); b) P. Cagniant and A. Deluzarche, *C. R. Acad. Sci.*, **223**, 677 (1946); *Chem. Abstr.*, **41**, 1669 h (1947).
5) R. C. Fuson and J. H. Koehneke, *J. Org. Chem.*, **14**, 706 (1949).
6) B. M. Trost and T. N. Salzmann, *J. Am. Chem. Soc.*, **95**, 6840 (1973).
7) K. Iwai, H. Kosugi, H. Uda, and M. Kawai, *Bull. Chem. Soc. Jpn.*, **50**, 242 (1977).
8) Y. S. Rao, *Chem. Rev.*, **76**, 625 (1975).
9) A. B. Hornfeldt, *Ark. Kemi.*, **29**, 229 (1968).

Halogenation with *N*-Halo-2-oxazolidinones. The Chain-carrying *N*-Centered Radicals

Toshihiko Migita,* Mitsumasa Nakayama, Toshiro Watanuki, Mikio Suzuki, and Masanori Kosugi

Department of Applied Chemistry, Faculty of Technology, Gunma University, 1-5-1, Tenjin-cho, Kiryu, Gunma 376

(Received August 12, 1980)

Selectivities in halogenation of 2,3-dimethylbutane, 1-chlorobutane and substituted toluenes with *N*-chloro- or *N*-bromo derivatives of 4,4-dimethyl-2-oxazolidinone (NXDMO), 2-oxazolidinone (NXO), and succinimide (NXS) were examined. In the presence of olefin, halogenation of the substituted butane by these *N*-halo reagents were found to proceed involving hydrogen abstraction by the *N*-centered radicals, since chlorination by the *N*-chloro reagents and bromination by the corresponding *N*-bromo reagents showed the same selectivities. The relative reactivity of a *t*-C–H bond compared with a *prim*-C–H bond RS_p^t markedly depends on the structure of the *N*-radical, being 200, 70, and 11 at 80 °C toward the radicals derived from NXDMO, NXO, and NXS, respectively. Reaction constant ρ of hydrogen abstraction from the toluenes by the *N*-radical from NXDMO was −1.0 at 130 °C.

There has been considerable controversy about the mechanism of halogenations by *N*-halo reagents. At first, for bromination by *N*-bromosuccinimide (NBS), Bloomfield proposed the radical chain mechanism involving the nitrogen centered imidyl radical.[1] In 1953 Goldfinger explained chlorination by *N*-chlorosuccinimide (NCS) by the mechanism in which actual halogenating agent is halogen molecule produced by the reaction of NCS with hydrogen chloride.[2]

Many subsequent studies showed that selectivities or isotope effects in halogenations by various *N*-halo compounds are almost the same as those in photohalogenations by elemental halogens, supporting that the Goldfinger mechanism, if not exclusively, is operative at least as the main path.[3–8]

Bloomfield mechanism

$$\rangle N\cdot + RH \longrightarrow \rangle N\text{-}H + R\cdot$$

$$R\cdot + \rangle N\text{-}X \longrightarrow R\text{-}X + \rangle N\cdot$$

Goldfinger mechanism

$$X\cdot + RH \longrightarrow R\cdot + HX$$

$$R\cdot + X_2 \longrightarrow R\text{-}X + X\cdot$$

$$HX + \rangle N\text{-}X \longrightarrow X_2 + \rangle N\text{-}H$$

Consequently hydrogen abstraction by *N*-radicals has received only a little attention,[9] except intramolecular abstraction and its application to synthetic chemistry.[10] Recently, however, it has been reported that in some cases selectivities in halogenations by *N*-halo compounds differ from those by elemental halogens. The cases are classified as follows: i) NBS bromination of substrates which are relatively unreactive toward bromine atom:[11] ii) using a good solvent for NBS, for example, CH_2Cl_2;[12] iii) presence of olefin or base which can trap halogen or hydrogen halide.[12,13]

These findings may suggest that under these conditions the Bloomfield mechanism plays an important role in the halogenation by *N*-halo compounds. However, discrepancy in selectivity in halogenation between by halogen and by *N*-halo compound is not necessarily an unequivocal evidence for the contribution of the nitrogen centered radical. Mosher and Estes, for example, demonstrated that selectivity of chlorination by *N*-chlorophthalimide depended on the reaction conditions, and explained the feature in terms of the Goldfinger mechanism complicated by the reversible hydrogen abstraction.[14]

$$X\cdot + RH \rightleftharpoons H\text{-}X + R\cdot$$

If the *N*-radicals are the true chain carrier, selectivity of chlorination by the *N*-chloro reagent should be the same to that of bromination by the corresponding *N*-bromo reagent. From the view of this criteria, in this work, selectivities in halogenations by several *N*-halo reagents were examined, aiming to elucidate the chemical nature of the *N*-radicals.

Besides NBS and NCS, we chose 3-halo-4,4-dimethyl-2-oxazolidinone(NXDMO) and 3-halo-2-oxazolidinone(NXO) as the reagents, since these two *N*-halides have been found to have "lower positive halogens," and to react with hydrogen halides, giving halogens, much slower relative to *N*-halosuccinimides,[15] and consequently are expected to have natures less favorable to take place the Goldfinger processes.

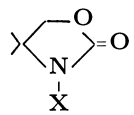

X: Cl (NCDMO)
Br (NBDMO)

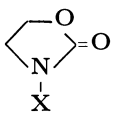

X: Cl (NCO)
Br (NBO)

Results and Discussion

Selectivities in halogenations of 2,3-dimethylbutane, 1-chlorobutane, and substituted toluenes by the *N*-halo reagents were determined by intra- and intermolecular competition methods.

2,3-Dimethylbutane. Halogenations initiated by benzoyl peroxide (BPO) were conducted at 80 °C by using 0.2 equivalent amounts of the *N*-halo regents to avoid dichlorination. In order to eliminate the occurence of the Goldfinger processes, the reaction was carried out in a good solvent for the *N*-halo reagents, CH_2Cl_2,[12] and in the presence of 3,3-dimethyl-1-butene as a halogen scavenger or γ-collidine as a hydrogen halide acceptor.[12,13]

Change in isomer distribution of monohalogenated products was examined as a function of the initial

Table 1. BPO-initiated halogenation of 2,3-dimethylbutane by the *N*-halo reagents (80 °C)

N-Halide	Additive	Product yield/%[b]			Halides
		prim-Halide	*t*-Halide	Amide or imide	Amide %
NCDMO	None	14	58	72	100
	t-BuCH=CH_2	3.1	36	59	66
	γ-Collidine	1.1	13	37	39
NBDMO	None	—[c]	71	79	90
	t-BuCH=CH_2	2.6	28	61	51
NCO	None	5.5	84	100	90
	t-BuCH=CH_2	1.9	55	100	57
NBO	None	—[c]	68	80	85
	t-BuCH=CH_2	1.5	36	100	38
NCS	None	29	36	83	78
	t-BuCH=CH_2	4.6	8.6	—[d]	—
	γ-Collidine	3.7	7.8	—[d]	—
NBS	None	—[c]	64	80	80
	t-BuCH=CH_2	4.3	7.6	—[d]	—

a) 2,3-Dimethylbutane 1.25 mmol, halogenating agent 0.25 mmol, BPO 0.01 mmol, additive 0.25 mmol, solvent: CH_2Cl_2 5 cm^3 80 °C 15 h. b) Determined by VPC, based on the reagent used. c) Only trace amounts were detected. d) Not determined.

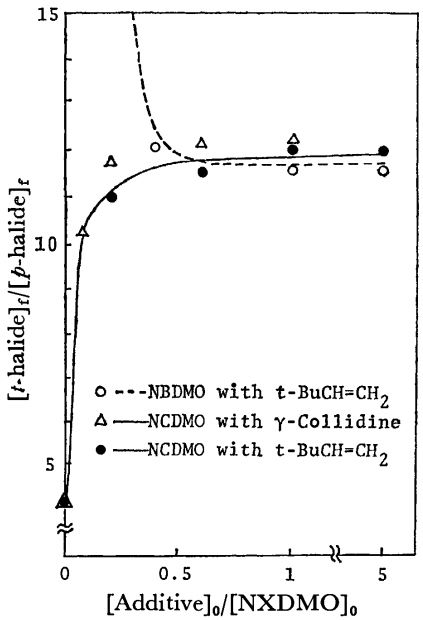

Fig. 1. Dependence of relative yield of tertiary halide to primary halide on relative concentration of additives.

concentration of the olefinic or basic additive. Typical tendencies observed in halogenation with NXDMO are shown in Fig. 1. In the absence of the additives NBDMO halogenated the tertiary C–H of the substrate almost exclusively, while chlorination by NCDMO gave the primary and the tertiary chloride in a ratio of 4:1.

A small amount of the additives brought about marked effects on the distribution of the product, and in the presence of their equimolar amount to the reagents, bromination by NBDMO and chlorination by NCDMO showed the almost same selectivity.

Table 2. Selectivity factor RS^t_p in halogenation of 2,3-dimethylbutane

Reagent	No additive	RS^t_p(80 °C) *t*-BuCH=CH_2 added	γ-Collodine added
NCDMO	25.8±3.6	70.5±1.1	70.8±3.0
NBDMO	—[a]	65.2±4.7	—[b]
NCO	91.6	175±15	—[b]
NBO	—[a]	206±7	—[b]
NCS	7.6±0.1	11.3±0.9	12.8±2.7
NBS	—[a]	10.7	—[b]

a) *prim*-C–H bonds are almost inactive. b) The reaction mixtures are too complex to be analyzed.

This shows, under these conditions both halogenations proceed almost exclusively through the Bloomfield mechanism, involving the common *N*-centered radical as a hydrogen abstracting species.

Table 1 shows the yields of the products of halogenation of 2,3-dimethylbutane by various halogenating agents in the absence and the presence of an equimolar amount of the olefin or the base. Apparently, the presence of the additives reduced the total yield of the halogenated products, and also lowered the relative amount of the halogenated products to the amides (or imide) produced. These facts indicate that the *N*-halo reagents can be consumed also by some side reactions, perhaps, with the additives. Particularly, the presence of γ-collidine gave the complicated mixture containing several unidentified by-products.

Neverthless, in all cases, relative yields of the tertiary to the primary halides fairly coincide with each other between bromination by the *N*-bromo reagent and chlorination by the corresponding *N*-chloro reagent. From the relative yield of the halides obtained in at least three runs for each reaction, selectivity factor between *t*- and *pirm*-C–H bonds, that is the reactivity

of a *t*-C–H bond relative to a *prim*-C–H bond in the substrate, RS^t_p was calculated to be as shown in Table 2.

In the absence of the additives, bromination hardly occurs on a *t*-C–H. The tendency is essentially the same to that in bromination by bromine.[16] Therefore, bromination by *N*-bromo amides or imide seems to mainly proceed through the Goldfinger mechanism. Selectivities of chlorination depend on the nature of *N*-chloro reagents and are different from that of chlorination by chlorine (RS^t_p=3—4).[17] Thus, chlorinations by *N*-chloro reagents may proceed through both of the Bloomfield and the Goldfinger mechanism.

In the presence of the olefin, halogenation proceed through the Bloomfield mechanism almost exclusively, since the selectivity depends on the structure of the amide or imide groups but not on the nature of halogen.

1-Chlorobutane. Based on the information obtained in the study of halogenation of 2,3-dimethylbutane described above, 1-chlorobutane was halogenated by the *N*-halo reagents in the presence of 3,3-dimethyl-1-butene. From the isomer distribution of the halogenated products, relative reactivity of a C–H bond at each position was estimated. In Table 3 the reactivity values refered to those of a C–H bond at 3-position were listed as well as the results of photochlorination[18] and bromination.[19]

TABLE 3. RELATIVE REACTIVITIES OF C–H BONDS OF 1-CHLOROBUTANE TOWARD HALOGENATIONS[a),b)]

Reagent	$Cl-CH_2-CH_2-CH_2-CH_3$			
NCDMO	0.48	0.37	1.00	0.12
NBDMO	0.88	0.40	1.00	0.13
NCO	0.69	0.65	1.00	0.09
NBO	0.70	0.46	1.00	0.12
NCS	0.17	0.56	1.00	0.25
NBS	0.25	0.61	1.00	0.22
Cl_2[c)]	0.09	0.40	1.00	0.19
Br_2(60 °C)[c)]	0.45	0.48	1.00	—

a) 1-Chlorobutane: 1.25 mmol. *N*-halogeno reagent: 0.25 mmol. 3,3-dimethyl-1-butene: 0.25 mmol. BPO: 0.01 mmol. solvent: CH_2Cl_2 5 cm³, 80 °C 15 h. b) Reactivity of a C–H bond at 3-position was taken as unity. c) Calculated from the results in the references.[18,19]

Relative reactivities of C–H bonds toward a *N*-chloro reagent are in tolerable agreement with those toward the corresponding *N*-bromo reagent, except abnormally high reactivity at 1-position toward NBDMO, the reason for which is not clear. It can be seen that the selectivities of these halogenation are quite different from these of photohalogenation, suggesting that hydrogen abstracting species are the *N*-centered radicals.

Selectivity in Hydrogen Abstraction by the N-*Radicals.* Recognizing that halogenations of aliphatic compounds by *N*-halo amide or imide proceed by the Bloomfield mechanism, the selectivities in the halogenation would reveal the relative rates of hydrogen abstraction by the *N*-centered radicals.

From the results of intramolecular competitive reactions of 2,3-dimethylbutane and 1-chlorobutane, relative reactivities of *prim*-, *s*-, and *t*-C–H bonds toward the *N*-centered radicals were found to be as shown in Table 4. Since polar effects of a chlorine substituent in 1-chlorobutane are only slightly operative on 3- and 4-positions,[20] relative reactivities of C–H bonds between these two positions may be used approximately for the selectivity factor between ordinary *s*- and *prim*-C–H bonds. For comparison, selectivity factors in hydrogen abstraction by other radicals are also shown in Table 4.

The *N*-centered radicals are found to be much less selective than bromine atom,[16] but more selective than chlorine atom,[17] *t*-butoxyl[21] and phenyl radicals.[22] The trend is understandable on the basis of the available values of dissociation energies of the bonds forming through hydrogen abstraction: H–Br

TABLE 4. RELATIVE RATE FACTORS IN HYDROGEN ABSTRACTION

Radical	Temp °C	*prim*-C–H	*s*-C–H	*t*-C–H	Ref.
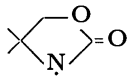	80	1	8	70	this work
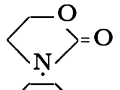	80	1	8—11	200	this work
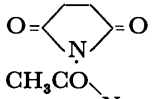	80	1	4	11	this work
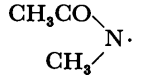	25	1	—	95	13
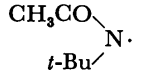	25	1	—	1.6	13
Cl·	25	1	3.5	4.2	17
Br·	150	1	80	1700	16
Ph·	60	1	9	44	21
t-BuO·	40	1	12	44	22

87, average N–H 93.4, *t*-BuOH 102, Ph–H 104, H–Cl 103 kcal mol^{-1}.[23] Comparing with the radicals derived from NXO and NXDMO, succinimidyl radical is less selective. This is perhaps due to that difference in effective electronegativity of the nitrogen atom affects on the bond energy of the forming N–H bond.

The radical derived from NXDMO appears less selective than that from NXO, especially in discrimination between *prim*- and *t*-C–H. This apparent less selectivity can be explained in terms of steric effects. Two methyl groups neighboring the radical center will sterically interfer the attack of the radical center on the more crowded position. As a result, reactivities of a C–H bond at more hindered positions, *e.g.* *t*-C–H, may be apparently lessered. More pronounced similar steric effects have been demonstrated in the selectivities of *N*-methyl- and *N*-*t*-butylacetamidyl radicals.[13] And these acyclic amidyl radicals seem less selective than the cyclic *N*-radicals studied in this work. These can be also considered to be the results of similar steric effects. In the acyclic systems blocking effects of the groups bonded to the nitrogen atom will be much larger. Consequently abstractions by the acyclic radicals are less selective, and more sensitive to steric hindrance by the groups in substrates, than those by the cyclic radicals.

Table 5. Halogenation of toluene by NXDMO

Reagent	Initiator	Temp °C	Time h	Yield of benzyl halide %
NCDMO	BPO	80	15	19
	AIBN	80	3	trace
	DTBP	130	22	73
NBDMO	BPO	80	15	69
	AIBN	80	3	69
	DTBP	130	22	70

Substituted Toluenes. In order to obtain preliminary information about polar selectivities of hydrogen abstraction by the *N*-radicals, substituted toluenes were intended to be halogenated competitively by the *N*-halo reagents in the presence of 3,3-dimethyl-1-butene.

Bromination of toluene by NBDMO was initiated by either BPO or AIBN, and the reaction (at 80 °C) gave benzyl bromide in a reasonable yield. However, chlorination by NCDMO was quite sluggish under these conditions and afforded benzyl chloride in a quite poor yield. Perhaps, this is due to dif-

Table 6. Competitive halogenation of substituted toluenes by NXDMO (130 °C)

$YC_6H_4CH_3$ Y=	NXDMO X=	(mol dm^{-3})	Olefin[a] (mol dm^{-3})	Substrates (mol dm^{-3}) $PhCH_3$	Substrates (mol dm^{-3}) $YC_6H_4CH_3$	Molar ratio $YC_6H_4CH_2X/PhCH_2X$	Relative rate const.
p-CH_3	C	0.040	—	0.800	0.402	1.64±0.1	1.63
	B	0.045	—	0.812	0.416	3.21±0.2	3.13
	C	0.041	0.045	0.818	0.600	2.44±0.04	1.83
	B	0.042	0.048	0.810	0.610	2.71±0.01	1.80
p-Cl	C	0.062	0.062	0.604	0.602	0.67±0.01	0.67
	B	0.062	0.074	0.608	0.612	0.76±0.03	0.70
p-CN	C	0.101	0.073	2.006	2.005	0.25±0.01	0.25
	B	0.088	0.104	2.035	1.996	0.25±0.01	0.25

a) 3,3-Dimethyl-1-butene.

Table 7. Competitive halogenation of substituted toluenes by NXO (130 °C)

$YC_6H_4CH_3$ Y=	NXO X=	(mol dm^{-3})	Olefin[a] (mol dm^{-3})	Substrates (mol dm^{-3}) $C_6H_5CH_3$	Substrates (mol dm^{-3}) $YC_6H_4CH_3$	Molar ratio $YC_6H_4CH_2X/PhCH_2X$	Relative rate const.
p-CH_3	C	0.044	—	1.02	0.479	1.70±0.03	1.88
	C	0.047	0.048	0.979	0.481	2.00±0.04	2.03
	C	0.042	0.049	1.04	0.447	1.68±0.05	1.95
	B	0.022	—	1.00	0.233	0.94±0.02	2.22
	B	0.022	0.025	1.03	0.238	0.90±0.03	1.93
p-Cl	C	0.043	—	0.426	0.796	1.16±0.01	0.62
	C	0.040	0.045	0.425	0.993	1.04±0.03	0.56
	C	0.046	0.045	0.407	0.429	0.49±0.04	0.46
	B	0.050	—	0.424	0.620	1.16±0.04	0.79
	B	0.049	0.041	0.405	0.592	1.21±0.04	0.83
p-CN	C	0.021	—	0.225	1.00	1.44±0.04	0.32
	C	0.022	—	0.220	1.00	1.38±0.03	0.30
	B	0.046	—	0.427	1.26	0.12±0.05	0.04
	B	0.041	0.046	0.414	1.30	0.17±0.10	0.06

a) 3,3-Dimethyl-1-butene.

Table 8. Competitive bromination of substituted toluenes by NBS (130 °C)

$YC_6H_4CH_3$ Y=	NBS (mol dm^{-3})	Olefin[a] (mol dm^{-3})	Substrates(mol dm^{-3}) $PhCH_3$	Substrates(mol dm^{-3}) $YC_6H_4CH_3$	Molar ratio $YC_6H_4CH_2Br/PhCH_2Br$	Relative rate const.
p-CH_3	0.044	—	1.00	0.390	2.92±0.07	3.75
	0.042	—	1.02	0.320	2.17±0.03	3.45
	0.040	0.039	1.01	0.400	2.61±0.02	3.24
p-Cl	0.042	—	0.435	0.818	1.22±0.01	0.67
	0.039	0.039	0.404	0.806	1.64±0.02	0.82
p-CN	0.023	—	0.214	2.02	0.83±0.03	0.087
	0.022	0.028	0.231	1.89	0.56±0.03	0.069

a) 3,3-Dimethyl-1-butene.

ficulty in chlorine abstraction from the N–Cl bond by the relatively stable benzyl radical. However, when the reaction was carried out at 130 °C using di-*t*-butyl peroxide (DTBP) as a radical generator, toluene was smoothly halogenated by either NCDMO or NBDMO, giving benzyl halides in good yields, as shown in Table 5. Even under these conditions NCS could not chlorinate toluene in an appreciable yield. On the basis of the observations, competitive experiments were conducted with NXDMO and NXO at 130 °C in CH_2Cl_2 solvent using DTBP as an initiator, and relative reactivities of substituted toluenes were compared between bromination and chlorination.

Table 6 shows the results obtained about halogenation by NXDMO. Relative reactivity of each substituted toluene was obtained with satisfactory reproducibility, and the values obtained for chlorination and bromination were coincide with each other. This obviously supports that the reagent attacking benzylic hydrogen in both reactions is the common *N*-radical, and the radical has fairly electron seeking nature ($\rho=-1.0$).

Competitive experiments with NXO gave, however, poorer reproducible results, as shown in Table 7. Although there can be seen the tendencies that the presence of the olefin makes the chlorination with NCO more selective and the bromination with NBO less selective, no numerical coincidence in relative reactivity was obtained between chlorination and bromination. This may arise probably from that both of the Bloomfield and the Goldfinger processes proceed concurrently even in the presence of the olefin. Contrasting with 3-halo-4,4-dimethyl-2-oxazolidinone, 3-halo-2-oxazolidinone, bearing α-hydrogens, is though to take place dehydrohalogenation at higher temperature.[10] Hydrogen halide thus formed will ac-

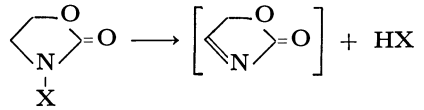

celarate the Goldfinger process through the reaction with NXO producing halogen molecule. Under the drastic conditions used in this study, therefore, halogen will form too rapidly to be entirely scavenged by the olefin added. Increasing the amount of the olefin might suppress the Goldfinger process. Under these circumstances, however, yield of the benzyl halides became too low for reliable competitive study.

Table 8 shows the results of bromination with NBS in the absence and the presence of the olefin. The reaction constant obtained in the absence of the olefin are derived to be *ca.* −1.8 ($r=0.95$), being somewhat larger negative compared with the values reported so far ($\rho=-1.46$,[4] $\rho^+=-1.38$[6] at 80 °C in CCl_4). This is perhaps due to that a more polar solvent, CH_2Cl_2 was used in this work. The presence of the olefin makes the reaction slightly more electron seeking ($\rho=-1.9$, $r=0.97$). We feel, this reveals the polar selectivity of hydrogen abstraction by the succinimidyl radical, although comparison with chlorination by NCS could not be accomplished owing to the difficulty described above.

Experimental

Materials. NCO and NCDMO were prepared by the modified known method.[24] The precipitated NCO was filtered, dried under reduced pressure, and crystallized from dichloromethane-petroleum ether. Yield 50%, mp 62.5—63.5 °C. The sample in a vacuum sealed tube wrapped with aluminum foil was reserved in a refrigerator. NCDMO was recrystallized from benzene–petroleum ether. Yield, 70%, mp 69—70 °C. NBDMO was prepared by the known method[15] and recrystallized from dichloromethane–petroleum ether. Yield 76%, mp 118—119 °C. NBO was prepared by bromination of 2-oxazolidinone (7 g) with *t*-butyl hypobromite[25] in dichloromethane. The crystal was filtered and recrystallized from dichloromethane–petroleum ether. The sample was reserved in a evacuated tube wrapped with aluminum foil. Yield 50%, mp 115—120 °C (partially decomposed).[15] NCS were prepared by the usual method.[26] NBS was commercially available and purified by recrystallizing from water. All substrates were purified by distilling the commercial materials.

Halogenation of 2,3-Dimethylbutane and 1-Chlorobutane. A solution of an *N*-halo reagent (0.25 mmol), 2,3-dimethylbutane (1.25 mmol), BPO (0.01 mmol), and γ-collidine or 3,3-dimethyl-1-butene (0.25 mmol) in dichloromethane (5 cm^{-3}) was taken in a reaction tube and degassed by successive freezing-thawing processes. The tube was sealed under vacuum, and immersed in a thermostat at 80 °C for 15 h. The products were collected by GLPC, identified spectroscopically and determined by GLPC. All products were well known in the literature.[3-8] The results were summarized in Tables 1—3.

Competitive Hologenation of Substituted Toluenes. In a

5 cm^{-3} graduated flask, an *N*-halo reagent (0.2—0.5 mmol), DTBP (0.2 mmol), 3,3-dimethyl-1-butene (0—0.5 mmol) and precisely weighed toluene (*ca.* 5 mmol) and a substituted toluene were taken, and the mixture was diluted with dichloromethane to 5 cm^{-3}. Then the solution was devided to 3—4 fractions. Each fraction was degassed in a tube, which then was evacuated and sealed. The tube was immersed in a thermostat at 130 °C at 15 h. Molar ratio of halogenated products was determined by GLPC using calibration curves. From the molar ratios of initial concentration of toluenes and final concentration of benzylic halides, relative reactivity of the substituted toluene was calculated. The results were tabulated in Tables 6—8. In the reaction with NXO, the fractions from the same solution did not necessarily give the results in reasonable agreement with each other.

References

1) G. F. Bloomfield, *J. Chem. Soc.*, **1944**, 114.
2) J. Adam, P. A. Gosselain, and P. Goldfinger, *Nature*, **171**, 704 (1953).
3) K. B. Wiberg and L. H. Shugh, *J. Am. Chem. Soc.*, **80**, 3033 (1958).
4) R. E. Pearson and J. C. Martin, *J. Am. Chem. Soc.*, **85**, 354, 3142 (1963).
5) G. A. Russell, C. Deboer, and K. M. Desmond, *J. Am. Chem. Soc.*, **85**, 365, 3139 (1963).
6) C. Walling, A. L. Rieger, and D. D. Tanner, *J. Am. Chem. Soc.*, **85**, 3129 (1963).
7) C. Walling and A. L. Rieger, *J. Am. Chem. Soc.*, **85**, 3134 (1963).
8) J. H. Ineremona and J. C. Martin, *J. Am. Chem. Soc.*, **92**, 627 (1970).
9) A. E. Fuller and W. J. Hickinbottom, *J. Chem. Soc.*, **1965**, 3228; T. R. Beebe and F. M. Haward, *J. Am. Chem. Soc.*, **91**, 3379 (1969).
10) S. F. Nelson, "Free Radicals," ed by J. K. Kochi, (1973), Vol. II, p. 534; R. S. Neale, *Synthesis*, **1971**, 1.
11) J. G. Trayham and Y. Lee, *J. Am. Chem. Soc.*, **96**. 3590 (1974).
12) J. C. Day, M. J. Lindstrom, and P. S. Skell, *J. Am. Chem. Soc.*, **94**, 5617 (1972); P. S. Skell and J. C. Day, *ibid.*, **100**, 1950, 1951 (1978); *Acc. Chem. Res.*, **11**, 381 (1978); P. S. Skell, J. C. Day, and J. P. Slange, *Angew. Chem. Int. Engl.*, **17**, 516 (1978).
13) R. A. Johnson and F. D. Green, *J. Org. Chem.*, **40**, 2192 (1975).
14) M. W. Mosher and G. N. Estes, *J. Am. Chem. Soc.*, **99**, 6928 (1977).
15) J. J. Kaminski and N. Bodor, *Tetrahedron*, **32**, 1097 (1976).
16) In a gas phase: $RS_p^t = 1700$. J. M. Tedder, *Quart. Rev, (London)*, **14**, 336 (1960).
17) G. A. Russell and H. C. Brown, *J. Am. Chem. Soc.*, **77**, 4031 (1955).
18) L. Horner and L. Schläfer, *Justus Liebigs Ann. Chem.*, **635**, 31 (1960).
19) W. Thaler, *J. Am. Chem. Soc.*, **85**, 2607 (1963).
20) P. S. Fredricks and J. M. Tedder, *J. Chem. Soc.*, **1960**, 144; **1961**, 3520; M. Kosugi, T. Migita, and Y. Nagai, *Nippon Kagaku Zasshi*, **92**, 477 (1971).
21) R. F. Bridger and G. A. Russell, *J. Am. Chem. Soc.*, **85**, 3754 (1964).
22) C. Walling and W. Thaler, *J. Am. Chem. Soc.*, **83**, 3877 (1961).
23) J. A. Kerr, *Chem. Rev.*, **66**, 496 (1966); J. D. Roberts and M. C. Caserio, "Basic Principle of Organic Chemistry," W. A. Benjamin Inc., New York (1965).
24) M. Kosugi, J. J. Kaminski, S. H. Selk, I. H. Pitman, N. Bodor, and T. Higuchi, *J. Pharm. Sci.*, **65**, 1743 (1976).
25) J. C. Joseph and Y. L. Chow, *Can. J. Chem.*, **54**, 3517 (1976).
26) H. Zimmer and L. F. Audrieth, *J. Am. Chem. Soc.*, **76**, 3856 (1954).

Carbon-13 NMR Study on the Cyclodextrin Inclusion Complexes in Solution

Makoto KOMIYAMA* and Hidefumi HIRAI

Department of Industrial Chemistry, Faculty of Engineering, The University of Tokyo, Hongo, Bunkyo-ku, Tokyo 113

(Received August 19, 1980)

A correlation between the penetration depth of the carbon atoms of 4-nitrophenolate, benzoic acid, 4-nitrophenol and 2,6-dimethyl-4-nitrophenolate in the cavity of α-cyclodextrin and the changes of their ^{13}C-chemical shifts has been investigated. By use of this relationship and the observed changes of the ^{13}C-chemical shifts of 3-nitrophenol on the complex formation with α-cyclodextrin, the time-averaged conformation of the α-cyclodextrin-3-nitrophenol complex is determined.

The attention to the catalyses by cyclodextrins, cyclic oligosaccharides composed of 6—8 glucose units, has been increasing. This mainly comes from the inclusion complex formation of cyclodextrins with the substrates prior to the catalytic function in the similar way as enzymatic reactions, resulting in specificities.[1]

Although almost all of the reactions catalyzed by cyclodextrins are carried out in aqueous solutions, little is known on the positions of the substrates in the cavities of cyclodextrins. The information on the structures of inclusion complexes is quite important, since the characteristics of the cyclodextrin-catalyzed reactions are mainly due to the formation of the complexes.

In the previous paper,[2] the time-averaged conformations of the complexes of α-cyclodextrin with 4-nitrophenol and benzoic acid as well as their anions were determined by fitting the changes of the ^{1}H-chemical shifts of α-cyclodextrin to the calculated values of the anisotropic shielding effects of the aromatic rings of the guest compounds.

This paper describes the extension of the previous study to the ^{13}C-NMR spectroscopy. The relationship between the positions of the carbon atoms of the guest compounds in the cavity of α-cyclodextrin and the changes of the ^{13}C-chemical shifts of these atoms is shown for the complex of α-cyclodextrin with 4-nitrophenolate, benzoic acid, 4-nitrophenol, and 2,6-dimethyl-4-nitrophenolate. Furthermore, the conformation of the complex of α-cyclodextrin with 3-nitrophenol is determined by use of this relationship.

Experimental

Materials. The guest compounds and α-cyclodextrin were purified by recrystallization. Deuterium oxide (the minimum purity 99.75%) from Merck Co. was used as the solvent for the ^{13}C- and ^{1}H-NMR measurements.

Spectrometry. ^{13}C-NMR spectra were taken at ambient temperature (about 25 °C) on a JEOL PFT-100 spectrometer operating at 25.03 MHz, connected with JEOL EC-100 computer. The ^{13}C-chemical shifts were determined with the accuracy of ±0.01 ppm by use of sodium formate as the internal standard. The assignments of the signals were made according to the literatures for 4-nitrophenolate,[3] benzoic acid[4] and 4-nitrophenol,[3] and by using the additivity rule[5] for 2,6-dimethyl-4-nitrophenol and 3-nitrophenol. The changes of the ^{13}C-chemical shifts of the guest compounds (Δ_c's) on the complex formation with α-cyclodextrin were determined with the accuracy of ±0.05 ppm by plotting the observed changes of the ^{13}C-chemical shifts *vs.* the concentration of α-cyclodextrin.

^{1}H-NMR spectra were measured at 60 °C by use of JEOL PS-100 spectrometer. Assignments of the signals of α-cyclodextrin followed the literature.[6]

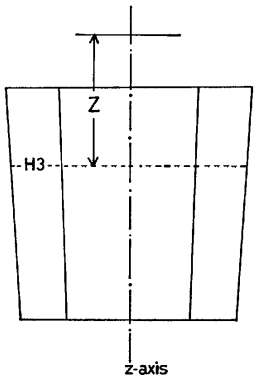

Fig. 1. Schematic drawing showing the definition of *Z*. ---H3--- shows the plane comprised of the six H-3 atoms of α-cyclodextrin.

Determination of the Time-averaged Position of the Guest Compound by ^{1}H-NMR Spectroscopy. The time-averaged position of the guest compound in the cavity of α-cyclodextrin was determined by the following method, the detailed description of which was made in the previous paper;[2]

1) The change of the ^{1}H-chemical shifts of the H-3 and H-5 atoms of α-cyclodextrin due to the complex formation with the guest compound were experimentally determined.

2) The magnitudes of the anisotropic shielding effects of the aromatic ring of the guest compound on the H-3 and H-5 atoms were calculated by using the table of Johnson and Bovey.[7]

3) The optimal position of the guest compound was determined by shifting the aromatic ring along the longitudinal axis (z-axis) of the cavity of α-cyclodextrin. In the optimal position, the calculated values of the shielding effects of the guest compound on the both H-3 and H-5 atoms show the maximal agreements with the corresponding observed values.

and

4) The optimal position was taken as the time-averaged position of the aromatic ring of the guest compound.

The position of the center of the aromatic ring and the carbon atoms of the guest compounds were expressed in terms of the heights (*Z*, in Å) from the plane comprised of the six H-3 atoms of α-cyclodextrin as shown in Fig. 1.

Results

Time-averaged Positions of the Guest Compounds in the Cavity Determined by the ^{1}H-NMR Spectroscopy. Table 1 shows the heights of the centers of the aromatic rings (*Z*-values) of 4-nitrophenolate, benzoic acid, 4-nitrophenol and 2,6-dimethyl-4-nitrophenolate, determined by the ^{1}H-NMR spectroscopy as described

Table 1. Penetration depth (the Z value) for the center of the aromatic ring of the guest compound and the observed and calculated changes of the ^{1}H-chemical shifts of the H-3 and H-5 atoms of α-cyclodextrin

Guest compound	Z of the center of the aromatic ring/Å[a]	^{1}H-Chemical shift change/ppm[b]			
		H-3		H-5	
		Obsd	Calcd	Obsd	Calcd
4-Nitrophenolate[c]	−1.1	+0.20	+0.21	−0.05	−0.08
Benzoic Acid[c]	−0.1	+0.41	+0.40	−0.08	−0.09
4-Nitrophenol[c]	−0.7	+0.25	+0.26	−0.04	−0.08
2,6-Dimethyl-4-nitrophenolate	−1.4	+0.15	+0.15	−0.06	−0.08

a) The negative sign refers to the shallower penetration with respect to the plane composed of the six H-3 atoms of α-cyclodextrin. b) The positive sign shows the increase in the shielding. c) From Ref. 2.

Table 2. Values of Δ_c and Z for the complex formation of α-cyclodextrin with various guest compounds

Guest compound	Carbon atom[a]	Δ_c/ppm[b]	Z/Å[c]
4-Nitrophenol	C-1	+0.25	−1.8
	C-2	−1.05	−0.4
Benzoic acid	C-3	−1.61	+0.6
	C-4	+0.14	−0.8
	C-5	−0.28	−1.5
4-Nitrophenol	C-6	−0.27	−1.3
	C-7	−1.26	0.0
2,6-Dimethyl-4-nitrophenolate	C-8	+0.59	−2.1
	C-9	+0.10	−0.8

a) The numbering system is shown in the legend for Fig. 2. b) The positive sign refers to the increase in the shilding. c) The negative sign shows the shallower penetration with respect to the plane comprised of the six H-3 atoms.

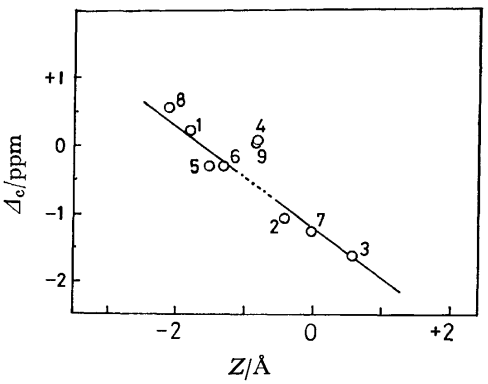

Fig. 2. Plot of the changes of the ^{13}C-chemical shifts (Δ_c in ppm) of the guest compounds on the inclusion complex formation with α-cyclodextrin *vs.* the penetration depth (Z in Å).
The positive sign in Δ_c shows the increase in the shielding, and the positive sign in Z shows the deeper penetration with respect to the plane (Z=0) comprised of the six H-3 atoms of α-cyclodextrin; the numbering system of the carbon atoms of the guest compounds are as follows;

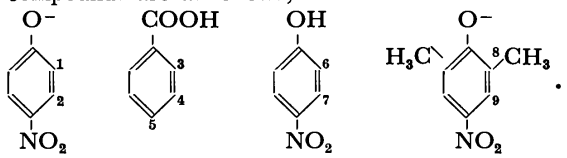

in the Experimental Section. The agreements between the observed values of the changes of the ^{1}H-chemical shifts and the calculated ones are fair for both the H-3 and H-5 atoms.

The conformations of the inclusion complexes can be definitely determined from the Z-values of the centers of the aromatic rings listed in Table 1, since the directions of the penetrations of the guest compounds were known.[8,9] 4-Nitrophenolate, 4-nitrophenol and 2,6-dimethyl-4-nitrophenolate form the complexes with α-cyclodextrin in which the nitro groups are located inside the cavity with the hydroxyl group and phenoxide oxygen atoms protruding from the secondary hydroxyl side of the cavity.[8] In the α-cyclodextrin–benzoic acid complex, the carboxyl group penetrates as a head from the secondary hydroxyl side.[9] Thus, the Z-values for all of the carbon atoms of the guest compounds were determined as shown in Table 2.

Relationship between the Penetration Depth and the Change of the ^{13}C-Chemical Shift. Table 2 lists the changes of the ^{13}C-chemical shifts (Δ_c) as well as the Z-values for the complex formations of α-cyclodextrin with 4-nitrophenolate, benzoic acid, 4-nitrophenol, and 2,6-dimethyl-4-nitrophenolate.

A fair correlation between Δ and Z are found as shown in Fig. 2. The seven points except for those of the C-4 and C-9 atoms showed linearity. As the carbon atom was included more deeply in the cavity, its chemical shift moved from the values in the absence of α-cyclodextrin towards the lower magnetic field to a greater extent. The C-4 and C-9 atoms, both of which have the Z-values of around −0.8 A, showed almost the identical Δ_c values (+0.1 ppm), although the corresponding points considerably deviated from the linear straight line for the other seven points.

The most important conclusion from Fig. 2 is that Δ_c is virtually governed only by the penetration depth in the cavity. The positions of the carbon atoms with respect to the substituents in the guest compounds are less important. Thus, the relationship in Fig. 2 is applicable to other guest compounds, especially to the substituted benzenes.

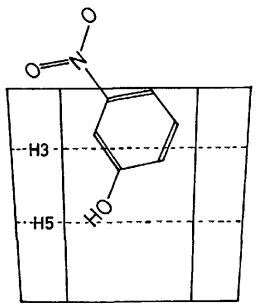

Fig. 3. The time-averaged conformation of the α-cyclodextrin-3-nitrophenol complex.
---H3--- and ---H5--- show the planes comprised of the six corresponding atoms of α-cyclodextrin.

Application of the Relationship between Δ_c and Z to the Complex Formation of α-Cyclodextrin with 3-Nitrophenol. The time-averaged position of 3-nitrophenol in the cavity of α-cyclodextrin can be estimated as shown in Fig. 3. Here, the Z-values of the carbon atoms of 3-nitrophenol are determined by use of the observed Δ_c's and the relationship in Fig. 2. The Δ_c's for the C-10, C-11, and C-13 atoms are evaluated from the straight line, and that for the C-12 atom, which is located at $Z=-0.9$ A, is taken as the average of the values for the C-4 and C-9 atoms. The agreements between the observed values of Δ_c and the calculated values are fair as shown in Table 3.

Supports for the conformation in Fig. 3 and thus the method for the determination were provided by the ^{1}H-NMR spectroscopy. The magnitudes of the anisotropic shielding effects of the aromatic ring of 3-nitrophenol on the H-3 and H-5 atoms, respectively, of α-cyclodextrin can be calculated to be +0.30 and −0.05 ppm. These values were determined by averaging the magnitudes of the shielding effects of the aromatic ring on the six H-3 or H-5 atoms, each of which are estimated by using the table of Johnson and Bovey.[7] These values are in fair agreements with the observed values (+0.29 and −0.05 ppm, respectively).

Penetration of the hydroxyl group of 3-nitrophenol in the cavity rather than the nitro group was further confirmed by the absorption spectroscopy. Table 4 shows the dissociation constant (K_d) of the inclusion complexes of α-cyclodextrin with 3-nitrophenol, 2-methyl-3-nitrophenol, and 4-methyl-3-nitrophenol, determined at 25 °C in 0.1 mol dm^{-3} HCl by using the change of the absorbance at 340 nm. The methyl substitution in the ortho position of the hydroxyl group prevents the complex formation with α-cyclodextrin, although the methyl substitution in the para-position of the hydroxyl group enhances it. These results are consistent with the conformation shown in Fig. 3, since the steric hindrance around the hydroxyl group shows larger effect on the complex formation than the steric hindrance around the nitro group does.

Table 3. Vales of Δ_c and Z for the α-cyclodextrin-3-nitrophenol complex

Carbon atom[a]	Z/Å[b]	Δ_c/ppm[c]	
		Obsd	Calcd
10	−0.4	−0.78	−0.92
11	−1.9	−0.13	+0.16
12	−0.9	0.00	+0.12
13	+0.4	−1.45	−1.48

a) The numbering system is as follows:

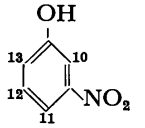

b) The negative sign shows the shallower penetration with respect to the plane composed of the six H-3 atoms. c) The positive sign shows the increase in the shielding.

Table 4. The equilibrium constant (K_d) of the dissociation of the inclusion complex of α-cyclodextrin[a]

Guest compound	K_d/10^{-2} mol dm^{-3}
3-Nitrophenol	1.7
2-Methyl-3-nitrophenol	2.2
4-Methyl-3-nitrophenol	0.065

a) At 25°C in 0.1 mol dm^{-3} HCl.

Discussion

It has been shown that the ^{13}C-NMR spectroscopy as well as the ^{1}H-NMR spectroscopy[2] can be applicable to the determination of the time-averaged positions of the guest compounds in the cavity. An advantage of the ^{13}C-NMR spectroscopy over the ^{1}H-NMR spectroscopy is that it can provide the direct informations on the positions of all the carbon atoms of the guest compounds and thus on the directions of the penetrations of the guest compounds in the cavity. However, only the position of the aromatic ring of the guest compound in the cavity can be determined by use of the ^{1}H-NMR spectroscopy. The positions of the carbon atoms of the guest compounds can be estimated by ^{1}H-NMR spectroscopy only when the directions of the penetrations are determined by other methods. In the complex formations of 4-nitrophenolate and 4-nitrophenol, for example, the absorption spectroscopy showed the penetration of the nitro group as a head, since the steric hindrance due to the methyl substitution(s) around the nitro group exhibited much larger suppression of the complex formations than the steric hindrance around the hydroxyl group or phenoxide ion does.

The deviations for the C-4 and the C-9 atoms from the straight line in Fig. 2 are associated with the secondary hydroxyl groups of α-cyclodextrin which are located around $Z=-1.0$ A. Apolar property near the hydroxyl groups is smaller than estimated from the Z-value.

The penetration of the hydroxyl group in the cavity in the α-cyclodextrin–3-nitrophenol complex is attributable to the attraction of the dipole of the nitro group of 3-nitrophenol mainly by the negative charge at

the O-2 oxygen atom of α-cyclodextrin. The O-2 oxygen atoms are located near the nitro group, since the corresponding secondary hydroxyl groups orient inside the cavity. In the α-cyclodextrin–4-nitrophenol complex, however, the interaction between the nitro group and the negative charge is less important because of the larger distance between them, resulting in the penetration of the more apolar nitro group in the cavity.

The conformation of the α-cyclodextrin–3-nitrophenol complex in solution in Fig. 3 is consistent with that in the crystal[10] where the benzene ring is located near the secondary hydroxyl side of the cavity. The complex in the crystal, however, has the nitro group inside the cavity, whereas that in solution has the hydroxyl group inside the cavity. This discrepancy is probably associated with the process of the crystallization.

Small discrepancies between the observed and calculated values of Δ_c's for the C-10 and C-11 atoms (Table 3) are due to the minor contribution of the inclusion complex where the nitro group penetrates the cavity as a head, in addition to the major contribution of the inclusion complex where the hydroxyl group penetrates the cavity as a head (Fig. 3).

Conclusion

1) A correlation between the penetration depth of the carbon atoms of the aromatic guest compounds and the changes of the ^{13}C-chemical shifts was found.
2) The time-averaged conformation of the α-cyclodextrin–3-nitrophenol complex in solution was determined by use of the relationship.

This work was partially supported by a Grant-in-Aid for Scientific Research from the Ministry of Education, Science and Culture.

References

1) M. L. Bender and M. Komiyama, "Cyclodextrin Chemistry," Springer-Verlag, Berlin (1978).
2) M. Komiyama and H. Hirai, *Polym. J.*, in press.
3) R. Bergeron and M. A. Channing, *Bioorg. Chem.*, **5**, 437 (1976).
4) A. M. Ihrig and J. L. Marshall, *J. Am. Chem. Soc.*, **94**, 1756 (1972).
5) J. B. Stothers, "Carbon-13 NMR Spectroscopy," Academic Press, New York (1972).
6) D. J. Wood, F. E. Hruska, and W. Saenger, *J. Am. Chem. Soc.*, **99**, 1735 (1977).
7) C. E. Johnson and F. A. Bovey, *J. Phys. Chem.*, **29**, 1012 (1958).
8) R. J. Bergeron, M. A. Channing, G. J. Gibeily, and D. M. Pillor, *J. Am. Chem. Soc.*, **99**, 5146 (1977).
9) R. J. Bergeron, M. A. Channing, and K. A. McGovern, *J. Am. Chem. Soc.*, **100**, 2878 (1978).
10) K. Harata, H. Uedaira, and J. Tanaka, *Bull. Chem. Soc. Jpn.*, **51**, 1627 (1978).

Acylchlorination and Related Reactions of Fluoroethenes Using $AlCl_3$ and $FeCl_3$

Nobuo Ishikawa,* Hiroshi Iwakiri, Kazuya Edamura, and Satoshi Kubota
Department of Chemical Technology, Tokyo Institute of Technology, Ookayama, Meguro-ku, Tokyo 152
(Received September 4, 1980)

Acylchlorination of mono-, 1,1-di-, and trifluoroethenes with carboxylic acid chlorides using $AlCl_3$ and $FeCl_3$ as a Lewis acid was investigated. In $AlCl_3$-catalyzed reactions, fluorine-chlorine exchange reaction always occurred in part, while in $FeCl_3$-catalyzed reactions Claisen-type condensation giving β-diketones was observed. Preparations of 2-chloro-2-fluoroethyl, 2-chloro-2,2-difluoroethyl, and 2-chloro-1,2,2-trifluoroethyl ketones are given.

Although the reactivity of fluoroethenes towards electrophiles is lowered by the presence of negative fluorine atoms, several examples of the electrophilic addition across the double bond of mono-, di-, and trifluoroethenes appeared in the literature.[1)]

As to the Friedel-Crafts acylhalogenations of the fluoroethenes, the additions of acyl chlorides or acetyl fluoride to 1,1-difluoroethene and trifluoroethene catalyzed by $AlCl_3$[2)] and SbF_5[3)] were reported by Soviet workers.

In this paper we wish to report on the reactions of various carboxylic acid chlorides with mono-, di-, and trifluoroethenes using $AlCl_3$ and $FeCl_3$ as a Lewis acid, and on the preparations of chlorofluoroethyl ketones and β-diketones, which are expected as useful intermediates for synthesis of fluorine containing organic compounds.

Results and Discussion

Acylchlorination of Fluoroethene. Among fluoroethenes, monofluoroethene is expected to be the most susceptible to the attack of electrophiles, however, only a few electrophilic reactions of fluoroethene, *e.g.* additions of fluorosulfuric acid[4)] and arenesulfenyl chlorides,[5)] are known. No reports on the acylchlorination of fluoroethene have appeared in literatures so far. We found that fluoroethene was readily acylchlorinated by various carboxylic acid chlorides in the presence of $AlCl_3$ or $FeCl_3$ even under mild conditions. For example, when fluoroethene gas was allowed to be absorbed in a mixture of excess acyl chlorides and $AlCl_3$ (4:1 mole ratio) at 0 °C, 2-chloro-2-fluoroethyl ketones (**1**) were obtained. However, 2,2-dichloroethyl ketones (**2**), formed by a halogen exchange reaction, were always found as a side product in the reaction mixture. Expecting to avoid this dichloroethyl ketone formation, dichloromethane was used as a solvent and equimolar amounts of acyl chloride and fluoroethene were made to react under the same conditions. The formation of **2**, however, could not be controlled by this method, and from benzoyl chloride, in particular, 2,2-dichloroethyl phenyl ketone (**3**) was formed in a yield of 43%. The fluorine-to-chlorine exchange reaction by $AlCl_3$ forming dichloroethyl ketones in these reactions was confirmed experimentally. For example, when a mixture of equimolar amounts of 2-chloro-2-fluoroethyl propyl ketone **1** (R=*n*-Pr) and $AlCl_3$ in dichloromethane was stirred at 0 °C for 40 min, **1** and **2** were found in a ratio 68:32, based on the ^1H NMR signal intensities, in the resulting mixture.

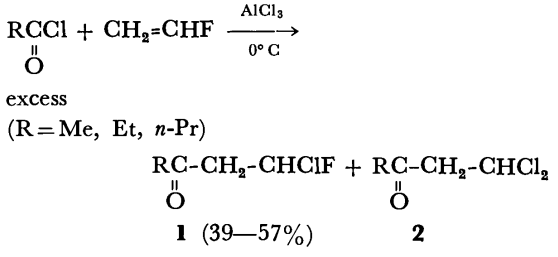

Then we carried out the acylchlorination of fluoroethene, using $FeCl_3$ instead of $AlCl_3$ in the above procedure, because $FeCl_3$ is known to be a milder Lewis acid than $AlCl_3$.[6,7)] By this method, the expected 2-chloro-2-fluoroethyl ketones were obtained exclusively in good yields (Table 1). Even aroyl chlorides afforded corresponding ketones in fairy good yields (≈50%). These 2-chloro-2-fluoroethyl ketones were readily dehydrochlorinated by heat or by a base, giving unstable vinyl ketones.

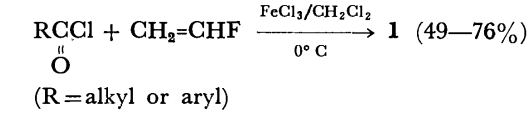

Acylchlorination of 1,1-Difluoroethene. More than twenty years ago Knunyants and his co-workers reported the addition of acetyl, propionyl, and butyryl chlorides to 1,1-difluoroethene using $AlCl_3$ in trichloromethane at low temperature (−10—−5 °C), affording 2-chloro-2,2-difluoroethyl ketones in rather low yields (33—48%).[2)] More recently, Belen'kii and German reported the reaction between acetyl fluoride and 1,1-difluoroethene in sulfur dioxide using SbF_5 as a Lewis acid, obtaining a normal adduct together with condensation products, a β-diketone and an ester.[3)]

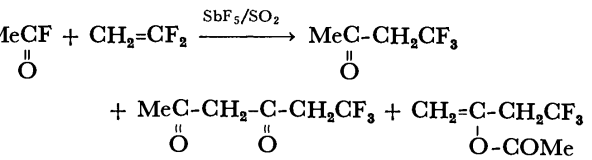

By tracing the procedure reported by Knunyants *et al.*, 2,2,2-trichloroethyl ketones (**5**) were formed as well as 2-chloro-2,2-difluoroethyl ketones (**4**) according

Table 1. Preparation of $RC(=O)-CH_2-CHClF$ (**1**)

R	Bp °C/mmHg [Mp °C]	Yield (%) (Method)[a]	^1H and ^{19}F NMR (δ ppm) α-H	β-H (J_{H-F} Hz)	β-F	IR (C=O) cm^{-1}	Found (Calcd) (%) C	H
Me	38—39/9	(A) 39 (B) 70	3.20 3.27	6.50 (50)	54.3	1720	38.84 (38.58)	4.66 (4.86)
Et	43—45/9	(A) 46	3.20 3.27	6.53 (50)	54.0	1720	43.13 (43.34)	5.46 (5.82)
n-Pr	53—54/5	(A) 57 (B) 76	3.10 3.17	6.45 (49)	54.3	1720	47.64 (47.23)	6.70 (6.61)
i-Pr	55—52/5	(A) 32	3.10 3.17	6.43 (49)	54.3	1720	47.64 (47.23)	6.70 (6.61)
n-C_5H_{11}	55-60/2.5	(B) 65	3.15 3.25	6.50 (50)	54.0	1720	53.67 (53.19)	7.67 (7.81)
Ph	[48.5—50]	(B) 50	3.63 3.72	6.65 (50)	53.3	1680	58.19 (57.93)	4.25 (4.32)
p-MeC_6H_4	[76—77]	(B) 49	3.60 3.70	6.70 (50)	53.3	1675	60.27 (59.86)	4.97 (5.02)

a) Method (A): $AlCl_3$ in excess RCOCl, (B): $FeCl_3$ in CH_2Cl_2. b) ^{19}F NMR was measured in neat and chemical shifts are given in δ ppm from ext. CF_3CO_2H. ^1H NMR was measured in CCl_4.

Table 2. Preparation of $RC(=O)-CH_2-CClF_2$ (**4**)

R	Bp °C/mmHg	Yield (%) (Method)[a]	^1H and ^{19}F NMR (δ ppm)[b] α-H	β-F	IR (C=O) cm^{-1}
Me	38—40/24[c]	(A) 59[c] (B) 46[f]	3.40	−29.7	1730
Et	59—60/29[d]	(A) 56[d]	3.38	−29.5	1730
n-Pr	60—62/20[e]	(B) 50[f]	3.33	−29.6	1720

a) Method (A): $AlCl_3$ in $CHCl_3$, (B): $FeCl_3$ in CH_2Cl_2. b) See Table 1, footnote b): ^1H NMR was measured in $CDCl_3$. c) Lit,[2] bp 40—41 °C/25 mmHg, 44.5%. d) Lit,[2] Bp 56—57 °C/30 mmHg, 48%. e) Lit,[2] bp 64—65 °C/22 mmHg, 33%. f) Contaminated with further acylated products (≈10%).

to the ^1H NMR spectra of reaction products, with the ratios shown below.

$$RC(=O)Cl + CH_2=CF_2 \xrightarrow[-10\text{—}-5\,^\circ C]{AlCl_3/CHCl_3} RC(=O)-CH_2-CClF_2 + RC(=O)-CH_2-CCl_3$$

4 **5**

R	Ratio **4**/**5**
Me	2.3
Et	2.5
Pr	4.0

Avoiding the halogen exchange between **4** and **5** with $AlCl_3$, we examined $FeCl_3$ instead of $AlCl_3$ in these cases again. Thus 1,1-difluoroethene was allowed to be absorbed into a mixture of acyl chlorides and $FeCl_3$ in dichloromethane at 0 °C. By this method, chlorodifluoroethyl ketones were obtained in 50% yield, and no formation of trichloroethyl ketone was observed in the reaction mixture (Table 2).

However, other unidentified by-products were always included in the main product and these contaminants were assumed to be further acylated condensation products such as β-diketone (**6**) or enol ester (**7**) as Belen'kii *et al.* observed in their reaction. The formation of these kind of condensation products is reasonable as $FeCl_3$ is known to accelerate Claisen-type condensation under acidic conditions.[8] Actually, when butyryl chloride was made to react with 2-chloro-2,2-difluoroethyl methyl ketone using $FeCl_3$, β-diketone was obtained though in a low yield.

$$RC(=O)Cl + CH_2=CF_2 \xrightarrow[0\,^\circ C]{FeCl_3/CH_2Cl_2} \quad (R=Me,\ n\text{-}Pr,\ n\text{-}C_5H_{11};\ R=R'CH_2)$$

$$\mathbf{4} + RC(=O)-CH(R')-C(=O)-CH_2-CClF_2 + R'CH=C(OCOR)-CH_2-CClF_2$$

6 **7**

$$n\text{-}PrC(=O)Cl + MeC(=O)-CH_2-CClF_2 \xrightarrow[\text{r.t., 24 h}]{FeCl_3/CH_2Cl_2} n\text{-}Pr-C(=O)-CH_2-C(=O)-CH_2-CClF_2$$

29%

Table 3. Preparation of $RC(=O)-\overset{\alpha}{C}HF-\overset{\beta}{C}ClF_2$ (**8**)

R	Bp °C/mmHg	Yield %	^1H and ^{19}F NMR (δ ppm)[a] α-H (J_{H-F} Hz)	α-F	β-F_2 (J_{F-F} Hz)	IR (C=O) cm^{-1}	Found (Calcd) (%) C	H
Me	98—100[b]	70[b]	4.83 (50)	116.5	−13.9, −16.1 (180)	1745	—	—
n-Pr	78.5—79/103	73	4.85 (48)	117.4	−14.4, −16.6 (174)	1755	38.62 (38.22)	4.16 (4.28)
n-C_5H_{11}	74—76/12	82	4.82 (48)	117.6	−13.9, −16.1 (178)	1765	44.09 (44.35)	5.51 (5.58)
n-C_9H_{19}	92.5—94.5/2.5	82	4.86 (48)	117.2	−14.2, −16.4 (173)	1740	53.34 (52.85)	7.31 (7.39)
Ph	58—59/1.5	13	5.65 (48)	113.3	−15.8, −16.8 (172)	1710	49.00 (49.00)	2.78 (2.74)

a) See, Table 1, footnote b). b) Lit,[2] bp 99—100 °C, yield 34%.

Table 4. Preparation of $RC(OH)=CH-\overset{\alpha}{C}(=O)-\overset{\beta}{C}HF-CClF_2$ (**9′**) (R=H)

R	Bp °C/mmHg	Yield (%) (Method)[a]	^1H and ^{19}F NMR (δ ppm) OH	α-H (J_{H-F} Hz)	α-F	β-F_2 (J_{F-F} Hz)	IR (C=O) cm^{-1}	Found (Calcd) (%) C	H
Me	70—74/23	(A) 40 (B) 70	14.2—15.0	5.00 (48)	117.9	−13.2, −15.5	1600 br	35.83 (35.58)	2.88 (2.99)
n-Pr	89/18	(B) 67	14.1—14.9	4.90 (47)	117.6	−13.9, −15.9	1600 br	41.19 (41.67)	4.37 (4.34)
n-C_5H_{11}	75—76/3	(B) 61	14.2—16.2	4.96 (46)	117.1	−13.7, −15.8	1600 br	46.63 (46.43)	5.35 (5.46)

a) Method (A): $RCOCl+C_2HF_3$ ($FeCl_3$), Method (B): $RCOCl+MeCOCHFCClF_2$ ($FeCl_3$).

Since, 1,1-difluoroethene is less reactive to electrophiles than fluoroethene, the acylchlorination must be sluggish, and it is natural that other side reactions likely occur. Further, aroyl chlorides, which are weaker electrophiles than aliphatic carboxylic acid chlorides, gave no reaction products either by $AlCl_3$ or by $FeCl_3$.

Reaction of Trifluoroethene with Acyl Chlorides. As trifluoroethene is even less susceptible to the Friedel-Crafts acylchlorination than mono- and difluoroethenes, it does not react with acyl chlorides under atmospheric pressure. Knunyants *et al.* made trifluoroethene react with an excess amount of acetyl chloride in a sealed vessel and obtained 2-chloro-1,2,2-trifluoroethyl methyl ketone in 34% yield.[2] Belen'kii also reported that the reaction between acetyl fluoride and trifluoroethene with SbF_5 in SO_2 resulted in the formation of the adduct and its further acylated products.

Various carboxylic acid chlorides were tried to use for the reaction with trifluoroethene using $AlCl_3$ in dichloromethane in a sealed vessel. By making them react at room temperature for a prolonged time, 2-chloro-1,2,2-trifluoroethyl ketones (**8**) were obtained in rather good yields (Table 3).

$$RC(=O)Cl + CHF=CF_2 \xrightarrow[\text{r.t., 20—48 h}]{AlCl_3/CH_2Cl_2} RC(=O)-CHF-CF_2Cl$$

(R=Me, *n*-Pr, *n*-C_5H_{11}, *n*-C_9H_{19}) **8** (70—82%)

However, a small amount of 1,1,1,2-tetrachloroethane was always formed as a side-product, which was assumed to have been formed by chlorination of trifluoroethene with $AlCl_3$ followed by hydrochlorination with HCl. This was confirmed experimentally by allowing trifluoroethene and $AlCl_3$ to react in the presence of a trace of water. Substantial amount of tetrachloroethane was obtained by this reaction.

$$CHF=CF_2 + AlCl_3 \longrightarrow [CHCl=CCl_2] \xrightarrow{HCl} CH_2ClCCl_3$$

As a matter of interest, when $FeCl_3$ was used instead of $AlCl_3$, β-diketones (**9**) were obtained as a main product and only a small or trace amount of acylchlorinated product was formed (Table 4-Method A).

$$RC(=O)Cl + CHF=CF_2 \xrightarrow{FeCl_3/CH_2Cl_2} [\mathbf{8}] \xrightarrow[FeCl_3]{RCOCl} RC(=O)-CH(R')-C(=O)-CHF-CF_2Cl$$

(R=R′CH_2) **9**

This also means that $FeCl_3$ worked as an effective catalyst for the Claisen-type condensation.

In order to prepare the β-diketones carrying an active CH_2 group, chlorotrifluoroethyl methyl ketone **8**, obtained by the $AlCl_3$ catalyzed reaction, was allowed to react with an acyl chloride using $FeCl_3$. Diketones **9** (R=Me, *n*-Pr, *n*-C_5H_{11}; R′=H) were obtained in considerable yields by this method (Table

4-Method B), and they existed in an enol form (**9'**) based on the ^1H NMR.

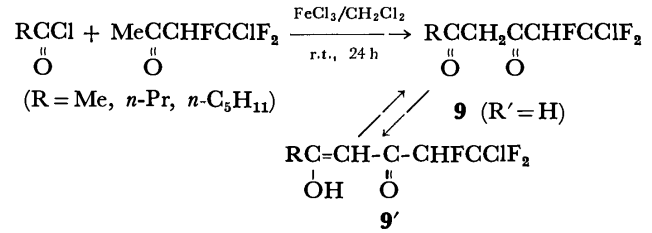

Consequently, it was concluded that trifluoroethene was acylchlorinated by using $AlCl_3$ under more vigorous conditions than the cases of mono- and difluoroethenes, and that when $FeCl_3$ was used, the formation of β-diketone occurred dominantly, presumably because the Claisen-type further acylation proceeded faster than the preceding acylchlorination.

Experimental

2-Chloro-2-fluoroethyl Methyl Ketone **1** *(R=Me). (A)*: Into a solution of $AlCl_3$ (13.3 g, 0.1 mol) in acetyl chloride (31.4 g, 0.4 mol), fluoroethene gas was introduced through the bottom of the vessel. The temperature was kept below 0 °C and the introduction was continued until no more absorption was observed (≈40 min). The reaction mixture was then poured into a mixture of ice (50 g) and concd hydrochloric acid (10 ml) and a separated oily material was extracted with diethyl ether. The extract was washed with aqueous solution of $NaHCO_3$ to remove a free carboxylic acid, then with water, and dried over $MgSO_4$. After evaporating the solvent, the residue was subjected to distillation under reduced pressure, giving **1** (R=Me) (5.0 g), bp 38—39 °C/9 mmHg**, in a yield of 39% based on the used $AlCl_3$.

(B): Into a suspension of $FeCl_3$ (19.4 g, 0.12 mol) in dichloromethane (100 ml), acetyl chloride (7.85 g, 0.10 mol) was added dropwise with cooling in an ice-bath. Then fluoroethene gas was introduced to the solution keeping the temperature below 0 °C until no more gas was absorbed (3 h). The reaction mixture was treated similarly as mentioned in (A) and distillation gave **1** (R=Me) (8.70 g) in 70% yield.

The other carboxylic acid chlorides were allowed to react with fluoroethene in similar procedures (Table 1). When the aroyl chlorides were used, the products came out as a solid after removal of the solvent, which were purified by recrystallization from cyclohexane. All of the 2-chloro-2-fluoroethyl ketones were readily dehydrochlorinated by distillation at high temperature. Therefore it was necessary to distill them at lower than 60 °C under reduced pressure. They gradually decomposed even kept in a refrigerator.

2,2-Dichloroethyl Phenyl Ketone (3). Into a mixture of benzoyl chloride (14.1 g, 0.10 mol), $AlCl_3$ (13.3 g, 0.10 mol) and dichloromethane (38 ml), fluoroethene gas was absorbed, and the reaction mixture was worked up as usual. After evaporation of the solvent, the residue was recrystallized from hexane, giving **3** (7.44 g, 43%), mp 58—59 °C; NMR (CCl_4): δ 3.82 (2H), 6.27 (H), 7.30—8.00 (5H); $\nu_{C=O}$; 1670 cm^{-1}. Found: C, 53.82; H, 3.95%. Calcd for $C_9H_{18}Cl_2O$: C, 53.23; H, 3.97%.

2-Chloro-2,2-difluoroethyl Methyl Ketone (4) (R=Me). (A): The reactions between acetyl chloride and 1,1-difluoroethene in chloroform were carried out after the Knunyants procedure. Somewhat higher yield was obtained (Table 2).

(B): 1,1-Difluoroethene was absorbed into a mixture of acetyl chloride, $FeCl_3$, and dichloromethane at 0 °C. The procedure was similar to that of fluoroethene mentioned above, though the reaction was sluggish and it took ≈5 h. The product, even after distillation, was contaminated with unidentified impurities and the purity of **4** was ≈90% from the signal intensities of ^1H NMR.

2-Chloro-1,2,2-trifluoroethyl Methyl Ketone (8) (R=Me). A mixture of $AlCl_3$ (16.0 g, 0.12 mol), acetyl chloride (7.85 g, 0.10 mol), and dichloromethane (100 ml) was placed in a pressure vessel, and was cooled in a Dry Ice–acetone bath. Liquefied trifluoroethene (9.0 g, 0.11 mol) was introduced into the vessel and the mixture was stirred at room temperature for 48 h and was poured onto a mixture of ice (100 g) and concd hydrochloric acid (10 ml). An oily layer was separated, washed with an aqueous solution of $NaHCO_3$, and dried over $MgSO_4$. After evaporating the solvent, distillation of the residue gave **8** (R=Me) (11.3 g), bp 98—100 °C (lit,[2] bp 99—100 °C), in 70% yield.

The reactions of trifluoroethene with other carboxylic acid chlorides using $AlCl_3$ were carried out in a similar manner. When benzoyl chloride was used, the product was separated by column chromatography on silica gel (solvent : hexane).

6-Chloro-5,6,6-trifluoro-2,4-hexanedione (9) (R=Me; R'=H). (A): Into a mixture of $FeCl_3$ (32.4 g, 0.2 mol), acetyl chloride (15.7 g, 0.2 mol), and dichloromethane (100 ml) was introduced liquefied trifluoroethene (8.2 g, 0.1 mol) as described above. The mixture was allowed to react for 20 h at room temperature and the reaction mixture was worked up as usual. β-Diketone **9** (R=Me; R'=H) (8.1 g), bp 70—74 °C/23 mmHg, was obtained in 40% yield.

(B): Into a suspension of $FeCl_3$ (1.95 g, 12 mmol) in dichloromethane (10 ml), a mixture of acetyl chloride (0.40 g, 5 mmol) and 2-chloro-1,2,2-trifluoroethyl methyl ketone (0.80 g, 5 mmol) was dropped and the mixture was stirred for 24 h at room temperature under atmospheric pressure. The reaction mixture was worked up giving a β-diketone **9** (R=Me; R'=H) (0.70 g) in 70% yield.

**1 mmHg≈133.3 Pa.

References

1) B. L. Dyatkin, E. P. Mochalina, and I. L. Knunyants, "Fluorine Chemistry Reviews," Marcel Dekker, New York, N.Y. (1969), Vol. 3, p. 45.

2) I. L. Knunyants, R. N. Sterlin, L. N. Pinkina, and B. L. Dyatkin, *Izv. Akad. Nauk SSSR, Ser. Khim.*, **1958**, 296.

3) G. G. Belen'kii and L. S. German, *Izv. Akad. Nauk SSSR, Ser. Khim.*, **1974**, 942.

4) G. A. Olah, J. Nishimura, and Y. K. Mo, *Synthesis*, **1973**, 661.

5) S. Kondo, T. Akasaka, and K. Tsuda, *Nagoya Kogyo Daigaku Gaku-ho*, **26**, 231 (1974).

6) G. A. Olah, S. J. Kuhn, S. H. Flood, and B. A. Hardie, *J. Am. Chem. Soc.*, **86**, 1044 (1064).

7) G. A. Olah, S. J. Kuhn, and B. A. Hardie, *J. Am. Chem. Soc.*, **86**, 1055 (1964).

8) B. M. Perfetti and R. Levine, *J. Am. Chem. Soc.*, **75**, 626 (1953).

The σ-Bonded Palladium(II) Complex of [π-(Dimethylaminomethyl)-cyclopentadienyl]tetraphenylcyclobutadienecobalt(I)

Taeko Izumi, Mitsugi Maemura, Kazuyoshi Endoh, Tadashi Oikawa, Satoshi Zakozi, and Akira Kasahara*

Department of Applied Chemistry, Faculty of Engineering, Yamagata University, Yonezawa 992

(Received September 8, 1980)

[π-(Dimethylaminomethyl)cyclopentadienyl]tetraphenylcyclobutadienecobalt(I) reacts with lithium tetrachloropalladate(II) in the presence of sodium acetate to give an ortho-palladated binuclear complex. The σ-bonded structure of the complex was confirmed by studies of the IR and ^{1}H-NMR spectra and of the reactions with triphenylphosphine, thallium(I) acetylacetonate, and lithium aluminum deuteride. The reactions of the σ-bonded complex with carbon monoxide and olefins have been examined.

Following the first observation by Cope and Siekman[1] that azobenzene reacts with palladium(II) chloride to give an intramolecular ortho-palladation product with a carbon-to-metal σ-bond, considerable interest developed in this area and numerous ortho-metalated complexes have been prepared.[2] In connection with the ortho-metalation, Alper[3] reported the first example of the intramolecular ortho-palladation of a metallocene by the reaction of thiopivaloylferrocene with sodium tetrachloropalladate(II); subsequently the intramolecular ortho-palladations of (dimethylaminomethyl)ferrocene,[4] acetylferrocene *N,N*-dimethylhydrazone,[5] 2-pyridylferrocene,[6] and (dimethylaminomethyl)ruthenocene[7] were also reported. In this report, we wish to report on the intramolecular ortho-palladation of [π-(dimethylaminomethyl)cyclopentadienyl]tetraphenylcyclobutadienecobalt(I) (**1**) and the reaction of the metalation product (**2**) with carbon monoxide and olefins.

Results and Discussion

In the presence of sodium acetate trihydrate, the reaction of **1** with mole equivalents of lithium tetra-

Table 1. The ^{1}H-NMR spectra (δ, ppm) of [π-(dimethylaminomethyl)cyclopentadienyl]-tetraphenylcyclobutadienecobalt(I) derivatives

Compound	-N-C<u>H</u>$_3$	-C<u>H</u>$_2$-	Cp-<u>H</u>	Other
1	2.23 (s, 6H)	2.71 (s, 2H)	4.63 (s, 4H)	7.10—7.65 (m, 20H, Ar-<u>H</u>).
3	2.43 (s, 3H) 2.82 (s, 3H)	3.00 (d, 1H) 3.18 (d, 1H)	4.61 (m, 3H)	7.02—7.90 (m, 35H, Ar-<u>H</u>).
4	2.20 (s, 3H) 2.62 (s, 3H)	2.75 (d, 1H) 3.25 (d, 1H)	4.20—4.60 (t, 3H)	1.67 and 1.82 (each s, 3H, C<u>H</u>$_3$ of Acac group), 5.11 (s, 1H, -C<u>H</u>- of Acac group), 7.07—7.62 (m, 20H, Ar-<u>H</u>).
6	2.11 (s, 6H)	2.78 (br-s, 2H)	4.93 (t, 3H)	1.02 (t, 3H, -COOCH$_2$C<u>H</u>$_3$), 3.63 (q, 2H, -COOC<u>H</u>$_2$CH$_3$), 7.13—7.47 (m, 20H, Ar-<u>H</u>).
7	2.15 (s, 6H)	2.98 (br-s, 2H)	4.68—4.94 (m, 3H)	6.35 (d, 1H, J=16 Hz, -C=C<u>H</u>-Ph), 6.71 (d, 1H, J=16 Hz, -C<u>H</u>=C-Ph), 7.25—770 (m, 25H, Ar-<u>H</u>).
8	2.15 (s, 6H)	2.99 (br-s, 2H)	4.72—4.98 (m, 3H)	1.91 (s, 3H, -CO-C<u>H</u>$_3$), 600 (d, 1H, J=16 Hz, -C=C<u>H</u>-CO-), 6.84 (d, 1H, J=16 Hz, -C<u>H</u>=C-CO-), 7.15—7.50 (m, 20H, Ar-<u>H</u>).
9	2.00 (s, 6H)	2.85 (br-s, 2H)	4.65—4.95 (m, 3H)	6.71 (d, 1H, J=16 Hz, -C=C<u>H</u>-CO-), 7.10—7.75 (m, 26H, Ar-<u>H</u>+-C<u>H</u>=C-CO-).
10	2.11 (s, 6H)	2.93 (br-s, 2H)	4.51—4.78 (m, 3H)	3.97—4.16 (m, 9H, Cp-<u>H</u> of ferrocene), 5.87 (d, 1H, J=16 Hz, -C=C<u>H</u>-Fc), 6.31 (d, 1H, J=16 Hz, -C<u>H</u>=C-Fc), 7.11—7.53 (m, 20H, Ar-<u>H</u>).
11	2.01 (s, 6H)	2.96 (br-s, 2H)	4.51—4.79 (m, 3H)	4.82 and 5.13 (each d-d, 2H, -C=C<u>H</u>$_2$), 5.99 (d-d, 1H, -C<u>H</u>=C), 7.09—7.56 (m, 20H, Ar-<u>H</u>).
12	2.44 (s, 12H)	3.17 (s, 4H)	4.74—4.90 (m, 3H)	7.16—7.51 (m, 42H, Ar-<u>H</u>+-C<u>H</u>=C<u>H</u>-).

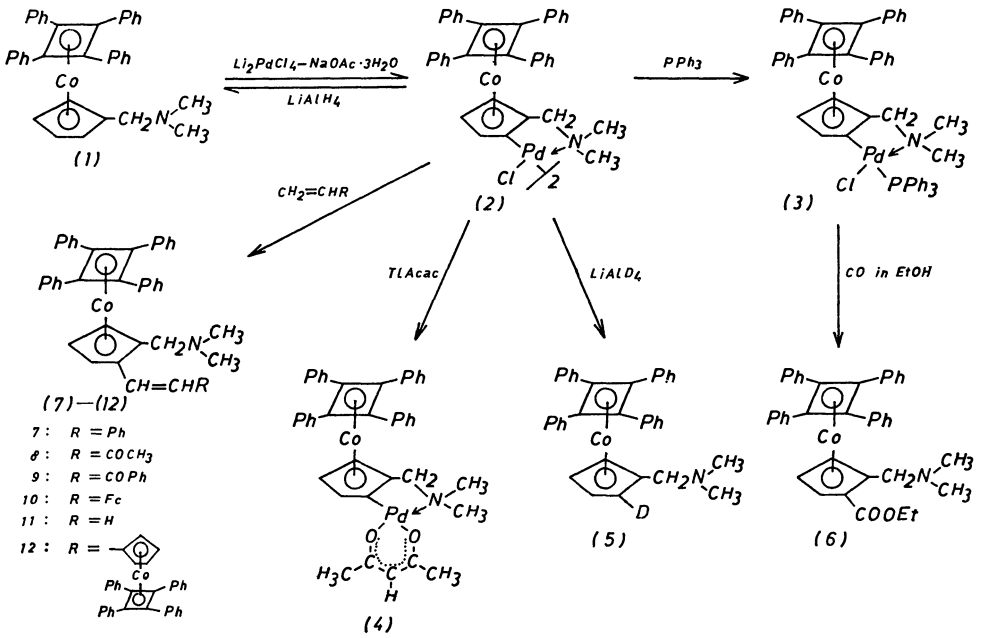

Fig. 1.

chloropalladate(II) gave di-μ-chloro-bis{[π-1-(dimethylaminomethyl)cyclopentadienyl-2*C*,*N*]tetraphenylcyclobutadienecobalt(I)}dipalladium(II) (**2**) in 96% yield. The complex **2** was shown to be an intramolecularly ortho-palladated complex on the bases of its reactions and of the microanalytical and spectroscopic results. Measurement of the molecular weight using a vapor pressure osmometer was not conducted because of the low solubility of **2** in all common solvents. However, the binuclearly σ-bonded structure of the complex **2** was supported by the bridged splitting reaction with triphenylphosphine and thallium(I) acetylacetonate to give readily soluble monomeric triphenylphosphine derivative **3** and a monomeric acetylacetonate derivative **4**, respectively. Moreover, the far-infrared spectrum of **2** showed a bridged Pd–Cl streching absorption at about 303, 275, and 255 cm^{-1}. The low solubility of **2** in all common solvents precluded any NMR studies at room temperature. However, the ^{1}H-NMR spectra of derivative **3** and **4** clearly demonstrated that Pd–C σ-bonds and Pd–nitrogen coordination bonds existed in these complexes (Table 1). *N*-Methyl and *N*-methylene protons of **1** appear as singlets, whereas in **3** and **4** the *N*-methyl protons appear as two singlets and the *N*-methylene protons as two doublets. The non-equivalence of the *N*-methyl and *N*-methylene protons in **3** and **4** can be explained in terms of a cyclic system in which the nitrogen is coordinated to the palladium and a palladium–carbon σ-bond is involved.[8] Furthermore, to ascertain the formation of the σ-bond between palladium and the cyclopentadienyl ring in **2**, **3**, and **4**, the compound **2** was reduced with lithium aluminum deuteride to give [π-1-(dimethylaminomethyl)cyclopentadienyl-2-*d*]tetraphenylcyclobutadienecobalt(I) (**5**). On the other hand, the lithium aluminum hydride reduction of **2** gave **1**, whose mass spectrum was identical with that of an authentic sample. The IR spectrum of the compounds prepared in this study is recorded in Table 2. In ferrocene derivatives, generally, 1,2-disubstituted derivatives exhibited one peak, while the 1,3-isomers showed two peaks in the region near 900 cm^{-1}; this was the characteristic absorption band of the C–H out-of-plane bending mode on the ferrocene ring.[9] The infrared frequencies of the C–H bending modes of ruthenocene derivatives are also similar to those ferrocene.[7,10] Compounds **2**, **3**, and **4** and another derivatives from **2** all exhibited a single peak in the 900 cm^{-1} region. Taking these results into account, it has been confirmed that **2**, **3**, and **4** are 1,2-disubstituted cyclopentadienyl derivatives.

The reactions of ortho-palladation products from α-aryl-nitrogen derivatives with numerous reagents have been reported.[2] The carbonylation of ortho-palladation products of azobenzene, Schiff bases, and *N*,*N*-dialkylbenzylamines usually gives a variety of heterocyclic compounds.[11,12] The derivative **3** in ethanol was readily carbonylated at 100 °C to produce an uncyclic ester [π-1-(dimethylaminomethyl)-2-ethoxycarbonylcyclopentadienyl]tetraphenylcyclobutadienecobalt(I) (**6**) in 42% yield. On the other hand, in the presence of triethylamine, the complex **2** reacted with simple olefins, such as styrene, methyl vinyl ketone, phenyl vinyl ketone, and vinylferrocene, in toluene at 100 °C, leading to the formation of [π-1-(dimethylaminomethyl)-2-alkenylcyclopentadienyl]-tetraphenylcyclobutadienecobalt(I) (**7**—**10**) in moderate yields. Moreover, the reaction of the complex **2** with ethylene led to the formation of vinyl derivative (**11**) and disubstituted ethylene derivative (**12**) in 78 and 1.5% yield, respectively. The IR and ^{1}H-NMR spectra of compounds **5**—**12** were all consistent with the proposed structures. The compounds **5**—**12** also exhibited a single peak absorption in the 900 cm^{-1} region characteristic of homoannularly 1,2-disubstituted metallocene derivatives.

Table 2. The IR absorption frequencies (cm^{-1}) of [π-(dimethylaminomethyl)cyclopentadienyl]-tetraphenylcyclobutadienecobalt(I) derivatives

Compound	917 Rule	Other bands
2	910	3050, 2900, 2850, 1600, 1500, 740, 690; 303, 275, 255 (bridged Pd-Cl).
3	910	3050, 2900, 2850, 1600, 1500, 745, 690: 345, 330 (terminal Pd-Cl).
4	905	3030, 2900, 2850, 1600, 1500, 750, 690; 1580, 1510 (Acac group), 1200 (H-C bending of Acac group).
6	910	3030, 2950, 2830, 1600, 1500, 750, 690; 1710 (ester).
7	910	3030, 2950, 2800, 1600, 1500, 745, 690; 960 (*trans* -CH=CH-).
8	910	3030, 2950, 2800, 1600, 1500, 750, 690; 1660 (-CO-CH=CH-), 960 (*trans* -CH=CH-).
9	910	3030, 2950, 2800, 1600, 1500, 750, 690, 1660 (-CO-CH=CH-), 960 (*trans* -CH=CH-).
10	910	3050, 2950, 2800, 1600, 1500, 745, 690; 1100, 1000 (Fc), 960 (*trans* -CH=CH-).
11	910	3020, 2900, 2800, 1600, 1500, 750, 690; 1620, 990 (-CH=CH_2).
12	910	3020, 2900, 2800, 1600, 1500, 750, 690; 1620, 965 (*trans* -CH=CH-).

Table 3. Properties and analysis of [π-1-(dimethylamenomethyl)cyclopentadienyl]-tetraphenylcyclobutadienecobalt(I) derivatives

Compound	
6	pale yellow crystals, mp 112—113 °C. Found: C, 76.71; H, 5.84; N, 2.13%. MS: *m/e* 609 (M^+). Calcd for $C_{39}H_{36}CoNO_2$: C, 76.83; H, 5.95; N, 2.29%; mol wt, 609.
7	pale yellow crystals, mp 86—88 °C. Found: C, 82.48; H, 5.86; N, 2.05%. MS: *m/e* 639 (M^+). Calcd for $C_{44}H_{38}CoN$: C, 82.61; H, 6.01; N, 2.18%; mol wt, 639.
8	pale yellow crystals, mp 109—111 °C. Found: C, 79.23; H, 5.88; N, 2.25%. MS: *m/e* 605 (M^+). Calcd for $C_{40}H_{36}CoNO$: C, 79.32; H, 5.99; N, 2.31%; mol wt, 605.
9	pale yellow crystales, mp 157—159 °C. Found: C, 80.61; H, 5.59; N, 1.88%. MS: *m/e* 667 (M^+). Calcd for $C_{45}H_{38}CoNO$: C, 80.79; H, 5.73; N, 2.09%; mol wt, 667.
10	reddish yellow crystals, mp 79—81 °C. Found: C, 76.87; H, 5.71; N, 1.73%. MS: *m/e* 747 (M^+). Calcd for $C_{48}H_{42}CoFeN$: C, 77.08; H, 5.67; N, 1.87%; mol wt, 747.
11	pale yellow crystals, mp 124—125 °C. Found: C, 80.90; H, 5.95; N, 2.33%. MS: *m/e* 563 (M^+). Calcd for $C_{38}H_{34}CoN$: C, 80.97; H, 6.07; N, 2.48%; mol wt, 536.
12	yellow crystals, mp 244—246 °C. Found: C, 80.77; H, 5.72; N, 2.45%; mol wt 1094 (in $CHCl_3$). Calcd for $C_{74}H_{64}Co_2N_2$: C, 80.86; H, 5.86; H, 2.54%; mol wt, 1099.

Experimental

Materials. All the melting points are uncorrected. [π-(Dimethylaminomethyl)cyclopentadienyl]tetraphenylcyclobutadienecobalt(I) (**1**) was prepared according to the method described by Rausch and Genetti.[13] Phenyl vinyl ketone[14] and vinylferrocene[15] were synthesized according to known procedures. The other olefins were obtained from commercial sources.

Measurements. The ^{1}H-NMR spectra were determined in $CDCl_3$ with a Hitachi R-22 spectrometer (90 MHz), using TMS as the internal standard (δ, ppm). The IR spectra were measured (4000—650 cm^{-1}) and Nujol mulls mounted on thin polythene windows (700—200 cm^{-1}) with Hitachi 215 and EPI-L spectrometers. The mass spectra were obtained on a Hitachi RMU-6M mass spectrometer, using a direct insertion probe at an ionization energy of 70 eV. The molecular weight was determined in $CHCl_3$ with a Hitachi 115 vapor pressure osmometer.

*Di-μ-chloro-bis{[π-1-(dimethylaminomethyl)cyclopentadienyl-2C,N]tetraphenylcyclobutadienecobalt(I)}dipalladium(II) (**2**).* A mixture of lithium tetrachloropalladate(II) (2.62 g, 10 mmol) and sodium acetate trihydrate (1.36 g, 10 mmol) in methanol (50 ml) was stirred for 30 min at room temperature. To the reaction mixture, a solution of **1** (5.37 g, 10 mmol) in methanol (100 ml) was added, and the mixture was stirred for 36 h at room temperature. The yellow precipitate which formed was filtered and washed successively with several portions of methanol and then ether. The solid (6.5 g, 96% yield) was insoluble in all common solvents; mp 208—210 °C (dec). Found: C, 60.68; H, 4.67; N, 2.02%. Calcd for $C_{64}H_{62}Cl_2Co_2N_2Pd_2$: C, 60.96; H, 4.95; N, 2.22%.

*Chloro(triphenylphosphine{[π-1-(dimethylaminomethyl)cyclopentadienyl-2C,N]tetraphenylcyclobutadienecobalt(I)}palladium(II) (**3**).* A mixture of the complex (5.0 g, 3.7 mmol) and triphenylphosphine (1.94 g, 7.4 mmol) in benzene (50 ml) was stirred for 12 h at room temperature. After removal of the solvent *in vacuo*, the column chromatography of the residue on silica gel ($CHCl_3$) gave triphenylphosphine derivative (**3**) (6.9 g, 99% yield); mp 235—237 °C (dec). Found: C, 67.33; H, 5.31; N, 1.71%; mol wt 884 (in $CHCl_3$). Calcd for $C_{50}H_{46}ClCoNPPd$: C, 67.27; H, 5.19; N, 1.55%; mol wt 892.

*Acetylacetonato{[π-1-(dimethylaminomethyl)cyclopentadienyl-2C,N]tetraphenylcyclobutadienecobalt(I)}palladium(II) (**4**).* A suspension of the complex **2** (0.80 g, 0.6 mmol) and thal-

lium(I) acetylacetonate (0.33 g, 1.2 mmol) in benzene (20 ml) was stirred for 24 h at room temperature. The filtrate was evaporated *in vacuo*, and the residue was purified by column chromatography on silica gel ($CHCl_3$) and gave the acetylacetonate derivative (**4**) (0.7 g, 80% yield); mp 219—221 °C (dec). Found: C, 64.15; H, 5.62; N, 2.17%; mol wt 686 (in $CHCl_3$). Calcd for $C_{37}H_{38}CoNO_2Pd$: C, 64.03; H, 5.51; N, 2.01%; mol wt 694.

Reduction of Complex 2 with Lithium Aluminum Hydride. Lithium aluminum hydride (0.08 g, 2 mmol) in dry ether (50 ml) was slowly added to a solution of the complex **2** (2.52 g, 2 mmol) in dry THF (50 ml). The resulting black mixture was stirred at 50 °C for 8 h; then water (20 ml) was added with cooling. The ether layer was washed with water and dried over anhydrous $MgSO_4$. After the removal of the solvent, **1** was obtained as yellowish needles from benzene–cyclohexane; mp 189—190 °C (lit,[13] mp 189—190 °C). The ^{1}H-NMR, IR, and mass spectra of **1** were consistent with those of an authentic sample.

Reduction of Complex 2 with Lithium Aluminum Deuteride. The reduction of the complex **2** (1.0 g) with lithium aluminum deuteride (0.035 g) was conducted under the same conditions as in the preceeding experiment. After recrystallization from benzene–cyclohexane, the product (mp 189—191 °C) was identified as [π-1-(dimethylaminomethyl)cyclopentadienyl-2-*d*]tetraphenylcyclobutadienecobalt(I) (**5**) on the basis of the following evidence; ^{1}H-NMR ($CDCl_3$): δ 2.23 (s, 6H, $-N(C\underline{H}_3)_2$), 2.71 (s, 2H, $-C\underline{H}_2-$), 4.63 (s, 3H, Cp–H), 7.10—7.65 ppm (m, 20H, Ar–H). MS: *m/e* 538 (M^+). Found: C, 80.16; H, 6.01; N, 2.45%. Calcd for $C_{36}H_{31}CoDN$: C, 80.27; H, 6.19; N, 2.60%; mol wt, 538.

Carbonylation of Complex 3 in Ethanol. In an autoclave, a suspension of the complex **3** (2.0 g, 2.1 mmol) in ethanol (80 ml) was stirred for 24 h at 100 °C under carbon monoxide pressure of 50 atm. The reaction mixture was filtered to remove precipitated palladium, and the filtrate was evaporated *in vacuo*. The residue was dissolved in $CHCl_3$ and column chromatographed on silica gel to afford [π-1-(dimethylaminomethyl)-2-ethoxycarbonylcyclopentadienyl]-tetraphenylcyclobutadienecobalt(I) (**6**): mp 112—113 °C, (0.41 g, 42% yield). The structure of **6** has been confirmed by elemental analysis and ^{1}H-NMR, IR, and mass spectra (Tables 1, 2, and 3).

General Procedure for the Reaction of Complex 2 with Olefins. In a closed vessel, a mixture of the complex **2** (1.26 g, 1 mmol), 3 mmol of olefin (styrene, methyl vinyl ketone, phenyl vinyl ketone, and vinylferrocene) and triethylamine (0.20 g, 2 mmol) in toluene (50 ml) was stirred for 8 h at 80 °C under a nitrogen atmosphere. The reaction mixture was cooled and filtered to remove precipitated palladium, and the filtrate was evaporated *in vacuo*. The residue was dissolved in $CHCl_3$ which had been washed with brine, and dried over anhydrous $MgSO_4$. After removal of the solvent, purification of the crude product by column chromatography (silica gel–$CHCl_3$) gave [π-1-(dimethylaminomethyl)-2-styryl-cyclopentadienyl]tetraphenylcyclobutadienecobalt(I) (**7**), [π-1-(dimethylaminomethyl)-2-(2-acetylvinyl)cyclopentadienyl]-tetraphenylcyclobutadienecobalt(I) (**8**), [π-1-(dimethylaminomethyl)-2-(2-benzoylvinyl)cyclopentadienyl]tetraphenylcyclobutadienecobalt(I) (**9**), and [π-1-(dimethylaminomethyl)-2-(2-ferrocenylvinyl)cyclopentadienyl]tetraphenylcyclobutadienecobalt(I) (**10**) in 30, 45, 57, and 40% yields, respectively.

In the case of the reaction with ethylene, a suspension of the complex **2** (2.52 g, 2 mmol) in triethylamine (30 ml) was stirred for 20 h at 100 °C under ethylene pressure of 50 atm in an autoclave. The crude products were purified by column chromatography on silica gel. First elution with $CHCl_3$ and recrystallization from benzene–cyclohexane afforded pale yellow crystals (78% yield), which were identified to [π-1-(dimethylaminomethyl)-2-vinylcyclopentadienyl]tetraphenylcyclobutadienecobalt(I) (**11**). Further elution with $CHCl_3$ and recrystallization from benzene–cyclohexane afforded yellow crystals, which were identified as μ-{bis[π-2-(dimethylaminomethyl)cyclopentadienyl]ethylene}-bis[tetraphenylcyclobutadienecobalt(I)] (**12**) (1.5% yield). The structure of the compounds (**7**—**12**) has been confirmed by elemental analysis and the ^{1}H-NMR, IR, and mass spectra (Tables 1, 2, and 3).

References

1) A. C. Cope and R. W. Siekman, *J. Am. Chem. Soc.*, **87**, 3272 (1965).
2) I. Omae, *Chem. Rev.*, **79**, 287 (1979).
3) H. Alper, *J. Organomet. Chem.*, **80**, C29 (1974).
4) J. C. Gaunt and B. L. Shaw, *J. Organomet. Chem.*, **102**, 511 (1975).
5) M. Nonoyama, *Inorg. Nucl. Chem. Lett.*, **12**, 709 (1976).
6) A. Kasahara, T. Izumi, and M. Maemura, *Bull. Chem. Soc. Jpn.*, **50**, 1878 (1977).
7) S. Kamiyama, T. Kimura, A. Kasahara, T. Izumi, and M. Maemura, *Bull. Chem. Soc. Jpn.*, **52**, 142 (1979).
8) A. C. Cope, J. M. Kliegman, and E. C. Friedrich, *J. Am. Chem. Soc.*, **89**, 287 (1967).
9) M. Rosenblum, "Chemistry of The Iron Group Metallocenes" John Wiley & Sons, Inc., New York, (1965), p. 38.
10) E. R. Lippincott and R. D. Nelson, *Spectrochim. Acta*, **10**, 307 (1958).
11) H. Takahashi and J. Tsuji, *J. Organomet. Chem.*, **10**, 511 (1967).
12) J. M. Thompson and R. F. Heck, *J. Org. Chem.*, **40**, 2667 (1975).
13) M. D. Rausch and R. A. Genetti, *J. Org. Chem.*, **35**, 3888 (1970).
14) W. G. Young and J. D. Roberts, *J. Am. Chem. Soc.*, **68**, 649 (1946).
15) M. D. Rausch and A. Siegel, *J. Organomet. Chem.*, **11**, 317 (1968).

"Naked" Hydrogencarbonate Ion as a Bifunctional Catalyst toward Amide Substrates.[1] Nucleophilic Ion Pairs. 9

Seiji SHINKAI,** Naotoshi NAKASHIMA, and Toyoki KUNITAKE*

Department of Organic Synthesis, Faculty of Engineering, Kyushu University, Naka-ku, Fukuoka 812

(Received September 16, 1980)

The cleavage of amide substrates(*p*-nitro-*N*-methyltrifluoroacetanilide and *p*-nitro-*N*-methyldichloroacetanilide) with anionic nucleophiles was studied at 30 °C in aprotic (acetonitrile and *N*,*N*-dimethylformamide) and protic(ethanol) media. Hydrogencarbonate ion acted as catalyst much more efficiently in the aprotic solvents (about 10^3 fold) than expected from its aqueous pK_a, but in ethanol, its reactivity was close to those of simple nucleophiles (*p*-cyanophenolate anion and *N*-hydroxysuccinimide anion) that possess analogous pK_a values in water. The reaction rate in the aprotic solvents was sensitive to small amounts of water. The kinetic isotope effect showed that proton transfer was involved (at least partially) in the rate-determining step. Thus, hydrogencarbonate ion behaves in aprotic media as a nucleophilic-general acid catalyst for the amide cleavage. The biochemical implication with regard to the action of biotin was discussed.

The catalytic hydrolysis of amide substrates has been of special concern as model systems of hydrolytic enzymes. Amide groups are generally very stable toward nucleophiles, so that investigation has been limited to the alkaline hydrolysis of amide substrates containing strongly electron-attracting groups.[2-5] In the previous publications of this series, we reported that the cleavage of amide linkages which was virtually impossible in aqueous systems did take place in very dry aprotic solvents with tetraalkylammonium hydroxamate ion pairs.[6,7] The rate augmentation observed reached 10^8—10^9 fold in comparison with that in the aqueous system. We proposed, on the basis of several pieces of evidence, that the amide cleavage is achieved due to (i) enhanced nucleophilicity of the hydroxamate anion(or probably oxide anions in general: RO^-) which is desolvated in aprotic solvents[8,9] and (ii) efficient proton transfer from poorly solvated water molecules to the tetrahedral intermediate.[6,7] Particularly, the second factor is characteristic of the amide cleavage, since it requires proton sources to avoid the formation of energetically-unfavorable amine anions.[10] Obviously, these are opposing factors: that is, factor (i) arises from enhanced basicity(nucleophilicity) of oxide anions and factor (ii) is related to the enhanced reactivity of water molecules as proton source. Thus, the combination of these two factors in a single reaction medium is not easy.

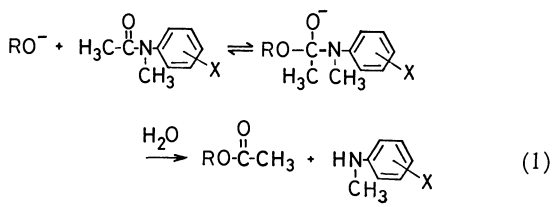

(1)

However, a tautomer which combines within a molecule structural characteristics of acid(s) (proton source) and base(s) (oxide anions) may serve as an efficient catalyst for the amide cleavage. Tautomeric catalysts have been extensively employed as bifunctional catalysts in mutarotation and acyl transfer reactions.[11] However, they cannot be applied directly to the amide cleavage, because their nucleophilic reactivities are not sufficiently large. Therefore, we adopted potassium hydrogencarbonate ($HCO_3^-K^+$) as a bifunctional catalyst which has an oxide anion group (pK_a=6.37 in H_2O)[12] as well as a dissociable OH group. As monofunctional nucleophiles, potassium *p*-cyanophenolate(*p*-$CNC_6H_4O^-K^+$: pK_a=7.95 in H_2O)[12] and potassium salt of *N*-hydroxysuccinimide(SIO$^-$K$^+$: pK_a=6.0 in H_2O)[13] were employed. These salts were solubilized in desired solvents with 10 times excess perhydrodibenzo-18-crown-6. Substrates employed are recorded below with their abbreviations.

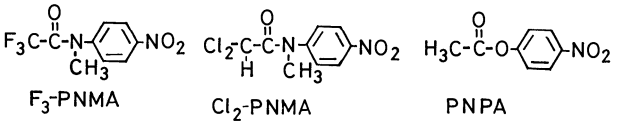

F_3-PNMA Cl_2-PNMA PNPA

Experimental

Materials. Equimolar amounts of *p*-cyanophenol and potassium hydroxide were mixed in methanol and the solvent was evaporated. The residue was recrystallized from acetonitrile and methanol to give monohydrate of potassium *p*-cyanophenolate. The potassium salt of *N*-hydroxysuccinimide was prepared in the same way. *p*-Nitro-*N*-methyltrifluoroacetanilide (F_3-PNMA) was prepared by Dr. T. Sakamoto in these laboratories from *p*-nitro-*N*-methylaniline and trifluoroacetic anhydride, mp 129—131 °C (lit,[14] 126.5—131 °C). *p*-Nitro-*N*-methyldichloroacetanilide (Cl_2-PNMA) was obtained from dichloroacetyl chloride and *p*-nitro-*N*-methylaniline in the presence of triethylamine in benzene. Recrystallization from benzene–hexane gave slightly yellow powders; mp 131—133 °C, Found: C, 41.38; H, 3.10; N, 10.59%. Calcd for $C_9H_8N_2O_3Cl_2$: C, 41.05; H, 3.07; N, 10.65%. The purification of solvents was described previously.[7]

Kinetics. The potassium salts were dissolved in desired solvents with 10 times excess perhydrodibenzo-18-crown-6 by sonication (1.5 h). All kinetic measurements were carried out at 30±0.1 °C in modified Thunberg cuvettes. The details of the procedure have been described elsewhere.[8,9] The progress of the reaction was monitored spectrophotometrically by following the increase in the absorption of *p*-nitro-*N*-methylaniline or that of *p*-nitrophenolate: 401 nm for PNPA and 390 nm for F_3-PNMA and Cl_2-PNMA. Since excess nucleophiles were present in all the cases, pseudo

** Present address: Department of Industrial Chemistry, Faculty of Engineering, Nagasaki University, Nagasaki 852.

first-order behavior was observed. The water content of the reaction medium was evaluated immediately after the reaction, using a coulometric Karl-Fisher apparatus (Hiranuma Aquacounter AQ-1). The water concentration listed is the average of two to three determinations (relative error, less than 10%).

Product Analysis. A mixture of potassium hydrogencarbonate (3.9×10^{-3} M) (1 M=1 mol dm^{-3}), perhydrodibenzo-18-crown-6 (3.9×10^{-2} M), F_3-PNMA (7.0×10^{-3} M), and aniline (1.0×10^{-2} M) in acetonitrile was refluxed for 3 h, and evaporated to dryness *in vacuo*. The residue taken in methanol was subjected to high-speed liquid chromatography (Hitachi type 635 instrument; solvent, methanol; column, Hitachi gel 3010; wavelength, 254 nm). The following peaks appeared in this order and were identified by comparison with authentic samples: trifluoroacetanilide, aniline, substrate, and *p*-nitro-*N*-methylaniline. The peak height of trifluoroacetanilide was almost the same as that of aniline.

On the other hand, trifluoroacetanilide was not detected in the reaction of aniline and trifluoroacetic acid (7.0×10^{-3} M) under the comparable reaction conditions. Salt formation occurred immediately after mixing as confirmed by UV spectroscopy.

Results

Nucleophilic vs. *General Base Attack of Hydrogencarbonate.* In order to assess whether HCO_3^- acts as a nucleophile or as a general base, the semi-quantitative product analysis was performed with a high-speed liquid chromatograph.

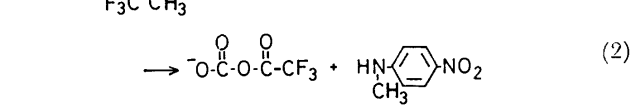

(2)

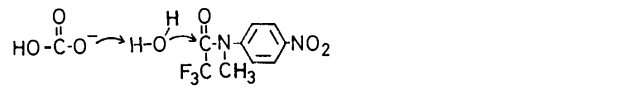

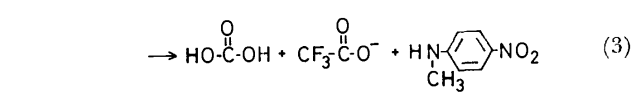

(3)

If HCO_3^- acts as a general base, it directly produces trifluoroacetate and *p*-nitro-*N*-methylaniline (Eq. 2). On the other hand, the nucleophilic reaction would give a mixed acid anhydride, $^-OCOOCOCF_3$ (Eq. 3), which then, decomposes rapidly to trifluoroacetate and hydrogencarbonate. The intermediacy of the mixed anhydride was confirmed by the aniline trap-

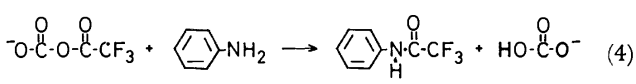

(4)

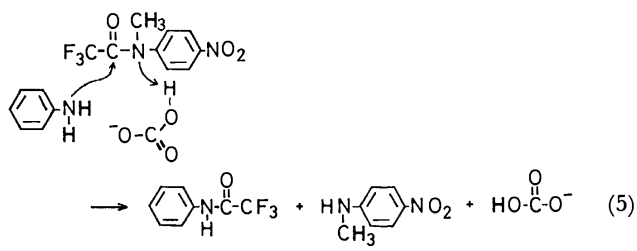

(5)

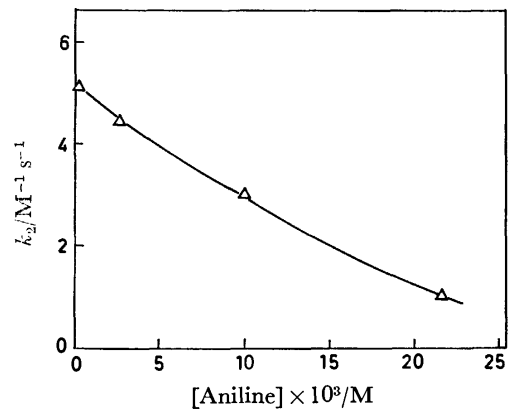

Fig. 1. Second-order rate constants for the reaction of HCO_3^- and F_3-PNMA in acetonitrile ([H_2O]=4±1 mM), plotted as a function of added aniline. [HCO_3^-]=1.28×10^{-3} M, [F_3-PNMA]=4.87×10^{-5} M.

ping experiment (Eq. 4) described in Experimental. It was confirmed in separate experiments that the trapping product, trifluoroacetanilide, was not formed directly by the reaction of aniline with F_3-PNMA substrate or with trifluoroacetic acid. The possibility that trifluoroacetanilide is formed *via* a mechanism related to the general base mechanism of Eq. 3 (Eq. 5) may be denied by the following argument. Provided that Eq. 5 is the predominant path, added aniline should accelerate the reaction. In Fig. 1, the second-order rate constant(k_2) for the reaction of HCO_3^- and F_3-PNMA is plotted as a function of added aniline. Since aniline retards the reaction, Eq. 5 is not likely to occur.

The presence of trifluoroacetanilide in the product of the aniline experiment, together with the rate-retarding effect of aniline, clearly indicates that the amide cleavage proceeds *via* direct attack of hydrogencarbonate ion on the amide substrate.

Absorption Spectra of Nucleophilic Anions. Prior to the kinetic examination, the relative absorbance of nucleophilic anions was measured as a function of water concentration in order to obtain reliable information on prototropic equilibria. *p*-Cyanophenol (*p*-CNC_6H_4OH) in very dry acetonitrile ([H_2O]=11.7 mM) possesses the absorption maximum at 243 nm with ε=18400, and the spectrum was not affected by added perhydrodibenzo-18-crown-6 (10 times excess). On the other hand, the absorption maximum of *p*-$CNC_6H_4O^-K^+$ solubilized in acetonitrile with 10 times excess of perhydrodibenzo-18-crown-6 appeared at 294 nm (ε=19800), which can be clearly differentiated from that of *p*-CNC_6H_4OH. The absorbance decreased only slightly with increasing water concentrations, the relative absorbance at [H_2O]=999 mM being 86% of the original value in very dry acetonitrile. At this water concentration a weak shoulder was observed at 243 nm which is ascribable to the absorption of *p*-CNC_6H_4OH. The relative amount of the neutral species calculated with ε=18400 was 12%, which is in good accord with the decrease of *p*-$CNC_6H_4O^-K^+$ ($\approx$14%) within the experimental error. Therefore, the increase in the water concentration causes a small shift in the prototropic equilib-

Table 1. Second-order rate constants for the cleavage of amide and ester substrates[a)]

Solvent[b)]	Nucleophile	$k_2/M^{-1}\,s^{-1}$		
		F_3-PNMA	Cl_2-PNMA	PNPA
DMF	HCO_3^-	59	3.7	19
DMF	p-$CNC_6H_4O^-$	1.3	0.51	26
DMF	SI-O^- [d)]	1.6	—	*ca.* 10^3
Acetonitrile	HCO_3^-	0.37—3.9[c)]	0.048—0.15[c)]	46
Acetonitrile	p-$CNC_6H_4O^-$	0.035	0.0033	22
Acetonitrile	SI-O^- [d)]	0.0030—0.032[c)]	—	400
Ethanol	HCO_3^-	1.5	0.16	0.38
Ethanol	p-$CNC_6H_4O^-$	1.1	0.085	0.32

a) [nucleophile] = (0.4—20) × 10^{-4} M, [substrate] = (5—20) × 10^{-5} M, [perhydrodibenzo-18-crown-6] = 10 × [nucleophile salt]. b) [H_2O]: 6.2—9.2 mM in DMF, 4.9—7.0 mM in acetonitrile, 100±15 mM in ethanol. c) The probable range of k_2 estimated from the non-linear plots. d) Potassium salt of *N*-hydroxysuccinimide.

rium between p-$CNC_6H_4O^-K^+$ and p-CNC_6H_4OH.

The absorption spectra of SI-O^-K^+ were somewhat more complicated. SI-O^-K^+ solubilized in very dry acetonitrile ([H_2O] = 14.1 mM) with 10 times perhydrodibenzo-18-crown-6 gave rise to two absorption maxima at 278 nm (ε 2320) and 294 nm (ε=2360). The absorption peak at 278 nm gradually increased upon addition of water and the peak at 294 nm disappeared almost completely at [H_2O] > 200 mM. However, the increase in the absorption of *N*-hydroxysuccinimide (ε=*ca.* 7000 at 210 nm (shoulder)) was not detected. This means that the spectral change cannot be ascribed to the prototropic equilibrium. Conceivably, added water may affect the nature of the ion pair which is reflected in the absorption spectrum.

Unfortunately, HCO_3^- ion does not have an absorption maximum in the UV region suitable to study the prototropic equilibrium. We thus measured the IR spectrum of $HCO_3^-K^+$ solubilized in acetonitrile with 10 times perhydrodibenzo-18-crown-6. The $\nu_{C=O}$ absorption band of the carboxylate group appeared at 1632 cm^{-1} which is comparable to that of solid $KHCO_3$ (KBr disc, $\nu_{C=O}$ 1628 cm^{-1}). The absorption peak hardly changed even in acetonitrile containing 1000 mM of water.

It is assumed from the above experimental data that the shift of prototropic equilibria due to small quantities of added water is not extensive, as compared with dramatic rate retardations observed (see below). Although a clear, quantitative analysis of prototropy was possible only in the p-CNC_6H_4OH system, the similarity in the aqueous pK_a values[12,13)] suggests that the prototropic equilibria for SI-O^- and HCO_3^- would not differ greatly from that for p-$CNC_6H_4O^-$.

Estimation of Rate Constants. In the presence of excess nucleophile, the formation of p-nitro-*N*-methylaniline from the amide substrates gave good first-order plots for up to 70% reaction, so that the reactions are first-order in substrates. The pseudo first-order rate constants(k_{obsd}) thus determined were plotted against the concentration of nucleophile. As shown in Fig. 2, plots of k_{obsd} *vs.* [nucleophile(hydrogencarbonate)] were not always linear. The second-order rate constants(k_2) were calculated as k_{obsd}/[nucleophile]

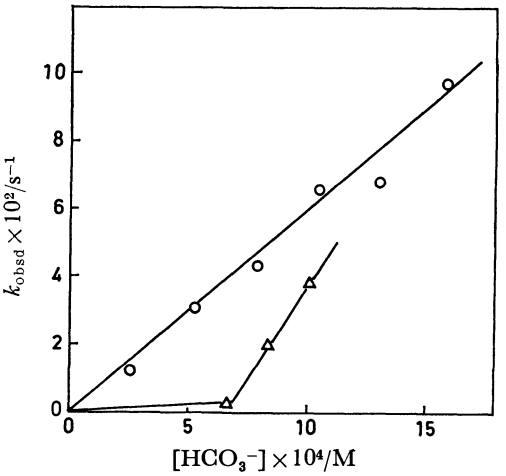

Fig. 2. Pseudo-first-order rate constants for the reaction of HCO_3^- and F_3-PNMA in DMF(○) and acetonitrile(△) plotted as a function of [HCO_3^-]. [F_3-PNMA] = 8.80 × 10^{-5} M. Water concentrations are recorded in Table 1.

and listed in Table 1. In the case of the non-linear plots, the probable range of k_2 is given.

In accordance to close pK_a values in aqueous solution, the second-order rate constants for the reaction of PNPA with HCO_3^- and p-$CNC_6H_4O^-$ are not much different in three solvents employed (two times difference at the largest). The much higher reactivity of SI-O^- toward PNPA may be attributed to the so-called α-effect. It is known that the nucleophilic attack is wholly rate-determining in water for phenyl esters with good leaving groups such as p-nitrophenolate.[10)] Whether or not this holds true in aprotic solvents is not clear at the moment. However, the relative reactivity of the nucleophiles used shows approximately parallel tendencies between the aqueous and aprotic media (Table 1).

Interestingly, HCO_3^- acted as the most efficient catalyst toward amide substrates: for example, the reaction of HCO_3^- and F_3-PNMA in DMF was faster by factors of 37—45 than the corresponding reactions with p-$CNC_6H_4O^-$ and SI-O^-. On the other hand, the rate difference between HCO_3^- and p-$CNC_6H_4O^-$ was very small in ethanol (protic solvent).

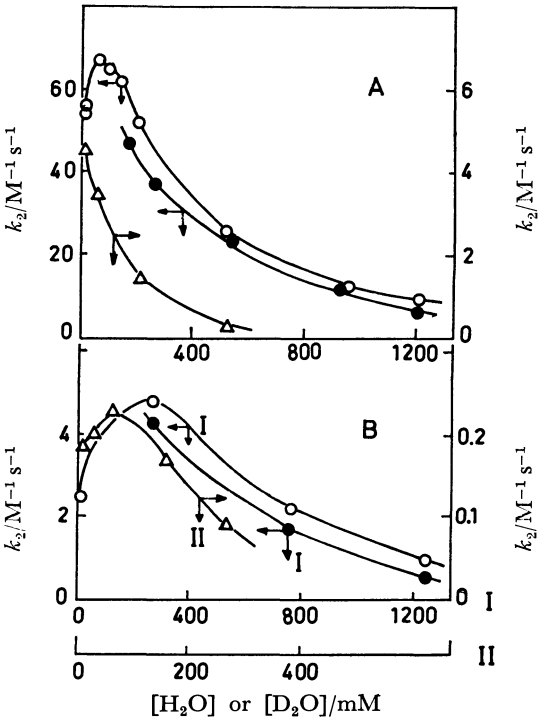

Fig. 3. Second-order rate constants for F_3-PNMA cleavage plotted as a function of [H_2O] or [D_2O]. (A) HCO_3^-+F_3-PNMA: ○; H_2O in DMF, ●; D_2O in DMF, △; H_2O in acetonitrile. (B) *p*-$CNC_6H_4O^-$+F_3-PNMA: symbols used stand for the same as above.

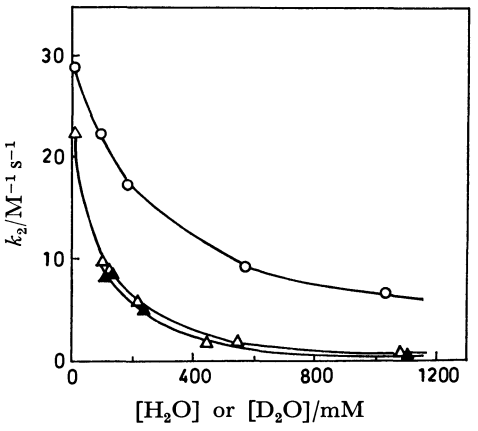

Fig. 4. Second-order rate constants for PNPA cleavage plotted as a function of [H_2O] or [D_2O]. ○: H_2O for *p*-$CNC_6H_4O^-$+PNPA in DMF, △: H_2O for HCO_3^-+PNPA in acetonitrile, ▲: D_2O for HCO_3^-+PNPA in acetonitrile.

Influence of Small Amounts of Water on Reaction Rates. The experiments described above were performed at almost constant water concentrations, which are recorded in the caption for Figures or in the footnote for Tables. Followingly, we determined the second-order rate constant as a function of water concentration in the respective reaction media. The results are illustrated in Figs. 3 and 4. It is clear that the rates are sensitive to small amounts of water. The rate constants are almost meaningless without accurate

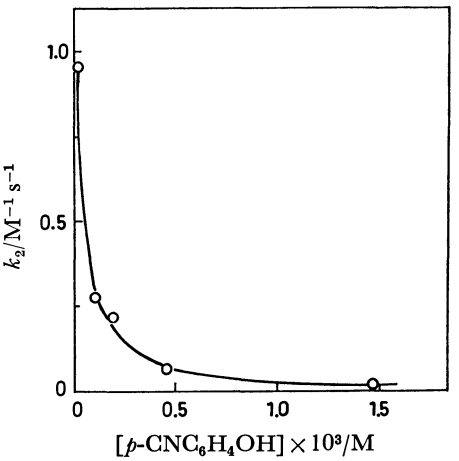

Fig. 5. Second-order rate constants for the reaction of *p*-$CNC_6H_4O^-$ and F_3-PNPA in DMF ([H_2O]= 4±2 mM) plotted as a function of added *p*-CNC_6H_4-OH. [*p*-$CNC_6H_4O^-$]=1.61×10^{-3} M, [F_3-PNMA]= 2.51×10^{-5} M.

indication of the water concentration. In some of the amide cleavage(HCO_3^-+F_3-PNMA in DMF, *p*-$CNC_6H_4O^-$+F_3-PNMA in DMF, and *p*-$CNC_6H_4O^-$+ F_3-PNMA in acetonitrile), rate maxima were observed at about 100—300 mM H_2O. On the other hand, F_3-PNMA cleavage by HCO_3^- in acetonitrile (Fig. 3A) and the nucleophilic reaction of HCO_3^- and *p*-$CNC_6H_4O^-$ toward PNPA (Fig. 4) did not provide such rate maxima. Thus, the phenomenon seems to be confined to the amide cleavage, but is not limited to the catalysis by HCO_3^-.

Water may suppress the reaction by neutralizing *p*-$CNC_6H_4O^-$ ion or by reducing reactivity of *p*-$CNC_6H_4O^-$ due to solvation.[7-9] If added water produces *p*-CNC_6H_4OH which then act as general acid in the amide cleavage, a rate maximum could arise from the cooperative action of *p*-$CNC_6H_4O^-$ and *p*-CNC_6H_4OH.

Figure 5 shows the second-order rate constant at the constant water concentration plotted against the concentration of added *p*-CNC_6H_4OH. The reaction rate diminished with increasing *p*-CNC_6H_4OH concentration, contrary to the expectation. *p*-CNC_6H_4OH quenches the reactivity of *p*-$CNC_6H_4O^-$ probably due to the hydrogen-bonded solvation, instead of assisting the reaction as general acid. Therefore, it appears that only the intramolecular proton in the tetrahedral intermediate of HCO_3^- and amide substrates is capable of acting as effective proton source (see Eqs. 7 and 8).

Kinetic Isotope Effects. If the rate-determining step involves proton transfer to the tetrahedral intermediate, the reaction will be retarded by replacing H_2O with D_2O. Figures 3 and 4 indicate that at the same water concentration the rate constants in the D_2O-containing medium are smaller than those in the H_2O-containing medium: $k_{2,H_2O}/k_{2,D_2O}=1.3\pm0.2$ for HCO_3^-+F_3-PNMA, 1.2±0.1 for *p*-$CNC_6H_4O^-$+ F_3-PNMA, and 1.10±0.06 for HCO_3^-+PNPA. Since the acyl transfer reaction with PNPA is considered not to be general acid catalyzed,[10] the isotope effect

of 1.1 may be associated with the simple nucleophilic step. The $k_{2,H_2O}/k_{2,D_2O}$ value for the F_3-PNMA is somewhat greater than this, and suggests the involvement of general acid catalysis.

The kinetic isotope effect was also assessed for the reaction in ethanol-*d*. The rate constants were relatively insensitive to the water concentration (or D_2O concentration in ethanol-*d*). Though the relative error of 10—20% must be assumed, the magnitude of $k_{2,EtOH}/k_{2,EtOD}$ for HCO_3^-+F_3-PNMA and HCO_3^-+Cl_2-PNMA (2.2 and 1.6, respectively) is greater than that for PNPA (1.1—1.5).

Discussion

Polyvalent inorganic salts have been considered to act as bifunctional catalyst, since they can accept and release proton simultaneously.[11] Cunningham and Schmir[15] and Barnett and Jencks[16] reported that intramolecular aminolysis is accelerated by hydrogencarbonate ion. The kinetic examination established that HCO_3^- partitions the zwitterionic tetrahedral intermediate in favor of the products. For example, the rate constant for hydrogencarbonate-catalyzed intramolecular aminolysis of *S*-(2-aminoethyl)thioacetate exhibits positive deviation of two orders of magnitude.[16] Thus, it is concluded that HCO_3^- interacts with the tetrahedral intermediate in a cyclic manner to accelerate its decomposition (Eq. 6).

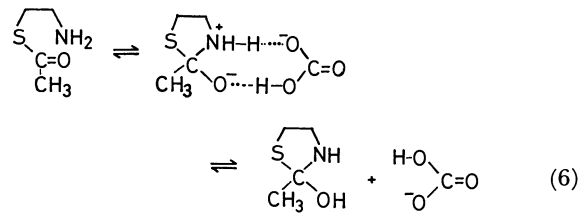

(6)

A similar acceleration of the breakdown of the tetrahedral intermediate by HCO_3^- was reported for the alkaline hydrolysis of trifluoroacetanilide,[4] but not for that of *p*-nitrotrifluoroacetanilide.[5] However, HCO_3^- by itself cannot cleave the amide substrate in an aqueous system. Since the nucleophilicity of anions is drastically enhanced in aprotic solvents,[7,17] HCO_3^- in aprotic solvents can act as a bifunctional catalyst toward amide substrates. The product analysis strongly indicates that HCO_3^- in acetonitrile directly attacks the amide group of F_3-PNMA. The rate data suggest that the OH group of HCO_3^- acts as general acid during the breakdown of the tetrahedral intermediate. The most reasonable reaction scheme would be the following.

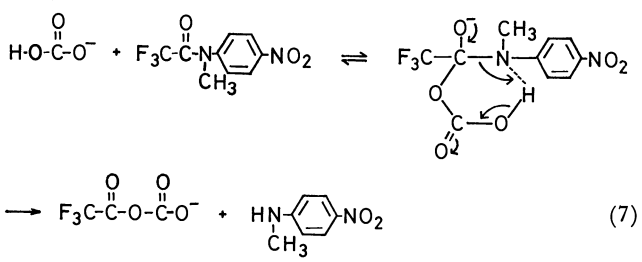

(7)

Table 2. Relative reaction rates and efficiency parameters for amide cleavage[a]

Solvent		F_3-PNMA	Cl_2-PNMA	PNPA
DMF	$k_{rel,CNC_6H_4O^-}$	45	7.3	0.73
	$k_{rel,SI-O^-}$	37	—	0.019
	$r_{CNC_6H_4O^-}$	62	10	1.0
	r_{SI-O^-}	*ca.* 1900	—	1.0
Acetonitrile	$k_{rel,CNC_6H_4O^-}$	11—110	15—45	2.1
	$k_{rel,SI-O^-}$	120	—	0.12
	$r_{CNC_6H_4O^-}$	5.2—52	7.1—21	1.0
	$r_{rel,SI-O^-}$	*ca.* 1000	—	1.0
Ethanol	$k_{rel,CNC_6H_4O^-}$	1.4	1.9	1.2
	$r_{CNC_6H_4O^-}$	1.2	1.6	1.0

a) $k_{rel}=k_2$ for HCO_3^-/k_2, $r=k_{rel}$ for amide/k_{rel} for PNPA. For detail see text (Eqs. 9, 10, and 11).

However, the bifunctional attack of hydrogencarbonate ion followed by efficient proton transfer (Eq. 8), if it occur, would not be differentiated kinetically.

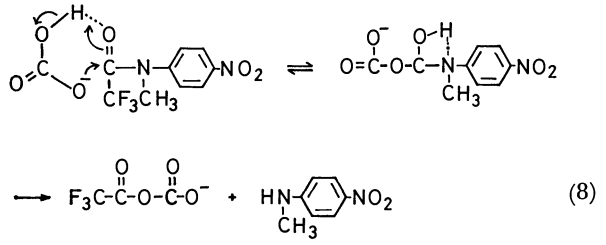

(8)

In Table 2, we summarize relative reaction rates (k_{rel}) and efficiency parameters (r) for the amide cleavage. The r value given by Eq. 11 stands for a measure

$$k_{rel,CNC_6H_4O^-} = \frac{k_2 \text{ for } HCO_3^-}{k_2 \text{ for } p\text{-}CNC_6H_4O^-} \quad (9)$$

$$k_{rel,SI-O^-} = \frac{k_2 \text{ for } HCO_3^-}{k_2 \text{ for SI-O}^-} \quad (10)$$

$$r = \frac{k_{rel} \text{ for a substrate}}{k_{rel} \text{ for PNPA}} \quad (11)$$

of relative efficiency of HCO_3^- catalysis for amide cleavage *versus* PNPA cleavage. The r value for PNPA is, of course, equal to unity. The data of Table 2 substantiates that (i) r-values in DMF and acetonitrile are always much greater than unity and r_{SI-O^-} amounts to 10^3; in contrast, (ii) r-values in ethanol are almost equal to unity. Therefore, in the present system, the general acid catalysis by the hydroxyl group of HCO^-_3 is effective only in aprotic solvents. Proton transfer from hydrogencarbonate hydroxyl group may not be particularly favorable in ethanol due to its hydrogen bonding with the solvent and/or due to proton transfer from solvent ethanol. In addition, SI–O$^-$ (highly nucleophilic toward PNPA) is not effective in the amide cleavage, which again points to the importance of proton transfer.

As shown in Figs. 4 and 5, the isotope effect for the amide cleavage is greater than that for PNPA cleavage. The corresponding data in organic media are scarce. Breslow and McClure[18] gave k_{H_2O}/k_{D_2O}= 1.47—2.27 for the general-acid catalyzed cleavage of maleamic acid in acetonitrile containing 1 M H_2O. Schowen *et al.*[19] also reported that, in the basic meth-

anolysis of amide substrates, $k_{2,EtOH}/k_{2,EtOD}$ approaches 2.0 when proton transfer becomes involved in the rate-limiting step. The isotope effects observed in the present study for the amide cleavage are: $k_{2,H_2O}/k_{2,D_2O}$ =1.3 (for F_3-PNMA) and $k_{2,EtOH}/k_{2,EtOD}$=1.6—2.2. These data are comparable to those observed for other general acid catalyses, and proton transfer is supposedly involved (at least partially) in the rate-limiting step in the present case.

The dependence of rate constants on the nucleophile and water concentrations is complicated. Among conceivable factors, (1) added water lowers the nucleophilicity of HCO_3^- and p-$CNC_6H_4O^-$ [5,6,8] and (2) added water changes the aggregation structure of the nucleophilic ion pairs, tightness of ion pairs, *etc.* The rate maximum observed is not amenable to simple interpretation. The non-linear dependence on nucleophile concentrations may reflect a similar phenomenon. In particular, HCO_3^- ion pairs may exhibit a strong association tendency in aprotic solvents as shown below.

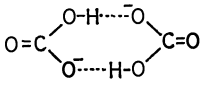

(12)

Finally, we would like to point out the analogy of the hydrogencarbonate catalysis with the action of biotin. Mg-ATP and HCO_3^- are believed to form mixed acid anhydride, which (in a stepwise manner or in a concerted manner) reacts with enzyme-bound biotin.[20] The present study would suggest that the efficiency of HCO_3^- as acyl-group (or probably phosphate-group) acceptor can be enhanced in the aprotic environment. We could prepare mixed acid anhydride from HCO_3^- and F_3-PNMA, but trifluoroacetyl group, not hydrogencarbonate, was transfered to aniline.

In conclusion, the present study substantiates that HCO_3^- in aprotic media acts as a proper nucleophilic-general acid catalyst in the cleavage of amide substrates.

References

1) Contribution No. 570 from Department of Organic Synthesis.
2) M. L. Bender, *Chem. Rev.*, **60**, 53 (1960).
3) C. A. Bunton, B. Nayak, and C. O'Connor, *J. Org. Chem.*, **33**, 572 (1968).
4) S. O. Erikson and C. Holst, *Acta Chem. Scand.*, **20**, 1892 (1966).
5) R. M. Pollack and T. C. Dumsha, *J. Am. Chem. Soc.*, **95**, 4463 (1973).
6) S. Shinkai and T. Kunitake, *Chem. Lett.*, **1976**, 109.
7) S. Shinkai, N. Nakashima, and T. Kunitake, *J. Am Chem. Soc.*, **100**, 5887 (1978).
8) S. Shinkai and T. Kunitake, *J. Chem. Soc., Perkin Trans. 2*, **1976**, 980.
9) S. Shinkai, Y. Okahata, N. Nakashima, K. Tamaki, and T. Kunitake, to be submitted.
10) W. P. Jencks, "Catalysis in Chemistry and Enzymology," McGraw-Hill, New York, N. Y. (1969), Chap. 10.
11) P. R. Rony, *J. Am. Chem. Soc.*, **91**, 6090 (1969).
12) W. P. Jencks and J. Regenstein, "Handbook of Biochemistry and Molecular Biology," ed by G. D. Fasman, CRC Press, Ohio (1976), p. 305.
13) D. E. Ames and J. F. Grey, *J. Chem. Soc.*, **1955**, 633.
14) L. O. Kershner and R. L. Showen, *J. Am. Chem. Soc.*, **93**, 2014 (1971).
15) B. A. Cunningham and G. L. Schmir, *J. Am. Chem. Soc.*, **89**, 917 (1967).
16) R. E. Barnett and W. P. Jencks, *J. Am. Chem. Soc.*, **91**, 2358 (1969).
17) A. J. Parker, *Chem. Rev.*, **69**, 1 (1969).
18) R. Breslow and D. E. McClure, *J. Am. Chem. Soc.*, **98**, 258 (1976).
19) R. L. Schowen, C. R. Hopper, and C. M. Bazikian, *J. Am. Chem. Soc.*, **94**, 3095 (1972).
20) H. G. Wood, *Trends Biochem. Sci.*, **1976**, 4.

The Photo-Beckmann Rearrangement of Steroidal β,γ-Unsaturated Ketone Oximes[1)]

Hiroshi SUGINOME,*,** Norio MAEDA, Yuko TAKAHASHI, and Nobuyoshi MIYATA
Department of Chemistry, Faculty of Science, Hokkaido University, Sapporo 060

(Received December 8, 1979)

The photoreaction of 4,4-dimethylcholest-5-en-3-one oxime, a β,γ-unsaturated ketone oxime, has given two lactams, 4a,4a-dimethyl-3-aza-*A*-homocholest-5-en-4-one and 4a,4a-dimethyl-4-aza-*A*-homocholest-5-en-3-one resulting from photo-Beckmann rearrangement. 4,4,6-Trimethylcholest-5-en-3-one oxime behaved analogously on photolysis, yielding two lactams but accompanied by 4,6-dimethyl-4-methylene-3,4-secocholest-5-ene-3-nitrile as a minor product. In contrast, major products in the ordinary Beckmann rearrangement are nitriles resulting from the second order Beckmann rearrangement.

Our previous studies on the photo-Beckmann rearrangement of several steroidal ketone oximes established that the chirality of the migrating group center is retained in the product lactams, indicating that the lactams are formed *via* a concerted reorganization of the intermediate oxaziridines and that the migrating group center does not become separated from the migration terminus in the course of the photo-rearrangement.[2-4)] This conclusion was further supported by our recent study on the photoreaction of a β,γ-cyclopropyl ketone oxime.[5)] We have found, however, that there are some exceptional cases[6)] in which ionic or radical species resulting from a cleavage of a bond α to their hydroxyimino group should be considered to be involved as intermediate species in the photochemical lactam formation from oximes. Moreover, the possibility of lactam formation occurring *via* coupling of radical pairs or biradical species has been suggested for photochemical lactam formation from some fused bicyclic oxaziridines.[7)]

In connection with these paths of the photochemical lactam formation, it is worth studying whether cyclic β,γ-unsaturated ketone oximes give lactams or nitriles and other products which originate from the radical pair or biradical species on photolysis. This group of oximes is considered to be particularly susceptible to the fission into biradical or ionic species by virtue of generation of stabilized allyl radicals or ions (*e.g.*, A).

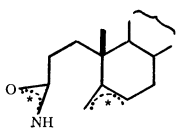

(A) * radical or ion

In this paper, the results on the photoreactions of two steroidal β,γ-unsaturated ketone oximes are described.

Results and Discussion

4,4-Dimethylcholest-5-en-3-one oxime (**1**) and 4,4,6-trimethylcholest-5-en-3-one oxime (**12**), prepared from the parent ketones (**2** and **11**)[8,9)] by the standard method, were chosen as steroidal β,γ-unsaturated ketone oximes. 4,4,6-Trimethylcholest-5-en-3-one (**11**)[9)] was prepared from 5,6α-epoxy-5α-cholestan-3β-ol (**6**) *via* 4 steps (Scheme 4).[10-12)] In the course of these preparations, it was found that the reaction of epoxide (**6**) with methylmagnesium iodide to yield 6β-methyl-5α-cholestane-3β,5α-diol (**7**)[12)] is accompanied by at least 6% yield of 3β-hydroxy-5α-cholestan-6-one (**8**)[12,13)] resulting from a hydride shift followed by isomerization.

^{1}H NMR spectroscopy proved that the conformation of the ring A of oximes **1** and **12** is a *quasi* boat, as in the corresponding ketones,[14)] and that the geometries of their hydroxyimino groups are *syn* with respect to their $C_{(2)}$–$C_{(3)}$ bond. Thus, the chemical shifts of the 19-H of the oximes **1** and **12** deviated considerably from those predicted by the additivity rule, indicating that their ring A is in a non-chair conformation; signals due to the 19-H of the oximes **1** and **12** were found at τ 9.14 and 9.19, whereas chemical shifts of their 19-H predicated by the additivity rule of deshielding effects[15)] are about τ 8.79 based on the chemical shift (τ 9.10) of the 19-H of (*E*)- and (*Z*)-5α-cholestan-3-one oximes,[16)] the ring A of which is in a chair conformation. Inspections of the Dreiding model indicated that when their ring A takes a *quasi* boat conformation, their hydroxyimino groups are almost eclipsed by their 2β-H. Thus, when the hydroxyl group is *syn* with respect to the $C_{(2)}$–$C_{(3)}$ bond, their 2β-H is deshielded.[2)] The ^{1}H NMR spectrum of oximes **1** and **12** showed one-proton multiplets at τ 6.78—7.26 and at τ 6.79—7.19. These signals are assigned to their 2β-protons in the *quasi* boat conformations.[17)] There were other one-proton double doublet centered at τ 7.59 (J=7.5 and 19.2 Hz) and at τ 7.68 (J=7.5 and 18.6 Hz) in the spectra of the oximes **1** and **12**. These signals are assigned to their 2α-proton on the basis of their chemical shifts and coupling constants.

A preliminary experiment showed that irradiation of oxime **1** in methanol until all the oxime was photolyzed would cause the secondary decompositions of appreciable amounts of product lactams. Therefore, irradiation was discontinued after three hours when TLC indicated that still about a half of the starting oxime remained unchanged. At this point, besides the starting oxime, spots due to the parent ketone (**2**) and two products were detected. Column chromatography afforded the parent ketone **2** (11%), the starting oxime **1** (53%), and two new products, **3** (10%) and **4** (9%) successively. The structures of

** Present address: Organic Chemistry Laboratory, Department of Chemical Process Engineering, Faculty of Engineering, Hokkaido University, Sapporo 060.

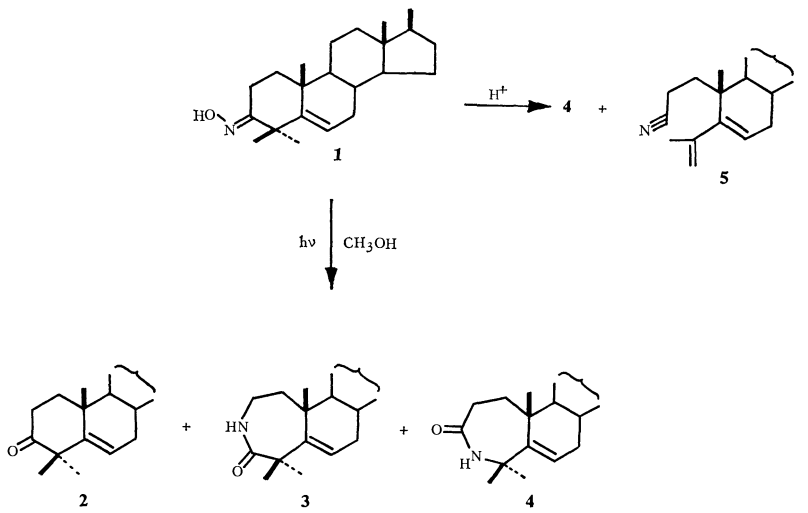

Scheme 1.

3 and **4** were determined to be 4a,4a-dimethyl-3-aza-*A*-homocholest-5-en-4-one (**3**) and 4a,4a-dimethyl-4-aza-*A*-homocholest-5-en-3-one (**4**) by their NMR, IR, and MS spectra (Scheme 1). The mass spectrum[18] of lactam **4** showed a weak molecular ion peak at *m/e* 427; the M^+-CH_3 fragment peak was the base peak assignable to an immonium species (a) in Scheme 2. In contrast, the mass spectrum of lactam **3** showed a distinct molecular ion peak at *m/e* 427 and the base peak at *m/e* 357. The intensity of the M^+-CH_3 peak (*m/e* 412) was only 13.5%, confirming the assigned structure. Scheme 3 shows the structure and a plausible genesis of this ion (b).

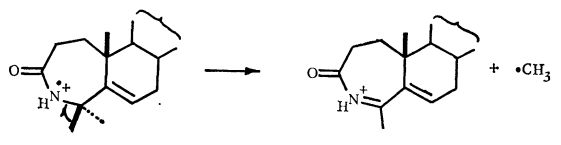

(a) *m/e* 402 (100%)

Scheme 2.

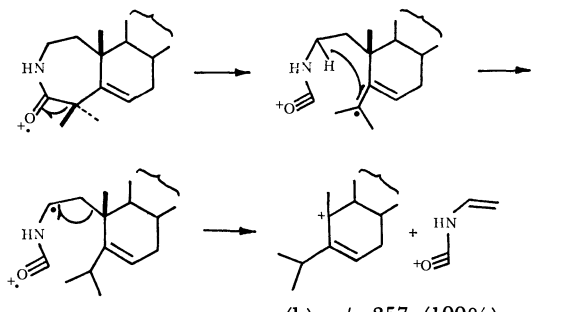

(b) *m/e* 357 (100%)

Scheme 3.

The ordinary Beckmann rearrangement of the oxime **1** with thionyl chloride afforded a product, which was shown to be a seconitrile (**5**) resulting from the second order Beckmann rearrangement by the MS, IR, and NMR (Table 1) spectra, and only a trace amount of the lactam **4** (Scheme 1). The mass spectrum of seconitrile **5** showed the molecular ion at *m/e* 409 as the base peak and only three distinct peaks at *m/e* 394 (M^+-CH_3), *m/e* 355, and *m/e* 296 ($M^+-C_{(17)}$ substituent) beyond *m/e* 200. The species *m/e* 355 is assignable to a species (c).

Photoreaction of the oxime **12** in methanol was performed under conditions similar to those used for the photoreaction of the oxime **1**. Three-hour irradiation gave an isomeric oxime (**13**) (10%), the starting oxime **12** (41%), 4,6-dimethyl-4-methylene-3,4-seco-

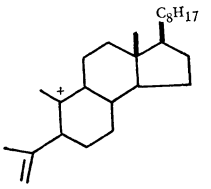

(c) *m/e* 355

cholest-5-ene 3-nitrile (**14**) (3%), 4a,4a,6-trimethyl-3-aza-*A*-homocholest-5-en-4-one (**15**) (16%), and 4a,4a,6-trimethyl-4-aza-*A*-homocholest-5-en-3-one (**16**) (11%) (Scheme 4). Structures of these products were confirmed by spectral analysis. The isomeric oxime showed M^+ of *m/e* 441 and M^+-CH_3 peak as the base peak in the MS spectrum. The nitrile **14** was obtained only as a mixture with 3-aza lactam **15**; the yield was estimated by NMR spectroscopy. The $C_{(2)}$ methylene protons in the ^1H NMR spectrum of 3-aza lactam (**15**) appeared as two broad signals centered at τ 6.48 and 7.05. After D_2O exchange of the NH proton, the signal at τ 6.48 changed to a broad triplet and the signal at τ 7.05 to a broad doublet. Irradiation at τ 8.41 changed the broad triplet to a sharper triplet with J=13.5 Hz and the broad doublet to a double doublet (J=13.5 and 4.5 Hz). The splittings and the results of the decoupling experiments exclude a *quasi* chair conformation and are consistent with a *quasi* boat conformation of the ring A, in which the C_6–CH_3 bond nearly bisects the angle between gem dimethyl at $C_{(4a)}$; the dihedral angles between the 1β- and 2β-protons, the 1β- and 2α-protons, the 1α- and 2β-protons, and the 1α- and 2α-protons are around 40°, 160°, 80°, and 40°, respectively. Assuming this conformation and that the signal at τ 8.41 arises

Table 1. NMR parameters (100 MHz) for 5α-cholestane derivatives, 4,4-dimethylcholest-5-en-3-one 4,4,6-trimethylcholest-5-en-3-one, their oximes, and the reaction products in $CDCl_3$ solution [chemical shifts (τ) and splittings (Hz; in parenthesis)]

Compound	2-Methylene	6-H	18-H	19-H	4-Methyl	4-Methylene	NH	Others
1	a)	4.38(dd) (1.8 and 4.5)	9.29(s)	9.14(s)	8.63(s) and 8.70(s)	—	—	
2	a)	4.50(bs)	9.31(s)	9.15(s)	8.77(s)	—	—	
3	a)	4.10(dd) (1.5 and 4.5)	9.28(s)	8.70(s)	8.47(s) and 8.76(s)	—	4.16(bs)	
4	6.1—7.2(m)	4.12(dd) (1.8 and 6.3)	9.32(s)	8.91(s)	8.53(s) and 8.63(s)	—	3.72(bt) (6.7)	
5	a)	4.35(bd)	9.33(s)	8.86(s)	8.07(s)	5.17(bd)(15.0 and 1)	—	
7	a)	a)	9.31(s)	8.93(s)	—	a)	—	3α-H, 5.88(bs)
8	a)	—	9.37(s)	9.24(s)	—	—	—	3α-H, 6.45(bs)
9	a)	a)	9.30(s)	8.76(s)	—	—	—	4α-H, 7.02(d) $J=13.5$ 4β-H, 7.99(d) $J=13.5$
10	a)	a)	9.31(s)	8.85(s)	—	4-H, 4.26(s)	—	6α-methyl, 8.96(d) $J=6.0$
11	a)	—	9.32(s)	9.25(s)	8.65(s) and 8.59(s)	—	—	6-methyl, 8.25(s)
12	2β-H, 6.79—7.19 (m), 2α-H, 7.68(dd) $J=7.5$ and 18.6 Hz	—	9.33(s)	9.19(s)	8.60(s) and 8.49(s)	—	—	6-methyl, 8.19(s)
13	a)	—	9.32(s)	8.91(s)	8.66(s) and 8.62	—	—	6-methyl, 8.23(s)
14	a)	—	9.32(s)	8.98(s)	8.15(s)	4.91(bs) $W_{1/2}=6$ Hz 5.47(bs) $W_{1/2}=6$ Hz	—	6-methyl, 8.15(s)
15	after D_2O exchange 6.48, 1H(bt) $J=14$ 7.05, 1H(bd) $J=15$	—	9.35(s)	8.95(s)	two of 8.14, 8.26 and 8.56(each s)	—	4.12(t) $J=6$	6-methyl, one of 8.14, 8.26 and 8.56(each s)
16	a)	—	9.32(s)	8.76(s)	two of 8.14, 8.17 and 8.47(each s)	—	4.31(s)	6-methyl, one of 8.14, 8.17 and 8.47(each s)

a) Unassignable.

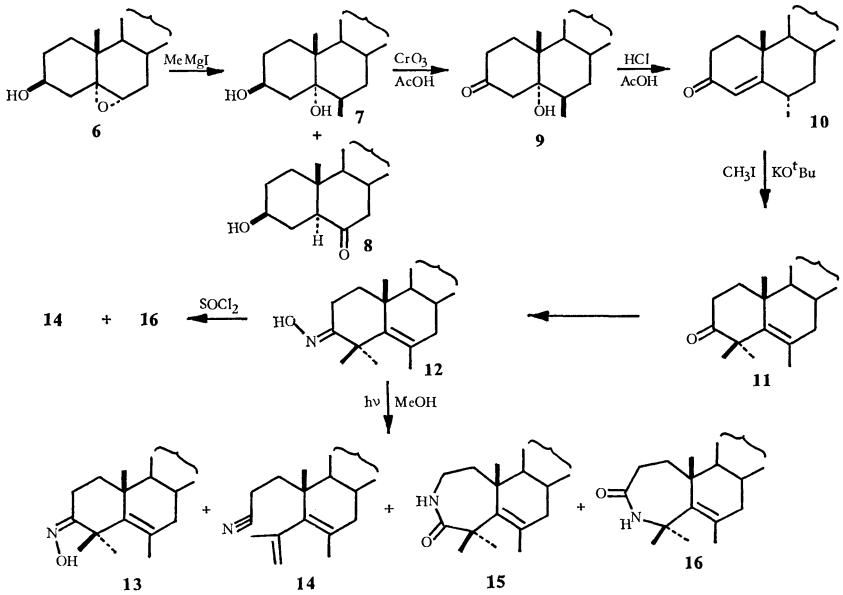

Scheme 4.

from the 1α-proton, the signals at τ 6.48 and 7.05 can be assigned to the 2α- and 2β-protons with $J_{2\alpha,2\beta}$ = 13.5 Hz, $J_{1\beta,2\alpha}$ = 13.5 Hz, and $J_{1\beta,2\beta}$ = 4.5 Hz respectively. Such assignments fit in with the coupling constants required by the above dihedral angles. Two 1,3-diaxial interactions of methyl groups are involved in the chair conformation of the 3-aza lactam. This interaction prohibits the lactam from taking the chair conformation. Fragmentations in the mass spectra of the nitrile **14** and the lactams **15** and **16** were entirely analogous to those of the nitrile **5** and the lactams **3** and **4**, respectively. Thus, the MS spectra of the lactams **15** and **16** showed their base peaks at *m/e* 371 and at *m/e* 426, corresponding to the species (b) and (a).

The ordinary Beckmann rearrangement of the oxime **12** was also studied. The treatment of oxime **1** with thionyl chloride gave two products, nitrile **14** and 4-aza lactam **15**, in 46 and 44% yields.

The present experiments confirmed that cyclic β,γ-unsaturated ketone oximes undergo photo-Beckmann rearrangements to lactams in yields comparable to those in the case of cyclic saturated ketone oximes.[2] Such results reinforce our previous conclusion[2,3] that the lactam formation resulting from the photo-rearrangement of cyclic saturated ketone oximes does not involve coupling of biradical or ions since, if a radical pair or ion pair were involved in the present photoreaction, these species would lead immediately to seconitriles; also, lactam formation by recombination of the cleaved species in the present case is very unlikely. Since there is a difference in the major products between acid-catalyzed reactions and photoreactions, the present photoreaction is of value for synthesis of unsaturated lactams (*e.g.*, **3** and **15**) which are not readily accessible by the ground state reactions.

Experimental

For instruments used and general procedures see Ref. 2. IR spectra were determined for Nujol mull with a JASCO IRA-1 spectrophotometer. The MS were recorded with a Hitachi JMS-D 300 spectrometer (direct inlet system, ion source temperature, *ca.* 180 °C, ionizing voltage, 70 eV) in the Faculty of Pharmaceutical Sciences or the Faculty of Agriculture. Only the Fragment peaks of the relative intensities over 20% for the lactams **3** and **4** and those over 30% for the seconitrile **5** are described.

Preparation of 4,4-Dimethylcholest-5-en-3-one Oxime (1). To a solution of 4,4-dimethylcholest-5-en-3-one (**2**) (800 mg) in methanol (200 ml) was added a solution of hydroxylamine hydrochloride (1 g) and sodium acetate trihydrate (1 g) in water (4 ml). The solution was stirred at 40 °C for 1.5 h and a further amount of methanol (100 ml) was added to the solution. The solution was refluxed for 2.5 h. The solvent was partly removed and the solution was extracted with diethyl ether. The diethyl ether solution was worked up in the usual way and evaporated. The residue was recrystallized from diethyl ether–methanol to afford the oxime **1** (726 mg), mp 223—226 °C. (Found: C, 81.26; H, 11.48; N, 3.14. Calcd for $C_{29}H_{49}NO$: C, 81.44; H, 11.55; N, 3.28%); IR 3304 (OH), 949 and 929 cm^{-1}; for NMR see Table 1; UV_{max} (MeOH) 207 nm (ε 5100).

The Photo-Beckmann Rearrangement of 4,4-Dimethylcholest-5-en-3-one Oxime (1). The oxime **1** (79 mg) in methanol (special grade, Wako) (230 ml) was irradiated with a Rayonet RPR-208 preparative photochemical reactor under an atmosphere of nitrogen for 3 h. TLC indicated four spots, due to the parent ketone **2**, the unchanged oxime **1**, and two lactams, in the order of their mobility. Three further photoreactions (80, 81, and 66 mg) were carried out under the same procedure. Products from the four photolyses were combined and subjected to column chromatography (Wako gel C-200, 10 g). Elution with a 3:1 mixture of benzene and hexane gave the parent ketone (32 mg). Further elutions with a 19:1 mixture of benzene and hexane and with pure benzene gave oxime **1** (162 mg). Successive elutions with a 4:1 mixture of benzene and ethyl acetate gave 3-aza lactam **3** (30 mg) which was recrystallized from methanol. Mp 175—177 °C. (Found: C, 81.30; H, 11.32; N, 3.10%. Calcd for $C_{29}H_{49}NO$: C, 81.44; H, 11.55; N, 3.28%); $[\alpha]_D^{18}$ −4.2° (*c* 0.5 $CHCl_3$); IR 1657 (lactam carbonyl), 3062 and 3198 cm^{-1} (NH); for NMR see Table 1;

MS *m/e* (rel intensity) 429 (M^+, 1.9), 427 (30.8), 358 (29.5), 357 (100), and 42 (24.2). Continued elutions with the same solvent mixture gave 4-aza lactam **4** (29 mg), which was recrystallized from methanol. Mp 198.5—201.0 °C. (Found: C, 80.86; H, 11.69; N, 3.21%. Calcd for $C_{29}H_{49}NO$: C, 81.44; H, 11.55; N, 3.28%); $[\alpha]_D^{20}$ −11.3° (*c* 1.0 $CHCl_3$); IR 1656 and 1611 (lactam carbonyl) 3062 and 3198 cm^{-1} (NH); for NMR see Table 1; MS *m/e* (rel intensity) 42 (M^+ 0.4), 427 (3.7), 413 (31.5), 412 (100), and 58 (26.6).

The Beckmann Rearrangement of 4,4-Dimethylcholest-5-en-3-one Oxime (1). To a solution of the oxime **1** (200 mg) in dioxan (10 ml) was added some freshly purified thionyl chloride (0.1 ml) at room temperature. The solution was stirred for 20 min at room temperature and poured into water. The mixture was neutralized with sodium hydrogencarbonate. The aqueous solution was extracted with diethyl ether. The diethyl ether solution was worked up as usual. TLC showed that the product (184 mg) (R_f= 0.8) is nearly a single compound, with only traces of minor products (R_f=0.1 and 0). The residue was subjected to preparative TLC with benzene. The more mobile major product (162 mg) was recrystallized from methanol to afford the nitrile (**8**), mp 43.5—45.0 °C, (54 mg). (Found: C, 84.68; H, 11.39; N, 3.41. Calcd for $C_{29}H_{47}N$: C, 85.02; H, 11.56; N, 3.42%); IR 2243 (C≡N), 1610 and 906 cm^{-1}; for NMR see Table 1; MS *m/e* (rel intensity) 409 (100, M^+), 394 (28.7), 296 (33.6), 147 (30.9), 145 (52.3), 121 (31.1), 107 (32.6), 105 (40.2), 95 (46.9), 93 (34.0), 81 (47.1), 69 (41.4), 57 (53.6), 55 (66.2), 43 (70.4), and 41 (55.3). The less mobile fraction (10 mg) was an unidentified gum. The least mobile fraction (R_f=0) (19 mg) was recrystallized from methanol to afford 4-aza lactam **4**, identical with the specimen obtained by the photo-Beckmann rearrangement.

Reaction of 5,6α-Epoxy-5α-cholestan-3β-ol (6) with Methylmagnesium Iodide.[11,12] A solution of epoxide **6** (18.8 g) in dry benzene (300 ml) was added to a solution of methylmagnesium iodide prepared with magnesium (4.6 g) and methyl iodide (30 ml) in dry diethyl ether (50 ml) and dry benzene (100 ml). The solution was refluxed for 5 h. After cooling, aqueous solution of ammonium chloride (300 ml) was added and the solution was extracted with diethyl ether (200 ml). After the usual work-up, the product was recrystallized from diethyl ether–ethanol to give 6β-methyl-5α-cholestane-3β,5α-diol **7** (3.3 g). The residue from the filtrate was subjected to column chromatography. (alumina, 660 g). Elutions with a 1:1 mixture of hexane and benzene and then benzene gave a fraction (2.78 g) which was recrystallized from methanol to give 3β-hydroxy-5α-cholestan-6-one (**8**) (1.12 g, 6%) mp 148—150 °C (lit,[11] 145—146 °C). The acetate, mp 129—131.5 °C (methanol) (lit,[12] 128—129 °C), was obtained in usual way. Continued elutions with benzene gave a second fraction which was recrystallized from dichloromethane–ethanol to give an additional 3β,5α-diol **7** (5.59 g), 182—183 °C (lit,[11] 182—183 °C). The total yield of the diol was 47%.

Preparation of 6α-Methylcholest-4-en-3-one (10).[9] Diol **7** (13 g) in acetic acid (240 ml) was oxidized with chromium trioxide.[10] The crude 5α-hydroxy-6β-methylcholestan-3-one (**9**) obtained was dissolved in acetic acid (100 ml). To this solution was added concd hydrochloric acid (10 mg). The solution was stirred for 13 h and was extracted with diethyl ether. The usual work-up afforded a residue which was subjected to column chromatography (Wako C-200, 400 g). Successive elutions with 1:3, 1:5, and 1:10 mixtures of hexane and benzene, benzene only, and a 1:10 mixture of benzene and diethyl ether gave a fraction which was once recrystallized from methanol to yield ketone **10**, mp 126—127 °C (lit,[9] 127—128.5 °C). For NMR spectrum see Table 1.

Preparation of 4,4,6-Trimethylcholest-5-en-3-one (11). The ketone **10** (360 mg) in dry *t*-butyl alcohol (6 ml) was added to potassium (110 mg) in the same solvent (100 ml) under a nitrogen atmosphere. Methyl iodide (0.33 ml) was added and the mixture was heated under reflux for 75 min. After the addition of methyl iodide (0.1 ml) the solution was heated under reflux for an additional 25 min. The solution was extracted with dichloromethane and the organic layer was worked up in the usual manner. The product was subjected to preparative TLC with benzene to yield ketone **11** (189 mg). Recrystallization from methanol gave the pure material, mp 134—136 °C. (Found: C, 84.39; H, 11.84%. Calcd for $C_{30}H_{50}O$: C, 84.44; H, 11.81%); $[\alpha]_D^{21}$ = −7.8° (*c* 1.1 $CHCl_3$); IR 1609 (carbonyl), and 1026 cm^{-1}.

Preparation of 4,4,6-Trimethylcholest-5-en-3-one Oxime (12). The ketone **11** (770 mg), hydroxylamine hydrochloride (2.5 g), and sodium acetate trihydrate (2.5 g) in a mixture of ethanol (300 ml) and water (15 ml) were refluxed for 2 d. After the addition of a further amount of hydroxylamine hydrochloride (1 g) in water (3 ml), the solution was refluxed for another 3 d. A part of the solvent was evaporated under a reduced pressure and the solution was extracted with diethyl ether. The ethereal solution was worked up in the usual way and the product was subjected to column chromatography (silica gel Wako C-200, 27 g). Elutions with a 1:3 mixture of hexane and benzene gave the starting material (384 mg after recrystallization from methanol) and continued elutions gave the oxime **12**. The oxime was recrystallized from aq methanol to yield crystals (339 mg, 43%), mp 179.0—180.5 °C. (Found: C, 81.17; H, 11.89; N, 3.33%. Calcd for $C_{30}H_{51}NO$: C, 81.57; H, 11.64; N, 3.17%); $[\alpha]_D^{21}$ −3.2 (*c* 1.0 $CHCl_3$); IR 3311 (OH), 949, 918, and 720 cm^{-1}; MS *m/e* (rel intensity), 441 (M^+, 32.9), 426 (M^+-CH_3, 82.7), 425 (M^+-O, 29.8), 424 (M^+-OH, 100), 369 (25.0), 95 (32.8), 57 (26.7), 55 (29.6), and 43 (33.3). For the NMR see Table 1. UV_{max}(MeOH) 208 nm (ε 7600).

The Photo-Beckmann Rearrangement of 4,4,6-Trimethylcholest-5-en-3-one Oxime (12). Oxime **12** (80 mg) in methanol (special grade, Wako) (230 ml) was irradiated with a preparative photochemical reactor under an atmosphere of nitrogen for 4 h. TLC indicated five spots due to an isomeric oxime (**13**), a recovered oxime **12**, nitrile **14**, and two lactams **15** and **16**, in the order of their mobility. The photoreaction was repeated three times under the same conditions as the first one (80, 81, and 81 mg) and the products were combined and subjected to column chromatography. Elutions with a 3:1 mixture of benzene and hexane gave four fractions: A (32 mg), B (146 mg), C (61 mg), and D (35 mg). Fraction A was isomeric oxime **13** and was recrystallized from methanol. Mp 145—148 °C. IR, 3450 cm^{-1} (OH); MS *m/e* (rel intensity) 441 (M^+, 14.0), 426 (M^+-CH_3, 100), 424 (M^+-OH), 411 (51.4), 410 (51.0), 369 (77.2), 327 (26.9), 95 (83.7), 57 (74.2), 55 (79.2), and 43 (96.5). For NMR spectra see Table 1. Fraction B was recovered oxime **12**. Fraction C was a mixture of seco-nitrile **14** and 3-aza lactam **15**, based on its NMR analysis. Its recrystallization from methanol gave pure 3-aza lactam **15** (42 mg), mp 197—199 °C. (Found: M^+, *m/e* 441.3969). Calcd for $C_{30}H_{51}NO$: M^+ 441.3969; $[\alpha]_D^{21}$ −33.6 (*c* 0.25 $CHCl_3$); IR 3250 (NH), 1677 and 1742 (lactam carbonyl), and 720 cm^{-1}; MS *m/e* (rel intensity) 441 (M^+, 0.4), 426 (M^+-CH_3, 2.1), 398 (1.0), 372 (20.0), and 371 (100); for NMR see Table 1.

The residue (19 mg) from the filtrate in the above re-

crystallization was a 1:1 mixture of nitrile **14** and 3-aza lactam **15**, as estimated by the relative intensities of the signals due to their 10β-methyl in the NMR spectrum. Fraction D was 4-aza lactam **16**, which was recrystallized from methanol. Mp 178—180 °C. (Found: C, 81.33; H, 11.72; N, 3.14%. Calcd for $C_{30}H_{51}NO$: C, 81.57; H, 11.64; N, 3.17%); $[\alpha]_D^{22}$ −31.7 (*c* 1.0 $CHCl_3$); IR 3240 (NH), 1685 (lactam carbonyl), and 774 cm^{-1}; MS *m/e* (rel intensity) 441 (M^+, 3.4), 426 (M^+-CH_3, 100), and 58 (55.0); for the NMR see Table 1.

The Beckmann Rearrangement of 4,4,6-Trimethylcholest-5-en-3-one Oxime. To oxime **12** (74 mg) in dry dioxane (3 ml) and dry diethyl ether (0.1 ml) was added thionyl chloride (0.5 ml) at 0 °C. The solution was stirred for 30 min at 10 °C. The solution was extracted with diethyl ether and the organic layer was washed with 5% sodium hydrogencarbonate and water successively and dried. The product was subjected to preparative TLC with benzene to give three major fractions: A (34 mg), B (10 mg), and C (33 mg), in the order of their mobility. Fraction A was an oil and was identified as seconitrile **14**. (Found: N, 3.34%. Calcd for $C_{30}H_{49}N$: N, 3.31%); MS *m/e* (rel intensity), 423 (M^+, 26.7), 408 (M^+-CH_3, 20.2), 369 ($M^+-C_{(10)}$ side chain, 100), 265 (9.8), and 57 (54.9); for NMR see Table 1. Fraction C was 4-aza lactam **16**, which was recrystallized from methanol to afford a pure specimen (18 mg). It was identical with **16** obtained by the photoreaction.

We thank Mrs. T. Okayama and Miss H. Maki for ^1H NMR measurements and spin decoupling experiments.

References

1) Photoinduced Transformations. Part 56. Part 55. H. Suginome, H. Ono, and T. Masamune, *Bull. Chem. Soc., Jpn.*, **54**, 852 (1981).

2) H. Suginome and H. Takahashi, *Bull. Chem. Soc. Jpn.*, **48**, 576 (1975); H. Suginome and F. Yagihashi, *J. Chem. Soc., Perkin Trans. 1*, **1977**, 2488.

3) For a review of the Photo-Beckmann Rearrangement, see H. Suginome, *Kagaku No Ryoiki*, **30**, 578 (1976).

4) H. Suginome and Chi-Ming Shea, *Synthesis*, **1980**, 229.

5) H. Suginome and Chi-Ming Shea, *J. Chem. Soc., Perkin Trans. 1*, **1980**, 2268.

6) H. Suginome and T. Uchida, *Bull. Chem. Soc., Jpn.*, **47**, 687 (1974); H. Suginome and T. Uchida, *Bull. Chem. Soc. Jpn.*, **53**, 2292 (1980).

7) L. S. Kaminsky and M. Lamchen, *J. Chem. Soc., C*, **1966**, 2295; J. Parello, M. Riviere, E. Desherces, and A. Lattes, *C. R. Acad. Sci.*, **273**, 1097 (1971); E. Desherces, M. Riviere, J. Parello, and A. Lattes, *ibid.*, Ser. C, **275**, 581 (1972); D. St. C. Black and K. G. Watson, *Aust. J. Chem.*, **26**, 2505 (1973); D. St. C. Black, N. A. Blackman, and A. B. Boscacci, *ibid.*, **32**, 1775 (1979).

8) R. B. Woodward, A. A. Patchett, D. H. R. Barton, D. A. J. Ives, and R. B. Kelly, *J. Chem. Soc.*, **1957**, 1131.

9) R. J. Abraham and J. S. E. Holker, *J. Chem. Soc.*, **1963**, 806.

10) R. B. Turner, *J. Am. Chem. Soc.*, **74**, 5362 (1952).

11) M. I. Ushakov and O. S. Madaeva, *J. Gen. Chem. (USSR)*, **9**, 436 (1939).

12) L. F. Fieser and J. Rigaudy, *J. Am. Chem. Soc.*, **73**, 4660 (1951).

13) I. M. Heilbron, H. Jackson, E. R. H. Jones, and F. S. Spring, *J. Chem. Soc.*, **1938**, 102.

14) a) M. Gorodetsky and Y. Mazur, *Tetrahedron Lett.*, **1966**, 227; M. Gorodetsky, A. Yogev, and Y. Mazur, *J. Am. Chem. Soc.*, **31**, 699 (1966); b) B. B. Dewhurst, J. S. E. Holker, A. Lablache-Combier, M. R. G. Leeming, J. Levisalles, and J. P. Pete, *Bull. Soc. Chim. Fr.*, **1964**, 3259; c) G. Ferguson, W. C. Marsh, J. M. Midgley, and W. B. Whalley, *J. Chem. Soc., Perkin Trans. 2*, **1978**, 272; d) U. Burkert and N. L. Allinger, *Tetrahedron*, **34**, 807 (1978).

15) J. N. Shoolery and M. T. Rogers, *J. Am. Chem. Soc.*, **80**, 5121 (1958); R. F. Zürcher, *Helv. Chim. Acta*, **44**, 1380 (1961).

16) C. W. Shoppee, G. Krüger, and R. N. Mirrington, *J. Chem. Soc.*, **1962**, 1050.

17) The conclusions on the conformations of the ring A and the geometries of hydroxyimino groups of oximes **1** and **12** are further supported by a study of the ^1H NMR spectrum of 17β-acetoxy-4,4-dimethyl-19-norandrost-5-en-3-one oxime prepared by A. Osada in this laboratory. The ring A of this oxime should be in a *quasi* chair conformation since no 1,3-diaxial interaction of methyl groups is involved in the molecule. In fact, its NMR spectrum showed a one-proton double doublet at τ 6.74 with $J=13.5$ and 4.5 Hz. The chemical shift and the coupling constants are in agreement with those of the 2α-proton deshielded by the adjacent hydroxyimino group in the ring A in a *quasi* chair conformation.

18) a) H. Budzikiewicz, C. Djerassi, and D. H. Williams, "Mass spectrometry of Organic Compounds," Holden-Day, Inc., San Francisco (1967), p. 353; b) H. Budzikiewicz, F. Compernolle, K. V. Cauenberghe, K. Schulze, H. Wolf, and G. Quinkert, *Tetrahedron*, **24**, 6797 (1968).

The Transformation of Jervine into 18-Functional *D*-Homo-*C*-norsteroids. IV.[1] The Transformation of Jervine into (20*R*)-18,20β-Epoxy-3β-hydroxy-17β-ethyletiojervan-18-one 3-Acetate *via* (20*R*)-18,20β-Epoxy-3β-hydroxy-12α,17β-ethyletiojervan-11-one 3-Acetate[2]

Hiroshi SUGINOME,*,** Hitoshi ONO, and Tadashi MASAMUNE*
Department of Chemistry, Faculty of Science, Hokkaido University, Sapporo 060
(Received March 29, 1980)

Catalytic hydrogenation of (22*S*,25*S*)-*N*-acetyl-3β,23β-dihydroxyveratra-5,13(17)-dien-11-one 3-acetate over rhodium-platinum catalyst in acetic acid gave (22*S*,25*S*)-N-acetyl-3β,23β-dihydroxyveratranin-11-one 3-acetate (**2**) in *ca* 70% yield, together with two minor products. Irradiation of **2** in benzene containing mercury(II) oxide and iodine gave 20-formyl-3β-hydroxy-12α,17β-ethyletiojervan-11-one 3-acetate (**5**) in 43% yield, accompanied by the 17-epimer of (22*S*,23*R*,25*S*)-N-acetyl-3β-hydroxy-5α-jervanin-11-one 3-acetate (4%). Aldehyde **5** was transformed into 3β-hydroxy-12α,17β-ethyletiojervane-11,20-dione 3-acetate (**15**) (79% yield) by photo- or copper-catalysed oxygenation of the corresponding enamine. Reduction of **15** with sodium borohydride gave 3β,20β-dihydroxy-12α,17β-ethyletiojervan-11-one 3-acetate (**17**) as a major product (69%), together with the 20-epimer. The hypoiodite reaction of **17** gave 18,20β-epoxy-3β-hydroxy-17β-ethyl-12α-etiojervan-11-one 3-acetate (**19**) in 92% yield. Hydrolysis of **19** resulted in the isomerization of the C/D ring junction to give 18,20β-epoxy-3β-hydroxy-17β-ethyletiojervan-11-one (**20**), the first 18-functional C/D *trans* *D*-homo-*C*-norsteroid ever prepared. Wolff-Kishner reduction of **20** gave the corresponding 11-deoxo compound; its acetylation followed by oxidation yielded 18,20β-epoxy-3β-hydroxy-17β-ethyletiojervan-18-one 3-acetate. The 11-oxo function of **19** can be reduced quite easily with lithium aluminum hydride to give the corresponding 11β-ol.

Despite the extensive studies on the synthesis of 18-functional steroids, little has been done on the synthesis of 18-functional *D*-homo-*C*-norsteroids which may be useful for the synthesis of biologically active compounds. In the previous paper,[1] we reported the transformation of jervine into 18-functional C/D *cis* fused *D*-homo-*C*-norsteroids.

In this paper, the transformation of jervine into an 18-functional C/D *trans* fused *D*-homo-*C*-norsteroid, (20*R*)-18,20β-epoxy-3β-hydroxy-17β-ethyletiojervan-18-one 3-acetate,[3] *via* a C/D *cis* fused 11-oxo-*D*-homo-*C*-norsteroid, is reported. The method involved a series of photoinduced reactions reported in the previous paper.[1]

Results

Catalytic hydrogenation of (22*S*,25*S*)-*N*-acetyl-3β,23β-dihydroxyveratra-5,13(17)-dien-11-one 3-acetate (**1**), derived from jervine *via* two steps,[4] over rhodium-platinum catalyst in acetic acid[1,5] gave a mixture of products from which a perhydro derivative, (22*S*,25*S*)-*N*-acetyl-3β,23β-dihydroxyveratranin-11-one 3-acetate (**2**), was obtained by a single recrystallization in 62% yield (Scheme 1). Hydrogenation of the mixture recovered from the reaction gave a further amount (10%) of perhydro derivative **2**. The structure of **2** was confirmed by the IR, NMR, and mass spectra. The NMR spectrum (Table 1) showed the absence of an olefinic proton and showed three doublets arising from three secondary methyl groups (the 18-H, 21-H, and 26-H). The assigned stereochemistry at C-5, C-13, and C-17 centers is based on a *cis* addition analogous to the closely related substrate.[1,4] TLC of the crude product in this catalytic hydrogenation indicated the presence of two minor products **3** and **4**, which are more mobile than the perhydro derivative **2**. The structure of crystalline product **3**, mp 218.5—219.5 °C, was ascertained to be (22*S*,25*S*)-*N*-acetyl-23β-hydroxyveratr-13(17)-en-11-one by the mass, IR, and NMR spectra. Its mass spectrum showed a M^+ peak at *m/e* 455 and a fragment ion of low abundance at *m/e* 299 due to a species resulting from the removal of the heterocyclic ring from the molecular ion. Its IR spectrum showed bands due to the 23β-hydroxyl, 11-oxo- and *N*-acetyl groups. The NMR spectrum showed no 3β-acetoxyl

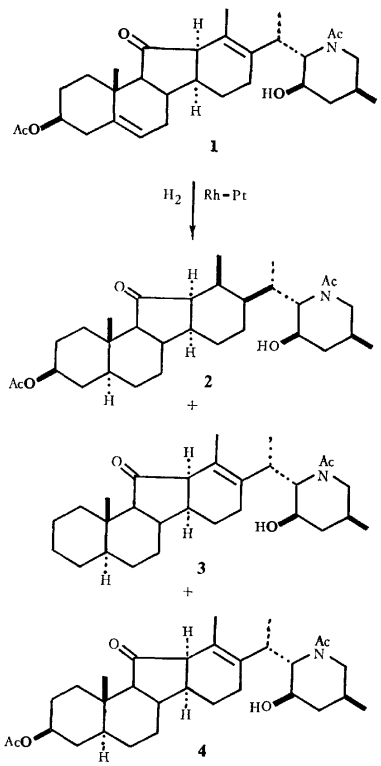

Scheme 1.

** Present address: Organic Chemistry Laboratory, Department of Chemical Process Engineering, Faculty of Engineering, Hokkaido University, Sapporo 060.

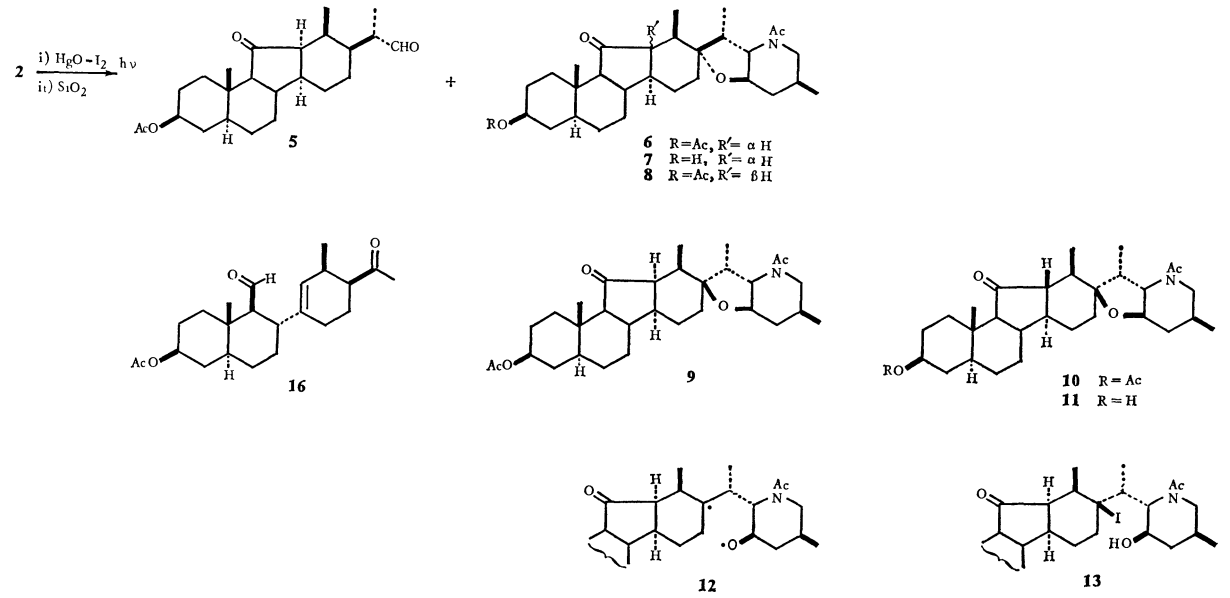

Scheme 2.

group and the presence of a 3H singlet at τ 8.14 due to the 18-H.

The structure of the amorphous product **4** was shown to be (22*S*,25*S*)-*N*-acetyl-3β,23β-dihydroxyveratr-13(17)-en-11-one 3-acetate by spectrometry. The mass spectrum showed a M^+ peak of *m/e* 513. The IR spectrum showed bands due to the 23β-hydroxyl, 11-oxo-, *N*-acetyl, and 3β-acetoxyl groups. The NMR spectrum showed a three-proton singlet at τ 8.14 due to the 13-methyl group and the absence of olefinic protons, proving the product to be the 5,6-dihydro derivative of the starting diene.

The transformation of the perhydro derivative **2** into a 12α-etiojervane **15** was accomplished by the series of photoinduced reactions described in the previous paper.[1,6] (Schemes 2 and 3) Irradiation of **2** in benzene containing three equivalents each of mercury(II) oxide and iodine with a 100-W high pressure mercury arc gave the expected crystalline aldehyde, 20-formyl-3β-hydroxy-12α,17β-ethyletiojervan-11-one 3-acetate (**5**), mp 144—146 °C, in 43% yield after column chromatography with silicic acid and recrystallization. The various spectra were in agreement with the structure assigned. The TLC of the crude photolysate showed the formation of a very minor product **6**, which was more mobile than aldehyde **2**. It was isolated by column chromatography in 4% yield and had mp 219—220 °C. Its mass spectrum (M^+ 513) and the elemental analysis were in agreement with the molecular formula $C_{31}H_{47}O_5N$, indicating it to be a product from an intramolecular hydrogen abstraction by a 23β-oxyl radical arising from the 23β-ol **2**. Hydrogens available for the intramolecular abstraction by the oxyl radical would be the 16α-H, the 17-H, and the 21-H and the abstraction reactions involving these hydrogens should take place *via* six or seven-membered cyclic transition state.[7] The ^{1}H NMR spectrum of **6** showed three three-proton doublets assigned to the 18-H, 21-H, and 26-H, excluding any structure arising from the abstraction of the 21-H. The ^{13}C NMR spectrum of **6**, aided with off-resonance spectrum, showed a signal at δ 86.64 ppm ascribed to a quarternary carbon carrying an oxygen.[8] This result proved that the 23β-oxyl radical abstracted the 17α-H, resulting in a N-acetyltetrahydrojervine O-acetate, the signal at 86.64 ppm thus arises from the C-17. A tetrahydro derivative of jervine, (22*S*, 23*R*, 25*S*)-*N*-acetyl-3β-hydroxy-5α-jervanin-11-one acetate, (**9**) and its 12β-isomer (**10**) (the C-17 signal at δ 86.52 ppm) have already been prepared by catalytic hydrogenation of jervine in acetic acid followed by acetylation.[9,10] The direct comparison showed that **6** is not identical with *N*-acetyltetrahydrojervine **9**.[9] Therefore, the structure of **6** should be the 17-epimer of (22*S*,23*R*,25*S*)-*N*-acetyl-3β-hydroxy-5α-jervanin-11-one 3-acetate. The mass spectra of **6** and **10** showed their base peaks at *m/e* 167 could be assigned to a fragment of structure (A)[11]

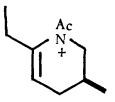

(A)

in accordance with the assigned structure. Hydrolysis of **6** with aqueous methanolic potassium hydroxide under reflux gave the corresponding 3β-ol (**7**). The C/D ring junction of **7** was proved to be *cis*, since **7** reverted back to **6** on acetylation. It is noteworthy that, while treatment of (22*S*,23*R*,25*S*)-*N*-acetyl-3β-hydroxy-5α-jervanin-11-one 3-acetate (**9**) with base readily causes an epimerization at the C-12 and gives the 12β-epimer (**11**), no isomerization of the C-12 hydrogen takes place in the basic hydrolysis of **6**. Inspection of Dreiding models of **6** and its 12β-epimer **8** showed that the most stable conformation of the ring D of **6** would be a *quasi* chair conformation with the 13-axial substituent, but that of the 12β-epimer **8** would be a *quasi* chair conformation with the 13-equatorial substituent. It also showed that the 13β-

Table 1. NMR parameters for
[chemical shifts (τ) and

Compound	3α-H	6-H	11α-H (11-H)	12α-H	18-H	19-H
1	5.44, br	4.62, bs	—	7.18, d (7.5)	8.15, s	9.02, s
2	5.36, br	*	—	*	9.29, d (6.0)	9.13, s
3	*	*	—	7.24, d (9.0)	8.14, s	9.23, s
4	5.39, br	*	—	7.23, d (9.0)	8.14, s	9.21, s
5	5.35, br	*	—	*	9.26, d (6.0)	9.10, s
6	5.34, br	*	—	*	9.21, d (6.0)	9.12, s
14	5.35, br	*	—	*	9.35, d (7.2)	9.10, s
15	5.45, br	*	—	*	9.34, d (7.5)	9.15, s
16	5.30, br	*	0.55, d (5.4)	4.52, d (3.0)	9.23, d (7.5)	8.93, s
17	5.33, br	*	—	*	8.80, d (6.0)	9.11, s
18	5.35, br	*	—	*	8.83, d (6.0)	9.11, s
19	5.36, br	*	—	*	18β-H, 6.84, dd, (10.5, 7.5) 18α-H, 6.12, t, (7.5)	9.17, s
20	6.43, br	*	—	*	18β-H, 5.64, d, (8.6) 18α-H, 6.17, dd, (8.6, 4.9)	9.18, s
21	—	*	—	*	18β-H, 5.75, d, (8.7) 18α-H, 6.15, dd, (8.7, 4.8)	8.99, s
22	a)	*	*	*	18β-H, 6.38, d, (8.4) 18α-H, 6.19, dd, (8.4, 4.8)	9.29, s
23	5.28, br	*	*	*	18β-H, 6.37, d, (8.4) 18α-H, 6.16, dd, (8.4, 4.8)	9.25, s
24	5.37, br	*	*	*	—	9.33, s
25	6.38, br	*	*	*	—	9.30, s
26	6.41, br	*	5.68, t (6.0)	*	18α- and β-H 6.07, s ($W1/2=5$)	8.99, s
27	5.33, br	*	5.70, t (6.0)	*	18α- and β-H 6.09, s ($W1/2=5$)	8.98, s
28	—	*	5.64, t (6.3)	*	18α- and β-H 6.09, s ($W1/2=5$)	8.80, s

a) Superimposed on 18-H. b) Superimposed on 18α-H. c) *d*, (9.0) after irradiation at τ 8.80. d) *d*, (9.3)

methyl and the 20α-methyl of **8** are nearly in a 1,3-diaxial relationship and therefore the 12β-epimer **8** (C/D *trans* isomer) appears to be less stable than the 12α-epimer **6**, in which the C(13)–C(18) and C(20)–C(21) bonds are in nearly orthogonal positions. On the other hand, there are no non-bonded interactions between the 13β-methyl and the 20α-methyl of **9** and its 12β-epimer **10**. Thus, the situation differs sharply from that of the pair of 17-epimers **6** and **8**.

The jervanine **6** may be formed *via* an intramolecular radical combination of a biradical intermediate **12**. In this step, the attack of the 23β-oxyl radical to the C-17 radical center from the β-face should be hindered by the presence of the 13β-methyl group and therefore the observed product **6** will result. The formation of **6** through an iodohydrin intermediate (**13**) is unlikely, since the combination of an iodine atom with the C-17 radical from the β-face would be severely hindered by the 13β-methyl group.

The aldehyde **5** was transformed into a crystalline enamine **14** with morpholine and *p*-toluenesulfonic acid in toluene under reflux in an almost quantitative yield. The enamine **14** was then subjected to a copper-catalysed oxygenation[12] or an oxidative cleavage with

ETIOJERVANE DERIVATIVES IN $CDCl_3$
splittings (Hz; in parentheses)]

20-H	21-H	22α-H (22-H)	23α-H	26-H	27-H	NAc, OAc
6.97, dq (6, 11)	8.83, d (6.3)	5.33, bd (10.5)	5.92, bs ($W1/2=7.5$)	9.02, d (6.5)	6.80, bs ($W1/2=6.6$)	8.00, s, and 8.03 s,
*	9.13, d (5.4)	6.72, bs	6.05, bs ($W1/2=18$)	8.95, d (6.0)	*	7.90, s, and 8.01, s
7.00, dq (6, 11)	8.85, d (6.3)	5.38, bd (11.3)	5.95, bs ($W1/2=7.5$)	8.98, d (6.6)	6.80, bs	7.98, s
7.00, dq (7, 12)	8.85, d (6.3)	5.39, d (10.5)	5.95, bs ($W1/2=7.5$)	8.99, d (6.6)	6.80, bs	8.00, s
*	8.98, d (7.2)	0.45, d	—	—	—	7.98, s
*	9.08, d (6.0)	*	*	9.01, d (6.6)	*	7.92, s, and 7.98, s
—	8.35, s	4.78, s	—	—	—	8.01, s
—	7.94, s	—	—	—	—	8.04, s
—	7.89, s	—	—	—	—	7.98, s
6.43, dq	9.20, d (6.6)	—	—	—	—	8.00, s
6.45, m	9.27, d (6.6)	—	—	—	—	8.00, s
6.32, dq	8.82, d (6.3)	—	—	—	—	8.00, s
ca. 6.2 b)	8.82, d (6.0)	—	—	—	—	—
6.18, dq c)	8.80, d (6.0)	—	—	—	—	—
a)	8.83, d (6.0)	—	—	—	—	—
a)	8.82, d (6.0)	—	—	—	—	8.01
5.65, dq d)	8.71, d (6.0)	—	—	—	—	8.07
5.60, dq (9.8, 6.0) e)	8.65, d (6.0)	—	—	—	—	—
6.12, dq (2.3, 6.0)	8.85, d (6.0)	—	—	—	—	—
6.12, dq	8.84, d (6.0)	—	—	—	—	7.99, s
6.13, dq (4.5, 6.0)	8.83, d (6.0)	—	—	—	—	—

after irradiation at τ 8.71. e) (9.8) after irradiation at τ 8.65.

dye-sensitized singlet oxygen[13] (Scheme 3).

In the copper-catalyzed oxygenation, oxygen was bubbled through a chloroform solution of the enamine **14** containing copper(I) chloride for 24 h under cooling. The expected product, 3β-hydroxy-12α,17β-ethyletiojervane-11,20-dione 3-acetate (**15**), mp 134—135 °C, was obtained in 91% yield after recrystallization from diethyl ether.

In the dye-sensitized oxidative cleavage, the enamine **14** in dry benzene containing Rose Bengal was irradiated with a 90-W high pressure mercury arc under an atmosphere of oxygen for 48 h. Column chromatography of the product gave dione **15**, which is identical with the dione obtained by the copper-catalyzed oxygenation, in 79% yield. Although this photochemical procedure was successful in most of the experiments with 90-W Hg arc, the irradiation was found in some experiments to lead to the exclusive formation of an aldehyde **16** resulting from α-fission of an excited 11-oxo group; in these experiments a lamp of a wattage slightly above 100-W was used. The structure of the aldehyde **16** was confirmed to be 3β-hydroxy-11,12-seco-17β-ethyletiojervane-11,20-dione 3-acetate by spectrometry. The high

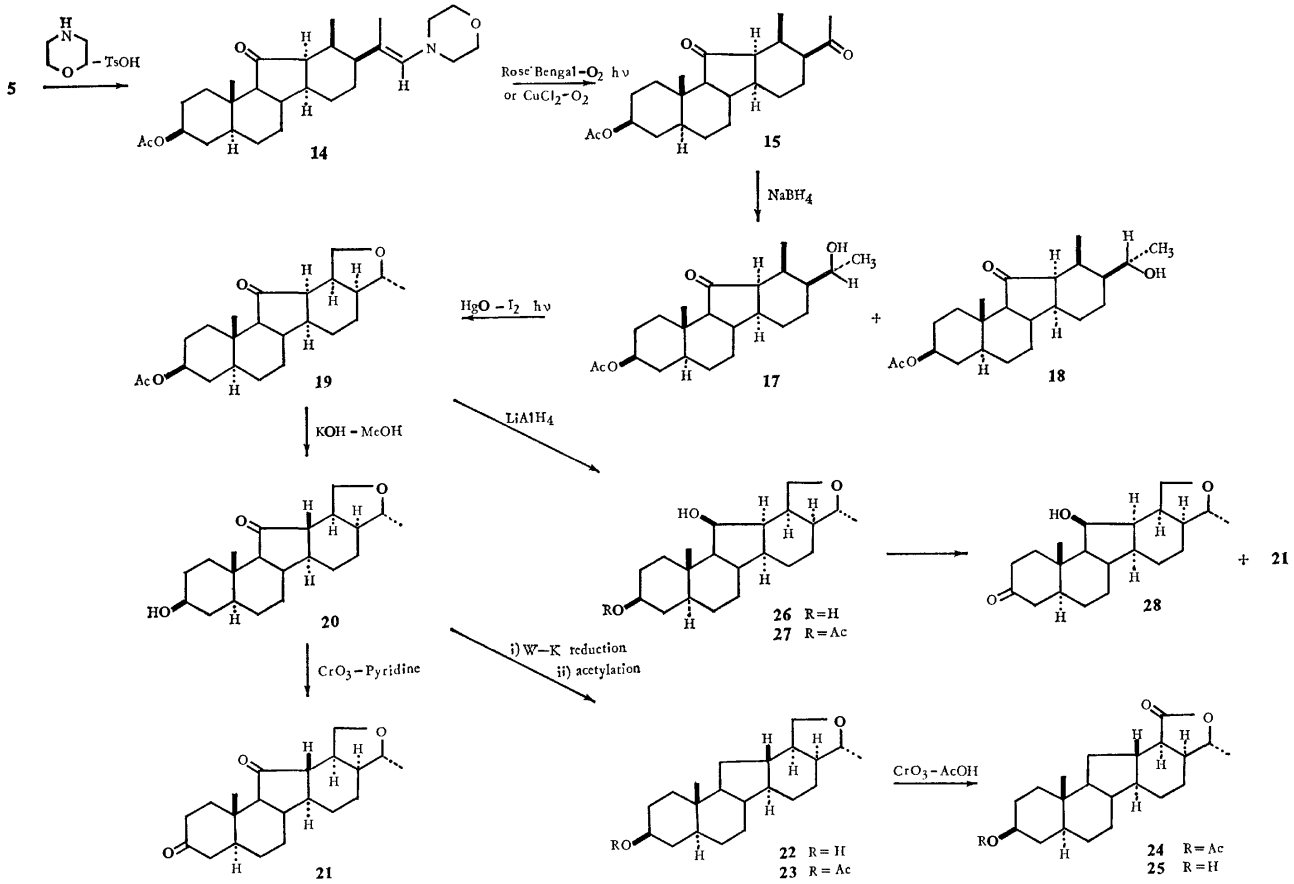

Scheme 3.

resolution mass spectrum of **16** indicated that it had the molecular formula $C_{23}H_{34}O_4$. The IR spectrum of **16** showed three bands arising from the acetoxyl, the formyl, and the acetyl groups. The NMR spectrum showed two one-proton doublets at τ 0.55 (J= 5.4 Hz) and at τ 4.52 (J=3.0 Hz) assignable to the C-11 hydrogen and the olefinic C-12 hydrogen, and other signals consistent with the assigned structure. The use of the high pressure Hg arc lamps of wattage as intense as 100 watts for the oxygenation seems to be just on a critical line for the cleavage and may be inappropriate, even though the excited 11-oxo group is being quenched by oxygen during oxygenation, which is a faster process than the α-fission.

The 20-oxo group of the 11,20-dione **15** was selectively reduced with sodium borohydride in ethanol containing ethyl acetate to give a mixture of 3β,20β-dihydroxy-17β-ethyletiojervan-11-one 3-acetate (**17**) and its 20α-epimer (**18**). Recrystallization and preparative TLC of the mixture gave 20β-ol **17**, mp 169—171 °C, and 20α-ol **18**, mp 175—176 °C, in 69 and 11% yields respectively. It was not possible to deduce the configurations at the C-20 centers of these compounds by NMR spectroscopy, since the differences in the splitting and the chemical shifts of their 20-H signals and the differences in the chemical shifts of their 18-H were too small to distinguish the configurations of their C-20 centers. However, consideration of the steric course of the reduction with complex metal hydrides, in a manner analogous to the case of the reduction of the 11-deoxo analogue[5] of dione **15**, allowed us to assign a 20β-configuration for the major product and a 20α- for the minor one. These assignments were further supported by an analysis of the NMR spectrum of 18,20β-epoxy-3β-hydroxy-17β-ethyletiojervan-11-one 3-acetate (**19**) obtained by the hypoiodite reaction of the alcohol **17** (*vide infra*). Interestingly, the 11-oxo group of **15** exerts an influence on the steric course of the reduction, as shown by the formation of an appreciable amount of 20α-isomer **18** from **15** and the exclusive formation of 20β-isomer from a 11-deoxo analogue of **15**.[5]

The 20β-ol **17** in benzene containing mercury(II) oxide and iodine was then irradiated for 2.5 h under an argon atmosphere.[1,7b] Column chromatography of the product gave **19** in 81% yield together with the recovered material (7%). Various spectra of the product was in agreement with (20*R*)-18,20β-epoxy-3β-hydroxy-17β-ethyl-12α-etiojervan-11-one 3-acetate (**19**). Thus, high resolution mass spectrometry confirmed the molecular formula $C_{23}H_{34}O_4$. IR spectrum showed the absence of any hydroxyl group and the presence of a superimposed band at 1732 cm^{-1} arising from the 3β-acetoxyl and the 11-oxo groups. The very intense molecular ion peak (67.8%) in the mass spectrum of **19** contrasts to that of the 11-deoxo analogue,[5] in which the intensity of the molecular ion is only 2% and M^+-CH_3 ion peak is intense. The NMR spectrum showed a three-proton doublet at τ 8.82 with J=6.3 Hz assigned to the 21-H. It also

showed a one-proton double quartet at τ 6.32. Irradiation at τ 8.82 caused a collapse of the double quartet at τ 6.32 to a doublet with J=4.2 Hz. On this basis, the signal at τ 6.32 is asigned to the 20-H. The NMR spectrum showed another double doublet at τ 6.84 with J=10.5 Hz and 7.5 Hz and a triplet at τ 6.12 with J=7.5 Hz; these are assigned to the 18β-H and the 18α-H respectively. Model inspection indicates that the dihedral angles between the 18α-H and the 13α-H, and the 18β-H and the 13α-H in a twisted boat conformation of the ring D are about 20° and 140° respectively, in accord with the observed magnitudes of the couplings. The relevant coupling constants are $J_{18\alpha,18\beta}$=7.5 Hz, $J_{18\beta,13\alpha}$=7.5 Hz, and $J_{18\beta,13\alpha}$=10.5 Hz. The Dreiding molecular model also shows that the dihedral angle between the 17α-H and the 20β-H is about 120° in the above conformation. The observed coupling constant 4.2 Hz allows us to assign the configuration of the methyl group at the C-20 to be α. Therefore, **17** should be the 20β-ol.

Hydrolysis of **19** with methanolic potassium hydroxide gave a crystalline alcohol **20**, mp 229—229.5 °C, the first 18-functional C/D *trans* *D*-homo-*C*-norsteroid ever prepared. The epimerization of the C-12 center of **19** was proved by the ^{1}H NMR spectrum of **20**. The ^{1}H NMR spectra of **20** and 3-oxo compound **21** showed an appreciable change of the splitting of the signals arising from their 18-methylene protons, in comparison with the correponding ones of C/D *cis* compound **19**. The spectrum of **20** showed a broad doublet at τ 5.64 with J=8.6 Hz and a double doublet at τ 6.17 with J=8.6 Hz and 4.9 Hz. The inspection of the model of C/D *trans* ketone **20** having the ring D in a *quasi* chair conformation indicated that the dihedral angle between the 18β-H and the 13α-H is about 90° and that between the 18α-H and the 13α-H is about 30°. On the other hand, the two corresponding dihedral angles in the model of C/D *trans* ketone having the ring D in a boat conformation were about 130° and 30°. The observed coupling constants are thus in agreement with the predicted ones for the hydroxy ketone having the ring D in a chair; the doublet at τ 5.64 and the double doublet at τ 6.17 are ascribed to the 18β-H and the 18α-H. A signal due to the 20β-H was superimposed on the signal arising from the 18α-H; the superimposed signal shape changed when a three-proton doublet at τ 8.82 (the 21-H) was irradiated. The isomerization of the C/D junction of **19** in the hydrolysis was finally confirmed by a comparison of its 11-deoxo compound (**23**) with (20*R*)-18,20β-epoxy-17β-ethyl-12α-etiojervan-3β-ol 3-acetate[1,5] previously prepared. This showed that the two compounds are not identical (*vide infra*).[1,5]

The ketone **20** was then oxidized to 18,20-epoxy-17β-ethyletiojervane-3,11-dione (**21**) with chromium trioxide-pyridine. Oxidation of **21** with chromium trioxide-acetic acid failed to give the lactone. It is almost certain that the 11-oxo group hinders the oxidation of the 18-methylene to a 18-oxo group, since the 18-methylene group of the corresponding 11-deoxo compound (**23**) can readily be oxidized to 18-oxo group (*vide infra*).

The 11-oxo group of **20** was removed by a modified procedure[14] of the Wolff-Kishner reduction. The reduction by this procedure gave 11-deoxo alcohol (**22**), mp 171—174 °C, as a single product. It gave an O-acetyl derivative (**23**), which was proved to be not identical with 18,20β-epoxy-17β-ethyl-12α-etiojervan-3β-ol 3-acetate reported previously.[1,5] The NMR spectra of **22** and **23** showed that the splittings of the signals arising from their 18-methylene protons were similar to those of their 11-oxo analogue **20**, with the exception that the doublet arising from the 18β-H shifted significantly to a higher field (Δ 0.74 ppm for **22**). Oxidation of **23** with chromium trioxide in acetic acid gave an amorphous γ-lactone (**24**) in 39% yield. The IR spectrum showed two bands due to an acetoxyl and a γ-lactone groups. Its NMR spectrum exhibited a double quartet at τ 5.65 due to the 20β-H and a doublet at τ 8.71 due to the 21-H. Irradiation at τ 8.71 caused a collapse of the former to a doublet with J=9.3 Hz. The mass spectrum showed only a weak molecular ion peak at *m/e* 374 (0.3%), a base peak at *m/e* 314, and a prominent peak at *m/e* 299 (35.7%). The last two fragments are attributable to $M^+-CH_3CO_2H$ and $M^+-CH_3CO_2H-CH_3$.

Hydrolysis of the lactone **24** in a mixture of chloroform and methanol with dilute hydrochloric acid at room temperature gave the corresponding 3β-ol **25**, mp 202—205 °C.

The aforementioned experiments indicated that the cyclic ether **19** with the C/D *cis* junction is a less stable isomer and readily isomerizes with a base to the more stable cyclic ether **20** with C/D *trans* junction. Attempts have been made to modify the 11-oxo function of **19** without affecting the stereochemistry of the C/D *cis* ring junction. Reduction of the 11-oxo function of **19** with lithium aluminum hydride for 1.5 h at room temperature gave 3β,11β-diol (**26**), mp 211—214 °C, as a single product. This remarkably facile reduction of the 11-oxo group is surprising. The conformation of the molecule **19** should be one in which the degree of steric hindrance around the 11-oxo group for the attack of hydride ion is appreciably reduced. The *cis* stereochemistry of the C,D-ring junction was supported by NMR spectroscopy. The NMR spectrum showed a one-proton triplet at τ 5.68 (J=6.0 Hz) assigned to the 11α-H, a two-proton singlet ($W_{1/2}$= 5 Hz) at τ 6.07 assigned to the 18-methylene protons, and a one-proton double quartet centered at τ 6.12 with J=2.3 and 6.0 Hz ascribed to the 20β-H. Apart from these signals it showed a one proton multiplet centered at τ 7.49 and a three-proton doublet at τ 8.85 (J=6.0 Hz) ascribed to the 17α-H and the 21-H. These assignments were supported by the following spin decoupling studies. Irradiation at τ 8.85 resulted in a collapse of the double quartet at τ 6.12 into a doublet with J=2.3 Hz. Irradiation at τ 7.49 decoupled the double quartet at τ 6.12 into a quartet with J=6.0 Hz. Finally, irradiation at τ 6.12 resulted in collapses of the doublet at τ 8.85 to a singlet and of the multiplet at τ 7.49 into a diffused triplet. On the basis of these results, the relevant coupling constants are $J_{21\text{-H},\,20\beta\text{-H}}$=6.0 Hz, $J_{20\beta\text{-H},\,17\alpha\text{-H}}$=2.3

Hz, $J_{18\alpha\text{-H},\,18\beta\text{-H}} \simeq J_{18\alpha\text{-H},\,13\alpha\text{-H}} \simeq J_{18\beta\text{-H},\,13\alpha\text{-H}} < 5$ Hz. The unusually small gem-coupling of the 18-methylene protons should be noted.

Acetylation of **26** by the standard procedure gave a 3-acetate **27**. To transform 3β-hydroxyl group into a 3-oxo group, diol **26** was subjected to the Oppenauer oxidation. However only a low yield of 3-oxo compound **28** was obtained, together with 3,11-dione **21**. An analysis of the signals arising from the 18-methylene protons and the 20β-proton of **28** is given in the Table.

Experimental

For instruments used and general procedures see Ref. 1. Low resolution mass spectra of compounds **2,4—7, 14, 15, 17, 18, 20—26**, and all the high resolution mass spectra were recorded at the Faculty of Agriculture of this University with a Hitachi JMS-D 300 spectrometer. Low resolution mass spectra of compounds **3, 18**, and **28** were recorded at the Faculty of Pharmaceutical Sciences with a Hitachi RMU-6E spectrometer.

Catalytic Hydrogenation of (22S, 25S)-N-Acetyl-3β,23β-dihydroxyveratr-5,13(17)-dien-11-one 3-Acetate (1). (*a*): Rhodium–platinum catalyst (38.65 g) in glacial acetic acid (350 ml) was shaken under an atmosphere of hydrogen for *ca.* 11.5 h. To this solution was added the diene **1** (25.0 g) dissolved in glacial acetic acid (250 ml). The resulting solution was shaken under an atmosphere of hydrogen for 43.5 h and then a further amount of freshly prepared catalyst (4 g) in glacial acetic acid (150 ml) was added. The solution was again shaken under an atmosphere of hydrogen for 18.5 h. During this period, 3.25 l of hydrogen were absorbed. After the removal of the catalyst and the solvent, water (300 ml) was added to the residue and the solution was neutralized with aq 10% sodium carbonate solution. The solution was then extracted with chloroform (500 ml × 3). The chloroform solution was washed with water and dried. After the usual work-up, the residue was recrystallized from acetone–diethyl ether to yield perhydro derivative **2**, mp 204—206 °C. (15.60 g) in colorless crystals in two crops. (Found: C, 72.24; H, 9.75; N, 2.67%. Calcd for $C_{31}H_{49}NO_5$: C, 72.19; H, 9.58; N, 2.72%); $[\alpha]_D^{25}$ −1.5° (*c* 1.5, $CHCl_3$); IR, 3319 (OH), 1734 and 1722 (5-membered ring ketone and OAc), 1606 (NAc), 1236 and 1015 cm^{-1}; MS, (70 eV) *m/e* (*rel intensity*), 515 (M^+, 0.4), 500 ($M^+ - CH_3$, 0.3) 472 (0.3), 198 (0.3), 185 (0.7), 156 (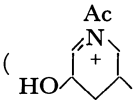 , 100), and 114 (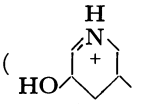 , 17.3); for NMR see Table 1.

Examination of the residue (9.4 g) from the filtrate by TLC indicated that it was a mixture of the starting material, which was the major component, and two other minor products. This residue in glacial acetic acid (200 ml) was again hydrogenated in the presence of rhodium–platinum catalyst (14.4 g). About 0.74 l of hydrogen were absorbed during 50 h. The product was recrystallized from diethyl ether to yield perhydro derivative **2** (0.794 g). The residue from the filtrate was subjected to column chromatography (Mallinckrodt silicic acid, 100 mesh, 100 g). Elutions with hexane, benzene, and a 1:1 mixture of chloroform and benzene gave a mixture (6.85 g). An analysis of a part of the mixture by preparative TLC (a 5:3 mixture of diethyl ether–chloroform as the solvent) indicated that it contained 1.01 g of perhydro derivative **2**. Further elutions with diethyl ether gave a fraction which gave the perhydro derivative **2** (0.505 g) after recrystallization from diethyl ether. The total yield of perhydro derivative **2** was thus 71.6%. Isolations of the minor products **3** and **4** are described in the following procedure (b).

(*b*): Rhodium–platinum catalyst (2.0 g) in glacial acetic acid (30 ml) was shaken under an atmosphere of hydrogen for 4 h. During this period, 578 ml of hydrogen were absorbed. To this solution was added diene **1** (2 g) in glacial acetic acid (30 ml) and the solution was shaken under an atmosphere of hydrogen for 46 h, 180 ml of hydrogen being absorbed. After removal of the catalyst and the solvent, the product was dissolved in chloroform and the solution was washed with water, then dried over anhydrous sodium sulfate. The residue (2.472 g) showed four spots on TLC (a 5:3 mixture of diethyl ether–chloroform). A part of the product (750 mg) was subjected to preparative TLC with a 5:3 mixture of diethyl ether and chloroform to give four fractions: A (69 mg), B (337 mg), C (62 mg), and D (388 mg) in the order of decreasing mobility. Fraction A was recrystallized from acetone–diethyl ether to yield product **3**, mp 218.5—219.5 °C (15 mg). (Found: C, 76.54; H, 9.94; N, 3.14%. Calcd for $C_{29}H_{45}O_3N$: C, 76.44; H, 9.95; N, 3.07%); IR 3314 (OH), 1725 (5-membered ring ketone), 1608 (NAc), 1254, and 1017 cm^{-1}; MS (80 eV), *m/e* (*rel intensity*), 455 (M^+, 0.3), 299 (1), 298 (0.9), 156 (100), 114 (45), 55 (9), and 43 (9); for NMR see Table 1.

Fraction B was identified as an olefin **4** but could not be induced to crystallize. (Found: *m/e* 513.3453. $C_{31}H_{47}NO_5$ requires M^+ 513.3453); $[\alpha]_D$ +1.64° (*c*, $CHCl_3$); IR, 3320 (OH), 1727 (OAc and 5-membered ring ketone), 1604 (NAc), 1240, and 1028 cm^{-1}; MS, (70 eV) *m/e* (*rel intensity*), 513 (M^+, 0.2), 357 ($M^+ - C - 20$ substituent, 0.5), 156 (100), and 114 (20.6); for NMR see Table 1.

Fraction C was a mixture; fraction D was recrystallized from acetone–diethyl ether to yield perhydro derivative **2**, (238 mg).

The Removal of Heterocyclic Moiety of (22S,25S)-N-Acetyl-3β,23β-dihydroxyveratranin-11-one 3-Acetate **2** by *Irradiation in the Presence of Mercury(II) Oxide and Iodine.* The perhydro compound **2** (13.5 g) in dry benzene (700 ml) in the presence of mercury(II) oxide (27.0 g) and iodine (33.8 g) was irradiated with a 100-W high pressure mercury arc while being stirred. After a period of 24 h, more iodine (3 g) and mercury(II) oxide (3 g) were added and the irradiation was continued for another 24 h. Precipitates were removed by filtration and washed with hot benzene. The solution and the washing were combined, washed with saturated aq sodium hydrogensulfite solution (300 ml) and water (500 ml × 2), and dried over anhydrous sodium sulfate. Removal of the solvent at below 40 °C gave a brown residue. TLC indicated that this was largely aldehyde **5**, together with a small amount of a less mobile compound **6**. The residue was subjected to column chromatography with Mallincrodt silicic acid (35 g). Elutions with a 1:1 mixture of benzene and hexane and then benzene only gave three fractions. The first fraction gave crystalline aldehyde **5**. Recrystallization from diethyl ether gave pure aldehyde **5** (4.0 g), mp 144—146 °C (Found: *m/e* 388.2608. Calcd for $C_{24}H_{36}O_4$: M^+ 388.2613); $[\alpha]_D^{25}$ −3.3° (*c* 0.4, $CHCl_3$); IR, 1731, (broad, CHO, OAc and 5-membered ring ketone), 1234, and 1020 cm^{-1}; MS, (70 eV) *m/e* (*rel intensity*) 388 (M^+, 34.1), 360 ($M^+ - CO$, 52.7), 345 (9.3), 330 ($M^+ - C -$ 17 substituent-H, 17.7), 328 ($M^+ - CH_3CO_2H$, 39.5), 300 ($M^+ - CO - CH_3CO_2H$, 77.4), 147 (89.0), 123 (70.3), 95 (73.2), 93 (87.8), 81 (75.8), 67 (61.8), 55 (70.4), and 43 (100); for NMR see Table 1.

The second fraction gave an amorphous mixture (800 mg), which was subjected to preparative TLC with a 20:1 mixture of chloroform and diethyl ether to give aldehyde **5** (300 mg) and a new compound **6** (479 mg). The aldehyde **5** was recrystallized from diethyl ether to give a pure specimen (259 mg). The new compound **6** was recrystallized from diethyl ether to give a pure specimen, mp 221—222 °C. (Found: C, 72.25; H, 9.18; N, 2.58%. Calcd for $C_{31}H_{47}NO_5$; C, 72.48; H, 9.22; N, 2.73%); $[\alpha]_D^{25}$ −2.7 (*c* 1.1, $CHCl_3$); IR, 1733 (OAc and 5-membered ring ketone) and 1671 cm^{-1} (NAc); MS, (70 eV) *m/e* (*rel intensity*), 513 (M^+, 11.9), 277 (5.2), 222 (20.3), 211 (31.5), 167 (100), 156 (24.5), 114 (9.8), and 43 (17.3); for NMR see Table 1.

Hydrolysis of Compound ***6***. Product **6** in methanol (5 ml) containing potassium hydroxide (250 mg) was heated under reflux and an atmosphere of nitrogen for 40 min. After the removal of methanol, water (20 ml) and 2 mol dm^{-3} hydrochloric acid (5 ml) were added to the residue. The solution was extracted with chloroform. The organic layer was worked up as usual. The amorphous residue (41 mg) was recrystallized from acetone–diethyl ether to give 3β-ol **7**, mp 242—244°. (Found: *m/e* 471.3334. Calcd for $C_{29}H_{45}NO_4$: M^+ 471.3346); MS ,(70 eV) *m/e* (*rel. intensity*), 471 (M^+, 19.7), 222 (18.5), 211 (31.2), 167 (100), and 156 (19.1).

Preparation of Enamine ***14*** *from 20-Formyl-3β-hydroxy-12α-17β-ethyletiojervan-11-one 3-Acetate.* Aldehyde **5** (4 g), morpholine (10 ml), and p-toluenesulfonic acid (200 mg) in dry toluene (150 ml) were heated under reflux in a flask fitted with a Dean Stark trap for 5.5 h. After the removal of the solvent, an oily residue was extracted with chloroform (200 ml×2). The solution was washed with an aq 5% sodium carbonate solution (100 ml) and water (100 ml×2) and dried over anhydrous sodium sulfate. Removal of the solvent left crystals of enamine **14** (4.45 g), mp 106—108 °C. This enamine **14** was used immediately for the next step without further purification. (Found: *m/e* 457.3203. Calcd for $C_{28}H_{43}NO_4$: M^+ 457.3192); $[\alpha]_D^{25}$ −4.4 (*c* 1.1, $CHCl_3$); IR, 1732 (OAc and 5-membered ring ketone), 1260, 1123, 1031, 874, and 735 cm^{-1}; MS, (70 eV) *m/e* (*rel intensity*) 457 (M^+, 72.0), 388 (11.2), 360 (18.9), 328 (18.5), 300 (31.3), 166 (100), 147 (38.9), 123 (34.3), 100 (43.9), 95 (44.3), 93 (42.8), 81 (39.4), 67 (31.2), 55 (36.6), and 43 (70.0); for NMR see Table 1.

*Preparation of 3β-Hydroxy-12α,17β-ethyletiojervane-11,20-dione 3-Acetate (****15****) from Enamine* ***14***. (*a*): Enamine **14** (500 mg) and copper(I) chloride (300 mg) in chloroform (100 ml) were cooled with ice–water and oxygen was bubbled through the solution for 9.5 h. After about 3 h, precipitates appeared in the yellow-green solution. At this point 10 ml of chloroform were added and the solution was allowed to stand under an atmosphere of oxygen for an additional 14.5 h. The precipitates were removed by filtration and washed with chloroform (100 ml). The filtrate and the washings were combined and worked up in the usual way. The crystalline residue was recrystallized from diethyl ether to yield dione **15** (343 mg), mp 134—135 °C. (Found: C, 73.99: H, 9.42%. Calcd for $C_{23}H_{34}O_4$: C, 73.76; H, 9.15%); $[\alpha]_D^{25}$ −1.4 (*c* 1.0, $CHCl_3$); IR, 1732 (OAc and 5-membered ring ketone), 1704 (Ac), 1242, 1024, 992, and 896 cm^{-1}; MS, (70 eV) *m/e* (*rel intensity*) 374 (M^+, 77.7), 359 (M^+-CH_3, 4.8), 314 ($M^+-CH_3CO_2H$, 19.5), 299 ($M^+-CH_3CO_2H-CH_3$, 25.2), 219 (9.8), 205 (10.3), 147 (18.3), 107 (14.7), 105 (16.6), 95 (57.3), 93 (20.3), 91 (15.8), 81 (15.5), 79 (16.4), 67 (17.7), 55 (17.4), and 43 (100); for NMR see Table 1.

(*b*): Enamine **14** (4.276 g) and Rose Bengal (100 mg) in dry benzene (600 ml) were irradiated with a 90-W high pressure mercury arc under an atmosphere of oxygen for 48 h. Oxygen was occasionally bubbled into the stirred solution. The solution was washed with water (300 ml×3) and dried over anhydrous sodium sulfate. After removal of the solvent, the crystalline residue (4.744 g), which was almost a single product, was subjected to column chromatography (Mallincrodt SiO_2, 7 g) to remove some polar substances. Elutions with benzene containing an increasing amount of chloroform gave dione **15**. It was recrystallized from diethyl ether to give 2.79 g in two crops.

(*c*): Enamine **14** (8.95 g) and Rose Bengal (250 mg) in dry benzene (1.3 l) were irradiated with a 103-W high pressure mercury arc for 48 h while oxygen was bubbled through slowly. After work-up as in procedure (b), the product (6.35 g) was subjected to column chromatography (Mallincrodt SiO_2, 15 g). Elutions with benzene gave a fraction which was recrystallized from diethyl ether–hexane to yield aldehyde (**16**) (3.4 g). The residue from the filtrate was subjected to preparative TLC with 50:1 chloroform–diethyl ether to yield a further amount of aldehyde (16) (0.31 g), mp 132—134 °C. (Found: *m/e* 374.2447. Calcd for $C_{23}H_{34}O_4$. M^+ 374.2455). IR, 1738 (OAc), 1726 (CHO), 1717 ($COCH_3$), and 1248 cm^{-1}. MS, *m/e* (*rel intensity*), 374 (M^+, 3.2), 346 (3.0), 286 (2.8), 271 (3.6), 253 (3.8), 107 (22.0), 105 (14.5), 95 (14.9), 93 (16.3), and 43 (100).

Reduction of Dione **15** *with Sodium Borohydride.* Dione **15** (600 mg) in absolute ethanol (60 ml) containing sodium borohydride (260 mg) and ethyl acetate (2 ml) was stirred for 2.5 h at room temperature. The reaction mixture was worked up as usual to give a residue (713 mg). Examination of the product by TLC with a 1:20 mixture of diethyl ether–chloroform showed it to be a mixture of a major product (R_f 4.4) and a minor product (R_f 5.5). Recrystallization from diethyl ether gave 3β,20β-dihydroxy-12α,17β-ethyletiojervan-11-one 3-acetate **17**, mp 169—171 °C, (349 mg). (Found: C, 73.22; H, 9.59%. Calcd for $C_{23}H_{36}O_4$. C, 73.36; H, 9.64%); $[\alpha]_D^{25}$ −0.62 (*c* 1.7, $CHCl_3$); IR, 3544 (OH), 1724 (OAc and 5-membered ring ketone), 1235, 1121, 1031, and 899 cm^{-1}; MS, (70 eV) *m/e* (*rel intensity*), 376 (M^+, 2.4), 358 (M^+-H_2O), 332 (45), 272 (100), 235 (27.4), 218 (31.8), 147 (43.9), 123 (32.4), 107 (36.1), 105 (32.6), 95 (92.2), 93 (58.5), 91 (31.9), 81 (41.6), 79 (36.2), 67 (40.6), 55 (38.4), and 43 (73.9); for NMR see Table 1.

Removal of the solvent from the filtrate gave a mixture of 20α- and 20β-ols (283 mg). The mixture was subjected to preparative TLC with a 1:20 mixture of diethyl ether–chloroform to give two fractions. The less mobile fraction (124 mg) was 20β-ol; this was recrystallized from diethyl ether to give pure 20β-ol **13** (64 mg). The more mobile fraction (68 mg) was recrystallized from diethyl ether to give 20α-ol **18**, mp 175—176 °C. (Found: C, 73.13; H, 9.54%. Calcd for $C_{23}H_{36}O_4$: C, 73.36; H, 9.64%); $[\alpha]_D^{25}$ −1.1 (*c* 1.2, $CHCl_3$); IR 3564 (OH), 1726 (OAc and 5-membered ring ketone), 1232, 1106, 1019, and 895 cm^{-1}; MS, (80 eV) *m/e* (*rel intensity*) 376 (M^+, 4), 358 (M^+-H_2O, 8), 332 (29), 272 (78), 218 (57), 177 (30), 147 (54), 123 (43), 107 (47), 105 (37), 95 (100), 93 (59), 91 (46), 81 (55), 79 (47), 67 (66), 55 (60), and 43 (95); for NMR see Table 1.

The Hypoiodite Reaction of 3β,20β-Dihydroxy-12α,17β-ethyletiojervan-11-one 3-Acetate ***17***. Alcohol **17** (267 mg) in dry benzene (40 ml) containing mercury(II) oxide (550 mg) and iodine (850 mg) was irradiated with a 100-W high pressure mercury arc through a Pyrex filter under an argon atmosphere. The solution was stirred during irradiation. The irradiation was discontinued after 2.5 h when the starting material disappeared as shown by TLC. The precipitates

were removed by filtration and washed with hot benzene (100 ml×2). The filtrate and the washings were combined and washed with 10% sodium hydrogen sulfite solution (30 ml) and then with water and dried over anhydrous sodium sulfate. Evaporation of the solvent left a residue (308 mg) which was subjected to column chromatography (Mallincrodt silicic acid, 2.6 g). Elution with a 1:1 mixture of hexane and benzene gave a fraction (10 mg); further elution with benzene, a 2:1 mixture of benzene and chloroform, and a 1:1 mixture of benzene and chloroform gave acetate **19** (216 mg). (Found: *m/e* 374.2438. Calcd for $C_{23}H_{34}O_4$: M$^+$ 374.2455); IR ($CHCl_3$) 1732 (OAc and 5-membered ring ketone), 1240, 1028, and 758 cm^{-1}; MS, (70 eV) *m/e* (*rel intensity*) 374 (M$^+$, 67.8), 359 (M$^+-CH_3$, 3.6), 314 (M$^+-CH_3CO_2H$, 9.9), 299 (M$^+-CH_3CO_2H-CH_3$, 12.9), 235 (7.7), 147 (26.7), 105 (25.1), 95 (35.0), 93 (30.7), 91 (29.0), 79 (33.3), 67 (25.1), 55 (19.7), and 43 (100).

The final fraction (19 mg) eluted with a 1:1 mixture of chloroform and diethyl ether was the starting material. Acetate **19** was subjected to hydrolysis without further purification.

*Hydrolysis of Acetate **19**.* Acetate **19** (560 mg) in methanol containing potassium hydroxide (2.5 g), water (0.5 ml), and chloroform (8 ml) was stirred for 2.5 h at room temperature and then warmed for another 0.5 h (bath temp 40 °C). The solvent was removed by a rotary evaporator and the residue in added water (30 ml) was neutralized with 2 mol dm^{-3} hydrochloric acid (*ca.* 50 ml) and extracted with chloroform (100 ml×3). The chloroform solution was washed with water and dried over anhydrous sodium sulfate. The residue (532 mg) was recrystallized from diethyl ether to yield 3β-hydroxy-12β-ketone **20**. Preparative TLC of the residue from the filtrate with a 1:1 mixture of diethyl ether and benzene gave a further amount of ketone **20** (27 mg), mp 229—229.5 °C. (Found: *m/e* 332.2352. Calcd for $C_{21}H_{32}O_3$. M$^+$ 332.2351); $[\alpha]_D^{25}-4$ (*c* 1.4, $CHCl_3$); IR 3410 (OH), 1724 (5-membered ring ketone), 1080, and 1041 cm^{-1}; MS, (70 eV), *m/e* (*rel intensity*) 332 (M$^+$, 100), 317 (M$^+-CH_3$, 6.2), 302 (M$^+-2CH_3$, 26.1), 147 (17.9), 110 (17.7), 109 (13.3), 107 (16.9), 105 (24.0), 97 (28.6), 96 (30.9), 93 (30.3), 91 (30.3), 79 (49.2), 67 (24.9), 55 (25.1), 43 (16.7), and 41 (25.0).

Oxidation of 3β-Hydroxy-12β-ketone with Chromium Trioxide–Pyridine. The 3β-ol **20** (150 mg) and chromium trioxide (150 mg) in pyridine (3 ml) were stirred for 3.5 h at room temperature. To this solution was added more (100 mg) of chromium trioxide in pyridine (1 ml) and the solution was stirred for another 1.5 h. After an excess of chromium trioxide was decomposed by adding saturated sodium hydrogensulfite solution (20 ml), the solution was extracted with chloroform (30 ml×3). The chloroform solution was worked up as usual. A product was recrystallized from acetone to yield 3,11-dione **21**, mp 127—129 °C. (Found: *m/e* 330.2193. Calcd for $C_{21}H_{30}O_3$. M$^+$ 330.2193); IR, 1706 (6-membered ring ketone), 1728 (5-membered ring, ketone), 1258, 1129, 1084, and 861 cm^{-1}; MS, (70 eV), *m/e* (*rel intensity*), 330 (M$^+$, 100), 315 (M$^+-CH_3$, 9.8), 300 (M$^+-2CH_3$, 37.5), 286 (11.5), 245 (24.2), 191 (18.5), 121 (17.4), 97 (38.3), 96 (42.0), 93 (31.0), 91 (22.5), 81 (21.0), 79 (44.6), 67(20.1), 55 (25.7), 43 (20.9), and 41 (22.9).

*Wolff-Kishner Reduction of Ketone **20**.* Ketone **20** (102 mg), hydrazine hydrate (1 ml), and hydrazine hydrochloride (280 mg) in triethylene glycol (7.2 ml) were heated at 130 °C for 4 h under an atmosphere of nitrogen. To this solution was added potassium hydroxide pellets (370 mg) and the solution was distilled until the temperature rose to 210 °C. The solution was heated at that temperature for another 2.5 h (bath temp 223 °C). After cooling, the solution was poured into a water–ice mixture. Crude 11-deoxo compound **22**, (78 mg), mp 158—165 °C, was collected by filtration. The specimen for analysis, mp 171—174 °C, was obtained by recrystallization from acetone–diethyl ether. (Found: C, 78.71; H, 10.72%. Calcd for $C_{21}H_{34}O_2$. C, 79.19; H, 10.76%); IR, 3400 (OH), 1084, and 1049 cm^{-1}; MS, (70 eV) *m/e* (*rel intensity*) 318 (M$^+$, 45.6), 303 (M$^+-CH_3$, 47.6), 300 (M$^+-H_2O$, 11.8), 285 (32.7), 274 (11.2), 259 (71.1), 241 (43.7), 149 (72.6), 148 (100), 147 (37.6), 107 (76.1), 105 (48.9), 95 (44.1), 93 (81.1), 91 (77.0), 81 (70.0), 79 (80.6), 67 (71.6), 55 (66.8), 43 (39.4), and 41 (62.1), for NMR see Table 1.

The 3-acetate **23**, mp 135—137 °C, was prepared in a usual manner. (Found: C, 76.68; H, 10.10%. Calcd for $C_{26}H_{36}O_3$: C, 76.62; H, 10.07%. (Found: *m/e* 360.2654. Calcd for $C_{26}H_{36}O_3$. M$^+$, 360.2664); IR, ($CHCl_3$) 1732 (OAc), 1243, 1087, 1031, and 762 cm^{-1}; MS, (70 eV) *m/e* (*rel intensity*) 360 (M$^+$, 10.5), 345 (19.2), 300 (100), 285 (45.1), 256 (23.9), 255 (23.3), 241 (80.8), 149 (39.0), 148 (53.0), 147 (33.0), 107 (47.0), 105 (33.9), 93 (51.5), 91 (40.6), 81 (40.9), 79 (43.8), 67 (36.7), 55 (32.9), and 43 (93.0).

*Preparation of the γ-Lactone **24** from Acetate **23** with Chromium Trioxide–Acetic Acid.* To a solution of acetate **23** (74 mg) in glacial acetic acid (8.5 ml), under reflux, was added chromium trioxide (234 mg) dissolved in glacial acetic acid (4.5 ml) and water (0.5 ml). The solution was heated under reflux for 2.5 h. After removal of the solvent at below 70 °C, the residue was extracted with chloroform (50 ml×3). The chloroform solution was worked up as usual to yield amorphous γ-lactone **24** (30 mg). All attempts to induce the lactone to become crystals were unsuccessful. (Found: *m/e* 314.2248. Calcd for $C_{21}H_{30}O_2$ (M$^+-CH_3CO_2H$ 314.2245). IR, 1729 (OAc), 1765 (γ-lactone), 1258, and 1023 cm^{-1}; MS, (70 eV) *m/e* (*rel intensity*) 374 (M$^+$, 0.3), 314 (100), and 299 (35.7); for NMR see Table 1.

*Hydrolysis of the γ-Lactone **24** with Hydrochloric Acid.* The γ-lactone **24** (40 mg) in methanol (8.1 ml) and chloroform (0.9 ml) containing 12 mol dm^{-3} hydrochloric acid (0.9 ml) was stirred for 17 h at room temperature. The solution was neutralized with aq 5% sodium carbonate solution and the solvent was partly removed by a rotary evaporator. The crystals of the 3β-hydroxy γ-lactone **25** were collected by filtration and recrystallized from methanol–water to yield **25**, mp 202—205 °C. (Found: *m/e* 332.2340. Calcd for $C_{21}H_{32}O_3$: M$^+$ 332.2350); IR 3400 (OH) and 1765 cm^{-1} (γ-lactone); MS, *m/e* (70 eV) (*rel intensity*) 332 (M$^+$, 27.4), 314 (M$^+-H_2O$, 95.8), 299 (22.2), 285 (10.2), 260 (45.1), 259 (30.2), 258 (100), 149 (12.8), 147 (25.5), 108 (14.3), 93 (23.7), 91 (24.6), 79 (24.3), 55 (22.1), and 41 (14.3).

*Reduction of Ketone **19** with Lithium Aluminum Hydride.* To 12α-ketone **19** (522 mg) in dry THF (30 ml) cooled by ice–water was added slowly lithium aluminum hydride (400 mg). The solution was stirred for 1.5 h at room temperature and an excess of lithium aluminum hydride was decomposed by addition of small amounts of ethyl acetate and methanol. To this solution were added water (50 ml) and chloroform (100 ml) and the two-layered solution was stirred for 30 min. The solution was filtered and the aqueous filtrate was extracted with chloroform (50 ml×20). The chloroform solution was worked up in the usual manner. The product was recrystallized from diethyl ether to yield **26** (241 mg), mp 211—214 °C. A residue (185 mg) from the filtrate was subjected to preparative TLC with a 1:1 mixture of chloroform–diethyl ether to yield a further amount of diol **26** (26 mg). (Found: M$^+$ *m/e* 334.2505. Calcd for

$C_{21}H_{34}O_3$: M^+ 334.2506); $[\alpha]_D^{25}$ −3.0 (*c* 0.75, $CHCl_3$); IR, 3428 (OH), 1040, and 851 cm^{-1}; MS, (70 eV) *m/e* (*rel intensity*) 334 (M^+, 6.6), 316 (M^+-H_2O, 100), 301 ($M^+-H_2O-CH_3$, 47.3), 298 (M^+-2H_2O, 10.6), 290 (41.0), 283 (34.6), 147 (66.6), 133 (33.0), 121 (37.6), 119 (37.1), 109 (36.7), 107 (76.8), 105 (66.6), 97 (37.4), 96 (41.1), 95 (77.2), 93 (94.0), 91 (78.1), 81 (75.1), 79 (95.3), 67 (80.7), 55 (80.8), 43 (71.3), and 41 (70.7).

The diol **26** (13 mg) and acetic anhydride (5 mg) in pyridine (0.5 ml) were stirred for 20 h at room temperature. At the time intervals of 1.5 h and 5 h, a more acetic anhydride (0.05 ml) was added. Work-up of the reaction mixture in the usual manner gave a product (13 mg), which was recrystallized from methanol to yield **27**, mp 170—171 °C. (Found: *m/e* 376.2612. Calcd for $C_{23}H_{36}O_4$: M^+ 376.2612), IR, 3490 (OH), 1734 (OAc), and 1242 cm^{-1}; MS *m/e* (*rel intensity*) 376 (M^+, 2.6), 358 (M^+-H_2O, 69.4), 343 (15.8), 316 ($M^+-CH_3CO_2H$, 18.6), 298 ($M^+-CH_3CO_2H-H_2O$, 35.2), 283 (39.9), 147 (43.8), 107 (60.9), 105 (40.0), 95 (55.8), 93 (69.2), 91 (43.9), 81 (55.9), 79 (61.8), 67 (42.5), 55 (38.1), and 43 (100%).

Oppenauer Oxidation of Alcohol ***26***. Alcohol **26** (288 mg) and aluminum isopropoxide (120 mg) in toluene (25 ml) and dry cyclohexanone (2.3 ml) were heated for 1 h under reflux (bath temp 120 °C). More aluminum isopropoxide (140 mg) was added to the solution. The mixture was heated under reflux for another 1 h and then subjected to a steam distillation to give 150 ml of a distillate. To the solution there were added chloroform (50 ml) and water; then the solution was stirred for 1 h. The aqueous layer was again extracted with chloroform. The combined chloroform solution was worked up as usual. The residue (260 mg) was recrystallized from acetone to yield ketone **28** (69 mg), mp 151—152 °C. The filtrate was evaporated and the residue (143 mg) was subjected to column chromatography (Mallincrodt silicic acid, 2.0 g). Elution with a mixture of a 2:1 benzene and hexane gave fraction (120 mg), which was recrystallized from acetone to yield more **28** (16 mg). The residue from the filtrate was subjected to preparative TLC with a 10:1 mixture of chloroform and diethyl ether to yield two fractions. The more mobile fraction gave dione **21** and the less mobile fraction (45 mg) was recrystallized to yield ketone **28** (35 mg), (Found: C, 75.81; H, 97.0%. Calcd for $C_{21}H_{32}O_3$: C, 75.86; H, 9.70%), $[\alpha]_D^{25}$ −2.0 (*c* 0.5, $CHCl_3$); IR ($CHCl_3$) 3416 (OH), and 1707 cm^{-1} (carbonyl); MS, (80 eV) *m/e* (*rel intensity*) 332 (M^+, 15), 314 (M^+-H_2O, 70), 299 (32), 288 (48), 95 (82), 93 (78), 91 (65), 79 (85), 67 (70), 55 (95), 43 (100), and 41 (78); for NMR see Table 1.

The authors thank Mrs. Tomoko Okayama in this laboratory for the measurements of the NMR spectra and the spin-decoupling experiments and Miss Yuko Chiba in the Faculty of Agriculture for the measurements of the mass spectra. The authors also wishes to thank Mr. Maki Kuramoto for his help in preparing some starting materials.

References

1) Part III: H. Suginome, N. Yonekura, and T. Masamune, *Bull. Chem. Soc. Jpn.*, **53**, 210 (1980).

2) Photoinduced Transformations. Part 55. A part of this work has been published in a preliminary form. H. Suginome, H. Ono, M. Kuramoto, and T. Masamune, *Tetrahedron Lett.*, **1973**, 4147. Part 54. H. Suginome and Chi-Ming Shea, *Bull. Chem. Soc. Jpn.*, **53**, 3387 (1980).

3) Throughout this paper, the name 17*β*-ethyletiojervane with the numbering given is used for the hydrocarbon framework (B). S. M. Kupchan and M. J. Abu El-Haj, *J. Org. Chem.*, **33**, 647 (1968); F. C. Chang and R. C. Ebersole, *Tetrahedron Lett.*, **1968**, 3521.

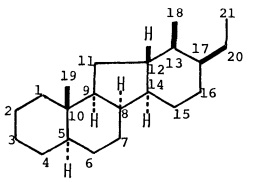

(B)

4) H. Suginome, M. Murakami, and T. Masamune, *Chem. Commun.*, **1966** 343; *Bull. Chem. Soc. Jpn.*, **41**, 468 (1968).

5) H. Suginome, N. Sato, and T. Masamune, *Tetrahedron Lett.*, **1969**, 2671; *Bull. Chem. Soc. Jpn.*, **52**, 3043 (1979).

6) H. Suginome, H. Umeda, and T. Masamune, *Tetrahedron Lett.*, **1970**, 4571; H. Suginome, H. Umeda, S Sugiura, and T. Masamune, *J. Chem. Res.*, (s), **1978**, 380; (M) 4520.

7) a) R. H. Hesse, "Advances in Free-Radical Chemistry," ed by G. H. Williams, Logos Press, London (1969), Vol. 3, p. 83; b) K. Heusler and J. Kalvoda, *Angew. Chem.*, **76**, 518 (1964); J. Kalvoda and K. Heusler, *Synthesis*, **1971**, 501.

8) P. W. Spraque, D. Doddrell, and J. D. Roberts, *Tetrahedron*, **27**, 4857 (1971).

9) T. Masamune, A. Murai, H. Ono, K. Orito, S. Numata, and H. Suginome, *Tetrahedron Lett.*, **1969**, 255; T. Masamune, A. Murai, K. Orito, H. Ono, S. Numata, and H. Suginome, *Tetrahedron*, **25**, 4853 (1969).

10) For nomenclature of the veratrum alkaloids see the IUPAC Corrected Tentative Rules. IUPAC Inform. Bull. No. 33, **1968**, 454.

11) H. Budzikiewicz, C. Djerassi, and D. H. Williams, "Structure Elucidation of Natural Products by Mass Spectrometry," Holden-Day, Inc., San Francisco (1964), Vol. 2, p. 21.

12) V. V. Rheenen, *Chem. Commun.*, **1969**, 314.

13) J. E. Huber, *Tetrahedron Lett.*, **1968**, 3271.

14) W. Nagata and H. Itazaki, *Chem. Ind.*, **27**, 1194 (1964).

Kinetic Studies of the Interaction of Bromphenol Blue with Bovine Serum Albumin by Pressure-jump Method

Kiyofumi MURAKAMI, Takayuki SANO, and Tatsuya YASUNAGA*

Department of Chemistry, Faculty of Science, Hiroshima University, Higashisenda-machi, Naka-ku, Hiroshima 730

(Received August 5, 1980)

The interaction of Bromphenol Blue (BPB) with bovine serum albumin (BSA) was studied statically, by spectrophotometry, and kinetically, by the pressure-jump method. The absorbance changes of BPB were monitored at 20 °C, pH 7.00 in 0.2 M† phosphate buffer. The static measurements showed that there were two binding classes. The number of binding sites and the binding constants for each class are $n_1=1$, $K_1=1.4\times10^7$ M^{-1} and $n_2=3$, $K_2=9.5\times10^4$ M^{-1}. Kinetically, the binding of BPB to the primary binding site of BSA proceeds *via* at least 4 steps. Two models are offered for the possible binding mechanism. In these models, a fast, probably diffusion controlled, second order step is followed by three first order steps. A correlation between the number of binding steps and the magnitude of the binding constant is discussed. The positive activation entropies associated with the backward reactions of the second and third steps show that these reactions proceed through disordered activation states. From the comparison of the present results to those for other ligands, it was found that the ligand is intimately involved in which activated configuration is adopted.

Albumin reversibly binds many kinds of small molecules such as fatty acids, bilirubin, amino acids, drugs and hormones, and plays important roles as carrier and buffer for these molecules. The binding of albumin with small molecules, therefore, is one important factor which determines the distribution, metabolism and excretion of small molecules in the body. It has been extensively studied by static methods.

On the other hand, until the past few years, the kinetics of the interactions of albumin with small molecules had not been extensively studied since the investigation of Froese *et al.*,[1] probably because the binding of small molecules with albumin was thought to be too fast to be a rate-limiting process in physiological phenomena.[2,3] However, recently, many kinetic studies have been performed in the attempt to elucidate the detailed binding mechanism of physiologically important substances such as bilirubin[4-8] and fatty acid.[9]

The interactions of organic dyes with albumin have often been studied as the model systems of protein-small molecule interaction. Besides the role of a model system, the binding of Bromphenol Blue with albumin has physiologically and clinically important applications such as the quantitative analyses of proteins[10] and the determination of the concentration of available bilirubin binding sites in serum[11,12] using the spectrum shift of Bromphenol Blue on binding to albumin. The investigation of the detailed binding mechanism may offer a better basis for such procedures.

In the present study, the binding mechanism of Bromphenol Blue to bovine serum albumin was investigated through both static and kinetic experiments. The kinetic study was concerned with binding to the highest affinity site, which is the most important site for physiological effects.

Experimental

Materials. Bovine serum albumin fraction V(BSA) was obtained from Armour Laboratories and was used without further purifications. The dimer content was about 5%, as determined by gel chromatography with Sephadex G-150. The fatty acid content was determined to be 0.33 mole per mole of protein by the method of Dole.[13] The BSA solutions were prepared by weight, assuming a molecular weight of 69000. Bromphenol Blue (BPB) was of special reagent grade from Wako Pure Chemical Industries, Ltd. and recrystallized from a mixture of acetone and acetic acid. All other chemicals used were reagent grade and used without further purification. All the sample solutions were prepared in 0.2 M phosphate buffer of pH 7.00.

Apparatus. The absorption spectra were measured with a Union Giken SM401 Spectrophotometer. The kinetic measurements were performed with an optical detection pressure-jump apparatus constructed in our laboratory. The pressure of the sample solution was suddenly decreased from 150 atm to 1 atm by rupture of brass film within a time of 100 μs. The light source used was a halogen lamp (250 W) and the path length of the cell was 10 mm. The details of the pressure-jump apparatus can be found elsewhere.[14] All measurements were performed at 20±0.2 °C with the exception of the experiments on the temperature dependence of the relaxation times.

Results

Spectrophotometric Studies. The absorption spectra of the BSA–BPB complex under the various polymer-to-dye ratios (P/D) are shown in Fig. 1. The peak of the spectrum of the free dye around 590 nm decreases with increasing P/D, and that of the complex at 610 nm increases. The increase of the absorbance in the whole range of wavelength with the change of P/D from 4 to 20 shows that the contribution of the absorbance of the protein can not be ignored. The binding parameters were determined from the absorbance change at 590 nm by applying the correction for the contribution of the protein. The extinction coefficients of the free and bound dyes were determined to be $\varepsilon_f=7.9\times10^4$ M^{-1} cm^{-1} and $\varepsilon_b=4.5\times10^4$ M^{-1} cm^{-1} respectively. The latter value was determined from the absorbance at the higher limit of P/D. The concentration of the free dye C and the average number of bound dye molecules per molecule of BSA $\bar{\nu}$ were determined from the equations:

† In this paper 1 M = 1 mol dm^{-3}.

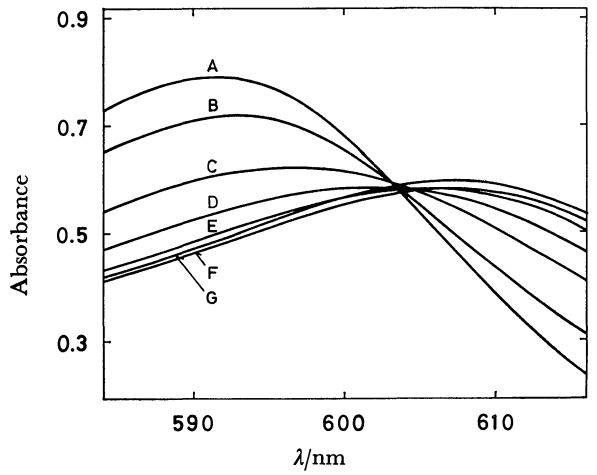

Fig. 1. P/D dependence of absorption spectra of BPB–BSA complex at 20 °C, pH 7.00 and $C_0=1\times10^{-5}$ M. A: Dye only, B: P/D=0.1, C: P/D=0.3, D: P/D=0.5, E: P/D=1, F: P/D=4, G: P/D=20.

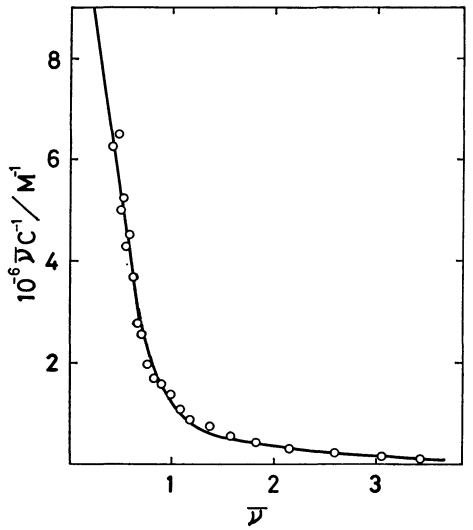

Fig. 2. Scatchard plot of the binding of BPB to BSA.

$$C=\frac{\varepsilon_{app}-\varepsilon_b}{\varepsilon_f-\varepsilon_b}C_0, \quad (1)$$

$$\bar{\nu}=\frac{C_0-C}{P_0}, \quad (2)$$

with

$$\varepsilon_{app}=\frac{A}{C_0 l},$$

where C_0 and P_0 are the total concentrations of the dye and the polymer, respectively, A is the absorbance at 590 nm, and l is the path length of the cell. The Scatchard plot[15] for the present system is shown in Fig. 2. The analysis of this plot yields the following binding parameters:

$$n_1=0.8, \qquad K_1=1.4\times10^7\ M^{-1},$$

$$n_2=3.4, \qquad K_2=9.5\times10^4\ M^{-1},$$

where n_1 and n_2 are the number, of binding sites for the primary and secondary binding sites, respectively. The solid line in Fig. 2 represents the theoretical curve calculated using these values. Good agreement can be seen between the observed and calculated curves. For the calculation of equilibrium concentrations, we used $n_1=1$, $n_2=3$, since these are the closest integers to 0.8 and 3.4.

In the present study, the number of binding sites and the equilibrium constants were determined using the absorbance at the wavelength 590 nm with the same extinction coefficient for all kinds of complexes. At this wavelength, the absorbance decreases to the saturation value with increasing concentration of BSA, and reaches saturation at P/D$\simeq$5. On the other hand, at the wavelength 610 nm, where the absorbance increases with the concentration of BSA, a gradual increase of the absorbance was observed above P/D$\simeq$5. This effect is probably due to dimer formation, which makes the environment around BPB more hydrophobic. This can also be presumed from the fact that the effect becomes more pronounced in more concentrated solutions.

The binding isotherm of BPB with BSA has also been investigated by other researchers. Bjerrum[16] has obtained $n_1=3$, $K_1=5\times10^5\ M^{-1}$, and $n_2=4$, $K_2=2.5\times10^4\ M^{-1}$ at 4.5 °C, pH 7.00 in 0.1 M phosphate buffer by the gel chromatography method. His studies were confined to values of $\bar{\nu}$ above 1; the primary binding sites in his study may thus correspond to the secondary binding sites in the present study. Peeters *et al.*[7] have reported $n_1=1$, $K_1=7.8\times10^5\ M^{-1}$, $n_2=3$, $K_2=7.6\times10^3\ M^{-1}$, $n_3=12$, $K_3=3.1\times10^2\ M^{-1}$ with the defatted BSA at 25 °C, pH 6.62 in 0.1 M phosphate buffer using the microcalorimetry method. The number of binding sites for both of the stronger two binding classes agrees with those of the present study, but the binding constants are about one order of magnitude smaller. The differences in the binding constants may be due to differences in the fatty acid content[7] and/or pH.[18]

Kinetic Studies. Four separate relaxation processes could be observed. The relaxation amplitudes were very small, and 4 to 20 repetitions were averaged to measure the relaxation times. Typical relaxation curves observed at 540 nm are shown in Fig. 3. These relaxations were observed from 400 nm to 560 nm. The relaxation time of the fastest process, which appears as the sudden decrease at $t=0$ in Fig. 3(a), was shorter than the time constant of the apparatus and could not be measured even at a temperature of 5 °C. To obtain the relaxation time of the fastest process, temperature-jump measurements with a temperature increase of about 2 degrees were tried for the same samples, but no relaxation was observed. The static absorption spectra were also insensitive to temperature. All relaxations were observed at 610 nm with opposite direction to and same relaxation times as those observed in the shorter wavelength region. In addition to these four relaxation processes, a relaxational phenomenon with a longer time constant, around 1 min, was observed. This phenomenon has a very small relaxation amplitude, and could be seen only for relatively concentrated samples. Therefore, this phenomenon was not discussed in the present study. These four relaxation processes were numbered 1, 2, 3, 4 in order of the relaxation times,

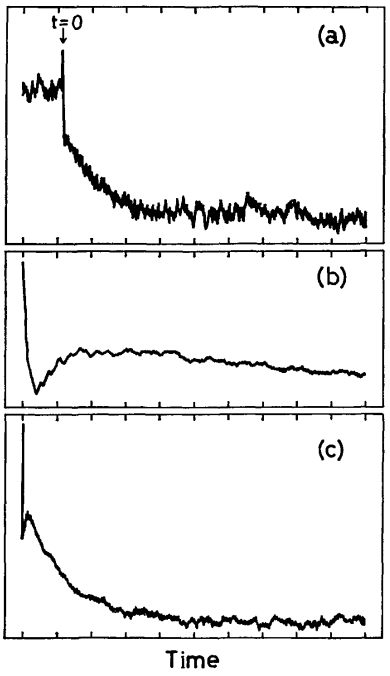

Fig. 3. Typical relaxation spectra of the BPB-BSA system at 20 °C, pH 7.00, λ=540 nm, $C_0=1\times10^{-5}$ M, and $P_0=2\times10^{-5}$ M.
(a) 2ms/div., (b) 40ms/div., (c) 400ms/div.

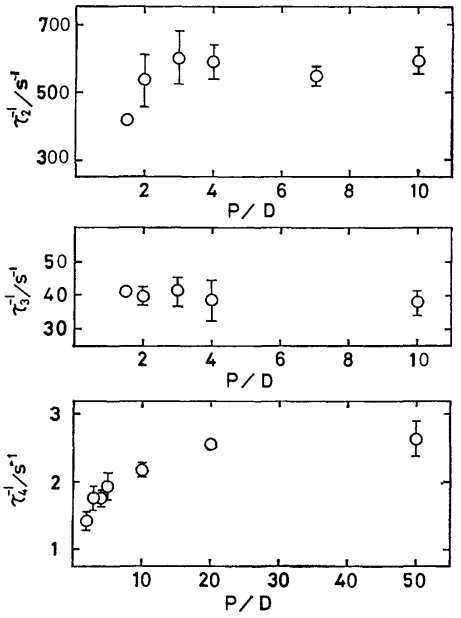

Fig. 4. P/D dependences of the reciprocal relaxation times for slower three processes.

from fast to slow.

Interpretation of the Kinetic Data. The P/D dependences of the relaxation times of the slower three processes, 2, 3, 4 in the region of P/D>1, where the binding of the dye to the highest affinity site of protein occurs, are shown in Fig. 4. All these processes show saturation behavior with P/D. This fact shows that these processes are essentially first order processes. Considering the existences of the very fast process and the three first order processes, the following six models, which are the simplest available under the assumption that the extinction coefficients of the complexes are equal, were examined.

First, the series model which is represented by Eq. 3 was examined.

Model 1

$$\mathrm{D} + \mathrm{P} \underset{k_{-1}}{\overset{K_1'}{\underset{k_1}{\rightleftarrows}}} \mathrm{C}_1 \underset{k_{-2}}{\overset{K_2'}{\underset{k_2}{\rightleftarrows}}} \mathrm{C}_2 \underset{k_{-3}}{\overset{K_3'}{\underset{k_3}{\rightleftarrows}}} \mathrm{C}_3 \underset{k_{-4}}{\overset{K_4'}{\underset{k_4}{\rightleftarrows}}} \mathrm{C}_4, \qquad (3)$$

very fast fast slow very slow

where D, P, and C_i denote free dye, free polymer and complexes of the dye and the polymer, respectively, K_i' is the equilibrium constant, and k_i and k_{-i} are the forward and backward rate constants, respectively. The relaxation times and the overall equilibrium constant for this model are expressed by

$$\tau_1^{-1} = k_1(C+P) + k_{-1} \qquad (4)$$

$$\tau_2^{-1} = k_2\frac{K_1'(C+P)}{1+K_1'(C+P)} + k_{-2} \qquad (5)$$

$$\tau_3^{-1} = k_3\frac{K_1'K_2'(C+P)}{1+K_1'(1+K_2')(C+P)} + k_{-3} \qquad (6)$$

$$\tau_4^{-1} = k_4\frac{K_1'K_2'K_3'(C+P)}{1+K_1'\{1+K_2'(1+K_3')\}(C+P)} + k_{-4} \qquad (7)$$

$$K_\Sigma = K_1'\{1+K_2'(1+K_3'(1+K_4'))\}. \qquad (8)$$

The relaxation time τ_1 of the fast bimolecular step could not be obtained in the present experiment, so that it is difficult to determine all the constants of each reaction step from the fast to slow step successively. Moreover, the experimental errors of the relaxation times are relatively large. Thus, the validity of the reaction mechanism was examined from the standpoint of determining whether proper constants satisfying the concentration dependences of the relaxation times could be chosen. First, from the data of τ_2 and τ_4, the allowable ranges of the combinations of the parameters were estimated as follows:

k_2K_1'	1×10^7—2.6×10^8 M^{-1} s^{-1}
K_1'	3.3×10^4—4.4×10^5 M^{-1}
k_{-2}	0—400 s^{-1}
$k_4K_1'K_2'K_3'$	3.1×10^4—2×10^5 M^{-1} s^{-1}
$K_1'\{1+K_2'(1+K_3')\}$	1.9×10^4—1×10^5 M^{-1}
k_{-4}	0—1.4 s^{-1}.

Next, we get $3.3\times10^4\ M^{-1}\leqslant K_1'\leqslant7\times10^4\ M^{-1}$ from the condition $K_3'\geqslant0$. Using $5\times10^4\ M^{-1}$ as the value of K_1' from the reduced range, the range of K_2' was estimated to be $0.5\leqslant K_2'\leqslant1$. In this range, the value of K_2' which satisfies the concentration dependence of τ_2 is 0.5 (k_2=200 s^{-1}, k_{-2}=400 s^{-1}). From the τ_3 data, we get $K_3'\leqslant0.05$($k_3\leqslant2$ s^{-1}, k_{-3}=40 s^{-1}) using the above values for K_1' and K_2'. Furthermore, we get $K_4'\geqslant1.1\times10^4$ ($k_4\geqslant160$ s^{-1}, 2.3×10^{-3} $s^{-1}\leqslant k_{-4}\leqslant1.5\times10^{-2}$ s^{-1}) using the overall equilibrium constant $K_\Sigma=1.4\times10^7\ M^{-1}$ which was determined as the equilibrium constant for the primary binding site by the spectrophotometric measurements. The results are summarized in Table 1. The comparison of the plots of the reciprocal relaxation times *versus* $K_1'(C+P)$/

Table 1. Equilibrium and rate constants and activation parameters for Models 1 and 5

Step	K_i'	k_i	$\frac{k_{-i}}{s^{-1}}$	$\frac{\Delta H_{-i}^*}{kcal\ mol^{-1}}$	$\frac{\Delta S_{-i}^*}{cal\ mol^{-1}\ K^{-1}}$
		Model 1			
1	$5\times10^4\ M^{-1}$	$>4\times10^8\ M^{-1}\ s^{-1}$	$>8\times10^3$		
2	0.5	$200\ s^{-1}$	400	19	17
3	$\leqslant 0.05$	$\leqslant 2\ s^{-1}$	40	36	71
4	$\geqslant 1.1\times10^4$	$\geqslant 160\ s^{-1}$	2.3×10^{-3}—1.5×10^{-2}		
		Model 5			
4	280	$1.5\ s^{-1}$	5.4×10^{-3}		

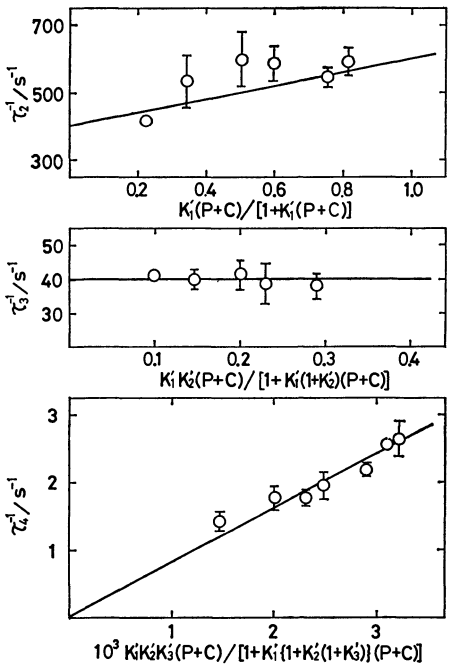

Fig. 5. Plots of the reciprocal relaxation times with Model 1.

$\{1+K_1'(C+P)\}$ for τ_2, $K_1'K_2'(C+P)/\{1+K_1'(1+K_2')(C+P)\}$ for τ_3, and $K_1'K_2'K_3'(C+P)/[1+K_1'\{1+K_2'(1+K_3')\}(C+P)]$ for τ_4 between observed and calculated relaxation times are shown in Fig. 5, in which the solid lines were calculated using the following values: $K_1'=5\times10^4\ M^{-1}$, $K_2'=0.5$ ($k_2=200\ s^{-1}$, $k_{-2}=400\ s^{-1}$), $K_3'=0.01$ ($k_3=0.4\ s^{-1}$, $k_{-3}=40\ s^{-1}$) and $K_4'=5.6\times10^4$ ($k_4=800\ s^{-1}$, $k_{-4}=1.5\times10^{-2}\ s^{-1}$). As can be seen, the theoretical and experimental plots agree relatively well. Therefore, Model 1 seems to be possible as the reaction mechanism of the present system.

Next, the branch model was examined.

Model 2

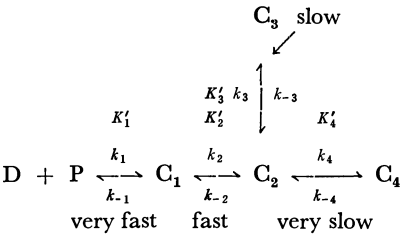

(9)

The relaxation times and the overall equilibrium constant for this model become

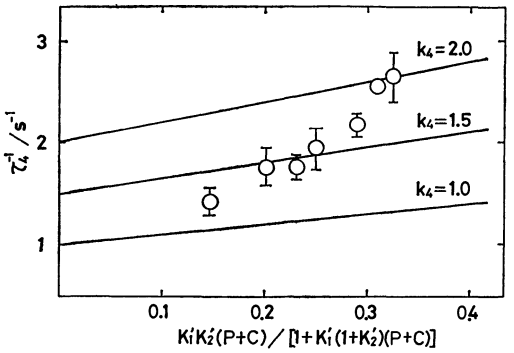

Fig. 6. Plot of τ_4^{-1} with Model 2.

$$\tau_1^{-1} = k_1(C+P) + k_{-1} \tag{10}$$

$$\tau_2^{-1} = k_2\frac{K_1'(C+P)}{1+K_1'(C+P)} + k_{-2} \tag{11}$$

$$\tau_3^{-1} = k_3\frac{K_1'K_2'(C+P)}{1+K_1'(1+K_2')(C+P)} + k_{-3} \tag{12}$$

$$\tau_4^{-1} = k_4\left\{\frac{K_1'K_2'(C+P)}{1+K_1'(1+K_2')(C+P)}+\frac{1}{1+K_3'}\right\} + k_{-4} \tag{13}$$

$$K_\Sigma = K_1'\{1+K_2'(1+K_3'+K_4')\}. \tag{14}$$

The parameters of the Model 2 were determined as follows from an analysis similar to that used in the case of Model 1.

K_1' $5\times10^4\ M^{-1}$

K_2' 0.5 ($k_2=200\ s^{-1}$, $k_{-2}=400\ s^{-1}$)

K_3' $\leqslant 0.05$ ($k_3\leqslant 2\ s^{-1}$, $k_{-3}=40\ s^{-1}$)

K_4' 560 ($1.2\ s^{-1}\leqslant k_4\leqslant 8\ s^{-1}$, $1.8\times10^{-3}\ s^{-1}\leqslant k_{-4}\leqslant 1.4\times10^{-2}\ s^{-1}$).

The expressions of the relaxation times of the faster three processes are the same as those of Model 1, so that the same results were obtained for these processes. Since the allowable values of K_3' and k_{-4} do not contribute to the value of τ_4^{-1}, the comparison of the plot of τ_4^{-1} against $K_1'K_2'(C+P)/\{1+K_1'(1+K_2')(C+P)\}$ between observed and calculated relaxation times for some allowable values of k_4 was made as shown in Fig. 6. Model 2 does not explain the concentration dependence of τ_4, so it may be excluded from possible mechanisms of the present system.

In the same way, the following models were also examined.

Model 3

$$\begin{array}{ccccccc} & & & & C_2 & & \\ & & & & \uparrow\downarrow \text{fast} & & \\ D + P & \longleftrightarrow & C_1 & \longleftrightarrow & C_3 & \longleftrightarrow & C_4 \\ & \text{very fast} & & \text{slow} & & \text{very slow} & \end{array}$$

Model 4

$$\begin{array}{ccccccc} & & & & C_3 & & \\ & & & & \uparrow\downarrow \text{slow} & & \\ D + P & \longleftrightarrow & C_1 & \longleftrightarrow & C_2 & \longleftrightarrow & C_4 \\ & \text{very fast} & & \text{fast} & & \text{very slow} & \end{array}$$

Model 5

$$\begin{array}{ccccccc} & & & & C_4 & & \\ & & & & \uparrow\downarrow \text{very slow} & & \\ D + P & \longleftrightarrow & C_1 & \longleftrightarrow & C_2 & \longleftrightarrow & C_3 \\ & \text{very fast} & & \text{fast} & & \text{slow} & \end{array}$$

Model 6

$$\begin{array}{ccccc} & & C_3 & & \\ & & \uparrow\downarrow \text{slow} & & \\ D + P & \longleftrightarrow & C_1 & \longleftrightarrow & C_2 \\ & \text{very fast} & \uparrow\downarrow & \text{fast} & \\ & & C_4 \text{ very slow} & & \end{array}$$

The concentration dependences of the relaxation times of the second and the third processes can be explained by all of those models, as in the cases of Model 1 and Model 2. Thus, the validity of these models was checked by calculating the concentration dependency of τ_4. The results are shown in Fig. 7 to 10 for the models from 3 to 6, respectively. In these models, only Model 5 can explain the concentration dependence of τ_4. The values of the parameters which were determined with Model 5 are summarized in Table 1, omitting the values for the faster three steps which are same as those of Model 1. From the above analyses, both Model 1 and Model 5 are left as the possible mechanisms from the point of view of the concentration dependences of the relaxation times.

The activation parameters were determined from the temperature dependences of the relaxation times. From the results of the analysis of the reaction mechanism, it was found that the relaxation times whose temperature dependences can be attributed to particular rate constants are τ_2 and τ_3, and the corresponding rate constants are k_{-2} and k_{-3}, respectively. The Eyring plots of those rate constants are shown in Fig. 11. From the slope and the intercept, the activation enthalpy ΔH_{-2}^{*} and the entropy ΔS_{-2}^{*} of the backward reaction of the second step were determined to be 19 kcal/mol and 17 cal/mol K, respectively, and those of third step ΔH_{-3}^{*} and ΔS_{-3}^{*} were determined to be 36 kcal/mol and 71 cal/mol K, respectively. The results are listed in Table 1.

Although the first second order process was too rapid for the values of the rate constants to be determined, the values of 4×10^{8} M^{-1} s^{-1} and 8×10^{3} s^{-1} were evaluated as the lower limit values of the forward and backward rate constants respectively. This calculation used the equilibrium constant $K_1'=5\times10^{4}$ M^{-1}

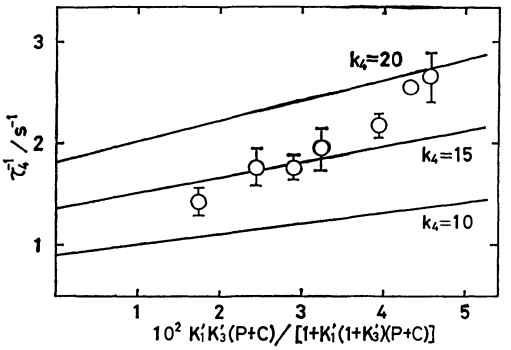

Fig. 7. Plot of τ_4^{-1} with Model 3.

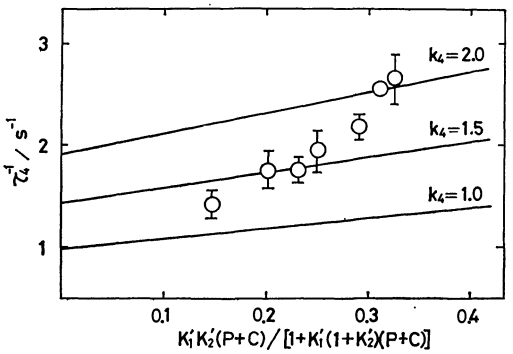

Fig. 8. Plot of τ_4^{-1} with Model 4.

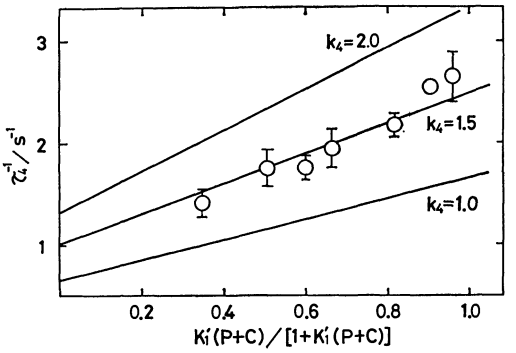

Fig. 9. Plot of τ_4^{-1} with Model 5.

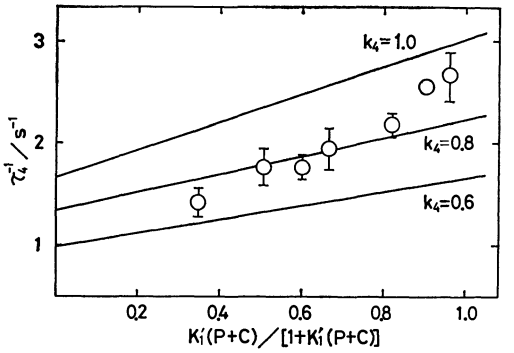

Fig. 10. Plot of τ_4^{-1} with Model 6.

Table 2. Binding constants of dyes to the highest affinity site of albumin

Bilirubin	Ref.	Bromphenol Blue	Ref.	Phenol Red	Ref.
7.0×10^{7} M^{-1} a)	21	1.5×10^{7} M^{-1} a)	23	1.1×10^{5} M^{-1} b)	24
2.7×10^{7} M^{-1} b)	5	1.4×10^{7} M^{-1} b)	present study	2.8×10^{4} M^{-1} a)	25
2.4×10^{7} M^{-1} a)	22	7.8×10^{5} M^{-1} b)	17	1.5×10^{4} M^{-1} a)	23
2.2×10^{7} M^{-1} b)	21				
1.5×10^{7} M^{-1} b)	22				

a) Human albumin. b) Bovin albumin.

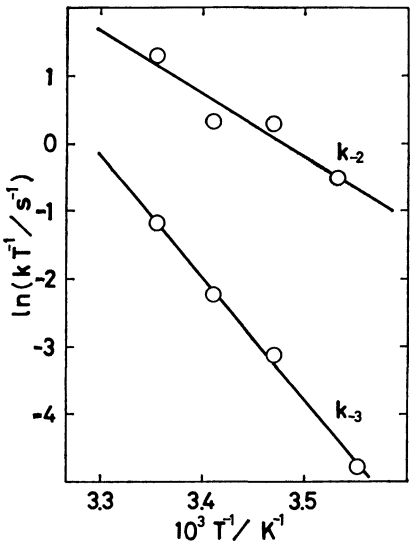

Fig. 11. Eyring plots of the rate constants.

estimated in the analysis of the slower processes, the time constant of the apparatus (100 μs), and the lowest observed concentration.

Discussion

The kinetic behaviour of the interaction of BPB with albumin is of interest in terms of competition binding with bilirubin. It was found from the present study that the binding of BPB to the primary binding site of BSA consists of many first order steps following a fast second order step. The multiplicity of the binding steps has also been observed in the case of the binding of bilirubin with albumin.[4,6] Reed *et al.*[19] have shown through peptic hydrolysis that bilirubin and Bromcresol Green bind to the same position on the BSA molecule, p-14 (residues 186—306). Bromphenol Blue and Phenol Red, which are sulfonphtalein dyes, have structures similar to that of Bromcresol Green, so that these dyes can be thought to bind to the same position. However, multiple binding steps for Phenol Red were not observed,[20] in contrast with the results of bilirubin and BPB. On the other hand, it can be seen from the comparison of the binding constants to the highest affinity site of albumin in Table 2 that the binding constants of bilirubin and BPB are about two or three orders of magnitude larger than that of Phenol Red. These facts seems to indicate the existence of a strong correlation between the multiplicity of the binding processes and the magnitude of the binding constant: that is, ligands having higher affinity bind in more steps than ligands having lower affinity. This can be interpreted as follows. The ligand molecule which has a large binding constant can migrate deeply into the hydrophobic crevice of the albumin molecule. For such a molecule, there must exist many barriers to be overcome during the migration. The existence of those barriers, which correspond to activated states, may yield multiple relaxations. This migration process seem to be driven by entropy rather than enthalpy, considering the insensitivity of the present system to temperature.

Although the reaction mechanism of the binding of BPB to BSA could not be uniquely determined from only the concentration dependences of the relaxation times, the series model (Model 1) seems to be more likely from the viewpoint of the stepwise migration of BPB into the deep site of the hydrophobic crevice of BSA molecule. The magnitude of the rate constant of the first association process was found to be larger than 4×10^{8} M^{-1} s^{-1} from the present analysis. This value suggests that the first association process is the diffusion controlled process. The rate constant of the dissociation process has also a relatively large value. Therefore, the first process can be thought of as the association-dissociation reaction of BPB at the cation rich hairpin turn located on the end of loop 2A[26] of the albumin molecule, which is governed by electrostatic forces. Moreover, the large value of K_1' suggests that there still exist complex formation processes in the longer time region. This can also be understood from the existence of the slow fifth process which was not analyzed in the present study.

From the analysis of the temperature dependences of the relaxation times, it was found that the activation entropies of the backward process in the second and third steps take positive values. This fact shows that those processes occur through the disordered activated states. On the other hand, Scheider[9] has reported for the association-dissociation reaction between oleate and human serum albumin that the first order process which follows the assumed fast second order process occurs with a negative activation entropy, that is, through the ordered activated state. He has pointed out two possibilities for the role of the ligand in the activated configuration. One possibility is that the ligand plays no role in activation *i.e.*, the protein can take the activated configuration on a purely probabilistic basis without any ligand help. The other is that the ligand is closely involved in the activation process *i.e.*, the ligand's movement on the exterior surface brings it to the mouth of the hydrophobic

crevice, facilitating the formation of the activated configuration. Considering both results, it can be seen that the different ligand species yield different activated configurations, and we may consider that the ligand is closely involved in the activation process. If the present argument is correct, the difference in albumin between the two studies may not be the decisive factor to explain the characteristically different results.

In the present analysis, it was assumed that the extinction coefficients of BPB in all the complexes have the same value. This assumption should be regarded as a first approximation. Strictly speaking, each extinction coefficient probably has a different value. To take account of this difference in the consideration of the reaction mechanism, ε_i, ΔV_i, K'_i, which are, respectively, the extinction coefficient of the ith complex, the volume change and the equilibrium constant of the ith process, must be determined by simulation using the data of the concentration dependence of the relaxation amplitudes along with the relaxation times. However, the relaxation amplitudes of the present system are too small for us to get data of enough accuracy to perform the above mentioned simulation.

References

1) A. Froese, A. H. Sehon, and M. Eigen, *Can. J. Chem.*, **40**, 1786 (1962).
2) J. M. Thorp, "Absorption and Distribution of Drugs," ed by T. B. Binns, E. & S. Livingstone L. T. D. Edinburgh and London (1964), Chap. 4.
3) M. C. Meyer and D. E. Guttman, *J. Pharm. Sci.*, **57**, 895 (1968).
4) R. F. Chen, *Arch. Biochem. Biophys.*, **160**, 106 (1974).
5) T. Faerch and J. Jacobsen, *Arch. Biochem. Biophys.*, **168**, 351 (1975).
6) T. Faerch and J. Jacobsen, *Arch. Biochem. Biophys.*, **184**, 282 (1977).
7) R. G. Reed, *J. Biol. Chem.*, **252**, 7483 (1977).
8) R. D. Gray and S. D. Stroupe, *J. Biol. Chem.*, **253**, 4370 (1978).
9) W. Scheider, *Proc. Natl. Acad. Sci. U. S. A.*, **76**, 2283 (1979).
10) R. Flores, *Anal. Biochem.*, **88**, 605 (1978).
11) H. Hertz, *Scand. J. Clin. Lab. Invest.*, **35**, 545 (1975).
12) H. Hertz, *Scand. J. Clin. Lab. Invest.*, **35**, 561 (1975).
13) V. P. Dole, *J. Clin. Invest.*, **35**, 150 (1956).
14) K. Hachiya, M. Ashida, M. Sasaki, H. Kan, T. Inoue, and T. Yasunaga, *J. Phys. Chem.*, **83**, 1866 (1979).
15) G. Scatchard, *Ann. N. Y. Acad. Sci.*, **51**, 660 (1949).
16) O. J. Bjerrum, *Scand. J. Clin. Lab. Invest.*, **22**, 41 (1968).
17) H. Peeters, M. Y. Rosseneu-Motreff, and F. Soeteway, *Protides Biol. Fluids, Proc. Colloq.*, **20**, 471 (1973).
18) L.-O. Anderson, A. Rehnström, and D. L. Eaker, *Eur. J. Biochem.*, **20**, 371 (1971).
19) R. G. Reed, R. C. Feldhoff, O. L. Clute, and T. Peters, Jr., *Biochemistry*, **14**, 4578 (1975).
20) D. E. Goldsack and P. M. Waern, *Can. J. Biochem.*, **51**, 1281 (1973).
21) R. F. Chen, "The Fluorescence of Bilirubin-Albumin Complexes," in "Fluorescence Techniques in Cell Biology," ed by A. A. Thaer and M. Sernetz, Springer-Verlag, New York (1972), p. 273.
22) J. Krasner, G. P. Giacoia, and S. J. Yaffe, *Ann. N. Y. Acad. Sci.*, **226**, 101 (1973).
23) U. Kragh-Hansen, J. V. Møller, and K. E. Lind, *Biochim. Biophys. Acta*, **365**, 360 (1974).
24) F. L. Rodkey, *Arch. Biochem. Biophys.*, **94**, 38 (1961).
25) F. L. Rodkey, *Arch. Biochem. Biophys.*, **94**, 526 (1961).
26) J. R. Brown, "Serum Albumin; Amino Acid Sequence," in "Albumin Structure, Function and Uses," ed by V. M. Rosenoer, M. Oratz, and M. A. Rothchild, Pergamon, New York (1977), p. 27.

Reexamination of the Molecular Size Dependence of Diffusivities of Hydrocarbons in Natural Rubber†

Mitsuyasu KAWAKAMI, Hideaki IWANAGA, and Shuichi KAGAWA*

Department of Industrial Chemistry, Faculty of Engineering, Nagasaki University, Nagasaki 852

(Received May 24, 1980)

Diffusion coefficients at zero concentration, D_0, for hydrocarbon vapors in natural rubber have been determined, and their dependence on the size and shape (or length) of the penetrants has been reexamined. For normal hydrocarbons, D_0 decreased gradually with increasing the number of carbon atoms up to 5 and then leveled off. For branched hydrocarbons, such as iso- and neo-paraffins, D_0 was considerably lower than that for the corresponding normal ones. The dependence of D_0 on the size and shape of penetrants could be explained by assuming that the principal resistance to diffusion is defined by the cross-sectional area at the most bulky portion of the major axis and also that an additional resistance due to the molecular length contributes for relatively lower hydrocarbons. The latter resistance was practically negligible for hydrocarbons with more than 4 carbon atoms in the major chain. The effective cross-sectional dimension could be estimated successfully in terms of the group dimension of Pauling.

Extensive studies of gas or vapor diffusion in polymers have been made for elucidating the mechanisms of diffusion and the microstructure of polymers. The free volume theory seems to succeed in interpreting diffusion phenomena in polymer substances (see, for example, Refs. 1—3). However, estimation of the critical size of a hole required for diffusion to take place has not been achieved.

Natural rubber is one of the materials studied from the earliest period because of its high permeability. For common gases, the general dependence of diffusion properties in natural rubber on the size of diffusant molecule seems to be fairly well established and predictable. For organic vapors, on the other hand, the phenomena are more complicated. The diffusion coefficient varies, in general, with the concentration of the vapor in the rubber. Therefore, the diffusion coefficient at zero concentration, D_0, has often been employed to estimate the diffusivity; it is found to be a function not only of the size but also of the shape of a given penetrant molecule.

According to information published earlier (see, for example, Refs. 4 and 5), the characteristic behavior of D_0 for hydrocarbons in rubber can be summarized as follows. (1) D_0 for normal hydrocarbons decreases with an increase in the number of carbon atoms up to 4 and then levels off, (2) D_0 for branched hydrocarbons such as iso- or neo-paraffins are remarkably lower than the values for the corresponding normal ones.

The effect of length or branching of a penetrant molecule on diffusivity has been studied, but few attempts have been made to explain all these effects together. It is the purpose of this work to reexamine the dependence of D_0 for hydrocarbons in rubber on the size and shape of penetrants, and to discuss how a penetrant molecule moves through rubber.

Experimental

The average permeability coefficient, $\bar{P}$ was determined by means of a conventional permeation apparatus.[6] That is, the pressure increase at the low pressure compartment due to vapor transport through a rubber film was measured as a function of time with a Pirani gauge which was calibrated previously through a McLeod gauge.[7] $\bar{P}$ was calculated, then, from the steady state permeation rate, $\Delta p/\Delta t$, using the expression

$$\bar{P} = \frac{273.2}{76T}\frac{V_c}{p_h}\frac{l}{A}\frac{\Delta p}{\Delta t}, \quad (1)$$

where V_c and T are the volume and temperature, respectively, of the measuring chamber, p_h is the applied pressure of the penetrant, and A and l are the effective area and the thickness of the membrane. The change of l due to swelling was not taken into account in the calculation of $\bar{P}$ from Eq. 1. However, the resulting effect on the diffusion coefficient will be compensated for when the average diffusion coefficient is extrapolated to zero concentration.

The solubility coefficient, S, is defined as

$$S = \frac{c}{p}, \quad (2)$$

where c is the equilibrium concentration of a penetrant in the film and p is the partial pressure at sorption equilibrium. When Henry's law is obeyed, S is a constant. Sorption isotherms were measured by a volumetric method. The apparatus used in this experiment was essentially the same as that of Aitken and Barrer.[8]

The average diffusion coefficient, $\bar{D}$, was calculated from $\bar{P}$ and the solubility coefficient, S_h at the high pressure side of the membrane using the relation

$$\bar{D} = \frac{\bar{P}}{S_h}, \quad (3)$$

where the sorption equilibrium is assumed to be established at the both surfaces of the film. A series of $\bar{D}$ was measured as a function of $c_h(=p_hS_h)$, and the diffusion coefficient at zero concentration, D_0, was obtained by extrapolating $\bar{D}$ to $c_h=0$.

The rubber film was prepared by casting a benzene solution of smoked sheet on a glass plate. This was first air dried, followed by vacuum drying at room temperature for at least 2 days. The average thickness of a film used in the measurements was determined from the density and the weight per unit area of the film. Six kinds of lower hydrocarbons of 99.0% minimum purities (Seitetsu Kagaku Co.) and four kinds of liquid ones of commercial reagent grade (Tokyo Kasei Kogyo Co.) were employed. They

† A preliminary report of this work was presented at the 40th National Meeting of the Chemical Society of Japan, Fukuoka, October 1979.

TABLE 1. DIFFUSIVITY AND SOLUBILITY DATA AT 298 K FOR HYDROCARBONS IN NATURAL RUBBER

Hydrocarbon	Symbol	$10^7 D_0$ / $cm^2 s^{-1}$		β [a]	S_0 / cm^3 (STP) cm^{-3} MPa^{-1}	α [a]
Methane	C_1	6.8	(8.9) [b]		3.35	
Ethane	C_2	4.7			6.78	
Propane	C_3	2.1	(2.1) [b]		52.9	
Butane	C_4	1.5		1.8	159	2.1
Pentane	C_5	1.3		7.3	640	2.3
Hexane	C_6	1.3		7.7	1520	3.0
Isobutane	iso-C_4	0.91		4.8	101	2.4
Isopentane	iso-C_5	0.70		7.5	362	2.9
Neopentane	neo-C_5	0.47		5.5	164	2.5
Neohexane	neo-C_6	0.43		4.3	701	3.1

a) These parameters have the unit of cm^3(rubber)cm^{-3}(penetrant as liquid). b) The values in parentheses represent the data of Michaels and Bixler.[13]

were subjected to repeated freeze-thaw cycles to remove dissolved gases before being introduced into the apparatus.

Results and Discussion

For lighter hydrocarbons such as methane, ethane, and propane, P did not show any pressure dependence in the applied pressure range (up to about 50 kPa for lighter hydrocarbons) and Henry's law was obeyed. In this case, the diffusion coefficient, D, is essentially independent of c and may be also determined directly from the time lag observed in the permeation measurement. Actually, the values of D obtained by the time lag method and those from Eq. 3 were in excellent agreement.

For heavier hydrocarbons, on the other hand, the concentration dependence of solubility coefficients was observed. Thus, Henry's law was no longer obeyed. In the range of measurements (the range was limited by the vapor pressure at room temperature for liquid hydrocarbons), the sorption isotherms could be well represented by the equation

$$S = S_0 \exp(\alpha c), \tag{4}$$

where S_0 is the solubility coefficient at zero concentration and α is a constant. Equation 4 can be derived from a simplified form of the Flory-Huggins equation

$$\ln a = \ln v + (1-v) + \chi(1-v)^2, \tag{5}$$

where a and v are the activity and the volume fraction of the penetrant, and χ is the interaction parameter. That is, assuming $a=p/p_0$ (where p_0 is the vapor pressure of the penetrant at the measuring temperature), making the substitutions and neglecting higher terms, we obtain the expression

$$S = S_0 \exp[2(1+\chi)c]. \tag{6}$$

Therefore, it is clear that the parameter α in Eq. 4 is approximately equal to $2(1+\chi)$.[9-12] The solubility coefficient, S_h required to calculate $\overline{D}$ from Eq. 3 was estimated from Eq. 4.

Average permeabilities, and therefore, average diffusion coefficients varied with the applied pressure for C_4 and higher hydrocarbons. The concentration dependence of $\overline{D}$ could be expressed fairly well by the equation

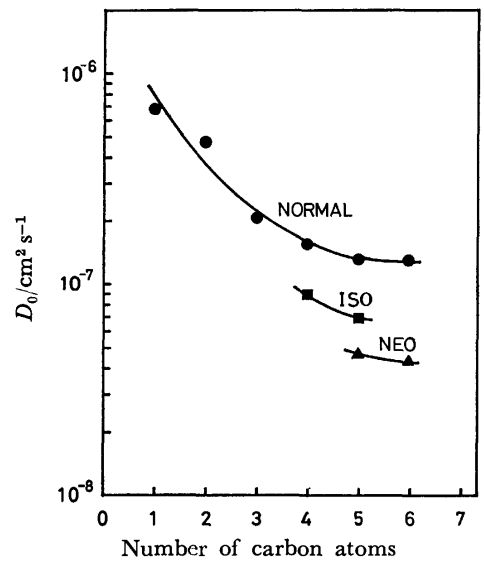

Fig. 1. Dependence of D_0 for hydrocarbons in natural rubber at 298 K on the number of carbon atoms.

$$\overline{D} = D_0 \exp(\beta c_h), \tag{7}$$

where β is a constant (see, for example, Refs. 9—12). Then, D_0 was determined readily by extrapolation of the ln $\overline{D}$ *vs.* c_h plot. The results are shown in Table 1. The vslues of D_0 for methane and propane are in fair agreement with those obtained by Michaels and Bixler.[13]

The values of S_0 satisfy the relation between S_0 and the boiling or critical temperature which has been reported earlier.[14] The parameter α can be taken as being roughly constant for the seven hydrocarbons examined. This means that the Flory-Huggins interaction parameters are also the same for the systems of these hydrocarbons and natural rubber. According to the free volume theory,[1-3] the concentration dependence parameter of D is a function of the critical size of the hole required for diffusion to take place. In the present work, however, the parameter β only represents the extent of the concentration dependence of $\overline{D}$ and has a complicated meaning. Moreover, these values can not be compared as such, be-

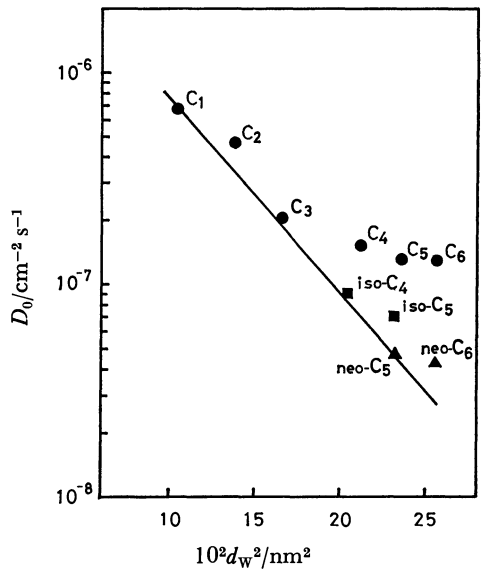

Fig. 2. Correlation of D_0 with d_W^2. Symbols refer to hydrocarbons given in Table 1.

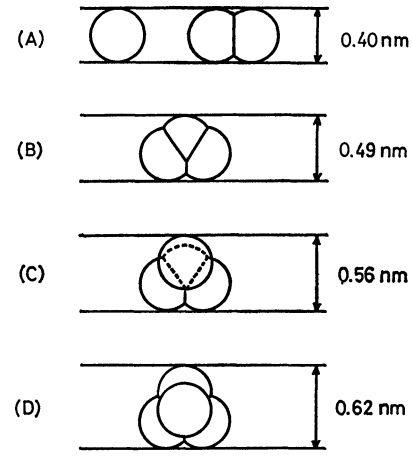

Fig. 3. Schematic drawing of the effective cross-sectional dimension, d_P. (A) Methane and Ethane, (B) Normal hydrocarbons above Propane, (C) Branched hydrocarbons with a single methyl group, (D) Branched hydrocarbons with two methyl groups on the same carbon atom.

cause the concentration ranges measured are appreciably different. The dependence of D_0 on the size of a penetrant molecule will now be discussed.

In Fig. 1, D_0 values are plotted against the number of carbon atoms. Obviously, D_0 for normal paraffins decreases with the chain length from C_1 to C_5, to reach a constant value at C_5 and higher homologues. Note also that the branching of a penetrant molecule increases somewhat its effective dimension and hence yields a lower value of D_0.

For diffusion in polymers it is generally accepted that the hole formation in a given polymer-diffusant system as a result of thermal fluctuations of the diffusant molecule and/or the polymeric jumping unit is responsible for the diffusivity. According to Fujita's free volume theory,[2,5] the diffusivity is proportional to the probability of finding a hole exceeding a critical volume, and can be described as

$$D = A_d \exp\left(-\frac{B_d}{f}\right), \tag{8}$$

where B_d is a parameter corresponding to the minimum hole required for diffusion, f is the average fractional free volume of the system, and A_d is a proportionality factor which is considered to be dependent primarily on the size and shape of the diffusant molecule. Some attempts have been made to correlate the diffusivities with the size and shape of diffusant vapors.

As one idea, the "diffusive cross-section" difined as the ratio of the molar volume $\bar{V}$ and the maximum molecular length $\bar{L}$ of the penetrant has been proposed for the diffusivities of organic vapors (see, for example, Refs. 15—17). This parameter, however, could not be applied to the present systems, as shown in Fig. 1. The value of D_0 decreases with the number of carbon atoms from C_3 to C_6 normal hydrocarbons, while that of $\bar{V}/\bar{L}$ is almost constant for them. This measure tends to overestimate the effective size, especially for lighter hydrocarbons.

In Fig. 2, D_0 is plotted against the square of the van der Waals diameter, d_W^2, instead of the number of carbon atoms. This dimension can be considered to represent the size of molecule regarded as spheres. In the figure, the points of methane (C_1) and neopentane (neo-C_5), whose the shapes are practically spherical, are connected by a solid line for convenience. It can be noted that all the points for other non-spherical hydrocarbons studied here are above this line. This means these hydrocarbons have more preferable shape for diffusion than a spherical molecule. The effective size of such penetrants, therefore, must be smaller than d_W^2.

As previously described, D_0 for normal paraffins decreases gradually with an increase in the number of carbon atoms and finally levels off for homologues higher than C_4. This implies a mode of diffusion in which the diffusant molecule moves through rubber with its major axis aligned with the diffusion direction. Under such circumstances the resistance to diffusion may be a function of the cross-sectional area normal to the main axis and the length of a given penetrant. When the cross-sectional dimension is not uniform along the axis, that at the most bulky part must become the predominant factor. Thus, for estimating such a dimension, an alternative measure, d_P, was proposed. Speculations on these dimensions in terms of the group dimension of Pauling[18] are illustrated in Fig. 3, where the diameters of methylene and methyne group have been both assumed to be 0.4 nm, which is the methyl group diameter.

The relationship between D_0 and d_P^2 is shown in Fig. 4, in which a line joining the points of C_1 and neo-C_5 is also drawn for convenience. This line can be considered to reflect the effective size of the spherical penetrant. For isomeric butanes and pentanes in cross-linked natural rubber, Aitken and Barrer[8] have demonstrated that D_0 decreased linearly with the size expressed as the product of the minimum dimension, l_1 and the next smallest dimension, l_2 of the molecule. Such a dimension $l_1 l_2$ may be a useful measure of

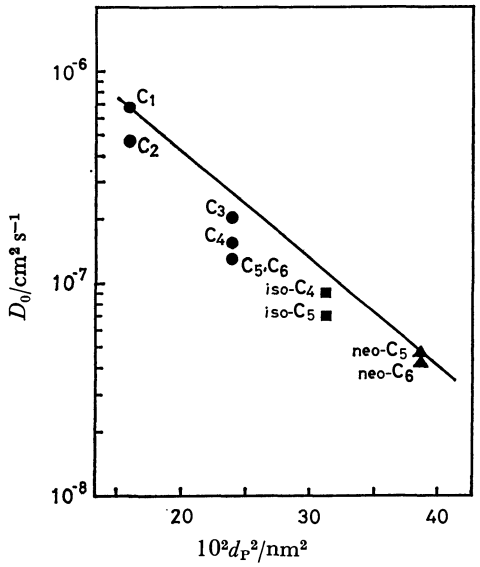

Fig. 4. Correlation of D_0 with d_P^2. Symbols refer to hydrocarbons given in Table 1.

the cross-section when the diffusant is not spherical. They have suggested that the maximum dimension has little significance, but did not explain further. We have also confirmed that a reasonably linear relationship holds between D_0 and $l_1 l_2$ for isomeric butanes, pentanes, and hexanes. The data for C_1 and C_2, however, deviated considerably from the rectilinear relationship. In addition, the appreciable difference between D_0 for C_1 and C_2 implies that the maximum length of the molecule has some significance. In Fig. 4, the distance along the ordinate between a certain point and the line may suggest the effect of the molecular length. It is inferred that the extent of this effect is more significant at the first increase in the number of carbon atoms in major axis, and then gradually diminishes with a subsequent increase in length. Thus, Fig. 4 is a convenient illustration for understanding the effects of both the size and shape (or length) of hydrocarbon penetrants on their diffusivities.

From above discussion, we obtain the following conclusions. A hydrocarbon molecule moves through rubber matrix with its major axis aligned in the diffusion direction. The largest resistance to diffusion is thus determined by the cross-sectional area at the most bulky part of the axis. An additional effect is caused by the length of major chain, but this effect practically diminishes for more than 4 carbon atoms. The effective cross-sectional area at the most bulky part can be estimated successfully using the group dimension concepts of Pauling.

References

1) M. H. Cohen and D. Turnbull, *J. Chem. Phys.*, **31**, 1164 (1959).
2) H. Fujita, *Fortshr. Hochpolym. Forsch.*, **3**, 1 (1961).
3) J. S. Vrentas, *J. Polym. Sci. Polym. Phys. Ed.*, **15**, 403 (1977).
4) G. J. van Amerongen, *Rubber Chem. Technol.*, **37**, 1065 (1964).
5) H. Fujita, "Diffusion in Polymers," ed by J. Crank and G. S. Park, Academic, New York (1968), Chap. 3.
6) R. M. Barrer and G. Skirrow, *J. Polym. Sci.*, **3**, 549 (1948).
7) In the present work, a McLeod gauge with a measuring capillary 1.5 mm in diameter and a measuring bulb of 60 cm^3 was employed. With this gauge the measurement was made over the range where the difference in the level of the mercury in the measuring capillary and the compensating capillary did not exceed about 10 cm. Over such a pressure range, condensation in capillary did not occur for any hydrocarbons studied.
8) A. Aitken and R. M. Barrer, *Trans. Faraday Soc.*, **51**, 116 (1955).
9) C. E. Rogers, V. Stannet, and M. Szwarc, *J. Polym. Sci.*, **45**, 61 (1960).
10) C. E. Rogers and S. Sternberg, *J. Macromol. Sci., Phys.*, **B5**, 189 (1971).
11) S. A. Stern, S.-M. Fang, and H. L. Frisch, *J. Polym. Sci., A-2*, **10**, 201 (1972).
12) M. S. Suwandi and S. A. Stern, *J. Polym. Sci. Polym. Phys. Ed.*, **11**, 63 (1973).
13) A. S. Michaels and H. J. Bixler, *J. Polym. Sci.*, **50**, 413 (1961).
14) M. Kawakami and S. Kagawa, *Bull. Chem. Soc. Jpn.*, **51**, 75 (1978).
15) R. C. Binning, R. J. Lee, J. F. Jennings, and E. C. Martin, *Ind. Eng. Chem.*, **53**, 45 (1961).
16) C. Y. Choo, "Advances in Petroleum Chemistry and Refining," Interscience, New York (1962), Vol. 6, Chap. 2.
17) R. Y. M. Huang and N. R. Jervis, *J. Appl. Polym. Sci.*, **14**, 2341 (1970).
18) L. Pauling, "The Nature of the Chemical Bond," Cornell Univ. Press, New York (1940), p. 189.

The Electronic Absorption and Emission Spectra of Biphenylene-2,3-dione in Solutions

Akira KUBOYAMA

National Chemical Laboratory for Industry, Tsukuba Research Center, Yatabe, Ibaraki 305

(Received June 12, 1980)

The electronic absorption and MCD spectra and phosphorescence spectra at 77 K, in solutions, have been studied by the use of P-P-P-method calculations. The longest-wavelength S–S $\pi\pi^*$ band, near 370 nm, is proved to consist of two $\pi\pi^*$ bands, the $^1A_1$ and $^1B_2$ bands. The $n\pi^*$ absorption, and phosphorescence bands in various kinds of solutions are compared in many respects with those of the *o*-quinones previously studied.

Previously, we have theoretically and experimentally studied the electronic absorption spectra of the *o*-quinones, *o*-benzoquinone,[1-3] and 1,2-naphthoquinone,[1,4,5] and the electronic absorption and emission spectra of the *o*-quinones, acenaphthenequinone,[4,6,7] and 9,10-phenanthrenequinone,[1,4,6,8,9] in solutions. Heretofore, however, the $n\pi^*$ absorption spectra of *o*-benzoquinones have not been studied in detail because of their instability. The emission spectra of *o*-benzoquinones and 1,2-naphthoquinones have never been reported, either, as far as we know. Biphenylene-2,3-dione[11,12] (BPD), which may be classified as a *o*-benzoquinone, is stable and is unique for its containing a fused four-membered ring. As for BPD, only the positions and intensities of its $\pi\pi^*$ absorption maxima in a solution have been reported. Therefore, we have studied the $\pi\pi^*$ and $n\pi^*$ absorption and emission spectra of BPD in solutions.

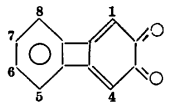

BPD

Experimental

Measurements. The absorption spectra in solutions were measured in the same manner as in previous works.[3-5,8] The magnetic circular dichroism (MCD) spectra in solutions were obtained by means of a J-20C recording spectropolarimeter of the Japan Spectroscopic Co., with a magnetic field of 0.93 T. The magnetic field was measured by means of a gauss meter. The phosphorescence spectra in solutions at 77 K were measured in the same manner as in previous works.[6,7,9] The dichroism of the phosphorescence spectrum in the 1-chlorobutane solution was measured by the photoselection method.[6,13]

Materials. BPD prepared by Sato *et al.*[12] was used (mp 213.5—214.5 °C).[14] Commercially available cyclohexane, methylcyclohexane, carbon disulfide, toluene, dioxane, methanol, 1,1,1,3,3,3-hexafluoro-2-propanol (HFP) of a spectro-grade, and 1-chlorobutane of Tokyo Kasei's Special Use grade were used without further purification. Commercially available chloroform of a special grade was washed five times with water, dried with calcium chloride, and distilled.

Results. The absorption, MCD, and phosphorescence spectra obtained are shown in Figs. 1—4. The wavelengths and molar absorption coefficients of the absorption maxima, and the oscillator strengths of the absorption bands are shown in Table 1. The band names in Table 1 will be presented later. The MCD spectra in the toluene and cyclohexane solutions were similar to that in the 1-chlorobutane solution in Fig. 3. The MCD spectra were obtained with a relatively high noise-level because a low magnetic field was used. However, their accuracy is thought to be

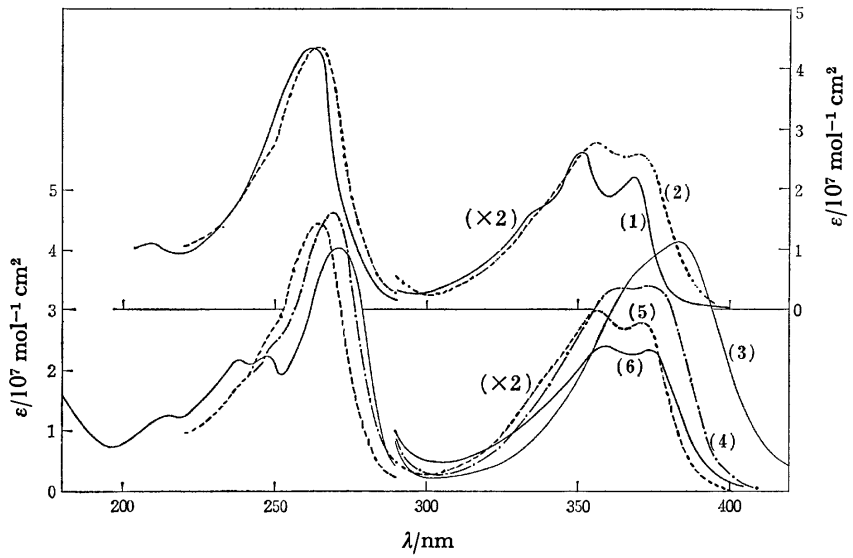

Fig. 1. Absorption spectra of biphenylene-2,3-dione in solutions.
Solvent: (1) methylcyclohexane, (2) dioxane, (3) 1,1,1,3,3,3-hexafluoro-2-propanol, (4) chloroform, (5) 1-chlorobutane, (6) toluene.
(In (1) the scale of the ordinate is arbitrary.)

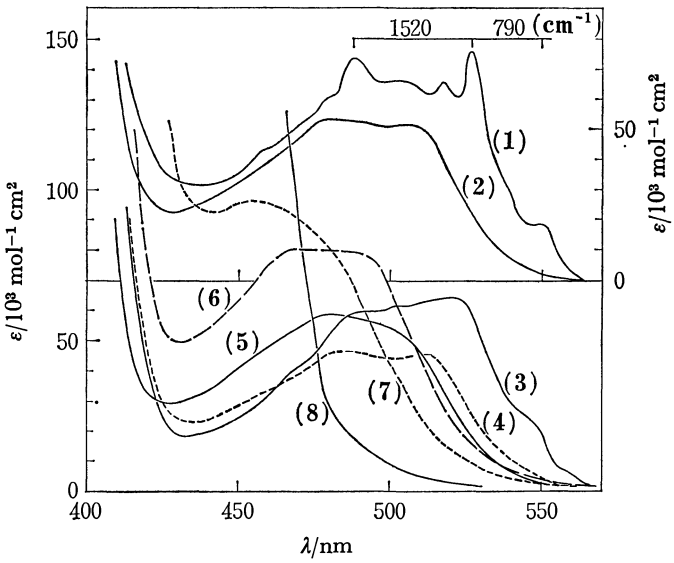

Fig. 2. Absorption spectra of biphenylene-2,3-dione in solutions.
Solvent: (1) methylcyclohexane, (2) 1-chlorobutane, (3) carbon disulfide, (4) toluene, (5) dioxane, (6) chloroform, (7) methanol, (8) 1,1,1,3,3,3,-hexafluoro-2-propanol.
(In (1) the scale of the ordinate is arbitrary.)

not so low as to affect the discussion in this work. The wavelengths of the phosphorescence maxima were 575, 579, and 584 nm for the 1-chlorobutane, dioxane, and toluene solutions respectively. As for the dichroism of the phosphorescence-excitation spectrum, the qualitative results to be presented later were obtained. The lifetimes of the phosphorescence bands have not yet been accurately obtained with the phosphoroscope, partly because these phos-

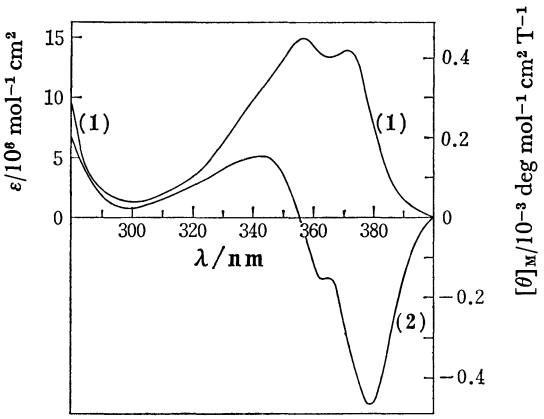

Fig. 3. Absorption and MCD spectra of biphenylene-2,3-dione in 1-chlorobutane.
(1) absorption spectrum, (2) MCD spectrum.

TABLE 1. WAVELENGTHS, ENERGIES, AND MOLAR-ABSORPTION COEFFICIENTS OF THE ABSORPTION MAXIMA AND OSCILLATOR STRENGTHS OF THE ABSORPTION BANDS

Solvent	λ / nm	E / eV	ε / 10^3 mol^{-1} cm^2	f	Band
Methylcyclohexane	550	2.25			
	527	2.35			nπ*
	517	2.40			
	488	2.54			
	369	3.36			a_1, a_2
	351	3.53			
	261	4.75			b
	210	5.90			d
1-Chlorobutane	505	2.45	51.5	0.00080	nπ*
	479	2.59	53.8		
	371	3.34	13850	0.242	a_1, a_2
	356	3.48	14850		
	265	4.68	44000	0.99	b
1,1,1,3,3,3-Hexafluoro-2-propanol	382.5	3.24	20600	0.34	a_1, a_2
	271	4.57	40500	0.63	b
	247.5	5.01	22350	0.48	c
	238	5.21	21700		
	213	5.82	11900	0.23	d
Chloroform	475		80.0	0.00120	nπ*
	374		16850		a_1, a_2
	362		16700		
	269.5		46100		b
Toluene	512.5		45.5	0.00068	nπ*
	481		46.0		
	372.5		11700		a_1, a_2
	359		11900		
Dioxane	479		58.5		nπ*
	370.5		12850		a_1, a_2
	355.5		13800		
	265		43550		b
Carbon disulfide	521		64.3	0.00092	nπ*
Methanol	456		96.2		nπ*

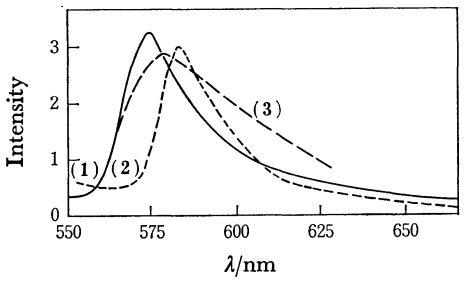

Fig. 4. Phosphorescence spectra of biphenylene-2,3-dione in solutions at 77 K.
Solvent: (1) 1-chlorobutane, (2) toluene, (3) dioxane.

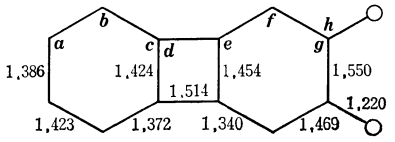

Fig. 5. Dimensions of biphenylene-2,3-dione.
a: 123°, b: 115°, c: 123°, d: 90°, e: 122.5°, f: 120°, g: 117.5°, h: 122°.

phorescence bands are weak and partly because their lifetimes are short. They were estimated to be around 0.3 ms on the basis of the observed relationships between the phosphorescence intensities and the rotational speeds of the phosphoroscope.

Calculations

Method. The electronic integral values for BPD in the P-P-P method[15] were the same as those previously used for other quinones,[3,5,8] except for those of the core-resonance integrals. Since BPD containes a fused four-membered ring, the core-resonance integrals between non-adjacent atoms were also included. The core-resonance integral (β_{ij}) between the i-th and j-th atoms was obtained according to the following formula;

$$\beta_{ij} = -31.35 \exp(-1.86 R_{ij}) \text{ (eV)},$$

except for those of the carbonyl bonds, which were taken as −2.5 eV, as in the previous works.[3,4,8] R_{ij} (Å) denotes the bond distance between the two atoms. This formula gives values close to those previously used for *o*- and *p*-benzoquinones and 9,10-anthraquinone,[3] −2.0, −2.5, and −2.3 eV for the conventional single and double bands and the benzene bonds respectively. The changes in the excitation energy of the lowest $\pi\pi^*$ states of BPD with the alkyl-group substitutions were also calculated in the same manner as in the previous works.[3,5,8] In the calculations, the thirty lowest singly excited configurations were included. The dimensions of BPD shown in Fig. 5, where the molecular structure of BPD is planar and has the C_{2v} symmetry,[16] were assumed considering the previously reported dimensions of *o*-benzoquinone[17] and biphenylene.[18]

Results. The calculated results for the lower singlet excited states are shown in Table 2. The molecular plane and symmetry axis of BPD are regarded as the yz-plane and the z-axis respectively. In this table, the first column denotes an order based on the magnitudes of the calculated excitation energies. Y and Z in the second column denote the directions of the elctronic-transition moments from the ground state. The assignment in the last column will be discussed later.

Table 2. The calculated results

No.	Symmetry	$\frac{E}{\text{eV}}$	f	Band
1	$^1B_2(Y)$	3.68	0.137	a_1
2	$^1A_1(Z)$	3.75	0.102	a_2
3	$^1B_2$	4.44	0.094	
4	$^1A_1$	4.51	0.003	
5	$^1A_1$	4.71	1.895	b
6	$^1B_2$	4.98	0.002	
7	$^1B_2$	5.37	0.206	c

Discussion

In Figs. 1 and 2, an $n\pi^*$ band is observed near 500 nm and four $\pi\pi^*$ bands appear to be near 370, 260, 240, and 210 nm, the 260 nm band being the strongest. These four $\pi\pi^*$ bands are denoted as the a-, b-, c-, and d-bands respectively. The largest red-shift of the a- and b-bands, and the large intensification of the a-band in the HFP solution in comparison with the cases of other solutions, are noticeable. Those facts may be attributed to the strong hydrogen-bond formation between BPD and HFP.[5,8] The fact that the intensity near 300 nm of the $\pi\pi^*$ absorption spectrum in the toluene solution is stronger than those in other solutions shows that, in this wavelength region, there is an intermolecular charge-transfer band between toluene and BPD. The emission bands in Fig. 4 may be assigned to the $n\pi^*$ phosphorescence band in view of their positions relative to those of the $n\pi^*$ absorption bands in Fig. 2 and their short lifetimes. Previously, similar $n\pi^*$ phosphorescence bands have been observed for 9,10-phenanthrenequinone[9] and acenaphthenequinone,[7] as will be discussed later. Therefore, the lowest triplet state of BPD may be the $n\pi^*$ state, as in the case of the other *o*-quinones.[6,7,9]

The MCD spectrum in Fig. 3, clearly shows that the a-band consists of two $\pi\pi^*$ bands, where the MCD signs of the longer and shorter wavelength bands are minus and plus respectively.[19,20] The observed dichroism of the phosphorescence-excitation spectrum is consistent with this fact and shows that the above-mentioned shorter wavelength band has its absorption maximum, which may be its 0-0 band, near the second peak of the a-band. These two $\pi\pi^*$ bands are denoted as the a_1- and a_2-bands for the longer and shorter wavelength bands respectively. Furthermore, the dichroism of the phosphorescence-excitation spectrum shows that the direction of the polarization of the a_1- and c-bands and that of the a_2- and b-bands are the same as, and different from, that of the phosphorescence band respectively.

The assignments of the a_1-, a_2-, b-, and c-bands are shown in the last column in Table 2. As may be seen from the comparison between the observed

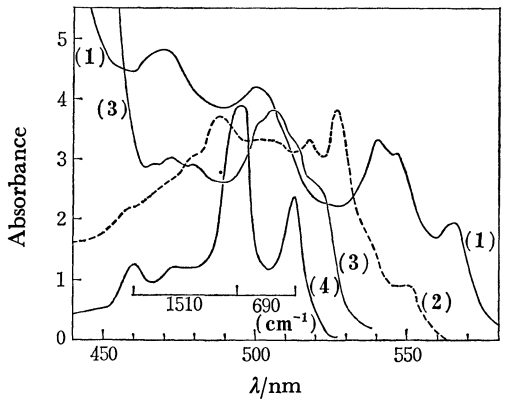

Fig. 6. nπ* Absorption bands of *o*-quinones in heptane solutions.
(1) 1,2-naphthoquinone, (2) biphenylene-2,3-dione, (3) 9,10-phenanthrenequinone, (4) acenaphthenequinone.
(In biphenylene-2,3-dione the solvent is methylcyclohexane.)

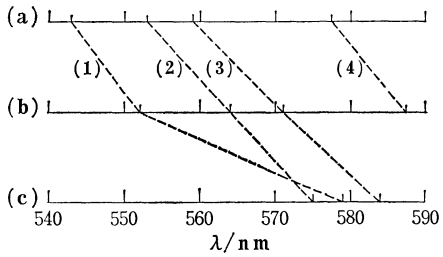

Fig. 7. Positions of nπ* phosphorescence bands of *o*-quinones in solutions.
(a) Acenaphthenequinone, (b) 9,10-Phenanthrenequinone, (3) Biphenylene-2,3-dione.
(1) Dioxane, (2) 1-chlorobutane, (3) toluene, (4) heptane.

and calculated results, these assignments seems reasonable. Therefore, the a_1- and c-bands and the phosphorescence band may be said to be polarized along the short axis (Y-axis) of BPD, and the a_2- and b-bands to be polarized along the long axis (Z-axis). The assignment of the d-band is ambiguous. The calculated results show that the excited state of the a_1-band is of the local excitation type in the benzoquinone group and is similar to that of the longest-wavelength ππ* ($^1B_2$) band (near 370 nm) of *o*-benzoquinone.[3] However, the intensity of the a_1-band is far larger than that of the corresponding band of *o*-benzoquinone.[1,10] As for the changes in the calculated excitation energy of the lowest ππ* states (the Nos. 1 and 2 states) of BPD with the symmetrical two-alkyl-group substitutions, a relatively large energy decrease in the No. 1 state of 1,4-dialkyl-BPD was found.

Since it is generally accepted, on the basis of the observed photoelectron spectra, that the energy difference between the n_+ and n_- orbitals[21] of α-dicarbonyls is *ca.* 2 eV,[22,23] where the n_+ orbital energy is higher, the nπ* bands of BPD in Fig. 2 may contain only the $\pi^* \leftarrow n_+$ transition band,[24] as in the case of the α-diketones.[23,25] The nπ* absorption bands of the *o*-quinones in saturated hydrocarbon solutions are situated in the following order from the longer wavelength side, as may be seen from a comparison of Figs. 2 and 6:

o-Benzoquinone > 1,2-Naphthoquinone > BPD
> 9,10-Phenanthrenequinone > Acenaphthenequinone.

The nπ* band of *o*-benzoquinone[1,10] is situated at far longer wavelengths than those of the other *o*-quinones.[4] This order is just the reverse of that in the numbers of carbon atoms in the π-electronic systems of these *o*-quinones, except for the case of acenaphthenequinone. A similar phenomenon is observed in the *p*-quinones[4,26] (*p*-benzoquinone, 1,4-naphthoquinone, and 9,10-anthraquinone).

As for the nπ* bands of BPD in Fig. 2, it is noticeable that its blue-shift in the dioxane solution, in comparison with the case of the saturated hydrocarbon solutions, is smaller than those in other *o*-quinones,[4] acenaphthenequinone, 9,10-phenanthrenequinone, and 1,2-naphthoquinone, which are remarkably large, and that its intensity remarkably increases with the hydrogen-bond formation between BPD and the protic solvents, as may be seen from a comparison between the cases of toluene and the protic solvents, chloroform, and methanol. The former point corresponds to a fact about the phosphorescence bands which will be presented later. This point may show that the charge-transfer interaction between dioxane and BPD is weaker than those between dioxane and other quinones. The calculated π-electronic structures of these *o*-quinones give no information about this difference between BPD and other *o*-quinones. As for the latter point, nothing similar is observed in acenaphthenequinone,[4] but in the thiocarbonyl nπ* band of styrene trithiocarbonate[27,28] there is a similarity. This intensity enhancement may be due to the symmetry degradation of the n_+ orbital of BPD and the increased mixing of the nπ* and its neighbouring ππ* states, accompanied by the decreased energy gap between them, resulting from the hydrogen-bond formation. Acenaphthenequinone's failure to show anything similar may be an interesting problem to be solved in future.

In the nπ* band in the methylcyclohexane solution, the energy difference between the longest-wavelength shoulder near 550 nm and the sharp peak at 527 nm is *ca.* 790 cm^{-1}, while the one between the two main peaks at 527 and 488 nm is *ca.* 1520 cm^{-1}, as is shown in Fig. 2. A similar vibrational structure is also observed in the case of acenaphthenequinone, though the intensity distributions are different, as may be seen in Fig. 6. The structures of 790 cm^{-1} and 1520 cm^{-1} may be assigned to the ring-breathing[29] and C–O stretching vibrations respectively.

In the nπ* phosphorescence bands in Fig. 4, only the 0-0 band appears clearly; this pattern is similar to those in 9,10-phenanthrenequinone[9] and acenaphthenequinone.[7] No phosphorescence band can be observed in saturated hydrocarbon solutions. The estimated lifetimes (*ca.* 0.3 ms) are far shorter than those in the above two *o*-quinones, which are around 10 ms.[6,7,9] A similar difference is observed between *p*-benzoquinone (*ca.* 0.08 ms)[30,31] and 9,10-anthraqui-

none (*ca.* 3 ms).[6,32] The phosphorescence band in the dioxane solution is situated between those in the 1-chlorobutane and toluene solutions, while in the above two *o*-quinones[7,9] it is at far shorter wavelengths than the others, as may be seen in Fig. 7. This fact is consistent with the before-mentioned fact about the $n\pi^*$ absorption band of BPD in the dioxane solution.

The author wishes to express his thanks to Profs. Seiji Ebine and Josuke Tsunetsugu of the Faculty of Science of Saitama University for their kindness in furnishing him with biphenylene-2,3-dione.

References

1) S. Nagakura and A. Kuboyama, *Nippon Kagaku Zasshi*, **74**, 499 (1953); *J. Am. Chem. Soc.*, **76**, 1003 (1954); A. Kuboyama, *Bull. Chem. Soc. Jpn.*, **32**, 1226 (1959).
2) A. Kuboyama and K. Wada, *Bull. Chem. Soc. Jpn.*, **38**, 1709, (1965); *Rep. Gov. Chem. Ind. Res. Inst., Tokyo*, **63**, 123 (1968).
3) A. Kuboyama, S. Matsuzaki, M. Takagi, and H. Arano, *Bull. Chem. Soc. Jpn.*, **47**, 1604 (1974); *J. Nat. Chem. Lab. Ind.*, **69**, 492 (1974).
4) A. Kuboyama, *Bull. Chem. Soc. Jpn.*, **33**, 1027 (1960); *Rep. Gov. Chem. Ind. Res. Inst., Tokyo*, **57**, 541 (1962).
5) A. Kuboyama and H. Arano, *Bull. Chem. Soc. Jpn.*, **49**, 1401 (1976); *J. Nat. Chem. Lab. Ind.*, **72**, 170 (1977); A. Kuboyama and H. Matsumoto, *Bull. Chem. Soc. Jpn.*, **52**, 1796 (1979).
6) A. Kuboyama and S. Yabe, *Bull. Chem. Soc. Jpn.*, **40**, 2475 (1967); *Rep. Gov. Chem. Ind. Res. Inst., Tokyo*, **64**, 105 (1969).
7) A. Kuboyama and S. Matsuzaki, *Nippon Kagaku Kaishi*, **1973**, 2248; *J. Nat. Chem. Lab. Ind.*, **69**, 69 (1974).
8) A. Kuboyama, F. Kobayashi, and S. Morokuma, *Bull. Chem. Soc. Jpn.*, **48**, 2145 (1975); *J. Nat. Chem. Lab. Ind.*, **71**, 180 (1976); A. Kuboyama, *Chem. Phys. Lett.*, **41**, 544 (1976); *J. Nat. Chem. Lab. Ind.*, **73**, 348 (1978).
9) A. Kuboyama and M. Anze, *Nippon Kagaku Kaishi*, **1972**, 229; *J. Nat. Chem. Lab. Ind.*, **67**, 165 (1972).
10) S. Goldschmidt and F. Graef, *Chem. Ber.*, **61**, 1858 (1928); H. J. Teuber and G. Staiger, *ibid.*, **88**, 802 (1955); DMS, "UV Atlas of Organic Compounds," Butterwoths (1968), B8/27.
11) J. M. Blatchly, J. F. W. McOmie, and S. D. Thatte, *J. Chem. Soc.*, **1962**, 5090.
12) M. Sato, H. Fujino, S. Ebine, and J. Tsunetsugu, *Bull. Chem. Soc. Jpn.*, **50**, 3076 (1977).
13) J. R. Lombardi, J. W. Raymonda, and A. C. Albrecht, *J. Chem. Phys.*, **40**, 1148 (1964); J. Czekalla, W. Liptay, and E. Döllefeld, *Ber. Bunsenges. Phys. Chem.*, **68**, 80 (1964).
14) The BPD was furnished by the courtesy of Prof. S. Ebine of the Faculty of Science of Saitama University.
15) R. Pariser and R. G. Parr, *J. Chem. Phys.*, **21**, 466, 767 (1953); J. A. Pople, *Trans. Faraday Soc.*, **49**, 1375 (1953).
16) H. Eyring, J. Walter, and G. E. Kimball, "Quantum Chemistry," John Wiley & Sons, New York (1944), p. 384.
17) A. L. Macdonald and J. Trotter, *J. Chem. Soc., Perkin Trans. 2*, **1973**, 476.
18) T. K. Fawcett and J. Trotter, *Acta Cristallogr.*, **20**, 87 (1966); T. C. W. Mak, *J. Chem. Soc.*, **1962**, 1.
19) Since BPD has no degenerate state, its MCD spectrum is of the B type (A. D. Buckingham and P. J. Stephens, *Ann. Rev. Phys. Chem.*, **17**, 399 (1966)).
20) A. Kuboyama, *Bull. Chem. Soc. Jpn.*, **52**, 329 (1979); *J. Nat. Chem. Lab. Ind.*, **75**, 315 (1980).
21) n_+ and n_- orbitals denote the bonding (+) and antibonding (−) combinations of the two high-energy nonbonding orbitals of the two oxygen atoms of BPD.
22) D. Dougherty, P. Brint, and S. P. McGlynn, *J. Am. Chem. Soc.*, **100**, 5597 (1978).
23) J. R. Swenson and R. Hoffmann, *Helv. Chim. Acta*, **53**, 2331 (1970).
24) Since the calculated energy of the lowest $\pi^*(b_1)$ orbital is lower by 0.86 eV than that of the second lowest $\pi^*(b_2)$ orbital, the $n\pi^*$ band may be the out-of-plane polarized $^1B_1$ band. Accordingly, the $n\pi^*$ phosphorescence band may also be the $^3B_1$ band.
25) J. F. Arnett, G. Newkome, W. L. Mattice, and S. P. McGlynn, *J. Am. Chem. Soc.*, **96**, 4386 (1974).
26) DMS, "UV Atlas of Organic Compounds," Butterworths (1968), B8/10.
27) Y. Jinnouchi, N. Kōno, and A. Kuboyama, The Abstracts of the 36th National Meeting of the Chemical Society of Japan (1977), p. 403.
28) In the $n\pi^*$ bands of 9,10-phenanthrenequinone and 1,2-naphthoquinone, the effect of the hydrogen-bond formation is difficult to examine because of the proximity of the $n\pi^*$ band and its neighbouring $\pi\pi^*$ band.
29) S. N. Singh and R. S. Singh, *Current Sci.*, **36**, 624 (1967); S. N. Singh, M. G. Jayswal, and R. S. Singh, *Bull. Chem. Soc. Jpn.*, **42**, 2048 (1969).
30) A. Kuboyama and S. Matsuzaki, The Abstracts of the 26th Annual Meeting of the Chemical Society of Japan (1972), p. 277.
31) G. Briegleb, W. Herre, and D. Wolf, *Spectrochim. Acta*, **25A**, 39 (1969).
32) A. Kuboyama, *Bull. Chem. Soc. Jpn.*, **43**, 3373 (1970); *Rep. Gov. Chem. Ind. Res. Inst., Tokyo*, **66**, 176 (1971).

The Reaction of Magnesium Hydroxide with Soluble Silica under Hydrothermal Conditions below the Critical Temperature

Haruto MURAISHI

Department of Chemistry, Fukuoka University of Education, Munakata-cho, Fukuoka 811-41

(Received July 14, 1980)

$Mg(OH)_2$ powder packed into a basket was placed apart from solid SiO_2 in an autoclave so that the SiO_2 might react with the solid $Mg(OH)_2$ in the state of soluble silica. At given temperatures of 250—360 °C, the $Mg(OH)_2$ changed into talc($Mg_3Si_4O_{10}(OH)_2$) through serpentine($Mg_3Si_2O_5(OH)_4$): the reaction was a first-order consecutive-irreversible reaction which can be represented as:

$$Mg(OH)_2 \xrightarrow{+SiO_2} Mg_3Si_2O_5(OH)_4 \xrightarrow{+SiO_2} Mg_3Si_4O_{10}(OH)_2.$$

The reaction rate of serpentine into talc as a single reaction was also first-order. The formation of serpentine was much faster than that of talc. The reaction rate depended on the silica concentration in the hydrothermal solution rather than on the reaction temperature. In the course of the reaction, the crystallite size of the $Mg(OH)_2$ and the serpentine was hardly changed. In addition, the crystallite size of $Mg(OH)_2$ did not affect that of the resulting serpentine. From these results, the rate-limiting step is presumed to be the formation of the crystal nuclei of the serpentine or talc.

The mechanism of the synthetic reaction of silicates under hydrothermal conditions is of interest, but it has not been investigated except for the syntheses of zeolite below 100 °C.[1-5] The purpose of this study is to gain some insight into the mechanism of silicate formation under high temperatures and high pressures. From this point of view, the rate of the formation of serpentine and talc from $Mg(OH)_2$ powder and soluble silica has been investigated at the vapor pressures of hydrothermal solutions.

In the previous investigations[6-9] of the synthetic reaction of the MgO–SiO_2–H_2O system, mixtures of solid MgO (or $Mg(OH)_2$) and solid SiO_2 were used as the starting materials. In this study, in order to observe more simply the reaction process, solid $Mg(OH)_2$ is placed apart from solid SiO_2 in an autoclave so that the SiO_2 may react with the solid $Mg(OH)_2$ surely in the state of soluble silica.

Experimental

The apparatus used for separating the two starting materials from each other is shown in Fig. 1. The silica gel or α-quartz powder used as the silica source was placed at the bottom of a modified Morey-type autoclave with a capacity of 30 ml, while the $Mg(OH)_2$ powder, packed naturally into a basket which was mounted on a holder, was placed above the silica source: distilled water was then introduced into the autoclave to fill it by 60%. The reaction was carried out in the temperature range of 250—360 °C at an autogeneous pressure of the autoclave. The heating rate up to a fixed temperature was 75 °C/h. After a definite time of heating, the autoclave was quenched rapidly with water. The reaction products were taken out of the basket and dried at 110 °C for 12 h. The products were identified by the use of the X-ray diffractometer and DTA. Their quantities could be determined with the gravimetric technique (TG), as will be shown in the following section. The solution was filtered off, and the soluble silica and magnesium ion in the solution were determined by means of the silico molybdate method[10] and EDTA titrimetry[11] respectively. The crystallite size of the reactant and products was measured by the X-ray diffraction method.[12] These methods have also been described fully in previous papers.[13,14]

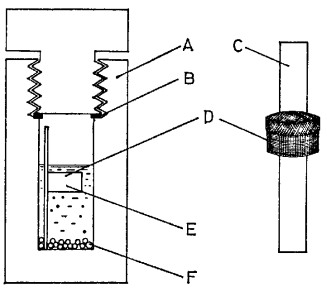

Fig. 1. Hydrothermal apparatus.
A: Hydrothermal vessel (stainless steel), B: silver gasket, C: basket holder, D: sample container (netted stainless steel basket, 160 mesh), E: reactant ($Mg(OH)_2$), F: reactant (SiO_2).

Results

Effects of Amount of Silica and $Mg(OH)_2$ on the Reaction Rate. Approximately 0.2 g of $Mg(OH)_2$, packed into a basket, was allowed to react with various amounts of 0.5—6.0 g of the silica source at 330 °C for 3 h. After each run, the conversion fraction was determined from the amount of remaining $Mg(OH)_2$. The results are shown as a function of the amount of silica in Fig. 2(a). It was found that, when 1 g or more of silica was used, the conversion fraction was independent of the amount of silica: it was 0.4 for silica gel and 0.2 for α-quartz under these conditions. The silica concentration in the solution during the reaction was about 1200 ppm for silica gel and 400 ppm for α-quartz: these values are approximately equal to their equilibrium solubilities at that temperature.[15,16] The distinction between the conversion fractions for silica gel and α-quartz can be explained in terms of the difference between their solubilities.

On the other hand, various amounts of $Mg(OH)_2$ (0.05—0.60 g) were allowed to react with a fixed amount of 2.0 g of silica at 360 °C for 6 h. The results were shown in Fig. 2(b). The conversion fraction diminished with an increase in the amount of $Mg(OH)_2$. In addition, it was found, from the deter-

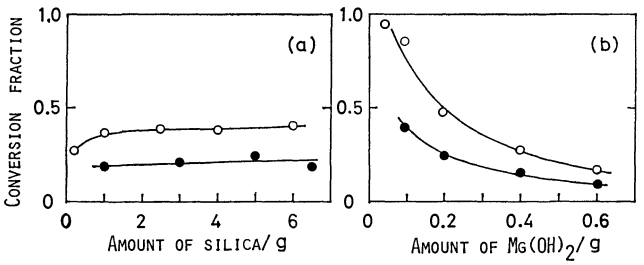

Fig. 2. Effect of amount of SiO_2 and $Mg(OH)_2$ on the conversion of $Mg(OH)_2$.
Silica gel (○) and α-quartz powder (●) were used as silica source. (a) is for a fixed amount of $Mg(OH)_2$ (0.2 g) and treatment at 330 °C for 3 h, and (b) for a fixed amount of SiO_2 (2.0 g) and treatment at 360 °C for 6 h.

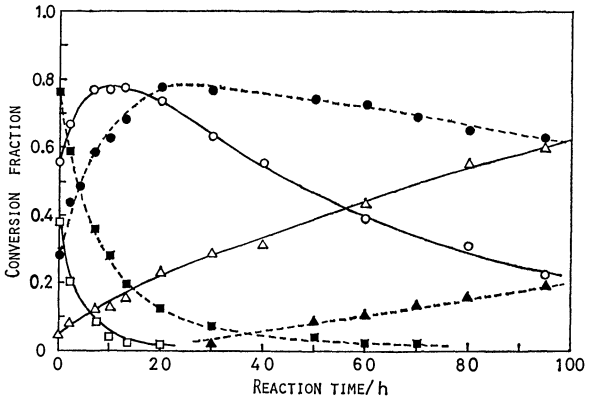

Fig. 3. Conversion curves for reaction of $Mg(OH)_2$ with soluble silica at 250° (----) and 360 °C (——). Silica source: silica gel. ■,□: $Mg(OH)_2$, ●,○: $Mg_3Si_2O_5(OH)_4$(serpentine), ▲,△: $Mg_3Si_4O_{10}(OH)_2$ (talc).

mination of silica concentration in the solution during the reaction, that the silica concentration decreased with an increase in the amount of $Mg(OH)_2$. The decrease in the silica concentration is explicable as a result of the faster rate of taking out of silica by $Mg(OH)_2$ than the rate of dissolution of silica. The relation between the silica concentration and the conversion was examined in detail. In the case of an amount of $Mg(OH)_2$ of 0.2 g or less, the solution was saturated with silica during the reaction (about 1400 ppm for silica gel and 500 ppm for α-quartz). The conversion fraction, however, was decreased with the amount of $Mg(OH)_2$. The drop in the conversion may be due to the fact that soluble silica penetrates slowly into the interior of the pack of $Mg(OH)_2$ powder. When the amount of $Mg(OH)_2$ was 0.05 g or below, the reaction went to completion too rapidly for us to measure the reaction rate. Therefore, 0.2 g of $Mg(OH)_2$ and 2.0 g of silica were employed as the standard amounts of reactants in order to keep the silica concentration constant throughout the reaction and in order to allow the reaction to proceed steadily and at a moderate speed.

Reaction Products. Under these experimental conditions, serpentine($Mg_3Si_2O_5(OH)_4$) and talc ($Mg_3Si_4O_{10}(OH)_2$) were identified as the products.

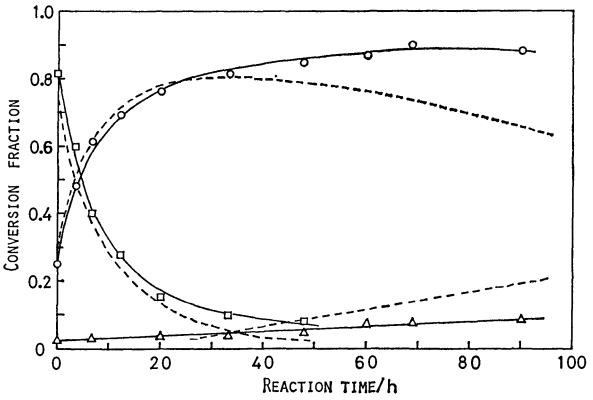

Fig. 4. Effect of temperature on the reaction rate. Reaction temperature: ----, 250 °C;[a] ——, 360 °C. Silica gel and α-quartz powder were used as silica source at 250 and 360 °C, respectively, and the silica concentration in the solution was 900 and 500 ppm. Symbols are the same as in Fig. 3.
a) This curve has been already shown in Fig. 3.

The results were compatible with the phase boundary in the phase diagram of the MgO–SiO_2–H_2O system presented by Bowen and Tuttle.[17] These silicates possess a layer structure and essential water analogues with $Mg(OH)_2$. It was found, from the TG and DTA curves of $Mg(OH)_2$ and synthesized serpentine and talc, that the essential water was quantitatively dehydrated and that the dehydration temperatures were 400, 640, and 860 °C respectively. These silicates, therefore, could be determined gravimetrically from mixtures of reactant and products.

Effect of the Temperature and Silica Concentration on the Reaction Rate. Figure 3 shows the conversion curves plotted against the time for the formation of serpentine and talc at the temperatures of 250 and 360 °C. When the autoclave reached a prescribed temperature (0 h of the reaction time), the reaction had proceeded considerably. Although the real initial stage could not be observed, it was found that both conversion curves obtained for serpentine reach a maximum in a certain time, and that for talc increases monotonously with the time throughout the reaction. Therefore, the reaction can be written as:

$$Mg(OH)_2 \xrightarrow{+SiO_2} \text{serpentine} \xrightarrow{+SiO_2} \text{talc}.$$

This is a typical consecutive two-stage reaction.

The two conversion curves at 250 and 360 °C shown in Fig. 3 are those obtained at different concentrations of silica as well as at different temperatures, since the equilibrium solubility of silica gel is dependent on the temperature (*e.g.*, the silica concentrations at 250 and 360 °C were about 900 and 1400 ppm respectively). As long as silica gel is used as the silica source, it is difficult to control the experimental conditions so as to keep the same silica concentration at the different reaction temperatures. Therefore, α-quartz powder, which has a different solubility[15] from silica gel, was also used as a silica source. The effect of the reaction temperature on the reaction rate was measured semiquantitatively under the conditions of a somewhat similar silica concentration but at dif-

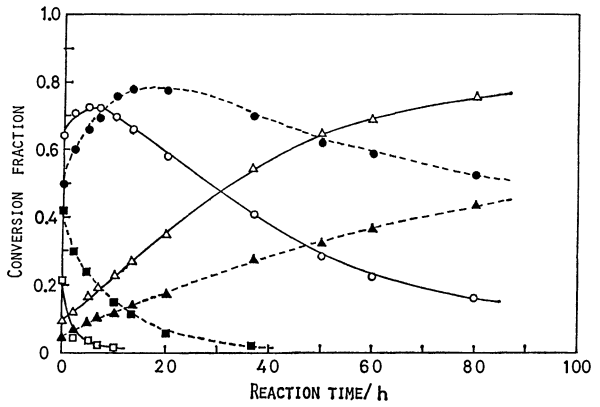

Fig. 5. Conversion for different parts of briquette of reactant in sample container.
Reaction temperature: 360 °C, Silica source: silica gel. ——: outer parts of the pack, ----: inner parts of the pack. Symbols are the same as in Fig. 3.

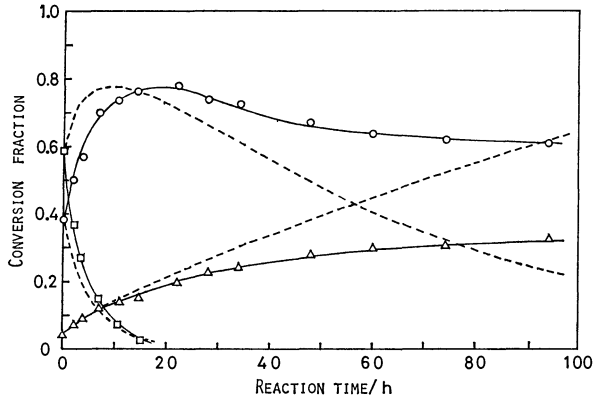

Fig. 6. Effect of crystallite size of starting $Mg(OH)_2$ on the reaction rate.
Reaction temperature: 360 °C, Silica source: silica gel. Crystallite size of starting $Mg(OH)_2$: ----, 16.4 nm;[a] ——, 58.0 nm. Symbols are the same as in Fig. 3.
a) This curve has been already shown in Fig. 3.

ferent temperatures. The results are shown in Fig. 4. There was no difference in the mode of the two conversion curves in the initial stage of the reaction, but in the later stage the position of the maximum of the curve for serpentine was shifted to the right in the case of lower silica concentrations, while the slope of the curve for talc became more gentle. In other words, the rate of the reaction of serpentine into talc may be more affected by the silica concentration than by the reaction temperature.

Effect of Diffusion of Soluble Silica. Since the two starting materials were separated from each other in the autoclave, and since $Mg(OH)_2$ powder was packed into the basket, there may be a concentration gradient of soluble silica in the solution and in the pack of $Mg(OH)_2$ powder. Therefore, two processes of the diffusion of soluble silica may be considered; one is the diffusion through the solution (intrasolution diffusion), and the other is the diffusion across the interstice constructed by $Mg(OH)_2$ particles (interstice diffusion). In order to study the effect of the former,

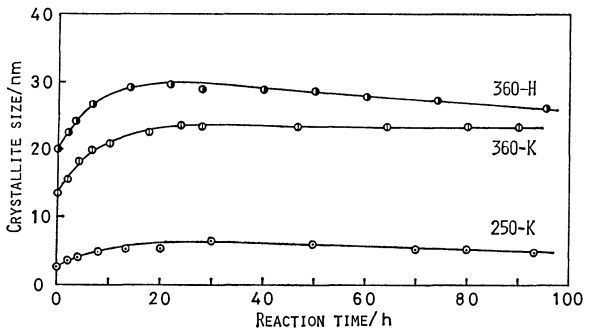

Fig. 7. Effect of reaction temperature and crystallite size of starting $Mg(OH)_2$ on the crystallinity of product (serpentine).
Silica source: silica gel.

Symbol	Reaction temperature	Crystallite size of starting $Mg(OH)_2$	Shorthand
⊙:	250 °C	16.4 nm	250-K
◫:	360 °C	16.4 nm	360-K
◑:	360 °C	58.0 nm	360-H

the distance between the silica on the bottom of the autoclave and the $Mg(OH)_2$ powder in the container was allowed to vary. The variation in the distance between them did not enable us to distinguish the conversion. In order to study the effect of the latter, a large amount of $Mg(OH)_2$ powder was used. The pack of $Mg(OH)_2$ powder was, after the reaction, divided into several parts beginning with the outside, and the conversion fraction of each part was measured. Consequently, the conversion fraction decreased with an increase in the distance from the outside, and thus the reaction rate was found to be influenced by the interstice diffusion. Some typical conversion curves obtained for the outside and inner parts of the pack are shown in Fig. 5.

Effect of Particle Size of $Mg(OH)_2$ on the Reaction Rate. Two kinds of $Mg(OH)_2$ with different particle sizes were used as reactants. These $Mg(OH)_2$ powders were about 35 and 18 m^2/g in surface area, while the crystallite sizes were about 16 and 58 nm respectively. The distinction of the reaction rate due to different particle size is shown in Fig. 6. The reaction rate for larger particles was slower, but the conversion curves obtained for them differed in form from those for small particles. The alteration in the form of the conversion curves suggests that a part of the reaction process varied in the case of larger particles, as will be described in the following section.

Effect of the Crystallite Size of $Mg(OH)_2$ and the Reaction Temperature on the Crystallinity of Serpentine. It has been reported that the crystallite size of the starting material influences the crystallinity of products in some solid reactions—for example, the hydration of MgO,[18] the oxidation of Fe_3O_4 into γ-Fe_2O_3[19] and the reaction of $MgO+Al_2O_3 \rightarrow MgO \cdot Al_2O_3$.[20] Similar behavior can also be expected for the serpentinization of $Mg(OH)_2$, since serpentine has a layer structure consisting of linked SiO_2 tetrahedra and Mg–O(OH) octahedra sheets,[21] like the structure of $Mg(OH)_2$. In order to examine this tendency, two kinds of $Mg(OH)_2$ with different crystallite sizes were allowed

Table 1. Effect of the crystallite size of $Mg(OH)_2$ on the crystallinity of products (serpentine)
Reaction temperature: 360 °C
Silica source: α-quartz blocks

Reaction time (week)	Crystallite size of serpentine (nm)	
	Starting material	
	$Mg(OH)_2$-K[a]	$Mg(OH)_2$-H[a]
1	25.3	26.4
2	28.0	28.7
3	29.8	30.5
4	31.9	31.3

a) The crystallite sizes of $Mg(OH)_2$-K and $Mg(OH)_2$-H are, respectively, 16.4 and 58.0 nm.

to react at 360 °C. The serpentine produced from large crystals (360-H) was slightly larger than that produced from small crystals (360-K), as is shown in Fig. 7. The distinction of the crystallinity may also have been caused by the variation in the reaction rate due to the different crystallite size. In order to minimize this effect, α-quartz blocks were used as the silica source because their slow dissolution rate may limit the rate of reaction. The results showed that the crystallite size of the resulting serpentine was not affected by that of $Mg(OH)_2$, as is shown in Table 1.

On the other hand, the reaction temperature apparently had an effect on the crystallinity of the products, as may be seen from the curves of 250-K and 360-K in Fig. 7. The crystallite size was about 5 nm at 250 °C and 23 nm at 360 °C for 30 h.

Discussion

As has been described above, the reaction of $Mg(OH)_2$ with soluble silica proceeds consequently in two stages as follows:

$$Mg(OH)_2 \xrightarrow{\text{(Reaction 1)}} \text{serpentine} \xrightarrow{\text{(Reaction 2)}} \text{talc}.$$

It is assumed that Reactions 1 and 2 proceed *via* a similar reaction process. The process may consist of the following steps:[22]

(1) Dissolution of silica.
(2) Diffusion of soluble silica in solution.
(3) Diffusion of soluble silica along interstices constructed by $Mg(OH)_2$ (or serpentine) particles.
(4) Adsorption of soluble silica on the $Mg(OH)_2$ (or serpentine) surface.
(5) Formation of crystal nuclei for serpentine (or talc).
(6) Crystal growth.

An excess of the silica source was used in this experiment, and the solution was kept saturated with silica throughout the reaction. As has been described above, under these conditions Steps (1) and (2) are not rate-limiting. Furthermore, Step (4), that is, surface reaction, proceeds much faster than the other steps, as has been reported in a previous paper.[14] Accordingly, Steps (3), (5), or (6) may be considered to be the rate-limiting steps.

The conversion curves obtained were analyzed on the basis of the kinetics in order to clarify the reaction mechanism. The full reaction scheme is represented as follows:

$$\begin{array}{lccccc} & Mg(OH)_2 & \xrightarrow[+SiO_2]{k_1} & Mg_3Si_2O_5(OH)_4 & \xrightarrow[+SiO_2]{k_2} & Mg_3Si_4O_{10}(OH)_2 \\ t=0 & [A]_0 & & 0 & & 0 \\ t=t & [A] & & [B] & & [C] \end{array} \quad (1)$$

where k_1 and k_2 are the rate constants, $[A]_0$ is the amount of $Mg(OH)_2$ at $t=0$, and [A], [B], and [C] are, respectively, the amounts of $Mg(OH)_2$, serpentine, and talc at $t=t$. Since the silica concentration is almost constant throughout the reaction, as has been described above, the silica concentration is not contained in the rate equation, but is one of the constant factors that are contained in the rate-constant term. The reaction rate also depends on the surface area of $Mg(OH)_2$ powder. However, the surface area is constant in the same sample.

If the reaction is a first-order reaction, the rate equation is expressed as follows:[23]

$$\frac{d[A]}{dt} = -k_1[A], \quad (2)$$

$$\frac{d[B]}{dt} = k_1[A] - k_2[B], \quad (3)$$

$$\frac{d[C]}{dt} = k_2[B]. \quad (4)$$

The above three simultaneous differential equations are solved as follows:

$$[A] = [A]_0 e^{-k_1 t}, \quad (5)$$

$$[B] = [B]_0 e^{-k_2 t} + \frac{k_1[A]_0}{k_2 - k_1}(e^{-k_1 t} - e^{-k_2 t}), \quad (6)$$

$$[C] = [C]_0 + [A]_0(1 - e^{-k_1 t}) + [B]_0\left(1 - e^{-k_2 t} - \frac{[A]_0/[B]_0}{1 - k_2/k_1}\right)(e^{-k_2 t} - e^{-k_1 t}), \quad (7)$$

where $[A]+[B]+[C]=1$ and the initial concentrations are $[A]_0=1$ and $[B]_0=[C]_0=0$. These equations can be simplified by writing $k=k_2/k_1$ and $\tau=k_1 t$:

$$[A] = e^{-\tau}, \quad (8)$$

$$[B] = (e^{-\tau} - e^{-k\tau})/(k-1), \quad (9)$$

$$[C] = \{k(1-e^{-\tau}) - (1-e^{-k\tau})\}/(k-1). \quad (10)$$

The values of [A], [B], and [C] are equal to the conversion fractions. They can be represented as a function of τ by changing the value of k in Eqs. 8, 9, and 10. When an appropriate k value was given, the conversion curves determined from Eqs. 8, 9, and 10 agreed with those obtained from this measurement. Some typical model curves determined to correspond to the experimental curves are shown in Fig. 8. Table 2 shows the experimental conditions under which these experimental conversion curves were obtained and also the k values selected to determine these model curves. From the k values, the conversion into serpentine was proved to be much faster than that into talc. Moreover, the dependence of the k values on the

Table 2. k values and experimental conditions of measured conversion curves

Silica source	Reaction temperature (°C)	Silica concentration (ppm)	Crystallite size of $Mg(OH)_2$ (nm)	k value	k_1	Ref.
α-quarts powder	360	500	16.4	0.03	0.080	Fig. 5
Silica gel	250	900	16.4	0.07	0.085	Fig. 4
	330	1200	16.4	0.10	0.102	—
	360	1400	16.4	0.09[a]	0.090	Fig. 6
				0.12[b]	0.107	Fig. 4
				0.19[c]	0.114	Fig. 6
	360	1400	58.0	—[d]	—	Fig. 7

a) Conversion of the inner parts of the sample pack. b) Conversion of whole sample. c) Conversion of the outer parts of the sample pack. d) Disagreement with theoretical conversion curve.

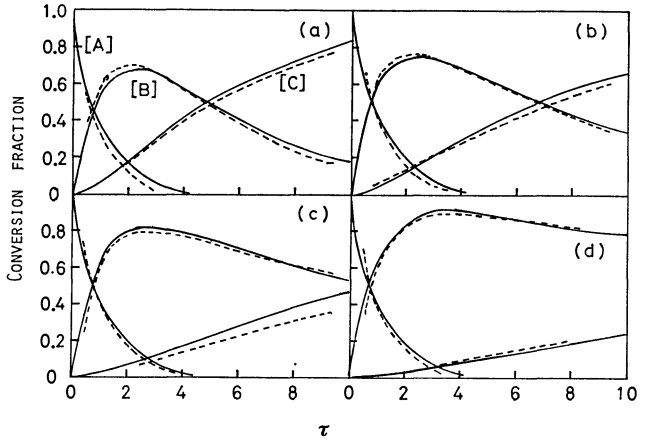

Fig. 8. Typical model curves for the first-order consecutive-irreversible two stage reaction $A \xrightarrow{k_1} B \xrightarrow{k_2} C$. $k=k_2/k_1$, $\tau=k_1t$. (a) $k=0.19$, (b) $k=0.12$, (c) $k=0.07$, (d) $k=0.03$. ——: Calculated conversion curve, ----: observed conversion curve.

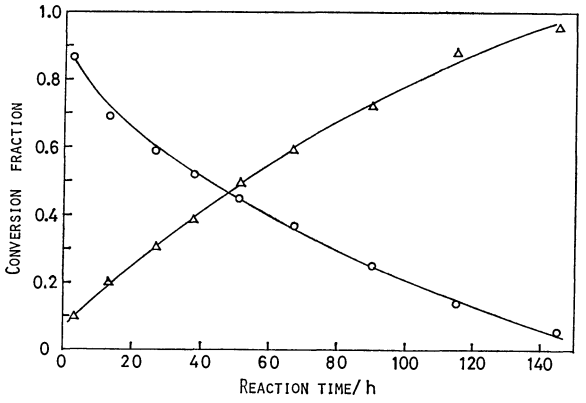

Fig. 9 Conversion curves for the reaction of synthesized serpentine with soluble silica.
Reaction temperature: 360 °C, Silica source: silica gel. Symbols are the same as in Fig. 3.

silica concentration showed that the k values become greater with an increase in the silica concentration. In other words, an increase in the silica concentration accelerates the formation of talc rather than that of serpentine.

When a larger quantity of $Mg(OH)_2$ was packed in the sample container, the rate of the reaction was slowed down toward the center of the pack of $Mg(OH)_2$ powder. Regardless of whether a part or the whole of the sample is involved, these rate equation could be applied only if the k value was varied. The reaction proceeded in a first-order manner at any part of the pack of $Mg(OH)_2$ powder, although there was a concentration gradient attributable to the interstice diffusion. This may be explained as follows. The term referring to the interstice diffusion rate as well as that of the silica concentration is contained in the rate constant k.

In order to measure the reaction rate of serpentine into talc as a single reaction, a synthesized serpentine was used as the starting material. The results are shown in Fig. 9. It was confirmed from the decrease in the amount of serpentine that the reaction of serpentine into talc is also first-order.

These results suggest that diffusion is not a rate-limiting step under the present experimental conditions, since diffusion is not represented by a first-order rate equation.[23] Therefore, Step (5), the formation of crystal nuclei, which is considered to be independent of the diffusion,[22] seems to be the rate-limiting step.

The change in the crystallite size of $Mg(OH)_2$ and serpentine with the reaction time was followed by the use of an X-ray diffractometer in order to obtain some further information about the reaction mechanism. The results for serpentine can be seen in Fig. 8. The amount of $Mg(OH)_2$ was reduced to one-half of its initial value after 1—5 h, while its crystallite size was hardly changed at all. Thus, in the $Mg(OH)_2$——→serpentine——→talc reaction, the crystallite of the reactions did not decrease despite the decrease in their amount as the reaction proceeded. In the course of the reaction, the reactants may be either completely transformed into products (serpentine or talc) or may still be kept in the initial state. This result suggests that the crystal growth, Step (6), will finish immediately following the formation of the nucleus, Step (5). Thus, this evidence supports the idea that the formation of nuclei is the rate-limiting step. This conception is reasonable, however, only in the case of $Mg(OH)_2$ powder with a small particle size, since the use of larger particles gives rise to an apparent deviation from the typical model curve described above. The reaction mechanism for large particles may be more complex than that for small par-

ticles.

It has been reported that solid-phase reactions, such as the crystallization of zeolite[1] and the dehydration of $Mg(OH)_2$[24] and kaolinite ($Al_2Si_2O_5(OH)_4$),[25,26] are first-order. In these reactions, the mechanism is thought to involve a rate-limiting heterogeneous nucleation. For the dehydration of larger particles of kaolinite,[27,28] however, the rate-limiting step is taken as the diffusion process and the reaction is not a first-order. These reports seem to support our proposal.

The author would like to express his hearty thanks to Professor Shigeto Kitahara for his valuable guidance and for his critical reading of this manuscript.

References

1) G. T. Kerr, *J. Phys. Chem.*, **70**, 1047 (1966).
2) J. Ciric, *J. Colloid Interface Sci.*, **28**, 315 (1968).
3) S. P. Zhdanov, *Adv. Chem. Ser.*, **101**, 20 (1971).
4) R. A. Cournoyer, W. L. Kranich, and L. B. Sand, *J. Phys. Chem.*, **79**, 1578 (1975).
5) H. Kacirek and H. Lechert, *J. Phys. Chem.*, **80**, 1291 (1976).
6) Von. W. Noll, *Z. Anorg. Chem.*, **261**, 1 (1950).
7) J. J. Hemley, J. W. Montary, C. L. Christ, and P. B. Hostetler, *Am. J. Sci.*, **277**, 322 (1977).
8) J. C. Yang, *J. Am. Ceram. Soc.*, **43**, 542 (1960).
9) G. L. Kalousec and D. Mui, *J. Am. Ceram. Soc.*, **37**, 38 (1954).
10) R. K. Iler, "The Chemistry of Silica," John Wiley & Sons, New York (1979), p. 96.
11) "Jikken Kagaku Koza," ed by The Chemical Society of Japan, Maruzen Press, Tokyo (1957), Vol. 15, p. 291.
12) K. Kubo, E. Suito, U. Nakagawa, and S. Hayakawa, "Funtai," Maruzen Press, Tokyo (1962), p. 186.
13) S. Kitahara and H. Muraishi, *Nippon Kagaku Kaishi*, **1978**, 555.
14) H. Muraishi and S. Kitahara, *Nippon Kagaku Kaishi*, **1978**, 1457.
15) A. J. Ellis and W. A. J. Mahon, "Chemistry and Geothermal Systems," Academic Press, New York (1977), p. 145.
16) R. K. Iler, "The Chemistry of Silica," John Wiley & Sons, New York (1979), p. 30.
17) N. L. Bowen and O. F. Tuttle, *Bull. Geol. Soc. Am.*, **60**, 439 (1949).
18) S. Kitahara, unpublished.
19) M. Kiyama, *Bull. Chem. Soc. Jpn.*, **47**, 1646 (1974).
20) R. C. Rossi and R. M. Fulrath, *J. Am. Ceram. Soc.*, **50**, 56 (1967).
21) L. G. Berry and B. Marson, "Mineralogy," W. H. Freeman and Co., San Francisco (1959), p. 504.
22) W. S. Fyfe, N. J. Price, and A. B. Thompson, "Fluids in The Earth's Crust," Elsevior Scientific Publishing Co., Amsterdam (1978), p. 89.
23) C. H. Banford and C. F. H. Tipper, "Chemical Kinetics, Vol. 2," Elsevior Scientific Publishing Co., Amsterdam (1969), p. 17.
24) R. S. Gordon and W. D. Kingery, *J. Am. Ceram. Soc.*, **58**, 8 (1967).
25) G. W. Brindley and M. Nakahira, *J. Am. Ceram. Soc.*, **40**, 346 (1957).
26) F. Toussaint, J. J. Fripat, and M. C. Gaetuche, *J. Phys. Chem.*, **67**, 26 (1963).
27) J. B. Holt, I. B. Culter, and M. E. Wadsworth, *J. Am. Ceram. Soc.*, **45**, 133 (1962).
28) R. E. Carter, *J. Chem. Phys.*, **34**, 2010 (1961); **35**, 1137 (1961).

Electrochemical Oxidation and Reduction of Flavin Mononucleotide Adsorbed on a Mercury Electrode Surface

Tadaaki KAKUTANI,* Kenji KANO, Shinji ANDO, and Mitsugi SENDA
Department of Agricultural Chemistry, Faculty of Agriculture, Kyoto University, Kyoto 606
(Received Augast 4, 1980)

The electrochemical redox reaction of flavin mononucleotide (FMN) adsorbed on a hanging mercury drop electrode was studied in a pH 6.9 phosphate buffer and a pH 4.9 acetate buffer by means of cyclic d.c. and phasese lective a.c. voltammetry. Both the oxidized and reduced forms of FMN are strongly adsorbed on the electrode surface, and a stable adsorption layer of FMN($(FMN)_{ad}$) is formed. The cyclic d.c. and a.c. voltammetric behavior of $(FMN)_{ad}$ is explained by equations for a two-step one-electron surface redox reaction. The formal standard redox potentials, semiquinone formation constants, and charge transfer-rate constants of the surface redox reaction of FMN at the mercury electrode were determined.

Recently an increasing number of papers have appeared regarding redox-modified electrodes, which are prepared by attaching redox species, by chemical binding or irreversible adsorption, to the surface of an electrode material (for reviews, see Refs. 1 and 2). Electrocatalysis and electroanalysis have been in particular considered as possible applications of these electrodes. In such applications, data are essential on the kinetics of the surface redox reaction, *i.e.*, the electrode processes exhibited by redox species confined to the electrode surface. In previous papers, we have presented theories of a.c. polarography and voltammetry for simple one-step[3] and two-step surface redox reactions.[4] The theories have also been applied to the electrode processes of ferredoxins irreversibly adsorbed on the mercury electrode surface.[5,6]

The electrochemical behavior of flavin mononucleotide(FMN) has been studied by many authors (for review, see Ref. 7). Senda *et al.*[8] have shown by a.c. polarography that both the oxidized and reduced forms of FMN are adsorbed on the mercury electrode surface; this was confirmed by Takemori[9] and by Hartley and Wilson.[10] However, these authors did not consider the surface redox reaction of FMN, which will be discussed below. In this work, the electrochemical redox reaction of FMN adsorbed on the surface of the hanging mercury drop electrode (HMDE) has been studied in terms of the surface redox reaction, using cyclic d.c. and a.c. voltammetric techniques. We have also determined the kinetic and thermodynamic parameters of the surface redox reaction of FMN. The results and discussion are presented here.

Experimental

Chemicals. Flavin mononucleotide(FMN), a reagent-grade chemical purchased from Nakarai Chemicals Co., was used without further purification. The supporting electrolyte salt and buffers were commercially available reagent-grade materials, used as received. Triply distilled water was used to prepare the electrolysis solution.

Electrochemical Measurements. Cyclic d.c. voltammograms were obtained with a potentiostat, Yanaco Model PE-21-TB2S, equipped with a function generator, YHP 3310B or Nikko Keisoku Model NFG-3. The a.c. voltammetric measurements were performed with a lock-in amplifier, NF LI-574, equipped with the above potentiostat system. A lock-in amplifier, NF LI-572B, was used as an a.c. signal generator. This instrumental system allows the simultaneous measurement of the real (in-phase) and imaginary(out-of-phase) components of the a.c. voltammetric current, which are recorded against the d.c. sweep voltage applied to a hanging mercury drop electrode (HMDE).

All the voltammetric measurements were made under potentiostatic conditions with a three-electrode system consisting of a hanging mercury drop working electrode, a coiled platinum wire auxiliary electrode, and a saturated calomel reference electrode(SCE). The HMDE was a Metrohm drop electrode E 410, the surface area of which was 0.0187 ± 0.0003 cm^2. Buffer solutions (0.2 mol dm^{-3} acetic acid–sodium acetate for pH 4.9 and 0.2 mol dm^{-3} sodium dihydrogenphosphate–disodium hydrogenphosphate for pH 6.9) were used as the base solutions. The ionic strength of a base solution was adjusted to 0.5 mol dm^{-3} with potassium nitrate. A fresh mercury drop from the HMDE was exposed to the electrolysis solution for a given period of time, to be referred to as the exposure time, t_{exp}, below, while the potential of the HMDE was controlled at a constant d.c. potential(E_i). Then the d.c. voltage scan was started from E_i, with scan rates of $v=0.091$ V s^{-1} for cyclic d.c. voltammetry and of $v=0.036$ V s^{-1} for a.c. voltammetry, unless otherwise stated. In a.c. voltammetry, the amplitude of the superimposed a.c. voltage was adjusted to 10 mV (peak to peak) throughout the frequency range of 100—500 Hz. To avoid possible photochemical decomposition of FMN, electrochemical measurements were performed in a dark box at 25 °C under a nitrogen atmosphere.

Results

In order to study the surface redox reaction of FMN, electrochemical measurements were performed at concentrations of FMN lower than 4×10^{-6} mol dm^{-3}, at which the current resulting from unadsorbed, diffusing FMN will be negligibly small.

Figure 1 shows a linear potential sweep voltammogram of 1.5×10^{-6} mol dm^{-3} FMN in a pH 6.9 phosphate buffer, which was recorded after $t_{exp}=2$ min at $E_i=+0.15$ V. At such a low concentration, FMN gave two peaked-shaped waves centered at +0.05 V and −0.41 V, but no ordinary diffusion wave was observed. According to Senda *et al.*[8] and Breyer and Biegler,[11] the reduction wave observed at +0.05 V may be due to the dissolution of the mercury electrode by FMN. Thus, in this study, the electrochemical behavior of the wave observed at −0.41 V was investigated in detail.

Cyclic D.c. Voltammetry. Figure 2A shows the cyclic voltammogram of 9×10^{-7} mol dm^{-3} FMN at

Table 1. Scan-rate dependence of the peak current, peak potential, and half-peak width of cyclic d.c. voltammograms of FMN adsorbed on a mercury electrode at pH 6.9[a)]

Scan rate/mV s^{-1}	$I_{pc}/\mu A$	$I_{pa}/\mu A$	E_{pc}^{DC}/V[b)]	E_{pa}^{DC}/V[b)]	$\Delta E_{p/2,c}^{DC}/mV$	$\Delta E_{p/2,a}^{DC}/mV$
34	0.068	0.073	−0.41	−0.41	68	68
47	0.100	0.104	−0.41	−0.41	68	68
91	0.180	0.181	−0.41	−0.41	68	68
181	0.335	0.336	−0.41	−0.41	70	69

a) $C_{FMN}=9\times10^{-7}$ mol dm^{-3}, $t_{exp}=3$ min at $E_i=-0.20$ V *vs.* SCE. b) V *vs.* SCE.

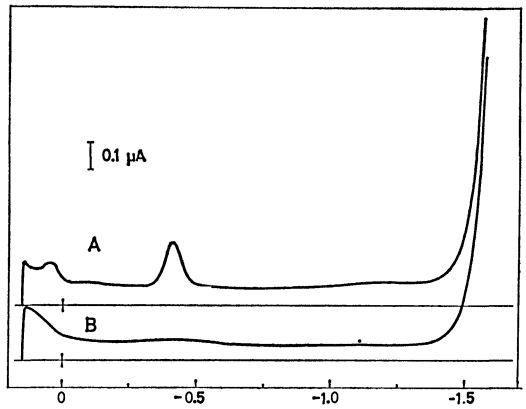

Fig. 1. Linear potential sweep voltammograms recorded after $t_{exp}=2$ min at $E_i=+0.15$ V *vs.* SCE in pH 6.9 phosphate buffer containing (A) 1.5×10^{-6} mol dm^{-3} FMN and (B) no FMN.

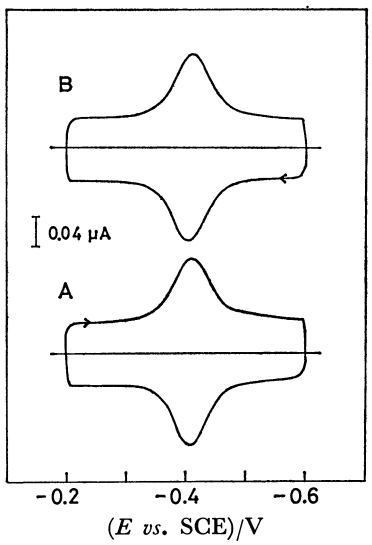

Fig. 2. Cyclic d.c. voltammograms of 9×10^{-7} mol dm^{-3} FMN in pH 6.9 phosphate buffer. Voltage scan was started after $t_{exp}=1$ min from (A) $E_i=-0.2$ V *vs.* SCE and (B) $E_i=-0.6$ V *vs.* SCE.

pH 6.9, which was recorded after $t_{exp}=1$ min at $E_i=-0.2$ V with the HMDE. A pair of cathodic and anodic waves was observed at −0.41 V. The shapes and heights of these two waves were practically identical expect for the opposite current sign. The waves grew to a certain limit, the maximum peak height I_{pc}^{max} or I_{pa}^{max}, with an increase in the concentration of FMN at a constant exposure time or with

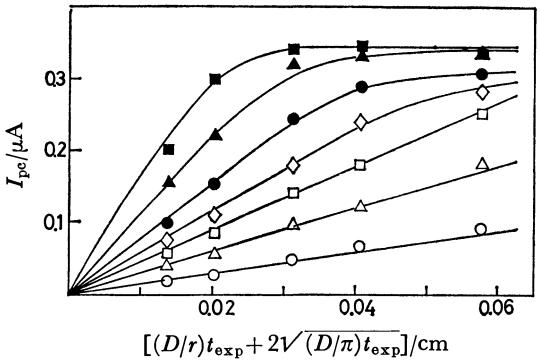

Fig. 3. Plot of I_{pc} against $[(D/r)t_{exp}+2(D/\pi)^{1/2}t_{exp}^{1/2}]$ in pH 6.9 phosphate buffer. FMN concentrations are: (○) 3×10^{-7} mol dm^{-3}; (△) 6×10^{-7} mol dm^{-3}; (□) 9×10^{-7} mol dm^{-3}; (◇) 1.2×10^{-6} mol dm^{-3}; (●) 1.8×10^{-6} mol dm^{-3}; (▲) 3×10^{-6} mol dm^{-3}; (■) 4×10^{-6} mol dm^{-3}.

an increase in the exposure time at a constant concentration of FMN, indicating that the waves are due to the FMN accumulated on the HMDE surface. The t_{exp} dependence of the cathodic peak height, I_{pc}, obtained with $E_i=-0.2$ V is shown in Fig. 3 for different FMN concentrations at pH 6.9. At lower concentrations, I_{pc} was proportional to the $[(D/r)t_{exp}+2(D/\pi)^{1/2}t_{exp}^{1/2}]$ function, where D is the diffusion coefficient of FMN, which was estimated by means of the Ilkovič equation to be 3.2×10^{-6} cm^2 s^{-1} in the pH range of 4.9—6.9, and where r is the radius of the HMDE, which was determined to be 0.038 cm. The slope of the plot was also proportional to the concentration of FMN. These results indicate the diffusion-controlled adsorption of FMN at the electrode surface.[5,13)] A similar dependence of the peak height on t_{exp} was observed also for the anodic wave. However, the maximum value of the anodic peak height, I_{pa}^{max}, was slightly larger than that of the cathodic peak height, I_{pc}^{max}; *i.e.*, $I_{pa}^{max}/I_{pc}^{max}\simeq1.1$ (see Fig. 5A).

Table 1 summarizes the peak heights, I_{pc} and I_{pa}; the peak potentials, E_{pc}^{DC} and E_{pa}^{DC}, and the half-peak widths, $\Delta E_{p/2,c}^{DC}$ and $\Delta E_{p/2,a}^{DC}$, of the cathodic and anodic waves respectively, which were recorded with various scan rates after $t_{exp}=3$ min at $E_i=-0.2$ V in a pH 6.9 phosphate buffer containing 9×10^{-7} mol dm^{-3} of FMN. Both I_{pc} and I_{pa} were proportional to the voltage scan rate, v. The I_{pa}/I_{pc} ratio was unity when corrected for the difference between the amounts of the adsorbed FMN at E_{pc}^{DC} and E_{pa}^{DC} due to the different t_{exp} values. E_{pc}^{DC} and E_{pa}^{DC} coincided with each other and are independent

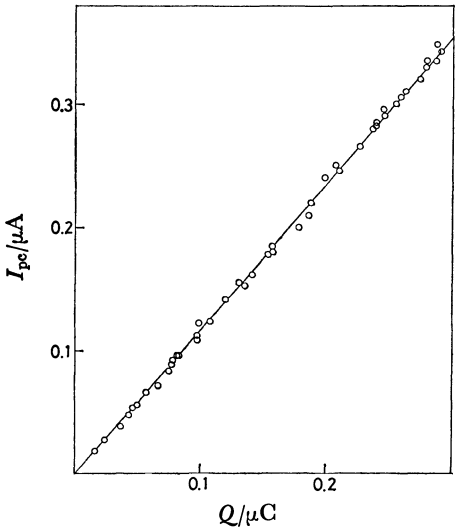

Fig. 4. Plot of I_{pc} against Q at pH 6.9.

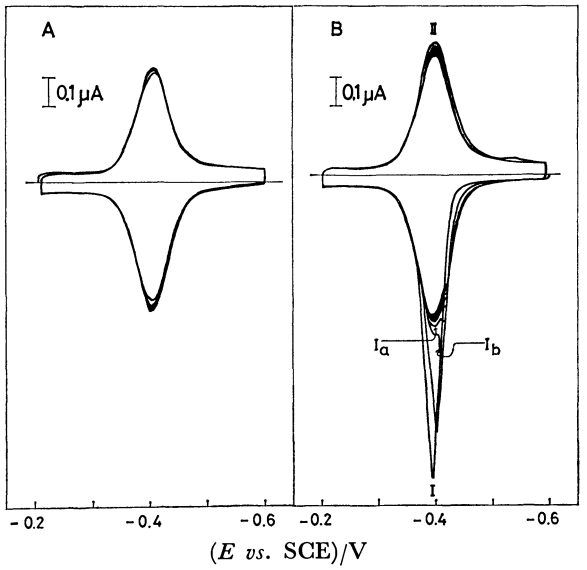

Fig. 5. Cyclic d.c. voltammograms of 4×10^{-6} mol dm^{-3} FMN in pH 6.9 phosphate buffer. Voltage scan was started after $t_{exp}=3$ min from (A) $E_i=-0.2$ V *vs.* SCE and (B) $E_i=-0.6$ V *vs.* SCE.

of the v. The half-peak widths were 68 mV over the scan rate range of 34 mV s^{-1} to 181 mV s^{-1}. The peak height of either wave was proportional to the electricity, Q, required to reduce or oxidize the FMN adsorbed on the electrode surface, which was estimated from the area under the wave, as is shown in Fig. 4. This indicates that the peak height is directly proportional to the amount of the FMN adsorbed on the electrode surface until the peak height reaches a maximum value. On the other hand, the peak potentials and half-peak widths were practically independent of the amount of the adsorbed FMN. These results indicate that the reaction corresponding to the waves is a reversible surface redox reaction.[4]

When the electrode was exposed to the FMN solution at potentials much more negative than the redox potential of the adsorbed FMN, *e.g.*, −0.6 V at pH

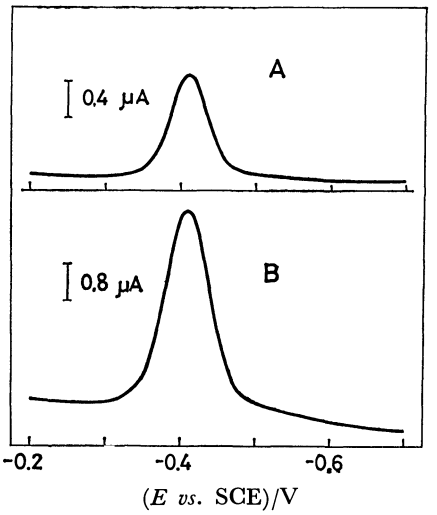

Fig. 6. A.c. voltammograms of 3×10^{-7} mol dm^{-3} FMN in pH 6.9 phosphate buffer at 300 Hz. D.c. voltage scan was started from $E_i=-0.2$ V *vs.* SCE after $t_{exp}=5$ min. (A): Real component, (B): imaginary component.

6.9, the adsorbed FMN was reduced to form an adsorbed layer of leuco-FMN on the electrode surface. The cyclic voltammetric behavior of this adsorbed leuco-FMN was the same as that of adsorbed FMN, provided that the surface coverage was low, as is shown in Fig. 2. However, as the surface coverage increased, the cyclic voltammograms observed were remarkably different in shape and height from that of the adsorbed FMN. Figure 5 shows the cyclic voltammograms of FMN at pH 6.9, which were recorded after the electrode had been exposed to a solution containing 4×10^{-6} mol dm^{-3} of FMN for $t_{exp}=3$ min at $E_i=-0.2$ V (Fig. 5A) and at $E_i=-0.6$ V (Fig. 5B). When FMN was adsorbed at $E_i=-0.2$ V, a symmetrical voltammogram was obtained as has been stated above; in succeeding cycles of the voltage scan between −0.2 V and −0.6 V, the peak heights and shapes of the cathodic and anodic waves remained practically unchanged (Fig. 5A). On the contrary, when FMN was adsorbed at $E_i=-0.6$ V, in the first voltage scan from −0.6 V to −0.2 V an asymmetric anodic wave was observed at −0.39 V (Wave I); its peak height was about three times that of the anodic wave in Fig. 5A. Upon the reversal of the voltage scan at −0.2 V, a symmetrical cathodic wave (Wave II) was observed at −0.40 V; its peak height was slightly larger than that of the cathodic wave in Fig. 5A. In the successive cycles of the voltage scan, Wave I decreased in height and split into two peaks, I_a and I_b, while Waves I_a, I_b, and II decreased in height until a steady state was attained. The steady-state cyclic voltammograms were nearly symmetric, and their peak heights were, though dependent on the bulk concentration of FMN, slightly higher than that of the wave in Fig. 5A, *i.e.*, the maximum peak height of the voltammogram produced by FMN adsorbed at $E_i=-0.2$ V. Similar behavior was observed also in the pH 4.9 acetate buffer.

A.c. Voltammetry. In the cyclic a.c. voltammetry

Table 2. Peak potential and half-peak width of a.c. voltammograms of FMN adsorbed on a mercury electrode at pH 6.9[a]

Frequency/Hz	E_p^{real}/V[b]	E_p^{imag}/V[b]	$\Delta E_{p/2}^{real}$/mV		$\Delta E_{p/2}^{imag}$/mV	
			Obsd	Calcd[c]	Obsd	Calcd[c]
100	−0.41	−0.41	53	52.4	68	67.0
200	−0.41	−0.41	54	53.1	69	68.3
300	−0.41	−0.41	55	54.2	71	70.4
400	−0.41	−0.41	56	55.6	73	73.3
500	−0.41	−0.41	59	57.3	78	76.7

a) $C_{FMN}=9\times10^{-7}$ mol dm^{-3}, $t_{exp}=2$ min at $E_1=-0.20$ V *vs.* SCE. b) V *vs.* SCE. c) Calculated by using $K=1.1$, $k_{sap}=4.9\times10^3$ s^{-1}, and $\theta_t=0.40$.

of FMN adsorbed at $E_1=-0.2$ V, the a.c. voltammogram of the cathodic scan was practically identical in height and shape with that of the anodic scan. Accordingly, the a.c. voltammetric behavior was studied only for the cathodic scan. Figure 6 shows a.c. voltammograms for FMN adsorbed on the HMDE at pH 6.9; the voltammograms were recorded after the electrode had been exposed to a solution containing 3×10^{-7} mol dm^{-3} FMN at $E_1=-0.2$ V for $t_{exp}=5$ min. In all the a.c. voltammograms recorded in this study, the peak potentials of the real and imaginary components, E_p^{real} and E_p^{imag}, were independent of the a.c. frequency between 100 and 500 Hz and independent of the amount of the adsorbed FMN; they coincided with each other and with the peak potentials of the corresponding cyclic d.c. waves, as is shown in Table 2. On the other hand, the peak currents, $\delta_1 I_p^{real}$ and $\delta_1 I_p^{imag}$, and the half-peak widths, $\Delta E_{p/2}^{real}$ and $\Delta E_{p/2}^{imag}$, of the real and imaginary components depended on the a.c. frequency and also on the amount of the adsorbed FMN, as may be seen in Fig. 8 and Table 2.

Discussion

Adsorption of FMN on the Mercury Electrode Surface. The present study has revealed that both the oxidized and reduced forms of FMN are strongly adsorbed on the HMDE surface; this finding is consistent with those of previous works.[8–10] The d.c. voltammetric data indicate that the adsorption of FMN is controlled by diffusion; at lower FMN concentrations, the peak height of the cyclic d.c. voltammogram is given by $I_p=kA\Gamma=kA[(D/r)t_{exp}+2(D/\pi)^{1/2}t_{exp}^{1/2}]C_{FMN}$, where k is the proportionality constant; A, the surface area of the HMDE; Γ, the surface concentration of FMN per unit of area; and C_{FMN}, the concentration of FMN in a bulk solution. At high concentrations, when the maximum current is attained, it is given by $I_p^{max}=kA\Gamma^{max}$, where Γ^{max} is the maximum value of Γ. By applying these two equations to such plots as are shown in Fig. 3, we estimated the maximum surface concentration of FMN adsorbed at -0.2 V, Γ_0^{max}, as $(6.7\pm0.1)\times10^{-11}$ mol cm^{-2} at pH 6.9 and $(9.5\pm0.4)\times10^{-11}$ mol cm^{-2} at pH 4.9. The Γ or Γ^{max} value can also be estimated from the area under the d.c. voltammetric wave, provided that m_1/n_1 and m_2/n_2 are assumed as unity;[3,4] $Q=nFA\Gamma$ and $Q_{max}=nFA\Gamma^{max}$, where n is the number of electrons transferred per molecule of FMN. For the cathodic wave this gave $\Gamma_0^{max}=(8.0\pm0.2)\times10^{-11}$ mole cm^{-2} at pH 6.9 and $(8.8\pm0.2)\times10^{-11}$ mol cm^{-2} at pH 4.9, by assuming $n=2$. The Γ_0^{max} values estimated by these two methods agree well with each other at either pH. When we assume that FMN is adsorbed on the electrode surface with its alloxazine-ring plane oriented parallel to the electrode surface, a CPK molecular model[14] gives $\Gamma_0^{max}=7.5\times10^{-11}$ mol cm^{-2}. On the other hand, when FMN was adsorbed at $E_1=-0.6$ V, the area under the anodic wave obtained with the first voltage scan increased with an increase in C_{FMN} and/or t_{exp} and did not attain a maximum value even at $C_{FMN}=4\times10^{-6}$ mol dm^{-3} and $t_{exp}=5$ min, at which the Γ_R estimated by $Q=nFA\Gamma$ was already larger than Γ_0^{max}. Accordingly, the maximum surface concentration of leuco-FMN, Γ_R^{max}, should be larger than Γ_0^{max}, but it could not be accurately estimated from the present d.c. voltammetric data.

The cyclic d.c. voltammetric behavior of FMN and leuco-FMN at high surface concentrations, shown in Fig. 5, should be interpreted as follows. Since $\Gamma_0^{max}<\Gamma_R^{max}$, the reduction of a complete monolayer of FMN would be followed by the further adsorption of FMN at potentials more negative than the redox potential of the adsorbed FMN, resulting in a higher surface concentration of leuco-FMN than the initial Γ_0^{max}. This would be explain why the anodic peak height is slightly larger than the preceding cathodic one for a complete monolayer of adsorbed FMN (see Fig. 5A). When the initial surface concentration of leuco-FMN, Γ_R, is larger than Γ_0^{max}, the oxidation of the monolayer of leuco-FMN should cause an immediate desorption of a part of the adsorbed FMN molecules. The distortion of the anodic wave (Wave I) and the appearance of Wave I_b, shown in Fig. 5B, may reflect the desorption process associated with the oxidation of the adsorbed leuco-FMN. Cyclic voltammograms of the repeated scans, illustrated in Fig. 5B, suggest that the desorption and adsorption processes are slow.

Surface Redox Reaction of FMN Adsorbed on HMDE. The cyclic d.c. and a.c. voltammetry behavior of FMN adsorbed on the electrode surface should be interpreted in terms of a two-step surface redox reaction:[7–10,12]

$$\begin{aligned} O_{ad} + n_1 e &\rightleftharpoons S_{ad} \\ S_{ad} + n_2 e &\rightleftharpoons R_{ad}. \end{aligned} \qquad (I)$$

When these two steps are d.c. reversible, the simplified equations (Case (I) in Ref. 4) of the cyclic d.c. voltammogram, I^{DC}, and the real and imaginary components of the a.c. current, $\delta_1 I_{corr}^{imag}$ and $\delta_1 I_{obsd}^{real}$, can be written, for $n_1=n_2=m_1=m_2=1$, as:

$$I^{DC} = I_F^{rev} = (F^2/RT)Av\Gamma_t \frac{[\rho^2(\sqrt{K}\rho+2)+\rho(\sqrt{K}+2\rho)]}{(1+\sqrt{K}\rho+\rho^2)^2}, \tag{1}$$

$$\delta_1 I_{obsd}^{real} = \delta_1 I_F^{real} = (F^2/RT)A\omega\Gamma_t\delta_1 E \frac{\sqrt{K}\rho\rho^{1/2}}{(1+\sqrt{K}\rho+\rho^2)} \times \frac{\lambda(\sqrt{K})^{1/2}(1+\rho)\{\sqrt{K}[\lambda^2\rho-(1+\sqrt{K}\rho+\rho^2)]+(\sqrt{K}+4\rho+\sqrt{K}\rho^2)(1+\sqrt{K})\}}{\{K[\lambda^2\rho-(1+\sqrt{K}\rho+\rho^2)]^2+\lambda^2(\sqrt{K})(1+\sqrt{K})^2(1+\rho)^2\rho\}}, \tag{2}$$

$$\delta_1 I_{corr}^{imag} = \delta_1 I_F^{imag} = (F^2/RT)A\omega\Gamma_t\delta_1 E \frac{\sqrt{K}\rho}{(1+\sqrt{K}\rho+\rho^2)} \times \frac{\{\rho\lambda^2(\sqrt{K})(1+\sqrt{K})(1+\rho)^2-\sqrt{K}[\lambda^2\rho-(1+\sqrt{K}\rho+\rho^2)](\sqrt{K}+4\rho+\sqrt{K}\rho^2)\}}{\{K[\lambda^2\rho-(1+\sqrt{K}\rho+\rho^2)]^2+\lambda^2(\sqrt{K})(1+\sqrt{K})^2(1+\rho)^2\rho\}}, \tag{3}$$

with:

$$K = \exp[(F/RT)(E'_{o1}-E'_{o2})]$$
$$\rho = \exp[(F/RT)(E-E'_o)]$$
$$E'_o = (E'_{o1}+E'_{o2})/2$$
$$\lambda = \omega/k_{sap}.$$

Here, it is further assumed that $\alpha_1=\alpha_2=\beta_1=\beta_2=0.5$ and $k_{sap}(1)=k_{sap}(2)=k_{sap}$, where α_i, β_i, and $k_{sap}(i)$ are the cathodic and anodic transfer coefficients and the apparent rate constant of the i-th charge transfer step respectively. In these equations, Γ_t is the total surface concentration per unit of area defined by $\Gamma_t=\Gamma_O+\Gamma_S+\Gamma_R$; E'_{o1} and E'_{o2} are the formal standard potentials of the first and second redox steps respectively, and ω and $\delta_1 E$ are the angular frequency and amplitude of the superimposed a.c. voltage respectively. E'_o corresponds to the formal standard potential of the adsorbed redox couple, O_{ad}/R_{ad}. The parameter K corresponds to the formation constant of the adsorbed semiquinone form, S_{ad}. The apparent rate constant, k_{sap}, depends on the adsorption parameters and on the total surface coverage, $\theta_t(\equiv\Gamma_t/\Gamma^{max})$; *i.e.*,

$$k_{sap} = k_{sap}(\theta_t\to 0)\exp(-a\theta_t), \tag{4}$$

where $k_{sap}(\theta_t\to 0)$ is the apparent rate constant at $\theta_t=0$.

When K is less than 16, Eq. 1 predicts that the cathodic and anodic d.c. voltammograms will have a maximum at E'_o, independently of v and Γ_t, *i.e.*, $E_{pc}^{DC}=E_{pa}^{DC}=E'_o$, and that the half-peak widths, $\Delta E_{p/2,c}^{DC}$ and $\Delta E_{p/2,a}^{DC}$, will have the same value, which is independent of v and Γ_t and which depends only on the K parameter:

$$\Delta E_{p/2,c}^{DC} = \Delta E_{p/2,a}^{DC} = (2RT/F)|\ln\xi|, \tag{5}$$

where ξ is the solution of the equation: $\xi^4-K\xi^3+(K-\sqrt{K}-6)\xi^2-K\xi+1=0$, and that the cathodic and anodic peak heights will be proportional to v and Γ_t:

$$I_{pc} = I_{pa} = 2(F^2/RT)A\Gamma_t v(2+\sqrt{K})^{-1} = (F/RT)vQ(2+\sqrt{K})^{-1}. \tag{6}$$

All the experimental results obtained in this work agreed well with these theoretical predictions (see Table 1 and Fig. 4). Thus, we determined the semiquinone formation constant, K, from the half-peak widths (Eq. 5) and from the slope of the I_p *vs.* Q plot (Eq. 6). The results are summarized in Table 3. The K values estimated by these two methods agreed well with each other at either pH.

Table 3. Semiquinone formation constants of FMN adsorbed on a mercury electrode at pH 6.9 and 4.9

pH	K	Method
6.9	1.2	$\Delta E_{p/2}^{DC}$
	1.0	I_{pc} *vs.* Q plot
4.9	0.82	$\Delta E_{p/2}^{DC}$
	0.62	I_{pc} *vs.* Q plot

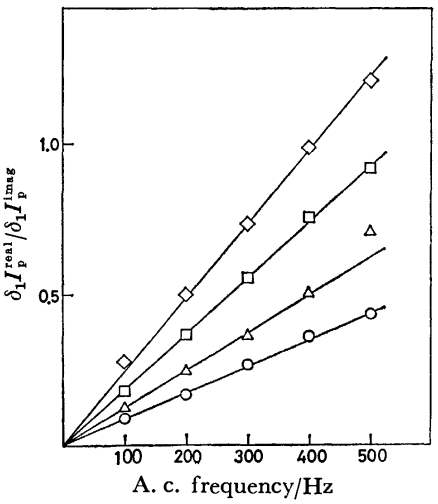

Fig. 7. Frequency dependence of the ratio of a.c. peak current, $(\delta_1 I_p^{real}/\delta_1 I_p^{imag})$, at various total surface coverages of FMN, θ_t, in pH 6.9 phosphate buffer. θ_t: (○) 0.24; (△) 0.40; (□) 0.84; (◇) 1.0.

According to Eqs. 2 and 3, the peak potentials of a.c. voltammograms, E_p^{real} and E_p^{imag}, should be independent of the a.c. frequency and should coincide with each other and with E'_o within a certain limited range of values of K and λ. Table 2 shows that the experimental results agree well with this prediction. In addition, the ratio of $\delta_1 I_F^{real}$ to $\delta_1 I_F^{imag}$ at $E=E'_o$ is given by:

$$(\delta_1 I_F^{real}/\delta_1 I_F^{imag})_{E=E'_o} = \omega/k_{sap}(K)^{1/4}. \tag{7}$$

Such a linear dependence of the current ratio on the a.c. frequency was proved for various total surface coverages, as is shown in Fig. 7, where θ_t was cal-

culated from the peak height of the corresponding cathodic d.c. voltammogram, *i.e.*, $\theta_t=(I_{pc}/I_{pc}^{max})$. The slope of this plot allows us to estimate the apparent rate constant, k_{sap}, provided that K is known. Table 4 summarizes the k_{sap} values estimated from such plots at various surface coverages using K values determined by d.c. voltammetry, *i.e.*, $K=1.1$ at pH 6.9 and $K=0.72$ at pH 4.9. Table 2 gives the experimental values of $\Delta E_{p/2}^{real}$ and $\Delta E_{p/2}^{imag}$ and the theoretical values calculated by using these values of K and k_{sap} at $\theta_t=0.4$. The a.c. peak currents are plotted against the a.c. frequency in Fig. 8, in which the solid lines are drawn by the use of Eqs. 2 and 3. The agreement between the experimental results and theoretical predictions is good. A good agreement between theory and experimental results was also obtained at other θ_t's. As may be seen from Eq. 4, a plot of ln k_{sap} against θ_t should yield a straight line with a slope of $-a$; this was experimentally verified, as is shown in Fig. 9. In conclusion, we can state that the cyclic d.c. and a.c. voltammetric behavior of the adsorbed FMN can be explained by the two-step surface redox mechanism (I). From E'_o and K, we can estimate the formal standard redox potentials of the first and second redox steps, E'_{o1} and E'_{o2}. Table 5 summarizes the values of $k_{sap}(\theta_t\rightarrow\theta)$ and a as well as the K, E'_o, E'_{o1} and E'_{o2} values determined above. For comparison, the standard redox potentials, E'_o(bulk), E'_{o1}(bulk), and E'_{o2}(bulk), and the semiquinone formation constant, K(bulk), for the redox reaction of FMN in a bulk solution[12] are given in Table 5. A comparison of the formal standard potentials of the surface redox reaction with those of the redox reaction in a bulk solution gives $\Delta E_1=E'_{o1}-E'_{o1}(\text{bulk})\simeq+70$ mV and $\Delta E_2=E'_{o2}-E'_{o2}(\text{bulk})\simeq+10$ mV at pH 6.9 and $\Delta E_1\simeq+60$ mV and $\Delta E_2\simeq0$ at pH 4.9. These results suggest that[4] the increasing adsorbability of FMN on the mercury electrode surface is in the order of the oxidized form<the semiquinone form≃the reduced form; this order is consistent with the findings of previous works.[7-10]

This work was supported by a Grant-in-Aid for Scientific Research No. 411706 from the Japanese Ministry of Education, Science and Culture.

Table 4. The apparent rate constants of the surface redox reaction of FMN adsorbed on a mercury electrode at pH 6.9 and 4.9

pH 6.9		pH 4.9	
θ_t	$k_{sap}/10^3$ s^{-1}	θ_t	$k_{sap}/10^3$ s^{-1}
0.17	7.9	0.20	7.9
0.25	7.1	0.25	7.7
0.40	4.9	0.33	6.5
0.75	3.4	0.49	4.9
0.84	3.3	0.59	4.6
0.88	3.2	0.79	3.8
1.0	2.4	0.89	3.5

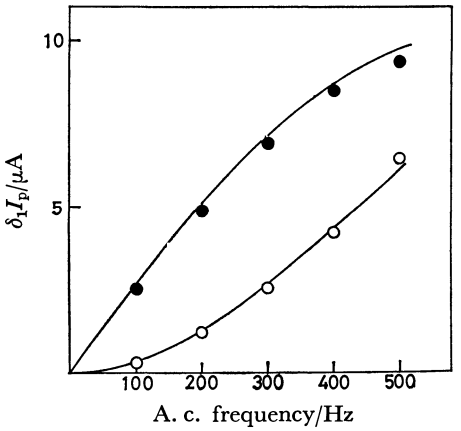

Fig. 8. Dependence of the a.c. peak currents of 9×10^{-7} mol dm^{-3} FMN on a.c. frequency at pH 6.9. A.c. voltammograms were recorded after $t_{exp}=2$ min at $E_i=-0.2$ V *vs.* SCE. ○: Real component, ●: imaginary component. Solid lines: theoretical curves ($K=1.1$, $k_{sap}=4.9\times10^3$ s^{-1} and $\theta_t=0.40$).

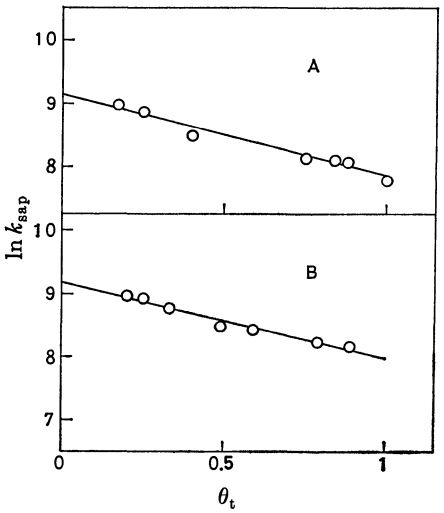

Fig. 9. Plots of ln k_{sap} against θ_t at (A) pH 6.9 and (B) pH 4.9.

Table 5. Electrochemical data of FMN adsorbed on a mercury electrode and in a bulk solution

pH	$k_{sap}(\theta_t\rightarrow0)$ / s^{-1}	a	K	E'_o *vs.* SCE / V	E'_{o1} *vs.* SCE / V	E'_{o2} *vs.* SCE / V	K(bulk)[a]	E'_o(bulk)[a] *vs.* SCE / V	E'_{o1}(bulk)[a] *vs.* SCE / V	E'_{o2}(bulk)[a] *vs.* SCE / V
6.9	9.5×10^3	1.3	1.1	−0.41	−0.41	−0.41	0.073	−0.45	−0.48	−0.42
4.9	9.7×10^3	1.2	0.72	−0.31	−0.31	−0.31	0.094	−0.34	−0.37	−0.31

a) Ref. 12.

References

1) W. R. Heineman and P. T. Kissinger, *Anal. Chem.*, **50**, 166R (1978).
2) K. D. Snell and A. G. Keenan, *Chem. Soc. Rev.*, **8**, 259 (1979).
3) T. Kakutani and M. Senda, *Bull. Chem. Soc. Jpn.*, **52**, 3236 (1979).
4) T. Kakutani and M. Senda, *Bull. Chem. Soc. Jpn.*, **53**, 1942 (1980).
5) T. Ikeda, K. Toriyama, and M. Senda, *Bull. Chem. Soc. Jpn.*, **52**, 1937 (1979).
6) T. Kakutani, K. Toriyama, T. Ikeda, and M. Senda, *Bull. Chem. Soc. Jpn.*, **53**, 947 (1980).
7) G. Dryhurst, "Electrochemistry of Biological Molecules", Academic Press, New York (1977).
8) M. Senda, M. Senda, and I. Tachi, *Rev. Polarogr. (Kyoto)*, **10**, 142 (1962).
9) Y. Takemori, *Rev. Polarogr. (Kyoto)*, **12**, 63 (1964).
10) A. M. Hartley and G. S. Wilson, *Anal. Chem.*, **38**, 681 (1966).
11) B. Breyer and T. Biegler, *Collect. Czech. Chem. Commun.*, **25**, 3348 (1960).
12) R. D. Draper and L. L. Ingraham, *Arch. Biochem. Biophys.*, **125**, 802 (1968).
13) J. Koryta, *Collect. Czech. Chem. Commun.*, **18**, 206 (1953).
14) R. A. Harie, "Molecules in Three Dimensions," Am. Soc. of Biol. Chem. Inc., Bethesda, Meryland, U.S.A.

The Crystal and Molecular Structures of Paracyclophadiynes

Hideo UEDA,† Chuji KATAYAMA, and Jiro TANAKA*

Department of Chemistry, Faculty of Science, Nagoya University, Chikusa-ku, Nagoya 464

(Received March 27, 1980)

The molecular structures of tetramethyl[3.3]paracyclophadine(I) and [3.4]paracyclophadiyne(II) have been determined by X-ray analysis. Both crystals are monoclinic, with the space group of $P2_1/c$. The crystal data are: $a=9.170(4)$, $b=9.208(3)$, $c=18.232(7)$ Å, $\beta=94.0(1)°$, $Z=4$ for (I) and $a=10.938(3)$, $b=9.173(2)$, $c=14.988(4)$ Å, $\beta=116.1(1)°$, $Z=4$ for (II). In both molecules, consisting of benzene and diacetylene groups linked by two methylene-bridges, the diacetylene chain is bent into a bow shape. The (I) molecule has Cs symmetry, and the distances (3.019—3.256 Å) between the atoms of the diacetylene group and the benzene plane are smaller than those of [3.3]paracyclophadiyne(Aono, Sakabe, Sakabe, Katayama, and Tanaka, 1975). The methylene-bridge of [3.4]paracyclophadiyne has a disordered structure.

Misumi and his collaborators[1] have synthesized a series of paracyclophadiyne derivatives, and the chemical and spectral properties[1-3] and the crystal structures[4,5] have been investigated. We have ourselves now determined the structures of tetramethyl[3.3]-paracyclophadiyne(I) and [3.4]paracyclophadiyne(II) in order to study the interactions between the diacetylene group and the benzene ring in more detail.

Experimental

The space group of the two colorless crystals were determined as $P2_1/c$ from the systematic absences on the oscillation and Weissenberg photographs. The unit-cell parameters were determined by the least-squares method, using twelve reflections measured on a Hilger & Watts four-circle diffractometer with Zr-filtered Mo $K\alpha$ radiation for (I) and Ni-filtered Cu $K\alpha$ radiation for (II). In order to confirm the stability of the crystal and counting systems, the intensities of three standard reflections were monitored after every 100 reflections. The standard reflections were stable within a 1% fluctuation in both crystals. Neither absorption nor extinction correction was made. The crystal data and their experimental conditions are shown in Table 1.

Table 1. Crystal data and experimental conditions

	Tetramethyl[3.3]-paracyclophadiyne	[3.4]Paracyclo-phadiyne
Molecular formula	$C_{20}H_{24}$	$C_{17}H_{18}$
Molecular weight	264.4	222.3
Crystal system	Monoclinic	Monoclinic
Space group	$P2_1/c$	$P2_1/c$
a	9.170(4) Å	10.938(3) Å
b	9.208(3) Å	9.173(2) Å
c	18.232(7) Å	14.988(4) Å
β	94.0(1)°	116.1(1)°
V	1535.7 Å^3	1350.5 Å^3
Z	4	4
D_c	1.143 g cm^{-3}	1.094 g cm^{-3}
μ	0.69 cm^{-1} (for Mo $K\alpha$)	4.66 cm^{-1} (for Cu $K\alpha$)
Crystal size	0.22×0.22×0.22 mm	0.25×0.25×0.35 mm
Scan technique	2θ-ω step scan	2θ-ω step scan
Range (ω)	1.2°	1.2°
Step	0.02°	0.02°
Counting time/step	2 s	2 s
Maximum 2θ	54°	144°

Determination and Refinement of the Structure

Tetramethyl[3.3]paracyclophadiyne. The structure was determined by the direct method with the MULTAN program,[12] using 188 reflections with $|E|\geqq 1.40$. An E map computed from the phase set with the highest figure of merit ($FOM=1.65$) revealed the locations of all the non-hydrogen atoms. The hydrogen atoms were found on a difference Fourier map computed after the refinement of the carbon atoms. The refinement was performed by the block-diagonal least-squares method with 1508 independent reflections of $|F_o|>3\sigma(F_o)$. The R index converged to 0.058 with an equal weight for each reflection.

[3.4]Paracyclophadiyne. The unit-cell parameters and the relative magnitude of the structure factors are very similar to those of [3.3]paracyclophadiyne-(III);[4] therefore, the two molecules seemed to take a similar structure in the crystals. All the non-hydrogen atoms were located on a Fourier map computed with the phases calculated for the crystal of (III), the structure was found to be disordered. The structure was refined by the block-diagonal least-squares method, with several different occupancies for the atoms of disordered trimethylene-bridge. The minimum R value of 0.083 was obtained when the occupancy factors of 0.55 and 0.45 were assigned to C(8a) and C(8b) respectively, while the R value calculated by the equal occupancy factors was 0.085. The hydrogen atoms of the aromatic ring and tetramethylene-bridge were found on a difference Fourier map after the anisotropic refinement for the non-hydrogen atoms, those of the disordered trimetylene-bridge were also located after the refinement of the other atoms. The refinement was carried out with an equal weight for 1504 independent reflections of $|F_o|\geqq 3\sigma(F_o)$.

The atomic scattering factors were taken from the "International Tables for X-Ray Crystallography."[13] The least-squares program used for the refinement was written by one of the present authors (C.K.). The

† Present address: Central Research Laboratory, Ube Industries, Ltd., Nishihon-machi, Ube, Yamaguchi 755.

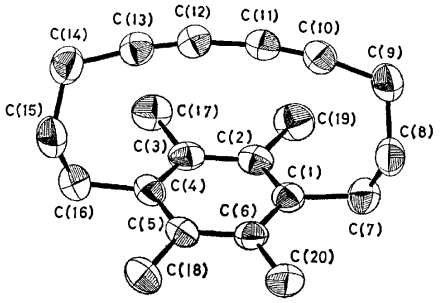

Fig. 1. The atomic numberings of tetramethyl[3.3]paracyclophdiyne.

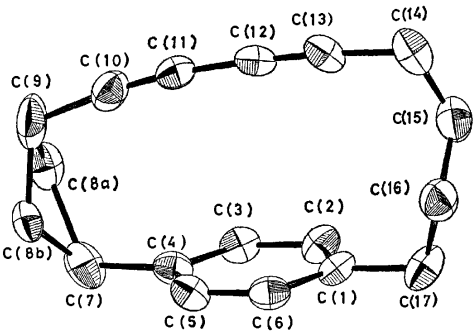

Fig. 2. The atomic numberings of [3.4]paracyclophadiyne.

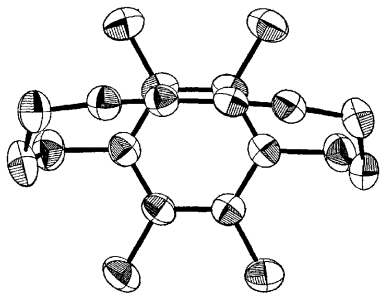

Fig. 3. The molecular structure of tetramethyl[3.3]-paracyclophadiyne projected onto the benzene ring.

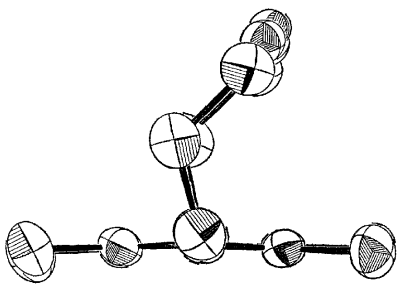

Fig. 4. The molecular structure of tetramethyl[3.3]-paracyclophadiyne viewed from the trimethylene bridge.

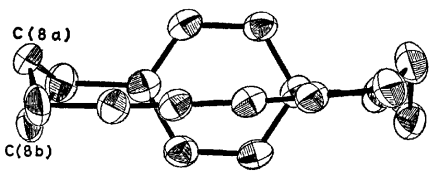

Fig. 5. The molecular structure of [3.4]paracyclophadiyne projected onto the benzene plane.

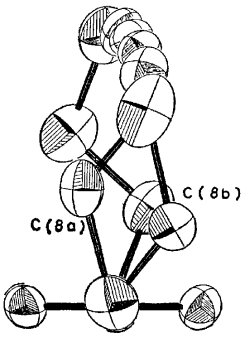

Fig. 6. The molecular structure of [3.4]paracyclophadiyne viewed from the disordered trimethylene bridge.

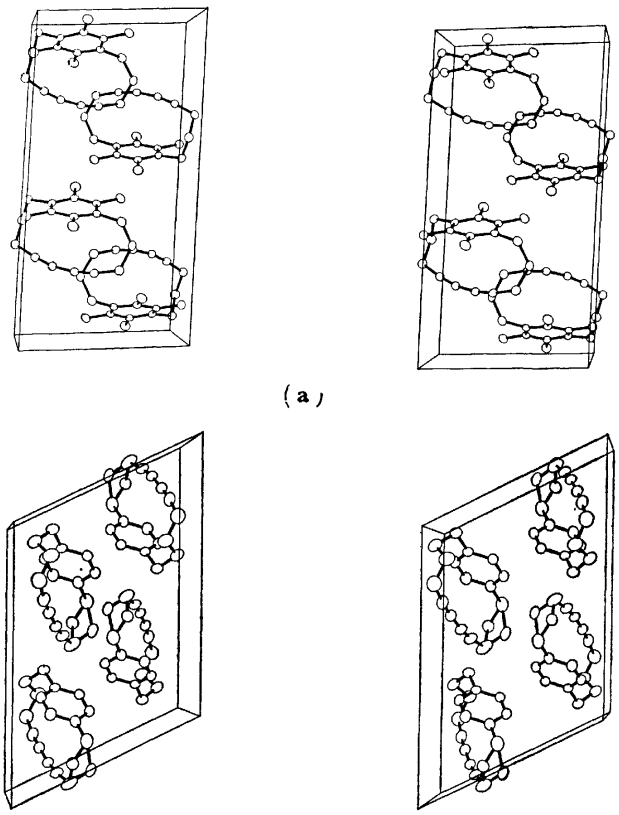

Fig. 7. The stereoscopic views of the crystals with the thermal ellipsoids as having 20% probability. For the origin at the lower rear right-hand corner, *a* is to the left, *b* is out, and *c* is up of the paper:
(a) tetramethyl[3.3]paracyclophadiyne,
(b) [3.4]paracyclophadiyne.

ORTEP program[14] was used for the drawing of Figs. 1—7. The computations were performed at the Nagoya University Computation Center and at Ube Industries. The observed and calculated structure factors are given in Tables 2 and 3.[15]

Results and Discussion

The molecular structures, with atomic numbering, are shown in Figs. 1 and 2, where each atom is represented by a thermal ellipsoid as having a 50% probability for (I) and a 20% one for (II). The

Table 4. Final atomic coordinates and e.s.d.'s($\times 10^4$) for carbon atoms
The standard deviations are given in parentheses and refer to the last decimal position of the respective values.

(I)				(II)			
	x	*y*	*z*		*x*	*y*	*z*
C (1)	5870 (4)	−239 (4)	3987 (2)	C (1)	2515 (4)	−23 (5)	1714 (3)
C (2)	7237 (4)	415 (4)	3919 (2)	C (2)	3880 (4)	−29 (5)	2405 (3)
C (3)	8519 (4)	−387 (4)	4076 (2)	C (3)	4368 (4)	1031 (5)	3137 (3)
C (4)	8450 (4)	−1833 (4)	4312 (2)	C (4)	3553 (4)	2107 (5)	3220 (3)
C (5)	7085 (4)	−2444 (4)	4436 (2)	C (5)	2190 (4)	2102 (5)	2515 (3)
C (6)	5807 (4)	−1651 (4)	4271 (2)	C (6)	1694 (4)	1067 (5)	1791 (3)
C (7)	4448 (4)	538 (4)	3738 (2)	C (7)	4104 (5)	3216 (5)	4052 (4)
C (8)	3708 (4)	−19 (5)	3013 (2)	C (8a)	4376 (8)	2519 (10)	5196 (6)
C (9)	4413 (4)	409 (5)	2311 (2)	C (8b)	3334 (10)	3350 (10)	4600 (7)
C (10)	5806 (4)	−336 (4)	2229 (2)	C (9)	3266 (6)	2082 (7)	5330 (4)
C (11)	6921 (4)	−991 (4)	2258 (2)	C (10)	2653 (5)	675 (6)	4824 (3)
C (12)	8201 (4)	−1762 (4)	2425 (2)	C (11)	2226 (4)	−400 (5)	4361 (3)
C (13)	9245 (4)	−2384 (4)	2680 (2)	C (12)	1797 (4)	−1583 (5)	3745 (3)
C (14)	10440 (4)	−3190 (5)	3065 (2)	C (13)	1471 (4)	−2562 (5)	3196 (4)
C (15)	10071 (5)	−3823 (5)	3792 (2)	C (14)	1152 (6)	−3720 (6)	2465 (5)
C (16)	9829 (4)	−2766 (5)	4424 (2)	C (15)	1770 (6)	−3380 (6)	1797 (4)
C (17)	9990 (4)	313 (5)	3964 (2)	C (16)	995 (5)	−2250 (6)	1059 (3)
C (18)	6984 (5)	3955 (5)	4762 (2)	C (17)	1972 (5)	−1175 (7)	910 (3)
C (19)	7335 (5)	1974 (4)	3660 (2)				
C (20)	4345 (4)	−2347 (5)	4401 (2)				

positional and thermal parameters of the non-hydrogen atoms are given in Tables 4 and 5.[15] The coordinates and isotropic thermal parameters of hydrogen atoms are given in Table 6.[15] The bond lengths and angles are listed in Tables 7 and 8 respectively.

Molecular Structure of Tetramethyl[3.3]paracyclophadiyne. The bond lengths in the benzene ring are 1.396—1.405 Å (mean 1.401 Å), somewhat longer than the value found for other paracyclophadiynes and close to those found for some cyclophanes[11] in which electron-donor-acceptor(EDA) interaction is considerable and for a complex of hexamethylbenzene with TCNE.[16] These results are reasonable, since some electrons in the bonding MO of the benzene ring are transfered to the vacant MO of the acceptor.

It has been reported that in the cyclophanes[6-11] and [3.3]paracyclophadiyne(III),[4] an angle of the carbon replaced by a methylene group is smaller by a few degree than the value of 120°, but the bond angles of C(2)–C(1)–C(6) and C(3)–C(4)–C(5) are very close to that of the normal sp^2 carbon. Therefore, it seems that the deformation of the benzene ring from the hexagonal shape is restricted by the repulsive forces between the methylene and methyl groups in the molecule. Although the substituent on the benzene ring has been reported to shrink the internal angle at the position of substitution,[17] the present molecule has substituent for all the atoms in the ring; therefore, the above effect might be cancelled.

The deviations of the atoms from the least-squares plane of the benzene ring are listed in Table 9. The C(1) and C(4) atoms in the ring deviate toward the diacetylene group, and the other atoms, C(2), C(3), C(5), and C(6), are displaced in the opposite direction. The deviations of the C(7) and C(16) atoms, which are the atoms of methylene groups substituted into the ring, are also displaced toward the diacetylene group. The dihedral angles between the least-squares plane composed of C(2), C(3), C(5), and C(6) and the planes through C(1), C(2), and C(6) and C(3), C(4), and C(5) are 4.3 and 4.0 °, respectively. The angles are greater than the value of 1.8° of (III).

A characteristic feature of the methyl groups attached to the benzene ring is the deviation from the benzene plane to the outer side of the molecule, not toward the center, as with the hydrogen of many paracyclophanes; this is perhaps due to the repulsion of the methyl and methylene groups. A similar displacement of the methyl group is found in tetramethyl quandruple-layered cyclophane.[10]

The bond lengths of the diacetylene group are almost the same as those of other paracyclophadiynes. The diacetylene chain is bent into a bow shape, which is characterized by the mean bond angle of 171.1° in the C(10), C(11), C(12), and C(13) atoms.

The molecular structures projected onto the benzene plane and from a trimethylene-bridge are shown in Figs. 3 and 4 respectively. The molecule has Cs symmetry, and the diacetylene group is nearly overlapped on the atoms of C(2) and C(3). The features of this molecules are distinct compared with those of (II) and (III), in which the diacetylene chaines are located on the mirror plane containing the C(1) and C(4) atoms.

It has been reported that the interaction between a methyl-substituted benzene and TCNE increases in

Table 7. Bond lengths (l/Å) and their standard deviations of nonhydrogen atoms

(a) Tetramethyl[3.3]paracyclophadiyne			
C(1) -C(2)	1.404(5)	C(1) -C(6)	1.402(5)
C(1) -C(7)	1.529(6)	C(2) -C(3)	1.400(5)
C(2) -C(19)	1.516(6)	C(3) -C(4)	1.403(5)
C(3) -C(17)	1.522(6)	C(4) -C(5)	1.405(5)
C(4) -C(16)	1.530(6)	C(5) -C(6)	1.396(5)
C(5) -C(18)	1.518(6)	C(6) -C(20)	1.519(6)
C(7) -C(8)	1.532(6)	C(8) -C(9)	1.526(6)
C(9) -C(10)	1.467(6)	C(10)-C(11)	1.185(5)
C(11)-C(12)	1.388(5)	C(12)-C(13)	1.182(5)
C(13)-C(14)	1.462(6)	C(14)-C(15)	1.506(6)
C(15)-C(16)	1.537(6)		
C(i)-H(i)			
Average	0.98		
Range	0.92—1.04		
(b) [3.4]Paracyclophadiyne			
C(1) -C(2)	1.392(7)	C(1) -C(6)	1.383(7)
C(1) -C(17)	1.513(8)	C(2) -C(3)	1.385(7)
C(3) -C(4)	1.372(7)	C(4) -C(5)	1.396(7)
C(4) -C(7)	1.514(8)	C(5) -C(6)	1.362(7)
C(7) -C(8a)	1.418(13)	C(7) -C(8b)	1.728(11)
C(8a)-C(9)	1.375(12)	C(8b)-C(9)	1.620(13)
C(9) -C(10)	1.497(9)	C(10)-C(11)	1.178(7)
C(11)-C(12)	1.367(7)	C(12)-C(13)	1.163(7)
C(13)-C(14)	1.454(9)	C(14)-C(15)	1.467(10)
C(15)-C(16)	1.481(9)	C(16)-C(17)	1.540(8)
C(i)-H(i)			
Average	1.00		
Range	0.73—1.19		

Table 8. Bond angles (ϕ/°) and their standard deviations of nonhydrogen atoms

(a) Tetramethyl[3.3]paracyclophadiyne			
C(2)-C(1)-C(6)	119.4(3)	C(2)-C(1)-C(7)	121.5(3)
C(6)-C(1)-C(7)	119.2(3)	C(1)-C(2)-C(3)	119.9(3)
C(1)-C(2)-C(19)	120.4(3)	C(3)-C(2)-C(19)	119.7(3)
C(2)-C(3)-C(4)	120.5(4)	C(2)-C(3)-C(17)	119.3(3)
C(4)-C(3)-C(17)	120.2(4)	C(3)-C(4)-C(5)	119.3(3)
C(3)-C(4)-C(16)	121.3(4)	C(5)-C(4)-C(16)	119.4(3)
C(4)-C(5)-C(6)	120.0(3)	C(4)-C(5)-C(18)	120.7(3)
C(6)-C(5)-C(18)	119.4(3)	C(5)-C(6)-C(1)	120.6(3)
C(5)-C(6)-C(20)	118.8(3)	C(1)-C(6)-C(18)	120.6(3)
C(1)-C(7)-C(8)	114.6(3)	C(7)-C(8)-C(9)	116.7(4)
C(8)-C(9)-C(10)	112.8(4)	C(9)-C(10)-C(11)	171.3(4)
C(10)-C(11)-C(12)	169.8(4)	C(11)-C(12)-C(13)	169.6(4)
C(12)-C(13)-C(14)	173.6(4)	C(13)-C(14)-C(15)	114.3(4)
C(14)-C(15)-C(16)	117.9(4)	C(4)-C(16)-C(15)	114.7(4)
(b) [3.4]Paracyclophadiyne			
C(2)-C(1)-C(6)	117.6(4)	C(2)-C(1)-C(17)	120.4(5)
C(6)-C(1)-C(17)	122.0(4)	C(1)-C(2)-C(3)	120.0(5)
C(2)-C(3)-C(4)	122.5(5)	C(3)-C(4)-C(5)	116.7(5)
C(3)-C(4)-C(7)	121.5(5)	C(5)-C(4)-C(7)	122.0(5)
C(4)-C(5)-C(6)	121.5(5)	C(1)-C(6)-C(5)	121.7(4)
C(4)-C(7)-C(8a)	113.6(5)	C(4)-C(7)-C(8b)	114.4(6)
C(7)-C(8a)-C(9)	118.4(7)	C(7)-C(8b)-C(9)	123.0(8)
C(8a)-C(9)-C(10)	113.9(6)	C(8b)-C(9)-C(10)	114.9(6)
C(9)-C(10)-C(11)	173.2(6)	C(10)-C(11)-C(12)	172.8(5)
C(11)-C(12)-C(13)	176.4(5)	C(12)-C(13)-C(14)	173.9(6)
C(13)-C(14)-C(15)	109.2(6)	C(14)-C(15)-C(16)	112.0(6)
C(15)-C(16)-C(17)	110.5(5)	C(1)-C(17)-C(16)	112.8(5)

response to a number of methyl groups.[18] In the molecule of (I), the distances of the atoms in the diacetylene group from the benzene plane are in the range from 3.019 to 3.256 Å, as is shown in Table 9, smaller than those of (III) by 0.01—0.04 Å. Some of the short intramolecular contacts are 3.203 of C(1)···C(10), 3.288 of C(2)···C(11), 3.259 of C(3)···C(12), and 3.153 Å of C(4)···C(13).

Since the methyl substituents on the benzene ring enhance the electron-donor property of the ring by reducing the I_p of the ring (7.86 eV in hexamethylbenzene as compared to 9.24 eV of benzene), the EDA interaction is apparently stronger for this molecule than for unsubstituted [3.3]paracyclophadiyne. For instance, the peak of the first electronic-absorption band appears at 34200 cm^{-1}, while it is 35300 cm^{-1} in the unsubstituted one, and the red shift of about 1100 cm^{-1} means that the inter-ring interaction is enhanced. The CT transition from the benzene ring to the diacetylene group was found in (III) at 42700 cm^{-1}, while it is observed in this molecule at 40500 cm^{-1}. The lowering of the transition energy by 2200 cm^{-1} is an indication of the stronger EDA interaction. The analysis of the MO involved in EDA interaction would seem to be of interest. As is shown in Fig. 8, the phase of the HOMO of hexamethylbenzene (which is degenerated) matches the LUMO of diacetylene. The HOMO-LUMO interaction which is necessary for the EDA complex is considerable for this system, while in other cyclophadiynes without methyl substituents, the EDA interaction is less favourable.

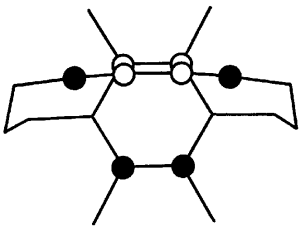

Fig. 8. Symmetries of MO. One of the HOMO of hexamethylbenzene and the LUMO of diacetylene groups are illustrated.

The mean value of the torsion angles around the methylene bridge is 70.5°, this indicates that the conformation are *gauche* as regards the internal rotation around the carbon-carbon bonds.

Molecular Structure of [3.4]*Paracyclophadiyne.* The

Table 9. Deviations (l/Å) from the least-squares plane of the benzene ring

Tetramethyl[3.3]paracyclophadiyne				[3.4]Paracyclophadiyne			
Deviations		Distances from the benzene plane		Deviations		Distances from the benzene plane	
C (1) a)	0.035	C (10)	3.076	C (1) a)	0.002	C (10)	3.185
C (2) a)	−0.022	C (11)	3.256	C (2) a)	−0.001	C (11)	3.473
C (3) a)	−0.012	C (12)	3.236	C (3) a)	−0.003	C (12)	3.642
C (4) a)	0.033	C (13)	3.019	C (4) a)	0.005	C (13)	3.718
C (5) a)	−0.020			C (5) a)	−0.003		
C (6) a)	−0.014			C (6) a)	0.000		
C (7)	0.187			C (2)	−0.021		
C (16)	0.163			H (3)	−0.060		
C (17)	−0.006			H (5)	−0.057		
C (18)	−0.110			H (6)	−0.020		
C (19)	−0.063			C (7)	0.055		
C (20)	−0.051			C (17)	0.004		

a) These atoms were included in the calculation of the least-squares plane.

average of the bond lengths of the benzene ring is 1.382 Å, which is shorter than the normal value (1.392—1.397 Å) and similar to that of (III). As in cyclophanes, it is observed that a benzene ring is distorted from a normal hexagon, with the endocyclic angle of C(1) and C(4) being 117.6 and 116.7° respectively, smaller than the rest by 4.3°. The carbon atoms of the benzene ring are almost coplanar, and no deviation of the hydrogen atoms toward the center of the molecule is found. The dihedral angles between the benzene plane and the planes through C(1), C(2), and C(6) and C(3), C(4), and C(5) are 0.6 and 0.2° respectively. The displacements of the carbon of para-substituted methylene are 0.004 Å for C(1) of the tetramethylene and 0.055 Å for C(17) of the trimethylene-bridge. These values are smaller than those of (III), and the benzene ring keeps a good planarity.

The bond lengths of the diacetylene group are the same as those of the other paracyclophadiynes. The bow-shape deformation, the mean bond angle of the carbon atoms of diacetylene, is 174.1°, smaller than in the case of (I) and (III) because of a less repulsive interaction due to a longer methylene-bridge and a larger spatial distances between the two groups. The larger bow-shape deformation compared to the benzene ring is due to the difference between the length and shapes in these two groups. The distances between the benzene ring and the C(10) and C(11) atoms of the moiety of the diacetylene group are 3.185 and 3.473 Å, and the shortest interatomic distance is 3.250 Å of C(4)···C(10). For the other moeity, the short intramolecular distances are 3.729 of C(1)···C(13), 3.747 of C(1)···C(12), and 3.769 Å of C(6)···C(12). As may be seen from the projection of the diacetylene group onto the benzene plane, the diacetylene group is nearly parallel to the direction of C(1)···C(4) of the benzene ring, the inclination being only 4°, similar to (III).

An unexpected feature of the structure is the disordered arrangement of the trimethylene-bridge. It is interesting that the disordered arrangement is found only on the trimethylene-bridge of the molecules of (II) and (III). The bond distances of this disordered methylene-bridge are 1.4—1.7 Å. The values of the bond lengths and angles, including those of the atoms of the disordered part, are less reliable. The average of the torsion angles of the two methylene-bridges is 67.2°, and it is apparent that the conformations are *gauche*, similar to those of other paracyclophadiynes.

The stereoscopic views of the crystal structure projected along the b-axis are shown in Fig. 7. All the intermolecular contacts are normal.

The authors are grateful to Professor Soichi Misumi and Drs. Yoshiteru Sakata and Takehiro Matsuoka of Osaka University for the gift of the samples.

References

1) T. Matsuoka, T. Negi, T. Otsubo, Y. Sakata, and S. Misumi, *Bull. Chem. Soc. Jpn.*, **45**, 1825 (1972).
2) T. Takabe, M. Tanaka, and J. Tanaka, *Bull. Chem. Soc. Jpn.*, **47**, 1917 (1974).
3) T. Kaneda and S. Misumi, *Bull. Chem. Soc. Jpn.*, **50**, 3310 (1977).
4) T. Aono, K. Sakabe, N. Sakabe, C. Katayama, and J. Tanaka, *Acta Crystallogr., Sect. B*, **31**, 2389 (1975).
5) K. Harata, T. Aono, K. Sakabe, N. Sakabe, and J. Tanaka, *Acta Crystallogr., Sect. A*, **28**, s14 (1972).
6) D. J. Cram and J. M. Cram, *Acc. Chem. Res.*, **4**, 204 (1971).
7) P. K. Gantzel and K. N. Trueblood, *Acta Crystallogr.*, **18**, 958 (1965).
8) H. Hope, J. Bernstein, and K. N. Trueblood, *Acta Crystallogr., Sect. B*, **28**, 1733 (1972).
9) N. L. Allinger, J. T. Sprague, and T. Liljefors, *J. Am. Chem. Soc.*, **96**, 5100 (1974).
10) H. Mizuno, K. Nishiguchi, T. Toyoda, T. Otsubo, S. Misumi, and N. Morimoto, *Acta Crystallogr., Sect. B*, **33**, 329 (1977).
11) Y. Kai, N. Yasuoka, and N. Kasai, *Acta Crystallogr., Sect. B*, **34**, 2840 (1978).
12) G. Germain, P. Main, and M. M. Woolfson, *Acta Crystallogr., Sect. A*, **27**, 368 (1971).

13) "International Tables for X-Ray Crystallography," Birmingham Kynoch Press (1974), Vol. IV, pp. 72—98.
14) C. K. Johnson, ORTEP, Report ORNL-3794, Ork Ridge National Laboratory, Tennessee, 1965.
15) Tables 2, 3, 5, and 6 are kept at the Office of the Editor of the Bulletin of the Chemical Society of Japan, Kanda-Surugadai, Chiyoda-ku, Tokyo (Document No. 8103).
16) M. Saheki, H. Yamada, H. Yoshida, and K. Nakatsu, *Acta Cristallogr., Sect. B*, **32**, 662 (1976).
17) A. Domenicano and A. Vaciago, *Acta Crystallogr., Sect. B*, **35**, 1382 (1979).
18) M. Rossi, U. Buser, and E. Haselbach, *Helv. Chim. Acta*, **59**, 1039 (1976).

Measurement and Analysis of the ν_4 Band of Fluoroform and Its Molecular Constants

Susumu SOFUE,† Kentarou KAWAGUCHI, Eizi HIROTA, and Tsunetake FUJIYAMA*

Institute for Molecular Science, Myodaiji, Okazaki 444

†*Department of Chemistry, Faculty of Science, Tokyo Metropolitan University, Setagaya-ku, Tokyo 158*

(Received August 30, 1980)

The ν_4 fundamental of fluoroform has been measured with a tunable diode-laser source spectrometer. The following molecular constants were determined: $\nu_0=1377.8458\ cm^{-1}$, $B_4=0.344788\ cm^{-1}$, $C_4=0.189134\ cm^{-1}$ $(C\zeta)_4=0.18619\ cm^{-1}$, $D_4^J=3.78\times10^{-7}\ cm^{-1}$, $D_4^{JK}=-5.73\times10^{-7}\ cm^{-1}$, $D_4^K=2.94\times10^{-7}\ cm^{-1}$, $\eta_4^J=1.44\times10^{-6}$ cm^{-1}, and $\eta_4^K=-8.2\times10^{-7}\ cm^{-1}$. Using the molecular constants of the $2\nu_3$, the Coriolis x-y interaction constant between the ν_4 fundamental and $2\nu_3$, $|\zeta_{334}|$, was estimated to be 0.065.

Although fluoroform is one of the most simple molecules belonging to the point group C_{3v}, only a few studies of its rotation-vibration spectra have been reported.[1-4] This is largely due to the deficiency in the resolving power of the spectrometers. Graner *et al.*[1] have observed the infrared spectra for the ν_6 and ν_3 fundamentals with an approximate resolution of 0.03 cm^{-1}. As for the ν_4 fundamental, the observations have been done under rather poor resolution. The molecular constants have been obtained from the analyses of the heads of the successive Q's in these works,[2-4] because the resolving power was not quite enough to resolve the successive Q branches into their fine structures. The present report concerns itself with the measurement of the rotation-vibration spectra for the ν_4 fundamental of fluoroform by the use of a tunable diode laser-source spectrometer and with the analysis of the rotation-vibration spectra.

Experimental

The sample used in this study was a commercial product and was used without further purification. The survey spectrum of the ν_4 band of fluoroform was recorded from 1350 to 1410 cm^{-1} using a Nicolet 7199A Fourier transform infrared spectrometer at a resolution of 0.06 cm^{-1}. The observation was made at room temperature using a 10 cm gas cell. The sample pressure was about 9 Torr.

The high resolution spectra were recorded from 1361 to 1385 cm^{-1} by the use of a tunable diode laser-source spectrometer (Laser Analytics, model LS 3). The sample pressure was 0.5—1.5 Torr. As the resolution of the instrument was estimated to be 10^{-4}—10^{-3} cm^{-1}, the line-width of the observed spectrum was governed by the Doppler broadening. About ten modes could be oscillated in the region cited above. In order to determine an accurate frequency value, the wavelengths of a few lines for each mode were measured by the use of a Michelson interferometer-type wavelength meter which was designed and constructed by Nagai *et al.*[5] The wavelengths of the other lines were determined relative to these frequencies by observing the interference fringes arising from a confocal germanium etalon. The free spectral range was calibrated to be $0.009929\pm0.000008\ cm^{-1}$ by the use of the OCS lines in the 870 cm^{-1} region. The precision of the wavelength measurement was about 0.0015 cm^{-1}. The accuracy of the wavelength measurement was restricted by the incomplete alignment of the reference He–Ne laser beam in parallel with the diode laser source.[5] It is believed to be better than 0.001 cm^{-1}.

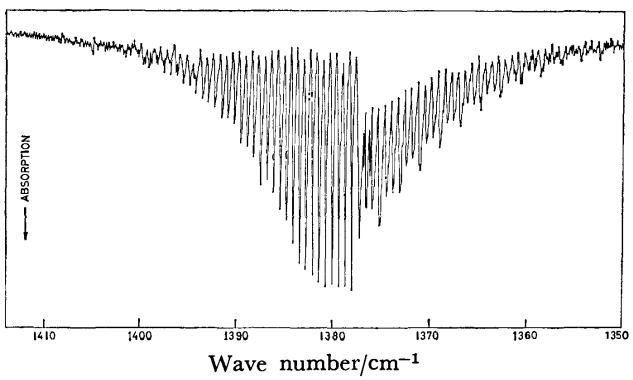

Fig. 1. The infrared absorption spectra for the ν_4 band of fluoroform recorded by the Fourier transform spectrometer.

Results and Discussion

Observed Spectra. The spectra for the ν_4 band recorded by the Fourier transform spectrometer is shown in Fig. 1. We can see the usual intensity alternation due to the three-fold symmetry for the sub-bands on the low frequency side (the 1377—1350 cm^{-1} region). These sub-bands may therefore be assigned to the successive ^RQ lines. In the high frequency region (the 1377—1400 cm^{-1} region), on the other hand, we cannot recognize any clear intensity alternations. This happens because these sub-bands on the high frequency side are mainly composed from

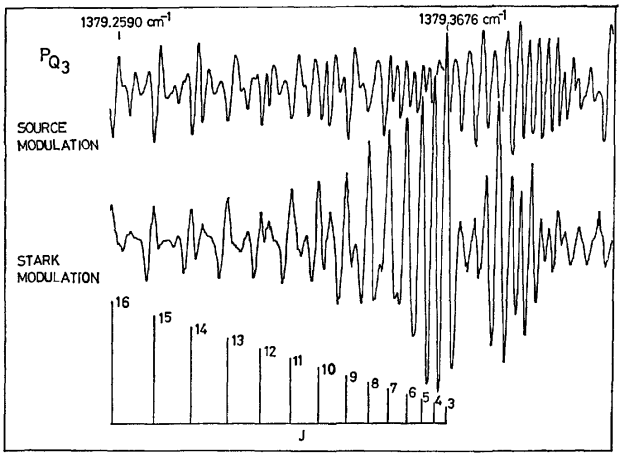

Fig. 2. The high resolution spectra observed by the diode laser-source spectrometer (upper: source modulation, lower: Stark modulation).

the ^{R}R lines instead of ^{P}Q lines. The ^{P}Q lines form only a background of the high frequency side.

Figure 2 shows the part of the high resolution spectra observed by the diode laser-source spectrometer which may be assigned to the $^{P}Q_3$ line series. The upper spectra were recorded by modulating the source diode by a sine wave of 5 kHz and detecting the absorption signal at 10 kHz by the use of a phase-sensitive detection method. The lower spectra were recorded by the use of the usual Stark modulation method. The modulation frequency and the electric field were 100 kHz and 200 V_{p-p}/cm (being superposed on the 200 V/cm DC field), respectively. The lower spectra were used for the J-number assignment.

The observed frequency values are summarized in Table 2, together with the assignments.

Assignment of the Observed Spectra. First, we calculated the synthetic spectra corresponding to the ν_4 fundamental by using the approximate molecular constants given in the references.[1,4] The spectral simulation showed that a group of lines having the same K value forms a localized sub-band, ^{P}Q or ^{R}Q, and that a group of lines having the same $(J-K)$ value form a localized sub-band, ^{P}P or ^{R}R. The comparison between the observed and the calculated frequencies leads to the rigorous assignments of K and $(J-K)$ numbers to the sub-bands ^{P}Q, ^{R}Q, ^{P}P, and ^{R}R. The sub-bands ^{P}P and ^{R}R can be identified from the sub-bands ^{P}Q and ^{R}Q, because the component lines of ^{P}P and ^{R}R show the intensity alternation due to the three-fold symmetry. The assignments of K numbers to the ^{P}Q and ^{R}Q sub-bands are confirmed by the low-resolution spectra of Fig. 1.

The assignment of J numbers to the component fine structure lines of each sub-bands can be done without ambiguity by using the Stark modulated spectra and the missing lines rule $(J \geq K)$. As the apparent intensity of a Stark modulated spectrum is observed to be stronger for lower J, the lines of the smallest J number in a sub-band is easily found. Therefore, the J number is rigorously assigned to the individual component lines in consideration of the missing lines rule and the already determined K and $(J-K)$ values. In this way we could identify about 100 lines and make a rigorous assignment of J and K numbers. Using these lines, trial molecular constants were obtained by least-squares method; these in turn were used in the spectral simulation to make further assignments.

Determination of the Molecular Constants. The vibration-rotation energy of a symmetric top in an E-vibrational state can be written in the form (for $v_4=1$):

$$\begin{aligned} E(J,k,l) = {} & \nu_0 + (C_4 - B_4)k^2 + B_4 J(J+1) - 2(C\zeta)_4 kl \\ & - D_4^J J^2(J+1)^2 - D_4^{JK} J(J+1)k^2 \\ & - D_4^K k^4 + \eta_4^J J(J+1)kl + \eta_4^K k^3 l, \end{aligned} \tag{1}$$

where ν_0 is the vibrational energy, C_4 and B_4 are the rotational constants, ζ is the Coriolis coupling constant, D_4^J, D_4^{JK}, and D_4^K are the centrifugal distortion constants, and η_4^J and η_4^K express the dependence of the Coriolis coupling on J and K.

From the selection rules for a perpendicular band ($\Delta k=+1$, $\Delta l=+1$, and $\Delta J=0, \pm 1$; or $\Delta k=-1$, $\Delta l=-1$, and $\Delta J=0, \pm 1$), the transition frequencies can be calculated as the differences between the energy levels of the upper and lower states. The energy of the ground state can be given by this formula:

$$\begin{aligned} E(J,k) = {} & (C_0 - B_0)k^2 + B_0 J(J+1) \\ & - D_0^J J^2(J+1)^2 - D_0^{JK} J(J+1)k^2 - D_0^K k^4. \end{aligned} \tag{2}$$

The B_0, D_0^J, D_0^{JK}, and C_0 values were obtained by the microwave studies[6,7] and/or by the analysis of the infrared spectra.[3,4,8] The D_0^K value was calculated from the harmonic force field.[7] After fixing all these molecular constants related with the ground state, the molecular constants of the excited state were determined by the least-squares method. The constants thus obtained are listed in Table 1 together with the fixed ground state values. The observed frequencies are listed in Table 2 with their assignments and the calculated frequencies.

Table 1. MOLECULAR CONSTANTS OF THE ν_4 BAND OF CHF_3 (cm^{-1})

ν_0	1377.84576(33)	η_4^J	$1.436(35)\times10^{-6}$
B_4	0.3447884(12)	η_4^K	$-8.20(28)\times10^{-7}$
C_4	0.18913390(54)		Ground State
$(C\zeta)_4$	0.186195(10)	B_0	0.34520105(7)
D_4^J	$3.7774(85)\times10^{-7}$	C_0	0.18925(10)
D_4^{JK}	$-5.735(18)\times10^{-7}$	D_0^J	3.779×10^{-7}
D_4^K	$2.941(12)\times10^{-7}$	D_0^{JK}	$-6.0375(134)\times10^{-7}$
q_4	$-1.115(12)\times10^{-4}$	D_0^K	3.72×10^{-7}

Numbers in parentheses denote the standard deviation σ.

l-type Doubling. In the case of the ν_4 fundamental, the effect of the l-type resonance is not so drastic as was observed for the ν_6 fundamental.[1] This is because the Coriolis coupling constant ζ_4 takes a positive value, which produces a repulsive effect on the interacting pair. As the precision of the frequency measurement exceeds the order of 10^{-3} cm^{-1}, it is possible to determine the l-type doubling constant, q_4. In our analysis, we take l-type resonace into account as well as l-type doubling.

The perturbed energies can be obtained from the diagonalization of a 2×2 matrix of this form:

$$\begin{bmatrix} E(K-1,\ l=-1) & W \\ W & E(K+1,\ l=+1) \end{bmatrix}, \tag{3}$$

where K is the absolute value of k. The off-diagonal element, W, has this form:

$$W = -\frac{q_4}{2}[J(J+1)-K(K+1)]^{1/2}[J(J+1)-K(K-1)]^{1/2}. \tag{4}$$

The explicit expression for the perturbed energy level can be written as

$$\begin{aligned} 2E_{\pm}(J,K\pm1,\pm1) = {} & E(J,K-1,-1) + E(J,K+1,+1) \\ & \pm \{E[(J,K-1,-1) - E(J,K+1,1)]^2 \\ & + q_4^2[J(J+1)-K(K+1)][J(J+1) \\ & - K(K-1)]\}^{1/2}, \end{aligned} \tag{5}$$

where E_+ and E_- correspond to the perturbed states of the upper and lower levels of the interacting pair, respectively. In order to determine the sign of q_4, the twelve lines which are definitely assigned to the

TABLE 2. OBSERVED AND CALCULATED FREQUENCIES OF THE ν_4 BAND

Assignment[a] K (J)	Observed frequency (cm^{-1})	Obsd − Calcd (cm^{-1})	Assignment[a] K (J)	Observed frequency (cm^{-1})	Obsd − Calcd (cm^{-1})	Assignment[a] K (J)	Observed frequency (cm^{-1})	Obsd − Calcd (cm^{-1})
PQ 3 (3)	1379.3676	0.0011	RQ 6(31)	1372.8314	-0.0008	PP25(33)	1371.3531	-0.0088
PQ 3 (4)	1379.3637	0.0006	RQ 6(32)	1372.8053	-0.0015	PP26(34)	1371.3270	-0.0142
PQ 3 (5)	1379.3596	0.0006	RQ 6(33)	1372.7799	-0.0007	PP27(35)	1371.2982	-0.0220
PQ 3 (6)	1379.3547	0.0008	RQ 6(34)	1372.7520	-0.0017			
PQ 3 (7)	1379.3487	0.0006	RQ 6(35)	1372.7238	-0.0021	PP 1(18)	1365.4570	0.0000
PQ 3 (8)	1379.3421	0.0007	RQ 6(36)	1372.6949	-0.0024	PP 2(19)	1365.4369	0.0001
PQ 3 (9)	1379.3350	0.0012	RQ 6(37)	1372.6659	-0.0020	PP 3(20)	1365.4162	-0.0001
PQ 3(10)	1379.3267	0.0012	RQ 6(38)	1372.6352	-0.0026	PP 4(21)	1365.3956	0.0001
PQ 3(11)	1379.3172	0.0010	RQ 6(39)	1372.6060	-0.0008	PP 5(22)	1365.3746	0.0002
PQ 3(12)	1379.3074	0.0012				PP 6(23)	1365.3531	0.0002
PQ 3(13)	1379.2967	0.0014	RQ 7 (8)	1372.5157	-0.0015	PP 7(24)	1365.3316	0.0005
PQ 3(14)	1379.2851	0.0015	RQ 7 (9)	1372.5088	-0.0013	PP 8(25)	1365.3100	0.0010
PQ 3(15)	1379.2724	0.0014	RQ 7(10)	1372.5009	-0.0013	PP 9(26)	1365.2872	0.0008
PQ 3(16)	1379.2590	0.0014	RQ 7(11)	1372.4920	-0.0016	PP10(27)	1365.2645	0.0010
PQ 3(17)	1379.2449	0.0015	RQ 7(12)	1372.4827	-0.0014	RP 1(16)	1365.4963	0.0003
PQ 3(18)	1379.2299	0.0015	RQ 7(13)	1372.4727	-0.0011	RP 2(15)	1365.5162	0.0010
PQ 3(19)	1379.2139	0.0014	RQ 7(14)	1372.4608	-0.0020	RP 3(14)	1365.5358	0.0016
PQ 3(20)	1379.1968	0.0011	RQ 7(15)	1372.4489	-0.0021			
PQ 3(21)	1379.1793	0.0011	RQ 7(16)	1372.4364	-0.0020	PP 1(19)	1364.7534	0.0001
PQ 3(22)	1379.1609	0.0011	RQ 7(17)	1372.4232	-0.0017	PP 2(20)	1364.7330	0.0007
PQ 3(23)	1379.1414	0.0008	RQ 7(18)	1372.4087	-0.0020	PP 3(21)	1364.7113	0.0002
PQ 3(24)	1379.1214	0.0009	RQ 7(19)	1372.3943	-0.0015	PP 4(22)	1364.6896	0.0001
PQ 3(25)	1379.1005	0.0009				PP 5(23)	1364.6674	-0.0002
PQ 3(26)	1379.0788	0.0009	RQ18(19)	1364.9547	-0.0009	PP 6(24)	1364.6453	-0.0001
PQ 3(27)	1379.0563	0.0009	RQ18(20)	1364.9396	-0.0010	PP 7(25)	1364.6228	0.0000
PQ 3(28)	1379.0321	0.0001	RQ18(21)	1364.9241	-0.0008	PP 8(26)	1364.6000	0.0002
PQ 3(29)	1379.0078	0.0000	RQ18(22)	1364.9068	-0.0017	PP 9(27)	1364.5771	0.0007
PQ 3(30)	1378.9831	0.0003	RQ18(23)	1364.8897	-0.0016	PP10(28)	1364.5538	0.0011
PQ 3(31)	1378.9573	0.0004	RQ18(24)	1364.8717	-0.0016	PP11(29)	1364.5296	0.0010
PQ 3(32)	1378.9305	0.0002	RQ18(25)	1364.8537	-0.0009	PP12(30)	1364.5050	0.0009
PQ 3(33)	1378.9031	0.0003	RQ18(26)	1364.8337	-0.0015	PP13(31)	1364.4808	0.0016
PQ 3(34)	1378.8747	0.0003	RQ18(27)	1364.8143	-0.0007	PP14(32)	1364.4558	0.0019
PQ 3(35)	1378.8452	-0.0001	RQ18(28)	1364.7932	-0.0009	PP15(33)	1364.4298	0.0016
			RQ18(29)	1364.7715	-0.0009	PP16(34)	1364.4032	0.0012
PQ 9(23)	1383.2575	0.0019	RQ18(30)	1364.7491	-0.0008	PP17(35)	1364.3765	0.0010
PQ 9(24)	1383.2357	0.0011	RQ18(31)	1364.7254	-0.0014	PP18(36)	1364.3486	0.0001
PQ 9(25)	1383.2142	0.0013	RQ18(32)	1364.7012	-0.0017			
PQ 9(26)	1383.1922	0.0020	RQ18(33)	1364.6765	-0.0017	RR30(33)	1380.0676	0.0027
PQ 9(27)	1383.1682	0.0015	RQ18(34)	1364.6512	-0.0016	RR31(34)	1380.0639	0.0023
PQ 9(28)	1383.1436	0.0013	RQ18(35)	1364.6251	-0.0015	RR32(35)	1380.0610	0.0030
PQ 9(29)	1383.1182	0.0012	RQ18(36)	1364.5978	-0.0019	RR33(36)	1380.0573	0.0030
PQ 9(30)	1383.0922	0.0013	RQ18(37)	1364.5698	-0.0022	RR34(37)	1380.0532	0.0028
PQ 9(31)	1383.0655	0.0016	RQ18(38)	1364.5423	-0.0013	RR35(38)	1380.0494	0.0031
PQ 9(32)	1383.0379	0.0019	RQ18(39)	1364.5134	-0.0011	RR36(39)	1380.0450	0.0029
PQ 9(33)	1383.0088	0.0015	RQ18(40)	1364.4832	-0.0014	RR37(40)	1380.0404	0.0027
PQ 9(34)	1382.9794	0.0017	RQ18(41)	1364.4523	-0.0017	RR38(41)	1380.0359	0.0028
PQ 9(35)	1382.9489	0.0017	RQ18(42)	1364.4215	-0.0011	RR39(42)	1380.0308	0.0025
PQ 9(36)	1382.9181	0.0022	RQ18(43)	1364.3889	-0.0016	RR40(43)	1380.0251	0.0018
PQ 9(37)	1382.8871	0.0034	RQ18(44)	1364.3554	-0.0022	RR41(44)	1380.0200	0.0018
PQ 9(38)	1382.8541	0.0035				RR42(45)	1380.0146	0.0016
PQ 9(39)	1382.8195	0.0028	PP28(28)	1377.0457	-0.0013	RR43(46)	1380.0084	0.0009
			PP29(29)	1377.0328	-0.0009	RR44(47)	1380.0026	0.0006
PQ11(13)	1384.7970	0.0007	PP31(31)	1377.0062	-0.0003	RR45(48)	1379.9960	-0.0002
PQ11(14)	1384.7843	0.0004	PP32(32)	1376.9924	-0.0001	RR46(49)	1379.9894	-0.0009
PQ11(15)	1384.7716	0.0009	PP33(33)	1376.9775	-0.0008	RR47(50)	1379.9831	-0.0012
PQ11(16)	1384.7575	0.0010	PP34(34)	1376.9628	-0.0010	RR48(51)	1379.9763	-0.0018
PQ11(17)	1384.7422	0.0008	PP35(35)	1376.9489	-0.0002	RR49(52)	1379.9661	-0.0057
PQ11(18)	1384.7264	0.0009	PP36(36)	1376.9343	0.0001	RR50(53)	1379.9538	-0.0115
PQ11(19)	1384.7098	0.0011	PP37(37)	1376.9193	0.0003			
PQ11(20)	1384.6922	0.0012	PP38(38)	1376.9035	-0.0000	RR18(23)	1381.4325	0.0010
PQ11(21)	1384.6745	0.0021	PP39(39)	1376.8880	0.0001	RR19(24)	1381.4297	0.0009
PQ11(22)	1384.6551	0.0021	PP40(40)	1376.8727	0.0008	RR20(25)	1381.4268	0.0009
PQ11(23)	1384.6348	0.0022	PP41(41)	1376.8571	0.0013	RR21(26)	1381.4239	0.0010
PQ11(24)	1384.6141	0.0027	PP42(42)	1376.8404	0.0010	RR22(27)	1381.4202	0.0006
PQ11(25)	1384.5917	0.0024	PP43(43)	1376.8239	0.0012	RR23(28)	1381.4167	0.0006
			PP44(44)	1376.8069	0.0010	RR24(29)	1381.4128	0.0005
RQ 0(27)	1377.0493	-0.0002	PP45(45)	1376.7891	0.0003	RR25(30)	1381.4089	0.0005
RQ 0(28)	1377.0290	-0.0006	PP46(46)	1376.7729	0.0015	RR26(31)	1381.4040	-0.0003
RQ 0(29)	1377.0092	0.0001	PP47(47)	1376.7551	0.0012	RR27(32)	1381.3995	-0.0005
RQ 0(30)	1376.9873	-0.0005	PP48(48)	1376.7375	0.0014	RR28(33)	1381.3948	-0.0006
RQ 0(31)	1376.9655	-0.0003	PP49(49)	1376.7190	0.0009	RR29(34)	1381.3894	-0.0013
RQ 0(32)	1376.9431	-0.0000	PP50(50)	1376.7003	0.0005	RR30(35)	1381.3835	-0.0022
RQ 0(34)	1376.8954	-0.0002	PP51(51)	1376.6809	-0.0004			
RQ 0(35)	1376.8708	-0.0000				RR42(50)	1383.2488	-0.0004
RQ 0(36)	1376.8453	0.0000	PP 1 (8)	1372.4545	-0.0016	RR44(52)	1383.2269	-0.0008
RQ 0(37)	1376.8195	0.0004	PP 2 (9)	1372.4414	-0.0024	RR46(54)	1383.2058	0.0003
RQ 0(38)	1376.7925	0.0004	PP 3(10)	1372.4296	-0.0016	RR48(56)	1383.1820	-0.0003
RQ 0(39)	1376.7642	-0.0003	PP 4(11)	1372.4169	-0.0014	RR50(48)	1383.1590	0.0006
			PP 5(12)	1372.4032	-0.0020	RR52(60)	1383.1335	-0.0001
RQ 6 (7)	1373.2028	-0.0007	PP 6(13)	1372.3894	-0.0024	RR54(62)	1383.1082	0.0003
RQ 6 (8)	1373.1964	-0.0008	PP 7(14)	1372.3768	-0.0013	RR56(64)	1383.0817	0.0002
RQ 6 (9)	1373.1892	-0.0008	PP 8(15)	1372.3626	-0.0015	RR57(65)	1383.0688	0.0008
RQ 6(10)	1373.1813	-0.0008	PP 9(16)	1372.3480	-0.0018	RR58(66)	1383.0546	0.0003
RQ 6(11)	1373.1725	-0.0009	PP10(17)	1372.3345	-0.0008	RR60(68)	1383.0267	0.0005
RQ 6(12)	1373.1630	-0.0009	PP11(18)	1372.3193	-0.0011			
RQ 6(13)	1373.1530	-0.0006	PP12(19)	1372.3051	-0.0001	RR 1(11)	1384.8550	0.0022
RQ 6(14)	1373.1414	-0.0011				RR 2(12)	1384.8518	0.0022
RQ 6(15)	1373.1296	-0.0010	PP 5(13)	1371.7069	0.0016	RR 3(13)	1384.8476	0.0015
RQ 6(16)	1373.1164	-0.0015	PP 6(14)	1371.6932	0.0021	RR 4(14)	1384.8439	0.0014
RQ 6(17)	1373.1030	-0.0014	PP 7(15)	1371.6779	0.0014	RR 5(15)	1384.8397	0.0011
RQ 6(18)	1373.0904	0.0003	PP 8(16)	1371.6633	0.0016	RR 6(16)	1384.8353	0.0008
RQ 6(19)	1373.0734	-0.0016	PP 9(17)	1371.6482	0.0016	RR 7(17)	1384.8310	0.0008
RQ 6(20)	1373.0579	-0.0013	PP10(18)	1371.6321	0.0009	RR 8(18)	1384.8266	0.0009
RQ 6(21)	1373.0400	-0.0025	PP11(19)	1371.6175	0.0020	RR 9(19)	1384.8216	0.0006
RQ 6(22)	1373.0234	-0.0016	PP12(20)	1371.6012	0.0017	RR10(20)	1384.8167	0.0006
RQ 6(23)	1373.0043	-0.0025	PP13(21)	1371.5845	0.0014	RR11(21)	1384.8109	-0.0000
RQ 6(24)	1372.9856	-0.0022	PP14(22)	1371.5683	0.0018	RR12(22)	1384.8058	0.0003
RQ 6(25)	1372.9656	-0.0023	PP15(23)	1371.5514	0.0019	RR13(23)	1384.7994	-0.0005
RQ 6(26)	1372.9451	-0.0022	PP16(24)	1371.5345	0.0023	RR14(24)	1384.7934	-0.0007
RQ 6(27)	1372.9242	-0.0017	PP17(25)	1371.5162	0.0016	RR15(25)	1384.7879	-0.0001
RQ 6(28)	1372.9022	-0.0015	PP18(26)	1371.4983	0.0016	RR16(26)	1384.7814	-0.0004
RQ 6(29)	1372.8792	-0.0014	PP19(27)	1371.4798	0.0013	RR17(27)	1384.7749	-0.0004
RQ 6(30)	1372.8552	-0.0016	PP20(28)	1371.4607	0.0008	RR18(28)	1384.7682	-0.0003
			PP21(29)	1371.4411	0.0001	RR19(29)	1384.7611	-0.0004
			PP22(30)	1371.4204	-0.0013	RR20(30)	1384.7541	-0.0002
			PP23(31)	1371.3993	-0.0028	RR21(31)	1384.7462	-0.0007
			PP24(32)	1371.3768	-0.0053	RR22(32)	1384.7386	-0.0006
						RR23(33)	1384.7304	-0.0009

TABLE 2. Continued

Assignment[a] $K(J)$	Observed frequency (cm^{-1})	Obsd−Calcd (cm^{-1})
RR24(34)	1384.7233	0.0001
RR25(35)	1384.7144	−0.0004
RR26(36)	1384.7062	−0.0000
RR27(37)	1384.6977	0.0004
RR28(38)	1384.6882	−0.0000
RR29(39)	1384.6800	0.0011
RR30(40)	1384.6706	0.0013
RR31(41)	1384.6604	0.0009
RR32(42)	1384.6510	0.0015
RR33(43)	1384.6403	0.0011
RR34(44)	1384.6309	0.0023
RR35(45)	1384.6203	0.0025
RR36(46)	1384.6101	0.0033
RR37(47)	1384.5987	0.0032
RR38(48)	1384.5877	0.0037

The standard deviation of the residuals $\sigma = 0.0023\ cm^{-1}$.

a) For example, PQ 3(3) denotes $^{P}Q_3(3)$.

$^{R}Q_0$ were carefully observed. The standard deviation arising in the least-squares fitting has shown that the negative sign was definitely preferable to the positive sign. The final result for q_4 is included in Table 1.[9]

x-y Type Coriolis Interaction. The standard deviation of $0.0023\ cm^{-1}$ for the overall least-squares fit is somewhat too large if we consider the precision of the wavelength measurement. This may hint at the existence of an x-y type Coriolis interaction between ν_4 and $2\nu_3$, because the band origin of $2\nu_3$ is expected to be about $1400\ cm^{-1}$. The intensity of the $2\nu_3$ band is so weak, in comparison with the ν_4 band, that we failed to pick up the lines of $2\nu_3$ in the $1400\ cm^{-1}$ region. Therefore, we attempted to consider the effect of such an x-y type Coriolis interaction by using the frequencies calculated for $2\nu_3$. The molecular constants were estimated from the results obtained for the $2\nu_3-\nu_3$.[1] The details are:

$$\nu = 700.1009 + 699.310 = 1399.411\ cm^{-1}$$

$$B = B_0 - 0.641\times10^{-3} - 0.6463\times10^{-3} = 0.343914\ cm^{-1}$$

$$C \simeq C_0 - 2\times1.700\times10^{-4} = 0.18852\ cm^{-1}$$

$$D^J = 3.52\times10^{-7}\ cm^{-1}$$

$$D^{JK} \simeq D_0^{JK} - 2\times(0.28\times10^{-8}) = -6.0935\times10^{-7}\ cm^{-1}$$

and

$$D^K \simeq D_0^K = 3.27\times10^{-7}\ cm^{-1}.$$

The matrix elements of the Hamiltonian for the Coriolis interaction between ν_4 and $2\nu_3$ are expressed as

$$\langle v_3 = 2, J, K|H_c|\ v_4 = 1,\ l = \pm1,\ J, K\pm1\rangle = \pm\xi_{334}[J(J+1)-K(K\pm1)]^{1/2}.$$

The ζ_{334} value is obtained from the ξ_{334} value by this relation:[10]

$$\xi_{334} = \left(\frac{1}{\sqrt{2}}\right)[(\nu_4/\nu_{33})^{1/2} + (\nu_{33}/\nu_4)^{1/2}]B\zeta_{334}.$$

By considering the x-y Coriolis interaction, the standard deviation value was reduced from $0.0024\ cm^{-1}$ to $0.0012\ cm^{-1}$. The final interaction parameters obtained are: $|\xi_{334}| = 0.03185\pm0.00054\ cm^{-1}$ and $|\zeta_{334}| = 0.065$. Other molecular constants did not change their magnitude very much, except for η_4^J and η_4^K. These values were obtained to be $(6.94\pm0.32)\times10^{-7}\ cm^{-1}$ and $(-1.30\pm0.24)\times10^{-7}\ cm^{-1}$, respectively. As this treatment of the x-y type Coriolis interaction is not complete, we have listed the molecular constant values which were obtained without considering this interaction in Table 1. However it must be concluded that the interaction parameter $|\zeta_{334}|$ takes the value of about 0.065 and that the molecular constants given in Table 1 are not affected much by the neglect of this type of interaction.

The authors are grateful to Dr. Jun Nakagawa of Hiroshima University for his helpful suggestions about the computer program.

References

1) G. Graner, R. Anttila, and J. Kauppinen, *Mol. Phys.*, **38**, 103 (1979).
2) L. C. Hoskins, *J. Chem. Phys.*, **53**, 4216 (1970).
3) A. Ruoff, H. Bürger, and S. Biedermann, *Spectrochim. Acta, Part A*, **27**, 1359 (1970).
4) N. J. Fyke, P. Lockett, J. K. Thomson, and P. M. Wilt, *J. Mol. Spectrosc.*, **58**, 87 (1975).
5) K. Nagai, K. Kawaguchi, C. Yamada, K. Hayakawa, Y. Takagi, and E. Hirota, *J. Mol. Spectrosc.*, (accepted, 1980).
6) T. E. Sullivan and L. Frenkel, *J. Mol. Spectrosc.*, **39**, 185 (1971).
7) Y. Kawashima and A. Peter Cox, *J. Mol. Spectrosc.*, **72**, 423 (1978).
8) F. N. Marsi and W. E. Blass, *J. Mol. Spectrosc.*, **39**, 98 (1971).
9) As for the definition of the sign of q_4, see the text book: G. Herzberg, "Molecular Spectra and Molecular Structure," D. Van Nostrand Company, Inc., London (1967), Vol. III, p. 91.
10) H. Matsuura and T. Shimanouchi, *J. Mol. Spectrosc.*, **60**, 93 (1976); C. di Lauro and I. M. Mills, *ibid.*, **21**, 386 (1966).

Phase Transition in Ammonium-d_4 Sulfate as Studied by Heat Capacity Measurements between 3 and 300 K†

Yoshiyuki HIGASHIGAKI†† and Hideaki CHIHARA*

Department of Chemistry and Chemical Thermodynamics Laboratory, Faculty of Science, Osaka University, Toyonaka 560

(Received September 17, 1980)

Molar heat capacities were determined of $(ND_4)_2SO_4$ between 2.8 and 301 K. The phase transition at 223.94±0.03 K is of the first-order with a long tail extending down to 160 K. The overall heat and entropy of transition are 4270 J mol^{-1} and 20.35 J K^{-1} mol^{-1}, respectively, the first-order portion contributing only 40%. The contraction of the molar volume at the transition was evaluated as 0.33 cm^3 mol^{-1}. The enthaply to misorient ions in an otherwise perfectly ordered lattice was derived from the low-temperature tail of the anomalous heat capacity. It was 12.0 kJ/mol of $(ND_4)_2SO_4$, in reasonable agreement with 16 kJ mol^{-1} derived from O'Reilly-Tsang's mean field theory. The present results support the order-disorder mechanism of the transition.

Ammonium sulfate is probably one of the most extensively studied ferroelectric crystals. Its phase transition had been known to exist at about −50 °C by calorimetric investigations[1-3] before the ferroelectricity was discovered by Matthias and Remeika[4] in 1956. Since then reports have been published on its properties by such measurements as dielectric,[5,6] calorimetric,[5] X-ray[7] and electron[8] diffractions, neutron diffraction,[9] infrared[10,11] and far-infrared absorption,[12] neutron[13,14] and Raman[12] scattering, proton[10,15-18] and deuteron[17,19] magnetic resonance.

In spite of these studies, the nature of the phase transition has not been established; the neutron diffraction studies and the deuteron resonance studies gave conflicting interpretations. Thus, Schlemper and Hamilton[9] stated that both the high- and low-temperature phases were ordered from their neutron diffraction experiments on a single crystal of $(NH_4)_2SO_4$ whereas O'Reilly and Tsang[17] proposed that the transition is of an order-disorder type from their deuteron resonance. Both techniques indicate that there are two crystallographically inequivalent ammonium ions but the main issue is that whereas the neutron diffraction results can be interpreted by static distortion of the hydrogen-bonded ammonium tetrahedra, the deuteron resonance has to show a double minimum potential on each ammonium across the mirror plane in the high-temperature phase. O'Reilly and Tsang[20] then developed a molecular field theory based on a three-sublattice model involving disorder of sulfate ions. High resolution inelastic neutron scattering experiments[14] also support the dynamic order-disorder model.

More recently, an X-ray diffraction study[21] suggested strongly that the low-temperature phase of $(NH_4)_2SO_4$ was more properly described as a ferrielectric state in which the two types of inequivalent ammonium ions might assume separate order parameters. Peculiarity of the spontaneous polarization[26] at low temperatures and smallness of the Curie-Weiss constant in the high-temperature phase were also the reason to suspect the crystal to be ferrielectric at low temperatures.

Previous heat capacity results[2,5] are not sufficiently accurate for detailed examination of the transition; the measurements reported in this paper are consistent with the order-disorder model of the transition.

Experimental

Material. Ammonium sulfate (Nakarai Chemicals, Ltd., stated purity better than 99.5%) was recrystallized from distilled water and dried in vacuo. Ammonium-d_4 sulfate was prepared by deuterium substitution of the recrystallized $(NH_4)_2SO_4$ in heavy water. Thus, the degassed heavy water with various deuterium concentrations (48.1—99.8%) was transfered onto solid in a vacuum apparatus to prevent pick-up of atmospheric water and then the aqueous solution was evaporated to dryness. The deuterium content of water which was distilled in vacuo was monitored with the integral proton intensity of the high resolution NMR at each substitution step. Water thus distilled at the final stage was found to have an isotopic purity of 99.6%. The $(ND_4)_2SO_4$ crystals thus obtained, however, showed a small thermal anomaly at about 250 K on DTA thermogram, which was likely to be due to D_2O occluded in the $(ND_4)_2SO_4$ specimen. These crystals were then pulverized and heated to 80 °C under vacuum but this small DTA peak did not

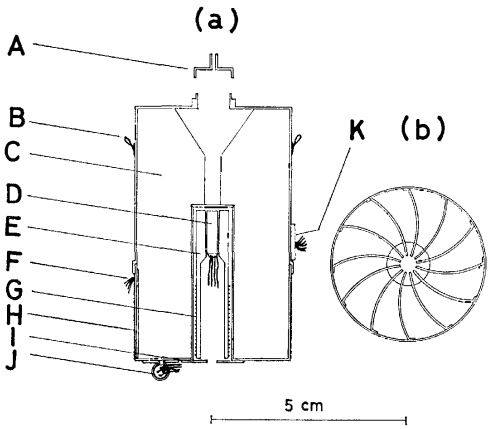

Fig. 1. Calorimeter vessel. (a) vertical cross-section (b) horizontal cross-section. A cap of vessel, B looped hook of copper, C gold-plated copper vane, D platinum thermometer, E thermometer/heater holder, F lead wire outlet, G KARMA heater, H lead wire wound non-inductively, I radiation trap, J germanium thermometer, K sleeve for differential thermocouples.

† Contribution No. 12 from Chemical Thermodynamics Laboratory, Faculty of Science, Osaka University.

†† Present address: Department of Chemistry, University of Utah, Salt Lake City, Utah 84112, U.S.A.

disappear completely. Therefore, the $(ND_4)_2SO_4$ crystals were dissolved in D_2O again, recrystallized by slow cooling, separated from the solution by filtration, and dried *in vacuo*. Crystals thus prepared still showed a smaller heat anomaly at the same temperature as before, which disappeared after several thermal cycles between room temperature and liquid nitrogen temperature in a vacuum. Deuterium content of this sample was determined to be 99.3% from the deuterium content of the water distilled from the last mother liquor. Found: N, 19.90; S, 22.95%. Calcd for: N, 19.98; S, 22.87%.

The powder samples were put into the gold-plated copper calorimeter vessel which will be described below, in a conventional dry-box to reject atmospheric moisture. Weight of specimen used for calorimetry was 48.668 g (*in vacuo*), amounting to 0.34717 mol.

Calorimeter and Cryostat. The apparatus used was a newly constructed cryostat of a design similar to the one reported in the literature.[22] Some modifications were made to permit continuous operation from 2.5 K to 300 K using both liquid helium and liquid nitrogen. Once charged fully in the lower refrigerant tank, the liquid helium lasted for 6 to 10 h according as the upper tank contained solid nitrogen or solid hydrogen.

The calorimeter vessel is made of copper (0.3 mm in wall thickness) with 12 vertical vanes of copper (0.2 mm thick) as shown in Fig. 1. Both outside and inside were gold-plated. The platinum resistance thermometer D (Minco Products, Inc., Model S1055-1, Laboratory designation α) was fitted to the copper holder E with soft solder around which the heater G (double-nylon insulated KARMA wire, Driver-Harris Co., B.S. #36) was wound non-inductively and fixed with G.E. 7031 adhesive. This thermometer/heater assembly was cast into the re-entrant well of the calorimeter vessel with Wood's alloy. Gold-plated radiation shield I covers most of the bottom to reduce direct heat exchange between the thermometer and the adiabatic shield that surrounds the calorimeter vessel. The germanium resistance thermometer J (CryoCal, Inc., Model CR 1000, Laboratory designation ε) was fitted into a copper sheath snugly with small amounts of silicone grease. The calorimeter vessel thus weighed 91 g including the attachments and its inside volume was 76 cm^3. In measurements of the heat capacity of the $(ND_4)_2SO_4$ sample, helium exchange gas less than 3.6×10^{-5} mol was used for Series from I to XII and 1.5×10^{-5} mol for Series from XIII to XV. Equilibration rates of the vessel containing $(ND_4)_2SO_4$ varied greatly. At temperatures below 20 K, the sample reached equilibrium in ten seconds to a few minutes. At higher temperatures it took about 15 min for equilibrium, except near the ferroelectric transition temperature where it was much longer. The sample contributed 23% to the total heat capacity at 3 K: the contribution increased to more than 60% above 100 K.

Temperature Scales. The platinum thermometer (α) was used above 14 K and the germanium thermometer (ε) below 15 K. They were calibrated prior to the measurements of heat capacity.

The temperature scale of the thermometer α was fixed based on the 1968 International Practical Temperature Scale (IPTS 68). The necessary resistance values at the eight defining fixed points from 13.81 to 373.15 K were obtained by comparison with the Leeds & Northrup platinum thermometer (Model 8164) whose scale was determined at the U.S. National Bureau of Standards on IPTS 68. The thermometer α proved to satisfy the condition for the SPRT; $R(100\ °C)/R(0\ °C)\geqq1.3925$. The necessary coefficients for the IPTS 68 scale below 0 °C were calculated according to the standard procedure.[23] To obtain the scale between 0 and 100 °C, the resistance values were measured from 255 to 380 K at intervals of 5 K instead of determining the value at the freezing point of tin or zinc. Observed values of temperatures based on the IPTS 68 and the resistances were fitted to the following empirical formula;

$$R(t) = R(0)\{1+At+Bt^2+C(t-100)t^3\},$$

where $t=T_{68}-273.15$.

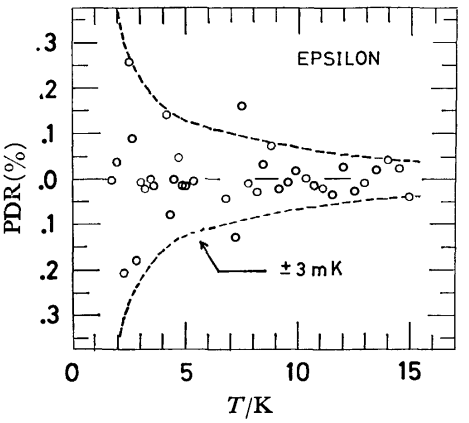

Fig. 2. Percent deviation (PDR) of calibration points from the smooth values of the germanium temperature scale.

The germanium thermometer ε was compared with the germanium thermometer (the same model, laboratory designation γ) which had been calibrated in our laboratory using the helium vapor pressures and gas thermometry on the IPTS 68. Resistance value of the thermometer ε was about 1 kΩ at 4.2 K and the calibration current of 5.7 μA was chosen to avoid the adverse effect of self-heating. To obtain the interpolation formula, a series expansion of the type

$$\log R = \sum_i A_i(\log T)^{k+i}$$

was used to fit the calibration data. The variance V given by

$$(M-1)V^2 = \sum_{j=1}^{M}\{R_j(\text{observed})-R_j(\text{smoothed})\}^2,$$

where M (=38) is the number of calibration points, and the temperature dependences of the first and second derivatives of log R with respect to log T were employed as a measure of fitting. The best fit was obtained when the power $k+i$ of the first term was taken as -2 and the number of the series expansion terms as 10. The temperature determined by the thermometer ε deviated less than 5 mK from the thermodynamic temperature between 1.8 and 15 K as shown in Fig. 2.

Results and Discussion

The experimental molar heat capacity is given in Table 1 in chronological sequence at the mean temperatures of determination. The temperature increment in each measurement was small as seen from the differences in the adjacent mean temperatures and hence no curvature correction was made. Corrections were not made either for the contribution from the helium exchange gas in calculating the heat capacity values because of negligible contribution. Scattering

TABLE 1. MOLAR HEAT CAPACITIES OF $(ND_4)_2SO_4$
Weight of specimen 48.668 g. Molecular weight 140.18. IPTS-68.

T/K	C_p/J K^{-1} mol^{-1}	T/K	C_p/J K^{-1} mol^{-1}	T/K	C_p/J K^{-1} mol^{-1}	T/K	C_p/J K^{-1} mol^{-1}	T/K	C_p/J K^{-1} mol^{-1}
Series I		158.533	142.34	222.842	304.90	217.347	250.33	49.969	36.92
58.928	47.25	160.864	144.48	223.675	939.0	218.696	259.07	51.380	38.52
60.517	49.09	163.162	146.75	223.934	17323	220.010	269.11	52.738	40.08
62.272	51.04	165.438	149.03	223.973	11975	221.282	281.20	54.058	41.54
64.032	53.09	167.696	151.32	224.291	704.52	222.502	297.61	55.344	43.07
65.698	54.97	169.437	153.72	225.365	177.25	223.499	482.00	56.600	44.50
67.403	56.85	172.152	155.84	227.013	175.99	223.921	12020	57.940	46.06
69.071	58.82	Series III		Series V		223.956	14578	59.351	47.68
70.609	60.50	161.730	144.67	(Transition region,		223.998	8796.6	Series XIII	
72.192	62.19	163.626	146.68	run 2. continuous		224.539	356.40	3.121	0.0121
73.746	63.87	165.597	148.74	heating)		225.922	175.58	3.546	0.0193
75.274	65.57	167.634	150.88	Series VI		227.655	175.74	3.988	0.0270
77.041	67.49	169.640	152.89	226.035	175.34	229.387	175.90	4.411	0.0401
78.705	69.34	171.618	155.24	227.674	175.31	Series IX		4.807	0.0504
80.170	70.88	173.571	157.23	229.314	175.89	(Transition region,		5.183	0.0625
81.710	72.74	175.496	159.48	230.872	175.90	run 3 and 4. conti-		5.571	0.0798
83.310	74.17	177.392	161.81	232.503	176.53	nuous heating)		Series XIV	
85.039	76.03	179.268	163.90	234.210	176.71	Series X		2.814	0.0083
86.765	77.82	181.110	165.88	235.985	176.78	14.104	1.839	3.117	0.0113
88.435	79.45	182.939	168.13	237.827	177.47	15.134	2.313	3.439	0.0167
90.147	81.13	184.748	170.72	239.670	177.90	16.220	2.885	3.756	0.0221
91.910	82.97	186.530	173.30	241.517	178.71	17.664	3.784	4.066	0.0294
93.689	84.96	188.293	175.73	243.450	179.44	20.500	5.903	4.368	0.0348
95.464	86.43	190.117	178.43	245.456	179.51	23.827	8.765	4.692	0.0450
97.234	88.09	191.999	181.54	247.394	180.36	Series XI		5.005	0.0547
99.020	89.76	193.861	184.63	249.345	180.83	14.033	1.806	5.334	0.0725
100.823	91.51	195.692	188.33	251.436	181.59	14.927	2.201	5.669	0.0847
102.703	93.18	197.494	191.16	Series VII		16.724	3.184	6.064	0.1014
104.572	95.04	199.285	194.80	251.347	181.54	17.722	3.818	6.502	0.1260
106.456	96.64	201.062	198.68	253.364	182.32	18.911	4.646	7.003	0.1567
Series II		202.812	202.79	255.769	182.99	20.191	5.619	7.579	0.2014
106.111	96.31	204.535	207.06	258.315	183.76	21.398	6.593	8.307	0.2747
107.979	97.98	206.229	211.27	260.849	184.54	22.526	7.559	9.179	0.3905
107.848	99.63	207.882	214.99	263.129	185.00	23.604	8.522	10.203	0.5751
111.738	101.34	209.515	219.23	265.391	186.08	Series XII		11.374	0.8543
113.643	103.20	211.123	224.11	267.893	187.13	24.117	9.017	12.523	1.191
115.560	104.54	212.699	229.43	270.474	187.74	25.106	9.949	13.637	1.605
117.493	106.33	214.247	234.81	273.136	188.73	26.086	10.90	Series XV	
119.437	108.07	215.832	239.68	275.800	189.40	27.166	11.94	3.948	0.0253
121.401	109.77	217.381	249.53	278.443	190.13	28.325	13.05	4.237	0.0346
123.386	111.16	Series IV		281.145	191.71	29.299	14.02	4.521	0.0422
125.397	113.70	(Transition region,		283.912	192.02	30.243	15.02	4.812	0.0535
127.429	114.96		run 1)	286.676	193.05	31.299	16.11	5.192	0.0699
129.478	116.96	204.289	205.81	289.426	193.96	32.453	17.25	5.675	0.0850
131.546	118.66	205.812	209.74	292.244	194.77	33.698	18.47	6.194	0.1081
133.610	120.52	207.387	214.12	295.120	195.62	34.990	20.20	6.765	0.1405
136.073	122.61	208.939	218.56	298.051	196.67	36.283	21.78	7.392	0.1855
138.614	124.75	210.466	222.70	301.049	197.74	37.493	23.21	8.165	0.2592
140.823	126.89	211.959	227.18	Series VIII		38.694	24.48	9.015	0.3683
142.997	128.65	213.422	233.37	(Transition region,		40.063	25.89	9.910	0.5179
145.136	130.53	214.928	238.64		run 3)	41.536	27.45	10.841	0.7174
147.530	132.60	216·397	247.09	210.335	223.03	42.917	28.45	11.747	0.9549
149.855	134.50	217.766	254.84	211.674	227.11	44.259	30.44	12.605	1.217
151.916	136.22	219.097	262.68	213.135	232.13	45.608	31.95	13.461	1.526
154.054	138.12	220.391	273.24	214.564	238.37	47.005	33.49	14.362	1.938
156.257	140.10	221.642	286.11	215.965	242.98	48.487	35.20		

TABLE 2. THERMODYNAMIC FUNCTIONS OF $(ND_4)_2SO_4$ TO 300 K

T / K	C_p° / J K^{-1} mol^{-1}	S° / J K^{-1} mol^{-1}	$(H_T^\circ - H_0^\circ)T^{-1}$ / J K^{-1} mol^{-1}	$-(G_T - H_0^\circ)T^{-1}$ / J K^{-1} mol^{-1}
5	0.0546	0.0180	0.0135	0.0045
10	0.5353	0.1584	0.1208	0.0376
15	2.233	0.6456	0.4999	0.1457
20	5.467	1.695	1.308	0.3871
25	9.833	3.367	2.561	0.8061
30	14.75	5.589	4.178	1.411
35	20.14	8.261	6.068	2.193
40	25.69	11.31	8.174	3.139
45	31.22	14.66	10.43	4.230
50	36.79	18.23	12.78	5.450
60	48.26	25.95	17.73	8.213
70	59.76	34.27	22.94	11.34
80	70.77	42.98	28.23	14.74
90	81.08	51.91	33.54	18.38
100	90.75	60.96	38.78	22.18
110	99.86	70.04	43.92	26.12
120	108.61	79.11	48.95	30.16
130	117.30	88.14	53.87	34.27
140	126.01	97.16	58.72	38.44
150	134.52	106.14	63.49	42.65
160	143.59	115.11	68.20	46.90
170	153.60	124.11	72.93	51.18
180	164.76	133.20	77.72	55.48
190	178.29	142.45	82.64	59.81
200	196.49	152.03	87.85	64.18
210	221.0	162.18	93.58	68.61
220	269.1	173.38	100.27	73.11
230	175.8	190.67	112.76	77.91
240	178.0	198.19	115.43	82.76
250	181.1	205.52	117.99	87.53
260	184.4	212.69	120.49	92.20
270	187.6	219.71	122.91	96.80
280	190.8	226.59	125.28	101.31
290	194.0	233.34	127.59	105.75
300	197.3	239.97	129.86	110.11
273.15	188.5	221.88	123.66	98.22
298.15	196.6	238.74	129.44	109.30

of results was within 15% below 8 K, decreasing to 2% between 8 and 15 K, within 1% between 15 and 50 K, and 0.5% above 50 K. When our results are compared with the data by Nitta and Suenaga,[2] their values are found systematically larger than ours by 13% in the low-temperature phase and by 8% in the high-temperature phase. Hoshino *et al.*[5] also reports values too large by 24% at 200 K and 15% at 250 K in a similar manner to the case of NH_4HSO_4.[24] The entire heat capacity curve is shown in Fig. 3.

The thermodynamic functions were evaluated from the smoothed values of the heat capacity and are summarized in Table 2 at rounded temperatures, including the contributions from the heat capacity below 3 K and near the transition region which will be discussed later.

Low Temperature Heat Capacity. From the C_pT^{-3} *versus* T^2 plot, the heat capacity values below 5 K were estimated by using the formula,

$$10^4\, C_pT^{-3} = 4.28 \pm 0.04 + 0.003\, T^2,$$

where C_p is in the units of J K^{-1} mol^{-1} and the coefficient of the second term has an uncertainty of about 20%. This coefficient is smaller by a factor of 25 than that of $(NH_4)_2SO_4$ for which it is 0.08. The Debye temperature at 0 K was found to be 238.8±0.7 K for $9N$ degrees of freedom and 165.6±0.5 K for $3N$ degrees of freedom.

'Normal' Behavior. We now attempt to separate the 'normal' portion of the observed heat capacity in order to assess the 'abnormal' portion associated with the phase transition and to see to what extent the normal portion may be rationalized in terms of harmonic vibrational spectrum. The best practical way in which to find the temperature at which the abnormal contribution begins to be seen is to plot the equivalent Debye temperature θ_D as a function of temperature (see Fig. 4) and then draw a smooth curve ignoring the transition region. The normal por-

Table 3. Estimated normal heat capacities of $(ND_4)_2SO_4$ at rounded temperatures

T/K	C_p/J K^{-1} mol^{-1}	T/K	C_p/J K^{-1} mol^{-1}	T/K	C_p/J K^{-1} mol^{-1}	T/K	C_p/J K^{-1} mol^{-1}
95	85.9	150	130.4	205	161.4	260	184.0
100	90.7	155	133.7	210	163.7	265	185.8
105	95.4	160	136.9	215	165.9	270	187.5
110	99.9	165	140.0	220	168.1	275	189.2
115	104.3	170	143.0	225	170.2	280	190.9
120	108.5	175	145.9	230	172.3	285	192.5
125	112.4	180	148.7	235	174.3	290	194.0
130	116.2	185	151.4	240	176.3	295	195.5
135	119.9	190	154.0	245	178.3	300	197.0
140	123.5	195	156.5	250	180.2	305	198.3
145	127.0	200	159.0	255	182.1	310	199.7

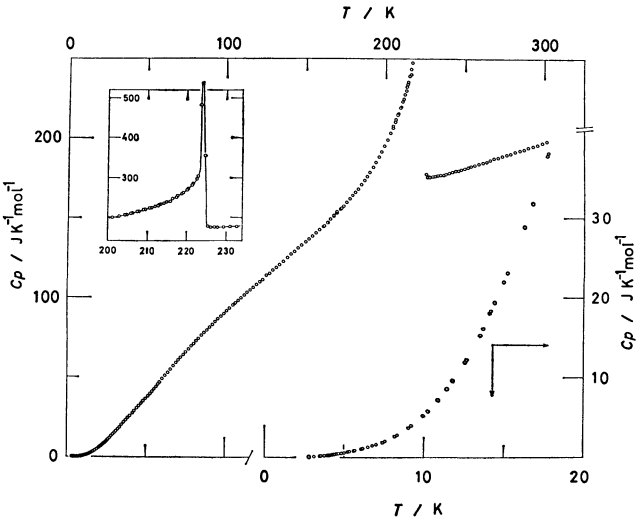

Fig. 3. Measured heat capacities of $(ND_4)_2SO_4$.

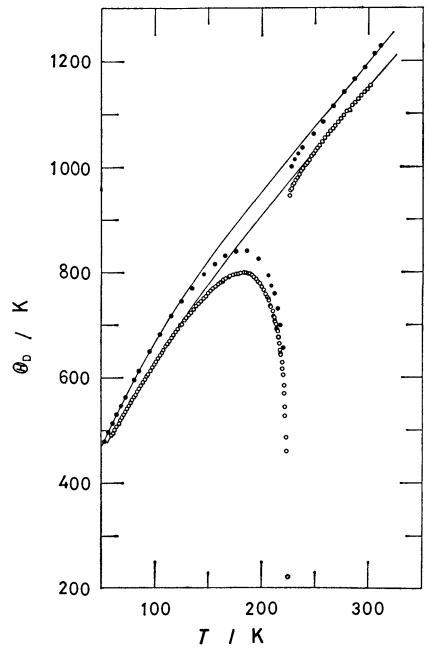

Fig. 4. Assessment of 'normal' heat capacities by the use of Debye temperature θ_D. Open circles for $(ND_4)_2SO_4$ and filled circles for $(NH_4)_2SO_4$.

tion of the heat capacity thus obtained is given in Table 3.

We may divide a total of $45N$ degrees of freedom into the $9N$ lattice vibrational modes, $3N$ librational modes of SO_4^{2-}, $6N$ librational modes of ND_4^+, $9N$ internal modes of SO_4^{2-} and 18 internal modes of ND_4^+, assuming that the intermolecular interactions are much weaker than the intramolecular interaction. The lattice vibrational contributions to the normal heat capacity may be derived from a Debye function with $\theta_D(0\,K)=238$ K. Other contributions can be estimated from the fundamental frequencies observed in the infrared and far infrared absorption spectra and also the Raman scattering; that is, for ND_4^+, $\nu_1(A_1)=2220$, $\nu_2(E)=1215$, $\nu_3(F_2)=2390$, $\nu_4(F_2)=1032$, $\nu_L=260$ and for SO_4^{2-}, $\nu_1(A_1)=973$, $\nu_2(E)=452$ and 464, $\nu_3(F_2)=1110$, $\nu_4(F_2)=614$ and 626, $\nu_L=102$ and 130 in units of cm^{-1}. Assuming that the librational modes of cations and anions are dispersion-less, the sum total of their modes accounts for most of the normal heat capacity above 120 K. However, such estimation exceeds the observed by about 10 J K^{-1} mol^{-1} at 80 K, which is outside of the experimental error. The anharmonic effects are usually too small to be seen at this temperature and, therefore, the discrepancy probably comes from inadequacy of the Debye approximation for the $9N$ degrees of freedom. The $9N$ degrees of 'lattice' freedom can further be divided into $3N$ acoustic modes and $6N$ optical modes. Since the translational optical mode frequencies are nearly independent of their wave vectors, compared with the acoustic modes, we tried to fix the average frequency of these optical modes by means of an Einstein function. As to the acoustic modes the value of $\theta_D(0\,K)=165.6$ K was used in the Debye approximation for $3N$ degrees of freedom. The best fit was obtained when the average optical frequency was chosen to be 185 ± 5 cm^{-1}. This value is consistent with the broad far infrared bands centering at 180 and 200 cm^{-1} which are assigned as the translational modes of ND_4^+ by our preliminary study[25] shown in Fig. 5. This value also shows a good agreement with the broad peak at 200 ± 16 cm^{-1} in the neutron inelastic scattering experiment,[13] the assignment of which is

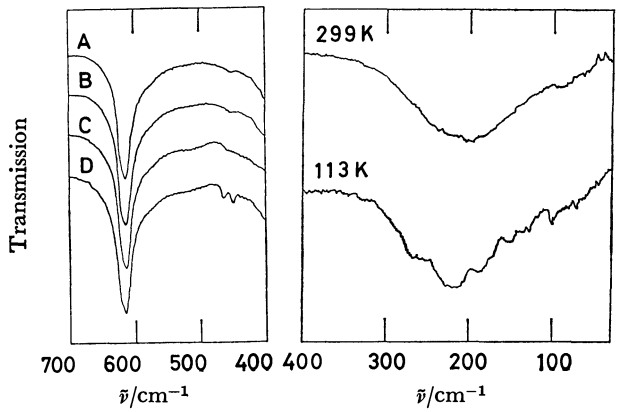

Fig. 5. Infrared and far infrared spectra of $(ND_4)_2SO_4$.

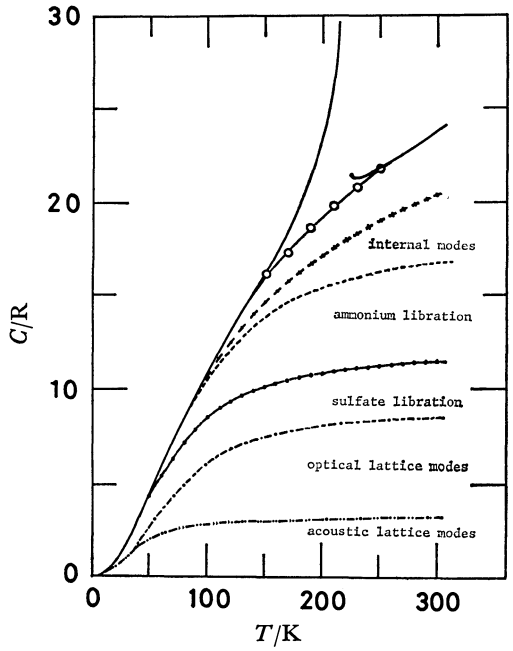

Fig. 6. Breakdown of the normal heat capacity into contributions.

the same as ours. Figure 6 shows the final result of the present analysis on the normal heat capacity of $(ND_4)_2SO_4$. Remaining discrepancy of about 10% of the normal C_p value at 200 K (14% at 300 K) is partly due to neglected C_p-C_V correction and partly due to the onset of anharmonic effects.

Ferroelectric (Ferrielectric) Phase Transition. The transition temperature of $(ND_4)_2SO_4$ was determined from the position of maximum heat capacity as 223.94± 0.03 K and is compared with previous determinations and with the results for $(NH_4)_2SO_4$ in Table 4. There is virtually no effect of deuterium substitution on the transition temperature. This fact indicates that the Gibbs energies on both sides of the transition change by the same magnitude upon deuteration. Because the modes of motion that suffer from the largest influence are those related to libration of ammonium ions, the potential energy surface which an ammonium ion sees when it rotates changes little on passing through the transition. In other words, there is little difference in the libration frequency between the low- and high-

TABLE 4. TRANSITION TEMPERATURES OF $(NH_4)_2SO_4$ AND $(ND_4)_2SO_4$

T_c/K of $(NH_4)_2SO_4$	T_c/K of $(ND_4)_2SO_4$
223.1[a]	223.6[a]
223.4[b]	
223.0[c]	223.7[c]
225.7[c]	225.2[c]
	223.94±0.03[d]

a) Ref. 2. b) Ref. 3. c) Ref. 5. d) Present research.

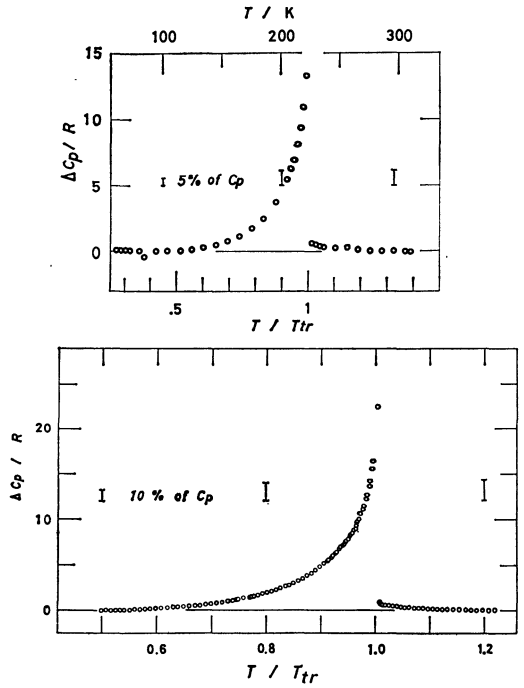

Fig. 7. Anomalous part of heat capacity. Top $(NH_4)_2SO_4$, Bottom $(ND_4)_2SO_4$.

temperature phases. This is consistent with the fact it was possible to draw a continuous smooth curve between the normal portions on the θ_D *vs.* T plot (Fig. 4). This also leads to an important notion that the transition mechanism can not be such as to accompany a substantial change in the librational state of the ammonium ions. If the ammonium ions are to play a leading role in the transition, it will be either order-disorder between almost equivalent orientations or translational displacement.

The transition is of first order with a long tail on the low-temperature side (down to $0.6T_c$). Other properties also show the first-order characteristics, like thermal hysteresis,[2] molar volume,[5] spin-lattice relaxation time of NMR,[17,19] and spontaneous polarization.[5] The present calorimetric study showed that the time for equilibration was extremely long in the transition region, as long as three hours. However, the latent heat and its corresponding entropy change account for only 40% of the overall heat and entropy of the transition (1.8 kJ mol^{-1} and 8.1 J K^{-1} mol^{-1}). The overall shape of the heat capacity anomaly is shown in Fig. 7. The inset of Fig. 3 depicts how the latent heat portion begins abruptly after very gradual rise of the heat capacity. The temperature

Table 5. Enthalpy and entropy of transition in $(NH_4)_2SO_4$ and $(ND_4)_2SO_4$

$(NH_4)_2SO_4$		$(ND_4)_2SO_4$	
ΔH_c / J mol^{-1}	ΔS_c / J K^{-1} mol^{-1}	ΔH_c / J mol^{-1}	ΔS_c / J K^{-1} mol^{-1}
3890[a]	18[a]	3890[a]	18[a]
—	16.7[b]	4270[c]	20.35[c]

a) Ref. 5. b) Ref. 3. c) Present research.

dependence between $0.6T_c$ and T_c is very much like that of dielectric anomaly[5,6]. Table 5 lists the thermodynamic quantities of the transition in comparison with corresponding results for $(NH_4)_2SO_4$. These are large, perhaps one of the largest among the ferroelectric transitions. Shomate[3] reported a value of 16.7 J K^{-1} mol^{-1} for the 'excess' entropy of $(NH_4)_2SO_4$ which is smaller than our value of 20.4 for $(ND_4)_2SO_4$ by as much as 18%. His value is based on an arbitrary assessment of the 'normal' curve and it is not possible to deduce from his published primary results a quantity which may be compared with our ΔS value. However, the θ_D curve calculated by using the Shomate's results for $(NH_4)_2SO_4$ is superimposable on the θ_D curve for $(ND_4)_2SO_4$ by slight vertical displacement (Fig. 4), which fact strongly suggests that what is occurring in $(ND_4)_2SO_4$ is also occurring in $(NH_4)_2SO_4$ in the same way.

If we formally apply the Clapeyron-Clausius equation to the transition excluding the gradual part, we obtain a value of 0.33 cm^3 mol^{-1} for the volume decrease from the low-temperature to the high-temperature phase by using the value[27] of $dT_c/dp = -4.0 \times 10^{-3}$ K kg^{-1} cm^2. There is no other data to compare with this figure but the almost corresponding quantity[5] for $(NH_4)_2SO_4$ is 0.69 cm^3 mol^{-1}.

Now, we will consider the mechanism of the transition. From neutron diffraction studies,[9] there are two kinds of inequivalent ammonium ions, types I and II, in both phases, each of which changes the hydrogen bond arrangements as well as the extent of distortion from regular tetrahedral structure. The most eminent structural feature of the transition is the replacement of the mirror symmetry (the ab plane of the high-temperature phase) with the two-fold screw axis (low-temperature phase). O'Reilly and Tsang[20] developed a molecular field treatment of the transition using three-sublattice model on the basis of their experimental results of deuteron magnetic resonance[17]. The theory assumes essentially an order-disorder mechanism in which the two types of ammonium ions assume random distribution of two orientations separated by $\pm 30°$ from the mirror plane in the high-temperature phase. They also assumed that sulfate ions, which occupy the third sublattice, are also disordered in a similar manner. They derived two energy parameters ε and $d\varepsilon/dn_\pm$ by fitting the theory to the temperature dependence of the crystal volume[5] in the low-temperature phase. Here ε is the energy of a misoriented (antiparallel) pair relative to a parallel pair and $d\varepsilon/dn_\pm$ is its dependence on the number of the antiparallel pairs. The values they

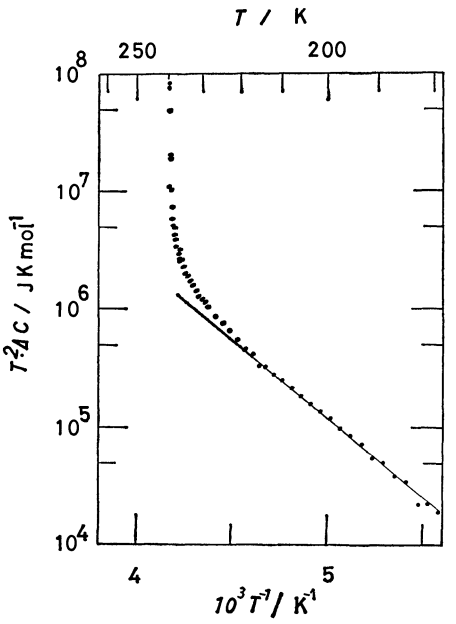

Fig. 8. Plot according to Eq. 1 for determination of enthalpy to form defects.

obtained were $\varepsilon = 0.92$ kJ mol^{-1} and $d\varepsilon/dn_\pm = 0.10$ kJ mol^{-1} for the case of six nearest neighbors.

The present thermodynamic results may be compared with the O'Reilly-Tsang theory in two ways. In the first place, the overall entropy of the transition is expected to be $\Delta S = 3R\ln 2 = 17.3$ J K^{-1} mol^{-1} according to the three-sublattice, order-disorder model in comparison with the experimental 20.4 J K^{-1} mol^{-1}. The difference is outside of the experimental error; although there is small uncertainty in the evaluation of the 'normal' portion of the heat capacity, it can not account for the difference. Therefore, there must be some other small contributions to the entropy such as coupling of translational modes of motion with librational degrees of the ions.

The other quantity that can be compared with the theoretical model is the enthalpy to form a defect in the otherwise perfectly ordered structure. Suppose an ammonium ion is misoriented to create six 'wrong' pairs in the ordered lattice. This process requires an additional enthalpy of 6ε per ion. Since there are three such ions a formula unit, the total enthalpy per mole would be $h = 18\varepsilon$. Let n be the number of such defects and the excess heat capacity due to this process of defect formation is given by

$$\Delta C_p = (\partial \Delta H/\partial T)_p = \partial(nh)/\partial T = (n_0 h^2/kT^2)\exp(-h/kT), \quad (1)$$

where the Boltzmann relation,

$$n = n_0 \exp(-h/kT),$$

has been used. Thus, a plot of $\ln(T^2\Delta C_p)$ *vs.* T^{-1} should give a straight line whose slope yields a value of h. Figure 8 shows such a plot for $(ND_4)_2SO_4$ and the straight line corresponds to

$$n/N = 88 \exp(-1451/T),$$

which gives $h = 12.0$ kJ mol^{-1} or $\varepsilon = 0.67$ kJ mol^{-1}. This is comparable in magnitude with 0.92 kJ mol^{-1} which O'Reilly and Tsang derived. The observed

points in Fig. 8 begin to deviate from the straight line at about 173 K where the fraction of the defects reaches 2%. The deviation reflects the cooperative nature of the defect formation, in other words h or ε depends on the number of defects already present.

A similar analysis on the Shomate's data on $(NH_4)_2SO_4$ gave $h=12.2$ kJ mol^{-1}, indicating that one sees the same phenomenon in the two crystals.

An attempt to find the critical index was not successful because a plot of $\ln\Delta C_p$ against $\ln(T-T_c)/T_c$ did not give any straight line region.

In conclusion, the phase transition, whether ferroelectric or otherwise, in $(ND_4)_2SO_4$ consists of a second-order portion and a first-order portion, the former contributing 60% to the total entropy of transition. The thermal properties are consistent with the three-sublattice, order-disorder model proposed by O'Reilly and Tsang including disordering of the sulfate ions. It will help understand the mechanism better if the quadrupole effects of ^{17}O resonance may be studied in the two phases.

References

1) J. L. Gronshaw and J. Ritter, *Z. Phys. Chem., B*, **16**, 143 (1932).
2) I. Nitta and K. Suenaga, *Bull. Chem. Soc. Jpn.*, **13**, 36 (1938).
3) C. H. Shomate, *J. Am. Chem. Soc.*, **67**, 1096 (1945).
4) B. T. Matthias and J. P. Remeika, *Phys. Rev.*, **103**, 262 (1956).
5) S. Hoshino, K. Vedam, Y. Okaya, and R. Pepinsky, *Phys. Rev.*, **112**, 405 (1958).
6) H. Ohshima and E. Nakamura, *J. Phys. Chem. Solids*, **27**, 481 (1966).
7) B. Singh, Dissertation, The Pennsylvania State University, 1962.
8) V. V. Vdalova and Z. G. Pinsker, *Soviet Phys.-Cryst.*, **8**, 433 (1964).
9) E. O. Schlemper and W. C. Hamilton, *J. Chem. Phys.*, **44**, 4498 (1966).
10) R. Blinc and I. Levstek, *J. Phys. Chem. Solids*, **12**, 295 (1960).
11) C. J. H. Schutte and A. M. Heyns, *J. Chem. Phys.*, **52**, 864 (1970).
12) B. H. Torrie, C. C. Lin, O. S. Binbrek, and A. Anderson, *J. Phys. Chem. Solids*, **33**, 697 (1972).
13) J. J. Rush and T. I. Taylor, Inelastic Scattering Neutrons Solids Liquids, Proc. Symposium, 3rd, Bombay, India, **2**, 333 (1965).
14) U. Dahlborg, K. E. Larsson, and E. Pirkmajer, *Physica*, **49**, 1 (1970).
15) R. E. Richards and T. Schaefer, *Trans. Faraday Soc.*, **57**, 210 (1961).
16) R. Miller, R. Blinc, M. Breuman, and J. S. Waugh, *Phys. Rev.*, **126**, 528 (1962).
17) D. E. O'Reilly and T. Tsang, *J. Chem. Phys.*, **46**, 1291 (1967).
18) R. R. Knispel, H. E. Petch, and M. M. Pintar, *J. Chem. Phys.*, **63**, 390 (1975).
19) D. W. Kydon, M. Pintar, and H. E. Petch, *J. Chem. Phys.*, **47**, 1185 (1967).
20) D. E. O'Reilly and T. Tsang, *J. Chem. Phys.*, **46**, 1301 (1967).
21) A. Onodera, H. Fujishita, and Y. Shiozaki, *Solid State Commun.*, **27**, 463 (1978).
22) P. Flubacher, A. J. Leadbetter, and J. A. Morrison, *Phil. Mag.*, **4**, 273 (1959).
23) J. L. Riddle, G. T. Furukawa, and H. H. Plumb, "Platinum Resistance Thermometry," NBS Monograph 126, 1973; *Metrologia*, **5**, 35 (1969).
24) Y. Higashigaki and H. Chihara, unpublished results.
25) Y. Higashigaki, Dissertation, Osaka University, 1977.
26) H. G. Unruh, *Solid State Commun.*, **8**, 1951 (1970).
27) S. Tsunekawa, Y. Ishibashi, and Y. Takagi, *J. Phys. Soc. Jpn.*, **33**, 862 (1972).

A Method of Estimating the Diffusion Coefficient of Disperse Dyes into Hydrophobic Fibers from the Initial Sorption Data of Dyeing by Means of the Polynomial Least-squares Method[1)]

Takao SHIBUSAWA

College of Technology, Gunma University, Kiryu, Gunma 376

(Received January 17, 1980)

For the initial and the medium stage of diffusion, Hill's equation was approximated by the simple polynomial in the form of $M_t/M_\infty \approx P_1(Dt/r^2)^{1/2} - P_2(Dt/r^2)$, where P_1 and P_2 are constants depending on the interval in which the approximation is used, while the other symbols have a usual meanings. On the other hand, several experimental M_t's were plotted against square root of t, and an experimental formula describing the regression curve passing through a discrete set of experimental points, $M_t = A_0 + A_1 t^{1/2} - A_2 t$, was obtained by means of curve fitting with a polynomial of degree 2. From the polynomial approximation and the experimental formula, the following equations which are capable of calculating the approximate value of M_∞ and D were obtained.

$$(D/r^2)^{1/2} \approx (A_2P_1)/(A_1P_2), \quad M_\infty \approx (A_1^2P_2)/(A_2P_1^2)$$

Then the method for obtaining more probable values of D and M_∞ was described, in this method the approximations to inverse function of Hill's equation and the curve fitting with polynomial of degree 2 were used.

The diffusion coefficient of a dye into a fiber is frequently calculated from the kinetic data of dyeing obtained in an infinite bath using Eq. 1 (Hill's equation)[2)] or its approximations.[3)]

$$\frac{M_t}{M_\infty} = 1 - \sum_{n=1}^{\infty} \frac{4}{q_n^2} \exp\left(-q_n^2 \frac{Dt}{r^2}\right) \tag{1}$$

where M_t and M_∞ are the quantities of dye taken up by a fiber of radius r at time t and equilibrium respectively, D is concentration independent diffusion coefficient and q_n's are positive roots of the Bessel function of the first kind of order zero, $J_0(q_n)=0$.

However, it is often difficult to determine a reasonable value of M_∞ experimentally, since the decomposition of dye and the degradation of polymer substrate are apt to occur during a long period of the dyeing. Therefore, several studies have been made regarding the method of estimating D without using M_∞.[4-7)]

In this paper, we propose a polynomial least-squares method which is capable of estimating the probable value of D and M_∞ from several values of M_t determined at the early stage of dyeing.

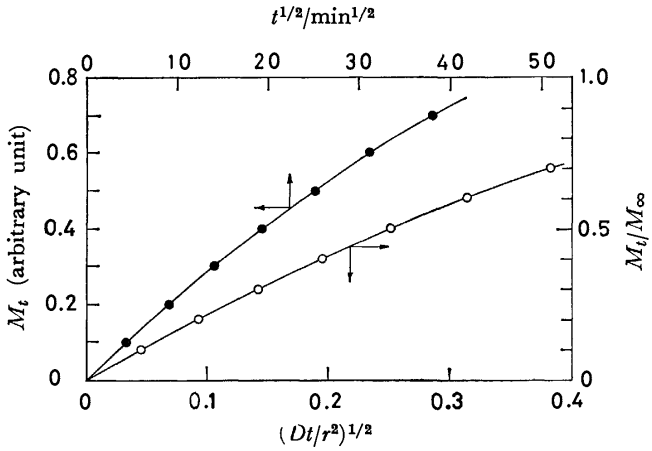

Fig. 1. Curve fitting by least squares with a polynomial of degree 2.
—●—: $M_t = A_0 + A_1 t^{1/2} - A_2 t$, —○—: $M_t/M_\infty = Q_0 + Q_1(Dt/r^2)^{1/2} - Q_2(Dt/r^2)$.

Theoretical

For the small and medium values of Dt/r^2, Eq. 1 can be approximated by simple polynomials in the form of Eq. 2.

$$\frac{M_t}{M_\infty} \approx P_1\left(\frac{Dt}{r^2}\right)^{1/2} - P_2\left(\frac{Dt}{r^2}\right) \tag{2}$$

P_1 and P_2, the coefficients of the polynomial, depend on the interval in which Eq. 2 is used as an approximation to Eq. 1. The values of the coefficients were determined by the minimum maximum error techniques as follows:

Interval	P_1	P_2	$\Delta\left(\frac{M_t}{M_\infty}\right)$
$0 < \frac{M_t}{M_\infty} < 0.6$	2.271	1.122	±0.0005
$0 < \frac{M_t}{M_\infty} < 0.7$	2.277	1.150	±0.001
$0 < \frac{M_t}{M_\infty} < 0.8$	2.297	1.222	±0.002
$0 < \frac{M_t}{M_\infty} < 0.9$	2.331	1.352	±0.005

where $\Delta(M_t/M_\infty)$ is the maximum deviation of Eq. 2 from Eq. 1 in M_t/M_∞ in the interval.

On the other hand, if the plot of the experimental M_t value *vs.* $t^{1/2}$ is made as is shown by the solid circles in Fig. 1, we can obtain Eq. 3 as an experimental formula expressing the rate of diffusion by the curve-fitting technique:

$$M_t \approx A_0 + A_1 t^{1/2} - A_2 t \tag{3}$$

empirical constants, A_0, A_1, and A_2, are determined in order to minimize S:

$$S = \sum_{i=0}^{n} \{M_{ti} - (A_0 + A_1 t_i^{1/2} - A_2 t_i)\}^2 \tag{4}$$

where, the data at origin ($t=0$, $M_t/M_\infty=0$) are weighted by a factor of ten. This weighting makes A_0 negligible and reduces the effect of the experimental error in the M_t determined at the early stage of dyeing

TABLE 1. EXAMINATION OF THE ACCURACY OF THE DIFFUSION COEFFICIENT ESTIMATED BY POLYNOMIAL LEAST-SQUARES METHOD

Time of dyeing / min	$t^{1/2}$ / $\text{min}^{1/2}$	M_t [a] / Arbitrary unit	M_t/M_∞ [b]	$\left(\frac{Dt}{r^2}\right)^{1/2}$ [c]
0	0	0	0	0
20.45	4.523	0.1000	0.10025	0.04533
85.53	9.248	0.2000	0.20049	0.09272
202.07	14.215	0.3000	0.30074	0.14254
379.35	19.477	0.4000	0.40099	0.19532
630.58	25.111	0.5000	0.50123	0.25184
976.31	31.246	0.6000	0.60148	0.31340
1453.42	38.124	0.7000	0.70173	0.38252
	$A_0=0.000095$		$Q_0=-0.000094$	
	$A_1=0.022785$		$Q_1=2.2786$	
	$A_2=0.00011544$		$Q_2=1.1549$	
	$M_\infty=0.9975_4$ [d]		$M_\infty=1.0003$	
	$(D/r^2)^{1/2}=0.01003_1$ $\text{min}^{-1/2}$ [d]		$(D/r^2)^{1/2}=0.009996$ $\text{min}^{-1/2}$	

a) Calculated by Eq. 1 using $M_\infty=1.0000$ and $(D/r^2)^{1/2}=0.01\ \text{min}^{-1/2}$. b) Calculated by using $M_\infty=0.9975_4$. c) Calculated using the M_t/M_∞ given in the fourth column by Eq. 7. d) Calculated by Eq. 6 using $P_1=2.277$ and $P_2=1.150$.

on the value of D estimated by this method.

A comparison of Eqs. 2 and 3 gives:

$$\left(\frac{D}{r^2}\right)^{1/2} \approx \frac{A_2P_1}{A_1P_2} \tag{5}$$

$$M_\infty \approx \frac{A_1^2P_2}{A_2P_1^2}. \tag{6}$$

Equation 5 enables us to estimate an approximate value of D without using M_∞. The appropriate P_1 and P_2 values in Eq. 5 are selected as follows. The rate of dyeing data given in the columns from the first to the third of Table 1 were calculated by Eq. 1 using $(D/r^2)^{1/2}=0.01000\ \text{min}^{-1/2}$ and $M_\infty=1.000$ (arbitrary unit) in order to examine the accuracy of D, estimated by this method. From the data given in the second and the third columns of Table 1, $A_0=0.000095$, $A_1=0.022785$, and $A_2=0.00011544$ are obtained as the empirical constants in Eq. 3 by means of curve fitting with a polynomial of degree 2. For this case, if we use $P_1=2.271$ and $P_2=1.122$(suitable for $M_t/M_\infty=0$—0.6), we get $M_\infty=0.9784$ by Eq. 6. By dividing the values of M_t by the M_∞ value obtained above, we can estimate that the M_t's range about $M_t/M_\infty=0$—0.715 and that the appropriate P_1 and P_2 values are that for $M_t/M_\infty=0$—0.7. Similarly, if $P_1=2.297$ and $P_2=1.222$(suitable for $M_t/M_\infty=0$—0.8) are used at first, we get $M_\infty\approx1.0416$ and find that P_1 and P_2 for $M_t/M_\infty=0$—0.7 are suitable for this case. The appropriate P_1 and P_2 values are thus determined. By using $P_1=2.277$ and $P_2=1.150$ which are suitable for $M_t/M_\infty=0$—0.7, approximate values, $(D/r^2)^{1/2}=0.01003\ \text{min}^{-1/2}$ and $M_\infty=0.9975$, are obtained by the use of Eqs. 5 and 6 respectively. This result shows that the use of appropriate P_1 and P_2 values gives an accurate value of D in Eq. 5. However, we can not always use values of P_1 and P_2 as appropriate as in the case of simulation described above, so that, in most cases, further calculations are required to get a more probable value of D, as will be described below.

An accurate value of $(Dt/r^2)^{1/2}$ yielding a given value of M_t/M_∞ in Eq. 1 can be obtained by the use of Eq. 7 or 8, which were derived by means of the method described by Hastings[8] as the approximations to the inverse function of Eq. 1.

For $M_t/M_\infty<0.855$,

$$\left(\frac{Dt}{r^2}\right)^{1/2} \approx \frac{0.44292M-0.480014M^2+0.069127M^3}{1-1.282686M+0.31912M^2}. \tag{7}$$

For $0.855<M_t/M_\infty<0.998$,

$$\left(\frac{Dt}{r^2}\right)^{1/2} \approx \left\{-\frac{0.36839+\ln(1-M)}{5.7836}\right\}^{1/2} \tag{8}$$

where $M\equiv M_t/M_\infty$; the maximum deviation of Eqs. 7 and 8 from the inverse function of Eq. 1 in $(Dt/r^2)^{1/2}$ are within ±0.000015 at the each interval.

By dividing the experimental M_t values by the M_∞ estimated by Eq. 6, we can get the series of M_t/M_∞ values given in the fourth column of Table 1. The value of $(Dt/r^2)^{1/2}$ yielding each M_t/M_∞ in Eq. 1 is obtained by the use of Eq. 7 or 8 as is shown in the fifth column of Table 1. The set of data: $\{(Dt_i/r^2),\ M_{t_i}/M_\infty,\ i=0,1,2,\cdots n\}$ is thus obtained. If the data are plotted as is shown by the empty circles in Fig. 1, we can get Eq. 9 as a regression equation passing through these points by means of the curve-fitting with polynomial of degree 2, where the data at origin, $\{(Dt/r^2)^{1/2}=0,\ M_t/M_\infty=0\}$, are also weighted by a factor of ten.

$$\frac{M_t}{M_\infty} = Q_0 + Q_1\left(\frac{Dt}{r^2}\right)^{1/2} - Q_2\left(\frac{Dt}{r^2}\right) \tag{9}$$

Q_1, Q_2, and Q_0 are the regression coefficients and constant respectively.

A comparison of Eqs. 3 and 9 gives:

$$\left(\frac{D}{r^2}\right)^{1/2} \approx \frac{A_2Q_1}{A_1Q_2} \tag{10}$$

and:

$$M_\infty \approx \frac{A_1^2Q_2}{A_2Q_1^2}. \tag{11}$$

More probable values of D and M_∞ are obtained by the use of Eqs. 10 and 11 respectively. For example, from the data given in the fourth and fifth columns of Table 1, the regression coefficients, $Q_1=2.2786$ and $Q_2=1.1549$, are obtained by means of the curve-fitting with polynomial of degree 2. By inserting this values into Eqs. 10 and 11, we get $(D/r^2)^{1/2}=0.009996\ \text{min}^{-1/2}$ and $M_\infty=1.0003$ respectively.

If we repeat the calculations described above using the M_∞ value obtained by means of Eq. 11 and the experimental M_t's, we can get a far more probable value of D, *e.g.*, in the case of the M_t's given the third column of Table 1, $Q_1=2.2784$, $Q_2=1.1540$ and $(D/r^2)^{1/2}=0.010003$ and $M_\infty=0.99979$. However, taking into account the precision with which the experimental M_t's can be obtained, repeated calculations are not required in most cases if the appropriate P_1 and P_2

Table 2. Estimation of the diffusion coefficient of C.I. disperse violet 1 into poly(ethylene terephthalate) fiber at 95 °C from the initial sorption data of dyeing

Time of dyeing / h	$t^{1/2}$ / $min^{1/2}$	M_t / (mol/kg) $\times 10^{-2}$	M_t a) / M_∞	$\left(\frac{Dt}{r^2}\right)^{1/2}$ b)	M_t c) / M_∞	D d) / ($cm^2 \cdot min^{-1}$) $\times 10^{-11}$
0	0	0	0	0		
1	7.75	0.40	0.0904	0.04077	0.091	1.30
2	10.95	0.53	0.1197	0.05434	0.121	1.16
5	17.32	0.81	0.1830	0.08427	0.185	1.12
12	26.83	1.25	0.2824	0.13320	0.285	1.16
25	38.73	1.78	0.4021	0.19591	0.406	1.21
45	51.96	2.26	0.5105	0.25729	0.516	1.16
70	64.81	2.73	0.6167	0.32330	0.623	1.18
285		4.11			0.938	1.12
409		4.38				Average = 1.18

a) Calculated by using $M_\infty = 4.427 \times 10^{-2}$ mol/kg. b) Calculated using the M_t/M_∞ given in the fourth column by Eq. 7. c) Calculated using $M_\infty = 4.38 \times 10^{-2}$ mol/kg. d) Calculated using the M_t/M_∞ given in the sixth column by Eq. 7 or 8.

values are used in Eq. 6.

The results of simulations using M_t's including experimental error show that the value of D estimated by this method is insensitive to the error in M_t at the early stage of diffusion, but relatively sensitive to that at the later stage. Therefore, by increasing the accuracy of the M_t determined at the last two or three points of measurement, we can get an accurate value of D without using M_∞.

Experimental

Materials. The dye used was purified C.I. Disperse Violet 1 (1,4-diaminoanthraquinone, mp: 271—272 °C, Found: N, 11.9%, Calcd for: N, 11.8%). The crystal of the dye was grounded in a ball mill with a dispersing agent for 48 h and then dispersed in water. The dispersing agent was thus removed from the dispersion by the use of a membrane filter (average pore size: 0.65 μm). The dispersion containing 0.5 g/l pure dye was used for dyeing.

The fiber used poly(ethylene terephthalate) spun yarn (40 s, pretreated in boiling water for 2 h, $r = 6.79 \times 10^{-4}$ cm).

Determination of Rate of Dyeing. About 10 mg of the fiber was dyed in the dye dispersion of one liter for a certain period at 95 °C using an apparatus similar to that used by Peters *et al.*[9] The dyed fiber was rinsed with cold acetone to remove the surface dye. Then the dye on the fiber was extracted with hot chlorobenzene, and the amount of dye in the fiber was determined colorimetrically using a Hitachi 101 spectrophotometer.

All the calculations were made using a Canon SX 110 programmable calculator.

Results and Discussion

The kinetic data of the dyeing were determined to be as given in the first three columns of Table 2. From the set of data given in the second and third columns of the table, the values of the empirical constants in Eq. 3 were calculated to be $A_1 = 0.050109$ and $A_2 = 0.0001234$ respectively by means of the polynomial least-squares method. Consequently, approximate values of $(D/r^2)^{1/2} \approx 0.00498_4$ $min^{-1/2}$, and $M_\infty \approx 4.42_7 \times 10^{-2}$ mol/kg were obtained by the use of Eqs. 5 and 6, where $P_1 = 2.271$ and $P_2 = 1.122$ were used. If we use $P_1 = 2.297$ and $P_2 = 1.222$, which are suitable for $M_t/M_\infty = 0$—0.8, we get $M_\infty \approx 4.71_3 \times 10^{-2}$ mol/kg from Eq. 6. However, by dividing the experimental M_t's by the M_∞ obtained above, we find that the values of M_t/M_∞ range about 0—0.58 and that the appropriate P_1 and P_2 values for this case are 2.271 and 1.122 respectively.

Therefore, the values of M_t/M_∞ were calculated using $M_\infty = 4.42_7 \times 10^{-2}$ mol/kg and the experimental M_t values given in the fourth column of Table 2. The values of $(Dt/r^2)^{1/2}$ yielding these M_t/M_∞ in Eq. 1 were calculated by the use of Eqs. 7 or 8, as listed in the fifth column. The application of the polynomial least-squares method to the set of data listed in the fourth and fifth columns of Table 2 gave these regression coefficients: $Q_1 = 2.2697$ and $Q_2 = 1.116_4$. The substitution of these values into Eqs. 10 and 11 gave $(D/r^2)^{1/2} \approx 0.00500_7$ $min^{-1/2}$, $D = 1.15_4 \times 10^{-11}$ $cm^2 \cdot min^{-1}$ and $M_\infty \approx 4.41_0 \times 10^{-2}$ mol/kg respectively.

If we use the M_t obtained at $t = 409$ h as M_∞, we get the values of D given in the last column of Table 2 by means of the standard method, which gives an average value of $D = 1.18 \times 10^{-11}$ $cm^2 \cdot min^{-1}$. This value agrees well with the value of D estimated by the polynomial least-squares method proposed in this paper.

Conclusions

Since the numerical calculations of Eqs. 7 and 8 and the curve-fitting with a polynomial of degree 2 can easily be carried out using one of the programmable pocket calculator commercially available today, the method of estimating D and M_∞ from the initial sorption data by the polynomial least squares-method is relatively simple. The values of D and M_∞ estimated by this method are accurate enough when the several experimental M_t's fall in the range wider

than $M_t/M_\infty=0$—0.6 and each M_t's are equally spaced within the range.

References

1) Part of this work was presented at the Annual Meeting of The Society of Fiber Science and Technology, Japan, held at Tokyo in June, 1979; see Abstr. p. 158.
2) A. V. Hill, *Proc. R. Soc. London, Ser. A*, **104 B**, 39 (1928).
3) T. Shibusawa, *J. Soc. Dyers Colour.*, **95**, 175 (1979).
4) H. Inoue and Y. Suda, *Sen'i Gakkaishi*, **24**, 88 (1968).
5) J. G. Blacker and D. Patterson, *J. Soc. Dyers Colour.*, **85**, 598 (1969).
6) N. Choji and M. Karasawa, *J. Polym. Sci., Polym. Phys. Ed.*, **15**, 1309 (1977).
7) J. Militky, *J. Soc. Dyers Colour.*, **95**, 327 (1979).
8) C. Hastings, "Approximations for Digital Computers," Princeton New Jersey, Princeton University Press (1955).
9) R. H. Peters, J. H. Peteropoulos, and R. McGregor, *J. Soc. Dyers Colour.*, **77**, 704 (1961).

NOTES

Bull. Chem. Soc. Jpn., 54, 913—914 (1981)

X-Ray Photoelectron Spectrum of Cr_2O_5

Takayoshi Tsutsumi, Isao Ikemoto, Tatsuru Namikawa,† and Haruo Kuroda*

Department of Chemistry and Research Centre for Spectrochemistry, Faculty of Science, The University of Tokyo, Hongo, Bunkyo-ku, Tokyo 113

†*The Graduate School of Engineering and Science, Tokyo Institute of Technology, Nagatsuta, Midori-ku, Yokohama 227*

(Received July 2, 1980)

Synopsis. The X-ray photoelectron spectrum of the powder of Cr_2O_5 was measured and compared with those of the related chromium compounds. It is concluded that Cr_2O_5 is a mixed-valence compound having Cr^{3+} and Cr^{6+} ions, possibly with the ratio of 1:2.

We have previously studied the X-ray photoelectron spectra of CrO_2, and related Cr compounds which contain Cr^{3+}, Cr^{4+} and Cr^{6+}.[1] One of the present authors (T. N.)[2] found that the powder of Cr_2O_5 can be obtained as an intermediate product in the process of preparing the ferromagnetic fine powder of CrO_2 by the hydrothermal decomposition of CrO_3 under a high oxygen pressure. The chemical composition of this oxide suggests the possibility that Cr ions in this oxide are in the valency state of Cr^{5+}. Thus it seemed of great interest to see if Cr ions are actually in the state of Cr^{5+} or in a mixed-valence state. We examined the X-ray photoelectron spectrum of the powder of Cr_2O_5 and found that this oxide is a mixed-valence compound having Cr^{6+} and Cr^{3+} ions with a ratio of 2:1.

Experimental

The powder of Cr_2O_5 was prepared by the following method. The powder of CrO_3 was heated at 350 °C for 2 h in the ordinary atmosphere, and, after cooled, the product was suspended in water to remove water-soluble components and ferromagnetic component, the latter being removed by applying a magnetic field to the suspension. The resultant product Cr_2O_5 was filtered off from the suspension and dried. The powder thus obtained was confirmed to be Cr_2O_5 by means of X-ray diffraction.

In the present study, we also measured the X-ray photoelectron spectra of Cr_2O_3, $K_2Cr_2O_7$, and KCr_3O_8. The first two compounds were commercially obtained and the last one was synthesized according to the literature.[3]

X-Ray photoelectron spectra were measured with a McPherson ESCA 36 photoelectron spectrometer using Mg $K\alpha$ (1253.6 eV) as the stimulating radiation. All measurements were done on the powder samples pressed onto aluminium plates. Binding energies of photoelectron peaks were calibrated by using Au $4f_{7/2}$ peak (84.0 eV) of gold deposited on the sample.

In the case of Cr_2O_5, the X-ray photoelectron spectrum was found to change gradually with X-ray irradiation. Thus, we collected the photoelectron data only within a short measuring time on each fresh sample, and, repeating such measurements on many fresh samples, we summed up the data to obtain the spectrum which can be regarded as the one having been little affected by X-ray irradiation.

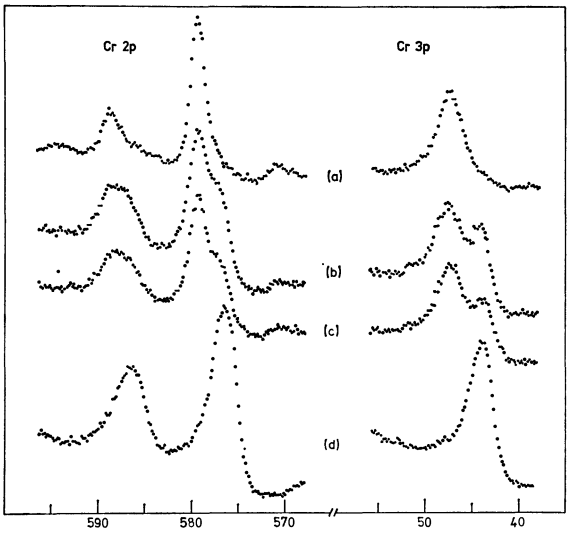

Fig. 1. The X-ray photoelectron spectra of Cr 2p and 3p peaks of (a) $K_2Cr_2O_7$, (b) Cr_2O_5, (c) KCr_3O_8, and (d) Cr_2O_3.

Results and Discussion

The Cr 2p and Cr 3p regions of the XPS spectrum of Cr_2O_5 are shown in Fig. 1 together with those of KCr_3O_8, $K_2Cr_2O_7$, and Cr_2O_3. The observed spectra are very much similar between Cr_2O_5 and KCr_3O_8. In these two cases, the Cr 3p peak exhibits a shape composed of two component peaks, the Cr $2p_{3/2}$ peak exhibits a shoulder at the low binding energy side of the main peak, again suggesting that two peaks are superimposed on each other, and the Cr $2p_{1/2}$ peak is very broad. All these facts indicate that Cr ions of two different valency states are contained in Cr_2O_5 as well as in KCr_3O_8, in other words, these materials are mixed-valence compounds. In effect, it is known from the X-ray crystal structure analysis that there are Cr^{6+} and Cr^{3+} sites with the ratio of 2:1 in the crystal lattice of KCr_3O_8.[4] Thus one can regard that, in the XPS spectrum of KCr_3O_8, each core electron peak associated with Cr ions, is a superposition of the peaks due to Cr^{6+} and Cr^{3+}, respectively. This can be seen in Fig. 1 by comparing the spectrum of KCr_3O_8 with those of Cr_2O_3 and $K_2Cr_2O_7$: Cr_2O_3 contains only Cr^{3+} and $K_2Cr_2O_7$ contains only Cr^{6+}. The fact that the profiles of the Cr 2p and Cr 3p peaks of Cr_2O_5 are very much similar to those of the corresponding peaks of KCr_3O_8, suggests that Cr_2O_5 is also a mixed-valence compound having Cr^{6+} and Cr^{3+} sites with a ratio roughly the same as that

Table 1. XPS Core-level binding energies of chromium compounds

	Binding energy/eV			
	$K_2Cr_2O_7$	Cr_2O_5	KCr_3O_8	Cr_2O_3
Cr $2p_{1/2}$	588.9	588.6	588.3	
		587.1	586.7	586.5
Cr $2p_{3/2}$	579.6	579.3	579.4	
		577.0	577.2	576.6
Cr 3p	47.4	47.7	47.3	
		44.1	43.5	43.8
O 1s	530.3	529.8	530.2	530.6

in KCr_3O_8.

Using the profiles of the Cr 2p and Cr 3p peaks of Cr_2O_3 as those characteristic of Cr^{3+} ion, and the profiles of the corresponding peaks of $K_2Cr_2O_7$ as those characteristic of Cr^{6+} ion, we tried to decompose the observed Cr 2p and Cr 3p peaks of KCr_3O_8 and Cr_2O_5 into the component peaks due to Cr^{6+} and Cr^{3+} ions, respectively. The procedure used here is the same as the one which we have adopted in the XPS study of organic mixed-valence compounds.[5]

The binding energies of the decomposed peaks are listed in Table 1 together with those of the corresponding peaks of Cr_2O_3 and $K_2Cr_2O_7$. In principle, one could determine the Cr^{6+}/Cr^{3+} ratio from this peak profile analysis. The analysis of the Cr 3p peak profile of KCr_3O_8 gave the Cr^{6+}/Cr^{3+} ratio as 2:1 in agreement with the ratio known from the crystal structure. In comparison with this, the Cr^{6+}/Cr^{3+} ratio obtained from the analysis of the Cr $2p_{3/2}$ peak of KCr_3O_8 was found to be rather anomalous, it being 1:1 in significant disagreement with the expected ratio. It should be noted that, in the obtained Cr $2p_{3/2}$ peak, the main peak corresponds to Cr^{6+} and its low-binding-energy shoulder correspond to Cr^{3+}, and the intensity ratio of the Cr^{6+} component to the Cr^{3+} component will be estimated to be 2—2.5 if we decompose the observed peak into the two components naively assuming the same peak width for the two components. On the other hand, it becomes 1:1 as we have mentioned when we use the Cr $2p_{3/2}$ peak profile of $K_2Cr_2O_7$ for the Cr^{6+} component and that of Cr_2O_3 for the Cr^{3+} component, the peak width of the former being significantly smaller than the latter. Seemingly it is inadequate to use the peak shapes of $K_2Cr_2O_7$ and Cr_2O_3 for decomposing the observed peak profile of a mixed valence compound. Probably we should better assume that the peaks of the Cr^{6+} and Cr^{3+} components are of nearly the same width. The situation will be the same in the case of Cr_2O_5. Since the observed profile of the Cr $2p_{3/2}$ peak of Cr_2O_5 is almost exactly the same as that of KCr_3O_8, one may conclude that the Cr^{6+}/Cr^{3+} ratio in Cr_2O_5 is also 2:1 as in KCr_3O_8. The observed profile of the Cr 3p peak of Cr_2O_5 is slightly different from that of KCr_3O_8 although they should be the same if the Cr^{6+}/Cr^{3+} ratio is identical between the two compounds as we have concluded from the Cr $2p_{3/2}$ peak shape. This may be due to the situation that, in the case of Cr_2O_5, it is rather hard to obtain the true Cr 3p peak profile without having been affected by X-ray irradiation since a considerably long measuring time is necessary to record Cr 3p peak while Cr_2O_5 is damaged with X-ray irradiation. Since Cr $2p_{3/2}$ peak is much stronger than Cr 3p peak, the observed 2p peak of Cr_2O_5 is likely to be more free from the radiation damage as compared with the Cr 3p peak.

In conclusion, the XPS data of Cr_2O_5 indicate that the chromium ions in Cr_2O_5 is not in the state of Cr^{5+} but in a mixed-valence state consisting of Cr^{6+} and Cr^{3+}, presumably with the ratio of 2:1.

References

1) I. Ikemoto, K. Ishii, S. Kinoshita, H. Kuroda, M. A. A. Franco, and J. M. Thomas, *J. Solid State Chem.*, **17**, 425 (1976).

2) T. Namikawa and M. Satou, *Nippon Kagaku Kaishi*, **1975**, 52.

3) J. J. Foster and A. N. Hambly, *Aust. J. Chem.*, **29**, 2137 (1976).

4) K. A. Wilhelmi, *Acta Chem. Scand.*, **12**, 1965 (1958).

5) I. Ikemoto, M. Yamada, T. Sugano, and H. Kuroda, *Bull. Chem. Soc. Jpn.*, **53**, 1871 (1980).

On the NMR Spectra of Some Substituted Pyridinium 2-Pyridylcarbonylmethylides

Gen-etsu MATSUBAYASHI

Department of Applied Chemistry, Faculty of Engineering, Osaka University, Yamadakami, Suita, Osaka 565

(Received June 7, 1980)

Synopsis. The partial double-bond character of the ylide carbon–pyridinium nitrogen bond is discussed on the basis of the ^1H and ^{13}C NMR spectra of 4-cyano- (Y_{CN}), 4-methyl- (Y_{pic}), and 3,5-dimethylpyridinium 2-pyridylcarbonylmethylide (Y_{lut}). The α-proton signals of the 4-cyanopyridinium ring of Y_{CN} have been separately observed at low temperatures, indicating a hindered rotation around the ylide carbon-pyridinium nitrogen bond.

Sulfur and phosphorus ylides can be stabilized by the carbanion delocalization to d-orbitals of the sulfur and phosphorus atoms.[1,2] On the other hand, the same effect is usually unexpected in nitrogen ylides, because nitrogen has no d-orbitals available for bond formation. Pyridinium ylides, however, are unique in being stabilized by the carbanion participation in the resonance of the pyridinium ring.[3] In the course of an investigation of the nucleophilic reactivity of several 2-pyridylcarbonylmethylides, $C_5H_4NC(O)\bar{C}H\overset{+}{Z}$ ($\overset{+}{Z}=\overset{+}{S}Me_2$, $\overset{+}{P}Ph_3$, and $\overset{+}{N}C_5H_4CH_3$-4), toward metal ions,[4–7] we have recently found some unique NMR spectral behavior of the substituted pyridinium 2-pyridylcarbonylmethylides. This paper will discuss the configurations of 4-cyano-(Y_{CN}), 4-methyl-(Y_{pic}), and 3,5-dimethylpyridinium 2-pyridylcarbonylmethylide (Y_{lut}) and the carbanion delocalization on the basis of the IR frequencies and the ^1H and ^{13}C NMR parameters.

The IR spectra of the 2-pyridylcarbonylmethylides gave ν(C=O) bands at fairly low frequencies compared with those of common organic carbonyl compounds: 1529, 1530, and 1530 cm^{-1} for Y_{pic}, Y_{lut}, and Y_{CN} respectively, indicating a considerable contribution of the canonical structure, **B**, besides **A**. Furthermore,

A **B**

X=4-CH_3, 3,5-$(CH_3)_2$, and 4-CN

assuming that the 2-pyridylcarbonyl group is almost planar, the ylides are likely to adopt a configuration avoiding some electronic repulsion between the negatively polarized pyridine–nitrogen and carbonyl–oxygen atoms.

The ^1H and ^{13}C NMR spectra of Y_{pic} in chloroform-*d* are depicted in Fig. 1. The proton signals have easily been assigned by comparison with the spectra of *N*-substituted 2-pyridylmethanimines[8] and 2,2′-bipyridine.[9] The ^{13}C-signal assignment has been performed by comparing the chemical shifts with those of 2-substituted pyridines[10] and the coupling constants between ^{13}C and directly bonded hydrogen atoms ($^1J(^{13}C–H)$).

The ylide-carbon signal is observed at an extremely low field (99.1 δ) compared with those of other

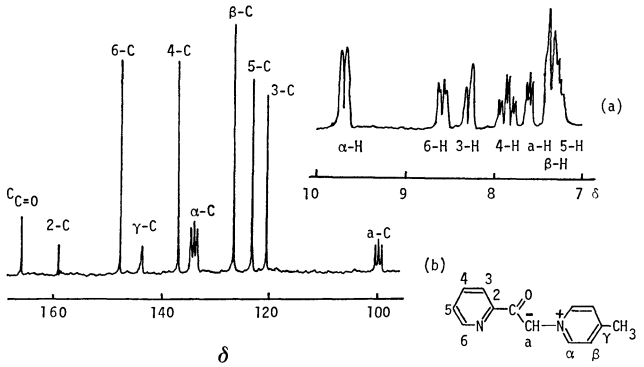

Fig. 1. The ^1H (a) and ^{13}C NMR (b) spectra of Y_{pic} in chloroform-*d*.

related phenacylides and 2-pyridylcarbonylmethylides: $PhC(O)\bar{C}H\overset{+}{P}Ph_3$ (50.4 δ),[11] $PhC(O)\bar{C}H\overset{+}{A}sPh_3$ (53.13 δ),[12] and $PyC(O)\bar{C}H\overset{+}{S}Me_2$ (53.8 δ).[13] This may be due to the strongly electron-withdrawing property of the 4-methylpyridinium group, as is shown in the resonance contributions, **C**—**E**.

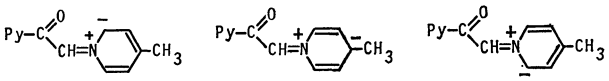

C **D** **E**

The ylide-proton signal of Y_{pic} appears at a fairly low field compared with that of 4-methylpyridinium phenacylide (6.64 δ);[14] this is because of the paramagnetic anisotropy effect of the lone-pair electrons of the pyridine nitrogen in the configurations, **A** and **B**, with the almost planar 2-pyridylcarbonyl group. Essentially the same situation was noticed in Y_{lut} (7.46 δ) and 3,5-dimethylpyridinium phenacylide (6.56 δ).

A characteristic feature is the clear appearance of a triplet signal of the ylide proton resulting from spin-spin coupling with the ^{14}N nucleus ($^2J(^{14}N–H_{ylide})$= 2.5 Hz). Furthermore, it is notable that the α-carbon signal, as well as the ylide-carbon signal, appears as a well-resolved triplet because of the ^{14}N coupling. In Y_{lut} and 3,5-dimethylpyridinium phenacylide, these carbon signals have also been observed as triplets ($^1J(^{14}N–^{13}C)$=8.8 and 8.3 Hz respectively). The relevant ^1H and ^{13}C NMR parameters of the ylides are summarized in Table 1.

Previously Phillips and Ratts[15] showed that the signals of the α-protons of the pyridinium ring of 4-substituted pyridinium phenacylides are shifted fairly downfield compared to those of the α-protons of the HBr salts of the phenacylides. These downfield shifts were attributed to the deshielding of α-H by the carbonyl function, as is depicted in **F**. This explanation may be based on the planarity of both the pyridinium ring and the phenacyl group. However, no separated

Table 1. Relevant NMR chemical shifts (δ) of the ylides[a)]

	6-H	a-H	α-H	6-C	a-C	α-C
Y_{pic}	8.52	7.50[b)]	9.61	147.2[c)] (178)	99.1[c)] (183)	133.4 (189)
Y_{lut}	8.49	7.46[b)]	9.31	147.6[c)] (178)	99.2[c)] (185)	131.3 (189)
Y_{CN}	8.56	7.82	9.39	d)	d)	d)

a) Measured in chloroform-d at 24 °C (^{1}H NMR) and at 34 °C (^{13}C NMR). The spin-spin couplings ($^1J(^{13}C-^1H)$, Hz) are shown in parentheses. b) $^2J(^{14}N-^1H) = 2.5$ Hz. c) $^1J(^{14}N-^{13}C) = 8.8$ Hz. d) Not measured because of its poor solubility.

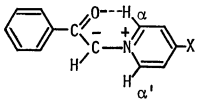

F

signals due to α-H and α′-H were observed, and only one signal occurred at an averaged field, because of the fast rotation around the ylide carbon-pyridinium nitrogen bond. This is the same as with the α-H signals of the pyridinium rings of both Y_{pic} and Y_{lut}, which exhibited the averaged chemical shifts of the α-H and α′-H signals at approximately 9.5 δ even at −70 °C in dichloromethane.

In Y_{CN} broad α-H signals are observed at 9.39 δ in chloroform-*d* at room temperature. At −50 °C, two widely separated α-H signals are noticed, as is illustrated in Fig. 2. This indicates the magnetic non-equivalence of the two α-protons, which seems to be attributable to the slow hindered rotation around the ylide carbon-pyridinium nitrogen bond on the NMR time scale. The Gibbs energy of activation (ΔG_{Tc}^{*}) for the rotation at the coalescence temperature (−20±5 °C) has been estimated to be 11.4(±0.3) kcal/mol using the approximate equation.[16)] The hindered rotation may be caused by the partial double-bond character of the ylide carbon-pyridinium nitrogen bond, which is ascribed to the contribution of the canonical structures, **C**—**E**.

Experimental

Preparation of 4-Cyanopyridinium 2-Pyridylcarbonylmethylide (Y_{CN}). 4-Cyanopyridine (1.25 g, 12 mmol) was added to a benzene (50 ml) solution of 2-(bromoacetyl)pyridine[17)] (2.0 g, 10 mmol), and the mixture was refluxed for 10 h to give white precipitates of Y_{CN}·HBr, which were subsequently collected by filtration (1.98 g, 66% yield). To an aqueous solution (10 ml) of the product was added a 30% K_2CO_3 aqueous solution (50 ml) to separate out red solids immediately. They were collected and recrystallized from a mixture of dichloromethane/diethyl ether (1/1 vol. ratio) to afford red crystals of Y_{CN} (0.59 g, 26% yield); mp 168 °C (dec). Found: C, 69.95; H, 4.06; N, 18.82%. Calcd for $C_{13}H_9N_3O$: C, 70.28; H, 3.77; N, 18.65%.

The preparation of Y_{pic} and Y_{lut} is described elsewhere.[5)]

Spectral Measurements. The IR and ^{1}H NMR spectra were measured as has been described previously.[14)] The ^{13}C NMR spectra were recorded in chloroform-*d* at 15.03 MHz, using the pulse Fourier transform technique on a JEOL FX 60 spectrometer at 34 °C. The chemical shifts were measured relative to TMS as the internal standard.

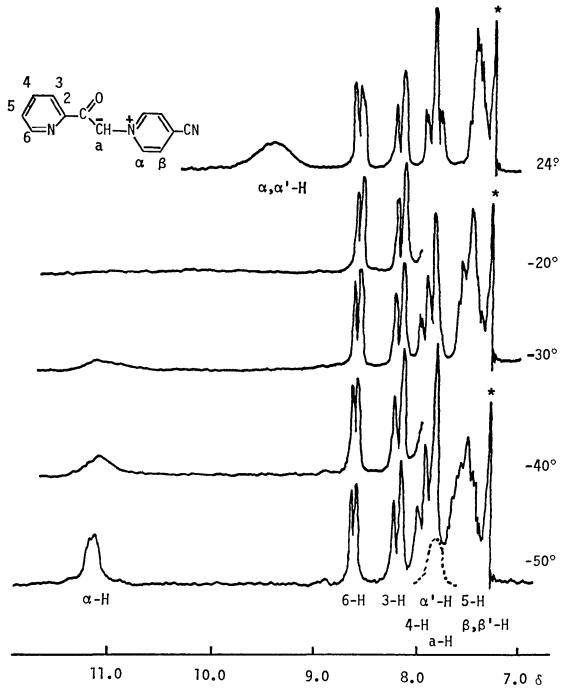

Fig. 2. Temperature-dependent ^{1}H NMR spectra of Y_{CN} in chloroform-*d* (*; $CHCl_3$).

The author wishes to express his hearty thanks to Professor Toshio Tanaka for his continuous encouragement throughout this study.

References

1) A. W. Johnson, "Ylid Chemistry," Academic Press, New York (1966).
2) B. M. Trost and L. S. Melvin, Jr., "Sulfur Ylides," Academic Press, New York (1975).
3) I. Zugravescu and M. Pelrovanu, "N-Ylid Chemistry," McGraw-Hill, New York (1976).
4) G. Matsubayashi, Y. Kondo, T. Tanaka, S. Nishigaki, and K. Nakatsu, *Chem. Lett.*, **1979**, 375.
5) G. Matsubayashi, Y. Kondo, and T. Tanaka, to be published.
6) G. Matsubayashi, I. Kawafune, T. Tanaka, S. Nishigaki, and K. Nakatsu, *J. Organomet. Chem.*, **187**, 113 (1980).
7) I. Kawafune, G. Matsubayashi, and T. Tanaka, to be published.
8) K. Kawakami, T. Ohara, G. Matsubayashi, and T. Tanaka, *Bull. Chem. Soc. Jpn.*, **48**, 1440 (1975).
9) T. McL. Spotwood and C. I. Tanzer, *Aust. J. Chem.*, **20**, 1227 (1967).
10) J. B. Stothers, "Carbon-13 NMR Spectroscopy," Academic Press, New York (1972).
11) T. A. Albright, M. D. Gordon, W. J. Freeman, and E. E. Schweizer, *J. Am. Chem. Soc.*, **98**, 6249 (1976).
12) P. Froyen and D. G. Morris, *Acta Chem. Scand. B*, **30**, 435 (1976).
13) G. Matsubayashi, unpublished results.
14) H. Koezuka, G. Matsubayashi, and T. Tanaka, *Inorg. Chem.*, **15**, 417 (1976).
15) W. G. Phillips and K. W. Ratts, *J. Org. Chem.*, **35**, 3144 (1976).
16) J. A. Pople, W. G. Schneider, and H. J. Bernstein, "High Resolution Nuclear Magnetic Resonance," McGraw-Hill, New York (1959), p. 233.
17) G. R. Clemo, W. McG. Morgan, and R. Rapper, *J. Chem. Soc.*, **1937**, 965.

A Molecular Orbital Study of the Conformation and *g*-Factors of the $H_2SSH_2^+$ and H_2SSH Radicals

Osamu KIKUCHI

Department of Chemistry, The University of Tsukuba, Sakura-mura, Ibaraki 305

(Received June 16, 1980)

Synopsis. The conformation and *g*-factors of the $H_2SSH_2^+$ and H_2SSH radicals were analyzed by means of a restricted open-shell SCF MO method with the semi-empirical MINDO/3 and INDO approximations, and the observed *g*-factors of the family of radicals consisting of $R_2SSR_2^+$, R_2SSR, and $RSSR^-$ were compared on the basis of their molecular and electronic structures.

Since the principal values of *g*-factors correlate strongly with the molecular structure of a radical, the theoretical analysis of the *g*-factors can clarify the molecular and electronic structure of the radical. We have elucidated the observed *g*-factors of the $HSSH^-$ radical anion in a previous paper.[1] Recently, much attention has been paid to the structure and stability of the S–S cation radicals.[2-4] In the present study, the *g*-factors of the $H_2SSH_2^+$ and H_2SSH radicals were examined, and the $H_2SSH_2^+$, H_2SSH, and $HSSH^-$ radicals are compared in terms of their molecular and electronic structures.

The MO's of the restricted doublet state were obtained by the use of the approximate SCF version proposed by Longuet-Higgins and Pople.[5] In the previous study of the $HSSH^-$ anion,[1] the MINDO/3 approximation was used. It is, however, uncertain whether MINDO/3 correctly predicts the *g*-factors of all of the neutral, anion, and cation radicals. Both the MINDO/3[6] and INDO[7] approximations were, thus, employed independently for the present calculation of $H_2SSH_2^+$ and H_2SSH. A more detailed description of the calculation of the *g*-factors has been reported elsewhere.[8-9]

$H_2SSH_2^+$ Radical. The observed $g_{av}(=(g_1+g_2+g_3)/3)$ values for the $R_2SSR_2^+$ radicals are $\simeq 2.01$;[2-3,10-11] no principal value has been reported. Since the 12 protons in $Me_2SSMe_2^+$ have equivalent hyperfine coupling constants,[10] the symmetric structures are examined. The MINDO/3 optimized $H_2SSH_2^+$ structures are I—IV. In all of the I—IV structures, the singly-occupied MO (SOMO) is the S–S antibonding σ^* orbital. The large g_y value of the planar structure, I, comes from the contribution of the π(S–S) bonding orbital; the highest occupied π^*(S–S) orbital makes no contribution because of its symmetry property. The other two principal values of I, g_x and g_z, are close to the free-spin value, g_f. The skewed structure, II, has two lone-pair orbitals at the sulfur atoms; these 3p lone-pair orbitals contribute to the large g_y and g_z values of II. These electronic structure and *g*-factors of II are very similar to those of the $HSSH^-$ anion radical.[1] In the bent structures, III and IV, mixing occurs among the σ^* SOMO and the π orbitals. This mixing reduces the g_y value and gives smaller g_{av} values for III and IV.

The INDO optimized structures are shown in Fig. 2, while their *g*-factors are listed in Table 2. The trend observed in the INDO *g*-factors of I'—IV' is similar to that in the MINDO/3 *g*-factors.

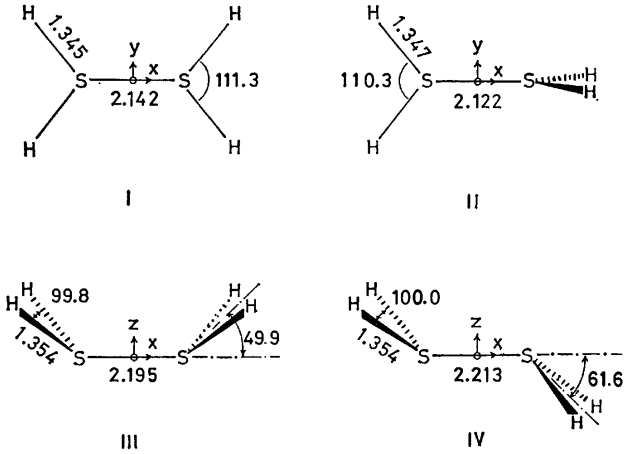

Fig. 1. The MINDO/3 optimized structures of the $H_2SSH_2^+$ radical. Bond lengths are in Å, and angles are in degrees.

TABLE 1. THE MINDO/3 *g*-FACTORS FOR FOUR OPTIMIZED STRUCTURES OF THE $H_2SSH_2^+$ RADICAL[a]

	I	II	III	IV
E_{total}/eV	−515.377	−515.483	−515.907	−515.903
g_x	2.0023	2.0023	2.0022	2.0023
g_y	2.0156	2.0125	2.0067	2.0071
g_z	2.0031	2.0125	2.0018	2.0017
g_{av}	2.0070	2.0091	2.0036	2.0037

a) The coordinate axes are shown in the optimized structures in Fig. 1.

The electronic structure of the $H_2SSH_2^+$ radical described above indicates that the g_y and g_{av} values depend largely on the S–S distance. The calculation showed that the increase in the g_{av} values of the planar and skewed structures, I and II, with an increase in the S–S distance was larger than that of the bent structures. The bent structure III with $R_{S-S}=2.542$ has $g_{av}=2.0118$. Since the principal values have not been reported for the $R_2SSR_2^+$ radical, it is difficult to derive any ultimate conclusion for the structure of the $H_2SSH_2^+$ radical from the present *g*-factor calculation. However, the present analysis of the *g*-factors suggests that the planar or skewed structure may correspond to the observed $R_2SSR_2^+$ structures. The present calculation shows a large difference in the principal values of the planar and skewed structures; the conformation of the $R_2SSR_2^+$ radicals may be determined if three principal values are determined experimentally.

H_2SSH Radical. The MINDO/3 optimized structure of H_2SSH is V. The calculated principal values of this structure are 2.036, 2.002, and 2.002.

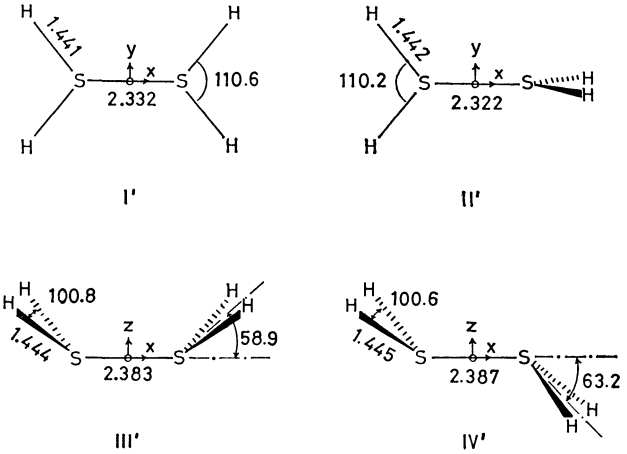

Fig. 2. The INDO optimized structures of the $H_2SSH_2^+$ radical.
Bond lengths are in Å, and angles are in degrees.

Table 2. The INDO g-factors for four optimized structures of the $H_2SSH_2^+$ radical[a)]

	I'	II'	III'	IV'
E_{total}/eV	−609.657	−609.713	−610.136	−610.153
g_x	2.0023	2.0023	2.0023	2.0023
g_y	2.0119	2.0080	2.0068	2.0074
g_z	2.0022	2.0080	2.0010	2.0010
g_{av}	2.0055	2.0061	2.0034	2.0036

a) The coordinate axes are shown in the optimized structures in Fig. 2.

Similar results were obtained by the INDO calculation; the optimized structure is V', and its g-factors are 2.053, 2.002, and 2.002. The radicals attributed to R_2SSR are H_2SSH (g_1=2.066, g_2=2.025, g_3=2.003),[12] EtHSSEt (g_1=2.063, g_2=2.027, g_3=1.999),[13] and RCH_2SSHCH_2R (g_1=2.063, g_2=2.010, g_3=2.000).[12,14] The two principal values are very large, while only one principal value is close to g_f. Since the two principal values of V and V' are very close to g_f, the V and V' structures can not explain the observed g-factors of the R_2SSR radicals. In the solid state, the environment effect may cause a deformation of the molecular structure of the radical. Thus, the dependence of the g-factors upon the conformation of H_2SSH was examined by means of MINDO/3. The g-factors were calculated by changing the S–S distance from 2.05 Å to 2.25 Å, the rotation angle about the S–S bond from −90° to +90°, the S–S–H angle from 100° to 140°, or the bending angle of the H_2S group from 0° to 60°. In all the conformations considered, the second largest principal values was less than 2.007. The results of this examination suggest that the observed principal values are possibly reproduced by the conformation with a very large SSH angle. The structures in Fig. 4 are the conformations for which the best agreement between the calculated and observed values was obtained. The g-factors of VI are 2.066, 2.023, and 2.000. The g-factors of VI' are 2.067, 2.021, and 2.002. Although the VI and VI' structures are more unstable than the optimized structures by 80 and 130 kJ mol^{-1} respectively, the present analysis of the g-factors suggests that the SSR* angle of the R_2SSR^* radical would be much larger than those to be expected for the $R_2SSR_2^+$ and $RSSR^-$ radicals.

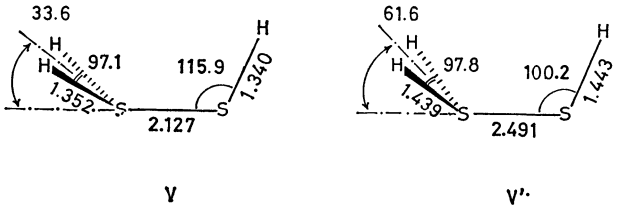

Fig. 3. The MINDO/3(V) and INDO(V') optimized structures of the H_2SSH radical.

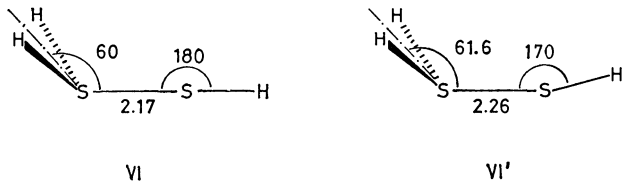

Fig. 4. The MINDO/3(VI) and INDO(VI') structures of the H_2SSH radical which give the best agreement between the calculated and observed g-factors.

References

1) O. Kikuchi, *Bull. Chem. Soc. Jpn.*, **51**, 315 (1978).
2) W. K. Musker and T. L. Wolford, *J. Am. Chem. Soc.*, **98**, 3055 (1976).
3) W. K. Musker, T. L. Wolford, and P. B. Roush, *J. Am. Chem. Soc.*, **100**, 6416 (1978).
4) K.-D. Asmus, D. Bahnemann, Ch.-H. Fischer, and D. Veltwisch, *J. Am. Chem. Soc.*, **101**, 5322 (1979).
5) H. C. Longuet-Higgins and J. A. Pople, *Proc. Phys. Soc.*, **68**, 591 (1955).
6) R. C. Bingham, M. J. S. Dewar, and D. H. Lo, *J. Am. Chem. Soc.*, **97**, 1285 (1975).
7) J. A. Pople, D. L. Beveridge, and P. A. Dobosh, *J. Chem. Phys.*, **47**, 2026 (1967).
8) O. Kikuchi, *Bull. Chem. Soc. Jpn.*, **42**, 1187 (1969).
9) T. Morikawa, O. Kikuchi, and K. Someno, *Theor. Chim. Acta*, **22**, 224 (1971).
10) B. C. Gilbert, D. K. C. Hodgman, and R. O. C. Norman, *J. Chem. Soc., Perkin Trans. 2*, **1973**, 1748.
11) M. C. R. Symons and R. L. Petersen, *J. Chem. Soc., Faraday Trans. 2*, **75**, 210 (1979).
12) M. C. R. Symons, *J. Chem. Soc., Perkin Trans. 2*, **1974**, 1618.
13) J. Skelton and F. C. Adam, *Can. J. Chem.*, **49**, 3536 (1971).
14) K. Akasaka, S. Ohnishi, T. Suita, and I. Nitta, *J. Chem. Phys.*, **40**, 3110 (1964).

Near-infrared Magnetic Circular Dichroism Studies on Iron(III) Horse Heart Cytochrome c

Nagao KOBAYASHI,** Tsunenori NOZAWA, and Masahiro HATANO*
Chemical Research Institute of Non-aqueous Solutions, Tohoku University, Sendai 980
(Received June 30, 1980)

Synopsis. Magnetic circular dichroism (MCD) spectra in the near-infrared region reported first for oxidized cytochrome c in its neutral (pH 5.58), alkaline (pH 11.62), and acidic (pH 1.88) forms exhibit temperature dependence, indicating that they are composed of Faraday C terms, except for the acidic form. The relation between the near-infrared MCD and the heme vicinity is discussed in terms of the structures for the heme chromophore of cytochrome c.

Near-infrared MCD spectra for heme chromophores are very sensitive to the oxidation, spin and ligand states of hemoproteins.[1,2] This is due to the fact that the bands ascribable to the charge-transfer transitions among iron, porphyrin and axial ligand, and d-d transitions of the iron ion can be easily resolved because of the absence of strong π-π^* transitions.[3,4] However, only a few studies[1,2,5-7] have been reported on the observation of near-infrared MCD, especially its temperature dependence, because of technical difficulties. The difficulties were overcome by use of a near-infrared MCD spectropolarimeter and deuterated solvents. We wish to report the accurate temperature dependence of near-infrared MCD for several forms of iron(III) cytochrome c.

Experimental

Materials. Cytochrome c from horse heart (Sigma type VI) was dissolved in deuterium oxide without further purification. Complete oxidation was attained by adding slight excess of freshly prepared deuterium oxide solution of potassium hexacyanoferrate(III). For the temperature variation experiments, an appropriate solution was diluted with hexadeutrated ethylene glycol at 60 (v/v) percent. The pH was adjusted by adding the least amount of concentrated sodium hydroxide or hydrochloric acid solution with stirring. The concentrations were determined on the basis of the heme molar concentrations from the visible absorption spectra.

Measurements. Absorption spectra were measured with a Hitachi EPS-3T spectrophotometer, MCD being recorded on a JASCO J-200 spectropolarimeter equipped with an electromagnet which affords up to 1.47 T magnetic field. MCD magnitude is expressed by the 10^{-4} molar ellipticity per Tesla ($[\theta]_M/10^{-4}$ °mol^{-1} dm^3 m^{-1} T^{-1} or 10^{-7} °m^2 mol^{-1} T^{-1}). Temperature was controlled by means of a stream of cold nitrogen gas. The path lengths of cells were 10 mm for the measurement at ambient temperature and 3 mm for that at cryogenic temperature.

Results and Discussion

MCD and absorption spectra are shown for iron (III) cytochrome c at neutral and at alkaline pH solutions in Figs. 1 and 2, respectively. The general spectral patterns of MCD are similar to those of absorption spectra, being characteristic for iron(III) low-spin heme complexes such as metmyoglobin cyanide.[1,6] The MCD spectra show the largest absorption peak. The positions of the strongest MCD peaks for neutral cytochrome c and alkaline cytochrome c are at 1720 and 1460 nm, respectively. The cyanide derivatives of metmyoglobin[1] and peroxidase[2] reveal MCD peaks at 1530 and 1680 nm, respectively. Since the iron (III) heme bands in the near-infrared region have been assigned as charge-transfer transitions from porphyrin a_{1u}, $a_{2u}(\pi)$ to $e_g(d\pi)$ orbitals ($E_u \leftarrow A_{1g}$) in D_{4h} symmetry, the energy differences in the peak positions for these low-spin species depend mostly on the energy levels of $e_g(d\pi)$ orbitals which vary more sensitively with the axial ligation mode than those of the porphyrin π orbitals. Theoretical consideration

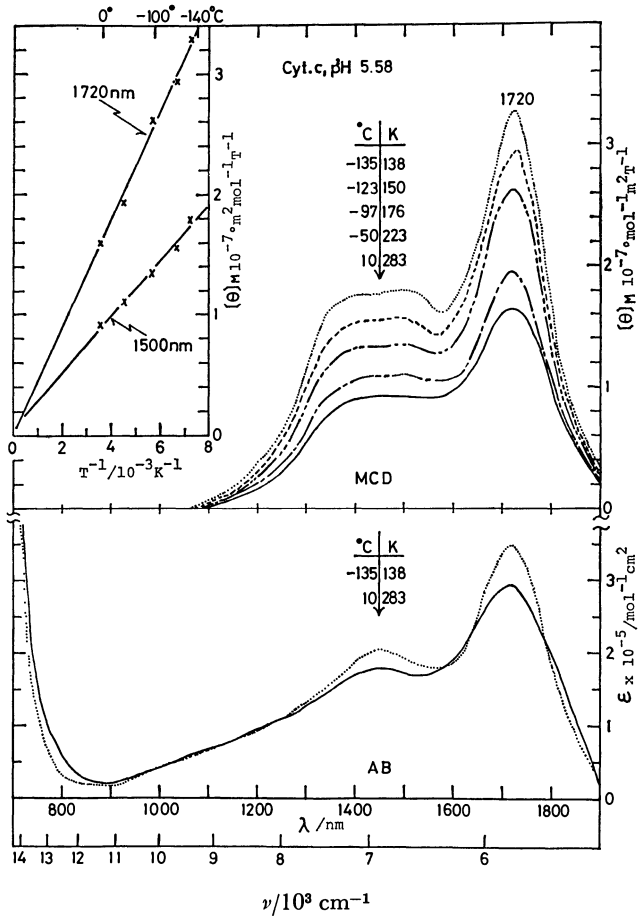

Fig. 1. MCD and absorption spectra of iron(III) cytochrome c at p^{2}H 5.58. Cell length; 0.3 cm, concentration; 4.5×10^{-3} mol dm^{-3}, field; 1.47 T. The inset shows plots of the MCD magnitudes at 1720 and 1500 nm *vs.* the reciprocal of the absolute temperature.

**Present address: Pharmaceutical Institute, Tohoku University, Aobayama, Sendai 980.

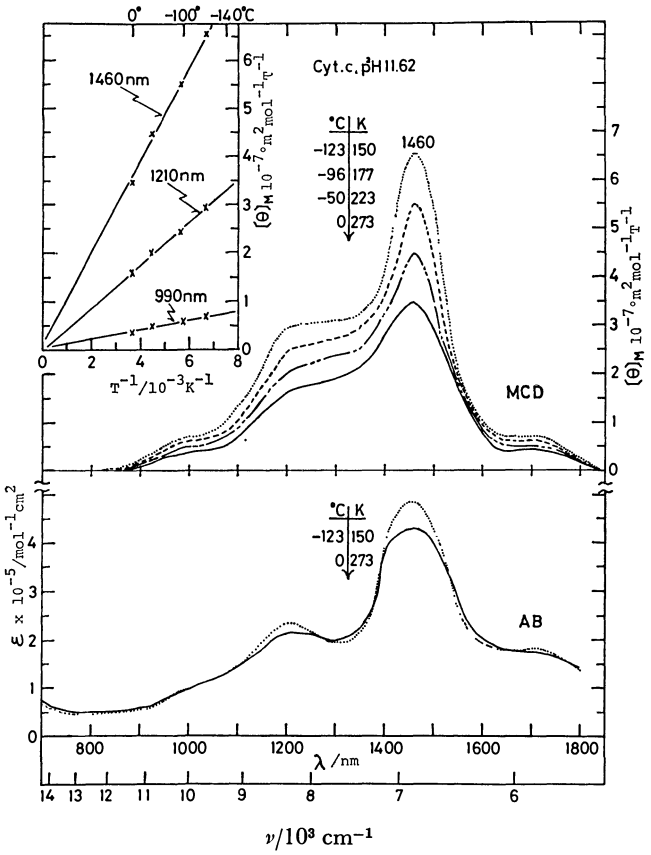

Fig. 2. MCD and absorption spectra of iron(III) cytochrome c at p²H 11.62. Other conditions are the same as for Fig. 1. The inset shows the MCD magnitudes of the peaks at 1460, 1210, and 990 nm *vs.* the reciprocal of the absolute temperature.

on the spectra of iron(III) low-spin heme derivatives[8] indicates that these peaks are composed mainly of the vibrational overtones superposed on the two electronic (charge-transfer) transitions.

The effect of wider temperature range on the near-infrared MCD of iron(III) cytochrome c is shown in Figs. 1 and 2. For metmyoglobin cyanide,[1] the shape of MCD did not change with lowering in temperature as in the Soret bands, while the MCD magnitude increased linearly with the reciprocal of absolute temperature. The extrapolation of temperature dependence at the peaks around 1720, 1500, 1460, 1210, and 990 nm approaches zero at infinite temperature, indicating that these bands are composed of pure Faraday C terms.

Figure 3 shows the MCD and absorption spectra of iron(III) cytochrome c in an acidic solution. A dispersion type MCD, characteristic of iron(III) high-spin heme, was obtained corresponding to the absorption peak at 1000 nm. For native metmyoglobin the

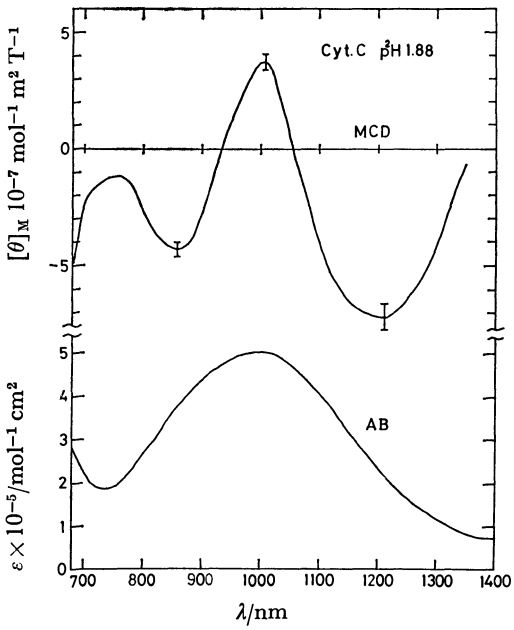

Fig. 3. MCD and absorption spectra of iron(III) cytochrome c at p²H 1.88. Cell length 1.0 cm. Concentration; 0.6×10^{-3} mol dm^{-3}. Temperature; 20 °C.

curve is non-symmetrical with respect to the line of $[\theta]_M=0$, differing from metmyoglobin fluoride which displays a clear S-shaped dispersion.[1] The MCD spectrum showed a slight change in magnitude with lowering in temperature. The band was confirmed to consist predominantly of Faraday A terms plus B terms. A similar spin state is suggested between this species and metmyoglobin from the near coincidence of the crossover points and relative intensities of the MCD peak (1010 nm) and trough (1210 nm).

References

1) T. Nozawa, T. Yamamoto, and M. Hatano, *Biochim. Biophys. Acta*, **427**, 28 (1976).
2) N. Kobayashi, T. Nozawa, and M. Hatano, *Biochim. Biophys. Acta*, **493**, 340 (1977).
3) D. W. Smith, and R. J. P. Williams, *Struct. Bonding*, **1**, 1 (1970).
4) M. Zerner, M. Gouterman, and H. Kobayashi, *Theor. Chim. Acta*, **6**, 363 (1966).
5) J. C. Cheng, G. A. Osborne, P. J. Stephens, and W. A. Eaton, *Nature*, **241**, 193 (1973).
6) W. A. Eaton, and E. Charney, *J. Chem. Phys.*, **51**, 4502 (1969).
7) J. Rawrings, P. J. Stephens, L. A. Nafie, and M. D. Kamen, *Biochemistry*, **16**, 1725 (1977).
8) P. J. Stephens, J. C. Sutherland, J. C. Cheng, and W. A. Eaton, "Proceedings of the International Conference on Excited States of Biological Molecules, Leiden," ed by J. Birks, Wiley-Interscience, New York (1976), p. 434.

Charge-transfer Interaction and Ground-state Energy Stabilization in Crystalline Complex Ion Radical Salts

Yôichi IIDA

Department of Chemistry, Faculty of Science, Hokkaido University, Sapporo 060

(Received July 2, 1980)

Synopsis. Although predominant cohesive energy is Madelung energy, the ground state of crystalline complex ion radical salt is further stabilized by the charge-transfer interaction between neutral molecule and ion radical, together with that between ion radicals. The magnitude of this stabilization energy was estimated with (Phenothiazine)$_2^{+\cdot}$ Br$^-$.

In crystalline simple ion radical salts, the planar ion radical molecules are known to form, in themselves, a segregated stacking into columns so as to make a large overlap between their half-occupied molecular orbitals.[1] Much attention has been paid to the prominent optical and magnetic properties of such ion radical salts.[1-6] In their optical properties, charge-transfer absorption due to the transition of unpaired electron between ion radical molecules appear in the low-energy region. As for the magnetic properties, antiferromagnetic spin exchange interaction acts between adjacent ion radicals, so that such a salt is considered as one-dimensional Heisenberg antifferomagnet. In previous papers,[2,3] we applied one-dimensional half-occupied Hubbard model to the segregated stack of ion radical molecules. This model is a simplification of the real crystal and is described by two parameters I and T. $T(<0)$ is the transfer matrix element of an unpaired electron which describes hopping between adjacent molecular ion radical sites, while I is the on-site Coulomb repulsion between two electrons with up and down spins on the same molecule. This model could well explain the reason why the charge-transfer absorption is observable in such ion radical salts.[2] The applicability of the Hubbard model is further justified by the fact that the one-dimensional half-occupied Hubbard model with $I \gg |T|$ becomes equivalent to one-dimensional Heisenberg antiferromagnet with exchange interaction $J=2T^2/I$.[7] Then, the ground-state energy of the one-dimensional system of ion radicals can be given by $E=-2NJ\ln 2=-(4NT^2/I)\ln 2$, where $N\to\infty$ is the number of ion radical molecules in the one-dimensional system.[3] This energy stabilization is caused by the charge-transfer interaction between unpaired electrons of adjacent ion radicals through non-zero $|T|$ value in segregated stack of ion radicals.

So far, we have considered simple ion radical salts, where each ion radical carries one unpaired electron. In the case of crystalline complex ion radical salts, the ion-radical and parent neutral molecules are known to stack together to form regular one-dimensional column, where each molecular site is occupied by less-than-one electron.[4-6] Then, we can apply regular one-dimensional less-than-half occupied Hubbard model to the segregated stack composed of ion-radical and neutral molecules in crystalline complex ion radical salts. Shiba and Klein-Seitz have shown that the magnetic susceptibility of a uniform stack of less-than-half occupied molecules (average number of unpaired electrons per site is $\rho<1$) is related to the magnetic susceptibility of a uniform stack of half-occupied molecules ($\rho=1$) in simple ion radical salt.[8,9] If the value of I is much larger than that of $|T|$, the less-than-half occupied one-dimensional Hubbard model becomes equivalent to an antiferromagnetic Heisenberg chain with exchange interaction,[10]

$$J=\frac{2T^2\rho}{I}\left(1-\frac{\sin 2\pi\rho}{2\pi\rho}\right). \tag{1}$$

Under the same condition, the lowest energy was also given by Shiba.[8] If we denote total number of molecular sites as N, the number of unpaired electrons is given by $N\rho$, and the lowest energy of the system, E, is expressed by

$$E/N|T| = -\left\{\frac{2}{\pi}\sin\pi\rho+\frac{4|T|\rho^2\ln 2}{I}\left(1-\frac{\sin 2\pi\rho}{2\pi\rho}\right)\right\}. \tag{2}$$

In the case of $\rho<1$, the E value of Eq. 2 is composed of two factors; one is the term, $E_1=-(2/\pi)N|T|\sin\pi\rho$, and the other, $E_2=-(4NT^2\rho^2/I)\ln 2\ (1-\sin 2\pi\rho/(2\pi\rho))$. The E_2 term is regarded as the stabilization energy due to the charge-transfer interaction between unpaired electrons. In terms of J in Eq. 1, E_2 is written as $-2NJ\rho\ln 2$. On the other hand, the E_1 term is characteristic of less-than-half occupied system. It becomes zero at $\rho=0$ or 1, but has the most negative value of $-(2/\pi)N|T|$ at $\rho=1/2$. E_1 is not a function of I, but is related only to $|T|$ and ρ. Therefore, E_1 corresponds to the stabilization energy due to the charge-transfer interaction between neutral and ion-radical molecules in one-dimensional system. If we consider the case of $\rho=1$, Eq. 1 is simply $J=2T^2/I$, and Eq. 2 is reduced to $E=E_2=-(4NT^2/I)\ln 2$ and $E_1=0$. As our model requires, the J and E values are found to be identical with those described previously in simple ion radical salt. In the case of half-occupied Hubbard model with $\rho=1$, each molecular site is occupied by one unpaired electron and there remains no neutral molecular site, so that there acts no charge-transfer interaction between neutral and ion-radical molecules in simple ion radical salts. This is the reason why $E_1=0$ at $\rho=1$. Therefore, the energy stabilization due to E_1 appears only in complex ion radical salts.

Next, we shall apply the above-mentioned approach to certain crystalline complex ion radical salt and estimate its ground-state stabilization energy. For purposes of comparison, we shall also examine the corresponding simple salt. For this purpose, we take simple cation radical salt of (Phenothiazine)$^{+\cdot}$ Br$^-$ and complex salt of (Phenothiazine)$_2^{+\cdot}$ Br$^-$. In pre-

vious papers,[6] we reported that the optical and magnetic properties of those phenothiazine (PT) cation radical salts were well explained by applying regular one-dimensional Hubbard model to the segregated stack of phenothiazines, and estimated the values of $I=12900\ cm^{-1}$ and $T\approx-2500\ cm^{-1}$ for the one-dimensional system of the simple salt of $PT^{+\cdot}\ Br^-$. Moreover, these parameter values could be commonly used for the one-dimensional system of the complex salt of $(PT)_2^{+\cdot}\ Br^-$. Then, the average number of unpaired electrons per site and the number of phenothiazine sites are $\rho=1$ and $N=N_A$ (Avogadro number) for one mole of $PT^{+\cdot}\ Br^-$, respectively, while they are $\rho=1/2$ and $N=2N_A$ for one mol of $(PT)_2^{+\cdot}\ Br^-$, respectively. In the case of the simple salt, by the use of $E=-(4NT^2/I)$ ln 2 together with the estimated I and T values, the stabilization energy due to the charge-transfer interaction between phenothiazine cation radicals was calculated to be $E=-16.0\ kJ\ mol^{-1}$. As for the complex salt, the stabilization energy, E, is given by two factors, E_1 and E_2. By using the E_2 equation together with $N=2N_A$, $\rho=1/2$, $I=12900\ cm^{-1}$ and $T\approx-2500\ cm^{-1}$, the value of E_2 was determined to be $-8.0\ kJ\ mol^{-1}$, whose magnitude was found to be just half of that of E in the simple salt. In the complex salt, however, the E_1 term due to the charge-transfer interaction between neutral and cation-radical phenothiazines was estimated to be $-38.0\ kJ\ mol^{-1}$ by the use of the E_1 equation. By summing E_1 and E_2, the ground-state stabilization energy of the complex salt was $E=-46.0\ kJ\ mol^{-1}$. We can see that, although the stabilization due to the charge-transfer interaction between phenothiazine cation radicals decreases, the total stabilization energy of the complex salt greatly increases in comparison with that of the simple salt. The reason for this is that the interaction between neutral and cation-radical phenothiazines plays an important role in the complex salt.

Since every ion radical salt belongs to a kind of ionic crystals, Madelung energy is the most important factor for the cohesive energy.[11] However, the ground-state energy stabilization due to the charge-transfer interactions between ion-radical molecules and between neutral and ion-radical molecules will be the next important factor for the total cohesive energy in crystalline ion radical salts.

References

1) See, for example, Z. G. Soos and D. J. Klein, "Molecular Association," ed by R. Foster, Academic Press, London, New York, San Francisco (1975), Vol. 1, Chap. 1; "Synthesis and Properties of Low-Dimensional Materials," ed by J. S. Miller and A. J. Epstein, The New York Academy of Sciences, New York (1978).
2) Y. Iida, *Bull. Chem. Soc. Jpn.*, **50**, 1445 (1977); **51**, 2523 (1978); **52**, 689, 2791 (1979).
3) Y. Iida, *Bull. Chem. Soc. Jpn.*, **52**, 3447 (1979); **53**, 1447 (1980).
4) Y. Iida, *Bull. Chem. Soc. Jpn.*, **42**, 637 (1969); **51**, 434 (1978).
5) S. Doi and Y. Matsunaga, *Bull. Chem. Soc. Jpn.*, **48**, 3747 (1975).
6) Y. Iida, *Bull. Chem. Soc. Jpn.*, **51**, 3637 (1978); **53**, 2397 (1980).
7) M. Takahashi, *Prog. Theor. Phys. (Kyoto)*, **42**, 1098 (1969).
8) H. Shiba, *Phys. Rev. B*, **6**, 930 (1972).
9) D. J. Klein and W. A. Seitz, *Phys. Rev. B*, **10**, 3217 (1974).
10) J. B. Torrance, "Synthesis and Properties of Low-Dimensional Materials," p. 210. See Ref. 1.
11) R. M. Metzger, *J. Chem. Phys.*, **64**, 2069 (1976).

Effect of Ionic Strength on the Metachromatic Behavior of Dye-Polymer Systems[1)]

Kiwamu YAMAOKA* and Mineo TAKATSUKI

Faculty of Science, Hiroshima University, Higashisenda-machi, Naka-ku, Hiroshima 730

(Received August 28, 1980)

Synopsis. The effect of added sodium chloride on the metachromatic interaction between cationic dyes (Crystal Violet, Trypaflavine, and 9-aminoacridinium chloride) and sodium polyphosphate and poly(ethylenesulfonate) was studied in aqueous solutions by measuring the visible absorption spectra and by determining the bound-dye spectra and the equilibrium constants with the principal component analysis.

Previous reports have shown that metachromatic changes of the absorption spectra of Crystal Violet (CV) and Trypaflavine (TF) in the presence of sodium polyphosphate (NaPP) are affected by addition of simple electrolytes.[2-4)] The degree of metachromasy was decreased with the increase of ionic strength, *i.e.*, the absorption spectra of dye–NaPP solutions returned to the original spectra of the NaPP-free dye solutions. On the basis of the ultrafiltration of dye–NaPP solutions, this result was attributed to the dissociation of bound-dye species from NaPP by competition with Na^+ ions.[3,4)]

Recent applications of the extended-principal-component-analysis (EPCA) procedure to a variety of dye–polymer solutions demonstrated that it is possible to determine the number of light-absorbing components, the equilibrium constant, the pure spectra of dye species bound to polymer, and the fraction of the bound-dye species from a family of experimental absorption spectra of a dye–polymer system.[5-8)] By utilizing this EPCA procedure, therefore, the amount of dye species dissociated from the polymer site by an increase of ionic strength can now be estimated on a precise and quantitative basis. In this Note, the effect of added NaCl on the metachromatic behavior of four different dye–polymer systems will be reported. In all dye–polymer combinations, the fractions of bound-dye species indeed decrease with an increase of added NaCl but, surprisingly, the spectra of the bound-dye species remain unchanged.

Experimental

Materials. Samples were sodium polyphosphate (NaPP)[5)] and sodium poly(ethylenesulfonate) (NaPES),[5)] and the chlorides of Crystal Violet (CV),[5)] Trypaflavine (TF),[5)] and 9-aminoacridinium chloride (AA).[8)]

Measurements and the Procedure for Data Analysis. Absorption spectra were measured at 25 °C.[8)] Optical titration of a dye solution, which contains either 1 mM ($=10^{-3}$ mol/dm^3) or 0.1 mM NaCl, was carried out by the dropwise addition of a polymer solution which contains the same amount of NaCl. The observed series of spectra of each dye–polymer system were analyzed by the EPCA procedure, which has been described together with other precautions.[5-9)] The molar absorption coefficient, ε, was defined as before.[5,8)]

Results and Discussion

Pure Spectra of Bound-dye Species and Equilibrium Constants. Figures 1a—d show the typical absorption spectra of dyes in the presence and the absence of polymers. In each dye–polymer system, optical titrations were carried out to obtain eight to nine experimental spectra over the P/D range 0—*ca.* 1, where P and D are the concentrations of a polymer in the residue unit and a dye respectively.[3)] (Not all spectra were drawn in each figure, but details are the same as were shown in Refs. 5—8.) Each family of spectra shows the presence of isosbestic points, which are independent of the concentration of added NaCl (*cf.* caption of Fig. 1), indicating that the dye–polymer solution consists of two light-absorbing components, probably, free- and bound-dye species. The result of the EPCA procedure applied to the experimental spectra revealed that each dye–polymer system, which contains either 1 mM or 0.1 mM NaCl, is composed

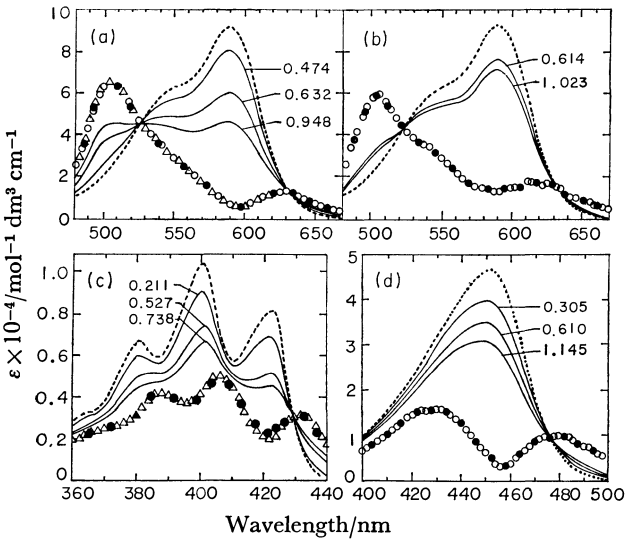

Fig. 1. Absorption spectra of CV–, AA–, and TF–polymer systems in the presence of NaCl and the corresponding pure spectra of dye species bound to the polymers. The experimental conditions are: (a) CV–NaPP with P/D 0—1.26 in 0.1 mM NaCl, (b) CV–NaPES with P/D 0—1.023 in 0.1 mM NaCl, (c) AA–NaPP with P/D 0—0.738 in 1 mM NaCl (precipitates appeared at the concentration of added NaCl higher than 5 mM), and (d) TF–NaPES with P/D 0—1.145 in 0.1 mM NaCl. The initial dye concentrations in μM are (a) 8.13, (b) 7.04, (c) 44.3, and (d) 9.43. Isosbestic points in nm are: (a) 639 and 529, (b) 641 and 526, (c) 429, (d) 476. In each figure, the spectrum of the polymer-free dye solution is shown by the dotted curve and the numerals indicate the P/D values. The bound spectra are denoted by either (○) in 0.1 mM or (△) in 1 mM NaCl and by (●) in NaCl-free solutions, the latter being cited from Ref. 5 for (a), (b), and (d) and from Ref. 8 for (c) for comparison.

Table 1. Effect of added NaCl on the empirical parameter α and the equilibrium constant K of dye-polymer systems at 25 °C

Dye-polymer	NaCl[a]	α	K[b]	K'[c]
CV-NaPP	0.1	2.1(1.5)[d]	1.0×10^{11}	1.4×10^{5}
CV-NaPP	1.0	1.9(1.5)	1.8×10^{9}	4.7×10^{4}
CV-NaPES	0.1	1.5(0.6)	5.2×10^{7}	1.4×10^{5}
AA-NaPP	1.0	1.6(1.2)	1.2×10^{8}	2.8×10^{5}
TF-NaPES	0.1	1.2(0.9)	1.5×10^{6}	1.5×10^{5}

a) The concentration in 10^{-3} mol/dm^3. b) The dimension in $[\mathrm{dm^3/mol}]^{\alpha}$. c) $K'=K[\mathrm{P}]^{\alpha-1}$ at $P/D=1$. d) The α values in parentheses are for NaCl-free systems and are taken from Ref. 5 or 8 for comparison.

of two absorbing species. The pure spectra of dye species bound to NaPP and NaPES were thus evaluated and are shown in Figs. 1a—d, together with those in NaCl-free solutions. Interestingly, the bound-dye spectra in the presence or the absence of added NaCl are essentially identical with each other.

Fractions of Bound-dye Species. The scheme for the binding reaction includes an empirical parameter, α, in such a way that $K=[\mathrm{DP^*}]([\mathrm{D}][\mathrm{P}]^{\alpha})^{-1}$. The notations are all the same as before.[5,8] Both α and K were estimated by the EPCA procedure and are given in Table 1. The values of α are larger than unity in all cases where NaCl is added, indicating that the optical titration curves change sigmoidally with P/D.[5,6] The values of α are also larger in the presence of NaCl than in its absence. It is thus clear that the empirical parameter α reflects the effect of ionic strength on the binding reaction.

The fraction of bound-dye species in each solution, f_b, may be calculated with the estimated α and K values and also directly from the EPCA method.[5-8] The results are shown in Fig. 2, where the fraction of free-dye species remaining in solution, $1-f_b$, is plotted against P/D. The amount of CV bound to NaPP decreases most markedly with the increase in NaCl (Fig. 2a), *i.e.*, only 20% of CV remain bound even at $P/D=1$ in 1 mM NaCl, while 50% of CV are bound in the salt-free solution. In contrast, the effect of added NaCl was negligible for the AA–NaPP system (Fig. 2c), *i.e.*, 75% of AA remain bound at $P/D=1$ in 1 mM NaCl. Similarly, CV bound to NaPES is affected more than TF by added NaCl (Figs. 2b and d). It is clear that, as compared with acridine dyes (TF and AA), CV dissociates from the polymer to a remarkable extent, probably as a result of competitive inhibition by Na^+ ions.[10] Our result is in accord with the cases of Proflavine–poly(glutamic acid),[10] CV–poly(methacrylic acid),[11] and Acridine Orange–poly(*p*-styrenesulfonate).[12]

In summary, we have clearly shown that the spectra of bound-dye species are not affected by added NaCl but the Na^+ ion competes with the bound dye for the polymer site from which the dye is forced to dissociate. These results imply several possibilities to be resolved: (1) If the dye molecules are stacked on a polymer chain, they remain so even when over

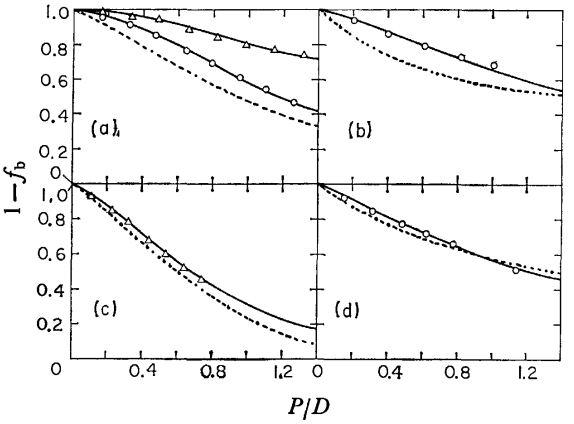

Fig. 2. The P/D dependence of the fraction of free-dye species remaining in solution, $1-f_b$, for four dye–polymer systems. (a) CV–NaPP, (b) CV–NaPES, (c) AA–NaPP, and (d) TF–NaPES. The solid curves were calculated from the values of α and K in Table 1 (*cf.* Eq. 2 in Ref. 6), while each point [(○) in 0.1 mM NaCl or (△) in 1 mM NaCl] was calculated by the EPCA method with 56 to 40 selected wavelengths (*cf.* Eq. 4 in Ref. 6). The dotted curves are the binding curves for NaCl-free systems for comparison (taken from Ref. 5 for (a), (b), and (d) and from Ref. 8 for (c)).

80% of them are liberated into the solution as free dye. (2) If the added salt enhances the degree of stacking[12] or aggregation of dye,[13] the bound-dye spectra may be so insensitive as not to reflect such changes of the bound-dye species. (3) The bound-dye species may exist in an unstacked state regardless of the amount of NaCl present in a solution.

We thank Mr. Kinya Nakata for his technical assistance.

References

1) Part VIII of *Metachromasy*. For the preceding paper of this series, see Ref. 8.
2) K. Yamaoka, T. Suenaga, A. Fujita, and M. Miura, *J. Sci. Hiroshima Univ., Ser. A-II*, **34**, 1 (1970).
3) K. Yamaoka, M. Takatsuki, K. Yaguchi, and M. Miura, *Bull. Chem. Soc. Jpn.*, **47**, 611 (1974).
4) K. Yamaoka, M. Takatsuki, and M. Miura, *Bull. Chem. Soc. Jpn.*, **48**, 2739 (1975).
5) K. Yamaoka and M. Takatsuki, *Bull. Chem. Soc. Jpn.*, **51**, 3182 (1978).
6) M. Takatsuki and K. Yamaoka, *Bull. Chem. Soc. Jpn.*, **52**, 1008 (1979).
7) M. Takatsuki, *Bull. Chem. Soc. Jpn.*, **53**, 1922 (1980).
8) K. Yamaoka, M. Takatsuki, and K. Nakata, *Bull. Chem. Soc. Jpn.*, **53**, 3165 (1980).
9) M. Takatsuki and K. Yamaoka, *J. Sci. Hiroshima Univ., Ser. A*, **40**, 387 (1976).
10) G. Schwarz, S. Klose, and W. Balthasar, *Eur. J. Biochem.*, **12**, 454 (1970).
11) V. Vitagliano, L. Costantino, and A. Zagari, *J. Phys. Chem.*, **77**, 204 (1973).
12) W. H. J. Stork, P. L. de Haseth, W. B. Schippers, C. M. Körmeling, and M. Mandel, *J. Phys. Chem.*, **77**, 1772 (1973).
13) Y. Sato, M. Hatano, and M. Yoneyama, *Bull. Chem. Soc. Jpn.*, **46**, 1980 (1973).

Vibrational Spectra and Normal Coordinate Calculations for Trimethylsilane

Yoshika IMAI* and Koyo AIDA

Department of Applied Science, Faculty of Engineering, Tohoku University, Sendai 980

(Received September 19, 1980)

Synopsis. Vibrational spectra of trimethylsilane-d_0, -d_1, -d_9, and -d_{10} have been obtained. Assignments for all the fundamentals have been made assuming C_{3v} molecular symmetry. Normal coordinate calculations have been carried out to confirm the assignments.

The vibrational studies of trimethylsilane have been made extensively.[1] For instance, Ball *et al.*[2] have reported the vibrational spectra of $(CH_3)_3SiH$ and $(CH_3)_3SiD$, and based on their data, Tenisheva *et al.*[3] have carried out the normal coordinate calculations. From these studies, it was found that there is a considerable coupling between the SiH bending and the methyl rocking vibrations, thus remaining some ambiguities in these assignments. Therefore, it is desirable to obtain the vibrational spectra of its methyl-d_9 homologues, $(CD_3)_3SiH$ and $(CD_3)_3SiD$, and to achieve the normal coordinate calculations using the data of these four isotopic species.

Experimental

The compounds were prepared by reduction of bromotrimethylsilane-d_0 or -d_9 with $LiAlH_4$ or $LiAlD_4$ and purified by vacuum distillation.

Infrared spectra (4000—300 cm^{-1}) were obtained on a Hitachi 345 spectrophotometer in the gas phase and in the solid films at liquid nitrogen temperature. Far-infrared spectra (400—80 cm^{-1}) were recorded on a Hitachi FIS-III spectrophotometer in the solid films at liquid nitrogen temperature. Raman spectra were recorded in the liquid state on a JEOL JRS S-1 laser Raman spectrophotometer equipped with a 50 mW NEC GLS 5800 He-Ne laser. Qualitative polarizations were also measured.

Results and Discussion

With C_{3v} symmetry, 24 normal vibrations are expected to distribute as $8A_1+4A_2+12E$. The A_1 and E modes are both infrared and Raman active, and the A_2 modes are inactive in both spectra. The observed frequencies for $(CD_3)_3SiH$ and $(CD_3)_3SiD$ are listed in Table 1. Those for $(CH_3)_3SiH$ and $(CH_3)_3SiD$ are nearly equal with those given by the previous authors.[2] The Raman spectra below 1000 cm^{-1} are shown in Fig. 1.

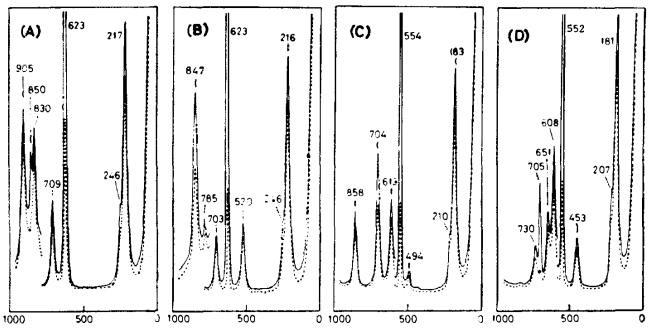

Fig. 1. Raman spectra of (A) $(CH_3)_3SiH$, (B) $(CH_3)_3SiD$, (C $(CD_3)_3SiH$, and (D) $(CD_3)_3SiD$. Solid line; parallel polarization, broken line; crossed polarization.

TABLE 1. OBSERVED AND CALCULATED FREQUENCIES (cm^{-1}) FOR $(CD_3)_3SiH$ and $(CD_3)_3SiD$[a]

	No.	$(CD_3)_3SiH$			$(CD_3)_3SiD$		
		Obsd	Calcd	PED	Obsd	Calcd	PED
A_1	1	2218	2213	$99S_1$	2217	2213	$99S_1$
	2	2119	2117	$90S_2$	2119	2118	$96S_2$
	3	2119	2126	$95S_3$	1544	1533	$100S_3$
	4	1038	1029	$98S_4$	1035	1029	$98S_4$
	5	992	988	$70S_5$ $15S_7$ $15S_2$	990	988	$71S_5$ $15S_7$ $15S_2$
	6	704	708	$66S_6$ $14S_7$ $15S_8$	705	703	$65S_6$ $13S_7$ $15S_8$
	7	554	546	$73S_7$ $12S_5$ $15S_6$	552	545	$74S_7$ $12S_5$ $14S_6$
	8	183	183	$62S_8$ $37S_6$	181	182	$62S_8$ $37S_6$
E	13	2218	2211	$64S_{13}$ $35S_{14}$	2217	2210	$68S_{13}$ $31S_{14}$
	14	2218	2212	$64S_{14}$ $35S_{13}$	2217	2212	$68S_{14}$ $31S_{13}$
	15	2119	2116	$97S_{15}$	2119	2117	$97S_{15}$
	16	1038	1029	$77S_{16}$ $22S_{17}$	1035	1029	$73S_{16}$ $25S_{17}$
	17	1038	1028	$76S_{17}$ $22S_{16}$	1035	1028	$73S_{17}$ $25S_{16}$
	18	992	986	$65S_{18}$ $14S_{15}$ $21S_{22}$	990	986	$65S_{18}$ $14S_{15}$ $21S_{22}$
	19	494	490	$79S_{19}$ $19S_{21}$	453	452	$59S_{19}$ $40S_{21}$
	20	613	591	$64S_{20}$ $27S_{22}$	608	590	$61S_{20}$ $31S_{22}$
	21	858	857	$90S_{21}$	651	648	$40S_{21}$ $19S_{20}$ $26S_{19}$
	22	704	700	$41S_{22}$ $31S_{20}$ $19S_{18}$	730	728	$33S_{22}$ $22S_{21}$ $20S_{20}$ $13S_{18}$
	23	210	213	$93S_{23}$	207	212	$92S_{23}$

a) The subscript number i in S_i corresponds with that in F_i given in Table 2.

TABLE 2. SYMMETRY FORCE CONSTANTS AND THEIR UNCERTAINTIES FOR TRIMETHYLSILANE[a)]

A_1 species				E species			
Mode			σ	Mode			σ
$\nu(CH_3)$	F_1	4.674	0.011	$\nu(CH_3)$	F_{13}	4.683	0.033
$\nu(CH_3)$	F_2	4.657	0.055	$\nu(CH_3)$	F_{14}	4.679	0.033
$\nu(SiH)$	F_3	2.584	0.009	$\nu(CH_3)$	F_{15}	4.664	0.077
$\delta(CH_3)$	F_4	0.527	0.003	$\delta(CH_3)$	F_{16}	0.525	0.005
$\delta(CH_3)$	F_5	0.524	0.016	$\delta(CH_3)$	F_{17}	0.520	0.005
$\rho(CH_3)$	F_6	0.359	0.016	$\delta(CH_3)$	F_{18}	0.499	0.022
$\nu(SiC_3)$	F_7	3.222	0.050	$\rho(CH_3)$	F_{19}	0.351	0.010
$\delta(SiC_3)$	F_8	0.731	0.065	$\rho(CH_3)$	F_{20}	0.459	0.008
				$\delta(SiH)$	F_{21}	0.549	0.012
	$F_{2,5}$	−0.414	0.064	$\nu(SiC_3)$	F_{22}	2.843	0.063
	$F_{5,7}$	−0.132	0.029	$\delta(SiC_3)$	F_{23}	0.620	0.025
	$F_{6,8}$	−0.275	0.023				
					$F_{15,16}$	−0.410	0.090
					$F_{16,22}$	−0.086	0.028
					$F_{19,21}$	0.113	0.006
					$F_{20,22}$	0.149	0.039

a) The stretching force constants are given in mdyn/Å, the deformation force constants in mdyn·Å, the stretching-deformation interaction constants in mdyn.

The observed spectra and the assignments for $(CH_3)_3SiH$ and $(CH_3)_3SiD$ are almost identical with those given by the previous authors.[2)] However, a discrepancy is found in the assignments for the methyl rocking vibrations. They have reported two Raman bands at 853 and 831 cm^{-1}, of which the latter was assigned to the A_1 mode from the polarization measurements. In agreement in frequency with their results, we have observed two bands at 850 and 830 cm^{-1}, but the former band, not the latter, is found to be polarized (Fig. 1. (A)). Therefore, the band at 850 cm^{-1} should be assigned to the A_1 methyl rocking mode and the latter to the E mode. This mis-assignments were probably caused by the fact that the polarization measurements were difficult in a photographic method with a Hg-arc as an excitation, especially in the case of closely separated bands.

For $(CD_3)_3SiH$ and $(CD_3)_3SiD$, the assignments can be easily made except the range between 1000 and 400 cm^{-1}. In the case of $(CD_3)_3SiD$, two polarized Raman bands are observed at 705 and 552 cm^{-1} in this region (Fig. 1. (D)) and can be assigned to the CD_3 rock(A_1) and to the SiC_3 stretch(A_1), respectively. These bands are observed nearly at the same frequencies in $(CD_3)_3SiH$, but the band at 704 cm^{-1} is now only partly polarized (Fig. 1. (C)). This suggests that some vibrations other than the CD_3 rock(A_1) coincide on this band. The most probable candidate is the asymmetric SiC_3 stretch, for this mode has been observed at *ca.* 700 cm^{-1} in $(CD_3)_3SiX$.[4)] This asymmetric SiC_3 stretch is found at 730 cm^{-1} in $(CD_3)_3SiD$.

The Raman band at 858 cm^{-1} in $(CD_3)_3SiH$ can be assigned to the SiH bending vibration, for it disappears in $(CD_3)_3SiD$. However, as a considerable coupling is expected between this mode and the methyl rock, the exact assignments can only be made with the aid of the normal coordinate calculations.

The normal coordinate calculations were carried out by Wilson's GF-matrix method on an ACOS 77/900 computer at the Computer Center, Tohoku University, using the iterative least-squares procedure in the usual manner. The G matrix was calculated by use of the molecular parameters determined from microwave study.[5)] The least-squares refinement[6)] was carried out in terms of the symmetry force constants, which were fitted to the Raman frequencies observed in the liquid, for the four isotopes simultaneously. The torsional mode was neglected in the E class. The symmetry force constants, together with uncertainties from the last cycle are given in Table 2. The average errors were 0.41 and 0.66% for the A_1 and E vibrations, respectively. The sum of the weighted squares of errors $\Sigma(\lambda_{obsd}-\lambda_{calcd})^2/\lambda_{obsd}$ was 1.8×10^{-3} for the A_1 and 4.9×10^{-3} for the E vibrations. The potential energy distributions are also given in Table 1.

The results of the calculations clearly indicate that the methyl rock, the SiH bending and the asymmetric SiC_3 stretch strongly couple with each other, especially in $(CD_3)_3SiD$.

The valuence force constant f(Si–C), derived from the symmetry force constants, is 2.97 mdyn/Å. This value is equal to that of CH_3SiH_3(2.97 mdyn/Å)[7)] and is slightly larger than that of $(CH_3)_4Si$(2.88 mdyn/Å).[8)] This is in agreement with what might be expected from their Si–C bond lengths; 1.868 Å in $(CH_3)_3SiH$,[5)] 1.867 Å in CH_3SiH_3,[9)] and 1.875 Å in $(CH_3)_4Si$.[10)]

This work was partly supported by a grant from the Asahi Glass Foundation for Industrial Technology to which our thanks are due. One of the authors (Y. I.) wishes to his thanks to Assist. Prof. Fumio Watari for the computer programs used in calculations.

References

1) L. M. Sverdlov, M. A. Kovner, and E. P. Krainov, "Vibrational Spectra of Polyatomic Molecules," John Wiley & Sons, New York (1974), p. 562.

2) D. F. Ball, P. L. Goggin, D. C. Mckean, and L. A. Woodward, *Spectrochim. Acta*, **16**, 1358 (1960).

3) T. F. Tenisheva, A. N. Lazarev, and R. I. Uspenskaya, *Izv. Akad. Nauk SSSR, Ser. Khim.*, **1978**, 344.

4) A. N. Lazarev and T. F. Tenisheva, *Izv. Akad. Nauk SSSR, Ser. Khim.*, 338 (1978).

5) L. Pierce and D. H. Petersen, *J. Chem. Phys.*, **33**, 907 (1960).

6) F. Watari, *J. Phys. Chem.*, **84**, 448 (1980).

7) J. L. Duncan, *Spectrochim. Acta*, **20**, 1807 (1964).

8) F. Watari, *Spectrochem. Acta, Part A*, **34**, 1239 (1978).

9) R. W. Kilb and L. Pierce, *J. Chem. Phys.*, **27**, 108 (1957).

10) B. Beagley, J. J. Monaghan, and T. G. Hewitt, *J. Mol. Struct.*, **8**, 401 (1971).

Separation of Metals on Sulfonated Diphenyl Phosphonate–Formaldehyde Resin in HCl–Organic Solvent Systems

Hidehiko MORI,* Yoshikazu FUJIMURA, and Yoshinobu TAKEGAMI†

Department of Industrial Chemistry, Chubu Institute of Technology, Matsumoto, Kasugai 487

†*Department of Hydrocarbon Chemistry, Faculty of Engineering, Kyoto University, Yoshida, Sakyo-ku, Kyoto 606*

(Received June 12, 1980)

Synopsis. The distribution coefficients of several metal ions have been measured on sulfonated diphenyl phosphonate–formaldehyde resin in HCl–water miscible organic solvent solutions. Differences in the distribution coefficients are large enough to develop multicomponent separations. Particularly in HCl–propanone systems the separation of a complex mixture, Cd(II)–Zn(II)–Pb(II)–Cu(II)–Co(II)–Mn(II)–Mg(II), can be carried out chromatographically by sequential elution.

In a previous paper,[1] a report was given on the cation exchange behavior of metal ions on sulfonated diphenyl phosphonate–formaldehyde resin (abbreviated to DFS resin) in an aqueous HCl system.

The numerous studies to improve the cation exchange separation of metal ion by addition of a water miscible organic solvent have been reported. Fritz and Rettig[2] studied the separation of metal ions using Dowex 50W-X8 resin by elution with 0.10—1.0 mol dm^{-3} HCl–60—92 vol% propanone systems. Strelow *et al.*[3] presented a procedure for the separation of metal ions using Bio-Rad AG 50W-X8 resin by elution with 0.20—1.0 mol dm^{-3} HCl–30—90 vol% propanone systems. However, the separation of Pb(II) has not been achieved. Kawazu *et al.*[4] performed the separation of Pb(II) from bivalent metal ions by elution with 1.2—1.4 mol dm^{-3} HCl–90 vol% 2 propanol system using Amberyst 15 cation exchanger.

We have selected ethanol, propanone and acetonitrile as water miscible organic solvent and examined the separation of several metal ions. In the HCl–propanone systems seven elements could be separated successfully from each other, the separation of Pb(II) being achieved. In the HCl–acetonitrile and –ethanol systems, neither Zn(II)–Pb(II) or Co(II)–Mn(II) could be separated. In both systems Pb(II) could be separated from bivalent metal ions except Zn(II).

Experimental

The DFS resin was prepared as described previously.[1] 1 cm^3 of sample solution containing 5 mg of metal as nitrate was used. The concentration of organic solvent is expressed in volume percentage and that of HCl in molarity. Procedures for the separation of metal ion mixtures are shown in Figs. 2—4. Metal ions were determined by atomic adsorption spectrometry and are given in mmol/25 cm^3.

TABLE 1. DISTRIBUTION COEFFICIENT IN HCl–ORGANIC SOLVENT MEDIA

Metal	Concentration of acid/mol dm^{-3}															
	0.10				0.20				0.30				0.40			
	Concentration of solvent/vol%															
	20	40	60	80	20	40	60	80	20	40	60	80	20	40	60	80
Propanone																
Cd(II)	300	160	20	0	35	5	0	0	20	0	0	0				
Zn(II)	420	380	150	20	190	130	10	0	60	0	0	0				
Pb(II)	670	630	180	40	200	140	30	0	80	0	0	0				
Mn(II)					190	250	280	330	200	250	270	290	50	70	100	150
Mg(II)					150	400	410	480	80	170	240	300	50	80	150	210
Cu(II)					300	330	470	1470	170	180	230	180	60	50	40	20
Acetonitrile																
Cd(II)	250	200	25	0	40	10	0	0	20	0	0	0				
Zn(II)	700	620	160	10	200	180	5	0	50	0	0	0				
Pb(II)	650	530	200	25	240	150	25	0	80	30	0	0				
Mn(II)					250	300	350	410	180	250	300	380	60	80	100	160
Mg(II)					320	330	710	930	100	280	280	460	40	80	140	190
Cu(II)					150	190	250	330	120	190	230	190	50	40	30	10
Ethanol																
Cd(II)	110	100	60	5	70	20	5	0	20	0	0	0				
Zn(II)	390	310	200	110	210	180	150	0	50	0	0	0				
Pb(II)	780	690	230	110	200	190	150	10	40	10	0	0				
Mn(II)					240	330	480	700	210	220	290	460	20	30	330	400
Mg(II)					500	600	650	730	420	520	550	630	30	50	430	600
Cu(II)					260	280	290	200	300	290	140	120	60	60	50	10

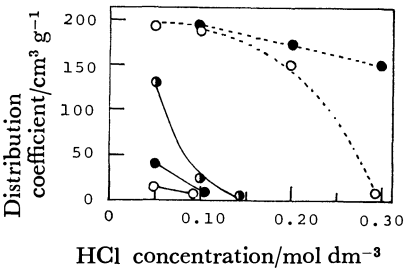

Fig. 1. Distribution coefficients as a function of acid concentration in 95 vol% organic solvent.
——: Propanone, ----: ethanol, ○: Cu(II), ●: Co(II), ◑: Mn(II).

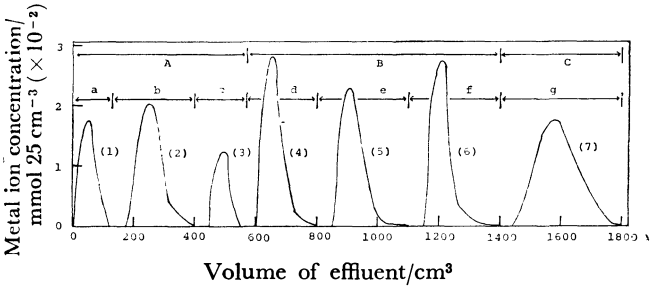

Fig. 2. Elution curves for a seven-component mixture in HCl–propanone system.
Propanone(vol%); A: 60, B: 95, C: 20, HCl(mol dm⁻³); a: 0.10, b: 0.14, c: 0.20, d: 0.025, e: 0.05, f: 0.10, g: 0.40,
(1): Cd(II), (2): Zn(II), (3): Pb(II), (4): Cu(II), (5): Co(II), (6): Mn(II), (7): Mg(II), yield of metal ion: over 99.0 wt%, column: 8ϕ×250 mm, flow rate: 2.5 cm³/min

Results and Discussion

Distribution Coefficient. The distribution coefficients of metal ions were measured in HCl–organic solvent media in the acid concentration range 0.10—0.40 mol dm^{-3} and solvent concentration range 20—80 vol% (Table 1). The coefficients of Cd(II), Zn(II), and Pb(II) decreased in the HCl concentration range 0.10—0.30 mol dm^{-3} with increase in solvent concentration. The coefficient of Cu(II) in 0.40 mol dm^{-3} HCl decreased with increase in solvent concentration. The coefficients of Mn(II) and Mg(II) gave the lowest value in 20 vol% organic solvent at 0.40 mol dm^{-3} HCl. The coefficients of Co(II), Ni(II), and Ca(II) were higher than under the conditions given in Table 1.

For the organic solvent concentration of 95 vol%, the coefficients of Cd(II), Zn(II), and Pb(II) were nearly 0 in 0.025 mol dm^{-3} HCl. On the other hand, in the HCl–propanone and –acetonitrile systems the coefficients of Cu(II), Co(II), and Mn(II) decreased sharply from 0.025 to 1.0 mol dm^{-3} HCl. In the HCl–ethanol system only the adsorption of Cu(II) decreased significantly from 0.10 to 0.30 mol dm^{-3} HCl. The results for Cu(II), Co(II), and Mn(II) in propanone and ethanol systems are given in Fig. 1.

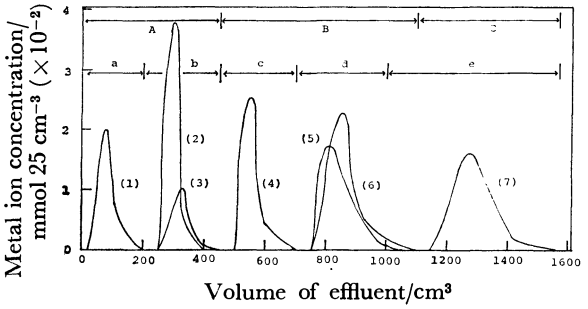

Fig. 3. Elution curves for a seven-component mixture in HCl–acetonitrile system.
Acetonitrile(vol%); A: 60, B: 95, C: 20, HCl(mol dm^{-3}); a: 0.10, b: 0.20, c: 0.05, d: 0.10, e: 0.40, (1): Cd(II), (2): Zn(II), (3): Pb(II), (4): Cu(II), (5): Co(II), (6): Mn(II), (7): Mg(II), yield of metal ion: over 99.0 wt%, column: 8ϕ×250 mm., flow rate: 2.5 cm³/min.

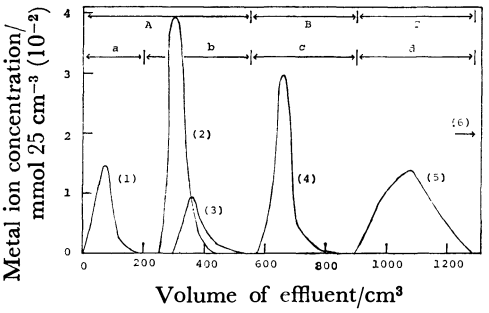

Fig. 4. Elution curves for a seven-component mixture in HCl–ethanol system.
Ethanol(vol%); A: 80, B: 95, C: 20, HCl(mol dm^{-3}); a: 0.10, b: 0.20, c: 0.30, d: 0.40, (1): Cd(II), (2): Zn(II), (3): Pb(II), (4): Cu(II), (5): Mg(II), (6): Co(II) and Mn(II), yield of metal ion: over 99.0 wt%, column: 8ϕ×250 mm, flow rate: 2.5 cm³/min.

Separation of Mixtures. Based on the relevant distribution coefficients, several procedures for the separation of Cd(II)–Zn(II)–Pb(II)–Cu(II)–Co(II)–Mn(II)–Mg(II) were developed. Cd(II)–Zn(II)–Pb(II) were stripped consecutively by elution with 0.10—0.20 mol dm^{-3} HCl–60—80 vol% organic solvent systems, then Cu(II)–Co(II)–Mn(II) with 0.025—0.30 mol dm^{-3} 95 vol%, and Mg(II) with 0.40 mol dm^{-3} —20 vol%. The elution curves with HCl–propanone, –acetonitrile, and –ethanol systems are shown in Figs. 2, 3, and 4, respectively.

References

1) H. Mori, Y. Fujimura, and Y. Takegami, *Nippon Kagaku Kaishi*, **1980**, 338.
2) J. S. Fritz and T. A. Rettig, *Anal. Chem.*, **34**, 1562 (1962).
3) F. W. E. Strelow, A. H. Victor, C. R. Van Zyl, and C. Eloff, *Anal. Chem.*, **43**, 870 (1971).
4) K. Kawazu, T. Matsueda, and H. Kakiyama, *Bunseki Kagaku*, **22**, 1301 (1971).

The ^{1}H NMR Spectra of $[(CH_3)_2SbCl_2(oxine)]$ in Several Solvents

Yoshikane KAWASAKI* and Masahiro KINOSHITA

Department of Petroleum Chemistry, Osaka University, Yamadakami, Suita, Osaka 565

(Received June 19, 1980)

Synopsis. The ^{1}H NMR spectra of dichlorodimethyl(8-quinolinolato)antimony(V), $[(CH_3)_2SbCl_2(oxine)]$, were measured in several solvents. Two methyl signals were observed in some aromatic and aliphatic solvents, although only one signal was detected in dichloromethane. The results were explained by the presence of two isomers in solution.

The structure of dichlorodimethyl(8-quinolinolato)-antimony(V), $[(CH_3)_2SbCl_2(oxine)]$, was studied by Meinema, Rivalora, and Noltes.[1] They reported that the IR spectrum of this compound shows one Sb–C and two Sb–Cl stretching bands in the solid state, while the ^{1}H NMR spectra in chloroform-*d* and dichloromethane give only one methyl signal, and no broadening of this signal is observed even at −100 °C. From these facts and the UV spectral data, they concluded that the compound has a hexacoordinate structure with a distorted *trans*-dimethyl configuration(**1**).[1]

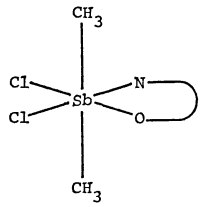

1

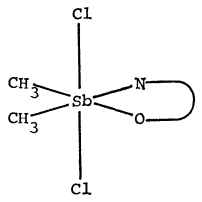

2

As we have been interested in the solvent dependence of the ^{1}H NMR spectra of several organometallic compounds,[2,3] we measured the ^{1}H NMR spectra of $[(CH_3)_2SbCl_2(oxine)]$ in several solvents in order to elucidate the solute-solvent interaction and structure in solution.

The ^{1}H NMR data of the compound are shown in Table 1. The chemical shifts of the 2-, 3-, and 4-protons of the 8-quinolinolato ligand move to a higher field in benzene as compared with those in nonaromatic solvents. Especially, the upfield shift of the 2-proton in a benzene solution has been explained in terms of the coordination of the nitrogen atom of the 8-quinolinolato ligand to the antimony atom.[3] This result is consistent with the UV spectral data of the compound.[1]

One of the most remarkable results of the solvent dependence of the ^{1}H NMR spectra of the compound is that two methyl proton signals were observed in some solvents (see Table 1). These results are different from those obtained by Meinema *et al.* in chloroform-*d* and dichloromethane.[1] The signal intensity at the higher field(I_h) is larger than that of the lower field(I_l) in nonpolar solvents. However, the opposite results were obtained in polar solvents. The signal contour and the intensity ratio(I_h/I_l) do not show any appreciable change upon a change in the temperature from the ambient temperature to −24 °C in carbon disulfide and to 58 °C in 1-chloronaphthalene. Figure 1 shows the methyl-proton chemical shifts and relative intensities of the higher-field methyl signal($I_h/(I_h+I_l)$) in mixed solvents of benzene and dichloromethane. The methyl-proton chemical sihfts move to a higher field as the relative volume of benzene ($V_b/(V_b+V_m)$) increases, but the intensity ratio is almost insensitive to the volume fraction of benzene in the 0.1—0.9 range. The relative intensity of the higher-field methyl signal, extrapolated to pure dichloro-

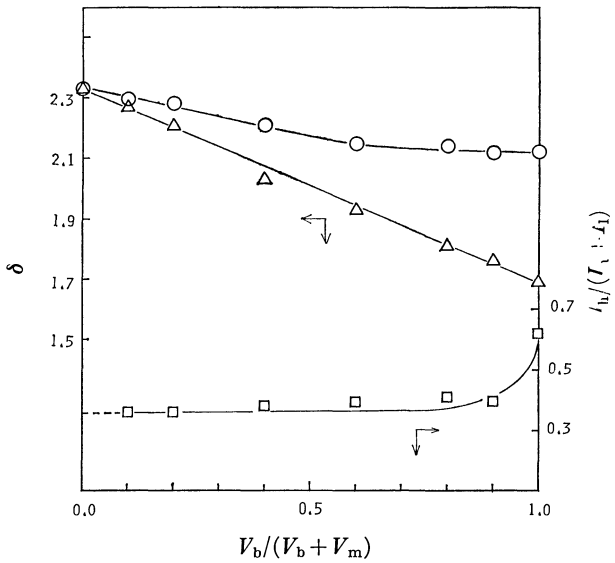

Fig. 1. Methyl proton chemical shifts and relative intensities of higher field methyl signal in mixed solvents of benzene and methylene chloride.

TABLE 1. ^{1}H NMR DATA OF $[(CH_3)_2SbCl_2(oxine)]$ IN SEVERAL SOLVENTS

Solvent	$\delta(CH_3)_h$	$\delta(CH_3)_l$	I_h/I_l[a]	δ(2-H)	δ(3-H)	δ(4-H)
CCl_4	2.23	2.29	0.55/0.45	9.28	7.59	8.47
CS_2	2.12	2.22	0.63/0.37	9.35	7.63	8.49
C_6D_6	1.70	2.11	0.62/0.38	8.82	6.31	7.32
$CDCl_3$[b]	2.38			9.36		8.64
CH_2Cl_2	2.33		(0.35/0.65)[c]	9.32	7.69	8.57
$C_{10}H_7Cl$(1-)	1.79	2.28	0.26/0.74			
CH_3NO_2	2.18	2.22	0.41/0.59			

a) Intensity ratio of high-field signal to low-field signal. b) Ref. 1. c) Extrapolated value.

methane, is found to be 0.35. This value is similar to that obtained in 1-chloronaphthalene. The observation of only one signal of the methyl protons of $[(CH_3)_2SbCl_2(oxine)]$ in dichloromethane, therefore, may be an accidental coincidence of the two methyl-proton signals.

The observation of the two methyl signals in the ^1H NMR spectra with unequal signal intensities seems to suggest that the compound has two isometic structures, probably **1** and **2**, in solution. The presence of two isomers in solution has also been reported for some hexacoordinate (acethylacetonato)diaryldihaloantimony(V) compounds,[4,5] although only one isomer with a *trans*-dimethyl configuration corresponding to **1** has been reported for (acetylacetonato)dihalodimethylantimony(V).[6,7]

Experimental

The compound, $[(CH_3)_2SbCl_2(oxine)]$, was prepared and purified by the method reported in the litarature.[1] The solvents used was purified by distillation. The ^1H NMR spectra were measured by using a JEOL JNM PS-100 spectrometer. The chemical shift was measured relative to the internal TMS.

References

1) H. A. Meinema, E. Rivarola, and J. G. Noltes, *J. Organomet. Chem.*, **17**, 71 (1969).
2) Y. Kawasaki, *Bull. Chem. Soc. Jpn.*, **49**, 2319 (1976).
3) Y. Kawasaki, *Mol. Phys.*, **12**, 287 (1967).
4) N. Nishii and R. Okawara, *J. Organomet. Chem.*, **38**, 335 (1972).
5) H. A. Meinema and J. G. Noltes, *J. Organomet. Chem.*, **16**, 257 (1969).
6) R. Okawara, Y. Matsumura, and N. Nishii, Abstracts, 4th International Conference on Organometallic Chemistry, Bristol (1969).
7) N. Kanehisa, K. Onuma, S. Uda, K. Hirabayashi, Y. Kai, N. Yasuoka, and N. Kasai, *Bull. Chem. Soc. Jpn.*, **51**, 2222 (1978).

Dehydration Associated with High-spin to Low-spin Conversion of 5,5,7,12,12,14-Hexamethyl-1,4,8,11-tetraazacyclotetradecane-nickel(II) Halide Dihydrate

Tasuku Ito,†,†† Yukie Tsutsumi,† Yukio Hiratsuka,† Katsura Mochizuki,† and Masatoshi Fujimoto*,†

†*Department of Chemistry, Faculty of Science, Hokkaido University, Sapporo 060*

††*Institute for Molecular Science, Okazaki 444*

(Received July 3, 1980)

Synopsis. The title compounds, orange, diamagnetic four-coordinate complexes, $[NiL]X_2 \cdot 2H_2O$ (X=Cl, Br, I for *meso*-L and X=Cl, Br for *rac*-L) were converted, upon dehydration by heating in the solid state, to violet, paramagnetic six-coordinate complexes, $[NiX_2L]$. The enthalpies of the dehydration reactions were close to those for many simple inorganic hydrates and that for the ice-water vapor equilibrium in spite of the presence of the large organic ligand.

Nickel(II) halides (Cl, Br, and I) and the *meso*-form of the title macrocyclic ligand ((7*RS*,14*SR*)-form) form orange low-spin complexes, $[Ni(meso\text{-}L)]X_2 \cdot 2H_2O$, and violet high-spin complexes, $[NiX_2(meso\text{-}L)]$.[1] The macrocyclic ligand is constrained by the steric requirements to coordinate in a single plane. From their electronic spectra and magnetic properties,[1] and the X-ray analyses of $[Ni(meso\text{-}L)]Cl_2 \cdot 2H_2O$,[2] $[NiCl_2(meso\text{-}L)]$,[2] and $[Ni(meso\text{-}L)]Br_2 \cdot 2H_2O$,[3] it has been shown that the orange dihydrate is a square-planar four-coordinate complex having a singlet ground state, whereas the violet paramagnetic anhydride is a *trans*-dihalogeno six-coordinate complex having a triplet ground state. The solid, violet, paramagnetic anhydrous complex readily reverts to $[Ni(meso\text{-}L)]X_2 \cdot 2H_2O$ when moisture is available.[1]

In the present study, the orange four-coordinate dihydrate was found to be converted to $[NiX_2(meso\text{-}L)]$ upon dehydration by heating in the solid state. The isomeric complex containing the racemic ligand ((7*RS*,14*RS*)-form),[4] $[Ni(rac\text{-}L)]X_2 \cdot 2H_2O$ (X=Cl and Br)[5] underwent exactly the same reaction, yielding the anhydrous six-coordinate complex, *trans*-$[NiX_2(rac\text{-}L)]$. In the present note, the enthalpies of the dehydration reactions are reported.

Figure 1 shows a typical example of the thermogravimetry (TG) and the differential scanning calorimetry (DSC). When $[Ni(meso\text{-}L)]Cl_2 \cdot 2H_2O$ was heated at a heating rate of 3 °C min^{-1}, the weight loss due to the dehydration began at 58 °C and constant weight attained at 110 °C. The weight loss of 8.2±0.2% was in accord with the calculated value for the loss of two mols of water (8.00%). Corresponding to the weight loss, an endothermic peak appeared on a DSC curve. The heat of dehydration was estimated to be 100±1 kJ mol^{-1} by comparing the peak area with that for melting of naphthalene crystals (ΔH=18.98 kJ mol^{-1}).[6] Experiments for other systems were carried out similarly. The results are summarized in Table 1. Values given in Table 1 are mean values for at least four experimental runs. The product was identified by elemental analysis, electronic spectrum,[1,7,8] and infrared spectrum.[8] All the results indicated that the reaction proceeds as follows:

$$[NiL]X_2 \cdot 2H_2O \xrightarrow{\Delta} [NiX_2L] + 2H_2O.$$

This is the reverse reaction reported by Busch[1] and involves the change in the coordination number from four to six, *viz.*, the singlet to triplet spin-state change.

As shown in Table 1, the ΔH values are not largely different from each other except for the iodide system of [Ni(*meso*-L)], though the difference in ΔH caused by the kind of halide ion and the ligand may be significant. It is worth while to mention that the enthalpies found in the present study can be compared to the calculated enthalpy value for sublimation of ice, where ΔH(sublimation)=51.9 kJ mol^{-1} at 25 °C.[9] (Note that the ΔH values given in Table 1 correspond to the loss of two mols of water.) Except for the iodide system, the enthalpy values found in the present study are significantly larger than those usually found for dehydration reactions of coordination compounds. For example, ΔH for dehydration of $[Ni(abi)_4]X_2 \cdot nH_2O$ (abi=2-aminobenzimidazole) has been reported to be 8.8 (X=Cl, n=3), 8.8 (X=Br, n=3), and 7.1

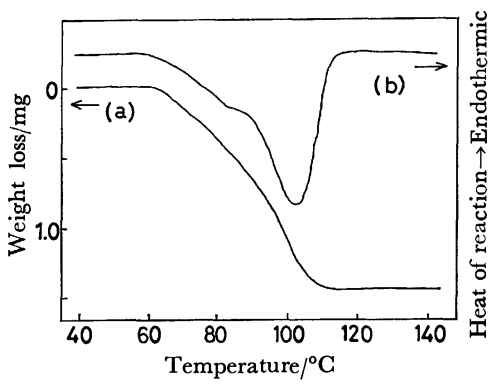

Fig. 1. TG (a) and DSC (b) curve for the thermal dehydration of $[Ni(meso\text{-}L)]Cl_2 \cdot 2H_2O$.
Heating rate: 3 °C min^{-1}. Sample: 18.52 mg.

Table 1. Enthalpy of the thermal dehydration reaction of $[NiL]X_2 \cdot 2H_2O$

L	X	$\Delta H(-2H_2O)$ / kJ mol^{-1}	Temperature of incipient reaction/°C[a]
meso-L	Cl	100±1	58
	Br	104±3	75
	I	78±2	58
rac-L	Cl	99±4	76
	Br	96±4	65

a) Heating rate: 3 °C min^{-1}.

kJ mol^{-1} (X=NO_3, n=1).[10] Fogel *et al.* studied dehydration reactions of many simple inorganic hydrates[9,11,12] and reported that, for many reactions, ΔH=55.2x kJ mol^{-1} (x designates mol number of lost water), which is close to what is observed for the ice system.[12] They concluded on this basis that, when only small structural changes occur during dehydration reactions, the thermodynamic value is close to that for the vaporization of ice.[9]

It is striking that the ΔH values given in Table 1 are close to those reported by Fogel and that for the sublimation of ice, even though the present complexes bear the large organic ligand. This indicates that the water molecules in the dihydrates of the present complexes are involved in the strong hydrogen-bonds such as those in ice and many simple inorganic hydrates. It has been shown that, in the crystals of [Ni(*meso*-L)]$Cl_2\cdot 2H_2O$[2] and [Ni(*meso*-L)]$Br_2\cdot 2H_2O$,[3] all the water molecules are disposed above the hydrogen atoms of N–H groups and are involved in the strong hydrogen-bonds, N–H···OH_2 and OH_2···X, forming hydrogen-bonded chelate rings of the type Ni–N–H···O–H···X···H–N. The magnitude of ΔH seems to reflect at least qualitatively the strength of the hydrogen-bonds in the hydrate, although many other factors affect the magnitude of ΔH. The small ΔH value for the iodide system probably indicates the weaker hydrogen-bond in the crystal as expected. Busch pointed out the importance of the role played by water in the spin-state conversions such as the anhydrous spin-free–hydrate spin-paired type.[13] When the anhydrous [NiX_2L] takes up the two water molecules from the atmospheric moisture to produce [NiL]$X_2\cdot 2H_2O$, the incorporated water molecules displace the halogen ions from the coordination sites but are not involved in the coordination in the product. This is unexpected in the light of the fact that water has much higher coordinating ability as compared with the halide ion. In view of the crystal structures of [Ni(*meso*-L)]$Cl_2\cdot 2H_2O$[2] and [Ni(*meso*-L)]$Br_2\cdot 2H_2O$,[3] the dispositions of the water molecules above the N–H bonds would be much more favorable over the hypothetical occupation by the water molecules at the axial coordination sites. This situation could be explained by the larger ΔH values observed in the present study. The N–H···OH_2 and OH_2···X hydrogen-bond networks operating in the vicinity of the nickel(II) ion are strong enough to prevent the coordination of water.

Experimental

Materials. Orange dihydrates, [Ni(*meso*-L)]$X_2\cdot 2H_2O$ (X=Cl, Br, and I) and [Ni(*rac*-L)]$X_2\cdot 2H_2O$ (X=Cl and Br), were prepared from the corresponding perchlorates[4] by ion exchange (Dowex 1-X8). Elemental analyses gave satisfactory results.

Measurements. Thermal analyses were carried out on a Rigaku Denki differential scanning calorimeter, Model 8001 SL/C.

Elemental Analyses of the Reaction Products. (a) [NiX_2(*meso*-L)]=$NiC_{16}H_{36}N_4X_2$. Found: C, 46.35; H, 8.89; N, 13.44; Cl, 17.16%. Calcd for X=Cl: C, 46.41; H, 8.76; N, 13.53; Cl, 17.12%. Found: C, 38.08; H, 7.30; N, 11.30; Br, 31.96%. Calcd for X=Br: C, 38.20; H, 7.21; N, 11.14; Br, 31.77%. Found: C, 31.96; H, 6.16; N, 9.42; I, 42.69%. Calcd for X=I: C, 32.19; H, 6.08; N, 9.39; I, 42.51%. (b) [NiX_2(*rac*-L)]=$NiC_{16}H_{36}N_4X_2\cdot$ Found: C, 45.53; H, 8.81; N, 12.89; Cl, 16.83%. Calcd for X=Cl: C, 46.41; H, 8.76; N, 13.53; Cl, 17.12%. [$NiBr_2$(*rac*-L)] is very sensitive to moisture. Accurate data for the anhydrous complex could not be obtained because of rapid absorption of water vapor during weighing the sample.

The authors wish to thank Professor Yoshio Matsunage for the kindness in the DSC measurements.

References

1) D. H. Busch, *Adv. Chem. Ser.*, **62**, 616 (1967).
2) T. Ito and K. Toriumi, submitted for publication in *Acta Crystallogr.*
3) T. Ito, K. Toriumi, and H. Ito, unpublished result.
4) L. G. Warner and D. H. Busch, *J. Am. Chem. Soc.*, **91**, 4092 (1969).
5) Mixture of the β-[4] and γ-form. See N. F. Curtis, D. A. Swann, and T. N. Waters, *J. Chem. Soc., Dalton Trans.*, **1973**, 1963.
6) J. P. McCullough, H. L. Finke, J. F. Messerly, S. S. Todd, T. C. Kincheloe, and G. Waddington, *J. Phys. Chem.*, **61**, 1105 (1957).
7) L. Y. Martin, C. R. Sperati, and D. H. Busch, *J. Am. Chem. Soc.*, **99**, 2968 (1977).
8) J. Karn, Ph.D. Thesis, The Ohio State University, Columbus, Ohio, U.S.A. (1966).
9) W. K. Grindstaff and N. Fogel, *J. Chem. Soc., Dalton Trans.*, **1972**, 1476.
10) Y. Ihara and R. Tsuchiya, *Bull. Chem. Soc. Jpn.*, **53**, 1614 (1980).
11) W. K. Grindstaff and N. Fogel, *Thermochim. Acta*, **6**, 299 (1973).
12) T. J. Nolan, H. Haralson, J. L. McAdams, and N. Fogel, *J. Chem. Soc., Dalton Trans.*, **1977**, 1608.
13) D. H. Busch, *Helv. Chim. Acta*, Fasciculus Extraordinarius Alfred Werner, 174 (1967).

Potential Gradient Detector for Capillary Type Isotachophoresis

Fumitaka NISHIYAMA, Takeshi HIROKAWA,* and Yoshiyuki KISO
Applied Physics and Chemistry, Faculty of Engineering, Hiroshima University, 3-8-2, Senda, Naka-ku, Hiroshima 730
(Received July 10, 1980)

Synopsis. The potential gradient detector previously reported has been improved as regards mechanical stability and the contaminated electrodes can be easily exchanged with new ones. The linearity of step-height holds below the electrode voltage of 1.2 V (0.005 mol dm^{-3} aq HCl). The detection limit was 2.5×10^{-10} mol for adipic acid.

In isotachophoresis, the ratio of potential gradients of sample zone (E_V) to leading zone (E_L) can be measured by means of a potential gradient detector (PGD). The ratio, R_E, correlates with the step-height (h) in the isotachopherogram and the effective mobility (m) of sample and leading ion as follows:

$$R_E = E_V/E_L = h_V/h_L = \bar{m}_L/\bar{m}_V, \quad (1)$$

where V and L denote the sample and leading zones, respectively.

The R_E values obtained are useful for the evaluation of aboslute mobility,[1,2] dissociation constants[2] and complex stability constants.[3] For the measurements of R_E, the drift of baseline in the isotachopherogram should be suppressed as little as possible. The drift might be due to the following: (A) Inadequate choice of electrolyte system and/or pH of leading electrolyte. (B) An undesirable electric pass among sensing electrodes and ground due to leak of electrolytes and/or high humidity. (C) The inactive electrodes of PGD contaminated by electrode reaction; An exchange of the damaged sensing electrodes is preferable, since the PGD once contaminated will not give a stable base line even when it is rinsed well. The defects due to acryl resin[2] were removed: The previous model was not strong mechanically; due to thermal melting on boring, it was difficult to pass electrolytes with a uniformed bore and no organic solvent could be used.

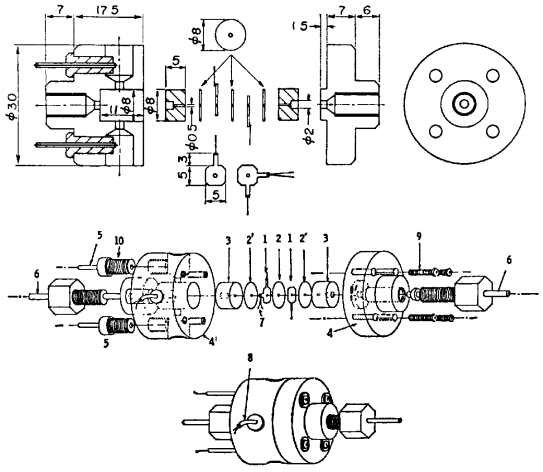

Fig. 1. Potential gradient detector.
1: Pt sensing electrodes, 2: PTFE insulator, 2′: PTFE gaskets, 3: PTFCE holders, 4 and 4′: Cell bodies (polycarbonate), 5: Lead wires, 6: PTFE capillary tube, 7 and 8: Cu-constantan thermocouple, 9: Fixing screws, 10: PTFE bushings.

Construction of PGD Cell. Figure 1 shows the mechanical construction and an exploded view of the PGD cell. The cell bodies (4,4′) are made of polycarbonate resin and turn on a rod, the holes in the bodies being for screws (9), and plugs to fit the capillary tube to the cell, and lead wires to the sensing electrodes (5). The sensing electrodes (1) are made of platinum disk of 20 μm thick. A copper-constantan thermocouple soldered to one of the electrodes (7) is to monitor the temperature of electrolyte. The holders (3) for sandwiching the electrodes are made of poly(trifluorochloroethylene) (PTFCE), which is harder than poly(tetrafluoroethylene) (PTFE). PTFE disks of 50 μm thick were used as an insulator of the electrodes (2) and gaskets (2′). The diameter of the pass of electrolyte is 0.5 mm. The bored electrodes were carefully trimmed with sandpaper (# 2000) and rinsed with water, 0.1 mol dm^{-3} HNO_3, distilled water and ethanol. The holders, insulators, and gaskets were also rinsed with ethanol and dried.

One of the holders (3) was inserted into the cell body (4′), a centering rod of 0.5 mmϕ being inserted into the holes. The gaskets, electrodes, insulator and the other holder were inserted and settled. The other body was then fixed tightly with the screws (9) and the rod was pulled out carefully. The lead wires, supported by PTFE bushings (10), were soldered to the sensing electrodes. When construction was complete, the pass was rinsed again.

Check on PGD. First, the linearity between the input voltage applied and the observed step-heights was checked using the recorder of an isotachophoretic analyzer (Shimadzu Seisakusho Ltd., IP-1B) and continuous voltage generator (0 to 2 V).

A 0.005 mol dm^{-3} aq HCl was used as an electrolyte in the pass of the capillary tube and the PGD. The pH was adjusted to 6 by addition of histidine. When there was no electric leakage and the sensing electrodes were clean, the base line of the electropherogram did not drift for 1 h with migration current of 50 μA (drift, less than a few percent of the step-height of base line). Sometimes, an upward drift due to electric leakage among the electrodes and ground, and a downward drift due to electric leakage between the electrodes or the contaminated electrodes were observed.

Since the electric resistance of the buffered electrolyte is constant in the thermostatted capillary tube, the migration current and the voltage detected should be linearly correlated until the sensing electrodes are polarised. The linearity of step-heights on migration was checked as follows. The migration current was varied from 25 to 200 μA at regular intervals of 25

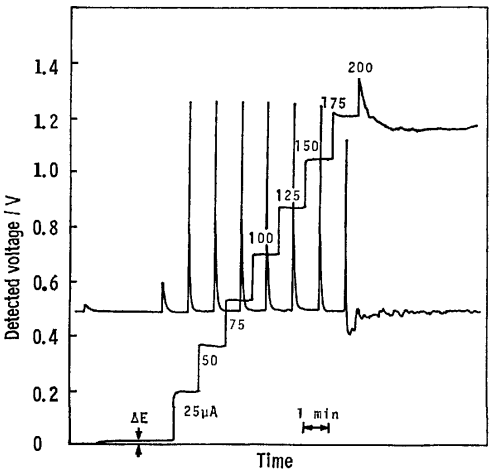

Fig. 2. Electropherogram for the check on linearity of step heights.

μA and the step-heights *vs.* time were recorded (Fig. 2). The irregular step-heights on migration due to polarisation of the electrodes were recorded at 200 μA. However, the linearity held below 175 μA, at which the electrode voltage corresponded to *ca.* 1.2 V. The value agrees with the decomposition voltage of aq HCl. If the electrodes were contaminated or the electric leakage took place in the pass of electrolyte, no normal linear relation could be obtained. Thus, the present PGD gives the correct R_E values of given samples, when the voltage between the sensing electrodes does not exceed the decomposition voltage of sample or solvent. ΔE in Fig. 2 shows an example of the asymmetrical potential which appears at the opening of a short-circuiting switch for PGD. Ideally, the value should be null, but sometimes a slight shift was observed. For estimation of the exact R_E value, the step-height of ΔE should be subtracted from the step-heights of leading, samples and terminating zones. Use of an internal standard will give more reliable R_E values.

Detection Limit. Adipic acid was used in order to check the quantitative limitation according to the procedure reported by Akiyama and Mizuno.[4] The leading electrolyte was 0.01 mol dm^{-3} aq HCl containing 0.2% Triton X-100, the pH of which was adjusted to 6.0 by adding histidine. The terminating electrolyte was 0.01 mol dm^{-3} glutamic acid. The pH was adjusted to *ca.* 6 by adding histidine. Figure 3 shows the differential curves of the isotachopherograms obtained for the injected sample. The quantitative limit was *ca.* 5×10^{-10} mol and the detection limit 2.5×10^{-10} mol.

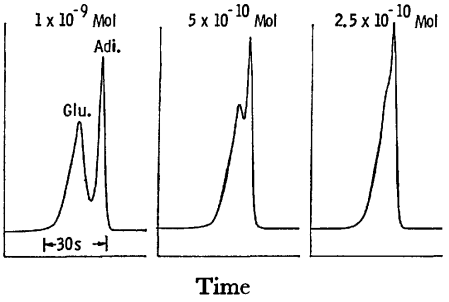

Fig. 3. Differential curves of isotachopherograms of adipic acid for the check on detection limit. Adi: adipic acid, Glu: glutamic acid.

According to a computer analysis of isotachophoresis for the injected sample of 1×10^{-9} mol, the total concentration in the sample zone and the zone length were estimated to be 0.00433 mol dm^{-3} and 0.1176 cm, respectively. The isotachophoretic velocity can be expressed as follows:

$$v = E_a\bar{m}_a = J\bar{m}_a/\kappa_a \text{ cm/s}, \quad (2)$$

where E_a is the potential gradient and $\bar{m}_a$ the effective mobility, J the current density and κ_a specific conductivity. When the current applied is 25 μA, J is 1.273×10^{-2} A/cm^2. The simulated $\bar{m}_a$ and κ_a were 42.96×10^{-5} cm^2/V s and $5.593\times10^{-4}/\Omega$ cm, respectively. Substitution of these values into Eq. 2 gives the isotachophoretic velocity 9.8×10^{-3} cm/s. The passing time of the zone through the detector expected was 12 seconds ($0.1176/9.8\times10^{-3}$). This agrees with the observed one (*ca.* 12 s.) as shown in Fig. 3. The maximum resolving power of 5×10^{-10} mol corresponds to the zone length of 588 μm, which is 8 times the effective gap of the electrodes of 70 μm.

The resolving power of 2.5×10^{-10} mol reported by Akiyama and Mizuno[4] for the same inner diameter and thickness of insulator is twice as large as that of our result. The difference may be due to the thickness of our electrodes (20 μm), since it would affect the degree of sharpness of differential curves. A better resolution might be obtained using thinner eletrodes, a smaller inner diameter of PGD, and lower concentration of leading electrolyte than those in the present experiment.

References

1) Y. Kiso and T. Hirokawa, *Chem. Lett.*, **1979**, 891.
2) Y. Kiso and T. Hirokawa, *Chem. Lett.*, **1980**, 323.
3) Y. Kiso and T. Hirokawa, *Chem. Lett.*, **1980**, 745.
4) J. Akiyama and T. Mizuno, *J. Chromatogr.*, **119**, 605 (1976).

The Core-level Binding Energies and the Structures of Nickel Complexes

Tooru YOSHIDA* and Kiyoshi YAMASAKI

Osaka Prefectural Industrial Research Institute, 2-1-35, Enokojima, Nishi-ku, Osaka 550

(Received July 28, 1980)

Synopsis. The X-ray photoelectron spectra of thirty-two nickel complexes were measured in order to examine the relation between the structures and the core-level binding energies of the complexes. The differences between the energies of Ni(2p) and Ni(3p) electrons for the complexes with an octahedral structure were about 1 eV larger than for those with a square planar one.

There have been many reports on X-ray photoelectron spectroscopic studies of nickel compounds.[1] It has been established that paramagnetic complexes show intense shake-up satellites on the higher energy side of the primary peaks in the Ni(2p) electron region, but that diamagnetic ones do not. However, there have been few studies of the relationship between the binding energy and the stereochemistry.[1d] The purpose of this study is to examine the relation between the structure of nickel complex, square planar or octahedral, and the binding energies of its core-electrons.

The X-ray photoelectron spectra were measured on an AEI ES200 spectrometer. Al $K\alpha$ (1486.6 eV) X-ray radiation was used as the excitation source. The samples were ground to powder and then dusted onto double-backed adhesive tape. The measurements were run at room temperature under a vacuum of about 10^{-7} Torr. The binding energy of the C(1 s) electron peak was used as the energy standard throughout the present experiments; it was taken to be 285.0 eV. The reproducibilities of the values thus obtained were ±0.1 eV. All the complexes used and their binding energies are given in Table 1. All the complexes were prepared based upon the literature.

The spectra in the Ni(2p)- and Ni(3p)-electron regions for the nickel complexes of 2-pyridinecarboxylic acid and dimethylglyoxime are shown in Fig. 1. E_b in the figure indicates the binding energy. The spectra of the 2-pyridinecarboxylic acid complex, like those of the complexes of Nos. 1—16 in Table 1, showed intense satellites on the higher energy side of each primary peak originating in the $2p_{1/2}$, $2p_{3/2}$, and 3p electrons, but the spectra of the dimetylglyoxime complex, like those of the complexes of Nos. 17—32, did not show such satellites. This suggests that the complexes of Nos. 1—16 are paramagnetic, while those of Nos. 17—32 are diamagnetic.

In general, the Ni(3p) spectrum does not show clear doublet peaks because of the small difference (about 2 eV)[2] between the binding energies of the Ni($3p_{1/2}$) and Ni($3p_{3/2}$) electrons. Therefore, the 3p binding energies in Table 1 correspond to the top of a main peak, as is shown in Fig. 1b.

On the basis of the results of X-ray structural analysis, IR, UV, and magnetic measurements, it has been proved that the structures of the complexes of Nos. 1,[3] 2,[4] 4,[5] 5,[5] 6,[5] 7,[6] 9,[7] 11,[8] 12,[8] 13,[8] 14,[9] 15,[8] and 16[10] are octahedral, while those of Nos. 18,[11] 23,[12] 24,[13] 25,[14] 26,[15] 27,[16] 29,[10] 30,[17] 31,[18]

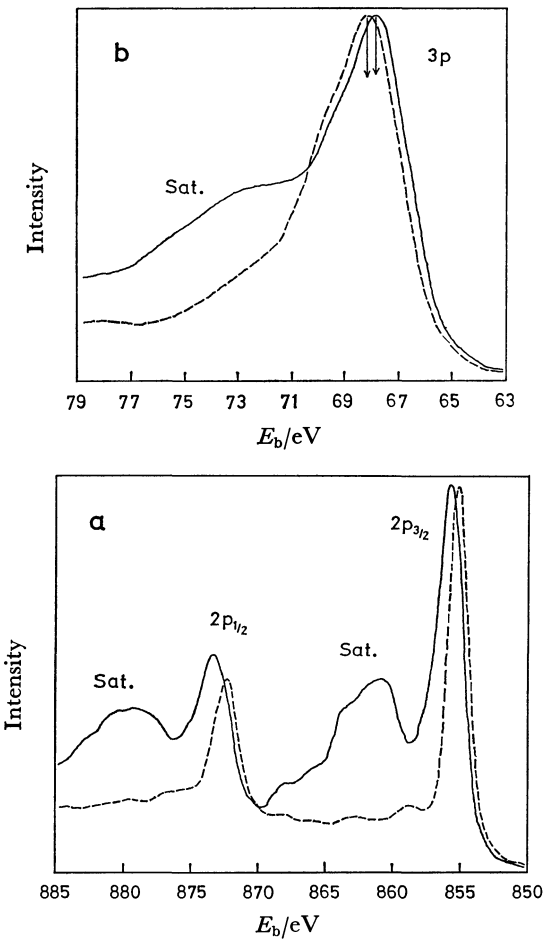

Fig. 1. XPS spectra of a: Ni(2p) and b: Ni(3p) electron regions. Solid line: *trans*-diaquabis(2-pyridinecarboxylato)Ni(II), broken line: bis(dimethylglyoximato)Ni(II).

and 32[19] are square planar. The structure of the No. 3 complex may be considered to be octahedral in view of the structures of the corresponding copper and zinc complexes.[20] It seems reasonable to consider that the structures of the complexes of Nos. 8 and 10 are octahedral, because 1-(2-pyridylazo)- and 1-(8-quinolylazo)-naphthols as well as 1-(2-thiazolylazo)-2-naphthol are tridentate ligands. Furthermore, it seems that the structures of the complexes of Nos. 17, 19—21, and 28 are square planar in view of the structures of the complexes of Nos. 18 and 25—27. The structure of the No. 22 complex seems to be square planar. The square planar structure for the complexes of Nos. 17—32 are supported by the absence of intense satellites in their Ni(2p) and Ni(3p) electron spectra.

It has been reported that, for the nickel complexes of NCS^- ligand, the Ni(2p) binding energies of octahedral compounds are a little higher than those of the square planar ones.[1d] Such a tendency was

Table 1. Measured binding energies

Sample No.	Ligand	Complex[a] formula	BE of Ni/eV			ΔE_1[c]	ΔE_2[c]
			$2p_{1/2}$	$2p_{3/2}$	3p[b]		
1	Ethylenediaminetetraacetic acid	A	872.7	855.1	67.2	805.5	787.9
2	Glycine	B	873.0	855.6	67.7	805.3	787.9
3	8-Quinolinol	B	873.6	856.0	68.0	805.6	788.0
4	2-Pyridinecarboxylic acid	B	873.4	855.7	67.9	805.5	787.8
5	3-Pyridinecarboxylic acid	C	873.7	856.1	68.3	805.4	787.8
6	4-Pyridinecarboxylic acid	C	873.9	856.2	68.4	805.5	787.8
7	2-Aminobenzoic acid	D	873.8	856.1	68.2	805.6	787.9
8	1-(2-Pyridylazo)-2-naphthol	D	873.1	855.6	67.9	805.2	787.7
9	1-(2-Thiazolylazo)-2-naphthol	D	873.3	855.7	68.0	805.3	787.7
10	1-(8-Quinolylazo)-2-naphthol	D	872.8	855.4	67.8	805.0	787.6
11	Ethylenediamine	E	872.4	855.0	67.2	805.2	787.8
12	Ethylenediamine	F	872.6	855.2	67.4	805.2	787.8
13	2,2'-Bipyridine	G	873.6	856.1	68.1	805.5	788.0
14	2,2'-Bipyridine	F	873.4	856.0	68.2	805.2	787.8
15	1,10-Phenanthroline	G	873.6	856.1	68.2	805.4	787.9
16	Biuret	F	874.3	856.9	68.9	805.4	788.0
17	2-(*p*-Nitrophenylazo)-4-methylphenol	D	872.6	855.5	68.6	804.0	786.9
18	1-Phenylazo-2-naphthol	D	872.7	855.5	68.6	804.1	786.9
19	1-(*p*-Methoxyphenylazo)-2-naphthol	D	872.6	855.4	68.5	804.1	786.9
20	1-(*p*-Nitrophenylazo)-2-naphthol	D	872.6	855.6	68.6	804.0	787.0
21	1-(1-Naphthylazo)-2-naphthol	D	872.5	855.3	68.4	804.1	786.9
22	1-(8-Quinolylazo)-2-naphthol	H	872.7	855.4	68.4	804.3	787.0
23	Salicylaldehyde oxime	D	873.4	856.1	69.0	804.4	787.1
24	Salicylideneamine	D	873.0	855.7	68.6	804.4	787.1
25	Dimethylglyoxime	D	872.3	855.1	68.2	804.1	786.9
26	2,3-Pentanedione dioxime	D	872.4	855.2	68.2	804.2	787.0
27	Benzil dioxime	D	872.9	855.9	68.8	804.1	787.1
28	1,2-Cyclohexanedione dioxime	D	872.7	855.5	68.4	804.3	787.1
29	Biuret	I	872.1	854.8	67.7	804.4	787.1
30	Rubeanic acid	J	871.8	854.5	67.4	804.4	787.1
31	2-Mercaptobenzothiazole	D	872.6	855.3	68.2	804.4	787.1
32	Diethyldithiocarbamic acid	D	871.6	854.3	67.4	804.2	786.9

a) A: $Ni(L\text{-}4H)Na_2 \cdot 2H_2O$, B: $Ni(L\text{-}H)_2 \cdot 2H_2O$, C: $Ni(L\text{-}H)_2 \cdot 4H_2O$, D: $Ni(L\text{-}H)_2$, E: $NiL_3Cl_2 \cdot 2H_2O$, F: NiL_2Cl_2, G: $NiL_3(ClO_4)_2$, H: Ni(L-H)Cl, I: $K_2Ni(L\text{-}2H)_2$, J: Ni(L-2H). L, L-H, L-2H, and L-4H in the above formulas indicate a free ligand and mono-, di-, and tetra-deprotonated ligands respectively. b) The binding energy of a main peak. c) ΔE_1 and ΔE_2 indicate the binding energy differences, $2p_{1/2}-3p$ and $2p_{3/2}-3p$ respectively.

not observed in this study. This is probably due to the comparison among the complexes of a variety of ligands. Therefore, in this study the differences between the binding energies of core-electrons for each complex were compared in order to reduce the effect of the variety of ligand on the binding energies.

Two kinds of differences, $\Delta E_1 = Ni(2p_{1/2}) - Ni(3p)$ and $\Delta E_2 = Ni(2p_{3/2}) - Ni(3p)$, are given in Table 1. The ΔE_1 and ΔE_2 values for Nos. 1—16 were 805.0—805.6 eV and 787.6—788.0 eV respectively. Those for Nos. 17—32 were 804.0—804.4 eV and 786.9—787.1 eV respectively. That is, the ΔE_1 and ΔE_2 values for the complexes of the former group were about 1 eV larger than those of the latter. This indicates that the differences between the binding energies of core-electrons give valuable information on the stereostructures of nickel complexes.

References

1) a) C. K. Jørgensen, *Chimica*, **25**, 213 (1971); b) L. J. Matienzo, W. E. Swartz, Jr., and S. O. Grim, *Inorg. Nucl. Chem. Lett.*, **8**, 1085 (1972); c) L. J. Matienzo and S. O. Grim, *ibid.*, **9**, 731 (1973); d) L. J. Matienzo, L. I. Yin, S. O. Grim, and W. E. Swartz, Jr., *Inorg. Chem.*, **12**, 2762 (1973); e) C. A. Tolman, W. M. Riggs, W. J. Linn, C. M. King, and R. C. Wendt, *ibid.*, **12**, 2770 (1973); f) M. Scrocco, *J. Electron Spectrosc. Relat. Phenom.*, **19**, 311 (1980).

2) T. A. Carlson, "Photoelectron and Auger Spectroscopy," Plenum Press, New York (1975), p. 339.

3) G. S. Smith and J. L. Hoard, *J. Am. Chem. Soc.*, **81**, 556 (1959).

4) A. J. Stosick, *J. Am. Chem. Soc.*, **67**, 365 (1945).

5) a) A. Takenaka, H. Utsumi, N. Ishihara, A. Furusaki, and I. Nitta, *Nippon Kagaku Zasshi*, **91**, 921 (1970); b) A. Kleinstein and G. A. Webb, *J. Inorg. Nucl. Chem.*, **33**, 405 (1971).

6) a) S. S. Sandhu, B. S. Manhas, M. R. Mittal, and S. S. Parmar, *Ind. J. Chem.*, **7**, 286 (1969); b) A. G. Hill and C. Curran, *J. Phys. Chem.*, **64**, 1519 (1960).

7) M. Kurahashi, *Bull. Chem. Soc. Jpn.*, **47**, 2067 (1974).

8) a) L. N. Swink and M. Atoji, *Acta Crystallogr.*, **13**, 639 (1960); b) A. S. Antsyshkina and M. A. Porai-Koshits, *Chem. Abstr.*, **57**, 2954f (1962); c) M. Nelson and J. Rodgers, *J. Chem. Soc., A*, **1968**, 272.

9) R. J. H. Clark and C. S. Williams, *Spectrochim. Acta, Part A*, **23**, 1055 (1967).

10) a) A. W. McLellan and G. A. Melson, *J. Chem. Soc., A*, **1967**, 137; b) H. C. Freeman, J. E. W. L. Smith, and J. C. Taylor, *Nature*, **184**, 707 (1959).

11) N. W. Alcock, R. C. Spencer, R. H. Prince, and O. Kennard, *J. Chem. Soc., A*, **1968**, 2383.

12) L. L. Merritt, Jr., C. Guare, and A. E. Lessor, Jr., *Acta Crystallogr.*, **9**, 253 (1956).

13) J. M. Stewart and E. C. Lingafelter, *Acta Crystallogr.*, **12**, 842 (1959).

14) L. E. Godycki and R. E. Rundle, *Acta Crystallogr.*, **6**, 487 (1953).

15) a) E. Frasson and C. Panattoni, *Acta Crystallogr.*, **13**, 893 (1960); b) R. H. Bowers, C. V. Banks, and R. A. Jacobson, *Acta Crystallogr., Sect. B*, **28**, 2318 (1972).

16) G. Maki, *J. Chem. Phys.*, **29**, 1129 (1958).

17) K. A. Jensen, *Z. Anorg. Chem.*, **252**, 227 (1944).

18) a) M. F. El-Shazly, T. Salem, M. A. El-Sayed, and S. Hedewy, *Inorg. Chim. Acta*, **29**, 155 (1978); b) I. P. Khullar and U. Agarwala, *Can. J. Chem.*, **53**, 1165 (1975).

19) M. Bonamico, G. Dessy, C. Mariani, A. Vaciago, and L. Zambonelli, *Acta Crystallogr.*, **19**, 619 (1965).

20) a) R. Kruh and C. W. Dwiggins, *J. Am. Chem. Soc.*, **77**, 806 (1955); b) L. L. Merritt, Jr., R. T. Cady, and B. W. Mundy, *Acta Crystallogr.*, **7**, 473 (1954); c) G. J. Palenik, *ibid.*, **17**, 696 (1964).

Synthesis and Absorption Spectra of Annelated 5-Amino-1,4-diazaanthraquinones and Related Compounds

Hiroyuki NAKAZUMI,* Kazuyoshi KONDO, and Teijiro KITAO

Department of Applied Chemistry, College of Engineering, University of Osaka Prefecture, Sakai, Osaka 591

(Received February 20, 1980)

Synopsis. New annelated 5-amino-1,4-diazaanthraquinones and related derivatives were prepared from 2,3,5-triamino-1,4-naphthoquinone or 5-amino-2,3-dichloro-1,4-naphthoquinone. Their visible absorption spectra were examined by the PPP-SCF-MO calculation with a variable β approximation.

1-Amino- and 1,4-diaminoanthraquinones are of great value as coloring matter. We have attempted to prepare new diazaanthraquinones for dyes. The visible absorption maximum of 5-amino-1,4-diazaanthraquinone **2** prepared from 2,3,5-triamino-1,4-naphthoquinone **1** is found at a longer wavelength than that of its carbon analogue.[1)]

In this paper, we wish to report the preparation and visible absorption spectra of annelated derivatives of **2** and related compounds. Annelated 5-amino-1,4-diazaanthraquinones **5**—**7** were prepared by the reaction of 1,2-quinones (1,2-naphthoquinone, acenaphthenequinone and 9,10-phenanthrenequinone) with **1** in 50—86% yields. Benzo derivative **4** was prepared from 5-amino-2(or 3)-chloro-3(or 2)-anilino-1,4-naphthoquinone **3** and sodium azide. Bromination of **2** afforded 5-amino-6,8-dibromo-1,4-diazaanthraquinone **8**. No monobromo derivative[1)] was isolated under the same conditions. 5-Amino-8-anilino derivative **9** was prepared by the Ullmann amination of **8** with aniline, along with 6(or 8)-bromo-5-amino derivative **10**, debrominated product of **8** in trace amounts.

The observed and calculated absorption maxima of new annelated compounds and **9** are summarized in Table 1. All the annelated compounds showed a pronounced bathochromic shift of λ_{max} in polar solvents. In this PPP calculation, the parameters for the solvent effect were not included. Annelation to 6,7-positions of some 1,4-disubstituted anthraquinones produces a small hypsochromic shift.[2)] The hypsochromic shifts of 4—8 nm are accurately predicted by the PPP calculation.[3)] The observed absorption

TABLE 1. THE ABSORPTION MAXIMA OF ANNELATED 5-AMINO-1,4-DIAZAANTHRAQUINONES AND RELATED COMPOUNDS

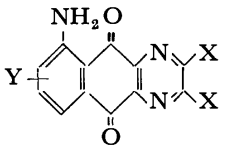

Compd No.	X, Y		λ_{max} (exptl)/nm ($\varepsilon \times 10^{-4}$)			λ_{max}(calcd)/nm (f[a)])
			Benzene[b)]	DMF	EtOH	
2[1)]	X = H	Y = H	476	489	500 (0.57)	423 (0.226)
4	2X = 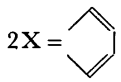	Y = H	464	475 (0.68)	484	422 (0.304)
5[c)]	2X = 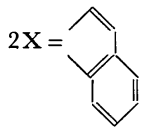	Y = H	471	486 (0.64)	493	419 (0.309)
6	2X = 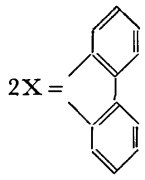	Y = H	473	489 (0.79)	498	420 (0.306)
7	2X = 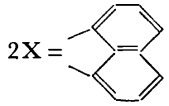	Y = H	485	501 (0.74)	511	422 (0.300)
9	X = H	Y = 6-Br-8-NHC_6H_5	598 634	598 634	598 (1.2) 636 (1.2)	—

a) Oscillator strength. b) The values of ε could not be measured due to the poor solubility. c) This structure was presumed by the comparison with the calculated λ_{max} of **5** and its isomer (2X = 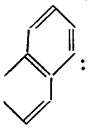 : 426 nm (f = 0.343).

maxima of annelated derivatives **4**—**6** were found at wavelengths somewhat shorter than those of the parent compound **2**. The calculated values of all annelated compounds were very close to the value of **2**. The calculated changes in π-electron density accompanying electronic excitation to the first excited state for **4**—**6** were mainly from aniline moiety to two carbonyl groups. The changes were similar to those for **2**.[1)]

On the other hand, the λ_{max} of **7** was observed at a longer wavelength than that of **2**. The absorption band corresponds to changes in π-electron density away from aniline moiety to an acenaphthene ring. Thus, it is predicted that the character of charge transfer for the first excitation for **7** differs from that of the other 5-amino-1,4-diazaanthraquinones.

The absorption maximum of 5-amino-8-anilino derivative **9** was found at the same wavelength as that of its carbon analogue (1-amino-2-bromo-4-anilinoanthraquinone: λ_{max} (benzene) 634 nm (ε, 1.35×10^4)).[4)] It is suggested that the substitution of a pyrazine ring for 1,4-disubstituted anthraquinone series produces no bathochromic shift.

Experimental

Most melting points of 1,4-diazaanthraquinones were not measured owing to the fact that no melting takes place below 300 °C. The absorption spectra were recorded on a Hitachi EPS-3T spectrophotometer, IR spectra on a Hitachi EPI-S_2 spectrophotometer, and mass spectra on a Hitachi RMU-6E mass spectrometer operating at 80 eV. Elemental analyses were recorded on a YANACO CHN recorder MT-2.

Method of SCF-MO Calculation. The calculations were carried out by the PPP-SCF-CI method with a variable β approximation, using the parameters reported,[1)] except for the core resonance integrals (β). The following β_{rs}'s were used for all the annelated compounds.

$$\beta_{CC}/\text{eV} = -1.81 - 0.51\,P_{CC}$$
$$\beta_{CN}/\text{eV} = -1.98 - 0.53\,P_{CN}$$
$$\beta_{CO}/\text{eV} = -2.17 - 0.56\,P_{CO}$$

5-Amino-2,3-benzo-1,4-diazaanthraquinone (4). A solution of aniline (3.5 g) in EtOH (8.3 ml) was added dropwise to a solution of 5-amino-2,3-dichloro-1,4-naphthoquinone (3.7 g)[5)] in EtOH (160 ml) at 75 °C. After the mixture had been refluxed for 3 h, the solid was separated. The filtrate was evaporated, and the combined solids were dissolved in pyridine and filtered. Water was added to the filtrate and the resulting solid was separated. The crude product was purified by dissolution in a minimum quantity of pyridine and reprecipitating with water to give **3**; yield 48%, mp 213—216 °C (dec), Found: C, 64.61; H, 3.76; N, 10.11%. Calcd for $C_{16}H_{11}N_2O_2Cl$: C, 64.32; H, 3.69; N, 9.38%. *m/e* (rel intensity), 300 (M+2, 30), 298 (M, 86), 264 (23), and 263 (100). A solution of NaN_3 (0.7 g) in water (2.2 ml) was added dropwise to a solution of **3** (2.2 g) in DMF (17 ml) at room temperature. The mixture was stirred at 120 °C for 4 h. After cooling, the resulting solid was separated, water being added to the first filtrate to precipitate crude product. The combined crude products were dissolved in EtOH and filtered. The filtrate was evaporated, and the residue was washed with hot xylene. Recrystallization from *o*-dichlorobenzene gave **4**; yield 18%, *m/e* (rel intensity), 275 (M, 100), 247 (35), 219 (35), and 192 (7), IR: 3400 and 3290 cm^{-1} (NH_2), 1670 and 1648 cm^{-1} (CO): Found, C, 69.17; H, 3.59; N, 14.39%. Calcd for $C_{16}H_9N_3O_2$: C, 69.82; H, 3.27; N, 15.27%.

Preparation of Annelated 5-Amino-1,4-diazaanthraquinones (5—7). 1,2-Naphthoquinone (0.93 g, 5.9 mmol) was added to a suspension of 2,3,5-triamino-1,4-naphthoquinone (1.0 g, 4.9 mmol) in 10% acetic acid (50 ml) at 80 °C. The mixture was stirred at 90 °C for 2.5 h. After cooling, the solid was separated and recrystallized from xylene to give **5**. No other isomer was observed by means of TLC. The other annelated compounds **6** and **7** were similarly prepared and recrystallized from DMF. **5**: yield 86%, *m/e* 325 (M, 100), 297 (27), and 269 (27), IR (KBr): 3420 and 3300 cm^{-1} (NH_2), 1689 and 1645 cm^{-1} (CO), Found: C, 74.20; H, 3.72; N, 11.69%. Calcd for $C_{20}H_{11}N_3O_2$: C, 73.85; H, 3.38; N, 12.92%. **6**: yield 51%, *m/e* 375 (M, 100), 347 (17), 319 (15), and 318 (10), IR (KBr): 3440 and 3325 cm^{-1} (NH_2), 1678 and 1650 cm^{-1} (CO), Found: C, 76.65; H, 3.36; N, 11.08%. Calcd for $C_{24}H_{13}N_3O_2$: C, 76.80; H, 3.47; N, 11.20%. **7**: yield 56%, *m/e* 349 (M, 100), 321 (22), and 293 (17), IR (KBr): 3430 and 3300 cm^{-1} (NH_2), 1670 and 1645 cm^{-1} (CO), Found: C, 75.51; H, 3.20; N, 11.60%. Calcd for $C_{22}H_{11}N_3O_2$: C, 75.64; H, 3.15; N, 12.03%.

5-Amino-6,8-dibromo-1,4-diazaanthraquinone (8). To a suspension of **2** (0.91 g) in *o*-dichlorobenzene (46 ml) was added bromine (1.62 g) dropwise at 130 °C for 1 h. The mixture was heated at 140—145 °C for 5 h. After cooling, the solid was separated and washed with benzene, methanol, and water. The crude product was suspended in water (150 ml) and treated with aqueous sodium sulfite, and recrystallized from xylene to give **8**; yield 47%, *m/e* 385 (M+4, 52), 383 (M+2, 100), 381 (M, 52), 357 (8), 355 (16), 353 (9), 286 (23), and 284 (28), IR (KBr): 3400 and 3280 cm^{-1} (NH_2), 1680 and 1640 cm^{-1} (CO), λ_{max} (EtOH): 492 nm (ε, 6.6×10^3), Found: C, 37.58; H, 1.52; N, 10.93%. Calcd for $C_{12}H_5N_3O_2Br_2$: C, 37.62; H, 1.31; N, 10.97%.

5-Amino-6-bromo-8-anilino-1,4-diazaanthraquinone (9). A mixture of **8** (0.94 g), $CuCO_3$ (0.06 g), potassium acetate (1.3 g), and aniline (8.0 g) was stirred at 130—140 °C for 1 h. After being cooled to 80—90 °C, methanol (8 ml) was added to the mixture. The resulting solid was separated, washed with water and methanol, and recrystallized from benzene. The crude product was separated by column-chromatography on silica gel (developing solvent: benzene–acetone (1:2)) to give **9** and **10** in yields of 31% and $\approx$0.1%, respectively. Compound **9** was again recrystallized from benzene. The first filtrate was steam distilled, and the residue solution evaporated. The crude product was recrystallized from water to give **10** (yield 0.3%). **9**: *m/e* 396 (M+2, 100) 394 (M, 100) 379 (43), 377 (47), and 298 (38), Found: C, 54.87; H, 3.01; N, 12.94%. Calcd for $C_{18}H_{11}N_4O_2Br$: C, 54.70; H, 2.79; N, 14.18%, mp 254 °C (sublimed). **10**: λ_{max} (EtOH): 488 nm (ε, 6.8×10^3), *m/e* 305 (M+2, 100), 303 (M, 100), 277 (24), 275 (25), 249 (14), 248 (12), 247 (12), 197 (13), and 196 (20), Found: C, 47.85; H, 2.20; N, 13.12%. Calcd for $C_{12}H_6N_3O_2Br$: C, 47.38; H, 1.97; N, 13.82%.

References

1) H. Nakazumi, T. Agawa, and T. Kitao, *Bull. Chem. Soc. Jpn.*, **52**, 2445 (1979).
2) M. Matsuoka, M. Kishimoto, and T. Kitao, *J. Soc. Dyers Colour.*, **94**, 439 (1978).
3) Y. Kogo, H. Kikuchi, M. Matsuoka, and T. Kitao, *J. Soc. Dyers Colour.*, **96**, 475, 526 (1980).
4) K. Konishi, M. Matsuoka, K. Takagi, S. Watanabe, T. Kitamura, and T. Kitao, *Kogyo Kagaku Zasshi*, **74**, 2118 (1971).
5) K. Fries, W. Pense, and O. Peeters, *Ber.*, **61**, 1395 (1928).

Phenalenones. III. The Anomalous Diazotization of 3-Substituted 2-Aminophenalenones

Masatane KUROKI* and Yutaka TSUNASHIMA

Department of Chemistry, Shibaura Institute of Technology, Fukasaku, Ohmiya, Saitama 330

(Received July 9, 1980)

Synopsis. The diazotization of 3-substituted 2-amino-1*H*-phenalen-1-ones (substituents=Cl, Br, PhS, or OH) gave 2-diazo-1*H*-phenalene-1,3(2*H*)-dione. It is most probable that the reaction involves the intramolecular rearrangement of a transient diazohydroxide intermediate and the consequent elimination of the substituent at the 3-position.

When 2-amino-3-bromo-1*H*-phenalen-1-one (**1a**) was treated with nitrous acid in concentrated hydrochloric acid, 2-diazo-1*H*-phenalen-1,3(2*H*)-dione (**2**) was unexpectedly obtained. Although the diazo diketone **2** had previously been prepared by the diazotization of 2-amino-3-hydroxy-1*H*-phenalen-1-one (**1e**),[1] the reaction of **1a** seemed to be different from that of **1e**. A bromine atom at the 3-position of **1a** is replaced by a carbonyl oxygen, whereas a hydrogen atom of the hydroxyl group is apparently eliminated in the case of **1e**. However, the reaction of **1e** may be understood similarly, if the hydroxyl group is considered to be a leaving group.

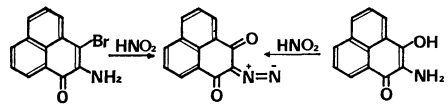

1a **2** **1e**

Scheme 1.

In order to clarify this, the diazotization of several 3-substituted 2-amino-1*H*-phenalen-1-ones was investigated.

Results and Discussion

The treatment of the amine **1a** with nitrous acid gave no clear solution, and no nitrogen gas evolved on the addition of phosphinic acid to the reaction mixture. In accordance with these observations, the reaction product was not the 3-bromo-1*H*-phenalen-1-one expected for a usual reductive deamination, but, rather, was diazo diketone **2**. The yields of **2** were independent of the presence of phosphinic acid.

Similarly, other 3-substituted 2-amino-1*H*-phenalen-1-ones (**1b**—**1e**) afforded the corresponding diazo diketones in good yields (Table 1).

TABLE 1. YIELDS OF **2a** AND **2d**

	1		2	
	R^1	R^2	R^2	Yield/%
a	Br	H	H	96
b	Cl	H	H	62
c	SPh	H	H	44
d	Br	Br	Br	97
e	OH	H	H	74
f	H	H	H	0

Eistert *et al.*[1] carried out the diazotization of the 3-hydroxy derivative **1e** by using nitrosyl hydrogensulfate in a homogeneous solution. The present reactions proceeded sufficiently in a suspension of the amines in hydrochloric acid.

An exceptional case was the reaction of 2-amino-1*H*-phenalen-1-one (**1f**) (R^1=H), which gave an unworkable polymer (mp>330 °C, partly soluble in an aqueous sodium carbonate solution). The treatment of the diazotized solution with phosphinic acid led to a partial decomposition to give a small amount of phenalenone, although the main product was a complicatedly polymerized mass. The formation of phenalenone indicates that normal diazotization occurred in part.

These reactions resemble those of 3-substituted 2-amino-1,4-naphthoquinones. Cajipe *et al.*[2] found that the diazotization of the amino quinones in acetic acid gave 3-diazo-1,2,4(3*H*)-naphthalenetrione. They postulated a reaction mechanism involving the nucleophilic attack of the acetate ion at the 3-position, followed by hydrolysis and the elimination of RH (R=Cl, CH_3O, N_3, and PhS), as is shown in Scheme 2.

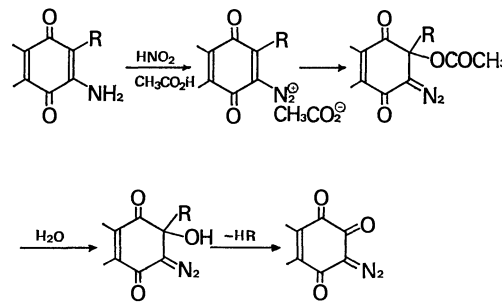

Scheme 2.

However, the application of Cajipe's mechanism to the present reaction seems to be less probable, since we did not use acetic acid as a solvent, and even if the nucleophile is the hydroxide ion, the concentration of the hydroxide ion could be extremely low in concentrated hydrochloric acid.

For our reactions, the participation of the diazohydroxide intermediate **3** and a sequent intramolecular rearrangement seem probable, as is outlined in Scheme 3. The existence of a diazohydroxide compound as a transient intermediate has been widely accepted in the diazotization of primary amines.[3] The hydroxyl group of **3** migrates to the 3-position of the phenalene ring, then HR^1 is released to give the diazo diketone **2**. Consistently with the reaction sequences benzenethiol was obtained as another reaction product in the reaction of **1c**. On the same basis, it is understandable that the unsubstituted 2-amino-1*H*-phenalen-

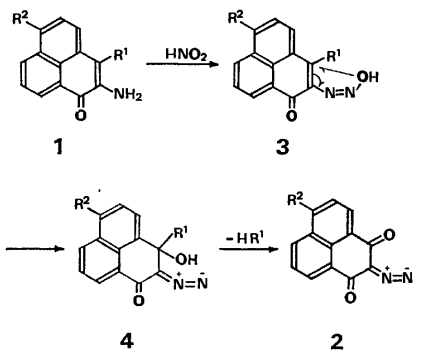

Scheme 3.

1-one **1f** did not give **2**, since the hydroxyl group of the intermediate **3f** can migrate only with difficulty because of the less positive nature of the carbon atom at the 3-position. In addition, even if migration occurs, the intermediate **4f** can not be converted to **2** unless dehydrogenation takes place. There is no possibility of dehydrogenation under the present reaction conditions.

The authers are grateful to Mr. Toshikatsu Sekine and Mr. Minoru Matsuzawa for their technical support.

Experimental

All the melting points are uncorrected. The IR spectra were taken on a JASCO IRA-1 spectrophotometer, while the UV spectrum was recorded on a Hitachi EPS-3T spectrophotometer. The NMR spectra were recorded with a JEOL JNM-PS-100 spectrometer (100 MHz), with TMS as the internal standard. The mass spectra were obtained at 70 eV using a Hitachi RMU-7M spectrometer.

*2-Amino-3-bromo-1*H*-phenalen-1-one (**1a**)* (mp 187—188.5 °C) and *2-amino-3,6-dibromo-1*H*-phenalen-1-one (**1d**)* (mp 213—215 °C) were prepared by the methods described in a previous paper.[4]

*2-Amino-3-chloro-1*H*-phenalen-1-one (**1b**).* Into 30 ml of a vigorously stirred solution of 2-amino-1*H*-phenalen-1-one[4] (0.50 g) in chlorobenzene we added, portion by portion, a chlorine solution in carbon tetrachloride containing 0.20 g of chlorine at 50 °C. After 30 min, a yellow precipitate was collected and washed with carbon tetrachloride. The free base was obtained by the treatment of the solid salt with a sodium carbonate aqueous solution. Red crystals of mp 214 °C (methanol) was obtained in a 36% yield. IR (KBr) 3467, 3347 (N-H) and 1622 cm^{-1} (C=O); NMR (DMSO-d_6) δ=7.95—7.52 (4H, m), 8.32 (1H, d, J=8 Hz), 8.46 (1H, d, J=8 Hz). Found: C, 67.76; H, 3.49; N, 6.12; Cl, 15.82%. Calcd for $C_{13}H_8ONCl$: C, 67.98; H, 3.51; N, 6.10; Cl, 15.44%.

*2-Amino-3-(phenylthio)-1*H*-phenalen-1-one (**1c**).* The solution of 2-amino-3-bromo-1*H*-phenalen-1-one (1.37 g) in 80 ml of an ethanol–dioxane mixture (2:1) was added by an ethanolic solution of sodium benzenethiolate which had been prepared from 1.10 g of benzenethiol and sodium methoxide; the mixture was then refluxed for 4 h. After the removal of a small amount of dark powder by filtration, the solution was concentrated to give 0.96 g of reddish brown crystals (63%); mp 147.5—149 °C. MS *m/e* 303 (M^+); IR (KBr) 3470, 3360 (N-H), and 1635 cm^{-1} (C=O); NMR (DMSO-d_6) δ=7.07—7.14 (5H, m), 7.48 (1H, t, J=7 Hz), 7.77 (1H, t, J=6 Hz), 7.82 (1H, d, J=6 Hz), 7.98 (1H, d, J=6 Hz), 8.32 (1H, d, J=7 Hz), and 8.51 (1H, d, J=7 Hz).

Found: C, 75.68; H, 4.31; N, 4.54; S, 10.32%. Calcd for $C_{19}H_{13}ONS$: C, 75.22; H, 4.32; N, 4.62; S, 10.57%.

*2-Diazo-1*H*-phenalene-1,3(2*H*)-dione (**2**).* Finely ground 2-amino-3-bromo-1*H*-phenalen-1-one (2.00 g) was added, portion by portion, to 20 ml of concentrated hydrochloric acid, after which we added 2.00 g of sodium nitrite dissolved in minimum volume of water; the mixture was then stirred at 5 °C for 1 h and allowed stand overnight. A yellow-brown solid was collected and washed with dilute aqueous ammonia and then with water. Recrystallization from benzene gave 1.05 g (65%) of **2** as pale yellow crystals of mp 197—199 °C dec. (lit,[1] mp 191—195 °C). MS *m/e* 222.0434 (M^+, Δ=0.5 m mass unit), 194.0041 (M^+−28, $-N_2$), and 166.0418 (M^+−56, -CO) IR (KBr) 2230, 2160 (N_2), and 1635 cm^{-1} (C=O); NMR ($CDCl_3$) δ=7.66 (2H, t, J=7 Hz), 8.12 (2H, d, J=7 Hz), 8.48 (2H, d, J=7 Hz); UV (λ_{max}^{EtOH}, nm, log ε) 235.5 (4.82), 298 (4.08), and 338 (4.05). Found: C, 69.91 H, 2.55; N, 12.11%. Calcd for $C_{13}H_6O_2N_2$: C, 70.27; H, 2.72; N, 12.61%.

Similar reactions on **1b**, **1c**, and **1e** afforded **2**, as is shown in Table 1. The addition of the diazotized reaction mixture to phosphinic acid did not affect the yields of diazo diketone.

In a run of the reactions on **1c**, benzenethiol was obtained besides **2**. The reaction mixture was filtered and washed with diethyl ether. The filtrate and washings were combined, and the solution was extracted with diethyl ether. The subsequent removal of the solvent left an oil, which was determined to be benzenethiol by a comparison of its IR and GLC with those of an authentic specimen (15% crude yield).

*6-Bromo-2-diazo-1*H*-phenalene-1,3(2*H*)-dione (**2d**).* Orange yellow crystals (benzene); mp 194—195.5 °C dec; MS *m/e* 302 (M^+); IR (KBr) 2230, 2150 (N_2), and 1644 cm^{-1} (C=O); NMR (pyridine-d_5) δ=7.81 (1H, t, J=9 Hz), 8.07 (1H, d, J=9 Hz), 8.39 (1H, d, J=9 Hz), 8.50 (1H, d, J=8 Hz), and 8.56 (1H, d, J=8 Hz). Found: C, 51.53; H, 1.67; N, 9.01; Br, 25.95%. Calcd for $C_{13}H_5O_2N_2Br$: C, 51.85; H, 1.67; N, 9.31; Br, 26.54%.

References

1) B. Eistert, W. Eifler, and H. Göth, *Chem. Ber.*, **101**, 2162 (1968).

2) G. J. B. Cajipe, G. Landen, B. Semler, and H. H. Moore, *J. Org. Chem.*, **40**, 3874 (1975).

3) H. Zollinger, "Azo and Diazo Chemistry," Interscience Publishers, New York (1961), p. 35.

4) M. Kuroki, T. Nakazawa, and M. Yokote, *Nippon Kagaku Kaishi*, **1974**, 2144.

Conversion of Quassin into 15β-[(*E*)-3,4-Dimethyl-2-pentenoyloxy]quassin. A *D*-Ring Analog of Bruceantin

Tatsushi MURAE and Takeyoshi TAKAHASHI*

Department of Chemistry, Faculty of Science, The University of Tokyo, Hongo, Bunkyo-ku, Tokyo 113

(Received July 29, 1980)

Synopsis. Quassin was transformed in five steps into 15β-[(*E*)-3,4-dimethyl-2-pentenoyloxy]quassin.

Bruceantin (**1**), a simaroubolide isolated from *Brucea antidysenterica* MILL., has been described to be a potent antileukemic tumor inhibitor, the importance of the α,β-unsaturated ester grouping for the antitumor activity of **1** being pointed out.[1] This paper deals with a conversion of quassin (**2**)[2] into its 15β-[(*E*)-3,4-dimethyl-2-pentenoyloxy] derivative (**3**), having the *D*-ring moiety of bruceantin (**1**).

Quassin (**2**) has been transformed, *via* neoquassin (**4**)[2,3] and anhydroneoquassin (**5**),[4] into hydroxyneoquassin (**6**) and hydroxyquassin (**7**) both in low yields, the configuration of the hydroxyl group at C-15 being undetermined for **6** and **7**.[2a] Synthesis of **3** starting from **2** was carried out as follows.

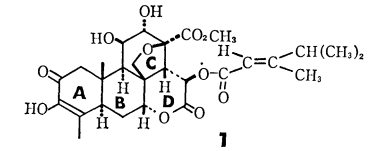

1

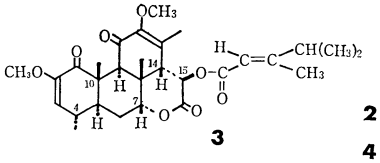

3

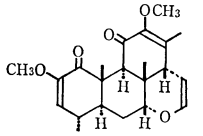

5

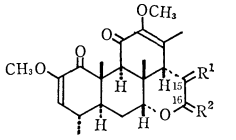

	R^1	R^2
2	H_2	O
4	H_2	OH, H
6	ξ-OH, ξ-H	OH, H
6a	β-OH, α-H	OH, H
7	ξ-OH, ξ-H	O
7a	β-OH, α-H	O

When quassin (**2**) was reduced with 1 equivalent mole of sodium borohydride in ethanol or 3 equivalent moles of diisobutylaluminium hydride in benzene, neoquassin (**4**) was obtained almost quantitatively. Treatment of **4** with hexamethylphosphoric triamide under reflux gave anhydroneoquassin (**5**) in 80% yield. The unsaturated ether (**5**) was oxidized with osmium(VIII) oxide in pyridine and then treated with sodium hydrogensulfite to give 15β-hydroxyneoquassin (**6a**) in 91% yield. On oxidation with silver(I) oxide, **6a** gave 15β-hydroxyquassin (**7a**) in 55% yield. In the ^{1}H-NMR spectrum of **7a**, the coupling constant between the C-14 and C-15 protons was observed to be 11 Hz. Thus the C-15 hydroxyl group was shown to be in a β-configuration for both **6a** and **7a**. By the improved procedure described above, 15β-hydroxyquassin (**7a**) was prepared from quassin (**2**) in *ca.* 40% yield.

Finally, acylation of **7a** gave 15β-[(*E*)-3,4-dimethyl-2-pentenoyloxy]quassin (**3**) in 83% yield. Inhibitory effect (ID_{50}) against growth of HeLa cells was 150 μg/ml for **3**. Further modification of the quassin molecule would be required for exhibition of strong activity.

Experimental

Melting points were measured on a Mel-temp capillary melting point apparatus (Laboratory Devices) and are uncorrected. High resolution mass spectra were measured with a JEOL JMS-D300 mass spectrometer. Other details are the same as described previoulsy.[5]

Reduction of Quassin (2) with Sodium Borohydride or Diisobutylaluminium Hydride. Quassin (**2**)[2] was isolated from *Picrasma ailanthoides* PLANCHON according to the procedure of Murae *et al.*[6] Sodium borohydride (38 mg, 1 mmol) was added to a solution of quassin (**2**) (388 mg, 1 mmol) in ethanol (50 ml), and the mixture was stirred at room temperature for 3.5 h. After addition of a few drops of acetic acid, the solvent was removed to give a residue. This was extracted with dichloromethane after addition of water. The organic solution was washed with brine, dried (Na_2SO_4) and evaporated, giving **4** (386 mg) in 99% yield as a colorless solid. Crystallization from a mixture of dichloromethane and ether gave colorless needles, mp 230.5—231 °C, identical with an authentic specimen of neoquassin (**4**).[2a,7]

Diisobutylaluminium hydride (22 mg, 0.15 mmol) in dry tetrahydrofuran (0.5 ml) was added to a solution of quassin (**2**) (20 mg, 0.05 mmol) in dry benzene (2 ml), and the mixture was stirred under nitrogen atmosphere at room temperature for 1 h. The reaction mixture was treated in the usual way to give a product (19 mg) in 95% yield identical with neoquassin (**4**).

Dehydration of Neoquassin (4). A mixture of neoquassin (**4**) (67 mg) and hexamethylphosphoric triamide (0.9 ml) was heated under reflux for 5 min. The reaction mixture was poured into a mixture of chloroform (20 ml) and brine (30 ml). The chloroform solution was separated, and the aqueous layer was extracted twice with chloroform (each 20 ml). The combined chloroform solution was dried (Na_2SO_4) and evaporated to give a residue, which was chromatographed on a column of silica gel (50 g). Elution with ether gave **5** (51.3 mg) in 80% yield. Crystallization from a mixture of chloroform and ether gave **5** as colorless prisms, mp 191—192 °C, IR (Nujol) 1705, 1668, 1643, and 1630 cm^{-1}, no absorption due to hydroxyl group; ^{1}H-NMR ($CDCl_3$) δ 1.11 (3H, d, J=7 Hz), 1.17 (3H, s), 1.59 (3H, s), 1.88 (3H, s), 3.12 (1H, s), 3.59 (3H, s), 3.63 (3H, s), 3.81 (1H, t, J=2 Hz), 4.59 (1H, dd, J=6 and J=2 Hz), 5.30 (1H, d, J=2 Hz), and 6.45 (1H, dd, J=6 and J=3 Hz). Found: *m/e* 372.1927. Calcd for $C_{22}H_{28}O_5$: M, 372.1935. The product was found to be identical with an authentic sample of anhydroneoquassin (**5**).[2a]

15β-Hydroxyneoquassin (6a). A solution of anhydroneoquassin (**5**) (496 mg) in pyridine (20 ml) was treated with osmium(VIII) oxide (369 mg) at room temperature for 4 h. After addition of a solution of sodium hydrogensulfite (1 g) in a mixture of water (40 ml) and pyridine (30 ml), the reaction mixture was extracted with chloroform. The chloroform solution was washed with water (30 ml) and brine (30 ml), dried (Na_2SO_4) and evaporated to give

6a (495 mg) in 91% yield. 15β-Hydroxyneoquassin (**6a**): amorphous solid; IR (Nujol) 3450, 1680, and 1632 cm^{-1}; UV (EtOH) λ_{max} 258 nm (ε 10100); ^{1}H-NMR ($CDCl_3$) δ 1.06 (3H, s), 1.07 (3H, d, J=6 Hz), 1.43 (1.5H, s), 1.46 (1.5H, s), 1.51 (3H, s), 3.18 (0.5H, s), 3.23 (0.5H, s), 3.53 (1.5H, s), 3.55 (1.5H, s), 3.65 (3H, s), 4.50 (0.5H, broad d, J=7.5 Hz), 5.19 (0.5H, d, J=4 Hz), and 5.26 (1H, d, J=2 Hz). Found: *m/e* 406.1963. Calcd for $C_{22}H_{30}O_7$: M, 406.1990. The hemiacetal (**6a**) of a neoquassin type exists as a mixture of diastereomers at C-16.

Oxidation of **5** was attempted with potassium permanganate to form **6** and **7**,[2a] but no consistent result was obtained due to the complicatedness of the reaction. Direct comparison of **6a** with **6** was not carried out.

15β-Hydroxyquassin (7a). 15β-Hydroxyneoquassin (**6a**) (444 mg) was dissolved in ethanol (20 ml) and water (15 ml), and treated with freshly prepared silver(I) oxide (1.4 g) under reflux for 19 h. The warm mixture was filtered through Celite, the solid on Celite being washed with methanol (50 ml). The filtrate and washings were combined and concentrated to a volume of 20 ml. This was extracted with chloroform. The chloroform solution was treated in the usual way to give a residue (408 mg), which was chromatographed on a column of silica gel (50 g). Elution with a mixture of benzene and acetone (7:3) gave **7a** (241 mg) in 55% yield. 15β-Hydroxyquassin (**7a**): mp 256—258 °C (crystallized from a mixture of ethyl acetate and light petroleum); IR (Nujol) 3490, 1740, 1699, 1681, and 1632 cm^{-1}; UV (MeOH) λ_{max} 257 nm (ε 10500); ^{1}H-NMR ($CDCl_3$) δ 1.12 (3H, d, J=7 Hz), 1.21 (3H, s), 1.52 (3H, s), 2.09 (3H, s), 2.41 (1H, d, J=11 Hz), 3.05 (1H, s), 3.59 (3H, s), 3.69 (3H, s), 4.35 (1H, m), 4.49 (1H, d, J=11 Hz), and 5.31 (1H, d, J=2 Hz). Found: *m/e* 404.1813. Calcd for $C_{22}H_{28}O_7$: M, 404.1832. Direct comparison of **7a** with **7**[2a] was not carried out.

(E)-3,4-Dimethyl-2-pentenoyl Chloride. Ethyl (*E*)-3,4-dimethyl-2-pentenoate was prepared according to the procedure of Jorgenson and Leung.[8] Potassium hydroxide (1 g) was added to a solution of ethyl (*E*)-3,4-dimethyl-2-pentenoate (2 g) in ethanol (10 ml), and the mixture was treated in the usual way to give an acid (1.5 g) in 91% yield. (*E*)-3,4-Dimethyl-2-pentenoic acid: a colorless oil, bp 114 °C/2.4 kPa; IR (neat) 3050 (broad), 1690, and 1619 cm^{-1}; ^{1}H-NMR (CCl_4) δ 1.10 (6H, d, J=7 Hz), 2.13 (3H, broad s), and 5.67 (1H, broad s). Found: *m/e* 128.0845. Calcd for $C_7H_{12}O_2$: M, 128.0837.

A mixture of carboxylic acid (1.5 g) and thionyl chloride (2.4 g) was heated under reflux for 1 h. The reaction mixture was distilled under reduced pressure giving an acid chloride (0.89 g) in 52% yield. (*E*)-3,4-Dimethyl-2-pentenoyl chloride: bp 70—72 °C/2.7 kPa; IR (neat) 1780 cm^{-1}. The acid chloride was used immediately for the following acylation.

15β-[(E)-3,4-Dimethyl-2-pentenoyloxy]quassin (3). A mixture of 15β-hydroxyquassin (**7a**) (100 mg) and (*E*)-3,4-dimethyl-2-pentenoyl chloride (1.5 g) in the presence of potassium carbonate (450 mg) was heated with stirring at 100 °C for 30 min. After addition of dichloromethane (10 ml), the reaction mixture was filtered and evaporated to give a residue, which was subjected to purification by dry column chromatography [18 g of silica gel; eluted with a mixture of light petroleum and ether (1:1) (240 ml) and then ether (180 ml)]. The fractions eluted with ether were combined and the solvent was removed to afford an ester (**3**) (106 mg) as a colorless solid in 83% yield. 15β-[(*E*)-Dimethyl-2-pentenoyloxy]quassin (**3**): mp 219—223 °C (crystallized from a mixture of benzene and light petroleum), $[\alpha]_D^{28}$ +152° (*c* 0.73, $CHCl_3$), IR (Nujol) 1753, 1718, 1702, 1690, 1635, and 1628 cm^{-1}, no absorption due to hydroxyl group; UV λ_{max} (MeOH) 226 nm (ε 19300) and 252 nm (ε 14800; shoulder); ^{1}H-NMR ($CDCl_3$) δ 1.10 (6H, d, J=6 Hz), 1.13 (3H, d, J=6 Hz), 1.22 (3H, s), 1.56 (3H, s), 1.92 (3H, s), 2.17 (3H, d, J=1 Hz), 2.63 (1H, d, J=10 Hz), 3.05 (1H, s), 3.60 (3H, s), 3.70 (3H, s), 4.55 (1H, m), 5.15 (1H, d, J=10 Hz), 5.31 (1H, d, J=2.5 Hz), and 5.80 (1H, broad s). Found: *m/e* 514.2511. Calcd for $C_{29}H_{38}O_8$: M, 514.2566. The fragment ion peak due to a loss of 3,4-dimethyl-2-pentenoic acid was observed at *m/e* 386.1720 as a base peak. Calcd for $C_{22}H_{26}O_6$: M−$C_7H_{12}O_2$, 386.1727.

The authors wish to thank Dr. Wataru Tanaka, Nippon Kayaku Co., for the biological assay.

References

1) S. M. Kupchan, R. W. Britton, M. F. Ziegler, and C. W. Sigel, *J. Org. Chem.*, **38**, 178 (1973).

2) a) Z. Valenta, S. Papadopoulos, and C. Podešva, *Tetrahedron*, **15**, 100 (1961); b) W. A. C. Brown and G. A. Sim, *Proc. Chem. Soc.*, **1964**, 293.

3) E. London, A. Robertson, and H. Worthington, *J. Chem. Soc.*, **1950**, 3431.

4) K. R. Hanson, D. B. Jaquiss, J. A. Lamberton, A. Robertson, and W. E. Savige, *J. Chem. Soc.*, **1954**, 4238; E. P. Clark, *J. Am. Chem. Soc.*, **59**, 2511 (1937).

5) H. Hirota, Y. Moriyama, H. Shirasaki, T. Tsuyuki, and T. Takahashi, *Bull. Chem. Soc. Jpn.*, **52**, 3755 (1979).

6) T. Murae, T. Tsuyuki, T. Ikeda, T. Nishihama, S. Masuda, and T. Takahashi, *Tetrahedron*, **27**, 1545 (1971).

7) T. Murae, T. Tsuyuki, T. Ikeda, T. Nishihama, S. Masuda, and T. Takahashi, *Tetrahedron*, **27**, 5147 (1971).

8) M. J. Jorgenson and T. Leung, *J. Am. Chem. Soc.*, **90**, 3769 (1968).

Synthesis of Thiol Esters by Carboxylic Trichlorobenzoic Anhydrides

Yasuhiro KAWANAMI, Yuichiro DAINOBU, Junji INANAGA, Tsutomu KATSUKI, and Masaru YAMAGUCHI*

Department of Chemistry, Faculty of Science, Kyushu University, Hakozaki, Higashi-ku, Fukuoka 812

(Received August 27, 1980)

Synopsis. Thiocarboxylic S-esters were obtained rapidly and in high yields by treating the mixed anhydrides prepared from 2,4,6-trichlorobenzoyl chloride and carboxylic acid, with various types of thiols in the presence of 4-dimethylaminopyridine.

Because of the distinctive properties of thiocarboxylic S-esters as activated esters in synthetic as well as biological reactions, considerable attention has recently been called to the mild and facile preparation of these compounds.[1] Recently we have shown that the combination of carboxylic 2,4,6-trichlorobenzoic anhydrides (**2**) and 4-dimethylaminopyridine[2] are very useful for the preparation of esters from alcohols as well as for macrocyclic lactonizations.[3] Now we wish to describe the synthesis of thiol esters using the same mixed anhydrides.

When the solutions prepared by mixing 2,4,6-trichlorobenzoyl chloride (**1**),[4] carboxylic acid and triethylamine in dichloromethane, were treated with thiols under the presence of 4-dimethylaminopyridine, the corresponding thiol esters were obtained in good yields. The reaction proceeded rapidly, and was usually completed within 30 min at room temperature. The results are summarized in Table 1.

$$R^1COOH + 2,4,6\text{-}Cl_3C_6H_2COCl \xrightarrow{Et_3N} \underset{\mathbf{1}}{} \quad 2,4,6\text{-}Cl_3C_6H_2COOCOR^1 \quad \underset{\mathbf{2}}{}$$

$$\mathbf{2} + R^2SH \xrightarrow[CH_2Cl_2]{\text{4-dimethylaminopyridine}} R^1COSR^2$$

As can be seen from these results, aliphatic, aromatic or heterocyclic thiol esters could be smoothly prepared. The sterically crowded thiol esters such as *S-t*-butyl 2,2-dimethylpropanethioate (entry 3, Table 1) were also prepared in good yields. Methyl hydrogen meso-2,4-dimethylglutarate was converted into the corresponding 2-methyl-2-propanethiol ester without any detectable epimerization (GLPC, entry 7).

When dimethylaminopyridine was replaced by pyridine or triethylamine, the reaction became very slow and, for example, only 3—4% of *S-t*-butyl 2-methylpentanethioate was formed after 1 h (*cf.* entry 2). Though the aromatic hydrocarbons such as benzene or toluene, were the best solvent for the esterification by the same reagents,[3] dichloromethane was the most effective solvent in the present thiol esterification. Acetonitrile or DMF was much less satisfactory.

The possibility of nucleophilic attack on the undesired carboxyl site is inherent to the mixed anhydride method. For example, when carboxylic pivalic anhydrides which have been sometimes used in peptide[5] or ketone synthesis,[6] were treated with 2-methyl-2-propanethiol or benzenethiol in the presence of 4-dimethylaminopyridine under the similar conditions, both the carboxyl sites were attacked as shown in Eqs. 1, 2, and 3. In the present method, however, thiol attacked exclusively on the desired carboxyl carbon except for one case where sterically crowded pivalic acid was converted into its benzenethiol ester (entry 5, Table 1).[7]

$$\begin{array}{l} C_6H_5COOCOC(CH_3)_3 \\ + \\ HSC(CH_3)_3 \end{array} \xrightarrow[\text{rt, 10 h}]{\text{DMAP (1 eq)}} \begin{array}{ll} C_6H_5COSC(CH_3)_3 & 60\% \\ + & \\ (CH_3)_3CCOSC(CH_3)_3 & 15\% \end{array} \quad \text{(GLPC)} \qquad (1)$$

$$\begin{array}{l} CH_3(CH_2)_2COOCOC(CH_3)_3 \\ + \\ HSC_6H_5 \end{array} \xrightarrow[\text{rt, 10 min}]{\text{DMAP (1 eq)}} \begin{array}{ll} CH_3(CH_2)_2COSC_6H_5 & 48\% \\ + & \\ (CH_3)_3CCOSC_6H_5 & 43\% \end{array} \quad (^1\text{H-NMR}) \qquad (2)$$

$$\begin{array}{l} (CH_3)_2CHCOOCOC(CH_3)_3 \\ + \\ HSC_6H_5 \end{array} \xrightarrow[\text{rt, 10 min}]{\text{DMAP (1 eq)}} \begin{array}{ll} (CH_3)_2CHCOSC_6H_5 & 48\% \\ + & \\ (CH_3)_3CCOSC_6H_5 & 38\% \end{array} \quad (^1\text{H-NMR}) \qquad (3)$$

The use of symmetrical anhydrides[8] or mixed anhydrides with phosphoric acid derivatives[9] has been reported for the synthesis of thiol esters. The main advantage of the present method is the rapidness and the mildness of the reaction, high yields, and the wide applicability.

Experimental

The preparation of *S-t*-butyl 2-methylpentanethioate (entry 2, Table 1) is described below as a typical example of the present thiol esterifications.

2,4,6-Trichlorobenzoyl chloride (80 μl, 0.5 mmol) was added to a stirred mixture of 2-methylpentanoic acid (63 μl, 0.5 mmol), triethylamine (70 μl, 0.5 mmol), and dichloromethane (0.8 ml). After 1 h, the reaction mixture was filtered through a dry celite column. To the filtrate were added 2-methyl-2-propanethiol (56.4 μl, 0.5 mmol) and 4-dimethylaminopyridine (61 mg, 0.5 mmol) and the mixture was stirred at room temperature. GLPC analysis showed the quantitative formation of the thiol ester after 30 min. The reaction mixture was diluted with ether, washed successively with 5% aqueous phosphoric acid, a saturated sodium hydrogencarbonate solution, and brine, dried with sodium sulfate, and distilled at 80 °C/15 mmHg[10] (bath temperature) giving *S-t*-butyl 2-methylpentanethioate in 86.3% yield.

This work was partially supported by a Grant-in-Aid for Scientific Research No. 443008 from the Ministry of Education, Science and Culture.

References

1) For recent reports see; T. Mukaiyama, T. Takeda,

Table 1. Reaction conditions and yields of thiol esters[a]

	Acid (0.5 mmol) R^1 in R^1COOH	Thiol (0.5 mmol) R^2 in R^2SH	DMAP[b] (mmol)	Time (min)	Yield(%)[c] R^1COSR^2
1	$CH_3(CH_2)_2$	C_2H_5	0.5	4	96 (82)[d]
2	$CH_3CH_2CH_2\underset{\vert}{C}HCH_3$	$(CH_3)_3C$	0.5	30	98 (86)[e]
3	$(CH_3)_3C$	$(CH_3)_3C$	0.5	120	96
4	$(CH_3)_2CH$	C_6H_5	0.5	4	87 (78)[f]
5	$(CH_3)_3C$	C_6H_5	0.5	5	60[g]
6	C_6H_{11} (cyclohexyl)	C_5H_4N[h]	0.5	10	(84)
7	$CH_3O_2CCH(CH_3)CH_2\underset{\vert}{C}HCH_3$[i]	$(CH_3)_3C$	0.5	10	96 (80)[j]
8	C_6H_5	$(CH_3)_3C$	0.5	3	93 (81)
9	$C_6H_5CH{=}CH$	$(CH_3)_2CH$	0.5	3	93 (81)[k]

a) All reactions were carried out in dichloromethane at room temperature. b) 4-Dimethylaminopyridine. c) The yields were determined by GLPC. Isolated yields were given in parentheses. d) A new compound: Bp 150 °C (bath temp). Found: C, 54.32; H, 9.17%. Calcd for $C_6H_{12}OS$: C, 54.50; H, 9.15%. ^{1}H-NMR (δ); 1.25 (t, 3H, J=7.0 Hz), 2.53(t, 2H, J=7.4 Hz). e) Bp 100 °C (10 mmHg, bath temp). Found: C, 63.48; H, 10.56%. Calcd for $C_{10}H_{20}OS$: C, 63.71; H, 10.70%. ^{1}H-NMR; 1.46(s, 9H), 2.50(m, 1H). f) Bp 140 °C (9 mmHg, bath temp). Found: C, 66.34; H, 6.68%. Calcd for $C_{10}H_{12}OS$: C, 66.63; H, 6.71%. ^{1}H-NMR; 1.26 (d, 6H, J=6.8 Hz), 7.38 (s, 5H). g) *S*-Phenyl 2,4,6-trichlorothiobenzoate [mp 119 °C, Found: C, 49.05; H, 2.29%. Calcd for $C_{13}H_7Cl_3OS$: C, 49.16; H, 2.22%. ^{1}H-NMR; 7.33(m, 2H), 7.49(m, 5H)] was also formed in 18% yield. h) 2-Pyridinethiol. i) Methyl hydrogen meso-2,4-dimethylglutarate. j) Found: C, 58.21; H, 8.92%. Calcd for $C_{13}H_{22}O_3S$: C, 58.50; H, 9.00%. ^{1}H-NMR; 1.46 (s, 9H), 3.68(s, 3H). k) Bp 180 °C (11 mmHg, bath temp). Found: C, 69.66; H, 6.86%. Calcd for $C_{12}H_{14}OS$: C, 69.86; H, 6.84%. ^{1}H-NMR; 1.35(d, 6H, J=6.7 Hz), 6.67(d, 1H, J=16.1 Hz), 7.61(d, 1H, J=16.1 Hz).

and K. Atsumi, *Chem. Lett.*, **1974**, 187; S. Masamune, S. Kamata, and W. Schilling, *J. Am. Chem. Soc.*, **97**, 3515 (1975); F. Souto-Bachiller, G. S. Bates, and S. Masamune, *J. Chem. Soc., Chem. Commun.*, **1976**, 719; Y. Watanabe, S. Shoda, and T. Mukaiyama, *Chem. Lett.*, **1976**, 741; R. P. Hatch and S. M. Weinreb, *J. Org. Chem.*, **42**, 3960 (1977); A. Pelter, T. E. Levitt, K. Smith, and A. Jones, *J. Chem. Soc., Perkin Trans. 1*, **1977**, 1672; H. -J. Gais, *Angew. Chem., Int. Ed. Engl.*, **16**, 244 (1977); K. Horiki, *Synth. Commun.*, **7**, 251 (1977); P. A. Grieco, Y. Yokoyama, and E. Williams, *J. Org. Chem.*, **43**, 1283 (1978); and Refs. 7 and 8.

2) G. Höfle and W. Steglich, *Synthesis*, **1972**, 619; H. Vorbrüggen, *ibid.*, **1973**, 301; G. Höfle, W. Steglich, and H. Vorbrüggen, *Angew. Chem., Int. Ed. Engl.*, **17**, 569 (1978).

3) J. Inanaga, K. Hirata, H. Saeki, T. Katsuki, and M. Yamaguchi, *Bull. Chem. Soc. Jpn.*, **52**, 1989 (1979).

4) R. C. Fuson, J. W. Bertetti, and Wm. E. Ross, *J. Am. Chem. Soc.*, **54**, 4380 (1932).

5) M. Zaoral, *Coll. Czech. Chem. Commun.*, **27**, 1273 (1962).

6) M. Araki and T. Mukaiyama, *Chem. Lett.*, **1974**, 663.

7) The thiol esterification of pivalic acid with benzenethiol by the present method is peculiar in that the reaction with triethylamine or morphorine in place of dimethylaminopyridine gives a quite similar result as that with dimethylaminopyridine in rate, yield, and product distribution. This indicates that the reaction presumably involves the direct attack of thiolate ion formed by the bases, on the mixed anhydride. Benzenethiol is much more acidic than the aliphatic thiols.

8) A. A. Schleppnik and F. B. Zienty, *J. Org. Chem.*, **29**, 1910 (1964).

9) S. Yamada, Y. Yokoyama, and T. Shioiri, *J. Org. Chem.*, **39**, 3302 (1974); S. Masamune, S. Kamata, J. Diakur, Y. Sugihara, and G. S. Bates, *Can. J. Chem.*, **53**, 3693 (1975); Y. Yokoyama, T. Shioiri, and S. Yamada, *Chem. Pharm. Bull.*, **25**, 2423 (1977).

10) 1 mmHg=133.322 Pa.

A Simple Method for the Synthesis of Exaltolide

Toshio SATO, Tatsuo KAWARA, Yasuchika KOKUBU, and Tamotsu FUJISAWA*

Chemistry Department of Resources, Mie University, Tsu, Mie 514

(Received September 8, 1980)

Synopsis. Copper-catalyzed reaction of β-propiolactone with 12-methoxydodecylmagnesium bromide, derived from 1,12-dodecanediol, gives 15-methoxypentadecanoic acid in a high yield, which is easily converted into exaltolide.

15-Pentadecanolide (exaltolide, **1**) is a component of the root oil of *Archangelica officianalis* Syn., which is known as a perfume of the most strong and elegant musk-like fragrance in the series of macrocyclic lactones. Among the numerous synthetic methods for exaltolide so far reported, the most common one is the cyclization of 15-hydroxy- or 15-bromopentadecanoic acid. These acids have been usually prepared from long-chain carboxylic acids arising from several plant oils, such as (*Z*)-13-docosenoic acid (erucic acid)[1] from rapeseed oil, 9,10,16-trihydroxyhexadecanoic acid (aleuritic acid)[2] from the resin of schellac, or 10-undecenoic acid from castor oil.[3] Recently cyclododecanone has been frequently used as a useful starting material of C_{12} unit because of easy availability from butadiene trimer, and various routes to exaltolide have been elaborated by C_3 extention of cyclododecanone.[4] A short-step synthesis of exaltolide (**1**) *via* 15-bromopentadecanoic acid (**4**) was investigated from easily available starting materials of β-propiolactone (**2**) and 1,12-dodecanediol (**3**).

In this route, the regioselective reaction of β-propiolactone with a Grignard reagent[5] containing an oxygen functionality was applied as a key step for the synthesis of exaltolide, *i.e.*, the three carbon homologation terminating in a carboxyl function was easily achieved by the copper catalyzed reaction of 12-methoxydodecylmagnesium bromide (**6**) with the lactone **2** to furnish 15-methoxypentadecanoic acid (**5**) which was smoothly converted into **4**. Thus, to a mixture of

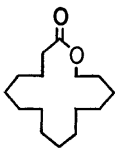

1

2

$HO(CH_2)_{12}OH$

3

$X(CH_2)_{14}CO_2H$
4 X=Br
5 X=MeO

$MeO(CH_2)_{12}Y$
6 Y=MgBr
7 Y=OH
8 Y=Br

the lactone **2** (1 equiv) and copper(I) iodide (0.02 equiv) in THF–Me_2S (8:1) was added **6** (1 equiv) at 0 °C. After the reaction mixture was stirred at 0 °C for 3 h, the desired acid **5** was obtained in a yield of 99%. Treatment of **5** with excess boron tribromide in CH_2Cl_2 at −25 °C for 4 d gave 15-bromopentadecanoic acid (**4**) in 78% yield. Then, according to the method of Mandolini *et al.*,[6] the ω-bromo acid was treated with potassium carbonate in dimethyl sulfoxide at 75 °C to furnish exaltolide (**1**) in 78% yield.

The Grignard reagent **6** of C_{12} unit was easily derived from the diol **3**. Chipped sodium was slowly added to an excess of **3** at 100 °C and then dimethyl sulfate was added dropwise. After stirring for 2 h at 120 °C, 12-methoxy-1-dodecanol (**7**) was obtained quantitatively. Bromination of **7** with phosphorus tribromide and pyridine at room temperature for 2 d gave 1-bromo-12-methoxydodecane (**8**) in a yield of 65%, which was easily transformed into the Grignard reagent **6** by the reaction with magnesium metal in refluxing ether.

As mentioned above, by the use of the regioselective reaction of the Grignard reagent of an oxygen functionality with β-propiolactone in the presence of a copper(I) catalyst, exaltolide was conveniently synthesized from the easily available materials.

Experimental

The IR spectra were recorded on a Hitachi EPI-G2 spectrometer. The NMR spectra were taken with a Varian A-60 spectrometer using TMS as an internal standard. All boiling points and melting points are uncorrected.

12-Methoxy-1-dodecanol (7). Chipped sodium (0.744 g, 31 mg atom) was slowly added to 1,12-dodecanediol (25 g, 124 mmol) at 100 °C. After the sodium was dissolved, dimethyl sulfate (3.9 g, 31 mmol) was added dropwise at 120 °C and the mixture was stirred for 2 h. The reaction mixture was cooled to room temperature, quenched with water and extracted with chloroform. The extracts were dried over anhydrous $MgSO_4$. The solvent was removed and the residue was extracted with hexane. Distillation of the hexane solution gave **7** (6.9 g, quant.): bp 120—124 °C/0.8 mmHg; IR (KBr) 3300 (OH) and 1120 cm^{-1} (C-O); NMR (CCl_4) δ 1.10—1.78 (20H, broad), 3.12—3.60 (5H, m), and 3.20 (3H, s).

1-Bromo-12-methoxydodecane (8). To a mixture of phosphorus tribromide (3.10 g, 11.4 mmol) and pyridine (0.048 g, 0.61 mmol) in dry ether (5 ml) was added dropwise **7** (7.45 g, 34.4 mmol) in pyridine (0.160 g, 2.02 mmol) at −20 °C. The reaction mixture was stirred at room temperature for 2 d. Hydrochloric acid (1 M) was added and the mixture was extracted with ether. The extracts were washed with 5% sodium hydrogencarbonate solution and dried over anhydrous $MgSO_4$. After removal of the solvent, distillation afforded **8** (6.24 g, 65%): bp 114—119 °C/0.5 mmHg; IR (KBr) 1120 (C-O), 645 and 560 cm^{-1} (C-Br); NMR (CCl_4) δ 1.3 (20H, m) and 3.12—3.60 (4H, m), 3.20 (3H, s).

15-Methoxypentadecanoic Acid (5). 12-Methoxydodecylmagnesium bromide (**6**) was prepared from magnesium (1.17 g, 48 mmol) and **8** (6.19 g, 22 mmol) in ether (24 ml), which was titrated by Eastham's method[6] (0.547 M, 74%).

To a THF (4 ml) solution of copper(I) iodide (3.8 mg, 0.02 mmol), dimethyl sulfide (0.5 ml) and β-propiolactone (72.2 mg, 1.00 mmol) was added the Grignard reagent **6** (0.55 ml, 1.01 mmol) at 0 °C. The reaction mixture was

stirred for 3 h, quenched with water and then made basic with 3 M aqueous sodium hydroxide solution. The white precipitate was filtered and the filtrate was washed with ether. The water layer was acidified with 6 M hydrochloric acid. The solid was dissolved in this acidic solution, which was extracted with ether. The extracts were dried over anhydrous $MgSO_4$ and the solvent was evaporated to afford **5** (268 mg, 99%): mp 47—48 °C; IR (KBr) 3300—2500, 1700 (CO_2H), and 1125 cm^{-1} (C-O); NMR (CCl_4) δ 1.10—1.72 (24H, m), 2.20 (2H, t, J=7 Hz), 3.20 (3H, s), 3.23 (2H, t, J=7 Hz), 9.20 (1H, s).

15-Bromopentadecanoic Acid (4). To a solution of **5** (0.234 g, 0.86 mmol) in dry CH_2Cl_2 (4 ml) was added dropwise boron tribromide (0.870 g, 3.47 mmol) in dry CH_2Cl_2 at −78 °C and the reaction mixture was stirred for 30 min. The solution was warmed to −25 °C and allowed to stand for 4 d. Sodium hydrogencarbonate (2.60 g, 3.09 mmol) was added at −25 °C. The mixture was then acidified with 3 M hydrochloric acid and extracted with ether. The extracts were dried over anhydrous $MgSO_4$. Removal of the solvent gave **4** (0,215 g, 78%): mp 66—67 °C (lit,[8] 66 °C); IR (KBr) 3500—2400, 1700 (CO_2H) and 650 cm^{-1} (C-Br); NMR (CCl_4) δ 1.20—2.00 (24H, m), 2.30 (2H, t, J=7 Hz), and 9.50 (1H, s).

Exaltolide (1). To a suspension of powdered potassium carbonate (0.563 g, 4.08 mmol) in dimethyl sulfoxide (11 ml) was added dropwise **4** (0.321 g, 1.00 mmol) in dimethyl sulfoxide (5 ml) at 75 °C in 4 h under vigorous stirring. After the mixture was cooled to room temperature, cold water (10 ml) was added and resulting mixture was extracted with hexane. The extracts were dried over anhydrous $MgSO_4$ and the solvent was evaporated. The crude product was purified by TLC on silica gel (hexane:ether=8:1) to afford **1** (0.189 g, 78%): mp 32 °C (lit,[1] 32 °C); IR (KBr) 1735 cm^{-1} (C=O); NMR (CCl_4) δ 1.00—2.00 (26H, m), 2.17 (2H, t, J=7 Hz), and 3.93 (2H, t, J=5 Hz). The spectral data were identical with those of an authentic sample.

The present work was partially supported by a Grant-in-Aid for Scientic Research No. 554144 from the Ministry of Education, Sciene and Culture.

References

1) V. V. Dhekne, B. B. Ghatge, U. G. Nayak, K. K. Chakravarti, and S. C. Bhattcharyya, *J. Chem. Soc.*, **1962**, 2343.

2) H. H. Mathur and S. C. Bhattcharyya, *J. Chem. Soc.*, **1963**, 3505.

3) H. Kurihara, T. Matsui, A. Hattori, and T. Moroe, Japan Patent 68-4262; *Chem. Abstr.*, **70**, 19927z (1969).

4) H. Nozaki, T. Mori, and M. Kawanisi, *Can. J. Chem.*, **46**, 3767 (1968); J. Becker and G. Ohloff, *Helv. Chim. Acta*, **54**, 2889 (1971); K. Bauer and A. Koerber, Ger. Offen, 2 731 573 (1979); *Chem. Abstr.*, **90**, 15167n (1979).

5) T. Sato, T. Kawara, M. Kawashima, and T. Fujisawa, *Chem. Lett.*, **1980**, 571.

6) G. Calli and L. Mandolini, *Gazz. Chim. Ital.*, **105**, 367 (1975).

7) S. C. Watson and J. F. Eastham, *J. Organomet. Chem.*, **9**, 165 (1975).

8) H. Hunsdiecker and C. Hunsdiecker, *Ber.*, **75**, 291 (1942).

Studies on the Synthesis of Sydnone Derivatives and Their Properties. XV. Synthesis of 4-Sydnonylmethyl Acetates

Mou-Yung YEH, Hsien-Ju TIEN,* Jiun-Tzer CHOU, and Tsutomu NONAKA**

Department of Chemistry, National Cheng Kung University, Tainan, Taiwan, Republic of China

***Department of Electronic Chemistry, Tokyo Institute of Technology, 4259, Nagatsuta, Midori-ku, Yokohama 227*

(Received September 26, 1980)

Synopsis. The convenient methods for the synthesis of 4-sydnonylmethyl acetates from *N*-(4-sydnonylmethyl)morpholines, 4-sydnonylmethanols, or bis(4-sydnonylmethyl) ethers are described.

Sydnones are typical mesoionic compounds and their chemical, physical, and biological properties are peculiar.[1] Generally, a sydnone ring is unstable to acid, alkali, and heat. Therefore, reaction conditions for the synthesis of sydnone compounds are considerably limited. For instance, no method to introduce electron-releasing groups, such as amino, hydroxyl, and alkoxy groups, into the 4-position of the sydnone ring has been found. It seems to be possible to substitute the 4-position by these groups in interposition of a methylene group. Imashiro and Masuda[2] synthesized many kinds of 4-sydnonylmethylamines and found that some of them have a biological activity. We also found the synthetic method of 4-sydnonylmethanols and bis(4-sydnonylmethyl) ethers.[3] Screening tests of some biological activities of these 4-sydnonylmethyl compounds are in progress.

We aim at synthesizing new derivatives of 4-sydnonylmethyl compounds, especially 4-sydnonylmethyl acetates in this work. The 4-sydnonylmethyl acetates may have a characteristic biological activity different from those of the previously synthesized 4-sydnonylmethyl compounds. The expectation of such a biological activity and an interest in reactivities of the 4-sydnonylmethyl compounds inspired us to develop the synthetic method of 4-sydnonylmethyl acetates.

For this purpose, three kinds of 4-sydnonylmethyl compounds, of which preparative methods had been reported,[2,3] were examined as starting compounds for the 4-sydnonylmethyl acetates.

The first attempt to synthesize the 4-sydnonylmethyl acetates was led by the reaction of *N*-(4-sydnonylmethyl)morpholines, which were prepared by the modified method of Imashiro and Masuda,[2] with acetic anhydride(Method A).

Method A:

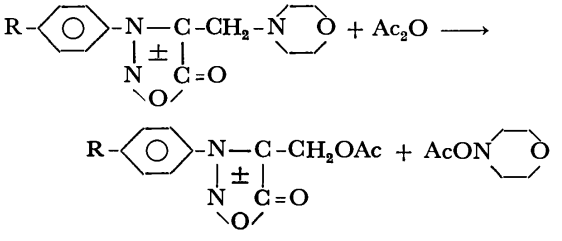

As shown in Table 1, though the desired 4-sydnonylmethyl acetates could be obtained, their yields were not high even in high reaction temperature and long reaction time. Since a sydnone ring is generally unstable as described above, mild conditions should be desirable in the synthesis of sydnone compounds.

Table 1. Synthesis of 4-sydnonylmethyl acetates

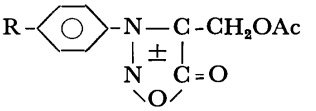

R	Method	Temp/°C	Time/min	Yield[a]/%
H	A	90—100	480	48
CH_3	A	90—100	480	42
Br	A	90—100	480	47
H	B	30	4	76
CH_3	B	30	4	81
Br	B	30	4	84
H	C	30	5	71
CH_3	C	30	5	80
Br	C	30	5	81

a) After purification.

The second attempt was done by acetylating directly 4-sydnonylmethanols[3] with acetic anhydride in the presence of a catalytic amount of sulfuric acid and was successful as expected. The acetylation was completed within a few minutes at room temperature (about 30 °C) and the 4-sydnonylmethyl acetates could be obtained in high yields as shown in Table 1 (Method B).

Method B:

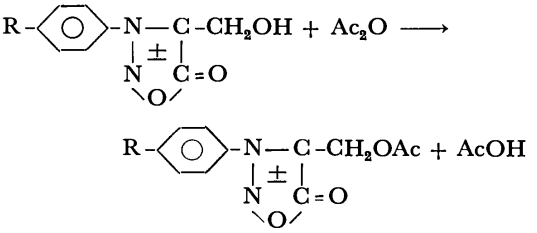

In the synthesis of the 4-sydnonylmethanols, considerable amounts of bis(4-sydnonylmethyl) ethers were formed as a by-product under a reaction condition.[3] The third attempt was the synthesis of the 4-sydnonylmethyl acetates from these ethers (Method C). The ethers also reacted with acetic anhydride in the presence of sulfuric acid to give the corresponding 4-sydnonylmethyl acetates in high yields comparable to those in Method B.

Method C:

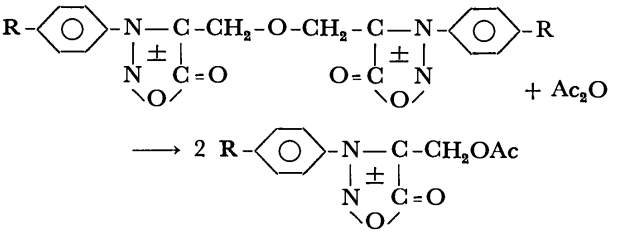

The above fact may suggest that the 4-sydnonylmethyl acetates can be efficiently and conveniently obtained from a mixture of the 4-sydnonylmethanols and the bis(4-sydnonylmethyl) ethers, without separation of the each component from mixed products in their syntheses.

In all the methods, the yield of the 4-sydnonylmethyl acetates was not affected by both an electron-releasing group (*p*-CH_3) and an electron-withdrawing one (*p*-Br) attached to the benzene ring of the starting sydnone compounds. This fact may suggest a potentiality of the general application of these methods to the synthesis of a variety of 4-sydnonylmethyl acetates, though few examples were given in the present work.

Experimental

Starting Materials. N-*(4-Sydnonylmethyl)morpholines*: *N*-(3-Phenyl-4-sydnonylmethyl)morpholine was prepared by the method of Imashiro and Masuda.[2] *N*-[3-(*p*-methylphenyl)-4-sydnonylmethyl]morpholine and *N*-[3-(*p*-bromophenyl)-4-sydnonylmethyl]morpholine were newly synthesized according to a similar procedure. The former compound: yield, 72%; appearance, colorless needles; mp, 118—120 °C. IR (KBr): 2810, 1740, 1730, 1240, and 1110 cm^{-1}. MS (70 eV): *m/e* 275 (M^+). Found: C, 61.15; H, 6.24; N, 15.44%. Calcd for $C_{14}H_{17}N_3O_3$: C, 61.09; H, 6.22; N, 15.26%. The latter compound: yield, 77%; appearance, colorless needles: mp, 128—130 °C. IR (KBr): 2830, 1730, 1235, and 1110 cm^{-1}. MS (70 eV): *m/e* 339 (M^+) and 341 (M^+). Found: C, 45.85; H, 4.08; N, 12.54; Br, 23.61%. Calcd for $C_{13}H_{14}N_3BrO_3$: C, 45.90; H, 4.15; N, 12.35; Br, 23.49%.

4-Sydnonylmethanols and Bis(4-sydnonylmethyl) Ethers: 3-Phenyl-4-sydnonylmethanol, 3-(*p*-methylphenyl)-4-sydnonylmethanol, bis(3-phenyl-4-sydnonylmethyl) ether, and bis[3-(*p*-methylphenyl)-4-sydnonylmethyl] ether were prepared by the method of the previous work.[3] 3-(*p*-Bromophenyl)-4-sydnonylmethanol and bis[3-(*p*-bromophenyl)-4-sydnonylmethyl] ether were newly synthesized by a similar method. The former compound: yield, 67%; appearance, colorless powder; mp 161—163 °C. IR (KBr): 3395, 1710, 1245, and 1010 cm^{-1}. MS (70 eV): *m/e* 270 (M^+) and 272 (M^+). Found: C, 39.74; H, 2.62; N, 10.14%. Calcd for $C_9H_7N_2BrO_3$: C, 39.87; H, 2.60; N, 10.34%. The latter compound: yield, 23%, appearance, pale yellow needles; mp, 175—176 °C. IR (KBr): 3080, 1735, 1260, 1250, 1040, and 1000 cm^{-1}. MS (70 eV): *m/e* 253 [1/2(M^+−16)] and 255 [1/2(M^+−16)]. Found: C, 41.19; H, 2.10; N, 10,65%. Calcd for $C_{18}H_{12}N_4Br_2O_5$: C, 41.25; H, 2.31; N, 10.69%.

Synthesis of 4-Sydnonylmethyl Acetates. Typical procedures for the synthesis of the titled compounds are shown below. *Method A*: One gram (3.6 mmol) of *N*-[3-(p-methylphneyl)-4-sydnonylmethyl]morpholine was added into 3 ml of acetic anhydride and the reaction mixture was heated at 90—100 °C in a water bath. After 8 h, the reaction mixture was poured into crushed ice. Recrystallization of the resulting solid from ethanol afforded 0.38 g (1.5 mmol, 42%) of pure 3-(*p*-methylphenyl)-4-sydnonylmethyl acetate as colorless needles. Mp, 129—131 °C. IR (KBr): 3050, 1740, 1230, and 1030 cm^{-1}. MS (70 eV): *m/e* 248 (M^+). NMR (chloroform-*d*): δ 2.06 (s, 3H), 2.52 (s, 3H), 4.91 (s, 2H), and 7.42 (s, 4H) ppm. Found: C, 58.35; H, 4.97; N, 11.30%. Calcd for $C_{12}H_{12}N_2O_4$: C, 58.06; H, 4.87; N, 11.29%.

Method B: One gram (5.3 mmol) of 3-phenyl-4-sydnonylmethanol was added into 3 ml of acetic anhydride containing one drop of sulfuric acid. After 4 min at room temperature, the reaction mixture was poured into crushed ice. Recrystallization of the resulting pale yellow solid from ethanol afforded 0.92 g (4.0 mmol, 76%) of pure 3-phenyl-4-sydnonylmethyl acetate as colorless needles. Mp, 97—98 °C. IR (KBr): 3060, 1750, 1220, and 1020 cm^{-1}. MS (70 eV): *m/e* 234 (M^+). NMR (chloroform-*d*): δ 2.08 (s, 3H), 4.95 (s, 2H), and 7.65 (m, 5H) ppm. Found: C, 56.29; H, 4.19; N, 11.69%. Calcd for $C_{11}H_{10}N_2O_4$: C, 56.41; H, 4.30; N, 11.96%.

Method C: One gram (1.9 mmol) of bis[3-(*p*-bromophenyl)-4-sydnonylmethyl] ether was added into 3 ml of acetic anhydride containing one drop of sulfuric acid. After 5 min at room temperature, the reaction mixture was poured into crushed ice. Recrystallization of the resulting solid from ethanol afforded 0.97 g (3.1 mmol, 81%) of pure 3-(*p*-bromophenyl)-4-sydnonylmethyl acetate as colorless needles. Mp, 88—91 °C. IR (KBr): 3060, 1750, 1215, and 1010 cm^{-1}. MS (70 eV): *m/e* 312 (M^+) and 314 (M^+). NMR (chloroform-*d*): δ 2.10 (s, 3H), 4.95 (s, 2H), and 7.66 (m, 4H) ppm. Found: C, 42.21; H, 2.28; N, 8.84; Br, 25.43%. Calcd for $C_{11}H_9N_2BrO_4$: C, 42.19; H, 2.90; N, 8.95; Br, 25.52%.

References

1) M. Ohta and H. Kato, "Non-benzenoid Aromatics," Academic Press, New York, N. Y. (1969), Vol. 1, Chap. 4.

2) Y. Imashiro and K. Masuda, Brit. Pat., 1207629 (1968) and 1215878 (1968).

3) M. -Y. Yeh and H. -J. Tien, *Bull. Cheng Kung Univ. Sci. and Eng. Sec.*, **14**, 23 (1979).

Effect of Ammonia Pre-treatment on Catalytic Activity of Metal Halide Catalyst for Reduction of Nitrogen Monoxide

Akio NISHIJIMA,* Yoshimichi KIYOZUMI, Minoru KURITA, Hiroyuki HAGIWARA, Akifumi UENO,** Toshio SATO, and Naoyuki TODO

National Chemical Laboratory for Industry, 1-1, Higashi, Yatabe, Ibaraki 305

(Received August 7, 1980)

Synopsis. Effects of ammonia pre-treatment on catalytic activities of metal halides for the reduction of nitrogen monoxide are investigated in order to obtain highly active catalysts at lower temperatures. By the pre-treatment with NH_3, some supported metal halide catalysts such as $CeCl_2$, $MnCl_2$, $TiCl_4$, $FeBr_3$, and $CuCl_2$, showed higher activities than untreated ones.

Among the various techniques proposed for reducing nitrogen oxides (NO_x) emitted from stationary combustion equipments, the catalytic reduction of nitrogen monoxide (NO) with ammonia (NH_3) has been considered to be one of the most favorable methods.[1-3] In this process, metal oxide supported catalysts such as V_2O_5, CuO, Fe_2O_3, and MoO_3 on γ-Al_2O_3 or TiO_2 have been applied for practical use. They are used at reaction temperatures over 300 °C in order to obtain effective reduction of NO_x. From economical point of view, catalysts active at lower temperatures are desirable since temperatures of flue gases emitted from a coke oven or sintering furnace are lower than 200 °C. The present authors have been trying to develope new type of catalysts having higher activities at temperatures as low as possible. Metal halide catalysts were found to show high activities at temperatures under 200 °C.[4] Another investigation showed that the most favorable electronic state of cations in the catalysts can be obtained by a proper combination of the cation with a counter anion and carrier for high activity.[5] In this work, it was found that supported metal halide catalysts pre-treated with NH_3 show higher activities than those of untreated ones.

Experimental

The catalyst used in this study were prepared by impregnating γ-Al_2O_3 spheres (diam. 1.5 mm, surface area 250 m^2/g, average pore radius 58 Å, alkali content 0.01 wt%) with aqueous solution of metal halides. After the impregnation, the catalysts were dried for 3 h at 120 °C and then for 2 h at 180 °C in air stream. The catalysts were then placed in a glass vessel containing gaseous ammonia for 10 h at room temperature. Activity measurements were carried out using a conventional flow reactor (stainless steel, length 200 mm, diam. 15 mm) under the space velocity of 15000 h^{-1}. As a standard feedstream, the gas mixture consisting of NO 300 ppm, NH_3 400 ppm, O_2 5 vol%, H_2O 9.2 vol%, SO_2 200 ppm, and N_2 balance was used. Analysis of NO and NH_3 were made by means of a chemiluminescence type NO_x analyzer and the chemical method (JIS-K-0099), respectively.

Results and Discussion

The effect of NH_3 pre-treatment on the activity of $CeCl_2$–Al_2O_3 catalyst for the reduction of NO is shown in Fig. 1. In the temperature region lower than 200 °C, $CeCl_2$–Al_2O_3 catalyst treated with ammonia showed higher activity than untreated ones. Figures 2 and 3 show results obtained on $MnCl_2$–Al_2O_3 and $TiCl_4$–Al_2O_3 catalyst, respectively. Though almost no activity was observed on untreated one on $TiCl_4$–Al_2O_3 catalyst, much higher activity was obtained after NH_3 pre-treatment. Similar effects were observed on some supported metal halide catalysts such as $FeBr_3$, and $CuCl_2$ on γ-Al_2O_3. These activities enhanced by NH_3 pre-treatment continued longer

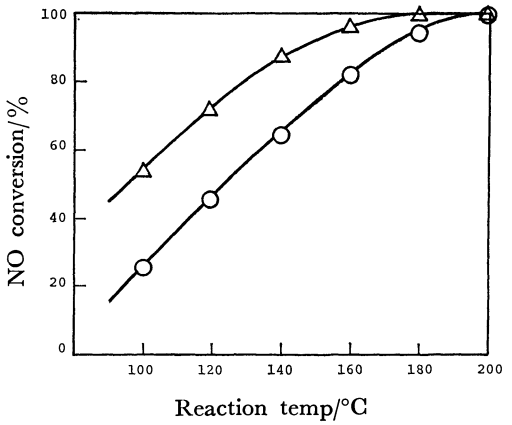

Fig. 1. Effect of NH_3 pre-treatment on activity of $CeCl_2$–Al_2O_3 catalyst.
△: Treated with NH_3, ○: untreated.
Reaction conditions; SV: 15000 h^{-1}, NO: 300 ppm, NH_3: 400 ppm, O_2: 5 vol%, H_2O: 9.2 vol%, SO_2: 200 ppm, N_2: balance.

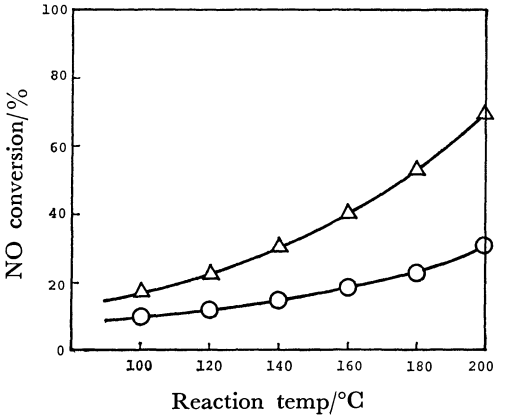

Fig. 2. Effect of NH_3 pre-treatment on activity of $MnCl_2$–Al_2O_3 catalyst.
△: Treated with NH_3, ○: untreated.
Reaction conditions; SV: 15000 h^{-1}, NO: 300 ppm, NH_3: 400 ppm, O_2: 5 vol%, H_2O: 9.2 vol%, SO_2: 200 ppm, N_2: balance.

**Present address: Toyohashi University of Technology, 1-1, Hibarigaoka, Senpaku, Toyohashi, Aichi 440.

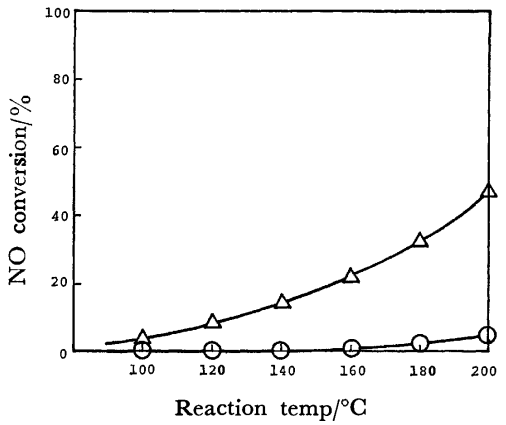

Fig. 3. Effect of NH_3 pre-treatment on activity of $TiCl_4$–Al_2O_3 catalyst.
△: Treated with NH_3, ○: untreated.
Reaction conditions; SV: 15000 h^{-1} NO: 300 ppm, NH_3: 400 ppm, O_2: 5 vol%, H_2O: 9.2 vol%, SO_2: 200 ppm, N_2: balance.

than 3 h.

Metal halides are well known to form metal halide ammonium complexes. The color of each catalyst changed to that of metal halide ammonium complex by NH_3 pre-treatment, indicating that metal halide ammonium complexes were formed on the catalysts. It is also known, however, that ammonium complexes are unstable at temperatures over 100 °C. The activities of the present catalysts pre-treated with NH_3 disappeared when they were heated over 300 °C. A thermogravimetric analysis showed that although the amount of NH_3 in these complexes decreased with the temperature elevated, NH_3 were still remained at temperatures over than 200 °C. These results show that NH_3 coordinates to metal ions in metal halides at lower temperatures, indicating the increase of the concentration of NH_3 available for the reduction of NO on active sites. On the other hand, previous study showed that proper amount of NO adsorption on catalyst is also essential as well as that of NH_3 adsorption for producing highly active state, and that the most favorable electronic state of the cation in the catalyst is required for this purpose.[5] NH_3 coordination is considered to affect on the electronic state of the cation. In fact, the binding energy of Fe $2p_{3/2}$ photoelectron peak on $FeBr_3$–Al_2O_3 catalyst measured by a photoelectron spectrometer(XPS) changed from 711.6 to 711.1 eV after NH_3 pre-treatment. These results will indicate that the enhancement of the activity by NH_3 pre-treatment is mainly due to the improvement of the electronic state of the cation. More research is now needed on such metal halide ammonium complex catalysts to fully understand the mechanism of the enhancement of the catalysts.

References

1) S. Jarros and J. Krizek, *Int. Chem. Eng.*, **8**, 261 (1968).
2) G. Chakrabarti and C. Chu, *Atmos. Environ.*, **6**, 279 (1972).
3) P. L. Klimisch and K. C. Taylor, *Env. Sci. Technol.*, **7**, 127 (1973).
4) N. Todo, A. Nishijima, A. Ueno, M. Kurita, H. Hagiwara, T. Sato, and Y. Kiyozumi, *Chem. Lett.*, **1976**, 897.
5) A. Nishijima, Y. Kiyozumi, A. Ueno, M. Kurita, H. Hagiwara, T. Sato, and N. Todo, *Bull. Chem. Soc. Jpn.*, **52**, 3724 (1979).

Hydration of Quaternary Phosphonium Bromides, $Bu_{4-n}Ph_nPBr$, in Chloroform[1]

Toshiki WAKABAYASHI* and Katsuko TAKAIZUMI
The College of General Education, Tohoku University, Kawauchi, Sendai 980

(Received January 5, 1980)

Studies have been carried out on the hydration of quaternary phosphonium bromides, $Bu_{4-n}Ph_nPBr$($n=0$—4), in the chloroform phase by means of distribution equilibrium and ^1H NMR spectroscopy, in order to clarify the difference between the alkyl- and aryl-substituted ions in ion–water interactions. The hydration constant for these bromides in the chloroform phase increases gradually from Bu_4PBr to Bu_2Ph_2PBr, and then rapidly to $BuPh_3PBr$ and to Ph_4PBr. The free energy of transfer from water to chloroform was evaluated for the non-hydrated species of the phosphonium bromides in the chloroform phase, the lowest being that for Bu_2Ph_2PBr. From ^1H NMR spectra for water in the chloroform phase, it is concluded that the hydrated water molecule is hydrogen bonded with the anion of the onium salts. In the case of phenyl-rich cations such as $BuPh_3P^+$, Ph_4P^+, and Ph_4As^+ the water molecule occupies a site so close to the central atoms that it undergoes diamagnetic effects of phenyl groups. With phenyl-rich cations such hydration will play a certain role in their aqueous solutions.

The ion–water interactions of the so-called hydrophobic ions, considerably large organic ions, have been widely investigated over the past two decades. Differences between the alkyl- and aryl-substituted ions in their interactions with water have been recognized.[2-4] In a similar way to those of hydrocarbons, the interactions of alkyl-substituted ions with water are tentatively explained by the concept of a structure-making effect on the solvent water, though not completely established so far.

On the other hand, with tetraphenyl ions such as Ph_4M^+ (M=P, As, Sb) and BPh_4^-, their interactions with water might be more complicated, due to some effects not present in the case of benzene such as the delocalized charges on the phenyl groups[8,9] and the hydration of the central atoms. Tetraphenyl borate is known to interact with water in a different way from Ph_4M^+ ions.[4-7] The penta-coordinate state of the central atom was suggested for Ph_4As^+ in water, but not for Ph_4P^+, by Orenberg *et al.*[10] who studied laser-Raman spectra. From a study of ^1H NMR for Ph_4M^+ and BPh_4^- ions in various solvents, Coetzee and Sharpe[7] concluded that the screening of the central atoms by essentially flat phenyl rings is not sufficient for elimination of the solvation effects. The effects are related to the failure to classify the ions as structure makers or structure breakers.[12]

An approach to the hydration of aryl-substituted ions would be to examine systematically the ions with mixed substituents of alkyl and aryl groups besides the tetraalkyl and tetraphenyl ions. Only tetraphenyl ions have been used as aryl-substituted ions, with only one exception.[11] A series of studies[13-15] deal with some quaternary phosphonium ions, $Bu_{4-n}Ph_nP^+$.

The hydration of these phosphonium ions might be influenced by two factors: (a) influence on the structure of the solvent water and (b) the interaction between the central atoms and water separated from the bulk of water. The effect of (b) might depend upon the nature of substituents as well as that of the central atom.

The present work was undertaken anticipating that the interaction with water separated from the bulk water would become conspicuous in a system containing water dissolved in a non-aqueous solvent. The methods used in this study are distribution equilibrium and ^1H NMR spectroscopy.

Experimental

Materials. All the phosphonium salts were synthesized from the phosphines except for commercial Ph_4PCl (DOTITE) and Ph_4AsCl. The synthesis, purification and purity of these salts are similar to those reported.[13] Water was redistilled after ion exchange. Chloroform was distilled just before use after being treated with aqueous solution of Na_2CO_3 and then with water. The other chemicals were all of G.R. grade.

Procedure. Distribution equilibria were attained by shaking chloroform solution of known concentration of phosphonium bromide with an equal volume of an aqueous solution of sodium bromide in an air-thermostat, the temperature being regulated to 25±0.5 °C. The concentration of NaBr was 0.08 and/or 0.125 mol dm^{-3}. The initial concentration of the phosphonium salts in chloroform phase was in the range 5×10^{-3}—2×10^{-1} mol dm^{-3}. The shaking time was 45 min, the same results being obtained by shaking for 20 min. The aliquots of the equilibrated chloroform phases were subjected to measurements for water content and ^1H NMR of water in the phase. The aqueous phases were analyzed for phosphonium salts. An aliquot of the aqueous phase was diluted and a part of it was transferred to a neutral aqueous solution containing sodium bromide (0.1 mol dm^{-3}) and Methyl Orange in a large excess in comparison with the phosphonium bromide (below 5×10^{-5} mol dm^{-3}). Phosphonium ion was then extracted into a fresh chloroform phase in a form of 1 : 1 ion-pair with the anion of Methyl Orange. The molar absorption coefficient of the ion-pair at 415 nm is around 2.6×10^5 dm^3 mol^{-1} cm^{-1} in chloroform for all the phosphonium salts examined. Lambert-Beer's law holds. All the phosphonium ions seemed to be almost quantitatively extracted into chloroform. For the sake of confirmation the standard solutions of each phosphonium salt were treated under the same conditions for calibration.

Measurement. The water contents in the chloroform phases were determined by Karl Fischer's method with a Hirama Rika recording automatic titrator.

The ^1H NMR spectra were obtained on a Hitachi R-20 (90MHz) spectrometer, equipped with a temperature controller. All the solutions were measured at 25±0.5 °C with the probe temperature established by a standard methanol calibration. Tetramethyl silane (TMS) was used as an internal standard at a concentration of 0.3% (v/v). The chemical shift for each solution is the mean from a minimum of three scannings for each solution.

Solubility of NaBr in Chloroform. The solubility of NaBr in chloroform was tested as follows: A 50 cm^3 volume

of chloroform was shaken with 0.125 mol dm^{-3} aqueous solution of NaBr, 30 cm^3 of the chloroform phase being separated and evaporated at room temperature in the dark, no residue remained. After adding of 10 cm^3 water titration was carried out with silver nitrate solution. No titrant was consumed.

Results

Water Content in Chloroform Phase. For all the onium salts examined, the water concentration in the organic phase increases linearly with increase in the analytical concentration of a given onium salt in the phase. Examples for Bu_2Ph_2PBr and Ph_4PBr, the ionic strength of aqueous phase being 0.125 (NaBr), are shown in Fig. 1. The linear relation between water concentration in the organic phase and the salt concentration indicates two kinds of water species, (a) free water dissolved in the solvent and (b) hydrated water accompanied by the onium salt. The average hydration number of the phosphonium salt is constant and nearly independent of its concentration in the organic phase. The average hydration number, α, for some onium salts (Table 1) was determined from the slopes of the straight lines in Fig. 1. For both aqueous phases of ionic strength of 0.08 and 0.125, the α values agree with each other within experimental error as expected, since the water activities for both ionic strengths are nearly the same, *i.e.*, 0.997 and 0.996 for aqueous solutions of NaBr of 0.08 and 0.125 mol dm^{-3}, respectively, evaluated from osmotic coefficients of NaBr at 25 °C in water.[16]

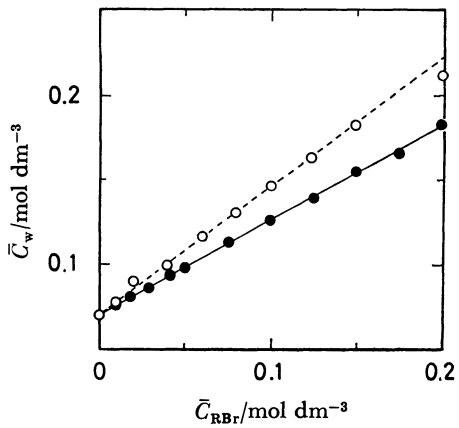

Fig. 1. The water concentration, $\bar{c}_w$, in chloroform phase equilibrated with aqueous phase of an ionic strength of 0.125 (NaBr), as a function of the analytical concentration of phosphonium bromide, $\bar{c}_{RBr}$, in the organic phase, at 25 °C. The open circles are for Ph_4PBr and closed circles, for Bu_2Ph_2Br.

Chemical Shift of Water Proton in Chloroform Phase. Single resonance of water proton is found in the ^{1}H NMR spectra of organic solutions of onium salts equilibrated with aqueous phase. Equilibrium is established in the organic phase between free water and hydrated water through a rapid exchange reaction in the NMR time scale. The observed chemical shifts are obtained for averaged proton by the process

$$H_2O(\text{hydrated}) \rightleftharpoons H_2O(\text{free})$$

and we thus have

$$\delta = x_f\delta_f + x_h\delta_h, \quad (1)$$

where δ is the observed chemical shift, x_f the fraction of the free water, δ_f the chemical shift of free water proton and subscript h refers to the hydrated water.

The chemical shift of free water proton in the presence of phosphonium salt would differ from that in the absence of the salt. The salt effect on the ^{1}H chemical shift can be expressed by

$$\delta_f = \delta_f^\circ + F(\bar{c}), \quad (2)$$

where $F(\bar{c})$ is a function of the gross concentration of a given salt and δ_f° the chemical shift of free water proton in the absence of the salt. In order to understand the F-function, the chemical shifts of water proton in chloroform phase were measured in the presence of hexane, butyl bromide, benzene, and chlorobenzene. The water concentration in these solutions was 0.0665 mol dm^{-3}, the same for all runs, the ratio to water solubility being *ca.* 0.9. The results are shown in Fig. 2.

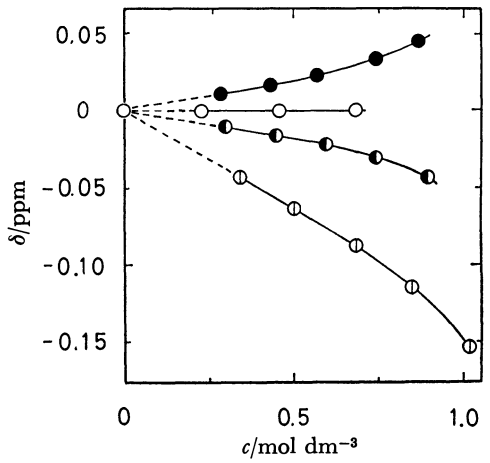

Fig. 2. Chemical shift of water proton in chloroform solutions of some solutes; butyl bromide (●), hexane (○), chlorobenzene (◐), and benzene (◑), as a function of solute concentration, at 25°C. The shifts are relative to that of water in pure chloroform at a concentration of 0.0665 mol dm^{-3}.

The ^{1}H chemical shifts of water are expressed by the relative value to that of water proton in pure chloroform measured against internal TMS. A linear relation with respect to the solute concentration holds for each solution, at least up to near 0.7 mol dm^{-3}. Equation 2 can thus be simplified to

$$\delta_f = \delta_f^\circ + \beta\bar{c}, \quad (3)$$

where β is a constant for a given salt. The hydrated water concentration is given by $\alpha\bar{c}$, x_h being equal to $(1-x_f)$ by definition. Combining Eqs. 1 and 3, we have

$$\delta = x_f\delta_f^\circ + (1-x_f)\left(\delta_h + \frac{\beta}{\alpha}\bar{c}_0\right), \quad (4)$$

where $\bar{c}_0$ is the solubility of water in chloroform (0.072 mol dm^{-3}, 25 °C). Since the last term in the second brackets is a constant for a given onium salt by the

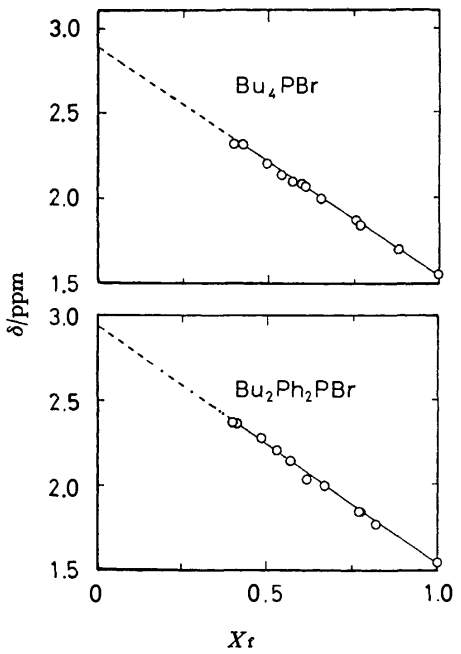

Fig. 3. ^1H chemical shifts of water in chloroform solutions of phosphonium bromides against internal TMS as a function of the fraction of free water to the total of water in the solution, at 25 °C.

Table 1. The ^1H chemical shifts of water solvated to phosphonium salts in chloroform, at 298 K

Salts	δ_h^f/ppm[a]	α[b]
Bu_4PBr	2.89	0.50
Bu_3PhPBr	2.90	0.52
Bu_2Ph_2PBr	2.92	0.55
$BuPh_3PBr$	2.85	0.67
Ph_4PBr	2.79	0.77
Ph_4PNO_3[c]	3.01	0.84
Ph_4PCl[d]	3.10	1.09
Ph_4AsBr	2.75	0.79

a) Average chemical shifts from protons of hydrated water, measured against internal TMS (see text). b) Average hydration number. c) Ionic strength of aqueous phase was adjusted by $NaNO_3$ (0.125). d) Ionic strength of aqueous phase was adjusted by NaCl(0.125).

above assumption, the plots of the observed chemical shifts against the free water fraction should give straight lines. Some of the plots are shown in Fig. 3, in which linearity holds. The values for the second brackets in Eq. 4 are obtained from the intercepts of these straight lines with the ordinate (Table 1).

The resonance of water proton, in the absence of salt in the chloroform phase, shifts gradually to high-field by dilution, *viz.*, 1.55, 1.54, and 1.51 ppm (relative to internal TMS) at water concentrations of 0.072, 0.036, and 0.014 mol dm^{-3}, respectively. It seems that the free water slightly associates in chloroform at the free water concentration of 0.072 mol dm^{-3}.

Distribution Ratios of Phosphonium Bromides at Zero Concentration. The distribution ratio, D, of a phosphonium bromide is defined by

$$D = \frac{\bar{c}_{RBr}}{c_{RBr}}, \quad (5)$$

where $\bar{c}_{RBr}$ and c_{RBr} are the analytical concentrations of the salt in the chloroform phase and in the aqueous phase, respectively. As an example, the distribution ratios of Bu_4PBr and Ph_4PBr are shown as a function of $\bar{c}_{RBr}$ in Fig. 4, where the ionic strength of aqueous phase is 0.125, adjusted by NaBr. From these curves the distribution ratios at zero concentration of the phos-

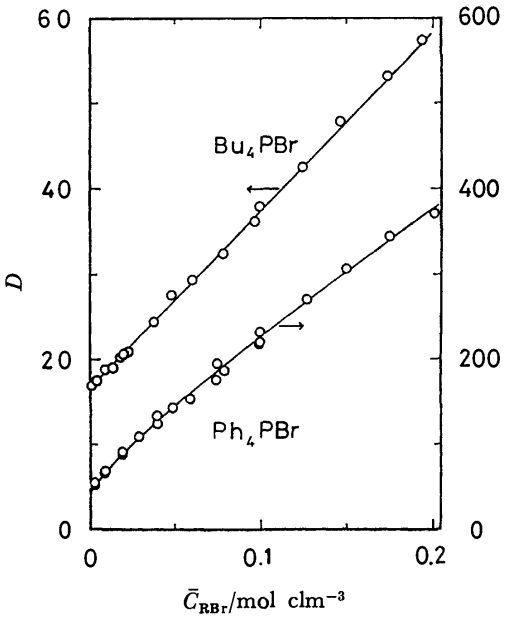

Fig. 4. Distribution ratios of phosphonium bromides between chloroform phase and aqueous phase of an ionic strength of 0.125 (NaBr) as functions of the analytical concentration of the salts in the organic phase, $\bar{c}_{RBr}$, at 25 °C.

Table 2. Hydration constants of phosphonium bromides in chloroform phase and distribution constants between chloroform and water at 298 K

		Hydration constant	Distribution constant				
			I=0.125(NaBr)		I=0.08(NaBr)		Mean value
Salts	α	K_h	D_o	$K_D\times10^{-2}$	D_o	$K_D\times10^{-2}$	$K_D\times10^{-2}$
Bu_4PBr	0.50	1.0_0	16.5	1.3	11.5	1.3	1.3
Bu_3PhPBr	0.52	1.0_8	28	2.1	18	1.9	2.0
Bu_2Ph_2PBr	0.55	1.2_2	42	3.0	30	3.0	3.0
$BuPh_3PBr$	0.67	2.0_3	41	2.1	29	2.1	2.1
Ph_4PBr	0.77	3.3_4	44	1.6	31	1.6	1.6

phonium bromides, D_o, are obtained by graphical extrapolation. These results are given in Table 2.

The D_o value is considered to be the distribution ratio for the undissociated and monomer species of the phosphonium bromide in the organic phase. The possible species in the organic phase are the dissociated ions, hydrated and non-hydrated monomer, and the aggregated species. The activity coefficients of RBr in aqueous phase are expected to be constant because of constant ionic strength in the aqueous phase. Hence, the increase in D with increase in $\bar{c}_{RBr}$ is attributed to the decrease in the activity coefficient of RBr in the chloroform phase, probably due to the aggregation of RBr[17-19]. The aggregation effect on D can be subtracted by extrapolation of D to zero concentration of RBr, the dissociation effect on D being considered insignificant. This can be judged from the behavior of D in the low concentration range of RBr. A tendency of increase in D toward zero concentration, which should be seen if the dissociation is significant, was not observed. An estimation for the degree of dissociation of RBr in chloroform phase saturated with water also supports the view. If we apply Bjerrum's equation,[20] the dissociation constant is estimated to be *ca.* 2×10^{-7} for phosphonium bromides. In the estimation the distance of closest approach is taken as 6.5 Å[21] and the dielectric constant of chloroform solution saturated with water, 5.[22] The dissociation constant thus obtained gives the degree of dissociation of the order of 0.01 at $\bar{c}_{RBr}$ of 0.001 mol dm^{-3}, which is lower than the lowest concentration examined. For dichloromethane as organic phase, the degree of dissociation is estimated as 0.14 even at 0.01 mol dm^{-3}. In fact, an increase in D for Ph_4PBr was found[25] at lower concentrations in dichloromethane.

It is reasonable concluded that the D_o values given in Table 2 are the overall distribution ratios for monomer species of hydrated and non-hydrated RBr in chloroform phase at zero concentration of RBr.

Discussion

Hydration Constant. The distribution equilibria in the present systems can be expressed as

$$H_2O \rightleftharpoons \overline{H_2O} \qquad (a)$$

$$R^+ + Br^- \rightleftharpoons \overline{RBr} \qquad (b)$$

$$\overline{RBr} + \overline{H_2O} \rightleftharpoons \overline{RBr\cdot H_2O}, \qquad (c)$$

where R^+ stands for the phosphonium ion, the bar indicating the species in chloroform phase. The aggregation process is neglected, the fact that the average hydration number is less than unity for all RBr examined being taken into account.

The hydration constant in chloroform phase, K_h, corresponding to the equilibrium (c), is given by

$$K_h = \frac{\alpha}{1-\alpha}\frac{1}{\bar{a}_w}\frac{\bar{y}_h}{\bar{y}_{RBr}}, \qquad (7)$$

where $\bar{a}_w$ is the water activity in chloroform phase, $\bar{y}_i$ the activity coefficient of species i in chloroform phase, referred to the concentration scale of mol dm^{-3}, and subscript h denotes the hydrated phosphonium bromide. With pure water chosen as a standard state for water in chloroform phase, $\bar{a}_w$ is equal to a_w. Since the water activity is close to unity, $\bar{a}_w$ is taken as unity. At infinite dilution of $\overline{RBr}$, the last factor in Eq. 7 becomes unity, and we obtain the hydration constant simply by replacing α with the numerical values given in Table 1. The hydration constants in chloroform phase at 25 °C are given in Table 2.

The K_h value increases gradually from Bu_4PBr to Bu_2Ph_2PBr and rapidly to $BuPh_3PBr$ and to Ph_4PBr. This suggests that the hydrated water molecule is stabilized through interactions with phenyl-rich cations ($n\geq3$) to a greater extent than butyl-rich cations ($n\leq1$).

Free Energy of Transfer of RBr from Water to Chloroform. In order to examine the effects of the substituent of phosphonium bromides upon distribution equilibria, it is essential to split the distribution constant, K_D, (equilibrium (b)), from the overall distribution ratios, D_o. Since the distribution ratio for the non-hydrated species of RBr in chloroform phase is given by $(1-\alpha)D$, we have

$$K_D = \frac{\bar{a}_{RBr}}{a_R a_{Br}} = \frac{(1-\alpha)D}{c_{Br}}\frac{\bar{y}_{RBr}}{\gamma^2_{RBr(NaBr)}}, \qquad (8)$$

where $\gamma_{RBr(NaBr)}$ is the mean activity coefficient of RBr in the aqueous phase in molality in the presence of NaBr, the small difference between the two concentration scales in aqueous solution being ignored. At zero concentration of RBr in the organic phase, we have

$$K_D = \frac{(1-\alpha)D_o}{c_{Br}}\frac{1}{\gamma^2_{(0)RBr}}, \qquad (9)$$

where $\gamma_{(0)RBr}$ is the activity coefficient of RBr at zero concentration in the presence of NaBr at the ionic strength of 0.08 and/or 0.125, in aqueous solution. In order to obtain the values for $\gamma_{(0)RBr}$, we need parameters, either the interaction parameters for mixed electrolyte solutions[26] or Harned's coefficients,[27] α_{ij}. So far they do not seem to have been reported. For the present purpose we can use the equation[27,28]

$$\log\gamma_{(0)MX} = \log\gamma_{(0)NX} = \frac{1}{2}\log\gamma_{MX(0)}\cdot\gamma_{NX(0)}, \qquad (10)$$

where $\gamma_{(0)MX}$ is the activity coefficient of MX at zero concentration in the presence of electrolyte, MX, at a given ionic strength, $\gamma_{MX(0)}$ and $\gamma_{NX(0)}$ being the activity coefficients of MX and NX in the pure solutions of MX and NX at the same ionic strength, respectively. The equation is found to be useful for some binary mixtures, including tetraalkyl ammonium bromides, at least for dilute solutions ($I\leq0.1$): For mixed aqueous solutions of HBr (1) and Bu_4NBr (2),[29] α_{12} are 0.3304 and 0.268 at ionic strengths of 0.1 and 0.25, respectively, which give the values 0.746 and 0.668 for $\gamma_{(0)HBr}$. Equation 10 gives the values 0.747 and 0.656, respectively. For α_{21} at ionic strength of 0.1, the reported value is −0.2057. This leads to the value 0.727 for $\gamma_{(0)Bu_4NBr}$, which is less by only 3% than the value estimated by means of Eq. 10. In the mixed solutions of KBr and $(C_3H_7)_4NBr$,[30] $\gamma_{(0)Pr_4NBr}$ values are determined to be 0.748 and 0.594 at ionic strengths of 0.1 and 0.5,

respectively, Eq. 10 giving 0.736 and 0.561, respectively.

By assuming Eq. 10, we can rewrite Eq. 9 as:

$$K_D = \frac{(1-\alpha)D_o}{a_{\pm(NaBr)}} \frac{1}{\gamma_{RBr(0)}}. \quad (11)$$

Since no activity coefficients for RBr in each of the pure solutions are known, some estimations must be made. Use of the activity coefficient of Bu_4NBr might be a good approximation for Bu_4PBr. The γ_{Bu_4NBr}[30] in aqueous solution at 25 °C fits the Debye-Hückel limiting law up to moderate concentration; *e.g.*, the deviations from the law amount to only 0.6% at 0.1 and 5% even at 0.4 mol dm^{-3}, though the consistence is regarded as accidental.[23] Thus, we obtain the value of 1.3×10^2 for K_D, which is common to both systems with different ionic strengths. For other phosphonium bromides, the limiting law was also applied to obtain $\gamma_{RBr(0)}$. The K_D values thus obtained are given in Table 2. The agreement between two values for K_D at different ionic strengths is good in spite of a considerable difference between D_o values. This supports the validity of the assumption.

From K_D, we obtain the free energy of transfer for RBr (non-hydrated in chloroform) from water to chloroform at 25°, $\Delta G_{C\leftarrow W}$, by means of

$$\Delta G_{C\leftarrow W} = -RT \ln K_D,$$

where a hypothetical solution of 1 mol dm^{-3} in each phase is taken as the standard state for RBr.

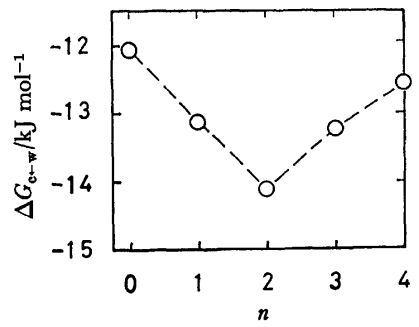

Fig. 5. The free energy of transfer for $Bu_{4-n}Ph_nPBr$ from water to chloroform as a function of n, at 25 °C. The standard state is taken as a hypothetical solution of 1 mol dm^{-3} of the salt.

$\Delta G_{C\leftarrow W}$ is shown as a function of n in Fig. 5. No additivity of group contributions to $\Delta G_{C\leftarrow W}$ is found; $\Delta G_{C\leftarrow W}$ is the lowest for Bu_2Ph_2PBr. This might be related to hydration processes in the aqueous phase, since there is no reason to expect that, of the phosphonium bromides, Bu_2Ph_2PBr interacts most effectively with the solvent chloroform. The state of cosphere water of phenyl groups differs from that of butyl groups. Different types of cospheres coexist in each cation with n=1—3. Thus, we find the interpretation for the variation of $\Delta G_{C\leftarrow W}$ with n in terms of the statement by Friedman and Krishnan:[2] adjacent cospheres interfere with each other so that the overall solvation is less energetic than one might guess from the properties of separate cospheres.

State of Hydration Water. Comparing δ'_h with the hydration number (Table 1), we find: (1) As found in a series of Ph_4PX's, δ'_h increases (low-field shift) in the order X^-, Br^-, NO_3^-, Cl^-, in accordance with that of the average hydration number; (2) with respect to a series of phosphonium bromides, the low-field shift remains nearly constant or gradually increases from Bu_4PBr to Bu_2Ph_2PBr with gradual increase in hydration number, and decreases to $BuPh_3PBr$ and to Ph_4PBr in spite of rapid increase in the hydration number (Fig. 6).

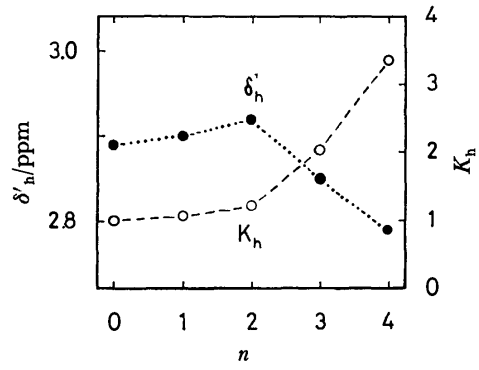

Fig. 6. ^1H chemical shift of water solvated to $Bu_{4-n}Ph_nPBr$ in chloroform phase and their hydration constants, as function of n, at 25 °C.

We infer from (1) that the hydrated water is hydrogen-bonded with anions of the phosphonium salts. Since the δ'_h values are the average values from two protons of hydrated water molecule, the chemical shift for the proton which participates in hydrogen bond, δ°_h, is roughly estimated from δ'_h by the relation

$$\delta^\circ_h = 2\delta'_h - \delta^\circ_f,$$

where assumptions are made that the chemical shift for the other proton is equal to that of non-hydrated water, the correction factor, $\bar{c}_o\beta/\alpha$, being relatively small as expected from Fig. 2. The values for δ°_h are, for example, 4.0, 4.4, and 4.7 ppm (against TMS), for Ph_4PBr, Ph_4PNO_3, and Ph_4PCl, respectively.

Let us examine the salt effect upon the chemical shift of free water proton: (a) polarization of free water due to the salts as electric dipoles, and (b) magnetic anisotropy due to phenyl groups and polarization of free water due to charges located on the phenyl groups. Effect (a) leads to the net low-field shift of free water proton (Fig. 2), the effect being expected to nearly the same degree for all onium bromides examined since their molal volumes are nearly the same[13] while effect (b) due to phenyl rings leads to net high-field shift. With the present onium salts, however, the phenyl groups may differ from benzene or chlorobenzene as regards their interactions with water because of geometric effects and charge delocalization effects. The π-electron donation from phenyl groups to phosphorus d-orbitals of quaternary phosphonium salts was shown by Gim and McFarlane.[8] The charge delocalization for Ph_4P^+ ion was estimated to be 0.18 electron unit per phenyl group.[9] When a water molecule is situated in the vicinity of the peripheries of phenyl rings, it will undergo deshielding effects due to the local magnetic

field of phenyl rings as well as possible polarization induced by delocalized charges. In contrast, high-field shift should be observed when the water molecule is located so close to the central atom that the proton undergoes the diamagnetic effect due to phenyl rings. In this case, however, the water molecule is not regarded as "free," but "hydrated." Onium salts lead to deshielding free water protons.

We can conclude from (2) that the hydrated water molecule interacts not only with anions but with cations, especially with phenyl-rich cations ($n \geq 3$), as evidenced by relatively large hydration constants for these salts. Starting with Bu_4PBr, we find the most favorable site for water molecule at $BuPh_3PBr$, since it is free from steric hindrance by butyl groups. For butyl-rich salts, no sites of this kind are available and thus their hydration constants are expected to be nearly the same.

The hydration constant for Ph_4AsBr seems to be somewhat larger than that for Ph_4PBr, in accordance with the less low-field shift for the former. This is consistent with the results obtained by Orenberg *et al.*[10]

References

1) A part of this paper was presented at the 40th National Meeting of the Chemical Society of Japan, Fukuoka, October, 1979.

2) H. L. Friedman and C. V. Krishnan, "Water," ed by F. Franks, Plenum Press (1973), Vol. 3, Chap. 1.

3) G. Kalfoglou and L. H. Bowen, *J. Phys. Chem.*, **73**, 2728 (1969).

4) C. Jolicoeur, N. D. The, and A. Cabana, *Can. J. Chem.*, **49**, 2008 (1971).

5) C. Jolicoeur, P. R. Philip, G. Perron, P. A. Leduc, and J. E. Desnoyers, *Can. J. Chem.*, **50**, 3167 (1972).

6) C. Jolicoeur and P. R. Philip, *J. Solution Chem.*, **4**, 3 (1975).

7) J. F. Coetzee and W. R. Sharpe, *J. Phys. Chem.*, **75**, 3141 (1971).

8) S. O. Gim and W. McFarlane, *Can. J. Chem.*, **46**, 2071 (1968).

9) E. Grunwald, G. Baughaman, and G. Kohnstam, *J. Am. Chem. Soc.*, **82**, 5801 (1960).

10) J. B. Orenberg, M. D. Morris, and C. V. Long, *Inorg. Chem.*, **10**, 933 (1971).

11) C. V. Krishnan and H. L. Friedman, *J. Phys. Chem.*, **73**, 3934 (1969).

12) K. Takaizumi and T. Wakabayashi, *Bull. Chem. Soc. Jpn.*, **49**, 2194 (1976).

13) K. Takaizumi and T. Wakabayashi, *J. Solution Chem.*, in press.

14) K. Takaizumi and T. Wakabayashi, *J. Solution Chem.*, in press.

15) T. Wakabayashi, K. Takizumi, and M. Yamamoto, Presented at the 40th National Meeting of the Chemical Society of Japan, Fukuoka, October, 1979.

16) R. A. Robinson and R. H. Stokes, "Electrolyte Solutions," 2nd ed, Butterworths (1970), p. 483.

17) Y. Marcus and A. S. Kertes, "Ion Exchange and Solvent Extraction of Metal Complexes," Wiley-Interscience (1969), Chap. 10.

18) T. Kato and T. Fujiyama, *Bull. Chem. Soc. Jpn.*, **51**, 1328 (1978).

19) J. S. Fok, Z. Z. Hugus, and E. B. Sandell, *Anal. Chim. Acta*, **48**, 243 (1969).

20) N. Bjerrum, *K. Danske Vidensk. Selsk.*, 7 (1926) No. 9; "Selected Papers," Einar Munksgaard, Copenhagen (1949), p. 108; Ref. 16, Chap. 14.

21) Stokes' radius for Ph_4P^+ is taken as 4.6 Å[3] and the ionic radius of Br^- as 1.95 Å.

22) The dielectric constant for chloroform, ε_r, is taken as 4.9[17] (25 °C) and the increment in ε_r due to water (0.072 mol dm^{-3}) was estimated as 0.1 from equations taken from: J. B. Hasted, "Water," ed by F. Franks, Plenum Press (1973), Vol. 2, Chap. 7.

23) The $\gamma_{R,NX(0)}$ values are considerably affected by the anion (X), and to some extent by the chain-length of alkyl groups. *Cf.* J. E. Desnoyers, M. Arel, G. Perron, and C Jolicoeur, *J. Phys. Chem.*, **73**, 3346 (1969).

24) R. M. Fuoss and C. A. Kraus, *J. Am. Chem. Soc.*, **55**, 1019 (1933).

25) The results obtained by a preliminary experiment.

26) H. L. Friesman, *J. Chem. Phys.*, **32**, 1134; 1351 (1960); H. L. Friedman, "Ionic Solution Theory," Interscience (1962).

27) H.S. Harned and B. B. Owen, "The Physical Chemistry of Electrolyte Solutions," Reinhold Publishing Corporation (1950), Chap. 14.

28) Ref. 16, Chap. 15.

29) R. N. Roy, J. J. Gibbons, C. Krueger, and T. White, *J. Chem. Soc., Faraday Trans. 1*, **72**, 2197 (1976).

30) W. Y. Wen, K. Miyajima, and A. Otsuka, *J. Phys. Chem.*, **73**, 3346 (1969).

  Bull. Chem. Soc. Jpn., 54, 957—961 (1981)

Photoelectrochemical Behavior of Chlorophyll a-Lipid Films on a Platinum Electrode in an Aqueous Electrolyte

Tsutomu MIYASAKA,* Akira FUJISHIMA, and Kenichi HONDA

Department of Synthetic Chemistry, Faculty of Engineering, The University of Tokyo, Hongo, Bunkyo-ku, Tokyo 113

(Received March 19, 1980)

The photoelectrochemical behavior of chlorophyll a-lipid mixed monolayers coated on a platinum electrode by the Langmuir-Blodgett technique was investigated under potentiostatic conditions in an aqueous electrolyte in the absence of redox agents. Under illumination, cathodic photocurrents were observed at electrodes coated with a sufficient number of monolayers. The quantum efficiency of the photocurrent was estimated to be about 10^{-4}, much lower than that obtainable for dye-sensitized photocurrent on semiconductor electrode. The cathodic photocurrent increased with lowering in the pH of electrolyte. The possibility of the photoreduction of water by excited triplet chlorophyll a is discussed on the basis of observed pH dependence and correlation of the redox potentials involved.

During the last decade an increasing number of studies have appeared on the photoelectrical and photoelectrochemical behavior of chlorophyll (Chl) in the form of solid layers coated on metal electrodes.[1-13] The photoconductive nature of solid Chl films in various forms, such as amorphous layers,[1,3,5] microcrystals,[2,4,5] and monolayer assemblies,[6,7] in contact with metal substrates has been established by the use of metal/Chl/metal sandwich-type photovoltaic cells. However, the organic semiconductivity inherent to solid-state Chl, postulated for the microcrystalline films[2,14] in order to explain the photoelectrical rectifying effects at metal/Chl contacts, is the subject of controversy;[4,15] in particular, it seems unlikely for the monolayer assemblies.[6,16,17] In photoelectrochemical cells employing metal electrodes (mostly platinum) coated with various forms of Chl films,[8-13] cathodic photocurrents have usually been obtained, presumably reflecting the *p*-type semiconduction formed within a bulk Chl layer. Water splitting reactions with use of Chl-coated platinum photocathodes have been demonstrated by several groups.[10,13] Such behavior is in contrast to the case of Chl-coated *n*-type semiconductor electrodes which produce anodic sensitized photocurrents.[18,19]

According to the principles of dye sensitization processes, the photocurrent of dye molecules adsorbed on a metal electrode should be incomparably less efficient than that obtained at a semiconductor electrode, owing mainly to the rapid energy quenching of dye excited states by free electrons in the metal, as reported by Memming[20] and Gerischer and Williug.[21] Ample efficiency for dye-sensitized photocurrent on a metal electrode could thus be expected in cases where the dye layer is thick enough to develop the bulk effects such as *p*-type photoconductivity. Typical of this case are solid films of metal phthalocyanines[22] and porphyrins[23] which are regarded as *p*-type organic semiconductors.

Reports have been given on the anodic sensitized photocurrents obtained for various monolayer assemblies (Langmuir-Blodgett films) of Chl coated on an SnO_2 semiconductor electrode,[19,24-26] where quantum efficiency of the photocurrent was investigated as a function of the surface concentration of Chl[19,24] and thickness of the monolayers.[25] For such a Chl-sensitized semiconductor photoanode, it was confirmed that the single monolayer film of Chl that is amply diluted in the surface concentration gives the highest quantum efficiency (≤ 0.25) for photocurrent generation.[26]

By means of the Langmuir-Blodgett technique which allows a precise and uniform control of the film thickness, we have investigated the photocurrent behavior at the thin monolayer assemblies of a Chl-lipid mixture on a platinum electrode. The behavior observed in this system, such as photocurrent-potential characteristics, pH dependence of photocurrent, and effect of the film thickness was found to be in contrast to the corresponding observations in a Chl multilayer/semiconductor system.[25]

Experimental

Pure Chl a was obtained from spinach leaves in the usual manner.[19] L-α-Dipalmitoyllectithin (DPL from Sigma Chemical.) was employed as a two-dimensional diluent for a Chl a monolayer,[24] in order to keep Chl a from possible photodegradation[27] as well as to suppress the energy dissipation within layers due to the concentration quenching characteristic of Chl a molecules.[28] A monomolecular layer consisting of Chl a and DPL at molar ratio 1/1 was prepared, using benzene as a spreading solvent, on an aqueous phosphate buffer (pH$\approx$ 8) in a Langmuir trough. The monolayers were then deposited on the surface of a platinum electrode substrate (0.05 mm thick, 2.5×2.5 cm^2), which had been treated with several organic solvents and hot sulfuric acid to make the surface hydrophilic, by serial dipping of the substrate across the supernatant monolayer under a surface pressure of 20 dyn cm^{-1} (1 dyn$=10^{-5}$ N); each monolayer coated on the substrate was vacuum-dried prior to the subsequent deposition. The deposition ratio for the Chl a–DPL mixed monolayer with respect to the platinum surface area was 0.7—1.0, indicating that the film was packed less densely on the electrode than on the water.[29]

Sodium sulfate (reagent grade) dissolved in doubly distilled water, 0.1 M (1 M$=1$ mol dm^{-3}), was used as a neutral electrolyte except when H_2SO_4 and/or NaOH was added for pH variation. The electrolyte solution was flushed with nitrogen which had been deoxygenated by passing over an activated copper column. The electrochemical cell employed was of one compartment including three electrodes; the potential of the Chl a–DPL film-coated platinum electrode was regulated with a Hokuto Denko Model HA-101 potentiostat, using a saturated calomel electrode (SCE) and a platinum wire as a reference electrode and a counterelectrode, respectively. Photo- and dark currents were measured on a Keithley Model 610 B

picoammeter. The light source was a 500-W Xe arc lamp in combination with a grating monochromator. The observed photocurrents were corrected for incident photon flux, corresponding to *ca.* 1.2×10^{16} photons s^{-1}. For details of the experimental setup as well as the monolayer deposition technique, refer to the previous paper.[19]

Results and Discussion

Photocurrent Characteristics. When a single Chl a-DPL monolayer on the platinum electrode was illuminated, almost no significant photocurrent was observed. This can be ascribed to the rapid energy-quenching of excited Chl a by free electrons in the metal[20,21] as well as to a reversible and simultaneous exchange of electrons *via* the metal/Chl a interface (no rectifying property). The former phenomenon, mainly responsible for the minimal photocurrent, has been elucidated by Kuhn[30] on the basis of fluorimetric studies.

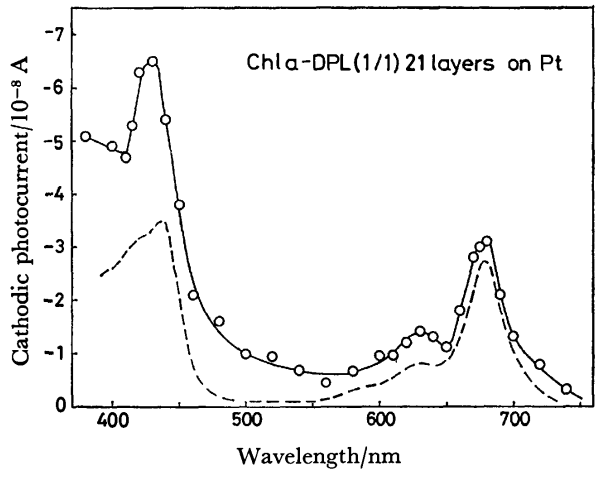

Fig. 1. Photocurrent action spectrum for Chl a-DPL (1/1) film consisting of 21 monolayers on a platinum electrode. Electrolyte, 0.1 M Na_2SO_4 (pH *ca.* 7); electrode potential, 0 V *vs.* SCE. The broken line shows the absorption spectrum of Chl a multilayer at solid-electrolyte interface in arbitrary units.[25] Photocurrent (solid line) is for the total area illuminated on the electrode (*ca.* 5 cm^2). Photocurrents plotted in figures hereinafter show an experimental error of *ca.* $\pm0.3\times10^{-8}$ A.

Electrodes coated with more than several monolayers were found to develop significant cathodic photocurrents upon illumination. Figure 1 shows the photocurrent action spectrum obtained for a film consisting of 21 monolayers with an absorption spectrum of a pure Chl a multilayer[25] for comparison. Apparently the cathodic photoresponse follows the absorption of Chl a, showing peaks at around 680 nm and 430 nm in the red and blue bands, respectively. The observed action spectrum suggests that the monomeric form of Chl a is the main species participating in the present photoelectrochemical reaction. No significant changes due to the formation and photochemical involvement of the hydrated Chl species absorbing in the far-red region (≈740 nm)[2,4,5,12,13] was detected, at least not in the action spectrum.

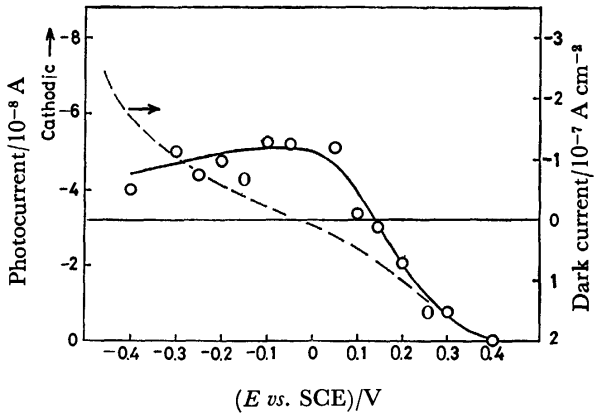

Fig. 2. Photocurrent-potential characteristics.
—○—: Photocurrent, ----: dark current. Illumination at 675 nm. Film and electrolyte composition are the same as in Fig. 1.

Figure 2 shows the dependence of the photocurrent on electrode potential. Cathodic photocurrent, *i.e.*, electron injection from the Pt/Chl a electrode to the solution, occurred at potentials more negative (cathodic) than +0.4 V *vs.* SCE, increasing with cathodic polarization until it became saturated at around 0 V.

Generation of cathodic photocurrent can be interpreted schematically in terms of the electron donation from excited Chl a molecules at the film-electrolyte interface to some reducible species (A) in the electrolyte and the subsequent reduction of the produced Chl a cation radical by free electrons of the electrode, namely,

$$\text{Chl a} \xrightarrow{h\nu} \text{Chl a}^* \quad (1)$$

$$\text{Chl a}^* + \text{A} \longrightarrow \text{Chl a}^+ + \text{A}^- \quad (2)$$

$$\text{Chl a}^+ + e^-_{Pt} \longrightarrow \text{Chl a}. \quad (3)$$

Such a mechanism is substantially the same as that proposed for an electron transfer process involved in dye sensitization on a *p*-type semiconductor photocathode.[31] The above reaction, however, hardly proceeds if the dye layer on a metal is not as thick as several monolayers, because of the quenching phenomenon as well as the absence of rectifying properties. This differs from the case of semiconductor electrode surface where only monolayer-thick adsorption of dye is sufficient to develop a considerable efficiency of photocurrent. In the semiconductor electrode, electron flow is rectified *via* the space charge layer in which energy transferred from the dye, if any, can be utilized for charge separation which leads to photocurrent generation. If, however, the dye layer on a metal is of sufficient thickness, the photooxidation of Chl a with an acceptor in solution (Eq. 2) can take place at the film/electrolyte interface where the quenching of excited dye by the metal can be suppressed by the spatial separation of its interface from the metal surface. The photooxidized Chl a may subsequently be reduced by electrons which migrate from the metal surface by hopping through the dye layer. Another reaction mechanism, applicable to the *p*-type semiconductor/dye interface, which involves the direct reduction of excited-state Chl a by electrode at the metal/film interface (Chl $a^*+e^-_{Pt}\rightarrow$

Chl a^{+}) is unlikely since reoxidation of Chl a^{+} into Chl a would occur simultaneously at the metal surface.

The proposed mechanism is compatible with the fact that the onset potential for the cathodic photocurrent, 0.4 V *vs.* SCE, was observed at a somewhat more negative potential than the oxidation potential of the ground state Chl a, *ca.* 0.54 V *vs.* SCE,[32] since the reaction process of reducing Chl a cation radical (Eq. 3) is expected to be promoted at potentials $<$*ca.* 0.54 V on an electrochemical basis. According to the mechanism, the observed onset potential further implies that the oxidation potential of Chl a, which has so far been estimated in nonaqueous media on account of the insolubility of Chl, would be situated at $\geq$0.4 V *vs.* SCE in the monolayer assembly in contact with an aqueous electrolyte.

In the present system, semiconduction in the solid Chl film is not important to explain the observed photoeffect because the monolayer assemblies of Chl are generally not regarded as good semiconductor materials,[16,17] unlike the amorphous or microcrystalline films which display significant photoconductivity.[1,2,5] It should be noted that the Chl a monolayers studied here were doped with lipid molecules which diminish the Chl–Chl electronic interaction needed for the developing of photoconduction.

A blank test was carried out by irradiating a platinum electrode free of Chl a with 680 nm and 430 nm light. No photocurrent was detected at electrode potentials below +0.4 V *vs.* SCE. A slight anodic photocurrent was detectable under 430 nm irradiation at *ca.* 0.4 V, but this intrinsic photoresponse of platinum was within experimental error and is negligible.

Effect of Film Thickness. The magnitudes of the cathodic photocurrents for various numbers of layers on the platinum were compared at an applied elecrode potential of 0 V *vs.* SCE where the photocurrent tends to be saturated (Fig. 2). The results are summarized in Fig. 3.

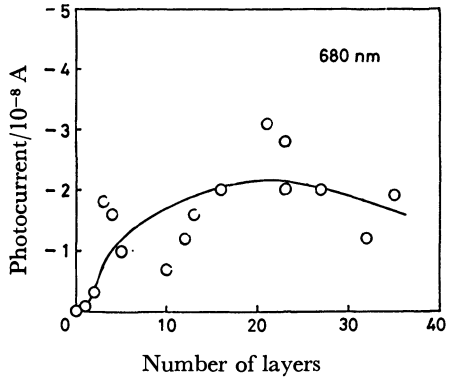

Fig. 3. Relation between cathodic photocurrent and the number of layers deposited on the platinum electrode. Illumination at 680 nm. Electrolyte, 0.1 M Na_2SO_4; electrode potential, 0 V *vs.* SCE.

No significant photocurrent was observed with a single monolayer film. Photocurrent, however, increased with an increase in the number of layers (*i.e.*, total film thickness), reaching a maximum at 20—30 layers. The increase may result from the spatial separation of the film/solution interface participating in the photooxidation reaction of Chl a with an acceptor in the electrolyte (Eq. 2) from the metal/film interface involved in the dark electron transfer (Eq. 3). Such a separation of the two interfaces by stacking a sufficient number of monolayers would thus suppress the energy dissipation of dye excited at the film/electrolyte interface due to energy transfer as well as back electron transfer[33] toward the metal. The observed saturation of photocurrent above 20 layers may be due to the increased electrical resistance within the film.

The quantum yields of steady state cathodic photocurrents obtained for 20—30 layers, estimated taking into account the surface reflectance of platinum (*ca.* 0.7) with respect to incident light, are of the order 10^{-4} electron/photon. This is incomparably lower than the value, 10^{-1} electron/photon, reported for dye-sensitized cathodic photocurrents at a *p*-type semiconductor.[31] Such a low efficiency is apparently due to the minimal rectifying properties of the metal electrode. Using platinum electrodes coated with microcrystalline Chl a aggregates, Fong and co-workers have reported relatively efficient cathodic photocurrents[12] and claimed evidence for water splitting reaction.[13] However, it is presumed that the electrodes used in their system, prepared by drastic treatments of the surface Chl a layers with repeated platinizations,[13] may involve a certain photocatalytic effect ascribed to some Chl a-Pt composite and the observed phenomena cannot be attributed simply to the light reaction of Chl aggregate itself.

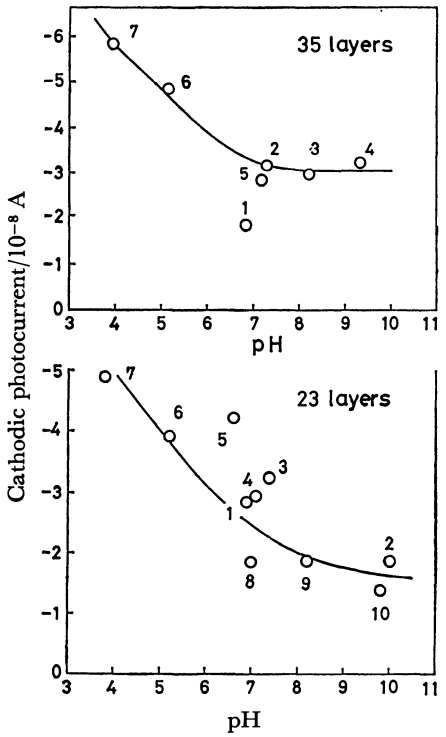

Fig. 4. Dependence of cathodic photocurrent on electrolyte pH. 35 layers and 23 layers on the platinum were examined under the same experimental conditions as in Fig. 3. The numbers on the plots stand for the experimental sequence.

Effect of pH on Photocurrent. The pH dependence of the photocurrent was investigated in order to clarify the nature of acceptor species involved in the photooxidation reaction of Chl a. Figure 4 shows the results obtained for films of 23 and 35 monolayers under a constant electrode potential of 0 V *vs.* SCE. In both cases, cathodic photocurrents tend to increase with lowering in pH. The increase occurs at pH's $<$*ca.* 7. Since the redox potential of Chl a can be regarded as almost independent of pH, the behavior clearly indicates that some protonic oxidant in the solution acts as an electron acceptor for excited Chl a. After a series of pH variation, an attempt was made to check the chemical degradation of Chl a by dissolving the illuminated samples in benzene. No significant change assigned to decomposed Chl a species, such as pheophytin, could be detected in the absorption spectrum, indicating that the chemical changes in Chl a during the course of pH variation is almost negligible.

In order to discuss the photooxidation reaction of Chl a with an acceptor, involvement of two donor states of Chl a, excited singlet and excited triplet states, should first be taken into account. It is known that the photoionization of Chl a by reaction with a redox agent in solution takes place exclusively *via* the excited triplet state, a long-lived species with a lifetime of *ca.* 2 ms.[34] A variety of oxidants[35] has thus far been found to react with the triplet state of Chl a producing Chl a radical cations. Using photovoltaic cells, Janzen and Bolton[6] found a large contribution of triplet state Chl a to the reduction of acceptor species immobilized in monolayer assemblies. Consequently, it is reasonable to assume that in the present system the photooxidation of Chl a (Eq. 2) takes place *via* the triplet state, from the viewpoint that an amply long lifetime of the excited state is needed to achieve the reaction with a dilute oxidant diffusing from the bulk of solution.

If we assume that the electrolyte used contains no impurities that can act as electron acceptors, water (proton) is the only possible oxidant involved because it can be reduced on an energetic basis by both the singlet and triplet excited states of Chl a which have oxidation potentials of -1.31 V and -0.79 V *vs.* SCE,[32] respectively. Here, the oxidation potential of the triplet state Chl a, the predominant species involved in the photooxidation process, is situated somewhat negative of the reduction potential of water at pH 7, namely -0.66 V *vs.* SCE. This suggests that the triplet Chl a cannot reduce water very efficiently in neutral solutions because of a rather small free energy change (overpotential). Since the lowering of pH brings about a positive shift in water redox potential which facilitates the reaction of triplet Chl a with a proton, the observed increase in photocurrent at pH's below 7 might result from the reduction of water by the excited triplet Chl a.

In contrast with the result shown in Fig. 4, the reverse behavior in pH dependence has been obtained with a Chl a multilayer-coated SnO_2 *photoanode*[25] using a similar electrolyte to that of the present system. Anodic sensitized photocurrent of Chl a observed was found to increase at pH's higher than 7. This was rationalized by the recognition that the oxidation potential of ground state Chl a, 0.54 V *vs.* SCE, is in the vicinity of the water oxidation potential at pH 7, 0.57 V *vs.* SCE, and the reduction by water of the Chl a cation radical produced by electron injection into SnO_2 is promoted by increasing of pH (*i.e.*, a negative shift in water oxidation potential).

The combination of both features of Chl a *photoanode* and *photocathode* in pH dependence brings us to the view that the oxidation and reduction of water by *in vitro* photoexcited Chl a, or at least by monomeric Chl a, would be difficult in *neutral* aqueous solutions owing to the absence of any overpotential (*i.e.*, free energy change) sufficient for an electron transfer reaction. Watanabe and Honda[36] have recently found that Chl a cation radical produced by electrolysis, which corresponds to the photooxidized form of Chl a produced at the photoanode, has an extremely low rate constant for the reaction with water in an organic solution, suggesting that the oxidation of water by excited Chl a is inefficient. Consequently, photosplitting of water by *in vitro* Chl a is thought to be feasible under either acidic or alkaline conditions which can promote, respectively, the photoreduction and photooxidation of water. This is in line with the demonstrations of hydrogen[10,13] and oxygen[37] evolutions at illuminated Chl electrodes with use of acidic and alkaline electrolyte solutions, respectively.

The authors wish to thank Dr. K. Itoh for his helpful discussion. This work was supported by a Grant-in-Aid from the Ministry of Education, Science and Culture.

References

1) I. S. Meilanov, V. A. Benderskii, and L. A. Blyumenfel'd, *Biofizika*, **15**, 822 (1970).
2) C. W. Tang and A. C. Albrecht, *Nature*, **254**, 507 (1975).
3) A. Ya Shkuropatov, K. B. Kurbanov, Yu. M. Stolovitski, and V. B. Yevstigneyev, *Biofizika*, **22**, 407 (1977).
4) G. A. Corker and I. Lundström, *Photochem. Photobiol.*, **26**, 139 (1977).
5) J.-P. Dodelet, J. Le Brech, and R. M. Leblanc, *Photochem. Photobiol.*, **29**, 1135 (1979).
6) A. F. Janzen and J. R. Bolton, *J. Am. Chem. Soc.*, **101**, 6342 (1979).
7) R. Jones, R. H. Tredgold, and J. E. O'Mullane, *Photochem. Photobiol.*, **32**, 223 (1980).
8) F. Takahashi and R. Kikuchi, *Bull. Chem. Soc. Jpn.*, **49**. 3394 (1976).
9) F. Takahashi, M. Aizawa, R. Kikuchi, and S. Suzuki, *Electrochim. Acta*, **22**, 289 (1977).
10) M. Aizawa, N. Suzuki, M. Hirano, and S. Suzuki, *Electrochimica Acta*, **23**, 1061 (1978).
11) J.-G. Villar, *J. Bioenerg. Biomembr.*, **8**, 199 (1976).
12) F. K. Fong, J. S. Polles, L. Galloway, and D. R. Fruge, *J. Am. Chem. Soc.*, **99**, 5802 (1977).
13) F. K. Fong and L. Galloway, *J. Am. Chem. Soc.*, **100**, 3594 (1978); D. R. Fruge, G. D. Fong, and F. K. Fong, *ibid.*, **101**, 3694 (1979).
14) A. N. Terenin, E. K. Putzeiko, and I. A. Akimov, *Discuss. Faraday Soc.*, **27**, 83 (1959).
15) T. Miyasaka and K. Honda, ACS Symp. Series 146, "Photoeffects at Semiconductor-Electrolyte Inferfaces," ed by A. J. Nozik, American Chemical Society, Washington, D. C.

(1981), p. 231.
16) K. J. McCree, *Biochim. Biophys. Acta*, **102**, 90 (1965).
17) P. J. Reucroft and W. H. Simpson, *Discuss. Faraday Soc.*, **51**, 202 (1971).
18) H. Tributsch and M. Calvin, *Photochem. Photobiol.*, **14**, 95 (1971); H. Tributsch, *ibid.*, **16**, 261 (1972).
19) T. Miyasaka, T. Watanbe, A. Fujishima, and K. Honda, *J. Am. Chem. Soc.*, **100**, 6657 (1978).
20) R. Memming, *Photochem. Photobiol.*, **16**, 325 (1972).
21) H. Gerischer and F. Willig, *Topics Curr. Chem.*, **61**, 31 (1976).
22) H. Meier, W. Albrecht, U. Tshirwitz, E. Zimmerhackl, and N. Geheeb, *Ber. Bunsenges. Phys. Chem.*, **81**, 592 (1977).
23) T. Kawai, K. Tanimura, and T. Sakata, *Chem. Phys. Lett.*, **56**, 541 (1978).
24) T. Miyasaka, T. Watanabe, A. Fujishima, and K. Honda, *Nature*, **277**, 638 (1979); **279**, 451 (1979).
25) T. Miyasaka, T. Watanabe, A. Fujishima, and K. Honda, *Photochem. Photobiol.*, **32**, 217 (1980).
26) T. Miyasaka and K. Honda, *Surface Sci.*, **101**, 541 (1980).
27) W. Stillwell and H. T. Tien, *Biochem. Biophys. Res. Commun.*, **76**, 232 (1977); K. Iriyama, *J. Membr. Biol.*, **52**, 115 (1980).
28) S. M. de B. Costa, J. R. Froines, J. M. Harris, R. M. Leblanc, B. H. Orger, and G. Porter, F. R. S., *Proc. R. Soc. London, Ser. A*, **326**, 503 (1972).
29) Compared to SnO_2 semiconducting glasses,[25] the platinum electrodes showed difficulty in depositing the monolayers with high surface concentration and uniformity of molecules.
30) H. Kuhn, *Naturwissenschaften*, **54**, 439 (1967).
31) R. Memming and H. Tributsch, *J. Phys. Chem.*, **75**, 562 (1971).
32) G. R. Seely, *Photochem. Photobiol.*, **27**, 639 (1978).
33) Electron transfer from excited dye to the metal would be accompanied simultaneously by the back electron transfer toward the oxidized dye, leading consequently to dissipation of the excitation energy.
34) N. N. Lebedev, J. Naus, and A. A. Krasnovskii, Jr., *Biofizika*, **21**, 393 (1976); A. Mau and M. Puza, *Photochem. Photobiol.*, **25**, 601 (1977).
35) J. M. Kelly and G. Porter, *Proc. R. Soc. London, Ser. A*, **319**, 319 (1970); R. G. Brown, A. Harriman, and L. Harris, *J. Chem. Soc., Faraday Trans. 2*, **74**, 1193 (1978).
36) T. Watanabe and K. Honda, *J. Am. Chem. Soc.*, **102**, 370 (1980).
37) M. Aizawa, M. Hirano, and S. Suzuki, *Electrochim. Acta*, **24**, 89 (1979).

The Crystal Structures of Hexamethyleneiminium *p*-Chlorobenzoate and Dimorphs of Hexamethyleneiminium *p*-Bromobenzoate

Setsuo KASHINO,* Norimitsu SASAHARA, Shin-ichi KATAOKA, and Masao HAISA

Department of Chemistry, Faculty of Science, Okayama University, Tsushima, Okayama 700

(Received June 12, 1980)

The crystal structures of hexamethyleneiminium *p*-chlorobenzoate (**1**), and the monoclinic [**2**(**m**)] and orthorhombic [**2**(**o**)] forms of hexamethyleneiminium *p*-bromobenzoate have been determined from visually estimated Cu $K\alpha$ data. The crystal data are: $P2_1/c$, $a=10.10(2)$, $b=16.78(1)$, $c=9.01(2)$ Å, $\beta=118.4(2)°$, $Z=4$ for **1**; C2/c, $a=25.47(2)$, $b=7.01(1)$, $c=16.29(1)$ Å, $\beta=109.1(1)°$, $Z=8$ for **2**(**m**); and Pbca, $a=11.55(1)$, $b=27.40(1)$, $c=8.57(1)$ Å, $Z=8$ for **2**(**o**). The structures of **1**, **2**(**m**), and **2**(**o**) were refined to R values of 0.072, 0.100, and 0.083 for 1628, 1009, and 1013 non-zero reflections, respectively. In the crystals of **1**, the type of hydrogen bond and the molecular arrangement in (010) plane are the same as those in piperazinediylium terephthalate. In **2**(**m**), two pairs of the base and acid ions related by a twofold axis are linked together by N–H···O hydrogen bonds. The crystal structure of **2**(**o**) is very similar to that of piperidinium and pyrrolidinium *p*-substituted benzoates in Pbca, but there is a difference in the combination mode of the base and acid ions participating in the hydrogen bonds. In all the crystals, the hydrogen bond extending along the long axis of the acid ion is shorter than that nearly perpendicular to the axis. Hexamethyleneimine rings in **1**, **2**(**m**), and **2**(**o**) take a similar twist-chair conformation.

It has been found for crystals of piperidinium and pyrrolidinium *p*-substituted benzoates that the N–H···O hydrogen bonds linking together the base and acid ions are usually formed around a 2_1 axis.[1-3] The crystal structures of the title compounds have been examined in order to ascertain whether the type of hydrogen bonds is maintained or not by the enlargement of the ring size of the base, to see what types of hydrogen bonds other than the 2_1 type are possible in the crystals, if any, and to determine the conformation of hexamethyleneimine ring in the crystals.

Experimental

Equimolar amounts of the base and the acid were dissolved in dry benzene. The crystals of hexamethyleneiminium *p*-chlorobenzoate (**1**) and of monoclinic form of hexamethyleneiminium *p*-bromobenzoate [**2**(**m**)] were grown from the solutions by slow evaporation. The crystals of orthorhombic form of hexamethyleneiminium *p*-bromobenzoate [**2**(**o**)] were grown from the filtrate of **2**(**m**) by slow evaporation. Crystal data and experimental details are given in Table 1. The systematic absences for **2**(**m**) showed the possible space group to be C2/c or Cc, but the latter was ruled out by the structure analysis.

The specimens were sealed in glass capillaries, since the crystals of the compounds decompose gradually. The intensity data were collected on equi-inclination Weissenberg photographs using Cu $K\alpha$ radiation. Intensities were estimated visually and corrected for Lorentz and polarization factors and spot shape.

Table 1. Crystal data and experimental details

	Hexamethyleneiminium *p*-chlorobenzoate (**1**) $(C_6H_{12}NH_2)^+(ClC_6H_4CO_2)^-$ $F.W.=255.7$	Hexamethyleneiminium *p*-bromobenzoate $(C_6H_{12}NH_2)^+(BrC_6H_4CO_2)^-$, $F.W.=300.2$	
		Monoclinic form [**2**(**m**)]	Orthorhombic form [**2**(**o**)]
Mp/°C	131—133	141—143	118—120
Morphology	Plates developed {010}	Plates developed {100}	Plates developed {010}
Space group	$P2_1/c$	C2/c	Pbca
a/Å	10.10(2)	25.47(2)	11.55(1)
b/Å	16.78(1)	7.01(1)	27.40(1)
c/Å	9.01(2)	16.29(1)	8.57(1)
β/°	118.4(2)	109.1(1)	
V/Å^3	1342(3)	2751(3)	2713(4)
Z	4	8	8
D_m/g cm^{-3}	1.26	1.46	1.47
D_x/g cm^{-3}	1.265	1.450	1.469
μ(Cu $K\alpha$)/cm^{-1}	24.5	44.5	44.8
Dimensions of crystals used/mm	0.50×0.15×0.25 0.25×0.15×0.60	0.20×1.20×0.35 0.25×0.35×0.55	0.70×0.15×0.20 0.30×0.10×0.50
Layers photographed	0*kl* to 6*kl* *hk*0 to *hk*6	*h*0*l* to *h*5*l* *hk*0 to *hk*6	0*kl* to 8*kl* *hk*0 to *hk*6
Non-zero reflections	1628	1009	1013
Percentage accessible	53	32	33
B/Å^2 from Wilson's plot	5.2	11.8	5.7

TABLE 2. FINAL ATOMIC PARAMETERS OF THE NON-HYDROGEN ATOMS ($\times 10^4$, except B_{eq}) AND THOSE OF THE HYDROGEN ATOMS ($\times 10^3$, except B_{iso}) WITH VALUES OF e.s.d. IN PARENTHESES

	x	y	z	B_{eq} or B_{iso}/Å^2
(a) Hexamethyleneiminium *p*-chlorobenzoate (**1**)				
C(1)	1737(4)	1408(2)	4606(4)	4.4(1)
C(2)	912(4)	698(2)	4130(5)	5.2(2)
C(3)	−104(5)	553(2)	2450(5)	5.3(2)
C(4)	−289(4)	1115(2)	1239(5)	5.2(2)
C(5)	485(4)	1824(2)	1687(5)	5.6(2)
C(6)	1493(5)	1970(2)	3363(5)	5.4(2)
C(7)	2856(4)	1547(2)	6430(4)	4.8(2)
O(8)	3685(3)	2139(2)	6811(3)	5.8(1)
O(9)	2869(4)	1043(2)	7487(3)	6.5(1)
Cl(10)	−1533(1)	937(1)	−868(1)	6.5(1)
N(11)	4506(4)	1466(2)	10739(4)	5.0(1)
C(12)	3894(6)	849(3)	11445(6)	6.4(2)
C(13)	4829(6)	643(3)	13285(6)	7.4(3)
C(14)	5677(6)	1313(3)	14460(6)	7.4(3)
C(15)	7168(5)	1517(3)	14500(6)	6.6(2)
C(16)	7050(5)	1893(3)	12890(6)	6.3(2)
C(17)	6131(5)	1439(3)	11266(6)	6.2(2)
H(2)	111(5)	28(3)	502(6)	6(1)
H(3)	−59(5)	5(3)	214(6)	6(1)
H(5)	33(5)	225(3)	91(6)	6(1)
H(6)	202(5)	246(2)	366(5)	4(1)
H(11A)	421(4)	202(2)	1099(5)	4(1)
H(11B)	401(7)	137(4)	945(7)	9(2)
H(12A)	366(5)	34(3)	1081(5)	5(1)
H(12B)	277(6)	107(3)	1127(7)	7(1)
H(13A)	580(7)	32(4)	1347(7)	9(2)
H(13B)	404(5)	41(3)	1357(6)	6(1)
H(14A)	489(5)	191(3)	1394(5)	5(1)
H(14B)	591(6)	121(3)	1573(7)	8(1)
H(15A)	778(7)	197(4)	1546(8)	9(2)
H(15B)	770(5)	97(2)	1476(5)	5(1)
H(16A)	818(6)	192(3)	1305(7)	7(1)
H(16B)	659(5)	243(3)	1271(6)	5(1)
H(17A)	642(5)	81(2)	1157(5)	4(1)
H(17B)	624(7)	159(4)	1020(8)	9(2)
(b) Hexamethyleneiminium *p*-bromobenzoate, monoclinic form [**2**(**m**)]				
C(1)	846(5)	7856(15)	1320(7)	7.9(6)
C(2)	1420(5)	7505(15)	1620(8)	8.2(6)
C(3)	1790(5)	8800(23)	1550(8)	9.5(7)
C(4)	1617(4)	10615(15)	1230(6)	7.2(5)
C(5)	1067(4)	11067(16)	913(6)	7.2(6)
C(6)	684(4)	9722(15)	977(6)	7.1(5)
C(7)	418(5)	6428(18)	1401(7)	8.4(7)
O(8)	626(3)	4976(11)	1864(5)	9.7(5)
O(9)	−75(4)	6855(13)	1054(7)	9.9(5)
Br(10)	2151(1)	12471(2)	1186(1)	10.3(1)
N(11)	−736(3)	4301(12)	1419(5)	7.2(4)
C(12)	−1300(5)	4969(19)	953(10)	10.1(8)
C(13)	−1764(6)	3682(25)	743(9)	10.8(9)
C(14)	−1731(6)	2092(21)	1388(12)	11.3(10)
C(15)	−1387(5)	407(18)	1355(9)	10.3(8)
C(16)	−780(5)	792(16)	1675(8)	8.6(7)
C(17)	−577(6)	2369(15)	1201(8)	8.6(7)
H(2)	157(5)	613(20)	194(7)	10(4)
H(3)	225(5)	859(20)	183(8)	9(3)
H(5)	96(5)	1245(12)	69(7)	5(3)
H(6)	25(4)	1012(17)	71(7)	7(3)
H(11A)	−70(5)	436(22)	214(8)	11(4)
H(11B)	−49(5)	526(18)	137(8)	10(4)
H(12A)	−139(6)	608(23)	105(9)	12(4)
H(12B)	−120(5)	543(20)	45(8)	11(4)
H(13A)	−208(5)	447(20)	63(8)	10(4)
H(13B)	−176(7)	300(22)	34(10)	12(5)
H(14A)	−217(5)	180(21)	128(8)	9(4)
H(14B)	−166(7)	271(18)	210(9)	11(5)
H(15A)	−149(6)	−71(23)	159(9)	13(5)
H(15B)	−154(5)	24(19)	69(7)	9(4)
H(16A)	−66(6)	135(23)	233(9)	12(4)
H(16B)	−58(6)	−52(25)	180(11)	15(5)
H(17A)	−74(5)	231(15)	63(8)	8(4)
H(17B)	−21(6)	240(15)	122(9)	9(4)
(c) Hexamethyleneiminium *p*-bromobenzoate, orthorhombic form [**2**(**o**)]				
C(1)	4236(8)	1210(3)	8712(9)	2.3(4)
C(2)	3925(9)	1646(3)	9513(12)	3.3(4)
C(3)	4633(9)	2063(3)	9332(11)	3.4(4)
C(4)	5603(10)	2048(4)	8450(13)	4.4(5)
C(5)	5900(10)	1640(4)	7675(13)	4.1(5)
C(6)	5228(9)	1212(3)	7837(9)	2.8(5)
C(7)	3477(9)	763(3)	8822(12)	3.4(5)
O(8)	2703(7)	748(3)	9829(8)	4.2(4)
O(9)	3720(8)	414(3)	7904(9)	5.2(4)
Br(10)	6493(2)	2619(1)	8244(2)	7.5(1)
N(11)	2386(7)	−376(2)	7831(9)	3.0(4)
C(12)	1183(11)	−238(4)	8122(13)	4.1(5)
C(13)	408(9)	−601(4)	9032(14)	3.8(4)
C(14)	492(10)	−1129(3)	8482(12)	4.0(5)
C(15)	1503(10)	−1405(4)	9173(14)	4.3(5)
C(16)	2685(10)	−1239(3)	8636(12)	3.9(5)
C(17)	2969(9)	−713(3)	9009(13)	3.4(4)
H(2)	320(9)	164(4)	1003(16)	3(3)
H(3)	441(13)	238(5)	1000(17)	6(4)
H(5)	672(13)	161(6)	710(18)	7(5)
H(6)	550(11)	92(4)	743(14)	3(3)
H(11A)	246(14)	−56(6)	679(17)	7(4)
H(11B)	285(12)	−7(5)	768(19)	6(3)
H(12A)	91(8)	−13(4)	707(11)	1(2)
H(12B)	122(15)	7(7)	861(20)	8(5)
H(13A)	−51(9)	−44(3)	888(13)	2(2)
H(13B)	55(13)	−59(6)	1015(17)	7(4)
H(14A)	−32(11)	−132(4)	872(15)	4(3)
H(14B)	52(11)	−112(4)	730(14)	4(3)
H(15A)	148(8)	−182(4)	897(14)	2(3)
H(15B)	135(10)	−140(5)	1032(17)	5(4)
H(16A)	281(11)	−131(4)	769(16)	4(3)
H(16B)	319(9)	−142(4)	912(14)	3(3)
H(17A)	263(10)	−61(4)	991(16)	4(3)
H(17B)	379(9)	−69(4)	896(13)	2(2)

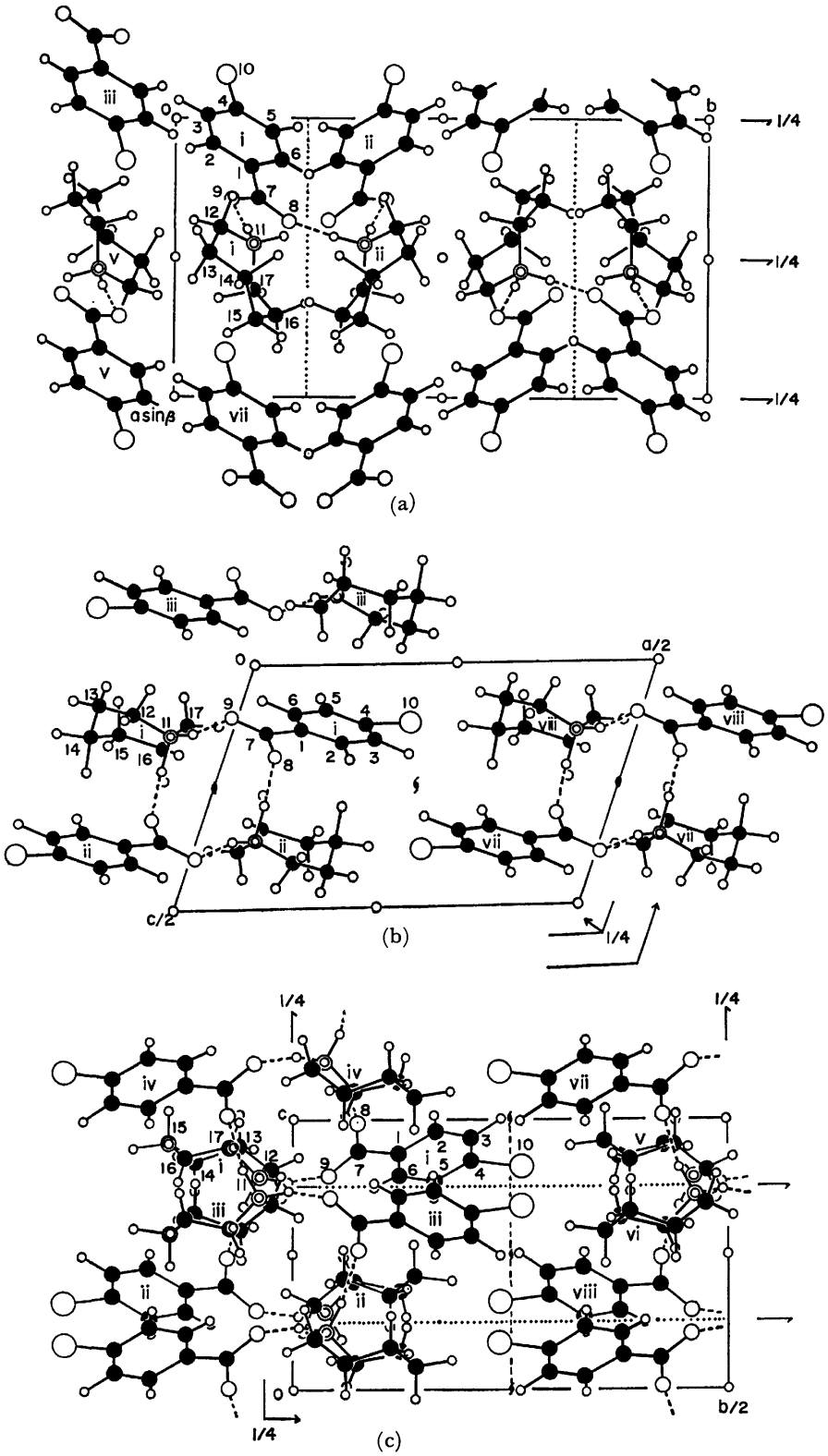

Fig. 1. Projections of the crystal structures and numbering of the non-hydrogen atoms. (a) **1** viewed along c, (b) **2**(**m**) viewed along b, and (c) **2**(**o**) viewed along a. Broken lines show hydrogen bonds.

Symmetry code: for **1**: (i) x, y, z; (ii) x, $1/2-y$, $1/2+z$; (iii) $-x$, $-y$, $-z$; (iv) $-x$, $-y$, $1-z$; (v) $1-x$, $-y$, $2-z$; (vi) $1-x$, $-y$, $3-z$; (vii) $1+x, y, 1+z$; (viii) $x, y, 1+z$; for **2**(**m**): (i) x, y, z; (ii) $-x, y, 1/2-z$; (iii) $-x, 2-y, -z$; (iv) $-x, 1-y. -z$; (v) $x, 1+y, z$; (vi) $-x, 1+y, 1/2-z$; (vii) $1/2-x, 1/2+y, 1/2-z$; (viii) $1/2+x, 1/2+y, z$; for **2**(**o**): (i) x, y, z; (ii) $1/2-x, -y, -1/2+z$; (iii) $1/2+x, y, 3/2-z$; (iv) $1-x, -y, 2-z$; (v) $1/2-x, 1/2+y, z$; (vi) $1-x, 1/2+y, 3/2-z$; (vii) $1/2+x, 1/2-y, 2-z$; (viii) $x, 1/2-y, -1/2+z$.

Structure Determination and Refinement

The structure of **1** was solved by the symbolic addition procedure and the structures of **2(m)** and **2(o)** by the Patterson method. Refinement was made by block-diagonal least-squares calculations. For **1** all the H atoms were located from a difference Fourier synthesis. Further refinement was carried out including the parameters of the H atoms. The weighting scheme used was $w=1.0$ for $0<|F_o|\leq F_{max}$, and $w=(F_{max}/|F_o|)^2$ for $|F_o|>F_{max}$, where $F_{max}=6.5$.

For **2(m)** and **2(o)**, the coordinates of nine and thirteen H atoms were determined from difference Fourier syntheses at the stages of $R=0.124$ and 0.110, respectively. The positional parameters of the remaining H atoms were calculated by assuming the usual geometry, and were included in the subsequent refinement. The same weighting scheme was used with $F_{max}=16.0$ for **2(m)** and 14.0 for **2(o)**. The final R values for the non-zero reflections were 0.072 for **1**, 0.100 for **2(m)**, and 0.083 for **2(o)**. The final atomic parameters are given in Table 2.[4]

The atomic scattering factors were taken from International Tables for X-Ray Crystallography.[5] Computations were carried out at the Okayama University Computer Center. The programs used were SIGM, TANG, HBLS-V, and DAPH.[6]

Results and Discussion

The projections of the crystal structures and the numbering of the atoms are shown in Fig. 1. Geometry of the hydrogen bonds is summarized in Table 3. Bond lengths and angles are given in Table 4.

Crystal Structures. In the crystals of **1**, the base and acid ions are linked together by two kinds of N–H···O hydrogen bonds to form a ribbon along a c glide plane. The type of hydrogen bond is the same as that found in piperazinediylium terephthalate (**3**).[7] The ribbons are stacked along a in alternate succession of the base and acid ions to form a sheet parallel to (010). The molecular arrangement in the sheet is also the same as that in **3**. The doubling of b occurs in **1** because of the loss of molecular symmetry $\bar{1}$ in the base and acid ions.

Table 3. Geometry of hydrogen bonds
Lengths in Å and angles in degrees.

Crystals	**1**	**2(m)**	**2(o)**
Type of hydrogen bonds	Glide	2	2_1
a) Hydrogen bond between base (i) and acid (i)			
N(11)···O(9)	2 686(5)	2.655(14)	2.658(12)
H(11B)···O(9)	1.68(7)	1.73(13)	1.68(16)
N(11)–H(11B)···O(9)	163(6)	168(12)	165(15)
N(11)···O(9)–C(7)	115.1(3)	111 0(9)	120.0(8)
b) Hydrogen bond between base (i) and acid(ii)			
N(11)···O(8)	2.804(5)	2.759(12)	2.769(11)
H(11A)···O(8)	1.79(5)	1.63(15)	1.77(18)
N(11)–H(11A)···O(8)	167(4)	167(13)	163(15)
N(11)···O(8)–C(7)	147.8(3)	128.4(8)	133.1(7)

Table 4. Bond lengths (l/Å) and angles (ϕ/°) with values of e.s.d. in parentheses

	1 (X=Cl)	**2(m)** (X=Br)	**2(o)** (X=B)
C(1)–C(2)	1.400(6)	1.404(18)	1.423(14)
C(2)–C(3)	1.388(7)	1.341(20)	1.414(15)
C(3)–C(4)	1.386(7)	1.392(19)	1.353(16)
C(4)–C(5)	1.375(6)	1.361(16)	1.344(17)
C(5)–C(6)	1.384(7)	1.385(16)	1.413(15)
C(6)–C(1)	1.393(6)	1.430(17)	1.370(14)
C(1)–C(7)	1.505(6)	1.517(18)	1.510(14)
C(7)–O(8)	1.238(5)	1.275(16)	1.244(13)
C(7)–O(9)	1.269(6)	1.234(17)	1.269(14)
C(4)–X(10)	1.732(5)	1.901(11)	1.881(12)
N(11)–C(12)	1.493(7)	1.465(19)	1.462(15)
N(11)–C(17)	1.476(6)	1.489(17)	1.524(14)
C(12)–C(13)	1.507(8)	1.439(25)	1.547(17)
C(13)–C(14)	1.502(9)	1.516(26)	1.525(17)
C(14)–C(15)	1.528(8)	1.483(24)	1.512(16)
C(15)–C(16)	1.534(8)	1.486(20)	1.511(17)
C(16)–C(17)	1.514(7)	1.533(20)	1.514(16)
N(11)–H(11A)	1.03(5)	1.15(15)	1.03(18)
N(11)–H(11B)	1.04(7)	0.94(13)	0.99(16)
C(1)–C(2)–C(3)	120.4(4)	122.2(13)	118.6(9)
C(2)–C(3)–C(4)	119.6(4)	120.3(14)	121.1(10)
C(3)–C(4)–C(5)	120.8(4)	121.1(11)	120.9(11)
C(4)–C(5)–C(6)	119.6(4)	118.3(10)	120.1(11)
C(5)–C(6)–C(1)	121.0(4)	122.2(11)	121.1(10)
C(6)–C(1)–C(2)	118.5(4)	115.5(11)	118.2(9)
C(3)–C(4)–X(10)	120.1(4)	119.8(9)	118.7(9)
C(5)–C(4)–X(10)	119.1(3)	119.1(8)	120.4(9)
C(2)–C(1)–C(7)	119.7(4)	123.4(11)	120.3(9)
C(6)–C(1)–C(7)	121.8(4)	121.0(11)	121.5(9)
C(1)–C(7)–O(8)	119.0(4)	114.1(11)	119.1(9)
C(1)–C(7)–O(9)	116.8(4)	116.9(12)	116.4(9)
O(8)–C(7)–O(9)	124.2(4)	128.9(12)	124.4(10)
N(11)–C(12)–C(13)	117.3(5)	120.9(14)	118.1(10)
C(12)–C(13)–C(14)	116.9(5)	116.2(15)	114.6(10)
C(13)–C(14)–C(15)	114.2(5)	117.4(15)	113.8(10)
C(14)–C(15)–C(16)	115.9(5)	113.7(13)	115.3(10)
C(15)–C(16)–C(17)	116.3(4)	116.0(12)	114.7(10)
C(16)–C(17)–N(11)	111.9(4)	111.9(11)	109.9(9)
C(17)–N(11)–C(12)	117.6(4)	117.7(10)	117.6(8)
H(11A)–N(11)–C(12)	108(3)	105(8)	111(10)
H(11B)–N(11)–C(12)	107(4)	108(8)	109(9)
H(11A)–N(11)–C(17)	111(2)	110(8)	104(10)
H(11B)–N(11)–C(17)	103(4)	112(8)	111(9)

In the crystals of **2(m)**, two pairs of the base and acid ions related by a twofold axis are linked together by two kinds of N–H···O hydrogen bonds. The hydrogen-bonded units are stacked along b in alternate succession of the base and acid ions to form a ribbon. The ribbons related by $\bar{1}$ are held together by van der Waals interactions and dipole-dipole interactions between the acid ions to form a sheet parallel to (100). The sheets are stacked along a by weak interactions.

In **2(o)** all atoms of the acid ion and a center of the base ion occupy positions similar to those of piperidinium *p*-substituted benzoates[1,2] and of pyrrolidinium *p*-substituted benzoates[3] in Pbca, but the position of N

differs by about $c/4$. This difference causes a change in the combination mode of the base and acid ions participating in the hydrogen bonds. In **2**(**o**) base ion (i) donates the hydrogen bonds to acid ions (i) and (ii), while in the others it is base ion (ii) that doantes the hydrogen bonds to the corresponding acid ions, where the symmetry code follows that given in Fig. 1(c) for all the crystals.

For the crystals of **1**, **2**(**m**), and **2**(**o**), all the intermolecular contacts correspond to those expected for the usual van der Waals interactions. The shortest contacts are found between C(7^{i}) and H($11B^{i}$): 2.42(7) Å for **1**, 2.44(13) Å for **2**(**m**) and 2.59(16) Å for **2**(**o**).

Geometry of the Hydrogen Bonds. Irrespective of the type of hydrogen bond, the bond N(11^{i})···O(9^{i}) extending nearly parallel to the long axis of the acid ion is shorter than the other one N(11^{i})···O(8^{ii}) lying nearly perpendicular to the long axis. A notable difference between the two hydrogen bonds is that the former is associated with the nearly tetrahedral C–O···N angle, while in the latter the angle takes a significantly larger value, especially for the glide type.

TABLE 5. THE LEAST-SQUARES PLANES AND DISPLACEMENTS (l/Å) OF THE ATOMS FROM THE PLANES $X=ax+cz\cos\beta$, $Y=by$, $Z=cz\sin\beta$.

	1 (X=Cl)	**2**(**m**) (X=Br)	**2**(**o**) (X=Br)
(I) Benzene ring			
1:	$0.898X-0.422Y-0.126Z+1.665=0$		
2(**m**):	$0.245X-0.335Y-0.910Z+3.343=0$		
2(**o**):	$-0.538X+0.285Y-0.793Z+7.620=0$		
C(1)[a]	0.011	0.007	0.008
C(2)[a]	−0.004	−0.013	−0.004
C(3)[a]	−0.008	0.021	0.005
C(4)[a]	0.013	−0.022	−0.010
C(5)[a]	−0.005	0.015	0.014
C(6)[a]	−0.007	−0.007	−0.012
C(7)	0.043	−0.049	0.056
O(8)	0.190	−0.288	−0.159
O(9)	−0.100	0.075	0.257
X(10)	0.032	−0.058	0.022
(II) Carboxylate group			
1:	$0.835X-0.538Y-0.111Z+1.860=0$		
2(**m**):	$0.305X-0.471Y-0.828Z+3.829=0$		
2(**o**):	$-0.636X+0.386Y-0.668Z+6.813=0$		
C(1)[a]	−0.001	−0.005	−0.005
C(7)[a]	0.004	0.018	0.017
O(8)[a]	−0.001	−0.006	−0.006
O(9)[a]	−0.001	−0.007	−0.006
(III) Hexamethyleneimine ring			
1:	$0.616X-0.762Y-0.201Z+3.560=0$		
2(**m**):	$0.404X-0.211Y-0.890Z+3.610=0$		
2(**o**):	$0.230X+0.294Y+0.928Z-6.571=0$		
N(11)[a]	−0.058	−0.034	−0.013
C(12)[a]	0.052	0.026	0.010
C(15)[a]	−0.059	−0.026	−0.009
C(16)[a]	0.068	0.035	0.012
C(13)	0.118	0.072	0.235
C(14)	−0.709	−0.682	−0.605
C(17)	0.765	0.762	0.808
Dihedral angle (ϕ/°) between planes (I) and (II)	7.6	9.8	10.9

a) Used for calculation of the planes.

Molecular Structures. *(a) Benzoate Ions*: The benzene rings and carboxylate groups are planar within experimental errors (Table 5). The C(1)–C(7)–O(9) angles remain constant in these crystals, the O(9) participating in shorter hydrogen bond. The corresponding angles in the related compounds also take a restricted range of values, 116.1—117.4°.[1-3,7] On the other hand, in **2**(**m**) the C(1)–C(7)–O(8) angle is smaller and the O(8)–C(7)–O(9) angle larger than the corresponding angles in **1** and **2**(**o**). A similar opening of the O–C–O angle has been observed in trifluoroacetic acid.[8] Shortening of the C(7)–O(9) bond in **2**(**m**) can be explained in terms of the *s*-character of the C(7) atom,[9] the C(7)–O(8) bond length in **2**(**m**) being unexpectedly large.

TABLE 6. THE TORSION ANGLES (ϕ/°) IN THE HEXAMETHYLENEIMINE RINGS

		1	**2**(**m**)	**2**(**o**)
χ_0	C(17)-N(11)-C(12)-C(13)	41.3	37.9	29.0
χ_1	N(11)-C(12)-C(13)-C(14)	36.4	33.2	46.3
χ_2	C(12)-C(13)-C(14)-C(15)	−81.8	−79.5	−83.4
χ_3	C(13)-C(14)-C(15)-C(16)	68.6	71.3	68.3
χ_4	C(14)-C(15)-C(16)-C(17)	−54.0	−58.3	−60.4
χ_5	C(15)-C(16)-C(17)-N(11)	70.8	72.7	79.3
χ_6	C(16)-C(17)-N(11)-C(12)	−86.7	−81.8	−84.4

(b) Hexamethyleneiminium Ions: Let $A(i)$ be the non-hydrogen atoms in the rings, where i is an integer from 11 to 17 and $A(i+7)=A(i)$ in the present numbering system. In each crystal of **1**, **2**(**m**) and **2**(**o**), the planarity through the four atoms $A(i)$, $A(i+1)$, $A(i+4)$, and $A(i+5)$ is the best when $i=11$ (Table 5). In each ring the C(14) and C(17) deviate from the plane in opposite directions. The torsion angles around each bond in the rings show the twist-chair conformation[10] (Table 6). The hexamethyleneimine rings in **1**, **2**(**m**), and **2**(**o**) take similar conformations irrespective of the crystallographic environment of the rings. For cycloheptane the conformation has been estimated to be more stable than the chair conformation by 5.9 kJ mol^{-1}.[10]

References

1) S. Kashino, Y. Sumida, and M. Haisa, *Acta Crystallogr., Sect. B*, **28**, 1374 (1972).

2) S. Kashino, *Acta Crystallogr., Sect. B*, **29**, 1836 (1973).

3) S. Kashino, S. Kataoka, and M. Haisa, *Bull. Chem. Soc. Jpn.*, **51**, 1717 (1978).

4) Lists of structure factors and anisotropic thermal parameters have been deposited at the Chemical Society of Japan (Document No. 8117).

5) "International Tables for X-Ray Crystallography," Kynoch Press, Birmingham (1974), Vol. IV, p. 72.

6) "The Universal Crystallographic Computing System-Osaka," The Computation Center, Osaka University (1973).

7) S. Kashino, M. Sasaki, and M. Haisa, *Bull. Chem. Soc. Jpn.*, **46**, 1375 (1973).

8) I. Nahringbauer, J.-O. Lundgren, and E. K. Andersen, *Acta Crystallogr., Sect. B*, **35**, 508 (1979).

9) S. Kashino and M. Haisa, *Acta Crystallogr., Sect. B*, **33**, 855 (1977).

10) J. B. Hendrickson, *J. Am. Chem. Soc.*, **89**, 7036 (1967).

  Bull. Chem. Soc. Jpn., 54, 967—970 (1981)

New Scale of the Ionic Character of the Chemical Bond Using Multiconfiguration SCF Wave Functions

Kazuhiro ISHIDA,* Shuichi KADOWAKI, and Teijiro YONEZAWA†

Department of Chemistry, Faculty of Science, Science University of Tokyo, Kagurazaka, Shinjuku-ku, Tokyo 162

†*Department of Hydrocarbon Chemistry, Faculty of Engineering, Kyoto University, Sakyo-ku, Kyoto 606 and Institute for Molecular Science, Okazaki 444*

(Received June 14, 1980)

Two-configuration SCF wave functions constructed with multiconfiguration SCF localized-orbitals are obtained for several molecules, cations, and anions. The weights of the valence-bond resonance-structures are obtained from the wave functions for these molecules and molecular ions. A new formula of the ionic character of a chemical bond is proposed using these weights. For these neutral molecules, the values calculated from this formula are consistent with Pauling's scale of the ionic character. The present formula is shown to be applicable even for molecular ions.

The ionic character is an important concept in understanding chemical bonds. Several scales of the ionic character in relation to the electronegativity difference were proposed by Pauling,[1] by Hannay and Smyth,[2] by Nethercot,[3] by Hinze, Whitehead, and Jaffe,[4] and by others. They are not so satisfactory. Coulson[5] defined a scale of the ionic character from the weight of the ionic structure in the valence-bond wave function. However, few calculations have been performed along this line, so that the validity of this scale has not been confirmed extensively.

In the present paper, we propose a new scale for the ionic character using the weights obtained from the two-configuration SCF wave function constructed with multiconfiguration SCF localized molecular orbitals (MCSCF-LMOs).[6,7] Properties of this wave function (referred to as Ψ[2c] from now on) and its relation to the ionic character are described in the second section. In the third section, we apply the new scale to simple molecules and molecular ions: LiF, LiH, HF, H_2O, NH_3, CH_4, H_2, OH^-, NH_2^-, CH_3^-, H_3O^+, and NH_4^+. The values calculated are compared with the observed partial charges[8] and other scales. The present scale is shown to be in an excellent agreement with Pauling's scale as improved by Nethercot[3] for these neutral molecules.

Theory

The Ψ[2c] is fully described in a previous paper.[7] It can be briefly sketched as follows:

A Ψ[2c] wave function to discuss the nature of a local bond, say A–B, in a polyatomic molecule can be expressed as

$$\Psi[2c] = a_1\|(\text{other MCSCF-LMOs})\sigma_{AB}\bar{\sigma}_{AB}\| + a_2\|(\text{other MCSCF-LMOs})\sigma^*_{AB}\bar{\sigma}^*_{AB}\|, \quad (1)$$

where σ_{AB} is the bonding orbital, σ^*_{AB} is the corresponding antibonding orbital, a_1 and a_2 are the configuration mixing coefficients. All orbitals are the MCSCF-LMOs and can be expanded in terms of atomic orbitals (AOs) χ_t. All LCAO coefficients and the configuration mixing coefficients are optimized variationally.

The bonding orbital σ_{AB} and the antiboding orbital σ^*_{AB} can be expressed as

$$\sigma_{AB} = \sum_p^{\text{on A}} \chi_p c_p + \sum_q^{\text{on B}} \chi_q c_q + \sum_r \chi_r c_r,$$
$$\sigma^*_{AB} = \sum_p^{\text{on A}} \chi_p d_p + \sum_q^{\text{on B}} \chi_q d_q + \sum_r \chi_r d_r, \quad (2)$$

where the subscript p denotes the numbering of AO's on atom A, q denotes that of AO's on atom B, and r denotes that of AO's on other atoms. Since σ_{AB} and σ^*_{AB} (also the other orbitals) are MCSCF-LMOs, all of c_r and d_r (which are the LCAO coefficients of AO's on the other atoms) can usually be neglected. Neglecting the last term in Eq. 2 and then substituting Eq. 2 into Eq. 1, we have the following equation, which clarifies the physical significance of the Ψ[2c]:

$$\Psi[2c] \simeq \Psi(A^-B^+) + \Psi(A^+B^-) + \Psi(A{:}B), \quad (3)$$

where

$$\Psi(A^-B^+) = \sum_p^{\text{on A}} \sum_{p'}^{\text{on A}} b_{pp'}\|(\text{other MCSCF-LMOs})\chi_p\bar{\chi}_{p'}\|, \quad (4)$$

$$\Psi(A^+B^-) = \sum_q^{\text{on B}} \sum_{q'}^{\text{on B}} b_{qq'}\|(\text{other MCSCF-LMOs})\chi_q\bar{\chi}_{q'}\|, \quad (5)$$

$$\Psi(A{:}B) = \sum_p^{\text{on A}} \sum_q^{\text{on B}} b_{pq}\|(\text{other MCSCF-LMOs})(\chi_p\bar{\chi}_q - \chi_p\bar{\chi}_q)/\sqrt{2}\|, \quad (6)$$

$$b_{pp'} = a_1c_pc_{p'} + a_2d_pd_{p'}, \quad b_{qq'} = a_1c_qc_{q'} + a_2d_qd_{q'},$$
$$b_{pq} = \sqrt{2}(a_1c_pc_q + a_2d_pd_q).$$

The $\Psi(A^-B^+)$ is an ionic structure in which two bonding-electrons belong to atom A (see Eq. 4). In the covalent structure $\Psi(A:B)$, those electrons are shared by the two atoms.

Let us define the following three weights, which include interference terms:

$$W(A^-B^+) = \|\Psi(A^-B^+)\|^2 + \langle\Psi(A^-B^+)|\Psi(A^+B^-) + \Psi(A{:}B)\rangle, \quad (7)$$

$$W(A^+B^-) = \|\Psi(A^+B^-)\|^2 + \langle\Psi(A^+B^-)|\Psi(A^-B^+) + \Psi(A{:}B)\rangle, \quad (8)$$

$$W(A{:}B) = \|\Psi(A{:}B)\|^2 + \langle\Psi(A{:}B)|\Psi(A^-B^+) + \Psi(A^+B^-)\rangle. \quad (9)$$

Using these weights of the structures, we can define a new scale of the ionic character for the local bond A–B as

$$\lambda_{AB} = [W(A^-B^+) - W(A^+B^-)] \times 100\%. \quad (10)$$

The more electronegative one of these two atoms should

be referred to as A in Eq. 10. Thus λ_{AB} happens to be negative when atom A happens to be more positive than atom B, as seen in Table 5 for the CH_3^- anion.

Results and Discussion

Ab initio calculations of the ionic character λ_{AB} were performed in the observed geometries with the 6-31G basis set[9] and with the STO-3G basis set[10] for neutral molecules: LiF, LiH, HF, H_2O, NH_3, CH_4, and H_2, and for molecular ions: H_3O^+, NH_4^+, OH^-, NH_2^-, and CH_3^-. The dipole moment (μ) was also computed directly for each of these neutral molecules with the same basis set (*i.e.*, not obtained from λ_{AB}).

Geometry optimization is omitted. The optimization will not greatly affect the ionic character, since the change of the bond length will be less than 0.01 Å in the 6-31G basis set.[11] Table 1 shows the geometries used in the present calculations.

TABLE 1. THE GEOMETRIES OF MOLECULES AND IONS

Molecule	Bond length / Å	Bond angle / °	Ref.
LiF	1.5639		a
LiH	1.5953		a
HF	0.917		a
H_2O	0.956	105.2	b
NH_3	1.0173	107.8	b
CH_4	1.0940		b
OH^-	0.970		c
NH_2^-	1.0173	107.8	d
CH_3^-	1.0940	109.5	e
H_3O^+	0.96	117.0	f
NH_4^+	1.032		g

a) F.J. Lovas and E. Tiemann, *J. Phys. Chem. Ref. Data*, **3**, 609 (1974). b) G. Herzberg, "Molecular Spectra and Molecular Structure," D. Van Nostrand, Princeton, New Jersey (1967), Vol. 3. c) K.P. Huber and G. Herzberg, "Molecular Spectra and Molecular Structure," Van Nostrand Reinhold, New York, N.Y. (1979), Vol. 4. d) Estimated from ammonia. e) Estimated from methane. f) Y.K. Yoon and G.B. Carpenter, *Acta Crystallogr.*, **12**, 17 (1959). g) J. A. Ibers and D. P. Stevenson, *J. Chem. Phys.*, **28**, 929 (1958).

TABLE 2. THE VALUE OF IONIC CHARACTER, λ_{AB}, THE DIPOLE MOMENT CALCULATED AND THAT OBSERVED, AND THE OBSERVED PARTICAL CHARGE. THE CALCULATIONS WERE PERFORMED WITH THE 6-31G BASIS SET

Molecule	λ_{AB} / %	μ_{calc} / Debye	μ_{obsd} / Debye	$[\mu/er_e]_{obsd}$ / %
LiF	94[a]	7.289[a]	6.28409[c]	83.675
LiH	49[b]	4.466[b]	5.8820[c]	76.762
HF	40	2.147	1.826526[c]	41.47
H_2O	32	2.504	1.94[d]	34.8
NH_3	24	2.228	1.468[d]	28.00
CH_4	11	0.0	0.0	...
H_2	0	0.0	0.0	...

a) P-type basis functions on lithium are excluded. b) P-type basis functions on lithium are excluded and a p_z-type basis function (α=0.25) on hydrogen is added. c) See footnote (a) of Table 1. d) B. Starck, Landolt-Börnstein Table, New Series, II/4, Springer (1967).

Table 2 shows the comparison of the λ_{AB} with the observed partial charge and the comparison of the calculated dipole moment with that observed for neutral molecules. The relative error of the dipole moment calculated to that observed is 50% at most. For a better agreement, polarization functions should be added to the basis set. The difference of the λ_{AB} from the observed partial charge is 10% at most (except for LiH). The λ_{AB} would be less sensitive than the dipole moment with respect to the absence of the polarization functions. In the case of the STO-3G basis set, the values of the λ_{AB} are too small in all molecules (*i.e.*, only 2% for LiF, 31% for LiH, 12% for HF, 11% for H_2O, and 10% for NH_3). Good λ_{AB} seems to require the 6-31G level basis-set at least.

The basis-set dependence of the λ_{HLi} for LiH was investigated by using various basis-sets. These results are in Table 3. In the STO-3G basis-set, the values of both the calculated dipole moment and the λ_{HLi} are extremely small. In the original 6-31G basis-set in which p-type basis functions on lithium (abbreviated to p(Li) from now on) are included, the calculated value of the dipole moment is in excellent agreement with the observed value, but the value of λ_{HLi} is in rather poor agreement with the observed partial charge.

TABLE 3. THE BASIS-SET DEPENDENCE OF THE VALUE OF THE IONIC CHARACTER FOR LiH MOLECULE

Basis set		E / Hartree	μ / Debye	λ_{HLi} / %
(I)	STO-3G[a]	−7.85446	1.798	8
(II)	STO-3G[b]	−7.86932	3.580	31
(III)	Dunning's [4s/2s] set[c]	−7.98381	4.089	36
(IV)	Dunning's [4s/3s] set[c]	−7.98488	4.227	38
(V)	(IV)+p_z-GTO(α=0.25) on H	−7.98994	4.270	47
(VI)	6-31G[d]	−7.99579	5.632	20
(VII)	(VI)+p_z-GTO(α=0.36) on H	−7.99808	5.564	26
(VIII)	6-31G[e]	−7.98415	4.479	42
(IX)	(VIII)+p_z-GTO (α=0.25) on H	−7.98887	4.466	49
Experiment			5.8820[f]	76.762[g]

a) The scale factor of 1s-GTO on H is 1.2. b) The scale factor of 1s-GTO on H is 1.0. c) Ref. 12. d) Ref. 9. e) P-type basis functions on lithium are excluded. f) See footnote (a) of Table 1. g) Observed partial charge (there is no bond-moment due to a lone-pair in the LiH molecule).

	Li–F	Li–H	H–F	H–OH	H–NH_2	H–CH_3	H–H
(A)	$Li^+:F^-$ 94%	$Li^+:H^-$ 50%	$H^+:F^-$ 44%	$H^+:OH^-$ 37%	$H^+:NH_2^-$ 31%	$H^+:CH_3^-$ 22%	$H^+:H^-$ 22%
(B)	$Li:^-F^+$ 0%	$Li:^-H^+$ 0%	$H:^-F^+$ 3%	$H:^-OH^+$ 5%	$H:^-NH_2^+$ 7%	$H:^-CH_3^+$ 11%	$H:^-H^+$ 22%
(C)	Li· ·F 6%	Li· ·H 50%	H· ·F 53%	H· ·OH 59%	H· ·NH_2 65%	H· ·CH_3 73%	H· ·H 55%

Fig. 1. The weights of resonance structures for a local bond in neutral molecules.

The function p(Li) extends into the bonding region, so it can improve the description of the region. The resulting description near the center of the electronic charge becomes reasonable (leads to a good dipole moment). However, the bonding electrons are accumulated in the p(Li) too much, so that the sharing ratio of the bonding electrons between Li and H is biased. In the 6-31G basis-set, the value of λ_{HLi} is remarkably improved by excluding the p(Li), as seen in Table 3 at basis-set (VIII). Further, the λ_{HLi} is improved by adding a p_z-type GTO on hydrogen to either the 6-31G set (without p(Li)) or the CGTO better values of λ_{HLi}, a larger basis set may be used and/or other configuration(s) may be taken into account.

Generally speaking, the λ_{AB} would be the sharing ratio of the bonding electrons between atoms A and B, so that λ_{AB} is sensitive to the balance of basis functions in the basis set used. Therefore, the p(Li) should be excluded from the 6-31G set for the calculations of λ_{XLi} as was done in the calculations for LiF and LiH.

Figure 1 shows the resonance-structures for a local-bond and their weights calculated for neutral molecules. The structures denoted by (A) and (B) are the ionic structures ($A:^- B^+$) and ($A^+ :B^-$), respectively. The covalent structure (A· ·B) is denoted by (C).**

The Ψ[2c] reduces to the Hartree-Fock wave function in the limit where a_2 goes to zero (see Eq. 1). The MCSCF-LMO reduce to the LMO in the limiting case. Therefore, the weights of resonance structures for the Hartree-Fock wave function can be calculated with the use of Eqs. 4—9 by seting a_2 to zero and using LMOs instead of MCSCF-LMOs. The results are as follows: The weights of the structures (A), (B), and (C) are 96, 0, and 4%, respectively, for LiF. For LiH, they are 66, 3, and 30%. For HF, they are 56, 6, and 38%. For H_2O, they are 47, 12, and 47%. For NH_3, they are 44, 15, and 52%. For CH_4, they are 36, 22, and 56%. They are 25, 25, and 50%, for H_2. In all molecules, the weight of the ionic structure calculated from the Hartree-Fock wave function is always larger than that calculated from the Ψ[2c] (see Fig. 1 for the values). The present weights calculated from the Ψ[2c] are reasonable, since the MO method usually overestimates the weights of the ionic structures.

Comparison with Other Scales. Several empirical relations between the ionic character and the electronegativity difference $|X_A - X_B|$, were proposed in the early days, for example, by Pauling[1] and by Hannay and Smyth;[2]

$$q_P = [1-\exp(-|X_A-X_B|^2/4)] \times 100\%, \quad (11)$$

$$q_{HS} = 16|X_A-X_B| + 3.5|X_A-X_B|^2 \ (\%), \quad (12)$$

where q_P is the ionic character determined by Pauling and q_{HS} is that determined by Hannay and Smyth. Nethercot[3] recently proposed an improved relation:

$$q_N = [1-\exp(-|X_A-X_B|^{3/2}/X_{GM}^{3/2})] \times 100\%, \quad (13)$$

where X_{GM} is the geometric mean of X_A and X_B. Table 4 shows the values of these scales in comparison with the present λ_{AB} for several molecules.

The present scale λ_{AB} is in an excellent agreement with the Nethercot scale (the improved Pauling scale), as seen in Table 4.

Table 4. The comparison of the present scale of the ionic character λ_{AB} with other scales: q_P by Pauling, q_{HS} by Hannay and Smyth, q_N by Nethercot. The observed partial charge is again listed for convenience

Molecule	q_P/%	q_{HS}/%	q_N/%	λ_{AB}/%	$[\mu/er_e]_{obsd}$/%
LiF	89	78	84	94	83.675
LiH	26	22	48	49	76.762
HF	59	43	42	40	41.47
H_2O	39	29	31	32	34.8
NH_3	18	17	19	24	28.00
CH_4	4	7	7	11	...
H_2	0	0	0	0	...

For Ionic Species. We further calculate λ_{AB} for several cation and anion molecules. It is difficult to obtain the "observed ionic character" of any bond in any ionic species. In addition, it will be difficult to extend any scale which makes use of the electronegativity difference to make it applicable to the ionic species. On the other hand, the λ_{AB} can be evaluated in the ionic species without any difficulty.

Table 5. The value of the ionic character λ_{AB} for anion and cation calculated with the 6-31G basis-set. The values for neutral molecules are again listed for convenience

Ion	λ_{OH}/%	Ion	λ_{NH}/%	Ion	λ_{CH}/%
OH^-	9	NH_2^-	0	CH_3^-	−12
H_2O	32	NH_3	24	CH_4	11
H_3O^+	50	NH_4^+	42		

Table 5 shows the values of λ_{AB} calculated with the 6-31G basis set for OH^-, NH_2^-, CH_3^-, H_3O^+, and NH_4^+ (geometries are shown in Table 1). In all cases, the λ_{XH} (X=C, N, O) shows an increase of about 20% from the neutral molecule to its cation (proton adduct), and also a decrease of about 20% to its anion (product from the elimination of a proton). Figure 2 shows the resonance structures and their weights for molecular

** The sum of values of these weights is not always unity, because all of the c_r and d_r values in Eq. 2 are not always zero. In other words, the MCSCF-LMO are not completely localized.

	$[O-H]^-$	$[H-NH]^-$	$[H-CH_2]^-$	$[H-OH_2]^+$	$[H-N_3]^+$
(A)	$H^+: O^{2-}$ 19%	$H^+: NH^{2-}$ 14%	$H^+: CH_2^{2-}$ 9%	$H^+: OH_2$ 52%	$H^+: NH_3$ 45%
(B)	$H:^- O$ 10%	$H:^- NH$ 14%	$H:^- CH_2$ 20%	$H:^- OH_2^{2+}$ 2%	$H:^- NH_3^{2+}$ 3%
(C)	$H\cdot\ \cdot O^-$ 70%	$H\cdot\ \cdot NH^-$ 73%	$H\cdot\ \cdot CH_2^-$ 76%	$H\cdot\ \cdot OH_2^+$ 43%	$H\cdot\ \cdot NH_3^+$ 53%

Fig. 2. The weights of resonance structures for a local bond in molecular ions.

ions. In Fig. 2, the structure denoted by (A) is the resonance structure in which two bonding-electrons belong to the more electronegative atom. The (B) is the resonance structure in which those electrons belong to the less electronegative atom. In structure (C), the bonding-electrons are shared between both atoms.

The weights of the resonance structures can also be evaluated from the Hartree-Fock wave function in the same manner as described in this section. The results are as follows: The weights of the structures (A), (B), and (C) are 32, 19, and 49%, respectively, for OH^-. For NH_2^-, they are 27, 28, and 54%. For CH_3^-, they are 9, 29, and 33%. For H_3O^+, they are 63, 5, and 35%. They are 57, 8, and 42% for NH_4^+. In all ions, the values of the weights of the ionic structures calculated from the Hartree-Fock wave function are always larger than those from the Ψ[2c] (see Fig. 2 for the values). In the case of molecular ions, the present weights calculated from the Ψ[2c] are reasonable (as well as for the case of neutral molecules).

Conclusion

The scale of the ionic character λ_{AB} presented here is reasonable not only for neutral molecules but also for molecular ions. One may apply this scale to systems with hydrogen bonding, organometalic compounds, complex ions, metal complexes, and so on. One may use an effective core-potential[13] in order to reduce the computational time. Even for this case, no modifications of the theory are needed.

To obtain good values of λ_{AB} requires that the 6-31G level basis-set ("double-zeta" level) be used and that some care be taken in the choice of the basis functions used in this basis set.

The authors wish to thank Prof. Dr. M. Kasha for his kind and valuable discussions. A part of this work was supported by a Grant-in-Aid for Scientific Research from the Ministry of Education, Science and Culture of Japan. Computations were carried out at the Computer Center of the University of Tokyo or at the Computer Center of the Institute for Molecular Science.

References

1) L. Pauling, "The Nature of the Chemical Bond," Cornell Univ., Ithaca, N.Y. (1960).
2) N. B. Hannay and C. P. Smyth, *J. Am. Chem. Soc.*, **68**, 171 (1964).
3) A. H. Nethercot, Jr., *Chem. Phys. Lett.*, **59**, 346 (1978).
4) J. Hinze and H. H. Jaffe, *J. Am. Chem. Soc.*, **84**, 540 (1962); J. Hinze, M. A. Whitehead, and H. H. Jaffe, *ibid.*, **85**, 148 (1963).
5) C. A. Coulson, "Valence," Oxford Univ., London (1952).
6) B. Levy, *Chem. Phys. Lett.*, **18**, 59 (1973).
7) K. Ishida, K. Kondo, and T. Yonezawa, *J. Chem. Phys.*, **66**, 2883 (1977).
8) The observed partial charge is obtained by dividing the observed dipole moment (μ) by the observed bond length (r_e) for diatomic molecules (the bond moment is used instead of the dipole moment for water and ammonia). The observed partial charge is not always the "observed ionic character," because the bond moments of lone-pairs make a large contribution to the dipole moment. Recently, Matcha and King [*J. Am. Chem. Soc.*, **98**, 3415 and 3420 (1976)] have discussed the relation between the dipole moment and the scale of the ionic character.
9) W. J. Hehre, R. Ditchfield, and J. A. Pople, *J. Chem. Phys.*, **56**, 2257 (1972); J. D. Dill and J. A. Pople, *ibid.*, **62**, 2921 (1975).
10) R. F. Stewart, *J. Chem. Phys.*, **52**, 431 (1970).
11) J. A. Pople, "A Priori Geometry Predictions," in "Applications of Electronic Structure Theory," ed by H. F. Schaefer, III., Modern Theoretical Chemistry, Plenum Press, New York (1977), Vol. 4.
12) T. H. Dunning, Jr., *J. Chem. Phys.*, **53**, 2823 (1970); **55**, 716 (1971).
13) For example, V. Bonifacic and S. Huzinaga, *J. Chem. Phys.*, **60**, 2779 (1974); P. Coffey, C. S. Ewig, and J. R. Van Wazer, *J. Am. Chem. Soc.*, **97**, 1656 (1975); L. R. Kahn, P. Baybutt, and D. G. Truhlar, *J. Chem. Phys.*, **65**, 3826 (1976).

  Bull. Chem. Soc. Jpn., 54, 971—974 (1981)

A New Interpretation of the Fast Relaxation in a Micellar Solution

Tohru INOUE,* Ryoichi TASHIRO, and Ryosuke SHIMOZAWA
Department of Chemistry, Faculty of Science, Fukuoka University, Fukuoka 814-01
(Received June 16, 1980)

Some contradictions are pointed out in the kinetic parameters of the fast relaxation in a micellar solution deduced from the previously proposed kinetic models. A modification of the previous models is proposed. The proposed model eliminates the contradictions and leads to a consistent interpretation of the experimental results.

In many surfactant solutions there exist two well-separated relaxation processes associated with micelle-monomer equilibria. The fast process has been attributed to the perturbation of the exchange equilibrium of the monomer between micellar and bulk phases. Thus far, two different kinetic models for this process have been widely accepted for the analysis of the fast relaxation data; one of them has been proposed by Wyn-Jones *et al.*,[1] and the other, by Aniansson and Wall.[2] However, as will be shown later, it seems that neither of the two models successfully lead to a consistent kinetic parameter from the experimental data. This paper will show that a consistent interpretation becomes possible by combining the two basic concepts incorporated in the previous models.

The Treatment of Wyn-Jones *et al.*

Wyn-Jones *et al.*[1b] have treated the monomer exchange just as the adsorption-desorption phenomena of a monomer from the bulk phase to the micelles. They assumed that the rate of the entering of the monomer into the micelle is proportional to the product of the monomer concentration in the bulk phase and the area of the micellar surface uncovered by the surfactant molecules, and that the rate of the escape of the monomer from the micelle is proportional to the area of the micellar surface covered by the surfactant molecules. On these assumptions, the rate of the disappearance of the monomer from the bulk phase is given by:

$$-\frac{dA_1}{dt} = k_1 A_1(1-\alpha)S - k_{-1}\alpha S, \quad (1)$$

where A_1 represents the monomer concentration in the bulk phase; k_1 and k_{-1}, the rate constants of the entering and escaping processes of the monomer; S, the sum of the surface area of micelles present in the solution, and α, the fraction of the surface area covered by monomers. Letting a_0 be the molar area of the micellized monomer at the micellar surface, S is given by the following expression:

$$S = \sum_i iA_i\frac{a_0}{\alpha} = \frac{a_0}{\alpha}(C_0 - A_1), \quad (2)$$

where A_i is the concentration of the micelle with the aggregation number i, and C_0, the total surfactant concentration. From Eqs. 1 and 2, the following expression is derived for the relaxation time:

$$\tau_1^{-1} = k_1 a_0\frac{1-\alpha}{\alpha}C_0 - k_{-1}a_0 = k_a C_0 - k_d, \quad (3)$$

where k_a and k_d are the apparent rate constants for the entering and escaping processes of the monomer. Furthermore, from the equilibrium condition, $k_d/k_a = \bar{A}_1 \simeq$ CMC, Eq. 3 is rearranged to:

$$\tau_1^{-1} = k_d\frac{C_0 - \mathrm{CMC}}{\mathrm{CMC}}. \quad (4)$$

Equation 4 well explains the experimental finding that τ_1^{-1} increases linearly with C_0. However, the experimental findings for various surfactant systems indicate that τ_1^{-1} has a positive intercept when the abscissa is taken as $(C_0 - \mathrm{CMC})$.[3-9] Thus, the Wyn-Jones model can only partly explain the experimental results.

The Treatment of Aniansson and Wall

Aniansson and Wall[2] have explicitly taken account of the distribution of the aggregation number, s, for micelles. They assumed that the association rate of the monomer with s-mer is proportional to the product of the concentrations of the monomer and s-mer, and that the dissociation rate of the monomer from s-mer is proportional to the concentration of s-mer. Thus, the rate of flow into the aggregation number, s, is expressed by:

$$\frac{dA_s}{dt} = k_s^+ A_1 A_{s-1} - k_s^- A_s - (k_{s+1}^+ A_1 A_s - k_{s+1}^- A_{s+1}), \quad (5)$$

where A_1 and A_s represent the concentrations of the monomer and s-mer; k_s^+, the rate constant of the formation of s-mer from the monomer and $(s-1)$-mer, and k_s^-, the rate constant of the degradation of s-mer into $(s-1)$-mer. Introducing the relative deviation from the equilibrium concentration, $\xi_s = (A_s - \bar{A}_s)/\bar{A}_s$, and assuming that the distribution curve of the aggregation number is continuous, Eq. 5 is transformed to Eq. 6, which is an analogue of the one-dimensional diffusion equation:

$$\bar{A}_s\frac{\partial\xi(s,t)}{\partial t} = \frac{\partial}{\partial s}k_s^-\bar{A}_s\left[\frac{\partial\xi(s,t)}{\partial s} - \xi_1\right]. \quad (6)$$

Solving Eq. 6 under appropriate boundary conditions and assumptions, the following expression for the relaxation time is finally obtained:

$$\tau_1^{-1} = \frac{k^-}{\sigma^2} + \frac{k^-}{n}\frac{C_0 - \bar{A}_1}{\bar{A}_1}. \quad (7)$$

Furthermore, $k^+\bar{A}_1\bar{A}_{s-1} = k^-\bar{A}_s$, the equilibrium condition, leads to:

$$k^+ \simeq k^-/\bar{A}_1 \simeq k^-/\mathrm{CMC}. \quad (8)$$

In Eqs. 7 and 8, k^- and k^+ are the dissociation and association rate constants, which are assumed to be independent of s for proper micelles, σ, the parameter

characterizing the width of the distribution curve of a micellar size, and n, the average aggregation number.

According to Eq. 7, τ_1^{-1} increases linearly with C_0 and has a definite value at the CMC, which corresponds to k^-/σ^2. This agrees with experimental findings on the behavior of τ_1^{-1} with C_0. In Table 1 the values of the kinetic parameters evaluated from Eqs. 7 and 8 are summarized for several surfactant systems. All the k^- and k^+ values are those reported by Hoffmann *et al.*[4,5,8] The E_A^+'s are the apparent activation energies for the association process, estimated from the temperature dependence of k^+. A precise examination of the kinetic parameters in Table 1 will be given in the subsequent descriptions, (i), (ii), and (iii).

TABLE 1. VALUES OF THE KINETIC PARAMETERS EVALUATED FROM ANIANSSON AND WALL THEORY

Surfactant	Temp/°C	k^{-1}/s^{-1}	k^+/mol^{-1} dm^3 s^{-1}	E_A^+/kJ mol^{-1}
DPI[a]	25	1.6×10^7	3.0×10^9	38
TPCl[a]	15	9.7×10^6	2.4×10^9	30
TPBr[a]	25	6.3×10^6	2.5×10^9	45
HPCl[a]	15	4.4×10^5	4.6×10^8	31
HPBr[a]	25	3.3×10^5	5.5×10^8	29
NaDS[b]	25	1.0×10^7	1.2×10^9	
NaTS[b]	25	9.6×10^5	4.7×10^8	
NaHS[b]	30	6×10^4	1.3×10^8	
$NiDS_2$[c]	25	3.9×10^6	1.6×10^9	44
$CoDS_2$[c]	25	2.6×10^6	1.1×10^9	49

DP=dodecylpyridinium, TP=tetradecylpyridinium, HP =hexadecylpyridinium, DS=dodecylsulfate, TS=tetradecyl sulfate, HS=hexadecyl sulfate.
The k^- and k^+ are those reported by Hoffmann *et al.* a) Ref. 4. b) Ref. 5. c) Ref. 8.

(i) According to Debye,[10] the rate constant to be expected for encounter-controlled ionic reaction is given by:

$$k = \frac{4\pi N_A z_A z_B e^2}{1000\varepsilon kT} \frac{D_A+D_B}{\exp(z_A z_B e^2/\varepsilon rkT)-1}, \quad (9)$$

where D and z are the diffusion coefficient and the electrovalency of the reacting species respectively, r is the center-to-center distance at which two reactants enter into the reaction, ε is the dielectric constant of the medium, and the other symbols have their usual meanings.

Applying Eq. 9 to the present association reaction between a single surfactant ion and a micelle in an aqueous solution, the rate constant is roughly estimated to be 3×10^9—1×10^8 mol^{-1} dm^3 s^{-1} at 25 °C using the appropriate numerical values; the diffusion coefficient of the monomer$\approx1\times10^{-5}$ cm^2 s^{-1}; the diffusion coefficient of the micelle is negligibly small compared with that of the monomer; the micelle radius is 15—20 Å; the micelle charge is $\pm$10—20;[11] the radius of the spherical monomer is 5 Å; hence, $r\approx$20—25 Å and $z_A z_B\approx+$10—20. Thus, the k^+ values in Table 1 imply that the association of the monomer with the micelle is controlled by the diffusion of the monomer to the micelle.

(ii) The apparent activation energy expected for a diffusion-controlled ionic reaction is estimated from Eq. 10:

$$E_A = -RT^2\frac{d\ln\eta}{dT} + RT\left\{LT+\frac{z_A z_B e^2}{\varepsilon rkT}(1-LT) \times[1-\exp(-z_A z_B e^2/\varepsilon rkT)]^{-1}\right\}. \quad (10)$$

Equation 10 is derived from Eq. 9, taking into account the fact that the diffusion coefficient is proportional to kT/η, where η is the viscosity of the medium, and that $\varepsilon=\varepsilon_0\exp(-LT)$, where L is a constant specific to the medium. In the case of an aqueous solution at 25 °C, $-RT^2d\ln\eta/dT\simeq17$ kJ mol^{-1} and $LT\simeq1.4$.[12] By substituting these numerical values into Eq. 10, one obtains E_A values of 13—17 kJ mol^{-1} for the diffusion-controlled association of the monomer with the micelle. The experimentally obtained activation energies listed in Table 1 are obviously too large to be attributed to a diffusion-controlled process.

(iii) It is expected from the conductance data that the diffusion coefficient of a surfactant ion increases by a factor of approximately 1.1 per methylene unit decrease in the chain.[13] On the other hand, as is shown in Table 1, the k^+ value for the homologous surfactant series is increased by a factor of about three to four per methylene unit decrease. Although the larger ionic strength due to the larger CMC of the shorter chain surfactant may cause a certain enhancement of the association rate, since the two reactants have the same sign of the charge, the variation of k^+ in Table 1 with alkyl chain length seems to be much larger than that expected for a diffusion-controlled association reaction.

The facts described in (ii) and (iii) are not in accordance with the order of the magnitude of k^+ estimated by means of the Aniansson and Wall theory. In order to obtain self-consistent rate constants and activation energies, an alternative approach will be proposed in the next section.

Alternative Treatment

Aniansson and Wall have considered that the dissociation rate is proportional to the micelle concentration, and that the association rate is proportional to the product of the monomer concentration and the micelle concentration. However, as assumed by Wyn-Jones *et al.*,[1a] it may be reasonable to regard the dissociation rate of the monomer as proportional to the concentration of the surfactant ion which can dissociate from the micelle, *i.e.*, the product of the concentration of the micelle and the aggregation number. Also, the association rate may be regarded as proportional to the product of the concentration of the monomer and the concentration of the site in the micellar phase into which the surfactant ion can enter. The concentration of the vacant site on the micellar surface may be expressed by a manner analogous to the treatment of Wyn-Jones *et al.* Let a_0 be the area occupied by a monomer on the micellar surface; α, the fraction of the surface area occupied by monomers, and m, the aggrega-

tion number. Then, the vacant area on the surface of a micelle is expressed by $m(1-\alpha)/\alpha \cdot a_0$. We assume here that the number of vacant sites per micelle is given by dividing the vacant area by a_0, *i.e.*, $m(1-\alpha)/\alpha$. Then, the concentration of the vacant site is expressed by $m(1-\alpha)/\alpha \cdot A_m$ for the micelle with the aggregation number m. Thus, the following relations are obtained:

$$\text{association rate} = k_{a,m+1}A_1 m\frac{1-\alpha}{\alpha}A_m = mk'_{a,m+1}A_1A_m \quad (11)$$

$$\text{dissociation rate} = mk_{d,m}A_m, \quad (12)$$

where $k_{a,m+1}$ and $k_{d,m}$ are the elementary rate constants for the monomer to enter into, and to escape from, the micelle with the aggregation number m, and where $k'_{a,m+1}=(1-\alpha)/\alpha \cdot k_{a,m+1}$. Taking account of the probable dependence of $k'_{a,m+1}$ and $k_{d,m}$ on m, and the size distribution of the micelle, the rate expression for the monomer-concentration change in the bulk phase induced by the exchange process is given by:

$$\frac{dA_1}{dt} = \sum_{m'}^{m''}[mk_{d,m}A_m-(m-1)k'_{a,m}A_1A_{m-1}], \quad (13)$$

where the aggregates with the aggregation numbers $m' \leq m \leq m''$ are regarded as micelles and where the concentrations of the oligomers are neglected. Then, according to the usual procedure of relaxation kinetics, one obtains:

$$\frac{d\Delta A_1}{dt} = \sum_{m'}^{m''}mk_{d,m}\left(\Delta A_m-\frac{\bar{A}_m}{\bar{A}_{m-1}}\Delta A_{m-1}-\frac{\bar{A}_m}{\bar{A}_1}\Delta A_1\right), \quad (14)$$

where $\Delta A_1=A_1-\bar{A}_1$, *etc.*; the bar indicates the concentration at the equilibrium for the fast relaxation process, *i.e.*, pseudo-equilibrium. If $k_{d,m}$ is assumed to be independent of m in the region of $m' \leq m \leq m''$ and is replaced by k_d, Eq. 14 leads to:

$$\frac{d\Delta A_1}{dt} = k_d\sum_{m'}^{m''}m\left(\Delta A_m-\frac{\bar{A}_m}{\bar{A}_{m-1}}\Delta A_{m-1}\right) - \frac{k_d}{\bar{A}_1}\sum_{m'}^{m''}m\bar{A}_m\Delta A_1. \quad (15)$$

If we choose the m'—m'' range properly, the first term on the right-hand side of Eq. 15 is transformed to:

$$k_d\sum_{m'}^{m''}m\left(\Delta A_m-\frac{\bar{A}_m}{\bar{A}_{m-1}}\Delta A_{m-1}\right) \simeq k_d\sum_{m'}^{m''}m\Delta A_m\left(1-\frac{\bar{A}_{m+1}}{\bar{A}_m}\right),$$

Assuming the distribution of the aggregates to be Gaussian, *i.e.*,

$$\bar{A}_m = \bar{A}_{\tilde{m}}e^{-(m-\tilde{m})^2/2\sigma^2},$$

where $\tilde{m}$ represents the average aggregation number at the pseudo-equilibrium, and σ^2, the variance of the distribution curve, we obtain:

$$\frac{\bar{A}_{m+1}}{\bar{A}_m} = e^{-1/2\sigma^2}e^{-(m-\tilde{m})/\sigma^2} \simeq 1-\frac{m-\tilde{m}}{\sigma^2}. \quad (16)$$

Equation 16 is obtained by expanding the exponential terms and neglecting the higher terms, since $\sigma \approx 10$, and $|m-\tilde{m}|$ is usually about 20 at most. Thus,

$$\sum_{m'}^{m''}m\left(1-\frac{\bar{A}_{m+1}}{\bar{A}_m}\right)\Delta A_m \simeq \frac{1}{\sigma^2}\sum_{m'}^{m''}m\left(m-\tilde{m}\right)\Delta A_m = \frac{1}{\sigma^2}\sum_{m'}^{m''}\left[\left(m-\tilde{m}\right)^2-\tilde{m}^2+m\tilde{m}\right]\Delta A_m. \quad (17)$$

In Eq. 17, $(m-\tilde{m})^2$ can be neglected compared with $m\tilde{m}$, and the $\tilde{m}^2$ term can be dropped out since $\sum_{m'}^{m''}\Delta A_m=0$ under the assumption that the distribution curve undergoes a parallel shift during the fast relaxation process. Then, under conditions of mass balance, $\Delta A_1+\sum_{m'}^{m''}m\Delta A_m \simeq 0$, the following relation is obtained from Eq. 17:

$$\text{First term of Eq. 15} = -\frac{\tilde{m}k_d}{\sigma^2}\Delta A_1. \quad (18)$$

Furthermore, the total concentration of the surfactant is expressed by:

$$C_0 \simeq \bar{A}_1+\sum_{m'}^{m''}m\bar{A}_m$$

since the concentrations of the oligomers are much smaller than those of the monomer and the micelle. Therefore,

$$\text{Second term of Eq. 15} = -k_d\frac{C_0-\bar{A}_1}{\bar{A}_1}\Delta A_1. \quad (19)$$

From Eqs. 15, 18, and 19, one obtains:

$$\frac{d\Delta A_1}{dt} = -\left(\frac{\tilde{m}k_d}{\sigma^2}+k_d\frac{C_0-\bar{A}_1}{\bar{A}_1}\right)\Delta A_1. \quad (20)$$

Thus, the reciprocal of the fast relaxation time is expressed by:

$$\tau_1^{-1} = \frac{\tilde{m}k_d}{\sigma^2}+k_d\frac{C_0-\bar{A}_1}{\bar{A}_1}, \quad (21)$$

which becomes equivalent to the expression of Aniansson and Wall (Eq. 7) when k_d in Eq. 21 is read as k^-/n. According to Eq. 21, the dissociation rate constant of the monomer from the micelle, k_d, is obtained from the slope of the τ_1^{-1} *vs.* C_0 plot. Here, $\bar{A}_1$ is the monomer concentration at the pseudo-equilibrium, but it may be practically assumed to be the CMC since the relaxation measurements are carried out under the condition of a small perturbation.

The equilibrium condition gives:

$$mk_d\bar{A}_m = (m-1)k'_a\bar{A}_1\bar{A}_{m-1}.$$

Since $\bar{A}_m \simeq \bar{A}_{m-1}$ for a broad distribution ($\sigma \approx 10$) and $m \simeq m-1$ for a usual, proper micelle, one obtains:

$$k'_a \simeq k_d/\bar{A}_1 \text{ and } k_a = \frac{\alpha}{1-\alpha}k'_a. \quad (22)$$

In the above expressions, k'_a and k_a are assumed to be independent of the aggregation number in the region of $m' \leq m \leq m''$. This assumption necessarily implies that α, the fraction of the occupied surface, is virtually invariant with m. Thus, from Eq. 22, k_a, the elementary association rate constant, can be determined if α is known. The precise value of α is not available at the present time, but an approximate estimation of it is possible. According to Tanford's calculation[14] based on geometrial considerations, S/m is 80—70 Å^2 in the range of $50 \leq m \leq 80$ for a globular micelle formed from the surfactant molecule with 12 carbon atoms. There-

TABLE 2. VALUES OF k_d AND k_a EVALUATED FROM Eqs. 21 AND 22

Surfactant	Temp/°C	k_d/s^{-1}	$k_a/mol^{-1}\,dm^3\,s^{-1}$
DPI	25	2.5×10^5	2.0×10^7
TPCl	15	1.1×10^5	1.2×10^7
TPBr	25	7.8×10^4	1.3×10^7
$TPC_3H_7SO_3$ [a]	15	9.6×10^4	1.4×10^7
$TPC_4H_9SO_3$ [a]	15	4.4×10^4	8.6×10^6
$TPC_5H_{11}SO_3$ [a]	15	2.0×10^4	6.0×10^6
HPCl	15	4.0×10^3	1.8×10^6
HPBr	25	3.3×10^3	2.4×10^6
NaDS	25	1.6×10^5	8.1×10^6
NaTS [b]	25	1.2×10^4	2.5×10^6
NaHS	30	6×10^2	5.6×10^5
$NiDS_2$	25	4.0×10^4	6.9×10^6
$CoDS_2$	25	2.4×10^4	4.2×10^6

a) From the data in Ref. 6. b) From the data in Refs. 5 and 9.

fore, taking the value of 2—3 Å as a radius of the head group, α can be estimated to be 0.2—0.4.

Table 2 lists the k_d and k_a values evaluated from Eqs. 21 and 22 for several surfactant systems. For the evaluation of k_a, we adopted $\alpha=0.3$. Although the k_a values have some uncertainty associated with α, they may be reliable at least to the order of magnitude. When α is varied from 0.2 to 0.4, k_a increases by a factor of 2.7.

As is shown in Table 2, the alternative treatment proposed in this work gives k_a values of the order of 10^6—10^7 $mol^{-1}\,dm^3\,s^{-1}$, smaller by about 10^2 than the k^+ values deduced from the Aniansson-Wall model. This difference in rate constants results from the m and α factors in Eq. 11 ($m\approx10^2$ and $\alpha\approx0.2$—0.4). These values of k_a suggest the non-diffusion-controlled association reaction of a monomer with a micelle and are reasonably consistent with the facts described in (ii) and (iii) of the preceding section.

It is considered that the association proceeds *via* the activated state, which exists in the course of the incorporation of a monomer present at the micellar surface into the interior. This activated state probably consists of the hydrocarbon tail of a monomer being partly inserted into the micellar hydrocarbon core, just to the depth where further incorporation tends to be favored by the hydrophobic interaction. For the attainment of this state, a vacant space must be formed in the hydrocarbon core where the terminal group of a hydrocarbon tail can enter. Furthermore, it is necessary for the water molecules attached to the hydrocarbon tail of the entering monomer to be released. Thus, it is likely that the energies required for such processes contribute mainly to the activation energy for the association reaction.

References

1) a) P. J. Sams, E. Wyn-Jones, and J. Rassing, *Chem. Phys. Lett.*, **13**, 233 (1972); b) J. Rassing, P. J. Sams, and E. Wyn-Jones, *J. Chem. Soc., Faraday Trans. 2*, **70**, 1247 (1974).

2) a) E. A. G. Aniansson and S. N. Wall, *J. Phys. Chem.*, **78**, 1024 (1974); b) E. A. G. Aniansson and S. N. Wall, *ibid.*, **79**, 857 (1975).

3) R. Folger, H. Hoffmann, and W. Ulbricht, *Ber. Bunsenges. Phys. Chem.*, **78**, 986 (1974).

4) H. Hoffmann, R. Nagel, G. Platz, and W. Ulbricht, *Colloid Polym. Sci.*, **254**, 812 (1976).

5) E. A. G. Aniansson, S. N. Wall, M. Almgren, H. Hoffmann, K. Kielmann, W. Ulbricht, R. Zana, J. Lang, and C. Tondre, *J. Phys. Chem.*, **80**, 905 (1976).

6) H. Hoffmann, H. Nüsslein, and W. Ulbricht, "Micellization, Solubilization, and Microemulsions," ed by K. L. Mittal, Plenum Press, New York (1977), Vol. 1, p. 263.

7) S.-K. Chan, U. Herrmann, W. Ostner, and M. Kahlweit, *Ber. Bunsenges. Phys. Chem.*, **81**, 396 (1977).

8) W. Baumüller, H. Hoffmann, W. Ulbricht, C. Tonder, and R. Zana, *J. Colloid Interface Sci.*, **64**, 418 (1978).

9) T. Inoue, Y. Shibuya, and R. Shimozawa, *J. Colloid Interface Sci.*, **65**, 370 (1978).

10) P. Debye, *Trans. Electrochem. Soc.*, **82**, 265 (1942).

11) K. Shinoda, T. Nakagawa, B. Tamamushi, and T. Isemura, "Colloidal Surfactants," Academic Press, New York (1963), p. 16.

12) E. A. Moelwyn-Hughes, "The Chemical Statics and Kinetics of Solutions," Academic Press, New York (1971), Chaps. 5 and 7.

13) a) A. N. Campbell and R. Lakshminarayanan, *Can. J. Chem.*, **43**, 1729 (1965); b) J. S. Clunie, J. F. Goodmann, and P. C. Symons, *Trans. Faraday Soc.*, **63**, 754 (1967).

14) C. Tanford, *J. Phys. Chem.*, **76**, 3020 (1072).

  Bull. Chem. Soc. Jpn., 54, 975—979 (1981)

A Magnetic Resonance Study of the Fe_2O_3/Al_2O_3 Catalyst in a CO-N_2O Reaction

Miki Niwa,* Kunihiko Yagi, and Yuichi Murakami

Department of Synthetic Chemistry, Faculty of Engineering, Nagoya University, Furo-cho, Chikusa-ku, Nagoya 464

(Received July 18, 1980)

A magnetic resonance study was performed in order to determine the phase of iron oxide supported on Al_2O_3 and to measure *in situ* the surface conditions during the reaction. The irreversible transition of α-Fe_2O_3 into Fe_3O_4 by the reduction of the supported catalyst and the reversible transition between Fe_3O_4 and γ-Fe_2O_3 were confirmed at 280 °C. The spectrum appearing at $g=2.03$ and having the line width of about 1000 gauss clearly showed ferrimagnetic behavior; it could be attributed to the ferrimagnetic resonance (FMR) of Fe_3O_4 and/or γ-Fe_2O_3. Kinetic study suggested that the CO–N_2O reaction took place in the oxidation-reduction mechanism. The concentration of γ-Fe_2O_3 was calculated from not only the kinetic equation, but also the *in situ* measurement of the FMR signal; these values were consistent. The γ-Fe_2O_3/Al_2O_3 had nearly the same activity as the α-Fe_2O_3/Al_2O_3, whereas the unsupported γ-Fe_2O_3 had a lower activity than the α-Fe_2O_3. Such a difference in catalytic activity was discussed in comparison with other oxidation reactions.

It is well known that iron and iron oxides are differentiated into ferromagnetic and paramagnetic inorganic compounds according to their chemical composition.[1] Fe metal, Fe_3O_4 (magnetite), and γ-Fe_2O_3 (maghemite) are ferromagnetic or ferrimagnetic, and they have large magnetic moments. A Magneto-chemical investigation of catalysts has been already carried out by Selwood.[2] However, it seems that such magnetic measurements should be replaced by magnetic-resonance studies because the latter have a higher sensitivity and greater availability. Nevertheless, only a few reports about magnetic resonance studies of catalysis or adsorption have been published. For example, Loy and Noddings have investigated the hydrogen chemisorbed on a nickel catalyst.[3] The ferro-magnetic resonance (FMR) of nickel is very simple, because nickel metal should be only ferromagnetic. On the other hand, iron compounds are fairly complex, because three different phases can be observed by the FMR, as has been described above. However, the magnetic resonance of iron oxides provides a unique phenomenon, and it is particularly suitable for the measurement of solids containing small quantities of these species.

The purpose of the present study is to demonstrate the usefulness of the FMR study of the CO–N_2O reaction on Fe_2O_3 supported by the Al_2O_3 catalyst. The FMR measurements as well as the kinetic study will be used to show the reaction mechanism and the transition of the solid phases during the CO–N_2O reaction. Furthermore, the difference in catalytic activity between α- and γ-Fe_2O_3 in this reaction will be discussed.

Experimental

Catalyst and Reagent. The Al_2O_3 (Sumitomo KHD) was calcined at 450 °C for 3 h and then dipped into a solution of $Fe(NO_3)_3 \cdot 9H_2O$. After drying at 110 °C, this was calcined at 450 °C for 2 h in the stream of an O_2–N_2 (1 : 4) mixture. The final Fe_2O_3 content in the supported Fe_2O_3/Al_2O_3 catalyst was in the range between 0.15 and 13.0 wt%. Unsupported iron oxide was prepared from precipitates of $Fe(OH)_3$ obtained by the neutralization of a $Fe(NO_3)_3 \cdot 9H_2O$ solution with ammonia water. The calcination was carried out at 500 °C for 5 h in the air.

The N_2O (99.8%) and CO (99.9%) were supplied from the Takachiho Chemical Co., Ltd., and were used without further purification.

Apparatus and Procedure. An *in situ* cell, made with a Pyrex glass outer tube (3 mm i.d.) and inner tube (1 mm o.d.) was placed in an ESR cavity and heated with temperature-variant equipment. A reactant gas cosisting of N_2O, CO, Ar, and He was allowed to flow into the reactor, and the products were directly analyzed by means of a gas chromatograph connected with the reactor cell. A Porapak Q column (2.8 m) for CO_2 and N_2O and Molecular Sieve 13X column (3.5 m) for Ar, N_2, and CO were used at room temperature for the separation. The ESR was measured by means of a JEOL X-band spectrometer (JEX-ME-1X).

A conventional pulse technique was performed with helium carrier gas deoxidized through a Ti-sponge bed at 700 °C.

The amount of CO adsorbed was measured gravimetrically with a quartz spring balance.

Results and Discussion

Measurement of Phases of Supported Fe_2O_3 by Magnetic Resonance and Stoichiometry. The Fe_2O_3 supported on Al_2O_3 catalysts with different loadings have been measured in the ESR cavity at room temperature up to 280 °C. Figure 1 shows the ESR spectra of the fresh Fe_2O_3/Al_2O_3 catalyst, with 6.7% by weight Fe_2O_3 loading, as an example. As is shown clearly, this spectrum can be fitted to the simulated one assuming three differenet species with Lorentz line shapes. The computation was performed with a FACOM 230-75 at Nagoya University Computation Center. Obviously, the signal showed a greater intensity at room temperature than at 280 °C, as is usually observed in the ESR measurement of paramagnetic species.

The spectrum observed here is approximately identical with the spectrum of the iron impurity in ammonium-exchanged NaY-zeolite previously reported by Derouane *et al.*[4] According to their identification, there are three distinct paramagnetic species, *i.e.*, Fe^{3+} species in the alumino-silicate framework at $g=4.3$, an exchangeable Fe^{3+} ion at $g=2.1$, and another precipitated Fe^{3+} compound with a strong spin-exchange interaction at $g=2.3$. Consequently, the observed spectrum in Fig. 1 may be composed of these identified species. The

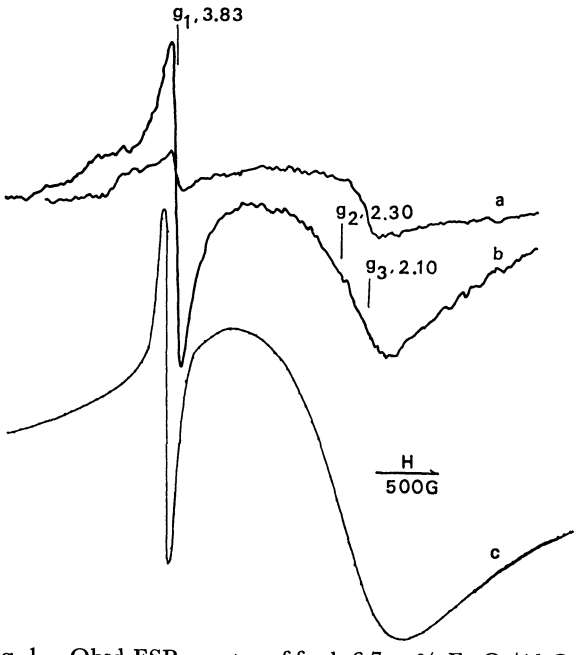

Fig. 1. Obsd ESR spectra of fresh 6.7 wt% Fe_2O_3/Al_2O_3 catalyst at 280 °C (a) and room temp (b) and simulated spectrum (c), which was obtained by the assumption of g_1, g_2, and g_3 signals whose parameters were 70, 1500, and 700 G (1 G = 10^{-4} T) as line width and 0.005, 0.933, and 0.062 as normalized coefficient of linear combination, respectively.

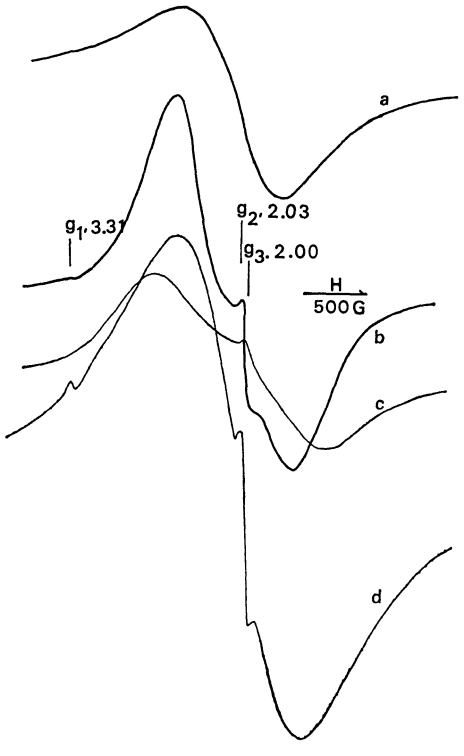

Fig. 2. Obsed ESR spectra of treated 6.7 wt% Fe_2O_3/Al_2O_3 catalyst in the reduced state at 280 °C (a) and in the oxidized state at 280 °C (b) and room temp (c). Simulated spectrum (d) was obtained by the assumption of g_1, g_2, and g_3 signals whose parameters were 50, 960, and 50 G (1 G = 10^{-4} T) as line width and 0.0002, 0.999, and 0.001 as normalized coefficient of linear combination, respectively.

substituted Fe^{3+} species may be shifted lower from g= 4.3 to g=3.8 because of the difference in the support.

The sample of Fe_2O_3 was then reduced by the current of CO at 280 °C; after confirming the steady state of ESR signal, it was reoxidized by N_2O at 280 °C. Such a treatment of the catalyst drastically changed the ESR spectrum, the intensity being magnified by about 100 times (Fig. 2). The spectrum of the oxidized sample in Fig. 2-b contained three different species, while that of the reduced sample lost the sharp signal at g=2.00. The oxidized one showed a broader signal at room temperature than at 280 °C.

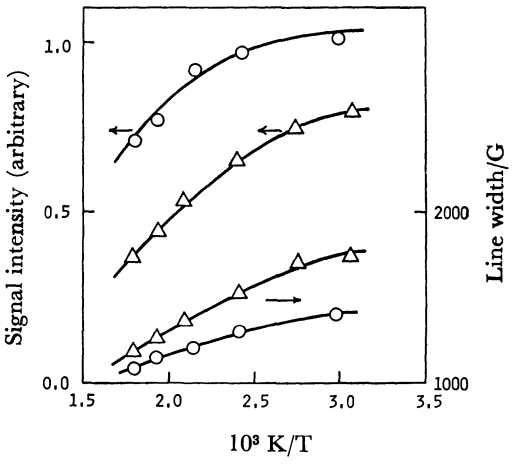

Fig. 3. Dependence of the signal intensity and the line width on the measurement temp using oxidized (○) and reduced (△) samples of the treated catalyst.

The spectra of such reduced and oxidized samples of the treated 6.7-wt% Fe_2O_3/Al_2O_3 were examined in more detail at different temperatures. After the sample had been reduced or oxidized with a CO–N_2 or N_2O–N_2 mixture at 280 °C respectively, it was sealed and subjected to measurement. In Fig. 3, the intensity and line-width of the g_2 signal are plotted against the reciprocal absolute temperature. Remarkably, the line width increased with a decrease in the temperature. Such a dependence does not indicate the paramagnetic property, but the ferro- (or ferri-) magnetic property of the samples. The small deviation from the linearity between the signal intensity and the reciprocal absolute temperature may also show the ferro- (or ferri-) magnetic property.

A pulse technique was then used to determine the phases of the treated Fe_2O_3/Al_2O_3. The injection of CO into the bed of reoxidized 6.7-wt% Fe_2O_3/Al_2O_3 formed CO_2 at 280 °C. Successive injections of CO reduced the catalyst by the depletion of the catalyst oxygen. The total amount of the CO_2 formed on 150 mg of the catalyst was 29.6 μmol. This was nearly in agreement with the expected value, 21 μmol, in which the iron oxide was assumed to be reduced to the magnetite; *i.e.*,

$$3Fe_2O_3 + CO \longrightarrow 2Fe_3O_4 + CO_2.$$

Consequently, the phase of the reduced catalyst may be identified as Fe_3O_4.

As has previously been indicated,[5] the unsupported

α-Fe_2O_3 was reduced by carbon monoxide to Fe_3O_4 at a low temperature such as 280 °C. However, the magnetite was not reversibly reoxidized to γ-Fe_2O_3 unless it was oxidized above 400 °C.[6] In other words, the reduction-reoxidation of the Fe_2O_3 can be described as;

$$\alpha\text{-}Fe_2O_3 \xrightarrow[\text{red}]{} Fe_3O_4 \underset{\text{red}}{\overset{\text{oxi}}{\rightleftharpoons}} \gamma\text{-}Fe_2O_3 .$$

The magnification of the signal by the reduction-reoxidation and its temperature dependence are, therefore, correlated with the change in the magnetic property, *i.e.*, from the paramagnetic Fe^{3+} ion to ferrimagnetic Fe_3O_4 and γ-Fe_2O_3. The sharpening of the line-width at a high temperature, as is the case of a treated catalyst, has already been indicated by Singer in the measurement of the magnetite.[7] Furthermore, it was found by the pulse method that the reoxidized catalyst could be only reduced to the level of the Fe_3O_4. Therefore, the signal at $g=2.03$ (g_2) of the treated catalyst is attributed to the ferrimagnetic-resonance (FMR) spectra of γ-Fe_2O_3 and Fe_3O_4 in the oxidized and reduced samples respectively. The g-values of γ-Fe_2O_3 and Fe_3O_4 were not distinguished from that of the pure oxide; they have been reported to be 1.96[8] and 2.13[9] respectively.

X-Ray diffraction, Mössbauer spectroscopy, or XPS has been used to distinguish the phases of iron oxide.[5,10] Infrared spectroscopy has also been recommended to identify them[11] However, these analytical methods can not be used for the supported catalysts, for the iron oxide content is too low to be detected. In fact, the X-ray diffraction of the Fe_2O_3/Al_2O_3 catalyst revealed only aluminum oxide as the support. Furthermore, it was found that the ir spectroscopy could not be used because of the intense absorption of the Al–O band. The ESR or the magnetic resonance is the most suitable for this case, for iron oxides should exhibit different resonances with high intensities depending on their magnetic properties.

On other samples of the Fe_2O_3/Al_2O_3 catalyst with a different loading of iron oxide, nearly the same spectrum as that shown in Fig. 1 was observed in the fresh condition. Although the intensities of the substituted Fe^{3+} ion at $g=3.8$ increased with the loading up to about 9 wt%, the principal signal at $g=2.3$ showed nearly the same intensity regardless of the iron-oxide content, while it turned into the FMR signal upon reduction-reoxidation treatment. The sharp signal of the treated catalyst at $g=2.00$ (g_3) which was observed in the oxidized condition became outstanding in the catalyst with a low iron content. Because this signal has a broader line-width at room temperature than at 280 °C, it might be attributed to ferromagnetic Fe metal, which may be considered to disappear upon the formation of $Fe(CO)_x$ in the reduction by CO.

In Situ *Measurement of the Reversible Transition between γ-Fe_2O_3 and Fe_3O_4.* By the use of an *in situ* cell, the FMR spectrum was measured *in situ* during the reduction and reoxidation of the catalyst at 280 °C. A Fe_2O_3/Al_2O_3 catalyst supported by 6.7-wt% Fe_2O_3 which had been treated by CO and N_2O was measured. The intensity of the signal at $g=2.03$ due to γ-Fe_2O_3

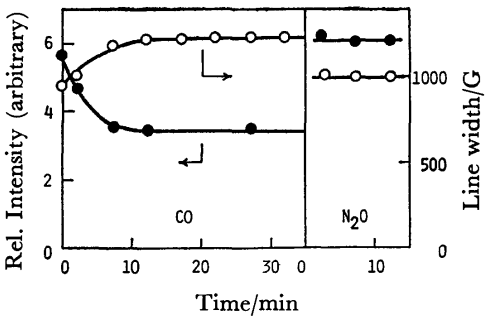

Fig. 4. Variation of signal parameters with the course of reduction by CO or oxidation by N_2O over the ferrimanetic Fe_2O_3/Al_2O_3 catalyst.

gradually decreased in flowing carbon monoxide (Fig. 4) and attained a steady state 15 min later. Simultaneously, the line-width also increased. As has been described above, the reduced state of the catalyst was attributed to Fe_3O_4. The reduced catalyst was then reoxidized by the flowing of N_2O. As is shown in Fig. 4, the signal intensity was increased rapidly by the reoxidation, and the resultant spectrum was in good agreement with the initial one. Consequently, it can be said that the transition between γ-Fe_2O_3 and Fe_3O_4 proceeds reversibly and that the rate of reoxidation is obviously faster than that of reduction. Furthermore, the intensity of Fe_3O_4 is evaluated to be 0.60 times that of γ-Fe_2O_3. The relative ratio of these signal intensities will be used in the next section of this paper to calculate the relative concentration of γ-F_2O_3. The relative intensity was measured over as wide a range of the spectrum as possible in order to minimize the error which would be contained in the evaluations of the intensity of the broad spectrum. *In situ* measurement afforded the advantage of the precise determination of the relative intensity, because the sample was measured under exactly the same conditions except for the oxidation state of the catalyst.

Kinetics and in Situ *Measurement of the CO–N_2O Reaction.* The reduction of dinitrogen monoxide by carbon

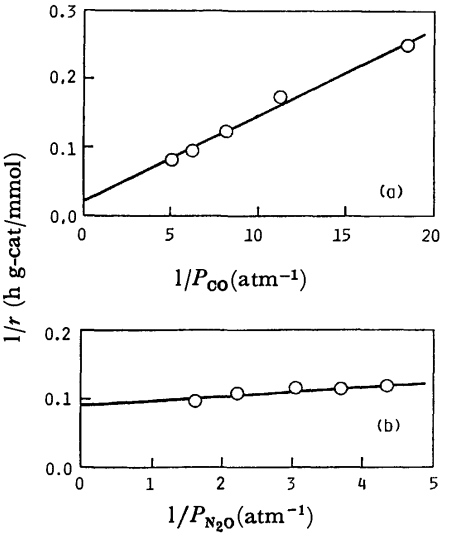

Fig. 5. Kinetics of the CO–N_2O reaction on the treated catalyst at 270 °C; Partial pressures of CO (a) or N_2O (b) were varied with other conditions kept const.

monoxide on the ferrimagnetic 6.7 wt% Fe_2O_3/Al_2O_3 catalyst was then investigated kinetically using the *in situ* cell. Simultaneously, the FMR spectrum was measured in order to monitor the condition of the catalyst.

Although the CO–N_2O reaction should form equimolar amounts of CO_2 and N_2, the CO_2 exceeded slightly the N_2 in this experiment. This was caused by the impurity of the oxygen in the cylinder of N_2O (0.16 vol%). Consequently, the rate of CO–N_2O reaction is here described by the rate of N_2 formation. Figure 5 shows the kinetics of the N_2O–CO reaction at 270 °C, in which the partial pressures of CO or N_2O are shown to vary in Fig. 5-a and Fig. 5-b respectively. The reciprocal plots between the rate of formation and the partial pressure both gave straight lines.

By taking into consideration the reversible transition between γ-Fe_2O_3 and Fe_3O_4, this reaction was assumed to proceed according to the following oxidation-reduction mechanism;

$$CO + \gamma\text{-}Fe_2O_3 \xrightarrow[k_1]{} CO_2 + Fe_3O_4 \quad (1)$$

$$N_2O + Fe_3O_4 \xrightarrow[k_2]{} N_2 + \gamma\text{-}Fe_2O_3. \quad (2)$$

In the stationary state, we abtain;

$$\frac{1}{r_{N_2}} = \frac{1}{k_1 P_{CO}} + \frac{1}{k_2 P_{N_2O}}, \quad (3)$$

where r_{N_2} denotes the rate of N_2 formation and where P_{CO} and P_{N_2O} show the partial pressures of CO and N_2O respectively. Furthermore, the concentration of γ-Fe_2O_3 during the reaction can be described as

$$\left[\gamma\text{-}Fe_2O_3\right] = \frac{1}{1 + \frac{k_1 P_{CO}}{k_2 P_{N_2O}}}. \quad (4)$$

Based on Eq. 3, the values of k_1 and k_2 can be calculated from the slope and intercept in Fig. 5. The k_1 and k_2 calculated from Fig. 5-a were 76 and 270 (mmol/h g-cat atm) respectively. Likewise, 84 and 170 (mmol/h g-cat atm) were obtained from Fig. 5-b as the values of k_1 and k_2. Because these values of the rate constant were approximately consistent, the mechanism described above seems reasonable.

The simultaneous observation of the FMR signal showed that the reaction proceeded in a state close to the γ-Fe_2O_3, for the signal intensity decreased only a little, even when there was more CO than N_2O in the gas phase. This is in agreement with the rapid reoxidation by N_2O described above and is supported by the greater value of k_2 (reoxidation step) than k_1 (reduction step).

The relative concentration of γ-Fe_2O_3 can be estimated from the kinetic equation (4) as well as from the observed FMR signal intensity (see the previous section); the concentrations of γ-Fe_2O_3 we have obtained are compared in Fig. 6. These are consistent, though a little deviation from linearity was observed in a reduced condition.

The precise determination of the concentration of γ-Fe_2O_3 from FMR is rather difficult in this case, for the signal does not vary much. Such an *in situ* measurement of the catalyst should, however, have a potential

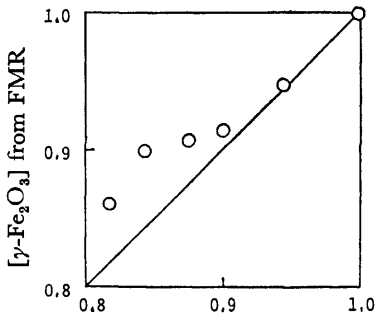

Fig. 6. Plot for the comaprison between calcd concns of γ-Fe_2O_3 based on the kinetics and the FMR signal.

ability to show direct evidence for help in solving a given problem. In this paper, the reaction mechanism shown above for the CO–N_2O reaction is supported by the *in situ* measurement of the FMR spectra.

Reactivity of α- and γ-Fe_2O_3. Misono *et al.* have already shown that γ-Fe_2O_3 has a higher activity for the oxidative dehydrogenation of 1-butene than does α-F_2O_3.[5] They suspected, because of its structural characteristics, that the high reactivity of γ-Fe_2O_3 probably originates from the rapid uptake and removal of oxygen. The reactivities of α- and γ-Fe_2O_3 were measured also in the CO–N_2O reaction. Figure 7 shows

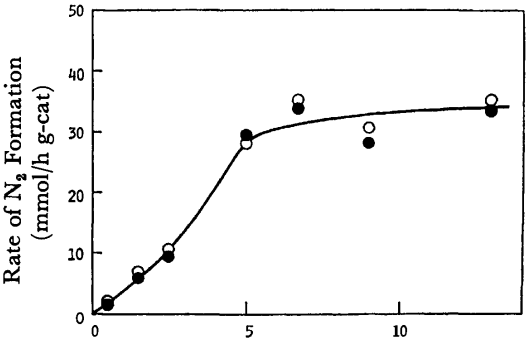

Fig. 7. Activity of α- (●) and γ- (○) Fe_2O_3/Al_2O_3 catalysts having different loadings in the CO–N_2O reaction at 280 °C in the *in situ* cell. Partial pressures of N_2O and CO were 0.23 and 0.22 atm, respectively, and 0.14 atm of Ar was contained as the internal standard for the chromatography.

the activity of α- and γ-Fe_2O_3/Al_2O_3 catalysts of various loadings in the CO–N_2O reaction. The reaction was performed in the *in situ* cell, and the phase of the catalyst was confirmed by ESR. The catalytic activity increased linearly with iron-oxide content up to about 5 wt%, while it kept nearly constant in higher concentrations. As is clearly shown, no difference was observed between the activities of α- and γ-Fe_2O_3/Al_2O_3.

In order to confirm this fact, various reactions, *i.e.*, the CO–N_2O reaction, the oxidative dehydrogenation of 1-butene, and the oxidation of hydrogen, were carried out on both supported and unsupported iron oxides by

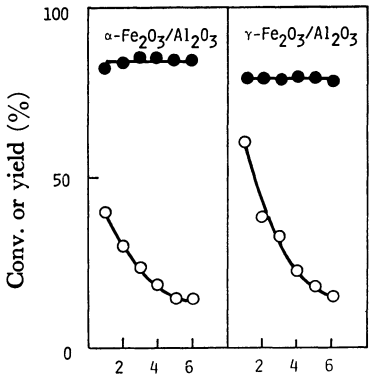

Fig. 8. Comparison of catalytic activities between α- and γ-Fe_2O_3/Al_2O_3 supported by 6.7 wt % Fe_2O_3; 0.2 ml of $CO-N_2O$ (1 : 1) (●) or 0.1 ml of 1-butene (○) was injected successively into the catalyst bed at 280 °C, and conversion into CO_2 and butadiene were plotted *vs.* number of pulse.

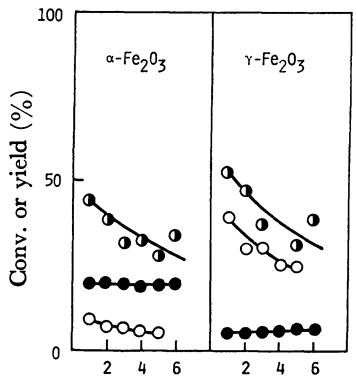

Fig. 9. Comparison of catalytic activities between α- and γ-Fe_2O_3 in the pulse reaction of $CO-N_2O$ (●), 1-butene (○) or H_2 (◑); Oxidation of hydrogen was done at 313 °C, and other were referred to in Fig. 8.

the pulse technique. Figure 8 shows the activities of α- and γ-Fe_2O_3/Al_2O_3 for the $CO-N_2O$ reaction and the oxidative dehydrogenation of 1-butene. Furthermore, Figure 9 shows the activity of unsupported oxide in these oxidation reactions. Both α- and γ-Fe_2O_3/Al_2O_3 had similar activities in the $CO-N_2O$ reaction (Fig. 8). In the case of pure iron oxide, on the other hand, α-Fe_2O_3 had a higher activity than γ-Fe_2O_3 in the $CO-N_2O$ reaction (Fig. 9). The high activity of γ-Fe_2O_3 in the oxidative dehydrogenation of 1-butene which was reported by Misono *et al.*[5] was reproducible also in this study. However, the difference between them was very small in the supported catalyst.

Not only the $CO-N_2O$ reaction, but also the oxidative dehydrogenation of 1-butene, is considered to take place in the oxidation-reduction mechanism, as has been mentioned above and described previously by Misono *et al.*[5] Furthermore, the specific surface areas of α- and γ-Fe_2O_3 were exactly the same, 18 m^2/g. Nevertheless, the catalytic activity of α- and γ-Fe_2O_3 was reversed in these reactions. Therefore, different characteristics controling these activities should be considered.

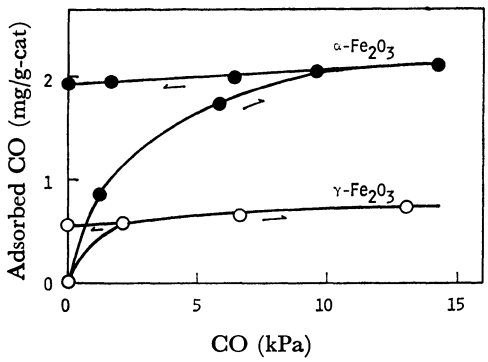

Fig. 10. Adsorption isotherms of CO on α- (●) and γ- (○) Fe_2O_3 at room temp, following the arrow in the figure.

The amount of CO adsorbed on iron oxides may be one of the reasons, because the saturated adsorbed amounts of CO on α- and γ-Fe_2O_3 at room temperature were 1.93 and 0.55 (mg/g-cat), and such a difference was analogous to the activity profile of the $CO-N_2O$ reaction. As is shown in Fig. 10, the adsorption of CO was irreversible at this temperature, and probably it was stabilized as a carbonyl complex with an exposed iron ion. In other words, the metal ions responsible for the adsorption of carbon monoxide are exposed on the surface of α-Fe_2O_3 more than on that of γ-Fe_2O_3 and seem to contribute to the high activity of the $CO-N_2O$ reaction.

As is shown in Fig. 9, γ-Fe_2O_3 had a higher activity than α-Fe_2O_3 also in the hydrogen oxidation, which can be regarded as the simplest oxidation reaction, and therefore as the reaction which is the most sensitive to the activity of surface oxygen. This adds support to the consideration by Misono *et al.* about the high activity of oxygen of γ-Fe_2O_3. On the other hand, the $CO-N_2O$ reaction may be influenced by the activation of carbon monoxide by the surface iron ion.

References

1) M. M. Scieber, "Experimental Magnetochemistry," Interscience Publ., New York (1967), p. 157.
2) P. W. Selwood, "Adsorption and Collective Paramagnetism," Academic Press, New York (1962).
3) B. R. Roy and C. R. Noddings, *J. Catal.*, **3**, 1 (1964).
4) E. G. Derouane, M. Mestdagh, and L. Vielvoye, *J. Catal.*, **33**, 169 (1974).
5) M. Misono, Y. Nozawa, and Y. Yoneda, Preprint of VIIth Intern. Congress on Catalysis, (1976), p. 386.
6) B. Klimaszewski and J. Pietrzak, *Bull. Acad. Sci. Ser. Sci. Math., Astr. Phys.*, **17**, 51 (1969).
7) L. S. Singer and D. N. Stamires, *J. Chem. Phys.*, **42**, 3299 (1965).
8) A. H. Morrish and E. P. Valstyn, *J. Phys. Soc. Jpn.*, **17** Suppl. B-1, 392 (1962); in the study of Klimaszewski *et al.*[6] also, the shift by the transition of Fe_3O_4 to γ-Fe_2O_3 was hardly observable.
9) L. R. Bickford, Jr., *Phys. Rev.*, **78**. 449 (1950).
10) D. V. Sokolskii, G. K. Alekseeva, A. S. Khlystov, V. I. Yashkevich, and G. K. Kotova, *Reac. Kinet, Catal. Lett.*, **6**, 59 (1977).
11) T. Maekawa and M. Terada, *Nippon Kinzoku Gakkai-shi*, **29**, 421 (1965).

The Effect of Crystallite Size of Nickel on the Enantioselectivity of Modified Nickel Catalysts

Yuriko NITTA, Fumimaro SEKINE, Toshinobu IMANAKA, and Shiichiro TERANISHI*

Department of Chemical Engineering, Faculty of Engineering Science, Osaka University, Toyonaka, Osaka 560

(Received August 6, 1980)

Enantioselective hydrogenation of methyl acetoacetate to methyl 3-hydroxybutyrate with various unsupported nickel catalysts modified by (2*R*,3*R*)-tartaric acid was studied under mild conditions in order to elucidate the dependence of the selectivity upon the surface states of the catalysts. The catalyst with the larger crystallite size has the higher enantioselectivity, presumably because of the higher probability to obtain large ensembles of regularly-arranged nickel atoms in the catalyst surface for the modifier to adsorb strongly and regularly. The nickel boride catalyst has very low enantioselectivity, mainly due to its amorphous structure. The detrimental effect of additives (B, P, and Al in Ni–B, Ni–P, and R–Ni catalysts) was explained as the effect of their lowering the crystallinity of the catalysts.

There have been many studies on the effects of the structure of modifiers, modifying conditions, and reaction conditions on the enantioselectivities of modified nickel catalysts, mainly for the hydrogenation of methyl acetoacetate (MAA) to methyl 3-hydroxybutyrate (MHB).[1-3] On the other hand, it is well known that the enantioselectivity of modified catalysts is affected strongly by the preparation methods or the conditions of pretreatments of the metal catalysts.[4-6] However, only a few studies have established a correlation of enantioselectivity to the structure or the surface state of the modified catalysts.

We have been studying the activities and selectivities of various nickel catalysts, such as nickel boride (Ni–B), nickel phosphide (Ni–P), Raney nickel (R-Ni), Urushibara nickel(U-Ni), and the other nickel blacks, for the hydrogenation of olefins, aldehydes, and ketones by comparing with the surface states of the catalysts.[7] In the present study, we examined the enantioselective hydrogenation over various nickel catalysts in order to establish the correlation between the selectivity and the surface structure of nickel catalysts. The enantioselective hydrogenation with heterogeneous catalysts has usually been investigated by using nickel catalysts and the reaction seems very sensitive to the structure of the catalysts. (2*R*,3*R*)-Tartaric acid (TA) and MAA were selected as a modifier and a reactant in this study because most previous experiments have used them.

The Ni–B catalyst, which is known to have similar activities and selectivities to the R-Ni catalyst in many hydrogenation reactions, has a very low enantioselectivity compared to that of the R-Ni catalyst. The reason for this low enantioselectivity will be discussed later.

Experimental

Catalyst Preparation. *Nickel Boride(Ni–B)*: $Ni(CH_3COO)_2 \cdot 4H_2O$ (4.24 g) in 50 ml of distilled water was reduced with 20 ml of $NaBH_4$ (1.94 g) aqueous solution at 30 °C with vigorous stirring (P-1 method according to Brown[8]). This catalyst is called Ni–B-1 here. After 10 min, the precipitated catalyst was washed 3 times with portions of 50 ml of distilled water before modification. The catalyst was separated by centrifugation after each wash. In order to vary the surface concentration of boron in the resulting catalyst,[7f] $NiCl_2 \cdot 6H_2O$ was used instead of nickel acetate. The Ni–B-2 catalyst was prepared in 95% ethanol instead of water (P-2 method).

Nickel Phosphide(Ni–P): Nickel hydroxide, obtained by the addition of NaOH aqueous solution into 30 ml of $NiCl_2 \cdot 6H_2O$ (4.1 g) aqueous solution, was reduced with NaH_2PO_2 (5.5 g) in water at about 72 °C according to a method described by Sada.[9] This catalyst is abbreviated as Ni–P-1. For the preparation of Ni–P-2 catalyst, the reduction of nickel hydroxide was carried out in 50% ethyl alcohol instead of water.[7f] The precipitated catalyst was washed in the same way as the Ni–B catalyst was.

Raney Nickel (R-Ni): Ni–Al (42 : 58) alloy (1.43 g) was added during 10 min in small portions to 60 ml of 20% NaOH aqueous solution, usually at 70 °C, and this mixture was kept at the temperature for 20 min with gentle stirring. The leached catalyst was washed 5 times with portions of 100 ml of distilled water by decantation. The alloy was also leached at different temperatures in order to make the catalysts with different surface states.[7g]

Nickel Blacks (D–Ni and H–Ni): D–Ni catalysts were prepared by decomposing $Ni(HCOO)_2 \cdot 2H_2O$ (9.5 g) at 300 °C for 1.5—6 h (usually 3 h) followed by hydrogen flushings. NiO (3.8 g) was reduced under a hydrogen stream of 8 l/h at 350 °C for 1.5 h to prepare H–Ni catalyst. After cooled to room temperature in the hydrogen atmosphere, the nickel black was washed twice with distilled water before modification.

Modification. The modification of a catalyst was carried out at 83 °C by soaking a freshly prepared catalyst in a 1.6% aqueous solution of TA(pH=5.1) for 1.5 h with occasional shaking according to the method described by Izumi *et al.*[1,10] Several kinds of amino acids were also used as modifiers to check the enantioselectivity of modified nickel boride catalyst. After the modification, the catalyst was rinsed once with water, twice with methanol, and then once with ethyl acetate (10 ml portion of each).

Hydrogenation. 10 ml of MAA was added to the described amount of catalyst in 10 ml of ethyl acetate and hydrogenated at 60 °C in a 50 ml glass autoclave (TEM-U-50, Taiatsu Glass Industry Co., LTD.) equipped with a 200 ml gas tube and with a magnetic stirring system. The starting pressure of hydrogen was 10 kg/cm² and the pressure dropped to about 3 kg/cm² at 100% conversion. Almost all conversions were 100%. Ethyl acetate, used as a solvent, was dried and distilled before use. All the reactants were obtained from commercial sources and used without further purification.

Analysis. The reaction product was filtered off and distilled under reduced pressure. The conversion and the purity of the distilled product was measured with GLC (Shimadzu model 4APT) with a 2 m column of 20% PEG

20M on Celite 545.

The optical rotation (α_D) of the distilled product was determined with a Union PM-101 automatic digital polarimeter at room temperature (about 25 °C) in a 0.1 dm cell. The optical yield (OY) of (−)-MHB was calculated from the observed α_D value by the equation $OY=(\alpha_D/22.95)\times 100$.[11]

The X-ray diffraction pattern of the catalyst filtered after the reaction was measured with a Shimadzu VD-1 diffractometer after wetting the catalyst with ethylene glycol to avoid the oxidation of nickel metal. The mean crystallite size of nickel (D_c) was calculated from the half width of the peak from the (111) plane of nickel metal.

BET surface areas of the catalysts were measured separately by N_2 adsorption at 77 K after washing with acetone and after evacuation by a diffusion pump for 4 h at ambient temperature.

The surface compositions of some catalysts used were estimated from the analysis of X-ray photoelectron spectra (XPS) with a Hitachi 507 photoelectron spectrometer. The detailed procedures were reported elsewhere.[7f]

The amount of TA adsorbed on the modified catalyst was determined colorimetrically with Hitachi 200-20 spectrophotometer by the method reported by Christian[12] and by Harada *et al.*[13]

Results and Discussion

For the enantioselective hydrogenation of MAA with Ni–B-1 catalyst modified by TA, preliminary experiments showed that the effects of modification conditions (pH, temperature, and modifying time) and of hydrogenation conditions (temperature, H_2 pressure) on the optical yields of MHB were similar to those for the hydrogenation with modified R-Ni catalyst reported previously.[1] However, as shown in Table 1, the enantioselectivity of the modified Ni–B catalyst was very low compared to that of modified R-Ni catalyst for all the substrates and modifiers examined. The enantioselectivity of Ni–P catalyst was also very low. The negative effect of water added to the reaction mixture on the optical yield of (−)-MHB was previously reported for the enantioselective hydrogenation of MAA with modified R-Ni.[14] Therefore, the effect of the water which was contained in larger quantities within the Ni–B than within the R-Ni catalyst was examined by drying the Ni–B catalyst after modification or by adding a small amount of molecular sieve to the reaction mixture to remove the water. The result showed that the water contained within the Ni–B catalyst was not the cause of the low enantioselectivity of the catalyst. No racemization of the product on the Ni–B catalyst under the reaction conditions was observed.

Using a modified R-Ni catalyst, Harada *et al.*[5] suggested that aluminum derivatives on the catalyst surface decrease the enantioselectivity of the catalyst and that the exclusion of aluminum or related metal compounds from the catalyst surface is an essential factor for obtaining a highly enantioselective catalyst.

Table 1. Product optical purities for some hydrogenations with modified nickel catalysts

Catalyst	Modifying variables			Hydrogenation variables		Conversion	Optical activity	
	Modifier	pH	Temp/°C	Substrate[a]	Time/h	%	$[\alpha]_D^{25}$	OY/%[b]
1 H–Ni	TA	5.1	83	MAA	147	94.5	−12.90	56.2
2 D–Ni	TA	5.1	83	MAA	188	100	−9.70	42.3
3 R–Ni	TA	5.1	83	MAA	41	100	−5.87	25.7
4 Ni–B-1	TA	5.1	83	MAA	21	100	−0.69	3.0
5[c] Ni–B-1	TA	5.1	83	MAA	19	100	−0.73	3.2
6 Ni–B-2	TA	5.1	83	MAA	22	100	−1.29	5.6
7 Ni–P-1	TA	5.1	83	MAA	43	99	−0.33	1.5
8 Ni–P-2	TA	5.1	83	MAA	44	97.2	−0.43	1.9
9 Ni–B-1	TA	5.1	0	MAA	22	99.2	−0.38	1.7
10 Ni–B-1	L-Glu	5.1	0	MAA	24	98.1	−0.37	1.6
11 Ni–B-1	L-Met	6.0	0	MAA	64	99	−0.58	2.5
12 Ni–B-1	L-Phe	6.3	0	MAA	19	100	+0.87	3.8
13 Ni–B-1	L-Glu	5.1	0	DAOH	168	99	+0.90	5.4
14[c] Ni–B-1	L-Met	7.3	0	DAOH	17	100	+0.71	4.3
15 Ni–B-1	L-Phe	5.7	0	DAOH	46	100	+0.58	3.5
16[c] D–Ni	TA	5.1	83	DAOH	97	35	−2.55	15.3
17[c] R–Ni	TA	5.1	83	DAOH	17	100	−1.11	6.7
18[c] Ni–B-2	TA	5.1	83	DAOH	18	100	−0.47	2.8
19[c] Ni–B-1	TA	5.1	83	DAOH	20	100	−0.44	2.7
20[c] Ni–P-1	TA	5.1	83	DAOH	19	100	−0.29	1.7
21 Ni–B-1	L-Phe	5.8	0	APH	25	100	+0.18	0.4
22 Ni–B-1	TA	5.1	83	APH	24	100	+0.11	0.2
23 Ni–B-1	TA	5.1	83	EAA	27	100	−0.82	3.4
24 Ni–B-1	TA	5.1	83	EMK	27	99	+0.05	0.4

a) MAA: Methyl acetoacetate, DAOH: Diacetone alcohol, APH: Acetophenone, EAA: Ethyl aceto acetate, EMK: Ethyl methyl ketone. b) Optical yields (OY) were calculated using the absolute rotations $[\alpha]_D^{25}=22.95$, 16.6, 44.3, 24, and 13 for the hydrogenation products of MAA, DAOH, APH, EAA, and EMK respectively. c) Hydrogenation was carried out under the initial H_2 pressure of 90 kg/cm^2 instead of 10 kg/cm^2.

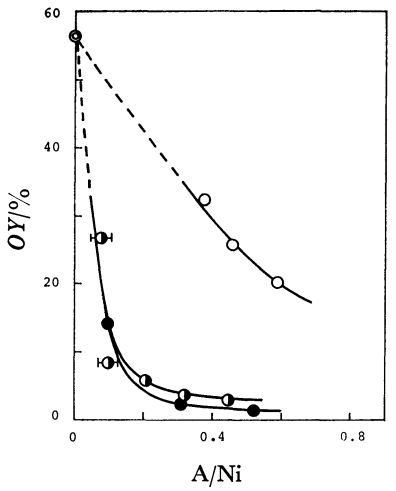

Fig. 1. Relation between optical yields and surface contents of additives in nickel catalysts. A/Ni: atomic ratio of Al, B, or P to Ni, ○: R-Ni, ◑: Ni-B, ●: Ni-P, ◎: H-Ni.

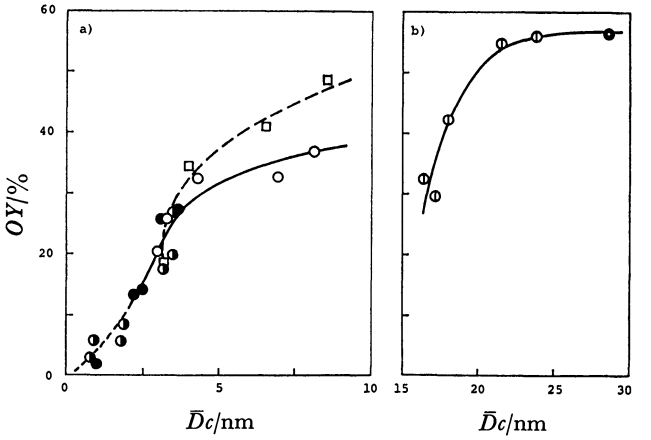

Fig. 2. Dependence of optical yields on mean crystallite sizes of nickel in various catalysts.
○: R-Ni, ◑: Ni-B, ●: Ni-P, ⓓ: D-Ni, ◎: H-Ni, —: R-Ni by Gross and Rys.[4]

Therefore, the relations between the enantioselectivity of R-Ni, Ni–B, and Ni–P catalysts and the surface contents of Al, B and P in each catalyst were investigated here. Since catalytic activities and selectivities should be compared with the states on the surface (not in the bulk) of the catalysts, we measured the surface contents of additives in various nickel catalysts by XPS.

It can be seen from Fig. 1 that the enantioselectivity of the Ni–B or Ni–P catalyst increases with decrease of the surface content of B or P in each catalyst similarly to the case of the R-Ni catalyst. The enantioselectivities of the catalysts refluxed in 20% NaOH aqueous solution for 2—6 h in order to remove the additives approach the selectivity of H–Ni catalyst, which has essentially no additives on the catalyst surface. However, the extents of the decrease in the selectivity of the Ni–B and Ni–P catalysts with the increase of additives are so large compared with that of the R-Ni catalysts that the low enantioselectivities of those catalysts are not directly attributable to the amount of additives.

On the other hand, the Ni–B and Ni–P catalysts have been reported to have amorphous structures considerably different from the structure of the R-Ni catalyst and to have similar selectivities in hydrogenation reactions.[7d,7h]

Fish and Ollis suggested, from their results on an electrochemical technique for measuring the surface coverage of TA on nickel, that a reactant molecule adsorbed on an optically selective site requires more metal surface area than one adsorbed at an optically nonselective site.[15] Alternatively this suggestion may be stated as follows: the optically selective site must consist of an ensemble of regularly-arranged nickel atoms for reactant molecules and modifiers to adsorb strongly and regularly. Accordingly, amorphous surfaces of catalysts, such as the Ni–B catalyst, are supposed to exhibit a low enantioselectivity because of the low probability of finding such ensembles. A higher optical yield is expected for a catalyst with a larger crystallite size, by assuming that the surface structure reflects directly the bulk structure of the catalyst.

With these considerations in mind, the dependence of the enantioselectivities of various nickel catalysts modified by TA upon the crystallite sizes of nickel metal in them has been investigated.

As can be seen from Fig. 2, the enantioselectivities of the catalysts are clearly related to the mean crystallite sizes of nickel in the catalysts, although the crystallite sizes in the Ni–B and Ni–P catalysts are too small to calculate exactly by the XRD method. In addition, the removal of Al, B, or P from the R–Ni, Ni–B, or Ni–P catalyst by refluxing the catalyst in 20% NaOH aqueous solution led to the larger crystallite size of nickel and correspondingly to the higher enantioselectivity of the catalyst. Also noteworthy is that the plots for the three kinds of catalysts of different preparative methods (*i.e.*, Ni–B, Ni–P, and R–Ni) in Fig. 2a) are almost all on the same line, while the plots in Fig. 1 are on different lines for the three kinds of catalysts. Moreover, the data of *OY* of (−)-MHB reported by Gross and Rys[4] for a similar enantioselective hydrogenation over various R-Ni catalysts, under slightly different experimental conditions from ours, were found to be in good correlation to the crystallite sizes of nickel in the catalysts, as shown in Fig. 2a). The relatively low enantioselectivities of the D–Ni catalysts with the crystallite sizes under 20 nm in Fig. 2b) are probably due to the impurities from decomposed nickel(II) formate still remaining on the nickel surface after the short decomposition time of 1.5—3 h. A similar dependence of enantioselectivity on the crystallite size of nickel was observed for the hydrogenation of diacetone alcohol (4-hydroxy-4-methyl-2-pentanone), as can be seen from Table 1 (Nos. 16—20).

These findings are in accordance with the report by Klabunovskii for the enantioselective hydrogenation of ethyl acetoacetate (EAA) on Ru/SiO_2 catalysts with the particle sizes of Ru smaller than 4.5 nm,[6c] although the enantioselectivity should be compared, not with the particle size, but with the crystallite size, because of the reason discussed above.

These results suggest that the size of ensembles of

regularly-arranged nickel atoms on the catalyst surface is a more important factor for a catalyst to be enantioselective than the surface content of additives is. The detrimental effect of additives (B, P, and Al) shown in Fig. 1 can be attributed to the effect of their lowering the crystallinity of the catalysts. The difference between the influence of Al and that of B or P is explained by the fact that the aluminum in R-Ni segregates in the catalyst as Al_2O_3[7g] and that it does not lower the crystallinity of the catalyst so much as B or P in the Ni–B or Ni–P catalyst.

Table 2. The amounts of adsorbed (2*R*,3*R*)-tartaric acid on various nickel catalysts

Catalyst	Sa[a]	Amount of adsorbed acid[b]		OY[c]
	m^2 g-Ni^{-1}	10^{-2} mmol × g-Ni^{-1}	10^{-3} mmol × m^{-2}	%
Ni–B-1	21.8	10.7	4.91	3.0
Ni–B-1[d]	21.8	4.65	2.13	0.7
Ni–B-2	38.2	7.03	1.84	5.6
Ni–B-2[e]	62.7	3.16	0.50	26.7
R-Ni	100.4	5.71	0.57	25.7
D-Ni	10.5	1.06	1.01	42.2
H-Ni	3.4	0.35	1.03	56.2

a) BET surface area. b) Modifying conditions: pH=5.1, 83 °C, 1.5 h. c) The optical yield of (−)-MHB. d) The catalyst was washed 6 times with water after modification instead of 2 times. e) The catalyst was refluxed for 6 h in 20% NaOH aq solution before modification.

In Table 2, the amounts of adsorbed TA on various nickel catalysts measured after modification are shown, together with the surface areas and the enantioselectivities of the catalysts. The amount of adsorbed TA on unit surface area of nickel in the Ni–B catalyst is rather more than the amount on the R-Ni or the other catalysts. When the Ni–B-1 catalyst was washed much more than usual after modification, it lost more than half of the adsorbed acid and there was a drastic decrease of the enantioselectivity of the catalyst. The remaining amount of the adsorbed acid was, however, still much more than that on the R-Ni catalyst. These facts suggest that the adsorption strength of the acid on Ni metal in the surface of the Ni–B catalyst is rather weak and that the adsorbed acid remaining after the heavy washing may be bound to the boron in the catalyst by esterification, contributing nothing to the enantioselectivity of the catalyst. On the other hand, the Ni–B-2 catalyst freed of the boron by refluxing in alkaline solution before modification had a much higher enantioselectivity than the untreated catalyst, in spite of the much smaller amount of the adsorbed acid on the treated catalyst. As for the catalysts in Table 2 other than the Ni–B, the increase of the adsorbed modifier results in the increase of the enantioselectivity.

These facts show that the total amount of the adsorbed modifier is not a direct factor affecting the enantioselectivity of modified catalysts, but the amount of the modifier adsorbed strongly and regularly on the surface of a large crystallite is important for the enantioselectivity. Thus, the poor enantioselectivities of modified Ni–B and Ni–P catalysts can be explained mainly by the exceedingly low crystallinity of these catalysts.

A binary boride catalyst, Co–Ni–B (Co : Ni=6 : 4), had only a negligible degree of enantioselectivity (OY=0.8%). This is also attributable to the more amorphous structure of the binary boride catalyst than that of Ni–B catalyst, as reported before.[16] The much lower enantioselectivity of Raney-Cu–Ru catalyst (Ru= 0.01—0.5%) than those of Raney-Cu and Raney-Ru catalysts reported by Klabunovskii[17] may also be explained in terms of the crystallite size of the catalyst.

From the discussion above, it can be concluded that the catalyst with the larger crystallite size has the higher enantioselectivity, presumably because of the higher probability to find ensembles of regularly-arranged nickel atoms (*i.e.*, optically selective sites) on the catalyst surface.

Recently, Klabunovskii[18] proposed a model of the active sites for enantioselective hydrogenation located not on the plane but on the edge in the catalyst surface. In order to make clear the more detailed structure of optically selective sites in the catalyst surface, further studies will be required.

As for the reaction rate, the catalyst of the higher enantioselectivity has the lower hydrogenation activity, as can be deduced from the data in Table 1. This is easily understandable from the fact that the catalyst with the larger crystallite size generally has the smaller specific surface area. In order to obtain a highly enantioselective catalyst with a high hydrogenation activity, it seems a good idea to use supported nickel catalysts. Moreover, the supported catalysts are very useful in order to elucidate the relation between the surface states and the enantioselectivities of the catalysts, since it is possible to vary the surface states or the size distribution of metal particles of the supported catalysts by employing various preparation methods. With these expectations in mind, further studies on the effect of preparation methods upon the enantioselectivity of supported nickel catalysts are now in progress.

The authors wish to thank Professors Yoshiharu Izumi and Akira Tai, Osaka University, for their helpful suggestions, and Dr. Yasuaki Okamoto of our laboratory for his valuable advice.

References

1) Y. Izumi and A. Tai, "Stereo-differentiating Reactions," Kodansha, Tokyo, and Academic Press, New York (1971), Sec. 5.1.1, and references cited therein.

2) Y. Orito, S. Niwa, and S. Imai, *Yuki Gosei Kagaku Kyokai Shi*, **34**, 236 and 672 (1976); **35**, 753 (1977).

3) G. V. Smith and M. Musoiu, *J. Catal.*, **60**, 184 (1979).

4) L. H. Gross and P. Rys, *J. Org. Chem.*, **39**, 2429 (1974).

5) T. Harada, S. Onaka, A. Tai, and Y. Izumi, *Chem. Lett.*, **1977**, 1131.

6) a) E. I. Klabunovskii, V. I. Neupokoev, and Yu. I. Petrov, *Izv. Akad. Nauk SSSR, Ser. Khim.*, **1971**, 2067; b) E. I. Klabunovskii, A. A. Vedenyapin, N. D. Zubareva, N. P. Sokolova, and Yu. M. Talanov, *React. Kinet. Catal. Lett.*, **2**, 291 (1975); c) A. A. Vedenyapin, E. I. Klabunovskii, Yu. M. Talanov, and G. Kh. Areshidze, *Izv. Akad. Nauk SSSR, Ser. Khim.*, **1976**, 2628.

7) a) Y. Murakami, S. Kishida, T. Imanaka, and S. Teranishi, *Nippon Kagaku Zasshi*, **89**, 263 (1968); b) Y. Nitta, T. Imanaka, and S. Teranishi, *Kogyo Kagaku Zasshi*, **74**, 777 (1971); c) T. Imanaka, Y. Nitta, and S. Teranishi, *Bull. Chem. Soc. Jpn.*, **46**, 1134 (1973); d) Y. Nitta, T. Imanaka, and S. Teranishi, *Nippon Kagaku Kaishi*, **1976**, 1362; e) Y. Nitta, Y. Okamoto, T. Imanaka, and S. Teranishi, *ibid.*, **1978**, 634; f) Y. Okamoto, Y. Nitta, T. Imanaka, and S. Teranishi, *J. Chem. Soc., Faraday Trans.* **1**, **75**, 2027 (1979); g) Y. Okamato, Y. Nitta, T. Imanaka, and S. Teranishi, *ibid.*, **76**, 998 (1980); h) Y. Okamoto, Y. Nitta, T. Imanaka, and S. Teranishi, *J. Catal.*, **64**, 397 (1980).

8) C. A. Brown and H. C. Brown, *J. Am. Chem. Soc.*, **85**, 1003 and 1005 (1963).

9) S. Sada, *Kogyo Kagaku Zasshi*, **71**, 957 (1968).

10) Y. Izumi, T. Harada, T. Tanabe, and K. Okuda, *Bull. Chem. Soc. Jpn.*, **44**, 1418 (1971).

11) T. Harada and Y. Izumi, *Chem. Lett.*, **1978**, 1195.

12) G. D. Christian, *Talanta*, **16**, 255 (1969).

13) T. Harada, A. Tai, M. Yamamoto, H. Ozaki, and Y. Izumi, *Proc. 7th Int. Congr. Catal., Tokyo*, **1980**, A24.

14) T. Ninomiya, *Bull. Chem. Soc. Jpn.*, **45**, 2545 (1972).

15) M. J. Fish and D. F. Ollis, *J. Catal.*, **50**, 353 (1977).

16) Y. Nitta, T. Imanaka, and S. Teranishi, *Bull. Chem. Soc. Jpn.*, **53**, 3154 (1980).

17) E. I. Klabunovskii, A. A. Vedenyapin, and G. Kh. Areshidze, *Izv. Akad. Nauk SSSR, Ser. Khim.*, **1975**, 2311.

18) E. I. Klabunovskii, A. A. Vedenyapin, E. I. Karpeiskaya, and V. A. Pavlov, *Proc. 7th Int. Congr. Catal., Tokyo*, **1980**, A26; E. I. Klabunovskii and A. A. Vedenyapin, *Zh. Fiz. Khim.*, **51**, 3005 (1977).

Studies on Chemiluminescent Compounds. I. Syntheses of Acyl-substituted Anthracene Derivatives and Their Chemiluminescence

Toshiyuki HIRAMATSU,* Toshiaki HARADA, and Teizo YAMAJI

Products Development Institute, Teijin Limited, 2-1 Hinode-cho, Iwakuni, Yamaguchi 740

(Received August 14, 1980)

New anthracene derivatives with a –COCH– group, such as 1,5-dipropionylanthracene, 1,8-dipropionylanthracene, 1,5-di-isobutyrylanthracene, 1,8-diisobutyrylanthracene, 1,5-bis[3-(methoxycarbonyl)propionyl]-anthracene, 1,8-bis[3-(methoxycarbonyl)propionyl]anthracene, 1,5-bis(cyclohexylcarbonyl)anthracene, 3,7-diisopropyl-1,5-diisobutyrylanthracene, and 5-dimethylamino-4-isobutyryl-1-methoxyanthracene (**10**) have been synthesized. Their direct chemiluminescences were studied by air oxidation in alkaline solutions. The properties of the chemiluminescence have been found to be influenced by not only the class of the C–H bond adjacent to the carbonyl group but also by the electronic properties of the aromatic ring system, the solvent, and the additive. **10** exhibited the longest chemiluminescence. This chemiluminescent phenomenon might be explained by a chemically initiated electron exchange luminescence (CIEEL) mechanism.

Since luminescence is an emission from an electronic excited state, the necessary excited molecule must be produced in any chemiluminescent reaction. Recent investigations suggest that effective excited molecules (singlet state) are produced in decomposition reactions of cyclic peroxides such as 1,2-dioxetanes, and 1,2-dioxetanones.[1] These intermediate peroxides are thought to exist also in bioluminescence. Most of the bioluminescence processes are remarkably efficient and show direct luminescence from the air oxidation of luciferins. The quantum yield for an enzymatic process as in a firefly is approximately 0.88 einstein mol^{-1}.[2]

Kamiya and Sugimoto studied indirect chemiluminescence: the transfer of energy from activated carbonyl intermediates in the oxidation of compounds having –COCH– groups to 9,10-dibromoanthracene or 9,10-diphenylanthracene. They observed strong luminescence when the C–H bond adjacent to the carbonyl group is tertiary C–H. They also reported that 4-hydroxy or 4-methoxy-substituted aromatic ketones gave effective singlet excited states. They did not, however, mention the effect of the catalyst and the additives on the chemiluminescence of the compounds mentioned above.[3] They recently reported the direct chemiluminescence of 9,10-diisobutyrylanthracene in the alkaline air oxidation, but they did not mention the effects of substitution in the anthracene ring, of basicity of the catalyst, and of the additives.[3]

In the practical use of chemiluminescence, the radiation of light of 500—520 nm is preferred because of strong human sensitivity to light in this region. Direct chemiluminescence in the benzene system fails to produce visible radiation of such a long wave length. But the use of anthracene compounds makes it possible to radiate the light of 500 nm and to make a practical light source for human beings. The lack of the investigation of details in the mechanism of chemiluminescence of anthracene type ketones motivated our present work.

We report in this paper the effects of substitution in anthracene ring, of basicity of catalyst, and of the additives, with the hope of the development of light for practical use.

To investigate the direct chemiluminescence mechanism, anthracene compounds **1**—**10** were synthesized and examined in various alkali catalyst oxidations with additives such as crown ether. We will discuss the chemiluminescence mechanism based on the observed chemiluminescence spectra. We suggest that an excited singlet state carbonyl may be generated by the air oxidation of these anthracenes. The mechanism is explained in terms of chemically initiated electron exchange luminescence (CIEEL).[4]

Results and Discussion

In order to investigate the substituent effects on the direct chemiluminescence from the air oxidation of anthracene derivatives, we newly synthesized several compounds listed in Tables 1, 2, and 3 using the usual Friedel-Crafts acylation.[5]

Reaction of Acyl Chloride with Anthracenes. The reaction of anthracene derivatives with several acyl chlorides and anhydrous aluminum chloride in anhydrous carbon disulfide afforded the corresponding compounds **1**—**10**. In most cases, carbonyl groups are introduced at the 1-position or at both 1 and 5-positions of anthracene.[6] However, in the reaction of anthracene with isobutyryl chloride, alkylation reaction also occurred in part to afford 3,7-diisopropyl-1,5-diisobutyrylanthracene (**9**). The reaction of isopropyl chloride with 1,5-diisobutyrylanthracene (**3**) in the presence of excess anhydrous aluminum chloride gave the same alkylated diketone **9**. A similar alkylation in the Friedel-Crafts acylation reaction has been reported by Rothstein and Saville.[7] They suggested that alkylation took place *via* the decarbonylated acyl chloride-aluminum chloride addition complex ($R^+ \cdot AlCl_4^-$) when less reactive aromatic compounds were used. Compound **9** might be produced in the same manner. Anthracene and more reactive anthracene derivatives such as 1-dimethylamino-5-methoxyanthracene were easily acylated. The acylation of 1,5-diisobutyrylanthracene did not proceed. The reaction gave only a dialkyl diacyl derivative. This might be due to the deactivation by two carbonyl groups.

Chemiluminescence in the Air Oxidation of Anthracenes. The direct chemiluminescence was observed upon adding potassium *t*-butoxide (^{t}BuOK) in *t*-butyl alcohol or potassium hydroxide (KOH) in water to these ketones in various aerated solvents, such as

TABLE 1. THE CHEMILUMINESCENCE WITH 1,5-DISUBSTITUTED ANTHRACENES BY AIR OXIDATION[a)]

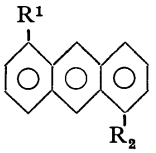

R_1, R_2		Base	Life time / min	Light emission	Colors of resulting solns
$COCH_3$	(1)	^{t}BuOK or KOH	≈0	none	dark purple (in DMSO)
$COCH_2CH_3$	(2)	^{t}BuOK or KOH	≈0	very weak	dark purple (in DMSO or DBP)
$COCH(CH_3)_2$	(3)	^{t}BuOK or KOH	≈0.5	medium	dark orange (in DMSO or DBP)
COC_6H_{11}	(4)	^{t}BuOK	≈0.5	medium	dark orange (in DMSO)
$COCH_2CH_2CO_2Me$	(5)	^{t}BuOKor KOH	≈0.5	weak	dark purple (in DMSO)

a) A solution of ^{t}BuOK (0.35 mmol) in *t*-butyl alcohol (1 ml) was added to a stirred solution of anthracenes (0.001 mmol) in dimethyl sulfoxide (1 ml) or dibutyl phthalate (1 ml) at 25 °C or a solution of KOH (0.35 mmol) in H_2O (0.1 ml) was added to a stirred solution of anthracenes (0.001 mmol) in dimethyl sulfoxide (1.9 ml) or dibutyl phthalate (1.9 ml) at 25 °C.

TABLE 2. THE CHEMILUMINESCENCE WITH 1,8-DISUBSTITUTED ANTHRACENES BY AIR OXIDATION[a)]

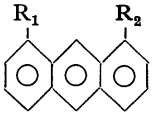

R_1, R_2		Base	Life time / min	Light emission	Colors of resulting solns
$COCH_2CH_3$	(6)	^{t}BuOK or KOH	≈0	very weak	dark purple (in DMSO)
$COCH(CH_3)_2$	(7)	^{t}BuOK or KOH	≈0.5	weak	dark orange (in DMSO)
$COCH_2CH_2CO_2Me$	(8)	^{t}BuOK	≈0	very weak	dark orange (in DBP)

a) Table 1 footnote a).

TABLE 3. THE CHEMILUMINESCENCE WITH 1,5-DISUBSTITUTED ANTHRACENES BY AIR OXIDATION[a)]

Compd		Base	Life time / min	Light emission	Colors of resulting solns
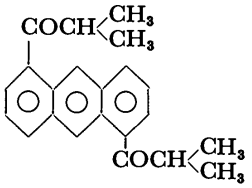	(3)	^{t}BuOK or KOH	≈0.5	medium	dark orange (in DMSO orDBP)
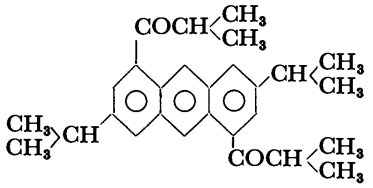	(9)	^{t}BuOK or KOH	≈1	very strong	orange (in DMSO)
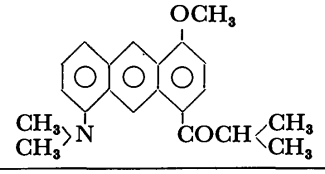	(14)	^{t}BuOK	≈30	very strong	greenish yellow (in DMSO)

a) Table 1 footnote a).

dimethyl sulfoxide (DMSO), *N,N*-dimethylformamide (DMF), benzene, or phthalic esters. The chemiluminescent responses were changed by the experimental conditions—*i.e.* by the solvent, by the concentrations of ketones and catalysts, more essentially by the electronic properties of the aromatic ring systems, and by the chemical structures of the ketones. The properties of chemiluminescence examined in DMSO or dibutyl phthalate (DBP) solution, using ^{t}BuOK or KOH as a base, are listed in Tables 1, 2, and 3 for 1,5-disubstituted, 1,8-disubstituted, and multi-substituted anthracenes, respectively, together with the colors of the resulting solutions. The results in the tables show that the efficiency of the emission is influenced both by the class of the C–H bond adjacent to the carbonyl group and by the electronic properties of the aromatic ring systems. The former was discussed by Kamiya *et al.*, who showed that a compound possessing a C–H bond adjacent to carbonyl group gave the most intensive chemiluminescence.[3] Our results showed the similar behavior of the chemiluminescent reaction. From Table 3, it can be seen that electron-donating groups such as dimethylamino or methoxy groups strongly increase quantum yield and lengthen chemiluminescence time. Thus, 5-dimethylamino-4-isobutyryl-1-methoxyanthracene (**10**) exhibits the most intensive and longest chemiluminescence among all of these ketones.

We also examined the fluorescence and chemiluminescence spectra of ketones **3**, **9**, and **10**, which are shown in Figs. 1, 2, and 3. In Figs. 1 and 2, the chemiluminescent spectra of the ketones **3** and **9** are red-shifted compared to those of the two air-oxidated products. Contrary to this, in Fig. 3, the chemiluminescent spectrum of ketone **10** shows a pattern closely similar to the fluorescent spectrum of the methyl ester of its air-oxidated product. The final products of the air oxidation of these ketones were the corresponding acids.

In order to obtain the best conditions for the chemi-

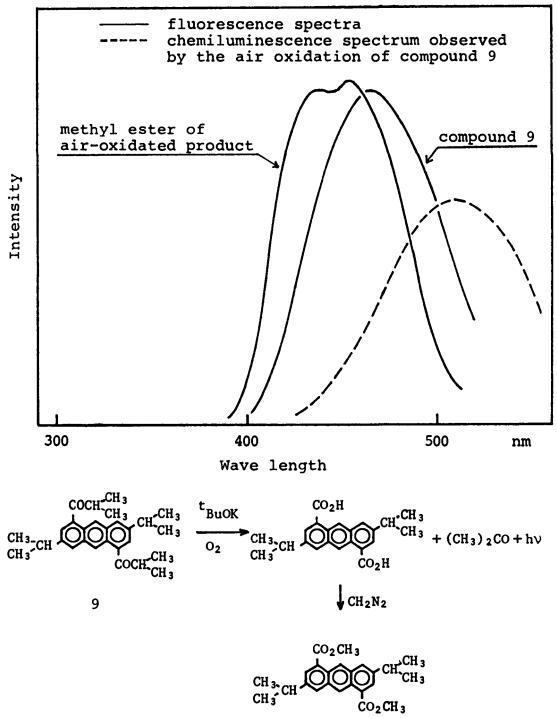

Fig. 2. Fluorescence and chemiluminescence spectra of 3,7-diisopropyl-1,5-diisobutyrylanthracene (**9**) and its oxidated product.

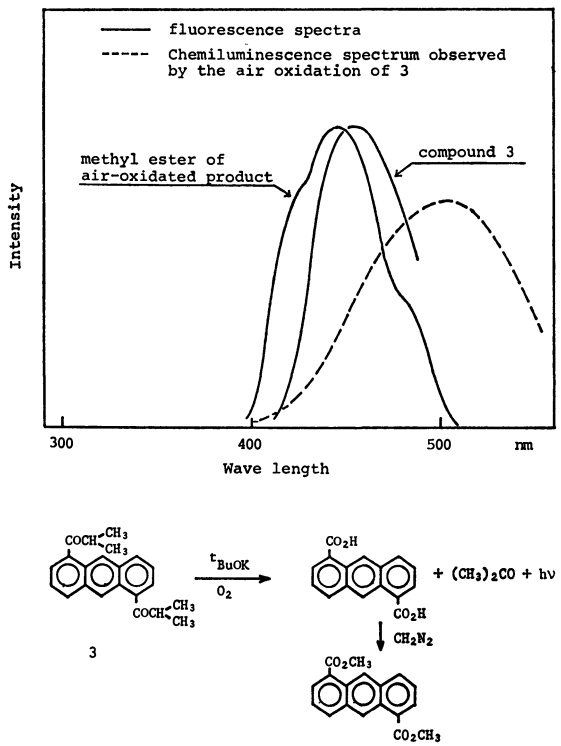

Fig. 1. Fluorescence and chemiluminescence spectra of 1,5-diisobutyrylanthracene (**3**) and its oxidated product.

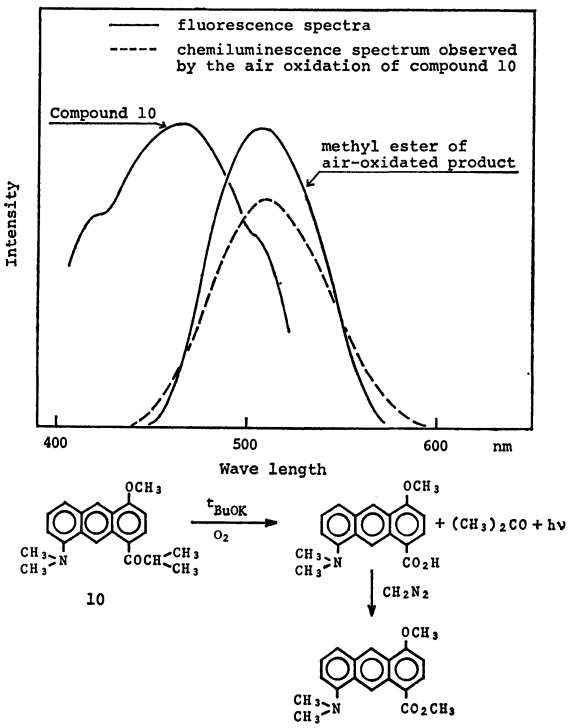

Fig. 3. Fluorescence and chemiluminescence spectra of 5-dimethylamino-4-isobutyryl-1-methoxyanthracene (**10**) and its oxidated product.

TABLE 4. THE EFFECTS OF BASE AND ADDITIVE (DICYCLOHEXANO-18-CROWN-6(C.E.)) ON THE EFFICIENCY OF EMISSION OF COMPOUND **10**

Condition	1[e]	2[e]	3[e]	4[f]
Base and additive	^{t}BuOK / ^{t}BuOH	^{t}BuORb / ^{t}BuOH	^{t}BuOCs / ^{t}BuOH	^{t}BuOK+ C.E.
i_{max}[a]	1.00	0.61	0.88	46.0
t_{max}[b]	10 min	20 min	11 min	0.5 min
$t_{1/4}$[c]	81 min	110 min	75 min	1.0 min
Quantum yield[d]	2.5%	2.0%	2.0%	4.6%

a) The relative intensity of the emission peaks; the intensity of the emission peak under conditions 1 was defined as 1.00. b) The time needed for the intensity of the emission to reach a maximum. c) The time for the intensity to decay to one-fourth of the maximum value. d) These were measured in benzene solution at 25 °C. e) To a stirred solution of compound **10** (0.002 mmol) in benzene (1 ml) was added a solution of ^{t}BuOM (0.35 mmol) in ^{t}BuOH (1 ml). f) To a stirred mixture of compound **10** (0.002 mmol), benzene (1.9 ml), and powdered ^{t}BuOK (40 mg) was added dicyclohexano-18-crown-6 (0.2 mmol).

luminescent reaction, we investigated the effects of solvent, of base, and of additives, using ketone **10**, which has the longest chemiluminescence. Nonpolar solvents such as benzene, toluene and xylene extended the life-time of the emission. The effects of the base and the additive are summarized in Table 4. When benzene was used as a solvent, the addition of dicyclohexano-18-crown-6 as an additive was the most effective: the quantum yield of chemiluminescence reached 0.046 einstein mol^{-1}. This value is approximately three-times as high as those produced using the Seliger-Lee luminol standard.[8] These results suggest that intermediate dioxetane species which will be generated by the oxygenation of the anion of ketones are formed as described in the following mechanism:

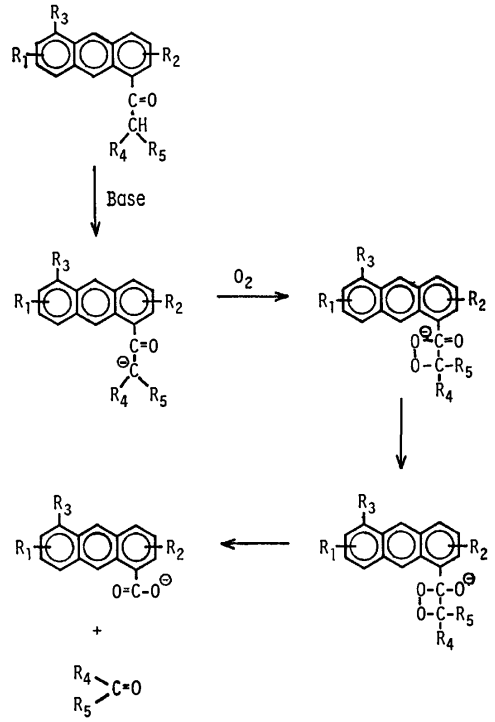

Conclusion

The efficiency of chemiluminescence increases when an electron-donating group is attached to the aromatic ring (**10**) and the chemiluminescent spectrum of ketone **10** shows a pattern closely similar to the fluorescent spectrum of its air-oxidated product. These findings suggest that this chemiluminescence may be generated *via* CIEEL mechanism. By contrast, the emission from ketones **3** and **9** may be generated from the intermediate intramolecular exciplex, because the chemiluminescent spectra are red-shifted compared to those of the air-oxidated products.

Werner *et al.* reported that, for anthracenes in general, the energy of the first excited singlet state (S_1) is observed to decrease as solvent polarity increases.[9] We think that the low efficiency of chemiluminescence in polar solvents is due to the efficient intersystem crossing from S_1 to T_1. Dicyclohexano-18-crown-6 may play an important role in dissolving the catalyst in a nonpolar solvent.

In summary, we have synthesized several anthracene derivatives which showed chemiluminescence by air-oxidation, using a base as a catalyst. 5-Dimethylamino-4-isobutyryl-1-methoxyanthracene (**10**) exhibits the most intensive chemiluminescence. This may be generated *via* CIEEL mechanism.

Experimental

Melting points were determined on a Yanagimoto micro melting point apparatus and are uncorrected. ^{1}H NMR spectra were run on a JEOL-MH-100 NMR spectrometer using $CDCl_3$ as a solvent and tetramethylsilane as an internal standard. ^{13}C NMR spectra were taken on a JEOL-FT-NMR spectrometer FX200 apparatus, using $CDCl_3$ as solvent and tetramethylsilane as an internal reference. Infrared spectra were recorded on Shimadzu IR-400 spectrometer as Nujol mulls. Mass spectra were determined on a JEOL-JMS-D-100. Chemiluminescence spectra were measured using a Shimadzu spectrofluorophotometer RF-520 and are uncorrected. Column chromatography was carried out using Wako silica gel C-200 with cyclohexane–benzene mixture from 1 : 0.1—1 : 3 or benzene as an eluent. The solvents for the column chromatography were obtained from Tokyo Kasei Co., Ltd. and were used without purification.

General Procedure for Friedel-Crafts Acylation of Anthracenes with Acyl Chlorides. A solution of anhydrous aluminum chloride (0.06 mol) and the acyl chloride (0.06 mol) in 30 ml of anhydrous carbon disulfide was added to a stirred solution of anthracene (3.6 g, 0.02 mol) in 35 ml anhydrous carbon disulfide at 20—25 °C and the mixture was stirred for 2—5 h at room temperature or at reflux. The reaction mixture was poured to a 200 ml beaker nearly filled with a mixture of crushed ice and concentrated hydrochloric acid. The organic layer was extracted with benzene, washed with 5% aqueous sodium hydrogencarbonate solution, and evaporated to dryness. Isolation and purification of each product were performed with column chromatography on silica gel.

Analyses and properties of the products are described below. Specific examples of the acylation are given in detail below.

1,5-Dipropionylanthracene (2): Yield 28%; mp 169—171.5 °C; IR 1675 cm^{-1}; NMR ($CDCl_3$): δ=1.32 (6H, t, J=9.0 Hz), 3.12 (4H, q, J=9.0 Hz), 7.45 (2H, dd, J=7.0 and 8.0

Hz), 7.96 (2H, d, J=7.0 Hz), 8.20 (2H, d, J=8.0 Hz), and 9.40 (2H, s). MS *m/e*: 290. Found: C, 82.70; H, 6.23%. Calcd for $C_{20}H_{18}O_2$: C, 82.73; H, 6.25%.

1,8-Dipropionylanthracene (6): Yield 13%; mp 169—171.5 °C; IR 1675 cm^{-1}; NMR ($CDCl_3$): δ=1.30 (6H, t, J=7.5 Hz), 3.08 (4H, q, J=7.5 Hz), 7.40 (2H, dd, J=7.0 and 7.5 Hz), 7.75 (2H, d, J=7.0 Hz), 8.04 (2H, d, J=7.5 Hz), 8.36 (1H, s), and 9.77 (1H, s). MS *m/e*: 290. Found: C, 82.91; H, 6.24%. Calcd for $C_{20}H_{18}O_2$: C, 82.73, H, 6.25%.

1,5-Bis(cyclohexylcarbonyl)anthracene (4): Yield 37%; mp 208—210 °C; IR 1690 cm^{-1}; NMR ($CDCl_3$): δ=1.20—2.10 (20H, m), 3.10—3.50 (2H, m), 7.46 (2H, dd, J=7.0 and 8.5 Hz), 7.86 (2H, d, J=7.0 Hz), 8.16 (2H, d, J=8.5 Hz), and 9.06 (2H, s). MS *m/e*: 398. Found: C, 84.26; H, 7.62%. Calcd for $C_{28}H_{30}O_2$: C, 84.38; H, 7.59%.

1,5-Bis[3-(methoxycarbonyl)propionyl]anthracene (5): Yield 23%; IR 1735 cm^{-1}; NMR ($CDCl_3$): δ=2.88 (4H, t, J=6.0 Hz), 3.48 (4H, t, J=6.0 Hz), 3.76 (6H, s), 7.52 (2H, dd, J=7.0 and 8.5 Hz), 8.12 (2H, d, J=7.0 Hz), 8.26 (2H, d, J=8.5 Hz), and 9.45 (2H, s). MS *m/e*: Found: C, 71.20; H, 5.32%. Calcd for $C_{24}H_{22}O_6$: C, 70.92; H, 5.46%.

1,8-Bis[3-(methoxycarbonyl)propionyl]anthracene (8): Yield 11%; mp 172.5—175 °C; IR 1730—1745 cm^{-1}; NMR ($CDCl_3$): δ=2.92 (4H, t, J=7.0 Hz), 3.45 (4H, t, J=7.0 Hz), 3.76 (6H, s), 7.45 (2H, dd, J=7.0 and 8.0 Hz), 8.02 (2H, d, J=7.0 Hz), 8.18 (2H, d, J=8.0 Hz), 8.50 (1H, s), and 9.92 (1H, s). MS *m/e*: 406. Found: C, 70.98; H, 5.42%. Calcd for $C_{24}H_{22}O_6$: C, 70.92; H, 5.46%.

Reaction of Anthracene with Isobutyryl Chloride. A solution of aluminum chloride (8.0 g) and isobutyryl chloride (6.4 g) in 30 ml of anhydrous carbon disulfide was added to a stirred solution of anthracene (3.6 g) in 35 ml anhydrous carbon disulfide at 20 °C and the mixture was stirred for 5 h at reflux. The reaction mixture was poured into a 200 ml beaker nearly filled with a mixture of ice and concentrated hydrochloric acid. The organic substances were extracted with benzene and washed with 5% aqueous sodium hydrogencarbonate. Then the solvent was evaporated to dryness. The obtained residue was subjected to column chromatography with benzene as an eluent. The crude crystalline products were separated and recrystallized from ethanol to afford three pure products:

1,5-Diisobutyrylanthracene (3): Yield 2.16 g (34%). Mp 124.5—126 °C; IR 1675 cm^{-1}; NMR ($CDCl_3$): δ=1.28 (12H, d, J=8.0 Hz), 3.69 (2H, sept, J=8.0 Hz), 7.44 (2H, dd, J=7.0 and 8.0 Hz), 7.83 (2H, d, J=7.0 Hz), 8.14 (2H, d, J=8.0 Hz), and 9.08 (2H, s). ^{13}C-NMR ($CDCl_3$): δ=18.9, 39.0, 124.1, 126.0, 127.5, 128.3, 133.0, 133.5, 135.5, and 208.2 Hz. MS *m/e*: 318. Found: C, 83.10; H, 6.88%. Calcd for $C_{22}H_{22}O_2$: C, 82.98; H, 6.96%.

1,8-Diisobutyrylanthracene (7): Yield 0.75 g (12%). Mp 102.5—104.5 °C; IR 1675 cm^{-1}; NMR ($CDCl_3$): δ=1.28 (12H, d, J=8.0 Hz), 3.54 (2H, sept. J=8.0 Hz), 7.43 (2H, dd, J=7.0 and 8.0 Hz), 7.67 (2H, d, J=7.0 Hz), 8.04 (2H, d, J=8.0 Hz), 8.40 (1H, s), and 9.18 (1H, s). MS *m/e*: 318. Found: C, 82.73; H, 6.99%. Calcd for $C_{22}H_{22}O_2$: C, 82.98; H, 6.96%.

3,7-Diisopropyl-1,5-diisobutyrylanthracene (9): Yield 0.12 g (1.5%). Mp 192—195 °C; IR 1680 cm^{-1}; NMR ($CDCl_3$): δ=1.27 (12H, d, J=8.0 Hz), 1.40 (12H, d, J=8.0 Hz), 3.08 (2H, sept, J=8.0 Hz), 3.56 (2H, sept, J=8.0 Hz), 7.65 (2H, s), 7.90 (2H, s), and 8.91 (2H, s). ^{13}C-NMR ($CDCl_3$): δ= 19.0, 23.5 34.1, 39.1, 125.0, 127.5, 128.1 128.2, 132.9, 135.7, 143.8, and 208.5 Hz. MS *m/e*: 402. Found: C, 83.38; H, 8.44%. Calcd for $C_{28}H_{34}O_2$: C, 83.54; H, 8.51%.

Reaction of 1,5-Diisobutyrylanthracene with Isobutyryl Chloride. To a stirred mixture of 1,5-diisobutyrylanthracene (4.8 g) and aluminum chloride (16 g) in anhydrous carbon disulfide (20 ml) was added a solution of isobutyryl chloride (8.0 g) in anhydrous carbon disulfide (5 ml) at 20 °C. The mixture was stirred overnight and treated as described above. Separation by column chromatography and recrystallization from ethanol–hexane afforded 3,7-diisopropyl-1,5-diisobutyrylanthracene (**9**): Yield 1.05 g (17.4%).

Reaction of 1-Isobutyrylanthracene with Isobutyryl Chloride. To a stirred mixture of 1-isobutyrylanthracene (2.5 g) and aluminum chloride (10.7 g) in anhydrous carbon disulfide (20 ml) was added a solution of isobutyryl chloride (8.5 g) in anhydrous carbon disulfide (5 ml) at 25 °C. The mixture was stirred overnight at 25 °C and treated as described above. Separation using column chromatography and recrystallization from ethanol–hexane afforded 1,5-diisobutyrylanthracene (**3**) (0.36 g, 11%), and 3,7-diisopropyl-1,5-diisobutyrylanthracene (**9**) (0.4 g, 10%).

Reaction of 1,5-Diisobutyrylanthracene with Isopropyl Chloride. To a stirred mixture of 1,5-diisobutyrylanthracene (1.6 g) and aluminum chloride (6.7 g) in anhydrous carbon disulfide (20 ml) was added a solution of isopropyl chloride (4.0 g) in anhydrous carbon disulfide (10 ml) at 25 °C. The mixture was stirred at 25 °C for 6 h, then for 2 d at reflux, and treated as described above. The starting 1.5-diisobutyrylanthracene was recovered (1.1 g) and 3.7-diisopropyl-1,5-diisobutyrylanthracene (**9**) (0.4 g, 19.4%) was separated out.

Reaction of 1-Dimethylamino-5-methoxyanthracene with Isobutyryl Chloride. A solution of anhydrous aluminum chloride (0.06 mol) and isobutyryl chloride (0.06 mol) in 30 ml of anhydrous carbon disulfide was added to a stirred mixture of 1-dimethylamino-5-methoxyanthracene (5.0 g, 0.02 mol) in 30 ml anhydrous carbon disulfide at 0—5 °C. The mixture was stirred at the same temperature for 3 h. The reaction mixture was treated as described above. Isolation and purification gave a greenish crystalline material identified as 5-dimethylamino-4-isobutyryl-1-methoxyanthracene; Yield 2.0 g (31.2%). Mp 134.5—139 °C; IR 1675 cm^{-1}; NMR ($CDCl_3$): δ=1.30 (6H, d, J=6.0 Hz), 3.00 (6H, s), 3.66 (1H, sept, J=6.0 Hz), 4.12 (3H, s), 6.66 (1H, d, J=8.5 Hz), 6.98 (1H, d, J=8.0 Hz), 7.38 (1H, dd, J=8.0 and 9.0 Hz), 7.66 (1H, d, J=9.0 Hz), 7.86 (1H, d, J=8.5 Hz), 8.80 (1H, s), and 9.58 (1H, s). MS *m/e*: 321. Found: C, 78.27; H, 7.10; N, 4.56%. Calcd for $C_{21}H_{23}O_2N$: C, 78.47; H, 7.21; N, 4.36%.

The Measurement of Chemiluminescence. Commercially available KOH (from Kanto Chemical Co., Inc.), and ^{t}BuOK (from Merck for synthesis) were used without further purification. Other alkali metal *t*-butoxides were prepared by dissolving an alkali metal in *t*-butyl alcohol. Luminol was recrystallized from dilute hydrochloric acid prior to use. All solvents used were purified by distillation. The luminescent reaction was initiated by adding a base to an aerated solution of ketone, with stirring, in a quartz cell (10×10×45 mm) which was situated in a thermostatically-controlled cell holder. The chemiluminescent intensity was measured on a Shimazu spectrofluorophotometer RF-520 with no exciting source. The total light emission was determined graphically from the *I-t* curves. A standard solution of luminol in anhydrous DMSO having an optical density at 359.5 nm (the absorption peak) of 0.010 (1.26×10^{-6} mol l^{-1}) was prepared, and the *I-t* curve of the chemiluminescence initiated by adding 0.2 ml of a ^{t}BuOK solution to 2 ml of the standard solution was measured on the same apparatus at 313 K. Using the value of 1.28×10^{-2} einstein mol^{-1} proposed by Lee *et al.* for the chemiluminescence exhibited from the luminol solution, the quantum yields for direct chemiluminescence from ketones were determined from the ratio of the total light emitted from the luminol solutionto the total measured light emission from the ketone

solutions.

Methyl Ester of the Air-oxidated Product of Compound **3**, **9**, *and* **10**. To a stirred solution of compound **3**, **9**, or **10** in benzene was added a solution of excess amount of potassium *t*-butoxide in *t*-butyl alcohol at 20 °C. Then chemiluminescence was observed. Water was added to the resulting mixture and stirred vigorously. The aqueous layer was separated, neutralized with acetic acid and extracted with chloroform. To this organic solution was added a solution of diazomethane in ethyl ether. After stirring for 1 h, the solvent was evaporated to dryness. The obtained residue was subjetced to column chromatography with benzene as an eluent. The methyl ester of compound **3**, **9**, or **10** was obtained.

1,5-Bis(methoxycarbonyl)anthracene: Mp 123—125 °C; IR 1710 cm^{-1}; NMR ($CDCl_3$): $\delta=4.06$ (6H, s), 7.54 (2H, t, $J=8.0$ Hz), 8.30 (4H, d, $J=8.0$ Hz), and 9.65 (2H, s). Found: C, 73.63; H, 4.53%. Calcd for $C_{18}H_{14}O_4$: C, 73.46; H, 4.80%.

3,7-Diisopropyl-1,5-bis(methoxycarbonyl)anthracene: Mp 149—151 °C; IR 1705 cm^{-1}; NMR ($CDCl_3$): $\delta=1.38$ (12H, d, $J=8.0$ Hz), 3.10 (2H, sept, $J=8.0$ Hz), 4.02 (6H, s), 8.00 (2H, s), 8.12 (2H, s), and 9.40 (2H, s). Found: C, 75.80; H, 7.02%. Calcd for $C_{24}H_{26}O_4$: C, 76.16; H, 6.93%.

5-Dimethylamino-1-methoxy-4-(methoxycarbonyl)anthracene: Mp 130—131 °C; IR 1700 cm^{-1}; NMR ($CDCl_3$): $\delta=3.00$ (6H, s), 3.96 (3H, s), 4.00 (3H, s), 6.58 (1H, d, $J=8.0$ Hz), 6.92 (1H, d, $J=8.0$ Hz), 7.32 (1H, t, $J=8.0$ Hz), 7.58 (1H, d, $J=8.0$ Hz), 8.14 (1H, d, $J=8.0$ Hz), 8.74 (1H, s), and 9.92 (1H, s). Found: C, 74.00; H, 6.02; N, 4.62%. Calcd for $C_{19}H_{19}O_3N$: C, 73.76; H, 6.19; N, 4.53%.

References

1) F. McCapra, *J. Chem. Soc., Chem. Commun.*, **1977**, 946; M. J. S. Dewar and L. Kirschner, *J. Am. Chem. Soc.*, **96**, 7578 (1974); D. R. Roberts, *J. Chem. Soc., Chem. Commun.*, **1974**, 683; G. Barnett, *Can. J. Chem.*, **52**, 3837 (1974); N. J. Turro and P. Lechtken, *J. Am. Chem. Soc.*, **95**, 264 (1973); M. A. Umbreit and E. H. White, *J. Org. Chem.*, **41**, 479 (1976); K. R. Kopecky J. E. Filby, C. Mumford, P. A. Lockwood, and J. Y. Ding, *Can. J. Chem.*, **53**, 1103 (1975).

2) H. H. Seliger and W. D. McElroy, *Biochem. Biophys. Res. Commun.*, **1**, 21 (1959); H. H. Seliger and W. D. McElroy *Arch. Biochem. Biophys.*, **88**, 136 (1960).

3) I. Kamiya and K. Aoki, *Bull. Chem. Soc. Jpn.*, **47**, 1744 (1974); I. Kamiya and T. Sugimoto, *Chem. Lett.*, **1976**, 33; I. Kamiya and T. Susimoto *Bull. Chem. Soc. Jpn.*, **50**, 2442 (1977); I. Kamiya and T. Sugimoto *Chem. Lett.*, **1978**, 335.

4) J. Y. Koo and G. B. Schuster, *J. Am. Chem. Soc.*, **99**, 6107 (1977); **100**, 4496 (1978); F. McCapra, *J. Chem. Soc., Chem. Commun.*, **1977**, 946; K. A. Zaklika, A. L. Thayer, and A.P. Schaap, *J. Am. Chem. Soc.*, **100**, 4916 (1978); K. A. Zaklika, P. A. Burns, and A. P. Schaap, *ibid.*, **100**, 318 (1978).

5) "Friedel-Crafts and Related Reactions," ed by G.A. Olah, Interscience, New York, N. Y. (1964), Vol. III, Part 1.

6) P. H. Gore and C. K. Thadani, *J. Chem. Soc., C*, **1966**, 1729.

7) E. Rothstein and R. W. Waville, *J. Chem. Soc.*, **1949**, 1961.

8) J. Lee, A. S. Wesley, J. F. Ferguson, and H. H. Seliger, "Bioluminescence in Progress," ed by F. H. Johnson and Y. Haneda, Princeton University Press, New Jersey (1966), p. 35.

9) T. C. Werner, T. Matthews, and B. Soller, *J. Phys. Chem.*, **77**, 1611 (1973).

  Bull. Chem. Soc. Jpn., 54, 991—997 (1981)

Observation of Mutual Diffusion Coefficients and Cooperative Motions in Binary Solutions of *t*-Butyl Alcohol-Water and 2-Butoxyethanol-Water

Nobuyuki Ito,† Koichi Saito,† Tadashi Kato, and Tsunetake Fujiyama*

Institute for Molecular Science, Myodaiji, Okazaki 444

†*Department of Chemistry, Faculty of Science, Tokyo Metropolitan University, Setagaya-ku, Tokyo 158*

(Received August 18, 1980)

Rayleigh scattering spectra were observed for the binary solutions of t-butyl alcohol(TBA)–water and 2-butoxyethanol (BE)–water. The observed line-widths were reduced to mutual diffusion coefficients. The observed concentration dependencies of the mutual diffusion coefficients were well explained by postulating the existence of "moving units"— a group of molecules which move together for a time much longer than the velocity auto-correlation time. The structure of the moving units which are formed in the TBA–water solution was $(H_2O)_{20}$TBA for $X_{TBA} \lesssim 0.05$, and $4(H_2O)_{20}$TBA for $X_{TBA} \gtrsim 0.05$, where X_{TBA} is the mole fraction of TBA. For the BE–water solution, the structure was found to be $(H_2O)_{50}$BE for $X_{BE} \lesssim 0.02$ and $3(H_2O)_{50}$BE for $X_{BE} \gtrsim 0.02$. These results were compared with the results which had been obtained from the concentration dependencies of the mean-square concentration fluctuation values.

Local fluctuations of concentration afford information which is useful for understanding the mixing of liquids from a molecular viewpoint. Since the mean-square amplitude of concentration fluctuation is related to the spatial correlation between positions of different molecules, it affords information about the local structure formation in solution. In our previous reports, we have discussed the local structures in various solutions on the basis of the quantitative analysis of the mean-square concentration fluctuation obtained from the Rayleigh scattering intensities.[1-9] The local structures were expressed in terms of the mean association number in the ordinary sense.

In order to discuss the state of mixing from a dynamical standpoint, however, the life-time of local structures should be taken into account along with the mean association number. Here, we define the "life-time" as the time during which the relative positions of molecules in a local structure change very little. Instead of observing the life-time directly, we introduced the concept of a "moving unit"—a group of molecules which move together for a time much longer than the velocity auto-correlation time—in our preceding report[10] as a useful concept for describing dynamical aspects of local structures. The mutual diffusion coefficient was theoretically expressed in terms of the self diffusion coefficients and the number of moving units. The theoretical results were applied to the study of the mutual diffusion coefficients for methanol–carbon tetrachloride and ethanol–carbon tetrachloride systems obtained from the intensity distribution measurements of Rayleigh lines. It was shown that the mean number of alcohol molecules which constitutes a moving unit was much smaller than the mean association number of alcohol, especially in the high concentration range of alcohol. This indicated that the hydrogen-bonded polymer of alcohol molecules cannot move without changing shape within the velocity auto-correlation time.

The present report concerns itself with the extension of this line of approach to the aqueous solutions of *t*-butyl alcohol (TBA hereafter) and 2-butoxyethanol (BE hereafter). Our expectation is that the life-times of the local structures formed in these solution are much longer than those in the ordinary binary solutions like methanol–carbon tetrachloride and ethanol–carbon tetrachloride.[10]

Recently, Iwasaki *et al.* have observed the light scattering spectra for the binary solution of *t*-butyl alcohol and water.[7,8] They have concluded that clathrate hydrate-like structures of the type $g[(H_2O)_{21}TBA]$ ($g=1$—5) exist in the solution, from the analysis of the observed concentration dependence of the mean-square concentration fluctuation. By considering the results of X-ray diffraction analyses for the structure of solid clathrate hydrate, it has been suggested that a TBA molecule is surrounded by water molecules which form a polyhedron. This result indicates that the life-time of these local structures in the TBA–water solution might be much longer than those observed in the carbon tetrachloride solutions of alcohols.[10] This expectation is confirmed by the measurement and analysis of the concentration dependence of the mutual diffusion coefficient, which is obtained from the line-width of Rayleigh line. The binary solution of water–BE is also included in the present study.

Experimental

The light scattering spectrometer (heterodyne detection) used in the present study was designed and constructed in our laboratory.[11] The light source is an argon ion laser (Spectra-Physics model 165-09) which produced 0.1—1 W power at 488 nm. The scattering angle, θ, was defined by two pinholes approximately 50 cm apart and 0.5 mm in diameter. The laser beam is focused into a rectangular scattering cell. Scattered light and local oscillator beam (scattered from the cell walls) are collected onto the surface of a photomultiplier tube (HTV R-374). The photocurrent is amplified and then fed to a spectrum analyzer (Takeda-Riken TR 4120S). This analyzer is designed for use in the spectral region 50 Hz—30 MHz. The out-put of the analyzer is averaged by a signal averager (Kawasaki Electronica M50E-TMC 600). The averaged spectrum is squared prior to recording, so that the final output signal is proportional to the power spectrum of the scattered light. Details of the spectrometer have been reported elsewhere along with the reliability of the observed

data.[11]

Light scattering spectra were recorded at the temperature of 25±1 °C in the scattering angle range of $5°<\theta<21°$.

All the chemicals were commercial products (Tokyo Kasei's Extra Pure). 2-Butoxyethanol was purified by distillation and *t*-butyl alcohol was used without further purification. Water was triply distilled. The binary mixtures of TBA and water were made dust free by the use of a Nuclepore filter with a pore size of 0.1 μm.

Results and Discussion

Mutual Diffusion Coefficients and Velocity Correlation between Different Molecules. The procedure for obtaining the mutual diffusion coefficient from the Rayleigh scattering spectra is the same as that described in the preceding report.[10] Figures 1 and 2 show the concentration dependences of the mutual diffusion coefficients for the binary solutions of TBA–water and BE–water, respectively.

The mutual diffusion coefficient for the binary solution whose components are molecules A and B is expressed in terms of velocity correlation functions as

$$D = QL \tag{1}$$

with

$$L = X_B D_A + X_A D_B + X_B(n_A - 1)\, V_{aa'} + X_A (n_B - 1)\, V_{bb'} - 2X_A X_B (n_A + n_B)\, V_{ab} \tag{2}$$

$$Q = \frac{X_A X_B}{N\langle(\Delta X)^2\rangle} \tag{3}$$

$$V_{ij} = \frac{1}{3}\int_0^\infty \langle \mathbf{v}_i(t)\cdot\mathbf{v}_j(0)\rangle dt \tag{4}$$

(i, j, = a, a', b or b').

The notations in these equations are the same as those used in the preceding report.[10]

In the case where velocity correlation between different molecules can be neglected, L is reduced to

$$L^\circ = X_B D_A + X_A D_B. \tag{5}$$

Equation 2 can be rewritten in terms of L° as

$$L \simeq L^\circ + X_A X_B (n_A + n_B)\,(V_{aa'} + V_{bb'} - 2V_{ab}), \tag{6}$$

where we have taken $n_A - 1 \simeq n_A$ and $n_B - 1 \simeq n_B$ because $n_A, n_B \gg 1$. Equation 6 indicates that L is larger than L° when the velocity correlation between same species is stronger than that between different species, that is, $V_{aa'}+V_{bb'} > 2V_{ab}$. In the case where $V_{aa'}+V_{bb'} < 2V_{ab}$, on the other hand, L takes a smaller value than L°.

Figures 3 and 4 show the concentration dependences of L calculated from the observed values of D and $N\langle(\Delta X)^2\rangle$ for the binary solutions of TBA–water and BE–water. The observed values of $N\langle(\Delta X)^2\rangle$ for the BE–water system are shown in Fig. 12. The observed values for the TBA–water system were already reported.[7,8] It is seen from Figs. 3 and 4, that L takes a minimum value at $X \approx 0.05$ for the TBA–water system and $X \approx 0.02$ for the BE–water system, where X is the mole fraction of TBA or BE.

The broken line of Fig. 3 shows the concentration dependence of L° calculated from Eq. 5 where experimental values of the self diffusion coefficients found in the literature[12,13] was used (see Fig. 5). It is seen from

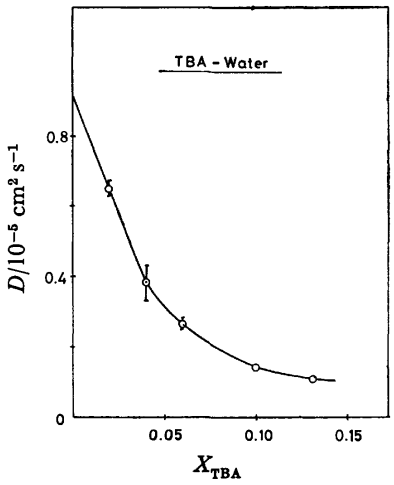

Fig. 1. Observed mutual diffusion coefficients for TBA–water system at 25 °C.

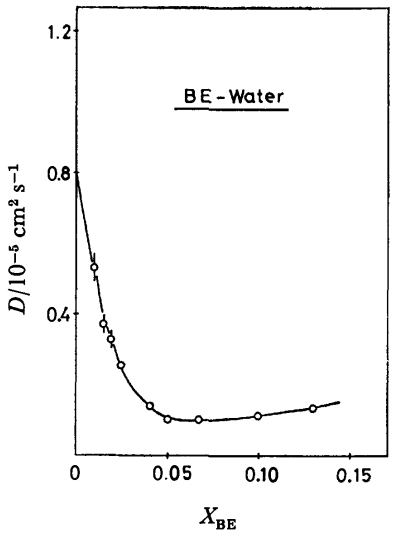

Fig. 2. Observed mutual diffusion coefficients for BE–water system.

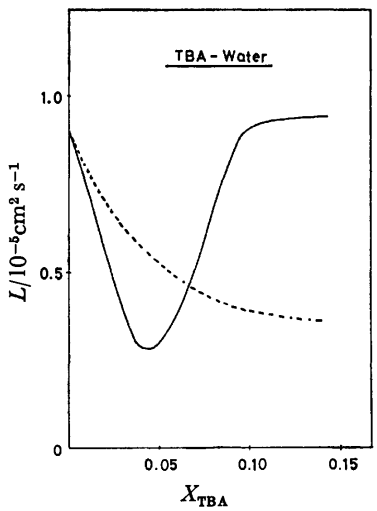

Fig. 3. Observed values of L (see Eqs. 1—3) for TBA–water system. The dashed line shows L° (see Eq. 5).

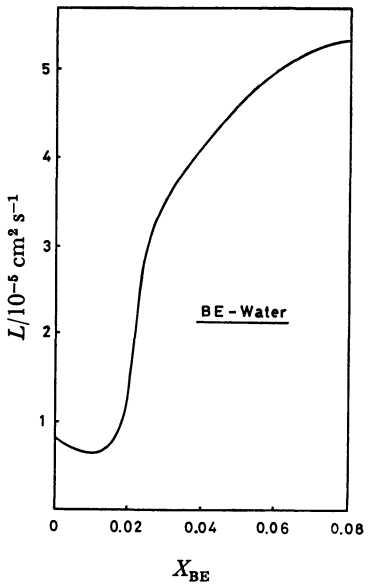

Fig. 4. Observed values of L (see Eqs. 1—3) for BE–water system.

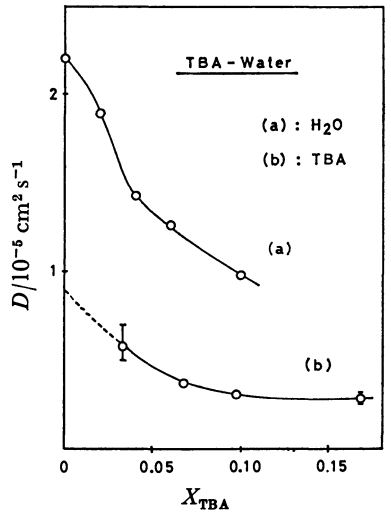

Fig. 5. Observed self diffusion coefficients for TBA–water system.

the figure that L is smaller than L° for $0<X<0.065$ and is larger than L° for $0.065<X$. These results suggest that $(V_{aa'}+V_{bb'}-2V_{ab})$ in Eq. 6 is not equal to zero for the present system.

Moving Unit in TBA–Water System. In the previous report,[10] we have introduced the concept of a moving unit in order to obtain information about the cooperative translational motion of molecules in solution. We will try to explain the observed concentration dependence of L by using this concept.

The analysis[7] of the Rayleigh intensities for the TBA–water system has shown the existence of clathrate hydrate-like structures of the type $(H_2O)_{21}TBA$ for $0<X<1/22$ and of the type $5[(H_2O)_{21}TBA]$ for $1/22<X$. Therefore, we consider first a moving unit of the A_lB-type where A and B represent water and TBA molecules, respectively. Then, L is expressed as

$$L = \frac{X_B}{n_A}\left[r^2 n_{A_r} D_{A_r} + l^2 n_{A_lB} D_{A_lB}\right] + \frac{X_A}{n_B}\left[n_{B_1} D_{B_1} + n_{A_lB} D_{A_lB}\right] - 2l\frac{n_{A_lB}}{n_A+n_B} D_{A_lB}, \quad (7)$$

where $n_\alpha(\alpha=A_lB$ *etc.*$)$ is the number of moving units of α-type and D_α the self diffusion coefficient of a moving unit α. In Eq. 7, a moving unit of the A_l-type has also been assumed to exist. Since the relations

$$n_A = rn_{A_r} + ln_{A_lB}$$
$$n_B = n_{B_1} + n_{A_lB} \quad (8)$$

hold, Eq. 7 is reduced to

$$L = X_B r D_{A_r} + X_A D_{B_1} + X_{A_lB}\left[\frac{X_B}{X_A} l\left(lD_{A_lB} - rD_{A_r}\right) + \frac{X_A}{X_B}\left(D_{A_lB} - D_{B_1}\right) - 2lD_{A_lB}\right] \quad (9)$$

$$X_{A_lB} = \frac{n_{A_lB}}{n_A + n_B}. \quad (10)$$

(a) L for a Model System Composed of A_l, A_lB, and B_1. In order to determine the l-dependence of L, we consider the special case where $r=l$ and $D_{A_lB}=D_{A_l}=D_{B_1}\equiv D^s$. We further assume that for $0\leq X_B\leq 1/(l+1)$ there exist only those moving units of the types A_l and A_lB and for $1/(l+1)\leq X_B$ only those of the types A_lB and B_1. This corresponds to the conditions $X_{A_lB}=X_B$ for $0\leq X_B\leq 1/(l+1)$, and $X_{A_lB}=X_A/l$ for $1/(l+1)\leq X_B$. Figure 6 shows the concentration dependences of L for $D^s=1$ and for various values. It is seen from the figure that there exists a specific concentration, X_l, at which L is zero. X_l is equal to $1/(l+1)$, which is the number ratio of B molecules to all the molecules in the moving unit A_lB. By comparing Fig. 6 with Fig. 3, we can see that the theoretical curve for $l=20$ in Fig. 6 explains the observed concentration dependence of L in the sense that L takes a minimum value at $X_B\sim 0.05$. However, the observed value of L does not go to zero at any concentration. This suggests the existence of other types of moving units than A_lB even at $X_B=$

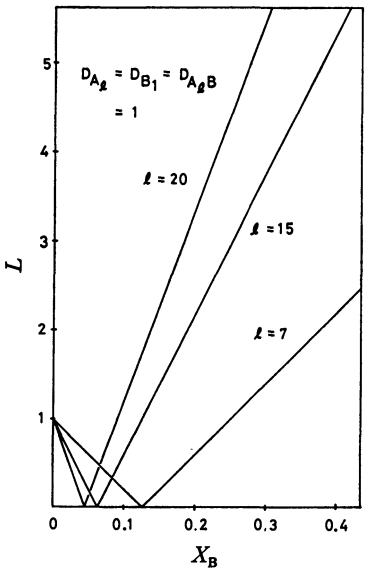

Fig. 6. Theoretical values of L calculated from Eq. 9 for $D_{A_lB}=D_{A_r}=D_{B_1}=1$ $(r=l)$ and for various l values.

$1/(l+1)$. Therefore, we consider the coexistence of the types A_l, A_lB, and B_1. In order to determine the concentration dependence of X_{A_lB}, we further assume the relation

$$\frac{n_{A_lB}}{N'} = K\frac{n_{A_l}}{N'}\frac{n_{B_1}}{N'}$$

$$N' = n_{A_l} + n_{A_lB} + n_{B_1}. \tag{11}$$

This corresponds to assuming the association equilibrium

$$A_l + B_1 \overset{K}{\rightleftharpoons} A_lB, \tag{12}$$

where K is an equilibrium constant. Then, X_{A_lB} can be expressed in terms of K as

$$X_{A_lB} = \frac{1}{2l}\left[\left(X_A + lX_B\right) - \left\{\left(X_A + lX_B\right)^2 - 4l\frac{K}{K+1}X_AX_B\right\}^{1/2}\right]. \tag{13}$$

Figure 7 shows the concentration dependences of L calculated from Eqs. 10 and 13 for $l=r=20$ and for various K values. It is seen from the figure that L takes a minimum value at $X_B \approx 0.05$.

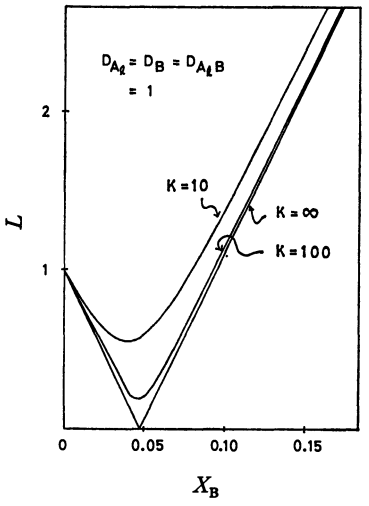

Fig. 7. Theoretical values of L calculated from Eqs. 10 and 13 for $l=r=20$ and for various K values.

(b) L for a Model System Composed of A_r, A_lB, and B_1. In the above analysis, we have assumed that the self diffusion coefficients of the moving units (D_{A_r}, D_{A_lB}, and D_{B_1}) are equal and independent on concentration. This assumption, however, is not quite reasonable, for the following reasons. The self diffusion coefficients, D_{A_r}, D_{A_lB}, and D_{B_1}, can be related to the self diffusion coefficients, D_A and D_B, which correspond to the species A and B by the equations

$$D_A = \frac{rn_{A_r}}{n_A}D_{A_r} + \frac{ln_{A_lB}}{n_A}D_{A_lB}$$

$$D_B = \frac{n_{A_lB}}{n_B}D_{A_lB} + \frac{n_{B_1}}{n_B}D_{B_1}. \tag{14}$$

Therefore, the above assumption is equivalent to assuming $D_A=D_B$ at any concentrations. Actually, the observed D_A and D_B values are different and depend on concentration (see Fig. 5).

In order to take into account the observed concentration dependences of D_A and D_B properly, we rewrite Eq. 11 by using Eq. 14 as

$$L = rX_BD_A + X_AD_B - lX_{A_lB}D_{A_lB} \times \left[2 - \frac{X_B}{X_A}\left(l - r\right)\right]. \tag{15}$$

As Eq. 15 has four unknown parameters, l, r, X_{A_lB}, and D_{A_lB}, on the right hand side, it is difficult to determine these parameters from the observed data uniquely. Fortunately, however, we can restrict the probable magnitudes of these parameter values as follows.

As the sizes and weights of A_r and B_1 are both smaller than those of A_lB, the lower limit of the D_{A_lB} value may be defined as: $D_{A_lB} \leq D_{A_r}$ and $D_{A_lB} \leq D_{B_1}$. We can also define the upper limits of D_{A_lB} and D_{B_1}, so that the probable magnitudes of these parameters are restricted by the relations

$$D_{A_lB} \leq D_{A_r} \leq aD_{A_lB}$$
$$D_{A_lB} \leq D_{B_1} \leq bD_{A_lB}. \tag{16}$$

The constants a and b of Eq. 16 are arbitraly. However, it is improbable that D_{B_1} is larger than $10D_{A_lB}$ because the self diffusion coefficient of a moving unit is inversely proportional to its weight, approximately,[14] and because the weight of A_lB is about six times as large as that of B_1. So, we set $b=10$. Similarly, we may set $a=40/r$ because the weight of B_1 is about $4/r$ times as large as that of A_r. D_{A_r} and D_{B_1} can be expressed in terms of D_A, D_B, and D_{A_lB} as

$$D_{A_r} = \frac{D_AX_A - lX_{A_lB}D_{A_lB}}{X_A - lX_{A_lB}} \tag{17a}$$

$$D_{B_1} = \frac{D_BX_B - X_{A_lB}D_{A_lB}}{X_B - X_{A_lB}}. \tag{17b}$$

Combination of Eqs. 16 and 17 gives the relations

$$D_A \geq D_{A_lB} \geq \frac{X_AD_A}{a\left(X_A - lX_{A_lB}\right) + lX_{A_lB}} \tag{18a}$$

$$D_B \geq D_{A_lB} \geq \frac{X_BD_B}{b\left(X_B - X_{A_lB}\right) + X_{A_lB}}. \tag{18a}$$

Therefore, we can define the smallest value, L_{min}, and the largest value, L_{max}, of L as

$$L_{min} = M - X_{A_lB}D_AH \tag{19}$$

$$L^a_{max} = M - \frac{X_AD_AX_{A_lB}}{a\left(X_A - lX_{A_lB}\right) + lX_{A_lB}}H \tag{20a}$$

$$L^b_{max} = M - \frac{X_BD_BX_{A_lB}}{b\left(X_B - X_{A_lB}\right) + X_{A_lB}}H \tag{20b}$$

$$M = X_BrD_A + X_AD_B$$
$$H = l[2 - X_B(l-r)/X_A] \quad (a=40/r,\ b=10)$$

if $H>0$. The values of L^a_{max} and L^b_{max} are determined from Eqs. 18a and 18b, respectively. The values of L_{min} are determined from Eq. 18 and the relation that $D_A>D_B$ (see Fig. 5). For $H<0$, L_{min} in Eq. 19 becomes a maximum value and L_{max} in Eq. 20 becomes a minimum value. Figures 8—10 show the domain of L calculated from Eqs. 19 and 20 for some values of r and K, where the concentration dependence of X_{A_lB} is assumed to be determined by Eq. 13. It is seen from these figures that the observed L values satisfy the inequality represented by Eqs. 19 and 20 for $r=4$ in the

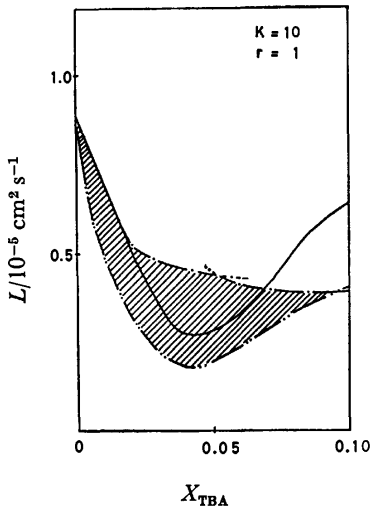

Fig. 8. Domain of L calculated from Eqs. 19 and for $l=20$, $r=1$, and $K=10$ (shaded area).

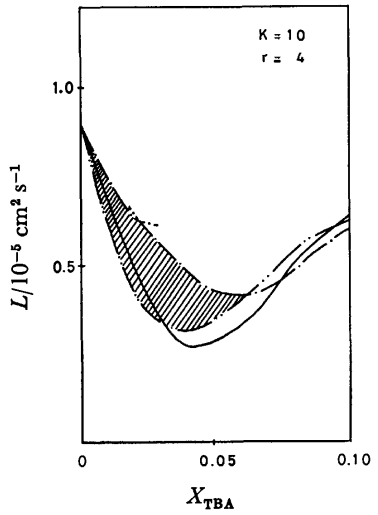

Fig. 9. Domain of L calculated from Eqs. 19 and 20 for $l=20$, $r=4$, and $K=10$ (shaded area).

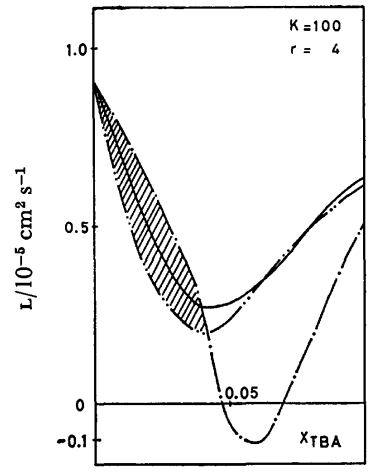

Fig. 10. Domain of L calculated from Eqs. 19 and 20 for $l=20$, $r=4$, and $K=100$ (shaded area).

low concentration range of TBA ($X<0.03$). In the high concentration range, however, the domain calculated for any r or K value does not cover the observed L values. This implies that the present model is not applicable in the high concentration range.

(c) L for a Model System Composed of A_r, gA_lB, and B_1. In the Rayleigh intensity analysis, the existence of the local structure of the type $5[(H_2O)_{l'}TBA]$ has been proposed for $1/(l'+1)<X_B(l'\approx 21)$. So we assume the coexistence of the moving units of the types gA_lB ($g=2, 3, ..$), A_r, and B_1 for $X_B>1(l+1)$. Then, L is expressed as

$$L = M + X_{A_lB}D_{gA_lB}H'$$

$$H' \equiv l\left[2g - \frac{X_B}{X_A}\left(gl - r\right)\right] - \left[\frac{X_A}{X_B}\left(g - 1\right)\right]$$

$$X_{A_lB} = gX_{gA_lB}. \tag{21}$$

In this case the relations corresponding to Eq. 16 are

$$D_{gA_lB} \leq D_{A_r} \leq \frac{ag}{r} D_{gA_lB} \tag{22a}$$

$$D_{gA_lB} \leq D_{B_1} \leq bgD_{gA_lB}. \tag{22b}$$

Therefore,

$$L_{min} = M - D_A X_{A_lB} H' \tag{23}$$

$$L^a_{max} = M - \frac{X_A D_A X_{A_lB}}{ag(X_A - lX_{A_lB}) + lX_{A_lB}} H' \tag{24a}$$

$$L^b_{max} = M - \frac{X_B D_B X_{A_lB}}{bg(X_B - X_{A_lB}) + X_{A_lB}} H' \tag{24b}$$

for $H'>0$. The domain of L calculated from Eqs. 23 and 24 for $r=1$, $K=10$, and $g=4$ is shown in Fig. 11, where the domain of L for $X_B<1/(l+1)$ is calculated from Eqs. 19 and 20. It can be seen from the figure that the calculated domain covers the observed values of $X>0.02$.

We could not find any other r and g values which give a domain of L which covers the observed values for $X<0.1$. However, for $X<0.075$, for example, the domain calculated for $r=1$ and $g=3$ also covers the observed L values. Similarly, for $X<0.07$, we can find

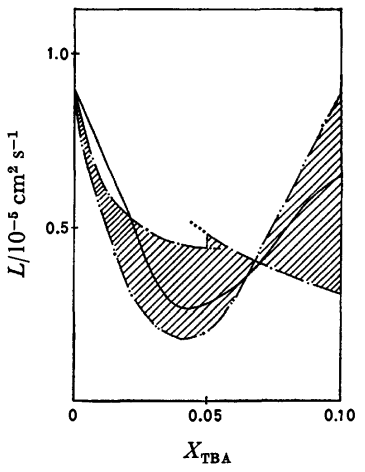

Fig. 11. Domain of L calculated from Eqs. 23 and 24 for $l=20$, $r=1$, $K=10$, and $g=4$ ($X\geq 0.02$) and that calculated from Eqs. 19 and 20 for $l=20$, $r=1$, and $K=10$ ($X\leq 0.02$).

that three sets of values: $(r, g)=(1, 4)$, $(1, 3)$, and $(2, 2)$, can produce domains which can cover the observed L. These results may suggest an increase of g and decrease of r with the increasing concentration of TBA.

From the above analysis, the following types of moving units can be expected in the TBA–water solution:

A_r ($r = 4$—10), $A_{20}B$, and B_1 for $0 < X_B \lesssim 0.05$

A_1, $4A_{20}B$, and B_1, for $0.05 \lesssim X_B$.

An approximate l value can be determined from the concentration at which L takes a minimum value.

Moving Unit in BE–Water System. We have analyzed the observed mean-square concentration fluctuation for the BE–water system by the same way as was used for the TBA–water system.[7] Our conclusion is that there are local structures of the type $(H_2O)_{55}BE$ for $0<X_{BE}<1/56$ and of the type $3(H_2O)_{55}$ BE for $1/56>X_{BE}$.

For the BE–water system, the self diffusion coefficients have not been reported. However, the observed concentration dependence of L in Fig. 4 suggests the existence of moving units similar to those in the TBA–water system, that is, the $(H_2O)_lBE$ type. From the concentration at which L takes a minimum value, the l value is obtained to be about 50.

Concluding Discussion. We have shown that moving units of the types $g[(H_2O)_{20}TBA]$ and $g'[(H_2O)_{50}BE]$ exist in the binary solution of TBA–water and BE–water, respectively. The analysis of the concentration dependences of the mutual diffusion coefficients gave these results. In the study of the mean-square concentration fluctuations for these systems, on the other hand, the existence of local structures of the types $g''[(H_2O)_{20}TBA]$ and $g'''[(H_2O)_{55}BE]$ has been suggested. With the help of the results of X-ray diffraction analyses for the structure of solid clathrate hydrate,[15] the following picture can be drawn for the mixing state of TBA–water mixtures. In the concentration range of $0<X_{TBA}<1/22$, a TBA molecule forms a polyhedron surrounded by water molecules and the polyhedra are dispersed in water. In the concentration range of $1/22<X_{TBA}<0.1$, the aggregates of five polyhedra are dispersed in TBA. Because the ratio of water molecules to a TBA molecule in a moving unit is nearly equal to that in the above polyhedron, it can be concluded that the life-time of the clathrate hydrate-like structure is much longer than the order of the velocity auto-correlation time (10^{-13}—10^{-12} s). This is in contrast with the results obtained for the binary solutions of methanol–carbon tetrachloride and ethanol–carbon tetrachloride. In these systems, a group of hydrogen-bonded alcohols cannot be a moving unit, especially in the high concentration range of alcohol ($X_{alcohol} \gg 0.1$). This result has been explained as follows. Consider the velocity correlation between two alcohols which form a linear hydrogen-bonded polymer. If these two molecules are adjacent to each other, the velocity correlation between them is expected to be strong. If these two molecules are not adjacent to each other, on the other hand, the velocity correlation between them becomes relatively weak. Therefore it is expected that

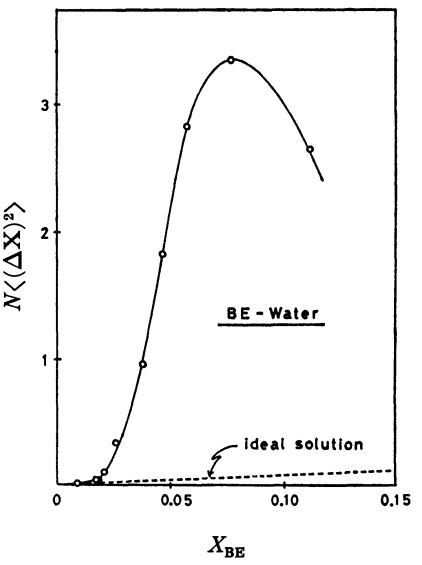

Fig. 12. Observed mean-square concentration fluctuation for BE–water system.

the number of alcohols which form a moving unit cannot exceed a certain number, no matter how large the association number of hydrogen-bonded polymer is. In other words, the long hydrogen-bonded polymer cannot be a moving unit.

The present results are not inconsistent with this viewpoint. In the TBA–water solution, the distances between the TBA molecule and each water molecule which form a polyhedron are almost the same. Therefore, the velocity correlation between the TBA molecule and each water molecule is expected to be strong. For the BE–water system, no picture for the mixing state has been drawn. We suggest the picture is similar to that in the TBA–water systems, because the present study has shown that the local structure predicted by the Rayleigh intensity analysis can be a moving unit itself.

References

1) K. Iwasaki, M. Tanaka, and T. Fujiyama, *Bull. Chem. Soc. Jpn.*, **49**, 2719 (1976).
2) K. Iwasaki, Y. Katayanagi, and T. Fujiyama, *Bull. Chem. Soc. Jpn.*, **49**, 2988 (1976).
3) T. Kato and T. Fujiyama, *J. Phys. Chem.*, **81**, 1560 (1977).
4) T. Kato and T. Fujiyama, *Bull. Chem. Soc. Jpn.*, **51**, 1328 (1978).
5) T. Kato, S. Hyodo, and T. Fujiyama, *J. Phys. Chem.*, **82**, 1010 (1978).
6) T. Fujiyama and M. Tanaka, *Bull. Chem. Soc. Jpn.*, **51**, 1655 (1978).
7) K. Iwasaki and T. Fujiyama, *J. Phys. Chem.*, **81**, 1908 (1977).
8) K. Iwasaki and T. Fujiyama, *J. Phys. Chem.*, **83**, 463 (1979).
9) T. Kato, T. Nakanishi, and T. Fujiyama, *Bull. Chem. Soc. Jpn.*, **53**, 2173 (1980).
10) T. Kato, N. Ito, and T. Fujiyama, *Bull. Chem. Soc. Jpn.*, **53**, 2167 (1980).

11) N. Ito, T. Kato, and T. Fujiyama, *Bunko Kenkyu*, **29**, 106 (1980).
12) F. Franks and J. Ravenhill, *Proc. R. Soc. London, Ser. A*, **319**, 189 (1970).
13) E. V. Goldammer and M. D. Zeidler, *Ber. Bunsenges. Phys. Chem.*, **73**, 4 (1969).
14) See Eq. 24 of Ref. 10.
15) D. N. Glew, H. D. Mak, and N. S. Rath, "Hydrogen-Bonded Solvent Systems," ed by A. K. Covington and P. Jones, Taylor and Francis, London (1968), p. 195.

Crystal and Molecular Structures of Octaethylporphinium(monocation) Triiodide and Its Benzene Hemisolvate

Noriaki HIRAYAMA, Akio TAKENAKA,* Yoshio SASADA, Ei-ichi WATANABE,†
Hisanobu OGOSHI,† and Zen-ichi YOSHIDA†

Laboratory of Chemistry for Natural Products, Tokyo Institute of Technology, Nagatsuta, Midori-ku, Yokohama 227
†*Department of Synthetic Chemistry, Kyoto University, Yoshida, Sakyo-ku, Kyoto 606*

(Received August 23, 1980)

The structure of the triclinic form of octaethylporphinium (monocation) triiodide was determined by X-ray analysis. The structure of the previously determined orthorhombic form was refined using diffractometer data. The final R values for the triclinic and the orthorhombic forms were 0.060 and 0.069, respectively. The present analysis has established the inherent structure of porphyrin monocations; three pyrrole rings are coplanar and the plane of the fourth ring is tilted from the mean plane of the other three. The magnitude of the tilt angle is 12.5° for the triclinic form and 16.1° for the orthorhombic form.

Porphyrins exist in solution as the free base, monocationic and/or dicationic species, each of which shows the characteristic absorption spectrum.[1] As the equilibrium between the free base and the monocation is sensitive to pH and other factors,[2] the cationic species could be present in a biological environment.[3] The resemblance of spectrum between the monocation and the reaction intermediate of metal incorporation[4] suggests that in the final stage of oxidation from porphyrinogen to porphyrin, which occurs in the mitochondoria or in cytoplasm,[5] the monocationic species plays a role in controlling the formation of metalloporphyrins.

For comprehensive studies in porphyrin stereochemistry, it is important to reveal the structure of porphyrin monocation, since structural studies have been done for the free base and dicationic species.[6,7] As a first example, we have previously reported the structure of the orthorhombic form of octaethylporphinium (monocation) triiodide crystal,[8] in which one pyrrole ring is inclined by 14° with respect to the plane of the remaining porphyrin nucleus. This is quite different from the typical structures of the other species; the free base is planar within ±0.05 Å,[6] whilst the dication is deformed considerably, assuming $\bar{4}$ symmetry.[7] Although the inner hydrogen atoms are expected to determine the stereochemistry of monocation, their positions were not directly obtained owing to the low accuracy of intensity data. We have tried to refine the structure using new diffractometer data. On the other hand, we obtained the triclinic crystals of octaethylporphinium(monocation) triiodide [$(H_3OEP)^+I_3^-$], in which benzene molecules are solvated. The structure of this crystal has been determined in order to examine the packing effect of the crystal upon the structural feature of the monocation. A comparison of the two structures in detail will give the inherent structure of porphyrin monocation.

Experimental and Structure Determination

Triclinic Crystal. Triclinic crystals of $(H_3OEP)^+I_3^-$, reddish brown plates, were obtained from a dichloromethane–benzene solution of octaethylporphinium(dication) tetraiodide, A crystal 0.16×0.16×0.32 mm³ was used for data collection on a Rigaku automated, four-circle diffractometer with graphite monochromated Mo $K\alpha$ (λ=0.71069 Å) radiation. Density measured by the flotation method suggested the benzene hemi-solvate. The unit-cell dimensions were determined by least-squares calculations with 47 high-angle reflexions. Intensities of the independent reflexions within the range $2\theta \leqq 55°$ were measured by use of the $\omega/2\theta$ scan mode with a scanning rate of 2° (2θ) min^{-1}. Stationary background counts were accumulated for 30 s before and after each scan. Periodic checks of the intensity values of five standard reflexions showed no significant X-ray damage or crystal decay. Corrections for absorption or extinction were not applied. A total of 9099 independent reflexions were obtained, of which 3096 were zero; the observed threshold value, F_{11m}, was 5.56. The space group $P\bar{1}$ was deduced by the intensity statistics.

The structure was solved by the heavy-atom method. The structural parameters were refined by block-diagonal least-squares techniques; the quantity minimized was $\sum w\Delta^2$, where $\Delta=|F_o|-|F_c|$. All the hydrogen atoms were found by the difference synthesis. The zero-reflexions, for which $|F_c|>F_{11m}$, were included in the least-squares calculation by assuming $F_o=F_{11m}$. The following weights were applied; $w=\exp(-(As^2+Bt^2+Cst+Ds+Et+F))$ where $s=|F_o|\times 10^2$ and $t=\sin\theta/\lambda$ for $|F_o|\geqq F_{11m}$. and $w=1/\langle\Delta^2\rangle$ for $|F_o|<F_{11m}$. The coefficients, A–F, were evaluated by least-squares calculation at each cycle of structure refinement so that $\langle w\Delta^2\rangle=1$ in (s, t) space; their values in the final stage of refinement were, −0.8951, 14.35, −0.2166, 7.782, −6.059, and 1.845, respectively. The final R value was 0.06 for 6829 reflexions ($|F_o|>3/\sqrt{w(s,t)}$). Atomic scattering factors were taken from "International Tables for X-Ray Crystallography" Vol.

Table 1. Crystal data

Triclinic form	Orthorhombic form
$C_{36}H_{47}I_3N_4\cdot 1/2C_6H_6$	$C_{36}H_{47}I_3N_4$
$F.W.$=955.6	$F.W.$=916.5
$P\bar{1}$	Cmca
a=16.047(6) Å	a=29.564(4) Å
b=15.762(4) Å	b=14.512(5) Å
c=14.251(6) Å	c=17.385(3) Å
α=122.69(2)°	U=7459(3) Å³
β=139.15(2)°	D_m=1.61 g cm^{-3}
γ=63.84(2)°	D_x=1.63 g cm^{-3}
U=1981(1) Å³	Z=8
D_m=1.60 g cm^{-3}	μ(Mo $K\alpha$)=26.7 cm^{-1}
D_x=1.602 g cm^{-3}	
Z=2	
μ(Mo $K\alpha$)=25.7 cm^{-1}	

4.[9] Anomalous dispersion effect was taken into account with f' and f'' for iodine atom.[10]

Table 2. Fractional coordinates and temperature factors (triclinic form)

The B values for non-hydrogen atoms are equivalent isotropic temperature factors calculated from anisotropic thermal parameters using the equation $B=8\pi^2(U_1+U_2+U_3)/3$, where U_1, U_2, and U_3 are the principal components of mean square displacement matrix U. The e.s.d.'s in ( ) refer to last dicimal places.

Atom	x	y	z	B/Å^2
I(1)	0.13695(6)	0.22348(6)	0.09973(9)	6.86
I(2)	0.30733(5)	0.24553(4)	0.41499(8)	6.64
I(3)	0.47593(7)	0.25735(6)	0.73001(9)	7.46
N(1)	1.0850(5)	0.1331(4)	0.6791(7)	3.7
N(2)	0.9480(5)	0.0498(4)	0.6738(7)	3.4
N(2*)	1.2519(5)	−0.0443(4)	0.6961(7)	3.6
N(3)	1.1114(5)	−0.1390(4)	0.6815(6)	3.3
C(1)	1.0267(7)	0.3012(5)	0.6922(8)	3.4
C(2)	1.0047(6)	0.2142(5)	0.6800(8)	3.2
C(3)	0.9097(6)	0.2177(5)	0.6722(8)	3.0
C(4)	0.8839(6)	0.1427(5)	0.6688(7)	2.9
C(5)	0.7892(6)	0.1454(5)	0.6623(8)	3.0
C(6)	0.7995(6)	0.0565(5)	0.6653(8)	3.1
C(7)	0.9030(6)	−0.0053(5)	0.6749(8)	3.2
C(8)	0.9467(7)	−0.1008(5)	0.6834(9)	3.8
C(9)	1.0479(7)	−0.1594(5)	0.6980(9)	3.4
C(10)	1.1152(8)	−0.2432(6)	0.748(1)	4.7
C(11)	0.9568(7)	0.4029(5)	0.700(1)	4.3
C(12)	1.004(1)	0.463(1)	0.856(1)	7.0
C(13)	0.7010(6)	0.2371(6)	0.6629(9)	3.6
C(14)	0.7587(8)	0.3110(6)	0.820(1)	5.1
C(15)	0.7240(8)	0.0264(6)	0.667(1)	4.3
C(16)	0.790(1)	0.037(1)	0.820(1)	6.7
C(17)	1.0898(1)	−0.284(1)	0.799(1)	5.8
C(18)	1.018(1)	−0.378(1)	0.679(2)	8.9
C(1*)	1.1253(1)	0.2705(6)	0.6992(8)	3.5
C(2*)	1.1602(6)	0.1677(5)	0.6939(8)	3.0
C(3*)	1.2621(7)	0.1072(5)	0.7035(8)	3.4
C(4*)	1.3060(6)	0.0118(5)	0.7083(8)	2.9
C(5*)	1.4126(6)	−0.0483(5)	0.7259(8)	3.0
C(6*)	1.4198(6)	−0.1388(5)	0.7240(8)	3.2
C(7*)	1.3175(6)	−0.1370(5)	0.7064(8)	3.1
C(8*)	1.2965(6)	−0.2120(5)	0.7074(9)	3.5
C(9*)	1.2074(6)	−0.2122(5)	0.7051(8)	3.3
C(10*)	1.2142(8)	−0.2758(6)	0.754(1)	4.4
C(11*)	1.1879(8)	0.3325(6)	0.7162(1)	4.6
C(12*)	1.295(1)	0.391(1)	0.880(1)	7.0
C(13*)	1.5042(7)	−0.0123(6)	0.7524(9)	3.8
C(14*)	1.6054(9)	0.0483(8)	0.918(1)	6.0
C(15*)	1.5184(7)	−0.2244(6)	0.7463(9)	4.1
C(16*)	1.6214(8)	−0.2237(8)	0.911(1)	5.9
C(17*)	1.3182(9)	−0.3573(8)	0.813(1)	5.8
C(18*)	1.290(1)	−0.451(1)	0.683(2)	8.4
CB(1)	0.389(1)	0.498(1)	0.357(2)	8.5
CB(2)	0.392(1)	0.473(1)	0.436(2)	7.6
CB(3)	0.500(1)	0.475(1)	0.577(2)	7.9
HN(2)	1.017(6)	0.033(5)	0.697(8)	0.0
HN(2*)	1.204(7)	−0.016(5)	0.710(8)	1.7
HN(3)	1.070(5)	−0.114(4)	0.617(7)	0.0

Table 3. Fractional coordinates and temperature factors (orthorhombic form)

The B values for non-hydrogen atoms are equivalent isotropic temperature factors calculated from anisotropic thermal parameters using the equation $B=8\pi^2(U_1+U_2+U_3)/3$, where U_1, U_2, and U_3 are the principal components of mean square displacement matrix U. The e.d.s.'s in ( ) refer to last dicimal places.

Atom	x	y	z	B/Å^2
I(1)	0.18254(8)	0.0	0.0	10.9
I(2)	0.18189(7)	0.1457(2)	0.1150(1)	12.8
N(1)	0.5	0.429(1)	0.3946(9)	2.2
N(2)	0.4285(6)	0.565(1)	0.412(1)	3.1
N(3)	0.5	0.709(2)	0.438(1)	3.1
C(1)	0.4771(5)	0.279(1)	0.3670(9)	2.6
C(2)	0.4626(7)	0.375(1)	0.385(1)	3.1
C(3)	0.4187(8)	0.401(2)	0.387(1)	3.0
C(4)	0.4012(6)	0.491(2)	0.402(1)	3.0
C(5)	0.3565(6)	0.521(2)	0.403(1)	3.6
C(6)	0.3567(7)	0.614(2)	0.417(1)	3.8
C(7)	0.4031(6)	0.641(2)	0.423(1)	2.9
C(8)	0.4194(9)	0.728(2)	0.435(1)	4.0
C(9)	0.4617(7)	0.765(2)	0.435(1)	2.8
C(10)	0.4769(5)	0.856(1)	0.426(1)	2.8
C(11)	0.4459(7)	0.199(1)	0.353(1)	4.5
C(12)	0.4321(7)	0.193(1)	0.268(1)	7.2
C(13)	0.3159(6)	0.458(1)	0.389(1)	4.6
C(14)	0.3050(7)	0.445(2)	0.306(1)	9.2
C(15)	0.3155(7)	0.676(1)	0.422(1)	5.0
C(16)	0.3093(6)	0.733(2)	0.348(1)	7.8
C(17)	0.4450(6)	0.938(1)	0.412(1)	4.5
C(18)	0.4290(6)	0.939(1)	0.330(1)	7.6
HN(2)	0.458(5)	0.55(1)	0.413(8)	0.0
HN(3)	0.5	0.66(2)	0.46(1)	0.0

Orthorhombic Crystal. Orthorhombic crystals, reddish brown hexagonal plates, were obtained from methylenechloride–benzene solution. A crystal with dimensions of $0.15\times0.10\times0.02$ mm^3 was used for data collection on the automated, four-circle diffractometer with graphite-monochromated Mo $K\alpha$ radiation. The unit-cell dimensions were determined by least-squares calculations with 34 high-angle reflexions. Diffraction intensities of all the independent reflexions within the range $2\theta\leqq40°$ were measured by use of the ω scan mode at a scanning rate of 1° min^{-1}. Stationary background counts were accumulated for 50 s before and after each scan. Periodic checks of the intensity of three standard reflexions showed no significant X-ray damage or crystal decay. Corrections for absorption and extinction were not applied. A total of 1784 independent reflexions were obtained, of which 731 were zero. The structural parameters, determined by photographic data,[8] were used as the initial values. They were refined by the full-matrix least-squares methods. All the hydrogen atoms were located by the difference synthesis. The final R value was 0.069 for 1345 reflexions ($|F_o|>3/\sqrt{w(s,t)}$). The atomic parameters of most of the hydrogen atoms were fixed during the refinement. Details of refinement including anomalous dispersion effect of iodine were the same as those for the triclinic crystal. $F_{\rm lim}$ was 9.00 and the weighting coefficients A—F were 0.4916, 22.01, −0.03600, −1.585, −6.020, and 6.661, respectively. Crystal data are summarized in Table 1, and the final coordinates of both crystals are

TABLE 4. BOND LENGTHS (l/Å) AND ANGLES (ϕ/°) IN TRICLINIC FORM

Some nonbonded distances of interest are also given. CB's denote the carbon atoms of the benzene molecule.

N(1)–C(2)	1.36(1)	C(6)–C(7)–N(2)	106.2(8)
N(1)–C(2*)	1.37(1)	C(6)–C(7)–C(8)	126.5(9)
N(2)–C(4)	1.37(1)	N(2)–C(7)–C(8)	127.3(9)
N(2)–C(7)	1.36(1)	C(7)–C(8)–C(9)	127.5(10)
N(2*)–C(4*)	1.36(1)	C(8)–C(9)–N(3)	125.0(9)
N(2*)–C(7*)	1.38(1)	C(8)–C(9)–C(10)	127.8(10)
N(3)–C(9)	1.39(1)	N(3)–C(9)–C(10)	106.9(9)
N(3)–C(9*)	1.37(1)	C(9)–C(10)–C(10*)	108.7(11)
C(1*)–C(1)	1.37(1)	C(10)–C(10*)–C(9*)	107.0(10)
C(1)–C(2)	1.46(1)	N(3)–C(9*)–C(10*)	107.8(9)
C(2)–C(3)	1.42(1)	C(8*)–C(9*)–C(10*)	126.5(10)
C(3)–C(4)	1.38(1)	N(3)–C(9*)–C(8*)	124.8(9)
C(4)–C(5)	1.43(1)	C(7*)–C(8*)–C(9*)	129.0(10)
C(5)–C(6)	1.36(1)	N(2*)–C(7*)–C(8*)	128.2(9)
C(6)–C(7)	1.50(1)	C(6*)–C(7*)–C(8*)	125.6(9)
C(7)–C(8)	1.38(2)	N(2*)–C(7*)–C(6*)	106.1(8)
C(8)–C(9)	1.38(2)	C(7*)–C(6*)–C(5*)	107.8(8)
C(9)–C(10)	1.42(2)	C(6*)–C(5*)–C(4*)	108.1(8)
C(10)–C(10*)	1.38(2)	C(5*)–C(4*)–N(2*)	107.2(8)
C(9*)–C(10*)	1.43(2)	C(5*)–C(4*)–C(3*)	128.9(9)
C(8*)–C(9*)	1.41(1)	C(3*)–C(4*)–N(2*)	123.9(9)
C(7*)–C(8*)	1.38(1)	C(2*)–C(3*)–C(4*)	128.2(9)
C(6*)–C(7*)	1.45(1)	N(1)–C(2*)–C(3*)	122.6(9)
C(5*)–C(6*)	1.37(1)	C(1*)–C(2*)–C(3*)	124.6(9)
C(4*)–C(5*)	1.44(1)	N(1)–C(2*)–C(1*)	112.9(8)
C(3*)–C(4*)	1.37(1)	C(2*)–N(1)–C(2)	103.7(8)
C(2*)–C(3*)	1.43(1)	C(4)–N(2)–C(7)	111.2(8)
C(1*)–C(2*)	1.44(1)	C(4*)–N(2*)–C(7*)	110.9(8)
C(1)–C(11)	1.50(2)	C(9*)–N(3)–C(9)	109.3(8)
C(11)–C(12)	1.50(2)	C(1*)–C(1)–C(2)	105.4(9)
C(5)–C(13)	1.51(1)	C(1)–C(2)–N(1)	112.5(9)
C(13)–C(14)	1.50(2)	C(1)–C(2)–C(3)	121.8(9)
C(6)–C(15)	1.50(2)	N(1)–C(2)–C(3)	125.7(9)
C(15)–C(16)	1.47(2)	C(2)–C(3)–C(4)	127.5(9)
C(10)–C(17)	1.53(2)	C(3)–C(4)–N(2)	125.6(9)
C(17)–C(18)	1.49(3)	C(2*)–C(1*)–C(1)	105.6(9)
C(1*)–C(11*)	1.51(2)	C(1*)–C(1)–C(11)	128.8(10)
C(11*)–C(12*)	1.50(2)	C(2)–C(1)–C(11)	125.8(9)
C(5*)–C(13*)	1.51(1)	C(1)–C(11)–C(12)	111.9(1)
C(13*)–C(14*)	1.50(2)	C(4)–C(5)–C(13)	123.5(8)
C(6*)–C(15*)	1.50(2)	C(6)–C(5)–C(13)	127.9(9)
C(15*)–C(16*)	1.54(2)	C(5)–C(13)–C(14)	113.3(9)
C(10*)–C(17*)	1.52(2)	C(5)–C(6)–C(15)	127.6(9)
C(17*)–C(18*)	1.48(3)	C(7)–C(6)–C(15)	124.5(9)
N(2)–HN(2)	0.83(10)	C(6)–C(15)–C(16)	114.1(11)
N(2*)–HN(2*)	0.82(10)	C(9)–C(10)–C(17)	125.3(11)
N(3)–HN(3)	0.83(8)	C(10*)–C(10)–C(17)	125.8(12)
HN(2)···HN(2*)	2.63(14)	C(10)–C(17)–C(18)	111.9(14)
HN(2)···HN(3)	2.06(13)	C(10)–C(10*)–C(17*)	127.9(12)
HN(2*)···HN(3)	2.28(14)	C(9*)–C(10*)–C(17*)	124.9(11)
N(1)···N(2)	2.96(1)	C(10*)–C(17*)–C(18*)	110.1(13)
N(1)···N(2*)	2.86(1)	C(7*)–C(6*)–C(15*)	123.9(9)
N(3)···N(2)	2.96(1)	C(5*)–C(6*)–C(15*)	128.2(9)
N(3)···N(2*)	3.05(1)	C(6*)–C(15*)–C(16*)	112.2(9)
N(2)···N(2*)	4.23(1)	C(6*)–C(5*)–C(13*)	127.2(9)
I(1)–I(2)	2.889(1)	C(4*)–C(5*)–C(13*)	124.6(9)
I(2)–I(3)	2.945(1)	C(5*)–C(13*)–C(14*)	111.6(10)
CB(1)–CB(2)	1.34(3)	C(2*)–C(1*)–C(11*)	127.1(10)
CB(2)–CB(3)	1.32(3)	C(1)–C(1*)–C(11*)	127.3(10)
CB(1)–CB(3′)	1.40(3)	C(1*)–C(11*)–C(12*)	112.9(11)
C(3)–C(4)–C(5)	128.2(9)	I(1)–I(2)–I(3)	176.77(5)
N(2)–C(4)–C(5)	106.3(8)	CB(1)–CB(2)–CB(3)	120.2(18)
C(4)–C(5)–C(6)	108.5(8)	CB(2)–CB(3)–CB(1′)	119.7(18)
C(5)–C(6)–C(7)	107.8(9)	CB(2)–CB(1)–CB(3′)	120.2(18)

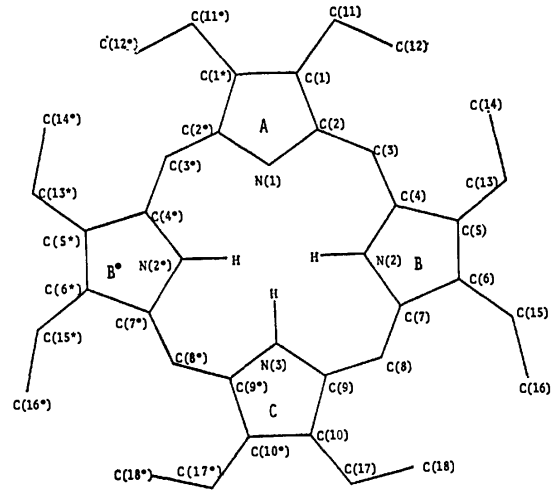

Fig. 1. The atom numbering system.

TABLE 5. BOND LENGTHS (l/Å) AND ANGLES (ϕ/°) IN ORTHORHOMBIC FORM

Some nonbonded distances of interest are also given.

N(1)-C(2)	1.37(2)	C(4)-N(2)-C(7)	110(2)
N(2)-C(4)	1.36(3)	C(9)-N(3)-C(9*)	109(2)
N(2)-C(7)	1.34(3)	C(1*)-C(1)-C(2)	107(1)
N(3)-C(9)	1.39(3)	C(1)-C(2)-N(1)	110(2)
C(1)-C(2)	1.49(3)	C(1)-C(2)-C(3)	123(2)
C(2)-C(3)	1.35(3)	N(1)-C(2)-C(3)	128(2)
C(3)-C(4)	1.43(3)	C(2)-C(3)-C(4)	127(2)
C(4)-C(5)	1.39(3)	C(3)-C(4)-N(2)	122(2)
C(5)-C(6)	1.38(3)	C(3)-C(4)-C(5)	129(2)
C(6)-C(7)	1.43(3)	N(2)-C(4)-C(5)	109(2)
C(7)-C(8)	1.37(3)	C(4)-C(5)-C(6)	108(2)
C(8)-C(9)	1.36(3)	C(5)-C(6)-C(7)	107(2)
C(9)-C(10)	1.41(3)	C(6)-C(7)-N(2)	108(2)
C(10)-C(10*)	1.37(3)	C(6)-C(7)-C(8)	127(2)
C(1)-C(1*)	1.36(3)	N(2)-C(7)-C(8)	125(2)
C(1)-C(11)	1.50(3)	C(7)-C(8)-C(9)	133(2)
C(11)-C(12)	1.54(3)	C(8)-C(9)-N(3)	121(2)
C(5)-C(13)	1.52(3)	C(8)-C(9)-C(10)	131(2)
C(13)-C(14)	1.49(3)	N(3)-C(9)-C(10)	107(2)
C(6)-C(15)	1.52(3)	C(9)-C(10)-C(10*)	109(2)
C(15)-C(16)	1.54(3)	C(11)-C(1)-C(1*)	128(2)
C(10)-C(17)	1.53(3)	C(1)-C(11)-C(12)	112(2)
C(17)-C(18)	1.51(3)	C(2)-C(1)-C(11)	125(2)
N(2)-HN(2)	0.88(14)	C(4)-C(5)-C(13)	124(2)
N(3)-HN(3)	0.82(18)	C(5)-C(13)-C(14)	113(2)
HN(2)···HN(2*)	2.50(28)	C(6)-C(5)-C(13)	128(2)
HN(2)···HN(3)	2.62(18)	C(5)-C(6)-C(15)	126(2)
N(1)···N(2)	2.90(2)	C(7)-C(6)-C(15)	127(2)
N(2)···N(3)	3.00(3)	C(6)-C(15)-C(16)	122(2)
N(2)···N(2*)	3.49(2)	C(9)-C(10)-C(17)	123(2)
I(1)-I(2)	2.910(3)	C(10*)-C(10)-C(17)	128(2)
C(2)-N(1)-C(2*)	107(1)	C(10)-C(17)-C(18)	110(2)
		I(1)-I(2)-I(3)	180

given in Tables 2 and 3.††

†† The tables of thermal parameters, hydrogen coordinates, and observed and calculated structure factors are kept as Document No. 8125 at the Chemical Society of Japan.

Results and Discussion

Cation. Figure 1 shows the atom numbering system used for both crystals. The monocation in the orthorhombic crystal has a crystallographic mirror plane perpendicular to the mean molecular plane through N(1) and N(3). Similar approximate local mirror symmetry is also observed in the triclinic monocation. The symmetry-related atoms are indicated with asterisk. The bond lengths and angles are listed in Tables 4 and 5 for triclinic and orthorhombic forms, respectively.

In the both crystals the imino hydrogen atoms are localized on rings B, B*, and C just as we postulated from the geometrical considerations in the previous paper on the orthorhombic form.[8] In the triclinic form, the C_α–N–C_α bond angle in the ring A, pyrrolenine ring, is 103.7°, while those of the ring B, B*, and C are 111.2, 110.9, and 109.3°, respectively. The corresponding values in the orthorhombic form are 107, 110, 110, and 109°, respectively. These values are consistent with those of pyrrole rings with and without attached hydrogen atoms.[11]

The stereoscopic drawings of the cations are shown in Fig. 2. Both cations take essentially the same architecture except the orientation of the peripheral ethyl groups. In the triclinic form the two ethyl groups attached to the ring C are oriented opposite to the other six ethyl groups with respect to the plane of the porphyrin nucleus, while all ethyl groups stick out on the same side in the orthorhombic form.

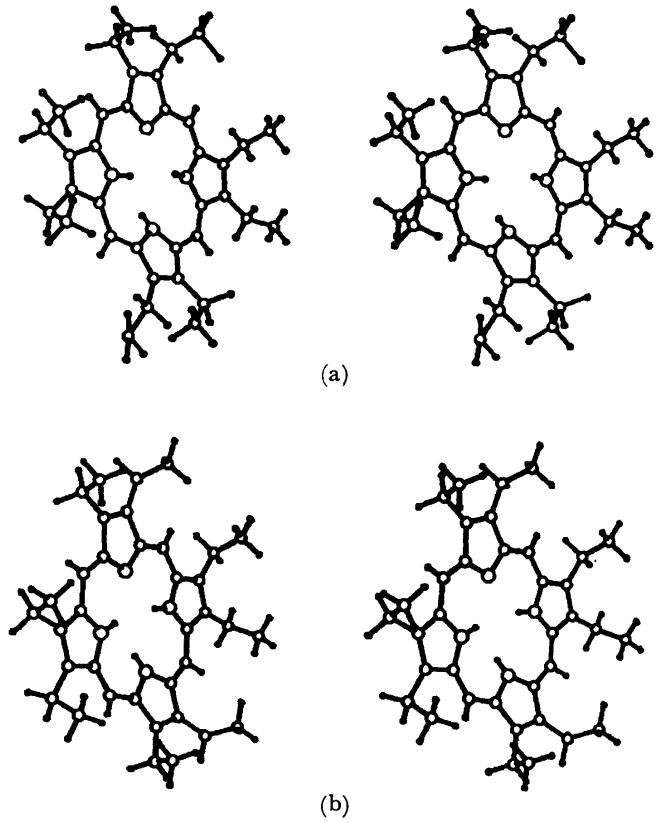

Fig. 2. The stereoscopic drawings of the molecules. (a) Triclinic form. (b) Orthorhombic form.

Table 6A. Least-squares planes in the orthorhombic monocation with displacements of atoms from these planes

(a) Displacements from the mean plane (l/Å)

Plane (1); N(1), N(2), C(1), C(2), C(3), C(4), C(5), C(6), C(7), C(8), N(2*), C(1*), C(2*), C(3*), C(4*), C(5*), C(6*), C(7*), C(8*)

N(1) 0.06, N(2) 0.02, C(1) −0.04, C(2) 0.03, C(3) −0.01, C(4) 0.03, C(5) −0.04, C(6) −0.02, C(7) 0.01, C(8) −0.01

Plane (2); ring A

N(1) −0.00, C(1) −0.00, C(2) 0.00

Plane (3); ring B

N(2) −0.01, C(4) 0.02, C(5) −0.01, C(6) 0.01

Plane (4); ring C

N(3) −0.02, C(9) 0.02, C(10) −0.01, HN(3) 0.24

(b) Plane equations in the form $Px+Qy+Rz=S$

	P	Q	R	S
(1)	0.000	−0.174	0.985	5.62
(2)	0.000	−0.216	0.976	5.36
(3)	−0.025	−0.171	0.985	5.35
(4)	0.000	0.106	0.994	8.68

(c) Angles (τ/°) between the planes. Estimated standard deviations are in parentheses.

(1)/(2) 2.4(5)	(1)/(3) 1.5(6)	(1)/(4) 16.1(6)
(2)/(3) 3.0(8)	(2)/(4) 18.5(7)	(3)/(4) 16.0(8)

Table 6B. Least-squares palnes in the triclinic monocation with displacements of atoms from these planes

(a) Displacements from the mean plane (l/Å)

Plane (1); N(1), N(2), C(1), C(2), C(3), C(4), C(5), C(6), C(7), C(8), N(2*), C(1*), C(2*), C(3*), C(4*), C(5*), C(6*), C(7*), C(8*)

N(1) −0.09, N(2) −0.03, N(2*) −0.07, C(1) −0.07, C(2) −0.02, C(3) −0.01, C(4) −0.02, C(5) −0.00, C(6) 0.02, C(7) 0.02, C(8) 0.06, C(1*) 0.06, C(2*) −0.02, C(3*) −0.02, C(4*) −0.01, C(5*) 0.07, C(6*) 0.04, C(7*) −0.03, C(8*) −0.01

Plane (2); ring A

N(1) −0.01, C(1) 0.00, C(2) 0.00, C(1*) −0.01, C(2*) 0.01

Plane (3); ring B

N(2) −0.01, C(4) 0.01, C(5) −0.00, C(6) −0.01, C(7) 0.01, HN(2) 0.15

Plane (4); ring B*

N(2*) −0.01, C(4*) 0.00, C (5*) 0.00, C(6*) −0.00, C(7*) 0.01, HN(2*) 0.21

Plane (5); ring C

N(3) 0.03, C(9) −0.02, C(10) 0.01, C(9*) −0.03, C(10*) 0.02, HN(3) −0.33

(b) Plane equations in the form $Px+Qy+Rz=S$

	P	Q	R	S
(1)	0.643	0.413	0.645	5.431
(2)	0.651	0.351	0.673	5.155
(3)	0.652	0.425	0.628	5.551
(4)	0.598	0.417	0.684	4.580
(5)	0.612	0.639	0.466	5.146

(c) Angles (τ/°) between the planes. Estimated standard deviations are in parentheses.

(1)/(2) 3.9(5)	(1)/(3) 1.3(11)	(1)/(4) 3.4(4)
(1)/(5) 16.7(3)	(2)/(3) 4.9(4)	(2)/(4) 4.9(4)
(2)/(5) 20.6(4)	(3)/(4) 4.5(4)	(3)/(5) 15.6(4)
(4)/(5) 17.9(4)		

The common feature of the cations in the two different crystalline field is of particular interest. As shown in Table 6, three of the four pyrrole rings, each of which are planar within the experimental errors, are approximately coplanar. The fourth ring C is tilted from the plane consisting of the three rings by 16.1(6) and 12.5(8)° for orthorhombic and triclinic forms, respectively. The difference between the two values may be due to the packing effects. Similar deformation mode is seen in octaethylporphinium tri-μ-chloro-hexacarbonyl-dirhenate[12] and in 21-ethoxycarbonylmethyl-2,3,7,-8,12,13,17,18-octaethylporphyrin.[13] In the former case the corresponding tilt angle is smaller (8.6°) probably due to the hydrogen bonding between the pyrrole nitrogen atoms and the water molecule of solvation. In the latter case the angle is much larger apparently due to the bulky alkyl substituents.

The tilt of the fourth pyrrole ring is believed to be due

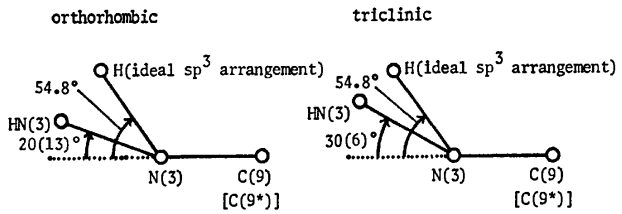

Fig. 3. Deviations of HN(3) atoms from the plane defined by N(3), C(9), and C(9*) atoms. The degree of deviations is expressed by the angle between N(3)→H vector and the plane. Estimated standard deviations are in parentheses.

mainly to the steric hindrance of the imino hydrogen atoms. As shown in Tables 4 and 5, H···H distances are 2.06 to 2.63 Å which indicate the relieved nonbonded H···H repulsion, if we take 1.9—2.0 Å as the minimum H···H nonbonded contact.[14] While HN(2)···HN(2*) distance are longer than 2.5 Å, HN(2)···HN(3) and HN(2*)···HN(3) distances are shorter than 2.3 Å. These distances suggest that the steric hindrance is effectively relieved by the tilt of the ring C. In addition, it is noted that the imino hydrogen atom of the ring C deviates from the plane of C_α–N–C_α. Figure 3 illustrates the angles between the N–H vector and the C_α–N–C_α planes for orthorhombic and triclinic cations, together with the N–H vector for the ideal sp^3 hybridization. Although these differences are not statistically significant enough, it may be concluded that the nitrogen atoms of the ring C have some sp^3 character. Such sp^3 character of N(3) is favourable for relieving the steric hindrance.

The values of corresponding bond lengths and angles in both cations are quite similar. In addition to this, the crystallographic and local mirror symmetries justify averaging equivalent bond lengths and angles to give the typical molecular dimensions as shown in Fig. 4.

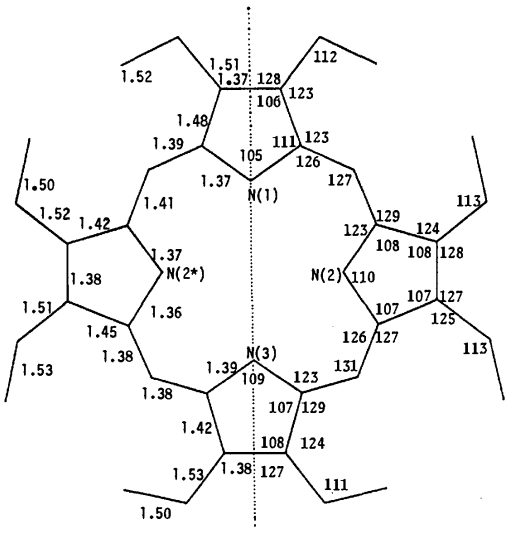

Fig. 4. Bond lengths and angles obtained by averaging equivalent halves of the two independent molecules. The dotted line reveals the crystallographic or local mirror plane.

The C_α–N distances are slightly longer in the ring C than in the other rings. The C_α–C_m–C_α angles, especially C(7)–C(8)–C(9), are larger than those normally found.[11] These features are similar to those of octaethylporphinium tri-μ-chloro-hexacarbonyldirhenate.[14] Other bond lengths and angles fall within the range tabulated by Hoard.[11]

The observed structures are the essential feature of monocationic species of porphyrins. Absorption spectra of many porphyrin monocations exhibit a similar pattern,[3,15] which reflects the common conjugate system determined by the present steric structure.

Anion and Molecular Packing. In the orthorhombic crystal, the central iodine atom of the triiodide anion is on the two-fold axis; therefore it has a symmetrical structure with the I–I distance of 2.910(3) Å and the I–I–I angle of 180°. In the triclinic crystal, on the other hand, the anion is free from any crystallographic restriction; the I(1)–I(2) distance of 2.889 Å is significantly shorter than the I(2)–I(3) of 2.945 Å, and I(1)–I(2)–I(3) angle is 176.77(5)°. The asymmetry may be due to the asymmetric environment around the anion in the crystal.[16] The gravity centre of benzene molecule in the triclinic crystal is placed on the centre of symmetry at (1/2, 1/2, 1/2).

The stereoscopic drawings of the crystal structures of both polymorphs are shown in Fig. 5. The common packing feature is "face-to-face" stacking of the porphyrin nuclei. There is no NH···N hydrogen bond between the faces. The similar packing mode is found in the crystal of other octaethylporphyrin derivatives.[12,13] This "face-to-face" stacking well explains the orientation of the terminal ethyl groups. The exceptional direction of the two ethyl groups attached to the C ring is seen in the triclinic crystal.

No unusual van der Waals contact is seen between the anion and the peripheral part of the cations. There is no charge transfer interaction between the benzene molecule and the anion in the triclinic crystal.

Figures 2 and 5 were drawn by TSD : XTAL, which is a computer-graphics interactive modeling programme for the NOVA3 computer.[17]

The present work was partially supported by a Grant-in-Aid for Scientific Research from the Ministry of Education, to which the authors's thanks are due.

References

1) K. M. Smith, "Porphyrins and Metalloporphyrins," Elsevier, Amsterdam (1975).
2) H. Baker, P. Hambright, and L. Wagner, *J. Am. Chem. Soc.*, **95**, 5942 (1973).
3) J. E. Falk, "Porphyrins and Metalloporphyrins," Elseveier, Amsterdam (1964).
4) D. A. Brisbin and R. J. Balahura, *Can. J. Chem.*, **46**, 3431 (1968).
5) S. Sano and S. Granick, *J. Biol. Chem.*, **236**, 1173 (1961); H. G. Schiefer, *Z. Physiol. Chem.*, **350**, 921 (1969).
6) S. J. Silvers and A. Tulinsky, *J. Am. Chem. Soc.*, **89**, 3331 (1967); B. L. Chen and A. Tulinsky, *ibid.*, **94**, 4144 (1972); P. W. Codding and A. Tulinsky, *ibid.*, **94**, 4151 (1972); J. W. Lauher and J. A. Ibers, *ibid.*, **95**, 5148 (1973).
7) A. Stone and E. B. Fleisher, *J. Am. Chem. Soc.*, **90**, 2735

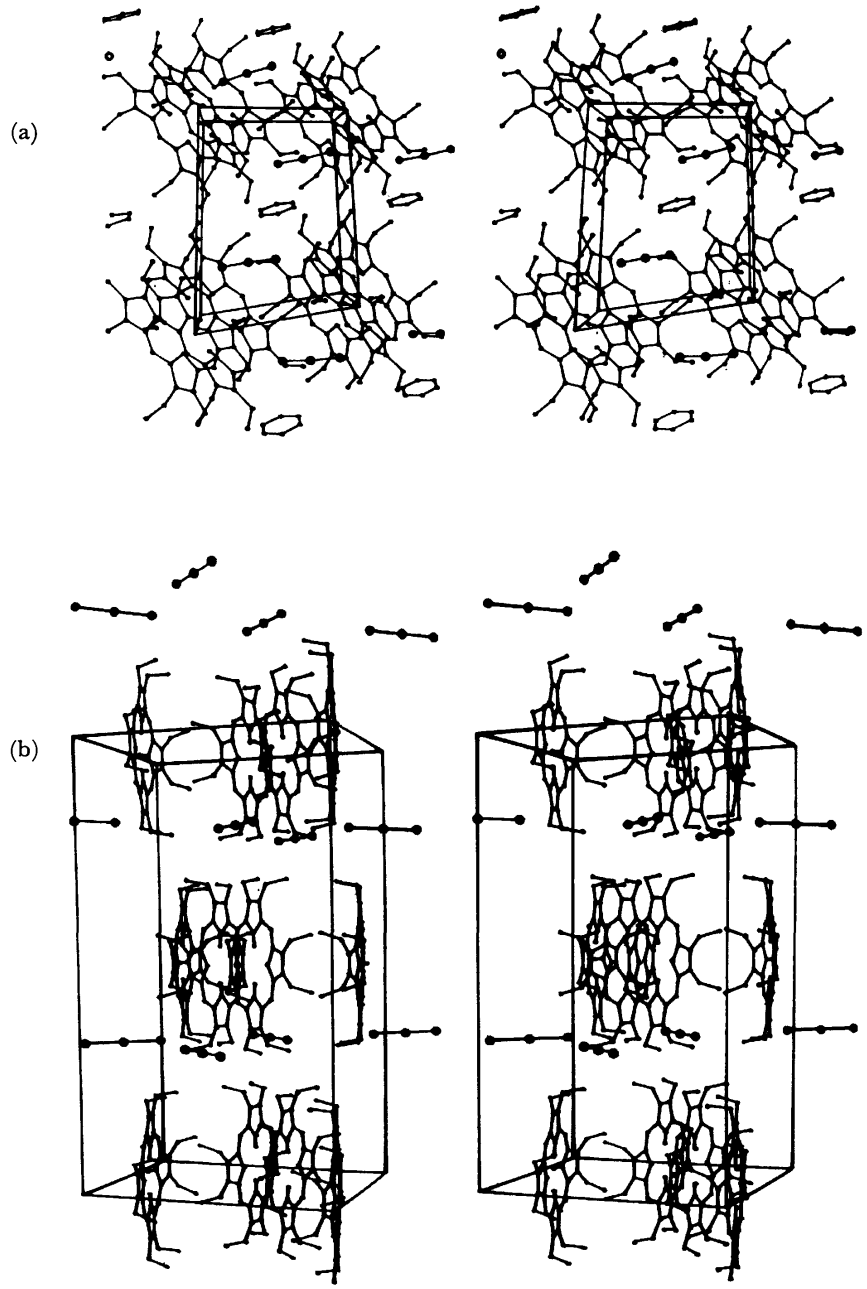

Fig. 5. The stereoscopic drawings of the crystal structures. (a) Triclinic form. The origin is at the lower left rear corner, c points to the viewer, b upward, and a rightward. (b) Orthorhomibc form. The origin is at the lower left rear corner, b points to the viewer, a upward, and c rightward.

(1968).

8) N. Hirayama, A. Takenaka, Y. Sasada, E. Watanabe, H. Ogoshi, and Z. Yoshida, *J. Chem. Soc., Chem. Commun.*, **1974**, 330.

9) "International Tables for X-Ray Crystallography," Kynoch Press, Birmingham (1974), Vol. IV, p. 71.

10) "International Tables for X-Ray Crystallography," Kynoch Press, Birmingham (1962), Vol. III, p. 213.

11) J. L. Hoard, "Porphyrins and Metalloporphyrins," Elsevier, Amsterdam (1975), p. 337.

12) C. P. Hrung, M. Tsutsui, D. L. Cullen, E. F. Meyer, Jr., and C. N. Morimito, *J. Am. Chem. Soc.*, **100**, 6068 (1978).

13) G. M. MacLaughlin, *J. Chem. Soc., Perkin Trans. 2*, **1974**, 136.

14) O. Ermer and J. D. Dunitz, *J. Chem. Soc., Chem. Commun.*, **1971**, 178.

15) H. Ogoshi, E. Watanabe, and Z. Yoshida, *Tetrahedron.* **29**, 3241 (1973).

16) V. H. Pritzkow and H. Hartl, *Acta Crystallogr., Sect. B*, **29**, 1777 (1973); J. Runsink, S. Swen-Walstra and T. Migchelsen, *ibid., B*, **28**, 1331 (1972).

17) A. Takenaka and Y. Sasada, *J. Cryst. Soc. Jpn.*, **22**, 214 (1980).

  Bull. Chem. Soc. Jpn., 54, 1005—1009 (1981)

The X-Ray Study of Several Reaction Products of Substituted Benzo-[1,2 : 4,5]dicyclobutene. II. 2,7-Di-*t*-butyl-11,12-dicyano-4,5,9,10-tetraphenyltetracyclo[4.4.2.$0^{1,8}$.$0^{3,6}$]dodeca-2,4,7,9-tetraene

Harumichi Tsukada, Hirotaka Shimanouchi, and Yoshio Sasada*

Laboratory of Chemistry for Natural Products, Tokyo Institute of Technology, Nagatsuta, Midori-ku, Yokohama 227

(Received September 16, 1980)

trans-1,2-Dicyanoethylene (DCNE) reacts with substituted benzo[1,2 : 4,5]dicyclobutene (**1**) to give only one adduct (**4**), the title compound, whereas tetracyanoethylene (TCNE) gives two isomers. Crystals of **4** are triclinic; space group P$\bar{1}$, a=13.505(2), b=14.118(2), c=10.722(1) Å, α=98.87(1), β=102.36(1), γ=111.71(1)° and Z=2. The structure was solved by the direct method and was refined by the block-diagonal least-squares method to the final R factor of 0.055 for 5479 observed reflections. The absence of two cyano groups in **4** makes less steric hindrance than **3**. Introducing the empirical parameters, non-bonded interaction energy was calculated for the approaching model of **1** and DCNE. The result well explains the addition of DCNE to the C(1)–C(6) position of **1**.

We have investigated a series of Diels-Alder adducts formed by the reaction of substituted benzo[1,2 : 4,5]-dicyclobutene (**1**)[1] and some dienophiles. In the first two papers, we reported the crystal structures of molecules **2** and **2a**[2,3] which are the first stable compounds with an *anti*-aromatic 8π electron benzo[1,2 : 4,5]-cyclobutene skeleton, and observed some degree of electron localization in agreement with a result of molecular orbital calculation. In the third paper,[4] we presented the crystal structure of **3**, a by-product of the addition reaction of **1** and tetracyanoethylene (TCNE). The analysis revealed the stereochemical differences between the main (**2**) and by-product (**3**) of this reaction. We calculated the electronic and steric interactions between approaching **1** and TCNE, and obtained an explanation for the bifurcate reactivity.

trans-1,2-Dicyanoethylene (DCNE) gives, on the contrary, only one product **4**.[5] The present study on the X-ray analysis of **4** is, therefore, not only an assertation of the proposed molecular structure, but also the stereochemical approach to a complicated organic reaction mechanism.

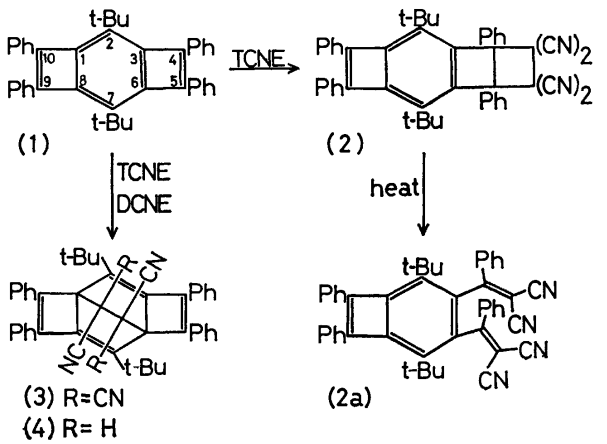

Experimental and Structure Determination

Colorless needles were recrystallized from acetone–methanol solution. Oscillation and Weissenberg photographs indicated triclinic symmetry. A crystal with dimensions 0.35×0.40×0.40 mm was mounted on a Rigaku automated four-circle diffratometer with graphite monochromated Mo $K\alpha$ radiation (λ=0.71069 Å). The crystal data are listed in Table 1. A total of 6317 independent reflections ($2\theta \leqq 50°$) was obtained in which 5479 had net intensities greater than the background. The intensities were corrected for Lorentz and polarization effects. The statistical distribution of the normalized structure factors, $|E|$'s, shows that the space group is P$\bar{1}$.

Table 1. Crystal data

2,7-Di-*t*-butyl-11,12-dicyano-4,5,9,10-tetraphenyltetracyclo-[4.4.2.$0^{1,8}$.$0^{3,6}$]dodeca-2,4,7,9-tetraene
$C_{46}H_{40}N_2$
M.W.=620.8
Crystal system: triclinic
Space group: P$\bar{1}$
a=13.505(2) Å
b=14.118(2) Å
c=10.722(2) Å
α=98.87(1)°
β=102.36(1)°
γ=111.71(1)°
U=1793 Å^3
D_m=1.148 g cm^{-3}
D_x=1.150 g cm^{-3}
Z=2

The structure was solved by the direct method.[6] All the 48 non-hydrogen atoms were found on the first E map calculated with 475 $|E|$'s greater than 1.6. The atomic parameters were refined by the block-diagonal least-squares method. Although hydrogen atoms were found by the difference Fourier synthesis, they were fixed at geometrically calculated positions, which were recalculated at the last stage of the refinement. Their isotropic thermal parameters were also fixed. Three reflections had $|F_o|$'s abnormally lower than $|F_c|$'s. As they seem to suffer from the secondary extinction, the final refinement was carried out without these reflections. The weighting scheme used was

$$w = 0.3 \quad \text{for } |F| = 0.0$$
$$w = 1/(1 + 0.44(4 - |F|)) \quad \text{for } 0 < |F| \leqq 4$$
$$w = 1 \quad \text{for } 4 < |F| \leqq 15$$
$$w = 1/(1 + 0.44(|F| - 15)) \quad \text{for } |F| > 15.$$

The final R factor was 0.55 for the observed reflections, and

Table 2. Fractional coordinates and equivalent isotropic temperature factors

B_{eq}'s are defined as $B_{eq}=8\pi^2(U_1+U_2+U_3)/3$.

Atom	x	y	z	B_{eq}/Å^2
C(1)	0.2235(1)	0.4218(1)	0.1104(1)	2.58
C(2)	0.2134(1)	0.5017(1)	0.0311(1)	2.61
C(3)	0.2818(1)	0.5977(1)	0.1111(1)	2.68
C(4)	0.3411(1)	0.7135(1)	0.1348(1)	3.05
C(5)	0.4020(1)	0.7262(1)	0.2602(1)	2.93
C(6)	0.3484(1)	0.6065(1)	0.2509(1)	2.66
C(7)	0.2689(1)	0.5476(1)	0.3251(1)	2.56
C(8)	0.2072(1)	0.4501(1)	0.2459(1)	2.56
C(9)	0.1255(1)	0.3396(1)	0.2213(1)	2.79
C(10)	0.1344(1)	0.3112(1)	0.0980(1)	2.78
C(11)	0.3467(1)	0.4329(1)	0.1387(1)	3.13
C(12)	0.4246(1)	0.5472(1)	0.2321(1)	3.20
C(13)	0.1428(1)	0.4735(1)	-0.1116(1)	3.20
C(14)	0.1946(2)	0.4243(2)	-0.2022(2)	5.60
C(15)	0.1394(1)	0.5723(1)	-0.1499(1)	4.12
C(16)	0.0216(1)	0.3948(1)	-0.1332(2)	5.24
C(17)	0.2622(1)	0.5918(1)	0.4602(1)	3.21
C(18)	0.3500(2)	0.5814(2)	0.5681(2)	6.05
C(19)	0.1464(1)	0.5299(1)	0.4733(1)	4.05
C(20)	0.2798(2)	0.7071(1)	0.4807(2)	5.63
C(21)	0.3463(1)	0.7879(1)	0.0503(1)	3.74
C(22)	0.2940(1)	0.8553(1)	0.0613(2)	5.01
C(23)	0.3014(2)	0.9259(2)	-0.0175(3)	6.80
C(24)	0.3593(2)	0.9287(2)	-0.1075(2)	7.30
C(25)	0.4116(2)	0.8620(2)	-0.1208(2)	7.02
C(26)	0.4065(2)	0.7909(1)	-0.0411(2)	5.41
C(27)	0.4985(1)	0.8142(1)	0.3563(1)	3.20
C(28)	0.5250(1)	0.9177(1)	0.3469(2)	4.47
C(29)	0.6182(2)	1.0006(1)	0.4366(2)	5.52
C(30)	0.6862(2)	0.9827(1)	0.5367(2)	5.49
C(31)	0.6605(1)	0.8810(1)	0.5485(2)	5.49
C(32)	0.5677(1)	0.7978(1)	0.4587(2)	4.52
C(33)	0.0743(1)	0.2788(1)	0.3096(1)	3.05
C(34)	-0.0394(1)	0.2367(1)	0.2939(2)	4.04
C(35)	-0.0814(2)	0.1806(1)	0.3814(2)	5.19
C(36)	-0.0110(2)	0.1670(1)	0.4838(2)	5.45
C(37)	0.1024(2)	0.2087(1)	0.4999(2)	4.90
C(38)	0.1451(1)	0.2641(1)	0.4132(1)	3.98
C(39)	0.0897(1)	0.2108(1)	-0.0028(1)	3.12
C(40)	-0.0191(1)	0.1366(1)	-0.0261(1)	4.13
C(41)	-0.0627(2)	0.0428(1)	-0.1246(2)	5.31
C(42)	0.0015(2)	0.0221(1)	-0.1993(2)	5.53
C(43)	0.1097(2)	0.0943(1)	-0.1763(2)	5.25
C(44)	0.1542(1)	0.1887(1)	-0.0789(2)	4.19
C(45)	0.3627(1)	0.3528(1)	0.2027(2)	4.29
C(46)	0.5099(1)	0.6033(1)	0.1720(2)	4.34
N(1)	0.3745(1)	0.2902(1)	0.2517(2)	7.15
N(2)	0.5745(1)	0.6456(1)	0.1233(2)	6.56

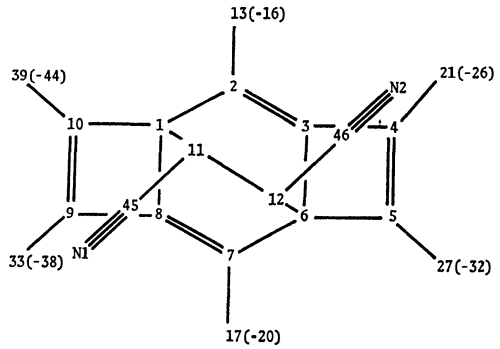

Fig. 1. Numbering scheme. Numbers in parentheses indicate the atoms of the substituents.

0.067 for all the reflections.† The atomic scattering factors were taken from "International Tables for X-ray Crystallography."[7] The final atomic parameters are listed in Table 2. The crystallographic numbering scheme is shown in Fig. 1.

Description of the Structure

Crystal structure viewed along the a axis is shown in Fig. 2. Stereoscopic views of the molecular framework are given in Fig. 3. There is no intermolecular distance shorter than van der Waals contacts. Bond lengths and angles are listed in Tables 3 and 4, respectively. As previously assigned from spectroscopic studies,[5] **4** has a framework formed by an addition of DCNE to C(1) and C(6) position of **1**. Although two isomers of cross

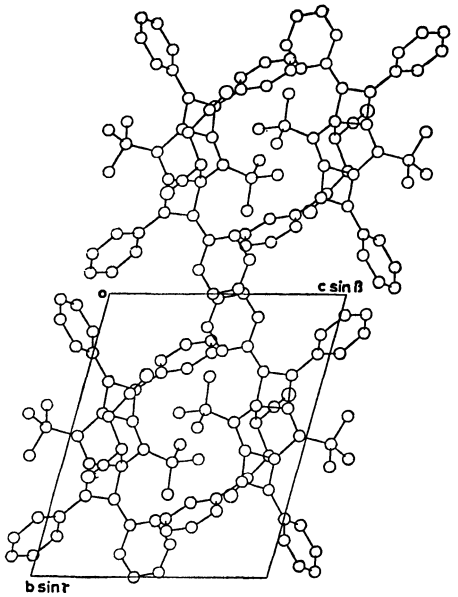

Fig. 2. Crystal structure projected along the a axis.

Table 3. Bond lengths (l/Å)

Standard deviations are given in parentheses.

C(1)–C(2)	1.541(3)	C(17)–C(20)	1.528(4)
C(1)–C(8)	1.531(3)	C(21)–C(22)	1.384(3)
C(1)–C(10)	1.543(3)	C(21)–C(26)	1.397(4)
C(1)–C(11)	1.568(3)	C(22)–C(23)	1.393(4)
C(2)–C(3)	1.342(3)	C(23)–C(24)	1.362(5)
C(2)–C(13)	1.520(3)	C(24)–C(25)	1.378(5)
C(3)–C(4)	1.481(3)	C(25)–C(26)	1.408(4)
C(3)–C(6)	1.534(3)	C(27)–C(28)	1.395(3)
C(4)–C(5)	1.363(3)	C(27)–C(32)	1.390(3)
C(4)–C(21)	1.482(3)	C(28)–C(29)	1.387(4)
C(5)–C(6)	1.549(3)	C(29)–C(30)	1.377(4)
C(5)–C(27)	1.461(3)	C(30)–C(31)	1.380(4)
C(6)–C(7)	1.545(3)	C(31)–C(32)	1.385(4)
C(6)–C(12)	1.573(3)	C(33)–C(34)	1.386(3)
C(7)–C(8)	1.340(3)	C(33)–C(38)	1.398(3)
C(7)–C(17)	1.521(3)	C(34)–C(35)	1.398(4)
C(8)–C(9)	1.481(3)	C(35)–C(36)	1.378(4)
C(9)–C(10)	1.365(3)	C(36)–C(37)	1.382(4)
C(9)–C(33)	1.484(3)	C(37)–C(38)	1.390(4)
C(10)–C(39)	1.467(3)	C(39)–C(40)	1.394(3)
C(11)–C(12)	1.582(3)	C(39)–C(44)	1.396(3)
C(11)–C(45)	1.468(3)	C(40)–C(41)	1.392(4)
C(12)–C(46)	1.473(3)	C(41)–C(42)	1.376(4)
C(13)–C(14)	1.535(4)	C(42)–C(43)	1.378(4)
C(13)–C(15)	1.528(3)	C(43)–C(44)	1.391(4)
C(13)–C(16)	1.542(3)	C(45)–N(1)	1.137(4)
C(17)–C(18)	1.536(4)	C(46)–N(2)	1.138(4)
C(17)–C(19)	1.533(3)		

† The tables of the structure factors and the other atomic parameters are kept as Document No. 8124 at the Chemical Society of Japan.

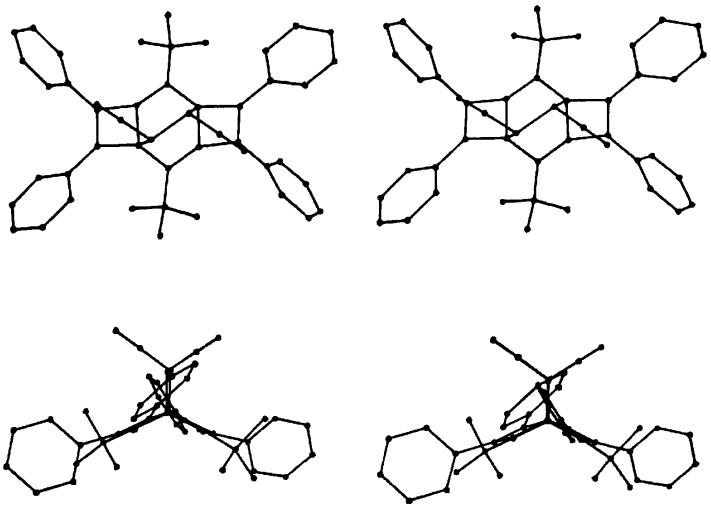

Fig. 3. Stereoscopic views.

TABLE 4. BOND ANGLES (ϕ/°)
Standard deviations are given in parentheses.

C(2)-C(1)-C(8)	110.9(1)	C(2)-C(13)-C(16)	111.6(2)
C(2)-C(1)-C(10)	128.1(2)	C(14)-C(13)-C(15)	108.8(2)
C(2)-C(1)-C(11)	107.2(1)	C(14)-C(13)-C(16)	109.2(2)
C(8)-C(1)-C(10)	84.5(1)	C(15)-C(13)-C(16)	107.8(2)
C(8)-C(1)-C(11)	105.8(1)	C(7)-C(17)-C(18)	109.3(2)
C(10)-C(1)-C(11)	115.8(1)	C(7)-C(17)-C(19)	110.1(2)
C(1)-C(2)-C(3)	106.2(2)	C(7)-C(17)-C(20)	111.6(2)
C(1)-C(2)-C(13)	125.4(2)	C(18)-C(17)-C(19)	108.7(2)
C(3)-C(2)-C(13)	128.4(2)	C(18)-C(17)-C(20)	110.1(2)
C(2)-C(3)-C(4)	151.4(2)	C(19)-C(17)-C(20)	107.0(2)
C(2)-C(3)-C(6)	119.0(2)	C(4)-C(21)-C(22)	121.4(2)
C(4)-C(3)-C(6)	89.2(1)	C(4)-C(21)-C(26)	119.2(2)
C(3)-C(4)-C(5)	93.4(2)	C(22)-C(21)-C(26)	119.5(2)
C(3)-C(4)-C(21)	134.1(2)	C(21)-C(22)-C(23)	120.5(2)
C(5)-C(4)-C(21)	132.0(2)	C(22)-C(23)-C(24)	120.3(3)
C(4)-C(5)-C(6)	93.0(2)	C(23)-C(24)-C(25)	120.3(3)
C(4)-C(5)-C(27)	133.5(2)	C(24)-C(25)-C(26)	120.4(3)
C(6)-C(5)-C(27)	132.2(2)	C(21)-C(26)-C(25)	119.0(3)
C(3)-C(6)-C(5)	84.4(1)	C(5)-C(27)-C(28)	120.8(2)
C(3)-C(6)-C(7)	110.2(1)	C(5)-C(27)-C(32)	121.3(2)
C(3)-C(6)-C(12)	105.8(1)	C(28)-C(27)-C(32)	117.9(2)
C(5)-C(6)-C(7)	128.9(2)	C(27)-C(28)-C(29)	120.6(2)
C(5)-C(6)-C(12)	115.1(1)	C(28)-C(29)-C(30)	120.6(3)
C(7)-C(6)-C(12)	107.5(1)	C(29)-C(30)-C(31)	119.6(3)
C(6)-C(7)-C(8)	105.9(2)	C(30)-C(31)-C(32)	119.9(2)
C(6)-C(7)-C(17)	126.8(2)	C(27)-C(32)-C(31)	121.4(2)
C(8)-C(7)-C(17)	127.3(2)	C(9)-C(33)-C(34)	123.1(2)
C(1)-C(8)-C(7)	119.4(2)	C(9)-C(33)-C(38)	117.8(2)
C(1)-C(8)-C(9)	89.2(1)	C(34)-C(33)-C(38)	119.1(2)
C(7)-C(8)-C(9)	151.1(2)	C(33)-C(34)-C(35)	119.8(2)
C(8)-C(9)-C(10)	93.0(1)	C(34)-C(35)-C(36)	120.8(3)
C(8)-C(9)-C(33)	132.3(2)	C(35)-C(36)-C(37)	119.8(3)
C(10)-C(9)-C(33)	133.4(2)	C(36)-C(37)-C(38)	120.0(3)
C(1)-C(10)-C(9)	93.2(1)	C(33)-C(38)-C(37)	120.6(2)
C(1)-C(10)-C(39)	132.0(2)	C(10)-C(39)-C(40)	120.4(2)
C(9)-C(10)-C(39)	134.3(2)	C(10)-C(39)-C(44)	120.9(2)
C(1)-C(11)-C(12)	107.0(1)	C(40)-C(39)-C(44)	118.7(2)
C(1)-C(11)-C(45)	111.7(2)	C(39)-C(40)-C(41)	120.4(2)
C(12)-C(11)-C(45)	110.1(2)	C(40)-C(41)-C(42)	120.3(3)
C(6)-C(12)-C(11)	107.6(1)	C(41)-C(42)-C(43)	119.9(3)
C(6)-C(12)-C(46)	111.3(2)	C(42)-C(43)-C(44)	120.4(3)
C(11)-C(12)-C(46)	109.7(2)	C(39)-C(44)-C(43)	120.2(2)
C(2)-C(13)-C(14)	109.1(2)	C(11)-C(45)-N(1)	179.6(3)
C(2)-C(13)-C(15)	110.3(2)	C(12)-C(46)-N(2)	178.7(3)

adducts of **1** and DCNE, **4** and **4a**, would be possible, the present analysis revealed that the former is the correct one. This stereoselectivity of the addition reaction will be discussed later.

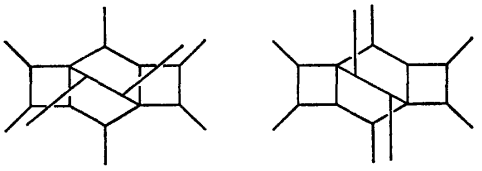

4 4a

The present structure is quite similar to that of **3** except that the latter has two more cyano groups on the central bridge. Therefore, the framework of **4** without terminal substituents also consists of three planar parts, which include C(1)–C(6) interatomic vector in common. Least-squares planes and deviations of the atoms from the planes are given in Table 5. Dihedral angles between these planes are shown in Table 6. The planes I and II make an angle of 125.7°. The plane III, formed by the addition of DCNE, bisects this dihedral angle. These were also the case in **3**; the corresponding value is 125.0°. But the detailed observation of the planarity and dihedral angle indicates some characteristic differences between **3** and **4**. A slight folding of the four-membered ring observed in **3** is reduced in **4**. Mean deviation from these planes is 0.014 Å in **3** and 0.007 Å in **4**. On the contrary, coplanarity between I and this four-membered ring is poorer in **4**; the dihedral angle between them is 4.6° in **4**, whereas it is 2.0° in **3**. The direction of this bending is upward to the cyano group just above the four-membered ring. However, the largest difference between these molecules is the deviation of *t*-butyl groups. The trend observed in **3** in which the *t*-butyl groups are bent away from the plane I opposite to the cyano group just above is greatly reduced in **4**. The mean deviation of C(13) of the *t*-butyl group from the plane I is up to 0.13 Å in **3**, and it is 0.048 Å in **4**.

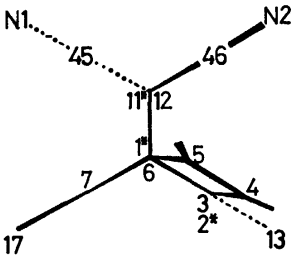

Fig. 4. Schematic drawing of the molecule projected along the C(1)–C(6) direction.

These differences may be consistently explained as follows. Figure 4 is a schematic drawing of the molecule projected along the C(1)–C(6) direction. Absence of the two cyano groups on the central bridge in the case of **4** reduces the repulsion with *t*-butyl groups and the latter can be nearly on the plane I. At the same time, the torsion angle along the C(11)–C(12) bond will be changed to be favourable against the other steric effect. The torsion angle C(1)–C(11)–C(12)–C(6) in **4** [121.2(1)°] is greater than that of **3** by 2.5°. Then the four-membered ring, C(3)–C(4)–C(5)–C(6), below this cyano group may slightly go upward so as to avoid the repulsion between the *t*-butyl group which is attached to the other plane II.

The lack of the two cyano groups also reduces the steric hindrance in the central bridge bond. The mean bond length C(1)–C(11) in **4** is 1.571 Å, which is 0.016 Å shorter than that of **3**. Moreover, the difference of the C(11)–C(12) distances between **3** and **4** is 0.042 Å. This shortening is partly due to the elimination of an electron withdrawing cyano group, but more important is the reduction of the repulsion between the cyano groups in the eclipse conformation.

TABLE 5. DEVIATIONS (l/Å) OF THE ATOMS FROM THE LEAST-SQUARES PLANES

Asterisks indicate the atoms defining the best plane.

Plane I		Plane II		Plane III	
C(1)*	−0.001	C(1)*	−0.006	C(1)*	0.015
C(2)*	0.001	C(8)*	0.012	C(11)*	−0.023
C(3)*	−0.001	C(7)*	−0.011	C(12)*	0.023
C(6)*	0.001	C(6)*	0.006	C(6)*	−0.015
C(13)	−0.049	C(17)	−0.048		
C(4)	−0.133	C(9)	0.138		
Plane IV		Plane V			
C(3)*	0.003	C(1)*	0.010		
C(4)*	−0.002	C(8)*	−0.011		
C(5)*	0.003	C(9)*	0.012		
C(6)*	−0.003	C(10)*	−0.012		
C(2)	−0.092	C(7)	0.033		
C(21)	−0.155	C(33)	0.274		
C(27)	−0.208	C(39)	0.096		

TABLE 6. DIHEDRAL ANGLES (ϕ/°)

	II	III	IV	V
I	125.7(1)	117.1(1)	4.9(1)	128.7(1)
II		117.2(1)	127.9(1)	4.3(1)
III			114.6(1)	114.1(1)
IV				130.6(1)

Discussion

In a previous paper,[4] we have shown a new approach to a reaction mechanism of complicated molecules. Its interaction energy was divided into two parts, a stabilization energy in the intermediate state[8] of the approaching molecules, and a steric effect of the bulky substituents estimated from the empirical non-bonded interaction parameters.[9] The former was calculated in the reaction intermediate of unsubstituted benzo[1,2 : 4,5]dicyclobutene and TCNE or ethylene. The preference of the cross addition of TCNE is expected from this result. However, it is overcome by the repulsion between the bulky substituents. These results are in good agreement with the observed reaction of **1** and TCNE. It is, therefore, quite important to carry out the same kind of calculation for the reaction of **1** and DCNE which is

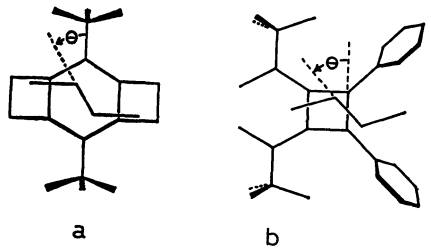

Fig. 5. Relative orientation θ in the (a) cross, and (b) linear approaching mode.

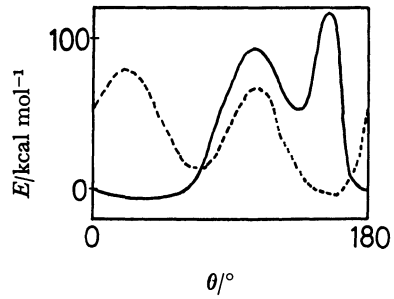

Fig. 6. Variations of the non-bonded interaction energy with the relative orientation θ at a constant distance (3.4 Å).

expected to be less repulsive than TCNE. The procedure is almost the same as that in the previous report. Since the electronic interaction energy was calculated without bulky substituents, the result is also applicable to that of DCNE. Relative orientation θ in the reaction intermediate is defined in Fig. 5. Non-bonded interaction energy in the case where the interplane distance is 3.4 Å is shown in Fig. 6. The solid curve refers to the cross addition (Fig. 5a). Its minimum is -6.6 kcal mol^{-1}†† at about 50° of θ. The dashed curve indicates the energy value of the linear addition (Fig. 5b). It has a minimum energy -5.0 kcal mol^{-1} when θ is $-10°$. In order to reduce the total number of parameters, terminal substituents are fixed as those in Fig. 5, which may be regarded as least repulsive conformations. Both of the minimum energy and the shape of the potential groove indicate that the cross approaching mode is less hindered than that of the linear approach. Taking the electronic interaction energy into account, we conclude that the cross addition is much preferable to the linear addition, and it is consistent with the reaction of **1** and DCNE.

The present calculation also explains why **4**, not a possible isomer **4a**, was actually formed. They correspond to the adducts with the θ value of 60° and 120° respectively. There is a local minimum at 120° in Fig. 6, but the energy value is high because of the repulsion between *t*-butyl groups and cyano groups.

The authors are grateful to Professor Fumio Toda of Ehime University for supplying the sample and also for his valuable suggestions.

†† 1 kcal mol^{-1}=4.184 kJ mol^{-1}.

References

1) F. Toda and M. Ohi, *J. Chem. Soc., Chem. Commun.*, **1975**, 506.
2) H. Tsukada, H. Shimanouchi, and Y. Sasada, *Bull. Chem. Soc. Jpn.*, **51**, 985 (1978).
3) H. Tsukada, H. Shimanouchi, and Y. Sasada, *Acta Crystallogr., Sect. B*, **33** 2951 (1977).
4) H. Tsukada, H. Shimanouchi, and Y. Sasada, *Bull. Chem. Soc. Jpn.*, **53**, 983 (1980).
5) F. Toda and T. Yoshioka, *Chem. Lett.*, **1977**, 561.
6) J. Karle and I. L. Karle, *Acta Crystallogr.*, **21**, 849 (1966).
7) "International Tables for X-Ray Crystallography," The Kynoch Press, Birmingham (1974), Vol. IV, pp. 72—98.
8) T. Fueno, *J. Syn. Org. Chem. Jpn.*, **29**, 1 (1971).
9) E. Giglio, *Nature*, **222**, 339 (1969).

Critical Phenomena in a Surfactant/Water/Oil System. Basic Study on the Correlation between Solubilization, Microemulsion, and Ultralow Interfacial Tensions

Hironobu KUNIEDA* and Stig E. FRIBERG†

Department of Applied Chemistry, Faculty of Engineering, Yokohama National University, Tokiwadai 156, Hodogaya-ku, Yokohama 240

†*Department of Chemistry, University of Missouri-Rolla, Rolla, Missouri, 65401 U.S.A.*

(Received September 1, 1980)

The phase equilibrium in $C_8H_{17}(OCH_2CH_2)_3OH$/water/decane system was studied at 13.6, 15.8, 21.5, 26.0, and 30.0 °C. An upper critical solution point for the surfactant and oil phases, and a lower critical solution point for the surfactant and water phases were found. Strong critical opalescence was observed in the vicinity of the critical points. In a temperature range between two critical points, a three-phase region appeared due to the superposition of three miscibility gaps, *i.e.*, 1) surfactant+water; 2) surfactant+oil, and 3) oil+water phases. The correlations between the phase equilibria and the ultralow interfacial tensions were straightforward. An ionic surfactant/cosurfactant/brine/oil system gave similar phase equilibria as the nonionic surfactant system, but the effect of temperature was the reverse.

In ordinary binary-liquid systems, mutual solubility of two phases increases with the increase of temperature and the compositions of the two phase coincide at the critical temperature, at which the interfacial tension between them becomes zero.[1-3] In a critical region, due to the large concentration fluctuation large clusters of molecules develop since the dimensions of the clusters are of the order of the wave length of light. Such systems scatter light strongly and the phenomenon is called critical opalescence.[4]

In surfactant solutions, the micelles present may be interpreted as large concentration fluctuations in a wider range of temperature than that in ordinary binary mixtures. According to the traditional interpretation[5-6] micelles grow with increasing temperature in nonionic surfactant aqueous solutions and their aggregation number becomes infinite in the vicinity of the solubility curve (cloud point curve), above which a surfactant and a water phases coexist. The recent NMR investigations by Tiddy and collaborators[7] have given results at variance with this interpretation. Their evaluation rather pointed to the presence of aggregates of flocculated micelles instead of larger ones.

In nonionic surfactant/water/oil systems, the surfactant mainly dissolves in water at lower temperature, whereas it dissolves in oil at higher temperature. At the transition temperature range of the surfactant from water-soluble to oil-soluble, there is a three-phase region consisted of a water phase, an oil phase and a surfactant phase which solubilizes a large amount of water and oil.[8-10] In this region, following phenomena are observed; 1) the amount of the solubilization of oil or water in a surfactant phase is attained to maximum, and the surfactant phase scatters a considerable amount of light, 2) ultralow interfacial tensions between the surfactant and oil (water) phases are obtained.[11] It is considered that these resemble critical phenomena in ordinary liquid systems. But the correlation between these phenomena and phase equilibria has not been clarified.

In this paper, solution behavior of $C_8H_{17}(OCH_2CH_2)_3OH$ in water and oil has been studied and compared with phase equilibria in ordinary binary or ternary mixtures. The solution behavior of ionic surfactant has also been evaluated for comparison.

Experimental

Materials. Pure $C_8H_{17}(OCH_2CH_2)_3OH$ was synthesized by POLA Research Laboratory and pure $C_{12}H_{25}(OCH_2CH_2)_5OH$ was synthesized by Nikko Chemicals; the high purity was confirmed by gas chromatographic analysis. *p*-$C_8H_{17}C_6H_4SO_3Na$ was kindly supplied by Kao Soap Company. Extra pure grade decane, hexadecane, 2,2,4-trimethylpentane were obtained from Tokyo Kasei Kogyo Company, and used without further purification.

Procedures. The procedures for the determinations of the phase diagrams were described in previous papers.[9-12]

Results and Discussion

$C_8H_{17}(OCH_2CH_2)_3OH$/Water/Decane System. Complicated phase equilibria are observed in long-chain surfactant/water/oil system, since liquid crystalline phases exist in a wide range of composition.[8-13] Therefore, the use of a short-chain surfactant is of advantage in order to understand the basic solution behavior of nonionic surfactant in oil and water. The short hydrocarbon chain is not sufficient to stabilize a liquid crystalline phase, hence the phase equilibria involving only liquid phases are more easily achieved.

With this fact in mind phase diagrams for $C_8H_{17}(OCH_2CH_2)_3OH$/water/decane system were determined at 13.6, 15.8, 21.5, 26.0, and 30.0 °C and are shown in Figs. 1(a)—(e).

There are two two-phase regions in Fig. 1(a). One contains a surfactant phase (D) and an aqueous phase (W) located in the vicinity of water apex. Compositions of coexisting D phase and W phase coincide at the plait point K (isothermal critical point) on the miscibility curve. Kc means the upper limit of K as described later. The other two-phase region is comprised of a surfactant (or water) phase and an oil phase (O). Compositions of both phases coincide at the plait point L on the miscibility curve, but the boundary between the surfactant phase and the water phase cannot be distinguished since there is no plait point between these phases.

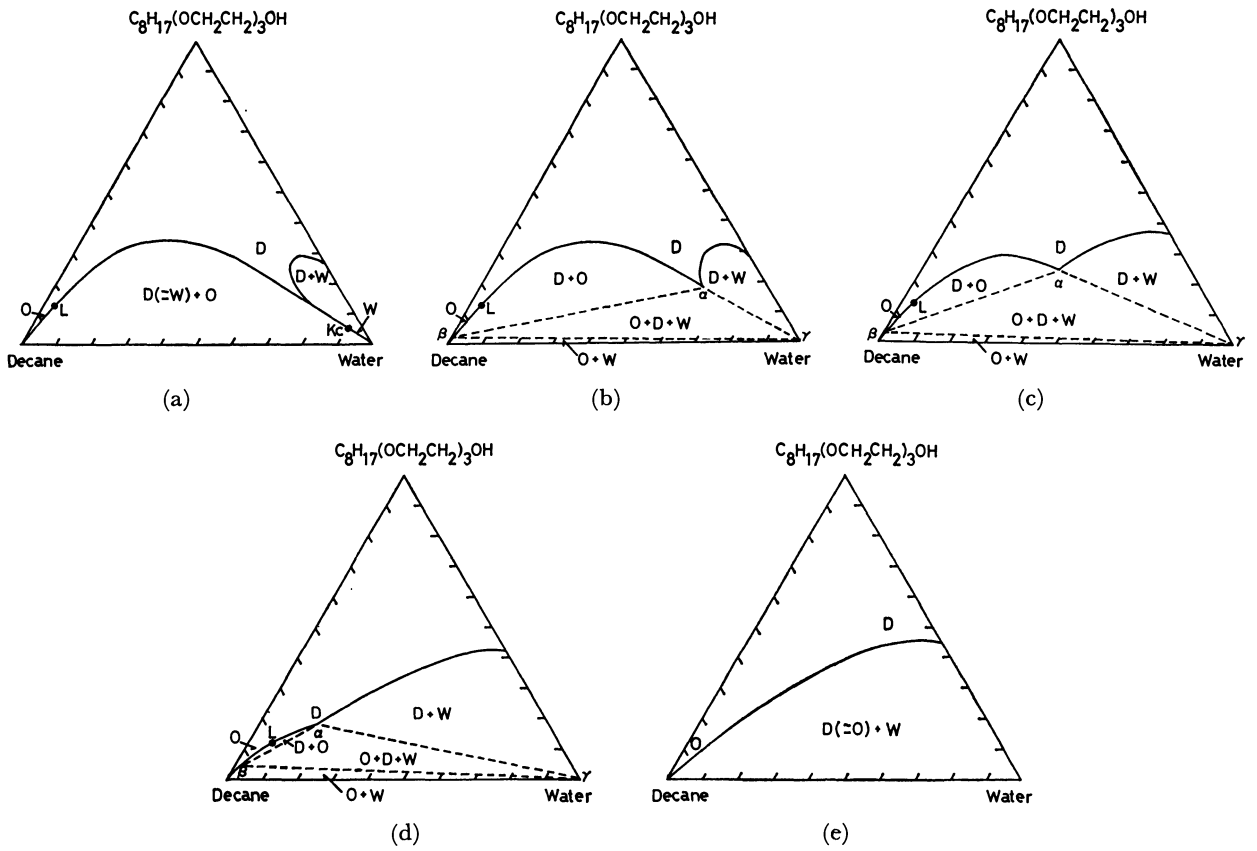

Fig. 1. Phase diagrams for $C_8H_{17}(OCH_2CH_2)_3OH$/water/decane system at various temperatures. (a) 13.6 °C, (b) 15.8 °C, (c) 21.5 °C, (d) 26.0 °C, (e) 30.0 °C. O, an oil phase; W, a water phase; D, a surfactant phase; α, β and γ, invariant points; K and L, plait points. Kc and Lc are upper limits of K and L (*cf.* Fig. 3).

The water phase continuously changes to the surfactant phase with increasing the content of a surfactant/decane solution of the ratio 1.2. Therefore, this latter two-phase region contains two miscibility gaps, *i.e.*, D+O and W+O so that the notation, D(≃W) is used. Below this temperature the two-phase D(≃W)+O region becomes wider, whereas D+W region becomes narrower and the plait point K approaches to water apex and the plait point L approaches the oil-surfactant axis (*cf.* Fig. 3).

Point Kc is still in contact with the miscibility curve between D(≃W) and O at 13.6 °C as shown in Fig. 1(a). Slightly above this temperature, the single-phase region splits into two realms, *i.e.*, the surfactant phase and the water phase at point Kc, and a three-phase region is formed consisted of a water, and oil and a surfactant phases. In other words, the equilibrium of three liquid phases causes the superposition of three miscibility gaps, *i.e.*, O+W, D+W, and D+O. The three coexisting liquids are the point, α, β, and γ as shown in Fig. 1(b).

This kind of phenomenon is also known in ordinary ternary systems, such as water/ether/succinonitrile systems.[14,15] The single water-phase region abruptly falls to the water apex in a very narrow range of temperature. The plait point Kc is the lower critical point between the surfactant and the water phases in the presence of oil. W or D phase in the vicinity of the plait point Kc scatters light and looks blue. The system is called a microemulsion.[10]

Point α shifts to the oil apex and the three-phase and D+W phase regions become wider with increasing temperature as shown in Fig. 1(c). Point α in Fig. 1(c) is the minimum concentration of $C_8H_{17}(OCH_2CH_2)_3OH$ to make equal amount of oil and water a single phase. Three points, α, β, and L approach each other with increasing temperature as shown in Fig. 1(d) and coalesce at 26.6 °C which is the upper critical point, (Lc) between the surfactant and the oil phases in the presence of water. Three-phase and D+O regions disappear and only the two-phase D(≃O)+W phase region is observed above this temperature as shown in Fig. 1(e).

Since the plait point does not exist on the miscibility curve in Fig. 1(e), the boundary between an oil phase and a surfactant phase cannot be distinguished. In other words, this two-phase region contains two miscibility gaps, *i.e.*, D+W and O+W so that the notation D(≃O) is used.

It is clear that the mutual dissolution between the surfactant phase and the water phase is increased with decreasing temperature, whereas that between the surfactant phase and the oil phase is increased with increasing temperature as shown in Figs. 1(a)—(e).

The correlations between phase equilibria and ultralow interfacial tensions are also made clear from Figs. 1(a)—(e). It is known that the interfacial tension

becomes zero at a critical point in ordinary liquid system.[3,16] The interfacial tension between the surfactant phase and the water phase approaches zero at the plait point K, because the compositions of both phases become equal. On the other hand, the interfacial tension between a surfactant phase and an oil phase approaches zero at the plait point L. Since no plait points exists above 26.6 °C as shown in Fig. 1(e), the interfacial tension does not become zero at any points in two-phase region. In three-phase region, the interfacial tension between a surfactant and a water phase becomes zero on the line at which the two lines, α-β and β-γ coalesce each other at 13.6 °C. On the other hand, the interfacial tension between a surfactant phase and an oil phase becomes zero on the line at which the two lines, α-γ and β-γ coalesce each other at 26.6 °C.

These results are in excellent accordance with those by Friberg and coworkers,[17,18] whose more complex equilibria were due to the influence of longer hydrocarbon chains. These favor the formation of lamellar phases.[19]

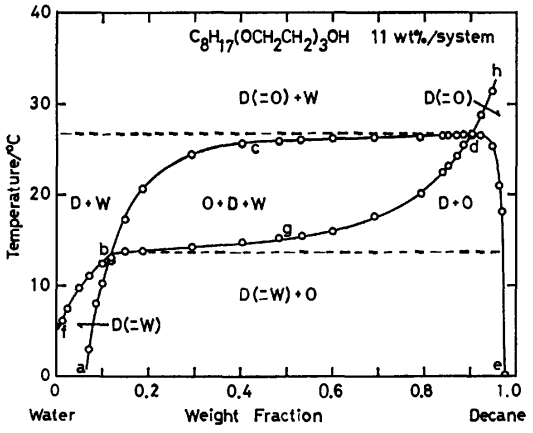

Fig. 2. Phase diagrams for water–decane containing 11 wt% of $C_8H_{17}(OCH_2CH_2)_3OH$/system as a function of temperature.

The effect of temperature on the phase equilibria of water-decane containing 11 wt% of $C_8H_{17}(OCH_2CH_2)_3$-OH was also studied and is shown in Fig. 2. This kind of phase diagrams have been extensively investigated by Shinoda and coworkers.[8-10] D($\simeq$O) and D($\simeq$W) are single-phase regions. (*cf.* Fig. 1). Above the curve a-b-c-d-e which is the miscibility curve of an oil and a surfactant phases, O and D phases cannot coexist in equilibrium. On the other hand, the surfactant phase and the water phase cannot coexist in equilibrium below the miscibility curve f-b-g-d-h. Hence the surfactant phase may coexist with the oil and the water phases only in the closed region, b-c-d-g. The curve a-b-c-d-e is smoothly continuous but the curve f-b-g-d-h has a break at point b in Fig. 2. From Fig. 2, it is clear that the solubilization of oil or water attains maximum in the vicinity of critical point (Kc or Lc).

Figure 3 is the polythermal projection of Figs. 1(a)—(e). Broken line means the locus of invariant point α and in the region of lower side of this line, a single liquid phasc does not appear at any temperatures.

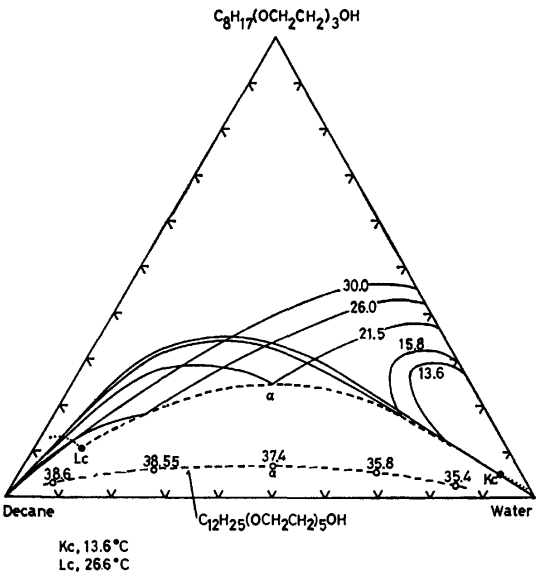

Fig. 3. Polythermal projection of Figs. 1(a)—(e). Dotted lines are the loci of plait points. —○— is a locus of α in $C_{12}H_{25}(OCH_2CH_2)_5OH$/water/decane system. Numerical numbers indicate the temperature (°C). Kc, $C_8H_{17}(OCH_2CH_2)_3OH$ 5 wt%, water 91 wt%, decane 4 wt%; Lc, $C_8H_{17}(OCH_2CH_2)_3OH$ 11 wt%, water 9 wt%, decane 80 wt%.

Dotted lines represent the loci of the plait points K and L. Since the locus of α is far from water–oil axis in $C_8H_{17}(OCH_2CH_2)_3OH$/water/decane system, the solubilizations of oil and water in surfactant phase are relatively small. The locus of α in $C_{12}H_{25}(OCH_2CH_2)_5$-OH/water/decane system (open circles) is also shown in Fig. 3. α is very close to oil–water axis so that the solubilization is very large. But, the composition of α is rapidly changed with increasing temperature.

The critical phenomenon at the composition of point Kc in Fig. 1(a) is captured in the sequence of the photographs shown in Figs. 4(a)—(d). Well above the critical temperature, both an upper surfactant phase and a lower water phase are clear and there is no appreciable scattered light. With decreasing temperature, the solubilization of water in a surfactant phase is increasing and D phase (upper) begins to scatter light as shown in Fig. 4(a). Just above the critical temperature, the dissolution of D phase in W phase will strongly increase and both show pronounced phases light-scattered as shown in Fig. 4(b). At the critical temperature (13.6 °C), the boundary between two phases suddenly disappears and the scattered light attains a maximum as shown in Fig. 4(c). Below this temperature, the light-scattering weakens and excess oil is separated from D($\simeq$W) phase as shown in Fig. 4(d). (See the meniscus). It is essential to point out that the scattered light observed in microemulsion systems[9] is a critical opalescence. Except these critical points, it is known that two critical phenomena exist on the oil-surfactant axis and the water-surfactant axis in nonionic surfactant system.[20-23]

Phase diagram of equal amount of oil and water containing $C_8H_{17}(OCH_2CH_2)_3OH$ as a function of temperature is shown in Fig. 5. The curve a-b-c-d is

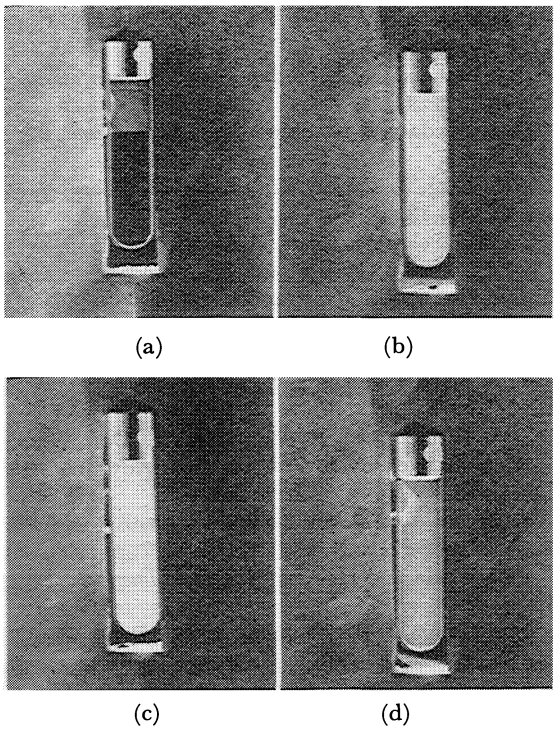

Fig. 4. The critical phenomenon captured in the sequence of the photographs at the composition of the lower critical point (Kc) in Fig. 1(a). (a) 14.0 °C, (b) 13.7 °C, (c) 13.6 °C, (d) 12.0 °C.

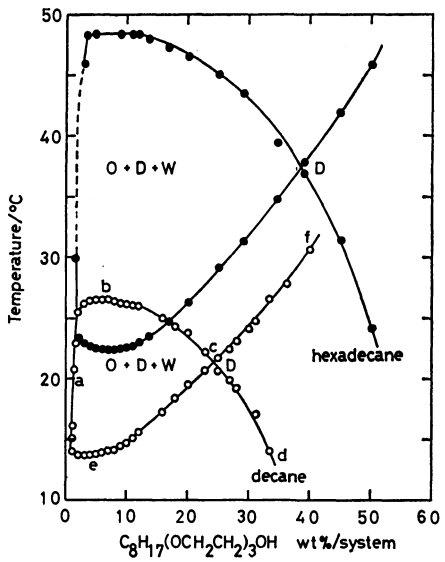

Fig. 5. The effect of the concentrations of $C_8H_{17}(OCH_2CH_2)_3OH$ on the equi-weight mixture of water and decane (or hexadecane) as a function of temperature.

the coexisting curve of the surfactant phase and the oil phase in the presence of water, whereas the curve a-e-c-f is that of the surfactant and the water phases in the presence of oil. If a molecular volume of oil is large (hexadecane), two coexisting curves shift to higher temperature as shown in Fig. 5. This fact means that a surfactant becomes more soluble in the water phase. Upper coexisting curve shifts more to higher temperature than the lower one does and the three-phase region becomes wider. Hence the minimum content of surfactant to make equal amount of oil and water a single phase is increased. This is in agreement with earlier solubilization studies.[17]

Ionic Surfactant/Cosurfactant/Brine/Oil System. Ordinary ionic surfactant dissolves in water and solubilizes a small amount of oil and the solubilization is little affected by temperature change.[19] Even hydrophile-lipophile balanced ionic surfactant, Aerosol OT (sodium 1,2-bis(2-ethylhexyloxycarbonyl)ethanesulfonate) dissolves mainly in water in dilute system, in which aqueous micellar solution phase coexists with an excess oil.[23-24] If brine is used instead of water, a three-phase region consisting of an oil, a water and a surfactant phases has been shown appearing in certain temperature ranges in Aerosol OT system as well as nonionic surfactant systems.[24-26] On the other hand, it is known that the solution behavior of Aerosol OT in water is similar to that of the appropriate mixture of ordinary ionic surfactant and cosurfactant such as long-chain alcohol.[27] Hence, it is expected that same solution behavior as that in Aerosol OT or nonionic surfactant systems appears in ordinary ionic surfactant systems if proper amounts of brine and cosurfactant are used. Phase diagram of p-$C_8H_{17}C_6H_4SO_3Na$, brine, 2,2,4-trimethylpentane and 1-hexanol as a function of temperature is shown in Fig. 6. Brine/2,2,4-trimethyl-

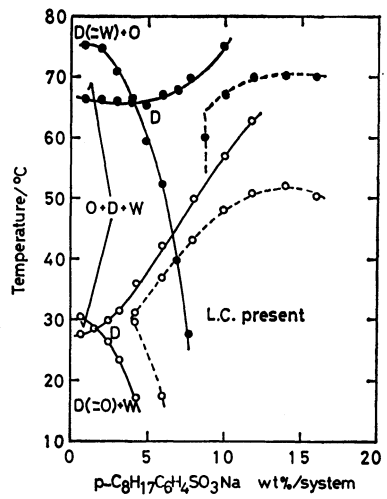

Fig. 6. The effect of the concentration of p-$C_8H_{17}C_6H_4$-SO_3Na on the equi-weight mixtures of brine (○, 1 wt% NaCl; ●, 3 wt% NaCl) and 2,2,4-trimethylpentane containing 30 wt% of 1-hexanol as a function of temperature.

pentane (containing 30 wt% of 1-hexanol) ratio is unity (W/W). Concentrations of salt in water are 1 wt% (open circles) and 3 wt% (filled circles) respectively. Below the temperature indicated by broken lines, liquid crystalline phase is separated. Below the curve which is concave downward, an excess water and a surfactant phase are separated, whereas an excess oil and a surfactant phase are separated above the curve which is concave upward. Therefore, three-phase consisted of a water, an oil and a surfactant phases appears in overlapping realm which is indicated by

O+D+W. From this result, it is clear that ionic surfactant becomes more hydrophilic with increasing temperature. Overlapping realm, *i.e.*, three-phase region shifts to lower temperature with decreasing salt content as shown in Fig. 6 and finally, it may disappear and a surfactant phase and an excess oil phase remain at room temperature in the absence of salt.

The authors thank Prof. Kōzō Shinoda for his stimulating discussion. Senior author thanks Sakko-kai Foundation for its financial support.

References

1) J. H. Hildebrand and T. F. Buehrer, *J. Am. Chem. Soc.*, **42**, 2213 (1920).
2) J. H. Hildebrand, J. M. Prausnitz, and R. L. Scott, "Regular and Related Solutions," Van Nostrand Reinhold Co., New York (1970), Chap. 10.
3) D. Atack and O.K. Rice, *Discuss. Faraday Soc.*, **15**, 210 (1953).
4) H. E. Stanley, "Introduction to Phase Transitions and Critical Phenomena," Oxford University Press, New York and Oxford (1971), pp. 1—21.
5) T. Nakagawa, K. Kuriyama, and H. Inoue, *J. Colloid Sci.*, **15**, 268 (1960).
6) K. Kuriyama, *Kolloid-Z.*, **180**, 55 (1962).
7) T. A. Bostack, M. P. McDonald, G. J. T. Tiddy, and L. Haring, "Surface Active Agents," Soc. Chem. Ind., London (1979), p. 181.
8) K. Shinoda and H. Saito, *J. Colloid Interface Sci.*, **26**, 70 (1968).
9) K. Shinoda and H. Kunieda, *J. Colloid Interface Sci.*, **42**, 381 (1973).
10) K. Shinoda and H. Kunieda, "Microemulsions," ed by L. M. Prince, Academic Press Inc., New York (1977), Chap. 4.
11) H. Saito and K. Shinoda, *J. Colloid Interface Sci.*, **32**, 647 (1970).
12) H. Kunieda and K. Shinoda, *J. Phys. Chem.*, **82**, 1710 (1978).
13) S. Friberg, I. Lapczynska, and G. Gillberg, *J. Colloid Interface Sci.*, **56**, 19 (1976).
14) F. A. H. Schreinemakers, *Z. Phys. Chem.*, **25**, 543 (1898).
15) J. E. Ricci, "The Phase Rule and Heterogeneous Equilibrium," D. Van Nostrand Co., Tronto, New York (1951), p. 214.
16) M. P. Brun, *C. R. Acad Sci.*, **184**, 966 (1927).
17) S. E. Friberg and I. Lapczynska, *Prog. Colloid Polym. Sci.*, **56**, 16 (1975).
18) S. E. Friberg, L. Rydhag, and T. Doi, "Lyotropc Liquid Crystals," ed by S. Friberg, ACS Adv. in *Chem. Sci.* **152**, 28 (1976).
19) P. Ekwall, "Advances in Liquid Crystals," ed by G. H. Brown, Academic Press, N. Y. (1974), Vol. 7, p. 1.
20) K. Shinoda and H. Arai, *J. Colloid Interface Sci.*, **20**, 93 (1965).
21) J. S. Clunie, J. F. Goodman, and P. C. Symons, *Trans. Faraday Soc.*, **65**, 287 (1969).
22) K. Shinoda, *J. Colloid Interface Sci.*, **34**, 278 (1971).
23) H. Kunieda and K. Shinoda, *J. Colloid Interface Sci.*, **70**, 577 (1979).
24) H. Kunieda and T. Sato, *Yukagaku*, **28**, 627 (1979).
25) H. Kunieda and K. Shinoda, *J. Colloid Interface Sci.*, **75**, 601 (1980).
26) H. Kunieda, *Yukagaku*, **29**, 510 (1980).
27) H. Kunieda, *Nippon Kagaku Kaishi*, **1977**, 1428.

  Bull. Chem. Soc. Jpn., 54, 1015—1018 (1981)

Hydrodimerization of Methyl Acrylate Catalyzed by Halogenotris(triphenylphosphine)cobalt

Hiroyoshi KANAI* and Keiji ISHII

Department of Hydrocarbon Chemistry, Faculty of Engineering, Kyoto University, Sakyo-ku, Kyoto 606

(Received September 4, 1980)

Methyl acrylate was hydrodimerized in a methanolic solution by $CoX(PPh_3)_3$ (X=halogen) into dimethyl adipate. The *in situ* prepared cobalt complexes from cobalt halides, triphenylphosphine, and zinc gave higher yields of the hydrodimer in the presence of alkali halides. A mechanism is proposed which involves the protonation of Co(I)–methyl acrylate π-complex to give (2-methoxycarbonylethyl)cobalt complex, followed by a further addition of methyl acrylate.

Olefins substituted with electron-withdrawing groups are dimerized to head-to-head or head-to-tail dimers by bases,[1,2] electrolytic coupling,[3] and transition metal complexes.[4,5] The head-to-head hydrodimerization has been extensively studied because head-to-head dimers are of considerable interest as starting materials for the preparation of monomers.[3,5] We have previously reported that acrylic esters were hydrodimerized by cobalt(I)–triphenylphosphine complexes and that the addition of alkali halides and zinc increased the yield.[5j] We wish to report our subsequent work on the development of good catalysts for and the mechanism of the hydrodimerization of methyl acrylate.

Experimental

All reagents were used directly as obtained commercially unless otherwise noted. Tetrahydrofuran (THF) and alcohols were refluxed over sodium and sodium alkoxides, respectively, distilled, and stored under an atmosphere of nitrogen. Methyl acrylate was distilled and stored under N_2 in a refrigerator. ^1H NMR spectra were obtained on a JEOL PM-60 spectrometer. A Shimadzu 6A gas chromatograph with a FID detector was used for most GLC analyses [PEG 20M (25% on celite 545), 4 m×3 mm i.d. column, 175°]

Cobalt Complexes. Cobalt (I) complexes were prepared by modifying the procedure used by Aresta *et al.*[6] slightly. A solution of cobalt iodide (0.30 g, 1 mmol) and triphenylphosphine (0.93 g, 3.5 mmol) in THF (15 ml) and ethanol (1 ml) was treated with zinc dust (0.36 g, 5.5 mmol) under stirring at room temperature for 1 h. The resulting green suspension was filtered and the filtrate was concentrated almost to dryness. Ethanol (25 ml) was added and the precipitate was washed with three portions of ethanol (6 ml) and dried. The yield was 0.69 g (60%). Anal. Found: C, 66.79; H, 4.66%. Calcd for $C_{54}H_{45}ICoP_3$: C, 66.68; H, 4.66%. Bromo- and chlorotris(triphenylphosphine)cobalt were obtained similarly. The yields were 42 and 22%, respectively. Their elementary analyses were in fair agreement with the calculated values.

Reactions. The complex (*ca.* 0.2 mmol) was placed in a 100-ml flask which was flushed with nitrogen. Tetrahydrofuran (8 ml), methanol (2 ml), and methyl acrylate (1.5 ml, 16.4 mmol) were added by syringes. The reaction mixture was stirred for 16—20 h at room temperature.

Reactions with in Situ *Prepared Complexes.* In a 100-ml flask were placed cobalt halide (1 mmol), triphenylphosphine (3 mmol), and zinc (8 mmol). Tetrahydrofuran (8 ml) and methanol (2 ml) were added and the solution was stirred for half an hour. To the resulting yellow-green solution was added methyl acrylate (16.4 mmol) and the reaction mixture was stirred for an adequate interval. The determination of yields was carried out by gas chromatography using an internal standard.

Results and Discussion

Stoichiometric Reactions. When methyl acrylate (MA) was treated with $CoX(PPh_3)_3$ (X=halogen) in THF–methanol, the yellow-green solution turned brown and finally blue. The former color change suggests an interaction between the Co(I) complex and MA. The products were identified as dimethyl adipate and methyl 2-methoxypropionate. The yield of dimethyl adipate is dependent upon halides and decreases in the order I>Br>Cl, as shown in Table 1. The higher

Table 1. Hydrodimerization of methyl acrylate catalyzed by $CoX(PPh_3)_3$[a]

X	mmol	MA mmol	Yield of dimethyl adipate Co base mol/g atom
Cl	0.26	16.4	0.15(0.15)[b]
Br	0.20	16.4	0.26(0.18)[b]
I	0.23	2.2	0.18
I	0.22	16.4	0.31(0.30)[b]

a) KX 5 mmol, THF 8 ml, CH_3OH 2 ml, r.t., 16—20 h.
b) In the absence of KX.

concentration of MA causes the increase of Co(I)–MA complex, resulting in the higher yield of the hydrodimer.

$$2\,CH_2{=}CHCO_2CH_3 + 2\,CH_3OH + CoX(PPh_3)_3 \longrightarrow H_3CO_2C(CH_2)_4CO_2CH_3 + XCo(OCH_3)_2(PPh_3)_n \quad (1)^{7)}$$

$$CH_2{=}CHCO_2CH_3 + CH_3OH \xrightarrow{XCo(OCH_3)_2(PPh_3)_n} H_3COCH_2CH_2CO_2CH_3. \quad (2)$$

The hydrodimerization was little affected by the addition of potassium halides. A Michael reaction (Eq. 2) is responsible for the catalysis of the cobalt methoxide formed.

Use of in Situ *Prepared Cobalt(I) Complexes in the Presence of Alkali Halides and Zinc.* Cobalt(I) complexes were prepared by the reaction of cobalt halides, triphenylphosphine (PPh_3), and zinc in THF–methanol at room temperature. If methoxyl group in $XCo(OCH_3)_2(PPh_3)_n$ is replaced by halogens, Co(I) complexes are expected to be regenerated in the presence of zinc. Catalytic hydrodimerization of MA was, in fact, carried out successfully by cobalt complexes in the

$$CoX_2 + 3\,PPh_3 + \frac{1}{2}Zn \longrightarrow CoX(PPh_3)_3 + \frac{1}{2}ZnX_2 \quad (3)$$

presence of alkali halides and zinc, as shown in Table 2. The addition of zinc affords dimethyl adipate in more than 100% yields, based on cobalt complexes, even in the absence of alkali halides. The reaction of $XCo(OCH_3)_2(PPh_3)_n$ and ZnX_2 in the presence of zinc might regenerate a Co(I) complex. The trend in the reactivity of $CoX(PPh_3)_3$ in the presence of zinc is the same as that in the isolated complexes. Alkali iodides and lithium chloride are effective and potassium iodide is the most effective among the alkali halides investigated. Although lithium salts are more soluble,[8] none of them exert any positive effect toward the hydrodimerization. It is not clear why potassium iodide is the most effective even though it is less soluble. Counter ions also play an important role in the hydrodimerization.[9]

TABLE 2. EFFECTS OF THE ADDITION OF ALKALI HALIDES ON THE HYDRODIMERIZATION OF METHYL ACRYLATE BY $CoX(PPh_3)_3$ IN THE PRESENCE OF ZINC[a]

X	Alkali halide	mmol	Conv. %	Yield of dimethyl adipate[b] Co base[c] mol/g atom
Cl[d]	—			1.51
Cl	LiCl	8.1	75	4.30 (70)[e]
Cl	KCl	8.0	25	0.54 (26)
Cl	NH_4Cl	7.9	50	2.97 (72)[f]
Cl[d]	$AgClO_4$	1.0		3.02
Cl[g]	KI	5.2		5.47
Br[h]	—			2.25
Br	LiBr	8.0	43	1.44 (41)[i]
Br	KBr	8.0	27	0.81 (36)
I	—		39	1.98 (62)
I[d]	LiI	4.8		4.12[j]
I	LiI	8.0	57	1.55 (33)[k]
I[d]	NaI	5.0		3.86
I	NaI	8.0	62	3.54 (69)
I	KI	5.0	55	4.09 (91)
I	KI	8.0	81	6.56 (98)
I	KI	15	80	5.16 (78)
I[d]	RbI	5.1		3.35
I	RbI	8.0	43	2.42 (69)
I[d]	CsI	5.0		3.48
I	CsI	8.0	54	3.91 (88)
I[d]	NH_4I	5.1		4.87
I	NH_4I	8.0	66	3.56 (66)[l]

a) $CoX(PPh_3)_3$ was prepared *in situ* from CoX_2 (1 mmol), PPh_3 (3 mmol), and Zn (10 mmol) in THF (10 ml) and CH_3OH (2 ml). MA (16.4 mmol), 20 °C, 2 h. b) The number in parentheses is the yield based on MA consumed. c) Yield based on cobalt complex. d) r.t., 20—24 h. e) Methyl 2-methoxypropionate 20%. f) Methyl propionate 12%. g) r.t., 2 d. h) r.t., 4 d. i) Methyl 2-methoxypropionate 5.4%. j) Methyl 2-methoxypropionate 50%. k) Methyl 2-methoxypropionate 2.7%. l) Methyl propionate 16%.

The yield of the hydrodimer is dependent upon the amount of alkali halides. The excess of alkali halides lowers both yield and selectivity. The appropriate amount of alkali halides nearly corresponds to that of the dimethyl adipate to be produced. A considerable amount of methyl 2-methoxypropionate and propionate were formed in the presence of lithium and ammonium salts, respectively.

TABLE 3. EFFECTS OF TEMPERATURE AND ADDITIVES ON THE HYDRODIMERIZATION OF METHYL ACRYLATE[a]

Temp °C	Additive KI mmol	Additive MeOH ml	Time h	Conv. %	Yield of dimethyl adipate[b] Co base mol/g atom
0	5.0	2	6	92	7.54 (99)
20	—	—	2	40	1.13 (34)
	5.0	—	2	68	1.61 (29)
	5.0	2	2	55	4.09 (91)
	5.0	2	6	83	5.87 (86)
40	5.0	2	6	46	2.81 (75)

a) Catalysts prepared *in situ* from CoI_2 (1 mmol), PPh_3 (3 mmol), and Zn (10 mmol) in THF (8 ml). MA 16.4 mmol. b) Yields are the same as those in Table 2.

The effects of methanol and temperature were examined as shown in Table 3. Even in the absence of methanol, hydrodimerization occurred, but the addition of methanol appreciably increased the yield of the hydrodimer. Low temperatures are preferable because catalytic species are so thermally unstable as to be easily decomposed.[6]

TABLE 4. SOLVENT EFFECTS ON THE HYDRODIMERIZATION OF METHYL ACRYLATE BY $CoX(PPh_3)_3$[a]

X	Solvent ml	Yield of dimethyl adipate Co base mol/g atom
Cl	THF 8, MeOH 2	1.51
	DMF 8, MeOH 2	2.89
	CH_3CN 8, MeOH 2	2.18
	MeOH 10	2.23
I	THF 8, MeOH 2	5.26
	THF 10	0.56
	CH_3CN 8, MeOH 2	0.67
	CH_3CN 10	1.20
	MeOH 10	0.45

a) $CoX(PPh_3)_3$ prepared *in situ* from CoX_2 (1 mmol), PPh_3 (3 mmol), and Zn (8—10 mmol) in solvents. MA 16.4 mmol, r.t., 20—90 h.

Tetrahydrofuran and *N,N*-dimethylformamide were found to be the most suitable solvents among several investigated in the catalysis of $CoI(PPh_3)_3$ and $CoCl(PPh_3)_3$, respectively (Table 4). Polar solvents are preferable. The reduction to the Co(I) complexes occurred in all solvents listed in Table 4, but it was accelerated by the addition of methanol. The effects of methanol on the hydrodimerization of MA in THF–methanol are shown in Fig. 1. The appropriate mole ratio of methanol to MA is 4—5. The Michael reaction took place in preference to the hydrodimerization in a large excess of methanol : methyl 2-methoxypropionate was obtained in a 52% yield in methanol as the sole solvent. Ethanol functions similarly to methanol in the hydrodimerization, but ester exchange occurs in it.

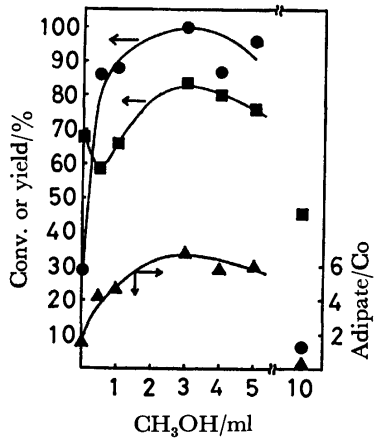

Fig. 1. Effects of the amount of methanol on the hydrodimerization of methyl acrylate by *in situ* prepared $CoI(PPh_3)_3$ in THF (8 ml)–methanol. (Methanol (10 ml) without THF.)
■: Conversion, ●: yield based on MA consumed, ▲: yield based on the cobalt complex.

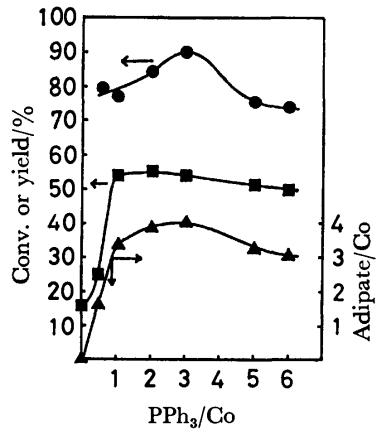

Fig. 2. Effects of the ratio of triphenylphosphine to cobalt on the hydrodimerization of methyl acrylate by *in situ* prepared $CoI(PPh_3)_3$. Symbols are the same as those in Fig. 1.

The effects of the ratio of PPh_3 to a cobalt complex are shown in Fig. 2. The optimum ratio is 3, which is in accord with the ratio of the isolated complexes. The excess of PPh_3 did not affect the conversion of MA, but lowered the yield of the hydrodimer. The coordination of MA is blocked by excess PPh_3 which, however, does not inhibit the Michael reaction.

Mechanism. The hydrodimer obtained in deuterated compounds was analyzed by ^1H NMR as shown in Table 5. Most of the hydrogen added originates from the hydroxyl hydrogen in methanol. The rest seems to be from solvents and MA itself, because we have not detected ortho-hydrogen of PPh_3 in the hydrodimer. No hydrogen attached to β-carbon of MA exchanged with that of solvents such as THF and benzene, but a part of the hydrogen exchanged with that of acetonitrile. Acetonitrile is sometimes split to H and CH_2CN radicals by oxidative addition to low-valent transition metal complexes.[10] Since $CoX(PPh_3)_3$, one of the low-valent d^8 complexes, is susceptible to oxidative addition,[11] deuterium incorporation into the hydrodimer may occur *via* deuterium atom abstraction of acetonitrile-d_3 by the Co(I) complex and the transfer of the deuterium.

Table 5. Analysis of hydrogen of dimethyl adipate produced by the reaction of MA with *in situ* prepared $CoX(PPh_3)_3$ in deuterated compounds

Catalytic system[a]	Deuterium source	Solvent	^1H NMR analysis[b] β-C	α-C
CoI_2P_2–P–Zn	CH_3OD	THF	2.05	1.24
$CoCl_2$–3P–Zn	CH_3OD–D_2O[c]	THF	2.06	1.22
CoI_2–P–Zn	CH_3OD	CH_3CN	2.03	1.68
CoI_2–3P–Zn	CH_3OD	C_6H_6	1.96	1.78
CoI_2–3P–Zn	$P(C_6D_5)_3$	CH_3CN	2.11	1.94
CoI_2–3P–Zn	CD_3CN	CD_3CN	1.76	1.95
CoI_2–3P–Zn	CH_3OD	CH_3CN	1.35	1.59

a) P=PPh_3. b) Based on the assumption that the number of hydrogens of the methoxy group is 3.00. c) Before the end of the reaction, D_2O was added.

Hydrodimerization of acrylonitrile by iron carbonyls and ruthenium complexes has been extensively investigated by Misono *et al.*,[5a-e] McClure *et al.*,[5f] and Billig and coworkers.[5g] They explained the reaction involving insertion of acrylonitrile into an M–H or M–cyanoethyl or an M–vinyl bond (M=Fe, Ru), some of which were isolated and characterized. The products are not only a hydrodimer but also propionitrile, 2-methylglutaronitrile, and *cis*- and *trans*-2-hexenedinitrile. The products from the reaction of MA with Co(I) complexes are a head-to-head hydrodimer, Michael adduct, and methyl propionate. We could not observe 2-methylglutarate and *cis*- and *trans*-2-hexenedioate at all. The products of the latter reaction are very similar to those derived from the electrolytic coupling.[3] The difference in products suggests that the hydrodimerization of MA by $CoX(PPh_3)_3$ proceeds by a mechanism different from that of the hydrodimerization of acrylonitrile by iron carbonyls and ruthenium complexes. Another characteristic feature is that the hydrogen incorporated into the hydrodimer in the Co(I) complex systems originates mainly from alcohols, but that in the ruthenium complex systems comes from atmospheric hydrogen.

The addition of MA to $CoX(PPh_3)_3$ in methanolic solution produces a red-brown color from a yellow-green one. A similar color change was observed between cobaloxime(I) and ethyl acrylate or acrylonitrile.[12] Spectroscopic study showed an interchange between the cobaloxime–ethyl acrylate π-complex and (2-ethoxycarbonylethyl)cobaloxime.[12b] However, a hydride $HCo(dmg)_2P(n\text{-}C_4H_9)_3$ (dmg=dimethylglyoximato) reacted with acrylonitrile or acrylates to yield the α-substituted ethylcobaloxime derivatives,[13] in contrast with β-substituted isomers from the protonation of the cobaloxime(I)–olefin π-complex (Scheme 1). The latter has been exemplified by the work on the rhodium–olefin complexes.[14]

We postulate a mechanism for the hydrodimerization of methyl acrylate by Co(I) complexes (Scheme 2). Red-brown species are responsible for the formation

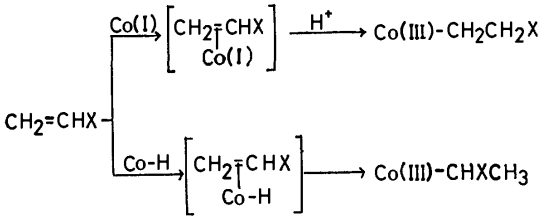

Co=cobaloxime, X=CN, CO_2R.

Scheme 1.

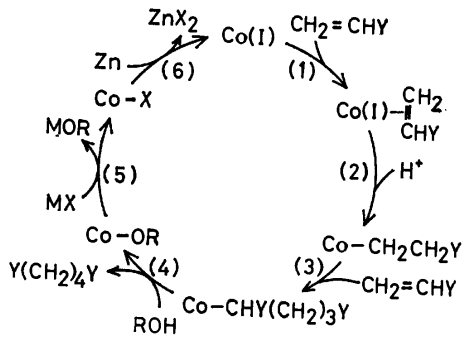

Co=$CoX(PPh_3)_n$, X=halogen,
Y=CO_2CH_3, M=alkali metal.

Scheme 2.

of Co(I)–MA π-complex. A β-substituted ethylcobalt complex is formed from the protonation of the Co(I)–MA π-complex with alcohol. Further addition of MA to the ethylcobalt complex gives 1,4-bis(methoxycarbonyl)butylcobalt complex, which is protonated to yield dimethyl adipate. No reverse reaction in (2) occurs because hydrogen exchange between MA and alcohol has not been observed. The susceptibility of protonation of the 1,4-bis(methoxycarbonyl)butylcobalt complex, in comparison with that of the β-substituted ethylcobalt complex, is correlated with the stability of the cobalt-carbon: alkylmetal complexes bearing primary carbons are more stable than those bearing secondary carbons.[15] The Co(I) complex can be regenerated by the reduction of the cobalt halide complex which is formed by replacing the alkoxyl group with alkali halides. Cobalt alkoxide or alkali metal alkoxide released in (5) causes the Michael reaction to occur.

The present work was partially supported by Grants-in-Aid for Scientific Research (Nos. 065100, 265235) from the Ministry of Education, Science and Culture.

References

1) H. R. Snyder and R. E. Putnam, *J. Am. Chem. Soc.*, **76**, 33 (1954); M. M. Baizer and J. D. Anderson, *J. Org. Chem.*, **30**, 1357 (1965); M. F. Semmelhack and R. D. Stauffer, *ibid.*, **40**, 3619 (1975); J. Shabtai, E. Ney-Igner, and H. Pines, *ibid.*, **43**, 4086 (1978); T. Miyakoshi, H. Omichi, and K. Saito, *Nippon Kagaku Kaishi*, **1978**, 473.

2) Y. Arad, M. Levy, and D. Vofsi, *J. Org. Chem.*, **34**, 3709 (1969).

3) M. M. Baizer, *J. Electrochem. Soc.*, **111**, 215 (1964); M. M. Baizer and J. D. Anderson, *ibid.*, **111**, 223 (1964); M. M. Baizer, *Chemtech*, **1980**, 161; D. E. Danly *ibid.*, **1980**, 302.

4) J. Kwiatek, I. L. Mador, and J. K. Seyler, *Adv. Chem. Ser.*, **37**, 201 (1963); T. Alderson, E. L. Jenner, and R. V. Lindsey, Jr., *J. Am. Chem. Soc.*, **87**, 5638 (1965); Y. Kobayashi and S. Taira, *Tetrahedron*, **24**, 5763 (1968); T. Saegusa, Y. Ito, H. Kinoshita, and S. Tomita, *Bull. Chem. Soc. Jpn.*, **43**, 877 (1970); G. Oehme and H. Pracejus, *Tetrahedron Lett.*, **1979**, 343.

5) a) A. Misono, Y. Uchida, K. Tamai, and M. Hidai, *Bull. Chem. Soc. Jpn*, **40**, 931 (1967); b) A. Misono, Y. Uchida, M. Hidai, and H. Kanai, *J. Chem. Soc., Chem. Commun.*, **1967**, 357; c) A. Misono, Y. Uchida, T. Saito, and M. Hidai, *Kogyo Kagaku Zasshi*, **70**, 1890 (1967); d) A. Misono, Y. Uchida, M. Hidai, H. Shinohara, and Y. Watanabe, *Bull. Chem. Soc. Jpn*, **41**, 396 (1968); e) A. Misono, Y. Uchida, M. Hidai, and I. Inomata, *J. Chem. Soc., Chem. Commun.*, **1968**, 704; f) J. D. McClure, R. Owyang, and L. H. Slaugh, *J. Organomet. Chem.*, **12**, P8 (1968); g) E. Billig, C. B. Strow, and R. L. Pruett, *J. Chem. Soc., Chem. Commun.*, **1968**, 1307; h) S. Hosaka and S. Wakamatsu, Japan Patent, 46-5689, *Chem. Abstr.*, **74**, 124867 (1971); i) G. Agnès, G. P. Chiusoli, and G. Cometti, *J. Chem. Soc., Chem. Commun.*, **1968**, 1515; j) H. Kanai and M. Okada, *Chem. Lett.*, **1975**, 167.

6) M. Aresta, M. Rossi, and A. Sacco, *Inorg. Chim. Acta*, **3**, 227 (1969).

7) The authors wish to thank a referee who kindly suggested the structure of the cobalt complex produced after the reaction.

8) E. Price, "The Chemistry of Non-aqueous Solvents," ed by J. J. Lagowski, Academic Press, New York and London (1966), Chap. 2, p. 70; J. Burgess, "Metal Ions in Solutions," Ellis Horwood Ltd. (1978), pp. 219—223.

9) Lithium iodide and sodium iodide are the most effective additives in the hydrodimerization of methyl acrylate by Co(I)–fumarate complexes and in that of methyl vinyl ketone by Co(I)–bipyridyl complexes, respectively. The congeniality has not been simply explained.

10) B.-K. Teo, A. P. Ginsberg, and J. C. Calabrese, *J. Am. Chem. Soc.*, **98**, 3027 (1976); J. A. Sofranko, R. Eisenberg, and J. A. Kampmeier, *ibid.*, **102**, 1163 (1980).

11) J. K. Kochi, "Organometallic Mechanisms and Catalysis," Academic Press, New York (1978), pp. 156—177.

12) G. N. Schrauzer, *Angew. Chem.*, **88**, 465 (1976); G. N. Schrauzer, J. H. Weber, and T. M. Beckham, *J. Am. Chem. Soc.*, **92**, 7078 (1970).

13) G. N. Schrauzer and R. J. Holland, *J. Am. Chem. Soc.*, **93**, 1505 (1971).

14) L. P. Seiwell, *Inorg. Chem.*, **15**, 2560 (1976).

15) T. Yamamoto, A. Yamamoto, and S. Ikeda, *J. Am. Chem. Soc.*, **93**, 3350 (1971); M. Tamura and J. K. Kochi, *J. Organomet. Chem.*, **29**, 111 (1971).

  Bull. Chem. Soc. Jpn., 54, 1019—1024 (1981)

Transport Number of Ions in Water/DMF Solvents and Reference Electrode for Electrochemical Measurements in Nonaqueous Media

Kazunori TAKAOKA* and Roger G. BATES**

Department of Industrial Chemistry, Fukui Technical College, Geshi-cho, Sabae, Fukui 916
***Department of Chemistry, University of Florida, Gainesville, Florida 32611, U.S.A.*

(Received October 17, 1980)

The transport number of the ions, $t^{\pm}$, of $(C_2H_5)_4NClO_4$, $NaClO_4$, NaCl, KCl, and HCl in *N,N*-dimethylformamide(DMF)–water solvents were determined by the agar–salt bridge method. In order to compare this method, t^+(HCl)'s in DMF–water media were measured by both the Hittorf method and the concentration cell method. Good agreement among these methods leads to the conclusion that t^+(KCl) and t^-(KCl) are nearly equal in the whole range of DMF–water media. The results suggest that potentials obtained in nonaqueous polarography with the bridged SCE by correcting the bridge potential with a slow flowing type aqueous SCE are always referred to the ordinary aqueous SCE.

It is desirable that all potentials be referred to a common aqueous scale, such as the ordinary calomel electrode, regardless of the fact that the medium is aqueous or nonaqueous. A few attempts to do this in nonaqueous polarography have been made.[1–4] On prolonged immersion of an aqueous saturated potassium chloride salt bridge in a nonaqueous medium, a plug of solid KCl formed on the tip of the bridge and caused a significant increase in the resistance of the cell[2,3] and an increase in the liquid junction potential.[4] This resulted in a drift of the potential with time.

The use of the reference redox couple such as rubidium ion-rubidium amalgam,[5] ferricinum ion-ferrocene,[6] tris-(phenanthroline)iron(II, III) complex,[7] $[Fe(bpy)_3]^+$–$[Fe(bpy)_3]^\circ$,[8] and the form R^--R^+ type[9] have an advantage for the purpose of comparing redox potentials of a given couple in different solvents. Those, however, are relative and contain some assumption concerning the solvation of couple ions or neutral particles.

Suitable reference electrodes in individual solvent systems are convenient,[10–13] but it is desirable, if possible, to use a common reference for emf measurements made in a variety of solvent systems.

In this connection, Fujinaga *et al.* have proposed a bridged SCE as an external reference electrode,[14] and polarographic behaviours of some compounds in the solvents of *N,N*-dimethylformamide (DMF)–water binary system have been studied with exact comparison of potentials referred to the bridged SCE.[15–18] One of the authors has investigated in detail the characteristics of the bridged SCE and emphasized its great utility,[19] showing that the potential drift during a period of polarographic scanning is less than 3 mV and that the potentials could be referred to the ordinary aqueous SCE with a precision of a few millivolts when the potentials were corrected for the bridged potential measured with a slow flowing-type aqueous SCE just after the scan was completed.

This conclusion is based on the coincidence of both the final bridge potential E_∞ and the calculated liquid junction potential $E_j(C_1, C_2)$ as tabulated in Table 1. The E_j were calculated by using the equation

$$E_j(C_1, C_2) = \frac{RT}{F}(t^- - t^+) \ln (C_2/C_1). \quad (1)$$

The differences in transport number $(t^- - t^+)$ were obtained from the slope of the bridge potential E *vs.* log (C_2/C_1) plots at each DMF concentration. If the transport number thus obtained is right, all the voltammetric measurements with the bridged SCE are always referred to the common aqueous SCE, when a correction for the bridge potential is applied.

Table 1. Bridge potential and recalculated liquid junction potential[19]

$v_1=v_2$[a]	C_1	C_2[b]	E_0	E_∞[c]	$(t^- - t^+)$[d]	$E_j(C_1,C_2)$[e]
0	0.1	0.24	11	4	0.160	3.6
40	0.1	0.5	38	8	0.174	7.2
70	0.1	0.5	75	14	0.268	11.1
100	0.1	0.5	122	38	0.773	32.0

a) The isometric volume % of DMF in the test soln(1) and in the tip of the bridge(2). b) Molarity of tetraethylammonium perchlorate (TEAP) in the test soln(1) and in the tip of the bridge(2). c) The bridge potential (mV) at the same day(0) and 30 d after the preparation of the bridge. d) Transport number of TEAP obtained from the slope of the E *vs.* log (C_2/C_1). e) Recalculated liquid junction potential at 25 °C by the help of Eq. 1.

In the present communication, the subject of the transport number was investigated in order to clarify the above point. The experimental methods available for measuring transport numbers fall into four categories: the Hittorf method, the concentration cell method, the moving boundary method, and the agar–salt bridge method.[20] The last of these is like that in the previous paper.[19] The purpose of this paper is, indeed, to compare the transport number obtained by the last method with those obtained by the first two methods.

Experimental

Preparation of the Test Solution in DMF–Water Media. Although it is a simple matter to prepare the solutions of a substance at various concentrations in different compositions of mixed solvent, it is difficult in practice to represent exactly and simultaneously both the solute and solvent composition. The present paper has solved this problem by introducing an isometric volume concentration, by which can be expressed a molarity, C, for the solute and a volume percent of either solvent composition. The conversion of the isometric volume percent to a weight percent or a mole fraction is easy.

Suppose a mixed solvent is prepared by adding V_A and V_B cm³ of pure solvents A and B whose densities d_A and d_B,

respectively. Then the total volume V_0 whose density d is

$$V_A d_A + V_B d_B = V_0 d. \quad (2)$$

When weight percent w_i and mole fraction X_i of solvent i are introduced into Eq. 2, we have

$$\frac{V_A}{V_0} = \frac{d}{d_A}\frac{w_A}{100} = \frac{d}{d_A}\frac{X_A M_A}{X_A M_A + X_B M_B}. \quad (3)$$

Equation 3 contains two unknown variables w_i and d, or X_i and d. Since the relation between w_i and d is measured experimentally, the isometric volume percent $v_i = 100\, V_i/V_0$ is easily converted to a weight percent w_i or mole fraction X_i. The conversion table for DMF–water binary system is shown in Table 2.

TABLE 2. RELATION BETWEEN THE ISOMERIC VOLUME PERCENT AND WEIGHT PERCENT OR MOLE FRACTION IN DMF–WATER MEDIA AT 25 °C

DMF wt% w_B	d[a]	Mole fraction of water, X_A	v_A	v_B[b]
0	0.9971	1.0000	100.00	0.00
5	0.9972	0.9869	95.01	5.28
10	0.9971	0.9733	90.00	10.56
15	0.9973	0.9583	85.02	15.85
20	0.9972	0.9419	80.01	21.13
25	0.9974	0.9260	75.02	26.42
30	0.9976	0.9044	70.04	31.71
35	0.9979	0.8828	65.05	37.00
40	0.9982	0.8588	60.07	42.30
45	0.9989	0.8322	55.10	47.62
50	1.0023	0.8022	50.26	53.09
55	1.0026	0.7685	45.25	58.42
60	1.0017	0.7301	40.18	63.67
65	0.9964	0.6860	34.98	68.62
70	0.9911	0.6349	29.82	73.50
75	0.9849	0.5749	24.70	78.26
80	0.9784	0.5035	19.62	82.92
85	0.9714	0.4172	14.61	87.48
90	0.9637	0.3107	9.67	91.89
95	0.9534	0.1759	4.78	95.96
98	0.9476[c]	0.0765	1.90	98.38
99	0.9457[c]	0.0394	0.95	99.19
99.9	0.9440[c]	0.0040	0.10	99.91
100	0.9439[d]	0.0003	0.01[d]	99.99

a) Density (g/cm³) of the mixed solvent from Ref. 21. b) Isometric volume % of water (A) and DMF (B). c) Values obtained by interpolating between w_B=95 and 100%. d) Ref. 26.

Electrolyte solutions were prepared, for example, by pipetting adequate amounts of aqueous stock solution of electrolyte and V_B cm³ of pure DMF, and then diluting with water in a V_0 cm³ volumetric flask. After reaching room temperature or thermostat temperature, the decrement is adjusted by adding water. Since the conductance of hydrochloric acid solutions in DMF–water media varies with time after its preparation, the potential measurement for the HCl solutions was carried out one day after preparation. In this paper, DMF volume percent means thus $v_B = 100\, V_B/V_0$, unless otherwise stated. This method is convenient to prepare a series of sample solutions with changing solute concentration and/or in varying solvent composition, contineously.

All electrolytes used were of extra-pure reagent grade. The solvents were purified as described previously.[14] Even 100% DMF contains water about 0.03% (*cf.* Table 2) in this experiment.

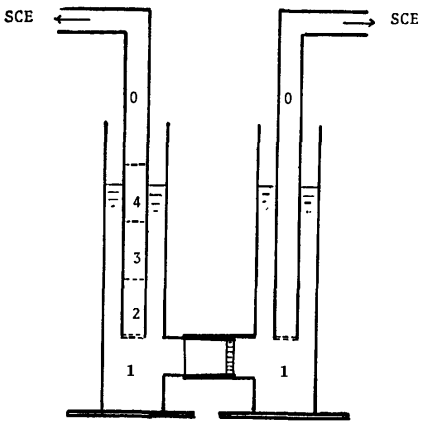

Fig. 1. Bridge potential measurement.
Phase 0, aq satd. KCl soln; 1, test soln (C_1, v_1); 2, DMF agar-salt bridge (C_2, v_2); 3, aq 0.5 M $NaClO_4$ agar bridge; 4, aq 1 M NaCl agar bridge.

Measurement of Transport Number. The Agar-Salt Bridge Method: Figure 1 shows the experimental set-up for measuring the bridge potential E. The agar-salt bridge, dipping into the left compartment of the H-type cell in the figure, was prepared according to the previous paper,[19] and the compositions in phase 2 are shown in Table 3. When not in use, the end of the phase 2 side of the bridge was stored in the renewed preserving solution, having C_2=0.1 mol/dm³ of the electrolyte and v_2 volume percent of DMF. A reference bridge, in the right-hand comaprtment, was an aqueous solution saturated with potassium chloride, which was allowed to flow very slowly into the test solution of phase 1, so as not to plug the tip of the bridge.

TABLE 3. COMPOSITION OF THE PHASE 2

Electrolyte	C / mol dm^{-3}	DMF vol%, v
TEAP[a]	0.1	0, 40, 70, 100
$NaClO_4$	0.1	0, 40, 70, 100
NaCl	0.1	0, 40, 70, 100
KCl	0.1	0, 40, 70, 100
HCl	0.1	0, 40, 70, 85

a) Tetraethylammonium perchlorate.

In Fig. 1, the cell is filled with a test solution (phase 1) which consists of C_1 mol/dm³ of an electrolyte and v_1 % of DMF. The potential difference E between two SCE's was measured within one minute after both bridges have been dipped at the same time (or the agar bridge later than the reference) into the test solution. The E's were measured every time in renewed test solution under the condition of various electrolyte concentrations C_1 but C_2=0.1 and at various DMF contents, but v_1 was always equal to v_2. In each DMF solvent, the E's thus obtained were plotted against log (C_2/C_1); the slope gives the difference of transport number of anion and cation by the equation

$$t^- - t^+ = \frac{F}{RT}\frac{dE}{d\ln(C_2/C_1)}. \quad (4)$$

The Hittorf Method: For simplicity in the determination, only hydrochloric acid was chosen as an electrolye in this method.

Two 1×1 cm^2 platinum plates were used as electrodes. The copper coulometer consisted of 150 g of copper sulfate, 50 cm^3 of 3 M sulfuric acid, 50 cm^3 of ethanol and 1 dm^3 of pure water. Electrolyses were performed at room temperature, and the electrolysis time was fixed between 90—150 min.

Volumetric determination of HCl concentration in both compartments, cathode and middle, was carried out by titration with aqueous sodium hydroxide solutions with phenolphthalein as an indicator, using a microburette. Since the color change at end-point was not clear in the solution containing more than 70% DMF, the solution were diluted with water appropriately. The decrement of HCl in the cathode compartment, Δn_c, is calculated by

$$\Delta n_c = (V_m - V_c)\frac{1}{b}N\frac{V}{1000}, \quad (5)$$

where V_m and V_c are the titer of N normality NaOH solution for b cm^3 of the respective middle and cathode compartments, V is the total amount in the cathode compartment. Hence the transport number of H^+ in HCl solution is

$$t^+(\mathrm{HCl}) = 1 - \Delta n_c \cdot \frac{F}{Q}, \quad (6)$$

where Q is the amount of electricity passed through the coulometer and F the Faraday constant.

The Concentration Cell Method: The potential E of Cell-1 without liquid junction

$$\mathrm{Ag|AgCl|HCl}(C_1)\mathrm{|H_2(Pt)|HCl}(C_2)\mathrm{|AgCl|Ag} \quad \text{Cell-1}$$

and the potential E_t of Cell-2 with liquid junction

$$\mathrm{Ag|AgCl|HCl}(C_1) \vdots \mathrm{HCl}(C_2)\mathrm{|AgCl|Ag} \quad \text{Cell-2}$$

are expressed by the equations

$$E = \frac{2RT}{F}\ln\frac{a_\pm(C_1)}{a_\pm(C_2)} \quad (7)$$

$$E_t = t^+\frac{2RT}{F}\ln\frac{a_\pm(C_1)}{a_\pm(C_2)}. \quad (8)$$

In each solution having a definite DMF content, the logarithmic terms in Eq. 7 and 8 are equal, hence the combination of the two equations gives a transport number

$$t^+(\mathrm{HCl}) = E_t/E. \quad (9)$$

Since the hydrogen electrodes and the silver-silver chloride electrodes have asymmetry potentials ΔE_h and ΔE_t, respectively, the equation 9 must be replaced in practice by

$$t^+(\mathrm{HCl}) = \frac{E_{t,\mathrm{exp}} - \Delta E_t}{E_{\mathrm{exp}} - (E_h - \Delta E_t)}. \quad (10)$$

Potential measurements were made with a Shimadzu Precision Potentiometer K-2 Type. The hydrogen electrodes, 1×1 cm^2 platinum plates, and Ag–AgCl electrodes, the electrolytic type and the thermal-electrolytic type, were prepared and stored according to the accepted methods.[22-24] The latter were kept in water saturated with AgCl for 3 d (for use in water) and 7 d (for use in DMF–water media) after preparation, in order to stabilize the asymmetry potential ΔE_t.

For the E_{exp} and $E_{t,\mathrm{exp}}$ measurements, the cell consists of four compartments (A, B, C, and D) connecting to a four-way stopcock. Two test solutions C_1 and C_2, whose DMF contents were the same, were placed in the compartments A, C and B, D, respectively. To A and B an appropriate amount of AgCl powder was added and stirred to saturate, and then the Ag–AgCl electrodes were inserted. The hydrogen electrodes were put into C and D compartments. The four compartments were bubbled with hydrogen gas (purified through pyrogallol solution) for 30—60 min. After the bubbling, the compartments A-C and B-D were connected by turning the four-way stopcock and the potential difference E_{exp} between A and B was measured (Cell-1). When two hydrogen electrodes were exchanged for a salt bridge or when the two compartments A and B were connected by the stopcock, the potential corresponds to $E_{t,\mathrm{exp}}$ (Cell-2).

The asymmetry potentials ΔE_h and ΔE_t were measured before each E_{exp} measurement, using, an H-type cell in which the concentrations of electrolyte in both compartments were fixed at C_2 and the other concentrations were the same as in the measurement of E_{exp}. The ΔE_t potentials have large values just after the Ag–AgCl electrodes have been transferred to DMF–water media from the aqueous preserving solution, but they decrease with time and stabilize after about half an hour in water and 1 h in DMF, respectively. The addition of solid AgCl is necessary because the silver chloride of the electrode is dissolved in DMF.[25]

Results

The Agar–Salt Bridge Method. The bridge potentials E were measured at room temperature by changing the electrolyte concentration C_1 of the test solution under the condition of $v_1 = v_2$. The results of plotting the E *va.* log (C_2/C_1) for several electrolytes at DMF contents of 0, 40, 70% and DMF-rich solutions are

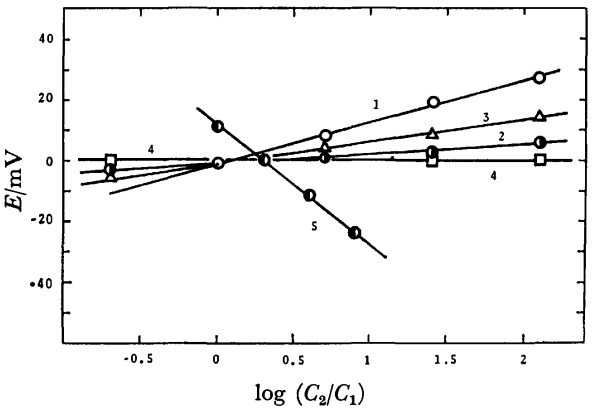

Fig. 2. Plots of E *vs.* log (C_2/C_1) at $C_2 = 0.1$ in water. Electrolyte: curve 1, TEAP; 2, $NaClO_4$; 3, NaCl; 4, KCl; 5, HCl.

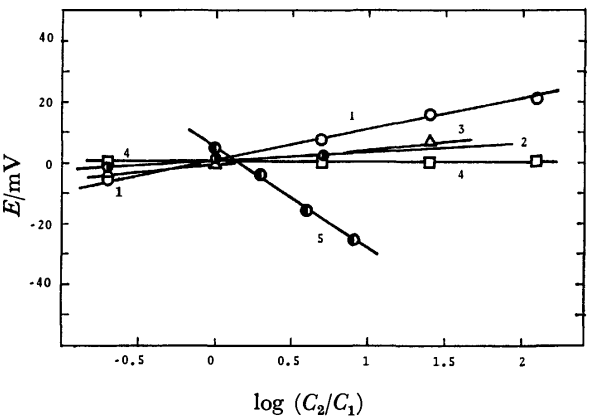

Fig. 3. Plots of E *vs.* log (C_2/C_1) at $C_2 = 0.1$ in 40% DMF. Electrolyte: curve 1, TEAP; 2, $NaClO_4$; 3, NaCl; 4, KCl; 5, HCl.

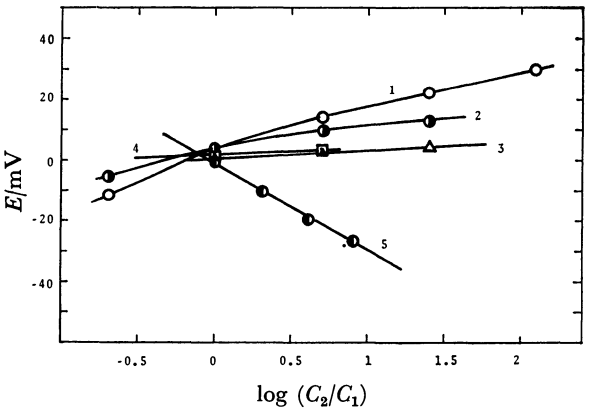

Fig. 4. Plots of E *vs.* log (C_2/C_1) at $C_2=0.1$ in 70% DMF.
Electrolyte: curve 1, TEAP; 2, $NaClO_4$; 3, NaCl; 4, KCl; 5, HCl.

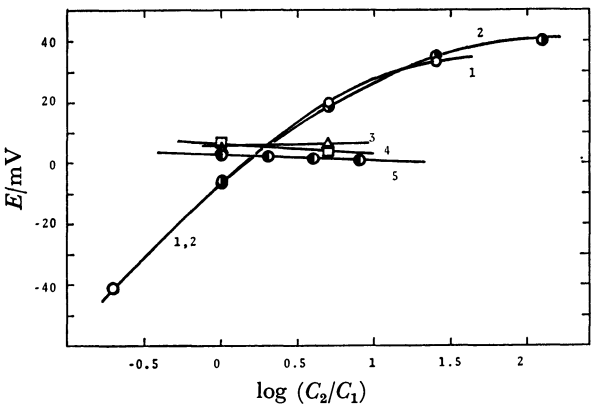

Fig. 5. Plots of E *vs.* log (C_2/C_1) at $C_2=0.1$ in DMF–water.
Electrolyte: curve 1, TEAP in DMF; 2, $NaClO_4$ in DMF; 3, NaCl in DMF; 4, KCl in DMF; 5, HCl in 85% DMF.

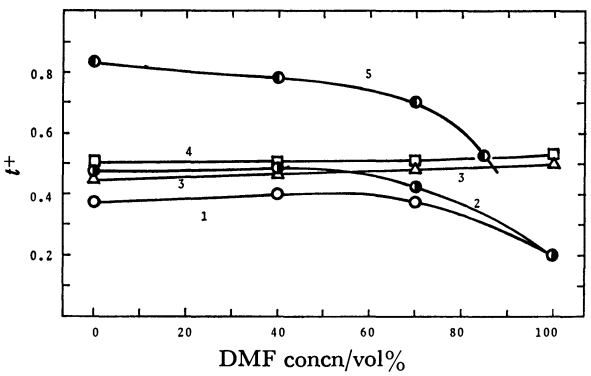

Fig. 6. Transport number of cations t^+ by the Agar–salt bridge method in DMF–water media at room temperature.
Electrolyte; curve 1, TEAP; 2, $NaClO_4$; 3, NaCl; 4, KCl; 5, HCl.

shown in Figs. 2, 3, 4, and 5, respectively. From these figures, one sees that good linear relations are found, except for tetraethylammonium perchlorate (TEAP) in solutions DMF content above 70% (curve 1 in Figs. 4

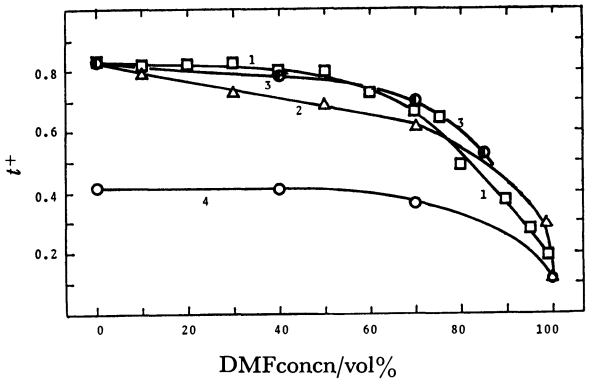

Fig. 7. Comparison of different methods of transport number in DMF–water media.
Curve 1, Hittofrt method t^+(HCl) at $C=0.1$, 2 Concn cell method t^+(HCl) at $C=0.01$—0.0005; 3, Agar–salt bridge method t^+(HCl) at $C=0.1$—0.02 from Fig. 6; 4, Agar–salt bridge method t^+(TEAP) at $C=0.5$—0.1.[19]

and 5) and for $NaClO_4$ in DMF (curve 2 in Fig. 5). By taking the slope between 0 and 0.7 in the abscissa and introducing this slope into Eq. 4, the transport number was calculated. In this way, the transport numbers of cation t^+ in each electrolyte were plotted against DMF content as shown in Fig. 6.

The Hittorf Method. Measurements were carried out at room temperature at a concentration of hydrochloric acid about 0.1 mol/dm^3 and in the range of DMF content $v=0$—99%. The amounts of electricity (Q) passed through the cell for a definite time were decreased with increase of DMF content from 50 coulombs in water to about 4 coulombs in 99% DMF media. The values of t^+(HCl) varied from 0.825 in water to 0.188 in 99% DMF media. A plot of the t^+(HCl) against DMF content is shown as curve 1 in Fig. 7.

The Concentration Cell Method. In order to compare with the Hittorf method, hydrochloric acid in DMF–water media was studied by this concentration cell method. All the cell electromotive forces E_{exp} and $E_{t,exp}$ were measured at the condition of $C_1=2C_2$, and the asymmetry potentials ΔE_h and ΔE_t were measured at the lower concentration of C_2. The data tabulated in Table 4 were obtained with a Ag–AgCl electrode made by the electrolytic method. The plot of these average values t^+(HCl) against the DMF content is shown as curve 2 of Fig. 7.

The t^+ in 99.9 wt% of DMF, about 0.11, is quite uncertain, due possibly to a failure of the hydrogen electrodes. From the limiting ionic conductances $\lambda_0(Cl^-)=55.1$[26] and $\Lambda_0(HCl)=(79.3+70+75.5)/3\fallingdotseq 74.9$,[27] the calculated transport number of the proton in hydrochloric acid in most carefully purified DMF is 0.26, a value obtained by dividing the difference $\Lambda(HCl)-\lambda_0(Cl^-)$ by the $\Lambda_0(HCl)$.

Discussion

Curves 1, 2, and 3 in Fig. 7 are transport numbers of the proton of HCl in DMF–water media, obtained by the three methods. Because of the dissimilarity in

Table 4. Transport number of the proton of HCl by the concentration cell method at $C_1=2C_2$ in DMF–water media at 24±0.5 °C

DMF vol% v_B	C_1 / mol dm^{-3}	Emf/mV				t^+(HCl)
		ΔE_h	ΔE_t	E_{exp}	$E_{t,ext}$	
0	0.01	0.03	0.11	25.78	21.28	0.8257
	0.005	0.07	0.12	22.37	18.41	0.8246
	0 001	0.03	0.13	21.91	18.06	0.8244
	0.0005	0.02	0.07	21.75	17.92	0.8241
10	0.01	0.03	0.41	21.14	17.01	0.8019
	0.005	0.06	0.38	22.63	17.43	0.7684
	0.001	0.08	0.40	22.18	17.87	0.8051
	0.0005	0.07	0.41	20.97	16.94	0.8067
30	0.01	0.05	0.98	20.66	15.41	0.7351
	0.005	0.08	0.90	19.43	14.41	0.7322
	0.001	0.09	1.00	20.27	14.98	0.7289
	0.0005	0.12	1.09	20.39	15.11	0.7310
50	0.01	0.03	0.50	17.04	11.78	0.6832
	0.005	0.09	0.49	16.72	11.40	0.6760
	0.001	0.08	0.48	16.26	11.31	0.6898
	0.0005	0.10	0.68	17.71	12.19	0.6799
70	0.01	0.09	0.69	16.22	8.56	0.5097
	0.005	0.10	0.68	15.64	8.26	0.5101
	0.001	0.12	0.65	16.43	8.46	0.4987
	0.0005	0.11	0.68	16.91	9.22	0.5298
98	0.0113	0.03	0.83	8.48	3.25	0.318
	0.0055	0.12	0.78	12.54	3.98	0.275
	0.0011	0.12	0.96	11.55	4.05	0.295
	0.0006	0.07	0.87	8.78	3.05	0.275
99.9[a)]	0.0113	0.05	0.98	6.40	1.38	0.075
	0.0055	0.07	1.03	4.11	1.48	0.150
	0.0011	0.03	0.95	5.14	1.47	0.125
	0.0006	0.04	0.83	5.72	1.23	0.083

a) Weight percent.

the concentration and in the temperature, a precise comparison among them is difficult. Nevertheless, one may conclude that the method of the agar–salt bridge (curve 3 in Fig. 7) is consistent with the other two methods (curves 1 and 2) of measuring the transport number. Consequently, the transport numbers shown in Fig. 6 for different electrolytes and the t^+(TEAP) in curve 4 of Fig. 7 (taken from the reference 19) are also correct.

It may be noted that curve 4 of Fig. 6 shows that the transport numbers t^+(KCl) and t^-(KCl) are nearly equal in the whole range of DMF–water binary solutions. Thus the liquid junction potential E_j is expected to be zero in terms of Eq. 1 for KCl solutions.

From the above discussion, it can be concluded that potentials obtained in nonaqueous polarography with a slow flowing-type aqueous SCE can be referred to the ordinary aqueous SCE exactly within a few millivolts.

The authors express their cordial gratitude to Professor Taitiro Fujinaga at Kyoto University for his continuing encouragement. Thanks are also given to Hideo Hattori, Hiroshi Yamamoto and Keiko Sasakawa for their assistance in parts of the experimental work.

References

1) H. Letaw, Jr., and A. H. Gropp, *J. Phys. Chem.*, **57**, 964 (1953); J. H. Hook, H. Letaw, Jr., and A. H. Gropp, *ibid.*, **58**, 81 (1954).

2) I. M. Kolthoff and J. F. Coetzee, *J. Am. Chem. Soc.*, **79**, 870 (1957).

3) R. C. Larson and R. T. Iwamoto, *J. Am. Chem. Soc.*, **82**, 3239 (1960).

4) J. F. Coetzee and G. R. Padmanabhan, *J. Phys. Chem.*, **66**, 1707 (1962).

5) V. A. Pleskov, *Zh. Fiz. Khim.*, **22**, 351 (1948).

6) H. M. Koepp, H. Wendt, and H. Strehlow, *Z. Elektrochem.*, **64**, 483 (1960).

7) I. M. Kolthoff and F. G. Thomas, *J. Phys. Chem.*, **69**, 3049 (1965).

8) N. Tanaka and T. Ogata, *Sci. Rep. Tohoku Univ.*, **17**, 57 (1974); *Inorg. Nucl. Chem. Lett.*, **10**, 511 (1974).

9) T. Kakutani, Y. Morihiro, M. Senda, R. Takahashi, and K. Matsumoto, *Bull. Chem. Soc. Jpn.*, **51**, 2847 (1978).

10) A. T. Popov and D. H. Geske, *J. Am. Chem. Soc.*, **79**, 2074 (1957).

11) R. C. Larson, R. T. Iwamoto, and R. N. Adams, *Anal. Chim. Acta*, **25**, 371 (1961).

12) D. J. G. Ives and G. J. Janz, "Reference Electrode,

Theory and Practice," Academic Press, N.Y. (1961), p. 433.
13) N. Tanaka, "Standardization of Electrode Reaction Measurements, Investigation and Proposal," Synthetic Research B (1977).
14) T. Fujinaga, K. Izutsu, and K. Takaoka, *J. Electroanal. Chem.*, **12**, 203 (1966).
15) T. Fujinaga, K. Izutsu, and K. Takaoka, *J. Electroanal. Chem.*, **16**, 89 (1968).
16) T. Fujinaga and K. Takaoka, *J. Electroanal. Chem.*, **16**, 99 (1968).
17) K. Takaoka, *Rev. Polarog. Jpn.*, **15**, 52 (1968).
18) T. Fujinaga, K. Takaoka, and Y. Yoshimura, *Res. Rep. Fukui Tech. Coll., Nat. Sci. and Eng.*, **2**, 55 (1969); T. Fujinaga, K. Takaoka, and Y. Kawae, *ibid.*, **4**, 45 (1971); K. Takaoka and T. Yoshimura, *ibid.*, **11**, 127 (1978).
19) K. Takaoka, *Rev. Polarog. Jpn.*, **14**, 63 (1966).
20) K. Takaoka, H. Yamamoto, H. Hattori, I. Taniguchi, and H. Nagata, 31th National Meeting of the Chemical Society of Japan, Sendai, October 1974, Abstr. No. 2B24.
21) B. E. Geller, *Zh. Fiz. Khim.*, **35**, 1105 (1961).
22) "Jikken Kagaku Koza I," ed by the Chemical Society of Japan, Maruzen, Tokyo (1957), Chap. 4.
23) R. G. Bates, "Determination of pH, Thery and Practice," 2nd ed, John Wiley & Sons (1973), Chap. 10.
24) R. A. Robinson and R. H. Stokes, "Electrolyte Solutions," Butterworths (1959), Chap. 8.
25) J. J. Lagowski, "The Chemistry of Nonaqueous Solvents II," Academic Press (1967), p. 244.
26) J. E. Prue and P. J. Sherrington, *Trans. Faraday Soc.*, **57**, 1795 (1961).
27) G. J. Janz and R. P. T. Tomkins, "Nonaqueous Electrolytes Handbook I," Academic Press (1972), p. 152.

  Bull. Chem. Soc. Jpn., 54, 1025—1030 (1981)

Deactivation of Excited 2-Naphthylamine Due to Hydrogen Bonding Interaction with Pyridines. Fluorescence and Picosecond Laser Photolysis Studies

Noriaki IKEDA, Tadashi OKADA, and Noboru MATAGA*

Department of Chemistry, Faculty of Engineering Science, Osaka University, Toyonaka, Osaka 560

(Received October 24, 1980)

The mechanism of the strong fluorescence quenching observed when two conjugated π-electron systems are directly connected by hydrogen bonding has been studied by means of transient absorption spectral measurements with ps as well as ns laser photolysis method and fluorescence measurement. The bimolecular rate constants of quenching of 2-naphthylamine fluorescence by pyridine and 4-cyanopyridine have been determined in various solvents. The bimolecular reaction rate of fluorescence quenching by pyridine is smaller than the diffusion controlled one in many cases and depends considerably upon the dipole moment and the ability of formation of hydrogen bonding chain of solvent. However, the quenching by 4-cyanopyridine is diffusion controlled in every solvent examined here. By means of ps laser photolysis method, the state formed by charge transfer from excited 2-naphthylamine to hydrogen bonded pyridine in the quenching process has been observed for the first time. The possibility of the hydrogen atom transfer due to the mechanism of charge transfer followed by proton transfer in hexane solution is also discussed.

Many investigations have been carried out on the inter- and intramolecular hydrogen bonding interactions from various viewpoints.[1]

Regarding the effect of hydrogen bonding interaction upon fluorescence yield, it has been observed frequently that, when two conjugate π-electronic systems are directly combined by hydrogen bonding interaction, fluorescence of proton donor or acceptor is strongly or thoroughly quenched.[1-7] Moreover, it has been confirmed in the cases of some systems that the hydrogen bonding interaction induces strong deactivation of S_1 state but does not lead to the enhanced intersystem crossing.[5,7] Especially detailed luminescence kinetic studies have been made for carbazole–pyridine systems[4,7,8] and the lifetime of the singlet excited state of carbazole–pyridine complex was estimated to be 28 ps.[8]

It was suggested that CT (charge transfer) interaction between proton donor and acceptor π-electron systems *via* hydrogen bond was responsible for the quenching.[2-4,6-8] Namely, the CT state in this case was assumed very weakly fluorescent or nonfluorescent.[8] Hydrogen atom transfer from proton donor to acceptor was also suggested as a possible mechanism of quenching.[9]

From the investigation of naphthol–pyridine system by means of absorption-emission flash technique, it has been concluded that the fluorescence quenching in this system is partly due to hydrogen atom transfer.[10] On the other hand, it has been proposed that the primary process in the hydrogen bonding system in the triplet state is the electron transfer followed by proton transfer between the proton donor and acceptor.[11] However, direct proof of the electron transfer mechanism has not yet been given.

In relation to this problem, we have made ps laser photolysis studies upon naphthylamine–pyridine systems in addition to detailed investigations of solvent effects upon fluorescence quenching due to hydrogen bonding interaction.[12]

Experimental

Materials. 2-Naphthylamine (GR grade, Tokyo Kasei) was recrystallized twice from ligroine, and sublimated in a vacuum. *N,N*-Dimethyl-2-naphthylamine (GR grade, Tokyo Kasei) was recrystallized three times from ethanol–water mixture and sublimated in a vacuum. Pyridine (spectro grade, Kishida) was refluxed over calcium hydride and distilled. 4-Cyanopyridine (GR grade, Nakarai) was recrystallized twice from ether–ligroine mixture and sublimated in a vacuum. Laboratory deionized water was distilled and redistilled by nonboiling type distillation apparatus. *N*-Methylformamide (GR grade, Tokyo Kasei) and the other solvents (spectro grade) were used as received. The solvents for solutions examined by laser photolysis were refluxed over appropriate desiccant and distilled before use. All sample solutions were deaerated by freeze-pump-thaw cycles.

Apparatus and Measurements. Absorption and fluorescence spectra were measured using respectively a JASCO UVIDEC-1 type spectrophotometer and an Aminco-Bowman spectrophotofluorometer. Fluorescence lifetimes were determined by using a pulsed nitrogen laser with 1 kW peak power as an exciting light source, combined with a monochromator, 1P28 photomultiplier, a sampling oscilloscope and a XY recorder. The time resolution of this system was about 2.5 ns. Nanosecond laser photolysis apparatus was the same as described elsewhere.[13]

Picosecond laser photolysis measurements were made as follows. Single picosecond pulse of the second harmonic from a mode-locked ruby laser was used for excitation. Pulse width was *ca.* 30 ps. Picosecond continuum for monitoring the transient absorption spectra was generated by focussing the single fundamental pulse into heated polyphosphoric acid solution, BK-7 glass or fused quartz plate. The generated picosecond continuum was split into two beams one of which was passed through the excited sample solution. Both beams were detected by multichannel detectors of photodiode arrays (abbreviated as MCPD) through polychromators, respectively. Both MCPD's were connected with a microcomputer system for data processing and transient absorption spectra at various delay times were stored in disk and displayed on a recorder or oscilloscope.

The transient absorption spectrum can be obtained by measuring intensities of monitoring light pulse in the presence

($I(\lambda)$) as well as in the absence ($I^0(\lambda)$) of exciting pulse, and by evaluating the absorbance $A(\lambda)$ at the wavelength λ according to the following equation. λ covers wavelength range of 200 nm in one measurement.

$$A(\lambda) = \log\{I_1(\lambda)/I_2(\lambda)\} - \log\{I_1^0(\lambda)/I_2^0(\lambda)\},$$

where the subscripts 1 and 2 mean the light intensities detected by MCPD1 and MCPD2, respectively, and MCPD2 receives the monitoring light passed through the sample solution. More details of the picosecond apparatus will be described elsewhere.[14]

Results and Discussion

(A) Hydrogen Bonding Equilibrium in the Ground State. The change of absorption spectra of 2-naphthylamine (NA) caused by hydrogen bonding interaction with pyridine (P) is not so large and the equilibrium constant K_g of the hydrogen bond formation in the ground state is rather small. For example, K_g of NA–P in hexane is 0.6 M^{-1} (1 M=1 mol dm^{-3}) at 20 °C, while it was reported that K_g=0.2 M^{-1} in benzene at 13 °C[3] and K_g=12 M^{-1} in cyclohexane at 15 °C.[4] In the case of NA–4-cyanopyridine (CNP) system in hexane solution, the absorption spectra of NA were little affected by the addition of CNP in the range of concentration (up to 4×10^{-2} M) used in the measurements. We have confirmed that the ability of CNP to make hydrogen bond with NA is considerably smaller than that of pyridine. Moreover, the hydrogen bonding interaction between NA and pyridine or NA and CNP in polar solvents becomes much weaker than in nonpolar solvents probably owing to solvation of NA as well as pyridines. Therefore, hydrogen bonding interaction in the ground state of these systems in polar solvents can be neglected.

(B) Fluorescence Quenching Reaction and Its Solvent Dependence. As is well-known, the hydrogen bonding ability of aromatic hydroxy and amine compounds is considerably larger in the lowest excited singlet state than in the ground state, which results the red shift of electronic spectra due to the hydrogen bonding interaction. Actually, in the case of naphthylamines and carbazole, the change of the fluorescence spectra caused by the hydrogen bonding interaction with proton acceptors in nonpolar solvents was confirmed to arise at much smaller concentrations of acceptor than those of absorption spectra.[3,4,8]

The progressive changes of fluorescence spectra of NA caused by adding pyridine in hexane solution are indicated in Fig. 1. In relation to the hydrogen bonding quenching of fluorescence, we have examined the *N,N*-dimethyl-2-naphthylamine (DMNA)–P system, and have confirmed that the fluorescence of DMNA is not quenched by pyridine in hexane. This result shows evidently that the hydrogen bonding interaction is essential for the quenching of NA–P system. In pure pyridine solution of NA, a very weak fluorescence band which is a little red-shifted compared with that of NA in hexane was observed. Analogous results were obtained also in the case of carbazole–pyridine system.[8] The very weak fluorescence band seems to be ascribed to the hydrogen bonded complex. In the case of the strong quenching by CNP, no red-shifted fluorescence band was observed. Moreover, CNP quenches not only the fluorescence of NA but also the fluorescence of DMNA in hexane, which indicates that the quenching by CNP is due to the molecular interaction other than hydrogen bonding, probably the direct charge transfer interaction.

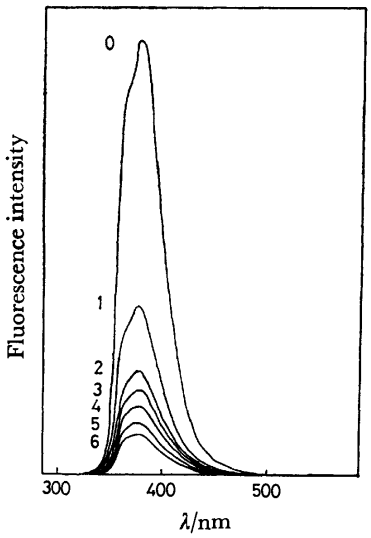

Fig. 1. Quenching of NA fluorescence caused by added P in hexane solution.
[NA]=3.6×10^{-4} M, [P]/M: 0. 0, 1. 0.004, 2. 0.008, 3. 0.012, 4. 0.016, 5. 0.020, 6. 0.030.

In general, for the fluorescence behaviors of hydrogen bonding as well as the other molecular complex forming systems, the following mechanism may be assumed.

$$\begin{array}{ccc} DH^* + A & \underset{k_{-q}}{\overset{k_q}{\rightleftharpoons}} & (DH\cdot A)^* \\ I_{abs}\cdot\delta \Big\downarrow (k_f+k_i) & & I_{abs}\cdot\delta' \Big\downarrow (k_f'+k_i') \\ DH + A & \underset{K_g}{\rightleftharpoons} & (DH\cdot A) \end{array} \qquad (1)$$

In the above scheme, I_{abs} is the total light quanta absorbed by the solution. δ and δ' are the fractions absorbed by free DH and complex, respectively. k_q and k_{-q} are rate constants of complex formation and decomposition reactions, respectively. k_f and k_i are rate constants of radiative and radiationless transitions of the excited free DH, respectively, and k_f' and k_i' are those of the excited complex.

When the equilibrium constant K_g of the complex formation in the ground state is very small and, moreover, $k_i' \gg k_f'$, $k_{-q'}$, simple Stern-Volmer equation may be valid approximately to reproduce the observed fluorescence yield.

$$I_f^0/I_f = 1 + k_q\tau_0[A], \qquad (2)$$

where $\tau_0=1/(k_f+k_i)$. Equation 2 holds approximately for NA–P and NA–CNP systems in various solvents, from which the quenching rate constants have been obtained.

As typical examples, the Stern-Volmer plots for NA–P and NA–CNP systems in hexane as well as aqueous solutions are shown in Fig. 2. Values of the quenching rate constant in various solvents are indicated in

Table 1. Solvent dependence of the fluorescence quenching rate constants (~25°C)

Solvent	μ/Debye[c]	$\varepsilon/\varepsilon_0$	τ_0/ns	k_q^P/M^{-1}s^{-1} [d]	k_q^C/M^{-1}s^{-1} [e]	k_d/M^{-1} s^{-1} [f]	k_q^P/k_d
Benzene	0	2.27	12	8.7×10^9	1.5×10^{10}	1.1×10^{10}	0.8
Hexane	0.085	1.9	14	2.4×10^{10}	2.9×10^{10}	2.2×10^{10}	1.1
Toluene	0.31	2.38	15	8.2×10^9	1.3×10^{10}	1.2×10^{10}	0.7
Ethanol	1.66(20 °C)	24.55	17	1.8×10^9	1.1×10^{10}	6.1×10^9	0.3
Water	1.84	78.4	21	4.0×10^9	9.3×10^9	7.4×10^9	0.5
Acetone	2.69(20 °C)	20.7	10	6.0×10^8	2.1×10^{10}	2.1×10^{10}	0.03
Methanol	2.87(20 °C)	32.7	16	3.2×10^9	1.9×10^{10}	1.2×10^{10}	0.3
Acetonitrile	3.44(20 °C)	37.5	19	3.5×10^8	1.9×10^{10}	1.7×10^{10}	0.02
NMF[a]	3.86	182.4	11	2.4×10^8	7.3×10^9	4.0×10^9	0.06
DMF[b]	3.86	36.7	18	8.2×10^7	1.0×10^{10}	8.2×10^9	0.01

a) *N*-Methylformamide. b) *N*,*N*-Dimethylformamide. c) 1 Debye=3.33564×10^{-30} Cm. d) k_q value of NA–P system. e) k_q value of NA–CNA system. f) $k_d=8RT/3000\eta$.

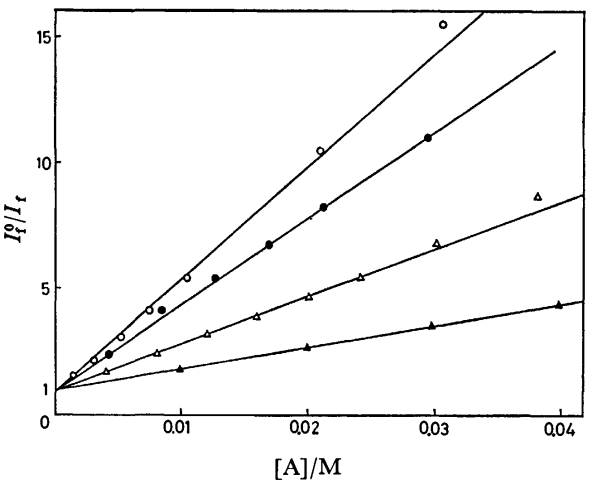

Fig. 2. I_f^0/I_f *vs.* [A] relation for NA–P and NA–CNP systems in hexane and water.
●: NA–P in hexane, ▲: NA–P in water, ○: NA–CNP in hexane, △: NA–CNP in water.

Table 1 together with those of solvent dielectric constant and dipole moment as well as τ_0 values of NA measured in various solvents. Moreover, k_q values are compared with the values of the diffusion controlled rate constant estimated by, $k_d=8RT/3000\,\eta$.

As can be seen from Table 1, the quenching by CNP is almost diffusion controlled in every solvent used here. Although the quenching by pyridine is also approximately diffusion controlled in nonpolar solvents, it shows remarkable solvent dependence in polar solvents. The dipole moment of the solvent molecule seems to be an appropriate parameter representing the solvent effect upon the interaction between pyridine and excited NA, except in the case of protic solvents. This result indicates that the solvation by polar solvent molecules hinders more or less the hydrogen bonding interaction. The quenching efficiency (k_q^P/k_d) changes about one order of magnitude around the value of the solvent dipole moment equal to that of pyridine (2.37 D).

The ability of solvent to form hydrogen bonding chains seems to affect also the quenching efficiency. For example, the quenching efficiency (k_q^P/k_d) in methanol (0.3) is much larger than that in acetone (0.03) which has dipole moment very close to that of methanol. Similar result can be seen in the case of NMF as compared to DMF solvents. Thus, the quenching efficiency in protic solvent is larger than in aprotic solvent which has dipole moment close to that of the protic solvent. This result suggests that the hydrogen bonding chains in solvents assist in some way the quenching of NA–P system.

In relation to this effect of hydrogen bonding solvent upon the NA–P hydrogen bonding quenching of fluorescence, we have confirmed that the fluorescence of DMNA is not quenched by P not only in nonpolar solvent but also in polar aprotic solvent, but even in the case of DMNA–P system, fluorescence is quenched remarkably in aqueous ($k_q=3.2\times10^9$ M^{-1} s^{-1}) and ethanol solutions, to almost the same extent as in the case of NA–P system. Thus, the important role of hydrogen bonding interaction among solvent molecules which assists the interaction between solute fluorescer and quencher leading to the fluorescence quenching has been confirmed, although its mechanism is not very clear at the present stage of investigation.

Contrary to the case of the quenching by pyridine, fluorescence of DMNA is quenched strongly by CNP not only in polar protic solvent ($k_q=7.4\times10^9$ M^{-1} s^{-1} in water), but also in polar aprotic solvent ($k_q=1.8\times10^{10}$ M^{-1} s^{-1} in acetonitrile) just as in the nonpolar solvent ($k_q=3.2\times10^{10}$ M^{-1} s^{-1} in hexane). These values of the bimolecular rate constant are rather similar to those of NA–CNP system in various solvents which are approximately diffusion controlled. As it is discussed already, this result shows that the quenching is due to the direct complex formation in the excited state rather than hydrogen bonding interaction.

(*C*) *Measurements of Transient Absorption Spectra by Means of Picosecond and Nanosecond Laser Spectroscopy.* If the charge transfer interaction between the hydrogen bonded pair in the excited state is responsible for the fluorescence quenching in the case of NA–P system, one may expect to observe the transient CT state by means of laser spectroscopy.

Results of ps laser photolysis measurements upon NA and NA–P systems in hexane solution are shown in Fig. 3. In Fig. 3, the spectra of NA cation radical[15] produced by γ-irradiation in *s*-butyl chloride solution at 77 K are indicated for the purpose of comparison. The spectra of NA in hexane at the delay time of 200

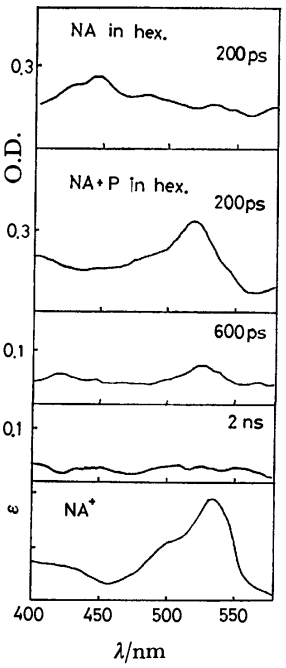

Fig. 3. Transient absorption spectra of NA and NA–P systems in hexane solution obtained by ps laser photolysis method.
[NA]$=3.45\times10^{-4}$ M, [P]$=0.37$ M.

ps may be due to the $S_n\leftarrow S_1$ transition. With addition of sufficient P, completely different spectra appeared. The spectra at 200 ps are similar to the spectra of NA cation radical. The delay time of 200 ps is necessary in order to convert completely the excited NA into the hydrogen bonded complexes at [P]$=0.37$ M. We have examined also the ps transient spectra of NA in pure pyridine solvent and observed again the band similar to that of NA cation radical.

The observed transient spectra are most probably due to the state formed by CT from excited NA to hydrogen bonded pyridine, ($D^{+\delta}$–H$\cdots A^{-\delta}$). Thus, we have directly demonstrated for the first time that the CT state is responsible for the deactivation of excited singlet hydrogen bonded species. The absorbance of the CT state decays during a few hundreds ps and at 2 ns we cannot recognize any characteristic band due to the CT state. We have examined also the very weak fluorescence of the hydrogen bonded complex by means of ps streak camera and obtained the decay time of a few hundred ps.[17]

The possibility of intermolecular electron transfer in the excited state may be examined by evaluating the standard free energy change ΔG° for the process, $D^*\cdots A\rightarrow D^+\cdots A^-$, in the encounter complex according to Eq. 3.

$$\Delta G^\circ = E(D/D^+) - E(A^-/A) - (e^2/\varepsilon R) - \Delta E + \Delta G_s$$

$$\Delta G_s = (e^2/2)\left(\frac{1}{R^+}+\frac{1}{R^-}\right)\left(\frac{1}{\varepsilon}-\frac{1}{37.5}\right), \qquad (3)$$

where $E(D/D^+)$ and $E(A^-/A)$ are respectively the oxidation potential (*vs.* SCE) of electron donor and the reduction potential of the electron acceptor in acetonitrile. R is the center to center distance between D^+ and A^- assumed to be 7 Å. ΔE is the electronic excitation energy of D and ΔG_s is the correction term for solvation energy of cation and anion with radius R^+ and R^-, respectively, in a solvent with dielectric constant ε. Values of $E(D/D^+)$ and $E(A^-/A)$ were taken from literatures[9,16,18] and ΔG° values were estimated for the present systems as shown in Table 2.

Table 2. ΔG° for NA–P and NA–CNP systems

	ΔG°/kcal mol^{-1}			
	Hexane	Acetonitrile	Water	Pyridine
NA–P	14.4	−8.1	−11.4	−4.4
NA–CNP	−13.3	−35.7	−39.0	—

For example, ΔG° value of NA–P system in hexane is estimated to be 14.4 kcal/mol, which means that the electron transfer in the encounter complex is not possible. Even if we take a little smaller encounter distance $R=5$ Å, ΔG° is estimated to be 4.4 kcal/mol, which means that the reaction is much slower than the diffusion-controlled one. Since the fluorescence quenching reaction was observed to be diffusion-controlled in the case of NA–P system and the quenching is caused by hydrogen bonding interaction as it is discussed in (*B*), the above result shows that the hydrogen bonding interaction assists the π-electronic CT state formation. It is expected that the hydrogen bonding decreases the ionization potential of NA and increases the electron affinity of pyridine.

Contrary to the case of NA–P system, the fluorescence quenching by CNP is almost diffusion-controlled not only in nonpolar solvents but also in polar solvents in both cases of NA and DMNA, which indicates the direct CT interaction without hydrogen bonding as it is discussed already in (*B*). Actually, we have observed by means of ps laser photolysis an absorption band which is very similar to that of DMNA cation in the case of DMNA–CNP system in benzene. This absorption band may be ascribed most probably to non-fluorescent heteroexcimer formed by excited DMNA and CNP. In the case of NA–CNP system in hexane as well as in benzene, however, the characteristic absorption band due to the CT state was not observed in the ps transient spectra. Very rapid deactivation process associated with the CT interaction seems to be predominant in this case.

We have examined the transient absorption spectra of NA–P system in hexane also by means of ns laser photolysis method. The results of measurements are indicated in Fig. 4. The spectra of NA in hexane at the delay time of 100 ns seems to be due to $T_n\leftarrow T_1$ transition. Similar absorption spectra were observed at the delay time of 100 ns also in the case of NA–P system in hexane. However, it might be possible to assign the band around 450 nm of the NA–P system to the absorption spectra of 2-naphthylaminyl radical which are similar to the $T_n\leftarrow T_1$ spectra of NA.[19,20]

If the observed spectra of NA–P system are due to the 2-naphthylaminyl radical, it may be produced by the mechanism of CT followed by proton transfer competing

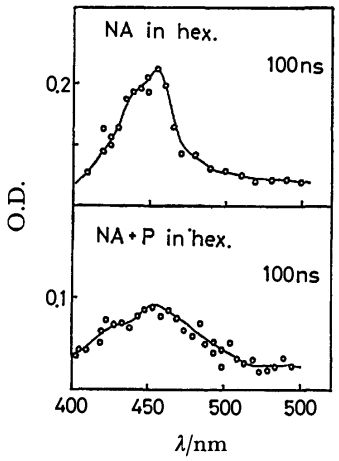

Fig. 4. Transient absorption spectra of NA and NA–P systems in hexane solution obtained by ns laser photolysis method at 100 ns. Concentrations of NA and P are respectively the same as in Fig. 3.

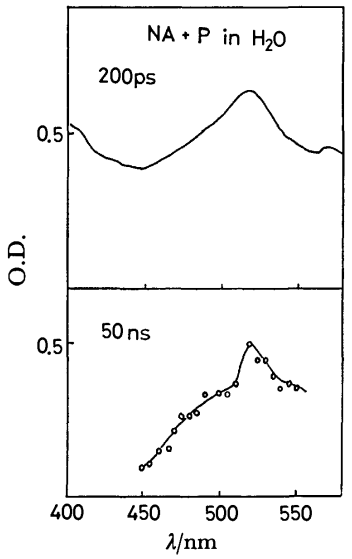

Fig. 5. Transient absorption spectra of NA–P system in water obtained by ps and ns laser photolysis method. [NA]=3×10^{-4} M, [P]=0.25 M.

with the deactivation to the ground state. This interpretation seems to be supported by the fact that the intersystem crossing rate constant is little influenced by hydrogen bonding interaction.[5,7,21] Namely, the $S_1 \rightsquigarrow T_1$ intersystem crossing seems to be negligible owing to the other overwhelming non-radiative processes from S_1 state of the NA–P hydrogen bonded complex. Thus, the formation of 2-naphthylaminyl radical from the CT state seems to be probable. Nevertheless the rise of its absorption band was not recognized clearly by means of ps laser photolysis at the delay time of 2 ns. This result may be due to the smaller extinction coefficient of 2-naphthylaminyl radical than that of NA cation and the lower power of exciting ps pulse compared with ns pulse.

We have examined also the transient spectra of NA–P and NA–CNP systems in polar solvents such as acetonitrile and water by means of ps as well as ns laser photolysis, and have observed clearly the spectra due to NA cation in both 100 ps and 10 ns —100 ns time regions. This result shows clearly that dissociated ion radicals are produced in these polar solvents. However, contrary to the case of nonpolar solvent, cation radicals can be produced not only by electron transfer from excited NA to pyridines followed by ionic dissociation but also by laser induced electron ejection to polar solvent. Therefore, more quantitative studies are necessary for the elucidation of the details of reaction mechanism. In Fig. 5, transient absorption spectra in water observed by means of ps and ns laser photolysis methods are indicated in the case of NA–P system.

Peculiar Nature of the Quenching by Pyridine. There is a definite relation between the bimolecular quenching rate constant k_q and the free energy change $\Delta G°$ of Eq. 3 in acetonitrile solution for some typical electron donor acceptor systems including heteroexcimers.[9] According to this relation between k_q and $\Delta G°$, the $\Delta G°$ value estimated for NA–P system in acetonitrile (−8.1 kcal/mol, Table 2) corresponds to almost diffusion-controlled value of k_q ($\approx 10^{10}$ M^{-1} s^{-1}), contrary to the observed value of 10^8 M^{-1} s^{-1}. Moreover, since the ionization potential of DMNA may be smaller than that of NA, the $\Delta G°$ value of DMNA–P system in acetonitrile seems to be more negative predicting diffusion-controlled k_q value. Actually, however, fluorescence of DNMA is not affected by added pyridine in acetonitrile solution. These results clearly show that the ordinary k_q-$\Delta G°$ relation of electron transfer quenching does not hold for the NA–P and DMNA–P systems. Thus, even if the reaction is sufficiently exothermic, the electron transfer reaction does not occur in the case of DMNA–P system in acetonitrile and the hydrogen bonding interaction is necessary in the case of NA–P system in acetonitrile. Although the reason for this result is not very clear at the present stage of investigation, one should note this specific nature of photochemical electron transfer.

The hydrogen bonding interactions between chromophores as well as between chromophores and environmental water seem to play important roles in biological systems. The present results may be of some importance also from such a point of view. More detailed fluorescence quenching and ionic photodissociation studies upon various hydrogen bonding systems are now going on in this laboratory.

The authors wish to express their thanks to Dr. T. Shida of Kyoto University for informing us of his unpublished result of the absorption spectra of NA cation radical. Thanks are also due to Mr. K. Kida for his help in the ps laser photolysis measurements. N. M. and T. O. acknowledge the support by Toray Science Foundation and Mitsubishi Foundation, and N. M. also acknowledges the support by Grant-in-Aid for special project research on photobiology from the Japanese Ministry of Education, Science and Culture.

References

1) See for example, N. Mataga and T. Kubota, "Molecular Interactions and Electronic Spectra," Marcel Dekker, New

York (1970).
2) N. Mataga and S. Tsuno, *Naturwiss.*, **10**, 305 (1956); *Bull. Chem. Soc. Jpn.*, **30**, 711 (1957).
3) N. Mataga, *Bull. Chem. Soc. Jpn.*, **31**, 481 (1958).
4) N. Mataga, Y. Torihashi, and Y. Kaifu, *Z. Phys. Chem. N. F.*, **34**, 379 (1962).
5) J. R. Merill and R. G. Bennett, *J. Chem. Phys.*, **43**, 1410 (1965).
6) N. Mataga and K. Ezumi, *Bull. Chem. Soc. Jpn.*, **40**, 1350 (1967).
7) N. Mataga, F. Tanaka, and M. Kato, *Acta Phys. Polon.*, **34**, 733 (1968).
8) M. M. Martin and W. R. Ware, *J. Phys. Chem.*, **82**, 2770 (1978).
9) D. Rehm and A. Weller, *Israel J. Chem.*, **8**, 259 (1970).
10) K. Kikuchi, H. Watarai, and M. Koizumi, *Bull. Chem. Soc. Jpn.*, **46**, 749 (1973).
11) S. Yamamoto, K. Kikuchi, and H. Kokubun, *Bull. Chem. Soc. Jpn.*, **49**, 2950 (1976).
12) A preliminary short report was published in *Chem. Phys. Lett.*, **62**, 251 (1980).
13) J. Hinatu, H. Masuhara, N. Mataga, Y. Sakata, and S. Misumi, *Bull. Chem. Soc. Jpn.*, **51**, 1032 (1978).
14) T. Okada, M. Migita, N. Mataga, Y. Sakata, and S. Misumi, unpublished.
15) T. Shida, private communication.
16) E. S. Pysh and N. C. Yang, *J. Am. Chem. Soc.*, **82**, 2124 (1963).
17) N. Ikeda, H. Miyasaka, T. Okada, and N. Mataga, unpublished.
18) The value of the reduction potential of CNP obtained *vs.* Ag: $AgClO_4$ (P. N. Rieger, I. Bernal, W. H. Reinmuth and G. K. Fraenkel, *J. Am. Chem. Soc.*, **85**, 683 (1963)) was corrected using equation by Chen and Wentworth (E. C. M. Chen and W. E. Wentworth, *J. Chem. Phys.*, **63**, 3183 (1975)).
19) E. J. Land and G. Porter, *Trans. Faraday Soc.*, **59**, 2077 (1963).
20) G. Jackson and G. Porter, *Proc. R. Soc. A*, **260**, 13 (1961).
21) We made a preliminary measurement upon phosphorescence of NA–P system in low temperature rigid solvent (methylcyclohexane–isopentane mixture) and observed the quenching due to hydrogen bonding.

Molecular Dynamics Study on Transport Properties of Fluids

Kazuo TOKIWANO† and Kiyoshi ARAKAWA*

Research Institute of Applied Electricity, Hokkaido University, Sapporo 060

†*Faculty of Engineering, Hokkaido University, Sapporo 060*

(Received November 13, 1980)

A molecular dynamics "experiment" has been performed for a system of 216 molecules interacting through a modified Lennard-Jones-type potential. The velocity autocorrelation functions and associated self-diffusion coefficients were computed for varying degrees of the steepness of the repulsive part in the pair potential. The dependence of these quantities upon the hardness of the core, and then the applicability of a perturbation approach to the transport theory, was elucidated. The computed self-diffusion coefficients were compared with the prediction of the Rice-Allnatt theory.

With the advent of computer experiment techniques, it has become possible to acquire useful information on dynamical processes in liquids by simulation. The velocity autocorrelation function $\Psi(t)$ is of particular interest, here, because it is the most important quantity for the description of the dynamics of liquids. Molecular dynamics experiments have been performed for the Lennard-Jones potential fluids by Rahman[1] and by Levesque-Verlet,[2] and, also for a rigid sphere fluid, those have been done by Alder-Wainwright and others.[3,4] The results have brought us some valuable information on $\Psi(t)$. Recent progress in the transport theory of liquids has been strongly promoted by these studies.[1-7]

The most important problem in the transport theory of liquids is to present a theoretical model amenable to the analytical treatment for various correlated motions of molecules in a liquid. In explaining the equilibrium properties of liquids, the perturbation approach has proved to be successful for the last decade.[8,9] The theory rests on the idea that the short range structure of liquids is governed primarily by a steep repulsive part of the intermolecular potential. Then, the attractive potential is regarded as a perturbation on a rigid sphere potential. Concerning transport properties, however, no successful perturbation theory has been proposed yet, and for the advancement of the theory, it is required to elucidate further the effect of the intermolecular potential upon the transport properties of fluids. Considerable efforts through computer experiments have been devoted to the presentation of a reference fluid, which is useful in predicting the transport properties of liquids. The predominant role of the repulsive interaction by hard cores in the dynamics of dense fluids has been confirmed through the molecular dynamics results.[6,10,11] Levesque *et al.*[2] stated that the transport coefficient for the Lennard-Jones fluids was practically explained in terms of a corresponding hard sphere model. On the other hand, concerning the effect of softness of the core, it seems that a soft core potential gives rise to remarked oscillations in $\Psi(t)$ while the diffusion coefficient is rather insensitive to the steepness of the repulsive core.[12] Then, for the elucidation of these properties of liquids, further examinations are required.

The purpose of the present work is to study the effect of the repulsive core on the transport properties of liquids with varying degrees of the steepness of the repulsive part of the potential. For that purpose, we consider a fluid system composed of molecules interacting through a modified Lennard-Jones-type potential: a parameter which shows the hardness of the repulsive core is introduced there. Velocity autocorrelation functions and associated self-diffusion coefficients for the systems are calculated by means of molecular dynamics experiments. The dependence of those quantities upon the hardness of the core and the applicability of a perturbation approach to the transport theory are investigated. Detailes of the results will be given in the following sections.

Molecular Dynamics Method

Description of the System. We consider a system composed of molecules interacting through a pair potential of the form

$$u(r_{ij}) = 4h\varepsilon\left[\left(\frac{\sigma}{r_{ij}}\right)^{12} - \left(\frac{\sigma}{r_{ij}}\right)^{6}\right] + (h-1)\varepsilon \quad r_{ij} \leq r_0$$
$$= 4\varepsilon\left[\left(\frac{\sigma}{r_{ij}}\right)^{12} - \left(\frac{\sigma}{r_{ij}}\right)^{6}\right] \quad r_{ij} > r_0, \quad (1)$$

where r_{ij} is the separation between molecules i and j, ε an energy parameter, and $r_0 = 2^{1/6}\sigma$. This potential function has a minimum of $-\varepsilon$ at r_0 and crosses the abscissa at the distance σ_0, and

$$\sigma_0 = [2(h - \sqrt{h})/(h-1)]^{1/6}\sigma \quad h \neq 1$$
$$= \sigma \quad h = 1. \quad (2)$$

h is a parameter which shows the hardness of the repulsive core. When $h=1$, $u(r_{ij})$ becomes a Lennard-Jonse 12-6 potential with parameters ε and σ. Figure 1 displays the potential curves for different values of h for the same ε and σ (Fig. 1-(a)) and those for the same ε and σ_0 (Fig. 1-(b)). For large values of h the potential may be regarded as a nearly rigid sphere potential with an attractive part.

Reduced quantities have been used throughout. There is some arbitrariness in choosing the reduction units for the present potential system. We have taken the reduced density ρ^* and the reduced temperature T^* as

$$\rho^* = N\sigma_0^3/V \text{ and } T^* = kT/\varepsilon, \quad (3)$$

respectively, where k is the Boltzmann constant.

The magnitude of ρ^* of the systems considered were taken to be not larger than 0.95. When exceeded this reduced density, the system actually lost its fluidity for the lowest temperature chosen, showing an adrupt

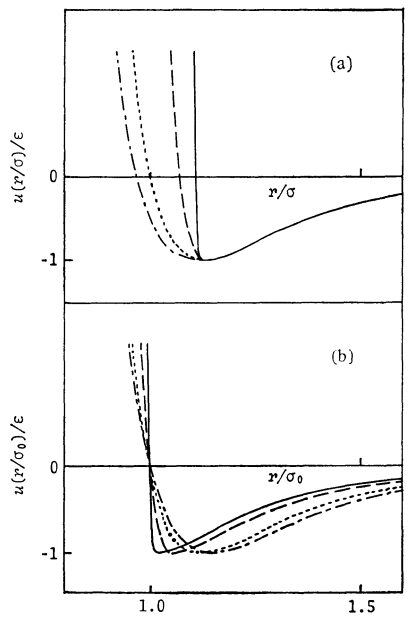

Fig. 1. Intermolecular potentials for varying degrees of the steepness of the repulsive potential.
(a): For constant ε and σ, (b): for constant ε and σ_0.
——: $h=200$, – – –: $h=10$, ·····: $h=1$, –·–·–: $h=0.5$.

drop in the diffusion coefficient. With respect to temperature, we have taken the range of T^* of 0.6—4.0, because we consider the liquids composed of molecules interacting with comparatively strong forces, such as H_2O, C_6H_6, CCl_4, CH_3OH *etc.*[13]

Computational Technique. Molecular dynamics calculations have been performed for the system of 216 molecules confined to a cubic box with volume V, interacting through the potential Eq. 1. Following the usual procedure in molecular dynamics studies, the periodic boundary conditions were employed and interactions beyond a cutoff distance r_c were ignored. The cutoff was placed at $r_c=2.5\,\sigma_0$. The technique due to Verlet[15] was used to integrate the $3N$ coupled Newton equations of motion,

$$m\frac{\mathrm{d}^2\boldsymbol{r}_i}{\mathrm{d}t^2} = -\nabla_i \sum_{i\neq j}^{N} u(r_{ij}). \tag{4}$$

The basic time increment for the numerical integration has been taken to be 0.012 (in $(m\sigma_0^2/\varepsilon)^{1/2}$), taking the conservation of total energy of the system into account. The number of time steps required to investigate a given thermodynamic state was about 12000 time steps; 2000 time steps were sufficient, usually, to reach equilibrium, and a period of 10000 time steps was utilized to form the statistical average. The results were stable and reproducible.

Radial Distribution Function. The radial distribution function gives the average local density of molecules at distance r from the central molecule, and is indicative of the local structure in a liquid.

Figure 2 displays the computed radial distribution functions, $g(r^*)$, *vs.* $r^*=r/\sigma_0$ at $\rho^*=0.80$ for varying h, including the result of Alder and Hecht on rigid spheres.[16] It is seen that the curve for $h=200$ agrees closely with that for the rigid spheres. As the softness

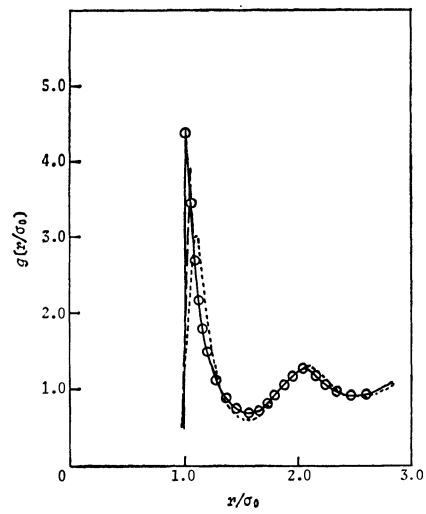

Fig. 2. Radial distribution functions at $\rho^*=0.80$ and $T^*\simeq 0.6$.
——: $h=200$, – – –: $h=10$, ·····: $h=1$, ○: rigid spheres for $V/V_0=1.7$ given by Alder and Hecht.[16] Refer to Fig. 1-(b) for the potentials.

of the repulsive core increases, the first peak of the distribution function is less sharp.[12,17] The $g(r^*)$ for $h=1$ can be compared with the distribution function of liquid Ar.[18] These results show the effectiveness of the present potential function.

Velocity Autocorrelation Function

The normalized velocity autocorrelation function at time t has been calculated as

$$\Psi(t) = \frac{\langle \boldsymbol{v}(0)\cdot\boldsymbol{v}(t)\rangle}{\langle \boldsymbol{v}^2\rangle} = \frac{\langle \frac{1}{N}\sum_i^N \boldsymbol{v}_i(t_0)\cdot\boldsymbol{v}_i(t_0+t)\rangle_{t_0}}{\langle \frac{1}{N}\sum_i^N \boldsymbol{v}_i(t_0)\cdot\boldsymbol{v}_i(t_0)\rangle_{t_0}}, \tag{6}$$

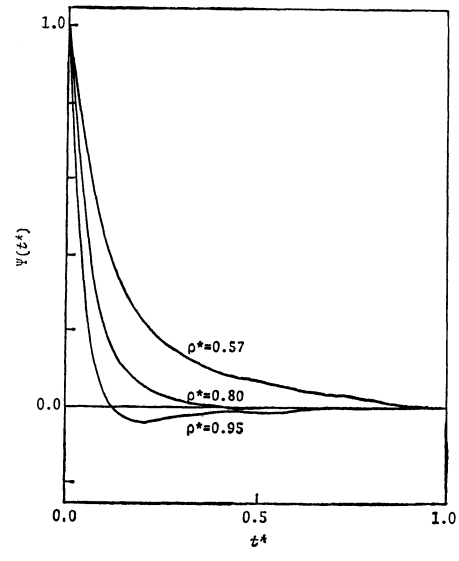

Fig. 3. Velocity autocorrelation functions for $h=200$ at $T^*\simeq 1.0$.

where $v_i(t)$ is the linear velocity of a molecule i at t, and the angular brackets $< >_{t_0}$ imply a mean value over time origins.

For a short time behavior of $\Psi(t)$, we have made a comparison of molecular dynamics computations with the values given by the Brownian and Gaussian approximations (see Appendix I).

Figure 3 shows the normalized velocity autocorrelation functions, $\Psi(t^*)$, computed by means of Eq. 6 for various values of ρ^* for $h=200$ and $T^*=1$, where t^* is the reduced time given by $t^*=t/(m\sigma_0^2/\varepsilon)^{1/2}$. The statistical error on the normalized velocity autocorrelation function is due mainly to the replacement of an equilibrium ensemble average by a time average over a finite time interval. In the present case, the error is estimated to be $\pm 0.015|\Psi(t)-1|$ by means of Zwanzig and Ailawadi's formula.[19]

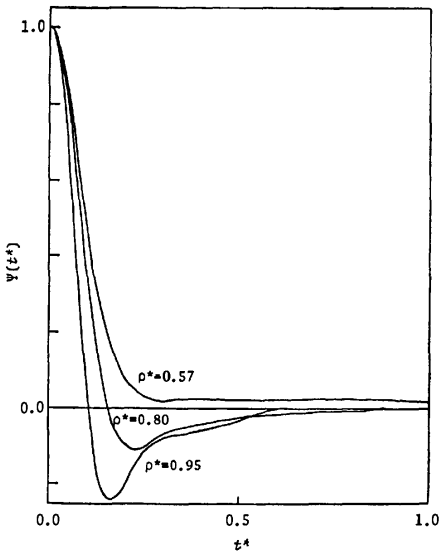

Fig. 4. Velocity autocorrelation functions for $h=1$ at $T^*\simeq 0.6$.

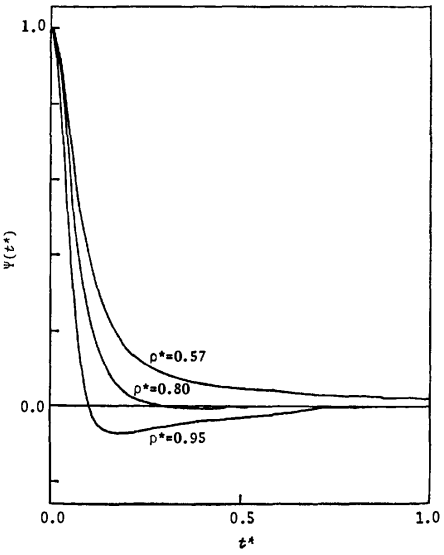

Fig. 5. Velocity autocorrelation functions for $h=10$ at $T^*\simeq 0.6$.

At low density $\Psi(t^*)$ decays steadily. When the density is higher, $\Psi(t^*)$ has a pronounced minimum attributed to the "back-scattering" of the diffusing molecule due to its collisions with surrounding molecules,[1,10] followed by a negative plateau. The level of the negative region rises up with decreasing density, becoming eventually positive at a low density. The qualitative behavior of $\Psi(t^*)$ is consistent not only with Alder and Wainwright's[4] computer results on rigid spheres but also with Levesque and Verlet's[2] results on the Lennard-Jones fluid.

We now examine the effect of the steepness of the repulsive core potential on the velocity autocorrelation function. Figures 4—9 present $\Psi(t^*)$ computed at the same reduced temperature ($T^*=0.6$) and different densities, for $h=0.1$, 0.5, 1, 10, and 200. The results

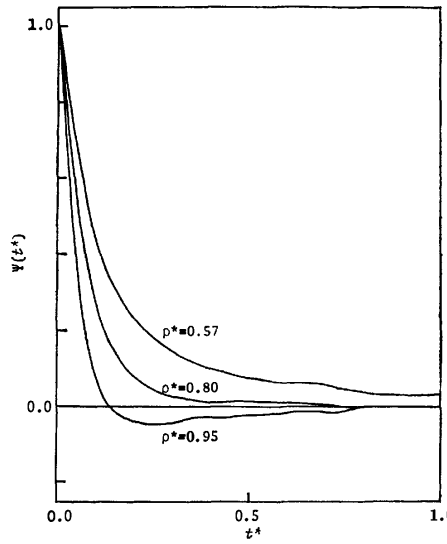

Fig. 6. Velocity autocorrelation functions for $h=200$ at $T^*\simeq 0.6$.

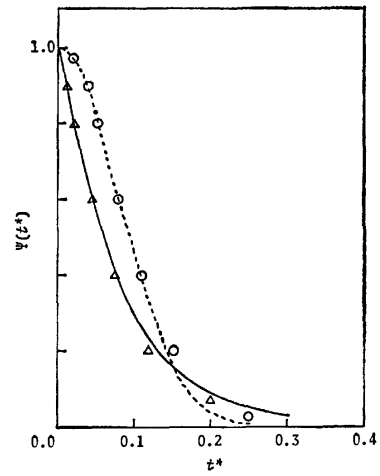

Fig. 7. Comparison of the velocity autocorrelation functions computed by molecular dynamics at $\rho^*=0.80$ and $T^*\simeq 0.6$ with those predicted by Brownian and Gaussian approximations.
△: $h=200$ by MD, ——: $h=200$ by Brownian approx. (Eq. AI-1), ○: $h=1$ by MD, ·····: $h=1$ by Gaussian approx. (Eq. AI-4). Refer to Fig. 1-(b) for the potentials.

are summarized as in the following (1)—(4).

(1) At short times, $\Psi(t^*)$ for large values of h has an appearence of the exponential or nearly exponential decay (Fig. 6). When h becomes smaller, the initial behavior of $\Psi(t^*)$ shows an extended Gaussian appearence (Fig. 4). The extent of the Gaussian decay at a soft core system can be understood intuitively as the effect of the duration of a collision. This is more clearly seen in Fig. 7. The figure displays the $\Psi(t^*)$ computed for the soft core ($h=1$), together with the curve predicted by the Gaussian approximation (Eq. AI-4), and also that for the hard core ($h=200$) with the curve obtained from the Brownian approximation (Eq. AI-1). The agreement between the computed and predicted values is very good.[20] It is confirmed that the initial decay of $\Psi(t^*)$ for $h=200$ is still Gaussian at extremely short times. The initial purely-Gaussian decay is attributed to a quasi-Brownian motion of the pair of molecules in the relatively weak, but rapidly fluctuating, field of all the neighboring molecules, in which the momentum transfer is understood to be small.[21]

(2) At intermediate times, $\Psi(t^*)$ at high density has a negative region with a long plateau. As seen in Figs. 4—6, the soft core potential has an effect enhancing the negative correlations. $\Psi(t^*)$ for large h shows the overdamped behavior and no oscillatory features. The oscillatory aspect of the self motion associated with the soft core is very weak in the Lennard-Jones case (Fig. 4). However, as Fig. 8 shows, $\Psi(t^*)$ of $h=0.1$ apparently shows the oscillatory behavior similar to that found in molecular dynamics experiments on liquid metals[12] and also has no longer an appreciably long plateau. The long plateau is not a consequence of an attractive potential tail but an essential feature for rigid sphere systems; it is generally believed to arise from repeated collisions between the two molecules due to the cage effect of its neighbors.[22]

(3) As seen in Fig. 9, when h increases at the same

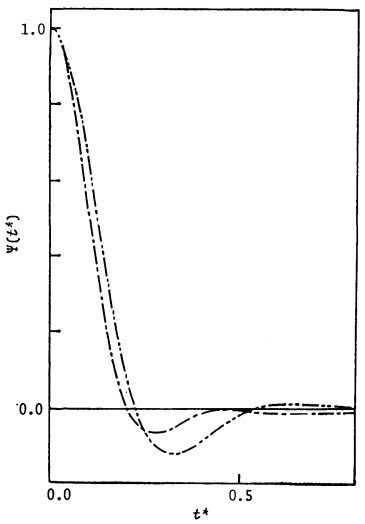

Fig. 8. Velocity autocorrelation functions for $h<1$ at $\rho^*=0.70$ and $T^*\simeq 0.6$.
——: $h=0.5$, – – –: $h=0.1$. Refer to Fig. 1-(b) for the potentials.

reduced density, the behavior of $\Psi(t^*)$ approaches that of $\Psi(t^*)$ for rigid spheres. The area under $\Psi(t^*)$ increases at small times with increasing softness of the core, but at intermediate times we observe an opposite trend on $\Psi(t^*)$ throughout three cases (a) ($\rho^*=0.57$), (b) ($\rho^*=0.85$), and (c) ($\rho^*=0.95$). In this respect, the three groups of curves given in Figs. 9(a), (b), and (c) may be said to have a similar trend of change with the increase of h over all the range of t^*. The decrease of $\Psi(t^*)$ at intermediate times is largely compensated for by its increase at small times. This is the reason why the self-diffusion coefficient, which is given by the integral of $\Psi(t)$, is rather insensitive to the shape of intermolecular potentials (Table 1). Figure 10 shows $\Psi(t^*)$ for varying h at $T^*=1.0$. The trend of change

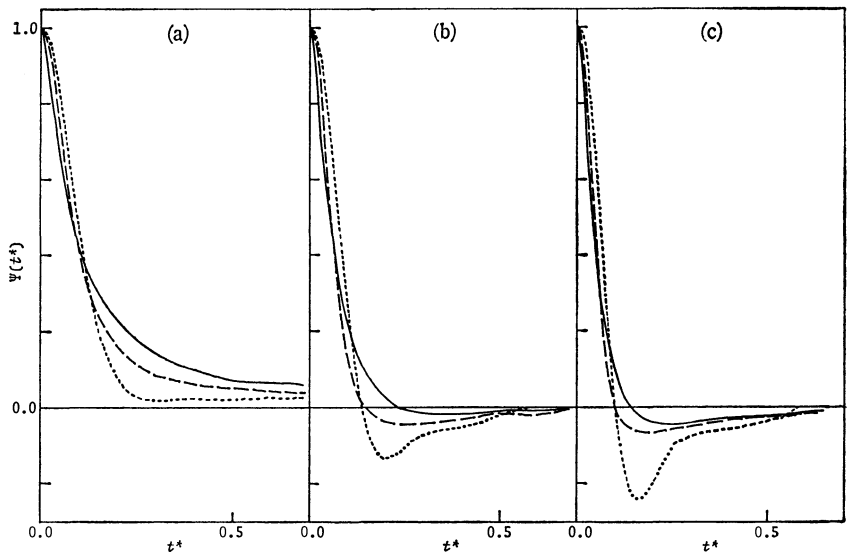

Fig. 9. Velocity autocorrelation functions for potential functions presented in Fig. 1-(b) at $T^*\simeq 0.6$.
(a): For $\rho^*=0.57$, (b): for $\rho^*=0.85$, (c): for $\rho^*=0.95$. ——: $h=200$, – – –: $h=10$, ……: $h=1$.

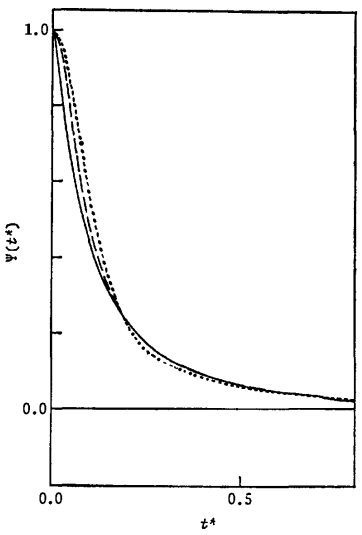

Fig. 10. Velocity autocorrelation functions at $\rho^*=0.57$ and $T^*=1.0$.
——: $h=200$, - - - -: $h=10$, ·····: $h=1$.

with the increasing h is found to be essentially similar to that at $T^*=0.6$, though its magnitude is small.

The fundamental behavior of velocity autocorrelation functions for continuous potential fluids may be explained by the extreme one of rigid spheres with an appropreate diameter at the same volume. The existence of such an extreme offer the basis of a perturbation approach in the transport theory. In Fig. 9 we have used simply σ_0 as a diameter of rigid spheres as a reference. A useful way to determine the rigid core diameter will be the one due to Dymond and Alder.[10]

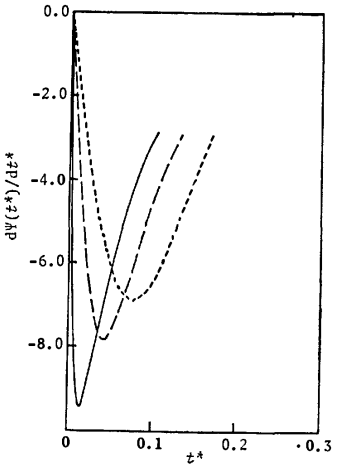

Fig. 11. First derivatives of the velocity autocorrelation functions at $\rho^*=0.57$ and $T^*\simeq 0.6$.
——: $h=200$, - - -: $h=10$, ·····: $h=1$. Refer to Fig. 1-(b) for the potentials.

(4) We present the first derivative $d\Psi(t^*)/dt^*$ in the region of initially fast decay for varying h in Fig. 11. The first minimum point of $d\Psi(t^*)/dt^*$ *vs.* t^* curves, or the first inflexion point of $\Psi(t^*)$ *vs.* t^* curves, gives the time at which the force autocorrelation function first passes through zero. As Fig. 11 shows, that is strongly dependent on the steepness of the core potential, going to zero as a rigid core limit as h becomes large.[23] The decay time of $\Psi(t^*)$ appears to be relatively insensitive to the steepness of the repulsive core potential in spite of the strong dependence of the force autocorrelation. This implies that the motion of a molecule in the systems considered is far from harmonic oscillations.

Here, we would mention the following point. The extreme of $h=\infty$ in the present potential may be closer to a square-well potential for the presence of an attractive part rather than to rigid spheres (see Fig. 1). The velocity autocorrelation functions for square-well potential fluids have been calculated by Michels and Trappeniers.[24] Unfortuately, their molecular dynamics calculations were made at too low densities to confirm the velocity autocorrelation at liquid densities. Einwohner and Alder[25] computed the free-path distributions and collision rates in square-well potential fluids as well as those in rigid sphere fluids, and made the comparison between the two cases. They found that at liquid density the majority of collisions were hard core collisions and the free-path distribution was nearly indifferent to the presence of an attractive potential. For the extreme of $h=\infty$ in the present potential, the velocity autocorrelation function is supposed to be approximately equal to the one for rigid spheres, except for low densities.

Self-diffusion Coefficient

Procedure of Calculations. The self-diffusion coefficient D is calculated either from the velocity autocorrelation function,

$$D=\frac{kT}{m}\int_0^\infty \Psi(t)\mathrm{d}t, \tag{7}$$

or from the long time limit of the mean-square displacement of a selected molecule i,

$$D=\lim_{t\to 0}\left[\frac{1}{6t}<[r_i(0)-r_i(t)]^2>\right]. \tag{8}$$

The evaluation of integral in Eq. 7 was carried out over the range of t, 0—2000 time steps. In the application of Eq. 8, we used the slope of the linear part of the curve for the mean-square displacement at 2000 time steps. The error of both results are considered to be of the order of 10%, and then, both results may be safely said to agree to each other within the range of errors. The diffusion coefficient for liquid Ar (at 94 °K and 1.374 g cm^{-3}) was calculated to be 2.44×10^{-5} cm^2 s^{-1} in agreement with Rahman's result.[1]

The self-diffusion coefficients, D_{MD}, calculated from the velocity autocorrelation function are listed in Table 1, where we have used as the reduced quantity

$$D^*=D/(\sigma_0^2\varepsilon/m)^{1/2}. \tag{9}$$

We can not make a direct comparison of the values for $h=1$ with the results of Levesque and Verlet[2] on the Lennard-Jones fluid. It is possible to compare those by the use of $(\sigma^2\varepsilon/m)^{1/2}(kT/\varepsilon)^{5/12}$ as a unit of D and $\rho'=(\rho\sigma^3/\sqrt{2})(\varepsilon/kT)^{1/4}$ as the reduced density.[26] Both results are confirmed to be quite similar each other

Table 1. Self-diffusion coefficients

ρ^*	h	T^*	D_{MD}^*
0.42	1	0.61	0.084
0.51	10	0.61	0.094
0.57	1	0.60	0.072
0.57	10	0.61	0.085
0.57	200	0.60	0.101
0.57	200	0.99	0.143
0.57	200	4.01	0.430
0.59	1	0.61	0.067
0.70	1	0.59	0.055
0.72	10	0.61	0.067
0.80	1	0.61	0.029
0.80	10	0.59	0.041
0.80	50	0.60	0.042
0.80	100	0.60	0.049
0.80	200	0.59	0.050
0.80	200	0.99	0.061
0.80	200	3.94	0.148
0.86	10	0.60	0.022
0.95	1	0.61	0.006
0.95	10	0.60	0.011
0.95	200	0.59	0.016
0.95	200	1.02	0.022
0.95	200	3.97	0.064

except for those at the low density ($\rho'<0.55$), showing that the scaling variables for the inverse 12-th power potential may be useful for the Lennard-Jones fluids.

Density Dependence of Self-Diffusion Coefficient. Figure 12 illustrates the density dependence of the self-diffusion coefficients at $T^*=0.6$ for a variety of the steepness of core potentials. The curves are found to shift along an arrow in the figure, when the hardness of the repulsive core increases.

We now attempt here an interpretation of this result by means of a rigid sphere model. The self-diffusion coefficient for rigid sphere gas of packing fraction

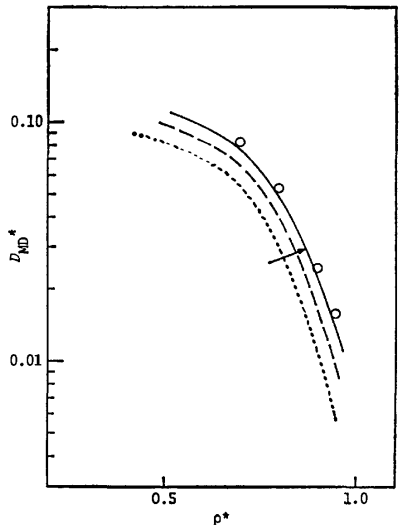

Fig. 12. Density dependence of self-diffusion coefficients at $T^*\simeq 0.6$.
——: $h=200$, — — : $h=10$, ·····: $h=1$, ○: D_∞^* calculated by means of Eq. 11.

$\xi(=(\pi/6)\rho d^3)$, where d is the diameter of spherical molecules, is given by the Enskog theory as

$$D_E=\frac{3}{8}\frac{1}{\rho d^2}\left(\frac{kT}{\pi m}\right)^{1/2}\Big/\left[\frac{3}{2\pi\rho d^3}(\chi(\xi)-1)\right], \qquad (10)$$

in which $\chi(\xi)$ $(=pV/NkT)$ is the compressibility factor of a rigid sphere system. We consider the extreme of $h=\infty$ in the present potential *i.e.* the nearly rigid sphere potential with an attractive potential well. Let us assume that the self-diffusion coefficient for the system is given by the Enskog's value corrected by the Alder-Wainwright factor as the ratio $(D_{MD}^H/D_E)_A$,[3,4] where D_{MD}^H is the molecular dynamics values of diffusion coefficients for rigid spheres. It is written as[2]

$$D_\infty^*=\frac{(\sqrt{\pi}/4)\sqrt{T^*}}{\chi(\xi)-1}\left(\frac{D_{MD}^H}{D_E}\right)_A, \qquad (11)$$

where D_∞^* is expressed as the reduced coefficient given by Eq. 9. $\chi(\xi)$ is given by the formula $\chi(\xi)=(1+\xi+\xi^2)/(1-\xi)^3$. D_∞^* calculated at $T^*=0.6$ are plotted against ρ^* in Fig. 12. We can see that the D_{MD}^* *vs.* ρ^* curve for $h=200$ nearly agrees with the D_∞^* *vs.* ρ^* one. That is, when the hardness of the core increases, the D_{MD}^* *vs.* ρ^* curve at a given temperature, shifting along the arrow in Fig. 12, approaches the extreme curve of rigid spheres at the same temperature. This confirms that the rigid sphere model expressed as Eq. 11 gives a good description of self-diffusion coefficients for realistic continuous potential systems. An appropriate evaluation of the equivalent rigid sphere diameter for the Lennard-Jones fluid was given by Verlet,[18] who took for it the value to fit the equilibrium structure factor to the Wertheim-Thiele solution of the PY equation for rigid spheres. Using the core diameter thus determined, Levesque *et al.*[2] calculated diffusion coefficients for Lennard-Jones fluids, which were found to be about 10% larger than those by molecular dynamics computations. According to Verlet,[18] at low temperatures, the equivalent diameter is larger than the original core size σ in the Lennard-Jones potential. The direction of the arrow in Fig. 12 is consistent with the result of Verlet.

In addition to the interpretation described above, it can also be said from Fig. 12 that the duration of collisions between molecules, associated with the finite steepness of the repulsive potential, brings an important perturbation on the dynamical behavior of molecules mainly determined by the rigid sphere potential.

Comparison with the Rice-Allnatt Theory. The basic assumption underlying the transport theory of Rice and Allnatt[21] is that the motion of a molecule in a fluid consists of a strongly repulsive binary encounter followed by a quasi-Brownian motion of the molecules in the fluctuating field of neighboring molecules. The successive repulsive encounters are assumed to occur independently. This assumption is in direct opposition to the van der Waals picture of transport processes discussed by Dymond and Alder and others,[10] in which the dynamical event consists of correlated collisions of rigid spheres. The real situation lies between these two extremes, probably.

We attempt here to test the Rice-Allnatt theory through the examination of self-diffusion coefficients

calculated for various degrees of the steepness of the repulsive potential.[27] In the theory,

$$V(r) = V^{H}(r) + V^{S}(r)$$
$$\begin{cases} V^{H}(r) = \infty, \quad V^{S}(r) = 0 & r \leq a \\ V^{H}(r) = 0 & r > a, \end{cases} \tag{12}$$

where V^S is the soft potential. The forces on the molecules in a liquid are working on two time scales: one corresponds to the large momentum and energy transfers which occur during rigid sphere collisions, and the other to the frequent small momentum transfers which occur during the quasi-Brownian motion of a molecule in the soft force field. Then, the friction coefficient is expressed as $\zeta=\zeta^H+\zeta^S$, and the self-diffusion coefficient is

$$D_{RA} = \frac{kT}{\zeta^H+\zeta^S}, \tag{13}$$

where the friction coefficients become

$$\zeta^H = \frac{8}{3}(\pi m k T)^{1/2}\rho a^2 g(a), \tag{14}$$

and

$$\zeta^S = -\frac{16\pi^4}{3}\rho\left(\frac{\pi m}{kT}\right)^{1/2}\int_0^\infty dq\, q^3 V_q^S G_q. \tag{15}$$

The Fourier transforms V_q^s and G_q are given by

$$V_q^S = \frac{1}{8\pi^3}\int d\boldsymbol{r}\, e^{-i\boldsymbol{q}\cdot\boldsymbol{r}} V^S(r), \tag{16}$$

and

$$G_q = \frac{1}{8\pi^3}\int d\boldsymbol{r}\, e^{-i\boldsymbol{q}\cdot\boldsymbol{r}}(g(r) - 1), \tag{17}$$

respectively. The rigid core contribution, Eq. 14, is the Enskog expression. The evaluation of ζ^S, Eq. 15, is identical with the friction coefficient given by Helfand by applying the linear trajectory approximation.[29] For the application of the Rice-Allnatt theory to the present system, there is obviously some arbitrariness in choosing the core diameter a in Eq. 12. In this work, the distance where the potential crosses abscissa has been taken as the diameter. Equation 1 is rewritten as follows,

$$V^H(x) = \infty, \quad V^S(x) = 0 \qquad x \leq x_0$$
$$V^H(x) = 0, \quad V^S(x) = u(\sigma x) \quad x > x_0, \tag{18}$$

where $x=r/\sigma$ and $x_0=\sigma_0/\sigma$.

It is difficult to calculate ζ^S using Eq. 15 because of the presence of the factor q^3 and the oscillating behavior due to G_q in the integrand. However, for the present potential (Eq. 18) we can invert Eq. 15 according to the procedure used by Helfand. The details of the inversion are described in Appendix II. If we use the dimensionless coefficient $\zeta_r^S=\zeta^S/\zeta^*$ where $\zeta^*=(8/3)\rho x_0^2(\pi m k T)^{1/2}$, ζ_r^S is given by

$$\zeta_r^S = \left(\frac{\varepsilon}{kT}\right)\int_{x_*}^\infty dx f(x)\,(g(\sigma x) - 1) - \left(\frac{\varepsilon}{kT}\right)\int_0^{x_*} dx f(x), \tag{19}$$

and

$$f(x) = (1-h)\left[\frac{11}{2^{11/6}}f_{12}\left(\frac{x}{2^{1/6}}\right) - \frac{5}{2^{5/6}}f_6\left(\frac{x}{2^{1/6}}\right)\right] + h\left[\frac{11}{x_0^{11}}f_{12}\left(\frac{x}{x_0}\right) - \frac{5}{x_0^5}f_6\left(\frac{x}{x_0}\right)\right], \tag{20}$$

where

$$f_n(x) = 2\sum_{j=1}^{n/2}\frac{x^{2j-1}}{2j-1} - x^{1-n}\ln\left|\frac{x+1}{x-1}\right|. \tag{21}$$

Table 2. Friction and self-diffusion coefficients given by the Rice-Allnatt theory at $T^*\simeq 0.6$

	ρ^*	ζ_r^H	ζ_r^S	$\zeta_{RA,r}$	D_{RA}^*	$\zeta_{MD,r}$
$h=1$	0.57	0.85	4.48	5.33	0.054	4.03
	0.59	0.94	4.38	5.32	0.052	4.16
	0.70	0.69	3.86	4.55	0.051	4.21
	0.80	0.89	3.84	4.73	0.031	5.02
	0.95	1.51	3.97	5.48	0.032	29.56
$h=10$	0.57	0.90	7.17	8.09	0.050	4.74
	0.72	0.72	6.53	7.25	0.032	3.40
	0.80	0.85	7.16	8.01	0.025	8.01
	0.86	0.90	7.32	8.22	0.024	8.82
	0.95	1.24	8.15	9.39	0.018	15.50
$h=200$	0.57	0.81	22.60	23.41	0.013	2.86
	0.80	0.80	22.43	23.23	0.009	4.04
	0.95	1.17	27.11	28.28	0.009	15.21

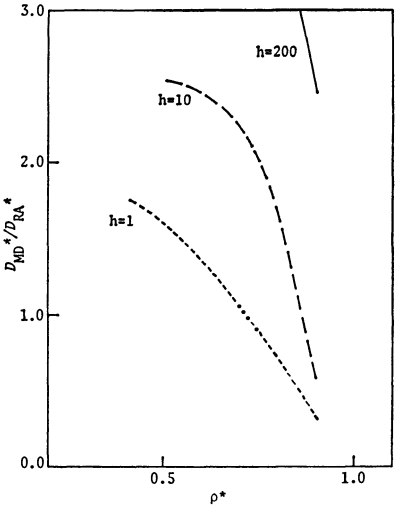

Fig. 13. Ratio of the values of self-diffusion coefficients at $T^*\simeq 0.6$ calculated by molecular dynamics to those predicted by the Rice-Allnatt thery.

$\zeta_r^H(=\zeta^H/\zeta^*)$, ζ_r^S, and D_{RA}^* are calculated by means of Eqs. 14, 19, and 13, respectively, using the radial distribution functions calculated by the molecular dynamics runs for the potential Eq. 1.[30] The results are given in Table 2, together with the molecular dynamics computations, $\zeta_{MD,r}^*(=(kT/D_{MD})/\zeta^*)$.

Figure 13 shows the D_{MD}^*/D_{RA}^* *vs.* ρ^* curves, for $h=1$, 10, and 200. As seen in Table 2 and Fig. 13, a good agreement between the predicted and computed values is obtained only for the Lennard-Jones potential ($h=1$) at a moderate density and also for the more rigid potential ($h=10$) at a high density. Too small values of D_{RA}^* for large h are evidently attributed to the overestimation of ζ_r^S about the contributions of the repulsive part, including the improperly strong repulsive contribution. The prediction of the Rice-Allnatt theory using the linear trajectory procedure is found to depend too sensitively upon how to separate the intermolecular potential. We have taken the diameter of rigid core to be equal to σ_0.

It is found from Fig. 13 that the ratio D_{MD}^*/D_{RA}^* for $h=1$ is smaller than 1 at high densities, and at low

densities we have an opposite result. This density dependence of the ratio D_{MD}^*/D_{RA}^* is supposed to be partly associated with that of the Alder-Wainwright ratio $(D_{MD}^H/D_E)_A$ for rigid spheres.

Concluding Remarks

By means of molecular dynamics calculations, we have examined the transport properties of a fluid composed of molecules interacting through the potential expressed in terms of three parameters: the depth of potential well ε, core size σ_0, and hardness parameter h. The results are summarized as follows.

(a) The essential feature of the behavior of velocity autocorrelation functions for continuous potential fluids can be explained by the extreme of rigid spheres with an appropriate diameter at the same volume. This implies that the rigid-sphere fluid can serve as a reference system suitable for the representation of dynamical properties of liquids.

(b) The detailed behavior of velocity autocorrelation functions is sensibly dependent upon the steepness of the repulsive core potential. The oscillatory behavior superimposed on the extreme behavior of rigid spheres becomes more pronounced as the softness of the core increases. Then, the decrease of the area under $\Psi(t)$ at intermediate times is largely compensated for by its increase at small times. This is the reason why the self-diffusion coefficient is rather insensitive to the shape of intermolecular potentials.

(c) The density dependence curve of self-diffusion coefficients in a continuous potential fluid shifts and approaches to that of rigid spheres at the same temperature with the increasing hardness of the core.

These results appear to offer a sound basis for the equivalent hard sphere model as well as for the applicability of the perturbation approach to the transport theory. The idea of separating the intermolecular potential into a rigid core part and a soft one, treating the latter as a perturbation, is considered to be essentially applicable to the transport theory of liquids. This is the basic physical assumption underlying the generalized van der Waals theory[10,31] and the dynamical model of liquids due to Rice and Allnatt. The results calculated by the use of the Rice-Allnatt model are also found to be strongly dependent of the arbitrariness in splitting the potential into two parts. At high densities and low temperatures, the correlated successive rigid core collisions of a pair of molecules is considered to have more important effects on the self-diffusion coefficients.

Appendix I

A Langevin type of velocity autocorrelation function arising from a Markovian velocity evolution is expressed as

$$\Psi(t) = \exp\left(-\frac{kT}{mD}t\right), \tag{AI-1}$$

where D is a self-diffusion coefficient. Equation AI-1 is expected to give a good description to $\Psi(t)$ for a hard core potential (large h) at a moderate density. It is evident that $\Psi(t)$ for a soft core potential (small h) is far from the simple exponential behavior. If the interaction potential is a smooth function where there is no rigid core, then $\Psi(t)$ can be assumed to be analytical in the neighborhood of $t=0$ and expanded in a Taylor series

$$\Psi(t) = 1 - \frac{\omega_e^2}{2!}t^2 + O(t^4), \tag{AI-2}$$

where the square of the Einstein frequency, ω_e^2, is given in terms of the average of the Laplacian of the total potential energy U:

$$\omega_e^2 = \frac{\langle \dot{v}^2 \rangle}{\langle v^2 \rangle} = \frac{1}{3m}\langle \nabla^2 U \rangle. \tag{AI-3}$$

Then, the Gaussian decay of $\Psi(t)$ is given by

$$\Psi(t) \simeq \exp\left[-\frac{\langle \nabla^2 U \rangle}{6m}t^2\right]. \tag{AI-4}$$

Since the potential function, Eq. 1, is continuous, the slope of $\Psi(t)$ at $t=0$ is zero and the decay at a small time should be Gaussian even for large values of h. For a completely rigid core, however, collisions are instantaneous and this results in a cusp of $\Psi(t)$ at $t=0$.

Appendix II

The inversion of the transforms in Eq. 15 can be made according to the same procedure as used by Helfand.[29] Equation 16 is integrated by parts to give

$$V_q^S = \frac{1}{2\pi^2}\int_0^\infty dq \frac{\cos(qr)}{q^2}\frac{d}{dr}[rV^S(r)]. \tag{AII-1}$$

Substitution of Eq. AII-1 into Eq. 15 gives

$$\zeta_r^S = -\frac{1}{4\sigma^2}\frac{1}{kT}\int_0^\infty dq\int_0^\infty dr\int_0^\infty dr'r'[\sin q(r'+r) + \sin q(r'-r)] \times [g(r') - 1]\frac{d}{dr}[rV^S(r)], \tag{AII-2}$$

Using the relation $\int_0^\infty \sin(qr)dq = p/r$, where p stands for the principal part, and introducting the change of variables $y = r/r'$ and $x = r'/\sigma$, we obtain from the integration over q of Eq. AII-2

$$\zeta_r^S = -\frac{1}{4}\frac{1}{kT}\int_0^\infty dx\int_{x_0/x}^\infty dy\left(\frac{p}{1+y}+\frac{p}{1-y}\right)x\frac{d}{dy}[yV^S(\sigma xy)][g(\sigma x) - 1]. \tag{AII-3}$$

For the potential function given by Eq. 18, Eq. AII-3 can be integrated over y explicitly to lead

$$\zeta_r^S = \left(\frac{\varepsilon}{kT}\right)\int_0^\infty dx f(x)[g(\sigma x) - 1], \tag{AII-4}$$

where $f(x)$ is given by Eq. 20. When $h=1$ and hence $x_0=1$, Eq. AII-4 is reduced to the expression of Helfand. Since $g(\sigma x)$ vanishes in the region $0<x<x_0$, Eq. AII-4 is rewritten as Eq. 19.

We acknowledge generous grants of computing time from Hokkaido University Computing Center.

References

1) A. Rhaman, *Phys. Rev.A*, **136**, 405 (1964).
2) D. Levesque and L. Verlet, *Phys. Rev. A*, **2**, 2514 (1970); D. Levesque, L. Verlet, and J. Kurkijarvi, *Phys. Rev. A*, **7**, 1690 (1973).
3) B. J. Alder and T. E. Wainwright, *Phys. Rev. Lett.*, **18**, 988 (1967); *Phys. Rev. A*, **1**, 18 (1970).

4) B. J. Alder, D. M. Gass, and T. E. Wainwright, *J. Chem. Phys.*, **53**, 3813 (1970).
5) J. P. Hansen and I. R. McDonald, "Theory of Simple Liquids," Academic Press, London (1976).
6) P. Schofield, "Statistical Mechanics," ed by K. Singer, Chem. Soc., London (1975), Vol. II.
7) S. Yip, *Ann. Phys. Chem.*, **30**, 547 (1979).
8) J. A. Barker and D. Henderson, *Rev. Mod. Phys.*, **48**, 587 (1976).
9) K. Arakawa, "Kagaku Sosetsu, No. 11, Ions and Solvents," (1976), p. 13.
10) J. H. Dymond and B. J. Alder, *J. Chem. Phys.*, **45**, 2061 (1966).
11) S. H. Chen and A. Rahman, *Mol. Phys.*, **34**, 1247, (1977); S. W. Haan, R. D. Mountain, C. S. Hsu, and A. Rahman *Phys. Rev. A*, **22**, 767 (1980).
12) D. Schiff, *Phys. Rev.*, **186**, 151 (1969).
13) In usual molecular dynamics studies of simple liquids, calculations have been made for the range of temperatures above the triple point of Ar, $T^*=0.70$. For the liquids composed of molecules with a comparatively strong interaction, if (ε/k) is assumed to be 500 K for example,[14] we have $T^*=0.6$ when $T=300$ K. In this paper, computations for $T^*=0.6$ are reported, and also some results for $T^*=1.0$ and 4.0 are given in Fig. 3, Fig. 10, and Table 1.
14) J. O. Hirschfelder, C. F. Curtiss, and R. B. Bird, "Molecular Theory of Gases and Liquids," Wiley, New York (1954).
15) L. Verlet, *Phys. Rev.*, **159**, 98 (1967).
16) B. J. Alder and C. E. Hecht, *J. Chem. Phys.*, **50**, 2032 (1969).
17) Y. Hiwatari, H. Matsuda, T. Ogawa, N. Ogita, and A. Ueda, *Prog. Theor. Phys.*, **52**, 1105 (1974).
18) L. Verlet, *Phys. Rev.*, **165**, 201 (1968).
19) R. Zwanzig and N. K. Ailawadi, *Phys. Rev.*, **182**, 280 (1969).
20) At lower densities, the agreement between the computed and predicted values is not good. This discrepancy is supposed to come from the effect of the attractive part of the potential, enhancing the correlation of the nearest neighbors at low densities.
21) S. A. Rice and P. Gray, "The statistical Mechanics of Simple Liquids," Wiley, New York (1965).
22) P. Schofield, "Molecular Motions in Liquids," ed by J. Lascombe, D. Reidel Publishing Co., Dordrecht, Holland (1974).
23) The binary collision time in force autocorrelation functions was discussed by Schofield *et al.* See Ref. 22.
24) J. P. J. Michels and N. J. Trappeniers, *Chem. Phys. Lett.*, **33**, 195 (1975).
25) T. Einwohner and B. J. Alder, *J. Chem. Phys.*, **49**, 1458 (1968).
26) W. T. Ashurst and W. G. Hoover, *Phys. Rev. A*, **11**, 658 (1975).
27) The effective potential theory due to Davis[28] incorporates the desirable features of the Rice-Allnatt theory, and is believed to be free from its several deficiencies. The contribution $\zeta^{H}_{(3)}$ in the Davis expression is very small (of the order of 1—0.1% for the present case), however, so that the Davis theory gives essentially the same numerical results as the Rice-Allnatt theory.
28) H. T. Davis, *Adv. Chem. Phys.*, **24**, 257 (1973).
29) E. Helfand, *Phys. Fluids*, **4**, 681 (1961).
30) Another choice of $g(r)$ is to use the molecular dynamics values for the modified potential, Eq. 18. From this calculation the contact value of $g(r)$ is somewhat larger than that for the unmodified potential.
31) H. C. Longuet-Higgins and B. Widom, *Mol. Phys.*, **8**, 549 (1964).

Effects of Salts on the Solubility of Elemental Mercury in Water

Isao SANEMASA,* Kenji HARAGUCHI, and Hideo NAGAI

Department of Chemistry, Faculty of Science, Kumamoto University, Kurokami 2-39-1, Kumamoto 860

(Received September 22, 1979)

The effects of 11 salts, NaCl, $NaNO_3$, Na_2SO_4, NaBr, NaSCN, NaF, $NaClO_4$, KCl, $BaCl_2$, $(CH_3)_4NBr$, and $(C_2H_5)_4NBr$, on the solubility of elemental mercury in water have been studied at 25 °C. Salting coefficients were determined and compared with those predicted by both the McDevit-Long equation and the scaled particle theory (SPT). The McDevit-Long equation gave reasonably good predictions except for NaBr, $NaClO_4$, and NaSCN. SPT is also applicable to prediction of the salt effect when the energy parameter of mercury determined from the Henry law constant of aqueous solubility of mercury vapor is employed. Attempts to predict the effects of tetraalkylammonium salts by SPT failed.

Attention is being paid to the influence of salts on the activity coefficients of nonelectrolytes in aqueous solutions from both experimental and theoretical interest and many reports have appeared.[1] However, few are concerned with elemental mercury as a nonelectrolyte except for the report by Glew and Hames, who restricted their study to conditions of 6.10 molal sodium chloride solution.[2]

It has been pointed out that there is an essential difference between the solution properties for inert gases and nonpolar molecules in water and in organic solvents. A similar anomaly of elemental mercury in water solvent was suggested by Spencer and Voigt.[3] They attributed this to the tendency of water molecules to form a structure around mercury atoms. The study of salt effects on the solubility of elemental mercury will help clarify the role of water.

The solubility of a nonelectrolyte in aqueous electrolyte solutions has been found to depend on the concentration and type of the salt present in the solution. In a sufficiently dilute nonelectrolyte solution, the activity coefficient of nonelectrolyte, f, in the salt solution of molar concentration, C, is given by

$$\log f = \log(S^\circ/S) = k_s C, \quad (1)$$

where S and S° denote the solubility of nonelectrolyte in salt and salt-free solutions, respectively, k_S being the salting coefficient.

In the present work, 11 salts showing no chemical reaction with elemental mercury were used. We have compared the values of observed k_S with those predicted from theoretical equations such as the McDevit-Long equation[4] and the scaled particle theory (SPT),[5] which have been accepted to give reasonably good predictions for inert gases and nonpolar nonelectrolyte.

Experimental

Electrolytes of analytical reagent grade were used except for a tetraethylammonium bromide of reagent grade. The salts were dissolved without further purification in redistilled water after drying at suitable temperatures. The concentrations of chloride, bromide, and thiocyanate salts were checked by the argentometric method. Purification of metallic mercury, the procedure of attaining saturated solubility of mercury vapor and measurements were the same as those described,[6] the solubility apparatus being essentially the same as that previously used except for a slight modification to include two identical 300 cm^3 solubility flasks instead of one flask. Mercury vapor was passed through a three-way stop-cock to each flask, and then combined with another three-way stop-cock attached to the outlet of each flask. One of the flasks was filled with pure water and the other with electrolyte solution. Saturated mercury solutions in both pure water and electrolyte solution can be obtained at the same time. It was confirmed by filling each flask with the same solution that concentrations of the saturated mercury solutions in the two flasks were identical with each other. A time of 30 min was found to be sufficient to attain the solubility equilibrium. The relative solubility of mercury in pure water and in the salt solution, S°/S, was measured directly by reading atomic-absorption peak-heights recorded on a chart for a set of samples withdrawn from the two solubility flasks. The value of S° was taken to be 63.9×10^{-6} g dm^{-3}.[6] Preliminary experiments for some electrolyte solutions revealed that the values of S thus estimated are in reasonably good agreement with those measured by addition of standard mercury (II) solutions. Determination of the S°/S ratios was repeated at least three times for each electrolyte concentration at 25 °C. No data were obtained for iodide; use of I^- ion gave abnormal results probably due to some chemical reaction with elemental mercury.

Results and Discussion

Experimental Salting Coefficients. The solubility ratios, S°/S, of elemental mercury obtained at each electrolyte concentration and salting coefficients, k_S, for 11 salts determined by the least-squares method according to Eq. 1 are given in Table 1, together with correlation coefficients for log (S°/S) *vs.* C plots and intercepts of these plots at $C=0$. We see that the salt effects are well represented by Eq. 1 over the concentration range examined. The value of k_S for 6.10 mol dm^{-3} NaCl, 0.0413 at 25 °C, determined by Glew and Hames[2] and expressed as reciprocal molality, is much lower than the present result. The apparent discrepancy can be attributed to the fact that a negative deviation from Eq. 1 occurs at such a high electrolyte concentration.

Salting Coefficients Calculated by the McDevit-Long Equation. Several theories have been given to explain the salt effects on the solubility of nonelectrolyte such as hydration, electrostatic, van der Waals force, internal pressure and scaled particle. The last two theories give a good prediction of the trend of the observed k_S value. Based on the internal pressure concept, McDevit and Long derived the equation[4]

$$k_s = \bar{V}_l^\circ(V_s - \bar{V}_S^\circ)/2.3\,\beta_o RT, \quad (2)$$

where $\bar{V}_l^\circ$ is the molar volume of the liquid nonelec-

TABLE 1. SOLUBILITY RATIOS AND SALTING COEFFICIENTS OF ELEMENTAL MERCURY IN AQUEOUS SALT SOLUTIONS
(Values in parentheses are those calculated using the energy parameter of elemental mercury, $\varepsilon_1/\kappa=851$ K given in Ref. 13.)

Salt	Concentration C/mol dm^{-3}	Solubility ratio S°/S[a]	log (S°/S) at $C=0$ (γ)[b]	Salting coefficient			
				Observed		Calculated	
				k_s	k_S^*[c]	k_s[d]	k_S^*[e]
NaCl	0.250	1.050					
	0.501	1.105	0.0025	0.0788	0.0872	0.071	0.0789
	0.752	1.154	(0.999)				(0.0187)
	1.00	1.204					
$NaNO_3$	0.250	1.037					
	0.500	1.074	−0.0002	0.0616	0.0652	0.047	0.0732
	0.753	1.106	(0.996)				(0.0088)
	1.00	1.156					
Na_2SO_4	0.125	1.104					
	0.250	1.216	0.0053	0.308	0.319	0.221	0.152
	0.375	1.314	(0.999)				(0.023)
	0.501	1.447					
NaBr	0.253	1.023					
	0.506	1.038	0.0063	0.0173	0.0227	0.060	0.0577
	0.750	1.046	(0.988)				(−0.0166)
	1.01	1.055					
NaSCN	0.266	0.977					
	0.531	0.964	0.0008	−0.0345	−0.0338	0.060	0.0436
	0.797	0.944	(0.987)				(0.0129)
	1.062	0.917					
NaF	0.250	1.102					
	0.500	1.207	0.0029	0.157	0.174	0.110	0.0732
	0.750	1.321	(0.999)				0.0129
$NaClO_4$	0.250	1.093					
	0.500	1.172	0.0098	0.117	0.114	0.035	0.0899
	0.750	1.252	(0.999)				(0.0363)
	1.00	1.338					
KCl	0.250	1.046					
	0.500	1.095	0.0018	0.0703	0.0743	0.055	0.0667
	0.750	0.120	(0.987)				(0.0023)
	1.00	1.188					
$BaCl_2$	0.250	1.080					
	0.500	1.148	0.0039	0.115	0.121	0.170	0.109
	0.750	1.233	(0.999)				(−0.0687)
$(CH_3)_4NBr$	0.250	0.968					
	0.500	0.923	0.0051	−0.0779	−0.112	−0.090	0.579
	0.750	0.886	(0.999)				(0.567)
	1.00	0.845					
$(C_2H_5)_4NBr$	0.250	0.933					
	0.500	0.870	−0.0022	−0.116	−0.176	−0.121	0.753
	0.746	0.812	(0.999)				(0.770)
	0.995	0.766					

a) S° and S denote pure water and salt solution, respectively. b) Correlation coefficient. c) Defined by $k_S^*=k_S+(0.036-\phi_0\times10^{-3})/2.30$, where ϕ_0 is the apparent molal volume of the salt. d) Calculated by the McDevit-Long equation. e) Calculated by the scaled particle theory.

trolyte, V_S the molar volume of pure (liquid) electrolyte, $\bar{V}_S^\circ$ the partial molar volume of the salt at infinite dilution, and β_0 the compressibility of pure water. The factor ($V_S-\bar{V}_S^\circ$) in Eq. 2 indicates electrostriction of the solvent caused by the salt, which is related to modification of the water structure by the salt added. The values of k_S calculated by using Eq. 2 are given in Table 1. The molar volume of liquid mercury 14.8 cm^3 was obtained by dividing atomic weight by density at 25 °C. The value of β_0 was taken to be 45.6×10^{-6} bar^{-1}.[4] All the V_S data were taken from the work of Lundén,[7] and the values for $\bar{V}_S^\circ$, the sum of partial

molar volumes of individual cation and anion, from that of Millero.[8]

The calculated k_s values are in reasonably good agreement with the observed values except for NaBr, NaSCN, and $NaClO_4$. In the McDevit-Long equation, the parameter concerned with nonelectrolyte is only its molar volume, hence the characteristic properties of nonelectrolyte such as nonelectrolyte-solvent and nonelectrolyte-electrolyte interactions are not taken into consideration. This probably causes the discrepancies observed for these three salts. The observed k_s values indicate that the increased interactions of mercury atoms with Br^- or SCN^- ions play an important role for NaBr or NaSCN salt and that the decreased interactions of mercury atoms with surrounding water molecules should be considered for $NaClO_4$ salt.

Salting Coefficients Calculated by the Scaled Particle Theory. In the SPT, which has been successfully applied to predict the solubility of nonelectrolyte in various solvents,[5] two steps are involved: (1) the creation of a cavity in the solvent of a suitable size to accommodate a nonelectrolyte molecule, and (2) the introduction of a nonelectrolyte into the cavity, the nonelectrolyte molecule interacting with the solvent and electrolyte species through repulsive, dispersion, and inductive forces. The SPT allows computations of the free energies involved in (1) and (2). The theory would reflect the characteristic properties of nonelectrolyte in its solubility in electrolyte solution more adequately than the McDevit-Long equation.

On the basis of SPT considerations given by Shoor and Guggins,[9] Masterton and Lee[10] have presented useful equations which enable one to estimate the salting coefficient k_S^*, defined by

$$k_S^* = \lim_{C\to 0} \frac{1}{C} \log \frac{X_0}{X}, \tag{3}$$

where X_0 and X denote the mole fraction solubility of nonelectrolyte in pure water and an electrolyte solution of molarity of C, respectively. The salting coefficient can be written as follows:

$$k_S^* = k_\alpha + k_\beta + k_\gamma, \tag{4}$$

where k_α and k_β are related to steps (1) and (2), respectively, and k_γ refers to the number densities of species present in the solvent. The expressions k_α, k_β, and k_γ are given by Eqs. 32, 19, and 11, respectively, in Ref. 10. These equations are expressed as functions of hard sphere diameter, σ, the energy parameter, ε/κ, polarizability, α, and apparent molal volume of salt at infinite dilution, ϕ_0. Subscripts 1, 2, 3, and 4 refer, respectively, to nonelectrolyte, water, cation, and anion. The hard sphere diameter is taken as twice that of the crystal ionic radius. Values of σ are given in Table 2, references being specified in the footnote. For water molecules, the following parameters are employed: $\sigma_2=0.275$ nm, $\varepsilon_2/\kappa=85.3$ K, and the dipole moment$=6.14\times10^{-30}$ C m. When values corresponding to ϕ_0, (σ_1, σ_3, σ_4), (α_1, α_3, α_4), and ε_1/κ are known, the value of k_S for a given nonelectrolyte-salt pair can be calculated. The value of ϕ_0 is taken as the sum of the partial molal volume, $\bar{V}_{ion}$, of cation and anion, that is $\phi_0=\bar{V}_3+\bar{V}_4$. Since the expression for k_S^* defined by Eq. 3 differs from the conventional k_S appearing in Eq. 1, the observed k_S is converted into k_S^* by means of the relation[11]

$$k_S^* = k_S + (0.036 - \phi_0 \times 10^{-3})/2.30. \tag{5}$$

In calculating k_S^* by the SPT, it is important to choose adequate parameters, since the calculated k_S^* value varies to a great extent with them. First, let us discuss the parameters for elemental mercury as a nonelectrolyte. The value 5.05×10^{-24} cm^3/molecule can be taken for α_1,[12] but it is difficult to select proper σ_1 and ε_1/κ values. We adopt here the value of 0.290 nm for the hard sphere diameter of mercury atom.[13] Calculations were first made using $\varepsilon_1/\kappa=851$ K but the results (Table 1) are unsatisfactory. An attempt was made to estimate the ε_1/κ value according to the derivation made by Pierotti,[14] who gave a relation between Henry's law constant, k_H, and the free energy changes in steps (1) and (2). Using $\sigma_1=0.290$ nm and $K_H=422$ atm at 25 °C,[6] we estimated the value ε_1/κ of elemental mercury to be 283 K, which is much smaller than the value obtained from viscosity data. The parameters used in the present calculation by the SPT are given in Table 2. The values of both observed and calculated k_S^* are given in Table 1.

If we employ the energy parameter derived from Henry's constant, the SPT is applicable, at least to an extent that the McDevit-Long equation can predict, to the salt effect on the elemental mercury solubility in water. Similarly to the McDevit-Long equation, the SPT approach gives poor agreement for NaBr and NaSCN salts. No reasonable interpretation can been given. The results of the SPT calculations for salt effects are sensitive to the ionic diameter of the electrolyte. It is difficult to estimate ionic diameters of polyatomic ions, since no accurate crystal ionic radii are

TABLE 2. PARAMETERS USED FOR CALCULATI NG SALTING COEFFICIENTS BY SCALED PARTICLE THEORY

Elemental Mercury: $\sigma=0.290$ nm,[a] $\alpha=5.05\times10^{-24}$ cm (molecule)$^{-1}$,[b] $\varepsilon/\kappa=851$[a], or 283 K[c]

Ion	σ / nm	$10^{24}\ \alpha$ / cm^3 mol^{-1}	$\bar{V}_{ion}$[d] / cm^3 mol^{-1}
Na^+	0.190[e]	0.21[f]	−6.21
K^+	0.266[e]	0.87[f]	4.02
Ba^{2+}	0.270[e]	1.73[g]	−22.47
$(CH_3)_4N^+$	0.694[h]	8.4[i]	84.57
$(C_2H_5)_4N^+$	0.800[h]	16.4[i]	144.12
F^-	0.272[e]	1.03[g]	3.84
Cl^-	0.362[e]	3.02[f]	22.83
Br^-	0.390[e]	4.17[f]	29.71
NO_3^-	0.406[j]	4.36[g]	34.00
SO_4^-	0.440[j]	5.83[g]	23.98
ClO_4^-	0.452[j]	5.24[g]	49.12
SCN^-	0.428[j]	7.56[k]	40.7

a) Ref. 13. b) Ref. 12. c) Estimated in this work. d) Ref. 8. e) Pauling crystal ionic radius.[18] f) Ref. 10. g) Calculated from mole refraction data cited in Ref. 20. h) Ref. 19. i) Ref. 21. j) Estimated from Hepler's equation.[15] k) Estimated in this work by measuring mole refraction.

known. In the present calculations, ionic radii adopted for polyatomic ions except for tetraalkylammonium ions are those estimated using Hepler's semiempirical equation.[15] It is not clear whether the equation can be properly extended to these ions. Masterton *et al.* tried to estimate the best ionic radii for SPT calculation which give the best fit to the observed salting coefficients.[11] In contrast with the McDevit-Long equation, the SPT gives great discrepancies between observed and calculated k_S^* for $(CH_3)_4NBr$ and $(C_2H_5)_4NBr$ salts. This can not be overcome even if diameters for tetraalkylammonium cations proposed by Masterton *et al.* are used. The failure of the SPT for tetraalkylammonium salts certainly does not lie solely with uncertainty of their ionic diameters, but should be ascribed to their abnormal physico-chemical properties for which the SPT does not account. The anomalous behavior exhibited by tetraalkylammonium ions has been revealed by many experimental observations and theoretical considerations.[16,17]

The authors wish to thank Dr. Toshio Deguchi, Kumamoto University, for valuable discussions. The present work was supported in part by a Grant-in-Aid for Scientific Research from the Ministry of Education, Science and Culture.

References

1) F. A. Long and W. F. McDevit, *Chem. Rev.*, **51**, 119 (1952).
2) D. N. Glew and D. A. Hames, *Can. J. Chem.*, **50**, 3124 (1972).
3) J. N. Spencer and A. F. Voigt, *J. Phys. Chem.*, **73**, 464 (1968).
4) W. F. McDevit and F. A. Long, *J. Am. Chem. Soc.*, **74**, 1773 (1952).
5) R. A. Pierotti, *Chem. Rev.*, **76**, 717 (1976).
6) I. Sanemasa, *Bull. Chem. Soc. Jpn.*, **48**, 1795 (1975).
7) B. Lunden, *Z. Phys. Chem.*, **192**, 345 (1943).
8) F. J. Millero, *Chem. Rev.*, **71**, 147 (1971). A value of -5.0 cm^3/mol is used for $\bar{V}_{H^+}$.
9) S. K. Shoor and K. E. Gubbins, *J. Phys. Chem.*, **73**, 498 (1969).
10) W. L. Masterton and T. P. Lee, *J. Phys. Chem.*, **74**. 1776 (1970).
11) W. L. Masterton, D. Bolocofsky, and T. P. Lee, *J. Phys. Chem.*, **75**, 2809 (1971).
12) E. A. Moelwyn-Hughes, "Physical Chemistry," 2nd rev ed, Pergamon Press, Oxford (1961), Chap. 9.
13) J. O. Hirshfelder, C. F. Curtiss, and R. B. Bird, "Molecular Theory of Gases and Liquids, " John Wiley and Sons, Inc., New York, N. Y. (1954), p. 1112, Table I-A.
14) R. A. Pierotti, *J. Phys. Chem.*, **69**, 281 (1965).
15) L. G. Hepler, *J. Phys. Chem.*, **61**, 1426 (1957). Appropriate corrections for $\bar{V}_{ion}$ were made based on his assumption that the partial molal volume of H^+ is equal to -0.2 cm^3/mol (see Ref. 8).
16) F. Hirata and K. Arakawa, *Bull. Chem. Soc. Jpn.*, **45**, 2715 (1972).
17) R. M. Diamond, *J. Phys. Chem.*, **67**, 2513 (1963).
18) L. Pauling, "Nature of the Chemical Bond," 2nd ed, Cornell University Press, Ithaca, N. Y. (1948).
19) R. A. Robinson and R. H. Stokes, "Electrolyte Solutions," 2nd ed, Butterworths, London (1959), pp. 124—125 (Cited from Ref. 11).
20) H. H. Landölt and R. Bornstein, "Zahlenwerte und Funktionen aus Physik-Chemie-Astronomie-Geophysik-Technik." (1950) Vol. I, Part 1.
21) W. R. Gilkerson and J. L. Stewart, *J. Phys. Chem.*, **65**, 1465 (1961).

Organopalladium(II) Complexes Derived from Chloro[4-[2-(diphenylphosphino)ethylamino]-3-penten-2-onato-*O,N,P*]palladium(II)

Katsuma Hiraki,* Toyohiko Masumoto, Yoshio Fuchita,* and Yasushi Zegi

Department of Industrial Chemistry, Faculty of Engineering, Nagasaki University, Bunkyo-machi, Nagasaki 852

(Received July 17, 1980)

A new tertiary phosphine containing α,β-unsaturated β-amino ketone, 4-[2-(diphenylphosphino)ethylamino]-3-penten-2-one (Hdpeap), reacts with sodium tetrachloropalladate(II) in the absence or presence of sodium ethoxide to give $[PdCl_2(Hdpeap)_2]$ or [PdCl(dpeap)] [dpeap ≡ 4-[2-(diphenylphosphino)ethylamino]-3-penten-2-onato-*O,N,P*], respectively. The latter complex reacts with terminal acetylenes in the presence of catalytic amounts of copper(I) iodide to produce alkynyl complexes, [Pd(C≡CR)(dpeap)]. Carbanions derived from active methylene compounds, and sodium dimethyldithiocarbamate also react with [PdCl(dpeap)] to afford [Pd(CHYY')(dpeap)] and $[Pd(S_2CNMe_2)_2]$, respectively.

Many investigations have been reported about the quadridentate Schiff bases derived from β-diketones and primary diamines[1] and about their transition metal complexes.[2] However, there have been only few papers on tridentate Schiff bases, derived from acetylacetone and primary monoamines containing a hetero atom on their β-position, except the diamines.[3-5] Uhlig and Gottschling[4] reported that 4-(2-picolylamino)-3-penten-2-one (Hpip), produced from acetylacetone and 2-picolylamine, forms univalent ONN-type tridentate chelates to nickel(II) and copper(II) ions. The previous paper from our laboratory dealt with the preparation of chloro[4-(2-picolylamino)-3-penten-2-onato-*O,N,N*]-palladium(II) and with the reactions of this complex with carbanions derived from active methylene compounds.[5]

In this paper, we present the preparation of a new, tertiary phosphine-containing tridentate α,β-unsaturated β-amino ketone, 4-[2-(diphenylphosphino)ethylamino]-3-penten-2-one (Hdpeap), and its reactions towards tetrachloropalladate(II) in the absence and presence of sodium ethoxide, resulting in the formation of $[PdCl_2(Hdpeap)_2]$ and [PdCl(dpeap)] [dpeap ≡ 4-[(2-diphenylphosphino)ethylamino]-3-penten-2-onato-*O,N,P*], respectively. In addition, the reactions of the latter complex with terminal acetylenes, carbanions, and sodium dimethyldithiocarbamate [Na(dmdc)] are reported.

Experimental

Materials and General Procedures. 2-(Diphenylphosphino)-ethylamine,[6] methyl propiolate,[7] and thallium(I) acetylacetonate [Tl(acac)][8] were prepared according to the published procedures. Solvents were dried by standard methods and distilled. The other reagents were commercial samples and were used without further purification.

Melting points were measured in capillary tubes on a Yanagimoto MP-S3 microstage apparatus and are uncorrected. IR and ^{1}H-NMR spectra were recorded according to the previous paper.[5] All preparative operations were performed in an atmosphere of dry nitrogen.

Preparation of Hdpeap. A benzene solution of 2-(diphenylphosphino)ethylamine (26 mmol) and acetylacetone (52 mmol) was heated under reflux for 3.5 h. After the reaction mixture had been evaporated to dryness, the residue was recrystallized from hexane to give crystalline solids, 4-[2-(diphenylphosphino)ethylamino]-3-penten-2-one (Hdpeap) **1**.

Reaction of Hdpeap with Sodium Tetrachloropalladate(II). An ethanol solution (100 ml) containing Hdpeap (3.93 mmol) and $Na_2[PdCl_4]$ (1.96 mmol) was stirred at room temperature for 15 h. After the solvent had been evaporated, the residue was extracted with 30 ml of benzene. The benzene-extract was evaporated *in vacuo*, and the resulting solids were recrystallized from THF and hexane to afford crystalline solids $[PdCl_2(Hdpeap)_2]$ **2**. Hdpeap (2.15 mmol) was added to an ethanol solution (40 ml) of sodium ethoxide (2.15 mmol). The resulting solution was added dropwise to an ethanol solution of $Na_2[PdCl_4]$ (2.36 mmol) for 2 h, and the reaction mixture was stirred at room temperature for 6 h. After filtration, the filtrate was concentrated to give a precipitate, which was collected by filtration and washed with diethyl ether to yield [PdCl(dpeap)] **3**.

Halogen Metathesis of 3. An acetone suspension (30 ml) containing **3** (0.66 mmol) and $LiBr \cdot H_2O$ (2.86 mmol) was heated under reflux for 10 h. The reaction mixture was evaporated to dryness, and the residue was extracted with benzene. The extract was diluted with diethyl ether to give a precipitate of [PdBr(dpeap)] **4**.

Reactions of 3 with Terminal Acetylenes. A diethyl ether solution (8 ml) of methyl propiolate (6.4 mmol) was added to a diethylamine solution (50 ml) containing **3** (1.28 mmol) and copper(I) iodide (3.8×10^{-2} mmol). The reaction mixture was heated under reflux for 31 h. After the volatile matters had been evaporated, the residue was washed with water and recrystallized from benzene and diethyl ether to give [Pd(C≡CCO$_2$Me)(dpeap)] **5**. Complex **3** reacted with phenylacetylene (at room temperature for 6.5 h) or 1-hexyne (under reflux for 13 h) in a diethylamine–diethyl ether mixture in the presence of a catalytic amount of copper(I) iodide followed by the similar recrystallization to yield [Pd(C≡C–Ph)(depeap)] **6** or [Pd(C≡C–*n*-C$_4$H$_9$)(dpeap)] **7**, respectively.

Reaction of 3 with Tl(acac). Thallium (I) acetylacetonate (0.51 mmol) was added to a dichloromethane solution (10 ml) of **3** (0.44 mmol). The resulting suspension was stirred at room temperature for 16.5 h. After filtration, the filtrate was concentrated and diluted with hexane to give a precipitate of [Pd{CH(COMe)$_2$}(dpeap)] **8**.

Reactions of 3 with Carbanions Formed from Active Methylene Compounds. A THF suspension containing **3** (0.44 mmol), malononitrile (0.55 mmol) and sodium methoxide (0.55 mmol) was stirred at room temperature for 24 h. After filtration, the resulting filtrate was evaporated *in vacuo*. The residue was recrystallized from dichloromethane–diethyl ether to afford [Pd{CH(CN)$_2$}(dpeap)] **9**. Complex **3** was analogously treated with carbanion formed from methyl cyanoacetate, followed by recrystallization from dichloromethane and hexane to yield [Pd{CH(CN)CO$_2$Me}(dpeap)] **10**.

Reaction of 3 with Sodium Dimethyldithiocarbamate-water (1/2). A dichloromethane suspension (30 ml) containing **3** (0.79 mmol) and sodium dimethyldithiocarbamate-water(1/2) (0.84 mmol) was stirred at room temperature for 27 h. The resulting solids were collected and washed with water and then diethyl ether to give yellow powders, $[Pd(S_2CNMe_2)_2]$ [in 54% yield, based on **3**, and in 100%, based on $Na(S_2CNMe_2)\cdot 2H_2O$]. Mp>300 °C (lit,[9] >300 °C).

Results and Discussion

Preparation of Hdpeap and its Palladium(II) Complexes. 2-(Diphenylphosphino)ethylamine and acetylacetone reacted easily in refluxing benzene to give a new tridentate Schiff base ligand, Hdpeap **1**. This ligand was treated with $Na_2[PdCl_4]$ in ethanol in the absence of alkali metal alkoxide, resulting in the formation of the adduct, $[PdCl_2(Hdpeap)_2]$, **2**. The Schiff base **1** reacted with equimolar amounts of sodium ethoxide and $Na_2[PdCl_4]$ in ethanol to afford [PdCl(dpeap)], **3**. Complex **3** reacted with $LiBr\cdot H_2O$, terminal acetylenes, Tl(acac), and carbanion formed from active methylene compounds, such as malononitrile and methyl cyanoacetate, giving new complexes **4**, **5**—**7**, **8**, and **9**—**10**, respectively. The yields, elemental analyses, and some physical properties of compounds **1**—**10** are summarized in Table 1. Complexes **2**—**7** are stable in the air and soluble in chloroform and dichloromethane.

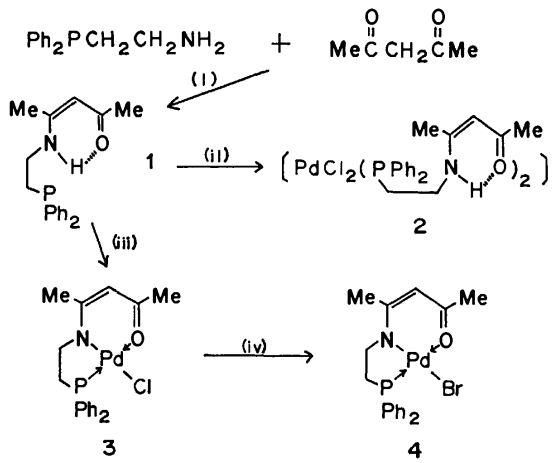

Scheme 1. Formation and reactions of Hdpeap, **1**.
i) Reflux in benzene; ii) $Na_2[PdCl_4]$; iii) $Na_2[PdCl_4]$+ NaOEt; iv) $LiBr\cdot H_2O$.

The Schiff base **1** and its adduct **2** showed a ν(NH) frequency at 3160 and 3400 cm^{-1}, respectively. Furthermore, they exhibited three bands near 1510, 1560, and 1590 cm^{-1}, characteristic of the 4-amino-3-penten-2-one moiety. The ^{1}H-NMR spectra of **1** and **2** showed a broad signal near δ 10.8, assignable to NH proton, in addition to three singlets near δ 1.77 (3H, Me), 1.93 (3H, Me), and 4.91 (1H, CH) and two multiplets near δ 2.3—2.7 (2H, CH_2P) and 3.43 (2H, CH_2N) (Table 3). These data confirm unambiguously that **2** retains the uncoordinated 4-amino-3-penten-2-one moiety. This was in contrast with the case of 4-(2-picolylamino)-3-penten-2-one, which had acted also as a proton acceptor.[5]

The IR spectra of **3**—**10** showed two bands near 1575 and 1505 cm^{-1}, attributable to the coordinated 4-amino-3-penten-2-onato-*N,O* group. The ^{1}H-NMR spectra of **3**—**10** exhibited three singlets near δ 2.0 (3H, Me), 2.1 (3H, Me), and 5.0 (1H, CH), and two double triplets in the ranges δ 2.2—2.7 [2H, CH_2P, ^2J(PH)=*ca.* 10 Hz, ^3J(HH)=*ca.* 6 Hz] and 3.0—3.7 [2H, CH_2N, ^3J(PH)=23—30 Hz]. These facts indicate that **3**—**10** have the tridentate dpeap group.

The Ethynyl Type Complexes 5—7. Complex **3** reacted smoothly with phenylacetylene at room temperature in the diethylamine–diethyl ether mixture in the presence of 1 mol percent of copper(I) iodide.[10] Complex **3** reacted fairly slowly with methyl propiolate in the same conditions, because about 30% of **3** remained unchanged after stirring at room temperature for 3.5 d. However, **3** did not react with 1-hexyne at room temperature even in the presence of CuI. It was found from the above results that the order of the reactivity of terminal acetylenes towards **3** was; phenylacetylene>methyl propiolate$\gg$1-hexyne. Taking the pK_a values of the terminal acetylenes [$Bu^nC{\equiv}CH$ (26.2[11])>$PhC{\equiv}CH$ (23.7,[11] 21[12])>$MeO_2CC{\equiv}CH$] into consideration, it seems likely that the ethynylation of **3** is influenced by two factors: one is the susceptibility of the acetylenes to deprotonation, resulting in the formation of the intermediates, ethynyl–copper complexes[10] and the other is the reactivity of the intermediates toward **3**.

Table 1. Yields and elemental analyses

Compound		Yield %	Color	Mp[a] °C	Found (Calcd) (%) C	H	N
Hdpeap	**1**	91	White	80—80.5	72.87(73.29)	7.20(7.12)	4.51(4.50)
$[PdCl_2(Hdpeap)_2]$	**2**	41	Pale yellow	90—95	56.70(57.05)	5.84(5.54)	3.58(3.50)
[PdCl(dpeap)]	**3**	65	Yellow	238—240	50.30(50.47)	4.75(4.68)	3.09(3.10)
[PdBr(dpeap)]	**4**	79	Yellow	241—242	44.92(45.94)	4.22(4.26)	2.70(2.82)
[[Pd(C≡CCO_2Me)(dpeap)]	**5**	34	Pale yellow	190	54.82(55.27)	4.75(4.84)	2.73(2.80)
[Pd(C≡CPh)(dpeap)]	**6**	46	Pale yellow	185—188	62.10(62.52)	5.11(5.06)	2.14(2.70)
[Pd(C≡C-C_4H_9)(dpeap)]	**7**	39	Pale yellow	165	60.31(60.31)	6.26(6.07)	2.74(2.81)
[Pd{$CH(COMe)_2$}(dpeap)]	**8**	80	Pale yellow	178—179	55.26(55.88)	5.46(5.47)	2.66(2.72)
[Pd{$CH(CN)_2$}(dpeap)]	**9**	80	Pale yellow	195—196	55.06(54.84)	4.57(4.60)	8.78(8.72)
[Pd{$CHCN(CO_2Me)$}(dpeap)]	**10**	75	Pale yellow	189—190	53.42(53.66)	4.87(4.89)	5.35(5.44)

a) With decomposition except for **1**.

TABLE 2. CHARACTERISTIC IR BANDS[a)]

Compound	ν(C≡C)	ν(C=O)	Others[b)]
1	—	—	3160[ν(NH)]
2	—	—	3400[ν(NH)]
5	2090	1655	1220[ν(C–O)]
6	2100	—	—
7	2120	—	—
8	—	1660,1635sh	—
9	—	—	2225[ν(C≡N)]
10	—	1715	2220[ν(C≡N)]

a) In cm^{-1}, in KBr disk. b) Assignment is given parentheses.

Complexes **5**—**7** showed a strong ν(C≡C) band near 2100 cm^{-1}, lower (*ca.* 35, 55, and 5 cm^{-1}, respectively) than those of the corresponding free acetylenes. Attempts to isolate **8**, **10**, and [Pd{$CHNO_2(CO_2Me)$}(dpeap)] by reactions of **7** with acetylacetone, methyl cyanoacetate, and methyl nitroacetate, respectively, were fruitless, **7** being recovered quantitatively after refluxing in THF for 5 h. The inertness of **7** toward the active methylene compounds is in contrast with phenylethynyl-[13] and 1-hexynyl[1,1,1-tris(diphenylphosphinomethyl)ethane]-copper(I).[14] However, the phenylethynyl complex **6** easily reacted with dimethyl acetylenedicarboxylate in dioxane at room temperature to afford an insertion product. It seems likely that this insertion reaction is comparable with that between halogeno(phenylethynyl)-bis(trialkylphosphine)palladium(II) and dimethyl acetylenedicarboxylate in dioxane at 85 °C.[15] Details of the former insertion reaction will be reported later.

The Disubstituted Alkyl Type Complexes ***8***—***10***.

The ^{1}H-NMR spectra of complexes **8**—**10** exhibited a doublet in the range δ 2.8—3.9 [1H, ^3J(PH)=2—5 Hz], characteristic of a palladium-bonded methine proton. The IR spectrum of **8** showed a strong ν(C=O) band at 1660 cm^{-1}, implying two free and equivalent acetyl groups. Complexes **9** and **10** showed a medium ν(C≡N) band near 2220 cm^{-1}, attributable to an uncoordinate cyano group. These data indicate unambiguously that the disubstituted alkyl groups were σ-bonded to palladium in an analogous fashion to those in [Pd(pip)-(CHYY')] type complexes.[5] Complexes **8**—**10** are stable in the solid state and in dichloromethane and chloroform and unreactive towards water or ethanol. The stability of **8**—**10** is possibly associated both with the electron delocalization effect to a π^* orbital of the conjugate 4-amino-3-penten-2-onato-*N*,*O* moiety and vacant d orbitals of the phosphorus atom in the dpeap ligand and with the electron-withdrawing effect of the substituents attached to the methine group, similar to the case of [Pd(pip)(CHYY')].[5]

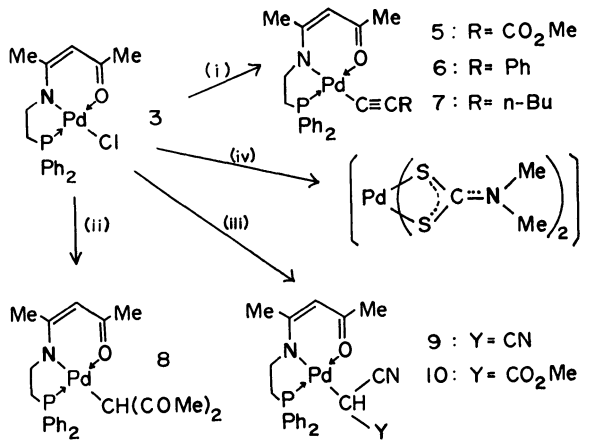

Scheme 2. Reactions of [PdCl(dpeap)], **3**.
i) HC≡CR+CuI (3 mol %) in $NHEt_2$; ii) Tl(acac); iii) $CH_2(CN)Y$+NaOMe; iv) $Na(S_2CNMe_2)\cdot 2H_2O$.

An attempt to isolate a dinuclear complex by the reaction between **8** and bis(acetylacetonato)palladium-(II) was unsuccessful, **8** being recovered quantitatively after heating under reflux in 1,2-dichloroethane for 6.5 h. The methine proton of the diacetylmethyl moiety in **8** is strongly bonded to the methine carbon, and does not give rise to tautomerism leading to 4-hydroxy-3-palladio-3-penten-2-one moiety, in contrast to the case of (2,2'-bipyridine)chloro(2,4-dioxopentyl)palladium(II).[15]

In contrast to the rapid reaction of **3** with Tl(acac), **3** reacted slowly with a carbanion formed from acetyl-

TABLE 3. ^{1}H-NMR DATA[a)]

Compound	1-Me[b)], 5-Me[b)]	3-CH[b)]	1'-CH_2N[c)]		2'-CH_2P[c)]		Others	
	δ/ppm	δ/ppm	δ/ppm	^3J(PH)/Hz	δ/ppm	^2J(PH)/Hz	δ/ppm	^3J(PH)/Hz
1	1.76, 1.92	4.92	3.43(m)	17	2.32(m)		10.87(b, 1H, NH)	—
2	1.78, 1.94	4.90	3·43(m)	—	2.71(m)	—	10.79(b, 1H, NH)	—
3	1.98, 2.03	4.91	3.50(dt)	29	2.32(dt)	11	—	—
4	2.02, 2.06	4.95	3.51(dt)	30	2.40(dt)	11	—	—
5	1.98, 2.07	4.96	3.59(dt)	26	2.51(dt)	10	3.51(s, 3H, OMe)	—
6	2.02, 2.16	5.04	3.69(dt)	28	2.62(dt)	11	7.21(s, 5H, Ph)	—
7	1.95, 2.09	4.90	3.50(dt)	26	2.48(dt)	10	0.56(t, 3H, 6''-Me)[c,d)]	—
							2.13(t, 2H, 3''-CH_2)[c)]	—
8	1.98, 2.02	4.98	3.33(dt)	26	2.25(dt)	10	3.82(d, 1H, CH)	5
							2.02(s, 6H, Me)	—
9	2.03, 2.06	5.04	3.04(dt)	25	2.51(dt)	10	2.81(d, 1H, CH)	2
10	1.99, 2.03	4.98	3.33(dt)	23	2.47(dt)	10	3.02(d, 1H, CH)	3
							3.38(s, 3H, OMe)	—

a) In $CDCl_3$. b) Appearing as a singlet. c) ^3J(H,H)=*ca.* 6 Hz. d) A multiplet near δ 1.1(4H) for 4''- and 5''-CH_2 protons was observed.

acetone and sodium methoxide, and gave a nearly 1 : 1 mixture of **3** and **8** after treatment with the carbanion in THF at room temperature for 24 h. However, **3** did not react with methyl nitroacetate in the presence of an equimolar amount of sodium methoxide. The reactivities of the carbanions toward **3** were ordered as follows.

$$^{-}CH(CN)CO_2Me \approx {}^{-}CH(CN)_2 >$$
$$^{-}CH(COCH_3)_2 \gg {}^{-}CH(NO_2)CO_2Me$$

This order is consistent with that of the nucleophilicity of the carbanions.[13,17]

*Reaction of **3** with Dimethyldithiocarbamate.* Complex **3** reacted with $Na(S_2CNMe_2)\cdot 2H_2O$ in dichloromethane, giving yellow powders. The IR spectrum of the powders lacked the bands characteristic of the dpeap ligand, and newly showed two bands at 1545 and 970 cm^{-1}, assignable to $\nu(C{=}N)$ and $\nu(S{=}C)$ frequencies, respectively. Accordingly, the powders were assigned to bis(dimethyldithiocarbamato)-palladium(II).[9] It is noteworthy that the tridentate dpeap ligand in **3** is substituted virtually quantitatively by bidentate dimethyldithiocarbamato ligands, which are soft themselves and are expected to be coordinated strongly to soft palladium(II) ion.

The authors thank Mrs. Hisako Mazume and Miss Yumi Kojima of Nagasaki University for their technical assistance.

References

1) H. Kanatomi, "Kirehto Kagaku," ed by K. Ueno, Nankodo, Tokyo (1975), Vol. 5, pp. 251—265, and literatures cited therein.

2) R. H. Holm, G. W. Everett, Jr., and A. Chakravorty, "Progress in Inorganic Chemistry," ed by F. A. Cotton, Interscience Publishers, New York (1966), Vol. 7, pp. 176—195, and literatures cited therein.

3) L. Wolf and E. G. Jaeger, *Z. Chem.*, **5**, 317 (1965).

4) E. Uhlig and E. Gottschling, *Z. Anorg. Allg. Chem.*, **376**, 113 (1970).

5) K. Hiraki, M. Onishi, and H. Matsuo, *J. Organomet. Chem.*, **185**, 111 (1980).

6) K. Issleib and H. Oehme, *Chem. Ber.*, **100**, 2685 (1967).

7) W. H. Perkin and J. L. Simonsen, *J. Chem. Soc.*, **91**, 833 (1907).

8) W. H. Nelson, W. J. Randall, and D. F. Martin, *Inorg. Synth.*, IX, 53 (1971).

9) C. G. Sceney and R. J. Magee, *Inorg. Nucl. Chem. Lett.*, **10**, 323 (1974).

10) K. Sonogashira, T. Yatake, Y. Tohda, S. Takahashi, and N. Hagihara, *J. Chem. Soc., Chem. Commun.*, **1977**, 291.

11) E. S. Petrov, M. I. Terekhova, A. I. Shatenshtein, and B. A. Trofimov, *Dokl. Akad. Nauk SSSR*, **211**, 1393 (1973).

12) O. A. Reutov, I. P. Belestskaya, and K. P. Butin, "CH-Acids," translated by T. R. Crompton. Pergamon Press, New York (1978), p. 11.

13) K. Hiraki, Y. Fuchita, and Y. Morita, *Bull. Chem. Soc. Jpn.*, **51**, 2012 (1978).

14) Y. Fuchita, Y. Morita, K. Hiraki, and K. Misono, Unpublished data.

15) Y. Tohda, K. Sonogashira, and N. Hagihara, *J. Chem. Soc., Chem. Commun.*, **1975**, 54.

16) a) S. Okeya, N. Yanase, Y. Nakamura, and S. Kawaguchi, *Chem. Lett.*, **1978**, 699; b) N. Yanase, Y. Nakamura and S. Kawaguchi, *Inorg. Chem.*, **17**, 2874 (1978).

17) Ref. 12, pp. 59 and 62.

The Crystal Structure and Luminescence Properties of Europium(II) Haloborates

Ken-ichi MACHIDA, Gin-ya ADACHI,* Yoshikazu MORIWAKI, and Jiro SHIOKAWA

Department of Applied Chemistry, Faculty of Engineering, Osaka University, Yamadakami, Suita, Osaka 565

(Received May 10, 1980)

The crystal structures of $Eu_2B_5O_9X$ (X=Cl and Br) were determined by the method of X-ray diffraction analysis and refined by the least-square method to give $R=0.054$ for 1967 observed reflections of $Eu_2B_5O_9Cl$ and $R=0.047$ for 1979 observed reflections of $Eu_2B_5O_9Br$. These haloborates are isostructural and belong to the orthorhombic (pseudotetragonal) system, with the *Pnn*2 space group and with four formula units in a cell of those dimensions: $a=11.364(3)$, $b=11.301(3)$, and $c=6.504(2)$ Å for $Eu_2B_5O_9Cl$, and $a=11.503(3)$, $b=11.382(3)$, and $c=6.484(2)$ Å for $Eu_2B_5O_9Br$. The structure consists of a three-dimensional $(B_5O_9)_\infty$ network, the B_5O_{12} groups of three BO_4 tetrahedra and two BO_3 triangles being linked together with one another. The Eu and X atoms are located alternately in tunnels of the $(B_5O_9)_\infty$ network extending along the c axis. Each Eu atom is surrounded by two X atoms and seven O atoms, and is isolated from the neighboring Eu atoms attributable to borate units and X atoms. This arrangement of anions around Eu atoms relates to the fact that the Eu^{2+}-activated phosphors of alkaline earth analogs give emissions with a high quantum efficiency.

Phosphors of Eu^{2+}-activated alkaline earth compounds give emissions based on the $4f^7-4f^65d$ transition or the $4f^7-4f^7$ transition of the Eu^{2+} ion.[1] Recently we have reported that the quantum efficiencies of compounds in the $EuO-B_2O_3$ system and their Eu^{2+}-activated strontium analogs depend greatly on the structural frameworks of borate units.[2] In the ternary system $EuO-EuX_2-B_2O_3$ (X=Cl and Br), $Eu_2B_5O_9$-type compounds have been obtained in attempts to prepare their boracite-type compounds,[3] they are paramagnetic and give blue emissions based on the $4f^7-4f^65d$ transition of the Eu^{2+} ion.[4] The compounds obtained by the dilution of the Eu^{2+} ions in the $Eu_2B_5O_9X$ matrix with alkaline-earth cations have been found to be efficient photoluminescent materials.[5] In this paper, we wish to report on the crystal structure of $Eu_2B_5O_9X$ and discuss their luminescence properties on the basis of X-ray structural analysis.

Experimental

Sample Preparation. Single crystals of $Eu_2B_5O_9X$ were prepared as follows: mixtures of EuB_2O_4 and B_2O_3 containing a large excess of EuX_2 as a flux were heated on molybdenum boats above the congruent melting points of haloborates (about 1100 °C) for 1—2 h in He gas; the molten samples were then allowed to cool at a rate of 3—5 °C/h. When the unreactive EuX_2 was then removed from the samples with washing with water, light-yellow crystals were obtained. Their crystal habits were prismatic for $Eu_2B_5O_9Cl$ and needle-like for $Eu_2B_5O_9Br$.

The Eu^{2+}-activated strontium haloborates, $Sr_2B_5O_9Cl$: Eu^{2+} and $Sr_2B_5O_9Br$: Eu^{2+}, were obtained by the following standard ceramic technique: appropriate amounts of SrX_2, H_3BO_3, and $SrCO_3$: Eu^{3+}, coprecipitated from a dilute HCl solution of $Sr(NO_3)_2$ and Eu_2O_3 (99.99%) by the slow addition of a $(NH_4)_2CO_3$ solution, were fully mixed, pelletized, and heated at 950 °C for 2 h in a stream of a reducing atmosphere, H_2.

Optical Measurements. The ultraviolet luminescence spectra were measured according to a technique described elsewhere.[2]

X-Ray Data Collection. Preliminary Weissenberg photographs and the Patterson syntheses showed that $Eu_2B_5O_9X$ belongs to the orthorhombic (pseudotetragonal) system, with a noncentrosymmetric space group *Pnn*2 and with $Z=4$.† The accurate cell parameters of $Eu_2B_5O_9Cl$ and $Eu_2B_5O_9Br$ were determined by least-square treatments of the X-ray powder diffraction patterns (Cu $K\alpha_1$), calibrated with high purity silicon. The crystal data are summarized in Table 1.

Table 1. Crystal data

	$Eu_2B_5O_9Cl$	$Eu_2B_5O_9Br$
F.W.	537.43	581.88
Orthorhombic		
Pnn2 ($0kl$, $k+l=2n+1$; $h0l$, $h+l=2n+1$)		
a/Å	11.364(3)	11.503(3)
b/Å	11.301(3)	11.382(3)
c/Å	6.504(2)	6.484(2)
V/Å^3	835.2(5)	848.9(4)
D_m/g cm^{-3}	4.30	4.53
D_x/g cm^{-3}	4.28	4.55
Z	4	4
$F(000)$	960	1032
Crystal size/mm^3	$0.14\times0.08\times0.17$	$0.10\times0.10\times0.20$
μ(Mo $K\alpha$)/mm^{-1}	15.283	19.264

The intensity data were measured on a Rigaku Denki automated four-circle diffractometer with Mo $K\alpha$ radiation ($\lambda=0.71069$ Å) monochromated with graphite. The ω-2θ scan technique was employed with a scanning rate of 4°/min. All the independent reflections were collected up to $2\theta=70°$. Three standard reflections were monitored every 50 or 60 reflections; no apparent decay in intensity was detected. The reflections with $F_o>3\sigma(F_o)$ were considered as observed: 1967 and 1979 observed reflections were obtained for $Eu_2B_5O_9Cl$ and $Eu_2B_5O_9Br$ respectively. The Lorentz and polarization corrections were applied, but the absorption correction was not.

Structure Determination and Refinements. The structures of europium (II) haloborates were solved by the conventional heavy-atom method and were refined by the method of block-diagonal least-squares (*HBLS*-V program[6]), the minimized function being $\sum w(|F_o|-|F_c|)^2$. From the three-dimensional Patterson syntheses, the coordinates of Eu and X atoms were determined: Eu(1) and Eu(2) atoms can be located on the general positions (4*c* site), while X(1) and X(2) atoms occupy

† The symmetry of $Eu_2B_5O_9Cl$ has been erroneously reported as tetragonal in a previous paper.[4]

TABLE 2. FINAL POSITIONAL AND THERMAL PARAMETERS FOR $Eu_2B_5O_9Cl$, WITH THEIR ESTIMATED STANDARD DEVIATIONS IN PARENTHESES

(a) Europium atoms ($\times 10^4$)

The form of the anisotropic thermal parameters ($\times 10^5$) is $\exp[-(\beta_{11}h^2+\beta_{22}k^2+\beta_{33}l^2+\beta_{12}hk+\beta_{13}hl+\beta_{23}kl)]$.

Atom	x	y	z	β_{11}	β_{22}	β_{33}	β_{12}	β_{13}	β_{23}
Eu(1)	2523(7)	475(6)	0	120(3)	106(3)	278(10)	25(6)	−61(12)	−61(14)
Eu(2)	255(6)	2403(6)	6624(12)	74(3)	149(3)	246(9)	−11(6)	−71(14)	17(17)

(b) Non-europium atoms ($\times 10^3$)

Atom	x	y	z	B/Å^2	Atom	x	y	z	B/Å^2
Cl(1)	0	0	862(6)	1.08(7)	O(7)	182(10)	269(10)	939(10)	0.21(11)
Cl(2)	0	500	613(6)	1.03(7)	O(8)	421(10)	207(10)	510(12)	0.53(12)
O(1)	244(10)	318(10)	594(10)	0.31(12)	O(9)	232(10)	114(10)	576(11)	0.46(12)
O(2)	211(10)	427(10)	1191(11)	0.60(13)	B(1)	274(14)	325(13)	809(15)	0.25(16)
O(3)	279(10)	225(10)	1255(10)	0.36(12)	B(2)	187(12)	299(12)	1162(20)	0.29(14)
O(4)	77(11)	270(11)	1263(11)	0.61(13)	B(3)	292(14)	217(13)	479(15)	0.31(16)
O(5)	286(11)	451(10)	853(12)	0.64(13)	B(4)	457(22)	231(21)	712(23)	1.40(27)
O(6)	384(12)	262(11)	856(12)	0.78(14)	B(5)	251(16)	497(15)	1035(15)	0.57(19)

TABLE 3. FINAL POSITIONAL AND THERMAL PARAMETERS FOR $Eu_2B_5O_9Br$, WITH THEIR ESTIMATED STANDARD DEVIATIONS IN PARENTHESES

(a) Heavy atoms ($\times 10^4$)

The form of the anisotropic thermal parameters ($\times 10^5$) is $\exp[-(\beta_{11}h^2+\beta_{22}k^2+\beta_{33}l^2+\beta_{12}hk+\beta_{13}hl+\beta_{23}kl)]$.

Atom	x	y	z	β_{11}	β_{22}	β_{33}	β_{12}	β_{13}	β_{23}
Eu(1)	2547(6)	501(6)	0	113(3)	118(3)	396(9)	35(6)	−62(11)	−52(12)
Eu(2)	307(6)	2374(6)	6572(10)	92(3)	140(3)	360(9)	−13(5)	−84(12)	7(15)
Br(1)	0	0	8769(27)	141(10)	163(11)	1146(46)	−58(18)	0	0
Br(2)	0	5000	6370(32)	112(9)	169(10)	1676(61)	6(16)	0	0

(b) Light atoms ($\times 10^3$)

Atom	x	y	z	B/Å^2	Atom	x	y	z	B/Å^2
O(1)	246(9)	318(9)	581(9)	0.40(11)	O(8)	423(7)	212(9)	500(11)	0.66(11)
O(2)	209(9)	427(9)	1182(10)	0.59(12)	O(9)	239(9)	115(9)	571(9)	0.62(12)
O(3)	279(9)	227(9)	1248(10)	0.59(12)	B(1)	275(12)	326(12)	805(13)	0.17(13)
O(4)	78(9)	267(9)	1254(10)	0.69(12)	B(2)	187(12)	299(12)	1167(17)	0.54(14)
O(5)	283(10)	454(9)	844(11)	0.76(12)	B(3)	295(12)	218(12)	471(13)	0.39(15)
O(6)	388(10)	266(10)	847(10)	0.76(12)	B(4)	462(14)	236(15)	699(14)	0.72(18)
O(7)	185(9)	271(8)	928(9)	0.35(10)	B(5)	248(12)	497(12)	1031(12)	0.29(14)

the special positions (2*a* and 2*b* sites). The remaining O and B atoms were located on the successive Fourier maps. The isotropic refinements gave a conventional R value of 0.06 for both compounds; further refinements with anisotropic thermal factors for heavy atoms reduced the R and R_w values to 0.054 and 0.068 for 1967 reflections of $Eu_2B_5O_9Cl$ and 0.047 and 0.053 for 1979 reflections of $Eu_2B_5O_9Br$, where $R_w=[\sum w(|F_o|-|F_c|)^2/\sum w(F_o)^2]^{1/2}$. The weighting schemes of $w=(F_{max}/F_o)^2$ for $F_o>F_{max}$ and $w=1.0$ for $F_o\leqq F_{max}$ ($Eu_2B_5O_9Cl$, $F_{max}=20.0$; $Eu_2B_5O_9Br$, $F_{max}=40.0$), were employed. The atomic scattering factors were taken from the International Tables for X-ray Crystallography.[7] The final positional and thermal parameters are listed in Tables 2 and 3.††

Results and Discussion

Since the final parameters of $Eu_2B_5O_9Cl$ are almost equal to those of $Eu_2B_5O_9Br$, the two europium(II) haloborates were considered to be isostructural with each other.

The interatomic distances and angles of $Eu_2B_5O_9Cl$ are given in Table 4. There are two types of B atoms: in the first type [B(1), B(2), and B(3)], each B atom is tetrahedrally coordinated with four oxygens with B–O distances from 1.44 to 1.49 Å, while the second type [B(4) and B(5)] are triangularly coordinated borons with B–O distances from 1.30 to 1.41 Å. The O–B–O angles are about 110° for the tetrahedra and about 120° for the triangles. Three BO_4 tetrahedra and two BO_3 triangles form a B_5O_{12} group with sharing O atoms, and these groups are linked together with one another to form a three-dimensional $(B_5O_9)_\infty$ network. The projection of the $Eu_2B_5O_9Cl$ structure viewed along the c axis is shown in Fig. 1. The Eu and Cl atoms are alternately located in tunnels of the $(B_5O_9)_\infty$ network, and each Eu atom is almost entirely isolated from neighboring Eu atoms because of the $(B_5O_9)_\infty$ network for the a and b directions and Cl atoms for the c direction.

Each Eu atom has four nearest Eu neighbors with the mean interatomic distance of 4.387 Å and four next-nearest Eu neighbors with the mean interatomic

†† The F_o-F_c Table is kept as Document No. 8111 at the Chemical Society of Japan.

TABLE 4. INTERATOMIC DISTANCES (Å) AND BOND ANGLES (°) IN $Eu_2B_5O_9Cl$

(a) The $(B_5O_9)_\infty$ network			
B(1)-tetrahedron		B(2)-tetrahedron	
B(1)-O(1)	1.44(2)	B(2)-O(2)	1.49(3)
-O(5)	1.46(2)	-O(3)	1.48(3)
-O(6)	1.47(2)	-O(4)	1.45(3)
-O(7)	1.48(2)	-O(7)	1.49(3)
O(1)-B(1)-O(5)	106(1)	O(2)-B(2)-O(3)	112(2)
O(1)-B(1)-O(6)	112(1)	O(2)-B(2)-O(4)	109(2)
O(1)-B(1)-O(7)	111(1)	O(2)-B(2)-O(7)	110(2)
O(5)-B(1)-O(6)	110(2)	O(3)-B(2)-O(4)	108(2)
O(5)-B(1)-O(7)	112(1)	O(3)-B(2)-O(7)	107(2)
O(6)-B(1)-O(7)	106(1)	O(4)-B(2)-O(7)	111(2)
		B(3)-tetrahedron	
B(3)-O(1)	1.48(2)	O(1)-B(3)-O(3)	115(1)
-O(3)	1.47(2)	O(1)-B(3)-O(8)	111(1)
-O(8)	1.49(2)	O(1)-B(3)-O(9)	103(1)
-O(9)	1.49(2)	O(3)-B(3)-O(8)	104(1)
		O(3)-B(3)-O(9)	115(1)
		O(8)-B(3)-O(9)	110(1)
B(4)-triangle		B(5)-triangle	
B(4)-O(4)	1.41(3)	B(5)-O(2)	1.36(2)
-O(6)	1.30(3)	-O(5)	1.36(2)
-O(8)	1.40(3)	-O(9)	1.36(2)
O(4)-B(4)-O(6)	117(2)	O(2)-B(5)-O(5)	122(2)
O(4)-B(4)-O(8)	120(2)	O(2)-B(5)-O(9)	118(2)
O(6)-B(4)-O(8)	123(2)	O(5)-B(5)-O(9)	120(2)
(b) Eu-Eu distances[a]			
Nearest neighbors		Next-nearest neighbors	
Eu(1)-Eu(2)	4.026(1)	Eu(1)-Eu(1^{i})	5.731(1)
-Eu(2^{i})	5.036(1)		5.833(1)
-Eu(2^{ii})	4.421(1)	Eu(2)-Eu(2^{i})	5.461(2)
-Eu(2^{iii})	4.063(1)		5.899(2)
		Eu(1)-Eu(2)	5.473(1)
		-Eu(2^{i})	6.253(1)
(c) Eu-Cl and Eu-O distances			
Eu(1)-polyhedron		Eu(2)-polyhedron	
Eu(1)-Cl(1)	3.052(7)	Eu(2)-Cl(1)	3.022(7)
-Cl(2)	2.958(6)	-Cl(2)	2.967(6)
-O(1)	2.665(10)	-O(1)	2.667(10)
-O(2)	2.465(11)	-O(3)	2.888(10)
-O(3)	2.621(10)	-O(4)	2.851(12)
-O(5)	2.581(12)	-O(6)	2.559(12)
-O(6)	3.000(12)	-O(7)	2.552(10)
-O(7)	2.662(10)	-O(8)	2.617(12)
-O(9)	2.866(11)	-O(9)	2.801(11)

a) Symmetry code: Eu(1^{i}), $(\bar{x},\bar{y},z)$; Eu(2^{i}), $(\bar{x},\bar{y},z)$; Eu(2^{ii}), $(1/2-x, 1/2+y, 1/2+z)$; Eu(2^{iii}), $(1/2+x, 1/2-y, 1/2+z)$.

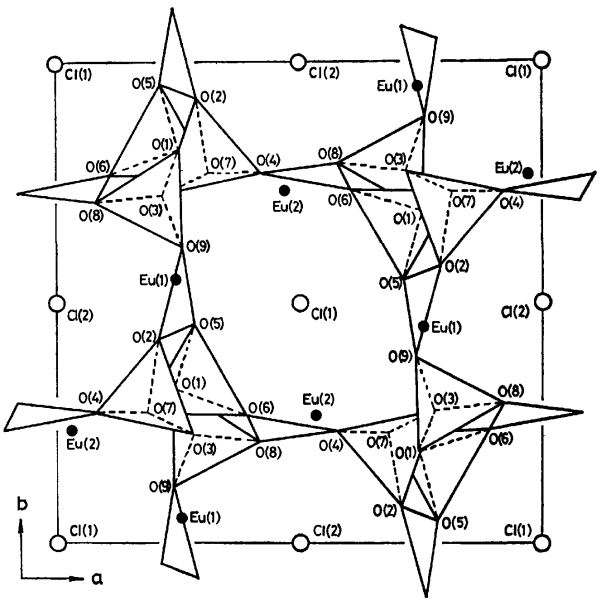

Fig. 1. A projection of the $Eu_2B_5O_9Cl$ structure along the c axis.

distance of 5.823 Å for the Eu(1) atom or 5.772 Å for the Eu(2) atom. These interatomic distances are long compared with those of other europium(II) compounds with magnetic transitions,[8] and are insufficient for the magnetic interactions between neighboring Eu^{2+} ions.[9] For example, the Eu–Eu distances in EuO (T_C=69 K) are 3.63 and 5.14 Å for the nearest and next-nearest Eu neighbors respectively. Therefore, $Eu_2B_5O_9X$ is paramagnetic even at low temperature.

The anion environments around Eu(1) and Eu(2) atoms in $Eu_2B_5O_9Cl$ are shown in Fig. 2. Both Eu(1) and Eu(2) atoms are surrounded with two Cl atoms and seven O atoms to form $Eu(1)O_7Cl_2$ and $Eu(2)O_7Cl_2$ polyhedra with Eu–Cl distances from 2.985 to 3.052 Å and Eu–O distances from 2.465 to 3.000 Å.

Peters *et al.*[5] and Fouassier *et al.*[3] have obtained $M^{II}_2B_5O_9X$ phases in their attempts to prepare boracite ($M^{II}_3B_7O_{13}X$)-type compounds .(M=Ca, Sr, Ba, Eu, and Pb). That is to say, these metal ions do not give boracite-type compounds. Each M^{2+} ion in boracites, which are formed in a ternary system, MO–MX_2–B_2O_3 (M=Mg, Cr, Mn, Fe, Co, Ni, Cu, Zn, and Cd), is surrounded by two X^- ions and four O^{2-} ions.[10] The fact that $M_2B_5O_9X$-type compounds are formed for M=Ca, Sr, Ba, Eu, and Pb may be due to their large ionic radii, since these ions hardly seem to occupy the sixfold sites of boracites.

The haloborates, $Eu_2B_5O_9Cl$ and $Eu_2B_5O_9Br$, give

TABLE 5. LUMINESCENCE AND STRUCTURAL DATA FOR Eu^{2+}-ACTIVATED Sr-COMPOUNDS

Compound	λ_{max}/nm[a]	(λ/2)/nm[b]	*Q.E.*/%[c]	*C.N.*[d]	Structural framework	Reference
$Sr_2B_5O_9Cl : Eu^{2+}$	425	30	50	9	$(B_5O_9)_\infty$ network	This work
$Sr_2B_5O_9Br : Eu^{2+}$	430	30	60	9	$(B_5O_9)_\infty$ network	This work
$SrB_2O_4 : Eu^{2+}$	367	20	≃2	8	$(BO_2)_\infty$ chain	2a
$SrB_4O_7 : Eu^{2+}$	367	20	40	9	$(B_4O_7)_\infty$ network	2a

a) λ_{max}=Peak position of the emission band at 300 K. b) λ/2=Half-width of emission band. c) *Q.E.*=Quantum efficiency of the Eu^{2+} concentration of a sample optimized under optimum excitation at 300 K. d) *C.N.*=Eu-coordination number.

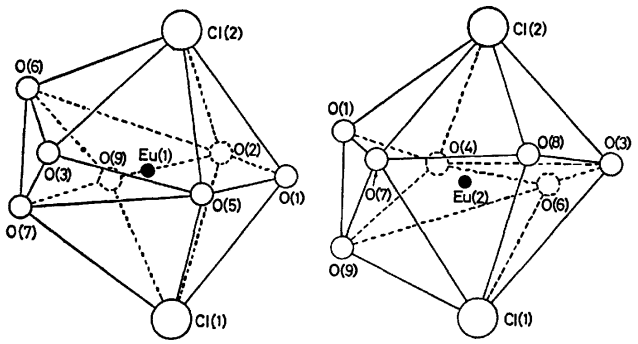

Fig. 2. Schematic illustrations of the $Eu(1)O_7Cl_2$ and $Eu(2)O_7Cl_2$ polyhedra in $Eu_2B_5O_9Cl$.

emissions at about 430 and 435 nm, and their Eu^{2+}-activated alkaline earth analogs are efficient phosphors. Since the ionic radius of the Sr^{2+} ion among alkaline earth cations is almost equal to that of the Eu^{2+} ion, strontium compounds are expected to be entirely isostructural with europium(II) analogs. Consequently, in order to discuss the relationship between the luminescence and structure of haloborates, we summarize the luminescence and structural properties for some Eu^{2+}-activated strontium compounds in Table 5.

The emission peak positions and shapes of Eu^{2+}-activated phosphors depend on the coordination numbers and symmetries of anions around Eu^{2+} ions, because the level of the $4f^65d$ excited state is affected by the crystal field. The haloborates, $Sr_2B_5O_9Cl : Eu^{2+}$ and $Sr_2B_5O_9Br : Eu^{2+}$, give emissions with a half-width of about 30 nm at 425—430 nm, while the emissions of $SrB_2O_4 : Eu^{2+}$ and $SrB_4O_7 : Eu^{2+}$ peak at about 367 nm. This must be because the symmetry of the EuO_7X_2 polyhedra (Fig. 2) is low compared with those[2a] of the EuO_8 and EuO_9 polyhedra in $SrB_2O_4 : Eu^{2+}$ and $SrB_4O_7 : Eu^{2+}$ because of the large X^- ions, although the Eu–O distances in these compounds are similar to one another (*e.g.*, 2.519 to 2.783 Å for EuB_2O_4[11] and 2.531 to 2.841 Å for EuB_4O_7[12]).

The quantum efficiencies of a series of Eu^{2+}-activated strontium borates greatly depend on the constructions of their borate units.[2] One of the quenching effects on Eu^{2+}-activated phosphors is a non-radiative process which proceeds by repeating the energy transfer *via* dipole-dipole interactions of Eu^{2+} ions.[13] Consequently, if the electrostatic shield effects of anions around the Eu^{2+} ions within them differ from one another, the values of their quantum efficiencies should vary with the degree of the shield effect. The Eu^{2+} ions in $SrB_2O_4 : Eu^{2+}$ are closely packed along $(BO_2)_\infty$ chains and are expected to interact easily with the neighboring Eu^{2+} ions on the (010) and (020) planes. The borate, $SrB_4O_7 : Eu^{2+}$, in which the Eu^{2+} ions are completely surrounded with the BO_4 tetrahedra of $(B_4O_7)_\infty$ network, gives a higher quantum efficiency than $SrB_2O_4 : Eu^{2+}$.

The quantum efficiency of $Sr_2B_5O_9X : Eu^{2+}$ is also very high compared with that of $SrB_2O_4 : Eu^{2+}$. The Eu^{2+} ions in $Sr_2B_5O_9X : Eu^{2+}$ are isolated from neighboring Eu^{2+} ions by the $(B_5O_9)_\infty$ network and X^- ions as well as those in $SrB_4O_7 : Eu^{2+}$; hence, the above-mentioned quenching effect can be expected to be small. Therefore, the high quantum efficiency of $Sr_2B_5O_9X : Eu^{2+}$ must be attributable to the arrangement of the borate units of the $(B_5O_9)_\infty$ network and X^- ions.

The authors wish to thank Dr. Noritake Yasuoka (Institute for Protein Research) and Professor Nobutami Kasai and Dr. Kunio Miki (Department of Applied Chemistry) for their helpful suggestions in connection with this study. The computations were carried out on an ACOS series 77 NEAC System 700 computer at the Crystallographic Research Center, Institute for Protein Research, Osaka University.

References

1) a) G. Blasse, *Phys. Status Solidi B*, **55**, K131 (1973); b) G. Blasse, "Structural and Bonding 26," Springer-Verlag, New York (1976), pp. 43—73.

2) a) K. Machida, G. Adachi, and J. Shiokawa, *J. Lumin.*, **21**, 101 (1979); b) K. Machida, G. Adachi, J. Shiokawa, M. Shimada, and M. Koizumi, *Inorg. Chem.*, **19**, 983 (1980).

3) C. Fouassier, A. Levasseur, and P. Hagenmuller, *J. Solid State Chem.*, **3**, 206 (1971).

4) K. Machida, T. Ishino, G. Adachi, and J. Shiokawa, *Mater. Res. Bull.*, **14**, 1529 (1979).

5) T. E. Peters and J. Baglio, *J. Inorg. Nucl. Chem.*, **32**, 1089 (1970).

6) T. Ashida, "The Universal Crystallographic Computing System-Osaka," The Computing Center, Osaka University (1979), pp. 53—59.

7) "International Tables for X-Ray Crystallography," Kynoch Press, Birmingham (1974), Vol. IV, pp. 72—102.

8) J. E. Greedan and G. J. McCarthy, *Mater. Res. Bull.*, **7**, 531 (1972).

9) T. R. McGuire and M. W. Shafer, *J. Appl. Phys.*, **35**, 984 (1964).

10) a) T. Ito, N. Morimoto, and R. Sadanaga, *Acta Crystallogr.*, **4**, 310 (1951); b) F. Jona, *J. Chem. Phys.*, **63**, 1750 (1959); c) F. Heide, G. Walter, and R. Urlau, *Naturwissenschaften*, **48**, 97 (1961); d) F. Heide and H. Beyrich, *Naturwissenschaften*, **52**, 181 (1965); e) J. Kobayashi, H. Schmid, and E. Ascher, *Phys. Status Solidi.*, **26**, 277 (1968); f) R. V. Pisarev, V. V. Druzhinin, S. D. Prochorova, N. N. Nesterova, and G. T. Andreeva, *Phys. Status Solidi*, **35**, 145 (1969); g) J. M. Trooster, *Phys. Status Solidi*, **32**, 179 (1969); h) W. J. Becker and G. Will, *Z. Kristallogr.*, **131**, 139 (1970); i) R. V. Pisrev, V. V. Druzhinin, N. N, Nesterova, S. D. Prochorova, and C. T. Andreeva, *Phys. Status Solidi*, **40**, 503 (1970); j) H. Schmid, *Phys. Status Solidi*, **37**, 209 (1970); k) T. A. Bither and H. S. Young, *J. Solid State Chem.*, **10**, 302 (1974).

11) K. Machida, G. Adachi, and J. Shiokawa, *Acta Crystallogr., Sect. B*, **35**, 149 (1979).

12) K. Machida, G. Adachi, and J. Shiokawa, *Acta Crystallogr., Sect. B*, **36**, 2008 (1980).

13) a) D. L. Dexter, *J. Chem. Phys.*, **21**, 836 (1953); b) G. Blasse, *Philips Res. Rep.*, **24**, 131 (1969); c) G. Blasse and A Bril, *Philips Tech. Rev.*, **31**, 304 (1970); d) A. L. N. Stevels and A. D. N. Schrama-de Pauw, *J. Electrochem. Soc.*, **123**, 691 (1976)

The Crystal Structure and Magnetic Property of Europium(II) Orthoborate

Ken-ichi MACHIDA, Gin-ya ADACHI,* Hajime HATA, and Jiro SHIOKAWA

Department of Applied Chemistry, Faculty of Engineering, Osaka University, Yamadakami, Suita, Osaka 565

(Received August 4, 1980)

The europium(II) orthoborate $Eu_3(BO_3)_2$ is trigonal, space group $R\bar{3}c$, with $a=9.069(1)$, $c=12.542(2)$ Å and $Z=6$. The structure has been refined to $R=0.082$ for 259 observed reflections with isotropic thermal parameters. The borate contains isolated and planar triangle BO_3^{3-} ions, the anions and Eu atoms being hexagonally packed along c. Each Eu atom is surrounded by 8 oxygens with Eu–O distances varying from 2.36 to 2.95 Å. The interatomic distances between Eu atoms are 3.509—4.200 Å for 8 nearest Eu neighbors and 4.831—5.450 Å for 6 second-nearest Eu neighbors. The 6 nearest Eu neighbors with the interatomic distances of 3.509 and 3.778 Å and the 4 second-nearest Eu neighbors with the Eu–O–Eu angle of 166.0° are effective for the magnetic exchange and superexchange interactions between Eu^{2+} ions, giving rise to ferromagnetism at low temperature.

Some europium(II) compounds have unique magnetic properties caused by the exchange and superexchange interactions between neighboring Eu^{2+} ions.[1] These interactions in oxides are closely related to the distances and angles *via* O^{2-} ions between the magnetic ions,[2] the arrangement of neighboring Eu^{2+} and O^{2-} ions around given Eu^{2+} ions being significant for interpreting their magnetic properties. For highly symmetrical compounds, *e.g.* EuO (rock salt type), $EuTiO_3$ (perovskite type) and Eu_2TiO_4 (K_2NiF_4 type), their magnetism has been discussed on the basis of their crystal structure.[3]

In a binary system $EuO-B_2O_3$, we have obtained a ferromagnetic compound, $Eu_3(BO_3)_2$, with $T_C=7.5$ K. This borate has been found to be isostructural with $Ca_3(BO_3)_2$,[4] which crystallizes in the trigonal system.[5] No three-dimensional structure analysis has been performed. The structures of other bivalent-cation orthoborates, $Zn_3(BO_3)_2$[6] and $Ni_3(BO_3)_2$,[7] have been determined. They consist of isolated triangle anions of BO_3 groups. Since the IR spectrum of $Eu_3(BO_3)_2$ is similar to that of zinc(II) and nickel(II) analogs,[8] $Eu_3(BO_3)_2$ is expected to contain BO_3^{3-} ions.

In this paper, we report the crystal structure of $Eu_3(BO_3)_2$ and discuss its magnetic property.

Experimental

Crystal Growth. The alkaline earth orthoborates [*e.g.* $Ca_3(BO_3)_2$ and $Sr_3(BO_3)_2$] have congruent melting points at 1400—1500 °C. However, $Eu_3(BO_3)_2$ has no melting point, decomposing into unknown compounds above 1400 °C. This might be due to the thermodynamic lability of Eu^{2+} ion.[9] The single crystals were prepared with use of a suitable flux: polycrystalline $Eu_3(BO_3)_2$ powder was mixed with a large excess of KCl, and the pelletized mixture was heated on a molybdenum boat at 1050 °C for 2 h in H_2 stream. The molten sample was allowed to cool to 750 °C at a rate of 3 °C/h, fine black hexagonal prisms being obtained by removing the flux with water.

Magnetic Susceptibility Measurements. The magnetic susceptibility of the powder sample was measured with a Shimadzu magnetic balance MB-11 (80—300 K) and a Faraday magnetic balance (2—80 K) constructed by Muneyuki Date and Ki-ichi Okuda (Department of Physics, Osaka University).

X-Ray Data Collection. Preliminary Weissenberg photographs showed that the crystals obtained belong to the trigonal system and that its space group is R3c or $R\bar{3}c$ from the systematic absence (*hkl*, $-h+k+l=3n+1$ and $3n+2$; *h0l*, $l=2n+1$). The cell parameters (Table 1) were determined by a least-squares treatment of the X-ray powder pattern (Cu $K\alpha$) calibrated with high purity silicon as an internal standard. The intensity data were measured on a Rigaku Denki automated four-circle diffractometer with Mo $K\alpha$ radiation monochromated with graphite. The ω-2θ scan method was employed at a scanning rate of 4°/min, the dimension of the crystal used being 0.08 mm (side to side of hexagonal cross section) × 0.04 mm (thickness). All possible reflections with the indices of hkl and *hkl* were collected up to $2\theta=70°$. Three standard reflections were monitored every 60 reflections, no apparent decay in intensity being detected. The intensity values for equivalent reflections were averaged and 259 nonzero reflections were used for analysis. The Lorentz and polarization corrections were applied, but not the absorption correction.

Table 1. CRYSTAL DATA

$F.W.=573.50$	$\lambda=0.71069$ Å
Trigonal	μ(Mo $K\alpha$)$=31.26$mm^{-1}
Space group $R\bar{3}c$	$D_m=6.31$ g cm^{-3}
$a=9.069(1)$ Å	$D_x=6.40$
$c=12.542(2)$	$Z=6$
$V=893.3(3)$Å^3	$F(000)=1482$

Structure Determination and Refinement. The structure was solved by the conventional heavy atom method and refined by the full-matrix least-square method (*FMLS* program[10]) based on the observed reflections, the minimized function being $\sum w(|F_o|-|F_c|)^2$ where $w=1$ for all $|F_o|$. From a three-dimensional Patterson synthesis, the centrosymmetric space group $R\bar{3}c$ was chosen and the coordinate of Eu atom determined to be at a special position (18e site). The remaining atoms (O and B) were located on the successive Fourier maps: O at the general position (36d site) and B at the 12c site on three-fold axis. Isotropic refinement for all atomic paramaters was carried out to give $R=0.082$ for 259 observed reflections. The atomic scattering factors for Eu, O, and B atoms were those given in International Tables for X-Ray Crystallography.[11] The final positional and thermal param-

Table 2. FINAL POSITIONAL AND THERMAL PARAMETERS[a] WITH THEIR STANDARD DEVIATIONS IN PARENTHESES

Atom	x	y	z	B/Å^2
Eu	3075(18)	0	2500	0.45(4)
O	164(23)	33(23)	396(18)	0.88(27)
B	0	0	39(6)	1.3(8)

a) The coordinates are multiplied by 10^4 for Eu atom, 10^3 for O atom and 10^2 for B atom.

eters are given in Table 2.†

Results and Discussion

The crystal structure of $Eu_3(BO_3)_2$ is shown in Fig. 1, and the bond lengths and angles are given in Table 3. The borate contains isolated and planar triangles of BO_3 groups with a B–O distance of 1.36 Å like other orthoborates,[6,7] the crystal consisting of Eu atoms and BO_3 groups hexagonally packed along c. The triangle planes of BO_3 groups are perpendicular to the c axis. Each Eu atom is surrounded by 8 oxygens to form an EuO_8 polyhedron with Eu–O distances varying from 2.36 to 2.95 Å (Fig. 2). An Eu atom has 8 nearest and 6 second-nearest neighboring Eu atoms with the mean interatomic distances 3.816 and 5.244 Å, respectively.

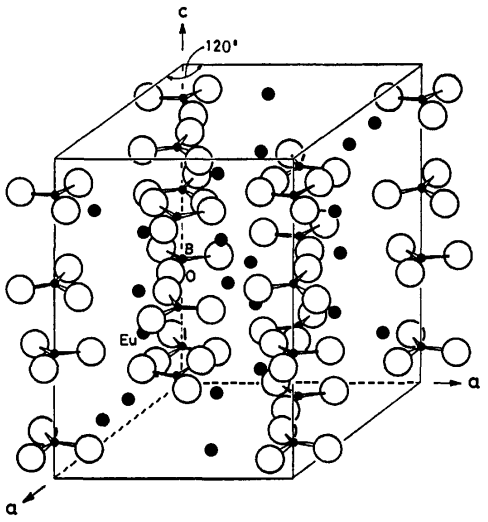

Fig. 1. Crystal structure of $Eu_3(BO_3)_2$.

TABLE3. INTERATOMIC DISTANCES (Å) AND BOND ANGLES (°)

(a) The BO_3 triangle			
B–O	1.36(6)	O–B–O	120(0)
(b) Eu–Eu distances			
Nearest neighbors		Second-nearest neighbors	
Eu–Eu^{i}	3.509(3)	Eu–Eu^{iv}	5.450(3)
–Eu^{ii}	3.778(3)	–Eu^{v}	4.831(3)
–Eu^{iii}	4.200(3)		
(c) Eu–O distances			
Eu–O^{i}	2.92(3)	Eu–O^{iii}	2.95(3)
–O^{ii}	2.58(3)	–O^{iv}	2.36(3)
(d) Eu–O–Eu angles			
Nearest neighbors		Second-nearest neighbors	
Eu–O–Eu^{i}	82.7(7)	Eu–O–Eu^{iv}	166.0(4)
–O–Eu^{ii}	80.1(6)		
	85.9(7)		
	99.8(8)		
–O–Eu^{iii}	103.9(8)		

Symmetry code: Eu^{i} $(1/3-x, -1/3, 1/6+z; 2/3-x, 1/3, 1/3-z)$, Eu^{ii} $(1/3, 2/3-x, 1/6+z; 1/3+x, -1/3+x, 1/6+z: 2/3, 1/3-x, 1/3-z; -1/3+x, -2/3+x, 1/3-z)$, Eu^{iii} $(-1/3+x, 1/3, 1/3+z; 1/3-x, 2/3-x, -1/3+z)$, Eu^{iv} $(1-x, 1-x, z; 1, x, z; 1-x, -x, z; 0, -1+x, z)$, Eu^{v} $(0, x, z; -x, -x, z)$, O^{i} $(x, y, z; x-y, -y, 1/2-z)$, O^{ii} $(2/3-x+y, 1/3+y, -1/6+z; 1/3-x, -1/3-y, 2/3-z)$, O^{iii} $(2/3-y, 1/3-x, -1/6+z; 1/3+x-y, -1/3+x, 2/3-z)$, O^{iv} $(2/3-x, 1/3-x+y, 5/6-z; 1/3-y, -1/3+x-y, 1/3+z)$.

† The F_o-F_c Table is kept as Document No. 8115 at the Chemical Society of Japan.

The temperature dependence of magnetization and susceptibility of $Eu_3(BO_3)_2$ are shown in Fig. 3. The borate is a ferromagnetic with a Curie point (T_C) of *ca.* 7.5 K and a paramagnetic Curie temperature (θ_C) of *ca.* 8 K. The magnetization per Eu^{2+} ion below the Curie point is saturated to *ca.* 7 μB.

Kasuya[2] suggested that the magnetism of europium-(II) compounds is attributable to the magnetic exchange and superexchange interactions taking place *via* the overlap of 4f and 5d orbitals between neighboring Eu^{2+} ions. The magnetism of highly symmetrical compounds, EuO (T_C=69 K),[1d] $EuTiO_3$ (T_N=5.3 K)[1f] and Eu_2TiO_4 (T_C=9 K),[3] has been interpreted in terms of the magnitude of the magnetic interactions between the nearest and second-nearest neighboring Eu^{2+} ions. The direct Eu^{2+}–Eu^{2+} interactions between the nearest Eu neighbors are responsible for the ferromagnetic interaction, the 90° Eu^{2+}–O^{2-}–Eu^{2+} superexchanging pairs undergoing the antiferromagnetic interaction *via*

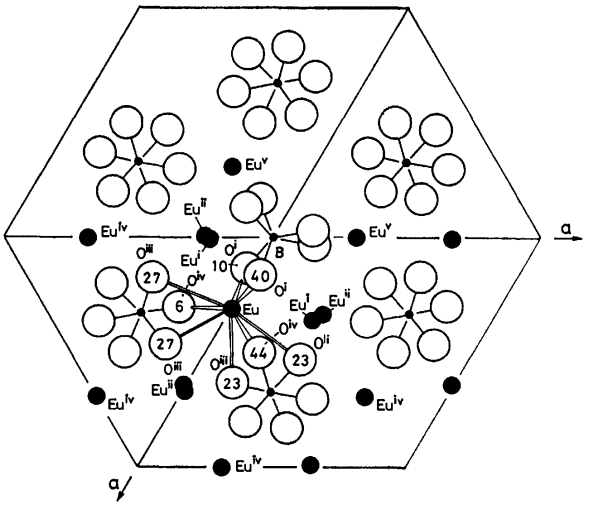

Fig. 2. A projection between z=0 and 0.5 of the $Eu_3(BO_3)_2$ structure viewed along the c axis. Numerical values give the fractional Z coordinates of O atoms.

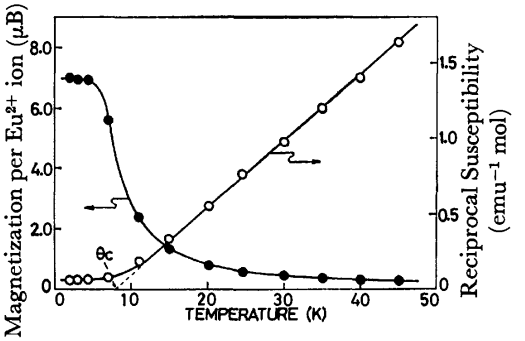

Fig. 3. Temperature dependences of magnetization and reciprocal susceptibility of $Eu_3(BO_3)_2$.

the O^{2-} ions at an angle of 90°. The 180° Eu^{2+}–O^{2-}–Eu^{2+} superexchange interactions between the second-nearest Eu neighbors contribute to the overall magnetism, ferromagnetically or antiferromagnetically, as the case may be. The difference among the magnetic properties of europium(II) compounds results from the difference in magnitude for the above-mentioned interactions.

From the Heisenberg model and molecular field approximation, McGuire *et al.*[1b,1d,1f] expressed the θ_C value as follows:

$$\theta_C = \frac{2}{3k} S\,(S+1)\,(Z_1J_1 + Z_2J_2), \qquad (1)$$

where J_1 and J_2 denote the effective exchange integrals between the nearest and second-nearest neighboring Eu^{2+} ions, respectively, and Z_1 and Z_2 the numbers of the nearest and second-nearest Eu neighbors, respectively. For the oxides, EuO, $EuTiO_3$, and Eu_2TiO_4, the direct Eu^{2+}–Eu^{2+} exchange and indirect 90° Eu^{2+}–O^{2-}–Eu^{2+} superexchange interactions are responsible for J_1, positively and negatively, respectively. The 180° Eu^{2+}–O^{2-}–Eu^{2+} superexchange interactions contribute to the value of J_2. The magnitude of direct exchange interactions is strongly influenced by the Eu–Eu distance, but that of superexchange interactions is not.

Each Eu^{2+} ion in $Eu_3(BO_3)_2$ has 8 nearest and 6 second-nearest neighboring Eu^{2+} ions. The nearest Eu neighbors with the interatomic distances of 3.509 and 3.778 Å contribute as the exchanging and superexchanging pairs, but not the nearest Eu neighbors with 4.200 Å, the distance of 4.200 Å appearing to be too great to interact with the neighboring Eu^{2+} ions as judged by the cases of other europium(II) compounds. For example, the mean distance between the nearest Eu neighbors in EuB_4O_7 (paramagnetic) is 4.338 Å and insufficient for the magnetic interactions.[12] In the nearest Eu neighbors, therefore, we can point out two kinds of effective exchanging pairs (Fig. 4). Type 1: the Eu–Eu^{i} pair with two 82.7° Eu^{2+}–O^{2-}–Eu^{2+}; Type 2: the Eu–Eu^{ii} pair with three 80.1—99.8° Eu^{2+}–O^{2-}–Eu^{2+}.

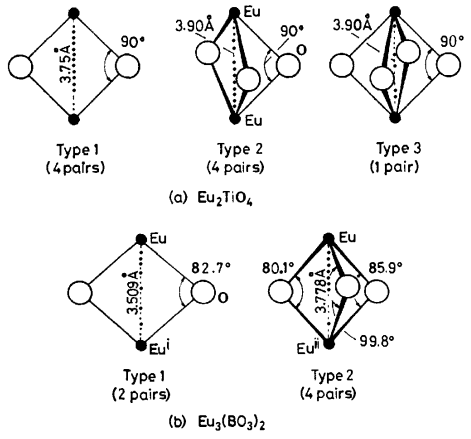

Fig. 4. Anions environments around exchanging pairs between nearest neighboring Eu^{2+} ions in Eu_2TiO_4 and $Eu_3(BO_3)_2$.

For the second-nearest Eu neighbors, four Eu–Eu^{iv} pairs *via* an O^{2-} ion at 166.0° correspond to the 180° Eu^{2+}–O^{2-}–Eu^{2+} superexchanging pairs in EuO, $EuTiO_3$ and Eu_2TiO_4, although the Eu–O–Eu angle somewhat deviates from the value of 180°. The remaining two Eu–Eu^{v} pairs can not be regarded as the superexchanging pairs because no oxygen occupies the position between them.

Greedan and McCarthy[3] estimated the values of exchange integrals J_1/k and J_2/k of Eu_2TiO_4 to confirm agreement with the experimental value (θ_C=10 K) using Eq. 1: J_1/k=0.07 and J_2/k=0.04 K (Table 4). An Eu^{2+} ion in Eu_2TiO_4 is surrounded by 9 nearest and 8 second-nearest neighboring Eu^{2+} ions with the interatomic distances of 3.75 to 3.90 Å and 5.51 Å, respectively. The Eu–Eu distances and Eu–O–Eu angles in Eu_2TiO_4 are closely similar to those of $Eu_3(BO_3)_2$.

In Eu_2TiO_4, there are three kinds of exchanging pairs between the nearest Eu neighbors, Types 1 and 2 correspond to those of $Eu_3(BO_3)_2$, the Eu–Eu distances in the borate being smaller than those in the titanate (Fig. 4). The exchanging pair (Type 3), not existing in $Eu_3(BO_3)_2$, is the pair with four 90° Eu^{2+}–O^{2-}–Eu^{2+} and contributing antiferromagnetically to the overall magnetism in a simillar manner to that of the exchanging pairs in $EuTiO_3$.[1f,3] Thus, $Eu_3(BO_3)_2$ is expected to give the greater values of J_1/k than Eu_2TiO_4. The superexchanging pairs between the second-nearest Eu neighbors in Eu_2TiO_4 and $Eu_3(BO_3)_2$ should give similar values of J_2/k from the similarity of the Eu–Eu distances and Eu–O–Eu angles. From the observed θ_C value of 8 K, we can estimate the values of J_1/k and J_2/k to be 0.10 and 0.04 K, substituting S=7/2,

TABLE 4. MAGNETIC EXCHANGE AND SUPEREXCHANGE INTERACTIONS IN Eu_2TiO_4 AND $Eu_3(BO_3)_2$

	Eu_2TiO_4[a]	$Eu_3(BO_3)_2$
T_c/K	9	7.5
θ_c/K[b]	10	8
Nearest neighbors	5 Eu^+ at 3.90 Å 4 Eu^+ at 3.75	2 Eu^+ at 3.509 Å 4 Eu^+ at 3.778
Second-nearest neighbors	8 Eu^+ at 5.51	4 Eu^+ at 5.450
Interactions contributing to J_1	Eu^{2+}–Eu^{2+}(+) 90°Eu^{2+}–O^{2-}–Eu^{2+}(−)	Eu^{2+}–Eu^{2+}(+) 80.1—99.8°Eu^{2+}–O^{2-}–Eu^{2+}(−)
Resultant J_1k^{-1}/K	0.07	0.10
Interactions contributing to J_2	180°Eu^{2+}–O^{2-}–Eu^{2+}	166.0°Eu^{2+}–O^{2-}–Eu^{2+}
Resultant J_2k^{-1}/K	0.04	0.04

a) Ref. 8. b) θ_c = paramagnetic Curie temperature.

$Z_1=6$ and $Z_2=4$ into Eq. 1. It is concluded that the 166.0° Eu^{2+}–O^{2-}–Eu^{2+} superexchanging pairs contribute ferromagnetically and the ferromagnetism of $Eu_3(BO_3)_2$ is attributable to the direct Eu^{2+}–Eu^{2+} and the 166.0° Eu^{2+}–O^{2-}–Eu^{2+} ferromagnetic interactions.

The authors wish to thank Mr. Ken-ichi Sakaguchi for the measurements on the four-circle X-ray diffractometer, and Dr. Noritake Yasuoka (Institute for Protein Research) and Prof. Nobutami Kasai and Dr. Kunio Miki (Department of Applied Chemistry) for their valuable suggestions. The computations were carried out on an ACOS series 77 NEAC System 700 computer at Crystallographic Center, Institute for Protein Research, Osaka University.

References

1) a) B. T. Matthias, R. M. Bozorth, and J. H. Van Vleck, *Phys. Rev. Lett.*, **7**, 160 (1961); b) T. R. McGuire, B. E. Argyle, M. W. Shafer, and J. S. Smart, *J. Appl. Phys.*, **34**, 1345 (1963); c) M. W. Shafer, T. R. McGuire, and J. C. Suits, *Phys. Rev. Lett.*, **11**, 251 (1963); d) T. R. McGuire and M. W. Shafer, *J. Appl. Phys.*, **25**, 984 (1964); e) M. W. Shafer, *J. Appl. Phys.*, **36**, 1145 (1965); f) T. R. McGuire, M. W. Shafer, R. J. Joenk, H. A. Alperin, and S. J. Pickart, *J. Appl. Phys.*, **37**, 981 (1966).

2) T. Kasuya, *IBM J. Res. Develop.*, **14**, 214 (1970).

3) J. E. Greedan and G. J. McCarthy, *Mater. Res. Bull.*, **7**, 531 (1972).

4) H. Hata, G. Adachi, and J. Shiokawa, *Mater. Res. Bull.*, **12**, 811 (1977).

5) J. Majling, V. Figusch, F. Hanic, V. Wiglasz, and J. Corba, *Mater. Res. Bull.*, **9**, 1379 (1974).

6) S. Garcia-Blanco and J. Fayos, *Z. Kristallogr.*, **127**, 145 (1968).

7) J. Pardo, M. Martinez-Ripoll, and S. Garcia-Blanco, *Acta Crystallogr., Sect. B*, **30**, 37 (1974).

8) C. E. Weir and R. A. Schroeder, *J. Res. Natl. Bur. Stand.*, **68A**, 465 (1964).

9) G. J. McCarthy and W. B. White, *J. Less-Common Met.*, **22**, 409 (1970).

10) T. Ashida, "The Universal Crystallographic Computing System-Osaka," The Computing Center, Osaka University (1979), p. 60.

11) "International Tables for X-Ray Crystallography," Kynoch Press, Birmingham (1974), Vol. IV, pp. 72—102.

12) K. Machida, G. Adachi, and J. Shiokawa, *Acta Crystallogr., Sect. B*, **36**, 2008 (1980).

Optical Resolution and Circular Dichroism Spectra of Mixed-diamine Palladium(II) Complexes with Configurational Chirality

Kazuhiko NAKAYAMA,* Takashi KOMORITA, and Yoichi SHIMURA

Department of Chemistry, Faculty of Science, Osaka University, Toyonaka, Osaka 560

(Received August 18, 1980)

Six square-planar complexes, [PdL(*meso*-stien)]$(ClO_4)_2$ (*meso*-stien=*meso*-1,2-diphenyl-1,2-ethanediamine; L=*N*,*N*-diethylethylenediamine, *N*,*N*-dimethylethylenediamine, 2-methyl-1,2-propanediamine, N^2,N^2-dimethyl-2-methyl-1,2-propanediamine, *N*,*N*-dimethyl-1,3-propanediamine, and (2*S*)-N^1,N^1-diethyl-1,2-propanediamine), were prepared and optically resolved (or separated in the case of the last named ligand) using diacetyl-*d*-tartaric anhydride as the resolving agent. Their electronic absorption and CD spectra were measured. A definite additivity has been confirmed between the configurational CD caused by the chiral configuration and the vicinal CD due to the asymmetric carbon atom in the (2*S*)-N^1,N^1-diethyl-1,2-propanediamine complex. Absolute configurations of this and the other five complexes have been assigned by examining molecular models and the CD spectra.

Circular dichroism (CD) of a metal complex in the d-d transition region generally arises from two kinds of main chirality, *i.e.*, the configurational one of the whole complex, and the vicinal one due to the asymmetric atoms of the ligands, the latter including the so-called conformational chirality of the chelate rings, if any. Although many kinds of Pt(II) and Pd(II) complex show d-d CD spectra owing to the vicinal effect,[1] only a limited number of square-planar complexes have been found to have the configurational chirality. The well-known complexes [M(2-methyl-1,2-propanediamine) (*meso*-stien)]$^{2+}$ (M=Pt[2] and Pd[3]) are unique examples of a successful optical resolution of the configurationally chiral complexes with square-planar coordination geometry. These complexes have a particular kind of configurational chirality, which arises from a combination of two types of bidentate ligands, an h-type which has a symmetry plane coplanar to the coordination square but none perpendicular to it in the conformationally averaged state, and a v-type which has the latter kind of symmetry plane but not the former kind (Fig. 1).

This paper reports the preparation, optical resolution, CD spectra, and absolute-configuration assignment of a series of such complexes, [Pd(h-type diamine) (*meso*-stien)]$^{2+}$. The ligands are given in Table 1. The complex [Pd(N^1,N^1-Et_2-(*S*)-pn) (*meso*-stien)]$^{2+}$ containing both kinds of chirality due to the asymmetric carbon atom and to the configuration was also examined in order to establish a criterion for the assignment of absolute configuration.

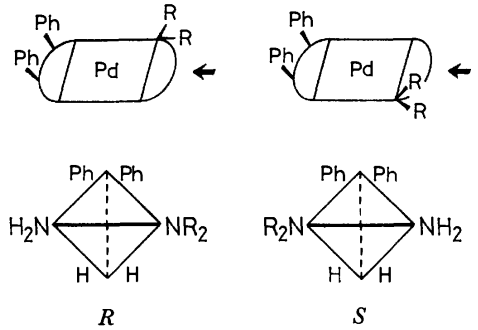

Fig. 1. Absolute configuration of the complex; the lower drawing shows the complex which is viewed along the arrow and regarded as a tetrahedron.

Table 1. Abbreviations and classification of the ligands

Abbreviation	Rational formula	Classification
N,*N*-Et_2en	$(C_2H_5)_2NCH_2CH_2NH_2$	h-type
N^1,N^1-Et_2-(*S*)-pn	$(C_2H_5)_2NCH_2CH(CH_3)NH_2$	——
N,*N*-Me_2en	$(CH_3)_2NCH_2CH_2NH_2$	h-type
C,*C*-Me_2en[a]	$H_2NC(CH_3)_2CH_2NH_2$	h-type
N,*N*,*C*,*C*-Me_4en[b]	$(CH_3)_2NC(CH_3)_2CH_2NH_2$	h-type
N,*N*-Me_2tn	$(CH_3)_2NCH_2CH_2CH_2NH_2$	h-type
meso-stien	$H_2NCH(Ph)CH(Ph)NH_2$	v-type
en	$H_2NCH_2CH_2NH_2$	——

a) 2-Methyl-1,2-propanediamine; the abbreviation is based on the name for a substituted ethylenediamine, specifying the atom to which the substituents attach. b) N^2,N^2-Dimethyl-2-methyl-1,2-propanediamine; abbreviation as in a).

Experimental

Ligands. *(1)* N,N,C,C-*Me_4en*: 2-Dimethylamino-2-methylpropanenitrile[4] (bp 54.3 °C/3.13 kPa; 56.6 g) in 130 cm^3 of anhydrous ether was added dropwise with stirring (at *ca.* −5 °C) to 25 g of lithium tetrahydridoaluminate suspended in 950 cm^3 of anhydrous ether. After the mixture had been stirred in an ice-bath for five hours, 28 cm^3 of water and 24 cm^3 of a 20% aqueous solution of potassium hydroxide were successively added with vigorous stirring. The ether layer was decanted from the slurry, from which the residue was extracted three times with 150 cm^3 portions of boiling ether. The combined mother liquor and extracts were treated with dry hydrogen chloride gas in an ice-bath. The white precipitate was mixed with a large excess of potassium hydroxide and a small amount of water, and the oil separated was extracted several times with boiling ether. The combined ether extracts were dried over potassium hydroxide pellets and then with sodium wire, and fractionally distilled. The fraction boiling at 61—62 °C/5.20 kPa was collected. Yield: 38.3 g.

(2) C,C-*Me_2en*: 2-Amino-2-methylpropanenitrile was obtained according to the method reported;[5] bp 61.5—62.0 °C/

3.60 kPa. The subsequent procedure was the same as described in *(1)*. bp 41.5 °C/2.87 kPa.

(3) Other Ligands: The following ligands were prepared by the methods reported: N^1,N^1-Et_2-(*S*)-pn[6] (bp 145—152 °C/100 kPa) and *meso*-stien[2,7] (Found: C, 79.25; H, 7.57; N, 13.19%).

Resolving Agent. Diacetyl-*d*-tartaric anhydride was obtained by the method of Chattaway and Parkes[8] (Found: C, 43.85; H, 3.88%).

[$PdCl_2L$]-type Complexes. (1) L=N,N-*Et_2en and* N^1,N^1-*Et_2-(S)-pn*: These complexes were prepared by a method similar to that of Suzuki and Nishida.[6] Found: C, 24.36; H, 5.52; N, 9.55%. Calcd for [$PdCl_2$(*N,N*-Et_2en)]=$C_6H_{16}N_2Cl_2Pd$: C, 24.55; H, 5.49; N, 9.54%. Found: C, 27.30; H, 5.92; N, 9.11%. Calcd for [$PdCl_2$(N^1,N^1-Et_2-(*S*)-pn)]=$C_7H_{18}N_2Cl_2Pd$: C, 27.34; H, 5.90; N, 9.11%.

(2) L=N,N-*Me_2en*, C,C-*Me_2en*, N,N,C,C-*Me_4en, and* N,N-*Me_2tn*: These complexes were obtained by a method similar to that for [$PdCl_2$(en)][9] as light orange to yellow crystals. Found: C, 18.01; H, 4.58; N, 10.56%. Calcd for [$PdCl_2$(*N,N*-Me_2en)]=$C_4H_{12}N_2Cl_2Pd$: C, 18.10; H, 4.56; N, 10.55%. Found: C, 18.09; H, 4.56; N, 10.65%. Calcd for [$PdCl_2$(*C,C*-Me_2en)]=$C_4H_{12}N_2Cl_2Pd$: C, 18.10; H, 4.56; N, 10.55%. Found: C, 23.06; H, 5.81; N, 8.97%. Calcd for [$PdCl_2$(*N,N,C,C*-Me_4en)]·H_2O=$C_6H_{18}N_2Cl_2OPd$: C, 23.13; H, 5.82; N, 8.99%. Found: C, 21.54; H, 5.07; N, 9.96%. Calcd for [$PdCl_2$(*N,N*-Me_2tn)]=$C_5H_{14}N_2Cl_2Pd$: C, 21.49; H, 5.05; N, 10.02%.

(3) L=meso-*stien*: When a methanol solution of *meso*-stien was mixed with an aqueous solution of K_2[$PdCl_4$] at *ca.* 60 °C (molar ratio 2 : 1), an ivory-colored insoluble precipitate was obtained. After two hours of heating and stirring, hydrochloric acid (equimolar with the *meso*-stien) was added to the mixture. The precipitate which had turned pale yellow was collected and washed with boiling water several times in order to remove *meso*-stien·2HCl (only slightly soluble). Found: C, 43.09; H, 4.15; N, 7.18%. Calcd for [$PdCl_2$(*meso*-stien)]=$C_{14}H_{16}N_2Cl_2Pd$: C, 43.16; H, 4.14; N, 7.19%.

[Pd(N)$_4$]-type Complexes. (1) [*Pd(*N,N-*Et_2en)(*meso-*stien)*]*(ClO_4)$_2$*: A hot methanol-solution (3 cm^3) containing 0.76 g of *meso*-stien was added (at *ca.* 55 °C) to an aqueous solution (30 cm^3) of [$PdCl_2$(*N,N*-Et_2en)] (1.05 g). The almost colorless solution was filtered and treated with an aqueous solution of sodium perchlorate (1.2 g), at *ca.* 50 °C with stirring. The desired complex precipitated during the course of addition of perchlorate drop by drop. The mixture was allowed to stand at room temperature and then in a refrigerator overnight. Very pale yellow crystals were collected, washed with water, and dried *in vacuo*. Yield: 2.0 g. This product is sparingly soluble in water, being more soluble in methanol. Found: C, 37.82; H, 5.12; N, 8.92%. Calcd for $C_{20}H_{32}N_4Cl_2O_8Pd$: C, 37.90; H, 5.09; N, 8.84%.

(2) [*Pd(*N^1,N^1-*Et_2-(S)-pn)(*meso-*stien)*]*(ClO_4)$_2$*: This was prepared by the same method as described in *(1)*. The crude product was purified by conversion into the corresponding chloride with an anion-exchange resin (Dowex 1×8, 200—400 mesh, Cl^- form) and then by reconversion into the perchlorate crystals. The yield was good. The product, labeled **2′**, is a mixture of *R*(*S*) and *S*(*S*) isomer, neither a pseudo racemate nor an equilibrium mixture. Found: C, 38.96; H, 5.35; N, 8.71%. Calcd for $C_{21}H_{34}N_4Cl_2O_8Pd$: C, 38.93; H, 5.29; N, 8.65%.

(3) [*Pd(*N,N-*Me_2en)(*meso-*stien)*]*(ClO_4)$_2$·H_2O*: To a suspension of [$PdCl_2$(*N,N*-Me_2en)] (1.00 g) in 35 cm^3 of water was added (at *ca.* 60 °C) 0.80 g of *meso*-stien dissolved in hot methanol (4 cm^3). When the mixture was stirred for a few minutes, the starting material was dissolved, the solution turning almost colorless. An aqueous solution of sodium perchlorate (1.2 g) was added to the filtered solution, at *ca.* 55 °C with stirring. The resulting cloudy solution was allowed to stand at room temperature for three hours, a powder product (very pale yellow; 0.82 g) being collected. The residual glassy solid adhering to the bottom of the beaker was dissolved again in the mother liquor at 70—75 °C, and the solution was allowed to stand at room temperature and then in a refrigerator overnight; an additional amount of the product was obtained (0.36 g). After removal of the potassium chloride by methanol extraction, further crops (0.52 and 0.31 g) were obtained from the mother liquor. Total yield: 2.01 g. The complex is more soluble in water and in methanol than the corresponding *N,N*-Et_2en complex. Found: C, 34.76; H, 4.83; N, 8.89%. Calcd for $C_{18}H_{30}N_4Cl_2O_9Pd$: C, 34.66; H, 4.85; N, 8.98%.

(4) [*Pd(*C,C-*Me_2en)(*meso-*stien)*]*(ClO_4)$_2$*: This was prepared by a method similar to that described in *(3)*, but is more difficult to crystallize. The yield was 1.63 g for 1.00 g of the starting material [$PdCl_2$(*C,C*-Me_2en)]. The solubility (in water and in methanol) is comparable to that of the corresponding *N,N*-Me_2en complex. Found: C, 35.67; H, 4.72; N, 9.22%. Calcd for $C_{18}H_{28}N_4Cl_2O_8Pd$: C, 35.69; H, 4.66; N, 9.25%.

(5) [*Pd(*N,N,C,C-*Me_4en)(*meso-*stien)*]*(ClO_4)$_2$*: This was obtained in the same way as described in *(3)*, and is more difficult to crystallize than the corresponding *C,C*-Me_2en complex. It tended to disproportionate to [Pd(*N,N,C,C*-Me_4en)$_2$]$^{2+}$ and [Pd(*meso*-stien)$_2$]$^{2+}$ during the course of preparation. The yield was 1.63 g for 1.30 g of the starting material [$PdCl_2$(*N,N,C,C*-Me_4en)]. Found: C, 38.09; H, 5.11; N, 8.77%. Calcd for $C_{20}H_{32}N_4Cl_2O_8Pd$: C, 37.90; H, 5.09; N, 8.84%.

(6) [*Pd(*N,N-*Me_2tn)(*meso-*stien)*]*(ClO_4)$_2$·0.5H_2O*: A methanol solution (3 cm^3) containing 0.26 g of *N,N*-Me_2tn was added to 0.985 g of [$PdCl_2$(*meso*-stien)] suspended in a water (23 cm^3)–methanol (7 cm^3) mixture. After the reaction mixture had been stirred at *ca.* 50 °C for 1.5 h, undissolved material was filtered off. The filtrate was treated with an aqueous solution of sodium perchlorate (0.80 g), and evaporated under reduced pressure to give a sirup. The sodium chloride was removed by extracting the complex with methanol, *ca.* 25 cm^3 of water being added to the extract (*ca.* 15 cm^3). The warmed mixture was allowed to stand at room temperature. The desired product was obtained as pale yellow needles (1.00 g). Total yield was 1.18 g, including another crop from the mother liquor. Found: C, 36.17; H, 4.99; N, 8.83%. Calcd for $C_{19}H_{31}N_4Cl_2O_{8.5}Pd$: C, 36.29; H, 4.97; N, 8.91%.

The anhydrous salt, [Pd(*N,N*-Me_2tn)(*meso*-stien)](ClO_4)$_2$ (pale yellow blocks), was also obtained by using [$PdCl_2$(*N,N*-Me_2tn)] as a starting material, the yield being low. Found: C, 36.91; H, 4.89; N, 8.96%. Calcd for $C_{19}H_{30}N_4Cl_2O_8Pd$: C, 36.82; H, 4.88; N, 9.04%.

(7) [*Pd(*N^1,N^1-*Et_2-(S)-pn)(en)*]Cl_2·H_2O (**7**): An aqueous solution containing 0.12 g of ethylenediamine was added at *ca.* 65 °C to 0.61 g of [$PdCl_2$(N^1,N^1-Et_2-(*S*)-pn)] suspended in 16 cm^3 of water. The reaction was fast. The almost colorless solution was filtered and evaporated under reduced pressure. The resulting sirup was dissolved in a small amount of ethanol and mixed with 15 cm^3 of acetone. The mixture was cooled in a refrigerator overnight to give very pale yellow needles. Yield: 0.60 g. The compound can be recrystallized from 95% ethanol by adding acetone, when necessary. Found: C, 28.02; H, 7.25; N, 14.63%. Calcd for $C_9H_{28}N_4Cl_2OPd$: C, 28.03; H, 7.32; N, 14.53%.

Optical Resolution and Separation. The diacetyl-*d*-tartrate

salts of all the configurationally chiral complexes were obtained as a sirup as follows.

General Procedure: A suspension of racemic perchlorate salt[10] (1.80 mmol) in 50 cm³ of water was stirred with an anion-exchange resin (Dowex 1×8, 200—400 mesh, Cl^- form) for one hour. After removal of the resin the reaction mixture was treated with silver carbonate (2.0 mmol) at room temperature for two hours in the dark. The silver chloride was filtered off and diacetyl-*d*-tartaric anhydride (1.75 mmol) was dissolved in the filtrate. The solution was evaporated under reduced pressure to give a sirup.

The subsequent procedure for individual complexes is as follows.

(1) $(+)^{CD}_{220}$-[*Pd*(N,N-*Et*$_2$*en*)(meso-*stien*)]$(ClO_4)_2$ (**1**): The sirup obtained by the general procedure was dissolved in methanol (6 cm³) and mixed with 20 cm³ of acetone. Almost white powder was deposited on scratching the wall of the beaker. It was collected and recrystallized twice from 90% methanol by adding acetone. An additional amount of the product was obtained from the mother liquor and repeatedly recrystallized. A high yield (91% based on the half of the racemate) was attained in total because of the moderately fast shift of the equilibrium ($R \rightleftharpoons S$) in the mother liquor. Found: C, 48.84; H, 6.18; N, 8.13%. Calcd for $(+)^{CD}_{220}$-[Pd(*N*,*N*-Et_2en)(*meso*-stien)](diac-*d*-tart)·H_2O[11] = $C_{28}H_{42}N_4O_9Pd$: C, 49.09; H, 6.18; N, 8.18%. The less-soluble diastereomer (0.18 g) was dissolved in 7 cm³ of water and treated with an aqueous solution (2 cm³) of sodium perchlorate (0.09 g). Very pale yellow crystals were collected after several hours, washed with water, and dried *in vacuo*. Yield: 0.135 g. Found: C, 37.93; H, 5.10; N, 8.84%. Calcd for $C_{20}H_{32}N_4Cl_2O_8Pd$: C, 37.90; H, 5.09; N, 8.84%.

(2) $(+)^{CD}_{220}$-[*Pd*(N^1,N^1-*Et*$_2$-(S)-*pn*)(meso-*stien*)]$(ClO_4)_2$ (**2**): The sirup obtained by the general procedure was crystallized from a 90% ethanol–acetone (2 : 1) mixture, giving a crude less-soluble diastereomer (diac-*d*-tart salt), which was recrystallized three times from 90% ethanol by adding acetone. Found: C, 48.38; H, 6.29; N, 7.79%. Calcd for $(+)^{CD}_{220}$-[Pd(*N*^{1},*N*^{1}-Et_2-(*S*)-pn)(*meso*-stien)](diac-*d*-tart)·$2H_2O$ = $C_{29}H_{46}N_4O_{10}Pd$: C, 48.57; H, 6.47; N, 7.81%. The resolving agent was removed by the same method as described in *(1)*. Found: C, 38.92; H, 5.29; N, 8.65%. Calcd for $C_{21}H_{34}N_4Cl_2O_8Pd$: C, 38.93; H, 5.29; N, 8.65%.

(3) $(+)^{CD}_{220}$-[*Pd*(N,N-*Me*$_2$*en*)(meso-*stien*)]$(ClO_4)_2 \cdot 0.5H_2O$ (**3**): A crude less-soluble diastereomer (diac-*d*-tart salt) was obtained from the corresponding sirup in the same manner as described in *(2)* and recrystallized twice from the same solvent as in *(1)*. Found: C, 47.66; H, 5.68; N, 8.48%. Calcd for $(+)^{CD}_{220}$-[Pd(*N*,*N*-Me_2en)(*meso*-stien)](diac-*d*-tart)·H_2O = $C_{26}H_{38}N_4O_9Pd$: C, 47.53; H, 5.83; N, 8.53%. The compound free from the resolving agent was obtained by the same method as in *(1)* but from a more concentrated solution. Found: C, 35.06; H, 4.63; N, 9.13%. Calcd for $C_{18}H_{29}N_4Cl_2O_{8.5}Pd$: C, 35.17; H, 4.75; N, 9.11%.

(4) $(-)^{CD}_{220}$-[*Pd*(C,C-*Me*$_2$*en*)(meso-*stien*)]$(ClO_4)_2 \cdot H_2O$ (**4**): A less-soluble diastereomer (diac-*d*-tart salt) was obtained by the method of Lidstone and Mills[3] with a slight modification. At first almost racemic[12] diacetyl-*d*-tartrate salt was obtained from the corresponding sirup in 95% ethanol by scratching the wall of the beaker, and recrystallized several times from the minimum quantity of water by adding ethanol, giving the corresponding optically pure salt. Found: C, 45.79; H, 6.23; N, 7.91%. Calcd for $(-)^{CD}_{220}$-[Pd(*C*,*C*-Me_2en)(*meso*-stien)](diac-*d*-tart)·$3H_2O$ = $C_{26}H_{42}N_4O_{11}Pd$: C, 45.06; H, 6.11; N, 8.08%. The resolving agent was removed by the same method as in *(3)*. Found: C, 34.67; H, 4.82; N, 9.02%. Calcd for $C_{18}H_{30}N_4Cl_2O_9Pd$: C, 34.66; H, 4.85; N, 8.98%.

(5) $(+)^{CD}_{220}$-[*Pd*(N,N,C,C-*Me*$_4$*en*)(meso-*stien*)]$(ClO_4)_2 \cdot H_2O$ (**5**): The sirup obtained by the general procedure was crystallized from a water–ethanol–acetone (1 : 3 : 14) mixture, giving a less-soluble diastereomer (diac-*d*-tart salt). Recrystallization was carried out four times from water by adding an ethanol–acetone (1 : 2) mixture. Found: C, 47.68; H, 6.48; N, 7.58%. Calcd for $(+)^{CD}_{220}$-[Pd(*N*,*N*,*C*,*C*-Me_4en)(*meso*-stien)](diac-*d*-tart)·$3H_2O$ = $C_{28}H_{46}N_4O_{11}Pd$: C, 46.64; H, 6.43; N, 7.77%. The product free from the resolving agent was obtained by the same method as in *(3)* but in water–methanol. Found: C, 37.06; H, 5.14; N, 8.59%. Calcd for $C_{20}H_{34}N_4Cl_2O_9Pd$: C, 36.85; H, 5.26; N, 8.60%.

(6) $(-)^{CD}_{220}$-[*Pd*(N,N-*Me*$_2$*tn*)(meso-*stien*)]Cl_2 *Solution* (**6**): A crude less-soluble diastereomer (diac-*d*-tart salt) was obtained from the corresponding sirup in a 90% ethanol–acetone (4 : 5) mixture, and recrystallized four times from the same solvent as described in *(5)*. Found: C, 49.47; H, 5.86; N, 8.56%. Calcd for $(-)^{CD}_{220}$-[Pd(*N*,*N*-Me_2tn)(*meso*-stien)](diac-*d*-tart) = $C_{27}H_{38}N_4O_8Pd$: C, 49.66; H, 5.87; N, 8.58%. No corresponding optically active perchlorate salt was obtained by a method similar to that for **1**, **3**, or **5**; the diastereomer was converted into the corresponding optically active chloride with a column containing an anion-exchange resin (Dowex 1×8, 200—400 mesh, Cl^- form). The CD spectrum of this complex was measured with the eluate, the concentration being calculated from the molar absorption coefficient of the corresponding racemic perchlorate.

Measurements. Electronic absorption spectra were recorded with a Hitachi 330 spectrophotometer and CD spectra with a JASCO MOE-1 spectropolarimeter. All the measurements were made in aqueous solutions at room temperature, except the electronic absorption spectrum of *meso*-stien measured in methanol and a water–methanol (9 : 1) mixture. A 10-cm cell was employed for the CD measurements in the long wavelength region. No spectral change was observed during the course of measurements.

Results and Discussion

Absolute Configuration. The enantiomeric configurations are denoted by *R* and *S* (Fig. 1) from analogy with the axial chirality[13] of organic compounds. The absorption spectrum of **2** is almost identical with that of **1** (Table 2 and Fig. 2). Both these optically pure complexes were derived from the less-soluble diastereomers. The CD spectra of both **1** and **2** contain a configurational contribution; in addition that of **2** contains the vicinal contribution due to the asymmetric carbon atom. Assuming the additivity of the configurational and vicinal contributions, a calculated vicinal CD curve can be obtained by subtracting the CD of **1** from that of **2**. The same configurational chirality of **1** and **2** was also assumed in the calculation, and justified by comparing the calculated vicinal CD with the CD spectrum of **7** containing the same asymmetric carbon atom as in **2** (Fig. 3); these two curves are of a similar pattern to each other, differing slightly in intensity.

The spectrum of **2′**[14] recorded immediately after dissolution can be reproduced by adding 0.25 part of the CD of **1** to the calculated vicinal CD of **2** (Fig. 4); this demonstrates the additivity of the configurational and vicinal CD. The CD spectrum of **2′** (*ca.* 10^{-3} mol dm^{-3}, in water) became constant in about five days at *ca.* 17 °C, indicating that the solution attained

Table 2. Absorption data of the complexes

No.	Complex	Spin-forbidden d-d σ_{max}[b] / 10^3 cm^{-1}	Spin-allowed d-d $\left(\log \frac{\varepsilon}{\text{mol}^{-1}\,\text{dm}^3\,\text{cm}^{-1}}\right)$	d-p or CT[a]
1	$(+)^{CD}_{220}$-[Pd(*N*,*N*-Et_2en)(*meso*-stien)]$^{2+}$	*ca.* 28.5sh (2.0)	34.2(2.79)	*ca.* 44.5sh
2	$(+)^{CD}_{220}$-[Pd(N^1,N^1-Et_2-(*S*)-pn)(*meso*-stien)]$^{2+}$	*ca.* 28.5sh (2.0)	34.1(2.81)	*ca.* 44.5sh
3	$(+)^{CD}_{220}$-[Pd(*N*,*N*-Me_2en)(*meso*-stien)]$^{2+}$	*ca.* 29sh (2.0)	34.5(2.75)	*ca.* 44.5sh
4	$(-)^{CD}_{220}$-[Pd(*C*,*C*-Me_2en)(*meso*-stien)]$^{2+}$	*ca.* 29sh (1.5)	34.9(2.65)	*ca.* 44.5sh
5	$(+)^{CD}_{220}$-[Pd(*N*,*N*,*C*,*C*-Me_4en)(*meso*-stien)]$^{2+}$	*ca.* 28.5sh (2.0)	34.3(2.77)	*ca.* 44.5sh
6	$(-)^{CD}_{220}$-[Pd(*N*,*N*-Me_2tn)(*meso*-stien)]$^{2+}$	*ca.* 28sh (2.0)	33.5(2.82)	*ca.* 44.5sh
7	[Pd(N^1,N^1-Et_2-(*S*)-pn)(en)]$^{2+}$	*ca.* 28.5sh (1.8)	34.2(2.65)	49.9(4.26)

a) See text. b) sh: shoulder.

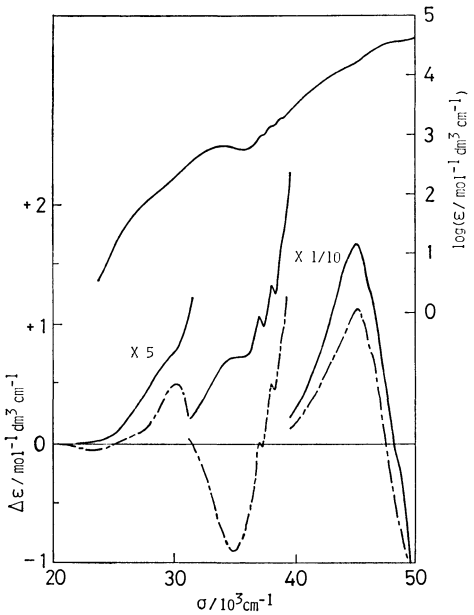

Fig. 2. Absorption and CD spectra of $(+)^{CD}_{220}$-[Pd(*N*,*N*-Et_2en)(*meso*-stien)]$^{2+}$, **1** (——) and CD spectrum of $(+)^{CD}_{220}$-[Pd(N^1,N^1-Et_2-(*S*)-pn)(*meso*-stien)]$^{2+}$, **2** (——).

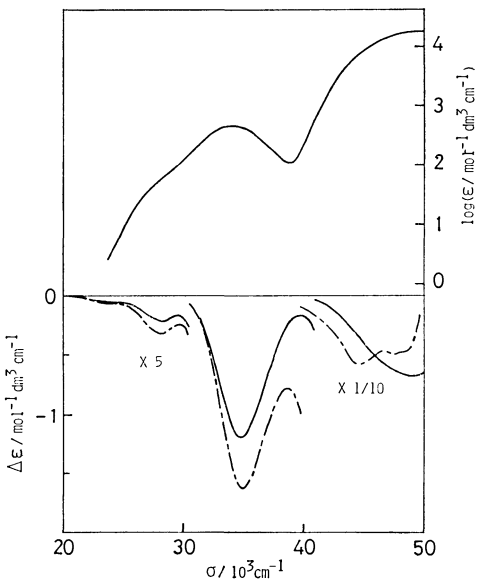

Fig. 3. Absorption and CD spectra of [Pd(N^1,N^1-Et_2-(*S*)-pn)(en)]$^{2+}$, **7** (——) and vicinal CD curve calculated from [$\Delta\varepsilon$(**2**)−$\Delta\varepsilon$(**1**)] (— — —).

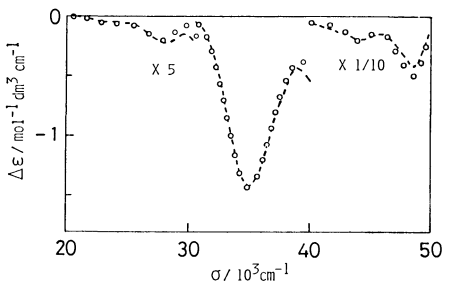

Fig. 4. CD spectrum of [Pd(N^1,N^1-Et_2-(*S*)-pn)(*meso*-stien)]$^{2+}$, **2′**, recorded immediately after dissolution (-----) and CD curve calculated from [0.25 $\Delta\varepsilon$(**1**)+ calcd $\Delta\varepsilon_{vicinal}$] (◦◦◦◦◦◦). The calcd $\Delta\varepsilon_{vicinal}$ is given in Fig. 3.

equilibrium. However, the CD spectrum could not be accurately measured in the region of wavelengths shorter than 250 nm because of the low intensity. This can be expained by the cancellation between the vicinal and the increasing configurational CD contribution. The CD additivity, therefore, was examined with the solution of **2′** immediately after dissolution over the range 500—200 nm. The configuration of the predominant isomer both in solid **2′** and in the equilibrium mixture is found to be the same as the absolute configuration of **1** from a comparison of the configurational CD. The abundance of the diastereomers in **2′** was estimated on the basis of CD additivity as follows: *R*(*S*), 62.5 and *S*(*S*), 37.5%[15] immediately after dissolution; *R*(*S*), 67.5 and *S*(*S*), 32.5% at equilibrium. The abundance at equilibrium was evaluated from $\Delta\varepsilon_{ext}$ at about 35000 cm^{-1}.

The absolute configuration predominating in aqueous solutions can be assigned by considering the steric

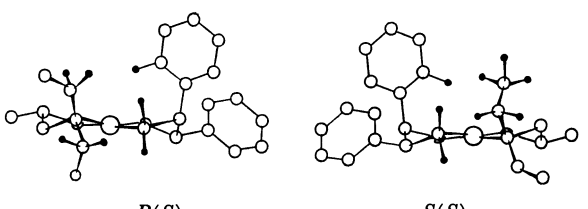

Fig. 5. A pair of diastereomers of [Pd(N^1,N^1-Et_2-(*S*)-pn)-(*meso*-stien)]$^{2+}$. Hydrogen atoms which are less concerned with the steric repulsions are omitted; one of two possible conformations of *meso*-stien is shown.

repulsions between the phenyl groups on *meso*-stien and one of the ethyl groups on N^1,N^1-Et_2-(*S*)-pn (Fig. 5). The ligand N^1,N^1-Et_2-(*S*)-pn is likely to be in almost pure δ-form, because of the repulsion between the *C*(*S*)-methyl and one of the two *N*-ethyl groups. As a result, the orientations of the two *N*-ethyl groups might be restricted. The steric interactions between the *N*-ethyl and the two phenyl groups should differ between the *R*(*S*) and the *S*(*S*) isomer. Thus, the repulsive interaction in *R* configuration is concluded to be smaller than that in *S*, and the predominant configuration in solid **2'** and in the equilibrium mixture can be assigned to *R*; consequently complex **1** has *R* configuration.

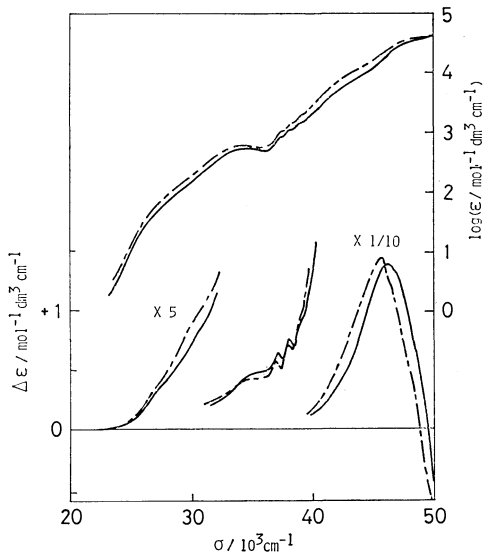

Fig. 6. Absorption and CD spectra of $(+)^{CD}_{220}$-[Pd(*N*,*N*-Me_2en)(*meso*-stien)]$^{2+}$, **3** (——) and $(+)^{CD}_{220}$-[Pd(*N*,*N*,*C*,*C*-Me_4en)(*meso*-stien)]$^{2+}$, **5** (—·—).

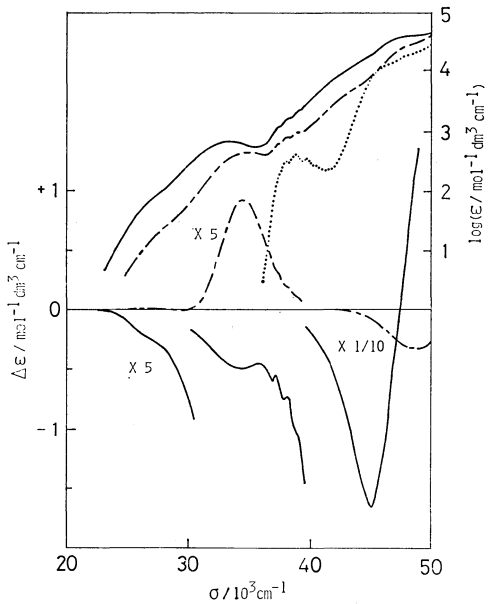

Fig. 7. Absorption and CD spectra of $(-)^{CD}_{220}$-[Pd(*C*,*C*-Me_2en)(*meso*-stien)]$^{2+}$, **4** (— — —) and $(-)^{CD}_{220}$-[Pd(*N*,*N*-Me_2tn)(*meso*-stien)]$^{2+}$, **6** (——); absorption spectrum of *meso*-stien in methanol (……).

The absolute configuration of **3** is easily assigned to *R* by comparing its CD curve with that of **1**; both CD patterns are very similar to each other throughout the range 500—200 nm, though the CD intensity is somewhat different (Figs. 2 and 6). However, the absolute configuration of **4** cannot be easily determined. The sign of the major CD band in the region of spin-allowed d-d transitions is the same as that for **1** or **3**, whereas the sign of the band at *ca.* 49000 cm^{-1} is opposite (Figs. 2, 6, and 7). In order to solve this problem complex **5** was prepared. The ligand *N*,*N*,*C*,*C*-Me_4en has four methyl substituents: two on a nitrogen, the other two on the carbon adjacent to the nitrogen atom (Table 1). From the fact complex **4** displays remarkably weak CD in comparison with **3**, the CD pattern of **5** is expected to be similar to that of **3**. Figure 6 shows the *R* configuration of **5**, indicating the validity of the expectation. The small deviation (from the CD curve of **3**) associated with the introduction of the *C*-methyl groups is considered to have a pattern similar to that of the CD spectrum of *R*-[Pd(*C*,*C*-Me_2en)(*meso*-stien)]$^{2+}$. Upon comparing the CD curves of **3** and **5**, the difference between their ligand-field-strengths should be taken into account. Quantitative estimation of the difference is not only difficult but also unnecessary. It is approximated by the energy difference in the d-d absorption maxima. In practice, the CD curve of **3** (27000—37000 cm^{-1}) is displaced to the side of lower energies by the difference (240 cm^{-1}) and then compared with the intact CD curve of **5** (Fig. 8). The positive (*ca.* 30000 cm^{-1}) and the negative (*ca.* 35000 cm^{-1}) deviation of the CD curve of **5** from that of **3** are visualized; the sign pattern is opposite that of the CD spectrum of **4** in the region. It is concluded that complex **4** has *S* configuration.

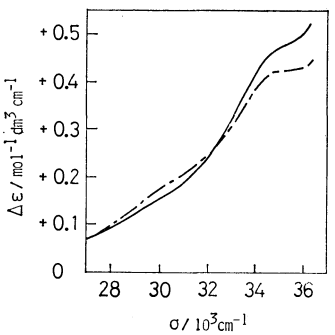

Fig. 8. CD curve of **3**, shifted by 240 cm^{-1} to the side of lower energies (——) and intact CD curve of **5** (—·—).

Complex **6** was similarly derived from the corresponding less-soluble diastereomer using the same resolving agent as used for **1**—**5**. The entire CD pattern, however, is enantiomeric to those of **1**, **3**, and **5**. No marked change is found in the CD pattern with increase in chelate-ring size (Figs. 6 and 7); we conclude that complex **6** has *S* configuration. The absolute configuration of the above six complexes are given in Table 3. The results can be summarized as follows: Positive sign of the first CD band in the region of wave numbers larger than 40000 cm^{-1} indicates *R* configuration.

Table 3. CD data of the complexes

No.	Complex	Spin-forbidden d-d σ_{ext}[b] / 10^3 cm^{-1}		Spin-allowed d-d $\Delta\varepsilon$ / mol^{-1} dm^3 cm^{-1}		d-p or CT[a]	
1	$R(+)^{CD}_{220}$-[Pd(N,N-Et$_2$en)(*meso*-stien)]$^{2+}$			*ca.* 30sh *ca.* 35sh	(*ca.*+0.15) (+0.73)	45.2	(+16.8)
2	$R(+)^{CD}_{220}$-[Pd(N^1,N^1-Et$_2$-(*S*)-pn)(*meso*-stien)]$^{2+}$	23.3 *ca.* 26.5sh	(−0.010) (*ca.*+0.014)	30.2 35.0	(+0.10) (−0.90)	45.2	(+11.3)
2′[c]	$(-)^{CD}_{220}$-[Pd(N^1,N^1-Et$_2$-(*S*)-pn)(*meso*-stien)]$^{2+}$	24sh 28.0	(−0.011) (−0.046)	35.0	(−1.42)	44.5 48.5	(−2.0) (−4.2)
3	$R(+)^{CD}_{220}$-[Pd(N,N-Me$_2$en)(*meso*-stien)]$^{2+}$	*ca.* 27.5sh	(+)	*ca.* 30.5sh *ca.* 35.5sh	(*ca.*+0.16) (+0.48)	46.2	(+13.9)
4	$S(-)^{CD}_{220}$-[Pd(C,C-Me$_2$en)(*meso*-stien)]$^{2+}$	26.7	(+0.002)	29.4 34.6	(−0.001) (+0.18)	49.0	(−3.2)
5	$R(+)^{CD}_{220}$-[Pd(N,N,C,C-Me$_4$en)(*meso*-stien)]$^{2+}$	*ca.* 27.5sh	(+)	*ca.* 30.5sh *ca.* 35.5sh	(*ca.*+0.18) (+0.43)	45.7	(+14.2)
6	$S(-)^{CD}_{220}$-[Pd(N,N-Me$_2$tn)(*meso*-stien)]$^{2+}$	*ca.* 27sh	(−)	34.4	(−0.49)	45.3	(−16.6)
7	[Pd(N^1,N^1-Et$_2$-(*S*)-pn)(en)]$^{2+}$	*ca.* 24.5sh 28.2	(−0.010) (−0.042)	34.8	(−1.19)	49.0	(−6.8)

a) See text. b) sh: shoulder. c) Recorded immediately after dissolution.

CD and Absorption Spectra. Absorption and CD data of the complexes are given in Tables 2 and 3, respectively, those concerning π-π^* intraligand transitions in Table 4. The complexes generally exhibit four configurational-CD bands (27000, 30000, 35000, and beyond 45000 cm^{-1}) within the range 20000—50000 cm^{-1}. The CD pattern of the complexes with *N*-alkyl substituents, however, is different from that for the *C*-alkyl analog. In the former complexes all of the four bands have the same sign (*i.e.*, plus for *R* isomer), whereas in the latter the sign pattern is −, +, −, and + (from the side of smaller wave numbers) for *R* isomer. For all of these complexes, the first band is assigned to a spin-forbidden d-d transition and the second and third to spin-allowed d-d transitions. The last band should be assigned to either d-p transition or nitrogen-σ-to-metal-d charge-transfer transition.

In the present series of complexes, h-type ligands were varied with the v-type ligand unchanged; the relative intensity of configurational CD varied in the following order: N,N-Et$_2$en > N,N-Me$_2$tn > N,N-Me$_2$en > C,C-Me$_2$en. This result indicates three factors determining the intensity, the size of alkyl substituent, the location of alkyl substituent and the size of chelate ring: (1) The CD intensity increases with increasing bulkiness of substituents. (2) Alkyl groups on the nitrogen atom cause CD intensity higher than those on the carbon atom. (3) The increase in chelate-ring size from five to six is accompanied by an increase in the CD intensity. The finding (1) can be explained in terms

Table 4. Absorption and CD data of π-π^* intraligand transitions

No.	Complex	α-bands: Absorption σ_{sh}[a] / 10^3cm^{-1}	α-bands: Absorption σ_{ext}[a] / 10^3cm^{-1}	α-bands: CD $\Delta\varepsilon$ / mol^{-1} dm^3 cm^{-1}		*p*-bands: Absorption σ_{sh}[a] / 10^3cm^{-1}	*p*-bands: CD σ_{sh}[a] / 10^3cm^{-1}
1	$R(+)^{CD}_{220}$-[Pd(N,N-Et$_2$en)(*meso*-stien)]$^{2+}$	*ca.* 37.4sh *ca.* 38.2sh *ca.* 39.0sh		37.1 38.1 *ca.* 39sh	(+1.07) (+1.33) (*ca.*+1.8)	*ca.* 47.3sh *ca.* 48.2sh	*ca.* 46.3sh *ca.* 48.5sh
2	$R(+)^{CD}_{220}$-[Pd(N^1,N^1-Et$_2$-(*S*)-pn)(*meso*-stien)]$^{2+}$	*ca.* 37.4sh *ca.* 38.2sh *ca.* 39.0sh		37.1 38.1 *ca.* 39sh	(+0.01) (+0.49) (*ca.*+0.9)	*ca.* 47.3sh *ca.* 48.2sh	*ca.* 46.3sh *ca.* 48.5sh
3	$R(+)^{CD}_{220}$-[Pd(N,N-Me$_2$en)(*meso*-stien)]$^{2+}$	*ca.* 37.4sh *ca.* 38.2sh *ca.* 39.0sh		37.1 38.0 *ca.* 39sh	(+0.65) (+0.76) (*ca.*+0.92)	*ca.* 47.4sh *ca.* 48.3sh	*ca.* 46.5sh *ca.* 48.5sh
4	$S(-)^{CD}_{220}$-[Pd(C,C-Me$_2$en)(*meso*-stien)]$^{2+}$	*ca.* 37.4sh 38.2(2.90)[b] 39.0(2.98)[b] *ca.* 40.0sh		*ca.* 37sh *ca.* 38sh	(+) (+)	*ca.* 47.4sh *ca.* 48.3sh	
5	$R(+)^{CD}_{220}$-[Pd(N,N,C,C-Me$_4$en)(*meso*-stien)]$^{2+}$	*ca.* 37.4sh *ca.* 38.2sh *ca.* 39.0sh		36.9 37.9 *ca.* 39sh	(+0.56) (+0.69) (*ca.*+1.0)	*ca.* 47.3sh *ca.* 48.2sh	*ca.* 46.3sh *ca.* 48.3sh
6	$S(-)^{CD}_{220}$-[Pd(N,N-Me$_2$tn)(*meso*-stien)]$^{2+}$	*ca.* 37.4sh *ca.* 38.2sh *ca.* 39.0sh		37.0 37.9 *ca.* 39sh	(−0.59) (−0.75) (*ca.*−1.0)	*ca.* 47.3sh *ca.* 48.1sh	*ca.* 46.1sh *ca.* 47.3sh

a) sh: shoulder. b) log (ε_{max}/mol^{-1} dm^3 cm^{-1}).

of the symmetry of complex cations. Although the present complexes have a square-planar coordination geometry around the central metal ion, the distribution of the peripheral substituents can be regarded as a tetrahedron: $Pd(\overline{Ph_2})(\overline{H_2})(\overline{NR_2})(\overline{NH_2})$ (Fig. 1). Thus the configurational-CD intensity increases with the bulkiness of R. Care should be taken for simultaneous operations of the factors producing mutually opposite CD signs. For example, complex **5** has a larger degree of the pseudo-tetrahedral chirality than **3**, but it exhibits a smaller CD intensity than the latter in *ca.* 34000—38500 cm^{-1}. This can be attributed to the *C*-methyl and *N*-methyl groups contributing to opposite CD signs in the region.

The CD intensity in the region of π-π^* intraligand transitions seems to depend upon another factor. The CD intensity of *C*-alkyl-substituted complex **4** considerably differs from those of the *N*-alkyl analogs **1**, **3**, and **6**. The former complex shows only very weak CD bands (shoulders) in the 36000—40000 cm^{-1} region, whereas the latter complexes show rather strong bands (Figs. 2, 6, and 7; Table 4). These bands have been assigned to α-bands[16] relating to the π-π^* transitions. The *N*-alkyl-substituted complexes give additional CD bands assigned to *p*-bands[16] in the 45000—49000 cm^{-1} region as very weak shoulders. In these complexes, the two phenyl groups are expected to interact with the *N*-alkyl group in a different way. It seems that the disposition of the two phenyl groups acquires a chirality, giving a strong CD in the region of the π-π^* intraligand transitions. For the *C*-methyl-substituted complex, however, no such a chirality around the two phenyl groups is expected since the *C*-methyl groups are remote from both phenyl groups; therefore complex **4** should exhibit only weak π-π^* CD as actually observed.

The vicinal CD due to the asymmetric carbon atom comprises four bands, as well as the configurational CD, in the range 20000—50000 cm^{-1}, but the band assignments in the two cases slightly differ. The weak CD bands at *ca.* 24500 and 28200 cm^{-1} and the strong band at 34800 cm^{-1} of complex **7** can be assigned to the spin-forbidden and -allowed d-d transitions, respectively, by comparing their positions with those of the corresponding absorption bands. Another CD band at 49000 cm^{-1}, which corresponds to the absorption peak at 49900 cm^{-1}, should be assigned to either d-p transition or nitrogen-σ-to-metal-d charge-transfer transition. The intensity of this CD band is significantly smaller than that of the corresponding bands in the configurational CD. This is fortunate in the assignment of absolute configuration for the complexes with asymmetric carbon atoms, such as **2**.

The absorption spectra apparently consist of three bands except those due to the π-π^* intraligand transitions. A shoulder at 28000—29000 cm^{-1} and a peak at 33500—35000 cm^{-1} can be assigned to the spin-forbidden and -allowed d-d transitions, respectively (Table 2). A bulge at *ca.* 45000 cm^{-1} is considered to be an apparent shoulder produced by the overlap of the *p*-bands with the band which has the same origin as the 49900 cm^{-1} band of **7**. In the absorption spectra of the present series of complexes the α-bands shift only slightly to lower energies and the *p*-bands by about 2000 cm^{-1} to higher energies than the absorption bands of *meso*-stien in a methanol solution[17] (Fig. 7). The bands in a water–methanol (9 : 1) mixture appear at almost the same places as in methanol. It is thus concluded that the shifts are caused by coordination and not by a solvent effect.

References

1) For example, T. Komorita, J. Hidaka, and Y. Shimura, *Bull. Chem. Soc. Jpn.*, **41**, 854 (1968); **44**, 3353 (1971); **52**, 1468 (1979); H. Ito, J. Fujita, and K. Saito, *ibid.*, **40**, 2584 (1967); **42**, 2863 (1969).

2) W. H. Mills and T. H. H. Quibell, *J. Chem. Soc.*, **1935**, 839.

3) A. G. Lidstone and W. H. Mills, *J. Chem. Soc.*, **1939**, 1754.

4) T. D. Perrine, *J. Org. Chem.*, **18**, 898 (1953).

5) H. T. Clarke and H. J. Bean, *Org. Synth.*, **11**, 4 (1931).

6) M. Suzuki and Y. Nishida, *Inorg. Chim. Acta*, **34**, 61 (1979).

7) O. F. Williams and J. C. Bailar, Jr., *J. Am. Chem. Soc.*, **81**, 4464 (1959); I. Lifshitz and J. G. Bos, *Recl. Trav. Chim.*, **59**, 173 (1940).

8) F. D. Chattaway and G. D. Parkes, *J. Chem. Soc.*, **1923**, 663.

9) H. D. K. Drew, F. W. Pinkard, G. H. Preston, and W. Wardlaw, *J. Chem. Soc.*, **1932**, 1895.

10) Diastereomeric mixture **2′** was used in the case of N^1,N^1-Et_2-(*S*)-pn complex.

11) diac-*d*-tart=diacetyl-*d*-tartrate=$C_8H_8O_8^{2-}$.

12) With respect to the complex cation.

13) *J. Org. Chem.*, **35**, 2849 (1970).

14) See Experimental.

15) The *R*(*S*) isomer content increases with the increasing yield in the preparation of **2′**. This suggests that solid **2′** is a mixture of *R*-[Pd(N^1,N^1-Et_2-(*S*)-pn)(*meso*-stien)]$(ClO_4)_2$ and pseudo racemic [Pd(N^1,N^1-Et_2-(*S*)-pn)(*meso*-stien)]$(ClO_4)_2$.

16) E. Clar, "Aromatische Kohlenwasserstoffe," 2 Aufl., Springer (1952), p. 25.

17) The *meso*-stien ligand is only slightly soluble in water.

Binuclear Metal Complexes. XXXVII.[1] Crystal and Molecular Structure of a Binuclear Manganese(III) Complex Bridged by Two Alkoxo Oxygens and Two Bidentate Acetate Ions

Masahiro MIKURIYA, Naoyuki TORIHARA, Hisashi OKAWA, and Sigeo KIDA*

Department of Chemistry, Faculty of Science, Kyushu University 33, Hakozaki, Higashi-ku, Fukuoka 812

(Received September 16, 1980)

The crystal structure of binuclear manganese(III) complex, Mn(spa)(ac) (H_2spa=3-salicylideneamino-1-propanol, ac=acetate), was determined by the single-crystal X-ray diffraction method. The crystals are triclinic, space group $P\bar{1}$, $a=8.804(3)$, $b=9.376(3)$, $c=8.671(3)$ Å, $\alpha=111.24(3)$, $\beta=101.34(3)$, $\gamma=65.00(3)°$, and $Z=1$. The structure was solved by the heavy atom method and refined by the block-diagonal least-squares method to an R factor of 0.034. The crystal structure consists of discrete binuclear clusters, where the two manganese atoms are bridged by two alkoxo oxygens of the spa ligands and two bidentate acetate ions. The structural detail is in conformity with the magnetic and spectral properties previously reported.

The chemistry of binuclear manganese(III) and manganese(IV) complexes is of importance in connection with the metalloenzymes in biological systems.[2,3] However, X-ray structural investigations on binuclear manganese complexes are very limited.[4-6]

In the previous paper of this series, we reported the synthesis and magnetic property of binuclear manganese(III) complexes with 3-salicylideneamino-1-propanol and its homologues, MnL(ac) and MnLX·H_2O (L=Schiff base dianion; ac=acetate ion; X=Cl, Br, N_3).[7] The temperature dependence of their magnetic susceptibilities (80—300 K) could be well interpreted in terms of the Van Vleck equation for the high-spin d^4-d^4 system based on the Heisenberg model, $\mathcal{H}=-2JS_1\cdot S_2$ ($J=-13.5$——20.4 cm^{-1}). Thus, it was thought that they possess a discrete binuclear structure in which an antiferromagnetic spin-exchange interaction is operating between a pair of manganese(III) ions. Based on the infrared and electronic spectral data, it was proposed that the binuclear complexes, MnL(ac) and MnLX·H_2O, are both bridged by an alcoholic oxygen. The antisymmetric and symmetric C–O stretching frequencies of the acetate group in the MnL(ac) led us to the conclusion that the acetate groups also bridge the two manganese(III) ions (Fig. 1). The binuclear structure consisting of two monatomic and two triatomic bridges as supposed for MnL(ac) is quite rare. Although such a mode of bridging has been observed for α-di-μ-hydroxo-bis[2-(2-dimethylaminoethyl)pyridine]dicopper(II) perchlorate,[8] to our knowledge it has not yet been documented in carboxylate chemistry. In order to confirm the bridging mode we have determined the crystal structure of Mn(spa)(ac) (H_2spa=3-salicylideneamino-1-propanol) by the single-crystal X-ray diffraction method.

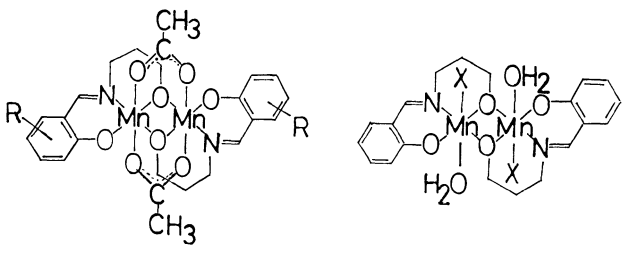

Fig. 1. Structures of MnL(ac) and MnLX·H_2O.

Experimental

Greenish black crystals of Mn(spa)(ac) were prepared by the method previously reported.[7] A crystal with dimensions of $0.23\times0.25\times0.50$ mm was used for the X-ray analysis. Preliminary Weissenberg photographs revealed no systematic absences and showed the triclinic symmetry. The cell parameters and intensities were measured on a Rigaku AFC-5 automated four-circle diffractometer with graphite-monochromated Mo $K\alpha$ radiation ($\lambda=0.71069$ Å).

Crystal data: $C_{24}H_{28}N_2O_8Mn_2$, F.W.=582.37, triclinic, $P\bar{1}$, $a=8.804$ (3), $b=9.376$ (3), $c=8.671$ (3) Å, $\alpha=111.24$ (3), $\beta=101.34$ (3), $\gamma=65.00$ (3)°, $D_m=1.59$ (by floatation in n-C_6H_{14}–CCl_4), $D_c=1.60$ gcm^{-3}, $Z=1$, μ(Mo $K\alpha$)=10.5 cm^{-1}.

Intensity data were collected by the 2θ-ω scan technique with a scan rate of 8 °min^{-1}. For weak reflections the peak scan was repeated up to four times depending on their intensities. The intensities of three standard reflections monitored every 100 reflections showed a good stability. A total of 2784 reflections with $2\theta<55°$ were collected. The intensity data were corrected for the Lorentz and the polarization effects, but not for absorption. 2614 Independent reflections with $|F_o|>3\sigma(|F_o|)$ were considered as "observed" and were used for the structure analysis.

Structure Determination and Refinement

The structure was solved by the heavy atom method. Of the two possible space groups, the centrosymmetric space group $P\bar{1}$ was assumed. Successful solution and refinement support this choice. The position of the manganese atom was obtained from a three-dimensional Patterson synthesis. Successive Fourier synthesis revealed all the nonhydrogen atoms. Refinement was carried out by the block-diagonal least-squares method. Anisotropic thermal parameters being introduced, the least-squares refinement yielded discrepancy factors $R_1=\sum||F_o|-|F_c||/\sum|F_o|=0.047$ and $R_2=[\sum\omega(|F_o|-|F_c|)^2/\sum\omega|F_o|^2]^{1/2}=0.075$. All the hydrogen atoms were located from the subsequent difference Fourier map. Further refinement with anisotropic thermal parameters for nonhydrogen atoms and isotropic temperature factors for hydrogen atoms gave final values of 0.034 and 0.052 for R_1 and R_2, respectively. In the least-squares refinement the function minimized was $\sum w(|F_o|-k|F_c|)^2$, where $w=(2.0+|F_o|+$

$0.016|F_o|^2)^{-1}$.[9] The final shifts in the atomic parameters of the nonhydrogen atoms were less than 0.13σ. The final difference Fourier synthesis showed no peaks higher than 0.77 e/Å^3.

The atomic scattering factors for Mn, O, N, C_{val}, and H and the anomalous dispersion corrections, $\Delta f'$ and $\Delta f''$ for Mn, were taken from the International Tables for X-Ray Crystallography.[10] All the calculations were carried out on the FACOM M-200 computer in the Computer Center of Kyushu University by the use of a local version[11] of the UNICS-II[12] and the ORTEP[13] programs.

The final positional and thermal parameters with their estimated standard deviations are given in Tables 1 and 2.***

TABLE 1. FRACTIONAL POSITIONAL PARAMETERS ($\times 10^4$) AND THERMAL PARAMETERS OF NON-HYDROGEN ATOMS WITH THEIR ESTIMATED STANDARD DEVIATIONS IN PARENTHESES

Atom	x	y	z	B_{eq}/Å^2
Mn	671.1(3)	412.8(3)	1675.5(3)	2.3
O(1)	397(2)	−1472(2)	37(2)	2.5
O(2)	951(2)	2320(2)	3083(2)	3.3
O(3)	3034(2)	− 564(2)	437(2)	3.1
O(4)	2015(2)	−1184(2)	−2206(2)	3.1
N	1675(2)	− 748(2)	3392(2)	2.6
C(1)	166(3)	−2769(3)	295(3)	3.2
C(2)	1527(3)	−3448(3)	1494(3)	3.9
C(3)	1453(4)	−2284(3)	3221(3)	4.0
C(4)	2510(3)	− 208(3)	4709(2)	2.9
C(5)	2725(2)	1341(3)	5262(2)	2.8
C(6)	1923(2)	2538(2)	4441(2)	2.7
C(7)	2119(3)	4061(3)	5129(3)	3.5
C(8)	3063(3)	4379(3)	6583(3)	4.1
C(9)	3871(3)	3185(4)	7387(3)	4.3
C(10)	3702(3)	1698(3)	6741(3)	3.7
C(11)	3195(2)	−1243(2)	−1102(3)	2.8
C(12)	4961(3)	−2209(3)	−1666(3)	3.9

TABLE 2. FRACTIONAL POSITIONAL PARAMETERS ($\times 10^3$) AND ISOTROPIC TEMPERATURE FACTORS OF HYDROGEN ATOMS WITH THEIR ESTIMATED STANDARD DEVIATIONS IN PARENTHESES

Atom	x	y	z	B/Å^2
H(C1A)	−99(3)	−245(3)	67(3)	3.7(5)
H(C1B)	20(3)	−365(3)	− 77(3)	3.5(5)
H(C2A)	137(3)	−440(3)	161(3)	3.5(5)
H(C2B)	275(3)	−380(3)	113(3)	3.8(5)
H(C3A)	14(3)	−185(3)	357(3)	3.8(5)
H(C3B)	224(3)	−279(3)	398(3)	3.5(5)
H(C4)	295(3)	− 88(3)	543(3)	3.0(5)
H(C7)	158(3)	487(3)	461(3)	3.3(5)
H(C8)	318(3)	541(3)	700(3)	3.7(5)
H(C9)	461(3)	344(3)	840(3)	3.6(5)
H(C10)	429(3)	86(3)	729(3)	3.5(5)
H(C12A)	500(3)	−261(3)	−280(3)	3.8(5)
H(C12B)	550(3)	−301(3)	−129(3)	4.0(6)
H(C12C)	547(3)	−166(3)	−158(3)	4.1(6)

*** Lists of structure factors and anisotropic thermal parameters have been deposited with the Chemical Society of Japan as a Document No. 8123.

Results and Discussion

The molecular structure is shown in Fig. 2. The bond distances and angles with their estimated standard deviations are listed in Table 3. Some least-squares planes with the deviations of atoms from the planes are given in Table 4.

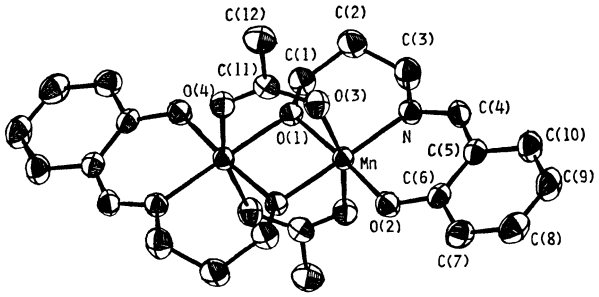

Fig. 2. Molecular Structure of Mn(spa)(ac) with thermal ellipsoids (50% probability level).

The crystal structure consists of discrete binuclear clusters, the closest intercluster contact being O(4)–C(9) (3.279(3) Å). Therefore, the binuclear clusters must be considered to be magnetically isolated. This is in harmony with the result of our magnetic investigation of MnL(ac).[7] The manganese atoms are bridged by the alcoholic oxygens. For the binuclear complexes with 3-salicylideneamino-1-propanol, alcoholic oxygen-bridged and phenolic oxygen-bridged binuclear structures are known.[14–27] As stated above, the infrared spectra of MnL(ac) and $MnLX\cdot H_2O$ suggest the alcoholic oxygen-bridged binuclear structures,[7] and this has been confirmed by the present X-ray structure analysis.

The coordination geometry around the manganese atom is an elongated octahedron. The approximate square plane involving the manganese atom at its center is formed by two alcoholic oxygen, imino nitrogen and phenolic oxygen atoms of the spa ligands (Table 4). The Mn–O(1) (1.899(2) Å), Mn–O(1)^i (1.951(2) Å), Mn–O(2) (1.849(2) Å) and Mn–N (2.006(2) Å) distances are normal for the in-plane bonds of manganese(III) complex.[4,6,28] The bond angles around the manganese atom vary from 82 to 97°. The axial Mn–O distances (2.208(2), 2.251(2) Å) are considerably longer than the in-plane Mn–O distances. Thus the coordination geometry around the manganese atom evidently deviates from a regular octahedron and this tetragonal elongation is attributable to the Jahn-Teller effect. Therefore, the ground ^5E_g and the excited $^5T_{2g}$ states for octahedral manganese(III) should split into sublevels. In fact, the diffuse reflectance spectrum of Mn(spa)(ac) shows d-d bands at 13000, 16400, 21200, and 22200 cm^{-1}.[7]

The four-membered Mn_2O_2 ring is exactly planar owing to the presence of an inversion center. The carbon atom, C(1), attatched to the bridging oxygen, O(1), deviates significantly from the plane of the four-membered Mn_2O_2 ring (Table 4). Each bond length in the spa ligand has a normal value.[29] The spa moiety

TABLE 3. INTERATOMIC DISTANCES (l/Å) AND BOND ANGLES (φ/°) WITH THEIR ESTIMATED STANDARD DEVIATIONS IN PARENTHESES

Symmetry code			
Superscript			
None	x	y	z
i	$-x$	$-y$	$-z$

(a) Manganese coordination spheres			
Mn···Mn^{i}	2.869(1)	Mn–O(3)	2.208(2)
Mn–O(1)	1.899(2)	Mn–O(4)	2.251(2)
Mn–O(1)^{i}	1.951(2)	Mn–N	2.006(2)
Mn–O(2)	1.849(2)		
O(1)–Mn–O^{i}(1)	83.66(7)	O(1)^{i}–Mn–N	176.57(8)
O(1)–Mn–O(2)	173.76(8)	O(2)–Mn–O(3)	94.28(8)
O(1)–Mn–O(3)	82.43(8)	O(2)–Mn–O(4)^{i}	97.07(8)
O(1)–Mn–O(4)^{i}	85.17(7)	O(2)–Mn–N	91.93(8)
O(1)–Mn–N	93.66(8)	O(3)–Mn–O(4)^{i}	164.00(5)
O(1)^{i}–Mn–O(2)	90.86(8)	O(3)–Mn–N	95.36(8)
O(1)^{i}–Mn–O(3)	86.42(7)	O(4)^{i}–Mn–N	95.49(8)
O(1)^{i}–Mn–O(4)^{i}	82.19(7)	Mn–O(1)–Mn^{i}	96.34(8)
(b) Spa moiety			
O(1)–C(1)	1.412(4)	C(10)–C(5)	1.412(3)
O(2)–C(6)	1.319(2)	C(1)–H(C1A)	1.02(3)
N–C(3)	1.485(4)	C(1)–H(C1B)	0.99(2)
N–C(4)	1.290(3)	C(2)–H(C2A)	1.00(3)
C(1)–C(2)	1.505(3)	C(2)–H(C2B)	1.06(3)
C(2)–C(3)	1.494(3)	C(3)–H(C3A)	1.11(3)
C(4)–C(5)	1.438(4)	C(3)–H(C3B)	0.95(3)
C(5)–C(6)	1.405(3)	C(4)–H(C4)	0.96(3)
C(6)–C(7)	1.406(4)	C(7)–H(C7)	0.93(3)
C(7)–C(8)	1.377(3)	C(8)–H(C8)	0.94(3)
C(8)–C(9)	1.393(4)	C(9)–H(C9)	1.01(3)
C(9)–C(10)	1.363(4)	C(10)–H(C10)	0.97(3)
Mn–O(1)–C(1)	127.4(1)	C(2)–C(1)–H(C1B)	110(1)
Mn^{i}–O(1)–C(1)	128.2(1)	H(C1A)–C(1)–H(C1B)	102(2)
Mn–O(2)–C(6)	129.9(1)	C(1)–C(2)–H(C2A)	108(1)
Mn–N–C(3)	120.8(1)	C(1)–C(2)–H(C2B)	113(2)
Mn–N–C(4)	123.1(2)	C(3)–C(2)–H(C2A)	104(1)
C(3)–N–C(4)	116.1(2)	C(3)–C(2)–H(C2B)	105(1)
O(1)–C(1)–C(2)	109.2(2)	H(C2A)–C(2)–H(C2B)	111(2)
C(1)–C(2)–C(3)	115.0(2)	N–C(3)–H(C3A)	105(2)
N–C(3)–C(2)	115.0(3)	N–C(3)–H(C3B)	108(2)
N–C(4)–C(5)	126.9(2)	C(2)–C(3)–H(C3A)	105(1)
C(4)–C(5)–C(6)	122.4(2)	C(2)–C(3)–H(C3B)	113(1)
C(4)–C(5)–C(10)	118.1(2)	H(C3A)–C(3)–H(C3B)	111(2)
C(6)–C(5)–C(10)	119.4(2)	N–C(4)–H(C4)	116(2)
O(2)–C(6)–C(5)	123.1(2)	C(5)–C(4)–H(C4)	117(2)
O(2)–C(6)–C(7)	118.3(2)	C(6)–C(7)–H(C7)	119(2)
C(5)–C(6)–C(7)	118.6(2)	C(8)–C(7)–H(C7)	120(2)
C(6)–C(7)–C(8)	120.7(2)	C(7)–C(8)–H(C8)	118(2)
C(7)–C(8)–C(9)	120.7(3)	C(9)–C(8)–H(C8)	121(2)
C(8)–C(9)–C(10)	119.7(2)	C(8)–C(9)–H(C9)	118(2)
C(5)–C(10)–C(9)	121.0(3)	C(10)–C(9)–H(C9)	122(2)
O(1)–C(1)–H(C1A)	114(2)	C(5)–C(10)–H(C10)	120(2)
O(1)–C(1)–H(C1B)	110(2)	C(9)–C(10)–H(C10)	119(2)
C(2)–C(1)–H(C1A)	111(2)		
(c) Acetate group			
O(3)–C(11)	1.261(3)	C(12)–H(C12A)	0.92(3)
O(4)–C(11)	1.263(3)	C(12)–H(C12B)	0.84(3)
C(11)–C(12)	1.505(3)	C(12)–H(C12C)	0.80(4)
Mn–O(3)–C(11)	124.6(1)	C(11)–C(12)–H(C12B)	113(2)
Mn^{i}–O(4)–C(11)	123.6(2)	C(11)–C(12)–H(C12C)	115(2)
O(3)–C(11)–O(4)	126.1(2)	H(C12A)–C(12)–H(C12B)	108(2)
O(3)–C(11)–C(12)	116.5(2)	H(C12A)–C(12)–H(C12C)	92(3)
O(4)–C(11)–C(12)	117.4(2)	H(C12B)–C(12)–H(C12C)	114(3)
C(11)–C(12)–H(C12A)	113(2)		

TABLE 4. DEVIATIONS OF THE ATOMS FROM LEAST-SQUARES PLANES (l/Å) AND DIHEDRAL ANGLES BETWEEN THE PLANES (φ/°)

(I) Plane through Mn, Mn^i, O(1), $O(1)^i$
$0.9246X+0.2240Y-0.4357Z=0$[a)]
[Mn 0.000, Mn^i 0.000, O(1) 0.000, $O(1)^i$ 0.000, O(2) 0.097, N −0.075, C(1) −0.558, C(2) −0.046, C(3) −0.513, C(4) 0.220, C(5) 0.512, C(6) 0.421, C(7) 0.640, C(8) 0.926, C(9) 1.029, C(10) 0.823][b)]

(II) Plane through O(1), $O(1)^i$, O(2), N
$0.9164X+0.1911Y-0.4269Z=0.0010$
[O(1) 0.042, $O(1)^i$ −0.044, O(2) 0.041, N −0.039, Mn −0.006, C(1) −0.472, C(2) 0.060, C(3) −0.430, C(4) 0.244, C(5) 0.490, C(6) 0.361, C(7) 0.538, C(8) 0.818, C(9) 0.959, C(10) 0.795]

(III) Plane through O(1), N, C(1), C(3)
$0.7956X-0.1269Y-0.3020Z=0.4082$
[O(1) 0.035, N −0.034, C(1) −0.040, C(3) 0.038, Mn −0.426, C(2) 0.680]

(IV) Plane through Mn, O(2), N, C(4), C(5), C(6)
$0.8399X+0.1269Y-0.5353Z=-0.3449$
[Mn 0.113, O(2) −0.107, N −0.080, C(4) −0.010, C(5) 0.077, C(6) 0.007]

(V) Plane through C(5), C(6), C(7), C(8), C(9), C(10)
$0.8207X+0.1485Y-0.5852Z=-0.5109$
[C(5) −0.003, C(6) 0.000, C(7) 0.005, C(8) −0.007, C(9) 0.003, C(10) 0.002]

(VI) Plane through Mn, Mn^i, O(3), O(4), C(11)
$0.2624X+0.9853Y-0.3629Z=0.0090$
[Mn 0.000, Mn^i −0.018, O(3) 0.033, O(4) 0.057, C(11) −0.072, $O(3)^i$ −0.052, $O(4)^i$ −0.075, $C(11)^i$ 0.054, C(12) −0.380, $C(12)^i$ 0.362]

(VII) Plane through O(3), O(4), C(11), C(12)
$0.4469X+0.9971Y-0.4280Z=0.5044$
[O(3) 0.000, O(4) 0.000, C(11) 0.000, C(12) 0.000, Mn −0.476, Mn^i −0.533, $O(3)^i$ −1.009, $O(4)^i$ −1.009, $C(11)^i$ −1.009, $C(12)^i$ −1.009]

Dihedral angles between the planes (φ/°)

(I) and (II)	1.9	(II) and (IV)	9.6
(I) and (III)	20.2	(II) and (V)	12.3
(I) and (IV)	10.5	(II) and (VI)	87.9
(I) and (V)	12.8	(III) and (IV)	17.6
(I) and (VI)	86.0	(IV) and (V)	3.4
(II) and (III)	18.3	(VI) and (VII)	11.8

a) The equation of the plane is expressed as $LX+MY+NZ=D$, where X, Y, and Z are in Å units referred to the crystallographic axes.
b) Deviations (l/Å) of atoms from the planes are listed in square brackets. Superscript (i) refers to the equivalent position $(-x, -y, -z)$.

forms two six-membered chelate rings with the manganese atom. The Mn–O(1)–C(1)–C(2)–C(3)–N chelate ring has a chair conformation, and Mn and C(2) are located 0.426 Å below and 0.680 Å above the plane defined by O(1), C(1), C(3) and N, respectively. On the other hand, the Mn–N–C(4)–C(5)–C(6)–O(2) chelate ring is nearly planar, the maximum deviation from the least-squares plane being 0.113 Å.

As was predicted,[7] the acetate groups are involved in the bridges in a syn-syn configuration. The acetate group is positioned above or below the Schiff base dimeric unit. The only example of two-acetate bridging in a similar fashion is found in di-μ-acetato-bis(diphenyltin), $Sn(Ph)_2(ac)$.[30] However, this complex is different from Mn(spa)(ac) in having a direct Sn–Sn bond and no monatomic bridging. Thus, the present complex, Mn(spa)(ac), including two monatomic and two triatomic bridges is unique in this regard. The manganese-carboxyl oxygen bonds deviate in several degrees from the axis perpendicular to the equatorial plane (Fig. 2), the O(3)–Mn–$O(4)^i$ bond angle being 164.00(5)°. This is due to the fact that the acetate bite (the O(3)–O(4) distance, 2.250(2) Å) is much less than the manganese-manganese distance (2.869(1) Å). The C(11)–O(3) and C(11)–O(4) distances are equal within experimental error. The $\begin{matrix}O\\O\end{matrix}\!>\!C-C$ plane retains its planarity (Table 4). Such planarity was also observed for dimeric copper(II) carboxylates.[31–36]

The authors wish to express sincere thanks to Professors Ikuhiko Ueda and Shigeaki Kawano of Kyushu University for their helpful advices and discussions. They are also grateful to Dr. Yuzo Nishida of Kyushu University for the help in data collection.

References

1) Part XXXVI: H. Okawa, W. Kanda, and S. Kida, *Chem. Lett.*, **1980**, 1281.
2) G. D. Lawrence and D. T. Sawyer, *Coord. Chem. Rev.*, **27**, 173 (1978).
3) W. M. Coleman and L. T. Taylor, *Coord. Chem. Rev.*, **32**, 1 (1980).
4) P. M. Plaskin, R. C. Stoufer, M. Mathew, and G. J. Palenik, *J. Am. Chem. Soc.*, **94**, 2121 (1972).
5) H. S. Maslen and T. N. Waters, *J. Chem. Soc., Chem. Commun.*, **1973**, 760.
6) A. Mangia, M. Nardelli, C. Pelizzi, and G. Pelizzi,

J. Chem. Soc., Dalton Trans., **1973**, 1141.
7) N. Torihara, M. Mikuriya, H. Okawa, and S. Kida, *Bull. Chem. Soc. Jpn.*, **53**, 1610 (1980).
8) D. L. Lewis, W. E. Hatfield, and D. J. Hodgson, *Inorg. Chem.*, **13**, 147 (1974).
9) D. W. J. Cruickshank, in "Computing Methods in Crystallography," ed by J. S. Rollet, Pergamon Press, Oxford (1965).
10) "International Tables for X-Ray Crystallography," Kynoch Press, Birmingham (1974), Vol. IV.
11) S. Kawano, *Rep. Comp. Cent. Kyushu Univ.*, **13**, 39 (1980).
12) T. Sakurai, H. Iwasaki, Y. Watanabe, K. Kobayashi, Y. Bando, and Y. Nakamichi, *Rep. Inst. Phys. Chem. Res.*, **50**, 75 (1972).
13) C. K. Johnson, Report No. 3794, Oak Ridge National Laboratory, Oak Ridge, Tennessee (1965).
14) S. Yamada, Y. Kuge, and K. Yamanouchi, *Inorg. Chim. Acta*, **1**, 139 (1967).
15) M. Kato, Y. Muto, H. B. Jonassen, K. Imai, and A. Harano, *Bull. Chem. Soc. Jpn.*, **41**, 1864 (1968).
16) J. A. Bertrand, J. A. Kelley, and J. L. Breece, *Inorg. Chim. Acta*, **4**, 247 (1970).
17) J. O. Miners and E. Sinn, *Bull. Chem. Soc. Jpn.*, **46**, 1457 (1973).
18) M. Kato, K. Imai, Y. Muto, T. Tokii, and H. B. Jonassen, *J. Inorg .Nucl. Chem.*, **35**, 109 (1973).
19) E. Sinn, *J. Chem. Soc., Chem. Commun.*, **1975**, 665.
20) J. A. Davis and E. Sinn, *J. Chem. Soc., Dalton Trans.*, **1976**, 165.
21) E. Sinn, *Inorg. Chem.*, **15**, 358 (1976).
22) J. A. Bertrand, J. L. Breece, A. R. Kalyanaraman, G. J. Long, and W. A. Baker, *J. Am. Chem. Soc.*, **92**, 5233 (1970).
23) J. A. Bertrand, J. L. Breece, and P. G. Eller, *Inorg. Chem.*, **13**, 125 (1974).
24) J. A. Bertrand and P. G. Eller, *Inorg. Chem.*, **13**, 927 (1974).
25) Y. Kuge and S. Yamada, *Bull. Chem. Soc. Jpn.*, **43**, 3972 (1970).
26) A. Syamal, E. F. Carey, and L. J. Theriot, *Inorg. Chem.*, **12**, 245 (1973).
27) H. A. O. Hill and N. Zarb-Adami, *J. Inorg. Nucl. Chem.*, **37**, 2443 (1975).
28) B. R. Stults, R. S. Marianelli, and V. W. Day, *Inorg. Chem.*, **14**, 722 (1975), and references therein.
29) "International Tables for X-Ray Crystallography," Kynoch Press, Birmingham (1962), Vol. III.
30) G. Bandoli, D. A. Clemente, and C. Panattoni, *Chem. Commun.*, **1971**, 311.
31) D. B. W. Yawney and R. J. Doedens, *Inorg. Chem.*, **9**, 1626 (1970).
32) G. M. Brown and R. Chidambaram *Acta Crystallogr., Sect. B*, **29**, 2393 (1973).
33) P. de Meester, S. R. Fletcher, and A. C. Skapski, *J. Chem. Soc., Dalton Trans.*, **1973**, 2575.
34) F. Hanic, D. Stempelova, and K. Hanicova, *Acta Crystallogr.*, **17**, 633 (1964).
35) G. Davey and F. S. Stephens, *J. Chem. Soc., A*, **1970**, 2803.
36) M. Mikuriya, S. Kida, I. Ueda, T. Tokii, and Y. Muto, *Bull. Chem. Soc. Jpn.*, **50**, 2464 (1977).

Study of the Mixed Ligand Complexes of Heavy Rare Earth Elements by Electromigration

Emiko Ohyoshi

Yatsushiro College of Technology, 2627, Hirayamashinmachi, Yatsushiro 866

(Received May 6, 1980)

The formation of the mixed ligand complexes of heavy rare earth elements with α-hydroxyisobutyric acid (AHIB or HA) and nitrilotriacetic acid (NTA or H_3L) was studied by electromigration. The equations expressing the zone mobility as a function of the concentrations of the two ligands were derived with or without the mixed ligand complexes, MLA^-. The experimental results showed that the MLA^- complexes were formed. The formation constants for the Tb(III), Dy(III), Ho(III), Er(III), Tm(III), Yb(III), and Lu(III) complexes were determined. The results obtained by using the two series of solutions, with varying $[L^{3-}]$ at a constant $[A^-]$ and with varying $[A^-]$ at a constant $[L^{3-}]$, were in good agreement. The stability trend was in an ordinary decreasing sequence of: Lu>Yb>Tm>Er>Ho>Dy>Tb.

The separation factor, the difference in the zone mobilities of two adjacent rare earth elements, is enhanced by the consecutive formation of complexes, ML_n.[1] This enhancement becomes more appreciable the closer the first and the second formation constants are to each other. This means that when various species, such as M, ML, and ML_2, are coexisting, more effective separation can be expected. If some mixed ligand complexes, such as MLA, were to be formed with another ligand A other than the binary complexes, ML_n, separation would be more improved. Therefore, it seems that a system containing two different ligands is more favorable for separating heavy rare earth elements than the conventional system. In this case, however, it is assumed that the formation constants of the mixed ligand complexes increase with increasing atomic number as observed in the case of the binary complexes, ML_n. To justify this assumption, it is necessary to obtain the data on the formation of the mixed ligand complexes of the heavy rare earth elements.

This work includes the results of a study on the mixed ligand complexes of the heavy rare earth elements with AHIB and NTA by paper electromigration.

Experimental

All chemicals used were of G.R. grade. The rare earth nitrate solutions of 2.0×10^{-2} mol dm^{-3} were prepared by dissolving the respective oxides in nitric acid. Mixed sample solutions of Tb(III), Dy(III), Er(III), and Yb(III), and of Tb(III), Ho(III), Tm(III) and Lu(III) at the same concentration of 1.5×10^{-4} mol dm^{-3} (pH≈1) were prepared. The other solutions were prepared as follows. Either AHIB(HA) or NTA (H_3L) was dissolved in chloroacetate buffer solution of pH 2.0 to give a concentration from 0.1 to 1.0 mol dm^{-3} or 10^{-3} to 10^{-2} mol dm^{-3}, respectively. By using the acid dissociation constants of AHIB[2] ($pK_{HA}=3.79$) and NTA[3] ($pK_{H_3L}=1.75$, $pK_{H_2L^-}=2.47$ and $pK_{HL^{2-}}=9.71$), the ligand ion concentrations are calculated to be $1.33-13.3\times10^{-3}$ mol dm^{-3} (A^-) and $2.33—23.3\times10^{-12}$ mol dm^{-3} (L^{3-}). The zone mobilities calculated by using these values of $[A^-]$ and $[L^{3-}]$ were found to agree well with the observed ones. In these concentration ranges, successive formation of the AHIB complexes proceeds, while that of the NTA complexes does not. The final ionic strength was adjusted to 0.1 with sodium chloride. In NaCl solution of 0.1 mol dm^{-3}, no appreciable complex formation of rare earth elements with chloride was observed.

Paper electromigration was carried out as described previously.[4]

Results and Discussion

The Effect of Two Ligands on the Zone Mobility of the Heavy Rare Earth Elements. At first, the experiment was carried out by using AHIB and NTA separately; the results are shown in Figs. 1a(AHIB) and 1b(NTA). In the ligand concentration ranges used here, the predominant complex species formed with NTA is ML, that is, the range of $[L^{3-}]$ is too low to form the ML_2 complex. On the other hand, various forms of complexes (MA^{2+}, MA_2^+, MA_3, and MA_4^-) are formed with increasing concentration of AHIB. In both cases, the zone mobility of each rare earth becomes close to each other with increasing ligand concentrations, but

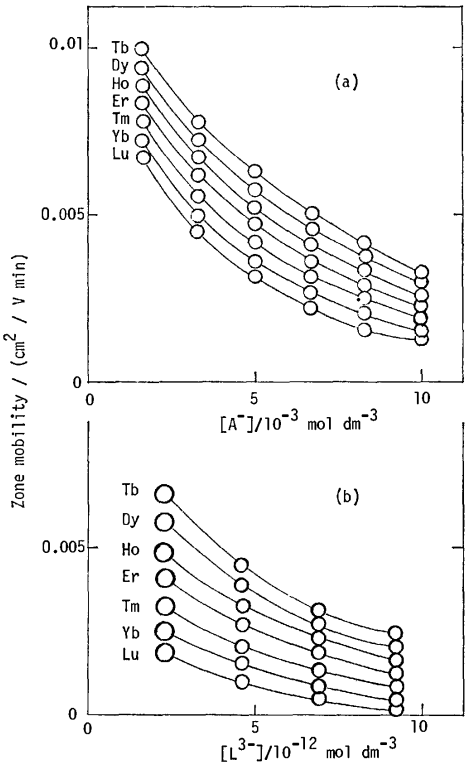

Fig. 1. Plots of the zone mobility *vs.* $[A^-]$(1a) or $[L^{3-}]$-(1b).

the range of AHIB concentration suitable for separation is broader than that of NTA. By lowering the concentration of NTA, the difference in the zone mobility becomes larger than that in the case of AHIB, but the zone width also becomes larger. This would be due to the large difference in the mobility between M^{3+} and ML. It may thus be concluded that AHIB generally gives better separation than NTA.

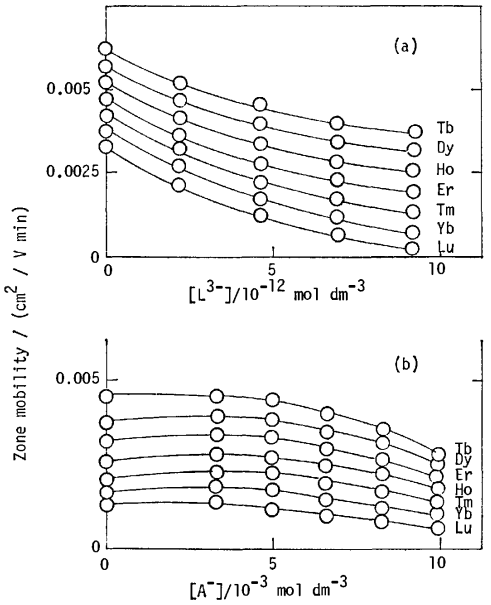

Fig. 2. (a): Plots of the zone mobility *vs.* $[L^{3-}]$ at $[A^-]=5.0\times10^{-3}$ mol dm^{-3}. (b): Plots of the zone mobility *vs.* $[A^-]$ at $[L^{3-}]=4.7\times10^{-12}$ mol dm^{-3}.

To examine the effect of mixed complexing agents on the zone mobility, experiments were done using mixtures of AHIB and NTA as electrolyte solutions. The results are shown in Fig. 2; $[L^{3-}]$ was varied at a constant $[A^-]$(2a) and $[A^-]$ was varied at a constant $[L^{3-}]$(2b). The zone location is found to be much more affected by increasing $[L^{3-}]$ than by increasing $[A^-]$. The formation of the neutral complexes with NTA considerably alters the zone mobility. In general, the zone is located between the limits found in cases where AHIB or NTA is separately used at the same concentration. With increasing concentration of AHIB, however, the zone mobility becomes lower than those in either case where the respective agent is separately used (Fig. 2b). This suggests that some mixed ligand complexes of the rare earth elements with NTA and AHIB, possibly as anionic species, might be formed, and that the zone mobility of each element is lowered.

Estimation of the Formation Constants of the Mixed Ligand Complexes. If there are no mixed ligand complexes in solutions containing M, H_3L, and HA, the species in equilibrium would be M, ML, MA, MA_2, MA_3, and MA_4 under the present experimental conditions (the charges are omitted for simplicity). When the equilibria among these species are rapidly attained under the electric field, the zone mobility u_{AL} can be related to the mobility and the amount of each species.[1,4,5]

$$u_{AL}([M]+[ML]+[MA]+[MA_2]+[MA_3]+[MA_4]) = u_M[M] + u_{ML}[ML] + u_{MA}[MA] + u_{MA_2}[MA_2] + u_{MA_3}[MA_3] + u_{MA_4}[MA_4], \quad (1)$$

where u means the mobility of the respective species. Using the overall formation constants of the above complexes, β's, Eq. 1 can be brought into the form:

$$u_{AL}(1+\beta_{ML}[L]+\beta_{MA}[A]+\beta_{MA_2}[A]^2+\beta_{MA_3}[A]^3+\beta_{MA_4}[A]^4) = u_M + u_{ML}\beta_{ML}[L] + u_{MA}\beta_{MA}[A] + u_{MA_2}\beta_{MA_2}[A]^2 + u_{MA_3}\beta_{MA_3}[A]^3 + u_{MA_4}\beta_{MA_4}[A]^4, \quad (2)$$

where $\beta_{ML}=[ML]/([M][L])$ and $\beta_{MA_n}=[MA_n]/([M][A]^n)$.

When H_3L or HA is separately used at the same concentrations as the above case, the appropriate following equation is applicable:

$$u_L(1+\beta_{ML}[L]) = u_M + u_{ML}\beta_{ML}[L] \quad (3)$$

$$u_A(1+\beta_{MA}[A]+\beta_{MA_2}[A]^2+\beta_{MA_3}[A]^3+\beta_{MA_4}[A]^4) = u_M + u_{MA}\beta_{MA}[A] + u_{MA_2}\beta_{MA_2}[A]^2 + u_{MA_3}\beta_{MA_3}[A]^3 + u_{MA_4}\beta_{MA_4}[A]^4, \quad (4)$$

where u_L or u_A is the zone mobility given by using H_3L or HA separately. Combining Eq. 2 with Eqs. 3 and 4, we obtain

$$(u_{AL}-u_L)(1+\beta_{ML}[L]) + (u_{AL}-u_A)(\beta_{MA}[A]+\beta_{MA_2}[A]^2 + \beta_{MA_3}[A]^3+\beta_{MA_4}[A]^4) + u_M - u_A = 0. \quad (5)$$

The left hand side of Eq. 5 can be calculated using the values of u_{AL}, u_L, u_A, and u_M obtained experimentally, as well as the overall formation constants of the respective complexes reported in the literature. The experimental results showed that Eq. 5 does not become zero, except for the case of Tb(III) at low values of [L] and [A]. Negative values which decrease with increasing [L] and [A] are obtained for all the elements. This indicates that the values of u_{AL} observed are smaller than those predicted by Eq. 5, which was derived by assuming that no mixed ligand complexes were formed. Hence, some mixed ligand complexes with negative charges other than the above complexes should be present in the mixed ligand solutions.

Assuming the mixed ligand complex to be MLA^-, Eq. 2 can be modified to the form:

$$u_{AL}(1+\beta_{ML}[L]+\beta_{MA}[A]+\beta_{MA_2}[A]^2+\beta_{MA_3}[A]^3+\beta_{MA_4}[A]^4 + \beta_{MLA}[L][A]) = u_M + u_{ML}\beta_{ML}[L] + u_{MA}\beta_{MA}[A] + u_{MA_2}\beta_{MA_2}[A]^2 + u_{MA_3}\beta_{MA_3}[A]^3 + u_{MA_4}\beta_{MA_4}[A]^4 + u_{MLA}\beta_{MLA}[L][A], \quad (6)$$

where u_{MLA} is the mobility of MLA and $\beta_{MLA}=[MLA]/([M][L][A])$. Combining Eq. 6 with Eqs. 3 and 4, we obtain

$$(u_{AL}-u_L)(u_{MLA}-u_{AL})^{-1}(1+\beta_{ML}[L])+(u_{AL}-u_A)(u_{MLA}-u_{AL})^{-1} \times (\beta_{MA}[A]+\beta_{MA_2}[A]^2+\beta_{MA_3}[A]^3+\beta_{MA_4}[A]^4) + (u_M-u_A)(u_{MLA}-u_{AL})^{-1} = \beta_{MLA}[L][A]. \quad (7)$$

If u_{MLA} is known, the left hand side of Eq. 7 can be obtained as a function of the product of [L] and [A]. If a linear relation is obtained between the left hand side of Eq. 7 and the product of [L] and [A], the formation constant of MLA^- can be determined from the slope of the line.

Various values have been reported for the formation constants of the rare earth complexes with NTA and AHIB. We tried to find the most suitable values by comparing the zone mobilities u_L and u_A calculated from Eqs. 3 and 4 with the observed ones. To estimate the mobilities of various complexes required for calculation, $u_{MA}^{2+}=0.007$ cm²/V min[4] and $u_{ML_2}^{-}=0.012\pm0.001$ cm²/V min measured at $I=0.1$ were used. When we consider that the value for u_{MA}^{2+} was measured with the presence of MA_2^+, the mobility is roughly proportional to the charge of the species. Hence, the following values might be given for the mobility of each species: $u_{ML}=0$, $u_{MA}^{2+}=0.008$, $u_{MA_2}^{+}=0.004$, $u_{MA_2}=0$, $u_{MA_4}=-0.004$, and $u_{MLA}^{-}=-0.004$ cm²/V min. The calculation of u_L and u_A was made by using the reported values for the formation constants of the rare earth complexes with NTA[6] and AHIB[7] determined at an ionic strength of 0.1. For all the elements the values calculated for u_L well agreed with those observed, whereas there were appreciable differences between the calculated and observed values of u_A. The values of u_A calculated by using another data for β_{MA_n} at higher ionic strength of 0.2[8] well agreed with the observed ones.

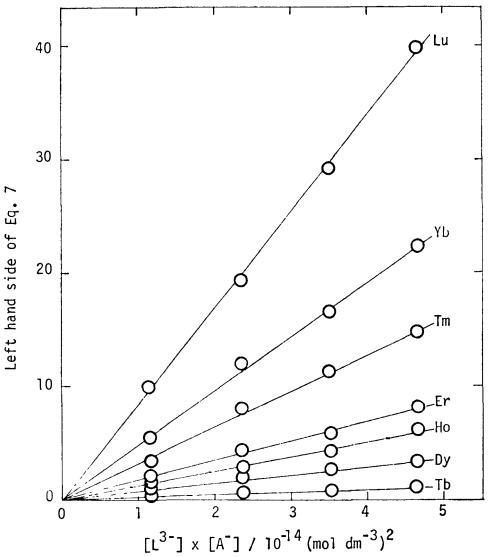

Fig. 3. Plots of the left hand side of Eq. 7 *vs.* $[L^{3-}]\times[A^-]$ at $[A^-]=5.0\times10^{-3}$ mol dm^{-3}.

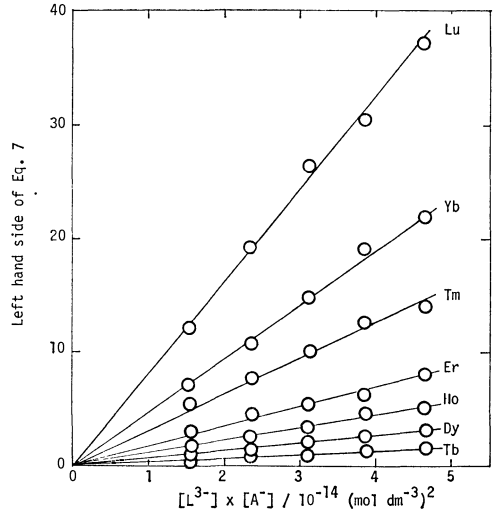

Fig. 4. Plots of the left hand side of Eq. 7 *vs.* $[L^{3-}]\times[A^-]$ at $[L^3]=4.7\times10^{-12}$ mol dm^{-3}.

Using the values of β_{ML},[6] β_{MA_n},[8] and u_{MLA} estimated above, the calculation of the left hand side of Eq. 7 was made. The results as a function of the product of [L] and [A] are shown in Figs. 3 and 4, where [A] or [L] is respectively kept constant. For all the elements, the plots in either Fig. 3 or 4 exhibit linear relations, indicating that the MLA^- complex is present in a mixture of NTA and AHIB solutions at the ligand concentrations studied. The values of β_{MLA}- for these rare earths were obtained from the slopes of the lines in both Figs. 3 and 4, as listed in Table 1. The two values obtained from Figs. 3 and 4 for each element are in good agreement. The stability trend was in an ordinary sequence, as expected. To obtain further information on the stability of the MLA^- complexes, the values of K^{ML}_{MLA} and K^{MA}_{MLA}, the equilibrium constants of Eqs. 8 and 9 and those of $\Delta\log K$ and $\log X$ defined by Sigel[9] (Eqs. 10 and 11) were calculated:

$$ML + A = MLA \quad k^{ML}_{MLA} = \beta_{MLA}/\beta_{ML}\ ^{6)} \tag{8}$$

$$MA + L = MAL \quad k^{MA}_{MAL} = \beta_{MLA}/\beta_{MA}\ ^{8)} \tag{9}$$

$$\Delta\log k = \log k^{ML}_{MLA} - \log\beta_{MA}\ ^{8)} = \log k^{MA}_{MAL} - \log\beta_{ML}\ ^{6)} \tag{10}$$

$$\log X = 2\log\beta_{MLA} - (\log\beta_{ML_2}\ ^{6)} + \log\beta_{MA_2}\ ^{8)}). \tag{11}$$

These results are also given in Table 1. For all the elements, $\Delta\log K$ values are nearly the same but $\log X$

Table 1. Formation constants of the mixed ligand complexes (MLA^-) of heavy rare earths at $I=0.1$(NaCl) and at 25 °C

Element	$\log\beta_{MLA}$- A[a]	B[b]	$\log K^{ML}_{MLA}$	$\log K^{MA}_{MAL}$	$\Delta\log K$	$\log X$
Tb(III)	13.4	13.5	1.86	10.53	−1.06	0.69
Dy(III)	13.8	13.8	2.06	10.86	−0.88	1.00
Ho(III)	14.1	14.0	2.15	11.07	−0.83	1.31
Er(III)	14.2	14.2	2.17	11.19	−0.84	1.41
Tm(III)	14.5	14.5	2.28	11.40	−0.82	1.76
Yb(III)	14.7	14.7	2.30	11.57	−0.83	1.88
Lu(III)	14.9	14.9	2.41	11.72	−0.77	1.84

a) Obtained from the plots in Fig. 3. b) Obtained from the plots in Fig. 4.

Table 2. Differences in logarithms of formation constants of the binary and the ternary complexes between adjacent rare earths

Element M_1–M_2	log $K(M_1)$ − log $K(M_2)$					
	$K=K_{MA}^{M}$ [8]	$K=K_{ML}^{M}$ [6]	$K=K_{MA_2}^{MA}$ [8]	$K=K_{ML_2}^{ML}$ [6]	$K=K_{MAL}^{MA}$	$K=K_{MAL}^{ML}$
Dy–Tb	0.02	0.15	0.19	0.03	0.33	0.20
Ho–Dy	0.04	0.16	0.05	−0.06	0.21	0.09
Er–Ho	0.03	0.13	0.13	−0.09	0.12	0.02
Tm–Er	0.09	0.19	0	−0.03	0.21	0.11
Yb–Tm	0.03	0.18	0.01	0.06	0.17	0.02
Lu–Yb	0.05	0.09	0.17	0.13	0.15	0.11

increases roughly with atomic number, indicating that the heavier the element is, the more the formation of the MLA^- complex is promoted.

Table 2 shows the differences in logarithms of the formation constants of the binary[6,8] and the ternary (Table 1) complexes between adjacent rare earth elements. There are considerable differences in both $\log K_{MAL}^{MA}$ and $\log K_{MLA}^{ML}$ between adjacent elements, suggesting that successive formation of the MLA complexes gives larger differences in the zone mobilities of adjacent elements. On the other hand, formation of the ML_2 complexes reduces the effect on the separation of the metals from dysprosium to thulium, since $K_{ML_2}^{ML}$ for these metals decrease with atomic number. Separation of the heavy rare earth elements would be improved by the formation of the MLA complexes other than the binary complexes ML and MA_n.

The author wishes to thank the Ministry of Education, Science and Culture for the financial support granted to this research (No. 364203).

References

1) E. Ohyoshi, *Bull. Chem. Soc. Jpn.*, **44**, 423 (1971).
2) R. S. Kolat, Doctoral Dissertation, Iowa State University, 1962.
3) H. M. N. H. Irving and M. G. Miles, *J. Chem. Soc., A*, **1966**, 727.
4) E. Ohyoshi, *Bull. Chem. Soc. Jpn.*, **43**, 1387 (1970).
5) V. P. Shvedov and A. V. Stepanov, *Radiokhimiya*, **1**, 62 (1959).
6) T. Moeller and R. Ferrús, *Inorg. Chem.*, **1**, 49 (1962).
7) J. E. Powell, R. H. Karraker, R. S. Kolat, and J. L. Farrell, "Rare Earth Research II," ed by K. S. Vorres, Gordon and Breach, New York (1964), pp. 509—522.
8) H. Deelstra and F. Verbeek, *Anal. Chim. Acta*, **31**, 251 (1964).
9) H. Sigel, *Chimia*, **21**, 489 (1967); R. Griesser and H. Sigel, *Inorg. Chem.*, **9**, 1238 (1970).

X-Ray Structures of Cu(II) Chelates of *cis*-1,3-Cyclohexanediamine

Keiko KAMISAWA, Keiji MATSUMOTO, Shun'ichiro OOI,* Reiko SAITO,** and Yoshinori KIDANI***

Department of Chemistry, Faculty of Science, Osaka City University, Sumiyoshi-ku, Osaka 558
***Aichi Junior College of Nursing, Kamishidanmi, Moriyama-ku, Nagoya 463*
****Faculty of Pharmaceutical Science, Nagoya City University, Tanabe-dori, Mizuho-ku, Nagoya 467*

(Received June 14, 1980)

The crystal structures of wine-red $[Cu(1,3\text{-chxn})_2]Br_2$ (**1**), $[Cu(1,3\text{-chxn})_2](NO_3)_2$ (**2**), and blue-violet $[CuCl(1,3\text{-chxn})_2]ClO_4$ (**3**) (1,3-chxn=*cis*-1,3-cyclohexanediamine) have been determined from the diffractometer data measured by the use of Mo $K\alpha$ radiation. The structures were solved by the Patterson-Fourier method and refined by the least-squares method to $R=0.042$ (**1**), 0.033 (**2**), and 0.057 (**3**) for 1309, 1210, and 776 nonzero reflections respectively. The Cu atoms in **1** and **2** have a square-planar coordination by 4 N atoms, while the complex ion in **3** has a 5-coordinate square-pyramidal geometry, with the Cl atom at the apical position. The 6-membered chelate rings in **1**, **2**, and **3** are of the chair, flattened-chair, and envelope conformations respectively. The complex ions in **1** and **2** have virtually a C_{2h} symmetry, the two-fold axis of which lies on the CuN_4 plane. The virtual symmetry for $[CuCl(1,3\text{-chxn})_2]^+$ is C_{2v}, the approximate two-fold axis being coincident with the Cu–Cl bond. The cyclohexane rings (chair conformation) in **2** and **3** are roughly perpendicular to the coordination plane, but that in **1** leans toward the central Cu(II) atom. The formation of such coordinatively unsaturated Cu(II) complexes as **1**—**3** is attributable to the steric hindrance of the bulky cyclohexane ring to the axial coordination site.

Although *cis*-1,3-cyclohexanediamine (1,3-chxn) is capable of chelating to a metal ion, as has been demonstrated by X-ray structure analyses of Pd(II) and Pt(II) chelates,[1,2] it has received much less attention in coordination chemistry than the *trans*-1,2-isomer, which is chiral and stereoselective for complex formation. Recently, however, the bis 1,3-chxn chelates of several metal ions have been prepared and characterized by means of the spectral method.[3] Of these chelates, $Cu(1,3\text{-chxn})_2X_2$-type compounds show various colors depending on the course of the preparation; *e.g.*, the recrystallization of the violet bromide from methanol yields wine-red crystals, whose color is unusual for the CuN_4X_2 chromophore, while the color of the bromide is unchanged by recrystallization from ethanol. The crystal structures of wine-red $Cu(1,3\text{-chxn})_2Br_2$ (**1**), $Cu(1,3\text{-chxn})_2(NO_3)_2$ (**2**), and blue-violet $Cu(1,3\text{-chxn})_2ClClO_4$ (**3**) have been investigated in order to reveal the stereochemical features of the 1,3-chxn as a ligand.

Experimental

The preparations of **1**, **2**, and **3** were described elsewhere.[3] The unit-cell dimensions of **1**, **2**, and **3** were determined from the least-squares analyses of 18, 16, and 12 θ values of the high-angle reflections measured on an automated diffractometer. Table 1 lists the crystal data and experimental details. The intensities were measured on the diffractometer using graphite-monochromated Mo $K\alpha$ radiation, and corrected for the Lp factor, but not for absorption. For each of the three compounds, the intensities of three standard reflections were monitored every 4 h, but they showed no ap-

Table 1. Summary of crystal data and experimental details

Compound	1	2	3
Color	Wine-red	Wine-red	Blue-violet
Crystal system	Monoclinic	Monoclinic	Orthorhombic
Space group	$P2_1/n$	C_m	Pbnm
a/Å	7.394(2)	10.059(3)	18.206(8)
b/Å	16.893(2)	9.278(3)	13.501(5)
c/Å	6.544(2)	10.428(3)	7.552(2)
β/°	90.34(6)	117.12(4)	
D_m/g cm^{-3}	1.83	1.59	1.51
D_c/g cm^{-3}	1.84	1.59	1.53
Z	2	2	4
μ(Mo $K\alpha$)/cm^{-1}	66.9	13.4	15.2
Crystal size/mm^3	0.09×0.15×0.24	0.25×0.12×0.30	0.06×0.24×0.18
Scan type	ω	ω	ω-2θ
Scan speed/° s^{-1}	0.017	0.025	0.008
Scan range/°	1.0+0.2 tan θ	0.8+0.2 tan θ	0.9
$2\theta_{max}$/°	60	60	46
Background estimation/s^{-1} (at each side of scan range)	20	15	Half of scan time
No. of unique reflections with $F_o^2 > 3\sigma(F_o^2)$	1309	1210	776
R	0.042	0.033	0.053
R_w	0.047	0.044	0.057

preciable decay.

The crystal structures were solved by the Patterson-Fourier method. The positional and thermal parameters were refined by the block-diagonal-matrix least-squares method. The minimized functions were $\sum w(F_o-|F_c|)^2$, where $w=1/\sigma^2(F_o)$. The systematic extinctions for **2** were indicative of three possible space groups: C2/m, C2, and Cm. Refinements for nonhydrogen atoms on the assumptions of the former two gave no further improvements over $R=0.098$ and 0.118, but R was reduced to 0.051 by the refinement based on the Cm space group. The systematic extinctions for **3**, $h+l=2n+1$ for $h0l$ and $k=2n+1$ for $0kl$, indicated two possible space groups, Pbnm and $Pbn2_1$; the former was confirmed by the successful refinement of the structure.

For **1**—**3**, peaks due to all H atoms were found from the difference syntheses after anisotropic refinement for nonhydrogen atoms. The positions of these H atoms were almost entirely in agreement with those calculated on the assumption that the C–H and N–H distances are 1.00 Å. The H atoms were included in the least-squares calculations, but their parameters were not refined. The isotropic temperature factors assigned to the H atoms were as follows:

	1	**2**	**3**
B_H/Å^2	4.5	$B_P+1.0$	$B_P+1.0$,

where B_p is the isotropic temperature factor of the nonhydrogen atom to which the H atom is bonded (the temperature factor obtained at the final cycle of isotropic refinement was used as the B_p).

The atomic scattering factors, with corrections for dispersion effects for Cu^0, Br^-, Cl^-, and Cl, were taken from Ref. 4. The atomic coordinates are listed in Table 2. The corodinates of the H atoms, the anisotropic thermal parameters, and the F_o-F_c tables for the three compounds are preserved by the Chemical Society of Japan (Document No. 8120). All the computations were performed by a FACOM 230-60 computer at Osaka City University using programs in the UNICS.[5]

Table 2. Positional and thermal parameters ($\times 10^4$)

Atom	x	y	z	B_{eq}[a]/Å^2
(**1**) $[Cu(1,3\text{-chxn})_2]Br_2$				
Cu	0	0	0	1.85
Br	2867.8(9)	991.7(4)	−4520.8(10)	2.62
N(1)	1139(6)	1076(3)	508(7)	2.2
N′(1)	−1393(7)	500(3)	−2316(7)	2.5
C(1)	−1019(8)	1908(3)	−1485(9)	2.3
C(2)	−43(8)	1787(3)	564(9)	2.4
C(3)	−1426(9)	1727(4)	2279(10)	3.2
C(4)	−2828(9)	1081(4)	1893(10)	3.3
C′(2)	−2377(8)	1260(3)	−1931(9)	2.6
C′(3)	−3718(9)	1162(4)	−200(11)	3.4
(**2**) $[Cu(1,3\text{-chxn})_2](NO_3)_2$				
Cu	0	0	0	2.29
N(1)	342(4)	1574(4)	1456(3)	3.29
N(2)	−343(4)	1569(4)	−1433(3)	3.34
C(1)	834(7)	0	3536(6)	4.4
C(2)	1266(5)	1359(5)	3046(4)	3.8
C(3)	2936(5)	1331(6)	3414(5)	4.2
C(4)	3366(7)	0	2895(7)	4.1
C(5)	−791(8)	0	−3534(7)	4.7
C(6)	−1260(5)	1364(5)	−3018(4)	3.8
C(7)	−2893(5)	1353(6)	−3402(5)	4.1
C(8)	−3344(7)	0	−2870(7)	4.2
N(3)	1838(5)	5000	1100(6)	4.0
O(1)	1360(8)	5000	1954(9)	8.3
O(2)	2075(4)	3829(4)	629(4)	5.5
N(4)	−1818(6)	5000	−1046(6)	3.9
O(3)	−1350(8)	5000	−1971(8)	8.0
O(4)	−2065(4)	3833(4)	−600(4)	5.0
(**3**) $[CuCl(1,3\text{-chxn})_2]ClO_4$				
Cu	752.9(9)	139.3(1)	2500	2.69
Cl(1)	−137(2)	−216(3)	2500	3.70
N(1)	1389(4)	844(5)	4468(10)	3.5
N(2)	145(4)	1999(5)	4450(10)	3.8
C(1)	1961(8)	−394(10)	2500	5.8
C(2)	2043(5)	197(7)	4158(15)	4.7
C(3)	2741(5)	838(9)	4133(17)	6.4
C(4)	2780(8)	1462(13)	2500	5.9
C(5)	−894(8)	2476(10)	2500	5.4
C(6)	−484(6)	2713(7)	4146(14)	4.8
C(7)	−176(6)	3765(7)	4141(16)	5.3
C(8)	267(10)	3962(10)	2500	6.2
Cl(2)	1729(2)	3288(3)	7500	5.7
O(1)	1188(11)	2584(13)	7500	13.2
O(2)	2100(11)	3135(9)	5999(27)	23.3
O(3)	1479(10)	4225(11)	7500	12.9

a) Equivalent isotropic temperature factor (W.C. Hamilton, *Acta Crystallogr.*, **12**, 609 (1959)).

Results and Discussion

Figure 1 shows a part of the crystal structure for each of the three compounds. The interatomic distances and bond angles are given in Table 3. In **1** the Br and its symmetry-related ions lying above and below the coordination plane participate in hydrogen bonding with the axial H atoms of NH_2 groups, but not in coordination with the Cu atom ($Cu\cdots Br^-=4.015(1)$ Å). The NO_3^- ions around the complex ion in **2** are distant from the Cu atom and take part in the hydrogen bonds with NH_2 groups. The complex ions in **1** and **2** thus have the 4-coordinate square-planar coordination. The Cl^- ion in **3** is bonded to the Cu atom, thus completing a 5-coordinate square-pyramidal configuration. Although the IR spectrum of **3** at the 1000—1200 cm^{-1} region is indicative of the participation of the ClO_4^- ion in the coordination sphere,[3] the structure analysis

Table 3. Interatomic distances and bond angles

Bond lengths (l/Å)	**1**	**2**	**3**
Cu–N	2.029(5)	2.020(4)	2.025(8)
Cu–N′(1)	2.013(5)		
Cu–N(2)		2.000(4)	2.015(8)
Cu–Cl(1)			2.710(4)
N(1)–C(2)	1.487(8)	1.499(6)	1.49(1)
N′(1)–C′(2)	1.498(8)		
N(2)–C(6)		1.494(6)	1.51(1)
C(1)–C(2)	1.533(8)	1.497(9)	1.49(2)
C(1)–C′(2)	1.513(8)		
C(2)–C(3)	1.526(9)	1.543(7)	1.54(2)
C′(2)–C′(3)	1.518(10)		
C(3)–C(4)	1.525(10)	1.489(9)	1.50(2)
C′(3)–C(4)	1.523(10)		
C(5)–C(6)		1.532(9)	1.48(2)
C(6)–C(7)		1.503(8)	1.53(2)
C(7)–C(8)		1.522(9)	1.50(2)

Selected intramolecular nonbonded distances (l/Å) [a]

	1	2	3
Cu···H_{ax}[C(4)]	2.28	2.61	
Cu···H_{ax}[C(8)]		2.61	
N(1)···N′(1)	2.798(7)	2.921(6)	2.97(1)
N(2)···N′(2)		2.912(6)	2.95(1)
C(2)···C′(2)	2.531(9)	2.521(7)	2.50(2)
C(6)···C′(6)		2.532(7)	2.49(2)
Cl(1)···C(1)			3.83(2)
Cl(1)···C(5)			3.89(2)
C(4)···C(8)			5.75(3)

The H···X distances (l/Å) in N–H···X hydrogen bonds[b]

N–H···X		1	2	3
N(1)	Br	2.64		
N(1)	Br^{I}	2.51		
N′(1)	Br	2.68		
N′(1)	Br^{I}	2.57		
N(1)	O(2)		2.08	
N(1)	$O(2)^{II}$		2.16	
N(2)	O(4)		2.10	
N(2)	$O(4)^{III}$		2.15	
N(2)	O(1)			2.13
N(1)	$Cl(1)^{IV}$			2.39
N(2)	$Cl(1)^{IV}$			2.45

Bond angles (ϕ/°)

	1	2	3
N(1)–Cu–N′(1)	87.6(2)	92.6(2)	94.4(3)
N(2)–Cu–N′(2)		93.4(2)	93.9(3)
Cl(1)–Cu–N(1)			92.7(2)
Cl(1)–Cu–N(2)			89.8(2)
Cu–N(1)–C(2)	119.0(4)	122.8(3)	123.7(6)
Cu–N′(1)–C′(2)	118.7(4)		
Cu–N(2)–C(6)		122.9(3)	124.3(6)
N(1)–C(2)–C(1)	111.1(5)	111.1(5)	111.4(10)
N′(1)–C′(2)–C(1)	109.3(5)		
N(2)–C(6)–C(5)		111.1(5)	111.7(9)
N(1)–C(2)–C(3)	111.2(5)	109.5(4)	109.4(9)
N′(1)–C′(2)–C′(3)	110.6(5)		
N(2)–C(6)–C(7)		110.1(4)	108.3(8)
C(1)–C(2)–C(3)	109.8(5)	110.7(5)	111.9(11)
C(2)–C(3)–C(4)	112.5(5)	112.7(5)	111.5(11)
C(3)–C(4)–C′(3)	112.0(6)	112.1(8)	111.2(17)
C(4)–C′(3)–C′(2)	113.6(6)		
C′(3)–C′(2)–C(1)	111.7(5)		
C′(2)–C(1)–C(2)	112.4(5)	114.7(8)	114.0(16)
C′(6)–C(5)–C(6)		111.5(6)	113.8(14)
C(5)–C(6)–C(7)		112.1(5)	112.5(10)
C(6)–C(7)–C(8)		112.3(5)	111.4(11)
C(7)–C(8)–C′(7)		111.1(8)	111.2(17)

Interplanar angles (Ψ/°)[c]

		1	2	3
[Cu,N(1),N′(1)]	[N(1),C(2),C′(2),N′(1)]	139.2	158.8	183.6
[Cu,N(2),N′(2)]	[N(2),C(6),C′(6),N′(2)]		159.3	176.4

a) The subscript ax indicates the axial H atom with respect to the cyclohexane ring. b) Roman-numeral superscripts refer to the following equivalent positions: I $x, y, 1+z$; II $-1/2+x, 1/2-y, z$; III $1/2+x, 1/2-y, z$; IV $-x, -y, 1-z$. c) The atom disposition in each [N,C,C′,N′] plane is completely planar in **2** and **3**; it is also planar in **1** within the limits of experimental error.

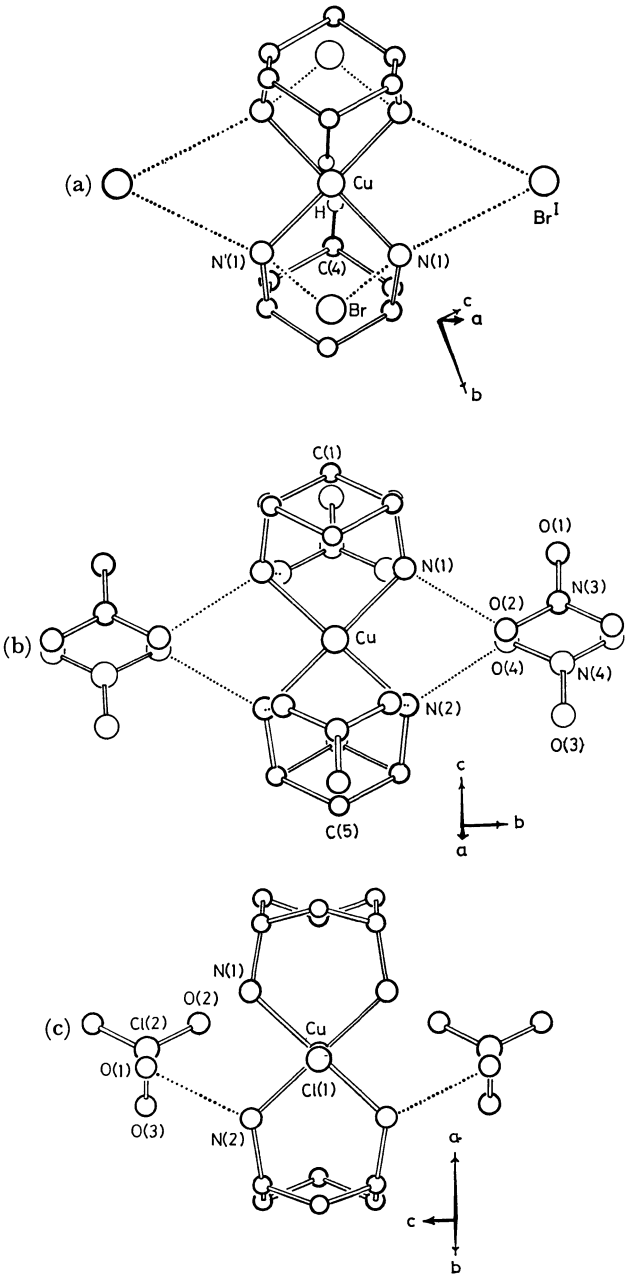

Fig. 1. Environments of the complex cations: (a) $[Cu(1,3\text{-chxn})_2]Br_2$, (b) $[Cu(1,3\text{-chxn})_2](NO_3)_2$, and (c) $[CuCl(1,3\text{-chxn})_2]ClO_4$. Each figure is the projection of a part of the crystal structure on the coordination plane defined by the 4 N atoms. The dotted lines indicate hydrogen bonds.

disclosed that one of the O atom [O(1)] of the ClO_4^- is linked to the H atom of the $N(2)H_2$ group. The ClO_4^- ion has no higher symmetry than the crystallographically imposed C_s symmetry, as was indicated by the examination of O–Cl–O bond angles,[6] and this low symmetry is responsible for the splitting of the IR band in that region.

The complex ions in **1** and **2** have strict C_i and C_s symmetries respectively, but both also have a virtual C_{2h} symmetry in which the two-fold axis bisects the N(1)–Cu–N(2) bond angle (for **1** N(2) stands for the

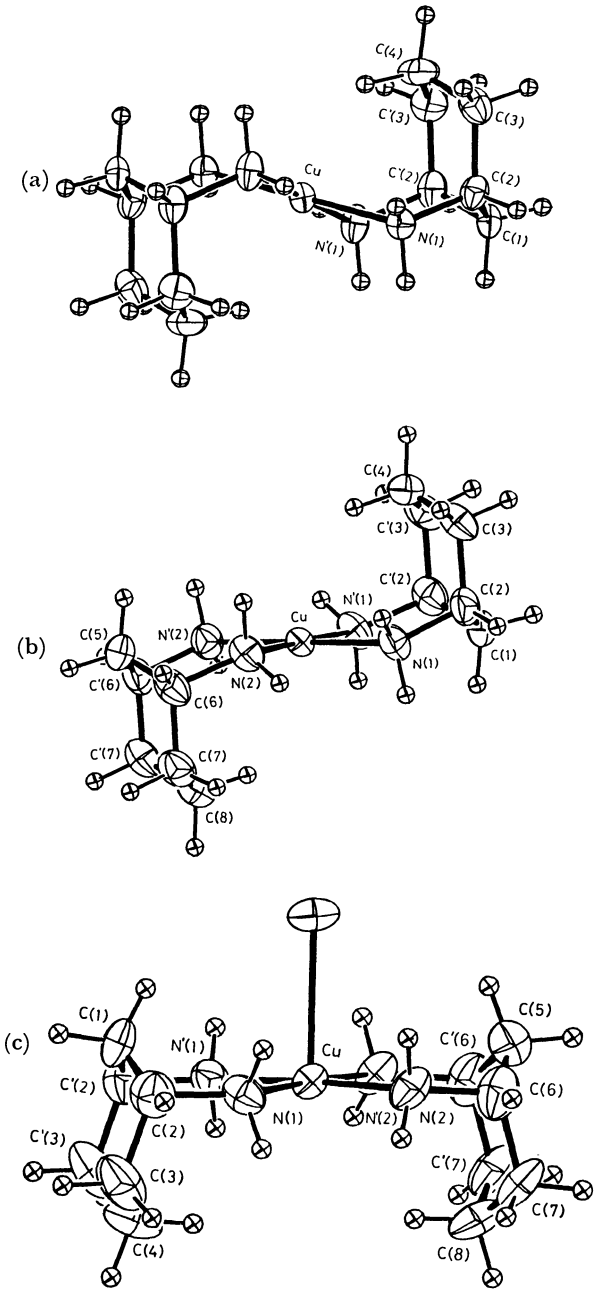

Fig. 2. Perspective views of (a) $[Cu(1,3\text{-chxn})_2]^{2+}$ in **1**, (b) $[Cu(1,3\text{-chxn})_2]^{2+}$ in **2**, and (c) $[CuCl(1,3\text{-chxn})_2]^{+}$ in **3**. Thermal ellipsoids are drawn at 50% probability level. Hydrogen atom is shown by a sphere with arbitrary radius.

equivalent of N'(1) at the $-x$, $-y$, $-z$ position). Above and below the coordination plane the most proximate atoms to the Cu are the axial H atom of $C(4)H_2$ and its symmetry-related (C_{2h}) atom [Fig. 2(a) and (b)], the Cu···H distances in **1** and **2** being 2.28 and 2.61 Å. The Cu···H vector in **1** intersects the CuN_4 plane at 79.1°, while those in 2 intersect it at 64.6° and 64.9°. The Cu–N bond lengths in **2** are slightly shorter than those in **1** and are comparable to the Cu–N (primary amine) length in the red form of bis(*N*,*N*-diethylethylenediamine)copper(II) perchlorate, in which the Cu atom has a square-planar coordination.[7] In general, however, the Cu–N distance in the planar complex is not appreciably different from those in 6-coordinate tetragonal and 5-coordinate square-pyramidal complexes.[7,8]

A perspective view of $[CuCl(1,3\text{-chxn})_2]^{+}$ is shown in Fig. 2(c). In addition to the crystallographically imposed mirror plane on which Cu, Cl(1), C(1), C(4), C(5), and C(8) lie, there is an approximate two-fold axis normal to the coordination plane; therefore, the virtual symmetry is regarded as C_{2v}. The Cu atom is displaced by 0.045 Å toward the apical atom, but this deviation is very small in comparison with that (0.33 Å) in chloro(2,7,12-trimethyl-3,7,11,17-tetraazabicyclo-[11.3.1]heptadeca-1(17),2,11,13,15-pentane)copper(II) nitrate dihydrate,[9] which involves the $CuClN_4$ coordination framework. Concomitantly, the Cu–Cl bond in **3** is much longer than that (2.50 Å) in the complex cited for comparison.[9] The $C(1)H_2$ and $C(5)H_2$ groups are in close contact with the Cl(1) atom and prevent the Cl atom from approaching Cu further. The visible spectrum of **3** in methanol ($\tilde{\nu}_{max}=18000\ cm^{-1}$) is somewhat different from that in the solid state ($\tilde{\nu}_{max}=18400\ cm^{-1}$), suggesting some change in the coordination sphere.

The 6-membered chelate rings in **1** and **2** are of the chair conformation, but those in **3** take the envelope conformation. The N–Cu–N′ coordination angles are greater than 90° in **2** and **3** and are comparable to that in $[Pd(1,3\text{-chxn})_2]Cl_2$.[1] The coordination angle in **1** is significantly smaller than those in **2** and **3**; it has a value of less than 90°. The [Cu,N,N′]–[N,C,C′,N′] interplanar angle in **1** is smallest (Table 3), but is comparable to that in $[Cu(tn)_2](NO_2)_2$ (132.5°)[10] (tn=1,3-propanediamine). In the chair ring, the increase in the interplanar angle gives rise to an enlargement of the coordination angle,[11] and the envelope ring has the largest angle (Table 3). The interplanar angle in the planar complex is thought to be susceptible to its surroundings. The different interplanar angles in **1** and **2** may result from the difference between the crystal packings.

As may be seen from Fig. 2, the 1,3-chxn ligand has the diaxial conformation, in which two C–NH_2 bonds are axial with respect to the cyclohexane ring. A CH_2 group at the 5-position ($C(4)H_2$ in **1**; $C(4)H_2$ and $C(8)H_2$ in **2** and **3**) is located close to the axial coordination site. A chelation of the diaxial 1,3-chxn thus situates the bulky cyclohexane moiety in the proximity of the metal ion, preventing the axial site from ligand access. This is in contrast to the case of the *trans*-1,2-isomer, whose cyclohexane ring is distant from the metal ion and has little influence on the adjacent coordination site.[12] The 1,3-chxn ligand, therefore, tends to give a coordinatively unsaturated complex and prefers a metal ion with tetragonal stereochemistry rather than one with an octahedral one. The steric hindrance of the cyclohexane moiety is responsible for the formation of the 4-coordinate planar Cu(II) complex unusual for the coordination geometry of $Cu(diamine)_2X_2$.

The reaction of $CuCl_2$ with twice as many mols of the 1,3-chxn in methanol yielded a violet compound,

$Cu(1,3\text{-chxn})_2Cl_2$; the violet bromide was also obtained by a similar reaction of $CuBr_2$ with the ligand in ethanol. The reflectance spectra of these compounds were indicative of a 6-coordinate tetragonal geometry.[3] The possible disposition of the 1,3-chxn ligands in this geometry is of the C_{2h} type (*vide supra*), since the C_{2v} disposition is unable to have a coordination number greater than 5 because of the steric interference of the cyclohexane rings. In the "6-coordinate C_{2h}" complex, however, the halide ligands are thought to be displaced greatly from the usual axial coordination sites to avoid the CH_2 groups at the 5-position of the 1,3-chxn. The distortion from tetragonal coordination geometry may be diminished if the cyclohexane ring assumes the boat conformation at the expense of the conformational energy. Unfortunately, no single crystals of the violet compounds have yet been obtained.

References

1) K. Kamisawa, K. Matsumoto, S. Ooi, H. Kuroya, R. Saito, and Y. Kidani, *Bull. Chem. Soc. Jpn.*, **51**, 2330 (1978).

2) F. E. Sarneski, A. T. Mcphail, and K. D. Onan, *J. Am. Chem. Soc.*, **99**, 7736 (1977).

3) R. Saito and Y. Kidani, *Bull. Chem. Soc. Jpn.*, **52**, 57 (1979).

4) "International Tables for X-Ray Crystallography," Kynoch Press, Birmingham (1974), Vol. IV, pp. 71, 148.

5) "The Universal Crystallographic Computation Progr. m System," Crystallographic Society of Japan (1969).

6) The bond lengths and angles in the ClO_4^- ion are as follows: Cl–O(1)=1.37(2), Cl–O(2), Cl–O′(2), Cl–O(3)=1.34(2) Å, O(1)–Cl–O(2)=105(1)°, O(1)–Cl–O′(2)=105(1)°, O(1)–Cl–O(3)=114(1)°, O(2)–Cl–O′(2)=116(2)°, O(2)–Cl–O(3)=108(1)°, O′(2)–Cl–O(3)=108(1)°.

7) M. M. Andio, J. D. Curet, and M. M. Muir, *Acta Crystallogr., Sect. B*, **32**, 3185 (1976); L. Grenthe, P. Paoletti, M. Sandström, and S. Glikberg, *Inorg. Chem.*, **18**, 2687 (1979), and the references cited therein.

8) T. G. Fawcett, S. M. Rudich, B. H. Toby, R. A. Lalancette, J. A. Potenza, and H. J. Schugar, *Inorg. Chem.*, **19**, 940 (1980), and the references cited therein.

9) M. R. Caira, L. R. Nassimbeni, and P. R. Woolley, *Acta Crystallogr., Sect. B*, **31**, 1334 (1975).

10) A. Pajunen and I. Belinskij, *Suom. Kemistil. B*, **43**, 70 (1970).

11) F. A. Jurnak and K. N. Raymond, *Inorg. Chem.*, **13**, 2387 (1974).

12) Y. Saito, "Inorganic Molecular Dissymmetry," Splinger-Verlag, Berlin (1979), Chap. IV.

Reactions of *trans*- and *cis*-Dichlorobis(benzonitrile)platinum(II) with Acetylacetonate and Benzoylacetonate Carbanions. Formation of *N*-Acetyl β-Ketoamine Complexes by the Acetyl Group Migration†

Toshihiko UCHIYAMA, Kazuhiko TAKAGI, Keiji MATSUMOTO, Shun'ichiro OOI, Yukio NAKAMURA,* and Shinichi KAWAGUCHI

Department of Chemistry, Faculty of Science, Osaka City University, Sumiyoshi-ku, Osaka 558

(Received September 11, 1980)

trans-Dichlorobis(benzonitrile)platinum(II) reacted with twice the molar amount of thallium(I) acetylacetonate and benzoylacetonate in dichloromethane at room temperature to afford mainly *N*-acetyl β-ketoamine chelates, *trans*-[Pt{N(COMe)=C(Ph)CH=COMe(and Ph)}$_2$] (**1a** and **3a**). This *N,O*-chelate structure of **1a** was determined by X-ray analysis. Reactions of *cis*-[$PtCl_2(PhCN)_2$] gave *C*-acetyl and *C*-benzoyl β-ketoamine chelates, *cis*-[Pt{NH=C(Ph)C(COMe(and Ph))=COMe}$_2$], together with other minor products. Formation of these β-ketoamine chelates is explained by the nucleophilic reactions of the β-diketonate carbanions at the coordinated cyanide carbon atom, followed by migration of the acetyl group or the methine proton of the nucleophiles onto the imino nitrogen atom formed during these reactions. In the presence of free β-diketones, migration of the acyl group was generally suppressed; this led to high yields of *C*-acyl complexes especially in reactions of *cis*-[$PtCl_2$-$(PhCN)_2$]. In each case, the reaction proceeded with retention of the geometrical configuration around the central metal atom. The structures of other products, including a compound obtained by acid hydrolysis of **1a**, were explored and discussed, based on IR and ^{1}H NMR data.

It is well known that nitriles in the coordination sphere of metal ions are very susceptible to nucleophilic attack and readily react with water, alcohols, and amines to yield the corresponding amides, imidic esters, and amidines, respectively.[1] Stephenson[2] examined the X-ray structure of the reaction product between [$PtCl_2(MeCN)_2$] and aqueous ammonia. The product originally formulated as [$Pt(NH_3)_4(MeCN)_2$]$Cl_2\cdot H_2O$ was shown to be an amidine complex of the stoichiometry [$Pt(NH_3)_2${$NHC(NH_2)Me$}$_2$]$^{2+}$ in which the imine nitrogens are bound to the platinum. Recently, Braunstein *et al.*[3] demonstrated that cyanide carbons in the benzonitrile analogue [$PtCl_2(PhCN)_2$] undergo the nucleophilic attack of carbanions Ph_2PCHY (Y= CO_2Et and CN) in tetrahydrofuran at 0 °C to afford *trans*-[Pt{P(Ph)$_2$C(Y)=C(Ph)NH}$_2$]. Similar reactions of metal complexes with β-diketonate ions have not been examined, although the nucleophiles are known to add to the coordinated unsaturated hydrocarbon[4-6] and imine[7] ligands. We have briefly reported[8] the reaction of [$PtCl_2(PhCN)_2$] with an acetylacetonate ion in dichloromethane at room temperature to give an *N*-acetyl β-ketoamine chelate, *trans*-[Pt{N(COMe)=C(Ph)CH=COMe}$_2$] (**1a**). It is noteworthy that the nucleophilic reaction occurred for [$PtCl_2(PhCN)_2$], which has been widely used as a starting material for the preparation of organoplatinum(II) complexes.[9] In our previous study,[10] the complex [$PtCl_2(PhCN)_2$] prepared by Kharasch's procedure[11] was found to exist as a mixture of *cis* and *trans* isomers, and both isomers were successfully isolated by column chromatography on silica gel. Details of reactions of *trans*- and *cis*-[$PtCl_2(PhCN)_2$] with thallium(I) acetylacetonate, Tl(acac), and benzoylacetonate, Tl(bzac), in dichloromethane at room temperature are presented here, together with the full account of the X-ray structure of **1a** as an example of products in these reactions.

† In this paper, the term "β-ketoamine" means an α,β-unsaturated β-amino ketone.

Experimental

Materials. The *trans*- and *cis*-[$PtCl_2(PhCN)_2$] complexes were prepared as described in the previous paper.[10] Thallium (I) salts of acetylacetone and benzoylacetone were synthesized according to the literature.[12] Dichloromethane over Molecular Sieve Type 3A was decanted, further dried over calcium hydride, and then distilled. For column chromatographic separation of reaction products, silica gel 60 F_{254} (Merck, 70-230 mesh) or aluminium oxide 60 (Merck, active, basic) was used as a packing. A technique of preparative layer chromatography (PLC) was applied in order to collect samples in the preparative scale, using the chromatoplate of silica gel 60PF_{254} containing $CaSO_4$ (Merck) or aluminium oxide 60PF_{254} (Merck, Type E). For the preparation of a PLC plate, one (25 g) of these adsorbents was suspended in deionized water (60 cm^3) and the mixture was applied on a glass plate (20×20 cm) and activated before use at 130—140 °C for 4 h.

Reaction of trans-[$PtCl_2(PhCN)_2$] *with Thallium (I) Acetylacetonate.* When Tl (acac) (376 mg, 1.24 mmol) was added to a yellow solution of *trans*-[$PtCl_2(PhCN)_2$] (293 mg, 0.62 mmol) in dichloromethane (20 cm^3) and the mixture was stirred for 1 h at room temperature, a white precipitate of thallium (I) chloride was formed and the solution turned brown-yellow. The mixture was passed through a short column (5×2 cm d) of silica gel, leaving thallium (I) chloride and a brown residue at the top of the column. The yellow eluent was concentrated and put on the PLC plate of silica gel. Development with benzene split the original band into two. The first band component with a large R_f value was extracted with benzene and the solvent was evaporated to dryness, leaving the yellow compound **1a** (26 mg, 7% yield). A dichloromethane-extract of the second band was concentrated and developed, once again, on the PLC plate in diethyl ether, resulting in two bands. Yellow compound **1b** (16 mg, 5% yield based on the platinum atom used) precipitated on addition of hexane to a diethyl ether-extract of the smaller R_f component. A trace amount of substance was obtained from

the larger R_f component; this was not characterized.

Reaction of cis-[$PtCl_2(PhCN)_2$] *with Thallium (I) Acetylacetonate.* Tl (acac) (413 mg, 1.36 mmol) was suspended in a dichloromethane solution (20 cm³) of *cis*-[$PtCl_2(PhCN)_2$] (320 mg, 0.68 mmol), and the mixture was stirred for 5 h at room temperature. After the volume of the solution was reduced by vacuum evaporation, the concentrate was mounted on the PLC plate of aluminium oxide without removal of thallium (I) chloride. Two bands appeared upon development with a benzene–acetone (20 : 1 by volume) mixture. The components with small and large R_f values were extracted separately with dichloromethane and the extracts were concentrated to obtain a yellow powder of **2a** (72 mg, 18% yield) and red crystals of **2b** (34 mg, 8% yield) on addition of diethyl ether, respectively. Reprecipitation of **2a** from acetone by adding diethyl ether gave yellow needles.

Reaction of trans-[$PtCl_2(PhCN)_2$] *with Thallium (I) Benzoylacetonate.* A mixture of *trans*-[$PtCl_2(PhCN)_2$](297 mg, 0.63 mmol) and Tl(bzac) (461 mg, 1.26 mmol) in dichloromethane (25 cm³) was stirred for 5 h at room temperature. After filtration of the precipitated thallium (I) chloride, the filtrate was concentrated to a small volume and placed on a PLC plate of silica gel. Development with benzene–hexane (3 : 2 by volume) resulted in three bands; each component was extracted with dichloromethane and isolated on addition of diethyl ether to the concentrated extract. Orange (**3a**) and yellow (**3a′**) powders were isolated from bands with middle and small R_f values, respectively, and another orange powder (**3b**) from that with a large R_f. The yields of **3a**, **3a′**, and **3b** were 48 mg (11%), 28 mg (6%), and 27 mg (6%), respectively.

Reaction of cis-[$PtCl_2(PhCN)_2$] *with Thallium (I) Benzoylacetonate.* *cis*-[$PtCl_2(PhCN)_2$] (282 mg, 0.60 mmol) was allowed to react with Tl(bzac) (439 mg, 1.20 mmol) in the same way as described above. After filtration of thallium (I) chloride, the concentrated orange-yellow solution was placed on the top of the column (40×2 cm d) of silica gel and developed with dichloromethane. The first fraction contained benzoylacetone (5 mg, 3% yield based on the Tl(I) salt used). After evaporation of the last and middle fractions to dryness, the resulting powders were recrystallized from acetone–petroleum ether and diethyl ether to give yellow needles of **4a** (19 mg, 4% yield) and red crystals of **4b** (14 mg, 3% yield), respectively.

Reactions of trans- *and* cis-[$PtCl_2(PhCN)_2$] *with Thallium (I) Acetylacetonate and Benzoylacetonate in the Presence of the Corresponding Free β-Diketones in Large Excess.* For example, in the case of reactions with Tl(acac), a mixed solvent of dichloromethane–acetylacetone (1 : 1 by volume) was used. Molar ratios of Tl(acac) and free acetylacetone to [$PtCl_2(PhCN)_2$] were 2 : 1 and *ca.* 350 : 1, respectively. After reactions for 5 h, adequate treatments were performed to isolate products. In the case of reaction with *trans*-[$PtCl_2(PhCN)_2$], yellow powders of **5a** and **5b** were obtained in 3 and 8% yields, respectively, while in the case of *cis*-[$PtCl_2(PhCN)_2$], compound **2a** was isolated in a 75% yield.

In the reactions with Tl(bzac), 2.5 g (*ca.* 15 mmol) of solid benzoylacetone was added to [$PtCl_2(PhCN)_2$] in dichloromethane prior to the reaction. Molar ratios of Tl(bzac) and free benzoylacetone to [$PtCl_2(PhCN)_2$] were 2 : 1 and *ca.* 24 : 1, respectively. Isolation of the reaction products without any contamination with benzoylacetone was somewhat difficult. After reactions for 7 h, compounds **3a** and **3a′** and yellow powder **6** were isolated from the reaction mixture with *trans*-[$PtCl_2(PhCN)_2$] in 15, 4, and 5% yields, respectively, while compound **4a** was obtained from the reaction mixture with *cis*-[$PtCl_2(PhCN)_2$] in a 57% yield.

Reaction of cis-[$PtCl_2(PhCN)_2$] *with Thallium (I) Acetylacetonate in the Presence of Excess* o-*Nitrophenol.* To examine the effect of protonic acids on the yield of **2a**, *o*-nitrophenol was used as a proton donor instead of acetylacetone. Ten times the molar amount of *o*-nitrophenol was added to *cis*-[$PtCl_2(PhCN)_2$] in dichloromethane and the mixture was allowed to react with twice the molar amount of Tl(acac) for 4 d, giving **2a** only in a 14% yield.

Acid Hydrolysis of ***1a*** *with Perchloric Acid.* Compound **1a** (88 mg, 0.15 mmol) was dissolved in a dichloromethane–acetone (1 : 1 by volume) mixture (160 cm³) and 60% $HClO_4$ (6 cm³) was added to the solution. After being stirred for 2.5 h, the solution was concentrated to 30 cm³ at room temperature under reduced pressure and allowed to stand overnight to deposit **7**. After addition of methanol to the mother liquor, the mixture was concentrated to a small volume and allowed to stand overnight again, depositing another crop of **7**. The total yield of golden crystals **7** was 58 mg, 76%. Attempts to detect acetic acid, which was thought to be produced in this reaction, were unsuccessful.

An Attempt to Synthesize Complex ***1a*** *by the Reaction of Bis(acetylacetonato)platinum(II) with Benzonitrile.* Although a mixture of bis(acetylacetonato)platinum (II) (92 mg, 0.23 mmol) and benzonitrile (2 cm³) in dichloromethane (7 cm³) was stirred at room temperature for **3d**, no reaction occurred and 40% of the starting platinum (II) complex was recovered. Even in benzonitrile at 100 °C for 5 h, 26% of the starting material was recovered with some decomposed black residue.

An Attempt to Synthesize 4-Acetylamino-4-phenyl-3-buten-2-one (the Ligand in ***1a****) by a Schiff Base Condensation.* Benzoylacetone (3.55 g, 22.0 mmol) was allowed to react with acetamide (1.30 g, 22.0 mmol) in refluxing ethanol (2.5 cm³) for 5 h, but no condensation occurred. Seventy-six per cent of the benzoylacetone used was recovered.

Crystal Data for ***1a****.* Crystals of **1a** suitable for X-ray crystallography were obtained by slow evaporation of a dichloromethane solution. They are monoclinic with $a=8.426(2)$, $b=9.347(3)$, $c=15.293(9)$ Å, $\beta=111.62(4)°$, $U=1119.8(9)$ Å³, $Z=2$, $D_c=1.77$, $D_m=1.76$ g·cm⁻³, μ(Mo $K\alpha$)=66.2 cm⁻¹, and space group $P2_1/c$. The Laue symmetries, space group, and approximate unit-cell dimensions were determined from oscillation and Weissenberg photographs taken with Cu $K\alpha$ radiation. The unit-cell dimensions were refined by the least-squares analysis of 30θ values measured on a Philips PW 1100 four circle diffractometer with Mo $K\alpha$ radiation.

X-Ray Data Collection. The intensity data with $2\theta \leq 55°$ were collected by the ω-scan mode with graphite-monochromated Mo $K\alpha$ radiation. The specimen size was 0.23× on a Philips PW 1100 four circle diffractometer with Mo $K\alpha$ 0.13×0.11 mm. A scan speed of 1°/min and a scan range of $(1.3+0.2\tan\theta)°$ were chosen. The background was counted for 20 s on each side of the scan range. Three standard reflections ($\bar{3}02$, 060, 002), measured every 4 h, showed no appreciable decay throughout the data collection. A total of 1433 independent reflections with $I>3\sigma(I)$ were classified as observed. The Lorenz-polarization corrections were applied and relative structure factors were derived.[13]

Structure Determination and Refinement. The structure of **1a** was solved by the heavy-atom technique. The positional and thermal parameters were initially refined isotropically by the block-diagonal least-squares method. Further refinement with an anisotropic temperature factor for the Pt atom gave an R value of 5.1%. At this stage, the absorption correction was applied.[14] The maximum and minimum transmission coefficients were 2.48 and 1.82, respectively. The convergence was attained with $R=3.9\%$. The function

Table 1. Positional and thermal parameters ($\times 10^4$)

Atom	x	y	z	U/Å^2
Pt	0	0	0	276(3)[a]
O(1)	757(10)	1746(8)	−470(5)	415(16)
O(2)	−112(11)	−3528(10)	−959(6)	532(20)
N	1171(11)	−1308(10)	−612(6)	376(18)
C(1)	2061(17)	3238(16)	−1244(9)	565(31)
C(2)	1674(13)	1746(12)	−986(7)	593(22)
C(3)	2302(15)	564(13)	−1284(8)	435(24)
C(4)	2114(13)	−903(11)	−1072(7)	341(20)
C(5)	1040(14)	−2872(12)	−442(7)	399(22)
C(6)	2400(17)	−3436(15)	427(9)	555(30)
C(7)	3045(14)	−1947(12)	−1457(7)	383(21)
C(8)	2170(15)	−3018(13)	−2093(8)	456(25)
C(9)	3113(17)	−3973(15)	−2433(9)	509(27)
C(10)	4864(17)	−3843(15)	−2119(9)	524(28)
C(11)	5713(19)	−2783(16)	−1516(10)	590(32)
C(12)	4810(16)	−1777(14)	−1164(8)	474(26)

a) Equivalent isotropic thermal parameter.

minimized was $\sum w(F_o-|F_c|)^2$, with $w=(54.0/F_o)^2$ for $F_o>54.0$, $w=1.0$ for $54.0\geq F_o\geq 17.3$, $w=0.6$ for $F_o>17.3$. The scattering factors for the neutral Pt, O, N, and C atoms were taken from Ref. 15. No attempt was made to locate hydrogen atoms. In the final cycle of the refinement all parameter shifts were less than 0.2σ. A final difference map showed no significant features. The atomic coordinates are presented in Table 1, along with their temperature factors. The observed and calculated structure factors are preserved by the Chemical Society of Japan (Document No. 8118). All the calculations were performed on a FACOM 230-60 computer at Osaka City University by the use of a local version of the UNICS.[16]

Measurements. IR spectra (4000—200 cm^{-1}) were measured in Nujol mull with a JASCO DS 701G spectrophotometer. ^{1}H NMR spectra were recorded at 100 M Hz on a JEOL JNM-MH 100 spectrometer. Molecular weights were determined with a vapor pressure osmometer manufactured by Knauer, West Berlin, West Germany.

Results and Discussion

In recent studies, we have found that $[PdCl_2(PhCN)_2]$ reacts with acetylacetone in acetone at room temperature to produce di-μ-chloro-bis(η^3-1-acetyl-2-hydroxyallyl)dipalladium(II), liberating benzonitrile molecules.[17] On the contrary, no reaction occurred between $[PtCl_2(PhCN)_2]$ and acetylacetone even in refluxing acetone, but the complex reacted with the acetylacetonate anion in dichloromethane at room temperature, giving rise to a nucleophilic attack on the cyanide carbons. A similar reaction occurred with the benzoylacetonate anion. Analytical data for all products isolated in this study are listed in Table 2, where compounds **1** and **2** represent products obtained by reactions of Tl(acac) with *trans*- and *cis*-$[PtCl_2(PhCN)_2]$, respectively, and **3** and **4** represent the corresponding reaction products of Tl(bzac). In each of these reactions, two or three compounds were isolated by PLC. Figure 1 depicts the structures proposed on the basis of spectroscopic data. Although compounds **3b** and **4b** were not obtained in amounts sufficient for measurements, the molecular weight data of all other compounds indicate

Table 2. Analytical data for products of nucleophilic attack of β-diketonate carbanions on benzonitrile–Pt (II) complexes

No.	Appearance	Yield %	Found(Calcd) C%	H%	N%	Mol wt[a]
1a	Yellow powder	7	48.8 (48.1)	4.04 (4.04)	4.63 (4.67)	580[b] (600)
1b	Yellow powder	5	41.8 (42.6)	3.21 (3.21)	5.10 (5.23)	508 (536)
2a	Yellow needles	18	48.0 (48.1)	4.04 (4.04)	4.67 (4.67)	619[c] (600)
2b	Red crystals	8	48.1 (48.1)	4.06 (4.04)	4.62 (4.67)	614 (600)
3a	Orange powder	11	56.0 (56.4)	4.02 (3.91)	3.73 (3.87)	757 (724)
3a′	Yellow powder	6	55.4 (56.4)	3.98 (3.91)	3.72 (3.87)	783 (724)
3b	Orange powder	6	56.4 (56.4)	3.90 (3.85)	4.07 (4.11)	
4a	Yellow needles	4	55.4 (56.4)	3.92 (3.91)	3.88 (3.87)	722[c] (724)
4b	Red crystals	3	55.5 (56.4)	3.90 (3.91)	3.60 (3.87)	
5a	Yellow powder	3	48.3 (48.1)	4.16 (4.04)	4.60 (4.67)	593 (600)
5b	Yellow powder	8	43.0 (42.6)	3.31 (3.21)	5.13 (5.23)	
6	Yellow powder	5	55.9 (56.4)	3.94 (3.91)	3.80 (3.87)	
7[d]	Golden crystals	76	46.7 (46.6)	3.89 (3.92)	5.43 (5.44)	488 (516)

a) In CH_2Cl_2 at 28 °C. b) At 37 °C. c) In $(CH_3)_2CO$ at 41 °C. d) Acid hydrolysis product of **1a**.

that these are mononuclear in each solvent used.

X-Ray Structure of Compound ***1a***. Two yellow compounds, **1a** and **1b**, were isolated from the reaction mixture of *trans*-$[PtCl_2(PhCN)_2]$ with Tl(acac) in dichloromethane at room temperature. Although compound **1a** was analyzed to have the composition of $Pt(acac)_2(PhCN)_2$, its X-ray structure analysis disclosed that the compound is the bis(*N*-acetyl β-ketoamine)-chelate of platinum(II), $[Pt\{N(COMe)=C(Ph)CH=CO\text{-}Me\}_2]$, as shown in Fig. 2. The Pt atom has a *trans* planar coordination by 2N and 2O atoms. The molecule has a crystallographically imposed center of symmetry. The six-membered chelate ring, phenyl group, and *N*-acetyl moiety are planar within ±0.03, ±0.01, and ±0.02 Å, respectively. The *N*-acetyl plane is perpendicular to the chelate ring plane (interplanar angle =89.7°). The C(6) and O(2) are in contact with the O′(1) atom, the C(6)···O′(1) and O(2)···O′(1) distances being 3.12(2) and 2.96(1) Å, respectively. Such a disposition of the acetyl group relative to the chelate ring imposes some restriction on the rotational orientation of the phenyl group about C(4)–C(7) axis: the short contact between the O(2) and the C(8) atoms makes the phenyl ring slant (59.2°) against the chelate ring plane. Much smaller angles (16° and 41°) between the phenyl and chelate rings are found in *cis*-bis(benzoylacetonato)palladium(II),[18] but in this case the disposition of the phenyl group relative to the chelate ring results from the intermolecular interaction. Bond

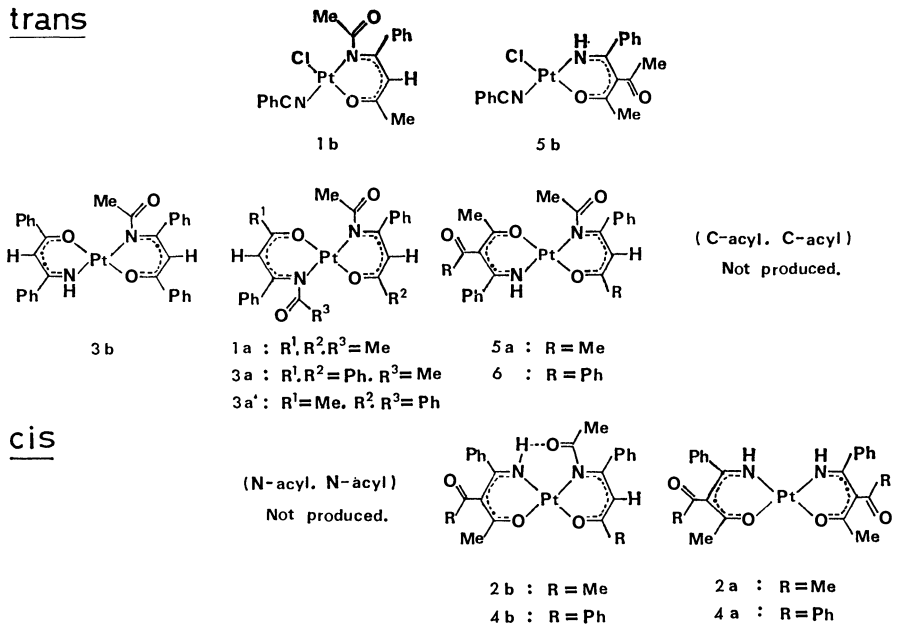

Fig. 1. Schematic drawings of the structure of reaction products between $[PtCl_2(PhCN)_2]$ and Thallium(I) β-diketonates. Numbering indicates products from the following reactions; **1**, *trans*-$[PtCl_2(PhCN)_2]$+Tl(acac); **2**, *cis*-$[PtCl_2(PhCN)_2]$+Tl(acac); **3**, *trans*-$[PtCl_2(PhCN)_2]$+Tl(bzac); **4**, *cis*-$[PtCl_2(PhCN)_2]$+Tl(bzac). **5** and **6** denote reaction products between *trans*-$[PtCl_2(PhCN)_2]$ and Tl(acac) or Tl(bzac), respectively, in the presence of the corresponding free β-diketones in large excess.

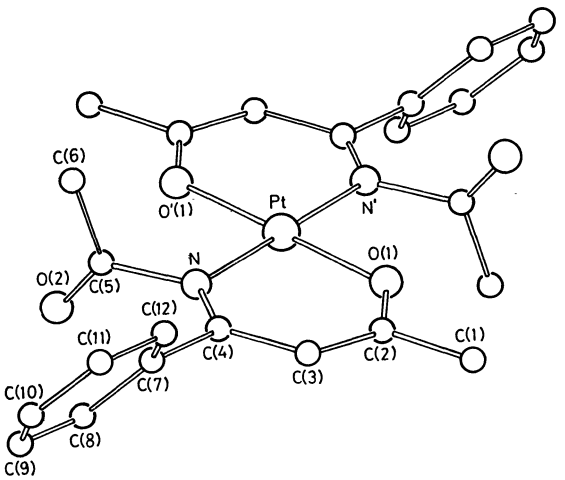

Fig. 2. A perspective view of **1a** with the atom numbering scheme.

distances and angles are summarized in Table 3.

Characterization of the Isolated Compounds by IR and ^1H NMR. Two compounds (**1a** and **1b**) were obtained by the reaction of *trans*-$[PtCl_2(PhCN)_2]$ with Tl(acac); the IR spectrum of **1a** showed no absorption due to the cyano group at around 2200 cm^{-1}, but instead a strong band at 1748 cm^{-1} and three medium to strong bands at 1580—1500 cm^{-1}, as shown in Table 4. Based on the molecular structure of **1a** given in the previous section, we can unequivocally assign the former band to the C=O stretching vibration of the *N*-acetyl group, although the frequency is a little higher than that of the amide I band of gaseous *N*-methylacetamide.[19] On the other hand, the latter three bands may be ascribed to the skeletal vibrations (ν(C=O), ν(C=N), and ν(C=C)) of the β-ketoamine chelate[20] and phenyl rings, but cannot be identified separately.

The ^1H NMR spectrum of **1a** in $CDCl_3$ showed one methine signal at 5.10 ppm and two methyl signals at 2.00 and 1.81 ppm, together with phenyl resonances as shown in Table 5. Of these, the methine signal and one of the methyl signals at 1.81 ppm are accompanied by ^{195}Pt satellites, the coupling constants, $^4J_{Pt-H}$ being 4 and 5 Hz, respectively; these two signals are assigned to the ring-proton and the methyl group attached to the β-ketoamine chelate ring, respectively. Similar couplings of methine and methyl protons to ^{195}Pt are observed to be 11 and 5 Hz, respectively, in the case of bis(acetylacetonato)platinum(II).[21] The other methyl signal at 2.00 ppm, with no coupling to ^{195}Pt was attributed to the *N*-acetyl protons. Compound **1b**, whose composition was $PtCl(acac)(PhCN)_2$, was easily identified to be the 1 : 1 reaction product, since it showed the same IR and ^1H NMR spectral patterns as those for **1a**, except the presence of ν(C≡N) and ν(Pt–Cl) bands in the IR spectrum.

If a similar nucleophilic reaction occurs between *cis*-$[PtCl_2(PhCN)_2]$ and Tl(acac), at least one of the products should show the same spectral patterns in IR and ^1H NMR as those of **1a**. Contrary to our expectation, both of the two products (**2a** and **2b**) isolated exhibited different IR and ^1H NMR patterns. Compound **2a** showed a single ν(C=O) band at 1675 cm^{-1}, much lower than 1748 cm^{-1} for **1a**, with an additional band of ν(NH) at 3270 cm^{-1}, indicating the absence of *N*-acetyl substituents. We can suppose the structure of **2a** to be that shown in Fig. 1 by ascribing

Table 3. Interatomic distances (l) and bond angles (ϕ)

Bond length

Bond	l/Å	Bond	l/Å
Pt–O(1)	1.98(1)	N–C(5)	1.50(1)
Pt–N	2.01(1)	O(2)–C(5)	1.18(1)
C(2)–O(1)	1.29(2)	C(5)–C(6)	1.50(2)
C(4)–N	1.30(2)	C(7)–C(8)	1.40(2)
C(2)–C(3)	1.37(2)	C(8)–C(9)	1.42(2)
C(3)–C(4)	1.43(2)	C(9)–C(10)	1.38(2)
C(1)–C(2)	1.52(2)	C(10)–C(11)	1.36(2)
C(4)–C(7)	1.50(2)	C(11)–C(12)	1.43(2)
		C(12)–C(7)	1.40(2)

Short contact

Contact	l/Å	Contact	l/Å
C(6)···O′(1)	3.12(2)	C(2)···C(8)^{I}	3.49
C(7)···O(2)	3.37(2)	C(9)···C(1)^{II}	3.48
C(8)···O(2)	3.06(2)	O(2)···C(11)^{III}	3.37
O(2)···O′(1)	2.95(1)		

Roman numeral superscripts refer to the following equivalent positions: I $-x$, $1/2+y$, $-1/2-z$; II $x, y-1, z$; III $x-1, y, z$

Bond angle

Angle	ϕ/°	Angle	ϕ/°
N–Pt–O(1)	93.1(4)	C(4)–N–C(5)	119(1)
Pt–O(1)–C(2)	124.5(7)	N–C(5)–O(2)	119(1)
Pt–N–C(4)	125.5(7)	N–C(5)–C(6)	115(1)
O(1)–C(2)–C(3)	126(1)	O(2)–C(5)–C(6)	126(1)
N–C(4)–C(3)	123(1)	C(7)–C(8)–C(9)	119(1)
C(2)–C(3)–C(4)	127(1)	C(8)–C(9)–C(10)	119(1)
O(1)–C(2)–C(1)	113(1)	C(9)–C(10)–C(11)	122(1)
C(1)–C(2)–C(3)	121(1)	C(10)–C(11)–C(12)	121(1)
N–C(4)–C(7)	122(1)	C(11)–C(12)–C(7)	117(1)
C(3)–C(4)–C(7)	115(1)	C(12)–C(7)–C(8)	122(1)
Pt–N–C(5)	116(1)	C(4)–C(7)–C(8)	121(1)
		C(4)–C(7)–C(12)	117(1)

Table 4. Characteristic IR bands [a)]

No.	ν(N–H)	ν(C≡N)	ν(C=O)				ν(C=O, C=N, C=C)	ν(Pt–Cl)
			N-COMe	*N*-COPh	*C*-COMe	*C*-COPh		
1a			1748s				1578m, 1548s, 1502s	
1b		2285w	1752s				1595w, 1550s, 1503s	346w
2a	3270s				1675s		1581m, 1547s	
2b	3270m		1680sh[b)]		1667s		1580m, 1540s, 1518s	
3a			1748s				1600w, 1586m, 1550s 1502s	
3a′			1750s	1698s			1600w, 1580m, 1548s 1502s	
3b	3350m		1750s				1600w, 1587m, 1552s 1516s, 1500s	
4a	3310w 3300m 3250m					1655s	1590w, 1580m, 1540sh 1535s	
4b	3290m		1700s[b)]			1650s	1580m, 1540s, 1520s	
5a	3320w		1743s		1658s		1580m, 1548s, 1503s	
5b	3340m	2280w			1688s		1590w, 1580m, 1553s	350w
6	3260m		1750s			1658s	1598m, 1582m, 1552s 1502s	
7	3360m						1588s, 1567s, 1513s	

a) Wave numbers in cm^{-1}. s: strong, m: medium, w: weak, sh: shoulder. b) Bands due to ν(C=O) of hydrogen-bonded N–C(Me)=O···H–N.

Table 5. ^{1}H NMR data[a]: Chemical shifts (δ) in ppm from internal TMS and coupling constants (J) in Hz.

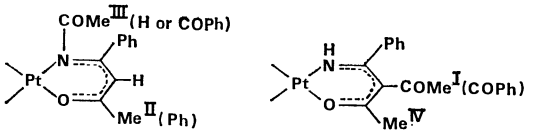

No.	CH_3[b]				CH	NH
	I	II	III	IV		
1a		1.81s $^4J_{Pt-H}=5$	2.00s		5.10s $^4J_{Pt-H}=4$	
1b		1.95s $^4J_{Pt-H}=2$	2.00s		5.16s $^4J_{Pt-H}=2$	
2a	1.60s			2.07s		c)
2b	1.64s	1.71s	2.10s	2.17s	5.42s	8.80br
3a			2.03s		5.84s	
3a′		1.86s	2.04s		5.19, 5.45s	
3b			2.06s		6.05d, 5.74s $^4J_{H-H}=3$	c)
4a				2.02s		7.89br
5a	1.63s	1.83s	1.92s	1.96s	5.01s	7.76br
5b	1.65s			2.02s		c)
6			1.92s	2.12s	5.88s	c)
7		1.88s			5.34d $^4J_{H-H}=4$	7.86br

a) In $CDCl_3$, except for **1b**, **3a**, **5b**, and **6**, whose spectra were recorded in CD_2Cl_2. Phenyl resonances are omitted for brevity. b) As shown above, I, II, III, and IV represent the following methyl resonances: I, *C*-acetyl; II, methyl on the *C*-unsubstituted chelate ring; III, *N*-acetyl; IV, methyl on the *C*-acetylated or -benzoylated chelate ring. c) Not detectable or overlapped with phenylsignals.

the band at 1675 cm^{-1} to vibration of the uncoordinated *C*-acetyl carbonyl. The uncoodinated acetyl carbonyls in the central-carbon-bonded acetylacetonate complex, $Na_2[PtCl_2(acac)_2]\cdot 2H_2O$,[22] absorb at 1652 and 1626 cm^{-1}, and those in the cobalt(III) tris-chelate of 3-acetyl-acetylacetone[23] at 1680 cm^{-1}.

In conformity with the proposed structure, no ring-methine signal appeared in the ^{1}H NMR spectrum of **2a**, although no signal assignable to the NH proton was detected, probably due to the H–D exchange with $CDCl_3$ used as the solvent.[24] Difficulty arose in finding any coupling to ^{195}Pt of the methyl signals at 2.07 and 1.66 ppm; this made it impossible to determine which signal is due to the methyl groups on the chelate rings. Collman *et al.*[23] examined ^{1}H NMR spectra of cobalt(III) tris-chelates of acetylacetone and 3-acetyl-acetylacetone in benzene and assigned peaks at 1.90 and 2.02 ppm to their corresponding ring-methyls. Such a downfield shift of the ring-methyl signal on acetylation at the central carbon atom of the chelate rings was also recognized in the case of rhodium(III) acetylacetonate in chloroform, and seems to be reasonable because of the electron-attracting nature of the acetyl substituent. If this relative resonance position of these two signals is valid in the case of the present β-ketoamine chelates, the methyl signal at 2.07 ppm, lower than 1.81 ppm found for **1a**, can be assigned to the methyl groups on the *C*-acetylated chelate rings of **2a**, while the signals at 1.66 ppm can be assigned to the uncoordinated *C*-acetyl groups.

These four methyl signals, including two for **1a**, resonate at their characteristic fields and can be classified into four types: I, II, III, and IV, as described in Table 5. This classification can facilitate structural assignments for other products. Thus compound **2b**, which exhibits four methyl signals at all these fields and a methine signal at 5.42 ppm in the intensity ratios of 3 : 3 : 3 : 3 : 1, was supposed to have the mixed-ligand chelate structure which comprises both chelate rings of *N*-acetyl and *C*-acetyl β-ketoamines, as shown in Fig. 1. The somewhat lower frequency in *N*-acetyl carbonyl stretching for **2b** may be caused by its hydrogen-bonded structure, indicating *cis* configuration around the platinum atom.

Compounds **4a** and **4b**, produced by the reaction between *cis*-$[PtCl_2(PhCN)_2]$ and Tl(bzac), exactly correspound to **2a** and **2b** in their structures, although the uncoordinated *C*-acyl groups are benzoyl instead of the acetyl groups in the former compounds. Unfortunately, the amount of **4b** obtained was not enough to allow recording of the ^{1}H NMR spectrum. However, the similarities in color and IR data of **4b** and **2b** support the structures depicted in Fig. 1.

Three compounds were produced by the reaction between *trans*-$[PtCl_2(PhCN)_2]$ and Tl(bzac). **3a** exhibits a single ν(C=O) band at 1748 cm^{-1} in its IR spectrum and one methine and one methyl signal at 5.84 and 2.03 ppm, respectively, in the intensity ratio of 1 : 3 in its ^{1}H NMR spectrum. These features are quite similar to those for **1a** except for the loss of a ring-methyl resonance, and hence a *trans*-bis-(*N*-acetyl β-ketoamine)chelate structure like **1a** was assigned for **3a**. On the contrary, **3a′** shows two ν(C=O) bands at 1750 and 1698 cm^{-1}, and two methine and two methyl

signals at 5.45 and 5.19 ppm and at 2.04 and 1.86 ppm, respectively, in the intensity ratios of 1 : 1 : 3 : 3. Especially, the presence of two methine signals and a ring-methyl signal suggests that the structure of **3a'** has different chelate rings of *N*-acetyl and *N*-benzoyl β-ketoamines (see Fig. 1).

The presence of *N*-acetyl carbonyl and NH bands in the IR spectrum of **3b** allowed us to presume that this compound was the *trans* counterpart of **4b**. No band appeared, however, in the region of *C*-benzoyl carbonyl stretching. A similar disparity also arose in the ^{1}H NMR spectrum of **3b**. No ring-methyl signal of type II is present, but a methyl signal of type III was observed along with two methine signals, in the intensity ratios of 3 : 1 : 1, indicating the presence of the *N*-acetyl group and the two central ring-methines of a different magnetic environment. Thus the structure shown in Fig. 1 was assigned for **3b**; this structure is in good agreement with its analytical data. Of the two methine signals resonating at 6.05 and 5.74 ppm, the downfield signal appeared as a doublet with $J=3$ Hz and was ascribed to the methine proton on the *N*-unsubstituted chelate ring based on the W-rule.[25]

Nucleophilic Reactions of β-Diketonate Carbanions at Coordinated Cyanide Carbons in trans- *and* cis-[$PtCl_2(PhCN)_2$]. Based on the confirmed structures of products, we suggest the following reaction course: 1) the initial step of these reactions involves the nucleophilic attack by a β-diketonate carbanion on the coordinated cyanide carbon atom; 2) the acetyl group or the central methine proton of the nuclephile migrates to the coordinated nitrogen atom in order to stabilize the imino anion formed in the initial step; 3) the carbonyl group in the residue coordinates to the metal to form the *N,O*-chelate ring, in cooperation with metal-assisted abstraction of the chloride ion. Thus the reaction path to produce **1a** can be formulated as below.

trans-[$PtCl_2(PhCN)_2$]+Tl(acac) ⟶

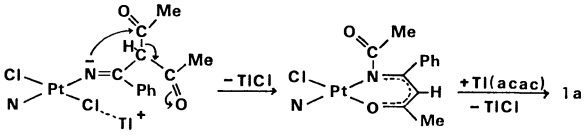

(1)

As was ascertained by X-ray analysis, *trans* configuration around the metal atom in the starting complex is kept in the reaction product **1a**. Although IR and ^{1}H NMR spectra were not helpful in deciding geometrical configurations for other reaction products, it was possible to confirm that neither of the products (**1** and **3**) from *trans*-[$PtCl_2(PhCN)_2$] is the same as either of those (**2** and **4**) from *cis*-[$PtCl_2(PhCN)_2$]. Moreover, the *cis*(*N,N*)-configuration was the most probable for the two products (**2b** and **4b**) from *cis*-[$PtCl_2(PhCN)_2$], on the basis of the IR data showing the presence of the hydrogen bond. Formation of the hydrogen bond will induce the *N*-acetyl group and the *N*-acetyl chelate ring to be coplanar. The red color of **2b** and **4b** might be brought about by the increased delocalization of π-electrons through these two planes. All these facts suport the above-mentioned reaction scheme, which proceeds with retention of the original configuration without breaking of the metal-nitrogen bond. No reaction to produce **1a** occurred between bis(acetylacetonato)platinum(II) and free benzonitrile even at 100 °C, although hexafluoro-2-butyne underwent 1,4-addition across palladium(II)–acetylacetonato rings on treating C_4F_6 with bis(acetylacetonato)-palladium(II).[26]

When *trans*-[$PtCl_2(PhCN)_2$] was reacted with β-diketonate anions, all products (**1** and **3**) were the *N*-acyl β-ketoamine chelates. In the case of reaction with a benzoylacetonate anion, only the former two complexes (**3a** and **3a'**) of all the possible (*N*-acetyl, *N*-acetyl)-, (*N*-acetyl, *N*-benzoyl)-, and (*N*-benzoyl, *N*-benzoyl)-complexes were isolated in 11 and 6% yields, respectively, indicating greater electrophilicity of the acetyl carbonyl carbon atom. On the contrary, the main products from *cis*-[$PtCl_2(PhCN)_2$] were (*C*-acyl, *C*-acyl)-(**2a** and **4a**) or (*C*-acyl, *N*-acyl)-(**2b** and **4b**)-complexes, and no (*N*-acyl, *N*-acyl)-complexes were obtained. These results may be due to steric hindrance at the *cis*-*N,N* positions to prevent an (*N*-acyl, *N*-acyl)-complex. Among these isolated compounds, **1a**, **2a**, and **2b** are isomers, and **3a**, **4a**, and **4b**, which are products from a benzoylacetonate anion, also are the corresponding isomers. These isomers which comprise the different combinations of *N*-acyl and *C*-acyl chelate rings are classified to summation isomerism.

The series of *N*-acetyl β-ketoamine chelates produced by the nucleophilic attack of β-diketonate carbanions on the cyanide carbons in *trans*- and *cis*-[$PtCl_2(PhCN)_2$] are a kind of Schiff base complexes having the acid amide moiety in the ligand. However, such an *N*-acetyl Schiff base has never been prepared by condensation of benzoylacetone and acetamide since the amide protons are generally protected against reactions by the acetyl group. This fact and the acid-lability of the *N*-acetyl bond (see later), together with the difficulty in separation of analogous complexes by PLC, cause the lowering in yields of the reaction products.

Table 6. Reaction products in the presence of excess free β-diketones or *o*-nitrophenol[a]

	Tl-(RCOCHCOMe)	Products (Yields/%)
trans-[$PtCl_2(PhCN)_2$]	R=Me	**5a** (3),**5b**(8)
	Ph	**3a** (15),**3a'**(4),**6**(5)
cis-[$PtCl_2(PhCN)_2$]	R=Me	**2a** (75)
	Me*	**2a** (14)
	Ph	**4a** (57)

a) The asterisk mark denotes the reaction in the presence of excess *o*-nitrophenol.

Reactions of trans- *and* cis-[$PtCl_2(PhCN)_2$] *with Thallium(I) β-Diketonate in the Presence of the Corresponding Excess Free β-Diketone or* o-*Nitrophenol.* With the exceptions of **5a**, **5b**, and **6**, each of the other compounds produced in these reactions is also found in the reaction products in the absence of free β-diketones. These products are summarized in Table 6 with their yields. **5a** and **5b** are compounds in which one *N*-acetyl chelate ring in **1a** and **1b** was formally replaced by a *C*-acetyl

chelate ring, respectively, and hence **5a** corresponds to the *trans* isomer of **2b**. Similarly, **6** and **4b** make another isomeric pair of *trans* and *cis*. From Table 6, we can see that the *C*-acyl compounds are main products in these cases; their amounts are increased especially in the reactions with *cis*-$[PtCl_2(PhCN)_2]$. The following process can produce such high yields of *C*-acyl products: protons from free β-diketone are used to stabilize imino nitrogens produced during the reaction; hence, migration of *C*-acyl groups onto the nitrogen atoms are suppressed; and then CH protons are accepted by the β-diketonate anions present in solution.

To examine the effect of other proton donors, *o*-nitrophenol instead of free β-diketone was used in the reaction of *cis*-$[PtCl_2(PhCN)_2]$ with Tl(acac), as an example. However, no increase in yield of *C*-acetyl product **2a** was found (see Table 6). The reason why the reagent has no effect has not yet been elucidated, but the rather strong acidity ($pK_a=7.2$) of *o*-nitrophenol compared with that of acetylacetone ($pK_a=9.0$) might be the reason for its inefficancy as catalyst.

Acid Hydrolysis of trans-N-*Acetyl Compound* **1a**. In the previous section, we showed that the presence of free β-diketone suppresses migration of the *C*-acyl group onto the imino nitrogen atom, affording *C*-acyl compounds, namely, *N*-unsubstituted β-ketoamine chelates in high yields. Next we examined the acid stability of the *N*-acetyl bonds in **1a**. This bond is readily hydrolyzed by aqueous perchloric acid to yield golden crystals of **7**. The compound did not show any

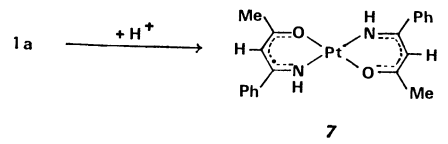

7 (2)

IR band in the carbonyl region higher than 1600 cm^{-1}, indicating the absence of uncoordinated acetyl carbonyl. The ^1H NMR spectrum exhibited only one methine and one ring-methyl signal at 5.34 and 1.88 ppm, respectively, together with one broad NH signal at 7.86 ppm in the intensity ratios of 1 : 3 : 1; this shows that the *N*-acetyl bonds in **1a** are hydrolyzed to the N-H. In fact, coupling ($^4J_{H-H}=4.0$ Hz) based on the W-rule[25] is again observed between the ring methine and the NH protons. Such an acid lability of the *N*-acetyl bonds might also play a part in the original reactions of $[PtCl_2(PhCN)_2]$ with β-diketonate anions. The compound **3b**, which is one of the reaction products between *trans*-$[PtCl_2(PhCN)_2]$ and Tl(bzac), might have been produced by the effect of a little amount of acid present accidentally in solution.

We are grateful to Mr. Junichi Gohda for the elemental analysis, and also to the Ministry of Education, Science and Culture for partial support by a Grant-in-Aid (Grant number 243014).

References

1) B. N. Storhoff and H. C. Lewis, Jr., *Coord. Chem. Rev.*, **23**, 1 (1977).
2) N. C. Stephenson, *J. Inorg. Nucl. Chem.*, **24**, 801 (1962).
3) P. Braunstein, D. Mutt, Y. Dusausoy, and J. Protas, *J. Chem. Soc., Chem. Commun.*, **1979**, 763.
4) B. F. G. Johnson, J. Lewis, and M. S. Subramanian, *J. Chem. Soc., A*, **1968**, 1993; B. F. G. Johnson, T. Keating, L. Lewis, M. S. Subramanian, and D. A. White, *ibid.*, **1969**, 1793.
5) See references cited in Tetrahedron Report No. 57, Pergamon Press (1979).
6) H. Kurosawa, *J. Chem. Soc., Dalton Trans.*, **1979**, 939.
7) B. T. Golding, J. MacB. Harrowfield, G. B. Robertson, A. M. Sargeson, and P. O. Whimp, *J. Am. Chem. Soc.*, **96**, 3691 (1974).
8) T. Uchiyama, K. Takagi, K. Matsumoto, S. Ooi, Y. Nakamura, and S. Kawaguchi, *Chem. Lett.*, **1979**, 1197. On p. 1198, lines 8 and 5 from bottom, the interplanar angles should read 59.2° and 89.7°, respectively.
9) F. R. Hartley, "The Chemistry of Platinum and Palladium," Applied Science Publishers, London (1973), p. 462.
10) T. Uchiyama, Y. Toshiyasu, Y. Nakamura, T. Miwa, and S. Kawaguchi, *Bull. Chem. Soc. Jpn.*, **54**, 181 (1981).
11) M. S. Kharasch, R. C. Seyler, and F. R. Mago, *J. Am. Chem. Soc.*, **60**, 882 (1938).
12) W. H. Nelson, W. J. Randall, and D. F. Martin, *Inorg. Synth.*, Vol. IX, 52 (1967).
13) J. Hornstra and B. Stubbe, PW1100 Data Processing Program, Philips Research Laboratories, Eindhoven, Holland.
14) L. Templeton and D. Templeton, Am. Cryst. Assoc., Storrs, Conn., 1973.
15) "International Tables for X-Ray Crystallography," Kynoch Press, Birmingham (1974), Vol. IV, pp. 71, 148.
16) "The Universal Crystallographic Computation Program System," ed by T. Sakurai, The Crystallographic Society of Japan (1969).
17) Z. Kanda, Y. Nakamura, and S. Kawaguchi, *Inorg. Chem.*, **17**, 910 (1978).
18) S. Okeya, H. Asai, S. Ooi, K. Matsumoto, S. Kawaguchi, and H. Kuroya, *Inorg. Nucl. Chem. Lett.*, **12**, 677 (1976).
19) L. J. Bellamy, "The Infrared Spectra of Complex Molecules," Methuen, London (1966), p. 209.
20) H. F. Holtzclaw, Jr., J. P. Collman, and R. M. Alire, *J. Am. Chem. Soc.*, **80**, 1100 (1958).
21) J. Lewis, R. F. Long, and C. Oldham, *J. Chem. Soc.*, **1965**, 6740.
22) G. T. Behnke and K. Nakamoto, *Inorg. Chem.*, **6**, 440 (1967).
23) J. P. Collman, R. L. Marshall, W. L. Young, III, and C. T. Sears, Jr., *J. Org. Chem.*, **28**, 1449 (1963).
24) S. Okeya, Y. Nakamura, and S. Kawaguchi, *J. Chem. Soc., Chem. Commun.*, **1979**, 914.
25) L. M. Jackman and S. Sternhell, "Applications of Nuclear Magnetic Resonance Spectroscopy in Organic Chemistry," 2nd ed, Pergamon Press (1969), p. 334.
26) D. R. Russell and P. A. Tucker, *J. Chem. Soc., Dalton Trans.*, **1975**, 1743.

  Bull. Chem. Soc. Jpn., 54, 1085—1095 (1981)

Bis(β-diketonato)-palladium(II) and -platinum(II) Complexes

Seichi OKEYA,*,† Shun'ichiro OOI, Keiji MATSUMOTO, Yukio NAKAMURA, and Shinichi KAWAGUCHI*

Faculty of Science, Osaka City University, Sumiyoshi-ku, Osaka 558
†Faculty of Education, Wakayama University, Masago-cho, Wakayama 640

(Received September 29, 1980)

A number of palladium(II) and platinum(II) bis-chelates have been prepared which contain one kind of symmetric or unsymmetric β-diketonate anions, or involve two different β-diketonate anions. Existence of the *cis* and *trans* isomers in solution of the binary chelates of unsymmetric β-diketones was confirmed by ^{1}H and ^{13}C NMR spectroscopy. Geometrical isomerization of the palladium(II) complexes to attain equilibrium in solution is fast, while the platinum(II) complexes are quite inert. The mixed-ligand chelates are stable in solution, showing no sign of disproportionation. The isomeric pairs of bis(1-phenyl-1,3-butanedionato)palladium(II), bis(2,4-hexanedionato)palladium(II), and bis(1,1,1-trifluoro-2,4-pentanedionato)platinum(II) were isolated, and molecular structure of the *cis* isomer of the first complex was determined by X-ray analysis.

2,4-Pentanedione and other β-dicarbonyl compounds (β-dikH) react with a wide variety of metal ions to form the (O,O') chelates[1] of the $[M(\beta\text{-dik})_n]$ type which are soluble in organic solvents, and are used frequently as analytical reagents. These complexes are useful not only for comparative studies of various metal ions, but also as starting materials for preparation of organometallic compounds and as catalysts for organic syntheses. Thus a huge number of papers have appeared concerning the complexes containing β-dicarbonyl compounds as a ligand.[2]

Although optical and geometrical isomerization of the octahedral $[M(\beta\text{-dik})_3]$ and related complexes have been studied extensively,[3] investigations on geometrical isomerism of the square-planar $[M(\beta\text{-dik})_2]$ complexes containing unsymmetrical β-dicarbonyl compounds are rather few. Recently two of the present authors have prepared bis(1-ethoxy-1,3-butanedionato)palladium(II) and showed that it exists as an equilibrium mixture of *cis* and *trans* isomers in chloroform.[4] This paper is concerned with preparation and spectroscopic studies of a number of palladium(II) and platinum(II) complexes of symmetric and unsymmetric β-dicarbonyl compounds including several mixed-ligand bis-chelates. A preliminary report on isolation of *cis*- and *trans*-bis(1-phenyl-1,3-butanedionato)palladium(II) and X-ray structure of the *cis* isomer was published in a short communication,[5] and the full account will be included in this paper.

Experimental

Preparation of Complexes. The palladium(II) and platinum(II) chelates of β-dicarbonyl compounds were prepared by one of the following four methods. (A) To an aqueous solution of sodium tetrachloropalladate(II), $Na_2[PdCl_4]$, was added more than twice moles of a ligand together with an appropriate amount of base. (B) Mercury(II) perchlorate and/or silver(I) perchlorate was added to $Na_2[PdCl_4]$ or potassium tetrachloroplatinate(II), $K_2[PtCl_4]$, in aqueous solution to prepare $[M(H_2O)_4]^{2+}$ ions *in situ*, which were allowed in turn to react with a sodium or potassium salt of the β-dicarbonyl compounds.[6] (C) To a methanol solution of sodium hexachlorodipalladate(II), $Na_2[Pd_2Cl_6]$, was added more than twice equivalents of a free ligand followed by an appropriate amount of sodium carbonate.[7] (D) The reaction between [PdCl(hfac)py] and Tl(β-dik) was convenient for preparation of the mixed-ligand palladium(II) chelates containing 1,1,1,5,5,5-hexafluoro-2,4-pentanedione (hfacH) and another β-diketone.

β-Dicarbonyl compounds were purchased and used without further purification except *t*-butyl acetoacetate which was prepared according to literature.[8] Aqueous solution of $Na_2[PdCl_4]$ was prepared by dissolving palladium(II) chloride and a two and half times molar amount of sodium chloride in a small amount of hot water and adjusting the complex concentration to 0.5 mol dm^{-3}. Methanol solution of $Na_2[Pd_2Cl_6]$ was prepared by dissolving palladium(II) chloride and an equimolar amount of sodium chloride in a small amount of hot methanol and then diluting the resultant solution to [Pd]=0.3 mol dm^{-3}.

*Bis(2,4-pentanedionato)palladium(II), [Pd(acac)$_2$] (**1a**):* An aqueous solution (4 cm^3) of sodium hydroxide (5 mol dm^{-3}) was added with stirring to a mixture of acacH (2.5 cm^3) and a solution (10 cm^3) of $Na_2[PdCl_4]$ (0.5 mol dm^{-3}) to form a yellow precipitate, which was filtered and washed three times each with small portions of water, methanol, and diethyl ether, successively. A yellow powder formed was dissolved in dichloromethane and filtered to avoid a small amount of insoluble material. The solvent was allowed to evaporate spontaneously at room temperature to leave large orange-red crystals (1.37 g) in a 90% yield. The yield is better than that (76%) reported in literature[9] using palladium(II) chloride as a starting material.

cis- *and* trans-*Bis(2,4-hexanedionato)palladium(II), cis- and* trans-*[Pd(hxd)$_2$] (**1f**):* The complex was prepared in a similar way as for **1a**. Recrystallization from hot toluene gave orange plates, while a mixture of orange plates and yellow needles was obtained from hot methanol. The yellow needles can conveniently be obtained by prompt evaporation of a dichloromethane solution under reduced pressure. They are geometrical isomers giving identical analyses and slightly different IR and NMR spectra. Orange plates were assigned to *cis* and yellow needles *trans*.

*Bis(1,1,1,5,5,5-hexafluoro-2,4-pentanedionato)palladium(II),[Pd(hfac)$_2$] (**1d**):* Yellow mercury(II) oxide (6.49 g, 30 mmol) was dissolved in a solution (60 cm^3) of perchloric acid (1 mol dm^{-3}). The solution of mercury(II) perchlorate thus prepared was added with stirring to a solution (20 cm^3) of $Na_2[PdCl_4]$ (0.5 mol dm^{-3}) kept at 0 °C. A greenish yellow precipitate appeared at once but stirring was continued for further several minutes. To the mixture was added dropwise a solution of Na(hfac) which had been prepared by dissolving hfacH (8 cm^3, 50 mmol) in a solution (20 cm^3) of sodium hydroxide (2 mol dm^{-3}). A precipitate was filtered, washed

several times with water, and dried *in vacuo*. The red-brown powder was treated with hexane and insoluble material was filtered off. The solvent was distilled away under reduced pressure to leave yellow fine needles (4.71 g) in a 91% yield. Recrystallization from hot hexane gave large red needles, while orange plates of trihydrate were obtained from methanol. When silver(I) nitrate was used instead of mercury(II) perchlorate, the yield was as low as 50%. Compound **1d** must be kept at cold place, since it gradually decomposes at room temperature.

Chloro(1,1,1,5,5,5-hexafluoro-2,4-pentanedionato)(pyridine)palladium(II), [PdCl(hfac)py]: A solution of **1d** (564 mg, 1.08 mmol) in dichloromethane (2 cm^3) was added to a solution of pyridinium chloride (130 mg, hygroscopic *ca.* 1 mmol) in methanol (5 cm^3) and the mixture was allowed to stand one day at room temperature to deposit red plates (318 mg). Hexane was added to the filtrate and the mixture was cooled to precipitate another crop (53 mg) of the product. The same procedure was repeated once more and the total yield of the product reached 92% (426 mg).

cis- *and* trans-*Bis(1-phenyl-1,3-butanedionato)palladium(II)*, cis- *and* trans-*[Pd(bzac)$_2$] (**1g**)*: The literature method[10] was improved to attain better yields. A solution (10 cm^3) of potassium hydroxide (1.5 mol dm^{-3}) was added to a solution of bzacH (2.6 g, 16 mmol) in methanol (20 cm^3). A solution (10 cm^3) of $Na_2[PdCl_4]$ (0.5 mol dm^{-3}) was added dropwise through a pipette to the above solution with stirring. A yellow precipitate was filtered, washed three times each with water, methanol, and diethyl ether, and dried *in vacuo*. Compound **1g** was obtained as a mixture of *cis* and *trans* isomers in a 90% yield (1.93 g). When the isomeric mixture was dissolved in dichloromethane and the solvent was evaporated spontaneously at room temperature, only the *trans* isomer was obtained quantitatively as orange-yellow needles. On the other hand, when ethyl acetate (20 cm^3) and petroleum ether boiling below 60 °C (several cm^3) were added to a solution of the *cis-trans* mixture (226 mg) in dichloromethane (25 cm^3) and the solution was kept in a shallow vessel to allow vaporization of solvents at room temperature, both of orange-red hexagonal plates of the *cis* isomer and orange-yellow needles of the *trans* isomer were left to be separated manually. Separation of the isomeric mixture by means of thin layer chromatography was tried over silica gel with dichloromethane as a developing solvent. The R_f values were 0.80 and 0.84 for *cis* and *trans*, respectively. Separation of isomers through a column was not successful because of rather fast isomerization reactions.

*Bis(1,1,1-trifluoro-2,4-pentandionato)palladium(II), [Pd(tfac)$_2$] (**1h**)*: To a methanol solution (20 cm^3) of $Na_2[Pd_2Cl_6]$ (0.15 mol dm^{-3}) was added tfacH (1.4 g, 9 mmol) with stirring. On addition of a fine powder of sodium carbonate in limited amounts to the solution, an increasing amount of a yellow precipitate appeared and *ca.* 20 cm^3 of methanol was added to make stirring easy. Addition of the base was stopped when no more precipitate was produced. The precipitate was filtered, washed three times each with water, methanol, and diethyl ether, successively and dried *in vacuo*. Recrystallization from dichloromethane–hexane gave orange-yellow needles (2.0 g) in an 81% yield.

*Bis(1,3-diphenyl-1,3-propanedionato)palladium(II), [Pd(dbm)$_2$] (**1b**), bis(2,2,6,6-tetramethyl-3,5-heptanedionato)palladium(II), [Pd(dpm)$_2$] (**1c**), bis-(3-phenyl-2,4-pentanedionato)palladium(II), [Pd(Ph-acac)$_2$] (**1e**), bis(1,1,1-trifluoro-5,5-dimethyl-2,4-hexanedionato)palladium(II), [Pd(pta)$_2$] (**1l**), and bis(1,1,1-trifluoro-4-(2-thienyl)-2,4-butanedionato)palladium(II), [Pd(tta)$_2$] (**1m**)*: These complexes were prepared by method C in a similar manner as for **1h**. Recrystallization of **1b**, **1c**, **1e**, and **1l** was performed from dichloromethane–hexane, benzene–hexane, dichloromethane, and diethyl ether, respectively. Compound **1m** is sparingly soluble in common solvents and was not recrystallized.

*Bis(1-t-butoxy-1,3-butanedionato)palladium(II), [Pd(buac)$_2$] (**1j**)*: *t*-Butyl acetoacetate (buacH, 1.5 cm^3, 10 mmol) was dissolved in a solution (10 cm^3) of potassium hydroxide (1 mol dm^{-3}). The solution was added drop by drop with stirring to a solution (10 cm^3) of $Na_2[PdCl_4]$ (0.5 mol dm^{-3}) to deposit a brown precipitate, which was filtered and dried *in vacuo*. The precipitate was dissolved in petroleum ether (bp$<$50 °C, 50 cm^3) and insoluble substance was filtered off. Then the solvent was allowed to evaporate spontaneously at room temperature to deposit light brown plates on the wall of vessel. The yield was 14% (295 mg). *Bis(1-ethoxy-1,3-butanedionato)palladium(II),*[4] *[Pd(etac)$_2$] (**1i**)* and *bis(1-phenyl-3-ethoxy-1,3-propanedionato)palladium(II), [Pd(etbz)$_2$] (**1k**)* were also prepared in a similar manner as above.

*2,4-Pentanedionato(1,1,1-trifluoro-2,4-pentanedionato)palladium(II), [Pd(acac)(tfac)] (**1n**)*: A methanol solution (20 cm^3) containing K(acac)·H_2O (0.97 g, hygroscopic, *ca.* 6 mmol) and K(tfac)·H_2O (1.35 g, 6.4 mmol) was added with stirring to a methanol solution (20 cm^3) of $Na_2[Pd_2Cl_6]$ (0.15 mol dm^{-3}) to deposit a yellow precipitate. After stirring of the mixture for 2 h, the precipitate was filtered, washed with water and methanol, successively, and dried *in vacuo* to give a yellow powder (1.85 g). Chromatographic separation of the crude product through a silica-gel column (70×3d cm) using a mixture of dichloromethane, benzene, and petroleum ether (4 : 1 : 1 by volume) as the developing solvent resulted in three fractions. The middle fraction gave yellow fine needles of **1n** (736 mg) in a 34% yield. The first and third eluents afforded [Pd(tfac)$_2$] (**1h**) and [Pd(acac)$_2$] (**1a**) in each 20% yields, respectively. The same preparative method was applied to various couples of acac, bzac, tfac, and hfac salts, but no mixed-ligand chelate was obtained successfully except the above acac-tfac case.

Alternatively, complex **1n** was also prepared by the partial substitution reaction of [Pd(tfac)$_2$]. To a solution of [Pd(tfac)$_2$] (500 mg, 1.21 mmol) in acetone (20 cm^3) was added with stirring a solution of K(acac)·H_2O (160 mg, *ca.* 1 mmol) in methanol (1 cm^3), when color of the solution changed from yellow to yellow-brown. After stirring of the mixture for 5 min, the solvent was evaporated under reduced pressure to leave a yellow powder, which was extracted with dichloromethane and the extract was subjected to the chromatographic separation as above. Complex **1n** was obtained in a 17% yield (72 mg). The residue which was insoluble in dichloromethane consisted mainly of K(tfac)·H_2O (210 mg, 1.0 mmol).

*1,1,1,5,5,5-Hexafluoro-2,4-pentanedionato(2,4-pentanedionato)palladium(II), [Pd(acac)(hfac)] (**1o**)*: A suspension of Tl(acac) (88 mg, 0.29 mmol) in dichloromethane (3 cm^3) was added with stirring to a solution of [PdCl(hfac)py] (152 mg, 0.36 mmol) in dichloromethane (1 cm^3) kept at −10 °C. After stirring of the mixture for 30 min, a white precipitate of thallium chloride was filtered off. Hexane was added to the filtrate and the solution was kept at −20 to −30 °C for 1 h. An additional precipitate of thallium chloride was separated by filtration and the solvent was distilled away under reduced pressure. The residue was dissolved in dichloromethane, hexane was added to the solution, and the mixture was cooled to deposit pale yellow crystals of $[Pd(py)_4](hfac)_2$ accompanied by a powder of thallium chloride. After separation of the precipitate, the solution was poured onto a column of silica gel. Development with dichloromethane gave rise to three zones and the first fraction gave lemon-yellow fine needles of

1o (28 mg) in a 18% yield on the basis of the starting complex. Substances recovered from the second and third fractions were not enough in amount to be identified.

1, 1, 1,5, 5, 5-Hexafluoro-2, 4-pentanedionato (1-phenyl-1, 3-butanedionato)palladium(II), [Pd(bzac)(hfac)] (1p): The same preparative method was used and the first fraction from the column chromatography gave **1p** in a 18% yield. The second fraction contained [Pd(bzac)$_2$] (**1g**) in a 7% yield. The substance in the third fraction was not identified.

Bis(2,4-pentanedionato)platinum(II), [Pt(acac)$_2$] (2a), bis-(1,1,1,5,5,5-hexafluoro-2,4-pentanedionato)platinum(II), [Pt-(hfac)$_2$] (2d), and cis- *and* trans-*bis(1,1,1-trifluoro-2,4-pentanedionato)platinum(II),* cis- *and* trans-*[Pt(tfac)$_2$] (2h)*: These complexes were prepared by the revised method B reported very recently.[6]

2,4-Pentanedionato(1, 1, 1-trifluoro-2, 4-pentanedionato) platinum-(II), [Pt(acac)(tfac)] (2n): Both of acacH (5 g, 50 mmol) and tfacH (7.7 g, 50 mmol) were dissolved in a solution (30 cm^3) of sodium hydroxide (5 mol dm^{-3}). To this solution was added with stirring a solution (500 cm^3) of [Pt(H$_2$O)$_4$](ClO$_4$)$_2$[6] (0.025 mol dm^{-3}) followed by a solution (73 cm^3) of sodium hydroxide (5 mol dm^{-3}) drop by drop from pipettes, respectively. A yellow-brown precipitate deposited gradually, which was filtered after being stirred for 15 h, washed three times with water, and dried *in vacuo*. The resultant yellow-brown powder was dissolved in dichloromethane, separated from insoluble material by filtration, and subjected to chromatographic separation through a column of silica gel (70× 3d cm) using dichloromethane as the eluent. The first fraction contained [Pt(tfac)$_2$] (**2h**) (656 mg, 10% yield) and the second gave **2n** (1.69 g), which was recrystallized from benzene–hexane to give yellow needles in a 29% yield (1.59 g).

1,1,1,5,5,5-Hexafluoro-2, 4-pentanedionato (2, 4-pentanedionato)-plantinum(II), [Pt(acac)(hfac)] (2o): In a similar manner as above, an equimolar mixture of Na(acac) and Na(hfac) was allowed to react with [Pt(H$_2$O)$_4$](ClO$_4$)$_2$ in aqueous solution and the crude product was subjected to chromatographic separation through a silica-gel column. Development with dichloromethane gave rise to four zones. The first fraction contained [Pt(hfac)$_2$] (547 mg, 7% yield) and the second gave purple fine needles of **2o** in a 15% yield (945 mg). The fourth fraction gave [Pt(acac)$_2$] (1067 mg, 22% yield) and the third a little amount of lemon-yellow substance which was not identified. An analogous preparative trial using a mixture of tfacH and hfacH was not successful in obtaining [Pt(tfac)-(hfac)].

Measurements. Infrared spectra were recorded in Nujol on Hitachi 295 and JASCO DS-701G spectrophotometers. JEOL JNM C60HL, MH-100, and FX-60Q instruments were used to obtain NMR spectra. Mass spectra were taken on a JEOL JMS-D300 mass-spectrometer. A vapor-pressure osmometer manufactured by Knauer in West Berlin, West Germany, was also used for molecular-weight determination.

X-Ray Analysis. X-Ray analysis of *cis*-[Pd(bzac)$_2$] (**1g**-*cis*) was performed. Laue symmetry and approximate cell dimensions were determined from Weissenberg photographs taken with Cu $K\alpha$ radiation. The cell dimensions were refined by the least-squares analysis of θ values of 16 reflections measured on an automated four-circle diffractometer with Mo $K\alpha$ radiation. Crystal data: Monoclinic, a=11.024(3), b=19.629(4), c=9.472(2) Å, β=119.78(2)°, space group P2$_1$/c, D_m=1.60, D_c=1.60 g cm^{-3}, Z=4, μ(Mo $K\alpha$)=10.5 cm^{-1}.

Intensity data were collected by the ω-2θ scan method by the diffractometer with graphite-monochromated Mo $K\alpha$ radiation, using a crystal specimen with size of 0.22×0.30×0.08 mm^3. The scan speed and scan width in ω were 0.017 s^{-1} and (0.7+0.2 tan θ)°, respectively. The background was counted for 20 s at each side of the scan range. A total of 1927 unique reflections having intensity $I_t-2\sqrt{I_t}>I_b$ was collected in the $2\theta\leq55°$ range (I_t, intensity at the peak of reflection; I_b, mean background intensity obtained from preliminary background measurement of 5 s at each side of the scan range). The intensities of three standard reflections monitored every 4 h showed no appreciable variation. Intensities were corrected for Lp factor but not for absorption. Of 1927 reflections 1814 with $F_o^2>3\sigma(F_o^2)$ were used for the structure analysis.

The crystal structure was solved by the heavy atom method, and the positional and thermal parameters were refined by the least-squares. The minimized function was $\sum w(F_o-|F_c|)^2$. The weighting scheme, w=0.82 for $F_o<35.7$, w=1.0 for $35.7\leq F_o\leq71.4$, and $w=(71.4/F_o)^2$ for $F_o>71.4$, were found to be optimal. All H atoms could be located on the difference Fourier map calculated after anisotropic refinement for nonhydrogen atoms. These H atoms were included in the least-squares refinement with isotropic temperature factor $B_H=B_p+1.0$ Å^2, the positional parameter being fixed (B_p, the isotropic temperature factor of nonhydrogen atom to which the H atom is bonded). The convergence was attained with R=0.033 and $R'(=[\sum w(F_o-|F_c|)^2/\sum wF_o^2]^{1/2})$=0.042.

Table 1. Final atomic parameters(×10^4)

	x	y	z	B[a]/Å^2
Pd	344.9(5)	1037.8(2)	927.6(5)	2.43(1)
O(1)	1476(4)	1564(2)	222(5)	2.9(1)
O(2)	−1213(4)	1702(2)	35(4)	2.6(1)
O(3)	1948(4)	406(2)	1883(5)	2.9(1)
O(4)	−802(4)	490(2)	1573(5)	2.6(1)
C(1)	1937(7)	2310(3)	−1348(9)	3.6(2)
C(2)	977(6)	2056(3)	−780(7)	2.8(2)
C(3)	−303(6)	2366(3)	−1310(7)	2.8(2)
C(4)	−1285(6)	2214(3)	−858(6)	2.6(1)
C(5)	−2555(6)	2653(3)	−1367(7)	2.8(2)
C(6)	−2643(7)	3306(3)	−1991(9)	3.6(2)
C(7)	−3829(8)	3694(4)	−2419(10)	4.4(2)
C(8)	−4917(8)	3449(4)	−2278(10)	4.7(2)
C(9)	−4803(8)	2808(5)	−1646(11)	5.1(3)
C(10)	−3630(7)	2409(4)	−1171(10)	4.1(2)
C(11)	3249(7)	−567(4)	3145(9)	4.1(2)
C(12)	1951(6)	−157(3)	2543(7)	2.9(2)
C(13)	865(6)	−404(3)	2760(7)	2.7(2)
C(14)	−413(6)	−89(3)	2285(6)	2.5(2)
C(15)	−1462(6)	−422(3)	2623(7)	2.6(2)
C(16)	−2867(7)	−411(4)	1477(8)	3.4(2)
C(17)	−3831(7)	−700(4)	1817(10)	4.2(2)
C(18)	−3401(8)	−1013(4)	3291(9)	3.8(2)
C(19)	−2017(7)	−1036(4)	4429(8)	3.7(2)
C(20)	−1034(7)	−756(3)	4088(7)	3.1(2)

a) Equivalent isotropic temperature factor.

Atomic scattering factors were taken from Ref. 11. Real part of the anomalous dispersion corrections were applied for Pd[0]. Atomic coordinates are given in Table 1. The anisotropic thermal parameters, H atom coordinates, and F_o-F_c tables are preserved by the Chemical Society of Japan (Document No. 8127). All computations were performed on a FACOM 230-60 computer at the Osaka City University using programs in the UNICS.[12]

Results and Discussion

Syntheses. A number of palladium(II) (**1**) and platinum(II) (**2**) bis-chelates of β-dicarbonyl compounds were prepared including the binary chelates of both the symmetric (**1a—1e**, **2a**, and **2d**) and unsymmetric (**1f—1m** and **2h**) β-dicarbonyl anions as well as the mixed-ligand chelates (**1n—1p**, **2n**, and **2o**). The appearance, preparative method, yield, decomposition temperature, and elemental analyses of the new compounds are listed in Table 2 together with some molecular-weight data.

Of the four preparative methods summarized at the outset, method A represented by Eq. 1 is suitable for

$$[MCl_4]^{2-} + 2(\beta\text{-dik})^- \longrightarrow [M(\beta\text{-dik})_2] + 4Cl^- \quad (1)$$

more basic anions such as those of acacH, bzacH, and the β-keto esters. Very low yields of the β-keto-ester chelates may be related to weaker basicity of the oxygen atoms than that of the central carbon atom in the ligand anions as exemplified by the low [enol]/[keto] values of the β-keto ester molecules.[13] The fact that both of the chelating ligands in [Pd(etac)$_2$] (**1i**) are readily transformed to the central-carbon-bonded state on reactions with nitrogen bases,[4] whereas only one of the acac anions in [Pd(acac)$_2$] (**1a**) is converted in similar reactions[14] also shows the difference in the preference of bonding modes between acac and β-keto ester anions.

In the platinum(II) case, method A affords [Pt(acac)$_2$] (**2a**) in a much lower yield (35%) than that for [Pd(acac)$_2$] together with the central-carbon-bonded by-products such as K[PtCl(acac)(acac-C^3)] and K[PtCl$_2$(acac-C^3)$_2$].[15] Furthermore the platinum(II) chelates of less basic tfac and hfac anions have not been obtained. The Pt–Cl bonds might be more stable than the Pt–(β-dik) chelate, resisting the ligand substitution. On this supposition, the chloride anions in $[MCl_4]^{2-}$ were displaced by virtue of mercury(II)[16] and/or silver(I) ions prior to reactions with the β-dik ligands.[6] Thus

Table 2. Newly prepared M(R^{1}COCXCOR^2)$_2$ complexes of palladium(II) (**1**) and platinum(II) (**2**)[a]

No.	Complex R^1 R^2	Appearance (Prep. method[b])	Yield %	Dec temp °C	Found (Calcd) C %	H %	Mol wt
1d[c]	[Pd(hfac)$_2$] CF_3 CF_3	Yellow needles (B)	91	46—55[d]	23.19 (23.07)	0.43 (0.39)	520[e] (520.5)
1e[f]	[Pd(Ph-acac)$_2$] CH_3 CH_3	Yellow plates (C)	96	230—235	57.89 (57.84)	4.80 (4.85)	
1f-*cis*	[Pd(hxd)$_2$] CH_3 C_2H_5	Orange plates (A)		120—121[d]	43.42 (43.32)	5.50 (5.45)	332[e] (332.7)
1f-*trans*		Yellow needles	90	114—115[d]	43.37	5.45	
1g-*cis*	[Pd(bzac)$_2$] CH_3 C_6H_5	Orange-red plates (A)	≈40	240—242	55.79 (56.02)	4.22 (4.23)	
1g-*trans*		Orange-yellow needles	90	238—240	55.67	4.22	
1h	[Pd(tfac)$_2$] CH_3 CF_3	Orange-yellow needles (C)	81	≈200	29.12 (29.11)	1.96 (1.95)	412[e] (412.6)
1j	[Pd(buac)$_2$] CH_3 $OC_4H_9^t$	Light brown plates (A)	14	≈103	45.25 (45.67)	6.33 (6.23)	407[g] (420.8)
1k	[Pd(etbz)$_2$] C_6H_5 OC_2H_5	Orange cryst (A)	≈3	145—150	53.87 (54.05)	4.54 (4.54)	531[g] (488.8)
1l	[Pd(pta)$_2$] CF_3 $C_4H_9^t$	Orange-yellow needles (C)	95	≈100[d]	38.23 (38.69)	4.01 (4.06)	496[e] (496.7)
1m	[Pd(tta)$_2$] CF_3 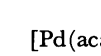	Yellow powder (C)	95	235—236	34.87 (35.02)	1.44 (1.47)	
1n	[Pd(acac)(tfac)]	Yellow fine needles (C)	34	90—92[d]	33.67 (33.49)	3.15 (3.09)	358[e] (358.6)
1o	[Pd(acac)(hfac)]	Yellow fine needles (D)	18	80—82[d]	29.06 (29.11)	1.97 (1.95)	412[e] (412.6)
1p	[Pd(bzac)(hfac)]	Yellow needles (D)	18	119—121[d]	38.04 (37.96)	2.16 (2.12)	474[e] (474.6)
2n	[Pt(acac)(tfac)]	Yellow needles (B)	29	≈114[d]	26.76 (26.85)	2.43 (2.48)	447[e] (447.3)
2o	[Pt(acac)(hfac)]	Purple fine needles (B)	15	≈78[d]	23.76 (23.96)	1.49 (1.61)	501[e] (501.2)

a) X=H except compound **1e** for which X=C_6H_5. b) See text. c) Trihydrate, orange crystals. Found: C, 20.99; H, 1.11%. Calcd: C, 20.90; H, 1.40%. d) Sublimation temperature. e) Parent peaks in mass spectra containing the ^{106}Pd or ^{195}Pt atom were used. f) The ligand is 3-phenyl-2,4-pentanedionate. g) Determined by the vapor pressure osmometry in chloroform at 42 °C.

the chelate formation reactions in method B are expressed by Eq. 2. [Pd(tfac)$_2$] (**1h**) was prepared in

$$[M(H_2O)_4]^{2+} + 2(\beta\text{-dik})^- \longrightarrow [M(\beta\text{-dik})_2] + 4H_2O. \quad (2)$$

a high yield by the reaction between $Na_2[Pd_2Cl_6]$ and tfacH in cooperation with sodium carbonate. Method C[7] is convenient and successfully applied to preparation of the [Pd(β-dik)$_2$] complexes other than **1d**.

$$[Pd_2Cl_6]^{2-} + 4(\beta\text{-dik})^- \xrightarrow[\text{in MeOH}]{} 2[Pd(\beta\text{-dik})_2] + 6Cl^- \quad (3)$$

By employing an equimolar mixture of two kinds of β-dicarbonyl compounds, [Pd(acac)(tfac)] (**1n**), [Pt(acac)(tfac)] (**2n**), and [Pt(acac)(hfac)] (**2o**) were obtained according to methods C, B, and B, respectively. In each of these cases binary bis-chelates were accompanied and separated by column chromatography. On the other hand, [Pd(acac)(hfac)] (**1o**) and [Pd(bzac)(hfac)] (**1p**) could not be prepared by this way, but were obtained by the metal-assisted ligand substitution reactions of [PdCl(hfac)(py)] with Tl(β-dik) (method D). Unfortunately the yield was low in either case and the desired reaction 4 seems to be accompanied by subsidiary reactions 5 and 6. The by-product [Pd-

$$[PdCl(hfac)(py)] + Tl(\beta\text{-dik}) \longrightarrow [Pd(hfac)(\beta\text{-dik})] + py + TlCl \quad (4)$$

$$[Pd(hfac)(\beta\text{-dik})] + Tl(\beta\text{-dik}) \longrightarrow [Pd(\beta\text{-dik})_2] + Tl(hfac) \quad (5)$$

$$[PdCl(hfac)(py)] + Tl(hfac) + 3py \longrightarrow [Pd(py)_4](hfac)_2 + TlCl \quad (6)$$

(py)$_4$](hfac)$_2$ was identified by comparison with the authentic sample prepared by the reaction between [Pd(hfac)$_2$] and pyridine.[17]

Geometrical isomerism is possible in the case of [M(β-dik)$_2$] complexes containing unsymmetrical β-dicarbonyl compounds as a ligand. The structures of *cis*-[VO(bzac)$_2$],[18] *cis*-[Zn(bzac)$_2$]·EtOH,[19] *trans*-[Cu(bzac)$_2$],[20] *trans*-[Pd(bzac)$_2$],[10] and *trans*-[Cu(etac)$_2$][21] were confirmed by X-ray analysis, but their geometrical isomers have not been reported and identification of isomers in solution has not been performed either, except for [Pd(etac)$_2$].[4] Recrystallization of [Pd(bzac)$_2$] (**1g**) from dichloromethane gave only orange-yellow needles of the *trans* isomer which had been reported.[10]

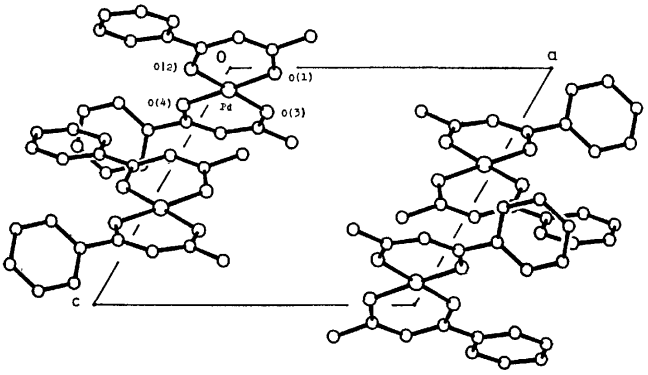

Fig. 1. The crystal structure of *cis*-[Pd(bzac)$_2$] viewed down the b axis.

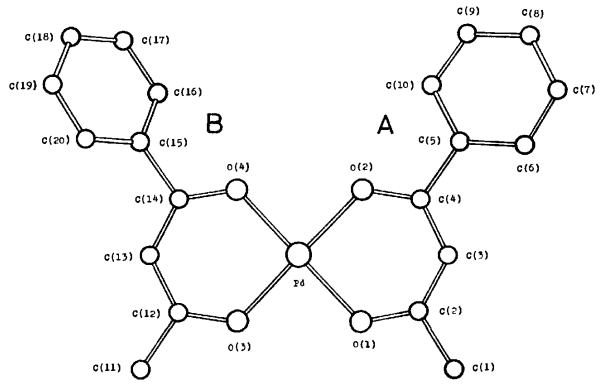

Fig. 2. The molecular structure of *cis*-[Pd(bzac)$_2$] viewed normal to the coordination plane.

Table 3. Bond lengths and angles

Bond lengths (l/Å)			
Pd–O(1)	1.974(5)	Pd–O(3)	1.973(5)
Pd–O(2)	1.980(4)	Pd–O(4)	1.974(5)
O(1)–C(2)	1.271(8)	O(3)–C(12)	1.270(8)
O(2)–C(4)	1.289(8)	O(4)–C(14)	1.282(8)
C(1)–C(2)	1.492(11)	C(11)–C(12)	1.487(11)
C(2)–C(3)	1.382(10)	C(12)–C(13)	1.398(9)
C(3)–C(4)	1.380(10)	C(13)–C(14)	1.392(9)
C(4)–C(5)	1.505(9)	C(14)–C(15)	1.495(9)
Bond angles (ϕ/°)			
O(1)–Pd–O(2)	94.0(2)	O(3)–Pd–O(4)	94.7(2)
Pd–O(1)–C(2)	122.5(4)	Pd–O(3)–C(12)	123.7(4)
Pd–O(2)–C(4)	123.4(4)	Pd–O(4)–C(14)	123.2(4)
O(1)–C(2)–C(3)	126.2(6)	O(3)–C(12)–C(13)	125.6(6)
C(2)–C(3)–C(4)	127.5(7)	C(12)–C(13)–C(14)	126.9(6)
C(3)–C(4)–O(2)	124.7(6)	C(13)–C(14)–O(4)	125.8(6)
O(1)–C(2)–C(1)	113.7(6)	O(3)–C(12)–C(11)	115.2(6)
C(1)–C(2)–C(3)	120.1(6)	C(11)–C(12)–C(13)	119.2(6)
O(2)–C(4)–C(5)	113.7(6)	O(4)–C(14)–C(15)	114.0(6)
C(3)–C(4)–C(5)	121.6(6)	C(13)–C(14)–C(15)	120.2(6)

Table 4. Deviations of atoms from mean planes and interplanar angles

Deviations (d) of atoms from planes[a]	
Plane	Deviation (d/Å)
(1)	O(1)* 0.035, O(2)* −0.035, O(3)* −0.034, O(4)* 0.036, Pd 0.004, C(1) 0.464, C(2) 0.272, C(3) 0.321, C(4) 0.115, C(5) 0.024, C(11) 0.029, C(12) 0.034, C(13) 0.087, C(14) 0.092, C(15) 0.140
(2)	O(1)* −0.020, O(2)* 0.031, C(2)* 0.018, C(3)* 0.014, C(4)* −0.041, Pd 0.233, C(1) 0.021, C(5) −0.217
(3)	O(3)* −0.001, O(4)* −0.000, C(12)* 0.003, C(13)* −0.003, C(14)* 0.002, Pd 0.065, C(11) −0.012, C(15) −0.018
(4)	C(5)* 0.010, C(6)* 0.003, C(7)* −0.013, C(8)* 0.009, C(9)* 0.003, C(10)* −0.011
(5)	C(15)* −0.017, C(16)* 0.007, C(17)* 0.003, C(18)* −0.003, C(19)* −0.010, C(20)* 0.019

a) Atoms marked with an asterisk were included in the calculation of the mean plane.

Interplanar angles (ϕ/°)	
(1)—(2)	170.1
(1)—(3)	177.0
(2)—(4)	17.0
(3)—(5)	41.1

On the other hand, orange-red hexagonal plates of the *cis* isomer accompanied by *trans* appeared from a mixture of dichloromethane, ethyl acetate, and petroleum ether. Detail of the X-ray structure of *cis*-[Pd(bzac)$_2$] is reported below. The isomeric pairs of [Pt(tfac)$_2$][6] and [Pd(hxd)$_2$] were also isolated and characterized. Isomers of the other [Pd(β-dik)$_2$] complexes of unsymmetric ligands were not isolated but were identified in solution by ^{1}H NMR spectroscopy as will be described in later sections.

X-Ray Structure of cis-[*Pd(bzac)*$_2$]. Figures 1 and 2 show the crystal structure and a view of the molecule normal to the coordination plane defined by four oxygen atoms. Bond lengths and angles are given in Table 3. Table 4 lists deviations of atoms from least-squares plane. The Pd atom has a usual square-planar coordination by four oxygen atoms. Both O–C–C–C–O planes in the six-membered chelate rings are slightly bent upward from the coordination plane, the interplanar angles being given in Table 4. The C(13) atom of the adjacent molecule ($-x$, $-y$, $-z$), the mean molecular plane of which is parallel to that of the molecule (x, y, z) under consideration, is located just above the Pd atom. The Pd···C(13) distance is 3.301(7) Å, and Pd···C(13) vector intersects the coordination plane at 80.8°.

The phenyl group is rotated about C–C bond joining the group to the chelate ring, being slant against the O–C–C–C–O plane. The torsion angle is 17.0° in the ligand A and 41.1° in B.[22] In the other metal chelates of the bzac the torsion angles are in the 4—23° range (6.5° and 19.0° in *cis*-[VO(bzac)$_2$],[18] 14.3° in *trans*-[Cu(bzac)$_2$],[20] 23° in *trans*-[Pd(bzac)$_2$],[10] 3.8° and 7.5° in *cis*-[Zn(bzac)$_2$]·EtOH.[19]). The ligand conformation for A is therefore thought to be preferred over that for B with larger torsion angle. The unfavorable conformation of B presumably results from crystal packing.

The approximate coplanarity of the phenyl and chelate rings in the preferred conformation suggests a conjugation of π systems between two rings. On the basis of the X-ray structures of the *trans* isomers of Cu and Pd complexes, Hon *et al.*[10] claimed that there is an effective inter-ring conjugation and that the chelate ring has a significant contribution from the following resonance structure. In the case of the *cis* isomer of Pd

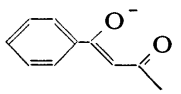

complex, however, the bond lengths in the O–C–C–C–O segment of A show no localization of π electrons. The C(4)–C(5) bond length, which may reflect the extent of the conjugation, is not different from the length for single C(sp^2)–C(sp^2) bond. Furthermore the structural parameters in A agree well with chemically equivalent ones in B of which larger torsion angle indicates smaller inter-ring conjugation; the extent of conjugation is not detectable from structural parameters. Bond lengths and angles in the chelate rings of *cis*-[Pd(bzac)$_2$] are rather in agreement with the corresponding ones in Pd(acac)$_2$(TTF)[23] (TTF=tetrathiafulvalene).

Thermal Stability and IR Spectra. Most of the chelates in Table 2 are thermally stable and the following features in volatility are noted which are similar to those observed for the β-dicarbonyl chelates of other metals.[2] (i) When the methyl groups in acac are replaced by the ethyl, *t*-butyl, and trifluoromethyl groups, volatility of the complex increases in this sequence. (ii) Substitution with phenyl and thienyl groups makes the complex less volatile. (iii) Sublimation temperature of a mixed-ligand chelate is intermediary of those for the two binary chelates. As is indicated in Table 2, molecular-weight data of volatile complexes were determined by mass spectrometry.

Infrared bands in the 1650—1500 and 830—770 cm^{-1} regions which are assigned to the ν(C=O)+ν(C=C) and chelate-ring π(CH) vibrations, respectively,[24] are listed in Table 5 together with some other characteristic vibrations. Substitution of the methyl group in the acac chelate with the electron-attracting trifluoromethyl group increases the ν(C=O)+ν(C=C) frequencies. IR spectra in the higher frequency region are not so sensitive to the geometry of complexes, but those in the region lower than 700 cm^{-1} show ap-

Table 5. Characteristic IR bands (cm^{-1}) in Nujol

No.	ν(C···O)+ν(C···C)	π(CH)	Other bands
1a[a]	1563vs, 1545vs, 1524vs	787s, 780s	
1b	1585m, 1530vs, 1520vs		
1c[b]	1589m, 1530vs, 1498vs	796s	
1d	1591vs, 1552m, 1529m	810vs	ν(C–F): 1260vs, 1210vs, br, 1145—1170vs, br
1e	1560—1540vs	774s	
1f-*cis*	1545vs, 1518vs	820s, 793s	
1f-*trans*	1560vs, br 1520vs	803m, 780s	
1g-*cis*	1582m, 1540—1510vs, br	785s	
1g-*trans*[c]	1584m, 1540—1510vs, br	772s	
1h-*trans*	1595vs, 1579vs, 1517s	799s	ν(C–F): 1228vs, 1183vs, 1155vs, 1038vs
1i[d]	1587vs, 1552s, 1515vs	785s	ν(C–O): 1181vs
1j	1582vs, 1560vs, 1510vs	800s	ν(C–O): 1178vs
1k	1590vs, 1560vs, 1515vs	777vs	ν(C–O): 1210vs
1l	1612m, 1581vs, 1536m, 1512s	807s	
1m	1585s, sh, 1560vs, br, 1530s, 1505m	794s, 785m	
1n	1605vs, 1568vs, 1519vs	799m, 790s, 780m	ν(C–F): 1230vs, 1190vs, br, 1145vs, br
1o	1620vs, 1597m, 1551vs, 1520vs	802s, 796s	ν(C–F): 1266vs, 1210vs, br, 1150vs
1p	1626vs, 1605vs, 1589vs, 1548vs, 1530vs, 1515vs		
2a[e]	1560vs, 1550vs, 1528vs	775vs	
2d[f]	1585vs, 1557w, 1533w	816s	ν(C–F): 1265vs, 1210vs, 1155vs
2h-*cis*[f]	1590vs, br, 1530vs	807vs	ν(C–F): 1235s, 1192vs, 1140vs, br
2h-*trans*[f]	1580vs, br, 1517vs	804vs	ν(C–F): 1190vs, 1160vs, br, 1140vs
2n	1601m, 1564s, 1525vs	798m, 790s, 780m,	ν(C–F): 1232s, 1188s, br, 1150vs
2o	1589s, 1550vs, 1529vs	802s	ν(C–F): 1275vs, 1262vs, 1201vs, 1154vs

a) Mikami, *et al.* recorded the corresponding bands at 1569, 1549, 1524, 786, and 779 cm^{-1} [M. Mikami, I. Nakagawa, and T. Shimanouchi, *Spectrochim. Acta, Part A*, **23**, 1037 (1967)]. b) The spectrum was shown in Ref. 7. c) Nakamoto, *et al.* recorded only the ν(Pd–O) band at 478 cm^{-1} for [Pd(bzac)$_2$] [K. Nakamoto, P. J. McCarthy, and A. E. Martell, *Nature*, **183**, 459 (1959)]. As is seen in Fig. 3, this band may be assigned to the *trans* isomer. d) Exact frequencies were not given in Ref. 4. e) The corresponding literature data probably in KBr are 1565s, 1555s, 1527s, and 774s cm^{-1} [J. Lewis, R. F. Long, and C. Oldham, *J. Chem. Soc.*, **1965**, 6740]. f) Ref. 6.

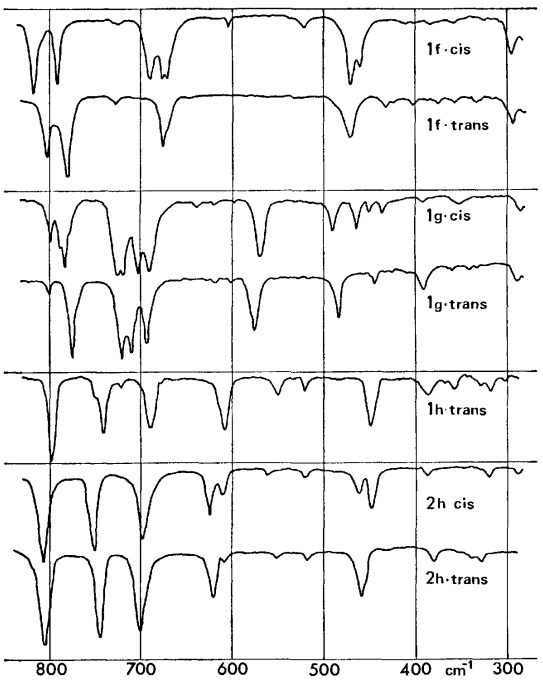

Fig. 3. IR spectra in Nujol in the lower-frequency region of [Pd(hxd)$_2$] (**1f**), [Pd(bzac)$_2$] (**1g**), [Pd(tfac)$_2$] (**1h**), and [Pt(tfac)$_2$] (**2h**).

preciable difference between the *cis* and *trans* isomers. Figure 3 compares the spectra of three isomeric pairs. In accordance with the lower symmetry, *cis* isomers of [Pd(hxd)$_2$] (**1f**), [Pd(bzac)$_2$] (**1g**) and [Pt(tfac)$_2$] (**2h**) exhibit more composite spectra than *trans* isomers. The spectrum of [Pd(tfac)$_2$] (**1h**) in this region shows a close resemblance to that of *trans*-**2h** and may be considered to be *trans*, although the *cis* isomer has not yet been isolated. As is seen in Fig. 3, orange plates of [Pd(hxd)$_2$] (**1f**) show more composite IR spectra than yellow needles and are tentatively assigned to the *cis* isomer.

IR spectrum of a mixed-ligand chelate [M(β-dik)(β-dik′)] looks like a superposition of spectra of the binary chelates [M(β-dik)$_2$] and [M(β-dik′)$_2$] and is complicated especially in the π(CH) and lower-frequency regions.

NMR Spectra. Tables 6—10 list the ^{1}H, ^{13}C, and ^{19}F NMR data. Substitution of the CH_3 group with CF_3 deshields the methine proton but increases shielding of the methine carbon. Inductive effect of the CF_3 group might shift the shared electrons of the C–H bond to the carbon side. It is noticed that C_6D_6 shows a remarkable effect on the ^{1}H NMR spectra, most signals showing substantial upfield shifts as compared with those taken in other solvents. Strange to say, the methyl protons of [M(acac)$_2$] (**1a** and **2a**)

Table 6. ^{1}H NMR data for the binary [M(R^1COCXCOR^2)$_2$] complexes of palladium(II) (**1**) and platinum(II) (**2**)[a]

No.	Solvent	δ[J(Pt-H)]		δ(J(H-H))	[*cis*]/[*trans*]
		CH_3	CH	Other	
1a	$CDCl_3$	2.07	5.43		
	C_6D_6	1.65	4.94		
	$(CD_3)_2CO$	1.97	5.49		
	$(CD_3)_2SO$	1.97	5.53		
1b	$CDCl_3$		6.77	C_6H_5: 7.5m, 8.0m	
1c	$CDCl_3$[b]		5.67	$C(CH_3)_3$: 1.14	
	C_6D_6		5.74	$C(CH_3)_3$: 1.13	
1d	$CDCl_3$		6.42		
	C_6D_6		5.92		
	CD_3OD		6.50		
	$(CD_3)_2CO$		6.60		
1e	$CDCl_3$	1.83		C_6H_5: 7.2m	
	C_6D_6	1.67		C_6H_5: 6.7m, 7.0m	
1f[c]	$CDCl_3$	2.08	5.43	CH_2-CH_3: 2.36q, 2.34q } −1.12t(7)	1/1[d]
	C_6D_6	1.71	5.08	CH_2-CH_3: 2.23q, 2.05q } −0.98t(7)	1/1[d]
1g-*cis*	$CDCl_3$	2.20	6.06	C_6H_5: 7.4m, 7.9m	2/1
1g-*trans*	$CDCl_3$	2.20	6.04	C_6H_5: 7 4m, 7.9m	
1h	$CDCl_3$	2.26	5.92		
	C_6D_6	1.36, 1.32	5.35		1/3
1i	$CDCl_3$	1.93, 1.98	4.78	CH_2-CH_3: 4.12q, 4.19q } −1.25t(7)	3/7
	C_6D_6	1.71	4.85	CH_2-CH_3: 3.88q− {0.84t(7), 0.91t(7)	1/1
1j	$CDCl_3$	1.92	4.63	$C(CH_3)_3$: 1.40	e)
1k[c]	$CDCl_3$		5.43	C_6H_5: 7.3m, 7.7m; CH_2-CH_3: 4.18q−1.29t(7), 4.27q−1.32t(7)	1/1
1*l*[c]	$CDCl_3$		6.01	$C(CH_3)_3$: 1.17	
	C_6D_6		5.87	$C(CH_3)_3$: 0.83, 0.78	6/5 or 5/6
2a	$CDCl_3$[f]	1.95[4.9]	5.54[10.7]		
	C_6D_6	1.49[4.9]	4.98[10.5]		
2d[g]	$CDCl_3$		6.50[10.5]		
2h-*cis*	$CDCl_3$[g]	2.08[3.9]	6.01[10.5]		
	C_6D_6	1.17[4]	5.54[10]		
2h-*trans*	$CDCl_3$[g]	2.09[4]	6.01[11]		
	C_6D_6	1.10[4]	5.40[10]		

a) X=H except **1e** for which X=C_6H_5. When two values of chemical shift are given for a signal from a mixture of geometric isomers, the former one refers to *cis* and the latter to *trans*. Chemical shifts are given in ppm from internal Me_4Si and *J* values in Hz. m, multiplet; q, quartet; t, triplet; others, singlet. b) The literature values are CH: 5.65 and $C(CH_3)_3$: 1.13 ppm.[7] c) Identification of isomers is not possible. d) The isomer ratio was determined based on the ^{13}C NMR spectra. e) Only one isomer seems to exist, but is not identified. f) The literature values are CH_3: 2.08[5] and CH: 5.53[11] [J. Lewis, R. F. Long, and C. Oldham, *J. Chem. Soc.*, **1965**, 6740]. g) Redetermined[6] on an FX-60Q instrument.

resonate at higher field in $CDCl_3$ but at lower field in C_6D_6 than those of [M(tfac)$_2$] (**1h** and **2h**), respectively. Similar reversion of the methyl-signal positions in the two solvents was also observed for similar Zr(IV), Hf(IV), Ce(IV), and Th(IV) complexes, and even for free ligands, acacH and tfacH.[25] The upfield shift in benzene may be attributed to the diamagnetic anisotropy of the solvent molecule interacting with the chelates and ligands, but reasonable rationalization of much more remarkable effect exerted on the tfac chelates than on the acac chelates is not possible at present.

NMR spectra are useful for distinguishing between geometrical isomers of bis-chelates of unsymmetrical ligands. The platinum(II) chelates are very inert and both isomers of [Pt(tfac)$_2$] (**2h**) showed no sign of isomerization in C_6D_6 for more than one month. The corresponding palladium(II) complex [Pd(tfac)$_2$] (**1h**) showed a single methyl signal at 1.32 ppm immediately after dissolution in C_6D_6, but a new signal at 1.36 ppm grew gradually with time at the expense of the 1.32 ppm signal to attain equilibrium within one day at the area ratio of 3 : 1. By reference to the spectra of **2h**

TABLE 7. ^{1}H NMR DATA FOR THE MIXED-LIGAND CHELATES [M(β-dik)(β-dik')] OF PALLADIUM(II) (**1**) AND PLATINUM(II) (**2**)[a]

No.	Solvent	β-dik	δ [J(Pt-H)]		
			CH_3	CH	Other
1n	$CDCl_3$	acac	2.08	5.44	
		tfac	2.19	5.83	
	C_6D_6	acac	1.59, 1.55	4.80	
		tfac	1.38	5.35	
1o	$CDCl_3$	acac	2.13	5.51	
		hfac		6.22	
1p	$CDCl_3$	bzac	2.26	6.15	C_6H_5: 7.5m, 7.8m
		hfac		6.25	
2n	$CDCl_3$	acac	1.99[≈5]	5.58[11.5]	
		tfac	2.03	5.96[9.8]	
	C_6D_6	acac	1.46[5], 1.41[5]	4.91[12]	
		tfac	1.15[4]	5.42[10]	
2o	$CDCl_3$	acac	2.02[5.6]	5.63[12.2]	
		hfac		6.30[9.0]	
	C_6D_6	acac	1.41[5.9]	4.89[12.2]	
		hfac		5.91[8.8]	

a) Chemical shifts in ppm from internal Me_4Si and J(Pt-H) values in brackets in Hz.

TABLE 8. $^{13}C\{^1H\}$ FT NMR DATA IN $CDCl_3$ FOR THE BINARY CHELATES[a]

No.	δ [J(Pt-C)] (J(F-C))					
	CH_3	CF_3	CH	$CH_3\underline{C}O$	$CF_3\underline{C}O$	Other[b]
1a[c]	25.4		101.6	187.2		
1a[d]	24.9		101.1	186.8		
1a[e]	25.0		101.4	j)		
1b			95.8	181.6		Ph: C^1, 136.6; C^2, 128.4; C^3, 127.6; C^4, 131.4
1c			91.8	196.2		*t*-Bu: C^1, 40.5; C^2, 28.6
1d		114.7q (284)	93.8m (1.6)		176.2q (37)	
1d[d]		115.1q (284)	93.6br		175.5q (37)	
1d[e]		115.8q (283)	94.9m (1.8)		176.5q (37)	
1e	26.9			186.1		Ph: C^1, 140.3; C^2, 128.9; C^3, 131.5; C^4, 127.2
1f-*cis*	25.5_0		99.9_3	191.2_4		$\underline{C}O\underline{C}H_2\underline{C}H_3$: 187.2_2, 32.2_5, 11.4_5
1f-*trans*	25.4_8		99.9_1	191.3_1		187.0_3, 32.2_2, 11.2_8
1f-*cis*[d]	25.0_0		99.9_1	190.9_1		187.0_6 } 32.2_3, 11.3_3
1f-*trans*[d]	24.9_6		99.8_9	190.9_0		187.0_3 }
1g-*cis*[f]	28.2_1		98.4_0	188.3_7		PhCO: C^1, 135.8_0; C^2, 127.4_2; C^3, 121.1_8; C^4, 131.3_2; CO, 179.9_9
1g-*trans*[f]	28.1_6		98.5_7	188.6_6		PhCO: C^1, 135.9_7; C^2, 127.4_2; C^3, 121.1_8; C^4, 131.2_2; CO, 179.9_9
1h	26.8	j)	97.8	195.4	j)	
1i[g]	24.6		86.3	187.1		CO_2Et: CO, 171.3(*cis*), 171.1(*trans*); CH_2, 61.8(*cis*), 61.6(*trans*); CH_3, 14.3.
1i[d]	24.5 } 24.4 }		86.4 } 86.2 }	187.6 } 187.9 }		CO_2Et: CO, 171.5, 171.9; CH_2, 61.9, 61.4; CH_3, 14.2
2a[h]	25.5 [43]		102.9 [74]	185.3 [25]		
2d		115.1q [67](283)	96.0 [77]		173.5q [24](37)	
2h-*cis*[i]	26.9 [45]	116.1q [67](283)	99.4 [76](≈2)	192.8 [26]	166.5q [≈23](34)	
2h-*trans*[i]	27.0 [46]	116.2q [j](281)	99.4 [74]	193.5 [24]	j)	

a) Chemical shifts in ppm from internal Me_4Si and J(Pt-C) in brackets and J(F-C) in parentheses in Hz. b) Numbering of the phenyl-ring carbons: quaternary, C^1; ortho, C^2; meta, C^3; para, C^4. Signal assignments to C^2 and C^3 might be inverted. Numbering of the *t*-butyl carbons: quaternary, C^1; primary, C^2. c) Similar data were recorded in literatures: T. Ito, T. Kiriyama, and A. Yamamoto, *Bull. Chem. Soc. Jpn.*, **49**, 3250 (1976); Y. Senda, A. Kasahara, A. Suzuki, *ibid.*, **49**, 3337 (1976). d) In C_6D_6. e) In $(CD_3)_2CO$. f) The major component in equilibrium was assigned to *cis*. g) The major component in $CDCl_3$ was assigned to *trans*, but the equi-intensity couples of signals in C_6D_6 can not be distinguished. h) Similar data for **2a** as well as for **1a** were reported by C. A. Wilkie and D. T. Haworth, *J. Inorg. Nucl. Chem.*, **40**, 195 (1978). i) At 48 °C. j) Indiscernible because of poor solubility of the complex.

Table 9. $^{13}C\{^1H\}$ FT NMR data in $CDCl_3$ for the mixed-ligand chelates[a]

No.	β-dik	δ [J(Pt-C)] (J (F-C))				
		CH_3	CF_3	CH	CH_3CO	CF_3CO
1n	acac	24.9		101.7	186.7, 187.5	
	tfac	27.2	116.3q (283)	97.5	195.1	168.2q (34)
1o	acac	24.4		101.8	187.0	
	hfac		115.6q (283)	92.6m (1.7)		175.0q (37)
2n	acac	25.2 [46]		103.1 [74]	185.5, 186.4 [26] [27]	
	tfac	27.3 [41]	116.5q [63](282)	99.5 [72]	192.4 [24]	165.9q [21](34)
2o	acac	24.8 [48]		103.1 [74]	186.7 [27]	
	hfac		116.3q [62](283)	95.8m [73](1.8)		171.5q [22](36)

a) Chemical shifts in ppm from internal Me_4Si and the J(Pt–C) in brackets and J(F–C) in parentheses in Hz.

Table 10. $^{19}F\{^1H\}$ NMR data[a]

No.	Solvent	δ [J(Pt-F)]
1d[b]	CH_2Cl_2	−73.8
1h[c]	$CDCl_3$	−69.5(*cis*), −69.6(*trans*)[d]
2d[b]	CH_2Cl_2	−73.8[17]
2h-*cis*[c]	$CDCl_3$	−69.8[18]
2h-*trans*[c]	$CDCl_3$	−69.9[18]

a) Chemical shifts in ppm downfield from $CFCl_3$ and the J (Pt–F) values in brackets in Hz. b) The chemical shifts were measured to be 4.68 and 4.74 ppm from external CF_3COOH for **1d** and **2d**, respectively, and converted to the $CFCl_3$ reference by means of the equation, $\delta_{CFCl_3}=\delta_{CF_3COOH}-78.5$ppm. c) The chemical shifts were measured from external C_6F_6[6] and converted to values referring to $CFCl_3$ by virtue of $\delta_{CFCl_3}=\delta_{C_6F_6}-162.9$ ppm. d) The more intense signal was assigned to *trans*.

in C_6D_6, the more intense upfield signal of **1h** was assigned to the *trans* isomer (Table 6) in accordance with the information from IR spectrum that crystalline **1h** is *trans* (Fig. 3). The ^{19}F NMR data for **1h** as compared with those for **2h** are consistent with this assignment, the more intense *trans* signal appearing in slightly higher field than the *cis* signal (Table 10).

The chemical shifts of methine protons in *cis*- and *trans*-[Pd(bzac)$_2$] (**1g**) are slightly different from each other in $CDCl_3$. Isomerization reaction between them was followed by virtue of these signals and found to attain equilibrium at [*cis*]/[*trans*]=2/1 within one day. Both isomers of **1g** also show different ^{13}C chemical shifts except for some of the benzoyl carbons (Table 8). The ^{13}C NMR spectrum of orange plates of [Pd(hxd)$_2$] (**1f**) in $CDCl_3$, which were assumed to be *cis* based on the IR spectra, changed with time to attain equilibrium after *ca.* 6 h at the isomer ratio of 1 : 1. The ^1H NMR spectra of [Pd(etac)$_2$] (**1i**) showed signal splitting for the acetyl methyl and $C\underline{H}_2$–CH_3 protons in $CDCl_3$ but only for the CH_2–$C\underline{H}_3$ protons in C_6D_6. The more abundant species in $CDCl_3$ was tentatively assigned to *trans* by reference to the previous studies on the d^8-metal chelates of *O*-ethyl 3-thioxobutanethioate.[26] Isomerization of **1i** in $CDCl_3$ is rapid, attaining equilibrium within 10 min at −40 °C.[4] The ^1H NMR spectrum of [Pd(etbz)$_2$] (**1k**) also shows coexistence of *cis* and *trans* isomers in $CDCl_3$.

Assignment of the ^1H and ^{13}C NMR signals for the mixed-ligand chelates to each β-diketonate ligand (Tables 7 and 9) was made by reference to the data for the respective binary bis-chelates. Methyl protons of the acac ligand in [M(acac)(tfac)] (**1n** and **2n**) exhibit two signals in C_6D_6 due to the unsymmetric nature of tfac. Unambiguous assignment of these signals to the two unequivalent methyl groups is difficult, since the *trans* influence of the trifluoroacetyl part relative to the other acetyl part of the tfac ligand is not certain on the basis of the present ^1H NMR data. Thus in C_6D_6, the methyl protons in [Pt(acac)(hfac)] (**2o**) resonate at 0.08 ppm upfield compared with those in [Pt(acac)$_2$] (**2a**), whereas the methyl protons in *cis*-[Pt(tfac)$_2$] (**2h**) resonate at 0.07 ppm downfield compared with those in the *trans* isomer, and the methyl signals for *cis*-[Pd(tfac)$_2$] (**1h**) are observed at 0.04 ppm lower field than those for *trans*.

The mixed-ligand palladium(II) and platinum(II) chelates are rather stable in solution, showing no appreciable change in their ^1H NMR spectra even after one month. On the other hand, refluxing of dichloromethane or methanol solution of two kinds of bis-chelates did not give rise to the mixed-ligand chelates, whereas the ligand exchange reactions have been reported for many β-diketonate chelates of Cu(II), Al(III), In(III), Ce(IV), Ti(IV), Zr(IV), Hf(IV), V(IV), Fe(III), Co(III), and Ni(II).[2] Thus the geometrical isomerization of bis(unsymmetric β-diketonato)palladium(II) complexes seems to proceed *via* a reaction pathway other than the intermolecular mechanism.

We wish to thank Mr. Junichi Gohda for elemental analyses and Mr. Tetsu Hinomoto of JEOL, Ltd for measurements of the ^{19}F NMR spectra. Assistance in preparation of complexes by Mr. Hiroyuki Sazaki, Mr. Fumiharu Egawa, Mr. Masato Oka, and Miss Hiroko Asai is also acknowledged. This work was partly supported by Grant-in-Aid for Scientific Research (Grant No. 243014) from the Ministry of Education, Science and Culture.

References

1) J. P. Fackler, Jr., *Prog. Inorg. Chem.*, **7**, 361 (1966).
2) R. C. Mehrotra, R. Bohra, and D. P. Gaur, "Metal β-Diketonates and Allied Derivatives," Academic Press, New York (1978); K. C. Joshi and V. N. Pathak, *Coord. Chem. Rev.*, **22**, 37 (1977).
3) J. J. Fortman and R. E. Sievers, *Coord. Chem. Rev.*, **6**, 331 (1971); N. Serpone and D. G. Bickley, *Prog. Inorg. Chem.*, **17**, 391 (1972).
4) S. Okeya and S. Kawaguchi, *Inorg. Chem.*, **16**, 1730 (1977).
5) S. Okeya, H. Asai, S. Ooi, K. Matsumoto, S. Kawaguchi, and H. Kuroya, *Inorg. Nucl. Chem. Lett.*, **12**, 677 (1976).
6) S. Okeya and S. Kawaguchi, *Inorg. Synth.*, **20**, 65 (1980).
7) D. A. White, *J. Chem. Soc., A*, **1971**, 143.
8) S.-O. Lawesson, S. Cronwall, and R. Sandberg, *Org. Synth.*, **42**, 28 (1962).
9) A. A. Grinberg and L. K. Simonova, *Zhur. Priklad. Khim.*, **26**, 880 (1953); *Chem. Abstr.*, **47**, 11060g (1953).
10) P. K. Hon, C. E. Pfluger, and R. L. Belford, *Inorg. Chem.*, **6**, 730 (1967).
11) "International Tables for X-Ray Crystallography," Kynoch Press, Birmingham (1974), Vol. 4.
12) "Universal Crystallographic Computing System," Crystallographic Society of Japan (1969).
13) The K=[enol]/[keto] values in neat liquid at 33 °C were reported to be 0.09, 0.21, and 0.28 for ethyl acetoacetate (etzcH), *t*-butyl acetoacetate (buacH), and ethyl benzoylacetate (etbzH), respectively in J. L. Burdett and M. T. Rogers, *J. Am. Chem. Soc.*, **86**, 2105 (1964).
14) S. Baba, T. Ogura, and S. Kawaguchi, *Bull. Chem. Soc. Jpn.*, **47**, 665 (1974).
15) A. A. Grinberg and I. N. Chapurskii, *Russ. J. Inorg. Chem.*, **4**, 137 (1959). The ligand acac-C^3 represents the central-carbon-bonded 2,4-pentanedionate anion.
16) L. I. Elding, *Inorg. Chim. Acta*, **20**, 65 (1976).
17) S. Okeya, Y. Onuki, Y. Nakamura, and S. Kawaguchi, *Chem. Lett.*, **1977**, 1305.
18) P. K. Hon, R. L. Belford, and C. E. Pfluger, *J. Chem. Phys.*, **43**, 1323 (1965).
19) R. L. Belford, N. D. Chasteen, M. A. Hitchman, P. K. Hon, C. E. Pfluger, and I. C. Paul, *Inorg. Chem.*, **8**, 1312 (1969).
20) P. K. Hon, C. E. Pfluger, and R. L. Belford, *Inorg. Chem.*, **5**, 516 (1966).
21) G. A. Barklay and A. Cooper, *J. Chem. Soc.*, **1965**, 3746; D. Hall, A. J. McKinnon, and T. N. Waters, *J. Chem. Soc., A*, **1966**, 615.
22) The H[C(3)]···H[C(6)] distance is 1.95 Å which is somewhat shorter than the value expected from van der Waals radius of H atom, while H[C(13)]···H[C(20)] is 2.20 Å, though no refinement was made of the positional parameters of H atoms.
23) A. R. Siedle, T. J. Kistenmacher, R. M. Metzger, C. S. Kuo, R. P. van. Duyne, and T. Cape, *Inorg. Chem.*, **19**, 2048 (1980).
24) K. Nakamoto, "Infrared and Raman Spectra of Inorganic and Coordination Compounds," 3rd ed, Wiley-Interscience, New York (1978), pp. 249—258.
25) T. J. Pinnavaia and R. C. Fay, *Inorg. Chem.*, **5**, 233 (1966).
26) A. R. Hendrickson and R. L. Martin, *Inorg. Chem.*, **12**, 2582 (1973).

The Role Played by Water in Spin State Variations among Nickel(II) Halide Complexes Containing (7*R*, 14*S*)-5,5,7,12,12,14-Hexamethyl-1,4,8,11-tetraazacyclotetradecane

Tasuku Ito,* Koshiro Toriumi, and Haruko Ito†

Institute for Molecular Science, Okazaki 444

(Received October 21, 1980)

A complex dihydrate formed with nickel(II) bromide and the title macrocyclic ligand (*meso*-Me_6[14]aneN_4) crystallizes in triclinic space group $P\bar{1}$ and in orthorhombic space group Pcab. The crystal and molecular structures of the two crystal modifications have been determined by single crystal X-ray diffraction. In each compound, the nickel(II) is surrounded by a square-planar array of nitrogen atoms, giving low-spin complexes. In both compounds, water of crystallization and bromide ions are located above the hydrogen atoms of N–H groups and form hydrogen-bonded chelate rings of the type Ni–N–H···Br^-···H–O···H–N. The N–H groups adjacent to the single methyl carbon and the geminal dimethyl carbon interact with bromide ion and water, respectively, in the $P\bar{1}$ form, whereas *vice versa* in the Pcab form. Water molecules in the present crystals and those in the previously reported crystal structure of [Ni(*meso*-Me_6[14]aneN_4)]$Cl_2\cdot 2H_2O$ are involved in the same type of specific hydrogen-bonds. Because of the specific hydrogen-bonding effects, the presence of water prevents coordination of not only water itself but also halide ions, yielding thereby low-spin four coordinate complexes.

Nickel(II) halide (Cl^- and Br^-) and the title macrocyclic ligand form orange low-spin complexes, [Ni(*meso*-Me_6[14]aneN_4)]$X_2\cdot 2H_2O$, and violet high-spin complexes, [NiX_2(*meso*-Me_6[14]aneN_4)].[1,2] The macrocyclic ligand *meso*-Me_6[14]aneN_4 is constrained by steric requirements to coordinate in a single plane. From their electronic spectra and magnetic properties[1] and the X-ray analyses on [Ni(*meso*-Me_6[14]aneN_4)]$Cl_2\cdot 2H_2O$ and [$NiCl_2$(*meso*-Me_6[14]aneN_4)],[3] it has been shown that the orange dihydrates are square-planar four coordinate complexes having a singlet ground state, whereas the violet anhydrides are *trans*-dihalogeno six coordinate complexes having a triplet ground state. The solid, orange diamagnetic dihydrates are converted upon heating to violet paramagnetic anhydrides.[4] Conversely, the solid, violet, paramagnetic anhydrous complexes readily revert to [Ni(*meso*-Me_6[14]aneN_4)]$X_2\cdot 2H_2O$ when moisture is available.[1] Of particular interest is the fact that the low-spin four coordinate complexes are dihydrates, whereas the six coordinate high-spin complexes are anhydrides. Although water has considerably high coordinating ability as compared with halide ion, the water molecules in the dihydrates are not involved in coordination.

Spin states of the complexes are affected also in the solution states by the presence or the absence of water. The anhydrous, violet high-spin complex dissolves in water to give an orange solution, which indicates that the complex turns to the low-spin four coordinate complex.[1] When the anhydrous high-spin complex is dissolved in freshly purified stabilizer-free chloroform, almost all the complexes remain high-spin six coordinate, but the solution contains a small amount of the four coordinate singlet form, giving an equilibrium mixture of the low- and high-spin species. The amount of the singlet species depends on the water content in the chloroform solution and increases with an increase in the amount of water in solution.[5]

Busch has pointed out the importance of the role played by water in the spin state variations and proposed a model for the interaction between water and the complex ions.[1,2]

The present study is a part of series of investigations on the spin state variations, *viz.*, coordination number isomerism among the nickel(II) complexes of the title and related macrocyclic ligands.[3–7] The main feature of interest in the present study is the elucidation of the role of water in spin-state variations. For this purpose, the crystal structures of two crystal modifications of [Ni(*meso*-Me_6[14]aneN_4)]$Br_2\cdot 2H_2O$ were determined by X-ray analyses. The dispositions of the water molecules in the vicinities of the nickel(II) ions in the present crystals and those in the previously reported crystal structures of [Ni(*meso*-Me_6[14]aneN_4)]$Cl_2\cdot 2H_2O$[3] and [NiF_2(*meso*-Me_6[14]aneN_4)]$\cdot 5H_2O$[7] were examined.

Experimental

Materials. The bromide dihydrate of the complex ion, [Ni(*meso*-Me_6[14]aneN_4)]$Br_2\cdot 2H_2O$, was prepared from the corresponding perchlorate salt [Ni(*meso*-Me_6[14]aneN_4)]$(ClO_4)_2$[8] by ion exchange (Dowex 1X8). Slow evaporation of the eluate from the column yielded mixture of orange needle ($P\bar{1}$) and large reddish orange plate (Pcab) crystals of [Ni(*meso*-Me_6[14]aneN_4)]$Br_2\cdot 2H_2O$. The orange and reddish orange forms can be separated mechanically under a microscope or more easily in carbon tetrachloride, using the difference in the crystal densities. The density of neat carbon tetrachloride ($D=1.59$ g cm^{-3}), in which the compounds are not soluble, is between densities of the crystals of the reddish orange ($D=1.57$ g cm^{-3}) and the orange ($D=1.62$ g cm^{-3}) form. The crystals of the compounds consists of 61% of the orange and 39% of the reddish orange form. Found for the orange ($P\bar{1}$) form; C, 35.56; H, 7.41; N, 10.24; Br, 30.09%. Found for the reddish orange (Pcab) form; C, 35.40; H, 7.44; N, 10.11; Br, 30.09%. Calcd for $NiC_{16}H_{40}N_4Br_2O_2$: C, 35.65; H, 7.48; N, 10.40; Br, 29.64%.

X-Ray Analyses. Preliminary X-ray work showed that the crystals of the orange complex belong to the triclinic space group $P\bar{1}$, whereas those of the reddish orange complex belong to the orthorhombic space group Pcab. Intensities of reflections were measured on a Rigaku automated four circle diffractometer AFC-5 with graphite monochromatized Mo $K\alpha$

† Present address: Department of Chemistry, Faculty of Science, Nagoya University, Chikusa-ku, Nagoya 464.

radiation (λ=0.71073 Å), the θ-2θ scan technique being employed.

For the orange P$\bar{1}$ form, a specimen with dimensions of 0.40×0.44×0.36 mm was used for the intensity measurements. A total of 5126 reflections was measured up to 2θ=70°. Of these, 3681 reflections with $|F_o|>3\sigma(|F_o|)$ were used in the calculations. Crystal data are: Triclinic, P$\bar{1}$, Z=1, a=8.650(1), b=9.417(1), c=7.813(1) Å, α=94.47(1), β=100.07(1), γ=115.39(1)°, U=557.1(1) Å^3, D_x=1.62, D_m=1.61g cm^{-3}, μ(Mo $K\alpha$)=46.84 cm^{-1}.

For the reddish orange Pcab form, a specimen shaped approximately into a sphere with a diameter of 0.42 mm was used for the intensity measurements. A total of 4935 intensities was measured up to 2θ=70°. Of these, 1938 reflections with $|F_o|>3\sigma(|F_o|)$ were used in the calculations. Crystal data are: Orthorhombic, Pcab, Z=4, a=14.146(2), b=15.739(2), c=10.338(2) Å, U=2301.7(5) Å^3, D_x=1.57, D_m=1.56 g cm^{-3}, μ(Mo $K\alpha$)=45.40 cm^{-1}.

The intensity data used in the structure refinements were corrected for Lorentz and polarization factors and for absorptions. In the absorption corrections, the specimen of the Pcab form was assumed to be a sphere, whereas, for the P$\bar{1}$ form, the numerical Gaussian integration method[9] was used. Both the structures were solved by the heavy atom method and refined by a block-diagonal least-squares method. The weighting scheme, $w=[\sigma_{count}^2+(0.015|F_o|)^2]^{-1}$, was employed. All hydrogen atoms were located by the difference Fourier syntheses, and included in the final refinements with the isotropic temperature factors. The scattering factors for non-hydrogen atoms were taken from International Tables for X-Ray Crystallography.[10] For hydrogen atom, the values given by Stewart *et al.* were used.[11] The final R indices were R=0.046 and R_w=0.051 for the P$\bar{1}$ form, and R=0.056 and R_w=0.046 for the Pcab form, respectively. Atomic parameters for each crystal are given in Table 1.[12]

The calculations were carried out on the HITAC M-180 computer at the Computer Center of the Institute for Molecular Science with Universal Crystallographic Computation Program System UNICS III.[13]

Table 1. Fractional atomic coordinates (×10^5) and equivalent isotropic thermal parameters (Å^2) for non-hydrogen atoms with their estimated standard deviations

Atom	x	y	z	B_{eq}/Å^2
A) Atomic parameters for the P$\bar{1}$ form				
Ni	50000(0)	50000(0)	50000(0)	1.8
Br	91122(4)	72142(4)	33329(4)	3.9
N(1)	54174(25)	71608(23)	59263(24)	2.3
N(2)	72047(24)	52436(23)	64421(23)	2.2
C(1)	30084(37)	63990(33)	34307(34)	3.2
C(2)	38078(38)	73363(34)	52526(37)	3.5
C(3)	62160(32)	78122(28)	78650(28)	2.5
C(4)	80462(31)	78877(30)	82557(30)	2.8
C(5)	81468(31)	63116(30)	82000(28)	2.6
C(6)	64483(43)	95240(33)	82922(39)	3.8
C(7)	50420(38)	67504(35)	89542(33)	3.4
C(8)	100766(36)	66409(37)	86415(37)	3.7
O	74235(33)	97034(32)	37985(34)	5.3
B) Atomic parameters for the Pcab form				
Ni	0(0)	0(0)	0(0)	2.3
Br	15510(4)	13181(3)	21769(6)	5.3
N(1)	−476(25)	−2571(21)	18432(34)	2.9
N(2)	10906(24)	−7357(20)	−3193(32)	2.7
C(1)	−10938(33)	9331(33)	17122(49)	4.0
C(2)	−9183(35)	1189(34)	24296(46)	4.3
C(3)	1689(30)	−11396(28)	23247(43)	3.2
C(4)	11532(33)	−13718(27)	18747(49)	3.5
C(5)	12810(33)	−15291(27)	4493(49)	3.5
C(6)	1662(42)	−11524(35)	38113(50)	5.3
C(7)	−5712(35)	−17573(33)	18117(55)	4.7
C(8)	22735(42)	−18691(35)	1991(52)	5.6
O	−22326(27)	−3748(24)	51086(37)	5.8

The equivalent isotropic thermal parameter is calculated using the expression $B_{eq}=4/3\ (\sum_i\sum_j a_i a_j \beta_{ij})$, where the a_i's are the unit-cell edges in direct space.

Results and Discussion

Description of the Molecular and Crystal Structures of [Ni(meso-Me$_6$[14]aneN$_4$)]Br$_2$·2H$_2$O. In both the P$\bar{1}$ and Pcab forms, the nickel(II) ions are required to lie on a center of symmetry. Table 2 lists bond lengths and angles within the complex ion in the two crystal modifications. As shown in Table 2, the structures of the complex ion, [Ni(*meso*-Me$_6$[14]aneN$_4$)]$^{2+}$, in the P$\bar{1}$

Table 2. Bond distances (l/Å) and angles (ϕ/°) with their standard deviations in parentheses

	The P$\bar{1}$ form	The Pcab form
(A) Bond lengths		
Ni–N(1)	1.961(2)	1.949(4)
Ni–N(2)	1.947(2)	1.957(3)
N(2)–C(1′)	1.491(4)	1.473(6)
N(1)–C(2)	1.482(4)	1.495(6)
N(1)–C(3)	1.508(3)	1.507(6)
N(2)–C(5)	1.501(3)	1.504(6)
C(1)–C(2)	1.490(4)	1.501(7)
C(3)–C(4)	1.528(4)	1.513(6)
C(4)–C(5)	1.521(4)	1.505(7)
C(3)–C(6)	1.538(4)	1.537(7)
C(3)–C(7)	1.523(4)	1.524(7)
C(5)–C(8)	1.530(4)	1.525(8)
(B) Bond angles		
N(1)–Ni–N(2)	93.5(1)	94.0(1)
Ni–N(1)–C(2)	108.6(1)	110.0(3)
Ni–N(2)–C(1′)	106.5(1)	107.0(3)
Ni–N(1)–C(3)	119.1(2)	120.5(3)
Ni–N(2)–C(5)	125.5(2)	122.9(3)
C(2)–N(1)–C(3)	113.8(2)	113.5(3)
C(1′)–N(2)–C(5)	109.9(2)	109.9(3)
N(2′)–C(1)–C(2)	106.3(2)	107.6(4)
N(1)–C(2)–C(1)	107.4(3)	105.9(4)
N(1)–C(3)–C(4)	107.3(2)	107.9(3)
N(2)–C(5)–C(4)	111.9(2)	111.0(4)
N(1)–C(3)–C(6)	110.3(2)	110.0(4)
N(1)–C(3)–C(7)	109.9(2)	109.5(4)
N(2)–C(5)–C(8)	110.6(2)	111.5(4)
C(3)–C(4)–C(5)	117.3(2)	116.8(4)
C(4)–C(3)–C(6)	107.6(2)	107.9(4)
C(4)–C(3)–C(7)	111.9(2)	111.8(4)
C(4)–C(5)–C(8)	109.3(2)	109.5(4)
C(6)–C(3)–C(7)	109.9(3)	109.8(4)

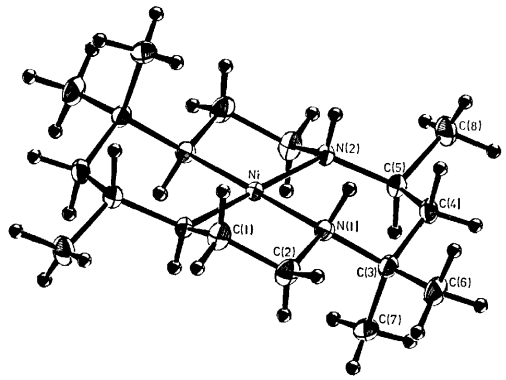

Fig. 1. A perspective drawing of [Ni(*meso*-Me_6[14]-$aneN_4$)]$^{2+}$ in the crystal structure of the P$\bar{1}$ form.

and Pcab forms are not significantly different. Figure 1 shows a perspective drawing of [Ni(*meso*-Me_6[14]-$aneN_4$)]$^{2+}$ in the P$\bar{1}$ form, which is essentially the same as those in the Pcab form and in [Ni(*meso*-Me_6[14]-$aneN_4$)]$Cl_2 \cdot 2H_2O$.[3] The nickel(II) is surrounded by four secondary nitrogen atoms of the macrocyclic ligand in a single plane, yielding a square-planar, diamagnetic nickel(II) complex. The average Ni–N bond distances are 1.954(7) Å for the P$\bar{1}$ form and 1.953(4) Å for the Pcab form, which are in the normal range for a low-spin nickel(II) complex with four planar nitrogen donors.[3,14,15] The macrocyclic skeleton adopts the most stable conformation: the six-membered chelate rings take the chair form with the C(5)–CH_3 bonds in equatorial positions; the five-membered rings are in the gauche conformation.

Three significant deviations from tetrahedral angles are noted. These are the large angles of Ni–N(1)–C(3), Ni–N(2)–C(5), and C(3)–C(4)–C(5) (see Table 2). These distortions are in common with six-membered chelate rings of metal complexes which have the title ligand in planar coordination.[3,7,16]

Figures 2(a) and 2(b) show dispositions of bromide ions and water of crystallization around the complex ions, as viewed along the normal to the coordination plane, in the P$\bar{1}$ and Pcab forms, respectively. The structures around the nickel(II) ions in the two different crystal modifications are very similar to each other as depicted in Fig. 2 in the following sense: (i) the bromide ions are located above the hydrogen atoms of N–H groups and the oxygen atoms of water lie also above the hydrogen atoms of the other crystallographically independent N–H groups; (ii) bromide ions and water molecules are involved in the hydrogen-bonds of the type shown in **1**, forming hydrogen-bonded chelate rings. The hydrogen-bond distances are normal (see Figs. 4(c) and 4(d)). Although the N–H···Y (Y=Br^- or H_2O) interactions in the two structures are very similar to each other in their features and lengths, the nitrogen atoms involved in such interactions are chemically different, N(1) and N(2) being hydrogen-bonded to the oxygen atom and bromide ion, respectively, in the

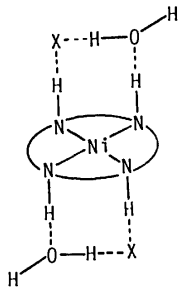

1

P$\bar{1}$ form, whereas *vice versa* in the Pcab form. A very similar situations has been found for the N–H···O interactions around the two crystallographically independent nickel(II) complexes in the crystals of [NiF_2(*meso*-Me_6[14]$aneN_4$)]$\cdot 5H_2O$ (see Figs. 4(e) and 4(f)).[7] The positions of bromide ions in [Ni(*meso*-Me_6[14]$aneN_4$)]$Br_2 \cdot 2H_2O$ are nearer to the axial coordination sites than that of the chloride ion in

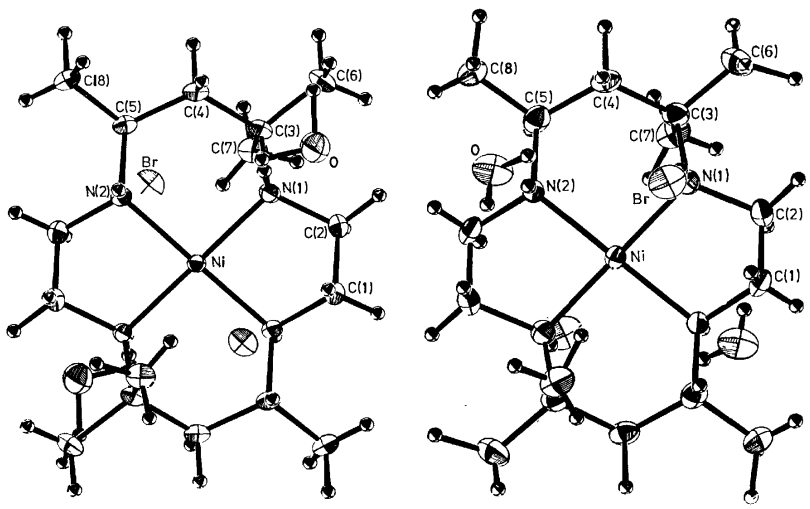

Fig. 2. Dispositions of bromide ions and water molecules around the nickel(II) ion in the crystal structures of the P$\bar{1}$ (a) and Pcab forms (b), as viewed along the normal to each of the coordination planes.

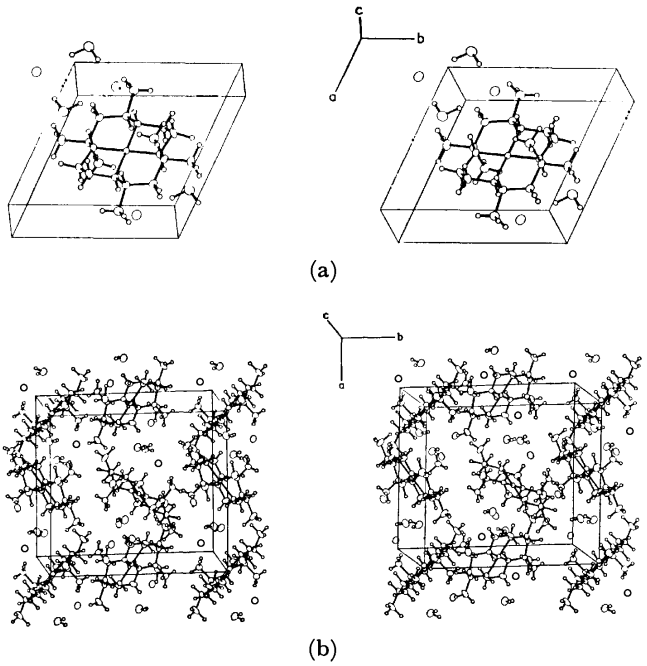

Fig. 3. Crystal structures of the $P\bar{1}$ (a) and Pcab forms (b).

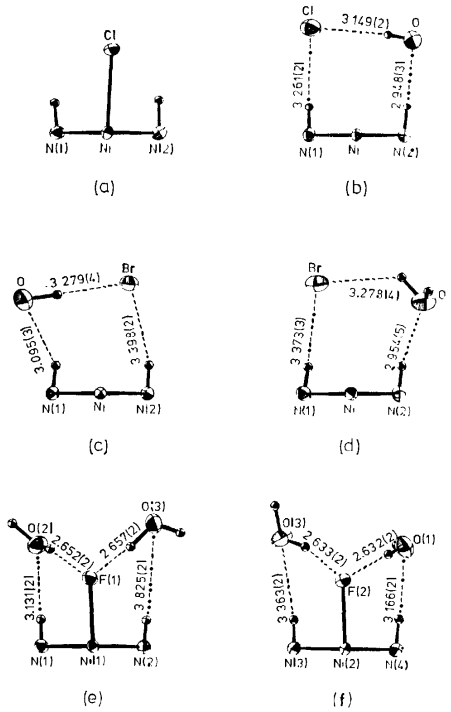

Fig. 4. Dispositions of halide ions and water of crystallization in the vicinities of the nickel(II) ions in $[NiCl_2(meso\text{-}Me_6[14]aneN_4)]\cdot 2CHCl_3$ (a),[3] $[Ni(meso\text{-}Me_6[14]aneN_4)]Cl_2\cdot 2H_2O$ (b),[3] $[Ni(meso\text{-}Me_6[14]aneN_4)]Br_2\cdot 2H_2O$ in the $P\bar{1}$ (c) and Pcab (d) form, and $[NiF_2(meso\text{-}Me_6[14]aneN_4)]\cdot 5H_2O$ ((e) and (f)).[7] In each compound, the nickel(II) ion sits on a crystallographic inversion center. In the fluoride system, there are two crystallographically independent complexes.[7] Hydrogen-bond distances corresponding to the lengths between donor and accepter atoms are given in Å.

$[Ni(meso\text{-}Me_6[14]aneN_4)]Cl_2\cdot 2H_2O$ (see Fig. 4). This may be related to the fact that $[NiBr_2(meso\text{-}Me_6[14]aneN_4)]$ reverts more easily to the bromide dihydrate than $[NiCl_2(meso\text{-}Me_6[14]aneN_4)]$ to the chloride dihydrate, when moisture is available.[1,5]

Stereoscopic views of the crystal structures for the $P\bar{1}$ and Pcab forms are presented in Figs. 3(a) and 3(b), respectively. Bromide ions and water molecules are further hydrogen-bonded with adjacent water molecules and bromide ions, respectively. Through these interactions the adjacent complex ions are held together, but the features of the interactions differ in the $P\bar{1}$ and Pcab forms. In the $P\bar{1}$ form, the interaction appears to be of the type shown in **2**, whereas that in the Pcab form, an infinite zigzag chain parallel to the c-axis as shown in **3**. The hydrogen-bond parameters are given in **2**, **3**, and Figs. 4(c) and 4(d). All other intermolecular contacts appear to be normal both in the two structures.

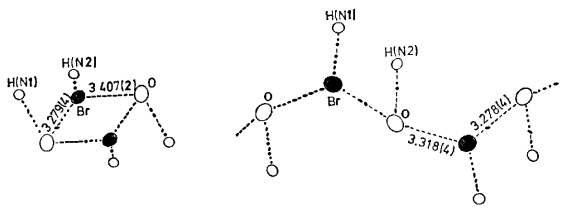

2 **3**

Specific Hydrogen-bonding Effects. The occurence of the spin-state variation is invariably associated with the presence or the absence of water. One exception is the fluoride system in the solid state, *trans*-$[NiF_2(meso\text{-}Me_6[14]aneN_4)]\cdot 5H_2O$, where fluoride ions occupy the axial coordination sites yielding a high-spin six coordinate complex in the hydrate.[7] Although water has high coordinating ability as compared with halogen ions for a nickel(II) ion in general, no evidence has been reported for coordination of water to a nickel(II) ion in the present systems.

Figure 4 shows the dispositions of water and halide ion in the vicinity of the nickel(II) ion found in the present study together with those in the crystal structures of $[Ni(meso\text{-}Me_6[14]aneN_4)]Cl_2\cdot 2H_2O$,[3] $[NiCl_2(meso\text{-}Me_6[14]aneN_4)]\cdot 2CHCl_3$,[3] and $[NiF_2(meso\text{-}Me_6[14]aneN_4)]\cdot 5H_2O$,[7] as viewed along each coordination plane. Note that all the nickel(II) ions in these complexes lie on centers of symmetry. Therefore, for simplicity, only the crystallographically independent two nitrogen atoms and a nickel(II) ion are depicted for each complex. In the fluoride system, there are two crystallographically independent complexes, which are shown in Figs. 4(e) and 4(f). Of particular interest in Fig. 4 is the fact that the dispositions of water and a halide ion and the features of the hydrogen-bond framework in the vicinity of the nickel(II) ion are very similar to each other in each hydrate. In all the hydrates except for the pentahydrate of the fluoro complex, water molecules and halide ions are located above the hydrogen atoms of N–H groups. As can be seen in Figs. 4(b), 4(c), and 4(d), hydrogen-bonded chelate rings of the type **1** are invariably formed.

Busch proposed that the halogen ions in the dihydrates occupy the axial coordination sites but are

displaced from the nickel(II) ion so that the ligand field of the halide ions cannot exert on the nickel(II) ions.[1] It was found in the present and previous studies that neither water molecules nor the halide ions are located near the axial coordination sites in the dihydrates. The specific hydrogen-bond effects such as the hydrogen-bonded chelate rings are undoubtedly responsible for failure of coordination of the water molecule. The occurence of such specific interactions would be much more favorable over the hypothetical occupation by the water molecules at the coordination sites. Because of the specific hydrogen-bonding effects, the presence of water not only prevents coordination of water itself but also prevents halide ions from coordinating, giving low-spin four coordinate complexes. Under water free circumstances such as in dry chloroform solutions or in solid states of the anhydride, halide ions can coordinate to nickel(II) to produce high-spin six coordinate complexes. These specific hydrogen-bonding effects also produce large enthalpy values for dehydrations of the hydrates of the present complexes.[4,7]

In the case of the fluoride system, axial coordination sites are occupied by fluoride ions even in the hydrate. Water molecules are located above the hydrogen atoms of all the N–H groups. Hydrogen-bonded chelate rings different from the type **1** can be seen in Figs. 4(e) and 4(f), which contain O–H···F–Ni bond. The reason for the change in geometry is most likely due to the ionic size of the fluoride ion. The fluoride ion is too small to form hydrogen-bonded chelate ring of the type **1**. In addition, a fluoride ion has high coordinating ability as compared with other halide ions for a nickel(II) ion.[1]

As described earlier, the spin state variations in solutions are also associated with the presence or the absence of water. In aqueous solutions or solutions of organic solvents containing water, hydrations take place around N–H groups. Structural feature of the hydration would be similar to the disposition of water molecules in solid state shown in Fig. 4. Water molecules involved in the hydration would play a role similar to water of crystallization in the solid dihydrates to give low-spin complexes.

References

1) D. H. Busch, *Adv. Chem. Ser.*, **62**, 616 (1967).
2) D. H. Busch, *Helv. Chim. Acta*, Fasciculus Extraordinarius Alfred Werner, 174 (1967).
3) T. Ito and K. Toriumi, *Acta Crystallogr., Sect. B*, **37**, 88 (1981).
4) T. Ito, Y. Tsutsumi, Y. Hiratsuka, K. Mochizuki, and M. Fujimoto, *Bull. Chem. Soc. Jpn.*, **54**, 931 (1981).
5) K. Mochizuki, T. Ito, and M. Fujimoto, unpublished study.
6) K. Mochizuki, M. Fujimoto, H. Ito, and T. Ito, *Bull. Chem. Soc. Jpn.*, **53**, 2535 (1980).
7) K. Toriumi and T. Ito, *Acta Crystallogr., Sect., B*, **37**, 240 (1981).
8) L. G. Warner and D. H. Busch, *J. Am. Chem. Soc.*, **91**, 4092 (1968).
9) W. R. Busing and H. A. Levy, *Acta Crystallogr.*, **10**, 180 (1957).
10) "International Tables for X-Ray Crystallography," Kynoch Press, Bermingham (1974), Vol. IV.
11) R. F. Stewart, E. R. Davidson, and W. T. Simpson, *J. Chem. Phys.*, **42**, 3175 (1965).
12) Tables of positional parameters for hydrogen atoms, anisotropic thermal parameters, and a list of the observed and calculated structure factors are kept in the office of the Chemical Society of Japan (Document No. 8129).
13) T. Sakurai and K. Kobayashi, *Rikagaku Kenkyusho Hokoku (Rept. Inst. Phys. Chem.)*, **55**, 69 (1979).
14) F. Madaule-Aubry, W. R. Busing, and G. M. Brown, *Acta Crystallogr., Sect. B*, **24**, 754 (1967).
15) S. W. Hawkinson and E. B. Fleischer, *Inorg. Chem.*, **11**, 2404 (1969).
16) K. B. Mertes, *Inorg. Chem.*, **17**, 49 (1978).

Models for Visual Pigments. The Effect of the Imidazolyl Group on the Absorption Maxima of the Retinal Schiff Base

Masato NANASAWA* and Hiroyoshi KAMOGAWA
Faculty of Engineering, Yamanashi University, Takeda, Kofu 400

(Received April 3, 1980)

The title effect has been investigated with the imidazolyl group either externally added or intramolecularly combined. *N*-Retinylidenebutylamine was protonated with imidazole derivatives under neutral conditions and was absorbed at longer wavelengths compared with carboxylic acids. The absorption peak with the imidazolyl group intramolecularly combined was highly affected by the structure, protonated N^{α}-retinylidene-L-histidine octadecylamide having an absorption maximum at 494 nm caused by the inductive effect and the polar imidazolyl group.

The absorption maxima of visual pigments bound to opsin by a Schiff-base linkage are observed at 500 nm, although the protonated products of synthetic analogues absorb at approximately 450 nm. As regards this bathochromic shift, a large number of interesting observations and theories have been reported: the polarizability of the micro environment,[1] the electrostatic effect of polar or charged groups in the vicinity of the chromophore,[2] and the twist or distortion of the π-conjugated system.[3] However, there are still many unsolved problems. Recently two synthetic models were reported which absorb at longer wavelengths by means of protonation with trifluoroacetic acid[4] or in an aqueous hydrochloric acid solution.[5] Since native photochromic processes proceed under mild conditions, we examined the effects of amino acids as protonating agents.[6] In this paper we intend to deal especially with the imidazolyl group of the histidine residue. The imidazolyl group is known to be responsible for a buffering capacity;[7] hence, it may be able to protonate the Schiff-base linkage in a physiological pH range and to mediate a charge relay system between protonated Schiff-base nitrogens and counter anions. On the basis of these assumptions, we have examined the protonation of *N*-retinylidenebutylamine(Bu–SB) with the salt of N^{α}-benzyloxycarbonyl-L-histidine butylamide (**1**) plus *N*-benzyloxycarbonyl-L-alanine (Z–α-Ala), N^{α}-octadecanoyl-L-histidine (**2**), and 4,5-imidazoledicarboxylic acid monohexadecyl ester (**3**). As Schiff-base models with the imidazolyl group, the following were synthesized, and the absorption maxima of the protonated products were determined:

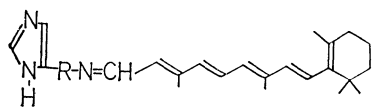

R = $-CH_2-$: **4**–SB. $-CH_2CH_2-$: **5**–SB.
$-CH_2\underset{|}{C}H-CONH-C_{18}H_{37}$: **6**–SB.
$-CH_2CH_2NHCOCH_2CH_2-$: **7**–SB.
$-CH_2CH_2-NHCO(CH_2)_5-$: **8**–SB.

Experimental

all-trans-Retinal was prepared by the oxidation of vitamin-A with MnO_2 and was recrystallized from petroleum ether;[8] mp 59—60 °C, λ_{max} 367.5, nm, E_1 % 1536 in petroleum ether. Isomerization to the *cis*-isomer was conducted by the irradiation of *all-trans*-retinal (1% in petroleum ether) containing iodine (1% to retinal), using a 150 W xenon lamp with a UV filter fitted as the light source;[9] λ_{max} 364.5 nm, $E_{1\%}$ 1259 in petroleum ether.

Preparation of N^{α}*-Benzyloxycarbonyl-L-histidinamide*: A mixture of N^{α},N^{im}-bis(benzyloxycarbonyl)-L-histidine(Z–His–Z 6.85 g, 15.5 mmol, the benzyloxycarbonyl group was abbreviated as Z) and dicyclohexylcarbodiimide(DCC 3.5 g, 17 mmol) in CH_2Cl_2 (50 ml) was stirred in an ice bath for 45 min, filtered, and washed with CH_2Cl_2. To the filtrate, alkylamine (31 mmol) in $CHCl_3$ (50 ml) was added, the mixture being stirred in an ice bath, allowed to stand overnight, and then refluxed for 30 min. While hot, the reaction mixture was filtered and washed with $CHCl_3$. The filtrate was dried over Na_2SO_4, concentrated to about 30 ml, and then cooled at −20 °C. The product thus precipitated was recrystallized from acetone or ethanol. **1**: yield, 62% mp; 143—145 °C. IR (KBr): 3300 (NH), 3150 (imidazole–NH), 1690 (carbamate C=O), 1650 cm^{-1} (amide C=O). ^{1}H-NMR ($CDCl_3$): 0.9—1.5 (m, 7H, $CH_3CH_2CH_2-$), 3.0 (m, 4H NH–C$\underline{H}_2$– and imi–CH_2–), 4.3 (q, 1H, α-CH), 5.2 (s, 2H, phenyl–C$\underline{H}_2$–), 6.9, 7.8 (s, 2H, imidazole ring), 7.3 ppm (8H, phenyl, NH). Found: C, 62.68; H, 7.32; N, 16.01%. Calcd for $C_{18}H_{23}N_4O_3$: C, 62.97; H, 6.31; N, 16.33%. MS (*m/e*): 343 (M^+, 11%). N^{α}-Benzyloxycarbonyl-L-histidine octadecylamide: yield, 36%; mp 151—154 °C.

N^{α}-Octadecanoyl-L-histidine (**2**) was prepared with octadecanoyl chloride; yield, 45%; mp 165—180 °C.[10] The 4,5-imidazoledicarboxylic acid monohexadecyl ester (**3**) was obtained by condensation with 4,5-bis(chloroformyl)imidazole[11] and hexadecyl alcohol; yield, 71%; mp 167—170 °C. In the IR of the salt containing **1** and Z–α-Ala (mp 125—126 °C), the absorption at 1710 cm^{-1} (COOH) no longer exists, and the salt peak is observed at 2000—2750 cm^{-1}. ^{1}H-NMR and elemental analyses made it posisble to identify the structure. 4-(Aminomethyl)imidazole (**4**) was obtained starting with D-fructose *via* 4-(hydroxymethyl)imidazole, oxidation with HNO_3 to aldehyde, conversion to oxime, and reduction with H_2 (5% Pd on charcoal) in methanol saturated with HCl.[12]

L-Histidine Octadecylamide (6): To N^{α}-Z–histidine octadecylamide (2.35 g, 4.4 mmol) in anhydrous acetic acid (5.0 ml), a 30% solution of hydrogen bromide in acetic acid (5.7 ml) was added with vigorous stirring at room temperature. The reaction mixture was stirred for 1 h and then poured into anhydrous ether (100 ml). **6**·HBr was filtered, thoroughly washed with ether, and then dissolved in ethanol (10 ml). The solution was basified with saturated aqueous Na_2CO_3. The product was extracted with ethanol and recrystallized from ethanol–ether, **6**: yield, 42%; mp 110—115 °C. Found: C, 70.79; H, 11.53; N, 13.73%. Calcd for $C_{24}H_{40}N_4O$: C,

70.93; H, 11.33; N, 13.79%.

Preparation of N-*(ω-Aminoalkanoyl)histamine (7, 8)*: A mixture of Z-β-Ala (3.94 g, 17.7 mmol) and DCC (4 g, 19.5 mmol) in a 1 : 2 mixture of dimethylformamide–acetonitrile (20 ml) was stirred in an ice bath for 45 min; the reaction mixture was then filtered and washed with dimethylformamide–acetonitrile (30 ml). To the filtrate, histamine dihydrochloride (3 g, 16.1 mmol) and NaOH (0.7 g) in H_2O (15 ml) were added in one portion; the mixture was vigorously stirred for 5 h, and then filtered. The filtrate was concentrated to about 40 ml and poured into cold 10^{-1} M hydrochloric acid (250 ml, 1 M= 1 mol dm^{-3}). The insoluble by-product (DCC urea, Z-β-Ala–DCC) was filtered off. The filtrate was basified with saturated aqueous Na_2CO_3 and cooled in a refrigerator overnight. The product thus precipitated was filtered, washed with H_2O, and then recrystallized from ethanol–ethyl acetate. *N*-(*N*-Benzyloxycarbonyl-β-alanyl)histamine: yield, 62%; mp 137—139 °C. *N*-[ω-(Benzyloxyamino)hexanoyl]-histamine: yield, 82%; mp 111—114 °C. Deblocking of the ω-amino group were conducted in a manner similar to that used for **6**. **7**: yield, 52%; mp 67—68 °C, Found: C, 52.89; H, 8.38; N, 29.94%. Calcd for $C_8H_{14}N_4O$: C, 52.75; H, 7.69: N, 30.77%. **8**: yield, 67%; mp 44—46 °C. Found: C, 59.04; H, 9.50; N, 24.32%. Calcd for $C_{11}H_{20}N_4O$: C, 58.93; H, 8.93; N, 25.00%.

The Schiff base was prepared by mixing solution of retinal (10^{-2} M) and imidazole derivatives (10^{-2} M) in absolute ethanol containing 3A molecular sive 1/16 in. pellets at room temperature for 8 h in the dark. In the case of **4** and **6**, the reaction time was prolonged to 24 h. The absorption spectra were recorded on a Hitachi 200-10 spectrophotometer, using quartz cells 1 mm and 10 mm in path length. The pH of the protonating solution (90% aqueous ethanol) was measured on a Horiba M-7E pH meter. The calibration curve for the protonated *N*-retinylidenebutylamine (Bu–SBH$^+$) satisfied the Lambert Law over the concentration range from 1.4×10^{-5} to 2.2×10^{-4} M.

Results and Discussion

Effect of Imidazole Derivatives on the Protonation of N-*Retinylidenebutylamine (Bu–SB).* Figure 1 shows the degree of protonation plotted against the pH values of the solution, in which the pH values were controlled by the addition of Z-α-Ala (10^{-2} M) to **1** (2.5×10^{-3} M) in 90% aqueous ethanol. The basic nitrogen of imidazole ring (N^3, pK_a 14.5) is, of course, neutralized with Z-α-Ala in a polar solvent, and some association may take place between **1** and Z-α-Ala. However, the absorption peak at 440 nm appeared even under neutral conditions, which indicates that undissociated imine hydrogen

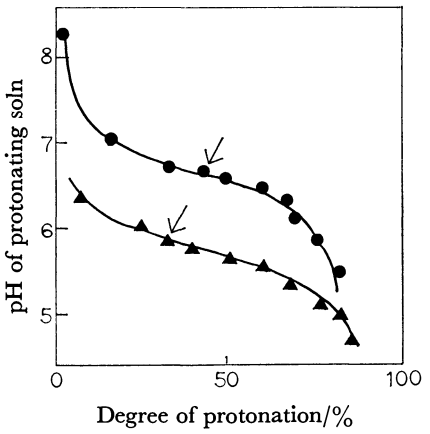

Fig. 1. Protonation of Bu–SB with amino acids.
●: With a mixture of **1** and Z-α-Ala, ▲: with Z-α-Ala only.
Bu–SB, 5×10^{-4} M. **1**, 2.5×10^{-3} M. Solvent, 90% aqueous ethanol. The arrows indicated the equimolar addition of Z-α-Ala to Bu–SB.

(N^1–H of imidazole ring) protonated the Schiff-base linkage.

In a nonpolar solvent such as chloroform, in which carboxylic acids with no steric hindrance at the α-position (Z-β-Ala, hexanoic acid) remain almost in undissociated or dimeric state, the extent of protonation increased upon the addition of **1** (5×10^{-3} M) to the

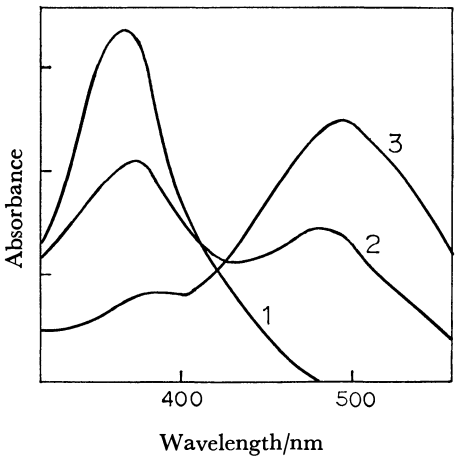

Fig. 2. Absorption spectra of **6**–SB
1: **6**–SB, 2: **6**–SBH$^+$, 3: **6**–SBH^{2+}. Concentration, 3.3×10^{-5} M; solvent, chloroform.

Table 1. Absorption maxima of imidazole derivatives

	λ_{max}/nm	SBH$^+$ a)			SBH_2^{2+} b)		
		λ_{max}/nm	$\Delta\lambda$ c)/nm	Absorbance	λ_{max}/nm	$\Delta\lambda$ c)/nm	Absorbance
4–SB	368	468	100	0.458	482	114	0.695
5–SB	366	467.5	101.5	0.595	479	113	0.747
6–SB	370	482	112	0.305	494	124	0.651
7–SB	367	464	97	0.505	470.5	103.5	0.779
8–SB	367	464	97	0.577	466.5	99.5	0.790
Bu–SB	366	460	94	0.848			

a) Monoprotonated Schiff base. b) Diprotonated Schiff base. c) The magnitude of shift against the Schiff base. Concentration, 3.3×10^{-5}M; solvent, chloroform.

mixture of Bu–SB (5×10^{-4} M) and Z–β-Ala (2.5×10^{-3} M). It is possible that the proton transfer from undissociated or dimeric carboxylic acid to **1** took place and that the resulting positive charge at the imidazole ring promoted the formation of Bu–SBH$^+$.

The protonation with **1** did not appear in ethanol or even in its aqueous solution (N^1–H, pK_a 7.2), whereas in chloroform a small absorption appeared at about 470 nm. The hydrogen bond at N^3 with a solvent presumably aided proton release at the N^1 of the imidazole ring. With **2** and **3** existing as an ion pair in chloroform, the absorption peaks were slightly shifted to longer wavelengths (**2**, 455 nm, **3**, 458 nm) than that with Z–α-Ala (450 nm). The red shift might be explained by Scheme 1, in which electrostatic energy[13] between the counter anion and the positive charge on the nitrogen of the Schiff-base linkage is decreased by the charge-relay system.

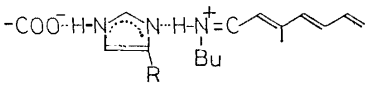

Scheme 1.

Absorption Maxima of the Protonated Schiff Base of Imidazole Derivatives. The 11-*cis*-retinal of rhodopsin is bound to an ε-amino group of a lysnine, and the bathochromic shift is caused by the placement of amino-acid residues near the protonated chromophore.[2] Schiff bases (**4**–SB—**8**–SB) with different distances between the Schiff-base linkage and the imidazole ring were synthesized in order to investigate the effect of the neighboring group on the absorption spectra. An attempt to synthesize a Schiff-base model with the least distance, such as a 4-aminoimidazole derivative, was unsuccessful because of the weak basicity of the amino group attached to the imidazole ring. It required 24 h to reach the constant absorption maxima of **4**–SB and **6**–SB after mixing, and their absorption peaks were slightly shifted to longer wavelengths compared with others; this shift was caused by the presence of an electron-withdrawing group at the α-position.[14] With one or two equivalents of Z–α-Ala, a protonated Schiff base did not indicate any absorption peaks, but only shoulders. With the intention of obtaining more obvious results, the protonation was conducted by the addition of an ethanolic solution containing one or two equivalents of hydrochloric acid to a Schiff base (2.5×10^{-2} M). Mono- and diprotonated Schiff bases were represented by SBH$^+$ and SBH^{2+} respectively; the pH values were 6.4 and 4.5 respectively in aqueous ethanol. The absorption maximum of the protonated *N*-retinylidene-L-alanine butylamide shifted to the red by approximately 106 nm, the magnitude of the shift against Bu–SBH$^+$ being large compared with that of the unprotonated product (SB: 371—366=5 nm, SBH$^+$: 477—460=17 nm). It seems reasonable to say that the carbonyl group at the α-position enhanced the electron-withdrawing character of the Schiff-base nitrogen.

The absorbance obtained by the addition of equimolar acid components was very small in the case of a Schiff base prepared with alkanediamines with short chains (ethylene, trimethylene) compared with that of imidazole derivatives. This denotes that the proton transfer from a Schiff-base linkage to primary amine might proceed, while in the latter case the transfer from the amphoteric imidazole ring is predominant. The red shifts caused by the neutral imidazolyl group (**4**–SBH$^+$, **5**–SBH$^+$) were approximately 7 nm compared with the absorption maximum of Bu–SBH$^+$, the magnitude of which was almost similar to that of Bu–SB with **2** and **3** externally added.

When the amount of acid was increased, the red shift was highly affected by the structure: shorter distances between two protonated sites might increase the repulsion between two cations (Scheme 2), thus bringing about an extrusion of the positive charge on the Schiff-base nitrogen to the ionane ring. The interaction of separated ions as observed in the absorption maxima was calculated over 8 Å on the basis of a molecular orbital theory.[15] The results of this calculation agree with those of our experiment, in which the maximum length affecting the red shift was six methylene chains (hexamethylenediamine–SBH$_2^{2+}$, 463 nm). The shifts caused by the protonated imidazole rings were larger than those of the corresponding model compounds, ethylenediamine–SBH$_2^{2+}$ (470 nm) and trimethylenediamine–SBH$_2^{2+}$ (468 nm).

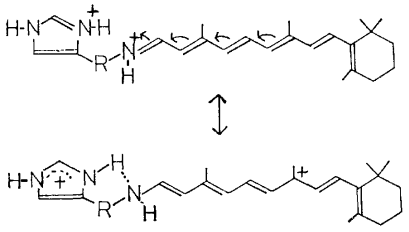

Scheme 2.

The magnitude of shift against the absorption maximum of Bu–SBH$^+$ was 19 nm in terms of the influence of the protonated imidazole ring and 12 nm in terms of the inductive effect of the α-carbonyl group, the large shift of **6**–SBH^{2+} being explicable by adding the two values.

When a *cis*-isomerized retinal was bound to the imidazole derivatives, some interaction could be postulated between rings (β-ionane–imidazole). However, the absorption maxima of the protonated products were almost consistent with those of the *all-trans*-retinal. In actual visual pigments, the twist or distortion of the retinal moiety and a complicating structure of opsin might cause the red shift up to 580 nm. It is experimentally impossible to make a highly selective and restrictive model until the complete structure is known. We have, therefore, synthesized simple models simulating visual pigments, in which the absorption spectra shifted toward longer wavelengths close to that of rhodopsin.

References

1) C. S. Ivring, G. W. Bayers, and P. A. Leermarers, *J. Am. Chem. Soc.*, **91**, 2141 (1969).

2) B. Honig, A. D. Greenberg, U. Dinur, and T. G.

Ebrey, *Biochemistry*, **21**, 4593 (1976).
3) P. Blatz and P. Liebman, *Expt. Eye Res.*, **17**, 573 (1973).
4) P. K. Das, R. S. Becker, D. Hannak, and E. Bayer, *J. Am. Chem. Soc.*, **101**, 239 (1979).
5) I. Tabushi, Y. Kuroda, and K. Shimokawa, *J. Am. Chem. Soc.*, **101**, 4759 (1979).
6) M. Nanasawa and H. Kamogawa, *Bull. Chem. Soc. Jpn.*, **52**, 1727 (1979).
7) T. Wieland and G. Schneidel, *Ann. Chem.*, **580**, 159 (1953).
8) C. D. Robeson, W. P. Blum, J. M. Dietele, J. D. Cawley, and J. G. Baxter, *J. Am. Chem. Soc.*, **77**, 4120 (1955).
9) R. Hubbard, *J. Am. Chem. Soc.*, **78**, 4662 (1956).
10) G. Gilter, *J. Am. Chem. Soc.*, **90**, 5004 (1968).
11) For a related procedure, see L. F. Fieser and M. Fieser for Organic Synthesis I," John Wiley & Sons, New York (1967), p. 286.
12) R. A. Turner, *J. Am. Chem. Soc.*, **71**, 2801 (1949).
13) P. E. Blatz, J. H. Mohler, and H. V. Navangul, *Biochemistry*, **11**, 848 (1972).
14) B. Rosenberg and T. M. Krigas, *Photochem. Photobiol.*, **6**, 769 (1967).
15) H. Suzuki, T. Komatzu, and H. Kitajima, *J. Phys. Soc. Jpn.*, **37**, 177 (1974).

  Bull. Chem. Soc. Jpn., 54, 1105—1107 (1981)

The Crystal and Molecular Structure of *N*-(Thioacetyl)tryptamine. A Radioprotective Indole Compound

Toshimasa ISHIDA,* Satomi SHIMIZU, Masatoshi INOUE, Kunihiro KITAMURA,**
Akio WAKAHARA,** Ken-ichi TOMITA,** and Masato SHINODA***

Osaka College of Pharmacy, Kawai, Matsubara, Osaka 580
***Faculty of Pharmaceutical Sciences, Osaka University, Yamadakami, Suita, Osaka 565*
****Hoshi College of Pharmacy, 2-4-41 Ebara, Shinagawa-ku, Tokyo 142*

(Received April 14, 1980)

The crystal structure of N-(thioacetyl)tryptamine, a radioprotective agent, has been determined by the X-ray method. The crystal is monoclinic, space, group $P2_1/c$ with the unit cell dimensions: $a=23.761(5)$, $b=5.553(1)$, $c=8.889(2)$ Å, and $\beta=94.04(4)°$. The structure was solved by the direct method and succesive Fourier syntheses, and refined by the block-diagonal least-squares method to give a final R-value of 0.072. In the crystal, the molecules are held together with van der Waals contacts between the nonpolar groups of adjacent molecules, and an intermolecular hydrogen bond between the sulfur and nitrogen atoms of the side chain (N–H···S=3.322 Å). The folded conformation observed in this compound could be related to the protection of DNA against irradiation.

Indolylalkylamines containing sulfur atoms could be expected to be rādioprotective agents in living cells, because other indolylalkylamines such as serotonin and tryptamine are well known to act as radioprotective agents,[1-4] and the sulfur compounds such as cysteine, cysteamine and 2-(2-aminoethyl) thiouronium salts are also used as radioprotective agents.[5-9] Shinoda *et al.*[10] examined the relationship between the chemical structures of these indolylalkylamines and their effects in protecting radiation damage, using mice irradiated with X-rays, and confirmed that *N*-(thioacetyl)tryptamine (TATP) was a potent radioprotective agent.

During a series of structural studies of the radioprotective indolylalkylamines,[11] we have determined the crystal structure of TATP; this will be reported in this paper.

Experimental

Preliminary oscillation and Weissenberg photographs showed the space group to be $P2_1/c$. The density was measured by the floatation method in a benzene–carbon tetrachloride mixture. The unit cell dimensions were refined on a Rigaku Denki automatic four-circle diffractometer with graphite-monochromated Cu $K\alpha$ radiation. The crystal data are shown in Table 1.

The intensity data were collected, using a single crystal with dimensions $0.5\times0.3\times0.2$ mm, on the diffractometer by $\omega/2\theta$ scanning technique within $\sin\theta/\lambda$ less than 0.595 Å^{-1}. Scan speed was 4°/min, background being measured for 5 s.

Table 1. Crystal data

Chemical formula	$C_{12}H_{14}N_2S$
Molecular weight	218.31
Crystal system	Monoclinic
Space group	$P2_1/c$
Cell constant	
a/Å	23.761(5)
b/Å	5.553(1)
c/Å	8.889(2)
β/°	94.04(4)
Volume/Å^3	1169.8(5)
Z	4
D_m/g cm^{-3}	1.233(1)
D_x/g cm^{-3}	1.240
F (0 0 0)	464

Intensities of 2009 independent reflections were corrected for Lorentz and polarization factors, but not for absorption. The intensities of four standard reflections, measured every 100 reflections, showed no deterioration during the course of the data collection.

All numerical calculations were carried out on an ACOS-700 computer of the Computation Center of Osaka University using UNICS program.[12] Atomic scattering factors in "International Tables for X-Ray Crystallography"[13] were used.

Determination and Refinement

The structure was solved by the direct method (program MULTAN[14]). An E-map computed using the 160 reflections with $|E|\geqq1.20$ (absolute figure of merit=1.14) revealed the positions of sulfur atom and non-hydrogen atoms of the indole ring. The coordinates of all the remaining non-hydrogen atoms were obtained by successive Fourier syntheses. The structure was refined by a block-diagonal least-squares method. From a difference map at the stage of R-value=0.12, the positions of all fourteen hydrogen atoms were

Table 3. Atomic coordinates ($\times10^4$) and their standard deviations

Atom	x	y	z
N(1)	8328(1)	12654(2)	10143(2)
C(2)	7779(1)	11757(3)	10008(2)
C(3)	7747(1)	9828(2)	9084(2)
C(4)	8528(1)	7783(2)	7671(2)
C(5)	9086(1)	7938(3)	7409(2)
C(6)	9426(1)	9732(3)	8069(2)
C(7)	9219(1)	11407(3)	9009(2)
C(8)	8656(1)	11265(2)	9279(2)
C(9)	8299(1)	9468(2)	8616(2)
C(10)	7237(1)	8343(3)	8482(3)
C(11)	6707(1)	9515(3)	8748(3)
N(12)	6231(1)	8178(2)	8083(2)
C(13)	5919(1)	8676(2)	6857(2)
S(13)	6049(0)	10946(1)	5713(1)
C(14)	5425(1)	7045(3)	6544(2)

Table 5. Hydrogen atom coordinates ($\times 10^3$) with their standard deviations

Atom	x	y	z
H(1)	847(1)	1381(3)	1071(2)
H(2)	747(1)	1244(3)	1051(2)
H(4)	828(1)	648(2)	719(2)
H(5)	927(1)	675(3)	669(2)
H(6)	984(1)	973(3)	784(2)
H(7)	946(1)	1269(3)	953(2)
H(10A)	727(1)	662(3)	909(2)
H(10B)	719(1)	834(2)	724(2)
H(11A)	671(1)	1135(3)	817(2)
H(11B)	682(1)	965(3)	1001(2)
H(12)	616(1)	675(3)	861(2)
H(14A)	554(1)	556(3)	622(2)
H(14B)	521(1)	682(4)	739(3)
H(14C)	512(1)	770(4)	574(2)

determined (peak height: 0.25—0.40 e·Å^{-3}); these positions were included in subsequent refinements with isotropic temperature factors.

In the later stage of refinement, the following weighting scheme was used: $w=0.71$ for $F_o=0.0$, $w=1.0$ for $0<F_o\leqq 15.0$ and $w=1.0/[1.0+0.095(F_o-15.0)]$ for $F_o>15.0$. In the last stage of refinement, none of the positional parameters shifted more than one-fourth of the estimated standard deviations. The final R-value excluding $F_o=0$ is 0.072. The residuals in the difference map were within the range of ± 0.2 e·Å^{-3}. The observed and calculated structure factors are listed in Table 2.[15] The final positional and thermal parameters for non-hydrogen atoms are given in Tables 3 and 4,[15] respectively. The coordinates for hydrogen atoms are given in Table 5.

Results and Discussion

Molecular Structure. The bond lengths and angles are given in Fig. 1, together with the atomic numbering used in this work. Their standard deviations are 0.004 to 0.009 Å for lengths and 0.3 to 0.5° for angles. The bond lengths of N–H or C–H are from 0.87 to 1.13 Å. The equations of the least-squares planes for the indole ring and the thioacetyl group and the deviations of atoms from these planes are listed in Table 6.

Table 6.

Equations of the best planes expressed by $m_1X+m_2Y+m_3Z=d$ in an orthogonal space

Plane	m_1	m_2	m_3	d
Indole ring	0.1669	−0.5961	0.7854	6.0448
Thioacetyl group	0.6013	−0.6039	−0.5233	2.0865

Deviations (Å) from the best planes:

Indole ring		Thioacetyl group	
N(1)*	0.025	N(12)*	0.019
C(2)*	0.011	C(13)*	−0.021
C(3)*	−0.004	S(13)*	−0.018
C(4)*	−0.021	C(14)*	0.019
C(5)*	0.012	C(11)	−0.083
C(6)*	0.005	H(12)	0.127
C(7)*	0.013		
C(8)*	0.022		
C(9)*	−0.021		
C(10)	−0.120		
H(1)	0.088		
H(2)	0.006		
H(4)	0.022		
H(5)	−0.018		
H(6)	0.014		
H(7)	0.042		

Atoms with asterisks define the plane.

The bond lengths and angles of the indole ring agree well with those found in the related indole derivatives within their standard deviations,[16] but the bond lengths of the side chain are significantly different: the C(10)–C(11) and C(11)–N(12) bonds are shorter than 1.511 and 1.463 Å of the average bond lengths found in the substituted tryptamine derivatives.[16] The shortening of the N(12)–C(13) bond indicates clearly the contribution of a resonance form:–N(12)=C(13)–S(13).

The indole ring is planar within a maximum deviation of 0.025 Å at the N(1) atom, whereas the C(10) atom deviates significantly from the plane, probably due to the effect of the crystal packing. The thioacetyl group is also planar and its plane makes a dihedral angle of 87.2° to the indole ring.

The conformation of TATP projected onto the indole ring plane is shown in Fig. 2. The bond sequence of C(3)–C(10)–C(11)–N(12) is the extended form, due

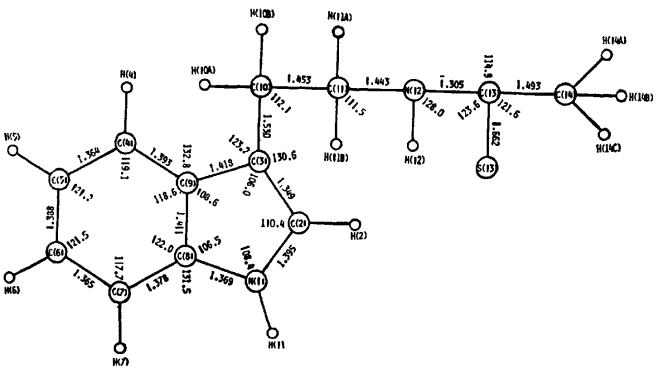

Fig. 1. The bond lengths and angles for non-hydrogen atoms.

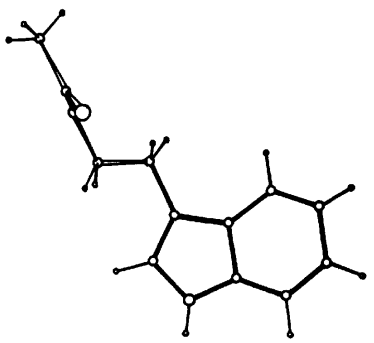

Fig. 2. The conformation of TATP molecule projected onto the indole ring.

to the attachment of the thioacetyl group to the N(12) atom; the torsion angles of C(2)–C(3)–C(10)–C(11) and C(3)–C(10)–C(11)–N(12) are 12.6° and 176.0°, respectively. A similar conformation is also found in the *N*-monosubstituted tryptamine such as melatonin.[17,18] On the other hand, the bond sequence of C(11)–N(12)–C(13)–S(13) takes the folded form: the torsion angles of C(10)–C(11)–N(12)–C(13) and C(11)–N(12)–C(13)–S(13) are −104.4° and 4.9°, respectively.

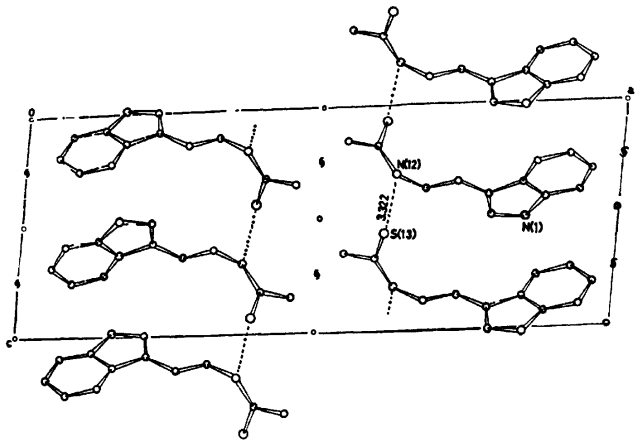

Fig. 3. Crystal packing of TATP viewed along the b-axis. The dotted lines represent possible hydrogen bonds.

Crystal Structure. Figure 3 shows the crystal structure viewed down the b-axis, where the hydrogen bonds are represented by the dotted lines. The indole rings related by c-glide form a zig-zag sheet which is stabilized by the van der Waals contacts with the neighboring sheets related by b-translation and inversion. The N(1) atom does not take part in any hydrogen bond. The 2-(thioacetylamino)ethyl side chains arranged parallel to the c-axis are linked by the hydrogen bonds between the N(12) and S(13) atoms (N(12)···S(13), 3.322 Å, H(12)···S(13), 2.42 Å, ∠N(12)–H(12)···S(13), 159.8°).

No stacking between the indole rings and no contacts shorter than 3.5 Å were observed.

The TATP molecule could exert its radioprotective effect in a manner similar to the mechanism proposed for indolylalkylamines:[19] the formation of the charge-transfer complex between nucleic acid bases and indole ring may protect the formation of peroxide radicals of the bases by irradiation. The role of the sulfur atom is thought to be the stabilization of the charge-transfer complex by the hydrogen bond between S(13) atom and the hydroxyl group of phosphate backbone of DNA, from the CPK model fitting based on the B-type DNA. Since the sulfur atom is said to act as a radical scavenger,[20] it may further protect the cleavage of the phosphodiester linkage of DNA.

References

1) Z. M. Bacq, *Acta Radiologica*, **41**, 47 (1954).
2) Z. M. Bacq and A. Herve, *Strahlentherapie*, **95**, 215 (1954).
3) H. Langendorff and R. Koch, *Strahlentherapie*, **98**, 245 (1955).
4) P. Dukor and R. Shuppli, *Experientia*, **17**, 257 (1961).
5) H. M. Patt, E. B. Tyree, R. L. Straube, and D. E. Smith, *Science*, **110**, 213 (1949).
6) H. Langendorff, R. Koch, and U. Hagen, *Strahlentherapie*, **95**, 238 (1954).
7) A. Herve and Z. M. Bacq, *Brit. J. Radiol.*, **24**, 617 (1951).
8) D. G. Doherty, W. T. Burnett. Jr., and R. Shapira, *Radiat. Res.*, **7**, 13 (1957).
9) B. G. Crough and R. R. Overman, *Science*, **125**, 1092 (1957).
10) M. Shinoda, S. Ohta, T. Hino, and S. Akaboshi, *Yakugaku Zasshi*, **94**, 1620 (1974).
11) M. Inoue, T. Sakaki, A Wakahara, and K. Tomita, *Biochim. Biophys. Acta*, **543**, 123 (1978).
12) The Universal Crystallographic Computing System-Osaka. The Computing Center, Osaka University (1973).
13) "International Tables for X-Ray Crystallography," Kynoch Press, Birmingham (1974), Vol. 4.
14) G. Germain, P. Main, and M. M. Woolfson, *Acta Crystallogr., Sect. A*, **27**, 368 (1971).
15) Tables 2 and 4 have been deposited at the Chemical Society of Japan (Document No. 8116).
16) T. Ishida, Dissertation, Faculty of Pharm. Sci., Osaka Univ., (1979).
17) A. Mostad and C. Römming, *Acta Chem. Scand., Sect. B*, **28**, 564 (1974).
18) A. Wakahara, T. Fujiwara, and K. Tomita, *Chem. Lett.*, **1972**, 1139.
19) K. Tomita, *Yuki Gosei Kagaku Kyokai Shi*, **31**, 747 (1973).
20) A. Hanaki and S. Akaboshi, *Japan Analyst*, **15**, 518 (1966).

Dynamic Structure of the Potent Uncoupler SF 6847 (3,5-Di-*t*-butyl-4-hydroxybenzylidenemalononitrile) and Its Derivatives

Kenichi YOSHIKAWA, Noriyuki KUMAZAWA, Hiroshi TERADA,*,† and Motoharu JU-ICHI††

College of General Education, University of Tokushima, Tokushima 770
†Faculty of Pharmaceutical Sciences, University of Tokushima, Tokushima 770
††Faculty of Pharmaceutical Sciences, Mukogawa Women's University, Edagawa-cho, Nishinomiya 663

(Received April 28, 1980)

The steric and electronic structures of the most potent uncoupler of oxidative phosphorylation known, SF 6847, and its derivatives were studied. ^{1}H and ^{13}C NMR measurements showed that the malononitrile moiety is not planar with the benzene ring and that its intramolecular motional freedom is reduced on acid dissociation of the phenolic proton. The activation energies of the tumbling motion of the malononitrile moiety in the anionic forms of SF 6847 and its derivatives were also determined from their ^{1}H NMR measured at various temperatures. The CNDO/2 and *ab initio* MO calculations of the model compounds of SF 6847 showed that the planar form is quite unstable and that the malononitrile moiety is twisted considerably relative to the benzene ring. The effect of the dynamic structure on the acidity of SF 6847 was discussed based on the above results.

It is widely known that phenols exhibit a wide variety of biological activities, such as fungicidal, bacteriocidal and acaricidal effects, probably due to uncoupling of the phosphorylation reaction from the oxidoreduction reaction in microorganisms and organelles.[1-4] Among phenols, 3,5-di-*t*-butyl-4-hydroxybenzylidenemalononitrile (SF 6847) was found to show the most potent uncoupling activity in mitochondria.[4] This compound is characterized by being hydrophobic and having a strong electron-withdrawing group (malononitrile group) and an acid dissociable proton (phenolic hydroxyl group). These features are common to other potent uncouplers of oxidative phosphorylation, such as carbonyl cyanide-*p*-trifluoromethoxyphenylhydrazone (FCCP), 4,5,6,7-tetrachloro-2-trifluoromethoxybenzimidazole (TTFB) and 5-chloro-3-*t*-butyl-2′-chloro-4′-nitrosalicylanilide (S-13).[5-7] However, the structural requirements of uncouplers required for their activities are not yet fully clarified, although considerable attention has been paid to this problem.[8-12]

The neutral molecular form of SF 6847 has an absorption band at about 365 nm and the anionic form has one at about 456 nm.[13,14] On binding of SF 6847 to mitochondria and liposomes with various phospholipid compositions, its absorption spectrum changes greatly.[13,14] Changes in spectral properties are also observed when this compound is dissolved in organic solvents or when it forms a dimer.[13-17] These results suggest that the structural properties of SF 6847 change greatly in different circumstances. This paper deals with the dynamic structure of SF 6847 and its derivatives examined by NMR spectroscopic and molecular orbital (MO) studies.

Experimental

All the 3,5-dialkylbenzylidenemalononitriles were prepared by the procedure of Horiuchi *et al.*[18] and purified by chromatography and repeated recrystallization.

Fourier-transformed ^{1}H and ^{13}C NMR spectra were obtained at 90 MHz and 22.5 MHz, respectively, with a JEOL FX-90Q NMR spectrometer.

Molecular orbital (MO) calculations were performed according to the CNDO/2 method.[19] Since the energy of the dissociated forms (anions) of SF 6847 derivatives did not converge in the usual CNDO/2 program, we adopted a modified program using the density matrix method proposed by McWeeny.[20] *Ab initio* (STO 3G) MO calculations were also carried out using the GAUSSIAN 70 program.[21] The standard bond angles and bond lengths were used in the calculation referring to the crystal geometry of SF 6847 determined by X-ray diffractometry.[22]

Results and Discussion

^{1}H and ^{13}C NMR. Figure 1A shows the 90 MHz ^{1}H NMR spectrum of the neutral (undissociated) form of SF 6847 in $CDCl_3$ at room temperature. From the signal intensity in the figure, all the signals are easily assigned; δ 1.46 (*t*-butyl), 6.04 (-OH), 7.65 (benzylidene), and 7.80 (aromatic). The chemical shift

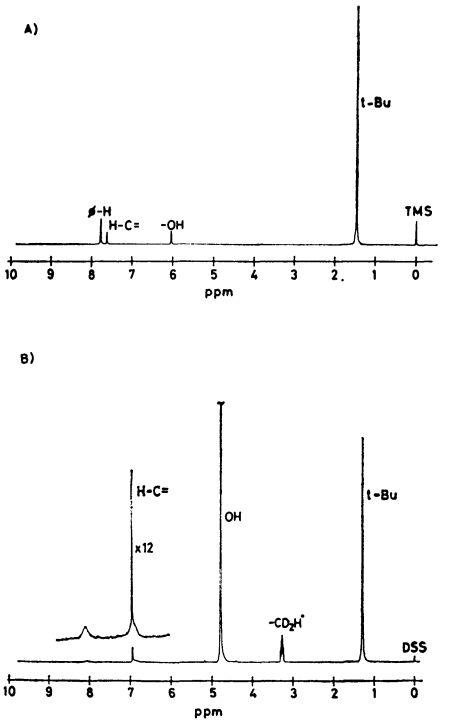

Fig. 1. 90 MHz ^{1}H NMR spectrum of SF 6847 in $CDCl_3$ (A) and in methanol-d_4 containing 0.1 mol dm^{-3} sodium hydroxide (B).

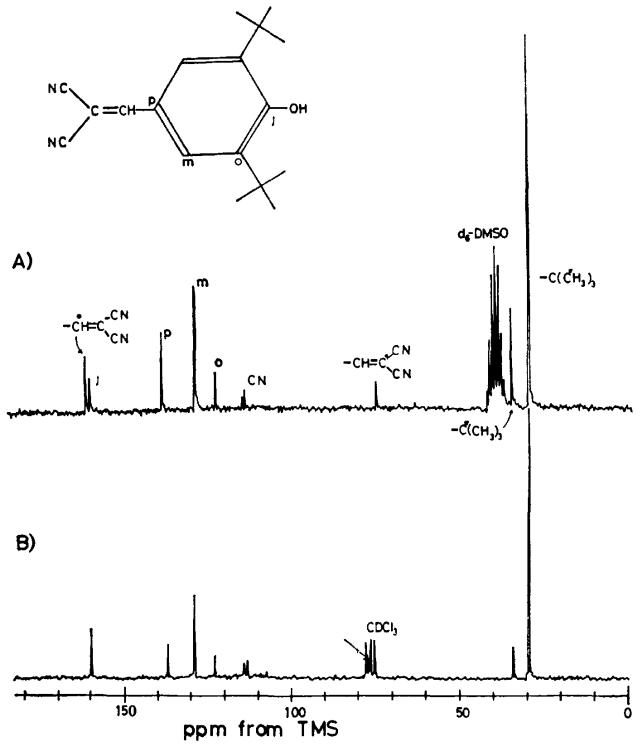

Fig. 2. 22.5 MHz ^{13}C NMR spectrum of SF 6847 in dimethyl-d_6 sulfoxide (A) and in $CDCl_3$ (B).

of the two aromatic protons (meta to the hydroxyl group) is the same in Fig. 1A, and this still exhibited a single resonance when the temperature was lowered to −90 °C in $CDCl_3$ (spectrum not shown). Figure 2 shows the ^{13}C NMR of the neutral form of SF 6847 in $CDCl_3$ (A) and in DMSO-d_6 (dimethyl-d_6 sulfoxide) (B). The carbon signals were assigned as shown in Fig. 2, with reference to the splitting pattern in the proton-coupled spectra (spectrum not shown). It is noted in the figure that the 2- and 3-carbons are equivalent to the 6- and 5-carbons, respectively. The ^1H and ^{13}C NMR spectra indicate that the malononitrile moiety of the neutral form of SF 6847 does not remain fixed in the same plane as the benzene ring.

On the other hand, the ^1H NMR spectrum of the anionic form of SF 6847 in alkaline methanol solution in Fig. 1B shows broad signals of the aromatic protons at 6.9 and 8.1 ppm from DSS. Figure 3 shows the temperature dependence of the ^1H NMR spectrum of the aromatic protons of SF 6847 in the anionic form. As can be seen, the two separate proton signals become narrower when the temperature is decreased to 0 °C from room temperature (23 °C), while they become broad (at 28 °C) and then coalescence into a single resonance (at 58 °C) when the temperature is raised from 23 °C. These results suggest that the malononitrile moiety of the anionic form is less mobile than that in the neutral form. Figure 3 also shows that the signal of the benzylidene proton shifts to a higher field when the temperature is raised. This is attributable to the change of the inter- or intramolecular anisotropic shielding effect of the benzene ring in SF 6847 molecules.

From the temperature dependence of the signal

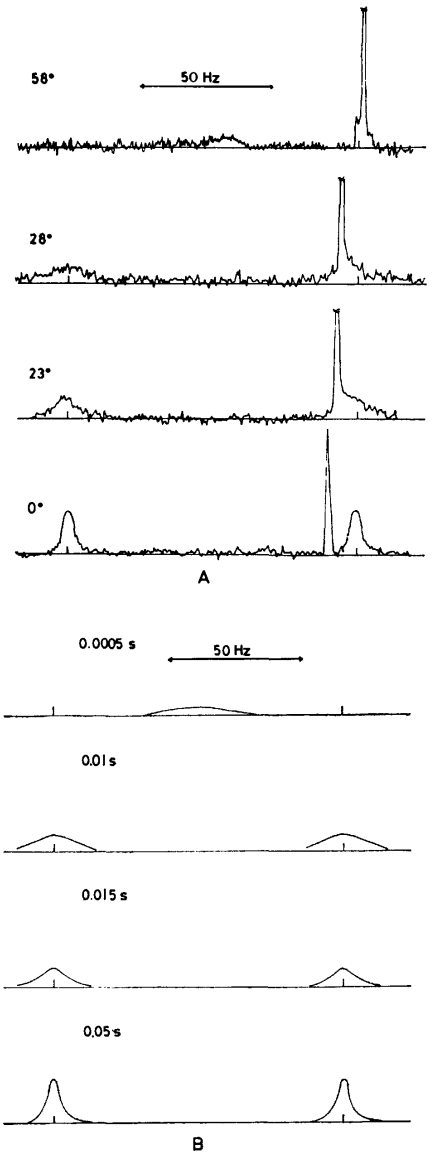

Fig. 3. (A) Temperature dependent ^1H NMR spectra of the benzylic protons of SF 6847 in methanol-d_4 containing 0.1 mol dm^{-3} sodium hydroxide. (B) Calculated spectra for the mean lifetime (τ) indicated. The sharp signal in (A) is due to the benzylic proton.

pattern of the aromatic protons, it is possible to calculate the activation energies of the rotational or tumbling motion around the C–C bond between the benzene ring and the malononitrile moiety. Table 1 gives the calculated activation energies based on a simple line-shaped analysis[23] for SF 6847 and its dialkyl derivatives (**1**—**5**), together with the differences of the chemical shifts between the two aromatic protons at low temperatures and the coalescence temperatures. Table 1

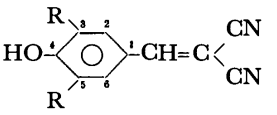

R = H	**1**
Methyl	**2**
Ethyl	**3**
Isopropyl	**4**
t-Butyl	**5**

indicates that the motional barrier tends to increase with increase in the bulkiness of the 3,5-dialkyl groups, and that the activation energy (E_a) of the di-*t*-butyl

Table 1. Activation energies (E_a) in the anionic forms of SF 6847 (**5**) and its derivatives

Compound	R	$\Delta\nu$[a] / Hz	T_c[b] / K	E_a / K J mol^{-1}	ΔE_a[c] / K J mol^{-1}
1	H	90	213	42±2	—
2	Methyl	90	233	46±2	4
3	Ethyl	93	251	50±2	4
4	Isopropyl	97	261	54±2	4
5	*t*-Butyl	109	327	64±3	10

a) Difference between the chemical shifts of the two aromatic protons at low temperatures. b) Coalescence temperature. c) Difference between E_a values due to introduction of an additional carbon atom.

derivative **5** (SF 6847) is higher than those of derivatives substituted with smaller alkyl groups (**1**—**4**). It is of interest to note that the energy difference of E_a between **4** and **5** is apparently greater than that between **1** and **2**, or **2** and **3**, or **3** and **4**, indicating that the "steric" effect of the *t*-butyl group is significant.

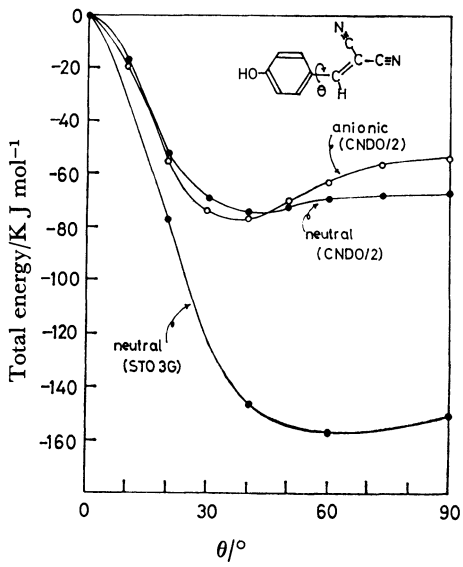

Fig. 4. Changes of the total energy with the angle θ between the benzene ring and the malononitrile moiety in the anionic and neutral forms of **1** calculated using CNDO/2 and *ab initio* (STO 3G) MO calculations. The total energy of the planar form (θ=0°) is standardized to zero.

MO Calculation. In order to gain further insight into the dynamic structure of the SF 6847 molecule, MO calculations were performed for **1**. The changes of the total energy with the angle θ between the benzene ring and the malononitrile moiety in the anionic and neutral forms of compound **1** are shown in Fig. 4. The CNDO/2 calculation shows that the "planar form" (θ=0°) is quite unstable and the minimum energy is found at about θ=40° for both molecular forms. As shown in Fig. 4, essentially the same results were obtained in the *ab initio* calculations, *i.e.*, the planar form is the most unstable conformation. However, the position at the minimum energy determined by the *ab initio* calculation is slightly shifted giving a greater angle θ than that in the CNDO/2 MO calculation. These MO results show clearly that the energy barrier at θ=90° is very small in the neutral form of **1** and a little greater in the anionic form. Similar angular dependence of the total energy based on the MO calculation has also been observed with compound **2**.[17] In view of these results, all the compounds in the series of 3,5-dialkyl derivatives of SF 6847 (compounds **3**, **4**, and **5**) can be regarded as having a similar profile of energy change with θ.

Dynamic Structure. From the above results obtained by NMR and MO calculations, the following conclusions can be drawn concerning the dynamic structure of SF 6847 (**5**) and its derivatives (**1**—**4**.)

(1) The planar conformation (θ=0°) is quite unstable.

(2) In the most stable conformation of these molecules the benzene ring and the malononitrile moiety are twisted.

(3) The energy barrier at θ=90° is rather small, and thus the malononitrile group can tumble beyond the barrier at θ=90°.

(4) The activation energy of the intramolecular tumbling motion of the malononitrile moiety is greater in the anionic form than in the neutral form.

Here it should be stressed that the degree of conjugation between the benzene ring and the malononitrile moiety in SF 6847 and its derivatives is quite small in solutions. A recent X-ray diffraction study on SF 6847 (**5**)[22] showed that **5** is almost planar in a single crystal. This may be due to the stressed packing of **5** in the crystal, because of the rather strong intermolecular interaction between the benzene ring and the malononitrile moieties of SF 6847 molecules.[22] Difference in the conformation between in crystalline and in solution was also reported for the case of biphenyl.[24]

On Acidity of SF 6847. Next with regard to the acidity of SF 6847 and its derivatives, it is well known[25,26] that introduction of *t*-butyl groups into a molecule near an acidic or basic site causes a large change in acidity or basicity of the molecule. The acid ionization constants (pK_a) of series of 4-substituted 2,6-di-*t*-butylphenols (I) and their unhindered analogues (II) in water and methanol have been reported by some workers.[25,26] It was reported that the hindered

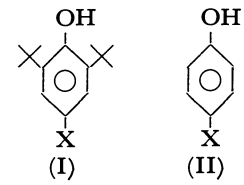

phenol (I) is a weaker acid than its unhindered analogue (II).[27,28] However, in the case of X=–CH=C(CN)$_2$, the acidity of the hindered phenol (R=*t*-butyl, SF 6847) is stronger than that of the unhindered one (R=H, the compound **1**), *i.e.*, the pK_a for SF 6847 is 6.83 and for its unhindered derivatives is 7.25.[27,28] This is explained as follows. As discussed above, in the dissociated (anionic) form the activation energy of the rotational motion around the C–C bond between the benzene ring and the malononitrile moiety of the hindered phenol, SF 6847, is higher than that of the corresponding

unhindered phenol (*cf.* Table 1). Thus, the non-planarity of the π conjugated system, *i.e.*, the angle between the benzene ring and the malononitrile moiety, is possibly reduced in the hindered form, accompanied with the increase in the activation energy at $\theta=90°$. This implies that the conjugation between the benzene ring and the malononitrile moiety is greater when di-*t*-butyl groups are introduced onto the 3,5-carbons of the benzene ring. Consequently the electron-withdrawing power of the malononitrile moiety is stronger in SF 6847 than in the unhindered analogue. Thus, the *t*-butyl groups electronically enhance the acidity of SF 6847, and this overcomes the steric effect of the bulky *t*-butyl groups which weaken the acidity. Therefore, SF 6847 is more acidic than the unhindered derivative.

It is sometimes pointed out that for exhibiting uncoupling activity, the anionic form of an uncoupler should be present in the hydrophobic biological membrane, and thus that a bulky hydrophobic group adjacent to the acid dissociable proton and the electron-withdrawing group is essential for a potent uncoupler.[7,12,29,30] The unique effect of the hydrophobic *t*-butyl group on the acid dissociation of SF 6847 will explain why SF 6847 is such a very potent uncoupler of oxidative phosphorylation.

One of the authors (K. Y.) wishes to express his thanks to Professor Michiya Itoh, Faculty of Pharmaceutical Science, Kanazawa University, for data on the molecular structure of SF 6847 determined by X-ray diffractometry. The authors are indebted to Messrs. Tadahiro Dohi, Hiroshi Fujiwara, and Yoshiaki Tsuda, Otsuka Pharmaceutical Factory Inc., for facilitating use of an NMR spectrometer. They are also grateful to Professor Akira Imamura, Siga University of Medical Science, for making his program available, and to Professor Kichisuke Nishimoto, Faculty of Science, Osaka City University, for helpful discussion. They would also like to thank members of the Computer Center of the Institute for Molecular Science for assistance. The present work was partially supported by Grants-in-Aid for Scientific Research No. 421324 and No. 311901 from the Ministry of Education, Science and Culture of Japan.

References

1) G. E. Blackman, M. H. Parke, and G. Garton, *Arch. Biochem. Biophys.*, **54**, 45 (1955).
2) A. Burger, "Medicinal Chemistry," 2nd ed, Interscience Publisher Inc., New York (1960), p. 1123.
3) C. Hansch and T. Fujita, *J. Am. Chem. Soc.*, **86**, 1616 (1964).
4) S. Muraoka and H. Terada, *Biochim. Biophys. Acta*, **275**, 271 (1972).
5) P. G. Hytler, *Biochemistry*, **2**, 357 (1963).
6) R. B. Beechey, *Biochem. J.*, **98**, 284 (1966).
7) R. L. Williamson and R. L. Metcalf, *Science*, **158**, 1694 (1967).
8) T. Fujita, *J. Med. Chem.*, **9**, 797 (1966).
9) M. Stockdale and M. J. Selwyn, *Europ. J. Biochem.*, **21**, 565 (1971).
10) H. Terada and S. Muraoka, *Mol. Pharmacol.*, **8**, 95 (1972).
11) H. Terada, S. Muraoka, and T. Fujita, *J. Med. Chem.*, **21**, 591 (1978).
12) H. Terada, M. Uda, F. Kametani, and S. Kubota, *Biochim. Biophys. Acta*, **504**, 237 (1978).
13) H. Terada, *Biochim. Biophys. Acta*, **387**, 519 (1975).
14) A. Yamaguchi, Y. Anraku, and S. Ikegami, *Biochim. Biophys. Acta*, **501**, 150 (1978).
15) K. Inoue and M. Itoh, *Bull. Chem. Soc. Jpn.*, **52**, 45 (1979).
16) M. Itoh, K. Inoue, T. Kuzuhara, and T. Kusui, *Bull. Chem. Soc. Jpn.*, **52**, 1010 (1979); H. Mizukoshi and M. Itoh, *ibid.*, **53**, 590 (1980).
17) K. Yoshikawa, N. Kumazawa, H. Terada, and K. Akagi, *Int. J. Quantum Chem.*, **18**, 539 (1980).
18) F. Horiuchi, K. Fujimoto, T. Ozaki, and Y. Nishizawa, *Agric. Biol. Chem.*, **35**, 2003 (1971).
19) J. A. Pople and M. S. Gordon, *J. Am. Chem. Soc.*, **89**, 4253 (1967).
20) R. McWeeny, *Proc. R. Soc. London, Ser. A*, **235**, 496 (1956).
21) W. J. Hehre, W. A. Lathan, R. Ditchfield, M. E. Newton, and J. A. Pople, Quantum Chem. Prog. Exchange, Program No. 236, Indiana Univ., Bloomington, I. N., U.S.A.
22) M. Itoh, Y. Tanimoto, and Y. Iitaka, *J. Chem. Phys.*, **69**, 816 (1978).
23) J. A. Pople, W. G. Schneider, and H. J. Bernstein, "High-resolution Nuclear Magnetic Resonance," McGraw-Hill Book Co., New York (1959), Chap. 10.
24) L. N. Ferguson, "The Modern Structural Theory of Organic Chemistry," translated by M. Ohki, M. Hirota, H. Iwamura, and K. Mutai, Tokyo-kagakudojin, Tokyo (1965), Vol. 1, Chap. 3.
25) L. A. Cohen and W. M. Jones, *J. Am. Chem. Soc.*, **85**, 3397 (1963).
26) C. H. Rochester and B. Rossall, *J. Chem. Soc., B*, **1967**, 986.
27) Unpublished results. The pK_a value of SF 6847 and the derivatives will be reported elsewhere together with their biological activities.
28) Similar abnormality in the acidity of the hindered phenol has been observed in the case of X=$-NO_2$ (4-nitro-2,6-di-*t*-butylphenol).[26]
29) V. P. Skulachev, A. A. Jasaitis, V. V. Navickaite, and L. S. Yaguzhinsky, *FEBS Symposium*, **17**, 275 (1969).
30) B. T. Storey, D. F. Wilson, A. Brachey, S. L. Rosen, and S. Stephenson, *FEBS Lett.*, **49**, 338 (1975).

Photoadducts of 2-Pyridones with Chloroethylenes and Their Derivatives

Kenichi SOMEKAWA,* Ryusuke IMAI, Ryuichi FURUKIDO, and Sanetada KUMAMOTO
Department of Applied Chemistry, Faculty of Engineering, Kagoshima University, Korimoto, Kagoshima 890
(Received May 6, 1980)

Sensitized photoirradiations of 2-pyridones with tetrachloroethylene or trichloroethylene gave chlorinated 3-azabicyclo[4.2.0]oct-4-en-2-ones (**1**) and 2-azabicyclo[4.2.0]oct-4-en-3-ones (**2** and **3**), 7,7,8-trichloro-2-methyl-2-azabicyclo[2.2.2]oct-5-en-3-one (**4**), and other products. The reaction with 1,1-dichloroethylene, though, gave only 7,7-dichloro-3-azabicyclo[4.2.0]oct-4-en-2-one. **1**, **2**, **3**, and **4** were reduced by zinc to give 7,8-dichloromethyl-3-azabicyclo[4.2.0]octa-4,7-dien-2-one, 2-azabicyclo[4.2.0]octa-4,7-dien-3-ones (**7**) and 6-chloro-2-methyl-2-azabicyclo[2.2.2]octa-5,7-dien-3-one respectively. Then, **7** thermally gave valence isomers, 7-azabicyclo[4.2.0]-octa-2,4-dien-8-ones, which were β-lactams.

Photocycloadditions between α,β : γ,δ-unsaturated cyclic compounds and unsaturated substances are very interesting because of the possibility of valence isomerizations,[1] and 1 : 2-cycloadditions,[2] followed by ring expansions.[3] 2-Pyridone is a typical heterocyclic α,β : γ,δ-unsaturated carbonyl compound and has a few novel features with regard to its photoreactions.[4] The objectives of the present research are to synthesize the photocycloadducts between 2-pyridones and chloroethylenes, reduce the adducts, and obtain the valence isomers.

Results and Discussion

Photochemical Cycloadditions. All of the preparative reactions described herein were conducted in benzene or methanol with irradiation by means of a 400 W high-pressure mercury lamp through a Pyrex filter. The photoadditions with trichloroethylene or 1,1-dichloroethylene demanded a sensitizer, as aid that with tetrachloroethylene. The progress of the reactions was traced by means of GC. After concentration, the residues were passed through silica-gel columns to give products given in Scheme 1. The data of the elemental analyses and mass spectra indicated that the products of the **1**, **2**, **3**, and **4b** types were the expected 1 : 1 cycloadducts of 2-pyridones with chloroethylenes, while **5a** was the 1 : 1 adduct between **1a** and water.

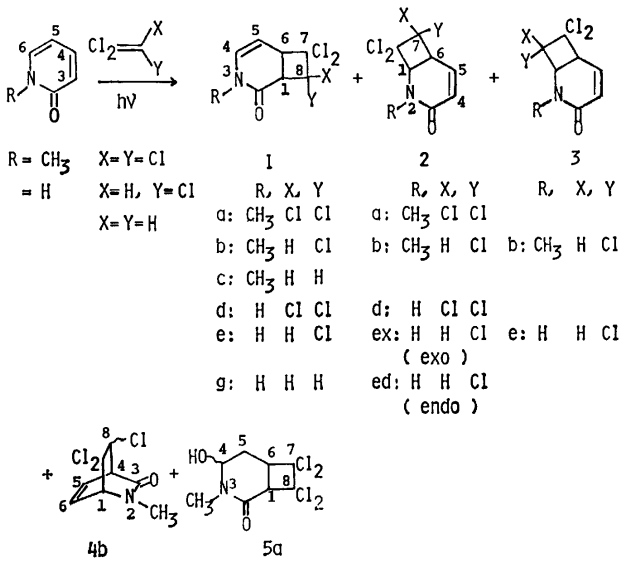

Scheme 1. Photoreactions and products.

The ^{1}H-NMR data of the products are shown in Table 1. The products, **1a—g**, have two absorption bands in the range of 1690—1650 cm^{-1} ($\nu_{C=O}$, $\nu_{C=C}$) and peaks of δ *ca.* 6.1 (4-H) and 5.0 ppm (5-H). On the basis of those data, the structures of 3-azabicyclo[4.2.0]-oct-4-en-2-ones (3,4-adducts), being consisting of [2+2]-cycloadducts at the C-3 and C-4 positions of 2-pyridones,[5] were determined. The orientational mode of the cycloaddition in Scheme 1 was confirmed from the ^{1}H-NMR coupling multiplicities of the angular methine protons.

The IR data of *ca.* 1680 ($\nu_{C=O}$) and 1630 cm^{-1} ($\nu_{C=C}$) and the ^{1}H-NMR data of δ *ca.* 6.0 (4-H) and 6.5 ppm (5-H) of **2a**, **2b**, **2d**, **2ex**, **2ed**, **3b**, and **3e** are characteristic of the rings of 2-azabicyclo[4.2.0]oct-4-en-3-ones (5,6-adducts).[5] The orientational features of the additions are apparent from the coupling patterns of the ^{1}H-NMR data, as is shown in Table 1. As the stereoisomers, **2ex** and **2ed**, suffered no change upon treatment with basic alumina, which was used to infer the steric structures with regard to bicyclo-alicyclic compounds,[4] the bridgeheads of these adducts were presumed to be *cis*-forms. The chemical shift (δ) of 7-H of **2ex** was smaller than that of **2ed**. This difference is caused by the magnetic-shielding effect of the double bond between C-4 and C-5 on **2ex**.[4] Accordingly, the configurations of **2ex** and **2ed** are, respectively, *exo* and *endo*, making the 7-Cl an target.

The ^{1}H-NMR data of δ 6.6 of two olefinic protons (5-H and 6-H) on **4b** is characteristic of the ring of 2-azabicyclo[2.2.2]oct-5-en-3-one, which is a [4+2]-cycloadduct.[6] **5a** had an IR peak of 3400 cm^{-1}, a ^{1}H-NMR peak of δ 3.27 ppm (which disappeared with hot D_2O), which was assigned to an OH group, and no ^{1}H-NMR peak of olefinic protons. By means of these facts and the characteristic peak of *m/e* 291 (=M$^+$), the structural feature was confirmed. The position of the OH group was determined by means of the ^{1}H-NMR coupling patterns ($J_{4,5}$=4 Hz).

The following properties of the present photoreactions consequently thus became apparent. The photoreaction with 1,1-dichloroethylene gave one regiospecific 3,4-adduct. That with trichloroethylene gave 3,4-adducts, 5,6-adducts, and a [4+2]adduct which was a new type of product,[4] the main products were 5,6-adducts, the regioselectivity of which was varied by the solvents. That with tetrachloroethylene gave 3,4-adducts and 5,6-adducts (main product); it also afforded a hydrate

Table 1. ^{1}H-NMR data of photoreaction products

Compound (R, X, Y)	1-H	2-H	3-H	4-H	5-H	6-H	7-H	8-H
	Coupling const., J/Hz							(δ/ppm)
1a	4.04		3.10	6.07	5.04	3.88		
(CH_3, Cl, Cl)	J; 1,6=10, 4,5=8, 5,6=4							
1b	3.80		3.05	6.12	5.00	3.80		5.00
(CH_3, H, Cl)	J; 4,5=8, 5,6=4							
1c	3.50		3.04	6.12	5.02	3.82		3.27
(CH_3, H, H)	J; 1,6=1,8=4,5=8, 5,6=4							
1d	4.0		7.81	6.07	5.02	3.9		
(H, Cl, Cl)	J; 3,4=6, 4,5=8							
1e	3.41		8.00	6.22	5.1	3.88		4.9
(H, H, Cl)	J; 3,4=4, 4,5=8, 1,6=1,8=7							
1g	3.3		7.84	6.08	4.94	3.76		3.3
(H, H, H)	J; 1,6=4,5=8, 3,5=5, 5,6=4							
2a	4.73	3.09		6.04	6.45	4.05		
(CH_3, Cl, Cl)	J; 1,6=11, 4,5=10, 5,6=4							
2b	4.68	3.07		5.94	6.46	3.44	4.54	
(CH_3, H, Cl)	J; 1,6=11, 4,5=10, 5,6=4, 6,7=4							
2d	4.76	8.38		5.80	6.50	4.27		
(H, Cl, Cl)	J; 1,2=4, 1,6=10, 4,5=9, 4,6=2, 5,6=3							
2ex : *exo*	4.62	6.6		5.92	6.58	3.31	4.62	
(H, H, Cl)	J; 4,5=9, 5,6=5, 6,7=7							
2ed : *endo*	4.58	6.5		6.02	6.49	3.70	4.98	
(H, H, Cl)	J; 1,2=4, 1,6=10, 4,5=9, 6,7=9							
3b	4.10	3.04		6.04	6.58	4.10		4.82
(CH_3, H, Cl)	J; 1,6=10, 1,8=8 (benzene-d_6)							
3e	4.66	6.5		6.06	6.50	3.94		4.94
(H, H, Cl)	J; 1,8=7, 4,5=10, 6,8=4							
4b	4.48	3.04		3.66	6.58	6.58		4.44
	J; 1,6=2, 4,5=6, 4,8=2, 5,6=10							
5a	3.98		2.87	5.04	2.04 2.10	3.57	4-OH=3.27	
	J; 1,6=10, 4,5=4,					5,6=10	(DMSO-d_6)	

Table 2. Relative product ratio of the reactions between *N*-methyl-2-pyridone and substituted ethylenes in the presence of xanthone or nothing

	$Cl_2C{=}CCl_2$	$ClC{=}CCl_2$	$C{=}CCl_2$	$ClC{=}CCl$	$C{=}C{-}CO_2CH_3$
Xanthone	0.1[a)]	0.5	6.5	0	1.0[b)]
Nothing	0.03	0	0	0	

a) The solution is, for example, a mixture of pyridone (2.3 mmol), tetrachloroethylene (23 mmol), xanthone (0.61 mmol), and benzene–acetonitrile (10 : 1) (20 ml). b) Ref. 4.

of the 3,4-adduct upon prolonged irradiation. All these photocycloadditions were promoted by sensitizers, Michler's ketone, thioxanthen-9-one, benzophenone, and xanthone, all of those triplet energies are over 62 kcal/mol. This phenomenon was similar to the triplet reactions of 2-pyridones with methyl acrylate.[4)]

The photoreactivity of *N*-methyl-2-pyridone with chloroethylenes in the presence of xanthone decreased in the following order, as is shown in Table 2: 1,1-dichloroethylene > trichloroethylene > tetrachloroethylene $\gg$ *trans*-dichloroethylene, *cis*-dichloroethylene. The reactions with both dichloroethylenes gave no product. The reaction with the more polar chloroethylene is more reactive. Those phenomena are contarry to those of 5,6-dihydro-2-pyridone, which was more reactive with 1,2-dichloroethylene and which had, photochemically, a likeness to α,β-unsaturated enones.[7)] Enones add effectively to electron-donating ethylenes, and the excited species are $n\pi^*$ triplets. The triplet species of the present cycloadditions are inferred to be the same as those of sensitized cycloadditions between 2-pyridones and electron-withdrawing ethylenes,[4)] because the reactivity was not diminished by protic solvents and both the triplet energies were the same. The direct photoexcitation of 2-pyridone hardly gave the triplet species.[4)] From the several findings and inferrences cited above, it is considered that the excited species of 2-pyridones are $\pi\pi^*$ triplets and that the 3,4-positions are more polar than the 5,6-positions.

In order to determine the true nature of the excited state responsible for the present cycloaddition reaction, further, detailed mechanistic investigations should be done.

Synthetic Applications. *Reductions of Photoadducts*:

Table 3. ^{1}H-NMR data of reduced products and valence isomers

Compound (R, X, Z)	1-H	2-H	3-H	4-H	5-H	6-H	7-H	8-H
	Coupling const., J/Hz							(δ/ppm)
6a	3.78		3.12	5.98	5.04	3.64		
	1,6=4, 4,5=8, 5,6=4							
7a	4.50	3.09		5.96	6.55	3.80		
(CH_3, Cl, Cl)	1,6=4, 4,5=8, 5,6=4							
7b	4.58	3.10		6.15	6.65	3.70		6.34
(CH_3, H, Cl)	1,6=6, 4,5=11, 5,6=4, 1,8≒0							
7e	4.60	7.36		5.86	6.69	3.60	6.22	
(H, Cl, H)	1,6=4, 4,5=10, 5,6=4, 6,7=0							
8b	4.56	2.94		4.27	6.57		6.86	6.86
	1,5=2, 1,7=3, 4,5=7, 4,8=3							
9a	4.26	6.15	6.15			4.48	3.04	
(CH_3, Cl, Cl)	1,2=6, 1,6=11				(1,2,4-trichlorobenzene)			
9b	4.3	6.0—6.1			6.44	4.4	3.02	
(CH_3, H, Cl)	1,2=6, 5,6=4						(DMSO-d_6)	
9e	4.22	5.8—5.9		6.12		4.34	6.46	
(H, Cl, H)	1,2=4, 1,6=8, 3,4=6							

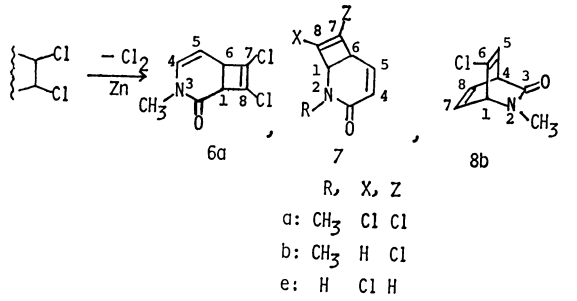

Scheme 2. Reductions of photoadducts.

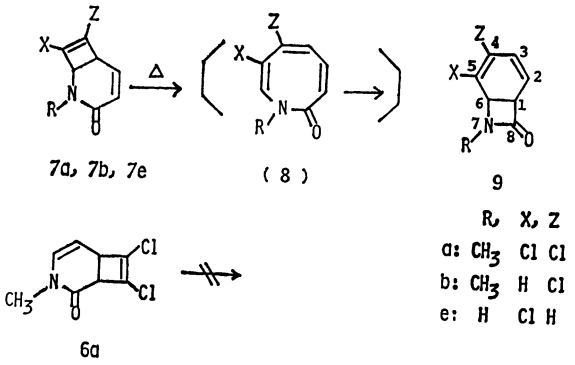

Scheme 3. Valence isomerizations of azabicyclo[4.2.0]-octadienones.

Mixtures of the photoadducts and zinc dust in the solvent were warmed at the refluxing temperature. After checking the disappearance of the reactants by TLC and the concentration of the filtrate, treatment by the use of column chromatography afforded the compounds shown in Scheme 2. That is, **1a**, **2a**, **3b**, **2ex**, and **4b** gave 7,8-dichloro-3-methyl-3-azabicyclo-[4.2.0]octa-4,7-dien-2-one (**6a**), chlorinated 2-azabicyclo[4.2.0]octa-4,7-dien-3-ones (**7a**, **7b**, and **7e**), and 6-chloro-2-methyl-2-azabicyclo[2.2.2]octa-5,7-dien-3-one (**8b**) respectively. The structures were confirmed by their elemental analyses and the spectral data. The increased IR peaks of 1635—1580 cm^{-1} and the ^{1}H-NMR data in Table 3 were exactly same as had been expected. The reactions are the normal eliminations of a chlorine molecule by zinc dust. The reactivities were as follows: **2a**, **3b**, **2ex**>**4b**>**1a**. That of the chlorinated 2-azabicyclo[4.2.0]oct-4-en-3-one ring is large. **7e** in refluxed benzene suffered valence isomerization.

Valence Isomerization of Azabicyclo[4.2.0]octa-4,7-dienes: The heating of the solution of **7a** and **7b** in the solvent at 120 °C, and that of **7e** at 90 °C, resulted in the complete disappearance of the materials and afforded 7-azabicyclo[4.2.0]octa-2,4-dien-8-ones (**9a**, **9b**, and **9e** respectively) in high yields; all were compounds of the β-lactam type. The structures in Scheme 3 were based on the IR peaks of 1745—1759 cm^{-1} ($\nu_{C=O}$ of β-lactam[8]) and 1635—1648 cm^{-1} ($\nu_{C=C}$) and on the ^{1}H-NMR data of the lower part of Table 3.

The intermediates of the reactions for **9** from **7** may be 2(1*H*)-azocinones (**8**), which are unstable.[9] The heating of **9a** and **9b** at 180 °C and that of **9e** at 120 °C gave the respective chlorobenzenes. These phenomena bore a close parallel to those shown by the MS data.

These results were distinctly different from the behavior of **6a**, which was stable in heating reactions up to 190 °C (Scheme 3).

Experimental

All the melting points were measured on a Yanagimoto Mel-temp apparatus and are uncorrected. The IR, ^{1}H-NMR, and mass spectra were recorded on JASCO A-3, JEOL JNM-MH-100 (100 MHz), and JEOL JMS-01SG spectrometers respectively. The ^{1}H-NMR spectra were recorded with TMS as an internal standard and $CDCl_3$ as the solvent, unless otherwise indicated. The reported values are on the cm^{-1} scale in IR and on the δ (ppm) scale in ^{1}H-NMR. All the photoaddition and synthetic application reactions were monitored by the use of GC, which was performed at 170—200 °C (column temp) on a Yanagimoto G80 instrument using a column of Silicone SE-30 (10%)/Chromosorb W(AW).

Photoreactions of N-Methyl-2-pyridone. (a) With Tetrachloroethylene: A solution of pyridone (45 mmol) and chloroethylene (225 mmol) in 200 ml of methanol was irradiated with a Rikō immersion-type 400 W high-pressure mercury

lamp through a Pyrex jacket for 31 h. The solvent was then removed by the use of a rotary evaporator, and the residue was chromatographed on a silica-gel (Wakogel C-200, 200 g) column with benzene, diethyl ether, and acetone (in this order) as the eluents. The materials obtained from the first and second fractions were recrystallized from benzene to give **1a** (mp 110—112 °C, 4%) and **2a** (mp 134—135 °C, 4%) respectively. The recrystallization of the third fraction from acetonitrile gave **5a** (mp 186—188 °C, 1%). The photoirradiation of the benzene solution of the same reactants, containing thioxanthen-9-one (1.5 mmol) as a sensitizer, gave **1a** and **2a** in 7 and 16% yields respectively. **1a**: IR (KBr) 1663—1650 (sh); MS 109 (M−C_2Cl_4, 100%). Found: C, 35.03; H, 2.61; N, 5.09%. Calcd for $C_8H_7NOCl_4$: C, 34.95; H, 2.57; N, 5.09%. **2a**: IR (KBr) 1675, 1630; MS 238 (M−Cl, 100%). Found: C, 35.05; H, 2.52; N, 5.08%. **5a**: IR (KBr) 1665; MS 291 (M^+, 5%). Found: C, 32.95; H, 3.24; N, 4.88%. Calcd for $C_8H_9NO_2Cl_4$: C, 32.80; H, 3.10; N, 4.78%.

(b) With Trichloroethylene: A solution of pyridone (57 mmol), chloroethylene (570 mmol), and benzophenone (10 mmol) in 200 ml of benzene was irradiated for 30 h and then worked up much as in the procedure described in (*a*). **1b** (mp 97—100 °C (benzene), 1%), **3b** (mp 126—128 °C (benzene), 7%), and **4b** (oil, 2%) were thus obtained. The **4b** was further purified by repeated column chromatography (diethyl ether). The photoirradiation of the methanol solution of the same reactants containing thioxanthen-9-one instead of benzophenone gave **1b** (2%), **2b** (mp 128—130 °C (benzene), 4%), and **4b** (0.5%). The non-sensitized irradiation in methanol gave no cycloadduct. **1b**: IR (KBr) 1658—1645 (sh); MS 239 (M^+, 10%). Found: C, 40.15; H, 3.31; N, 5.83%. Calcd for $C_8H_8NOCl_3$: C, 39.95; H, 3.35; N, 5.82%. **2b**: IR (KBr) 1690, 1633; MS 239 (M^+, 1%). Found: C, 39.91; H, 3.25; N, 5.72%. **3b**: IR (KBr) 1683, 1623; MS 239 (M^+, 2%). Found: C, 39.98; H, 3.33; N, 5.82%. **4b**: IR (neat) 1690, 1622; MS 239 (M^+, 1%). Found: C, 39.93; H, 3.34; N, 5.91%.

(c) With 1,1-Dichloroethylene: A solution of pyridone (28 mmol), chloroethylene (280 mmol), and xanthone (7 mmol) in 200 ml of benzene was irradiated for 6 h and then worked up much as in the procedure described in (*a*). Benzene–diethyl ether (2 : 1) was used as the eluent of the column chromatography. **1c** (oil, 28%) was thus obtained. IR (neat) 1662; MS 205 (M^+, 1%). Found: C, 46.95; H, 4.33; N, 6.85%. Calcd for $C_8H_9NOCl_2$: C, 46.63; H, 4.40; N, 6.80%.

Photoreactions of 2-Pyridone. (a) With Tetrachloroethylene: A solution of pyridone (40 mmol), chloroethylene (400 mmol), and benzophenone (13 mmol) in 200 ml of methanol was irradiated for 15 h and then worked up much as in the procedure of column chromatography described above (*a*). As the eluents, benzene and diethyl ether were used; **1d** (mp 172—175 °C, 9%) and **2d** (mp 212—218 °C, 16%) respectively were thus obtained. **1d**: IR (KBr) 1692, 1663; MS 259 (M^+, 1%). Found: C, 32.30; H, 1.98; N, 5.36%. Calcd for $C_7H_5NOCl_4$: C, 32.21; H, 1.93; N, 5.37%. **2d**: IR (KBr) 1683, 1623; MS 224 (M−Cl, 5%). Found: C, 32.18; H, 1.90; N, 5.25%.

(b) With Trichloroethylene: A solution of pyridone (57 mmol), chloroethylene (570 mmol), benzophenone (10 mmol), and methanol (200 ml) was irradiated for 23 h, the work-up described in (*a*) (eluents: benzene, diethyl ether, and acetone) then gave **1e** (mp 84—86 °C, 5%), **2ex** (mp 172—175 °C, 9%), **2ed** (mp 192—195 °C, 2%), and **3e** (mp 155—158 °C, 7%). **2ex** (0.5 mmol) and **2ed** (0.05 mmol) were passed through a basic alumina (Merck) column (ϕ8 mm × 30 mm), using chloroform as the eluent, and the solutions were concentrated. The ^{1}H-NMR analysis showed that there was no change during this treatment, confirming the *cis* four-six ring fusions. **1e**: IR (KBr) 1670—1650; MS 155 (M−2Cl, 3%). Found: C, 37.08; H, 2.69; N, 6.27%. Calcd for $C_7H_6NOCl_3$: C, 37.12; H, 2.67; N, 6.18%. **2ex**: IR (KBr) 1690, 1623: MS 190 (M−Cl, 10%). Found: C, 37.13; H, 2.69; N, 6.05%. **2ed**: IR (KBr) 1688, 1618. Found: C, 37.15; H, 2.67; N, 5.96%. **3e**: IR (KBr) 1679, 1621; MS 190 (M−Cl, 10%). Found: C, 37.40; H, 2.70; N, 6.02%.

(c) With 1,1-Dichloroethylene: After the irradiation of a solution of pyridone (32 mmol), chloroethylene (320 mmol), and benzophenone (6 mmol) in 200 ml of benzene for 32 h, the same work-up as above gave **1g** (mp 139—141 °C, 10%). IR (KBr) 1683, 1657. Found: C, 44.23; H, 3.70; N, 6.94%. Calcd for $C_7H_7NOCl_2$: C, 43.78; H, 3.67; 7.29%.

Reactivities of Photoreactions: After solutions of *N*-methyl-2-pyridone (2.3 mmol), chloroethylene (23 mmol), a predetermined amount of sensitizers[4] (or none), and benzene–acetonitrile (10 : 1) (20 ml) in Pyrex reaction tubes (ϕ20) had been irradiated by the use of a Rikō Rotary 400 W high-pressure mercury lamp, the relative product ratio was determined by removing aliquots with a syringe and examining them by means of GC.

Reductions of Photoadducts by Zinc. (a) The Reaction of 1a: A mixture of **1a** (370 mg) and zinc dust (550 mg) in 20 ml of benzene was refluxed for 60 h. After the concentration of the filtrate, the precipitate was recrystallized from benzene to give **6a** (mp 91—93 °C, 67%). IR (KBr) 1670, 1635; MS 203 (M^+, 50%). Found: C, 46.83; H, 3.47; N, 6.73%. Calcd for $C_8H_7NOCl_2$: C, 47.09; H, 3.46; N, 6.86%.

(b) The Reactions of 2a, 3b and 2ex: A mixture of **2a** (770 mg) and zinc dust (700 mg) in 35 ml of benzene was refluxed for 4 h. After the concentration of the filtrate, the residue was chromatographed on a silica-gel column (benzene, diethyl ether) to give **7a** (mp 83—87 °C, 75%). IR (KBr) 1740, 1670, 1615; MS 203 (M^+, 30%). Found: C, 46.72; H, 3.64; N, 6.76%. Calcd for $C_8H_7NOCl_2$: C, 47.09; H, 3.46; N, 6.86%.

The refluxing of a mixture of **3b** (300 mg) and zinc (1.2 g) in 20 ml of benzene for 7 h, and of **2ex** (720 mg) and zinc (1.0 g) in 50 ml of methanol for 20 h, followed by treatment by the use of column chromatography similar to that described above, gave **7b** (oil, 80%) and **7e** (mp 124—128 °C, 45%) respectively. **7b**: IR (neat) 1663, 1610—1580. Found: C, 57.05; H, 4.78; N, 8.20%. Calcd for C_8H_8NOCl: C, 56.83; H, 4.74; N, 8.29%. **7e**: IR (KBr) 1674, 1613, 1582; MS 155 (M^+, 3%). Found: C, 54.06; H, 3.94; N, 9.04%. Calcd for C_7H_6NOCl: C, 54.04; H, 3.89; N, 9.00%.

(c) The Reaction of 4b: A mixture of **4b** (140 mg) and zinc (400 mg) in 10 ml of benzene was refluxed for 17 h. Subsequent treatment similar to that given (*b*) afforded **8b** (oil, 58%). IR (neat) 1681, 1623, 1580. Found: C, 56.80; H, 4.79; N, 8.36%. Calcd for C_8H_8NOCl: C, 56.83; H, 4.74; N, 8.29%.

Valence Isomerizations of 7a, 7b, and 7e. (a) The Reactions of 7a and 7b: The heating of **7a** (1.0 mmol) or **7b** (1.0 mmol) in 10 ml of 1,2,4-trichlorobenzene at 120 °C for 5 h resulted in the complete disappearance of the starting materials. The residues were chromatographed on a silica-gel column, with benzene and diethyl ether as eluents, to give **9a** (oil, 70%) and **9b** (oil, 73%) respectively. The reactions, monitored by the use of TLC and ^{1}H-NMR, were almost quantitative. The **9a** and **9b** were decomposed by heating them at 180 °C in glass tubes to give dichlorobenzene and chlorobenzene respectively. **9a**: IR (neat) 1759, 1635; MS 203 (M^+, 2%). Found: C, 47.17; H, 3.50; N, 6.89%. Calcd for $C_8H_7NOCl_2$:

C, 47.09; H, 3.46; N, 6.86%. **9b**: IR (neat) 1750, 1640. Found: C, 56.90; H, 4.85; N, 8.27%. Calcd for C_8H_8NOCl: C, 56.83; H, 4.74; N, 8.29%.

(b) The Reaction of ***7e***: A solution of **7e** (1.0 mmol) in benzene (15 ml) was refluxed for 10 h. The residue was chromatographed in a manner similar to the above to give **9e** (mp 86—90 °C, 45%). The half-life time of **7e** was 50 min at 90 °C, and the generated **9e** was decomposed by heating at 120 °C to give chlorobenzene. IR (KBr) 1745, 1648; MS 155 (M^+, 5%), 112 (M−NHCO, 100%). Found: C, 53.87; H, 3.93; N, 8.87%. Calcd for C_7H_6NOCl: C, 54.04; H, 3.89; N, 9.00%.

The heating reaction of **6a** (1.0 mmol) in 1,2,4-trichlorobenzene (10 ml) was attempted up to 190 °C, and the progress was monitored by similar methods. However, no reaction occurred.

References

1) J. G. Atkinson, D. E. Ayer, G. Büchi, and E. W. Robb, *J. Am. Chem. Soc.*, **85**, 2257 (1963).

2) K. Kraft and G. Kortzenburg, *Tetrahedron Lett.*, **1967**, 4723.

3) A. G. Anastassiou, E. Reichmanis, S. J. Girgenti, and M. Schaefer-Ridder, *J. Org. Chem.*, **43**, 315 (1978).

4) K. Somekawa and S. Kumamoto, *Nippon Kagaku Kaishi*, **1977**, 1489.

5) K. Somekawa, T. Shimou, H. Muta, and S. Kumamoto, *Nippon Kagaku Kaishi*, **1976**, 1443.

6) K. Somekawa, T. Watanabe, and S. Kumamoto, *Nippon Kagaku Kaishi*, **1978**, 412.

7) S. Kumamoto, K. Somekawa, and R. Imai, 11th Congress of Heterocyclic Chemistry, Abstr., Kanazawa, October (1978), p. 137.

8) R. M. Silverstein, G. C. Bassler, and T. C. Morrill, "Spectroscopic Identification of Organic Compounds," 3 rd ed, John Wiley & Sons, New York (1974), p. 102.

9) L. A. Paquette, T. Kakihana, and J. F. Kelly, *J. Org. Chem.*, **36**, 435 (1971).

Preparation of Several 1,5,5,11,11-Pentamethyltricyclo-[6.2.1.0^{2,6}]undecane Derivatives

Yoshinobu INOUYE,* Chikara FUKAYA, and Hiroshi KAKISAWA

Department of Chemistry, The University of Tsukuba, Sakura-mura, Niihari-gun, Ibaraki 305

(Received June 12, 1980)

1,6-Diketone, available in eight steps from homocamphorquinone, was converted into 1,5,5,11,11-pentamethyltricyclo[6.2.1.0^{2,6}]undecan-7-one by treatment with potassium *t*-butoxide and then lithium dimethylcuprate, while α,α-dimethyl-γ-valerolactone, prepared in five steps from homocamphor, was converted into 1,5,5,11,11-pentamethyltricyclo[6.2.1.0^{2,6}]undec-2-en-4-one by treatment with diphosphorus pentoxide–methanesulfonic acid.

Taxinine (**1**), the major component isolated from the Japanese *Taxus cuspidata*,[1] has a unique carbon skeleton, named "taxane," containing an 8-membered ring as a part of the bicyclo[5.3.1]undecane system. Several attempts[2-4] to synthesize this compound have been reported, but none have succeeded.

In the course of our synthetic approach to this skeleton,[4] we were faced with the necessity to prepare a compound **2** having a 5-alkyl-1,5,11,11-tetramethyltricyclo[6.2.1.0^{2,6}]undecane system. This compound was thought to be derivable from a homocamphor framework by creating a 5-membered ring on it. The readily available ketone **3**, prepared by Büchi *et al.*[5] during their investigation of the synthesis of pachouli alcohol, was at first attractive, but our preliminary attempts at the conversion of **3** into **2** were unsuccessful, especially in the introduction of two alkyl groups at the C-5 position of the tricyclo[6.2.1.0^{2,6}]undecane system.

The present paper will describe the syntheses of two 1,5,5,11,11-pentamethyltricyclo[6.2.1.0^{2,6}]undecane derivatives (**26** and **39**) as possible model compounds for **2**. The synthetic efforts were mainly concentrated on the creation of a 5-membered ring with a geminate dimethyl group on the homocamphor framework.

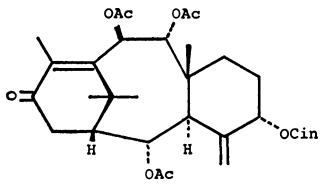

1

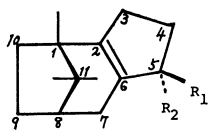

2 R_1=CH_3, R_2=Alkyl

3 R_1=R_2=O

Construction of a 5-Membered Ring Prior to the Introduction of a Methyl Group. One of the methods most widely used to create the cyclopentane ring is an intramolecular aldol condensation of 1,4-diketones. An initial effort was directed at preparing a cyclopentenone, 1,5,11,11-tetramethyltricyclo[6.2.1.0^{2,6}]undec-5-en-4-one (**14**), from the 1,4-diketone **12**. The preparation of **12** from the easily avairable unsaturated alcohol **4**[5] is shown in Schemes 1 and 2.

The alcohol **4** was oxidized to the epoxy alcohol **5** by treatment with *m*-chloroperbenzoic acid. The direct dehydration of this epoxy alcohol **5** with phosphoryl chloride or thionyl chloride in pyridine gave no fruitful results; however, the introduction of a chlorine atom was recognized from the analysis of the mass spectrum. This is thought to arise from the participation of the epoxy group.[7] The trouble was overcome by opening the epoxy ring prior to the dehydration. Thus, when **5** was treated with lithium dimethylcuprate in ether, the diol **6** was obtained in 89% yield as a result of the selective opening of the epoxy ring into a secondary alcohol.[8] After the secondary hydroxyl group had been protected by acetylation, the tertiary one was dehydrated with phosphoryl chloride in pyridine to give a mixture of an unsaturated acetate **7** and a

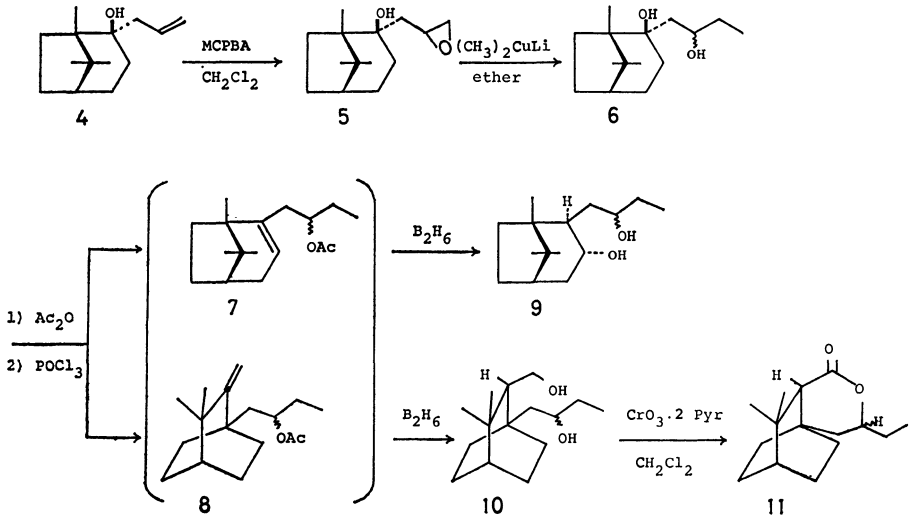

Scheme 1.

rearranged acetate **8**. The mixture, without the separation of its components, was converted into two diols, **9** and **10** (49 and 14% yields respectively from **6**), by hydroboration with diborane.[9] The structure of the rearranged diol **10** was determined by NMR spectroscopy. In the NMR spectrum of the diacetate of **10**, only two tertiary methyl signals are observed, at 0.99 and 1.04 ppm, while one -CH-OAc group and one $-CH_2-OAc$ group are recognized at 4.8 and 4.1 ppm respectively. The structure was finally confirmed by the oxidation of **10** with chromium trioxide to afford a δ-lactone **11** [$\nu(CCl_4)$: 1740 cm^{-1}; δ ($CDCl_3$): 4.0 (m, 1H) and 1.95 (s, 1H)]. The configurations at the newly formed asymmetric centers of the major diol are assigned as in **9** by considering the less-hindered-side attack of diborane.[10]

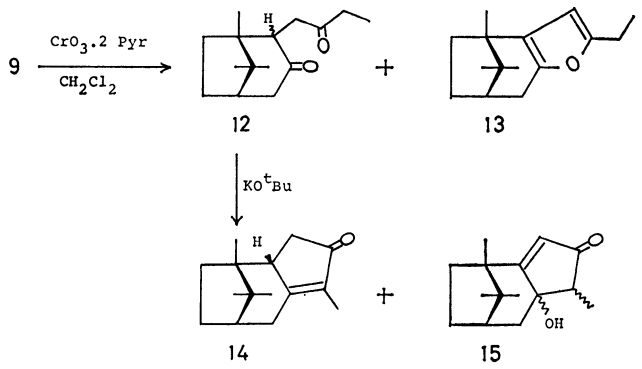

Scheme 2.

The oxidation of the major diol **9** gave the desired 1,4-diketone **12** in 72% yield, accompanied by a small amount (17%) of a furan derivative **13**. When **12** was treated with potassium *t*-butoxide in *t*-butyl alcohol at room temperature (30 min), 1,5,11,11-tetramethyl-[6.2.1.$0^{2,6}$]undec-5-en-4-one (**14**) and 6-hydroxy-1,5,11,-11-tetramethyltricyclo[6.2.1.$0^{2,6}$]undec-2-en-4-one (**15**) were obtained in 79 and 9% yields respectively. The methyl group attached to the double bond of the major product **14** was recognized at 1.59 ppm in the NMR spectrum. The structure of the minor product **15** was deduced from the presence of one secondary methyl doublet (1.08 ppm, J=7 Hz) and one proton singlet on the double bond (5.77 ppm), which has no allylic proton coupled to it (*cf.* **39**). The stereochemistry of C-2 in **14** was assigned as is shown by the conformational analysis of the molecule. The mechanism for the formation of **15** during the cyclization of the diketone **12** was not clarified.

Several attempts to introduce an alkyl group into the C-5 position of **14** were unsuccessful: the treatment of **14** with allyl bromide–sodium hydride gave a 3-allyl derivatives, while a protected **14**, the 3,3-butylthiomethylene derivative, did not react with allyl bromide–sodium hydride in benzene or diglyme.

Another approach to the title compound is summarized in Scheme 3. Here, a 1,6-diketone **24** was chosen as the precursor because no epimerization at C-2 was anticipated during the alkaline cyclization.

The treatment of homocamphorquinone with cyclohexanol led to the regiospecific production of an enol

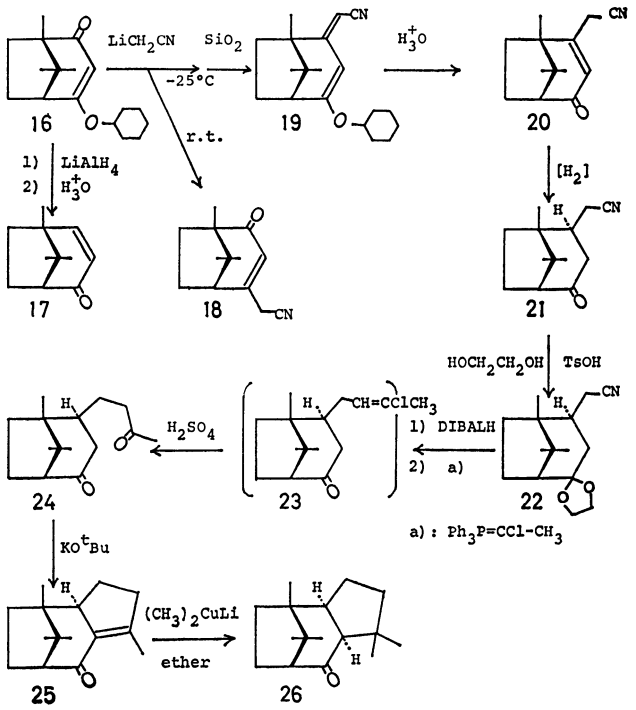

Scheme 3.

ether **16** in 73% yield, ν(KBr): 1650 and 1600s cm^{-1}. None of the other isomers was detected in the reaction product. The structure of **16** was confirmed by reduction with lithium aluminum hydride, followed by hydrolysis with hydrochloric acid, to convert it into the known unsaturated enone **17**.[11] The lithioacetonitrile, prepared[12] from acetonitrile and butyllithium, was treated with the enol ether **16** at −78 °C, after which the mixture was brought to room temperature to give a cyanomethyl enone **18** in 95% yield. The structure of **18** was determined by comparison of its spectra with those of an isomer **20** (see below). The formation of **18** resulted from the 1,4-addition of the reagent to an α,β-unsaturated ketone. When the reaction was controlled at lower temperatures (−25——30 °C), the reaction proceeded by means of the 1,2-addition of the reagent; the initial product was dehydrated during the isolation procedure (silica gel chromatography) to give **19** exclusively. The NMR spectrum of **19** shows the presence of a cyclohexyloxy group (multiplet at 4.2 ppm) and two vinylic protons (singlets at 4.53 and 5.53 ppm). A similar temperature-dependence of the 1,2- *vs.* 1,4-addition of a reagent to an α,β-unsaturated ketone system has recently been reported.[13]

The acid hydrolysis of **19** afforded the desired cyanomethyl enone **20**. The double bond in **20** was readily hydrogenated over a palladized charcoal catalyst. The configuration of the side chain in the dihydro-compound **21** was postulated from the known reactions;[10] the hydrogen approaches **20** from the α-side of the molecule.

After protecting the carbonyl group with ethylene glycol, the acetalized nitrile **22** (mp 83—84 °C) was reduced with diisobutyl aluminum hydride,[14] after which the intermediate imine was hydrolyzed in aqueous ammonium chloride, giving an aldehyde

[$\nu(CCl_4)$: 2700 and 1720 cm^{-1}; and $\delta(CDCl_3)$: 9.7 ppm (t, 1H)] in 90% yield. The treatment of the crude aldehyde with (1-chloroethylidene)triphenylphosphorane, a new reagent prepared according to the procedure of Seyferth *et al.*,[15] and the subsequent hydrolysis of the acetal group afforded a mixture of chlorovinyl ketones, **23** (a mixture of *E*- and *Z*-isomers), in 70% yield. **23** was then hydrolyzed with concentrated sulfuric acid to afford a crystalline 1,6-diketone **24**; mp 59—60 °C; ν(KBr): 1705 and 1690 cm^{-1}.

The cyclization of **24** was effected by the use of potassium *t*-butoxide to give 1,5,11,11-tetramethyltricyclo-[6.2.1.0^{2,6}]undec-5-en-7-one (**25**); $\nu(CCl_4)$: 1675 and 1615 cm^{-1}: $\delta(CCl_4)$: 0.85, 0.90, 0.96 (each s, 3H), and 2.12 (br. s, 3H). The enone **25** was unstable, and even when it was left in an icebox under nitrogen, some unidentifiable crystalline substances resulted. **25** was, therfore, promptly converted into a stable compound, **26**; the freshly purified **25** was treated with lithium dimethylcuprate to afford the expected 1,5,5,11,11-pentamethyltricyclo[6.2.1.0^{2,6}]undecan-7-one (**26**) in 91% yield by the conjugate addition of methyl to an α,β-unsaturated ketone.[16]

Introduction of a Geminate Dimethyl Group Prior to the Formation of a 5-Membered Carbocyclic Ring. Another approach to the title compound was to introduce a geminate dimethyl group before the construction of a 5-membered carbocyclic ring. γ-Lactones, such as **30** and **36**, were chosen as the starting materials.

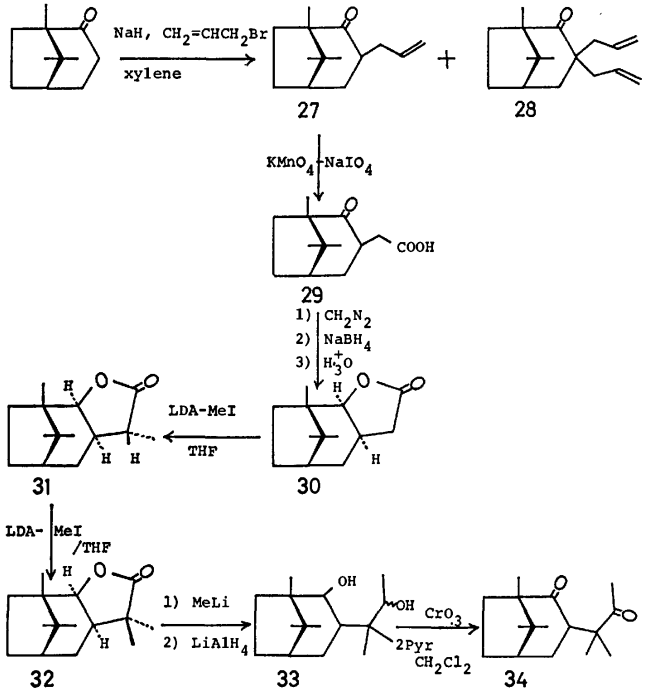

Scheme 4.

The allyl group was introduced into the C-2 position of homocamphor according to Fried's procedure.[17] The resulting **27**, separated from the dially derivative **28** by fractional distillation, was subjected to Lemiux's oxidation, thus giving a keto acid **29**. The methyl ester of **29** was then reduced with sodium borohydride in methanol, followed by acid treatment, to afford a γ-lactone **30** in 90% yield from **27**. The stereochemistry of **30** was deduced from the facts that the coupling constant, J=5 Hz, between the protons on the ring junctures of the lactone ring requires a *cis* relationship of these two protons, and that the hydride in the sodium borohydride reduction of **29** attacks from the rear side of the molecule.[10] The methylation of **30** with one equivalent of lithium diisopropylamide (LDA)[18] and methyl iodide afforded α-methyl-γ-lactone **31** in a quantitative yield. Because of the concave shape of **30**, reagents were expected to attack exclusively from the convex side of the molecule. The further treatment of **31** with excess LDA–methyl iodide gave dimethyl-γ-lactone **32**. The conversion of **32** into a diketone **34** was achieved by successive treatment with methyllithium in ether, lithium aluminum hydride in ether, and chromium trioxide–pyridine complex in dichloromethane.

Several attempts at the cyclization of **34** to cyclopentenone under alkaline (*t*-BuOK/*t*-BuOH, NaH/benzene, or NaOH/EtOH) or acid conditions ($Et_3N\cdot C_6H_5COOH$/xylene or TsOH/benzene) were unsuccessful. This failure is thought to have arisen from a severe steric repulsion in the transition state as a result of changing the hybridization of the C-2 carbon from sp^2 to sp^3. These difficulties were finally overcome by using the γ-valerolactone derivative described in Scheme 5 and by cyclizing under acid conditions, where the carbon bearing the oxygen atom changes hybridization from sp^3 to sp^2.

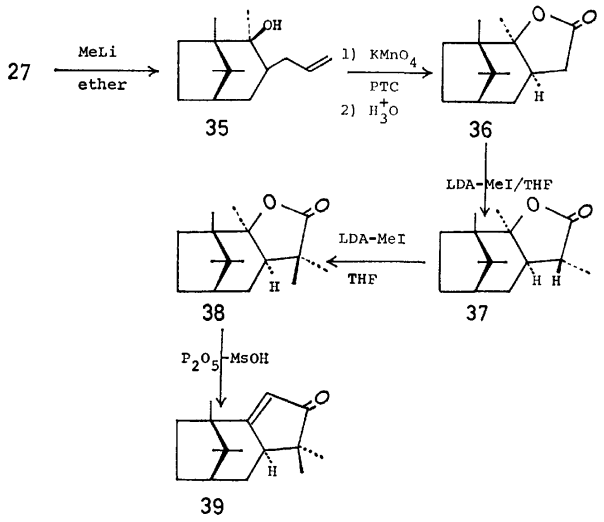

Scheme 5.

Allylhomocamphor (**27**) was treated with methyllithium to give an alcohol **35**. The stereochemistry of **35** was deduced from the rear-side attack of the reagent. **35** was oxidized with potassium permanganate in the presence of alkyldimethylbenzylammonium chloride[19] to afford a γ-valerolactone derivative **36**. The methylation with LDA–methyl iodide proceeded much as in the case of **30**; the dimethyl derivative **38** was thus obtained in a quantitative yield.

The transformation of γ-valerolactone into cyclopentenone had been reported by only Fisini and Manjean; 7a-methylperhydro-2-benzofuranone was con-

verted into hexahydroindenone by treatment with polyphosphoric acid, but in only 25% yield, accompanied by the same amount of a rearranged product.[20] As will be shown in the Experimental section, we used diphosphorus pentoxide–methanesulfonic acid, a more effective reagent[21] than polyphosphoric acid; the yield of hexahydroindenone could thus be raised to 59%.

The treatment of **38** with diphosphorus pentoxide–methanesulfonic acid at 70 °C for 2 h afforded the expected 1,5,5,11,11-pentamethyltricyclo[6.2.1.$0^{2,6}$]-undec-2-en-4-one (**39**) in 50% yield; $\nu(CCl_4)$: 1700 and 1605 cm^{-1}. Besides five methyl singlets, at 0.78, 0.91, 0.98, 1.03, and 1.12 ppm, one vinylic proton is recognized at 5.51 ppm; it couples to an allylic proton with a coupling constant of 2 Hz.

In conclusion, 1,5,5,11,11-pentamethyltricyclo-[6.2.1.$0^{2,6}$]undecane derivatives have been successfully prepared through two different routes (**16**→**24**→**26** and **36**→**38**→**39**). Further investigations of the conversion of an appropriate intermediate (*e.g.*, 5α-allyl instead of 5α-methyl in **38**) to a taxane framework *via* **2** are in progress.

Experimental

All the melting points are uncorrected. The NMR spectra were obtained with Hitachi H-60 and JEOL MH-100 spectrophotometers, using TMS as the internal standard; the chemical shifts are given in δ values. The IR spectra were taken on a Hitachi 215 grating spectrophotometer. *dl*-Camphor was used in all cases.

Epoxidation of the Unsaturated Alcohol **4**. To a cooled mixture of **4** (4.4 g, prepared according to Büchi's procedure[5]) in 40 ml of dichloromethane there was added a solution of *m*-chloroperbenzoic acid (4.3 g) in 80 ml of dichloromethane. After having been stirred overnight at room temperature, the mixture was extracted with ether. The extract was washed with aqueous sodium hydroxide (10%), water, and brine, and was dried over anhydrous sodium sulfate. The subsequent evaporation of the solvent afforded a crystalline epoxide, **5** (4.5 g, 94%), which was recrystallized from pentane; mp 61—62 °C; $\nu(CHCl_3)$: 3500, 2950, 1260, and 1240 cm^{-1}; $\delta(CDCl_3)$: 0.87 (s, 3H), 0.90 (s, 3H), 1.22 (s, 3H), 2.45 (dd, 1H, J=4.5 and 2 Hz), 2.80 (t, 1H, J=4.5 Hz), and 3.17 (m, 1H). Found: C, 75.02; H, 10.63%. Calcd for $C_{14}H_{24}O_2$: C, 74.95; H, 10.78%.

Reaction of **5** *with Lithium Dimethylcuprate.*[22] To a suspension of 6.46 g (34 mmol) of copper(I) iodide in 40 ml of anhydrous ether at 0 °C, there was added 88 ml (68 mmol) of a methyllithium–ether solution over a 15-min period. After 10 more min of stirring, a solution of 1.99 g (9 mmol) of **5** in 30 ml of ether was added over a 10-min peroid, and the mixture was stirred at 0—5 °C for 20 h.[8] The whole was treated with aqueous ammonium chloride (30 ml), and the products were extracted with ether. The extract was washed with water and brine, and then dried over anhydrous sodium sulfate. The solvent was evaporated to give a crystalline diol, **6**, (1.93 g 89%), which was subsequently recrystallized from ethyl acetate to afford a pure **6**; mp 104 °C; ν(KBr): 3430, 3360, 2950, 1390, 1380, 1370, 1080, 1060, and 1030 cm^{-1}; $\delta(CDCl_3)$: 0.85 (s, 3H), 0.95 (s, 3H), 0.95 (t, 3H, J=7 Hz), 1.22 (s, 3H), 2.7 (br. s, 2H), and 3.9 (m, 1H). Found: C, 74.82; H, 12.00% Calcd for $C_{15}H_{28}O_2$: C, 74.95; H, 11.74%.

A Mixture of Two Unsaturated Acetates, **7** *and* **8**. A solution of 3.15 g of **6** in 15 ml of pyridine and 15 ml of acetic anhydride was allowed to react for 17 h at room temperature. A subsequent, usual work-up gave 3.68 g of a monoacetat $\nu(CCl_4)$: 3580, 3500, 2950, 1740, 1390, 1370, 1250, 1230, 1110, 1080, 1020, and 960 cm^{-1}; $\delta(CDCl_3)$: 0.85 (s, 3H), 0.89 (t, 3H, J=7 Hz), 0.93 (s, 3H), 1.20 (s, 3H), 2.07 (s, 3H), 4.8 (m, 1H), and 5.1 (m, 1H). The monoacetate (3.68 g) was placed in a sturdy flask with 80 ml of pyridine, 16 ml of phosphoryl chloride was then added, the flask was stoppered tightly, and the contents were heated on an oil bath at 95 °C for 6 h. After colling, the dark mixture was cautiously poured onto 500 g of ice and stirred briefly. The mixture was extracted with pentane, and the extract was washed with water, dried, and evaporated to yield an oil (3.05 g). By chromatography on silica gel (50 g), 2.75 g of a mixture of unsaturated acetates (**7** and **8**) were obtained; $\nu(CCl_4)$: 2950, 1730, 1630w, 1380, 1370, 1245, 1020, and 960 cm^{-1}. The oil showed two peaks on VPC (5% OV-1, glass column 3φ× 1.7 m, 170 °C), but was used directly in the subsequent reaction without any separation of the components.

Hydroboration of the Mixture of **7** *and* **8**. A solution of 2.87 g of the mixture (**7** and **8**) in 50 ml of THF was treated with diborane as usual[9] to give an oil (2.94 g). The oil was chromatographed on silica gel (three times with 20 g each). From hexane–ethyl acetate (100 : 10) eluates, 385 mg (14%) of **9** were obtained. From hexane–ethyl acetate (50 : 50), 1.28 g of **10** resulted.

9, mp 113.5—116 °C (from hexane); ν(KBr): 3200br, 1045, 1005, 980, 970, and 955 cm^{-1}; δ(100 MHz, $CDCl_3$): 0.89 (t, 3H, J=7 Hz), 0.90 (s, 3H), 1.04 (s, 3H), 3.60—3.8 (m, 5H; the addition of D_2O changes the area to 3H). Found: C, 74.80; H, 11.95%. Calcd for $C_{15}H_{28}O_2$: C, 74.94; H, 11.74%.

Diacetate of **9**, bath temp 136—139 °C/0.25 mmHg (Kugelrohr dist); $\nu(CCl_4)$: 1735 and 1240 cm^{-1}; δ(100 MHz, CCl_4): 0.84 (t, 3H, J=7 Hz), 0.99 (s, 3H), 1.04 (s, 3H), 1.90 (s, 3H), 1.96 (s, 3H), 4.1 (m, 2H), and 4.8 (m, 1H). Found: C, 70.22; H, 9.93%. Calcd for $C_{19}H_{32}O_4$: C, 70.33; H, 9.94%.

10, mp 131—133.5 °C (from hexane); ν(KBr): 3300br, 1035, and 960 cm^{-1}; δ(100 MHz, $CDCl_3$): 0.81 (s, 3H), 0.86 (s, 3H), 0.88 (s, 3H), 0.94 (t, 3H, J=7 Hz), 2.9 (br. s, 2H, -OH×2), 3.8 (m, 1H), 3.86 (br. d, 1H, J=6 Hz). Found: C, 74.93; H, 12.07%. Calcd for $C_{15}H_{28}O_2$: C, 74.94; H, 11.74%.

Diacetate of **10**, bath temp 127—130 °C/0.25 mmHg (Kugelrohr dist); $\nu(CCl_4)$: 1730 and 1250 cm^{-1}; δ(100 MHz, CCl_4): 0.83 (s, 3H), 0.88 (t, 3H, J=7 Hz), 0.91 (s, 6H), 1.91 (s, 3H), 1.97 (s, 3H), 4.7 (m, 1H), and 4.82 (br. d, 1H, J= 6 Hz). Found: C, 70.23; H, 9.99%. Calcd for $C_{19}H_{32}O_4$: C, 70.33; H, 9.94%.

Oxidation of **9**. To a solution of 300 mg of chromium trioxide and 0.49 ml of pyridine in 8 ml of dichloromethane[23] there was added a solution of 60 mg of **9** in 5 ml of dichloromethane in one portion. After stirring for 3 h at room temtemperature, the solution was decanted and the residue was washed with 10 ml of ether. The combined organic solutions were washed successively with 5% aqueous sodium hydroxide (3×5 ml), 5% hydrochloric acid (5 ml), 5% aqueous sodium hydrogencarbonate (5 ml), and saline, and were dried over anhydrous sodium sulfate. The subsequent evaporation of the solvent afforded an oil, which was then chromatographed on silica gel (5 g). From hexane–ethyl acetate (100 : 2), 29 mg (49%) of a crystalline **11** were obtained. Recrystallization from hexane gave a pure **11**; mp 77—78 °C; $\nu(CCl_4)$: 1740, 1200, and 1195 cm^{-1}; δ(100 MHz, $CDCl_3$): 0.96 (t, 3H, J=7 Hz), 1.10 (s, 3H), 1.37 (s, 3H), 1.95 (s, 1H), and 4.0 (m, 1H). Found: C, 76.28; H, 10.35%. Calcd for $C_{15}H_{24}O_2$:

C, 76.22; H, 10.24%.

1,5,11,11-Tetramethyltricyclo[6.2.1.0^{2,6}]undec-5-en-one (14). By the same procedure as in the case of **10**, **9** (240 mg) was oxidized with 1.2 g of chromium trioxide. The crude oil was chromatographed on silica gel (5 g) to give 38 mg (17%) of a furan derivative **13** from the hexane eluates. Pure **13**, mp 65—66 °C (from pentane, at −70 °C); ν(KBr): 1620, 1560, 930, and 800 cm^{-1}; δ(CCl_4): 0.82 (s, 3H), 0.94 (s, 3H), 1.08 (s, 3H), 1.18 (t, 3H, J=7 Hz), 2.53 (q, 2H, J=7 Hz), and 5.62 (s, 1H); Found: C, 82.43; H, 10.27%. Calcd for $C_{15}H_{22}O$: C, 82.51; H, 10.15%. Further elution with hexane–ethyl acetate (10 : 1) gave 171 mg (72%) of **12**, ν(CCl_4): 1710 and 1690 cm^{-1}; two peaks on VPC.

A solution of the diketone **12** (171 mg), without any separation of the components, in 5 ml of *t*-butyl alcohol was added to a stirred solution of potassium *t*-butoxide (prepared from 53 mg of potassium) in 5 ml of *t*-butyl alcohol, after which the mixture was stirred at room temperature for 30 min. Water was added, and the products were extracted with ether. The ether layer was washed with water and dried over anhydrous sodium sulfate. By flash chromatography (hexane–ethyl acetate=5 : 1), 124 mg (79%) of a cyclopentenone **14** were obtained. Bath temp: 99—101 °C/0.2 mmHg (Kugelrohr dist); mp 44—46 °C from pentane, at −70 °C); ν(CCl_4): 1700 and 1645 cm^{-1}; δ (CCl_4): 0.87 (s, 3H), 0.94 (s, 3H), 1.12 (s, 3H), and 1.59 (br. s, 3H). Found: C, 82.40; H, 10.18%. Calcd for $C_{15}H_{22}O$: C, 82.51; H, 10.15%.

When the residue was eluted with hexane–ethyl acetate (3 : 1), 16 mg (9%) of 6-hydroxy-1,5,11,11-tetramethyltricyclo[6.2.1.0^{2,6}]undec-2-en-4-one (**15**) were obtained in a crystalline form; mp 141—142 °C (from pentane); ν(CCl_4): 3500, 1700, and 1600 cm^{-1}; δ($CDCl_3$): 0.74 (s, 3H), 1.00 (s, 3H), 1.08 (d, 3H, J=7 Hz), 1.13 (s, 3H), and 5.77 (s, 1H). Found: C, 77.16; H, 9.66%. Calcd for $C_{15}H_{22}O_2$: C, 76.88; H, 9.46%.

*Preparation of the Enol Ether **16**.* In a flask fitted with a water separator there was placed a solution of 1.03 g of homocamphorquinone, 50 mg of *p*-toluenesulfonic acid, and 0.6 ml of cyclohexanol in 90 ml of toluene. The mixture was then heated to boiling, the azeotrope composed of toluene and water being removed continuously. Several hours later, the water separator was filled with a molecular sieve of the 4A type and heating was continued for 2 more days. The solution was washed with 10% aqueous sodium hydroxide (10 ml×2), water (10 ml×3), and brine. After having been dried over anhydrous sodium sulfate, the solvent was evaporated to give an oil, which crystallized when chilled in pentane (1.1 g, 73%). Recrystallization from pentane gave a pure **16**; mp 74—76 °C; ν(CCl_4): 1650, 1600, and 1210 cm^{-1}; δ($CDCl_3$): 0.94 (s, 6H), 1.07 (s, 3H), 4.1 (br. m, 1H), and 5.14 (br. s, 1H). Found: C, 77.95; H, 9.98%. Calcd for $C_{17}H_{26}O_2$: C 77.82; H, 9.99%.

*Conversion of **16** to the Known Enone **17**.* A solution of 100 mg of **16** in 10 ml of dry THF was refluxed for 1 h with $LiAlH_4$. After the excess reagents had then been decomposed by the careful addition of water, a 5-ml portion of 10% sulfuric acid was added and the mixture was stirred at room temperature for 30 min. The products were taken up in ether, and the ether extract was evaporated to give an oil, which was subsequently chromatographed on alumina (10 g). From the benzene eluates, 47 mg (75%) of the enone **17** were obtained. The NMR spectrum of **17** [δ($CDCl_3$): 0.92 (s, 6H), 1.14 (s, 3H) 5.88 (dd, 1H, J=10 and 1.5 Hz), 6.73 (d, 1H, J=10 Hz) was in accord with the previously reported value.[11]

*Treatment of **16** with Lithioacetonitrile. A) At −25—−30 °C:* A solution of 5.25 g (18.4 mmol) of **16** in 25 ml of THF was added, drop by drop, over a 5-min period to 4 eq of $LiCH_2CN$ (prepared from 56 ml of a 1.6 M buthyllithium–hexane solution and 4.2 ml of acetonitrile in 30 ml of THF at −78 °C)[12] at −78 °C, after which the mixture was stirred at that temperature for 1.5 h. The temperature was then raised to −25 °C and stirring was continued for 3 h at −25 ——30 °C. A saturated ammonium chloride solution (30 ml) was added, drop by drop, while the temperature was kept below −25 °C by the occasional cooling of the flask. Water (30 ml) was added, and an organic layer was separated. The aqueous layer was extracted with ether, and the combined extracts were washed with a small portion of water and saline, and dried over anhydrous sodium sulfate. The evaporation of the solvent gave an oil, which was then chromatographed on silica gel (150 g). Elutions with 50% benzene–hexane and then with benzene gave 3.64 g (64%) of **19**.

19, mp 76—77 °C (from pentane); ν(CCl_4): 2210, 1610, and 1215 cm^{-1}; δ(CCl_4): 0.85 (s, 3H), 0.95 (s, 3H), 1.05 (s, 3H), 4.2 (m, 1H), 4.53 (s, 1H), and 5.53 (br. s, 1H). Found: C, 80.08; H, 9.62; N, 5.18%. Calcd for $C_{19}H_{27}NO$: C, 79.95; H, 9.53; N, 4.90%.

B) At Room Temperature: A mixture of 130 mg of **16** and 10 eq of $LiCH_2CN$ was stirred at −78 °C for 1.5 h, at −25 ——30 °C for 3 h, and finally at room temperature for 1 h. By a subsequent work-up as in A), 95 mg (95%) of **18** were obtained.

18, mp 67—70 °C (from ether); ν($CHCl_3$): 2220 and 1670 cm^{-1}; δ($CDCl_3$): 0.90 (s, 3H), 0.99 (s, 3H), 1.07 (s, 3H), 3.31 (d, 2H, J=2 Hz), and 6.00 (br. s, 1H). Found: C, 76.93; H, 8.49; N, 6.89%. Calcd for $C_{13}H_{17}NO$: C, 76.80; H, 8.42; N, 6.89%.

*Cyanomethyl Enone **20**.* A solution of 5.13 g of **19** in 110 ml of methanol and 30 ml of water containing 2 ml of concd sulfuric acid was stirred at room temperature for 20 h. After the addition of solid sodium hydrogencarbonate (6.3 g), the solution was neutralized with aqueous sodium hydrogencarbonate and diluted with 80 ml of water. The **20** thus precipitated (2.18 g) was collected, and the filtrate was extracted with ethyl acetate. Evaporating the solvent afforded solids, from which a further 0.96 g of **20** was obtained by recrystallization from benzene–hexane. The total yield was 3.14 g (86%).

20, mp 117—118 °C (from ether); ν(KBr); 2250, 1660, and 1610 cm^{-1}; δ($CDCl_3$): 0.95 (s, 3H), 0.99 (s, 3H), 1.18 (s, 3H), 3.3 (d, 2H, J=2 Hz), and 6.17 (q, 1H, J=2 Hz). Found: C, 76.80; H, 8.44; N, 6.73%. Calcd for $C_{13}H_{17}NO$: C, 76.80; H, 8.42; N, 6.89%.

*Hydrogenation of **20**.* A mixture of 2.17 g of **20** and 1 g of 10% Pd-C in 120 ml of ethanol was shaken under a hydrogen atmosphere. The hydrogen uptake ceased after 305 ml of hydrogen had been absorbed (27 h). The catalyst was removed by filtration, and the filtrate was evaporated to give an oil, which was then purified through alumina (40 g). From the benzene eluates, 2.03 g (92%) of **21** were obtained.

21, mp 114—115 °C (from ether): ν(KBr): 2230 and 1700 cm^{-1}; δ($CDCl_3$): 0.95 (s, 6H) and 1.10 (s, 3H). Found: C, 75.80; H, 9.27; N, 6.64%. Calcd for $C_{13}H_{19}NO$: C, 76.05; H, 9.33; N, 6.82%.

*Acetalization of **21**.* A solution of 3.45 g of **21**, 100 mg of *p*-toluenesulfonic acid, and 5 ml of ethylene glycol in 120 ml of benzene was heated under reflux *via* a water separator. After 40 ml of an azeotropic distilate had been removed, a molecular sieve (4A) was placed in the water separator and heating was continued for further 20 h. The mixture was then cooled and diluted with water. The organic phase thus separated was washed with aqueous sodium hydrogen-

carbonate, water, and brine. The subsequent evaporation of the solvent gave a crude acetal (4.09 g), which was chromatographed on alumina (90 g). Elution with hexane–benzene (1 : 1) gave 3.38 g (81%) of a solid acetal, **22**; mp 83—84 °C (from pentane); ν(KBr): 2240 cm^{-1}; δ($CDCl_3$): 0.83 (s, 3H), 0.98 (s, 3H), 1.10 (s, 3H), and 4.85 (m, 4H). Found: C, 72.25; H, 9.22; N, 5.42%. Calcd for $C_{15}H_{23}NO_2$: C, 72.25; H, 9.30; N, 5.62%.

(1-Chloroethyl)triphenylphosphonium Bromide. According to Seyferth's procedure,[15] 30 g (0.115 mol) of triphenylphosphine and 12.9 g (0.13 mol) of 1,1-dichloroethane in 200 ml of anhydrous ether were treated at −30——40 °C by the drop-by-drop addition of a butyllithium–hexane solution (0.10 mol) under vigorous stirring. When the cooling bath was then removed and hydrogen bromide was bubbled into the flask, the orange colour was immediately lost and white solids were formed. The solids were collected on a glass filter, washed with benzene and petroleum ether, and dried *in vacuo* at 70 °C overnight. The dried product weighed 44 g.

The purification was done as follows: a 40-ml portion of water was added to 2.0 g of the crude product, and the undissolved materials were removed by filtration. The filtrate was evaporated to give solids (1.0 g), which were then recrystallized from water (6 ml) to afford 0.5 g of pure (1-chloroethyl)-triphenylphosphonium bromide. An analytical sample was obtained by repeated recrystallizations from water and by heating at 100 °C over P_2O_5 *in vacuo* for 24 h; mp 203—205 °C. Found: C, 59.40; H, 4.56%. Calcd for $C_{20}H_{19}PClBr$: C, 59.21; H, 4.72%.

The reagent should be dried at 80 °C *in vacuo* just before use.

Conversion of 22 into the Diketone 24. To a solution of 1.00 g of **22** in 4 ml of toluene, 3.5 ml (1.5 eq) of a DIBAL-H solution was added, drop by drop, at −78 °C, after which the mixture was stirred at that temperature for 1 h. Methanol (0.3 ml) was then added, the cold bath was removed, and 5 ml of a saturated ammonium chloride solution was added. The whole was stirred at room temperature for 1 h. The ether extract was evaporated to give an oil, from which an oily, acetalized aldehyde [900 mg, 90%; ν(CCl_4): 2700, 1720, and 1090 cm^{-1}] was isolated by chromatography on silica gel (20 g) with benzene–ethyl acetate (19 : 1). The aldehyde was used directly in the next reaction without any further purification.

To a suspension of 1.34 g (3.3 mmol) of (1-chloroethyl)-triphenylphosphonium bromide in 5 ml of THF, 2.2 ml (3.2 mmol) of a butyllithium–hexane solution was added, drop by drop, at −78 °C, after which the dark red mixture was stirred for 30 min at that temperature. A solution of 410 mg (1.6 mmol) of the acetalized aldehyde in 2 ml of THF was added, and the whole was stirred at −78 °C for 30 min, at room temperature for 30 min, and finally under reflux for 2 h. After cooling, 4 ml of 6 M hydrochloric acid was added, and the mixture was stirred for 30 min. The products were taken up in ether, and the ether extract was evaporated to give an oil which contained some triphenylphosphine oxide. The residue was heated with 10 ml of hexane, and the hexane solution was chromatographed on silica gel (20 g). The benzene eluates afforded a mixture of vinyl chloride **23** (295 mg, 71%; two peaks on VPC). The components are separable by repeated chromatography (see below).

A mixture of vinyl chloride, **23**(295 mg), was stirred overnight with 5 ml of concd sulfuric acid. The red solution was then poured onto ice, and the products were taken up in ether. The ether extract was evaporated to give an oil, which was subsequently purified by flash chromatography (hexane–ethyl acetate=5 : 3) to afford a crystalline diketone **24** (208 mg, 76%); mp 59—60.5 °C (from pentane); ν(KBr): 1705br and 1690 cm^{-1}; δ ($CDCl_3$): 0.90 (s, 3H), 0.92 (s, 3H), 1.08 (s, 3H), and 2.12 (s, 3H). Found: C, 76.28; H, 10.27%. Calcd for $C_{15}H_{24}O_2$: C, 76.22; H, 10.23%.

Separation of Z and E Isomers of 23. **23** was chromatographed repeatedly on silica gel; two vinyl chlorides were thus isolated in a pure state.

(**A**): liquid, δ($CDCl_3$): 0.91 (s, 6H), 1.06 (s, 3H), 2.03 (br.s, 3H), and 5.38 (br. t, 1H, J=7 Hz).

The acetal, prepared with ethylene glycol and *p*-toluenesulfonic acid in benzene, of (**A**): mp 51—52 °C (from pentane, at −78 °C). Found: C, 68.63; H, 9.16%. Calcd for $C_{17}H_{27}ClO_2$: C, 68.32; H, 9.10%.

(**B**): liquid; δ($CDCl_3$): 0.90 (s, 3H), 0.95 (s, 3H), 1.07 (s, 3H), 2.08 (br. s, 3H), and 5.33 (br. t, 1H, J=7 Hz).

The acetal of (**B**): mp 66—67 °C (from pentane, at −78 °C). Found: C, 68.23; H, 9.14%. Calcd for $C_{17}H_{27}ClO_2$: C, 68.32; H, 9.10%.

1,5,11,11-Tetramethyltricyclo[6.2.1.0^{2,6}]undec-5-en-7-one (25). To a stirred portion of potassium *t*-butoxide (1 mmol) in 5 ml of *t*-butyl alcohol, 133 mg (0.5 mmol) of **24** in 2 ml of *t*-butyl alcohol was added, after which the mixture was stirred at room temperature for 30 min. The whole was then poured into ether, and the solution was well washed with water. After drying over anhydrous sodium sulfate and after the solvent had been evaporated, a crude oil (120 mg) was chromatographed on silica gel (5 g). From hexane–ethyl acetate (100 : 1), 107 mg (88%) of an enone **25** was obtained; ν(CCl_4); 1675 and 1615 cm^{-1}; δ(CCl_4): 0.85 (s, 3H), 0.90 (s, 3H), 0.96 (s, 3H), and 2.12 (br. s, 3H).

25 can be purified by flash chromatography (hexane–ethyl acetate=10 : 1), but it is apt to change to an unidentified crystalline material even when standing overnight under nitrogen and in an ice-box. Therefore, freshly purified **25** was used immediately in the subsequent reaction.

1,5,5,11,11-Pentamethyltricyclo[6.2.1.0^{2,6}]undecan-7-one(26). To a stirred suspension of 190 mg (1 mmol) of copper (I) iodide in 5 ml of dry ether, 5 ml of a methyllithium–ether solution (2 mmol) was added, drop by drop, at 0 °C. A solution of 107 mg (0.5 mmol) of **25** in 5 ml of ether was then added to this almost colorless solution . The resulting yellow suspension was stirred for 30 min at 0 °C. After then being allowed to warm to room temperature (5 min), the whole was poured into 50 ml of a saturated ammonium chloride solution. The solids were removed by filtration, and the products were extracted with ether. Evaporating the solvent gave an oil, which was chromatographed on silica gel (5 g) to afford 103 mg (91%) of **26**; bath temp 79—83 °C/0.1 mmHg (Kugelrohr dist); ν(CCl_4): 1710 and 1695 cm^{-1}; δ(CCl_4): 0.87 (s, 3H), 0.93 (s, 3H), 1.01 (s, 3H), 1.08 (s, 3H), and 1.20 (s, 3H). Found: C, 81.45; H, 11.24%. Calcd for $C_{16}H_{26}O$: C, 81.99; H, 11.18%.

2-Allylhomocamphor (27). Homocamphor[24] (6.66 g) was dissolved in 70 ml of xylene, and then 40 ml of the xylene was distilled off.[17] To the solution, a 4-g portion of 50% sodium hydride (washed two times with xylene) was added, after which the mixture was refluxed for 2 h. After it had then cooled to room temperature, a 8-ml portion of allyl bromide was added and the whole was heated to 130 °C, whereupon massy precipitates resulted. Heating was continued at that temperature for 20 h. After the solution had then cooled to room temperature, water was added and the organic layer was separated. The aqueous layer was extracted with ether, and the combined organic extracts were washed with water and saline. The subsequent evaporation of the solvent gave an oil, which distilled fractionally at 3

mmHg to give 2-allylhomocamphor (**27**) (bp 75—90 °C; 5 g) and 2,2-diallylhomocamphor (**28**) (bp>110 °C).

27, bp 110—113 °C/8 mmHg; $\nu(CCl_4)$: 3070, 1700, 1635, 990, and 910 cm^{-1}; $\delta(CCl_4)$: 0.71 (s, 3H), 0.91 (s, 6H), and 4.7—6.2 (m, 3H); *m/e*: 206 (M^+), 191, 163, 95. Found: C, 81.38; H, 10.62%. Calcd for $C_{14}H_{22}O$: C, 81.49; H, 10.74%.

28, bp 113—116 °C/3 mmHg; $\nu(CCl_4)$: 3070, 1695sh, 1685, 1630, 985, and 910 cm^{-1}; $\delta(CCl_4)$: 0.78 (s, 3H), 0.93 (s, 6H), and 4.7—6.2 (m, 6H). *m/e*: 246 (M^+), 231, 95.

2-(Carboxymethyl)homocamphor (29). 2-Allylhomocamphor (**27**, 4.1 g) in 500 ml of *t*-butyl alcohol was mixed with a solution of 24 g of $NaIO_4$ and 100 mg of $KMnO_4$ in 1 liter of water. To the mixture there was then added 40 ml of 5% aqueous potassium carbonate, and the whole was stirred at room temperature for 2 d.[25] The products were taken up in ether, and the acidic materials were extracted with a 5% aqueous sodium hydroxide solution to give a crystalline **29** (4.4 g, 100%).

29, mp 94—94.5 °C (from pentane); ν(KBr): 3300—2400 and 1695br cm^{-1}. Found: C, 69.39; H, 8.85%. Calcd for $C_{13}H_{20}O_3$: C, 69.61; H, 8.99%.

γ-Lactone 30. **29** (1.0 g) was converted into its methyl ester by treating it with ethereal diazomethane. After evaporating off the ether, a residual oil (1.07 g) was dissolved in 20 ml of methanol and was treated with 400 mg of $NaBH_4$ at 0 °C. After 2 h, a further 200 mg of $NaBH_4$ was added and stirring was continued for another 2 h. Concd hydrochloric acid (2 ml) was then added, drop by drop, and the whole was stirred for 10 min. After it had then been concentrated to a small volume, the products were extracted with ether. The extract was evaporated to give a crystalline oil (918 mg), from which 772 mg (89%) of γ-lactone **30** was collected.

30, mp 85—86 °C (from pentane); ν(KBr): 1755sh, 1735, and 1410 cm^{-1}; $\delta(CDCl_3)$: 0.89 (s, 3H), 1.00 (s, 3H), 1.10 (s, 3H), and 4.08 (d, 1H, J=5.5 Hz). Found: C, 74.95; H, 9.57%. Calcd for $C_{13}H_{20}O_2$: C, 74.96; H, 9.68%.

α-Methyl-γ-lactone 31. To a mixture of 5 ml of dry THF and 3.4 ml of a butyllithium–hexane solution (5.6 mmol) there was added 0.8 ml (5.7 mmol) of diisopropylamine (freshly distilled over NaH) at 0 °C, after which the mixture was stirred at that temperature for 45 min.[18] The whole was then cooled to −78 °C, and 1.03 g (5 mmol) of **30** in 10 ml of THF was added, drop by drop, during a 15-min period. Some excess methyl iodide (1 ml) was added all at once, and the mixture was stirred for 15 min. A saturated ammonium chloride solution (5 ml) was added to the mixture, and the products were taken up in ether. The ether extract was evaporated to give a crystalline residue (1.12 g). Recrystallization from pentane gave α-methyl-γ-lactone **31** (1.07 g, 97%); mp 116—117 °C (sublimable); ν(KBr): 1750 cm^{-1}; $\delta(CDCl_3)$: 0.87 (s, 3H), 0.99 (s, 3H), 1.10 (s, 3H), 1.27 (d, 3H, J=7.5 Hz), and 4.17 (d, 1H, J=5.5 Hz). Found: C, 75.43; H, 9.92%. Calcd for $C_{14}H_{22}O_2$: C, 75.67; H, 9.97%.

Dimethyl-γ-lactone 32. To lithium diisopropylamide (5.6 mmol) prepared as above, 972 mg (4.4 mmol) of **31** in 10 ml of THF was added, drop by drop, at −78 °C; the mixture was then stirred at that tempreature for 15 min. After 0.5 ml of HMPA had then been added, the whole was warmed to room temperature and 1 ml of methyl iodide was added. After 30 min stirring, 5 ml of a saturated ammonium chloride solution was added and the products were extracted with ether. The ether was evaporated to give a crystalline oil (1.01 g). Crystallization from pentane gave 909 mg (88%) of the dimethyl-γ-lactone, **32**, mp 106—107 °C; ν(KBr): 1755 cm^{-1}; $\delta(CDCl_3)$: 0.88 (s, 3H), 0.98 (s, 3H), 1.10 (s, 3H), 1.16 (s, 3H), 1.27 (s, 3H), and 4.13 (d, 1H, J=5.5 Hz). Found: C, 75.94; H, 10.17%. Calcd for $C_{15}H_{24}O_2$: C, 76.22; H, 10.23%.

Diol 33. To a solution of 845 mg of **32** in 20 ml of dry ether, an excess methyllithium–ether solution was added at 0 °C; the mixture was then stirred unitl **32** disappeared (VPC analysis). A large excess (1 g) of $LiAlH_4$ was added to the mixture, and the whole was refluxed for 1.5 h. After cooling to room temperature, the excess $LiAlH_4$ was carefully decomposed by the addition of ethyl acetate, and then an aqueous ammonium chloride solution. The ether extract, when evaporated, gave crystals (905 mg, 100%). The crystals showed two spots on TLC, and two recrystallizations from pentane afforded one isomer; mp 94—95 °C; ν(KBr): 3300br, 1110, and 1075 cm^{-1}; $\delta(CDCl_3)$: 0.82 (s, 3H), 0.89 (s, 3H), 0.98 (s, 6H), 1.14 (s, 3H), 1.17 (d, 3H, J=7 Hz), 3.60 (br. d. 1H J=4 Hz), and 3.82 (q, 1H, J=7 Hz). Found: C, 75.53; H, 11.91%. Calcd for $C_{16}H_{30}O_2$: C, 75.53; H, 11.88%.

Diketone 34. To a stirred solution of 2.4 g (24 mmol) of chromiun trioxide and 3.9 g (48 mmol) of pyridine in 60 ml of dichloromethane, 490 mg (1.9 mmol) of **33** in 10 ml of dichloromethane were added all at once, after which the mixture was stirred at room temperature for 15 min. The black materials were removed by filtration, and the filtrate was evaporated to give a brown residue. The residue was heated under reflux with 50 ml of pentane, and the undissolved material was removed by filtration. The filtrate was then evaporated to give colorless crystals (415 mg). Recrystallization from pentane afforded 280 mg of a diketone **34**. The mother liquor was chromatographed on silica gel (5 g, hexane–benzene=1 : 1) to give a further 78 mg of **34**.

34, mp 114—115 °C; ν(KBr): 1690sh and 1685 cm^{-1}: $\delta(CDCl_3)$: 0.73 (s, 3H), 0.88 (s, 3H), 0.92 (s, 3H), 1.15 (s, 3H), and 2.18 (s, 3H). Found: C, 76.59; H, 10.40%. Calcd for $C_{16}H_{26}O_2$: C, 76.75; H, 10.46%.

γ-Valerolactone 36. To a cooled solution (0 °C) of 3.82 g of **27** in 60 ml of dry ether, 20 ml of a 5% methyllithium–ether solution was added, drop by drop, after which the whole was stirred at room temperature for 1 h. An aqueous ammonium chloride solution was then added, and the products were taken up in ether. Evaporating the solvent gave a crude **35** (3.95 g); $\delta(CCl_4)$: methyl signals at 0.82, 0.92, 1.12, and 1.15.

To a stirred solution of 3.16 g of $KMnO_4$ in 12 ml of water and 6 ml of benzene containing 75 mg of $R(CH_3)_2C_6H_5CH_2N^+Cl^-$, 1.06 g of the above alcohol **35** was added, drop by drop, during a 10-min period. The temperature of the mixture was kept at 35—40 °C during addition. The mixture was then stirred at that temperature for 1 h,[19] and the precipitates were removed by filtration. The products were divided into a neutral part (0.81 g) and an acid part; the former was chromatographed on silica gel (10 g) to give a pure lactone **36** (0.48 g, 45%) in a crystalline form.

36, mp 95—97 °C (from pentane, in a sealed tube); ν(KBr): 1750 and 930 cm^{-1}; $\delta(CCl_4)$: 0.92 (s, 3H), 1.02 (s, 3H), 1.08 (s, 3H), 1.34 (s, 3H), 2.0 (d, 1H, J=17 Hz), 2.8 (dd, 1H, J=17 and 7 Hz). Found: C, 75.45; H, 9.70%. Calcd for $C_{14}H_{22}O_2$: C, 75.63; H, 9.97%.

α-Methyl-γ-valerolactone 37. To a stirred lithium diisopropylamide (0.65 mmol) in THF, 135 mg (0.61 mmol) of **36** in 15 ml of THF were added, drop by drop. After 15 min, 0.2 ml of methyl iodide was added all at once and stirring was continued for a further 15 min. A saturated ammonium chloride solution was added, and the products were taken up in ether to give crystalline **37** (143 mg, 100%).

37, mp 72—74 °C (from pentane, sublimable); ν(KBr): 1750 cm^{-1}; $\delta(CCl_4)$: 0.92 (s, 3H), 0.98 (s, 3H), 1.08 (s, 3H),

TABLE 1. REACTIONS OF 7a-METHYLPERHYDRO-2-BENZOFURANONE WITH P_2O_5–METHANESULFONIC ACID

Lactone(vi)	P_2O_5–MsOH	t/°C	h	Yield/%		Ratio vii/viii	Remarks
mg	g			vii	viii		
500	5	80	1	59	34	1.7	
503	5	50	24	56	23	2.4	Some recovery
510	5	30	143	52	8	6.5	12% recovery
	PPA[19]	70—80	3	25	25	1.0	
	PPA[19]	120	vacuum dist	5	20	0.3	20% indane

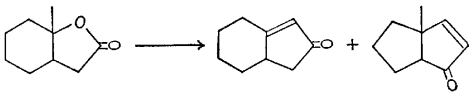

vi vii viii

1.42 (d, 3H, J=7 Hz), 1.43 (s, 3H), and 2.32 (br. q, 1H, J= 7 Hz). Found: C, 76.18; H, 10.25%. Calcd for $C_{15}H_{24}O_2$: C, 76.22; H, 10.24%.

Dimethyl-γ-valerolactone 38. α-Methyl-γ-valerolactone **37** was converted into the dimethyl derivative, **38**, in a quantitative yield when treated with excess lithium diisopropylamide and methyl iodide in the presence of HMPA.

38, mp 99—100 °C (from pentane); ν(KBr): 1740 cm^{-1}; δ(CCl_4): 0.88 (s, 3H), 0.90 (s, 3H), 1.08 (s, 3H), 1.23 (s, 3H), 1.46 (s, 3H), and 1.56 (s, 3H). Found: C, 76.71; H, 10.51%. Calcd for $C_{16}H_{26}O_2$: C, 76.75; H, 10.47%.

P_2O_5–Methanesulfonic Acid Treatment of 7a-Methylperhydro-2-benzofuranone (vi). General procedure: The lactone (vi) was heated at a given temperature with 10 parts (weight) of a P_2O_5–methanesulfonic acid (1 : 10) solution.[21] The dark red solution was then poured into ice water, and the products were taken up in ether. The ether extract was washed with water and saline, and dried over anhydrous sodium sulfate. In every case, only two products (vii) and (viii) were recognized on VPC. The products were separated by column chromatography on silica gel. The results are shown on Table 1.

1,5,5,11,11-Pentamethyltricyclo[6.2.1.0^{2,6}]undec-2-en-4-one (39) To a stirred solution of 10 g of P_2O_5–methanesulfonic acid, there was added 395 mg of **38**, after which the mixture was heated at 70 °C for 2 h. After cooling, the red solution was poured into water (50 ml) and extracted with chloroform. The chloroform layer was washed with water, aqueous sodium hydrogencarbonate, and saline and dried over anhydrous sodium sulfate. The subsequent evaporation of the solvent gave an oil (380 mg), which was then chromatographed on silica gel (20 g). The elution with chloroform afforded 195 mg (50%) of a cyclopentenone **39** as an oil.

39, bath temp 83—86.5 °C/0.05 mmHg (Kugelrohr dist); mp 38—40 °C (from pentane, −78 °C); ν(CCl_4): 1700 and 1605 cm^{-1}; δ(CCl_4; the Δ values show the pseudocontact shift upon the addition of 0.05 eq of Eu-FOD): 0.78 (s, 3H, Δ 0.17), 0.91 (s, 3H, Δ 0.52), 0.98 (s, 3H, Δ 0.07), 1.03 (s, 3H, Δ0.51), 1.12 (s, 3H, Δ0.11), 2.58 (ddd, 1H, J=2, 9, and 11.5 Hz, Δ 0.38), and 5.51 (d, 1H, J=2 Hz, Δ 0.97). Found: C, 82.68; H, 10.49%. Calcd for $C_{16}H_{24}O$: C, 82.70; H, 10.41%.

The present work was partially supported by a Grant-in-Aid for Scientific Research No. 164147 from the Ministry of Education, Science and Culture.

References

1) a) M. Kurono, Y. Nakadaira, S. Onuma, K. Sasaki, and K. Nakanishi, *Tetrahedron Lett.*, **1963**, 2153; b) K. Nakanishi, M. Kurona, and N. S. Bhacca, *ibid.*, **1963**, 216; c) K. Ueda, S. Uyeo, Y. Yamamoto, and Y. Maki, *ibid.*, **1963**, 2167.

2) a) S. Kumazawa, Y. Nakano, T. Kato, and Y. Kitahara, *Tetrahedron Lett.*, **1974**, 1757; b) T. Kato, H. Takayanagi, T. Suzuki, and Y. Uyehara, *ibid.*, **1978**, 1201.

3) I. Kitagawa, H. Shibuya, H. Fujioka, A. Kajiwara, Y. Yamamoto, A. Takagi, K. Suzuki, and M. Hori, Symposium Papers, 22nd Symposium on the Chemistry of Natural Products, Fukuoka, October, 1979, p. 132.

4) A part of the work was preliminarily reported: Y. Inouye, C. Fukaya, and H. Kakisawa, Abstr. No. 2I27, 35th Annual Meeting of the Chemical Society of Japan, Sapporo, August, 1976. The retrosynthetic analysis of a taxane framework we planned is as follows:

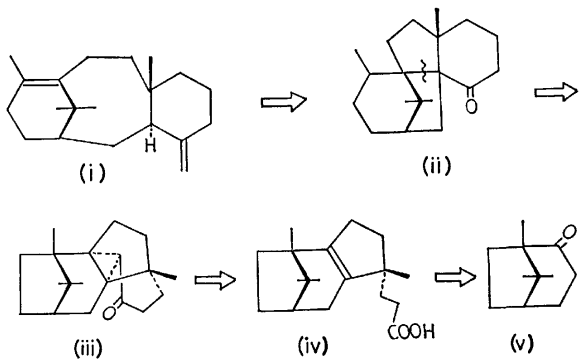

5) G. Büchi, W. D. MacLeod, Jr., and J. Padillao, *J. Am. Chem. Soc.*, **86**, 4438 (1964).

6) Taken in part from the Doctoral Thesis of C. Fukaya, Tokyo Kyoiku University, 1977.

7) J. D. White and P. S. Manchand, *J. Org. Chem.*, **38**, 720 (1973).

8) a) R. H. Herr, D. M. Wieland, and C. R. Johnson, *J. Am. Chem. Soc.*, **92**, 3813 (1970); b) R. H. Herr and C. R, Johnson, *ibid.*, **92**, 4979 (1970).

9) G. Zweifel and H. C. Brown, *Org. React.*, Vol. 13, 1 (1963).

10) Numerous examples of rear-side attack of reagents on the geminate dimethyl groups in camphor or pinene have been reported. See, for example, "Rodd's Chemistry of Carbon Compounds," II C (1969).

11) K. Matoka, K. Yoshii, M. Yoshioka, T. Yamazaki, and Y. Sasaki, *Yakugaku Zasshi*, **89**, 506 (1969).

12) a) E. M. Kaiser and C. R. Hauser, *J. Org. Chem.*, **33**, 3402 (1968); b) D. N. Crouse and D. Seebach, *Chem. Ber.*, **101**, 3113 (1968).

13) A. G. Schulty and Y. K. Yee, *J. Org. Chem.*, **41**, 4045 (1976).

14) a) J. A. Marshall, N. H. Andersen, and J. W. Schlicher,

J. Org. Chem., **35**, 858 (1970); b) A. E. G. Miller, J. W. Biss, and L. H. Schwartzman, *ibid.*, **24**, 627 (1959).
15) D. Seyferth, S. O. Grim, and T. O. Read, *J. Am. Chem. Soc.*, **83**, 1617 (1961).
16) H. O. House, W. L. Respess, and G. W. Whitesides, *J. Org. Chem.*, **31**, 3128 (1966).
17) J. H. Fried, A. N. Nutile, and G. E. Arth, *J. Am. Chem. Soc.*, **82**, 5704 (1960).
18) a) G. H. Posner and G. L. Loomis, *J. Chem. Soc., Chem. Commun.*, **1972**, 892; b) J. L. Herrman and R. H. Schlessinger, *ibid.*, **1971**, 711.
19) *Cf.* C. M. Starks, *J. Am. Chem. Soc.*, **93**, 195 (1971).
20) J. Ficini and A. Manjean, *Bull. Soc. Chim. Fr.*, **1972**, 4392.
21) P. E. Eaton, G. R. Carlson, and J. T. Lee, *J. Org. Chem.*, **38**, 4071 (1973).
22) H. Gilman, R. G. Jones, and L. A. Woods, *J. Org. Chem.*, **17**, 1630 (1952).
23) R. Ratchiffe and R. Rodehorst, *J. Org. Chem.*, **35**, 4000 (1970).
24) H. Favre and J.-C. Richer, *Can. J. Chem.*, **37**, 417 (1959).
25) J. W. ApSimon, A. S. Y. Chan, W. G. Craig, and H. Krehm, *Can. J. Chem.*, **45**, 1439 (1967).

Reaction Paths of the Photochemical Electrocyclic Reaction of Acrylaldehyde. A Possible Path *via* a Zwitterion

Osamu KIKUCHI,* Hiroshi KUBOTA, and Keizo SUZUKI
Department of Chemistry, The University of Tsukuba, Sakura-mura, Ibaraki 305
(Received June 16, 1980)

The photochemical electrocyclic reaction paths of *s-cis*-acrylaldehyde to oxetene were examined on the basis of the potential surfaces obtained by the MINDO/3 CI calculation, and compared with those of the corresponding conjugated hydrocarbon system. The strong S_0-S_2 interaction, which appears in the disrotatory mode of the cyclization of butadiene, was not observed in the acrylaldehyde–oxetene system. There appears to be a step-by-step path, in which the $\pi\rightarrow\pi^*$ induced rotation of the methylene group is followed by the ring-closing step. The zwitterion in which the positive charge is localized on the terminal carbon atom is involved in this step. Since the σ lone-pair electrons of the oxygen atom play a key role in the ring-closing step, this path is characteristic of the hetero-atom conjugated system and cannot be deduced by analogy or by a simple extension of the concepts established for the photoreactions of all-hydrocarbon conjugated systems. The possible decay paths from acrylaldehyde in the excited states were also discussed.

Orbital symmetry arguments[1] and calculated reaction paths[2] have well elucidated the thermal and photochemical electrocyclic reactions of the all-hydrocarbon conjugated system, **1**→**2**. Little attention, however, has been paid to the electrocyclic processes of the hetero-atom conjugated system, in which one of the terminal methylene groups is replaced by a hetero atom. The formal photochemical electrocyclic reaction of *s-cis*-acrylaldehyde **3**→**4**, for example, has been considered to proceed by means of a mechanism similar to that of *s-cis*-butadiene, **1**→**2**, if the $\pi\rightarrow\pi^*$

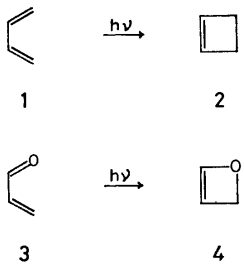

1 2

3 4

excited state is involved.[3] However, there are two essential differences between the **1**→**2** and **3**→**4** reactions. The first is the mode of rotation of the methylene groups. In the conjugated hydrocarbon system, the disrotatory and conrotatory modes give very different shapes of the potential cuves, while there is no distinction between these two modes in the **3**→**4** reaction, since only one methylene group is involved in the acrylaldehyde–oxetene system. It is thus impossible to consider the photochemical reaction mechanism of the **3**→**4** reaction by simple analogy with the disrotatory cyclization of the **1**→**2** reaction.

The second difference is the existence of the lone-pair electrons of the terminal hetero atom. Since the lone-pair electrons are distributed on the σ framework where the new σ bond is being formed, the lone-pair electrons should participate in the electrocyclic reaction mechanism of the hetero-atom conjugated system, even if the photochemical reaction proceeds from the $\pi\rightarrow\pi^*$ excited state. Because of these essential differences, the electron behavior during the **3**→**4** reaction cannot be understood sufficiently well by analogy with the **1**→**2** reaction; therefore, it is worthwhile to investigate the reaction processes of the **3**→**4** reaction and to compare the reaction mechanism with that of the all-hydrocarbon system, **1**→**2**.

The experimental evidence applicable to the **3**→**4** reaction has been reported by Friedrich and Schuster.[4] The irradiation of 3,4-dimethyl-3-penten-2-one in a hexane solution through a Pyrex filter gave no observable reaction, while the irradiation with Vicor-filtered UV light gave cyclic compound, the oxetene. They also investigated the thermal ring-opening reaction of the methyl-substituted oxetene and compared it with that of the cyclobutene derivatives.[4b]

In the present study, the potential curves for the ground and several excited states of the **3**→**4** reaction were obtained by means of the semi-empirical MINDO/3[5] CI calculations. On the basis of these potential surfaces, the possible photochemical paths of the **3**→**4** reaction are discussed. Attention is mostly paid to the clarification of the differences between the reaction mechanisms of the **1**→**2** and **3**→**4** reactions, and also to the comparison between the theoretical and experimental results.

Method of Calculation

The structures of Compounds **1**—**4** were optimized by the SCF (without CI) calculation; Fletcher's variable metric method[6] was employed. They are shown in Fig. 1. The potential surfaces for the **1**→**2** and **3**→**4** reactions are the functions of many geometrical variables. In the present study, the potential surfaces were calculated with respect to two independent parameters. One of these is the rotation algle, θ, of the methylene group(s). All the other geometrical variables were allowed to vary simultaneously from their inital to final values. This variation is expressed by the second parameter, d, which varies from 0.0(initial) to 1.0(final). In the CI calculation, 47 and 43 configuration functions were selected from the singly- and doubly-excited configurations for the singlet and triplet states respectively. MINDO/3 underestimates the strain energy of small cyclic compounds, while it overestimates the heats of formation of acrylaldehyde and butadiene.[5] The

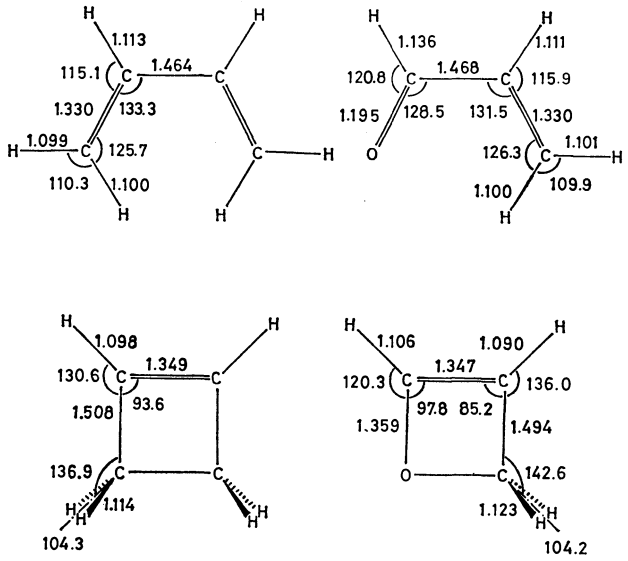

Fig. 1. Molecular structures of *s-cis*-butadiene, cyclobutene, *s-cis*-acrylaldehyde, and oxetene optimized by the MINDO/3 method. Bond lenghts are in Å, bond angles are in degrees.

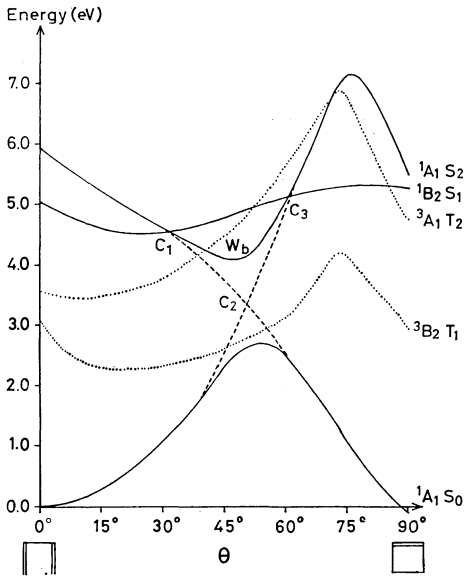

Fig. 2. Potential energy curves for the disrotatory mode of the butadiene–cyclobutene system. All the geometrical variables are varied simultaneously between the optimized structures of butadiene and cyclobutene.

Table 1. Excitation energies (eV) of *s-trans*-butadiene and *s-trans*-acrylaldehyde as calculated by the MINDO/3 CI method

State	MINDO/3	*ab initio*[2c]	Obsd	
Butadiene				
^1B_u	5.11	7.69	5.92[7a]	6.05[7b]
^3A_g	3.35	6.22	4.91[7a]	
^3A_u	3.11	4.28	3.20[7a]	3.32[7c]
Acrylaldehyde				
$^1n\rightarrow\pi^*$	3.48		3.21[7d]	
$^1\pi\rightarrow\pi^*$	5.70		6.41[7d]	
$^3\pi\rightarrow\pi^*$	3.27		3.01[7d]	

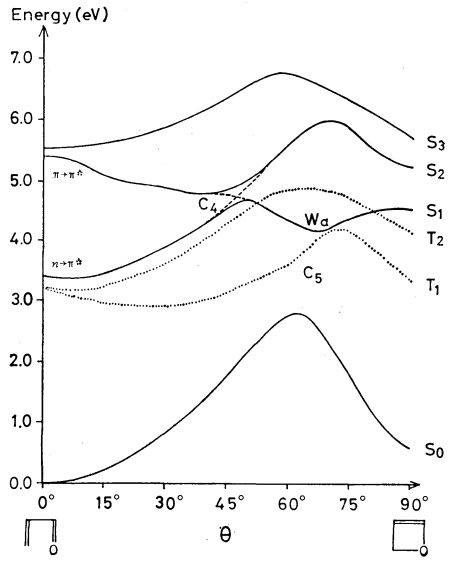

Fig. 3. Potential energy curves for the acryladehyde–oxetene system. All the geometrical variables are varied simultaneously between the optimized structures of acryladehyde and the oxetene.

excitation energies as calculated by MINDO/3 CI were compared with the experimental values (Table 1). Although the MINDO/3 and MINDO/3 CI calculations do not give sufficiently good results for the energetics of the present systems, we feel that the present objectives can be achieved satisfactorily on the basis of the MINDO/3 calculations.

Results and Discussion

Linear Variation of Geometrical Variables. First let us consider the concerted path in which the θ and d parameters are changed simultaneously. Figure 2 shows the potential curves of several electronic states for the disrotatory mode of the butadiene–cyclobutene system. Their shapes are very similar to those obtained previously by semi-empirical[2b] and *ab initio*[2c] methods. Notice two important features which appear in Fig. 2. The first is a true crossing at C_1 which takes place at the beginning of the cyclization and which involves the $\pi\rightarrow\pi^*$ singly-excited B_2 state and its doubly-excited counterpart. The second is an avoiding crossing at C_2 involving the ground state and the $\pi\rightarrow\pi^*$ doubly-excited state. The cyclobutene formation from the $\pi\rightarrow\pi^*$ state of butadiene can be understood in terms of these two crossings; the $\pi\rightarrow\pi^*$ state of butadiene populates the W_b well through the C_1 crossing, and this well is a leakage channel[8] from the excited state to the ground state.

Figure 3 shows the corresponding potential curves for the *s-cis*-acrylaldehyde–oxetene system. In this system, there is no distinction between the disrotatory and conrotatory modes of the methylene rotation,[9] and both the thermal and photochemical processes can be considered on the basis of these potential curves. The thermal ring-opening reaction of the substituted

oxetene has been studied by Friedrich and Schuster.[4b] The activation enthalpy of 1,2,3,3-tetramethyloxetene was found to be 100—105 kJ mol^{-1} (solvent dependent),[4b] while that of 1,2,3,4-tetramethylcyclobutene is 152 kJ mol^{-1}.[4b] The calculated values 213 kJ mol^{-1} for the oxetene and 242 kJ mol^{-1} for cyclobutene,[10] are somewhat larger than the observed values for the substituted compounds. This discrepancy comes partially from a deficiency in the MINDO/3 approximation, which overestimates the heats of formation of butadiene and acrylaldehyde, while underestimating the strain energy of the cyclic compounds. However, the faster thermal ring opening of the oxetene in comparison with that of cyclobutene is reflected in the calculated values.

The S_1 and T_1 states of acrylaldehyde are the singlet and triplet $n\rightarrow\pi^*$ states which are missing in butadiene. The S_2 and T_2 states are the $\pi\rightarrow\pi^*$ states which correspond to the B_2 singlet and triplet states of butadiene respectively. The most important feature observed in the potential curves of the acrylaldehyde–oxetene system is the absence of the crossings related to the doubly-excited configuration; they appear at C_1 and C_2 in the case of the butadiene–cyclobutene system. This is due to the non-symmetric property of acrylaldehyde with respect to the vertical plane; no crossing occurs between the π_2 and π_3 orbitals. Two new types of crossings are observed in the acrylaldehyde–oxetene system. They are the C_4 crossing between the $n\rightarrow\pi^*$ and $\pi\rightarrow\pi^*$ states, and the C_5 crossing between S_0 and S_1 states at the later part of cyclization. The concerted cyclization path of *s-cis*-acrylaldehyde may be elucidated as follows: the reaction proceeds from the $\pi\rightarrow\pi^*$ excited state of acrylaldehyde, this state reaches the W_a well through the C_4 crossing, and the non-adiabatic transition from W_a to the ground state gives the oxetene. As will be described later, the W_a well is not a clear well on the two-dimensional S_1 surface, and the transition from the W_a well to the ground state is expected to be much more inefficient than that from the W_b well to the ground state in the butadiene–cyclobutene system.

The $n\rightarrow\pi^*$ excited acrylaldehyde cannot reach the W_a well because of the high activation energy, and no appreciable formation of the oxetene is expected from the $n\rightarrow\pi^*$ state of acrylaldehyde. This agrees well with the experimental evidences.[4b]

Step-by-step Path via *a Zwitterion.* The rotation of methylene occurs easily in the $\pi\rightarrow\pi^*$ excited state of acrylaldehyde to give the twisted acrylaldehyde. The lower electronic states of the twisted acrylaldehyde involve the diradical,[11] $D_{\sigma\pi}$, and two zwitterions, Z_+ and Z_-.[12] The energies of several states of the twisted

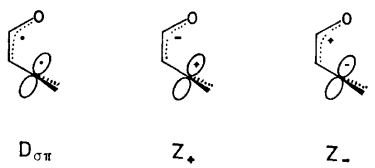

acrylaldehyde are shown in Fig. 4. The Z_+ zwitterion, in which the positive charge is located at the terminal

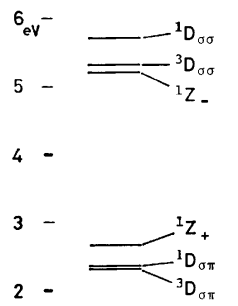

Fig. 4. Energy levels for several lower states of the twisted acrylaldehyde.

carbon atom, can undergo ring closing very easily, since a strong attraction is expected between the positive charge and the lone-pair electrons of the oxygen atom. The step-by-step path in which the

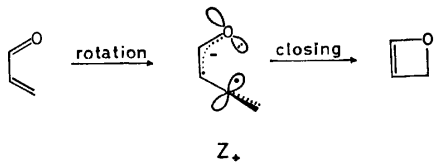

rotation of the methylene group is followed by the ring-closing is expected to exist. The state correlation diagram for this path is shown in Fig. 5.[13] As may be seen from Fig. 5, the excited Z_+ state correlates with the ground state of the oxetene. It can thus be expected that, if the Z_+ state of the twisted acrylaldehyde is formed from the $\pi\rightarrow\pi^*$ excited state of acrylaldehyde, the oxetene formation proceeds without any activation

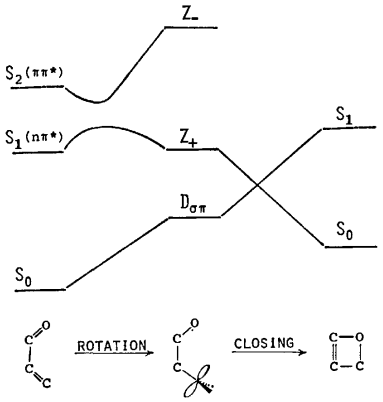

Fig. 5. State correlation diagram for the acrylaldehyde–twisted acrylaldehyde–oxetene system.

energy or with only a small activation energy. The potential curves along the suggested path are shown in Fig. 6. The molecule has a distinctive zwitterionic character between A and C on the Z_+ potential curve.[15] Figure 6 indicates that the internal conversion from the Z_+ state to the $D_{\sigma\pi}$ state occurs efficiently at the twisted acrylaldehyde; this results in the reproduction of the ground state of acrylaldehyde, and no formation of oxetene is expected. However, if the Z_+ zwitterion is formed from the $\pi\rightarrow\pi^*$ excited state[16] and has a high

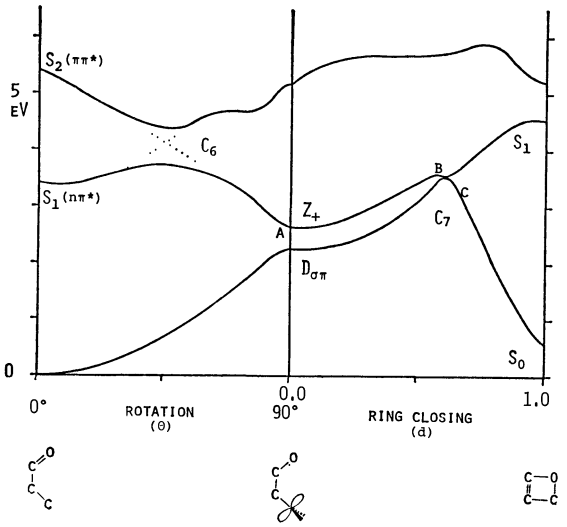

Fig. 6. Potential curves for the step-wise path of the acrylaldehyde–oxetene system. Only three lower singlet states are shown. θ is the rotation angle of the terminal methylene and d represents the simultaneous change in all the geometrical variables other than θ.

vibration energy, it can cyclize to form the oxetene *via* the C_7 crossing.

An important role of the zwitterion has been pointed out by Dauben *et al.*[14,17] and by Salem[18] in the photochemical cyclization of non-symmetric polyenes. In

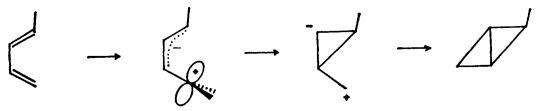

5 6

the **5→6** reaction, the primary step is the photoinduced rotation of the terminal methylene, which gives the zwitterion. This step is followed by the 1,3 ring closing of the anionic allyl group by another rotation about the C–C bonds. The reaction scheme of the zwitterion in the present **3→4** reaction is clearly different from that proposed for the **5→6** process. In the **3→4** reaction, the ring closing occurs between the positive carbon atom and the lone-pair electrons of the terminal hetero atom, without another rotation. This path can occur only if the terminal atom has the lone-pair electrons and is characteristic of the hetero-atom conjugated system.

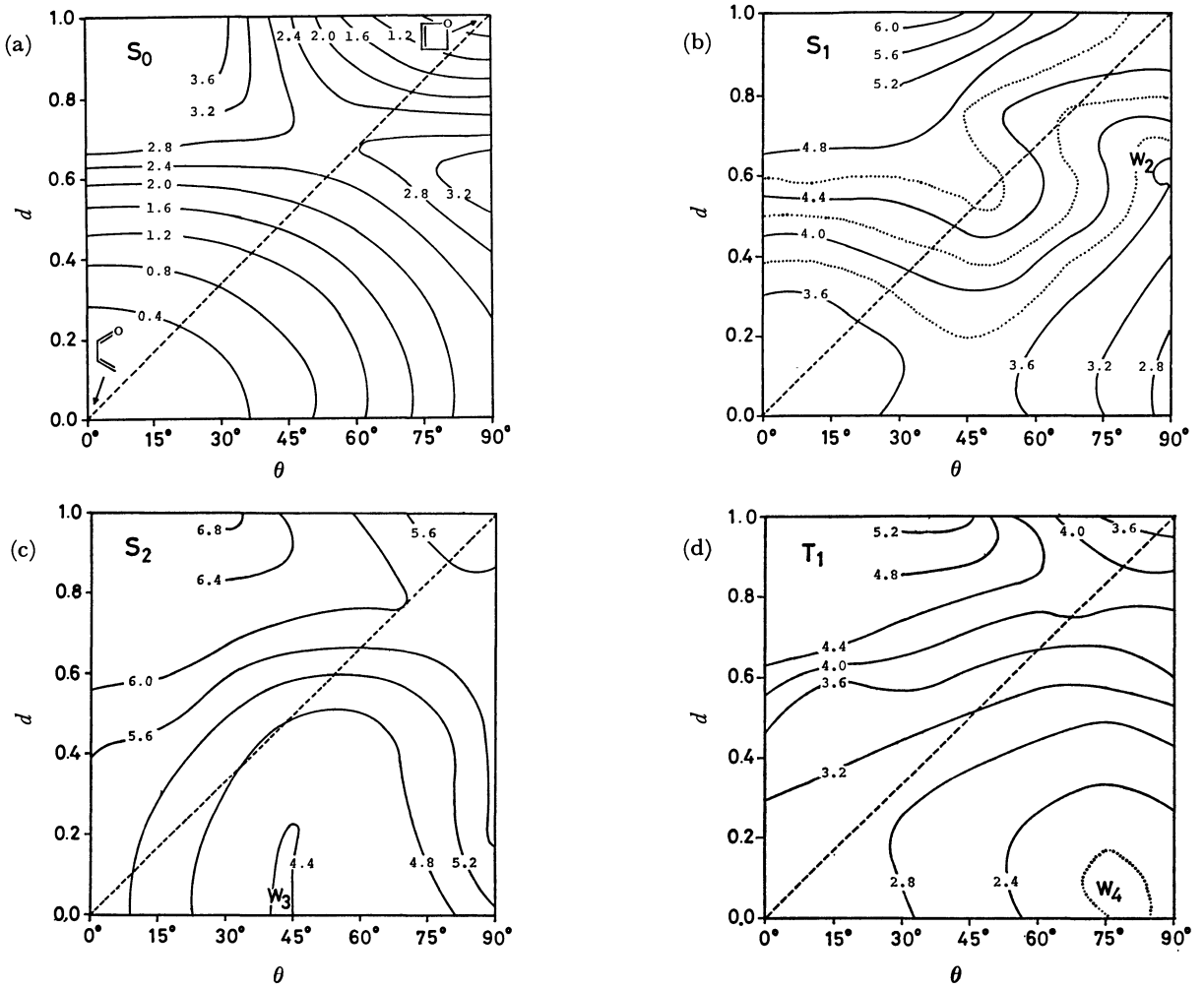

Fig. 7. Two-dimensional potential surfaces of (a) S_0, (b) S_1, (c) S_2, and (d) T_1 states of the acrylaldehyde–oxetene system. The energies (eV) are relative values with respect to that of the ground state of *s-cis*-acrylaldehyde.

Two-dimensional Potential Surfaces. The potential surfaces of several electronic states of the acrylaldehyde–oxetene system were obtained as the function of two geometrical parameters, θ and d. They are shown in Fig. 7. Although two-dimensional surfaces are still only a distant approximation of the real multi-dimensional hypersurfaces, they give much more information than one-dimensional ones; they are useful as confirmation of and complement to the results obtained from the one-dimensional potential curves. The $n\rightarrow\pi^*$ singlet state of acrylaldehyde is located at the energy minimum on the S_1 surface and is stable even when the molecular structure is deformed (Fig. 7-b). An important characteristic of this S_1 surface is the absence of the W_a well which appears in one-dimensional curves (Fig. 3). Instead, the W_a well in Fig. 3 is a part of the shallow well, W_2, the minimum point of which is located at the C_7 crossing point in Fig. 6. The transition from the W_2 region to the ground state occurs very easily to form the oxetene.

From Fig. 7-c, it may be seen that acrylaldehyde in its $\pi\rightarrow\pi^*$ excited state can move around most ($0.0<\theta<0.6$, and $0°<d<90°$) of the S_2 surface. The transition from the W_3 well to the S_1 state produces the normal acrylaldehyde or the twisted acrylaldehyde. However, Fig. 7-b indicates that the S_1 species formed from the W_3 well is capable of access to the W_2 well. In this case, the oxetene is formed *via* the Z_+ zwitterion. The smallest energy separation between the S_1 and S_2 surfaces is observed at the central region of the two-dimensional maps; this region corresponds to the C_4 crossing region in Fig. 3. The strong coupling between S_1 and S_2 is suggested by the calculated CI coefficients, and an appreciable transition from S_2 to S_1 is expected in this region. As may be seen from Figs. 7-b and 7-c, the Z_+ zwitterion (corresponding to the W_2 well) is formed from the S_1 species generated from S_2 through the C_4 crossing. From the analysis of the two-dimensional surfaces, it is confirmed that there is a path through the Z_+ zwitterion in the **3→4** photochemical process.

Figure 7-d shows the potential surface of the T_1 triplet state. The acrylaldehyde side of this surface corresponds to the $\pi\rightarrow\pi^*$ triplet state of acrylaldehyde. The rotation of methylene occurs easily in this state and gives the twisted acrylaldehyde, the triplet diradical, $^3D_{\sigma\pi}$. The crossing of this surface with the lowest S_0 state occurs near the W_4 well, and the reproduction of the ground state of acrylaldehyde proceeds from the triplet T_1 state through this singlet-triplet crossing. This path corresponds to the photochemical *cis-trans* isomerization of acrylaldehyde. The intersystem crossing rate between the $^3D_{\sigma\pi}$ and $^1D_{\sigma\pi}$ states is not expected to be particularly fast, but the intersystem crossing is still an efficient process, since the triplet is at a minimum.[14]

Conclusion

The possible decay paths for the photochemically excited *s-cis*-acrylaldehyde have been considered on the basis of the potential surfaces obtained by MINDO/3 CI calculations. Two possible paths have been predicted for the photochemical electrocyclic reaction of *s-cis*-

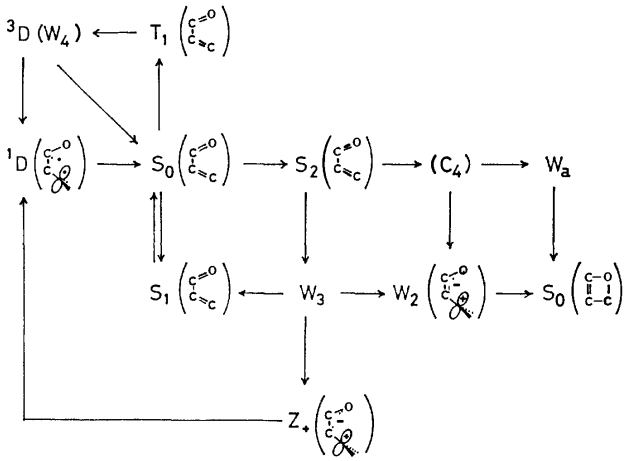

acrylaldehyde into oxetene. The concerted type of cyclization proceeds from the $\pi\rightarrow\pi^*$ state: acrylaldehyde $\rightarrow S_2\rightarrow C_4\rightarrow W_a\rightarrow$oxetene. The step-by-step path, in which the Z_+ zwitterion is involved, also proceeds from the $\pi\rightarrow\pi^*$ state: acrylaldehyde$\rightarrow S_2\rightarrow(C_4$ or $W_3)\rightarrow W_2\rightarrow$ oxetene. Since no quantitative examinations were performed for the transition probability between the electronic states, the efficiency of the above two possible paths to form the oxetene can not be determined from the present study. The W_a well appearing in the concerted path is actually a part of the W_2 well which corresponds to the Z_+ zwitterion. Therefore, the Z_+ zwitterion also plays an important role in the concerted-type pathway. The path *via* the Z_+ zwitterion proposed in this study is a new type of mechanism for the formal photochemical electrocyclic reactions. Since the lone-pair electrons play a key role in the ring-closing step, this path can not be deduced by analogy or a simple extension of the concepts established for the all-hydrocarbon conjugated systems.

References

1) R. B. Woodward and R. Hoffmann, *J. Am. Chem. Soc.*, **87**, 395 (1965); H. C. Longuet-Higgins and E. W. Abrahamson *ibid.*, **87**, 2045 (1965); K. Fukui, *Bull. Chem. Soc. Jpn.*, **39**, 498 (1966).

2) a) W. Th. A. M. van der Lugt and L. J. Oosterhoff, *J. Am. Chem. Soc.*, **91**, 6042 (1969); b) O. Kikuchi, *Bull. Chem. Soc. Jpn.*, **47**, 1551 (1974); c) D. Grimbert, G. Segal, and A. Devaquet, *J. Am. Chem. Soc.*, **97**, 6629 (1975); d) K. Hsu, R. J. Buenker, and S. D. Peyerimhoff, *ibid*,. **94**, 5639 (1972).

3) N. J. Turro, "Modern Molecular Photochemistry," Benjamin/Cummings, Menlo Park, Calif. (1978), p. 508.

4) a) L. E. Friedrich and G. B. Schuster, *J. Am. Chem. Soc.*, **91** 7204 (1969); b) **93**, 4602 (1971); c) **94**, 1193 (1972).

5) R. C. Bingham, M. J. S. Dewar, and D. H. Lo, *J. Am. Chem. Soc.*, **97**, 1285 (1975).

6) R. Fletcher, *Computer J.*, **13**, 317 (1970).

7) a) O. A. Mosher, W. M. Flicker, and A. Kuppermann, *Chem. Phys. Lett.*, **19**, 332 (1973); b) W. C. Pryce and A. D. Walsh, *Proc. R. Soc. London, Ser. A*, **174**, 220 (1940); c) D. F. Evans, *J. Chem. Soc.*, **1960**, 1735; d) G. Herzberg, "Molecular Spectra and Molecular Structure III," D. Van Nostrand Co., Inc., Toronto (1967), p. 648.

8) J. Michl, *J. Mol. Photochem.*, **4**, 243 (1972).

9) Since only one methylene group is involved in acrylaldehyde, there is no distinction between the conrotatory and disrotatory modes, which can be defined by means of the relative motion of the two terminal methylene groups. However, it may be interesting to illustrate the change in the orbital shape on the oxygen atom, which is induced by the rotation of the terminal methylene. The two highest occupied MO's, ϕ_{10} and ϕ_{11}, and the lowest unoccupied MO, ϕ_{12}, are shown here for acrylaldehyde, and also for the structure in which the terminal methylene group is twisted by 30°. When the terminal methylene group is rotated, the lone-pair orbital (ϕ_{11}) and the occupied π orbital (ϕ_{10}) of acryladehyde mix well to give the ϕ_{10} and ϕ_{11} MO's of the twisted structure, while the OCC part of the LUMO is unchanged. From these MO shapes, we may say that the orbital fragments on the oxygen atom in the occupied ϕ_{10} and ϕ_{11} MO's rotate in a disrotatory-like manner with respect to the methylene group. However, it should be noted again that we cannot define the methylene rotation in acrylaldehyde as the disrotatory rotation: only one kind of rotation exists in acrylaldehyde,.

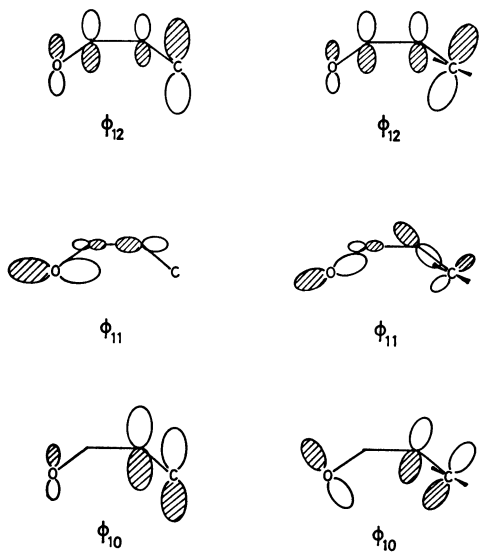

Planar 30° Twisted

10) The value was obtained from the potential curves for the conrotatory mode of the isomerization of butadiene.

11) L. Salem and C. Rowland, *Angew. Chem. Int. Ed. Engl.*, **11**, 92 (1972).

12) The Z_+ zwitterion has the same symmetry property as the D_{oo} diradical, in which two unpaired electrons occupy the carbon 2p AO and the lone-pair orbital of the oxygen atom. The Z_+ zwitterion is lower in energy than the D_{oo} diradical in the twisted acrylaldehyde.

13) The correlation between the twisted structure and the cyclic one can be determined simply by counting the σ and π electrons on the reaction centers.[14)]

14) W. G. Dauben, L. Salem, and N. J. Turro, *Acc. Chem. Res.*, **8**, 41 (1975).

15) The HOMO of the A(θ=90°, d=0), B(θ=90°, d=0.5), or C(θ=90°, d=2/3) conformation is the second (nonbonding type) π orbital, and the LUMO is the σ AO of the terminal carbon atom. The net charges at the terminal carbon atom in the A, B, and C conformations are in the range of + 0.65—+0.75.

16) The experimental evidence reported by Friedrich and Schuster[4a)] suggests that the photochemical cyclization of methyl-substituted acrylaldehyde occurs from the $\pi\rightarrow\pi^*$ state.

17) W. G. Dauben and J. S. Ritsher, *J. Am. Chem. Soc.*, **92**, 2925 (1970).

18) L. Salem, *Acc. Chem. Res.*, **12**, 87 (1979).

Dehydrooligopeptides. II. The Synthesis of Dehydrodehydrodipeptides by Direct Coupling and Base-catalyzed β-Elimination[1]

Chung-gi SHIN,* Yasuchika YONEZAWA, Masatoshi TAKAHASHI, and Juji YOSHIMURA†

Laboratory of Organic Chemistry, Faculty of Technology, Kanagawa University, Rokkakubashi, Kanagawa-ku, Yokohama 221

†*Laboratory of Chemistry for Natural Products, Faculty of Science, Tokyo Institute of Technology, Nagatsuta, Midori-ku, Yokohama 227*

(Received June 19, 1980)

The direct coupling between N-protected α-dehydroamino acid (**1**) and N-free α-dehydroamino acid ester (**2**) by the acid-chloride method was carried out to give several dehydrodehydrodipeptides (**7**). Furthermore, the two kinds of dehydrodipeptides with a hydroxyl group, obtained by the coupling of **1** with a serine or threonine ester, and that of N-protected serine or threonine with **2**, followed by mesylation and subsequent base-catalyzed β-elimination gave a number of **7** substances in good yields. The configurational structures of **7** obtained by both direct condensation and elimination were found to have (*Z*,*Z*)-geometry.

Much attention has been focused on the correlation between the structure and the bioactivity of dehydrooligopeptides containing one or more α-dehydroamino acid (DHA or ⊿AA)[2] residues.[3-7] Recently, antibiotic berninamycin A, a cyclodehydrodecapeptide with two dehydrodehydrodipeptide (⊿DHP) sequences and seven DHA moieties, has been isolated from a culture of *Streptomyces bernensis*, and the primary structure confirmed, by Liesch and Rinehart.[8] However, concerning the synthesis of ⊿DHP, few reports have been published on its preparation by means of the base-catalyzed β-elimination or by the direct coupling between two different DHA's, these being the indirect and restricted preparative methods from unsaturated azlactone.[9,10]

In a previous communication,[11] we briefly reported on the synthesis of the N-protected ⊿DHP ester by the coupling of benzyloxycarbonyl (Cbz)–DHA (**1**) with the N-free DHA ester (**2**) by the acid-chloride method. Here, we wish to report on a method of synthesis featuring the base-catalyzed β-elimination to dehydrodipeptide with a leaving group; we wish also to describe the direct method in detail.

Results and Discussion

Coupling of (Z)-DHA with β-Hydroxy α-Amino Acid. In order to prepare a dehydrodipeptide containing a Ser or Thr residue at the C- or N-terminus according to the method previously reported by us,[1,12] first, the coupling of **1** with α-amino acid ester was performed. The (*Z*)-**1** compound, as a carboxyl component, readily reacted with a racemic Ser or Thr ester by the usual peptide synthetic method [mixed anhydride (MA), dicyclohexylcarbodiimide (DCC), acid chloride, and azide method] to give Cbz–(*Z*)-α-dehydroaminoacyl–Ser and –Thr esters (**3**) respectively, as a colorless syrup or crystals, in *ca.* 70% yields. Therefore, although the yield was not significantly different, the preparation of **3** by the DCC method was found to be superior to that by the other methods. In Table 1, the yield of **3** by the DCC method is listed.

On the other hand, N-protected Ser or Thr was also coupled with (*Z*)-**2** as an amine component by the similar DCC method to give Cbz–Ser– and –Thr–(*Z*)-α-dehydroamino acid esters (**4**) respectively as colorless crystals in *ca.* a 34% yield. However, because of the weak basicity of the amino group in the amine component, the yield was lower than that of **3**, and the coupling of the α-dehydrophenylalanine ester with Cbz–Ser or –Thr was found to proceed to only a very small degree.

In the IR spectral data, the characteristic differences between **3** and **4** could not be recognized. The absorption bands of the hydroxyl and NH (3475—3175 cm^{-1}), ester carbonyl (1760—1720 cm^{-1}), secondary amide (1665—1625 cm^{-1}), and carbon-carbon double bond (1670—1620 cm^{-1}) functions are consistent with the assignment of the dehydrodipeptide structure.

The chemical shifts and the coupling constants of **3** and **4** were assigned as is shown in Tables 1 and 2. In the NMR spectrum of **3**, the signals at δ 4.56—4.76 as double doublets or double triplets, at δ 7.07—7.53 as doublets, and at δ 2.84—3.80 as broad singlets are attributable to methine, NH, and hydroxyl protons of the α-AA residue, respectively and the signals at δ 5.34—6.08, 6.37—7.10, and 6.76—7.52 regions as singlets, to vinyl, olefinic, and NH protons of the ⊿AA

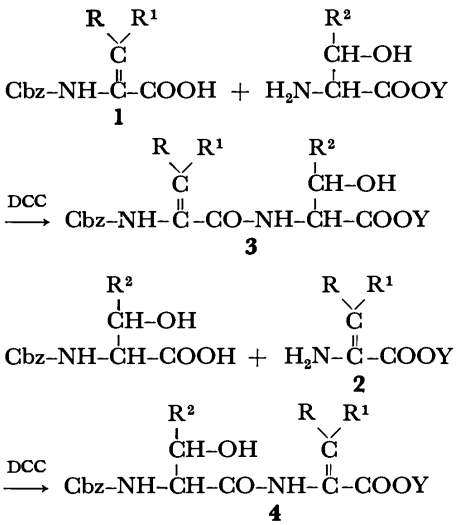

DHA and DHA residues = ⊿Ala, ⊿But, ⊿norVal, ⊿Val, ⊿norLeu, ⊿Leu, and ⊿Phe; R^2 = H and CH_3; Y = CH_3 and C_2H_5.

Scheme 1.

residue respectively. On the other hand, in the case of **4**, the corresponding signals appeared at δ 4.30—4.35 (methine) as multiplets, at δ 6.01—6.19 (NH) as doublets, and at δ 3.40—3.88 (hydroxyl) as broad singlets of the α-AA residue, and at δ 6.55—6.81 and at δ 7.96—8.15 (vinyl and olefinic protons) regions as broad singlets of the ⊿AA residue. As a result, it was found that the IR and NMR spectral patterns of **3** were remarkably similar to those of **4**.

According to the method confirmed previously,[1] the configurations of **3** and **4** could be readily determined to have (*Z*)-geometry.

The yields, physical constants, and NMR spectral data of **3** and **4** are summarized in Tables 1 and 2.

Preparation of Dehydro-dehydrodipeptides. In order to carry out the following base-catalyzed β-elimination easily, the mesylation of the hydroxyl group in **3** and **4** was performed. We followed a procedure reported

Table 1. Cbz-(*Z*)-⊿AA-Ser- and -Thr-OY (**3**)

Cbz-⊿AA-AA(OH)-OY	Yield[a] %	Mp/°C	Formula	Found (Calcd), % C	H	N	NMR spectrum, δ in $CDCl_3$ Olefinic-proton(J_{Hz})	α-Proton[h] (J_{Hz})	NH	OH
Cbz-⊿Ala-Ser-OMe	67	syrup[b]								
Cbz-⊿But-Ser-OMe	64	syrup	$C_{16}H_{20}N_2O_6$	57.45 (57.13	6.12 5.99	8.15 8.33)	6.52q, (7.5)	4.62dt, (3.0, 7.0)	7.04s, 7.26d	3.72
Cbz-⊿norVal-Ser-OMe	70	syrup	$C_{17}H_{22}N_2O_6$	58.49 (58.27	6.45 6.33	8.03 8.00)	6.43t, (7.3)	4.62m,	7.01s, 7.26d	3.80
Cbz-⊿norLeu-Ser-OMe	65	syrup	$C_{18}H_{24}N_2O_6$	59.51 (59.33	6.82 6.64	7.68 7.69)	6.45t, (7.3)	4.66m,	6.82s, 7.20d	3.20
Cbz-⊿Leu-Ser-OMe	86	100—101[c]	$C_{18}H_{24}N_2O_6$	59.42 (59.33	6.58 6.64	7.71 7.69)	6.41d, (10.0)	4.66dt, (3.0, 7.0)	7.07s, 7.40d	3.69
Cbz-⊿Phe-Ser-OMe	65	107—108[d]	$C_{21}H_{22}N_2O_6$	63.23 (63.31	5.56 5.57	7.11 7.03)	7.10s,	4.67dt, (3.0, 8.0)	6.76s, 7.24d	3.26
Cbz-⊿Ala-Thr-OMe	45	syrup	$C_{16}H_{20}N_2O_6$	57.51 (57.13	6.23 5.99	8.19 8.33)	5.34t, 6.08d	4.56dd, (2.5, 9.0)	7.07s, 7.53d	2.94
Cbz-⊿But-Thr-OMe	67	62—64[e]	$C_{17}H_{22}N_2O_6$	58.21 (58.27	6.45 6.33	7.91 8.00)	6.56q, (7.3)	4.56dd, (3.0, 8.8)	7.00s, 7.07d	3.34
Cbz-⊿norVal-Thr-OEt	61	65—66[e]	$C_{19}H_{26}N_2O_6$	60.12 (60.30	7.02 6.93	7.44 7.40)	6.46t, (7.2)	4.57dd, (3.0, 8.8)	7.00s, 7.09d	3.25
Cbz-⊿norLeu-Thr-OEt	76	54—56[f]	$C_{20}H_{28}N_2O_6$	61.07 (61.21	7.28 7.19	7.19 7.14)	6.51t, (7.5)	4.58dd, (3.0, 8.8)	6.86s, 7.09d	3.20
Cbz-⊿Leu-Thr-OMe	77	58—60[f]	$C_{19}H_{26}N_2O_6$	60.51 (60.30	7.11 6.93	7.32 7.40)	6.37d, (10.8)	4.61dd, (2.8, 9.0)	6.79s, 7.09d	2.84
Cbz-⊿Phe-Thr-OEt	84	110—111[f]	$C_{23}H_{26}N_2O_6$	64.56 (64.77	6.32 6.15	6.86 6.57)	7.40—7.55[g],	4.76dd, (3.0, 9.0)	7.14s, 7.40—7.55[g]	3.27

a) Yield by the DCC method. b) Ref. 1. c) Colorless prisms from benzene. d) Colorless prisms from CCl_4. e) Colorless needles from propyl ether. f) Colorless needles from CCl_4. g) Overlapped with phenyl protons. h) α-Proton of α-AA residue.

Table 2. Cbz-Ser- and Thr-(*Z*)-⊿AA-OEt (**4**)

Cbz-AA(OH)-⊿AA-OEt	Yield[a] %	Mp/°C[b]	Formula	Found (Calcd), % C	H	N	NMR spectrum, δ in $CDCl_3$ Olefinic-proton(J_{Hz})	α-Proton[c]	NH	OH
Cbz-Ser-⊿Val-OEt	51	155—157	$C_{18}H_{24}N_2O_6$	59.39 (59.33	6.58 6.64	7.77 7.69)	—	4.30m,	6.10d, 7.96bs	3.40
Cbz-Ser-⊿norLeu-OEt	26	64—66	$C_{19}H_{26}N_2O_6$	60.25 (60.30	7.05 6.93	7.39 7.40)	6.72t, (7.0)	4.35m,	6.19d, 8.04bs	3.75
Cbz-Ser-⊿Leu-OEt	33	107—108	$C_{19}H_{26}N_2O_6$	60.51 (60.30	7.23 6.93	7.34 7.40)	6.55d, (10.0)	4.35m,	6.10d, 7.96bs	3.75
Cbz-Thr-⊿But-OEt	21	88—90	$C_{18}H_{24}N_2O_6$	59.32 (59.33	6.79 6.64	7.79 7.69)	6.81q, (7.0)	4.30m,	6.16d, 8.15bs	3.70
Cbz-Thr-⊿norVal-OEt	25	99—100	$C_{19}H_{26}N_2O_6$	60.51 (60.30	6.87 6.93	7.29 7.40)	6.68t, (7.0)	4.30m,	6.06d, 8.00bs	3.80
Cbz-Thr-⊿Val-OEt	50	159—161	$C_{19}H_{26}N_2O_6$	60.33 (60.30	7.11 6.93	7.23 7.40)	—	4.35m,	6.01d, 7.96bs	3.84
Cbz-Thr-⊿norLeu-OEt	28	95—97	$C_{20}H_{28}N_2O_6$	60.98 (61.21	7.32 7.19	7.19 7.14)	6.73t, (7.0)	4.30m,	6.08d, 8.10bs	3.88
Cbz-Thr-⊿Leu-OEt	38	100—101	$C_{20}H_{28}N_2O_6$	61.23 (61.21	6.89 7.19	7.22 7.14)	6.55d, (10.0)	4.30m,	6.06d, 7.96bs	3.88

a) Yield by the DCC method. b) Colorless fibrous from CCl_4. c) α-Proton of α-AA residue.

previously,[13] treating a solution of **3** and methanesulfonyl (mesyl) chloride in CH_2Cl_2 with excess triethylamine but, unexpectedly, ⊿DHP (**7**) as a colorless syrup or crystals was obtained directly in *ca.* a 74% yield, without any yield of the corresponding mesyloxy intermediates (**5**).

On the other hand, a similar treatment of **4** with mesyl chloride gave the corresponding stable mesyloxy derivative (**6**) as colorless crystals in *ca.* an 80% yield. The subsequent elimination reaction of the **6** isolated purely was attempted in the presence of triethylamine, but the reaction did not proceed at all. In consequence, the treatment of a solution of **6** in THF in the presence of 1,8-diazabicyclo[5.4.0]undec-7-ene (DBU), a stronger base than triethylamine, was carried out successfully, and the desired **7** was obtained in *ca.* a 65% yield.

In the spectrum of **6**, the disappearance of the hydroxyl absorption and in the 3260—3300 cm^{-1} region and the appearance of characteristic strong sulfonyl function bands in the 1345—1360 and 1160—1190 cm^{-1} regions indicate unambiguously the formation of the mesyloxy derivative. Moreover, the IR spectrum of **7** showed bands in the 3280—3400 and 3200—3300 cm^{-1} regions due to the NH group, bands in the 1680—1728 and 1500—1540, and 1620—1650 and 1490—1500 cm^{-1} regions due to two secondary amide functions, and a weak band in the 1620—1670 cm^{-1} region due to the carbon-carbon double bond.

On the other hand, from the NMR spectral data of **7** listed in Tables 4 and 5, it was found that the signals in the δ 4.46—7.74 and 7.61—8.61 regions as broad singlets due to two NH protons, and the characteristic signals at δ 5.26—6.76 and at δ 6.30—7.24 due to vinyl and olefinic protons of the ⊿AA-⊿AA moeties respectively, are consistent with the assignment of the dehydrodehydrodipeptide structure. In consequence, it can be said that the appearance of two olefinic proton signals indicates unambiguously the formation of **7**.

As a result, it was found that the IR and NMR spectral patterns of **7** derived from **3** *via* **5** were in fairly good agreement with those of **7** from **4** *via* **6**.

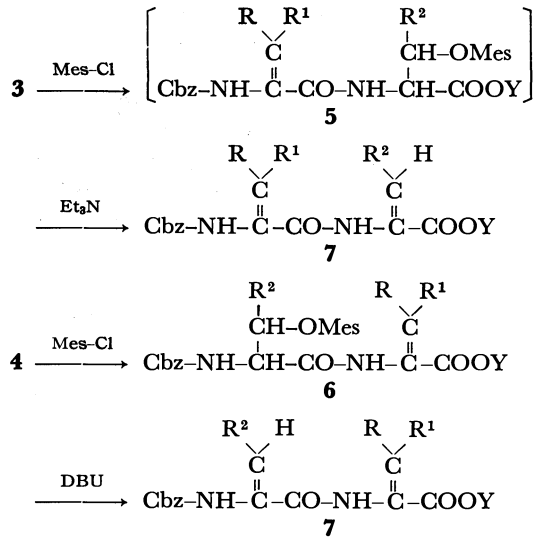

DHA residues = ⊿Ala, ⊿But, ⊿norVal, ⊿Val, ⊿norLeu, ⊿Leu, and ⊿Phe; Y = CH_3 and C_2H_5

Scheme 2.

The yields, physical constants, and NMR spectral data of **6** and **7** are summarized in Tables 3, 4, and 5.

The geometric structure of **7** could be readily determined to have (*Z*,*Z*)-geometry, since the chemical shifts and the spectral patterns of the individual ⊿AA residue in **7** were quite similar to the starting, (*Z*)-configurational **1** and **2**.[13,14] The above determination was further confirmed independently by the following direct coupling between two different (*Z*)-DHA's.[11]

The equimolar coupling of (*Z*)-**1** as a carboxyl component with (*Z*)-**2** as an amine component by the usual acid-chloride method gave the desired ⊿DHP (**7**) in *ca.* a 50% yield; its structure was completely in agreement with that of **7** derived from **3** and **4** respectively. Therefore, it was further ascertained that the (*Z*)-geometry of the DHA and DHA residues was maintained during the peptide-formation reaction and the base-catalyzed β-elimination reaction.

TABLE 3. Cbz-Ser(Mes)- AND Thr(Mes)-(*Z*)-⊿AA-OEt (**6**)

Cbz-AA(Mes)-⊿AA-OEt	Yield %	Mp/°C[a]	Formula	Found (Calcd), % C	H	N	NMR spectrum, δ in $CDCl_3$ Olefinic-proton(J_{Hz})	α-Proton[b] (J_{Hz})	NH
Cbz-Ser(Mes)-Val-OEt	80	135—136	$C_{19}H_{26}N_2O_8S$	51.38 (51.58	6.12 5.92	6.38 6.33)	—	4.60m,	6.12d 7.90bs
Cbz-Ser(Mes)-⊿Leu-OEt	78	107—108	$C_{20}H_{28}N_2O_8S$	52.39 (52.62	6.17 6.19	6.23 6.14)	6.58d, (10.0)	4.60m,	6.00d 7.70bs
Cbz-Thr(Mes)-⊿But-OEt	75	131—132	$C_{19}H_{26}N_2O_8S$	51.45 (51.58	6.01 5.92	6.39 6.33)	6.88q, (7.0)	4.60dd, (3.5, 8.0)	6.00d 7.86bs
Cbz-Thr(Mes)-⊿norVal-OEt	85	130—131	$C_{20}H_{28}N_2O_8S$	52.71 (52.62	6.08 6.19	6.19 6.14)	6.74t, (7.0)	4.60dd, (3.5, 8.3)	6.04d 7.86bs
Cbz-Thr(Mes)-⊿Val-OEt	88	159—160	$C_{20}H_{28}N_2O_8S$	52.66 (52.62	6.38 6.19	6.24 6.14)	—	4.52dd, (3.5, 8.3)	5.86d 7.60bs
Cbz-Thr(Mes)-⊿norLeu-OEt	80	132—133	$C_{21}H_{30}N_2O_8S$	53.88 (53.61	6.39 6.43	5.99 5.95)	6.76t, (7.0)	4.60dd, (3.5, 8.3)	6.00d 7.86bs
Cbz-Thr(Mes)-⊿Leu-OEt	76	127—130	$C_{21}H_{30}N_2O_8S$	53.66 (53.61	6.51 6.43	6.12 5.95)	6.58d, (10.0)	4.54dd, (3.5, 8.3)	5.88d 7.61bs

a) Colorless needles from CCl_4. b) α-Proton of α-AA residue.

Table 4. Cbz-(*Z*)-⊿AA-(*Z*)-⊿AA-OY (**7**) from **3**

Cbz-⊿AA-⊿AA-OY	Yield %	Mp/°C[a]	Formula	Found (Calcd), % C	H	N	NMR spectrum, δ in $CDCl_3$ CH_2= Me-CH=(J_{Hz})	R-CH= (J_{Hz})	NH
Cbz-⊿Ala-⊿Ala-OMe	62	syrup	$C_{15}H_{16}N_2O_5$	59.41 (59.20)	5.23 (5.30)	9.13 (9.21)	5.26dd, 6.18d	5.94d[b] 6.58s	7.51bs 8.43bs
Cbz-⊿But-⊿Ala-OMe	63	61—62	$C_{16}H_{18}N_2O_5$	60.33 (60.37)	5.58 (5.70)	8.97 (8.80)	5.36t, 6.22d	6.88q[c] (7.4)	7.54bs 7.67bs
Cbz-⊿norVal-⊿Ala-OMe	62	87—88	$C_{17}H_{20}N_2O_5$	61.34 (61.43)	5.89 (6.07)	8.44 (8.43)	5.84d, 6.60s	6.43t, (7.2)	6.60bs 8.40bs
Cbz-⊿norLeu-⊿Ala-OMe	76	100—101	$C_{18}H_{22}N_2O_5$	62.42 (62.41)	6.56 (6.40)	7.89 (8.09)	5.86d, 6.60s	6.47t, (7.2)	6.63bs 8.60bs
Cbz-⊿Leu-⊿Ala-OMe	91	86—87	$C_{18}H_{22}N_2O_5$	62.56 (62.41)	6.32 (6.40)	7.97 (8.09)	6.01d, 6.76s	6.46d, (10.2)	6.85bs 8.61bs
Cbz-⊿Phe-⊿Ala-OMe	86	115—116	$C_{21}H_{20}N_2O_5$	66.23 (66.30)	5.12 (5.30)	7.25 (7.37)	5.95d, 6.70s	7.22s, —	6.67bs 8.61bs
Cbz-⊿Ala-⊿But-OMe	65	syrup	$C_{16}H_{18}N_2O_5$	60.54 (60.37)	5.81 (5.70)	8.97 (8.80)	6.68q, (7.2)	5.36t,[b] 6.22d	7.54bs 7.67bs
Cbz-⊿But-⊿But-OMe	71	syrup	$C_{17}H_{20}N_2O_5$	61.23 (61.43)	5.98 (6.07)	8.55 (8.43)	6.77q, (7.2)	6.55q,[c] (7.2)	6.96bs 7.78bs
Cbz-⊿norVal-⊿But-OEt	76	syrup	$C_{19}H_{24}N_2O_5$	63.11 (63.32)	6.79 (6.71)	7.59 (7.77)	6.77q, (7.2)	6.47t, (7.5)	6.93bs 7.78bs
Cbz-⊿norLeu-⊿But-OEt	69	syrup	$C_{20}H_{26}N_2O_5$	63.89 (64.15)	6.89 (7.00)	7.57 (7.48)	6.80q, (7.2)	6.52t, (7.2)	6.76bs 7.73bs
Cbz-⊿Leu-⊿But-OMe	86	89—90	$C_{20}H_{26}N_2O_5$	63.53 (64.15)	6.68 (7.00)	7.90 (7.48)	6.77q, (7.2)	6.30d, (10.2)	6.46bs 7.61bs
Cbz-⊿Phe-⊿But-OEt	79	79—81	$C_{23}H_{24}N_2O_5$	67.60 (67.63)	6.08 (5.92)	7.11 (6.86)	6.82q, (7.2)	7.24s, —	6.72bs 7.85bs

a) Colorless needles from CCl_4. b) Vinyl protons. c) 1-Propenyl protons.

Table 5. Cbz-(*Z*)-⊿But-(*Z*)-⊿AA-OEt (**7**) from **6**

Cbz-⊿AA-⊿AA-OEt	Yield %	Mp/°C[a]	Formula	Found (Calcd), % C	H	N	NMR spectrum, δ in $CDCl_3$ CH_2= Me-CH=(J_{Hz})	R-CH= (J_{Hz})	NH (bs)[b]
Cbz-⊿But-⊿But-OEt	61	syrup	$C_{18}H_{22}N_2O_5$	62.45 (62.41)	6.38 (6.40)	7.97 (8.09)	6.57q, (7.2)	6.77q, (7.2)	6.96 7.78
Cbz-⊿But-⊿norVal-OEt	65	syrup	$C_{19}H_{24}N_2O_5$	63.45 (63.32)	6.88 (6.71)	7.70 (7.77)	6.70q, (7.2)	6.77t, (7.5)	7.30 8.06
Cbz-⊿But-⊿Val-OEt	67	69—70	$C_{19}H_{24}N_2O_5$	63.22 (63.32)	6.89 (6.71)	7.98 (7.77)	6.56q, (7.2)	—	6.95 7.71
Cbz-⊿But-⊿norLeu-OEt	65	45—46	$C_{20}H_{26}N_2O_5$	63.98 (64.15)	6.09 (7.00)	7.48 (7.48)	6.60q, (7.2)	6.71t, (7.5)	6.90 7.75
Cbz-⊿But-⊿Leu-OEt	66	67—68	$C_{20}H_{26}N_2O_5$	64.33 (64.15)	6.89 (7.00)	7.37 (7.48)	6.70q, (7.5)	6.57d, (7.2)	6.96 7.78

a) Colorless needles from cyclohexane. b) Broad singlet.

Table 6. Cbz-(*Z*)-⊿AA-(*Z*)-⊿AA-OEt (**7**) from **1** and **2**

Cbz-⊿AA-⊿AA-OEt	Yield/%	Mp/°C
Cbz-⊿But-⊿But-OEt[a]	40	syrup
Cbz-⊿But-⊿norVal-OEt[a,b]	41	syrup
Cbz-⊿But-⊿Val-OEt[a]	68	69—70
Cbz-⊿Leu-⊿norVal-OEt[b]	43	syrup[c]
Cbz-⊿norVal-⊿norLeu-OEt[b]	51	syrup[d]
Cbz-⊿But-⊿Leu-OEt[a,b]	65	67—68

a) See Table 5. b) Ref. 11. c) Found: C, 65.15; H, 7.40; N, 7.09%. Calcd for $C_{21}H_{28}N_2O_5$: C, 64.93; H, 7.27; N, 7.21%. d) Found: C, 65.33; H, 7.41; N, 7.10%. Calcd for $C_{21}H_{28}N_2O_5$: C, 64.93; H, 7.27; N, 7.21%.

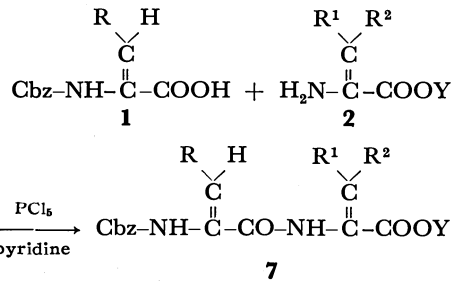

DHA residues = ⊿But, ⊿norVal, ⊿norLeu, ⊿Val, and ⊿Leu; Y = CH_3 and C_2H_5

Scheme 3.

The yields, physical constants, and NMR spectral data of **7** obtained by the direct coupling are summarized in Table 6.

Experimental

All the melting points are uncorrected. The IR spectra were recorded with a Hitachi EPI-G3 Spectrometer. The NMR spectra were measured with a JNM-PS-100 Spectrometer (Japan Electron Laboratory Co., Ltd.), using tetramethylsilane as the internal standard.

Starting Materials. The starting (*Z*)-**1** and (*Z*)-**2** were prepared by the methods reported previously.[1,11,12]

Preparation of ***3***. Into a solution of (*Z*)-**1** (10 mmol) and the Ser or Thr ester (10 mmol) in DMF (10 ml), we stirred DCC (11 mmol) under cooling. After stirring at room temperature for 12 h, the dicyclohexylurea deposited was filtered off and washed well with ethyl acetate. The filtrate was poured into water (70 ml), and the aqueous solution was extracted twice with ethyl acetate (60 ml). The combined extracts were successively washed with 2% aqueous HCl, water, saturated aqueous $NaHCO_3$, and water, and finally dried over anhydrous Na_2CO_3. The subsequent evaporation of the ethyl acetate under reduced pressure gave crude crystals or a syrup, subsequently purified on a silica gel column using benzene–ethyl acetate (4 : 1 v/v) to give **3**. See Table 1.

Preparation of ***4***. Into a solution of (*Z*)-**2** (10 mmol) and Cbz–Ser or –Thr (10 mmol) in CH_2Cl_2 (10 ml), we vigorously stirred DCC (11 mmol), portion by portion, below 0 °C. After stirring at room temperature for 20 h, the reaction solution was worked-up exactly according to the above treatment procedure to give **4**. See Table 2.

Preparation of ***6***. Into a solution of **4** (4 mmol) and mesyl chloride (5 mmol) in CH_2Cl_2 (20 ml) we stirred triethylamine (12 mmol), drop by drop, at 0 °C for 1 h, and then the stirring was continued at room temperature for 2 more h. The reaction solution was then poured into CH_2Cl_2 (50 ml), and the resulting solution was washed once with chilled 1 M HCl (50 ml) and twice with water and finally dried over anhydrous $MgSO_4$. The subsequent evaporation of the solvent gave a crude syrupy residue, which was crystallized with CCl_4 to give **6** as colorless needles. See Table 3.

Preparation of ***7***. *From Ser Derivatives (**3**)*: Into a solution of **3** (4 mmol) and mesyl chloride (5 mmol) in CH_2Cl_2 (20 ml) we stirred triethylamine (12 mmol), drop by drop, at 0—2 °C for 0.5 h, and then the stirring was continued at room temperature for 1.5 more h. Dichloromethane (40 ml) was further added to the reaction solution, and the resulting solution was washed with chilled 1 M HCl till the washing solution reached pH 4 and twice with water, and finally dried over $MgSO_4$. The subsequent evaporation of the CH_2Cl_2 gave **7** as a colorless syrup or crystals. See Table 4.

*From Thr Derivatives (**3**)*: Similarly, the treatment of **3** (4 mmol) with mesyl chloride (5 mmol) in the presence of triethylamine (20 mmol) was worked-up for 1 h; it was then stirred at room temperature for 12 h to give a crude syrupy substance, which was purified on a silica gel column using a mixture of benzene–ethyl acetate (3 : 1 v/v) as the eluent to give **7** as a colorless syrup or crystals. See Table 4.

From ***6***: Into a solution of **6** (4 mmol) in THF (20 ml) we stirred DBU (4.5 mmol) under cooling. After stirring at the same temperature for 2 h, the evaporation of THF gave a crude reaction product; this product was dissolved in ethyl acetate (20 ml) and chilled 1 M HCl (40 ml), and then the residual solution was well shaked. The organic layer thus separated was washed with water and dried over anhydrous Na_2SO_4. After the removal of the ethyl acetate under reduced pressure, the residual syrup thus obtained was chromatographed on a silica-gel column, using a mixture of benzene–ethyl acetate (4 : 1 v/v) as the eluent, to give **7** from the second fraction. See Table 5.

From ***1*** *and* ***2***: Into a solution of **1** (10 mmol) in dry THF (20 ml) we successively stirred PCl_5 (11 mmol), portion by portion, at 0 °C and then, after 20 min, a chilled solution of **2** (10 mmol) in dry pyridine (15 ml), drop by drop, all below 5 °C. The reaction mixture was continuously stirred at room temperature for 3 more h, and then the resulting solution was poured into ice water (100 ml). The resulting aqueous solution was extracted three times with ethyl acetate (180 ml). The extracts were washed once with 3 M HCl (50 ml) and three times with water (100 ml), and then dried over anhydrous Na_2SO_4. After the evaporation of the ethyl acetate under reduced pressure, the residual syrup thus obtained was purified on a silica-gel column, using a mixture of benzene–ethyl acetate (8 : 1 v/v) as the eluent, to give **7** as a pure colorless syrup or crystals. See Table 6.

References

1) Part I: Y. Yonezawa, C. Shin, Y. Ono, and J. Yoshimura, *Bull. Chem. Soc. Jpn.*, **53**, 2905 (1980).

2) In this paper, the symbol Δ indicates a double bond of the α-position in the DHA or DHA residue, while AA represents α-amino acid or its residue.

3) T. Kitagawa, T. Tamura, and H. Taniyama, *J. Biochem.*, **81**, 1757 (1977).

4) "Bioactive Peptides Produced by Microorganisms," ed by H. Umezawa, T. Takita, and T. Shiba, Kodansha, Tokyo (1978).

5) Y. Shimohigashi and N. Izumiya, *Yuki Gosei Kyokaishi*, **36**, 1023 (1970).

6) B. Anderson, D. C. Hodgkin, and M. A. Viswamutra, *Nature*, **225**, 233 (1970).

7) a) E. Gross, H. H. Kiltz, and E. Nebelin, *Hoppe-Seyler's Z. Physiol. Chem.*, **354**, 810 (1973). b) E. Gross and J. L. Morell, *J. Am. Chem. Soc.*, **93**, 4634 (1971).

8) J. M. Liesch and K. L. Rinehart, Jr., *J. Am. Chem. Soc.*, **99**, 1645 (1977).

9) D. G. Doherty, J. E. Tietzmann, and M. Bergmann, *J. Biol. Chem.*, **147**, 617 (1943).

10) M. L. English and C. H. Stammer, *Biochem. Biophys. Res. Commun.*, **83**, 1464 (1978).

11) C. Shin, Y. Yonezawa, and J. Yoshimura, *Tetrahedron Lett.*, **1979**, 4085.

12) C. Shin, Y. Yonezawa, K. Unoki, and J. Yoshimura, *Tetrahedron Lett.*, **1979**, 1049.

13) C. Shin, Y. Yonezawa, K. Unoki, and J. Yoshimura, *Bull. Chem. Soc. Jpn.*, **52**, 1657 (1979).

14) C. Shin, M. Hayakawa, T. Suzuki, A. Ohtsuka, and J. Yoshimura, *Bull. Chem. Soc. Jpn.*, **51**, 550 (1978).

α,β-Unsaturated Carboxylic Acid Derivatives. XIX. The Convenient Synthesis of α-Alkoxy-, α-Hydroxy-α-amino Acid, and Its Cyclic Dipeptide from α-Dehydroamino Acid[1]

Chung-gi SHIN,* Yoshiaki SATO, Hisao OHMATSU, and Juji YOSHIMURA†

Laboratory of Organic Chemistry, Faculty of Technology, Kanagawa University, Rokkakubashi, Kanagawa-ku, Yokohama 221

†*Laboratory of Chemistry for Natural Products, Faculty of Science, Tokyo Institute of Technology, Nagatsuta, Midori-ku, Yokohama 227*

(Received July 22, 1980)

The facile conversion of α-dehydroamino acid into α-alkoxy-α-amino acid and its cyclic dipeptide is described. The reaction of *t*-butyl 2-acetylamino-2-alkenoate or 1-benzyl-3-ethylidene-2,5-piperazinedione with alcohol, water, or acetic acid in the presence of NBS or NCS, followed by reduction with 10% Pd-C, gives *t*-butyl 2-alkoxy-, 2-hydroxy-, and 2-acetoxy-2-(acetylamino)alkanoates, and 3-alkoxy-3-ethyl-2,5-piperazinedione respectively. All the new compounds were characterized by spectroscopic analysis.

Recently, increasing interest has been directed to the synthesis of ergot alkaloids and cyclic peptide antibiotics containing an α-alkoxy- or α-hydroxy-α-amino acid moiety as an very important constituent or precursor.[2-5]

So far, several syntheses of α-alkoxy- and α-hydroxy-α-amino acids from α-amino acid[6-9] and from α-aminoacrylic acid,[10-13] as well as the semi-synthesis of 6-alkoxypenicillins and 7-alkoxycephalosporins,[14] have been reported. However, it seems that no facile and general synthetic method for α-alkoxy- and α-hydroxy-α-amino acids and their cyclic dipeptides has yet been achieved.

Previously, we reported briefly on the addition of alcohol to α,β-unsaturated α-amino acid (α-dehydroamino acid; DHA) in the presence of *N*-bromosuccinimide (NBS).[15] In order to apply and extend the addition reaction in a more versatile manner, various reactions of *t*-butyl 2-acetylamino-2-alkenoate (**1**) or 1-benzyl-3-ethylidene-2,5-piperazinedione (2,5-piperazinedione=PDO) (**21**) with several alcohols, acetic acid, or water in the presence of NBS or *N*-chlorosuccinimide (NCS) have here been studied thoroughly. As a result, the synthetic route for α-alkoxy- and α-hydroxy-α-amino acids and their cyclic dipeptides was established.

More recently, after the completion of our work,[16,17] Ottenheijm *et al.* reported a similar addition of methanol to acylimine intermediates.[18,19]

Results and Discussion

α-Alkoxy-α-amino Acid. A one-pot reaction of DHA (**1**: **a**; R=CH_3, **b**; R=C_2H_5) with an appropriate alcohol in the presence of NBS or NCS at room temperature gave directly the desired *t*-butyl 2-alkoxy-3-halo-2-(acetylamino)alkanoate (**6**—**13**) in an excellent yield. On the other hand, a similar reaction of *t*-butyl 2-acetylamino-2-butenoate (**1a**) with water in DMF barely proceeded to give *t*-butyl 2-hydroxy-3-bromo-2-(acetylamino)butanoate (**5a**) in a poor yield, whereas

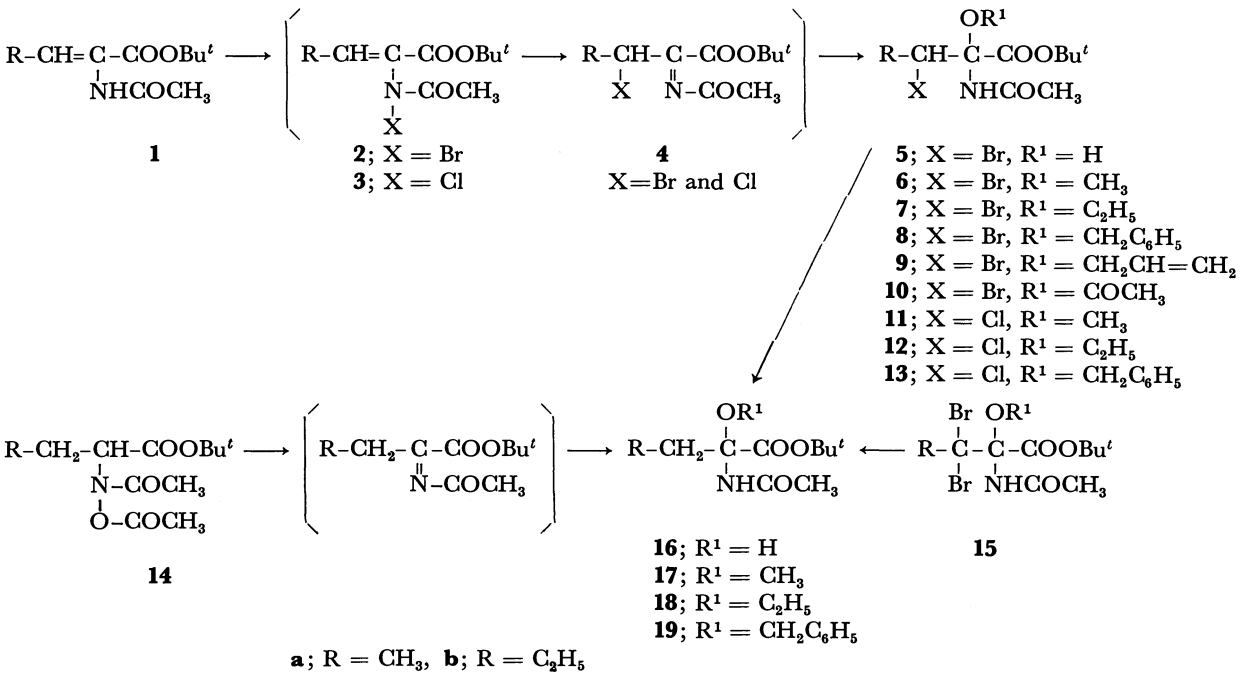

Scheme 1.

the reaction of **1** with glacial acetic acid was worked-up similarly to give *t*-butyl 2-acetoxy-3-bromo-2-(acetylamino)alkanoate (**10**) in *ca.* a 51% yield.

Subsequently, an attempt at the catalytic reduction of bromine at the 3-position of the **5**—**8** thus obtained with 10% Pd-C and equimolar triethylamine in methanol was successful; the expected *t*-butyl 2-alkoxy-2-(acetylamino)alkanoate (**16**—**19**) was thus obtained as colorless crystals in a fairly good yield. A similar reduction was further applied to *t*-butyl 3,3-dibromo-2-alkoxy-2-(acetylamino)alkanoate (**15**), prepared and reported previously,[15] using 10% Pd-C and two molar triethylamine to give **16**—**19** in an almost quantitative yield.

Moreover, it was found that *t*-butyl 2-benzyloxy-2-(acetylamino)alkanoate (**19**) was hydrogenolyzed with 10% Pd-C in the absence of triethylamine to give **16** in *ca.* a 60% yield.

On the other hand, in order to prepare independently and to confirm the structure of **16**—**19**, *t*-butyl 2-(*N*,*O*-diacetyl-hydroxyamino)alkanoate (**14**)[20] was subjected to the elimination of acetic acid and the subsequent addition of alcohol to the acylimine thus formed as an intermediate. When a solution in an appropriate alcohol was treated with sodium alkoxide, the expected elimination-addition reaction was carried out to give α-alkoxy derivative, which was found to be completely identical with **17** and **18**. This method, however, was found to be ineffective for the preparation of an α-hydroxy- or α-benzyloxy-α-amino acid moiety, *e.g.*, *t*-butyl 2-hydroxy- and 2-benzyloxy-2-(acetylamino)-alkanoate (**16** and **19**), which were thought to be very

TABLE 1. *t*-BUTYL 2-SUBSTITUTED 3-BROMO-2-(ACETYLAMINO)ALKANOATES (**5**—**10**)

Compd No.	R[1]	Yield/%	Mp/°C	Formula	Found (Calcd), %			NMR spectrum, δ[f]		
					C	H	N	NH	(OH)	3-Proton
5a	H	18	99.5—100[a]	$C_{10}H_{18}NO_4Br$	40.77 (40.56	6.00 6.13	4.54 4.73)	6.66,	(5.10),	4.30
6a[g]	CH_3	89	90—91[b]	$C_{11}H_{20}NO_4Br$	42.48 (42.59	6.59 6.50	4.32 4.52)	6.46,	6.98,	4.48 5.30
6b		91	syrup[c]					6.49,	6.95,	4.21 4.98
7a	C_2H_5	86	85.5—86.5[b]	$C_{12}H_{22}NO_4Br$	44.40 (44.46	6.87 6.84	4.26 4.32)	6.42,	6.94,	4.43 5.29
7b		93	syrup[c]					6.50,	6.96,	4.20 4.98
8a[g]	$CH_2C_6H_5$	92	115—116[b]	$C_{17}H_{24}NO_4Br$	52.92 (52.86	6.30 6.26	3.58 3.63)	6.42,	7.02,	4.45 5.38
8b		62	86—87[d]	$C_{18}H_{26}NO_4Br$	53.79 (54.01	6.82 6.55	3.62 3.50)	6.50,	7.02,	4.27 5.14
9a	$CH_2CH=CH_2$	80	85—86[b]	$C_{13}H_{22}NO_4Br$	46.69 (46.44	6.54 6.59	3.97 4.13)	6.45,	6.96,	e)
9b		80	syrup[c]					6.53	6.95	
10a	$COCH_3$	53	77—78[b]	$C_{12}H_{20}NO_5Br$	42.68 (42.65	5.94 5.96	4.24 4.14)	7.06,	7.24	5.04 5.56
10b		49	82—83[b]	$C_{13}H_{22}NO_5Br$	44.63 (44.33	6.28 6.30	3.98 3.98)	7.11,	7.25	4.71 5.28

a) Colorless needles from methanol–water. b) Colorless needles from hexane. c) Unstable. d) Colorless needles from ethanol–water. e) Overlapped with allyl protons. f) Measured in $CDCl_3$. g) Ref. 15.

TABLE 2. *t*-BUTYL 2-SUBSTITUTED 3-CHLORO-2-(ACETYLAMINO)ALKANOATES (**11**—**13**)

Compd No.	R[1]	Yield/%	Mp/°C	Formula	Found (Calcd), %			NMR spectrum, δ[e]		
					C	H	N	NH		3-Proton
11a	CH_3	89	83—84[a]	$C_{11}H_{20}NO_4Cl$	49.53 (49.72	7.56 7.59	5.27 5.27)	6.45,	6.94,	4.40 5.18
11b		94	syrup[b]	$C_{12}H_{22}NO_4Cl$	51.56 (51.52	7.91 7.93	5.13 5.01)	6.52,	6.92,	4.12 4.85
12a	C_2H_5	90	66—69[b]	$C_{12}H_{22}NO_4Cl$	51.56 (51.52	7.96 7.93	5.19 5.01)	6.48,	6.94,	4.37 5.17
12b		89	syrup[b]	$C_{13}H_{24}NO_4Cl$	53.28 (53.15	8.09 8.23	4.62 4.77)	6.54,	6.96,	4.12 4.86
13a	$CH_2C_6H_5$	88	107—108[c]	$C_{17}H_{24}NO_4Cl$	59.53 (59.73	7.02 7.08	4.26 4.10)	6.42,	6.98,	4.40 5.23
13b		68	126—127[d]	$C_{18}H_{26}NO_4Cl$	60.74 (60.75	7.41 7.36	4.09 3.94)	7.02,	6.52,	4.17 4.95

a) Colorless needles from hexane. b) Colorless amorphous or colorless syrup purified on a silica-gel column using benzene–ethyl acetate (15 : 1 v/v). c) Colorless needles from ethanol–water. d) Colorless needles from dibutyl ether. e) Measured in $CDCl_3$.

Table 3. *t*-butyl 2-alkoxy- and 2-hydroxy-2-(acetylamino)alkanoates (**16**—**19**)

Compd No.	Yield/% A[a]	B[b]	C[c]	D[d]	Mp/°C	Formula	Found (Calcd), % C	H	N	IR spectrum, cm^{-1} [e] NH (OH)	CO	NMR, δ[f] 3-Proton (J_{Hz})	NH (OH)
16a	62	65		66	78.5—79.5[g]	$C_{10}H_{19}NO_4$	55.31 (55.28)	8.91 (8.82)	6.44 (6.45)	(3420) 3340	1725 1655	1.82t (7.0)	(4.80) 6.95
16b				84	69—70[g]	$C_{11}H_{21}NO_4$	57.22 (57.12)	9.23 (9.15)	6.02 (6.06)	(3420) 3345	1725 1655	2.42m 1.75m	(4.83) 6.94
17a	87	97	56		137—138[h]	$C_{11}H_{21}NO_4$	57.36 (57.12)	9.44 (9.15)	6.03 (6.06)	3300	1745 1690	2.56m 1.90m	6.64
17b	83	99	62		109—110[i]	$C_{12}H_{23}NO_4$	58.78 (58.75)	9.63 (9.45)	5.53 (5.71)	3300	1745 1690	2.61m 1.86m	6.68
18a	84	96	21		144.5—145[i]	$C_{12}H_{23}NO_4$	58.80 (58.75)	9.34 (9.45)	5.70 (5.71)	3300	1745 1695	2.42m 1.85m	6.76
18b	86	93	22		110.5—111[i]	$C_{13}H_{25}NO_4$	60.31 (60.20)	9.81 (9.72)	5.32 (5.40)	3310	1750 1695	2.41m 1.87m	6.81
19a	92	96			90.5—91[i]	$C_{17}H_{25}NO_4$	66.17 (66.42)	8.32 (8.20)	4.56 (4.56)	3380	1730 1675	2.54m 1.87m	6.70
19b	94	93			71.5—72.5[i]	$C_{18}H_{27}NO_4$	67.34 (67.26)	8.50 (8.47)	4.22 (4.36)	3380	1740 1680	2.55m 1.86m	6.66

a) From **5**—**8**. b) From **15**. c) From **14**. d) From **19**. e) Recorded in KBr. f) Measured in $CDCl_3$. g) Colorless needles from dibutyl ether. h) Colorless needles from ethyl acetate. i) Colorless needles from hexane.

important segments in many of the natural products mentioned above.

In consequence, a convenient synthetic method for α-alkoxy-α-amino acid in a 75% overall yield was established by only two steps from DHA (**1**).

As is shown in Scheme 1, a formation mechanism of **5**—**13** was deduced in which, at first, the substitution of halogen to the nitrogen atom of **1** yielded *t*-butyl 2-(*N*-haloacetylamino)-2-alkenoate (**2** and **3**), followed by the 1,3-shift of the halogen to form *t*-butyl 3-halo-2-(acetylimino)alkanoate (**4**) as an unstable intermediate, to which immediately the present protic solvent was added. This deduction has already been supported by the fact that, to the *t*-butyl 3,3-dibromo-2-(acetylimino)-alkanoate isolated stably, we added alcohols to give **15**.[15]

In the IR spectral data of **5**—**13** and **16**—**19**, the characteristic absorption bands of the NH, ester carbonyl, and secondary amide functions appeared in the 3260—3390, 1730—1760, and 1660—1700 cm^{-1} regions respectively. Moreover, from the NMR spectral data, the disappearance of the characteristic olefinic proton signals in the δ 6.59—7.13 region of **1** and the appearance of the C-3 proton signals of **5**—**13** and **16**—**19** in the δ 4.12—5.56 and δ 1.66—2.78 regions respectively, resonating in a considerably higher magnetic field, are consistent with the formation of the α-substituted-α-amino acid structure.

The yields, physical constants, and NMR spectral data of **5**—**13** and **16**—**19** are summarized in Tables 1, 2, and 3.

3-Alkoxy-2,5-piperazinedione. In order to apply extensively and generalize the protic reagent-addition utilizing the halogen migration, 3-alkylidene-PDO was for instance, employed. Exactly, according to the synthetic method for α-alkoxy-α-amino acid, the starting 1-benzyl-3-ethylidene-PDO (**21**), which has been prepared by the cyclization of ethyl 2-iodoacetylamino-2-butenoate (**20**)[21] with benzylamine in a good yield, was treated with an appropriate alcohol in the

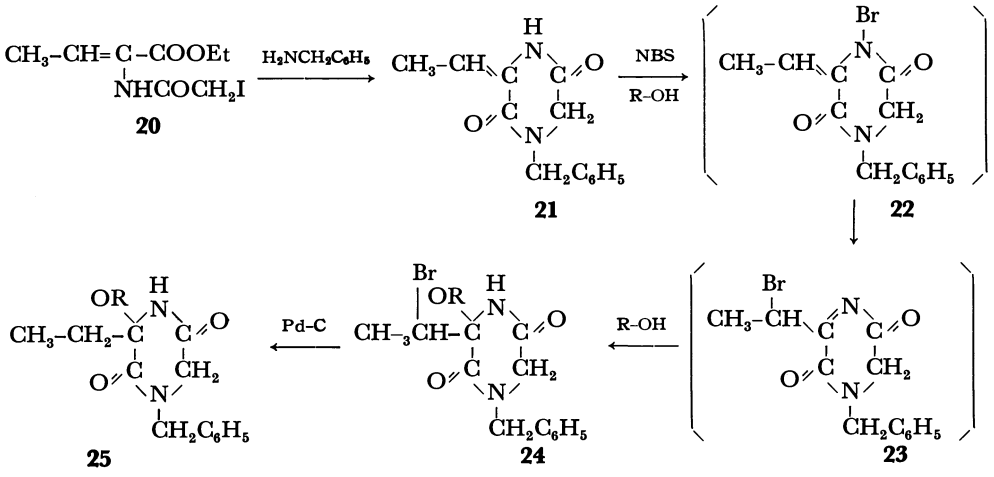

26; R = H **a**; R = CH_3, **b**; R = C_2H_5, **c**; R = $CH_2C_6H_5$

Scheme 2.

TABLE 4. 1-BENZYL-3-ETHYLIDENE- AND 1-BENZYL-3-ALKOXY-3-ETHYL-PDO (**21**, **24**, **25**, AND **26**)

Compd No.	Yield %	Mp/°C	Formula	Found (Calcd), % C	H	N	IR spectrum, cm^{-1} e) NH (OH)	CONH	C=C	NMR spectrum, δ f) -CH=	-CH- (-CH_2-)	NH (OH)
21	62	134—136a)	$C_{13}H_{14}N_2O_2$	67.84 (67.81	6.39 6.13	12.24 12.17)	3180	1675	1635	6.29		9.60
24a	88	129—130b)	$C_{14}H_{17}N_2O_3Br$	49.36 (49.28	5.09 5.02	8.38 8.21)	3170	1690 1670	—	—	4.72	8.27
24b	82	133—134b)	$C_{15}H_{19}N_2O_3Br$	50.72 (50.72	5.45 5.39	7.72 7.88)	3180	1680 1655	—	—	4.73	8.16
24c	61	116—117c)	$C_{20}H_{21}N_2O_3Br$	57.61 (57.56	5.12 5.07	6.78 6.71)	3200	1690 1660	—	—	4.78	8.45
25a	92	89—90c)	$C_{14}H_{18}N_2O_3$	64.06 (64.10	6.88 6.92	10.60 10.68)	3210	1690 1645	—	—	(2.02)	8.06
25b	90	138—139d)	$C_{15}H_{20}N_2O_3$	64.79 (65.19	7.24 7.30	10.08 10.14)	3220	1690 1640	—	—	(2.01)	7.72
25c	89	137—138c)	$C_{20}H_{22}N_2O_3$	70.89 (70.98	6.50 6.55	8.22 8.28)	3180	1680	—	—	(2.08)	7.98
26	90	145—146d)	$C_{13}H_{16}N_2O_3$	62.66 (62.89	6.47 6.50	11.09 11.28)	3210 (3260)	1680 1635	—	—	(1.96)	7.86 (4.8—5.6)

a) Colorless prisms from ethyl acetate–diethyl ether. b) Colorless needles from benzene–hexane. c) Colorless prisms from benzene–hexane. d) Colorless needles from benzene. e) Recorded in KBr. f) Measured in $CDCl_3$.

presence of NBS to give 1-benzyl-3-(1-bromoethyl)-3-alkoxy-PDO (**24**) as colorless crystals in *ca.* an 80% yield. The subsequent catalytic reduction of **24** with Pd–C and triethylamine was also carried out to give the desired 1-benzyl-3-alkoxy-3-ethyl-PDO (**25**) in a 90% yield.

Furthermore, the catalytic hydrogenolysis of **25** with 10% Pd–C was performed smoothly to give 1-benzyl-3-ethyl-3-hydroxy-PDO (**26**) in *ca.* a 90% yield.

From the above results, the yield of the each step from **21** to **26** was found to be excellent; the overall yield reached to *ca.* 50%.

As was illustrated in Scheme 2, the formation mechanism of **24** was also supposed that the initial substitution of bromine to the 4-position of **21** (**22**), followed by the immediate migration to the 2-position of exocyclic carbon, gave acylimine (**23**); finally, the addition reaction of alcohol to **23** occurred to give **24**.

Judging from the IR and NMR spectral data of **21** and **24**—**26**, the appearance of the carbon-carbon double bond at 1635 cm^{-1} and the olefinic proton signal at δ 6.29 in **21**, and the appearance of exocyclic 1-methine proton signals resonating at comparatively higher magnetic fields (at δ 4.72—4.78 in **24** and in the δ 1.96—2.08 region in **25** and **26**), indicate unambiguously the formation of 3-alkoxy- and 3-hydroxy-PDO structures.

All the new compounds thus obtained gave satisfactory results in their elemental analyses as well as in the spectroscopy.

The yields, physical constants, and NMR spectral data of **21**, **24**, **25**, and **26** are summarized in Table 4.

It is noteworthy that the addition reaction of protic reagent *via* the substitution and the subsequent migration in one pot is also applicable to linear and cyclic acylenamines, as is shown below (Fig. 1).

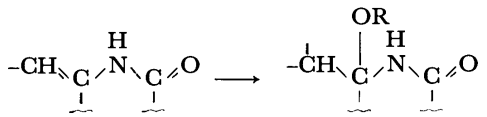

Fig. 1.

Experimental

All the melting points are uncorrected. The IR spectra were recorded with a Hitachi EPI-G3 Spectrometer. The NMR spectra were measured with a JNM-PS-100 Spectrometer (Japan Electron Optics Laboratory Co., Ltd.), using tetramethylsilane as the internal standard.

Preparation of ***5a***. Into a solution of **1a** (10.0 mmol) in water–DMF (15 ml, 1 : 9 v/v) we stirred NBS (11.0 mmol), portion by portion, at room temperature for 3 h. The reaction solution was poured into saturated aqueous NaCl (30 ml), and then the crystals deposited were collected by filtration. The recrystallization of the crystals from methanol–water gave colorless needles identified as *t*-butyl 3-bromo-2-hydroxy-2-(acetylamino)butanoate (**5a**).

Preparation of ***6***. Similarly, **1** and methanol (20 ml), in the presence of NBS, were worked-up for 2 h. The reaction solution was concentrated under reduced pressure to give a residue, which was subsequently dissolved in diethyl ether (30 ml). The resulting solution was washed twice with water and then dried over anhydrous Na_2SO_4. The evaporation of the ether gave colorless crystals or a syrup identified as *t*-butyl 3-bromo-2-methoxy-2-(acetylamino)alkanoate (**6**).

Preparation of ***7***. Similarly, a solution of **1** and NBS in ethanol (20 ml) was worked-up to give colorless crystals or a syrup identified as *t*-butyl 3-bromo-2-ethoxy-2-(acetylamino)-alkanoate (**7**).

Preparation of ***8***. A solution of **1a** in benzyl alcohol (6 ml) in the presence of NBS was similarly worked-up for 40 min to yield colorless crystals, which were then collected and washed with 50% ethanol. The crystals were identified as *t*-butyl 2-benzyloxy-3-bromo-2-(acetylamino)butanoate (**8a**).

Similarly, a solution of **1b** and NBS in benzyl alcohol was worked-up. The reaction solution was poured into water (250 ml), and then the aqueous solution was extracted three times with petroleum ether (180 ml). The combined extracts were washed three times with water, dried over anhydrous

Na_2SO_4, and then concentrated under reduced pressure to give colorless crystals identified as *t*-butyl 2-benzyloxy-3-bromo-2-(acetylamino)pentanoate (**8b**).

Preparation of ***9***. A solution of **1** in allyl alcohol (6 ml) in the presence of NBS was similarly worked-up for 10 h; to the reaction mixture we then added cyclohexane (60 ml). The resulting solution was washed twice with water and dried over anhydrous Na_2SO_4. The evaporation of the cyclohexane under reduced pressure gave colorless crystals or a syrup identified as *t*-butyl 2-allyloxy-3-bromo-2-(acetylamino)-alkanoate (**9**).

Preparation of ***10***. Into a solution of **1** (10.0 mmol) in acetic acid (5 ml) we stirred NBS (11.0 mmol), portion by portion, at room temperature for 3 h. To the reaction solution thus obtained we added hexane (100 ml). After the resulting solution had been washed twice with water, the crystals which separated out were collected by filtration. The filtrate was further washed twice with water and then dried over anhydrous $MgSO_4$. The removal of the hexane gave more of the crystals obtained above. The combined crystals were recrystallized from hexane to give colorless needles identified as *t*-butyl 3-bromo-2-acetoxy-2-(acetylamino)alkanoate (**10**).

Preparation of ***11***. A solution of **1a** in methanol (40 ml) in the presence of NCS (11.0 mmol) was similarly worked-up for 5 h to give colorless crystals identified as *t*-butyl 3-chloro-2-methoxy-2-(acetylamino)butanoate (**11a**).

In a similar manner, the reaction of **1b** with methanol and NCS for 24 h gave a syrupy residue, which was then purified on a silica gel column, using a mixture of benzene–ethyl acetate (15 : 1 v/v) as the eluent. The fraction thus obtained was concentrated under reduced pressure to give a colorless syrup identified as *t*-butyl 3-chloro-2-methoxy-2-(acetylamino)pentanoate (**11b**).

Preparation of ***12***. Similarly, a solution of **1** in ethanol (20 ml) in the presence of NCS was worked-up for 20 h to give a residual syrup. The crude syrup was purified on a silica gel column, using a mixture of benzene–ethyl acetate (15 : 1 v/v) as the eluent, to give a colorless amorphous substance or a syrup identified as *t*-butyl 3-chloro-2-ethoxy-2-(acetylamino)alkanoate (**12**).

Preparation of ***13***. Similarly, a solution of **1a** and NCS in benzyl alcohol (30 ml) was worked-up for 3 h to give colorless crystals identified as *t*-butyl 3-chloro-2-benzyloxy-2-(acetylamino)butanoate (**13a**).

In a similar manner, the treatment of **1b** with benzyl alcohol (10 ml) in the presence of NCS for 24 h gave a reaction solution which was then poured into water (400 ml). The resulting aqueous solution was extracted three times with petroleum ether (150 ml). The combined extracts were washed three times with water and then dried over anhydrous Na_2SO_4. The removal of the ether under reduced pressure gave colorless crystals identified as *t*-butyl 3-chloro-2-benzyloxy-2-(acetylamino)pentanoate (**13b**).

Preparation of ***16—19***. *a) From* ***5—8***: A solution of **5—8** (5.0 mmol) and triethylamine (5.5 mmol) in methanol (70 ml) was reduced in the presence of 10% Pd-C (500 mg). After 15 min, the catalyst was filtered off, and the reaction solution was concentrated under reduced pressure to give a residue, which was subsequently dissolved in chloroform (50 ml). The resulting solution was washed three times with water and then dried over anhydrous $MgSO_4$. The evaporation of the chloroform gave colorless crystals identified as *t*-butyl 2-alkoxy- and 2-hydroxy-2-(acetylamino)alkanoate (**16—19**).

b) From ***15***: A similar treatment of **15** (5.0 mmol) with triethylamine (10.5 mmol) in the presence of 10% Pd-C (500 mg) was worked-up to give the expected **16—19.**

c) From ***14***: Into a solution of **14** (10.0 mmol) in an appropriate alcohol (10 ml) we stirred sodium alkoxide (12.0 mmol) in alcohol (5 ml), drop by drop, below 10 °C. After the solution had been stirred for 2 h, the reaction solution was concentrated under reduced pressure to give a residue which was subsequently dissolved in chloroform (30 ml). The resulting solution was washed twice with water and then dried over anhydrous $MgSO_4$. The removal of the chloroform gave **17** and **18**.

Preparation of ***16*** *from* ***19***. A solution of **8** (3.8 mmol) in methanol (30 ml) was hydrogenolyzed in the presence of 10% Pd-C (100 mg) at room temperature for 1 h. After the removal of the catalyst, the resultant solution was concentrated to give a residual pale yellow syrup. The crude syrup was purified on a silica-gel column, using a mixture of benzene–ethyl acetate (5 : 2 v/v) as the eluent. The fraction was concentrated under reduced pressure to give colorless crystals, in agreement with the **16** prepared above.

Preparation of ***21***. Into a solution of **20** (6.73 mmol) in ethanol (20 ml) we stirred benzylamine (16.84 mmol), drop by drop, at room temperature. After the mixture had been stirred for 3 h, the reaction solution was concentrated under reduced pressure to give a residue, which was subsequently dissolved in 1 M HCl (50 ml). The aqueous solution was extracted three times with benzene (60 ml). The combined extracts were washed twice with saturated aqueous NaCl and then dried over anhydrous Na_2SO_4. The removal of the benzene under reduced pressure gave colorless crystals identified as 1-benzyl-3-ethylidene-PDO (**21**).

Preparation of ***24***. Into a solution of **21** (2.17 mmol) in an appropriate alcohol (5 ml) we stirred NBS (2.17 mmol), portion by portion, at room temperature. After the mixture had been stirred for 10 min, the reaction solution was concentrated under reduced pressure to give a residue, which was then dissolved in chloroform (20 ml). The resulting solution was washed twice with water and then dried over anhydrous Na_2SO_4. The removal of the chloroform gave colorless crystals identified as 1-benzyl-3-alkoxy-3-(1-bromoethyl)-PDO (**24**).

Preparation of ***25***. A solution of **24** (1.69 mmol) and triethylamine (2.03 mmol) in methanol (30 ml) was reduced in the presence of 10% Pd-C (170 mg) at room temperature for 1 h. After the removal of the catalyst, the reaction solution was concentrated under reduced pressure to give a residue, which was then dissolved in dichloromethane (20 ml). The resulting solution was washed twice with water and then dried over anhydrous Na_2SO_4. The evaporation of the dichlorome thane gave colorless crystals identified as 1-benzyl-3-alkoxy-3-ethyl-PDO (**25**).

Preparation of ***26***. A solution of 1-benzyl-3-benzyloxy-3-ethyl-PDO (**25c**; 2.07 mmol) in methanol (40 ml) was hydrogenolyzed in the presence of 10% Pd-C (500 mg) at room temperature for 24 h. After the removal of the catalyst, the resultant solution was concentrated under reduced pressure to give colorless crystals identified as 1-benzyl-3-ethyl-3-hydroxy-PDO (**26**).

References

1) Part XVIII: C. Shin, M. Hayakawa, H. Kato, K. Mikami, and J. Yoshimura, *J. Chem. Soc., Perkin Trans. 1*, **1980**, 419.

2) a) A. Stoll, A. Hofmann, and T. Petrizilka, *Helv. Chim. Acta.*, **34**, 1544 (1951); b) A. Hofmann, A. J. Frey, and H. Ott, *Experimentia*, **17**, 206 (1961).

3) a) T. Miyoshi, N. Miyairi, H. Aoki, M. Kohsaka, H.

Sasaki, and H. Imanaka, *J. Antibiotics*, **25**, 569 (1972); b) J. Fayos, D. Lokensgard, J. Clardy, R. J. Cole, and J. W. Kirksey, *J. Am. Chem. Soc.*, **96**, 6785 (1974); c) M. Yamazaki, S. Suzuki, and K. Miyaki, *Chem. Pharm. Bull. (Tokyo)*, **19**, 1739 (1971).

4) E. O. Stapley, M. Jackson, S. Hernandez, C. B. Zimmermann, S. A. Currie, S. Mochales, J. M. Mata, H. B. Woodruff, and D. Hendlin, *Antimicrob. Agents Chemother.*, **2**, 122 (1972).

5) E. P. Abraham and G. G. F. Newton, *Biochem. J.*, **79**, 377 (1961).

6) M. M. Chemiakine, E. S. Tchman, L. I. Denisova, G. A. Ravdel, and W. J. Rodionow, *Bull. Soc. Chim. Fr.*, **26**, 530 (1959).

7) U. Zoller and D. Ben-Ishai, *Tetrahedron*, **31**, 863 (1975).

8) a) H. Poisel and U. Schmidt, *Chem. Ber.*, **108**, 2547 (1975); b) H. Poisel, *ibid.*, **110**, 948 (1977).

9) T. Iwasaki, H. Horikawa, K. Matsumoto, and M. Miyoshi, *J. Org. Chem.*, **42**, 2419 (1977); *Bull. Chem. Soc. Jpn.*, **52**, 806 (1979).

10) G. Lucente and D. Rossi, *Chem. Ind. (London)*, **1973**, 324.

11) R. K. Olsen and A. J. Kolar, *Tetrahedron Lett.*, **1975**, 3597.

12) C. Gallina, M. Maneschi, and A. Romeo, *J. Chem. Soc., Perkin Trans. 1*, **1973**, 1134.

13) S. Nakatsuka, H. Tanino, and Y. Kishi, *J. Am. Chem. Soc.*, **97**, 5008 (1975).

14) a) M. M. Hoehn, W. M. Stark, and J. G. Whitney, *J. Am. Chem., Soc.*, **93**, 2308 (1971); b) R. A. Firestone and B. G. Christensen, *J. Org. Chem.*, **38**, 1436 (1973).

15) C. Shin, Y. Sato, and J. Yoshimura, *Bull. Chem. Soc. Jpn.*, **49**, 1909 (1976).

16) C. Shin, *J. Syn. Org. Chem. Jpn.*, Review A, "Synthesis of α-Dehydroamino Acid," **37**, 830 (1979).

17) a) C. Shin, Y. Sato, K. Sugizaki, K. Nanjo, and J. Yoshimura, 33rd National Meeting of the Chemical Society of Japan, Fukuoka, October 1975, Abstr. II, p. 910; b) C. Shin, Y. Sato, Y. Okazaki, T. Katakura, J. Sugano, and J. Yoshimura, 36th National Meeting of the Chemical Society of Japan, Osaka, April 1977, Abstr. II, p. 1222.

18) J. D. M. Herscheid, R. J. F. Nivard, M. W. Tijhuis, H. P. H. Scholten, and H. C. J. Ottenheijm, *J. Org. Chem.*, **45**, 1880 (1980).

19) J. D. M. Herscheid, R. J. F. Nivard, M. W. Tijhuis, and H. C. J. Ottenheijm, *J. Org. Chem.*, **45**, 1885 (1980).

20) C. Shin, K. Nanjo, E. Ando, and J. Yoshimura, *Bull. Chem. Soc. Jpn.*, **47**, 3109 (1974).

21) C. Shin, M. Hayakawa, T. Suzuki, A. Ohtsuka, and J. Yoshimura, *Bull. Chem. Soc. Jpn.*, **51**, 550 (1978).

22) C. Shin, K. Nanjo, T. Nishino, Y. Sato, and J. Yoshimura, *Bull. Chem. Soc. Jpn.*, **48**, 2492 (1975).

The Preparation of Optically Active β-Keto Sulfoxides by Means of an Enantiomer-differentiating Reaction of α-Lithio Aryl Methyl Sulfoxides with Chiral Carboxylates[1)]

Norio KUNIEDA,* Akira SUZUKI, and Masayoshi KINOSHITA

Department of Applied Chemistry, Faculty of Engineering, Osaka City University, Sumiyoshi-ku, Osaka 558

(Received June 26, 1980)

The reaction of α-lithio aryl methyl sulfoxides with a limited amount of chiral carboxylates (R^2–CO–O–R*) was found to be an enantiomer-differentiating reaction, affording the corresponding optically active β-keto sulfoxides (**3**), together with optically active aryl methyl sulfoxides which have the opposite configuration. The optical purity and the predominant configuration of **3** obtained were assigned by means of a combination of polarimetric analysis and NMR. The degree of enantioselectivity of this reaction was affected by the nature of the ester moiety R^2, indicating an increase in optical yields, from 1.3%, where R^2 was ethyl (**3b**), to 70.3%, where R^2 was *t*-butyl (**3f**). The stereochemical course of the reaction has been discussed by considering a six-membered cyclic transition state. Furthermore, the repeated recrystallizations of several β-keto sulfoxides thus obtained, such as (−)-**3e**, (−)-**3f**, (−)-**3g**, and (−)-**3p**, were found to give the corresponding highly optically pure β-keto sulfoxides.

β-Keto sulfoxides are useful as key synthetic intermediates.[2)] Previously, we have found that optically active β-keto sulfoxides can serve as good chiral precursors in the asymmetric synthesis of optically active alcohols.[3c)] The optically active β-keto sulfoxides hitherto reported have generally been prepared by either the reaction of carboxylic esters with α-sulfinyl carbanions, which are derived from optically active sulfoxides,[1,3c)] or by the oxidation of optically active β-hydroxy sulfoxides, which are prepared from optically active sulfoxides and aldehydes,[3e,4b)] exclusive of microbiological methods.[4)] However, these procedures involve the rather hard task of synthesizing optically active sulfoxides as the starting materials.[5)]

During the course of our research concerned with the asymmetric induction by the chiral sulfinyl group,[3)] we recently reported that 2 equivalents of a racemic α-sulfinyl carbanion reacted with a (−)-menthyl (*S*)-arenesulfinate to yield a diastereomeric mixture of (*R*,*S*)- and (*R*,*R*)-β-disulfoxides in a ratio of about 6 : 4.[3b)] In view of this finding, we considered that the reaction of a racemic α-sulfinyl carbanion with a limited amount of a chiral carboxylate might provide a kinetic resolution of the α-sulfinyl carbanion, together with the production of optically active β-keto sulfoxide. As expected, we have now found that the reaction of 2 equivalents of racemic α-lithio aryl methyl sulfoxides (**1**)[8)] with chiral carboxylates(**2**) affords the corresponding optically active β-keto sulfoxides(**3**), together with the optically active aryl methyl sulfoxides (Scheme 1). We wish herein to report on the application of this method to the synthesis of some optically active β-keto sulfoxides and the determination of their optical purities and absolute configurations.

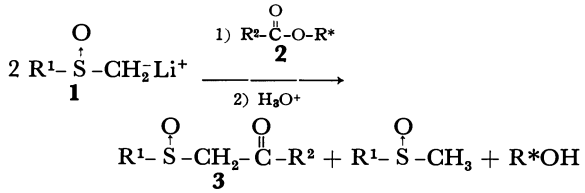

1a: R^1 = *p*-$CH_3C_6H_4$
b: R^1 = C_6H_5

2a: R^2 = CH_3, R* = (−)-Menthyl
b: R^2 = C_2H_5, R* = (−)-Menthyl
c: R^2 = *n*-C_3H_7, R* = (−)-Menthyl
d: R^2 = *n*-C_9H_{19}, R* = (−)-Menthyl
e: R^2 = *i*-C_3H_7, R* = (−)-Menthyl
f: R^2 = *t*-C_4H_9, R* = (−)-Menthyl
g: R^2 = C_6H_{11}, R* = (−)-Menthyl
h: R^2 = C_6H_5, R* = (−)-Menthyl
i: R^2 = *p*-$CH_3C_6H_4$, R* = (−)-Menthyl
j: R^2 = *o*-$CH_3C_6H_4$, R* = (−)-Menthyl
k: R^2 = 3,5-$(t\text{-}C_4H_9)_2C_6H_3$, R* = (−)-Menthyl
l: R^2 = α-$C_{10}H_7$, R* = (−)-Menthyl
m: R^2 = 2,4,6-$(CH_3)_3C_6H_2$, R* = (−)-Menthyl
n: R^2 = *t*-C_4H_9, R* = (−)-Bornyl
o: R^2 = C_6H_5, R* = (−)-Bornyl
p: R^2 = *t*-C_4H_9, R* = (+)-1-Methylheptyl
q: R^2 = C_6H_5, R* = (+)-1-Methylheptyl
r: R^2 = C_6H_5, R* = (−)-1-Methylheptyl

3a: R^1 = *p*-$CH_3C_6H_4$, R^2 = CH_3
b: R^1 = *p*-$CH_3C_6H_4$, R^2 = C_2H_5
c: R^1 = *p*-$CH_3C_6H_4$, R^2 = *n*-C_3H_7
d: R^1 = *p*-$CH_3C_6H_4$, R^2 = *n*-C_9H_{19}
e: R^1 = *p*-$CH_3C_6H_4$, R^2 = *i*-C_3H_7
f: R^1 = *p*-$CH_3C_6H_4$, R^2 = *t*-C_4H_9
g: R^1 = *p*-$CH_3C_6H_4$, R^2 = C_6H_{11}
h: R^1 = *p*-$CH_3C_6H_4$, R^2 = C_6H_5
i: R^1 = *p*-$CH_3C_6H_4$, R^2 = *p*-$CH_3C_6H_4$
j: R^1 = *p*-$CH_3C_6H_4$, R^2 = *o*-$CH_3C_6H_4$
k: R^1 = *p*-$CH_3C_6H_4$, R^2 = 3,5-$(t\text{-}C_4H_9)_2C_6H_3$
l: R^1 = *p*-$CH_3C_6H_4$, R^2 = α-$C_{10}H_7$
m: R^1 = *p*-$CH_3C_6H_4$, R^2 = 2,4,6-$(CH_3)_3C_6H_2$
n: R^1 = C_6H_5, R^2 = CH_3
o: R^1 = C_6H_5, R^2 = *i*-C_3H_7
p: R^1 = C_6H_5, R^2 = *t*-C_4H_9
q: R^1 = C_6H_5, R^2 = C_6H_5

Scheme 1.

Results and Discussion

To cite a typical reaction, (*R*)-(−)-menthyl benzoate (**2h**), $[\alpha]_D^{20}$ −90.5°(C_2H_5OH), was treated with 2 equivalents of α-lithiomethyl *p*-tolyl sulfoxide(**1a**), derived from racemic methyl *p*-tolyl sulfoxide and lithium diethylamide(Et_2NLi), in tetrahydrofuran (THF) at −78 °C in an atmosphere of nitrogen. After 2 h reaction, the work-up, followed by a preparative

TABLE 1. REACTIONS OF α-LITHIO SOLFOXIDES (**1**) WITH CHIRAL CARBOXYLATES (**2**)[a]

Chiral carboxylates	α-Lithio sulfoxides	Base	Reaction time/h	β-Keto sulfoxides				
					Yield/%[c]	$[\alpha]_D$[d]	Config.	%o.p.[e]
(*R*)-(−)-**2a**	**1a**	Et_2NLi	3	**3a**	89	+25.0°[f]	*R*	12.7[g] (12.0)[h]
(*R*)-(−)-**2b**	**1a**	Et_2NLi	2	**3b**	93	+3.5°	*R*	1.3
(*R*)-(−)-**2c**	**1a**	Et_2NLi	2	**3c**	90	−13.5°	*S*	5.3
(*R*)-(−)-**2d**	**1a**	Et_2NLi	2	**3d**	92	−13.2°	*S*	7.1
(*R*)-(−)-**2e**	**1a**	Et_2NLi	3	**3e**	90	−19.0°	*S*	7.4
(*R*)-(−)-**2f**	**1a**	Et_2NLi	5	**3f**	85	−185°	*S*	70.3 (67.5)[h]
(*R*)-(−)-**2f**	**1a**	b)	5	**3f**	76	−174°	*S*	66.2
(*R*)-(−)-**2g**	**1a**	Et_2NLi	2.5	**3g**	96	−52.0°	*S*	21.7
(*R*)-(−)-**2h**	**1a**	Et_2NLi	2	**3h**	94	+35.5°	*R*	13.4
(*R*)-(−)-**2h**	**1a**	b)	2	**3h**	90	+32.0°	*R*	12.1
(*R*)-(−)-**2i**	**1a**	Et_2NLi	2	**3i**	94	+43.8°	*R*	16.9
(*R*)-(−)-**2j**	**1a**	Et_2NLi	3	**3j**	70	+20.3°	*R*	7.6
(*R*)-(−)-**2k**	**1a**	Et_2NLi	3	**3k**	80	+45.1°	*R*	26.5
(*R*)-(−)-**2l**	**1a**	Et_2NLi	3	**3l**	82	+36.0°	*R*	15.2
(*R*)-(−)-**2m**	**1a**	Et_2NLi	1	**3m**	60	+12.0°	*R*	3.8
(*R*)-(−)-**2a**	**1b**	Et_2NLi	2	**3n**	80	+22.7°	*R*	14.6[j] (13.0)[h]
(*R*)-(−)-**2e**	**1b**	Et_2NLi	3	**3o**	83	−12.0°	(*S*)[k]	
(*R*)-(−)-**2f**	**1b**	Et_2NLi	5	**3p**	83	−152°	(*S*)[k]	(50.0)[h]
(*R*)-(−)-**2h**	**1b**	Et_2NLi	2	**3q**	92	+50.2°	(*R*)[k]	
(*R*)-(−)-**2n**	**1a**	Et_2NLi	3.5	**3f**	81	−69.0°	*S*	26.2 (27.0)[h]
(*R*)-(−)-**2o**	**1a**	Et_2NLi	3	**3h**	93	−68.5°	*S*	25.8
(*S*)-(+)-**2p**	**1a**	Et_2NLi	2.5	**3f**	72	+50.4°	*R*	19.2
(*S*)-(+)-**2q**	**1a**	Et_2NLi	2.5	**3h**	90	+22.0°	*R*	8.3
(*R*)-(−)-**2r**	**1a**	Et_2NLi	2.5	**3h**	90	−21.8°	*S*	8.2

a) In THF at −78 °C. b) $(i\text{-}C_3H_7)_2NLi$. c) Yields are based on the starting carboxylic esters (**2**). d) Average values of 2—7 experiments (in acetone, at 18—30 °C). e) Calculated on the basis of the specific rotations for the corresponding authentic β-keto sulfoxides (see Table 2). f) Determined in methanol. g) This value was calculated using the reported specific rotation of (*R*)-(+)-α-(*p*-tolylsulfinyl)acetate, $[\alpha]_D^{29}$ +197° (CH_3OH) (Ref. 4b). h) Evaluated by NMR using Eu(TFC)$_3$. i) Overnight at room temperature. j) Calculated using the reported specific rotation of (*R*)-(+)-α-(phenylsulfinyl)acetate, $[\alpha]_D$ +156° (Ref. 4a). k) Assigned on the basis of the absolute configuration of methyl phenyl sulfoxide which was produced concomitantly by the reaction.

TLC(diethyl ether), afforded dextrorotatory α-(*p*-tolylsulfinyl)acetophenone (**3h**) (93% yield, $[\alpha]_D^{20}$ +35.0° (*c* 0.622, acetone), 13.2% optical purity, (*R*)-rich) and (*S*)-(−)-methyl *p*-tolyl sulfoxide (92% yield, $[\alpha]_D^{20}$ −19.5° (*c* 0.995, acetone), 13.4% optical purity). By a similar procedure, a series of reactions were conducted using thirteen (*R*)-(−)-menthyl carboxylates (**2a—m**), two (*R*)-(−)-bornyl carboxylates (**2n—o**), and three (*R*)-(−)- and (*S*)-(+)-1-methylheptyl carboxylates (**2p—r**). The results are summarized in Table 1. The resultant β-keto sulfoxides (**3a—q**), which possess a variety of R^2 groups, were characterized by means of NMR, IR, mass-spectrum, and elemental analyses.

In order to get a clue as to the optical purity as well as the absolute configuration of the β-keto sulfoxides obtained, we synthesized, as authentic samples, twelve dextrorotatory alkyl and aryl α-(*p*-tolylsulfinyl)methyl ketones (**3b—m**) by the reactions of α-lithiomethyl *p*-tolyl sulfoxide, which has been derived from optically pure (*R*)-(+)-methyl *p*-tolyl sulfoxide, with the corresponding ethyl carboxylates. The specific rotations of the authentic β-keto sulfoxides are compiled in Table 2. Since the formation of carbanions from optically active aryl methyl sulfoxides has been known to take place without any loss of stereochemical integrity,[3b,10,13] and since the reaction of the carbanions with carboxylates is sure to proceed through the complete retention of the configuration at sulfur, the dextrorotatory, β-keto sulfoxides synthesized by the above method should be in an optically pure form with a (*R*)-configuration. This assignment may also be confirmed by the following reaction. That is, the treatment of (*R*)-(+)-α-(*p*-

TABLE 2. SPECIFIC ROTATIONS OF THE AUTHENTIC β-KETO SULFOXIDES (*p*-$CH_3C_6H_4$-SO-CH_2-CO-R^2)

β-Keto sulfoxides(R^2)	Specific rotations in acetone (*c*)
(*R*)-(+)-**3b** (C_2H_5)	$[\alpha]_D^{23}$ +265° (0.194)
(*R*)-(+)-**3c** (*n*-C_3H_7)	$[\alpha]_D^{22}$ +256° (0.266)
(*R*)-(+)-**3d** (*n*-C_9H_{19})	$[\alpha]_D^{15}$ +186.5° (0.222)
(*R*)-(+)-**3e** (*i*-C_3H_7)	$[\alpha]_D^{22}$ +258° (0.196)
(*R*)-(+)-**3f** (*t*-C_4H_9)	$[\alpha]_D^{25}$ +263° (0.275)
(*S*)-(−)-**3f** (*t*-C_4H_9)	$[\alpha]_D^{25}$ −263° (0.300)
(*R*)-(+)-**3g** (C_6H_{11})	$[\alpha]_D^{14}$ +240° (0.224)
(*R*)-(+)-**3h** (C_6H_5)	$[\alpha]_D^{25}$ +265.5° (0.264)
(*S*)-(−)-**3h** (C_6H_5)	$[\alpha]_D^{25}$ −265° (0.500)
(*R*)-(+)-**3i** (*p*-$CH_3C_6H_4$)	$[\alpha]_D^{25}$ +258.5° (0.280)
(*R*)-(+)-**3j** (*o*-$CH_3C_6H_4$)	$[\alpha]_D^{20}$ +268° (0.320)
(*R*)-(+)-**3k** (3,5-(t-C_4H_9)$_2$$C_6H_3$)	$[\alpha]_D^{15}$ +170° (0.446)
(*R*)-(+)-**3l** (α-$C_{10}H_7$)	$[\alpha]_D^{15}$ +237° (0.366)
(*R*)-(+)-**3m** (2,4,6-(CH_3)$_3$$C_6H_2$)	$[\alpha]_D^{15}$ +319° (0.263)

Table 3. Effects of temperature on the reactions of **1a** with (−)-menthyl carboxylates (**2f** and **2h**) in THF

(−)-Menthyl carboxylates	Temp °C	β-Keto sulfoxides	$[\alpha]_D$[a]	%o.p.[b]	$\Delta\Delta G^*$ kJ mol^{-1}	$-\Delta\Delta H^*$ kJ mol^{-1}	$\Delta\Delta S^*$ J K^{-1} mol^{-1}
2f	−78	**3f**	−185°±7°(3)	70.3	2.84	3.51	−3.4
	−35		−157°±6°(2)	59.7	2.73		
	0		−134°±6°(3)	51.0	2.56		
2h	−78	**3h**	+35.5°±2.3°(7)	13.4	0.44	0.58	−0.75
	−35		+26.4°±1.2°(2)	9.9	0.39		
	0		+21.6°±1.0°(3)	8.1	0.37		
	25		+19.5°±0.8°(2)	7.3	0.36		

a) Average values of 2—7 experiments. The number of experiments is shown in parentheses. b) o.p.=Optical purities which were determined by comparison with the specific rotations for the authentic β-keto sulfoxides listed in Table 2.

tolylsulfinyl)acetophenone (**3h**), $[\alpha]_D^{25}$ +265.5° (acetone), with methylmagnesium iodide in THF yielded (*S*)-(−)-methyl *p*-tolyl sulfoxide, $[\alpha]_D^{25}$ −145°(acetone) (99.3% optical purity) *via* a normal S_N2-type process, with a complete inversion of the configuration at sulfur.[14] In addition, the optical purities, in the cases of the authentic **3b**, **3e**, and **3f**, were confirmed with the aid of NMR using the chiral-shift reagent tris[3-(trifluoromethylhydroxymethylene)-*d*-camphorato]europium(III) [Eu(TFC)$_3$] (see Experimental). By a similar procedure, optically pure (*S*)-(−)-**3f** and (*S*)-(−)-**3h** were also prepared using α-lithiomethyl *p*-tolyl sulfoxide derived from optically pure (*S*)-(−)-methyl *p*-tolyl sulfoxide.

Accordingly, the optical purities and the predominant configurations of the β-keto sulfoxides listed in Table 1 were assigned mainly by comparison with the specific rotations for the corresponding authentic substances. In the cases of **3a**, **3f**, **3n**, and **3p**, their optical purities were further confirmed by NMR using Eu(TFC)$_3$.

The degree of enantioselectivity of the reaction was dependent on the reaction temperature (see Table 3). In the reactions of **1a** with **2f** and **2h**, the decrease in temperature favored the formation of the predominant enantiomers, (*S*)-(−)-**3f** and (*R*)-(+)-**3h** respectively, and the plot of $1/T$ *vs.* $\ln(R)/(S)$ (for **3h**) or $\ln(S)/(R)$ (for **3f**) gave a linear relationship with a positive slope. For both the reactions either the $\Delta\Delta H^*$ value or the $\Delta\Delta S^*$ value exhibited a negative sign.

Table 1 reveals that the degree of enantioselectivity varies drastically from 1.3% to 70.3% depending on the nature of the ester moiety, R^2. Generally, the extent of the enantioselectivity is higher when the inducing chiral moiety is menthyl rather than bornyl and 1-methylheptyl, and the chiral carboxylates which have a bulky R^2 group (R^2=phenyl, naphthyl, 3,5-di-*t*-butylphenyl, cyclohexyl, or *t*-butyl) give a relatively high degree of enantioselectivity. The best result has been obtained from the reaction of (*R*)-(−)-menthyl pivalate (**2f**) with **1a**, affording (*S*)-(−)-**3f** of a 70.3% optical purity.

The reactions of two kinds of (*R*)-(−)-bornyl carboxylates, **2n** (R^2=*t*-butyl) and **2o** (R^2=phenyl), with **1a** both gave (*S*)-rich β-keto sulfoxides, (−)-**3f** and (−)-**3h**. From the reactions of both (*S*)-(+)-1-methylheptyl pivalate(**2p**) and (*S*)-(+)-1-methylheptyl benzoate (**2q**) with **1a**, the (*R*)-rich β-keto sulfoxides, (+)-**3f** and (+)-**3h**, were produced preferentially. However, a reversal in the configuration with the variation in the ester moiety, R^2, is observed in the series of reactions of (*R*)-(−)-menthyl carboxylates with **1a**. That is, the carboxylates (−)-**2a**(R^2=methyl), (−)-**2b**(R^2=ethyl), and (−)-**2h**—**m** (R^2=aryl) preferentially react with (*R*)-**1a** to yield an excess of (*R*)-β-keto sulfoxides, while the carboxylates (−)-**2c** (R^2=propyl), (−)-**2d** (R^2=nonyl), (−)-**2e** (R^2=isopropyl), (−)-**2f** (R^2=*t*-butyl), and (−)-**2g**(R^2=cyclohexyl) preferentially react with (*S*)-**1a** to afford the (*S*)-β-keto sulfoxides in excess.

The oxygen atom of sulfoxides is known to have a donor ability towards electron acceptors.[15] Furthermore, in connection with the stereochemistry of the electrophilic substitution reactions of α-lithiosulfoxides, Marquet *et al.*[16] and Biellmann *et al.*[17] have proposed that an electrophilic assistance (a chelation) by the lithium cation on the α-lithiosulfoxides towards the electrophiles plays an important role. By considering this evidence together with a B_{AC} 2-type of mechanism for the reactions of carbanions with carboxylic esters,[18] it appears that the stereochemical course of this reaction can be explained by a six-membered cyclic transition state, as in the case of the reaction of (*R*)-(+)-α-(*p*-tolylsulfinyl)acetophenone with alkyl Grignard reagents reported previously.[19] Therefore, the stereochemical feature of the reaction can be illustrated in terms of the

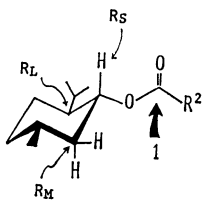

(*R*)-(−)-**2a**—**m**

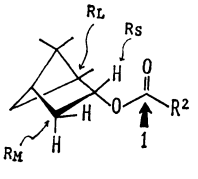

(*R*)-(−)-**2n**, **o**

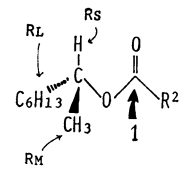

(*R*)-(−)-**2r**

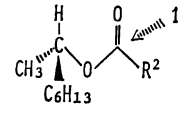

(*S*)-(+)-**2p**, **q**

(The symbols R_S, R_M, and R_L indicate small, medium, and large groups respectively.)

Scheme 2.

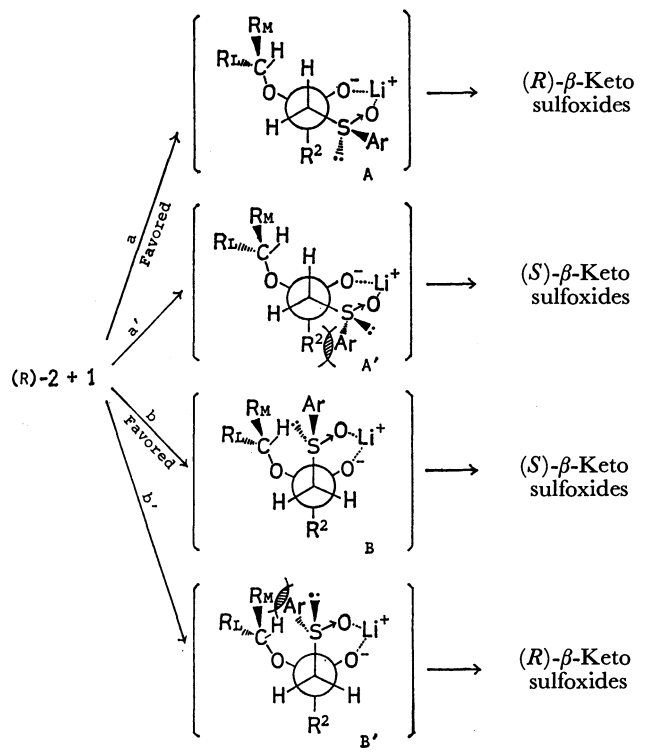

Scheme 3.

following schemes (Schemes 2 and 3). At first, by analogy with the empirical model predictions derived from Prelog's rule[20] and Cram's rule,[21] it can be recognized that the preferential attack of the α-lithiosulfoxides (**1**) towards the carbonyl carbon takes place from the less hindered diastereotopic face of the chiral carboxylates(**2**),[22] as indicated by the arrows (see Scheme 2). Next, the following four reaction paths, (a), (a'), (b), and (b'), involving the respective six-membered cyclic transitions, A, A', B, and B', are conceivable for the substitution reaction of (*R*)-**2** and **1** (see Scheme 3). However, the steric requirements in the transition states seem to indicate that Path (a) or (b) is the most likely possibility, while Paths (a') and (b') are unfavorable, since the significantly greater interactions of the arenesulfinyl group *vs.* the R^2 group or the substituents of the chiral alcohol moiety should contribute to the crowding of the transition states A' and B'. The (*R*)-β-keto sulfoxides will then be produced *via* the transition state A (Path a), while the reactions which proceed *via* the transition state B (Path b) will give the (*S*)-β-keto sulfoxides, and the direction and the degree of enantioselectivities of the reactions should depend upon the magnitudes of the mutual interactions among the arenesulfinyl group, the R^2 group, and the substituents of the chiral alcohol moiety (especially, the R_M group acts as an effective bulk to influence the steric course of the reaction) in the A and B transition states. In the cases of the reactions of **1** with (*R*)(—)-bornyl carboxylates (**2n** and **2o**) and (*R*)-(—)-1-methylheptyl benzoate (**2r**), Path b will predominate, since the sterical interaction between the arenesulfinyl group and the R_M group is considered to be smaller than that between the arenesulfinyl group and the bulky R^2 group. The reactions of the (*R*)-(—)-menthyl carboxylates, **2e**, **2f**, and **2g**, which have rather bulkier R^2 groups, will preferentially take place *via* the transition state B to yield the (*S*)-rich β-keto sulfoxides as well. On the other hand, in the cases of the reactions of the (*R*)-(—)-menthyl carboxylates, **2a** and **2b**, which have smaller R^2 groups, Path a will predominate, since the interaction between the arenesulfinyl group and the R_M group should be larger than that between the arenesulfinyl group and the R^2 group in this case. Actually, most of the experimental results in Table 1 agree fairly well with these predictions. The reversal in configuration from (*R*) to (*S*) in going from **3b** to **3c** may be attributed to the fact that the differences in magnitudes of the interactions of the arenesulfinyl group *vs.* the R^2 group and of the arenesulfinyl group *vs.* the R_M group are reversed with the change in the R^2 group from ethyl to propyl. On the other hand, contrary to our expections, the experimental results from the reactions of (*R*)-(—)-menthyl carboxylates (**2h**—**m**), which have aryl groups, indicate that the reactions proceed *via* the A transition state rather than B. We have now considered that, compared with the aryl groups, the R_M moiety of the menthyl group involving a C-2 equatorial hydrogen and a C-1 methyl group would act more effectively as a steric bulk towards the arenesulfinyl group in this case.

Further investigations, including kinetic experiments, are now under way in an effort to obtain detailed knowledge of the stereochemistry of the reaction.

Finally, we have now found that some of the β-keto sulfoxides thus obtained, **3e**, **3f**, **3g**, **3h**, **3n**, and **3p**, increase their optical purities upon repeated recrystallizations. As is shown in Table 4, especially, the repeated recrystallizations of the partially optically pure **3e**, **3f**, **3g**, and **3p** from a mixture of diethyl ether and hexane

Table 4. Results of the repeated recrystallizations of some β-keto sulfoxides obtained[a]

β-Keto sulfoxides	Specific rotation in acetone at 25 °C	
	Starting (%o.p.)[b]	After recrystallization(%o.p.)[b]
(−)-**3e**	−12.8° (*c* 0.530) (5.0)	−256° (*c* 0.190) (99.2)
(−)-**3f**	−180° (*c* 0.500) (68.4)	−262° (*c* 0.200) (99.6)
(−)-**3g**	−51.0° (*c* 0.680) (21.3)	−240° (*c* 0.331) (100)
(+)-**3h**	+32.3° (*c* 0.690)(12.2)	+55.0° (*c* 0.218) (20.7)
(−)-**3p**	−163°(*c* 0.460)	−266° (*c* 0.294)[c]

a) The recrystallization was repeated three times by the use of a mixture of diethyl ether and hexane. b) o.p.=Optical purities which were determined by comparison with the specific rotations for the authentic β-keto sulfoxides listed in Table 2. c) A single enantiomer was detected by NMR using $Eu(TFC)_3$.

supplied the corresponding β-keto sulfoxides with optical purities higher than 99%. While, the β-keto sulfoxides, **3a**, **3b**, **3c**, and **3j**, decreased in their optical purities to nearly zero upon repeated recrystallizations from diethyl ether or a mixture of diethyl ether and hexane. In these cases, the crystals obtained from the mother liquid exhibited a larger specific rotation than that of the starting β-keto sulfoxides.

In summary, we suppose at present that the present reaction, in combination with the recrystallization procedure, should be satisfactorily applicable to the synthesis of optically active β-keto sulfoxides, provided that the appropriate chiral carboxylates are used.

Experimental

General. The optical rotations were measured with a JASCO DIP-4 type polarimeter. The IR spectra were obtained with a JASCO IR-G type spectrometer. All the melting points are uncorrected. The NMR spectra were determined with a Hitachi-Perkin-Elmer R-20 or JEOL PS-100 spectrometer; the chemical shifts are reported in δ units, using tetramethylsilane as the internal reference. The CD spectra were determined for ethanol and cyclohexane solutions with a JASCO ORD/CD-5 spectrophotometer. The mass spectra were taken on a JEOL JMS 06 spectrometer.

Starting Materials. *(R)-(+)-Methyl* p-*Tolyl Sulfoxide* was prepared from (−)-menthyl (*S*)-(−)-*p*-toluenesulfinate, mp 107—107.5 °C, $[\alpha]_D^{25}$ −200°(*c* 0.520, acetone), and methylmagnesium iodide according to the method developed by Andersen;[6a] mp 74.5 °C, $[\alpha]_D^{20}$ +146°(*c* 0.460, acetone) [lit,[6b] mp 73—74.5 °C, $[\alpha]_D$ +145.5°(acetone)]. *(S)-(−)-Methyl* p-*Tolyl Sulfoxide* was prepared by the hydrolysis of the ethoxysulfonium salt of (*R*)-(+)-methyl *p*-tolyl sulfoxide according to the method of Johnson and McCants;[26] mp 74.5 °C, $[\alpha]_D^{20}$ −146° (*c* 0.325, acetone). *Racemic Methyl* p-*Tolyl Sulfoxide* and *Methyl Phenyl Sulfoxide* were prepared by the periodate oxidation of the corresponding sulfides.[27] C_6H_5-SO-CH_3; bp 98—99 °C/1 Torr (1 Torr=133.322 Pa)(lit,[28] bp 84 °C/0.25 Torr). *p*-$CH_3C_6H_4$-SO-CH_3; mp 43 °C (lit,[29] 42—43 °C). (−)-*Menthol* (Hoei Chemicals, $[\alpha]_D^{20}$ −50° (C_2H_5OH)) and (−)-*Borneol* (Aldrich, $[\alpha]_D^{20}$ −35.3° (C_2H_5OH)) used here are of a commercial grade. *(R)-(−)-* and *(S)-(+)-1-Methylhepty Alcohol* were prepared by the resolution of racemic 2-octyl alcohol.[30] (*R*)-(−)-1-Methylheptyl alcohol; $[\alpha]_D^{20}$ −10.1° (*c* 2.00, C_2H_5OH)(lit,[30] $[\alpha]_D^{17}$ −9.9° (neat)). (*S*)-(+)-*1*-Methylheptyl alcohol; $[\alpha]_D^{20}$ +10.0° (*c* 2.00, C_2H_5OH)(lit,[30] $[\alpha]_D^{17}$ +9.9° (neat)). *Optically Active Carboxylates* were prepared by treating optically active alcohols with the corresponding carboxylic acid chlorides in diethyl ether in the presence of pyridine. *(R)-(−)-Menthyl Corboxylates*: (−)-$C_{10}H_{19}$-O-CO-R^2; [R^2, mp or bp, Specific rotation (*c*, solvent)], CH_3(**2a**); 108.5—109.5 °C/15 Torr (lit, [31] 117.5—118 °C/25 Torr), $[\alpha]_D^{19}$ −85.0° (1.32, C_2H_5OH) (lit,[34] $[\alpha]_D$ −85.23° (C_2H_5OH)), C_2H_5 (**2b**); 136 °C/29 Torr (lit,[32] 118 °C/15 Torr), $[\alpha]_D^{20}$ −81.0° (1.45, C_2H_5OH)(lit,[32] $[\alpha]_D$ −76.66° (C_2H_5OH)), *n*-C_3H_7 (**2c**); 152 °C/30 Torr (lit,[33] 126 °C/12.5 Torr), $[\alpha]_D^{20}$ −76.0° (1.56, C_2H_5OH)(lit,[32] $[\alpha]_D$ −72.91° (C_2H_5OH)), $[\alpha]_D^{20}$ −72.4° (1.00, benzene) (lit,[33] $[\alpha]_D^{20}$ −70.56° (benzene)), C_9H_{19} (**2d**); 145 °C/2 Torr, $[\alpha]_D^{22}$ −55.8° (2.00, C_2H_5OH), *i*-C_3H_7 (**2e**); 121 °C/13 Torr (lit,[33] 116—117 °C /12 Torr), $[\alpha]_D^{20}$ −76.8° (1.20, C_2H_5OH), $[\alpha]_D^{22}$ −72.0° (1.00, benzene) (lit,[33] $[\alpha]_D^{20}$ −72.05 °(benzene)), *t*-C_4H_9 (**2f**); 124.5 °C/13.5 Torr, $[\alpha]_D^{20}$ −76.4° (1.85, C_2H_5OH), C_6H_{11} (**2g**); 48.3 °C (lit,[32] 48 °C), $[\alpha]_D^{17}$ −65.5° (0.531, C_2H_5OH) (lit,[32] $[\alpha]_D$ −59.11° (C_2H_5OH)), C_6H_5 (**2h**); 54.5 °C (lit,[32] 55 °C), $[\alpha]_D^{20}$ −90.5°(1.53, C_2H_5OH) (lit,[32] $[\alpha]_D^{20}$ −83.53° (C_2H_5OH)), *p*-$CH_3C_6H_4$ (**2i**); 140—141 °C/2 Torr (lit,[35] 196—198 °C/11 Torr), $[\alpha]_D^{22}$ −85.3° (1.26, C_2H_5OH) (lit,[35] $[\alpha]_D^{20}$ −89.9° (neat)), *o*-$CH_3C_6H_4$ (**2j**); 145 °C/3 Torr (lit,[35] 213—215 °C/25 Torr), $[\alpha]_D^{20}$ −81.0° (1.54, C_2H_5OH) (lit,[35] $[\alpha]_D^{20}$ −84.35° (neat)), 3,5-(*t*-C_4H_9)$_2C_6H_3$ (**2k**); 167—169 °C/2 Torr, $[\alpha]_D^{20}$ −67.5° (0.550, C_2H_5OH), α-$C_{10}H_7$ (**2l**); 185 °C/2 Torr (lit,[32] 231—232 °C/11 Torr), $[\alpha]_D^{20}$ −84.5° (1.59, C_2H_5OH) (lit,[32] $[\alpha]_D$ −79.08° (C_2H_5OH)), Mesityl (**2m**); 156—157 °C/2 Torr, $[\alpha]_D^{20}$ −65.0° (0.735, C_2H_5OH). *(R)-(−)-Bornyl Carboxylates*: (−)-$C_{10}H_{17}$-O-CO-R^2; [R^2, bp, Specific rotation], *t*-C_4H_9(**2n**); 74.0 °C/1 Torr, $[\alpha]_D^{15}$ −39.5° (1.68, C_2H_5OH), C_6H_5 (**2o**); 129—130 °C/1 Torr, $[\alpha]_D^{15}$ −42.7° (1.69, C_2H_5OH). *(S)-(+)-1-Methylheptyl Carboxylates*: (+)-C_8H_{17}-O-CO-R^2; [R^2, bp, Specific rotation (*c*, solvent)]; *t*-C_4H_9(**2p**); 61.0 °C /1 Torr, $[\alpha]_D^{20}$ +11.3° (2.00, C_2H_5OH), C_6H_5(**2q**); 109 °C/1 Torr (lit,[36] 171 °C/20 Torr), $[\alpha]_D^{20}$ +40.0° (3.04, C_2H_5OH) (lit,[36] $[\alpha]_D^{20}$ +33.27° (neat)). *(R)-(−)-1-Methylheptyl Benzoate*; 109 °C/1 Torr, $[\alpha]_D^{20}$ −40.1° (*c* 2.18, C_2H_5OH).

Reaction of α-Lithiosulfoxides (1) with Optically Active Carboxylates (2). A typical procedure is as follows. A 50-ml, two-necked, round-bottomed flask containing a magnetic stirring bar was equipped with a rubber septum and a nitrogen-inlet tube. After flusing with dry nitrogen, 15 cm³ of tetrahydrofuran (THF) (freshly distilled over $LiAlH_4$), 3.2 cm³ of a 100 mg/cm³ solution of butyllithium in hexane, and 370 mg of diethylamine were successively injected into the flask through the septum *via* a syringe at 0 °C. The flask was then cooled to −78 °C with a dry ice–acetone bath, a solution of 5 mmol of an aryl methyl sulfoxide in 2.5 cm³ of dry THF was added, and the solution was stirred vigorously for 30 min. A solution of an optically active carboxylate (**2**) (2.5 mmol) in 2.5 cm³ of dry THF was injected *via* a syringe, drop by drop, into the solution. After being stirred for an adequate time at −78 °C (the progress of the reaction was checked from time to time by TLC), water (10 cm³) was added; the mixture was then acidified (*ca.* pH 3) with 10% hydrochloric acid and extracted with chloroform(3×30 cm³). The combined extracts were then washed with brine, dried (Na_2SO_4), and evaporated under a vacuum. The residue was chromatographed on silica gel using a preparative thin-layer chromatoplate. Elution with diethyl ether yielded optically active aryl methyl sulfoxide and the corresponding β-keto sulfoxide(**3**). These products, which exhibited satisfactory NMR and IR spectra, were subjected to optical rotation measurements. The optical purities and the predominant configurations of the β-keto sulfoxides listed in Table 1 were assigned mainly by direct comparison with the specific rotations for the corresponding authentic β-keto sulfoxides.

The NMR spectral non-equivalence was observed for the enantiomers of several β-keto sulfoxides in the presence of

Table 5. Chemical-shift differences induced by $Eu(TFC)_3$ for some alkyl-substituted β-keto sulfoxides

β-Keto sulfoxides	Alkyl groups	$\Delta\Delta\delta$/Hz[a]
3a	$C\underline{H}_3$	3.5
3b	$CH_2C\underline{H}_3$	3.8
3e	$CH(C\underline{H}_3)_2$	2.7
3f	$C(C\underline{H}_3)_3$	1.8(5.0)[b]
3n	$C\underline{H}_3$	4.0
3p	$C(C\underline{H}_3)_3$	(3.0)[b]

a) $\Delta\Delta\delta=|\Delta\delta_R-\Delta\delta_S|$Hz. β-Keto sulfoxides =0.1mol/dm³ solution in CCl_4, $Eu(TFC)_3$=0.7 equiv. b) $Eu(TFC)_3$=1.0 equiv.

$Eu(TFC)_3$.[37] The chemical-shift differences for the resonances of alkyl substituents of β-keto sulfoxides are summarized in Table 5. The optical purities for **3a**, **3f**, **3n**, and **3p** were also evaluated from the NMR spectra by the integration of the respective signals (see Table 1).

By careful, repeated recrystallizations of the resulting **3e**, **3f**, **3g**, and **3p**, the corresponding highly optically pure β-keto sulfoxides were obtained. That is, when a 440 mg of (−)-**3f** ($[\alpha]_D^{25}$ −180° (*c* 0.500, acetone)) was recrystallized three times from a mixture of diethyl ether and hexane (1 : 3 volume ratio), highly optically pure (−)-**3f** (230 mg, $[\alpha]_D^{25}$ −262° (*c* 0.200, acetone), 99.6% optical purity) was obtained. Its physical properties were found to be identical with those of the authentic (*S*)-(−)-**3f**. Three recrystallizations of (−)-**3e** (1.06 g, $[\alpha]_D^{25}$ −12.8° (*c* 0.530, acetone)) and (−)-**3g** (800 mg, $[\alpha]_D^{25}$ −51.0° (*c* 0.680, acetone)) from a mixture of diethyl ether and hexane afforded (−)-**3e** (36 mg, $[\alpha]_D^{25}$ −256° (*c* 0.170, acetone), 99.2% optical purity) and optically pure (−)-**3g** (110 mg, $[\alpha]_D^{25}$ −240° (*c* 0.311, acetone)) respectively. Similarly, from the partially optically pure (−)-**3p** (380 mg, $[\alpha]^{25}$ −163° (*c* 0.460, acetone)), (−)-**3p** (146 mg, $[\alpha]_D^{25}$ −266° (*c* 0.294, acetone)) was obtained. Although the specific rotation for the optically pure (−)-**3p** has never been determined, one enantiomer of **3p** is detected by NMR using $Eu(TFC)_3$. The β-keto sulfoxide **3h** also increased its optical purity upon repeated recrystallizations from a mixture of diethyl ether and hexane. Three recrystallizations of (+)-**3h** (900 mg, $[\alpha]_D^{25}$ +32.3° (*c* 0.690, acetone)), which has been prepared by the reaction of **1a** with (−)-**2h**, afforded a 20.7% optically pure (+)-**3h** (320 mg, $[\alpha]_D^{25}$ +55.0° (*c* 0.218, acetone)). However, in the case of **3h**, we have not found a solvent for recrystallization effective enough to give a highly optically pure **3h**.

Preparation of Authentic Optically Active β-Keto Sulfoxides (p-$CH_3C_6H_4$–SO–CH_2–CO–R^2). The same experimental setup as has been described above was used. (*R*)-(+)-Methyl *p*-tolyl sulfoxide (1.54 g, 10 mmol) was treated with a solution of Et_2NLi (prepared from 6.4 cm^3 of a 100 mg/cm^3 solution of butyllithium in hexane and 740 mg of diethylamine) in 20 cm^3 of dry THF at 0 °C under nitrogen. After 30 min, a solution of an ethyl carboxylate (5 mmol) in 2.5 cm^3 of dry THF was added, and the mixture was stirred for 1—5 h. To the solution was then added water (10 cm^3); the mixture was acidified (*ca.* pH 3) with 10% hydrochloric acid and extracted with chloroform (3×30 cm^3). The combined extracts were washed with brine, dried (Na_2SO_4), and evaporated under a vacuum. The residue was chromatographed using a preparative thin-layer chromatoplate on silica gel; subsequent elution with diethyl ether gave the corresponding dextrorotatory β-keto sulfoxide. The recrystallization of the product from diethyl ether or ethyl acetate afforded the analytically pure β-keto sulfoxide. The β-keto sulfoxides obtained by the above procedure exhibited the following preperties.

(*R*)-(+)-**3b**; mp 68—68.5 °C. $[\alpha]_D^{23}$ +265° (*c* 0.194, acetone). NMR ($CDCl_3$): δ 1.01 (t, 3H, *J*=7 Hz, $-CH_2C\underline{H}_3$) 2.41 (s, 3H, $-CH_3$), 2.50 (q, *J*=7 Hz, 2H, $-C\underline{H}_2CH_3$), 3.76, 3.82 (dd, 2H, *J*=14 Hz, $-CH_2-$), 7.36, 7.53 (dd, 4H, aromatic). IR (KBr): 2900, 1704, 1365, 1270, 1105, 1090, 1053, 1029, 1017, 810 cm^{-1}. UV (C_2H_5OH) max: 220 nm (log ε 3.97), 245 nm (log ε 3.72). CD ($[\theta]\times10^{-4}$): in C_2H_5OH 220 nm (−10.8), 249 nm (+7.55), in cyclohexane 223 nm (−11.2), 260 nm (+5.78). MS: 210 (M^+).

Found: C, 62.65; H, 6.74%. Calcd for $C_{11}H_{14}SO_2$: C, 62.83; H, 6.71%.

(*R*)-(+)-**3c**; mp 60 °C. $[\alpha]_D^{22}$ +256° (*c* 0.266, acetone). NMR ($CDCl_3$): δ 0.87 (t, *J*=7 Hz, 3H, $-CH_2CH_2C\underline{H}_3$), 1.56 (six, *J*=7 Hz, 2H, $-CH_2C\underline{H}_2CH_3$), 2.43 (s, 3H, $-CH_3$), 2.48 (t, *J*=7 Hz, 2H, $-C\underline{H}_2CH_2CH_3$), 3.82, 3.86 (dd, *J*=14 Hz, 2H, $-CH_2-$), 7.43, 7.62 (dd, 4H, aromatic). IR (KBr): 2900, 1700, 1088, 1033, 1026, 1013, 810 cm^{-1}. UV (C_2H_5OH) max: 218 nm (log ε 4.00), 243.5 nm (log ε 3.83). CD ($[\theta]\times10^{-4}$): in C_2H_5OH 220 nm (−9.98), 248 nm (+7.18), in cyclohexane 223 nm (−12.16), 260 nm (+6.45). MS: 224 (M^+).

Found: C, 64.46; H, 7.24%. Calcd for $C_{12}H_{16}SO_2$: C, 64.25; H, 7.19%.

(*R*)-(+)-**3d**; mp 75 °C. $[\alpha]_D^{15}$ +186.5° (*c* 0.222, acetone). NMR ($CDCl_3$): δ 0.60—1.70 (b, 17H, $-CH_2(C\underline{H}_2)_7C\underline{H}_3$), 2.44 (s, 3H, $-CH_3$), 2.46 (t, *J*=7 Hz, 2H, $-C\underline{H}_2(CH_2)_7CH_3$), 3.80, 3.86 (dd, *J*=14 Hz, 2H, $-CH_2-$), 7.39, 7.61 (dd, 4H, aromatic). IR (KBr): 2880, 1700, 1470, 1090, 1045, 1025, 1010, 810 cm^{-1}. UV (C_2H_5OH) max: 217.5 nm (log ε 4.04), 242.5 nm (log ε 3.73). CD ($[\theta]\times10^{-4}$): in C_2H_5OH 220 nm (−11.34), 250 nm (+7.85), in cyclohexane 223 nm (−15.12), 258 nm (+8.33). MS: 308 (M^+).

Found: C, 69.89; H, 9.15%. Calcd for $C_{18}H_{28}SO_2$: C, 70.09; H, 9.15%.

(*R*)-(+)-**3e**; mp 68 °C. $[\alpha]_D^{22}$ +258° (*c* 0.196, acetone). NMR ($CDCl_3$): δ 1.01 (d, *J*=7 Hz, 3H, $-CH\langle^{C\underline{H}_3}_{CH_3}$), 1.09 (d, *J*=7 Hz, 3H, $-CH\langle^{CH_3}_{C\underline{H}_3}$), 2.43 (s, 3H, $-CH_3$), 2.60 (septet, 1H, $-C\underline{H}(CH_3)_2$), 3.85, 3.97 (dd, *J*=14 Hz, $-CH_2-$), 7.36, 7.58 (dd, 4H, aromatic). IR (KBr): 2900, 1696, 1380, 1088, 1055, 1035, 800 cm^{-1}. UV (C_2H_5OH) max: 220 nm (log ε 3.94), 245 nm (log ε 3.71). CD ($[\theta]\times10^{-4}$): in C_2H_5OH 222 nm (−9.88), 249 nm (+6.87), in cyclohexane 224 nm (−12.15), 260 nm (+6.54). MS: 224 (M^+).

Found: C, 64.53; H, 7.33%. Calcd for $C_{12}H_{16}SO_2$: C, 64.25; H, 7.19%.

(*R*)-(+)-**3f**; mp 112.5—113 °C. $[\alpha]_D^{25}$ +263° (*c* 0.275, acetone). NMR ($CDCl_3$): δ 1.07 (s, 9H, $-C(CH_3)_3$), 2.40 (s, 3H, $-CH_3$), 3.83, 4.15 (dd, *J*=15 Hz, 2H, $-CH_2-$), 7.34, 7.59 (dd, 4H, aromatic). IR (KBr): 2900, 1697, 1360, 1041, 810 cm^{-1}. UV (C_2H_5OH) max: 217 nm (log ε 3.99), 244 nm (log ε 3.73). CD ($[\theta]\times10^{-4}$): in C_2H_5OH 220 nm (−12.16), 247.5 nm (+8.31), in cyclohexane 223 nm (−14.22), 261 nm (+7.34). MS: 238 (M^+).

Found: C, 65.26; H, 7.63%. Calcd for $C_{13}H_{18}SO_2$: C, 65.51; H, 7.61%.

(*R*)-(+)-**3g**; mp 113 °C. $[\alpha]_D^{14}$ +240° (*c* 0.224, acetone). NMR ($CDCl_3$): δ 1.0—2.3 (b, 11H, cyclohexyl), 2.44 (s, 3H, $-CH_3$), 3.85, 4.00 (dd, *J*=14 Hz, 2H, $-CH_2-$), 7.42, 7.63 (dd, 4H, aromatic). IR (KBr): 2900, 1697, 1450, 1370, 1087, 1043, 810 cm^{-1}. UV (C_2H_5OH) max: 220 nm (log ε 3.90), 245 nm (log ε 3.68). CD ($[\theta]\times10^{-4}$): in C_2H_5OH 221 nm (−10.85), 250 nm (+7.72), in cyclohexane 223 nm (−12.83), 262 nm (+6.60). MS: 264 (M^+).

Found: C, 68.30; H, 7.70%. Calcd for $C_{15}H_{20}SO_2$: C, 68.15; H, 7.63%.

(*R*)-(+)-**3h**; mp 89 °C. $[\alpha]_D^{25}$ +265.5° (*c* 0.264, acetone). NMR ($CDCl_3$): δ 2.40 (s, 3H, $-CH_3$), 4.26, 4.51 (dd, *J*=14 Hz, 2H, $-CH_2-$), 7.18—7.96 (m, 9H, aromatic). IR (KBr): 2950, 1676, 1593, 1447, 1257, 1085, 1062, 1041, 820, 725 cm^{-1}. UV (C_2H_5OH) max: 248.5 nm (log ε 4.08). CD ($[\theta]\times10^{-4}$): in C_2H_5OH 217 nm (−9.35), 248 nm (+6.01). MS: 258 (M^+).

Found: C, 69.47; H, 5.33%. Calcd for $C_{15}H_{14}SO_2$: C, 69.74; H, 5.46%.

(*R*)-(+)-**3i**; mp 122—122.5 °C. $[\alpha]_D^{25}$ +258.5° (*c* 0.280, acetone). NMR ($CDCl_3$): δ 2.39 (s, 6H, 2×$-CH_3$), 4.27, 4.53 (dd, *J*=14 Hz, 2H, $-CH_2-$), 7.17—7.90 (m, 8H, aromatic). IR (KBr): 2920, 1674, 1606, 1300, 1190, 1041, 810 cm^{-1}.

Found: C, 70.21; H, 5.82%. Calcd for $C_{16}H_{16}SO_2$: C, 70.56; H, 5.90%.

(*R*)-(+)-**3j**; mp 77—77.5 °C. $[\alpha]_D^{20}$ +268°(*c* 0.320, acetone). NMR ($CDCl_3$): δ 2.38 (s, 3H, *o*-CH_3), 2.45 (s, 3H, *p*-CH_3), 4.29, 4.50 (dd, *J*=14 Hz, 2H, $-CH_2-$), 7.13—7.78 (m, 8H, aromatic). IR (KBr): 2950, 1666, 1300, 1253, 1033, 750 cm^{-1}.

Found: C, 70.38; H, 5.83%. Calcd for $C_{16}H_{16}SO_2$: C, 70.56; H, 5.90%.

(*R*)-(+)-**3k**; mp 100.5—101 °C. $[\alpha]_D^{15}$ +170°(*c* 0.446, acetone). NMR ($CDCl_3$): δ 1.32 (s, 18H, 2×$-C(CH_3)_3$), 2.35 (s, 3H, $-CH_3$), 4.36, 4.56 (dd, *J*=14 Hz, 2H, $-CH_2-$), 7.17—7.65 (m, 7H, aromatic). IR (KBr): 2950, 1676, 1058, 1045, 810 cm^{-1}. UV (C_2H_5OH) max: 260 nm (log ε 4.17).

Found: C, 74.59; H, 8.27%. Calcd for $C_{23}H_{30}SO_2$: C, 74.55; H, 8.16%.

(*R*)-(+)-**3l**; mp 110—110.5 °C. $[\alpha]_D^{15}$ +237°(*c* 0.366, acetone). NMR ($CDCl_3$): δ 2.32 (s, 3H, $-CH_3$), 4.34, 4.58 (dd, *J*=14 Hz, 2H, $-CH_2-$), 7.08—8.72 (m, 11H, aromatic). IR (KBr): 2900, 1672, 1290, 1080, 1040, 940, 815, 800 cm^{-1}. UV (C_2H_5OH) max: 242 nm (log ε 4.30), 320 nm (log ε 3.88).

Found: C, 73.77; H, 5.35%. Calcd for $C_{19}H_{16}SO_2$: C, 74.00; H, 5.23%.

(*R*)-(+)-**3m**; mp 89.5 °C. $[\alpha]_D^{15}$ +319° (*c* 0.263, acetone). NMR ($CDCl_3$): δ 2.14 (s, 6H, 2×*o*-CH_3), 2.23 (s, 3H, mesityl *p*-CH_3), 2.38 (s, 3H, *p*-CH_3), 3.98, 4.22 (dd, *J*=15 Hz, 2H, $-CH_2-$), 6.77 (s, 2H, aromatic), 7.29, 7.55 (dd, *J*=8 Hz, 4H, aromatic). IR (KBr): 2900, 1700, 1608, 1087, 1041, 985, 797 cm^{-1}. UV (C_2H_5OH) max: 252 nm (log ε 3.92).

Found: C, 71.97; H, 6.75%. Calcd for $C_{18}H_{20}SO_2$: C, 71.97; H, 6.71%.

*Preparation of (S)-(−)-α-(p-Tolylsulfinyl)acetophenone (**3h**).* Using a procedure similar to that described for (*R*)-(+)-**3h**, the treatment of α-lithiomethyl *p*-tolyl sulfoxide derived from (*S*)-(−)-methyl *p*-tolyl sulfoxide (771 mg, 5 mmol) and LDA (5 mmol)) with 375 mg (2.5 mmol) of ethyl benzoate in 20 cm^3 of dry THF at 0 °C afforded levorotatory α-(*p*-tolylsulfinyl)acetophenone (**3h**) (565 mg, 87.5% yield) after the usual work-up and chromatography on silica gel, with elution with diethyl ether. Subsequent recrystallization from diethyl ether gave analytically pure (S)-(−)-**3h**; mp 89 °C. $[\alpha]_D^{20}$ −265° (c 0.500, acetone). NMR ($CDCl_3$): δ 2.40 (s, 3H, $-CH_3$), 4.26, 4.51 (dd, *J*=14 Hz, 2H, $-CH_2-$), 7.18—7.95 (m, 9H, aromatic).

*Reaction of (R)-(+)-**3h** with Methylmagnesium Iodide.* An ethereal solution of methylmagnesium iodide (7 mmol; 1 mmol/cm^3 solution) was added, drop by drop, to a solution of 517 mg (2 mmol) of (*R*)-(+)-**3h**, $[\alpha]_D^{25}$ +265.5° (*c* 0.264, acetone), in 50 cm^3 of dry THF; the mixture was then stirred for 3 h at −5—0 °C under nitrogen, followed by the careful addition of 10 cm^3 of a saturated solution of ammonium chloride. After the separation of the ethereal layer, the aqueous layer was extracted with chloroform (3×30 cm^3). The combined organic layers were dried(Na_2SO_4) and evaporated under a vacuum. The subsequent preparative TLC of the residue on silica gel, eluting with diethyl ether, afforded (*S*)-(−)-methyl *p*-tolyl sulfoxide (62 mg, 20% yield, $[\alpha]_D^{25}$ −145° (*c* 0.300, acetone), together with the recovery of 370 mg of (*R*)-(+)-**3h**.

References

1) Part of this work was presented as a preliminary communication: N. Kunieda, H. Motoki, and M. Kinoshita, *Chem. Lett.*, **1978**, 713.

2) For example, B. M. Trost, *Acc. Chem. Res.*, **11**, 453 (1978), and the references cited therein.

3) a) N. Kunieda, J. Nokami, and M. Kinoshita, *Chem. Lett.*, **1973**, 871; b) N. Kunieda, J. Nokami, and M. Kinoshita, *Bull. Chem. Soc. Jpn.*, **49**, 256 (1976); c) N. Kunieda, J. Nokami, and M. Kinoshita, *Chem. Lett.*, **1974**, 369; d) N. Kunieda, J. Nokami, and M. Kinoshita, *ibid.*, **1977**, 289; e) J. Nokami, Doctoral Thesis, Osaka City University (1976).

4) a) R. L. Crumbie, D. D. Ridley, and G. W. Simpson, *J. Chem. Soc., Chem. Commun.*, **1977**, 315; b) S. Iriuchijima and N. Kojima, *Agric. Biol. Chem.*, **42**, 451 (1978).

5) To our knowledge, asymmetric syntheses (Andersen's method)[6] and the microbiological oxidation of sulfides[7] are applicable to the preparation of optically pure aryl methyl sulfoxides.

6) a) K. K. Andersen, *Tetrahedron Lett.*, **1962**, 93; b) K. Mislow, M. M. Green, P. Laur, J. T. Melillo, T. Simmons, and A. L. Ternay, Jr., *J. Am. Chem. Soc.*, **87**, 1958 (1965).

7) E. Abushanab, D. Reed, F. Suzuki, and C. J. Sih, *Tetrahedron Lett.*, **1978**, 3415.

8) α-Lithio aryl methyl sulfoxides can readily be prepared from aryl methyl sulfoxides by treatment with phenyl lithium[9] or lithium diethylamide(Et_2NLi),[10] without any side reactions such as the partial decomposition[11] or the displacement of aryl group from the sulfoxides by the lithium reagents.[9,12]

9) J. P. Lockard, C. W. Schroeck, and C. R. Johnson, *Synthesis*, **1973**, 485.

10) G. Tsuchihashi, S. Iriuchijima, and M. Ishibashi, *Tetrahedron Lett.*, **1972**, 4605.

11) J. Jacobus and K. Mislow, *J. Am. Chem. Soc.*, **89**, 5228 (1967); K. Mislow, *Record of Chemical Progress*, **28**, 217 (1967).

12) H. Gilman and S. H. Eidt, *J. Am. Chem. Soc.*, **78**, 3848 (1956).

13) Y. H. Khim, W. Tagaki, M. Kise, N. Furukawa, and S. Oae, *Bull. Chem. Soc. Jpn.*, **39**, 2556 (1966).

14) This result was presented as a preliminary communication: J. Nokami, N. Kunieda, and M. Kinoshita, *Chem. Lett.*, **1977**, 249.

15) R. H. Figueroa, E. Roig, and H. H. Szmant, *Spectrochem. Acta*, **22**, 1107 (1966); R. S. Drago, B. Wayland, and R. L. Carlson, *J. Am. Chem. Soc.*, **85**, 3125 (1963); P. Klaeboe, *Acta Chem. Scand.*, **18**, 999 (1964).

16) G. Chassaing, R. Lett, and A. Marquet, *Tetrahedron Lett.*, **1978**, 471.

17) J. F. Biellmann and J. J. Vicens, *Tetrahedron Lett.*, **1978**, 467.

18) C. K. Ingold, "Structure and Mechanism in Organic Chemistry," Cornell University Press, Ithaca and London (1969), p. 1170.

19) N. Kunieda, J. Nokami, and M. Kinoshita, *Chem. Lett.*, **1974**, 369.

20) V. Prelog, *Helv. Chim. Acta*, **36**, 308 (1953).

21) D. J. Cram and F. A. Abd Elhafez, *J. Am. Chem. Soc.*, **74**, 5828 (1952); T. J. Leitereg and D. J. Cram, *ibid.*, **90**, 4019 (1968).

22) The preferred conformations for the chiral carboxylates (**2**) illustrated in Scheme 2 were postulated on the basis of the X-ray crystallographic data of carboxylic esters of cyclohexanols,[23] the dipole moments of some carboxylic esters,[24] and the ORD and/or CD spectral data of some chiral carboxylic esters.[25]

23) A. McL. Mathieson, *Tetrahedron Lett.*, **1965**, 4137.

24) R. J. B. Marsden and L. E. Sutton, *J. Chem. Soc.*, **1936**, 1383.

25) M. Legrand and M. J. Rougier, "Application of the Optical Activity to Stereochemical Determinations," in "Stereochemistry Fundamentals and Methods," ed by H.B. Kagan, Georg Thieme Publishers, Stuttgart (1977), Vol. 2,

p. 130.
26) C. R. Johnson and D. McCants, Jr., *J. Am. Chem. Soc.*, **87**, 5404 (1965).
27) N. J. Leonard and C. R. Johnson, *J. Org. Chem.*, **27**, 282 (1962).
28) K. K. Andersen, W. H. Edmonds, J. B. Biasotti, and R. A. Strecker, *J. Org. Chem.*, **31**, 2859 (1966).
29) A. Cerniani and G. Modena, *Gazz. Chim. Ital.*, **89**, 834 (1959).
30) J. Kenyon, *Org. Synth.*, Coll. Vol. 1, 418 (1964).
31) K. Sisido, K. Kumazawa, and H. Nozaki, *J. Am. Chem. Soc.*, **82**, 125 (1960).
32) H. Rupe, *Justus Liebigs Ann. Chem.*, **327**, 157 (1903).
33) H. Rupe, *Justus Liebigs Ann. Chem.*, **369**, 311 (1909).
34) J. Kenyon and B. H. Pickard, *J. Chem. Soc.*, **107**, 35 (1915).
35) J. B. Cohen and H. W. Dudley, *J. Chem. Soc.*, **97**, 1732 (1910).
36) J. Kenyon and B. H. Pickard, *J. Chem. Soc.*, **107**, 115 (1915).
37) H. L. Goering, J. N. Eikenberry, and G. S. Koermer, *J. Am. Chem. Soc.*, **93**, 5913 (1971).

Reactions of Perfluoro-2-methyl-2-pentene with Carboxylic Acids, Alcohols, and Some Cyclic Amides. A New Fluorinating Reagent

Shozo YANAGIDA,* Yukihiro NOJI, and Mitsuo OKAHARA

Department of Applied Chemistry, Faculty of Engineering, Osaka University, Yamadakami, Suita, Osaka 565

(Received July 1, 1980)

Perfluoro-2-methyl-2-pentene (PMP) reacts with carboxylic acids, alcohols, and 2-pyridone, giving Michael-type addition products, 1,1,1,3,4,4,5,5,5-nonafluoro-2-trifluoromethyl-3-acyloxypentane, 1,1,1,3,4,4,5,5,5-nonafluoro-2-trifluoromethyl-3-alkoxypentane, 1,1,1,3,4,4,5,5,5-nonafluoro-2-trifluoromethyl-3(2-pyridyloxy)pentane, respectively, in good yields. In the presence of bases, carboxylic acids give acid fluorides, 1,1,1,4,4,5,5,5-octafluoro-2-trifluoromethyl-3-pentanone, and 1,1,1,4,4,5,5,5-octafluoro-2-trifluoromethyl-3-acyloxy-2-pentene (**4**), the yields changing with base, solvent, phase-transfer catalyst, and their combination. In the presence of triethylamine, fluorination occurs exclusively, producing acid fluorides in good yields. Alcohols and 2-pyridone are converted into alkyl fluorides and 2-fluoropyridine, respectively, with use of triethylamine as a base with an aprotic solvent. The reactions of PMP with 4-pyridone and 6-chloro-2-ethyl-5-methyl-4(3*H*)-pyrimidone were also examined. The fluorination reactions were rationalized by preferential replacement of the vinylic fluorine of PMP and a good leaving function of the perfluoro enol group of the intermediates such as **4**.

Since the discovery of oligomerization of tetrafluoroethylene and hexafuluoropropylene, studies on their oligomers have drawn much attentions.[1-5] Among the oligomers, perfuluoro-2-methyl-2-pentene (PMP) (**1**), a dimer of hexafluoropropene, is very susceptible to attack by nucleophiles. This high reactivity is attributable to the mesomeric assistance of the vinylic fluorine, the presence of two electrone-withdrawing trifluoromethyl groups which stabilize intermediate carbanion leading to polarization similar to that in the acid fluoride as shown below:[6]

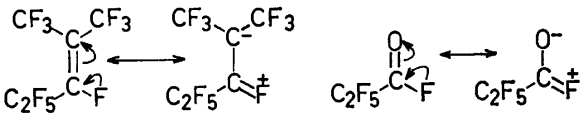

PMP can be regarded as a homolog of perfluoropropionyl fluoride. On the other hand, perfluoro carboxylic acid esters are labile since perfluorocarboxylates are good leaving groups. Thus, the reaction products of PMP with hydroxyl compounds through replacement of the vinylic fluorine are also labile and undergo further reactions under appropriate reaction conditions. We have investigated the reactions of PMP with some carboxylic acids, alcohols, and cyclic amides and found that PMP acts as a fluorinating agent to replace the hydroxyl group with fluorine.

Results and Discussion

Reactions with Carboxylic Acids. Carboxylate anions react readily with PMP (**1**) either in a dipolar aprotic solvent (DMSO, DMF, acetone, or acetonitrile) or under nonaqueous phase-transfer catalysis conditions, giving acid fluorides (**2**) in good yields along with 1,1,1,4,4,5,5,5-octafluoro-2-trifluoromethyl-3-pentanone (**3**), 1,1,1,4,4,5,5,5-octafluoro-2-trifluoromethyl-3-acyloxy-2-pentene (**4**), 1,1,1,3,4,4,5,5,5-nonafluoro-2-trifluoromethyl-3-acyloxypentane (**5**), and the HF addition product (**6**) (Scheme 1).[5] Further investigation has revealed that the reaction products are strongly dependent on the choice of base, solvent, phase-transfer catalysts and their combination.

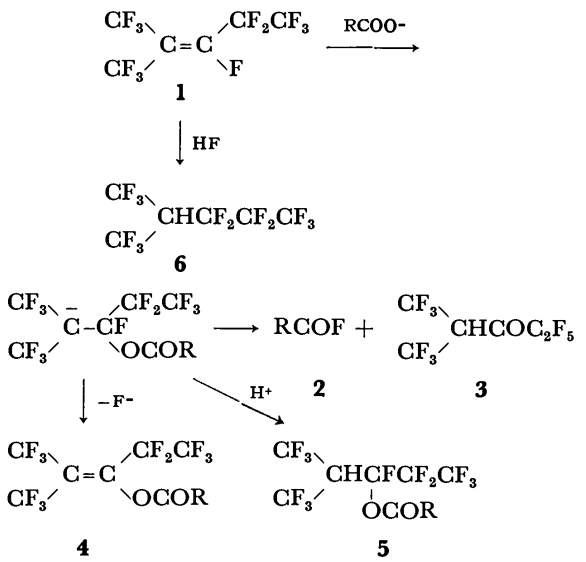

Scheme 1.

The results obtained by use of inorganic bases are summarized in Table 1. While the reaction of benzoic acid in acetone in the absence of base gave the Michael type addition product (**5**) (R=Ph) in moderate yield (run 1), K_2CO_3–acetone (run 2), K_2CO_3–acetonitrile–18-crown-6 (run 3), and K_2CO_3–benzene–octaglyme (run 6) reaction systems gave good yields of benzoyl fluoride. In the K_2CO_3–CH_2Cl_2–18-crown-6 (run 5) and K_2CO_3–CH_2Cl_2–quaternary ammonium salts (runs 9 and 10) reaction systems, the esters **4** and **5** (R=Ph) were formed concomitantly with benzoyl fluoride. The cases are typical for all reactions using Na_2CO_3 as a base. In spite of the strong interaction of Na^+ with 12-crown-4,[7] no significant difference was observed in the catalysis as compared with that of 18-crown-6 (runs 12 and 13). Use of $CaCO_3$ or CaO led to the exclusive formation of the saturated ester **5**, the reaction of calcium benzoate giving the unsaturated ester **4** selectively. The preferential formation of either the ester **4** or **5** in the presence of Na_2CO_3 or $CaCO_3$ is apparently due to the absence of an active fluoride anion in solution because of the low solubility of NaF and CaF_2.

The fluorination reactions were rationalized by assuming that the reaction goes through the esters **4** and **5**.[5] In fact, the reaction of the enol ester **4** (R=$PhCH_2$) with KF gave the benzoyl fluoride. The reaction, however, was slower than that of the saturated ester **5** (R=$PhCH_2$) with K_2CO_3, suggesting that intramolecular fluoride transfer is also possible (Path a, Scheme 2). The reaction mechanism is similar to that proposed in the fluorination reactions by 2-fluoropyridinium salts[8] and by picryl fluoride.[9]

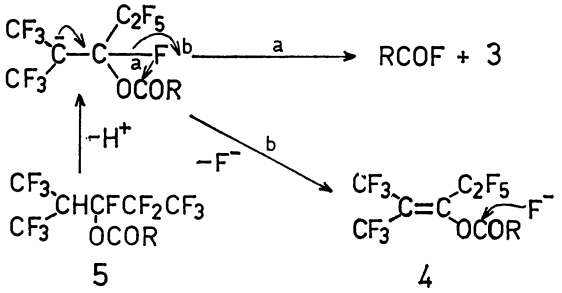

Scheme 2.

When triethylamine was used instead of inorganic bases, the reaction occurred within 1 h, giving acid fluorides with triethylammonium perfluoro-2-methyl-1-ethyl-1-propenolate (**7**) almost quantitatively. (Scheme 3 and Table 2).

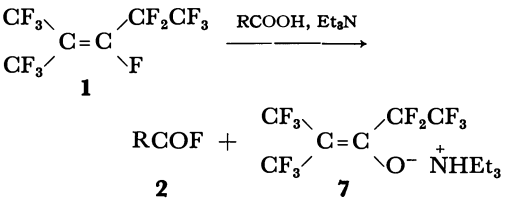

Scheme 3.

Enolate **7** was stable to distillation and characterized by mass, IR, ^{19}F NMR, and ^1H NMR spectra. Martini and Schumann[10] reported its formation by the reaction of PMP with water.

Employment of insoluble polystyrene-bound tertiary amines **8** (Amberlite IRA 68) and **9** gave acid fluorides in good yields (Table 2, runs 8—13). Even a catalytic

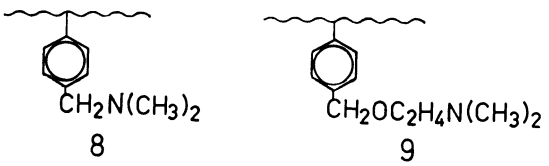

amount of the tertiary amine (run 13) gave acid fluorides in reasonable yield. The fluorination reactions using PMP and the insoluble resins (Table 1, run 10) are very simple, acid fluorides being readily obtained solely by filtration of the resins and the evaporation of solvent.

The reaction in the presence of triethylamine were extended to formic acid and perfluorooctanoic acid but were unsuccessful.

Reactions with Alcohols. Alcohols such as methanol, ethanol, and phenol react with PMP in the presence of triethylamine, yielding the following Michael-type addition products, 1,1,1,3,4,4,5,5,5-nonafluoro-2-trifluoromethyl-3-alkoxypentane (**10**) and their HF elimination products, 1,1,1,4,4,5,5,5-octafluoro-2-trifluoromethyl-3-alkoxy-2-pentene (**11**) (Scheme 4).[2c]

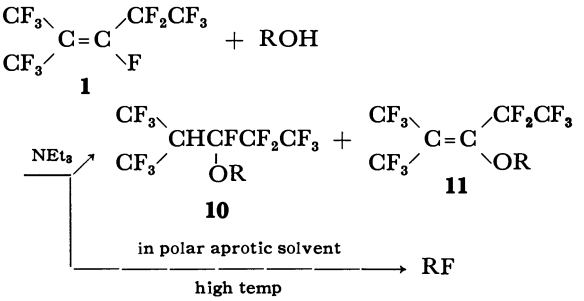

Scheme 4.

It has been found that PMP fluorinates alcohols in the presence of an equimolar amount of triethylamine in an aprotic polar solvent at high reaction temperatures, giving alkyl fluorides in fair to good yields (Scheme 4).

When a mixture of 1-dodecanol, PMP, and triethylamine in a 1 : 1 : 1 mole ratio was made to react in acetonitrile at 80 °C for 8 h, 1-fluorododecane was formed in 28% yield with the enol ether **11** (R=n-$C_{12}H_{25}$). The yield was almost unchanged even when the mole ratio was varied to 1 : 1 : 2, 1 : 2 : 1, and 1 : 2 : 2. Reaction of the mixture in 1 : 1 : 1 mole ratio was examined in various solvents (Table 3). Dipolar aprotic solvents such as DMF and sulfolane, when coupled with higher reaction temperatures, were favorable for the fluorination of alcohols. 2-Octanol was also fluorinated in one-step in moderate yield (runs 15 and 16).

The course of fluorination reaction can be monitored by ^{19}F NMR spectroscopy. In the reaction with 1-octanol, the perfluoro ethers **10** and **11** (R=n-C_8H_{17}) were formed initially in 26 and 56% yields, respectively, the prolonged reaction in sulfolane at 120 °C giving 1-fluorooctane in 74% yield. When the isolated ether **11** (R=n-$C_{12}H_{25}$) was reacted with triethylamine and PMP, 1-fluorododecane was formed in 45—58% yields. This indicates that the fluorination proceeds *via* the attack of fluoride ion on the perfluoro enol ethers **11**.

In the reactions with benzyl alcohol (runs 17 and 18), benzyl fluoride was formed in poor yields. Use of potassium carbonate as a base with 18-crown-6 in dichloromethane led to preferential formation of the perfluoroenol ether **11** (R=$PhCH_2$) (84% yield). Use of excess triethylamine gave rise to the formation of a viscous oily product without givin benzyl fluoride

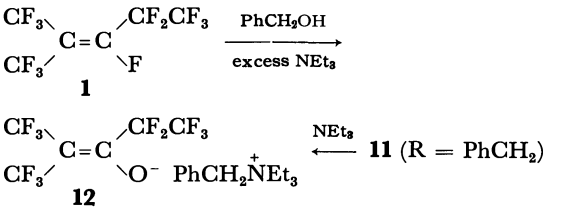

Scheme 5.

and the enol ether **11**. The oily product was identical with the product readily obtained by mixing the enol ether **11** (R=$PhCH_2$) with triethylamine, and identified as benzyltriethylammonium perfluoro-2-methyl-1-ethyl-1-propenolate (**12**) (Scheme 5).

^{19}F NMR analysis of the reaction of the enolate **12** with trifluoroacetic acid showed that the ketones **3** and **13** are formed in a 2 : 1 ratio (Scheme 6). The acid degradation of the triethylammonium enolate **7** also gave the two products.[7] Enolate **12** reacts slowly with benzyl alcohol, giving the two esters **14** and **15** (Scheme 6). These facts well explain the low yield of benzyl fluoride.

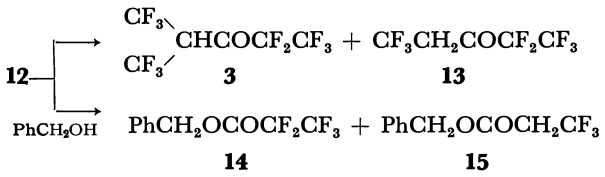

Scheme 6.

Reactions with Some Cyclic Amides. It was claimed in a Japanese patent[11] that 2-pyridone and 4-pyridone react with hexafluoropropene in the presence of potassium carbonate, giving the *N*-substituted products **16** and **17**, respectively. When 4-pyridone was made to

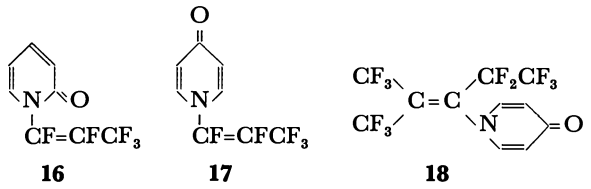

react with excess PMP in the absence of base in acetone at room temperature for 48 h, the *N*-substituted product **18** was formed quantitatively with the HF addition product **6**. However, a similar treatment of 2-pyridone in acetone gave *O*-substituted product, 1,1,1,3,4,4,5,5,5-nonafluoro-2-trifluoromethyl-3-(2-pyridyloxy)pentane (**19**) (Michael-type addition product) in 84% yield. Another *O*-substituted product **20** was formed in 64% yield in dichloromethane in the presence of potassium carbonate and 18-crown-6. When triethylamine was employed as a base and the reaction was conducted in acetonitrile under reflux for 24 h, 2-fluoropyridine was formed in 73% yield with the *N*-substituted product **21** (25% yield) (Scheme 7). Use of DMF as a solvent also gave rise to the formation of 2-fluoropyridine (69% yield) after reaction at 120 °C for 2 h.

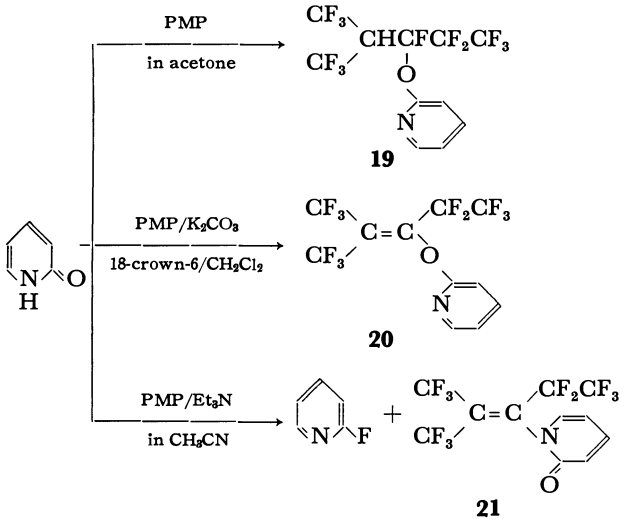

Scheme 7.

GLPC analysis of the course of the fluorination revealed that the *O*-substituted pyridine **20** and the *N*-substituted 2-pyridone **21** are initially formed, 2-fluoropyridine being gradually produced at the expence of **20**. Treatment of **20** with PMP and triethylamine in acetonitrile at 80 °C for 12 h gave 2-fluoropyridine in 90% yield (^{19}F NMR). No reaction took place in the absence of PMP. The reaction of **19** with triethylamine gave 2-fluoropyridine in 75% yield (^{19}F NMR). These facts clearly indicate that the fluorination occurs through the *O*-substituted pyridines **19** and **20**, and that active fluoride ion can also be formed by the degradation of PMP by triethylamine.

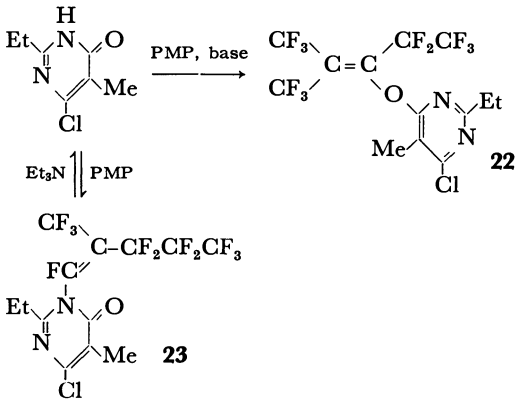

Scheme 8.

Fluorination by PMP in the presence of bases was extended to two pyrimidinones and cyanuric acid. 6-Hydroxy-2-methyl-4(3*H*)-pyrimidinone and cyanuric acid were recovered unchanged by the reaction in dichloromethane at room temperature for 48 h. By a similar treatment of 6-chloro-2-ethyl-5-methyl-4(3*H*)-pyrimidinone with excess PMP in the presence of base, the *O*-substituted product **22** was obtained in good yield (Scheme 8). No fluorination was observed even in the presence of triethylamine in dry sulfolane.

Close examination of the early stage of the reaction shows that the *N*-substituted products having larger retention volume are also formed as a mixture of at least three isomers, two of which were confirmed to be the unexpected *cis* and *trans* isomers **23** (Scheme 8). The attack of nucleophiles on the trifluoromethyl of PMP, *i.e.* the replacement of the allylic fluorine of PMP followed by rearrangement, was also observed in the cyclization reaction of PMP with *N,N*-dimethylhydrazine.[12] When a mixture of the *O*-substituted and *N*-substituted products was treated with triethylamine at room temperature, the *N*-substituted products gradually decomposed into the starting pyrimidinone, the *O*-substituted product **22** remaining unchanged.

Conclusion. The fluorination reactions of PMP

consist of two reactions, (a) replacement of the vinylic fluorine by carboxylates, alkoxides, or enolates leading to the perfluoropropenol esters or ethers, and (b) perfluoro enol oxygen-carbon fission followed by displacement by fluoride ion. The preferential fission of the enol oxygen-carbon was also observed in the isopropenyl derivatives.[13] Triethylammonium fluoride formed during the course of reactions in the presence of triethylamine might be the source of active fluoride ion causing an effective enol oxygen-carbon fission. The present fluorination reactions can be conducted in conventional glass vessels, the by-products being easily separable low-boiling substances and salts. Stable, storable, and low toxic PMP can be easily prepared from hexafluoropropene and is very easy to handle.[14] PMP appears to be advantageous as a small-scale fluorinating reagent as compared with *N,N*-diethyl-2-chloro-1,1,2-trifluoroethylamine,[15] SF_4–amine reagents,[16] HF–amine reagents,[17] and selenium tetrafluoride.[18] From the fact that most perfluoro enol derivatives with boiling points lower than expected are stable against distillation, PMP like trimethylsilyl chloride is promising as a protecting reagent of hydroxyl groups.

TABLE 1. REACTIONS OF BENZOIC ACID WITH PERFLUORO-2-METHYL-2-PENTENE (PMP) IN THE PRESENCE OF INORGANIC BASES WITH AND WITHOUT PHASE-TRANSFER CATALYSIS[a]

Run No.	Base	Solvent	Phase-transfer catalyst (mol %)	Reaction time/h (Rection temp)	Yield/% Reaction product		
					2	**4** and **5**	total
1	—	CH_3COCH_3	—	24 (room temp)	0	1(**4**) 35(**5**)	36
2	K_2CO_3	CH_3COCH_3	—	6(room temp)	74	—[b]	74
3	K_2CO_3	CH_3CN	18-crown-6(4%)	8(reflux)	68	trace	68
4	K_2CO_3	CH_2Cl_2	18-crown-6(38%)	24(reflux)	81	13	94
5	K_2CO_3	CH_2Cl_2	18-crown-6(4%)	8(reflux)	18	34	52
6	K_2CO_3	C_6H_6	octaglyme(10%)	8(reflux)	68	trace	68
7	K_2CO_3	CH_2Cl_2	octaglyme(14%)	8(reflux)	45	52	97
8	PhCOOK	CH_2Cl_2	octaglyme(14%)	8(reflux)	31	43	74
9	K_2CO_3	CH_2Cl_2	$(C_8H_{17})_3\overset{+}{N}CH_3Cl^-$	2(reflux)	39	48	87
10	K_2CO_3	CH_2Cl_2	Amberlite IRA-900(42%)	72(reflux)	47	21	68[c]
11	Na_2CO_3	CH_3COCH_3	—	3(reflux)	8	28(**4**) 28(**5**)	64
12	Na_2CO_3	CH_2Cl_2	12-crown-4(10%)	3(reflux)	5	53(**4**) 11(**5**)	69
13	Na_2CO_3	CH_2Cl_2	18-crown-6(10%)	2(reflux)	16	42(**4**) 13(**5**)	71
14	$CaCO_3$	CH_3COCH_3	—	12(reflux)	trace	3(**4**) 73(**5**)	76
15	CaO	CH_3COCH_3	—	18(reflux)	trace	3(**4**) 67(**5**)	70
16	$(PhCOO)_2Ca$	CH_2Cl_2	18-crown-6(10%)	4(room temp)	trace	58(**4**) 13(**5**)	71

a) PhCOOH (1.22 g, 10 mmol) and PMP (3 g, 10 mmol) were reacted in the presence of base (10 meq). b) Not determined. c) Benzoic acid anhydride was formed in 15% yield.

TABLE 2. FLUORINATION OF CARBOXYLIC ACIDS WITH PMP IN THE PRESENCE OF TERTIARY AMINES[a]

Run No.	Carboxylic acid	Tertiary amine	Solvent	Reaction time/h (Reaction temp)	Yield/%[b] RCOF
1	C_6H_5COOH	$N(Et)_3$	CH_3COCH_3	3(room temp)	86
2	*p*-$NO_2C_6H_4COOH$	$N(Et)_3$	CH_3COCH_3	3(reflux)	73
3	C_2H_5COOH	$N(Et)_3$	$CH_3C_6H_5$	3(room temp)	60
4	C_2H_5COOH	$N(Et)_3$	CH_2Cl_2	1(room temp)	96[c]
5	$CH_3(CH_2)_4COOH$	$N(Et)_3$	CH_2Cl_2	0.5(room temp)	64
6	$CH_3(CH_2)_4COOH$	$N(Et)_3$	CH_2Cl_2	1(room temp)	94[c]
7	$CH_3(CH_2)_6COOH$	$N(Et)_3$	CH_2Cl_2	1(room temp)	88[d]
8	C_6H_5COOH	resin **8**[e]	CH_3COCH_3	48(room temp)	68
9	C_6H_5COOH	resin **9**[f]	CH_3COCH_3	96(room temp)	42[g,h]
10	$CH_3(CH_2)_6COOH$	resin **8**[e]	CH_3COCH_3	48(room temp)	81
11	$CH_3(CH_2)_6COOH$	resin **9**[f]	CH_3COCH_3	96(room temp)	50[g,i]
12	$CH_3(CH_2)_6COOH$	resin **9**[f]	C_6H_6	120(room temp)	52[c,j]
13	$CH_3(CH_2)_6COOH$	resin **9**[k]	C_6H_6	48(room temp)	90[c,l]

a) Carboxylic acid(10 mmol) and PMP (10 mmol) were reacted in the presence of triethylamine (10 mmol). b) Isolated yield. c) NMR yields combined with GLPC analysis. d) After distillation three times. e) Amberlite IRA-68 (1 g) used (amino unit, 56 mol%). f) 0.25 g used (*ca.* 5 mol%). g) GLPC yield. h) The esters (**4** the main ester) were formed in 12% yield, the unreacted acid (41%) being recovered. i) The ester **5** was formed in 3% yield, the unreacted acid (44%) being recovered. j) The esters (**5** the main ester) were formed in 22% yield, the unreacted acid (26%) being recovered. k) 0.5 g used (10 mol%). l) The ester **5** was formed in 10% yield.

Table 3. Fluorination of alcohols by PMP and triethylamine[a)]

Run No.	Alcohol	Reaction conditions			Yield/%[b)] R–F
		Solvent	Temp/°C	Time/h	
1	$CH_3(CH_2)_{11}OH$	CH_3COCH_3	reflux	8	23
2	$CH_3(CH_2)_{11}OH$	CH_3CN	reflux	8	40
3	$CH_3(CH_2)_{11}OH$	$CH_3C_6H_5$	reflux	8	41
4	$CH_3(CH_2)_{11}OH$	xylene	reflux	8	40
5	$CH_3(CH_2)_{11}OH$	dioxane	reflux	8	48
6	$CH_3(CH_2)_{11}OH$	DMF	120	2	62
7	$CH_3(CH_2)_{11}OH$	DMF	120	8	58
8	$CH_3(CH_2)_{11}OH$	DMF	130	2	63
9	$CH_3(CH_2)_{11}OH$	DMF	140	2	64
10	$CH_3(CH_2)_{11}OH$	DMF	150	2	64
11	$CH_3(CH_2)_{11}OH$	sulfolane	120	2	56
12	$CH_3(CH_2)_{11}OH$	sulfolane	130	2	68(67)[c)]
13	$CH_3(CH_2)_{11}OH$	sulfolane	140	2	73
14	$CH_3(CH_2)_7OH$	sulfolane	130	2	75
15	2-octanol	sulfolane	130	2	39
16	2-octanol	CH_3COCH_3	reflux	8	36
17	$C_6H_5CH_2OH$	CH_3COCH_3	reflux	24	12
18	$C_6H_5CH_2OH$	DMF	120	2	15

a) See Experimental. b) ^1H NMR yield using triphenylmethane as internal references. c) Isolated yield.

Experimental

^1H NMR and ^{19}F NMR spectra were recorded with a JEOL LMN-PS-100 spectrometer, ^{19}F NMR spectra being obtained in the presence of 1,1,2-trichlorotrifluoroethane as an internal standard and peak center positions being given in ppm upfield from trichlorofluoromethane. Mass spectra were determined with a Hitachi RMU-6E mass spectrometer, GC–Mass spectra with a Hitachi RMU-6MG spectrometer at 20 eV connected with a Hitachi M-5201 apparatus using 3 m $\times$3 mm column of 5% Silicone OV-1 on Uniport KS, and IR spectra with a JEOL IR-E spectrophotometer. GLPC analysis and preparative scale GLPC were carried out on a Yanagimoto G-8 model instrument equipped with a thermal conductivity detector. The columns were Silicone SE-30 on a Diasolid L (60—80 mesh) (1.5 m$\times$4 mm) and Silicone OV-1 on a Uniport KS (60—80 mesh) (3 m$\times$4 mm).

Materials. Perfluoro-2-methyl-2-pentene (PMP) (supplied from Neos Co. Kobe) was used after distillation. All inorganic bases were used after being ground to powder and dried in a vacuum oven at 100 °C for 24 h. 6-Chloro-2-ethyl-5-methyl-4(3*H*)-pyrimidinone was prepared from propionitrile, phosgene and hydrogen chloride.[16] Amberlite IRA-900 (ammonium chloride type) and IRA-68 (tertiary amine type) (resin **8**) were used after washing and drying. Other commercial chemicals were used after purification.

Preparation of the 2-(Dimethylamino)ethoxy Resin **9**. 2-(Dimethylamino)ethanol (5.5 g, 61.8 mmol) and 40 ml of toluene were placed in a 100 ml three-necked flask equipped with a magnetic stirrer, reflux condenser, thermometer, and an inlet tube for nitrogen gas. Into this was added sodium hydride (2.0 g, *ca.* 42 mmol) under nitrogen. After the solution had been stirred at room temperature until the evolution of hydrogen gas ceased, 3.0 g of chloromethylated poly (styrene) (6.48 mmol) (2% DVB) (100—200 mesh) (Nakarai Chemical Co.) was added. The flask was then placed in an oil bath maintained at 85 °C and the mixture was stirred for 48 h under nitrogen. The resulting resin (**9**) was collected by filtration, washed successively with 350 ml of 4 : 1 THF : H_2O and 500 ml of THF, and washed continuously with THF using a Soxhlet apparatus for 48 h and then dried *in vacuo* at 100 °C. The resin (3.13 g) was obtained. Found: C, 86.09; H, 8.00; N, 2.35; Cl, 0.29%. Calcd for: C, 85.79; H, 8.33; N, 2.61; Cl, 0.29%. Calulation is based on chloromethyl unit mole of the starting resin, the degree of cross-linking by 2% DVB, and the unreacted chlorine content of the resin. Dimethylamino unit: 1.87 mmol/g-resin (dry).

Reactions. The technique used in each reaction was almost the same. Hydroxyl compounds (10 mmol), base (equivalent), and solvent (10 ml) were placed in a 30 ml-flask equipped with a magnetic stirrer and a reflux condenser. When necessary, phase transfer catalysts (4—56 mol%) were added. Stirring was started and the slurry was cooled down to 0 °C with an ice-water bath. PMP (10 mmol or more) was added dropwise and the reaction mixture was then warmed to room temperature or higher. After an appropriate reaction time the solid products and/or solid catalysts were filtered off and the filtrate was concentrated, distilled and analyzed by GLPC, ^1H NMR, and ^{19}F NMR spectroscopy. In case of the reaction mixture containing high-boiling solvent and/or ammonium salts, the products were extracted continuously with pentane using a liquid-liquid extraction apparatus. Most products were known compounds, giving ^1H NMR, ^{19}F NMR, IR, and mass spectra in line with their structures. The following are representative examples (Tables 1, 2, and 3.)

Reaction of Benzoic Acid with PMP in the Presence of K_2CO_3 and Octaglyme (Table 1 and run 7). Benzoic acid (1.22 g, 10 mmol), PMP (3 g, 10 mmol), K_2CO_3 (0.7 g, 5 mmol) and octaglyme (1 g) were made to react in CH_2Cl_2 (10 ml) under reflux for 8 h. After removal of solvent, the concentrate was distilled under reduced pressure, giving two fractions (Fr-1 2.49 g, Fr-2 0.16 g). GLPC analysis showed that each fraction consists of the benzoyl fluoride (**2**, R=Ph) and the ester **4** (R=Ph). Thus the fractions were quantitatively analyzed by GLPC (Silicone SE-30, toluene as an internal reference. *cf.* Table 1). In another reaction under similar conditions, a very small amount of the ester **5** (R=Ph) with a larger retention volume than that of **4** (R=Ph), was also observed with a trace of an unidentified product having the

largest retention volume.

Reaction of Benzoic Acid with PMP in the Presence of $CaCO_3$ (run 14). Benzoic acid (1.22 g) was treated with $CaCO_3$ (0.5 g) and PMP (3 g) in acetone (10 ml) under reflux for 12 h. The reaction mixture was concentrated and distilled under reduced pressure, giving a distillate (3.2 g). GLPC analysis indicated that it consists of the ester **5** (R=Ph), a small amount of the ester **4** (R=Ph), and traces of benzoyl fluoride and an unidentified product.

Reaction of Benzoic Acid with PMP in the Presence of Triethylamine (Table 2 and run 1). Benzoic acid (1.22 g) was treated with triethylamine (1.0 g) and PMP (3 g) in acetone (30 ml) at room temparature for 3 h. After removal of solvent, the concentrate was distilled under reduced pressure, yielding benzoyl fluoride (1.2 g, 86%) and triethylammonium perfluoro-2-methyl-1-ethyl-1-propenolate (**7**) (1.2 g, 30%). The latter product gave IR, ^{19}F NMR, and mass spectra in line with those of the product obtained by the reaction of PMP with triethylamine and water in acetonitrile. (bp 40—55 °C/0.1—0.2 Torr, lit,[8] 44.5 °C/0.2 Torr). (1 Torr=133.322 Pa).

Reaction of Octanoic Acid with PMP in the Presence of the Amberlite-IRA-68 (resin 8) (Table 2 and run 10). Octanoic acid (1.44 g, 10 mmol), PMP (3.0 g, 10 mmol), and Amberlite IRA-68 (1 g, 5.6 mmol of the amino unit) was made to react in 10 ml of acetone at room temperature for 48 h. The reaction mixture was filtered, concentrated, and distilled under reduced pressure, giving octanoic acid fluoride (1.31 g, 81%).

Reaction of Octanoic Acid with PMP in the Presence of the Resin 9 (Table 2 and run 13). Octanoic acid (0.144 g), PMP (0.3 g), and the resin **9** (0.05 g, 0.1 mmol) were allowed to react in benzene (1 ml) at room temparature for 48 h. The reaction mixture was filtered, concentrated, and analyzed by GLPC and ^1H NMR. GLPC analysis showed the disappearance of the starting octanoic acid and the absence of the ester **4** ($R=C_8H_{17}$). On the basis of ^1H NMR analysis, 90% yield of octanoic acid and 10% yield of the ester **5** ($R=C_8H_{17}$) were confirmed.

Reaction of 1-Dodecanol with PMP in the Presence of Triethylamine (Table 3 and run 2). A mixture of 1-dodecanol (1.86 g, 10 mmol), triethylamine (1.0 g, 10 mmol), and PMP (3.0 g, 10 mmol) was treated in acetonitrile (10 ml) under reflux for 8 h. After removal of the solvent, the product was extracted with pentane using a liquid-liquid extraction apparatus (8 h). The extract was concentrated to *ca.* 20% solution and analyzed by ^1H NMR spectroscopy. 40% yield of dodecyl fluoride was confirmed. By vacuum distillation, a mixture (2.03 g) of dodecyl fluoride and 1,1,1,4,4,5,5,5-octafluoro-2-trifluoromethyl-3-dodecyl-2-pentene (**11**) was obtained. The latter product (*ca.* 29% yield), confirmed on the basis of ^1H NMR and GLPC analysis, was isolated by preparative GLPC: IR (neat) 2940 (CH_2), 1640 (C=C), 1100—1400 (C–F) cm^{-1}; MS (70 eV), *m/e* (rel intensity, fragmentation), 466 (<1, M^+), 423 (<1, $M^+-C_3H_7$), 409 (<1, $M^+-C_4H_9$), 395 (<1, $M^+-C_5H_{11}$), 381 (<1, $M^+-C_6H_{13}$), 281 (<1, C_6F_{11}), 259 (<1, C_6F_9O), 181 (<1, C_4F_7), 179 (<1, C_4F_6HO), 169 (<1, $C_{12}H_{25}$), 168 (<1, $C_{12}H_{24}$), 159 (2, C_4F_5O), 140 (1, $C_{10}H_{20}$), 128 (4, C_9H_{20}), 119 (1, C_2F_5), 113 (9, C_8H_{17}), 112 (1, C_8H_{16}), 111 (2, C_8H_{15}), 99 (14, C_7H_{15}), 98 (3, C_7H_{14}), 97 (6, C_7H_{13}), 86 (4, C_6H_{14}), 85 (31, C_6H_{13}), 84 (4, C_6H_{12}), 83 (9, C_6H_{11}), 82 (2, C_6H_{10}), 72 (3, C_5H_{12}), 71 (79, C_5H_{11}), 70 (8, C_5H_{10}), 69 (15, CF_3), 68 (3), 67 (3), 58 (5), 57 (100), 56 (9), 55 (27), 54 (3), 53 (2), 44 (3), 43 (78), 42 (10), 41 (35), 39 (15): ^{19}F NMR ($CDCl_3$) $\delta_a=56.9$, $\delta_b=60.0$, $\delta_c=114.5$, $\delta_d=81.2$, $J_{a-b}=9.8$, $J_{a-c}=20.2$, $J_{a-d}=3.3$ Hz.

Fluorination of 1-Dodecanol with PMP (Table 3 and run 12). 1-Dodecanol (1.86 g, 10 mmol) was treated with triethylamine (1.0 g, 10 mmol) and PMP (3.0 g, 10 mmol) in 5 ml of sulfolane at room temperature until the reaction mixture became homogeneous. The mixture was further reacted at 130 °C for 2 h. After removal of the low-boiling products, the residue was extracted with pentane using a liquid-liquid extraction apparatus (6 h). The extarct was distilled to give 1.26 g of pure dodecyl fluoride (67% yield).

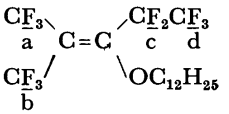

11 (P = $C_{12}H_{25}$)

Reaction of Benzyl Alcohol with PMP in the presence of K_2CO_3 and 18-Crown-6. To a slurry of benzyl alcohol (0.54 g, 5 mmol), K_2CO_3 (0.35 g, 2.5 mmol), and CH_2Cl_2 (10 ml) were added PMP (1.5 g, 5 mmol) and 18-crown-6 (0.13 g, 0.5 mmol). The mixture was refluxed for 4 h. The solid products were filtered and the filtrate was concentrated and distilled under reduced pressure, giving 1,1,1,4,4,5,5,5-octafluoro-2-trifluoromethyl-3-benzyloxy-2-pentene (**11**) (1.63 g, 84% yield): bp 56 °C/4 Torr; IR (neat) 1640 ($(CF_3)_2C$=C), 1100—1400 (C–F); MS (70 eV), *m/e* (relintensity, fragmentation), 388 (<1, M^+), 181 (2, C_4F_7), 179 (2, C_4F_5HO), 159 (2, C_4F_5O), 119 (2, C_2F_5), 107 (5, $PhCH_2O$), 91 (100, $PhCH_2$); ^{19}F NMR ($CDCl_3$) $\delta_a=56.6$, $\delta_b=59.6$, $\delta_c=114.3$, $\delta_d=81.3$, $J_{a-b}=9.5$, $J_{a-c}=20$, $J_{a-d}=3.3$, $J_{b-d}\simeq 1$, $J_{c-d}\simeq <1$ Hz.

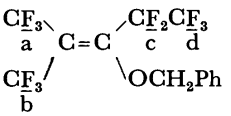

11 (R = $PhCH_2$)

Isolation of Benzyltriethylammonium Perfluoro-2-methyl-1-ethyl-1-propenolate (12). Benzyl alcohol (1.08 g, 10 mmol) was treated with PMP (3.0 g, 10 mmol) and triethylamine (1.01 g, 10 mmol) in dichloromethane (10 ml) at room temperature for 24 h. The reaction mixture was concentrated and distilled under reduced pressure. The distillate (0.723 g) consists of the enol ether **11** (R=$PhCH_2$) and the ammonium enolate **7** as a minor component. The residue is identical with benzyltriethylammonium perfluoro-2-methyl-1-ethyl-1-propenolate (**12**), which was obtained quantitatively by the 1 : 1 reaction of the enol ether **11** and triethylamine in CH_2Cl_2: IR (neat) 1600 ($(CF_3)_2C$=C), 1100—1400 (C–F) cm^{-1}; MS (70 eV, DI), *m/e* (rel intensity, fragmentation), 163 (13, $PhCH_2NEt_2$), 148 (48, $PhCH_2NEtCH_2$), 91 (100, $PhCH_2$); ^1H NMR ($CDCl_3$) δ=1.4 (9H, t), 3.2 (6H, q), 4.4 (2H, s), 7.7 (5H, s); ^{19}F NMR ($CDCl_3$) $\delta_a=49.8$, $\delta_b=55.3$, $\delta_c=117.3$, $\delta_d=81.6$, $J_{a-b}=10.7$, $J_{a-c}=19.6$, $J_{a-d}=1.4$, $J_{b-c}=2.0$, $J_{b-d}<1$, $J_{c-d}<1$, Hz.

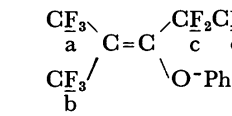

12

The chemical shift at 166.9 ppm observed can be assigned to the fluoride ion of triethylammonium fluoride formed during the course of reaction.

Reaction of the Benzyltriethylammonium Enolate 12 with Benzyl Alcohol. The ammonium enolate **12** (0.389 g, 0.08 mmol) was reacted with benzyl alcohol (0.11 g, 0.1 mmol) in 1 ml of CH_2Cl_2 at room temperature for 3 d. GC mass analysis showed that benzyl perfluoropropionate (**14**) and benzyl 3,3,3-trifluoropionate (**15**) are formed with a small amount of benzyl fluoride. Products **14** and **15** were isolated by preparative GLPC and analyzed. Benzyl perfluoropropionate (**14**): IR (neat) 1780 (C=O), 1215, 1155 (C–F), 1025 (C–O ester) cm^{-1}; MS (70 eV), *m/e* (rel intensity, fragmentation), 254 (57, M^+), 204 (1, $M^+-C_2F_5$), 119 (10, C_2F_5), 107

(11, $PhCH_2O$), 91 (100, $PhCH_2$), 90 (93, PhCH); ^1H NMR ($CDCl_3$) $\delta=5.32$ (2H, s), 7.34 (5H, s); ^{19}F NMR ($CDCl_3$) $\delta=84$ (3F, t), 122.6 (2F, q), $J=1.8$ Hz. Benzyl 3.3.3-trifluoropropionate (**15**): IR (neat) 1755 (C=O) cm^{-1}; MS (70 eV) *m/e* (rel intensity, fragmentation), 218 (42, M^+), 198 (4, M^+-HF), 111 (6, CF_3CH_2CO), 108 (100, $PhCH_2OH$ or $C_3F_2H_2O_2$), 107 (20, $PhCH_2O$), 91 (70, $PhCH_2$ or C_3F_2OH), 90 (84, PhCH, or C_3F_2O); ^1H NMR ($CDCl_3$) $\delta=3.16$ (2H, q, $J_{H-F}=10$ Hz), 5.16 (2H, s), 7.34 (5H, s); ^{19}F NMR ($CDCl_3$) $\delta=64.3$ (t, $J_{F-H}=10$).

Reaction of 4-Pyridone with PMP. 4-Pyridone having one mole of water of crystalization (0.452 g, 4 mmol) was treated with PMP (3 g, 10 mmol) in acetone (10 ml) at room temperature for 6 h. GLPC analysis indicated the formation of a single product. After the reaction mixture was evaporated to dryness, the solid product was purified by sublimation under reduced pressure (1 Torr, 120—140 °C), giving 1-(perfluoro-2-methyl-1-ethyl-1-propenyl)-4-pyridone (**18**) (0.82 g, 55% yield): mp 90—93 °C; IR (KBr disk) 1660 (shoulder) ($(CF_3)_2$-C=C), 1635 (C=O) cm^{-1}; MS (70 eV), *m/e* (rel intensity, fragmentation), 375 (10, M^+), 356 (1, M^+-F), 347 (7, M^+-CO), 337 (5, M^+-F_2), 328 (2, M^+-CFO), 318 (1, M^+-3F), 309 (3, M^+-CF_2O), 124 (100, C_6H_3FNO), 105 (48, C_6H_3NO), 96 (59, C_5H_3FN), 77 (37, C_5H_3N), 69 (13, CF_3), 51 (22, C_4H_3), 50 (19, CF_2), 44 (100, CH_2NO); ^1H NMR (acetone-d_6) $\delta_1=7.87$ (d), $\delta_2=6.26$ (d), $J_{12}=ca.$ 9 Hz; ^{19}F NMR (acetone-d_6) $\delta_a=58.1$, $\delta_b=60.5$, $\delta_c=112.7$, $\delta_d=80.5$, $J_{a-b}=10.8$, $J_{a-d}=9.7$, $J_{b-d}<1$, $J_{b-c}<1$, $J_{c-d}=2.0$ Hz. The same reaction (4-pyridone, 22.6 mg (0.2 mmol) and PMP, 300 mg (1 mmol) in acetone-d_6 (1 ml))was monitored by ^1H NMR and GLPC analysis. Quantitative formation of **6** and **18** was confirmed, suggesting that PMP acts as a scavenger of HF.

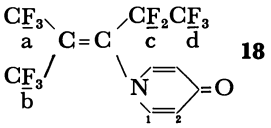

18

Reaction of 2-Pyridone with PMP in the absence of Base. 2-Pyridone (0.95 g, 10 mmol) was treated with PMP (6 g, 20 mmol) in acetone (15 ml) at room temparature for 3 h. After removal of the solvent, the unreacted 2-pyridone was filtered and the residue distilled unde reduced pressure, giving 1,1,1,3,4,4,5,5,5-nonafluoro-2-trifluoromethyl-3(2-pyridyloxy)-pentane (**19**) (3.31 g, 84% yield): bp 66—66.5 °C/5 Torr; IR (neat) 1600 (ring), 1170—1300 (C–F) cm^{-1}; MS (70 eV), *m/e* (rel intensity, fragmentation), 395 (1, M^+), 376 (1, M^+-F), 356 (1, M^+-HF_2), 306 (8, M^+-CHF_4), 300 (3, C_6F_{12}), 281 (27, C_6F_{11}), 231 (35, C_5F_9), 212 (5, C_5H_8), 193 (4, C_5F_7), 181 (100, C_4F_7), 162 (2, C_4F_6), 159 (3, C_4F_5O), 143 (9, C_4F_5), 97 (16, C_5H_4FN), 95 (47, C_5H_5NO), 78 (90, C_5H_4N), 69 (90, CF_3), 51 (13, CF_2H); ^1H NMR ($CDCl_3$) $\delta_1=6.20$ (heptulet), $\delta_2=6.90$ (d), $\delta_3=7.76$ (mc), $\delta_4=7.17$ (mc), $\delta_5=8.21$ (dd), $J_{1a}=J_{1b}=8.6$, $J_{1-e}=8.6$, $J_{23}=ca.$ 8, $J_{34}=ca.$ 8, $J_{45}=ca.$ 5; ^{19}F NMR ($CDCl_3$) $\delta_a,\delta_b=60.1$ (mc), $\delta_c=122.1$ (m), $\delta_d=79.5$ (d), $\delta_e=115.3$ (m), $J_{a-c}=J_{b-c}=ca.$ 26, $J_{d-e}=12$ Hz.

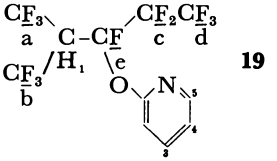

19

Reaction of 2-Pyridone with PMP in the presence of K_2CO_3 and 18-Crown-6. 2-Pyridone (0.476 g, 5 mmol) was treated with PMP (3.0 g, 10 mmol) in CH_2Cl_2 (10 ml) in the presence of K_2CO_3 (0.7 g, 5 mmol) and 18-crown-6 (0.15 g, 0.56 mmol) at room temparature for 24 h. The reaction mixture was worked up as described above, giving 1,1,1,4,4,5,5,5-octafluoro-2-trifluoromethyl-3(2-pyridyloxy)-2-pentene (**20**) (1.21 g, 64% yield): bp 57 °C/10 Torr; IR (neat) 1665 ($(CF_3)_2$-C–C), 1600, 1580 (ring), 1100—1300 (C–F) cm^{-1}. MS (70 eV), *m/e* (rel intensity, fragmentation), 375 (<1, M^+), 356 (8, M^+-F), 337 (<1, M^+-F_2), 318 (1, M^+-F_3), 306 (68, M^+-CF_3), 287 (1, M^+-CF_4), 268 (7, M^+-CF_5), 237 (16, $M^+-C_2F_6$), 218 (2, $M^+-C_2F_7$), 206 (1, $M^+-C_3F_7$), 181 (<1, C_4F_7); 159 (1, C_4F_5O), 119 (1, C_2F_5), 97 (4, C_5H_4FN), 78 (100, C_5H_4N), 69 (10, CF_3), 51 (26, C_4H_3); ^1H NMR ($CDCl_3$) $\delta_1=8.14$ (mc), $\delta_2=7.14$ (mc), $\delta_3=7.74$ (mc), $\delta_4=6.96$ (d), $J_{12}=ca.$ 4.5, $J_{23}=ca.$ 7, $J_{34}=ca.$ 9 Hz; ^{19}F NMR ($CDCl_3$) $\delta_a=57.7$, $\delta_b=61.1$, $\delta_c=113.4$, $\delta=81.4$, $J_{a-b}=9.9$, $J_{a-c}=20.1$, $J_{a-d}=6.2$, $J_{b-c}=1.9$, $J_{c-d}=1.5$ Hz.

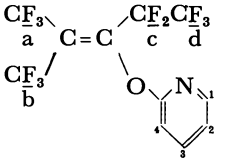

20

Reaction of 2-Pyridone with PMP in the Presence of Triethylamine. 2-Pyridone (0.95 g, 10 mmol), triethylamine (1.0 g, 10 mmol) and PMP (3.0 g, 10 mmol) were treated in 15 ml of acetonitrile under reflux for 24 h. Quantitative analysis by ^{19}F NMR using trifluoromethylbenzene as an internal standard revealed the formation of 2-fluoropyridine (73%) and 1-(perfluoro-2-methyl-1-ethyl-1-propenyl)-2-pyridone (**21**) (25%). The reaction mixture was concentrated under reduced pressure, each product being isolated by preparative GLPC (Silicone SE-30) and analyzed. 2-Fluoropyridine was identified by IR comparison. 1-(perfluoro-2-methyl-1-ethyl-1-propenyl)-2-pyridone (**21**): mp 61—65 °C; IR (KBr disk) 1695 ($(CF_3)_2C=C$), 1610 (ring), 1100—1300 (C–F); MS (70 eV), *m/e* (rel intensity, fragmentation), 375 (2, M^+), 356 (4, M^+-F), 318 (19, M^+-F_3), 306 (33, M^+-CF_3), 268 (100, M^+-CF_3), 243 (8, $M^+-C_3F_5H$), 237 (6, $M^+-C_2F_6$), 78 (86, C_5H_4N), 69 (25, CF_3), 51 (22, C_4H_3); ^1H NMR ($CDCl_3$) $\delta_1=6.54$ (d), $\delta_2=7.38$ (m), $\delta_3=6.24$ (t), $\delta_4=7.0$ (d), $J_{12}=ca.$ 10, $J_{23}=ca.$ 7, $J_{34}=ca.$ 7, $J_{24}=ca.$ 2 Hz; ^{19}F NMR ($CDCl_3$) $\delta_a=58.5$, $\delta_b=61.4$, $\delta_c=110.7$, $\delta_d=80.2$, $J_{a-b}=10.9$, $J_{a-c}=20.7$, $J_{a-d}=9.8$ Hz.

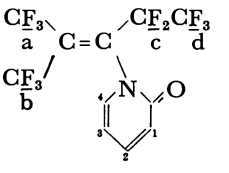

21

Reaction of 6-Chloro-2-ethyl-5-methyl-4(3H)-pyrimidinone with PMP in the presence of Triethylamine. The pyrimidinone (0.518 g, 3 mmol), triethylamine (1.0 g, 10 mmol) and PMP (3.0 g, 10 mmol) were reacted in CH_2Cl_2 (10 ml) at room temparature for 48 h. The reaction mixture was subjected to the usual work-up. Pure 6-chloro-2-ethyl-5-methyl-4-(perfluoro-1-ethyl-2-methyl-1-propenoxy)pyrimidine (**22**) was obtained by vacuum distillation (1.27 g, 94% yield): bp 59 °C/1 Torr; IR (neat) 1675 ($(CF_3)_2C=C$), 1610, 1535 (ring) cm^{-1}; MS (70 eV), *m/e* (rel intensity, fragmentation), 452 (19, M^+), 433 (7, M^+-F), 383 (100, M^+-CF_3), 345 (31, M^+-CF_5), 334 (17, $M^+-C_2H_3F_3Cl$), 171 (6, $M^+-C_6F_{11}$), 155 (40, $M^+-C_6F_{11}O$), 69 (17, CF_3); ^1H NMR ($CDCl_3$) $\delta=1.25$ (3H, t), 2.28 (3H, s), 2.84 (2H, q), $J=8$ Hz; ^{19}F NMR ($CDCl_3$) $\delta_a=57.9$, $\delta_b=61.3$, $\delta_c=113.5$, $\delta_d=81.7$, $J_{a-b}=10$, $J_{a-c}=20.5$, $J_{a-d}=6.2$, $J_{b-d}=-1$, $J_{b-c}=1.3$, $J_{c-d}=1.5$ Hz.

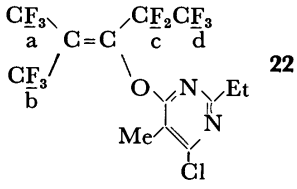

22

Reaction of 6-Chloro-2-ethyl-5-methyl-(3H)-pyrimidinone with PMP in the presence of K_2CO_3 and 18-crown-6. The pyrimidinone (0.518 g, 3 mmol) was reacted with PMP (3.0 g, 10 mmol) in CH_2Cl_2 (10 ml) in the presence of K_2CO_3 (0.7 g, 5 mmol) and 18-crown-6 (0.08 g, 0.3 mmol) at room temparature for 8 h. The reaction mixture was worked up in the usual manner, 0.86 g of the oil products being obtained by vaccum distillation. GLPC analysis (Silicone OV-1, 120 °C, 60 ml (H_2)/min) showed the formation of one major product (retention volume 64 ml) with three minor components (retention volume: peak a, 90 ml, peak b, 110 ml, peak c, 130 ml, peak area ratio a : b : c = 1 : 4 : 6). Each component was isolated by preparative GLPC. The major product was identified as **22** and the components b and c as isomers of 6-chloro-5-ethyl-2-methyl-3-(perfluoro-2-methyl-1-pentenyl)-4(3H)-pyrimidinone (**23**). component b: IR (neat) 1710 (RfC=CF and C=O), 1605 and 1530 (ring) cm^{-1}. MS (70 eV), *m/e* (rel intensity, fragmentation), 452 (13, M^+), 433 (<1, M^+-F), 383 (1, M^+-CF_3), 333 (1, C_2F_5), 283 (17, $M^+-C_3F_7$), 181 (<1, C_4F_7), 171 (1, $M^+-C_6F_{11}$), 155 (100, $M^+-C_6F_{11}O$), 69 (6, CF_3); ^1H NMR ($CDCl_3$) $\delta=1.30$ (3H, t), 2.86 (2H, q), 2.27 (3H, s), $J=8$ Hz; ^{19}F NMR ($CDCl_3$) $\delta_a=57.5$, $\delta_b=51.9$, $\delta_c=109.2$, $\delta_d=126.5$, $\delta_e=81.3$, $J_{a-b}=25.4$, $J_{a-c}=12.2$, $J_{a-d}=6.6$, $J_{b-c}=10.3$, $J_{c-e}=10.3$ Hz. Component c: IR (neat) 1710 (RfC=CF), 1610, 1535 (ring)

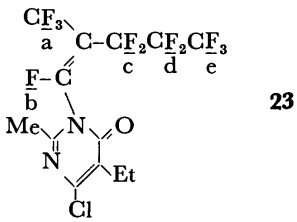

23

cm^{-1}; MS (70 eV), *m/e* (rel intensity, fragmentation), 452 283 (16, $M^+-C_3F_7$), 181 (<1, C_4H_7), 155 (100, $M^+-C_6F_{11}O$), 69 (5, CF_3); ^1H NMR ($CDCl_3$) $\delta=1.28$ (3H, t), 2.30 (3H,s), 2.85 (2H, q), $J=8$ Hz; ^{19}F NMR ($CDCl_3$) $\delta_a=58.0$, $\delta_b=53.3$, $\delta_c=109.5$, $\delta_d=127.4$, $\delta_e=81.2$. The spectrum was less amenable to analysis due to the combined effects of many unresolved couplings; component a was only analyzed by GC-mass spectrum: MS (20 eV) *m/e* (rel intensity, fragmentation), 452 (100, M^+), 433 (8, M^+-F), 383 (23, M^+-CF_3), 333 (17, $M^+-C_2F_5$), 281 (22, C_6F_{11}), 171 (46, $M^+-C_6F_{11}$), 155 (18, $M^+-C_6F_{11}O$), 69 (4, CF_3).

The authors wish to express their thanks to Prof. Daniel Swern, Temple University, for his encouragement and helpful suggestion. They are also grateful to the Neos Co. Ltd. for the supply of the fluorocompounds. The present work was partially supported by a Grant-in-Aid for Scientific Research from the Ministry of Education, Science and Culture.

References

1) J. Hutchinson, *Fette, Seifen, Anstrichm.*, **76**, 158 (1974).
2) a) N. Ishikawa, A. Nagashima, and A. Sekiya, *Chem. Lett.*, **1974**, 1225; b) N. Ishikawa and A. Nagashima, *Bull. Chem. Soc. Jpn.*, **49**, 502 (1976); c) N. Ishikawa and A. Nagashima, *ibid.*, **49**, 1085 (1976).
3) a) R. D. Chambers, A. A. Lindley, and P. D. Philpot, *J. Chem. Soc. Perkin Trans. 1*, **1979**, 214; b) R. D. Chambers, "Fluorine in Organic Chemistry" Weiley-Interscience, New York, 1973 and references contained.
4) a) R. N. Haszeldine, I-ud-D. Mir, and A. E. Tipping, *J. Chem. Soc., Perkin Trans. 1*, **1976**, 2349; b) R. N. Haszeldine, I-ud-D. Mir, and A. E. Tipping, *ibid.*, **1979**, 565 and a series of their studies.
5) a) S. Yanagida, Y. Noji, and M. Okahara, *Tetrahedron Lett.*, **1977**, 2337; b) S. Yanagida, Y. Noji, and M. Okahara, *ibid.*, **1977**, 2893.
6) a) N. Ishikawa, K. Inukai, and H. Muramatsu, *Kagaku Sosetsu*, **27**, 135 (1980); b) W. A. Sheppard and C. M. Smarts, "Organic Fluorine Chemistry," W. A. Benjamine, Inc., New York (1969), p. 300; c) W. A. Bernett, *J. Org. Chem.*, **28**, 1008 (1963); d) J. D. Park, L. H. Wilson, and J. R. Lacher, *ibid.*, **28**, 1008 (1963).
7) S. Yanagida, K. Takahashi, and M. Okahara, *Bull. Chem. Soc. Jpn.*, **51**, 311 (1978).
8) T. Mukaiyama and T. Tanaka, *Chem. Lett.*, **1976**, 303.
9) H. Kotake, K. Inomata, H. Kinoshita, K. Tanabe, and O. Miyano, *Chem. Lett.*, **1977**, 647.
10) T. Martini and C. Schumann, *J. Fluorine Chem.*, **8**, 535 (1976).
11) Japan Kokai, 48-80568 (1973).
12) I. Ikeda, T. Tsukamoto, and M. Okahara, *Chem. Lett.*, **1980**, 583.
13) a) E. S. Rothman, *J. Am. Oil Chem. Soc.*, **45**, 189 (1969); b) E. S. Rothman, G. G. Moore, and J. M. Chirinko, *ibid.*, **48**, 376 (1972).
14) a) N. Ishikawa and A. Sekiya, *Nippon Kagaku Kaishi*, **1972**, 2214; b) R. D. Dresdner, F. N. Tlumac, and J. A. Young, *J. Org. Chem.*, **30**, 3524 (1965); c) W. Brunskill, W. T. Flowers, R. Gregory, and R. N. Haszeldine, *J. Chem. Soc., Chem. Commun.*, **1970**, 1444; d) T. Mizuno, Japan Kokai, 50-117727 (1975), 51-11084 (1976).
15) a) N. Ishikawa, T. Kitazume, and A. Takaoka, *Yuki Gosei Kagaku Kyokai Shi*, **37**, 606 (1979); b) N. N Yarovenko and M. A. Rakusha, *Zh. Obshch. Khim.*, **29**, 2159 (1959).
16) a) W. J. Middletone, *J. Org. Chem.*, **40**, 574 (1975); b) W. J. Middleton and E. M. Bingham, *Org. Synth.*, **57**, 50 (1977).
17) G. A. Olah, M. Nojima, and I. Kerekes, *Synthesis*, **1973**, 786.
18) G. A. Olah, M. Nojima, and I. Kerekes, *J. Am. Chem. Soc.*, **96**, 925 (1974).
19) S. Yanagida, M. Ohoka, M. Okahara, and S. Komori, *J. Org. Chem.*, **34**, 2972 (1969).

  Bull. Chem. Soc. Jpn., 54, 1159—1162 (1981)

Sulfonation of 4*H*-Cyclopenta[*def*]phenanthrene and Its Carbonyl Derivative

Masaaki Yoshida,* Makoto Kobayashi, Masahiro Minabe, and Kazuo Suzuki

Department of Industrial Chemistry, Faculty of Engineering, Utsunomiya University, Ishiicho, Utsunomiya 321

(Received July 10, 1980)

The sulfonation of 4*H*-cyclopenta[*def*]phenanthrene gave 1-sulfonic acid accompanied by formation of 2-, 3-, and 8-analogues. The reaction of 8,9-dihydro derivative with sulfuric acid in acetic anhydride yielded exclusively the 2-acid. Also, 4*H*-cyclopenta[*def*]phenanthren-4-one afforded the 8-acid as the main product, and 1- and 2-isomers as minor products. The formation of the keto 2-sulfonic acid would be controlled thermodynamically and that of the 8-isomer is controlled kinetically.

The hydrocarbon 4*H*-cyclopenta[*def*]phenanthrene (**1**) is a characteristic arene. It was the subject of some interesting studies at its active methylene[1,2] and at its C_8–C_9 bond.[3] The reactivity in electrophilic substitution of **1** differs somewhat from those of phenanthrene and of fluorene during nitration,[4] bromination,[5] and acetylation.[6] Sulfonation of phenanthrene[7] and anthracene[8] has been investigated in detail and the distribution for the reaction products has been described.

The present work deals with sulfonation of **1**, 8,9-dihydro-4*H*-cyclopenta[*def*]phenanthrene (**2**), and 4*H*-cyclopenta[*def*]phenanthren-4-one (**3**) in order to clarify the property of the skeleton of **1** toward electrophile.

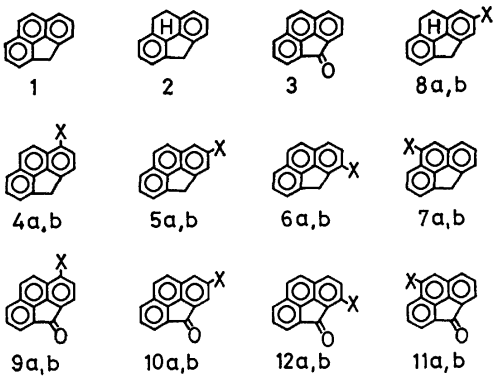

Scheme 1. (Descriptions **a** shows X=SO_3H and **b** is X=SO_3Et.)

Results and Discussion

The sulfonation of **1** afforded 4*H*-cyclopenta[*def*]-phenanthrene-1- (**4a**), -2- (**5a**), -3- (**6a**), and -8-sulfonic acids (**7a**), as is shown in Table 1 (Scheme 1). The assignment of these compounds was established by comparison of their ^1H NMR spectra with those of their nitro[4] and acetyl analogues.[6] The proportion of each isomer was determined by comparison of liquid phase chromatograms (HLPC) of the ester mixture derived from the reaction products with those of pure esters, **4b**, **5b**, **6b**, and **7b**. The error of the yield was within ± 3 (%) as the average of several experiments and the error of proportion was smaller than ± 1 (%) of the standard.

The predominant formation of **4a** would be explained by asserting that the electron density of the 1-position is higher than those of the other positions; this accords with the other electrophilic substitutions.[4–6]

The proportion of **4a** decreases and that of **6a** increases with elevation of the reaction temperature. In sulfonation of phenanthrene, 1-isomer is obtained moderately at low temperature.[7] These results suggest that the formation of **4a** is controlled kinetically and that of **6a** is controlled thermodynamically. Acid **6a** could be stabilized partially due to the hydrogen bond between the active methylene and the sulfonyl group at the 3-position as in the case of 9*H*-fluorene-1-carboxylic acid.[9]

The sulfonation of **2** gave 8,9-dihydro-4*H*-cyclopenta-[*def*]phenanthrene-2-sulfonic acid (**8a**) exclusively, as occurred with fluorene. Other electrophilic attacks to **2** behave in the same way. This tendency can also be seen in the reaction of 1,2,3,3a-tetrahydro-4*H*-cyclopenta[*def*]phenanthrene with electrophiles. This reaction takes place mainly at the 8-position, which corresponds to the 5-position of acenaphthene.[10]

The electron density at the 1- and 3-positions of ketone **3** would be reduced due to the carbonyl group. The reactivity at the 2- and 8-positions may be important. Sulfonation of **3** was examined using 30% oleum–

Table 1. Sulfonation of 4*H*-cyclopenta[*def*]phenanthrene (**1**)

Reaction conditions				Sulfonic acid					Recovd **1**
					Proportion/%				
Agent	Solvent	Temp °C	Time min	Yield %	**4a**	**5a**	**6a**	**7a**	%
H_2SO_4	Ac_2O	0	10	14	86	1	12	1	63
H_2SO_4	Ac_2O	30	10	58	77	1	21	1	10
$ClSO_3H$	dioxane	15	60	24	89	1	10	trace	53
$ClSO_3H$	dioxane	60	10	22	79	2	18	1	55
$ClSO_3H$	dioxane	100	3	29	75	2	22	1	49

Table 2. Sulfonation of 4*H*-cyclopenta[*def*]phenanthren-4-one (**3**)

Run	Reaction conditions			Sulfonic acid					Recovd **3**
				Mono-				Di-	
	Agent	Temp	time	yield	proportion/%			yield	%
		°C	min	%	**9a**	**10a**	**11a**	%	
1	10%oleum	40	20	68	*	4	96	1	25
2	100%H_2SO_4	40	20	28	*	5	95	0	66
3	100%H_2SO_4	40	60	41	*	8	92	0	50
4	100%H_2SO_4	40	1440	98	1	8	91	1	1
5	100%H_2SO_4	60	20	67	*	8	92	0	30
6	100%H_2SO_4	80	20	98	*	9	91	2	0
7	100%H_2SO_4	100	20	83	*	10	90	6	0
8	90%H_2SO_4	120	20	74	*	18	82	9	0
9	80%H_2SO_4	160	20	43[a)]	2	24	74	42	0

* The yield is smaller than 1% as the average. a) A trace amount of **12a** was found.

80% sulfuric acid at 0—160 °C for time periods between 20 min and 24 h. The formation of 4-oxo-4*H*-cyclopenta[*def*]phenanthrene-1- (**9a**), -2- (**10a**) and -8-sulfonic acids (**11a**) was confirmed by comparison of their HLPC with those of pure compounds. Table 2 shows typical runs of sulfonation of **3**. The experimental error of the yield is smaller than ±3 (%) and that of the proportion is within ±2 (%).

The major formation of **11a**, accompanied by **10a**, would be expected because of the influence of the 4-carbonyl group. The proportion of **11a** decreases with extension of the reaction time (runs 2—4), with elevation of reaction temperature (runs 2, 5—7), and with the combination of dilution of the acid and elevation of the temperature (runs 1, 6, 8, and 9). On the contrary, the proportion of **10a** increases.

The reaction of **3** using 20% oleum at 0 °C afforded **11a** (72%) and disulfonic acids (5%). Treatment of **11a** in sulfuric acid at 140 °C yielded **10a**. This finding would suggest that the formation of **11a** is kinetically controlled, that the production of **10a** is governed thermodynamically, and that **10a** forms by isomerization of **11a** under these conditions.

Notice that the positions thermodynamically controlled, that is, the 3-position of **1** and 2-position of **3**, correspond to the positions controlled thermodynamically in naphthalene[11] and phenanthrene.[12]

The π-π^* transition at *ca.* 255 nm on UV spectrum of **5a** shows a larger red shift than those of the other derivatives. This would suggest that the resonance is enlarged by replacement at the 2-position of **1**.[5,6]

The stretching vibrations on IR spectra of **6a** and **6b** show broad and complex peaks due to symmetrical and unsymmetrical S–O bonds. The NMR spectra of the 4-methylene protons of **6a** and **6b** shift to lower fields than those of the other isomers. These findings may be interpreted as due to a combination of an electronic effect and the steric factor between the SO_2 group and methylene group.

The carbonyl absorption of 4-oxo-4*H*-cyclopenta[*def*]-phenanthrene-3-sulfonic acid (**12a**) shifts in frequency about 10 cm^{-1} beyond the shifts those of the others; the UV shows a blue shift at *ca.* 370 nm, beyond that of the parent **3**. These shifts can be explained by the fact that the resonance between the 3-sulfonic acid and the 4-carbonyl group is disturbed both sterically and electronically.

Experimental

All the melting points are uncorrected. The IR spectra were measured on a JASCO IR-G spectrophotometer as KBr disks and the ^1H NMR were determined with a JEOL JNM-C60-HL spectrometer (60 MHz) in D_2O using TSP as internal reference for the sulfonic acids or in $CDCl_3$ using TMS for the esters. The UV spectra were obtained with a JASCO ORD/UV-5 apparatus in H_2O with a scanning speed of 0.76 s/nm. Mass spectra were recorded on a Hitachi RMU-6E apparatus by means of a direct inlet system.

The HLPC data were obtained on an FLC-150 instrument (JASCO) equipped with a UV detector using a reversed phase partition type SS-10-ODS column (JASCO, 25 cm). The elemental analyses of the sulfonic acids show that these crystals have waters of crystallization in the range of 1 to 3 mol, according to the degree of drying.

Sulfonation of 4H-Cyclopenta[def]*phenanthrene (1).* *(a) Quantitative Treatment*: To a solution of **1** (190 mg, 1 mmol) in Ac_2O (9 ml) there was added a mixture of H_2SO_4 (95%, 0.1 ml) and Ac_2O (1 ml); the resulting mixture was stirred for 10 min. After dilution with cold water (100 ml), the precipitate was filtered to give unreacted **1**. The aqueous layer was treated with NaCl and the deposited materials were filtered and ion-exchanged over a cation exchange resin (Amberlite IR-120). The eluate was evaporated off and the residue was extracted with benzene (50 ml). Hexane (150 ml) was added to the solution and the precipitate was filtered. The precipitate was dissolved in water and a part of the solution was titrated with aqueous NaOH (2 mmol/l) to estimate the total yield of the sulfonic acids.

An equimolar amount of NaCl was added to the rest of the solution, which was evaporated, and the residue was treated with $POCl_3$ (2 ml) at 100 °C for 10 min. The reaction mixture was diluted with water and the precipitate was esterified with EtOH (50 ml) in the presence of pyridine (0.5 ml) at 5 °C for 3 h. The ester mixture was applied to HPLC to determine the ratio of isomers. The mobile phase used was (*a*) 2,2,4-trimethylpentane–EtOAc (89/11 volume ratio) or (*b*) hexane–dioxane (92/8). The retention time and the

sensitivity were as follows: **1** (internal standard, 6.1 min for *a*, 6.2 min for *b*, 1.00), **4b** (*a*, 13.5 min, 0.69), **5b** (*a*, 12.5 min, 1.00), **6b** (*b*, 11.1 min, 0.60), and **7b** (*b*, 11.8 min, 0.70).

The reaction mixture of **1** (190 mg, 1 mmol) in dioxane (9 ml) with $ClSO_3H$ (0.2 ml, 3 mmol) in dioxane (1 ml) was treated in a manner similar to that described above.

(b) Separation of ***4a***: A solution of **1** (1.90 g, 10 mmol) in dioxane (50 ml) was refluxed with $ClSO_3H$ (1 ml, 15 mmol) for 10 min and the resulting mixture was poured into cold water (200 ml) containing NaCl (60 g). The precipitate was treated with $POCl_3$ to afford 2.208 g (77%) of the sulfonyl chlorides; these were estirified to give 2.065 g (69%) of the ethyl esters. The ester mixture was recrystallized from benzene–cyclohexane (1/1 volume ratio) to yield 1.082 g (47% based on **1**) of ethyl 4*H*-cyclopenta[*def*]phenanthrene-1-sulfonate (**4b**), mp 159.5—160.5 °C; IR, 1350 and 1165 cm^{-1}; NMR δ 1.23 (3H, t, J=7.2 Hz), 4.11 (2H, q), 4.41 (2H, s), 7.68—7.93 (4H, m), 8.04 (1H, d, J=9.0 Hz, H_8), 8.32 (1H, d, J=7.8 Hz, H_2), and 8.44 (1H, d, J=9.0 Hz, H_9); MS, *m/e*, 298 (M^+), 269, 244, and 189. Found: C, 68.51; H, 4.81%. Calcd for $C_{17}H_{14}O_3S$: C, 68.43; H, 4.73%.

The mother liquor was evaporated to dryness and the residue was dissolved in CCl_4 (100 ml) and chromatographed on a silica gel: the lower band on the column gave 15 mg (1%) of ethyl 4*H*-cyclopenta[*def*]phenanthrene-2-sulfonate (**5b**), mp 167—168 °C; IR, 1349 and 1171 cm^{-1}; NMR δ 1.30 (3H, t, J=7.2 Hz), 4.16 (2H, q), 4.39 (2H, s), 7.64—7.91 (5H, m), 8.13 (1H, s, H_3), and 8.45 (1H, s, H_1); MS, *m/e*, 298 (M^+), 269, and 189. Found: C, 68.57; H, 4.93%. Calcd for $C_{17}H_{14}O_3S$: C, 68.43; H, 4.73%.

The upper band afforded 152 mg (7%) of ethyl 4*H*-cyclopenta[*def*]phenanthrene-3-sulfonate (**6b**), mp 98.5—99.5 °C; IR, 1354 and 1178 cm^{-1}; NMR δ 1.30 (3H, t, J=7.2 Hz), 4.17 (2H, q), 4.67 (2H, s), and 7.67—8.14 (7H, m); MS, *m/e*, 298 (M^+), 269, 253, 244, 205, and 189. Found: C, 68.37; H, 4.86%. Calcd for $C_{17}H_{14}O_3S$: C, 68.43; H, 4.73%.

Sulfonation of 8,9-Dihydro-4H-cyclopenta[def]*phenanthrene (2).* A solution of H_2SO_4 (100%, 0.2 ml) and Ac_2O (1 ml) was added to **2** (576 mg, 3 mmol) in Ac_2O (14 ml). The resulting mixture was stirred for 10 min at room temperature. By a treatment similar to that given above, 506 mg (56% based on **2**) of ethyl 8,9-dihydro-4*H*-cyclopenta[*def*]phenanthrene-2-sulfonate (**8b**) was isolated, mp 144—145 °C; IR, 1357 and 1168 cm^{-1}; NMR δ 1.46 (3H, t, J=7.2 Hz), 3.40 (4H, s), 4.13 (2H, s), 4.30 (2H, q), 7.07—7.40 (3H, m), 7.64 (1H, s, H_1), and 7.78 (1H, s, H_3); MS, *m/e*, 300 (M^+), 271, 245, 207, and 191. Found: C, 67.80; H, 5.29%. Calcd for $C_{17}H_{16}O_3S$: C, 67.97; H, 5.37%.

Sulfonation of 4H-Cyclopenta[def]*phenanthren-4-one (3).*

(a) Quantitative Treatment: A mixture of **3** (204 mg, 1 mmol) and H_2SO_4 (1 ml) was shaken for a prescribed time at a suitable temperature. After dilution with water, the precipitate was filtered to give unreacted **3**. The aqueous layer was treated with NaCl and the deposited materials were ion-exchanged. The eluate was evaporated off and the residue was extracted with EtOAc (50 ml). Hexane (150 ml) was added to the EtOAc solution. The precipitate formed was dissolved in water (200 ml) and submitted to titration and HLPC to estimate the yield of acids and the ratio of isomers, respectively. The mobile phase used in HLPC comprised dioxane (35%) and aqueous Bu_4NBr (5 mmol/l, 65%). The retention time and sensitivity were as follows: **9a** (13.0 min, 45.5), **10a** (14.8 min, 47.1), **11a** (11.5 min, 35.3), **12a** (9.8 min, 36.1), disulfonic acids (*ca.* 5 min, 38.5), and *p*-toluenesulfonic acid (as reference sample, 5.3 min, 1.0).

(b) Separation of ***11b***. A mixture of **3** (2.04 g, 10 mmol) and H_2SO_4 (85%, 10 ml) was stirred for 50 min at 140 °C. After treatment with aqueous NaCl, the sodium salt was refluxed gently with $POCl_3$ (40 ml) for 15 min, giving 2.58 g (85%) of the sulfonyl chloride.

The resulting chloride (3.0 g, 10 mmol) was esterified with dry EtOH (1000 ml) in the presence of pyridine (40 ml) at 5 °C for 7 h and the reaction mixture was poured into cold water. The precipitate was chromatographed on a silica-gel column. The lower band afforded 2.24 g (74% based on sulfonyl chloride) of ethyl 4-oxo-4*H*-cyclopenta[*def*]-phenanthrene-8-sulfonate (**11b**), mp 218—219 °C; IR, 1710 (C=O), 1352, and 1167 cm^{-1}; NMR δ 1.29 (3H, t, J=7.2 Hz), 4.17 (2H, q), 7.51—8.09 (5H, m), 8.42 (1H, d, J=7.8 Hz, H_7), and 8.55 (1H, s, H_9); MS, *m/e*, 312 (M^+), 283, 257, 220, 219, 204, and 203. Found: C, 65.27; H, 3.67%. Calcd for $C_{17}H_{12}O_4S$: C, 65.37; H, 3.87%.

The upper band on the column gave 637 mg (22%) of ethyl 4-oxo-4*H*-cyclopenta[*def*]phenanthrene-2-sulfonate (**10b**) mp 208—209 °C; IR, 1710 (C=O), 1360 and 1173 cm^{-1}; NMR δ 1.33 (3H, t, J=7.2 Hz), 4.21 (2H, q), 7.64—8.03 (5H, m), 8.17 (1H, s, H_3), and 8.53 (1H, s, H_1); MS, *m/e*, 312 (M^+), 283, 257, 220, 219, 204, and 203. Found: C, 65.29; H, 3.93%. Calcd for $C_{17}H_{12}O_4S$: C, 65.37; H, 3.87%.

Isomerization of ***11a***. Acid **11a** (323 mg, 1 mmol) in H_2SO_4 (85%, 1 ml) was heated at 140 °C for 30 min. Upon similar treatment to that described above, 5% of **10a** and 92% of **11a** were detected by HLPC.

Oxidation of Sulfonic Acid Mixture. Hydrocarbon **1** (1.90 g, 10 mmol) was sulfonated with 20% oleum (2 ml) in dioxane (50 ml) under refluxing for 2 h, followed by salting-out, chlorination, and esterification. The yield was 787 mg (26% based on **1**) of the ethyl esters. In addition, 845 mg (44%) of **1** was recovered.

The ester mixture in aqueous EtOH (90%, 110 ml) was heated for 6 h and the solution was evaporated off. The residue was refluxed with MnO_2 (1 g) in water (50 ml) for 30 min. After filtration, the filtrate was added to a solution of $BaCl_2$ (20 g) in water (100 ml) to form the barium salt, which was treated with $POCl_3$, followed by esterification with EtOH. The keto ester was chromatographed on a silica-gel column with benzene. The first eluate afforded 151 mg (5.1% based on **1**) of ethyl 4-oxo-4*H*-cyclopenta[*def*]phenanthrene-1-sulfonate (**9b**), mp 185—186 °C; IR, 1712 (C=O), 1362, and 1172 cm^{-1}; NMR δ 1.30 (3H, t, J=7.2 Hz), 4.16 (2H, q), 7.50—8.04 (5H, m), 8.21 (1H, d, J=7.2 Hz, H_2), and 8.40 (1H, d, J=9.0 Hz, H_9); MS, *m/e*, 312 (M^+), 283, 257, 220, 219, 204, and 203. Found: C, 65.44; H, 3.83%. Calcd for $C_{17}H_{12}O_4S$: C, 65.37; H, 3.87%.

The second eluate gave 8 mg (0.3%) of **10b**, mp 208—209 °C.

The third eluate yielded 43 mg (1.4%) of ethyl 4-oxo-4*H*-cyclopenta[*def*]phenanthrene-3-sulfonate (**12b**), mp 182.5—183.0 °C; IR, 1722 (C=O), 1360, and 1182 cm^{-1}; NMR δ 1.40 (3H, t, J=7.2 Hz), 4.46 (2H, q), and 7.48—8.04 (7H, m); MS, *m/e*, 312 (M^+), 283, 220, 204, and 203. Found: C, 65.43; H, 3.66%. Calcd for $C_{17}H_{12}O_4S$: C, 65.37; H, 3.87%.

Reduction of ***11b***. Ester **11b** (312 mg, 1 mmol) in EtOH (100 ml) was refluxed with $N_2H_4 \cdot H_2O$ (90%, 0.5 ml) for 12 h to give the corresponding hydrazone. The hydrazone was warmed in ethylene glycol (40 ml) containing KOH (2 g) at 170 °C for 3 min and the mixture was poured into water. The precipitate was treated with $POCl_3$ and the chloride was converted into ethyl 4*H*-cyclopenta[*def*]phenanthrene-8-sulfonate (**7b**), yield 164 mg (55%), mp 137—138 °C; IR, 1351 and 1171 cm^{-1}; NMR δ 1.25 (3H, t, J=7.2 Hz), 4.12 (2H, q), 4.37 (2H, s), 7.64—8.00 (5H, m), 8.19—8.44 (1H, m, H_7), and 8.64 (1H, s, H_9); MS, *m/e*, 298 (M^+), 269, 243, and

189. Found: C, 68.70; H, 4.67%. Calcd for $C_{17}H_{14}O_3S$: C, 68.43; H, 4.73%.

By a similar procedure, **10b** (312 mg, 1 mmol) was reduced to **5b** (196 mg, 66%), and **9a** (312 mg, 1 mmol) afforded **4a** (154 mg, 52%).

Hydrolyses of the Esters into the Corresponding Sulfonic Acids. Ester **4b** (298 mg, 1 mmol) was refluxed in EtOH (100 ml) containing water (10 ml) for 6 h to give acid **4a**, yield 287 mg (94%), mp 191—194 °C (dec); IR, 1222, 1165, 1082, and 1034 cm^{-1}; UV_{max} 225 nm (log ε 4.47), 249 (4.62), 293 (3.86), 305 (3.85), 331 (2.95), and 347 (2.87); NMR δ 3.52 (2H, s), 7.01—7.51 (4H, m), 7.71 (1H, d, J=9.0 Hz, H_8), 8.09 (1H, d, J=7.2 Hz, H_2), and 8.28 (1H, d, J=9.0 Hz, H_9); MS, *m/e*, 270 (M^+), 205, and 189.

Acid **5a** was obtained from **5b**, by a method similar to that described above, in a 76% yield, mp 180—183 °C (dec); IR, 1205, 1178, 1095, and 1040 cm^{-1}; UV, 216 (4.52), 256 (4.79), 299 (3.88), 331 (2.54), and 350 (2.40); NMR δ 3.50 (2H, s), 7.03—7.36 (5H, m), 7.90 (1H, s, H_3), and 8.14 (1H, s, H_1); MS, *m/e*, 270 (M^+) and 189.

Acid **6a** was derived from **6b**, yield 95%, mp 175—179 °C (dec); IR, 1257—1128 (broad), 1081, and 1036 cm^{-1}; UV, 225 (4.66), 250 (4.55), 292 (3.96), 304 (3.95), 332 (2.77), and 348 (2.65); NMR δ 4.24 (2H, s), 7.08—7.51 (5H, m), 7.64 (1H, d, J=7.8 Hz, H_1), and 8.02 (1H, d, J=7.8 Hz, H_2); MS, *m/e*, 270 (M^+), 222, 205, and 189.

Acid **7a** was prepared from **7b**, yield 78%, mp 179—183 °C (dec); IR, 1198, 1080, and 1030 cm^{-1}; UV, 226 (4.73), 254 (4.58), 294 (3.78), 304 (3.75), 333 (2.85), and 351 (2.81); NMR δ 3.53 (2H, s), 7.05—7.84 (5H, m), 8.24 (1H, s, H_9), and 8.29 (1H, d, J=7.8 Hz, H_7); MS, *m/e*, 270 (M^+), 205, and 189.

Acid **8a** was obtained from **8b**, yield 86%, mp 179.5—181.0 °C (dec); IR, 1205, 1180, 1097, and 1035 cm^{-1}; UV, 211 (4.58) and 282 (4.16); NMR δ 2.83 (4H, s), 3.46 (2H, s), 6.96—7.23 (3H, m), 8.03 (1H, s, H_1), and 8.21 (1H, s, H_3); MS, *m/e*, 272 (M^+) and 191.

Acid **9a** was derived from **9b**, yield 98%, mp 254—256 °C (dec); IR, 1708 (C=O), 1256, 1224, 1172, 1084, and 1034 cm^{-1}; UV, 235 (5.29), 300 (3.79), and 381 (2.58); NMR δ 6.11—6.93 (5H, m), 7.37 (1H, d, J=9.0 Hz, H_9), and 7.47 (1H, d, J=7.2 Hz, H_2); MS, *m/e*, 284 (M^+), 204, and 203.

Acid **10a** was prepared from **10b**, yield 93%, mp 225—227 °C (dec); IR, 1708 (C=O), 1195, 1188, 1094, and 1049 cm^{-1}; UV, 239 (5.22) and 386 (2.59); NMR δ 6.09—6.81 (6H, m) and 7.23 (1H, s, H_1); MS, *m/e*, 284 (M^+), 204, and 203.

The acid **10a** was also obtained by the acidic hydrolysis of the corresponding sulfonyl chloride in a 79% yield.

Acid **12a** was derived from **12b**, yield 95%, mp 249—255 °C (dec); IR, 1716 (C=O), 1222, 1204, 1094, and 1034 cm^{-1}; UV, 238 (4.96), 275 (4.03), 320 (3.76), and 370 (2.37); NMR δ 6.60—6.89 (5H, m), 7.23 (1H, d, J=8.4 Hz, H_1), and 7.48 (1H, d, J=8.4 Hz, H_2); MS, *m/e*, 284 (M^+), 204, and 203.

Acid **11a** was prepared from **11b**, yield 99%, mp 245—251 °C (dec); IR, 1706 (C=O), 1231, 1202, 1061, and 1021 cm^{-1}; UV, 236 (5.27), 279 (3.94), and 366 (2,38); NMR δ 5.98—7.20 (5H, m), 7.29 (1H, s, H_9), and 7.68 (1H, d, J=7.8 Hz, H_7); MS, *m/e*, 284 (M^+), 204, and 203.

References

1) T. Kimura, M. Minabe, and K. Suzuki, *J. Org. Chem.*, **43**, 1247 (1978).
2) T. Kimura, M. Minabe, and K. Suzuki, *Bull. Chem. Soc. Jpn.*, **52**, 1447 (1979).
3) M. Yoshida, A. Kadokura, M. Minabe, and K. Suzuki, *Tetrahedron*, **35**, 2237 (1979).
4) M. Yoshida, S. Nagayama, M. Minabe, and K. Suzuki, *J. Org. Chem.*, **44**, 1915 (1979).
5) M. Yoshida, M. Minabe, and K. Suzuki, *J. Org. Chem.*, **44**, 3029 (1979).
6) M. Yoshida, K. Hishida, M. Minabe, and K. Suzuki, *J. Org. Chem.*, **45**, 1783 (1980).
7) L. F. Fieser, *J. Am. Chem. Soc.*, **51**, 2460 (1929).
8) H. Cerfontain, A. Koeberg-Telder, C. Ris, and C. Schenk, *J. Chem. Soc., Perkin Trans. 2*, **1975**, 966.
9) P. H. Grantham, E. K. Weisburger, and J. H. Weisburger, *J. Org. Chem.*, **26**, 1008 (1961).
10) M. Yoshida and K. Suzuki, unpublished results.
11) T. Shimura and E. Manda, *Nippon Kagaku Kaishi*, **1978**, 1532.
12) R. B. Girdler, P. H. Gore, and C. K. Thadani, *J. Chem. Soc., C*, **1967**, 2619.

Enzymatic Oxidation of Alkyl Sulfides by Cytochrome P-450 and Hydroxyl Radical

Yoshihito WATANABE, Tatsuo NUMATA, Takashi IYANAGI,** and Shigeru OAE*

Department of Chemistry, University of Tsukuba, Sakuramura, Ibaraki 305

***Division of Biochemistry, School of Medicine, University of Tsukuba, Ibaraki 305*

(Received July 11, 1980)

The oxidation of alkyl sulfides, sulfoxides, and sulfones was examined with either rabbit liver microsomes or a reconstituted system containing purified cytochrome P-450, *S*-dealkylation being found to take place more readily with alkyl sulfides bearing a higher acidic α-hydrogen. Similar results were obtained in the oxidation of alkyl sulfides by hydroxyl radical. Both *S*-dealkylation and *S*-oxygenation products are presumed to be formed *via* the cation radical intermediate.

N- and *O*-Dealkylation with hepatic microsomes and the reconstituted system with purified cytochrome P-450 has been studied with many substrates.[1] However, *S*-dealkylation with hepatic microsomes was observed only with a few anticancer agents such as 6-(methylthio)-purine and its analogues by Mazel *et al.*[2-4] who focused their attention on the effect of inhibitors and the dependency of inducers on *S*-dealkylase activity. They observed the formation of formaldehyde but not that of other products. 6-(Methylthio)purine was reported to be metabolized *in vivo* in man giving 6-mercaptopurine as a urinary metabolite.[5] However, the product analysis was incomplete, and the general nature of *S*-dealkylation has remained unexplored. We found a markedly large structural dependency of alkyl sulfide in the *S*-dealkylation with a few biomimetic oxygenase systems.[6,7]

The enzymatic hydroxylation of hydrocarbons by cytochrome P-450 which has recently been examined,[8,9] is suggested to proceed *via* homolytic process involving hydrogen abstruction by iron-bound "oxenoid" species such as $(P\text{-}450\cdot FeO)^{3+}$ analogous to Compound I of peroxidase.[10,11] On the other hand, the oxygenation of sulfur atom of cyclic and acyclic sulfides by cytochrome P-450 seems to result by the electrophilic attack of active oxygen bound to the active site of the heme iron,[12] as suggested by Ullrich and Duppel.[13] We have observed that neither singlet oxygen ($^1O_2$) nor hydrogen peroxide is the active oxygenating species in view of the lack of inhibition with both DABCO (1,4-diazabicyclo[2.2.2]octane, inhibitor for singlet oxygen), and catalase in the reaction with the reconstituted system.[12]

Chemical oxygenation using model systems has been studied,[14-17] the best-studied being Fenton's reagent (hydroxyl radical) which catalyzes the hydroxylation of a variety of substrates.[17]

Gilbert *et al.*[18] and others[19,20] examined the reaction of alkyl sulfides with hydroxyl radical generated by treating hydrogen peroxide with transition metal ions of low oxidation state such as Fe(II) and Ti(III) by means of UV and ESR spectroscopic studies, and found that the cation radical intermediate (III) is formed as the key intermediate in the reaction of sulfides with hydroxyl radical.

We have extended our study on the oxygenation of various sulfides, sulfoxides, and sulfones with phenobarbital-induced rabbit liver microsomes and also with a reconstituted system of purified cytochrome P-450 in order to understand the whole mechanistic feature of the enzymatic oxygenation of organosulfur compounds. We found that both *S*-dealkylation and *S*-oxygenation take place simultaneously, the acidity of α-hydrogen of alkyl sulfides playing an important role in determining the mode of the enzymatic oxygenation (Scheme 1).

We also carried out the oxidation of sulfides by hydroxyl radical and found that a similar mode of oxidation to that in the enzymatic oxygenation takes place.

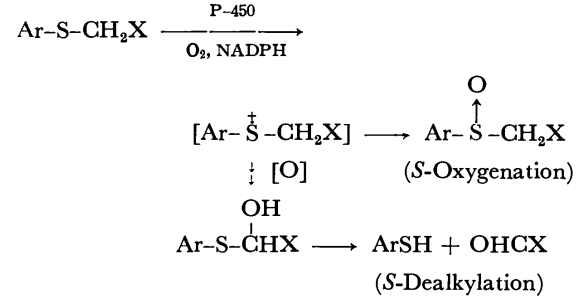

Scheme 1.

Experimental

Reagents. The following commercial compounds were used. $NADP^+$, D-glucose 6-phosphate (G6P), and D-glucose 6-phosphate dehydrogenase (G6P-DH) (Oriental Yeast); 16% Titanium trichloride solution (Kanto Chemicals); 30% Hydrogen peroxide, diphenyl disulfide, thioanisole, and thiophenol (Wako Chemicals).

Organic Synthesis. All the sulfides except thioanisole, diphenyl disulfide, and 4-(*p*-chlorophenyl)thiane were prepared by treating thiophenol with alkyl halides in the presence of sodium hydroxide in good yields,[21] and isolated by SiO_2 column chromatography (Merck Kieselgel 60, benzene as eluent). ^1H NMR (δ-value in $CDCl_3$, ppm) $PhSCH_2COPh$[22]; 4.05 (2H, s), 7.2—7.6 (8H, m), 7.8—8.0 (2H, m): $PhSCH_2\text{-}C_6H_4\text{-}NO_2\text{-}p$[23]; 4.01 (2H, s), 7.06 (5H, brs), 7.23 (2H, d, J=8.0), 7.93 (2H, d, J=8.0): $PhSCH_2CN$[24]; 3.44 (2H, s), 7.3—7.5 (5H, m): $PhSCH_2Ph$;[25] 4.11 (2H, s), 7.25 (10H, brs).

Deuterated sulfide, $PhSCD_2COPh$, was synthesized by the following method. Twenty equivalent of deuterium oxide (Merck, min 99.75%) was placed into a pyridine solution containing 2 mmol of phenacyl phenyl sulfide (5 ml) under argon atmosphere. The mixture was stirred at room temperature for 2 d, acidified (pH≈3) by adding 4 M HCl at 0 °C, and then extracted three times with chloroform (60 ml). The chloroform layer was washed with 1 M HCl (20 ml) to

remove a small amount of residual pyridine and dried over anhydrous magnesium sulfate. Chloroform was evaporated under reduced pressure and the deuterium content of phenacyl phenyl sulfide was determined from the ^1H NMR spectrum (95%-D_2). 4-(*p*-Chlorophenyl)thiane was prepared by the procedure described by Johnson.[26] ^1H NMR ($CDCl_3$) 2.1 (4H, m), 2.4 (1H, m), 2.8 (4H, m), 7.10 (2H, d, J=8.25), 7.25 (2H, d, J=8.25). All the sulfoxides used for the reactions and authentic samples were synthesized by the oxidation of corresponding sulfides with hydrogen peroxide in acetic acid.[27] ^1H NMR ($CDCl_3$), $PhS(O)CH_2COPh$;[28] 4.23 (1H, d' J=14.3), 4.25 (1H, d, J=14.3), 8—7.4 (10H, m): $PhS(O)CH_2$-C_6H_4-NO_2-*p*;[23] 4.0 (1H, d, J=12.8), 4.16 (1H, d, J=12.8), 7.1 (2H, d, J=9.0), 7.4 (5H, brs), 8.05 (2H, d, J=9.0): $PhS(O)CH_2CN$;[24] 3.70 (1H, d, J=15), 3.88 (1H, d, J=15), 7.6 (5H, m): $PhS(O)CH_2Ph$;[29] 4.0 (2H, brs), 7.4—6.9 (10H, m): $PhS(O)CH_3$;[30] 2.68 (2H, brs), 7.3—7.8 (5H, m), *trans*- and *cis*-4-(*p*-Chlorophenyl)thiane 1-oxide were separated by recrystallization (AcOEt) prior to Al_2O_3 column chromatography[31] (Wako, Alumina activated 200 mesh, AcOEt: $CHCl_3$=4 : 1 as eluent): *trans* sulfoxide; 2.0 (4H, m), 2.7 (1H, m), 2.7 (2H, dt, J=3.0, 12.0), 3.36 (2H, dt, J=2.4, 12.0), 7.0 (2H, d, J=7.5), 7.22 (2H, d, J=7.5): *cis* sulfoxide; 1.8 (2H, m), 2.6 (5H, m), 3.1 (2H, m), 7.11 (2H, d, J=7.5), 7.23 (2H, d, J=7.5). Sulfones were prepared by the treatment of corresponding sulfoxides with hydrogen peroxide in acetic acid.[23] ^1H NMR ($CDCl_3$) $PhS(O_2)CH_2$-C_6H_4-NO_2-*p*;[23] 4.4 (2H, s), 7.3 (2H, d, J=9.0), 7.6 (5H, m), 8.13 (2H, d, J=9.0): $PhS(O_2)CH_3$;[34] 3.05 (3H, s), 7.5—7.7 (3H, m), 7.8—8.1 (2H, m).

All the substrates were distilled or recrystallized prior to use. ^1H NMR spectra described above were recorded on a Parkin Elmer Hitachi R 20 (60 MHz).

Preparation of Microsomes, Purified Cytochrome P-450, and NADPH-Cytochrome P-450 Reductase. The hepatic microsomes (cytochrome P-450, 2.54 nmol/mg protein) were obtained from male rabbit (2—3 kg) pretreated with sodium phenobarbital (50 mg/kg of body weight, each day for 5 d) according to the procedure reported,[12] the purified cytochrome P-450 being obtained by the method of Imai and Sato.[35] NADPH-cytochrome P-450 reductase was purified by the method of Iyanagi *et al.*[36]

Enzyme Assay. The standard reaction mixture for assaying the *S*-dealkylation and *S*-oxygenation activities was made to contain 150—300 μmol of the substrates, the hepatic microsomes (130 mg protein), the NADPH generating system [30 μmol of $NADP^+$, 300 μmol of G6P (2 Na salt), and 36 units of G6P-DH], and phosphate buffer (pH 7.4, 0.1 M) in a final volume of 20 ml. The reaction mixture, except for G6P-DH, was incubated for 10 min at 36 °C to dissolve the substrates, prior to the addition of G6P-DH to the mixture. After the reaction mixture had been incubated at 36 °C for 2 h in the air, the reaction was stopped by adding 10 ml of acetone and 0.5 M of trichloroacetic acid (to pH 3) to the mixture which was cooled at 0 °C for 10 min in order to precipitate protein. After centrifugation (3000 rpm) of the mixture for 15 min, the supernatant layer was separated, neutralized by adding aqueous KOH solution, and then extracted 4 times with chloroform (200 ml). The chloroform layer was dried over anhydrous magnesium sulfate and concentrated under reduced pressure. The residue was diluted with acetone and analyzed by gas chromatography (GLC: Hitachi 163 Gas Chromatograph, 1 m glass column, 10% SE-30) and thin layer chromatography (TLC: Merck, Kieselgel 60-GF_{254}, and Aluminiumoxid GF-254, 60/E). The oxidation products were isolated by preparative TLC (chloroform was used as eluent), and identified by comparison with authentic samples. Formaldehyde was determined by the Nash reagent.[37]

Oxidation of Sulfides with Reconstituted System Containing Purified Cytochrome P-450. After a mixture of 35 nmol of cytochrome P-450, 38 nmol of the reductase and 0.3 ml of 1% detergent (Emalgen 913, KAO-ATRAS Chemicals) had been kept standing at room temperature for 5 min, 134 nmol of catalase, 22 ml of phosphate buffer (pH 7.4, 0.1 M), 250 μmol of G6P, 5 μmol of $NADP^+$, and 36 units of G6P-DH were added to the mixture. The substrate (480 μmol) was then suspended into the reaction mixture and the whole solution was incubated at room temperature for 1 h in the air. After the usual work-up, the products obtained were analyzed by GLC.

Measurement of the Difference Spectra Caused by the Addition of Substrates to the Purified Cytochrome P-450. Cytochrome P-450 (3.6 μM in 0.1 M of phosphate buffer containing 20% glycerol) was placed in 10 mm cuvettes for spectrometric recording. The substrate was dissolved in methanol (0.5—30 μl), into which was added the sample solution. The same volume of methanol was placed in the reference cuvette.

Analytic Procedure. The amount of protein in the microsomes was determined by the method of Lowry *et al.*[38] using bovin serum albumine. The concentration of cytochrome P-450 was determined by the carbon monoxide-difference spectrum of dithionite treated liver microsomes. The absorbance between 450 and 490 nm ($\Delta A_{450-490}$) was used for calculation of cytochrome P-450 content (ε, 91 mM^{-1} cm^{-1}).[39,40] The concentration of purified cytochrome P-450 was determined by measuring the absorption of the oxidized form ($\Delta A_{418-500}$), which has a molar extinction coefficient of 107 mM^{-1} cm^{-1}.[35] (UV: JASCO UVIDEC-1)

Oxidation of Sulfides by Iron(II) Perchlorate–Hydrogen Peroxide System. A mixture of sulfide (0.2 mmol) and iron(II) perchlorate (250 mg, 1 mmol) in methanol–7% perchloric acid aqueous solution (10 ml–5 ml) was stirred at room temperature under argon atomsphere for 5 min. 7% Perchloric acid (5 ml) containing 0.2 ml of hydrogen peroxide (30% solution in water) was then added dropwise slowly to the ethanolic solution and the reaction mixture was stirred for 10 min. The reaction mixture was extracted three times with chloroform (100 ml). The products were determined by GLC and SiO_2-TLC (eluent; $CHCl_3$).

Oxidation of Sulfides by Titanium Trichloride–Hydrogen Peroxide System. A mixture of sulfide (0.25 mmol) and methanol (10 ml) was stirred at room temperature under argon atmosphere for 5 min. Titanium trichloride solution (16% solution, 0.5 ml) was added in one portion to the mixture which was stirred for 1 min prior to the addition of hydrogen peroxide (30%, 0.2 ml) dissolved in 5 ml of H_2O, and the reaction mixture was stirred further for 5 min. The reaction was stopped by adding 30 ml of water and the mixture was subjected to the usual work-up.

Preparation of ^{18}O-Labeled Hepatic Microsomes. The hepatic microsome obtained above was diluted with $H_2{}^{18}O$ which contains 1.5% excess ^{18}O while phosphate buffer was prepared with $H_2{}^{18}O$-containing 1.5% excess ^{18}O (The British Oxygen Company Limited).

Oxidation of Sulfides by ^{18}O-Labeled Titanium Trichloride–Hydrogen Peroxide System. Five ml of ^{18}O-labeled (1.5 atom % excess) water was used instead of ordinary water.

^{18}O-Analyses. All the ^{18}O-labeled substrates were placed in a breakable glass tube together with well-dried $HgCl_2$ and $Hg(CN)_2$. The tube was evacuated by diffusion pump for 15 min, and sealed. The sealed tube was heated at 500 °C for 12 h. The gas (CO_2) produced was distilled repeatedly 3 times and transferred into a sampler of the mass spectrometer (Hitachi RMU 6MG). The ^{18}O-content of carbon dioxide

Table 1. Oxidation of sulfides by microsomes and reconstituted cytochrome P-450

Material	(μmol)	System[a]	Products (nmol/nmol P-450)
1a	(290)	A	**2a** (100) **3a** (5.7)[b]
1b	(180)	A	**2b** (100)
1c	(240)	A	**2c** (78) **5** (44)[c]
		B	**2c** (33) **5** (4.0)
1d	(170)	A	**2d** (30) **3d** (30) **4d** (91)[d] **5** (60)
		B	**2d** (12) **4d** (25) **5** (4.3)
1e	(170)	A	**2e** (91) **4e** (4.7) **5** (100)
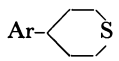	(153)	A	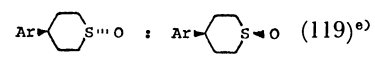 (119)[e]
1f			**2f-*t*** **2f-*c*** 66 : 34

a) System A; microsomes, system B; reconstituted system. b) Formaldehyde was measured in a separate experiment by using the Nash reagent. c) Isolated yields for the sulfoxides and sulfones by SiO_2 or Al_2O_3 PTLC. d) Yields determined by GLC described in Experimental. e) *Trans-cis* ratio determined by GLC (OV-1, 1m glass column).

was calculated from the height of flat peaks of *m/e* 44 and 46.

Measurement of Cyclic Voltammogram. Cyclic voltammograms of substrates were obtained in 0.1 M n-Bu_4NClO_4/CH_3CN solution. (scan rate: 300, 150, and 50 mV/s) (Hokuto Denko Ltd., Potentiostat Galvanostat HA-301).

Results

When the β-keto sulfide (**1e**) was incubated with the hepatic microsomes, *S*-dealkylation and *S*-oxygenation took place simultaneously, giving aldehyde (**4e**) and diphenyl disulfide (**5**) as the *S*-dealkylated products and the corresponding sulfoxide (**2e**) as the *S*-oxygenated product (Table 1). Similarly, *p*-nitrobenzyl phenyl sulfide (**1d**) gave *p*-nitrobenzaldehyde (**4d**) together with a comparable amount of **5**, accompanied by sulfoxide (**2d**) and sulfone (**3d**) as the *S*-oxygenated products. This is in contrast to the chemical oxidation of the sulfides (**1d**, **1e**) with hydrogen peroxide or *m*-chloroperbenzoic acid which gave only sulfoxides (**2d**, **2e**). Compounds **2d** and **3d**, microsomal oxidation products, were separated by Al_2O_3-PTLC (eluent; $CHCl_3$: AcOEt=1 : 1) and identified by comparison of mass spectra and GLC with those of authentic samples.

In the oxidation of thioanisole (**1a**) and benzyl

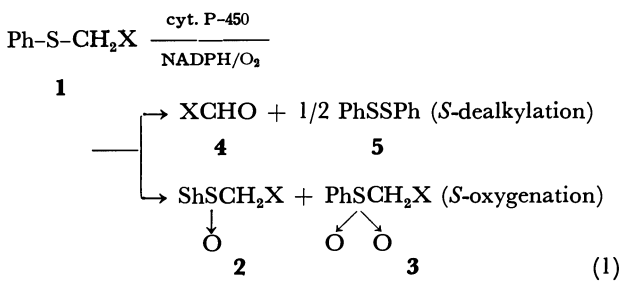

(1)

X: **a** = H, **b** = Ph, **c** = CN, **d** = C_6H_4-NO_2-*p*, **e** = COPh

phenyl sulfide (**1b**), *S*-oxygenation was found to take place predominantly giving the corresponding sulfoxides (**2a** and **2b**), respectively.

Thus, in the microsomal oxidation of alkyl sulfides, the mode of the reaction appears to depend markedly on the structure of the alkyl group; *viz.*, the ratio between the *S*-dealkylation and the *S*-oxygenation was found to increase with the increase of the acidity of α-hydrogen of the alkyl sulfide. (Tables 1 and 8). This trend is analogous to that in the biomimetic oxidation of the same sulfides with both Co^{II}(bzacen)–O_2 system and Udenfriend's system.[6,7]

Table 2. Relative S-dealkylation and S-oxygenation activity of rabbit liver microsomes

Additions		Products[a] PhSCH$_2$COPh (O)	Products[a] PhSSPh
Complete system	Ms. + O_2 + NADPH generating system	100	100
Complete system	minus NADPH generating system	0	0
Complete system	minus Ms. plus boiled Ms	0	0
Complete system	plus 50% CO	80	71

a) Products were compared in final yields determined by GLC described in Experimental part.

The requirements for cofactors in the reaction of the β-keto sulfide (**1e**) are given in Table 2. NADPH was required in the enzymatic reaction while boiled microsomes completely lost activities for both *S*-dealkylation and *S*-oxygenation. Carbon monoxide also inhibited enzymatic activity for both *S*-dealkylation and *S*-oxygenation of **1e**, respectively. This indicates that both *S*-dealkylation and *S*-oxygenation reactions are typical oxidation reactions promoted by cytochrome P-450.

Cyanomethyl phenyl sulfide (**1c**) and *p*-nitrobenzyl phenyl sulfide (**1d**) were metabolized with a reconstituted system, containing purified cytochrome P-450, NADPH-cytochrome P-450 reductase, 1% detergent and a NADPH generating system, and retaining similar activities for both *S*-dealkylation and *S*-oxygenation.

The sulfide (**1d**), however, was insoluble in a reconstituted system so that the net activity was low, and yet the oxidation of **1d** with the reconstituted cytochrome P-450 system was found to proceed in the two types of oxidation as denoted by cytochrome P-450.

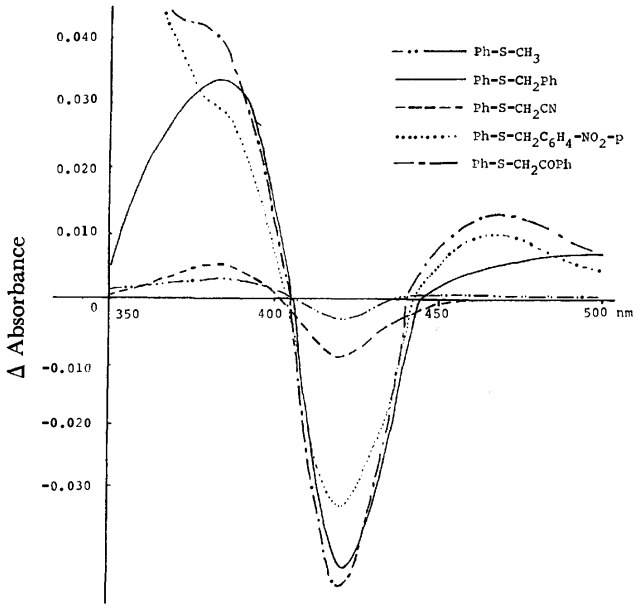

Fig. 1. Cytochrome P-450 from phenobarbital-treated rabbit were diluted to 3.6 μmol in 0.1 M phosphate buffer. After establishment of a base line of equal light absorbance, methanolic solution of sulfide (0.2 mM) was added to the sample cuvvett.

When methanolic solutions (0.5—30 μl) of these sulfides (**1a—e**) were added to the buffer solution of purified cytochrome P-450 (2 ml), and the difference spectra with iron(III) heme were found to be typical type I,[41,42] having a maximum at 385—390 nm and a minimum at 420 nm (Fig. 1), suggesting that the mode of the whole interaction between the sulfides and the hemoprotein is similar during the course of enzymatic oxidation.

The microsomal oxidation of sulfoxides (**2a**, **d**) and sulfones (**3a**, **d**) was performed for further assay of both *S*-oxygenation and *S*-dealkylation (Table 3). However, neither sulfoxides nor sulfones, both of which possess higher acidic α-hydrogen than the corresponding sulfides (see Table 8), underwent facile *S*-dealkylation, *e.g.*, *p*-nitrobenzyl phenyl sulfoxide (**2d**) gave both *S*-dealkylated product (**4d**) and *S*-oxygenated product (**3d**). However, the reaction was slow and the product ratio between the former and the latter is *ca.* 1/3 while in the oxygenation of the corresponding sulfide (**1d**) the ratio is *ca.* 4/3 (Table 3).

Table 3. Microsomal oxidation of sulfides, sulfoxides, and sulfones

Material (μmol)		Products (nmol/nmol P-450)[a]	Recovered (%)
1a	(290)	**2a** (100) **4a** (5.7)[b]	67
2a	(330)	**3a** (182) **4a** (trace)	64
3a	(280)	**4a** (trace)	95
1d	(170)	**2d** (30) **3d** (30) **4d** (91)[c]	75
		5 (60)	75
2d	(180)	**3d** (38) **4d** (14)[c]	89
3d	(150)	**4d** (2.8)[c]	96

a) Isolated yields by SiO_2 or Al_2O_3 PTLC. b) Determined in a separate experiment by using the Nash reagent. c) Determined by GLC as described in Experimental.

In the reaction of the sulfoxide to sulfone with microsomal cytochrome P-450, diphenyl disulfide (**5**) was not obtained as *S*-dealkylated product, despite the formation of the aldehyde, ruling out the possibility of the normal Pummerer rearrangement involving sulfoxide as the reaction intermediate for the *S*-dealkylation of sulfide.

$$\mathrm{Ph\text{-}S\text{-}CH_2X} \xrightarrow[\mathrm{NADPH/O_2}]{\text{cyt. P-450}} \mathrm{Ph\text{-}\overset{\overset{\mathrm{O}}{\uparrow}}{S}\text{-}CH_2X} \xrightarrow[\text{rearragement}]{\text{Pummerer type}} \mathrm{Ph\text{-}S\text{-}CHX} \xrightarrow[\mathrm{OH}]{[H_2O]} \mathrm{PhSH\ (+\ HCHO)} \xrightarrow{[O]} \mathrm{PhSSPh} \qquad (2)$$

Thioanisole (**1a**) and benzyl phenyl sulfide (**1b**) were found to react with hydroxyl radical generated by the reaction of iron(II) or titanium(III)–hydrogen peroxide system, giving only *S*-oxygenated products (**2a** and **2b**) in contrast to the oxidation of (**1c—e**), which gave both *S*-oxygenated products (**2c—e**) and *S*-dealkylated product (**4**) (Tables 4 and 5). The ratio of **5**/**2** increased from **1c** to **1e**. This is in line with the results given in both the microsomal and the purified cytochrome P-450 oxidations of alkyl sulfides (Table 1). The ratio between *S*-dealkylation and *S*-oxygenation

Table 4. The reaction of sulfides with hydroxyl radical generated from iron(II) perchlorate–hydrogen peroxide system

Substrate[a]	System[b]	Products (μmol)[c]
1a	A	**2a** (14)
1b	A	**2b** (9.3)
	B	**2b** (13)
	C	**2b** (14)
1c	A	**2c** (7.5) **5** (0.23)
	B	**2c** (6.7) **5** (0.8)
	C	**2c** (8.2) **5** (1.1)
1d	A	**2d** (8.0) **5** (2.8)
	B	**2d** (21) **5** (3.7)
	C	**2d** (10) **5** (4.7)
1e	A	**2e** (4.6) **5** (4.8)
	B	**2e** (24) **5** (4.6)
	C	**2e** (8.2) **5** (15)
1f[d]	A	**2f**-*t* : **2f**-*c* (87)[e] 80 : 20

a) 0.2 mmol of sulfides were used in all cases. b) System A; see Experimental. System B; H_2O was used instead of 7% perchloric acid aq solution. System C; buffer (pH= 7.0) was used instead of 7% perchloric acid solution. c) Determined by GLC and SiO_2 TLC. d) 212 mg (1.2 mmol) of sulfide used. e) Determined by GLC (10% OV-1, 1m glass column).

Table 5. Reaction of sulfides with hydroxyl radical generated from titanium trichloride–hydrogen peroxide system

Substrate[a]	Products (μmol)[b]	
1a		**2a** (250)
1b		**2b** (247)
1c	**2c** (226)	**5** (1.0)
1d	**2d** (109)	**5** (2.0)
1e	**2e** (57)	**5** (8.5)

a) 250 μmol of sulfides was suspended in all cases. b) Determined by GLC and SiO_2 TLC.

was found to vary in different media (Table 4, systems A, B, and C), while the tendency for *S*-dealkylation remained unchanged. The difference between the microsomal and the reconstituted systems can be explained on the basis of varying conditions of media used.

When the 95% deuterated sulfide (**1e**-d_2, $PhSCD_2COPh$) was incubated with hepatic microsomes in the complete system at 36 °C, both *S*-dealkylation and S-oxygenation proceeded concurrently. In this reaction only a small kinetic isotope effect ($k_H/k_D \fallingdotseq 1.2$) was observed while the ratio **5**/**2** remained nearly the same with both **1e** and **1e**-d_2. The k_H/k_D values were computed approximately by [**5**/**2**]/[**5**-d_2/**2**-d_2] for both microsomal and Fenton's oxidation. In the reaction with Fenton's system (system A), k_H/k_D was 1.3, being analogous to that in the oxidation (Table 6). The deuterium label of the recovered sulfide (**1e**-d_2) remained in both cases (measured by ^1H NMR).

When the oxidation of sulfide (**1c**) by both the microsomal and Fenton's oxidation systems was carried out in ^{18}O-labeled phosphate buffer solution, only 1.3 and 4.7% of oxygen were found to be incorporated into the sulfoxide (**2c**) from heavy water, $H_2{}^{18}O$ used (Table 7).

Table 6. Kinetic isotope effect for the oxidation of phenacyl phenyl sulfide by both rabbit liver microsomes and iron(II)–hydrogen peroxide system

System	Substrate $PhSCH_2COPh$ $PhSCD_2COPh$ products[b] **2e**	**5**	**2e**-d_2	**5**-d_2	k_H/k_D[a]
Microsomes	29	32	27	24	1.2
$Fe(II)$–H_2O_2	4.6	4.8	3.9	3.2	1.3

a) Estimated roughly by [**5**/**2e**]/[**5**-d_2/**2e**-d_2]. b) Yields measured by GLC (μmol).

Table 7. ^{18}O-Contents of phenyl methyl sulfoxide produced by both liver microsomes and Fenton's system

	$H_2{}^{18}O$ (A) used (%)	$PhS\overset{\overset{O}{\uparrow}}{C}H_3$ (B) (%)	O-content from water (B/A×100) (%)
Liver microsomes	1.05[a]	0.014[a]	1.3
$TiCl_3$–H_2O_2	1.32[b]	0.062[a]	4.7

a) Observed values. b) Calculated values (see Experimental).

Discussion

A multienzyme system containing cytochrome P-450 located in liver microsomes, and a reconstituted system of the purified cytochrome P-450 and its reductase from liver microsomes of phenobarbital-treated rabbit and NADPH were found to catalyze readily both *S*-dealkylation and *S*-oxygenation of common sulfides and only sluggishly those of sulfoxides and sulfones.

The relatively higher acidity of the α-hydrogen is required for *S*-dealkylation, though other factors are also necessary, since sulfoxides (**2**) and sulfones (**3**) having more acidic α-hydrogen are less reactive than the sulfides for *S*-dealkylation (Tables 1 and 8).

Free radicals are stabilized substantially when the central carbon is substituted by a divalent sulfur atom but less stabilized by an adjacent α-sulfinyl or α-sulfonyl group.[43] This is in line with the trend of the Q-values of substituted vinyl compounds. Vinyl sulfoxide possesses the smallest Q-value in copolymerization as suggested by the stability of α-substituted free radicals ($RS\dot{C}HR' > RS(O_2)\dot{C}HR' \geq RS(O)\dot{C}HR'$ in Table 8). Cyano, *p*-nitrophenyl, and carbonyl groups have larger Q-values than benzyl, and methyl groups.[44] Such a free radical-stabilizing effect of sulfenyl group may be partially responsible for the facile *S*-dealkylation of sulfides.

Several substrates, which are deuterated prior to hydroxylation at aliphatic sites have been tested with hepatic microsomes. Groves *et al.*[8] suggested that hydroxylation by highly purified liver microsomal cytochrome P-450 involves the direct hydrogen abstraction by iron-bound "oxenoid" species $(P\text{-}450\cdot FeO)^{3+}$, which is analogous to Compound I of peroxidase,[11] to generate the carbon radical intermediates on the basis of their observed kinetic isotope effects ($k_H/k_D = 11.5 \pm 1$)[8] and $k_H/k_D = 11 \pm 1$ for benzylic hydroxylation of 1,3-diphenylpropane (and 1,1-dideuterio derivative) by Hjelmeland *et al.*[9]

Sulfides are good substrates for the oxygenation with cytochrome P-450 enzyme system to give sulfoxides.[12,45] Since the "oxenoid" intermediate should be highly electron deficient, *S*-oxygenation is expected to be initiated by an electron transfer from divalent sulfur atom to "oxenoid" species, generating sulfenium cation radical. The oxygenation of alkyl sulfides with a highly purified cytochrome P-450 gave kinetic evidence for one-electron transfer mechanism.[46]

$$Ar\text{–}S\text{–}CH_3 \xrightarrow[\text{rate determining step}]{\text{cyt. P-450 } (FeO)^{3+}} Ar\overset{+}{S}\text{–}CH_3 + (FeO)^{2+} \longrightarrow Ar\text{–}S(\overset{\overset{O}{\uparrow}}{})\text{–}CH_3 + Fe(III) \quad (3)$$

In the oxidative dealkylation of tertiary amine by enzymes, a similar cation radical intermediate seems to be involved.[47] The oxygenation of aminopyrine by horseradish peroxidase has been suggested to involve the cation radical intermediate on the basis of ESR spectroscopic studies.[48]

TABLE 8. pK_a-VALUES OF METHANE DERIVATIVES OF ELECTRON-WITHDRAWING GROUP AND THE Q-VALUES OF VINYL DERIVATIVES IN RADICAL COPOLYMERIZATION

Compound	pK_a	Compound	Q
$PhCO\underline{CH_3}$[a]	24.7	$CH_2=CHCOPh$[b]	1.4
$NC\underline{CH_3}$[a]	31.3	$CH_2=CH-C_6H_4-NO_2$-p[b]	1.63
$Ph\underline{CH_3}$[c]	40.9	$CH_2=CHCN$[b]	1.78
$CH_3-\underline{H}$[c]	48	$CH_2=CHPh$[b]	1.0
$CH_3S(O)\underline{CH_3}$[c]	33	$CH_2=CH_2$[b]	0.015
$CH_3S(O_2)\underline{CH_3}$[c]	29	$CH_2=CHSCH_3$[d]	0.34
$PhS\underline{CH_3}$[a]	48	$CH_2=CHS(O)CH_3$[d]	0.06—0.01
$PhS(O_2)\underline{CH_3}$[a]	29	$CH_2=CHS(O_2)CH_3$[a]	0.11

a) E. Block, "Reactions of Organosulfur Compounds," Academic Press, New York (1978). b) "Kyojugo," ed by Kobunshi-gakkai, Baifukan, Tokyo (1975), Vol. 1, p. 396. c) T.H. Lowry and K.S. Richardson, "Mechanism and Theory in Organic Chemistry," Harper and Row Publishers, New York (1976). d) W. Tagaki, "Organic Chemistry of Sulfur," ed by S. Oae, Plenum Press, New York (1977), p.231.

$$\begin{aligned} &R_2N\text{-}CH_2R \xrightarrow{-e^-} R_2\overset{+}{N}\text{-}CH_2R \xrightarrow{-H^+} \\ &\qquad\qquad \downarrow (\text{or } -H\cdot) \\ &R_2N\text{-}\dot{C}HR \xrightarrow{-e^-} R_2\overset{+}{N}{=}CHR \xrightarrow{H_2O} \\ &[R_2N\text{-}\underset{\displaystyle OH}{\underset{|}{C}}HR] \longrightarrow R_2NH + RCHO \end{aligned} \qquad (4)$$

α-Hydroxyl sulfides (III) are formed as the intermediates *via* initial electron-transfer, subsequent proton removal, and final hydroxylation in the *S*-dealkylation (Eq. 5), and the formation of the α-sulfenyl radical (II) by direct hydrogen abstraction by electron deficient $(FeO)^{3+}$ is unlikely, since the ease of the *S*-dealkylation was found to be correlated not with the order of radical-stabilizing effect of α-substituent but with the acidity of α-hydrogen of the alkyl sulfides used.[49,50]

$$R\text{-}S\text{-}CH_2R' \xrightarrow[NADPH/O_2]{\text{cyt. P-450}} \underset{\text{(III)}}{R\text{-}S\text{-}\underset{\displaystyle OH}{\underset{|}{C}}HR'} \xrightarrow{H_2O} RSH + R'CHO \qquad (5)$$

The kinetic isotope effect observed for the *S*-dealkylation of phenacyl phenyl sulfide (**1e**) was rather small ($k_H/k_D=1.2$), differing from the results obtained by Groves *et al.*[8] and Hjelmeland *et al.*[9] A similar trend was observed in the reaction of sulfides with hydroxyl radical (Table 6).

Hydroxyl radical is an electrophilic species, reacting readily with electron rich sulfenyl sulfur, and giving the corresponding sulfenium cation radicals.

$$R\text{-}S\text{-}R' + \cdot OH \longrightarrow R\text{-}\overset{+}{S}\text{-}R + OH^- \qquad (6)$$

The reaction of sulfides with hydroxyl radical has been studied extensively by Gilbert *et al.*[18] and others[19,20] by means of UV and ESR and is illustrated in the following scheme (Scheme 2).

In this Scheme, step 4 should definitely be accelerated by either an electron-withdrawing substituents R′ or a group which stabilizes the intermediate radical (II), or by both. The Scheme is in line with our results with Fenton's oxidation system. In many ways, the reaction of step 4 can be considered as a 1,2 elimination of Elcb type,[51] and somewhat similar to the Pummerer rearrangement which shows a secondary kinetic isotope effect.[52] In the oxidation of tertiary amines, the deprotonation (Eq. 4) from nitrogen cation radical intermediate gives a kinetic isotope effect ($k_H/k_D=2.2$).[53]

Observation on the *S*-dealkylation can be interpreted, if we assume that the sulfenium cation radical initially formed is the common intermediate for both *S*-dealkylation and *S*-oxygenation through one electron transfer from divalent sulfur atom to the highly electron deficient "oxenoid." Electron-withdrawing substituent R′ would

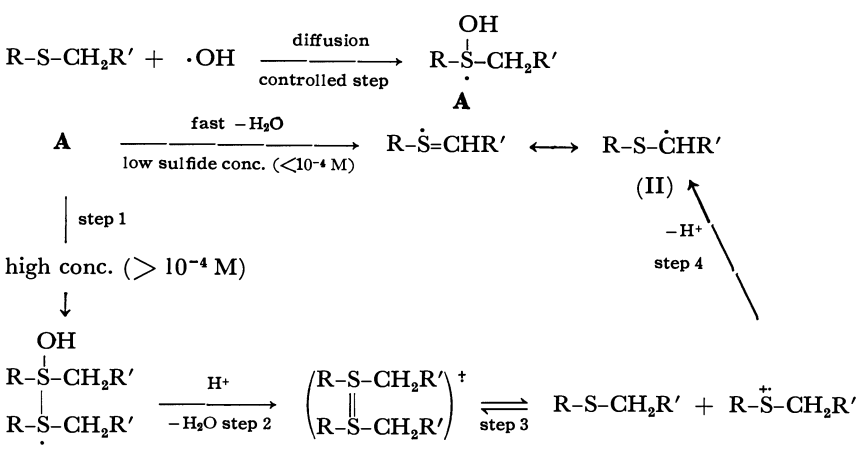

Scheme 2.

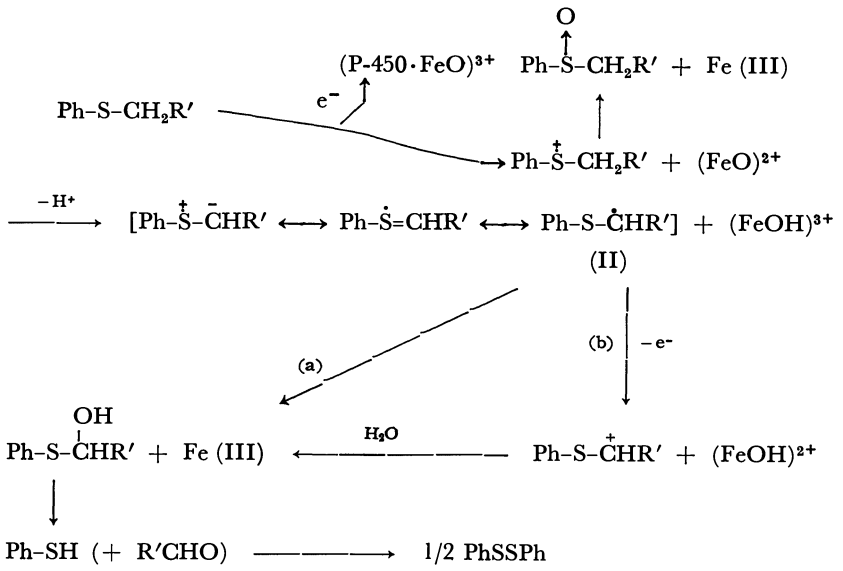

Scheme 3.

facilitate the α-proton removal to form the α-sulfenyl radical (II) which upon subsequent hydroxylation would undergo facile hydrolysis to afford the aldehyde and thiophenol which is readily oxidized further to diphenyl disulfide (Scheme 3). The cyclic voltammograms of sulfides (Fig. 2) show the ready α-proton removal from the sulfenium cation radicals as suggested by Sato and Kamada.[56] However, we cannot rule out the possibility of path (b) in Scheme 3.

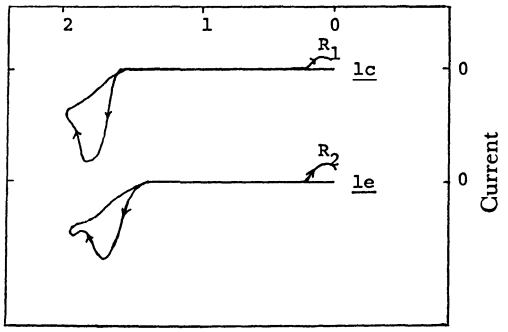

Potential (V *vs.* SCE)

$$PhSCH_2R' \xrightarrow{-e^-} PhSCH_2R'^{+\cdot} \xrightarrow{-H^+} PhS\dot{C}HR'$$

Fig. 2. Cyclic voltammograms for sulfides in CH_3CN *vs.* SCE. Cathodic peaks (R_1 and R_2) suggest the abstraction of a proton.[56]

One way to demonstrate the generation of the sulfenium cation radical as the reaction intermediate by chemical procedure is to examine whether or not the oxygen of the sulfoxide formed by both microsomal and Fenton's oxidation originates not only from the "oxenoid" bound to iron of heme protein but also from water. The reaction of the sulfenium cation radicals of sulfides with water has been examined somewhat in detail and shown by Evans and Blount[54] and Murata and Shine[55] to give the corresponding sulfoxides stoichiometrically.[7] However, in the reaction of thioanisole (**1a**) with Ti(III)–H_2O_2 system, the amount of ^{18}O incorporated into the sulfoxide (**2a**) was only

$$2\,R_2S^{+\cdot} + H_2O \longrightarrow R_2S{\rightarrow}O + R_2S + 2\,H^+ \quad (7)$$

4.7% of $H_2{}^{18}O$ used. This indicates that the cation radical reacts with hydroxyl radical preferentially even though the cation radical is surrounded by water of the medium.

The incorporation of ^{18}O into the sulfoxide through the microsomal oxygenation was only 1.3% of $H_2{}^{18}O$ used. In the oxygenation of sulfides with cytochrome P-450, the substrate seems to be tightly coordinated to the active site; the amount of water around the reaction site of the enzyme is too small to compete with "oxenoid" bound to the enzymatic active site so that the ^{18}O incorporation would be smaller than that with Fenton's system. The slight incorporation of ^{18}O into the sulfoxide from $H_2{}^{18}O$ water used in the microsomal oxygenation suggests that the transient intermediate, presumably the sulfenium cation radical, is still tightly held in the cavity of the enzyme which lacks enough water and eventually reacts oxygen bound to the enzyme. The ^{18}O experiment gave no information whether the key active sulfur intermediate is the sulfenium cation radical or dication. However, involvement of the dication species is quite unlikely in view of our earlier work, in which *p*-substituted thioanisole derivatives were oxygenated by a reconstituted system of purified cytochrome P-450, V_{max}'s of oxygenation being correlated nicely with Hammett σ^+-values rather than σ-values ($\rho^+ = -0.16$), and also with one electron oxidation potential of sulfides.[46]

In this study, we found a large structural dependency of alkyl sulfide in the *S*-dealkylation with both microsomal and hydroxyl radical oxidation systems. The over-all reaction may be explained by the generation of cation radical species as the common intermediate for both *S*-dealkylation and *S*-oxygenation as suggested in the enzymatic *N*-dealkylation.

References

1) Leading references see: Y. Imai and R. Sato, *Biochem. Biophys. Res. Commun.*, **75**, 420 (1977); T. Kamataki and H.

Kitagawa, *ibid.*, **76**, 1007 (1977).
2) P. Mazel, J. F. Henderson, and J. Axelrod, *J. Pharmacol. Exp. Therap.*, **143**, 1 (1964).
3) J. F. Henderson and P. Mazel, *Biochem. Pharmacol.*, **13**, 207 (1964).
4) J. F. Henderson and P. Mazel, *Biochem. Pharmacol.*, **13**, 1471 (1964).
5) G. B. Elion, S. Callaha, R. W. Rundles, and G. H. Hitchings, *Cancer Res.*, **23**, 1207 (1963).
6) T. Numata, Y. Watanabe, and S. Oae, *Tetrahedron Lett.*, **1978**, 4933.
7) T. Numata, Y. Watanabe, and S. Oae, *Tetrahedron Lett.*, **1979**, 1411.
8) J. T. Groves, G. A. McClusky, R. E. White, and M. J. Coon, *Biochem. Biophys. Res. Commun.*, **81**, 154 (1978).
9) L. M. Hjelmeland, L. Aronow, and J. R. Trudell, *Biochem. Biophys. Res. Commun.*, **76**, 541 (1977).
10) L. P. Hager, D. L. Doubek, R. M. Silverstein, and J. H. Martin, *J. Am. Chem. Soc.*, **94**, 4364 (1976).
11) G. A. Hamilton, "Molecular Mechanisms of Active Oxygen," ed by O. Hayaishi, Academic Press, New York (1974), p. 405.
12) D. Fukushima, Y. H. Kim, T. Iyanagi, and S. Oae, *J. Biochem.*, **83**, 1019 (1978).
13) V. Ullrich and W. Duppel, "The Enzymes," ed by P.D. Boyer, Academic Press, New York (1975), Vol. 12, p. 284.
14) T. Matsuura, *Tetrahedron*, **33**, 2869 (1977).
15) C. K. Chan and Ming-Shang Kuo, *J. Am. Chem. Soc.*, **101**, 3413 (1979).
16) J. T. Groves, T. E. Nemo, and R. S. Myers, *J. Am. Chem. Soc.*, **101**, 1032 (1979).
17) C. Walling, *Acc. Chem. Res.*, **8**, 125 (1975).
18) G. C. Gilbert, D. K. C. Hodgeman, and R. O. C. Norman, *J. Chem. Soc., Perkin Trans. 2*, **1973**, 1748; G. C. Gilbert, J. P. Larkin, and R. O. C. Norman, *ibid.*, **1973**, 272.
19) M. Bonifačič, H. Möckel, D. Bahnemann, and K. D. Asmus, *J. Chem. Soc., Perkin Trans. 2*, **1975**, 675.
20) W. Bose, E. Lengfelder, M. Saran, C. Fuchs, and C. Michel, *Biochem. Biophys. Res. Commun.*, **70**, 81 (1976).
21) R. B. Wagner and H. D. Zook, "Synthetic Organic Chemistry," John Wiley, New York (1953), p. 787.
22) W. J. Kenny, J. A. Walsh, and D. A. Davenport, *J. Am. Chem. Soc.*, **83**, 4619 (1961).
23) G. Leandri, A. Mangini, and R. Passertini, *J. Chem. Soc.*, **1957**, 1368.
24) G. Tsuchihashi, S. Iriuchijima, M. Nagatome, and Y. Kurosu, Japan Kokai 7475720.
25) Beil., **6**, 454.
26) C. R. Johnson, *J. Am. Chem. Soc.*, **85**, 1020 (1963).
27) L. I. Denisova and V. A. Batyakina, *Khim. Farm. Zh.*, **4**, 9 (1970).
28) N. Kunieda, Y. Fujiwara, J. Nokami, and M. Kinoshita, *Bull. Chem. Soc. Jpn.*, **49**, 575 (1976).
29) B. J. Auret, D. R. Boyd, H. B. Henbest, and S. Ross, *J. Chem. Soc., C*, **1968**, 2371.
30) J. Drabowiz, W. Mirura, and M. Mikolajczyk, *Synthesis*, **1979**, 39.
31) C. R. Johnson and McCants, Jr., *J. Am. Chem. Soc.*, **87**, 1109 (1965); B. J. Hutchinson, K. K. Andersen, and A. R. Katritzky, *ibid.*, **91**, 3839 (1969).
32) C. M. Sutter, "The Organic Chemistry of Sulfur," John Wiley, New York (1944), p. 683.
33) S. Ghersetti, *Bull. Sci. Fac. Chim. Ind. Bologna.*, **21**, 228 (1963).
34) A. H. Blatt, *Org. Synth.*, Coll. Vol. 4, 676 (1963).
35) Y. Imai and R. Sato, *Biochem. Biophys. Res. Commun.*, **60**, 8 (1973).
36) T. Iyanagi, F. Koici, Y. Imai, and H. S. Mason, *Biochem.*, **17**, 2224 (1978).
37) T. Nash, *Biochem. J.*, **55**, 416 (1953).
38) O. H. Lowry, N. J. Rosebrough, A. L. Farr, and R. J. Randall, *J. Biol. Chem.*, **193**, 265 (1951).
39) S. P. Colowick and N. O. Kaplan, "Method in Enzymology," ed by S. Fleisher and L. Packer, Academic Press, New York (1978), Vol. 52, p. 215.
40) T. Omura and R. Sato, *J. Biol. Chem.*, **239**, 2370 (1964).
41) W. Nastainzky, H. H. Ruf, and V. Ullrich, *Eur. J. Biochem.*, **60**, 615 (1975).
42) J. B. Schenkman, H. Remmer, and R. W. Estabrook, *Mol. Pharmacol.*, **3**, 113 (1967).
43) a) W. Tagaki, "Organic Chemistry of Sulfur," ed by S. Oae, Plenum Press, New York (1977), p. 231; b) K. Uneyama, H. Namba, and S. Oae, *Bull. Chem. Soc. Jpn.*, **41**, 1928 (1968); c) W. Tagaki, T. Tada, R. Nomura, and S. Oae, *ibid.*, **41**, 2082 (1968).
44) "Kyojugo," ed by Kobunshi-gakkai, Baifukan, Tokyo (1975), Vol. 1, p. 369.
45) T. Takahashi, Y. H. Kim, D. Fukushima, K. Fujimori, T. Iyanagi, and S. Oae, *Heterocycles*, **10**, 229 (1978).
46) Y. Watanabe, T, Iyanagi, and S. Oae, *Tetrahedron Lett.*, **21**, 3685 (1980).
47) a) Y. L. Chow, W. C. Danen, S. F. Nelsen, and D. H. Rosenblatt, *Chem. Rev.*, **78**, 243 (1978); b) G. Galliani and B. Rindone, *J. Chem. Soc., Perkin Trans. 1*, **1978**, 456.
48) B. W. Griffin and P. L. Ting, *Biochem.*, **17**, 2206 (1978).
49) T. H. Lowry and K. S. Richardson, "Mechanism and Theory in Organic Chemistry," Harper and Row Publisher, New York (1976).
50) E. Block, "Reactions of Organosulfur Compounds," Academic Press, New York (1978).
51) Elcb; unimolecular elimination of conjugate base.
52) a) H. Kobayashi, N. Furukawa, T. Aida, K. Tsujihara, and S. Oae, *Tetrahedron Lett.*, **1971**, 3109; b) T. Numata and S. Oae, *ibid.*, **1977**, 1337.
53) F. D. Lewis and Tong-Ing Ho, *J. Am. Chem. Soc.*, **102**, 1751 (1980).
54) J. F. Evans and H. N. Blount, *J. Org. Chem.*, **42**, 976 (1977).
55) Y. Murata and H. Shine, *J. Org. Chem.*, **34**, 3368 (1969).
56) T. Sato and M. Kamada, *J. Chem. Soc., Perkin Trans. 2*, **1977**, 384.

The Application of Field-ionization and Field-desorption Mass Spectrometry to the Analysis of Coal-derived Oil

Tadashi Yoshida,* Yosuke Maekawa, Tetsuo Higuchi,** Eiji Kubota,** Yasuhiro Itagaki,** and Susumu Yokoyama***

Government Industrial Development Laboratory, Hokkaido, Sapporo 061-01
***JEOL, Ltd., 1418 Nakagami, Akishima, Tokyo 196*
****Faculty of Engineering, Hokkaido University, Sapporo 060*

(Received July 28, 1980)

Field-ionization (FI) and field-desorption (FD) mass-spectroscopic techniques have been applied to the analysis of ring-type fractions of coal-derived oil, obtained by liquid chromatography. These techniques produce only the molecular ion and its isotopic signals, free from fragment ions, of a molecule, consequently the exact molecular-weight-distribution profiles of chromatographic fractions. The peak intensities are reproducible within a variation coefficient ($\sigma/\bar{x}$) of about 5—8% on repeated runs. The number-average molecular weights ($\overline{Mn}$) of the ring-type fractions, as calculated from the peak intensities, are close to those obtained by means of a vapor-pressure osmometer (VPO). These techniques, on the whole, give reliable mass spectra of coal-derived oil, although the isotope-ion ratios are overestimated compared to the theoretical natural abundances. The group-type analysis of the ring-type fractions has been made on the basis of their mass spectra, and the skeletal structures corresponding to each mass z series have been proposed.

In recent yeras, the shortage in energy resources has become a serious problem all over the world. Therefore, coal has been recognized again as one of the most valuable energy resources, and the development of an economical coal liquefaction process has been attempted.

Coal-derived oil is a multicomponent mixture of aromatic and hydroaromatic hydrocarbons. To date, however, there has been very little information on the mass distribution of the individual components, and coal-derived oil has generally been characterized as having an average molecular weight. Since a large portion of the coal-derived oil consists of low-volatile fractions, such as heavy oil and asphaltene, the use of a gas chromatograph-mass spectrometer (GC-MS) equipped with an electron-impact (EI) ion source has been severely limited.

On the other hand, the FI and FD techniques[1,2] produce only molecular ions and their isotopic peaks of the components in a mixture. The FD technique especially does not require the vaporization process of the sample for ionization, in contrast to the EI and FI techniques; consequently, it permits the analysis of thermally labile or nonvolatile substances. The usefulness of these techniques has already been proved in the analysis of biochemical substances[3] and aromatic hydrocarbons.[4] They can also be expected to be useful for the compositional analysis and determination of the molecular-weight distribution of coal-derived oil.

The purposes of the present work are to perform a quantitative mass analysis of coal-derived oil and to determine the types of hydrocarbons and their distribution in the coal-derived oil based on group-type analysis. The determination of the sensitivity coefficients of the hydrocarbons is beyond the scope of this work.

Experimental

The coal sample used in the present work was obtained from Akabira, Hokkaido. The sample was hydrogenated over Adkins catalyst at 400 °C for 60 min under an initial hydrogen pressure of 100 kg/cm^2. The hydrogenated product was extracted with hexane in a Soxhlet extractor. The extracted coal-derived oil was separated into five fractions on the liquid chromatograph by means of a modification of the Bureau of Mines-API 60 method:[5] saturates(Fr-P), monocyclic aromatics(Fr-M), bicyclic aromatics(Fr-D), tri- and tetracyclic aromatics(Fr-T), and polycyclic aromatics and polar compounds(Fr-PP). The Fr-PP fraction was further subdivided into eight fractions by gel-permeation chromatography(GPC). The volatile fractions were subjected to FI analysis by the direct-inlet method; they were charged into a glass tube with active alumina powder. On the other hand, the nonvolatile fraction(Fr-PP-8) was subjected to FD analysis by loading about 1 μg of a sample on the emitter with a microsyringe. The emitter was prepared by Beckey's method.[6] The FI and FD mass spectra were measured by means of a JMS-D300 double-focusing mass spectrometer equipped with an EI/FI/FD-combination ion source(JEOL Ltd). Ions were detected through an electrical detector connected to a data-analysis system, JMA-2000. The emitter current was kept at 5 mA for the FI analysis in order to prevent any condensation of the sample on the emitter and was elevated at a rate of 4 mA/min for the FD analysis. The scan speed for the mass range of m/z 100—550 was 5 s/cycle. Scanning was repeated 300—400 times in the FI and 40—50 times in the FD. The chamber temperature was maintained at 200 °C for the FI and at 60 °C for the FD. Throughout this work, homologs are assumed to have identical sensitivity coefficients.[7]

The average molecular weight was determined by the VPO (Knauer) method. Chloroform was used as the solvent.

Results and Discussion

Aspects of FI and FD Mass Spectra of Coal-derived Oil. Since any ring-type fraction of coal-derived oil is a multicomponent mixture, a sample must be introduced into an ion source without changing the composition of the mixture. However, the boiling points of these fractions cover a wide temperature range; therefore, a special technique is needed to effect simultaneous evaporation.

Figure 1 compares the total ion-current profiles (TICP) with the mass spectra of the Fr-P fraction as obtained by means of the FI and FD techniques. The TICP in FI with a direct-inlet probe suggests that the

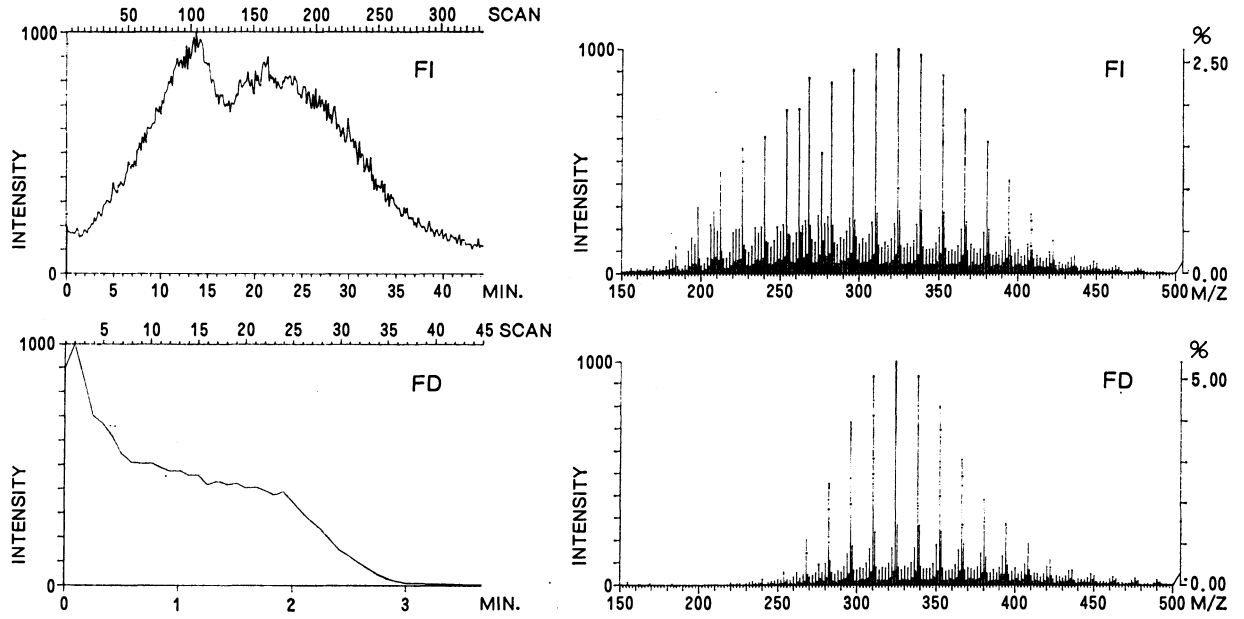

Fig. 1. Comparison of total ion current profiles with mass spectra of Fr-P for FI and FD techniques.

Table 1. Reproducibility of peak intensities in the FI and FD mass spectra of Fr-P and T

	Sample : Fr-P FI			
m/z	(1)	(2)	(3)	$\sigma/\bar{x}$(%)
196	270.1	286.1	269.5	3.4
212	631.3	751.3	735.8	9.2
226	742.9	831.5	830.2	6.5
240	759.8	820.7	854.5	5.9
254	857.5	925.0	965.0	5.9
268	1000.0	1000.0	1000.0	0
282	983.3	914.3	986.6	4.2
296	977.6	903.7	983.8	4.7
310	983.3	930.5	994.7	3.5
324	955.3	906.4	986.6	4.3
338	932.9	879.6	897.6	3.0
352	877.1	836.8	816.7	3.6
366	684.4	716.6	652.3	4.7
380	580.1	596.2	525.5	6.5
394	488.8	454.5	396.2	10.5
	Sample : Fr-T FD			
m/z	(1)	(2)	(3)	$\sigma/\bar{x}$(%)
192	523.0	544.0	503.2	3.9
206	742.1	820.3	772.7	5.1
220	665.6	712.1	704.0	3.6
232	1000.0	1000.0	1000.0	0
246	951.2	952.4	951.1	0.1
256	696.5	708.5	716.4	1.4
258	916.9	904.6	918.7	0.8
270	669.9	677.5	681.4	0.8
282	384.8	391.1	389.0	0.8
284	589.0	607.3	624.5	2.9
298	515.4	521.2	558.6	4.4
312	428.4	445.3	475.8	5.3
324	350.1	373.2	367.0	3.3
336	269.6	266.0	305.1	7.7
350	250.6	243.6	263.9	4.1

sample in a glass tube was not vaporized until the probe was heated enough. No residue was found in the tube after measurement. In contrast, the TICP in FD indicates that the majority of the sample molecules had vaporized *in vacuo* before the mass measurements started. The resulting FD mass spectrum reveals the absence of volatile components in the low-mass range. Thus, the FI technique with the direct-inlet probe was found to be suitable for the measurements of the volatile fractions,[8] which comprise about 30 wt% of coal-derived oil (hexane extract), while the FD technique was found to be suitable for the measurements of nonvolatile fractions and polar substances containing phenolic OH and nitrogen atoms.

Few quantitative studies of the FI and FD mass spectra of multicomponent mixtures have been reported.[9-12] The components of coal-derived oil have larger and more complex chemical structures than the model compounds, and the preparation of a multicomponent "model mixture" for coal-derived oil is practically impossible. Therefore, we abandoned our attempts to estimate the sensitivity coefficients of the components and to perform quantitative FI and FD mass analysis using the "model mixture." For this reason, the ring-type fractions of coal-derived oil, which have their own structural characteristics, were used as samples in the present work. Since the compositions of the ring-type fractions used are unknown, the reproducibility of the peak intensities, the isotope-ion ratios, and the number-average molecular weights, as calculated from the intensities of the peaks, were studied.

The reproducibility of the peak intensities in the FI and FD mass spectra of the Fr-P and T fractions is shown in Table 1. The reproducibility is expressed by the variation coefficient ($\sigma/\bar{x}$), defined by the following equation:

$$\sigma/\bar{x}(\%) = \frac{100}{\bar{x}}\sqrt{\frac{\Sigma(x-x_i)^2}{N-1}},$$

where $\bar{x}$ is the arithmetic mean value calculated from N

measured values of x_i. The variation coefficients of the peaks with high ion intensities are approximately 8% for FI and approximately 5% for FD. In both spectra, the variation coefficients increased with the decrease in the peak intensity. On the whole, the reproducibility of the FD mass spectra is better than that of the FI mass spectra. Both mass spectra generally tended to improve the reproducibility of the peak intensity with an increase in the amount of ions detected.

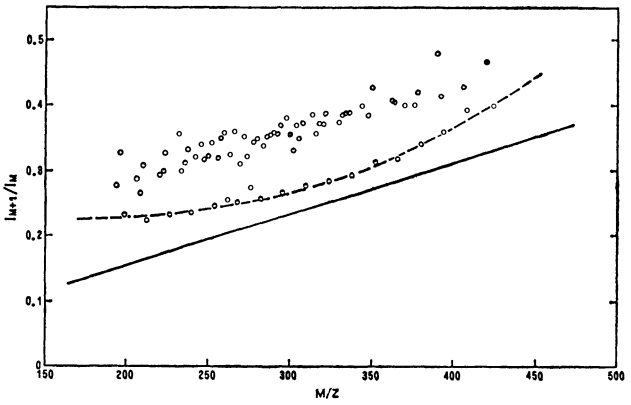

Fig. 2. Comparison of observed and calculated isotope ion ratios.

The reliability of the peak intensity was investigated by comparing the observed and calculated isotope-ion ratios. The isotope ratios in the FI mass spectrum of the Fr-P fraction are compared with the natural abundance (straight line) in Fig. 2. The observed isotope ratios are close to natural abundance when the peak intensities are high (broken line), but they tended to increase with the decrease in the peak intensity. The isotope ratios of peaks with small ion intensities are overestimated. These tendencies were observed in the FI and FD mass spectra of every ring-type fraction. Further studies are needed to elucidate the phenomenon. As a whole, the intensities of the peaks in the FI and FD mass spectra were well reproduced, although the isotope ratios deviated slightly from their natural abundances.

The FI and FD techniques give the molecular-weight-distribution profiles of mixtures. The reliability of the profiles was tested in terms of the number-average molecular weight, as calculated from the intensities of the mass peaks. The number-average molecular weight obtained from the mass spectrum is defined by the following equation:

$$Mn = \frac{\Sigma M_i I_i}{\Sigma I_i},$$

where M_i is the mass of the i th peak and where I_i is the intensity of the i th peak. The number-average molecular weights calculated from the FI and FD mass spectra of the Fr-P and T fractions are shown in Table 2. The molecular weight, like the peak intensity, is reproduced better in the FD mass spectra than in the FI mass spectra.

Furthermore, the calculated number-average molecular weights were compared with those measured by the VPO method in order to check whether or not the spectral patterns of mixtures corresponded to their real molecular-weight distributions. The number-average molecular weights of the ring-type fractions (Fr-P, -M, -D, -T, and -PP-8) were calculated from the FI and FD mass spectra in Figure 3 and are summarized in Table 3. The volatile fractions (Fr-P, -M, -D, and -T) were measured by FI, and the nonvolatile fraction (Fr-PP-8), by FD. In all the mass spectra of the ring-type fractions, ions were scarcely detected in the mass range below m/z 150, where the appearance of fragment ions was anticipated. Table 3 shows that the calculated molecular weights of all fractions but Fr-PP-8 are slightly greater than the VPO values. The overestimation is probably caused by an increase in the sensitivity coefficient with the number of carbon atoms in the molecule.[7] The great overestimation of the Fr-PP-8 fraction must be caused by the increase in the sensitivity coefficient and by the vaporization of the volatile components in this fraction. Table 3 suggests that most of the peaks in the mass spectra can be assigned to molecular and isotopic ions alone. Thus, the FI and FD mass spectra are suitable for the compositional analysis and for the determination of the molecular-weight distribution of coal-derived oil.

In conclusion, we advise that the FI technique is applied to the analyses of volatile fractions, and the FD technique, to the analyses of nonvolatile fractions, of coal-derived oil. These techniques provide more precise and useful data than those obtained by conventional analytical methods, such as GPC and VPO, and may be one of the most powerful tools for elucidating the components of coal-derived oil, although several problems must be solved before we can obtain fully quantitative FI and FD mass spectra.

Group-type Analysis of Ring-type Fraction. As discussed in the preceding section, ring-type fractions

Table 2. Number-average molecular weights as calculated from FI and FD mass spectra of Fr-P and T

Sample :	Fr-P FI	Fr-T FD
1st	301	277
2nd	297	277
3rd	313	288
4th	293	278
5th	301	284
Mean	301	281

Table 3. Comparison of number-average molecular weights of ring-type fractions obtained by FI/FD-MS and VPO

Fr	Yield %		$\overline{Mn}$ MS	$\overline{Mn}$ VPO
P	8.2	FI	301	270
M	6.4	FI	273	240
D	10.1	FI	231	220
T	7.2	FI	283	270
PP-8	7.7	FD	332	270

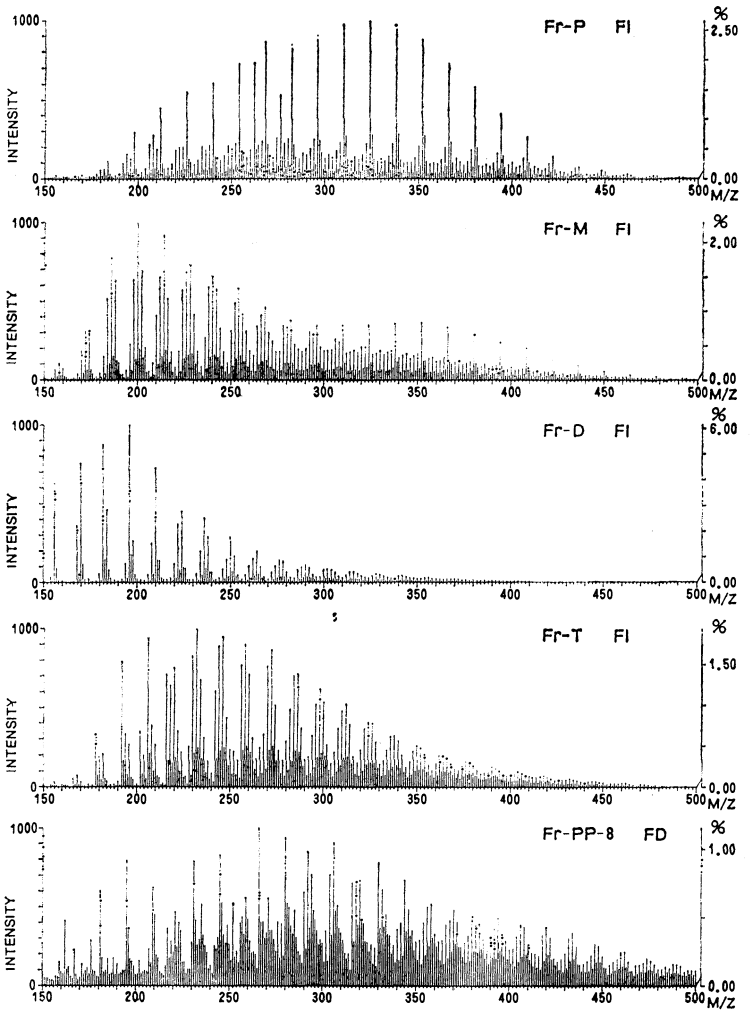

Fig. 3. FI and FD mass spectra of ring-type fractions.

of coal-derived oil can be analyzed semiquantitatively by the combined use of FI and FD techniques. The resulting spectra show their molecular-weight distribution profiles and number-average molecular weights. The group-type analysis based on the molecular weights of components should give information on their chemical structures. That is, the molecular weight of hydrocarbon is expressed by the following equation: $M=12C_n+H_{2n+z}$, and the components in coal-derived oil can be assigned to several group types by the use of the value of z.

In the present work, the ring-type fractions of coal-derived oil separated beforehand by liquid chromatography were used as samples in order to get more detailed structural information. As is shown in Fig. 3, the molecular-weight distributions of all the ring-type fractions but Fr-PP-8 cover the mass range between m/z 150 and 450, with the dominant components of the Fr-M, -D, and -T fractions being distributed in the low-mass range of m/z 200—250. In the Fr-PP-8 fraction, the high-mass ions of nonvolatile components were detected; this proves that the FD technique is suitable for the measurement of nonvolatile components.

The FI mass spectrum of the Fr-P fraction was characterized by the regular occurrence of molecular ions and isotopic ions at m/z 14 intervals. These ions were assigned to $z=2$, that is, paraffins. Other ions with a small ion intensity can be assigned to $z=0$, -2, -4, -6, -8, and -10, that is, cycloparaffins and olefins. Thus, the Fr-P fraction is a mixture of various types of paraffins (C_{13-33}), plus small amounts of cycloparaffins and olefins. The mass spectra of the Fr-M, -D, -T, and -PP-8 fractions were more complicated than Fr-P. The Fr-M fraction consists predominantly of alkyl-substituted monocyclic aromatics, such as 1,2,3,4,4a,9,9a,10-octahydroanthracene ($z=-10$) and 1,2,3,4,5,9,10,11,12,15-decahydropyrene ($z=-12$), and is contaminated by small amounts of the components in the Fr-P fraction. Judging from the values of z, most of the peaks beyond m/z 280 must be paraffins and cycloparaffins. The FI mass spectrum of the Fr-D fraction is comparatively simple, and the dominant components are alkyl-substituted biphenyl ($z=-14$) and alkyl-substituted bicyclic aromatics such as 1,2,3,4-tetrahydrophenanthrene ($z=-14$). The components of the Fr-T fraction have more complicated skeletal structures than Fr-M and -D. The ^{1}H-NMR spectrum of the Fr-T fraction indicates that the average skeletal structure of Fr-T is not a cata type such as anthracene, but a phenanthrene type.[13] Since the Fr-PP-8 fraction

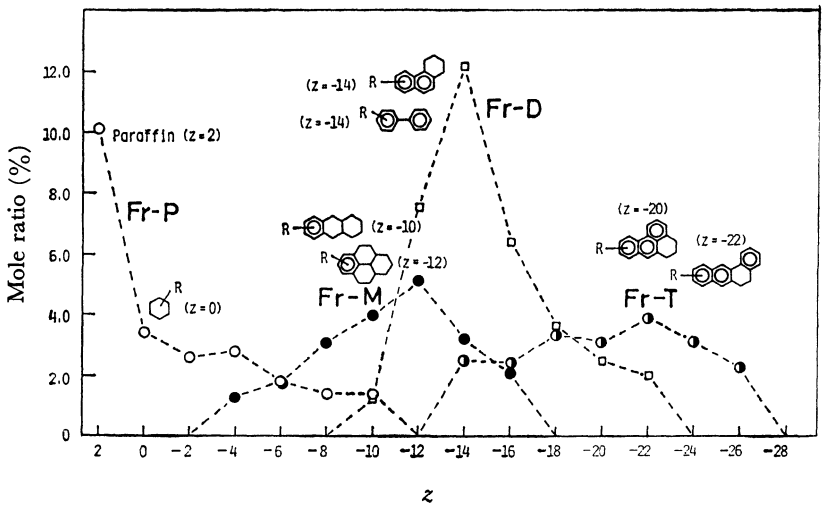

Fig. 4. Distribution of mass z series and an example of probable chemical structures for each z value.

contains the hetero atoms (oxygen and nitrogen), the assignments of the peaks must be made by using a high-resolution mass spectrometer. The distribution of the mass z series and an example of a probable chemical structure for each z value are illustrated in Fig. 4.

The FI and FD mass analysis of coal-derived oil made it possible not only to determine the molecular-weight-distribution profile, but also to speculate on the skeletal structures of components by means of group-type analysis.

References

1) M. G. Inghram and R. Gomer, *J. Chem. Phys.*, **22**, 1279 (1954).

2) H. D. Beckey, *Int. J. Mass Spectrom. Ion Phys.*, **2**, 500 (1969).

3) For example, H. D. Beckey and H.-R. Schulten, *Angew. Chem. Int. Ed. Engl.*, **14**, 403 (1975).

4) T. Yoshida, R. Yoshida, Y. Maekawa, Y. Yoshida, and Y. Itagaki, *Fuel*, **58**, 153 (1979).

5) S. Yokoyama, N. Tsuzuki, T. Kato, and Y. Sanada, *Nenryo Kyokai Shi*, **57**, 748 (1978).

6) H.-R. Schulten and H. D. Beckey, *Org. Mass Spectrom.*, **6**, 885 (1972).

7) H. D. Beckey, "Principles of Field Ionization and Field Desorption Mass Spectrometry," Pergamon Press (1977), p. 248.

8) M. Anbar and G. A. St. John, *Fuel*, **57**, 105 (1978).

9 H. D. Beckey and G. Wagner, *Z. Anal. Chem.*, **197**, 58 (1963).

10) H. D. Beckey, *Z. Anal. Chem.*, **197**, 80 (1963).

11) S. Pfeifer, H. D. Beckey, and H.-R. Schulten, *Z. Anal. Chem.*, **284**, 193 (1977).

12 H. Ishijima, K. Nojima, E. Kubota, T. Aoyama, and Y. Itagaki, "Proceedings of the 13th Organic Mass Spectrometry Conference," (1978), p. 75.

13) T. Yoshida, Y. Maekawa, H.Uchino, and S. Yokoyama, *Anal. Chem.*, **52**, 817 (1980).

  Bull. Chem. Soc. Jpn., 54, 1176—1182 (1981) [Vol. 54, No. 4

Photolysis of Organic Azides. VI.[1] 1,4-Diacetoxy-2,3-diazidonaphthalene. Formation of Isoquinoline Structure from α,α'-Dicyano-o-xylylene

Akira YABE

National Chemical Laboratory for Industry, Yatabe-Higashi 1-1, Tsukuba, Ibaraki 305

(Received July 29, 1980)

Transient absorbing in the 400—450 nm range was observed in the photolysis of 1,4-diacetoxy-2,3-diazidonaphthalene in rigid matrices at 77 K. The transient was assigned as α,α'-diacetoxy-α,α'-dicyano-*o*-xylylene by comparison with the low-temperature photolysis of the other precursors, 1,2-diacetoxy-1,2-dicyano-1,2-dihydrobenzocyclobutenes. The three *o*-xylylene stereoisomers showed differences in the longest-wavelength absorption maxima. Continued irradiation of the *o*-xylylenes converted them to 2-acetoxy-2-methyl[1,3]dioxolo[4,5-*c*]-isoquinoline-5-carbonitrile as the result of the reaction of a cyano group with the *o*-xylylene system and the migration of an acetoxyl group. The rate of formation of the isoquinoline in rigid matrices depends on the viscosity of glassy solvents and the configuration of the intermediate *o*-xylylenes. The room-temperature photolysis of the diazide gave 2,3-diacetamido-1,4-naphthoquinone as the main product and compounds *via* the *o*-xylylene as minor products. A mechanism involving two competitive reactions is discussed.

There has been considerable interest in the structures and properties of *o*-xylylene (*o*-quinodimethane: 5,6-dimethylene-1,3-cyclohexadiene) and its various derivatives.[2-4] In a previous paper we reported the formation of α,α'-dicyano-*o*-xylylenes (**1**) by the photolysis of 2,3-diazidonaphthalenes (**2**).[5] Among the three derivatives,

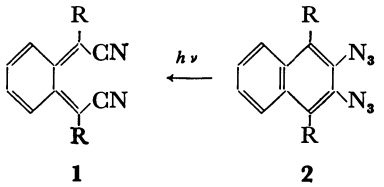

1 **2**

a: R = H
b: R = $OCOCH_3$
c: R = OCH_3

2b gave efficiently an unknown photoproduct *via* **1b** by prolonged irradiation at low temperature in rigid medium, while continued irradiation of the others, **1a** or **1c**, resulted in almost no reaction. We now report a new photochemical reaction of the *o*-xylylene system at low temperature in rigid medium.

In addition, the room-temperature photolysis of **2b** was investigated in connection with the low-temperature photolysis. Pearce *et al.*[6] found the formation of *cis*- and *trans*-1,2-diacetoxy-1,2-dicyano-1,2-dihydrobenzocyclobutenes (**3** and **4**, respectively) and 1,4-diacetoxy-3-isoquinoline (**5**) by the thermal decomposition of **2b**.

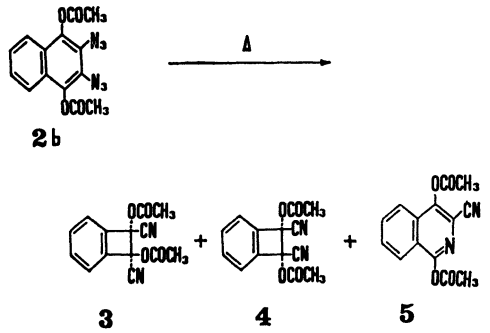

2b

3 (23%) **4** (<3%) **5** (39%)

On the other hand, the room-temperature photolysis of **2b** was quite complicated and considerably different from the thermolysis or the low-temperature photolysis. A new reaction involving the migration of acyl groups to nitreno groups has been found in addition to the formation of **3** *via* **1b**, while **5** has not been produced. The mechanism of the room-temperature *vs.* low-temperature photolysis will be discussed, and a characterization of the photoproducts will be given.

Results and Discussion

Low-temperature Photolysis. A rigid glassy solution of **2b** in EPA (diethyl ether/isopentane/ethanol, 5 : 5 : 2) was irradiated at 77 K with a 500-W super high-pressure mercury lamp through a 300 nm cutoff filter. Figure 1 shows the photochemical process followed by absorption spectroscopy. The absorbance in the range of 424—450 nm increased in the early stage of irradiation. At this stage, warming of the glassy solution to room temperature resulted in disappearance of the absorption. This transient absorbing in the 400—450 nm range was tentatively identified as the α,α'-dicyano-*o*-xylylene (**1b**) in the previous paper,[5] by analogy to the low-temperature photolysis of the parent 2,3-diazidonaphthalene. Continued irradiation resulted in the disappearance of the absorption in the 400—450 nm range and in the appearance of a new absorption in the 355—380 nm range. In the cases of the other diazidonaphthalenes, **2a** and **2c**, the conversion from the *o*-xylylenes, **1a** and **1c**, proceeded even after prolonged irradiation. The secondary photoproduct having absorption bands at 355—380 nm was stable at room temperature. By a separate irradiation of **2b** on a preparative scale, a product with two fewer nitrogen molecules than the starting material was isolated in an almost quantitative yield. Although the product was presumed to be an isoquinoline derivative, on the basis of the IR, ^{1}H-NMR, and ^{13}C-NMR spectra, its final identification was difficult because its UV absorption spectrum (longest-wavelength: λ_{max} 376, 368, 358, 355 sh nm) was considerably different from that (λ_{max} 304 nm) of the isoquinoline (**5**) given by the thermal treatment. Therefore, an X-ray crystal structure analysis was made of a single-crystal grown from dichloromethane–ethanol. The structure was established as 2-acetoxy-

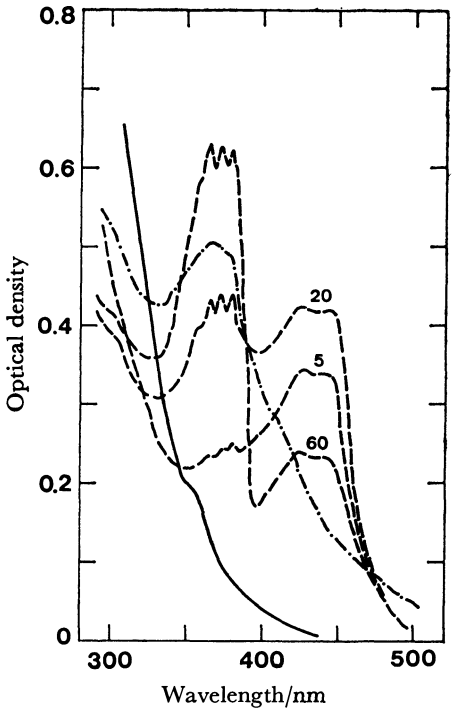

Fig. 1. Absorption spectra of **2b** in EPA at 77 K before (——) and after (----) irradiation. Numbers refer to irradiation times in min. Absorption spectrum (—·—) of **2b** recorded at room temperature after irradiation for 60 min.

2-methyl[1,3]dioxolo[4,5-*c*]isoquinoline-5-carbonitrile (**6**).[7] The formation of such an isoquinoline derivative by the photolysis in a rigid matrix was quite unexpected.

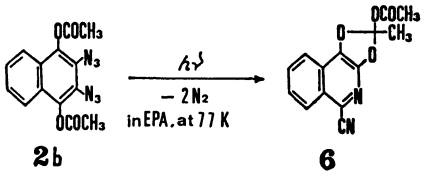

2b **6**

In addition, it is interesting that the electronic absorption spectra of isoquinoline derivatives depend highly on the position of the cyano group and on the presence of the dioxolane ring fused with the isoquinoline nucleus.

Irradiation of **2b** at 77 K was carried out in various media. The reaction proceeded as in the case of EPA. Figure 2 shows the relation between the irradiation time and the yield of the secondary photoproduct **6**, which was measured by monitoring the peak height of the 362 nm UV absorption due to **6** during stepwise photolysis. From a consideration of the viscosity of media as given in Table 1, it was found that the rate of formation decreased with the increase of the viscosity in a series of mixed solvents of isopentane and 3-methylpentane. In the case of EPA, the highly efficient formation, compared with other nonpolar media, may be attributed to solvent polarity.

Low-temperature photolyses of *trans*- and *cis*-1,2-diacetoxy-1,2-dicyano-1,2-dihydrobenzocyclobutenes (**3** and **4**, respectively) were carried out in order to confirm the intermediate and to study the mechanism of low-temperature photolysis of **2b**. Figures 3 and 4 show

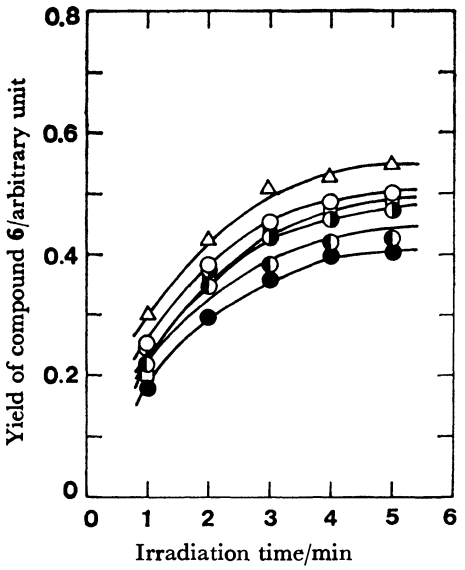

Fig. 2. Relation between the irradiation time and the yield of **6** by the photolysis of **2b** (0.1 mol m^{-3}) at 77 K in various solvents (shown in Table 1). Runs 1 (○), 2 (◑), 3 (◐), 4 (●), 5 (□), and 6 (△). The yields of the compound **6** correspond to the absorbances (λ 362 nm) due to **6**.

Table 1. Viscosity of the media in the photolysis of **2b** at 77 K

Run	Solvent (Composition in parts by volume)	Viscosity / Pa s	Ref.
1	Isopentane, 3-methylpentane (97 : 3)	8.9×10^{4}	a)
2	Isopentane, 3-methylpentane (3 : 2)	1.8×10^{7}	a)
3	Isopentane, 3-methylpentane (1 : 9)	2.4×10^{10}	a)
4	3-Methylpentane	9.4×10^{10}	a)
5	Methylcyclohexane, isopentane (1 : 3)	1.0×10^{7}	b)
6	Ether, isopentane, ethanol (5 : 5 : 2)	8.0×10^{7}	b)

a) J. R. Lombardi, J. Raymonda, and A. C. Albrecht, *J. Chem. Phys.*, **40**, 1148 (1964). b) Estimated from Fig. 2 in the literature: H. Greenspan and E. Fischer, *J. Phys. Chem.*, **69**, 2466 (1965).

the photochemical processes of **3** and **4**, respectively, in EPA at 77 K. As in the case of **2b**, the longer-wavelength transient absorptions appear in the range of 400—450 nm in the early stage of irradiation, and a new absorption in the range of 355—380 nm begins to appear with the increase of irradiation time. Moreover, the prolonged irradiation with longer-wavelength light (>300 nm) results in the increase of that absorption, together with the decrease of the 400—450 nm absorption. The absorption peaks in the 355—380 nm range are completely consistent with those of **6**. However, the peaks of the transients generated from **3** and **4** are shifted to slightly shorter wavelengths than those of the intermediate generated from **2b**. This spectral shift could be explained in terms of the different configurations of the *o*-xylylenes. The intermediate generated

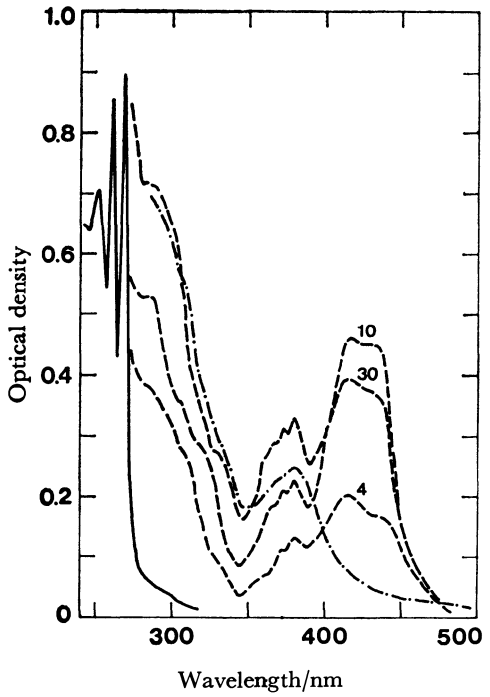

Fig. 3. Absorption spectra of **3** in EPA at 77 K before (——) and after (----) irradiation. Numbers 4 and 10 mean irradiation times (min) with a low-pressure mercury lamp, and 30 means irradiation time with a high-pressure mercury lamp (20 min) in addition to the 10 min irradiation. Absorption spectrum (—·—) recorded at room temperature after 30 min irradiation.

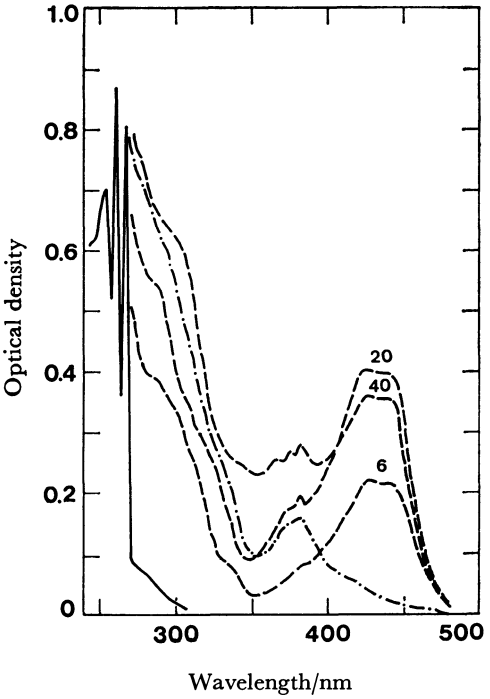

Fig. 4. Absorption spectra of **4** in EPA at 77 K before (——) and after (----) irradiation. Numbers 6 and 20 mean irradiation times (min) with a low-pressure mercury lamp, and 40 means irradiation time with a high-pressure mercury lamp (20 min) in addition to the 20 min irradiation. Absorption spectrum (—·—) recorded at room temperature after 40 min irradiation.

from **2b** must be the *E,E*-form stereoisomer (**1b**(*E,E*)) of α,α′-diacetoxy-α,α′-dicyano-*o*-xylylenes, as described in the previous paper[5] by analogy to the case of 1,2-diazidobenzene. The intermediates generated from **3** and **4** are presumed the *E,Z*-form **1b**(*E,Z*), and the

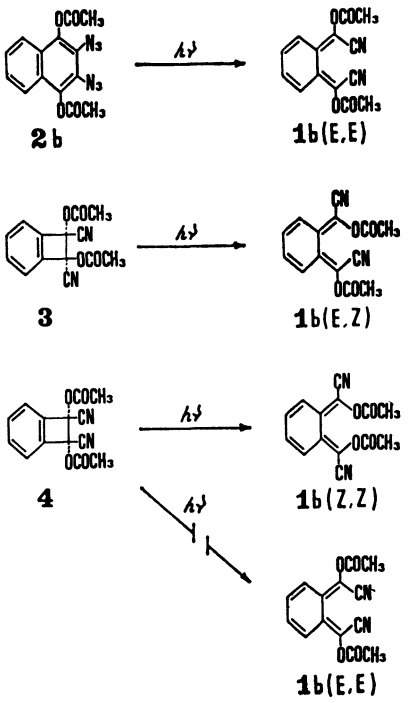

Z,Z-form **1b**(*Z,Z*) or *E,E*-form **1b**(*E,E*), respectively, from a consideration of the orbital symmetry rule. In the case of **4**, the intermediate structure must be **1b**(*Z,Z*)', because the absorption peaks generated from **4** are not identical with those generated from **2b**. The spectral shifts of these stereoisomers are consistent with those of the *o*-xylylene derivatives. The absorbing peaks of the *o*-xylylene stereoisomers are summarized in Table 2.

The secondary photoproduct from **3** or **4** is identified as **6** on the basis of the spectral properties of the crystals isolated from a separate irradiation on a preparative scale. The results of this photochemical reaction show that final product **6** is formed by a similar mechanism from the different stereoisomers of **1b**. A plausible mechanism which accounts for the formation of the isoquinoline (**6**) is depicted in Scheme 1.

Although the formation of **6** *via* **1b** from **2b** proceeds efficiently with the irradiation of a high-pressure mercury lamp, the rate of formation of **6** from **3** or **4** is very slow during irradiation of a low-pressure mercury lamp. In particular, the formation of **6** in the case of **4** occurs in a lower yield, compared with the case of **3**, after 10 min irradiation, as shown in Figs. 3 and 4. When the concentration of the intermediate **1b** was increased appropriately after 10 min irradiation, prolonged irradiation was carried out with a high-pressure mercury lamp (>300 nm). However, the rate of formation of **6** from **4** was much lower than that of **6** from **3** or, particularly, from **2b**. In the isoquinoline

Table 2. Absorbing peaks of *o*-xylylene stereoisomers (Absorption above 350 nm, at 77 K)

Substituents	Solvent	Absorbing peaks / nm		
		(*E*, *E*)	(*Z*, *Z*)	(*E*, *Z*)
α,α′-Diphenyl-[3e]	Methylcyclohexane	465		455
α,α′-Dicyano-[5]	EPA		432 458	432 454
α,α′-Diacetoxy-α,α′-dicyano-	EPA	424 448	423 444	415 435

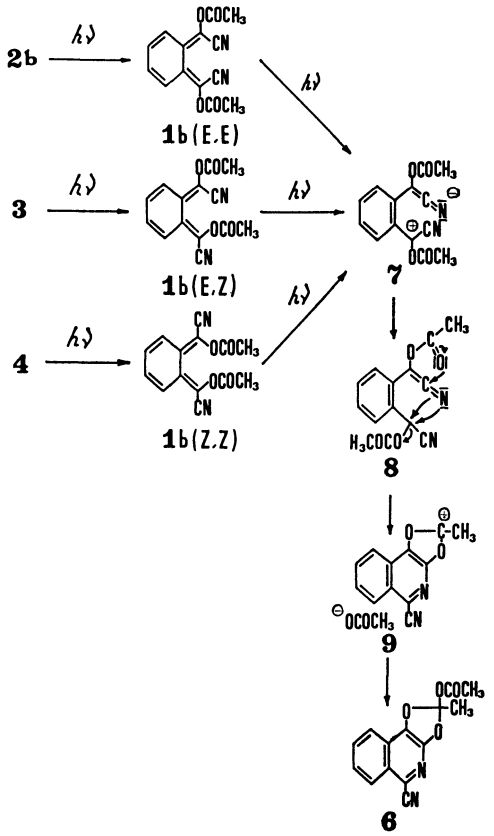

Scheme 1.

formation, the *o*-xylylene derivatives **1b**(*E*,*E*) and **1b**(*E*,*Z*) would have more favorable configurations than **1b**(*Z*,*Z*). The rigid medium at low temperature would control large rotational motions in each stereoisomer. The rigidity effects of glassy solvents have also been observed in the photolysis of **2b**, as shown in Fig. 2 and Table 1. The π-electrons of the *o*-xylylene system are delocalized by the substitution of the two cyano groups, and consequently the aromatization is liable to occur. The deactivation of the *o*-xylylene system by the cyano groups is consistent with the fact that the attempt to trap **1b** with dienophiles, such as *N*-phenylmaleimide or maleic anhydride, has failed. The formation of the isoquinoline structure is accomplished *via* the dipolar intermediate **7**, as shown in Scheme 1. The formation of the dioxolane ring is accompanied by the formation of the C–N bond, and the cleavage of the acetoxyl group follows. Finally, the migration of the acetate anion to the positive carbon atom of the dioxolane ring proceeds in the cage of rigid medium.

Although various photochemical and thermal reactions of *o*-xylylenes have been reported, it is interesting that the cyano groups conjugated with *o*-xylylene system participate in the reaction of *o*-xylylene structure. Moreover, it should be noted that the reactions involving a large rotational motion and a migration of the large acetoxyl group proceed readily in the rigid matrices at low temperature.[8]

Room-temperature Photolysis. A methanol solution of **2b** (0.52 mol m^{-3}) was irradiated at room temperature with a 400-W high-pressure mercury lamp through Pyrex. The photoproducts showed very complicated spots on a thin layer chromatogram of silica gel. As a major product, 2,3-diacetamido-1,4-naphthoquinone (**10**) was isolated in a 46% yield, together with the dihydrobenzocyclobutene **3** (25%) and the compound **6** (8%). Interestingly, the yield of the dihydrobenzocyclobutene **4** was only less than 1%, and 1,4-diacetoxy-3-cyanoisoquinoline (**5**), the main product in the case of the thermal decomposition of **2b**, was not detected.

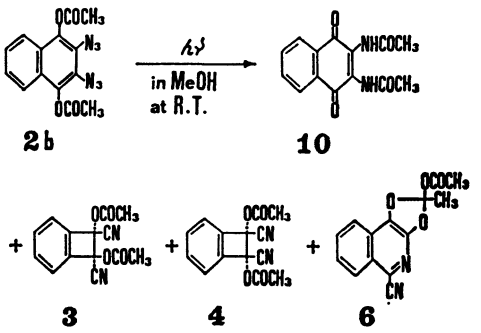

Irradiation of **2b** in hexane gave a new compound instead of **10** as a main product, together with **6** as a minor product. Its structure was identified as 2,3-dihydro-2-imino-3-acetylimino-1,4-naphthoquinone (**11**) based on the spectral properties.

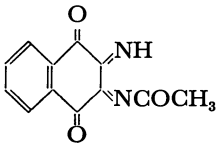

11

The product distributions were sensitive to the solvent used. The results for the room-temperature photolysis of **2b** in various solvents are summarized in Table 3. An unknown photoproduct having UV absorption bands at 362 and 285—325 nm was observed in the case of hexane, and was the main product in the case of benzene. This was not characterized, although it is

TABLE 3. ROOM-TEMPERATURE PHOTOLYSIS OF 1,4-DIACETOXY-2,3-DIAZIDONAPHTHALENE (**2b**)

Solvent	Concn/mol m^{-3}	Irrad time/min	Yield/%				
			3	**4**	**6**	**10**	**11**
Methanol	0.52	120	25	1	8	46	
2-Propanol	0.52	120	18	trace	6	45	
Diethyl ether	0.52	90	15		8	40	
Benzene	0.52	120	6		10	5	6
Hexane	0.26	30	3		12	3	48

presumed to be 1,2,3,4-naphthalenetetrone derivative (IR absorption bands at 1798, 1725, and 1690 cm^{-1}). It is certain that the products **3**, **4**, and **6** were given *via* the *o*-xylyelene **1b**, and **10** and **11** were formed by a different mechanism. Furthermore, in these room-temperature photolyses, the dihydrobenzocyclobutene, the product *via* the *o*-xylylene **1b**(*E*,*E*), was exclusively the *trans*-isomer (**3**). A consideration of the orbital symmetry rule shows that the cyclization of the *o*-xylylene is not a photoinduced but a thermal reaction.

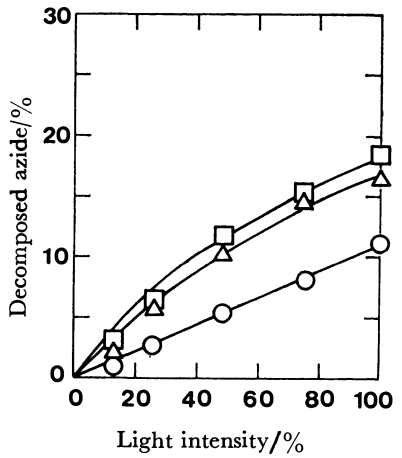

Fig. 5. Relation between the decomposed azide **2b** and light intensity. Photolyses (○) in EPA at 77 K, (△) in methanol at room temp, and (□) in hexane at room temp.

The dependence of the rate of decomposition of **2b** on the light intensity was examined. The amounts (%) of the decomposed azide were calculated on the basis of the measurement of the decrease in absorbance after 10 s irradiation. The results involving the low-temperature photolysis are shown in Fig. 5. In the previous paper,[5] it was found that the formation of **1a** or **1c** from **2a** or **2c**, respectively, was a monophotonic process. Similarly, the decomposition of **2b** in a rigid matrix at 77 K would lead quantitatively to the *o*-xylylene **1b**. Therefore, the relationship between the rate and the light intensity shows good linearity, suggesting a monophotonic reaction. On the other hand, the relationship deviates from linearity and displays downward curvature in the cases of the photolyses in methanol and in hexane. This indicates the participation of a biphotonic process. Therefore, the formation of **10** and **11** would be interpreted by the mechanism involving the stepwise decomposition of the two azido groups. Thus, there are two competitive reactions (Paths (a) and (b)) after the first azido group was decomposed. The process of the room-temperature photolysis is depicted in Scheme 2.

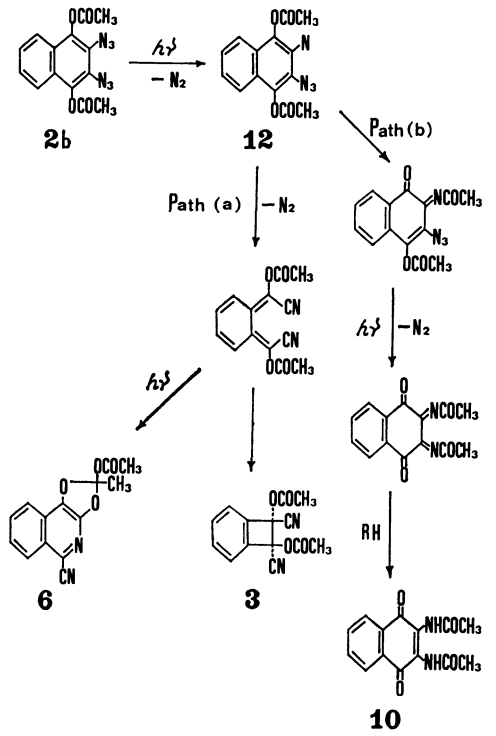

Scheme 2.

In Path (b), the attack of the nitreno groups upon the neighboring acetoxyl groups has been observed in the thermal decomposition of 1,4-diacetoxy-2-azidobenzenes.[6] The migration of acyl groups proceeded in a high yield (45—89%) for the reported compounds, although **5** was given as a main product and **10** was not given completely in the thermal decomposition of **2b**. In the room-temperature photolysis of **2b**, the migration of the acyl groups (Path (b)) has become the main process, taking the place of the formation of the *o*-xylylene (Path (a)) or **5**. Along Path (a), the cyclization to the dihydrobenzocyclobutene has become the main process, as a typical reaction of *o*-xylylene system.

The room-temperature photolysis of **2b** in the presence of some additives was carried out in order to study the factors governing the two competitive processes and the spin state of the nitrene **12**. The results are summarized in Table 4. The presence of dichloromethane (known to enhance singlet processes[9]) or iodomethane (heavy atom effect) gave nearly the same

product distribution as in the case of the direct irradiation (Runs 1 and 2). However, the addition of pyrene (a triplet quencher and singlet promoter[10]) in methanol raised the yield of **10** to 58%, while the yields of **3** and **6** were decreased (Run 3). The addition of benzophenone or acetophenone (triplet sensitizers[10]) seemed to show no remarkable effects (Runs 4 and 5). Based on the results of Run 3, one could predict that Paths (a) and (b) were divided into triplet-derived and singlet-derived processes, respectively. That is to say, the spin state of the nitrene (**12**) which attacks the neighboring acetoxyl group is singlet, whereas the nitrene (**12**) which attacks the remaining azido group is in the triplet state. The direct observations of actual precursors and quenching rates are lacking, so this conclusion cannot be confirmed yet.

Table 4. Room-temperature photolysis of **2b** in the presence of additives

Run	Conditions[a]	Yield / %		
		3	**6**	**10**
1	MeOH/CH_2Cl_2 (50%)	25	8	46
2	MeOH/CH_3I (10%)	25	6	42
3	MeOH/Pyrene (8.2 mol m^{-3})	3	<1	58
4	Benzene/Acetophenone (10%)	5	8	5
5	Benzene/Benzophenone (9.2 mol m^{-3})	6	15	<1

a) Concentration of **2b**: 0.52 mol m^{-3}. Irradiation time: 120 min.

Some differences in the low-temperature *vs.* room-temperature photolysis have been found in the processes of the attack by a nitreno group upon an acetoxyl group and the cyclization of the *o*-xylylene to the benzocyclobutene. The suppression of these processes in the low-temperature photolysis could be ascribed to a rigidity-controlled and activation-energy-controlled field.

Experimental

Measurements. The melting point is uncorrected. The IR and UV/VIS spectra were recorded on Hitachi Model 260-30 and Shimadzu Model UV-300 spectrophotometers respectively. The ^1H NMR and ^{13}C-NMR spectra were recorded on Varian Model XL-100-12 (100 MHz) and JEOL Model FX-100 (25 MHz) spectrometers respectively using TMS as an internal standard. The mass spectra were recorded on a Hitachi Model RMU-6M spectrometer. The microanalysis was performed at the Institute of Physical and Chemical Research.

Materials. 1,4-Diacetoxy-2,3-diazidonaphthalene (**2b**), and *cis*- and *trans*-1,2-diacetoxy-1,2-dicyano-1,2-dihydrobenzocyclobutenes were prepared according to the literature.[6]

Irradiations of 2b in Rigid Media at 77 K. Irradiation on preparative scale was carried out in a doughnut-shaped Pyrex vessel (volume: about 160 ml; thickness: 7 mm) which was immersed in liquid nitrogen with a 400-W high-pressure mercury lamp (Riko UVL-400HA) protected with a transparent quartz Dewar vessel. A solution of **2b** in 160 ml of EPA (0.37 mol m^{-3}) was irradiated for 10 min. Upon warming to room temperature, the solution was condensed on a rotary evaporator. Preparative-TLC (Merck Silica-gel 60 F_{254}) analysis of the concentrate gave the starting material (about 40%) and yellow crystals (55%). The crystals were recrystallized from dichloromethane–ethanol. Mp 146 °C (dec). IR (KBr): 2230, 1778, 1598, 1448, 1440, 1388 cm^{-1}. UV (Hexane): 376 (ε 3800), 368 (4500), 358 (4500), 355 sh (4100), 308 (6200), 296 (4600), 233 (19000) nm. ^1H-NMR ($CDCl_3$) δ: 2.09 (s, 3H, CH_3), 2.18 (s, 3H, $COCH_3$), 7.5—7.9 (m, 3H, aromatic), 8.20 (s, 1H, aromatic) ppm. ^{13}C-NMR ($CDCl_3$) δ: 21.6 (q), 24.7 (q), 116.0 (s), 119.9 (d), 121.4 (s), 122.0 (s), 125.5 (d), 125.9 (s), 128.2 (d), 129.3 (s), 130.9 (d), 136.0 (s), 150.8 (s), 167.0 (s) ppm. MS: *m/e* 270 (M^+), 218, 214, 212, 211, 186. Found: C, 62.33; H, 3.75; N, 10.45%. Calcd for $C_{14}H_{10}N_2O_4$: C, 62.22; H, 3.73; N, 10.37%. The structure of the crystals was determined as *2-acetoxy-2-methyl[1,3]-dioxolo[4,5-c]isoquinoline-5-carbonitrile* based on the spectral properties as described above and finally on the results of X-ray crystallography.

Irradiation for spectroscopy was carried out with a cell (path length: 10 mm) which had been immersed in liquid nitrogen in a quartz Dewar vessel equipped with optical windows on opposite sides. The light source was an Ushio USH-500D 500-W super high-pressure mercury lamp which transimitted through a 300 nm cutoff filter.

Irradiation of 3 or 4 in EPA at 77 K. Irradiation on a preparative scale was performed in the doughnut-shaped quartz vessel which was immersed in liquid nitrogen with a 160-W low-pressure mercury lamp (Riko UVL-160LA) protected with a transparent quartz Dewar vessel. A solution of **3** in 160 ml of EPA (0.44 mol m^{-3}) was irradiated for 2 h. The starting material and yellow crystals were isolated by a similar procedure to that for **2b**. The crystals were identical with those formed by the photolysis of **2b**.

Irradiation of **3** or **4** for spectroscopy was carried out in a manner like that described above for **2b**. The light source was a 15-W low-pressure mercury lamp (Toshiba GL-15).

Irradiation of 2b in Fluid Media at Room Temperature. Irradiation was performed under bubbling of nitrogen in a conventional immersion well-type reactor (volume: about 1200 ml) equipped with a 400-W high-pressure mercury lamp (Riko UVL-400HA) through Pyrex. The separation of the photoproducts was performed by the preparative TLC, and the yield determination was carried out by UV analysis (Tables 3 and 4).

The main photoproduct from the photolysis in methanol was precipitated in condensed solution (46% yield). The crystals were recrystallized from acetone–methanol, yielding yellow needles, mp 249 °C (dec). This product was identified as 2,3-diacetamido-1,4-naphthoquinone (**10**) by comparing the absorption spectrum with that of an authentic sample[11] and by the following spectral data. IR (KBr): 3310 (NH), 1668, and 1650 (quinone CO, acetamido CO) cm^{-1}. ^1H-NMR ($CDCl_3$) δ: 2.3 (s, 6H, CH_3), 7.6—7.9 (m, 2H, aromatic), 8.0—8.2 (m, 2H, aromatic), 8.5 (s, broad, NH) ppm. ^{13}C-NMR ($CDCl_3$) δ: 23.8 (q), 126.9 (d), 128.1 (s), 130.8 (s), 134.3 (d), 167.4 (q) ppm.

The main product from the photolysis in hexane was precipitated in condensed solution (48% yield). The crystals were recrystallized from acetone–dichloromethane. Yellow crystals, mp 180 °C (dec). It was identified as 2,3-dihydro-2-imino-3-acetylimino-1,4-naphthoquinone (**11**) on the basis of the following spectral data. IR (KBr): 1674 and 1640 (quinone CO, acetimino CO) cm^{-1}. MS: *m/e* 228 (M^+), 186 (M—ketene), 132. ^1H-NMR (DMSO-d_6) δ: 2.45 (s, 3H, CH_3), 7.8—7.9 (m, 2H, aromatic), 8.4—8.6 (m, 2H, aromatic), 12.8 (broad, 1H, NH) ppm. ^{13}C-NMR (DMSO-d_6) δ: 13.1 (q), 120.4 (s), 129.8 (s), 129.9 (s), 132.6 (s), 133.0 (s), 133.4 (s), 136.0 (s), 151.2 (s), 155.0 (s), 162.9 (s), 176.0 (s) ppm.

Preparative TLC (Merck Silica-gel 60 F_{254}) of the filtrates from the condensed solutions gave the photoproducts shown in Table 3.

The author wishes to thank to Professor Michio Kobayashi (Tokyo Metropolitan University) for helpful discussions, Professor Tamaichi Ashida (Nagoya University) and Mr. Yukishige Kitano (Toray Research Center) for X-ray crystal structure analyses, and Dr. Ikuo Sakai (Toray Research Center) for NMR spectral analyses.

References

1) Part V: A. Yabe, *Bull. Chem. Soc. Jpn.*, **53**, 2933 (1980).

2) a) C. R. Flynn and J. Michl, *J. Am. Chem. Soc.*, **95**, 5802 (1973); b) C. R. Flynn and J. Michl, *ibid.*, **96**, 3280 (1974), and references cited therein; c) R. D. Miller, J. Kolc, and J. Michl, *ibid.*, **98**, 8510 (1976); d) W. R. Dolbier, Jr., K. Matsui, and D. V. Horák, *ibid.*, **99**, 3876 (1977); e) K. L. Tseng and J. Michl, *ibid.*, **99**, 4840 (1977); f) R. P. Steiner, R. D. Miller, H. J. Dewey, and J. Michl, *ibid.*, **101**, 1820 (1979).

3) a) G. Quinkert, K. Opitz, W.-W. Wiersdorff, and J. Weinlich, *Tetrahedron Lett.*, **1963**, 1863; b) G. Quinkert, K. Opitz, W.-W. Wiersdorff, and M. Finke, *ibid.*, **1965**, 3009; c) G. Quinkert, W.-W. Wiersdorff, M. Finke, K. Opitz, and F.-G. von der Haar, *Chem. Ber.*, **101**, 2302 (1968); d) G. Quinkert, M. Finke, J. Palmowski, and W.-W. Wiersdorff, *Mol. Photochem.*, **1**, 433 (1969); e) K. H. Grellmann, J. Palmowski, and G. Quinkert, *Angew. Chem.*, **83**, 209 (1971); f) G. Quinkert, J. Palmowski, H.-P. Lorenz, W.-W. Wiersdorff, and M. Finke, *ibid.*, **83**, 210 (1971).

4) a) K. K. de Fonseka, J. J. McCullough, and A. J. Yarwood, *J. Chem. Soc., Chem. Commun.*, **1977**, 721; b) K. K. de Fonseka, C. Manning, J. J. McCullough, and A. J. Yarwood, *J. Am. Chem. Soc.*, **99**, 8257 (1977); c) K. K. de Fonseka, J. J. McCullough, and A. J. Yarwood, *ibid.*, **101**, 3277 (1979).

5) A. Yabe, *Bull. Chem. Soc. Jpn.*, **52**, 789 (1979). Configurational nomenclature of these isomers has now been reversed owing to the introduction of acetoxyl groups into the corresponding parent isomers described in the previous paper.[5]

6) D. S. Pearce, M-S. Lee, and H. W. Moore, *J. Org. Chem.*, **39**, 1362 (1974).

7) Details of the structure determination will be reported in a separate paper, together with data of X-ray crystallography.

8) Hirayama and his coworkers have reported that a large rotational motion of a group equal to or greater than an acetyl (or propionyl) group is strongly prohibited at 77 K. (S. Hirayama, *Bull. Chem. Soc. Jpn.*, **50**, 491 (1977); T. Matsumoto, M. Sato, and S. Hirayama, *Chem. Phys. Lett.*, **27**, 237 (1974)).

9) J. M. Lindley, I. M. McRobbie, O. Meth-Cohn, and H. Suschitzky, *Tetrahedron Lett.*, **1976**, 4513.

10) J. S. Swenton, T. J. Ikeler, and B. H. Williams, *J. Am. Chem. Soc.*, **92**, 3103 (1970).

  Bull. Chem. Soc. Jpn., 54, 1183—1185 (1981)

The Mechanism of the Reactions of Alkoxy- and Aryloxytrimethylsilanes with Sulfinyl Chlorides. A Doubt about 4-Center Mechanism for the Bimolecular IVb–VIb Bond Cleavages[1)]

Seizi KOZUKA* and Tetsuji HIGASHINO

Department of Applied Chemistry, Faculty of Engineering, Osaka City University, Sugimoto-cho, Sumiyoshi-ku, Osaka 558

(Received August 2, 1980)

Kinetic studies have been conducted for the reactions of ethoxytrimethylsilane with benzenesulfinyl chloride and aryloxytrimethylsilane with methanesulfinyl chloride. Both the reactions were found to obey second order rate equation. A clear negative ρ value was observed for the reaction of aryloxytrimethylsilane. The solvent effects suggested that both the two reactions were quite similar in their mechanisms. Nucleophilic addition of silyl-oxygen atom to sulfinyl group has been suggested for these two reactions.

Recently, Harpp *et al.* conducted kinetic studies for the reaction of alkoxytrimethylsilanes with benzenesulfinyl chloride.[2)] They observed that the reaction was rather insensitive to the solvent polarity and sensitive to the steric effect of the alkoxyl group. A *four-centered nonionic transition state* (I) has been suggested for the reaction.

$$\mathrm{RO\text{-}SiMe_3 + PhS(O)Cl \longrightarrow \left[\begin{array}{l} O \\ \| \\ Ph\text{-}S\cdots Cl \\ \vdots \quad \vdots \\ RO\cdots SiMe_3 \end{array}\right] \longrightarrow PhS(O)OR + ClSiMe_3} \quad (1)$$

R = Me, Et.

I

The mechanism has widely been accepted to explain the course of the reaction involving the IVb element at the reaction center,[3)] however, only few were supported by kinetic and/or stereochemical evidences.[4,5)] Restricting to bimolecular IVb–VIb bond cleavage reactions as expressed by the following general formula (Eq. 2),[6)]

$$\equiv\mathrm{IVb\text{-}VIb\text{-}} + \mathrm{E\text{-}Nu} \longrightarrow \equiv\mathrm{IVb\text{-}Nu} + \mathrm{E\text{-}VIb\text{-}} \quad (2)$$

IVb = Si, Ge, Sn *etc.* VIb = O, S, Se *etc.*

E-Nu = H_2O, ROH, RCO_2H, RX, RCOX, RS(O)X *etc.*

the reaction of alkoxysilane reported by Harpp *et al.* is the only one reaction involving the mechanism supported by kinetic evidence.[2)]

We have reexamined the reaction of alkoxysilane with sulfinyl chloride in order to obtain additional kinetic aspects of the bimolecular *nonionic four-centered reaction*, or to take a new look at the mechanism and found that the reaction involved *ionic* nucleophilic attack of the silyl-oxygen atom.

Results and Discussion

Examination of the substituent effect of the *nonionic four-centered reaction* would be of interest or important to clarify the reaction mechanism. Thus, we tried to prepare substituted-benzenesulfinyl chlorides to examine the substituent effect of the reaction shown in Eq. 1. The substituted-sulfinyl chlorides can be prepared either from the corresponding disulfides[7a)] or from sodium sulfinates,[7b)] however, it was found to be difficult to prepare them in pure forms enough for kinetic experiments. Alternatively, the reaction of aryloxytrimethylsilane with methanesulfinyl chloride was chosen for our study. The reaction was found to give methanesulfinate and chlorotrimethylsilane in nearly quantitative yields.

$$p\text{-X-}C_6H_4OSiMe_3 + MeS(O)Cl \longrightarrow p\text{-X-}C_6H_4OS(O)Me + Me_3SiCl \quad (3)$$

The rate of the reaction was measured by monitoring ^{1}H NMR trimethyl signals of the starting aryloxysilane and the formed chlorosilane at time. A good second order kinetic plot was obtained with satisfactory reproducibility. The results are given in Table 1.

Table 1. Rate of the reaction of $Me_3SiOC_6H_4X$-*p* (0.19 mol/dm^3) with MeS(O)Cl (0.23 mol/dm^3) in PhCN

X	Temp/°C[a)]	k/dm^{3}mol^{-1} s^{-1}	Remarks
OMe	28	1.62×10^{-3}	
OMe	34	2.35×10^{-3}	$\Delta H^{\ddagger}=43.9$ kJ mol^{-1}
OMe	41	3.25×10^{-3}	$\Delta S^{\ddagger}=-151$ J K^{-1} mol^{-1}
OMe	47	5.06×10^{-3}	
OMe	—	2.96×10^{-3}	
Me	—	1.39×10^{-3}	Hammett plot
H	—	1.03×10^{-3}	$\rho(\sigma)=-1.44$
Cl	—	6.60×10^{-4}	($\gamma=0.984$)
Br	—	6.30×10^{-4}	
NO_2	—	7.04×10^{-5}	

a) JEOL PS-100, VT Probe was used for measurement of activation parameters. Temperatures were calibrated. Substituent effect was measured on Hitachi R-20, at magnet temperature (36 °C); not calibrated.

The activation parameters appeared as normal magnitude for the reactions of this type shown in Eq. 2; not particular from the reactions involving either 5-coordination of the IVb element[8)] or nucleophilic attack of the VIb atom.[9)] More clear evidence in support of an *ionic mechanism* for the reaction is the substituent effect. A clearly negative ρ value was observed for the reaction in almost the same magnitude with those of the analogous reactions of (arylthio)trimethylstannanes with haloalkane (-1.40)[9a)] and with benzoyl chloride (-1.6)[9b)] in which nucleophilic attacks of the stannyl-sulfur atoms have been suggested for the reactions based on kinetic

and stereochemical results. The value is also pretty close to that of sulfonium salt formation which undoubtedly involves nucleophilic attack (-1.2).[10] In addition to these similarities, the magnitude of the entropy of activation is in accordance with that of the sulfonium salt formation (-138 J K^{-1} mol^{-1}).[10] These results would suggest a rate-determining nucleophilic attack of the silyl-oxygen atom giving oxonium intermediate for the reaction of aryloxytrimethylsilane with sulfinyl chloride (Eq. 3). Thus, the mechanism shown below would be the most plausible for the reaction.

$$Me_3SiOAr + MeS(O)Cl \xrightarrow{slow} \left[\begin{array}{c} Cl \\ | \\ Me_3SiO^+\text{–}SMe \\ | \quad | \\ Ar \quad O^- \end{array}\right] \quad \text{II}$$

$$\xrightarrow{fast} Me_3SiCl + ArOS(O)Me \qquad (4)$$

The detailed mechanism leading to the product from the onium intermediate (II) is not clear but *ionic four-centered transition state* (III) for the step is unlikely based on the similarities of the ρ and entropy values as discussed above.

$$\left[\begin{array}{c} Me_3Si\ldots Cl \\ \vdots \quad \vdots \\ ArO^+\text{–}S\text{–}Me \\ | \\ O^- \end{array}\right] \quad \text{III}$$

The remaining question is whether the nucleophilic addition mechanism is applicable to the reaction of Harpp *et al.* shown in Eq. 1.[2] Different mechanisms for the two reactions (Eqs. 1 and 3) are unlikely since the nucleophilic mechanism has been suggested even for the reaction of less nucleophilic aryloxy-oxygen atom. The more nucleophilic alkoxy-oxygen would attack the sulfinyl group in the same manner. Solvent effects on both the reactions were examined in order to prove the similarity of their mechanisms. The rates of the reactions were measured in various solvents including carbon tetrachloride and dichloromethane which have been employed by Harpp *et al.* The effect presently observed [$k(CH_2Cl_2)/k(CCl_4)=3.8$] is in accordance with that of them (5) as shown in Table 2.[11]

Both the rates of the reactions were clearly accelerated in polar solvents. The observed solvent effect for the reaction of aryloxysilane [Eq. 3, X=MeO; $k(Ph_6CN/k(CCl_4)=70$] is pretty close to that observed for the reaction of arylthiostannane with halo-alkane [$k(PhCN)/k(C_6H_6)=ca.$ 100] in which nucleophilic attack was suggested as the mechanism.[9a] The effect, however, appeared substantially smaller for the reaction of ethoxysilane (Eq. 1, R=Et). The difference in the magnitudes of the solvent effects is not clear; may perhaps due to difference in charge delocalization in the intermediates or in solvations, but both the rates in various solvents exhibit clearly linear correlation as shown in Fig. 1. The linear correlation ($\gamma=0.998$) would reveal that these two reactions proceed in a similar manner *i.e.*, the nucleophilic addition mechanism. The *nonionic four-center mechanism* suggested by Harpp *et al.*[2] has thus been ruled out also for the reaction of alkoxysilane (Eq. 1).

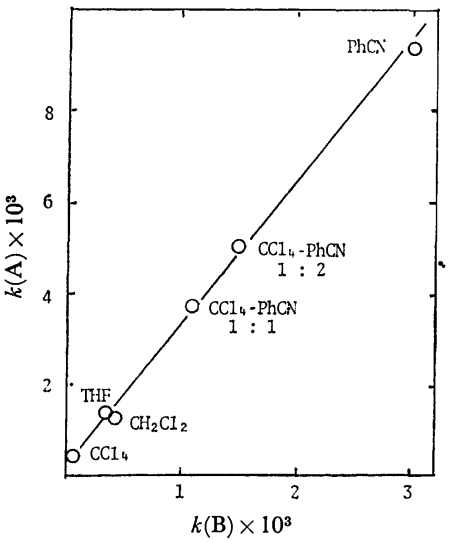

Fig. 1. Plot of the rates of the reaction A (Eq. 3, X=OMe) *vs.* reaction B (Eq. 1, R=Et) in various solvents.

The evidences cited by them in support of their mechanism were the solvent effect and the steric effect.[2] They examined five different solvents but all nonpolar ones. They compared their result with that of cheleotropic denitrogenation reaction of a caged diazo compound[12] in support of their *nonionic mechanism.* The auther claimed that the solvent effect of the reaction of alkoxysilane [$k(CH_2Cl_2)/k(C_6D_{12})=9$] was pretty close

Table 2. Rates of the reactions; $Me_3SiOC_6H_4OMe$-*p* (0.19 mol/dm^3)+MeS(O)Cl (0.23 mol/dm^3) [A] and Me_3SiOEt (0.16 mol/dm^3)+PhS(O)Cl(0.20 mol/dm^3) [B] in various solvents at 36 °C[a]

Solvent	Reaction [A][b]		Reaction [B]		
	k[d]	k_{rel}	k[d]	k_{rel}	k_{rel}[c]
CCl_4	4.34×10^{-5}	1.00	2.89×10^{-4}	1.00	1
Tetrahydrofuran	3.64×10^{-4}	8.4	1.23×10^{-3}	4.3	—
CH_2Cl_2	4.03×10^{-4}	9.3	1.11×10^{-3}	3.8	5
CCl_4–PhCN (1 : 1)[e]	1.03×10^{-3}	24	3.62×10^{-3}	12.5	—
CCl_4–PhCN (1 : 2)[a]	1.49×10^{-3}	34	4.93×10^{-3}	17	—
PhCN	2.96×10^{-3}	68	9.25×10^{-3}	32	—

a) Hitachi R-20 NMR magnet temperature; not calibrated. b) Reaction A and B are correspond to the reactions shown in Eqs. 3 and 1 in the text, respectively. c) Data from Ref. 2; initial concentrations were not recorded. d) Second order rate in dm^3 mol^{-1} s^{-1}. e) v/v Mixture.

to that of the cheleotropic reaction which was studied over a wide variety of solvents and a small solvent effect ($\simeq$15-fold) was noted.[2] The effects, however, appeared opposite. The rates of the cheleotropic reaction appeared no correlation to the solvent polarity; rather accelerated in nonpolar solvent (2-Me-heptane) and depressed in polar solvent (96% EtOH).[12] On the other hand, the rates of the reaction of alkoxysilane were apparently accelerated in a polar solvent (CH_2Cl_2).[2] In the present study, it was shown to be accelerated more in more polar solvent.

The steric effect of the alkoxy moiety [k(EtO)/k(MeO)=10] indicates that the reaction is sensitive to the steric hindrance as they claimed.[2] The sensitivity to the steric hindrance, however, is also acceptable to the steric crowd in the onium intermediate (IV), bearing bulky trimethylsilyl group and trigonal bipyramid sulfur functionality.

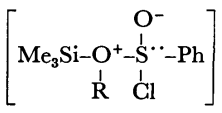

R = Me, Et,

IV

The *nonionic four-centered mechanism* has been ruled out for the reactions of (arylalkoxy)silanes with sulfinyl chlorides. None of the bimolecular reactions of this type shown in Eq. 2, has been known to proceed *via* either *ionic* or *nonionic four-center transition state* which has been supported by any evidence.

Experimental

Materials. Trimethylphenoxysilane was prepared from hexamethyldisilazane (5.0 g) and phenol (4.7 g) in the presence of imidazole,[2] bp 41 °C/2 mmHg (1 mmHg=133.332 Pa), 88% yield. Other aryloxytrimethylsilanes were prepared similarly. Methanesulfinyl chloride was prepared by chlorination of dimethyl disulfide in acetic anhydride,[7a] bp 38—41 °C/14 mmHg, 84% yield. Benzenesulfinyl chloride was prepared from sodium benzenesulfinate and thionyl chloride,[7b] 77 °C/1 mmHg, 95% yield.

Product Analysis. An equimolar mixture of methanesulfinyl chloride and trimethylphenoxysilane (10 mmol) in dichloromethane (4 ml) was heated at 45 °C for 20 h in a sealed tube. The solvent and volatile product were distilled off. Only chlorotrimethylsilane was detected in the distillate. ^{1}H NMR spectrum of the residue was consisted of the signals due to the remaining trimethylphenoxysilane and phenyl methanesulfinate with trace amounts of impurities which probably derived from thermal decomposition of the sulfinate ester. Signals were identified by comparing with those of the authentic phenyl methanesulfinate prepared from methanesulfinyl chloride and phenol in the presence of pyridine.[13] Attempts to isolate the sulfinate from the remaining trimethylphenoxysilane were failed due to its thermal instability. Accordingly, the conversion was obtained by integration of the NMR signals of the reaction mixture, 70%. Other aryloxytrimethylsilanes gave similar results. Substituent, reaction conditions, and conversion were: p-OMe, 45 °C 5 h, 80%; p-NO_2, 45 °C 24 h, 50%.

Kinetics. The procedure is essentially the same as that employed for the acyloxyl exchange reaction of acetoxysilane.[8a] Trimethylphenoxysilane (21 mm^3, 0.121 mmol) and methanesulfinyl chloride (10 mm^3, 0.143 mmol) were dissolved in the solvent (600 mm^3) and the reaction was monitored by following ^{1}H NMR trimethyl signals of the starting trimethylphenoxysilane (δ 0.27 ppm) and the product, chlorotrimethylsilane (δ 0.40 ppm) with time.

References

1) Preliminal results have been reported, S. Kozuka and T. Higashino, *Tetrahedron Lett.*, **21**, 2067 (1980).

2) D. N. Harpp, B. T. Friedlander, C. Larsen, K. Steriou, and A. Stockton, *J. Org. Chem.*, **43**, 3481 (1978).

3) For example, P. C. Paul, K. K. Soni, and P. Narula, *J. Organomet. Chem.*, **40**, 355 (1972).

4) H. Kwart and W. E. Barnett, *J. Am. Chem. Soc.*, **99**, 614 (1977) and references cited therin.

5) J. Stutsky and H. Kwart, *J. Am. Chem. Soc.*, **95**, 8678 (1973) and references cited therin

6) Kinetic studies of the reactions of this type have shown bimolecular nature of the reactions although kinetic behavior of some has not been uncovered yet. See Refs. 1, 2, 8, and 9.

7) a) I. B. Douglass and R. V. Norton, *J. Org. Chem.*, **33**, 2014 (1968). As was noted in the lit., aromatic sulfinyl chlorides should not be distilled. Purification of the sulfinyl chlorides without distillation was difficult; b) F. Kurger, *Org. Synth.*, Coll. Vol. **4**, 934 (1963).

8) a) $R_3SiOCOMe+R'COOH \longrightarrow R_3SiOCOR'+MeCOOH$; S. Kozuka, T. Kitamura, N. Kobayashi, and K. Ogino, *Bull. Chem. Soc. Jpn.*, **52**, 1950 (1979); b) $R_3SiSR''+R'COOH \longrightarrow R_3SiOCOR'+R''SH$; S. Kozuka and T. Kitamura, *Bull. Chem. Soc. Jpn.*, **52**, 3384 (1979); c) $Me_3SiSPh+PhCOCH_2Br \longrightarrow Me_3SiBr+PhSCH_2COPh$; $\Delta H^{\ddagger}=54.0$ kJ mol^{-1}, $\Delta S^{\ddagger}=156$ J K^{-1} mol^{-1}, S. Kozuka, T. Higashino, and T. Kitamura, *Bull. Chem. Soc. Jpn.*, **54**, in press.

9) a) $Me_3SnSR+R'X \longrightarrow Me_3SnX+RSR'$; S. Kozuka and S. Ohya, *Bull. Chem. Soc. Jpn.*, **51**, 2651 (1978); b) $Me_3SnSR+PhCOCl \longrightarrow Me_3SnCl+PhCOSR$; S. Kozuka and I. Naribayashi, *Bull. Chem. Soc. Jpn.*, **52**, 3638 (1979).

10) S. Kozuka, S. Taniyasu, A. Kikuchi, and K. Ogino, *Chem. Lett.*, **1979**, 129.

11) The rates of the reaction in CCl_4 and CH_2Cl_2 reported by Harpp *et al.* could not be reporduced, *e.g.*, 5×10^{-5} and 2.7×10^{-4} in CCl_4 and CH_2Cl_2, respectively,[2] although the k_{rel} appeared quite similar. These deviations in the k values may be due to the difference in the initial concentrations of the substrates and also in temperatures which were not calibrated.

12) J. P. Snyder and D. N. Harpp, *J. Am. Chem. Soc.*, **98**, 7821 (1976).

13) L. Senatore, E. Ciuttarin, A. Fave, and G. Levita, *J. Am. Chem. Soc.*, **95**, 2918 (1973).

The Nitration of Acylpentamethylbenzenes and 1,3-Diacyltetramethylbenzenes Bearing, as the Acyl Components, Pivaloyl, Trichloroacetyl, and Tribromoacetyl Groups. Exclusive Attack on the Methyl Group at the Most Crowded Site[1]

Hitomi SUZUKI,* Mitsuyuki HASHIHAMA,** and Tadashi MISHINA**

Department of Chemistry, Faculty of Science, Ehime University, Bunkyo-cho, Matsuyama 790

***Department of Chemistry, Faculty of Science, Hiroshima University, Higashi-sendamachi, Naka-ku, Hiroshima 730*

(Received August 4, 1980)

When treated with concentrated nitric acid in dichloromethane at room temperature, the title compounds undergo an exclusive attack on the methyl group at the most crowded site, giving 6-acyl-2,3,4,5-tetramethylbenzyl nitrates, and 2,6-diacyl-3,4,5-trimethylbenzyl nitrates and/or (2,6-diacyl-3,4,5-trimethylphenyl)nitromethanes respectively, as the major products. While the predominant mode of the side-chain substitution reactions is nitrooxylation for acylpentamethylbenzenes and 1,3-dipivaloyl-2,4,5,6-tetramethylbenzene, it shifts to nitration for 1,3-bis(trihalogenoacetyl)-2,4,5,6-tetramethylbenzenes. Nitrodeacylation is seen to some extent for pivaloylbenzenes, but not for trihalogenoacetylbenzenes. The exclusive attack on the methyl group at the most hindered position can be explained by a sequence involving the attachment of a nitronium ion at the site *meta* to the acyl group, followed by a proton release from the resulting arenium ion to form a nitromethylenecyclohexadiene intermediate, which is then transformed into the benzylic compounds *via* a benzyl cation/nitrite anion pair.

When treated with nitric acid at a low temperature, polyalkylated aromatic compounds often suffer the side-chain substitution to give benzylic compounds in addition to the normal nuclear substitution products. The side-chain reaction is characterized by a peculiar orientation and high regiospecificity in the products, which stand in marked contrast to the ordinary side-chain substitution occurring through a homolytic mechanism. The puzzling features of this reaction have been a subject of numerous recent studies,[2] but its mechanism still remains a matter of controversy and speculation. Recently, we have made a systematic investigation of the nitration of hexamethylbenzene and presented the first quantitative data of the product distribution; these data favor the S_Nl' mechanism, in which the side-chain substitution products are formed from the methylenecyclohexadiene intermediate through the intervention of an ion-pair.[3] To obtain further information about the character of the reaction, especially the steric effect of the substituent group on the course of the side-chain substitution, a series of acylpentamethylbenzenes and 1,3-diacyl-2,4,5,6-tetramethylbenzenes bearing bulky acyl groups, such as pivaloyl, trichloroacetyl, and tribromoacetyl groups, have been prepared, and their reactions with concentrated nitric acid have been investigated.

Experimental

All the melting points were determined on a hot-stage apparatus and are uncorrected. The infrared spectra were run as Nujol mulls on a Hitachi 215 spectrophotometer, and only prominent peaks were recorded. The ^{1}H-NMR spectra were measured in chloroform-*d* with a Varian T-60 apparatus and a JEOL MH-100 apparatus, using TMS as the internal standard, unless otherwise stated. The mass spectra were obtained on a Hitachi RMS-4 mass spectrometer, with an ionizing current of 70 eV.

Materials. *1,3-Dipivaloyl-2,4,5,6-tetramethylbenzene (7b)* was prepared from 1,3-dipropanoylbenzene (**6**) by repeated treatment with potassium *t*-butoxide and methyl iodide.[4]

Pentamethylpivalophenone (3b). Into a mixture of pivaloyl chloride (3.4 g, 28.2 mmol), aluminium chloride (6.5 g, 48.7 mmol), and carbon disulfide (20 ml), pentamethylbenzene (**1**; 5.0 g, 33.7 mmol) in carbon disulfide (15 ml) was stirred under ice-salt-bath cooling during the course of 0.3 h. After the addition, the brown viscous mixture was stirred for a further 0.7 h at room temperature and then decomposed with dilute hydrochloric acid. The organic layer was separated, the carbon disulfide was removed, and the residual solid product was collected by filtration and subjected to chromatography over silica gel, using hexane as a solvent. The unchanged hydrocarbon and then the ketone **3b** were eluted, and the latter was recrystallized from ethanol. White needles, mp 129—130 °C. Yield, 2.8 g (42% based on the pivaloyl chloride used).

1,3-Bis(tribromoacetyl)-2,4,5,6-tetramethylbenzene (7d).[5] Bromine (8.0 g, 50 mmol) was stirred into a solution of sodium hydroxide (8.0 g, 200 mmol) in water (70 ml). The temperature was kept below 10 °C during the addition. To the resulting solution, 1,3-diacetyl-2,4,5,6-tetramethylbenzene (**5**; 1.1 g, 5 mmol) dissolved in benzene (15 ml) was added; the mixture was then heated with vigorous stirring at 60 °C, while the progress of the reaction was monitored by means of ^{1}H-NMR. After 40 h, a further amount of aqueous sodium hypobromite (50 mmol) was added; heating was then continued for an additional 20 h. The organic layer was then separated, washed thoroughly with aqueous sodium hydrogensulfite and then water, and dried over magnesium sulfate. The solvent was removed, and the residue was recrystallized from benzene to give **7d** as colorless prisms; mp 195—197 °C. Yield, 2.28 g (65%).

1,3-Bis(trichloroacetyl)-2,4,5,6-tetramethylbenzene (7c) was similarly prepared by treating **5** with a large excess of aqueous sodium hypochlorite at 60 °C. It was recrystallized from benzene to give white needles; mp 138—139 °C. Yield, 37%.

Procedures for Nitration of Acylpentamethylbenzenes and 1,3-Diacyl-2,4,5,6-tetramethylbenzenes. Some typical examples are shown below for the nitration of α,α,α-trichloropentamethylacetophenone (**3c**) and 1,3-bis(trichloroacetyl)-2,4,5,6-tetramethylbenzene (**7c**).

i): Nitric acid (d=1.5; 0.63 g, 10 mmol) in dichloromethane (2 ml) was added to a vigorously stirred suspension of **3c** (0.50 g, 1.7 mmol) in dichloromethane (4 ml). The

mixture was stirred at room temperature for 1.5 h and then diluted with water. The organic layer was separated, and the aqueous layer was extracted with dichloromethane. The combined organic solutions were washed thoroughly with water, dried over magnesium sulfate, and evaporated to leave a solid residue, which was recrystallized several times from hexane to give **4c** as white crystals; mp 106—109 °C. Yield 0.27 g (45%).

ii): A suspension of 1,3-bis(trichloroacetyl)-2,4,5,6-tetramethylbenzene (**7c**; 1.0 g, 2.35 mmol) in dichloromethane (5 ml) was cooled to −10—0 °C, after which fuming nitric acid (d=1.5; 1.48 g, 23.5 mmol) was stirred in over a period of 5 min. The resulting brown mixture was stirred at room temperature for 3 h and then diluted with water. The organic layer was separated and worked up as usual to give a light brown, pasty solid, which was then passed through a short silica-gel column to obtaine the unchanged substrate (0.67 g) and a product mixture (0.151 g). The latter was then chromatographed on a thin-layer silica-gel plate, using hexane as the eluant. Two main bands were scraped off from the glass plate and extracted with ether; *1,3-bis(trichloroacetyl)-2-nitrooxymethyl-4,5,6-trimethylbenzene* (**9c**; 22 mg, 6%) was obtained from the fast moving band, and *1,3-bis(trichloroacetyl)-2-nitromethyl-5,4,6-trimethylbenzene* (**8c**; 39 mg, 11%), from the slow moving band.

In an alternative way, the product mixture was dissolved in a minimum amount of pentane, after which the solution was kept in a refrigerator for several days. Compounds **8c** and **9c** crystallized out as prisms and needles, respectively and were partially separated by hand-picking.

Results and Discussion

Acylbenzenes undergo nitration mainly at the position *meta* to the acyl group, as would be expected from the deactivating effect of the acyl group. Some examples of an acyl group being replaced by a nitro group are also well known.[6] However, the literature so far contains no report on the nitration of fully methylated acylbenzenes and diacylbenzenes.

Pentamethylacetophenone (**2**) reacted slowly with concentrated nitric acid in dichloromethane at −5—0 °C to give a four-component mixture, from which the major product was isolated and identified as 6-nitrooxymethyl-2,3,4,5-tetramethylacetophenone (**4a**). On similar treatment, 1,3-diacetyl-2,4,5,6-tetramethylbenzene (**5**) gave a complex mixture of products, one component of which was isolated by TLC and identified as 5-nitro-2,3,4,6-tetramethylacetophenone (**14**). The general pattern of the reaction was similar to those found in the nitrations of pentamethylbenzoic acid[7] and pentamethylbenzamide.[8] The nitrating agent seems to attack the acetyl group partially, making the products more complicated and difficult to separate.

Based on the results obtained from these preliminary experiments, we turned to the nitration of the title hindered mono- and diketones in order to see if the replacement of the acetyl group by a bulky acyl group, such as the pivaloyl and trihalogenoacetyl groups, may produce any effect on the course of the reaction or the product distribution. Pentamethylpivalophenone (**3b**) was obtained by the Friedel-Crafts acylation of pentamethylbenzene (**1**) with pivaloyl chloride. 1,3-Dipivaloyl-2,4,5,6-tetramethylbenzene (**7b**) could not be obtained by the similar acylation of 1,2,3,5-tetramethylbenzene; after several unsuccessful attempts, it was, however, prepared by the exhaustive methylation of 1,3-dipropanoyl-2,4,5,6-tetramethylbenzene (**6**) with potassium *t*-butoxide and methyl iodide. α,α,α-Trihalogenopentamethylacetophenones (**3c** and **3d**) and 1,3-bis(trihalogenoacetyl)-2,4,5,6-tetramethylbenzenes (**7c** and **7d**) were obtained following the routes outlined in Schemes 1 and 2. The halogenation with sodium hypohalite of the **2** and **5** ketones proceeded quite slowly, and the repeated treatment of partially halogenated ketones with a fresh batch of aqueous sodium hypohalite was necessary to obtain **7c** and **7d** in acceptable yields. All of these mono- and diketones are well-crystallized solids and are poorly soluble in ordinary non-polar solvents.

The treatment of acylpentamethylbenzenes **3b**—**3d** with an excess of nitric acid (d=1.5) in dichloromethane at room temperature, followed by the chromatography of the product over silica gel, gave the corresponding 6-nitrooxymethyl-2,3,4,5-tetramethylacylbenzenes **4b**—**4d** in 40—60% yields. The characteristic appearance of benzylic protons as a pair of doublets at δ 5.0—5.3 and 5.4—5.5 ppm indicated the presence of a nitrooxymethyl group adjacent to the bulky acyl group. Thus, irrespective of any difference in bulkiness or electron-withdrawing ability, the propensity of the acyl group to direct an entering group on the adjacent alkyl side-chain

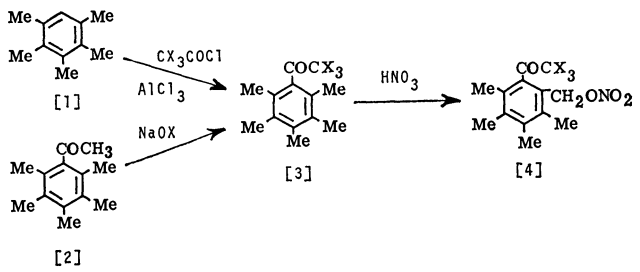

Scheme 1.

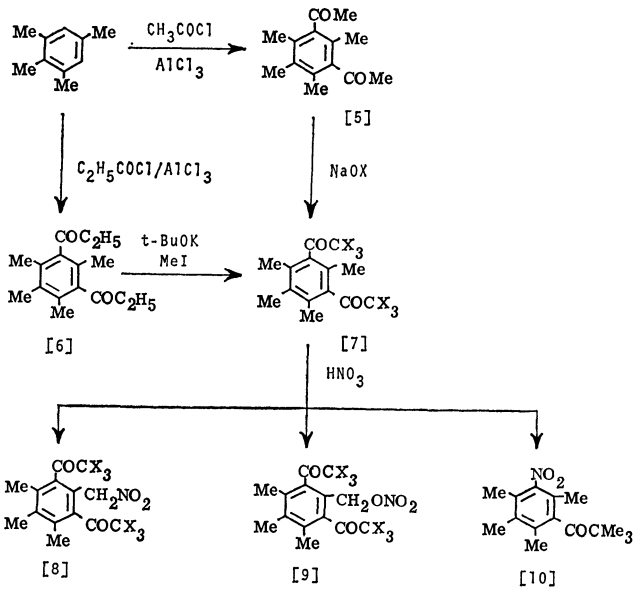

Scheme 2.

Table 1. Physical and spectral data for some polysubstituted acylbenzenes and 1,3-diacylbenzenes

Compound	Mp/°C	IR spectra ν_{max}/cm^{-1}	^{1}H-NMR spectra δ/ppm	Found (%)	Calcd (%)
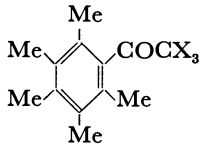					
[2] X=H	83—85	1700, 1300, 1170	2.07 (s, 2Me), 2.13 (s, 3Me)* 2.30 (s, MeCO)	—	—[9]
[3b] X=Me	129—130	1690, 1100, 910	1.17 (s, Me_3CCO), 2.02 (s, 2Me),* 2.15 (s, 2Me), 2.19 (s, Me)	C 82.6 H 10.6	82.7 10.4
[3c] X=Cl	91—92	1735, 1095, 840, 785	2.17—2.33 (br. s, 5Me)*	C 52.9 H 5.2	53.2 5.2
[3d] X=Br	131—133	1725, 1090, 910, 795, 740	2.20, 2.23, 2.28 (incompletely* resolved, 5Me)	C 36.5 H 3.5	36.6 3.5
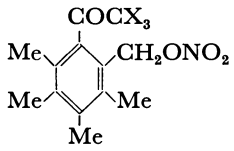					
[4a] X=H	100—101	1690, 1615, 1275, 860	2.13 (s, Me), 2.23 (s, 2Me),* 2.27 (s, Me), 2.40 (s, MeCO), 5.32 (s, CH_2)	C 61.9 H 6.9 N 5.5	62.1 6.8 5.6
[4b] X=Me	100—101	1690, 1630, 1270, 840	1.16 (s, Me_3CCO), 2.08 (s, Me),* 2.23 (br. s, 3Me), 5.03 (d, CH_2; J=11Hz), 5.37 (d, CH_2; J=11 Hz)	C 65.5 H 7.9 N 4.5	65.5 7.9 4.8
[4c] X=Cl	106—109	1730, 1620, 1270, 1095, 855, 800	2.20—2.42 (br. s,4Me), 5.25* (d, CH_2; J=11.5 Hz), 5.38 (d, CH_2; J=11.5 Hz)	C 44.1 H 4.0 N 3.9	44.0 4.0 4.0
[4d] X=Br	115—117	1715, 1630, 1275, 850	2.29, 2.33 (incompletely resolved,* 4Me), 5.35 (d, CH_2; J=12 Hz), 5.48 (d, CH_2; J=12 Hz)	C 32.0 H 2.9 N 2.7	32.0 2.9 2.9
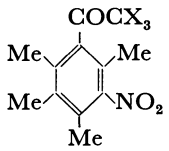					
[14] X=H	106—108	1690, 1525, 1255, 1155, 840	2.05 (s, Me), 2.15 (s, 2Me),* 2.18 (s, Me), 2.38 (s, MeCO)	C 65.2 H 7.0 N 6.3	65.1 6.8 6.3
[10] X=Me	104—105	1680, 1525, 1090, 920, 850	1.25 (s, Me_3CCO), 2.08 (s, Me),* 2.15 (s, Me), 2.20 (s, 2Me)	C 68.2 H 8.2 N 5.2	68.4 8.0 5.3
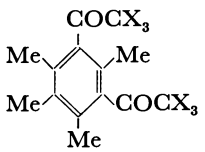					
[5] X=H	126—128	1695, 1350, 1200	1.98 (s, Me), 2.12(br. s, 3Me),* 2.35 (s, MeCO)	—	—[9]
[7b] X=Me	166—168	1690, 1300, 1100, 930, 910	1.21 (s, Me_3CCO), 1.24 (s, Me_3CCO), 2.00 (s, Me), 2.13 (br, s, 3Me)	C 79.7 H 10.2	79.4 10.0
[7c] X=Cl	138—139	1730, 1110, 965, 850, 770	2.23 (s, Me), 2.32 (s, 3Me)	C 39.5 H 2.8	39.6[5] 2.9
[7d] X=Br	195—197	1720, 1100, 950, 780, 730	2.23 (s, Me), 2.40 (s, 2Me), 2.47 (s, Me)	C 24.6 H 1.8	24.3[5] 1.8
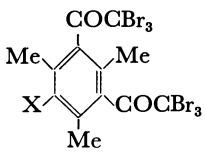					
[15] X=H	162—165	1730, 1240, 970, 795	2.48 (s, 2Me), 2.52 (s, Me), 7.10 (s, H_{arom})	C 23.3 H 1.5	23.0 1.5

Compound	Mp/°C	IR spectra ν_{max}/cm^{-1}	^{1}H-NMR spectra δ/ppm	Found (%)	Calcd (%)
[16] X=NO_2	215—217	1715, 1525, 1240, 790, 760	2.40 (s, 2Me), 2.53 (s, Me)	C 22.0 H 1.3 N 2.0	21.6 1.3 1.9
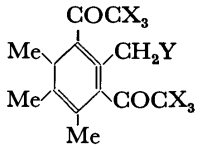					
[9b] X=Me, Y=ONO_2	143—145	1685, 1635, 1280, 845	1.22 (s, Me_3CCO), 1.25 (s, Me_3CCO), 2.17 (s, 2Me), 2.21 (s, Me), 5.00 (d, CH_2; J=11 Hz), 5.06 (s, CH_2), 5.15 (d, CH_2; J=11 Hz)	C 66.4 H 8.3 N 3.5	66.1 8.0 3.9
[9c] X=Cl, Y=ONO_2	93—95	1735, 1625, 1270, 840	2.30 (s, Me), 2.37 (s, 2Me), 5.24 (d, CH_2; J=12 Hz), 5.31 (s, CH_2), 5.43 (d, CH_2; J=12 Hz)	C 34.5 H 2.2 N 2.4	34.6 2.2 2.8
[9d] X=Br, Y=ONO_2	163—165	1730, 1615, 1270, 855	2.33 (s, Me), 2.45 (s, 2Me), 5.37 (d, CH_2; J=12 Hz), 5.47 (s, CH_2), 5.68 (d, CH_2; J=12 Hz)	C 22.4 H 1.5 N 1.5	22.3 1.4 1.8
[8b] X=Me, Y=NO_2	177—178	1690, 1560, 1300, 1090, 940	1.23 (s, Me_3CCO), 1.27 (s, Me_3CCO), 2.00 (s, Me), 2.12 (s, 2Me), 5.13 (br. s, CH_2)	C 69.2 H 8.5 N 4.0	69.1 8.4 4.0
[8c] X=Cl, Y=NO_2	217—220	1740, 1565, 1310,1110, 970, 805, 780	2.33 (s, Me), 2.38 (s, 2Me), 5.38 (d, CH_2; J=18 Hz), 5.42 (s, CH_2), 5.51 (d, CH_2; J=18 Hz)	C 35.9 H 2.4 N 2.9	35.8 2.4 3.0
[8d] X=Br, Y=NO_2	199—202	1730, 1565, 1310, 1095, 960, 775, 730	2.33 (s, Me), 2.45 (s, 2Me), 5.43 (d, CH_2; J=17 Hz), 5.64 (s, CH_2), 5.86 (d, CH_2; J=17 Hz)	C 23.2 H 1.5 N 1.7	22.8 1.5 1.9

* Determined in carbon tetrachloride.

was maintained through the whole series of four acylpentamethylbenzenes **3a**—**3d**. Nitrodeacylation was observed to some extent with pivalophenone, **7b**, but not at all with α,α,α-trihalogenoacetophenones, **7c** and **7d**. By similar treatment, 1,3-dipivaloyl-2,4,5,6-tetramethylbenzene (**7b**) gave 2,6-dipivaloyl-3,4,5-trimethylbenzyl nitrate (**9b**) as a side product (10—20%), in addition to the expected nitrodeacylation product, 5-nitro-2,3,4,6-tetramethylpivalophenone (**10**). Only the methyl group, flanked on both sides by bulky pivaloyl groups, suffered side-chain nitrooxylation. Those results, together with those obtained from the nitration of acylpentamethylbenzenes, **3b**—**3d**, present a striking contrast to the ordinary aromatic substitutions, which are quite sensitive to the bulkiness of the substituent groups.

The action of nitric acid upon the diacyl compounds, **7c**—**7d**, afforded a mixture of (2,6-diacyl-3,4,5-trimethylphenyl)nitromethanes, **8c**—**8d**, and 2,6-diacyl-3,4,5-trimethylbenzyl nitrates, **9c**—**9d**; the yields, as estimated from the ^{1}H-NMR peak integration, were 40—45 % and 20—25%, respectively, based on the unrecovered starting materials. With these halogeno-ketones, no nitrodeacylation was observed. The methyl group between two bulky acyl groups was exclusively attacked again. In these cases, however, the major mode of the side-chain reaction changed from nitrooxylation to nitration. Such a marked change produced by a slight modification of the substituent groups was unexpected, and we can find no parallel previously in the reported literature.

At room temperature the benzylic protons of the

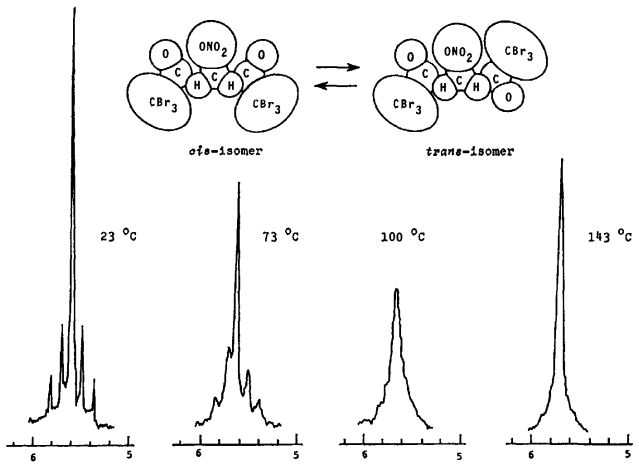

Fig. 1. Selected variable temperature ^{1}H-NMR signals (100 MHz) for benzylic protons of *cis*/*trans* isomers of 2,6-bis(tribromoacetyl)-3,4,5-trimethylbenzyl nitrate (**9d**) in *o*-dichlorobenzene.

nitrates, **9b**—**9d** and nitromethanes, **8c**—**8d**, appear as a peak cluster consisting of one double doublet signal and one singlet signal in the ^{1}H-NMR spectrum (Table 1). In the high-temperature spectrum, however, this peak cluster converges into a new single peak which occurs at the average position of the corresponding peaks in the low-temperature spectrum, indicating that these nitrates and nitromethanes exist in a pair of stable conformations resulting from the *cis*/*trans* isomerism due to restricted rotation about carbonyl groups. A variable-

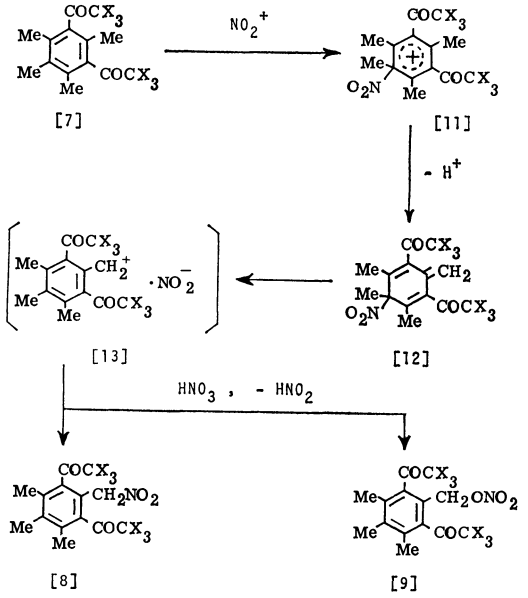

Scheme 3.

temperature ^{1}H-NMR spectrum of the **9d** nitrate is shown in Fig. 1. Clearly, at room temperature and below **9d** exists in the form of *cis/trans* isomers, the ratio of which is estimated to be 2.6 from the peak-area integration. The details of this interesting isomerism will be described elsewhere.

An examination of the CPK molecular models of the **7b—7d** ketones indicates the difficulty of a direct attack by a solvated electrophile on a methyl group flanked on both sides by bulky acyl groups. Thus, the nitration and nitrooxylation occurring exclusively on the methyl group at the most crowded site can be explained by the indirect sequence depicted in Scheme 3: an *ipso* attack of a nitronium ion on the most reactive ring site of **7** to form the arenium ion (**11**) is followed by a proton release from the activated methyl group *para* to the site of attack to give the triene (**12**), which is then transformed into the benzylic compounds, **8** and **9** *via* the assumed ion-pair (**13**).[3]

The authors wish to thank Dr. Tetsuo Ohtsuki of Kyoto University for measuring the variable-temperature ^{1}H-NMR spectra of hindered ketones described herein.

References

1) The reaction of polysubstituted aromatics. Part LIX. Part LVIII: H. Suzuki and K. Ohnishi, *Nippon Kagaku Kaishi*, **1981**, 245.

2) For a review of non-conventional nitration, see H. Suzuki, *Synthesis*, **1977**, 217; R. B. Moodie and K. Schofield, *Acc. Chem. Res.*, **9**, 287 (1976); S. R. Hartshorn, *Chem. Soc. Rev.*, **3**, 167 (1974).

3) H. Suzuki, T. Mishina, and T. Hanafusa, *Bull. Chem. Soc. Jpn.*, **52**, 191 (1979).

4) H. Suzuki, Y. Aomori, T. Mishina, and T. Hanafusa, *Bull. Chem. Soc. Jpn.*, **51**, 3393 (1978).

5) A. R. Gray, J. T. Walker, and R. C. Fuson, *J. Am. Chem. Soc.*, **53**, 3494 (1931).

6) A. H. Salway, *J. Chem. Soc.*, **95**, 1155 (1909); V. J. Harding, *ibid.*, **105**, 2790 (1914).

7) H. Suzuki and K. Nakamura, *Bull. Chem. Soc. Jpn.*, **44**, 227 (1971).

8) I. S. Isaev, L. A. Ostashevskaya, A. A. Morozov, L. M. Beschemnova, and V. A. Koptyug, *Zh. Org. Khim.*, **7**, 2321 (1971).

9) L. I. Smith and C. O. Guss, *J. Am. Chem. Soc.*, **59**, 804 (1937).

Synthesis and Reactions of Perylenecarboxylic Acid Derivatives. VIII. Synthesis of *N*-Alkyl-3,4:9,10-Perylenetetracarboxylic Monoanhydride Monoimide

Yukinori NAGAO* and Takahisa MISONO

Department of Industrial Chemistry, Faculty of Science and Technology, Science University of Tokyo, Yamazaki, Noda 278

(Received August 6, 1980)

The condensations of 3,4 : 9,10-perylenetetracarboxylic dianhydride with alkylamines (isobutyl-, pentyl-, hexyl-, and octylamines) were spectroscopically determined. Under all of the reaction conditions employed, *N*-alkyl-3,4 : 9,10-perylenetetracarboxylic monoanhydride monoimide (**2a—d**) (alkyl=a; isobutyl, b; pentyl, c; hexyl, d; octyl) were obtained. As the reaction proceeded, the yield of **2a—d** increased at an initial stage but decreased gradually after reaching a maximum. This maximum yield of **2a—d** was: **2a**; 85—88%, **2b**; 85—89%, **2c**; 78—84%, **2d**; 79—85%. The kinetics of the reaction were also examined.

In general, 3,4 : 9,10-perylenebis(dicarboximide) derivatives are synthesized by the condensation of 3,4 : 9,10-perylenetetracarboxylic dianhydride (**1**) with amines,[1-4] and have excellent resistance to light, heat, and solvents. Some of them are used as dyes or pigments. In previous papers[5,6] we described the preparation of unsymmetrical 3,4 : 9,10-perylenebis(dicarboximide)s having different substituents on N and N′ atoms by the reaction of 3,4 : 9,10-perylenetetracarboxylic monoanhydride monoimide (**2**), which was prepared by the condensation of **1** with an alkylamine, with arylamines. In the condensation of **1** with alkylamines, higher alkylamines appeared to be favorable for the formation of **2**. This suggests a possibility of selective formation of **2** in the condensation of **1** with amines by using higher or branched alkylamines. In this paper, we report the formation of **2** from isobutyl-, pentyl-, hexyl-, and octylamines and the kinetical study of the reaction by spectroscopic techniques.

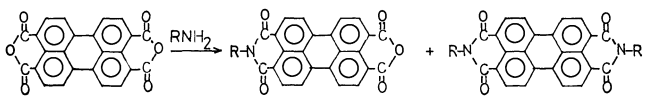

1 2a~d 3a~d

R = a; $CH_2CH(CH_3)_2$, b; $(CH_2)_4CH_3$, c; $(CH_2)_5CH_3$, d; $(CH_2)_7CH_3$

Experimental

Materials. **1** was supplied by BASF. Isobutyl-, pentyl-, hexyl-, and octylamines were obtained commercially.

Preparation of N-Alkyl-3,4 : 9,10-perylenetetracarboxylic Monoanhydride Monoimide (2a—d) and N,N′-Dialkyl-3,4 : 9,10-perylenebis(dicarboximide) (3a—d). ***2a—d***: Into a solution of an amine in an appropriate solvent was added **1** with stirring at a definite temperature. The mixture was stirred vigorously for an appropriate reaction time. The reaction conditions for each reaction are given in Table 1. The reaction mixture was acidified with 10% hydrochloric acid, and the precipitate formed was filtered, washed with water to remove amine, dissolved in 1% hot potassium hydroxide, and filtered to remove insoluble precipitates of **3a—d**. The soluble material which remained in the precipitate was again dissolved in 1% hot potassium hydroxide. The combined filtrate was heated again to dissolved the precipitate which had formed in cooling, and filtered to remove the small amount of the floating precipitate of **3a—d** which had passed through the filter. To the filtrate was added potassium chloride until 10% concentration, and the precipitated potassium salt of **2a—d** was filtered. The solid was dissolved in water and acidified with 10% hydrochloric acid, and the precipitate formed was filtered, washed with water, and dried to yield **2a—d**.

3a—d: **3a—d** was prepared by the treatment of **1** with a corresponding amine solution at 200 °C for 10 h in an autoclave. Unreacted **1** and **2a—d** were dissolved in hot 1% potassium hydroxide solution and removed from the precipitate of **3a—d**.

IR, visible spectra, mass spectra, and analysis data are given in Table 2. Samples for elementary analysis were obtained by a sublimation at 300—350 °C/3—5 mmHg.

Condensation of 1 with Amines. To a flask containing **1** 0.50 g (1.27×10^{-3} mol) and 30 ml solvent (isobutyl- and pentylamines; water, hexyl- and octylamines; water : 1-propanol=2 : 1 and 1 : 1), and maintained at the optimum temperature in a thermostat was added an amine solution 20 ml (optimum amine was dissolved in the same solvent) maintained at the same temperature with stirring. The reaction mixture showed a complicated suspension and not a homogeneous solution. This was stirred vigorously to maintain a homogeneous solution. Samples were collected at regular intervals and acidified with 10% hydrochloric acid. The precipitate was centrifuged, dried, and dissolved in 95% sulfuric acid, and the absorbances were measured. The composition of the reaction mixture were calculated from the absorbances. The optimum wavelengths (510 nm and λ_{max} of **2a—d** and **3a—d**) for the determination were decided from the standard 95% sulfuric acid solution of **1**, **2a—d**, and **3a—d**.

Measurements and Calculations. Paper Chromatography: Samples were dissolved in 1% potassium hydroxide or DMSO, placed on the paper, and developed by a mixture of equal volumes of 1-butanol, pyridine, 28% ammonia, and water.

The composition and rate ratio (K) were calculated using an IBM 370 computer. Mass spectra were recorded on a Hitachi RMU-7M mass spectrometer. Visible spectra were recorded on a Hitachi 124 spectrometer for solutions in concd sulfuric acid, and IR spectra on a Nippon Bunko IR-E spectrometer.

Results and Discussion

Preparation of 2a—d and 3a—d. Table 1 gives the reaction conditions, and the yields of **2a—d** and the by-product **3a—d**. The analytical and spectral data for **2a—d** and **3a—d** are given in Table 2. λ_{max}

TABLE 1. REACTION CONDITIONS FOR THE PREPARATION OF 3,4 : 9, 10-PERYLENETETRACARBOXYLIC MONOIMIDE (**2a—d**)

R	Amine (RNH_2) concn mol/l	Amine ml	**1** g	Temp °C	Time min	Yield/% **2a—d**		Yield/% **3a—d**	
$CH_2CH(CH_3)_2$	(0.204)	50[a]	0.500	60	220	80	**2a**	9	**3a**
	(0.304)	50[a]	0.500	60	210	80		9	
	(0.204)	100[a]	1.00	60	220	80		10	
	(0.306)	100[a]	1.00	60	210	80		10	
$(CH_2)_4CH_3$	(0.204)	50[a]	0.500	60	210	85	**2b**	11	**3b**
	(0.306)	50[a]	0.500	60	180	84		13	
	(0.204)	100[a]	1.00	60	210	85		9	
	(0.306)	100[a]	1.00	60	180	84		12	
$(CH_2)_5CH_3$	(0.306)	100[b]	1.00	60	420	73	**2c**	15	**3c**
$(CH_2)_7CH_3$	(0.306)	100[c]	1.00	60	420	75	**2d**	15	**3d**

a) Solvent; H_2O. b) Solvent; H_2O : *n*-PrOH=2 : 1. c) Solvent; H_2O : *n*-PrOH=1 : 1.

TABLE 2. ANALYTICAL AND SPECTRAL DATA FOR 3,4 : 9,10-PERYLENETETRACARBOXYLIC MONOANHYDRIDE MONOIMIDE (**2a—d**) AND 3,4 : 9,10-PERYLENEBIS(DICARBOXIMIDE) (**3a—d**)

2a—d and **3a—d** R		Found (Calcd) % C	H	N	$\lambda_{max}^{H_2SO_4}$/nm	IR(KBr)$\nu_{C=O}$/cm^{-1} Anhydride	Imide	MS/(*m*/*e*) (M^+)
2a	$CH_2CH(CH_3)_2$	74.77	3.65	3.09	581	1767	1693	447
		(75.16	3.83	3.13)		1725	1650	
2b	$(CH_2)_4CH_3$	75.41	3.84	3.81	580	1768	1695	461
		(75.48	4.12	3.04)		1727	1654	
2c	$(CH_2)_5CH_3$	75.26	4.19	3.06	580	1765	1690	475
		(75.78	4.45	2.98)		1725	1650	
2d	$(CH_2)_7CH_3$	76.32	4.99	2.98	580	1765	1690	503
		(76.33	5.00	2.78)		1725	1650	
3a	$CH_2CH(CH_3)_2$	76.41	5.02	5.51	599		1691	502
		(76.48	5.21	5.57)			1652	
3b	$(CH_2)_4CH_3$	77.45	5.60	5.11	598		1693	530
		(76.96	5.70	5.18)			1651	
3c	$(CH_2)_5CH_3$	77.31	5.98	4.96	598		1695	558
		(77.40	6.13	5.01)			1655	
3d	$(CH_2)_7CH_3$	77.51	6.50	4.70	598		1690	614
		(78.15	6.89	4.56)			1650	

TABLE 3. THE MAXIMUM YIELDS OF 3,4 : 9,10-PERYLENETETRACARBOXYLIC MONOANHYDRIDE MONOIMIDE (**2a—d**)

Amine (RNH_2) R	Temp °C	Mole ratio of amine; Amine/**1** The maximum yields of **2a—d**/% (The reaction time/min) 4	6	8	10	12	14	24
$CH_2CH(CH_3)_2$	40	83	86	85	88	82[a]	87	88
		(3600)	(1800)	(1380)	(1140)	(690)	(720)	(320)
$(CH_2)_4CH_3$	60	82	85	84	88	87	89	69
		(420)	(260)	(180)	(180)	(180)	(120)	(75)
$(CH_2)_5CH_3$	60	84	84	81	78	78	77	71
		(630)	(660)	(480)	(340)	(340)	(320)	(190)
$(CH_2)_7CH_3$	60	85	85	84	84	83	82	79
		(480)	(540)	(480)	(350)	(300)	(300)	(210)

1; 1.27×10^{-3} mol/50 ml. a) The maximum yields have not been reached.

in visible spectra of 95% concd sulfuric acid solution is 580—581 nm for **2a—d** and 598—599 nm for **3a—d**. *N*-Alkyl substituents in **2a—d** or **3a—d** caused no significant difference in the λ_{max}. IR spectra indicate that $\nu_{C=O}$ of anhydride and imide both exist in **2a—d**, and only $\nu_{C=O}$ of imide exists in **3a—d**. Mass spectra showed the corresponding molecular ion peak.

*Condensation of **1** with Amine.* In the reactions at 40—80 °C, the reaction mixture, after the amine was removed, has been proved to give no other products than the **2a—d** and **3a—d** by paper chromatography. The molar ratios, $C_A/(C_A+C_M+C_I)$, $C_M/(C_A+C_M+C_I)$,

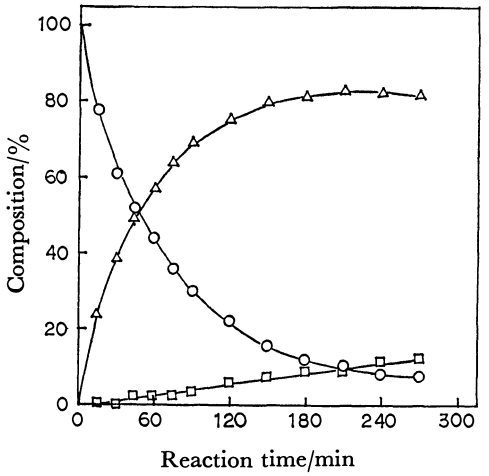

Fig. 1. Reaction of 3,4: 9,10-perylenetetracarboxylic dianhydride (**1**) with isobutylamine.
1; 1.27×10^{-3} mol/50 ml H_2O, temp; 60 °C, mole ratio (amine/**1**); 10. ○; 3,4: 9,10-Peryleneteracarboxylic dianhydride (**1**), △; *N*-Isobutyl-3,4: 9,10-perylenetetracarboxylic monoanhydride monoimide (**2a**), □; *N,N'*-Diisobutyl-3,4: 9,10-perylenebis(dicarboximide) (**3a**).

$C_I/(C_A+C_M+C_I)$, were determined by spectrometry, where C_A, C_M, and C_I are the concentrations of **1**, **2a—d**, and **3a—d**, respectively. Figure 1 shows a typical time-conversion curve showing that the reaction proceeded in successive manner. The maximum yields of **2a—d** on the time-conversion cuves, at the best temperature, are given in Table 3 for the reactions at 40—80 °C. Lower temperatures were favorable for selective preparation of **2c** and **2d**.

Plots of $\ln(C_A/C_{Ao})$, where C_{Ao} is the initial concentration of **1**, *vs.* time were linear, and the rate constants k_1 for the reaction of **1** to **2a—d**, were calculated from the slopes. Then the rate ratios $K(=k_2/k_1)$, where k_2 is the rate constant of **2a—d** to **3a—d** were calculated from Eq. 1.[5] Most of the K values in each reaction were constant. These results indicated that the reaction followed a pseudo first order process of **1**→**2a—d**→**3a—d**.

$$C_M/C_{AO} = \{1/(1-K)\}\{(C_A/C_{AO})^K - (C_A/C_{AO})\} \quad (1)$$

Figure 2 shows the variation of the maximum yield of **2a—d** and K with the number of carbon atoms in amine. As the number of carbon atoms in amine increases, the maximum yields of **2** increase in the reaction of **1** with methyl-, ethyl-, propyl-, and butylamines.[5] Though there is an increasing of the maximum yields of **2a—b** in isobutyl- and pentylamines, it is followed by an approximately constant in hexyl- and octylamines. It also indicate the pseudo first order reaction that the small K value increase the maximum yields of **2a—d**.

Figure 3 shows the variation of k_1 with the number of carbon atoms. This result shows that k_1 decreases with an increasing of the number of carbon atoms in all amines except octylamine. The reactions with methyl-, ethyl-, propyl-, and butylamines gave a similar results.[5] Lower k_1 in isobutylamine shows that the steric hindrance of alkyl group affects this reaction. The mixture

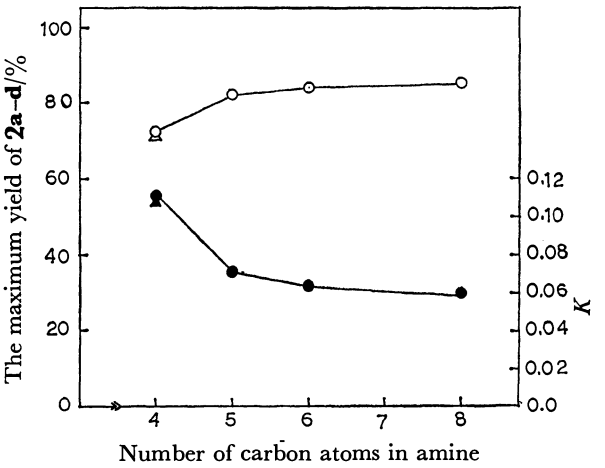

Fig. 2. Variation of the maximum yields of 3,4: 9,10-perylenetetracarboxylic monoanhydride monoimide (**2a—d**) and K with the number of carbon atoms in amine.
1; 1.27×10^{-3} mol/50 ml solvent, temp; 60 °C, mole ratio (amine/**1**); 4. The maximum yields of **2a—d**: ○; butyl-, pentyl-, hexyl-, and octylamines, △; isobutylamine. K: ●; butyl-, pentyl-, hexyl-, and octylamines, ▲; isobutylamine.

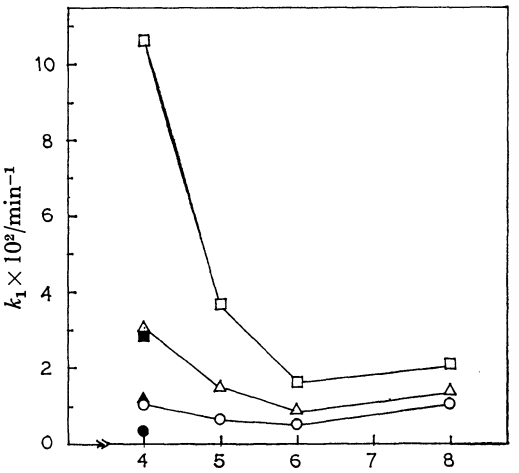

Fig. 3. Variation of k_1 with the number of carbon atoms in amine.
1; 1.27×10^{-3} mol/50 ml solvent, temp; 60 °C. Mole ratio (amine/**1**): 4: ○; butyl-, pentyl-, hexyl-, octylamines, ●; isobutylamine. 10: △; butyl-, pentyl-, hexyl-, octylamines, ▲; isobutylamine. 24: □; butyl-, dentyl-, hexyl-, octylamines, ■; isobutylamine.

of water and propanol was used for the solvent in the reaction with hexyl- and octylamines because of their poor solubility in water. Then the solvent effects have to be considered in these amines: the increasing k_1 in octylamine is explained as the effect of the solvent.

References

1) M. Kordos, *D.R.P.*, 276357, 276956 (1913).
2) T. Maki and H. Hashimoto, *Kogyo Kagaku Zasshi*, **54**, 479, 544 (1951).

3) T. Maki and H. Hashimoto, *Bull. Chem. Soc. Jpn.*, **25**, 411 (1952); **27**, 602 (1954).
4) W. Bradley and F. W. Pexton, *J. Chem. Soc.*, **1954**, 4432.
5) Y. Nagao, Y. Tanabe, and T. Misono, *Nippon Kagaku Kaishi*, **1979**, 528.
6) Y. Nagao, N. Ishikawa, Y. Tanabe, and T. Misono, *Chem. Lett.*, **1979**, 151.

Catalysis of Metal(II) Acetate-2,2'-Bipyridine Complexes in the Aldol Condensations

Kazuo IRIE and Ken-ichi WATANABE*

Department of Chemistry, Faculty of Science, Tokyo Metropolitan University, Fukazawa, Setagaya-ku, Tokyo 158

(Received September 30, 1980)

The rate of the condensation of benzaldehyde with excess acetophenone catalyzed by Co(II) acetate-2,2'-bipyridine complex was obtained by GLC analysis. The rate increased in proportion as the amount of the complex catalyst. 2,2'-Bipyridine ligand in the Co(II) complex enhanced the catalytic activity remarkably, though the ligand itself had no activity. When the molar ratio of Co(II): bpy was 1 : 1 or 1 : 2, the highest activity was observed. The activation energy of the complex (1 : 1) catalyzed reaction was calculated as 13.7 kcal/mol. The catalysis of the complex behaved like a base catalyst. Briefly, the relation of the complex catalyzed aldol condensations with the enzymatic reaction of Class II aldolase is also described.

The aldol condensation reactions are generally catalyzed by strong acids or bases. In preceding paper, we have reported that many kinds of the condensation are catalyzed by metal(II) complexes under neutral conditions and afford only cross condensation products, α,β-unsaturated ketones, in satisfactory yields.[1,2] The potent catalysts are complexes of 2,2'-bipyridine(bpy) and the first-row transition metal acetates, particularly Co(II), Ni(II), Cu(II), and Zn(II), and DMF is an excellent solvent.

In this paper, we describe the kinetics of the condensation of the benzaldehyde with acetophenone in DMF containing $Co(OAc)_2$–bpy complex and features of M(II)acetate–bpy complex. As this study might be connection with the catalysis of Class II aldolase governing the aldol condensation in microorganism, some considerations are also described briefly.

Results and Discussion

Catalytic Behavior of the Metal(II) Complexes. In order to examine the catalytic behavior of the metal complexes in the reaction, the condensations of benzaldehyde with acetophenone(excess) in the presence of $Co(OAc)_2$–bpy complex were carried out. In the case of this reaction system, dehydration of the addition product occurred immediately to give 1,3-diphenyl-2-propen-1-one(chalcone) without any by-product. The yields of chalcone were determined by GLC analysis.

$$PhCH(=O) + CH_3C(=O)Ph \xrightarrow[DMF]{Co(OAc)_2\text{-bpy}} PhCH{=}CHC(=O)Ph \quad \text{(Chalocone)}$$

The correlation of the yield(%) with reaction time was observed as a curve line shown in left hand of Fig. 1 which is a typical example. The ln plot of $(a-x)$ (a: initial concentration of the aldehyde, x: concentration of the chalcone produced) *versus* reaction time was shown as a straight line (right hand in Fig. 1). This meant the first order reaction for the concentration of the aldehyde used. The observed rate constant (k'_{obsd}) was calculated from the slope. Thus similar reaction profile was observed in other examples as mentioned below, and therefore, these rate constants were compared to elucidate the catalytic activity.

Firstly, the dependence of k'_{obsd} on the concentration of the complex was examined. The reaction and the catalyst used were similar to that mentioned above, and the concentrations of the catalyst employed were 8 mmol/l, 4 mmol/l, and 2 mmol/l to that of the aldehyde 200 mmol/l. The $k'_{obsd}\times 10^5$ (s^{-1}) were 12.3, 2.66, and 0.65, respectively, and the reaction rate was dependent apparently on the concentration of the complex catalyst. Thus, it has been shown that Co(II)–bpy complex has worked as true catalyst in this reaction.

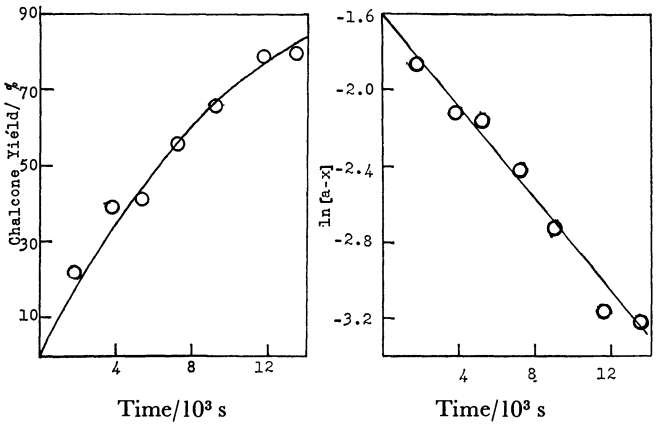

Fig. 1. Reaction profile of the aldol condensation catalyzed by $Co(OAc)_2$–bpy(1: 1)complex in DMF at 82 °C. [catalyst]=0.008 mol/dm³, [benzaldehyde]=0.2 mol/dm³, [acetophenone]=4 mol/dm³.
a: Initial concentration of the aldehyde, x: concentration of the chalcone produced.

Next, the effect of the molar ratio of bpy to the Co(II) on the catalytic activity was examined in the similar reaction as was shown in Table 1. According to the table, it was observed that the activities increased with

Table. 1 Effect of the molar ratio of bpy to Co (II) on the rate constants of the aldol condensation[a)]

$cat=\frac{(bpy)_n}{Co(II)}$	$k'_{obsd}\times 10^5/s^{-1}$
$n=0$	1.26
$n=0.5$	4.83
$n=1$	12.3
$n=2$	10.9
$n=3$	2.65

a) The reaction of benzaldehyde with acetophenone[b)] was carried out in DMF at 82 °C. b) [cat]=0.008 mol/dm³, [aldehyde]=0.2 mol/dm³, [ketone]=4 mol/dm³.

an increase in the amount of bpy to a certain extent. When the molar ratio was $n=1$ or $n=2$, the highest activity was observed. However, when the molar ratio increased to $n=3$, the activity decreased remarkably. The suppressed reaction can be explained in terms of that the molar ratio of $n=3$ is enough amount to occupy the residual vacant coordination sites in Co(II) and that bpy as bidentate ligand can coordinate to Co(II) more easily than the substrates as monodentate ligand. Therefore, the assumption may be made that the reaction proceeds *via* a mixed ligand complex between the substrates and Co(II)–bpy$_n$ complexes.

Furthermore, the effect of the reaction temperature on the reaction was examined in the similar reaction mentioned above. As the result, the $k'_{obsd}\times 10^5$ (s^{-1}) were 1.27 at 62 °C, 2.53 at 72 °C and 12.3 at 82 °C, respectively. Thus, the correlation of the log k'_{obsd} and three different reaction temperatures was shown as a straight line in Fig. 2 and the activation energy was calculated as 13.7 kcal/mol.

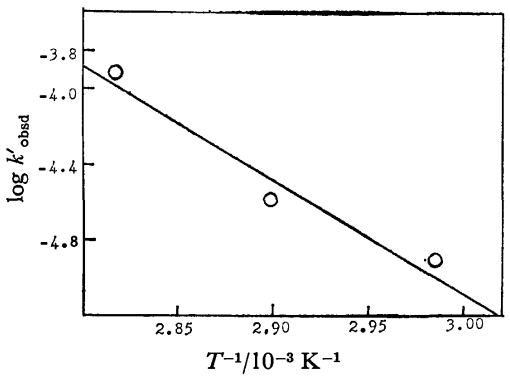

Fig. 2. Arrhenius plot for the aldol condensation of benzaldehyde with acetophenone catalyzed by Co(OAc)$_2$–bpy(1: 1) complex.
[cat.]=0.008 mol/dm^3, [aldehyde]=0.2 mol/dm^3, [ketone]=4 mol/dm^3 in DMF.

Effects of Kind of the Ligand. The complex catalyzed aldol condensations are largely affected by the kind of ligand in the complex, and such ligand as bpy or 1,10-phenanthroline is fairly effective to give the reaction products in high yield.[2] Therefore, the effects of ligands on the catalytic activity of the Co(II) complexes were examined in detail at 82 °C in the similar reaction system mentioned above. The k'_{obsd} of the reactions catalyzed by Co(II)–L(bpy, en, 4-dm-bpy, and 6-dm-bpy) complexes and by Co(OAc)$_2$ itself are shown in Table 2.

TABLE 2. LIGAND EFFECT ON THE RATE CONSTANTS OF THE ALDOL CONDENSATION

Cat[b,c]	$k'_{obsd}\times 10^5/s^{-1}$
Co(II)	1.26
Co(II)–bpy	12.3
Co(II)–en	1.41
Co(II)–4-dm-bpy	1.49
Co(II)–6-dm-bpy	0.33
Mn(II)–bpy	0.85

a) The reaction of benzaldehyde[b] with acetophenone[b] was carried out in DMF at 82 °C. b) [cat]=0.008 mol/dm^3, [aldehyde]=0.2 mol/dm^3, [ketone]=4 mol/dm^3. c) The molar ratio of the ligand molecule to anhydrous Co(II)acetate is 1.

It is observed that the catalytic activity of Co(II)–bpy complex in the reaction increases remarkably in comparison with the k'_{obsd} of Co(OAc)$_2$, while bpy itself has no catalytic activity at all. The activity of Co(II)–ethylenediamine(en) complex is almost similar to that of Co(OAc)$_2$. The effect of 4,4′-dimethyl-2,2′-bipyridine ligand(4-dm-bpy) containing methyl groups as electrodonative substituent is surprisingly low. Furthermore, 6,6′-dimethyl-2,2′-bipyridine ligand(6-dm-bpy) deactivates the catalytic activity of the complex extremely probably owing to steric hindrance of the ligand molecule to the reaction. With regard to the enhanced effect of 2,2′-bipyridine on the metal complex catalysts, seveal studies on other organic catalytic reactions were already reported.[3] According to their accounts, the net plus charge of M(II) will increase by π-back donation of M(II) to 2,2′-bipyridine in the complex, then the resulting enhanced coordination force of substrates to M(II) naturally accelerate the reactions. The ligand effects on the aldol condensations are also explainable by the similar π-back donation between M(II) and bpy. Table 2 also shows low catalytic activity of Mn(II)–bpy complex in comparison with that of Co(II)-bpy complex. It is assumed that this result is due to the different stabilities of general complexes in Irving-Williams series.[4]

The Feature of the Catalysis. In order to show a feature of the complex catalysts, two different reactions catalyzed by the complex catalyst were investigated. One example is the condensation of benzaldehyde with 2-butanone. It was known that the base-catalyzed reaction gave, preferentially, the condensation product at C_1 of the ketone, while the acid-catalyzed reaction occurred preferentially at C_3.[5] In our reaction system

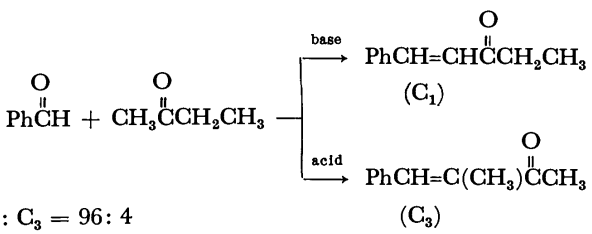

C_1: C_3 = 96: 4

with Co(OAc)$_2$–bpy complex, the regioselective condensation product at C_1-position was obtained in high yield as well as that with base catalysts.

Another reaction, the decomposition of 4-hydroxy-4-methyl-2-pentanone, which has been also known to take place only by the use of base catalysts,[6] was examined in the presence of Zn(OAc)$_2$–bpy (1 : 1) complex in the NMR tube. It was observed that the reaction proceeded smoothly as follows:

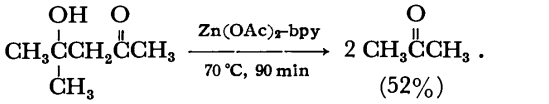

These findings show that the complex catalysts behave as a base catalyst. Both reactions do not commonly

proceed in the presence of bpy itself. Accordingly, it is assumed that the basic function in the complex catalyst is not by bpy ligand but by the counter ion, AcO^-, of the metal salts. It is widely recognized that the metal ion is considered as an acid and the counter ion is considered as a base.

Consideration of the Reaction Process. It has been known that enolization of ketone is the first stage in the aldol condensation catalyzed by acid or base.[5] In our reaction system with M(II)–bpy complexes, H-D exchange reaction of acetophenone with deuterium oxide in the presence of $Zn(OAc)_2$–bpy catalyst was carried out in order to ascertain the formation of enolate

$$PhCCH_3 \xrightarrow[70\,^\circ C,\ 18\,h]{Zn(II)\text{-}bpy} PhC{=}CH_2 \xrightarrow{D_2O} PhCCH_nD_{3-n} \quad (57\%)$$

anion. The reaction was remarkably catalyzed and the ratio of H-D exchange was 57% determined by NMR. When bpy itself was used, however, the reaction did not proceed.

At the second stage, it has been known that the reaction of aldehyde with the enolated ketone affords β-hydroxy ketone (aldol type product). However, the compound is easily dehydrated to give α,β-unsaturated ketone. In order to ascertain the formation of the aldol type product, the condensation of benzaldehyde with acetone in the place of acetophenone was carried out in the presence of Co(II)–bpy complex (1 : 1) at 80 °C in DMF for 3 h. The reaction gave yellow oil that was analyzed by ^{1}H-NMR and GC-MS spectra, and two kinds of product, 4-hydroxy-4-phenyl-2-butanone(**1**) and benzylideneacetone(**2**) were determined as follows:

$$PhCH + CH_3CCH_3 \xrightarrow[DMF,\ 80\,^\circ C,\ 3\,h]{Co(II)\text{-}bpy} PhCHCH_2CCH_3 + PhCH{=}CHCCH_3$$

1 **2**

25%	11%
NMR: 2.10 (CH_3)	: 2.28 (CH_3)
MS: 164 (M^+)	: 146 (M^+)

When the similar reactions were carried out for longer time, it was observed that the yields of **1** decreased with the increasing yields of **2**. Consequently, it was assumed that the reaction afforded the product **1** in the first instance which was succesively dehydrated to give the product **2** as well as acid or base catalyzed reaction.

Consideration of Coordination. A coordination of aldehyde to the metal ion was examined by absorption spectroscopy. A solution of nickel(II) acetate in DMF showed an absorption maximum at 430 nm as shown in Fig. 3. When bpy was added to this solution, an absorption maximum appeared at 630 nm, which was attributed to the d-d band of Ni(II)–bpy chelation. When benzaldehyde was added to this solution of Ni(II)–bpy complex, the absorption maximum at 630 nm shifted to 622 nm. The fact might suggest that the carbonyl oxygen atom of aldehyde entered the first coordination sphere of Ni(II). While, no similar shift was observed by addition of acetophenone to the Ni(II)–bpy system.

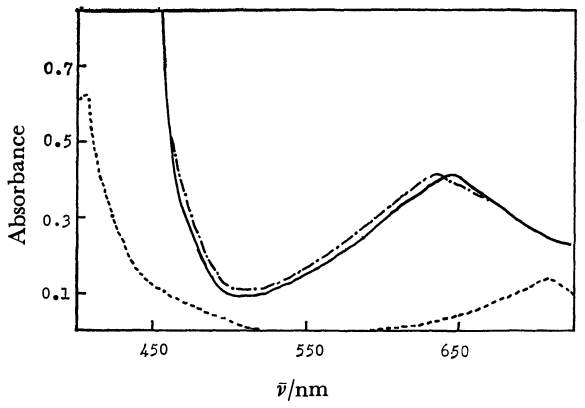

Fig. 3. Electronic absorption spectra of nickel (II) acetate–bpy–benzaldehyde and nickel (II) acetate–bpy–acetophenone complexes in DMF. $[Ni(OAc)_2]=0.060$ mol/dm^3, $[bpy]=0.060$ mol/dm^3, $[aldehyde]=0.075$ mol/dm^3, $[ketone]=0.075$ mol/dm^3.
·····: $Ni(OAc)_2$ (λ_{max} 430 nm), ——: $Ni(OAc)_2$–bpy (λ_{max} 630 nm) and $Ni(OAc)_2$–bpy acetophenone (λ_{max} 630 nm), —·—: $Ni(OAc)_2$–bpy–benzaldehyde (λ_{max} 622 nm).

Since acetophenone was enolized by M(II)–bpy complex, the interaction between acetophenone and M(II) seemed to be extremely weak. In other words, the ketone may be located in far distance from the metal ion. Considering in connection with the results described above, the aldol condensation reaction may proceed *via* a coordination of aldehydes to the M(II).

It has been known that aldol condensation in biological system are catalyzed by aldolase enzymes, Class I and II.[7] Class II aldolase is a metalloenzyme containing Zn(II) in the active site. In the reaction of Class II aldolase, however, catalysis of the enzyme has not been elucidated enough although some models of the reaction mechanism were presented by biochemists.[8–12] Therefore, our reaction system with Zn(II)–bpy complex may present a new example for understanding of the Zn(II) catalysis in Class II aldolase from a side of organic catalytic reactions.

Some information withdrawn from our study on the catalysis of M(II)–bpy complex are summerized as follows:

(1) 2,2'-Bipyridine ligand in the Co(II) complex enhanced the catalytic activity remarkably, though the ligand itself had no activity.

(2) M(II)–bpy complex showed a feature of basic catalyst. Such effect of (1) may be important in the metalloenzyme if there is interaction between the metal ion and imidazole ring of a histidine residue, since imidazole as well as bpy can form π-bonding by coordinating to the M(II). Ingram reported that Class II aldolase showed a basic catalysis.[8] Further, it was suggested that the basic group may be an appropriately located β-COO^- of aspartic acid or γ-COO^- of glutamic acid.[8] However, from a viewpoint of our metal(II)–bpy complex catalysis(2), another suggestion that basic group is the counter ion of the metal ion being located at active center of the metalloenzyme may be permitted. Further, a detail investigation of a model reaction of Class II aldolase is now in progress.

Experimental

Kinetics of Aldol Condensation. In order to study the rate of the aldol condensation of benzaldehyde with acetophenone, a sample of catalyst (for example; $Co(OAc)_2$ (0.0142 g, 0.08 mmol) and 2,2′-bipyridine (0.0125 g, 0.08 mmol)) was weighed into a volumeric flask (10 ml) and DMF (3 ml) was added to the flask to dissolve the catalyst. The solution was stirred at room temperature for 21 h. Benzaldehyde (0.212 g, 2 mmol) and acetophenone (4.8 g, 40 mmol) were poured in this flask and DMF was added to the mark. The solution was poured in each ampoule (1 ml×8). The sealed ampoules were heated at 82 °C and were withdrawn from time to time and then were quenched in a freezer. *p*-MeO–$C_6H_4COCH_2C_6H_5$ as an internal standard was added to the solution in opened ampoules which were analyzed by GLC (column temp at 220 °C, 1 m, Carbowax 20 M). The solution showed only one product (chalcone) other than unreacted benzaldehyde and acetophenone. The amount of chalcone was determined by comparing the relative peak area of chalcone *vs.* the internal standard with those of the calibration chart.

Regioselectivity in the Reaction of Benzaldehyde with 2-Butanone. A DMF (5 ml) solution of benzaldehyde (1.875 mmol), 2-butanone (5 ml), $Co(OAc)_2$ (0.300 mmol), and 2,2′-bipyridine (0.300 mmol) was stirred at a reflux temperature for 6 h. After the completion of the reaction, the solvent was removed *in vacuo* and the residue was extracted with ether–water system. The organic layer was dried over anhydrous sodium sulfate and was evaporated to give a mixture of 1-phenyl-1-penten-3-one (a) and 3-methyl-4-phenyl-3-buten-2-one (b) in 95% yield. The ratio (a) : (b) was 96 : 4 which was determined by NMR spectra.

Decomposition Reaction of 4-Hydroxy-4-methyl-2-pentanone (DAA). DAA (2 mmol) was added to a solution of anhydrous zinc acetate (0.1 mmol) and 2,2′-bipyridine (0.1 mmol) in DMSO-d_6 (0.09 ml) in NMR tube. The tube was sealed off and heated at 70 °C for 90 min. For the calculation of the amount of unreacted DAA determined by NMR, 1,1,2,2-tetrachloroethane as an internal standard was added to the reaction mixture and DAA was decomposed in 52%.

H-D Exchange of Acetophenone. A solution of acetophenone (1.0 mmol), $Zn(OAc)_2$ (0.1 mmol), D_2O (2.75 mmol), and CD_3CN (0.4 ml) in sealed NMR tube was heated at 70 °C for 18 h. The integration ratio of methyl proton *versus* aromatic proton was determined by NMR and the H-D exchanged ratio of methyl group of acetophenone was calculated in 54%.

References

1) K. Irie and K. Watanabe, *Chem. Lett.*, **1978**, 539.
2) K. Irie and K. Watanabe, *Bull. Chem. Soc. Jpn.*, **53**, 1366 (1980).
3) G. W. Watt and D. G. Upcharch, *J. Am. Chem. Soc.*, **90**, 914 (1968); P. R. Huber, R. Griesser, B. Prijs, and H. Sigel, *Europ. J. Biochem.*, **10**, 238 (1969).
4) H. Irving and R. J. P. Williams, *J. Chem. Soc.*, **1953**, 3192.
5) A. T. Nielsen and W. J. Houlihan, *Org. React.*, Vol. 16 (1968).
6) K. Yonai, S. Okazaki, Y. Fukuda, and K. Tanabe, *Nippon Kagaku Zasshi*, 815 (1971).
7) B. L. Horecker, O. Tsales, and C. Y. Lai, "The Enzymes," 3rd ed, ed by P. D. Boyer, Academic Press, New York and London (1972), Vol. 7, pp. 213—258.
8) J. M. Ingram, *Can. J. Biochem.*, **45**, 1909 (1967).
9) R. D. Kobes, R. T. Simpson, B. L. Vallee, and W. J. Rutter, *Biochem.*, **8**, 585 (1969).
10) D. E. Morse and B. L. Horecker, *Advances in Enzymology*, **31**, 125 (1968).
11) A. S. Mildvan, R. D. Kobes, and W. J. Rutter, *Biochem.*, **10**, 1191 (1971).
12) J. F. Riordan and P. Christen, *Biochem.*, **8**, 2381 (1969).

Restricted Rotation Involving the Tetrahedral Carbon. XXXVIII. Barriers to Rotation and Population Distributions of 9-(8-Methyl-1-naphthyl)fluorene and Its 1-Methyl Derivative[1)]

Teruo Mori and Michinori Ōki*

Department of Chemistry, Faculty of Science, The University of Tokyo, Hongo, Bunkyo-ku, Tokyo 113

(Received October 31, 1980)

The title compounds were prepared to see the effect of an 8-methyl group on the populations and the barriers to rotation of rotamers. As expected, the substituent destablized the *syn* conformation to a considerable extent, although the extent appeared to be a little less than that of a 2-*t*-butylphenyl group. Atropisomers of 1-methyl-9-(8-methyl-1-naphthyl)fluorene were isolated. The barriers to rotation were discussed with reference to related compounds.

In one of the previous papers, we have demonstrated that the conformational equilibrium of 9-(2-*t*-butylphenyl)fluorene is lop-sided: since the ground state of the *ap* conformation is so energy-rich that it rotates slowly at room temperature, although it can be made, to form the corresponding *sp* isomer, of which isomerization to the *ap* is practically nonexistent at room temperature.[2)] This finding aroused our interest in investigating the effect of an 8-methyl-1-naphthyl group in the 9-position of fluorene on the barriers to rotation and population equilibriums, because the bulkiness of a *t*-butyl group is often compared with that of an 8-methyl-1-naphthyl substituent: the compound may give stable atropisomers. It is also interesting to see how atropisomers become stable when we introduce a methyl group into 1-position of the fluorene ring, since such an operation is known to raise the barriers to rotation to a considerable extent.[3,4)]

Syntheses of the compounds were carried out in the following way. Fluorenones were added to a Grignard or a lithium compound derived from 1-bromo-8-methylnaphthalene (**1**) and the resultant 9-aryl-9-fluorenols (**2** and **3**) were reduced with hydriodic acid at room temperature to afford 9-(8-methyl-1-naphthyl)fluorenes (**4** and **5**).

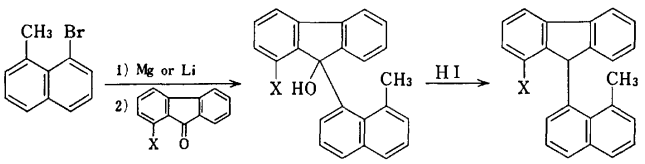

1 2 : X=H 3 : X=CH3 4 : X=H 5 : X=CH3

The syntheses afforded an isomer exclusively: **2** gave *syn*-**4** whereas **3** gave *anti*-**5**. Thus *syn*-**4** had to be converted to *anti*-**4** to examine the barrier to rotation. It was accomplished by taking advantage of the fact that protonation after lithiation of the 9-position proceeds from the less hindered side.[2,5)]

This paper reports the findings on the equilibriums of rotamers of 9-(8-methyl-1-naphthyl)fluorene and its 1-methyl derivative in addition to the syntheses and compares the barriers and populations of rotamers, which are affected by the substituents, with related compounds.

Experimental

syn-9-(8-Methyl-1-naphthyl)fluorene (syn-**4**). A solution of 279 mg (1.26 mmol) of 1-bromo-8-methylnaphthalene (**1**)[6)] in 30 mL of tetrahydrofuran was refluxed with 33 mg (1.4 mmol) of magnesium until most of the magnesium disappeared (*ca.* 3 h). Fluorenone (346 mg or 1.92 mmol) was added to the solution in the form of powder and the whole was refluxed for 2 h. The resultant mixture was treated in a usual manner and the desired product (**2**) was obtained in 28% yield. ^{1}H NMR ($CDCl_3$, δ): 1.40 (3H, s), 2.17 (1H, s), 7.0—7.8 (13H, m), 8.67 (1H, q). This compound must exist as an *anti* form from the ^{1}H NMR data.

A solution of 100 mg of **2** in 20 mL of acetic acid was mixed with 3 mL of 57% hydriodic acid and stirred for 6 h at room temperature. The solution was poured into water, treated with aqueous sodium dithionite and then with aqueous sodium hydrogencarbonate, and extracted with ether. The product was chromatographed on silica gel to afford *syn*-**4**, oil, in 90% yield. The purity was checked by a ^{1}H NMR spectrum and a high resolution mass spectrum. MS: found (M^+) 306.1399; calcd for $C_{24}H_{18}$, 306.1409. ^{1}H NMR ($CDCl_3$, δ): 3.17 (3H, s), 6.40 (1H, s), 6.62 (1/2H, d), 6.73 (1/2H, d), 7.0—7.8 (13H, m).

anti-9-(8-Methyl-1-naphthyl)fluorene (anti-**4**). A solution of 20 mg of *syn*-**4** in 0.4 mL of tetrahydrofuran was mixed with 0.5 mmol of butyllithium in hexane at room temperature. The mixture was heated at 60 °C for 3 h and was quenched with trifluoroacetic acid. The mixture was quickly treated in a usual manner and the product was purified by TLC on a silica gel plate at 0 °C. The operation afforded a mixture of *syn*-**4** and *anti*-**4** (*ca.* 3 : 7), which was directly used for the measurements of rates of isomerization. The following ^{1}H NMR data ($CDCl_3$, δ) were obtained by subtracting the signals due to *syn*-**4**: 1.32 (3H, s), 5.40 (1H, s).

anti-1-Methyl-9-(8-methyl-1-naphthyl)fluorene (anti-**5**). A mixture of 1.2 g (5.4 mmol) of **1** and 95 mg (14 mmol) of lithium in 20 mL of ether was refluxed until a reddish brown solution was obtained (*ca.* 2 h). To the solution was added 1.12 g (5.8 mmol) of 1-methyl-9-fluorenone[7)] in 20 mL of benzene over a period of 20 min. The solution was refluxed for 3 h and treated in a usual manner. The product was purified by silica-gel chromatography to afford 51% oil (**3**), which existed as *anti* conformation only as judged from its ^{1}H NMR spectrum ($CDCl_3$, δ): 1.44 (3H, s), 1.54 (3H, s), 2.30 (1H, s), 6.7—7.9 (12H, m), 8.76 (1H, q).

A solution of **3** in acetic acid was treated with hydriodic acid as described above to afford *anti*-**5**, mp 126—128 °C, in 93% yield. Found: C, 93.99; H, 6.10%. Calcd for $C_{25}H_{20}$: C, 93.71; H, 6.29%. ^{1}H NMR ($CDCl_3$, δ): 1.32 (3H, s), 1.71

(3H, s), 5.36 (1H, s), 6.7—8.0 (13H, s). ^{13}C NMR ($CDCl_3$, ppm from TMS): 19.3, 21.5, 59.8, 118.0, 120.2, 123.8, 126.8, 127.0, 127.7, 129.0, 129.4, 129.6, 130.4, 133.1, 134.4, 134.9, 135.0, 135.6, 135.9, 139.8, 146.3, 148.9.

syn-*1-Methyl-9-(8-methyl-1-naphthyl)fluorene* (syn-**5**). An equilibrium mixture of *syn* and *anti* forms of **5** was obtained by the kinetic study described below. The solution was evaporated and the residue was crystallized from dichloromethane-hexane. Mp 123—125 °C. Found: C, 93.66; H, 6.04%. Calcd for $C_{25}H_{20}$: C, 93.71; H, 6.29%. ^1H NMR ($CDCl_3$, δ): 1.90 (3H, s), 3.23 (3H, s), 6.47 (1H, s), 6.8—8.0 (13H, m). ^{13}C NMR ($CDCl_3$, ppm from TMS): 19.4, 27.2, 50.7, 118.0, 120.0, 124.8, 125.3, 126.2, 126.8, 127.1, 127.4, 128.5, 128.9, 130.8, 132.1, 133.3, 134.6, 135.7, 137.3, 140.2, 141.3, 147.6, 149.8.

Spectral Measurements. ^1H NMR spectra were measured on a Hitachi R-20B spectrometer and ^{13}C NMR with a JEOL FX-60 spectrometer. ^{13}C NMR spectra of *syn*- and *anti*-**5** were obtained at −20 °C to avoid isomerization of the latter during the measurement. A high resolution mass spectrum was obtained with a JEOL JMS-D-300 spectrometer.

Measurements of Rates of Rotation. Kinetic measurements were carried out with solutions of chloroform-*d*. Measurements which were necessary for both determination of the rates of rotation and equilibrium constants were carried out using ^1H NMR spectra where appropriate. In the cases where one isomer was so predominant that the errors involved in the measurements by the NMR spectra were large, a Waters HPLC instrument which was equipped with a UV detecter was used for the analysis. The correspondence of the peak areas in HPLC to the real populations was checked by comparing those with the populations obtained by the NMR spectra, where the latter was applicable. The correspondence was found to be satisfactory without considering the difference in absorption strengths per molecule of the isomers. The kinetic data were treated as a reversible unimolecular reaction to afford satisfactory results. The errors in rate constants are given for 95% confidence intervals in the least squares method, adopting t-distribution.

Results and Discussion

The first problem we wish to discuss is the nomenclature of the conformers concerned. If the fluorene ring is unsubstituted or symmetrically substituted, there is no problem in designating the rotational isomers by the present IUPAC rule E.[8] Namely we do have *ap* and *sp* isomers of 9-(8-methyl-1-naphthyl)fluorene (**4**) and they involve no ambiguities. The same is true for 9-(1-naphthyl)fluorene (**6**) and 9-(2-methyl-1-naphthyl)-fluorene (**8**). However, as soon as a methyl group is introduced into the 1-position of fluorene, we come across a difficulty. One may designate the conformation of 1-methyl-9-(8-methyl-1-naphthyl)fluorene (**5**), which corresponds to the *ap* conformation of **4**, as $\pm sc$. However, there is another conformation which is $\pm sc$ in this case: if we consider a conformation in which the 8-methyl-1-naphthyl group eclipses the bond connecting C_9 and an aromatic carbon of which ring bears no substituent, the conformation is also $\pm sc$ if the prefered side, in the sequence rule,[9] of the naphthyl moiety is close to the 1-methyl group. This type of ambiguity arises always when a conformation involves at least one chiral center. We must specify the configuration of the chiral center, in addition to the conformation, to avoid ambiguities. Thus the conformation becomes $[-sc(R)]+[+sc(S)]$.[10] In practice, however, comparing the *ap* form of **4** and $[-sc(R)]+[+sc(S)]$ form of **5** may be too complicated in writing and may cause confusion. Therefore, in designation of conformations concerned, we prefer to commonly use "*syn*" for the conformation in which a prefered group in the sequence rule is synclinal to the C_9–H bond (C_9–OH in the case of **2** and **3**). This nomenclature is conventional but is more convenient in the present case.

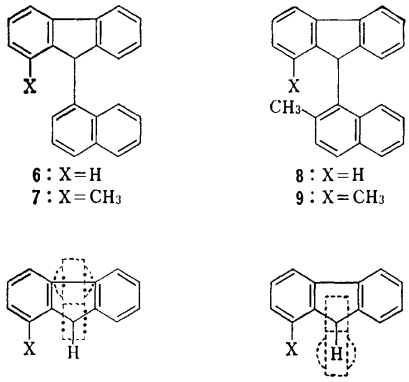

6: X=H
7: X=CH3
8: X=H
9: X=CH3

ap or $-sc(R)$ *sp* or $+ac(R)$

(Only one enantiomer is shown when X is CH_3.)

9-(8-Methyl-1-naphthyl)-9-fluorenols. The assignment of the conformation is straightforward, because the methyl group substituting the naphthyl moiety is expected to give a signal at a high magnetic field in the ^1H NMR spectrum if it is *anti* and that, in the *syn*, it must give a signal at a lower field. It is interesting to note that the *anti* isomer overwhelms in **2** and **3** in contrast to the fact that, in 9-(2-*t*-butylphenyl)-9-fluorenol, the *syn* isomer is overwhelming.[2] The distribution of conformers in **2** and **3** is similar with the cases of other 9-(2-alkylphenyl)-9-fluorenols. Probably the repulsive interaction between the *t*-butylphenyl group and the fluorene ring is much more severe than that between the 8-methylnaphthyl group and the fluorene. This is reflected in the equilibrium constants of the hydrocarbons also (*vide infra*).

It is well documented that substitution of the 9-hydrogen in 9-arylfluorenes by other groups decreases the barrier to rotation.[11] Thus it is not possible to isolate rotational isomers of 9-(2-methyl-1-naphthyl)-9-fluorenol (**10**), although rotamers of its parent hydrocarbon (**8**) were isolated.[2,12] However, Ford *et al.* reported that the introduction of a methyl group into the 1-position of the fluorene ring of **10** caused the increase in the rotational barrier (in **11**) and suggested that the barrier would be over 26 kcal/mol (1 kcal= 4.18 kJ):[3] the value is high enough for isolation of rotamers at room temperature. Indeed, Kajigaeshi *et al.* were able to isolate one of the rotamers of a benzo-annelated derivative of **10**, the barrier ($\Delta G^{\ddagger}_{323}$) being 24.6 kcal/mol.[13]

We found a similar situation for **3**, though to a lesser degree of enhancement of the barrier. The ^1H NMR spectra of the compound suggested the presence of a negligible amount of the *syn* isomer and overwhelming population of the *anti* isomer at room temperature.

Table 1. Kinetic and thermodynamic data for the rotation about the C_9–C_{Ar} bond of 9-(1-naphthyl)fluorenes and 9-(2-*t*-butylphenyl)fluorene

Comopund	Substituent		Rate Constant for Rotation (*anti*→*syn*)[a] ($\times 10^5$ s^{-1})	$\Delta G^{\ddagger}$[a] kcal mol^{-1}	Equilium Constant[a] (*syn*/*anti*)	Reference
	Fluorene	Naphthalene				
12	—	—	39(272)	20.1(307)[b]	>100(273)	2
4	H	8-CH_3	5.6±4.2(307) 170±20(327)	23.9(307)	25[c]	This work
5	1-CH_3	8-CH_3	0.80±0.03(307) 11.5±0.7(327)	25.2(307)	33[c]	This work
6	H	H		17.4(307)[b] 17.7(307)[b]	2[d] 2(303)	18 12
7	1-CH_3	H		21.4(433)	2[e]	4
8	H	2-CH_3		29.2(393)	1(373)	12
9	1-CH_3	2-CH_3		33.3(429)	1(429)	3

a) Numericals in parentheses are temperatures in Kelvin. b) Calculated from available data. c) These values were independent of temperatures examined. d) At room temperature and below. e) At room temperature.

However, on raising the temperature, we found that the signal due to the methyl group broadened considerably at about 120 °C to suggest that coalescence of two signals took place. The barriers to rotation in **3** is not certain, because we could not detect the signal due to the *syn* isomer, but is of the order of 20 kcal/mol.

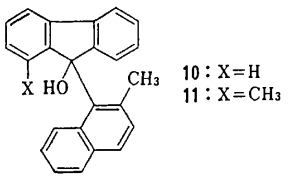

10 : X=H
11 : X=CH_3

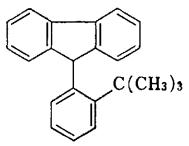

12

Populations of 9-(8-Methyl-1-naphthyl)fluorene Rotamers. Assignment of the conformations was carried out both from the ^1H NMR features as described above and from the mode of protonation. It is interesting to note that the unstable *anti* form of **5** was prepared preferentially, whereas the stable *syn*-**4** was the sole product in the preparation of **4**. This must be caused because **5** gave the kinetially controlled product owing to its high barrier to rotation whereas **4** gave the thermodynamically controlled product due to its low barrier to rotation. Although the mechanisms of the reaction are not well understood, the reaction conceivably proceeds *via* an iodide followed by a reaction with complex iodide anions.[14] In both cases, a bulky iodide ion is involved in the reaction and the approach from the less hindered side is favored to produce *anti*-**5**.

Equilibrium constants between the rotamers of **4** and **5** are summarized in Table 1 together with those of related compounds. From the molecular models, the 8-methyl group is expected to give severe steric interaction with the fluorene ring when the molecule has the *anti* conformation. This effect is apparent if one compares the equilibrium constants of **4** and **5** with those of the compounds which do not possess a methyl in the 8-position but do or do not carry a methyl in a position other than 8 of the naphthyl group. The ground states of **4** and **5** are raised to a considerable extent.

If one compares the equilibrium constants of **4** and **5** with that of 9-(2-*t*-butylphenyl)fluorene (**12**), however, one notices an interesting point. That is, although the steric effect of the *t*-butyl group given to the *o*-position of a phenyl group is often compared with that of the 8-methyl group given to the 1-position of naphthalene and the latter is often referred to be larger than the former because of rigidity, the data in Table 1 suggest that the ground state of the *anti* conformations of **4** and **5** are, relatively speaking, more stable than that of *anti*-**12**.

This is also reflected to the ^{13}C–^1H coupling constants of the NMR spectra: the coupling constants are 115.4 Hz[2] and 120.2 Hz for the *anti* forms of **12** and **5**, respectively. The coupling constants in the *syn* conformations of 9-(2-alkylphenyl)fluorenes are reported to be 128±1 Hz[2] and the *syn* form of **5** is no exception. The ^{13}C–^1H coupling constant is known to reflect the *s*-character of the carbon orbital:[15] the smaller coupling constant is due to higher *p*-character of the bonding orbital concerned. The geometry of the 9-carbon of the fluorene ring is more flattened than others in the *anti* conformation due to the steric compression between the fluorene ring and the *t*-butyl or 8-methyl group. The ^{13}C chemical shift data support the idea that the C_9 configuration has moved toward the trigonal in the *anti*-conformation of **5**: the chemical shift of the C_9 in *anti*-**5** is 9.1 ppm down field relative to that in *syn*-**5**. Therefore the anomaly in the *anti* conformations must be attributed to the steric strain rather than the electronic effect.

The smaller J_{C-H} of the *t*-butyl compound (**12**) than **5** may be taken as a reflection of the fact that the *anti* conformation of **12** has more severe steric interaction than *anti*-**5**. The reason for these phenomena is not apparent at present but may be connected to the fact that the 8-methyl-1-naphthyl group is thinner than the 2-*t*-butylphenyl group.

The effect of the 1-methyl group in the fluorene ring on the equilibrium constants seems to be very small. The difference between **4** and **5** may not be taken significant. This is in agreement with others[4,16] which generally show no difference in the equilibrium constants between a parent compound and a 1,4-dimethyl derivative. There is but one case, 9-(2-methylphenyl)-fluorene and its 1,4-dimethyl derivative, which shows a significant dependence of the equilibrium constant

on the 1-methyl group.[2,17]

Rotational Barriers. Kinetic data of internal rotation (*anti*→*syn*) of **4** and **5** are shown in Table 1 with those of related compounds. It is interesting to note that the introduction of a methyl group into the 8-position of the 1-naphthyl group raised the barrier to a considerable extent relative to the parent hydrocarbon (**6**). Since the ground state of *anti*-**4** is of high energy relative to *anti*-**6**, the high barrier for *anti*-**4** must be attributed to the steric repulsion involving the C–H group in the 1-position of the fluorene and the 8-methyl group in the transition state for rotation.

The effect of the 8-methyl group on the transition state seems to be larger than that of the 2-methyl in the naphthyl moiety, from the molecular model considerations. It seems to be reflected to the relatively high barriers to rotation of *anti*-**4** with respect to that of 9-(2-methyl-1-naphthyl)fluorene (**8**), when the very unstable ground state of *anti*-**4** is considered. Introduction of a methyl group into the 1-position of the fluorene ring caused the increase in barriers of *ca.* 3 kcal/mol and *ca.* 4 kcal/mol for the pairs of **6** : **7** and **8** : **9**, respectively, whereas the increase for the pair of **4** : **5** is 1.3 kcal/mol. The relative unimportance of the 1-methyl in *anti*-**5** in determining the barrier height may be attributed to two factors. The first is the rise of the ground state of *anti*-**5**: this will make the difference in energies between the *anti* and the transition state smaller. The second is the geometry of the transition state. The molecular model indicates that **5** can assume a transition state for rotation in which the 8-methyl group of the naphthyl avoids the 1-methyl of the fluorene. Then the transition state for rotation of **5** is very similar with that of **4**, unlike the case of a pair of **8** and **9**. The situation is rather close to that of **6** and **7** pair. Combination of these factors can give the smallest difference in barriers to rotation in the pair of **4** and **5**, if the difference is compared with others in Table 1.

References

1) Part XXXVII: G. Yamamoto and M. Ōki, *Chem. Lett.*, **1980**, 1523.
2) M. Nakamura, N. Nakamura, and M. Ōki, *Bull. Chem. Soc. Jpn.*, **50**, 2986 (1977).
3) W. T. Ford, T. B. Thompson, K. A. T. Snoble, and J. M. Timco, *J. Am. Chem. Soc.*, **97**, 95 (1975).
4) S. Kajigaeshi, S. Fujisaki, N. Sumiya, M. Kondo, and K. Ueda, *Nippon Kagaku Kaishi*, **1979**, 239.
5) M. Nakamura, H. Kihara, N. Nakamura, and M. Ōki, *Org. Magn. Reson.*, **12**, 702 (1979).
6) L. F. Fieser and A. M. Seligman, *J. Am. Chem. Soc.*, **61**, 136 (1939).
7) S. Kajigaeshi, unpublished results. We thank Professor Kajigaeshi for giving us information on the synthesis prior to publication.
8) L. C. Cross and W. Kylne, *Pure Appl. Chem.*, **45**, 11 (1976).
9) R. S. Cahn, C. Ingold, and V. Prelog, *Angew. Chem. Int. Ed. Engl.*, **5**, 385 (1966).
10) We thank Professor V. Prelog for discussion on the nomenclature.
11) E. A. Chandross and C. F. Sheley, Jr., *J. Am. Chem. Soc.*, **90**, 4345 (1968): A. Rieker and H. Kessler, *Tetrahedron Lett.*, **1969**, 1227.
12) T. H. Sidall, III, and W. E. Stewart, *J. Org. Chem.*, **34**, 233 (1969).
13) S. Fujisaki, M. Fujimoto, N. Fujii, M. Umeno, and S. Kajigaeshi, *Nippon Kagaku Kaishi*, **1979**, 739.
14) K. Ichikawa and E. Miura, *Nippon Kagaku Zasshi*, **74**, 798 (1953).
15) J. B. Stothers, "Carbon-13 NMR Spectroscopy," Academic Press, New York (1972), Chap. 10.
16) 9-[2-(Methoxymethyl)phenyl]fluorene and 9-[2-(dimethoxymethyl)phenyl]fluorene are examples which do not show significant difference in population ratios with their 1,4-dimethyl derivatives. Others seem to contain large errors which make the comparison meaningless. H. Tsukada, Ph. D. Thesis, The University of Tokyo, 1980.
17) H. Iwamura, *Chem. Lett.*, **1974**, 1205.
18) K. D. Bartle, P. M. G. Bavin, D. W. Jones, and R. L'Amie, *Tetrahedron*, **26**, 911 (1970).

Emission Spectra of Aromatic Hydrocarbons by Controlled Electron Impact

Teiichiro OGAWA,* Naoki YAMAMI, Masaharu TSUJI, and Yukio NISHIMURA
Department of Molecular Science and Technology, Kyushu University, Hakozaki, Fukuoka 812
(Received July 25, 1980)

The emission spectra of benzene, toluene, ethylbenzene, xylenes, trimethylbenzenes, cymene, and naphthalene were investigated under controlled electron-impact excitation. These aromatic hydrocarbons showed a characteristic band in the 250—400 nm region and several bands of such excited fragment species as H and CH. The characteristic bands are similar to those of fluorescence spectra obtained by optical excitation and, thus, were assigned to fluorescence emissions of the parent molecules. The intensity of the fluorescence emission of benzene decreased at higher electron energies, and fragment emissions became dominant above 100 eV. However, its vibrational structure did not change for electron energies of 5—60 eV. This indicates that cascade processes from high-lying states are negligible for benzene. The fluorescence emission of naphthalene shifted to a shorter wavelength for low electron energies. Together with a theoretical estimation based on the Born approximation, cascade effects from higher excited states (S_2 and S_3) are found to be the major source of the fluorescence emission of naphthalene.

The emission spectrum excited by the controlled electron beam provides valuable information for a detailed analysis of the mechanism of the excitation and fragmentation of molecules at very low pressures where the effect of collisions is greatly reduced.[1] A large molecule does not usually show photoemissions from its own excited state, but, instead, shows various fragment emissions, since non-radiative processes become more dominant for a large molecule. The aromatic molecules, however, give intense photoemissions of the parent molecules in the ultraviolet region. The emission spectra of benzene,[2-4] toluene,[2,4,5] xylenes,[2,5] and naphthalene[6,7] have been measured, and the similarity of their spectra with the fluorescence spectra has been pointed out.[2-7] The spectra and the lifetime of benzene emission by electron impact have also been studied.[8,9]

The fluorescence emission of aromatic molecules can be observed either by direct excitation into the fluorescing state or through the cascade process from the initially prepared states to the lower fluorescing state. These excitation processes have been studied with the Bethe theory.[10-12] The excitation cross section to a particular excited state is proportional to the molecular oscillator strength from the ground state to that excited state; on the other hand, the probability of photoemission from a specified state is expressed by the quantum yield of fluorescence.[3,4,6] The cascade effects from the S_n state to the S_1 state may be studied by photoexcitation; however, the electron-impact method can be applied to molecules at very low pressures, since a more intense beam is available and the cross section is large.

In the present paper, the emission spectra of nine aromatic hydrocarbons are described as an extension of previous investigations.[2,6] The electron energy dependence of the spectra was studied for two basic molecules. The excitation processes of these aromatic hydrocarbons are also discussed.

Experimental

A schematic diagram of the apparatus is shown in Fig. 1. The collision chamber was made of stainless steel, with its inside covered with soot to suppress secondary electrons and any stray light. Thermal electrons from a tungsten filament were accelerated, collimated, and introduced into the collision region through a hole (4 mm in diameter). The sample molecule was jetted into the collision region through a needle valve and a multichannel nozzle (0.5 mm × 40). The collision chamber was continuously evacuated with two oil-diffusion pumps; the base pressure was of the order of 10^{-7} Torr, while the operating pressure was of the order of 10^{-4} Torr (uncorrected ion gauge reading). The photoemission produced in the collision region was observed through a quartz window at a angle of 90° with respect to the electron beam.

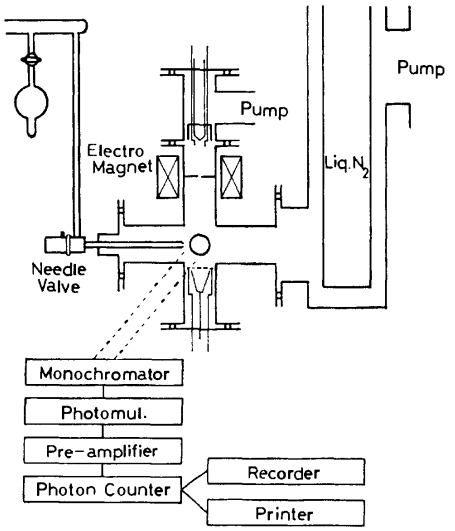

Fig. 1. Schematic diagram of the apparatus.

The emission spectra were observed with a JASCO CT-50 monochromator equipped with a 1200 grooves/mm grating blazed at 300 nm. The photons were measured with an HTV R212UH photomultiplier and a Burr-Brown 3421K OP amplifier or with an HTV R585 photomultiplier and an NF PC-545A photon counter. The wavelength dependence of the instrumental response was not corrected.

All the spectra were measured in a region where the intensity was proportional to both the gas pressure and the electron-beam current. In the case of the $6_1^0 1_2^0$ band of benzene, the intensity was linear in the region below 600 μA and 7.0×10^{-4} Torr. The effect of secondary electrons was estimated from the ratio of the emission intensity of the first negative band of N_2^+ (391.4 nm) to that of the second positive band of N_2 (337.1 nm);[13] the result is shown in Fig. 2.

All the compounds used were of a research grade; they were

deaerated before use by repeated freeze-pump-thaw cycles.

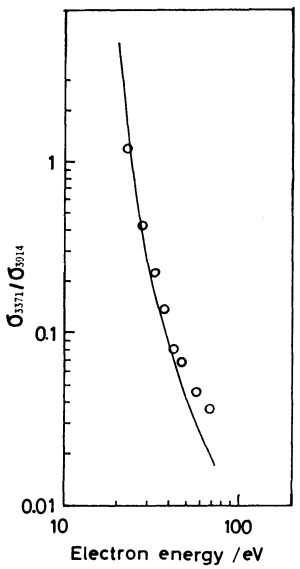

Fig. 2. Ratio of the emission intensity of N_2 (3371 Å) to that of N_2^+ (3914 Å). ○: This work.
The solid line is the estimated one.[13] The result indicates the effect of secondary electrons can be ignored below *ca.* 50 eV. The electron-beam current was 1 μA and the gas pressure was 1×10^{-4} Torr.

Results

The emission spectra of benzene, toluene, ethylbenzene, *o*- and *p*-xylenes, mesitylene, 1,2,3-trimethylbenzene, *p*-cymene, and naphthalene by controlled electron impact were measured; they are shown in Fig. 3. The energy of the incident electrons was 40 eV, and the spectral resolution was about 1 nm. All the aromatic hydrocarbons thus far studied have shown a characteristic band in the 250—400 nm region.[1] The fluorescence spectra taken in the gas phase and in the dilute solution were found to correspond well to the observed emission spectra. Thus, the characteristic bands observed in the present study were assigned to the fluorescence transition from the lowest excited singlet state (S_1) to the ground state (S_0); in the case of benzene, this is the symmetry forbidden $^1B_{2u}$—$^1A_{1g}$ transition.[2-4] Since Vroom and de Heer reported that the excitation cross sections of the Balmer line from various hydrocarbons differ little,[14] the relative intensity of the fluorescence emission can be estimated approximately from Fig. 3.

The spectrum of benzene has a striking dependence on the electron energy, as is shown in Fig. 4. The photoemission of the parent molecule becomes weaker at higher electron energies and almost disappears above

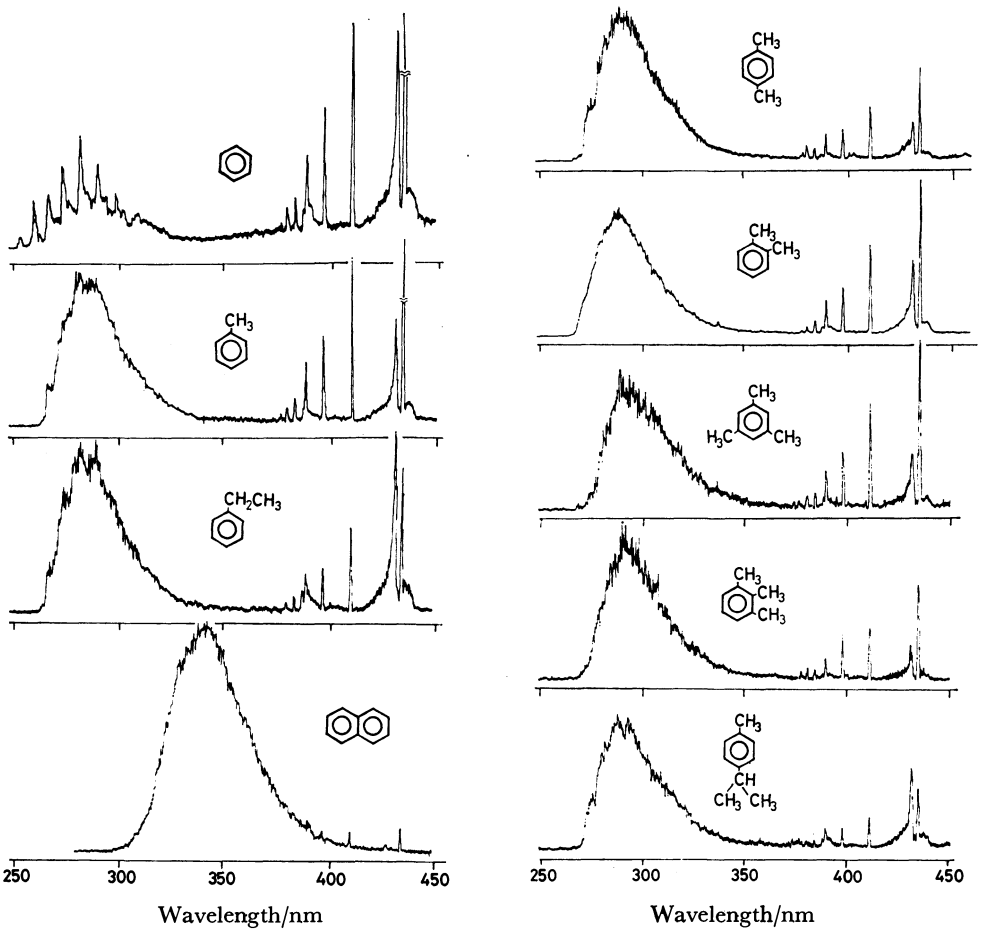

Fig. 3. Emission spectra of aromatic hydrocarbons by controlled electron impact.

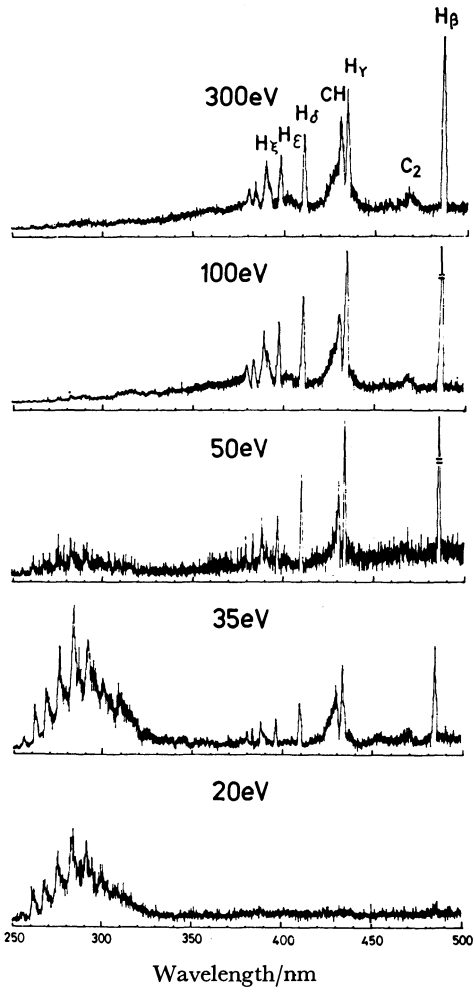

Fig. 4. Electron energy depence of the emission spectra of benzene.

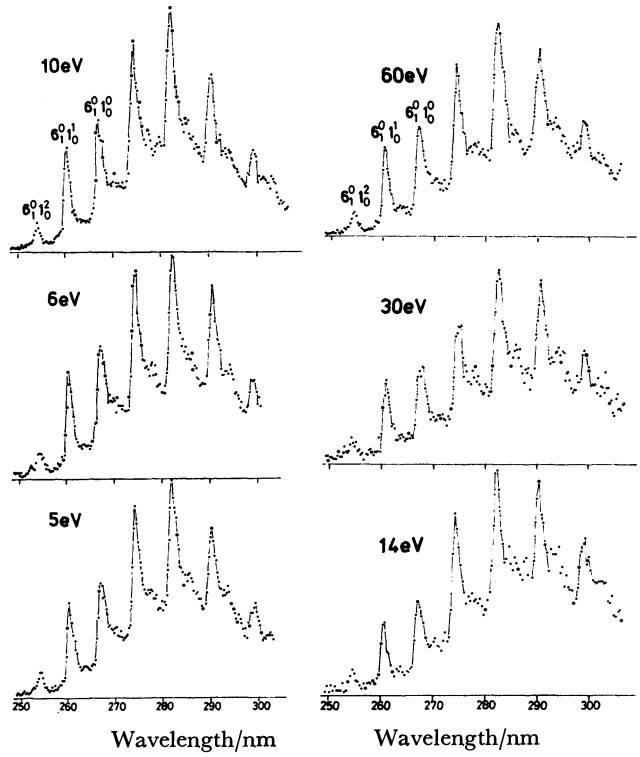

Fig. 5. Electron energy dependence of the vibrational structure of the fluorescence emission of benzene.

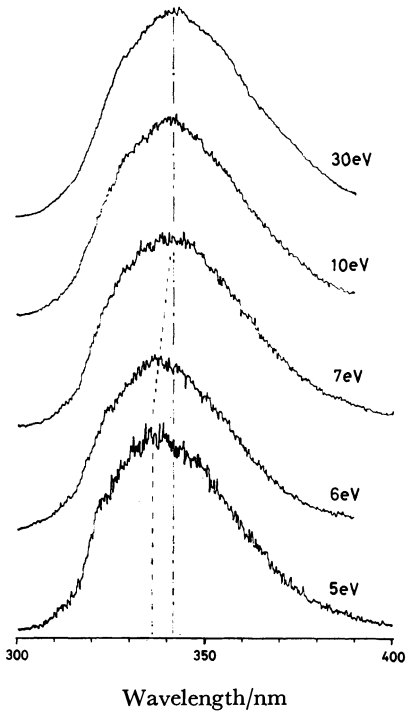

Fig. 6. Electron energy dependence of the fluorescence emission of naphthalene.

100 eV, as was shown by Smyth *et al.*[4] The spectrum of naphthalene, however, did not show such a dependence, and the band of its parent molecule could be observed even at 300 eV.

The shape and structure of this fluorescence emission were observed at various electron energies, as is shown in Fig. 5 for benzene and in Fig. 6 for naphthalene. The vibrational structure of the benzene emission did not change in the optical resolution of 1 nm at 5—60 eV; however, the peak of the band of naphthalene shifted to a shorter wavelength for lower electron energies.

The Balmer series of hydrogen and the $B^2\Sigma^- - X^2\Pi$ transition and the $A^2\Delta - X^2\Pi$ transition of CH were also observed in the 370—440 nm region, as is indicated in Fig. 4. In addition, the $C^2\Sigma^+ - X^2\Pi$ transition of CH (about 315 nm) and the bands of CH^+ (423 nm and 350—370 nm) were identified in the spectrum of benzene taken at a higher sensitivity. The Schüler's T spectrum of $C_4H_2^+$ and the C_2 Swan bands were also observed in the 430—570 nm region.[15]

In all the cases measured, the intensity of the fluorescence emissions was directly proportional to the electron-beam current and to the gas pressure. This indicates that the excited states of these aromatic hydrocarbons were all produced in a one-electron primary collision process.

Discussion

Spectrum of the Fluorescence Emission. The emission spectrum excited by controlled electron impact resembles the discharge spectrum and the equilibrated fluorescence;[16,17] all of these have a prominent vibrational

TABLE 1. ESTIMATION OF CONTRIBUTIONS OF THE S_1, S_2, AND S_3 EXCITATION PROCESSES TO THE OBSERVED FLUORESCENCE EMISSION

	Benzene				Naphthalene			
	E_i/eV	f_i	ϕ_i	Γ_i[a]	E_i/eV	f_i	ϕ_i	Γ_i[a]
$S_1 \rightarrow S_0$	4.9	0.0013	0.16	1.0	4.1	0.003	0.75	13
$S_2 \dashrightarrow S_1 \rightarrow S_0$	6.2	0.090	$<8\times10^{-4}$	<0.27	4.7	0.109	0.32	176
$S_3 \dashrightarrow S_1 \rightarrow S_0$	7.0	0.90	$<10^{-5}$	<0.03	6.0	1.3	0.01	52
$S_2 \rightarrow S_0$	6.2	0.090	8×10^{-6}	0.003	4.7	0.109		
$S_3 \rightarrow S_0$	7.0	0.90			6.0	1.3	2×10^{-5}	0.01

a) Value relative to the $S_1 \rightarrow S_0$ process of benzene. $\rightarrow$Radiative process. $\dashrightarrow$Non-radiative process.

structure and a broad background continuum. The present spectrum of benzene, however, clearly indicates the $6^0_1 1^2_0$ and $6^0_1 1^1_0$ transitions at 255 and 260 nm, which are not appreciable in the equilibrated fluorescence. The resonance fluorescence spectrum of benzene reveals a group of sharp lines,[17,18] whereas the present spectrum is broader and has a more vibrational structure. These facts indicate that the electron energy is large enough to excite many vibronic levels of the S_1 state simultaneously because of the non-resonant character of the electron excitation; however, the pressure is so low that the excited molecules undergo no collisional deactivation, and the vibrational population is not distributed in a 300 K Boltzman distribution. The electron impact spectrum is, thus, similar to the one excited by the irradiation of white light, whose maximum photon energy is that of the electrons.

The equilibrated fluorescence of toluene,[19] and the resonance fluorescence of toluene and xylenes[17] have previously been reported. The comparison of the present spectra with them leads to a conclusion similar to that in the case of benzene; the emission spectrum by controlled electron impact has some vibrational structure, including one above the 0-0 transition, and a broad background continuum. In the case of naphthalene, the vibrational structure becomes very diffuse, and the broad background continuum consists of the major part of the spectrum.

The fluorescence emissions of the other hydrocarbons may be compared with those of the fluorescence spectra taken in solution.[20] For all of the aromatic hydrocarbons studied, the emission spectra by controlled electron impact are more similar to the equilibrated fluorescence spectra in the gas phase or to the fluorescence spectra in solutions than to the resonance fluorescence in a low pressure gas.

Estimation of Excitation Processes. For most molecules, the bulk of the oscillator strength of the valence shell electrons lies at very great values of the excitation energy.[11] Thus, the most important primary processes of the electron-molecule collisions are high-lying electronic excitations of the valence electrons. If the intramolecular radiationless relaxation is very fast, the primarily-excited high-lying states can fall to the lowest excited singlet (S_1) state and contribute to the observed photoemission.

When the energy of the incident electrons for the excitation substantially exceeds the threshold energy of the molecule, the Born approximation is applicable;[10,12] the cross section of the excitation into the ith level (σ_i) is expressed by the optical oscillator strength (f_i) and the transition energy (E_i). The probability of photoemission from this level is proportional to the fluorescence quantum yield (ϕ_i). Thus, the contribution of the photoemission process involving the ith level on the total photoemission (Γ_i) is given as follows:[6]

$$\Gamma_i = b'\sigma_i\phi_i = b\phi_i f_i/E_i, \quad (1)$$

where b is a proportionality constant. Thus, Eq. 1 allows an estimation of the excitation and cascade processes with the available spectroscopic parameters. In actuality, the transition to a particular excited state is not very discrete, and both ϕ_i and f_i are dependent on the excitation energy; however, average values can be used for an order of magnitude estimation.

The very high-lying states seem not to be important for the observed fluorescence emission, since the spectra do not change above 7 eV (Figs. 5 and 6). Accordingly, the estimation of the cascade processes has been confined to the lower three excited states (S_1, S_2, and S_3). The dipole oscillator strength can be obtained from the electron energy loss spectrum.[21,22] The electron energy loss spectrum is closely related with the photoabsorption; the optical values[23] were used for benzene because of the lack of an explicit value of f in the electron energy loss spectrum. The quantum yields were taken from the vapor fluorescence of benzene[24-26] and naphthalene.[27-30] The results are shown in Table 1. The preliminary result[6] was revised by using more recent spectroscopic parameters.

Excitation Processes of Benzene and Naphthalene. The calculation (Table 1) shows that the direct excitation into the S_1 state is the most important process for benzene, while the contribution of the cascade process from the S_2 and S_3 states into the S_1 state is more predominant for naphthalene.

The observed spectrum of benzene has a characteristic vibrational structure, which does not change upon 5—60 eV excitation. This finding leads to the conclusion that the fluorescing S_1 state, whose excitation energy is about 5 eV, does not originate from a cascading process from the higher excited states. The smaller contribution of the higher excited states is due to the faster photochemical process of benzene and/or the direct internal conversion to the ground state, when benzene is excited into the S_2 or S_3 states.[24,25]

The vibrational structure of the fluorescence emission of naphthalene is less pronounced. The intramolecular internal conversion from the higher excited states causes a high vibrational excitation of the emissive S_1

state and makes the appearance of the spectrum more diffuse. The onset of the emission of naphthalene was found at 4.45 eV, which is the spectroscopic energy of the S_2 state.[7] Since a radiationless relaxation of the higher excited states results in the formation of the vibrationally highly-excited S_1 state, the Franck-Condon transition energy from such a highly-excited S_1 state is smaller than that of the directly excited S_1 states. The peak shift (Fig. 6) can be ascribed to the decrease in the contribution of cascading for the low energy excitation. The optical measurement also indicated that the fluorescence shifts to the red and becomes increasingly diffuse as the excitation energy increases.[31] Thus, the calculated and the observed findings are consistent.

The fact that the intensity of the fluorescence emission of benzene decreases rapidly as the increase of the electron energy and becomes negligibly small at a higher electron energy (Fig. 4) indicates that the major process of the excitation is neither a typical optically-allowed nor a typical symmetry-forbidden transition, since a Fano plot of an optically-allowed or a symmetry-forbidden transition has a positive or a zero slope. This finding indicates that another excitation process plays a more important role than those calculated. Smyth *et al.*[5] suggested the contribution of the resonance. Klump and Lassettre[32] indicated the importance of an electric octupole transition. Whereas, Doering,[33] and Wilden and Comer[34] showed the formation of the $^3E_{1u}$ state in this energy region; Matsuzawa[35] calculated that the excitation cross section to the $^3E_{1u}$ state is as large as that to the $^1B_{2u}$ state at a low incident energy and at a large angle. Such processes may be important in the excitation of the fluorescing S_1 ($^1B_{2u}$) state of benzene.

The spectroscopic data for other hydrocarbons in the vapor phase are so scanty that it is difficult to carry out similar estimations for them. However, the spectroscopic parameters obtained for the dilute solution often agree approximately with those in the gas phase, and the oscillator strength and the quantum yield in the dilute solution can be carried over to the rough estimation of the excitation processes. Those of some substituted aromatic molecules have been discussed in this approximation.[36,37]

The authors with to thank Professor Nobuhiko Ishibashi for his encouragment and Morihide Higo for his discussion.

References

1) K. Hirota, M. Hatada, and T. Ogawa, *Int. J. Radiat. Phys. Chem.*, **8**, 205 (1976).
2) T. Ogawa, M. Tsuji, M. Toyoda, and N. Ishibashi, *Bull. Chem. Soc. Jpn.*, **46**, 2637 (1973).
3) C. I. M. Beenakker, F. J. de Heer, and L. J. Oosterhoff, *Chem. Phys. Lett.*, **28**, 320, 324 (1974).
4) K. C. Smyth, J. A. Schiavone, and R. S. Freund, *J. Chem. Phys.*, **61**, 1782, 4747 (1974).
5) T. Ogawa, M. Tsuji, M. Toyoda, and N. Ishibashi, *Chem. Lett.*, **1972**, 233, 1157.
6) M. Tsuji, T. Ogawa, and N. Ishibashi, *Chem. Phys. Lett.*, **26**, 586 (1974).
7) K. C. Smyth, J. A. Schiavone, and R. S. Freund, *J. Chem. Phys.*, **62**, 136 (1975).
8) W. H. Smith, *J. Chem. Phys.*, **54**, 4169 (1971).
9) H. J. Hartfuß, *Z. Naturforsch.*, **29a**, 1489 (1974).
10) M. Inokuti, *Rev. Mod. Phys.*, **43**, 297 (1971).
11) R. L. Platzman, *Vortex*, **23**, 372 (1962).
12) F. J. de Heer, *Int. J. Radiat. Phys. Chem.*, **7**, 137 (1975).
13) M. Higo and T. Ogawa, *Eng. Sci. Reports, Kyushu. Univ.*, **1**, 19 (1979); W. L. Borst and E. C. Zipf, *Phys. Rev. A*, **1**, 834 (1970); M. Imami and W. L. Borst, *J. Chem. Phys.*, **61**, 1115 (1974).
14) D. A. Vroom and F. J. de Heer, *J. Chem. Phys.*, **50**, 573 (1969).
15) M. Tsuji, T. Ogawa, T. Imasaka, Y. Nishimura, and N. Ishibashi, *Bull. Chem. Soc. Jpn.*, **49**, 53 (1976).
16) H. F. Kemper and M. Stockburger, *J. Chem. Phys.*, **53**, 268 (1970).
17) J. M. Blondeau and M. Stockburger, *Ber. Bunsenges. Phys. Chem.*, **75**, 450 (1971).
18) C. S. Parmenter and M. W. Schuyler, *J. Chem. Phys.*, **52**, 5366 (1970).
19) C. S. Burton and W. A. Noyes, Jr., *J. Chem. Phys.*, **49**, 1705 (1968).
20) I. B. Berlman, "Handbook of Fluorescence Spectra of Aromatic Molecules," 2nd ed, Academic Press (1971).
21) R. H. Huebner, R. J. Celotta, S. R. Mielczarek, and C. E. Kuyatt, ANL Report 75-3, Part **1**, 45 (1973); E. E. Koch and A. Otto, *Chem. Phys. Lett.*, **12**, 476 (1972).
22) R. H. Huebner, S. R. Mielczarek, and C. E. Kuyatt, *Chem. Phys. Lett.*, **16**, 464 (1972).
23) E. Pantos, J. Philis, and A. Bolovinos, *J. Mol. Spectrosc.*, **72**, 36 (1978).
24) W. A. Noyes, Jr., W. A. Mulac, and D. A. Harter, *J. Chem. Phys.*, **44**, 2100 (1966); M. G. Rockley, *Chem. Phy. Lett.*, **50**, 427 (1977).
25) S. A. Lee, J. M. White, and W. A. Noyes, Jr., *J. Chem. Phys.*, **65**, 2805 (1976).
26) C. W. Lawson, F. Hirayama, and S. Lipsky, *J. Chem. Phys.*, **51**, 1509 (1969); F. Hirayama, T. A. Gregory, and S. Lipsky, *ibid.*, **58**, 4696 (1973); C. L. Braun, S. Kato, and S. Lipsky, *ibid.*, **39**, 1645 (1963).
27) W. A. Noyes, Jr., and D. A. Harter, *J. Am. Chem. Soc.*, **91**, 7585 (1969).
28) J. C. Hsieh, C. S. Huang, and E. C. Lim, *J. Chem. Phys.*, **60**, 4345 (1974).
29) L. M. Hall, T. F. Hunter, and M. G. Stock, *Chem. Phys. Lett.*, **44**, 145 (1976).
30) T. A. Gregory, F. Hirayama, and S. Lipsky, *J. Chem. Phys.*, **58**, 4697 (1973).
31) J. O. Uy and E. C. Lim, *Chem. Phys. Lett.*, **7**, 306 (1970).
32) K. N. Klump and E. N. Lassettre, *Chem. Phys. Lett.*, **51**, 99 (1977).
33) J. P. Doering, *J. Chem. Phys.*, **67**, 4065 (1977).
34) D. G. Wilden and J. Comer, *J. Phys., B*, **13**, 627 (1980).
35) M. Matsuzawa, *J. Chem. Phys.*, **51**, 4705 (1969).
36) M. Tsuji, T. Ogawa, Y. Nishimura, and N. Ishibashi, *Bull. Chem. Soc. Jpn.*, **50**, 2432 (1977).
37) T. Ogawa, N. Miyamoto, and N. Ishibashi, *Bull. Chem. Soc. Jpn.*, **51**, 394 (1978).

The Electronic Absorption Spectra of Fatty Acid Mono-, Bi-, and Multilayers with Bivalent Metal Ions

Yukio NAGAHIRA,*,† Kazunori MATSUKI, and Hideo FUKUTOME
Department of Physics, Faculty of Science, Kyoto University, Sakyo-ku, Kyoto 606
(Received August 28, 1980)

The electronic absorption spectra of fatty acid multilayers with bivalent metal ions were studied in the vacuum ultraviolet (VUV) to ultraviolet (UV) energy region below 8 eV; they are due to transitions in the carboxylic acid and metal carboxylate moieties. Infrared (IR) absorptions due to the C–O stretching vibration in the carboxylate moiety are also studied. Stearic acid multilayers without metal ions are shown to form hydrogen-bonded dimers. The spectra of multilayers with metal ions show a marked dependence on the subphase pH which is different for different kinds of adsorbed metal ions. Their VUV spectra are conspicuously dependent on the kind of metal ions adsorbed. All the multilayers with alkaline earth metals, metals of the 2B group, transition metals, Cu, and Pb have at least two bands in the VUV region, 7.3—6.3 eV. The polarization spectra of the Ba stearate multilayer suggest that the two transitions may be the intramolecular π-π^* and n-π^* transitions in the carboxylate anion moiety. The multilayers with Cu and Pb have another band in the UV region. The spectra of the UV bands of the Pb and Cu stearate mono-, bi-, and multilayers were studied. In the Pb stearate layers, the positions of the UV bands in the bi- and multilayers are the same, but those in the monolayers are at considerably shorter wavelengths. The positions of the UV band in the Cu stearate mono-, bi-, and multilayers are successively red shifted. The polarization spectra of the UV bands of the mono- and bilayers showed that they are charge-transfer bands between the Pb or Cu ion and the coordinated carboxylate moiety.

In an accompanying paper[1] (hereafter we will refer to it as I), we have shown that the vacuum ultraviolet (VUV) absorption spectra of fatty acid multilayers in the energy region below 10 eV consist of two parts, a strong absorption in the region above 8 eV (Region 1) and a weaker absorption in the region below 8 eV (Region 2). From the chain length and pH dependences of the spectra, we have assigned the absorption in Region 1 to the σ-σ^* transitions in the alkane chain moiety, and that in Region 2 to the transitions in the carboxylic acid and metal carboxylate moieties.

In this paper, we wish to present the results of our detailed studies of the absorption spectra of fatty acid multilayers and monolayers in Region 2. Fatty acid multilayers prepared on the water subphase containing metal ions adsorb the metal ions to a varying extent, depending on the pH of the subphase.[2,3] The pH profile of the metal ion adsorption is characteristic of the kind of metal ion. The physical properties of fatty acid monolayers such as the π-A profiles and the surface potential are dependent of the kind and amount of adsorbed metal ions. However, little direct information has been obtained about the interaction of metal ions with carboxylic acid moieties in fatty acid mono- and multilayers. The absorption spectra in Region 2 of fatty acid multilayers, that are due to the electronic transitions in the carboxylic acid and metal carboxylate moieties, provide direct information about the interaction of metal ions with fatty acid monolayers. In this paper, we will study the pH and metal ion dependencies and polarization of the spectra in Region 2. We will study also the infrared (IR) absorptions due to the carboxylic acid and carboxylate moieties.

Experimental

Materials. The fatty acids and other materials used in the present study were the same as those described in I. The spectrograde acetic acid and dichlorodimethylsilane were purchased from Nakarai Chemicals, Ltd. Optically flat quartz plates were obtained from the Takahashi Giken Co.

Methods. Fatty acid multilayers with metal ions and pure stearic acid multilayers were deposited on CaF_2 plates, as has been described in I. Monolayers of Cu stearate and Pb stearate were deposited on quartz plates with hydrophilic surfaces, as has been described by Matsuki *et al.*[4] Bilayers of Cu stearate and Pb stearate were deposited on quartz plates whose surfaces had been made hydrophobic by rinsing with a dichlorodimethylsilane solution.[5] All the multilayers and monolayers were prepared at 19 ± 0.5 °C.

The measurements of VUV absorption spectra were performed as has been described in I. The IR spectra were measured on Shimadzu-IRG and JASCO-IRA-2 spectrometers; the latter apparatus was five times more sensitive than the former. The measurements of the ultraviolet (UV) spectra of the monolayers and bilayers of Cu stearate and Pb stearate were performed on a high-sensitivity spectrometer using the single-beam and sample in-sample out technique described by Matsuki *et al.*[4] The apparatus was equipped with a CaF_2 Glan-Thompson prism for measurements of the polarized spectra.

The UV spectra of $PbCl_2$, $Pb(CH_3COO)_2$, and $Cu(CH_3COO)_2$ in water and acetic acid were measured with a Shimadzu-UV-180 spectrometer. To minimize the absorption of the solvent, acetic acid, the spectra were measured for solutions of high concentrations in the order of 10^{-2} M with the use of a thin cell, with the path length of 12 microns and the cell was made of two quartz plates and a polyethylene film spacer.

All the measurements of the VUV spectra in Region 2 (below 8 eV) and of the IR specrta in the region from 1000 cm^{-1} to 4000 cm^{-1} were performed for multilayers prepared by 15 dippings of the substrate.

The efficiency of the deposition of multilayers may change from sample to sample depending on the subphase pH, the kinds of metal ions, and the substrate.[6–10] In order to avoid uncertainty in the deposition ratio, we measured both the VUV and IR spectra for each multilayer sample. We nomalized the deposition ratio using the 2910 cm^{-1} IR band, which is attributable to the antisymmetric stretching vibration

† Present address: Osaka University of Economics and Law, Yao, Osaka 581.

of the CH_2 groups in the alkane chain moiety.[2,11-13] The 2910 cm^{-1} IR band of the Ba heneicosanoate multilayer was used as the standard for the normalization of the deposition ratio. The Ba heneicosanoate multilayer prepared at a neutral pH forms Y layers with a nearly perpendicular molecular arrangement.[1,13] Its deposition on a CaF_2 plate coated with Fe stearate was confirmed by the linearity of the VUV[14] and IR spectra to the dipping number. The number, L, of fatty acid layers deposited on a plate by 15 dippings was calculated by means of:

$$L = 60 \times \frac{20}{n} \times \mathrm{OD}(2910\ \mathrm{cm}^{-1})/\mathrm{OD}(2910\ \mathrm{cm}^{-1}\ \mathrm{Ba\ heneicosanoate}),$$

where n is the carbon number in the alkane chain, we assumed the deposition of 4 layers of Ba heneicosanoate on the substrate per dipping into the subphase.

For pure stearic acid and Zn stearate multilayers with molecular arrangements tilted against the normal of the layer plane, the intensity of the 2910 cm^{-1} band was corrected for the tilting of molecular axes by the method of Akutsu *et al.*[15]

All the VUV and UV spectra of multilayers except for Fig. 1 are normalized to the per-layer value. The molar extinction coefficient, ε, is obtained from the per-layer absorption, A, by means of:

$$\varepsilon = A \cdot a \cdot N = 12 \times 10^5 \times A,$$

where N is the Avogadro's number and a is the area (in cm^2) occupied by a fatty acid molecule, which is estimated to be about 20×10^{-16} cm^2 from the limiting area in the π-A profile of fatty acid monolayers.[16,17]

Results and Discussion

VUV Spectrum of Pure Stearic Acid Multilayer. The deposition of the pure stearic acid monolayer, which was spread on the subphase without any metal ions at acid pH (3.1), onto the CaF_2 plate was most uncertain, as was mentioned in I. The number of deposited layers appropriate for the measurements of the VUV spectra in Region 1 was limited to only a few layers because of the strong absorption of Region 1, so the intensity of the 2910 cm^{-1} IR band was too weak to use for the nomalization of the deposition ratio. However, in the measurements of the spectra in Region 2 much thicker multilayers could be used because of the weaker absorptions in that region, so the 2910 cm^{-1} IR band could be effectively used in the normalization of the deposition ratio. The pure stearic acid multilayer prepared at the acid pH was reported to have a molecular arrangement with chain axes tilted against the normal of the layer plane by about 30°.[12] The VUV spectrum in Region 1 also gave a tilting angle of about 30°, as has been discussed in I. Therefore, in the normalization of the deposition ratio, the intensity of the 2910 cm^{-1} band was corrected for the tilting by assuming the tilting angle of 30°. The Region 2 VUV spectrum of the pure stearic acid multilayer is shown in Fig. 1, as well as the spectra of the acetic acid dimer and the monomer in the gas state obtained by Barnes and Simpson.[18] The spectrum of the pure stearic acid multilayer has a band at 7.7 eV which resembles, in position and strength, the lowest energy band of the acetic acid dimer, but which has no absorption in the region near 7.2 eV where the absorption of the acetic acid monomer exists. This

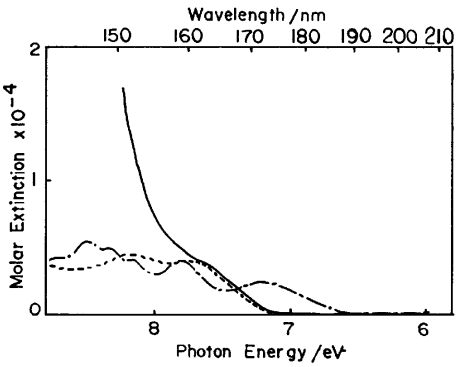

Fig. 1. Spectrum of pure stearic acid multilayer in molar extinction scale (——). The multilayer was prepared on the subphase without metal ions at pH 3.1. The spectra of acetic acid monomer (-·-) and dimer (----) obtained by Barnes and Simpson[18] were also shown.

shows that the carboxylic acid moieties in the pure stearic acid multilayer are not in the monomeric states but form hydrogen-bonded dimers. The existence of hydrogen bonding in pure fatty acid multilayers was also suggested by Koyama *et al.* from the broadness of the 1700 cm^{-1} IR band.[19]

pH *Dependencies of the VUV and IR Spectra of Fatty Acid Multilayers with Bivalint Metal Ions.* Fatty acid multilayers prepared on the subphase with metal ions adsorb the metal ions to a varying extent, depending on the pH of the subphase.[2,3] Corresponding to the pH dependencies of the metal ion adsorptions, the VUV spectra in Region 2 of the multilayers show marked dependencies on the subphase pH. In Figs. 2a and 3a we show the pH dependencies of the Region 2 spectra of the arachidic acid multilayers with Sr^{2+} and Cd^{2+} ions respectively.

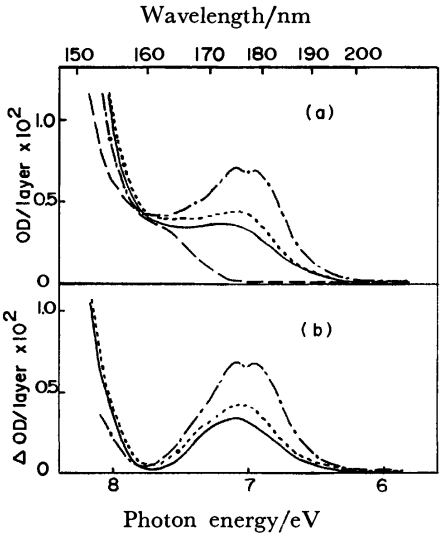

Fig. 2. (a): The pH dependence of the spectra of arachidic acid multilayers with Sr^{2+} ions prepared on the subphases with 10^{-4} M $SrCl_2$ at pH 6.6 (——), at pH 9.3 (----) and pH 10.7 (— - —). The spectrum of pure stearic acid multilayer prepared at pH 3.1 (——) is also shown. (b): The difference spectra presentation of the spectra in (a) with the reference of the pure stearic acid multilayer spectrum. The notation is the same as (a).

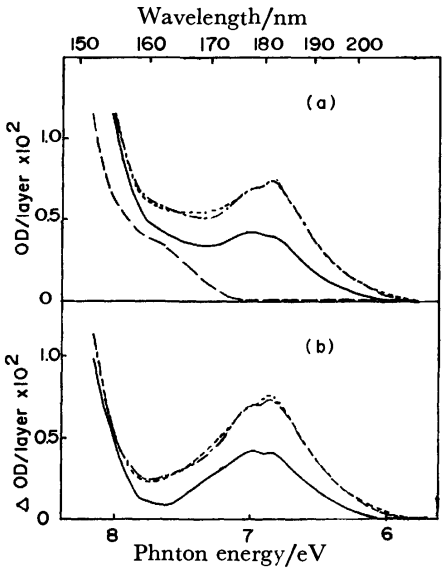

Fig. 3. (a): The pH dependence of the spectra of arachidic acid multilayers with Cd^{2+} ions prepared on the subphases with 10^{-4} M $CdCl_2$ at pH 6.15 (——), at pH 6.9 (----) and at pH 8.15 (— — —). The spectrum of pure stearic acid multilayer prepared at pH 3.1 is also shown (——). (b): The difference spectra presentation of the spectra in (a) with the reference of the pure stearic acid multilayer spectrum. The notation is the same as (a).

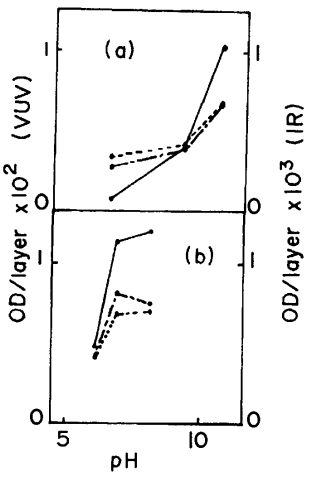

Fig. 4. (a): The pH dependences of the intensities of the VUV bands at 7.10 eV (——) and 6.95 eV (—·—) and of the IR band at 1515 cm^{-1} (——) of arachidic acid multilayers with Sr^{2+}. (b): Those of the VUV bands at 7.00 eV (— — —) and 6.85 eV (—·—) and of the IR band at 1546 cm^{-1} (——) of arachidic acid multilayer with Cd^{2+}.

At pH 3.1 little adsorption of these ions took place, and the spectra in Region 2 were almost the same as that of pure stearic acid multilayer. As the subphase pH was increased up to the pH region where the adsorption of the metal ions took place, however, new bands appeared in the energy region around 7 eV, where little absorption existed at pH 3.1, and their intensities increased with an increase in the pH. To establish the shapes of the new bands more clearly, in Figs. 2b and 3b we show the difference spectra with reference to the pH 3.1 spectra. The new bands depend on the kinds on metal ions adsorbed. At least two peaks can be discriminated for the multilayers with both Sr^{2+} and Cd^{2+} ions, at 7.10 and 6.95 eV for Sr^{2+} and at 7.00 and 6.85 eV for Cd^{2+}.

We show in Fig. 4 the pH dependencies of the absorption strengths at the positions of the two peaks. We note that the shapes of the spectra had a dependence on the pH. The relative strength of the lower energy peak to the higher energy one increased with the increase in the pH. This suggests that the metal ion dependent absorption around 7 eV contains contributions from at least two different molecular species.

To elucidate the nature of the molecular species responsible for the absorption, we inspected the pH dependencies of the IR spectra of the same multilayer samples in the wavenumber region from 1350 to 1850 cm^{-1} (Figs. 5 and 6). In this wavenumber region, there were two bands with marked pH dependencies, the broad band at 1700 cm^{-1} and the band at 1515 cm^{-1} (Sr^{2+}) or 1546 cm^{-1} (Cd^{2+}). The intensity of the 1700 cm^{-1} band was maximal at an acid pH and decreased with the increase in the pH. Its position was independent of the kinds of metal ions adsorbed. The 1700 cm^{-1} band can be assigned to the C=O stretching vibration in the unionized carboxylic acid moiety, because its position is identical with that of the C=O stretching band in the stearic acid crystal.[11] The metal ion dependent band at 1515 cm^{-1} (Sr^{2+}) or 1546 cm^{-1} (Cd^{2+}), on the other hand, was absent at an acid pH, but emerged in the pH region where the adsorption of the metal

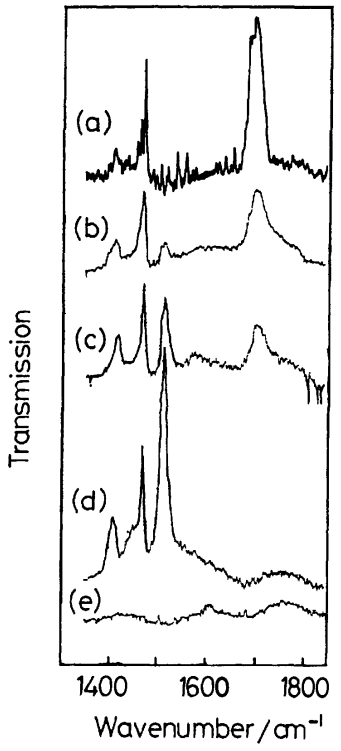

Fig. 5. IR spectra in the region 1850—1350 cm^{-1} of arachidic acid multilayers with Sr^{2+} ions prepared at pH 6.6 (b), at pH 9.3 (c), and at pH 10.7 (d). The spectrum of the pure stearic acid multilayer is also shown (a). (e) is the base line of the spectra.

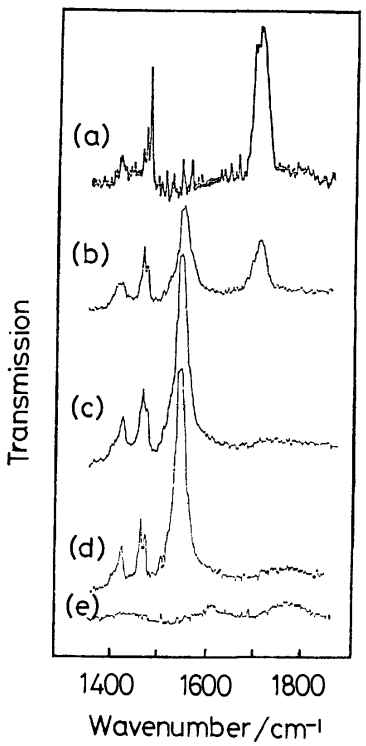

Fig. 6. IR spectra in the region 1850—1350 cm^{-1} of arachidic acid multilayers with Cd^{2+} ions prepared at pH 6.15 (b), pH 6.9 (c), and pH 8.15 (d). The spectrum of the pure stearic acid multilayer is also shown (a). (e) is the base line of the spectra.

ions begun to occur, and its intensity increased with the increase in the pH. The band can be assigned to the COO^- antisymmetric stretching vibration in the metal carboxylates moiety, because its position is very close to the position, 1514 cm^{-1} or 1548 cm^{-1}, of the vibration mode in Sr or Cd stearate crystal respectively.[11] The intensity of the band, therefore, is considered to be proportional to the amount of the metal ions adsorbed to the multilayer.

We show in Fig. 4 the pH dependencies of the 1515 cm^{-1} and 1546 cm^{-1} IR bands. One may see in Fig. 4 that there is a difference in the pH dependencies of the VUV and IR absorptions. The strength of the VUV absorption relative to that of the IR absorption was larger in the lower pH region, where the adsorption of the metal ions was incomplete, than in the high pH region, where the adsorption of the metal ions had been completed. This indicates that a molecular species which is present in the pH region with a partial adsorption of the metal ions contributes to the VUV absorption, but not to the IR band. This molecular species is considered to be unionized fatty acid molecules unhydrogen-bonded in their carboxylic acid moieties. As is shown in Fig. 1, the carboxylic acid moieties in pure fatty acid multilayers form hydrogen-bonded dimers. As the pH of the subphase is increased, a fraction of the fatty acid molecules is ionized and adsorbs metal ions. Therefore, the hydrogen bonds in a fraction of the remaining unionized molecules may be broken by the disturbance of the regular structure of the multilayer by the partial adsorption of metal ions. The unionized fatty acid monomers thus produced will have an absorption near 7.2 eV, as judged from the absorption spectrum of the acetic acid monomer shown in Fig. 1, and will contribure to the VUV absorption, but not to the IR band due to the metal salts of fatty acids. This mechanism can explain also the pH dependent change in the shape of the VUV absorption. The two peaks in the VUV spectra which were most clearly seen in the high pH region are

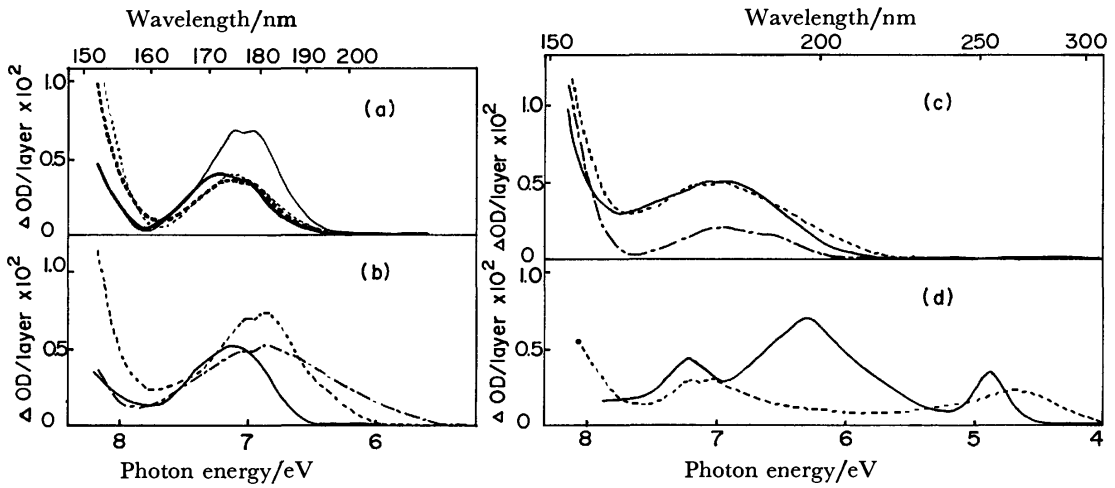

Fig. 7. The VUV difference spectra of fatty acid multilayers with alkaline earth metals (a), with 2B group metals (b), with transition metals (c), and with Cu and Pb (d). The reference is the spectrum of pure stearic acid multilayer prepared at pH 3.1. The metal ions and the pH's of the subphases are (a) Mg^{2+}, pH 10.1 (——), Ca^{2+}, pH 7.6 (- - -), Sr^{2+}, pH 10.7 (——), and Ba^{2+} at pH 9.6 (— — —), (b) Zn^{2+}, pH 7.3 (——), Cd^{2+}, pH 8.15 (— — —), and Hg^{2+}, pH 5.4 (—·—), (c) Mn^{2+}, pH 8.4 (——), Co^{2+}, pH 8.4 (— — —), and Ni^{2+}, pH 5.8 (—·—) and (d) Pb^{2+}, pH 5.7 (——) and Cu^{2+}, pH 5.4 (— — —). All the subphases contained 10^{-4} M metal chloride except for the Pb case with 6×10^{-7} M $PbCl_2$. The fatty acids used are indicated in Table 1. In the case of the multilayer with Zn^{2+} ions, the layer number was calculated assuming the tilted arrangement of molecules with the angle 26°[1,11] against the normal of the layer plane.

TABLE 1. POSITIONS OF THE ELECTRONIC ABSORPTION BANDS AND THE COO^- ANTISYMMETRIC STRETCHING VIBRATIONS OF FATTY ACID MULTILAYERS WITH BIVALENT METAL IONS

	Metal ions	Carbon[a] number	Metal[b] adsorption %	Electronic bands eV			The COO^- band cm^{-1}	Crystals[c] The COO^- band/cm^{-1}	Crystals[c] State of hydration
Alkaline earth metals	Mg	17	100	7.22	7.00		1560(b)	1564(b)	$3H_2O$
	Ca	17	50	7.15	6.95		1540, 1575	1540, 1581	H_2O
	Sr	19	100	7.10	6.95		1515(s)	1514(s)	Anhydrous
	Ba	20	50	7.10	6.85		1510, 1530	1513	Anhydrous
2B group metals	Zn	17	100	7.30	7.10		1540(s)	1540	Anhydrous
	Cd	19	100	7.00	6.85		1546(s)	1548	Anhydrous
	Hg	17	50	7.00	6.85		1590(s)	1570	Anhydrous
Transition metals	Mn	17	100	7.10	6.85		1560(b)	1550(sh), 1574	H_2O
	Co	17	100	7.20	6.95		1550(b)	1530(b)	H_2O
	Ni	17	100	7.00	6.60		1550(b)	1550(b)	$2H_2O$
Others	Cu	17	—	7.20	7.05	4.70	1590(s)	1588	Anhydrous
	Pb	17	—	7.20	6.30	4.86	1510(s)	1512	Anhydrous

(b): broad band, (s): sharp band, (sh): shoulder. a) The carbon number of the alkane chain of fatty acids used as the multilayer samples. b) Calculated from the intensity of the 1700 cm^{-1} IR band. c) The IR and hydration data for metal stearate crystals obtained by R. Matsuura.[11]

considered to be due to the metal carboxylate moieties. The absorption due to the unionized monomer carboxylic acid moieties is superimposed on them in the low pH region, so that a pH dependent change in the spectral shape is produced. The swelling near 7.2 eV present only in the low pH VUV spectra may be due to the absorption of the unionized monomer species.

Metal Ion Dependence of Region 2 Spectra of Fatty Acid Multilayers. The Region 2 spectra of fatty acid multilayers with bivalent metal ions have a conspicuous dependence on the kinds of metal ions adsorbed. We show in Fig. 7 the difference spectra of the multilayers with metal ions of an alkaline earth group (Fig. 7a), the 2B group (Fig. 7b), a transition metal group (Fig. 7c), and Cu^{2+} and Pb^{2+} (Fig. 7d). The reference was the spectrum of the pure stearic acid multilayer prepared at pH 3.1. The depositions of the multilayers were performed at the pH's where the adsorptions of the metal ions were almost complete, except in a few cases in which the efficiency of deposition was not so good in such a pH region. The spectra, therefore, represent the absorptions of the metal carboxylate moieties. In Table 1 we list the positions of the absorption peaks which could be clearly discriminated.

We measured also the IR spectra of the same samples. In Table 1 we list the positions of the IR bands which were assigned to the COO^- antisymmetric stretching vibration in the metal carboxylate moieties. We show also the data of the positions of the vibration mode in the metal stearate crystals.[11] Several multilayers have two bands for the vibration mode that may be ascribed to different hydration states. It has previously been reported that, in crystals, the band width of the vibration mode was broadened by hydration to metal carboxylate moieties.[11] We show also the qualitative data about the band width and the data of hydration in crystals. We may see in Table 1 that there are good correspondences between multilayers and crystals in the band positions and the states of hydration, as judged by the band splitting and the band width. We also show in Table 1 the extent of metal ion adsorption in the multilayers, as estimated by the intensity of the 1700 cm^{-1} IR band.

We may see in Fig. 7 and Table 1 that all the multilayers have a band in the 7.0—7.3 eV energy region. This band may have a common origin in all the multilayers. A possible origin is the intramolecular π-π^* transition in the carboxylate anion moiety. The spectrum of the carboxylate anion has not been obtained. Barnes and Simpson suggested, from their observation of its absorption edge, that the π-π^* transition of the carboxylate anion may lie near 7.2 eV.[18] The position of the π-π^* transition may be shifted a little depending on the kind of bound metal ion.

All the multilayers also have another band in the 6.3—7.1 eV energy region. The assignment of this second band is not clear. In the Ba stearate multilayer it has a polarization perpendicular to the first band, as we shall show in the next section. Hence, it may be due to an intramolecular transition in the carboxylate anion moiety, possibly the n-π^* transition. The intensity of the n-π^* transition may be enhanced by the distortion of the n electron orbital caused by the interaction with bound metal ions. In the case of the multilayer with Pb^{2+}, the intensity of the second band is too strong to be assigned to the n-π^* transition, though, its position is shifted to a much lower energy compared to the other multilayers. The nature of the second band in the multilayer with Pb^{2+} may, therefore, be different from those of the other multilayers. To obtain a certain assignment of the transitions, further studies seem to be necessary.

The absorptions of the multilayers with Cu^{2+} and Pb^{2+} extend up to the UV region and have their bands at

4.70 and 4.86 eV respectively. The UV band is due to the charge-transfer transition between the carboxylate anion moiety and the bound metal ion, as we shall show later by means of the polarization spectra in the UV region.

The absorption edges of the multilayers with transition metals and 2B group metals, except for Zn, extend to a much lower energy region (up to about 5.5 eV) than do the multilayers with alkaline earth metals. The low energy tails of the absorptions of those multilayers may, therefore, contain weak transitions with the charge-transfer character.

Polarization Spectra of the Ba Stearate Multilayer. We show in Fig. 8 the polarization spectra of the Ba stearate multilayer measured with a 45° angle incidence of plane polarized lights. The absorption of the light polarized perpendicularly to the plane of incidence (S-polarization) was stronger than that of the light polarized parallel to the plane of incidence (P-polarization) throughout the energy region. The Ba stearate multilayer has been reported to have a layer structure with molecular axes arranged perpendicularly to the layer plane.[13,20-25] Assuming the perpendicular molecular arrangement and using Akutsu *et al.*'s method, we calculated the angle, θ, of the transition moment against the molecular axis. In the calculation, we used as the refractive index, n, of the multilayer both the value, $n=1.70$, of quartz near 7.0 eV[26] and the value, $n=1.50$, of the multilayer in the visible region,[20] as we have done in I. The theoretical value of the dichroic ratio, $R=A_S/A_P$, where A_S and A_P are the absorbances for S and P polarized lights respectively, became maximal for $\theta=90°$. The theoretical maximal value of R is 1.21 for $n=1.70$ and 1.29 for $n=1.50$. In all the energies, the observed dichroic ratio was close to the theoretical maximal value; for instance, $R=1.29$ at 7.1 eV. Therefore, we can conclude that $\theta=90°$ within the limits of experimental error.

This result shows that the transitions near 7 eV in the Ba stearate multilayer are intramolecular transitions in the carboxylate anion moiety. The π-π^* transition in the carboxylate anion has its direction along the line connecting the two oxygen atoms, and the n-π^* transition is perpendicular to the carboxylate plane, so that they are polarized perpendicularly to the molecular axis. The charge-transfer transition between the carboxylate anion moiety and the bound metal ion, on the other hand, is expected to have its direction of the transition moment not perpendicular to the molecular axis, because bound metal ions are arranged outside

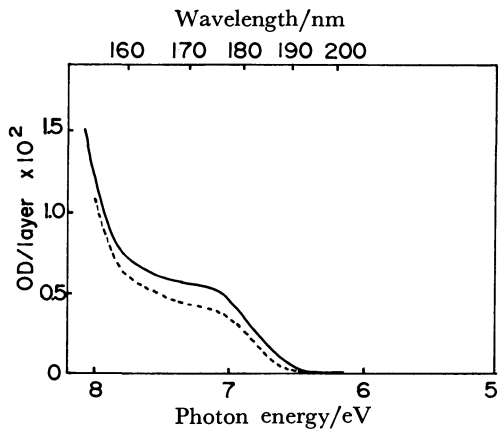

Fig. 8. Polarized absorption spectra of stearic acid multilayers with Ba^{2+} ions prepared on the subphase with 3×10^{-5} M $BaCl_2$ at pH 7.2 with 45° angle incidence of the light plane polarized perpendicularly (——), or parallely (– – –) to the plane of incidence.

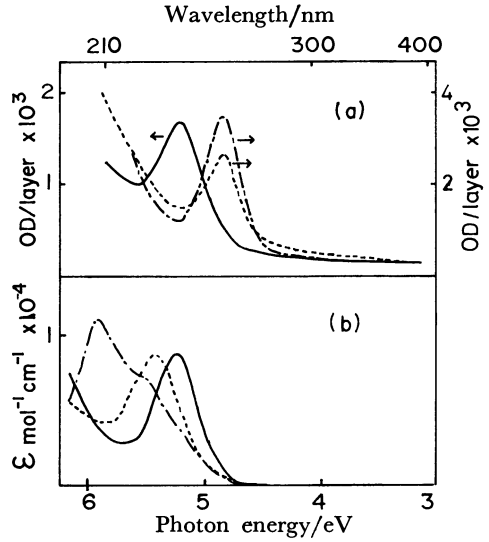

Fig. 9. (a): UV spectra of stearic acid mono- (——), bi- (– – –) and multi- (—·—) layers prepared on the water subhases with 1.2×10^{-6} M $PbCl_2$ at pH 5.4 (mono-) and 5.7 (bi- and multilayers). (b): UV spectra of $Pb(CH_3COO)_2$ (0.03 M) in CH_3COOH (——) and H_2O (– – –) solutions and $PbCl_2$ (0.02769 M) in H_2O (—·—) solution. The path length of the cell was 12 microns.

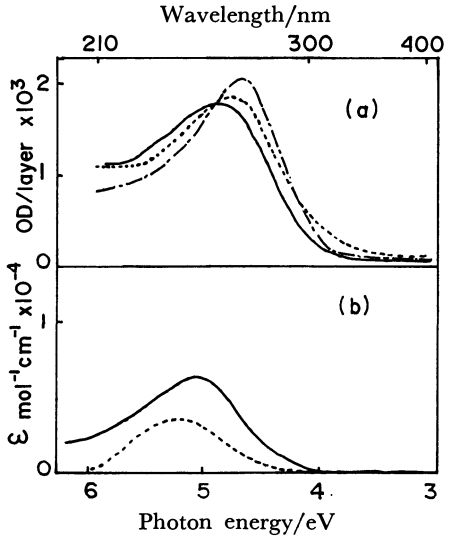

Fig. 10. (a): UV spectra of stearic acid mono- (——), bi- (– – –) and multi- (—·—) layers with Cu^{2+} ions prepared on the water subphase with 5×10^{-4} M $CuCl_2$ at pH 5.1 for the mono- and bilayers and with 10^{-4} M $CuCl_2$ at pH 5.4 multilayer. (b): UV spectra of $Cu(CH_3COO)_2$ (0.05 M) in H_2O (– – –), CH_3COOH (——) solutions. The path length of the cell was 12 microns.

TABLE 2. THE UV BANDS OF MONO-, BI-, AND MULTILAYERS OF Pb AND Cu STEARATE AND OF Pb AND Cu ACETATE AND $PbCl_2$ IN SOLUTION

Ion	Sample	Position/nm	OD/layer	ε[a)]/mol^{-1} cm^{-1}
Pb	Multilayer	254	3.3×10^{-3}	6300
	Bilayer	255	2.4×10^{-3}	6400
	Monolayer	237	1.6×10^{-3}	4100
	$Pb(CH_3COO)_2$ in CH_3COOH	237	—	8700
	$Pb(CH_3COO)_2$ in H_2O	228	—	8700
	$PbCl_2$ in H_2O	208 225	—	11000 —
Cu	Multilayer	263	2.1×10^{-3}	5000
	Bilayer	260	1.9×10^{-3}	4600
	Monolayer	254	1.8×10^{-3}	4300
	$Cu(CH_3COO)_2$ in CH_3COOH	245	—	3600
	$Cu(CH_3COO)_2$ in H_2O	235	—	6600

a) The molar extinctions of the L B layers were calculated as has been described in the Materials and Methods section.

the layer plane of the carboxylate anion moieties. The above conclusion is considered to be valid for the multilayers with alkaline earth metals. However, for the multilayers with metal ions of other kinds, further studies to check the validity of the assignment are necessary because their electronic structures are so different from those of alkaline earth metals that their interactions with the carboxylate anion moiety may be different from the interaction of the alkaline earth metals.

UV Spectra of Pb Stearate and Cu Stearate Mono- and Bilayers. As is shown in Fig. 7d, the Pb and Cu stearate multilayers have an absorption band in the UV region. The UV absorptions of the mono- and bilayers as well as those of the multilayers can be measured by using the high-sensitivity spectrometer for thin layers with the sample-in, sample-out technique developed in Kuhn's laboratory.[27] We show in Figs. 9a and 10a the UV spectra of the Pb and Cu stearate mono-, bi-, and multilayers. We also show, in Figs. 9b and 10b, the UV spectra of Pb acetate, $PbCl_2$ and Cu acetate in acetic acid and water solutions. The positions and molar extinctions of the UV bands are listed in Table 2.

The positions of the UV band in the bi- and multilayers with Pb ions were the same, though the breadth of the band was a little different, perhaps because of the larger light scattering in the bilayer. The coincidence of the peak position suggests that the structure and arrangement of the chromophores in the bilayer were unchanged by the formation of multilayer. The intensity of the absorption was larger in multilayer than in bilayer. This hyperchromicity of the multilayer may be due to the interlayer excitonic interaction of chromophores, as we shall discuss later. The peak position in the monolayer, on the other hand, was at a considerably shorter wavelength than those of the bi- and multilayers, and the intensity was stronger than that of the bilayer. This shows that the structure of coordination in the Pb carboxylate moieties is different between the mono- and bilayers. The peak position and the band width were almost the same in the monolayer and Pb acetate in an acetic acid solution. Therefore, the coordination of Pb ions in the monolayer is considered to be similar to that in an acetic acid solution.

The peak position of the UV band in the Cu stearate multilayer was red shifted a little against that of the bilayer, and the absorption intensity was a little stronger in the multilayer, showing that the structure and arrangement of chromophores in the bilayer are affected by the formation of the multilayer. The UV band in the bilayer was red shifted against that of the monolayer. This indicates that there is a difference between the mono- and bilayers in the coordination of Cu ions with the surrounding carboxylate anion moieties. The position of the UV band of the monolayer was closest to the UV band of Cu acetate in the acetic acid solution, though it was at a little longer wavelength position. Therefore, the coordination of Cu ions in the monolayer is considered to be similar to, but not identical with, the coordination in the acetic acid solution.

In order to determine the directions of the transition moments of the UV bands in Pb and Cu stearate mono- and bilayers, we measured their polarization spectra with the 45° oblique angle incidence of plane polarized lights, as is shown in Figs. 11 and 12. The absorption for the S-polarized light was stronger than that for the P-polarized lights, in all the cases. From the dichroic

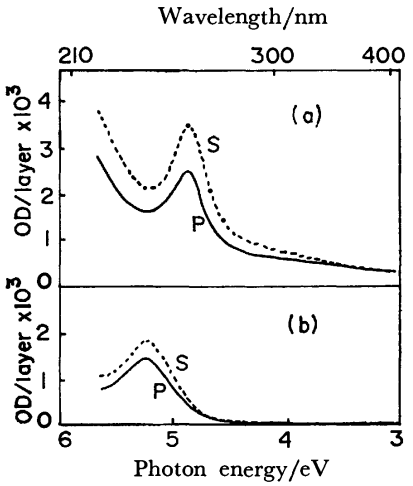

Fig. 11. UV polarization spectra of stearic acid bilayer (a) and monolayer (b) with Cu^{2+} prepared on the subphases containing 6×10^{-7} M $PbCl_2$ at pH 5.4 and 5.7, respectively. The angle of incidence was 45° with the lights plane polarized perpendicularly (---) and parallely (——) to the plane of incidence.

Table 3. The direction of the transition moment of the UV bands of Pb and Cu stearate mono- and bilayers

Ion	Layer number	R_{app} [a]	R [b]	n [c]	θ [d]
Pb	Monolayer	1.28 (at 237 nm)	1.07	1.515	59°
	Bilayer	1.41 (at 255 nm)	1.18	1.505	69°
Cu	Monolayer	1.37 (at 254 nm)	1.15	1.506	65°
	Bilayer	1.30 (at 260 nm)	1.09	1.503	61°

a) The apparent dichroic ratio at the wavelength in parentheses. b) The dichroic ratio after the correction for the interference effect.[27] c) The refractive index of quartz at the peak position that was used in the calculation as the refractive index of the mono- or bilayer. d) The angle of the transition moment against the normal of the layer plane

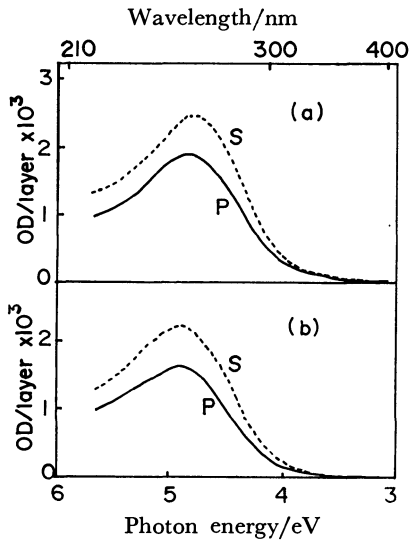

Fig. 12. UV polarization spectra of stearic acid bilayer (a) and monolayer (b) with Cu^{2+} prepared on the subphase containing 5×10^{-4} M $CuCl_2$ at pH 5.1. The angle of incidence was 45° with the lights plane polarized perpendicularly (---) and parallely (——) to the plane of incidence.

ratios at the peak positions, we calculated the angle, θ, of the transition moment against the molecular axis (Table 3). In the calculation, the molecular axes were assumed to be arranged perpendicularly to the layer plane; we used as the refractive index of the mono- and bilayers the values of quartz[26] at the peak positions, since we had no data about the refractive index at the peak positions and since quartz had a refractive index with a value close to those of the fatty acid multilayers at the Na D line, as was mentioned in I. We also made a correction for the interference effect[27] according to Matsuki *et al.*,[4] because, in the present systems, chromopores are arranged in a restricted layer.

The directions of the transition moments are tilted against the normal of the layer plane, as may be seen in Table 3. From the X-ray data of the Pb stearate multilayer,[28] we can estimate as about 40° the angle of the direction connecting the Pb ion and the oxygen atom in a lead(II) carboxylate complex against the normal of the layer plane. This angle is smaller than the angles of the transition moment obtained by us. However, the X-ray value is not so reliable because of the technical difficulty in the X-ray analysis of multilayers.

The tilting of the transition moments against the normal of the layer plane shows that the transitions are of a charge-transfer character. The same assignment was made for the UV bands of $PbCl_2$ and $CuCl_2$ in an aqueous solution.[29]

The θ angle in the Pb stearate bilayer is larger by about 10° than that in the Pb stearate monolayer. This shows that the lead(II) carboxylate complexes in the bilayer are distorted compared to the complexes in the monolayer in a manner to arrange the Pb ions closer to the layer plane of the carboxylate anions. The large red shift of the peak position in the bilayer may be due to this distortion, that may accompany an increase in the coordination number.[29]

The θ angles in Cu stearate mono- and bilayers are nearly the same. The small red shift in the peak position of the bilayer suggests that there may be a small distortion in the copper(II) carboxylate complexes, accompanied by the formation of a bilayer. Our data about the θ angle are consistent with the smallness of the red shift, but, unfortunately, are not of so high a precision as to enable us to detect conclusively such a small change in θ as only a few degrees.

It was shown that hyperchromicity is produced by the excitonic interaction of chromophores when they are packed in a head to tail arrangement of their transition moments.[30,31] The hyperchromicity of Pb and Cu stearate multilayers against the bilayers may be due to the interlayer excitonic interaction of the Pb and Cu carboxylate complexes. The tilting of the transition moments against the layer plane may produce a head to tail like packing of them. The interlayer distance is too long to produce a strong excitonic interaction between individual chromophores. However, in multilayers, chromophores form infinitely wide, two-dimensional layers, so that the integrated excitonic interaction between layers may become strong in spite of the weak interaction between individual chromophores. To elucidate the origin of the hyperchromocity, it is necessary to develop theory for excitonic interaction and its optical consequences in multilayers.

The authors would like to express their thanks to Professor Katsunosuke Machida for allowing us to use the JASCO-IRA-2 spectrometer in his laboratory and to Professor Rizo Kato for allowing us to use the VUV polarizer in his laboratory.

References

1) Y. Nagahira, K. Matsuki, and H. Fukutome, *Bull. Chem. Soc. Jpn.*, **54**, 1217 (1981).
2) J. W. Ellis and J. L. Pauley, *J. Coll. Sci.*, **19**, 755 (1964).
3) T. Sasaki and M. Muramatsu, *Bull. Chem. Soc. Jpn.*, **29**,

35 (1956).
4) K. Matsuki, Y. Nagahira, and H. Fukutome, *Bull. Chem. Soc. Jpn.*, **53**, 1817 (1980).
5) H. Bucher, O. V. Elsner, D. Möbius, P. Tillman, and J. Wiegand, *Z. Phys. Chem.* **65**, 152 (1969).
6) K. B. Blodgett, *J. Am. Chem. Soc.*, **56**, 1007 (1935).
7) Ronald D. Neuman and J. W. Swanson, *J. Colloid Interface Sci.*, **74**, 244 (1980).
8) Ronald D. Neuman, *J. Colloid Interface Sci.*, **63**, 106 (1978).
9) J. A. Spink, *J. Colloid Interface Sci.*, **23**, 9 (1967).
10) E. P. Honig, J. H. Th. Hengst, and D. Den Engelsen, *J. Colloid Interface Sci.*, **45**, 92 (1973).
11) R. Matsuura, *Nihon Kagaku Zasshi*, **86**, 560 (1965).
12) T. Takenaka, K. Nogami, H. Gotoh, and R. Gotoh, *J. Colloid Interface Sci.*, **35**, 395 (1971).
13) T. Takenaka, K. Nogami, and H. Gotoh, *J. Colloid Interface Sci.*, **40**, 409 (1972).
14) Y. Nagahira, Y. Jido, and H. Fukutome, *Chem. Phys. Lett.*, **34**, 95 (1975).
15) H. Akutsu, Y. Kyogoku, H. Nakahara, and K. Fukuda, *Chem. Phys. Lipids*, **15**, 222 (1975).
16) G. L. Gaines, Jr., "Insoluble Monolayers at Liquid-Gas Interfaces," Wiley Interscience, New York (1966), p. 187.
17) A. E. Alexander, *Trans. Faraday Soc.*, **37**, 426 (1941).
18) E. E. Barnes and W. T. Simpson, *J. Chem. Phys.*, **3**, 670 (1963).
19) Y. Koyama, M. Yanagishita, S. Toda, and T. Matsuo, *J. Colloid Interface Sci.*, **61**, 438 (1977).
20) K. B. Blodgett and I. Langmuir, *Phys. Rev.*, **51**, 964 (1937).
21) G. L. Gaines, Jr., "Insoluble Monolayers at Liquid-Gas Interfaces," Wiley Interscience, New York (1966), p. 341.
22) L. H. Germer and K. H. Stokes, *J. Chem. Phys.*, **6**, 280 (1938).
23) E. Havinga and J. de Wael, *Rec. Trav. Chim.*, **56**, 375 (1937).
24) J. de Wael and E. Havinga, *Rec. Trav. Chim.*, **59**, 770 (1940).
25) S. Bernstein, *J. Am. Chem. Soc.*, **62**, 374 (1940).
26) T. Sasaki, H. Fukutani, and K. Ishiguro, *Jpn. J. Appl. Phys.*, **4**, 527 (1965).
27) H. Kuhn, D. Möbius, and H. Bücher, "Technique of Chemistry," ed by A. Weissberger and B. W. Rossiter, Wiley Intersciences, New York (1972), Vol. 1.
28) J. F. Stephens and C. T. Lee, *J. Appl. Crystallogr.*, **2**, 1 (1969).
29) H. Fromherz and K. Lih, *Z. Phys. Chem., A*, **153**, 321 (1931).
30) I. Tinoco, *J. Am. Chem. Soc.*, **82**, 4787 (1960).
31) W. Rhodes, *J. Am. Chem. Soc.*, **83**, 3609 (1961).

The Vacuum Ultraviolet Absorption Spectra of Fatty Acid Multilayers

Yukio NAGAHIRA,*,† Kazunori MATSUKI, and Hideo FUKUTOME
Department of Physics, Faculty of Science, Kyoto University, Sakyo-ku, Kyoto 606
(Received August 28, 1980)

The electronic absorption spectra of fatty acid multilayers were measured in the vacuum ultraviolet region with an energy below 10 eV. From the chain length dependence of the spectra, the strong absorption (above 8 eV) was assigned to the σ-σ^* transitions in the alkane chain moiety, and the weaker one (below 8 eV), to the transitions in the carboxylic acid and metal carboxylate moieties. The polarized spectra of the Ba stearate multilayer showed that the band near 8.8 eV was polarized perpendicularly to the alkane chain. The spectra of the stearic acid multilayer without metal ions and the multilayer of the Zn stearate showed that their alkane chains were titled against the normal of the layer plane.

Fatty acid multilayers prepared by the Langmuir-Blodgett technique[1] are excellent objects for the measurement of the electronic absorption spectra of long alkane chains. In multilayers, the alkane chain and carboxylic acid moieties of fatty acids are arranged in regular two-dimensional layers, and the number of the layer can be controlled at any desired value. This property of multilayers makes it possible to measure the spectra of long alkane chains, which are difficult to measure in crystalline samples. The electronic absorption spectra of alkane chains and carboxylic acids lie in the vacuum ultraviolet (VUV) region. However, by depositing multilayers on a LiF or CaF_2 plate, spectra up to 10 eV can be measured. In a previous paper[2] we reported preliminary results for the VUV spectra of fatty acid multilayers. The VUV spectra of fatty acid multilayers provide information about the structures of multilayers and their interaction with metal ions, as well as basic information about the electronic structures of alkane chains. In this and an accompanying paper, we present the results of a systematic study of the VUV spectra of fatty acid multilayers. In this paper we deal mainly with the contribution of the alkane chain moiety in the VUV spectra. Studies of the chain length dependence and the polarization of the spectra are the main subjects of this paper. The application of the VUV spectra to the study of the molecular arrangement in multilayers is also made. Studies of the spectra of metal carboxylate moieties will be presented in an accompaying paper.[20]

Experimental

The crystalline stearic acid ($C_{17}H_{35}COOH$) was purchased from the Merck Co. The arachidic acid ($C_{19}H_{39}COOH$), heneicosanoic acid ($C_{20}H_{41}COOH$), and behenic acid ($C_{21}H_{43}COOH$) were purchased from Nakarai Chemicals, Ltd. The melting points of theses fatty acids were 70.0 °C, 76.0 °C, 74.0 °C, and 79.0 °C respectively, they agreed with the reported values[3] within an error of 1 °C. Guaranteed-reagent grade metal chlorides and spectrograde benzene were purchased from Nakarai Chemicals, Ltd. These chemicals were used without further purification. Twice-distilled water was used in all the experiments. A single crystal of CaF_2 was purchased from the Hursh Co., Ltd.

The fatty acid multilayers were prepared according to the Langmuir-Blodgett method[1] at 19±0.5 °C in a thermostated room. The pH of the water subphase was adjusted by the use of $KHCO_3$, HCl, or KOH. The fatty acids were spread on the water surface as a 0.1% (w/v) benzene solution, and caster oil was used as the piston oil (pressure, 16.5 dyn/cm). Plates of CaF_2 cleaved from a CaF_2 single crystal by a clean razor were used as the depositing plates. The CaF_2 plates were transparent up to 10 eV; their absorption was confirmed to be unchanged by dipping into water.

The deposition of fatty acid multilayers with bivalent metal ions was performed using CaF_2 plates coated with one layer of Fe stearate by the Langmuir method[4] and on the water subphase containing 10^{-4} M metal chloride at a neutral pH. Under these conditions with $BaCl_2$ and $CdCl_2$ multilayers were deposited as Y layers.[1,4-6] The deposition of multilayers was confirmed by the observation of the meniscus of the subphase near the dipping plate and by the linearity of the VUV absorption strength of the deposited multilayers to the number of times the plates were dipped into the subphase.[2]

The stearic acid monolayer on the subphase without metal ions at an acid pH could not be deposited on the CaF_2 plate coated with one layer of Fe stearate. To make the deposition possible, 4 layers of stearic acid with Ba ions were pre-deposited on the plate from the subphase with 10^{-4} M $BaCl_2$ at a neutral pH. After this treatment of the plate, the deposition of stearic acid multilayers at an acid pH became possible, but not so surely as the deposition at a neutral pH. From the observation of the meniscus when the plate was dipped only a few times, the stearic acid multilayer prepared at an acid pH without metal ions appeared to be of X-type layers.

The VUV absorption spectra were measured with a Shimadzu-SGV-50 VUV spectrometer (Seya-Namioka type with 50 cm focus concave grating blazed at 1500 Å and with 1200 rulings/mm. Light source, Tousey-type hydrogen discharge arc.). The apparatus was equipped with a beam splitter made of grazing incidence mirrors, and both the reference and sample signals were recorded. We used as the reference a CaF_2 plate coated with one layer of Fe stearate, so that the reflection at the surface of the sample plate was almost completely compensated for. A spectrum was measured after a plate with a multilayer had stood *in vacuo* for about three hours. An LiF polarizer with the Brewster angle reflection was used to obtain plane polarized VUV light. The polarizer was inserted between the light source and the entrance slit of the monochrometer.

Plates deposited with 8 layers of fatty acid (with 2 dippings of the plates for Y-type layers or 4 dippings for X-type layers) were used in all the spectral measurements to make the optical density in an appropriate range. The background spectra due to the pre-coating of the plates were substrated from the apparent spectra. All the spectra shown in this paper are those normalized to the per-layer value except for that of the pure stearic acid multilayer prepared at an acid pH, in which

† Present address: Osaka University of Economics and Law, Yao, Osaka 581.

the deposition at each dipping is not sure (see text).

Results and Discussion

We show in Fig. 1 the VUV absorption spectra of the stearic acid, arachidic acid, and behenic acid multilayers prepared on the water subphase containing Ba ions at a neutral pH. The spectra can be divided into two regions; the region of high absorption above 8 eV (Region 1), and the region of weaker absorption below 8 eV (Region 2). The spectra in Region 2 all have the same strength and shape, which do not depend on the carbon number, n, of the alkane chain moiety. The spectra in Region 1, on the other hand, have a broad maximum near 8.8 eV, and their strengths increase with the carbon number, n, though their shapes are homologous. We show in Fig. 2 the n dependence of the absorption in Region 1 (at 9 eV). The multilayers were prepared on the subphase containing Ba, Sr, Mg, Mn, or Cd ions at a neutral pH. In all the cases, the shapes of the spectra in Region 1 were homologous. We show in Fig. 2 that the absorption in Region 1 is proportional to n except for the stearic acid ($n=17$) multilayers with Mn, Sr, or Ba. The absorptions of these stearic acid multilayers, which showed deviations from the proportionality to n, were found to decrease slowly with the time, keeping their spectral shapes homologous in the whole wavelength region when they were kept *in vacuo*. This shows that stearic acids in the multilayers sublime slowly *in vacuo*, leading to the formation of a skeletal film.[4] The sublimation of stearic acids from the multilayers can explain the deviation from the proportionality to n.

From these results, we can assign the absorption in the Region 1 mainly to the σ-σ^* transitions in the alkane chain moiety, and that in Region 2, to the transitions in the carboxylic acid and metal carboxylate moieties. The absorption edge of polyethylene was reported to lie at 7.5 eV. The edge of the strong absorption of Region 1 is at the same position as the absorption edge of polyethylene, supporting our assignment.

In order to ascertain the polarization of the σ-σ^* transitions of the alkane chain moiety in Region 1, we measured the polarization spectra of a stearic acid multilayer with Ba ions prepared at a neutral pH (Fig. 3). The polarization spectra of normal incidence had no anisotropy, showing that the multilayer was uniaxial. The polarization spectra of 45° angle incidence showed a stronger absorption for the light with an electric field vector perpendicular to the plane of incidence (S-polarization) than the light with an electric field vector parallel to it (P-polarization) in both the regions, 1 and 2. We show in Table 1 the photon energy dependence of the dichroic ratio, A_S/A_P,

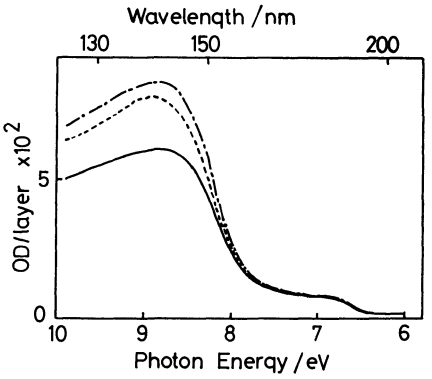

Fig. 1. Per layer absorption spectra of the stearic acid (——), arachidic acid (– – –) and behenic acid (—·—) multilayers prepared on the subphase with 10^{-4} M $BaCl_2$ at pH 7.6.

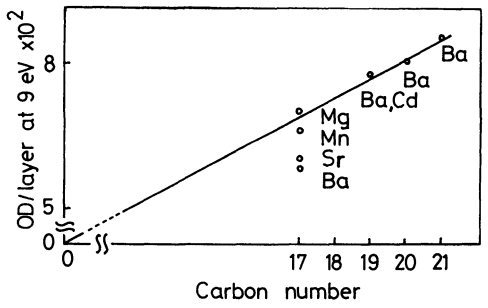

Fig. 2. Dependence of the per layer absorption strength at 9.0 eV of fatty acid multilayers on the carbon munber n of the alkane chain moiety. The multilayers were prepared on the subphase with 10^{-4} M metal chloride at neutral pH.

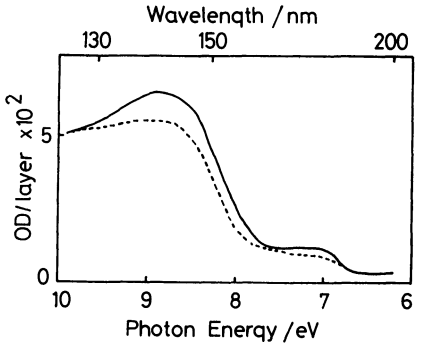

Fig. 3. Per-layer polarized spectra at 45° incidence of the stearic acid multilayer prepared on the subphase with 3×10^{-5} M $BaCl_2$ at pH 7.2. The spectrum for S polarized light (——) and the one for P polarized light (– – –).

Table 1. The angle of the transition moments of region 1 against the molecular axis

Photon energy/eV	$R(=A_s/A_p)$	$\theta(n=1.70)$	$\theta(n=1.50)$
8.3	1.30	90°[a]	90°[b]
8.4	1.29	90°[a]	90°
8.5	1.29	90°[a]	90°
8.6	1.22	90°[a]	73°
8.7	1.22	90°[a]	73°
8.8	1.20	82°	71°
8.9	1.17	74°	67°
9.0	1.16	72°	66°
9.1	1.15	70°	65°

a) The observed value of R exceeds the theoretical value, 1.21, for $\theta=90°$. b) The observed value of R exceeds the theoretical value, 1.29, for $\theta=90°$.

in Region 1, where A_S and A_P are the absorption strengths for the S and P polarized lights respectively. In the present system, the apparant dichroic ratio, A_S/A_P, represents the true dichroic ratio because the chromophores, *i.e.*, the alkane chains, are distributed nearly uniformly in the multilayer, and so no correction for the interference effect,[7] such as is necessary for multilayers with chromophores distributed only in a restricted layer, is necessary.

Stearic acid multilayers with Ba ions prepared at a neutral pH have been reported to have a layer structure with the molecular axes arranged near perpendicularly to the layer plane.[1,4,6,8-11] Assuming a perpendicular arrangement of alkane chains, and using the method of Akutsu *et al.*,[12] we calculated, from the observed dichroic ratio, the angle, θ, between the chain axis and the transition moment of the σ-σ^* transition near the absorption maximum of Region 1. (Akutsu *et al.*'s method assumes that the alkane chains in a monolayer have a uniform uniaxial distribution in their directions, with a tilting angle, γ, against the normal of the layer plane and that the transition moments with an angle, θ, against the chain axis, also have a uniform distribution around chain axis). The results are shown in Table 1. In the calculation of the angle, the value of the refractive index, n, in the VUV region is necessary. However, no data are available for it, and so we used $n=1.70$, that is, the value of quartz near 8 eV.[13] Since quartz has a refractive index with a value in the visible region similar to that of the fatty acid multilayer ($n=1.46$ for quartz and $n=1.49$—1.51, depending on the mixing ratio of stearic acid and metal stearate, for the fatty acid multilayer at the visible wavelength of 5890 nm[4,13]), and has an absorption edge near 7.5 eV, that is, close to that of the Region 1 absorption of fatty acid multilayers, the refractive index of fatty acid multilayers in the VUV region is considered to have a value similar to that of quartz. For the sake of comparison, we also show in Table 1 the results of the calculation using the value of $n=1.50$ in the visible region.

One may see in Table 1 that the dichroic ratio is nearly constant and that the angle between the transition moment and the chain axis calculated with $n=1.70$ is nearly perpendicular in the energy region from 8.6 eV to 8.8 eV. The angle calculated with $n=1.50$ is somewhat smaller. It is certain that the refractive index is larger in the VUV region than in the visible region and that the true value of the angle is larger than the one calculated with $n=1.50$.

Thus, the present measurement of the polarized spectra leads to the conclusion that the σ-σ^* transitions forming the absorption maximum in Region 1 are polarized perpendicularly to the molecular axis. The dichroic ratio begins to decrease in the higher energy region over 9 eV and becomes unity at 9.94 eV. This suggests that weak σ-σ^* transitions polarized in a parallel direction are present in this energy region or that the low energy tail of a strong σ-σ^* transition polarized in a parallel direction which may be present in the high energy region over 10 eV extends up to this energy region.

Based on the intramolecular exciton theory, Partridge estimated that the lowest parallel and perpendicular σ-σ^* transitions in polyethylene lie at 8.16 eV and 10.08 eV respectively.[14] Therefore, his estimates contradict our data. Based on the interband transition theory, McCubbin calculated that the lowest three transitions in polyethylene lie at 12.6, 13.6, and 16.9 eV and that all of them have perpendicular polarization.[15] The calculated peak positions are too high, but the direction of the transition moments is consistent with our data.

The polarization of the σ-σ^* transitions in Region 1 can be used for the study of the molecular arrangement in fatty acid multilayers. We show in Fig. 4 the normal incidence spectrum of the stearic acid multilayer prepared on the subphase with Zn ions at a neutral pH. The spectrum in Region 1 is apparently different from that of the stearic acid multilayer with Ba ions, with a weaker absorption strength in the energy region near 8.8 eV. We show in Table 2 the ratio of the absorption of the multilayer with Zn to that of the multilayer with Ba in the energy region near the absorption maximum. The ratio is nearly constant, though there is a weak decrease with the photon energy. The difference in the spectral shape can be ascribed to the fact that the multilayer with Zn ions has a tilting of the alkane chain axes against the normal of the layer plane. Assuming that the alkane chain axes in the multilayer with Ba ions are arranged perpendicularly to the layer plane, and that the σ-σ^* transitions near the absorption maximum are perpendicularly polarized against the chain axis, we calculated from the ratio the angle, γ, of the tilting of the chain axes in the multilayer with Zn ions using the method of Akutsu *et al.*[12] The results are shown in Table 2. The calculation gives angles of tilting in the range from 20° to 28°. The X-ray data about Ba stearate and Zn stearate crystals[16] showed that the inter-layer distances in these crystals were 47.5 Å and 42.6 Å respectively. The inter-layer distance of the Ba stearate crystal is consistent with the perpendicular packing of molecules against the layer plane. On the other hand, the inter-layer distence of the Zn stearate crystal shows that the axes of molecules are tilted against the normal of the layer plane. Assuming the perpendicular arrangement of molecules in the Ba stearate crystal, the angle, γ, of the tilting in the Zn

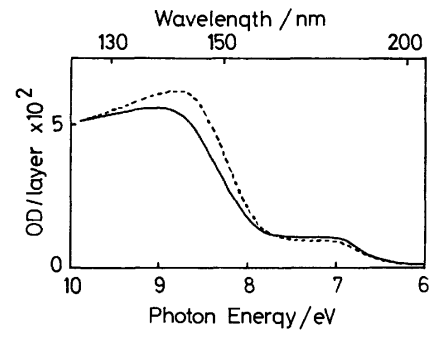

Fig. 4. Per-layer absorption spectrum of the stearic acid multilayer prepared on the subphase with 10^{-4} M $ZnCl_2$ at pH 6.5 (——). The per-layer spectrum of the stearic acid multilayer prepared on the subphase with 10^{-4} M $BaCl_2$ at pH 6.9 is also shown (– – –).

TABLE 2. THE TILTING ANGLE OF THE MOLECULAR AXIS AGAINST THE NORMAL OF THE LAYER PLANE IN THE Zn STEARATE MULTILAYER

Photon energy/eV	t[a)]	γ[b)]
8.4	0.90	19°
8.5	0.87	21°
8.6	0.85	23°
8.7	0.82	25°
8.8	0.80	27°
8.9	0.78	28°

a) t is the ratio of the per-layer absorptions of the Zn stearate multilayer to the Ba stearate multilayer. b) γ is the tilting angle of the molecular axis calculated from t.

stearate crystal is estimated from the $\cos\gamma=42.6/47.5$ relation to be $\gamma=26°$. The tilting angle estimated from our spectral data is in agreement with this X-ray value. We note also that the spectrum of the multilayer with Zn ions has the same intensity as that of the multilayer with Ba ions at the photon energy of 9.94 eV, just the energy where the S and P polarized spectra at the 45° incidence of the multilayer with Ba ions have the same strength (Fig. 3). This fact is also consistent with our interpretation that the change in the spectral shape of the multilayer with Zn ions is due to a change of polarization caused by a tilting of the molecular axis.

The spectrum in Region 1 of a pure stearic acid multilayer prepared on the subphase without metal ions at an acid pH is also different from that of the multilayer with Ba ions, as is shown in Fig. 5. In the case of the pure stearic acid multilayer, the deposition of monolayers on the plate is not so sure as in the case of the multilayers with bivalent metal ions. Furthermore, observation of the meniscus showed that the deposition occurred in such a manner as to give X-type layers for the first several dippings of the plate, but they became Y-type layers after several dippings. Therefore, it is difficult to determine the number of deposited layers in a pure stearic acid multilayer. The multilayers of our samples, prepared with only four dippings, are too thin to apply the interference and infrared techniques in measuring their thicknesses. Therefore, we normalized the spectrum of the pure stearic acid multilayer by the following indirect method.

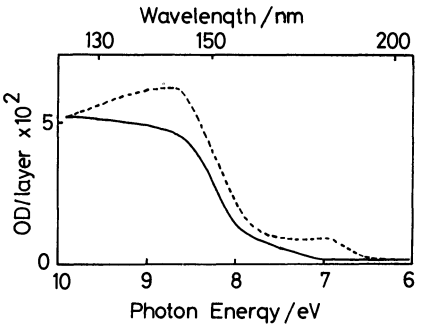

Fig. 5. Absorption spectrum of the stearic acid multilayer prepared on the subphase without metal ions at pH 3.0 (——). For the normalization of the spectrum, see text. The per layer spectrum of the stearic acid multilayer prepared on the subphase with 10^{-4} M $BaCl_2$ at pH 6.9 is also shown (----).

As may be seen in Figs. 3 and 4, the absorption of the alkane chain of stearic acid has the same strength at 9.94 eV irrespective of the polarization of incident light or the tilting of the chain axis. Hence, the photon energy of 9.94 eV is considered to be the isosbestic point for stearic acid multilayers with different directions of the σ-σ^* transition moments. Therefore, we normalized the spectrum of the pure stearic acid multilayer so as to have the same absorption strength at 9.94 eV as the multilayer with Ba ions.

We show in Table 3 the ratio of the absorption strength of the pure stearic acid multilayer thus normalized to the absorption strength of the stearic acid multilayer with Ba ions in the energy region near the absorption maximum. The ratio is fairly constant in this energy region. We calculated from the ratio the tilting angle of alkane chain axis in the pure stearic acid multilayer (Table 3). The calculation showed that alkane chain axes in the pure stearic acid multilayer are tilted by about 30° against the normal of the layer plane. This tilting is in good agreement with the reported value, ≈30°, measured with the infrared spectra.[17]

TABLE 3. THE TILTING ANGLE OF THE MOLECULAR AXIS AGAINST THE NORMAL OF THE LAYER PLANE IN THE PURE STEARIC ACID MULTILAYER

Photon energy/eV	t[a)]	γ[b)]
8.4	0.74	31°
8.5	0.76	30°
8.6	0.73	32°
8.7	0.75	30°
8.8	0.76	30°
8.9	0.78	28°

a) t is the ratio of the per-layer absorptions of the pure stearic acid multilayer to the Ba stearate multilayer. b) γ is the same as Table 2.

The spectrum in Region 2 of the stearic acid multilayer lacks the absorption near 7 eV which is present in the spectrum of the multilayer with Ba ions. The absence of the band near 7 eV cannot be explained by the tilting of the molecules, rather, it is attributable to the difference in the state of the carboxylic acid moiety. The former multilayer consists only of unionized stearic acids, but the latter is a mixture of Ba stearate and unionized stearic acid.[18,19] As we shall show in the accompanying paper, the band near 7 eV can be ascribed to the Ba carboxylate and unhydrogen-bonded carboxylic acid moieties, but the carboxylic acid moieties in the pure stearic acid multilayer are hydrogen-bonded. We stress that the marked pH dependence (and the metal ion dependence discussed in the accompanying paper) of the absorption in Region 2 support the assignment of it to the transitions in the carboxylic acid and metal carboxylate moieties.

References

1) K. B. Blodgett, *J. Am. Chem. Soc.*, **57**, 1007 (1935).
2) Y. Nagahira, Y. Jido, and H. Fukutomo, *Chem. Phys.*

Lett., **34**, 95 (1975).
3) "The Merck Index," 9th ed by M. Windholz, Merck and Co., U.S.A. (1976): Monograph number 8582, 792, 1029.
4) K. B. Blodgett and I. Langmuir, *Phys. Rev.*, **51**, 964 (1937).
5) H. H. Race and S. I. Reynolds, *J. Am. Chem. Soc.*, **61**, 1425 (1939).
6) G. L. Gains, Jr., "Insoluble Monolayers at Liquid-Gas Interfaces," Wiley Interscience, New York (1966), p. 341.
7) H. Kuhn, D. Möbius, and H. Bücher, "Physical Methods of Chemistry," ed by A. Weissberger and B. W. Rossiter, Wiley-Interscience (1972), Vol. 1, Pt. III B, Chap. VII.
8) L. H. Germer and K. H. Stokes, *J. Chem. Phys.*, **6**, 280 (1938).
9) E. Havinga and J. de Wael, *Rec. Trav. Chim.*, **56**, 375 (1937).
10) J. de Wael and E. Havinga, *Rec. Trav. Chim.*, **59**, 770 (1940).
11) S. Bernstein, *J. Am. Chem. Soc.*, **62**, 374 (1940).
12) H. Akutsu, Y. Kyogoku, H. Nakahara, and K. Fukuda, *Chem. Phys. Lipids.* **15**, 222 (1975).
13) T. Sasaki, H. Fukutani, and K. Ishiguro, *Jpn. J. Appl. Phys.*, **4**, 527 (1965).
14) R. H. Partridge, *J. Chem. Phys.*, **49**, 3656 (1968).
15) W. T. McCubbin, "Electronic Structure of Polymers and Molecular Crystals," ed by J. M. Andre and J. Latik, Plenum, New York (1975), p. 171.
16) R. Matsuura, *Nihon Kagaku Zasshi*, **86**, 560 (1965).
17) T. Takenaka, K. Nogami, H. Gotoh, and R. Gotoh, *J. Coll. Inter. Sci.*, **35**, 395 (1972).
18) I. Langmuir and V. J. Schaefer, *J. Am. Chem. Soc.*, **58**, 284 (1936).
19) J. W. Ellis and J. L. Pauley, *J. Coll. Sci.*, **19**, 755 (1964).
20) Y. Nagahira, K. Matsuki, and H. Fukutome, *Bull. Chem. Soc. Jpn.*, **54**, 1208 (1981).

Kinetic Isotope Effect of Chemically Activated Vinyl Radicals

Ken-ichi KOWARI, Ko-ichi SUGAWARA, Shin SATO,* and Shigeru NAGASE†

Department of Applied Physics, Tokyo Institute of Technology, Ookayama, Meguro-ku, Tokyo 152

†Chemistry Division, Faculty of Education, Yokohama National University, Hodogaya-ku, Yokohama 240

(Received September 1, 1980)

The apparent decay rates of hydrogen and deuterium atoms in the reactions with acetylene-d_0 and -d_2 in helium in the pressure range from 100 to 800 Torr (1 Torr=133.3 Pa) have been measured by the pulse radiolysis-Lyman-α absorption method at 300±2 K. The helium pressure dependence of the rate constants was well interpreted in terms of the RRKM theory including a tunneling effect, using the geometry and force constants of the activated complex and vinyl radical estimated by the *ab initio* calculation. (S. Nagase and C. W. Kern, *J. Am. Chem. Soc.*, **101**, 2544 (1979).)

The reaction of hydrogen atoms with acetylene has been investigated during the last half century.[1-10] The primary reaction mechanism established may be expressed as follows:

$$H + C_2H_2 \leftrightarrows C_2H_3^* \xrightarrow{+M} C_2H_3$$

Here $C_2H_3^*$ denotes an energized vinyl radical which can re-form reactants or be deactivated to a stable vinyl radical by a collision with a third body.

Recently Keil *et al.* reported two kinds of experiments:[11] one used a mass spectrometer in a flow system for the measurement of the rate constants of the reactions $H+C_2H_2$, $H+C_2D_2$, $D+C_2H_2$, and $D+C_2D_2$ in the pressure range from 1 to 7 Torr, and the other used a time-resolved Lyman-α photometric method for the measurement of the decay rate of H atoms in the reaction with C_2H_2 in flowing helium in the pressure range from 1 to 742 Torr. In order to explain the pressure dependence of these rate constants, they applied the RRKM theory, in which various parameters such as the geometry and vibrational frequencies of an activated complex were estimated by a somewhat arbitrary method.

In a previous investigation,[12] we measured the rate constants of the reactions $H+C_2H_2$, $H+C_2D_2$, $D+C_2H_2$, and $D+C_2D_2$, by means of the pulse radiolysis-Lyman-α absorption method. In that measurement, the hydrogen pressure was varied from 300 to 1200 Torr and no pressure dependence of the rate constants was observed. In the present study, we used helium as the third body and found the pressure dependence similar to that observed by Keil *et al.*

The recent development of the *ab initio* calculation has been considerable and the potential energy surfaces calculated for some simple reactions are believed to be not far from the real ones. Nagase and Kern have calculated the potential energy surface for the $H+C_2H_2$ reaction and predicted the geometry and force constants of the activated complex and of the vinyl radical.[13] We tried to use these calculated results to explain the kinetic isotope effects observed in the present experiments in terms of the RRKM theory. In the present calculation, however, there is an important assumption, which should in fairness be stated at the outset. The energy barrier for the reaction of $H+C_2H_2$ calculated by Nagase and Kern was 6.2 kcal/mol (1 kcal=4.184 kJ). This value seemed to be too large and was not used in the following calculation.

Experimental

The apparatus and procedures used in this study are the same as those described in a previous paper,[14] so we mention here only the major features.

Figure 1 shows the apparatus schematically. A mixture of 5 Torr H_2 or D_2 and a small amount of C_2H_2 or C_2D_2 (50—130 mTorr) diluted with He (100—800 Torr) was irradiated with an electron pulse (pulse width, 3 ns; upper limit of energy, 600 keV) generated by a Febetron 706 (Hewlett Packard Co.). The time dependence of the concentration of H or D atoms was measured by the absorption of Lyman-α (121.57 nm for H and 121.53 nm for D). The transmitted light was directly detected with a head-on type photomultiplier (Hamamatsu TV Co., R976), which was monitored with an oscilloscope (Tektronix 465). As has been discussed in previous papers,[14,15] the optical density used for the measurement is proportional to the atom concentration in this technique.

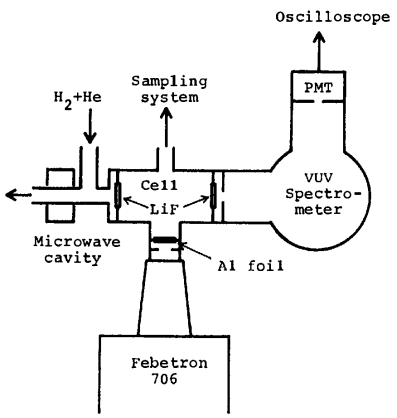

Fig. 1. Schematic diagram of the apparatus.

The high-purity dried He (Nihon Helium Co.) was passed through a trap filled with molecular sieve 4A at 77 K before use. Research grade H_2, D_2, and C_2H_2 (Takachiho Shoji Co.) were used without further purification. C_2D_2 was synthesized by the reaction of D_2O (above 99.99%, Merck Co.) with CaC_2 (Tokyo Kasei Co.), which was heated at about 500 °C for 70 h in vacuum prior to use. The C_2D_2 thus obtained was shaken with sulfuric acid for 1 h. The mass and infrared spectra showed that the purity of C_2D_2 was better than 99%.

Results

In the absence of acetylene, practically no change of the atom concentration could be observed in the time

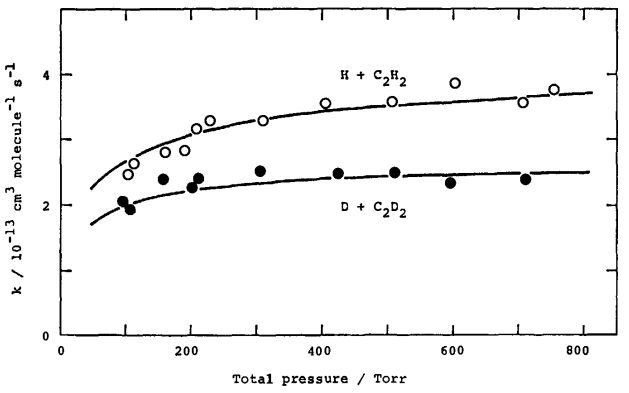

Fig. 2. The apparent decay rates of H atoms in the H+C_2H_2 reaction (○), and of D atoms in the D+C_2D_2 reaction (●) as functions of the total pressure. Solid curves were theoretically calculated.

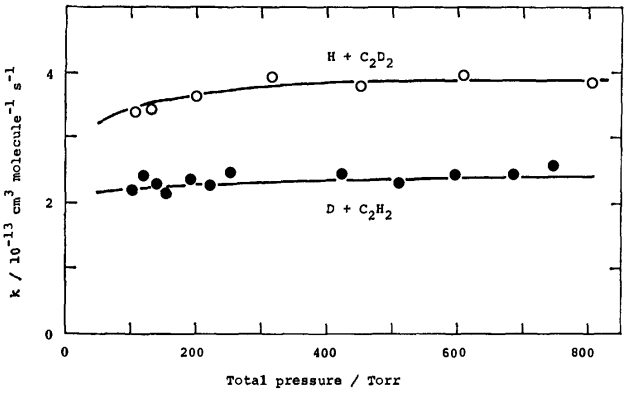

Fig. 3. The apparent decay rates of H atoms in the H+C_2D_2 reaction (○), and of D atoms in the D+C_2H_2 reaction (●) as functions of the total pressure. Solid curves were theoretically calculated.

range of 10 ms, while in the presence of 50 mTorr acetylene, the atoms decayed completely within 10 ms. From this first-order decay curve and the concentration of acetylene used, the rate constant of the reaction could be estimated.

Figures 2 and 3 show the rate constants obtained for the reactions of H+C_2H_2, D+C_2D_2, D+C_2H_2, and H+C_2D_2 as functions of total pressure. Below 100 Torr of helium, the atom concentration was too small for the measurement of the time dependence. It should be noted that the rate constant of the H+C_2H_2 reaction is strongly dependent upon helium pressure, while that for the D+C_2H_2 reaction is almost independent of helium pressure.

Theoretical Calculation

The treatment of the RRKM theory has been fully discussed in a book by Robinson and Holbrook.[16] The present experiments correspond to one of the chemical activations discussed in that book.

Let us consider the following reaction:

$$R + R' \leftrightarrows A^\dagger \leftrightarrows A^* \xrightarrow{+M} A.$$

Here, R and R′ denote reactants, $A^\dagger$ an activated complex, A* an energized product, and A a stabilized product. In the nomenclature used by Robinson and Holbrook, the bimolecular rate constant of the reaction between R and R′ may be expressed as follows:

$$k = k_\infty \int_0^\infty \frac{\omega f(E)}{\omega + k_a(E)} dE. \quad (1)$$

Here ω is the collision frequency between A* and the third body, $k_a(E)$ the rate constant of the decomposition of A*, $f(E)$ the non-equilibrium distribution of energy of A*, and k_∞ the bimolecular rate constant in the limit of high pressure.

In order to calculate these parameters, we have to use many approximations, which appear in the RRKM theory. Since many different degrees of approximation are introduced in the book of Robinson and Holbrook, the minimum number of equations used in the present calculation will be given below without any detailed interpretations.

$$\omega = \beta_c z p \quad (2)$$

$$z = \sigma_d^2 (8\pi N_A/\mu kT)^{1/2} \quad (3)$$

Here β_c is the collisional efficiency, z the collision frequency at 1 Torr of the third body, p the pressure, σ_d the collision radius, μ the reduced mass of A* and the third body, T the temperature, N_A Avogadro's number, and k the Boltzmann constant.

$$k_a(E) = L^\dagger (Q^\dagger/Q)[1/hN(E)] \times \left[\sum_{E_{vr}^\dagger=0}^{E} \kappa(E - E_{vr}^\dagger) P(E_{vr}^\dagger)\right] \quad (4)$$

$L^\dagger$ is the reaction path degeneracy and $Q^\dagger$ and Q the partition functions for the over-all rotations of $A^\dagger$ and A. The term $\kappa(E-E_{vr}^\dagger)$ is the transmission coefficient, which was not discussed in the book of Robinson and Holbrook; however, recent theoretical calculations on the hydrogen atom-molecule reaction revealed that the tunneling effect cannot be ignored even at room temperature, if a hydrogen atom is transferred in the reaction.[17] There are several ways to estimate the tunneling effect. One of the simplest ways is to use the transmission coefficient for the inverted parabolic potential barrier in one dimension.

$$\kappa(E) = (1 + \exp[2\pi(E - V_0)/h\nu])^{-1} \quad (5)$$

Here V_0 is the barrier height and $h\nu$ is the magnitude of the immaginary vibrational quanta. This expression has already been discussed by Kato and Morokuma in the unimolecular decomposition of CH_2CH_2F radicals.[18] $P(E_{vr}^\dagger)$ denotes the number of vibrational-rotational quantum states of $A^\dagger$ with vibrational-rotational non-fixed energy equal to $E_{vr}^\dagger$, h the Planck's constant, and $N(E)$ the density of quantum states of A* with energy between E and $E+dE$. Since in the H+C_2H_2 reaction, no active rotation is involved in $A^\dagger$, the term $P(E_{vr}^\dagger)$ becomes simply $P(E_v^\dagger)$, a value which has been counted directly. The $N(E)$ has been calculated by using the Whitten-Rabinovitch approximation:

$$N(E) = \frac{Q_r}{(kT)^{r/2}} \frac{(E + aE_z)^{s+r/2-1}}{\Gamma\left(s + \frac{r}{2}\right) \Pi h\nu_i} \left[1 - \beta\left(\frac{dw}{dE'}\right)\right]. \quad (6)$$

Here, Q_r is the partition function for the active rotations

in A*, r and s the number of active rotations and vibrations, E_z the sum of zero-point energies, ν_i the frequency of the i-th mode, and $E'=E/E_z$. According to Whitten and Rabinovitch, a, β, and w can be expressed as follows:

$$a = 1 - \beta w(E') \tag{7}$$

$$\left.\begin{aligned}(0.1<E'<1.0)\ \mathrm{d}w/\mathrm{d}E' &= -(5.00+1.365\,E'^{-0.75})w^2\\ (1.0<E'<8.0)\ \mathrm{d}w/\mathrm{d}E' &= -(0.60478E'^{-0.75})w\end{aligned}\right\} \tag{8}$$

$$\beta = \frac{s-1}{s}\,\frac{s+\frac{r}{2}}{s}\,\frac{\langle\nu^2\rangle}{\langle\nu\rangle^2}. \tag{9}$$

Here $\langle\nu\rangle$ and $\langle\nu^2\rangle$ are the mean frequency and mean-square frequency of A. In the present calculation, all vibrations and the rotation around the C–C bond in vinyl radical were taken as active. If the rotation was taken as inactive, we had to assume an extraordinarily large collision radius.

The distribution function $f(E)$ can be derived by using the principle of detailed balance:

$$f(E) = k_a(E)K(E)/\int_0^\infty k_a(E)K(E)\mathrm{d}E\,. \tag{10}$$

Here $K(E)$ is the Boltzmann distribution function of A.

$$K(E) = N(E)\exp(-E/kT)/\int_0^\infty N(E)\exp(-E/kT)\mathrm{d}E \tag{11}$$

To perform the RRKM calculation, we need the moments of inertia and the vibrational frequencies of the activated complex and the vinyl radical, the barrier height, and the minimum energy of the energized product, E_{min}, together with the molecular diameters of He (0.257 nm) and the vinyl radical (0.423 nm); the latter was assumed to be the average of acetylene and ethylene.[19] The *ad initio* calculation of Nagase and Kern using the 4-31G basis set provides the necessary data. Figure 4 shows the geometry of the activated complex and the vinyl radical. Table 1 summarizes the moments of inertia and the fundamental vibrational frequencies calculated by the GF-matrix method using the force constants reported. Here it should be noted that the activated complexes C_2H_2–D* and C_2HD–H* are different. Similarly two vinyl radicals, $\overset{D}{H}\!>\!C\!=\!C\!<^{H}$ and $\overset{D}{H}\!>\!C\!=\!C\!<^{H}$, should be taken as different radicals at the temperature of absolute zero, but, in the present calculation, these two radicals were assumed to be the same, since these two radicals are known to be in equilibrium even at 93 K.[20] In fact, the partition functions for these two radicals are the same in value within the limits of the calculation.

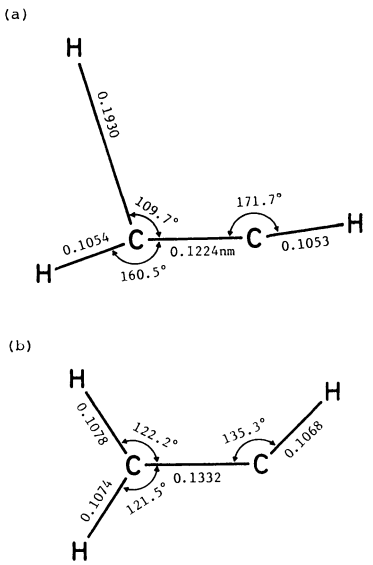

Fig. 4. The geometry of activated complex in the reaction of $H+C_2H_2$ (a) and of vinyl radical (b).

There is some uncertainty in the value of E_{min} because the heat of formation of vinyl radicals and the activation energy for the $H+C_2H_2$ reaction have not been established. We tentatively adopted 40 kcal/mol for the E_{min} of C_2H_3*. Since the $N(E)$ value is not strongly dependent on E_{min} around 40 kcal/mol, the adoption of this value does not restrict the conclusions of the following discussion. In the present calculation, the barrier height V_0 was also assumed to be equal to E_{min}. Table 1 contains the values of E_{min} for other isotopic vinyl radicals, which were calculated by taking into account the zero-point energies of each vinyl radical.

In order to calculate the absolute values of k, we need the values of k_∞ for each reaction. Table 2 summarizes the k_∞ values used in the present calculation. Since we have not measured the temperature dependence of the rate constants, we will not discuss the k_∞ values theoretically.

Reactions of $H+C_2H_2$ and $D+C_2D_2$. The calculation of Eq. 1 is now straight-forward for the $H+C_2H_2$ reaction. An adjustable parameter is the collisional frequency β_c in Eq. 3. The upper solid curve shown in Fig. 2 was drawn by assuming $\beta_c=0.078$. The scattering of the experimental results allowed us to estimate this value only within the error limit of $\pm15\%$. A similar calculation can be carried out for the $D+C_2D_2$ reaction. The lower solid curve in Fig. 2 was drawn by using the same collisional efficiency.

Reactions of $H+C_2D_2$ and $D+C_2H_2$. In these reactions, we have to consider two processes for the decomposition of energized vinyl radicals:

$$\begin{aligned}H + C_2D_2 &\rightarrow C_2D_2H^*\\ C_2D_2H^* &\rightarrow H + C_2D_2 \qquad k_{aH}(E)\\ &\rightarrow D + C_2DH \qquad k_{aD}(E)\\ &\overset{\omega}{\rightarrow} C_2D_2H.\end{aligned}$$

Consequently, the pressure dependence of the decay rate of H atoms should be expressed as follows:

$$k = k_\infty\int_0^\infty \frac{[\omega + k_{aD}(E)]f(E)}{\omega + k_{aH}(E) + k_{aD}(E)}\,\mathrm{d}E\,. \tag{12}$$

A similar equation can easily be constructed for the case of $D+C_2H_2$. The solid curves shown in Fig. 3 were calculated by using these equations. The same collisional efficiency was used. Although the scatter of the experimental data precludes any detailed comparison between experiment and theory, the trend of the pressure dependence could be reproduced by the calculation.

TABLE 1. PARAMETERS USED FOR CALCULATION

Species	Vibrational frequencies / cm^{-1}	Moments of inertia kg $m^2 \times 10^{-47}$ I_a	I_b	I_c	Critical energy E_{min} / kcal mol^{-1}
C_2H_3	3421	26.25	29.81	3.56*	
	3348				
	3253				
	1642				
	1421				
	1209				
	981				
	893				
	843				
C_2H_3†	3645	26.63	31.97	5.35	40.00
	3578				
	1764				
	884				
	793				
	703				
	577				
	479				
	890i				
C_2D_3	2534	34.91	41.75	6.84*	
	2487				
	2365				
	1457				
	1125				
	981				
	779				
	670				
	610				
C_2D_3†	2798	38.40	48.61	10.21	38.22
	2628				
	1611				
	634				
	600				
	576				
	467				
	355				
	698i				
C_2H_2D	3421	28.43	33.39	4.96*	
	3332				
	2403				
	1539				
	1364				
	1109				
	937				
	827				
	763				
C_2H_2--D†	3645	30.44	39.33	8.89	38.39
	3578				
	1757				
	824				
	793				
	699				
	554				
	384				
	723i				
C_2HD--H†	3622	30.35	36.16	5.81	36.81
	2707				
	1687				
	764				
	705				
	585				
	577				
	478				
	858i				
C_2D_2H	3274	33.14	38.10	4.96*	
	2533				
	2445				
	1523				
	1355				
	1002				
	894				
	674				
	644				
C_2D_2--H†	2799	35.29	41.15	5.86	39.85
	2628				
	1619				
	699				
	601				
	580				
	515				
	417				
	856i				
C_2DH--D†	3605	34.98	44.23	9.24	41.44
	2724				
	1682				
	809				
	727				
	600				
	467				
	356				
	719i				

*Active rotation.

TABLE 2. k_∞ USED FOR CALCULATION

Reaction	$k_\infty/10^{-13}$ cm^3 $molecule^{-1}$ s^{-1}
$H+C_2H_2$	4.0
$D+C_2D_2$	2.6
$D+C_2H_2$	2.5
$H+C_2D_2$	4.0

Discussion

As has been discussed in a previous paper,[12] the rate constant of the $H+C_2H_2$ reaction we obtained in the limit of high pressure is more than twice that reported by Payne and Stief (1.56×10^{-13} cm^3 $molecule^{-1}$ s^{-1}).[10] The result of Keil *et al.* is consistent with theirs. We therefore reconsidered this discrepancy. One possible reason is the participation of the reaction of

vinyl radicals in the decay of hydrogen atoms in our reaction system.

$$H + C_2H_2 \rightarrow C_2H_3 \quad (a)$$
$$C_2H_3 + H \rightarrow C_2H_2 + H_2 \quad (b)$$
$$2\,C_2H_3 \rightarrow C_2H_2 + C_2H_4 \quad (c)$$

The apparent decay rate of hydrogen atoms may be expressed as follows:

$$k_{app} = k_a\left(1 + \frac{k_b[C_2H_3]}{k_a[C_2H_2]}\right) = k_a\gamma. \quad (12)$$

The correction factor γ ranges from 1 to 2. The time dependence of $[C_2H_3]$ can be calculated by the Runge-Kutta integration procedure if the ratios of k_b/k_a and k_c/k_a and the initial concentration of H and C_2H_2 are known. Such calculations have already been made in a previous paper, in which the reaction between hydrogen atoms and ethylene has been discussed.[15] In the present experiments, we may approximate that $k_a \approx 4\times10^{-13}$, $k_b \approx 6\times10^{-11}$, and $k_c \approx 10^{-11}$ in units of cm^3 $molecule^{-1}$ s^{-1}, and the initial concentration of hydrogen atoms is in the order of 10^{12} cm^{-3} and $[C_2H_2]$, larger than 2×10^{15} cm^{-3}. The substitution of these data gives a γ factor of less than 1.1, *i.e.*, no correction seems to be necessary. However, the electron pulse-irradiation might produce an inhomogeneous distribution of atoms in the reaction cell, which cannot easily be estimated. If this occurred, the value of the γ factor would become close to 2. Consequently, it may be safe at present to retain the final conclusion until new evidence can be obtained. The measurement of the activation energy is now being undetraken.

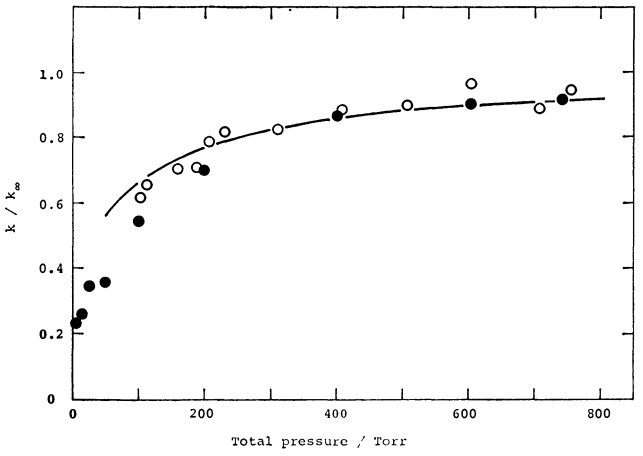

Fig. 5. Comparison of experiments obtained by Keil *et al.* (●) and by the present work (○) with theoretical curve. The value of k_∞ for the data of Keil *et al.* was assumed to be 1.7×10^{-13} cm^3 $molecule^{-1}$ s^{-1}.

Comparison with the Data of Keil et al. In Fig. 5, we plotted the pressure dependence of the k/k_∞ ratios for the $H+C_2H_2$ reaction obtained by Keil *et al.* and by us. Both experiments are in fair agreement with theoretical curve. According to Keil *et al.*, their RRKM calculation well explained this pressure dependence.[11] This fact probably means that the differences between the parameters of the moments of inertia and of the vibrational frequencies for the activated complex and vinyl radicals are not large enough to cause any difference in the pressure dependence of the rate constant. Since there is an adjustable parameter, β_c, in the theory, we cannot make a definite comparison. Incidentally, Keil *et al.* took the value of 0.25 for β_c.

Tunneling Effect. In the above treatment, we introduced a tunneling effect into the RRKM calculation. The calculation without a tunneling effect has also been carried out, and similar agreement between experiment and theory could be obtained, although the adjustable parameter, β_c, increased to 0.21. As far as the consistency between experiment and theoretical calculation is concerned, no substantial difference could be found between including and excluding the tunneling effect. Probably this effect will become a crucial problem when k_∞ is discussed theoretically.

References

1) K. F. Bonhoeffer and P. Harteck, *Z. Phys. Chem.*, **139**, 64 (1928).
2) E. W. R. Steacie, "Atomic and Free Radical Reactions," Renhold, New York (1954), Vol. 1. Early studies are reviewed.
3) E. L. Tollefson and D. J. LeRoy, *J. Chem. Phys.*, **16**, 1057 (1948).
4) J. R. Dingle and D. J. LeRoy, *J. Chem. Phys.*, **18**, 1632 (1950).
5) H. Girouard, F. M. Graber, and B. F. Mayers, General Dynamics-Astronautical Rept. No. N64-13061, San Diego (1963) NASA CR 52376.
6) G. G. Volpi and F. Zocchi, *J. Chem. Phys.*, **44**, 4010 (1966).
7) J. V. Michael and R. E. Weston, Jr., *J. Chem. Phys.*, **45**, 3632 (1966).
8) J. V. Michael and H. Niki, *J. Chem. Phys.*, **46**, 4969 (1967).
9) K. Hoyermann, H. G. Wagner, and J. Wolfrum, *Ber. Bunsenges. Phys. Chem.*, **75**, 22 (1971).
10) W. A. Payne and L. J. Stief, *J. Chem. Phys.*, **64**, 1150 (1976).
11) D. G. Keil, K. P. Lynch, J. A. Cowfer, and J. V. Michael, *Int. J. Chem. Kinet.*, **8**, 825 (1976).
12) Y. Ishikawa, K. Sugawara, and S. Sato, *Bull. Chem. Soc. Jpn.*, **52**, 3503 (1979).
13) S. Nagase and C. W. Kern, *J. Am. Chem. Soc.*, **101**, 2544 (1979).
14) K. Sugawara, Y. Ishikawa, and S. Sato, *Bull. Chem. Soc. Jpn.*, **53**, 1344 (1980).
15) Y. Ishikawa, M. Yamabe, A. Noda, and S. Sato, *Bull. Chem. Soc. Jpn.*, **51**, 2488 (1978).
16) P. J. Robinson and K. A. Holbrook, "Unimolecular Reactions," John Wiley and Sons, Inc., New York (1972).
17) B. C. Garrett and D. G. Truhlar, *J. Chem. Phys.*, **72**, 3460 (1980).
18) S. Kato and K. Morokuma, *J. Chem. Phys.*, **72**, 206 (1980).
19) J. O. Hirschfelder, C. F. Curtiss, and R. B. Bird, "Molecular Theory of Gases and Liquids," John Wiley and Sons, Inc., New York (1964).
20) R. W. Fessenden and R. H. Schuler, *J. Chem. Phys.*, **30**, 2147 (1963).

  Bull. Chem. Soc. Jpn., 54, 1227—1232 (1981)

Chlorination of Polyacrylonitrile and Analysis of Its Products

Masao Okamoto,* Ryōji Yamada, and Osamu Ishizuka

Department of Fiber and Polymer Engineering, Faculty of Engineering, Yamagata University, Jonan, Yonezawa 992

(Received July 8, 1980)

Chlorination of polyacrylonitrile (PAN) was carried out by passing dried chlorine gas through a tetrahydrothiophene 1,1-dioxide (sulfolane) solution of PAN or a powdery mixture of PAN with sodium chloride. The chlorinated products were examined by comparison with acrylonitrile–α-chloroacrylonitrile (CAN) copolymers corresponding to α-chlorinated PANs. In solution the reaction proceeded easily below 100 °C, but due to side reactions analysis of the products was difficult. In the powdery mixture hardly any reaction took place below 100 °C, but in the range 120—140 °C, the reaction proceeded smoothly and its rate became *ca.* 2.7 times in proportion as its temperature was raised by 10 °C. The chlorinated products were investigated by means of infrared and thermal analyses. The chlorinated moiety consists mainly of α,β-dichlorinated units, which seem to result from the addition of chlorine to the double bonds produced by dehydrochlorination after β-chlorination. These chlorinated products were dehydrochlorinated at lower temperature than acrylonitrile–CAN copolymers, but in many respects they resemble each other in the behavior of thermal degradation.

Grassie and McGuchan[1] carried out bulk copolymerization of acrylonitrile with α-chloroacrylonitrile (CAN) and recognized from the favorable thermoanalytical behavior of the copolymers obtained that the copolymers can be used for carbon fiber processing. They correspond to the partially α-chlorinated polyacrylonitrile (PAN). Chlorination of PAN remains to be investigated. However, if it proceeds preferentially on the α-carbon of the PAN molecule, its products should assume the same thermal behavior as copolymers.

Chlorination of PAN was studied in three different states: (1) dispersed powder in carbon tetrachloride, (2) solute in tetrahydrothiophene 1,1-dioxide (sulfolane), and (3) dispersed powder in sodium chloride powder. The reaction did not proceed in the first state but the chlorinated products could be obtained in the second and third states. In this work, these products were examined in comparison with acrylonitrile–CAN copolymers.

Experimental

Preparation of PAN. Two hundred and ninety grams of freshly distilled acrylonitrile was dissolved in 400 cm³ of *N,N*-dimethylformamide (DMF). This solution and 0.8 g of α,α′-azobisisobutyronitrile (AIBN) dissolved in 40 cm³ of DMF were put into a three-necked flask which had been evacuated with an oil pump and flushed with nitrogen several times. Stirring was started. The temperature inside the flask was maintained at 47 °C; it rose to 52 °C immediately after addition of AIBN. After 11.5 h, the reaction mixture was diluted with 400 cm³ of DMF containing 0.01 g of hydroquinone, and then poured into 20 dm³ of distilled water. The precipitate was filtered, washed with methanol and distilled water at 70 °C, and dried in a vacuum at 50 °C to constant weight. The yield was 92.7 g. The intrinsic viscosity, $[\eta]$, in DMF at 35 °C was 2.54.

Preparation of Acrylonitrile–CAN Copolymers. The method was reported in a previous work.[2]

Chlorination of PAN in A Solution State. Sulfolane (bp 122 °C at 4 mmHg (1 mmHg≈133.3 Pa)) was used as a solvent. Chlorination was carried out by passing dried chlorine gas at *ca.* 25 cm³/min through a polymer solution consisting of 0.2 g of PAN and 40 cm³ (at 100 °C) of sulfolane. The solution was bubbled with nitrogen for 15 min prior to the admission of chlorine gas. A magnetic stirrer was used and the solution was illuminated with a 100-W National Electric street lamp. After the lapse of reaction time (Table 1), the reaction system was purged with nitrogen and the solution was poured into 1 dm³ of methanol. The precipitate was filtered, washed with methanol for 18 h using a Soxhlet extractor, and dried at 30 °C in a vacuum oven to constant weight.

Chlorination of PAN in a Solid State. One gram of PAN powder was dispersed in 50 g of sodium chloride powder. The mixture was thoroughly dried and then charged in a U tube

Table 1. Chlorination of PAN in a solution state

Reaction temperature / °C	Reaction time / h	Chlorine content of product / wt%
55	10	9.17
80	10	16.10
110	10	22.20
120	3	9.84
120	10	23.70
135	2	6.64
135	3	9.70
135	10	23.10

Table 2. Chlorination of PAN in a solid state

Reaction temperature / °C	Reaction time / h	Chlorine content of product / wt%
100	20	4.49
120	4	4.03
120	7	7.32
120	10	9.85
130	2	2.70
130	3	4.35
130	5	10.81
130	10	20.82
140	2	5.73
140	3	10.84
140	5	22.45
140	8	34.84
140	10	42.11
140	20	49.54

The process of chlorination was similar to that for solution state. The reaction temperature and time are given in Table 2. After the reaction, the mixture was washed with distilled water until no chloride ion could be detected. The product obtained was dried in a vacuum at 30 °C to constant weight.

Chlorine Analysis and Measurement of Infrared Absorption Spectra. The methods were reported in a previous work.[3]

Thermomechanical Analysis (TMA). The measurement was carried out under tension at a heating rate of 10 °C/min with a Shimadzu TMA-20 Thermomechanical Analyzer. The sample was cut from the casting film (15—40 μm thick), the measurement being carried out with 5 g load.

Differential Thermal Analysis (DTA). A Rigaku CAT. No. 8001 Thermoflex was used. Fifty milligrams of sample was employed in each experiment and heated at a 5 °C/min rate under nitrogen.

Results and Discussion

Infrared Absorption Spectra of Acrylonitrile–CAN Copolymers. Acrylonitrile–CAN copolymers,[2] corresponding to α-chlorinated PANs, were studied before examining the chlorination of PAN. The infrared spectrum of a copolymer, shown in Fig. 1, is similar to the combination of spectra of PAN[2] and poly(α-chloroacrylonitrile)[3] (PCAN). In the copolymers, the bands at 2240 and 500 cm^{-1} were chosen as the characteristic bands of acrylonitrile and CAN[4] units, respectively. The absorbances and whether the molar extinction coefficients were affected by copolymerization were determined. Each absorbance was normalized by the equation

$$A = \frac{a}{w} \times \left(1 + \frac{34.445\,x}{3545.3 - 34.445\,x}\right), \qquad (1)$$

where A is the normalized absorbance, a the observed absorbance for w mg of sample, and x the chlorine content of sample.

The relationship between the number of chlorine atoms in 100 monomer units (N_{Cl}) and the absorbances at 2240 and 500 cm^{-1} (A_{2240} and A_{500}) is shown in Figs. 2 and 3 by solid lines. N_{Cl} was calculated by the equation

$$N_{Cl} = \frac{53.064\,x}{3545.3 - 34.445\,x} \times 100. \qquad (2)$$

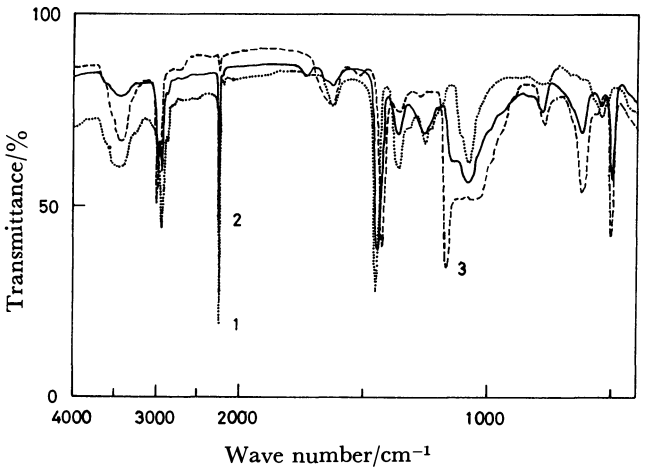

Fig. 1. Infrared absorption spectra of (1) PAN, (2) acrylonitrile–CAN copolymer (chlorine content: 20.25 wt%), and (3) PCAN.

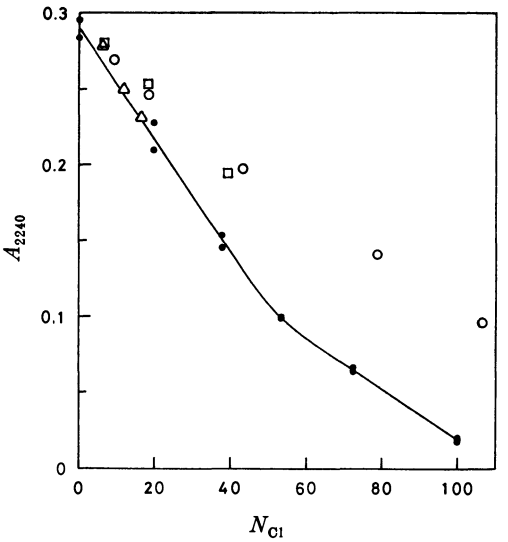

Fig. 2. Relationship between the number of chlorine atoms in 100 monomer units and the absorbance at 2240 cm^{-1}. ●: Acrylonitrile–CAN copolymers. △, □, and ○: Products chlorinated at 120, 130, and 140 °C, respectively, in a solid state.

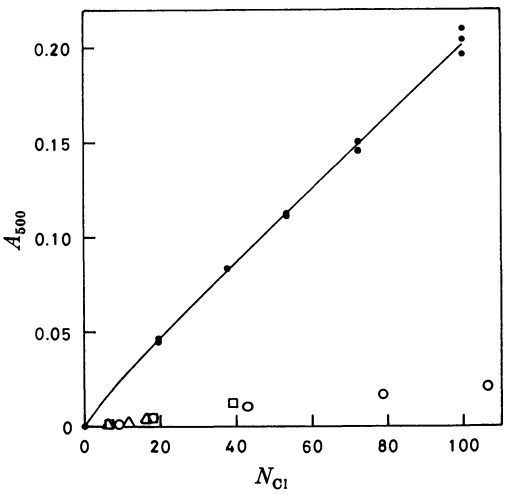

Fig. 3. Relationship between the number of chlorine atoms in 100 monomer units and the absorbance at 500 cm^{-1}. The symbols used here are the same as those in Fig. 2.

We see that the result for the band at 2240 cm^{-1} deviates considerably from the combination of absorbances of homopolymers, while at 500 cm^{-1} they are nearly equal. The chemical environment of acrylonitrile units in copolymer changes with position in the chain. In such cases, band broadening may occur. However, none was observed, indicating that the molar extinction coefficient of the 2240 cm^{-1} band in the copolymer is smaller than that in PAN, and that great care should be taken when using the absorbance of the band at 2240 cm^{-1} for determining the mole fraction of acrylonitrile units in a chlorinated PAN.

If only α-chlorination takes place during the course of chlorination of PAN, methylene groups do not change in number. However, with change in their chemical

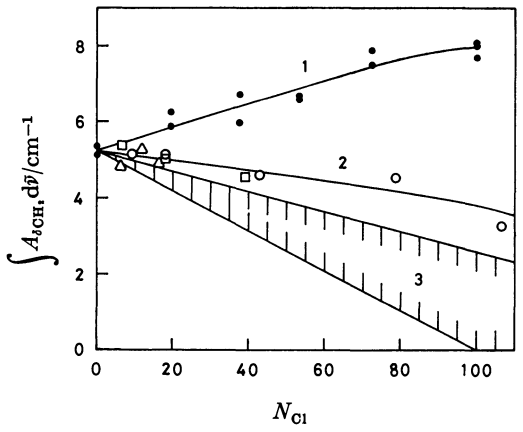

Fig. 4. Relationship between the number of chlorine atoms in 100 monomer units and the areal intensity of methylene scissoring vibration band. The symbols used here are the same as those in Fig. 2. Curves 1 and 2 express the changes which follow α-chlorination and the chlorination in a solid state, respectively. Area 3 is the expected one for β-chlorination (including β,β-dichlorination).

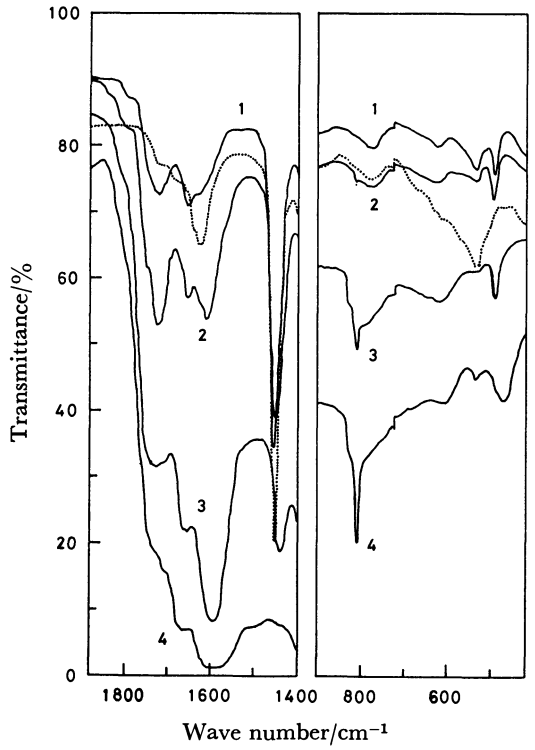

Fig. 5. Infrared absorption spectra of products chlorinated in sulfolane.
1, 2, 3, and 4: Products chlorinated at 55, 80, 110, and 135 °C, respectively, for 10 h. ·····: PAN heated at 150 °C for 10 h in sulfolane under nitrogen flow.

environment both methylene stretching and bending vibrations are affected (Fig. 1). The methylene scissoring vibration band appears at 1455 cm^{-1} in PAN and 1430 cm^{-1} in PCAN. In the copolymers, the integrated intensity of this band, $\int A_{\delta CH_2} d\bar{\nu}$, was calculated in the range 1540—1400 cm^{-1} (Fig. 4). Here, $A_{\delta CH_2}$ is the absorbance of methylene scissoring vibration band at a wave number ($\bar{\nu}$). We see from Curve 1 that the integrated intensity increases with the progress of α-chlorination, being nearly equal to the combination of the intensities in PAN and PCAN.

Chlorination of PAN in a Solution State and Analysis of Its Products. The chlorine content and infrared spectra of chlorinated products are shown in Table 1 and Fig. 5, respectively. In the case of chlorination above 100 °C, there is a ceiling in the chlorine content (Table 1). Although the 500 cm^{-1} band appears, its intensity is weak in comparison with that in the copolymer which has a corresponding chlorine content (see Fig. 1). In addition, strong absorptions are observed in the range 1800—1500 cm^{-1}. The absorptions in the neighborhood of 1700 cm^{-1} show that cyano groups have been transformed into carboxyl or carbamoyl groups. Since the formation of these groups was hardly observed without the admission of chlorine gas (Fig. 5), some side reaction should proceed simultaneously with chlorination.[5] The absorption at *ca.* 1600 cm^{-1} shows the progress of polymerization of cyano groups. A conspicuous absorption appears at *ca.* 810 cm^{-1} which seems to correspond to the characteristic band appearing in the heat-treatment of PAN in the air.[7] Chlorination is accompanied by several side reactions, making the analysis of chlorinated products difficult. The side reactions seem to cause the above-mentioned ceiling in the chlorine content.

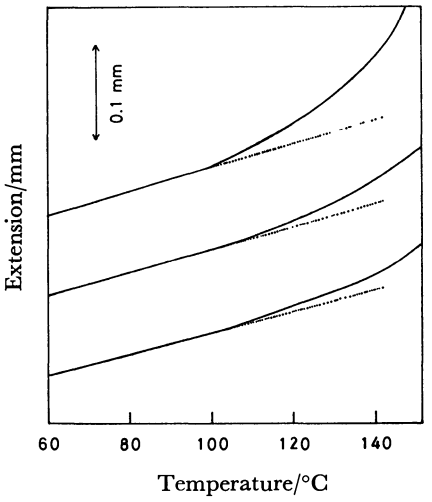

Fig. 6. TMA curves for PAN.

Chlorination of PAN in a Solid State and Analysis of Its Products. Change of Chlorine Content Following Chlorination: The chlorine content of chlorinated products is given in Table 2. It was found that the reaction scarcely proceeds at 100 °C. The reaction in a solid state should be accompanied by diffusion of chlorine into PAN granules. The rate of diffusion in a rubbery material is expected to be considerably higher than in a glassy one. Figure 6 shows TMA curves for original PAN. The rates of extension are equal below 100 °C but start to change at 100—110 °C, the glass transition temperature being *ca.* 100 °C. The reaction proceeded smoothly at 120, 130, and 140 °C. In the reaction at 140 °C, one chlorine atom per monomer unit was incorporated

after *ca.* 10 h, chlorination proceeding further.

The degree of chlorination is proportional to the weight gain resulting from chlorination, since no side reaction which brings about the change in sample weight was observed during the course of chlorination. The weight gain is expressed by the following equation:

$$\text{Weight gain} = \frac{34.445x}{3545.3-34.445x} \times 100(\%), \qquad (3)$$

where x is the chlorine content of chlorinated PAN. The relationship between chlorination time and weight gain is shown in Fig. 7. The rate of chlorination above 120 °C becomes *ca.* 2.7 times in proportion as the reaction temperature was raised by 10 °C.

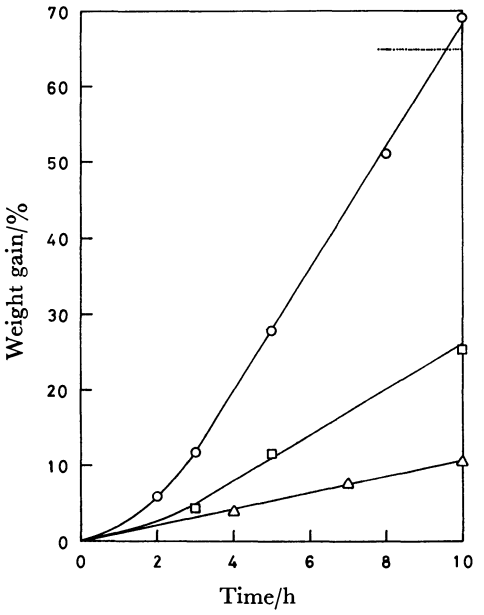

Fig. 7. Weight gain due to chlorination in a solid state. Chlorination temperatures are 120 (△), 130 (□), and 140 °C (○). A dotted line indicates the level of weight gain due to substitution of one hydrogen atom per monomer unit with one chlorine atom.

Infrared Analysis of Chlorinated Products: Infrared spectra of chlorinated products are shown in Fig. 8. No absorption related with side reactions was observed except in the neighborhood of 1600 cm^{-1}. New absorptions appearing in the neighborhood of 800 cm^{-1} and increasing with the progress of chlorination can be assigned to C–Cl stretching vibrations. A slight polymerization of the cyano groups proceeds simultaneously with chlorination but sample weight is changed by only chlorination. Thus each infrared absorption band can be quantitatively treated by means of the weight gain which follows chlorination.

A_{2240}, A_{500}, and $\int A_{\delta CH_2}d\bar{\nu}$ were calculated using Eq. 1. The results shown in Figs. 2, 3, and 4, respectively, indicate that a preferential α-chlorination hardly occurs. Here, β-chlorination should be considered. In this case, $\int A_{\delta CH_2}d\bar{\nu}$ is an effective measure. When only β-chlorination (including β,β-dichlorination) proceeds, the value should be in Area 3. However, Curve 2

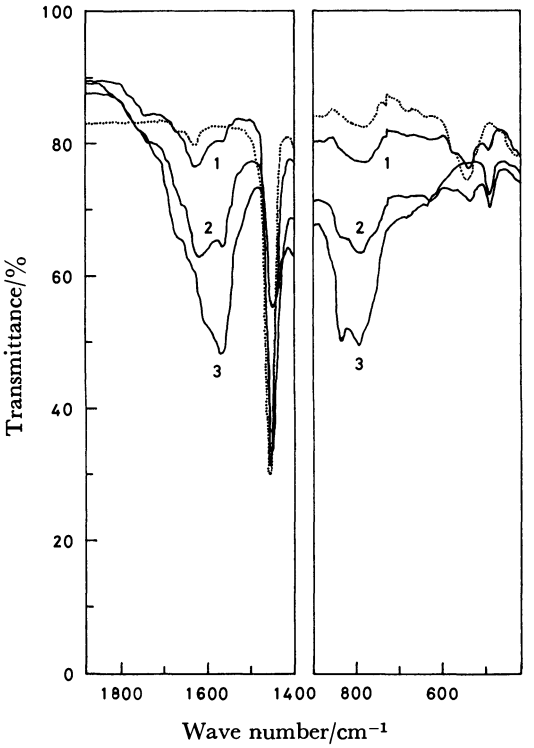

Fig. 8. Infrared absorption spectra of products chlorinated in a solid state.
1, 2, and 3: Products chlorinated at 120, 130, and 140 °C, respectively, for 10 h. ·····: PAN heated at 130 °C for 10 h in sodium chloride powder under nitrogen flow.

expresses the change of this value which follows chlorination at 120, 130, and 140 °C. It is in agreement with the change in PAN which undergoes nearly equal chlorination on both CH_2 and CH groups. If the chlorination on CH groups proceeds independently of that on CH_2 groups, absorbance of the 500 cm^{-1} band should become much higher than that in Fig. 3. It seems that the chlorinated moiety consists mainly of α,β-dichlorinated units. Figure 2 is not contradictory, since the rate of decrease in the absorbance is about half of that in α-chlorination. Such a substitution of two chlorine atoms per monomer unit would still leave many monomer units even if 100 chlorine atoms per 100 monomer units were incorporated, making further chlorination possible.

Thermal Analysis of Chlorinated Products: Figure 9 shows the DTA curves for products chlorinated at 130 and 140 °C for 10 h. The differential temperature, ΔT, is very small, exothermic reaction taking place at a temperature lower than that of the reactions in PCAN, acrylonitrile–CAN copolymers,[1] and PAN. When these two chlorinated products were heated at a rate of 5 °C/min under nitrogen in the DTA apparatus, their chlorine contents changed (Table 3). Since the number of chlorine atoms in 100 monomer units changes with dehydrochlorination following heating, its value, N'_{Cl}, was calculated by the following equation:

$$N'_{Cl} = \frac{\left(53.064-2.016\times\frac{N_{Cl}}{100}\right)x'}{3545.3-36.461x'} \times 100, \qquad (4)$$

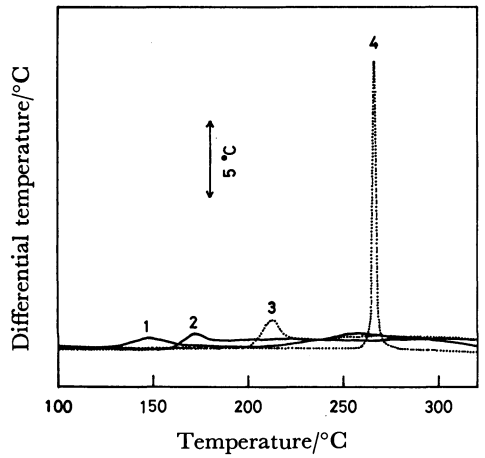

Fig. 9. Comparison in DTA curves between products chlorinated in a solid state (1 and 2) and PCAN (3) or PAN (4). 1 and 2: Products chlorinated at 130 and 140 °C, respectively, for 10 h.

Table 3. Change of chlorine content in chlorinated PAN during heating process[a)]

Sample[b)]	Temperature °C	Chlorine content wt%
1	Before heating	20.82
	127	18.94
	149	15.68
	172	11.53
	197	8.27
	222	5.32
	259	3.25
	320	1.57
2	Before heating	42.11
	156	39.57
	185	35.03
	217	29.52
	251	22.03
	284	18.01
	320	11.71
	390	7.20

a) Heating was carried out at a rate of 5 °C/min under nitrogen in DTA apparatus. b) Samples 1 and 2 were chlorinated at 130 and 140 °C, respectively, for 10 h in sodium chloride powder.

where x' is the chlorine content of heated sample. The values obtained are shown in Fig. 10. From a comparison of Figs. 9 and 10, it was found that thermal dehydrochlorination starts at about the initiation temperature of exothermic reaction. The mode resembles that in PCAN and acrylonitrile–CAN copolymers.[1,4,8)] This indicates that, even in chlorinated PANs, the initiation of polymerization of cyano groups takes place as a side effect of the thermal dehydrochlorination.[1)] On the other hand, dehydrochlorination in chlorinated PANs occurs at a temperature lower than that in acrylonitrile–CAN copolymers[1)] and PCAN. This indicates that β-substituted chlorine atoms are easily dehydrochlorinated at lower temperature than α-chlorine atoms. It seems that α,β-dichlorinated units

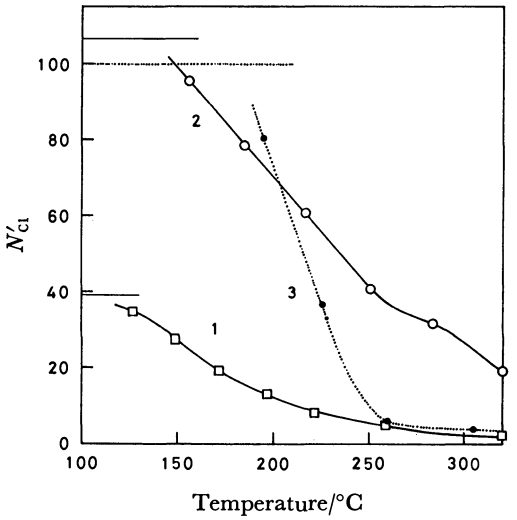

Fig. 10. Changes of the number of chlorine atoms in 100 monomer units during heating process.
1 and 2: Products chlorinated at 130 and 140 °C, respectively, for 10 h in a solid state, 3: PCAN.

result from the addition of chlorine to the double bonds produced by dehydrochlorination after β-chlorination. The dehydrochlorination shown in Fig. 10 is nearly completed in both PCAN and slightly chlorinated PAN, but not in highly chlorinated PAN before the sample temperature reaches 300 °C. This can be interpreted by considering the α,β-dichlorinated unit as a chlorinated moiety. A chlorinated moiety is usually easily dehydrochlorinated. The reaction can be expressed by

$$-CH_2-\underset{Cl}{C}(C\equiv N)-\underset{Cl}{CH}-CH(C\equiv N)- \longrightarrow$$
$$-CH=C(C\equiv N)-CH=C(C\equiv N)- + 2\,HCl.$$

When dehydrochlorination took place, three new infrared absorption bands appeared, corresponding to the characteristic bands of dehydrochlorinated PCAN.[3)] However, complete dehydrochlorination is difficult in highly chlorinated PAN, since there should be chlorine atoms not subjected to intramolecular dehydrochlorination. An example is the case of chlorine atom 1 or 2 in

$$-CH_2-\underset{Cl}{C}(C\equiv N)-\underset{Cl}{\underset{1}{CH}}-CH(C\equiv N)-\underset{Cl}{\underset{2}{CH}}-\underset{Cl}{C}(C\equiv N)-.$$

In order to examine the change of thermal behavior which follows chlorination, DTA curves were constructed for the products chlorinated at 130 °C (Fig. 11). In the case of the sample of low chlorine content, ΔT is still fairly high, the exothermic peak temperature

Table 4. Chlorination of PCAN in a solid state

Reaction temperature °C	Reaction time h	Chlorine content of product wt%
No chlorination		39.37[a)]
120	5	38.99
130	10	40.45
150	4	38.73

a) See Reference 9.

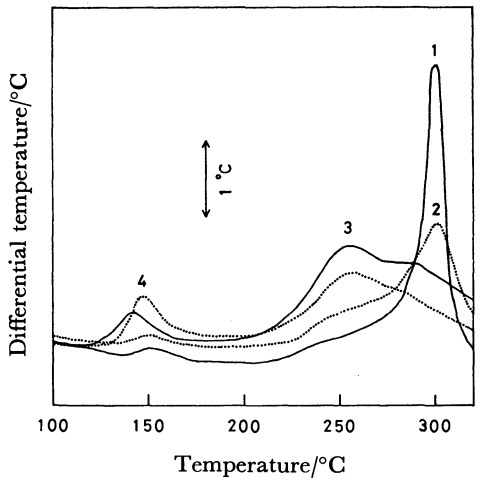

Fig. 11. DTA curves for products chlorinated at 130 °C in a solid state.
1, 2, 3, and 4: Products chlorinated for 2, 3, 5, and 10 h, respectively.

becoming higher than in PAN. Highly chlorinated samples exhibit broad complex exotherms at lower temperatures. Such DTA behavior is similar to that in acrylonitrile–CAN copolymers.[1] Although chlorinated PAN differs from acrylonitrile–CAN copolymer in chemical structure, they resemble each other as regards the mode of thermal degradation.

Possibility of The Chlorination or Hydrochlorination of Cyano Groups: There is a possibility that cyano groups in PAN undergo chlorination or hydrochlorination during the course of chlorination of PAN in a solid state. It is difficult to confirm whether cyano groups are chlorinated in the case of PAN; the groups in PCAN[9] are not chlorinated under similar conditions (Table 4). There might be a similarity in the case of PAN. If hydrochlorination takes place, a band would appear at *ca.* 1690 cm^{-1},[6] but no such band was observed (Fig. **9**).

References

1) N. Grassie and R. McGuchan, *Eur. Polym. J.*, **9**, 507 (1973).
2) M. Okamoto and O. Ishizuka, *Bull. Chem. Soc. Jpn.*, **53**, 3012 (1980).
3) M. Okamoto, C. Aoki, and O. Ishizuka, *Nippon Kagaku Kaishi*, **1977**, 103.
4) M. Okamoto, C. Aoki, and O. Ishizuka, *Nippon Kagaku Kaishi*, **1978**, 433.
5) Hydrogen chloride seems to play an important role in the occurrence of its side reaction.[6] The greater part of hydrogen chloride is produced when sulfolane is chlorinated.
6) S. Tazuke, K. Hayashi, and S. Okamura, *Kobunshi Kagaku*, **22**, 259 (1965).
7) a) R. T. Conley and J. F. Bieron, *J. Appl. Polym. Sci.*, **7**, 1757 (1963); b) K. Miyamichi, M. Okamoto, O. Ishizuka, and M. Katayama, *Sen'i Gakkai Shi*, **22**, 538 (1966); c) A. J. Clarke and J. E. Bailey, *Nature*, **243**, 146 (1973); d) M. M. Coleman and R. J. Petcavich, *J. Polym. Sci., Polym. Phys. Ed.*, **16**, 821 (1978).
8) N. Grassie and R. McGuchan, *Eur. Polym. J.*, **8**, 243 (1972).
9) PCAN used here was explained: M. Okamoto, T. Suzuki, and O. Ishizuka, *Nippon Kagaku Kaishi*, **1979**, 259.

Structure of the Galacturonate and Glucuronate Complexes with Copper(II) in Aqueous Solution. A Calorimetric Study

Roberto ARUGA

Institute of Analytical Chemistry, University of Turin, via *P. Giuria 5, 10125 Turin, Italy*

(Received October 13, 1979)

Heat and entropy of reaction of copper(II) with galacturonate and glucuronate anions have been determined by calorimetry. The measurements were performed in an aqueous medium at 25 °C and ionic strength $I=1$ M ($NaNO_3$). The results indicate a bidentate action of the two ligands towards copper. The carboxylate group as well as the oxygen atom of the ring, the latter by means of an outer-sphere electrostatic bond, seem to interact with the cation.

Acid polysaccharides are of importance among the polyelectrolytes of biological interest.[1] Complex formation of these polysaccharides with metal ions gives rise to particular structures and biological functions. Our knowledge of the structures and bonding sites is fragmentary. Data are insufficient for the reactions of not only polysaccharides but also the corresponding acid monosaccharides such as uronic acids. Of the few studies on the metal associations of uronic acids in solution, those of Anthonsen *et al.*[2-4] and Makridou *et al.*[5] may be cited. As regards the bond nature for galacturonate with some metals, the results of the above works do not agree. The NMR data suggest a tridentate behavior towards metal ions of large dimensions, the potentiometric results indicating a monodentate action with only the $-COO^-$ group bound to the metal. The latter conclusion, particularly for copper, appears curious. Thermodynamic studies on the association between this metal and some hydroxy and alkoxy carboxylic acids showed that some groups such as ethereal oxygen or alcoholic –OH group, in particular positions, can form bonds with copper.[6,7]

Taking into consideration the disagreement of these conclusions and the absence of calorimetric studies on metal-uronic acid reactions, it was thought of interest to extend the calorimetric investigations to the reaction of copper(II) with galacturonate and glucuronate (Fig. 1). The results obtained refer to the aqueous medium at 25 °C and $I=1$ M.

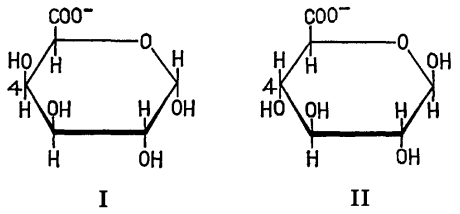

I II

Fig. 1. Galacturonate ion (I) and glucuronate ion (II).

Experimental

Materials. Copper(II) nitrate (C. Erba RPE) was used. The concentration of metal was determined by complexometric titration with EDTA (0.1 M solution, C. Erba RPE). Solutions of the ligands were prepared by D(+)-galacturonic acid monohydrate Fluka puriss and D-glucuronic acid Fluka purum. The purity of the acids was checked by potentiometric titration. Inert electrolyte: sodium nitrate (C. Erba RPE).

Equipment. Calorimetric measurements were carried out at 25.00 °C with an LKB 8700-2 Precision Calorimetry System and an LKB 8726-1 100-ml titration vessel equipped with a standard resistor (50Ω) and a thermistor (2000Ω). The accuracy of the instrument was checked by measuring the molar enthalpy of the reaction between tris(hydroxymethyl)methylamine and HCl in aqueous solution. The calorimeter was also equipped with a Radiometer ABU 12b autoburet for the addition of titrant. The calorimetric experiments were carried out in a room whose temperature was kept constant within ±0.3 °C. For the pH measurements a Metrohm Compensator E 388 potentiometer was used at 25 °C.

Procedure. For each ligand several sets of measurements of the reaction and dilution heats were carried out, each set being performed in the following way. 2.5±0.002 ml of 4×10^{-1} M copper nitrate solution was added in succession to 88.00 ml of the uronic acid solution contained in the calorimetric cell, the heat being measured for each addition. The pH of the copper solution was made 3.6± 0.1 in order to avoid the metal hydrolysis. The ligands were partly transformed into sodium salt by adding NaOH to pH=4.55±0.02. The ionic strength of all the solutions was brought to 1 M with sodium nitrate. The corresponding heat of dilution was measured by adding the same amounts of copper nitrate solution to 88.00 ml of 1 M $NaNO_3$, without ligand, at pH=4.55. The following results were obtained. (a) Formation of only the ML^+ complex species; in fact, the presence of only the ML^+ species was shown up to a C_L/C_M ratio of 2.[5] (b) Absence of polynuclear species.[5] (c) A negligible neutralization heat between H^+ and OH^-. The pH value in the cell, after each addition of titrant, was measured potentiometrically by means of titration performed in the same manner as the calorimetric one.

Treatment of the Experimental Data. Owing to the pH difference between metal and ligand solutions, a slight protonation process of the latter took place. The protonation heat was calculated by means of the acid ionization enthalpy of both glycolic acid (0.15 kcal mol^{-1})[8] and acetic acid (0.09 kcal mol^{-1}).[9] It was found to be lower than 0.7% of the measured heat, with no influence on the $\Delta H°$ values, and was thus neglected. Data for one series of the measurements: initial concentration of ligand (C_l) and initial pH (pH_l) in the cell, cumulative volume of titrant added (ΣV_T), pH in the cell (pH_f) and concentration of the species (C_{ML^+}, C_{L^-}, C_{HL}) after each addition of titrant, and cumulative heat corrected for the dilution (ΣQ_c) are given as an example in Table 1.

The molar enthalpy of association was determined from the heat (ΣQ_c) experimentally obtained and the complex species concentrations, the latter being obtained from the stability constants.[5] The calculation of $\Delta H°$ was carried out by two methods:[7,10] (a) the numerical method of minimization of the error square sum, and (b) the graphical

Table 1. Data for the mixing of Cu(II) with galacturonate and glucuronate solutions

Ligand	C_i / 10^{-2} M	pH_i	$\sum V_T$ / ml	pH_f	C_{ML^+} / 10^{-3} M	C_{L^-} / 10^{-2} M	C_{HL} / 10^{-4} M	$-\sum Q_c$ / cal
Galacturonate ion	2.50	4.57	2.505	4.33	5.81	1.73	12.1	0.318
			5.010	4.20	9.69	1.28	12.1	0.518
Glucuronate ion	2.51	4.56	2.505	4.43	4.11	1.96	6.50	0.309
			5.010	4.31	7.00	1.60	6.99	0.533

Table 2. Thermodynamics for the reaction: $Cu^{2+} + L^- \longrightarrow CuL^+$, in aqueous solution at 25 °C and $I = 1$ M

L^-	log K	$-\Delta G°$ [a] / kcal mol^{-1}	$\Delta H°$ / kcal mol^{-1}	$\Delta S°$ / gibbs mol^{-1}	(log K)/pK_a	Ref.
Galacturonate	1.81±0.02[b]	2.46±0.03	0.60±0.04	10.3±0.2	0.57	This work
Glucuronate	1.48±0.03	2.01±0.04	0.82±0.01	9.5±0.1	0.50	This work
Methoxyacetate	1.83	2.49	0.74±0.04	10.8	0.56	6)
Ethoxyacetate	1.80±0.02	2.45±0.03	0.50±0.02	9.9±0.1	0.51	7)
Pyruvate	1.59	2.17	−0.05±0.01	7.1	0.50	6)
Glycolate	2.17	2.96	−0.35±0.01	8.7	0.62	6)
Acetate	1.33	1.81	1.24±0.02	10.2	0.30	6)

a) The results are expressed by means of the thermochemical calorie, equal to 4.1840 absolute J. b) The uncertainty in each case is given as the estimated standard deviation.

method derived from the equations of Leden and Fronaeus for the overall formation constants. The results agree. The entropy was obtained by means of: $\Delta S° = 10^3(\Delta H° - \Delta G°)/T$.

Results and Discussion

The molar thermodynamic quantities for the reactions of copper(II) with galacturonate and glucuronate are given in Table 2. For the sake of comparison, the values obtained for a series of monocarboxylic ligands[6,7] (under the same conditions of T and I) are also given.

The values in Table 2 for the uronate anions show that only the entropy factor is favorable for the association but not $\Delta H°$. The positive values of these parameters can be caused by two factors: (a) partial solvent destruction accompanying the charge association, and (b) the displacement of at least one water molecule by carboxylate from the metal hydration sphere.[11] Nevertheless, the crystal fields produced by oxygen coordinating ligands are quite similar to those of the water molecules.[11] As regards the entropy variation, the displacement of one water molecule is counterbalanced by the metal-ligand association. Consequently it seems that both $\Delta H°$ and $\Delta S°$ are mainly influenced by factor (a).

One of the following arrangements might take place as regards the metal-ion interaction: (a) monodentate behavior of the uronate ions, with carboxylate group as the only bonding site, the structure being proposed on the grounds of the formation constants values;[5] (b) bidentate behavior, with $-COO^-$ and $-OH$ on C-4 as bonding sites; (c) bidentate action as in (b), but with $-COO^-$ and the ethereal oxygen of the ring taking part in the binding; (d) a tridentate action, by means of $-COO^-$, $-OH$ on C-4 and the oxygen of the ring, the structure being suggested for the association of galacturonate with Ca(II) and Eu(III) ions.[2]

Considering the fact that the log K values for uronate ions are greater than those for acetate (in spite of the latter's greater basicity towards proton), assumption (a) appears to be questionable. For the sake of illustration the values of (log K)/pK_a are given for each ligand (Table 2). The (log K)/pK_a ratio allows a comparison, for each ligand, between the stability of its association with copper and with proton. If a ligand acts as a monodentate towards copper (*i.e.*, the bond only through carboxylate is formed), the other groups in the ligand molecule have the same solvent ordering ability both in the case of copper and of proton. If a ligand acts as a bidentate towards the metal, another hydrophilic group besides carboxylate is neutralized by the metal charges. Consequently, the solvent ordering ability of this group is different before and after the reaction. In this case its external contribution to $\Delta G°$ of association with copper differs from that with proton. In the same way, the ratio (log K)/pK_a should differ as compared with the former case. Therefore the value of this ratio should be determined by a mono- or bidentate behavior of the ligand towards copper (last column, Table 2). For acetate the value is 0.30, while the other ligands (for which a bidentate action was demonstrated) give values in the range 0.50—0.62. The values of (log K)/pK_a for uronate ions (0.57 and 0.50) tend to discard the hypothesis of a monodentate action of galacturonate and glucuronate towards copper.

As regards hypothesis (b), it must be considered that in uronic acids the respective positions of $-OH$ on C-4 and $-COO^-$ are the same as in 3-hydroxypropionic acid. The monodentate action of this

ligand towards Cu(II) and other bivalent cations, and the consequent non-participation of –OH in the β-position in the binding of metal were demonstrated.[12,13] Considering also that –OH group, if taking part in complex formation, leads to exothermic values of $\Delta H°$ (the values for glycolate, Table 2), the suggestion in (b) may be unlikely.

The structure in (d) does not seem very reliable, both for the preceding considerations on –OH in β-position and for the following reasons. In a tridentate structure there is a strong difference in stability between the galacturonate complex (more stable) and that of glucuronate. This might be due to the different positions, in the molecule of the two ligands, of the hydroxyl group on C-4, which is axial and equatorial, respectively.[5] On the contrary, similar values of log K, $\Delta H°$, and $\Delta S°$ (Table 2) lead to the conclusion that both uronate ligands have the same behavior. Moreover, in the case of galacturonate, it was found[2] that a structure with three bonding sites fits the cations of particular dimensions, as Eu(III) and Ca(II) (crystalline radii: 0.95 and 0.99 Å, respectively), while Cu(II) is markedly smaller (0.72 Å, Ref. 14).

The structure given in (c) seems to be probable, considering the fact that the respective positions of ethereal oxygen and carboxylate group are the same as in methoxy- and ethoxyacetate, and that the participation of ethereal oxygen in the chelation of Cu(II) was confirmed for these two ligands.[6,7] In this case the metal-ethereal oxygen bond appeared to be of electrostatic character, and limited to the outer sphere of the cation. Similar values of log K, $\Delta H°$, and $\Delta S°$ between the two uronic and the two alkoxyacetic ligands (in particular, the values for galacturonate are between those for the two alkoxyacetates), support the last hypothesis.

References

1) A. Veis, "Biological Polyelectrolytes," Dekker, New York (1970).
2) T. Anthonsen, B. Larsen, and O. Smidsrød, *Acta Chem. Scand.*, **26**, 2988 (1972).
3) T. Anthonsen, B. Larsen, and O. Smidsrød, *Acta Chem. Scand.*, **27**, 2671 (1973).
4) H. Grasdalen, T. Anthonsen, B. Larsen, and O. Smidsrød, *Acta Chem. Scand.*, **B 29**, 17, 99 (1975).
5) C. Makridou, M. Cromer-Morin, and J. P. Scharff, *Bull. Soc. Chim. Fr.*, **1977**, 59.
6) R. Aruga, *Ann. Chim.*, **64**, 659 (1974).
7) R. Aruga, *J. Inorg. Nucl. Chem.*, **39**, 2159 (1977).
8) J. J. Christensen, J. L. Oscarson, and R. M. Izatt, *J. Am. Chem. Soc.*, **90**, 5949 (1968).
9) L. Nelander, *Acta Chem. Scand.*, **18**, 973 (1964).
10) L. G. Sillén, *Acta Chem. Scand.*, **16**, 159 (1962).
11) G. H. Nancollas, "Interactions in Electrolyte Solutions," Elsevier, Amsterdam (1966).
12) J. Savić, M. Savić, and I. Filipović, *Croat. Chem. Acta*, **44**, 305 (1972).
13) R. Aruga, *Atti Accad. Scienze Torino*, **109**, 361 (1974—1975).
14) F. Basolo and R. G. Pearson, "Mechanisms of Inorganic Reactions," J. Wiley, New York (1958).

Taft's Plot for the Co-pyrolysis of 2-Chloroethyl Compound and Methanol on Activated Alumina

Kiyonori SHINODA
Toyama Technical College, Hongo, Toyama 930-11
(Received August 12, 1980)

Synopsis. For the co-pyrolysis of 2-chloroethyl compounds with methanol on activated alumina, the ρ^* value was +0.49, indicating a nucleophilic reaction mechanism.

For the pyrolysis of chloroethanes on activated alumina, ρ^* values were negative, indicating an electrophilic reaction mechanism.[1] On the other hand, positive ρ^* values were observed for the elimination of hydrogen chloride from chloroethanes with sodium hydroxide in ethanol, as well as in the co-pyrolysis with methanol on activated alumina.[1,2]

The effect of the molecular structure on the consumption rate of the substrate was studied by carrying out the co-pyrolysis of 2-chloroethyl compounds and methanol on activated alumina.

Results and Discussion

It has been reported that the co-pyrolysis of organic chlorides and methanol on activated alumina proceeded according to good first-order kinetics.[3] Even if two organic chlorides were competitively co-pyrolyzed with methanol on activated alumina, it seemed reasonable to assume that the consumption rates were first-order in each substrate.

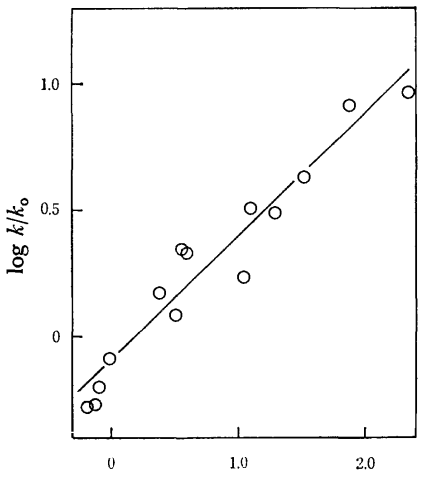

Fig. 1. Taft's plot for co-pyrolyses of 2-chloroethyl compounds and methanol on activated alumina at 250 °C.

In order to investigate the effect of the polar nature of the substituent upon the reactivity in the co-pyrolysis of organic chlorides with methanol on activated alumina, Taft's plot was applied to this heterogeneous catalysis:

$$\log k/k_0 = \rho^*\sigma^*, \quad (1)$$

where k/k_0 is the relative rate constant with respect to the standard reaction (1,1,2,2-tetrachloroethane in this case) and where σ^* represents the polar substituent parameter, which is a measure of the inductive effect.[4] A linear free-energy relationship was found to exist between the reactivity and Taft's σ^*, as is shown in Fig. 1. A value of ρ^* was calculated by the method of least squares to be +0.49.

Experimental

Materials. The 4-chlorobutyronitrile was prepared by the reaction of 1-bromo-3-chloropropane and potassium cyanide described in the literature.[5] The 1-chloro-3-methoxypropane was prepared from 1-bromo-3-chloropropane by modifying the method of Henne and Haeckl.[6] All of the other reagents used in this work were purchased from the Tokyo Kasei Kogyo Co. except for methanol and ethanol, which were obtained from Nakarai Chemicals. All the chemicals were used without further purification. The activated alumina used as catalyst (KHD-24) was supplied by the Sumitomo Chemical Co.: the particle diameter was in the range from 2 to 4 mm.

General Procedure for Co-pyrolysis. The flow-type reaction system of a previous work[7] was used. The organic chlorides were mixed with methanol in the volume ratio of 1.0 : 1.0 : 5.0. In all runs, two organic chlorides were competitively pyrolyzed at 250 °C to check the balance of such volatile products as propylene and to keep the effect of the time factor and the concentration of methanol constant.

References

1) K. Shinoda and S. Anzai, *Nippon Kagaku Kaishi*, **1974**, 1945.
2) K. Shinoda, *Bull. Chem. Soc. Jpn.*, **47**, 2406 (1974).
3) K. Shinoda, *Bull. Toyama Technical College*, **12**, 67 (1978).
4) M. S. Newman, "Steric Effects in Organic Chemistry," John Wiley and Sons, New York, N. Y. (1956), p. 618.
5) F. H. Allen, *Org. Synth.*, Coll. Vol. I, 156 (1956).
6) A. L. Henne and F. W. Haeckl, *J. Am. Chem. Soc.*, **63**, 2692 (1941).
7) K. Shinoda, *Nippon Kagaku Kaishi*, **1977**, 1989.

Synthesis and Electrical Resistivity of TCNQ Radical Anion Salts with 4,5-Disubstituted *N,N*-Dimethyl-1,3-dithiolan-2-iminium Cations

Futoshi KATO and Toshio TANAKA*

Department of Applied Chemistry, Faculty of Engineering, Osaka University, Suita, Osaka 565

(Received October 31, 1980)

Synopsis. The title salts with the formula $[S\text{-}CHR^1\text{-}CHR^2\text{-}S\text{-}C{=}\overset{+}{N}Me_2](TCNQ)_n^{\cdot}$ (R^1,R^2=Me, H; Et, H; Ph, H; Me, Me; and Me, Br; n=1 and 2) were prepared. Electrical resistivities, electronic spectra, and magnetic susceptibilities of these salts in the solid state are reported.

Recently, one of the authors reported the preparation of a series of 7,7,8,8-tetracyanoquinodimethane (TCNQ) radical anion salts with *N,N*-dialkyl-1,3-dithiolan-2-iminium cations, $[S(CH_2)_2SC{=}\overset{+}{N}R_2](TCNQ)_n^{\cdot}$ (R= Me, Et, *n*-Pr, *n*-Bu, *n*-C_6H_{13}, and *n*-C_8H_{17}; n=1 and 2, but not all combinations),[1,2] whose electrical resistivities increase with the bulkiness of substituents on the iminium nitrogen atom for each series of n=1 and 2, respectively.[2] The present work was undertaken to examine the effect of substituents on the dithiolane ring on the resistivity of $TCNQ^{\cdot}$ radical anion salts. This note reports the preparation and the electrical resistivities of some simple and complex salts of $TCNQ^{\cdot}$ radical anion with 4,5-disubstituted *N,N*-dimethyl-1,3-dithiolan-2-iminium cations, $[S\text{-}CHR^1\text{-}CHR^2\text{-}S\text{-}C{=}\overset{+}{N}Me_2](TCNQ)_n^{\cdot}$ (R^1,R^2=Me,H; Et,H; Ph,H; Me,Me; and Me,Br; n=1 and 2). Electronic spectra and magnetic susceptibilities of these salts are described in terms of the modes of stacking of TCNQ in the solid state. For the sake of abbreviation, the following numbers are used for compounds appeared in this note.

Compound	Number	R^1	R^2	X
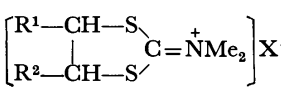	**1a**	Me	H	Br
	1b	Et	H	Br
	1c	Ph	H	Br
	1d	Me	Me	PF_6
	1e	Me	Br	Br

Compound	Number	R^1	R^2	*n*
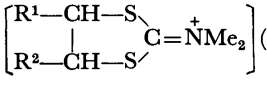	**2a**	Me	H	1
	2b	Et	H	1
	2c	Ph	H	1
	2d	Me	Me	1
	2e	Me	Br	1
	3a	Me	H	2
	3b	Et	H	2
	3c	Ph	H	2
	3d	Me	Me	2
	3e	Me	Br	2

Experimental

Materials. Compounds **1a**—**c** were prepared by the reactions of sodium dimethyldithiocarbamate, $Na(S_2CNMe_2)$, with 1,2-dibromopropane, 1,2-dibromobutane, and 1-phenyl-1,2-dibromoethane, respectively, in refluxing acetone by the procedure described elsewhere.[3] The reaction of $Na(S_2CNMe_2)$ with 2,3-dibromobutane in refluxing acetone yielded an oily product, which was dissolved in ethanol, followed by the addition of an equimolar ethanol solution of $NaPF_6$ to give white microcrystals of **1d**. Recrystallization was carried out from dichloromethane–petroleum ether (1 : 1). Compound **1e** was obtained according to the literature method.[4]

Preparation of Simple Salts ***2a—e.*** To a filtered solution of $Li^+TCNQ^{\cdot}$ (0.74 g, 3.5 mmol) in boiling ethanol (40 cm^3) was added a hot ethanol (20 cm^3) solution of **1a** (0.85 g, 3.5 mmol). The mixture was allowed to stand in a refrigerator overnight. The resulting precipitate was collected by filtration and recrystallized from ethanol to afford purple plates of **2a** in 85% yield. Similarly, purple needles or plates of **2b—e** were prepared in 60—80% yields by the equimolar reactions of $Li^+TCNQ^{\cdot}$ with **1b—e**, respectively, in ethanol.

Preparation of Complex Salts ***3a—e.*** To a hot acetonitrile (30 cm^3) solution of **2a** (0.52 g, 1.4 mmol) was added a solution of neutral TCNQ (0.29 g, 1.4 mmol) in boiling acetonitrile (30 cm^3). The mixture was allowed to stand in a refrigerator overnight, giving black microcrystals of **3a**, which was recrystallized from acetonitrile, 68% yield. Dark violet or black crystals of **3b—e** were obtained similarly in 45—76% yields by the reaction of neutral TCNQ with the appropriate simple salts in acetonitrile.

TABLE 1. MELTING POINT AND ANALYTICAL DATA OF THE $TCNQ^{\cdot}$ SALTS

Salt	Mp(dec) °C	%C Found (Calcd)	%H Found (Calcd)	%N Found (Calcd)
2a	174—177	59.06 (58.99)	4.20 (4.40)	19.36 (19.11)
2b	139—141	59.75 (59.98)	4.57 (4.77)	18.18 (18.41)
2c	166—168	64.51 (64.46)	4.13 (4.23)	16.45 (16.34)
2d	166—168	59.78 (59.98)	4.60 (4.77)	18.43 (18.41)
2e	174—176	48.40 (48.54)	3.22 (3.39)	15.63 (15.72)
3a	231—233	62.84 (63.14)	3.45 (3.53)	22.02 (22.09)
3b	218—221	63.64 (63.68)	3.48 (3.79)	21.38 (21.56)
3c	211—214	66.27 (66.44)	3.38 (3.50)	19.83 (19.92)
3d	238—240	63.82 (63.68)	3.48 (3.79)	21.82 (21.56)
3e	185—186	55.43 (55.47)	2.75 (2.95)	19.45 (19.41)

Physical Measurements. Electrical resistivities, electronic and infrared absorption spectra, and magnetic susceptibilities were measured as described previously.[2]

Results and Discussion

All the simple and complex salts obtained are stable

Table 2. Electrical resistivity(ρ), activation energy (E_a), magnetic susceptibility(χ_M), and absorption maxima (λ_{max}) of the $TCNQ^{\cdot}$ salts

Salt	$\rho_{25°C}$ / Ω cm	E_a [a] / eV	χ_M [b] / 10^{-4}emu mol^{-1}	λ_{max} [c] / 10^3cm^{-1}			
2a	2.1×10^8	0.77	−1.9	8.3	14.7	23.8	
2b	1.2×10^8	0.80	−1.9	11.1	14.1	25.0	
2c	1.3×10^7	0.46	−2.0	11.1	14.2	25.4	
2d	2.2×10^6	0.42	−1.5	8.5	14.2	24.3	
2e	8.8×10^5	0.44	−1.8	8.9	15.2	24.4	
3a	36	0.068	+3.8	10.0 11.1	15.4	24.6	
3b	10	0.038	+4.3	10.0 11.4	16.0	25.3	
3c	5.1	0.046	+1.7	10.0 11.5	(18.2)	25.6	
3d	3.8	0.11	+4.9	9.9 10.8	16.0	25.4	
3e	520	0.13	+7.8	10.3 11.9	15.4	25.6	

a) Calculated from the expression $\rho=\rho_o\exp(E_a/kT)$. b) Measured at room temperature. c) Measured in Nujol mulls, and shoulder in parenthesis.

to air. Plots of log ρ (ρ: electrical resistivities as compacted sample) *vs.* the reciprocal temperature ($1/T$) for each salt show a good linear relation in the 20—90 °C range, indicating that all the salts are typical semiconductors in the temperature range measured. The ρ values of simple salts **2a**—**e** and complex salts **3a**—**e** at 25 °C (Table 2) are the same order of magnitude as or larger by one or two orders of magnitude than those of the iminium salts without substituents on the 1,3-dithiolane ring, $[\overline{S(CH_2)_2SC}{=}\overset{+}{N}Me_2](TCNQ)_n^{\cdot}$ (8.7×10^5 Ω cm for $n=1$ and 3.8 Ω cm for $n=2$),[1] respectively. In view of these results, there may be a trend that the introduction of substituents on the 1,3-dithilane ring results in occasional increases of the resistivity of the $TCNQ^{\cdot}$ radical anion salts depending on the nature of substituents, although no detail of the trend is evident in this study.

The electronic absorption spectra of simple salt **2a** and complex salt **3a** in the solid state (Fig. 1) resemble well those of the iminium salts without substituents on the 1,3-dithiolane ring, as one may expect. The spectral patterns similar to **2a** and **3a** were obtained for simple salts **2b**—**e** and complex salts **3b**—**e**, respectively, except that the lowest frequency bands of **2b** and **2c**, assignable to charge-transfer (CT) transitions between the $TCNQ^{\cdot}$ radical anions,[5] are shifted to higher frequencies than that of **2a** (Table 2). In addition, all the complex salts exhibited a broad absorption band in the 4000—2500 cm^{-1} range, which is due to the CT transition between the $TCNQ^{\cdot}$ radical anion and neutral TCNQ.[5] These results can be subjected to the same discussion as that given previously,[1] which leads us to the conclusion that simple salts **2a**—**e** involve the $(TCNQ)_2^{2-}$ dimer, whereas complex salts **3a**—**e** contain monomeric $TCNQ^{\cdot}$ radical anions in their columnar structure in the solid state. This is consistent with the facts that simple and complex salts show diamagnetic and paramagnetic properties, respectively, at room temperature (Table 2).

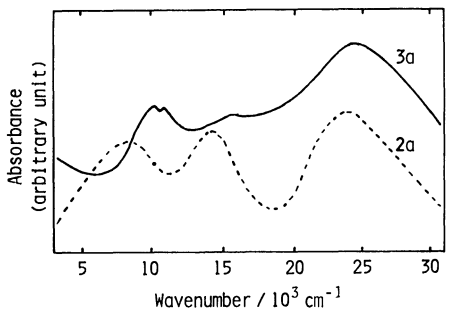

Fig. 1. Absorption spectra of **2a** and **3a** in Nujol mulls.

References

1) S. Araki, H. Ishida, and T. Tanaka, *Bull. Chem. Soc. Jpn.*, **51**, 407 (1978).
2) S. Araki and T. Tanaka, *Bull. Chem. Soc. Jpn.*, **51**, 1311 (1978).
3) T. Nakai, Y. Ueno, and M. Okawara, *Bull. Chem. Soc. Jpn.*, **43**, 156 (1970).
4) K. Hirotani, H. Shino, and M. Okawara, *Chem. Lett.*, **1973**, 867.
5) Y. Iida, *Bull. Chem. Soc. Jpn.*, **42**, 71, 637 (1969).

Adsorption of Pyranine onto Cationic Liposomal Membranes as Evidenced by Fluorescence Polarization†

Tadashi NOMURA, Hiroki KONDO, and Junzo SUNAMOTO*

Department of Industrial Chemistry, Faculty of Engineering, Nagasaki University, Nagasaki 852

(Received October 21, 1980)

Synopsis. A trianionic fluorescent probe, pyranine, was found to bind to positively charged liposomes as evidenced by a linear increase in the fluorescence polarization with the liposome concentration. Addition of perchlorate ion reduced the polarization of fluorescence, suggesting that perchlorate and pyranine compete for the same binding site on the surface of cationic liposomal membranes.

A knowledge of properties of membrane surface is essential to understand various phenomena occurring on membranes, because in biological systems most of events begins with the adsorption of a substance onto and permeation into membranes.[1] The surface of liposomal membranes as well as natural biomembranes has been characterized by a variety of techniques such as NMR[2] or neutron diffraction.[3] A focus has been on the negatively charged membranes to which cations bind through electrostatic interaction with a different degree of specificity.[4-6] In this work we would like to describe the interaction of positively charged liposomes with an anionic fluorescent probe, pyranine (trisodium 8-hydroxy-1,3,6-pyrenetrisulfonate), by means of fluorescence polarization. An advantage of utilizing this particular probe lies in the fact that it emits strong fluorescence at 510 nm and that it can bind to a charged membrane surface through the electrostatic interaction.[7,8] When the probe adsorbs onto the membrane surface the molecular motion of the probe will be depressed, possibly giving rise to a significant increase in the polarization of fluorescence.

Experimental

Pyranine was obtained from Eastman Kodak Co. and its purity was assessed before use by TLC on silica gel in butanol–water (6 : 1 by volume). Its concentration was determined on the basis of molar extinction coefficient of 1.02×10^4 M^{-1} cm^{-1} (1 M = 1 mol dm^{-3}) at 405 nm. Single-compartment liposomes of egg lecithin were prepared as described previously.[9,10] In the preparation of positively charged liposomes, hexadecylamine (20 mol% to lecithin) was added.[9] The pH of the liposome suspension was adjusted to 5 with either 0.6 mM CH_3CO_2H–1.4 mM CH_3CO_2Na or 5.4 mM $HClO_4$–9.6 mM $NaClO_4$. Fluorescence spectra were taken on a Hitachi 650-10 spectrofluorometer with 1 nm bandpaths for both excitation and emission sides. Fluorescence polarization was determined on a Union FS-501 fluorescence depolarization instrument which was connected to a Sord Microcomputer M 200 Mark II. Pyranine was excited at 405 nm and its fluorescence polarization was determined at 510 nm[11] The vertical and horizontal components of the emission were funneled through a Y-46 cut-off filter (50% transmittance at 460 nm). Fluorescence polarization is defined by Eq. 1:[9]

$$p = \frac{I_{VV} - C_f \cdot I_{VH}}{I_{VV} + C_f \cdot I_{VH}} \quad (1) \qquad C_f = I_{HV}/I_{HH},$$

where C_f is the grating correction factor[11] and I stands for the collected intensity of fluorescence at parallel and perpendicular positions of the polarizer. Subscripts V and cH refer to vertical and horizontal beams, respectively. For example, I_{VH} means the intensity of horizontal component of fluorescence when excited by the vertically polarized beam. All measurements were made at 25.0 °C under aerobic conditions.

Results and Discussion

The polarization of pyranine fluorescence was determined in the presence of neutral or positively charged liposomes in an aqueous buffered solution (pH 5) containing acetate or perchlorate ions (Fig. 1).

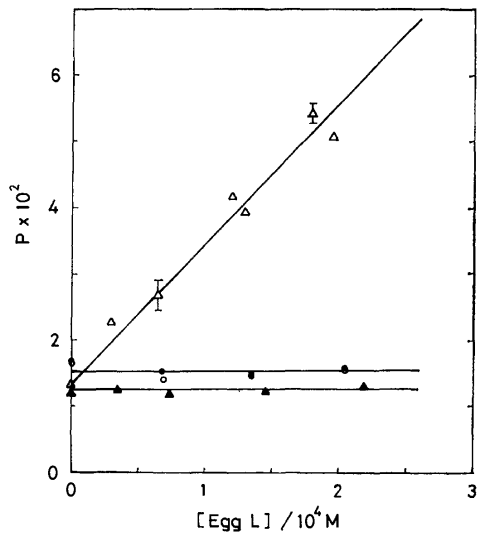

Fig. 1. Fluorescence polarization of pyranine as a function of egg lecithin concentration at pH 5 and 25.0 °C. Experiments were carried out using neutral liposomes in an aqueous acetate (▲) or perchlorate (●) solution and positively charged liposomes in an aqueous acetate (△) or perchlorate (○) solution. The concentration of pyranine was 2×10^{-6} M in all the runs.

For neutral liposomes the polarization did not vary over the liposome concentration range studied. This trend was common to the two salts adopted. These results indicate that no significant interaction takes place between pyranine and neutral liposomes. In the case of cationic liposomes in an acetate buffer, on the other hand, the polarization of pyranine fluorescence increased linearly with increasing liposome concentration. However, this was not the case for the perchlorate solution, suggesting that perchlorate ion interferes with the adsorption of pyranine onto the liposome surface. This was confirmed by the following experiment. When sodium perchlorate was further added to a cationic liposome suspension containing pyranine and acetate ion, the polarization decreased with an increase in the

† Liposomal Membranes, Part X from this laboratory.

Table 1. Effect of perchlorate anion on the fluorescence polarization of pyranine in the egg lecithin single-walled and positively charged liposome suspension at 25.0 °C and pH 5[a)]

$[NaClO_4]$/M	$p \times 10^2$
0	5.0(1.1)[b)]
2.0×10^{-3}	2.9
6.1×10^{-3}	1.9(1.2)

a) A liposome suspension contains 0.10 M NaCl, 1.4 mM CH_3CO_2Na, and 0.6 mM CH_3CO_2H. [Pyranine] $=2.0 \times 10^{-6}$ M; [Egg L] $=2.4 \times 10^{-4}$ M. b) Numbers in parentheses are p-values of pyranine in the absence of liposomes.

perchlorate concentration (Table 1).

From the result that the polarization of pyranine increases in the presence of cationic liposome, it is now evident that pyranine binds to the surface of positively charged liposomes through the electrostatic interaction and consequently the molecular motion of the probe is considerably hindered. It is of special interest that perchlorate ion competes for the same binding site whereas acetate ion does not. This difference seems to arise from the difference in the mode of hydration to these anions. It is presumed that the hydration to perchlorate is weaker than that to acetate, because the charge delocalization is more extensive for the former.[12)] This means that the weakly hydrated perchlorate ion may more easily form an ion pair with (more strongly binds to) the positive site of liposomal membranes. Certainly, the binding of these anions to positively charged liposomes follows a closely similar order to that for their interaction with anion exchange resins[13)] or acetyltetraglycine ethyl ester;[14)] perchlorate> sulfonate>acetate. The high lyophilicity as well as trianionic character of pyranine may make the probe to show the affinity for the cationic membrane surface.

It should be mentioned that the emission maxima and intensity of fluorescence from pyranine were not much affected upon the binding to liposomes. Thus the relative ratio of fluorescence intensity in the presence and absence of liposomes, I/I_0, changed by less than 10% over the egg lecithin concentration range $\approx$400 μM. The relative intensity was also independent of the probe concentration at least in a range of 1—5 μM. These results imply that quenching of pyranine fluorescence upon the binding to liposomes is negligible under the present experimental conditions. This is in contrast to the previous findings in which the concentration quenching of fluorescence was observed through the ionic probe aggregation on the surface of charged membranes.[15,16)] This also supports the contention that hexadecylamine molecules are dispersed evenly in the phospholipid bilayers and that no significant phase separation occurs even by the adsorption of the polyanionic probe.

We are grateful to Dr. Kaoru Tsujii, Tochigi Research Laboratories, Kao Soap Co. Ltd., for his helpful comments. This work was supported by a Grant-in-Aid for Scientific Research No. 447068, from the Ministry of Education Science and Culture.

References

1) P. L. Yeagle, *Acc. Chem. Res.*, **11**, 321 (1978).
2) J. Seeling, *Biochim. Biophys. Acta*, **515**, 105 (1978).
3) B. P. Schoenborn, *Biochim. Biophys. Acta*, **457**, 41 (1976).
4) R. J. Kurland, M. Hammoudah, S. Nir, and D. Papahadjopoulos, *Biochem. Biophys. Res. Commun.*, **88**, 927 (1979).
5) M. Eiserberg, T. Gresalfi, T. Riccio, and S. McLaughlin *Biochemistry*, **18**, 5213 (1979).
6) J. Sunamoto and M. Shironita, *Bull. Chem. Soc. Jpn.*, **53**, 2778 (1980).
7) K. Kano and J. H. Fendler, *Biochim. Biophys. Acta*, **509**, 289 (1978).
8) T. Nomura, J. R. Escabi-Perez, J. Sunamoto, and J. H. Fendler. *J. Am. Chem. Soc.*, **102**, 1484 (1980).
9) J. Sunamoto, K. Iwamoto, H. Kondo, and S. Shinkai, *J. Biochem.*, **88**, 1219 (1980).
10) J. Sunamoto, H. Kondo, and A. Yoshimatsu, *Biochim. Biophys. Acta*, **510**, 52 (1978).
11) P. Puchs, A. Parola, P. W. Bobbins, and E. R. Blout, *Proc. Natl. Acad. Sci. U.S.A.*, **72**, 3351 (1975).
12) W. P. Jencks, "Catalysis in Chemistry and Enzymology," McGraw-Hill, New York, N. Y. (1969), Chap. 7.
13) H. P. Gregor, J. Belle, and R. A. Marcus, *J. Am. Chem. Soc.*, **77**, 2713 (1955).
14) D. R. Robinson and W. P. Jencks, *J. Am. Chem. Soc.*, **87**, 2470 (1965).
15) C. Lee, *Biochemistry*, **10**, 4375 (1971).
16) A. Azzi, A. Fabbro, M. Santato, and P. L. Gherardini, *Eur. J. Biochem.*, **21**, 404 (1971).

The Effect of Polar Solvent on the $^1J_{CH}$ Spin-Spin Coupling Constants in Halomethanes and Haloethylenes

Shosuke WATANABE*,† and Isao ANDO

Department of Polymer Chemistry, Tokyo Institute of Technology, Ookayama, Meguro-ku, Tokyo 152

(Received March 31, 1980)

Synopsis. The solvent effect on the ^{13}C–^1H nuclear spin-spin coupling constants ($^1J_{CH}$) of halomethanes and haloethylenes is calculated by means of the finite perturbation theory based on the CNDO/2 approximations incorporating the 'solvaton' theory. The results of the calculation explained the tendency of the observed solvent effect data in the literature.

Nuclear spin-spin coupling constants are known to be solvent-dependent,[1] and Johnston and Barfield[2–4] have handled the observed solvent effect on spin-spin coupling constants by means of the so-called reaction field model,[2] the cluster model[3] and the rotating-point dipole model.[4] So far as $^1J_{CH}$ is concerned, that is, they have numerically estimated the solvent effect on the $^1J_{CH}$ values of fluoromethanes only.

Most recently,[5,6] we have quantitatively calculated the solvent effect of the one-bond ^{13}C–^1H coupling constant($^1J_{CH}$) by applying the finite perturbation theory (FPT)[7] with the INDO and CNDO/2 MO methods incorporating Klopman's solvaton theory.[8] This approach successfully offers a quantitative description of the solvent effects on the $^1J_{CH}$ values of some small organic compounds (*e.g.*, methane derivatives,[5] acrylonitrile,[5] $CHCl_2CHCl_2$,[6] and $CHCl_2CH_2Cl$[6]).

In the present work we applied the FPT method which we have developed ourselves[5,6] to estimate the substitution effects on the solvent effect of $^1J_{CH}$ coupling constants in such rigid molecules as halomethanes (fluoro- and chloro-) and haloethylenes (fluoro- and chloro-). The results of the calculation are compared with the tendency of the observed solvent effects in the literature.

Results and Discussion

In all the calculations of this work, $S_C^2(0)S_H^2(0) = 2.2240$ a.u. was used as the value of the integral product.

Table 1 shows the results of the calculation of fluoromethanes using the experimental values reported by Cox and Smith[9] and of that on chloromethanes using the experimental values obtained by Watts and Goldstein.[10]

It is evident from the results in Table 1 that the calculated results agree qualitatively well with such observed results as that the solvent-induced change in the $^1J_{CH}$ value increases as the number of substituted fluorine or chlorine atoms increases, or that the $^1J_{CH}$ value increases as the dielectric constant (ε) of the solvent increases.

It is also evident from Table 1 that the respective $^1J_{CH}$ values increase in the order of mono-, di- and trihalogen-substituted compounds, and also that, when the number of substituting halogen atoms is equal in the molecules under consideration, the fluorine deriva-

Table 1. Dependence of $^1J_{CH}$ spin-coupling constants of fluoromethanes and chloromethanes upon the dielectric constant(ε)

Solute	Solvent	ε	Observed		Calculated	
			$^1J_{CH}$/Hz	Δ^1J_{CH}/Hz	$^1J_{CH}$/Hz	Δ^1J_{CH}/Hz
CH_3F		2.02	—	—	161.62	0.0
		20.5	—	—	163.01	1.39
		46.0	—	—	163.16	1.54
CH_2F_2	Cyclohexane	2.02	182.10[a]	0.0	197.58	0.0
	Acetone	20.5	184.80[a]	2.70	201.61	4.03
	DMSO	46.0	186.50[a]	4.40	201.87	4.29
CHF_3	Cyclohexane	2.02	238.10[a]	0.0	257.72	0.0
	Acetone	20.5	245.35[a]	7.25	263.54	5.82
	DMSO	46.0	247.30[a]	9.20	264.15	6.43
CH_3Cl	Cyclohexane	2.02	148.58[b]	0.0	148.05	0.0
	CCl_4	2.23	149.64[b]	1.06	148.26	0.21
	DMF	35.0	150.40[b]	1.82	150.20	2.15
CH_2Cl_2	Cyclohexane	2.02	176.48[b]	0.0	160.91	0.0
	CCl_4	2.23	178.75[b]	2.27	160.97	0.06
	DMF	35.0	180.55[b]	4.07	164.69	3.78
$CHCl_3$	Cyclohexane	2.02	208.11[b]	0.0	178.49	0.0
	CCl_4	2.23	208.26[b]	0.15	178.96	0.47
	CMF	35.0	216.46[b]	8.35	183.57	5.08

a) R. H. Cox and S. L. Smith, *J. Magn. Reson.*, **1**, 432 (1969). b) V. S. Watts and J. H. Goldstein, *J. Phys. Chem.*, **70**, 3887 (1966). c) The calculated values represent the differences between the values in the indicated solvent and in cyclohexane.

† Permanent address: Minato High School of Technology, 18-13, Nishi-shinbashi 3-chome, Minato-ku, Tokyo 105.

TABLE 2. DEPENDENCE OF $^1J_{CH}$ SPIN-COUPLING CONSTANTS OF CHLOROETHYLENES UPON THE DIELECTRIC CONSTANT(ε)

Solute	Solvent	ε	Observed[a]		Calculated	
			$^1J_{CH}$/Hz	Δ^1J_{CH}/Hz[b]	$^1J_{CH}$/Hz	Δ^1J_{CH}/Hz[b]
$CH_2=CCl_2$	Cyclohexane	2.02	166.3	0.0	195.57	0.0
	DMF	35.0	167.0	0.7	199.36	3.79
cis-$C_2H_2Cl_2$	Cyclohexane	2.02	197.1	0.0	203.66	0.0
	DMF	35.0	200.1	3.0	208.57	4.91
trans-$C_2H_2Cl_2$	Cyclohexane	2.02	198.4	0.0	203.21	0.0
	DMF	35.0	200.8	2.4	207.45	4.24
C_2HCl_3	Cyclohexane	2.02	200.5	0.0	205.73	0.0
	DMF	35.0	204.2	3.7	211.48	5.75

a) V. S. Watts, J. Loemker and J. H. and J. H. Goldstein, *J. Mol. Spectrosc.*, **17**, 348(1965). b) The calculated values represent the differences between the values in the indicated solvent and in cyclohexane.

TABLE 3. DEPENDENCE OF $^1J_{CH}$ SPIN-COUPLING CONSTANTS OF DICHLOROFLUOROETHYLENES UPON THE DIELECTRIC CONSTANT(ε)

Solvent	ε	Observed[a]		Calculated	
		$^1J_{CH}$/Hz	Δ^1J_{CH}/Hz[b]	$^1J_{CH}$/Hz	Δ^1J_{CH}/Hz[b]
			(*Z*)-1,2-Dichlorofluoroethylene		
Cyclohexane	2.02	195.6	0.0	198.8	0.0
Benzene	2.26	198.0	2.4	199.4	0.6
$CHCl_3$	4.63	199.6	4.0	201.7	2.9
Acetone	20.0	199.5	3.9	203.4	4.6
DMF	35.0	202.5	6.9	203.7	4.9
DMSO	46.0	202.0	6.4	203.7	4.9
			(*E*)-1,2-Dichlorofluoroethylene		
Cyclohexane	2.02	201.7	0.0	207.9	0.0
Benzene	2.26	204.0	2.3	208.5	0.6
$CHCl_3$	4.63	203.8	2.1	211.0	3.1
Acetone	20.0	205.9	4.2	212.9	5.0
DMF	35.0	208.6	6.9	213.3	5.4
DMSO	46.0	208.1	5.4	213.3	5.4

a) C. L. Bell and S. S. Danyluk, *J. Mol. Spectrosc.*, **35**, 376 (1970). b) The calculated values represent the differences between the values in the indicated solvent and in cyclohexane.

tives exhibit a larger $^1J_{CH}$ value than the chlorine derivatives. This may be due to the greater electronegativity of the fluorine atom. This tendency agrees with the observed result.

The calculated results of the solvent effect on the $^1J_{CH}$ calculation of dichloroethylenes and trichloroethylene are tabulated in Table 2 in comparison with the corresponding experimental values reported by Watts *et al.*[11] It is now clear that the $^1J_{CH}$ value of 1,1-dichloroethylene is smaller than those of the 1,2-dichloroethylenes and that those of its *trans*- and *cis*-forms are nearly equal to each other. It is found that the trisubstituted ethylene has a larger $^1J_{CH}$ value than the disubstituted one and that, in both cases, its values depend highly on ε.

Table 3 shows the calculated results of the solvent effect on the $^1J_{CH}$ for 1,2-dichlorofluoroethylenes, together with the corresponding experimental data reported by Bell and Danyluk.[12] The (*E*) form exhibits a larger $^1J_{CH}$ value than the (*Z*) form, and both values depend on ε. The calculated results agree well with the experimental findings.

The authors wish to thank Professor Riichirô Chûjô of our department for his helpful suggestions and discussions.

References

1) a) M. Barfield and M. D. Johnston, Jr., *Chem. Rev.*, **73**, 53 (1973), b) S. L. Smith, *Fortscher. Chem. Forsch.*, **27**, 117 (1972).

2) M. D. Johnston and M. Barfield, *J. Chem. Phys.*, **54**, 3083 (1971).

3) M. D. Johnston and M. Barfield, *J. Chem. Phys.*, **55**, 3483 (1971).

4) M. D. Johnston and M. Barfield, *Mol. Phys.*, **22**, 831 (1971).

5) M. Kondo, S. Watanabe, and I. Ando, *Mol. Phys.*, **37**, 1521 (1979).

6) S. Watanabe and I. Ando, *Bull. Chem. Soc. Jpn.*, **53**, 1257 (1980).

7) J. A. Pople, J. W. McIver, and N. S. Ostlund, *J. Chem. Phys.*, **49**, 2965 (1967).

8) a) G. Klopman, *Chem. Phys. Lett.*, **1**, 200 (1967). b) G. Klopman, *J. Am. Chem. Soc.*, **90**, 223 (1968).

9) R. H. Cox and S. L. Smith, *J. Magn. Reson.*, **1**, 432 (1969).

10) V. S. Watts and J. H. Goldstein, *J. Phys. Chem.*, **70**, 3887 (1966).

11) V. S. Watts, J. Loemker, and J. H. Goldstein, *J. Mol. Spectrosc.*, **17**, 348 (1965).

12) C. L. Bell and S. S. Danyluk, *J. Mol. Spectrosc.*, **35**, 376 (1970).

^{1}H NMR Study of Dissociation and Re-association of Apoferritin and Ferritin

Noboru IMAI,* Yoji ARATA, and Shizuo FUJIWARA
Department of Chemistry, Faculty of Science, The University of Tokyo, Hongo, Bunkyo-ku, Tokyo 113
(Received November 4, 1980)

Synopsis. The processes of dissociation and re-association of apoferritin and the protein part of ferritin were investigated by ^{1}H NMR. It was suggested that the re-association of ferritin occurs more easily than that of apoferritin.

Ferritin is an iron storage protein consisting of 24 subunits around the iron core which is the polymerized iron (the composition is $(FeOOH)_8(FeOOPO_3H_2)$) and contains 0—4000 iron atoms.[1] Apoferritin, the protein part of ferritin (M.W. 445000), can be dissociated to subunits by sodium dodecyl sulfate,[2] 7 M (1 M=1 mol dm^{-3}) guanidinium chloride[3] and 67% (v/v) acetic acid.[4] It has been shown that the dissociation of apoferritin is reversible; However a significant degree of hysteresis is known to exist in the re-association process.[5] In a previous paper,[6] we have applied the technique of nuclear magnetic resonance (NMR) to the study of ferritin to discuss the state and role of the phosphate group on the surface of the iron core. In the present experiment, it will be shown that the processes of dissociation and re-association of the protein assembly in ferritin and apoferritin can be followed by ^{1}H NMR. The NMR signal from the protein part can be observed only after the protein part dissociates into subunits (M.W. 18500). Of special advantage of NMR over other methods is the fact that, in the case of ferritin, the iron core influences only little the NMR signal of the protein. The process of dissolution of the iron core to iron(III) ion will also be discussed using the linewidth of the peak of solvent water. On the basis of these results, we will discuss a possible role of the iron core in the processes of dissociation and re-association of ferritin.

Horse spleen ferritin (Nutritional Biochemicals Corporation, twice recrystallized, Cd free) was dialyzed against dilute EDTA solution. All reagents used are of reagent grade. The concentration of iron was determined by using atomic absorption[6] and that of protein by Lowry method.[7] ^{1}H NMR spectra were recorded using a JEOL PS-100 spectrometer operating at 100 MHz.

The pH of sample solution was changed in either of the following two ways: For the study of dissolution of the iron core to iron(III) ion, a small amount of ferritin solution (0.35 M, as iron) was added to a glycine–HCl buffer solution with pH pre-adjusted, and the linewidth of the NMR signal of water in the solution was measured. Before and after the above treatment, no precipitation occurred and very little change in pH was observed. 2) For the study of the dissociation of protein part for apoferritin and ferritin, the pH of sample solutions was changed by dialyzing for 24 h against a 10 mM glycine–HCl buffer. In the experiment of re-association, the solution, which had been dialyzed for 24 h against a 10 mM glycine–HCl buffer at pH 1.8, was further dialyzed for 24 h against the same buffer at higher pH.

Dissociation of the Protein Assembly in Ferritin and Apoferritin. The NMR signal of the protein part becomes observable when the pH of solutions of ferritin or apoferritin decreases below 3.5, suggesting that the protein part dissociates into subunits. The aliphatic region of the NMR spectrum of the protein part is shown in Fig. 1A. The signal indicated by an arrow is presumably due to the methyl groups of leucine, isoleucine, and valine. The height of the peak reaches maximum below pH 1.8; the extent of dissociation of the protein part was determined by measuring the height of these peaks. The dissociation curves for apoferritin and ferritin thus obtained are shown in Fig. 1B and Fig. 2, respectively; no significant difference was observed between ferritin and apoferritin.

The Process of Dissolution of the Iron Core to Iron(III) Ion. The red color of the ferritin solution fades when the pH decreases below 2.0, where the linewidth of H_2O signal greatly increases. This is most likely because the iron core dissolves and the amount of aqueous iron(III) ion increases at low pH, resulting in a large increase in the interaction of water molecule with the paramagnetic iron(III) ion. This suggests that the process of the dissolution of the iron core to iron(III) ion may

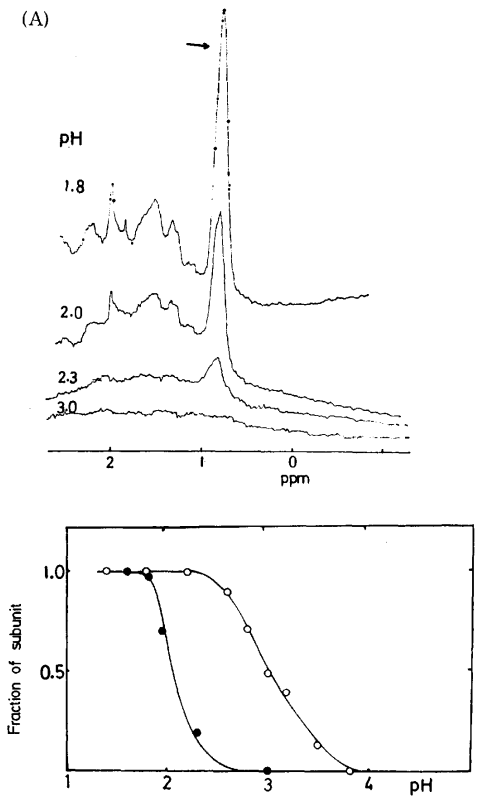

Fig. 1. (A) The aliphatic region of 100 MHz NMR spectra of apoferritin at low pH. The protein concentration was 12 mg/ml. (B) Dissociation and re-association of apoferritin at low pH.
●: Dissociation, ○: re-association.

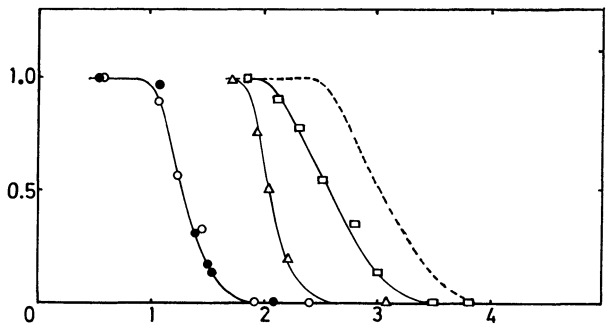

Fig. 2. Dissociation and re-association of ferritin at low pH.
○: Dissolution of iron core (NMR), ●: ($OD_{410\ nm}$), △: dissociation, □: re-association.

be followed quantitatively by observing the linewidth of the water signal. In the present experiment, the concentration of the ferritin solutions was 5 mM (as iron); at this concentration the solution is clear and there is no precipitation nor aggregation observed with the dissolution of the iron core. The results shown in Fig. 2 indicate that the iron core begins to dissolve at pH 1.8 and dissolves completely at pH 1.0. This process was also followed by the measurement of $OD_{410\ nm}$ and the result is in good agreement with that obtained by the NMR measurement. See Fig. 2. The results in Fig. 2 suggest that the protein part of ferritin begins to dissociate at pH 3.5 and dissociates completely at pH 1.8, but the iron core itself remains intact above pH 1.8. It is of interest that in a narrow range around pH 1.8 the protein part dissociates completely with the intact iron core.

Re-association of Subunits of Ferritin and Apoferritin. With an increase in pH of the solutions of ferritin or apoferritin where the protein part has been dissociated at low pH, the NMR signals of the protein part becomes undetectable, suggesting that the subunits re-associate. The fraction of re-association was determined from the peak height as in the case of dissociation. The re-association curve of apoferritin is shown in Fig. 1B. In this experiment, 0.01 M glycine–HCl buffer was used in dialysis at pH 1.8 to dissociate and at higher pH to re-associate the protein part. A similar experiment was carried out using ferritin. The re-association curve for ferritin is also included in Fig. 2. The broken line is the re-association curve of apoferritin. The curve of re-association for ferritin, which has already been dissociated at pH 1.8, deviates greatly from that for apoferritin. This suggests that re-association of the protein part occurs more easily in the case of ferritin than in the case of apoferritin.

References

1) R. R. Crichton, *Struct. Bonding (Berlin)*, **17**, 67 (1973).
2) K. Ishitani, Y. Niitsu, and I. Listowsky, *J. Biol. Chem.*, **250**, 3142 (1975).
3) I. Listowsky, G. Blauer, S. Englard, and J. J. Betheil, *Biochemistry*, **11**, 2176 (1972).
4) P. M. Harrison and D. W. Gregory, *Nature*, **220**, 578 (1968).
5) R. R. Crichton and C. F. A. Bryce, *Biochem. J.*, **133**, 289 (1973).
6) N. Imai, H. Terada, Y. Arata, and S. Fujiwara, *Bull. Chem. Soc. Jpn.*, **51**, 2538 (1978).
7) O. H. Lowry, N. J. Rosebrough, A. L. Farr, and R. J. Randall, *J. Biol. Chem.*, **193**, 265 (1951).

Generalized Graph-theoretical Formula for London Diamagnetism

Jun-ichi AIHARA

Department of Chemistry, Faculty of Science, Hokkaido University, Sapporo 060

(Received December 4, 1980)

Synopsis. The previous graph-theoretical formula for London diamagnetism was improved so as to include all kinds of cyclic conjugated systems. Bicyclo[6.2.0]decapentaene was then found to be diatropic but antiaromatic even though the central π bond was elongated.

Diamagnetic susceptibility due to ring currents is one of the key quantities in aromatic chemistry.[1] In 1937 London formulated it in quantum-mechanical terms,[2,3] so it has been called the London diamagnetism.[1] Recently I reformulated it[4,5] by means of Sachs' graph-theoretical theorem.[6] The obtained formula enabled us to estimate susceptibility contributions from individual π-electron rings in a conjugated system.[5] However, I later found that this formula was applicable only to conjugated hydrocarbons with no bond alternation. In this note, I would like to generalize the graph-theoretical formula for London diamagnetism so as to include not only conjugated hydrocarbons with appreciable bond alternation but also heterocycles.

Let us consider the conjugated system G placed perpendicularly in the external magnetic field H. The ith π-electron ring in G is denoted by r_i, which is identical with the ith ring component in Sachs' theorem.[6,7] The area of r_i is denoted by S_{r_i}. For simplicity, we define

$$\Theta_{r_i} = \frac{eS_{r_i}}{\hbar c}, \tag{1}$$

where e, $\hbar$, and c are the standard constants with these symbols. A characteristic polynomial for G is a function of H, so it is denoted by $P_G(X,H)$.[6,7] When there is no external field, the contribution of r_i to the coefficients of the characteristic polynomial is given by[7]

$$C(r_i, 0) = 2\prod_s^{r_i} k_s. \tag{2}$$

Here, k_s is a Hückel bond parameter for the sth π bond in G, and s runs over all π bonds in r_i. If the field H is applied to G, it should become[4,5]

$$C(r_i, H) = 2\cos(\Theta_{r_i}H)\prod_s^{r_i} k_s. \tag{3}$$

With this expression in mind and by analogy with Hosoya's way of expanding Hückel secular determinants,[8] $P_G(X,H)$ can be expanded as

$$P_G(X,H) = R_G(X) - 2\sum_i^G R_{G-r_i}(X)\cos(\Theta_{r_i}H)\prod_s^{r_i} k_s + 2^2\sum_{i<j}^G R_{G-r_i-r_j}(X)\cos(\Theta_{r_i}H)\cos(\Theta_{r_j}H)\prod_s^{r_i} k_s\prod_s^{r_j} k_s - \cdots. \tag{4}$$

Here, $R_G(X)$ is a reference polynomial defined for G, *i.e.*, a characteristic polynomial for the olefinic reference structure of G;[5,6,9] G-r_i is a subgraph of G, obtained by deleting r_i and all π bonds adjacent to it; G-r_i-r_j is a subgraph of G, obtained by deleting a pair of disjoint π-electron rings r_i and r_j and all π bonds adjacent to r_i and/or r_j; the first summation is practiced over all π-electron rings, and the second one over all possible pairs of disjoint π-electron rings.

Since the applied field H can be treated as a small perturbation,

$$\cos(\Theta_{r_i}H) \approx 1 - \frac{1}{2}\Theta_{r_i}^2H^2. \tag{5}$$

By applying this approximation to Eq. 4, the following expression can be derived:

$$\begin{aligned} P_G(X,H) &= R_G(X) - 2\sum_i^G R_{G-r_i}(X)\left(1-\frac{1}{2}\Theta_{r_i}^2H^2\right)\prod_s^{r_i} k_s \\ &\quad + 2^2\sum_{i<j}^G R_{G-r_i-r_j}(X)\left(1-\frac{1}{2}\Theta_{r_i}^2H^2\right)\left(1-\frac{1}{2}\Theta_{r_j}^2H^2\right) \\ &\quad \times \prod_s^{r_i} k_s\prod_s^{r_j} k_s - \cdots \\ &= P_G(X,0) + H^2\sum_i^G P_{G-r_i}(X,0)\Theta_{r_i}^2\prod_s^{r_i} k_s. \end{aligned} \tag{6}$$

In deriving the last expression, we used the relationship in this form:

$$P_G(X,0) = R_G(X) - 2\sum_i^G R_{G-r_i}(X)\prod_s^{r_i} k_s + 2^2\sum_{i<j}^G R_{G-r_i-r_j}(X)\prod_s^{r_i} k_s\prod_s^{r_j} k_s - \cdots. \tag{7}$$

This is nothing other than a generalized form of Hosoya's formula for obtaining $P_G(X,0)$.[8]

After a simple treatment of Eq. 6, analogous to that presented in Ref. 5, the diamagnetic susceptibility attributable to the mth orbital is given by

$$\chi_m = -2\beta\sum_i^G \frac{P_{G-r_i}(X_m^\circ, 0)}{P_G'(X_m^\circ, 0)}\Theta_{r_i}^2\prod_s^{r_i} k_s, \tag{8}$$

where X_m° is the mth largest root of the equation $P_G(X,0)=0$. Then, the overall susceptibility due to ring currents is

$$\chi = 2\sum_{m=1}^{m_0}\chi_m. \tag{9}$$

Here, m_0 indicates the highest occupied orbital. Unfortunately, Eq. 8 does not hold for degenerate orbitals. In this case, $P_G(X,0)$ is rewritten as

$$P_G(X,0) = U_G(X)(X-X_{m^*}^\circ)^2, \tag{10}$$

where m* indicates the degenerate orbitals. According to the mathematical treatment similar to that of Pullman and Pullman,[3] the diamagnetic susceptibility attributable to each of these orbitals becomes

$$\chi_{m^*} = \frac{U_G'(X_{m^*}^\circ)V_G(X_{m^*}^\circ) - U_G(X_{m^*}^\circ)V_G'(X_{m^*}^\circ)}{U_G(X_{m^*}^\circ)^2}, \tag{11}$$

where

$$V_G(X) = \sum_i^G P_{G-r_i}(X,0)\Theta_{r_i}^2\prod_s^{r_i} k_s. \tag{12}$$

Now the graph-theoretical formulation of London diamagnetism has been completed. We can easily evaluate the susceptibility of any cyclic conjugated

system by means of these expressions, but without any knowledge of graph theory. They are really applicable to any kind of conjugated systems, including heterocycles.

As an example, it is instructive to calculate the susceptibility of the bicyclo[6.2.0]decapentaene conjugated system (I). Oda *et al.* showed that this compound

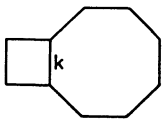

I

has relatively small alternation of the peripheral π bonds and a rather elongated central π bond.[10] Therefore, the susceptibility was calculated as a function of the bond parameter of the central π bond (k). The susceptibilities obtained according to Eq. 8 are 0.352 for $k=1.00$, 0.422 for $k=0.90$, 0.478 for $k=0.80$, 0.523 for $k=0.70$, 0.559 for $k=0.60$, and 0.587 for $k=0.50$, all in units of $\Theta_0^2\beta$. Here, Θ_0 is $e/\hbar c$, multiplied by the area of the benzene ring, and $\beta=|\beta|$. In this connection, the resonance energies due to aromatic stabilization[9] are -0.642 for $k=1.00$, -0.509 for $k=0.90$, -0.396 for $k=0.80$, -0.298 for $k=0.70$, -0.212 for $k=0.60$, and -0.137 for $k=0.50$, all in units of β. These results clearly indicate that the bicyclo[6.2.0]decapentaene conjugated system is diamagnetic but antiaromatic in nature. This conclusion is independent of the magnitude of the k value. Therefore, we might say that this compound is a diatropic antiaromatic compound. Diatropicity has been supported by experiment.[10] It is noteworthy that diatropicity and antiaromaticity coexist in such a bicyclic conjugated system.

The use of the facilities of the Hokkaido University Computing Center is gratefully acknowledged.

References

1) H. J. Dauben, Jr., J. D. Wilson, and J. L. Laity, "Nonbenzenoid Aromatics," ed by J. P. Snyder, New York, N. Y. (1971), Vol. II, Chap. 3.
2) F. London, *J. Phys. Radium*, **8**, 397 (1937).
3) B. Pullman and A. Pullman, "Les Théories Electroniques de la Chimie Organique," Masson et Cie, Paris (1952), Chap. 9.
4) J. Aihara, *J. Am. Chem. Soc.*, **101**, 558 (1979).
5) J. Aihara, *J. Am. Chem. Soc.*, **101**, 5913 (1979).
6) H. Sachs, *Publ. Math. (Debrecen)*, **11**, 119 (1964); A. Graovac, I. Gutman, N. Trinajstić, and T. Živković, *Theor. Chim. Acta*, **26**, 67 (1972).
7) J. Aihara, *J. Am. Chem. Soc.*, **98**, 6840 (1976).
8) H. Hosoya, *Theor. Chim. Acta*, **25**, 215 (1972).
9) J. Aihara, *J. Am. Chem. Soc.*, **98**, 2750 (1976); I. Gutman, M. Milun, and N. Trinajstić, *ibid.*, **99**, 1692 (1977).
10) C. Kabuto and M. Oda, *Tetrahedron Lett.*, **1980**, 103; M. Oda and H. Oikawa, *ibid.*, **1980**, 107.

The Crystal Structure of Di-μ-Bromo-tris(triphenylphosphine)dicopper(II)

Hisao NEGITA,* Morio HIURA, Yoshihiko KUSHI, Masahiro KURAMOTO, and Tsutomu OKUDA

Department of Chemistry, Faculty of Science, Hiroshima University, Higashisenda-machi, Naka-ku, Hiroshima 730

(Received June 5, 1980)

Synopsis. The crystal structure of the $Cu_2Br_2(PPh_3)_3 \cdot 1.5C_6H_6$ complex has been determined by three dimensional X-ray analysis. The crystals are monoclinic, and the space group is $P2_1/c$, with unit-cell parameters of $a=14.122$ (3), $b=19.573$ (4), $c=25.985$ (7) Å, $\beta=128.99$ (1)°, and $Z=4$. In the $Cu_2Br_2(PPh_3)_3$ molecule, one copper atom is three-coordinate, and the other, four-coordinate.

It has been known that copper(I) halides form a number of complexes with tertiary phosphine. A particularly interesting series is the 2 : 3 complexes, $Cu_2X_2(PPh_3)_3$, in which three- and four-coordinated copper atoms are both present and in which the stabilities of the two atoms are similar.[1-3] In this work, the bromide complex is investigated by means of the X-ray crystal analysis and the structure and bonding are discussed in connection with the NQR study.[4]

Experimental

Preparation. $Cu_2Br_2(PPh_3)_3 \cdot 1.5C_6H_6$, prepared as has been described in the literature,[5] was recrystallized from a mixed solvent of benzene and heptane (benzene : heptane = 3 : 1). Found: C, 62.94; H, 4.55%. Calcd for $C_{63}H_{54}Cu_2Br_2P_3$: C, 63.54; H, 4.57%.

X-Ray Data Collection. All the cell constants were determined by a least-squares treatment of the setting of 24 reflections measured on a Rigaku four-circle diffractometer, AFC-5, with Mo $K\alpha_1$ radiation ($\lambda_1=0.70926$ Å); $a=14.122$ (3), $b=19.573$ (3), $c=25.985$ (7) Å, $\beta=128.99$ (1)°. $Z=4$, and calculated density $\rho(\text{calcd})=1.42$ g cm^{-3}. The intensity data were collected by the ω-2θ scan technique to a maximum 2θ value of 42° at a scan rate of 16°/min (50 KV, 170 mA). The intensities of 4890 independent reflections were collected. Reflections for which the intensities were less than three times their standard deviations were regarded as "unobserved" and were not included in subsequent calculations. Thus, 4538 independent reflections were used for the structure determination. Their intensities were corrected for Lorentz and polarization factors, but no absorption corrections were made since the μ-values were low ($\mu=25.9$ cm^{-1}).

Structure Determination. The crystal structure was (solved by the heavy-atom technique, and the refinement was performed by a block-diagonal least-squares calculation. The quantity minimized was $w(|F_o|-k|F_c|)^2$. Cruickshank's weighting scheme was used, where $w=1/(a+|F_o|+b|F_o|^2)$, with $a=6.5$ and $b=0.019$. The atomic scattering factors from the International Tables for X-Ray Crystallography[6] were used. The effects of the anomalous dispersion of the P, Cu, and Br atoms for Mo $K\alpha$ radiation were included in the calculation. The final R value was 0.070. A list of observed and calculated structure factors is preserved by the Chemical Society of Japan (Document No. 8114). The final atomic coordinates are summarized in Table 1.

TABLE 1. FINAL ATOMIC PARAMETERS FOR $Cu_2Br_2(PPh_3)_3 \cdot 1.5C_6H_6$, WITH ESTIMATED STANDARD DEVIATIONS

Atom	x	y	z	Atom	x	y	z
Cu(1)	0.58856(12)	0.18115(8)	0.18994(7)	C(55)	0.7956(14)	0.3619(8)	0.0158(7)
Cu(2)	0.74821(12)	0.21919(7)	0.15925(7)	C(56)	0.7971(13)	0.3070(7)	0.0527(7)
Br(1)	0.55725(11)	0.28104(6)	0.12707(7)	C(61)	0.8504(9)	0.1334(5)	0.0873(5)
Br(2)	0.74503(11)	0.10785(6)	0.21339(7)	C(62)	0.9130(10)	0.1507(6)	0.0630(6)
P(1)	0.4461(3)	0.1564(2)	0.1972(1)	C(63)	1.0093(11)	0.1081(7)	0.0806(6)
P(2)	0.7220(3)	0.1845(2)	0.0682(1)	C(64)	1.0476(12)	0.0547(7)	0.1219(6)
P(3)	0.9001(3)	0.2800(2)	0.2479(1)	C(65)	0.9867(12)	0.0368(7)	0.1473(6)
C(11)	0.3619(10)	0.2259(6)	0.2184(5)	C(66)	0.8864(11)	0.0780(6)	0.1293(6)
C(12)	0.4759(12)	0.2787(7)	0.2571(7)	C(71)	0.9297(10)	0.3633(6)	0.2289(5)
C(13)	0.4418(15)	0.3322(9)	0.2789(8)	C(72)	0.8279(11)	0.4032(6)	0.1806(6)
C(14)	0.3260(15)	0.3348(9)	0.2615(8)	C(73)	0.8433(13)	0.4684(7)	0.1643(7)
C(15)	0.2423(14)	0.2851(8)	0.2210(8)	C(74)	0.9647(13)	0.4921(8)	0.1956(7)
C(16)	0.2733(13)	0.2287(7)	0.1986(7)	C(75)	1.0616(12)	0.4528(7)	0.2402(7)
C(21)	0.3141(9)	0.1300(6)	0.1142(5)	C(76)	1.0486(11)	0.3880(6)	0.2594(6)
C(22)	0.2847(11)	0.0615(6)	0.0972(6)	C(81)	1.0505(10)	0.2386(6)	0.3001(5)
C(23)	0.1872(13)	0.0440(8)	0.0302(7)	C(82)	1.0699(12)	0.1874(7)	0.2712(6)
C(24)	0.1245(14)	0.0954(8)	−0.0164(8)	C(83)	1.1853(13)	0.1540(8)	0.3084(7)
C(25)	0.1504(13)	0.1625(8)	−0.0008(7)	C(84)	1.2736(13)	0.1740(8)	0.3705(7)
C(26)	0.2484(12)	0.1821(7)	0.0664(7)	C(85)	1.2596(16)	0.2234(9)	0.4013(9)
C(31)	0.4685(10)	0.0855(6)	0.2484(6)	C(86)	1.1422(14)	0.2585(8)	0.3658(7)
C(32)	0.5664(13)	0.0423(7)	0.2717(7)	C(91)	0.8674(10)	0.2996(6)	0.3043(6)
C(33)	0.5817(16)	−0.0186(9)	0.3093(9)	C(92)	0.8751(13)	0.2451(8)	0.3411(7)
C(34)	0.5005(15)	−0.0319(8)	0.3194(8)	C(93)	0.8386(14)	0.2556(8)	0.3823(8)
C(35)	0.4085(14)	0.0110(8)	0.2988(8)	C(94)	0.7942(14)	0.3204(8)	0.3803(7)
C(36)	0.3872(12)	0.0697(7)	0.2608(7)	C(95)	0.7859(14)	0.3734(8)	0.3442(7)
C(41)	0.5921(10)	0.1304(6)	0.0094(5)	C(96)	0.8227(11)	0.3627(7)	0.3041(6)
C(42)	0.4929(12)	0.1347(7)	0.0092(6)	C(101)	0.5697(15)	0.4116(9)	−0.0197(8)
C(43)	0.3858(13)	0.0909(8)	−0.0400(7)	C(102)	0.5486(14)	0.4350(8)	0.0045(8)
C(44)	0.3905(13)	0.0497(7)	−0.0810(7)	C(103)	0.4785(15)	0.4438(8)	0.0244(8)
C(45)	0.4871(12)	0.0451(7)	−0.0794(7)	C(111)	0.0157(24)	0.0735(14)	0.4320(13)
C(46)	0.5901(11)	0.0861(7)	−0.0335(6)	C(112)	0.1246(24)	0.0987(13)	0.4495(13)
C(51)	0.7084(10)	0.2526(6)	0.0183(6)	C(113)	0.2160(22)	0.1275(13)	0.5157(12)
C(52)	0.6190(12)	0.2580(7)	−0.0503(7)	C(114)	0.1923(22)	0.1372(13)	0.5591(12)
C(53)	0.6174(15)	0.3155(9)	−0.0853(8)	C(115)	0.0808(28)	0.1144(16)	0.5384(15)
C(54)	0.7076(14)	0.3638(8)	−0.0517(8)	C(116)	−0.0062(28)	0.0855(16)	0.4775(15)

Table 2. Selected interatomic distances (Å) and angles (deg.) for $Cu_2Br_2(PPh_3)_3 1.5CH$, with estimated standard deviations in parentheses

Distanes				Angles			
Cu(1)–Cu(2)	2.992(2)	Cu(2)–Br(2)	2.610(2)	Cu(1)–Br(1)–Cu(2)	71.88(5)	Br(2)–Cu(1)–P(1)	127.03(9)
Br(1)···Br(2)	4.009(2)	Cu(1)–P(1)	2.190(3)	Cu(1)–Br(2)–Cu(2)	71.66(5)	Br(2)–Cu(2)–Br(2)	101.44(5)
Cu(1)–Br(1)	2.404(2)	Cu(2)–P(2)	2.252(3)	Br(1)–Cu(1)–Br(1)	114.26(6)	Br(2)–Cu(2)–P(2)	105.41(8)
Cu(1)–Br(2)	2.370(2)	Cu(2)–P(3)	2.260(3)	Br(1)–Cu(1)–P(1)	116.91(9)	Br(2)–Cu(2)–P(3)	102.60(8)
Cu(2)–Br(1)	2.569(2)			Br(1)–Cu(2)–P(2)	110.76(8)	P(2)–Cu(2)–P(3)	130.66(11)
				Br(1)–Cu(2)–P(3)	102.27(8)		

Results and Discussion

Crystals of $Cu_2Br_2(PPh_3)_3 \cdot 1.5C_6H_6$ are composed of discrete molecular units of $Cu_2Br_2(PPh_3)_3$ and benzene. The interatomic distances and bond angles, along with their estimated standard deviations, are listed in Table 2. The molecular structure obtained and the labelling of atoms are illustrated in Fig. 1. Two kinds of benzene molecules are present in this crystal. One benzene occupies interstitial sites in the structure centered at 1/2, 1/2, 0. In the other benzene, some degree of disorder is suggested by the large thermal parameters.

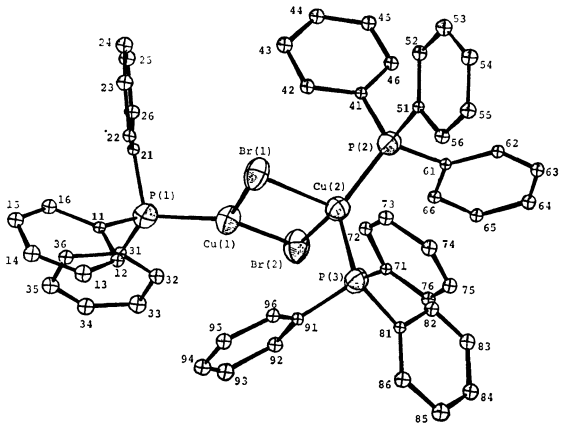

Fig. 1. View of the molecule $Cu_2Br_2(PPh_3)_3$ (drawn by use of ORTEP). The symbol, C, for each carbon atom has been omitted for clarity.

The structure of $Cu_2Br_2(PPh_3)_3$ consists of both three- and four-coordinated copper atoms. The geometry about Cu(I) is approximately trigonal planar, and the copper atom lies 0.183 Å above the plane including P(1), Br(1), and Br(2). The Cu(1)–P(1) distance, 2.190 Å, is nearly equal to the values observed cases where only one phosphine ligand is linked to the copper atom.[7,8] The environment of Cu(2) is distorted in a tetrahedral direction, and a marked departure from an idealized tetrahedral geometry is seen in the P(2)–Cu(2)–P(3) angle, which is 130.66°. The Cu(2)–P distances, 2.252 and 2.260 Å, are longer than the Cu(1)–P(1) distance in the three-coordinated copper atom.

The Cu–P distances involving the same kind of phosphines are dramatically influenced by the number of phosphine ligands bonded to the copper atom, whereas they are only slightly influenced by the coordination number of the copper atom.[7,8] In the ^{63}Cu NQR studies of $Cu_2X_2(PPh_3)_3$ (X=Cl, Br, and I),[4] the observed quadrupole coupling constant (e^2Qq/h) and the orientations of the efg principal axes of the three-coordinated copper atoms are mainly interpreted in terms of an sp^2-hybridization scheme. However, the observed frequencies are slightly higher than the maximum value expected for the sp^2 bonding. This discrepancy can be explained in terms of a bonding scheme involving 3d orbital mixing. This bonding scheme is applicable to the present compound, because the bromide complex is similar to the chloride and iodide complexes in the molecular structure as well as in ^{63}Cu NQR frequencies. In the case of the four-coordinated copper atom, the observed low frequency can be explained by sp^3 mixing only. However, from the distorted tetrahedral structure obtained in this compound, it seems likely that the Cu→P back-bonding exists and that it contributes to the Cu–P distance to some extent.

The Cu–Br distances in the four-coordinated copper atom are 0.203 Å (on the average) longer than those in the three-coordinated copper atom. In comparison with the case of the Cu–P distances, the copper-halogen distances increase with the copper coordination number. In the NQR studies of the $Cu_2X_2(PPh_3)_3$ series, it is observed that the e^2Qq/h values of the three-coordinated copper atoms decrease from X=Cl to I. This order is the reverse of the expectation for the sp^2 mixing scheme. This conflict can be explained by the existence of copper p_π-halogen p_π bonding; this π-bonding will reduce the e^2Qq/h value in this order; I>Br>Cl.[4] Therefore, the shortening of the copper-halogen distances in the three-coordinate copper atom is considered to be caused by the mixture of π-bonding.

References

1) D. F. Lewis, S. J. Lippard, and P. S. Wecker, *J. Am. Chem. Soc.*, **92**, 3805 (1970).

2) V. G. Albano, P. L. Bellon, G. Ciani, and M. Manassero *J. Chem. Soc., Dalton Trans.*, **1972**, 171.

3) P. G. Eller, G. J. Kubas, and R. R. Ryan, *Inorg. Chem.*, **16**, 2454 (1977).

4) H. Negita, M. Hiura, K. Yamada, and T. Okuda, *J. Mol. Struct.*, **58**, 205 (1980).

5) G. Costa, E. Reisenhofer, and L. Stefani, *J. Inorg. Nucl. Chem.*, **27**, 2581 (1965).

6) "International Tables for X-Ray Crystallography," Kynoch Press, Birmingham (1968), Vol. III, pp. 201—206.

7) S. J. Lippard and G. J. Palenik, *Inorg. Chem.*, **10**, 1322 (1971).

8) A. Camus, N. Marsich, G. Nardin, and L. Randaccio, *J. Chem. Soc., Dalton Trans.*, **1975**, 2560.

The Correlation between the Relative Retention Behavior and the Number of Chlorine Substituents in the Phenol Ring

Sukeo ONODERA

Faculty of Pharmaceutical Sciences, Tokyo University of Science, 12 Ichigaya-funagawara, Shinjuku-ku, Tokyo 162

(Received July 11, 1980)

Synopsis. The gas-chromatographic behavior of chlorinated phenols, *m*-cresols, and 3,5-xylenols on polar and nonpolar columns connected to either FID or ECD has been studied. The relative retention times (t_R) for individual homologous series were determined as a function of the number of chlorine substituents in the molecule. It was found, for the homologous series of these chlorinated compounds, that a relationship between log t_R and the number of chlorine substituents is of only limited use in the identification of individual chlorinated phenols.

Gas-liquid chromatography (GLC) is a rapid, specific, and sensitive method for the separation and determination of a variety of such volatile compounds as organic contaminants in the environment. The identification of the chromatographic separated components is, though, a complex problem, one which requires the use of many standards or a combination of gas chromatography and mass spectrometry (GC–MS). Some attempts to identify the compounds being chromatographed on the basis of their relative retention times (t_R) have been made, and it has been found that the plots of log t_R for many substituted phenols,[1] paraffins,[2] and organometalic compounds[3] against the number of carbon atoms in the molecule give straight lines. The corresponding relationships for organochlorine compounds have not yet been established, however.

Chlorination is extensively practiced in waste-water treatment in order to disinfect the effluent prior to discharge, particularly where the water may subsequently be used for recreational purposes or as a source of potable water. One class of compounds recognized as a major source of pollutants in the environment is the phenols. Phenols are introduced into the environment in several ways; directly as industrial effluents and indirectly as transformation products from natural and synthetic chemicals. It has now became evident that the treatment with chlorine of water which has been polluted with phenols leads to the formation of a variety of chlorinated phenols and quinones.[4] The aim of the present work is to reveal the relationships between the relative retention behavior of chlorinated phenols, *m*-cresols, and 3,5-xylenols and the number of chlorine substituents in the phenol ring, using both polar and nonpolar stationary phases. We then intend to use this relationship to identify the unknown samples in the environment.

Experimental

The chlorinated derivatives of phenol, *m*-cresol, and 3,5-xylenol used for the present work were obtained from various commercial sources; they are summarized in Table 1. These compounds were checked by GLC and mass spectrometry and were then used without further purification .

A Model 20-KE gas chromatograph (Japan Electron Optic Laboratory) equipped with an electron-capture detector (ECD, ^{63}Ni 10 mCi) and a Shimadzu GC-6A gas chromatograph equipped with a flame ionization detector (FID) were used with nitrogen as the carrier gas. Two coiled glass tubes (2 m × 3 mm I. D), one packed with 10% Apiezon L/Chromosorb-W (AW-DMCS, 60—80 mesh) as the nonpolar stationary phase and the other packed with 5% DEGS + 1% H_3PO_4/Chromosorb-W (AW-DMCS, 60—80 mesh) as the polar one, were used for the present work.

TABLE 1. CHLORINATED PHENOLS, *m*-CRESOLS, AND 3,5-XYLENOLS EXAMINED IN THIS INVESTIGATION

Index number	Compound	Index number	Compound
1	Phenol	14	*m*-Cresol
2	2-Chlorophenol	15	4-Chloro-m-cresol
3	3-Chlorophenol	16	6-Chloro-m-cresol
4	4-Chlorophenol	17	4,6-Dichloro-m-cresol
5	2,3-Dichlorophenol	18	2,4,6-Trichloro-m-cresol
6	2,4-Dichlorophenol		
7	2,5-Dichlorophenol	19	3,5-Xylenol
8	2,6-Dichlorophenol	20	2-Chloro-3,5-xylenol
9	3,4-Dichlorophenol	21	4-Chloro-3,5-xylenol
10	2,4,5-Trichlorophenol	22	2,4-Dichloro-3,5-xylenol
11	2,4,6-Trichlorophenol		
12	2,3,4,6-Tetrachlorophenol	23	2,4,6-Trichloro-3,5-xylenol
13	2,3,4,5,6-Pentachlorophenol		

Results and Discussion

In the present work, both polar and nonpolar stationary phases, connected to either FID and ECD, were tested for the direct chromatography of chlorinated derivatives of phenol, *m*-cresol, and 3,5-xylenol. The t_R values for these compounds are presented graphically in Figs. 1 and 2 as a plot of log t_R against the number of chlorine substituents in the molecule. Although GLC's of several chlorinated phenols have been reported by earlier workers,[5] the present results appear to be the first detailed GLC data for these compounds.

Since it is known that plots of log t_R for many organic compounds against their boiling points give approximately straight lines,[6] the t_R values of compounds with lower numbers of chlorine substituents and with low boiling points may be expected to be smaller that those of compounds with higher numbers and high boiling points when the compounds are chromatographed on a nonpolar column. Figures 1 and 2 show that plots of log t_R against the number of chlorine substituents in the molecule give approximately straight lines for each homologous series of these chlorinated phenols, *m*-cresols, and 3,5-xylenols, with few exceptions.

Figures 1 and 2 also show that the smallest t_R values are found for compounds with chlorine atoms, at least

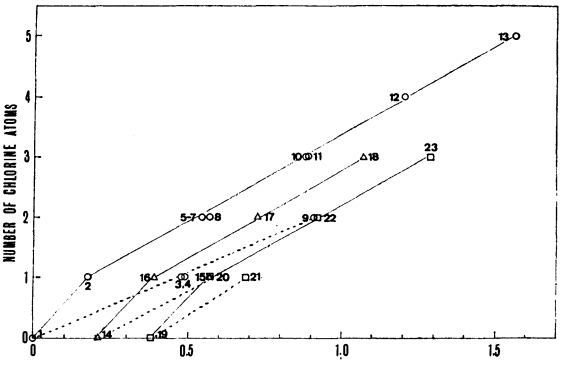

Fig. 1. Plot of log t_R against number of chlorine substituents in the molecule, using nonpolar column at 200 °C and 50 ml/min of N_2 as the carrier gas.
Chlorinated phenols; ○, chlorinated *m*-cresols; △, chlorinated 3,5-xylenols, □. Compound numbers, as in Table 1.

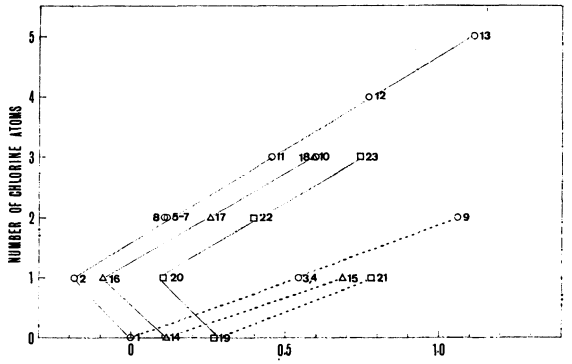

Fig. 2. Plot of log t_R against number of chlorine substituents in the molecule, using polar column at 160 °C and 50 mlmin of N_2 as the carrier gas.
Chlorinated phenols; ○, chlorinated *m*-cresols; △, chlorinated 3,5-xylenols; □. Compound numers, as in Table 1.

one of which is substituted on the ortho-position in the phenol ring (Solid lines) in comparison with those of the meta- and/or para-chlorinated isomers (dashed lines). In addition, these compounds (Points 3, 4, 9, 15, and 21) are characterized by larger t_R values on the polar column than those of the corresponding compounds with higher numbers of chlorine substituents. These results can be explained in terms of the steric shielding of the hydroxyl groups in phenols by chlorine atoms substituted on the ortho-position in the phenol ring, which prevents the formation of a hydrogen bond between the polar stationary phase and the chlorinated compounds.

Unfortunately, poor separations of *m*-chlorophenol from the para-isomer and of 2,3- from 2,4- and 2,5-dichlorophenol on both polar and nonpolar columns were observed, for these compounds have similar polarities and boiling points. In addition, the peaks of some compounds (*e.g.*, 2,6-dichlorophenol and 2-chloro-3,5-xylenol) overlapped when a mixture of these compounds was chromatographed on both polar and nonpolar columns. However, dichlorinated compounds among a mixture of mono- and dichloro-derivatives with similar t_R values on the columns could be assigned on the basis of the differences in ECD responses, because well-defined ECD peaks are observed for the ng order of a sample injected in the column connected to ECD, though these were very small ECD peaks for monochlorinated compounds in spite of the μg order of sample injection.

The response data indicated that the sensitiveties of FID for the chlorinated phenols became smaller with an increase in the number of chlorine substituents in the molecule, while those of ECD became larger. Similar relative ECD responses have been reported previously[7] for other aromatic halogeno and nitro compounds. These results can be explained in terms of the reduction of the flame-ionization current with organochlorine compounds, or as an increase in the electron-capture reactions with these compounds, which were, chromatographed on the column and then introduced into the detector.[8]

The apparent differences in the FID and ECD sensitivities for the chlorinated derivatives of phenol, *m*-cresol, and 3,5-xylenol chromatographed on both polar and nonpolar columns may also arise as a result of peak broadening or narrowing associated with increases or decreases in t_R.

These results suggest that both the plots of log t_R against the number of chlorine substituents and the differences in ECD responses for the subject compounds can be used to investigate the chemical structure of chlorinated aromatic compounds formed during the chlorination of a variety of phenol compounds with aqueous hypochlorite.

References

1) P. Buryan, J. Macak, and J. Hrivnak, *J. Chromatogr.*, **137**, 425 (1977); P. Buryan and J. Macak, *ibid.*, **130**, 69 (1977).
2) A. Wehrei and E. Kovatos, *Helv. Chim. Acta*, **42**, 2709 (1959).
3) S. Ishikura and S. Onodera, *Bunseki Kagaku*, **16**, 16 (1967).
4) R. H. Burttschell, A. A. Rosen, F. M. Middleton, and M. B. Ettinger, *J. Am. Water Works. Assoc.*, **51**, 205 (1959); J. Eliasek and A. Jungwirt, *Collect. Czech. Chem. Commun.*, **28**, 2163 (1963); O. M. Ali, *Water Res.*, **2**, 587 (1968); H. Thielmann, *Mikrochim. Acta*, **1972**, p. 665; K. L. Murphy, R. Zaloum, and D. Fulford, *Water Res.*, **9**, 389 (1975); J. G. Smith, S.-F. Lee, and A. Campus, *ibid.*, **10**, 985 (1976); J. G. Smith and S.-F. Lee, *J. Environ. Sci. Health*, **A13**, 61 (1978); S. Onodera, J. Kato, Y. Kamonzeki, and Ishikura, *Eisei Kagaku*, **23**, 331 (1977); R. A. Larson and A. L. Rockwell, *Environ. Sci. Technol.*, **13**, 325 (1979); Y. Nagawa, K. Uematsu, and S. Tokunaga, *Nippon Kagaku Kaishi*, **1970**, 1244.
5) J. A. Barry, R. C. Vasishth, and F. J. Shelton, *Anal. Chem.*, **34**, 67 (1962); R. H. Kolloff, L. J. Breuklander, and L. B. Barkley, *ibid.*, **35**, 1651 (1963); J. Ress and G. R.. Higginbotham, *J. Chromatogr.*, **47**, 474 (1970); C. Rappe and C.-A. Nilsson, *ibid.*, **67**, 247 (1972); W. Krugsman and C. G. Van De Kamp, *ibid.*, **131**, 412 (1977).
6) H. M. Tenny, *Anal. Chem.*, **30**, 2 (1958).
7) W. L. Zielinski, Jr., and L. Fishbein, *J. Chromatogr.*, **28**, 293 (1967); W. L. Zielinski, Jr., L. Fishbein, and R. O. Thomas, *ibid.*, **30**, 77 (1967); Y. Hattori, Y. Kuge, and S. Nakagawa, *Bull. Chem. Soc. Jpn.*, **51**, 2249 (1979).
8) A. J. Andreatch and R. Feinand, *Anal. Chem.*, **32**, 1021 (1960).

Uptake of Zinc Ion by Hydrous Manganese (IV) Oxide

Eiichi NARITA* and Taijiro OKABE

Department of Applied Chemistry, Faculty of Engineering, Tohoku University, Aramaki, Sendai 980

(Received August 1, 1980)

Synopsis. The uptake of zinc ion by hydrous manganese(IV) oxide in ammonium chloride solution containing zinc ion was investigated. The uptake of zinc ion was found to be proportional to the potassium content in the hydrous manganese(IV) oxide, the molar ratio of the sorbed Zn^{2+} to the released K^+ being *ca.* 1 : 2.

Adsorption studies of zinc ion on various kinds of anhydrous manganese(IV) oxides have been carried out in a 2 M† NH_4Cl solution containing zinc ion. An adsorption mechanism was postulated in order to explain the ion exchange reaction based on a surface chelation on the hydrated oxide.[1,2] Investigations have been carried out on the mode of metal adsorption by natural and synthetic manganese(IV) oxides as regards the characterization of oxides,[2,3] catalysis[4] and oceanology.[5] However, the effect of the chemical composition of manganese(IV) oxides on the mode of adsorption still remains unclarified.

Hydrous manganese(IV) oxide obtained by reduction and disproportionation of alkaline manganate(V), (VI), and (VII) solution usually contains a large amount of alkali and chemically bound water, exhibiting unusual properties differing a great deal from the anhydrous manganese(IV) oxides prepared by pyrolysis or oxidation of manganese(II) in acid solutions.[6]

In this study, the uptake of zinc ion by hydrous manganese(IV) oxide was investigated and the results were discussed in relation to the replacement of potassium ion present in the sorbent.

Experimental

The measurement of the uptake of zinc ion by hydrous manganese(IV) oxide was carried out in a way similar to that described by Kozawa.[1] The hydrous manganese(IV) oxide was dried by heating at 110 °C. 0.1 g of the sample was then added to 50 ml of zinc solution prepared by dissolving 0.01 M ZnO in 1.5 M NH_4Cl (pH 6.8). The hydrous manganese(IV) oxide suspended in an Erlenmeyer flask was stirred magnetically for 18 h at room temperature and then centrifuged. The supernatant layer was analyzed for zinc ion by titration. The uptake of zinc ion by the hydrous manganese(IV) oxide was calculated from the zinc ion concentrations in solution before and after the uptake was affected.

The preparation and characterization of the hydrous manganese(IV) oxide sample were the same as reported.[6]

Results and Discussion

The zinc ion uptake data and the chemical composition of hydrous manganese(IV) oxides are given in Table 1, together with those of manganese(IV) oxides of other types.

The uptake of zinc ion by typical amorphous and hydrous manganese(IV) oxides (Table 1, 1—4 and 7) was extremely high as compared to that of anhydrous manganese(IV) oxides (12—14). The hydrous manganese(IV) oxides prepared in a solution of high pH showed an approximately constant composition with the formula $K_2O \cdot 4MnO_2 \cdot 4H_2O$. Variation in chemical

TABLE 1. ZINC ION UPTAKE DATA AND CHEMICAL COMPOSITION OF THE MANGANESE (IV) OXIDES

No.	Preparation			Composition[a]				Zn^{2+} sorbed
	Procedure	pH	Temp °C	MnO_2 wt%	x in MnO_x	K_2O wt%	H_2O wt%	mol/g × 10^4
1	H_2O_2 reduction of $KMnO_4$ soln[b]	12.8	30	69.4	1.99	16.9	13.7	18.68
2	K_2SO_3 reduction of $KMnO_4$ soln[b]	12.6	50	68.2	1.98	18.4	13.4	20.39
3	KNO_2 reduction of $KMnO_4$ soln[b]	12.1	30	70.1	1.98	15.8	14.1	20.24
4	Disproportionation of K_2MnO_4 soln[b]	13.0	30	68.8	1.99	17.7	13.5	20.89
5	Disproportionation of K_2MnO_4 soln[b]	4.1	50	80.5	1.94	8.8	10.7	9.91
6	Disproportionation of K_2MnO_4 soln[b]	2.5	50	87.1	1.91	4.7	8.2	5.71
7	Disproportionation of K_3MnO_4 soln[c]	>13	50	66.1	2.01	19.2	14.8	21.74
8	2M HNO_3 treatment of sample No. 1	<1	30	87.9	1.89	4.0	8.1	5.76
9	Heating of sample No. 1	—	200	71.0	1.97	17.5	11.5	11.52
10	Heating of sample No. 1	—	300	73.8	1.94	17.7	8.0	6.71
11	Heating of sample No. 1	—	700	76.4	1.87	18.3	5.3	2.99
12	(α-MnO_2)			89.3	1.97	6.8	3.9	0.53
13	(β-MnO_2)			99.5	2.00	0	0.5	0.31
14	(γ-MnO_2)			97.8	1.97	0	2.2	1.69

a) The calculated chemical composition of the $K_2O \cdot 4MnO_2 \cdot 4H_2O$ formula is 18.3 K_2O, 67.7 MnO_2 and 14.0 H_2O(wt%), (1—8: amorphous, 9—11: tetramanganese dipotassium octaoxide[7]). b) The procedure is given in detail in a previous paper.[6] c) The reaction was performed by dilution of a (0.2M K_3MnO_4 + 10M KOH) solution with large amount of distilled water.

† 1 M = 1 mol dm^{-3}.

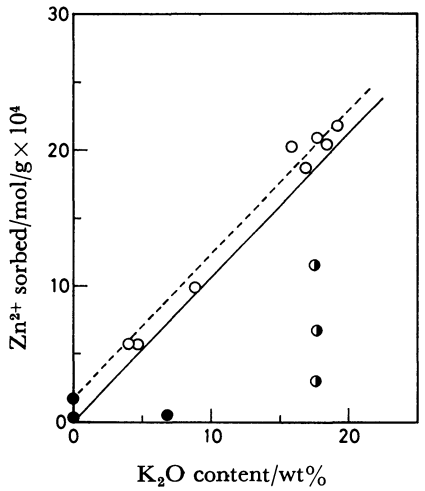

Fig. 1. Relationship between the uptake of Zn^{2+} and the K_2O content of MnO_2 substances.
○: Hydrous MnO_2 (Sample Nos. 1—10), ◑: Heated substances (Sample Nos. 9—11), ●: Crystalline MnO_2 (Sample Nos. 12—14). ——: (Zn^{2+} sorbed/K^+ content) m.r.=0.5.

composition remarkably influenced the zinc ion uptake. For example, the reduction in the K_2O content in the hydrous manganese(IV) oxides prepared by disproportionation (5 and 6) and by acid treatment (8) gave rise to the reduction of the uptake capacity of zinc ion. Potassium in the hydrous manganese(IV) oxide is responsible for the zinc ion uptake. It seems that potassium ions are replaced by zinc ions *via* ion-exchange mechanism. After the uptake reaction, the hydrous manganese(IV) oxide was found to be free from potassium. Figure 1 shows a linear relation between the zinc uptake and the K_2O content in the hydrous manganese(IV) oxide samples. The molar ratio, sorbed Zn^{2+}/released K^+, is slightly higher than 0.5. This can be attributed to the coexistence of H^+ with K^+ on the surface of the hydrated manganese(IV) oxide. γ-MnO_2 contains only H^+ and no K^+ (14).

At pH 6.8, under which most of the Zn^{2+} uptake reactions took place, ammonium ion dominates according to

$$\frac{a_{NH_3}}{a_{NH_4^+}} = 10^{(pH-9.27)}$$

Under these conditions, we see that $(ZnCl_4)^{2-}$ is the most stable zinc ion. It seems that the tetrachlorozincate ion acts on the hydrous manganese(IV) oxide as a bindetate as in the case of a previous study[1] in which H^+ instead of K^+ was the major concern.

On heating, the hydrous manganese(IV) oxide gradually crystallized into tetramanganese dipotassium octaoxide,[7] $K_2Mn_4O_8$ (9—11). This caused decrease in the uptake capacity of zinc ion. The same trend was found in the case of α-MnO_2 (12), showing a low uptake capacity due to its high crystallinity.

One of us (E. N) wishes to thank Prof. K. N. Han for his helpful discussions.

References

1) A. Kozawa, *J. Electrochem. Soc.*, **106**, 552 (1959).
2) A. Kozawa, *Denki Kagaku*, **43**, 618 (1975).
3) A. Regner, V. Ettel, and J. Vepřek-Šiška, *Collect. Czech. Chem. Commun.*, **28**, 2854 (1963).
4) T. Kaji, N. Yamazoe, and T. Seiyama, *Denki Kagaku*, **46**, 673 (1978).
5) V. M. Rutkouskiy, *Oceanology*, **17**, 46 (1977).
6) E. Narita and T. Okabe, *Bull. Chem. Soc. Jpn.*, **53**, 525 (1980).
7) X-Ray powder data file (ASTM card 16-205).

The Synthesis of Potassium Pentacyanohydroxochromate(III)

Yuzuru SAKABE* and Yoshio MATSUMOTO

Department of Chemistry, Faculty of Hygienic Science, Kitasato University, Asamizodai, Sagamihara, Kanagawa 228

(Received August 6, 1980)

Synopsis. The crystals of $K_3[Cr(CN)_5(OH)]\cdot H_2O$ have been obtained by making $[CrCl(NH_3)_5]Cl_2$ react with KCN, followed by purification on a Sephadex gel column.

On the cyano-hydroxo- and aqua-cyano- mixed-coordinated chromate(III) complexes, there have been only a few works reported.[1-4] All the experiments in those studies had been made on samples of the complexes formed in the aquation process of the $[Cr(CN)_6]^{3-}$ ion in an aqueous solution.

Accordingly, the works have more or less had difficulties in the isolation as well as in the identification of the complexes under consideration, which were yielded very scantly and had the property of continuing the sequential release of coordinating cyano ligands in an aqueous solution.

By the use of a new method quite different from the earlier processes, the present authors have obtained $K_3[Cr(CN)_5(OH)]\cdot H_2O$ in crystals. This product proved to be just the complex which had been presumed in one of the reports to have been formed in the reviewed aquation process;[3] this fact affords solid ground for the satisfactory settlement of an intriguing problem with regard to the spectrum-identification of the aqua-cyano-coordinated chromate(III) complexes.

The unit cell dimensions of the crystal were determined by means of X-ray diffraction.

Experimental

Potassium cyanide (25.5 g, 0.415 mol) and $[CrCl(NH_3)_5]Cl_2$ (15.0 g, 0.072 mol) were added to 170 cm³ of water, after which the mixture was boiled while being stirred. A considerable amount of undissolved $[CrCl(NH_3)_5]Cl_2$ which was at first observed disappered qiuckly at the beginning of the boiling, and the solution's color changed from deep-red to orange-yellow. The temperature of the oil-bath was maintained at about 140 °C, and the boiling was continued for 2—3 min after the disappearance of the solid $[CrCl(NH_3)_5]Cl_2$. Attention must be paid to the reaction time, since if the boiling is prolonged, most of the products are decomposed rapidly to form a black precipitate, and the desired complex is not obtained. The reaction mixture was cooled and evaporated to about one-half volume by means of a rotary evaporator. The concentrate, after the removal of a small amount of the black substance, was passed through a Sephadex G-15 gel column (5.5×49 cm). The fractionation of the products on the Sephadex column is illustrated in Fig. 1. The separated orange-yellow fraction which contained the desired complex was refined twice more by means of the same Sephadex column. The purified $K_3[Cr(CN)_5(OH)]$ solution was then evaporated to dryness in a rotary evaporator (the temperature being kept below 35 °C); 7.6 g of orange-yellow crystals as small needles were thus obtained. The crude crystals (2 g) were recrystallized by dissolving them in 2 cm³ of water and by slowly evaporating the solution thus formed in a KOH desiccator. About two days later, the deposited needle crystals were collected by filtration, washed with ethyl alcohol containing 20% water, and dried in a vaccum desiccator with sodium hydroxide: yield, 1.2 g. Analytical result, Found: Cr, 15.28; C, 17.72; H, 1.03; N, 21.05; K, 35.0; H_2O, 5.3%. Calcd for $K_3[Cr(CN)_5(OH)]\cdot H_2O$: Cr, 15.55; C, 17.96; H, 0.90; N, 20.94; K, 35.1; H_2O, 5.4%. The water of crystallization was determined by thermobalance analysis although the results varied to some extent corresponding to the conditions of drying applied to the crystals. The infrared spectrum is illustrated in Fig. 2.

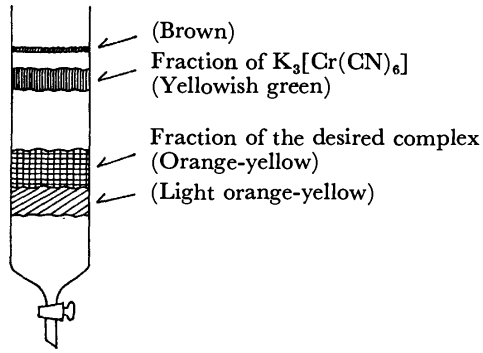

Fig. 1. Separation of the reaction products on Sephadex G-15 gel column.

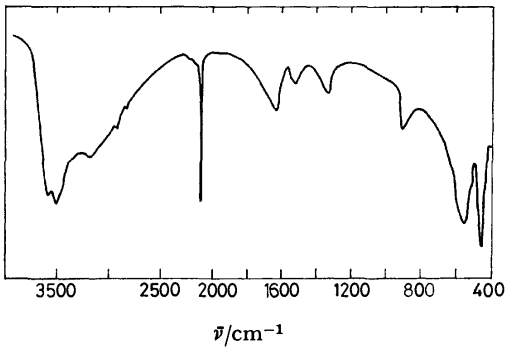

Fig. 2. Infrared spectrum of $K_3[Cr(CN)_5(OH)]\cdot H_2O$ in the 4000—400 cm^{-1} region.

Results and Discussion

The complex, $[CrCl(NH_3)_5]Cl_2$, was first made to react with KCN on the presumption that $K_3[CrCl(CN)_5]$ might be obtained, because an analogous cobaltate(III) complex, $K_3[CoCl(CN)_5]$, had been prepared[5] by making $[CoCl(NH_3)_5]Cl_2$ react with 5 mol of KCN. The complex isolated from the reaction products, however, was found to be not a chloro, but a hydroxo, complex, $K_3[Cr(CN)_5(OH)]$. In the past, the isolation of the pure substance of this complex was difficult, as has previously been explained, and the crystal could not be obtained. Accordingly, the properties of the complexes have been solely investigated on their aqueous solutions, the identification of the complexes being made mainly by means of the electronic spectra and the molar ratio, CN^-/Cr, of the solution.

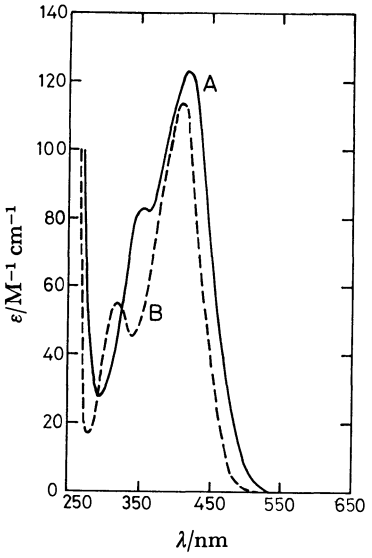

Fig. 3. Absorption spectra of $K_3[Cr(CN)_5(OH)]\cdot H_2O$ at pH 10.3 (——), and at pH 4.2 (– – –) in an aqueous solution.

Now, by virtue of the markedly increased yield by the new reaction process and the excellent ability of Sephadex gel to act as a molecular sieve, the complex has been obtained in crystals.

As a proof of the presence of a OH^- ligand in this complex, a 0.04 mol dm^{-3} (as $K_3[Cr(CN)_5(OH)]$) solution (pH=10.3) was titrated with 0.05 mol dm^{-3} amidosulfuric acid. A single break with a pK value of 8.8 was observed on the titration curve, indicating that the complex was a base with 1 g equivalent/mol. When the solution was made acidic, the complex varied to $K_2[Cr(CN)_5(H_2O)]$, and at pH 4.2 the electronic spectrum of the solution was observed to have been shifted in the direction of the shorter wave length from its initial position at pH 10.3, reinforcing our account of the OH^- ligand, as is illustrated in Fig. 3.

With respect to the spectrum of the cyano-aqua-mixedly coordinated complex of chromium(III), two arguments have been advanced by pioneers. The spectrum, which is identical to the B curve in Fig. 3, has been taken by Schaap *et al.*[1-2] as the spectrum of $[Cr(CN)_4(H_2O)_2]^-$, while the same spectrum was concluded to be that of $[Cr(CN)_5(H_2O)]^{2-}$ by Jeftić and Feldberg.[3] To the investigating made by the foregoing investigators, however elaborate, the result of our work can add adequate evidence which they wanted. The presented method would be of great value in preparing the authentic sample in crystals in quantity. On the three dimensional X-ray diffraction data collected by counter methods, the crystal was found to be monoclinic, with a unit cell of the dimensions: $a=4.45$, $b=8.29$, $c=20.23$ Å, $\beta=105.52°$, $Z=2$. Details of the crystal structure will be presented in another paper.

The authors are very grateful for the aid of Dr. Haruo Ogura, Professor of the Faculty of Pharmaceutical Sciences in Kitasato University, in performing the X-ray analysis of the crystal.

References

1) W. B. Schaap, R. Krishnamurthy, D. K. Wakefield, and W. F. Coleman, "Coordination Chemistry," ed by S. Kirschner, Plenum Press, New York, N. Y. (1969), p. 177.

2) R. Krishnamurthy, W. B. Schaap, and J. R. Perumareddi, *Inorg. Chem.*, **6**, 1338 (1967).

3) L. Jeftić and S. Feldberg, *J. Am. Chem. Soc.*, **92**, 5272 (1970).

4) A. Chiang and A. W. Adamson, *J. Phys. Chem.*, **72**, 3827 (1968).

5) A. W. Adamson, *J. Am. Chem. Soc.*, **78**, 4260 (1956).

The Molecular Structure of Δ-*cis*-α-[(*S*)-*N*,*N*′-Bis(2-pyridylmethyl)-propylenediamine]dichlorochromium(III) Chloride

Yasuo HATA,† Yukihiro YAMAMOTO,* and Yoichi SHIMURA

Department of Chemistry, Faculty of Science, Osaka University, Toyonaka, Osaka 560

†*Institute for Protein Research, Osaka University, Yamadakami Suita, Osaka 565*

(Received September 5, 1980)

Synopsis. The molecular structure of Δ-*cis*-α-[$CrCl_2$-(*S*-picpn)]$^+$ (*S*-picpn=(*S*)-*N*,*N*′-bis(2-pyridylmethyl)propylenediamine) was determined by X-ray analysis, the absolute configuration being confirmed to coincide with that assigned from the circular dichroism spectrum.

Two diastereomers, $(+)_{600}^{CD}$ and $(-)_{600}^{CD}$ ones of *cis*-α-[$CrCl_2$(*S*-picpn)]$^+$ complex (*S*-picpn=(*S*)-*N*,*N*′-bis(2-pyridylmethyl)propylenediamine), were isolated and their absolute configurations assigned from the circular dichroism (CD) spectra.[1] The present note deals with the X-ray structure analysis of a chloride of the more stable isomer, $(+)_{600}^{CD}$ one, which has been assigned to a Δ configuration from its CD spectrum.

Experimental

Ruby-red needle-like single crystals suitable for X-ray analysis were prepared by slow evaporation of an aqueous solution of the complex $(+)_{600}^{CD}$-[$CrCl_2$(*S*-picpn)]Cl at room temperature. Systematic absence indicated the monoclinic space group $P2_1$. Unit cell dimensions obtained by least-squares refinement of the setting angles of 11 reflections measured on a diffractometer were a=8.46 (2), b=15.68 (1), c=7.20 (1) Å and β=103.6 (1) °. The observed density 1.48 g cm^{-3} (by flotation in benzene-carbon tetrachloride) coincides with the calculated value 1.48 g cm^{-3} for Z=2. A crystal of the dimension 0.36×0.15×0.11 mm was used for the intensity measurement. Intensities were measured on a Rigaku automated four-circle diffractometer with graphite-monochromated Mo $K\alpha$ radiation (λ=0.71069 Å). The θ—2θ scan mode with a scan speed of 4 °min^{-1} in 2θ was employed. The scan range was calculated to be (1.0+0.35 tanθ)°. Intensities of 1704 independent reflections were collected in the range $1.0 \leq 2\theta \leq 50.0°$. Of these reflections 209 were measured as $|F_o|=0.0$. The intensities were corrected for Lorentz and polarization factors. No absorption correction was made [μ(Mo $K\alpha$)=1.072 mm^{-1}].

The structure was solved by the heavy atom method. The positions of chromium and two coordinated chlorine atoms were determined from a Patterson map. An electron density map based on the phases calculated from these atomic parameters revealed all the non-hydrogen atoms. The parameters were refined by the block-diagonal least-squares program HBLS-5,[2] with anisotropic thermal factors. The reliability factors $R=\sum||F_o|-|F_c||/\sum|F_o|$ and $Rw=[\sum w(|F_o|-|F_c|)^2/\sum w|F_o|^2]^{1/2}$ were 0.077 and 0.088, respectively, for 1495 non-zero reflections. The final weighting scheme for minimization of $\sum w(|F_o|-|F_c|)^2$ was $w=[\sigma^2(F_o)+0.00022|F_o|+0.00357|F_o|^2]^{-1/2}$. The positions of the hydrogenes were not determined.

Results and Discussion

Final atomic parameters, bond distances and angles are given in Tables 1, 2, and 3, respectively. The F_o-F_c data and final thermal parameters are deposited as Document No. 8119 at the Office of the Chemical Society of Japan. The quadridentate ligand takes an α configuration, the two chloro ligands occupying *cis* positions. There is no significant difference between the distances of chromium to amine nitrogens and chromium to pyridine nitrogens. Angles N(1)–Cr–N(2) of the central chelate ring and Cl(1)–Cr–Cl(2) are 83.9° and 95.1°, respectively, the coordination geometry being slightly distorted from a regular octahedron.

A stereoscopic view of the complex cation drawn by PLUTO[4] is shown in Fig. 1. The absolute configuration of the complex was determined during the course of synthesis from the fact that the asymmetric carbon atom C(8) adopts the (*S*)-configuration,[1] without using the anomalous dispersion technique. The Δ configuration coincides with that assigned from the CD data.[1]

The least-squares planes and the dihedral angles between the planes are given in Table 4. The two

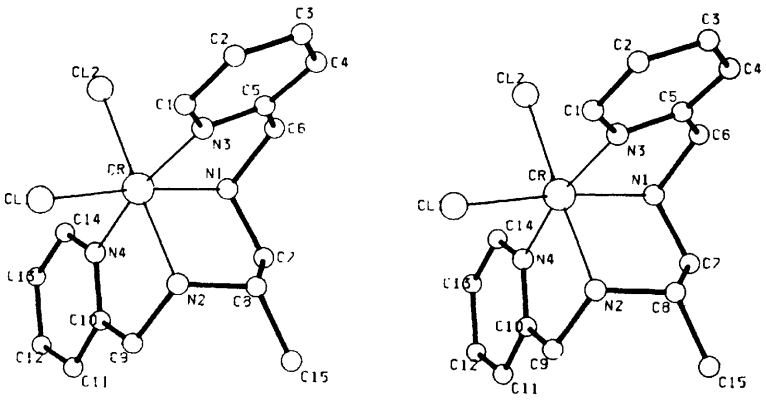

Fig. 1. Stereoview of the complex cation Δ-*cis*-α-[$CrCl_2$(*S*-picpn)]$^+$ and the numbering scheme of the atoms.

Table 1. Final positional parameters and their standard deviations (in parentheses)

	x	y	z	B_{eq}[a)]/Å^2
Cr	0.1947(2)	0	0.4004(2)	1.60
Cl(1)	0.1647(4)	0.0850(2)	0.1363(4)	2.82
Cl(2)	0.4313(3)	−0.0645(2)	0.3632(5)	2.93
Cl(3)	−0.1864(6)	0.2333(2)	0.3428(7)	6.21
N(1)	0.1980(11)	−0.0676(7)	0.6457(13)	2.85
N(2)	−0.0217(10)	0.0481(15)	0.4433(12)	1.70
N(3)	0.3300(10)	0.0837(6)	0.5937(14)	2.82
N(4)	0.0400(11)	−0.0916(6)	0.2499(13)	2.27
C(1)	0.3756(17)	0.1631(8)	0.5510(20)	4.00
C(2)	0.4783(17)	0.2090(10)	0.6928(22)	4.66
C(3)	0.5314(17)	0.1773(11)	0.8762(22)	4.96
C(4)	0.4811(15)	0.0980(10)	0.9181(20)	4.23
C(5)	0.3862(13)	0.0497(8)	0.7721(17)	2.79
C(6)	0.3415(15)	−0.0407(9)	0.8040(16)	3.09
C(7)	0.0371(15)	−0.0578(8)	0.6997(18)	3.06
C(8)	−0.0258(13)	0.0328(7)	0.6473(15)	2.30
C(9)	−0.1619(12)	0.0139(7)	0.2928(15)	2.29
C(10)	−0.1181(12)	−0.0722(7)	0.2224(15)	2.15
C(11)	−0.2387(16)	−0.1261(9)	0.1180(19)	3.53
C(12)	−0.1951(17)	−0.2015(10)	0.0404(23)	4.85
C(13)	−0.0275(17)	−0.2201(8)	0.0687(21)	3.92
C(14)	0.0854(16)	−0.1649(8)	0.1794(17)	3.03
C(15)	−0.1933(15)	0.0475(10)	0.6921(17)	3.60

a) B_{eq} is calculated by the method of Hamilton.[3)]

Table 2. Bond distances (Å) and their standard deviations (in parentheses)

Cr–Cl(1)	2.286(3)	C(6)–N(1)	1.52(2)
Cr–Cl(2)	2.314(4)	N(1)–C(7)	1.51(2)
Cr–N(1)	2.06(1)	C(7)–C(8)	1.53(2)
Cr–N(2)	2.07(1)	C(8)–C(15)	1.54(2)
Cr–N(3)	2.06(1)	C(8)–N(2)	1.50(1)
Cr–N(4)	2.07(1)	N(2)–C(9)	1.51(1)
N(3)–C(1)	1.36(2)	C(9)–C(10)	1.53(2)
C(1)–C(2)	1.38(2)	C(10)–C(11)	1.40(2)
C(2)–C(3)	1.38(2)	C(11)–C(12)	1.39(2)
C(3)–C(4)	1.37(2)	C(12)–C(13)	1.42(2)
C(4)–C(5)	1.39(2)	C(13)–C(14)	1.39(2)
C(5)–N(3)	1.37(2)	C(14)–N(4)	1.35(2)
C(5)–C(6)	1.50(2)	N(4)–C(10)	1.34(1)

terminal chelate rings take distorted λ envelope conformations. The two pyridine rings are nearly planar within error and make an angle 75.9° with each other. The two planes P1 and P3 are nearly perpendicular to plane P2. The central chelate ring CrN(1)C(7)C(8)N(2) has a distorted δ conformation with an equatorial methyl carbon C(15), carbon C(8) being more deviated than C(7) from plane P2.

Table 3. Bond angles (in degrees) and their standard deviations (in parentheses)

Cl(1)–Cr–Cl(2)	95.1(1)	N(3)–C(1)–C(2)	118.2(13)
Cl(1)–Cr–N(1)	172.7(3)	C(1)–C(2)–C(3)	121.8(15)
Cl(1)–Cr–N(2)	89.0(3)	C(2)–C(3)–C(4)	119.1(15)
Cl(1)–Cr–N(3)	97.3(3)	C(3)–C(4)–C(5)	119.0(14)
Cl(1)–Cr–N(4)	92.1(3)	C(4)–C(5)–N(3)	120.6(12)
Cl(2)–Cr–N(1)	92.1(3)	C(5)–N(3)–C(1)	121.0(11)
Cl(2)–Cr–N(2)	175.2(3)	C(4)–C(5)–C(6)	121.5(12)
Cl(2)–Cr–N(3)	89.9(3)	N(3)–C(5)–C(6)	117.9(11)
Cl(2)–Cr–N(4)	95.4(3)	C(5)–C(6)–N(1)	109.5(11)
N(1)–Cr–N(2)	83.9(4)	C(6)–N(1)–C(7)	113.0(10)
N(1)–Cr–N(3)	81.7(4)	N(1)–C(7)–C(8)	108.3(10)
N(1)–Cr–N(4)	88.3(4)	C(7)–C(8)–C(15)	111.7(11)
N(2)–Cr–N(3)	92.2(4)	C(7)–C(8)–N(2)	107.6(9)
N(2)–Cr–N(4)	81.8(4)	C(15)–C(8)–N(2)	114.5(10)
N(3)–Cr–N(4)	168.8(4)	C(8)–N(2)–C(9)	117.0(8)
Cr–N(1)–C(6)	110.4(8)	N(2)–C(9)–C(10)	110.1(9)
Cr–N(1)–C(7)	109.7(8)	C(9)–C(10)–C(11)	120.8(11)
Cr–N(2)–C(8)	108.2(6)	C(10)–C(11)–C(12)	120.0(13)
Cr–N(2)–C(9)	109.8(6)	C(11)–C(12)–C(13)	117.9(14)
Cr–N(3)–C(1)	125.0(9)	C(12)–C(13)–C(14)	119.0(13)
Cr–N(3)–C(5)	113.7(8)	C(13)–C(14)–N(4)	121.8(12)
Cr–N(4)–C(10)	114.0(7)	C(14)–N(4)–C(10)	120.0(10)
Cr–N(4)–C(14)	126.0(8)	N(4)–C(10)–C(11)	121.3(11)
		N(4)–C(10)–C(9)	117.7(10)

Table 4. The least-squares planes with displacements of atoms from the planes (Å)
$X=ax+cz\cos\beta$, $Y=by$, and $Z=cz\sin\beta$.

Plane P1					
$-0.8830X+0.4615Y+0.0863Z=-0.6157$					
Cr	0	N(1)	0	N(3)	0
C(5)	−0.2925	C(6)	−0.5461		
Plane P2					
$0.3815X+0.7455Y+0.5465Z=1.9013$					
Cr	0	N(1)	0	N(2)	0
C(7)	0.2326	C(15)	−0.2301	C(8)	−0.4572
Plane P3					
$0.0855X+0.5475Y-0.8324Z=-2.2486$					
Cr	0	N(2)	0	N(4)	0
C(9)	0.5033	C(10)	0.2160		
Plane P4 (Pyridine Ring)					
$0.8815X-0.3913Y-0.2644Z=-0.0408$					
C(1)	0.0020	C(2)	0.0131	C(3)	−0.0092
C(4)	−0.0373	C(5)	0.0387	N(3)	0.0062
Plane P5 (Pyridine Ring)					
$0.2433X+0.4896Y-0.8373Z=-2.1955$					
C(10)	0.0040	C(11)	−0.0042	C(12)	−0.0066
C(13)	0.0181	C(14)	−0.0193	N(4)	0.0083
Dihedral angles between planes (°)					
P1 ∧ P2	93.11	P2 ∧ P4	84.27		
P1 ∧ P3	83.96	P2 ∧ P5	90.01		
P1 ∧ P4	169.01	P3 ∧ P4	85.34		
P1 ∧ P5	93.50	P3 ∧ P5	9.64		
P2 ∧ P3	89.19	P4 ∧ P5	75.87		

References

1) Y. Yamamoto and Y. Shimura, *Bull. Chem. Soc. Jpn.*, **53**, 395 (1980).

2) T. Ashida (1973), "The Universal Crystallographic Computing System-Osaka," The Computation Center, Osaka Univ, pp. 55—61.

3) W. C. Hamilton, *Acta Crystallogr.*, **12**, 609 (1959).

4) W. D. Motherwell (1976). *PLUTO*. A program for plotting molecular and crystal structures. University Chemical Laboratory, Cambridge, England.

An Evaluation of Ion-exchange Membrane Electrodes

Hirokazu HARA, Satoshi OKAZAKI, and Taitiro FUJINAGA*

Department of Chemistry, Faculty of Science, Kyoto University, Sakyo-ku, Kyoto 606

(Received September 8, 1980)

Synopsis. The potentiometric response behavior and selectivity characteristics of ion-exchange membrane electrodes have been investigated. Nernstian responses were obtained for inorganic anions such as perchlorate, nitrate, and chloride with each form of Selemion ASV membrane. Highly selective exclusions of the divalent sulfate and large organic sulfonate anions were observed with those membranes.

There have been many reports on the use of ion-exchange resins as heterogeneous resin membranes, which were made of ion-exchange resins embedded into high polymer or silicone rubber binders.[1-3] The electrodes of these types, however, have not shown good selectivity among individual ions and have been of little utility. Recently, a hydrophobic anion-exchange resin electrode having a wide selectivity range has been developed by Jyo *et al.*[4] On the other hand, a homogeneous ion-exchange membrane has never been successfully used as an ion-sensing material. Birch and Clarke have reported on a surfactant selective electrode with an Asahi anion-exchange membrane, which showed only a poor response to surfactant anions.[5]

In this paper, the authors examined commercially available ion-exchange membranes as ion-sensing materials and found that these membranes showed linear and quick responses for inorganic univalent anions, such as perchlorate, nitrate, and chloride over the concentration range from 10^{-1} M (1 M=1 mol dm^{-3}) to nearly 10^{-4} M. These membranes exhibited a highly selective exclusion of the divalent sulfate and large organic anions such as *p*-toluenesulfonate (TsO^-) and benzenesulfonate ($PhSO_3^-$), in contrast to liquid membrane electrodes. The differences of the selectivity characteristics among these membranes were discussed qualitatively on the basis of their membrane structures.

Experimental

Reagents. The ion-exchange membranes used were Selemion ASV, AMV, and DMV produced by the Asahi Glass Co. Ltd. AMV is an anion permselective membrane for the use of electrodialysis, having an ion-exchange site of $-N(CH_3)_3^+$. ASV is a univalent anion permselective membrane having not only a functional group similar to AMV but also a cation exchange site, which can effectively repel polyvalent anions.[6] DMV is an anion permselective membrane for use in diffusion dialysis, having functional groups of $-NH_3^+$ and $>NH_2^+$. Cations, except proton and nondissociative organic molecules cannot pass through a DMV membrane. The substrates of these membranes are made of polystyrene–butadiene copolymer.[6] The ClO_4^-, NO_3^-, and TsO^- forms of these membranes were made by soaking their original chloride forms in an aqueous solution of a sodium salt of the objective anion. The air-dried chloride form of ASV has been soaked in 1-decanol or nitrobenzene for 3 d in order to examine the effects of the impregnated solvents on membrane selectivity. Sodium hydroxide and *p*-toluene–sulfonic acid were used to control the pH of the sample solution.

Apparatus. A membrane electrode of the double junction type with an outer filling solution of 0.1 M sodium salt of each anion was used. The electrode potentials were measured by an Orion Digital Ionalyzer Model 601 connected to a Matsushita Penrecorder Model VP654A. All measurements were carried out by stirring at 25±0.5 °C.

Results and Discussion

The potentiometric response characteristics of ClO_4^-, NO_3^-, Cl^-, and TsO^- forms of ASV and DMV membranes with respect to the sensitivity, slope of the calibration curve, and response time are summarized in Table 1. Each value listed in the table is a mean value of four independent measurements. The ΔE_{1-4} denotes the potential difference between the solutions of 10^{-1} M and 10^{-4} M, which was used as an index of sensitivity. The slopes were estimated by a regression analysis in the concentration range of from 10^{-1} M to 10^{-3} M. The response time was defined as a period of time when the electrode was dipped until the membrane potential reached a steady value within ±0.5 mV, and was listed as a mean value obtained from 10^{-1} M to 10^{-4} M.

Table 1. Potentiometric response behavior of ion-exchange membrane electrodes

Membrane and form	ΔE_{1-4} / mV	Slope / mV/pa	Response time / min
ASV : ClO_4^-	174±3.5	59.8	0.87
DMV : ClO_4^-	160±5.2	58.6	1.4
ASV : NO_3^-	168±3.0	60.1	0.54
DMV : NO_3^-	159±2.0	59.9	0.82
ASV : Cl^-	162±2.4	60.2	0.78
DMV : Cl^-	154±3.7	59.1	0.89
ASV : TsO^-	148±6.1	55.9	4.2
DMV : TsO^-	168±4.6	61.0	0.73

Each form of ASV and DMV, except the TsO^- form of ASV, gave the Nernstian response over the concentration range of from 10^{-1} M to nearly 10^{-4} M, and considerably quick response at concentrations above 10^{-3} M. ASV was superior to DMV in sensisivity for the inorganic univalent anions, while DMV showed a better response to TsO^- than ASV did. The TsO^- form of ASV gave a poor response in both sensitivity and response time. This phenomenon was attributed not only to the repulsion between the surface cation exchange layer and an organic sulfonate anion but also to the steric hindrance between the ASV membrane and a large organic anion. The response characteristics of AMV were almost the same as those of DMV.

Table 2 summarizes the selectivity characteristics of these membranes. The selectivity coefficients, log $K_{i,j}^{pot}$ of the ClO_4^-, NO_3^-, Cl^-, and TsO^- forms of ASV and DMV were measured by the separate solution

TABLE 2. SELECTIVITY COEFFICIENTS, log K^{pot}_{i-j} OF ION-EXCHANGE MEMBRANE ELECTRODES

Membrane and form (Sensing anion, i)	Interfering anion, j					
	ClO_4^-	NO_3^-	Cl^-	$PhSO_3^-$	TsO^-	SO_4^{2-}
ASV : ClO_4^-	0	−0.72	−1.40	−2.11	−2.21	−3.00
DMV : ClO_4^-	0	−0.38	−0.60	−0.73	−0.80	−1.40
ASV : NO_3^-	0.60	0	−0.28	−1.28	−1.70	−1.53
DMV : NO_3^-	0.28	0	−0.10	−0.33	−0.37	−0.46
ASV : Cl^-	1.11	0.27	0	−0.85	−1.35	−1.09
DMV : Cl^-	0.37	0.05	0	−0.25	−0.30	−0.47
ASV : TsO^-	1.48	0.95	0.48	0.05	0	−1.02
DMV : TsO^-	0.87	0.48	0.25	0.03	0	−0.58

Concn of interfering anion; 10^{-2}M

method. The reproducibility of the value was within ±0.08.

The order of the magnitude of the selectivity coefficients among the univalent anions was $ClO_4^- > NO_3^- > Cl^- > PhSO_3^- > TsO^-$. This sequence of interference was different from the results reported with the liquid membrane electrodes of *o*-dichlorobenzene, *i.e.*, $ClO_4^- > TsO^- > PhSO_3^- > NO_3^- > Cl^-$.[7] It was found that organic anions, such as $PhSO_3^-$ or TsO^-, caused less interference with the ion-exchange membranes than with the liquid membranes. However, the sequence of the interference among the inorganic anions was similar to that of the liquid membrane. ASV suffered less from the interference of a divalent sulfate anion than DMV owing to its univalent permselectivity. The selectivity characteristics of these membranes were examined more extensively with their chloride forms, as shown in Fig. 1. The selectivity range was widest in ASV and decreased in the order of ASV≫AMV>DMV. From the results, the degree of quaternization of the ion-exchange site seems to exert a smaller effect on the selectivity range than the presence of the surface cation-exchange site. Almost all organic anions tested caused less interference with these membranes than the inorganic anions. This result may be attributed to the difficulty in diffusion of the large organic anions into these compact membranes owing to their strong interaction with the high polymer chains.

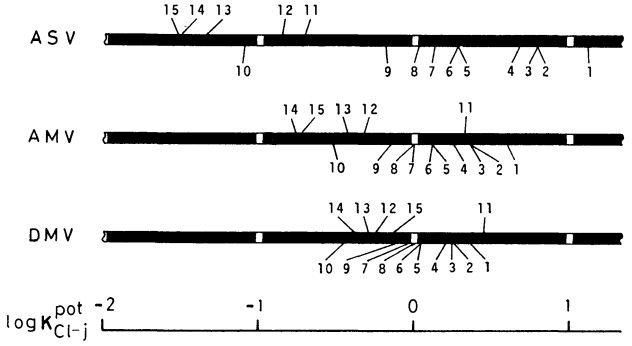

Fig. 1. Selectivity coefficient diagrams of Cl^- form ion-exchange membranes.
Interfering anion: (1) ClO_4^-, (2) BF_4^-, (3) SCN^-, (4) I^-, (5) NO_3^-, (6) Br^-, (7) ClO_3^-, (8) NO_2^-, (9) BrO_3^-, (10) SO_4^{2-}. (11) $C_8H_{17}OSO_3^-$ (octyl sulfate), (12) $PhSO_3^-$ (benzenesulfonate), (13) TsO^- (*p*-toluenesulfonate), (14) $C_8H_{17}SO_3^-$ (1-octanesulfonate), (15) 1-naphthalenesulfonate.

The effect of pH of the sample solution on the membrane potentials of the ClO_4^- forms of these membranes was examined. ASV sustained a constant potential over a wide pH range from 5.0 to 11.0, whereas DMV did so only in the range of from pH 6.0 to 9.0. This difference in the accessible pH range between ASV nad DMV is due to the degree of quaternization of their ion-exchange sites.

It has been reported by Jyo *et al.* that the selectivity range of the liquid membrane electrodes were influenced more by the membrane solvents than the ion-exchange sites.[8] The selectivity coefficients of the Cl^- form of ASV, however, were affected little by the impregnation of the membrane with 1-decanol. Nitrobenzene seemed to damage the high polymer chains of ASV.

In conclusion, though the ion-exchange membranes did not show a special advantage in sensitivity and in selectivity, in a conventional sense, over the liquid membranes, they did seem to have the following advantages: A high polymer membrane is very strong mechanically and has a very long life time. And in particular, a high polymer membrane has the possibility of making its selectivity highly specific for a certain ion by introducing a particular functional group into the high polymer chains, just as ASV showed a specific repulsion to divalent sulfate by its surface cation-exchange site, or to large organic sulfonate anions owing to their strong interaction with the high polymer chains.

References

1) M. R. J. Wyllie and H. W. Patnode, *J. Phys. Chem.*, **54**, 204 (1950).
2) M. Adhikali and G. G. Biswas, *J. Ind. Chem. Soc.*, **47**, 339 (1970).
3) E. Pungor and E. Papp, *Acta Chim. Acad. Sci. Hung.*, **66**, 19 (1970).
4) A. Jyo, T. Imato, K. Fukamachi, and N. Ishibashi, *Chem. Lett.*, **1977**, 815.
5) B. J. Birch and D. E. Clarke, *Anal. Chim. Acta*, **60**, 473 (1974).
6) T. Ebara, "Kōbunshimaku," ed by M. Nagasawa and A. Takizawa, Chijin Shokan, Tokyo (1975), Chap. 4.
7) T. Fujinaga, S. Okazaki, and H. Hara, *Chem. Lett.*, **1978**, 1201.
8) A. Jyo, M. Torikai, and N. Ishibashi, *Bull. Chem. Soc. Jpn.*, **47**, 2862 (1974).

Studies on the Chlorinated α-Santonins. III.[1] Revised Structure of α-Santonin Chlorohydrin

Hiroaki TAKAYANAGI, Haruo OGURA,* and T. BRIAN H. McMURRY††

School of Pharmaceutical Sciences, Kitasato University Shirokane, Minato-ku, Tokyo 108

††*Chemistry Department, Trinity College, Dublin 2, Ireland*

(Received June 30, 1980)

Synopsis. The molecular structure of α-santonin chlorohydrin is revised to 5β-chloro-4α-hydroxysantonin from 4α-chloro-5α-hydroxysantonin (Hendrickson and Bogard) by X-ray analysis of the corresponding 5β-chloro-4α-methoxysantonin.

Hendrickson and Bogard[2] have re-examined the products derived from chlorination, epoxidation and subsequent changes of α-santonin (**1**), and assigned structures to the various products. We have revised their structure of dichloro-α-santonin to **2**, based on an X-ray analysis of the derived tetrachloro-α-santonin (**3**).[3]

In this paper we wish to report a further revision, that of santonin chlorohydrin from **4'** to **4**, on the basis of an X-ray analysis of the related 5β-chloro-4α-methoxysantonin (**5**), and the ready conversion (HI, 90°) of **5** to **4**.

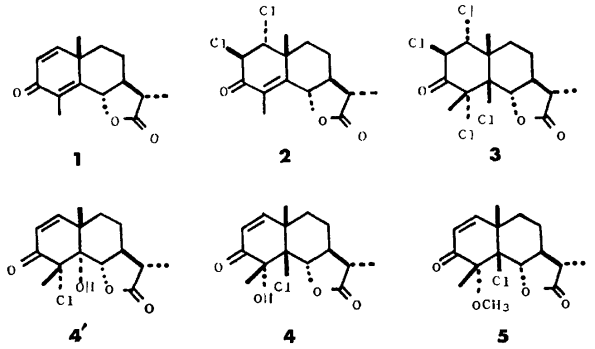

1 **2** **3**

4' **4** **5**

Experimental

5β-Chloro-4α-methoxysantonin (5). Dry chlorine was passed into α-santonin (5.0 g) in methanol (20 ml) at 0° for 20 min. The methanol was evaporated, and the residue was crystallized from methanol to give **5** (2.84 g) as colorless plates, mp 216—219 °C. Except for the unchanged material, no other isomeric products were found by TLC and NMR spectral examination of the residue. IR ($CHCl_3$) 1782, and 1691 cm^{-1}; UV(EtOH) λ_{max} 231 nm (ε=6300); NMR($CDCl_3$) δ 6.30 (1H, d, $J_{1,2}$=11 Hz, 1-H), 5.89 (1H. d, $J_{2,1}$=11 Hz, 2-H), 4.41 (1H, d, $J_{6,7}$=12 Hz, 6-H), 3.10 (3H, s, OMe), 1.69 (3H, s, 4-Me), 1.48 (3H, s, 10-Me), and 1.23 (3H, d, J=7 Hz, 11-Me). Found: C, 61.28; H, 6.88; Cl, 11.54%; M^+, 312. Calcd for $C_{16}H_{21}ClO_4$: C, 61.44; H, 6.77; Cl, 11.33%; M, 312.

5β-Chloro-4α-hydroxysantonin (4) from 5. A suspension of **5** (1.0 g) in 57% hydriodic acid (20 ml) was kept heating at 80—90 °C for 10 h. After filtrating the precipitate, water was added to the filtrate to give a crystalline precipitate, which was dried and chromatographed over silica gel. Elution with chloroform gave **4** (0.2 g), which was recrystallized from methanol to give colorless plates, mp and mixed mp 235—237 °C (dec) with the products prepared by Wedekind and Tettweiler.[4] The IR and NMR spectra of the two samples were identical. No other isomeric products except the unchanged starting material were found by TLC and NMR spectral examination of the mother liquor.

Crystallographic Measurement. The crystal of **5** belongs to the orthorhombic space group $P2_12_12_1$, a=8.458 (7), b=27.100 (8), c=6.796 (3) Å, Dm=1.34 g cm^{-3}, Dc=1.334 g cm^{-3}, and Z=4. The three-dimensional intensity data were collected on a Rigaku automatic four-circle diffractometer with graphite monochromated Cu $K\alpha$ radiation . Reflections having an intensity exceeding the corresponding standard deviations by a factor of three were treated as observed. 981 reflections with $2\theta \leqq 139°$ were retained and corrected for Lorentz and polarization factors but not for absorption and extinction factors.

Determination and Refinement of the Structure. The structure was determined by the heavy atom method. From the three-dimensional Patterson map, the position of the chlorine atom was easily deduced. From the Fourier synthesis with the chlorine phases, all the 20 non-hydrogen atoms in the asymmetric unit were obtained. The oxygen atoms were identified by structural consideration. Refinement of atomic parameters was carried out by the block-diagonal least-squares method, the quantity minimized being $\sum\omega(|F_o|-|E_c|)^2$, with ω=1.0 for all the reflections used . All the hydrogen atoms except the 12 hydrogen atoms on the methyl groups were located on the difference map. The final R value was 0.081.

Table 1. Final atomic parameters (×10^4) and thermal parameters

Standard deviations are given in parentheses. The B_{eq} values are the equivalent isotropic temperature factors.[a]

Atom	x	y	z	B_{eq}/Å^2
Cl	5687(4)	3755(1)	7537(5)	5.9
C(1)	6714(16)	4663(4)	4369(19)	4.1
C(2)	5195(16)	4797(4)	4699(22)	4.2
C(3)	3923(15)	4439(4)	4931(17)	4.3
C(4)	4250(14)	3925(4)	4111(15)	4.4
C(5)	5946(14)	3765(4)	4894(13)	3.8
C(6)	6538(13)	3247(3)	4355(15)	2.8
C(7)	6997(12)	3187(4)	2193(15)	2.9
C(8)	8418(15)	3522(4)	1752(18)	4.3
C(9)	7966(14)	4060(4)	2153(19)	3.3
C(10)	7291(14)	4142(4)	4408(17)	3.8
C(11)	7159(13)	2626(4)	2110(19)	3.4
C(12)	5813(15)	2482(4)	3510(17)	3.0
C(13)	8760(15)	4107(5)	5811(21)	5.0
C(14)	2909(13)	3546(4)	4628(22)	2.8
C(15)	7028(18)	2392(5)	51(22)	6.0
C(16)	3067(17)	4190(6)	1050(19)	7.1
O(1)	2653(10)	4550(3)	5680(14)	5.4
O(2)	5492(9)	2845(3)	4738(11)	3.9
O(3)	5085(10)	2100(3)	3450(14)	4.0
O(4)	4403(9)	3969(3)	2006(10)	4.5

a) W.C. Hamilton, *Acta Crystallogr.*, **12**, 609 (1959).

Table 2. Bond lengths and bond angles
Standard deviations are given in parentheses.

Bond lengths (l/Å)			
C(1)–C(2)	1.35(2)	C(7)–C(8)	1.54(2)
C(1)–C(10)	1.49(2)	C(7)–C(11)	1.53(1)
C(2)–C(3)	1.46(2)	C(8)–C(9)	1.53(2)
C(3)–C(4)	1.53(2)	C(9)–C(10)	1.65(2)
C(3)–O(1)	1.23(2)	C(10)–C(13)	1.57(2)
C(4)–C(5)	1.59(2)	C(11)–C(12)	1.53(2)
C(4)–C(14)	1.57(2)	C(11)–C(15)	1.54(2)
C(4)–O(4)	1.44(2)	C(12)–O(2)	1.32(1)
C(5)–C(6)	1.54(2)	C(12)–O(3)	1.21(1)
C(5)–C(10)	1.56(2)	C(16)–O(4)	1.43(2)
C(6)–C(7)	1.53(2)	C(5)–Cl	1.81(1)
C(6)–O(2)	1.43(2)		
Bond angles (ϕ/°)			
C(10)–C(1)–C(2)	124(1)	C(7)–C(8)–C(9)	109(1)
C(1)–C(2)–C(3)	123(1)	C(8)–C(9)–C(10)	112(1)
C(2)–C(3)–C(4)	116(1)	C(1)–C(10)–C(5)	113(1)
C(2)–C(3)–O(1)	122(1)	C(1)–C(10)–C(9)	103(1)
C(4)–C(3)–O(1)	122(1)	C(1)–C(10)–C(13)	109(1)
C(3)–C(4)–C(5)	107(1)	C(5)–C(10)–C(9)	111(1)
C(3)–C(4)–C(14)	113(1)	C(5)–C(10)–C(13)	114(1)
C(3)–C(4)–O(4)	108(1)	C(9)–C(10)–C(13)	106(1)
C(5)–C(4)–C(14)	114(1)	C(7)–C(11)–C(12)	99(1)
C(14)–C(4)–O(4)	106(1)	C(7)–C(11)–C(15)	116(1)
C(4)–C(5)–C(6)	118(1)	C(12)–C(11)–C(15)	114(1)
C(4)–C(5)–C(10)	114(1)	C(11)–C(12)–O(2)	111(1)
C(6)–C(5)–C(10)	108(1)	C(11)–C(12)–O(3)	125(1)
C(5)–C(6)–C(7)	114(1)	O(2)–C(12)–O(3)	124(1)
C(5)–C(6)–O(2)	117(1)	C(4)–O(4)–C(16)	115(1)
C(6)–C(7)–C(8)	109(1)	C(4)–C(5)–Cl	103(1)
C(8)–C(7)–C(11)	121(1)	C(10)–C(5)–Cl	108(1)
C(7)–C(6)–O(2)	105(1)	C(6)–C(5)–Cl	105(1)
C(5)–C(4)–O(4)	106(1)		

The final atomic parameters are given in Table 1. Anisotropic thermal parameters of non-hydrogen atoms and atomic parameters of hydrogen atoms and the complete Fo–Fc data are kept at the Chemical Society of Japan (Document No. 8131).

Results and Discussion

A perspective view of the molecule with numbering of the atoms is given in Fig. 1. The bond lengths and angles are given in Table 2. No abnormal lengths and angles were found in the structure.

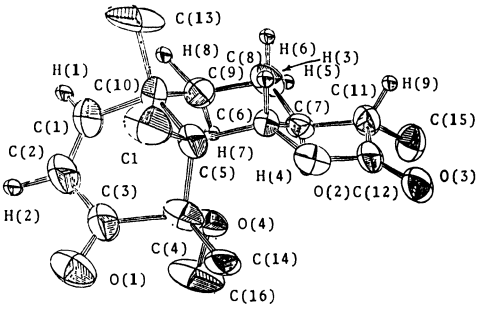

Fig. 1.

References

1) Part II: H. Takayanagi, H. Ogura, and Y. Iitaka, *Chem. Pharm. Bull.* (*Tokyo*), **26**, 2729 (1978).
2) J. B. Hendrickson and T. L. Bogard, *J. Chem. Soc.*, **1962**, 1678.
3) H. Ogura, H. Takayanagi, A. Yoshino, and T. Okamoto *Chem. Pharm. Bull.* (*Tokyo*), **22**, 1433 (1974).
4) E. Wedekind and K. Tettweiler, *Ber.*, **64**, 387, 1796 (1931).

Synthesis of 1,2,3,6,7,8-, 1,3,4,5,6,8-, and 1,2,3,5,6,8-Hexamethoxyxanthene

Heitaro OBARA,* Jun-ichi ONODERA, Tsutomu SHIBATA, and Kimio SHIBAYAMA

Department of Applied Chemistry, Faculty of Engineering, Yamagata University, Yonezawa 992

(Received May 19, 1980)

Synopsis. Three hexamethoxyxanthene isomers, 1,2,3,6,7,8-, 1,3,4,5,6,8-, and 1,2,3,5,6,8-hexamethoxyxanthene, were synthesized from the condensation products of 2,6-dimethoxyhydroquinone, 2,5-dimethoxyresorcinol, or 1,2,-3,5-benzenetetrol respectively with formaldehyde or ethyl formate.

In connection with the synthetic studies of carthamin,[1] the synthesis of three isomers of hexamethoxyxanthene, 1,2,3,6,7,8-, 1,3,4,5,6,8-, and 1,2,3,5,-6,8-hexamethoxyxanthene (**4**, **9**, and **12**), was accomplished. Although many methods of preparing xanthenes have been known,[2] no detailed study has been reported on the synthesis of hexahydroxyxanthene derivatives.

1,2,3,6,7,8-Hexamethoxyxanthene (**4**) was obtained by the methylation of 1,3,6,8-tetramethoxy-2,7-xanthenediol (**3**), which had itself been prepared by the dehydration of 2,2′,4,4′-tetramethoxydiphenylmethane-3,3′,6,6′-tetrol (**2**), obtained by the condensation of 2,6-dimethoxyhydroquinone (**1**)[3] with formaldehyde. Two aromatic protons of this symmetrical hexamethoxyxanthene, **4**, appeared as a singlet at 6.33 ppm in its ^{1}H-NMR spectrum.

In a similar manner, we attempted the synthesis of 1,3,4,5,6,8-hexamethoxyxanthene (**9**) from 2,5-dimethoxyresorcinol (**5**),[4] however, the attempt at the dehydration of 3,3′,6,6′-tetramethoxydiphenylmethane-2,2′,4,4′-tetrol (**6**) was unsuccessful.

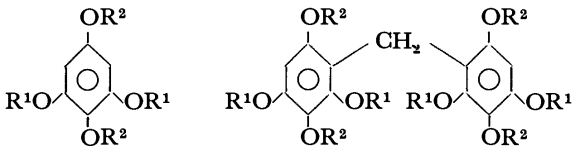

1 R^1 = Me, R^2 = H
2 R^1 = Me, R^2 = H
5 R^1 = H, R^2 = Me
6 R^1 = H, R^2 = Me
13 $R^1 = R^2$ = H

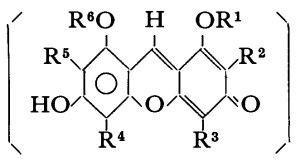

7 $R^1 = R^6$ = Me, $R^2 = R^5$ = H, $R^3 = R^4$ = OMe
10 $R^1 = R^3 = R^5$ = H, $R^2 = R^4$ = OMe, R^6 = Me
14 $R^1 = R^3 = R^5 = R^6$ = H, $R^2 = R^4$ = OH
15 $R^1 = R^3 = R^4 = R^6$ = H, $R^2 = R^5$ = OH

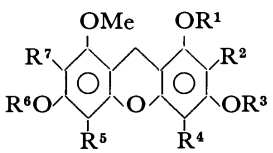

3 $R^1 = R^3 = R^6$ = Me, $R^2 = R^7$ = OH, $R^4 = R^5$ = H
4 $R^1 = R^3 = R^6$ = Me, $R^2 = R^7$ = OMe, $R^4 = R^5$ = H
8 R^1 = Me, $R^2 = R^3 = R^6 = R^7$ = H, $R^4 = R^5$ = OMe
9 $R^1 = R^3 = R^6$ = Me, $R^2 = R^7$ = H, $R^4 = R^5$ = OMe
11 $R^1 = R^3 = R^4 = R^6 = R^7$ = H, $R^2 = R^5$ = OMe
12 $R^1 = R^3 = R^6$ = Me, $R^2 = R^5$ = OMe, $R^4 = R^7$ = H

Compound **9** and, an unsymmetrical isomer, 1,2,3,5,-6,8-hexamethoxyxanthene (**12**), were obtained by the methylation of 1,4,5,8-tetramethoxy-3,6-xanthenediol (**8**) and 2,5,8-trimethoxy-1,3,6-xanthenetriol (**11**), respectively, obtained by the hydrogenation of the condensed-ring compound of 2,5-dimethoxyresorcinol (**5**) with ethyl formate. Two aromatic protons of **9** in the 2- and 7-positions appeared as a singlet at 6.21 ppm, while the 4- and 7-protons of **12** were observed at 6.18 and 6.48 ppm respectively in their ^{1}H-NMR spectra. Consequently, it is thought that the above crude condensed-ring compound was a mixture of 6-hydroxy-1,4,5,8-tetramethoxy- and 1,6-dihydroxy-2,5,8-trimethoxy-3*H*-xanthen-3-one (**7** and **10**).

Compound **12** was also obtained, along with **4**, by the methylation of the unstable hydrogenated products of the crude condensed-ring compound of 1,2,3,5-benzenetetrol (**13**)[5] with ethyl formate. The formation of 1,2,5,6,8- and 1,2,6,7,8-pentahydroxy-3*H*-xanthen-3-one (**14** and **15**) is also assumed in the above condensation.

From these results, significant information regarding the synthetic studies of hexamethoxyxanthene derivatives of carthamin[6] was obtained.

Experimental

All the melting points are uncorrected. The ^{1}H-NMR spectra were measured with a Hitachi R-22 spectrometer (90 MHz), using tetramethylsilane as the internal standard. The mass spectra were obtained on a Hitachi RMU-6M mass spectrometer.

2,2′,4,4′-Tetramethoxydiphenylmethane-3,3′,6,6′-tetrol (2). To a mixed solution of 2,6-dimethoxyhydroquinone (**1**) (3.7 g) and formalin (37%) (1.2 g) in ethanol (20 ml), we added one drop of concd hydrochloric acid. The reaction mixture was allowed to stand overnight, and the resulting colorless needles (**2**) were filtered and washed with water. Mp 180 °C (dec), 2.4 g (63%). Found: C, 57.67; H, 5.80%; M^+, 352. Calcd for $C_{17}H_{20}O_8$: C, 57.95; H, 5.72%; M, 352.

1,3,6,8-Tetramethoxy-2,7-xanthenediol (3). A mixed solution of **2** (240 mg) and phosphoryl chloride (100 mg) in dry toluene (140 ml) was refluxed for 2 h. The reaction mixture was then washed with water and dried over anhydrous sodium sulfate. The solvent was evaporated *in vacuo*, and the residue was chromatographed on silica gel. Elution with benzene–ethyl acetate (4 : 1) afforded **3** as light yellow needles; mp 204 °C (38 mg, 17%). Found: C, 60.81; H, 5.45%; M^+, 334. Calcd for $C_{17}H_{18}O_7$: C, 61.07; H, 5.43%; M. 334.

1,2,3,6,7,8-Hexamethoxyxanthene (4). A mixed solution of **3** (50 mg), dimethyl sulfate (47 mg), and anhydrous potassium carbonate (65 mg) in dry acetone (6.5 ml) was refluxed for 10 h. The reaction mixture was then worked up in the usual manner, and the crude product was chromatographed on a column of silica gel with benzene–ethyl acetate (10 : 1) to give **4** (10 mg, 18%) (mp 115—116 °C (from ether–petroleum ether)) as colorless needles. ^{1}H-NMR ($CDCl_3$) δ 3.76 (2H, s, $-CH_2-$), 3.82 (12H, s, $-OMe \times 4$), 3.93 (6H, s, $-OMe \times 2$), 6.33 (2H, s, $C_{4,5}-H$), Found: C, 62.87; H, 6.12%; M^+,

362. Calcd for $C_{19}H_{22}O_7$: C, 62.98; H, 6.07%; M, 362.

3,3',6,6'-Tetramethoxydiphenylmethane-2,2',4,4'-tetrol (6). This compound was prepared from 2,5-dimethoxyresorcinol (**5**) and formalin (37%) in a 72% yield by a manner similar to that used for **2**; mp 195 °C. Found: C, 57.89; H, 5.73%; M^+, 352. Calcd for $C_{17}H_{20}O_8$: C, 57.95; H, 5.73%; M, 352. The dehydration of this compound by a manner similar to that used for **2** was, however, unsuccessful.

1,4,5,8-Tetramethoxy-3,6-xanthenediol (8) and 2,5,8-Trimethoxy-1,3,6-xanthenetriol (11). Into a solution of 2,5-dimethoxyresorcinol (**5**) (1.0 g) in ethyl formate (8.0 ml), dry hydrogen chloride gas was stirred for 4 h under cooling with ice water. The reaction mixture was then allowed to stand for 2 d at 0 °C. The resulting deep purple-red ppt (850 mg) was filtered and washed with ether. The above condensation product was hydrogenated in ethanol (40 ml) with 5% palladium charcoal (980 mg) for 6 h. The reaction mixture was then filtered, and the solvent was removed *in vacuo*. The residue was chromatographed on a column of silica gel with benzene–ethyl acetate (2 : 1) to give **8** (85 mg, 10%) (mp 183 °C (from ether–petroleum ether)) from the first eluent. Found: C, 60.78; H, 5.41%; M^+, 334. Calcd for $C_{17}H_{18}O_7$: C, 61.07; H, 5.43%; M, 334. Compound **11** (400 mg, 49%) (mp 239°C (dec) (from toluene)) was obtained from the second eluent. Found: C, 59.72; H, 4.96%; M^+, 320. Calcd for $C_{16}H_{16}O_7$: C, 60.00; H, 5.03%; M, 320.

1,3,4,5,6,8-Hexamethoxyxanthene (9). A mixed solution of **8** (100 mg), dimethyl sulfate (0.12 ml), and anhydrous potassium carbonate (200 mg) in dry acetone (13 ml) was refluxed for 6 h. The reaction mixture was then worked up in the usual manner, and the crude product was chromatographed on a column of silica gel with benzene–ethyl acetate (10 : 1) to afford **9** (70 mg, 65%); mp 138—139 °C (from ether–petroleum ether). ^{1}H-NMR ($CDCl_3$) δ 3.65 (2H, s, $-CH_2-$), 3.82, 3.88, and 3.94 (each 6H, s, $-OMe\times6$), 6.21 (2H, s, $C_{2,7}-H$). Found: C, 62.60; H, 6.14%; M^+, 362. Calcd for $C_{19}H_{22}O_7$: C, 62.98; H, 6.07%; M, 362.

1,2,3,5,6,8-Hexamethoxyxanthene (12). This compound, **12**, was obtained by the methylation of **11** in a manner similar to that used for **9**; mp 120—121 °C (from ether–petroleum ether). ^{1}H-NMR ($CDCl_3$) δ 3.72 (2H, s, $-CH_2-$), 3.82 (9H, s, $-OMe\times3$), 3.85 and 3.87 (each 3H, s, $-OMe\times2$), 3.93 (3H, s, –OMe), 6.18 (1H, s, C_7-H), 6.48 (1H, s, C_4-H). Found: C, 62.94; H, 6.12%; M^+, 362. Calcd for $C_{19}H_{22}O_7$: C, 62.98; H, 6.07%; M, 362.

1,2,3,6,7,8- and 1,2,3,5,6,8-Hexamethoxyxanthene (4 and 12) from 1,2,3,5-Benzenetetrol (13). The condensation product (2.6 g) of 1,2,3,5-benzenetetrol (**13**) with ethyl formate, which was obtained in a manner similar to that used for **8**, was hydrogenated in ethanol (240 ml) with 5% palladium charcoal (20 g) for 6 h. The reaction mixture was then filtered, and the solvent was removed *in vacuo* to give an unstable reduction product (1.7 g), a mixture of **14** and **15**. A mixed solution of the above reduction product (100 mg), dimethyl sulfate (0.32 ml), and anhydrous potassium carbonate (460 mg) in dry acetone (15 ml) was refluxed for 6 h. The reaction mixture was then worked up in the usual manner, and the crude product was chromatographed on a column of silica gel with benzene–ethyl acetate (10 : 1). From the first eluent, **4** (59 mg, 44%) (mp 115—116 °C) was obtained. Similarly, **12** (6.0 mg, 4.6%) (mp 120—121 °C) was obtained from the second eluent.

The authors wish to express their thanks to Mr. Kazuaki Sato for the microanalyses.

References

1) H. Obara and J. Onodera, *Chem. Lett.*, **1979**, 201.
2) S. Wawzonek, "Heterocyclic Compounds," ed by R. C. Elderfield, Wiley and Sons, New York (1951), Vol. II, p. 419.
3) E. Chapman, A. G. Perkin, and R. Robinson, *J. Chem. Soc.*, **1927**, 3028; W. Baker, *ibid.*, **1941**, 662.
4) W. Baker, R. Nodzu, and R. Robinson, *J. Chem. Soc.*, **1929**, 77.
5) J. Onodera and H. Obara, *Nippon Kagaku Kaishi*, **1973**, 1808.
6) J. Onodera, T. Saito, and H. Obara, *Chem. Lett.*, **1979**, 1327.

Ammonolysis of *N*-Acylpyroglutamic Acid. Permanganate-oxidation of Peptides. II.

Keisuke TORIGOE, Yoshiaki MOTOKI, and Ichiro MURAMATSU*

Department of Chemistry, College of Science, Rikkyo University, Nishi-ikebukuro, Toshima-ku, Tokyo 171

(Received July 22, 1980)

Synopsis. The reaction of *N*-acylpyroglutamic acid with ammonia proceeds in two pathways. The one results in *N*-acylglutamine as a product, and the other in pyroglutamic acid and an amide formed from the *N*-acyl group. The ratio of the yields of the two reactions changes with the *N*-acyl group, being correlated with the acidity of the carboxylic acid from which the *N*-acyl group is derived, and also with the steric hindrance of the group.

In a previous paper,[1] it was reported that Z–Pro–OH[2] was oxidized to Z–pGlu–OH with $KMnO_4$ in the presence of strong acid. In further study, it has been found that Bz–Pro–OH is also oxidized to give Bz–pGlu–OH, and that the ammonolysis of Bz–pGlu–OH gives H–pGlu–OH as a main product. The latter result is in contrast to the well-known fact that Z–pGlu–OH is ammonolyzed to give Z–Gln–OH.[3] That is to say, two pathways seem possible in the ammonolysis of *N*-acyl–pGlu–OH.

In order to elucidate the factors determining the pathway, we synthesized several *N*-acyl–pGlu–OH's and their amides, and investigated the relationship between the *N*-acyl group and the reaction pathway.

Results and Discussion

The pathways in the ammonolysis of *N*-acyl–pGlu–OH are shown in Fig. 1. The reaction proceeds to produce *N*-acyl-Gln–OH with accompanying ring-opening in path I, and H–pGlu–OH and the amide in path II.

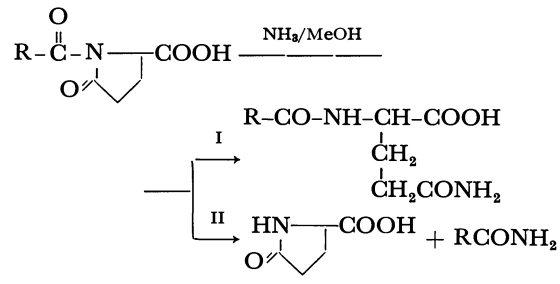

Fig. 1.

The results of ammonolysis are summarized in Table 1. Boc–pGlu–OH gave Boc–Gln–OH quantitatively, while pNBz–pGlu–OH gave H–pGlu–OH. The products vary with the acidity of the carboxylic acid from which the *N*-acyl group was derived. Namely, path II becomes predominant over I with increasing acidity of the carboxylic acid.

When the tosyl group was used as an *N*-protector, the product was Tos–Gln–OH only, although TosOH is a strong acid, showing deviation from the above correlation.

Ammonolysis of (A) Z–Ala–pGlu–NH_2 and (B) Z–Val–pGlu–NH_2 was carried out. In the case of (A), the peptide bond was cleaved almost quantitatively to give Z–Ala–NH_2 and H–pGlu–NH_2 (path II). In the case of (B), the reaction proceeded in two pathways, giving Z–Val–NH_2 and H–pGlu–NH_2 (path II), and Z–Val–Gln–NH_2 (path I) in the ratio 7 : 3.

Table 1. Ratio of the products in ammonolysis of *N*-acyl–pGlu–OH[a]

Acyl group	*N*-acyl–Gln–OH (Path I)	H–pGlu–OH (Path II)		pK_a[4]
Boc	1.00	0		
Z	0.83	0.17		
Ac	0.60	0.40	AcOH	4.67(5.84)[b]
Bz	0.15	0.85	BzOH	4.21(5.42)[b]
pNBz	0.04	0.96	pNBzOH	3.44(4.55)[b]
Tos	1.00	0	TosOH	1.70

a) Optically active (L-) in case of Boc, Z, and Tos; optically inactive in case of Ac, Bz, and pNBz. b) Measured in 50% MeOH at 27 °C.

The pK_a of Z–Ala–OH in 50% MeOH at 27 °C was determined to be 4.96, smaller than that of BzOH. Consequently the result of the ammonolysis of Z–Ala–pGlu–NH_2 is compatible with that of *N*-acyl–pGlu–OH. The pK_a of Z–Val–OH was 5.00 under the same conditions. It is conceivable that the ammonolysis of Z–Val–pGlu–NH_2 would give a similar result to that of Z–Ala–pGlu–NH_2. However, path I in the reaction of the valine peptide was not negligible. This shows that not only acidity but also steric hindrance of the *N*-acyl group affects the reaction pathway.

Z–Ala–pGlu–NH_2 and Z–Val–pGlu–NH_2 used in this study were obtained by the oxidation of Z–Ala–Pro–NH_2 and Z–Val–Pro–NH_2 by the method reported.[1]

Experimental

All melting points were uncorrected. NMR spectra were obtained on a Hitachi-Perkin Elmer R-20A Spectrometer, and IR spectra on a Hitachi Grating Infrared Spectrophotometer, Model 215. All *N*-acyl–pGlu–OH compounds were synthesized by the method reported.[3,5] All amino acids in peptide amides were of the L-series.

Ac–pGlu–OH·DCHA: Recrystallized from EtOH–EtOAc; yield[6] 32%; mp 174—175 °C; NMR (measured as free acid in $CDCl_3$) δ 2.54 (3H, s, CH_3–CO), 2.00—2.90 (4H, m, CH–CH_2–CH_2–CO), 4.73 (1H, m, >CH–COOH); IR (KBr) 1630, 1695, 1735 cm^{-1} (>C=O). Found: C, 64.83; H, 9.54; N, 8.11%. Calcd for $C_{19}H_{32}O_4N_2$: C, 64.74; H, 9.15; N, 7.95%.

Bz–pGlu–OH: Purified with a column of Sephadex LH-20 (solvent, benzene–EtOH–H_2O, 50 : 15 : 1), and recrystallized from EtOH–EtOAc; yield[6] 38%; mp 142—144 °C; NMR ($CDCl_3$–CD_3OD) δ 2.00—2.80 (4H, m, CH–CH_2–CH_2–CO), 4.88 (1H, m, >CH–COOH), 7.20—7.80 (5H, m, C_6H_5–CO); IR (KBr) 1655, 1710, 1730, 1770 cm^{-1} (>C=O). Found: C, 61.43; H, 4.63; N, 5.95%. Calcd for $C_{12}H_{11}O_4N$: C, 61.80;

H, 4.75; N, 6.01%.

pNBz–pGlu–OH: Recrystallized from EtOAc; yield[6] 41%; mp 180—181 °C; NMR ($CDCl_3$–CD_3OD) δ 1.80—2.80 (4H, m, CH–C$\underline{H}_2$–C$\underline{H}_2$–CO), 4.92 (1H, m, >C$\underline{H}$–COOH), 7.50—8.40 (4H, m, NO_2–$C_6\underline{H}_4$–CO); IR (KBr) 1695, 1705, 1750 cm^{-1} (>C=O). Found: C, 51.60; H, 3.34; N, 10.23%. Calcd for $C_{12}H_{10}O_6N_2$: C, 51.81; H, 3.62; N, 10.07%.

Z–Ala–pGlu–NH$_2$: Recrystallized from EtOAc–ether; yield[7] 38%; mp 156—158 °C; $[\alpha]_D^{26}$ −67.6° (*c* 1.0, EtOH); NMR ($CDCl_3$–CD_3OD) δ 1.37 (3H, d, >CH–C$\underline{H}_3$), 1.90—2.80 (4H, m, CH–C$\underline{H}_2$–C$\underline{H}_2$–CO), 4.56 (1H, m, >C$\underline{H}$–$CONH_2$), 5.06 (2H, s, C_6H_5–C$\underline{H}_2$O), 5.43 (1H, q, NH–C$\underline{H}$–CO), 7.31 (5H, s, $C_6\underline{H}_5$–CH_2); IR (KBr) 1670, 1690, 1745 cm^{-1} (>C=O). Found: C, 57.79; H, 6.05; N, 12.44%. Calcd for $C_{16}H_{19}O_5N_3$: C, 57.65; H, 5.75; N, 12.61%.

Z–Val–pGlu–NH$_2$: Purified with a column of silica gel (solvent, $CHCl_3$–EtOAc, 1 : 4), and recrystallized from EtOAc–hexane; yield[7] 17%; mp 145—147 °C; $[\alpha]_D^{26}$ −33.1° (*c* 1.2, MeOH); NMR ($CDCl_3$–CD_3OD) δ 0.80 (3H, d, CH–C$\underline{H}_3$), 1.05 (3H, d, CH–C$\underline{H}_3$), 1.90–2.80 (5H, m, CH–C$\underline{H}_2$–C$\underline{H}_2$–CO and CH_3–C$\underline{H}$–CH_3), 4.65 (1H, m, >C$\underline{H}$–$CONH_2$), 5.09 (2H, s, C_6H_5–C$\underline{H}_2$–O), 5.50 (1H, m, NH–C$\underline{H}$–CO), 7.34 (5H, s, $C_6\underline{H}_5$–CH_2); IR (KBr) 1670, 1685, 1745 cm^{-1} (>C=O). Found: C, 60.08; H, 6.46; N, 11.89%. Calcd for $C_{18}H_{23}O_5N_3$: C, 59.82; H, 6.42; N, 11.63%.

Method for Ammonolysis and Analysis of Products. To 1—3 mg of samples was added NH_3-saturated MeOH at 0 °C. The resulting solutions were allowed to stand at 0 °C overnight, and concentrated *in vacuo*. The products were identified with authentic samples[8] by TLC[9] on Kieselgel 60F-254 plate. The products were separated also by preparative TLC.[10] Silica gel layers at the position containing the products were raked up and treated with 6 M HCl for 10 h at 110 °C for hydrolysis. The ratios of amino acids in the hydrolyzates were determined by an amino acid analyzer (JEOL JLC-6AS).

We wish to thank Mr. Akira Ide for technical assistance and the staff of the Research Laboratory of Toyo Jozo Co. Ltd. for elemental analyses.

References

1) I. Muramatsu, Y. Motoki, Y. Yabuuchi, and H. Komachi, *Chem. Lett.*, **1977**, 1253.

2) Z=benzyloxycarbonyl; Boc=*t*-butoxycarbonyl; Ac=acetyl; Bz=benzoyl; pNBz=*p*-nitrobenzoyl; Tos=*p*-toluenesulfonyl; H-pGlu-OH=pyroglutamic acid. The abbreviation for amino acids and peptides is in accordance with the rules of the IUPAC-IBU Commission of Biochemical Nomenclature.

3) H. Gibian and E. Klieger, *Ann. Chem.*, **640**, 145 (1961).

4) J. A. Dean, "Handbook of Chemistry," 11th ed McGraw Hill Company (1973).

5) E. Schröder and E. Klieger, *Ann. Chem.*, **673**, 196 (1964).

6) From *N*-acyl–Glu–OH.

7) From *N*-acyl–Pro–NH_2.

8) Z–Val–Gln–NH_2 was prepared from Z–Val–Glu–$(OMe)_2$ by treatment with NH_3; mp 274—276 °C; $[\alpha]_D^{26}$ −18.3° (*c* 0.6, AcOH). Found: C, 56.85; H, 7.08; N, 14.51%. Calcd for $C_{18}H_{26}O_5N_4$: C, 57.13; H, 6.93; N, 14.81%.

9) Solvents for *N*-acyl–pGlu–OH; *n*-BuOH–HCOOH–H_2O, 4 : 1 : 1; *n*-BuOH–AcOH–H_2O, 4 : 1 : 1; *n*-BuOH–pyridine–AcOH–H_2O, 4 : 1 : 1 : 2; for *N*-acyl–pGlu–NH_2; $CHCl_3$–MeOH–AcOH, 18 : 2 : 1; $CHCl_3$–EtOH–HCOOH, 18 : 2 : 1; $CHCl_3$–MeOH–AcOH–pyridine, 18 : 2 : 1 : 1.

10) Solvent for *N*-acyl–pGlu–OH; *n*-BuOH–HCOOH–H_2O, 4 : 1 : 1; for *N*-acyl–pGlu–NH_2; $CHCl_3$–MeOH–AcOH, 18 : 2 : 1.

The Transition-metal Catalyzed Dehalogenation of Aromatic Halides by NaOH–Alcohols. A Facile Method of Destroying Aromatic Polyhalides

Tadashi OKAMOTO* and Shinzaburo OKA
Institute for Chemical Research, Kyoto University, Uji 611
(Received July 25, 1980)

Synopsis. Aromatic halides are dehalogenated by heating with NaOH in alcoholic solvents in the presence of transition metal salts, such as rhodium(III) chloride or palladium(II) acetate and triphenylphosphine. Bis(pentabromophenyl) ether was converted into diphenyl ether in 2-propanol when treated for 5 h at 355 K with a catalytic cycle of more than 80.

Lately transition metal catalysts have been found to be useful for the substitution of aromatic halides.[1] Dehalogenation is the simplest type of these reactions, and many reports on the catalysis of palladium, rhodium, or nickel complexes using borohydride, formate, alkoxide, or secondary alcohols as the hydrogen source have been published.[2] These methods in the literature usually require low-valent metal complexes or powerful reducing agents such as borohydride. There has been one report on a dehalogenation catalyzed by rhodium(III) chloride using Na_2CO_3 in ethanol, but the substrate is limited to such activated halides as α-keto halides or benzyl halide.[3] In this report we wish to present a facile and inexpensive method of dehalogenation. Aromatic halides were heated with sodium hydroxide in alcoholic solvents in the presence of transition metal salts and triphenylphosphine to give dehalogenated aromatic compounds in moderate to excellent yields. No previous preparation of a low-valent catalyst or alkoxide was necessary.

Results and Discussion

The results for various substrates are listed in Table 1. The reactivity of bromide is higher than that of chloride, and electron-releasing substituents on the aromatic ring retard the reaction, as in the case of the oxidative-addition reaction of aryl halides with low-valent transition-metal complexes.[4] Palladium acetate–$2P(C_6H_5)_3$ was a better catalyst than $RhCl_3$ hydrate–$2P(C_6H_5)_3$. $NiBr_2[P(C_6H_5)_3]_2$ or $CoCl_2$ hydrate–$2P(C_6H_5)_3$ was ineffective for the reaction. This trend of reactivity is in accordance with that of the reduction potential (E_o) of metal salts.[5] These observations suggest that a low-valent metal complex is generated *in situ* and reacts with aromatic halides to give oxidative-addition products, which are then reduced by the alkoxide ion (or alcohol) according to the scheme shown by Eqs. 1—3, where X represents an anion such as a halide or acetate ion:

$$M^{n+}X_n \xrightarrow{R'_2CHO^- \text{ (or } R'_2CHOH)} M^{(n-2)+}X_{n-2} \quad (1)$$

$$M^{(n-2)+}X_{n-2} + ArY \longrightarrow M^{n+}(Ar)X_{n-2}Y \quad (2)$$

$$M^{n+}(Ar)X_{n-2}Y + R'_2CHO^- \text{ (or } R'_2CHOH) \xrightarrow{-Y^- \text{ (or } HY)} M^{(n-2)+}X_{n-2} + R'_2CO + ArH \quad (3)$$

Table 1. Rhodium(III)-catalyzed dehalogenation of aromatic halides[a]

Substrate	Solvent	Yield of[b] arenes/%
Bromobenzene	MeOH	30
Bromobenzene	EtOH	78
4-Bromoanisole	EtOH	65[c]
4-Bromoanisole	*i*-PrOH	69
4-Bromoanisole	EtOH	27[d]
β-Bromostyrene	EtOH	65
3-Bromopyridine	EtOH	64
4-Bromoacetophenone	EtOH	15[e]
4-Bromoacetophenone	EtOH	25[f]
4-Bromobenzoicacid	EtOH	44[g]
4-Chlorobenzoic acid	EtOH	0[g]
1-Chloro-1-phenylethane	EtOH	h

a) Reactions were carried out at 335 K for 16 h with a substrate/catalyst of 50 and a NaOH/substrate of 1.5. Catalyst : $RhCl_3$–$2P(C_6H_5)_3$. b) Determined by gas chromatography based on the amount of substrate used. c) The reaction temperature was 351 K. d) Na_2CO_3 was used instead of NaOH; 73 h. e) Accompanied by 1-phenylethanol (7%). f) Accompanied by diphenylmethanol (*ca.* 25%). g) The NaOH/substrate was 2.5. h) The products were ethylbenzene and styrene, with the relative ratio being around 1. The yields were not determined.

There is a substantial difference in the reactivity of alcohols, MeOH<EtOH<*i*-PrOH. The slower reaction with Na_2CO_3 compared with NaOH suggests that NaOH is effective not only in neutralizing the hydrogen halide generated, but also in facilitating the reduction of metal complexes in some way.[6]

As may be seen from Table 1, the reaction is applicable to pyridine derivatives and also to vinyl halides. An aliphatic saturated halide such as 1-chloro-1-phenylethane was dehalogenated to give ethylbenzene, but it was accompanied by a substantial amount of styrene, the elimination product. The reduction of the carbonyl group is another side reaction; 4-bromobenzophenone gave almost equimolar amount of diphenylmethanol and the normal dehalogenation product of benzophenone.

Polyhalogenated aromatic compounds are dehalogenated by this system easily. The results are summarized in Table 2. Bis(pentabromophenyl) ether was converted to diphenyl ether (92% yield) by the catalysis of palladium acetate–$2P(C_6H_5)_3$ over a 5 h period at 355 K with a catalytic cycle of more than 80. Although polychlorinated biphenyl (Kanechlor) was dehalogenated more sluggishly than the bromide, the present reaction is suitable for the purpose of destroying

Table 2. Dehalogenation of polyhalogenated aromatic compounds[a)]

Substrate (mmol)	Catalyst	Time/h	Dehalogenation (%)[b)]
Bis(pentabromophenyl) ether (1.9)	$Pd(OAc)_2$–$2P(C_6H_5)_3$	5	100
	$Pd(OAc)_2$–2Pyridine	56	94
	$RhCl_3$–$2P(C_6H_5)_3$	21	74
	$RhCl_3$–2DPE[c)]	56	87
Kanechlor 600 (4.3)	$Pd(OAc)_2$–$2P(C_6H_5)_3$	45	50
	$RhCl_3$–$2P(C_6H_5)_3$	19	33

a) The reaction was carried out at 355 K with a 20% excess of NaOH and 0.20 mmol of the catalyst in 10 ml of 2-propanol. b) Determined by the elemetal analysis of the product (mixture). c) Ethylenebis(diphenylphosphine).

environment-contaminating aromatic polychlorides, because highly chlorinated compounds, which are known to be difficult to destroy, were dehalogenated preferentially, as is illustrated in Fig. 1 for the dehalogenation of 2,3,4,5,6-pentachloroanisole. The figure further suggests the step-by-step mechanism of the dehalogenation reaction. There is no indication of a benzyne intermediate with a simultaneous elimination of two halogen atoms.

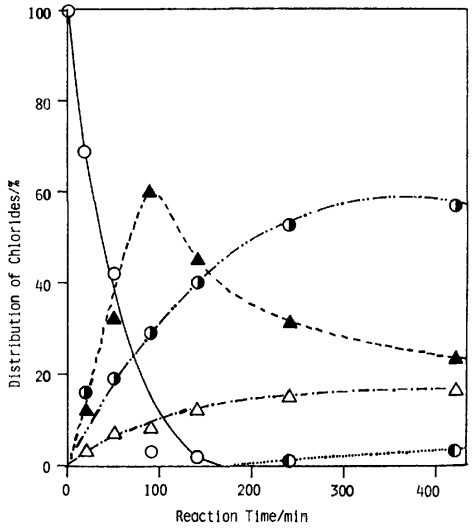

Fig. 1. Dehalogenation of 2,3,4,5,6-Pentachloroanisole. ○ Pentachloride, ▲ Tetrachloride, ◑ Trichloride, △ Dichloride, and ◐ Monochloride. $Pd(OAc)_2$, 0.27 mol; triphenylphosphine, 0.39 mmol; NaOH, 22.75 mol; substrate, 2.30 mmol in 10 ml of 2-propanol at 355 K. Product distribution was determined by gas chromatography.

Experimental

The palladium acetate was prepared by the method of Wilkinson.[7)] The other reagents were analytical-grade.

Dehalogenation of Aromatic Monohalides by $RhCl_3 \cdot 6H_2O$ and Triphenylphosphine. $RhCl_3 \cdot 6H_2O$ (20 mg), triphenylphosphine (40 mg), and NaOH (300 mg) were placed in a flask and deaerated. Into the flask we then added 5 mmoles of a substrate and 10 ml of a solvent, subsequently the mixture was stirred at 335 K for a specified period. The yields were determined by gas chromatography.

Dehalogenation of Bis(pentabromophenyl) Ether. Bis(pentabromophenyl) ether 1.78 g (1.9 mmol), NaOH 0.91 g (22.8 mmol), and the catalyst (0.2 mmol) were placed in a flask, and the mixture was flushed with nitrogen. Deaerated 2-propanol (10 ml) was then added to the flask, and the solution was refluxed for the specified period under stirring. The reaction mixture was then diluted with a 10-ml portion of H_2O and extracted by means of three 10-ml portions of hexane. The extract was concentrated and subsequently purified on a silica-gel column (hexane) from the base-promoted condensation products of acetone. The hexane effluent, which contained diphenyl ether and/or partly brominated diphenyl ethers, was concentrated and weighed. The average extent of dehalogenation was determined by the elemental analysis of the residue. The material balance of the reaction, as determined from the weight and the extent of dehalogenation of the residue, was generally good.[8)]

The dehalogenation of Kanechlor was carried out in a similar manner except for the amounts of the substrate and NaOH.

References

1) R. Cramer and D. R. Coulson, *J. Org. Chem.*, **40**, 2267 (1975); K. Takagi, T. Okamoto, Y. Sakakibara, A. Ohno, S. Oka, and N. Hayama, *Bull. Chem. Soc. Jpn.*, **48**, 3298 (1975).

2) N. A. Cortese and R. F. Heck, *J. Org. Chem.*, **42**, 3491 (1977): A. Zask and P. Helquist, *ibid.*, **43**, 1619 (1978): S.-T. Lin and J. A. Roth, *ibid.*, **44**, 309 (1979): Y. Tamaru, Y. Yamamoto, Y. Yamada, and Z. Yoshida, *Tetrahedron Lett.*, **1970**, 1401.

3) R. Grigg, T. R. B. Mitchell, and S. Sutthivayakit, *Tetrahedron Lett.*, **1979**, 1067.

4) T. T. Tson and J. K. Kochi, *J. Am. Chem. Soc.*, **101**, 6319 (1979), and the references cited therein.

5) J. P. Jesson and E. L. Muetterties, "Chemist's Guide," Marcel Dekker, New York (1969), p. 7.

6) The contribution of bases to the oxidation-reduction of transition-metal complexes was known, but the mechanisms were not clearly understood. See, for example, J. A. Switzer and J. F. Endicott, *J. Am. Chem. Soc.*, **102**, 1181 (1980), and the references cited therein.

7) T. A. Stephenson, S. M. Morehouse, A. R. Powell, J. R. Heff, and G. Wilkinson, *J. Chem. Soc.*, **1965**, 3632.

8) The material balance was 90—100% except for the reaction catalyzed by $RhCl_3$–2DPE (85%).

A Simple Method for the Esterification of Carboxylic Acids Using Chlorosilanes

Ren NAKAO,* Kunio OKA, and Tsugio FUKUMOTO
Radiation Center of Osaka Prefecture, Shinke-cho, Sakai, Osaka 593
(Received July 28, 1980)

Synopsis. Various carboxylic esters, including some with bulky substituents, are prepared in good yields from carboxylic acids and alcohols under mild conditions by the use of trimethylchlorosilane, dimethyldichlorosilane, methyltrichlorosilane, or tetrachlorosilane.

The esterification of carboxylic acids with alcohols is one of the most important reactions in organic synthesis, and quite a number of methods have been investigated. Among them, 2-halopyridinium salts,[1] (chloromethylene)dimethylammonium chloride,[2] 1-(sulfonyloxy)benzotriazoles[3] and graphite bisulfate[4] have been used successfully as coupling reagents for the reaction. In the course of the study of the reaction of acetoxytrimethylsilane with alcohols in the presence of hydrogen chloride,[5] we found that trimethylchlorosilane was a convenient reagent for the esterification of carboxylic acids with alcohols.

In this note, we wish to report some results of the esterification carried out by the use of chlorosilanes. The esterification was performed under the following standard conditions: $(CH_3)_3SiCl$ (1.7 mmol) was added to a mixture of RCOOH (3.3 mmol) and R'OH (5.0 mmol) in 2-methyltetrahydrofuran. After the reaction mixture had been allowed to stand for 15 min at room temperature, the products were analysed by GLPC. In a neat reaction, the starting homogeneous reaction mixture progressively separates into two layers as the reaction proceeds. Therefore, the solvent was chosen so as to be keep the reaction mixture homogeneous and to be favorable for GLPC analysis.

The results obtained with various carboxylic acids and alcohols by the use of trimethylchlorosilane are given in Table 1. In all cases, the production of hexamethyldisiloxane was confirmed. Although the esterification with secondary alcohols is slower than that with primary alcohols, the yields of all the esters, including sterically hinderd isobutyl pivalate, are very high. Therefore, trimethylchlorosilane can be said to be a very efficient and convenient reagent for the esterification of carboxylic acids with primary and secondary alcohols at room temperature. When, however, *t*-butyl alcohol and phenol were subjected to a reaction with acetic acid in the presence of trimethylchlorosilane, the reaction products were complicated and the yields of *t*-butyl acetate and phenyl acetate were only 9 and 19% respectively.

The rate of esterification decreases with the decrease in the amount of trimethylchlorosilane added. However, it must be emphasized that 1 mol of trimethylchlorosilane serves to produce more than 1 mol of the ester. This indicates that trimethylchlorosilane does not participate only as a hydrogen chloride source and/or a dehydrating agent in the reaction. When methoxytrimethylsilane, which is expected to be formed by the reaction of trimethylchlorosilane and methanol, was allowed to react with acetic acid in the presence of hydrogen chloride, methyl acetate was obtained in a 93% yield, along with the production of hexamethyldisiloxane. Therefore, the following scheme seems to be most probable for the esterification with trimethylchlorosilane:

$$(CH_3)_3SiCl + R'OH \longrightarrow (CH_3)_3SiOR' + HCl \quad (1)$$

$$RCOOH + (CH_3)_3SiOR' \xrightarrow{HCl} RCOOR' + (CH_3)_3SiOH \quad (2)$$

$$(CH_3)_3SiOH + R'OH \xrightarrow{H^+} (CH_3)_3SiOR' + H_2O \quad (3)$$

$$2(CH_3)_3SiOH \longrightarrow (CH_3)_3SiOSi(CH_3)_3 + H_2O \quad (4)$$

Table 1. Esterification of various carboxylic acids with alcohols using $(CH_3)_3SiCl$[a] $RCOOH + R'OH \xrightarrow{(CH_3)_3SiCl} RCOOR'$

R	R'	$\frac{[(CH_3)_3SiCl]}{[RCOOH]}$	Solvent	Reaction time	Yield of ester/%
CH_3	CH_3	0.13	2-Me-THF	30 min	72
CH_3	CH_3	0.13	2-Me-THF	110 min	87
CH_3	CH_3	0.5	2-Me-THF	15 min	97
C_2H_5	CH_3	0.5	2-Me-THF	15 min	95
$(CH_3)_2CH$	CH_3	0.5	THF	15 min	98
C_2H_5	CH_3	0.5	2-Me-THF	100 h	93
$(CH_3)_3C$	CH_3	0.5	THF	15 min	91
$(CH_3)_3C$	$(CH_3)_2CHCH_2$	0.5	2-Me-THF	15 min	90
CH_3	C_2H_5	0.5	2-Me-THF	15 min	92
CH_3	CH_2=$CHCH_2$	0.6	2-Me-THF	15 min	92
CH_3	$(CH_3)_2CH$	0.5	2-Me-THF	15 min	37
CH_3	$(CH_3)_2CH$	0.5	2-Me-THF	24 h	93
CH_3	$C_2H_5(CH_3)CH$	0.5	2-Me-THF	48 h	95
CH_3	*c*-C_6H_{11}	0.5	*n*-$C_{11}H_{24}$	48 h	81

a) Reactions were performed at room temperature.

In the initial stage of the reaction where alcohol remains in a large quantity, Eq. 3[6] may be faster than Eq. 4. However, in the final stage, Eq. 4 may become favorable. During the reaction, the alkoxytrimethylsilane produced in Eq. 3 participates repeatedly in the esterification of carboxylic acid *via* Eq. 2.

Other chlorosilanes can be used in this esterification as well as trimethylchlorosilane. By using dimethyldichlorosilane ($[(CH_3)_2SiCl_2]/[CH_3COOH]=0.25$), methyltrichlorosilane ($[CH_3SiCl_3]/[CH_3COOH]=0.17$) and tetrachlorosilane ($[SiCl_4]/[CH_3COOH]=0.13$) in the reaction of acetic acid and methanol, methyl acetate was obtained in 98, 97, and 96% yields respectively.

Experimental

The gas-chromatographic analyses were made by a Yanagimoto GCG-5DH apparatus on a 3-m column containing 30% dioctyl phthalate on Celite 545 or a 2.5-m column containing 25% silicon DC-200 on Celite 545, using helium as the carrier gas. The NMR spectrum was obtained on a JEOL JNM-100 apparatus, with tetramethylsilane as the internal standard.

All of the reagents and solvents were used after distillation. The products were identified and estimated by GLPC. Commercial materials were used as the standerds except for *s*-butyl pivalate. The *s*-butyl pivalate used as a standard was prepared by the reaction of pivalic acid and *s*-butyl alcohol using $(CH_3)_3SiCl$: bp 150 °C, NMR (CCl_4); δ 0.92 (d, 6, $CH(C\underline{H}_3)_2$), 1.15 (s, 9, $C(CH_3)_3$), 1.88 (m, 1, CH), 3.72 (d, 2, OCH_2).

Reaction of Acetic Acid with Methoxytrimethylsilane. CH_3COOH (1.2 mmol), $(CH_3)_3SiOCH_3$ (1.2 mmol), dry HCl (0.6 mmol), and 2-methyltetrahydrofuran (0.33 cm^3) were transferred from individual bulbs to a glass tube under a vacuum. The tube, after being sealed, was allowed to stand overnight at room temperature. The products were analysed by GLPC. Methoxytrimethylsilane was prepared from trimethylchlorosilane and methanol, using pyridine as the hydrogen chloride acceptor.

References

1) a) T. Mukaiyama, M. Usui, E. Shimada, and K. Saigo, *Chem. Lett.*, **1975**, 1045; *b*) T. Mukaiyama, H. Toda, and S. Kobayashi, *Chem. Lett.*, **1976**, 13; *c*) K. Saigo, M. Usui, K. Kikuchi, E. Shimada, and T. Mukaiyama, *Bull. Chem. Soc. Japan*, **50**, 1863 (1977).

2) P. A. Stadler, *Helv. Chim. Acta*, **61**, 1675 (1978).

3) M. Itoh, D. Hagiwara, and J. Notani, *Synthesis*, **1975**, 456.

4) J. Bertin, H. B. Kagan, and J. L. Luche, *J. Am. Chem. Soc.*, **96**, 8113 (1974).

5) R. Nakao, K. Oka, and T. Fukumoto, *Ann. Rept. Rad. Ctr. Osaka*, **19**, 83 (1978).

6) V. Bazant, V. Chvalovsky, and J. Rathousky, "Organosilicon Compounds," Academic Press, New York and London (1965), Vol. 1, p. 56; the reaction of silanols with an excess of methanol is of importance for determining the Si–OH bands. The equilibrium is rapidly established under acid catalysis and shifts toward the right by the removal of the water released. In our reaction, the equilibrium of Eq. 3 is shifted in the same direction by the removal of alkoxytrimethylsilane by means of Eq. 2.

Synthesis and Reactions of Perylenecarboxylic Acid Derivatives. VII. Hydrolysis of *N,N'*-Dialkyl-3,4 : 9,10-Perylenebis(dicarboximide) with Sulfuric Acid

Yukinori NAGAO* and Takahisa MISONO

Department of Industrial Chemistry, Faculty of Science and Technology, Science University of Tokyo, Yamazaki, Noda 278

(Received August 6, 1980)

Synopsis. The hydrolysis of *N,N'*-dialkyl-3,4 : 9,10-perylenebis(dicarboximide) (alkyl=CH_3, CH_2CH_3, $CH_2CH_2CH_3$, and $CH_2CH_2CH_2CH_3$) with sulfuric acid at 180—200 °C gave *N*-alkyl-3,4 : 9,10-perylenetetracarboxylic monoanhydride monoimide (alkyl=CH_3, CH_2CH_3, $CH_2CH_2CH_3$, and $CH_2CH_2CH_2CH_3$). The kinetics of the reaction were determined spectroscopically.

Previous work has shown that 3,4 : 9,10-perylenetetracarboxylic monoanhydride monoimide (**2a**—**e**) can be prepared by the condensation of 3,4 : 9,10-perylenetetracarboxylic dianhydride (**3**) with alkylamine.[1] The condensation of **2a**—**e** with arylamine gave *N*-alkyl-*N'*-aryl-3,4 : 9,10-perylenebis(dicarboximide).[2] This work was undertaken to examine whether **2b**—**e** could be prepared from *N,N'*-dialkyl-3,4 : 9,10-perylenebis(dicarboximide) (**1b**—**e**). **2a** was prepared by the hydrolysis of 3,4 : 9,10-perylenebis(dicarboximide) (**1a**) with sulfuric acid.[3] The formation of **2b**—**e** in the hydrolysis of **1b**—**e** with sulfuric acid was then determined.

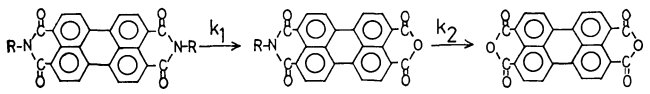

1a~e 2a~e 3

R = a; H, b; CH_3, c; CH_2CH_3, d; $CH_2CH_2CH_3$, e; $CH_2CH_2CH_2CH_3$

Experimental

Materials. **1b**—**e**, **2b**—**e**, and **3** were prepared by the procedures reported before.[1]

Hydrolysis. A flask containing 50.0 ml of 95%-sulfuric acid was set in a thermostated bath at the reaction temperature. To the flask was added 50 mg of finely powdered **1b**—**e** with stirring, and the reaction mixture was stirred to provide complete mixing. A small amount of the mixture was taken at an appropriate time interval. One half of the sample was used for measurement of absorbance after dilution with 95.0%-sulfuric acid and another half of the sample was poured into water to precipitate organic materials. These were separated by contrifugation, dried, dissolved in 1% potassium hydroxide, and analyzed by paper chromatography.

Measurements and Calculations. Absorbances were measured with a Hitachi 101 Spectrophotometer. The determination of the reaction mixture and paper chromatography were carried out as in the experiment reported before.[1] The calculations of composition or rate ratio $K(=k_2/k_1)$ were made by IBM 370 computer.

Results and Discussion

In the reactions at 180—200 °C, all the reaction mixtures have been proved to contain only three components, **1b**—**e**, **2b**—**e**, and **3** by paper chromatography. The compositions in the reaction mixture were determined by spectroscopy. The contents, $C_I/(C_I+C_M+C_A)$, $C_M/(C_I+C_M+C_A)$, and $C_A/(C_I+C_M+C_A)$ where C_I, C_M, and C_A are the concentrations of **1b**—**e**, **2b**—**e**, and **3**, respectively, were obtained from the standard absorbances of **1b**—**e**, **2b**—**e**, and **3**. Figure 1 shows a typical reaction curve. The pattern was similar in all reactions. As the reactions proceed, the yields of **2b**—**e** initially increased, but decreased after reaching a maximum. The maximum yields of **2b**—**e** were compared. Table 1 gives the maximum yields of **2b**—**e** in the reactions at 180, 190, and 200 °C. It is shown

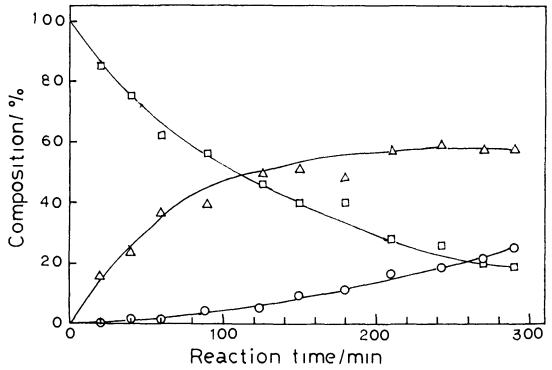

Fig. 1. Reaction of *N,N'*-dipropyl-3,4 : 9,10-perylenebis (dicarboximide) (**1d**) with H_2SO_4.
Reaction temp: 180 °C. □: *N,N'*-Dipropyl-3,4: 9,10-perylenebis(dicarboximide) (**1d**), △; *N*-Propyl-3,4: 9,10-perylenetracarboxylic monoahydride monoimide (**2d**), ○: 3,4: 9,10-Peryleneteracarboxylic dianhydride (**3**).

Table 1. The maximum yields of *N*-alkyl-3,4: 9,10-perylenetetracarboxylic monoanhydride monoimide (**2b**—**e**)

N,N'-Dialkyl-3,4 : 9,10-perylenebis-(dicarboximide)(**1b**—**e**) R		Temp °C	Time min	Maximum yield of **2b**—**e** %	
1b	CH_3	180	270	44	**2b**
		190	200	48	
		200	100	47	
1c	CH_2CH_3	180	220	55	**2c**
		190	140	49	
		200	40	45	
1d	$CH_2CH_2CH_3$	180	240	58	**2d**
		190	80	56	
		200	40	50	
1e	$CH_2CH_2CH_2CH_3$	180	180	53	**2e**
		190	150	47	
		200	40	40	

that all the values are in the range of 40—60%; the value is the smallest in **1b** and increases a little at lower temperature. The yields of **2b**—**e** isolated from the reaction mixture at 180 °C were **2b** : 31%, **2c** : 31%, **2d** : 31%, **2e** : 41%. Thus the yields of separable **2b**—**e** are lower than the spectroscopic yields in Table 1, because of the difficulty of their separation.

There was a scattering of the data points on a reaction curve as the concentration of **1b**—**e** increased over 100 mg/50 ml sulfuric acid; this became more serious at higher temperature, and was the largest in **1b** and the smallest in **1d**. In the reaction of **1a**,[3] no scattering was observed in ten times the concentration (500 mg/50 ml). This was attributed to the fact that the solubility of **1b**—**e**, which has an alkyl group, is smaller than that of **1a**. For these reasons, more sulfuric acid is necessary for the preparation of **2b**—**e** from **1b**—**e** than that from **1a**.

Plots of $\ln(C_I/C_{Io})$, where C_{Io} is the initial concentration of **1b**—**e**, *vs.* time are linear in the reaction of 50 mg **1b**—**e** at 180 °C. The rate constants k_1, for the reaction of **1b**—**e** to **2b**—**e**, were calculated from the slope. The rate ratios $K(k_2/k_1)$, where k_2 is the rate constant of **2b**—**e** to **3**, were calculated from Eq. 1.[1] Most of the values in each reaction were constant. These results indicated that the reaction followed a pseudo-first-order process. The rate constants k_1 and

$$C_M/C_{Io} = \{1/(1-K)\}\{(C_I/C_{Io})^K - (C_I/C_{Io})\} \quad (1)$$

rate ratio K are given in Table 2. All the rate constants are in the range of $0.45—0.95\times10^{-2}$ min^{-1}, and the rate ratio K are in the range of 0.35—0.50. A longer alkyl chain decreased the rate constants and ratios in the condensation of **3** with alkylamine,[1] but there was no such significant effect of alkyl groups in this reaction. All the k_1 values of **1b**—**e** were smaller than that of **1a** ($k_1=1.06\times10^{-2}$ min^{-1}).[3] Polar substituent constant σ^* are : H : +0.490, CH_3 : 0.000, C_2H_5 : −0.100, n-C_3H_7 : −0.115, n-C_4H_9 : −0.130.[4] The large k_1 value in **1a** is related to the polar effects of *N*-substituents.

Table 2. Rate constant k_1 and rate ratio $K(=k_2/k_1)$
Reaction temp, 180 °C

N,*N*-Dialkyl-3,4 : 9,10-perylene-bis(dicarboximide) (**1b**—**e**)	R	$k_1\times10^2$ / min^{-1}	$K(=k_2/k_1)$
1b	CH_3	0.472	0.420
1c	CH_2CH_3	0.929	0.420
1d	$CH_2CH_2CH_3$	0.572	0.360
1e	$CH_2CH_2CH_2CH_3$	0.920	0.500

References

1) Y. Nagao, Y. Tanabe, and T. Misono, *Nippon Kagaku Kaishi*, **1979**, 528.
2) Y. Nagao, N. Ishikawa, Y. Tanabe, and T. Misono, *Chem. Lett.* **1979**, 151.
3) Y. Nagao and T. Misono, *Kogyo Kagaku Zasshi*, **74**, 2500 (1971).
4) R. W. Taft, Jr., *J. Am. Chem. Soc.*, **75**, 4231 (1953).

Carbon-13 Chemical Shifts of Polychlorobicyclo[2.2.1]heptene Derivatives

Akira SERA,* Kazuhiro TAKAGI, Michiko NAKAMURA, and Kazuyoshi SEGUCHI**

Department of Chemistry, Faculty of Science, Kobe University, Kobe 657

***Faculty of Home Economics, Mukogawa Women's University, Nishinomiya 663*

(Received September 1, 1980)

Synopsis. The ^{13}C chemical shifts of 5-substituted polychlorobicyclo[2.2.1]heptene derivatives were determined. The chlorine, 5-*endo* and 5-*exo* substituent effects on the chemical shifts were discussed. The differences in the C_3 and C_7 chemical shifts are shown to be helpful for the identification of the *endo* and *exo* isomers. A possible operation of the interaction of pi electrons with a carbon-chlorine dipole is also discussed.

Because of their rigid molecular structures and fixed geometry, bicyclo[2.2.1]heptene derivatives have been extensively investigated by means of the ^1H and ^{13}C nuclear magnetic resonance methods.[1-3] The polar substituent effect on the ^1H and ^{13}C chemical shifts has been actively discussed as well as the molecular geometry effect on spin-coupling phenomena. Some chlorine nuclear quadrupole resonance (NQR) spectra of chlorobicyclo[2.2.1]heptenes were measured, and the ^{35}Cl NQR frequencies were discussed in terms of the charge density on the chlorine atoms.[4,5] However, the ^{13}C chemical shifts of chlorobicyclo[2.2.1]heptenes seem to have been reported only sporadically. In connection with our research project concerning high-pressure Diels-Alder reactions, we wish to report here some results of the systematic ^{13}C NMR examination of 5-substituted polychlorobicyclo[2.2.1]heptenes. The assignment of the C_5-*endo* and *exo* isomers by means of the ^{13}C NMR spectra is one of the purpose of the present investigation. Discussion will also be focused on the evidence of the interaction of the pi-electrons with a carbon-chlorine dipole.

Results and Discussion

The compounds employed in this work were synthesized by the usual Diels-Alder reactions and are listed in the Scheme. The proton chemical shifts of the compounds have been given elsewhere.[6] All the compounds gave nicely resolved ^{13}C NMR spectra. In most instances, the assignment of the signals to specific carbons was straightforward on the basis of the earlier results,[1-3] together with off-resonance decoupled spectra. In some cases, however, the assignment was made by using the substituent parameters of Lippmaa *et al.*[1]

Substituent Effect. The introduction of chlorine atoms onto C_1, C_4, and C_7 induced a pronounced paramagnetic effect on the substituted atoms and the neighbors. However, the chlorine atoms on C_2 and C_3 exerted a diamagnetic influence on the shifts of the substituted sp^2 carbon atoms.

For compounds **1** and **1'**, three carbons are in γ-positions with respect to the 5-substituent, and the orientation of the substituent affects the shieldings of the γ-carbon atoms (C_1, C_3, and C_7). The steric perturbation caused by the 5-substituent can be anticipated at C_3 by

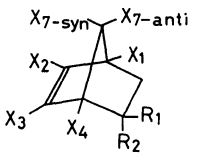

	X_1	X_2	X_3	X_4	X_7 (*syn*)	X_7 (*anti*)	R_1	R_2
1n	H	H	H	H	H	H	H	CO_2Me
1x	H	H	H	H	H	H	CO_2Me	H
2n	Cl	Cl	Cl	Cl	H	H	H	CO_2Me
2x	Cl	Cl	Cl	Cl	H	H	CO_2Me	H
3n	Cl	Cl	Cl	Cl	H	Cl	H	CO_2Me
4n	Cl	Cl	Cl	Cl	Cl	H	H	CO_2Me
4x	Cl	Cl	Cl	Cl	Cl	H	CO_2Me	H
5n	Cl	Cl	Cl	Cl	Cl	Cl	H	CO_2Me
1'n	H	H	H	H	H	H	H	CN
1'x	H	H	H	H	H	H	CN	H
2'n	Cl	Cl	Cl	Cl	H	H	H	CN
2'x	Cl	Cl	Cl	Cl	H	H	CN	H
5'n	Cl	Cl	Cl	Cl	Cl	Cl	H	CN
5'x	Cl	Cl	Cl	Cl	Cl	Cl	CN	H

Scheme 1.

the *endo* 5-substituent, and at C_7 by the *exo* one. Thus, for each *endo* isomer, the C_3 resonance appeared at a higher field than the C_3 of the corresponding *exo* isomer. This shielding effect of the *endo* 5-substituent decreased with the increase in the numbers of the chlorine substituents. On the contrary, the C_7 nuclei were indeed shielded by the *exo* 5-substituent, while the *endo* 5-substituent appeared to cause a slight deshielding of the C_7 atoms.[7] These effects increased in the presence of the chlorine substituents (except for **5'**). These differences, which are real but small, may provide an approach for the assignment of the *endo-exo* isomer pairs.

Pi Electron-Dipole Interaction. The observed high-field shifts of the C_2 and C_3 carbons of the polychloro derivatives can be explained in terms of the electromeric effect of the chlorine atoms.[8] Particularly, the pentachloro derivative with the *anti* chlorine atom on C_7(**3n**) exhibited both the C_2 and C_3 signals at lower fields than the corresponding 7-syn-Cl isomer (**4n**) did. In contrast, the C_7 of **3n** was observed at a higher field than that of **4n**. Because the usual inductive and electromeric effects of the chlorine atom are expected to be quite similar for **3n** and **4n**, and because the double-bond anisotropy can not explain the difference in the bridged methylene ^{13}C chemical shifts of these compounds, this observation implies the operation of some sort of charge delocalization from the double bond to the C_7 carbon atom of the *anti* isomer(**3n**). The high solvolytic reactivity of *anti*-7-norbornenyl chloride has been interpreted in terms of pi-participation. In this connection, Chihara[4] reported the ^{35}Cl NQR frequencies of *anti*-7-

Table 1. Carbon-13 chemical shifts of bicyclo[2.2.1] heptene derivatives (ppm from TMS)

Compound	C_1	C_2	C_3	C_4	C_5	C_6	C_7	CO_2–CH_3	
1n	42.7	137.5	132.7	45.7	43.2	29.4	49.7	173.6	51.1
1x	41.8	138.1	135.9	46.6	42.8	30.4	46.5	175.2	51.3
2n	69.3	134.5	131.5	72.2	54.0	41.8	63.9	169.2	52.4
2x	68.8	136.3	133.8	72.4	51.9	43.6	57.9	170.8	52.4
3n	72.5	133.4	130.7	75.1	51.1	38.5	77.7	169.0	52.5
4n	73.8	131.6	128.6	76.6	50.9	39.0	80.6	168.6	52.8
4x	73.3	133.3	130.8	76.9	50.0	40.8	76.3	170.4	52.9
5n	78.6	132.5	129.7	81.0	50.5	38.3	102.7	168.3	52.7
								CN	
1'n	42.5	138.7	133.0	45.8	27.1	32.5	48.6	122.1	
1'x	42.0	138.1	134.4	47.6	27.4	32.3	47.4	122.2	
2'n	68.6	135.5	132.2	71.4	41.0	43.6	61.5	116.4	
2'x	68.4	136.2	132.2	71.4	39.5	44.2	59.5	117.0	
5'n	78.2	133.6	130.6	80.5	38.3	40.5	100.7	115.2	
5'x	78.3	133.8	131.7	79.7	36.9	39.0	100.2	114.7	

and *syn*-7-norbornenyl chlorides. The results clearly showed that the s-character of the carbon orbital in the C–Cl bond of the latter was larger than that of the former. This conclusion agrees with the ^{13}C chemical shifts and $J_{^{13}C-H}$ values of the C_7 carbon atoms.[9,10] Since this pi-participation involves the transfer of the charge from the double bond to the polarized C_7–Cl bond, this participation may be inhibited by the chlorine substituents on C_2 and C_3, which make the double bond less nucleophilic. The difference in the ^{13}C chemical shift of C_7 between **3n** and **4n** is 2.9 ppm, whereas that between *anti*-7- and *syn*-7-norbornenyl chlorides is 5.4 ppm;[10] this indicates a weaker pi-participation for the 2,3-dichlorinated derivative, **3n**.

Experimental

All the ^{13}C NMR spectra were recorded on a JEOL PS-100 FT spectrometer. The chemical shifts were recorded in ppm from TMS. The compounds employed in this work were prepared from the corresponding dienes and methyl acrylate or acrylonitrile by the Diels-Alder reaction. The details were reported elsewhere.[6] Each isomeric adduct was obtained by preparative glc using a Yanagimoto GCG-3 or a Shimadzu GC-6A gas chromatograph.

References

1) E. L. Lippmaa, T. Pehk, J. Paasivirta, N. Belikova, and A. Plate, *Org. Magn. Reson.*, **2**, 581 (1970).
2) J. B. Grutzner, M. Jautelat, J. B. Dence, R. A. Smith, and J. D. Roberts, *J. Am. Chem. Soc.*, **92**, 7107 (1970).
3) J. B. Stothers, C. T. Tan, and K. C. Teo, *Can. J. Chem.*, **51**, 2893 (1973).
4) H. Chihara and N. Nakamura, *Bull. Chem. Soc. Jpn.*, **42**, 3034 (1969).
5) M. J. S. Dewar, M. L. Herr, and A. P. Marchand, *Tetrahedron*, **27**, 2371 (1971).
6) K. Seguchi, A. Sera, and K. Maruyama, *Bull. Chem. Soc. Jpn.*, **49**, 3558 (1976).
7) The reported chemical shifts for bicyclo[2.2.1]heptene: C_1, 41.8; C_2, 135.2; C_5, 24.6; C_7, 48.5 ppm.[3]
8) G. Miyajima and K. Takahashi, *J. Phys. Chem.*, **75**, 331 (1971).
9) The ^{13}C–H coupling constants were found to be 175 and 166 Hz for **3n** and **4n**, respectively.
10) Private communication from Dr. Kazuo Tori, Research Laboratory, Shionogi and Co., Ltd.: for *anti*-7-chlorobicyclo-[2.2.1]heptene; C_2, 135.4; C_7, 68.2 ppm; $J_{^{13}C-H}$ of C_7, 165.5 Hz: for the *syn*-7 isomer; C_2, 132.0; C_7, 73.6 ppm; $J_{^{13}C-H}$ of C_7, 157.0 Hz.

Selectivity in the *N*- and/or *C*-Alkylation of Schiff Bases Catalyzed by Crown Ether

Sadatoshi AKABORI,* Michiko OHTOMI, Kazuhide SHIMADA, and Ayami TAKEMURA

Department of Chemistry, Faculty of Science, Toho University, Funabashi, Chiba 274

(Received September 3, 1980)

Synopsis. The reaction of anions derived from Schiff bases (*N*-(α-methylbenzylidene)aniline and *N*-cyclohexylideneaniline) with ethyl iodide or diethyl sulfate in aprotic solvents, in the presence of 18-crown-6, is found to give a high ratio of $N/(N+C)$ or $C/(N+C)$ alkylation when conducted in benzene or in dioxane.

It is well known that the separation of ion-pairs and thus the anion activation can be obtained through the selective complexation of cations by organic ligands. This is dramatically shown by the enhancement in reaction rates by addition of crown ethers[1] and cryptands to homogeneous or heterogeneous reaction media. In previous papers,[2,3] we have shown that alkylation of sodium 2-naphtholate and sodium phenolate, in the presence of macrocyclic polyethers, is found to give high ratios of $O/(O+C)$ alkylation when conducted in aprotic solvents and in water. Heiszwolf *et al.*[4] found that ambident anions, derived from the reaction of a Schiff base with a strong base, could be alkylated with alkyl halide or dialkyl sulfate in aprotic solvents and that the nature of the solvent and of the alkylating agent played a decisive role in determining the reaction course of the ambident anion. Thus, in analogy with sodium phenolate or sodium 2-naphtholate,[2,3] it may be expected that in the presence of these macrocyclic polyethers the alkylation in solvents having low dielectric constants will result in predominant formation of the *N*- or *C*-alkylation product. Therefore, we have investigated the effect of 18-crown-6 on the yield and on the $N/(N+C)$ ratios of alkylation products in the reaction of anions (**2**), derived from Schiff bases, with ethyl iodide and diethyl sulfate under mild reaction conditions.

The following alkylations of ambident anions (**2a** and **2b**) derived from Schiff bases (**1a** and **1b**) with ethyl iodide or diethyl sulfate were run in aprotic solvents with or without added 18-crown-6 at appropriate temperatures. Table 1 summarizes the results of alkylation, where the effects of 18-crown-6 on the yields and on the $N/(N+C)$ ratios of the products can be seen. As the data in Table 1 show, the addition of 18-crown-6 to the reaction mixtures affects the $N/(N+C)$ ratios of the products to remarkable extents. In the absence of 18-crown-6, the reaction of Schiff base with ethyl iodide in benzene gave no alkylation products, whereas in the presence of 18-crown-6 the reaction occurs to give the *C*-alkyl derivative as the main product. These results may be interpreted on the basis that ionization of **1a** did not occur due to the low solubility of sodium hydride in benzene. Indeed, we could not observe any deep color change of the reaction mixture due to ambident anion formation when the reaction of **1a** with sodium hydride was carried out in benzene for several h at 80 °C. Furthermore, in the presence of 18-crown-6, the reactivity of the carbon site is enhanced relative to that of the nitrogen site of the ambident anion. These results can be explained as follows. Sodium hydride is solubilized in benzene to produce a "crowned" ion pair, in which Na^+ is linked coordinately to both the crown ether and the more electronegative nitrogen atom of the ambident anion. But the possibility of *C*-alkylation due to formation of a free naked anion cannot be ruled out. The *C*-alkylation is thought to take place as the main process.

In the reaction of the ambident anion (**2**) with diethyl sulfate in dioxane, the $N/(N+C)$ alkylation ratio is rather low; however, in the presence of 18-crown-6, the reaction under similar conditions gives a high yield of the *N*-alkylation, together with a low yield of the *C*-alkylation. These finding suggest that in the absence of 18-crown-6, the ambident anion (**2**), in analogy with sodium naphtholate[2] in dioxane and THF, exists as ion pairs and aggregates of a relatively high order; in the presence of 18-crown-6, however, the resulting ambident anion exists as an almost free anion due to solvation of the "crowned" sodium cation by dioxane because of the *N*-alkylation takes place. In support of this

Table 1. Alkylation of schiff bases[a]

Substrate	Alkylating agent	Solvent	18-Crown-6	Ionization time / h	Ionization temp / °C	Products, Yield/%[b] *C*-alkylation		*N*-alkylation		Total	$N/N+C$ ratio
1a	EtI	C_6H_6	presence	25	80	**3a**	58	**4a**	5	63	0.08
1a	EtI	C_6H_6	absence	25	80	**3a**	0	**4a**	0	0	
1a	Et_2SO_4	dioxane	presence	2	80	**3a**	5	**4a**	68	73	0.93
1a	Et_2SO_4	dioxane	absence	4	80	**3a**	56	**4a**	6	62	0.10
1b	EtI	C_6H_6	presence	16	80	**3b**	67	**4b**	11	78	0.14
1b	EtI	C_6H_6	absence	16	80	**3b**	0	**4b**	0	0	
1b	Et_2SO_4	dioxane	presence	2	100	**3b**	7	**4b**	84	91	0.92
1b	Et_2SO_4	dioxane	absence	2	100	**3b**	52	**4b**	19	71	0.27

a) The alkylations of ambident anions with ethyl iodide or diethyl sulfate were carried out at 15 °C for 60 min. b) These results were obtained by GLC.

explanation, the reaction in Diglyme, in which the dissociation of sodio-derivative (**2**) takes place, fails to show any effect of the 18-crown-6 on the product ratio. It is quite remarkable that *C*-alkylation of Schiff bases proceeds smoothly to afford **3a** and **3b** in good yields. Furthermore, in the case of **1b**, the yield of *N*-alkylation products **4b** (84%) was higher than the yield reported from the described procedures,[4] whereas for **1a** yields were relatively low compared with those obtained by reported methods. Our method, however, requires milder conditions of the reaction than alkylation by means of Et_3OBF_4 in Ethyl Cellosolve and ethyl iodide in xylene.[4]

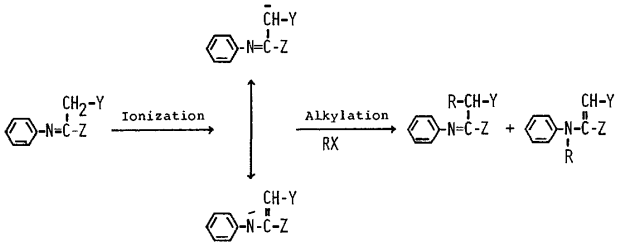

1a Y=H, Z=C_6H_5 **3a** Y=H, Z=C_6H_5
1b Y,Z=$-(CH_2)_4-$ **3b** Y,Z=$-(CH_2)_4-$
2a Y=H, Z=C_6H_5 **4a** Y=H, Z=C_6H_5
2b Y,Z=$-(CH_2)_4-$ **4b** Y,Z=$-(CH_2)_4-$

Experimental

The products were analyzed on a Hitachi-023 gas chromatography equipped with a flame-ionization detector. We used a 2 m×3 mm stainless steel column packed with 60—80 mesh Chromosorb-W NAW (washed with acid and treated with dimethyldichlorosilane) coated with 20% Apiezon-T (for the analysis of alkylation products of *N*-(α-methylbenzylidene)-aniline at *ca.* 222 °C) or a 1 m×3 mm stainless steel column packed with 60—80 mesh Chromosorb-W NAW (washed with acid and treated with dimethyldichlorosilane) coated with 20% Versamide (for the analysis of alkylation products of *N*-cyclohexylideneaniline at *ca.* 140 °C).

Materials. *N*-(α-methylbenzylidene)aniline,[5] *N*-cyclohexylideneaniline,[5] and authentic samples (*N*-(α-propylbenzylidene)aniline,[5] *N*-ethyl-*N*-(α-methylbenzylidene)-aniline,[6] *N*-(2-ethylcyclohexylidene)aniline[5] and *N*-(1-cyclohexenyl)-*N*-ethylaniline[6]) were prepared according to the procedures described in the literature. Sodium hydride and 18-crown-6 were of commercial origin and were used without further purification. Ethyl iodide and diethyl sulfate were purified by distillation, as were the solvents.

General Procedure. Typical procedures for the reaction of ethyl iodide or diethyl sulfate with *N*-(α-methylbenzylidene)-aniline and *N*-cyclohexylideneaniline follow.

Alkylation of N-*(α-Methylbenzylidene)aniline with Ethyl Iodide in Benzene.* Into a 50 ml round-bottomed flask equipped with a magnetic stirring bar, 60% sodium hydride in oil (7.5 mmol), *N*-(α-methylbenzylidene)aniline (6.2 mmol), 18-crown-6 (7.6 mmol), and 13 ml of benzene were introduced. The reaction mixture was stirred at 80 °C. There was evolution of hydrogen, which ceased after 25 h. The resulting turbid brown solution was cooled to 15 °C and ethyl iodide (13 mmol) was added with cooling. The color changed to light yellow at the end of the addition. The reaction mixture was stirred for a further 1.0 h and then filtered to remove inorganic salts and the filtrate was analyzed by GLC. GLC analysis revealed the presence of three components, which were identified as **4a** (5%), unreacted Schiff base **1a** (37%), and **3a** (58%); the relative retention times of these three components were 1.00 : 1.08 : 1.30.

Alkylation of N-*cyclohexylideneaniline with Ethyl Iodide in Benzene.* A solution of **1b** (9.2 mmol) and 18-crown-6 (9.1 mmol) in 20 ml of benzene was stirred with 60% sodium hydride in oil (13 mmol) at 80 °C for 16 h. There was evolution of hydrogen, which ceased after 16 h. The resulting turbid yellow-brown solution was then cooled to 15 °C and treated with diethyl sulfate (9.3 mmol). The color changed to light yellow at the end of the addition of diethyl sulfate. After the reaction mixture was stirred for 10 h, the inorganic salts were filtered off and the filtrate was analyzed by GLC. The analysis by GLC revealed the presence of **4b** (11%), **1b** (18%), and **3b** (67%); the relative retention times of these compounds were 1.00 : 0.28 : 1.20.

References

1) C. J. Pedersen and H. K. Frensdorff, *Angew. Chem. Int. Ed.*, **11**, 16 (1972); J. J. Christensen, D. J. Eatough, and R. M. Izatt, *Chem. Rev.*, **75**, 351 (1974).

2) S. Akabori and H. Tuji, *Bull. Chem. Soc. Jpn.*, **51**, 1197 (1978).

3) S. Akabori, S. Miyamoto, and H. Tanabe, *J. Polym. Sci. Polym. Lett. Ed.*, **16**, 533 (1978); S. Akabori, S. Miyamoto, and H. Tanabe, *J. Polym. Sci. Polym. Chem. Ed.*, **17**, 3933 (1979).

4) S. J. Heiszwolf and H. Kloosterziel, *Rec. Trav. Chim.*, **89**, 1217 (1970).

5) G. Reddelien, *Ber.*, **43**, 2476 (1910).

6) J. Hoch, *C.R. Acad. Sci.*, **200**, 938 (1935).

Azadi-π-methane Rearrangement Involving an Oxime Group

Makoto NITTA,* Ichiro KASAHARA, and Tomoshige KOBAYASHI

Department of Chemistry, School of Science and Engineering, Waseda University, Shinjuku-ku, Tokyo 160

(Received September 3, 1980)

Synopsis. Photoreaction of *exo*-6-methoxy-1,5,6-trimethyl or *exo*-6-methoxy-1,3,5,6-tetramethyltricyclo[3.2.1.-$0^{2,7}$]oct-3-en-8-one oxime underwent azadi-π-methane rearrangement leading to endo-7-methoxy-2,6,7-trimethyl or endo-7-methoxy-1,2,6,7-tetramethyltetracyclo[3.3.0.0.$^{2,8}0^{4,6}$]octan-3-one oxime. However, the one-carbon ring enlarged 5,8-dimethyl-9-methylenetricyclo[3.3.1.$0^{2,8}$]nona-3-en-6-one oxime underwent photo-Beckmann rearrangement to afford 5-aza-2,6-dimethyl-10-methylenetricyclo[4.3.1.$0^{2,9}$]deca-7-en-4-one.

Oximes undergo photoreactions leading to nitriles[1] or oxaziridine which rearranges to amides and/or lactams (photo-Beckmann rearrangement).[2] In a previous paper, we reported the photochemical reaction of 1,5-dimethyl- and 1,3,5-trimethyl-6-methylenetricyclo[3.2.1.$0^{2,7}$]oct-3-en-8-one oximes (**1a** and **1b**). These compounds underwent two types of di-π-methane rearrangement to afford **2a**, **2b**, and **2c**. The former two photoproducts are considered to be derived from the azadi-π-methane rearrangement involving the oxime moiety.[3] To examine the complementary effect of the ring size and chromophore on the azadi-π-methane rearrangement, we investigated the photochemistry of *exo*-6-methoxy-1,5,6-trimethyl and *exo*-6-methoxy-1,3,5,-6-tetramethyltricyclo[3.2.1.$0^{2,7}$]oct-3-en-8-one oximes (**3a** and **3b**) and 5,8-dimethyl-9-methylenetricyclo-[3.3.1.$0^{2,8}$]nona-3-en-6-one oxime (**4**), which is an one-carbon ring enlarged oxime of **1a**.

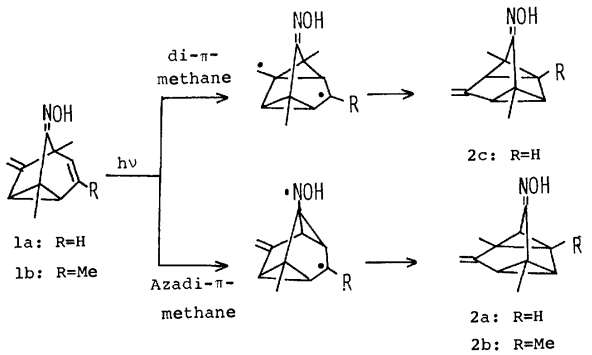

Scheme 1.

The required oximes **3a**, **3b**, and **4** were synthesized from the known ketones by the standard method (see Experimental). Direct preparative irradiation of **3a** and **3b** in anhydrous acetonitrile with 254 nm lamps afforded **8a** and **8b** in 20% and 57% yields, respectively. The NMR spectrum of **8a** exhibited four protons of cyclopropane ring at δ 1.90 (d, J=6.0 Hz), 1.92 (d, J=6.0 Hz), 2.25 (d, J=6.0 Hz), 2.29 (d, J=6.0 Hz) and hydroxyl proton at δ 8.90 (broad s) in addition to the protons of three methyl groups and methoxyl group at δ 1.09, 1.17, 1.35, and 3.26. The NMR spectrum of **8b** exhibited three protons of cyclopropane ring at δ 1.44 (d, J=6.0 Hz), 1.82 (d, J=6.0 Hz), 2.04 (s) and hydroxyl proton at δ 8.20 (broad s), in addition to the protons of four methyl groups and methoxyl group at δ 1.06, 1.20, 1.29, 1.35, and 3.29. These chemical shifts, the coupling patterns of these photoproducts, and the comparison of these data with those of **2a**, **b**, **c**[3] and their related compounds[7] are in good agreement with the proposed structures. The formations of **8a**, **b** are ascribed to be an azadi-π-methane rearrangement involving the oxime group. Since the photorearrangement did not proceed in the presence of acetophenone or acetone as the sensitizer, the singlet excited state might be involved in the photorearrangement of **3a**, **b**.

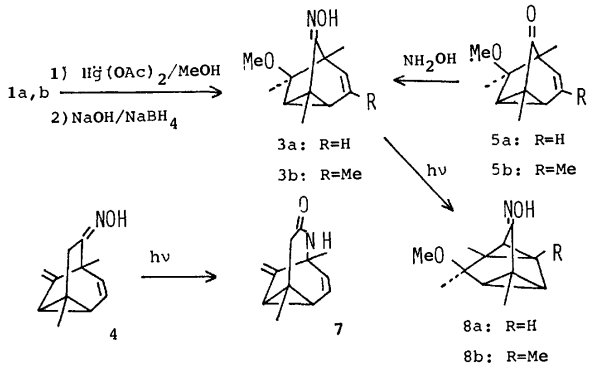

Scheme 2.

On the other hand, the direct irradiation of **4** in anhydrous acetonitrile with 254 nm lamps afforded 5-aza-2,6-dimethyl-10-methylenetricyclo[4.3.1.$0^{2,9}$]deca-7-en-4-one (**7**) in 60% yield. The absorption due to a carbonyl group at 1695 cm^{-1} suggests the existence of an amide function. The NMR spectrum of **7** exhibited the existence of a divinylcyclopropane moiety (see Experimental) similar to **4**. Each signal and coupling constant could be assigned with the help of a decoupling technique. The relatively high chemical shift at δ 2.44 (2H, s) for hydrogens of methylene group is suggestive of α-methylene of carbonyl group;[2d,e] thus the structure of **7** was deduced. This photoproduct **7** might be derived from the intermediate of oxaziridine and subsequent photoinduced migration of an alkyl group.[2]

The oximes **3a**, **b** which have azadi-π-methane systems in similar skeletons to the oxime **1a**, **b** underwent azadi-π-methane rearrangement. An attempted photoreaction of bicyclo[2.2.1]hept-2-en-5-isopropylimine did not undergo azadi-π-methane rearrangement.[8] As is shown in the present study, the oxime **4** which has two di-π-methane systems in the one-carbon ring enlarged skeleton, underwent photo-Beckmann rearrangement. The present results provide a complementary support for the first example of azadi-π-methane rearrangement of **1a**, **b**[3] as well as suggesting that the azadi-π-methane rearrangement might be controlled by the effect of suitable chromophoric interaction and/or the rigidity of the molecular framework.

Experimental

Preparation of exo-*6-Methoxy-1,5,6-trimethyltricyclo[3.2.1.0^{2,7}]-oct-3-en-8-one Oxime (***3a***).* *Method A*: To the stirred solution of mercury (II) acetate (6.4 g, 20 mmol) in anhydrous methanol (40 cm^3) was added **1a** (3.5 g, 20 mmol). After 30 min, 20 cm^3 of 3 mol dm^{-3} aqueous sodium hydroxide, then 380 mg (10 mmol) of sodium borohydride in 20 cm^3 of 3 mol dm^{-3} aqueous sodium hydroxide were added to the reaction mixture. This reaction mixture was stirred an additional 15 min and extracted with ether. The dried (Na_2SO_4) organic portion was evaporated *in vacuo*, and the residue was separated by preparative TLC on alumina with chloroform as the eluent. The first band from the TLC plates gave a colorless crystalline solid of **3a**: mp 161—163 °C (from EtOH); IR ($CHCl_3$): 3580, 1680, 1115 cm^{-1}; NMR ($CDCl_3$): δ 1.00 (3H, s), 1.06 (3H, s), 1.8—2.0 (2H, m), 1.68 (3H, s), 3.32 (3H, s), 5.45 (1H, d×d, J=9.0, 3.5 Hz), 5.96 (1H, d×d, J=9.0, 5.0 Hz), 8.54 (1H, broad s); UV (EtOH): 240 nm (end absorption, ε 4000); MS *m/e* (rel intensity): 207 (38, M$^+$), 43 (100). Found: C, 69.43; H, 8.00; N, 6.74%. Calcd for $C_{12}H_{17}O_2N$: C, 69.54; H, 8.27; N, 6.76%.

Method B: The mixture of **5a**[4,5] (1.78 g, 9.3 mmol), hydroxylamine hydrochloride (1.3 g, 18.6 mmol), and 5 cm^3 of pyridine was heated for 4 h at 100 °C. The reaction mixture was then poured into 50 cm^3 of water, followed by ether extraction. The dried (Na_2SO_4) ethereal portion was filtered and evaporated *in vacuo* to give 1.35 g (70%) of **3a**.

Preparation of exo-*6-Methoxy-1,3,5,6-tetramethyltricyclo[3.2.1.-0^{2,7}]oct-3-en-8-one Oxime (***3b***).* *Method A*: Exactly the same procedure as *Method A* in the case of **3a** was applied to **1b**. The colorless crystalline solid of **3b** (47%) was obtained: mp 162—163 °C (from EtOH); IR (KBr): 3226, 1686, 1111 cm^{-1}; NMR ($CDCl_3$): δ 1.00 (3H, s), 1.03 (3H, s), 1.29 (1H, d, J=6.0 Hz), 1.68 (3H, s), 1.70 (overlapped with methyl signal, 1H), 1.80 (3H, s), 3.31 (3H, s), 5.13 (1H, m), 8.35 (1H, broad s); UV (EtOH): 230 nm (end absorption, ε, 3900); MS *m/e* (rel intensity): 221 (10, M$^+$), 188 (100). Found: C, 70.21; H, 8.51; N, 6.14%. Calcd for $C_{13}H_{19}O_2N$: C, 70.55; H, 8.65; N, 6.33%.

Method B: Exactly the same procedure as *Method B* in the case of **3a** was applied to **5b**,[5] and **3b** was obtained in 65% yield.

Irradiation of **3a**. A solution of **3a** (240 mg, 0.76 mmol) in a quartz vessel with 254 nm lamps (Rayonet Photoreactor, MGR-100) in a nitrogen atmosphere. After removal of the solvent, the residue was separated by preparative TLC on alumina with chloroform–ethyl acetate (5/2) as the eluent to give 11 mg of **3a** and colorless crystals of **8a** (146 mg, 20%): mp 119—120 °C (from EtOH); IR ($CHCl_3$): 1580, 1115 cm^{-1}; NMR ($CDCl_3$): δ 1.09 (3H, s), 1.17 (3H, s), 1.35 (3H, s), 1.90 (1H, d, J=6.0 Hz), 1.92 (1H, d, J=6.0 Hz), 2.25 (1H, d, J=6.0 Hz), 2.29 (1H, d, J=6.0 Hz), 3.26 (3H, s), 8.90 (1H, broad s); MS *m/e* (rel intensity): 207 (6, M$^+$), 160 (100). Found: C, 69.46; H, 8.63; N, 6.95%. Calcd for $C_{12}H_{17}O_2N$: C, 69.54; H, 8.27; N, 6.76%.

Irradiation of **3b**. A solution of **3b** (150 mg, 0.68 mmol) in anhydrous acetonitrile (50 cm^3) was irradiated for 3.6 h in a quartz vessel with 254 nm lamps in a nitrogen atmosphere. After removal of the solvent, the residue was separated by preparative TLC on silica gel with chloroform–ethyl acetate (5/2) as the eluent to give 85 mg (57%) of **8b**: mp 118—120 °C (from EtOH); IR ($CHCl_3$): 1580, 1115 cm^{-1}; NMR ($CDCl_3$): δ 1.06 (3H, s), 1.20 (3H, s), 1.29 (3H, s), 1.35 (3H, s), 1.44 (1H, d, J=6.0 Hz), 1.82 (1H, d, J=6.0 Hz), 2.04 (1H, s), 3.29 (1H, s), 8.20 (1H, broad s); MS *m/e* (rel intensity): 221 (3, M$^+$), 190 (100). Found: C, 70.94; H, 8.27; N, 6.36%. Calcd for $C_{13}H_{19}O_2N$: C, 70.55; H, 8.65; N, 6.33%.

Irradiation of **4**. A solution of **4**[6] (150 mg, 0.8 mmol) in anhydrous acetonitrile (50 cm^3) was irradiated for 3 h in a quartz vessel with 254 nm lamps in a nitrogen atmosphere. After removal of the solvent, the residue was separated by preparative TLC on silica gel with chloroform as the eluent. The first band from the TLC plates contained **7** (68 mg, 60% based on consumed **4**): mp 139—140 °C (from EtOH); IR ($CHCl_3$): 3290, 1695 cm^{-1}; NMR ($CDCl_3$): δ 1.06 (6H, s), 2.25 (1H, t, J=6.0 Hz), 2.41 (1H, d, J=6.0 Hz), 2.44 (2H, s), 4.77 (1H, s), 4.90 (1H, s), 5.88 (1H, d×d, J=8.0, 6.0 Hz), 6.26 (1H, broad d, J=8.0 Hz), 8.95 (1H, broad s); MS *m/e* (rel intensity): 189 (5, M$^+$), 131 (100). Found: C, 76.45; H, 7.92; N, 7.02%. Calcd for $C_{12}H_{15}ON$: C, 76.15; H, 7.99; N, 7.40%.

Sensitized Irradiation of **3a**. Three Pyrex vessels, which contained **3a** (30 mg, 0.14 mmol) in (a) acetonitrile (10 cm^3), (b) acetone (10 cm^3), and (c) acetonitrile contained acetophenone (35 mg, 0.29 mmol) were irradiated with 300 nm lamps (Rayonet photoreactor, MGR-100) for 10 h in a nitrogen atmosphere. The reactions were monitored by GC (5% SE-30 on Rhromosorb W, 130 °C), but no new peak was observed. After removal of the solvents, each of the residues was purified by preparative TLC on alumina with chloroform as the eluent to give the starting oxime **3a** in 80% (a), 80% (b), and 90% (c) yield.

We thank the Science and Engineering Research Laboratory of Waseda University for their financial support.

References

1) a) T. Sato and H. Obase, *Tetrahedron Lett.*, **1967**, 1633; b) A. Stijilikovic and R. Tasovac, *Tetrahedron Lett.*, **1970**, 1405.

2) a) J. H. Amin and P. de Mayo, *Tetrahedron Lett.*, **1963**, 1585; b) I. Izawa and P. de Mayo, *Can. J. Chem.*, **47**, 51 (1969); c) T. Oine and T. Mukai, *Tetrahedron Lett.*, **1969**, 157; d) H. Suginome and H. Takahashi, *Bull. Chem. Soc. Jpn.*, **48**, 576 (1975); e) H. Suginome and F. Yagihashi, *J. Chem. Soc., Perkin Trans.* **1**, **1977** 2488 and references cited therein.

3) M. Nitta, O. Inoue, and M. Tada, *Chem. Lett.*, **1977**, 1065.

4) J. P-Katalinic, J. Zindely, and H. Schmid, *Helv. Chim. Acta*, **57**, 223 (1974).

5) M. Nitta, A. Omata, and H. Sugiyama, unpublished results.

6) M. Nitta, A. Omata, and H. Sugiyama, submitted to *Bull. Sci. Eng. Res. Rab.* (Waseda Univ).

7) M. Nitta, O. Inoue, and M. Tada, *Chem. Lett.*, **1977**, 59.

8) R. G. Weiss and G. S. Hammond, *J. Am. Chem. Soc.*, **100**, 1172 (1978).

Studies on Heterocyclic Analogs of Azulene. VIII.[1] Reaction of 2-Alkoxycyclohepta[*b*]pyrroles with Dimethyl Acetylenedicarboxylate

Noritaka ABE* and Tarozaemon NISHIWAKI

Department of Chemistry, Faculty of Sciences, Yamaguchi University, Yamaguchi 753

(Received October 16, 1980)

Synopsis. 2-Alkoxycyclohepta[*b*]pyrroles reacted with dimethyl acetylenedicarboxylate to give tetramethyl 2-alkoxy-3*H*-2a-azacyclopenta[*ef*]heptalene-3,4,5,6-tetracarboxylates in benzene and dialkyl 2-(2-alkoxycyclohepta[*b*]pyrrol-1-yl)fumarate in alcoholic solvents.

We have previously reported that ethyl 2-chlorocyclohepta[*b*]pyrrole-3-carboxylate (**1a**) reacts with dimethyl acetylenedicarboxylate (DMAD) in benzene giving 1-ethyl 3,4,5,6-tetramethyl 2-chloro-3*H*-2a-azacyclopenta[*ef*]heptalene-1,3,4,5,6-pentacarboxylate (**2a**) *via* a 1,8-dipolar intermediate.[2,3] As nature of substituents and/or reaction conditions appear to play important roles for the cycloadditions of nitrogen-heterocycles with DMAD,[4] we studied the reactions of 2-alkoxycyclohepta[*b*]pyrroles with DMAD in both of benzene and alcoholic solvents.

Treatment of ethyl 2-ethoxycyclohepta[*b*]pyrrole-3-carboxylate (**1b**) with an excess of DMAD in benzene gave 59% yield of 1-ethyl 3,4,5,6-tetramethyl 2-ethoxy-3*H*-2a-azacyclopenta[*ef*]heptalene-1,3,4,5,6-pentacarboxylate (**2b**) along with 29% yield of cyclohepta[*b*]-pyrrol-2(1*H*)-one (**3a**).[5] The structure of **2b** was assigned from the similarity of its spectroscopic properties with those of **2a**.[3] When the reaction of **1b** with DMAD was carried out in boiling abs MeOH, dimethyl 2-(3-ethoxycarbonyl-2-oxo-1,2-dihydrocyclohepta[*b*]pyrrol-1-yl)fumarate (**3b**) was obtained in 94% yield, whose structure was assigned by means of its spectroscopic properties as well as elemental analyses. The ester groups are presumed to have a (*E*)-configuration from the chemical shift of a vinyl proton ($\delta=7.40$) [*e.g.* the vinyl proton of dimethyl 2-(2-oxo-1,2-dihydro-1-pyridyl)fumarate is seen at $\delta=7.05$].[6] Reaction of **3a** with DMAD yielded **3b**, and this supports the structure. Compound **3b** was also obtained in excellent yield from the reaction of **1a** with DMAD in abs MeOH.

Whilst the reaction of 2-methoxycyclohepta[*b*]pyrrole-3-carbonitrile (**1d**) with DMAD in benzene proceeded less efficiently to give only 25% yield of **2c**, with 84% of the starting **1d** being recovered, the reaction in abs EtOH is accompanied by transesterification to furnish diethyl 2-(3-cyano-2-oxo-1,2-dihydrocyclohepta[*b*]pyrrol-1-yl)fumarate (**3d**) despite the absence of acidic or basic materials. Reaction of **3c** with diethyl acetylenedicarboxylate (DEAD) to give **3d**, and this supports the structure.

When the acetylenic ester was absent, **1** did no change in an alcoholic solvent.

It is obvious that the reactions of 2-alkoxycyclohepta[*b*]pyrroles with DMAD give a cycloadduct in benzene, but they follow a different course in alcohols. It is conceivable that the yilde (**4**) reacts with an alcohol to produce an acetal (**5**), which must be hydrolyzed to cyclohepta[*b*]pyrrol-2(1*H*)-one (**3**) by a trace amount of water fortuitously present in the reaction mixture.

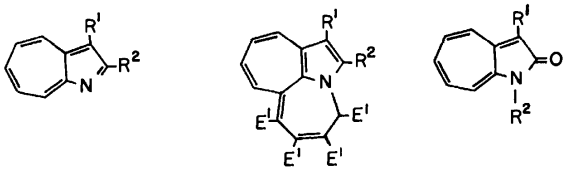

1 **2** **3**

$E^1=CO_2Me$, $E^2=CO_2Et$

1a: $R^1=E^2$, $R^2=Cl$
1b: $R^1=E^2$, $R^2=OEt$
1c: $R^1=CN$, $R^2=Cl$
1d: $R^1=CN$, $R^2=OMe$
2a: $R^1=E^2$, $R^2=Cl$
2b: $R^1=E^2$, $R^2=OEt$
2c: $R^1=CN$, $R^2=OMe$
3a: $R^1=E^2$, $R^2=H$
3b: $R^1=E^2$, $R^2=(E)$-$CE^1=CHE^1$
3c: $R^1=CN$, $R^2=H$
3d: $R^1=CN$, $R^2=(E)$-$CE^2=CHE^2$

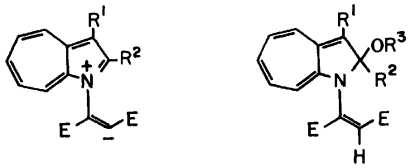

4 **5**

Experimental

Melting points were uncorrected. ^1H NMR spectra were taken with Hitachi R-24B spectrometer (60 MHz) for solutions in $CDCl_3$ with TMS as internal standard. UV spectra were measured for solutions in $CHCl_3$ and IR spectra for Nujol mulls. Kieselgel 60 was used for chromatography unless otherwise stated. Yields are based on consumed starting materials.

Synthesis of ***1b***. **1a** (1.00 g) was added to a sodium ethoxide solution prepared from Na (0.40 g) and abs EtOH (20 ml). The mixture was heated under reflux for 2 h, cooled, acidified with dil HCl, and extracted with chloroform. The extracts were washed with water, dried (Na_2SO_4), and evaporated. The residue was chromatographed on alumina with benzene–chloroform to give **1b** [0.914 g, 82%, yellow needles (from petroleum ether), mp 68—69 °C. UV_{max} 289 nm (log ε 4.67), 335 (3.82), 348 (3.71), 368 (3.61), 424 (3.27), 428 (3.26). IR 1675 cm^{-1} (C=O). ^1H NMR $\delta=1.45$ (3H, t, $J=7$ Hz, Me), 1.57 (3H, t, $J=7$ Hz, Me), 4.43 (2H, q, $J=7$ Hz, CH_2), 4.77 (2H, q, $J=7$ Hz, CH_2), 7.5—7.9 (3H, m, H-5,6,7), 8.15—8.4 (1H, m, H-8), 9.1—9.4 (1H, m, H-4). Found: C, 68.51; H, 6.20; N, 5.80%. Calcd for $C_{14}H_{15}NO_3$: C, 68.55; H, 6.16; N, 5.71%].

Synthesis of ***1d***. 2-Chlorocyclohepta[*b*]pyrrole-3-carbonitrile[7] (**1c**) (2.00 g) was added to a sodium methoxide solution prepared from Na (1.20 g) and abs MeOH (50 ml). The mixture was heated under reflux for 2 h and worked up as for **1b** to give **1d** [1.84 g, 94%, yellow needles (from MeOH), mp 186—187.5 °C. UV_{max} 285 nm (log ε 4.65), 334 (3.72), 347 (3.63), 369 (3.58), 423 (3.25), 430 (3.25). IR

2200 cm^{-1} (CN). ^1H NMR δ=4.32 (3H, s, OMe), 7.7—8.0 (3H, m, H-5,6,7), 8.2—8.5 (2H, m, H-4,8). Found: C, 71.68; H, 4.41; N, 15.25%. Calcd for $C_{11}H_8N_2O$: C, 71.73; H, 4.38; N, 15.21%].

Reaction of ***1b*** *with DMAD.* (*a*): A mixture of **1b** (1.00 g) and DMAD (4.06 g) in benzene (30 ml) was heated under reflux for 8 d. The solvent was evaporated and the residue was chromatographed with benzene–ethyl acetate (95 : 5) to give **1b** (0.305 g) followed by **2b** (0.873 g, 59%), which crystallized from cyclohexane as red prisms, mp 140—141 °C [UV_{max} 258 nm (log ε 4.37), 320^{sh} (3.89), 465 (4.01), IR 1740, 1730, 1710, and 1695 cm^{-1} (C=O), ^1H NMR δ= 1.37 (3H, t, J=7 Hz, Me), 1.41 (3H, t, J=7 Hz, Me), 3.72 (3H, s, OMe), 3.75 (3H, s, OMe), 3.83 (6H, s, OMe), 4.23 (2H, q, J=7 Hz, CH_2), 4.34 (2H, q, J=7 Hz, CH_2), 6.3—6.95 (3H, m, H-7,8,9), 6.48 (1H, s, H-3), 7.82 (1H, dd, J=10 and 3 Hz, H-10). Found: C, 49.51; H, 6.39; N, 3.18%. Calcd for $C_{26}H_{27}NO_{11}$: C, 49.43; H, 6.34; N, 3.26%]. Elution with ethyl acetate gave **3a** (0.147 g, 29%), yellow needles (from EtOH), mp 188.5—190 °C (lit,[5] mp 189—190 °C).

(*b*): A mixture of **1b** (1.00 g) and DMAD (4.06 g) in abs MeOH (50 ml) was heated under reflux for 4 d. The solvent was evaporated and the residue was chromatographed with benzene to give **1b** (0.13 g). Elution with chloroform gave **3b** (1.195 g, 94%), which crystallized from cyclohexane as yellow prisms, mp 119—121 °C [UV_{max} 277 nm (log ε 4.48), 432 (4.26), IR 1735, 1695, and 1670 cm^{-1} (C=O), ^1H NMR δ=1.42 (3H, t, J=7 Hz, Me), 3.63 (3H, s, OMe), 3.80 (3H, s, OMe), 4.43 (2H, q, J=7 Hz, CH_2), 6.8—7.75 (4H, m, H-5,6,7,8), 7.40 (1H, s, vinyl-H), 9.28 (1H, d, J=10 Hz, H-4). Found: C, 60.17; H, 4.78; N, 3.79%. Calcd for $C_{18}H_{17}NO_7$: C, 60.16; H, 4.77; N, 3.90%].

Reaction of ***3a*** *with DMAD.* A mixture of **3a** (1.00 g) and DMAD (2.00 g) in benzene (80 ml) was heated under reflux for 2 d. The solvent was evaporated and the residue was chromatographed with chloroform to give **3b** (1.030 g, 78%). Elution with ethyl acetate gave **3a** (0.205 g).

Reaction of ***1a*** *with DMAD.* A mixture of **1a** (1.00 g) and DMAD (4.22 g) in abs MeOH (40 ml) was heated under reflux for 6 h. The solvent was evaporated and the residue was chromatographed with chloroform to give **3b** (1.465 g, 98%).

Reaction of ***1d*** *with DMAD.* (*a*): A mixture of **1d** (1.00 g) and DMAD (4.00 g) in benzene (70 ml) was heated under reflux for 6 d. The solvent was evaporated and the residue was chromatographed with benzene–ethyl acetate (95 : 5) to give **1d** (0.837 g) followed by **2c** (0.101 g, 25%), which crystallized from cyclohexane as red needles, mp 101—103 °C [UV_{max} 285^{sh} nm (log ε 4.05), 459 (3.75), IR 2200 (CN) and 1740 and 1725 cm^{-1} (C=O), ^1H NMR δ=3.70 (3H, s, OMe), 3.73 (3H, s, OMe), 3.80 (6H, s, OMe), 4.30 (3H, s, OMe), 6.40 (1H, s, H-3), 6.7—7.1 (3H, m, H-7,8,9), 7.6—7.8 (1H, m, H-10). Found: C, 59.09; H, 4.39; N, 5.84%. Calcd for $C_{23}H_{20}N_2O_9$: C, 58.97; H, 4.30; N, 5.98%].

(*b*): A mixture of **1d** (0.500 g) and DMAD (2.00 g) in abs EtOH (70 ml) was heated under reflux for 2 d. The solvent was evapoated and the residue was chromatographed with benzene to give **1d** (0.140 g). Elution with benzene–chloroform (1 : 1) gave **3d** (0.367 g, 55%), which crystallized from ligroine–dichloromethane as yellow leaflets, mp 118—119 °C [UV_{max} 276 nm (log ε 4.37), 430 (4.10), IR 2210 (CN) and 1730 and 1690 cm^{-1} (C=O), ^1H NMR δ=1.13 (3H, t, J=7 Hz, Me), 1.29 (3H, t, J=7 Hz, Me), 4.12 (2H, q, J= 7 Hz, CH_2), 4.31 (2H, q, J=7 Hz, CH_2), 7.15—7.85 (4H, m, H-5,6,7,8), 7.40 (1H, s, vinyl-H), 7.93 (1H, d, J=10 Hz, H-4). Found: C, 63.76; H, 4.71; N, 8.46%. Calcd for $C_{18}H_{16}N_2O_5$: C, 63.52; H, 4.74; N, 8.23%]. Elution with MeOH gave **3c** (0.098 g, 29%), yellow needles (from ethyl acetate), mp 313 °C (lit.[7] mp 313 °C).

Reaction of ***3c*** *with DEAD.* A mixture of **3c** (0.100 g) and DEAD (0.35 g) in benzene (60 ml) was heated under reflux for 2 d and cooled. The product crystallized out of the solution was collected and recrystallized to give **3c** (0.087 g). The mother liquid was evaporated and the residue was chromatographed with chloroform to give **3d** (0.016 g, 80%). Elution with MeOH gave **3c** (0.003 g).

We thank Dr. Masafumi Yasunami, Tohoku University, for NMR spectral determination.

References

1) Part VII: N. Abe and T. Nishiwaki, *Bull. Chem. Soc. Jpn.*, **53**, 1773 (1980).

2) N. Abe, Y. Tanaka, and T. Nishiwaki, *J. Chem. Soc., Perkin Trans. 1*, **1978**, 429.

3) For a review in this field see T. Nishiwaki and N. Abe, *Heterocycles*, **15**, 547 (1981).

4) For a review see R. M. Acheson and N. F. Elmore, *Adv. Heterocycl. Chem.*, **23**, 263 (1978).

5) T. Nozoe, S. Seto, S. Matsumura, and T. Terasawa, *Chem. Ind.*, **1954**, 1356.

6) R. M. Acheson and P. A. Tasker, *J. Chem. Soc., C*, **1967**, 1542.

7) T. Nozoe, S. Seto, and S. Nozoe, *Proc. Jpn. Acad.*, **32**, 472 (1956).

Reduction of Ketones and Aldehydes *via* Catalytic Hydrosilylation Using Triethoxysilane and Trimethoxysilane

Hideyuki MATSUMOTO, Yoshikazu HOSHINO, and Yoichiro NAGAI*

Department of Chemistry, Gunma University, Kiryu, Gunma 376

(Received October 30, 1980)

Synopsis. It was found that ketones and aldehydes can be effectively reduced *via* catalytic hydrosilylation using triethoxysilane and trimethoxysilane in the presence of $RhCl(PPh_3)_3$ or $RuCl_2(PPh_3)_3$, followed by ethanolysis or methanolysis.

Reduction of carbonyl compounds *via* hydrosilylation catalyzed by group VIII metal complexes has been extensively investigated.[1,2] In most of the previous work alkyl- and arylsilanes were employed (*e.g.*, Et_3SiH, Et_2SiH_2, $PhMe_2SiH$, and Ph_2SiH_2, *etc.*), and only few examples of the corresponding hydrosilylation by alkoxysilanes have been reported to date.[3] Recently, it has been reported that trialkoxysilanes such as $(EtO)_3SiH$ and $(MeO)_3SiH$ can be readily prepared in large quantities by the direct reaction of silicon with the corresponding alcohols.[4] With such situation in view, we felt it pertinent to explore the reduction of carbonyl compounds by these trialkoxysilanes in some detail. We report herein our finding that various ketones and aldehydes can be smoothly hydrosilylated by $(EtO)_3SiH$ and $(MeO)_3SiH$ in the presence of $[RhCl(PPh_3)_3]$ or $[RuCl_2(PPh_3)_3]$ as catalyst and that alcoholysis of the resultant adducts with the respective alcohol gave desired reduction products in good yields.

$$R^1COR^2 + (R^3O)_3SiH \xrightarrow[\text{Ru(II)}]{\text{Rh(I) or}} R^1CH(OSi(OR^3)_3)R^2 \xrightarrow{R^3OH} R^1CH(OH)R^2 + (R^3O)_4Si \quad (1)$$

Results for the reduction of ketones and aldehydes studied in the present work are summarized in Table 1. The addition of $(EtO)_3SiH$ and $(MeO)_3SiH$ to diethyl ketone, cyclopentanone, cyclohexanone, acetophenone, and benzaldehyde was conducted using the ruthenium complex $[RuCl_2(PPh_3)_3]$ as a catalyst. The reaction in the presence of 0.5 mol% of the catalyst at temperatures of 60—120 °C reached completion after 3—10 h to give the corresponding adducts in high yields. It has been reported that the ruthenium(II) complex catalyzes the reaction of Et_3SiH and $Ph(1\text{-}C_{10}H_7)SiH_2$ with ketones (*e.g.*, acetophenone) and aldehydes (*e.g.*, benzaldehyde), but that it is not as effective a catalyst as $[RhCl(PPh_3)_3]$.[5] We found that this particular ruthenium complex is much more selective than the rhodium(I) complex in the present addition reactions. For instance, the ruthenium(II)-catalyzed reaction of $(EtO)_3SiH$ with acetophenone produced the adduct in 85% yield whereas the rhodium(I)-catalysis was accompanied by the concurrent formation of a considerable amount of the silyl enol ether.

$$PhCOCH_3 + (EtO)_3SiH \xrightarrow{\text{Rh(I)}} \underset{(40\%)}{PhCH(OSi(OEt)_3)CH_3} + \underset{(27\%)}{PhC(OSi(OEt)_3)=CH_2} \quad (2)$$

The desilylation of the resulting silyl enol ethers was also studied. The method commonly employed for the desilylation involves acid- or base-catalyzed hydrolysis.[2] However, this method would be inconvenient in the present case, because such procedure would result in the formation of a complex mixture of siloxanes. This

TABLE 1. REDUCTION OF KETONES AND ALDEHYDES *via* THE HYDROSILYLATION BY TRIETHOXYSILANE (A) OR TRIMETHOXYSILANE (B) IN THE PRESENCE OF $[RhCl(PPh_3)_3]$ OR $[RuCl_2(PPh_3)_3]$[a)]

Carbonyl compound	Silane	Conditions[b]	Product	Yield/%
$CH_3CH_2COCH_2CH_3$	A	Ru, 100 °C, 3 h	$CH_3CH_2CH(OH)CH_2CH_3$	88
	A	Ru, 60 °C, 5 h	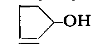	89
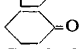	A	Ru, 100 °C, 10 h	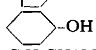	86
$C_6H_5COCH_3$	A	Ru, 120 °C, 10 h	$C_6H_5CH(OH)CH_3$	84
CH_5CHO	A	Ru, 120 °C, 6 h	CH_5CH_2OH	89
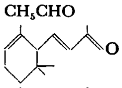	A	Rh, 50 °C, 2 h	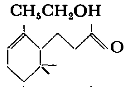	84
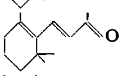	B	Rh, 60 °C, 4 h	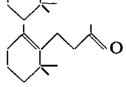	84(79)
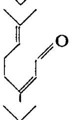	A	Rh, 70 °C, 3 h	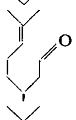	93
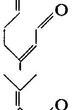	B	Rh, 70 °C, 5 h	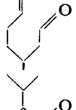	88(75)
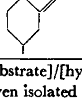	B	Rh, 80 °C, 4 h	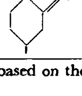	90

a) [Substrate]/[hydrosilane]/[catalyst] = 1/1.2/0.005. b) For hydrosilylation. c) Determined by GLC (based on the carbonyl compound charged); in parentheses are given isolated yields.

complication arises as a consequence of the high susceptibility of the ethoxyl and methoxyl groups on silicon to hydrolysis.[6] In fact, Kagan and coworkers obtained 1-Phenylethanol in at most 60% chemical yield (*via* GLC) from the reduction of acetophenone with $(EtO)_3SiH$ in the presence of a supported chiral rhodium complex after the treatment of the resulting silyl ether with an aqueous HCl–acetone solution.[3a] We found that the clean desilylation of the adducts of $(EtO)_3SiH$ or $(MeO)_3SiH$ can be achieved by ethanolysis or methanolysis in the presence of a catalytic amount of HCl or NaOH. The counter product, $(EtO)_4Si$ or $(MeO)_4Si$ can be readily removed by simple distillation in many cases. Thus, the corresponding alcohols were obtained in excellent yields *via* the hydrosilylation with the trialkoxysilanes.

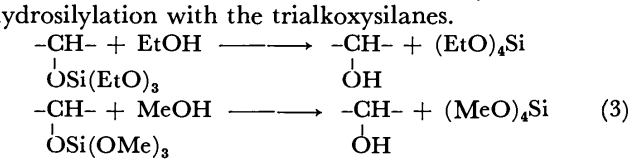

(3)

An attempt was also made to reduce α,β-unsaturated terpene carbonyl compounds with the trialkoxysilanes. The regioselective reduction of α,β-unsaturated terpene ketones and aldehydes *via* hydrosilylation catalyzed by $[RhCl(PPh_3)_3]$ was reported by Ojima and coworkers who found that the reduction with monohydrosilanes (*e.g.*, Et_3SiH) gave only or mainly saturated ketones *via* 1,4-addition while dihydrosilanes (*e.g.*, Et_2SiH_2) afforded allylic alcohols *via* 1,2-addition.[7] More recently, it has been also reported by Lappert and Nile that the hydrosilylation of *trans*-crotonaldehyde with $(EtO)_3SiH$ in the presence of $[RhCl(PPh_3)_3]$ proceeds

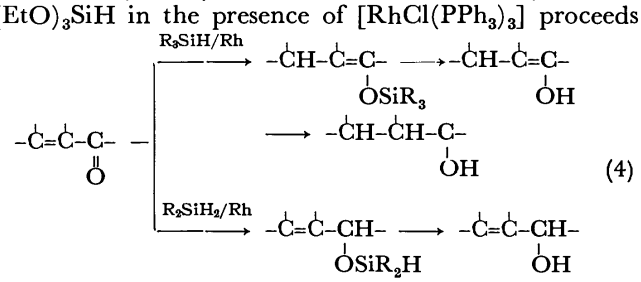

(4)

through 1,4-addition while the same reaction in the presence of $[Ni(COD)_2]$ takes place *via* 1,2-addition.[3b] We found that the rhodium(I)catalyzed hydrosilylation of several conjugated terpene enones with $(EtO)_3SiH$ or $(MeO)_3SiH$ also proceeded smoothly in a manner of 1,4-addition as in the case of the rhodium-catalyzed reduction of crotonaldehyde. Thus, the reduction of α-ionone, β-ionone, citral, and pulegone gave exclusively α-dihydroionone, β-dihydroionone, citronellal, and menthone in over 80% yields, respectively.

Incidentally, the reduction of α,β-unsaturated terpene ketones with trialkoxysilanes seems to show somewhat higher regioselectivity compared to that with triorganohydrosilanes; it was reported that the reduction of pulegone with Et_3SiH or $PhMe_2SiH$ gave a mixture of menthone and the allylic alcohol in a ratio of 50 : 50 or 75 : 25, respectively.[7]

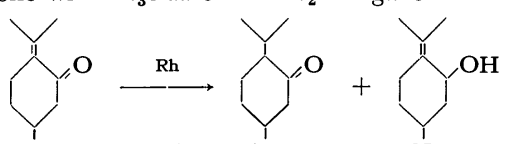

(5)

$PhMe_2SiH$	75	25
$(MeO)_3SiH$	100	0

Experimental

$(EtO)_3SiH$ and $(MeO)_3SiH$ were supplied by Mitsubishi Kasei Industry Co., Ltd. Ketones and aldehydes were commercially available and used without further purification. Ethanol and methanol were purified by standard methods.[8] The complexes $[RhCl(PPh_3)_3]$[9] and $[RuCl_2(PPh_3)_3]$[10] were prepared according to literature directions.

The following reduction products were identified by comparison of their physical properties (GLC retention times, and IR and NMR spectra) with those of commercial authentic samples or literature;[11] 3-pentanol, cyclopentanol, cyclohexanol, 1-phenylethanol, benzyl alcohol, α-dihydroionone, β-dihydroionone,[11] citronellal, and menthone.

General Procedure for the Reduction of Ketones and Aldehydes. All runs were conducted in essentially the same manner; therefore, only the reduction of β-ionone by $(MeO)_3SiH$ is described in detail.

A mixture of 9.7 g (50 mmol) of β-ionone, 7.4 g (60 mmol) of $(MeO)_3SiH$, and 0.23 g (0.25 mmol) of $[RhCl(PPh_3)_3]$ was heated at 60 °C for 4 h under nitrogen with stirring. The reaction mixture was then poured into methanol (30 ml) containing a small amount of sodium hydroxide, and the resulting mixture was stirred at room temperature for 12 h. GLC analysis of the mixture disclosed the formation of β-dihydroionone in 84% yield. Evaporation of the alcohol and subsequent distillation gave 7.3 g (79% yield) of the product boiling at 93 °C/5 mmHg[12] (lit,[11] bp. 105 °C/10 mmHg).

We thank Mitsubishi Kasei Industry Co., Ltd., for gifts of trialkoxysilane.

References

1) For reviews, see a) I. Ojima, K. Yamamoto, and M. Kumada, "Aspects of Homogeneous Catalysis," ed by R. Ugo, Reidel Publishing Co., (1977), Vol. 3, p. 186; b) I. Ojima, *J. Syn. Org. Chem. Jpn.*, **32**, 687 (1974); c) Y. Nagai, *Org. Prep. Proc. Intl.*, **12**, 13 (1980).

2) For recent reports, see a) R. J. P. Corriu and J. J. E. Moreau, *J. Organometal. Chem.*, **127**, 7 (1977); b) I. Ojima, T. Kogure, and M. Kumagai, *J. Org. Chem.*, **42**, 1671 (1977) and references cited therein; c) R. J. P. Corriu, J. Boyer, P. Perz, and C. Reye, *J. Organometal. Chem.*, **172**, 143 (1979).

3) a) W. Dumont, J.-C. Poulin, T.-P. Dang, and H.B. Kagan, *J. Am. Chem. Soc.*, **95**, 8295 (1973); b) M. F. Lappert and T. A. Nile, *J. Organometal. Chem.*, **102**, 543 (1975); c) A. J. Cornish, M. F. Lappert, G. L. Filatovs, and T. A. Nile, *J. Organometal. Chem.*, **172**, 153 (1979).

4) a) T. Suzuki, T. Imaki, and T. Yamaura, Jpn. Kokai, 55-2641 (1980); *Chem. Abstr.*, **93**, 71945 (1980); b) T. Suzuki, T. Imaki, and T. Yamaura, Jpn. Kokai, 55-11538, 55-28928, 55-28929 (1980); c) T. Imaki, T. Nakanome, and T. Yamaura, Jpn. Kokai, 55-33457 (1980).

5) a) C. Eaborn, K. Odell, and A. Pidcock, *J. Organometal. Chem.*, **63**, 93 (1973); b) R. J. P. Corriu and J. J. E. Moreau, *J.C.S. Chem. Comm.*, **1973**, 38.

6) C. Eaborn, "Organosilicon Compounds," Butterworths, London (1960), Chap. 6.

7) I. Ojima, T. Kogure, and Y. Nagai, *Tetrahedron Lett.*, **1972**, 5085.

8) J. A. Riddick and W. B. Bunger, "Organic Solvents," Wiley, New York (1980) p. 636.

9) J. A. Osborn, F. H. Jardine, J. F. Young, and G. Wilkinson, *J. Chem. Soc., A*, **1966**, 1711.

10) T. A. Stephenson and G. Wilkinson, *J. Inorg. Nucl. Chem.*, **28**, 945 (1966).

11) G. P. Boldrine and A. U. Ronchi, *Synthesis*, **1976**, 596.

12) 1 mmHg=13.595 1×980.665×10^{-2} Pa.

Ketone Synthesis from Acid Chloride by Means of Organometallic Reagent Derived from R_3Al-$Cu(acac)_2$-PPh_3 System

Kazuhiko TAKAI, Koichiro OSHIMA,* and Hitosi NOZAKI

Department of Industrial Chemistry, Faculty of Engineering, Kyoto University, Yoshida, Sakyo-ku, Kyoto 606

(Received November 18, 1980)

Synopsis. Reaction of acid chlorides or thiocarboxylic *S*-esters with the title reagent in tetrahydrofuran provides ketones in good to excellent yields. The coupling reactions with allylic halides to form alkene derivatives are also disclosed.

Synthetic reactions with organoaluminium reagent have received considerable attention recently.[1] The transformation[2] of R'COCl into R'COR fails, however, by means of plain R_3Al, as they react easily with the resultant ketones.[3] Now we wish to report that an organometallic reagent generated from trialkylaluminium, copper(II) bis(acetylacetonate), and triphenylphosphine in 2 : 1 : 2 molar ratio reacts cleanly with carboxylic acid derivatives to give the corresponding ketones, although the identity of the reactive species is not known yet.[4]

Addition of trialkylaluminium to a mixture of copper(II) bis(acetylacetonate) and triphenylphosphine in tetrahydrofuran produced a homogeneous solution. The absence of triphenylphosphine resulted in a suspension which did not react as expected. Treatment of an acid chloride with the resulting organometallic reagents gave the corresponding ketone in good yield. The results are summarized in Table 1. The reaction proceeded similarly with thiocarboxylic *S*-esters as shown in run 4, 5, 9, and 10. The simplicity and mildness of experimental conditions make the method as useful as other organometallic reagents.[2]

TABLE 1. KETONE SYNTHESIS FROM CARBOXYLIC ACID DERIVATIVES BY MEANS OF ORGANOMETALLIC REAGENT DERIVED FROM R_3Al-$Cu(acac)_2$-PPh_3 SYSTEM[a]

Run	R'COX R'	X	R	Reaction time/h	Yield/%[b] of R'COR
1	Ph	Cl	Me	0.5	95
2			Et	1	88
3			^{i}Bu	2	55
4	Ph	SPh	Me	1	76
5			Et	1	80
6	CH_2=$CH(CH_2)_8$–	Cl	Me	0.5	90
7			Et	1	91
8			^{i}Bu	1	71
9	CH_2=$CH(CH_2)_8$–	SPh	Me	1	92
10			Et	1	88

a) 2 mol of R_3Al, 1 mol of $Cu(acac)_2$, and 2 mol of PPh_3 were employed per mol of R'COX. b) Isolated yields.

The reagents readily reacted with cinnamyl chloride to provide the cross-coupling products as shown:[5]

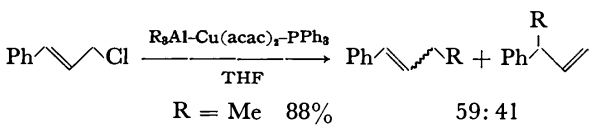

R = Me	88%	59 : 41
R = Et	80%	24 : 76

Experimental

The IR spectra were determined on a Shimadzu IR-27-G spectrometer; the mass spectra, on a Hitachi RMU-6L machine. The NMR spectra were recorded on a Varian EM-390H spectrometer, using TMS as an internal standard. The analyses were performed at the Elemental Analyses Center of Kyoto University. Tetrahydrofuran (THF) was dried on benzophenone ketyl and distilled. All the experiments were carried out under an argon atmosphere. Purification of the product was performed by preparative thin layer chromatography (TLC) or column chromatography on silica gel (Merck Kiesel gel 60). *S*-Phenyl benzenecarbothioate and *S*-phenyl 10-dodecenethioate were prepared by the reaction of the acid chlorides with an excess of thiophenol in pyridine.

Preparation of Methyl Ketones by Means of Me_3Al-$Cu(acac)_2$-PPh_3 System: A dry flask was charged with copper(II) bis(acetylacetonate) (0.26 g, 1.0 mmol), triphenylphosphine (0.52 g, 2.0 mmol), and THF (10 ml). To the stirred blue suspension at −78 °C was added slowly a hexane solution of trimethylaluminium (1.0 M, 2.0 ml, 2.0 mmol). The mixture was allowed to warm to 0 °C and stirring was continued until the copper(II) salt was completely dissolved and a pale yellow homogeneous solution was obtained (10 min). A solution of acid chloride or thiocarboxylic *S*-ester (1.0 mmol) in THF (2 ml) was added. After stirring at 0 °C for an appropriate time described in Table 1, the resulting mixture was diluted with ether (10 ml) and the ethereal extracts were washed with 1 M hydrochloric acid (20 ml) and brine (2×20 ml), dried over anhydrous sodium sulfate, and concentrated. The crude product was purified by silica gel column chromatography (hexane–ether 20 : 1) and distillation under reduced pressure.

The same procedure was employed for the preparation of organometallic reagents from Et_3Al and $^iBu_3Al$. Dark green and dark brown homogeneous solutions were obtained, respectively.

Isobutyl Phenyl Ketone: Bp 85 °C (bath temp, 2 Torr, 1 Torr = 133.322 Pa); IR (neat) 2955, 1690, 1600, 1584, 1450, 1365, 1210, 1005, 750, 688 cm^{-1}; NMR (CCl_4) δ 1.02 (d, 6H, J= 7 Hz), 2.29 (qt, 1H, J=7 Hz), 2.76 (d, 2H, J=7 Hz), 7.30—8.05 (m, 5H); MS *m/e* (%) 162 (M^+, 13), 147 (6), 120 (28), 105 (100), 77 (54), 51 (24). The compound was identical with the authentic sample.[6]

11-Dodecen-2-one: Bp 85 °C (bath temp, 2 Torr), IR (neat) 2940, 2860, 1724, 1644, 1358, 1160, 990, 908 cm^{-1}; NMR (CCl_4) δ 1.15—1.70 (m, 12H), 1.85—2.20 (m, 2H), 2.04 (s, 3H), 2.32 (t, 2H, J=6 Hz), 4.88 (d, 1H, J=9 Hz), 4.94 (d, 1H, J=18 Hz), 5.50—6.00 (m, 1H); MS *m/e* (%) 182 (M^+, 1), 124 (6), 82 (13), 71 (27), 58 (63), 55 (35), 43 (100), 41 (44).

Found: C, 79.07; H, 12.29%. Calcd for $C_{12}H_{22}O$: C, 79.06; H, 12.16%.

12-Tridecen-3-one: Bp 87 °C (bath temp. 2 Torr); IR (neat) 2925, 2850, 1715, 1642, 1460, 1108, 990, 904 cm^{-1}; NMR (CCl_4) δ 1.00 (t, 3H, J=7 Hz), 1.15—1.75 (m, 12H), 1.85—2.15 (m, 2H), 2.15—2.50 (m, 4H), 4.90 (d, 1H, J= 10 Hz), 4.94 (d, 1H, J=18 Hz), 5.50—6.00 (m, 1H); MS *m/e* (%) 196 (M^+, 1), 167 (6), 149 (11), 139 (8), 85 (26), 83 (26), 72 (76), 57 (100), 55 (73).

Found: C, 79.29; H, 12.58%. Calcd for $C_{13}H_{24}O$: C, 79.53; H, 12.32%.

2-Methyl-13-tetradecen-4-one: Bp 108 °C (bath temp, 2 Torr); IR (neat) 2940, 2860, 1712, 1642, 1468, 1365, 988, 905 cm^{-1}; NMR (CCl_4) δ 0.89 (d, 6H, J=7 Hz), 1.10—1.80 (m, 12H), 1.80—2.36 (m, 7H), 5.88 (d, 1H, J=10 Hz), 5.94 (d, 1H, J=18 Hz), 5.50—6.00 (m, 1H); MS *m/e* (%) 224 (M^+, 2), 209 (3), 167 (10), 149 (11), 113 (13), 100 (19), 85 (86), 69 (25), 67 (22), 58 (80), 57 (100).

Found: C, 80.11; H, 12.72%. Calcd for $C_{15}H_{28}O$: C, 80.29; H, 12.58%.

Methylation of Cinnamyl Chloride by Means of Me_3Al–$Cu(acac)_2$–PPh_3 System: A pale yellow organometallic reagent derived from trimethylaluminium (2.0 mmol), copper(II) bis-(acetylacetonate) (0.26 g, 1.0 mmol), and triphenylphosphine (0.52 g, 2.0 mmol) in THF (10 ml) was prepared as described above. A solution of cinnamyl chloride (0.15 g, 1.0 mmol) in THF (2 ml) was added slowly to the solution at 0 °C, and the resulting mixture was stirred at the same temperature for an additional 15 min. The mixture was diluted with ether (10 ml) and the ethereal extracts were washed with 1 M hydrochloric acid (20 ml) and brine (2×20 ml), dried over anhydrous sodium sulfate, and concentrated. The crude product was purified by preparative TLC with hexane as an eluent to give two isomeric methylated products (0.12 g, 88%) whose ratio was determined by GLPC (20% PEG 6000, 2 m, 100 °C). 1-Phenyl-1-butene (T_r=16.1 min, 59%) and 3-phenyl-1-butene (T_r=6.3 min, 41%) were identical with the authentic samples.[7]

The same procedure was employed for the coupling reaction of cinnamyl chloride and the organometallic reagent derived from triethylaluminium. GLPC (20% PEG 6000, 2 m, 100 °C) indicated two peaks, T_r=9.3 min (3-phenyl-1-pentene, 76%) and T_r=25.7 min (1-phenyl-1-pentene, 24%).

References

1) H. Yamamoto and H. Nozaki, *Angew. Chem., Int. Ed. Engl.*, **17**, 169 (1978); E. Negishi, "Organometallics in Organic Syntheses," John Wiley and Sons Inc., New York (1980), Vol. 1, pp. 286—393.

2) A variety of organometallics are reported to react with acid halides to give ketones. a) Mg, Mn, and Cu: B. M. Trost and E. Vedejs, "Organic Synthesis Part II," ACS Audio Courses (1979), p. 23 and references cited therein; b) Sn–Pd: M. Kosugi, Y. Shimizu, and T. Migita, *Chem. Lett.*, **1977**, 1423; D. Milstein and J. K. Stille, *J. Am. Chem. Soc.*, **100**, 3636 (1978).

3) T. Mole and E. A. Jeffery, "Organoaluminium Compounds," Elsevier Publishing Co., Amsterdam (1972), pp. 311—317; F. Sato, H. Kodama, Y. Tomuro, and M. Sato, *Chem. Lett.*, **1979**, 623.

4) Alkylcopper(I) complex can be an active species. A. Miyashita and A. Yamamoto, *Bull. Chem. Soc. Jpn.*, **50**, 1102, 1109 (1977).

5) F. Sato, H. Kodama, and M. Sato, *J. Organomet. Chem.*, **150**, C30 (1978).

6) E. Fourneu and M. C. E. Barrelet, *Bull. Soc. Chim. Fr.*, **47**, 72 (1930).

7) Y. Yamamoto, S. Yamamoto, H. Yatagai, and K. Maruyama, *J. Am. Chem. Soc.*, **102**, 2318 (1980) and references cited therein.

  Bull. Chem. Soc. Jpn., 54, 1283—1287 (1981)

Conditional Monte Carlo Trajectory Calculation of Elementary Gas Reaction Rates

Ryuichi MINAMI† and Takashi OKADA*

Information Processing Research Center, Kwansei Gakuin University, Uegahara, Nishinomiya, Hyogo 662

(Received October 26, 1979)

A new Monte Carlo trajectory method is proposed to estimate the rate constants of elementary molecular reactions. In this study, we have introduced the conditional Monte Carlo technique and obtained the following advantages. First, the procedure of calculation has been simplified. That is, the trajectory data have been accumulated as only one data set, from which the rate constants at any temperature have been reduced easily. Secondly, the necessary number of trajectories has been decreased by employing appropriate conditional distribution functions. Lastly, the error estimation has become possible on a reasonable base. This method has been applied to the (H_2, H_2) direct exchange reaction as an example and the result is reported briefly.

Karplus, Porter, and Sharma have demonstrated the usefulness of the Monte Carlo trajectory method through the calculation of the rate constants of the (H, H_2) exchange reaction.[1] Since then, it has been frequently applied to the dynamics of various elementary molecular collisions.[2,3] In this procedure, the reaction cross sections are first estimated by the Monte Carlo trajectory calculation. Then, the rate constants are computed from the cross sections by the numerical integration method.

The cross sections are specified by the initial vibration-rotational quantum state and by the initial translational energy. Therefore, if we have to take account of many quantum states to estimate the rate constant, the necessary number of trajectory calculations becomes enormous. Some chemists have tried to get away from this trouble, but the results have been not so effective.[4,5]

The rate constant was originally defined as proportional to the expected value of the product of the relative velocity and the probability that a trajectory goes into the reaction channel. This aspect suggests that the calculation of cross sections can be bypassed and that the reaction rate may be computed directly from trajectory data. In this paper, the above idea is developed by introducing the conditional Monte Carlo method,[6] and the new technique is applied to the (H_2, H_2) direct exchange reaction[7] as an example.

Reaction Rate Calculation by the Conditional Monte Carlo Method

In this section, we discuss the development of the Monte Carlo trajectory method, using as an example the simplest exchange reaction **a**: A+BC→**b**: AB+C. Here, the collision system is identified by the vibration-rotational quantum state of the BC molecule, (v, j), and by the relative translational energy E_t. Other types of reactions can be treated in a similar way.

The overall thermal rate constant at temperature T is defined by

$$k_{a,b}(T) = N_A\left(\frac{8}{\pi\mu k_B{}^3T^3}\right)^{1/2} Q_{vib}{}^{-1}Q_{rot}{}^{-1}\sum_{v,j} g_j(2j+1) \times \exp\left(-\frac{E_v+E_j}{k_BT}\right)\int_0^\infty S_{a,b}(E_t, j, v) \times \exp\left(-\frac{E_t}{k_BT}\right)E_t dE_t, \quad (1)$$

where N_A is Avogadro's number, k_B is the Boltzmann constant, μ is the reduced mass of the A+BC system, Q_{vib} and Q_{rot} are the partition functions for the vibrational and the rotational motion, E_v and E_j are the vibrational and rotational energies of the BC molecule at the quantum states v and j, respectively, g_j is the statistical weight of the rotational state j, and $S_{a,b}(E_t, j, v)$ is the reaction cross section at the (E_t, j, v) state.[4] According to the quasiclassical trajectory theory, the cross section $S_{a,b}(E_t, j, v)$ is equal to the averaged probability that a trajectory with the (E_t, j, v) initial state goes into the reaction channel and is given by

$$S_{a,b}(E_t, j, v) = \frac{\pi\hbar^2}{\mu^2V_t{}^2}\sum_{l=0}^{\infty}(2l+1)\frac{1}{16\pi^3}\int_0^\pi d\theta\int_0^{2\pi}d\phi\int_0^{2\pi}d\phi \times\int_0^{2\pi}d\eta\sin\theta P_{a,b}(\theta, \phi, \psi, \eta, l, E_t, j, v), \quad (2)$$

where l is the orbital quantum number of the initial collision system, V_t is the initial collision velocity, (θ, ϕ) and ψ are the orientation angles for the BC axis and the instantaneous rotational angular momentum, respectively, η is the vibrational phase angle,[8] and $P_{a,b}(\cdots\cdots)$ is the probability that a trajectory goes into the reaction channel, **a**→**b**.

Substituting the above expression for $S_{a,b}(E_t, j, v)$ in Eq. 1 yields a relation between the rate constant and $P_{a,b}$ of each trajectory. If we wish to estimate directly a rate constant by using the Monte Carlo trajectory method,[9] the dynamical equations of trajectories are numerically solved according to the initial conditions generated from the natural distribution functions G's. Then the expression of $k_{a,b}(T)$ takes the following Monte Carlo integration form:[10]

$$k_{a,b}(T) = \pi N_A b_m{}^2\frac{1}{N}\sum_{i=1}^{N} V_t(i)\cdot P_{a,b}(i), \quad (3)$$

where b_m is the characteristic impact parameter that is large enough to include all reactive trajectories, i points out the i-th sample in an N-trajectories set, and the value of $P_{a,b}(i)$ becomes 1 for a case that i-th trajectory passes through the channel **a**→**b** and is 0 for the other cases. To estimate the rate constant

† Visiting fellow. Present address: Department of Chemistry, School of Science and Engineering, Waseda University, Okubo, Shinjuku-ku, Tokyo 160.

at a temperature, we need only perform the Monte Carlo integration of Eq. 3. However, if the most of $V_t(i)P_{a,b}(i)$'s are expected to be zero and only a few samples with non-zero value contribute to $k_{a,b}(T)$, this method also requires numerous sample trajectories.

The conditional Monte Carlo method has been proposed to estimate the expected value of a given function of a random variable by a comparatively small number of samplings.[6,11] The values of random variables are generated not according to the natural distribution functions but to the conditional distribution functions. The initial state (l, E_t, j, v) of a trajectroy is determined by the conditional Monte Carlo choice, while all initial phases (θ, ϕ, ψ and η) of the BC molecule are determined by the analog Monte Carlo choice.[11,12] In the introduction of the conditional Monte Carlo method, we first have to set up adequate forms of the conditional distribution functions F's. Next, the calculations of trajectories with the above initial conditions are performed numerically and the necessary results are stored in one data set. This data set is independent of temperature. Then the rate constant at any temperature can be estimated by the following equation, which has been transformed from Eq. 3 according to the conditional Monte Carlo integration: (See Appendix I.)

$$k_{a,b}(T) = \pi N_A b_m^2 \frac{1}{N} \sum_{i=1}^{N} V_t(i) P_{a,b}(i) J_i(T), \tag{4}$$

where $J_i(T)$ is the Jacobian determinant of the G's with respect to the F's. If there are strong correlations among the random variables, we have to evaluate fully the terms of $J_i(T)$. However, in cases of no correlation, as is usually assumed, $J_i(T)$ is simply estimated by

$$J_i(T) = \frac{G^{orb}_{l(i)} - G^{orb}_{l(i)-1}}{F^{orb}_{l(i)} - F^{orb}_{l(i)-1}} \cdot \frac{G^{vib}_{v(i)}(T) - G^{vib}_{v(i)-1}(T)}{F^{vib}_{v(i)} - F^{vib}_{v(i)-1}} \cdot \frac{G^{rot}_{J(i)}(T) - G^{rot}_{J(i)-1}(T)}{F^{rot}_{J(i)} - F^{rot}_{J(i)-1}} \cdot \frac{\partial G(E_t(i), T)/\partial E_t(i)}{\partial F(E_t(i))/\partial E_t(i)}, \tag{5}$$

where (G^{orb}_l, $G(E_t, T)$, $G^{rot}_J(T)$, $G^{vib}_v(T)$) and (F^{orb}_l, $F(E_t)$, F^{rot}_J, F^{vib}_v) are the natural and conditional distribution functions for (l, E_t, j, v), respectively. In this procedure, it is expected that the necessary number of trajectories is greatly decreased, since the rate constant estimation at any temperature requires no additional trajectory data, and since the forms of the conditional distribution functions may be taken so as to decrease the number of samples within the limitation of the required accuracy.

Reasonable error estimates of the calculated rate constants are readily possible in the conditional Monte Carlo method. If the variances of the sampled data set, $\sigma_{a,b}(T)^2$, are calculated, the relative errors of the calculated rate constant can be estimated in terms of the central limit theorem.[13] Then, the deviation at the α% confidence level is given by

$$|\pm\Delta k(T)| = \Phi^{-1}(\alpha/200)\sigma_{a,b}(T)N^{-1/2}, \tag{6}$$

where the function Φ^{-1} is the inverse function of the normal distribution function. Here, the sample variance $\sigma_{a,b}(T)^2$ is estimated by the following conditional Monte Carlo integration:

$$\sigma_{a,b}(T)^2 = (\pi N_A b_m^2)^2 \frac{1}{N-1} \left\{ \frac{1}{N} \sum_{i=1}^{N} [V_t(i)P_{a,b}(i)J_i(T)]^2 - \left[\frac{1}{N} \sum_{i=1}^{N} V_t(i)P_{a,b}(i)J_i(T) \right]^2 \right\}. \tag{7}$$

The conditional distribution functions should be formed so as to minimize the above variance.

Application to the (H_2, H_2) Exchange Reaction

We take up the (H_2, H_2) direct exchange reaction as a typical example among the AB+CD→AC+BD reactions. The determination of the conditional distribution functions F's for this reaction, the process of rate calculation, and the results will be briefly described below.

The Forms of F's. This exchange reaction happens with higher probability when the large energy present originates in vibrational and/or translational motions.[14] Now, if we adopt the thermal distribution functions at a representative temperature, there are few sample trajectories in the region where the reaction probability is comparatively high and the effect on the magnitude of rate constant is significant. On the other hand, the reaction probability is nearly zero where the density functions take large values and the samples are numerous. Therefore, we intend to adopt the conditional distribution functions so that the number of trajectories does not decrease in the high reactive conditions. The forms of F's for the various modes of motion are separately discussed as follows.

For Vibrational Quantum Number v: Since large vibrational energy is favourable for a trajectory to go into the reaction channel, it is desirable to provide many samples in the high energy levels. The simplest treatment would be to assign an equal weight factor to each vibrational level. Then we construct the conditional distribution function in the following simple form:

$$F^{vib}_v = (v+1)/(v_m+1) \qquad (0 \le v \le v_m \le v_{max}), \tag{8}$$

where v_m denotes the largest vibrational quantum number considered in the trajectory calculations and v_{max} means the dissociation limit of the hydrogen molecule, which has been assumed to be the Morse oscillator. We must choose the value of v_m carefully, because a too large v_m value gives many sample trajectories that are hardly expected in the thermal distribution, and because a too small v_m value neglects the samples necessary for the estimation of the rate constant.

For Rotational Quantum Number j: The rotational effect on this reaction is expected to be weak. Therefore, the conditional distribution function F^{rot}_J is assumed to be the thermal equilibrium distribution function G^{rot}_J at a representative temperature T_0.

$$F^{rot}_J = G^{rot}_J(T_0). \tag{9}$$

Here, $G^{rot}_J(T)$ is given by

$$G_j^{\mathrm{rot}}(T) = Q_{\mathrm{rot}}(T)^{-1} \sum_{j'=0}^{j} g_{j'}(2j'+1) \exp(-E_{j'}/k_{\mathrm{B}}T), \tag{10a}$$

$$Q_{\mathrm{rot}}(T) = \sum_{j'=0}^{\infty} g_{j'}(2j'+1) \exp(-E_{j'}/k_{\mathrm{B}}T), \tag{10b}$$

where the magnitude of statistical weight g_j is noted in Ref. 15. In the case of homonuclear diatomic molecule, the procedure to determine the j-value from the rotational distribution function F_j^{rot} is somewhat complex and is explained in Appendix II.

For Translational Energy E_t: For the same reason as for the vibrational motion, we have employed the following conditional distribution function:

$$F(E_t) = \begin{cases} E_t/E_{t,m} & : \ 0 \le E_t \le E_{t,m} \\ 1 & : \ E_{t,m} \le E_t \end{cases} \tag{11}$$

where $E_{t,m}$ is a sufficiently large value of E_t, similarly to v_m.

For Orbital Quantum Number l: The following form is assumed as in the vibrational case, because the smaller value of l is expected to give the higher reaction probability:

$$F_l^{\mathrm{orb}} = (l+1)/(l_m+1) \qquad (0 \le l \le l_m). \tag{12}$$

Here l_m denotes the maximum orbital quantum number for a given translational energy and is calculated by the following equation if the characteristic impact parameter b_m is fixed:

$$l_m = \left[\frac{\{1 + b_m(8\mu E_t)^{1/2}/\hbar\}^{1/2} - 1}{2} \right]_{\mathrm{int}}. \tag{13}$$

Here $[\ ]_{\mathrm{int}}$ means to omit the decimal part. Once l is chosen, the impact parameter b, which is necessary for trajectory calculation, is estimated by

$$b = \hbar\{l(l+1)/2\mu E_t\}^{1/2}. \tag{14}$$

We add the remark that a similar technique has already been applied for the orbital motion.[4,16]

Calculating Procedure. Two FORTRAN IV programs were written to estimate the rate constants. The first program initializes the trajectories according to the given conditional distribution functions, integrates the Hamilton equation numerically, and then writes out the results into a data file. The second program reads the trajectory data in the file, and then estimates the rate constant at an optional temperature by use of Eq. 4.

The parameter values of the conditional distribution functions are set to those shown in Table 1. T_0 shows a representative value in the range of 500 to 5000 K. The values of v_m, $E_{t,m}$, and b_m have been determined by analyzing the results of the 4000 trajectories test run which has employed sufficiently large values for them. The LEPS type potential

Table 1. Parameters adopted in the conditional distribution functions for the (H_2, H_2) direct exchange reaction

$v_m = 4$
$T_0 = 1000$ K
$E_{t,m} = 125$ kcal mol^{-1}
$b_m = 2.25$ au

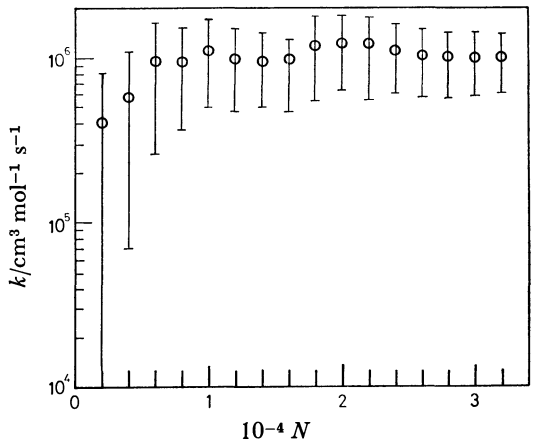

Fig. 1. The calculated rate constant of (H_2, H_2) direct exchange reaction at 2000 K *vs.* the number of sample trajectories, N. The error bars depict the 90% confidence limits.

surface devised by Raff *et al.*[17] and the parameter values by Porter *et al.*[4] are used to specify the Hamilton equation of the system. Numerical integration has been performed by the Adams-Moulton fifth-order predictor, sixth-order corrector method, and the time increment is set to 2×10^{-16} s. More details of trajectory calculation can be found elsewhere.[2,8]

Results. The calculated rate constants at a temperature of 2000 K are plotted as a function of the number of sample trajectories in Fig. 1. The confidence intervals at the 90% level are also depicted by the error bars, the lengths of which tend to decrease with the increase of N.

Here, we will estimate the necessary number of trajectories to attain accuracy within an order of magnitude:

$$\frac{\Delta k(T)}{k(T)} \le 0.9 \ . \tag{15}$$

Since the relative error at the α% confidence level inherent in the N-samplings is evaluated by Eq. 6, the relative standard deviation $\sigma(T)/k(T)$ can be related to Eq. 15 as follows:

$$\sigma(T)/k(T) \le 0.9N^{1/2}/\Phi^{-1}(\alpha/200). \tag{16}$$

Therefore, we will seek the number N which satisfies the above relation. The procedure can be traced in Fig. 2, where the calculated $\sigma(T)/k(T)$'s at $T=$ 1000 K and 2000 K are plotted against $N^{1/2}$, and three straight lines are drawn to show the equality of Eq. 16 for $\alpha=90$, 95, and 99(%). If a calculated point of $\sigma(T)/k(T)$ lies below each line, the $k(T)$ value is regarded to have the desired accuracy at the corresponding degree of confidence. For instance, it can be seen from this figure that 4000 and 18000 trajectories are enough to reach the 90% level at $T=2000$ and 1000 K, respectively.

The Arrhenius plot of the calculated rate constants and their 90% confidence limits at 32000 trajectories are shown in Fig. 3. This plot tends to be slightly concave and an activation energy of *ca.* 67 kcal/mol has been evaluated by fitting the Arrhenius equation to this slope. We also note the tendency that the

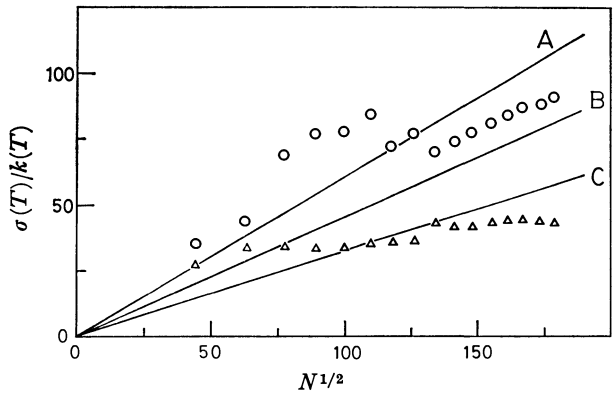

Fig. 2. Plot of $\sigma(T)/k(T)$ *vs.* $N^{1/2}$.
The marks ○ and △ represent the points of $\sigma(T)/k(T)$ at $T=1000$ and 2000 K, respectively. The straight lines A, B, and C mean the limits which satisfy the equality of Eq. 16 for $\alpha=90$, 95, and 99 (%), respectively.

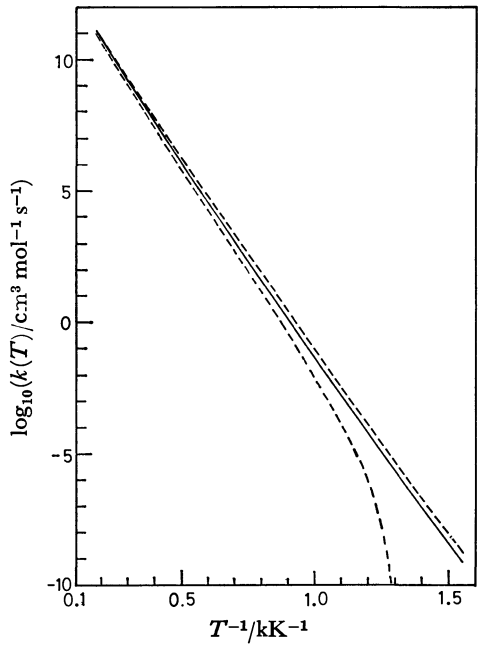

Fig. 3. Arrhenius plot for the (H_2, H_2) direct exchange reaction. The full line represents the Arrhenius plot calculated from 32000 trajectories. Two dotted lines show the 90% confidence limits.

accuracies attained at lower temperatures are poorer than those at higher ones. However, such results simply come from our choice of conditional distribution functions. Different tendencies are expected for other functional forms.

In this trial calculation, we have not determined the optimum functional forms of F's. Generally, a great number of test runs would be required to carry it out.[12] Therefore, we adopted appropriate forms of F's and performed a reasonable error estimation to determine the necessary number of trajectories.

Conclusion

We have presented a new technique for the numerical trajectory calculation of the rate constant for the elementary gas phase reaction. The conditional Monte Carlo method employed here has provided the following advantages. First, the dependence of the accuracy of the calculated rate constant on the number of sample trajectories has become clearer than that found in the conventional way. Next, the estimating procedure has become simpler. That is, the trajectory data are put into only one data set, from which the rate constant at any temperature can be calculated immediately. Lastly, even the smaller number of trajectories can give a fairly good estimation of rate constants, if the conditional distribution functions are formed well. Hence, the analysis of the collision process of complex molecules may be possible in the present method, while the necessary number of cross sections grows prohibitively with the increase of the intramolecular freedom of reactants in the conventional method.

One of the authors (M) is most grateful to Professor Keniti Higasi of Waseda University for his kind encouragement.

Appendix I. Conditional Monte Carlo Integration

The derivations of Eqs. 4 and 5 are inferred from analogy with the expected value of a function $P(x,n)$ of two random variables (x, n) which are generated according to natural distribution functions $G(x)$ and G_n, where x and n stand for continuous and integral values, respectively. The expected value of $P(x,n)$ is given by

$$\langle P(x,n)\rangle = \sum_{n=0}^{n(\max)} \int_0^1 P(x,n)\mathrm{d}G(x)(G_n - G_{n-1}), \tag{A1}$$

where the integral is a Rieman-Stieltjes type and G_{-1} and $G_{n(\max)}$ are defined by 0 and 1, respectively. If we want the values of random variables to be generated according to conditional distribution functions ($F(x)$, F_n), Eq. A1 should be reformulated as follows:

$$\langle P(x,n)\rangle = \sum_{n=0}^{n(\max)} \int_0^1 P(x,n)J(x,n)\mathrm{d}F(x)(F_n - F_{n-1}), \tag{A2}$$

where $J(x,n)$ is the Jacobian:

$$J(x,n) = \frac{\mathrm{d}G(x)}{\mathrm{d}F(x)} \cdot \frac{G_n - G_{n-1}}{F_n - F_{n-1}}. \tag{A3}$$

Employing the analog Monte Carlo method,[12] we can choose an N-samples set ($(x_i, n(i))$, $i=1,\ldots,N$) from the distribution according to the ($F(x)$, F_n)-functions and can simultaneously establish the corresponding set ($P(x_i,n(i))$ $J(x_i,n(i))$, $i=1,\ldots,N$). Then, Eq. A2 is approximated by

$$\langle P(x,n)\rangle = \frac{1}{N}\sum_{i=1}^{N} P(x_i,n(i))J(x_i,n(i)), \tag{A4}$$

where i-th sample values (x_i, $n(i)$) are derived from two uniform random numbers ξ_i and η_i using the following equations:

$$\begin{cases} x_i = F^{-1}(\xi_i) & (0 \le \xi_i < 1), \\ F_{n(i)-1} \le \eta_i < F_{n(i)} & (0 \le \eta_i < 1). \end{cases} \tag{A5}$$

Appendix II. Monte Carlo Choice of the Rotational State for Homonuclear Diatomic Molecule

The summation in Eq. 10 is first divided into two series with even and odd j-number, and these troublesome summations are carried out in the approximations of integral expression[8] as follows:

$$F_j^{\mathrm{rot}} = Q_{\mathrm{rot}}^{-1}\left\{g_{\mathrm{even}} \sum_{\mathrm{even}\ j'} (2j'+1)\exp\left(-\frac{\hbar^2 j'(j'+1)}{2Ik_{\mathrm{B}}T_{\mathrm{o}}}\right) + g_{\mathrm{odd}} \sum_{\mathrm{odd}\ j'} (2j'+1)\exp\left(-\frac{\hbar^2 j'(j'+1)}{2Ik_{\mathrm{B}}T_{\mathrm{o}}}\right)\right\}$$
$$= Q_{\mathrm{rot}}^{-1}\left\{g_{\mathrm{even}}\int_0 (8x+2)\exp\left(-\frac{\hbar^2 x(2x+1)}{Ik_{\mathrm{B}}T_{\mathrm{o}}}\right)\mathrm{d}x + g_{\mathrm{odd}}\int_0 (8x+6)\exp\left(-\frac{\hbar^2 (x+1)(2x+1)}{Ik_{\mathrm{B}}T_{\mathrm{o}}}\right)\mathrm{d}x\right\}, \quad \text{(A6)}$$

where I is the moment of inertia and the upper bounds of summations and integrals are limited by j-value. By calculating the above integrals between the interval $(0,\infty]$, Q_{rot} is expressed as

$$Q_{\mathrm{rot}} = Q_{\mathrm{rot}}(\mathrm{even}) + Q_{\mathrm{rot}}(\mathrm{odd}), \quad \text{(A7)}$$

$$Q_{\mathrm{rot}}(\mathrm{even}) = g_{\mathrm{even}}(2Ik_{\mathrm{B}}T_{\mathrm{o}}/\hbar^2), \quad \text{(A8a)}$$

$$Q_{\mathrm{rot}}(\mathrm{odd}) = g_{\mathrm{odd}}(2Ik_{\mathrm{B}}T_{\mathrm{o}}/\hbar^2)\exp\left(-\hbar^2/Ik_{\mathrm{B}}T_{\mathrm{o}}\right). \quad \text{(A8b)}$$

Then, F_j^{rot} is represented by the following formulae:

$$F_j^{\mathrm{rot}} = Q_{\mathrm{rot}}^{-1}\{Q_{\mathrm{rot}}(\mathrm{even})F_j^{\mathrm{rot}}(\mathrm{even}) + Q_{\mathrm{rot}}(\mathrm{odd})F_j^{\mathrm{rot}}(\mathrm{odd})\}, \quad \text{(A9)}$$

$$F_j^{\mathrm{rot}}(\mathrm{even}) = 1 - \exp\left(-\frac{\hbar^2 j(j+1)}{2Ik_{\mathrm{B}}T_{\mathrm{o}}}\right), \quad \text{(A10a)}$$

$$F_j^{\mathrm{rot}}(\mathrm{odd}) = 1 - \exp\left(-\frac{\hbar^2 (j-1)(j+2)}{2Ik_{\mathrm{B}}T_{\mathrm{o}}}\right), \quad \text{(A10b)}$$

where $F_j^{\mathrm{rot}}(\mathrm{even})$ and $F_j^{\mathrm{rot}}(\mathrm{odd})$ are considered to be distribution functions for even and odd rotational states alone, respectively.

In order to determine the quantum number j, we first distinguish whether it belongs to the even or the odd j-series by introducing a uniform random number η. Then, by use of another uniform random number ξ, the value of j in the respective series can be assigned as follows:
if $0 \leq \eta < Q_{\mathrm{rot}}(\mathrm{even})/Q_{\mathrm{rot}}$, even j-series:

$$j = \left[\frac{-1+(1-A)^{1/2}}{2}\right]_{\mathrm{even}}, \quad \text{(A11a)}$$

if $Q_{\mathrm{rot}}(\mathrm{even})/Q_{\mathrm{rot}} \leq \eta < 1$, odd j-series:

$$j = \left[\frac{-1+(9-A)^{1/2}}{2}\right]_{\mathrm{odd}}, \quad \text{(A11b)}$$

where A is given by

$$A = (8Ik_{\mathrm{B}}T_{\mathrm{o}}/\hbar^2)\ln\xi, \quad \text{(A12)}$$

and $[\ ]_{\mathrm{even}}$ and $[\ ]_{\mathrm{odd}}$ mean to adopt the maximum number in the even and the odd integer sequence below the given value, respectively.

The case of heteronuclear diatomic molecule has already been treated in Ref. 8.

References

1) M. Karplus, R. N. Porter, and R. D. Sharma, *J. Chem. Phys.*, **43**, 3259 (1965).
2) R. N. Porter and L. M. Raff, "Dynamics of Molecular Collisions, part B," ed by W. H. Miller, Plenum Press, New York (1976), Chap. 1, pp. 1—52.
3) D. L. Thompson, *Acc. Chem. Res.*, **9**, 338 (1976).
4) R. N. Porter, L. B. Sims, D. L. Thompson, and L. M. Raff, *J. Chem. Phys.*, **58**, 2855 (1973).
5) I. W. M. Smith and P. M. Wood, *Mol. Phys.*, **25**, 44 (1973).
6) J. M. Hammersley, *J. Assoc. Comp. Mach.*, **3**, 73 (1956).
7) K. Morokuma, L. Pedersen, and M. Karplus, *J. Am. Chem. Soc.*, **89**, 5064 (1967).
8) L. M. Raff, D. L. Thompson, L. B. Sims, and R. N. Porter, *J. Chem. Phys.*, **56**, 5998 (1972).
9) R. Minami and T. Fueno, *Chem. Lett.*, **1979**, 343.
10) J. M. Hammersley and D. S. Handscomb, "Monte Carlo Methods," Wiley, New York (1950).
11) D. W. Drawbaugh, *Nucl. Sci. Eng.*, **9**, 185 (1961).
12) O. Miyatake and T. Nakayama, "Monte Carlo Method," Nikkan Kogyo Shinbun, Tokyo (1966), Appendix 1.
13) W. Feller, "An Introduction to Probability Theory and Its Applications," Wiley, New York (1956), Vol. 1; A. Papoulis, "Probability, Random Variables and Stochastic Processes," McGraw-Hill, New York (1965).
14) L. L. Poulsen, *J. Chem. Phys.*, **53**, 1987 (1970).
15) G. Herzberg, "Molecular Spectra and Molecular Structure, I. Spectra of Diatomic Molecules," 2nd ed, Van Nostrand, New York (1950).
16) C. A. Parr, J. C. Polanyi, and W. H. Wong, *J. Chem. Phys.*, **58**, 5 (1973).
17) L. M. Raff, L. Stivers, R. N. Porter, D. L. Thompson, and L. B. Sims, *J. Chem. Phys.*, **52**, 3449 (1970).

Kinetic Studies on the Strictly Catalytic Acetylation of Mesitylene with Acetic Anhydride by HCl and Metal Chlorides in Acetic Acid

Tohr YAMANAKA* and Takashi IMAI

Central Research Laboratory of Takasago Perfumery Co., Ltd., Kamata, Ohta-ku, Tokyo 144

(Received June 13, 1980)

On the acetylation of mesitylene (**1**, 0.5—1 mol dm^{-3}) with acetic anhydride (Ac_2O, 0.5—1.5 mol dm^{-3}) at 30—90 °C in acetic acid as solvent, $SbCl_5$, $FeCl_3$, $SnCl_4$, or $ZnCl_2$ (each of 0.02—0.2 mol dm^{-3}) under the co-catalytic effect of HCl (0—0.75 mol dm^{-3}) showed a continuous catalytic activity. The product was exclusively 2′,4′,6′-trimethylacetophenone for conversions of **1** in the range of 0—90%. The reaction was first order with respect to **1** and Ac_2O. The rate constants were proportional to 1—1.4th power of the concentration of the metal chloride. The apparent activation energy was 18.8 kcal mol^{-1} for all the catalysts. The catalytically active species are thought to be the conjugate acids from the metal chloride and HCl. Relative catalytic activities of the metal chlorides varied in parallel with their relative Lewis acid-strengths.

With a few exceptions,[1a,2] the past Friedel-Crafts acylations of aromatic hydrocarbons with acid halides, acid anhydrides, or acids required[3-7] more than equimolar amounts of metal halides (MX_n) to the acyl component, because the resulting ketone combined with MX_n to form a complex.[7,8] Although a recent patent suggests an acylation by a *catalytic amount* of $FeCl_3$, namely by 0.05—0.1 mol of $FeCl_3$ for each mol of acetyl chloride (AcCl),[2] the efforts to reduce the amount of the catalyst were concentrated on dissociating the complexes by means of elevating the reaction temperature beyond the boiling point of the starting hydrocarbons, and the yield of ketones was not high.

Catalytic amounts of strong inorganic oxoacids are known to catalyze continuously the acetylation of thiophene,[1b] furan,[1b] and anisole[9] with acetic anhydride (Ac_2O). In the case of anisole,[9] the addition of acetic acid (AcOH) made the reaction mild and it prevented the formation of resinous products. These results should be compared with conventional acylations[3,4,10b] which required 2—3 times the molar quantity of metal halides such as $AlCl_3$ to acid anhydrides. Solutions of $SnCl_4$ or $ZnCl_2$ in AcOH, without undergoing solvolysis, form complex acids with the solvent, *e.g.*, $H_2ZnCl_2(OAc)_2$.[10a] In the system of $ZnCl_2$–HCl–AcOH, an acid stronger than $HClO_4$, H_2ZnCl_4 arises.[11] A Brönsted acid (HY) such as HCl, H_2O, and AcOH often functions as a co-catalyst in the systems of MX_n in an aprotic solvent, where a conjugate acid HMX_nY with a strong ability of proton donation was thought to be the catalytically active species.[12-15]

Prior to the present study there has been neither a kinetic study of Friedel-Crafts acylation with anhydrides, nor a catalytic study of the acylation of an aromatic hydrocarbon with anhydrides. Recently the authors found a new acetylation of cyclic sesquiterpenes with Ac_2O in the presence of a *catalytic amount* of ZnO or Fe_2O_3, and HCl in AcOH as solvent.[16] This paper deals with the kinetic study of the acetylations of mesitylene (**1**) with Ac_2O in the presence of *catalytic amounts* of various metal chlorides (MCl_n) and HCl in AcOH as solvent.

Experimental

Catalysts. $ZnCl_2$ of a guaranteed reagent grade, $SnCl_4$ and $FeCl_3$ of a purity greater than 99 wt%, and $SbCl_5$ of an electronics grade were used as the catalysts without further purification.

Materials. **1** of a purity greater than 98.5 wt% (by GLC), and Ac_2O, AcCl, and AcOH of a guaranteed reagent grade were used without further purification. (In one particular case, 6 mol dm^{-3} HCl was used instead of AcCl, water contained in which was predicted to react quantitatively with Ac_2O to form AcOH.)

Procedure. The acylation was carried out under an atmosphere of dry N_2 in a 30 ml three-necked flask equipped with a condenser which was connected to a bubble column sealed with concd H_2SO_4. N_2 was introduced through a side arm and discharged through the condenser. The desired amounts of AcCl or 6 mol dm^{-3} HCl, Ac_2O, and **1** were weighed into a 20 ml-measuring flask, and AcOH was added to the mixture to make the total amount 20 ml at room temperature. The desired amount of a catalyst (MCl_n) was weighed quickly into the reaction flask and the above AcOH solution was added to it. Immediately, the mixture was stirred vigorously by a magnetic stirrer in a water bath with a thermostat. At each reaction time, *ca.* 1.5 ml sample of the reaction mixture was taken out, diluted with 25 ml of 20 wt% NaCl aqueous solution to stop the reaction, and extracted with 10 ml of diethyl ether. The water layer was extracted again with 10 ml of diethyl ether. Both extracts were then combined, washed with NaCl-saturated water and, after concentration, used for the GLC analysis. Occasionally the N_2 flow was stopped. Each time, no bubbles were found in the bubble column. This showed that any losses of HCl or AcCl from the reactor were not substantial. AcCl or HCl (0—0.75 mol dm^{-3}), 0.5—1 mol dm^{-3} of **1**, 0.35—1.35 mol dm^{-3} of Ac_2O, and 0.02—0.2 mol dm^{-3} of a catalyst were used. The reaction temperature was between 30 and 90 °C. The reference volume of the reaction mixture used to express the concentration of components was taken at 25 °C.

GLC Analysis. Quantitative analysis was done by means of an internal standard method, using a Shimadzu GC-6A apparatus on a 1 m×2 mmϕ column packed with 5 wt% of FFAP on Chromosorb W,AW-DMCS of 80—100 mesh. The column temperature was elevated from 80 to 250 °C by 10 °C min^{-1}, N_2 was used as the carrier at 40 ml min^{-1}, and the injection temperature was 230 °C. Cyclododecane (extra pure reagent) was used as the standard. Compositions of products determined by the GLC analysis are shown in Table 1.

Table 1. Compositions of products[a)]

θ/h	Contents/wt%			
	1	2	Diacetyl-mesitylene	Others[b)]
0	98.5	0	0	1.5
2	26.3	70.5	trace	4.1
4	12.0	85.1	0.4	2.5
6	6.8	89.6	0.5	3.3
8	3.8	92.9	0.6	2.8

a) At 70 °C, $C_{1,0}=0.500$ mol dm^{-3}, $C_{Ac_2O,s}=1.20$ mol dm^{-3}, $C_{AcCl,s}=0.300$ mol dm^{-3}, and $C_{FeCl_3,s}=0.100$ mol dm^{-3}. b) Isomeric trimethylbenzenes, their monoacetylated prcducts, and an unknown product are included.

Identification of the Products. From the reaction mixture, **1**, 2′,4′,6′-trimethylacetophenone(**2**), and 2,4-diacetylmesitylene were identified by means of gas chromatography-mass spectroscopy(Hitachi M-80).

Results

Rate Equation. All the acetylation runs of **1** yielded 2′,4′,6′-trimethylacetophenone (**2**) exclusively. The initial rate of the acetylation was proportional to the initial concentration of **1** and also to the sum of the starting concentrations of AcCl and Ac_2O, in the reactions with 0.1 mol dm^{-3} of $FeCl_3$, 0.5—1 mol dm^{-3} of **1**, 0.35—1.35 mol dm^{-3} of Ac_2O, and 0.15 mol dm^{-3} of AcCl at 70 °C. When HCl and Ac_2O were adopted instead of using the equivalent amount of AcCl, the rate did not change. It was estimated that AcCl was rapidly solvolyzed by AcOH to form Ac_2O and HCl, and then participated in this reaction:

$$AcCl + AcOH \rightleftharpoons Ac_2O + HCl. \quad (1)$$

Therefore, the rate is proportional to the concentration of **1** and the effective concentration of Ac_2O *in the reaction system.* The rate of the acetylation was defined as $dC_2/d\theta$ and was expressed by the 2nd order rate equation(2):

$$dC_2/d\theta = k_2C_1C_{Ac_2O} = k_2(C_{1,0}-C_2)(C_{Ac_2O,s}+C_{AcCl,s}-C_2), \quad (2)$$

where θ, C, k_2, and 0 represent the time, the concentration of the species defined by the suffix, the second order rate constant, and $\theta=0$ respectively; the suffix s represents a starting concentration defined by: {the amount of the material or the catalyst used for the reaction}×{the volume of the reaction system}$^{-1}$. When $C_{1,0}\neq C_{Ac_2O,s}+C_{AcCl,s}$, integration of Eq. 2 gives

$$\log((C_{Ac_2O,s}+C_{AcCl,s}-C_2)/(C_{1,0}-C_2)) = k_2\theta(C_{Ac_2O,s}+C_{AcCl,s}-C_{1,0}) + \log((C_{Ac_2O,s}+C_{AcCl,s})/C_{1,0}). \quad (3)$$

The rate equation(2) fitted for reactions by each catalyst up to any conversion of **1** in the range of 0—90%, as illustrated by straight lines in Fig. 1. This is consistent with the above estimation that the equilibrium in Eq. 1 lies well to the right. This also indicates that the concentration of the catalytically active species does not change with the formation of **2**. Therefore, the present reaction medium avoids the deactivation of catalysts due to the complex formation[7)] between the Lewis acid and the product ketone(**2**).

Temperature Dependency of k_2. In Fig. 2, Arrhenius plots for k_2 by each catalyst are shown. The apparent activation energies are the same in all cases, *i.e.*, 18.8 kcal mol^{-1}. Therefore, relative activities of the catalysts must entirely be due to the pre-exponential factors of k_2. The constant activation energy suggests that each catalyst causes the same change of

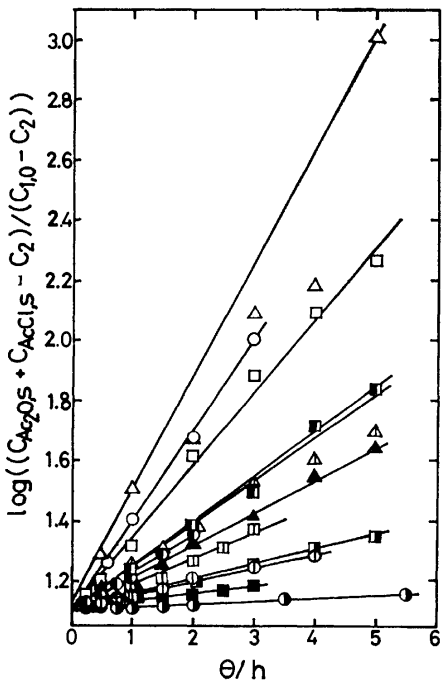

Fig. 1. Correlations between $\log((C_{Ac_2O,s}+C_{AcCl,s}-C_2)/(C_{1,0}-C_2))$, the left hand side of Eq. 3 and θ. $C_{1,0}=0.500$ mol dm^{-3}, $C_{Ac_2O,s}=1.350$ mol dm^{-3}, and $C_{AcCls,s}=0.150$—0.170 mol dm^{-3}. $FeCl_3$ 0.100 mol dm^{-3}, at 70 °C(○), 60 °C(◐), 50 °C(ⓓ), and 30 °C(◑); $SnCl_4$ 0.102 (□), 0.053 (▣), and 0.023 mol dm^{-3} (■) at 90 °C; $SnCl_4$ 0.201 (◧) and 0.101 mol dm^{-3} (◨) at 70 °C; $SbCl_5$ 0.108 (△) and 0.054 mol dm^{-3} (◬) at 70 °C; $SbCl_5$ 0.107 (▲) at 55 °C.

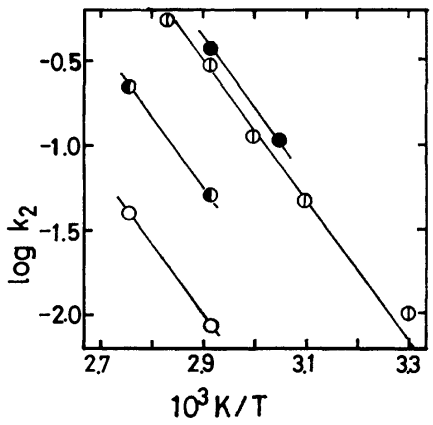

Fig. 2. Arrhenius plots of k_2 with 0.100 mol dm^{-3} of $SbCl_5$ (●), $FeCl_3$ (ⓓ), $SnCl_4$ (◐), and $ZnCl_2$ (○); $C_{AcCl,s}=0.150$ mol dm^{-3}.

the structure of species to form an activated complex in a rate determining step.

Dependency on the Catalyst Amount. In Fig. 3, the log k_2 values are plotted against the log $C_{MCl_n,s}$ of each catalyst. In the linear correlations of slope= 1—1.4, Fig. 3 shows that each k_2 is proportional to $C_{FeCl_3,s}^{1.0}$, $C_{SbCl_5,s}^{1.3}$, or $C_{SnCl_4,s}^{1.4}$. The slopes of $SnCl_4$ at 70 and 90 °C are the same. The specific activity of a catalyst, k_2', was estimated by the extrapolation of the straight line to the point where $C_{MCl_n,s}=1$ mol dm^{-3} in Fig. 3.

Effect of the Acid Strength of the Catalyst. In Fig. 4, log k_2' is plotted against the infrared spectroscopic shifts in carbonyl stretching frequencies ($\Delta\nu_{CO}$) between free xanthone and its complexes with metal halides.[17] These $\Delta\nu_{CO}$ values indicate the relative Lewis acid-strength of the catalysts. The correlation in Fig. 4 suggests that Lewis acid-strength is an important factor of the catalytic activity.

Effect of HCl-Concentration. Figure 5 indicates

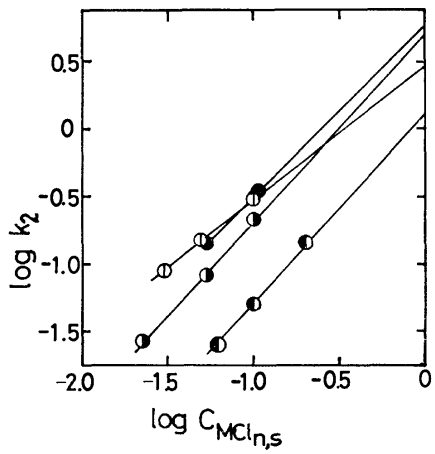

Fig. 3. Correlations between k_2 and the starting concentration of catalysts, $C_{MCl_n,s}$. $C_{AcCl,s}=0.150$ mol dm^{-3}.
●$SbCl_5$, ⦶$FeCl_3$, and ◐$SnCl_4$ at 70 °C; ◑$SnCl_4$ at 90 °C.

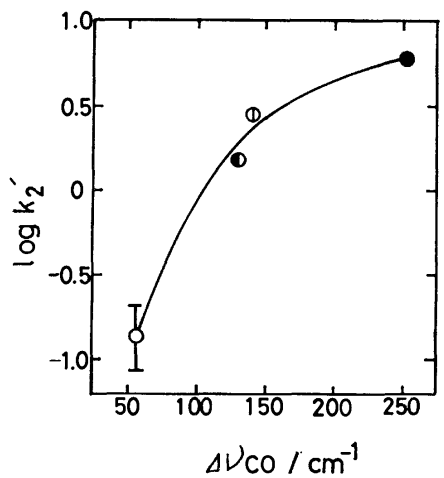

Fig. 4. Correlation between specific activity of catalysts, k_2' at 70 °C and $\Delta\nu_{CO}$. $C_{AcCl,s}=0.150$ mol dm^{-3}.
●$SbCl_5$, ⦶$FeCl_3$, and ◐$SnCl_4$. |-O-|$ZnCl_2$; the estimated value as (k_2 at $C_{ZnCl_2,s}=0.100$)/$(0.100^{1-1.4})$.

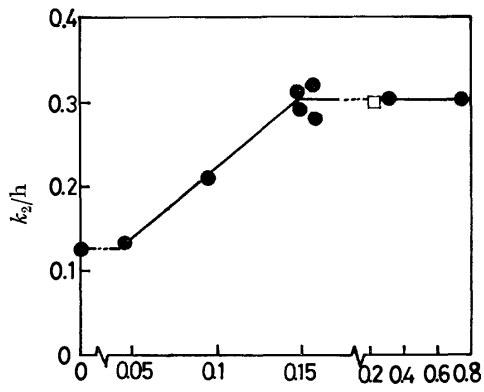

Fig. 5. Effect of C_{HCl} on k_2 of $FeCl_3$ at 70 °C.
$C_{FeCl_3,s}=0.100$ mol dm^{-3}. □$C_{AcCl,s}=0$; ●$C_{HCl,s}=0$.

the effect of C_{HCl} on the k_2 value of $FeCl_3$. The total HCl concentration was defined as the $\{C_{AcCl,s}+C_{HCl,s}\}$ value and was denoted by $C_{HCl,t}$. In Fig. 5, k_2 values vary with the $C_{HCl,t}$ value roughly along the same line. $FeCl_3$ still effected a catalytic activity when $C_{HCl,t}=0$. The k_2 value appears constant in the range of $C_{HCl,t}=0$—0.05 mol dm^{-3}, increases proportionally to the increase of $C_{HCl,t}$ in the range from 0.05 to 0.15 mol dm^{-3}, and attains approximately a maximum when $C_{HCl,t}\geq 0.15$ mol dm^{-3}.

Figure 5 shows that the catalytic activity of $FeCl_3$ when $C_{HCl,t}\approx 0.15$ mol dm^{-3} is 2.4 times as high as the one in the absence of HCl.

Discussion

Co-catalytic Action of HCl and AcOH on $FeCl_3$. In Friedel-Crafts acylations, the co-catalytic effects[12] of Brönsted acid(HY) on a metal halide have not been studied. Figure 5 suggests that the co-catalytic activity of AcOH is lower than that of HCl. The activity order seems parallel to the order of the reactivities of Brönsted acids HY in their hydrogen isotope exchange with aromatic solvents in the presence of $SnCl_4$ found by Satchell:[15] namely, HCl>H_2O>AcOH. He explained these observations by the co-catalytic effect of HY on $SnCl_4$.

Figure 5 shows that HCl prevails as the co-catalyst when $C_{HCl,t}\geq 0.15$ mol dm^{-3}, and that AcOH prevails when $C_{HCl,t}\leq 0.05$ mol dm^{-3}. Details of the k_2 value should be expressable by Eq. 4. When $C_{FeCl_3,s}=0.1$ mol dm^{-3},

$$k_2 = 0.126(1-C_{[FeCl_3\cdot HCl]}/C_{FeCl_3,s}) + 0.304\,C_{[FeCl_3\cdot HCl]}/C_{FeCl_3,s}, \quad (4)$$

where [$FeCl_3$·HCl] denotes the catalytically active species formed by $FeCl_3$ and HCl. The first term of the right hand side represents the co-catalytic effect of AcOH; the second term, that of HCl. If [$FeCl_3$·HCl] consists of $FeCl_3$ and HCl in the stoichiometric ratio of 1:1, and if it is formed quantitatively only when $C_{HCl,t}>0.05$, then $C_{[FeCl_3\cdot HCl]}$ equals the smaller value of $C_{FeCl_3,s}$ or $\{C_{HCl,t}-0.05\}$. Eq. 4 then agrees with the line in Fig. 5.

$HAlCl_4$ and $HAlBr_4$ are considered to be capable of being present in non-polar ternary systems of Lewis acid-catalyst/Brönsted acid-co-catalyst/solvent only when the solvent functions as a H^+-acceptor base.[12-14] If HCl and/or AcOH function(s) as co-catalyst(s) *via* the conjugate acid(s) $HFeCl_4$ and/or $HFeCl_3(OAc)$, they exist as ion pairs $AcOH_2^+FeCl_4^-$(**3**) and $AcOH_2^+$-$FeCl_3(OAc)^-$.[10a,11] This is because the present Ac_2O/AcOH–solvent system is polar and has a low dielectric constant, and the dissociation of the acid is suppressed.[18]

The equilibrium in Eq. 1 essentially lies to the left.[10b] When HCl is replaced by a strong acid such as perchloric or sulfonic acid, the equilibrium is shifted well to the right.[9,10a] Like $HAlCl_4$ and $HAlBr_4$, the conjugate acid $HFeCl_4$ formed by the interaction of Lewis and Brönsted acids presumably functions as an exceedingly strong acid and may be non-existent in the free state.[12,13] Then the observation in kinetics that the equilibrium in Eq. 1 lies well to the right can be interpreted in terms of the conjugate acid formation(5):

$$HCl + FeCl_3 + AcOH \overset{K_1}{\rightleftharpoons} AcOH_2^+FeCl_4^-. \quad (5)$$

Catalytic Action of the $FeCl_3$–HCl/AcOH System. In the results shown in Figs. 1—4, $C_{HCl,t}$ was 0.15—0.17, which was greater than $\{C_{FeCl_3,s}+0.05\}$ in every case. In those cases, k_2 of $FeCl_3$ is proportional to $C_{FeCl_3,s}$ but independent of $C_{HCl,t}$; $K_1 \gg 1$ is deduced from the analyses of Figs. 3 and 5.

According to Burton and Praill,[9] mixtures of perchloric and acetic acids which contain protons or solvated hydrogen ions, $AcOH_2^+$, are not O- or C-acetylating agents. Addition of Ac_2O to such mixtures leads to the formation of acetylium (Ac^+) and/or diacetoxyoxonium ion (Ac_2OH^+):

$$AcOH_2^+ + Ac_2O \rightleftharpoons Ac_2OH^+ + AcOH$$
$$\rightleftharpoons Ac^+ + 2AcOH.$$

These ions are both C-acetylating agents.[9] Because $C_{AcOH} \gg C_{Ac_2O}$ in the present medium, Ac_2OH^+ is estimated to prevail as the acetylating agent.[9,10] Therefore the acetylation in Scheme 1 is proposed; this proceeds *via* the formation of the diacetoxyoxonium ion pair(**4**):[9,10a]

$$\left.\begin{array}{ll} Ac_2O + \mathbf{3} \overset{K_2}{\rightleftharpoons} \underset{(\mathbf{4})}{Ac_2OH^+FeCl_4^-} + AcOH & (6) \\ \mathbf{1} + \mathbf{4} \longrightarrow \mathbf{2} + \mathbf{3} & (7) \end{array}\right\} \text{Scheme 1.}$$

This mechanism, with the pre-equilibrium(6) lying to the left, accounts formally for the observed kinetics of the first order dependence on Ac_2O, as in the O-acetylation of 2-naphthol.[10a] Provided that $K_2 \ll 1$ and that Step (7) is rate-determining in Scheme 1, the 2nd order rate expression (Eq. 2) is obtained. $FeCl_3$ functions strictly catalytically, because **3** is repeatedly regenerated. The suggestion by Burton *et al.*[9] that the formation of Ac_2OH^+ should be essential to the continuous activity of the acid catalysts seems to be kinetically proved in the present study. Because $FeCl_3$ does not exist in the free state, it does not form a complex[7] with the product ketone (**2**). The present results also kinetically support the suggestion by Hartough and Kosak for the acetylation of thiophene and furan that *catalytic amounts* of Lewis acid catalyst are sufficient in the absence of the complex formation.[1]

Catalytic Actions of $SbCl_5$, $SnCl_4$, and $ZnCl_2$. The same apparent activation energy and the observed first order dependency on Ac_2O suggest that the acetylations by $SbCl_5$, $SnCl_4$, and $ZnCl_2$ will also proceed *via* a diacetoxyoxonium ion pair like **4**. It seems reasonable to postulate that $SbCl_5$, $SnCl_4$, and $ZnCl_2$ function *via* steps similar to Scheme 1, as the active complex acid catalysts: $AcOH_2^+SbCl_6^-$ and $AcOH_2^+$-$SbCl_5(OAc)^-$, $AcOH_2^+HSnCl_6^-$ and $AcOH_2^+$-$HSnCl_5(OAc)^-$, or $AcOH_2^+HZnCl_4^-$ and $AcOH_2^+$-$HZnCl_3(OAc)^-$.[10a,11]

The observations in Fig. 3 suggest that the scheme of complex acid formation is somewhat different for each MCl_n. This should be responsible for variations in the degrees of the association and the solvation of the MCl_n's, variations in the stoichiometric compositions of the complex acids, and variations in the magnitudes of the equilibrium constants for the complex acid formations. Meanwhile, the observation of Fig. 4 suggests that Lewis acid-strength of MCl_n primarily effects the ability of proton donation to Ac_2O.

Providing that an attack of Ac_2OH^+ on the aromatic nucleus is the rate-determining step, and that the variation in the overall energy barriers of steps corresponding to Steps (6—7) by different MCl_n is negligibly small, the same apparent activation energy of each catalyst will be realized.

We wish to thank the Takasago Perfumery Co., Ltd., for its permission to publish this article.

References

1) a) H. D. Hartough and A. I. Kosak, *J. Am. Chem. Soc.*, **69**, 1012 (1947); b) H. D. Hartough and A. I. Kosak, *ibid.*, **69**, 3093 (1947).

2) Y. Takada, T. Matsuda, and R. Wakasa, Japan Patent SHO 48-19622.

3) P. H. Gore, "Friedel Crafts and Related Reactions," ed by G. A. Olah, Interscience Publishers, New York, London, Sydney (1964), Vol. 3, Part 1, p. 1.

4) K. Tanabe and T. Takeshita, "San Enki Shokubai," (Japanese), Sangyo Tosho, Tokyo (1966), p. 357.

5) G. A. Olah and S. Kobayashi, *J. Am. Chem. Soc.*, **93**, 6964 (1971).

6) P. H. Gore and J. A. Hoskins, *J. Chem. Soc., C*, **1970**, 517.

7) F. R. Jensen and G. Goldman, "Friedel Crafts and Related Reactions," ed by G. A. Olah, Interscience Publishers, New York, London, Sydney (1964), Vol. 3, Part 2, p. 1003.

8) L. Friedman and R. J. Honour, *J. Am. Chem. Soc.*, **91**, 6344 (1969).

9) H. Burton and P. F. G. Praill, *J. Chem. Soc.*, **1950**, 1203, 2034; **1953**, 837.

10) a) D. P. N. Satchell, *J. Chem. Soc.*, **1962**, 1894; b) D. P. N. Satchell, *Quart. Rev. Chem. Soc.*, **17**, 160 (1963); c) D. P. N. Satchell, *J. Chem. Soc.*, **1962**, 1899.

11) D. Betchell, V. Gold, and D. P. N. Satchell, *J. Chem. Soc.*, **1958**, 1918.

12) G. A. Olah, "Friedel Crafts and Related Reactions," Interscience Publishers, New York, London (1963), Vol. 1, pp. 205, 873.
13) H. Burton and P. F. G. Praill, *Chem. Ind.*, **1954**, 90.
14) H. Brown and H. W. Pearsall, *J. Am. Chem. Soc.*, **74**, 191 (1952).
15) D. P. N. Satchell, *Proc. Chem. Soc.*, **1960**, 355; *J. Chem. Soc.*, **1960**, 4388; **1961**, 1453, 3822.
16) T. Imai, T. Yamanaka, and Y. Yoshida, Japan Kokai 79-154740.
17) D. Cook, *Can. J. Chem.*, **41**, 522 (1963).
18) I. M. Kolthoff and S. Bruckenstein, *J. Am. Chem. Soc.*, **78**, 1 (1956).

An MO Study of the Reaction Mechanism of Photoisomerization from Isoxazole *via* Azirine Intermediate to Oxazole

Hidetsugu TANAKA, Yoshihiro OSAMURA, Toshio MATSUSHITA, and Kichisuke NISHIMOTO*

Department of Chemistry, Faculty of Science, Osaka City University, Sumiyoshi-ku, Osaka 558

(Received June 23, 1980)

The reaction mechanism of photoisomerization of isoxazoles and the wavelength dependent photochemistry of azirine intermediates which are the photoisomerization reaction intermediates are investigated theoretically by means of *ab initio* MO-CI calculation. The present calculation shows that the lowest excited singlet state, S_1, of azirine intermediate is an ($n\rightarrow\pi^*$) state localized at the carbonyl chromophore, while the S_2 state is assigned to be an ($n\rightarrow\pi^*$) state localized at the ketimine chromophore. Intersystem crossing from S_1 to T_1 states of azirine intermediate causes the N–C bond rupture of azirine ring and leads to isoxazole. On the other hand, azirine intermediate in the S_2 state proceeds to the C–C bond break of azirine ring and converts to oxazole *via* intersystem crossing to the T_1 state.

Some of five-membered heterocycles undergo the isomerization reactions in which two of ring atoms interchange their positions under the influence of UV-visible light. For instance, 2-substituted thiophenes were found to rearrange into 3-substituted thiophenes,[1] and 1,4-dimethylimidazoles into 1,2-dimethylimidazoles.[2] These reactions have been supposed to proceed *via* bridged-valence intermediates similar to those in the photochemical rearrangements of benzene derivatives.[3] Singh and his co-workers have studied the photochemical isomerization of diarylisoxazoles (**1**) to diaryloxazoles (**3**) and proposed an alternative

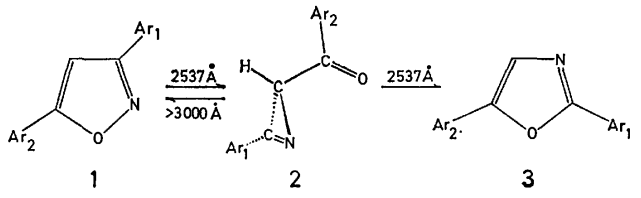

1 2 3

mechanism which proceeds *via* the three-membered intermediates.[4] This reaction is of compelling interest both experimentally and theoretically, since 2-aroyl-3-aryl-2*H*-azirines(**2**) have the reactivity strongly depending upon the wavelength of irradiation light.[4c]

In the present study, *ab initio* MO-CI calculations have been carried out for isoxazole (**1a**) (a: Ar_1=Ar_2=H, see Fig. 1), 2*H*-azirine-2-carbaldehyde (**2a**), and oxazole (**3a**) which are the parent molecules of **1**, **2**, and **3**, respectively.[5] On the basis of the calculated results, the reaction scheme and the wavelength dependency of the reactivity of **2** are discussed.

Calculations

Ab initio MO calculations of **1a**, **2a**, and **3a** are carried out with the STO-3G minimal basis set using the GAUSSIAN 70 program package.[6] The excited states of these species are calculated within the singly excited configuration interaction (SECI) procedure. In the SECI calculations, all the singly excited configurations are included except the inner-shell excitations.

The ground-state geometries of **1a**, **2a**, and **3a** are optimized using the STO-3G minimal basis set. Figure 2 shows the optimized geometries and those

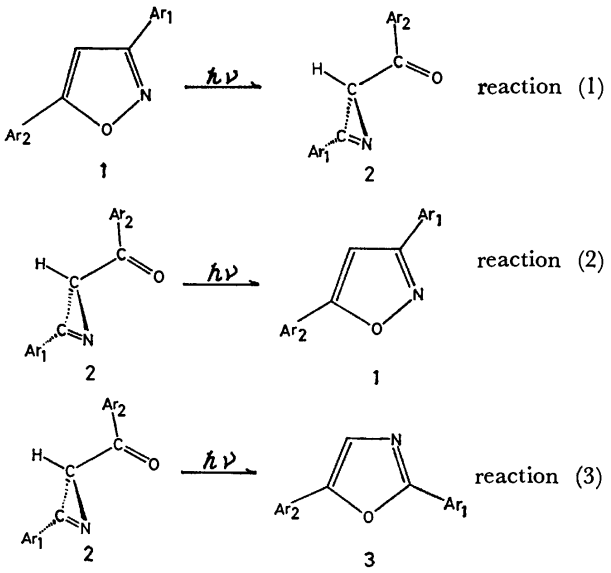

Fig. 1. Steps in the photoisomerization of isoxazole to oxazole.

determined by means of double resonance modulated microwave spectroscopy[7] in parentheses. The agreement between the calculated and the observed geometry is satisfactory.

The numbering of atoms of **1a** and **2a** is as follows.

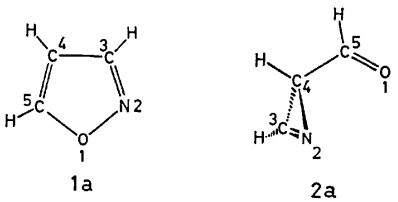

1a 2a

Results and Discussion

Excited States of 1a. The energy levels and their assignments of the ground (S_0) and some low-lying excited states of **1a**, **2a**, and **3a** at the optimized ground-state geometries are shown in Fig. 3.

Before discussing the mechanism of the reactions

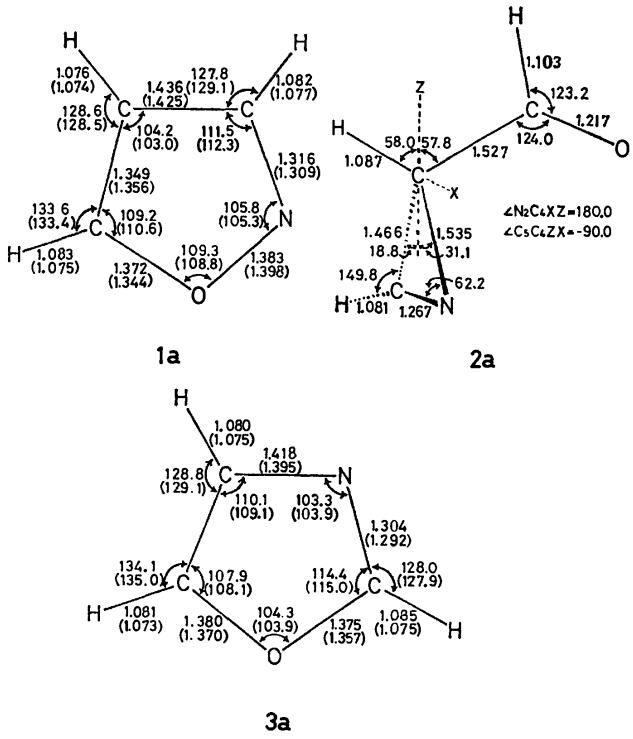

Fig. 2. Optimized ground-state geometries of **1a**, **2a**, and **3a**. **1a** and **3a** have a C_s symmetry. Values in parentheses are those determined by the experiments, see Ref. 7. Units are shown in Å and degree.

(1), (2), and (3) (see Fig. 1), it is of interest to examine the relation between the geometrical deformations and the state energy variation in the low-lying states of **1a** and **2a**. Several geometrical parameters are varied independently from the ground-state geometry. In **1a**, it is found that all of three geometrical variations, the C_5–C_4–C_3–N_2 torsional angle θ (by which the N_2 atom rises from the molecular plane and the O_1–N_2 bond is weakened), the C_3–C_4–C_5–O_1 torsional angle η (by which the O_1 atom stands up from the molecular plane and the O_1–N_2 bond is weakened), and the rotational angle with respect to the perpendicular

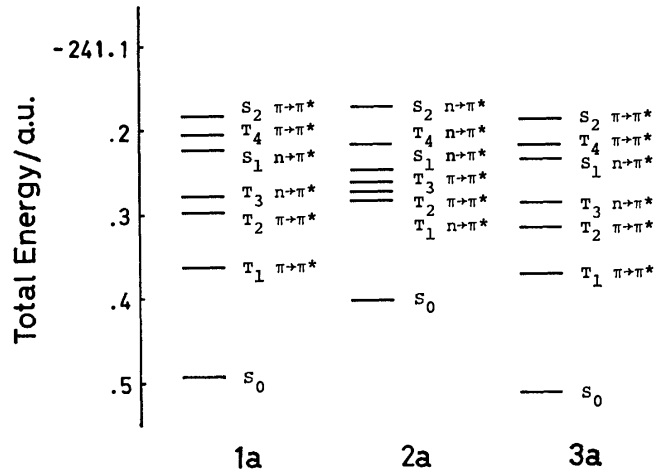

Fig. 3. State energies of the ground(S_0) and some low-lying excited states calculated by vertical excitation approximation.

bisector of the C_3–N_2 bond γ (by which the O_1–N_2 and the C_3–C_4 bonds are weakened simultaneously), give the rather flat potential curves in every excited states (see Figs. 4(a)—4(c)). The results of the independent geometrical variations show that the minima in the potential curves of the S_1 state appear at θ= 12.3° (depth is *ca.* 1.0 kcal mol^{-1}), η=17.2° (*ca.* 2.3 kcal mol^{-1}), and γ=9.9° (*ca.* 0.7 kcal mol^{-1}).

Excited States of ***2a***. T_1 and S_1 states of this intermediate are (n→π^*) states of the carbonyl chromophore and the T_4 and S_2 states are (n→π^*) states of the ketimine chromophore. Since the C_5=O_1 and the C_3=N_2 parts are perpendicular to each other, the excited states related these parts do not mix.

There are two ways of the reaction in the excited azirine intermediate. One is the N_2–C_4 bond break and the O_1–N_2 bond formation (reaction (2)), and the other is the C_3–C_4 bond break and the O_1–C_3 bond formation (reaction (3)). The former is described by the change of the N_2–C_3–C_4 bond angle δ (which causes the N_2–C_4 bond scission) and the out-of-plane torsional angle of the azirine ring (the C_4–

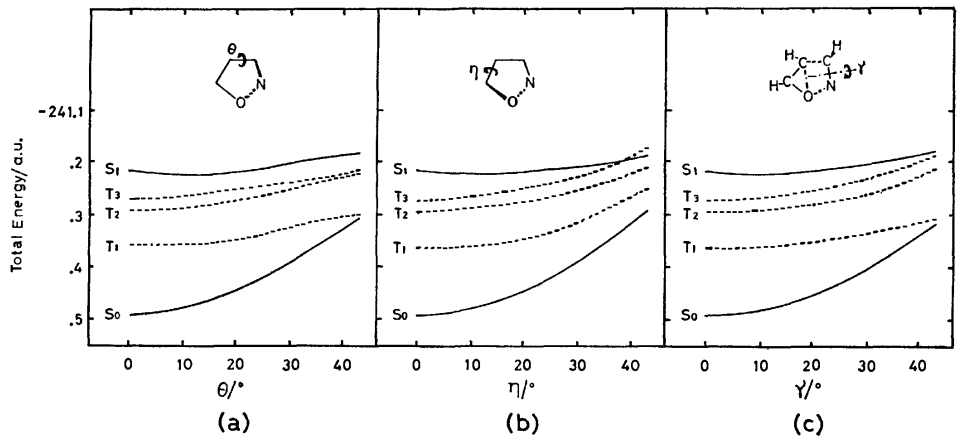

Fig. 4. State energy variations of **1a** by the deformations of (a) the C_5–C_4–C_3–N_2 torsional angle θ, (b) the C_3–C_4–C_5–O_1 torsional angle η, and (c) the rotational angle with respect to the perpendicular bisector of the N_2–C_3 bond γ relative to the ground-state geometry.

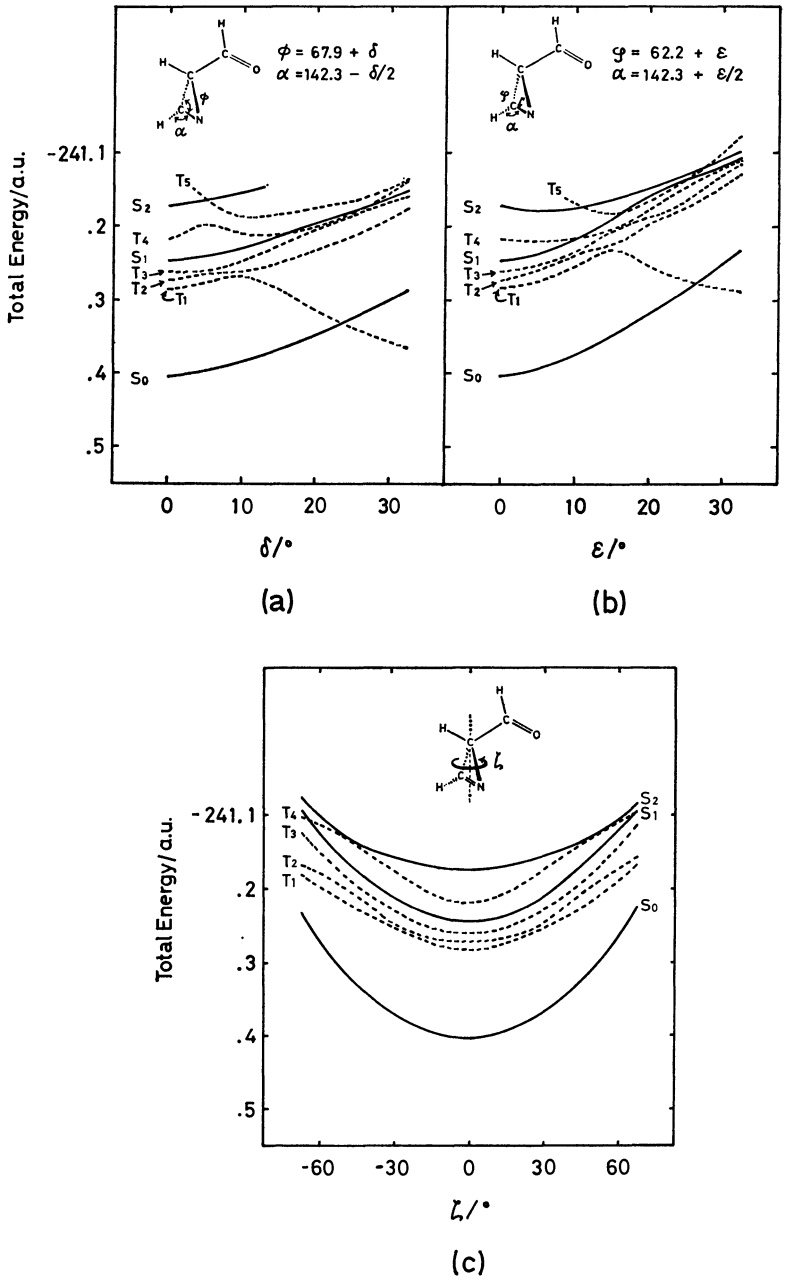

Fig. 5. State energy variations of **2a** by the deformations of (a) the N_2–C_3–C_4 bond angle δ, (b) the C_3–N_2–C_4 bond angle ε, and (c) the out-of-plane torsional angle of azirine ring (the C_4–N_2–C_3 plane) ζ relative to the ground-state geometry.

N_2–C_3 plane) ζ. The latter is described by the change of the C_3–N_2–C_4 bond angle ε (which causes the C_3–C_4 bond scission) and the geometrical parameter ζ. These three geometrical parameters are varied independently from the ground-state geometry. The results for some low-lying states are given in Fig. 5. Other geometrical parameters are also varied, but such geometrical deformations destabilize considerably any state. Therefore, only the geometrical parameters δ and ε can contribute to the initial stage in the reactions (2) and (3). In other words, the character of the reaction coordinate is varied from δ or ε to ζ gradually as the reaction proceeds.

While the S_1 state does not mix with the S_2 state at $\delta=\varepsilon=0$, the geometrical deformations cause the mixing of excited states each other. Let us consider the mechanism of the N_2–C_4 bond scission due to the geometrical deformation δ. As Fig. 5(a) shows, the T_1 state becomes more stable at large δ. Therefore, this state promotes the N_2–C_4 bond scission. Since both the S_1 and T_1 states are ($n\rightarrow\pi^*$) states of the carbonyl chromophore, and their energy separation is rather small, the intersystem crossing (ISC) between these states may rapidly occur. Thus, the excitation to the S_1 state leads to the N_2–C_4 bond scission *via* ISC to the T_1 state.

On the other hand, the geometrical deformation ε makes both the T_1 and S_1 states unstable, while it makes the S_2 state stable (see Fig. 5(b)). But the T_1 state becomes much stable at large ε. Therefore,

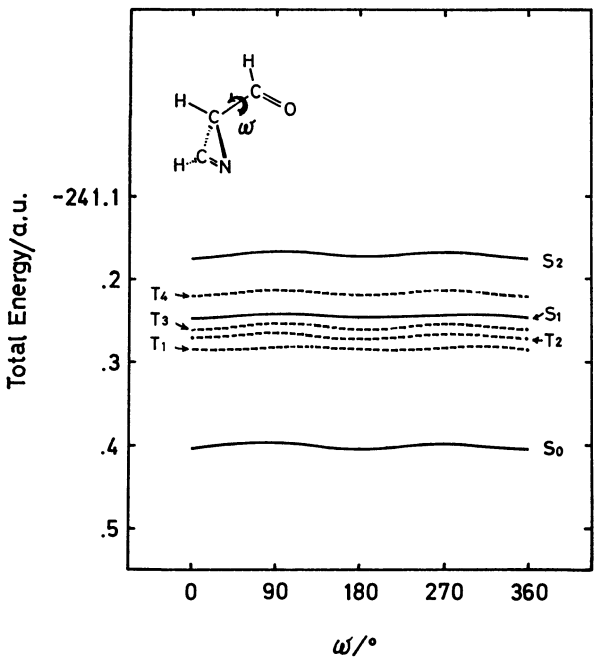

Fig. 6. State energy variation of **2a** by the rotation of CHO group ω. When $\omega=0°$ or 360°, **2a** is *s-trans* form. When $\omega=180°$, it is *s-cis* form.

the C_3–C_4 bond scission occurs *via* ISC from the S_2 to T_1 states.

In the ground state, the *s-trans* form of **2a** is slightly stable than the *s-cis* form (*ca.* 0.5 kcal mol^{-1}). However, the *s-cis* form is of advantage to initiate the reactions. Energy variation with the rotation of the CHO group in the low-lying states is given in Fig. 6. The rotational barriers are calculated to be *ca.* 5.2 kcal mol^{-1}, *ca.* 2.6 kcal mol^{-1}, and *ca.* 5.1 kcal mol^{-1} for the S_0, S_1, and S_2 states of **2a**, respectively. These energy barriers are rather small and, therefore, might obstruct the initiation of reaction.

Reaction (1): ***1a*→*2a***. In order to estimate the reaction path and the height of the barrier roughly, the geometies in the excited states are partly optimized (only several geometrical parameters are chosen) along the reaction paths which are infered from the results of independent variations of geometrical parameters given in Figs. 4 and 5.

It is well known that the bond break and creation cannot be described correctly in terms of singly excited configurations only. Thus, all valence singly excited configurations and the doubly and triply excited configurations from three highest occupied (HO) MO's to three lowest unoccupied (LU) MO's ((S+D+T)-ECI) are included in the present optimization procedure. As a result of partial optimization, the energy in S_1 state of **1a** descents along the reaction path. On the other hand, the T_1 state has an energy hill (the roughly estimated height is about 40 kcal mol^{-1}, see Fig. 8), so that this reaction would proceed hardly in the triplet state. These results are in good agreement with the experimental results that the reaction (1) could not be sensitized with benzophenone, acetophenone, or acetone.[4]

As Fig. 4 shows, the O_1–N_2 bond of **1a** becomes loose in the excited states. This is in accordance with the experiments that the compounds containing the O and N atoms adjacently such as isoxazoline derivatives are easily cleft at the O–N bond under the influence of UV-visible light.[8]

Let us consider this reaction in terms of the concept of orbital interaction.[9] The σ-type LUMO in **1a** is the *anti*-bonding orbital located at the O_1–N_2 bond. When a planar molecule such as isoxazole distorts with the out-of-plane motion, the σ-type LUMO becomes to mix with the occupied π MO's. In addition, since both O and N atoms have negative net charges and lone pair electrons, they repel each other by the electrostatic force. Thus, this force may be helpful for the twisting out-of-plane motion at the O_1–N_2 bond. This is the same as in the case of peroxides and hydrazines in which O–O and N–N bonds are broken very easily. In the excited states, the orbital mixing easily occurs because the σ-type LUMO is close energetically to π^* orbital and the out-of-plane distortion easily occurs, so that the O_1–N_2 bond break is promoted.

At the S_1 state of **1a**, the O_1–N_2 bond is cleft and a biradical might be formed at the N_2–C_3–C_4 part. Subsequently, the internal conversion (IC) into the ground state leads to the ring closure at the N_2 and C_4 atoms. Consequently, one can expect that the O_1–N_2 bond scission and the N_2–C_4 bond formation occur with nearly concerted manner.

Reaction(2): ***2a*→*1a***. As Fig. 5(a) shows, this reaction is favor to start from the S_1 or T_1 states which are (n→π^*) states localized at the C_5=O_1 chromophore. Therefore, in these excited states, electron charge density accumulates on the C_5 atom. The negative charge populated on the C_5 atom might delocalize into the σ-type LUMO of the three-membered ring which is the *anti*-bonding orbital (σ^*_{C-N}) of the N_2–

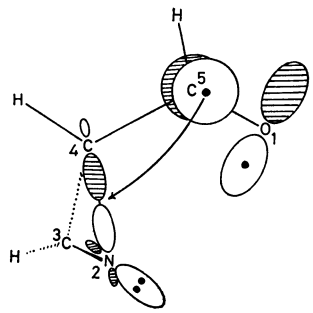

C_4 bond. Thus, this type of orbital interaction and also the strain of the three-membered ring promote the N_2–C_4 bond scission. Since σ^*_{C-C} orbital of the azirine ring lies much higher than σ^*_{C-N} orbital, it does not mix with π^*_{C-O} orbital so efficiently as σ^*_{C-N} orbital. The reaction does not experience nitrene be-

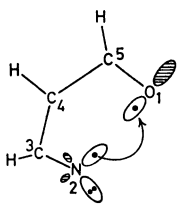

cause one of unpaired electrons is on the O_1 atom. That is, this reaction proceeds by above mentioned manner.

Reaction (3): ***2a→3a.*** As Fig. 5(b) shows, ($n\rightarrow\pi^*$) states of the $C_3{=}N_2$ chromophore, S_2 and T_4 states, become stable with the increase in the C_3–N_2–C_4 bond angle, because the hybridization on the N atom is varied from sp^2 to sp due to the removal of an electron from the lone-pair orbital of N atom (Walsh's rule).[10] Bigot *et al.* have shown that the ring opening of 2*H*-azirine occurs *via* ISC from $^1(n\rightarrow\pi^*)$ to $^3(n\rightarrow\pi^*)$ states.[11] The present results accord with theirs. But this ring opening would not occur with retaining the plane of azirine ring. The fol lowing motion would be also helpful for the ring opening. In fact, the present calculation shows that this conrotatory motion gives the descending potential curve in the T_1 state and leads to the O_1–C_3 bond formation.

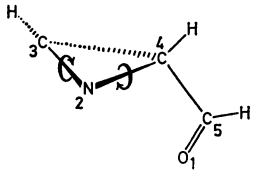

Padwa *et al.*[12] and Schmid *et al.*[13] have reported that 2*H*-azirines undergo the irreversible ring opening at the C–C bond to give nitrile ylides as the reactive intermediates. These intermediates can be intercepted

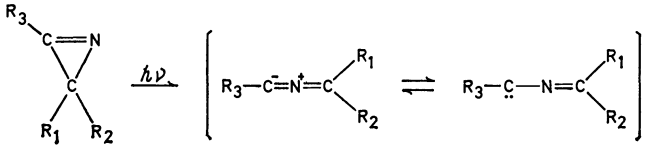

with dipolarophiles to form five-membered heterocyclic rings or other type of isomers.[14] With this analogy, Ullman and Singh have proposed nitrile ylide intermediates as the precursor of oxazole in the reaction (3).[4b,15] In order to examine whether the reaction (3) proceeds *via* this intermediate or not, the state energy variation due to the deformation of the C_3–N_2–C_4 bond angle of the nitrile ylide intermediate χ is calculated. The result is shown in Fig. 7. The decrease of χ in the ground state indicates the slow energy ascent. One can expect that the nitrile ylide intermediate in the ground state transforms to an oxazole with relative low activation energy.

However, the ground-state nitrile ylide has a linear structure at the C_3–N_2–C_4 part, while the lowest excited state nitrile ylide is carbenic and has a bent structure such as

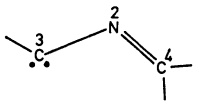

The ring opened form of **2a** in the triplet state seems to be biradical. If the ground-state nitrile ylide is formed during the reaction, the bond formation between O_1 and C_3 atoms requires too much motion of nuclei, which contravenes the principle of least

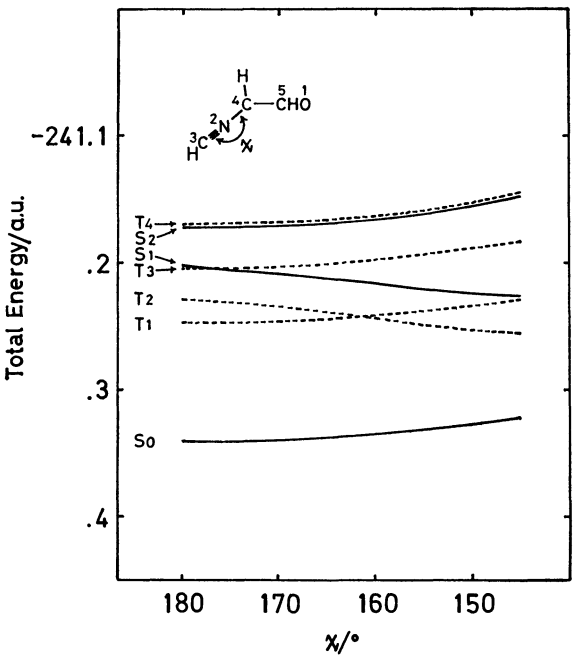

Fig. 7. State energy variation of nitrile ylide intermediate by the decrease of the C_3–N_2–C_4 bond angle χ.

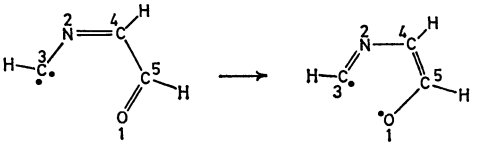

motion.[16] Therefore, it might be concluded that **3a** is formed without any intermediacy, that is, with almost one-step reaction.

Concluding Remarks

As Figs. 4 and 5 show, any geometrical deformation greatly destabilizes the ground states of both **1a** and **2a**, which suggests that these reactions hardly occur thermally.

As mentioned above, the azirine intermediate has different two reactive states, S_1 and S_2 states. These states are almost localized at the C=O and C=N chromophores, respectively, and lead to different reaction products each other *via* different reaction paths. This is the reason why the azirine intermediate has the wavelength dependent photochemistry.

From the calculated results, the mechanism of the photoisomerization of isoxazole can be summarized as follows;

Reaction (1): Isoxazole in the lowest $^1(n\rightarrow\pi^*)$ state interconverts to azirine intermediate in the ground state through the N_2–C_3–C_4–C_5 torsional deformation which leads to the O_1–N_2 bond scission and the N_2–C_4 bond formation simultaneously.

Reaction (2): The S_1 state of azirine intermediate is an ($n\rightarrow\pi^*$) state of the carbonyl chromophore. The deformation of the N_2–C_3–C_4 bond angle in the T_1 state produced through the ISC from the S_1 state causes the N_2–C_4 bond rupture. Subsequently, odd electrons on the O_1 and N_2 atoms combine to form the O_1–N_2 bond, leading to the formation of isoxazole.

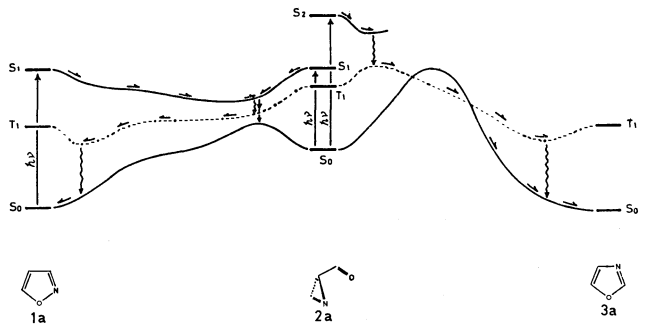

Fig. 8. The possible mechanism of the photoisomerization of isoxazole to oxazole infered from the present (S+D+T)ECI calculation.

This reaction does not experience nitrene.

Reaction (3): Azirine intermediate in S_2 state which is an ($n\rightarrow\pi^*$) state of the ketimine chromophore causes the C_3–C_4 bond rupture by the deformation of the C_3–N_2–C_4 bond angle. It is possible to follow the conrotatory motion in such a ring opening process. The transformation to oxazole proceeds *via* ISC from the S_2 to T_1 states. The doubly and triply excited configurations have an effect of small modification in this reaction.[5] This reaction does not experience any intermediacy.

The possible reaction path of photoisomerization reaction of isoxazoles to oxazoles through azirine intermediates can be shown pictorially in Fig. 8.

The authers would like to express their gratitude to the Computer Center of Institute for Molecular Science and to the Data Processing Center of Kyoto University, for the use of the HITAC M-180 and FACOM M-200 computers. They also thank Dr. Shinichi Yamabe, Nara University of Education, for the use of the GAUSSIAN 70 program.

References

1) a) H. Wynberg and H. van Driel, *J. Am. Chem. Soc.*, **87**, 3998 (1965); b) H. Wynberg, R. M. Kellogg, H. van Driel, and G. E. Beekhuis, *ibid.*, **89**, 3501 (1967).

2) P. Beak and W. Messer, *Tetrahedron*, **25**, 3287 (1969).

3) a) A. W. Burgstahler and P. L. Chien, *J. Am. Chem. Soc.*, **86**, 5281 (1964); b) K. E. Wilzbach and L. Kaplan, *ibid.*, **87**, 4004 (1965).

4) a) E. F. Ullman and B. Singh, *J. Am. Chem. Soc.*, **88**, 1844 (1966); b) B. Singh and E. F. Ullman, *ibid.*, **89**, 6911 (1967); c) B. Singh, A. Zweig, and J. B. Gallivan, *ibid.*, **94**, 1199 (1972).

5) In order to compare the electronic structure of **1a** and **2a** with those of **1** and **2**, CNDO/S-CI calculations are carried out for 3,5-diphenylisoxazole and 2-benzoyl-3-phenyl-2*H*-azirine($Ar_1=Ar_2=C_6H_5$ in Fig. 1). See, H. Tanaka, T. Matsushita, Y. Osamura, and K. Nishimoto, *Int. J. Quantum Chem.*, **18**, 463 (1980).

6) W. J. Hehre, W. A. Lathan, M. Ditchfield, M. D. Newton, and J. A. Pople, GAUSSIAN 70, Program No. 236, Quantum Chemistry Program Exchange, Indiana University, Bllomington, Indiana.

7) a) O. L. Stiefvater, *J. Chem. Phys.*, **63**, 2560 (1975); b) A. Kumar, J. Sheridan, and O. L. Stiefvater, *Z. Naturforsch., Tail A*, **33A**, 145 (1978).

8) a) T. Matsuura and Y. Ito, *Tetrahedron Lett.*, **1973**, 2283; b) T. Mukai, T. Kumagai, and O. Seshimoto, *Pure Appl. Chem.*, **49**, 287 (1977).

9) K. Fukui, "Theory of Orientation and Stereoselection," Springer-Verlag, New York (1975).

10) A. D. Walsh, *J. Chem. Soc.*, **1953**, 2260.

11) B. Bigot, A. Sevin, and A. Devaquet, *J. Am. Chem. Soc.*, **100**, 6924 (1978).

12) A. Padwa, M. Dahran, J. Smolanoff, and S. I. Wetmore Jr., *Pure Appl. Chem.*, **33**, 269 (1973).

13) P. Claus, T. Doppler, N. Gakis, M. Georgarakis, H. Giezendanner, P. Gilgen, H. Heimgartner, B. Jackson, M. Markey, N. S. Narasimhan, H. J. Rosenkranz, A. Wunderli, H. J. Hansen, and H. Schmid, *Pure Appl. Chem.*, **33**, 339 (1973).

14) A. Padwa, *Acc. Chem. Res.*, **9**, 371 (1976), and references cited therein.

15) E. F. Ullman, *Acc. Chem. Res.*, **1**, 353 (1968).

16) F. O. Rice and E. Teller, *J. Chem. Phys.*, **6**, 489 (1938).

ESR and ENDOR Studies of Azulenophane Anion Radicals

Masamoto Iwaizumi,* Yoshimasa Fukazawa,† Nobuo Kato,† and Shô Itô†

Chemical Research Institute of Non-Aqueous Solutions, Tohoku University, Katahira, Sendai 980

†*Department of Chemistry, Faculty of Science, Tohoku University, Aramaki Aoba, Sendai 980*

(Received August 4, 1980)

The anion radicals of *syn*- and *anti*-[2.2](2,6)azulenophane, (**1**) and (**2**), [2.2](1,3)azulenophane, (**3**), and [2](1,3)-azuleno[2]paracyclophane, (**4**), all produced by alkali metal reduction in various solvents, have been investigated by ESR and ENDOR spectroscopy. They exist in the ion pair with cations in the solutions, except for $\mathbf{4}^{\cdot-}$ which exists in 1,2-dimethoxyethane with Na^+. Their ion pairing tendency is appreciably higher than that of the naphthalenophane anion radicals. The unpaired electron in these ion pairs localizes mostly on an azulene ring (in $\mathbf{1}^{\cdot-}$, $\mathbf{2}^{\cdot-}$, and $\mathbf{3}^{\cdot-}$, close to a cation). The polarization effects due to the pairing with the cations are much larger than those in the naphthalenophane anion radicals, and increase in the order $\mathbf{1}^{\cdot-} \leq \mathbf{2}^{\cdot-} \leq \mathbf{3}^{\cdot-}$, indicating that the smaller the inter-layer orbital overlap, the larger the polarizability. The unpaired electron of $\mathbf{4}^{\cdot-}$ localizes mostly on the azulene ring even in the free anion.

Extensive studies have been carried out during the past decade on the distribution of unpaired electron in the anion radicals of paracyclophanes, because of the general interest in the transannular interaction in these layered compounds.[1-9] However, the compounds studied so far contain only alternant hydrocarbons with a few exceptions. In this paper, we describe the result of ESR and ENDOR spectroscopic studies on the anion radicals of *syn*- and *anti*-[2.2]-(2,6)azulenophanes (**1** and **2**), [2.2](1,3)azulenophane (**3**) and [2](1,3)azuleno[2]paracyclophane (**4**), all containing azulene rings. Investigation of these compounds seems significant, since they contain, as aromatic moieties, azulene which is a typical non-alternant hydrocarbon known to have unique physicochemical properties different from alternant hydrocarbons. We were interested in the evaluation of the difference in the unpaired electron delocalization found for $\mathbf{1}^{\cdot-}$ and $\mathbf{2}^{\cdot-}$ with opposite orientation of the azulene ring.

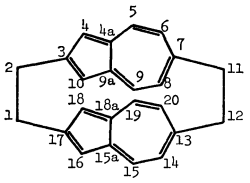

1

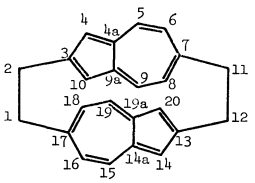

2

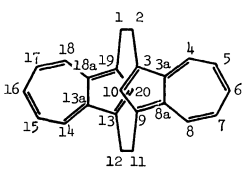

3

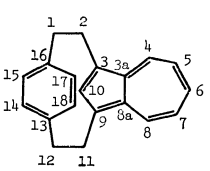

4

Experimental

Compounds **1**, **2**, **3**, and **4** were synthesized by the method reported.[10] In order to prepare the anion radicals of the compounds, reduction with sodium or potassium in 1,2-dimethoxyethane (DME), tetrahydrofuran (THF), 2-methyltetrahydrofuran (MTHF), and mixture of the former two was carried out. ESR and ENDOR spectra of the anion radicals were measured with Varian E112 ESR and E1700 ENDOR spectrometers. However, no radicals $\mathbf{1}^{\cdot-}$, $\mathbf{2}^{\cdot-}$, and $\mathbf{3}^{\cdot-}$ could be detected in DME because of their instability at *ca.* −85 °C, the freezing point of the solution.

Results and Discussion

ESR Spectra. All the ESR spectra of anion radicals produced from **1**—**4** at temperatures below −90 °C in various solvents are well defined (Figs. 1—4). However, in mixed DME–THF with concentration of DME higher than 3:1 (volume), radical

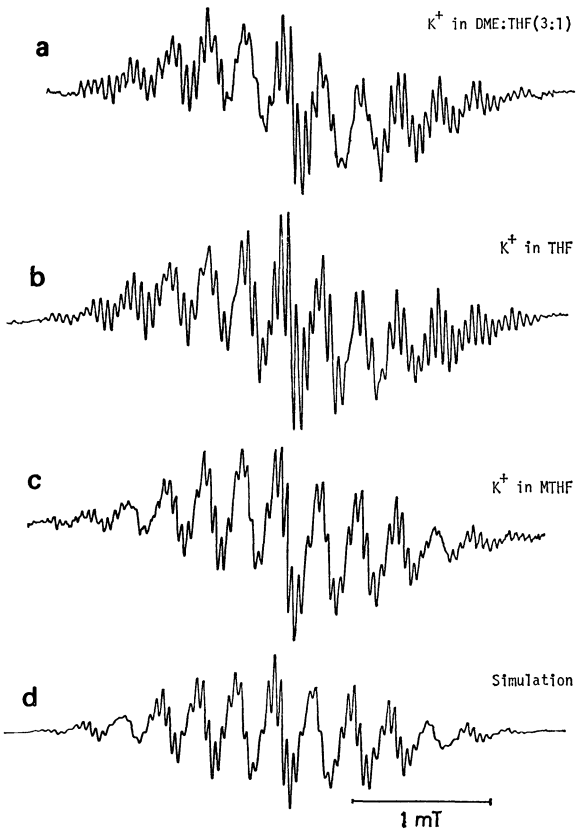

Fig. 1. ESR spectra of $\mathbf{1}^{\cdot-}$ observed at −95 °C in a) K^+ in DME:THF (3:1), b) K^+ in THF, and c) K^+ in MTHF, and d) simulated spectrum for c) using the hf coupling constants in Table 1.

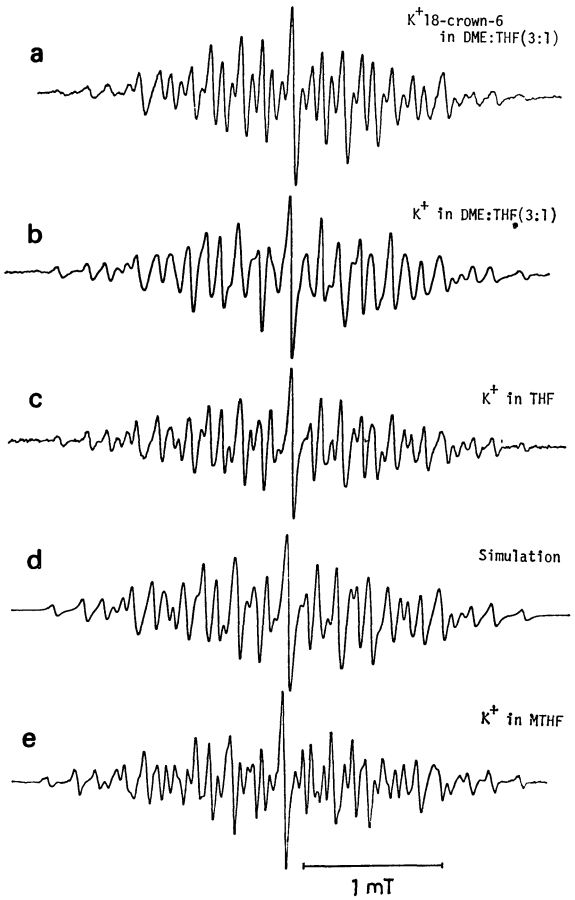

Fig. 2. ESR spectra of $\mathbf{2}^{\cdot-}$ observed at −95 °C in a) K^+ 18-crown-6 in DME:THF (3:1), b) K^+ in DME:THF (3:1), c) K^+ in THF and e) K^+ in MTHF, and d) simulated spectrum for c) using the hf coupling constants in Table 2.

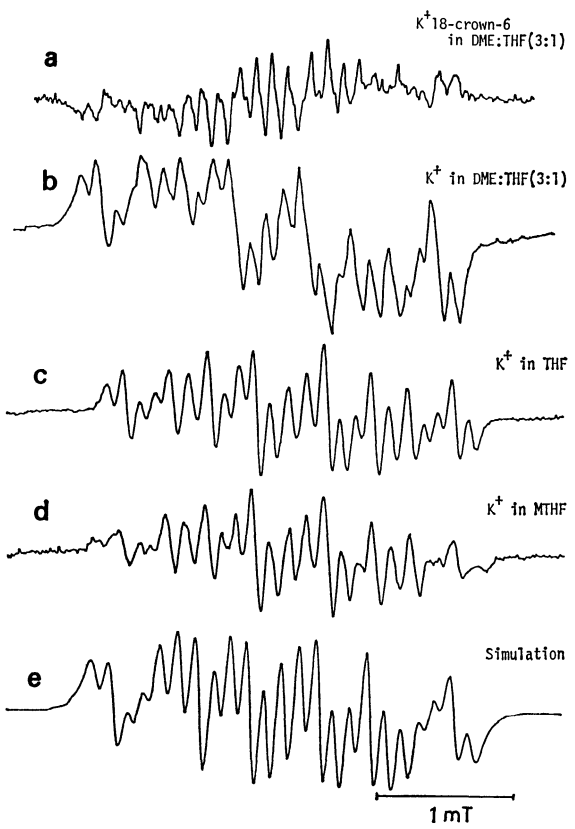

Fig. 3. ESR spectra of $\mathbf{3}^{\cdot-}$ observed at −95 °C in a) K^+ 18-crown-6 in DME:THF (3:1), b) K^+ in DME:THF (3:1), c) K^+ in THF, d) K^+ in MTHF, and e) simulated spectrum for d) using the hf coupling constants in Table 3.

species produced from **1** displayed different hf structure and smaller total spread (2.7 mT) than the spectra shown in Fig. 1. Furthermore, on reduction with sodium, **1** and **2** exhibit spectra due to two different radical species, one showing a very broad pattern with no hf splitting and the other a sharp one with many hf lines. In all cases, no reliable analysis was possible and no radical species could be identified.

From Figs. 1—4 we see that the spectra of $\mathbf{1}^{\cdot-}$ and $\mathbf{3}^{\cdot-}$ are hardly affected at all by solvents, the spectrum of $\mathbf{2}^{\cdot-}$ changing slightly, while that of $\mathbf{4}^{\cdot-}$, which is similar to that of $\mathbf{3}^{\cdot-}$, changes a great deal with solvent. The spectrum of $\mathbf{4}^{\cdot-}$ also changes with temperature. The hf pattern produced with potassium in DME at −50——60 °C is very similar to that in THF or MTHF, but on cooling to *ca.* −85 °C, the pattern becomes similar to that in DME with sodium ion.

ENDOR Spectra. Measurements of ENDOR spectra of $\mathbf{1}^{\cdot-}$—$\mathbf{4}^{\cdot-}$ were undertaken, but except for $\mathbf{4}^{\cdot-}$ no spectra could be obtained because of insufficient radical concentration. A typical spectrum observed for $\mathbf{4}^{\cdot-}$ is shown in Fig. 5.

Analysis of the ESR Spectra. The ESR spectra of $\mathbf{1}^{\cdot-}$ can be interpreted in terms of six sets of triplet splittings, those of $\mathbf{2}^{\cdot-}$ by four sets of triplets and those of $\mathbf{3}^{\cdot-}$ and $\mathbf{4}^{\cdot-}$ by two sets each of triplets and doublets. This indicates that the unpaired electrons in $\mathbf{1}^{\cdot-}$, $\mathbf{2}^{\cdot-}$, and $\mathbf{3}^{\cdot-}$ are distributed unequally on the two azulene rings in the molecules since the quintet splittings would be observed if the unpaired electrons are distributed equally on the two azulene rings. The observed distribution suggests that the anion radicals interact with the counter ion in the solutions. $\mathbf{4}^{\cdot-}$ is also considered to have interaction with the counter ion. The coupling constants were determined from the ESR and ENDOR (for $\mathbf{4}^{\cdot-}$) spectra and assigned to the respective protons on the basis of MO calculation (*vide infra*), referring to the hf interaction in the azulene anion radical ($\mathbf{5}^{\cdot-}$), since the relative ratio of the spin densities in the azulene should not change so much by the transannular interaction or ion pairing. No calculation was carried out for $\mathbf{3}^{\cdot-}$, but the assignment was easily made by comparison with that of $\mathbf{4}^{\cdot-}$, which gives very similar ESR spectra.

MO Calculation for the Hf Coupling Constants. The unpaired electron distribution and the hf coupling constants of the anion radicals in the ion pair form were calculated by the method reported.[9] The geometry of the anion radicals was estimated from the X-ray data for the neutral molecules,[10] the exchange integrals being assumed to be proportional to the overlap integrals, and the proportional constant for the exchange integrals between the layers one and half times the constant within the layers. Only the sets of atomic orbitals which gave larger overlap in-

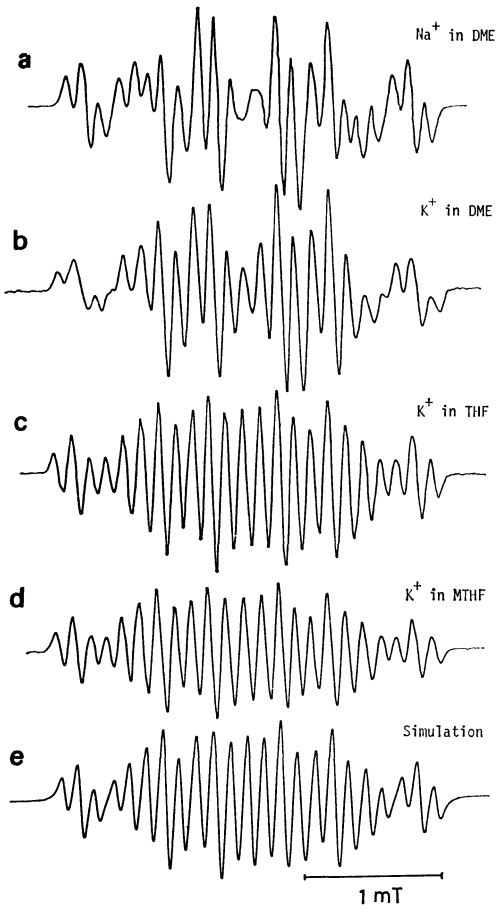

Fig. 4. ESR spectra of $\mathbf{4}^{\cdot-}$ a) Na^+ in DME at −90 °C, b) K^+ in DME at −90 °C, c) K^+ in THF at −95 °C, and d) K^+ in MTHF, and e) simulated spectrum for c) using the hf coupling constants in Table 4.

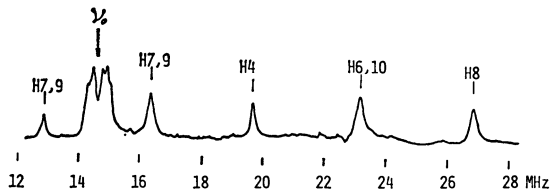

Fig. 5. ENDOR spectrum of $\mathbf{4}^{\cdot-}$, K^+ in MTHF at −95 °C.

tegrals than 0.02 were taken into account for the interlayer exchange integrals.

The potential energy maps for the cation placed at a distance of 0.38 nm above the nearest azulene ring were calculated for ion pairs of $\mathbf{1}^{\cdot-}$, $\mathbf{2}^{\cdot-}$, and $\mathbf{4}^{\cdot-}$. The results are shown in Fig. 6, together with a similar map for $\mathbf{5}^{\cdot-}$. Another model of $\mathbf{4}^{\cdot-}$ examined in which the cation was placed above the benzene ring gave less stable potential energies. The results show that the most stable position of cation in $\mathbf{1}^{\cdot-}$ is above the center of the five-membered ring. The position shifts toward the seven-membered ring on going from $\mathbf{1}^{\cdot-}$ to $\mathbf{2}^{\cdot-}$ and then to $\mathbf{4}^{\cdot-}$.

The spin density distribution and the hf coupling constants were calculated[11] as a function of the distance between the cation and the anion radicals by

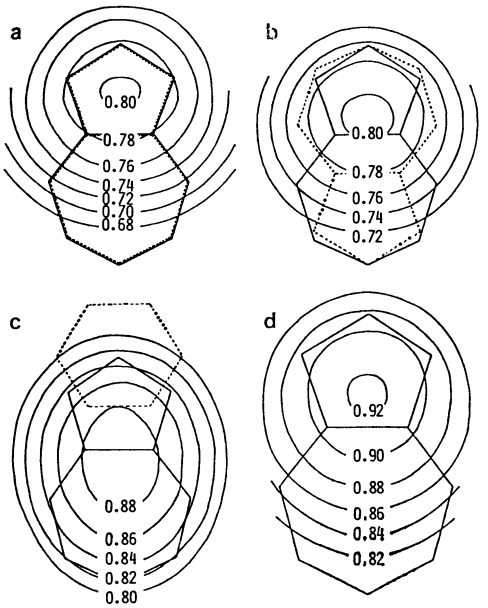

Fig. 6. Electrostatic interaction energies between a cation and anion radicals, a) $\mathbf{1}^{\cdot-}$, b) $\mathbf{2}^{\cdot-}$, c) $\mathbf{4}^{\cdot-}$, and d) $\mathbf{5}^{\cdot-}$ (in unit of β). The cation is placed at the distance of 0.38 nm from the nearest aromatic plane (drawn by solid lines).

placing the former above the potential minimum points. The potential minimum position of the cation has been shown to change slightly with distance which may cause some effect on the hf constants.[12] However, such an effect was ignored because it would not be so large as to give a wrong assignment of the hf coupling constants.

Spin Distribution in $\mathbf{1}^{\cdot-}$ and $\mathbf{2}^{\cdot-}$. The observed proton hf coupling constants could reasonably be assigned to the protons (Tables 1 and 2) of the anion radicals in the ion pair form on the basis of the above calculation. The MO calculation showed that the hf coupling constants change drastically with the distances between the cation and the anion radicals. The calculated coupling constants are for the distance 0.35 nm which give the best fit with the experimental values.

In order to observe the ESR spectra of $\mathbf{1}^{\cdot-}$ and $\mathbf{2}^{\cdot-}$ in the free anion state, generation of the anion radicals

Table 1. Hf coupling constants of $\mathbf{1}^{\cdot-}$

Position, i	$\lvert a_i^H \rvert$/mT			
	DME:THF, (3:1) K^+	THF, K^+	MTHF, K^+	Calcd[a]
5, 9	0.557	0.567	0.568	0.6010
11	0.517	0.524	0.523	0.5180
2	0.291	0.292	0.292	0.2689
6, 8	0.251	0.247	0.252	0.1503
15, 19	0.094	0.095	0.091	0.1245
12	0.050	0.050	0.047	0.0908
1	—	—	—	0.0601

a) The distance between the cation and the anion radical was taken to be 0.35 nm.

Table 2. Hf coupling constants of $2^{\cdot-}$

Position, i	$\lvert a_i^H \rvert$/mT				
	DME:THF(3:1), K^+-(18-crown-6)	DME:THF, K^+ (3:1)	THF, K^+	MTHF, K^+	Calcd[a]
5, 9	0.5826	0.5993	0.6029	0.6095	0.6487
11	0.5048	0.5046	0.5081	0.5187	0.5495
2	0.3600	0.3485	0.3589	0.3633	0.2875
6, 8	0.2177	0.2216	0.2167	0.2139	0.1671
15, 19	—	—	—	—	0.1317

a) The distance between the cation and the anion radical was taken to be 0.35 nm.

Table 3. Hf coupling constants of $3^{\cdot-}$

Position, i	$\lvert a_i^H \rvert$/mT			
	DME:THF(3:1), K^+-(18-crown-6)	DME:THF, K^+ (3:1)	THF, K^+	MTHF, K^+
6	0.832		0.840	
4, 8	0.590		0.610	
10	0.362		0.367	
5, 7	0.115		0.110	

in the presence of 18-crown-6 was examined. However, the ESR spectrum observed for $2^{\cdot-}$ was still due to the ion pair, and that attributable to $1^{\cdot-}$ was not observed under these conditions.

It is apparent from the hf coupling constants obtained that the unpaired electron largely localized on the azulene ring at the cation side. By comparison with the hf coupling constants of the azulene anion radical ($a_{1,3}^H=0.0274$ mT, $a_2^H=0.3948$ mT, $a_{4,8}^H=0.6219$ mT, $a_{5,7}^H=0.1338$ mT, $a_6^H=0.8829$ mT),[13] the unpaired electron densities on the azulene ring at the cation side were estimated to be *ca.* 87—91% for $1^{\cdot-}$ and 89—93% for $2^{\cdot-}$. The [2.2](1,4)naphthalenophane anion radical also shows a similar large polarization in the spin distribution by the formation of ion pairs.[5b] In the ion pair of the *syn* isomer($6^{\cdot-}$), the unpaired electron densities on the naphthalene ring close to a cation can be estimated as *ca.* 72—77% by comparison of its hf coupling constants with those of naphthalene anion radical.[14] The polarization in the azulenophane anion radicals is appreciably larger than that in the naphthalenophane anion radical.

The hf coupling constants of 11 position in $1^{\cdot-}$ is larger than that for the corresponding position in $2^{\cdot-}$, while that of 2 position in $1^{\cdot-}$ is smaller than that for the same position in $2^{\cdot-}$, indicating that the unpaired electron distribution in $1^{\cdot-}$ is polarized more from the head position (3 position) to the tail (7 position) than in $2^{\cdot-}$.

Spin Distribution in $3^{\cdot-}$. The observed hf coupling constants (Table 3) apparently show that the unpaired electrons are mostly distributed on one of the azulene ring. The situation did not change with the presence of 18-crown-6. As in $1^{\cdot-}$ and $2^{\cdot-}$, the observed polarization in the spin distribution can be attributed to the ion pairing of the anion radical. From a comparison with the hf coupling constants of the azulene anion radical, the unpaired electron densities on the azulene ring at the cation side are estimated to be *ca.* 94—95%; larger polarization than that in $1^{\cdot-}$ and $2^{\cdot-}$.

Spin Distribution in $4^{\cdot-}$. The ESR spectrum at −50—−60 °C of $4^{\cdot-}$ in DME with potassium ion is similar to spectra observed for $4^{\cdot-}$ in THF or MTHF, becoming similar to that observed in DME with sodium ion with lowering in temperature. This suggests that $4^{\cdot-}$ in DME with sodium ion exists mostly as a free anion; it is associated with the cation in THF and MTHF, and $4^{\cdot-}$ in DME with potassium ion is in an equilibrium between these two forms. The equilibrium shifts toward the free anion state by lowering in temperature. The hf coupling constants obtained for $4^{\cdot-}$ both in the free anion and in the ion pair are given in Table 4.

We see that the unpaired electrons are distributed mostly on the azulene ring even when the anion radical is in a free anion state. By ion pairing the spin density is polarized more from the benzene ring to the azulene ring. This indicates that the cation is associated with $4^{\cdot-}$ at the azulene ring side, in line with the result of calculation of the cation-anion interaction energies. The unpaired electron densities on the azulene ring are *ca.* 91—95% in the free anion state and *ca.* 98—99% in the ion pair form.

In contrast to the increase of spin density of the azulene ring as a whole, the density of carbon 10 is reduced by the interaction with the counter ion. Such polarization effect by ion pairing can be shown by MO calculation using the ion-pair model in which the cation is placed above the potential minimum point. The calculation using the other ion pair model does not reproduce the observed effect (Table 4).

Polarization of Unpaired Electron Distribution and the Interlayer Interaction. The unpaired electron in $1^{\cdot-}$, $2^{\cdot-}$, and $3^{\cdot-}$ is localized in one of the azulene rings. The unpaired electrons in the anion radical of [2.2]-

Table 4. Hf coupling constants of $4^{\cdot-}$

Position, i	$\lvert a_i^H \rvert$/mT			Effect of Cation, $\Delta\lvert a_i^H \rvert$/mT[a]			
	DME, Na^+	MTHF, K^+	Calcd[b]	Obsd	Calcd[b]		
					Model I[c]	II[c]	III[c]
6	0.8357	0.8746	0.8575	+0.0383	−0.0091	−0.0041	−0.0023
4, 8	0.5751	0.6180	0.6910	+0.0429	+0.0791	+0.0357	−0.0391
10	0.3865	0.3612	0.2777	−0.0253	−0.0031	−0.0141	+0.0011
5, 7	0.1070	0.1254	0.1546	+0.0184	+0.0587	+0.0094	−0.0360
2, 11[d]	0.0328	0.0294	0.0636	−0.0034	−0.0283	−0.0033	+0.0245
14, 15[d]	0.0241	0.0220	0.0046	−0.0021	−0.0018	−0.0007	+0.0000
17, 18[d]	0.0162	0.0106	0.0023	−0.0056	−0.0001	−0.0001	+0.0001
1, 12	—	—	0.0018	—	+0.0025	+0.0057	+0.0089

a) The difference between the hf coupling constants of the free anion state and the ion pair form. b) The distance between the cation and the anion radical was taken to be 0.35 nm. c) In models I, II, and III, the cation is placed above the center of the five-membered ring, the potential minimum point and the center of the seven-membered ring, respectively. d) The empirical hf coupling constants were tentatively assigned to the proton positions. The hf interactions were not observed in the ESR spectra and the coupling constants were obtained from the ENDOR specta.

paracyclophanes with the identical aromatic rings are distributed equally on both rings unless there is interaction with a counter ion.[1-7] The observed localization (polarization) might arise from such an interaction. The results indicate that polarization due to a cation increases in the order $\mathbf{1}^{\cdot-} \leq \mathbf{2}^{\cdot-} < \mathbf{3}^{\cdot-}$. Since the geometry of these molecules indicates the decreasing order $\mathbf{1}^{\cdot-} > \mathbf{2}^{\cdot-} > \mathbf{3}^{\cdot-}$ in the interlayer π-π interaction,[10] the observed order of the polarization shows that smaller interlayer π-π interaction gives larger polarization in the electron spin distribution.

The unpaired electron in $\mathbf{1}^{\cdot-}$ and $\mathbf{2}^{\cdot-}$ is polarized to a greater extent than in $\mathbf{6}^{\cdot-}$. Such a difference may be attributed to the nature of the two aromatic ring systems.

Tendency to Ion Pairing. While $\mathbf{6}^{\cdot-}$ exists as a free anion in THF with potassium ion,[5b] $\mathbf{1}^{\cdot-}$ and $\mathbf{2}^{\cdot-}$ exist in the ion pair form under the same conditions. This indicates that $\mathbf{1}^{\cdot-}$ and $\mathbf{2}^{\cdot-}$ have higher tendency of ion pairing than $\mathbf{6}^{\cdot-}$. It seems of interest to compare the ion pairing tendencies of the azulenophane anion radicals with those of other relating anion radicals. By taking into account the fact that anion radicals tend to associate more at higher temperature with the alkali metal cations in various solvents in the order $Li^+ < Na^+ < K^+$, and DME < THF < MTHF, the following order for ion pairing tendency is estimated: $\mathbf{6}^{\cdot-}$ < *anti*-[2.2](1,4)naphthalenophane$^{\cdot-}$ ($\mathbf{7}^{\cdot-}$) < $\mathbf{1}^{\cdot-}$, $\mathbf{2}^{\cdot-}$, $\mathbf{3}^{\cdot-}$, $\mathbf{4}^{\cdot-} \leq$ naphthalene$^{\cdot-}$ ($\mathbf{8}^{\cdot-}$) < $\mathbf{5}^{\cdot-}$.[15] Thus, the anion radicals corresponding azulene rings have higher tendency of ion pairing than the naphthalene counterparts. Such a pronounced tendency of ion pairing of azulenophane anion radicals may be mainly attributed to the nature of the azulene ring which tends to accumulate a high negative charge on its five-membered ring. The estimated order for the ion pairing agrees with the order in the electrostatic interaction energies calculated for the most stable ion pair structures for the anion radicals: $\mathbf{6}^{\cdot-}$(0.752) < $\mathbf{7}^{\cdot-}$(0.787) < $\mathbf{1}^{\cdot-}$(0.802) ≤ $\mathbf{2}^{\cdot-}$(0.806) < $\mathbf{4}^{\cdot-}$(0.893) < $\mathbf{8}^{\cdot-}$(0.895) < $\mathbf{5}^{\cdot-}$(0.920).[16]

Table 5. Calculated spin densities in $\mathbf{1}^{\cdot-}$ and $\mathbf{2}^{\cdot-}$ in the free anion state

Position	$\mathbf{1}^{\cdot-}$	$\mathbf{2}^{\cdot-}$
3	0.0729	0.0694
4, 10	−0.0099	0.0028
4a, 9a	0.0376	0.0195
5, 9	0.1497	0.1610
6, 8	−0.0308	−0.0372
7	−0.1338	0.1382

Spin Distribution in $\mathbf{1}^{\cdot-}$ and $\mathbf{2}^{\cdot-}$ in the Free Anion State. The spin density distributions in $\mathbf{1}^{\cdot-}$ and $\mathbf{2}^{\cdot-}$ in the free anion state were not clarified experimentally in the present work. However, the electron spin distribution (Table 5) predicted by MO calculation shows that the unpaired electron in $\mathbf{2}^{\cdot-}$ is localized more on the seven-membered ring than in $\mathbf{1}^{\cdot-}$, in view of the finding that in ion pairs the unpaired electron in $\mathbf{2}^{\cdot-}$ is localized more on the five-membered ring than in $\mathbf{1}^{\cdot-}$.

References

1) S. I. Weissman, *J. Am. Chem. Soc.*, **80**, 6462 (1958).
2) A. Ishitani and S. Nagakura, *Mol. Phys.*, **12**, 1 (1967).
3) a) K. Ishizu, Y. Sugimoto, Y. Sakata, and S. Misumi, *Bull. Chem. Soc. Jpn.*, **50**, 2801 (1977); b) F. Nemoto, K. Ishizu, T. Toyoda, Y. Sakata, and S. Misumi, *J. Am. Chem. Soc.*, **102**, 654 (1980).
4) a) F. Gerson, G. Kaupp, and H. Ohya-Nishiguchi, *Angew. Chem.*, **89**, 666 (1977); b) Ch. Elschenbroich, F. Gerson, and J. A. Reiss, *J. Am. Chem. Soc.*, **99**, 60 (1977).
5) a) F. Gerson and W. B. Martin, Jr., *J. Am. Chem. Soc.*, **91**, 1883 (1969); b) F. Gerson, W. B. Martin, Jr., and Ch. Wydler, *ibid.*, **98**, 1318 (1976).
6) T. Hayashi, M. Mataga, Y. Sakata, and S. Misumi, *Bull. Chem. Soc. Jpn.*, **48**, 416 (1975).
7) D. J. Williams, J. M. Pearson, and M. Levy, *J. Am. Chem. Soc.*, **93**, 5483 (1971).
8) F. Gerson, W. B. Martin, Jr., and Ch. Wydler, *Helv. Chim. Acta*, **59**, 1365 (1976).

9) M. Iwaizumi, S. Kita, T. Isobe, M. Kohno, T. Yamamoto, H. Horita, T. Otsubo, and S. Misumi, *Bull. Chem. Soc. Jpn.*, **50**, 2074 (1977).

10) N. Kato, Y. Fukazawa, and S. Itô, *Tetrahedron Lett.*, **1976**, 2045; N. Kato, H. Matsunaga, S. Oeda, Y. Fukazawa, and S. Itô, *ibid.*, **1979**, 2419; Y. Fukazawa, M. Aoyagi, and S. Itô, *ibid.*, **1978**, 1299, **1979**, 1055.

11) It was assumed that $Q_{alkyl}=2.30$ mT and $Q_{arom.}=2.25$ mT for $\mathbf{1}^{\overline{\cdot}}$, $\mathbf{2}^{\overline{\cdot}}$, and $\mathbf{3}^{\overline{\cdot}}$, and $Q_{alkyl}=2.30$ mT and $Q_{arom.}=2.50$ mT for $\mathbf{4}^{\overline{\cdot}}$.

12) M. Iwaizumi, M. Suzuki, T. Isobe, and H. Azumi, *Bull. Chem. Soc. Jpn.*, **40**, 1325 (1967).

13) I. Bernal, P. H. Rieger, and G. K. Fraenkel, *J. Chem. Phys.*, **37**, 1489 (1962); 1, 2, 3, 4, 5, and 6 positions in the azulene anion radical correspond to 10, 3, 4, 5, 6, and 7 positions in $\mathbf{1}^{\overline{\cdot}}$ and $\mathbf{2}^{\overline{\cdot}}$, respectively.

14) a) N. M. Atherton and S. I. Weissman, *J. Am. Chem. Soc.*, **83**, 1330 (1961); b) M. Iwaizumi, M. Suzuki, T. Isobe, and H. Azumi, *Bull. Chem. Soc. Jpn.*, **41**, 732 (1968).

15) The order of tendency among $\mathbf{1}^{\overline{\cdot}}$, $\mathbf{2}^{\overline{\cdot}}$, $\mathbf{3}^{\overline{\cdot}}$, and $\mathbf{4}^{\overline{\cdot}}$ has not been made clear in the present work.

16) In unit of β. The cation-anion distances are taken to be 0.38 nm.

  Bull. Chem. Soc. Jpn., 54, 1305—1307 (1981)

A Sandwich Photocell Using Chlorophyll Electrodes

Fujio TAKAHASHI* and Tetuo KOMORI

Faculty of Engineering, Utsunomiya University, Utsunomiya 321

(Received August 22, 1980)

A sandwich-type photocell was made by placing an electrolyte between two electrodes. A transparent electrode, a glass plate coated with In_2O_3, was used for one electrode. A mixture of chlorophyll and 2-(*cis*-10-heptadecenyl)-6-methoxy-*p*-benzoquinone was spread onto this transparent electrode. A Pt plate covered by chlorophyll or a mixture of chlorophyll and riboflavin tetrabutyrate was used as the other electrode. The electrolyte contained flavin mononucleotide in a phosphate buffer. The potential difference between the two electrodes was 314 mV and the maximum photovoltage under illumination was 176 mV. The photocell is compact and can produce a photocurrent for more than 90 h.

Recently there have been many papers concerning the energy conversion from light to electricity by photocells using a chlorophyll-coated electrode.[1,2] We reported already that the photovoltage and the photocurrent were obtainable by light irradiation on a system of a chlorophyll-quinone electrode immersed into an electrolyte.[3] This system consisted of two chambers separated by a porcelain diaphragm; each chamber contained a different electrolyte. The composition of electrolyte in each chamber was changed when the photoelectrolytic reaction was carried out. It was thought that such a photocell had to be made of two electrodes immersed into one electrolyte.

A sandwich-type photocell in which chlorophyll was placed between two different species of metals was found to generate a photovoltage caused by the difference of contact potential barrier on the two interfaces of chlorophyll and metal.[4] If we modeled on this system, a photocell using the electrolyte could be made in a compact shape.

This paper will present the results concerning a sandwich type photocell in which the electrolyte was placed between two different chlorophyll electrodes. This should be more compact than the two-chamber-type photocell, and could be expected to keep the composition of electrolyte constant during a cycle in which the redox compound in the electrolyte was reduced at the cathode and in turn the equivalent amount of reduced compound was oxidized at the anode to recover the original form.

Experimental

Materials. Chlorophyll and 2-(*cis*-10-heptadecenyl)-6-methoxy-*p*-benzoquinone (IQ) were obtained as described in the previous paper.[5] Riboflavin tetrabutyrate (RTB) was made by Wakamoto Pharmaceutical Co. Glutathione (abbreviated GSH or GSSG as the reduced or the oxidized form), flavin mononucleotide (FMN) and the other chemicals were of reagent grade or the best commercially available.

Photocell. A glass plate coated by In_2O_3 containing 5% SnO_2, or a silver or platinum plate (2 cm × 4 cm each) was used as the electrode. One electrode was prepared by covering a layer of a mixture of chlorophyll and IQ (molar ratio 1:5). The layer contained 0.03 μmol/cm² of chlorophyll. The other electrode was covered by chlorophyll alone or by a mixture of chlorophyll and RTB. A sheet of parafilm (American Can Co.; 2 cm × 2 cm × 0.013 cm) hollowed out in one part (1 cm × 1 cm) was placed on the electrode and the hollow was filled by the electrolyte. Then another electrode was placed on top of it to set up a sandwich-type photocell.

Measurements. The potential was measured by a Kikusui Denshi volt-ammeter model 116 connected to a recorder. A projector lamp (100 V, 150 W) was used for the source of light. The light of shorter wavelength than 460 nm was cut off by a color filter, V-Y46, and the heat wave band was cut off by a water filter.

Results and Discussion

Various Combination of Electrodes. It was observed that the photovoltage was generated by photocells made up by various combinations of two electrodes under illumination. The electrolyte used was composed of 0.1 M KCl solution containing 1 mM GSH and 1/2 mM GSSG. Glutathione was used because it gave the highest photovoltage among several redox compounds in the electrolyte as reported in the previous paper.[5] The results are summarized in Table 1.

In the case that two In_2O_3 electrodes were used for the photocell, the potential of the chlorophyll electrode was found to shift to a positive state with respect to the chlorophyll-IQ electrode when the light was turned on. This is in accord with the result in the previous paper.[5] The In_2O_3 electrode acted as an anode in the system of In_2O_3 and Ag electrodes, but as a cathode in the system of In_2O_3 and Pt electrodes. On the system of Ag|Chl|electrolyte|Chl, IQ|In_2O_3, and the system of In_2O_3|Chl|electrolyte|Chl,IQ|Pt, the potential differences between two electrodes became lower after the light was turned on, because the photopotential of chlorophyll electrode against chlorophyll-IQ electrode was always positive.

Table 1. The potentials of the photocells of

$$M_1|Chl\left|\begin{matrix}1\text{ mM GSH}\\0.5\text{ mM GSSG}\\0.1\text{ M KCl}\end{matrix}\right|Chl,\ IQ\ (1:5)|M_2$$

M_1	M_2	Potential (mV *vs.* M_2)		
		Dark (d)	Light (l)	Photovoltage (l) − (d)
In_2O_3	In_2O_3	15	84	69
In_2O_3	Ag	134	225	91
Ag	In_2O_3	−172	−149	23
In_2O_3	Pt	−98	−88	10
Pt	In_2O_3	175	228	53

3×10^4 lx, 20—24 °C.

The highest photovoltage was obtained with the system of In_2O_3|Chl|electrolyte|Chl,IQ|Ag. However this system was unstable. The photovoltage reduced with the lapse of time. Therefore the system of Pt|Chl|electrolyte|Chl,IQ|In_2O_3 was chosen for this work. This system produced a 0.05 $\mu A/cm^2$ photocurrent. It was thought that same other redox compound should be used instead of glutathione in order to obtain higher photovoltage and higher photocurrent.

The Photocells with FMN in Electrolyte. It is known that FMN can photoexcite and oxidize NADH, EDTA, or catecholamine easily.[6,7] Therefore, FMN rather than GSSG in the electrolyte might take the electron away from the chlorophyll electrode under illumination. The photoresponse-time curves of the photocell using FMN in the electrolyte were obtained and are shown in Fig. 1. Chlorophyll was coated on the In_2O_3 electrode. Another In_2O_3 electrode without coating was used as a counter electrode. The electrolyte contained 0.1 M KCl and 5 mM FMN in all cases.

The potential-time curve at the top in Fig. 1 shows that the potential shifted to a positive state at the beginning of light irradiation. Then the potential turned over into a negative state. It was assumed that photoexcited FMN might decompose to produce some substance whose isoalloxazine ring was reduced to form a hydroquinone type.[8] If so, the potential of the system containing EDTA, which reduced FMN under illumination,[6] should shift to a negative state more rapidly. It seems that the second curve in Fig. 1 sustains the above assumption. In order to keep the potential positive, the decomposition of FMN had to be avoided. Tryptophan is known to be effective for the suppression of FMN decomposition.[6] As seen at the bottom in Fig. 1, the potential of the system containing an equimolar mixture of FMN and tryptophan remained in the positive state during light irradiation.

A plate of Ag, Pt, or In_2O_3 covered by chlorophyll was used for one electrode. The other one was lined with a mixture of chlorophyll and IQ on In_2O_3 electrode. The electrolyte contained FMN and tryptophan. The results are summarized in Table 2. The potential difference between Ag and In_2O_3 electrodes was 40 mV under illumination. This value was the smallest. The potential difference of the Pt–In_2O_3 system was twice as great as that of the In_2O_3–In_2O_3 system.

It was found that the magnitude of the photovoltage was influenced by the pH of electrolyte. The pH-photovoltage curves obtained from the system of Pt|Chl|electrolyte|Chl,IQ|In_2O_3 are shown in Fig. 2. The maximum photovoltage appeared around pH 7 for the FMN-tryptophan electrolyte. The glutathione result is also shown in Fig. 2.

For the promotion of electron transfer at the surface of the chlorophyll electrode, RTB was mixed with chlorophyll on a Pt electrode. RTB was expected to relay the electron from chlorophyll on the electrode to FMN in the electrolyte. The photovoltages on the system of Pt|Chl,RTB|FMN,Trp|Chl,IQ|In_2O_3 are shown in Fig. 3. The results show 176 mV as the maximum photovoltage and 314 mV as the potential difference between the two electrodes.

At the optimum condition of the above photocell, the current shown in Fig. 4 was produced. The current began to reduce gradually with the lapse of time and finally reached an almost constant value.

TABLE 2. THE POTENTIALS OF THE PHOTOCELLS OF

M_1|Chl| 5 mM FMN, 5 mM Tryptophan, 0.1 M KCl |Chl, IQ (1 : 5)|M_2

M_1	M_2	Potential (mV *vs.* M_2) Dark (d)	Light (l)	Photovoltage (l) − (d)
In_2O_3	In_2O_3	45	141	96
Ag	In_2O_3	−23	40	63
Pt	In_2O_3	146	289	143

3×10^4 lx, 20—26 °C

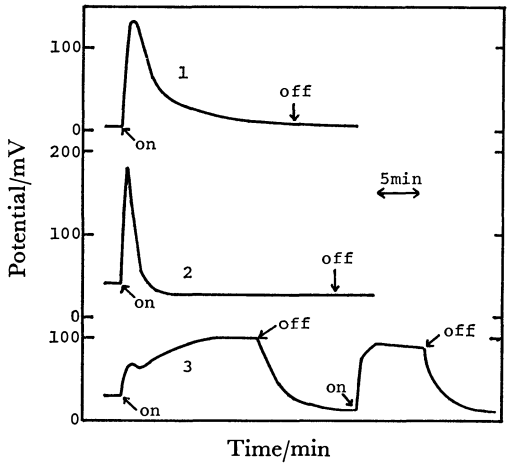

Fig. 1. The potential-time curves of the photocell using FMN in electrolyte.
In_2O_3|Chl|0.1 M KCl, 5 mM FMN, X|In_2O_3.
X: 1; none, 2; 2.5 mM EDTA, 3; Tryptophan.
Chl: 0.03 $\mu mol/cm^2$, 20—23 °C, 3×10^4 lx,

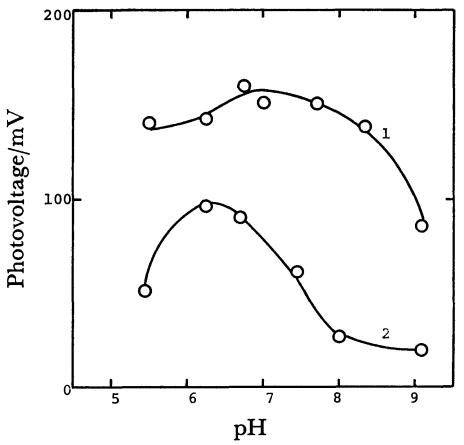

Fig. 2. The influence of pH to the photovoltage.
1: Pt|Chl|5 mM FMN, 5 mM Trp|Chl, IQ|In_2O_3,
2: Pt|Chl|1 mM GSH, 1/2 mM GSSG|Chl, IQ|In_2O_3, Chl: 0.03 $\mu mol/cm^2$, Chl:IQ=1:5, 19—24 °C, 3×10^4 lx.

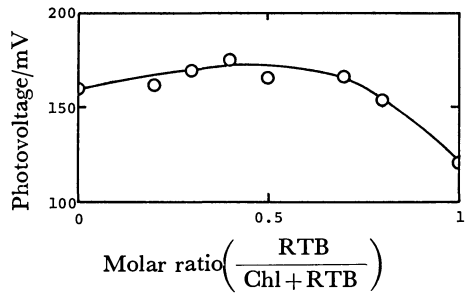

Fig. 3. The influence of molar ratio to the photovoltage.
Pt|Chl, RTB|5 mM FMN, 5 mM Trp (pH 6.7)|Chl, IQ|In_2O_3. Chl: 0.03 μmol/cm², Chl:IQ=1:5, 25—31 °C, 3×10^4 lx.

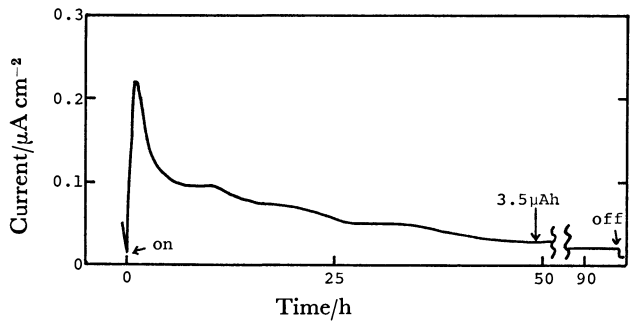

Fig. 4. The photocurrent.
Pt|Chl, RTB|5 mM FMN, 5 mM Trp (pH 6.7)|Chl, IQ|In_2O_3. Chl: 0.03 μmol/cm², Chl:RTB=1:1, Chl:IQ=1:5, 31—32 °C, 3×10^4 lx.

A steady state was found to exist after the current which had been passed reached the theoretical amount for the reduction of FMN in the electrolyte (3.5 μA h).

It is plausible from Fig. 1 that FMN in the electrolyte is reduced at the chlorophyll-RTB electrode and the photopotential shifts to a negative state, and thus the photocurrent becomes smaller. The reduced FMN, which is a strong reducing agent,[9] is susceptible to being oxidized to reproduce FMN at the chlorophyll-IQ electrode. Therefore it is very possible that a steady state was obtained during the photoelectrochemical reaction.

As a conclusion, the electron transfer process of the photocell may be the following:

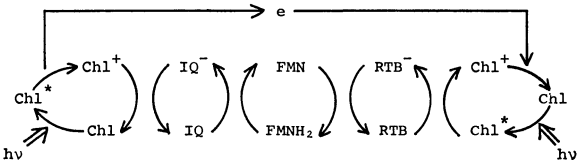

References

1) H. Tributsch and M. Calvin, *Photochem. Photobiol.*, **14**, 95 (1971); V. B. Evstigneev *et al.*, *Biofizika*, **19**, 810, 820, 997 (1974); F. K. Fong and N. Winograd, *J. Am. Chem. Soc.*, **98**, 2287 (1976); T. Miyasaka, T. Watanabe, A. Fujishima, and K. Honda, *J. Am. Chem. Soc.*, **100**, 6657 (1978).

2) A. F. Janzen and J. R. Bolton, *J. Am. Chem. Soc.*, **101**, 6342 (1979).

3) F. Takahashi and R. Kikuchi, *Biochim. Biophys. Acta*, **430**, 490 (1976); F. Takahashi and R. Kikuchi, *Bull. Chem. Soc. Jpn.*, **49**, 3394 (1976); F. Takahashi, M. Aizawa, R. Kikuchi, and S. Suzuki, *Electrochim. Acta*, **22**, 289 (1977).

4) C. W. Tang and A. C. Albrecht, *J. Chem. Phys.*, **62**, 2139 (1975); **63**, 953 (1975).

5) F. Takahashi, K. Seki, R. Kaneko, S. Sato, and Y. Kusumoto, *Bull. Chem. Soc. Jpn.*, **54**, 387 (1981).

6) G. K. Radda and M. Calvin, *Biochemistry*, **3**, 184 (1964); G. K. Radda, *Biochim. Biophys. Acta*, **112**, 448 (1966).

7) F. Takahashi, M. B. Rahman, and H. Maeda, *Bull. Chem. Soc. Jpn.*, **49**, 716 (1976).

8) "Riboflavin," ed by R. S. Rivlin, Plenum Press, New York and London (1975), p. 12.

9) "Progress in Bioorganic Chemistry," ed by E. T. Kaiser and F. J. Kézdy, John Wiley & Sons, New York (1976), Vol. 4, p. 44.

  Bull. Chem. Soc. Jpn., 54, 1308—1313 (1981) [Vol. 54, No. 5

Heterogeneous Reactions of Nitrogen Monoxide on Titanium Dioxide Photocatalysts in Solutions

Hiroshi Yoneyama,* Hisashi Shiota, and Hideo Tamura
Department of Applied Chemistry, Faculty of Engineering, Osaka University, Yamadakami, Suita, Osaka 565
(Received August 28, 1980)

Heterogeneous reactions of nitrogen monoxide on illuminated TiO_2 catalysts in 1 mol dm^{-3} $HClO_4$ were studied by electrochemical analysis. Nitrogen monoxide was reduced to ammonia and hydrazine. The main reaction was found to be a chemical reaction of hydroxylamine as a reaction intermediate with nitrogen monoxide to give molecular nitrogen. Nitrate was detected as an oxidation product formed by the counterpart reaction of the reduction of nitrogen monoxide.

Heterogeneous reactions on semiconductor photocatalysts in solutions are of interest in view of solar energy utilization. Fundamental mechanisms of the photocatalysts have been elucidated,[1–6] and several reaction systems in line with the established view have recently been reported.[7–14]

According to Guth and Schrauzer,[15] the reduction of molecular nitrogen to ammonia and hydrazine takes place on illuminated moist TiO_2 powders with simultaneous evolution of oxygen. However, the yield was poor. Causes for this might be: (1) the reaction terminates in the gas phase, when adsorbed active water is consumed, and (2) the reaction requires large positive Gibbs energy changes.

$$1/2N_2 + 3/2H_2O \longrightarrow NH_3 + 3/4O_2 \quad (1)$$
$$\Delta G^0_{298} = 382.5 \text{ kJ/mol}$$
$$N_2 + 2H_2O \longrightarrow N_2H_4 + O_2 \quad (2)$$
$$\Delta G^0_{298} = 625.7 \text{ kJ/mol}$$

In view of thermodynamics, the reduction of nitrogen monoxide to ammonia and hydrazine should take place more easily.

$$NO + 3/2H_2O \longrightarrow NH_3 + 5/2O_2 \quad (3)$$
$$\Delta G^0_{298} = 292.6 \text{ kJ/mol}$$
$$2NO + 2H_2O \longrightarrow N_2H_4 + 2O_2 \quad (4)$$
$$\Delta G^0_{298} = 448.1 \text{ kJ/mol}$$

The present study was undertaken to investigate reactions of NO on illuminated TiO_2 photocatalysts in solution.

Experimental

A tank NO gas (99.9% purity) was passed through 5 mol dm^{-3} KOH and then through 5 mol dm^{-3} H_2SO_4 to remove N_2O and NO_2.

TiO_2 powder of the rutile modification (Fuji Titanium Co.) was used in a commercially available form and a partially reduced one. The powder was soaked in a dilute HCl solution overnight, washed with twice distilled water several times, and then dried in a drying oven. Partial reduction was carried out under a stream of H_2 at 700 °C for 30 min. Platinization of the powder was carried out by means of photodeposition.[16] The powder was suspended in a HCl solution containing H_2PtCl_6. Illumination with a 500 W xenon lamp was carried out under N_2 atmosphere until the yellow color of the solution completely faded. The amount of platinum deposited on the powder surface was 21.8 mg/g of TiO_2, its specific surface area being 14.2 m^2/g as determined by the BET method. The amount of deposited Pt was comparable to that required for a monolayer coverage of the powder when the surface exposed to solution is the (001) face.

A TiO_2 single crystal, reduced in a stream of H_2 at 600 °C for 30 min, was used as an electrode as well as a photocatalyst. The (001) face was chosen as the electrode surface. Platinization of the electrode surface was carried out by means of electrodeposition.[17] The amount of deposited platinum was estimated by measuring the charge passed during the course of deposition, and converted into equivalent monolayers.[17]

Polarization measurements were carried out in the usual beaker type cell or in a H type cell with a potentiostat (Hokuto Denko, model HA 101). Experiments of the heterogeneous reaction were carried out in a beaker cell of *ca.* 10 ml capacity equipped with a gas inlet in the side wall near the bottom and with a gas outlet in the top of the cell. Illumination was made with focusing light from a 500 W xenon lamp. The powder catalyst was agitated with a magnetic stirrer during the course of illumination, NO gas being continuously bubbled into the solution.

Quantitative analysis of NH_3, N_2H_4, NH_2OH, NO_3^-, and NO_2^- was carried out by colorimetry. Solutions in the heterogeneous reaction vessel were transferred to a volumetric flask and diluted to 25 ml. In the case of powder photocatalysts, the solution was separated from the catalyst by filtration, and then diluted to the same volume. The diluted solutions were used as the sample solutions. The amount of NH_3 was determined by the method of Kruse and Mellon.[18] 10 ml of the sample solution was subjected to distillation in a micro-Kjeldahl apparatus. The ammonia in the distillate was collected in 0.01 mol dm^{-3} H_2SO_4, and determined. N_2H_4 was determined in 10 ml of the sample solution with *p*-dimethylamminobenzaldehyde.[19] For the determination of NH_2OH,[20] 5 ml of the sample solution was mixed with 1 ml of 10% NaOH, and then with 0.25 ml ethyl acetate. After the color of the ester had faded the solution was acidified with 25% HNO_3 making the volume of solution 25 ml. 1 ml of a 8% $FeCl_3$ solution was then added and the absorbance was measured at 505 nm. NO_3^- was determined by the nitration of sodium salicylate in the presence of H_2SO_4.[21] In order to eliminate interference from NO_2^-, 1 ml of the sample solution was diluted to 10 ml, and 1 ml of a sulfanilamide solution (1 g of sulfanilamide/100 ml of 1% HCl) was added to it. After standing for 15 min, 1 ml of a *N*-(naphthyl)ethylenediamine solution (0.1 g of *N*-(naphthyl)ethylenediamine/100 ml of water) was added, and the absorbance was measured at 530 nm after shaking for 20 min.[22]

N_2 originated from NO was determined by gas chromatography with the use of a helium carrier and a 70 cm length

molecular sieve 5 A column. In order to eliminate any error introduced by N_2 in air, experiments for collection of gases were carried out under Ar atmosphere. Since the chromatograms of N_2 and NO_2 overlapped at room temperature, the column was cooled down to −76 °C by dipping in a mixture of dry ice and acetone, the sample gas being then injected. After the chromatogram of Ar appeared, the coolant was removed to warm up the column to room temperature. During this time, N_2, NO, and NO_2 appeared successively in the chromatograms.[23,24]

Results and Discussion

Electrochemical Reactions of NO on TiO_2 Electrodes. According to the results obtained by Dutta and Landoldt on Pt electrodes in 4 mol dm^{-3} H_2SO_4,[25] the electrochemical reduction of NO occurs with two waves. The first wave starting at 0.6 V *vs.* SCE was postulated to be due to the formation of an intermediate having an oxidation state identical with that of N_2O such as $H_2N_2O_2$ or NO^-, and the second one to further reduction of the intermediate to NH_3OH^+. If the intermediate is assumed to be $H_2N_2O_2$, then the reactions are represented by

$$2NO + 2H^+ + 2e^- = H_2N_2O_2, \quad (5)$$

$$E^0 = 0.71 \text{ V } vs. \text{ SHE}^{26}$$

$$H_2N_2O_2 + 6H^+ + 4e^- = 2NH_3OH^+. \quad (6)$$

$$E^0 = 0.39 \text{ V } vs. \text{ SHE}^{23}$$

Figure 1 shows cyclic voltammograms for the reduction of NO in 1 mol dm^{-3} $HClO_4$ at a Pt electrode. Two waves appear by cathodic polarization up to 0.1 V *vs.* SCE. The formation of NH_3OH^+ is conceivable at potentials equal to or more negative than 0.1 V *vs.* SCE. The overall reaction for the reduction of NO is then represented by

$$NO + 4H^+ + 3e^- = NH_3OH^+. \quad (7)$$

Steady state current-potential curves obtained at the TiO_2 single crystal electrode are shown in Fig. 2, and those at a platinized electrode in Fig. 3. Measurements were carried out under both NO and N_2 atmosphere. The cathodic curves were obtained in the dark, while anodic ones under illumination. The cathodic current is enhanced by introduction of NO into the electrolyte, suggesting that the cathodic reaction is mainly due to the reduction of NO when it is present in the solution. The enhancement of the cathodic current is great when the electrode is platinized. On the other hand, a slight suppression of the anodic photocurrent is observed by introduction of NO. This seems to be due to the absorption of near-ultraviolet light in the electrolyte, causing a decrease in light quanta incident on the electrode. As shown in Fig. 4, NO-saturated 1 mol dm^{-3} $HClO_4$ shows relatively high absorption in wavelengths 340—400 nm which are effective for excitation of TiO_2.

In order to study the anodic photocurrents, constant

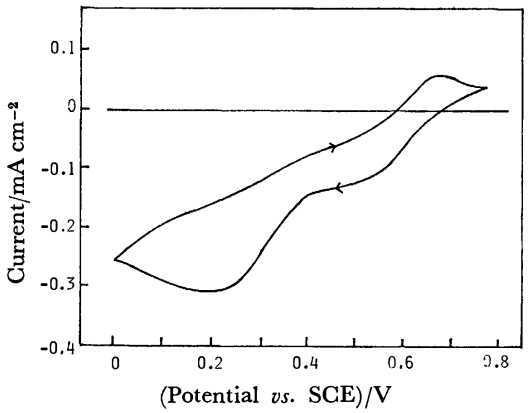

Fig. 1. Current-potential curves of a Pt electrode in 1 mol dm^{-3} $HClO_4$ under bubbling NO.
Sweep rate: 50 mV/s.

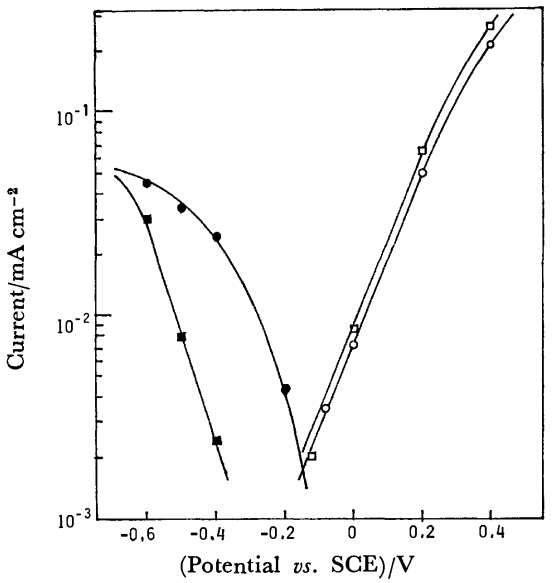

Fig. 2. Steady state current-potential curves of a single crystal TiO_2 electrode under illumination and in the dark.
Open symbols: under illumination, filled in symbols: in the dark. (○, ●): NO-bubbled 1 mol dm^{-3} $HClO_4$, (□, ■): 1 mol dm^{-3} $HClO_4$ under N_2 atmospheres.

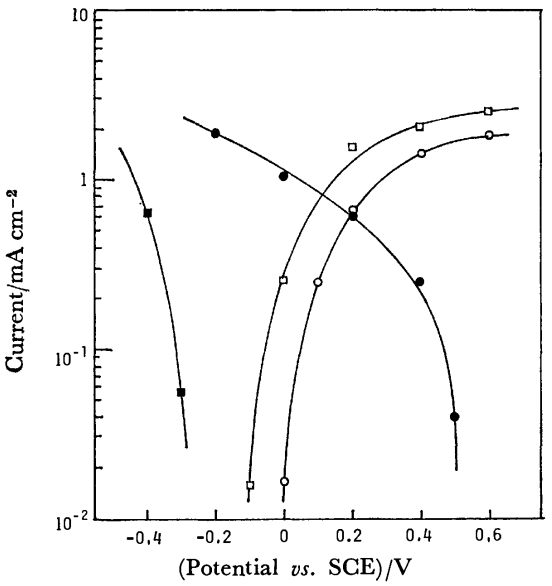

Fig. 3. As in Fig. 2, but for Pt(θ=100)/TiO_2 electrode.

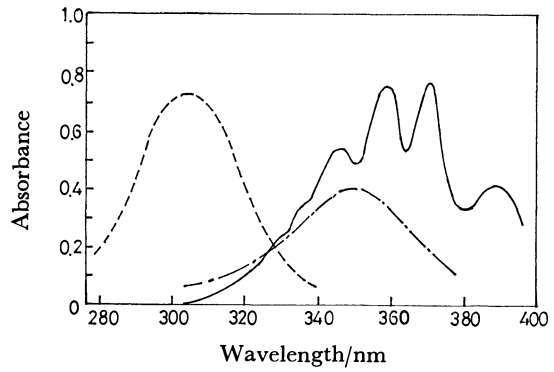

Fig. 4. Absorption spectra of 1 mol dm^{-3} $HClO_4$ containing oxide species of nitrogen.
(——): The solution bubbled NO for 5 min, (·——·): 0.01 mol dm^{-3} $NaNO_2$, (— —): 0.1 mol dm^{-3} KNO_3.

potential electrolysis at 0.5 V *vs.* SCE was carried out in 1 mol dm^{-3} $HClO_4$ in the presence and absence of NO, and the volume of gases evolved from the anodic compartment of an H type cell was compared with those predicted theoretically from the following equation on the basis of the consumed electrolytic charge.

$$2H_2O + 4p^+ \longrightarrow O_2 + 4H^+, \quad (8)$$

where p^+ denotes a photo-generated positive hole. The results are given in Table 1. When NO was dissolved in the electrolyte, gas evolution was appreciably suppressed, resulting in a low current efficiency for the oxygen evolution reaction. Not only water but also NO should participate in the photoanodic processes.

Reduction of NO gives rise to hydroxylamine.[25,26] However, by constant potential electrolysis of TiO_2 electrodes in the dark in NO-saturated solutions under various polarization conditions, ammonia and hydrazine, but not hydroxylamine, were produced regardless of whether or not the platinization of the electrode was made. The results are given in Table 2, in which the results obtained at Pt electrodes are also given. No formation of hydroxylamine was formed even by use of Pt electrode. If we assume that both ammonia and hydrazine are produced by the electrochemical reduction of hydroxylamine, then the reactions would be represented by Eqs. 9 and 10. We see from the

$$NH_3OH^+ + 2H^+ + 2e^- = NH_4^+ + H_2O, \quad (9)$$
$$E^0 = 1.35 \text{ V } vs. \text{ SHE}^{28)}$$

$$2NH_3OH^+ + H^+ + 2e^- = N_2H_5^+ + 2H_2O. \quad (10)$$
$$E^0 = 1.41 \text{ V } vs. \text{ SHE}^{28)}$$

results (Table 2) the following. (1) The ammonia production increases with a cathodic shift of the electrode potential. At the extreme of the shift of 0.5 V *vs.* SCE, however, hydrogen evolution seems to occur competitively, as judged from the onset potential of the cathodic current in alkaline solutions.[17] Even at 0.25 V *vs.* SCE, the same would be true for the platinized electrode, though the competition would occur to a much smaller extent. Adsorbed hydrogen on the electrode surface is essential for the production of ammonia and hydrazine in appreciable amounts. Theoretically, the reactions given by Eqs. 9 and 10 should occur easily, since the standard electrode potentials are positive. However, the actual rates of the reactions are so low[27] that a large overpotential is needed for the reactions to occur with appreciable rates. (2) The platinized TiO_2 is the most active for the conversion of NO to ammonia and hydrazine. Physical and chemical nature of the deposited platinum on TiO_2 has not so far been characterized. A high capability of sorbing hydrogen might be related to the observed high activity, since electrodeposited platinum has a high activity for the hydrogen electrode reaction.

Judging from electrochemical analysis on the reduction of NO on Pt electrodes,[25,26] there is no doubt as to the formation of hydroxylamine. However, this is not the case in electrolyte solutions. The current efficiency for the production of ammonia and hydrazine, determined on the basis of Eqs. 7, 9, and 10,

Table 1. Current efficiency for the evolution of oxygen at illuminated TiO_2 electrode in 1 mol dm^{-3} $HClO_4$ with and without dissolved NO

Atmosphere	Volume of gas / ml	Consumed charge / C	Current efficiency / %
N_2	0.82	14.1	100
NO	0.52	15.0	60.1

Table 2. Electrolytic reduction of NO at TiO_2 electrodes in the dark in 1 mol dm^{-3} $HClO_4$

Run No.	Electrode	Potential *vs.* SCE / V	Consumed charge / C	Produced substance			Total current[a] efficiency / %
				NH_3 / μmol	N_2H_4 / μmol	N_2 / μmol	
1	Pt	0.00	50.0	0.93	n.d.[b]	n.d.	0.90
2	Pt	−0.50	12.5	2.1	0.66	n.d.	12.2
3	TiO_2	−0.25	12.4	0.60	0.12	n.d.	3.08
4	TiO_2	−0.50	12.5	2.8	0.11	n.d.	11.5
5	$Pt(\theta=100)/TiO_2$[c]	−0.25	12.7	0.76	1.87	n.d.	14.3
6	$Pt(\theta=100)/TiO_2$	−0.50	12.5	5.13	1.87	n.d.	31.4
7	TiO_2	−0.20	12.7	0.55	0.08	34.1	80.3

a) Calculated on the basis of the determined substance. b) Not determined. c) TiO_2 electrode covered with deposited Pt the amount of which roughly corresponds to 100 monolayers coverage.

was found to be low, suggesting that a large fraction of the produced hydroxylamine is consumed in another reaction.

Gas bubbles stick to the electrode surface during the course of electrolysis even at potentials at which no hydrogen evolution is conceivable. The formation of N_2 was postulated as a principal reduction reaction. For the sake of confirmation determination of N_2 originating from NO was attempted. Electrolysis was carried out in a sealed cell with atmosphere of NO, the cell being kept in Ar during the course of electrolysis. After electrolysis at -0.2 V *vs.* SCE for 30 h, where the evolution of hydrogen is thermodynamically impossible, N_2 in the sealed cell was determined. As expected, N_2 was produced by electrolysis (Table 2). The reaction schemes for the formation of N_2 can be given by either one or both of the following equations.

$$NH_3OH^+ + 2NO = N_2 + HNO_2 + H_3O^+, \quad (11)$$
$$\Delta G^0 = -407.6 \text{ kJ/mol}$$
$$4/3NH_3OH^+ + 2/3NO + 2/3H^+ = N_2 + 2H_3O^+. \quad (12)$$
$$\Delta G^0 = -214.6 \text{ kJ/mol}$$

If the N_2 production is due to the reduction given by Eqs. 7 and 11, then the total current efficiency for the formation of ammonia, hydrazine and N_2 amounts to 80.3%. If Eqs. 7 and 12 are used, the value is 106%.

Table 3 shows the decrease in the amount of NH_3OH^+ by bubbling NO into the solution. The results show that even ammonia and hydrazine, when produced, are consumed to evolve N_2, causing a decrease in current efficiency for the formation of these substances. NO_2^- is formed by bubbling NO into 1 mol dm^{-3} $HClO_4$, possibly by the equation,

$$2NO + H_2O = NOH + HNO_2. \quad (13)$$

Heterogeneous Reactions on TiO_2 Single Crystal Photocatalysts. In heterogeneous reactions on n-type semiconductor photocatalysts, reduction process and photosensitized oxidation process proceed mainly on the non-illuminated and illuminated surfaces, respectively.[28,29] Electrochemical prediction of occurring heterogeneous reactions can be made by means of the current-potential curves of semiconductor photocatalysts in the photocatalytic reaction systems,[3,4] (Figs. 2 and 3). The current-potential curve due to the reduction of NO intersects with photoanodic curves,

Table 3. Decrease of NH_2OH, NH_3 and N_2H_4 by chemical reactions with NO

Substance[a]	Amount[b] Initial (μmol)	Final (μmol)	Decrease (μmol)	Produced NO_2^- (μmol)
NH_3	27.6	13.4	13.6	70.7
N_2H_4	112.0	0.7	111.3	59.9
NH_2OH	150.0	65.3	84.7	83.9
blank[c]	—	—	—	55.1

a) Dissolved in the base solution 1 mol dm^{-3} $HClO_4$. b) Solution volume 5 ml, NO gas bubbled for 2 h. c) NO gas bubbled in 1 mol dm^{-3} $HClO_4$.

Table 4. Heterogeneous reaction of NO on single crystal TiO_2 photocatalyst[a]

Pt coverage (monolayers)	Oxidation process Amount of NO_3^- (μmol)	Reduction process Amount of NH_3 (μmol)	Reduction process Amount of N_2H_4 (μmol)
0	91.0	0.96	0.15
100	36.5	2.93	2.28
300	21.4	1.69	1.62

a) Experiments were carried out under illumination, made on the platinum-free surface, for 15 h for a solution volume of 5 ml.

suggesting that heterogeneous reactions should occur on the illuminated TiO_2. By comparison of Figs. 2 and 3 we see that the platinization of TiO_2 photocatalysts mainly effects the reduction process. Experiments were carried out by illuminating the non-platinized surface, the platinized surface not being illuminated. Illumination was carried out for 15 h under bubbling NO into 5 ml of 1 mol dm^{-3} $HClO_4$, and the solution was analyzed for NO_3^- as an oxidation product, and for ammonia and hydrazine as reduced ones. The results are given in Table 4.

The platinized photocatalysts give a lower amount of NO_3^- but higher amounts of ammonia and hydrazine than the non-platinized catalysts, in line with the results given in Table 2 when a comparison of results is made at the same potential.

Heterogeneous Reactions on Powder Photocatalysts. The formation of NO_3^- by oxidation and of NH_3 by reduction was investigated by using TiO_2 powder photocatalysts. As the photocatalysts, a commercially available powder, a partially reduced powder and a platinized powder subjected to no reduction were used. The degree of platinization was so low as to give a monolayer coverage, differing from the cases of single crystal catalysts. Photodeposition to give a much higher coverage was unsuccessful.

The results on the heterogeneous reactions on the powder photocatalysts are given in Table 5. The NO_3^- production was suppressed but NH_3 production seemed to increase with platinization as observed in single crystal photocatalysts. However, the effect of platinization was not so obvious as in the case of single crystal catalysts mainly due to the low coverage of deposited Pt. The effects of the partial reduction of the catalyst are not clear. The results obtained are greatly scattered, making it difficult to give conclusions on the effect of illumination time and the amount of catalyst loadings on the production of NO_3^- and NH_4^+. Since chemical reactions (Eqs. 11 to 13) are involved in the heterogeneous reaction, slight differences in bubbling conditions of NO might greatly influence the yield.

The results given in Figs. 4 and 5 indicate that the amount of ammonia produced is higher in the powder photocatalysts than in the single crystals. The ammonia production may require the adsorbed hydrogen on the catalysts surface. A large surface area of powder photocatalysts is advantageous. The attack

TABLE 5. HETEROGENEOUS REACTION OF NO ON TiO_2 POWDER PHOTOCATALYSTS[a)]

Catalyst	Sp. surface area / $m^2\ g^{-1}$	Amount of powder / g	Illumination time / h	NO_3^- / μmol	NH_3 / μmol
Unreduced TiO_2	14.2	0.2	8	40.7	5.91
		0.2	15	43.9	6.22
		0.1	15	71.4	8.25
Reduced TiO_2[b)]	16.9	0.2	8	18.4	18.6
		0.2	15	26.3	7.66
		0.1	15	31.0	1.43
Platinized TiO_2[c)]	16.0	0.2	8	6.79	6.73
		0.2	15	8.04	9.31
		0.1	15	10.7	4.05
No catalyst			13.5		0.18

a) Solution: 5 ml of 1 mol dm^{-3} $HClO_4$. b) H_2 reduction at 700 °C for 30 min. c) Amount of Pt: 21.8 mg Pt/g of TiO_2, corresponding roughly to a monolayer coverage.

of NO on the ammonia produced would not take place with the same rate in the powder and single crystal catalyst systems, since experimental conditions differ.

Summary of the Heterogeneous Reactions of NO. It was confirmed that NO dissolved in 1 mol dm^{-3} $HClO_4$ undergoes heterogeneous reactions on TiO_2 photocatalysts, the reaction schemes being complicated. From the current-potential curves of TiO_2 single crystal electrodes (Figs. 2 and 3), we see that heterogeneous reaction takes place on single crystal catalysts following electrochemical mechanism. This might be the case also for powder photocatalysts, since as regards ZnO[30)] and TiO_2[17,31)] there is close similarity in photoelectrochemical properties of semiconducting powders to those of single crystals. The reaction schemes can be estimated on the basis of anodic and cathodic reactions at TiO_2 electrodes.

The oxygen evolution occurs as the main anodic reaction (Table 1). The oxygen evolved would easily react with NO to give NO_2, and the resulting NO_2 would dissolve into solutions to give NO_3^- with a disproportionation reaction. The current efficiency for the oxygen evolution decreases in the presence of NO. This is partly attributable to the contribution of the chemical reaction with NO. The electrochemical oxidation of NO to finally give NO_3^- should also be taken into consideration. NO is oxidized to NO_3^- at high anodic potentials on Pt electrodes.[32)]

The oxidation processes are postulated on the basis of the electrolysis experiments. The main difference expected between the electrolysis experiments and photocatalytic experiments would result from the difference in the magnitude of the electric field built in the semiconductor surface, the magnitude being usually small in the cases of heterogeneous reaction systems. The weak electric field enhances the recombination of photo-generated positive holes with electrons as majority charge carriers, resulting in a low utilization efficiency of light quanta as demonstrated by Ohnishi *et al.*[33)] To our present knowledge this effect is the only one expected for the change of surface electric field. No change would be predicted in the nature of electrochemical reactions when variation arises in the electric field of semiconductor surfaces.

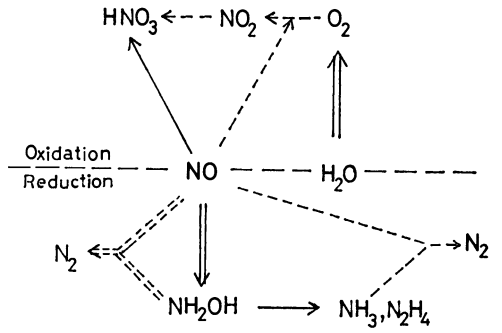

Fig. 5. Schematic illustrations of heterogeneous reactions of NO on illuminated TiO_2 in 1 mol dm^{-3} $HClO_4$.
Double lines stand for the main reaction path. Solid line: electrochemical reaction path, dashed line: chemical reaction path.

If there were any change the proposed reaction schemes would then become invalid.

As a cathodic process which should occur to keep the electrical neutrality of the photocatalysts, the reduction of NO to hydroxylamine would take place. A fraction of the hydroxylamine produced escapes from the chemical reaction with NO, and is subjected to further reduction to ammonia and hydrazine. A part of the produced ammonia and hydrazine would be decomposed into N_2 by the chemical reaction of NO. These routes are illustrated in Fig. 5.

In view of electrochemistry, the production of ammonia and hydrazine from NO seems promising in the heterogeneous reaction systems on illuminated TiO_2 if the entire processes are governed by electrochemical mechanisms. Actually, however, several chemical reactions are involved, and as a result N_2 is produced as the main substance.

The present study was supported by Grant-in-Aid for Scientific Research No. 505008 from the Ministry of Education, Science and Culture.

References

1) S. R. Morrison and T. Freund, *J. Chem. Phys.*, **47**, 1543 (1967).

2) T. Freund and W. P. Gomes, *Catal. Rev.*, **3**, 1 (1969).
3) H. Yoneyama, Y. Toyoguchi, and H. Tamura, *J. Phys. Chem.*, **76**, 3460 (1972).
4) F. Möllers, H. J. Tolle, and R. Memming, *J. Electrochem. Soc.*, **121**, 1160 (1974).
5) M. Miyake, H. Yoneyama, and H. Tamura, *Bull. Chem. Soc. Jpn.*, **50**, 1492 (1977).
6) A, J. Bard, *J. Photochem.*, **10**, 59 (1979); *Science*, **207**, 139 (1980).
7) S. N. Frank and A. J. Bard, *J. Phys. Chem.*, **81**, 1484 (1977).
8) H. Reiche and A. J. Bard, *J. Am. Chem. Soc.*, **101**, 3127 (1979).
9) B. Kraeutler and A. J. Bard, *J. Am. Chem. Soc.*, **100**, 2239, 5985 (1978).
10) T. Kawai and T. Sakata, *Nature*, **282**, 283 (1979).
11) H. Yoneyama, Y. Yamashita and H. Tamura, *Nature*, **282**, 817 (1979).
12) T. Watanabe, T. Takizawa, and K. Honda, *J. Phys. Chem.*, **87**, 1845 (1977).
13) F. D. Saeva and G. R. Olin, *J. Chem. Soc., Chem. Commun.*, **1978**, 417.
14) T. Inoue, A. Fujishima, S. Konishi, and K. Honda, *Nature*, **277**, 637 (1979).
15) G. N. Schrauzer and T. D. Guth, *J. Am. Chem. Soc.*, **99**, 7189 (1977).
16) B. Kraeutler and A. J. Bard, *J. Am. Chem. Soc.*, **100**, 4317 (1978).
17) K. Kogo, H. Yoneyama, and H. Tamura, *J. Phys. Chem.*, **90**, 1705 (1980).
18) J. Kruse and M. G. Mellon, *Anal. Chem.*, **25**, 1188 (1953).
19) G. W. Watta and J. D. Chrisp, *Anal. Chem.*, **24**, 2006 (1952).
20) "Bunseki Kagaku Binran," ed by Nippon Bunseki Kagakukai, Maruzen, Tokyo (1971), p. 193.
21) A. D. Dolance and P. W. Healy, *Ind. Eng. Chem. Anal. Ed.*, **17**, 718 (1945).
22) "Muki Oyo Hishoku Bunseki," ed by The Editorial Board of Muki Oyo Hishoku Bunseki, Kyoritsu Shuppan, Tokyo (1974), Vol. 3, p. 430.
23) J. M. Trowell, *Anal. Chem.*, **37**, 1152 (1965).
24) E. Moretti, G. Leofanti, D. Andreazza, and N. Giordano, *J. Chromatogr. Sci.*, **12**, 64 (1974).
25) D. Dutta and D. Landoldt, *J. Electrochem. Soc.*, **119**, 1320 (1972).
26) W. J. Plieth, "Encyclopedia of Electrochemistry of the Elements," ed by A. J. Bard, Marcel Dekker, New York, N. Y. (1978), Vol. VIII, pp. 322—377.
27) W. M. Latimer, "Oxidation Potentials," 2nd ed, Prentice Hall, Englewood Cliffs, N. J. (1952), p. 97.
28) H. Reiche, W. W. Dunn, and A. J. Bard, *J. Phys. Chem.*, **83**, 2248 (1979).
29) H. Yoneyama, N. Nishimura, and H. Tamura, *J. Phys. Chem.*, in press.
30) M. Micka, *J. Electroanal. Chem.*, **42**, 447 (1973).
31) B. Kraeutler and A. J. Bard, *J. Am. Chem. Soc.*, **100**, 5985 (1978).
32) D. Dutta and D. Landolt, *J. Electrochem. Soc.*, **119**, 1320 (1972).
33) T. Ohnishi, Y. Nakato, and H. Tsubomura, *Ber. Bunsenges. Phys. Chem.*, **79**, 523 (1975).

Neutron Diffraction Study of Aqueous Hydrochloric and Hydrobromic Acid Solutions

Norio Ohtomo,† Kiyoshi Arakawa,* Makoto Takeuchi,††
Toshio Yamaguchi,†† and Hitoshi Ohtaki††

Research Institute of Applied Electricity, Hokkaido University, Sapporo 060
†*Faculty of Engineering, Hokkaido University, Sapporo 060*
††*Department of Electronic Chemistry, Tokyo Institute of Technology, Nagatsuta-cho, Midori-ku, Yokohama 227*

(Received September 5, 1980)

The structure factors $S_m(Q)$ over a wide range of Q (1.7—25 Å^{-1}) for aqueous solutions of DCl and DBr (*ca.* 1 M) at room temperature have been determined by means of LINAC-TOF neutron diffraction. The intramolecular structures of D_2O and D_3O^+ in the solutions are found to be identical with those in the "revised watery model" for water. Applying the subtraction method of analysis to diffraction data for the solutions, we have obtained the following results with respect to the structure of the nearest hydration shell around ions in the DCl and DBr solutions: (a) D_3O^+ is tetrahedrally coordinated with four water molecules and Cl^- and Br^- are octahedrally coordinated with six ones, (b) the O–O distances between the central oxygen atom and that of hydrated water molecules for D_3O^+ are 2.88±0.05 Å, (c) the anion-oxygen distances are 3.10±0.05 Å for Cl^- and 3.21±0.05 Å for Br^-, and (d) around cations (D_3O^+) water molecules take the configuration to orient the axis of one of the two lone-pair hybrids on a straight line joining an oxygen atom and the cation, while around anions (Cl^- and Br^-) those take the configuration to orient the vector which bisects the D–O–D angle on a straight line joining an oxygen atom and the cation.

With respect to the structural studies of aqueous ionic solutions, X-ray diffraction techniques have been widely used and a rather large amount of knowledge with respect to the structure of the hydration shell around ions have been accumulated. These X-ray results are summarized in recent review articles.[1,2] The results obtained, such as the coordination numbers, *etc.*, however, are diverse and no precise determination of the orientational configuration of hydrated water molecules has been made by the X-ray diffraction studies.

Then, the neutron diffraction method, which has a unique advantage for determination of the positions of light atoms such as hydrogen (deuterium) contained in the molecules within liquids,[3] has been applied to the study of aqueous solutions. Narten *et al.* carried out X-ray and neutron diffraction studies on aqueous LiCl[4] and DCl[5] solutions, and in the latter they used a well-known conventional method developed for steady state experiment at reactor. Enderby *et al.*, using the same reactor conventional method, investigated aqueous solutions of $NiCl_2$, NaCl, and $CaCl_2$.[2,6,7] The authors carried out studies on alkali chloride (LiCl, NaCl, KCl, and CsCl) solutions by the use of a TOF neutron diffraction method at LINAC.[8,9] These works have the following remarkable features. First, the resolving power of neutron diffraction in structural studies of aqueous solutions has turned out to be superior to that of X-ray diffraction.[1,2] The neutron studies are sufficiently effective to distinguish between various possible ion-water configurations. Second, for structural studies of liquids, the accuracy of a LINAC-TOF neutron diffraction method has been raised in comparison with that of the reactor conventional method.[8,9,10–14] Consequently, associated with the proposition of improved correction procedures for inelastic scattering, the authors' works for hydrogenous molecular liquids have made it possible to provide more detailed knowledge.[8,9,13,14]

Concerning neutron diffraction data of aqueous ionic solutions, there is no definite procedure for the analysis. Three procedures have been proposed recently: the near-neighbor model approach by Narten *et al.*,[4,5] the first- and second-order-difference spectroscopy by Enderby *et al.*,[2,6,7] and the subtraction method by the authors.[8,9] The subtraction method has been found to be useful in order to elucidate the structure of the nearest neighbor shell around ions in more dilute aqueous solutions,[8,9] while Enderby *et al.*'s method using isotopes is clearly restricted in its practical utility.[15] As regards the method of Narten *et al.* especially on the fundamental nature of the near-neighbor model itself, important criticism has been raised by several workers.[13,15,16]

In the present paper, the result of a neutron diffraction study on aqueous solutions of DCl and DBr at *ca.* 1 M is given. With respect to concentrated DCl solutions X-ray[17,18] and neutron[5] diffraction studies have been made recently. However, the diffraction study for its more dilute aqueous solutions has never been carried out, which is required for the elucidation of the fundamental structure of hydration. Then, in order to investigate the hydrated structures around ions in dilute solutions, we have made an experiment for *ca.* 1 M solutions of DCl and DBr.

Experimental

Procedures for Measurements. The experiment was performed by the TOF neutron diffraction method by LINAC at Hokkaido University. Details of the apparatus and procedures were reported.[13,19,20] Experimental accuracy has been raised to a more satisfactory level by recent improvements: the resolving powder $\Delta Q/Q$ of less than a few % and the statistical errors of smaller than 1% in the whole range of Q can be easily attained at present ($Q=(4\pi\sin\theta)/\lambda$)[19,20]

Measurements on the DCl and DBr solutions and pure

D_2O at room temperature (16 °C) were carried out at a scattering angle, $2\theta=90°$. Data for pure heavy water are required for analysis of the data of aqueous ionic solutions. The time-of-flight of neutrons was analyzed by a multichannel time analyzer with a channel width of 10 μs. Thin-walled cylindrical quartz vessels were used as a container of samples.

Samples. Two acid solutions were prepared by the addition of deuterated hydrochloric and hydrobromic acids with the purity of deuteration of 99% to heavy water. The concentration and density of the DCl solution at 25 °C were 1.097 M and 1.125 g cm^{-3}, and those of the DBr solution were 1.038 M and 1.160 g cm^{-3}.

Corrections and Calibrations of Raw Scattering Data. For the determination of the structure factor $S_m(Q)$, corrections for multiple scattering, absorption, background counting, and inelastic scattering are necessary and absolute normalization of data was performed by the use of the scattering data from a standard vanadium rod of the same shape and dimensions as those of the sample.[8,9,13,14] Above all the correction for the inelastic scattering of neutrons is the most important for hydrogenous molecular liquids including light nuclei like deuterium. In order to compensate for this effect, we can apply the correction method being used successfully in our recent studies on liquid D_2O and CD_3COCl.[13,14] In the present study the Placzek correction method[21] was used in a lower Q region and the Wick correction method[22] in a higher Q region.

Calibration of absolute values for high Q data was performed according to the limiting procedure that $S_m(Q)\rightarrow \sum b_n^2/(\sum b_n)^2$ as $Q\rightarrow\infty$, where n ranges over all the nuclei in a molecule. Calibration of low Q data was made by overlapping the $S_m(Q)$ curves in the range 6—10 Å^{-1} for the two corrected data.[14] Thus, combining the data sets, we obtained the final $S_m(Q)$ curve for a wide range of Q, 1.7—25 Å^{-1}. In Fig. 1, the $S_m(Q)$ curves of DCl and DBr solutions together with that of D_2O are given.

The resolving powder $\Delta Q/Q$ was 0.03 in the Q range 1—8 Å^{-1} and 0.04 in the range of Q greater than 10 Å^{-1}.

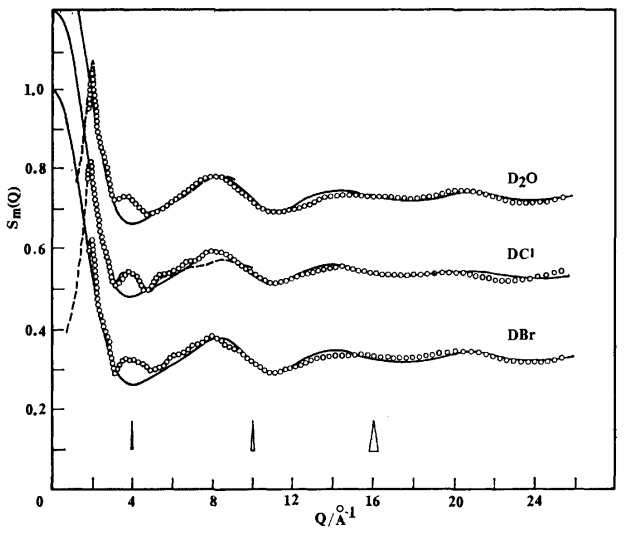

Fig. 1. Observed structure factors for DCl and DBr solutions at 1.10 M and 1.04 M, respectively, compared with the factor for D_2O.
○: $S_m(Q)$ observed, ----: $S_m(Q)$ observed previously (for D_2O by the authors[8,13] and for DCl solution by Triolo and Narten[5]), ——: $f_1^W(Q)$ for D_2O and $S_m^{(1)}(Q)$ for DCl and DBr solutions.

The magnitudes of resolution ΔQ are shown as triangles along the abscissa. The statistical error was found to be smaller than 1% in the whole range of Q.

Results. For the sake of comparison, the $S_m(Q)$ data for heavy water reported by the authors (dashed line)[8,13] are indicated in Fig. 1 overlapping the present data (open circles). Two sets of data agree fully with each other in the range of Q, 1.7—9 Å^{-1}, though slight differences in the main peak at 2 Å^{-1} and a broader peak at *ca.* 8 Å^{-1} are observed. Taking experimental uncertainties as well as the small difference in temperature into consideration, the $S_m(Q)$ data for D_2O are found to agree with other data (Page and Powles'[23] and Narten's[24] data at reactor, and the authors' at LINAC[8,13]). Thus, the reproducibility of the neutron data for D_2O is confirmed with sufficient accuracy.

Furthermore, the data for hydrochloric acid solution at *ca.* 1 M reported by Triolo and Narten (dashed line)[5] are indicated in Fig. 1 overlapping the present data (open circles). Their data in the figure are normalized to the value at the first peak of the structure factor obtained in the present work. A small deviation of Triolo and Narten's data from ours at 6—10 Å^{-1} is observed. Values of rms deviations for D_2O and D_3O^+ in their least-square analysis are, thus, supposed to be too large. Except for this point, their data are found to be essentially identical with our data in the range of Q, 1.7—6 Å^{-1}, and then the reproducibility of the data has been confirmed.

From the above-mentioned fact, reliability of the data required to elucidate the structure of the solutions is attained. Thus, with the help of the subtraction method in the analysis of lower Q data, the configurations of water molecules within the first hydration shell can be studied, and the molecular structure of D_2O and D_3O^+ within the solutions can be determined by the use of the $S_m(Q)$ data in a wide range of Q.[14]

Results and Discussion

Intramolecular Contribution to $S_m(Q)$. The structure factor $S_m(Q)$ for molecular liquids consists of an intramolecular contribution $S_m^{(1)}(Q)$ and an intermolecular one $S_m^{(2)}(Q)$, and is expressed as

$$S_m(Q) = S_m{}^{(1)}(Q) + S_m{}^{(2)}(Q). \quad (1)$$

Structure factors for higher Q region are dominated by the intramolecular contribution, *i.e.* $S_m(Q)\rightarrow S_m^{(1)}(Q)$. Then, the $S_m^{(1)}(Q)$ for the DCl and DBr solutions becomes

$$S_m{}^{(1)}(Q) = (1-x_+-x_-)f_1^W(Q)+x_+f_1^C(Q)+x_-f_1^A(Q). \quad (2)$$

$f_1^W(Q)$ is the intramolecular contribution from water molecules constituting a tetrahedral pentamer (the "revised watery model"[8,13]). $f_1^C(Q)$ and $f_1^A(Q)$ are the intramolecular contributions from the species constituting the first hydration shell around D_3O^+ and anions, respectively.[8] x_+ and x_- are mole fractions of D_2O molecules coordinated in the first shell around cations and anions.

The calculated curves $f_1^W(Q)$ for D_2O, $S_m^{(1)}(Q)$ for the DCl solution, and $S_m^{(1)}(Q)$ for the DBr solution are indicated in Fig. 1, in comparison with the observed data. The agreement between the calculated curves and the observed data at high Q region ($Q\gtrsim 8$ Å^{-1}) is satisfactory. The agreement in our results is found to be over a wider range of Q (8—25 Å^{-1})

than that in Triolo and Narten's work (8—13 Å^{-1}).[5] Thus, it has been confirmed that the intramolecular structures of D_2O within liquid heavy water are specified by those in the revised watery model.[8,13] Likewise, the structures of D_2O and D_3O^+ in the DCl and DBr solutions at 1 M have been found to be identical with those in the revised watery model.[8,13,25]

Significant differences between the $S_m(Q)$ data of D_2O and those of DCl and DBr solutions in the lower Q region (<7 Å^{-1}) can be ascribed mainly to contributions from the ion-water and water-water interactions within the structure of the first hydrated shell around ions.

Structure of the First Hydration Shell around Ions. A determination of the structure of the nearest hydration shell around ions has been made by comparing calculated values with observed data according to the subtraction method described in the preceding paper.[8,9] The method was proposed for the analysis of the data of comparatively dilute aqueous solutions, and its availability for the determination of the structure was demonstrated.[8,9] The outline of the subtraction method is as follows.

Determination of $\Delta S_m(Q)_{obsd}$: This factor is obtained by subtracting the structure factor $S_m(Q)_{D_2O}$ of D_2O multiplied by an appropriate fraction from the observed total structure factor $S_m(Q)_{total}$ for solution. Thus, in an aqueous solution as dilute as 1 M, the remaining factor for the hydrated structure $\Delta S_m(Q)_{obsd}$ becomes

$$\Delta S_m(Q)_{obsd} = S_m(Q)_{total} - (1-x)S_m(Q)_{D_2O} - axS_m(Q)_{D_2O}, \quad (3)$$

where x is the mole fraction of D_2O molecules coordinated in the first hydration shell, $x=c(n_+ + n_-)/55.3$: n_+ and n_- are the coordination numbers around cations and anions, respectively, and c is the concentration in M. The second term in Eq. 3 is the contribution from bulk water outside of the hydration shell, and the third one that from pairs between the molecules within the shell and bulk water molecules. The magnitude of a was estimated to be 1/2 in a preceding paper.[9]

Calculation of $\Delta S_m(Q)_{calcd}$: The structure of the hydration shell is specified by several parameters, such as coordination numbers, ion-oxygen distances, O–D···O distances, and orientational arrangements of water molecules around ions. Coordination numbers and ion-oxygen distances reported so far are given in Table 1 (see also Tables 1 and 2 in Ref. 8). As regards the configuration of water molecules around ions, two forms, "linear" and "bifurcated,"[8] are assumed for cations where lone-pair electrons are located in the vicinity of ions (Figs. 5(a) and (b) in Ref. 8), and also for anions where deuterium atoms in the vicinity of the ions (Figs. 5(c) and (d) in Ref. 8).

We calculated $\Delta S_m(Q)_{calcd}$ for a number of structure models in which the magnitudes of parameters were varied (Table 2). The expression for $\Delta S_m(Q)_{calcd}$ is given Eq. 4 of Ref. 9.

For each of the DCl and DBr solutions, 42 different types of structures with respect to varieties of coordination numbers and orientational configurations are assumed. In the case of D_3O^+, for the tetrahedral configuration three cases were taken into consideration: 1) all peripheral water molecules take the linear con-

TABLE 1. COORDINATION NUMBERS, O–O DISTANCES, AND ION-OXYGEN DISTANCES FOR D_3O^+, PROTON (H_3O^+), AND Br^- DETERMINED FROM X-RAY (X) AND NEUTRON (N) DIFFRACTION STUDIES AS WELL AS FROM MOLECULAR DYNAMICS (MD) CALCULATION

Ion	Coordination number	O-H···O distance/Å	Solute	Concentration	Method	Reference
D_3O^+	4	2.52	HCl, DCl	0.58—13.9 m	X, N	i[a]
Proton		2.56—2.75	HCl	2—6 M	X	ii
(H_3O^+)		2.5—2.6	HCl	7.48—12.28 M	X	iii
Ion	**Coordination number**	**Ion-oxygen distance/Å**	**Solute**	**Concentration**	**Method**	**Reference**
Br^-	6.6—8.9	3.37—3.43	LiBr	2.5—10 m	X	iv
		3.36	NH_4Br	7.3 m	X	v
	7.4—9.5	3.40	LiBr	3.80 M	X	vi
		3.40	NaBr	3.65 M		
	6	3.287—3.293	LiBr	2.1—5.6 M	X	vii
	6, 8	3.316—3.342	$CaBr_2$	1.2—2.0 M	X	viii
		3.14±0.1	$CuBr_2$	0.056 m	X	ix
		3.14±0.1	NaBr			
	5				MD	x
		3.5	$LaBr_3$	2.26, 2.95 m	X	xi

i) Ref. 5. ii) Ref. 17. iii) Ref. 18. iv) R. M. Lawrence and R. F. Kruh, *J. Chem. Phys.*, **47**, 4758 (1967). v) I. M. Shapovalov and I. V. Radchenko, *J. Struct. Chem.*, **10**, 804 (1969). vi) G. Licheri, G. Piccaluga, and G. Pinna, *J. Appl. Crystallogr.*, **6**, 392 (1973). vii) G. Licheri, G. Piccaluga, and G. Pinna, *Chem. Phys. Lett.*, **35**, 119 (1975). viii) G. Licheri, G. Piccaluga, and G. Pinna, *J. Chem. Phys.*, **63**, 4412 (1975). ix) P. Eisenbager and Kincaid, *Chem. Phys. Lett.*, **36**, 134 (1975). x) C. L. Briant and J. J. Burton, *J. Chem. Phys.*, **64**, 2888 (1976). xi) L. S. Smith and D. L. Wertz, *J. Inorg. Nucl. Chem.*, **39**, 95 (1977).

a) Triolo and Narten's "structure parameters for the hydrated ions were those found for the most concentrated solutions" (Ref. 5) in their study,

TABLE 2. RANGE OF PARAMETERS FOR STRUCTURE MODELS

Ion	Coordination number, n	O–O distance/Å	Type of configuration around ion (Hydrogen-, Non-hydrogen-bonded)
D_3O^+	4 (Tetrahedral)	2.70—2.94 (Interval of 0.03)	(Linear, Linear)
	3 (Pyramidal, Planar)		(Linear, Bifurcated) (Bifurcated, Linear)
Ion	**Coordination number, n**	**Ion-oxygen distance/Å**	**Type of configuration around ion**
Cl^-	4 (Tetrahedral) 6 (Octahedral) 8 (Cubic)	3.00—3.20 (Interval of 0.05)	Linear, Bifurcated
Br^-	4 (Tetrahedral) 6 (Octahedral) 8 (Cubic)	3.15—3.50 (Interval of 0.05)	Linear, Bifurcated

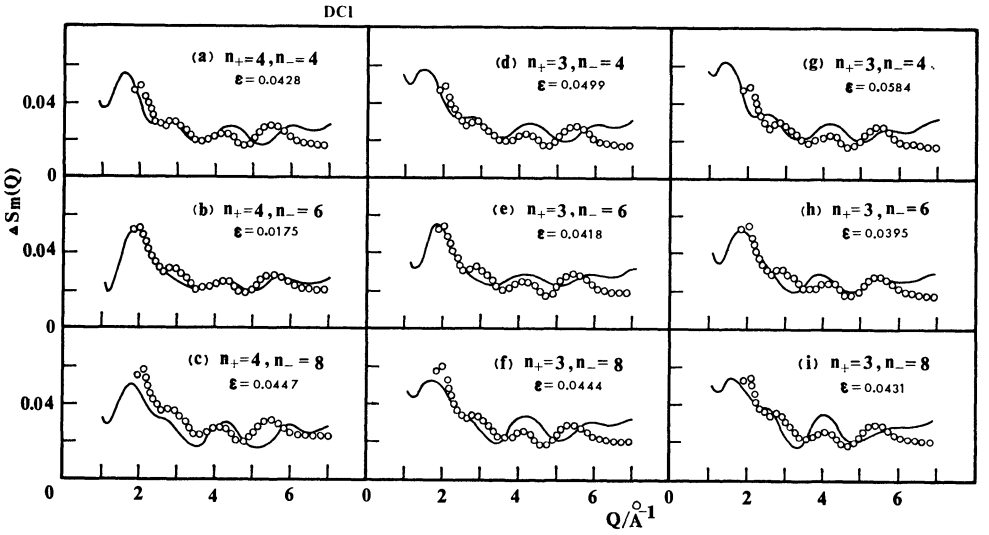

Fig. 2. Changes in the $\Delta S_m(Q)_{calcd}$ with variation of the coordination number for DCl solution. ○: $\Delta S_m(Q)_{obsd}$, ——: $\Delta S_m(Q)_{calcd}$, tetrahedral ($n_+=4$): (a) $n_-=4$, (b) $n_-=6$, and (c) $n_-=8$, pyramidal ($n_+=3$): (d) $n_-=4$, (e) $n_-=6$, and (f) $n_-=8$, planar ($n_+=3$): (g) $n_-=4$, (h) $n_-=6$, and (i) $n_-=8$.

figuration, 2) all those take the bifurcated one, and 3) one non-hydrogen-bonded molecule takes the bifurcated one and others the linear, and also for the pyramidal and/or planar configurations, two cases, 1) and 2), were taken. Distances were varied successively at intervals of 0.03 Å for the O–O distances and 0.05 Å for other ion-oxygen ones. As a whole, we calculated the $\Delta S_m(Q)_{calcd}$ curves for 516 different structure models of the first hydration shell in the DCl solution and those for 625 different models in the DBr solution, and then determined the best structure model by the comparison of $\Delta S_m(Q)_{calcd}$ with $\Delta S_m(Q)_{obsd}$ for both solutions.

Determination of the Best Fit Model: The procedure for determination of the best fit structure model is as follows. First the $\Delta S_m(Q)_{calcd}$ calculated by the above-mentioned procedures were compared by a rough estimation with the $\Delta S_m(Q)_{obsd}$ in the range of Q, 2—5 Å^{-1} and the models which gave appreciable deviations of the $\Delta S_m(Q)_{calcd}$ curves from the $\Delta S_m(Q)_{obsd}$ were excluded. Next, for the remaining $\Delta S_m(Q)_{calcd}$ curves, we calculated the deviations expressed as

$$\varepsilon = \{\sum_{i=1}^{N}[\Delta S_m(Q_i)_{obsd} - \Delta S_m(Q_i)_{calcd}]^2\}^{1/2} / \sum_{i=1}^{N}[\Delta S_m(Q_i)_{obsd}], \quad (4)$$

where N is the number of data points in the fitting region, and used ε as a measure for the fitness of the model. In the present study, the fitting region with respect to $\Delta S_m(Q)$ is taken to be Q=2—7 Å^{-1}.

In Figs. 2 and 3, the $\Delta S_m(Q)_{calcd}$ for different sets of coordination numbers are compared with the $\Delta S_m(Q)_{obsd}$ data for the DCl and DBr solutions. The values of ε calculated for each case are indicated. The ε_{min} is 0.0175 and 0.0347 for the DCl and DBr solutions, respectively. Thus, the best fit curve with $\Delta S_m(Q)_{obsd}$ is obtained in the case of $n_{D_3O^+}=4$ and $n_{Cl^-}=6$ for the DCl solution (Fig. 2(b)) and also obtained in the case of $n_{D_3O^+}=4$ and $n_{Br^-}=6$ for the DBr solution (Fig. 3(b)). The curves other than the best fit one deviate appreciably from the $\Delta S_m(Q)_{obsd}$ ($\varepsilon > \varepsilon_{min}$). In the case of $n_{D_3O^+}=3$, all curves are found to deviate from the observed ones ($\varepsilon > \varepsilon_{min}$) appreciably, and, thus, the structure models with

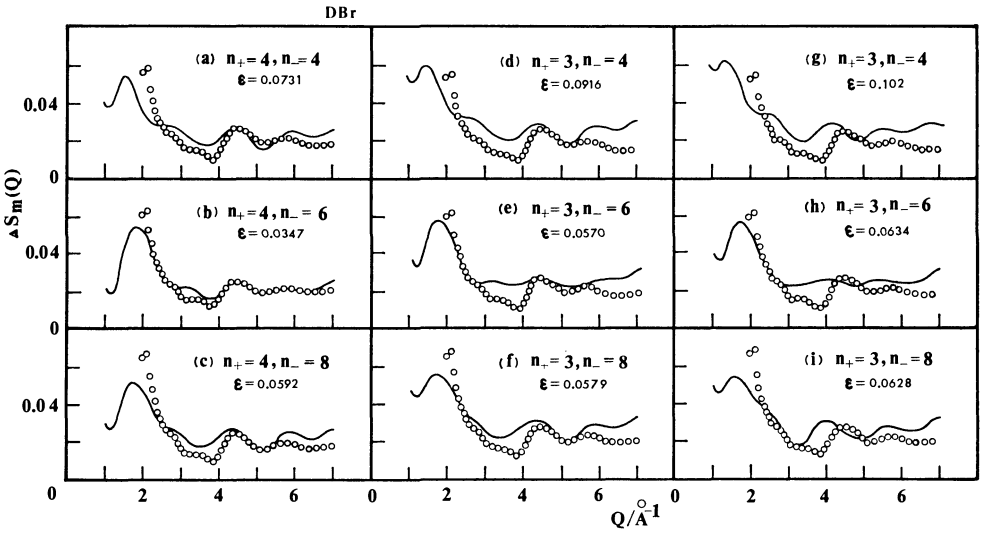

Fig. 3. Changes in the $\Delta S_m(Q)_{calcd}$ with variation of the coordination number for DBr solution. ○: $\Delta S_m(Q)_{obsd}$, ——: $\Delta S_m(Q)_{calcd}$, tetrahedral ($n_+=4$): (a) $n_-=4$, (b) $n_-=6$, and (c) $n_-=8$, pyramidal ($n_+=3$): (d) $n_-=4$, (e) $n_-=6$, and (f) $n_-=8$, planar ($n_+=3$): (g) $n_-=4$, (h) $n_-=6$, and (i) $n_-=8$.

$n_{D_3O^+}=3$ are rejected.

For $n_+=4$ and $n_-=6$, the $\Delta S_m(Q)_{calcd}$ curves with various magnitudes of the distances (r_{O-O}, r_{Cl^--O}, and r_{Br^--O}) are shown in Figs. 4(a)—(d), together with the parabolic curves in Figs. 4(a')—(d') required for locating the value of ε_{min}. For the distance r_{O-O} the ε_{min} exists at $r_0=2.88$ Å in both solutions, and that for r_{Cl^--O} and r_{Br^--O} exists at $r_0=3.10$ Å and $r_0=3.21$ Å in the DCl and DBr solutions, respectively. If we can introduce a range of allowance for ε, variations of distances can be determined. Then, taking account of the experimental errors, we set up the range, $\varepsilon<0.02$ for the DCl solution and $\varepsilon<0.035$ for the DBr solution. As a result, the deviations are found to be ±0.05 Å for all the distances.

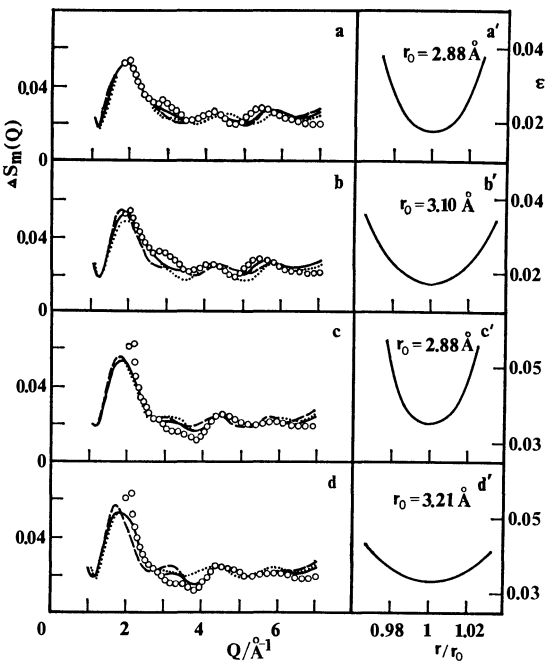

Fig. 4. Changes in the $\Delta S_m(Q)_{calcd}$ with variation of the O–O distance and the ion-oxygen distance for DCl (a, b) and DBr (c, d) solutions, and variation of ε with distances (a'—d').
○: $\Delta S_m(Q)_{obsd}$, (a), (c) r_{O-O} (all other parameters are identical with those given in Table 3), ……: 2.82 Å, ——: 2.88 Å, ----: 2.94 Å, (b) r_{Cl^--O} (all other parameters are identical with those given in Table 3), ……: 3.00 Å, ——: 3.10 Å, ----: 3.20 Å, (d) r_{Br^--O} (all other parameters are identical with those given in Table 3), ……; 3,15 Å, ——: 3.25 Å, ----: 3.35 Å.

In Figs. 5(a)—(d), the $\Delta S_m(Q)_{calcd}$ curves with various orientational configurations for the same set of coordination numbers ($n_+=4$ and $n_-=6$) are shown. Applying the same criterion ($\varepsilon<0.02$ for the DCl solution and $\varepsilon<0.035$ for the DBr solution) to these cases, linear configurations for D_3O^+ and bifurcated ones for anions are accepted as the best fit for both solutions.

The $\Delta S_m(Q)_{calcd}$ curves of the best models thus determined are given in Figs. 2(b) and 3(b) for the DCl and DBr solutions, respectively. The magnitudes of parameters and orientational configurations for the best fit models of the first hydration shell are given in Table 3.

Concerning the configurations of water molecules within the first hydration shell around D_3O^+, it is

TABLE 3. COORDINATION NUMBERS, O-O DISTANCES, ION-OXYGEN DISTANCES, AND ORIENTATIONAL CONFIGURATIONS AROUND IONS DETERMINED IN THE PRESENT STUDY

Ion	Coordination number	O-O and ion-oxygen distance/Å	Configuration around ion
D_3O^+	4	O-O: 2.88±0.05	Linear
Cl^-	6	Cl⁻-O: 3.10±0.05	Bifurcated
Br^-	6	Br⁻-O: 3.21±0.05	Bifurcated

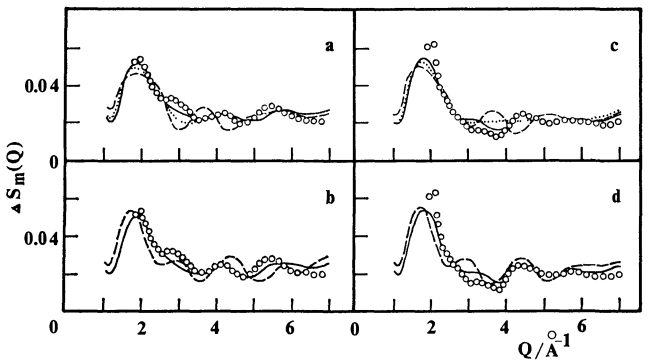

Fig. 5. Changes in the $\Delta S_m(Q)_{calcd}$ with variation of orientational configurations around ions for DCl (a, b) and DBr (c, d) solutions. ○: $\Delta S_m(Q)_{obsd}$, (a) confifurations around D_3O^+ (all other parameters are identical with those in Table 3), ……: one non-hydrogen-bonded water molecule takes the bifurcated configuration and others are the linear (ε=0.0252), ——: all peripheral water molecules take the linear configuration (ε=0.0175), ----: all peripheral water molecules take the bifurcated configuration (ε=0.0351), (b) configurations around Cl^- (all other parameters are identical with those given in Table 3), ——: bifurcated (ε=0.0175), ----: linear (ε=0.0432), (c) configurations around D_3O^+ (all other parameters are identical with those given in Table 3), ……: one non-hydrogen-bonded water molecule takes the bifurcated configuration and others are the linear (ε=0.0376), ——: all peripheral water molecules take the linear configuration (ε=0.0347), ----: all peripheral water molecules take the bifurcated configuration (ε=0.0507), (d) configurations around Br^- (all other parameters are identical with those given in Table 3), ——:bifurcated (ε=0.0347), ----: linear (ε=0.0554).

concluded that the "linear" type[8,9] of all water molecules is predominant for both solutions (Figs. 5(a) and (c)). On the other hand, with respect to the configurations around anions, it is concluded that the "bifurcated" type[8,9] is predominant for both solutions (Figs. 5(b) and (d)). The structure of the first shell around Cl^- in the DCl solution is found to be identical with those in aqueous alkali chloride solutions previously determined by the authors.[8,9] With respect to the coordination number around Cl^-, Triolo and Narten assigned the value of n_{Cl^-}=4 in their analysis (Ref. 5). However, as clearly seen in Figs. 2(a), (d), and (g), the tetrahedral coordination for Cl^- is rejected and n_{Cl^-}=6 is assigned. This difference between our results and those by Triolo and Narten is attributed to the difference in the concentration of solution.

In the present application of the "subtraction method" by using Eq. 3 we have taken the magnitude of

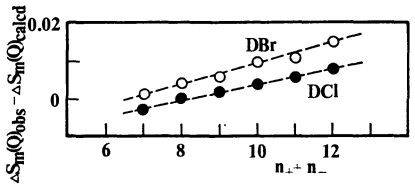

Fig. 6. $\Delta S_m(Q)_{obsd} - \Delta S_m(Q)_{calcd}$ plotted against $(n_+ + n_-)$.

a for 1/2 described above. In Fig. 6, the differences $\Delta S_m(Q)_{obsd} - \Delta S_m(Q)_{calcd}$[9] are plotted again against $(n_+ + n_-)$. The differences are substantially zero within the maximum range of 0.01. This supports the adequacy of the assignment of a as 1/2 (see Fig. 8 in Ref. 9).

References

1) J. F. Karnicky and C. J. Pings, *Adv. Chem. Phys.*, XXXIV, 157 (1976).

2) J. E. Enderby and G. W. Neilson, "Water-A Comprehensive Treatise," ed by F. Franks, (1979), Vol. 6, Chap. 1.

3) G. E. Bacon, "Neutron Diffraction," 3rd ed, Clarendon Press, Oxford (1975).

4) A. H. Narten, F. Vaslow, and H. A. Levy, *J. Chem. Phys.*, **58**, 5017 (1973); A. H. Narten and H. A. Levy, *Science*, **165**, 447 (1969).

5) R. Triolo and A. H. Narten, *J. Chem. Phys.*, **63**, 3624 (1975).

6) A. K. Soper, G. W. Neilson, J. E. Enderby, and R. A. Howe, *J. Phys. C, Solid State Phys.*, **10**, 1793 (1977).

7) S. Cummings, J. E. Enderby, and R. A. Howe, *J. Phys. C, Solid State Phys.*, **13**, 1 (1980).

8) N. Ohtomo and K. Arakawa, *Bull. Chem. Soc. Jpn.*, **52**, 2755 (1979).

9) N. Ohtomo and K. Arakawa, *Bull. Chem. Soc. Jpn.*, **53**, 1789 (1980).

10) J. C. Dore, G. Walford, and D. I. Page, *Mol. Phys.*, **29**, 565 (1975); J. H. Clarke, J. C. Dore, and R. N. Sinclair, *ibid.*, **29**, 581 (1975); J. H. Clarke, J. C. Dore, G. Walford, and R. N. Sinclair, *ibid.*, **31**, 883 (1976); G. W. Stanton, J. H. Clarke, and J. C. Dore, *ibid.*, **34**, 823 (1977); J. H. Clarke, J. C. Dore, and H. Egger, *ibid.*, **39**, 533 (1980).

11) G. Walford, J. H. Clarke, and J. C. Dore, *Mol. Phys.*, **36**, 1581 (1978); J. H. Clarke, J. R. Granada, and J. C. Dore, *ibid.*, **37**, 1263 (1979); I. P. Gibson and J. C. Dore, *ibid.*, **37**, 1281 (1979); J. R. Granada, G. W. Stanton, J. H. Clarke, and J. C. Dore, *ibid.*, **37**, 1297 (1979); J. R. Granada, J. C. Dore, and J. H. Clarke, *ibid.*, **39**, 175 (1980).

12) Y. Ishikawa and N. Watanabe, *Nippon Butsuri Gakkai Shi*, **28**, 461 (1973).

13) N. Ohtomo and K. Arakawa, *Bull. Chem. Soc. Jpn.*, **51**, 1649 (1978).

14) N. Ohtomo and K. Arakawa, *Bull. Chem. Soc. Jpn.*, **53**, 1510 (1980).

15) J. G. Powles, *Adv. Phys.*, **22**, 1 (1973).

16) G. Pálinkás, T. Radnai, and F. Hajdu, *Z. Naturforsch., Teil A*, **35**, 107 (1980); In this paper, starting from the analysis of the X-ray data, Pálinkás *et al.* arrived at the same conclusion as ours in Ref. 13 that the magnitude of r_c, the most important parameter[4] specifying Narten's model, was too small.

17) S. C. Lee and R. Kaplow, *Science*, **169**, 477 (1970).

18) D. L. Wertz, *J. Solution Chem.*, **1**, 489 (1972).

19) a) T. Matsumoto, N. Ohtomo, and M. Senda, *J. Nucl. Sci. Technol.*, **15**, 863 (1978); b) T. Matsumoto, N. Ohtomo, and M. Senda, *Bull. Fac. Engi. Hokkaido University*, **93**, 11 (1979).

20) N. Ohtomo and K. Arakawa (Internal Report: unpublished).

21) G. Placzek, *Phys. Rev.*, **86**, 377 (1952); J. G. Powles, *Mol. Phys.*, **37**, 623 (1979).

22) G. C. Wick, *Phys. Rev.*, **94**, 1228 (1954); T. Matsumoto, *J. Nucl. Sci. Technol.*, **16**, 401 (1979).

23) D. I. Page and J. G. Powles, *Mol. Phys.*, **21**, 901 (1971).

24) A. H. Narten, *J. Chem. Phys.*, **56**, 5681 (1972).

25) As regards the hydrated water molecules around ions, the intramolecular structure of those is assumed to be identical with that in the vapor phase, while the structure of D_3O^+ itself is assumed to be heavy ice-I-like.[13]

A Theoretical Approach to the Dielectric Relaxation of Alcohol Solutions

Ryuichi MINAMI, Koichi ITOH,* Hiroshi SATO, Hiroaki TAKAHASHI, and Keniti HIGASI

Department of Chemistry, School of Science and Engineering, Waseda University, Okubo, Shinjuku-ku, Tokyo 160

(Received September 10, 1980)

The dielectric relaxation mechanism of primary alcohols in solutions of various solvents with and without a hydrogen-bonding capacity was theoretically studied using the concept of the chemical equilibrium between hydrogen-bonded chain multimers and that between the multimers and solvents. The dipole-inversion processes originating from the successive rotation of the hydroxyl groups of the hydrogen-bonded multimers were considered to play the dominant role in the dielectric relaxation of alcohol solutions. By applying the one-dimensional random-walk process to the dipole inversion, we estimated the effect of dilution upon the dielectric relaxation times of primary alcohol in solution. The results of our calculation appear to explain the experimental data.

The dielectric relaxation of liquid alcohols was first studied by Mizushima[1] in 1926; since then, the theoretical explanation of its mechanism has become a long-standing problem which has never been solved clearly.[2-4] For the last decade some of the present authors have joined in examining the effect of dilution on the principal relaxation times of several alcohols, using inert solvents (*e.g.*, benzene) as well as those with functional groups (*e.g.*, pyridine and dioxane) as diluents.[5-8] In spite of these studies, it has still been difficult to give a simple molecular model for the dipole-inversion process of alcohol solutions in which various sorts of intermolecular hydrogen-bond interactions and steric hindrances are supposed to exist.[9] On the other hand, the theoretical explanation of the static dielectric constants of liquid alcohols has successfully been performed by several authors.[10-12] For example, Dannhauser[13] experimentally determined the values of the Kirkwood correlation factor,[11] g, for eight isomers of octanols and analyzed the data in terms of the thermodynamic equilibrium constants for cyclic-dimer and open-chain multimer formations.

Recently we ourselves proposed a new theoretical treatment of the dielectric relaxation process of pure liquid alcohols.[14] Following Dannhauser's treatment,[13] we assumed that liquid alcohol molecules exist in an association equilibrium involving both hydrogen-bonded cyclic dimers and open-chain n-mers, and, further, that each of the n-mers alters or reverses its dipole moment by the successive rotation of the indivisual hydroxyl group, as is shown in Scheme 1. This inversion process was assumed to be the main mechanism of the dipole relaxation of the hydrogen-bonded chain n-mers. Scheme 2 shows an intermediate state of the dipole inversion from the left multimer to the right one in Scheme 1. The hydroxyl group with an asterisk in Scheme 2 indicates a rotationally activated state. The dipole inversion of the n-mers is considered always to originate at the terminal molecules because, in order to activate one of the terminal segments, it needs to break only one

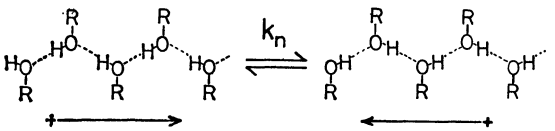

Scheme 1.

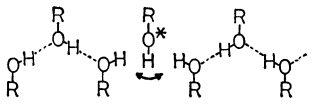

Scheme 2.

hydrogen bond, while two hydrogen bonds must be broken to activate an intermediate segment. Therefore, the inversion process can be regarded as the most probable process by which the activated state propagates from the left end to the right end, or from the right end to the left end. In our treatment, we applied the one-dimensional random-walk model with two absorption walls to these dipole inversion processes,[15] and concluded that the relaxation time, τ_n, of the n-mer is given by:

$$\tau_n = (n+1)\tau_H, \quad (1)$$

where τ_H is the reciprocal of k_H, the rate in which the terminal hydroxyl groups of the n-mer are activated rotationally. By using Eq. 1 and the values of the thermodynamic equilibrium constants for the cyclic dimer and chain n-mer formations, we calculated the complex permitivities as a function of the angular frequency, ω, of the field. The results are in fair agreement with the dielectric dispersion observed for liquid 1-heptanol.[16]

Sack also developed a theory for the relaxation process of a system containing linear chains of dipoles and applied it to explain the high dielectric constants and losses of long-chain alcohols in the solid state.[17] He assumed that there exists, at most, one discontinuity where two anti-parallel arrangements of the hydroxyl groups of alcohols face each other, and that the wandering of this discontinuity along each chain is the main mechanism of the dipole relaxation. It was concluded that the effective relaxation time of a linear chain n-mer is proportional to $(n+1)^2$. This mechanism, however, cannot be applied to the dielectric relaxation process of liquid alcohols because, immediately after a discontinuous point appears, a pair of anti-parallel chains should separate and move away from each other in the liquid state.

In this paper we extend the above-mentioned theory to include the effect of the addition of inert solvents as well as those with functional groups, which form hydrogen bonds, on the dielectric relaxation mechanism of alcohols. We also give a theoretical prediction regarding the dilution effect on the re-

laxation times of alcohol solutions. The results are compared with the experimental data.

Stoichiometry of Association Equilibria between Alcohol Monomers and Multimers and between Multimers and Solvents

The binary solutions of primary alcohols and solvents are assumed to consist of alcohol monomers, A_1; solvent molecules, B; hydrogen-bonded cyclic dimers,† A_c; hydrogen-bonded open-chain n-mers, A_n, and, if B has proton-acceptor groups, open-chain n-mers hydrogen-bonded with the solvent at one end, A_nB. As is the case with pure alcohols, the association equilibria can be expressed as follows:

i) Cyclic dimer: $A_1 + A_1 \overset{K_c}{\rightleftharpoons} A_c$,

ii) open-chain n-mer: $A_{n-1} + A_1 \overset{K_n}{\rightleftharpoons} A_n \quad (n \geqq 2)$,

where K_c and K_n are the equilibrium constants of the formation of the cyclic dimer and the open-chain n-mer respectively. When the solvent molecule, B, can form a hydrogen bond with the hydroxyl group of alcohols, we also assume the following equilibrium between A_n and B:

iii) addition compound: $A_n + B \overset{K_{nb}}{\rightleftharpoons} A_nB \quad (n \geqq 1)$,

where K_{nb} is the equilibrium constant of the association between A_n and B. As the mole fraction of the solvent molecules with the hydrogen-bond capacity is increased, the average degree of the association of alcohol multimers is decreased. This can be seen in the following stoichiometric calculations.

The stoichiometric relationships for the association equilibria mentioned above have been studied extensively,[13] and the volume fractions[18] of A_1, A_c, A_n, A_nB, and B, which are expressed as ϕ_1, ϕ_c, ϕ_n, ϕ_{nb}, and ϕ_b, are related to each other by the following equations:

$$\left.\begin{aligned} \phi_c &= K_c\phi_1^2, \\ \phi_n &= (K\phi_1)^{n-1}\phi_1, \\ \phi_{nb} &= (K\phi_1)^{n-1}\phi_1 K_b\phi_b, \end{aligned}\right\} \tag{2}$$

where we assumed that:[19]

$$K \equiv K_2 = K_3 \ldots = K_n = \ldots,$$

and

$$K_b \equiv K_{1b} = K_{2b} = \ldots = K_{nb} = \ldots .$$

The sum of the volume fractions is equal to one, giving this equation:

$$\sum_{n=1}^{\infty} \phi_n + \phi_c + \sum_{n=1}^{\infty} \phi_{nb} + \phi_b = 1. \tag{3}$$

The total mole fraction of the solvent B, x_B, can be expressed as follows:

$$\sum_{n=1}^{\infty} \phi_{nb}/(n+1) + \phi_b = x_B. \tag{4}$$

From Eqs. 2, 3, and 4, we derive the following transcendental equations:

$$(1+K_b\phi_b)\phi_1/(1-K\phi_1) + K_c\phi_1^2 + \phi_b = 1, \tag{5}$$

$$\phi_b - \{\ln(1-K\phi_1) + K\phi_1\}K_b\phi_b/K^2\phi_1 = x_B. \tag{6}$$

The numerical calculations[20] using Eqs. 5 and 6 give the ϕ_1 and ϕ_b values as functions of x_B for the assumed K, K_c, and K_b values. On the substitution of the ϕ_1 and ϕ_b values into Eq. 2 we can obtain the ϕ_c, ϕ_n, and ϕ_{nb} values as functions of x_B.

Dielectric Relaxation of Alcohol Solutions

The dielectric dispersion observed for alcohol solutions is the sum of the contributions from the dielectric relaxations of A_n, A_nB, and A_1 (and B, if it is a polar molecule.) The cyclic dimer A_c has no permanent dipole moment, and it does not contribute to the dielectric dispersion. The dielectric relaxation times of all the polar solvent molecules are, in general, very much smaller than those of the multimers. For this reason, the contribution from the solvent can also be neglected. We applied the one-dimensional random walk model also to the dipole inversion process of A_nB. The mechanism of its stochastic process, however, is a little different from that of the dipole inversion process of A_n. The reason for this is that activating the alcohol segment neighboring B requires a mechanism different from that required to activate one of the end segments in A_n. Therefore, we use the $\tau_{H'}$, symbol for the activation of the alcohol segments at the ends of A_nB instead of the symbol, τ_H, for the activation of the end segment of A_n. The relaxation time of the dipole inversion of A_nB, τ_{nb}, is expressed by:

$$\tau_{nb} = (n+1)\tau_{H'}. \tag{7}$$

The weights of the contributions of the multimers, A_n and A_nB, to the dielectric dispersion are proportional to the values of ϕ_n/n and $\phi_{nb}/(n+1)$, which represent the proportions of A_n and A_nB respectively, and are also proportional to the expected values of their squared dipole moments, $\langle\mu_n^2\rangle$ and $\langle\mu_{nb}^2\rangle$ respectively. In this paper we assume that μ_n is approximately equal to μ_{nb} and that $\langle\mu_n^2\rangle$ is proportional to n^2.†† On the basis of these considerations, we obtain the following equations:

$$\frac{\varepsilon^*-\varepsilon_\infty}{\varepsilon_0-\varepsilon_\infty} = Z^{-1}\left\{\frac{\phi_1}{1+i\omega\tau_1} + \sum_{n=2}^{\infty}\frac{n\phi_n}{1+i\omega(n+1)\tau_H} + \sum_{n=1}^{\infty}\frac{n^2\phi_{nb}/(n+1)}{1+i\omega(n+1)\tau_{H'}}\right\}, \tag{8a}$$

$$Z \equiv \sum_{n=1}^{\infty}(n\phi_n + n^2\phi_{nb}/(n+1)) = \phi_1/(1-K\phi_1)^2 + K_b\phi_b[K\phi_1^2/(1-K\phi_1)^2 - \{\ln(1-K\phi_1)+K\phi_1\}/K^2\phi_1], \tag{8b}$$

where ε^*, ε_0, and ε_∞ are the complex, static, and limiting high-frequency permitivities respectively.

† Cyclic trimers, cyclic tetramers, *etc.* are not considered here, after Dannhauser.[13]

†† For an extremely large n, $\langle\mu_n^2\rangle$ and $\langle\mu_{nb}^2\rangle$ would be proportional to n instead of n^2.[21] Our calculation, however, indicates that the average numbers $\langle n\rangle$, are 6.6, 8.7, and 10.8 for K=20, 30, and 40 respectively. For A_n and A_{nb} with these small n values, it is reasonable to assume that $\langle\mu_n^2\rangle$ and $\langle\mu_{nb}^2\rangle$ are proportional to n^2.

As is well known, the dielectric constants and losses of most of the liquid alcohols measured in the low-frequency region conform very well to the simple relaxation pattern of Debye. (This dispersion is often called "the principal dielectric dispersion", and the relaxation time corresponding to this dispersion, "the principal relaxation time".) On the other hand, some strong deviation from the simple Debye dispersion have been detected in the high-frequency region.[3] If we limit our discussion only to the low-frequency dispersions or the principal dispersions, we can express the measured complex permitivities of alcohol solutions by the well-known Debye equation:

$$(\varepsilon^*-\varepsilon_\infty)/(\varepsilon_0-\varepsilon_\infty) = 1/(1+i\omega\tau_p), \quad (9)$$

where τ_p is the principal relaxation time. By equating the right-hand side of Eq. 8a to that of Eq. 9, τ_p can be calculated as a function of ω. The results of calculation for several sets of the assumed values of K, K_b, K_c, and τ_H (assuming that τ_H is equal to $\tau_{H'}$) indicate that the calculated values of τ_p do not depend on ω so long as ω is less than $1/\tau_H$. On the basis of this result, we obtained the analytical equation of τ_p at the low-frequency limit(: $\omega\to 0$) as follows:

$$\tau_p = Z^{-1}\left\{\sum_{n=2}^{\infty} n(n+1)\tau_H\phi_n + \sum_{n=1}^{\infty} n^2\tau_H\phi_{nb}\right\}$$
$$= (\tau_H\phi_1/Z)[\{2+(1+K\phi_1)K_b\phi_b\}/(1-K\phi_1)^3-2], \quad (10)$$

where the contribution of alcohol monomers to the dielectric dispersion is neglected because τ_1 is much smaller than τ_n and τ_{nb} ($n\geqq 2$). This equation allows us to calculate the principal dielectric relaxation times of alcohol solutions for the assumed K, K_b, K_c, and τ_H values.

Effect of Dilution on Dielectric Relaxation Times of Alcohol Solutions

When an inert solvent is used as a diluent of alcohol solution, it can be assumed that K_b is equal to zero. Since primary alcohols associate strongly with each other, K is expected to be much larger than one, giving the condition $K\cdot x_A \gg 1$ (x_A denotes the total mole fraction of alcohol molecules, *viz.*, $x_A = 1-x_B$; its value is set so as to be always larger than 1/2.) A tentative assumption that K_c is equal to zero is also made because the K_c value of primary alcohol was experimentally found to be much smaller than the K value, and also because the cyclic dimers do not contribute to the dielectric dispersion of alcohol solutions.[13] Under these conditions, we can derive the analytical expression for ϕ_1 from Eqs. 5 and 6:

$$\phi_1 = x_A/(1+Kx_A). \quad (11)$$

On the substitution of Eq. 11 into Eq. 10, we obtain an approximate expression for τ_p defined by Eq. 9:

$$\tau_p = 2(1+Kx_A)\tau_H. \quad (12)$$

As can be seen from Fig. 1, the observed principal dielectric relaxation times of 1-propanol decrease linearly as the mole fractions of benzene are increased. From the variation in the observed principal dielectric relaxation times of 1-propanol and 1-butanol caused by the addition of benzene,[5,6] we can determine the values of K and τ_H. The results are summarized in Table 1.[22]

When the solvent has a functional group or groups which form a hydrogen bond or bonds with alcohols, K_b becomes much different from zero. In this case, we must use Eq. 10 in order to estimate the principal relaxation times of the solutions. Assuming that K is equal to 30 (*cf.* Table 1), we calculated the principal relaxation times of 1-propanol as functions of x_B, while varying the K_b from 0.5 to 30.0. The results are

Table 1. Experimental principal relaxation times, τ_p, for an alcohol/benzene mixture and estimated values of K and τ_H[a]

1-Propanol (25 °C)[b]		1-Butanol (25°C)[b]	
x_A[c]	τ_p/ps	x_A	τ_p/ps
1.0	338	1.0	504
0.920	324	0.899	472
0.886	294	0.806	422
0.788	279	0.670	353
0.691	235	0.620	314
K	τ_H/ps	K	τ_H/ps
30	5.5	41	6.1

a) The values of K and τ_H are evaluated by using the least-squares method applied to Eq. 12. b) Ref. 6. c) Mole fraction of alcohol.

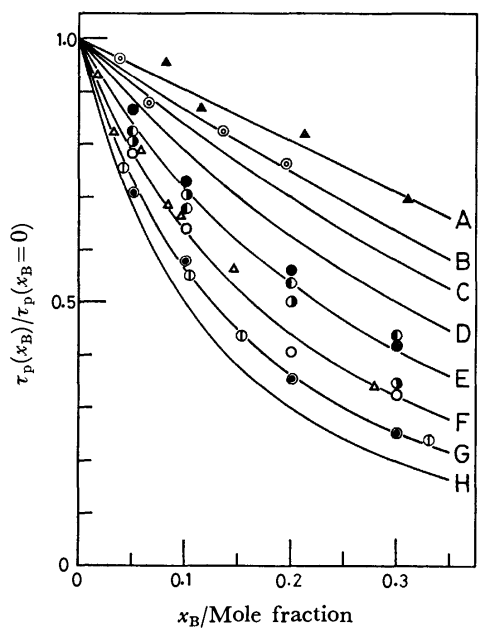

Fig. 1. Variation of principal dielectric relaxation times due to dilution with various solvents. Solid curves are theoretical results obtained from Eq. 10 with $K=30$ and $K_c=0$. The values of K_b for curves (A), (B),.., (H) are 0, 0.5, 1.0, 2.0, 4.0, 8.0, 15.0, and 30.0, respectively. The experimental data are for the 1-propanol solutions at 25 °C which are diluted with the following solvents.[5,6,8]
▲: Benzene, ◎: chlorobenzene, ●: water, ◐: camphor, ◑: cyclohexanone, △: pyridine, ○: 3-pentanone, ◉: acetone, ⓘ: dioxane.

shown by solid curves in Fig. 1. Into this figure we add also the result of calculation for the case when K_b is equal to zero. This theoretical curve (*i.e.*, (A)), which decreases linearly with the increase in x_B, compares well with the data of the principal relaxation time observed for the 1-propanol/benzene mixtures. Our previous papers[5-8] have shown that, when solutions are diluted with solvents having a hydrogen-bond capacity, the principal relaxation times of the solutions change in quite different manners from those in which the relaxation times of alcohol solutions change as they are diluted with inert solvents. As the results summerized in Fig. 1 show, the principal relaxation times of mixtures of 1-propanol and solvents with a hydrogen-bond capacity do not exibit a linear decrease with dilution, and this decrease is more pronounced than that observed for the 1-propanol/benzene system. The results of calculation for the K_b in the range from 4 to 15 correspond very well to the abovementioned observation.

Conclusion

Our mechanism, which was originally proposed to explain the anomalous dielectric relaxation behavior of pure primary alcohols, has now been extended to an examination of the effect of dilution upon the principal dielectric relaxation of 1-propanol using both inert and hydrogen-bonding solvents. The results obtained so far are in fair agreement with the experiments, confirming that our theory is valid for the dielectric relaxation of the liquid primary alcohols.

We are grateful to Dr. R. J. Meakins for providing us with valuable materials on his and Dr. Sack's work.

References

1) S. Mizushima, *Bull. Chem. Soc. Jpn.*, **1**, 47, 83, 115, 143, 163 (1926); *Physik. Z.*, **28**, 418 (1927).
2) K. Higasi, "Dipole, Molecule and Chemistry," *Monogr. Ser. Res. Inst. Appl. Elec. Hokkaido Univ.*, No. 13, Chap. 1 (1965).
3) S. K. Garg and C. P. Smyth, *J. Phys. Chem.*, **69**, 1294 (1965).
4) J. Crossley, *Adv. Mol. Relax. Processes*, **2**, 69 (1970).
5) E. Arie, M. Nakamura, H. Takahashi, and K. Higasi, *Chem. Lett.*, **1973**, 533.
6) T. Koshii, E. Arie, M. Nakamura, H. Takahashi, and K. Higasi, *Bull. Chem. Soc. Jpn.*, **47**, 618 (1974).
7) H. Sato, T. Koshii, H. Takahashi, and K. Higasi, *Chem. Lett.*, **1974**, 579; **1975**, 491.
8) H. Sato, H. Takahashi, and K. Higasi, *Chem. Lett.*, **1976**, 623.
9) C. Brot, *Ann. Phys. (Paris)*, **13-2**, 714 (1957); *J. Chim. Phys.*, **56**, 1036 (1959).
10) P. Debye, "Polar Molecules," Chemical Catalog Co., New York, N. Y. (1929).
11) H. Fröhlich, "Theory of Dielectrics," Oxford Univ., Oxford (1949).
13) W. Dannhauser, *J. Chem. Phys.*, **48**, 1911 (1968); see also W. Dannhauser and L. W. Bahe, *ibid.*, **40**, 3058 (1964).
14) R. Minami, K. Itoh, H. Takahashi, and K. Higasi, *J. Chem. Phys.*, **73**, 3396 (1980).
15) S. Karlin, "A First Course in Stochastic Processes," Academic Press, New York (1969).
16) J. Middelhoek and C. J. F. Böttcher, "Molecular Relaxation Processes," *Chem. Soc. Spec. Publ.*, **20**, 69 (1966).
17) R. A. Sack, *Aust. J. Sci. Res.*, **A5**, 135 (1952); *Trans. Faraday Soc.*, **59**, 1672 (1963); see also R. J. Meakins, *ibid.*, **58**, 1953 (1962).
18) K. Shinoda, "Solutions and Solubilities," Maruzen, Tokyo (1974); P. J. Flory, "Principles of Polymer Chemistry," Cornell Univ. Press, Ithaca (1953).
19) I. Prigogine and R. Defay, "Chemical Thermodynamics," Longmans Green, London (1954).
20) G. E. Forsythe, M. A. Malcolm, and C. B. Moler, "Computer Methods for Mathematical Computations," Englewood Cliffs, Prentice-Hall, New Jersey (1977), Chap. 7.
21) P. J. Flory, "Statistical Mechanics of Chain Molecules," John Wiley and Sons, New York (1969), Chap. 1.
22) A maximum in τ_p *vs.* x_B curves was observed by Sagal[23] and Komooka[24] for alcohol–cyclohexane solutions. This suggests that the nature of benzene as a solvent is different from that of inert solvents, such as cyclohexane and hexane.[25] We can suspect that the properties of a solvent cause the dependency of τ_H in Eq. 12 upon the atmosphere surrounding alcohol molecules or, rather, surrounding the end OH group of the molecule. In this case, we can tentatively put $\tau_H=\tau_H(A)x_A+\tau_H(B)x_H$, where $\tau_H(A)$ is associated with the hydrogen-bonded chain in pure alcohols, and $\tau_H(B)$, with that isolated from each other with solvent molecules. On the basis of this assumption, we calculated τ_p *vs.* x_B while varying the $\tau_H(B)/\tau_H(A)$ ratio. The result of calculation shows a maximum in fair agreement with the observations of Sagal and Komooka.
23) M. W. Sagal, *J. Chem. Phys.*, **36**, 2437 (1962).
24) H. Komooka, *Bull. Chem. Soc. Jpn.*, **45**, 1696 (1972).
25) K. Higasi, *Bull. Chem. Soc. Jpn.*, **25**, 159 (1952).

Theoretical and Experimental Studies of the Membrane Permeabilities to Ions in Liquid Membrane

Kazuo NOMURA,* Akira MATSUBARA, and Hideo KIMIZUKA†

Laboratory of Chemistry, College of General Education, Kyushu University 01, Ropponmatsu, Fukuoka 810

†*Department of Chemistry, Faculty of Science, Kyushu University 33, Hakozaki, Fukuoka 812*

(Received September 18, 1980)

A theory for the ion transport across liquid ion-exchange membrane was presented on the basis of nonequilibrium thermodynamics with the assumptions that the carrier ions and complexes were present only in the membrane phase, and that there was no volume flow and all chemical reactions were at equilibrium. The equations for "total" fluxes of membrane-permeable ions at steady state were derived from a set of the equations for "individual" fluxes of all mobile species present in the liquid membrane where the complexes were assumed to be partially dissociated. The "total" phenomenological coefficients were able to be expressed in terms of the "individual" coefficients. The diffusional and electroconductional membrane permeabilities to a selective ion in the liquid membrane–single electrolyte system were found to be in the same form as those in the fixed-site membrane–single electrolyte system, if the mean diffusion coefficient and mean mobility of the free species and its complex were used. The rate constants in the permeation process were also related to the diffusional membrane permeability. The experimental examination was made on a liquid cation-exchange membrane–aqueous single electrolyte system at 25 °C. The solution of calcium hexadecyl sulfate in 1-octanol and calcium chloride were used as the liquid membrane and the electrolyte, respectively. All the measured quantities were consistently interpreted by the presented theory.

Since the carrier model was introduced into the transport phenomena across cell membranes, liquid membranes having carrier species have been extensively studied by many investigators.[1,2] On the other hand, various ion-selective electrodes using liquid membranes have been devised and commercialized, because of their high selectivity to a particular ion.[3] Current research has been carried out to provide the underlying principle for the separation of metal ions by liquid membranes.[4,5]

In spite of numerous experimental works, theories proposed for the ion transport across liquid membrane are not as many as for the fixed-site membrane. The theory of Eisenman and his coworkers[6–9] has usually been applied to analyze the ion transport phenomena through liquid membranes, but it has been derived from the Nernst-Planck equation with some assumptions. A rigorous theory for the ion transport across fixed-site membrane has been presented in a previous paper on the basis of nonequilibrium thermodynamics without any assumptions concerning the distributions of concentration and potential within membrane.[10]

In the preceding paper,[11] an electrochemical study of the ion permeation has been made on a liquid membrane–aqueous single electrolyte system. The membrane permeabilities to the membrane-permeable ion p in the presence and absence of electric current, P_p and P_p^0, have been estimated according to the previous theory.[10] A remarkable discrepancy between P_p and P_p^0 has been observed and explained in terms of the permeability matrix. The theory of Eisenman *et al.* can not distinguish these two permeabilities since their theory is based on the Nernst-Planck equation which possesses only one transport coefficient for an ion.

In the preceding paper,[11] the theory of ion transport for the fixed-site membrane has been applied to estimate P_p and P_p^0 in the liquid membrane since the equation describing the ion transport can be deduced to have the same form for both systems.[12] However, the entities of physical representations for the membrane permeabilities, P_p and P_p^0, for the liquid membrane are supposed to be different from those for the fixed-site membrane, because the site ion as well as the complex is mobile in the liquid membrane.

Thus a theory for the liquid membrane was presented on the basis of nonequilibrium thermodynamics by taking into account the movements of the site ions and complexes in the liquid membrane. The experimental examination was also made with a liquid membrane–aqueous single electrolyte system.

Theoretical

System and Assumptions. We shall consider the ion transport phenomena in the system illustrated in Fig. 1. An aqueous phase I is separated by a liquid ion-exchange membrane from another aqueous phase II. The membrane phase is bounded by two planes normal to the x-axis at $x=0$ and $x=d$. There are stagnant layers on both sides of the membrane phase and their surfaces are in contact with the phase I at $x=-a$ and phase II at $x=b$, respectively. The two aqueous phases I and II are homogeneous be-

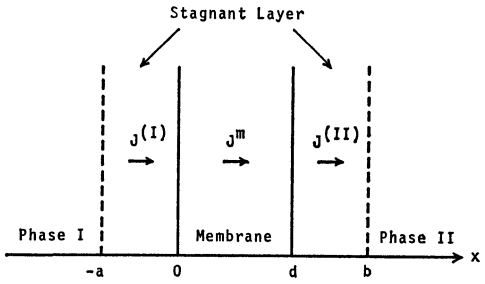

Fig. 1. Schematic diagram of the liquid membrane–aqueous electrolyte system.

cause of being well stirred. It is assumed that the system is isothermal and in a steady state in which there is no volume flow (Assumption 1), and the ion fluxes are constant. Moreover, all the chemical reactions are assumed to be at equilibrium anywhere within the membrane phase (Assumption 2) and a free carrier ion and its electrically neutral complexes are present only within the membrane phase (Assumption 3).

Flux Equation for Individual Species. Only counter- and co-ions can permeate across the liquid membrane, although all the species within membrane are mobile. The total flux of a permeable ion is the sum of the flux of free species and those of complexes. We shall first derive the flux equation for individual species in the membrane which will later be correlated with the total flux for the membrane-permeable species.

According to nonequilibrium thermodynamics, the flux of individual species, j_α, is given as a linear function of all forces that are negative gradients of the total chemical potentials

$$j_\alpha = -\sum_\beta l_{\alpha\beta}\nabla\bar{\mu}_\beta, \tag{1}$$

where α and β refer to all species in the membrane and $l_{\alpha\beta}$ indicates a phenomenological coefficient and satisfies the reciprocal relation of Onsager. Under the condition of chemical equilibrium, we have

$$\bar{\mu}_i = \sum_\gamma \nu_{\gamma i}\bar{\mu}_\gamma, \tag{2}$$

where the subscript i refers to the electrically neutral complex formed in the i-th reaction and $\nu_{\gamma i}$ denotes the stoichiometric coefficient of the free species γ in the i-th reaction. Since the complex is electrically neutral, we have

$$Z_i = \sum_\gamma Z_\gamma \nu_{\gamma i} = 0. \tag{3}$$

By substituting Eq. 2 into Eq. 1, the term for the force due to the complex can be eliminated, and the flux equations for all species can be written in terms of the forces for free species as follows:

$$j_\alpha = -\sum_\gamma l'_{\alpha\gamma}\nabla\bar{\mu}_\gamma, \tag{4}$$

where

$$l'_{\alpha\gamma} = l_{\alpha\gamma} + \sum_i \nu_{\gamma i} l_{\alpha i}. \tag{5}$$

The total chemical potential for species α, $\bar{\mu}_\alpha$, is expressed as[10]

$$\bar{\mu}_\alpha = \eta_\alpha + RT\ln a_\alpha + Z_\alpha F\psi = RT\ln\bar{\lambda}_\alpha, \tag{6}$$

where

$$\eta_\alpha = \mu_{\alpha,0} + p\bar{V}_\alpha + \xi_\alpha. \tag{7}$$

$\mu_{\alpha,0}$ denotes the standard chemical potential; a, the activity; ψ, the electric potential; p, the hydrostatic pressure; $\bar{V}$, the partial molar volume; ξ, the excess free energy; $\bar{\lambda}$, the absolute activity; and F, the Faraday constant.

By use of local electric potential, ψ, and equilibrium local electric potential for free ion γ, ψ_γ, the gradient of $\bar{\mu}_\gamma$ can be expressed alternatively as

$$\nabla\bar{\mu}_\gamma = Z_\gamma F\nabla(\psi-\psi_\gamma). \tag{8}$$

Using Eqs. 4 and 8, the individual ionic current for species α is given by

$$i_\alpha = Z_\alpha F j_\alpha = -\sum_\gamma \kappa'_{\alpha\gamma}\nabla(\psi-\psi_\gamma), \tag{9}$$

where $\kappa'_{\alpha\gamma}$ denotes a part of electric conductivity produced by the effective driving force of ion γ, $\nabla(\psi-\psi_\gamma)$ and given as

$$\kappa'_{\alpha\gamma} = Z_\alpha Z_\gamma F^2 l'_{\alpha\gamma}. \tag{10}$$

Electric Conductivity for Individual Species. According to Eq. 9, the electric conductivity of species α, κ'_α, is given by[13,14]

$$\kappa'_\alpha = \sum_\gamma \kappa'_{\alpha\gamma} = \sum_\gamma Z_\alpha Z_\gamma F^2 l_{\alpha\gamma} = (Z_\alpha F)^2 u_\alpha C_\alpha, \tag{11}$$

where u_α and C_α denote the absolute mobility and concentration of species α, respectively.

Now, the total flux for each free species in the membrane, J^m_γ, may be written as

$$J^m_\gamma = j_\gamma + \sum_i \nu_{\gamma i} j_i, \tag{12}$$

where the superscript m refers to the membrane phase. When the steady state is attained, the following relation can be realized:

$$J^m_\gamma = J^{(I)}_\gamma = J^{(II)}_\gamma \equiv J_\gamma, \tag{13}$$

where $J^{(I)}$ and $J^{(II)}$ denote the fluxes in the stagnant layers in phases I and II, respectively. According to Eqs. 12 and 13, the total ionic current for each free species, $I_\gamma = Z_\gamma F J_\gamma$, is seen to be expressed in terms of individual fluxes of the free species and of the complexes as follows:

$$I_\gamma = Z_\gamma F j_\gamma + Z_\gamma F\sum_i \nu_{\gamma i} j_i = i_\gamma + \sum_i i_i^{(\gamma)}, \tag{14}$$

where $i_i^{(\gamma)}$ represents the part of the ionic current of species γ carried by the form of complex i.

According to Eq. 14, it is seen that the flux of the complex contributes to the total ionic currents of free species from which the complex is formed even when the complex is electrically neutral. By using Eq. 4, $i_i^{(\gamma)}$ can be represented by

$$i_i^{(\gamma)} = Z_\gamma F\nu_{\gamma i} j_i = -\sum_\delta Z_\gamma Z_\delta F^2 \nu_{\gamma i} l'_{i\delta}\nabla(\psi-\psi_\delta), \tag{15}$$

where the subscript δ refers to the free species. According to Eqs. 14 and 15, the part of the electric conductivity of species γ due to the complex i, $\kappa_i^{(\gamma)}$, can be expressed as

$$\kappa_i^{(\gamma)} = \sum_\delta Z_\gamma Z_\delta F^2 \nu_{\gamma i} l_{i\delta} = (Z_\gamma F)^2 \nu_{\gamma i} u_i C_i. \tag{16}$$

It is evident from Eq. 16 that the contribution of the diagonal term l_{ii} to $\kappa_i^{(\gamma)}$ vanishes when the complex i is electrically neutral.[14] $\kappa_i^{(\gamma)}$ is correlated with the electric conductivity of the complex i, κ'_i, as follows:

$$\kappa'_i = \sum_\gamma \kappa_i^{(\gamma)} = 0, \tag{17}$$

where the superscript γ refers to the membrane-permeable ion as well as the carrier ion.

Total-Flux Equation for Free Species γ. Substituting Eq. 4 into Eq. 12, we have under the condition of the steady state

$$J_\gamma = -\sum_\delta l''_{\gamma\delta}\nabla\bar{\mu}_\delta, \tag{18}$$

where

$$l''_{\gamma\delta} = l'_{\gamma\delta} + \sum_1 \nu_{\gamma 1} l'_{1\delta}. \tag{19}$$

We see in Eq. 19 that the new phenomenological coefficient, $l''_{\gamma\delta}$, is expressed in terms of individual coefficients, $l_{\alpha\beta}$'s, and that the reciprocal relation for individual coefficients verifies that the $l''_{\gamma\delta}$'s also satisfy the reciprocal relation.

According to Eq. 18, the total ionic current for free species γ, I_γ, is expressed as

$$I_\gamma = -\sum_\delta \kappa''_{\gamma\delta}\nabla(\phi-\phi_\delta), \tag{20}$$

where

$$\kappa''_{\gamma\delta} = Z_\gamma Z_\delta F^2 l''_{\gamma\delta} = Z_\delta Z_\gamma F^2 l''_{\delta\gamma} = \kappa''_{\delta\gamma}. \tag{21}$$

Total Electric Conductivity for Free Species γ. According to Eq. 20, the total electric conductivity for ion γ, κ''_γ, is given by

$$\kappa''_\gamma = \sum_\delta \kappa''_{\gamma\delta}. \tag{22}$$

Substituting Eq. 19 into Eq. 21 and using Eqs. 11 and 16, Eq. 22 can be rewritten as

$$\kappa''_\gamma = \kappa'_\gamma + \sum_1 \kappa_1^{(\gamma)} = (Z_\gamma F)^2(u_\gamma C_\gamma + \sum_1 \nu_{\gamma 1} u_1 C_1). \tag{23}$$

Since the carrier species are completely trapped within the membrane phase, the total flux as well as total electric current of carrier species, J_s and I_s, should be zero at the steady state, *i.e.*,

$$J_s^m = J_s^{(I)} = J_s^{(II)} \equiv J_s = 0, \tag{24}$$

and

$$I_s = Z_s F J_s = 0, \tag{25}$$

where one kind of free carrier species, s, is assumed to be present in the membrane. According to Eq. 25, the total electric conductivity for the carrier species, κ''_s, is also zero. Using Eqs. 23 and 17, we obtain

$$\kappa''_s = \kappa'_s + \sum_1 \kappa_1^{(s)} = \kappa'_s - \sum_1\sum_\gamma \kappa_1^{(\gamma)} = 0 \quad (\gamma \neq s). \tag{26}$$

By means of Eq. 24, Eq. 18 can be reduced to a phenomenological relation

$$J_p = -\sum_q l^*_{pq}\nabla\bar{\mu}_q, \tag{27}$$

where

$$l^*_{pq} = l''_{pq} - \frac{l''_{ps} l''_{sq}}{l''_{ss}}, \tag{28}$$

and p and q refer to the membrane-permeable ions. The reciprocal relation of Onsager can be satisfied by l^*_{pq} as well as $l''_{\gamma\delta}$. According to Eq. 27, we have

$$I_p = -\sum_q \kappa^*_{pq}\nabla(\phi-\phi_q), \tag{29}$$

where

$$\kappa^*_{pq} = Z_p Z_q F^2 l^*_{pq} = Z_q Z_p F^2 l^*_{qp} = \kappa^*_{qp}. \tag{30}$$

The total electric conductivity for species p, κ''_p, given by Eq. 22 can also be expressed by using κ^*_{pq} as follows:

$$\kappa''_p = \sum_q \kappa^*_{pq}, \tag{31}$$

provided Eq. 26 holds.

Single Electrolyte System. Now, we shall apply our theory to the system in which only a single strong electrolyte, $M_{\nu'_M}A_{\nu'_A}$, is present in the aqueous phases. Moreover, the carrier ion is assumed to react only with counter ion to form a neutral complex in the membrane phase. As a result, the components present in the membrane phase are counter ion, M^{z_M+}, co-ion, $A^{|z_A|-}$, carrier ion, $S^{|z_s|-}$, and complex, C.

According to Eq. 29, the ionic current can be expressed as

$$I_p = -\sum_q \kappa^*_{pq}\nabla(\phi-\phi_q) \qquad (p, q; M, A). \tag{32}$$

Therefore, Eq. 23 can be written as

$$\kappa''_M = \kappa'_M + \kappa_c^{(M)} = (Z_M F)^2 \bar{u}_M C_M^{to}, \tag{33}$$

and

$$\kappa''_A = \kappa'_A, \tag{34}$$

where

$$\kappa'_M = (Z_M F)^2 u_M C_M, \quad \kappa_c^{(M)} = (Z_M F)^2 \nu_M u_c C_c, \tag{35}$$

and

$$\bar{u}_M \equiv f u_M + \nu_M(1-f)u_c. \tag{36}$$

C_M^{to} and f denote the total concentration and dissociated fraction of ion M ($f = C_M/C_M^{to}$), respectively, and the subscript c refers to the complex.

If κ^*_{pq} is independent of the externally applied field, Eq. 32 leads to

$$I_p - I_p^0 = -\kappa''_p\nabla(\phi-\phi^0) \qquad (p; M, A), \tag{37}$$

where the superscript 0 refers to the zero electric current. Under the condition of steady state, Eq. 37 can be integrated to give

$$(I_p - I_p^0)\int_{-a}^{b}\frac{dx}{\kappa''_p} = -(V-V^0), \tag{38}$$

where V^0 denotes the membrane potential at zero electric current. Therefore, the ionic membrane conductance of ion p, g_p, is expressed as

$$\frac{1}{g_p} = \int_{-a}^{b}\frac{1}{\kappa''_p}dx. \tag{39}$$

The contribution of carrier species to the ionic conductance vanishes outside the membrane.

At zero electric current, the following relation must hold

$$I_M^0 + I_A^0 = 0. \tag{40}$$

By means of Eq. 40, one of the forces in Eq. 32 can be eliminated to give

$$I_p^0 = -\kappa_p^0\nabla(\phi^0-\phi_p) \qquad (p; M, A), \tag{41}$$

where

$$\kappa_p^0 = \frac{\kappa^*_{pp}\kappa^*_{qq} - (\kappa^*_{pq})^2}{\kappa''_q} \qquad (p, q; M, A). \tag{42}$$

According to Eq. 41, the flux equation at zero electric current is given by

$$J_p^0 = -\frac{\kappa_p^0}{(Z_p F)^2}\nabla\bar{\mu}_p^0, \tag{43}$$

where $\bar{\mu}_p^0$ denotes the total chemical potential at zero electric current. Since Eq. 43 should be of the form of the Nernst-Planck equation, it can be written as

$$J_p^0 = -\frac{\bar{D}_p C_p^{to}}{RT}\nabla\bar{\mu}_p^0, \tag{44}$$

where $\bar{D}_p$ and C_p^{to} denote the diffusion coefficient and the total concentration of ion p, respectively, and

$$\frac{\kappa_p^0}{(Z_pF)^2} = \frac{\bar{D}_p C_p^{to}}{RT}. \tag{45}$$

Comparing Eq. 45 with Eqs. 33, 35, and 36, we have

$$\bar{D}_M = f(\kappa)\bar{u}_M RT = fD_M + (1-f)D_c, \tag{46}$$

and

$$D_A = f(\kappa)u_A RT, \tag{47}$$

where

$$f(\kappa) = 1 - \kappa_{MA}^*\left(\frac{1}{\kappa_M''} + \frac{1}{\kappa_A''}\right) = \frac{\kappa_p^0}{\kappa_p''}, \tag{48}$$

and D_M and D_c denote the diffusion coefficients of ion M, and of complex C, respectively. As seen in Eq. 48, the total electric conductivity at zero electric current, κ_p^0, is different from the total electric conductivity, κ_p'', unless the cross term κ_{pq}^* is zero. Under the condition of the steady state, Eq. 41 can also be integrated to give

$$I_p^0\int_{-a}^{b}\frac{dx}{\kappa_p^0} = -(V^0 - V_p), \tag{49}$$

where V_p denotes the equilibrium membrane potential of ion p. Therefore, κ_p^0, can be related to the ionic membrane conductance at zero electric current, g_p^0, as follows:

$$\frac{1}{g_p^0} = \int_{-a}^{b}\frac{1}{\kappa_p^0}dx. \tag{50}$$

Experimental

The materials, the apparatus and the procedures for measuring membrane potential, membrane conductance and salt flux were described in detail in the preceding paper.[11]

Partition of $CaCl_2$ between 1-Octanol and Aqueous Phases. The partition ratio, R^{wm}, was determined as the ratio of equilibrium concentration of $CaCl_2$ in 1-octanol phase to that in aqueous phase. The measurements were carried out both in the presence and absence of carrier species in 1-octanol phase. Preconditioned 1-octanol was layered on the aqueous $CaCl_2$, of which the initial concentration was 0.964 mol dm^{-3}. Whole system was vigorously shaken for thirty hours at 25 °C and allowed to stand until both phases became clear, then the sample was pipetted from 1-octanol phase for determining the equilibrium concentration of $CaCl_2$. The concentration was determined with a Nippon Jarrell-Ash atomic absorption spectrophotometer Model AA-8500. The partition ratio obtained for the system without carrier species was 1.7×10^{-4} which agreed well with the value obtained by the radiotracer method.[15] The partition ratio for the system with carrier species was 6.2×10^{-4}, where the concentration of calcium hexadecyl sulfate in 1-octanol phase was 2.5×10^{-3} mol dm^{-3}.

Molar Conductivity Measurement of Calcium Hexadecyl Sulfate in 1-Octanol. The electric conductivity of calcium hexadecyl sulfate in water-saturated 1-octanol was measured by use of a Yanagimoto conductivity outfit Model MY-7. The measurements were carried out with a pair of Pt–Pt electrodes immersed in 1-octanol solution of calcium hexadecyl sulfate at 25 °C. The cell constant, *ca.* 0.05, was determined by use of a standard solution of KCl. The molar conductivity is plotted against the square root of concentration in Fig. 2.

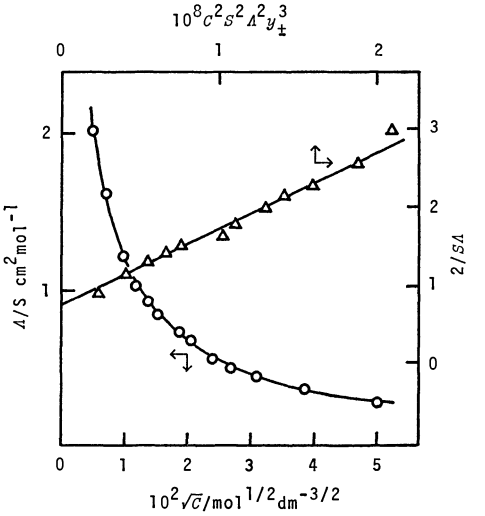

Fig. 2. Molar conductivity of calcium hexadecyl sulfate in 1-octanol as a function of square root of the concentration (○) and Shedlovsky's plot (△).

The limiting molar conductivity, Λ^∞, and the dissociation constant, K_1, were determined from Shedlovsky's plot,[16,17] $2/S\Lambda$ *vs.* $C^2S^2\Lambda^2y_\pm^3$, where

$$S = [z/2 + \{1 + (z/2)^2\}^{1/2}]^2, \tag{51}$$

and

$$z = \frac{2A'}{(\Lambda^\infty)^{3/2}}\sqrt{C\Lambda}. \tag{52}$$

A' is Onsager's coefficient; C, the concentration; $y_\pm$, the mean activity coefficient; and Λ, the molar conductivity. For the calculation of A', the values of viscosity[18] and relative permittivity[19] for pure solvent, *i.e.*, $\eta=0.0721$ P and $\varepsilon=9.85$, were used, respectively. The limiting transport number was assumed to be equal to that in water, $t_{Ca}^\infty=0.76$.[20] The mean activity coefficient was calculated by means of the Debye-Hückel equation in which the diameter of sodium hexadecyl sulfate, 9.9 Å, was used as an ion parameter. The diameter was estimated from its partial molar volume in water obtained by the extrapolation of the values for sodium alkyl sulfates of C_2–C_{12}.[21,22]

The Shedlovsky plot is also shown in Fig. 2. The values of Λ^∞ and K_1 obtained from the plot were 2.8 S cm^2 mol^{-1} and 4.1×10^{-9} mol^2 dm^{-6}, respectively. The degree of dissociation, θ, was 0.25 at 2.5×10^{-3} mol dm^{-3}, *i.e.*, the concentration of calcium hexadecyl sulfate in the liquid membrane studied.

Diffusion across Water–Octanol Interface. The kinetics of diffusion of $CaCl_2$ across the water–1-octanol interface was studied, where the concentration of carrier species in 1-octanol phase was 2.5×10^{-3} mol dm^{-3}. The modified apparatus of the type proposed by Davies[23], which is shown in Fig. 3, was used. The diffusion area was *ca.* 12.6 cm^2. Concentration change in aqueous phase was followed by measuring the electric conductance. A known amount of preconditioned 1-octanol was layered on the aqueous $CaCl_2$ solution with the initial concentration of 3.86×10^{-4} mol dm^{-3}. After the conductance of an aqueous phase became constant, 1-octanol solution of $CaCl_2$ was injected into the oil phase. The initial concentration of $CaCl_2$ in 1-octanol phase was 1.05×10^{-4} mol dm^{-3}. The measurement was carried out at 25 °C, and both phases were stirred at the

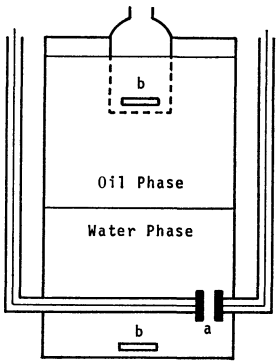

Fig. 3. Schematic diagram of the glass cell used for the measurement of diffusion across the oil–water interface. a: Pt–Pt electrodes, b: magnetic spin bar.

same rate as used for the salt flux measurements.

Results and Discussion

The membrane permeabilities evaluated from the electrical data, P_{Ca} and P_{Cl}, and those at zero electric current evaluated from the membrane potential and flux data, P^0_{Ca} and P^0_{Cl}, have already been reported in the preceding paper.[11] These values were again evaluated in the present study and are shown in Fig. 4. The general features of this figure are similar to those of the preceding paper, but somewhat lower values were obtained with P_{Ca} and P_{Cl}, being due to lower membrane conductance. After repeated measurements, it turned out to be essential for obtaining consistent membrane conductance that the liquid height of the membrane solution in the reservoir was kept constant. We shall, therefore, adopt the present results for analyzing the membrane permeability according to the presented theory.

Since the system is close to equilibrium with respect to calcium ion, we have[10]

$$P_{Ca} \approx \frac{RT}{(Z_{Ca}F)^2}\frac{g_{Ca}}{(a^{I}_{Ca}a^{II}_{Ca})^{1/2}}, \tag{53}$$

where superscripts I and II refer to the aqueous phases I and II, respectively. We shall assume that the ion transport is membrane-controlled. From Eqs. 33 and 39, the ionic conductance, g_{Ca}, can be expressed in terms of the absolute mobilities and concentrations of free calcium ion and its complex:

$$\frac{1}{g_{Ca}} = \int_0^d \frac{dx}{(Z_{Ca}F)^2(u_{Ca}C_{Ca} + \nu_{Ca}u_cC_c)}. \tag{54}$$

Combining Eq. 53 with Eq. 54, we have

$$\frac{1}{P_{Ca}} \approx \frac{(Z_{Ca}F)^2}{RT}(a^{I}_{Ca}a^{II}_{Ca})^{1/2}\int_0^d \frac{dx}{(Z_{Ca}F)^2(u_{Ca}C_{Ca} + \nu_{Ca}u_cC_c)}. \tag{55}$$

Since carrier species are completely trapped within membrane, we can obtain from Eq. 26

$$\kappa''_s = (Z_sF)^2u_sC_s - (Z_{Ca}F)^2\nu_{Ca}u_cC_c = 0. \tag{56}$$

Using Eq. 56, the term for the complex in Eq. 55 can be replaced by that for carrier ion, s,

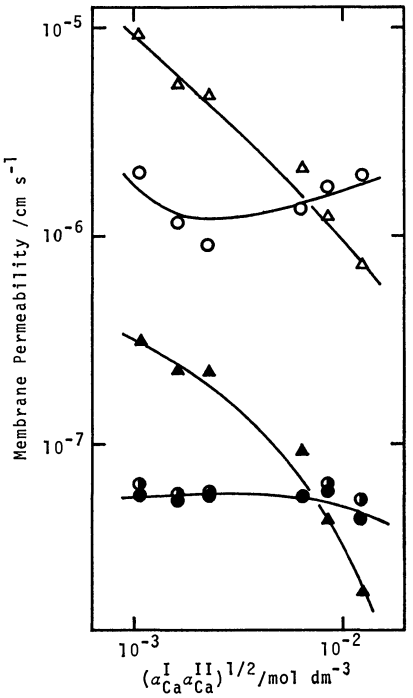

Fig. 4. The membrane permeabilities as a function of geometric mean of the activities of phases I and II. ○: P^0_{Ca}, ●: P^0_{Cl}, △: P_{Ca}, ▲: P_{Cl}. The membrane permeability to salt, P^0_{sa}, is also shown, ◑. The concentration of $CaCl_2$ in phase II was kept at 4×10^{-3} mol dm^{-3} and that in phase I being varied from 4×10^{-4} to 10^{-1} mol dm^{-3}. Solid lines indicate P^0_p and P_p calculated from P_{pq} according to Eqs. 6 and 7 in Ref. 11, respectively.

$$\frac{1}{P_{Ca}} \approx \frac{(Z_{Ca}F)^2}{RT}(a^{I}_{Ca}a^{II}_{Ca})^{1/2}\int_0^d \frac{dx}{(Z_{Ca}F)^2u_{Ca}C_{Ca} + (Z_sF)^2u_sC_s} \tag{57}$$

$$= \frac{(Z_{Ca}F)^2}{RT}\frac{(a^{I}_{Ca}a^{II}_{Ca})^{1/2}d}{(Z_{Ca}F)^2\tilde{u}_{Ca}\tilde{C}_{Ca} + (Z_sF)^2\tilde{u}_s\tilde{C}_s}, \tag{58}$$

where $\tilde{u}$ and $\tilde{C}$ denote the mean absolute mobility and mean concentration within membrane, respectively.

From the observed values of θ and R^{wm}, we see that the concentration of Donnan salt is negligible compared with that of free calcium ion. Under this condition, *i.e.*, $C_{Ca} \gg C_{Cl}$, Eq. 58 can be reduced to

$$P_{Ca} \approx \frac{RT}{(Z_{Ca}F)^2}\frac{\tilde{\Lambda}^1\tilde{\theta}\tilde{C}^{to}_{Ca}}{(a^{I}_{Ca}a^{II}_{Ca})^{1/2}d}, \tag{59}$$

$$\Lambda^1 = \nu_{Ca}\Lambda_{Ca} + \nu_s\Lambda_s, \tag{60}$$

where Λ_{Ca} and Λ_s denote the molar conductivity of calcium ion and of carrier ion, respectively, and Λ^1 is the hypothetical molar conductivity that the complex would have if it be completely dissociated and is related to the observed molar conductivity, Λ, as follows:[24]

$$\theta\Lambda^1 = \Lambda. \tag{61}$$

The molar conductivity within liquid membrane, $\tilde{\Lambda}$, must be independent of the external concentrations, because the total concentration of calcium ion within membrance is nearly constant, as stated above. Therefore, the dependence of P_{Ca} on the external

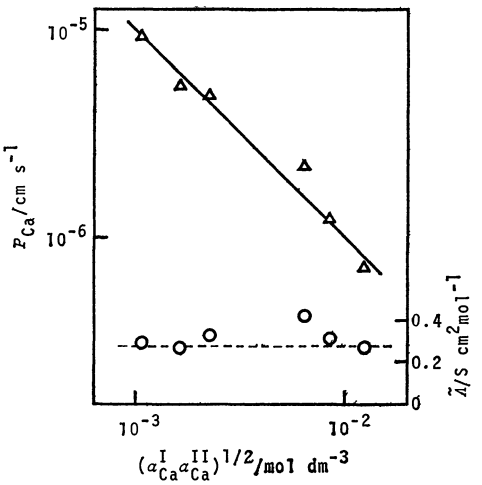

Fig. 5. The membrane permeability, P_{Ca} (△), and the molar conductivity in the liquid membrane estimated from P_{Ca}, $\tilde{\Lambda}$(○), as a function of the geometric mean of the activities of calcium ion in the aqueous phases I and II. Broken line indicates the molar conductivity of calcium hexadecyl sulfate measured in the bulk solution.

concentrations shown in Fig. 5 can well be described by Eq. 59. According to Eq. 59, $\tilde{\Lambda}$ was calculated from P_{Ca} and is compared with the molar conductivity measured in the 1-octanol solution of calcium hexadecyl sulfate in the same figure. We see from this figure that the agreement is satisfactory. This result implies that the electroconductional process of calcium ion is membrane-controlled and the effect of co-ion on this process is negligible.

From Eqs. 45 and 50, the diffusional ionic conductance at zero electric current, g^0_{Ca}, can be expressed as

$$\frac{1}{g^0_{Ca}} = \int_{-a}^{b} \frac{RT}{(Z_{Ca}F)^2 \bar{D}_{Ca} C^{to}_{Ca}} dx. \tag{62}$$

The membrane permeability of calcium ion at zero electric current is related to g^0_{Ca} as[10]

$$P^0_{Ca} \approx \frac{RT}{(Z_{Ca}F)^2} \frac{g^0_{Ca}}{(a^{I}_{Ca}a^{II}_{Ca})^{1/2}}, \tag{63}$$

when the system is close to equilibrium for calcium ion. Combining Eq. 63 with Eq. 62, P^0_{Ca} is expressed in terms of the mean diffusion coefficient, $\tilde{\tilde{D}}_{Ca}$, and mean total concentration, $\tilde{C}^{to}_{Ca}$, as

$$P^0_{Ca} \approx \frac{\tilde{\tilde{D}}_{Ca}\tilde{C}^{to}_{Ca}}{(a^{I}_{Ca}a^{II}_{Ca})^{1/2}d}, \tag{64}$$

provided the diffusion of calcium ion is membrane-controlled.

According to Eq. 64, $\tilde{\tilde{D}}_{Ca}$ was calculated from P^0_{Ca} and is shown in Fig. 6. We see from the small value of partitioning of $CaCl_2$, $R^{wm}=6.2\times10^{-4}$, and the concentrations of external $CaCl_2$ solutions less than 10^{-1} mol dm^{-3} that the concentration of Donnan salt is negligible. The mean total concentration of calcium ion in the membrane is nearly equal to 2.5×10^{-3} mol dm^{-3} which is a half of the concentration of membrane site and is almost independent of the external

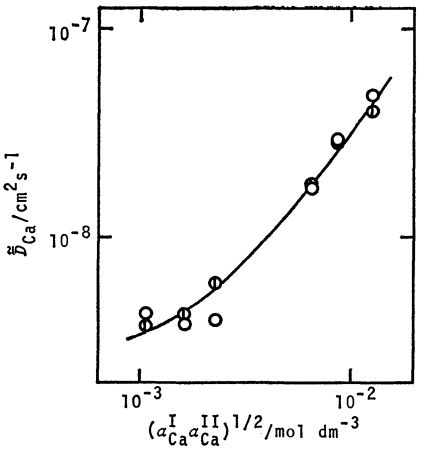

Fig. 6. Diffusion coefficient, $\tilde{\tilde{D}}_{Ca}$, as a function of the geometric mean of the activities in phases I and II. ○: Estimated from the observed P^0_{Ca}. ⓘ: Estimated from P^0_{Ca} calculated from P_{pq} according to Eq. 6 in Ref. 11.

electrolyte concentration. Therefore, the diffusion coefficient of calcium ion in the membrane phase would be almost independent of the external concentration of $CaCl_2$. Contrary to the expectation, a remarkable concentration dependence was found as shown in Fig. 6. A similar result has been obtained with an ion-exchange resin membrane and has been explained by assuming the energy barrier at the interface.[25] Thus the observed concentration dependence of $\tilde{\tilde{D}}_{Ca}$ may be attributed to the presence of energy barrier at the interface.

The diffusion of $CaCl_2$ across the interface was studied in the two-phase system of water and 1-octanol with carrier species. The flux of calcium ion at zero electric current can be expressed by Eq. 44. By substituting Eq. 6 into Eq. 44, we have

$$J^0_{Ca} = -\frac{\bar{D}_{Ca}C^{to}_{Ca}}{\bar{\lambda}_{Ca}} \nabla\bar{\lambda}_{Ca}. \tag{65}$$

Integrating Eq. 65 under the condition of steady state, we derive the equation for the flux across phase boundary as follows:

$$J^0_{Ca} = -P^{(b)}_{Ca}\{a^{w}_{Ca} \exp[(Z_{Ca}F\psi^{w} + \eta^{w}_{Ca} - Z_{Ca}F\psi^{m} - \eta^{m}_{Ca})/2RT] - a^{m}_{Ca} \exp[-(Z_{Ca}F\psi^{w} + \eta^{w}_{Ca} - Z_{Ca}F\psi^{m} - \eta^{m}_{Ca})/2RT]\}, \tag{66}$$

where

$$\frac{1}{P^{(b)}_{Ca}} = \left(\frac{a^{m}_{Ca}a^{w}_{Ca}}{\bar{\lambda}^{m}_{Ca}\bar{\lambda}^{w}_{Ca}}\right)^{1/2} \int \frac{\bar{\lambda}_{Ca}}{\bar{D}_{Ca}C^{to}_{Ca}} dx. \tag{67}$$

The integration extends over the boundary region interposing the interface. The superscript (b) refers to the boundary region, m and w, to the oil and aqueous phases, respectively. Equation 66 can be rewritten as[26]

$$J^0_{Ca} = -k_1C^{w}_{Ca} + k_2C^{m}_{Ca}, \tag{68}$$

where

$$k_1 = P^{(b)}_{Ca}y^{w}_{Ca} \exp\{[(Z_{Ca}F\psi^{w} + \eta^{w}_{Ca}) - (Z_{Ca}F\psi^{m} + \eta^{m}_{Ca})]/2RT\}, \tag{69}$$

and

$$k_2 = P_{Ca}^{(b)} y_{Ca}^{m} \exp\{[(Z_{Ca}F\psi^{m}+\eta_{Ca}^{m}) - (Z_{Ca}F\psi^{w}+\eta_{Ca}^{w})]/2RT\}. \quad (70)$$

y_{Ca} denotes the activity coefficient of calcium ion.

Assuming that the degree of dissociation of calcium hexadecyl sulfate in the membrane phase is not so much affected by the addition of a small amount of $CaCl_2$, the conservation law of mass holds for free calcium ion:

$$C_{Ca}^{m}v^{m} + C_{Ca}^{w}v^{w} = C_{Ca}^{m(e)}v^{m} + C_{Ca}^{w(e)}v^{w}, \quad (71)$$

where v denotes the volume of each phase and the superscript (e) refers to the equilibrium state. At the equilibrium state, we have from Eq. 68

$$\frac{k_2}{k_1} = \frac{C_{Ca}^{w(e)}}{C_{Ca}^{m(e)}}. \quad (72)$$

By means of Eqs. 71 and 72, Eq. 68 can be converted into a convenient form:[26,27]

$$\frac{dC_{Ca}^{w}}{dt} = k(C_{Ca}^{w(e)} - C_{Ca}^{w}), \quad (73)$$

where

$$k = A\left(\frac{k_1}{v^{w}} + \frac{k_2}{v^{m}}\right), \quad (74)$$

and t and A denote time and the diffusion area, respectively. By integrating Eq. 73 and replacing the concentration with the resistance of aqueous phase, R, we have

$$\ln\left(\frac{1}{R^{e}} - \frac{1}{R}\right) = -kt + \text{const.}, \quad (75)$$

where R^{e} denotes the resistance of aqueous phase at equilibrium. According to Eq. 75, k can be obtained from the slope of the logarithmic plot shown in Fig. 7. By using Eqs. 72 and 74, k_1 and k_2 were estimated and it was found that $k_1 = 2.8\times10^{-6}$ cm s^{-1}, and $k_2 = 2.3\times10^{-6}$ cm s^{-1}. In order to verify the relation of Eq. 72, the estimated values of k_1 and k_2 were substituted into Eq. 68 which was derived without the above assumption and J_{Ca}^{0} was calculated. The agreement between the calculated and observed J_{Ca}^{0}'s was excellent.

Combining Eq. 69 with Eq. 67, we have

$$\frac{y_{Ca}^{w}}{k_1} = \left[\exp\left(-\frac{Z_{Ca}F\psi^{w}+\eta_{Ca}^{w}}{2RT}\right)\right]\left(\frac{a_{Ca}^{w}}{\bar{\lambda}_{Ca}^{w}}\right)^{1/2}\int\frac{\bar{\lambda}_{Ca}}{\bar{D}_{Ca}C_{Ca}^{to}}dx, \quad (76)$$

$$= \int\frac{a_{Ca}\exp(U/RT)}{\bar{D}_{Ca}C_{Ca}^{to}}dx, \quad (77)$$

where U denotes the free energy of partition as

$$U \equiv Z_{Ca}F\psi + \eta_{Ca} - (Z_{Ca}F\psi^{w}+\eta_{Ca}^{w}). \quad (78)$$

According to a previous paper,[25] $\bar{D}_{Ca}$ can be expressed as

$$\bar{D}_{Ca} = \bar{D}_{Ca}^{0}\exp[(U-E)/RT], \quad (79)$$

where $\bar{D}_{Ca}^{0}$ and E denote the diffusion coefficient of calcium ion in bulk phase and the energy barrier at the interface, so that $E-U$ could be considered the apparent energy barrier for the diffusion of calcium ion. Substituting Eq. 79 into Eq. 77, we have

$$\frac{y_{Ca}^{w}}{k_1} = \int\frac{a_{Ca}/C_{Ca}^{to}}{D_{Ca}^{0}\exp(-E/RT)}dx. \quad (80)$$

We see from Eq. 80 that y_{Ca}^{w}/k_1 may almost be independent of the concentration of the external aqueous phase, since $\bar{D}_{Ca}^{0}$, E and a_{Ca}/C_{Ca}^{to} can be regarded as constant. This agrees well with the experimental observation[28] that k_1 is almost constant independent of the concentration of aqueous phase.

We shall compare k_1 with P_{Ca}^{0} determined from the salt flux across membrane. There are two interfaces in the liquid membrane–aqueous electrolyte system. Thus, the system may be regarded as that composed of the two o/w systems. The first consists of phase I and a half of the membrane, the second, phase II and another half of the membrane. According to Eq. 76, we find for the former system

$$\frac{y_{Ca}^{I}}{k_1^{(I)}} = \left[\exp\left(\frac{Z_{Ca}\Phi^{0}}{2}\right)\right]\left(\frac{a_{Ca}^{I}a_{Ca}^{II}}{\bar{\lambda}_{Ca}^{I}\bar{\lambda}_{Ca}^{II}}\right)^{1/2}\int_{-a}^{d/2}\frac{\bar{\lambda}_{Ca}}{\bar{D}_{Ca}C_{Ca}^{to}}dx, \quad (81)$$

where $-a$ and $d/2$ indicate the positions of the surface of the stagnant layer and of the middle of the membrane, respectively, and

$$\Phi^{0} = F(\phi^{II}-\phi^{I})RT. \quad (82)$$

Similarly we obtain

$$\frac{y_{Ca}^{II}}{k_1^{(II)}} = \left[\exp\left(-\frac{Z_{Ca}\Phi^{0}}{2}\right)\right]\left(\frac{a_{Ca}^{I}a_{Ca}^{II}}{\bar{\lambda}_{Ca}^{I}\bar{\lambda}_{Ca}^{II}}\right)^{1/2}\int_{d/2}^{b}\frac{\bar{\lambda}_{Ca}}{\bar{D}_{Ca}C_{Ca}^{to}}, \quad (83)$$

where b indicates the position of the surface of the stagnant layer in phase II. On the other hand, the

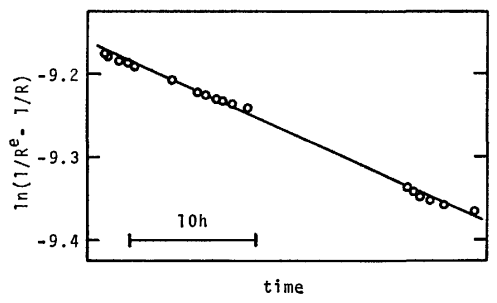

Fig. 7. Plot of $\ln(1/R^{e}-1/R)$ *versus* time.

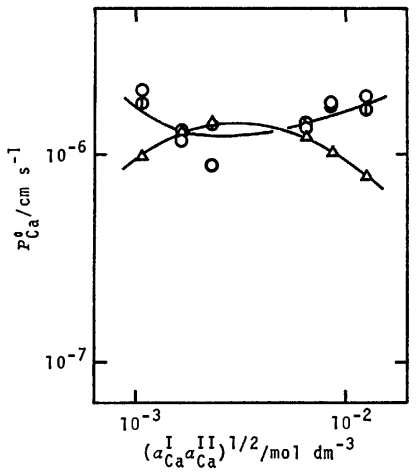

Fig. 8. Comparison of P_{Ca}^{0} estimated from k_1 according to Eq. 85 (△) with P_{Ca}^{0} observed in the liquid membrane–aqueous electrolyte system (○). P_{Ca}^{0} calculated from P_{pq} according to Eq. 6 in Ref. 11 (◫) is also shown.

diffusional membrane permeability to calcium ion can be obtained from Eq. 65 in a similar way to that described previously:[10]

$$\frac{1}{P^0_{Ca}} = \left(\frac{a^{I}_{Ca}a^{II}_{Ca}}{\bar{\lambda}^{I}_{Ca}\bar{\lambda}^{II}_{Ca}}\right)^{1/2}\int_{-a}^{b}\frac{\bar{\lambda}_{Ca}}{\bar{D}_{Ca}C^{to}_{Ca}}dx. \quad (84)$$

Comparing Eq. 84 with Eqs. 81 and 83, we have

$$\frac{1}{P^0_{Ca}} = \frac{y^{I}_{Ca}\exp(-Z_{Ca}\Phi^0/2)}{k_1^{(I)}} + \frac{y^{II}_{Ca}\exp(Z_{Ca}\Phi^0/2)}{k_1^{(II)}}. \quad (85)$$

According to Eq. 85, P^0_{Ca} can be estimated from k_1. The estimated P^0_{Ca} is compared with the observed P^0_{Ca} determined from the salt flux measurement on the membrane–electrolyte system in Fig. 8. We see from this figure that the estimated value agrees well with the observed one.

Thus the fact that the diffusional membrane permeability is less dependent on the external aqueous concentration can be attributed to the presence of an apparent energy barrier at interface. The diffusional fluxes of ions across liquid membranes have been measured by some workers.[15,29,30] However, they have not fully investigated the concentration dependence of the membrane permeability.

This research has been supported in part by a Grant-in-Aid for Scientific Research No. 247009 from the Ministry of Education, Science and Culture.

References

1) G. M. Shean and K. Sollner, *Ann. N. Y. Acad. Sci.*, **137**, 759 (1966).
2) J. Sandblom and F. Orme, "Membranes," ed by G. Eisenman, Marcel Dekker, Inc., New York (1972), Vol. I, Chap. 3.
3) J. W. Ross, "Ion Selective Electrode," ed by R. A. Durst, Dept. of Commerce, National Bureau of Standards Special Publication 314, Washington, D. C. (1969), Chap. 2.
4) E. L. Cussler and D. F. Evans, *J. Membrane Sci.*, **6**, 113 (1980).
5) J. D. Lamb, J. J. Christensen, and R. M. Izatt, *J. Chem. Educ.*, **57**, 227 (1980).
6) F. Conti and G. Eisenman, *Biophys. J.*, **6**, 227 (1966).
7) J. Sandblom, G. Eisenman, and J. L. Walker, Jr., *J. Phys. Chem.*, **71**, 3862 (1967).
8) J. Sandblom, G. Eisenman, and J. L. Walker, Jr., *J. Phys. Chem.*, **71**, 3871 (1967).
9) J. Sandblom, *Arkiv Fisik*, **35**, 329 (1967).
10) H. Kimizuka and K. Kaibara, *J. Colloid Interface Sci.*, **52**, 516 (1975).
11) K. Nomura, A. Matsubara, and H. Kimizuka, *Bull. Chem. Soc. Jpn.*, **51**, 1037 (1978).
12) A. Yamauchi, T. Minematsu, and H. Kimizuka, *Maku* (Membrane, in Japanese), **2**, 69 (1977).
13) A. Katchalsky and P. F. Curran, "Nonequilibrium Thermodynamics in Biophysics," Harvard Univ. Press, Cambridge, Mass. (1965), Chap. 11.
14) J. G. Kirkwood, "Ion Transport Across Membrane," ed by H. T. Clarke, Academic Press (1954), p. 119.
15) E. Pefferkorn and R. Varoqui, *J. Colloid Interface Sci.*, **52**, 89 (1975).
16) T. Shedlovsky, *J. Franklin Inst.*, **225**, 739 (1938).
17) R. M. Fuoss and T. Shedlovsky, *J. Am. Chem. Soc.*, **71**, 1496 (1949).
18) "International Critical Tables," McGraw-Hill Book Co., New York (1930), Vol. VII, p. 220.
19) A. M. Shkodin, L. P. Sadovnichaya, and V. A. Podolyanko, *Ukr. Khim. Zh.*, **35**, 144 (1969).
20) A. Lottermoser and F. Püschel, *Kolloid-Z.*, **63**, 175 (1933).
21) J. M. Corkill, J. F. Goodman, and T. Walker, *Trans. Faraday Soc.*, **63**, 768 (1967).
22) M. Tanaka, S. Kaneshina, W. Nishimoto, and H. Takabatake, *Bull. Chem. Soc. Jpn.*, **46**, 364 (1973).
23) J. T. Davies, *J. Phys. Colloid Chem.*, **54**, 185 (1950).
24) R. A. Robinson and R. H. Stokes, "Electrolyte Solutions," 2nd ed revised, Butterworths, London (1970), p. 338.
25) H. Kimizuka, K. Kaibara, E. Kumamoto, and M. Shirōzu, *J. Membrane Sci.*, **4**, 81 (1978).
26) H. Kimizuka and L. G. Abood, *J. Pharm. Sci.*, **62**, 740 (1973).
27) H. Kimizuka, T. Hideshima, and L. G. Abood *Mem. Fac. Sci., Kyushu Univ. Ser. C*, **9**, 143 (1974).
28) T. Hideshima, A. Yamauchi, and H. Kimizuka, *Biochim. Biophys. Acta*, **448**, 155 (1976).
29) H. L. Rosano, P. Duby, and J. H. Schulman, *J. Phys. Chem.*, **65**, 1704 (1961).
30) A. Ilani, *Isr. J. Chem.*, **4**, 105 (1966).

Reduction-Reoxidation Behavior of Silver(I) Ions in X-Type Zeolites

Masakazu IWAMOTO, Tsuneyasu HASHIMOTO, Toshikazu HAMANO, and Shuichi KAGAWA*

Department of Industrial Chemistry, Faculty of Engineering, Nagasaki University, Bunkyomachi, Nagasaki 852

(Received September 27, 1980)

The reduction of Ag^+ ions in X zeolites by hydrogen, the reoxidation of Ag atoms by oxygen, and the formation of silver particles were studied kinetically. The reduction is suggested to be a catalyzed reaction requiring an activation of hydrogen at some specific sites on the basis of the influence of exchange levels and hydrogen pressures on the reduction rates. At elevated temperatures the reduction of Ag^+ ions proceeded quantitatively and resulted in formations of Ag particles with a diameter between 10 and 25 nm and of highly dispersed Ag clusters. The clusters were easy to be reoxidized by oxygen at 473 K or below, while the particles were difficult to revert into the zeolite matrix. The diameter of the Ag particles was dependent on the reduction temperature and ion-exchange level and independent on the reduction time. It is discussed that this is due to the slow nucleation and the fast nuclear growth of Ag particles.

Many efforts have been made to develop finely dispersed metal clusters or particles upon reduction of transition metal ions in zeolites.[1,2] These zeolites can be used as highly active and/or bifunctional catalysts for a wide range of chemical reactions. Interest was stirred when Rabo *et al.*[3] reported an active catalyst consisting of Pt metal supported in a Y-type zeolite. To date, X and Y zeolites containing several metals such as Ni,[4] Cu,[5] and Pt[3,6] have been well investigated. The following reaction stoichiometry has been suggested to the hydrogen reduction of a metal ion in the zeolite. Here, Me^{x+} represents a transition metal ion. It is also reported that variations of methods in preparing supported metal catalysts affect a dispersion of the metal particles and an activity of the catalyst.

$$Me^{x+} + {}^1/_2xH_2 \longrightarrow Me^0 + xH^+ \quad (1)$$

An endeavor to form small silver clusters or particles in or on zeolite framework is very interesting and desirable, since silver metal is a highly active catalyst for not only the epoxidation reaction of ethene but also oxidations of various organic compounds. In fact, Kagawa *et al.*[7] reported an active silver catalyst which was prepared by the reduction of Ag^+ ions in X zeolites followed by the dissolution of zeolite matrix with a concentrated alkali solution. Tsutsumi and Takahashi[8] found that Ag^+ ions in Y zeolites could be reduced to particles of Ag atoms with a diameter 15—30 nm upon a treatment with alkylbenzenes and alcohols. Riekert[9] reoxidized Ag–Y zeolites reduced with hydrogen and found the reproduction of the original Ag^+–Y zeolites. Beyer *et al.*[10] also performed a kinetic and physicochemical study on the reduction of Ag^+ ions in Y zeolites. Recently, Kimm and Seff[11] reported the formation of small silver clusters in A zeolites without reducing agents. Upon an evacuation and oxidation at elevated temperatures, Ag^+ ions were found to form Ag_6 clusters surrounded by 8 Ag^+ ions.

Since the number of metal ions exchangeable in a unit cell of X zeolites is greater than that of Y zeolites, the redox behavior of silver ions in X zeolites is of interest though the X-type lattices are less stable than the Y-type lattices. In the present paper, therefore, a systematic study has been carried out on various Ag^+–X zeolites to clarify the following problems: the kinetics of the reduction and reoxidation of Ag^+ ions in X zeolites, the mechanism of Ag particles formation, and the influence of an extent of exchange between Ag^+ and Na^+ ions on the reduction. This would serve to further progress in the standardization of methods of catalyst preparations.

Experimental

Materials. Eight AgNaX samples with different Ag^+ contents were prepared from Linde NaX zeolite of a composition $Na_{86}(AlO_2)_{86}(SiO_2)_{106}$. The zeolite was washed with diluted $NaNO_3$ solution in order to eliminate cation deficiency, ion-exchanged in aqueous silver nitrate solutions with adequate concentrations,[12] washed with water and dried at 473 K. The respective exchange levels of Ag^+ ions were analyzed by conventional analytical procedures. The compositions of the samples are summarized in Table 1. All the samples obtained were sieved to 30—60 mesh for use.

Hydrogen, oxygen, and nitrogen gases were of high purity grade (above 99.9% purity). Before use in reduction-reoxidation experiments, these gases were passed through a cold trap cooled at the liquid nitrogen temperature for removal of a trace amount of water.

Methods and Procedures. Reduction by hydrogen and reoxidation by oxygen were carried out in two ways of a static system and a flow system.

(a) Static System: An uptake of hydrogen could be followed accurately as a function of time by measuring the pressure drop in a static system. Reoxidation was also investigated by measuring the oxygen consumption in the same apparatus. The change of pressure was followed on a mercury manometer. A liquid nitrogen cold trap was

TABLE 1. THE AgNaX ZEOLITES USED

Sample	Exchange level (%)	Number of Ag^+ ions per unit cell	Amount of silver supported (g-Ag/g-AgNaX)
AgNaX- 6	5.6	4.8	0.038
15	14.7	12.6	0.094
24	24.4	21.0	0.149
39	38.6	33.2	0.221
45	45.1	38.8	0.250
72	71.8	61.7	0.357
84	83.8	72.1	0.398
99	98.6	84.8	0.444

equipped between a reactor and a vacuum pump to avoid a possibility of contamination due to vapors flowing backward from the pump. In the reactor, each zeolite sample was degassed at 673 K for more than 1 h, exposed to oxygen at the same temperature for more than 30 min, and then reevacuated for 5 min. This pretreatment[13] was always carried out for a fresh sample in order to remove water, carbon dioxide, and possible hydrocarbon impurities on the zeolite surface. Following the pretreatment, the sample was cooled to a chosen temperature in static vacuum and exposed to hydrogen at a desired pressure for a prescribed time. Subsequently, the sample was evacuated for 30 min and subjected to X-ray analysis or reoxidation. Reoxidation was carried out at a prescribed temperature, period, and pressure in the presence of oxygen. In this paper, the experiments were performed by this procedure unless otherwise specified.

(b) Flow System: After being mounted in a reactor, samples were purged with nitrogen at ambient temperature and an atmospheric pressure, and then heated to a chosen temperature. At that temperature a mixture of nitrogen and hydrogen diverted to flow through the reactor. A constant flow of the mixture, 30 cm^3/min, were maintained for a prescribed period. The reduced samples were cooled down to ambient temperature in a nitrogen atmosphere. This procedure was applied to the study on the formation of silver particles under severe reduction conditions.

Characterization of Samples. In order to ascertain the change of the zeolite framework and to determine the average size of Ag particles formed, a X-ray diffraction pattern was taken on each sample after the reduction or the reoxidation. The line width of (111) reflection of the Ag crystal was used to determine the average size of the Ag particles by a simplified Scherrer relation.

Results and Discussion

Kinetics of the Reduction. Amounts of hydrogen consumption over AgNaX-45 are shown in Fig. 1 as functions of the reaction temperature and time. A reduction level was evaluated from a theoretical uptake of hydrogen based on Eq. 1. Evidently the rate and the amount of hydrogen uptake increased at the higher temperatures. At 723 K the sample consumed an amount of hydrogen corresponding to complete reduction of the Ag^+ ions within a few minutes and there was no further consumption of hydrogen. In each case the catalyst turned black from white with a progress of the hydrogen consumption, indicating the reduction of Ag^+ ions to Ag atoms. The plots of the logarithm of initial rates of the reduction, calculated from the amount of hydrogen consumption for 10 s, versus reciprocal absolute temperatures between 273 and 471 K gave a straight line. This linearity would indicate that the mechanism is essentially unchanged in the initial stage of the reduction between 273 and 471 K; therefore, the apparent activation energy was evaluated to be 23.4±1.6 kJ/mol. This value seems to be reasonable because the activation energy of reduction of copper ions in X zeolites has been reported to be 49 kJ/mol[14] and silver ions are well known to be reduced more easily than copper ions. However, it should be noted that this value (23.4 kJ/mol) might be lower than the average value of activation energies for the whole

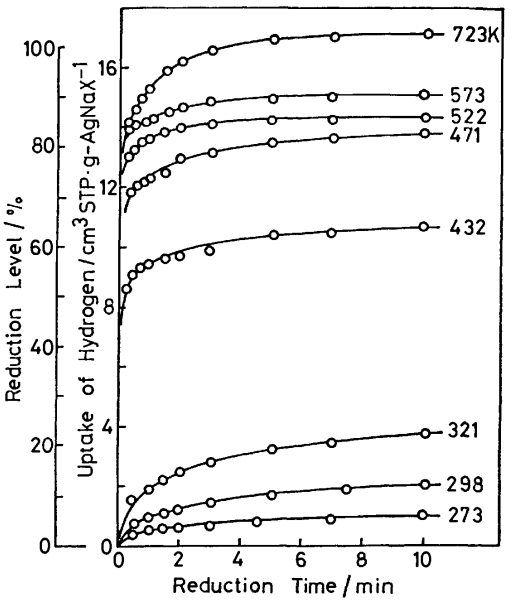

Fig. 1. Kinetic curves of the reduction of AgNaX-45 at various temperatures. The initial pressure of hydrogen was 13.3 kPa.

silver ions, since first the distribution of Ag^+ ions is somewhat heterogeneous as suggested by the dependence of the achievable degree of the reduction on the reaction temperature, and secondly the extent of reduction at 471 K for 10 s was about 50% which was too much to measure the initial reduction rate.

It was confirmed in a separate experiment that the rate of the reduction at 323 K did not depend on the partial pressure of hydrogen in the range 6.7—40.0 kPa. Beyer *et al.*[10] have reported that the reduction rate was proportional to the hydrogen pressure. However, it is very difficult to discuss the difference between these two results, since there was no description about the pressure range of hydrogen in their paper.

All samples reduced in the experiments of Fig. 1 were subjected to X-ray analyses. The reduction of AgNaX-45 at a temperature of 471 K or below did not give peaks in the diffraction pattern which are attributable to metallic silver particles. By contrast, the diffraction pattern of the sample reduced at a temperature higher than 522 K for 10 min showed a significant peak corresponding to the (111) reflection of metallic silver particles. These results lead to the conclusion that, under such mild reduction conditions as a treatment at 471 K for 10 min, the growth of silver particles should not proceed, or should stop below *ca.* 3.5 nm[15] in diameter.

The effect of an exchange level on the initial reduction rate of Ag^+ ions is depicted in Fig. 2. The reduction rate was calculated approximately from the amounts of hydrogen consumption during an initial short period, 10 sec, at 323 K. It was found that the reduction rate exhibited a characteristic correlation with the exchange level; the rate was very small for low-exchanged AgNaX zeolites until it increased rapidly above *ca.* 20% of the exchange level. This

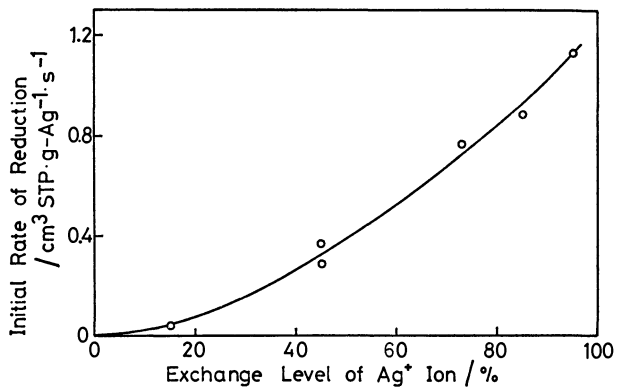

Fig. 2. Dependence of the initial rate of reduction at 323 K on the exchange level of silver(I) ions.

fact reflects that the reduction rate relates to the distribution of Ag^+ ions on several exchange sites in the zeolite framework. Ag^+ ions exhibit a tendency to occupy the interior sites (S_I or S_I') in dehydrated zeolites.[16] It is reasonable that the Ag^+ ions located at S_I and S_I' sites are difficult to be reduced with hydrogen. The influence of the exchange level and hydrogen pressure on the reduction rates at elevated temperatures could not be clarified, since the reduction rates were too fast to measure it accurately.

On the basis of the relation in Fig. 2, the activation energy of the reduction process, and the independency of the reduction rate on the hydrogen pressure, it is likely that the reduction is a catalyzed reaction in which the activation of hydrogen at some specific site S is required. This mechanism is acceptable

$$S + H_2 \rightleftharpoons S\text{-}H_2 \quad (2)$$

$$S\text{-}H_2 + Ag^+ \longrightarrow SH\text{-}Ag + H^+ \quad (3)$$

$$SH\text{-}Ag \longrightarrow SH + Ag \quad (4)$$

$$SH + Ag^+ \longrightarrow S\text{-}Ag + H^+ \quad (5)$$

$$S\text{-}Ag \longrightarrow S + Ag \quad (6)$$

if the exchange reaction of a Ag^+ ion with a H atom (Eq. 3) is a rate determining step. This cooperative exchange would be the reason for the lower activation energy of the process than that of a sole migration of univalent cations[17] (74.2 and 90.3 kJ/mol for Na^+ and Li^+ ions, respectively). This can explain the phenomenon shown in Fig. 2; that is, the reduction rate increased rapidly when Ag^+ ions began to situate inside or on the periphery of the supercage where Eq. 3 would become easy. The active species would be hydrogen atoms, since the hydrogen atoms have an average diameter small enough (0.1 nm)[18] to enter in the hexagonal or sodalite cavities through the hexagonal windows whose diameter is 0.22 nm,[19] while the diameter of hydrogen molecules is 0.24 nm.[20] Very recently, Che *et al.*[21] have reported that the reducing power of hydrogen atoms was higher than that of hydrogen molecules. In addition, in work on the equilibration of H_2–D_2 mixture over Y zeolites Heylen *et al.*[22] have shown that impurities such as iron ions are centers for the activation of hydrogen. These two findings support our assumption that the reduction is a catalyzed reaction requiring activation of the hydrogen at the site S. In the reduction process of Ag^+ ions located in S_I or S_I', it might be suggested that the generated Ag atoms are centeres for the activation of hydrogen and a spillover step of a hydrogen atom becomes significant.

Prior to the reduction experiments water vapor was introduced onto the sample which was dehydrated in the pretreatment. The reduction process was greatly inhibited in the presence of water, as shown in Fig. 3. This would result from the hydration of the active sites S or Ag^+ ions itself.

Kinetics of the Reoxidation. Reoxidation were performed on AgNaX reduced by a treatment with hydrogen at 573 K for 10 min. The uptakes of oxygen are illustrated in Fig. 4 as a function of time at dif-

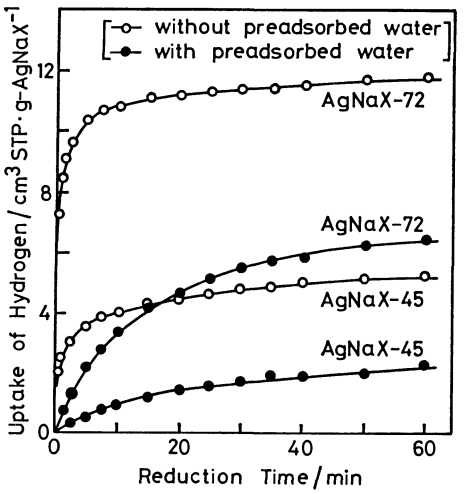

Fig. 3. Influence of the water addition on the reduction process of AgNaX-45 at 323 K. Water was introduced at 2.6 kPa into the system prior to the reduction and briefly evacuated at reaction temperature.

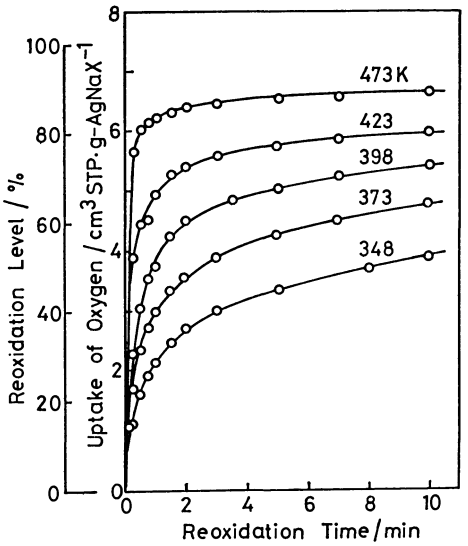

Fig. 4. Kinetic curves of the reoxidation of AgNaX-45 pre-reduced at 573 K for 10 min. The numerical values in the figure are the reoxidation temperatures. The initial pressure of oxygen was 13.3 kPa.

ferent temperatures. The reoxidation was slow at low temperatures. The achievable degree of reoxidation was nearly constant over the temperature range 348—473 K. For example, the uptake of oxygen in the reoxidation at 348 K for 2 h was 6.61 cm^3 STP/g-AgNaX-45, which was the same as that (6.65 cm^3 STP/g-AgNaX-45) at 473 K for 30 min within the experimental error. The apparent activation energy of the reoxidation, 20.1±2.0 kJ/mol, was calculated from the initial rates of Fig. 4 in the manner similar to that of the reduction. The extent of the reoxidation, evaluated from the amount of consumed oxygen on the basis of Eq. 7, was also graduated in Fig. 4. The

$$Ag + H^+ + {}^1/_4O_2 \longrightarrow Ag^+ + {}^1/_2H_2O \qquad (7)$$

reoxidation of the sample reduced at 573 K could not be achieved completely.

The stoichiometry of the reduction and reoxidation is quantitatively summarized in Table 2. Here, the reductions were carried out at two different temperatures for comparison. The amounts of reduced Ag^+ ions and reoxidized Ag atoms were determined by the quantities of the hydrogen and oxygen consumptions, respectively. The silver particles were defined here as the aggregates of silver metal which was detectable by X-ray analysis. Its quantities were measured by the method described in the following section. The remained Ag atoms were treated as silver clusters existing in the zeolites.

The hydrogen reduction of AgNaX-45 at 323 K for 30 min resulted in the production of 13.9 Ag atoms per unit cell. The formation of silver particles was not observed. Upon the treatment of this sample with oxygen at 473 K for 10 min, 3.01 cm^3 of oxygen was consumed and 14.0 Ag atoms were reoxidized to Ag^+ ions. This value is actually identical with the number of the produced Ag atoms. It is concluded that under these experimental conditions the reduction and reoxidation of Ag^+ ions in the zeolite are completely reversible. In contrast, among 34.8 Ag atoms generated by the reduction at 573 K 4.0 Ag atoms were found to form silver particles. Upon the reoxidation the amount of Ag^+ ions regenerated (30.9) is in fair agreement with that of silver clusters before the reoxidation (30.8). This is well interpreted by finding both amounts of silver particles before and after the reoxidation to be the same. These results lead to the conclusion that the silver particles remained unchanged even after the treatment of oxygen at 473 K and the reoxidation affected only the silver clusters presumably located inside the large cavities of the zeolite.

It is perhaps worthy of remark that there was no induction period in the reoxidation process and no effect of water addition on the reoxidation rate, in contrast to the observations for Ag–Y zeolites reported by Beyer *et al.*[10]

Formation of Metallic Silver Particles. The rates of particle formation during the reduction in the static system were evaluated from the increment of peak areas of Ag(111) diffraction pattern in the range 522—573 K. The apparent activation energy of the particle formation was 74.0±5.8 kJ/mol.

Next the reduction of Ag^+ ions was performed under severe conditions, *i.e.*, a treatment with hydrogen at 673 K and 101.3 kPa for 1 h in the flow system. The results were plotted in Fig. 5. The amounts of silver particles shown in Fig. 5A were essentially equal to those obtained when the reduction temperature and time were set to 773 K and 5 h. In addition, a good linear correlation evidently exists between the amounts of Ag^+ ions supported in the zeolite and the quantities

Table 2. Stoichiometry of reduction and reoxidation of AgNaX-45 sample

Run	A	B
Reduction		
Temperature/K	323	573
Time/min	30	10
Uptake of H_2/cm^3 STP	5.99	14.97
Reduced Ag^+ ions[a] /atoms per unit cell	13.9	34.8
Silver particles[b]	0	4.0
Silver clusters	13.9	30.8
Reoxidation		
Temperature/K	473	473
Time/min	10	30
Uptake of O_2/cm^3STP	3.01	6.65
Reoxidized Ag atoms[c] /atoms per unit cell	14.0	30.9
Silver particles[b] /atoms per unit cell	0	4.0

a) This value was evaluated from the amount of hydrogen consumption. b) This value was calculated from the peak area of a Ag(111) diffraction line. c) This value was evaluated from the amount of oxygen consumption.

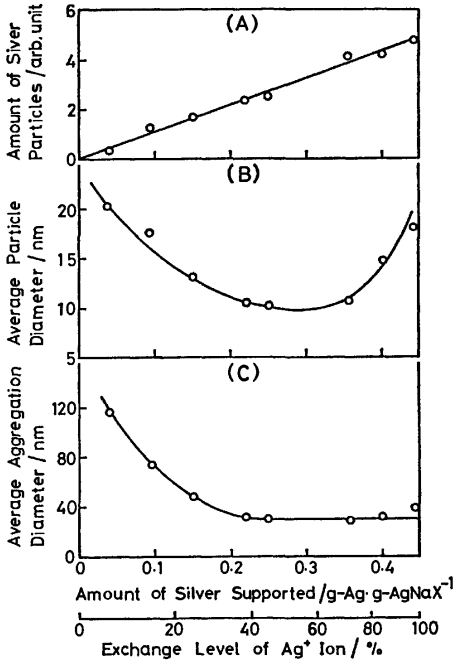

Fig. 5. Changes of amount of silver particles(A), particle diameter(B), and average aggregation diameter(C) with amount of silver supported. Reduction was performed at 673 K for 1 h by 101.3 kPa of hydrogen in the flow system.

of silver particles formed. Based on these facts, it was concluded that all Ag^+ ions were transferred into Ag particles. In Table 2, the amounts of Ag atoms converted into Ag particles were estimated by using this relation as a calibration.

In the experiments of Fig. 5, an irreversible destruction of the zeolite framework during the severe reduction was indicated by change in X-ray diffraction patterns. The diffraction patterns attributable to the zeolite structure were eliminated in proportion to the exchange level. After the reduction of AgNaX-99, for example, the diffraction patterns from the zeolites were completely disappeared and the formation of an amorphous phase was shown by the appearance of very broad and not intense peak. Under mild reduction conditions, however, the extent of the destruction was not so thorough, though the quantitative analysis concerning this phenomenon was not carried out.

The average diameters of the silver particles deduced from the line widths are shown in Fig. 5B. The diameter varied specifically with the Ag^+ ion-exchange level. It was approximately 20 nm for the low-exchanged AgNaX samples and decreased gradually with an increase in exchange level. The diameter increased after passing a minimum around 50% of the exchange level. The particle diameter were in the range 10—21 nm under these conditions. This value is in good agreement with 21 nm observed by Beyer *et al.*[10] and 15—30 nm by Tsutsumi and Takahashi.[8] Average aggregation diameters were evaluated by the following method from the results of Fig. 5B.

Since the crystal lattice of silver is of F. C. C., the number of Ag atoms included in a silver particles is given by $2\pi D_1^3/3A^3$ where D_1 represents the diameter of the silver particles and A is the lattice constant of silver crystal (0.4086 nm). On the other hand, the number of Ag^+ ions located in a unit cell of the X zeolite is $86E$, where E is an exchange level of Ag^+ ions. Therefore, writing the lattice constant of the zeolite (2.49 nm) as B, all silver ions situated in a volume of the zeolite given by $(2\pi D_1^3/3A^3)$ $(B^3/86E)$ were required to aggregate in order to form the silver particle. With an introduction of D_2 as a diameter of a sphere, whose volume is the same as that calculated above, Eq. 8 is

$$\frac{4}{3}\pi\left(\frac{D_2}{2}\right)^3=\left(\frac{2\pi D_1^3}{3A^3}\right)\left(\frac{B^3}{86E}\right) \tag{8}$$

$$D_2=\frac{D_1B}{A}\left(\frac{2}{43E}\right)^{1/3} \tag{9}$$

set up and then Eq. 9 is derived. Here, D_2 is named an average aggregation diameter. This value indicates a range of the migration and aggregation of silver in the reduction process to yield a silver particle.

The results of the calculation using Eq. 9 are shown in Fig. 5C. The aggregation diameter took a large value as 120 nm at the low exchange level and gradually decreased with increasing the exchange level. In order to understand this phenomenon and gather more informations about the process of particles formation, following experiments were performed. Amounts and

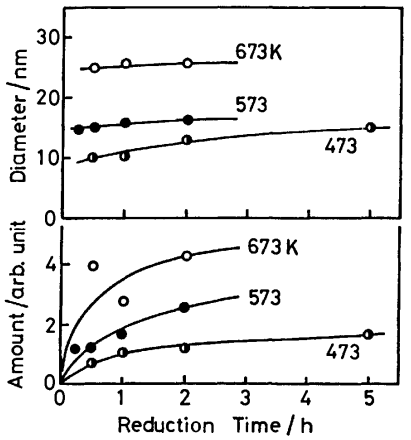

Fig. 6. Variations of amount and diameter of silver particles with reduction time at various temperatures. The reduction was performed by hydrogen at 10.1 kPa on AgNaX-99 in the flow system.

diameters of silver particles produced by the reduction of AgNaX-99 with 10.1 kPa of hydrogen in the flow system are plotted in Fig. 6 as functions of the reaction temperature and time. Clearly the amount of silver particles increased with the reaction time, while the particle diameters remained approximately constant irrespective of the reaction time. Moreover, the diameter showed a tendency to become larger at the higher temperatures.

The above observations suggest that in the formation of silver particles a step of nucleation is rate-determining and a process of subsequent nuclear growth is relatively fast. The constant particle diameters independent on the reduction time in Fig. 6 would be understood as a result of a phenomenon that once a nucleus generates, all silver ions located in the aggregation diameter are rapidly gather to its nucleus. At the higher reaction temperatures the nucleation becomes more difficult because of the unstability of nucleus and the rate of the nuclear growth is more facilitated. These result in the formation of larger particles at the higher reduction temperatures, as shown in Fig. 6. In a similar manner to the above, the low exchange level of the Ag^+ ions makes the nucleation more difficult. This is the reason why the average aggregation diameter changed with the extent of the Ag^+ ion-exchange in Fig. 5C.

Conclusions

The reduction of the Ag^+ ions and the reoxidation of Ag atoms in X zeolites are found to proceed with ease, while the silver particles with a diameter of 10—25 nm produced in the severe reduction are difficult to be reoxidized. The processes are summarized in Eq. 10, where E_a represents an activation energy

$$Ag^+ \underset{E_a=20.1\pm2.0}{\overset{E_a=23.4\pm1.6}{\rightleftarrows}} Ag^0 \xrightarrow{E_a=74.0\pm5.8} Ag(\text{particle}) \tag{10}$$

of each step (kJ/mol). The reduction requires a catalytic activation of hydrogen at specific sites in the zeolites. Upon mild reduction some of the reduced silver atoms would form clusters in the supercage of

the zeolites. The cluster might have a partial charge by the participation of unreacted silver ions, in a manner analogous to suggestions by Beyer *et al.*[10] or Kimm and Seff.[11] In the process of the particle formation it is suggested that the nucleation is rate-determining and its rate is varied with the reaction conditions. Che *et al.*[21] have recently found that Ni^{2+} ions in X zeolites were reduced to Ni atoms at very low temperatures (77—273 K) by hydrogen atoms and that the growth of clusters was achieved by gradually heating of the reduced sample above the reduction temperatures. These results indicate the possibility that the formations of Ag clusters and particles might be carried out by a migration of Ag atoms.

The authors wish to thank to Messrs. K. Kuroiwa and S. Miyazaki for carrying out some of the kinetic determination.

References

1) Kh. M. Minachev and Ya. I. Isakov, *ACS Monograph*, **171**, 552 (1976).

2) P. A. Jacobs, "Carboniogenic Activity of Zeolites," Elsevier Scientific, Amsterdam, Oxford, London (1977), p. 194.

3) J. A. Rabo, V. Schomaker and P. E. Pickert, "Proc. 3rd. Int. Congr. Catal.," North Holland, Amsterdam (1965), Vol. 2, p. 1264.

4) For example, P. A. Jacobs, J. P. Linart, H. Nijs, and J. B. Uytterhoeven, *J. Chem. Soc., Faraday Trans. 1*, **73**, 1745 (1977); P. A. Jacobs, H. Nijs and J. Vendonck, *ibid.*, **75**, 1196 (1979).

5) For example, R. G. Herman, J. H. Lunsford, H. Beyer, P. A. Jacobs, and J. B. Uytterhoeven, *J. Phys. Chem.*, **79**, 2388 (1975); P. A. Jacobs, W. de Wide, R. A. Schoonheydt, and J. B. Uytterhoeven, *J. Chem. Soc., Faraday Trans. 1*, **72**, 1221 (1976).

6) For example, P. Gallezot, *Catal. Rev. -Sci. Eng.*, **20**, 121 (1979); M. Uchida, H. Arai, and H. Tominaga, *Shokubai*, **22**, 310 (1980).

7) S. Kagawa, T. Seiyama, N. Nagao, K. Fujita, and I. Nakamori, *Kogyo Kagaku Zasshi*, **72**, 2151 (1969).

8) K. Tsutsumi and H. Takahashi, *Bull. Chem. Soc. Jpn.*, **45**, 2332 (1972).

9) L. Riekert, *Ber. Bunsenges. Phys. Chem.*, **73**, 331 (1973).

10) H. Beyer, P. A. Jacobs, and J. B. Uytterhoeven, *J. Chem. Soc., Faraday Trans. 1*, **72**, 674 (1976).

11) Y. Kimm and K. Seff, *J. Am. Chem. Soc.*, **99**, 7055 (1977).

12) R. A. Schoonheydt, L. J. Vandamme, P. A. Jacobs, and J. B. Uytterhoeven, *J. Catal.*, **43**, 292 (1976).

13) It is well known that Ag^+ ions are easily reduced upon evacuation at a higher temperature. However, the amount of Ag atoms produced in the present pretreatment should have been negligible because the sample did not turn black and the stoichiometry of reduction-reoxidation was undoubtedly confirmed as shown in Table 2.

14) S. J. Gentry, N. W. Hurst, and A. Jones, *J. Chem. Soc., Faraday Trans. 1*, **75**, 1688 (1979).

15) T. E. White, Jr., *Catal. Rev. -Sci. Eng.*, **8**, 177 (1973).

16) G. R. Eulenberger, J. G. Keil and D. P. Shoemaker, *J. Phys. Chem.*, **71**, 1812 (1967).

17) F. J. Jansen and R. A. Schoonheydt, *J. Chem. Soc., Faraday Trans. 1*, **69**, 1338 (1973).

18) F. A. Cotton and G. Wilkinson, "Advanced Inorganic Chemistry," Wiley, New York (1972), p. 151.

19) J. V. Smith, *Adv. Chem. Ser.*, **101**, 171 (1971).

20) K. Kuchitsu, "Kagaku Benran," ed by The Chemical Society of Japan, Maruzen, Tokyo (1975), p. 1408.

21) M. Che, M. Richard, and D. Olivier, *J. Chem. Soc., Faraday Trans. 1*, **76**, 1526 (1980).

22) C. F. Heylen, P. A. Jacobs, and J. B. Uytterhoeven, *J. Catal.*, **43**, 99 (1976).

Crystal and Molecular Structure of Antibiotic Gilvocarcin M

Noriaki HIRAYAMA,* Keiichi TAKAHASHI, Kunikatsu SHIRAHATA,
Yuji OHASHI,† and Yoshio SASADA†

Tokyo Research Laboratory, Kyowa Hakko Kogyo Co., Ltd., 3-6-6 Asahimachi, Machida, Tokyo 194

†*Laboratory of Chemistry for Natural Products, Tokyo Institute of Technology, Nagatsuta, Midori-ku, Yokohama 227*

(Received November 8, 1980)

The structure of gilvocarcin M, $C_{26}H_{26}O_9$, an antibiotic with a novel carbon skeleton, has been determined by single crystal X-ray analysis. The space group is $P2_1$ with $a=15.063(5)$, $b=16.162(4)$, $c=4.905(2)$ Å, $\beta=91.47(3)°$, and $Z=2$. The structure was solved by direct methods, and least-squares refinement using 1734 reflexions gave the final R value of 0.054. The title compound is composed of a unique aglycone and a fucofuranose, which are linked together through a C–C glycosyl linkage. The furanose ring takes the °E conformation.

Gilvocarcin M and V are antibiotics produced by *Streptomyces gilvotanareus* and *Streptomyces griseologilbus*.[1] They were called previously DC-38.[2] Their structures have been elucidated on the basis of their chemical nature and spectroscopic data.[3] The structural difference between M and V is that a methyl group at C(22) in the former is replaced by a vinyl group in the latter. The structure of gilvocarcin M and the numbering system is shown in Fig. 1. In spite of many efforts with various kinds of NMR techniques including proton-proton spin decoupling and ^{13}C-NMR with long range selective proton decoupling, there has still remained some ambiguity especially around the asymmetric carbons of the furanose. To determine the structure of gilvocarcins unequivocally, we have undertaken an X-ray analysis of gilvocarcin M. This paper will describe the crystal structure of the antibiotic.

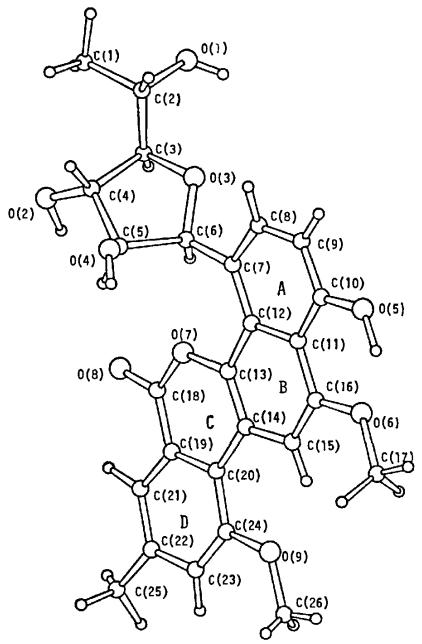

Fig. 1. The numbering system of gilvocarcin M.

Experimental and Structure Determination

Yellow prismatic crystals of gilvocarcin M were obtained from a DMSO–ethanol solution. A crystal, $0.5\times0.13\times0.05$ mm^3, was used for data collection on a Rigaku four-circle automated diffractometer with Ni-filtered Cu $K\alpha$ radiation. Preliminary unit cell dimensions and space group were obtained from oscillation and Weissenberg photographs. The space group was determined from systematic absences ($0k0$ for odd k). Accurate cell dimensions were determined by a least-squares calculation with 2θ values of 16 high-angle reflexions measured on the diffractometer. Crystal data are summarized in Table 1. All independent reflexions within the range $2\theta\leqq120°$ were collected by use of the ω-2θ scan mode with a scanning rate of $4°(2\theta)\text{min}^{-1}$. Stationary background counts were accumulated for 10 s before and after each scan. Periodic checks of the intensity values of three standard reflexions showed no significant X-ray damage. Corrections for absorption or extinction were not applied. Out of 1847 independent reflexions obtained, 1735 for which $|F_o|>3.0\sigma(|F_o|)$ were used.

TABLE 1.

$C_{26}H_{26}O_9\cdot0.4C_2H_6O$	$b=16.162(4)$ Å
$M.W.=500.9$	$c=4.905(2)$ Å
$P2_1$	$\beta=91.47(3)°$
$Z=2$	$D_x=1.393$ g cm^{-3}
$a=15.063(5)$Å	μ(Cu $K\alpha$)$=21.47$ cm^{-1}

The phases of 339 reflexions with $|E_o|\geqq1.2$ were assigned with MULTAN.[4] The best set of phases was used to calculate an E-map, which gave 21 chemically significant peaks. Other 15 non-hydrogen atoms were found by the successive Fourier syntheses. The structural parameters were refined by block-diagonal least-squares with a modified HBLS programme. All the hydrogen atoms and a molecule of the ethanol solvent without hydrogen atoms were found by the difference syntheses. Refinement gave the final R value 0.054 for 1734 reflexions. The atoms of the solvent molecules with the occupancy of 0.4 were refined isotropically. The weighting system used in the final stage was $w=0.3$ for $|F_o|<1.782$ and $|F_o|>17.82$, and $w=(0.00115(F_o)^2-0.12675|F_o|+4.48559)^{-1}$ for $1.782\leqq|F_o|\leqq17.82$. A strong reflexion, 020, was excluded because it seemed to suffer from secondary extinction. Atomic scattering factors were taken from "International Tables for X-Ray Crystallography."[5] The final positional and thermal parameters are given in Table 2. The tables of anisotropic temperature factors and observed and calculated structure factors are kept as a Document No. 8132 at the Chemical Society of Japan.

Results and Discussion

Molecular Structure. Bond lengths and angles are tabulated in Table 3. A stereoscopic drawing of the molecule is shown in Fig. 2. The two bonds C(15)–C(16) and C(18)–O(7), which correspond to K region of phenantherene,[6] show rather high double bond character. There is an intramolecular hydrogen bond between O(5) and O(6) atoms; O(5)···O(6)= 2.547(6) Å, H(O(5))···O(6)=1.68(7) Å, and O(5)–H···O(6) angle is 141.2°. Although the reason is not clear, the C(24)–O(9) length is significantly shorter than the C(16)–O(16).

The C–C glycosyl bond length, C(6)–C(7), is somewhat longer than the corresponding values (1.492—1.501 Å) in formycin.[7] In usual nucleosides C(4')–O(1') is significantly longer than C(1')–O1(1'). In gilvocarcin M, however, C(6)–O(3) is significantly longer than C(3)–O(3). There are two short intramolecular non-bonded contacts; O(3)···C(8)=2.622(7) Å and O(7)···C(6)=2.682(6) Å.

The least-squares planes of interest and the dihedral angles between them are tabulated in Table 4. The aglycone part except the substituents is planar within ±0.1 Å. Although every six-membered rings are planar, the planarity of the D ring is best (±0.008 Å) and that of the C ring is worst (±0.035 Å). The dihedral angles between the rings A and B, between rings B and C, and between rings C and D are 1.9, 2.3, and 2.4°, respectively. These values show a smooth convex character of the aglycone part, as seen in Fig. 3, the side view of the molecule. The dihedral angles between the least-squares planes of furanose ring and the aglycone part is 53.5°.

The O(3) atom deviates by 0.531 Å from the plane determined by the C(3), C(4), C(5), and C(6) atoms, and the puckering parameters P and θ_m[8] are 94.8 and 39.9°, respectively. This indicates that the furanose ring takes an unusual $^{\circ}E$ conformation. It is probable that the $^{\circ}E$ conformation is related to the above-mentioned bond length reversion at the C(3)–O(3) and C(6)–O(3) bonds. The conformation around the C(2)–C(3) bond is *gauche-trans*, and the χ_{cc} angle of 19.7° is in the *anti* region. Torsional angles are listed in Table 5.

Crystal Structure. A stereoscopic drawing of the crystal structure viewed along the c axis is shown in Fig. 4. There are three intermolecular OH···O hydrogen bonds as listed in Table 6. Between the

Table 2. Fractional atomic coordinates with their standard deviations and temperature factors

Atom	x	y	z	B_{eq} or B/Å^2	Atom	x	y	z	B_{eq} or B/Å^2
C(1)	−0.0849(4)	0.2055(5)	0.0166(19)	6.40	O(7)	0.3602(2)	0.3430(2)	0.0540(7)	2.81
C(2)	−0.0406(4)	0.2852(5)	0.1113(14)	4.97	O(8)	0.3800(2)	0.2557(2)	−0.2808(7)	3.31
C(3)	0.0574(3)	0.2879(4)	0.0555(12)	3.63	O(9)	0.6652(3)	0.4619(3)	0.2373(9)	4.89
C(4)	0.1124(4)	0.2152(3)	0.1634(11)	3.47	HAC(1)	−0.165(5)	0.215(5)	−0.163(17)	7.6
C(5)	0.2000(3)	0.2542(3)	0.2703(10)	3.00	HBC(1)	−0.077(5)	0.192(5)	−0.163(17)	9.4
C(6)	0.1897(3)	0.3471(3)	0.1973(10)	2.96	HCC(1)	−0.061(5)	0.151(5)	0.114(16)	8.0
C(7)	0.2292(3)	0.4112(3)	0.3907(10)	2.92	HC(2)	−0.057(4)	0.297(5)	0.303(12)	6.3
C(8)	0.1720(4)	0.4471(4)	0.5688(11)	3.55	HC(3)	0.072(3)	0.295(3)	−0.127(9)	2.8
C(9)	0.1985(4)	0.5083(4)	0.7573(12)	3.75	HC(4)	0.080(3)	0.187(3)	0.330(11)	3.9
C(10)	0·2830(4)	0.5353(3)	0.7661(10)	3.35	HC(5)	0.254(3)	0.232(3)	0.171(8)	1.7
C(11)	0.3473(3)	0.5021(3)	0.5896(10)	2.93	HC(6)	0.216(4)	0.354(4)	0.016(11)	4.7
C(12)	0.3192(3)	0.4377(3)	0.3988(10)	2.66	HC(8)	0.114(3)	0.435(3)	0.592(9)	2.3
C(13)	0.3890(3)	0.4053(3)	0.2321(10)	2.88	HC(9)	0.158(3)	0.531(3)	0.887(11)	3.5
C(14)	0.4758(3)	0.4291(3)	0.2402(9)	2.63	HC(15)	0.557(3)	0.515(3)	0.412(9)	2.9
C(15)	0.4989(4)	0.4946(4)	0.4242(10)	3.34	HAC(17)	0.578(4)	0.643(4)	0.634(12)	5.5
C(16)	0.4369(4)	0.5278(3)	0.5845(10)	3.15	HBC(17)	0.552(9)	0.658(9)	1.008(28)	11.7
C(17)	0.5517(4)	0.6122(4)	0.8013(14)	4.82	HCC(17)	0.597(5)	0.562(1)	0.838(15)	7.6
C(18)	0.4140(3)	0.3061(3)	−0.1233(10)	2.67	HC(21)	0.531(4)	0.240(4)	−0.391(12)	6.0
C(19)	0.5081(3)	0.3254(3)	−0.1118(10)	2.84	HC(23)	0.750(3)	0.362(3)	−0.091(3)	3.7
C(20)	0.5397(3)	0.3874(3)	0.0683(10)	2.98	HAC(25)	0.768(4)	0.280(5)	−0.473(13)	7.0
C(21)	0.5640(3)	0.2817(4)	−0.2811(10)	3.26	HBC(25)	0.701(5)	0.240(6)	0.365(16)	9.3
C(22)	0.6537(4)	0.2965(4)	−0.2789(11)	3.53	HCC(25)	0.739(5)	0.202(4)	−0.368(14)	7.1
C(23)	0.6872(3)	0.3582(4)	−0.1044(12)	3.76	HAC(26)	0.775(5)	0.498(5)	−0.005(15)	8.8
C(24)	0.6324(3)	0.4025(4)	0.0649(12)	3.45	HBC(26)	0.759(4)	0.464(4)	0.273(11)	4.6
C(25)	0.7152(4)	0.2476(5)	−0.4535(12)	8.03	HCC(26)	0.764(5)	0.528(5)	0.353(15)	8.0
C(26)	0.7590(5)	0.4812(6)	0.2429(20)	8.03	HO(1)	−0.062(5)	0.404(5)	0.009(15)	7.8
O(1)	−0.0856(3)	0.3500(4)	−0.0246(16)	8.92	HO(2)	0.170(5)	0.168(5)	−0.165(16)	9.2
O(2)	0.1247(3)	0.1515(3)	−0.0341(8)	4.16	HO(4)	0.264(4)	0.240(5)	0.590(13)	6.1
O(3)	0.0943(2)	0.3590(2)	0.1823(8)	3.43	HO(5)	0.368(4)	0.613(4)	0.939(13)	6.0
O(4)	0.2064(2)	0.2401(3)	0.5590(7)	3.54	O_{et}	0.0302(8)	0.0132(8)	−0.2667(25)	5.5
O(5)	0.3038(3)	0.5948(3)	0.9560(8)	4.29	$C(1)_{et}$	0.0250(11)	0.0083(12)	0.0333(38)	6.0
O(6)	0.4600(3)	0.5913(3)	0.7694(8)	4.44	$C(2)_{et}$	0.0469(14)	0.0021(13)	0.1974(38)	10.1

Table 3. Bond lengths (l/Å) and angles (ϕ/°)

C(1)-C(2)	1.517(12)	C(2)-O(1)	1.406(11)	C(2)-C(3)	1.509(10)
C(3)-C(4)	1.524(8)	C(4)-C(5)	1.543(8)	C(4)-O(2)	1.429(7)
C(5)-C(6)	1.549(8)	C(5)-O(4)	1.435(7)	C(6)-O(3)	1.449(7)
C(3)-O(3)	1.415(7)	C(6)-C(7)	1.517(7)	C(7)-C(8)	1.371(8)
C(8)-C(9)	1.405(8)	C(9)-C(10)	1.346(8)	C(10)-C(11)	1.421(8)
C(11)-C(12)	1.455(7)	C(12)-C(7)	1.421(7)	C(10)-O(5)	1.369(7)
C(16)-O(6)	1.407(7)	O(6)-C(17)	1.426(8)	C(12)-C(13)	1.447(7)
C(13)-C(14)	1.363(7)	C(14)-C(15)	1.428(8)	C(15)-C(16)	1.348(8)
C(16)-C(11)	1.413(7)	C(13)-O(7)	1.394(6)	C(14)-C(20)	1.461(7)
C(18)-O(7)	1.343(6)	C(18)-O(8)	1.225(6)	C(18)-C(19)	1.451(7)
C(19)-C(20)	1.410(7)	C(20)-C(24)	1.418(8)	C(19)-C(20)	1.391(8)
C(21)-C(22)	1.373(8)	C(22)-C(23)	1.399(9)	C(22)-C(25)	1.502(10)
C(23)-C(24)	1.385(8)	C(24)-O(9)	1.363(7)	C(26)-O(9)	1.445(11)
$C(1)_{et}$-$C(2)_{et}$	1.46(2)	$C(2)_{et}$-O_{et}	0.87(2)	C(1)-C(2)-C(3)	113.2(6)
C(1)-C(2)-O(1)	106.5(7)	O(1)-C(2)-C(3)	110.8(7)	C(2)-C(3)-C(4)	116.1(5)
C(2)-C(3)-O(3)	108.6(5)	C(4)-C(3)-O(3)	105.7(5)	C(3)-C(4)-C(5)	104.8(5)
C(3)-C(4)-O(2)	113.5(5)	C(5)-C(4)-O(2)	113.6(4)	C(4)-C(5)-C(6)	103.7(4)
C(4)-C(5)-O(4)	107.8(4)	C(6)-C(5)-O(4)	112.7(4)	C(5)-C(6)-O(3)	103.6(4)
C(5)-C(6)-C(7)	118.8(4)	O(3)-C(6)-C(7)	108.2(4)	C(3)-O(3)-C(6)	107.0(4)
C(6)-C(7)-C(8)	116.4(5)	C(6)-C(7)-C(12)	125.6(5)	C(8)-C(7)-C(12)	118.0(5)
C(7)-C(8)-C(9)	123.0(5)	C(8)-C(9)-C(10)	120.2(5)	C(9)-C(10)-C(11)	121.1(5)
C(10)-C(11)-C(12)	118.0(5)	C(11)-C(12)-C(7)	119.7(5)	C(9)-C(10)-O(5)	116.7(5)
C(11)-C(10)-O(5)	122.2(5)	C(10)-C(11)-C(16)	124.5(5)	C(7)-C(12)-C(13)	125.6(5)
C(11)-C(12)-C(13)	114.7(4)	C(12)-C(13)-C(14)	126.3(5)	C(13)-C(14)-C(15)	116.5(5)
C(14)-C(15)-C(16)	120.1(5)	C(15)-C(16)-C(11)	124.7(5)	C(16)-C(11)-C(12)	117.5(5)
C(11)-C(16)-O(6)	115.1(5)	C(15)-C(16)-O(6)	120.2(5)	C(16)-O(6)-C(17)	117.8(5)
C(12)-C(13)-O(7)	113.4(4)	C(15)-C(14)-C(20)	123.5(5)	O(7)-C(13)-C(14)	120.3(5)
C(13)-O(7)-C(18)	122.9(4)	O(7)-C(18)-C(19)	118.9(4)	C(18)-C(19)-C(20)	119.5(5)
C(19)-C(20)-C(14)	118.1(5)	C(20)-C(14)-C(13)	119.9(5)	C(7)-C(18)-O(8)	117.0(4)
C(19)-C(18)-O(8)	124.1(5)	C(18)-C(19)-C(21)	118.2(5)	C(14)-C(20)-C(24)	126.2(5)
C(20)-C(19)-C(21)	122.3(5)	C(19)-C(21)-C(22)	121.1(5)	C(21)-C(22)-C(23)	117.9(6)
C(21)-C(22)-C(25)	121.6(6)	C(23)-C(22)-C(25)	120.5(6)	C(22)-C(23)-C(24)	121.7(6)
C(23)-C(24)-C(20)	121.3(5)	C(24)-C(20)-C(19)	115.6(5)	C(20)-C(24)-O(9)	117.1(5)
C(23)-C(24)-O(9)	121.6(5)	C(24)-O(9)-C(26)	120.1(6)	$C(1)_{et}$-$C(2)_{et}$-O_{et}	154(2)

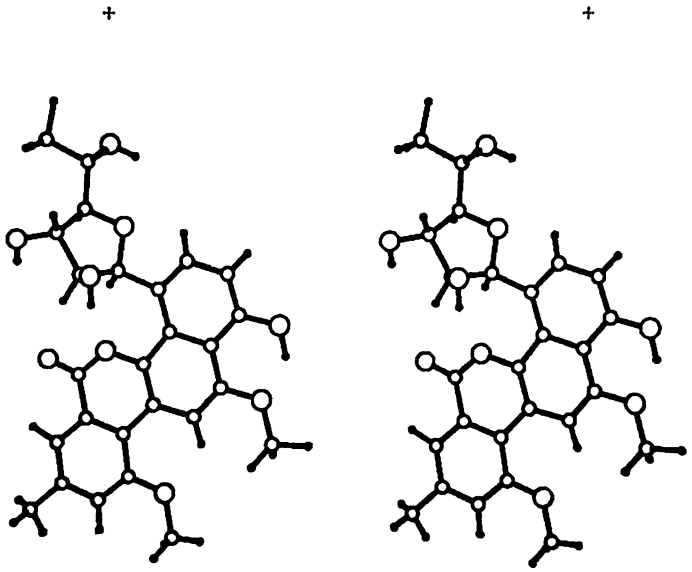

Fig. 2. Stereoscopic drawing of gilvocarcin M.

Table 4. Least-squares planes and dihedral angles (Ψ/°) between them

The asterisked atoms are included in the calculation of the planes and the values in the parentheses are the deviations ($\times 10^3$ Å) from the plane. x, y, and z are in Å

Plane 1.	C(3)*[−604], C(4)*[−38], C(5)*[−82], C(6)*[−192], O(3)*[−238]
	$0.347x-0.008y-0.938z+0.161=0$
Plane 2.	C(3)*[−14], C(4)*[20], C(5)*[−20], C(6)*[13], O(3)[−531]
	$0.405x-0.154y-0.901z+0.599=0$
Plane 3.	C(7)*[−4], C(8)*[−4], C(9)*[7], C(10)*[−3], C(11)*[−4], C(12)*[8]
	$0.211x-0.703y+0.679z+2.653=0$
Plane 4.	C(11)*[19], C(12)*[−8], C(13)*[−10], C(14)*[17], C(15)*[−6], C(16)*[−12]
	$0.200x-0.683y+0.703z+2.495=0$
Plane 5.	O(7)*[25], C(13)*[6], C(14)*[−24], C(18)*[−35], C(19)*[15], C(20)*[13]
	$0.161x-0.694y+0.701z+2.816=0$
Plane 6.	C(19)*[0], C(20)*[4], C(21)*[−5], C(22)*[6], C(23)*[−2], C(24)*[−3]
	$0.124x-0.685y+0.718z+3.045=0$
Plane 7.	C(7)*[10], C(8)*[73], C(9)*[107], C(10)*[57], C(11)*[−10], C(12)*[−12], C(13)*[−50], C(14)*[−61], C(15)*[−98], C(16)*[−80], O(7)*[−43], C(18)*[−99], C(19)*[−30], C(20)*[−19], C(21)*[23], C(22)*[100], C(23)*[99], C(24)*[43], C(6)[−42], O(5)[101], O(6)[−92], C(17)[24], O(9)[59], C(26)[109], O(8)[−168]
	$0.173x-0.689y+0.704z+2.649=0$

Dihedral angles (Ψ/°)

Plane	2	3	4	5	6	7
1	9.3	56.1	54.2	53.4	51.3	53.5
2		65.3	63.4	62.6	60.6	62.7
3			1.9	3.1	5.5	2.7
4				2.3	4.5	1.6
5					2.4	0.8
6						3.0

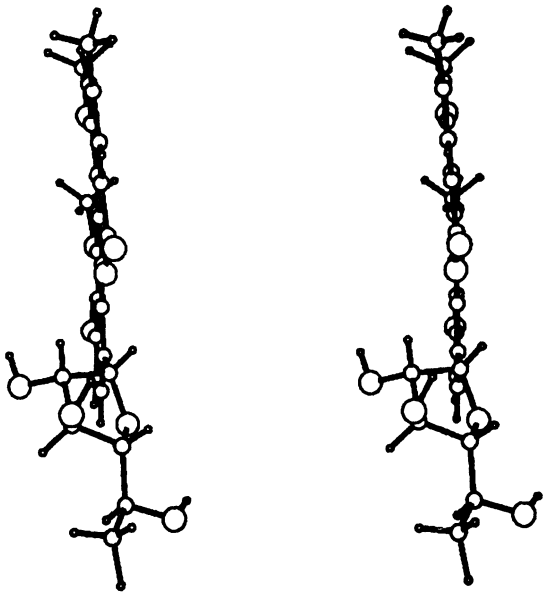

Fig. 3. Stereoscopic side view of gilvocarcin M.

molecules along the c axis, there are two hydrogen bonds; O(2)···O(4) and O(4)···O(8). The third hydrogen bond is formed between the O(1) atom and the oxygen atom of the solvent ethanol. In other part the molecules are stacked mainly by van der Waals interactions. The interplanar separation between the aglycone moieties along the c axis is 3.45 Å.

The solvent molecule of ethanol is disordered, which might be explained by the large cavity around it.

Structure Activity Relationship. It is assumed that the biological activity of gilvocarcins comes mainly from the interaction of the compounds with DNA.[1] It is conceivable from the stereochemical point of view, because gilvocarcins have geometrical prerequisites to interact with DNA. The dimensions and the planarity of the aglycone, and the delocalization of π electrons through the aglycone part are the common structural features found in most antibiotics which interact with DNA through the intercalation mode. It is interesting that gilvocarcins possess partial structures corresponding to K region and bay region[9]

Table 5. Torsional angles (τ/°)

C(1)-C(2)-C(3)-C(4)	−53.5	O(1)-C(2)-C(3)-O(3)	68.0
C(1)-C(2)-C(3)-O(3)	−172.4	O(1)-C(2)-C(3)-C(4)	−173.1
O(3)-C(3)-C(4)-C(5)	−20.1	C(2)-C(3)-C(4)-C(5)	−140.6
O(3)-C(3)-C(4)-O(2)	−144.6	C(2)-C(3)-C(4)-O(2)	94.9
C(3)-C(4)-C(5)-C(6)	−3.3	C(3)-C(4)-C(5)-O(4)	116.4
O(2)-C(4)-C(5)-C(6)	121.1	O(2)-C(4)-C(5)-O(4)	−119.2
C(4)-C(5)-C(6)-O(3)	24.9	C(4)-C(5)-C(6)-C(7)	144.9
O(4)-C(5)-C(6)-O(3)	−91.5	O(4)-C(5)-C(6)-C(7)	28.5
C(5)-C(6)-O(3)-C(3)	−39.4	C(7)-C(6)-O(3)-C(3)	−166.4
C(6)-O(3)-C(3)-C(4)	37.7	C(6)-O(3)-C(3)-C(2)	163.0
C(5)-C(6)-C(7)-C(8)	−97.9	C(5)-C(6)-C(7)-C(12)	83.1
O(3)-C(6)-C(7)-C(8)	19.7	O(3)-C(6)-C(7)-C(12)	−159.3
O(5)-C(10)-C(11)-C(16)	−1.9	C(10)-C(11)-C(16)-O(6)	−0.6
C(15)-C(16)-O(6)-C(17)	−6.7	C(11)-C(16)-O(6)-C(17)	171.5
C(20)-C(24)-O(9)-C(26)	−179.5	C(23)-C(24)-O(9)-C(26)	1.2

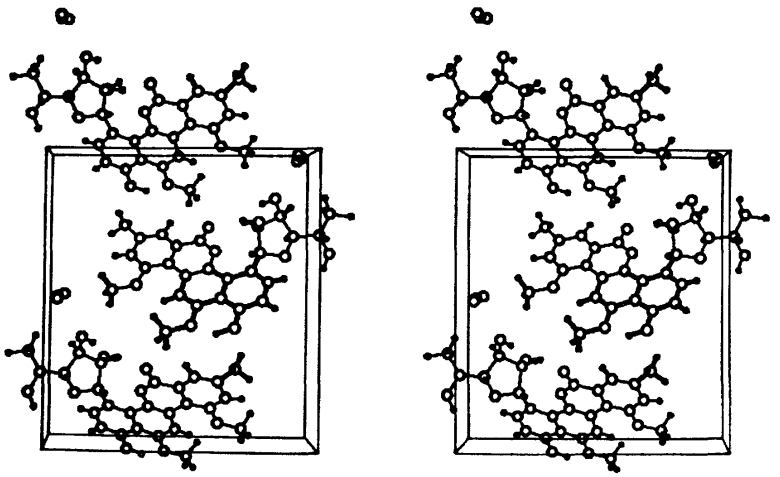

Fig. 4. Crystal structure viewed along c axis.

Table 6. Hydrogen bond distances (l/Å) and angles (ϕ/°)

A-H···B	A···B	∠A-H···B
O(5)-H^{I}···O(6)^{I}	2.547(6)	141(6)
O(1)-H^{I}···O$_{et}^{II}$	2.669(8)	142(6)
O(4)-H^{I}···O(8)^{III}	2.722(5)	168(5)
O(2)-H^{III}···O(4)^{I}	2.770(6)	149(5)
Symmetry code		
I: (x y z)		
II: ($-x$ 0.5+y $-z$)		
III: (x y 1.0+z)		

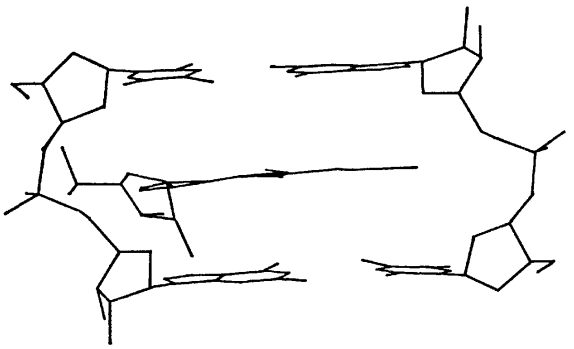

Fig. 5. A hypothetical intercalation mode of gilvocarcin M between the base pairs in DNA.

in the aglycone.

In this connexion, it should be noted that when the methyl group at C(22) is replaced by a vinyl group (gilvocarcin V), the activity is enhanced.[1] The vinyl group is of less bulkiness than the methyl group to intercalate between the base pairs in DNA. In addition to the relief of the steric hindrance, the vinyl group would electronically increase the reactivity of the compound to DNA.

A hypothetical way of the intercalation of gilvocarcin M between the base pairs in DNA is shown in Fig. 5. The structure of the fragment of the unwound DNA is taken from the results of the X-ray analysis of ethidium/dinucleoside monophosphate complex.[10] This figure illustrates that gilvocarcin M has molecular dimensions suitable for intercalation between the base pairs in DNA.

Figures 2, 3, and 4 were drawn by TSD:XTAL, which is a computer-graphics interactive modelling programme for the NOVA3 computer.[11]

References

1) H. Nakano, Y. Matsuda, K. Ito, S. Ohkubo, M. Morimoto, and F. Tomita, *J. Antibiot.*, **34**, 266 (1981).
2) F. Tomita, Y. Matsuda, K. Shirahata, K. Takahashi, H. Nakano, T. Sato, S. Ohkubo, and N. Nakamura, Japan Kokai Koho, 80—57586, April 28 (1980).
3) K. Takahashi, M. Yoshida, F. Tomita, and K. Shirahata, *J. Antibiot.*, **34**, 271 (1981).
4) G. Germain, P. Main, and M. M. Woolfson, *Acta Crystallogr., Sect. A*, **27**, 368 (1971).
5) "International Tables for X-Ray Crystallography," Kynoch Press, Birmingham (1974), Vol. IV, pp. 72—102.
6) A. Pullman and B. Pullman, *Adv Cancer Res.*, **3**, 117 (1955).
7) G. Koyama, H. Nakamura, H. Umezawa, and Y. Iitaka, *Acta Crystallogr., Sect. B*, **32**, 813 (1975).
8) C. Altona and M. Sundaralingam, *J. Am. Chem. Soc.*, **94**, 8205 (1972).
9) D. E. Zacharias, J. P. Glusker, P. P. Fu, and R. G. Harvey, *J. Am. Chem. Soc.*, **101**, 4043 (1979).
10) C. Tsai, S. C. Jain, and H. M. Sobell, *J. Mol. Biol.*, **114**, 301 (1977).
11) A. Takenaka and Y. Sasada, *J. Cryst. Soc. Jpn.*, **22**, 214 (1980).

  Bull. Chem. Soc. Jpn., 54, 1343—1347 (1981)

Intermolecular Potential, Vibrational Spectra, and Structures of Amino Acid Crystals. I. Distortion of Molecules and Equilibrium Crystal Structure

Katsunosuke MACHIDA* and Yoshihiro KURODA

Faculty of Pharmaceutical Sciences, Kyoto University, Sakyo-ku, Kyoto 606

(Received November 15, 1980)

A general method of the crystal packing optimization is developed for the molecular crystals consisting of non-rigid molecules. The intramolecular potential is described as a general harmonic force field in terms of a suitable set of internal symmetry coordinates, and the intermolecular potential as a sum of the pairwise atom-atom interaction terms. The adjustable structure parameters are those among the six cell constants, a, b, c, α, β, and γ, and the translations and the rotations of the molecules which maintain the crystal symmetry. The intermolecular force is separated into two parts, one of which determines the location of the center of mass and the orientation of the principal axes of each molecule and the other leads to a certain molecular distortion. The calculated distortion may be used, in addition to the difference between the calculated and the observed crystal structures, as a check point of the reliability of the model potential. The importance of this separation in the rigid molecule approximation is pointed out.

In order to search for the equilibrium structure of a given molecular crystal by taking account of all the degrees of freedom of atomic motions in the asymmetric unit, we should pay attention to both the intramolecular (internal) and the intermolecular (external) parts of the potential function. Any molecular crystals maintain their structures on the balance of the forces expressed as the gradients of these two parts. Confining the discussion to those crystals in which all the molecules are symmetrically equivalent, we shall denote the intramolecular and the intermolecular potentials per molecule as $V_{\rm in}$ and $V_{\rm ex}$, respectively. The contribution of $V_{\rm in}$ to the forces acting on the atoms may be estimated if the atomic displacements on the change from the gaseous state to the crystal are known experimentally and also the change of $V_{\rm in}$ on the change of state is assumed to be negligible. Warshel and Lifson carried out extensive calculations of this type for a number of hydrocarbons using the Cartesian coordinates of atoms as the working coordinates.[1] This method cannot be applied to amino acids for which the structures in the isolated zwitterionic form are unknown. Neither is the rigid molecule approximation applicable in this case, since the low-frequency intramolecular vibrations of amino acids couple appreciably with the lattice modes. The internal rotations around single bonds have been taken into account by several authors in the conformation analyses of molecular crystals.[2,3] In a series of studies on vibrational spectra of simple amino acids, however, we observed that some of the skeletal deformation frequencies were lower than the torsional frequencies of the NH_3^+ and the CH_3 groups.[4-7]

In this report, we propose a convenient procedure of the potential energy minimization for the crystals of amino acids and similar non-rigid molecules. General expressions for the increments of the structure parameters in the Newton-Raphson iteration are given by taking account of the effect of $V_{\rm in}$ without any knowledge on the structure of the isolated molecules. Application of the method to α-glycine, L-alanine and DL-alanine crystals will be given in the subsequent paper.

Theory

Molecular Distortion. The $3N$ degrees of freedom of motions of a non-linear N atomic molecule may be described by a set of $3N-6$ internal symmetry coordinates, denoted in a vector form as $\boldsymbol{S}_{\rm in}$, and 6 external coordinates, $\boldsymbol{S}_{\rm ex}$, representing the translation and the rotation of the whole molecule. These coordinates can be constructed from the Cartesian displacement coordinates $\boldsymbol{x}$ of the atoms through the transformations

$$\boldsymbol{S}_{\rm in} = \boldsymbol{B}_{\rm in}\boldsymbol{x} \quad \text{and} \quad \boldsymbol{S}_{\rm ex} = \boldsymbol{B}_{\rm ex}\boldsymbol{x}. \tag{1}$$

The matrix $\boldsymbol{B}_{\rm in}$ is related to the well known $\boldsymbol{G}$ matrix by

$$\boldsymbol{G} = \boldsymbol{B}_{\rm in}\boldsymbol{m}^{-1}\tilde{\boldsymbol{B}}_{\rm in}, \tag{2}$$

where $\boldsymbol{m}$ is a $3N\times 3N$ diagonal matrix consisting of the atomic masses.[8] Since $\boldsymbol{S}_{\rm ex}$ is so chosen as to fulfill the Eckart condition and is normalized,[9] it follows that

$$\boldsymbol{B}_{\rm in}\,\boldsymbol{m}^{-1}\,\tilde{\boldsymbol{B}}_{\rm ex} = \boldsymbol{0} \tag{3}$$

and

$$\boldsymbol{B}_{\rm ex}\,\boldsymbol{m}^{-1}\,\tilde{\boldsymbol{B}}_{\rm ex} = \boldsymbol{E}, \tag{4}$$

where $\boldsymbol{E}$ is a 6×6 identity matrix. Next we denote the vector of the external forces along the Cartesian coordinates by

$$\boldsymbol{f}_x^{\rm ex} = [-\partial V_{\rm ex}/\partial x_1 \; -\partial V_{\rm ex}/\partial y_1 \cdots -\partial V_{\rm ex}/\partial z_N]^{\rm T},$$

and introduce the vectors of generalized forces $\boldsymbol{f}_{\rm ex}^{\rm ex}$ and $\boldsymbol{f}_{\rm in}^{\rm ex}$ corresponding to the coordinates $\boldsymbol{S}_{\rm ex}$ and $\boldsymbol{S}_{\rm in}$, respectively. In accordance with Eq. 1, the transformation from the generalized forces to $\boldsymbol{f}_x^{\rm ex}$ is expressed as

$$\boldsymbol{f}_x^{\rm ex} = \tilde{\boldsymbol{B}}_{\rm in}\,\boldsymbol{f}_{\rm in}^{\rm ex} + \tilde{\boldsymbol{B}}_{\rm ex}\,\boldsymbol{f}_{\rm ex}^{\rm ex}. \tag{5}$$

Premultiplying Eq. 5 by $\boldsymbol{G}^{-1}\boldsymbol{B}_{\rm in}\,\boldsymbol{m}^{-1}$ and using Eqs. 2 and 3, we obtain

$$\boldsymbol{f}_{\rm in}^{\rm ex} = \boldsymbol{G}^{-1}\boldsymbol{B}_{\rm in}\,\boldsymbol{m}^{-1}\,\boldsymbol{f}_x^{\rm ex}. \tag{6}$$

Similarly, the use of Eqs. 3 and 4 after premultiplying by $\boldsymbol{B}_{\rm ex}\,\boldsymbol{m}^{-1}$ leads to

$$\boldsymbol{f}_{\rm ex}^{\rm ex} = \boldsymbol{B}_{\rm ex}\,\boldsymbol{m}^{-1}\,\boldsymbol{f}_x^{\rm ex}. \tag{7}$$

Equations 6 and 7 enable us to partition the external

force into two parts, one tending to distort the molecule and the other tending to displace and rotate it. At the equilibrium position, f_{ex}^{ex} should vanish while f_{in}^{ex} is not necessarily a zero vector since it can be offset by the internal force, f_{in}^{in}, which arises from a certain distortion of the molecule associated with the change of the environment from the isolated state into the crystal, *i.e.*,

$$f_{in}^{ex} = -f_{in}^{in}. \tag{8}$$

Kurittu and Pawley gave a general expression of this distortion in terms of the normal coordinates of the free molecule.[10] An alternative way, being applicable to the cases where the molecular structure in the free state is unknown, is to express the distortion in terms of the internal symmetry coordinates S_{in} of the molecules in the crystal. Denoting such a distortion by S_{in}^{c} and using Eqs. 6 and 8, we have

$$S_{in}^{c} = -F^{-1} f_{in}^{in} = F^{-1} G^{-1} B_{in} m^{-1} f_{x}^{ex}, \tag{9}$$

where F is the usual potential energy matrix for the internal vibrations defined by

$$2V_{in} = \tilde{S}_{in} F S_{in}.$$

The Cartesian components of the internal force are given by

$$f_{x}^{in} = \tilde{B}_{in} f_{in}^{in}, \tag{10}$$

since f_{ex}^{in} vanishes from the definition in contrast to the case of f_{ex}^{ex} in Eq. 5. When the F matrix does not change on going from the gaseous state to the crystal, S_{in}^{c} represents the structure change of the molecule on the change of state. In the procedure of Kurittu and Pawley,[10] one starts from the geometry of the undistorted molecule, and calculates the external force iteratively at the varying atomic positions until the final balance between V_{in} of the distorted molecule and V_{ex} is attained. On the other hand, the calculation in the present formulation is performed once for the distorted molecule, and the structure of the isolated molecule is inferred by subtracting S_{in}^{c} from the structure in the crystalline state. Obviously, our method is valid only for infinitesimal distortions while that of Kurittu and Pawley is applicable to larger ones. An advantage of our method is that we can incorporate all the degrees of freedom of atomic motions implicitly in the conformation analysis of molecular crystals, using the same number of adjustable parameters as the rigid molecule approximation, *viz.*, the lattice constants and the translations and the rotations of the whole molecule.

Changes of Lattice Constants and External Coordinates. The potential energy per unit cell of a uniformly deformed molecular crystal under a small strain may be expressed as

$$V = V_0 - \tilde{f}_{\sigma}\sigma - \tilde{f}_{x}x_{\rho} + (1/2)(\tilde{\sigma}F_{\sigma\sigma}\sigma + \tilde{x}_{\rho}F_{xx}x_{\rho}) + \tilde{\sigma}F_{\sigma x}x_{\rho}, \tag{11}$$

where σ is the strain vector,

$$\sigma = [\sigma_{xx}\ \sigma_{yy}\ \sigma_{zz}\ \sigma_{yz}\ \sigma_{zx}\ \sigma_{xy}]^{T},$$

which leads to the macroscopic deformation of the crystal, and x_{ρ} is the vector of the microscopic Cartesian displacements of the atoms in the unit cell.[11] We retain the linear terms in Eq. 11 considering the cases when no minima of the adopted model potential correspond to the experimentally determined structure. The vector f_x is the sum of the external and the internal forces, and is given by

$$f_{x} = f_{x}^{ex} + f_{x}^{in} = (E - \tilde{B}_{in} G^{-1} B_{in} m^{-1}) f_{x}^{ex} \tag{12}$$

from Eqs. 6, 8, and 10. The matrix F_{xx} is equivalent to the F matrix for the optical active crystal vibrations in terms of the Cartesian displacements, and can be diagonalized by the transformation into the normal coordinates,

$$x_{\rho} = L_{x} q_{\rho}. \tag{13}$$

In order to determine f_{σ}, $F_{\sigma\sigma}$, and $F_{\sigma x}$ in Eq. 11 and then to calculate the derivatives of V with respect to the lattice constants and the external coordinates, it is useful to follow the treatment of elastic constants of molecular crystals due to Shiro and Miyazawa in a slightly modified manner including the linear terms.[12]

Specifying each unit cell with an index vector L, we can express the Cartesian displacements of the ith atom in the cell L (denoted as the atom Li hereafter) of the uniformly deformed lattice as

$$x_{i}(L) = D^{i}(L)\sigma + E^{i} x_{\rho}, \tag{14}$$

where $D^{i}(L)$ consists of the Cartesian coordinates of the atom Li evaluated with reference to the origin of the cell $\mathbf{0}$ when $\sigma=\mathbf{0}$, $X_{i}^{0}(L)$, $Y_{i}^{0}(L)$, and $Z_{i}^{0}(L)$, *viz.*,

$$D^{i}(L) = \begin{bmatrix} X_{i}^{0}(L) & 0 & 0 & 0 & Z_{i}^{0}(L)/2 & Y_{i}^{0}(L)/2 \\ 0 & Y_{i}^{0}(L) & 0 & Z_{i}^{0}(L)/2 & 0 & X_{i}^{0}(L)/2 \\ 0 & 0 & Z_{i}^{0}(L) & Y_{i}^{0}(L)/2 & X_{i}^{0}(L)/2 & 0 \end{bmatrix},$$

and the elements of E^{i} are given in terms of Kronecker's delta as

$$(E^{i})_{jk} = \delta_{k-j,3(i-1)}.$$

The atomic displacement vector for the cell L is obtained by collecting $x_{i}(L)$ columnwise, and is written in the form

$$x(L) = D_{x}(L)\sigma + x_{\rho}, \tag{15}$$

where

$$D_{x}(L) = \Sigma_{i}\tilde{E}^{i}D^{i}(L).$$

The pairwise interaction potential between the atoms $\mathbf{0}i$ and Lj may be expanded as the power series of the relevant Cartesian displacements in the form

$$V^{ij}\{r_{ij}(L)\} = V^{ij}\{r_{ij}^{0}(L)\} - \tilde{f}_{ij}(L)\{x_{i}(\mathbf{0}) - x_{j}(L)\} + \frac{1}{2}\{\tilde{x}_{i}(\mathbf{0}) - \tilde{x}_{j}(L)\}F_{ij}(L)\{x_{i}(\mathbf{0}) - x_{j}(L)\}, \tag{16}$$

where $r_{ij}(L)$ is the distance between $\mathbf{0}i$ and Lj, and the superscript 0 denotes the value when $\sigma=\mathbf{0}$. The linear and the quadratic coefficients in Eq. 16 are given by

$$f_{ij}(L) = -\{\partial V^{ij}/\partial r_{ij}(L)\}e_{ij}^{0}(L)$$

and

$$\boldsymbol{F}_{ij}(\boldsymbol{L}) = \{\partial V^{ij}/\partial r_{ij}(\boldsymbol{L})\}\{\boldsymbol{E}-\boldsymbol{e}_{ij}{}^0(\boldsymbol{L})\tilde{\boldsymbol{e}}_{ij}{}^0(\boldsymbol{L})\}/r_{ij}{}^0(\boldsymbol{L}) + \{\partial^2 V^{ij}/\partial r_{ij}(\boldsymbol{L})^2\}\boldsymbol{e}_{ij}{}^0(\boldsymbol{L})\tilde{\boldsymbol{e}}_{ij}{}^0(\boldsymbol{L}),$$

respectively, where $\boldsymbol{e}_{ij}{}^0(\boldsymbol{L})$ denotes the unit vector along the direction from $\boldsymbol{L}j$ to $\boldsymbol{0}i$. Substituting Eq. 14 into Eq. 16, dividing by $1+\delta_{ij}$ and summing over all the intermolecular atom pairs $\boldsymbol{0}i$ and $\boldsymbol{L}j$ such that $i \leqq j$, we obtain the portion of the potential energy in Eq. 11 arising from V_{ex}. Since we are dealing with a homogeneous deformation, the contribution of V_{in} to Eq. 11 can be evaluated by writting down V_{in} for the cell $\boldsymbol{0}$ in terms of the Cartesian displacements as

$$V_{\text{in}} = -\tilde{\boldsymbol{f}}_x{}^{\text{in}}\boldsymbol{x}(\boldsymbol{0}) + (1/2)\tilde{\boldsymbol{x}}(\boldsymbol{0})\boldsymbol{F}_{xx}{}^{\text{in}}\boldsymbol{x}(\boldsymbol{0}),$$

and substituting Eq. 15. Carrying out these calculations, we have

$$\boldsymbol{f}_\sigma = \sum_{i\leqq j,\boldsymbol{L}}\sum (1+\delta_{ij})^{-1}\tilde{\boldsymbol{D}}^{ij}(\boldsymbol{L})\boldsymbol{f}_{ij}(\boldsymbol{L}) + \tilde{\boldsymbol{D}}_x(\boldsymbol{0})\boldsymbol{f}_x{}^{\text{in}}, \tag{17}$$

$$\boldsymbol{F}_{\sigma\sigma} = \sum_{i\leqq j,\boldsymbol{L}}\sum (1+\delta_{ij})^{-1}\tilde{\boldsymbol{D}}^{ij}(\boldsymbol{L})\boldsymbol{F}_{ij}(\boldsymbol{L})\boldsymbol{D}^{ij}(\boldsymbol{L}) + \tilde{\boldsymbol{D}}_x(\boldsymbol{0})\boldsymbol{F}_{xx}{}^{in}\boldsymbol{D}_x(\boldsymbol{0}) \tag{18}$$

and

$$\boldsymbol{F}_{\sigma x} = \sum_{i\leqq j,\boldsymbol{L}}\sum (1+\delta_{ij})^{-1}\tilde{\boldsymbol{D}}^{ij}(\boldsymbol{L})\boldsymbol{F}_{ij}(\boldsymbol{L})(\boldsymbol{E}^i-\boldsymbol{E}^j) + \tilde{\boldsymbol{D}}_x(\boldsymbol{0})\boldsymbol{F}_{xx}{}^{in}, \tag{19}$$

where

$$\boldsymbol{D}^{ij}(\boldsymbol{L}) = \boldsymbol{D}^i(\boldsymbol{0}) - \boldsymbol{D}^j(\boldsymbol{L}).$$

Substituting Eq. 13 into Eq. 11, and using the condition that the potential energy is stationary with respect to the microscopic deformation, we have

$$\boldsymbol{q}_\rho = \boldsymbol{\Lambda}^{-1}\tilde{\boldsymbol{L}}_x\boldsymbol{f}_x - \boldsymbol{\Lambda}^{-1}\tilde{\boldsymbol{L}}_x\tilde{\boldsymbol{F}}_{\sigma x}\boldsymbol{\sigma}, \tag{20}$$

where $\boldsymbol{\Lambda}$ is the diagonal matrix of the eigenvalues of $\boldsymbol{m}^{-1/2}\boldsymbol{F}_{xx}\boldsymbol{m}^{-1/2}$ corresponding to the genuine normal modes, and the eigenvectors for the translations of the whole crystal are excluded from $\boldsymbol{L}_x$. By eliminating $\boldsymbol{q}_\rho$ from Eqs. 13 and 20 and substituting the result into Eq. 11, the potential energy is rewritten as

$$V = V_0 - (\tilde{\boldsymbol{f}}_\sigma - \boldsymbol{L}_x\boldsymbol{\Lambda}^{-1}\tilde{\boldsymbol{L}}_x\tilde{\boldsymbol{F}}_{\sigma x})\boldsymbol{\sigma} + (1/2)\tilde{\boldsymbol{\sigma}}(\boldsymbol{F}_{\sigma\sigma} - \boldsymbol{F}_{\sigma x}\boldsymbol{L}_x\boldsymbol{\Lambda}^{-1}\tilde{\boldsymbol{L}}_x\tilde{\boldsymbol{F}}_{\sigma x})\boldsymbol{\sigma}. \tag{21}$$

The quadratic part of Eq. 21 divided by the volume of the unit cell gives the matrix of the elastic constants as derived by Shiro and Miyazawa.[12]

Let a set of infinitesimal changes of the cell dimensions be denoted in a vector form

$$\Delta\boldsymbol{a} = [\Delta a\ \Delta b\ \Delta c\ \Delta\alpha\ \Delta\beta\ \Delta\gamma]^{\text{T}},$$

and those required to eliminate the linear terms in Eq. 21 be $\Delta\boldsymbol{a}^*$. By differentiating Eq. 21 with respect to $\boldsymbol{\sigma}$ and using the transformation

$$\boldsymbol{\sigma} = \boldsymbol{A}\,\Delta\boldsymbol{a}, \tag{22}$$

the vector $\Delta\boldsymbol{a}^*$ is derived to be

$$\Delta\boldsymbol{a}^* = (\tilde{\boldsymbol{f}}_\sigma - \tilde{\boldsymbol{f}}_x\boldsymbol{L}_x\boldsymbol{\Lambda}^{-1}\tilde{\boldsymbol{L}}_x\tilde{\boldsymbol{F}}_{\sigma x})(\boldsymbol{F}_{\sigma\sigma} - \boldsymbol{F}_{\sigma x}\boldsymbol{L}_x\boldsymbol{\Lambda}^{-1}\tilde{\boldsymbol{L}}_x\tilde{\boldsymbol{F}}_{\sigma x})^{-1}\boldsymbol{A}^{-1} \tag{23}$$

Derivation of the transformation matrix $\boldsymbol{A}$ and its inverse is given in Appendix.

The first term of Eq. 20 represents those microscopic displacements of the atoms which are required to minimize the energy of a stress-free crystal in the first-order approximation. These displacements may also be expressed in terms of the internal symmetry and the external coordinates in the form

$$\boldsymbol{S}_{\text{in}}^* = -\boldsymbol{B}_{\text{in}}\boldsymbol{L}_x\boldsymbol{\Lambda}^{-1}\tilde{\boldsymbol{L}}_x\boldsymbol{f}_x \tag{24}$$

and

$$\boldsymbol{S}_{\text{ex}}^* = -\boldsymbol{B}_{\text{ex}}\boldsymbol{L}_x\boldsymbol{\Lambda}^{-1}\tilde{\boldsymbol{L}}_x\boldsymbol{f}_x. \tag{25}$$

Iterative minimization of the potential energy can now be carried out by the Newton-Raphson method in which $\Delta\boldsymbol{a}^*$ and $\boldsymbol{S}_{\text{ex}}^*$ are used as the correction vectors.[13] The normalized external coordinates are not so convenient to visualize the actual position and orientation of each molecule in the unit cell. Instead, we may use the translations along the principal axes of inertia, T_1^*, T_2^*, and T_3^*, and the rotations around those axes, R_1^*, R_2^*, and R_3^*. Denoting the vector of these quantities as $\boldsymbol{T}_{\text{ex}}^*$ and introducing a 6×6 diagonal matrix

$$\boldsymbol{M}^{-1/2} = \text{diag}[M^{-1/2}\ M^{-1/2}\ M^{-1/2}\ I_1^{-1/2}\ I_2^{-1/2}\ I_3^{-1/2}],$$

where M is the molecular mass and I_1, I_2, and I_3 are the principal moments of inertia of the molecule, we have

$$\tilde{\boldsymbol{T}}_{\text{ex}}^* = [T_1^*\ T_2^*\ T_3^*\ R_1^*\ R_2^*\ R_3^*] = \tilde{\boldsymbol{S}}_{\text{ex}}^*\boldsymbol{M}^{-1/2}. \tag{26}$$

When the unit cell has any symmetry elements, calculation of Eq. 25 for the non-totally symmetric species of the factor group can be avoided by using a set of properly chosen symmetry coordinates. If all the rotations R_i^* are small, the combined rotation is defined uniquely as their vector sum, the magnitude of which is

$$\theta = |R_1^{*2}+R_2^{*2}+R_3^{*2}|^{1/2},$$

and the direction cosine between the axis of the rotation and the ith principal axis is

$$l_i = R_i^*/\theta.$$

In the frame of the principal axes, the rotation is performed by using the transformation matrix familiar in crystallography[14] which consists of the diagonal elements

$$\theta_{ii} = \cos\theta + l_i^2(1-\cos\theta)$$

and the off-diagonal elements

$$\theta_{ij} = l_il_j(1-\cos\theta) + (j-i)(-1)^{i+j}l_{6-i-j}\sin\theta/|i-j|.$$

The Cartesian coordinates of the kth atom in the molecule after the correction of the structure according to $\Delta\boldsymbol{a}^*$ and $\boldsymbol{T}_{\text{ex}}^*$ are calculated from those before the correction, $x_k{}^0$, $y_k{}^0$, and $z_k{}^0$, by

$$x_k^* = \sum C_{xi}[\sum\theta_{ij}\{C_{xj}(x_k{}^0-x_g{}^0)+C_{yj}(y_k{}^0-y_g{}^0)+C_{zj}(z_k{}^0-z_g{}^0)\}+T_i^*]+(1+\sigma_{xx})x_g{}^0+\sigma_{xy}y_g{}^0+\sigma_{zx}z_g{}^0, \tag{27}$$

where C_{xi} is the direction cosine between the x axis and the ith principal axis, and $x_g{}^0$, $y_g{}^0$, and $z_g{}^0$ are the coordinates of the center of mass of the molecule before the correction, and similar expressions for the y and the z components.

Discussion

In the procedure described above, the internal correction vector S^*_{in} is excluded from the iteration and the internal structure of the molecules is accordingly kept unchanged throughout the energy minimization. If the matrix $L_x A^{-1} \tilde{L}_x$ is positive definite, the force f^{ex}_{ex} tends to vanish when the external correction vector S^*_{ex} diminishes according to Eq. 25, since

$$f_x = \tilde{B}_{ex} f^{ex}_{ex}$$

and the matrix $B_{ex} L_x A^{-1} \tilde{L}_x \tilde{B}_{ex}$ has an inverse, and S^*_{in} in Eq. 24 is made automatically a zero vector at a potential minimum. This condition is fulfilled by any model potential for which all the calculated lattice frequencies are real. In this respect, the present scheme of the crystal packing analysis resembles that based on the rigid molecule approximation in which the molecular structure can be chosen in the same way as that determined experimentally. The present method affords, however, a useful information not available from the rigid molecule approximation, *i.e.*, the molecular distortion vector S^c_{in}, which may be compared with the structure data in the gaseous state or the results of theoretical calculations on the electronic states of the isolated molecule.

The use of Eqs. 12 and 17 including f^{in}_x is essential in the calculation of Δa^* even when the rigid molecule approximation is adopted. In this case, the terms arising from V_{in} should be excluded from Eqs. 18 and 19, and the elements of A and L_x in Eq. 23 related to the internal modes should be absent. Since the rigid molecule approximation is the limiting case that the diagonal elements of F become infinite, the distortion S^c_{in} turns out to be infinitesimal but the product

$$f^{in}_{in} = -F S^c_{in}$$

remains undiminished because it is determined purely by the external force. This point has so far been overlooked and f^{ex}_x instead of f_x has been used as the net force acting on the atoms by many investigators who have adopted the rigid molecule approximation.

In contrast to the case of Δa^*, the effect of f^{in}_{in} on T^*_{ex} is expected to be important only for non-rigid molecules. If we use f^{ex}_x in place of f_x in Eq. 25, it follows from Eq. 5 that

$$S^*_{ex} = -B_{ex} L_x A^{-1} \tilde{L}_x (\tilde{B}_{in} f^{ex}_{in} + \tilde{B}_{ex} f^{ex}_{ex}). \quad (28)$$

If the internal and the external modes do not couple with each other, the matrix of the coefficients of f^{ex}_{in} in Eq. 28 vanishes and f^{ex}_x leads to the same T^*_{ex} as f_x does. This condition is approximately fulfilled when the crystal consists of nearly rigid molecules, whereas there are no simple conditions for the cancellation of the contributions of f^{in}_x to f_x and f_a in Eq. 23.

In order to check the effect of the internal force on the packing analysis of α-glycine, L-alanine, and DL-alanine crystals, the correction vectors Δa^* and T^*_{ex} were calculated from Eqs. 23 and 25, respectively, and also from the same equations in which f^{in}_x was set equal to zero. In this calculation, the atomic coordinates, the potential parameters and the ranges of the lattice sums were taken in the same way as those in our previous studies on the crystal vibrations of these amino acids.[5,7] As shown in Table 1, the correction vectors of each amino acid calculated for the cases $f^{in}_x \neq 0$ and $f^{in}_x = 0$ are roughly parallel to each other. As to the individual components of Δa^* and T^*_{ex}, however, there is no systematic trend in signs and relative magnitudes of the differences between the values obtained from the two calculations. Some of the components of T^*_{ex} change quite sensitively when f_x is replaced by f^{ex}_x, owing probably to the coupling between the internal and the external modes. These results suggest that we should take account of the internal force of non-rigid molecules correctly in searching for the crystal structure corresponding to the energy minimum for a given model potential. Similar consideration may be required when we try to adjust the potential parameters in such a way as to minimize the correction vectors.

We wish to express our sincere thanks to Prof. Kenji Osaki and Prof. Takeo Matsubara of Kyoto University for their valuable advices. The numerical calculations were carried out on FACOM 230-75 and M200 computers at the Data Processing Center of Kyoto University.

TABLE 1. COMPONENTS OF CORRECTION VECTORS Δa^* AND T^*_{ex}

f^{in}_x	α-Glycine		L-Alanine		DL-Alanine	
	$\neq 0$	$=0$	$\neq 0$	$=0$	$\neq 0$	$=0$
Δa^*	0.414	0.401	−0.353	−0.145	1.003	0.650
Δb^*	1.013	1.158	1.063	0.754	−0.388	−0.278
Δc^*	−0.270	−0.353	0.082	0.107	−0.409	−0.308
$\Delta \beta^*$	0.032	0.031				
T_1^*	0.048	0.049	0.026	0.020	−0.020	−0.019
T_2^*	0.486	0.473	0.099	0.066	0.048	0.051
T_3^*	−0.491	−0.444	−0.091	−0.021	−0.007	−0.007
R_1^*	−0.063	−0.038	0.020	0.042	−0.070	−0.060
R_2^*	0.070	0.072	0.010	0.037	−0.017	−0.013
R_3^*	−0.036	−0.013	0.082	0.095	0.133	0.131

Δa^*, Δb^*, Δc^*, and T_i^* are in Å, and $\Delta \beta^*$ and R_i^* are in radian.

Appendix

Let the Cartesian coordinates of the atoms in a unit cell be defined in the framework where the x axis coincides with the a axis and the y axis lies on the ab plane. Then the matrix of the transformation from the fractional coordinates along the cell axes to the Cartesian coordinates is given by

$$\boldsymbol{C} = \begin{bmatrix} a & b\cos\gamma & c\cos\beta \\ 0 & b\sin\gamma & -c\sin\beta\cos\alpha^* \\ 0 & 0 & c\sin\beta\sin\alpha^* \end{bmatrix}, \tag{A1}$$

where the asterisk denotes the lattice constants of the reciprocal lattice.[14] By labelling the quantities at the equilibrium under vanishing stress with the subscript 0, the inverse of $\boldsymbol{C}$ at the equilibrium is expressed as

$$\boldsymbol{C}_0^{-1} = \begin{pmatrix} \dfrac{1}{a_0} & \dfrac{\cos\gamma_0}{a_0\sin\gamma_0} & \dfrac{\cos\beta_0^*}{a_0\sin\gamma_0\sin\beta_0^*} \\ 0 & \dfrac{1}{b_0\sin\gamma_0} & \dfrac{\cos\alpha_0^*}{b_0\sin\gamma_0\sin\alpha_0^*} \\ 0 & 0 & \dfrac{1}{c_0\sin\beta_0\sin\alpha_0^*} \end{pmatrix}. \tag{A2}$$

The elements of the matrix $\boldsymbol{C}\boldsymbol{C}_0^{-1}$ are related to the strain components by

$$(\boldsymbol{C}\boldsymbol{C}_0^{-1})_{ij} = \delta_{ij} + \sigma_{ij}, \tag{A3}$$

where δ_{ij} is Kronecker's delta and the subscripts 1, 2, and 3 for σ_{ij} represent x, y, and z, respectively.[15] Substituting Eqs. (A1) and (A2) into Eq. (A3), expanding each of the six independent elements of $\boldsymbol{C}\boldsymbol{C}_0^{-1}$ as a power series of the variations of the lattice constants and neglecting the higher-order terms, we obtain Eq. (22) in the text. The transformation matrix can be factored into two matrices

$$\boldsymbol{A}_1 = \begin{pmatrix} 1 & 0 & 0 & 0 & 0 & 0 \\ 0 & 1 & 0 & 0 & 0 & c \\ 0 & 0 & 1 & -r & -p & -pr \\ 0 & r & -r & -1 & c & cr-p \\ p & cr & b/s & 0 & -1 & -r \\ -c & c & 0 & 0 & 0 & -1 \end{pmatrix},$$

where

$$p = \cot\beta_0^*/\sin\gamma_0, \quad r = \cot\alpha_0^*, \quad s = \sin\alpha_0^*,$$
$$b = \cot\beta_0 \quad \text{and} \quad c = \cot\gamma_0$$

and

$$\boldsymbol{A}_2 = \mathrm{diag}[a_0^{-1}\, b_0^{-1}\, c_0^{-1}\ (\sin\gamma_0\sin\beta_0^*)^{-1}\ (\sin\alpha_0^*)^{-1}\ 1],$$

and is written as $\boldsymbol{A} = \boldsymbol{A}_1\boldsymbol{A}_2$. By a straightforward manipulation, an expression for the inverse of $\boldsymbol{A}_1$ was obtained as

$$\boldsymbol{A}_1^{-1} = \sin^2\gamma_0 \begin{pmatrix} 1+c^2 & 0 & 0 & 0 & 0 & 0 \\ c^2 & 1 & 0 & 0 & 0 & c \\ 0 & 0 & 0 & 0 & 0 & 0 \\ pc & -pc & 0 & 0 & 0 & p \\ 0 & 0 & 0 & 0 & 0 & 0 \\ -c & c & 0 & 0 & 0 & -1 \end{pmatrix}$$
$$+ \sin^2\beta_0 \begin{pmatrix} 0 & 0 & 0 & 0 & 0 & 0 \\ 0 & 0 & 0 & 0 & 0 & 0 \\ b^2 & a^2 & s^2 & -as & bs & -ab \\ bq & a(s-bp) & ws & (bp-s)s & qs & -aq \\ -b/s & arb & bs & -ab & -1 & r \\ 0 & 0 & 0 & 0 & 0 & 0 \end{pmatrix},$$

where

$$q = (pr-c)s = \cot\gamma_0^*/\sin\beta_0, \quad a = rs = \cos\alpha_0^*$$

and

$$w = bc - rs = \cos\alpha_0/\sin\beta_0\sin\gamma_0.$$

Since $\boldsymbol{A}_2$ is diagonal, it follows immediately that

$$\boldsymbol{A}_2^{-1} = \mathrm{diag}\,[a_0\ b_0\ c_0\ \sin\gamma_0\ \sin\beta_0^*\ \sin\alpha_0^*\ 1],$$

and we can express the inverse of $\boldsymbol{A}$ analytically as $\boldsymbol{A}^{-1} = \boldsymbol{A}_2^{-1}\boldsymbol{A}_1^{-1}$.

References

1) A. Warshel and S. Lifson, *J. Chem. Phys.*, **53**, 582 (1970).
2) D. E. Williams, *Acta Crystallogr., Sect. A*, **28**, 629 (1972).
3) F. A. Momany, L. M. Carruthers, and H. A. Scherage, *J. Phys. Chem.*, **78**, 1621 (1974).
4) K. Machida, A. Kagayama, Y. Saito, Y. Kuroda, and T. Uno, *Spectrochim. Acta, Part A*, **33**, 569 (1977).
5) K. Machida, A. Kagayama, Y. Saito, and T. Uno, *Spectrochim. Acta, Part A*, **34**, 909 (1978).
6) K. Machida, A. Kagayama, and Y. Saito, *J. Raman Spectrosc.* **7**, 188 (1978).
7) K. Machida, A. Kagayama, and Y. Saito, *J. Raman Spectrosc.* **8**, 133 (1979).
8) E. B. Wilson, Jr., *J. Chem. Phys.*, **7**, 1047 (1939); **9**, 76 (1941).
9) C. Eckart, *Phys. Rev.*, **47**, 552 (1935).
10) J. Krittu and G. S. Pawley, *Acta Crystallogr., Sect. A*, **29**, 615 (1973).
11) M. Born and K. Huang, "Dynamical Theory of Crystal Lattices," Oxford University Press, London (1954), Chap. 3.
12) Y. Shiro and T. Miyazawa, *Bull. Chem. Soc. Jpn.*, **44**, 2371 (1971).
13) See for example, Ref. 1.
14) G. S. Pawley, "Advances in Structure Research by Diffraction Methods," Pergamon Press, Oxford (1972), Vol. 4, pp. 1—64.
15) J. L. Schlenker, G. V. Gibbs, and M. B. Boisen, Jr., *Acta Crystallogr., Sect. A*, **34**, 52 (1978).

Intermolecular Potential, Vibrational Spectra, and Structures of Amino Acid Crystals. II. α-Glycine, L-Alanine, and DL-Alanine Crystals

Katsunosuke MACHIDA,* Akira KAGAYAMA, and Yoshihiro KURODA
Faculty of Pharmaceutical Sciences, Kyoto University, Sakyo-ku, Kyoto 606
(Received November 15, 1980)

The lattice energies, the deviations of the structure parameters from the model equilibrium, the molecular distortions due to the intermolecular interaction and the vibrational frequencies of α-glycine, L-alanine and DL-alanine crystals were calculated from three sets of parameters for the pairwise atom-atom interaction potential functions. By comparing the calculated quantities with the observed ones, the combination of the exp-6 type non-bonded potential and the Lippincott type hydrogen bond stretching potential is shown to afford a better model of the intermolecular interaction in these crystals than the combination of the Lennard-Jones 6-12 potential and the general hydrogen bond 10-12 potential.

Evaluation of the intermolecular forces acting in amino acid crystals is an indispensable step for the conformational study of proteins. We have recently investigated the polarized Raman spectra of single crystals of glycine (α-form), L-alanine and DL-alanine,[1-4] and have obtained a common set of potential parameters with which the observed vibrational frequencies of these amino acids can be elucidated fairly well. The intermolecular potential of amino acid crystal is very complicated, however, owing to the presence of many terms due to the exchange repulsion and dispersion force, the hydrogen bonding and the Coulomb interaction between atomic charges. Even the simplest description of these forces requires too many parameters to be estimated from the vibrational spectra alone.

The present work has been undertaken to check if the potential parameters used in our previous analyses of the vibrational spectra are compatible with the crystal structure itself. By taking account of the non-rigidity of the molecule as described in the preceding paper,[5] the lattice energies, the equilibrium crystal structures, the molecular distortions due to the intermolecular force, the elastic constants and the vibrational frequencies have been calculated and a modification of a few potential parameters has been attempted. For the sake of comparison, the same calculations have been carried out by using the model potential proposed by Momany *et al.* on the basis of their extensive analyses of the conformations of amino acid crystals.[6]

Calculation

The potential energy per molecule was written in the same functional form as those used in our previous analyses of the vibrational spectra of α-glycine, L-alanine, and DL-alanine crystals.[1-4] The intramolecular part, $V_{\rm in}$, is the simple Urey-Bradley type quadratic force field supplemented with the diagonal terms in the CO_2^- out-of-plane deformation coordinate and the internal rotation coordinates around the N–C and the C–C bonds.[7] The intermolecular part, $V_{\rm ex}$, is the sum of the pairwise potential terms of the three types,

$$V_1 = \frac{1}{2}\sum_i\sum_j [-A_{ij}r_{ij}^{-6} + B_{ij}\exp(-C_{ij}r_{ij})]$$

$$V_2 = -\frac{1}{2}\sum_i\sum_j D_{ij}\exp[-k_{ij}r_{ij}^e(r_{ij}-r_{ij}^e)^2/2D_{ij}r_{ij}]$$

and

$$V_3 = \frac{1}{2}\sum_i\sum_j e_ie_j\,\mathrm{erfc}(\sqrt{\pi}Kr_{ij})/r_{ij},$$

where r_{ij} is the distance between the atoms i and j, the index i runs over a single molecule and j over the others. The potential V_1 represents the exchange-repulsion and dispersion interaction for the atom pairs H···H, C···H, C···C, O···H(C), and N···O. V_2 is the Lippincott type stretching potential[8] of the hydrogen bonds (N)H···O, and V_3 arises from the Coulomb interaction between the atomic charges e_i and e_j. The vector of the molecular distortion, $\boldsymbol{S}_{\rm in}^e$, the correction vector for the lattice constants, $\Delta\boldsymbol{a}^*$, and that for the molecular translation and rotation, $\boldsymbol{T}_{\rm ex}^*$, were calculated from Eqs. 9, 23, and 26, respectively, in the preceding paper,[5] and $V_{\rm in}$ from

$$V_{\rm in} = (1/2)\tilde{\boldsymbol{S}}_{\rm in}^e\boldsymbol{F}\boldsymbol{S}_{\rm in}^e,$$

where $\boldsymbol{F}$ is the potential energy matrix for the intramolecular vibrations. The lattice energy was then calculated from

$$V = V_{\rm in} + V_{\rm ex}.$$

An order-of-magnitude estimation of the zero point energy per molecule was made according to

$$V_0 = (1/2n)\sum_{i=1}^{6n-3}\nu_i^{\rm calcd},$$

where n is the number of molecules per primitive unit cell and $\nu_i^{\rm calcd}$ is the calculated value of the ith optical-active lattice frequency.

The calculation was carried out for two sets of potential parameters, Sets I and II. Both the sets consist of the same parameters as those used in our unified treatment of the vibrational spectra of α-glycine and DL-alanine crystals,[4] except that the parameters A_{ij} and C_{ij} for the N···O contact in Set II were taken as 3266.1 kJ mol^{-1} Å^6 and 37.11 Å^{-1}, respectively. The meaning of this adjustment will be given in the next section. The summation limit for V_1 was taken to be 8 Å. The limit of 6 Å used previously is sufficient for the convergence of the vibrational frequencies, but causes truncation errors up to 10% for the lattice energy. According to Williams,[9] the Coulomb potential V_3 was written in the form including the complementary error function as a con-

vergence factor. In a preliminary survey of the Coulombic lattice sum, we recognized little indication of the convergence of V_3 on extending the summation limit to 40 Å in the absence of the convergence factor. When the convergence constant K was taken to be 0.20 and 0.05, however, the energy converged with enough accuracy at the summation limits of 20 Å and 40 Å, respectively. We calculated the complete Coulomb energies for several representative choices of K by Bertaut's method,[10] and estimated the errors due to the neglect of the reciprocal lattice sum to be about 4 kJ mol^{-1} for α-glycine and L-alanine crystals and about 13 kJ mol^{-1} for DL-alanine crystal. The comparatively large error for DL-alanine may be ascribed to the residual dipole moment of the unit cell resulting from the polar structure of this crystal.[11]

In order to compare the behaviors of various types of the model potential functions, the same calculations as described above were carried out for the model potential proposed by Momany *et al.* in their conformation analysis of amino acid crystals.[6] In these authors' model, which will be abbreviated as MCS model hereafter, V_1 is given by the Lennard-Jones 6—12 potential, V_2 by the general hydrogen bond 10—12 potential and V_3 is written in the form including the reciprocal of the effective dielectric constant in place of the convergence factor. All the potential parameters and the atomic charges were taken from the original works.[6]

In the calculation with Sets I and II, the atomic coordinates were taken from the neutron diffraction study for α-glycine crystal[12] and the X-ray analyses for L-alanine[13] and DL-alanine[11,14] crystals. The positions of the hydrogen atoms of alanine were then adjusted by scaling the bond vectors in such a way that the averages of the C–H and the N–H bond lengths in each crystal became equal to those in α-glycine crystal, 1.09 Å and 1.039 Å, respectively. The same coordinates were used in our previous analyses of the crystal vibrations.[1-4] The atomic coordinates for MCS model were calculated from those for Sets I and II in the following two steps. First we shortened the N–H bondlengths of glycine and alanine and the C–H bondlengths of glycine to 1.00 Å without changing the valence angles and the internal rotation angles relevant to these bonds. The lattice constants of α-glycine and L-alanine crystals were next changed from the experimental values to those reported to give the minimum energy of the model potential according to the calculation of Momany *et al.*[6] In this adjustment of the lattice constants, the fractional coordinates of the center of mass of each molecule along the crystal axes were kept unchanged from the experimental values. No adjustment of the lattice constants were made for DL-alanine crystal.

Results and Discussion

The calculated values of the lattice energies, the components of the correction vectors $\boldsymbol{T}^*_{ex}$ and $\Delta\boldsymbol{a}^*$ and the diagonal elastic constants are listed in Tables 1 and 2 for the three sets of potential parameters investigated. The contributions of V_{in} and V_0 to the total energy are very small compared to those of V_{ex}, and may be disregarded at the present level of approximation. In support of the correctness of our

Table 1. Lattice energy, components of Δa^* and T^*_{ex}, and diagonal elastic constants of α-glycine crystal

	Set I		Set I′ [a]	Set II	MCS model[a]
R_{max}[b]/Å	40.0	20.0	40.0	40.0	20.0
K/Å^{-1}	0.05	0.20	0.05	0.05	0.00
V/kJ mol^{-1}	−222.4	−212.4	−203.6	−216.0	−100.3
V_{in}/kJ mol^{-1}	7.8	6.4	8.8	4.3	1.5
V_0/kJ mol^{-1}	3.4	3.4	3.1	4.0	3.5
Δa^*/Å	0.421	0.423	0.109	−0.005	−0.046
Δb^*/Å	0.860	0.930	0.091	0.076	0.065
Δc^*/Å	−0.251	−0.253	0.061	−0.167	0.018
$\Delta\beta^*$/radian	0.029	0.027	0.057	0.054	−0.019
T_1^*/Å	0.044	0.045	0.091	0.016	0.063
T_2^*/Å	0.504	0.494	0.031	0.145	−0.060
T_3^*/Å	−0.507	−0.497	0.007	−0.098	0.008
R_1^*/radian	−0.072	−0.068	0.009	−0.053	0.001
R_2^*/radian	0.063	0.064	0.099	0.076	−0.010
R_3^*/radian	−0.038	−0.036	−0.034	−0.018	0.043
C_{11}/kJ cm^{-3}	42.91	43.02	38.98	54.38	30.30
C_{22}/kJ cm^{-3}	22.71	21.74	22.65	32.88	27.25
C_{33}/kJ cm^{-3}	46.01	45.37	47.41	73.99	69.43
C_{44}/kJ cm^{-3}	7.16	7.16	6.17	7.88	−0.62
C_{55}/kJ cm^{-3}	9.18	8.95	9.35	12.61	11.56
C_{66}/kJ cm^{-3}	4.89	4.62	−13.73	10.61	8.79

a) Non-bifurcated hydrogen bond model. b) The summation limit for V_3.

TABLE 2. LATTICE ENERGY, COMPONENTS OF $\Delta\boldsymbol{a}^*$ AND $\boldsymbol{T}^*_{ex}$, AND DIAGONAL ELASTIC CONSTANTS OF L-ALANINE AND DL-ALANINE CRYSTALS

	L-Alanine			DL-Alanine		
	Set I	Set II	MCS model	Set I	Set II	MCS model
V	−202.8	−194.4	−101.2	−200.5	−192.1	−50.1
V_{in}	11.8	9.3	2.8	7.3	5.7	5.0
V_0	3.3	3.7	3.0	3.2	3.5	3.9
Δa^*	−0.345	−0.267	0.255	0.654	−0.080	1.041
Δb^*	0.892	0.159	−0.076	−0.160	−0.074	−0.577
Δc^*	0.123	−0.029	0.025	−0.045	−0.131	−0.387
T_1^*	0.026	0.035	−0.026	−0.017	−0.013	−0.017
T_2^*	0.097	−0.064	−0.150	0.045	−0.141	−0.265
T_3^*	−0.095	−0.230	−0.060	−0.007	0.029	0.047
R_1^*	0.021	0.018	−0.003	−0.050	−0.018	−0.006
R_2^*	0.008	0.012	−0.039	−0.026	−0.042	−0.046
R_3^*	0.082	0.063	0.034	0.130	0.088	0.097
C_{11}	16.73	17.38	11.00	19.31	25.07	35.13
C_{22}	20.58	27.39	27.69	17.60	18.79	13.62
C_{33}	34.04	44.92	51.94	36.51	46.80	66.77
C_{44}	6.30	5.12	−0.17	10.14	10.24	7.22
C_{55}	6.90	6.48	3.53	11.59	10.84	6.93
C_{66}	6.57	5.24	2.89	6.83	6.05	3.21

The summation limit for V_3 is 40 Å for Sets I and II, and 20 Å for MCS model. K for Sets I and II is 0.05 Å^{-1}. The units are the same as those in Table 1.

algorithm, the lattice energies calculated for MCS model are comparable with those reported by the original authors.[6] Recently, Gaffney *et al.* have estimated the heat of sublimation of glycine into the gaseous zwitterions by adding their mass-spectroscopic data of the heat of evaporation to the *ab initio* energy difference between the classical and the zwitterionic structures.[15] The value of *ca.* 218 kJ mol^{-1} obtained by these authors agrees very well with the lattice energy calculated for both Sets I and II.

The components of $\Delta\boldsymbol{a}^*$ of DL-alanine crystal calculated for MCS model were large because we used the lattice constants not adapted to this model. As to the components of $\boldsymbol{T}^*_{ex}$, MCS model seems to give an excellent result although these degrees of freedom have been left out of consideration by the original authors in determining the potential parameters.[6] MCS model were found, however, to give negative values of the elastic constant C_{44} of α-glycine and L-alanine crystals, failing to keep these crystals stable against the shearing stress along the bc (bc* for α-glycine crystal) plane. In such a case, the correction vectors $\Delta\boldsymbol{a}^*$ and $\boldsymbol{T}^*_{ex}$ indicate the direction of a pathway not toward a minimum but toward a saddle point on the potential supersurface. A large negative value of C_{66} was obtained for α-glycine crystal when the longest hydrogen bond, *i.e.*, one of the bifurcated hydrogen bonds with the bond distance 2.365 Å, was excluded from V_2 of Set I. This hydrogen bond is suggested accordingly to play an important role of stabilizing the crystal against the shearing stress along the ab plane. In a trial calculations without V_2 or V_3, some of C_{11}, C_{22} and C_{33} became negative, indicating that such a model cannot hold the crystal from expansion. The correction vector $\Delta\boldsymbol{a}^*$ of L-alanine calculated for MCS model has a fairly large component despite the use of the energy-minimizing lattice constants reported by Momany *et al.*[6] A possible origin of such a discrepancy between these authors' calculation and the present result is the effect of the microscopic deformation which partly relaxes the macroscopic stress. A slight difference in the assumed molecular geometry or in the scheme of taking the lattice sum may also result in different equilibrium structures.

For each of the three amino acid crystals, the largest of Δa^*, Δb^*, and Δc^* calculated for Set I is positive in sign and is associated with the axis along the longest edge of the unit cell. Since about half of the hydrogen bonds per unit cell of each crystal are roughly directed along this axis, the largest deviation is attributable to deficiency of the potential parameters for the hydrogen bonds. Only worse results were obtained, however, in various trials to adjust the parameters in V_2 or to replace the Lippincott potential by the 10-12 potential. Accordingly, we tried to modify the exp-6 type potential in V_1 related to the N···O contact, for which the original parameters had been estimated from those for the N···N and the O···O contacts involving no hydrogen bonds.[16] After the failure of several attempts to change the depth and the curvature of the potential curve, Set II was obtained by shifting the minimum to the same internuclear distance as that of the 10-12 potential used by Momany *et al.*[6] The revision was readily carried out by expressing the potential in terms of the parameters ε, ρ, and μ introduced by Taddei *et al.*,[17] and changing only ρ from 3.125 Å to 3.500 Å. As seen from Table 1, Set II was successful in confining all the elements

Table 3. Distortions of skeletal deformation coordinates, δ[a] and ρ,[b] and internal rotation coordinates, t[c] (in degree)

		Theor.[d]	Set I[e]	Set II[e]	MCS model[e]
α-Glycine	δ(C′-C-N)	5.65	2.39	1.00	0.54
	δ(O-C′-O)	−6.25	−3.00	−2.61	−1.54
	ρ	2.33	1.75	0.41	0.62
	t(C-C′O_2)	19.15	7.86	−0.29	8.44
	t(C-NH_3)	−2.43	−3.57	−1.73	0.73
L-Alanine	δ(C′-C-N)	4.07	3.22	2.62	1.22
	δ(O-C′-O)	−6.10	−2.96	−2.63	−1.58
	ρ	3.23	2.13	2.25	0.63
	t(C-C′O_2)	−16.95	−11.49	−6.44	−5.10
	t(C-NH_3)	−0.74	−1.98	−1.25	−1.96
	t(C-CH_3)	−1.74	−13.91	−15.25	−7.19
DL-Alanine	δ(C′-C-N)	2.11	2.26	1.69	−1.07
	δ(O-C′-O)	−6.27	−2.04	−2.24	1.08
	ρ	6.22	1.97	2.03	1.14
	t(C-C′O_2)	−14.14	−10.13	−4.92	−2.09
	t(C-NH_3)	−0.73	−0.03	0.75	1.54
	t(C-CH_3)	−6.70	−3.67	−5.01	−6.33

a) The change of the valence angle shown in the parentheses. b) $\rho=(1/2)[\delta(\text{C-C'-O}_t)-\delta(\text{C-C'-O}_c)]$, where O_t and O_c are the oxygen atoms at the trans and the cis positions, respectively, of the nitrogen atom. c) The definition is given in Ref. 7. t(C-C′O_2) is zero when O_c is at the exact cis position of the nitrogen atom. t(C-NH_3) and t(C-CH_3) are zero for the staggered conformations. d) The experimental (X-ray or neutron diffraction) value minus the *ab initio* value. e) The lattice sums for V_3 were taken as in Table 2.

of $\Delta\boldsymbol{a}^*$ and $\boldsymbol{T}^*_{ex}$ within the range between −0.27 Å and 0.16 Å.

Table 3 shows the calculated distortions of the skeletal deformation and the internal rotation coordinates brought about by the balance between the internal and the external forces. The distortions of the stretching coordinates are all smaller than the uncertainty in the corresponding bondlengths reported in the literature on the X-ray analyses,[11-14] and are not given here. For the deformation coordinates, an alternative set of $\boldsymbol{S}^c_{in}$ is available from the crystallographic data[11-14] by subtracting therefrom the theoretical values of the equilibrium structure parameters of the isolated zwitterionic glycine based on an *ab initio* LCMO-SCF method.[18] The signs of all the calculated distortions for Sets I and II agree with those predicted from the combination of the results of the crystallographic and the quantum-mechanical studies. As to the distortions of the internal rotation angles, all the signs calculated for Set I agree with those derived by assuming that the equilibrium structure of the isolated zwitterionic amino acids takes the staggered conformation around the N-C and the (CH_3)-C bonds and the planar conformation around the C-(CO_2) bond. Set II gave the wrong sign to the distortion of the internal rotation angle of the CO_2 group of α-glycine crystal, while MCS model predicted the sign of this distortion of the three amino acids correctly. At present, accuracy of this sort of calculation seems to be far from sufficient for discussing the difference in the molecular structure between L-alanine and DL-alanine crystals.

An iterative search for the minimum of the model potential according to the Newton-Raphson method[19] was carried out by taking the summation limit and the convergence constant for V_3 as 20 Å and 0.20, respectively. This limit was not large enough to disregard the effect of the neglected reciprocal sum, but was chosen in order to save computing time. Whenever the energy did not decrease in a single step, the correction vectors $\Delta\boldsymbol{a}^*$ and $\boldsymbol{T}^*_{ex}$ were multiplied by a damping factor 0.5. The iteration was repeated until all the elements of $\Delta\boldsymbol{a}^*$ and $\boldsymbol{T}^*_{ex}$ became less than 0.001 Å for the length and 0.001 radian for the angle. Set I failed to give any convergence of this procedure for L-alanine, leading to destruction of the crystal with negative infinite energy. Diverging results were obtained for the three amino acid crystals also by using MCS model. The success of this model for α-glycine and L-alanine crystals reported by Momany *et al.*[6] may be ascribed accordingly to the fixing of some degrees of freedom of molecular motions. The calculated equilibrium structures for the converging cases are described in Table 4 in terms of the lattice constants, the coordinates of the centers of masses and the Eulerian angles which define the principal axes of inertia of the molecules with reference to the unit cell axes. The maximum and the average distances between the calculated and the experimental atomic positions are also shown for the sake of comparison. Although the Eulerian angles seem to indicate that the calculated and the experimental orientations of the molecules are quite different from each other, the average deviations of the atomic positions are not too large, expecially for Set II, in comparison with the thermal motions of atoms in usual crystals. It is worth noting that these structures satisfy the equilibrium condition for all the degrees of freedom

TABLE 4. EXPERIMENTAL AND CALCULATED STRUCTURE PARAMETERS[a] AT EQUILIBRIUM

		α-Glycine			L-Alanine		DL-Alanine		
		Obsd	Set I	Set II	Obsd	Set II	Obsd	Set I	Set II
Lattice constants	a/Å	5.105	5.014	5.120	6.032	6.368	12.060	11.574	12.133
	b/Å	11.969	11.991	12.036	12.343	12.127	6.05	6.496	6.204
	c/Å	5.465	5.384	5.569	5.784	5.816	5.82	5.564	5.829
	β/°	111.70	108.65	109.22					
Coordinates of centers of masses	x_g/Å	0.679	0.806	0.769	3.184	3.331	1.621	1.591	1.636
	y_g/Å	1.411	1.299	1.357	1.641	1.642	1.662	1.875	1.619
	z_g/Å	−0.090	−0.060	−0.056	2.702	2.575	1.700	1.627	1.703
Eulerian angles[b]	ϕ/°	8.64	2.62	3.16	31.05	36.33	115.42	144.92	124.77
	θ/°	48.39	47.99	46.40	10.95	9.91	11.96	10.19	11.67
	χ/°	77.64	72.17	73.58	52.57	44.37	120.08	156.84	134.17
Δr/Å[c]	average		0.176	0.132		0.224		0.355	0.127
	max.		0.259	0.218		0.286		0.574	0.204

a) The experimental structures are taken from Refs. 11—13. b) The Eulerian angles are defined according to Ref. 20 with the convention that $I_1 > I_2 > I_3$. c) The distance between the experimental and the calculated atomic positions.

TABLE 5. CO_2 TORSIONAL FREQUENCIES AND LATTICE FREQUENCIES/cm^{-1}

α-Glycine				L-Alanine				DL-Alanine			
Obsd	I	II	MCS	Obsd	I	II	MCS	Obsd	I	II	MCS
	a_g				a				a_1		
194	*194*	*202*	229	190	*190*	219	277	180	*181*	205	262
178	170	184	*177*		160	*185*	*200*	145	141	*170*	193
155	136	164	145	137	130	145	145	115	121	136	*183*
	117	143	119	112	107	129	127	102	93	122	137
109	104	118	95	103	87	84	85		89	79	56
74	74	73	55	47	49	42	34		47	40	21
51	44	68	34		45	37	0		b_1		
	a_u				b_1				*180*	*211*	253
226	*217*	*218*	231	192	*184*	206	*245*	150	137	164	*191*
	139	185	*188*	157	158	*176*	*193*	122	125	141	180
	130	149	146	138	129	151	171	117	111	107	111
	87	122	69	112	102	119	130	90	84	93	89
	66	68	57	103	87	114	106	72	78	77	51
	43	43	10		83	86	91		a_2		
	b_g				b_2			180	*176*	204	248
	208	*210*	230		*193*	*224*	252	160	160	*171*	191
178	166	180	*191*	144	137	162	*181*	145	119	148	*173*
163	134	167	146	112	123	143	137	115	98	111	154
109	122	136	117	86	99	104	117	98	88	105	116
84	99	114	96	73	80	80	80	90	81	84	81
74	83	101	68	48	76	74	65		74	70	54
51	60	75	27		b_3				b_2		
	b_u			190	*199*	*224*	*247*		*190*	*214*	*251*
	210	*225*	230	137	140	169	194	150	136	171	231
175	170	185	*164*	128	130	143	162	115	115	122	143
140	140	167	133	103	112	124	126	98	98	106	105
91	112	137	114	98	105	99	93	90	80	77	74
	83	96	95	47	83	79	64	72	79	74	63

The calculated frequencies to which the CO_2 torsional mode contributes dominantly are shown in italics.

of atomic motions under the influence of the internal and the external forces of the model. The numbers of iterations required to reach the energy minimum were 9 to 10 for Set I and 6 to 7 for Set II, being even smaller than the number of the adjustable parameters in the latter case.

The deviation of the calculated lattice constants from the observed values in Table 4 differs considerably from the initial guess of the corresponding elements of Δa^* in Tables 1 and 2. The inversion of signs is encountered in many cases and the structure of α-glycine crystal can be predicted by Sets I and II equally well after the iteration. Such discrepancies between the initial guess and the final result are attributable to the higher-order elastic constants as well as to the correlation between Δa^* and T^*_{ex}, both neglected in the present treatment.

The calculated and the observed frequencies of the lattice vibrational modes and the CO_2 torsional mode are shown in Table 5. In each symmetry species of the three amino acid crystals, the CO_2 torsional mode is the lowest-frequency internal mode and apts to couple appreciably with the lattice modes. Among the three sets of the potential parameters, Set I gave the closest fit between the calculated and the observed frequencies, and Set II ranks next. There are systematic deviations of the calculated frequencies for Sets I and II toward the lower- and the higher-frequency sides, respectively, of the observed values. For about half the data in Table 5, the observed frequency falls between the corresponding frequencies calculated from these two sets. On the other hand, MCS model failed to reproduce the observed frequencies between 200 and 140 cm^{-1} of L-alanine and DL-alanine crystals, and led to a vanishing frequency in the totally symmetric species of L-alanine. As to the factor group splittings of the deformation modes of the alkyl groups, the results for Sets I and II are essentially the same as those reported previously.[1-3] Compared to these sets, MCS model gave too large splittings of about 30 cm^{-1} for the CH_3 asymmetric deformation mode of DL-alanine crystal, and too small splittings of about 3 cm^{-1} for the CH_2 bending mode of α-glycine crystal. This result seems to reflect the difference in the dependence of $\partial^2 V/\partial^2 r$ on r between the 6-12 and the exp-6 potentials for the H···H contact. By substituting the potential parameters used in this work, we have confirmed that the former falls off more rapidly than the latter in the range between 2.3 and 3.0 Å in which the nearest-neighbor H···H distances of the alkyl groups of α-glycine, L-alanine and DL-alanine crystals are included.

According to the present calculation, the combination of the exp-6 type non-bonded atom-atom interaction potential and the Lippincott type hydrogen bond stretching potential gives more reasonable results with respect to the lattice energy, the crystal structure and the vibrational frequencies of the three amino acid crystals, than the combination of the Lennard-Jones 6-12 type and the 10-12 type general hydrogen bond potential. There is no assurance, however, as to whether the Lippincott potential is the best representation of the hydrogen bond stretching of amino acids in general. Furthermore, our choice of the parameter r^e_{ij}, which is the intrinsic equilibrium distance of the hydrogen bond, in V_2 (2.0 Å)[4] is very different from the original value of Lippincott and Schroeder (0.97 Å),[8b] and is rather similar to the equilibrium distance of the 10-12 general hydrogen bond potential given by Momany *et al.*[6] Further studies on the other amino acid crystals should be carried out extensively in order to settle this controversy.

The numerical calculations were carried out on a FACOM M200 computer at the Data Processing Center of Kyoto University.

References

1) K. Machida, A. Kagayama, Y. Saito, Y. Kuroda, and T. Uno, *Spectrochim. Acta, Part A*, **33**, 569 (1977).
2) K. Machida, A. Kagayama, Y. Saito, and T. Uno, *Spectrochim. Acta, Part A*, **34**, 909 (1978).
3) K. Machida, A. Kagayama, and Y. Saito, *J. Raman Spectrosc.*, **7**, 188 (1978).
4) K. Machida, A. Kagayama, and Y. Saito, *J. Raman Spectrosc.*, **8**, 133 (1979).
5) K. Machida and Y. Kuroda, *Bull. Chem. Soc. Jpn.*, **54**, 1343 (1981).
6) a) F. A. Momany, L. M. Carruthers, R. F. McGuire, and H. A. Scheraga, *J. Phys. Chem.*, **78**, 1595 (1974); b) F. A. Momany, L. M. Carruthers, and H. A. Scheraga, *J. Phys. Chem.*, **78**, 1621 (1974).
7) T. Miyazawa and K. Fukushima, *J. Mol. Spectrosc.*, **15**, 308 (1965).
8) a) E. R. Lippincott, *J. Chem. Phys.*, **21**, 2070 (1953); b) E. R. Lippincott and R. Schroeder, *J. Chem. Phys.*, **23**, 1099 (1955).
9) D. E. Williams, *Acta Crystallogr., Sect. A*, **27**, 452 (1971).
10) F. Bertaut, *J. Phys. Radium*, **13**, 499 (1952).
11) J. Donohue, *J. Am. Chem. Soc.*, **72**, 949 (1950).
12) P. G. Jönsson and Å. Kvick, *Acta Crystallogr., Sect. B*, **28**, 1827 (1972).
13) H. J. Simpson and R. E. Marsh, *Acta Crystallogr.*, **20**, 550 (1966).
14) H. A. Levy and R. B. Corey, *J. Am. Chem. Soc.*, **63**, 2095 (1941).
15) J. S. Gaffney, R. C. Pierce, and L. Friedman, *J. Am. Chem. Soc.*, **99**, 4293 (1977).
16) V. G. Dashevsky, V. T. Struchykov, and Z. A. Akoppayan, *Zh. Strukt. Khim.*, **7**, 594 (1966).
17) G. Taddei, R. Righini, and P. Manzelli, *Acta Crystallogr., Sect. B*, **33**, 626 (1977).
18) Y.-C. Tse, M. D. Newton, S. Vishveshwara, and J. A. Pople, *J. Am. Chem. Soc.*, **100**, 4329 (1978).
19) A. Warshel and S. Lifson, *J. Chem. Phys.*, **53**, 582 (1970).
20) E. B. Wilson, Jr., J. C. Decius, and P. C. Cross, "Molecular Vibrations," McGraw-Hill, New York (1955), Appendix I.

  Bull. Chem. Soc. Jpn., 54, 1354—1359 (1981) [Vol. 54, No. 5

Adsorption of Neutral α-Amino Acids at the Mercury–Aqueous Solution Interface and Hydrophobicity Scales of Amino Acid Side Chains at the Electrified Interfaces

Takashi KAKIUCHI and Mitsugi SENDA*

Department of Agricultural Chemistry, Faculty of Agriculture, Kyoto University, Sakyo-ku, Kyoto 606

(Received December 5, 1980)

The adsorption of glycine, DL-serine, L-threonine, L-asparagine, L-glutamine, L-valine, L-leucine, L-methionine, and L-tryptophan at the mercury-aqueous sodium fluoride solution interface has been studied by measuring differential capacities, potentials of zero charge, pzc, and surface tensions at the pzc. The standard adsorption free energies for these amino acids and for the amino acids previously studied have been used to deduce hydrophobicity scales of amino acid side chains at positively charged, negatively charged, and uncharged interfaces. The hydrophobicity scale at the uncharged interface was basically similar to that of Nozaki and Tanford. When the surface was charged positively, the positions of serine and alanine, and of threonine and α-aminobutyric acid, in the scale were reversed. This reversion was primarily ascribed to the difference in the positions of maximum adsorption potentials between the amino acids with an aliphatic side chain and those with a hydroxyl group in the side chain.

In previous papers we have reported the adsorption properties of four α-amino acids with normal hydrocarbon side chains[1] and of phenylalanines[2] at the mercury–aqueous solution interface. This paper is concerned with the adsorption behavior of nine neutral amino acids, *i.e.*, glycine, DL-serine, L-threonine, L-asparagine, L-glutamine, L-valine, L-leucine, L-methionine, and L-tryptophan, at the mercury–aqueous sodium fluoride solution interface.

The primary interest of this study is to find a hydrophobicity scale of amino acid side chains at the electrified interface. In recent years the electrochemical properties of proteins and enzymes at electrode interfaces have been a subject of intense studies.[3] Increasing attention has also been paid to the behavior of proteins and enzymes at the interfaces of two immiscible liquids. Since every interface is invariably electrified due to electric charges and/or oriented dipoles at the interface and the physicochemical properties of the interface largely depend on its electrical state, the hydrophobicity of amino acid side chains at electrified interface is expected to give important information for understanding electrochemical behavior of proteins and enzymes at such interfaces.

Nozaki and Tanford[5] have proposed a hydrophobicity scale of amino acid side chains based on the solubility measurements of amino acids in water and aqueous organic solvents. Aboderin[6] used the relative mobilities of amino acid derivatives in paper chromatography to estimate the hydrophobicity of amino acid side chains. These hydrophobicity scales resort to the physicochemical properties of amino acids in homogeneous bulk phases. On the other hand, the depression of the surface tension of the air–aqueous solution interface caused by the adsorption of amino acids was used by Bull and Breese[7] as a measure of the hydrophobicity. They found fairly good agreement between their hydrophobicity scale and that of Nozaki and Tanford. In the case of air–solution interfaces, however, it is not feasible to control its electrical state. In contrast, the mercury–aqueous solution interface behaves in a certain range of electrode potential as an ideally polarized electrode having an additional degree of freedom for an electrical variable,[8] which enables us to specify and control accurately its electrical state. In addition, the mercury in contact with aqueous solution provides an electrode surface of hydrophobic nature.[9,10] Therefore, the transfer free energies of amino acids from an aqueous bulk phase to the mercury–aqueous solution interface are expected to serve for a measure to estimate the hydrophobicity of amino acid side chains at electrified interfaces.

Experimental

Reagent grade glycine, DL-serine, L-threonine, L-asparagine, L-glutamine, L-valine, L-leucine, L-methionine, and L-tryptophan were obtained from Nakarai Chem. Co., Japan and were twice recrystallized from aqueous ethanol (for glycine, serine, and threonine) or from triple distilled water (for other amino acids). Sodium fluoride, a standard-reagent-for-analysis grade from Hashimoto Chem. Co., Japan, was used as the base electrolyte without further purification.

Test solutions were deaerated by bubbling purified nitrogen gas through the solution for 30 min and kept under nitrogen atmosphere during the measurement. Electrode potential was measured against a saturated calomel electrode (SCE). Procedures for measuring the potential of zero charge, surface tension at this potential, and double layer capacity for the amino acids at the dropping mercury electrode–aqueous solution interface are described elsewhere.[2] All measurements were made at 25±0.2 °C.

Results

The potentials of zero charge(pzc) and surface tensions at this potential for glycine, DL-serine, L-threonine, L-asparagine, L-glutamine, L-valine, L-leucine, L-methionine, and L-tryptophan in 0.500 mol l^{-1} sodium fluoride are summarized in Tables 1 and 2. The relative surface excesses of the amino acids at the pzc were calculated from the surface tension *vs.* logarithm of the amino acid concentration curves by using the basic electrocapillary equation.[11] Differentiation involved in the calculation was made numerically.[12] We assumed that the activity of sodi-

Table 1. Potentials of zero charge, E_{pzc}, of mercury in contact with aqueous 0.5 mol l^{-1} sodium fluoride solution containing amino acid at 25 °C

c / mol l^{-1}	E_{pzc}/V (*vs.* SCE)								
	Gly	L-Try	DL-Ser	L-Thr	L-Asn	L-Gln	L-Val	L-Leu	L-Met
0.005	—	0.596	—	—	—	—	—	—	—
0.008	—	—	—	—	—	—	—	—	0.449
0.010	—	0.608	0.430	—	0.431	0.432	0.430	0.432	0.450
0.012	—	0.615	—	—	—	—	—	—	—
0.015	—	0.615	—	—	—	—	0.430	0.433	0.452
0.020	—	0.622	0.430	0.431	0.431	0.434	0.430	0.432	0.455
0.025	—	0.620	—	—	—	—	—	0.433	—
0.030	—	0.622	—	—	0.433	0.434	0.428	0.431	0.457
0.040	—	—	0.431	0.431	0.433	0.435	0.431	0.433	0.462
0.050	0.432	—	—	—	—	—	—	0.432	—
0.060	—	—	0.432	0.432	0.435	0.437	0.427	0.432	0.465
0.080	—	—	—	—	—	—	—	—	0.467
0.100	0.432	—	0.433	0.432	0.437	0.439	0.429	—	0.469
0.120	—	—	—	—	0.439	0.440	—	—	0.470
0.150	0.433	—	0.434	0.434	0.442	0.442	0.426	—	0.472
0.200	0.433	—	0.436	0.435	—	0.445	0.423	—	0.473
0.250	—	—	—	—	—	—	0.420	—	—
0.300	0.433	—	0.438	0.437	—	—	0.417	—	—
0.400	0.435	—	0.440	—	—	—	—	—	—
0.500	—	—	—	0.438	—	—	—	—	—
0.600	0.435	—	—	—	—	—	—	—	—
0.700	—	—	—	0.440	—	—	—	—	—
0.800	0.437	—	—	—	—	—	—	—	—
1.000	0.440	—	—	—	—	—	—	—	—

Table 2. Surface tensions of mercury at the potential of zero charge, γ_{pzc}, in contact with aqueous 0.5 mol l^{-1} sodium fluoride containing amino acid at 25 °C

c / mol l^{-1}	γ_{pzc}/mN m^{-1}								
	Gly	L-Try	DL-Ser	L-Thr	L-Asn	L-Gln	L-Val	L-Leu	L-Met
0.005	—	395.3	—	—	—	—	—	—	—
0.008	—	—	—	—	—	—	—	—	424.2
0.010	—	392.4	427.3	—	427.2	426.9	426.8	426.5	423.6
0.012	—	391.6	—	—	—	—	—	—	—
0.015	—	389.8	—	—	—	—	426.7	426.5	422.5
0.020	—	388.4	427.2	427.0	427.2	426.7	426.7	426.3	421.4
0.025	—	387.0	—	—	—	—	—	426.2	—
0.030	—	385.8	—	—	427.1	426.4	426.5	425.8	419.7
0.040	—	—	427.1	426.9	426.9	426.2	426.3	425.7	418.4
0.050	427.1	—	—	—	—	—	—	425.2	—
0.060	—	—	427.1	426.8	426.7	425.7	426.0	425.0	416.2
0.080	—	—	—	—	—	—	—	—	414.5
0.100	427.1	—	427.0	426.7	426.2	424.9	425.5	—	412.9
0.120	—	—	—	—	426.0	424.5	—	—	411.8
0.150	427.2	—	427.0	426.4	425.7	424.0	424.7	—	410.0
0.200	427.1	—	426.9	426.3	—	423.1	423.7	—	407.7
0.250	—	—	—	—	—	—	423.3	—	—
0.300	427.1	—	426.8	426.0	—	—	422.7	—	—
0.400	427.0	—	426.7	—	—	—	—	—	—
0.500	—	—	—	425.3	—	—	—	—	—
0.600	427.0	—	—	—	—	—	—	—	—
0.700	—	—	—	424.5	—	—	—	—	—
0.800	427.0	—	—	—	—	—	—	—	—
1.000	427.0	—	—	—	—	—	—	—	—

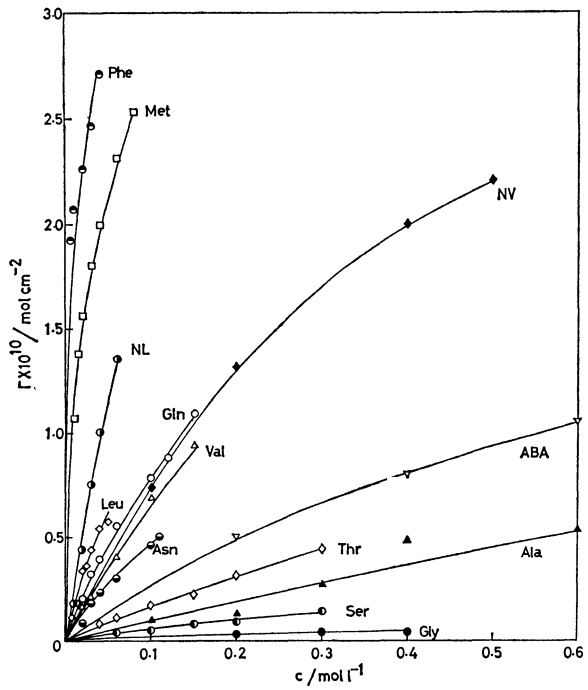

Fig. 1. Adsorption isotherms of amino acids at the mercury–aqueous 0.5 mol l^{-1} sodium fluoride solution interface at the potential of zero charge at 25 °C. See Table 3 for abbreviated name of the amino acids indicated by each line.

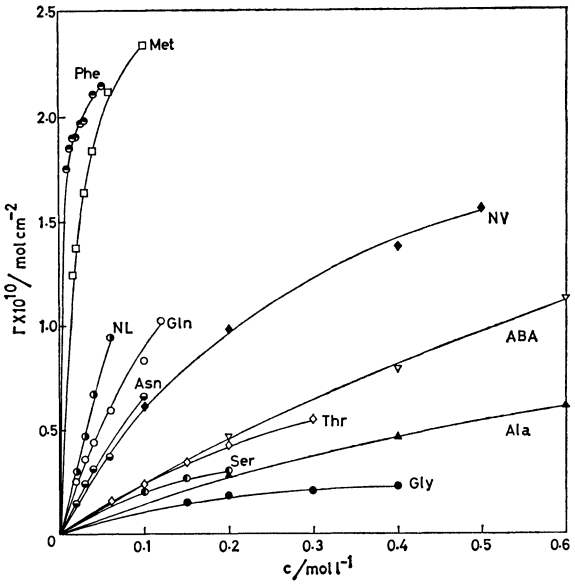

Fig. 2. Adsorption isotherms of amino acids at the positively charged mercury–aqueous 0.5 mol l^{-1} sodium fluoride solution interface (−0.1 V *vs.* SCE) at 25 °C.

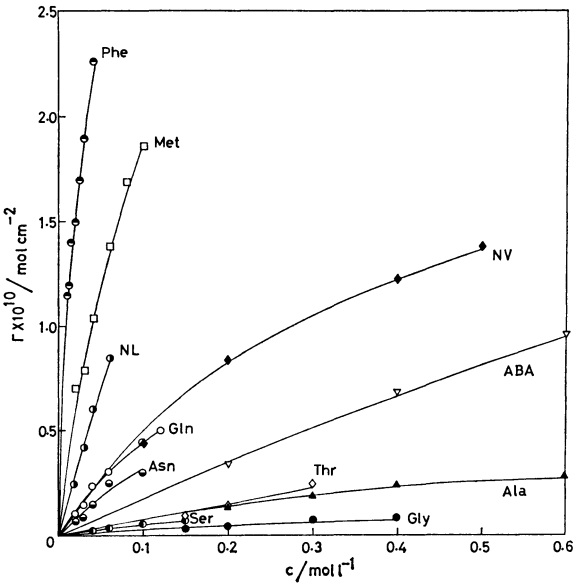

Fig. 3. Adsorption isotherms of amino acids at the negatively charged mercury–aqueous 0.5 mol l^{-1} sodium fluoride solution interface (−0.9 V *vs.* SCE) at 25 °C.

um fluoride and the activity coefficients of amino acids did not change over the experimental range of the amino acid concentration.[13] Figure 1 shows the relative surface excess of the amino acids, except tryptophan, plotted against their molar concentration. The relative surface excess of tryptophan seemed to reach a saturation value already at 0.005 mol l^{-1}, the lowest concentration studied; the surface tension *vs.* logarithm of tryptophan concentration plot was linear between 0.005 and 0.030 mol l^{-1}. The slope of this plot gave a relative surface excess of 2.4×10^{-10} mol cm^{-2} which was in agreement with the maximum surface concentration of 2.5×10^{-10} mol cm^{-2} calculated from a space filling model (CPK) of the tryptophan molecule adsorbed with its aromatic ring plane oriented parallel to the electrode surface. Figure 1 also includes the previous results for DL-alanine, DL-α-aminobutyric acid, DL-norvaline, DL-norleucine,[1] and L-phenylalanine.[2]

In order to obtain the surface excess of the amino acids at the electrically charged interfaces, differential capacities of the interface were measured for glycine, DL-serine, L-threonine, L-asparagine, L-glutamine, and L-methionine as functions of the electrode potential and amino acid concentration. Electrocapillary curves were obtained by numerical integration of the differential capacity *vs.* electrode potential curves and were used to calculate the surface excess of the amino acids at various electrode potentials. We chose for further analysis the electrode surfaces at −0.1 and −0.9 V (*vs.* SCE) as the representatives of positively charged and negatively charged interfaces, respectively. In 0.500 mol l^{-1} sodium fluoride base solution, the surface charge densities at −0.1 and −0.9 V were determined as 8.9 and −9.3 μC cm^{-2}, respectively. The relative surface excesses of the amino acids at −0.1 and −0.9 V are shown in Figs. 2 and 3 as a function of the amino acid concentration. These figures also include the previous results obtained for four aliphatic amino acids[1] and L-phenylalanine.[2]

Since the bulk concentrations of the amino acids used in this study are not high, as much as 1 mol l^{-1} for glycine at the highest, the relative surface excess of the amino acid may be regarded as the surface concentration of the adsorbed amino acid per unit area, Γ, without introducing significant error.[14] Then,

TABLE 3. LIMITING SLOPES OF ADSORPTION ISOTHERMS, $B\Gamma_m$, AND ADSORPTION FREE ENERGIES OF AMINO ACIDS, ΔG_a°, AT POSITIVELY CHARGED(−0.1 V), UNCHARGED(pzc) AND NEGATIVELY CHARGED(−0.9 V) MERCURY-AQUEOUS 0.5 mol l^{-1} SODIUM FLUORIDE SOLUTION INTERFACE AT 25 °C

Amino acids	$B\Gamma_m \times 10^{10}$/cm			$\Gamma_m \times 10^{10}$ c)	ΔG_a°/kJ mol^{-1}		
	−0.1 V	pzc	−0.9 V	mol cm^{-2}	−0.1 V	pzc	−0.9 V
Glycine (Gly)	1.1	0.2	0.3	6.6	4.4	9.0	8.0
DL-Serine (Ser)	2.1	0.6	0.6	5.9	2.6	5.8	6.0
DL-Alanine (Ala)[a]	1.5	1.2	0.7	5.9	3.3	4.0	5.1
L-Threonine (Thr)	2.7	1.8	0.7	4.2	1.1	2.1	4.4
DL-α-Aminobutyric acid (ABA)[a]	2.4	2.7	1.7	5.0	1.8	1.5	2.6
L-Asparagine (Asn)	8.0	5.9	3.7	3.7	−1.9	1.2	0.0
L-Valine (Val)	—	9.8	—	4.3	—	−2.0	—
DL-Norvaline (NV)[a]	6.9	10.2	4.6	4.3[d]	−1.2	−2.1	−0.1
L-Glutamine (Gln)	13.0	13.0	5.6	3.2	−3.5	−3.5	−1.4
L-Leucine (Leu)	—	16.2	—	3.8	—	−3.6	—
DL-Norleucine (NL)[a]	17.5	22.0	15.6	3.8	−3.8	−4.3	−3.5
L-Methionine (Met)	91.5	127.5	36.0	3.7	−7.9	−8.8	−5.6
L-Phenylalanine (Phe)[b]	245	390	127	3.2	−10.7	−11.9	−9.1

a) Data from Ref. 1. b) Data from Ref. 2. c) Calculated from CPK model of amino acid. d) Experimental value from Ref. 1.

the relative surface excess *vs.* concentration curve shown in Figs. 1, 2, and 3 can be considered as the surface concentration *vs.* bulk concentration curves for the amino acids at the pzc, −0.1, and −0.9 V, respectively. In dilute concentration region the adsorption isotherm generally obeyes Henry's law[15]

$$Bc = \Gamma/\Gamma_m, \quad (1)$$

where B is the adsorption coefficient, c the bulk concentration of an adsorbate and Γ_m the maximum surface concentration of an adsorbate. The adsorption coefficient is related to the standard adsorption free energy, ΔG_a°, by

$$-\Delta G_a^\circ = RT \ln B, \quad (2)$$

where R is the gas constant and T the absolute temperature. The standard adsorption free energy in Eq. 2 is defined as the free energy change accompanied with the transfer of an adsorbate from a bulk phase at infinite dilution to an adsorption phase at infinite dilution. In this definition the adsorption free energy of an enantiomer and that of the correponding racemate must be the same[2] and, hence, will not be distinguished hereafter. We graphically evaluated the limiting slopes of the adsorption isotherms, $(\partial\Gamma/\partial c)_{c=0}$, in Figs. 1, 2, and 3 to obtain $B\Gamma_m$. The values are summarized in Table 3. The maximum surface concentrations of amino acids in the fifth column of Table 3 were calculated by using the CPK model of the amino acid molecules adsorbed with their side chains oriented parallel to the electrode surface. The ΔG_a° values evaluated from these data by using Eq. 2 are given in the last three columns in Table 3.

Discussion

The standard adsorption free energies for glycine and a series of aliphatic α-amino acids, alanine, α-aminobutyric acid, norvaline, and norleucine, at the pzc are plotted in Fig. 4 against the number of carbon atom in the side chain, n. The linear plot in Fig. 4 provides an experimental basis for dividing the standard adsorption free energy of an α-amino acid into two contributions, a contribution from a zwitterion group and that from a side chain group. The decrement of ΔG_a° per one methylene group in the side chain was found to be 2.9 kJ mol^{-1}. This may be comparable with 3.3 kJ mol^{-1} [16] obtained for the adsorption of normal aliphatic alcohols at the mercury–aqueous solution interface and 3.1 kJ mol^{-1} [17] for the adsorption of normal aliphatic acids at the copper–aqueous solution interface.

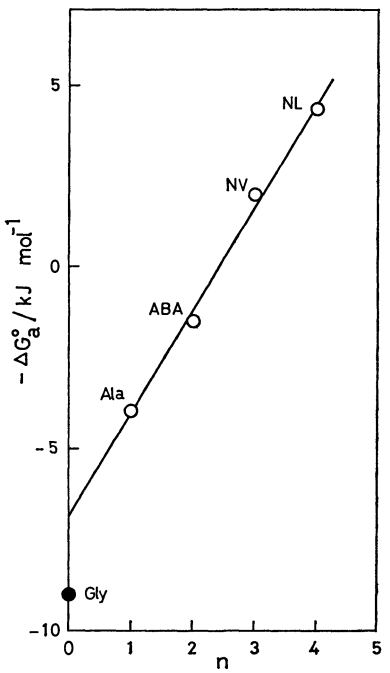

Fig. 4. Standard adsorption free energies of normal aliphatic α-amino acids and glycine as a function of the number of carbon atom, n, in the side chain.

TABLE 4. TRANSFER FREE ENERGY OF AMINO ACID SIDE CHAIN, $\Delta G^{\circ}_{a,s}$, FROM AQUEOUS BULK PHASE TO THE MERCURY–AQUEOUS SODIUM SULFATE SOLUTION INTERFACE AT 25 °C AS A HYDROPHOBICITY SCALE OF AMINO ACID SIDE CHAINS ON POSITIVELY CHARGED(−0.1 V), UNCHARGED(pzc), AND NEGATIVELY CHARGED(−0.9 V) INTERFACES

Amino acid side chains	$-\Delta G^{\circ}_{a,s}$/kJ mol^{-1}		
	−0.1 V	pzc	−0.9 V
Serine	1.8	3.2	2.0
Alanine	1.1	5.0	2.9
Threonine	3.3	6.9	3.6
α-Aminobutyric acid	2.6	7.5	5.4
Asparagine	6.3	7.8	8.0
Valine	—	11.0	—
Norvaline	5.6	11.1	8.0
Glutamine	7.9	12.5	9.4
Leucine	—	12.6	—
Norleucine	8.2	13.3	11.5
Methionine	12.3	17.8	13.6
Phenylalanine	15.1	20.9	17.1

The transfer free energy of an amino acid side chain from aqueous bulk phase to the interface, $\Delta G^{\circ}_{a,s}$, was calculated by subtracting ΔG°_{a} for glycine from ΔG°_{a} for each amino acid. Table 4 summarizes the $\Delta G^{\circ}_{a,s}$ values thus estimated at the pzc, −0.1 V and −0.9 V (*vs.* SCE). These series of the transfer free energies of the side chains may be regarded as interfacial hydrophobicity scales at electrified interfaces. The major trend in the series of $\Delta G^{\circ}_{a,s}$ at the uncharged interface (at the pzc) is essentially similar to that found by Nozaki and Tanford,[5] as illustrated in Fig. 5 in which $\Delta G^{\circ}_{a,s}$'s at the pzc are plotted against the transfer free energies of amino acid side chains from water to organic solvents, ΔG°_{tr}.[5] As seen in this figure serine, threonine, alanine, valine, leucine, and norleucine fall around the straight line of unit slope.

There are, however, a few facts in Table 4 and Fig. 5 which do not conform to the results by Nozaki and Tanford. In their scale, threonine is less hydrophobic than alanine whereas the converse is true in the interfacial hydrophobicity scale at the pzc. Introduction of a hydroxyl group into a hydrocarbon side chain decreases the hydrophobicity of the side chain by 1.8 kJ mol^{-1} (for an alanine and serine pair) and 0.6 kJ mol^{-1} (for an α-aminobutyric acid pair). These values are appreciably smaller than 3.4 kJ mol^{-1} estimated by Nozaki and Tanford[5] as a contribution of a hydroxyl group to the transfer free energy. At the interface the hydroxyl group of serine or threonine is probably only partially dehydrated because a part of the adsorbed molecule should be exposed to the aqueous phase, whereas on transfer of the molecule from water to nonaqueous solvent the hydroxyl group must completely be dehydrated and surrounded by nonaqueous medium. Table 4 also shows that glutamine is more hydrophobic than asparagine. This is contrary to the result obtained by Nozaki and Tanford who found that glutamine was apparently

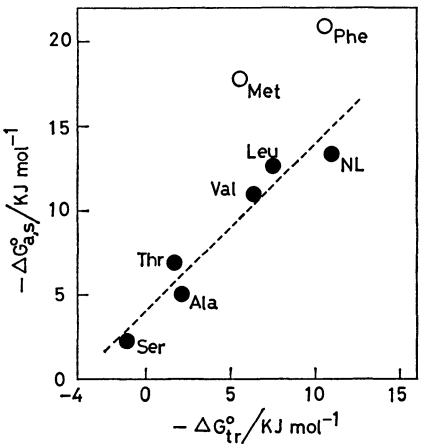

Fig. 5. Plot of the free energies of transfer of amino acid side chains from aqueous bulk phase to the uncharged mercury surface in contact with aqueous phase, $\Delta G^{\circ}_{a,s}$, against the free energies of transfer of amino acid side chain from aqueous bulk phase to pure organic solvents, ΔG°_{tr}, taken from Ref. 5.

less hydrophobic than asparagine. They have suggested that the formation of an intramolecular hydrogen bond in asparagine molecule in nonaqueous phase is responsible to the abnormal position of asparagine with respect to glutamine in their hydrophobicity scale. In adsorption layer asparagine molecules will not form an intramolecular hydrogen bond but remain to hold hydrogen bonding with adjacent water molecules. Figure 5 shows that methionine and phenylalanine have higher values of $\Delta G^{\circ}_{a,s}$ than those expected from the line of unit slope. Since sulfur atom has strong affinity with mercury,[18] such a chemical interaction should be involved in the observed high surface activity of methionine. Phenylalanine interacts with mercury surface through not only the hydrophobic interaction but also the charge transfer interaction due to π-electron in the aromatic ring.[2] Specific interaction also seems to exist between the amide group in asparagine and the mercury surface. Among the amino acid side chains studied only asparagine side chain showed higher surface activity at the negatively charged surface than at the pzc.

Table 4 shows that when the mercury surface is charged either positively or negatively, $\Delta G^{\circ}_{a,s}$'s for all the amino acid side chains but asparagine side chain at −0.9 V are increased; their surface activity becomes lower when the surface comes to bear excess charges. The change of $\Delta G^{\circ}_{a,s}$ with the change of the electrical state of the interface is illustrated in Fig. 6 for ten amino acid side chains. The effect of electrode charge on $\Delta G^{\circ}_{a,s}$ for alanine, α-aminobutyric acid, norvaline, and norlecuine, which we refer as group I, is appreciably asymmetrical with respect to the pzc, but the effect is almost symmetrical for serine and threonine (group II). This difference in the dependence of $\Delta G^{\circ}_{a,s}$ on electrode charge between groups I and II causes the reversion of the mutual positions of serine and α-alanine, and of threonine and α-aminobutyric acid in their interfacial hydrophobicity scale at the positively charged electrode surface.

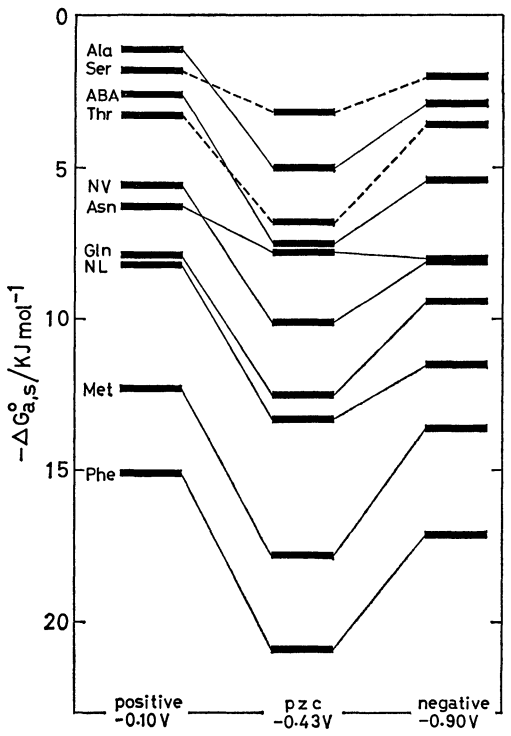

Fig. 6. Schematic representation of the change of the interfacial hydrophobicity of amino acid side chains with the change of the electrical state of the mercury–aqueous 0.5 mol l^{-1} sodium fluoride solution interface at 25 °C.

According to the theory of Frumkin[19] and Butler[20] on the adsorption of organic compounds at electrified interface, the dependence of the adsorption free energy, ΔG°_{a}, of an organic compound on electrode potential is described by

$$\Delta G^{\circ}_{a} = \Delta G^{\circ}_{a,max} + RT\alpha(E-E_{max})^2, \quad (3)$$

where $\Delta G^{\circ}_{a,max}$ is ΔG°_{a} at $E=E_{max}$, E the electrode potential, E_{max}, the electrode potential at which the adsorption maximum occurs, and α the constant represented by

$$\alpha = \frac{C_0-C_1}{2RT\Gamma_m}. \quad (4)$$

In Eq. 4 C_0 is the double layer capacity in the absence of adsorption ($\theta=0$) and C_1 is the double layer capacity at the full coverage of the electrode with adsorbate ($\theta=1$). The maximum adsorption potential in Eq. 3 is given by[21]

$$E_{max}-E^{\circ}_{pzc} = \frac{C_1(E^{\theta=1}_{pzc}-E^{\circ}_{pzc})}{C_1-C_0}, \quad (5)$$

where $E^{\theta=1}_{pzc}$ and E°_{pzc} are the potentials of zero charge at $\theta=1$ and $\theta=0$, respectively.

In view of Eqs. 3, 4, and 5, the difference in the effect of the electrode potential on $\Delta G^{\circ}_{a,s}$ between groups I and II is probably due primarily to the different values of E_{max} for groups I and II. Group II seems to have E_{max} values around the pzc, whereas the E_{max} values for group I seem to be located in more negative potential region with respect to E°_{pzc}. The presumption of $E_{max}-E^{\circ}_{pzc}<0$ for group I implies[1] that water dipoles are oriented with their negative end pointing toward the electrode surface,[9,10] because in this group the effective dipole moment of the side chain should be small, if any. The more positive E_{max} for group II compared with that of group I indicates the orientation of the hydroxyl group dipole with its negative end pointing toward the electrode surface.

According to Eqs. 3 and 4, the change of $\Delta G^{\circ}_{a,s}$ with the change of the electrical state of the interface depends also on the magnitude of the double layer capacities of the interface. The double layer capacities in the presence and absence of the adsorption are generally a function of the electrical state of the interface due to the change in the orientation mode of adsorbed molecules as well as solvent molecules in the compact layer of the double layer with the change of the electrical state.[22] Therefore, the change of the capacities may partly contribute to the observed dependence of $\Delta G^{\circ}_{a,s}$ on the electrical state of the interface.

References

1) T. Kakiuchi and M. Senda, *J. Electroanal. Chem. Interfacial Electrochem.*, **88**, 219 (1978).
2) T. Kakiuchi and M. Senda, *Bull. Chem. Soc. Jpn.*, **54**, 535 (1981).
3) M. Senda, T. Ikeda, K. Kakutani, H. Kinoshita, and K. Kano, *Bioelectrochem. Bioenerg.*, in press.
4) I. R. Miller and D. Bach, "Surface and Colloid Science," ed by E. Matijevic, John Wiley & Sons, New York (1973), Vol. 6, p. 185.
5) Y. Nozaki and C. Tanford, *J. Biol. Chem.*, **246**, 2211 (1971).
6) A. A. Aboderin, *Int. J. Biochem.*, **2**, 537 (1971).
7) H. B. Bull and K. Breese, *Ach. Biochem. Biophys.*, **161**, 665 (1974).
8) D. C. Grahame, *Chem. Rev.*, **41**, 441 (1947).
9) S. Trasatti, *J. Electroanal. Chem. Interfacial Electrochem.*, **33**, 351 (1971).
10) A. Frumkin, B. Damaskin, N. Grigoriev, and I. Bagotskaya, *Electrochim. Acta*, **19**, 69 (1974).
11) D. M. Mohilner, "Electroanalytical Chemistry," ed by A. Bard, Marcel Dekker, New York, (1966), Vol. 1, p. 241.
12) P. R. Mohilner and D. M. Mohilner, "Computer in Chemistry and Instrumentation," ed by J. S. Mattson, H. B. Mark, Jr., and H. C. MacDonald, Jr., Marcel Dekker, New York (1971), Vol. 2, p. 3.
13) A. DeBattisti and S. Trasatti, *J. Electroanal. Chem. Interfacial Electrochem.*, **54**, 1 (1974).
14) B. B. Damaskin, O. A. Petrii, and V. V. Batrakov, "Adsorption of Organic Compounds on Electrodes," Plenum Press, New York (1971), Chap. 1.
15) Ref. 14, p. 86.
16) Ref. 14, p. 165.
17) R. O. Loutfy, *J. Electroanal. Chem. Interfacial Electrochem.*, **41**, 27 (1973).
18) R. Parsons, *Proc. R. Soc. London, Ser. A*, **261**, 70 (1961).
19) Ref. 14, Chap. 3.
20) J. A. V. Butler, *Proc. R. Soc. London, Ser. A*, **122**, 399 (1929).
21) M. Senda and I. Tachi, *Rev. Polargr. (Kyoto)*, **10**, 79 (1962).
22) B. B. Damaskin and A. N. Frumkin, *J. Electroanal. Chem. Interfacial Electrochem.*, **34** 191 (1972).

The Effect of Iron(III) on the Cadmium Ion-selective Electrode

Sachiko SAKURA*,† and Rauno VIRTANEN

Chemical Laboratory, Technical Research Centre of Finland, Biologinkuja 7, SF-02150, Espoo 15, Finland

(Received March 7, 1980)

Iron(III) interferes with the operation of a cadmium, lead and copper ion-selective electrode. The cadmium ion-selective electrode (CdS/Ag_2S) showed a potential shift to the positive direction of more than 100 mV for a decade change of iron(III) concentration. However, the exact mechanism for this interference is not known, though it is expected to be the oxidation of sulfide ion by Fe(III). The mechanism of interference by iron(III) was studied by using the cadmium ion-selective electrode, flow-through cell, pH buffer solutions, potentiometric titrations, and atomic absorption spectrophotometry measurements. It was found that iron(III) promotes dissolution reaction of cadmium ions from the solid cadmium sulfide electrode and that flow conditions of samples have no effect on the iron(III) interference.

An important group of ion-selective electrodes is composed of metal sulfide membranes such as pure silver sulfide or silver sulfide mixed with other metal sulfides (*e.g.* CuS, PbS, CdS).[1] As a rule, these electrodes are interfered with by ions which can react with the membrane. For example, Ag^+ and Hg^{2+} interfere with the determination of Cu^{2+} with CuS/Ag_2S membrane electrode. Other interference is caused by the dissolution of the membrane to form a soluble complex with some ion in the membrane. For example, the cyanide ion interferes with all silver salt membranes. Actually, silver salt membranes can be used as cyanide ion selective electrode on the basis of this phenomenon. Another kind of interference is caused by oxidizers. For example, iron(III) oxidizes sulfide ions on the electrode membrane and thus affects the membrane potential.

The effect of oxidation by iron(III) on CdS/Ag_2S electrode has been noted by Brand *et al.*,[2] Mascini and Liberti,[3] and Kivalo *et al.*[4] In the case of PbS/Ag_2S electrode, the potential of PbS electrode changed about 59 mV by a decade change in the iron(III) concentration.[5] By the use of a reductant, iron(III) interference could be eliminated in low level analysis of copper(II) ion with CuS/Ag_2S electrode.[6] The effect of iron(III) on mixed sulfide electrode (CuS/Ag_2S) was used for quantitative determination of iron(III) in the range of (10^{-5}—10^{-2}) M (1 M=1 mol dm^{-3}) iron(III).[7] Kivalo *et al.* measured the interference of iron(III) on PbS/Ag_2S electrode,[8] and Bixler *et al.* found a large interference of iron(III) on Ag_2S electrode.[9]

Under different oxidizing conditions without iron(III), Johansson and Edström discussed corrosion of CuS/Ag_2S electrode.[10]

The purpose of this work is to study the mechanism of oxidation by iron(III) on the CdS/Ag_2S membrane, by measuring the rate of oxidation reaction by iron(III), the effect of pH buffer solution, the concentration of iron(III), and the amount of Cd(II) which was dissolved from CdS-membrane.

Experimental

Equipment. The electrodes used were Orion cadmium electrode 94-48A (CdS/Ag_2S) and Orion double junction reference electrode 90-02. Potentials were measured with an Orion 801A digital pH/mV-meter and recorded with a Goerz Servogor RE 511 strip chart recorder. The stabilization of electrode potential was followed with the aid of the chart recorder. Potential measurements were made either in a dip cell or in a thermostated flow-through cell (Fig. 1), both at 298 K.

Measurements in the Dip Cell: The dip cell was a polyethylene vessel with volume of 2000 cm^3. The solution was stirred at constant speed with a teflon propellor.

Measurements in the Flow-through Cell: The reference electrode was dipped in the outlet of the sample solution about 10 cm from the cadmium ion-selective electrode. Flow rate was from 0 $cm^3\ min^{-1}$ to 45.1 $cm^3\ min^{-1}$. Possible streaming potential was checked by using two calomel electrodes, one in the place of the indicator electrode and the other in the place of the reference electrode. No streaming potential developed in the flow-through cell, at any flow rate, in the solutions at pH 2, 3, or 5, either in the presence or in the absence of iron(III).

Cadmium ions dissolved from CdS was determined by an Hitachi model 518 atomic absorption spectrophotometer equipped with a cadmium hollow cathode lamp (229.0 nm).

Solutions. Chemicals used were of analytical purity. The ionic strength of solutions was adjusted to 0.1 M. The pH was adjusted with buffers (pH 2; potassium chloride

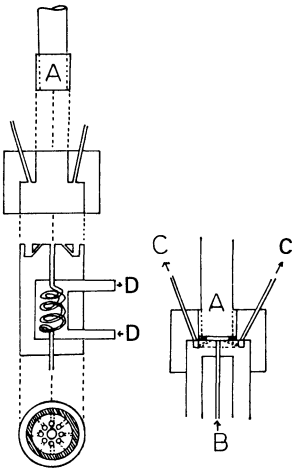

Fig. 1. The flow-through cell.
A: Cadmium ion-selective electrode, B: inlet of the solution, C: reference electrode and outlet of the solution, D: water to control the temperature (298 K).

† Present address: Department of Chemistry, Faculty of Medicine, Hamamatsu University School of Medicine, Hamamatsu 431-31.

and hydrochloric acid, pH 3 and 5; potassium phthalate) or by nitric acid and potassium hydroxide (unbuffered solutions). The cadmium and iron(III) salts used were nitrates. Powder cadmium sulfide was the guaranteed reagent by Nakarai Co. Ltd.

Results

Figure 2 showed the results of the effect of iron(III) in the dip cell at buffered pH 2. The very severe effect of iron(III) is noticeable from the slope (115 mV for a decade change of iron(III) concentration). The selectivity coefficient for iron(III) of the cadmium electrode ($K=[Cd^{2+}]/[Fe^{3+}]^{2/3}$) was determined with the mixed solution method with constant activity of Cd^{2+} and varying activity of Fe^{3+} similar to the method recommended by IUPAC.[11] At pH 2, the value of K was 46 $mol^{1/3}\,dm^{-1}$. And iron(III) began to interfere at concentrations of about 10^{-6} M. Table 1 shows the numerical values of the dip cell measurements at pH 2, 3, and 5 (all were buffered solutions). As the pH decreased, the effect of iron(III) became more severe. This pH effect is attributed to the increase of the activity of free iron(III) ion with decreasing pH.

The interference of iron(III) still remained at pH 5 ($K=7.8$ $mol^{1/3}\,dm^{-1}$), although a large decrease in interference could be expected on the ground of pH change. At pH 5 the ratio of free iron(III) to the hydroxide complex is only $10^{-3.7}$ in the absence of other ligands except OH^-.[12]

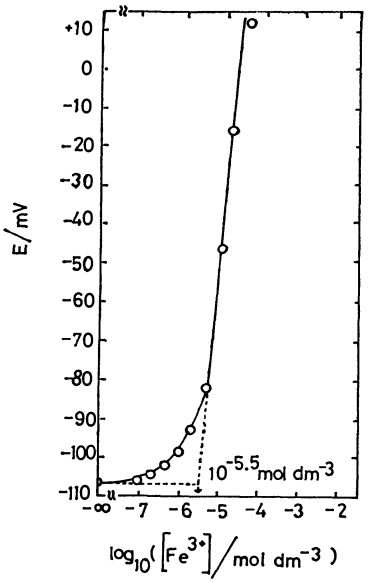

Fig. 2. The effect of iron (III) on the cadmium electrode in the dip cell in pH 2 buffered solution. Concentration of Cd^{2+} was 10^{-2} M.

Table 1. The effect of pH on the interference of iron(III) on the cadmium electrode potential in the dip cell (10^{-2} M Cd^{2+})

pH	Slope / mV	$[Fe^{3+}]$[a] / mol dm^{-3}	K[b] / $mol^{1/3}\,dm^{-1}$
5.0	37.5	4.57×10^{-5}	7.8
3.0	125.0	1.59×10^{-5}	16
2.0	115.0	3.16×10^{-6}	46

a) Concentration at the break point.[11] b) Selectivity coefficient, $K=[Cd^{2+}]/[Fe^{3+}]^{2/3}$.

In the dip cell measurement, if the electrode was dipped in the iron(III) solution for a short time, the response time[11] (the time until the change of potential is less than 1 mV min^{-1}) was short (about 1 or 2 s), although the change of the potential to the positive direction was large.

When the electrode was kept in 10^{-6} M iron(III) solution for a few seconds then rinsed by water, and the potential was measured in 10^{-2} M cadmium(II) solution, the potential was 10 mV lower than expected. When the electrode was polished with three successively finer grades of aluminium oxide (The German earth clay Nos. 1, 2, and 3, Jean Wirtz, Düsseldorf), it recovered.

If the electrode was kept some minutes in iron(III) solution (10^{-6} to 10^{-4} M), its potential in 10^{-2} M Cd^{2+} solution was found to have risen considerably, sometimes over 200 mV. And the response time[11] was very long (10 to 20 min). Slight polishing did not restore the potential to its original level. It was only after repeated polishing that the anomaly was removed. This result suggests that iron(II) has an interference effect on the deep interior of the CdS electrode membrane.

Measurements in the Flow-through Cell. The flow-through cell was used to study the effect of the flow conditions of the sample solution. Flow conditions are more easily and reproducibly effected in a flow-through cell than in the dip cell. The flow rate had no effect on the potential in the presence and absence of iron(III), either at buffered or unbuffered pH solution. The response time was as long as 120—150 min in the case of unbuffered pH 2 with 10^{-4} M iron(III). The response time at buffered pH 5 with 10^{-4} M iron(III) was also long (30—60 min). These results suggest that the oxidation of CdS is not controlled by the flow conditions in the solution, but by the reaction in the inside of solid CdS electrode.

The effect of iron(III) on the cadmium electrode was tested in buffered and unbuffered solutions at different pH at a fixed flow rate (5 cm^3/min). The concentration of Cd^{2+} was 10^{-3} M. Figure 3 shows that at pH 2, the effect of iron(III) on the potential was very pronounced both in buffered and unbuffered solutions, though in buffered solution the effect started at about 10 times lower concentration. At pH 5 there was no interference in unbuffered solution, but in buffered solution interference began at 10^{-5} M iron(III). The behaviour is the same as in the dip-cell experiments, *i.e.* buffering of solution preserves the attack by iron(III) on the membrane even at higher pH-values. It seems that by complex formation of phthalate ion with iron(III), iron(III) is still kept in solution even at pH 5 and the penetration of iron(III) into CdS electrode is easy. In fact, in unbuffered solution at pH 5 incipient precipitation of $Fe(OH)_3$ could be seen and no interference of iron(III) was observed.

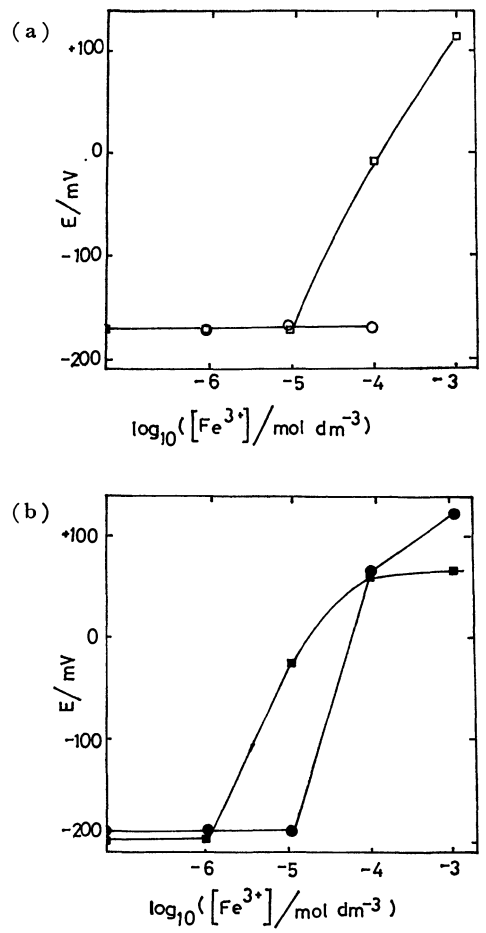

Fig. 3. The effect of iron(III) on the cadmium electrode in the flow-through cell, at pH 2 and pH 5. Concentration of Cd^{2+} was 10^{-3} M. Flow rate: 5 cm^3/min. (a): In unbuffered solution. □: pH 2, ○: pH 5. (b): In buffered solution. ■: pH 2, ●: pH 5.

Potentiometric Titrations and Atomic Absorption Spectrometry (AAS) Measurements. To determine whether the oxidation of CdS by iron(III) takes place, a suspension of CdS powder (guaranteed CdS was commercially obtained or wet CdS was obtained by freshly precipitation from equivalent $Cd(NO_3)_2$ and Na_2S) was titrated by iron(III) using platinum electrode. Titrations were performed in a nitrogen atomosphere. No noticeable oxidation of CdS took place, regardless of whether the CdS powder was dried or freshly precipitated. Obviously the oxidation of CdS by iron(III) is slow. On the other hand, the same titration curve of S^{2-} by iron(III) was obtained as was given in Ref. 13. Oxidation of S^{2-} by iron(III) takes place rapidly and quantitatively.

To measure the dissolution of Cd^{2+} from CdS, CdS powder was mixed with a deaerated solution; after one day the solution was filtered, and the concentration of cadmium in the filtrate was measured. If iron(III) was involved, fairly large amounts of Cd^{2+} were found in pH 2 solution (both for buffered and unbuffered solutions). Even in buffered pH 5 solution, a considerable amount of Cd^{2+} was found in the filtrate, though in unbuffered pH 5 solution, the dissolved Cd^{2+} in the presence of iron(III) was found to be just the same as in the absence of iron(III). The fact that a considerable amount of Cd^{2+} from CdS was found in buffered pH 5 solution in the presence of iron(III) supports the assertion that iron(III) and phthalate ion form stable complexes which remain in the solution.

Discussion

If oxidation of cadmium sulfide by iron(III) takes place according to the following reaction:

$$2Fe^{3+} + CdS \longrightarrow Cd^{2+} + S + 2Fe^{2+} \quad (1)$$

the equilibrium constant is obtained to be 2.1×10^{14}, by calculating from various standard potentials.[14] The reaction proceeds completely to the right. The equilibrium constants for the oxidation of different sulfides, calculated by reactions analogous to (1), are as follows: PbS, 5.5×10^{13}; CuS, 18; and Ag_2S, 7.1×10^{-9}. Ignoring kinetic aspects, one may thus deduce that interference of iron(III) is most pronounced at a CdS/Ag_2S electrode and least pronounced at a pure Ag_2S electrode.

From Table 1, the change of the potential for a decade change of iron(III) concentration at pH 2 was 115 mV in the case of cadmium electrode. The value of this slope is remarkably larger than those in the cases of lead or copper electrodes (59 mV for the lead electrode[5] and 25 mV for the copper electrode[7]).

In the case of a copper ion-selective electrode, it is reported that the potential drifts in the negative direction after prolonged use in high concentrations of iron(III).[7] When the cadmium electrode was dipped in lower concentrations of iron(III) for a short time, the potential drifted in the negative direction like a copper electrode. When the cadmium electrode was kept in high concentrations of iron(III) for a few minutes, the potential drifted in the positive direction; extended polishing was needed to remove the anomaly. These facts support the conclusions that reaction(1) takes place and suggest that the iron(III) exerts an influence on the deep interior of the electrode membrane, according to the dipping time and concentration of iron(III).

This oxidation reaction(1) was not controlled by the flow conditions of iron(III); the reaction rate was very slow and the reaction proceeded even with the complexed iron(III).

The authors would like to express their thanks to Prof. Dr. Pekka Kivalo, chief director of the Finnish Technical Inspectorate, former head of Chemical Laboratory of the Technical Research Centre of Finland, for his helpful suggestions and for arranging this work and to Mr. Tauno Mikkola for his kindly preparing the flow-through cell. The authors would also like to express their thanks to Prof. Dr. Norio Ichinose for his kind offer of the atomic absorption spectrophotometer. This work is supported in part by the Grant-in-Aid for Scientific Research from the Finnish Ministry of Education.

References

1) K. Cammann, "Das Arbeiten mit ionenselektiven Elektroden," Springer-Verlag, Berlin (1977), Vol. 2, p. 73.
2) M. J. D. Brand, J. J. Militello, and G. A. Rechnitz, *Anal. Lett.*, **2**, 523 (1969).
3) M. Mascini and A. Liberti, *Anal. Chim. Acta*, **64**, 63 (1973).
4) P. Kivalo, R. Virtanen, K. Wickström, M. Wilson, E. Pungor, K. Toth, and G. Sundholm, *Anal. Chim. Acta*, **87**, 387 (1976).
5) M. Mascini and A. Liberti, *Anal. Chim. Acta*, **60**, 405 (1972).
6) M. J. Smith and S. E. Manahan, *Anal. Chem.*, **45**, 836 (1973).
7) Y. Fung and K. W. Fung, *Anal. Chem.*, **49**, 497 (1977).
8) P. Kivalo, R. Virtanen, K. Wickström, M. Wilson, E. Pungor, G. Horvai, and K. Toth, *Anal. Chim. Acta*, **87**, 401 (1976).
9) J. W. Bixler, R. Nee, and S. P. Perone, *Anal. Chim. Acta*, **99**, 225 (1978).
10) G. Johansson and K. Edström, *Talanta*, **19**, 1623 (1972).
11) IUPAC, "Recommendations for Nomenclature of Ion-selective Electrodes," *Pure Appl. Chem.* **48**, 127 (1976).
12) A. Ringbom, "Complexation in Analytical Chemistry," Interscience Publishers, New York (1963), p. 356.
13) F. A. Cotton and G. Wilkinson, "Advanced Inorganic Chemistry," 3rd ed, Interscience, New York (1972), p. 864.
14) W. M. Latimer, "Oxidation Potentials," 2nd ed, Prentice-Hall, Inc., New York (1952).

A Sensitive Atomic Absorption Spectrometric Method for Copper Employing the Direct Introduction of Chelating Resin into a Carbon Tube Atomizer

Akinori Isozaki,* Naoki Soeda, and Satori Utsumi

Department of Industrial Chemistry, College of Science and Technology, Nihon University, 1-8-14, Kanda-Surugadai, Chiyoda-ku, Tokyo 101

(Received May 14, 1980)

A new and simple method for the determination of ppb levels of copper by electrothermal atomic absorption spectrometry was established. The main feature of the proposed method is that chelating resin, a preconcentration agent for copper, is introduced directly as a "resin-suspension" into the carbon tube atomizer without drying and weighing of the resin. To a 250 cm^3 sample solution containing up to 1.0 μg of copper, 0.10 g of chelating resin (below 400 mesh) is added, and the mixture is stirred for about 20 min. After the separation of the resin from the aqueous phase through a membrane filter, 5.0 cm^3 of resin-suspension is prepared by adding water to the resin. Then, 10 μdm^3 (resin: 0.2 mg) of the suspension is introduced into an atomizer, and the copper peak-height is measured under the optimum operating conditions. The calibration graph was linear over the concentration range from 0.1 ppb to 4.0 ppb of copper. The relative standard deviation was 2.3% from 10 repeated measurements; a mean value of 1.08 ppb copper was obtained for a sea water sample.

Atomic absorption spectrometry with an electrothermal atomizer and a deuterium background corrector is today an useful analytical tool: the determinations of trace metal elements in both liquid and solid samples can be carried out rapidly and easily. The direct analysis of a solid sample has been applied to biological tissues[1,2] and plastic containers.[3]

Chitosan,[4] a natural chelating polymer with anion-exchange behavior, has been used for the separation of transition elements from alkali and alkaline-earth salts. By combining the concentration of vanadium (VO_3^-) on chitosan with the direct introduction of its powder into the atomizer, Muzzarelli *et al.*[5] proposed a sensitive method for the determination of vanadium in sea water; however, the method requires the drying and weighing of VO_3-adsorbed chitosan powder. Atomization methods which use direct heating of the metal-adsorbed ion-exchange resin have also been examined as ways to determine copper[6] and mercury[7] concentrations; these methods make it possible to analyze an extremely dilute solution, but the precisions are not satisfactory.

For the preconcentration and separation of trace metal ions in sample solution, the chelating resin[8] has been used because of its selectivity in forming stable chelates: for instance, Sato *et al.*[9] proposed a determination method for copper by Flameless A. A. S. which included preliminary treatment by the resin.

The present authors[10] have briefly reported a determination method for copper in which chelating resin was introduced as a "resin-suspension" into a carbon tube atomizer, after the adsorption of copper ions on it under a batchwise operation. Highly purified chelating resin contains no copper, and its smoke does not affect the value of the atomic absorption of copper or the base line. The method does not require drying and weighing of the resin, nor elution of copper from the resin. We did some experiments on the effect of foreign ions on the method: magnesium and calcium ions in as small an amount as 0.1 ppm caused lower results for the atomic absorption of copper. It was found that the interferences of these ions can be eliminated by adding cobalt nitrate to the sample solution; there will be no adsorptions of these ions on the resin.

The proposed method for the determination of copper in a matrix of chelating resin was studied in detail and applied to determine copper ion concentrations in water samples.

Experimental

Apparatus. A Nippon Jarrell-Ash FLA-100 carbon tube atomizer was used in conjunction with a Nippon Jarrell-Ash Model AA-8500 two channel atomic absorption spectrophotometer. A single-element copper hollow cathode lamp (Hamamatsu TV. Co. L-233) was employed as a light source, and peak-heights were recorded with a Rikadenki Co. B-34 recorder. Resin-suspension was injected into the atomizer by using a micropipette (Eppendorf Co. Model 3130) fitted with disposable plastic tips. A centrifuge tube (volume: 15 cm^3) with a glass stopper was used, and a 5.0 cm^3 mark was etched on the tube.

Reagents. All chemicals were of super-special grade. Deionized water was passed through a column packed with Chelex-100 (NH_4-form, 50—100 mesh) prior to use.

Standard Copper Solution: The copper stock solution (1000 ppm) was made by dissolving 0.5000 g of copper metal grain (99.99% purity) in nitric acid and then diluting to 500 cm^3 with water. The working solutions were prepared by diluting the stock solution properly.

Chelating Resin: Chelex-100 (Bio-Rad laboratories, Richmond, Calf., Na-form) prepared to grain size below 400 mesh was used. After the removal of fine particles in the resin by decantation, 500 cm^3 of 2 mol dm^{-3} hydrochloric acid was added to about 50 g of resin in a beaker. The mixture was stirred for about 30 min, and the resin was washed with water by decantation. Then, 500 cm^3 of 4 mol dm^{-3} ammonia water was added to the resin, and the mixture was stirred for 2 h. The resin was filtered through a glass filter (3G4), washed with water, and dried in vacuum for four hours at 60 °C.

Ammonium Tartrate Solution (10%): Ammonium tartrate was dissolved in water to give a 20% solution. The solution was passed through a column packed with Chelex-100 (NH_4-form), and diluted to 10%.

Buffer Solution: 0.8 mol dm^{-3} sodium acetate solution was purified by use of Chelex-100 (Na-form), and diluted to 0.4 mol dm^{-3}. 0.2 mol dm^{-3} acetic acid-sodium acetate solution was used as a buffer solution (pH: 4.7),

Cobalt Nitrate Solution (2.5%): 5.0% cobalt nitrate solution was purified by use of Chelex-100 (Co-form), and diluted to 2.5%.

Water Samples. Samples were acidified to about pH 2 with nitric acid, and stored in polyethylene bottles.

Analytical Procedure. To a sample solution (250 cm^3) containing less than 1.0 μg of copper, 5 cm^3 of 2.5% cobalt nitrate solution and 10 cm^3 of 10% ammonium tartrate solution are added. The solution is adjusted to about pH 5 with (1+10) ammonia water and acetic acid, and 5 cm^3 more of buffer solution is added to the solution. Then, 0.10 g of chelating resin is added to the solution, and the mixture is stirred for 20 min by a magnetic stirrer. After the resin has been separated from the mixture through a membrane filter (pore size: 2.0 μm) or glass filter (3G4), the resin is transferred into a centrifuge tube by using about 10 cm^3 of water and the tube is centrifuged. The supernatant liquid is decanted, being careful to leave the resin in the tube, and 5.0 cm^3 of "resin-suspension" is prepared by adding water to the resin in the tube. Then, 10 μdm^3 (resin: 0.2 mg) of the suspension, which has been mixed thoroughly to prepare a uniformly suspended solution, are introduced into a carbon tube atomizer. The atomic absorption of copper, its peak-height, is measured under the instrumental operating conditions shown in Table 1.

Table 1. Instrumental operating conditions

Operating step	Current A	Time s	Mode	Final temp °C
Drying	35	20	Ramp	*ca.* 300
Ashing	110	60	Ramp	*ca.* 1200
Atomization	250	10	Flash	*ca.* 2500

Wavelength: 324.75 nm, lamp current: 5 mA, argon gas flow rate: 3 dm^3/min, damping: 1, sensitivity: 0.

The calibration graph was linear over the concentration range from 0.1 ppb to 4.0 ppb of copper. It was confirmed by using standard copper solution that the copper ions in a sample solution (250 cm^3) are almost all adsorbed by the chelating resin (resin-suspension: 5.0 cm^3) under the conditions of this procedure; that is, the concentration ratio is found to be about 50:1.

Results and Discussion

Ashing of Chelating Resin. Figure 1 shows the typical profiles of absorption for copper-adsorbed resin and copper-free resin in a carbon tube under the instrumental operating conditions. In the case of copper-adsorbed resin, the first peak appeared in an ashing step owing to a smoke evolution of the resin, and then the second peak, which is based on the atomization of copper, was obtained. In copper-free resin, although the first peak appeared as before, there were neither the second peak nor any absorption by the deuterium lamp during the atomization step. Therefore, no correction is necessary for background absorption in measuring the second peak.

The Effect of Ashing Current. Figure 2 shows the effect of ashing current on the absorbance of copper. In the case of copper-adsorbed resin, the absorbance at an ashing current of 70 A was higher than those at the current range from 100 to 130 A, and the absorbance at 140 A was lower. The increase of absorbance at 70 A is due to an absorption by smoke evolution of the resin resulting from an incomplete ashing. This is seen by observing that the copper-free resin also has an absorption at the same current. On the other hand, the decrease of absorbance at 140 A is due to the loss of copper by its partial volatilization during the ashing step; in the case of an aqueous solution, the absorbance of copper also shows a similar decrease. As shown in Table 1, an ashing current of 110 A was adopted before the atomization step. It was observed that the resin acts as a sensitizer for copper during the atomization step; that is, the absorbance of copper-adsorbed resin at an ashing current of 110 A increases about 35% in comparison with that of copper in an aqueous solution. Similar sensitization was observed when a fine activated carbon was added instead of the resin to the aqueous solution. Yoshimura and Noda[11] have reported that an activated carbon is effective for the deoxidation of metal oxides (Cu_2O, CuO, PbO_2, ZnO, ZnO_2) in the direct atomization of these oxides during the flame A. A. S.

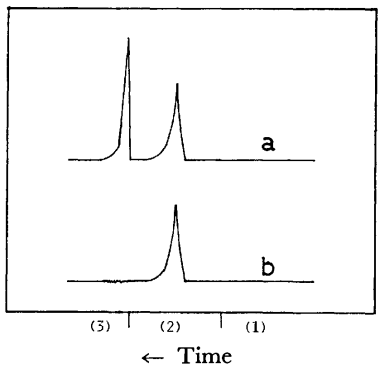

Fig. 1. Typical profiles of absorption for copper-adsorbed resin and copper-free resin.
(a): Cu-adsorbed resin (b): Cu-free resin (1): Drying, (2): Ashing, (3): Atomization.

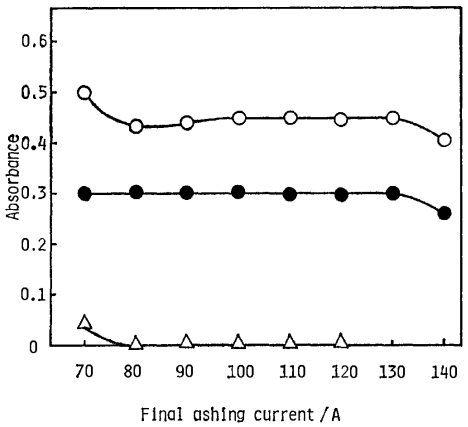

Fig. 2. Effect of ashing current on absorbance of copper.
Resin-suspension: 0.10 g/5 cm^3 H_2O, injecting volume: 10 μdm^3. ○: Cu-adsorbed resin (Cu: 0.75 μg), △: Cu-free resin, ●: aqueous soln (Cu: 0.75 μg/5 cm^3).

The Effect of the Amount of Chelating Resin and of the Stirring Time. We examined the effects of the

amount of chelating resin and of the stirring time in the procedure on the adsorption of copper on the resin. Since the absorbance of copper gave a constant value for amounts from 0.05 to 0.50 g, 0.10 g of the resin was added to a 250 cm^3 sample solution. Stirring for 20 min by a magnetic stirrer was sufficient to allow copper and cobalt ions to be adsorbed on the chelating resin from a sample solution. The resin transformed into NH_4-form was used in the procedure, because the rate of adsorption for copper ion on NH_4-form resin was faster than that on H-form resin.

The Effect of the Amount of Cobalt. Chelex-100[8] has a very strong attraction for transition metals. The selectivity series for cations in an acetate buffer system at pH 5 is:

$$Hg^{2+} > Cu^{2+} \gg Pb^{2+} > Ni^{2+} > Co^{2+} > Mn^{2+} \gg Mg^{2+} = Ca^{2+} \gg Na^{+} > NH_4^{+} > H^{+}.$$

In general, when a large amount of cobalt ion exists in a sample solution containing the resin, magnesium or calcium ions are not adsorbed by the resin, but a small amount of copper ion is quantitatively adsorbed by it. From some experiments, the addition of 5.0 cm^3 of 2.5% cobalt nitrate solution to a 250 cm^3 sample solution showed satisfactory results for copper ions in the presence of about 100 ppm of magnesium ions.

The Effect of PH on the Adsorption of Copper. As is seen in Fig. 3, the absorbance (△) decreased appreciably with the increase in pH, because of incomplete adsorption of copper due to the formation of hydrolysis products such as $Cu(OH)^+$ or $Cu(OH)_2$. The absorbance (●) also decreased as the pH increased from 4 to 7, but those at pH 9 and 10 increased again through the formation of ammine complexes such as $[Cu(NH_3)_4]^{2+}$. The absorbance (○) gave a constant value over the pH range from 2.5 to 10, because the hydrolysis of copper was prevented by the addition of 10 cm^3 of 10% ammonium tartrate solution. The effect of pH on the adsorption of cobalt ion was also examined: the amount of cobalt ion adsorbed by the chelating resin gave a maximum and constant value over the pH range from 4 to 7. Therefore, the buffer solution with pH 4.7 was used in the procedure.

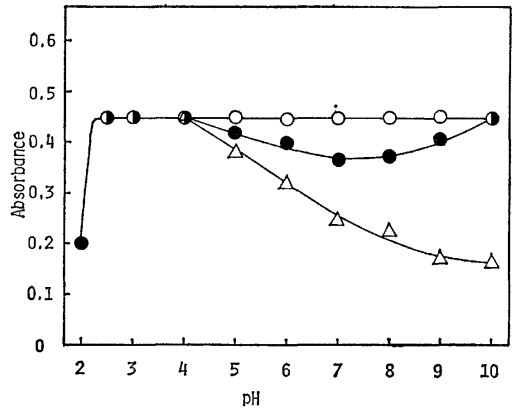

Fig. 3. Effect of pH on the adsorption of copper. Cu: 0.75 μg/250 cm^3, reagents used for pH adjustment; ○: CH_3COOH, NH_3–water, $(NH_4)_2C_4H_4O_6$, ●: CH_3COOH, NH_3–water, HNO_3, △: CH_3COOH, NaOH.

The Effect of Foreign Ions. The effect of foreign ions on the procedure were examined under the presence of 3.0 ppb copper ion, both in the case of the addition of a cobalt nitrate solution and in the case of no such addition. The experimental results are given in Table 2. When the cobalt nitrate solution was not added to a sample solution, strontium, iron(II) and chromium(III) ions in small amount such as 1 ppm gave lower results for the absorbance of copper. Further, magnesium and calcium ions interfered remarkably even at 0.1 ppm. On the other hand, the addition of a cobalt nitrate solution was found to be very effective in eliminating the interferences of these ions. Most anions did not interfere, even when 1000 ppm of them were present, regardless of the presence or absence of cobalt ion during the procedure.

Table 2. Effect of foreign ions

Ion	Proposed method		Without Co^{2+}	
	Amount/mg	Absorbance	Amount/mg	Absorbance
—	—	0.450	—	0.450
Na^+	2500	0.455	250	0.438
K^+	2500	0.445	250	0.439
Mg^{2+}	250	0.460	0.0025	0.449
Ca^{2+}	250	0.458	0.0025	0.446
Sr^{2+}	250	0.447	0.025	0.436
Ba^{2+}	250	0.449	0.25	0.447
Fe^{2+}	250	0.459	0.025	0.452
Mn^{2+}	250	0.452	250	0.442
Ag^+	250	0.455	250	0.458
Al^{3+}	250	0.451	2.5	0.441
Cr^{3+}	0.25	0.452	0.025	0.452
Zn^{2+}	25	0.445	25	0.449
Pb^{2+}	2.5	0.443	2.5	0.455
Hg^{2+}	25	0.449	25	0.454

Copper ion: 0.75 μg, Sample volume: 250 cm^3.
The amount of foreign ions means the amount of those ions which does not show any deviation larger than the error allowed(of ±3%) from the absorbance(0.450) of copper.

Table 3. Analytical results of copper in various water samples

Sample	Cu added / ppb	Cu found / ppb
Town water; Chiyoda-ku, Tokyo (Feb. 12, 1980)	—	3.40
River water; Kamuiwatsuka-river Hokkaido (Aug. 15, 1979)	—	3.36
Sea water;[a]		
Aburatsubo-bay	—	1.08
Kanagawa Pref. (Nov. 24, 1979)	1.0	2.07
Deionized water[b]	—	0.12

a) Sample was taken about 2 km away from the coast.
b) Sample volume taken: 1000 cm^3.

The Determination of Copper in Various Water Samples. The results obtained by the procedure for water samples are shown in Table 3. The mean copper content of a sea water sample was 1.08 ppb from 10 repeated measurements and the relative standard deviation was 2.3%. The content was also confirmed by adding known amounts of copper to the sea water; good recovery of these amounts was achieved. Some experiments were performed on different volumes (100, 500, 1000 cm^3) of a sample solution containing 0.75 μg of copper ions; these absorbances of copper agreed, within the experimental error allowed, with that obtained by use of a sample volume of 250 cm^3. The proposed method is therefore applicable to the determination of copper ions in water samples over a wide concentration range. That is, the content of a deionized water used in this laboratory was determined to be 0.12 ppb by using a 1000 cm^3 sample volume instead of 250 cm^3 as in the standard procedure.

In addition, it is possible to increase the apparent sensitivity for the determination of copper by changing the volume (5.0 cm^3) of resin-suspension or the volume (10 μdm^3) injected into the atomizer. The procedure is relatively simple to use, and few chemicals are required. The proposed technique may be applied not only to the determination of copper, but also to that of other metals at ppb levels.

References

1) L. Gillis and J. Gillis, *Talanta*, **21**, 257 (1974).
2) K. Fujiwara, Y. Umezawa, Y. Numata, K. Fuwa, and S. Fujiwara, *Bunseki Kagaku*, **26**, 735 (1977).
3) P. Girgis-Takla and I. Chroneos, *Analyst (London)*, **103**, 122 (1978).
4) R. A. A. Muzzarelli, "Natural chelating polymers," Pergamon, Oxford (1973), p. 144.
5) R. A. A. Muzzarelli and R. Rocchetti, *Anal. Chim. Acta*, **70**, 283 (1974).
6) K. Nakano, T. Takada, and T. Kakuta, *Bunseki Kagaku*, **28**, 325 (1979).
7) K. Nakano, T. Takada, and K. Fujita, *Chem. Lett.*, **1979**, 869.
8) "Separating metal using Chelex-100 chelating resin," Bio-Rad laboratories product information (1976).
9) A. Sato, T. Oikawa, and N. Saitoh, *Bunseki Kagaku*, **24**, 584 (1975).
10) A. Isozaki, N. Soeda, T. Okutani, and S. Utsumi, *Nippon Kagaku Kaishi*, **1979**, 549.
11) C. Yoshimura and Y. Noda, *Nippon Kagaku Kaishi*, **1978**, 561.

Sublimation Behavior of Tris(2,2,6,6-tetramethyl-3,5-heptanedionato)lanthanoid(III)

Ryohei Amano,* Akiko Sato,** and Shin Suzuki**

School of Paramedicine, Kanazawa University, Kodatsuno 5, Kanazawa 920

***The Research Institute for Iron, Steel and Other Metals, Tohoku University, Katahira 2, Sendai 980*

(Received June 20, 1980)

Two fundamental experiments (to determine vapor pressures and vacuum sublimation-recrystallizing temperature zones) were undertaken on a series of remarkably volatile and thermally stable lanthanoid(III) chelates of 2,2,6,6-tetramethyl-3,5-heptanedione ($Ln(thd)_3$) in order to obtain information about their sublimation behavior. Vapor pressures of these chelates were measured from 100 to 150 °C by means of a modified Knudsen effusion technique. Vacuum sublimation-recrystallizing temperatures were determined by using a sublimation apparatus with a continuous temperature gradient along its sublimation tube. The obtained enthalpies of sublimation were classified into three groups (La to Gd, Tb and Dy, and Ho to Lu), and the vacuum sublimation-recrystallizing temperature zones were divided into two sets (La to Tb, and Dy to Lu). The Tb and Dy chelates were also found to change thermally from a dimeric form to a monomeric form at a definite temperature. These results are explained in terms of the two different crystallizing forms of $Ln(thd)_3$ chelates. Furthermore, the regularity in their sublimation behavior is discussed as a function of the atomic numbers of the lanthanoid metals, using thermochemical considerations.

The volatile lanthanoid chelates of 2,2,6,6-tetramethyl-3,5-heptanedione are very useful as gasoline antiknock additives and catalysts for the removal of carbon deposits,[1] and as sources of metal chelate vapors.[2] They are also useful in trace metal analysis by gas chromatography and sublimatography.[3–5] It is therefore important to study the thermal properties of these chelates over a wide temperature range. Sicre *et al.* have determined the vapor pressures of the $Ln(thd)_3$ chelates (Ln=lanthanoid ion, thd=2,2,6,6-tetramethyl-3,5-heptanedione) by means of the isoteniscope technique over the temperature range of 150 to 250 °C and have mentioned the regularity in their thermochemical behavior.[4] Radiochemical studies on the $Ln(thd)_3$ and $An(thd)_n$ (An=actinoid ion) have been carried out by vacuum sublimation method; their sublimation-recrystallizing temperature zones were found to be in the range of 70 to 150 °C.[6] These vacuum sublimatographic results prompted us to study the vapor pressures of these chelates over the temperature range lower than 150 °C.

A modified Knudsen effusion method has been chosen for the measurements of vapor pressures of $Eu(thd)_3$ and $^{243}Am(thd)_3$ chelates over a relatively low temperature range (100—150 °C).[7] This technique was found to be effective for a highly specific radioactive compound.

In the present study, the vapor pressure were determined as a function of temperature for 13 $Ln(thd)_3$ chelates by means of the Knudsen effusion technique, and their vacuum sublimation-recrystallizing temperatures were also determined by a sublimation apparatus with a continuous temperature gradient. Our purpose was to find what regularity might exist in the sublimation behavior. Some aspects of the sublimation behavior of $Ln(thd)_3$ chelates will be also discussed.

Experimental

Preparation of $Ln(thd)_3$ Chelates Labeled with Radioisotope. The purified lanthanoid oxides (99.9%) of La_2O_3, Pr_6O_{11}, Sm_2O_3, Eu_2O_3, Gd_2O_3, Tb_4O_7, Dy_2O_3, Ho_2O_3, Er_2O_3, Tm_2O_3, Lu_2O_3, and Y_2O_3 were each dissolved in a concentrated nitric acid solution. This was heated almost to dryness, then diluted with distilled water to make each stock solution. The gadolinium chloride of the radioisotope ^{153}Gd was purchased from The Radiochemical Centre (England). Other radioisotopes of ^{140}La, ^{142}Pr, ^{147}Nd, ^{153}Sm, ^{152}Eu, ^{160}Tb, ^{159}Dy, ^{166}Ho, ^{169}Er, ^{170}Tm, ^{169}Yb, and ^{177}Lu were produced from an (n,γ) nuclear reaction by irradiating each lanthanoid oxide with thermal neutrons in the reactor of Kyoto University. Yttrium radioisotope ^{88}Y was produced from a (γ,n) reaction by bremsstrahlung which was performed by using the LINAC of Tohoku University. Each radioisotope was dissolved in a minimum amount of concentrated nitric acid. Each radioisotope solution was added into the above stock solution of the same lanthanoid ion to make each solution be labeled with a radioisotope. The metal concentration and specific radioactivity of the solution were 10^{-2}—10^{-1} M and 10^{-3}—10^{2} μCi/μg of Ln, respectively.

The lanthanoid chelates, $Ln(thd)_3$, were prepared by the method of Eisentraut and Sievers[3] with a slight modification. The Ln nitrate solution (0.002 mol) labeled with radioisotopes was heated to dryness. The residue was dissolved in a minimum amount of 99% methanol, and pH of the resultant solution was adjusted between 3 and 5 by dropwise addition of 2 M NH_4OH solution. A solution of Hthd chelating agent (0.006 mol) in 10 ml of 99% methanol was then added to the above solution. The mixture was adjusted to the desired pH. The precipitate was filtered off, dried in a desiccator, then purified by recrystallization from chloroform and by two vacuum sublimations.

Vapor Pressure Measurements. Vapor pressures of the $Ln(thd)_3$ chelates were measured by a modified Knudsen effusion method. The major modifications from the normal Knudsen effusion method were as follows: (1) the $Ln(thd)_3$ chelate sublimated was collected stepwise at each temperature; (2) the amount of chelate on a collecting foil was determined by a radioactivity measurement. This method has the advantage that the spurous effluents caused by decomposition of the sample and/or volatile impurities have no corresponding lanthanoid metal and will not be counted. The relation between the amount of collected $Ln(thd)_3$ and the collecting time at a given temperature was linear

beyond 5 min, as previously described in a preliminary work on the vapor pressure measurement of Eu(thd)$_3$ chelate.[7] The effusion rate of each Ln(thd)$_3$ chelate was determined from more than 4 weight-time data points at each temperature. For example, a series of measurements at the intervals of 5, 15, 8, and 10 min was carried out at the same temperature.

The Knudsen cell was made of 18-8 stainless steel, nearly cylindrical, 1.3 cm high, and 1.2 cm in diameter. Orifice parameters were photographed and measured on a microscope. An orifice with an area of 0.0021 cm^2 and a height of 0.032 cm was used.[8] The cell was attached to the bottom of a molecular still of the cold-finger type. The glass still with the above effusion cell was connected to a vacuum system. The pressure inside the vacuum line, as measured by a penning gauge, Daia Vacuum Engineering Model CT-2P, fell below 1×10^{-3} Torr (1 Torr=133.3224 Pa) within 30 s. The cell containing each Ln(thd)$_3$ chelate sample was heated by an oil bath, whose temperature was measured by a standard thermometer. The difference in temperature between the oil bath and the cell was calibrated by simultaneous measurement of the temperature of another cell within an enclosed thermometer in the same oil bath.

The effusion cell was loaded with 50 mg of sample, transported into the still, and evacuated to a vacuum of 1×10^{-5} Torr. The cell containing the sample chelate was exposed to the argon atomosphere. After the cell was heated for 1 h at a constant temperature in an argon atomosphere, it was evacuated. The effusion chelate gas collected on a water-cooled Al foil for more than 5 min. Effusing of the chelate gas was stopped by introducing argon into the vacuum line. The temperature of the oil bath and the collecting time of chelate gas were recorded. The collecting foil was replaced with a new aluminum foil.

The above procedure was repeated for a series of collecting intervals at a given temperature; the same repetitions were applied to various temperatures.

The collecting foil was dissolved in diluted hydrochloric acid. Radioactivity of each lanthanoid solution was measured by a NaI(Tl) scintillation counter, or by a Ge(Li) semiconductor detector. By using the specific radioactivity of the sample, the total weight of the collected chelate on the foil, W, was calculated. The rate of sublimation, m, is obtained by dividing the total weight of the collected chelate by the area of the orifice, the collecting time, and the Clausing factor: *i.e.* $m=W/atK$, where a is the area of the orifice, t is the collecting time, and K is the Clausing factor.[8]

Measurements of Vacuum Sublimation-recrystallizing Temperatures. A schematic drawing of the vacuum sublimation apparatus for the measurement of the vacuum sublimation-recrystallizing temperatures of the Ln(thd)$_3$ chelates is shown in Fig. 1. The apparatus has the advantage that the continuous temperature gradient along the sublimation tube can be obtained by sliding a electric furnace gently (1 °C/cm) or steeply (10 °C/cm) along the outer porcelain tube (5.8 cm in outer diameter and 166 cm in length), which consists of a copper tube (1.6 cm in outer diameter and 180 cm in length) covered with air and aluminum. The sublimation tube for introducing Ln(thd)$_3$ sample (10 mg) was evacuated to 1—10×10^{-3} Torr, and placed in a definite position inside the sublimation apparatus. This had been heated and held at 180 °C before inserting the sublimation tube. The temperature gradients along the sublimation tube at various elapsed times are shown in Fig. 2. The sublimation of all Ln(thd)$_3$ chelates was carried out for 2 h under the above conditions. The radioactivity of the sublimate was

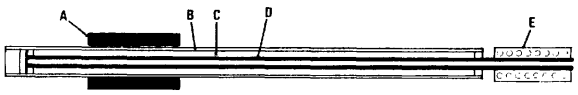

Fig. 1. Vacuum sublimation apparatus with continuous temperature gradient.
A: Electric furnace, B: outer porcelain tube, C: enclosed air and Al foil, D: copper tube, E: cooler.

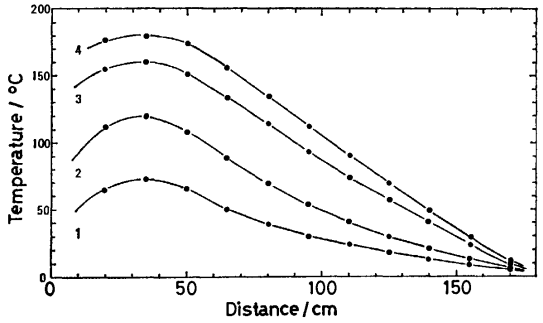

Fig. 2. Temperature gradient along vacuum sublimation tube at elapsed time.
1: 10 min, 2: 20 min, 3: 35 min, 4: 60—120 min.

scanned along the sublimation tube by sliding it on the lead slit of a NaI(Tl) scintillation detector. The highest temperature of the deposition zone on the wall of the sublimation tube was taken as a relative measure of the vacuum sublimation-recrystallizing temperature.

IR and X-Ray Powder Diffraction Measurements. IR spectra of the Ln(thd)$_3$ chelates were obtained with a JASCO Model DS-701G spectrometer in the range of 4000 to 400 cm^{-1} by using the KBr pellet technique. X-Ray powder diffraction data were taken with nickel-filtered Cu $K\alpha$ radiation and recorded with a Rigaku Denki Diffractometer.

Results and Discussion

The rate of sublimation of each Ln(thd)$_3$ chelate was constant for collecting times longer than 5 min at a given temperature. Figure 3 shows that the relationship in the Eu(thd)$_3$ chelate between the weight of the collected chelate and the collecting time is linear at each temperature, and the slope of the straight lines is given as the apparent rate of sublimation of the Eu chelate. A slight amount of the collected chelate was easily measured by the radioactive tracer technique.[7] The rate of sublimation of each Ln(thd)$_3$ chelate was obtained over the temperature range of 100 to 150 °C

Vapor pressure, P, is calculated from the rate of sublimation, m, according to the following equation:[8]

$$P = m\{(2\pi RT)/M\}^{1/2}, \quad (1)$$

where R is the gas constant; T, the absolute temperature of the sample; M, the molecular weight of the effusing gas. The units of m and P were chosen in g/(cm^2 s) and Torr, respectively (1 Torr=133.3224 Pa). The equation

$$P = 17.144\times m(T/M)^{1/2} \quad (2)$$

is obtained. The vapor pressures of each Ln(thd)$_3$ chelate were fitted to the following equation:

$$\log P = -(A/T) + B \quad (3)$$

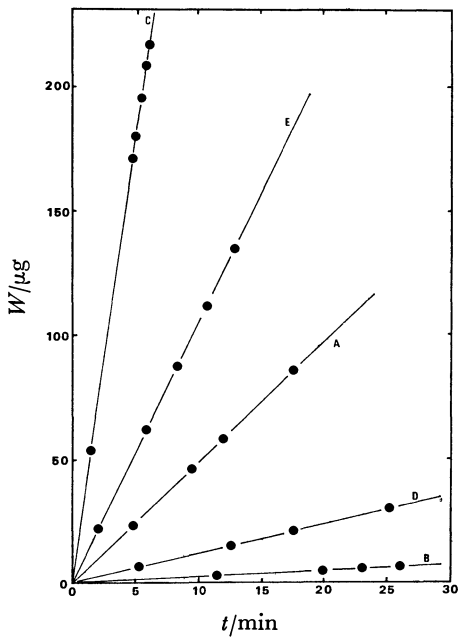

Fig. 3. Relation between amounts of collected Eu(thd)$_3$ chelate and collecting times at various temperatures.
A: 125.4 °C, B: 103.7 °C, C: 140.8 °C, D: 115.2 °C, E: 131.1 °C.

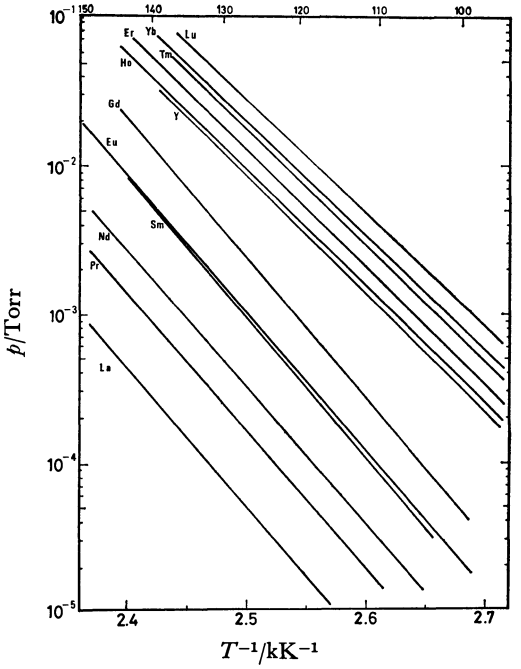

Fig. 4. Clausius-Clapeyron plots 11 Ln(thd)$_3$ and Y(thd)$_3$ chelates.

by a least square method. Heats of sublimation, ΔH_T, and entropies of sublimation, ΔS_T, were taken by equating the above experimental equation to the thermochemical equation

$$\ln(P/760) = (\Delta H_T - T\Delta S_T)/(-RT). \quad (4)$$

Thus, $\Delta H_T = 2.303 \times AR$ and $\Delta S_T = 2.303 \times R$(B-log 760) were obtained.

The Clausius-Clapeyron plots of a series of Ln(thd)$_3$ (expect Tb(thd)$_3$ and Dy(thd)$_3$) and Y(thd)$_3$ chelates are shown and compared in Fig. 4. Table 1 summarizes the thermochemical constants obtained. The plots of the Tb and Dy chelates were found to break at definite temperatures. The vapor pressures of these two chelates were measured in more detail in the temperature-descending process (160→100 °C), and the temperature-ascending process (100→160 °C). Figure 5 shows the Clausius-Clapeyron plots obtained in both processes for these chelates. Table 2 gives their thermochemical constants. The vapor pressures of the Ln(thd)$_3$ chelates have been found to increase with atomic number of lanthanoid ion, according to Sicre *et al.*[4] Figure 4 shows the same phenomena. The enthalpies of sublimation of the chelates of La to Gd, and Ho to Lu are slightly different from those of Sicre *et al.*

However, the Clausius-Clapeyron plots obtained in the temperature-ascending process of the Tb(thd)$_3$ chelate were found to break at 147 °C, where the crystal structure of this chelate changed thermally

TABLE 1. VAPOR PRESSURES AND ENTHALPIES OF SUBLIMATION OF LANTHANOID AND Y CHELATES

(1 cal=4.184 J)

Sample	A[a]	B[a]	Error %	Limit °C	ΔH_T° kcal mol^{-1}	ΔS_T° cal K^{-1} mol^{-1}
$La_2(thd)_6$	9382.7	19.149	4	115—150	42.9	74.4
$Pr_2(thd)_6$	9333.5	19.553	3	110—150	42.7	76.3
$Nd_2(thd)_6$	9248.1	19.622	3	105—150	42.3	76.6
$Sm_2(thd)_6$	9440.4	20.573	3	105—145	43.2	81.0
$Eu_2(thd)_6$	9400.3	20.496	2	90—160	43.0	80.6
$Gd_2(thd)_6$	9242.4	20.468	3	100—145	43.3	80.5
Ho(thd)$_3$	7978.1	17.917	2	90—145	36.5	68.8
Er(thd)$_3$	8041.0	18.202	3	90—145	36.8	70.1
Tm(thd)$_3$	8159.3	18.650	3	90—140	37.3	72.2
Yb(thd)$_3$	8145.9	18.677	3	90—145	37.3	72.3
Lu(thd)$_3$	8085.2	18.672	3	90—140	37.0	72.3
Y(thd)$_3$	8211.7	18.463	2	90—140	37.5	71.3

a) $\text{Log } P(\text{Torr}) = -(A/T) + B$.

Table 2. Vapor pressures and enthalpies of sublimation of Tb and Dy chelates

(1 cal=4.184 J)

Sample	A[a]	B[a]	Error %	Limit °C	ΔH_T° kcal mol^{-1}	ΔS_T° cal K^{-1} mol^{-1}
$Tb_2(thd)_6$	9072.6	20.238	3	100—147	41.5	79.4
$Tb(thd)_3$	7897.3	17.464	3	100—160	36.1	66.7
$Dy_2(thd)_6$	8963.8	20.390	6	100—115	41.0	80.1
$Dy(thd)_3$	7934.2	17.627	3	100—140	36.3	67.5

a) $\mathrm{Log}\, P(\mathrm{Torr}) = -(A/T) + B$.

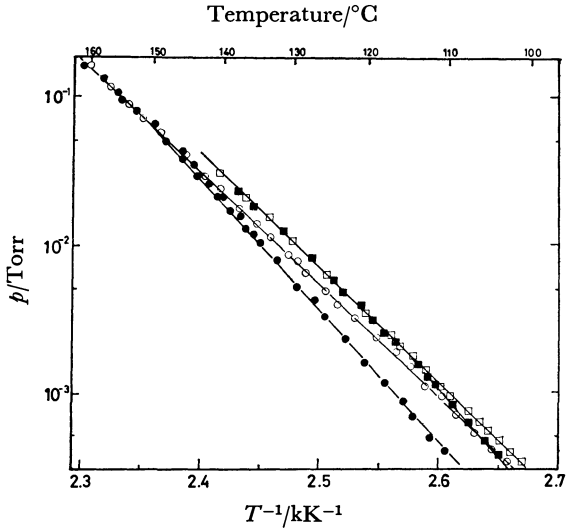

Fig. 5. Clausius-Clapeyron plots of $Tb(thd)_3$ and $Dy(thd)_3$ chelates.
●: Temperature-ascending process of the Tb chelate,
○: temperature-descending process of the Tb chelate,
■: temperature-ascending process of the Dy chelate,
□: temperature-descending process of the Dy chelate.

from a monoclinic dimer to an orthorhombic monomer.[9] The enthalpy of sublimation of the Tb chelate in lower temperature range (100—147 °C) was similar to those of lighter lanthanoids (La to Gd), and the enthalpy in upper temperature range (147—160 °C) resembled those of heavier lanthanoids (Ho to Lu) and yttrium. On the other hand, the Clausius-Clapeyron plots in the temperature-descending procesess did not break at 147 °C and followed a straight line. The enthalpy of sublimation obtained from this line was the same as those in the upper temperature range (147—160 °C) of the ascending process, and almost equal to those of heavier lanthanoid chelates. The sublimation behavior of $Dy(thd)_3$ chelate is similar to that of the Tb chelate. The Dy chelate also changed its crystal structure at about 115 °C. The thermal transitions of the Tb and Dy chelates were found to be irreversible. The thermal behaviors of the $Ln(thd)_3$ chelates were found to be classified into three groups: La to Gd, Tb and Dy, and Ho to Lu. Figure 6 gives a relationship between the enthalpy of sublimation and the atomic number. The difference in enthalpy of sublimation between the lighter lanthanoids (La to Gd) and the heavier ones (Ho to Lu) is 6—8 kcal/mol (1 cal=4.184 J), which appears to correspond to the transition enthalpy of dimer to monomer of

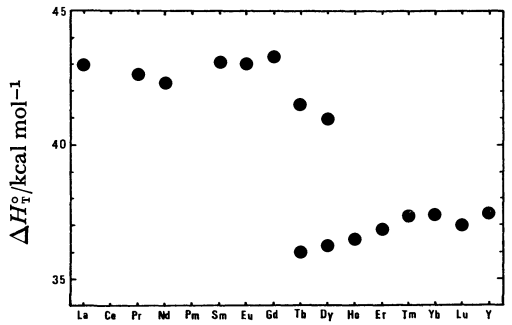

Fig. 6. Enthalpies of sublimation of $Ln(thd)_3$ as a function of atomic number.

the Tb and Dy chelates.

Partial X-ray powder patterns of the $Ln(thd)_3$ chelates are compared in Table 3. The patterns of the lighter lanthanoid chelates of La to Gd were different from those of heavier ones of Ho to Lu and yttrium. Erasmus and Boeyens reported the Pr chelate to be a monoclinic dimer.[10] The crystal structure of $Er(thd)_3$ and $Lu(thd)_3$ chelates have also been reported to be those of an orthorhombic monomer.[11,12] The crystal structure of the Tb chelate is the same as those of the lighter lanthanoid chelates. In the previous work,[9] the freshly sublimated Tb chelate has been found to change in crystallographic modification from a monoclinic dimer to an orthorhombic monomer at 147 °C, by means of differential scanning calorimetric technique and X-ray powder diffraction at elevated temperature. The breaking point on the Clausius-Clapeyron line of the Tb chelate corresponds to the temperature of its thermal transition. Fresh $Dy(thd)_3$ chelate was obtained in two different X-ray crystallographic systems by vacuum sublimation: a monoclinic dimer form and an orthorhombic monomer form. Vapor of the Dy chelate crystallizes in orthorhombic monomer form under the sublimation condition with a gentle temperature gradient, although it deposits in the monoclinic dimer form on the cooler of the molecular still if sublimed with a steep temperature gradient (100 °C/cm). Infra-red spectra of the freshly prepared lighter lanthanoid chelates were different from those of the heavier ones at 1300—1250 cm^{-1}, 1250—1100 cm^{-1}, 970—940 cm^{-1}, 810—770 cm^{-1}, and 510—450 cm^{-1}, as shown in Fig. 7. The spectral shape of the fresh Tb chelate was compared with those of lighter lanthanoid (La, Pr-Gd) chelates and found to be identical over the range of 4000 to 600 cm^{-1}. On the other hand, the IR spectra

Table 3. Partial X-ray powder patterns of some lanthanoid and Y chelates (d, Å)

$La_2(thd)_6$	$Pr_2(thd)_6$	$Nd_2(thd)_6$	$Eu_2(thd)_6$	$Gd_2(thd)_6$	$Tb_2(thd)_6$	$Dy(thd)_3$	$Ho(thd)_3$	$Er(thd)_3$	$Yb(thd)_3$	$Y(thd)_3$
14.72 w	14.48 w	14.48 w	14.48 w	14.48 w	14.48 w					
13.59 w		13.59 w								
12.22 s	11.94 s	12.02 s	11.94 s	12.05 s	11.94 s					
11.40 s	11.25 m	11.32 s	11.32 s	11.32 s	11.18 s					
10.84 s	10.84 s	10.84 s	10.91 s	10.91 s	10.91 s					
						10.84 s	10.80 s	10.79 s	10.77 s	10.77 s
	10.21 w		10.16 w	10.21 w	10.10 w					
9.66 m	9.60 w		9.60 w	9.66 m	9.60 w					
9.11 w	9.20 w	9.30 w	9.30 w	9.28 m	9.20 m	9.30 s	9.28 s	9.30 s	9.20 s	9.25 s
							9.06 m	9.06 m	9.06 m	9.06 m
8.88 w	8.93 m	8.93 m	8.93 m	8.93 m	8.88 m					
						8.84 m	8.84 s	8.84 s	8.79 s	8.84 s
						7.37 m	7.37 m	7.37 m	7.34 m	7.37 m
						6.91 m	6.91 m	6.91 s	6.86 s	6.91 m
						6.80 m	6.80 m	6.83 m	6.80 m	6.80 m
	5.69 w	5.71 w	5.71 w	5.73 w	5.71 w	5.68 w	5.69 w	5.71 w	5.64 w	5.68 w
	5.38 w	5.37 w	5.35 w	5.37 w	5.34 w	5.37 w	5.35 w	5.34 w	5.34 w	5.34 w
						5.17 s	5.15 s	5.15 s	5.11 s	5.15 s
	5.00 w	5.00 w	5.00 w	5.00 w	4.98 w	5.00 m	5.03 m	5.03 m	5.00 m	5.02 m
4.75 w	4.74 w					4.71 m	4.72 m	4.72 m	4.71 m	4.72 m
4.67 w	4.67 m	4.67 m	4.65 m	4.67 m	4.64 m	4.64 m	4.64 m	4.64 m	4.61 m	4.64 m
4.62 w	4.62 m	4.59 m	4.58 m	4.59 m	4.57 m	4.55 s	4.55 m	4.58 m	4.55 m	4.57 m
							4.50 w	4.50 w	4.46 w	4.49 w
						4.39 m	4.39 s	4.39 s	4.39 s	4.40 s
		4.32 w	4.31 w	4.31 w	4.27 w					
		4.20 w	4.22 w	4.19 w	4.21 w	4.17 m	4.18 m	4.21 m	4.16 m	4.18 m
						4.05 m	4.05 m	4.05 w	4.04 m	4.05 m

s=Strong; m=medium; w=weak.

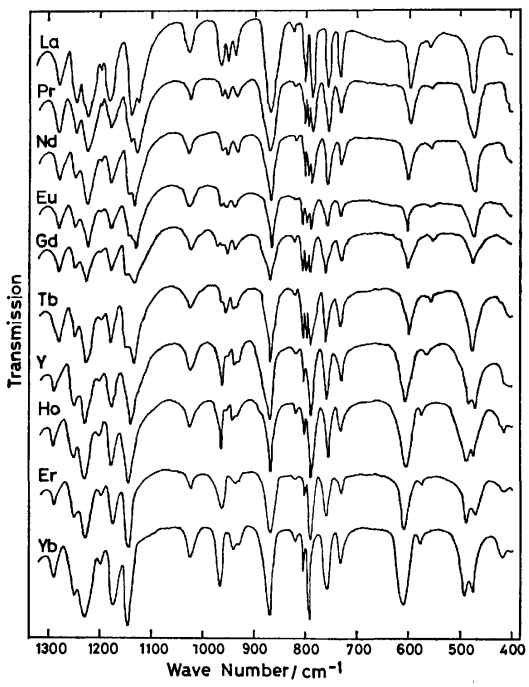

Fig. 7. IR spectra of the freshly sublimated $Ln(thd)_3$ and $Y(thd)_3$ chelates.

of the pre-heated Tb and Dy chelates were identical with those of the heavier lanthanoid (Ho–Lu) chelates.

Table 4. Vacuum sublimation-recrystallizing temperature ranges of lanthanoid and Y chelates

Sample	Temperature range/°C
$La_2(thd)_6$	88—141
$Pr_2(thd)_6$	88—139
$Nd_2(thd)_6$	86—137
$Sm_2(thd)_6$	87—129
$Eu_2(thd)_6$	79—126
$Gd_2(thd)_6$	74—125
$Tb_2(thd)_6$	66—117
$Dy(thd)_3$	46—75
$Ho(thd)_3$	49—74
$Er(thd)_3$	49—74
$Tm(thd)_3$	48—71
$Yb(thd)_3$	45—66
$Lu(thd)_3$	46—67
$Y(thd)_3$	52—80

Vacuum sublimation-recrystallizing temperature zones can be observed discretely and reproducibly at the higher temperature site of the deposition zone, while the tailing appears in its lower temperature site. The vacuum sublimation-recrystallizing temperature zones of the $Ln(thd)_3$ chelates are summarized in Table 4. Figure 8 shows the plots of the highest temperature of vacuum sublimation-recrystallizing zone

Table 5. Critical values of lanthanoid and Y chelates

Sample	$P_{180\,°C}$[a]	$P_{v.s.r.}$[b]	γ[c]
$La_2(thd)_6$	2.7×10^{-2}	3.0×10^{-4}	9.0×10^{1}
$Pr_2(thd)_6$	8.9×10^{-2}	7.9×10^{-4}	1.1×10^{2}
$Nd_2(thd)_6$	1.6×10^{-1}	1.2×10^{-3}	1.3×10^{2}
$Sm_2(thd)_6$	5.4×10^{-1}	1.2×10^{-3}	4.5×10^{2}
$Eu_2(thd)_6$	5.6×10^{-1}	8.6×10^{-4}	6.5×10^{2}
$Gd_2(thd)_6$	1.2	1.8×10^{-3}	6.7×10^{2}
$Tb_2(thd)_6$	1.1	1.6×10^{-3}	6.9×10^{2}
$Dy(thd)_3$	1.3	6.7×10^{-6}	1.9×10^{5}
$Ho(thd)_3$	2.0	8.4×10^{-6}	2.4×10^{5}
$Er(thd)_3$	2.8	1.1×10^{-5}	2.5×10^{5}
$Tm(thd)_3$	4.4	8.5×10^{-6}	5.2×10^{5}
$Yb(thd)_3$	5.0	4.4×10^{-6}	1.1×10^{6}
$Lu(thd)_3$	6.7	7.8×10^{-6}	8.6×10^{5}
$Y(thd)_3$	2.2	1.6×10^{-5}	1.4×10^{6}

a) $P_{180\,°C}$ indicates the pressure of chelate gas which is taken as the vapor pressure of the chelate at the temperature of heating site(180 °C). b) $P_{v.s.r.}$ is the saturated vapor pressure of the chelate at the highest site of vacuum sublimation-recrystallizing temperature. c) γ is the critical value calculated from the equation, $\gamma=P_{180\,°C}/P_{v.s.r.}$.

as a function of the atomic number of the corresponding lanthanoid. The plots can be classified in two distinct groups (La to Tb, and Dy to Lu) that coincided with the two different crystal structures observed from X-ray powder diffraction patterns. The $Dy(thd)_3$ chelate purified under the gentle temperature gradient belonged to a class of heavier lanthanoids. The lighter lanthanoids (La to Tb) form a monoclinic dimer system, and heavier ones (Dy to Lu) recrystallize in orthorhombic form on purification from the vapor phase. The vacuum sublimation-recrystallizing temperature can be explained on the basis of crystallization in the dimeric or monomeric system from the chelate vapor. Monomeric chelate gas of the lanthanoid will solidify to form a dimer system according to either of the following equations:

$$2Ln(thd)_3(gas) \rightarrow Ln_2(thd)_6(gas) \rightarrow Ln_2(thd)_6(solid), \quad (5)$$

or

$$2Ln(thd)_3(gas) \rightarrow 2Ln(thd)_3(solid) \rightarrow Ln_2(thd)_6(solid). \quad (6)$$

The enthalpies of the above two reactions are larger than that of the reaction of monomeric gas to monomeric solid. The enthalpy of sublimation of a monomeric $Ln(thd)_3$(solid) nearly equals 36 kcal/mol, and that of dimeric chelate is about 43 kcal/mol. From these results, the difference in the enthalpy of sublimation corresponds to the transition enthalpy of the following reaction:

$$Ln_2(thd)_6(soid) \rightarrow 2Ln(thd)_3(solid), \quad (7)$$

where the transition enthalpy of the reaction nearly equals 7 kcal/mol. In fact, the dimeric Tb and Dy chelates change to the monomeric chelates endothermically.[9] The enthalpies of both processes of (6)

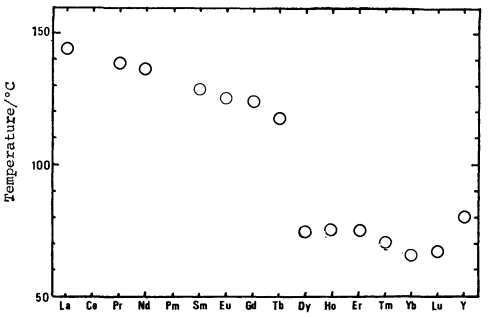

Fig. 8. Vacuum sublimation-recrystallizing temperatures of $Ln(thd)_3$ as a function of atomic number.

can be calculated from the thermochemical data obtained in this experiment. The volatilization process of the lighter lanthanoid chelate, $Ln_2(thd)_6$, is represented by the reverse of reaction (5) or (6). The lighter chelate thus requires more energy to vaporize than the heavier one. Deposition temperature is derived from overall sublimation-recrystallization processes. The lighter chelate deposits in a higher temperature zone than the heavier one. In general, the growth of crystals can be definitely observed at the "critical temperature."[13] Moreover, the ratio $\gamma=P_h/P_c$, where P_h is the pressure of vapor phase and P_c is the saturated vapor pressure at the critical temperature, have a characteristic value for each sample; this value is called the "critical value."[13] The vacuum sublimation-recrystallizing temperature in this paper corresponds to the critical temperature. The critical values have been calculated to the individual lanthanoid chelates to find out what regularity may exist in vacuum sublimation-recrystallization behavior; their values are given in Table 5. The critical values of the lanthanoid chelates were classified into two groups (La to Tb, and Dy to Lu) that coincided with the groupings of the vacuum sublimation-recrystallizing temperature. To estimate vacuum sublimation-recrystallizing temperatures of a variety of β-diketonato chelates, it would be necessary to collect the data of vapor pressures over the temperature range of deposition zone and critical values for these compounds.

The authors wish to express their thanks to Professor Eishin Kyuno of Hokuriku University for his kind permission to use the IR instruments. The present work was partially supported by a Grant-in-Aid for Scientific Research No. 374189 and No. 574227 from the Ministry of Education, Science and Culture.

References

1) R. E. Sievers and J. E. Sadlowski, *Science*, **201**, 217 (1980); W. F. Libby, *ibid.*, **171**, 499 (1971); L. A. Pedersen and W. F. Libby, *ibid.*, **176**, 1355 (1972); R. C. Vickery, *ibid.*, **172**, 86 (1971); R. J. H. Voorhoeve, J. P. Remeika, P. E. Freeland, and B. T. Matthias, *ibid.*, **177**, 353 (1972).

2) R. L. Van Hemert, L. B. Spendlove, and R. E. Sievers, *J. Electrochem. Soc.*, **112**, 1123 (1965); S. C. Chattoraj, A. G. Cupka, Jr., and R. E. Sievers, *J. Inorg. Nucl. Chem.*, **28**, 1937 (1966).

3) K. J. Eisentraut and R. E. Sievers, *J. Am. Chem. Soc.*, **87**, 5254 (1965).

4) J. E. Sicre, J. T. Dubois, K. J. Eisentraut, and R. E. Sievers, *J. Am. Chem. Soc.*, **91**, 3476 (1969).
5) E. W. Berg and J. J. C. Acosta, *Anal. Chim. Acta*, **40**, 101 (1968).
6) M. Sakanoue and R. Amano, "Transplutonium 1975," ed by W. Müller and R. Lindner, North-Holland Publ. Co., (1976), p. 123.
7) R. Amano, A. Sato, and S. Suzuki, *Radiochem. Radioanal. Lett.*, **39**, 441 (1979).
8) P. Clausing, *Ann. Phys.*, **12**, 961 (1932); S. Saito and M. Kinoshita, "Jiken-kagaku-kōza, Zoku-2, Bunri-to-seisei," Maruzen, Tokyo (1967), p. 69; T. Sata, "Shin-jiken-kagaku-kōza, 2, Netsu-atsuryoku," Maruzen, Tokyo (1977), p. 371.
9) R. Amano, A. Sato, and S. Suzuki, *Chem. Lett.*, **1980**, 537.
10) C. S. Erasmus and J. C. A. Boeyens, *Acta Crystallogr., Sect. B*, **26**, 1843 (1970).
11) J. P. R. Villiers and J. C. A. Boeyens, *Acta Crystallogr., Sect. B*, **28**, 2335 (1972).
12) S. Onuma, H. Inoue, and S. Shibata, *Bull. Chem. Soc. Jpn.*, **49**, 644 (1976).
13) M. Knudsen, *Ann. Phys.*, **50**, 472 (1916); R. W. Wood, *Phil. Mag.*, **32**, 364 (1916); K. Yoshimura, *Jpn. Anal.*, **11**, 397, 400 (1962).

The Temperature Dependence of the Trapped and Averaged-valence State in Mono-oxidized Dialkylbiferrocenes

Sei'ichiro IIJIMA,† Ritsuko SAIDA, Izumi MOTOYAMA, and Hirotoshi SANO*

Department of Chemistry, Faculty of Science, Tokyo Metropolitan University, Fukasawa, Setagaya-ku, Tokyo 158

(Received August 4, 1980)

An interesting temperature dependence of the valence state was observed in the Mössbauer spectra of the mixed-valence salts of 1′,1‴-dialkylbiferrocenes, measured at various temperatures from 4.2 K to 300 K. A mechanistic consideration of the temperature dependence has been carried out assuming a conformational change of the monocation salts induced both by the variation in the temperature and by the kind of counter anion.

The monocation salts of binuclear ferrocenes are so-called "mixed-valence" compounds, in which, formally, two kinds of iron atoms, Fe(II) and Fe(III), are simultaneously contained. It is known that the monocation salts can be classified into two types, a trapped-valence type (or a mixed-valence type, in a narrow sense) and an averaged-valence one, by means of Mössbauer spectroscopy.[1-7] The former type gives two different states of irons, corresponding to bi- and tervalent irons, while the latter gives iron atoms in an equivalent state averaged between these two kinds of valence states. As for biferrocene derivatives, various monocation salts of biferrocene itself have been reported to be of the trapped-valence type,[1,4] while 1′,1‴-diiodobiferrocenium triiodide is of the averaged-valence type.[4]

In the present paper, results will be reported on the temperature dependence of valence states in mono-oxidized 1′,1‴-diethyl- and 1′,1‴-dipropylbiferrocenes†† investigated by means of Mössbauer spectroscopy.

Results and Discussion

The biferrocene derivatives used in this study are listed in Table 1, all the compounds, **1**—**8**, were identified by means of elemental analyses (**1** and **5** were also identified by NMR), the results of which are summarized in Table 2. The Mössbauer data for the neutral species, 1′,1‴-diethylbiferrocene (**1**) and 1′,1‴-dipropylbiferrocene (**5**), are shown in Table 3, along with the data for unsubstituted biferrocene. The Mössbauer spectra of **1** and **5** at 78 K are shown in Fig. 1. The Mössbauer parameters of the substituted biferrocenes are actually identical to those of unsubstituted biferrocene at the same temperature, indicating that the replacement of hydrogens by alkyl groups does not affect the Mössbauer parameters of biferrocene.

The Mössbauer parameters for the dication salts, 1′,1‴-diethylbiferrocenium$^{2+}(BF_4^-)_2$ (**3**), 1′,1‴-diethylbiferrocenium$^{2+}(DDQH^-)_2$ (**4**), and 1′,1‴-dipropylbiferrocenium$^{2+}(BF_4^-)_2$ (**8**), are listed in Table 4, along with those for biferrocenium$^{2+}(BF_4^-)_2$. The Mössbauer spectra of these dication salts, **3**, **4**, and **8** show broad singlet peaks with very small quadrupole splittings, which are assignable to the ferrocenium-like tervalent iron, although generally no quadrupole splittings are found in the Mössbauer spectra of most mononuclear ferrocenium salts.[8] The 78 K spectra of **3** and **8** are shown in Fig. 2. The Mössbauer parameters of the dications of the diethylbiferrocene, **3** and **4**, with BF_4^- and $DDQH^-$ respectively as the counter ion, are essentially identical at the same temperature. Therefore, no effect of the counter anion was found on the parameters of these dication salts. These results agree with the fact that little difference can be detected in the Mössbauer parameters of mononuclear ferrocenium salts containing various anions as the counter ion.[8] Furthermore, the Mössbauer parameters of **3**, **4**, and **8** are quite similar to those of biferrocenium$^{2+}(BF_4^-)_2$ at the same temperature. Thus, no effect of the alkyl substitution was found on the Mössbauer parameters of the dications.

Table 1. Compounds

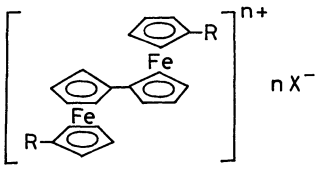

Compound	R	*n*	X⁻
1′,1‴-Diethylbiferrocene (**1**)	C_2H_5	0	
1′,1‴-Diethylbiferrocenium$^+I_3^-$ (**2**)	C_2H_5	1	I_3^-
1′,1‴-Diethylbiferrocenium$^{2+}(BF_4^-)_2$ (**3**)	C_2H_5	2	BF_4^-
1′,1‴-Diethylbiferrocenium$^{2+}(DDQH^-)_2$ (**4**)	C_2H_5	2	$DDQH^-$ [a]
1′,1‴-Dipropylbiferrocene (**5**)	C_3H_7	0	
1′,1‴-Dipropylbiferrocenium$^+I_3^-$ (**6**)	C_3H_7	1	I_3^-
1′,1‴-Dipropylbiferrocenium$^+(TCNQ)_2^{\pm}$ (**7**)	C_3H_7	1	$(TCNQ)_2^{\pm}$ [b]
1′,1‴-Dipropylbiferrocenium$^{2+}(BF_4^-)_2$ (**8**)	C_3H_7	2	BF_4^-

a) $DDQH^-\equiv$ 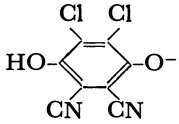 .

b) $(TCNQ_2)^{\pm}\equiv$ 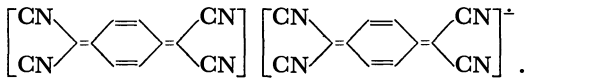 .

† Present address: Research Institute for Polymers and Textiles, Yatabe-Higashi, Tsukuba, Ibaraki 305.

†† The proper name of this type of compound is 1′,1‴-dialkyl-1,1″-biferrocenyl according to the nomenclature followed by the tentative IUPAC rule.

Table 2. Analytical data

Compound	Calcd (%)		Found (%)	
	C	H	C	H
1′,1‴-Diethylbiferrocene (**1**)	67.64	6.15	67.67	6.39
1′,1‴-Diethylbiferrocenium$^{+}I_3^{-}$ (**2**)[a]	35.75	3.25	35.66	3.21
1′,1‴-Diethylbiferrocenium$^{2+}(BF_4^{-})_2$ (**3**)	48.06	4.37	47.99	4.40
1′,1‴-Diethylbiferrocenium$^{2+}(DDQH^{-})_2$ (**4**)[b]	54.46	3.20	54.90	3.40
1′,1‴-Dipropylbiferrocene (**5**)	69.36	7.12	68.75	6.66
1′,1‴-Dipropylbiferrocenium$^{+}I_3^{-}$ (**6**)	37.40	3.62	37.49	3.72
1′,1‴-Dipropylbiferrocenium$^{+}(TCNQ)_2^{\pm}$ (**7**)[c]	69.62	4.44	69.59	4.52
1′,1‴-Dipropylbiferrocenium$^{2+}(BF_4^{-})_2$ (**8**)	49.67	4.85	49.77	4.82

a) Iodine analysis: Calcd, 47.18%; Found, 47.39%. b) Nitrogen analysis: Calcd, 6.35%; Found, 6.40%. c) Nitrogen analysis: Calcd, 12.99%; Found, 13.00%.

Table 3. Mössbauer data for 1′,1‴-diethylbiferrocene (**1**), 1′,1‴-dipropylbiferrocene (**5**), and biferrocene

Compound	Temperature/K	δ[a]/mm s^{-1}	ΔE_Q/mm s^{-1}
1′,1‴-Diethylbiferrocene (**1**)	300	0.45	2.30
	78	0.55	2.34
1′,1‴-Dipropylbiferrocene (**5**)	300	0.44	2.30
	78	0.55	2.31
Biferrocene	298	0.45[b]	2.30[b]
		0.45[c]	2.30[c]
	78	0.55[b]	2.34[b]
		0.52[c]	2.36[c]

a) Isomer-shift data are reported with respect to metallic iron foil. b) See Ref. 9. c) See Ref. 17.

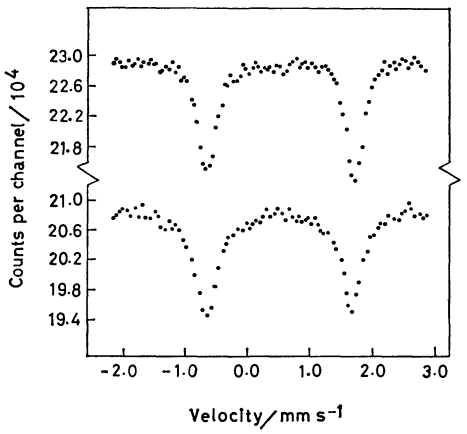

Fig. 1. Mössbauer spectra at 78 K of 1′,1‴-diethylbiferrocene (**1**) (top) and 1′,1‴-dipropylbiferrocene (**5**) (bottom).

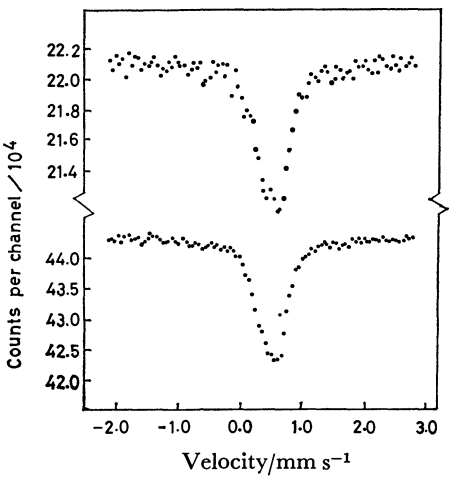

Fig. 2. Mössbauer spectra at 78 K of 1′,1‴-diethylbiferrocenium$^{2+}(BF_4^{-})_2$ (**3**) (top) and 1′,1‴-dipropylbiferrocenium$^{2+}(BF_4^{-})_2$ (**8**) (bottom).

Mössbauer measurements of the monocation salt, 1′,1‴-diethylbiferrocenium$^{+}I_3^{-}$ (**2**), were carried out at ten different temperatures between 4.2 to 300 K. The Mössbauer data for **2** are summarized in Table 5, along with those for the related compounds, while the spectrum at each temperature is shown in Figs. 3 and 4. As can be seen from Figs. 3 and 4, the shape of the spectrum greatly depends upon the temperature of the measurement. The spectrum at 4.2 K consists of inner and outer doublets in a nearly 1:1 ratio; these doublets are ascribed to the ferrocenium-like tervalent and ferrocene-like bivalent iron in **2** respectively. This spectrum is of the typical trapped-valence type. With an increase in the temperature, however, the quadrupole splitting of the inner doublet increases, while that of the outer doublet decreases gradually. Eventually, at 275 and 300 K, **2** shows typical averaged-valence spectra which consist of a single quadrupole doublet.

The Mössbauer data for 1′,1‴-dipropylbiferrocenium$^{+}I_3^{-}$ (**6**), are summarized in Table 6. The temperature dependence of the Mössbauer spectra of **6** was found to be very similar to that of **2**, but the typical averaged-valence spectrum appears at a temperature

TABLE 4. MÖSSBAUER DATA FOR 1′,1‴-DIETHYLBIFERROCENIUM^{2+}(BF_4^-)$_2$ (**3**), 1′,1‴-DIETHYLBIFERROCENIUM^{2+}($DDQH^-$)$_2$ (**4**), 1′,1‴-DIPROPYLBIFERROCENIUM^{2+}(BF_4^-)$_2$ (**8**), AND BIFERROCENIUM^{2+}(BF_4^-)$_2$

Compound	Temperature/K	δ[a]/mm s^{-1}	ΔE_Q/mm s^{-1}
1′,1‴-Diethylbiferrocenium^{2+}(BF_4^-)$_2$ (**3**)	78	0.54	0.17
1′,1‴-Diethylbiferrocenium^{2+}($DDQH^-$)$_2$ (**4**)	300	0.38	0.17
	78	0.48	0.17
1′,1‴-Dipropylbiferrocenium^{2+}(BF_4^-)$_2$ (**8**)	300	0.35	*ca.* 0.1
	78	0.54	0.14
Biferrocenium^{2+}(BF_4^-)$_2$	77	0.497[b]	0.163[c]

a) Isomer-shift data are reported with respect to metallic iron foil. b) See Ref. 1.

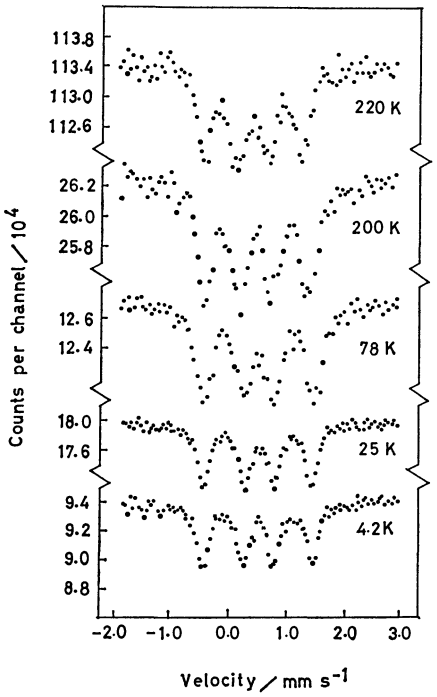

Fig. 3. Mössbauer spectra of 1′,1‴-diethylbiferrocenium$^+I_3^-$ (**2**) in the temperature range 4.2—220 K.

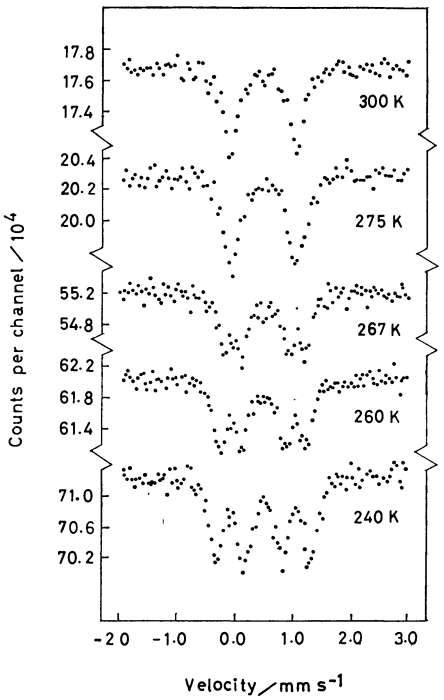

Fig. 4. Mössbauer spectra of 1′,1‴-diethylbiferrocenium$^+I_3^-$ (**2**) in the temperature range 240—300 K.

about 25—30 degrees lower than that in the case of **2**, as is shown in Fig. 5.

As was mentioned in the Introduction, the Mössbauer spectra of biferrocenium$^+I_3^-$ and 1′,1‴-diiodobiferrocenium$^+I_3^-$ are of the trapped-valence and averaged-valence types respectively, neither of which is temperature-dependent. Consequently, it is obvious that these monocation salts of the dialkylbiferrocenes, **2** and **6**, are an additional type of "mixed-valence" compound, the valence state of which changes from the trapped-valence state to the averaged-valence one with the elevation of the temperature. Furthermore, from the Mössbauer spectroscopic behavior of the four monocation salts just discussed above, it can be said that the valence state of the mono-oxidized biferrocene system is greatly affected by the kind of substituent on the biferrocene system, while little effect of the substitution is found on the Mössbauer parameters of the neutral and dioxidized species.

In previous papers we reported that the monocation salt of *as*-indacenebis(cyclopentadienyliron) was the first example of a binuclear ferrocene salt which shows a remarkably temperature-dependent Mössbauer spectrum, that is, a trapped-valence-type spectrum at a lower temperature and an averaged-valence-type one at higher temperature.[9,10] This temperature dependence was interpreted successfully in terms of an electron-hopping process, in which the thermal electron-transfer takes place between two iron atoms and the electron-transfer increases with the increase in the temperature. However, the behavior of **2** and **6** observed in this study cannot be explained by using such an electron-hopping process, because the line-broadening of the Mössbauer spectrum at intermediate temperatures, which is characteristic of such a process,[9,11—13] was not found for **2** and **6**. It was previously suggested that the difference in valence state between biferrocenium$^+I_3^-$ and 1′,1‴-diiodobiferrocenium$^+I_3^-$ was attributable to the conformational difference between these monocations.[4] It was also suggested that the diiodo-monocation is in a *trans* or *cis* conformation with respect to the iron atoms, which would enhance the interaction between the two iron centers. The change in valence state observed for **2** and **6** seems to be understandable according to the following assumptions regarding the monocations:

that the conformation of the monocation of **2**, as well as that of **6**, at low temperatures (below about 200 K for **2**) differs from that at high temperatures (above about 270 K for **2**), and that the latter conformation, probably similar to that of the diiodo-monocation, causes strong interaction between the two iron atoms, that is, a full delocalization of electrons between the iron centers. At an intermediate temperature, it can be concluded that the conformation of the 1′,1‴-diethylbiferrocenium and 1′,1‴-dipropylbiferrocenium monocation varies gradually from the low-temperature-type conformation to the high-temperature-type one with an increase in the temperature.

TABLE 5. MÖSSBAUER DATA FOR 1′,1‴-DIETHYLBIFERROCENIUM$^+I_3^-$ (**2**)

Temperature/K	δ[a]/mm s^{-1}	ΔE_Q/mm s^{-1}	$\Gamma_{1/2}$/mm s^{-1}
300	0.47	1.17	0.27
275	0.47	1.16	0.33
267	0.46	0.87	0.29
	0.45	1.42	0.27
260	0.46	0.80	0.30
	0.46	1.51	0.29
240	0.46	0.68	0.31
	0.47	1.64	0.30
220	0.50	0.58	0.33
	0.50	1.72	0.30
200	0.49	0.56	0.34
	0.48	1.80	0.32
78	0.57	0.50	0.36
	0.55	1.88	0.32
25	0.54	0.52	0.36
	0.54	1.91	0.34
4.2	0.53	0.51	0.37
	0.54	1.93	0.35

a) Isomer-shift data are reported with respect to metallic iron foil.

As indicated by the data cited in Table 6, the anion-substituted monocation salt of 1′,1‴-dipropylbiferrocene, 1′,1‴-dipropylbiferrocenium$^+$(TCNQ)$_2^-$ (**7**), was found to give averaged-valence-type Mössbauer spectra, which are not temperature-dependent. As has been described above, we found little effect of anions on the Mössbauer parameters for the mononuclear ferrocenium salts; this was also demonstrated for the dioxidized 1′,1‴-diethylbiferrocene of Mössbauer spectra in the present work. The difference observed in the temperature dependence of the Mössbauer spectra between **6** and **7** may suggest that the conformation of the 1′,1‴-dipropylbiferrocenium mono-

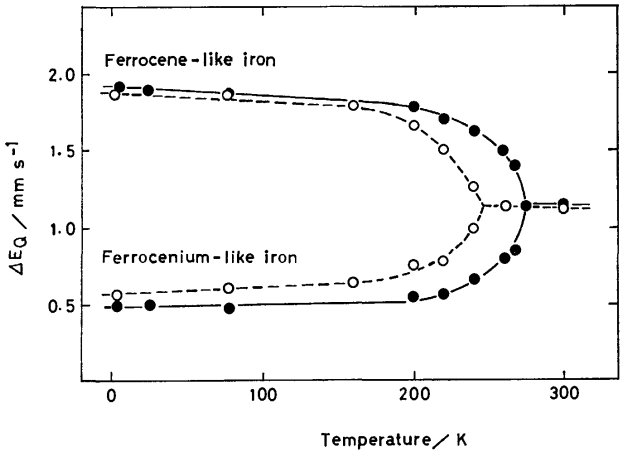

Fig. 5. Temperature-dependence of the quadrupole splittings of 1′,1‴-diethylbiferrocenium$^+I_3^-$ (**2**) and 1′,1‴-dipropylbiferrocenium$^+I_3^-$ (**6**).
—●—●— 1′,1‴-Diethylbiferrocenium$^+I_3^-$ (**2**),
—○—○— 1′,1‴-dipropylbiferrocenium$^+I_3^-$ (**6**).

TABLE 6. MÖSSBAUER DATA FOR 1′,1‴-DIPROPYLBIFERROCENIUM$^+I_3^-$ (**6**) AND 1′,1‴-DIPROPYLBIFERROCENIUM$^+$(TCNQ)$_2^-$ (**7**)

Compound	Temperature/K	δ[a]/mm s^{-1}	ΔE_Q/mm s^{-1}	$\Gamma_{1/2}$/mm s^{-1}
1′,1‴-Dipropylbiferrocenium$^+I_3^-$ (**6**)	300	0.44	1.16	0.25
	260	0.45	1.16	0.33
	240	0.46	0.97	0.27
		0.46	1.27	0.27
	220	0.47	0.78	0.32
		0.45	1.51	0.31
	200	0.49	0.75	0.32
		0.49	1.68	0.31
	160	0.50	0.64	0.33
		0.50	1.81	0.32
	78	0.54	0.60	0.34
		0.54	1.90	0.33
	4.2	0.54	0.57	0.35
		0.53	1.92	0.33
1′,1‴-Dipropylbiferrocenium$^+$(TCNQ)$_2^-$ (**7**)[b]	300	0.45	0.84	0.31
	78	0.52	1.20	0.36
	4.2	0.55	1.27	0.43

a) Isomer-shift data are reported with respect to metallic iron foil. b) The presence of a small amount of the dioxidized species of 1,1‴-dipropylbiferrocene was detected.

cation in the crystalline state is considerably influenced by the counter ion and controls the extent of interaction between the metal centers.

Experimental

Mössbauer Measurements. As the radioactive source for Mössbauer measurements a $^{57}Co(Pt)$ moving in a constant-acceleration mode was used. The Mössbauer spectra of **2**, **5**, and **6** were obtained by using an Austin Science Associates Mössbauer spectrometer and a proportional counter. The other spectra were obtained by using a Shimadzu Mössbauer spectrometer and a NaI scintillator. The isomer shifts are determined relative to metallic iron foil. The experimental errors of the Mössbauer parameters are estimated to be ± 0.03 mm/s.

Materials. The 1′,1‴-diethylbiferrocene **1** was prepared by the Ullmann coupling of 1-ethyl-1′-bromoferrocene,[14] which had itself been obtained from the $LiAlH_4$-$AlCl_3$ reduction of 1-acetyl-1′-bromoferrocene.[15]

The 1′,1‴-dipropylbiferrocene **5** was prepared by the Ullmann coupling of 1-propyl-1′-bromoferrocene, which had itself been obtained from the reduction of 1-propionyl-1′-bromoferrocene. 1-Propyl-1′-bromoferrocene (2.5 g, 8.1 mmol) mixed with 10 g of copper powder was heated to 120—130 °C for 18 h in a sealed glass tube. **5** was rapidly separated from the starting materials by using column chromatography on alumina; it was then obtained as reddish needles upon recrystallization from hexane. Mp 67—68 °C. ^1H NMR δ 0.90 (6H, t), 1.46 (4H, m), 2.16 (4H, t), 3.90 (8H, s), 4.16 (4H, t), and 4.30 (4H, t).

The 1′,1‴-dipropylbiferrocenium$^+$(TCNQ)$_2^{\cdot-}$ (**7**) was synthesized according to the procedure used for the preparation of ferrocenium$^+$(TCNQ)$_2^{\cdot-}$,[16] as follows. To a refluxing solution of 82 mg (0.4 mmol) of TCNQ in 30 ml of acetonitrile, a 91 mg portion (0.2 mmol) of **5** was added. After the reaction mixture had been refluxed for 15 min, **7** was separated out as blue-black needles, but in a low yield, on cooling. **5** did not react with TCNQ in boiling dichloromethane in place of acetonitrile.

The 1′,1‴-diethylbiferrocenium$^+I_3^-$ (**2**), 1′,1‴-diethylbiferrocenium$^{2+}(BF_4^-)_2$ (**3**), 1′,1‴-diethylbiferrocenium^{2+}-$(DDQH^-)_2$ (**4**), and 1′,1‴-dipropylbiferrocenium$^{2+}(BF_4^-)_2$ (**8**) were synthesized according to the procedures previously reported for the preparation of the corresponding salts of unsubstituted biferrocene.[1,2,4]

The analytical data for all the compounds described above are listed in Table 2.

References

1) D. O. Cowan, R. L. Collins, and F. Kaufman, *J. Phys. Chem.*, **75**, 2025 (1971).
2) W. H. Morrison, Jr., and D. N. Hendrickson, *J. Chem. Phys.*, **59**, 380 (1973).
3) W. H. Morrison, Jr., and D. N. Hendrickson, *Chem. Phys. Lett.*, **22**, 119 (1973).
4) W. H. Morrison, Jr., and D. N. Hendrickson, *Inorg. Chem.*, **14**, 2331 (1975).
5) I. Motoyama, M. Watanabe, and H. Sano, *Chem. Lett.*, **1978**, 513.
6) M. Watanabe, S. Iijima, I. Motoyama, and H. Sano, *J. Phys. (Paris), Colloq.*, **C2**, 392 (1979).
7) J. A. Kramer, F. H. Herbstein, and D. N. Hendrickson, *J. Am. Chem. Soc.*, **102**, 2293 (1980).
8) See, for example, Ref. 5 and R. H. Collins, *J. Chem. Phys.*, **42**, 1072 (1965).
9) S. Iijima, I. Motoyama, and H. Sano, *Bull. Chem. Soc. Jpn.*, **53**, 3184 (1980).
10) S. Iijima, I. Motoyama, and H. Sano, *Chem. Lett.*, **1979**, 1349.
11) O. Berkooz, M. Malamud, and S. Shtrikman, *Solid State Commun.*, **6**, 185 (1968).
12) G. A. Sawatzky, J. M. D. Coey, and A. H. Morrish, *J. Appl. Phys.*, **40**, 1402 (1969).
13) D. Lupu, D. Barb, G. Filoti, M. Moratiu, and D. Tarina, *J. Inorg. Nucl. Chem.*, **34**, 2803 (1972).
14) A. N. Nesmeyanov, V. N. Dorzd, V. A. Sazonova, V. I. Romanenko, A. K. Prokof'ef, and L. A. Nikonova, *Izvest. Akad. Nauk SSSR, Otdel. Khim. Nauk*, **1962**, 47.
15) D. W. Hall and J. H. Richards, *J. Org. Chem.*, **28**, 1549 (1963).
16) L. R. Melby, R. J. Harder, W. R. Hertler, W. Mahler, R. E. Benson, and W. E. Mochel, *J. Am. Chem. Soc.*, **84**, 3374 (1962).
17) G. K. Wertheim and R. H. Herber, *J. Chem. Phys.*, **38**, 2106 (1963).

The Solution Chemistry of Organotin Compounds. I. A ^{1}H NMR Study of the Complex Formation between Methyltin Trichloride and 4-Substituted Pyridines

Hideaki FUJIWARA,* Fumihiko SAKAI, Miyoko TAKEYAMA, and Yoshio SASAKI

Faculty of Pharmaceutical Sciences, Osaka University, 133-1 Yamadakami, Suita, Osaka 565

(Received August 11, 1980)

The formation of donor-acceptor complexes between $MeSnCl_3$ and 4-substituted pyridines has been investigated by analyzing the concentration dependence of NMR parameters. The formation of 1($MeSnCl_3$):2(pyridine) and 1:1 complexes has been proved, and the equilibrium constants(K_1 and K_2) and complex formation shifts (Δ_{AB} and Δ_{AB_2}) are determined for the successive formation of these complexes. log K_1 and log K_2 are in a good linear correlation with each other, and they have a tendency parallel with that of pK_a of the pyridine derivative, suggesting a predominant contribution of σ-bonding in the donor-acceptor bond. Both Δ_{AB} and Δ_{AB_2} indicate a high-field shift on the formation of the complex, which is consistent with the expected electron transfer in the donor-acceptor bond. However, Δ_{AB} varies inversely to the basicity of the pyridines; the anisotropy effect of the pyridine ring is suggested as the reason for this. The results are also discussed in relation to Hammett's substituent constant.

Among a variety of organometallic compounds, organotins are particularly stable and so are widely used in industry and in pharmaceuticals. They are used, for example, as stabilizers and catalysts for synthetic polymers and such biocides as fungicides, bacteriostasis, and insecticides.[1,2] These facts have stimulated recent studies of the related compounds by means of modern physical techniques.[2,3] In these studies, the physico-chemical properties and geometries of the compounds as well as of their complexes with bases have been the main subject. However, studies from the standpoint of solution chemistry are equally inevitable for a full understanding of the nature of these substances. We are interested in the intermolecular interaction in solution and have, therefore, set about studying the equilibria and thermodynamics as well as the dynamics of the complex formation of organotin compounds.

In the present work the complex formation of methyltin trichloride ($MeSnCl_3$) with several 4-substituted pyridines is investigated by means of analyzing the concentration dependence of the NMR chemical shift, and the equilibrium constant and the complex-formation shift are determined for the 1($MeSnCl_3$):1(pyridine) and 1:2 complexes. The results are discussed in relation to the basicity of pyridines as well as to the substituent effect.

Experimental

The $MeSnCl_3$ and 4-nitropyridine were synthesized from Me_2SnCl_2[4] and 4-nitropyridine *N*-oxide[5] respectively. The other materials were from commercial sources. The $MeSnCl_3$ was purified by sublimation under reduced pressure at $\approx$30 °C. The NMR spectra showed an impurity of Me_2SnCl_2 of less than 1%. The pyridines were distilled over BaO under normal pressure (pyridine and 4-methylpyridine) and under reduced pressure (4-acetyl- and 4-(methoxycarbonyl)pyridines). The 4-cyanopyridine was sublimed at $\approx$70 °C, and the 4-nitropyridine was recrystallized several times from petroleum ether. The nitrobenzene was dried over BaO and distilled under reduced pressure. All the materials were stored in desiccators, and all operations of the above distillation and sample preparation for the NMR measurement were made in dry boxes under a relative humidity of <20%. The ^{1}H NMR spectra were observed with a Hitachi R-22 spectrometer operating at 90 MHz and 34.1 °C. The chemical shifts and coupling constants were measured by means of a frequency counter within an error of $\pm$0.1 Hz. As an internal reference, $\approx$0.02 vol% Me_4Si was added to the solvent. The calculations were done on a NEAC S-900 computer at the Computation Center, Osaka University.

Results and Discussion

$MeSnCl_3$ is known to form a 1:2 donor-acceptor complex with pyridine, as evidenced by the isolation of the complex from solution.[6,7] Therefore, in interpreting the equilibrium property of these systems, it is necessary to take into account the concurrent formation of 1:1 and 1:2 complexes. Although equilibrium studies have often been reported with regard to the complex formation of methyltin halides,[6] there have been very few analyses of the simultaneous formation of 1:1 and 1:2 complexes.[8] We have made a computer program, CONDEP,[9] which minimizes the standard deviation(σ) between the observed and calculated NMR parameters—such as the chemical shift and the coupling constant—on the basis of the equilibrium of 1) A+B=AB, 2) A+2B=AB_2, and 3) A+B=AB and AB+B=AB_2. In this program the NMR parameter can be measured on the side of either A or B, and several selections of the number of adjustable parameters are made possible. The calculations below are made through the use of this program.

Composition of the Complex Formed in Solution. Job plots are shown in Fig. 1 for the $MeSnCl_3$+4-methyl-, +4-acetyl-, and +4-cyanopyridine systems. In the $MeSnCl_3$+4-methylpyridine system, the errors are relatively large in the shift measurement and ^2J(SnH) is difficult to observe because of the signal broadening. The Job plots of this system are almost the same in pattern when the solvent is changed to CH_2Cl_2 from nitrobenzene. Job plots were not obtained for the $MeSnCl_3$+pyridine system because of precipitation during the sample preparation. The Job plots of the $MeSnCl_3$+4-methoxycarbonyl- and +4-nitropyridine systems are similar to those of the $MeSnCl_3$+4-acetyl- and +4-cyanopyridine systems (Figs. 1b and 1c) re-

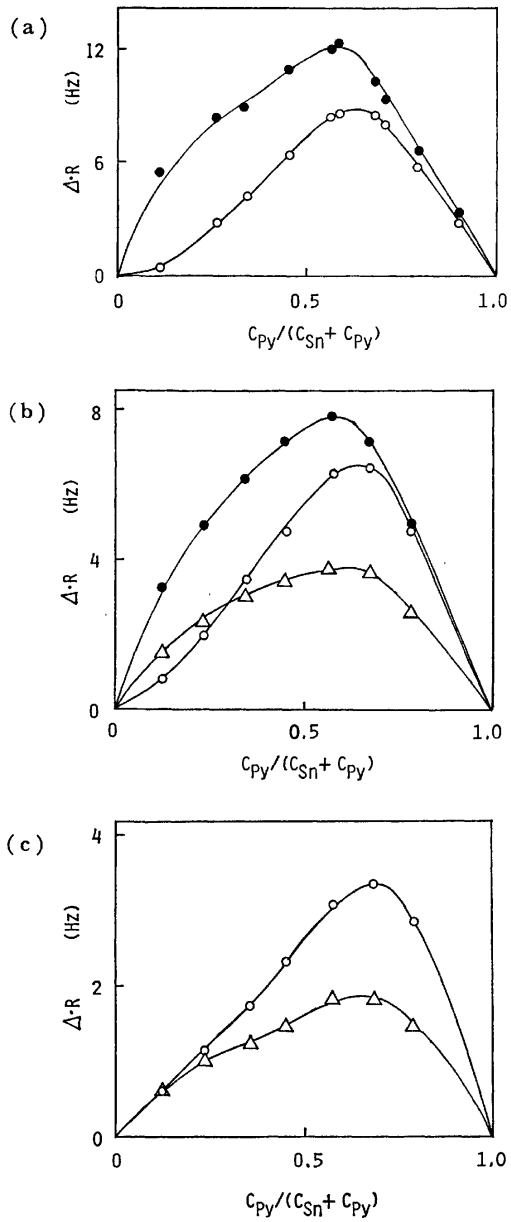

Fig. 1. Job plots for the a) $MeSnCl_3$+4-methylpyridine, b) $MeSnCl_3$+4-acetylpyridine, and c) $MeSnCl_3$+4-cyanopyridine systems.
C_{Sn} and C_{py} are molarities of $MeSnCl_3$ and the pyridines, respectively. $C_{Sn}+C_{py}\simeq 0.1$ mol dm^{-3}. Δ is equal to the variation in NMR parameters from a free state of the molecule under observation. R indicates mole fraction of the molecule under observation. $\Delta \cdot R$ is negative for δ (CH_3 in base) and $^2J(^{119}SnH)$, but absolute value is plotted. ●: Experimental point for $\delta_H(CH_3$ in base), △: experimental point for $^2J(^{119}SnH)$, ○: experimental point for $\delta_H(SnCH_3)$.

spectively. In all these systems, the plots show a plateau between 0.6—0.7 mole fraction of the base, irrespective of the NMR parameters observed, *i.e.*, $\delta_H(SnCH_3)$, δ_H(base), and ^2J(SnH), supporting the idea of the formation of a 1:2 complex in solution as well. On the other hand, the presence of a 1:1 complex is only inferred from the mole fraction corresponding to the plateau, which is a little smaller than 0.67. This is ascertained below from the simulation of the NMR concentration dependences based on several models of the equilibrium. Hitherto, little has been reported about the 1:1 complex.

Determination of the Equilibrium Constant and Complex-formation Shift. The equilibrium constant (K) and the complex-formation shift (Δ), the latter being equal to the variation in chemical shift when complex formation occurs, can be obtained from the simulation of the concentration dependence in the NMR shifts. For this purpose, the concentration of $MeSnCl_3$ is held constant at an appreciably low molarity ($\approx$0.005 M), while that of the base is varied. In this manner, the concentration dependence of δ ($SnCH_3$) is obtained as depicted in Fig. 2. This is analysed on the basis of the equilibrium of 1) $A+2B=AB_2$ and 2) $A+B=AB$ and $AB+B=AB_2$, considering the results of the above Job plots, which strongly support the 1:2 complex. The calculation based on the $A+2B=AB_2$ is shown in Table 1. In this table, the σ

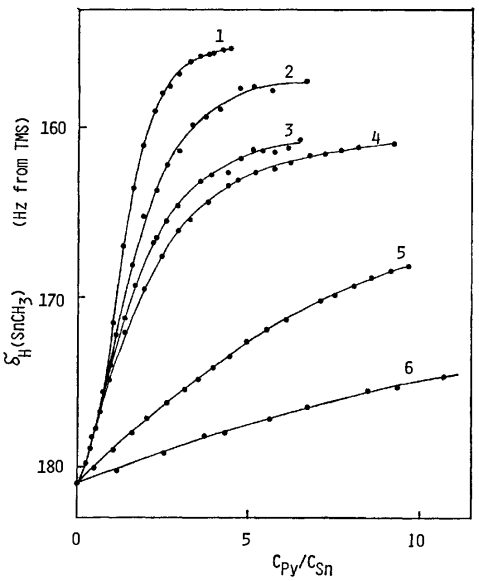

Fig. 2. Concentration dependence of $\delta_H(SnCH_3)$ in the systems of $MeSnCl_3$+4-substituted pyridines.
Substituent: 1; CH_3, 2; H, 3; $COCH_3$, 4; $COOCH_3$, 5; CN, 6; NO_2. C_{Sn} is held constant at $\approx$0.005 mol dm^{-3}.

Table 1. Simulation of the NMR concentration dependence according to the equilibrium of $A+2B=AB_2$

4-Substituent in pyridine	log K[a]	Δ_{AB}[b]	σ[c]
CH_3	5.42	26.1	1.05
H	5.16	23.8	0.49
$COCH_3$	5.22	19.4	0.44
$COOCH_3$	4.74	20.0	0.54
CN	3.63	14.2	0.49
NO_2	2.85	11.4	0.54

a) Equilibrium constants, K, in a unit of (dm^3 mol^{-1})^2. b) In a unit of Hz. c) σ=standard deviation between the shifts of observation and calculation(Hz).

Table 2. Simulation of the NMR concentration dependence according to the equilibrium of A+B=AB and AB+B=AB_2

4-Substituent in pyridine	log K_1[a]	log K_2[a]	Δ_{AB}[b]	Δ_{AB_2}[b]	σ[c]
CH_3	4.07±0.63	3.15±0.11	−6.3±1.2	−26.4±0.5	0.46
H	3.66±0.92	2.79±0.17	−5.8±0.8	−25.3±0.4	0.31
$COCH_3$	3.43±0.34	2.36±0.03	−6.9±0.4	−22.3±0.3	0.19
$COOCH_3$	2.61±0.04	2.35±0.06	−9.2±1.0	−21.7±0.3	0.09
CN	1.51±0.01	1.31±0.01	−13.9±0.2	−22.0±0.3	0.08
NO_2	1.03±0.01	0.83±0.03	−14.8±0.3	−17.4±0.5	0.11

a) K_1 and K_2 in a unit of $dm^3\,mol^{-1}$. b) In a unit of Hz. c) See footnote c) in Table 1.

amounts to 0.4—1.1 Hz. Furthermore, the deviation between the observed and calculated shifts is found to change systematically with the molarity of the base. These facts indicate the inadequacy of the model adopted. When the equilibrium of A+B=AB(K_1) and AB+B=AB_2(K_2) is assumed, four parameters have to be taken into account, *i.e.*, K_1, K_2, δ_{AB}, and δ_{AB_2}, the latter two being identified as the $\delta_H(SnCH_3)$ in the AB and AB_2 species respectively. Under these conditions, it proved necessary to obtain a rough estimate of the four parameters for the simultaneous determination of these parameters in the simulation. That is, the same final values were not always reached if the corresponding initial values were considerably changed. This is not the case in the above two-parameter calculation; it can be interpreted by saying that a small variation in one parameter is compensated for by that in others, with the σ almost unchanged, if the number of adjustable parameters is increased.[10] When the concentration of the base was increased further in Fig. 2, $\delta_H(SnCH_3)$ was found to level off. This ultimate value of $\delta_H(SnCH_3)$ should correspond to δ_{AB_2}, and so a three-parameter calculation becomes feasible, eliminating δ_{AB_2} from the variables. The values of the 4 parameters thus estimated are next used as the initial ones in the four-parameter calculation. Thus, a final set of all the parameters is obtained (Table 2). Errors are also estimated in the CONDEP program for each parameter as equal to the 95% confidence range, which makes the σ^2 larger by 1.96 times when a parameter under consideration is varied, whereas the others are held constant. The average of such errors was usually a little larger than the reproducibility of each parameter in several repeated experiments; it is also depicted in Table 2. The relatively large σ's in the $MeSnCl_3$+4-methylpyridine and +pyridine systems are due to signal broadening. The relatively large errors in log K_1 are caused by the experimental concentration conditions; that is, our experimental concentrations were rather suitable for the precise determination of small values of K_1 and K_2, but they were too high for the large value of K_1 to be determined more accurately.

Equilibrium Constant. A linear correlation is observable between the stability constants of the 1:1 and 1:2 complexes (Fig. 3). A least-squares fit by means of the $y=ax$ equation proves the satisfactory linearity between them:

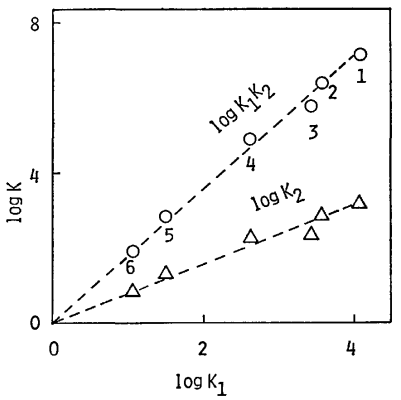

Fig. 3. Plots of log K_1K_2 and log K_2 against log K_1. The numbering corresponds to that in Fig. 2.

$$\log K_1K_2 = 1.78 \log K_1, \qquad \sigma = 0.20. \tag{1}$$

This equation also implies a linear relation between log K_1 and log K_2, a least-squares fit leading to log K_2=0.78 log K_1, and σ=0.20. These equations are reflections of the colinearity in the free-energy changes in the formation of 1:1 and 1:2 complexes; the latter equation also means that the absolute value of the free-energy change in the second step is decreased to *ca.* 3/4 of that in the first step. Such a simple relation may be understood as indicative of the absence of a particular derivative in the pyridines treated here, which exerts a specific steric effect or which behaves differently in the complex formation.

It may be seen from Fig. 4 that log K_1, log K_2, and log K_1K_2 change in parallel with pK_a.[12] The fact that they are not in a strictly linear relation is obvious from the plots of log K_2, for which the experimental accuracy is excellent. Such deviation is a little improved if log K_2 is plotted against the effective substituent constant($\bar{\sigma}$) determined from the Menschutkin reaction of pyridines with ethyl iodide in nitrobenzene[13] (Fig. 5). The Hammett ρ value can be determined from the log K/K_0 *vs.* $\bar{\sigma}$ plots and is 2.9, which is equal to the value for the Menschutkin reaction, *i.e.*, 2.94.[13] This indicates that the donor-acceptor bond formation is less sensitive to changes in electron density on the N atom than is the dissociation of pyridinium ions (ρ=6.01[12] and 6.24[14]). This is a reasonable result, because the ionicity in the present donor-acceptor bond should be smaller than that in the N^+–H bond of the pyridinium ion. As

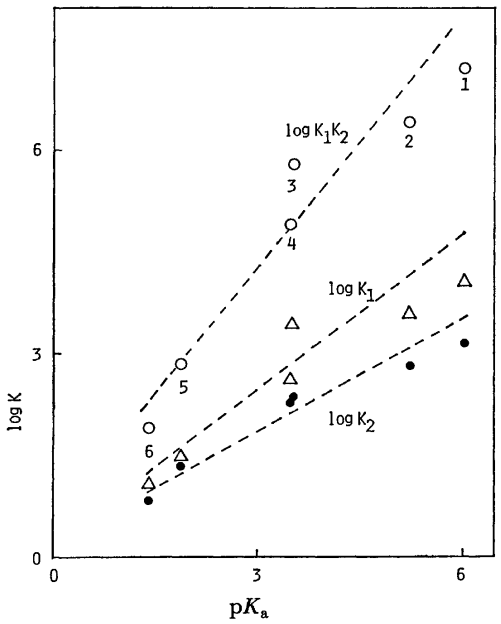

Fig. 4. Correlation between the equilibrium constant and basicity of the pyridine (pK_a).
The numbering corresponds to that in Fig. 2. pK_a's are cited from Ref. 12.

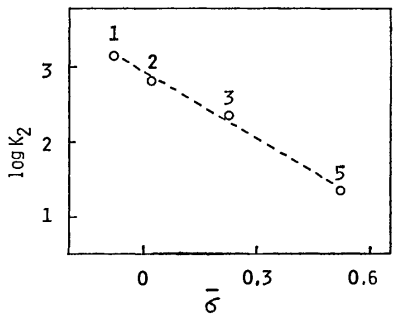

Fig. 5. Correlation between log K_1 and $\bar{\sigma}$ in nitrobenzene.
The numbering corresponds to that in Fig. 2. $\bar{\sigma}$ is cited from Ref. 13 and is available for the four derivatives among the ones treated here.

far as the electron-accepting group is concerned, the σ-effect is known to be a dominant factor in the substituent effect on the dissociation of the pyridinium ion[12,15] and on the above Menschutkin reaction.[13] Therefore, a parallel tendency between the log K's and pK_a as well as $\bar{\sigma}$ can be interpreted as indicating dominant σ-bonding in the formation of the present donor-acceptor complexes.

The distribution curve of $MeSnCl_3$ is shown in Fig. 6 for the $MeSnCl_3$+4-methylpyridine and +4-cyanopyridine systems. This figure clearly demonstrates that an appreciable amount of the 1:1 complex is formed in the solution. In Fig. 6a) the distribution to the free species of $MeSnCl_3$ rapidly falls off with the increase in the molar ratio, $C_{Py}/_{Sn}C$. This is responsible for the relatively large error in log K_1 in this system. If the initial concentration of $MeSnCl_3$ is reduced further, the fall-off will become slower, making the value of K_1 more accurate. However,

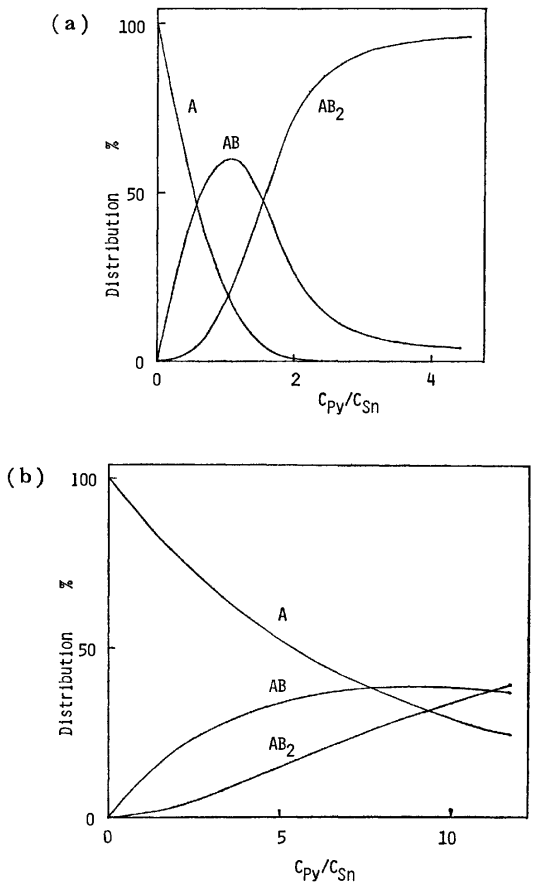

Fig. 6. Distribution curves of $MeSnCl_3$ in the a) $MeSnCl_3$+4-methylpyridine and b) $MeSnCl_3$+4-cyanopyridine systems.
C_{Sn} and C_{Py} are molarities of $MeSnCl_3$ and the pyridines, respectively. C_{Sn} is held constant at $\approx$0.005 mol dm^{-3}. A=$MeSnCl_3$. B=Pyridine derivative.

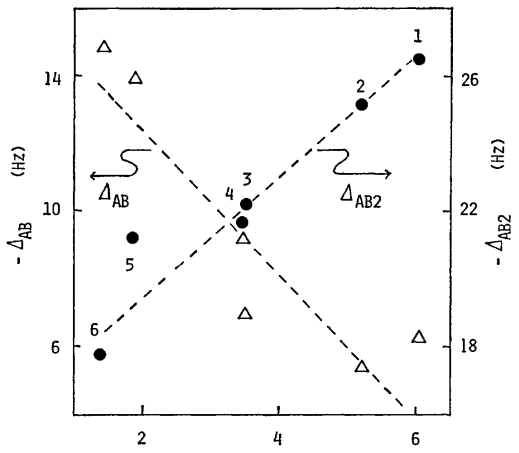

Fig. 7. Plots of Δ_{AB} and Δ_{AB2} against pK_a.
The numbering corresponds to that in Fig. 2. pK_a is cited from Ref. 12. See text for the definition of Δ_{AB} and Δ_{AB2}.

such an experiment is beyond the sensitivity of the spectrometer used here.

Complex-formation Shift. The complex-formation shifts, Δ_{AB} and Δ_{AB2}, which are defined as Δ_{AB}=

$\delta_{AB}-\delta_A$ and $\Delta_{AB2}=\delta_{AB2}-\delta_A$, are all negative, indicating a high-field shift on the formation of the complex. This is consistent with the expectation from the electron transfer in the donor-acceptor bond. When Δ_{AB} and Δ_{AB2} are plotted against pK_a, a nearly linear relation is obtained (Fig. 7). It is reasonable that Δ_{AB2} is varied to the high-field side by the more basic pyridine derivative. On the contrary, Δ_{AB} is seen to vary inversely with the basicity of the pyridine derivative, although the plots in Fig. 7 are scattered, reflecting the relatively large errors in $\log K_1$. As a reason for this inverse dependency, the anisotropy of the pyridine ring may be pointed out; it originates from the ring current effect. That the anisotropy effect really acts is also suggested by the variation of $\delta_H(SnCH_3)$ in Me_2SnCl_2, which moves toward the low-field side on the addition of pyridine, contrary to the case when DMSO or HMPA is added. A detailed analysis of this effect will be worthwhile for the elucidation of structural problems in solution; it will be the subject of further work.

References

1) I. G. A. Luijten, "Applications and Biological Effects of Organotin Compounds," in "Organotin Compounds," ed by A. K. Sawyer, Marcel Dekker, New York (1972), Vol. 3, Chap. 12.

2) "Organotin Compounds; New Chemistry and Applications," ed by J. J. Zuckerman, *Adv. Chem. Ser.*, **157**, Am. Chem. Soc., Washington (1976).

3) Y. K. Ho and J. J. Zuckerman, *J. Organomet. Chem.*, **49**, 1 (1973).

4) H. W. Jung, R. Maul, S. Kintopf, W. Kloss, and R. Knapp, Ger. Patent 2437586 (1975); *Chem. Abstr.*, **83**, 10404n (1975).

5) E. Ochiai, *J. Org. Chem.*, **18**, 534 (1953).

6) V. S. Petrosyan, N. S. Yashina, and O. A. Reutov, *Adv. Organomet. Chem.*, **14**, 63 (1976).

7) E. V. Van den Berghe and G. P. Van der Kelen, *J. Organomet. Chem.*, **11**, 479 (1968).

8) A graphic method and a trial-and-error method have been reported regarding the infrared data in $SnCl_4$+benzonitrile systems (Ref. a) and the calorimetric titration data in organotin compound+Lewis base systems (Ref. b) respectively. a) T. L. Brown and M. Kubota, *J. Am. Chem. Soc.*, **83**, 331 (1961). b) Y. Farhange and D. P. Graddon, *J. Organomet. Chem.*, **87**, 67 (1975).

9) H. Fujiwara, F. Sakai, and Y. Sasaki, to be submitted; see Ref. 10. The SCD program in Ref. 10 is extended to apply also for the observation from the side of B, and it is revised to use a minimization procedure of Simplex and a modification of the Davidon-Fletcher-Powell method.

10) H. Fujiwara, F. Sakai, and Y. Sasaki, *J. Phys. Chem.*, **83**, 2400 (1979).

11) This fact is consistent with the results in the Me_2SnCl_2+pyridine system (Ref. 10).

12) A. Fisher, W. J. Galloway, and J. Vaughan, *J. Chem. Soc.*, **1964**, 3591.

13) A fisher, W. J. Galloway, and J. Vaughan, *J. Chem. Soc.*, **1964**, 3596.

14) M. Sawada, M. Ichihara, Y. Yukawa, T. Nakachi, and Y. Tsuno, *Bull. Chem. Soc. Jpn.*, **53**, 2055 (1980).

15) The σ-effect is about 3 times stronger than the π-effect for electron-accepting groups, according to the equation in Ref. 14:

$$\Delta pK_a = 6.49\sigma_i + 9.50\sigma_\pi^+ + 2.20\sigma_\pi^- - 0.04.$$

The Thermal Decomposition of Sodium Nitrate and the Effects of Several Oxides on the Decomposition

Yoshio Hoshino,* Taizo Utsunomiya, and Osami Abe

Research Laboratory of Engineering Materials, Tokyo Institute of Technology, Nagatsuta, Midori-ku, Yokohama 227

(Received August 15, 1980)

The thermal decomposition of sodium nitrate and the effects of several oxides, such as silica, titania, zirconia, alumina, and magnesia, on the decomposition were studied up to 900 °C by means of the thermal analysis, gas analysis, and chemical analysis of the reaction products. The reaction of sodium nitrate and silica was especially investigated in some detail over a wide composition range. The thermal decomposition of sodium nitrate started at about 450 °C. The gases formed were O_2, NO, and N_2, the formation of N_2 being detected above 680 °C. The thermal decomposition of sodium nitrate was supposed to consist of the following three successive or concurrent reaction processes, according to the degree of the reaction: (I) the decomposition of sodium nitrate to nitrite and oxygen, (II) the first-order liquid-phase reaction, with some kind of quantitative relationship between nitrate and nitrite, and (III) the formation reaction of sodium oxide, expressed by the Avrami-Erofe'ef equation. The (II) and (III) reaction processes can be reasonably interpreted if the existence of the peroxide ion is assumed. Acidic oxides, such as silica and titania, were supposed to lower the activation energy of the (III) reaction process by forming stable salts with sodium nitrate and/or its intermediate reaction products. The effects of these oxides on the thermal decomposition of sodium nitrate could be interpreted by the relative scale of the acidity of oxides.

Sodium nitrate is one of the most important components used in the chemical industry. In recent years, it has been used as the source of the sodium used in multi-component glass fibers for optical waveguides.[1] This is because sodium nitrate has some advantages, such as oxidation and clarification effects, a low melting point, and a low decomposition temperature. However, few studies have been made of the reaction of sodium nitrate and several oxides. Furthermore, in the studies of the thermal decomposition of sodium nitrate,[2-6] there are some disagreement concerning the decomposition temperature and/or the kind of gas formed.

In the previous paper,[7] the following results were obtained with regard to the reaction of sodium nitrate and silica: (1) the formed gases in this system up to 800 °C were O_2 and NO; (2) 3 to 7 wt% sodium nitrite was present in the reaction system just before the formation of gas ceased; (3) the reaction products were sodium metasilicate (Na_2SiO_3) and disodium disilicate ($Na_2Si_2O_5$), depending on the silica content in the sample mixtures, and (4) the history of preparation and the relative surface area of the silica scarcely affect this reaction. However, the mechanism of the thermal decomposition of pure sodium nitrate was not investigated, since this decomposition appeared to be difficult to investigate in view of the creep-out of the melt of sodium nitrate from a platinum reaction vessel. In relation to the decomposition of sodium nitrate, disagreements among the other workers' paper[2-6] seem to be caused by not taking account of the possibility of the effect of the experimental conditions, such as the measuring atmosphere and the material of the reaction vessel, on the decomposition, and by not setting up precise conditions of gas analysis.

In this study, the thermal decomposition of sodium nitrate and the effects of silica, titania, zirconia, alumina, and magnesia on the decomposition were investigated by a simultaneous measurement of thermogravimetry (TG), differential thermal analysis (DTA), differential thermogravimetry (DTG), and gas chromatograpy (GC), by which the gas formed could be analysed directly in a short time. Furthermore, the effect of silica addition was investigated over a relatively wide range of silica compositions.

Experimental

Samples. Reagent-grade sodium nitrate, titania, zirconia, and magnesia from the Wako Chemical Industries, Ltd., and alumina from the Nishio Industries, Co., Ltd., were ground under 100 mesh in an agate mortar and dried in an oven at 100 °C. Commercially available α-quartz was also ground under 100 mesh by means of a ball mill, washed with acid and distilled water, and dried in the oven. Sodium nitrate was mixed with one of these oxides by dry-blending at each run. The composition of sample is indicated by the atomic ratio, X_i (=i/Na; i=Si, Ti, Zr, Al, or Mg), in each sample mixture.

Apparatus and Procedure. The TG-DTA measurement was carried out with a high-temperature thermobalance from the Rigaku Denki Co., Ltd. The DTG was carried out with a differentiator from the Rikadenki Kogyo Co., Ltd., in order to differetiate the TG curve. A GC-2C-type gas chromatograph from the Shimadzu Seisakusho, Ltd., was used for quantitative gas analysis, in which silica-gel and molecular-sieve 5A were used as the column-packing reagents after treatment by the method descrived by Sakaida *et al.*[8]

The simultaneous measurement of TG-DTA, DTG, and GC was carried out as follows. At first ,the sample mixture (less than 80 mg) was weighed in a reaction vessel (5 mm in diameter, 5 mm in depth), and this vessel was placed on a sample holder in the thermobalance; then, the ambient gas was introduced into the measuring system and adjusted to the desired flow rate (50 $cm^3\ min^{-1}$). Secondly, the sample was heated at 20 °C min^{-1} and then held at 250 °C for about one hour. By this procedure, a trace amount of adsorbed water could be removed. The sample was then heated up to the desired temperature at the rate of 5 °C or 20 °C per min. In gas chromatography, argon was used as the carrier gas, and the gas formed from the sample was introduced into the gas chromatograph every 2 min

It took less than one minute from gas formation to gas sampling.

On the other hand, the reaction products were identified by X-ray powder diffractometry with Cu $K\alpha$ radiation. These reaction products were also used for quatitative analysis. About 100 mg of the reaction products were dissolved in water for one hour and then filtered. The unreacted silica was determined from the amount of dissolution residue. The silicates and total sodium were determined by atomic absorption spectrometry and flame emission spectrometry respectively. The sodium nitrate and sodium nitrite were determined by using a nitrate-ion electrode from the Toa Electronics, Ltd., and by UV spectrometry with sulfanilic acid respectively.

Results and Discussion

Effect of Experimental Condition on the Thermal Decomposition of Sodium Nitrate. In order to investigate the thermal decomposition of sodium nitrate and the effects of several oxides on the reaction, various factors which seemed to affect the reaction were investigated. They are, for example, the amount of the sample mixture, the heating rate, the ambient gas and its flow rate, and the material of the reaction vessel. The use of a small amount of the sample would result in a better thermal response. Taking the accuracy of the measurement into consideration, a sample mixture containing 8.5, 10.0 or 17.0 mg of sodium nitrate was used. In the binary system of sodium nitrate and silica, the similar shapes of the TG and DTG curves, and also the similar behavior of gas formation, were shown for the sample with the same value of X_{Si} in the ranges from 14.5 mg to 58.0 mg ($X_{Si}=1.0$) and from 38.0 mg to 77.0 mg ($X_{Si}=5.0$). The heating rate and the flow rate of the ambient gas scarecely affected the decomposition in the range investigated here; therefore, they were not important experimental factors. It is well known that a quartz or Pyrex-glass reaction vessel affects the decomposition. The reason for this is that sodium nitrate reacts with these vessels to form stable salts. On the other hand, platinum and stainless steel vessels seldom affect the decomposition; however, a creep-out of the fused sample from the vessel sometimes occurs. The reactivity of the vessels and the creep-out of the sample were investigated with platinum, gold, and two kinds of sintered magnesia vessels (MgO-A vessel: pressed at 9.3×10^3 kg cm^{-2} and heated at 1000 °C for one day; MgO-B vessel: pressed at 1.85×10^4 kg cm^{-2} and heated at 1000 °C for two days). There are no appreciable difference among these reaction vessels. Figure 1 shows the DTG curves and the behavior of the gas formation when a platinum or MgO-B vessel was used. The rate of weight loss, $d\alpha/dt$, is the differential of the fraction of weight loss, α, with respect to the reaction time, t. R_{O_2}, R_{NO}, and R_{N_2} are the formation rates of O_2, NO, and N_2, respectively per mole of sodium nitrate. These results resemble each other below 700 °C. If the MgO-B vessel affected the decomposition, this behavior when a MgO-B vessel is used would be similar to that in the reaction of sodium nitrate and magnesia, which will be described later. When the sodium nitrate

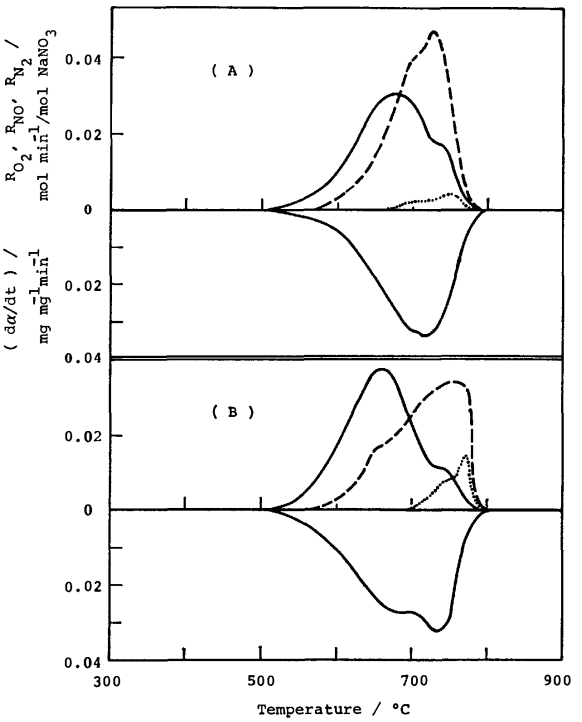

Fig. 1. DTC curves and the behavior of gas formation for the thermal decomposition of sodium nitrate with platinum (A) or MgO-B (B) reaction vessel in argon atmosphere. The solid line, the interrupted line and the dotted line indicate the formation rate of O_2 (R_{O_2}), NO (R_{NO}), and N_2 (R_{N_2}), respectively.

was held at a constant temperature, the MgO-B vessel, where no creep-out of the melt occurred, was used because it required a long time for measurement (for example, it took 260 min at 592 °C).

Then, the effect of the heating atmosphere, such as argon, nitrogen, oxygen and air on the reaction of the binary system of sodium nitrate and silica was investigated at the flow rate of 50 cm^3 min^{-1}. Figure 2 shows the TG curves and DTG curves for the reaction in argon (a) and oxygen (b). The TG and DTG curves for the reaction in nitrogen showed a shape similar to those obtained in argon. In air, they showed an intermediate shape between (a) and (b). The DTG curve of (b) showed peaks at 730 °C and 755 °C and shifted to a higher temperature than that of (a). From these results, it is evident that the partial pressure of oxygen (perhaps also nitrogen monoxide) affects the decomposition.

Thermal Decomposition of Sodium Nitrate. Figure 3 shows the results of the simultaneous measurement of TG-DTA, DTG, and GC on the thermal decomposition after heating at 5 °C min^{-1}. The DTA curves show the endothermic peaks at 278 °C and 308 °C which correspond to the transformation and melting. The TG and DTG curves indicate that the decomposition finished at 800 °C. It is found from the behavior of gas formation that, at first, sodium nitrate generates O_2, secondly, O_2 and NO, and then, over 680 °C, O_2 NO, and N_2. On the decomposition of sodium nitrite, the formation of N_2 was scarecely detected, so the formation must be caused by the reaction pro-

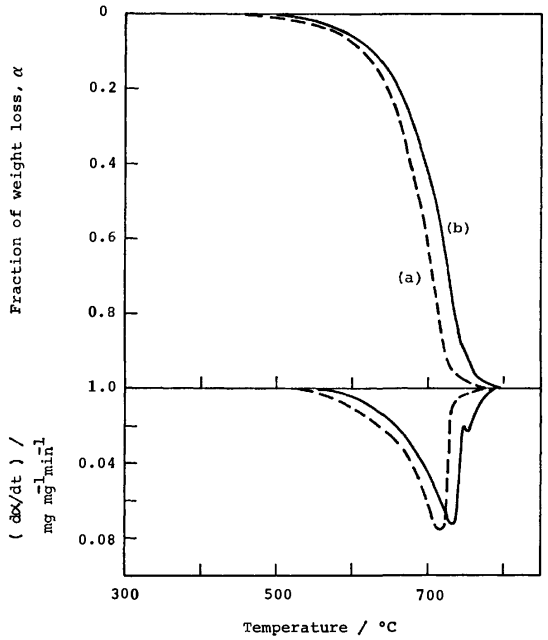

Fig. 2. TG and DTG curves for the reaction of sodium nitrate and silica ($X_{Si}=1.0$) in argon (a) or in oxygen (b).

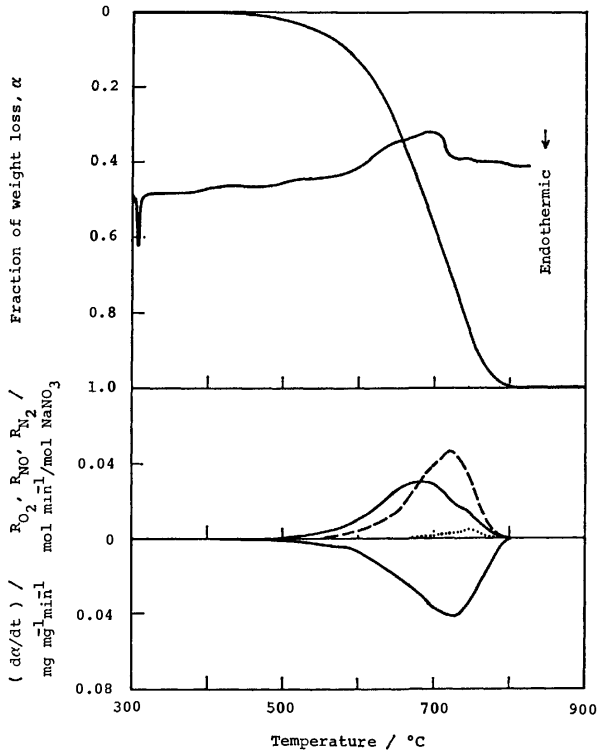

Fig. 3. TG, DTA, and DTG curves, and the behavior of gas formation for the thermal decomposition of sodium nitrate in argon atmosphere. The solid line, the interrupted line and the dotted line indicate R_{O_2}, R_{NO}, and R_{N_2}, respectively.

cess that sodium nitrate directly decomposes or reacts with its reaction products.

Furthermore, the decomposition was investigated at various constant temperatures in the range from 592 °C to 703 °C. Figure 4 and 5 show the TG curves

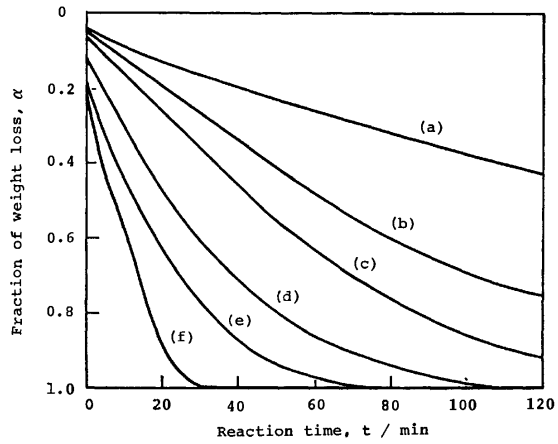

Fig. 4. TG curves for the thermal decomposition of sodium nitrate in argon.
(a): 592 °C, (b): 611 °C, (c): 625 °C, (d): 648 °C, (e): 672 °C, (f): 703 °C.

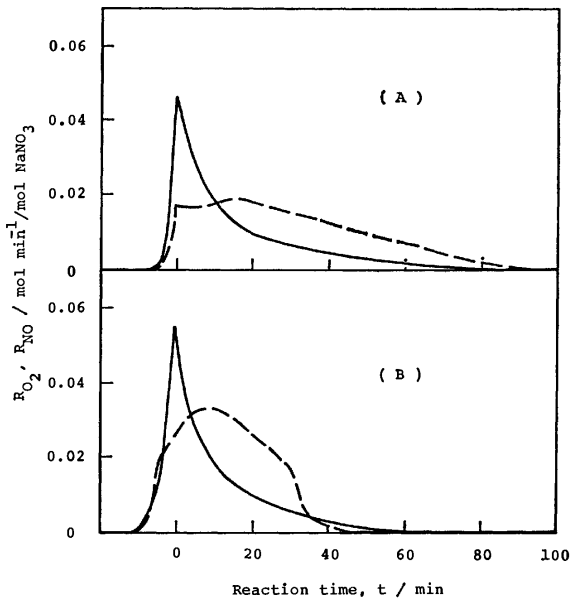

Fig. 5. The behavior of gas formation for the thermal decomposition of sodium nitrate at 648 °C (A) and 672 °C (B). The solid line and interrupted line indicate R_{O_2} and R_{NO}, respectively.

and the behavior of gas formation respectively.

The TG curves in Fig. 4 were analysed by the method described by Hancock and Sharp.[9] This method is based on the Avrami-Erofe'ef equation (Eq. 1):

$$(-\ln(1-\alpha))^{1/n} = kt, \quad (1)$$

where α is the fraction reacted, k is the kinetic constant, and t is the reaction time. The n value is a constant peculiar to this type of reaction; usually, it is an integer larger than 2. Hancock showed that, when $\ln(-\ln(1-\alpha))$ is plotted against ($\ln t$), an approximately linear relation is observed for many kinds of solid-state reactions and the first-order and zeroth-order reactions. For the first- and zeroth-order reactions, the n slopes equal unity and 1.24 respectively. Figure

6 illustrates the ln (−ln (1−α)) *vs.* (ln *t*) plots for the decomposition of sodium nitrate. Figure 6 shows the ranges in which the kinetic equation of the first-order reaction is valied ($\alpha \leqq 0.85$) and in which the Avrami-Erofe'ef equation with $n=3$ is valid ($\alpha \geqq 0.85$). In the α ranges mentioned above, the TG curves being

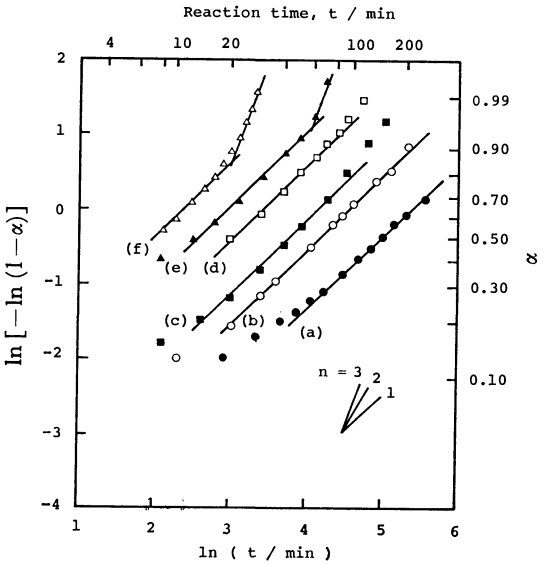

Fig. 6. ln(−ln(1−α)) versus (ln *t*) plot for the thermal decomposition of sodium nitrate.
(a): 592 °C, (b): 611 °C, (c): 625 °C, (d): 672 °C, (d): 703 °C.

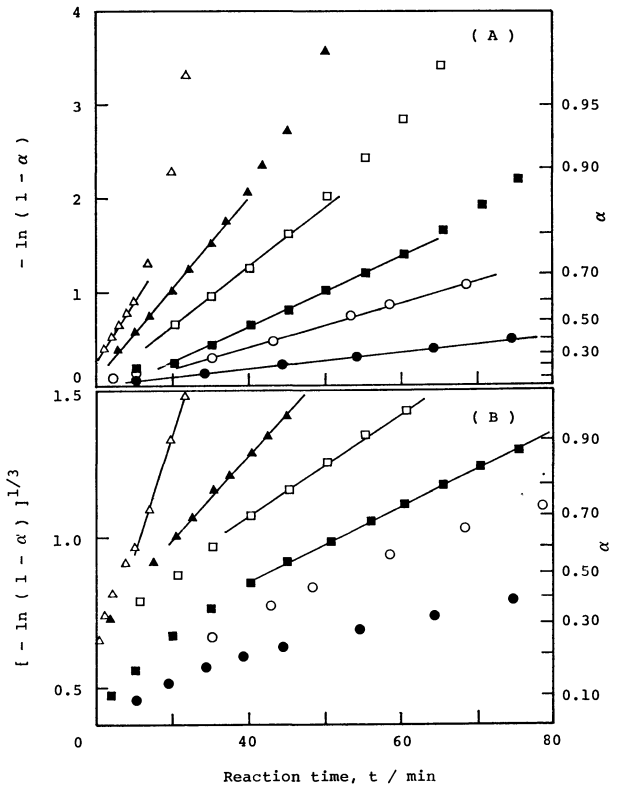

Fig. 7. Estimation of TG curves with the kinetic equation of the first order reaction (A) and Avrami-Erofe'ef equation with $n=3$ (B) for the thermal decomposition of sodium nitrate.

estimated with the kinetic equation of the first-order reaction and the Avrami-Erofe'ef equation, Fig. 7 obtained. They give approximately linear plot. The kinetic constants were obtained from these slopes. From their Arrhenius plot, the apparent activation energy was calculated to be 223 kJ mol^{-1} for the first-order reaction below 648 °C and 243 kJ mol^{-1} for the $n=3$ range above 672 °C.

The behavior of gas formation was analysed by the method of plotting the formation ratio of O_2 to NO *versus* α. They are illustrated in Fig. 8, which shows that the formation of O_2 is remarkable at the initial and final stages of the reaction. In the middle stage of the reaction, the R_{O_2}/R_{NO} value is nearly constant in the α range from 0.25 to 0.75. This strongly suggests that it is reasonable to divide the thermal decomposition of sodium nitrate into three successive or concurrent reaction processes. From the analysis of the solid-state reaction products, it was found that the amount of sodium nitrite in the melt increased at the initial stage of the reaction and decreased at the middle and final stages. The three predominant reaction processes in the initial, middle and final stages of the reaction may be summalized as follows:

Process I (predominant in the initial stage); the thermal decomposition of sodium nitrate to nitrite and oxygen (Eq. 2)

$$NaNO_3 = NaNO_2 + 1/2O_2. \quad (2)$$

This reaction process has been studied by several workers.[2-6]

Process II (predominant in the middle stage); the first-order liquid-phase reaction with some kind of quantitative relationship between nitrate and nitrite in the melt; the reverse reaction of sodium nitrite to form nitrate also occured. This can reasonably be interpreted if the existence of sodium peroxide or

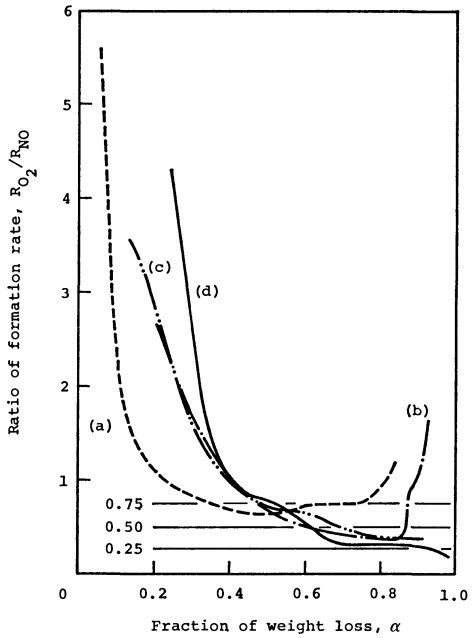

Fig. 8. The ratio of the formation rate of O_2 to NO, R_{O_2}/R_{NO} at various constant temperatures.
(a): 611 °C, (b): 648 °C, (c): 672 °C, (d): 703 °C.

hyperoxide as an intermediate during the decomposition of sodium nitrate is assumed. Paniccia *et al.*[10] reported that sodium peroxide was the main basic species in (sodium–potassium) nitrate eutectic *in vacuo*. Under the argon flow, peroxide is also considered to be the main basic species. This reaction process is expressed by the following equations:

$$NaNO_2 = 1/2Na_2O_2 + NO \quad (3)$$

$$Na_2O_2 = Na_2O + O \quad (4)$$

$$NaNO_2 + O = NaNO_3 \quad (5)$$

$$Na_2O_2 + O = NaO + O_2. \quad (6)$$

As the equilibrium constant of the I reaction process (Eq. 2) increases with an increase in the temperature, the R_{O_2}/R_{NO} value of the II precess will be close to 0.25, which is the formation ratio of O_2 to NO in Eq. 7:

$$NaNO_2 = 1/2Na_2O + NO + 1/4O_2 \quad (7)$$

Precess III (predominant in the final stage); the reaction process to form sodium oxide. Eq. 1 was applied to the solid-state reaction by taking account of the nucleation at various places in a crystal and the gradual piling up of these nuclei with the progress of the reaction. However, in the III process, it is reasonable to conclude that the reaction proceeds by means of a mechanism by which oxide precipitates are formed from the melt and the precipitate becomes the nuclei of the subsequent reaction. This process was remarkable at higher temperatures.

Effects of Several Oxides on the Decomposition. From the viewpoint of the Lux-Flood acid-base theory, sodium nitrate is considered to act as a base in the reaction with acidic oxides. Therefore, the effects of oxides with different acidities on the thermal decomposition of sodium nitrate was investigated at a constant heating rate. The results obtained are shown in Figs. 9 and 10.

The DTA curves in Fig. 9 show the relatively large endothermic peaks for the reactions at about 700 °C, 640 °C, and 690 °C in the systems containing silica (b), titania (c), and zirconia (d) respectively. In the (b) system, the endothermic peak at 575 °C indicates the transformation of α- to β-quartz.

To understand the effects of oxides in detail, the $2Z_i/r$ values were calculated as one of the scale of the acidity of oxides: here, Z_i is the charge of the metal ion, M^{Z_i+}, and r is the interatomic distance. The values of r were calculated from the data of Pauling.[11] The $2Z_i/r$ values express the relative bond strength between M^{Z_i+} and O^{2-}, the larger value indicating the stronger acidity. These values for several oxides are shown in Table 1. In Fig. 10, the behavior of the gas formation in the reaction of binary systems

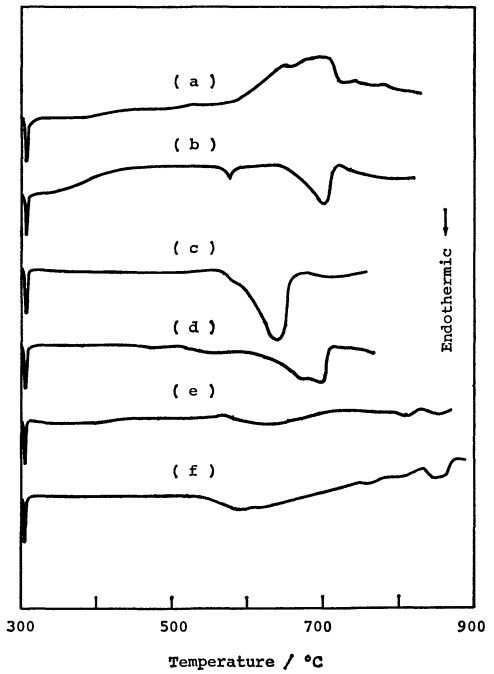

Fig. 9. DTA curves for mixtures of binary system including sodium nitrate (0.2 mmol) with $X_i=2.0$.
(a): Sodium nitrate, (b): $NaNO_3+SiO_2$, (c): $NaNO_3+TiO_2$, (d): $NaNO_3+ZrO_2$, (e): $NaNO_3+Al_2O_3$, (f): $NaNO_3+MgO$.

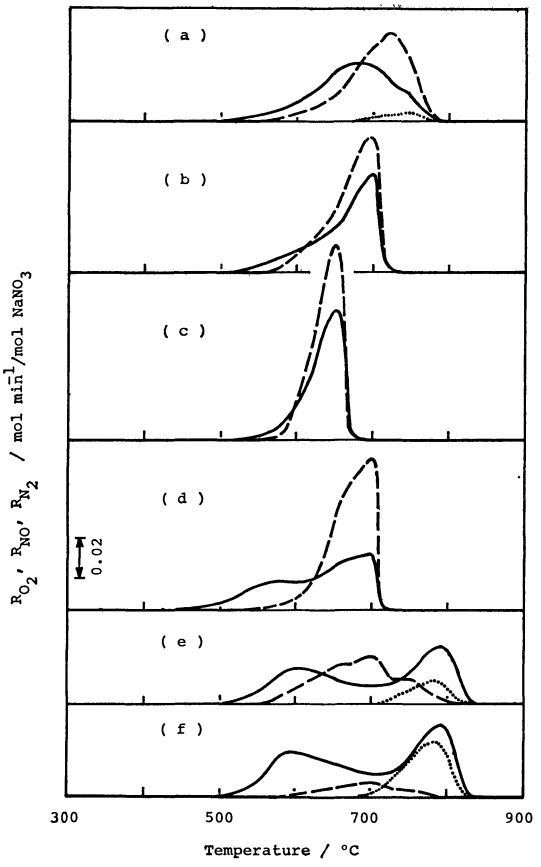

Fig. 10. The behavior of gas formation by the reaction in binary system containing sodium nitrate (0.2 mmol) with $X_i=2.0$.
(a): Sodium nitrate, (b): $NaNO_3+SiO_2$, (c): $NaNO_3+TiO_2$, (d): $NaNO_3+ZrO_2$, (e): $NaNO_3+Al_2O_3$, (f): $NaNO_3+MgO$.

TABLE 1. $2Z_i/r$ VALUES FOR SEVERAL OXIDES

Na_2O	MgO	Al_2O_3	ZrO_2	TiO_2	SiO_2
0.83	1.95	3.26	3.54	3.81	4.71
weak	←	acidity		→	strong

containing silica (b), titania (c), zirconia (d), alumina (e), and magnesia (f), arranged in the order of acidity, is shown. The thermal decomposition of pure sodium nitrate (a) is also presented for the sake of comparison. Strong acidic oxides, such as silica and titania, remarkably accelerate the thermal decomposition of sodium nitrate ((b) and (c)). In the reaction of sodium nitrate and such basic oxides as magnesia (f), the formation of O_2 in the temperature range from 500 °C to 600 °C is characteristic. When the basic oxides are characterised by the formation rate of O_2 at 600 °C, this decreases in the order of: (f), (e), (d), and (c)≈(b). This trend agrees well with the order of acidities in Table 1. From the values in Table 1, the behavior of gas formation in the (c) system would be expected to show an appearance intermediate between (b) and (c), but Fig. 10 shows that the reaction in (c) is more accelerated than in (b). The reason for this is that the titania used in this experiment was very fine (the volume avarage particle size: 4 μm).

Reaction of Sodium Nitrate and Silica. Silica is an important material in the glass industry. Therefore, the reaction in the binary system of sodium nitrate (0.1 or 0.2 mmol) and silica was investigated at various constant temperatures from 570 °C to 700 °C and over a relatively wide range of silica composition. The results of the analysis of the reaction products (X_{Si}=0.5 to 5.0) were similar to those in the previous report.[7] Figure 11 shows the behavior of gas formation at 650 °C. When the X_{Si} value is 1.0, the range in which the R_{O_2} and R_{NO} values are both constant exists at the reaction times from 12 to 38 minutes. Even if the X_{Si} value is 0.5, the reaction is accelerated by silica, and when X_{Si} is 3.0 and 5.0, the reaction is more accelerated than the reaction with X_{Si}=1.0. In all cases, a range of nearly constant R_{NO} values was observed. Figure 12 shows the DTG curves of these systems. They also indicate the increase of the rate of weight loss with the increase in the X_{Si} value. The characteristic acceleration of the reaction was found at the final stage of the reaction. The peak based on this acceleration shifted to the shorter-reaction-time side with the increase in X_{Si} value, until it could not be detected at all at X_{Si}=5.0. When the $(d\alpha/dt)_{\alpha=0.25}$ values, which is the rate of weight loss at α=0.25, were plotted versus X_{Si} as a scale of the effect of silica, Fig. 13 was obtained. The larger X_{Si} value gives the larger $(d\alpha/dt)_{\alpha=0.25}$ value. Nearly constant $(d\alpha/dt)_{\alpha=0.25}$ values were obtained at $X_{Si}\geqq 5.0$ and $X_{Si}\leqq 1.0$. These results indicate that, at $X_{Si}\leqq 1.0$, the acceleration of the decomposition reaction of sodium nitrate by the addition of silica is scarcely observed in the first stage of the reaction ($\alpha\leqq 0.25$), but it becomes evident with the increase in the X_{Si} value, while at $X_{Si}\geqq 5.0$ the degree of acceleration is almost constant.

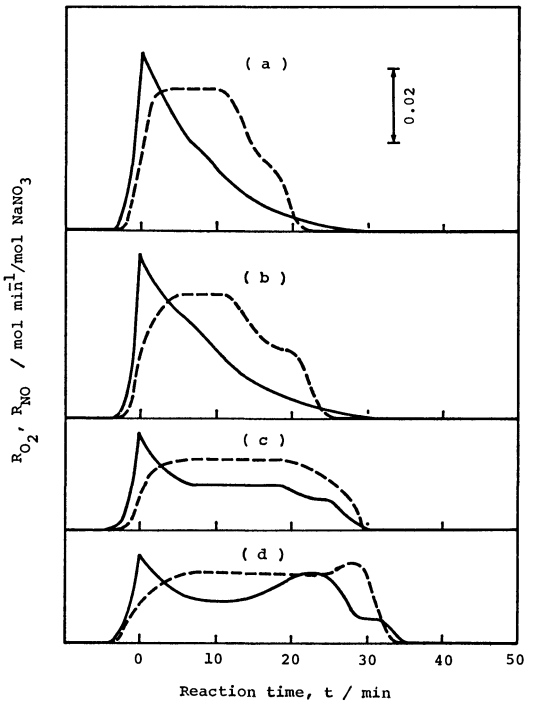

Fig. 11. Effect of silica on the behavior of gas formation at 650 °C.
(a): X_{Si}=5.0, (b): X_{Si}=3.0, (c): X_{Si}=1.0, (d): X_{Si}=0.5. The solid line and interrupted line indicate R_{O_2} and R_{NO}, respectively.

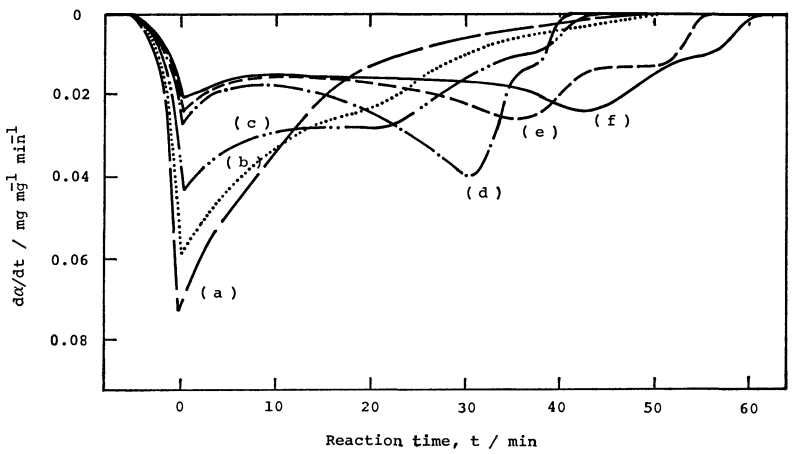

Fig. 12. Effect of silica on DTG curves at 650 °C. (a): X_{Si}=5.0, (b): X_{Si}=4.0, (c): X_{Si}=3.0, (d): X_{Si}=2.0, (e): X_{Si}=1.0, (f): X_{Si}=0.5.

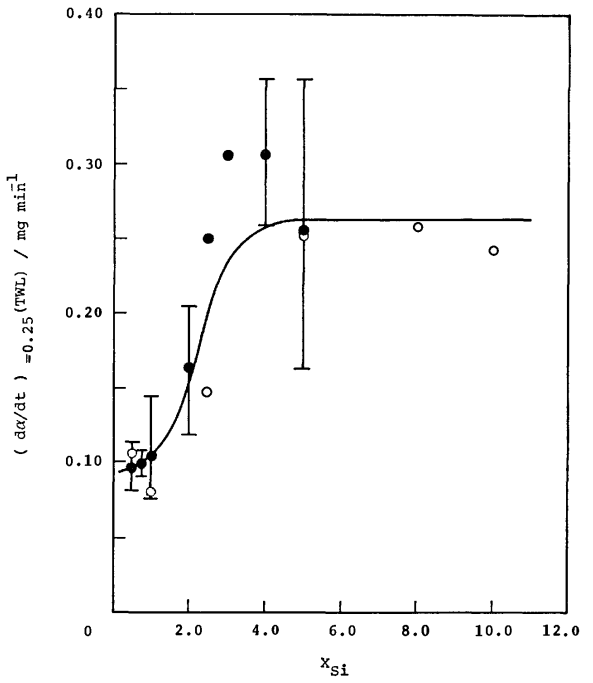

Fig. 13. $(d\alpha/dt)_{\alpha=0.25}$ (TWL) values for various X_{Si} values at 650 °C. (TWL) means the total amount of weight loss.
Open circle: 0.1 mmol $NaNO_3$, closed circle: 0.2 mmol $NaNO_3$.

By analysing TG curves by means of Hancock and Sharp's method, the n value was obtained as close to 3 at $\alpha \geqq 0.25$. This indicates that the reaction of sodium nitrate and silica is expressed by Avrami-Erofe'ef equation with $n=3$ and that the diffusion of Na^+ into silica ($n=0.54$ to 0.62) or the phase-boundary reaction ($n=1.07$, 1.11) is not a rate-determining step. Thus the mechanism of the reaction of this system is considered to be one in which the main basic species, sodium peroxide, reacts with a strong acidic oxide, silica, and forms the precipitate of silicate, and that they then grow in the melt. The apparent activation energy, ΔE, and the frequency factor, k_0, are shown in Table 2 for various X_{Si} values. The increase in k_0 supports the above-mentioned mechanism. ΔE is lower at $X_{Si}=1.0$ and 3.0 compared to that of the thermal decomposition of pure sodium nitrate. The reason for this is probably that silica, which is a strong acidic oxide, reacts with the basic species, such as sodium peroxide, and so lowers the activation energy of the reaction. Sodium metasilicate and disodium disilicate were identified as the reaction products. It is easily supporrted that these reaction products also affect the decomposition of sodium nitrate. At $X_{Si}=4.0$ and 5.0, a large amount of silicates would be formed and precipitated in the melt and at the boundary in the early stage on the reaction. These silicates are considered to cover a part of the surface of silica and to interfere with the effective contact of melt and silica. The increase in activation energy at $X=4.0$ and 5.0 might thus be caused. If so, about the same value of $(d\alpha/dt)_{\alpha=0.25}$ at $X_{Si} \geqq 5.0$ is considered to result from the competitive effects of covering and acceleration.

Table 2. Apparent activation energy, ΔE, and frequency factor, k_0, for the reaction of sodium nitrate and silica

X_{Si}		ΔE/kJ mol^{-1}		$\ln(k_0/\text{min}^{-1})$	
		a	b	a	b
0	$n=1$	—	223	—	25.5
	$n=3$	243	—	26.7	—
1.0		179	179	20.5	20.5
3.0		204	179	22.9	19.9
4.0		226	198	25.2	22.3
5.0		229	177	25.8	19.8

a: $\alpha \geqq 0.85$.
b: $0.25 \leqq \alpha \leqq 0.85$.

Sodium nitrate in this system may be supposed to decompose through the reactions expressed in Eqs. 2 to 6, but silica would react with sodium peroxide to form sodium metasilicate *via* disodium disilicate.

References

1) S. Ikeda, *Denshi Zairyo*, **1974**, 40.
2) H. R. Bartos and J. L. Margave, *J. Phys. Chem.*, **60**, 256 (1956).
3) J. C. Casanova, *Bull. Soc. Chim. Fr.*, **1959**, 429.
4) E. S. Freeman, *J. Phys. Chem.*, **60**, 1487 (1956).
5) B. D. Bond and P. W. M. Jacobs, *J. Chem. Soc.*, A, **1966**, 1265.
6) R. N. Kust and J. D. Burke, *Inorg. Nucl. Chem. Lett.*, **6**, 333 (1970).
7) Y. Hoshino, T. Utsunomiya, G. Utsugi, and O. Abe, *Nippon Kagaku Kaishi*, **1980**, 690.
8) R. R. Sakaida, R. G. Rinker, R. F. Cuffel, and W. H. Corcoran, *Anal. Chem.*, **33**, 32 (1961).
9) J. D. Hancock and J. H. Sharp, *J. Am. Chem. Soc.*, **55**, 74 (1972).
10) F. Paniccia and P. G. Zambonin, *J. Phys. Chem.*, **78**, 1693 (1974).
11) L. Pauling, "The Nature of the Chemical Bond," 3rd ed, Cornell University, Ithaca (1960), p. 514.

Structural Interpretation of Plasma-polymerized Tetrafluoroethylene

Keiichiro Hozumi,* Keisuke Kitamura, and Tatsuya Kitade
Kyoto College of Pharmacy, Misasagi Nakauchi-cho Yamashina-ku, Kyoto 607

(Received September 4, 1980)

Structural interpretation of plasma-polymerized tetrafluoroethylene produced in a glow discharge chamber is given by referring to ^{19}F-NMR and IR spectroscopy, elemental analysis, and number-average molecular weight determination. The polymer is hardly soluble in the usual organic solvents because of its highly branched structure, making NMR spectroscopy and molecular weight determination impossible. However, the polymer is soluble in 1,2-dibromo-1,1,2,2-tetrafluoroethane and the following structural interpretation could be obtained. The number-average molecular weight is 3600 for the majority of the polymer, consisting of 96 carbon and 129 fluorine atoms within a unit molecule. The IR spectrum shows evidence of some C=C groups and the ^{19}F-NMR spectrum a highly branched and cross-linked structure in which a large number of quaternary carbons are involved in the polymer matrix as compared with CF_2 and CF carbons. The plasma-polymerized tetrafluoroethylene has been characterized in a somewhat different way from the plasma-polymerized ethylene, involving a small number of quaternary carbons.

Polymer thin films deposited on solid substrates by means of plasma polymerization in which monomer gases are exposed to glow discharge have a highly branched and cross-linked structure, uniform film thickness, and are pinhole free. By selective use of the monomer gases we can alter the physico-chemical properties of the polymer films, such as surface free energy, optical transmittance, and electric specificities.[1-3]

Plasma-polymerized fluorocarbons have an extraordinarily low surface free energy and a good optical transparency throughout the visible and infrared regions. Deposition of the plasma-polymer was successfully applied to the hydrophobic coating of ion-crystal windows installed in various infrared instruments and the anti-reflection coating of certain organic lenses.[4-6] We recently reported the use of tetrafluoroethylene (TFE) as a monomer gas by which solid materials of fine and complicated structure such as ashed residue of biological specimens were effectively coated by the hydrophobic plasma-polymer eliminating the initial hygroscopic nature and preserving the three-dimensional microstructures.[7] The results suggest further application of the plasma-polymer to the hydrophobic coating of porous surfaces or granular materials.

We have undertaken to obtain structural interpretation of plasma-polymerized tetrafluoroethylene (PPTFE) mainly by means of ^{19}F-NMR spectroscopy, also by infrared and ESR spectroscopy, elemental analysis, and number-average molecular weight determination. This paper reports a hypothetical model of the atom configration within the polymer molecule having average molecular weight.

Experimental

Monomer Gas. TFE was stored in a pressure tank and supplied to the plasma chamber through a flow meter and a needle valve. The purity was confirmed by a gas chromatograph incorporated with a Porapack column giving no signal of impurity.

Plasma System. A schematic diagram of the apparatus for the plasma polymerization, which is the same as reported[7] is shown in Fig. 1. A valve introducing air was incorporated with the system for occasional cleaning of the polymer film deposited on the inside wall of the plasma chamber by plasma oxidation. The gas pressure in the system was monitored by a MacLeod gauge attached to a three-way manifold located between the plasma chamber and a rotary pump. The plasma in the chamber was initiated and sustained by controlling high-frequency electric power supplied from a 100 W generator operating at 13.56 MHz. Typical operating conditions for the film deposition were 2—3 ml(1 atm)/min for the TFE flow, 20 W for the effective input power, and 0.2—0.4 Torr (13.322 Pa) for the gas pressure. Vapor pressure osmometer, Knauer Dampfdruck Osmometer; IR spectrometer, Shimadzu Model IR-400; ESR spectrometer, JEOL Model JES-FE-3X; ^{19}F-NMR spectrometer, Varian Model EM-390.

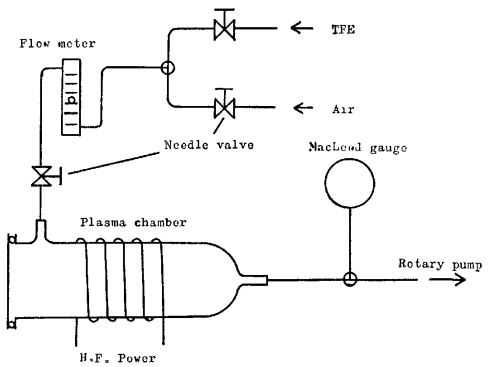

Fig. 1. Schematic diagram of plasma-polymerization apparatus.

Results and Discussion

Solubility of PPTFE in Organic Solvents. TFE monomer gas was polymerized for 60 min in an empty chamber. Solid film was always deposited on the inside wall of the chamber under the plasma conditions employed without forming other types of polymer such as oil or powder. The solid film deposited in the chamber was scraped off and extracted with acetone. However, a large portion of the polymer, obviously of higher degree polymer, remained insoluble. Various other polar or nonpolar organic solvents were examined for removal of the insoluble substance. No usual organic solvent was found to be more effective than acetone.

1,2-Dibromo-1,1,2,2-tetrafluoroethane(DF114B$_2$) was found to be an effective solvent, supposedly because

of the chemical analogy within the two. TFE could be prepared simply by reacting sodium hydroxide with $DF114B_2$.

$DF114B_2$ still left a small fraction of insoluble substance which suggested an extremely high degree of cross-linking. The fraction was rejected from further application to NMR or molecular weight determination.

The acetone and $DF114B_2$ extracts were vacuum-evaporated at room temperature. The dried extracts together with the insoluble residue were weighed in order to determine the weight percent compositions of the initial polymer substance; acetone extract=15%, $DF114B_2$ extract=81%. Only 4% was left as insoluble residue. The acetone extract was dark brown, the $DF114B_2$ extract and the insoluble residue being amber colored.

The acetone and $DF114B_2$ dissolved the respective fractions of the polymer in high concentrations until forming viscous fluid, no quantitative solubility could be obtained. The solubility was therefore determined by use of organic solvents having much less solubility to the individual fractions. The powder sample was put in a centrifuge tube with an organic solvent. The mixture was stirred at room temperature and the resulting suspension was centrifuged (3500 rpm) for 5 min. 5 ml of the supernatant layer was transferred to a weighed beaker which was then vacuum-evaporated at room temperature. The beaker was weighed and the solubility calculated. The solubility data are given in Table 1.

The acetone extract was practically insoluble in nonpolar solvents, but somewhat soluble in polar solvents. On the other hand, the $DF114B_2$ extract was insoluble in all the solvents examined. The difference in behavior between the two extracts is probably due to the shape of the molecules, *i.e.*, the acetone extract consisting of smaller molecules is more or less polarized due to the branched structure of the plasma-polymer, while the $DF114B_2$ extract of larger molecules exhibits no orientation of the branching effects which were dispersed in all directions resulting in a perfectly nonpolar characteristic. It is understandable that the acetone extract is somewhat soluble in the polar solvents.

Thermal Property and Average Molecular Weight. Each of the three fractions of the polymer was powdered and the individual melting point was measured on a hot stage. Melting took place in a wide range of temperature, half-liquified point being taken as the melting point. The results are given in Table 2.

Table 1. Solubility data of two solvent extracts of PPTFE in different organic solvents

Solvent	Acetone extract (%)	$DF114B_2$ extract (%)
Petroleum ether	0.01	0.00
Carbon tetrachloride	0.01	0.00
Hexane	0.01	0.00
Toluene	0.01	0.00
Benzene	0.00	0.00
Chloroform	0.02	0.00
Diethyl ether	1.29	0.00
Ethanol	2.71	0.01
Methanol	1.23	0.00

Table 2. Physical and chemical properties of three fractions derived from PPTFE

Item of determination	Fractions: Acetone extract	$DF114B_2$ extract	Insoluble residue
Melting point/°C	80—105	141—150	190—225
Average molecular weight	900	3600	—
Elemental composition F (%)	56.4	67.8	64.0
Elemental composition C (%)	—	32.0	—

The insoluble residue showed the highest melting point but lower than that of the conventional Teflon resin by *ca.* 100 °C. This is understandable if we assume that the PPTFE we obtained has a lower molecular weight than that of the conventional Teflon and/or the intermolecular force was reduced by the three-dimensional molecular structure resulting from the high branching of carbon chain developed during the course of plasma polymerization.

Vapor pressure osmometry was carried out for the acetone and $DF114B_2$ solutions of respective extracts. The number-average molecular weight was calculated for the individual polymer extracts employing benzyl as a standard (Table 2). The molecular weight of the $DF114B_2$ extract was 3600, the majority of PPTFE thus not being polymerized as highly as expected.[8—10] The insoluble residue was polymerized and cross-linked to a greater extent.

Elemental Analysis. Elemental analysis was carried out with a carbon-hydrogen-nitrogen analyzer and fluorine determination with an oxygen flask. Mean values are given in Table 2. Fluorine content of PPTFE was significantly lower than that of Teflon, supporting the highly branched structure.

The result of elemental analysis made it possible to determine the number of carbon and fluorine atoms in a unit molecule when a hypothetical molecule having the average molecular weight was assumed. For acetone extract we have C:F=30:30, and for $DF114B_2$ extract C:F=96:129. It is of interest that the F/C ratios of the two extracts were both much smaller than the H/C ratio of plasma-polymerized ethylene evaluated by Tibbit *et al.*[10] Higher concentrations of quaternary or tertiary carbons should be assumed for the former molecules.

IR Spectrum. A pressed KBr tablet was placed in the plasma chamber and coated with PPTFE in 10000 Å thickness. Each of the two extracts and the insoluble residue were powdered and mixed with KBr to form a tablet. The IR spectrum of the PPTFE film (Fig. 2) shows a strong resemblance to that of the other three fractions, indicating that the structural characteristics of the three fractions of the polymer are essentially the same.

The wide absorption band at 950—1500 cm^{-1} was

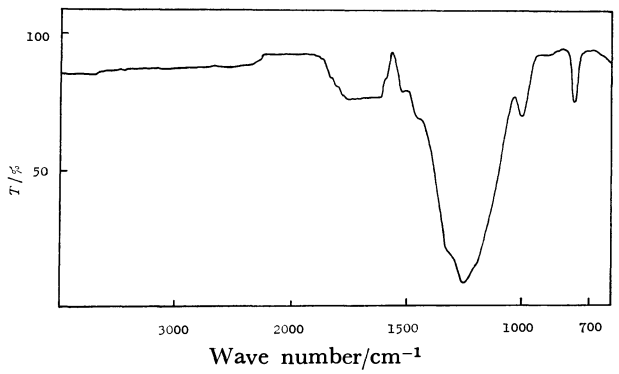

Fig. 2. IR spectrum of PPTFE.

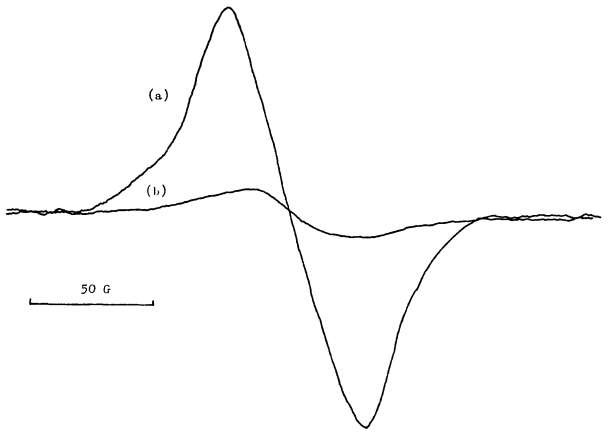

Fig. 3. Relative signal intensities of ESR spectra of freshly prepared PPTFE and its DF114B$_2$ extract.

assigned to C–F stretching vibration modified by various modes of neighboring atom groups. A weak absorption band at 1540—1800 cm^{-1} was tentatively assigned to C–C stretching vibration shifting considerably to higher wave number induced by the fluorinated carbon chain. Similarly the C=O absorption band appearing usually at *ca.* 1715 cm^{-1} is expected to shift towards much higher wave number for the same reason. The IR spectrum gave no signal of detectable C=O group. This is in line with the result of elemental analysis (Table 2). An intense and single band observed at 740 cm^{-1} is attributed to $-CF_2-$ bending vibration associated to adjacent $-CF_3$ terminal.

ESR Spectrum. Freshly prepared PPTFE was subjected to ESR spectroscopy. High concentration of unpaired spins, a characteristic of plasma-polymers, was observed as anticipated. The ESR spectrum of PPTFE was sealed in a standard 3.0 mm I.D. quartz tube filled with argon (Fig. 3(a)). The ESR signal showed a single and almost symmetrical wave form with a magnitude of 175 G having a *g*-value of 2.0038. The signal intensity decayed very slowly, reaching its half-intensity after 48 days at room temperature. A relative intensity of the ESR spectrum of the DF114B$_2$ extract is shown in Fig. 3-(b). A rough evaluation shows that the freshly prepared PPTFE contains *ca.* 20 folds higher concentration of free radicals than the DF114B$_2$ extract. This can be explained in terms of intense intermolecular collisions sustained during the course of extraction by the solvent DF114B$_2$ and

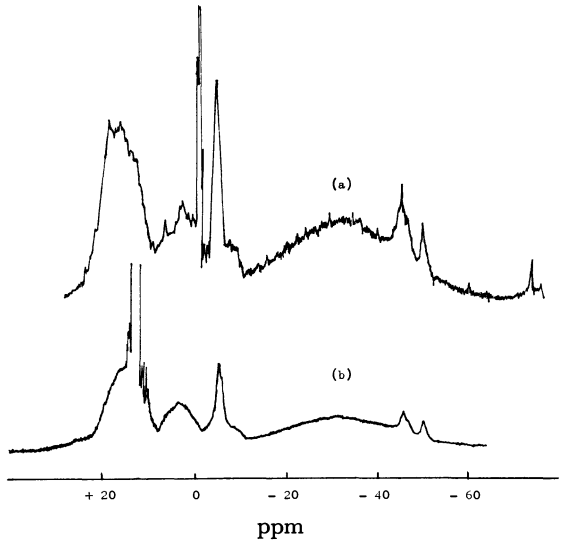

Fig. 4. ^{19}F-NMR spectra of PPTFE.

the resulting rapid termination of free radicals in the polymer. No quantitative determination was possible because of the lack of standard material. One free radical would be involved in a few plasma-polymer molecules.[11] In such a large molecule the radical site could be ignored for determining the chemical structure of the polymer molecule.

^{19}F-NMR Spectrum. ^{19}F-NMR spectra of the acetone extracts were measured with use of trifluoroacetic acid as an internal reference (Fig. 4(a)) and those of DF114B$_2$ extracts with the DF114B$_2$ itself (Fig. 4(b)).

The reference peaks are indicated at 0 and 16 ppm in the spectra (a) and (b), respectively. Eliminating these reference signals, the two spectra exhibit similar characteristics. It seems that the chemical structure of the two extracts are basically the same except for the difference in molecule size.

The individual signals were assigned from the lower magnetic field to the higher as follows:[6]

δ	30— 10 ppm	$\underline{CF_3}$-C
δ	10— 10 ppm	$\underline{CF_3}$-CF
δ	0——10 ppm	$\underline{CF_3}$-CF_2
δ	−10——60 ppm	CF_2 and CF_3
δ	−44 ppm	-$\underline{CF_2}$-CF_3
δ	−49 ppm	-$\underline{CF_2}$-CF_2-

Signal intensities of the CF_3 group derived from the DF114B$_2$ extract, the majority of PPTFE, were measured in order to calculate the relative abundance of different modes of adjacent carbon groups. From the result the following composition is obtained.

$$\underline{CF_3}\text{-C} : \underline{CF_3}\text{-CF} : \underline{CF_3}\text{-}CF_2 = 79 : 16 : 20$$

We see that the $\underline{CF_3}$–C group occupies a large majority of the overall CF_3 group within the polymer, in contrast to plasma-polymerized ethylene where the $\underline{CH_3}$–CH group is the major constituent, hardly any of the $\underline{CH_3}$–C group being found in the ^{13}C-NMR spectrum.[10] Thus it seems that the molecular structure of PPTFE consists of irregular sequences of very

highly branched aliphatic chains.

Hypothetical Model of Molecular Structure. If we assume that a polymer molecule has the average molecular weight derived from the DF114B$_2$ extract, an interpretation of its chemical structure can be given in reference to spectral data and the elemental analysis. Atom constitution of a unit molecule was calculated to be 96 carbon and 129 fluorine atoms, the existence of some C=C groups being presumed by IR spectrometry.

^{19}F-NMR spectroscopy clarified the constitution of fluorocarbon groups in the molecule. The signal intensities of the following underlined groups gave the ratio:

$$\underline{CF_3}\text{-C} : \underline{CF_3}\text{-CF} : \underline{CF_3}\text{-}\underline{CF_2} : \underline{CF_2} + \underline{CF} = 79 : 16 : 20 : 69$$

This indicates that equal numbers of CF_2 and CF groups are involved in one molecule. The signal intensity of CF_2+CF could be allocated to CF_2 and CF groups with 2/3 and 1/3 portions, respectively. If we denote the number of CF_3, CF_2, and CF groups within a unit molecule by x, y, and z, respectively, the relative abundance of these groups can be obtained.

$$x : y : z = \frac{79+16+20}{3} : \frac{69\times 2/3}{2} : \frac{69\times 1/3}{1}$$

$$= 38 : 23 : 23$$

Since the number of fluorine atoms in a unit molecule is 129, we have

$$3x + 2y + z = 129.$$

Solving the two equations, we get

$$x = 26.8, \quad y = 16.2, \quad z = 16.2.$$

The number of quaternary carbon is calculated by subtracting the number of carbons belonging to CF_3, CF_2, and CF groups from 96 the total number of carbon.

$$96 - (27+16+16) = 37$$

Rearranging the data, we get

$$CF_3 = 27, \quad CF_2 = 16, \quad CF = 16, \quad C = 37.$$

Signal intensities of CF_3 groups adjacent to different carbon groups were allocated in proportion to the numbers of adjacent carbon groups.

$$\underline{CF_3}\text{-}CF_2 = 4.5 \quad \underline{CF_3}\text{-CF} = 4.5 \quad \underline{CF_3}\text{-C} = 19$$

The composition of the atom groups within a unit molecule is as follws:

$$\underline{CF_3}\text{-}CF_2 = 4\text{—}5, \quad \underline{CF_3}\text{-CF} = 4\text{—}5, \quad \underline{CF_3}\text{-C} = 19,$$
$$CF_2 = 16, \quad CF = 16, \quad C = 37.$$

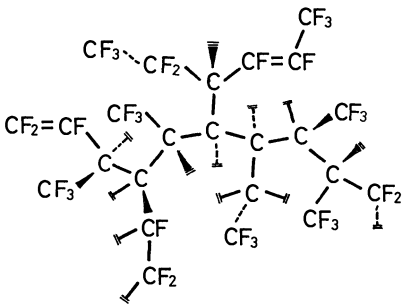

Fig. 5. Atom configuration of PPTFE depicted as 1/4 portion of unit molecule having average molecular weight.

A hypothetical model of a quarter of a unit molecule is shown in Fig. 5.

The structure is not yet established, since the abundance of the C–C group was roughly estimated by IR spectroscopy.

The authors wish to thank Dr. Y. Sugiura for carrying out ESR spectroscopy with PPTFE at the Department of Pharmaceutical Sciences, Kyoto University. They are indebted to Daikin Kogyo Co. Ltd. for the supply of TFE as a monomer gas and DF114B$_2$ as an effective solvent of PPTFE.

References

1) "Techniques and Applications of Plasma Chemistry," ed by J. R. Hollahan and A. T. Bell, John Wiley and Sons, Inc., New York (1974).

2) "Low-Temperature Plasma Chemistry," ed by K. Hozumi, Nankodo, Tokyo (1976).

3) "Plasma Chemistry of Polymers," ed by M. Shen, Marcel Dekker, New York (1976).

4) J. R. Hollahan and T. Wydeven, *Appl. Opt.*, **13**, 1844 (1974).

5) T. Wydeven and R. Kubacki, *Appl. Opt.*, **15**, 132 (1976).

6) O. Tsuji, T. Wydeven, and K. Hozumi, *Microchem. J.*, **22**, 229 (1977).

7) K. Hozumi, K. Kitamura, and T. Kitade, *Yakugaku Zasshi*, **99**, 521 (1979).

8) H. Kobayashi, A. T. Bell, and M. Shen, *J. Appl. Polym. Sci.*, **17**, 885 (1973).

9) H. Kobayashi, A. T. Bell, and M. Shen, *Macromolecules*, **7**, 277 (1974).

10) J. M. Tibbit, M. Shen, and A. T. Bell, *J. Macromol. Sci., Chem.*, **A10**, 1623 (1976).

11) M. M. Millard, J. J. Windle, and A. E. Pavlath, *J. Appl. Poly. Sci.*, **17**, 2505 (1973).

The Determination of Alkaline Phosphatase Activity in Serum by Means of Flow-through Analysis with an Ion-selective Electrode

Tadashi HARA,* Masakatsu IMAKI,** and Motohiro TORIYAMA

Department of Chemical Engineering, Faculty of Engineering, Doshisha University, Karasuma Imadegawa, Kamigyo-ku, Kyoto 602

***Horiba, Ltd., Kissyoin, Minami-ku, Kyoto 601*

(Received September 11, 1980)

In order to determine continuously the alkaline phosphatase activity in a serum sample, a potentiometric method using a newly prepared phosphate ion-selective electrode has been established by the authors for the first time. The alkaline phosphatase activity was determined by measuring the concentration of the phosphate ion which was liberated by the enzymatic hydrolysis of disodium phenyl phosphate in the presence of alkaline phosphatase. The measurement of the phosphate ion with an ion-selective electrode was seriously interfered with by protein and the halide ion, but the interference could be removed by covering the electrode surface with a cellulose acetate membrane and by separating the chloride ion from a serum sample by gel chromatography. The present method was applied to the determination of alkaline phosphatase activity in serum; the results obtained showed a satisfactory correlation with those obtained by the conventional method. The method was found to be useful for practical diagnosis based on the activity of alkaline phosphatase.

The present study was carried out with the object of establishing a simple, rapid, and economical method by which alkaline phosphatase activity(APA) in a transparent as well as an opaque sample solution could be determined continuously with a phosphate ion-selective electrode(PISE) by the use of an arbitrary substrate.

As can be seen from the following examples, the determination of APA is very important in various fields, such as biochemistry, analytical chemistry, clinical examination, and diagnosis: 1) APA in serum is significant for the diagnoses of cancer of the liver and malignant bone tumor, since there seems to be a close relationship between APA and the beforementioned diseases, and 2) the exact determination of APA is indispensable for the enzyme immunoassay, in which alkaline phosphatase is used as a labeling enzyme.

In the conventional determination of APA, the methods proposed by Bodansky,[1] Kind-King,[2] and Bessey-Lowry[3] have been used. All these methods are based on the absorptiometric determination of phosphoric acid,[1] phenol,[2] and *p*-nitrophenol,[3] which are formed by the enzymatic hydrolysis of the corresponding substrates in the presence of alkaline phosphatase. Nowadays, complicated autoanalyzers designed on the basis of these measurement principles are commercially available. These methods have, however, the following defects: 1) the measurement becomes complicated, since coloring and deproteinizing agents are added; 2) the fluctuation of the blank value is large, since the substrate is unstable; 3) the apparatus is complicated and expensive; 4) the method is not applicable to opaque samples, and 5) the concentration range suitable for the measurement is narrow, less than twenty times.

Though ion-selective electrodes have been used in several papers[4–11] for a simple and rapid estimation of enzyme activity, no reports have been published pertaining to the potentiometric determination of APA with a PISE. From this standpoint, the authors have newly made a PISE and applied it to the continuous determination of APA in serum with a simple and inexpensive apparatus; favorable results were obtained.

Experimental

Reagents. The buffers and the base solution were prepared from analytical-grade reagents without further purification. A substrate solution was prepared as a 1.0×10^{-2} mol/dm^3 disodium phenyl phosphate in a buffer solution (pH 10.15) consisting of disodium carbonate (3.18 g/dm^3) and sodium hydrogencarbonate (1.68 g/dm^3). The alkaline phosphatase was obtained from Sigma, and its standard solution was prepared by diluting 1.1 U/mg of alkaline phosphatase (Type 1) with distilled water. Sephadex G-25 was used as a packing agent in gel chromatography. Serum samples were offered by the Kyoto Prefectural University of Medicine; their APA values were certified to be around the normal values.

Apparatus. A PISE[12] in which trisilver phosphate was used as the active substance of a soild membrane was built up newly by the authors in order to estimate the amount of phosphate ions. A solid membrane composed of trisilver phosphate and disilver sulfide in the weight ratio of 4:1 was found to be the best with regard to the mechanical strength, the electromotive force of the electrode, the plasticity of the membrane, and the life of the electrode. The electrode responded to the phosphate-ion concentration in the range of 1.0×10^{-5}—1.0×10^{-1} mol/dm^3. The electrode has a serviceable life of at least six months. The determination of the phosphate ions was found to be seriously affected by chloride, thiocyanate, and sulfite. The other instrumental units used were as follows: 1) an Atto Perista mini-pump, type SJ 1211; 2) a thermostat manufactured by Netsudenshi Kogyo; 3) a Horiba 2535—05 T reference electrode, and 4) a model VP6521A recorder (Matsushita Communication Industrial Co., Ltd.).

Procedure. The determination of APA was done with the apparatus shown in Fig. 1. A 0.5-cm^3 serum sample is added with a pipette to the top(l) of a 290×8 mm i.d. column(a), which is then charged with Sephadex G-25 and cooled at 0 °C in a thermostat. By passing the substrate solution through the column at the rate of 0.5 cm^3/min, chloride and alkaline phosphatase are separated and eluted out of the column in the order shown in Fig. 3. The portion containing alkaline phosphatase is sent to a Teflon-made reaction tube by way of a four-way cock(c) at the rate of 0.5 cm^3/min by means of the pump(b_1). Since

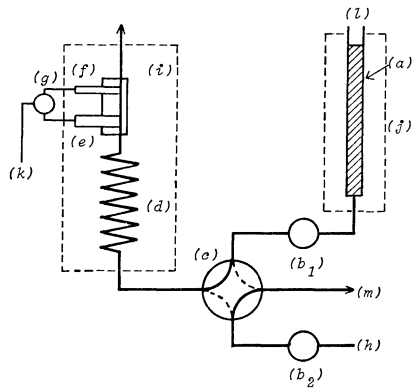

Fig. 1. Schematic flow diagram.
a: Gel column, b_1: pump, b_2: pump, *c*: four-way cock, *d*: reaction tube(Teflon), *e*: indicator electrode, *f*: reference electrode, *g*: voltmeter, *h*: inlet, *i*: thermostat (37.0 °C), *j*: thermostat (0 °C), *k*: recorder, *l*: sample, and *m*: exit.

the reaction tube, 10 m long and 1 mm i.d., is being held at 37.0±0.2 °C in a thermostat(*i*), the enzymatic hydrolysis of phenyl phosphate in the presence of alkaline phosphatase proceeds to form phosphate ions. The concentration of phosphate ions is measured with a voltmeter(*g*) as an electromotive force of a cell consisting of a PISE(*e*) and a reference electrode(*f*), and its value is recorded with a recorder (*k*). By turning a four-way cock(*c*) at a definite time after the addition of a serum sample, the portion containing chloride is removed by way of the exit(*m*), while the substrate solution is sent to the reaction tube by means of the pump(b_2) by way of the inlet(*h*) at the rate of 0.5 cm³/min. The APA in serum is estimated from the calibration curve on the basis of the peak height on a recorder chart.

Results and Discussion

Interference of Serum Proteins. Ion-selective electrodes for chloride and silver ions in which disilver sulfide is used as a constituent in an active solid membrane have been reported[13,14] to be interfered with by about 6% proteins consisting of albumin, globulin, and so on in serum. Since the present PISE is made of trisilver phosphate and disilver sulfide, it was expected to be interfered with by serum proteins. As can be seen from Fig. 2, the present PISE was interfered with by albumin in bovine serum (Fig. 2(d)). Therefore, the PISE is not applicable to the determination of APA in serum without removing the interference of protein.

It has been already reported[15] that the interference of protein can be removed by covering a electrode with a semi-permeable membrane. Several membranes were tested, but the best result was obtained when a cellulose acetate membrane (0.0203 mm thick, 2.4 nm pore size) was used; the interference of albumin was thus almost completely removed (Fig. 2(b)). In all the following experiments, the PISE covered with a cellulose acetate membrane was used.

Removal of Chloride. As can be foreseen from the solubility product of silver chloride and silver thiocyanate, the PISE is seriously interfered[12] with by chloride and thiocyanate ions. Since the concentration of chloride in serum is about 0.1 mol/dm³,

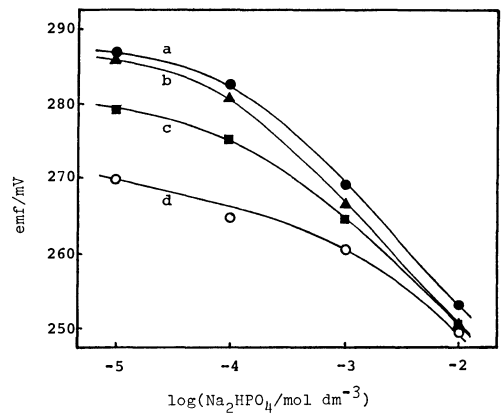

Fig. 2. Response of the PISE in sample solutions containing albumin.
a: Albumin free, b: covered with cellulose acetate, c: covered with nitrocellulose, and d: not covered with a membrane.

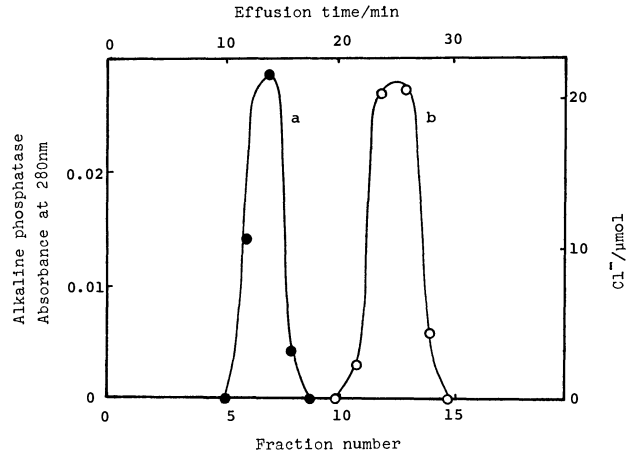

Fig. 3. Gel separation of alkaline phosphatase from a chloride ion on a Sephadex G-25 column.
a: Alkaline phosphatase, b: chloride ion.

the removal of chloride is indispensable for the determination of APA in serum.

The separation of alkaline phosphatase from chloride was examined by means of gel chromatography. A 0.5-cm³ sample solution containing sodium chloride (0.1 mol/dm³) and alkaline phosphatase (1 mg/cm³) was treated in order to separate its components by passing a buffer solution through the column at the rate of 0.5 cm³/min; the results are shown in Fig. 3. Here the flow rate of the buffer solution was chosen to be maximal so long as the gel particle was not crushed. The amounts of alkaline phosphatase and chloride in each 1-cm³ fraction were determined by the absorption at 280 nm and by the precipitation titration based on Mohr's procedure respectively. On the basis of Fig. 3, the following procedure is recommended for the separation of alkaline phosphatase from chloride: the eluent obtained from the column (Fig. 1(*a*)) in 0—16 min is introduced into the reaction tube(*d*), and the eluent obtained after 16 min is drawn out of the exit(*m*) by turning a four-way cock(*c*). By this procedure, the portion of chloride-free alkaline

phosphatase is sent to a measuring chamber equipped with a PISE.

Calibration Curve. The hydrolysis of disodium phenyl phosphate in the presence of alkaline phosphatase proceeds in accordance with Eq. 1:

$$C_6H_5OPO_3Na_2 + H_2O \xrightarrow{\text{phosphatase}} C_6H_5OH + Na_2HPO_4. \quad (1)$$

It is possible to estimate the APA by measuring the formation rate of phosphate ions, since the APA is generally represented by the reaction rate of Eq. 1. If the reaction of Eq. 1 proceeds as zero-order with respect to the concentration of disodium phenyl phosphate, the reaction rate of Eq. 1 is given by the concentration of phosphate ions at a definite time. To examine whether or not the reaction of Eq. 1 proceeds as a zero-order one, a PISE was dipped in a 1.0×10^{-2} mol/dm^3 disodium phenyl phosphate solution which contained 5.5—110 U/dm^3 alkaline phosphatase and was held at 37.0 °C in a thermostat; the relationship between the reaction time and the concentration of phosphate ions was thus obtained (Fig. 4). It may be concluded from Fig. 4 that the reaction of Eq. 1 proceeds as zero-order with respect to the concentration of disodium phenyl phosphate, since there is a linear relationship between the reaction time and the concentration of phosphate ions for the APA values of more than 20 U/dm^3. The present results, obtained at 10^{-2} mol/dm^3 disodium phenyl phosphate, seem to be quite reasonable considering that the Km value in the reaction of Eq. 1 is around 10^{-3} mol/dm^3.[16]

A calibration curve (Fig. 5) was obtained as a peak height against each standard solution of alkaline phosphatase. The curvature corresponding to 2.2—22 U/dm^3 alkaline phosphatase in the calibration curve is attributed to: 1) the deviation of an electrode potential from the Nernst equation at 10^{-4}—10^{-5} mol/dm^3 phosphate ion (Fig. 2(a)); 2) the deviation of the enzyme reaction rate from a zero-order one for the APA values less than 20 U/dm^3, 3) the broadening of a phosphate ion peak by the diffusion and/or mixing in a flowing solution, etc. For the practical determination of the APA, the part of the straight line in the calibration curve can be used satisfactorily, since the APA in serum is usually more than 20 U/dm^3.

Effect of Serum Matrix. To examine whether or not the present method can be applied to the determination of the APA in serum, different APAs were added to 0.5 cm^3 control serum and their APAs were estimated by the present method; the result thus obtained are shown in Fig. 6. Figure 6 shows that, there was a good relationship between the activities of the added alkaline phosphatase and the potentiometrically measured ones. The value at the intersection of the straight line on the abscissa in Fig. 6 corresponded exactly to the APA in the control serum. It became clear from the results that the present method could be satisfactorily applied to the determination of the APA in serum.

Serum Samples. The relationship between the APA values in serum samples measured by the present method and those measured by means of a Hitachi autoanalyzer, type 400, based on absorptiometry was examined (Fig. 7). As can be seen from Fig. 7, there was a fairly good correlation between them; the correlation factor was calculated to be 0.88.

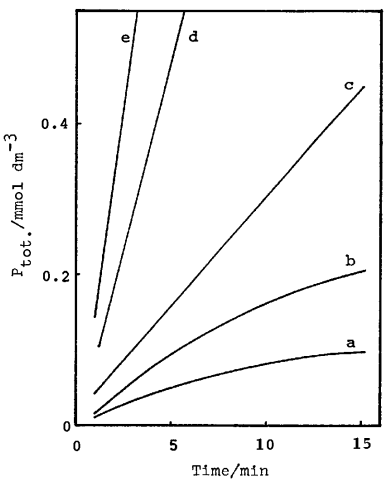

Fig. 4. Relationship between reaction time and $P_{tot.}$. Measured at 37.0 °C in a 1.0×10^{-2} mol/dm^3 disodium phenyl phosphate solution containing alkaline phosphatase.
a: 5.5 U/dm^3, b: 11 U/dm^3, c: 22 U/dm^3, d: 55 U/dm^3, e: 110 U/dm^3. $P_{tot.}=H_3PO_4+H_2PO_4^-+HPO_4^{2-}+PO_4^{3-}$.

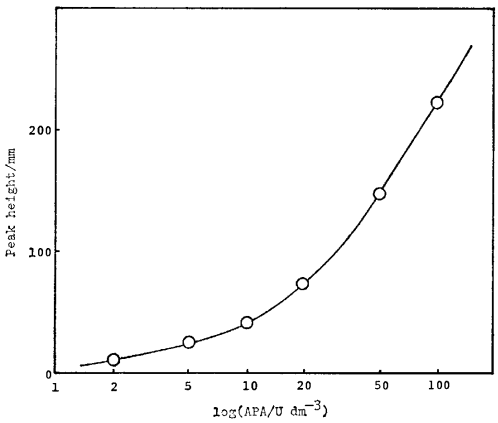

Fig. 5. Calibration curve.

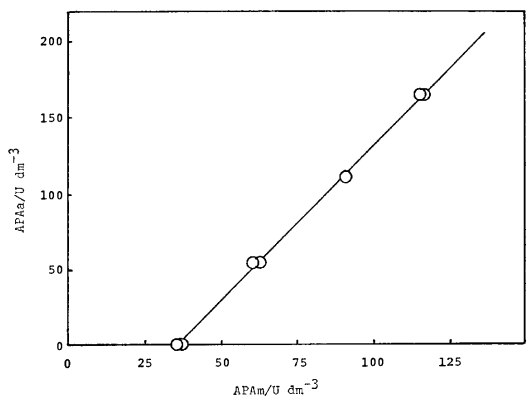

Fig. 6. Relationship between potentiometrically measured APA(APAm) and added APA(APAa).

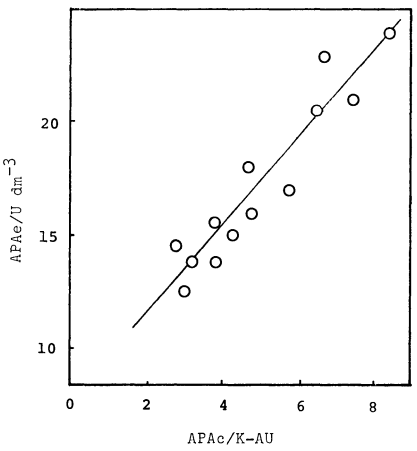

Fig. 7. Correlation between the APAs in serum samples measured by the PISE method(APAe) and by the conventional method(APAc).

Judging from the facts that: 1) the APA in serum sample used in this experiment corresponds to that of alkaline phosphatase in a healthy human, and 2) the APA in a liver patient is much larger than that value, the present method can be said to be sensitive enough for a practical diagnosis based on the APA.

According to the present method, it takes about 30 min for the analysis of one sample. However, many samples can be treated effectively and continuously by arranging a number of columns in parallel with column(*a*), because the time-consuming step in the present method is the separation of alkaline phosphatase from chloride ions. A system by which information concerning APA is obtained from a much smaller serum sample is now being developed.

References

1) A. Bodansky, *J. Biol. Chem.*, **101**, 93 (1933).
2) P. R. N. Kind and E. J. King, *J. Clin. Path.*, **7**, 322 (1954).
3) O. A. Bessey, O. H. Lowry, and M. J. Brock, *J. Biol. Chem.*, **164**, 321 (1946).
4) G. Baum, *Anal. Biochem.*, **39**, 65 (1971).
5) R. A. Llenado and G. A. Rechnitz, *Anal. Chem.*, **44**, 468 (1972).
6) R. A. Llenado and G. A. Rechnitz, *Anal. Chem.*, **44**, 1366 (1972).
7) R. A. Llenado and G. A. Rechnitz, *Anal. Chem.*, **45**, 826 (1973).
8) H. Booker and J. Haslam, *Anal. Chem.*, **46**, 1054 (1974).
9) D. P. Nikolelis and H. A. Mottola, *Anal. Chem.*, **50**, 1665 (1978).
10) H. Nakamura, M. Takagi, and K. Ueno, *Talanta*, **26**, 921 (1979).
11) C. R. Gebauer, M. E. Meyerhoff, and G. A. Rechnitz, *Anal. Biochem.*, **95**, 479 (1979).
12) M. Imaki, M. Toriyama, I. Higashiguchi, K. Hirata, and T. Hara, *Sci. Eng. Rev. Doshisha Univ.*, **21**, 18 (1980).
13) P. D'Orazio and G. A. Rechnitz, *Anal. Chem.*, **49**, 41 (1977).
14) Y. Morishita and K. Nakane, *Eiseikensa*, **28**, 1069 (1979).
15) K. Takahara, *Kensa To Gijyutsu*, **7**, 937 (1979).
16) T. Hashimoto, T. Okubo, H. Suzuki, S. Moriuchi, K. Higashino, and K. Nose, *Taisya*, **13**, 279 (1976).

  Bull. Chem. Soc. Jpn., 54, 1400—1402 (1981) [Vol. 54, No. 5

Determination of Hyperoxide in Dimethyl Sulfoxide by Photometric Titration with Iodine

Katsumi KITAMURA, Koichi HASEGAWA, Katsura MOCHIZUKI,
Taira IMAMURA,* and Masatoshi FUJIMOTO*
Department of Chemistry, Faculty of Science, Hokkaido University, Sapporo 060
(Received September 26, 1980)

The concentration of hyperoxide, O_2^-, in dimethyl sulfoxide (DMSO) was determined by photometric titration with iodine. The validity of the method was confirmed on the basis of stoichiometry by use of the standardized hyperoxide solution in the reaction of the complex, MoO(tpp)NCS, with methanol, where TPP denotes α,β,γ,δ-tetraphenylporphyrin.

Hyperoxide solutions prepared from potassium hyperoxide solubilized in aprotic solvents by crown ether[1] have been used for the syntheses of many organic compounds[2] and for reactions of metal complexes.[3] However, for determination of hyperoxide in aprotic solvents, only two reliable methods have been reported:[4] (1) determination of the dioxygen evolved first upon mixing a hyperoxide solution with water, then by the addition of catalase to the mixed solution,[6] and (2) measurement of the absorbance at 250 nm of the solution of potassium hyperoxide solubilized by 18-crown-6 ether in DMSO.[7]

In the kinetic study of the reaction of cobalt(III) complex with hyperoxide in aprotic solvents, we proposed a simple method for the determination of hyperoxide in DMSO according to the reaction[8]

$$I_2 + 2\,O_2^- \longrightarrow 2\,I^- + 2\,O_2. \qquad (1)$$

The reaction proceeds quantitatively[7] because of a large difference in the redox potential of iodine ($E^\circ = 0.54$ V)[9] and that of hyperoxide ion ($E^\circ = -0.5$—-0.6 V).[10] The validity of the proposed method was confirmed by applying the hyperoxide solution to the reaction between the complex, MoO(tpp)NCS, and CH_3OH in CH_2Cl_2.

Experimental

Materials. Potassium hyperoxide (KO_2, ICN Pharmaceuticals) and 18-crown-6 (Nippon Soda) were used without further purification. Potassium content in the hyperoxide specimen was determined to be 95.7% by the Kalibor-Zephiramine method.[11] The solution of hyperoxide was prepared in an argon atmosphere from potassium hyperoxide solubilized by 18-crown-6 in DMSO. About 10 h is required for the preparation of *ca.* 10^{-2} mol dm^{-3} solution.

Reagent grade iodine was purified by repeated sublimation. In order to avoid any loss of iodine in the preparation of the standard solution, the following procedure was adopted. A small amount of DMSO was taken in a well-stoppered volumetric flask, and weighed. A desired amount of iodine was carefully taken in the volumetric flask and completely dissolved. The amount of dissolved iodine was determined from the difference in weight. Then the solvent was added to a mark on the flask and mixed to prepare a standard solution. Since the absorbance at 365 nm, λ_{max} of the solution, gradually increases (*ca.* 10% for 2.0×10^{-3} mol dm^{-3} I_2 in 3 d), and decreases in the presence of 18-crown-6 (*ca.* 5% in 40 h), the standard DMSO solution of iodine should always be prepared immediately before use.

Dimethyl sulfoxide was kept with CaH_2 for several days, distilled under reduced pressure, and stored in an argon atmosphere. The water content in the purified DMSO was determined to be less than 0.03% by the Karl-Fischer method.

Dichloromethane was distilled and passed through an alumina column. The pre-purified solvent was distilled immediately before use. The complexes, MoO(tpp)NCS and MoO(tpp)Br, were synthesized.[12]

Results and Discussion

Photometric Titration with Iodine. The concentration of O_2^- in DMSO was determined as follows. A 3.00-cm^3 hyperoxide solution (2×10^{-5}—9×10^{-3} mol dm^{-3}) is taken into an optical cell in an argon atmosphere. The optical cell is sealed at once with a serum cap. A small amount of iodine solution (5×10^{-4}—1×10^{-1} mol dm^{-3}) is then injected into the optical cell with a 100 mm^3 microsyringe or a micropipet. The absorbance at 400 nm, λ_{sh} of the iodine solution, is measured and plotted against the volume of the iodine solution injected. A typical change in absorbance at 400 nm is shown in Fig. 1. The absorbance gradually decreases until the end point depicted by A in Fig. 1 is reached. After the point A, the absorbance is measured 15 min after each addition of the solution of iodine in order to complete the reaction. The concentration of hyperoxide, x, is calculated by $x=2VC/3$, where V is the volume of the iodine solution consumed and C the concentration of iodine. The 10-fold change in the concentration ratio of 18-crown-6 and weighed amount of KO_2 does not affect the

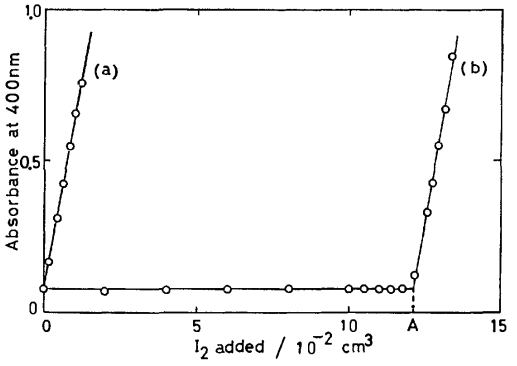

Fig. 1. Typical change in absorbance of hyperoxide solution at 400 nm by addition of an iodine solution. $[I_2]_0=3.98\times10^{-2}$ mol dm^{-3}. (a): $[O_2^-]_0=0$ and [18-crown-6]$_0=6.0\times10^{-3}$ mol dm^{-3}. (b): $[O_2^-]_0=3.12\times10^{-3}$ and [18-crown-6]$_0=6.0\times10^{-3}$ mol dm^{-3}.

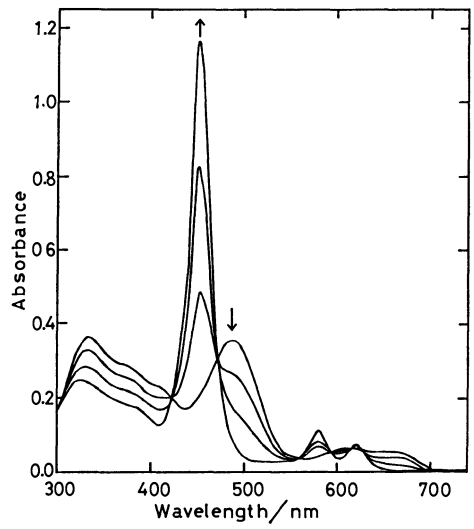

Fig. 2. Change in spectra for the reaction among MoO(tpp)NCS, CH_3OH, and O_2^- in CH_2Cl_2 containing 2%(v/v) CH_3OH, 1%(v/v) DMSO, and $[MoO(tpp)NCS]_0 = 7.54 \times 10^{-6}$ mol dm^{-3} at 25 °C.

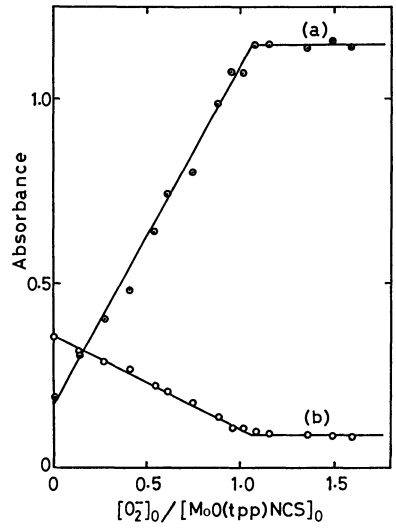

Fig. 3. Molar-ratio method for the reaction among MoO(tpp)NCS, CH_3OH, and O_2^- at 25 °C. (a): At 452 nm. (b): At 488 nm.

determination of O_2^-. Reproducibility of the data was estimated to be within ±1%.

Reaction among MoO(tpp)NCS, CH_3OH, and O_2^-. The solution of hyperoxide was applied to the reaction between the complex, MoO(tpp)NCS, and CH_3OH in order to confirm the validity of the proposed method. When the solution of hyperoxide is added to a dichloromethane solution of the complex, MoO(tpp)NCS, containing 2%(v/v) methanol, the spectrum changes with isosbestic points at 423 and 472 nm (Fig. 2).[13] The final spectrum agrees with the spectrum of the complex, $MoO(tpp)OCH_3$, synthesized from the complex, MoO(tpp)Br. The reaction should be written as follows.

$$Mo^{V}O(tpp)NCS + CH_3OH + O_2^- \longrightarrow Mo^{V}O(tpp)OCH_3 + HO_2 + NCS^- \quad (2)$$

The stoichiometry of the reaction was determined to

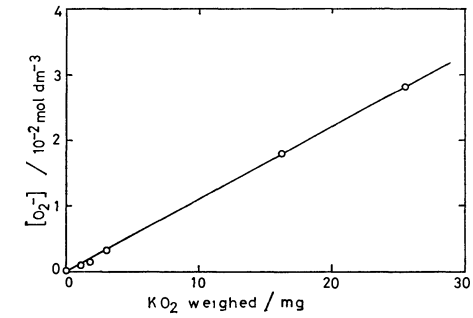

Fig. 4. Concentrations of O_2^- in DMSO *vs.* weighed amounts of KO_2. Two-fold excess of 18-crown-6 is contained over KO_2.

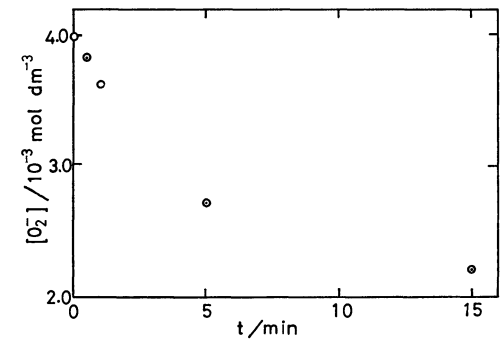

Fig. 5. Decomposition of hyperoxide solution in a flask placed in the ultrasonic cleaner (Bransonic, B-220, 45 kHz, 100 W).

be $MoO(tpp)NCS:O_2^- = 1:1.05$ by the molar-ratio method (Fig. 3). The absorbance at 452 nm, λ_{max} of the spectrum of the complex, $MoO(tpp)OCH_3$, increased in proportion to the concentration of O_2^- with an excess of the complex, MoO(tpp)NCS, and CH_3OH. This confirms the high accuracy of the determination of O_2^- in DMSO by means of the photometric titration with iodine.

Stability of O_2^- in DMSO. The concentration of hyperoxide in a stock solution was *ca.* 70% of that calculated from the weighed amount of KO_2, showing the decomposition of *ca.* 30% of O_2^- during the course of preparation of the solution (Fig. 4). The concentration gradually decreased *ca.* 2% a day.

When 1 volume of a 3.51×10^{-3} mol dm^{-3} hyperoxide solution was accurately diluted to 10 volumes with DMSO, a 3.19×10^{-4} mol dm^{-3} solution was obtained, which indicates partial decomposition of O_2^- by the addition of DMSO. Thus a hyperoxide solution should be standardized immediately before use.

A decrease in the concentration of O_2^- in DMSO was also observed when the solution was treated in an ultrasonic cleaner (Fig. 5).

References

1) J. S. Valentine and A. B. Curtis, *J. Am. Chem. Soc.*, **97**, 224 (1975); R. A. Johnson and E. G. Nidy, *J. Org. Chem.*, **40**, 1680 (1975).

2) E. Lee-Ruff, *Chem. Soc. Rev.*, **6**, 195 (1977); C. I. Chern, R. DiCosimo, R. D. Jenus, and J. S. Filippo, Jr., *J. Am. Chem. Soc.*, **100**, 7317 (1978); R. A. Johnson, E. G.

Nidy, and N. V. Merritt, *ibid.*, **100**, 7960 (1978).

3) J. A. Fee and J. S. Valentine, "Superoxide and Superoxide Dismutase," ed by A. M. Michelson, J. M. McCord, and I. Fridovich, Academic Press, New York, N. Y. (1977); J. S. Valentine and A. E. Quinn, *Inorg. Chem.*, **15**, 1997 (1976); J. S. Valentine, Y. Tatsuno, and M. Nappa, *J. Am. Chem. Soc.*, **99**, 3522 (1977); J. Stein, J. P. Fackler, Jr., G. J. McClume, J. A. Fee, and L. T. Chan, *Inorg. Chem.*, **18**, 3511 (1979); M. Nappa, J. S. Valentine, A. R. Miksztal, H. J. Schugar, S. S. Isied, *J. Am. Chem. Soc.*, **101**, 7744 (1979); R. F. Pasternack and B. Halliwell., *ibid.*, **101**, 1026 (1979).

4) Nitrotetrazolium Blue (NBT) was used to assay O_2^- in DMSO solutions of tetramethylammonium hyperoxide.[5] The spectra of the products in the reaction of NBT with O_2^- in DMSO change with the concentrations of O_2^-; with increase in the concentration of O_2^-, the absorption peak at 680 nm shifted to 725 nm. Beer's law does not hold at 680 nm.

5) C. S. Foote, F. C. Shook, and R. A. Abakerli, *J. Am. Chem. Soc.*, **102**, 2503 (1980).

6) J. A. Fee and P. G. Hildenbrand, *FEBS Lett.*, **39**, 79 (1974).

7) S. Kim, R. DiCosimo, and J. S. Filippo, Jr., *Anal. Chem.*, **51**, 679 (1979).

8) K. Mochizuki, T. Imamura, and M. Fujimoto, *Bull. Chem. Soc. Jpn.*, **53**, 1757 (1980).

9) W. M. Latimer, "Oxidation Potentials," 2nd ed, Prentice-Hall, Inc., Englewood Cliffs, N. J. (1952).

10) D. T. Sawyer and J. L. Roberts, Jr., *J. Electroanal. Chem.*, **12**, 90 (1966); M. E. Reover and B. S. White, *Electrochim. Acta*, **11**, 1061 (1966); D. L. Maricle and W. G. Hodgson, *Anal. Chem.*, **37**, 1562 (1965); E. L. Johnson, K. H. Pool, and R. E. Hamm, *ibid.*, **38**, 183 (1966); J. Chevelet, F. Rovelle, L. Gierst, and J. P. Lambert, *J. Electroanal. Chem.*, **39**, 201 (1972).

11) E. M. Epps and J. C. Burden, *Anal. Chem.*, **30**, 1882 (1958); K. Ueno, M. Saito, and K. Tamaoku, *Bunseki Kagaku*, **18**, 81 (1969).

12) T. Imamura, M. Terui, Y. Takahashi, T. Numatatsu, and M. Fujimoto, *Chem. Lett.*, **1980**, 89; T. Imamura, T. Numatatsu, M. Terui, and M. Fujimoto, *Bull. Chem. Soc. Jpn.*, **54**, 170 (1981).

13) When methanol is absent in the reaction system, the complex, MoO(tpp)NCS, is reduced by O_2^- to form the complex, $Mo^{IV}O(tpp)$.

Formose Reactions. XIV. A Selective Formose Reaction in the Presence of a Slight Amount of Calcium Ions

Yoshihiro SHIGEMASA,* Tsuyoshi TAJI, Eiichi WAKI, and Ruka NAKASHIMA
Department of Industrial Chemistry, Faculty of Engineering, Tottori University, Tottori 680
(Received July 4, 1980)

It was found that a formose reaction in the presence of small amounts of calcium and D-fructose gave rise to three products, 2-(hydroxymethyl)glycerol, 3-(hydroxymethyl)pentitol, and 2,4-bis(hydroxymethyl)pentitol, with a high selectivity. Various factors affecting the selectivity were also discussed: [Ca], pH, [D-fructose], the reaction temperature, co-catalysts, and metal hydroxides. The amount of formaldehyde relative to [Ca] is the most important factor in obtaining the selective formation of the three-branched sugar alcohols. Under these reaction conditions, the α,β-enediol structure is required in an effective co-catalyst for the formose reaction. 2-(Hydroxymethyl)glycerol, 3-(hydroxymethyl)pentitol, and 2,4-bis(hydroxymethyl)pentitol were formed with a high selectivity in the formose reactions catalyzed by KOH, $Mg(OH)_2$, $Fe(OH)_3$, and LiOH.

In the preceding papers,[1-3] which dealt with various factors affecting formose reactions catalyzed by $Ca(OH)_2$ in a batch reactor, the continuous measurement of the oxidation-reduction potential (ORP) of the reaction mixture has proven usefull for distinct discrimination among the induction, the sugar-forming, and the sugar-decomposing periods by means of an ORP minimum and maximum appearing at the end of the induction period and at the end of the sugar-forming period respectively. The T_{min} and T_{max} symbols correspond to the times of the end of the induction and the sugar-forming periods respectively.

In the course of our recent kinetic studies of $Ca(OH)_2$-catalyzed formose reactions, we found that three kinds of branched sugar alcohols, 2-(hydroxymethyl)glycerol (2-HG), 2,4-bis(hydroxymethyl)pentitol (2,4-DHP), and most probably a diastereomeric mixture of 3-(hydroxymethyl)pentitol (3-HP), are obtained with a high selectivity when most of the dissolved calcium ions are removed as hardly soluble salts or stable chelates at the end of the induction period (T_{min}).[4,5]

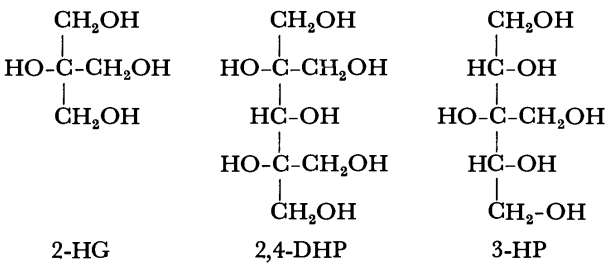

When the formose reaction was carried out in the presence of small amounts of calcium ions and D-fructose by adjusting the pH of the reaction mixture to 12.0 with potassium hydroxide, it was found to give rise to the same products. Under these reaction conditions, furthermore, the reaction mixture is homogeneous, so the analysis of the reaction is easier than in the heterogeneous system.

The purpose of this paper is to explore the reaction conditions which give a similar selective formation of the above three kinds of branched sugar alcohols. Particular attention is placed on the following factors: the calcium-ion concentration; the formaldehyde concentration; the kind of promoters, such as D-fructose and D-glucose; the D-fructose concentration; the pH of the reaction mixture; the reaction temperature, and the kind of metal hydroxide.

Experimental

The apparatus and the experimental procedure were virtually the same as those described previously.[1,2] The formaldehyde solutions were prepared from paraformaldehyde by refluxing for 4 h, followed by the filtration of the insoluble substances. The reaction was started by adding given amounts of $CaCl_2$ and D-fructose, immediately after which the pH of the reaction mixture was adjusted with concd KOH. The pH of the reaction mixture was maintained by adding concentrated aqueous KOH during the reaction.

The total saccharides were determined using the phenol-sulfuric acid method[6] and were calculated as glucose from a previously prepared calibration curve. The sugar yield was calculated according to the following equation: Sugar yield (%) = [sugars as glucose]/([HCHO]$_0$ + [D-fructose]) × 100. The formaldehyde was determined by the method of Bricker *et al.*;[7] only the optical density was measured at 579 nm, while the ORP was measured by the method described in a previous paper.[1]

The products were trimethylsilylated by Sweeley's method,[8] and the trimethylsilyl (TMS) derivatives were analyzed by gas chromatography, as has been described previously.[9] The products were numbered according to their retention time as GP-13, GP-18, *etc.* The yield of the products (GLC%) were given by measuring the peak areas.

The calcium salts and other reagents were of an analytical grade.

Results and Discussion

Effect of the Calcium-ion Concentration. In the previous papers,[4,5] it was suggested that the concentration of the dissolved calcium ions ([Ca]) at the formose-forming step was a very important factor in the selective product formation. It was found that the formose reaction in the presence of small amounts of calcium and D-fructose gave rise to similar selectivities (Table 1).

Table 1 shows the effects of [Ca] on formose reactions carried out at various pHs (9.5—12.0) of the reaction mixture. At any pH, the T_{max} value at which the consumption of formaldehyde reaches over 90% decreases, and the sugar yield increases with an increase in the amount of calcium. At [Ca] = 0.025 M, a similar relationship between T_{max} and the sugar yield with an increase in the pH of the reac-

TABLE 1. EFFECTS OF $CaCl_2$ CONCENTRATION ON THE DISTRIBUTION OF PRODUCTS[a]

Run No.	pH	$CaCl_2$ mM	T_{max} min	Sugar yield %	Products (GLC%)[e] 2-HG	18	3-HP	25	2,4-DHP	T_{3p}[b]
1	9.5	25		$(20.3)^{d)}_{270}$						
2	9.5	350	181	49.7	12.0	c)	45.4	4.9	18.7	76.1
3	9.5	500	84	59.1	8.1	5.2	36.5	20.8	6.9	51.5
4	9.5	650	59	58.7	2.6	3.4	39.1	20.0	3.1	44.8
5	9.5	900	40	63.2	c)	7.8	28.0	18.6	c)	30.0
6	10.5	25	108	43.3	15.1	c)	28.6	c)	37.2	80.9
7	10.5	50	54	55.0	9.1	5.9	24.4	12.2	12.7	46.8
8	10.5	100	27	68.3	9.3	6.2	26.4	15.3	1.8	37.5
9	10.5	250	9	69.1	1.9	9.9	9.4	19.0	c)	12.3
10	11.0	5		$(67.3)^{d)}_{180}$						
11	11.0	10	57	40.8	13.3	c)	23.4	3.0	5.14	88.1
12	11.0	25	36.5	47.1	12.0	c)	25.7	4.8	23.0	60.7
13	11.0	50	12.5	65.5	5.9	5.9	29.6	15.4	4.5	40.0
14	11.0	100	9.5	69.2	4.5	9.9	21.2	19.0	2.5	32.2
15	11.5	5	56.0	31.8	9.2	2.0	21.8	4.1	47.6	78.6
16	11.5	25	8.5	55.3	9.8	4.5	21.4	9.7	11.0	42.2
17	12.0	5	26.5	37.7	8.4	3.3	22.2	6.1	34.4	65.0
18	12.0	25	5.5	67.5	4.7	7.3	13.8	10.5	7.6	26.1

a) [HCHO]=1.0 M; [D-fructose]=0.01 M; the pH was adjusted by concd KOH; temp=60 °C; total volume=200 ml. b) Total yield of 2-HG, 3-HP, and 2,4-DHP. c) GLC was below 1%. d) The number in parentheses is the HCHO consumption(%) at the time (min) shown by the subscript. e) 2-HG: 2-(hydroxymethyl)glycerol, 3-HP: 3-(hydroxymethyl)pentitol, 2,4-DHP: 2,4-bis(hydroxymethyl)pentitol; 18 and 25: products which were shown by the peak numbers of 18 and 25 respectively in a gas chromatogram of the TMS derivatives.

tion mixture is observed (Runs 1, 6, 12, and 18): the sugar yield increases as T_{max} decreases. These phenomena are in fairly good agreement with the results reported previously.[2,3] In this case, it could easily be considered that the sugar yield is affected by the amount of formaldehyde consumed by the Cannizzaro reaction. The sugar yield, however, is influenced by the product composition: the sugar yield decreases with an increase in the total yields of 2-HG, 3-HP, and 2,4-DHP, which are sugar alcohols. A sugar alcohol usually has little reducing power. Therefore, the sugar yield which is determined using the phenol-sulfuric acid method and calculated as glucose is useful only when the product composition is similar.

Here, the total yield (T_{3p}) of 2-HG, 3-HP, and 2,4-DHP is used as an indicator of the selectivity of the formose reaction. As is shown in Table 1, T_{3p} increases with a decrease in the pH of the reaction mixture and [Ca]. Although the yields of 2-HG and 3-HP are not affected by the pH of the reaction mixture, the yield of 2,4-DHP increases greatly with a decrease in the pH. The yield of 3-HP is not so much affected by [Ca]. The yields of 2,4-DHP and 2-HG increase with a decrease in [Ca], while the yield of GP-25, which is one of products shown by the peak number of 25 in a gas chromatogram of the TMS derivatives,[4,5] increases with an increase in [Ca]. These results led us to conclude that the formation of 2,4-DHP and GP-25 is competitive or that GP-25 is an intermediate of 2,4-DHP.

Figure 1 shows the effects of [Ca] on the sugar yield, T_{max}, and T_{3p} at given formaldehyde concentrations. The relationship between T_{max} and the sugar yield is quite similar to that shown in Table 1. Furthermore, the sugar yield increases with a decrease in the formaldehyde concentration at the same ratio of [Ca]/[HCHO]. This phenomenon is in fairly good agreement with the result reported previously.[2]

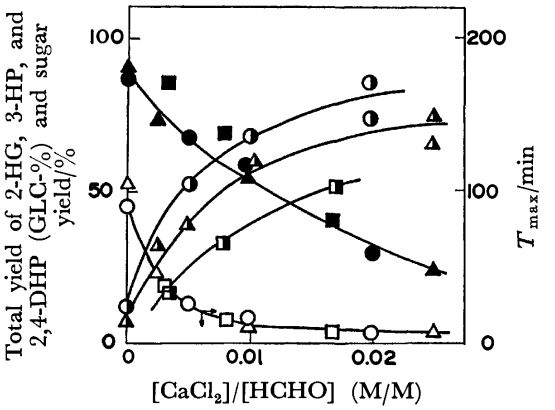

Fig. 1. Effects of $CaCl_2$ concentration on the selectivity, T_{max}, and sugar yield.
[D-Fructose]=0.01 M; pH=12.0 (adjusted by concd KOH); temp=60 °C; total volume=200 ml. T_{3p}, [HCHO](M): ●, 0.5; ▲, 1.0; ■, 3.0. T_{max}, [HCHO] (M): ○, 0.5; △, 1.0; □, 3.0. Sugar yield, [HCHO] (M): ◑, 0.5; ◭, 1.0; ◨, 3.0.

In Fig. 1, it is clear that the selectivity (T_{3p}) increases with a decrease in [Ca], and that at any formaldehyde concentrations the same [Ca]/[HCHO] ratios give similar total yields of 2-HG, 3-HP, and 2,4-DHP (T_{3p}). On the other hand, when the formaldehyde

concentration is varied at a given [Ca], the relationship between the ratio of [Ca]/[HCHO] and T_{3p} is also similar (Fig. 2) to that described above. These results suggest that these branched sugar alcohols of 2-HG, 3-HP, and 2,4-DHP are end products under these reaction conditions and that the ratio of the formaldehyde concentration to [Ca] is the most important factor in selective formation of these products. In this case, however, there is another important factor is the selective formation of the three branched sugar alcohols, namely, the role of D-fructose as a co-catalyst,

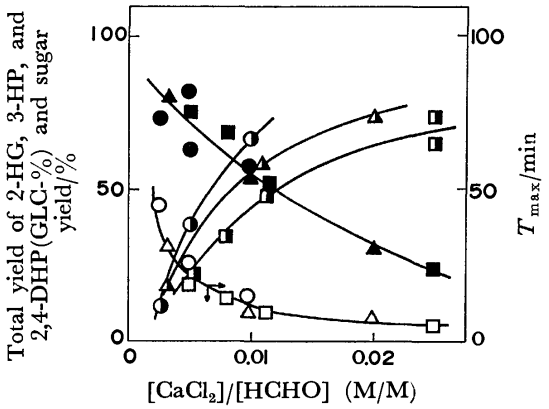

Fig. 2. Effects of HCHO concentration on T_{3p}, T_{max}, and sugar yield.
[D-Fructose]=0.01 M; pH=12.0 (adjusted by concd KOH); temp=60 °C; total volume=200 ml. T_{3p}, [$CaCl_2$] (M): ●, 0.005; ▲, 0.01; ■, 0.025. T_{max}, [$CaCl_2$] (M): ○, 0.005; △, 0.01; □, 0.025. Sugar yield, [$CaCl_2$] (M): ◑, 0.005; ◭, 0.01; ◨, 0.025.

for it diminishes the induction period and offers reaction conditions similar to those at T_{min}, which is the time of the beginning of the formose-forming step in the formose reaction catalyzed by calcium hydroxide.[4,5]

Therefore, large amounts of 2-HG, 3-HP, and 2,4-DHP can be easily obtained at one time by starting the reaction under the usual conditions ([$Ca(OH)_2$]= 0.1 M, [HCHO]=1.0 M, and temp=60 °C), followed by continuously adding a given amount of formaldehyde and adjusting the pH of the reaction mixture after T_{min}, at which the ORP curve shows a minimum. The details of these results will be presented in a subsequent paper.

Effect of the Fructose Concentration. In order to clarify the functions of D-fructose in the formose reaction, the relationship among the D-fructose concentration, [Ca], T_{max}, the sugar yield, and the product distribution was studied. The results are summarized in Table 2.

At the concentration of calcium ions ([Ca]) below 5×10^{-3} M, an increase in the D-fructose concentration led to decrease in T_{max} and to an increase in both the sugar yield and T_{3p}. At 25×10^{-3} M of [Ca], T_{3p} increases with an increase in the D-fructose concentration; however, the T_{max} and the sugar yield are little affected by the D-fructose concentration.

For a constant D-fructose concentration (10×10^{-3} or 50×10^{-3} M), an increase in [Ca] led to a decrease in both T_{max} and T_{3p} and to an increase in the sugar yield. These phenomena are the same as those described previously (Table 1). T_{3p} (2-HG, 3-HP, and 2,4-DHP) decreases, however, GP-25 increases with an increase in [Ca].

Table 2. Effects of fructose concentration[a]

[$CaCl_2$] mM	D-Fructose mM	T_{max} min	Sugar yield %	Products (GLC%)[d] 2-HG	3-HP	25	2,4-DHP	T_{3p}
2.5	0	$(81.9)^{b)}_{200}$						
2.5	1	94.2	19.2	7.0	15.9	c)	43.8	66.7
2.5	5	56.2	22.5	11.0	10.4	c)	47.9	69.3
2.5	10	41.0	23.9	11.3	19.0	4.8	44.1	74.4
2.5	20	35.0	26.6	12.4	20.7	2.7	46.3	79.4
2.5	50	20.2	35.7	15.7	18.9	1.8	49.8	84.4
5.0	0	$(86.6)^{b)}_{210}$						
5.0	0.5	73.2	19.7	4.9	20.8	6.0	22.3	48.0
5.0	1	56.5	23.7	5.1	23.0	4.5	27.3	55.4
5.0	5	30.5	35.6	7.5	21.8	3.1	32.5	61.8
5.0	10	26.5	37.7	8.4	22.2	6.1	34.4	65.0
5.0	20	22.5	37.5	8.5	20.7	6.2	38.2	67.4
5.0	30	21.2	34.8	8.1	22.6	2.1	40.3	71.0
5.0	50	18.0	41.3	10.6	20.2	4.9	38.4	69.2
5.0	100	12.0	41.9	7.9	13.4	8.5	33.6	54.9
25.0	0	$(77.9)^{b)}_{60}$						
25.0	10	5.7	67.5	4.7	13.8	10.5	7.6	26.1
25.0	25	6.8	65.8	5.0	12.0	12.5	9.7	26.7
25.0	50	7.3	61.7	5.9	12.6	13.4	15.4	33.9
25.0	100	7.1	59.3	5.6	14.2	10.7	20.8	40.6

a) [HCHO]=1.0 M; [$CaCl_2$]=0.005 M; [metal hydroxide]=0.1 M; [D-fructose]=0.01 M; pH=12.0 (adjusted by concd KOH); temp=60 °C; total volume=200 ml. b) pH=11.5, while the other reaction conditions were the same as in a). c) GLC was below 1%. d) See Table 1.

Furthermore, the TMS derivative of D-fructose was a minor one. In another experiment, *ca.* 50% of added D-fructose was found to decompose or change to other compounds in 10 min and *ca.* 70% of D-fructose in 20 min under these reaction conditions: [D-fructose] $=10\times10^{-3}$ M, [$CaCl_2$] $=5\times10^{-3}$ M, pH= 12.0 adjusted by concd potassium hydroxide, and temp=60 °C. These results led us to suggest that D-fructose added as a co-catalyst would react with formaldehyde or would decompose to some products, such as reductone,[10] which may then act effectively as co-catalysts.

Time Course of the Selective Formose Reaction in the Presense of a Small Amount of Calcium Ions. Figure 3 shows a typical time course of the formaldehyde consumption, the sugar yield, and ORP in the formose reaction which gives rise to 2-HG, 3-HP, and 2,4-DHP with a high selectivity when the reaction is catalyzed by potassium hydroxide and a small amount of calcium ions in the presence of D-fructose. Formaldehyde was consumed at a rather uniform rate,

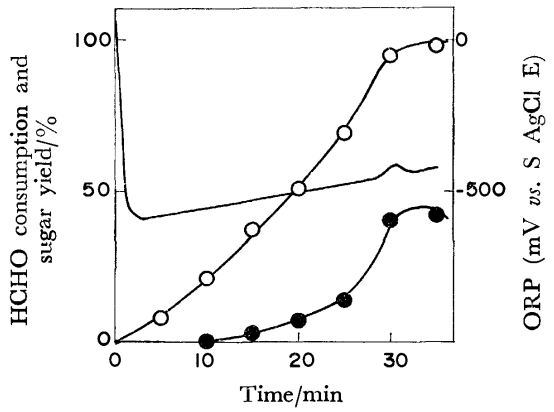

Fig. 3. Time course of HCHO consumption, sugar yield, and ORP.
[HCHO]=1.0 M; [$CaCl_2$]=0.005 M; [D-fructose]= 0.01 M; pH=12.0 (adjusted by concd KOH); temp= 60 °C; total volume=200 ml. ○: HCHO consumption, ●: sugar yield, —: ORP.

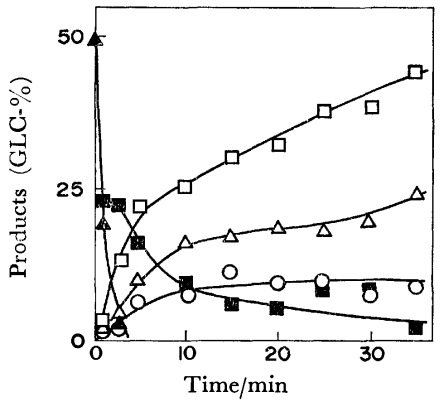

Fig. 4. Time course of selective formose reaction products.
[HCHO]=1.0 M; [$CaCl_2$]=0.005 M; [D-fructose]= 0.01 M; pH=12.0 (adjusted by concd KOH); temp= 60 °C; total volume=200 ml. ○, 2-HG, △, 3-HP, □, 2,4-DHP, ■, 25; ▲, fructose.

although the usual formose reaction catalyzed by calcium hydroxide consumed formaldehyde auto-catalytically.[1,11] This consumption curve is also different from that given by the formose reaction which is catalyzed by calcium oxide in the presence of various co-catalysts.[12]

In this reaction system, the maximum ORP is found to be useful for the indicator of the end point of the reaction (T_{max}) at which the sugar yield is at its maximum. The same relationship has been observed in the usual formose reaction catalyzed by calcium hydroxide alone.[1,11]

Figure 4 shows the time course of the main products; 2-HG, 3-HP, 2,4-DHP, GP-25, and D-fructose. The added D-fructose disappears rapidly and becomes of minor importance at the end of the reaction, as has been described above. 2,4-DHP, 3-HP, and 2-HG are formed selectively even at the initial stage. Although 2-HG early reaches a constant proportion (*ca.* 10 GLC%), 2,4-DHP and 3-HP increase continuously as the reaction proceeds.

Quite importantly, GP-25 is formed with a high selectivity as one of the initial products; it then disappears with the simultaneous increase in both 2,4-DHP and 3-HP. These results suggest that GP-25 might be an intermediate of 2,4-DHP or 3-HP.

In our previous paper,[13] we have already proposed a scheme of possible pathways for the selective formation of these three branched sugar alcohols (2-HG, 3-HP, and 2,4-DHP), which may be explained by a conventional mechanism[14] involving cumulative aldol condensations, followed by the cross-Cannizzaro reaction of their aldose precursors. In addition, it has been already reported that the reduction of 2,4-bis(hydroxymethyl)-3-pentulose (2,4-DH-3-P) with sodium borohydride[15] or formaldehyde in the presence of a base[16] give 2,4-DHP. A modified scheme of possible pathways for the selective formose formation is proposed in Scheme 1. There has previously been no reasonable explanation for the occurrence of the selective formose reaction.

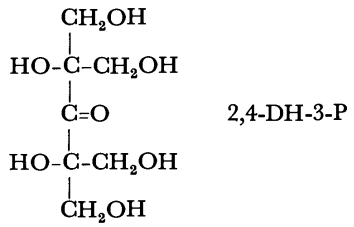

2,4-DH-3-P

Effect of Reaction Temperature. The formose reaction was carried out at various temperatures; the results are summarized in Table 3. T_{max} decreases with an increase in the reaction temperature, so with the decrease in T_{max} the sugar yield increases, as has been described previously.[2,3] At 80 °C, however, the sugar yield is not so high in spite of the short reaction time, because the resulting sugars easily decompose as a result of the high reaction temperature. Three branched sugar alcohols (T_{3p}) are formed with a high selectivity (*cf.* Table 3), although the increase in the reaction temperature leads to tendency for T_{3p} to decrease.

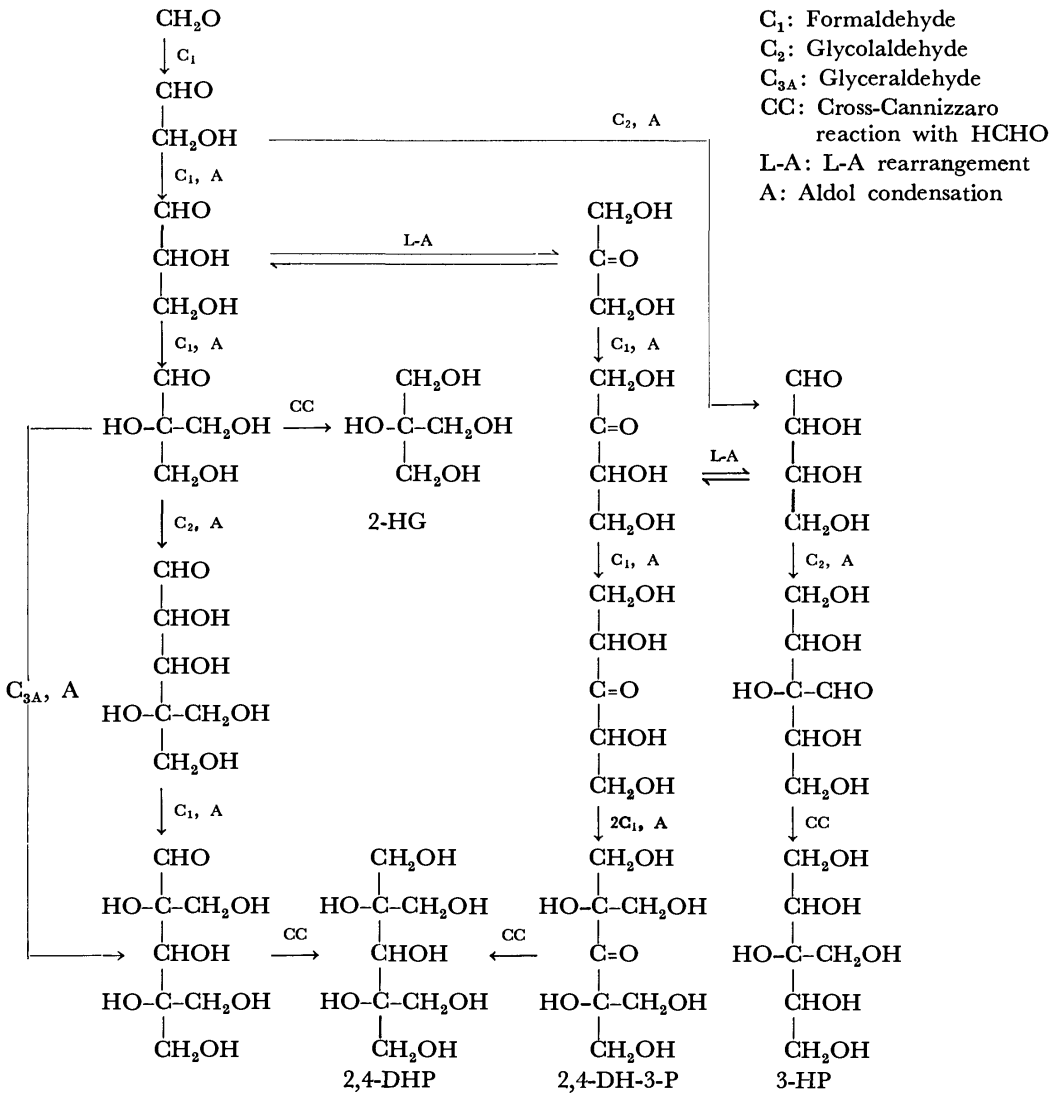

Scheme 1. Possible pathways for the selective formose formation.

Table 3. Effects of reaction temperature[a)]

Reaction temp °C	T_{max} min	Sugar yield %	Products (GLC%)[b)] 2-HG	3-HP	25	2,4-DHP	T_{3p}
50	334	33.5	16.8	27.4	16.2	31.0	75.2
60	45	42.1	13.1	18.9	5.8	45.5	77.5
70	6.3	49.3	7.7	27.7	1.0	30.4	65.8
80	1.0	45.6	11.7	18.9	1.8	22.3	52.9

a) [HCHO]=1.0 M; [$CaCl_2$]=0.005 M; [D-Fructose]=0.01 M; pH=11.5; total volume=200 ml. b) See Table 1.

On the other hand, Tambawala *et al.*[17)] reported that, at 50% and lower conversion levels, the C_4 and C_5 aldose and ketose products are practically pure straight chains at 40 °C and practically pure branched chains at 60 °C. At higher conversion levels as much as 40% branched chains are present at 40 °C. Furthermore, as has been mentioned above, the three branched sugar alcohols are formed selectively even at the initial stage, at which the formaldehyde consumption is only 10%. It would be supposed that these differences are mainly attributable to the amount of calcium ions. At any rate, there is a remarkable effect of the reaction temperature, that is, the formation of GP-25, which might be an intermediate of 2,4-DHP or 3-HP and which increases with a decrease in the reaction temperature. Efforts are under way to separate and identify GP-25. The formation of GP-25 under various reaction conditions is also under investigation in detail.

Effect of Various Co-catalysts on the Selectivity of Products. Since Kusin[18)] and Langenbeck[12)] reported that the induction period can be eliminated or shortened by the addition to the reaction mixture of small amounts of carbohydrates, the formose reaction in the presence

of carbohydrates or other compounds with an enediol form has been studied: the reaction is accelerated to a small extent, and the induction period is shortened greatly, by the addition of glycolaldehyde and glyceraldehyde; the catalytically active species is not the hydroxide of an alkaline earth metal, but its complex with a carbohydrate.[19-21]

However, there have been few reports which have discussed the effects of a formose-reaction-promoting-co-catalyst on the selectivity of products. Although we have already reported the effects of various co-catalysts on the formose reaction in the presence of a small amount of calcium ions,[22] a few other co-catalysts have been investigated in terms of how they affect the product distribution. The results are summarized in Table 4.

As has been described previously,[22] the formose reaction in the presence of acetoin or benzoin is found to give GP-13 and -14 or 1,2-diphenylglycerol respectively with a high selectivity and to give a low sugar yield as glucose. From these results, one can easily suppose that acetoin and benzoin do not act as co-catalysts, but only as substrates which are easily hydroxymethylated with formaldehyde to give a stable and unreactive compound.

On the other hand, other co-catalysts give rise to similar T_{max} values, sugar yields, and product distributions, although in the case of L-ascorbic acid the T_{max} is relatively long. In addition, phenacyl alcohol was found to form GP-16 (*ca.* 10 GLC%), which could not be detected without phenacyl alcohol. Hence, these co-catalysts would seem to function similarly to each other both as co-catalysts and substrates.

Furthermore, when DL-glyceraldehyde or dihydroxyacetone is used as a co-catalyst, the total yield of 2-HG, 3-HP, and 2,4-DHP (T_{3p}) is very high (*ca.* 80 GLC%). This results led us to assume that DL-glyceraldehyde and dihydroxyacetone would function both as co-catalysts and as substrates which especially act as intermediates of the above three branched sugar alcohols.

On the basis of the above results, we propose that the enediol form of a co-catalyst is very important in promoting the formose reaction: the $R-\overset{HO}{\overset{|}{C}}=\overset{OH}{\overset{|}{C}}-H$ type is effective, but the $R_1-\overset{HO}{\overset{|}{C}}=\overset{OH}{\overset{|}{C}}-R_2$ (R_1, $R_2 \neq H$) type is not effective in promoting the reaction. The same assumption has already been presented by Sakai *et al.*[23] The relatively long T_{max} with L-ascorbic acid is attributable to the time necessary to convert an enediol form of L-ascorbic acid, $R_1-\overset{HO}{\overset{|}{C}}=\overset{OH}{\overset{|}{C}}-R_2$, to the effective type, $R-\overset{HO}{\overset{|}{C}}=\overset{OH}{\overset{|}{C}}-H$.

Effect of Various Metal Hydroxides. In the presence of a slight amount of calcium ions, the formose reactions were carried out by various metal hydroxides in order to examine the effect of the kind of metal cation on the reaction. The results are summarized in Table 5. Judging from the results (T_{max} values, the sugar yields, and the product distributions), the catalytic activity of $Sr(OH)_2$ is very similar to that of $Ca(OH)_2$. The catalytic activity, furthermore, decreases in the following order: $Ca(OH)_2$, $Sr(OH)_2$> $Ba(OH)_2$>$Mg(OH)_2$. These results are the same as those reported by Partridge *et al.*,[24] who supposed that the intermediate complexes must contain a carbohydrate molecule in addition to formaldehyde molecules in the coordination sphere of the catalytically active cation. In Table 5, furthermore, $Mg(OH)_2$, $Fe(OH)_3$, and $Pb_2O(OH)_2$ have a longer T_{max} than that of the control experiment.

In the cases of $Cu(OH)_2$ and LiOH, in spite of their short T_{max} values, the sugar yield is low. Pfeil *et al.*[25] reported that LiOH catalyzes the Cannizzaro reaction rather than the formose reaction. In the presence of $Cu(OH)_2$, metal copper separated out from the reaction mixture, so one can easily suppose that $Cu(OH)_2$ would be reduced by formaldehyde to metal copper and that formaldehyde would be oxidized to formic acid. Hence, the low sugar yield in these formose reactions is attributable to the large consumption of formaldehyde to formic acid.

2-(Hydroxymethyl)glycerol (2-HG), 3-(hydroxy-

TABLE 4. EFFECTS OF VARIOUS CO-CATALYSTS[a]

Co-catalyst	T_{max}	Sugar yield	Products (GLC%)[e]						
	min	%	2-HG	13	14	3-HP	1,2-DPG[b]	2,4-DHP	T_{3p}
D-Fructose	26.5	40.0	8.4	c)	c)	22.2	c)	34.4	65.0
D-Glucose	29.7	34.8	7.4	c)	c)	24.0	c)	35.0	66.4
D-Xylose	26.9	39.3	8.1	c)	c)	23.2	c)	31.9	63.7
Triose reductone	32.8	34.7	10.7	c)	c)	20.7	c)	33.3	64.7
DL-Glyceraldehyde	24.0	35.6	9.5	c)	c)	27.3	c)	41.4	78.2
Dihydroxyacetone dimer	28.6	30.8	10.1	c)	c)	26.4	c)	45.5	82.0
L-Ascorbic acid	50.7	29.4	10.0	c)	c)	24.9	c)	28.6	63.5
Phenacyl alcohol	25.3	39.1	8.0	c)	c)	20.7	c)	30.7	59.4
Acetoin	177.0	8.3	c)	14.4	33.4	c)	c)	c)	c)
Benzoin	94.3	11.2	c)	c)	c)	c)	89.1	c)	c)

a) [HCHO]=1.0 M; [co-catalyst]=0.01 M; [$CaCl_2$]=0.005 M; pH=12.0 (adjusted by concd KOH); temp=60 °C; total volume=200 ml. b) 1,2-(Diphenyl)glycerol is abbreviated as 1,2-DPG. c) GLC was below 1%. e) See Table 1.

Table 5. Effects of various metal hydroxides[a)]

Metal hydroxide	T_{max} min	Sugar yield %	Products (GLC%)[d)] 2-HG	18	3-HP	25	2,4-DHP	T_{3p}
	24.0	44.6	12.8	c)	29.0	2.3	41.9	83.7
$Mg(OH)_2$	36.8	38.5	12.0	c)	31.2	2.1	40.8	84.0
$Sr(OH)_2$	3.5	65.7	2.5	6.3	16.1	12.3	7.2	25.8
$Ba(OH)_2$	6.8	63.9	2.7	6.4	20.8	8.6	27.7	51.2
$Pb_2O(OH)_2$	76.0	26.5	1.3	10.4	22.4	5.5	1.3	25.0
$Cu(OH)_2$	8.0	7.7	8.8	4.1	18.0	4.8	18.0	44.8
$Fe(OH)_3$	70.0	14.6	19.3	c)	18.8	c)	51.8	89.9
LiOH[b)]	10.0	25.2	5.2	c)	44.0	c)	31.6	80.8
b)	45.0	38.6	13.5	c)	19.4	5.9	46.7	79.6

a) [HCHO]=1.0 M; [$CaCl_2$]=0.005 M; [metal hydroxide]=0.1 M; [D-fructose]=0.01 M; pH=12.0 (adjusted by concd KOH); temp=60 °C; total volume=200 ml. b) pH=11.5, while the other reaction conditions were the same as in a). c) GLC was below 1%. d) See Table 1.

methyl)pentitol (3-HP), and 2,4-bis(hydroxymethyl)-pentitol (2,4-DHP) are formed with a high selectivity (T_{3p}, 80 GLC%) in the formose reaction catalyzed by KOH, $Mg(OH)_2$, $Fe(OH)_3$, and LiOH in the presence of small amounts of calcium ions and D-fructose. Especially, $Fe(OH)_3$ is found to give 52 GLC% of 2,4-DHP only. $Pb_2O(OH)_2$, furthermore, give rise to an unknown product, GP-18; efforts are under way to isolate and identify this product. These results are in fair agreement with those results[5)] obtained from a modified formose reaction.

Under the same reaction conditions as in Table 5, but without calcium ions, furthermore, the formose reaction was found to give a longer T_{max} value than that in the presence of calcium ions, but the product distributions were quite similar to each other. For example, when no metal hydroxide was added, only adjusting the pH of the reaction mixture to 12.0 with concd KOH aq; the T_{max} was 182 min; at barium hydroxide, the T_{max} was 23 min.

References

1) Y. Shigemasa, M. Shimao, C. Sakazawa, and T. Matsuura, *Bull. Chem. Soc. Jpn.*, **48**, 2099 (1975).
2) Y. Shigemasa, T. Fujitani, C. Sakazawa, and T. Matsuura, *Bull. Chem. Soc. Jpn.*, **50**, 1527 (1977).
3) Y. Shigemasa, M. Shimao, C. Sakazawa, and T. Matsuura, *Bull. Chem. Soc. Jpn.*, **50**, 2138 (1977).
4) Y. Shigemasa, O. Nagae, C. Sakazawa, R. Nakashima, and T. Matsuura, *J. Am. Chem. Soc.*, **100**, 1309 (1978).
5) Y. Shigemasa, M. Kawahara, C. Sakazawa, R. Nakashima, and T. Matsuura, *J. Catal.*, **62**, 107 (1980).
6) M. Bubois, K. A. Gilles, J. K. Hamilton, P. A. Rebers, and F. Smith, *Anal. Chem.*, **28**, 350 (1956).
7) C. E. Bricker and H. R. Johnson, *Ind. Eng. Chem.*, **17**, 400 (1945); M. Lambert and A. C. Neish, *Can. J. Res.*, **28B**, 83 (1950).
8) C. C. Sweeley, R. Bentley, M. Makita, and W. W. Wells, *J. Am. Chem. Soc.*, **85**, 2497 (1963).
9) Y. Shigemasa, Y. Matsuda, C. Sakazawa, and T. Matsuura, *Bull. Chem. Soc. Jpn.*, **50**, 222 (1977).
10) H. Omura, A. Fujita, M. Sato, M. Otsuki, and M. Isao, *Sci. Bull. Far. Agric. Kyushu Univ.*, **28**, 79 (1974); H. Obata, K. Shikata, and T. Tokuyama, *Agric. Chem. Soc. Jpn.*, **50**, 593 (1976).
11) T. Matsuura, Y. Shigemasa, and C. Sakazawa, *Chem. Lett.*, **1974**, 713.
12) W. Langenbeck, *Naturwissenschaften*, **30**, 30 (1942).
13) Y. Shigemasa, C. Sakazawa, R. Nakashima, and T. Matsuura, Origin of Life, (1978), p. 211.
14) T. Mizuno and A. H. Weiss, *Adv. Carbohydr. Chem. Biochem.*, **29**, 137 (1974).
15) Y. Shigemasa, S. Akagi, R. Nakashima, and S. Saito, *Carbohydr. Res.*, **80**, C1 (1980).
16) Y. Shigemasa, S. Akagi, E. Waki, and R. Nakashima, 40th Fall Meeting of the Chem. Soc. Jpn., Fukuoka, October 1979, Abstr. No. 3G28.
17) H. Tambawala and A. H. Weiss, *J. Catal.*, **26**, 388 (1972).
18) A. Kusin, *Ber.*, **69**, 619, 1495, 2169 (1935).
19) O. V. Krylov, Yu. I. Sinyak, A. A. Berlin, and I. L. Shulgina, *Dokl. Akad. Nauk. SSSR*, **119**, 643 (1971).
20) K. Fujino, J. Kobayashi, and I. Higuchi, *Nippon Kagaku Kaishi*, **1972**, 2292.
21) Ya. B. Gorokhovat-skii, N. P. Evmenko, and V. F. Gaevskii, *Kinet. Katal.*, **18**, 558 (1971).
22) Y. Shigemasa, Y. Suetoki, E. Waki, and R. Nakashima, *Rep. Fac. Eng. Tottori Univ. Jpn.*, **10**, 112 (1979).
23) T. Sakai, M. Takahashi, H. Kato, M. Ishizaki, and M. Goto, 38th Fall Meeting of the Chem. Soc. Jpn., Nagoya, October, 1978, Abstr. No. 4I11.
24) R. D. Patridge, T. I. Khomenko, O. A. Golovina, M. M. Sakharov, A. H. Weiss, and O. V. Krylov, *Kinet. Katal.*, **18**, 557 (1977).
25) E. Pfeil and G. Schroth, *Chem. Ber.*, **85**, 293 (1952).

The Conformational Analysis of a Series of 4,8-Dimethyl-6-phenyl-5,6,7,8-tetrahydro-4*H*-1,3,2,6-dioxathiazocine 2-Oxides Using NMR

Tomihiro NISHIYAMA, Yasushi NAKAI, Hideaki SHISHIBORI, and Fukiko YAMADA*

Department of Applied Chemistry, Faculty of Engineering, Kansai University, Senriyama, Suita, Osaka 564

(Received August 1, 1980)

The title compounds were prepared, and their ^{1}H- and ^{13}C-NMR spectra were examined. On the basis of the data for the benzene-solute collision complexes and the magnitudes of the γ shifts, five isomeric conformations of the compounds were discussed.

Recently, a number of conformational analyses of ethylene and trimethylene sulfites have been reported.[1-4] For example, Green and Hellier[1] have used the IR technique of the S=O stretching vibrations to study the conformation of trimethylene sulfites. They concluded that the higher wave number band (*ca.* 1195 cm^{-1}) is attributable to the chair form with an axial S=O function and/or flexible twist forms, while the lower wave number band (*ca.* 1234 cm^{-1}) is to be assigned to the chair form with an equatorial S=O group. Buchanan *et al.*[4] reported ^{13}C-NMR data on trimethylene sulfites and ten alkyl derivatives and concluded that these compounds exist in the chair form with an axial or equatorial S=O function and twist conformations.

In a previous paper,[5] we ourselves reported the reaction of *N*,*N*-bis(2-hydroxyethyl)anilines with thionyl chloride giving the 6-phenyl-5,6,7,8-tetrahydro-4*H*-1,3,2,6-dioxathiazocine 2-oxides, which had a structure similar to that of the trimethylene sulfite skeleton. In order to obtain more stereochemical information about the 1,3,2,6-dioxathiazocine 2-oxide system, it seems desirable to prepare 1,3,2,6-dioxathiazocine 2-oxides with a ortho-, meta-, para-substituent on the *N*-phenyl ring and methyl group on the C-4 and C-8. In this paper we wish to report the conformational analyses of 4,8-dimethyl-6-phenyl-5,6,7,8-tetrahydro-4*H*-1,3,2,6-dioxathiazocine 2-oxides (**1**—**7**) by means of NMR spectroscopy.

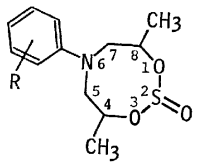

1, R=H
2, R=*o*-CH_3
3, R=*m*-CH_3
4, R=*p*-CH_3
5, R=*o*-Cl
6, R=*m*-Cl
7, R=*p*-Cl

Experimental

Measurements. All the melting points are uncorrected. All the NMR spectra were determined at 100- and 60-MHz with JEOL JNM-PS-100 and JNM-PMX-60 spectrometers respectively. The ^{13}C-NMR spectra were obtained using a JNM-PS-100/EC-100 Fourier transform spectrometer operating at 25.15 MHz, with complete proton decoupling. The pulse width and repetition time were 10.2 μs for a 45° pulse and 6 s respectively. The spectra were observed as

TABLE 1. CHARACTERIZATION DATA OF THE 1,3,2,6-DIOXATHIAZOCINE 2-OXIDES

Compd No.	Yield/%	Mp/°C	IR, S=O ν/cm^{-1}	Found (Calcd) %		
				C	H	N
1a	18	205.0—206.0	1193	56.36 (56.45)	6.65 (6.71)	5.42 (5.48)
1b	8	122.0—122.7	1190	56.34	6.75	5.47
1c	6	88.2— 88.8	1182	56.24	6.80	5.47
2d	23	109.5—110.0	1190	58.09 (57.97)	7.14 (7.11)	5.11 (5.20)
2e	5	—a)	1200	58.56	7.24	5.08
3a	2	137.8—138.0	1187	57.62	7.28	5.15
3b	13	80.2— 81.5	1187	58.20	7.14	5.05
3c	6	46.1— 47.0	1200	58.21	7.22	5.15
4a	50	182.0—182.9	1190	57.74	7.07	5.18
4b	8	93.9— 94.1	1182	57.12	7.35	5.13
4c	17	78.0— 79.0	1192	57.65	7.19	5.14
5d	12	87.5— 89.5	1187	49.64 (49.74)	5.55 (5.57)	4.89 (4.83)
5e	15	—a)	1200	49.15	5.47	4.93
6a	5	158.0—158.9	1202	49.66	5.57	4.89
6b	7	125.0—125.5	1190	49.44	5.42	4.77
6c	15	90.0— 90.6	1200	49.78	5.43	4.78
7a	9	163.4—164.2	1195	49.43	5.51	4.79
7b	20	99.5—100.0	1190	49.45	5.54	4.79
7c	21	137.0—137.3	1198	49.56	5.43	4.88

a) Liquid.

2 mmol cm^{-3} solutions in $CDCl_3$ with a spectral width of 6250 Hz (data points : 8192). The chemical shifts were referred to the internal TMS as the standard. The IR spectra were recorded on a Shimadzu Model 27-G grating spectrophotometer on a KBr for the solid materials or on a NaCl plate for the liquid materials.

Compounds. The series of **1**—**7** was prepared by the reaction of the corresponding *N,N*-bis(2-hydroxypropyl)-anilines with thionyl chloride, as has been described in our previous paper.[5] The purification of the crude product by the use of a short silica gel column, with hexane or a hexane–benzene (1:1) mixture as an eluent, and subsequent recrystallization afforded two or three pure isomers as colorless crystals; these compounds gave satisfactory results for mass spectra and elemental analyses. The physical properties of the compounds of **1**—**7** are listed in Table 1.

Results and Discussion

S=O Frequencies. The IR spectra of **1**—**7** showed a characteristic band of the S=O function at 1190—1200 cm^{-1} (Table 1). Trimethylene sulfites prefer the chair form with an axial S=O group, and the same conformational preference is found for six-membered-ring sulfoxides.[6,7] In the case of trimethylene sulfites,[8] the S=O stretching band at 1190 cm^{-1} (CCl_4) to 1198 cm^{-1} (C_6H_{12}) indicates a axial S=O conformer, while 1233 (CS_2) to 1234 cm^{-1} (C_6H_{12}) is a equatorial conformer. Twist conformations apparently give intermediate values.

If this consideration can be extended to Compounds **1**—**7**, the position of the S=O stretching band of 1190—1120 cm^{-1} would indicate a predominance of the axial conformer or the twist conformer.

^{1}H-NMR Spectra. The NMR spectra of the heterocyclic protons of **5d**, **5e**, **7a**, **7b**, and **7c** are shown in Fig. 1. The NMR spectra of **7a** and **7b** consist of four distinct sets of multiplets, at *ca.* δ 4.7—4.9(m), 3.7—3.8(q), 3.1(q), and 1.3—1.4(d), for which a straightforward analysis was possible. In contrast, in Compounds **5d**, **5e**, and **7c**, the methylene protons for H-5 and H-7 gave complicated multiplets and were not easily analyzed. Striking differences in Compounds **5e** and **7c** compared with Compounds **5d**, **7a**, and **7b** are recognizable in the signals of the methine protons for H-4 and H-8. That is, two kinds of methine protons of H-4 and H-8 for **5e** and **7c** appeared at *ca.* δ 5.1 and 4.6 ppm. We subdivided the spectra into five types—A, B, C, D, and E, as can be seen in Fig. 1. The spectra of the compounds with an ortho-substituent may all be considered to belong to types A and B. Similarly, those without a substituent or with meta- and para-substituents belong to types C, D, and E. The methine proton for H-4 and/or H-8 of **5d**, **7a**, and **7b** shows one set of multiplets, while compounds of **5e** and **7c** show two sets of multiplets. We have, therefore, suggested that, in the case of Compounds **5d**, **7a**, and **7b**, the possible comformations are in the symmetric form, while, in contrast, Compounds **5e** and **7c** are asymmetric forms.

From the above considerations, the possible conformations of Types A, C, and D are illustrated in Scheme 1. For discussing the eight-membered-ring

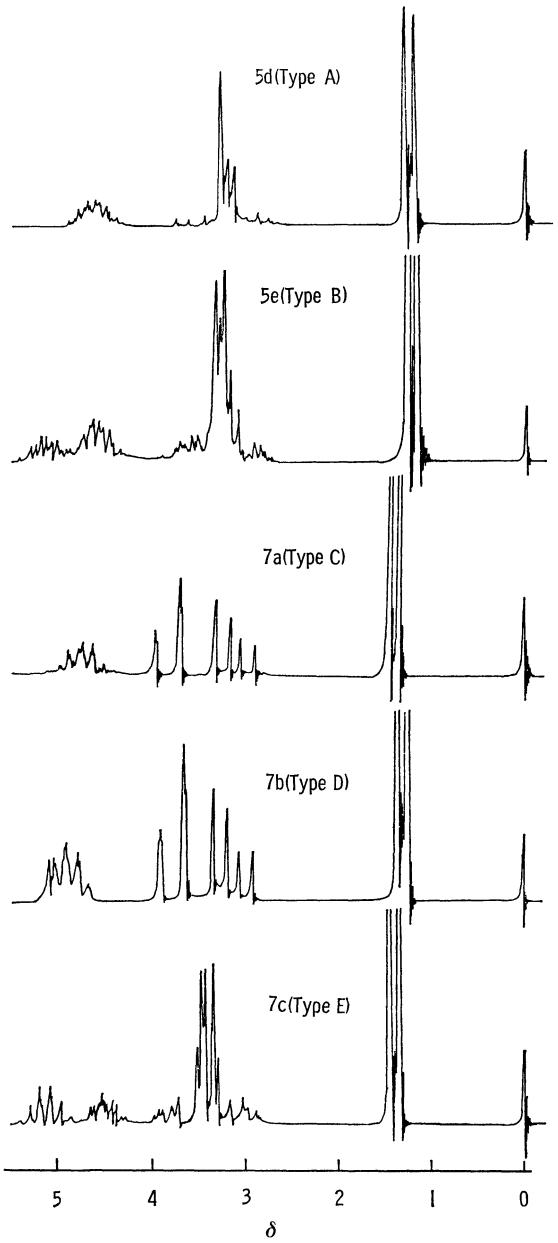

Fig. 1. NMR spectra of the heterocyclic and methyl protons of **5** and **7** in $CDCl_3$.

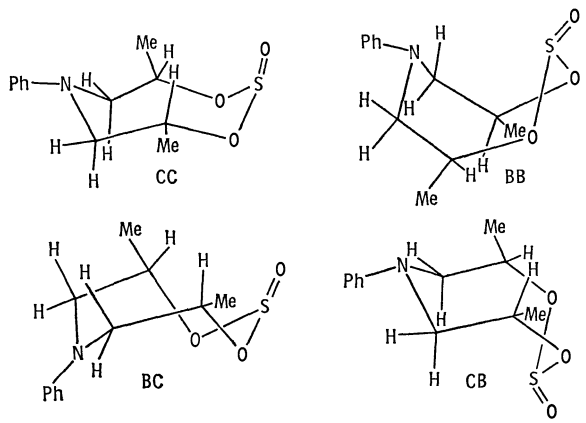

Scheme 1. Possible conformations of types A, C, and D.

stereochemistry, we used the nomenclature established for cyclooctane.[9]

For the geometry of solute-solvent collision complexes, Ledaal[10] proposed a common model with the dipole axis of the solute molecule located along the sixfold-symmetry axis of a benzene nucleus, with the positive end of the dipole nearest, and the negative end farthest away from, it. As for the aromatic solvent effect on the sulfoxides, our recent papers have also described the same type of collision complexes in connection with the stereochemistry of the 3-aryl-1,2,3-oxathiazolidine 2-oxides.[11,12]

Assuming that collision complexes of a similar geometry are formed between the benzene molecule (solvent) and the S=O bond in the compounds for chair-chair (CC), boat-boat (BB), boat-chair (BC), and chair-boat (CB) conformations, the following considerations are presented. For the CC conformation, benzene association should take place from the H-5 and H-7 axial protons of the solute molecule, *i.e.*, from the positively polarized end of the S=O bond. Consequently, the H-4 and H-8 axial protons are strongly deshielded. In the BB conformation, the benzene molecule should be formed from the H-4, H-5, H-7, and H-8 axial protons of the solute molecule; consequently, it is anticipated that all the protons of the heterocyclic ring will experience strong shielding effects in a benzene solution. Similar considerations are possible for the BC and CB conformations. That is, the axial protons of H-4, H-5, H-7, and H-8 are more deshielded than the remaining equatorial protons and methyl protons for the BC conformation. In the CB conformation, all the protons are shielded.

Table 2 shows the benzene-induced shift (Δ=

TABLE 2. ^{1}H-NMR CHEMICAL SHIFTS AND BENZENE-INDUCED SOLVENT SHIFTS FOR **1—7**

Compd No.	Chemical shifts, δ						
	H-4	H-8	H-5 and H-7		CH_3-4	CH_3-8	R
			axi-H	eq-H			
1a	4.78(m) (0.57)		3.85(q, J_{gem}=15.7, J_{vic}=1)[a] (0.57)[b]	3.08(q, J_{vic}=9.1) (0.60)	1.38(d, J=6.2) (0.52)		
1b	4.97(m) (0.01)		3.83(q, J_{gem}=15.0, J_{vic}=1) (0.33)	3.20(q, J_{vic}=8.5) (0.47)	1.28(d, J=6.2) (0.36)		
1c	5.10(m) (0.23)	4.53(m) (0.36)	3.8—3.1(m) (0.4—0.5)		1.37(d, J=6.2) (0.30)	(0.45)	
2d	4.60(m) (0.27)		3.34—3.01(m) (0.3)		1.20(d, J=6.0) (0.23)		2.27(s) (0.17)
2e	5.12(m) (0.09)	4.43(m) (0.28)	3.65—2.73(m) (0.3)		1.18(d, J=6.0) (0.20)	(0.26)	2.30(s) (0.09)
3a	4.73(m) (0.34)		3.85(q, J_{gem}=15.8, J_{vic}=1) (0.51)	3.04(q, J_{vic}=9.0) (0.49)	1.39(d, J=6.2) (0.46)		2.32(s) (0.09)
3b	4.93(m) (0.03)		3.80(q, J_{gem}=16.0, J_{vic}=1) (0.32)	3.08(q, J_{vic}=8.5) (0.42)	1.26(d, J=6.2) (0.40)		2.36(s) (0.16)
3c	5.10(m) (0.12)	4.57(m) (0.40)	3.98—2.85(m) (0.3—0.4)		1.42(d, J=6.0) (0.32)	(0.47)	2.32(s) (0.10)
4a	4.77(m) (0.42)		3.81(q, J_{gem}=15.9, J_{vic}=1) (0.55)	3.06(q, J_{vic}=9.0) (0.65)	1.38(d, J=6.1) (0.54)		2.23(s) (0.02)
4b	4.95(m) (0.01)		3.80(q, J_{gem}=16.1, J_{vic}=1) (0.30)	3.08(q, J_{vic}=9.0) (0.35)	1.27(d, J=6.1) (0.37)		2.23(s) (0.00)
4c	5.15(m) (0.17)	4.57(m) (0.39)	3.81—2.98(m) (0.4)		1.38(d, J=6.2) (0.31)	(0.45)	2.25(s) (0.05)
5d	4.60(m) (0.40)		3.45—2.87(m) (0.3—0.4)		1.25(d, J=6.0) (0.40)		
5e	5.19(m) (0.08)	4.60(m) (0.29)	3.77—2.85(m) (0.3)		1.23(d, J=6.2) (0.06)	(0.25)	
6a	4.77(m) (0.54)		3.83(q, J_{gem}=16.0, J_{vic}=1) (0.63)	3.10(q, J_{vic}=9) (0.60)	1.25(d, J=6.0) (0.38)		
6b	4.90(m) (0.07)		3.80(q, J_{gem}=16.0, J_{vic}=1) (0.52)	3.20(q, J_{vic}=9.2) (0.59)	1.30(d, J=6.2) (0.50)		
6c	5.16(m) (0.28)	4.53(m) (0.53)	3.9—2.9(m) (0.5)		1.36(d, J=6.1) (0.35)	(0.49)	
7a	4.73(m) (0.53)		3.79(q, J_{gem}=16.0, J_{vic}=1) (0.53)	3.07(q, J_{vic}=9.0) (0.63)	1.39(d, J=6.2) (0.54)		
7b	4.89(m) (0.13)		3.77(q, J_{gem}=16.0, J_{vic}=1) (0.54)	3.14(q, J_{vic}=8.2) (0.53)	1.32(d, J=6.2) (0.49)		
7c	5.13(m) (0.23)	4.48(m) (0.47)	3.7—2.9(m) (0.4—0.5)		1.36(d, J=6.0) (0.33)	(0.43)	

a) Coupling constants, Hz. b) Benzene-induced solvent shifts, $\Delta=(\delta_{CDCl_3}-\delta_{C_6D_6})$.

$\delta_{CDCl_3}-\delta_{C_6D_6}$) with the chemical shift of Compounds **1**—**7** in $CDCl_3$. As can be seen in Table 2, the 4,8-protons of Compound **7b** are deshielded (the mean value is *ca.* +0.13 ppm). Only the CC conformation in Scheme 1 is compatible with these observations; therefore, compounds of Type D are considered to take the CC conformation. The spectra of Compounds **1b**, **3b**, **4b**, **6b**, and **7b** may all be considered to belong to Type D. On the other hand, all the protons of Compounds **5d** and **7a** are strongly deshielded (the mean values are *ca.* +0.4 and +0.5 ppm, respectively). Therefore, the BB or CB conformation is compatible with the above observations discussed for Compounds **5d** and **7a**. The differences between the signal patterns of Types A and C may be due to the different conformations of Compounds **5d** and **7a**. We thought, therefore, that, in Type C, the most reasonable conformation is BB in Scheme 1. In contrast, in the case of Type A, the CB conformation is more suitable than the BB conformation because of the steric hindrance between the S=O group and the ortho-substituent. The spectra of Compounds **1a**, **3a**, **4a**, **6a**, and **7a** may all be considered to belong to Type C, and those of Compounds **2d** and **5d**, to Type A.

On the other hand, some possible conformations of Types B and E are illustrated in Scheme 2; that is, the CC and BB conformations are obtained by the replacement of *syn*-axial hydrogen by a methyl group in the CC and BB conformations in Scheme 1, while TCB and TBB are twist forms of CB and BB. If we consider that the CC or BB conformations in Scheme 2 are for Types B and E, the chemical shifts of the axial and equatorial methyl protons may be said to appear at different positions because of the anisotropy of the S=O bond. Nikander *et al.*,[2] in reporting on chemical shifts for methyl-substituted 1,3,2-dioxathiane 2-oxides in which the methyl group is *syn*-axial to the S=O bond, said that there is only a minor shielding effect relative to its equatorial counterpart. As can be seen in Fig. 1 or Table 2, the two methyl groups attached to C-4 and C-8 of Types B and E are almost equivalent magnetically in $CDCl_3$, while the two methine protons are not. Marked differences between compounds of Types B and E are shown in the benzene-induced shifts of the two methine protons and two methyl protons attached to C-4 and/or C-8. For the compounds of Type B, the methine and methyl protons attached to C-4 or C-8 are shielded, while the remaining methine and methyl protons are only marginally affected. Judging from the examination of the molecular model, the TCB conformation will give rise to severe nonbonded interactions between the ortho-substituent of the phenyl ring and the S=O group. Thus, we concluded that compounds of Type B exist in the TCB conformation. The spectra of Compounds **2e** and **5e** may all be considered to belong to Type B. On the other hand, in the case of compounds of Type E, two methine and methyl protons are shielded. Therefore, it can be considered that compounds of Type E exist in the TBB conformation. The spectra of Compounds **1c**, **3c**, **4c**, **6c**, and **7c** may all be considered to belong to Type E.

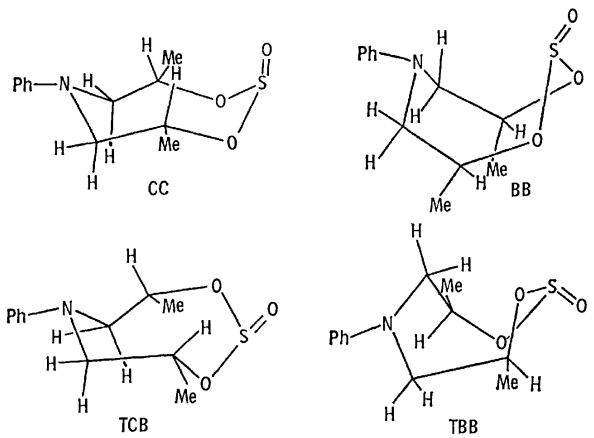

Scheme 2. Possible conformations of types B and E.

^{13}C-NMR Spectra. The conformations of Compounds **1**—**7** are further illustrated by means of ^{13}C-NMR. The ^{13}C-NMR chemical shifts for the Compounds, **1**—**7**, examined in $CDCl_3$ solutions are presented in Table 3. The assignments of the carbons were made on the basis of: (1) the relative signal intensity, (2) the off-resonance decoupling technique, and (3) a comparison with the published data for trimethylene sulfites and ethylene sulfites.

The upfield shifts of 6—9 ppm at C-4 and/or C-8 of the CC-conformation compared with those in the CB and BB conformations are due to the γ-relationship between the axial S=O and axial hydrogens at the C-4 and/or C-8 in Scheme 1. Nonbonded interactions between the axial oxygen in CC conformation and the axial hydrogens at C-4 and/or C-8 are probably sufficient to perturb the electron distribution about

Table 3. ^{13}C chemical shifts of compounds **1**—**7**

Compd No.	Chemical shifts, δ				
	C-4	C-5 or C-7	C-8	4-Me or 8-Me	R
1a	74.0	60.1	74.0	18.3	—
1b	65.3	58.1	65.3	18.4	—
1c	67.5	55.9 55.5	71.2	19.8 19.1	—
2d	77.8	65.0	77.8	18.1	18.4
2e	69.7	61.6 60.2	73.6	19.6 19.4	18.6
3a	74.1	60.1	74.1	18.3	22.1
3b	65.4	58.2	65.4	18.4	22.1
3c	67.8	56.0 55.6	71.4	19.7 19.1	21.9
4a	74.1	60.1	74.1	18.2	20.1
4b	65.3	58.2	65.3	18.4	20.1
4c	68.1	56.2 55.9	71.5	19.7 19.1	20.1
5d	77.5	64.3	77.5	18.1	—
5e	69.5	60.0 59.4	73.4	19.5 19.2	—
6a	73.7	60.0	73.7	18.3	—
6b	65.0	58.2	65.0	18.4	—
6c	66.6	55.6 55.3	70.6	19.8 19.3	—
7a	73.7	60.1	73.7	18.3	—
7b	64.9	58.3	64.9	18.4	—
7c	66.9	55.8 55.6	70.7	19.8 19.2	—

C-4 and/or C-8 and increase their shieldings. These γ-shifts have already been reported for ethylene sulfites and propylene sulfites.[4,13] For example, Buchanan *et al.*[14] reported upfield shifts of 9.9 and 6.6 ppm at C-4 and C-6 of 4-phenyl-1,3,2-dioxathiane 2-oxide with an axial S=O bond relative to that of the equatorial S=O type. On the contrary, the chemical shifts of C-4 and C-8 in the TCB and TBB conformations appeared at different positions, as is shown in Table 3. The upfield shifts in C-4 indicate that the S=O function turned away to the axial hydrogen at C-4.

We concluded, in the light of all the available evidence, that Compounds **1**—**7** exist in five conformations, that is, CC, BB, CB, TCB, and TBB, as is shown in Schemes 1 and 2.

References

1) C. H. Green and D. G. Hellier, *J. Chem. Soc.*, **1972**, 458.
2) H. Nikander, V. Mukkala, T. Nurmi, and K. Pihlaja, *Org. Magn. Reson.*, **8**, 375 (1976).
3) D. G. Hellier and F. J. Webb, *Org. Magn. Reson.*, **9**, 347 (1977).
4) G. W. Buchanan, J. B. Stothers, and G. Wood, *Can. J. Chem.*, **51**, 3746 (1973).
5) T. Nishiyama, K. Ido, and F. Yamada, *J. Heterocycl. Chem.*, **16**, 597 (1979).
6) K. W. Buck, A. B. Foster, W. D. Pardoe, M. H. Qadir, and J. M. Webber, *J. Chem. Soc., Chem. Commun.*, **1966**, 759.
7) C. R. Johnson and D. McCants, Jr., *J. Am. Chem. Soc.*, **86**, 2935 (1964); J. C. Martin and J. J. Uebel, *ibid.*, **86**, 2936 (1964).
8) D. G. Hellier and F. J. Webb, *J. Chem. Soc.*, **1977**, 612.
9) F. A. L. Anet and J. Krane, *Tetrahedron Lett.*, **1973**, 5029.
10) T. Ledaal, *Tetrahedron Lett.*, **1968**, 1683.
11) T. Nishiyama and F. Yamada, *Bull. Chem. Soc. Jpn.*, **44**, 3073 (1971).
12) F. Yamada, T. Nishiyama, and H. Samukawa, *Bull. Chem. Soc. Jpn.*, **48**, 1878 (1975).
13) G. W. Buchanan and D. G. Hellier, *Can. J. Chem.*, **54**, 1428 (1976).
14) G. W. Buchanan, C. M. E. Cousineau, and T. C. Mundell, *Tetrahedron Lett.*, **1978**, 2775.

  Bull. Chem. Soc. Jpn., 54, 1415—1419 (1981)

The Methylation of Nucleic Acids. The Analysis of Methylated Ribonucleosides by Means of High-performance Liquid ODS-Silica Gel[1] and Cation-exchange Chromatography

Toshizumi TANABE, Kiyoshi YAMAUCHI,* and Masayoshi KINOSHITA
Department of Applied Chemistry, Osaka City University, Sumiyoshi-ku, Osaka 558
(Received August 2, 1980)

The quantitative determination of adenosine, guanosine, inosine, cytidine, uridine, and their methylated derivatives was studied by means of a high-performance liquid chromatographic method using ODS-silica gel, cation-exchange, and anion-exchange resins as column packings. The method was applied to the analysis of yeast-RNA, which was methylated by trimethyl phosphate at pH 7 and 9.

Nucleic acids, especially tRNA and mRNA, contain a variety of modified nucleosides.[2,3] A mutagenic study of the action of alkylating agents on nucleic acids has shown them to give polymers with various alkylated nucleosides.[4] The rapid and quantitative analysis of such rare nucleosides has, therefore, been actively sought. Although two-dimensional thin-layer chromatography and ion-exchange chromatography,[2,5-7] which are coupled with a scintillation-counting technique, have frequently been employed, the chromatographic procedures are complex and time-consuming. These drawbacks may be avoided by utilizing high-performance liquid chromatography (HPLC). There have been reports on the HPLC of such major nucleosides as Ado, Guo, Cyd, and Urd.[8-11] However, only a limited number of papers have dealt with the HPLC of rare nucleosides of nucleic acids.[9,12]

In this paper, we wish to report the HPLC of a variety of methylated ribonucleosides, *etc.*, using ODS-silica gel, cation-exchange, and anion-exchange resins as column packings. The application of the HPLC method to the analysis of the enzymatic hydrolysates of methylated RNA will also be described.

Results and Discussion

The following nucleosides were studied for the HPLC analysis: Ado, m^1Ado, m^6Ado, Guo, m^1Guo, m^6Guo, m^7Guo, Ino, m^1Ino, Cyd, m^3Cyd, Urd, and m^3Urd.[13] The methylated substances include not only the constituents of tRNA, but also the products furnished easily upon the treatment of RNA with methylating agents. In addition to these compounds, 7-methylguanine and the imidazole ring-opened m^7Guo[14] were examined, since m^7Guo has been known to give the former by a depurination reaction, and the latter, by hydrolysis under weakly alkaline conditions.[15]

Although previous HPLC studies of the rare nucleosides of RNA used ion-exchange columns exclusively,[9-12] we found that a ODS-silica gel column was most useful in fractionating these compounds. Of the various solvent systems investigated as the mobile phase, a buffer [triethylamine–acetic acid–water (0.3–0.3–100 v/v)] containing 2% acetonitrile gave the optimum results. Figure 1a shows a typical elution

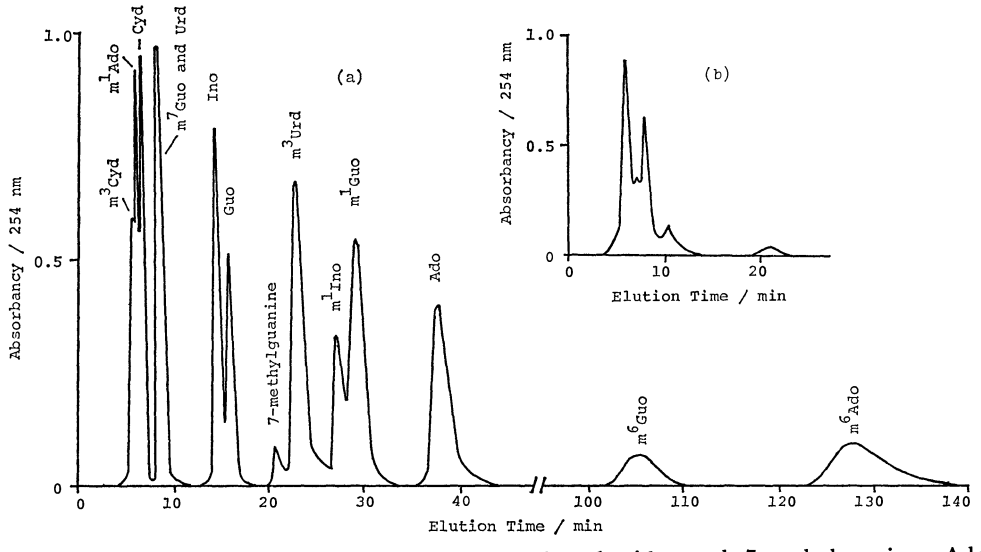

Fig. 1. (a): ODS silica gel HPLC of a mixture of nucleosides and 7-methylguanine; Ado; 3.33; m^1Ado, 2.10; m^6Ado, 1.81; Guo, 1.77; m^1Guo, 2.95; m^6Guo, 1.68; m^7Guo, 3.00; 7-methylguanine, 1.40; Ino, 3.33; m^1Ino, 1.94; Cyd, 3.33; m^3Cyd, 3.50; Urd, 3.33; m^3Urd, 4.36 (mmol/l). Injected volume, 15 μl. Solvent, triethylamine–acetic acid–water–acetonitrile= 0.3—0.3—100—2 v/v; pH 8.9; flow rate, 0.73 ml/min; column pressure, 40 kg/cm^2.
(b): ODS silica gel HPLC of imidazole ring opened m^7Guo (15 mmol/l). Injected volume, 15 μl. For chromatographic conditions see Fig. 1a.

pattern. The addition of acetonitrile to the buffer decreased the retention times considerably and resulted in a higher sensitivity (or height of the peaks) than the same solvent system without the organic solvent. The increase in the content of the amine in the solvent (for instance, triethylamine–acetic acid–water=0.5—0.8–0.3–100 v/v, 2% acetonitrile) resulted in a decreased resolution, especially for Urd, m^3Urd, m^1Guo, and Guo. The imidazole ring-opened m^7Guo may exist as a mixture of various compounds,[14] and its elution pattern overlaps with the peaks of Cyd, m^3Cyd, m^1Ado, m^7Guo, *etc.* (Fig. 1b).

This drawback in the silica gel column was, however, solved by the use of a cation-exchange column. The gradient chromatography achieved by changing the solvent was not employed here because of the time-consuming process needed for the reequilibration of the column after each sample application. As the mobile phase, an ammonium formate buffer (0.05 mol dm^{-3} with respect to the HCO_2^- concentration, pH 4.2) gave good results. A typical elution pattern furnished by the cation-exchange column is shown in Fig. 2a using the sample used in Fig. 1a. It is apparent that the ion-exchange column complemented

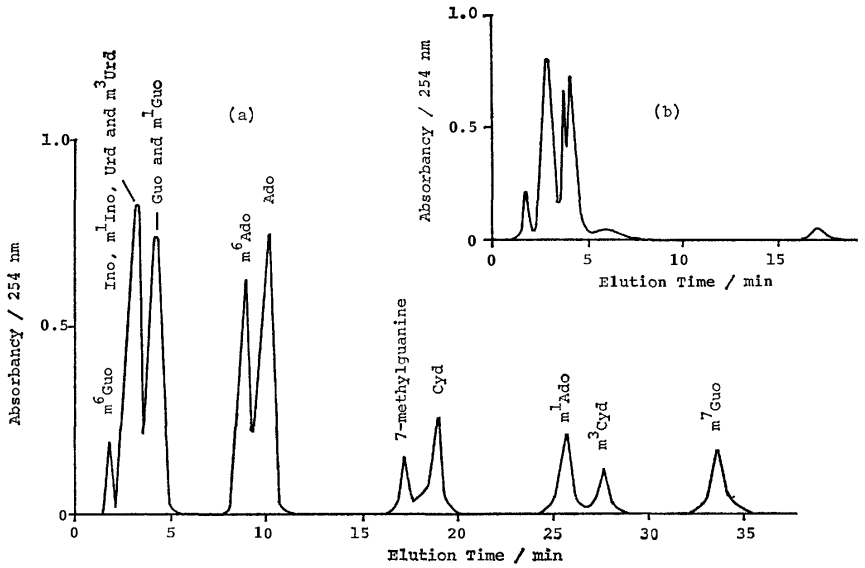

Fig. 2. (a): Cation-exchange HPLC of a mixture of nucleosides and 7-methylguanine. See Fig. 1a for the sample. Injected volume, 10 μl. Solvent, ammonium formate buffer (0.05 M, pH 4.2); flow rate, 0.67 ml/min; column pressure, 75 kg/cm².
(b): Cation-exchange HPLC of imidazole ring-opened m^7Guo (15 mmol/l). Injected volume, 10 μl. For chromatographic conditions see Fig. 2b.

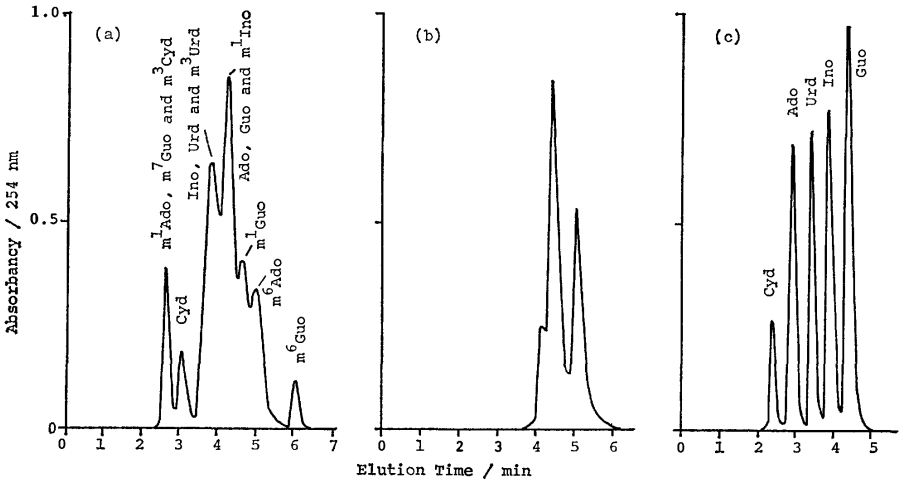

Fig. 3. (a): Anion-exchange HPLC of a mixture of nucleosides and 7-methylguanine. See Fig. 1a for the sample. Injected volume, 7 μl. Solvent, potassium phosphate buffer (0.03 M, pH 3.9); flow rate, 1.00/min; column pressure, 50 kg/cm².
(b): Anion-exchange HPLC of imidazole ring-opend m^7Guo (15 mmol/l). Injected volume, 5 μl. For chromatographic conditions see Fig. 3a.
(c): Anion-exchange HPLC of a mixture of Ado (0.83 mmol/l), Guo (1.37), Ino (0.95), Cyd (0.85) and Urd (1.00). Injected volume, 25 μl. Solvent, potassium phosphate buffer (0.03 M, pH 2.9); flow rate, 0.53 ml/min; column Pressure, 23 kg/cm².

Table 1. Retention data of nucleosides and 7-methylguanine[a)]

Compound	pK_a	Retention volume/ml (time/min)		
		Silica gel pH 8.9	Cation resin pH 4.2	Anion resin pH 3.9
Ado	3.5	27.9 (38.2)	6.4 (10.0)	4.2 (4.2)
m^{1}Ado	8.8	4.3 (5.9)	17.3 (25.8)	2.6 (2.6)
m^{6}Ado	4.0	93.4 (128)	5.9 (8.8)	5.0 (5.0)
Guo	1.6, 9.2	11.3 (15.5)	2.9 (4.4)	4.2 (4.2)
m^{1}Guo	2.4	21.3 (29.3)	2.9 (4.4)	4.6 (4.6)
m^{6}Guo	2.4	78.1 (107)	1.3 (2.0)	6.2 (6.2)
m^{7}Guo	7.0	5.7 (7.8)	22.5 (33.6)	2.6 (2.6)
Ring-opened m^{7}Guo	—	4.1—15.3 (5.6—21)	1.3—4.2, 11.7 (2.0—6.2, 17.4)	4.0—4.9 (4.0—4.9)
7-Methylguanine	3.5, 9.9	15.3 (21.0)	11.7 (17.4)	4.8 (4.8)
Ino	8.8, 1.2	10.2 (14.0)	2.1 (3.2)	3.9 (3.9)
m^{1}Ino	—	20.1 (27.6)	2.1 (3.2)	4.1 (4.1)
Cyd	4.2	4.5 (6.1)	12.1 (18.0)	3.1 (3.1)
m^{3}Cyd	8.7	3.9 (5.4)	18.5 (27.6)	2.6 (2.6)
Urd	9.2	5.7 (7.8)	2.1 (3.2)	3.6 (3.6)
m^{3}Urd	—	17.0 (23.3)	2.1 (3.2)	3.8 (3.8)

a) See the Experimental section for chromatographic conditions.

the silica gel column in separating characteristics. Thus, the group of compounds which eluted simultaneously with the imidazole ring-opened m^{7}Guo in the silica gel column (*vide supra*) were resolved fairly well by the cation-exchange column except for Urd. Although the peaks of m^{6}Guo, m^{1}Guo, Guo, and m^{3}Urd were overlapped by the complex peaks of the imidazole ring-opened m^{7}Guo, as is shown in Fig. 2b, the silica gel column separated these compounds well (Fig. 1a).

As is to be expected from the pK_a values (Table 1) of the nucleosides examined, the increase in the pH value of the buffer to 4.4—4.6 in the cation-exchange column resulted in the peak-coherence of m^{6}Ado with Ado, of Cyd with m^{7}Guo, and of m^{1}Ado with m^{3}Cyd.

An anion-exchange column, on the other hand, was not as useful as the silica-gel column and the cation-exchange column. The elution patterns of various nucleosides are shown in Figs. 3a—3c, using a potassium phosphate buffer (0.03 mol dm^{-3} with respect to the $H_2PO_4^-$ concentration). The retention volume (R_v)-difference between the initial peak and the last peak was small (*ca.* 3.7 ml) in comparison with the R_v of the initial peak (2.6 ml). It thus appeared that the anion-exchange column was suitable for the analysis of a mixture of major nucleosides of RNA (Fig. 3c).

The lowest concentration of samples for quantitative determination was found to be better than *ca.* 0.5 μmol/l (R_v 3—12 ml)—*ca.* 8 μmol/l (R_v 15—28 ml) for the ODS–silica gel column, *ca.* 0.5 μmol/l (R_v 1.3—7 ml)—5 μmol/l (R_v 11—23 ml) for the cation-exchange column, and *ca.* 0.5 μmol/l for the anion-exchange column. The retention data are summarized in Table 1.

As an application of the present HPLC method, yeast RNA was methylated with trimethyl phosphate at pH 7 and 9, and its enzymatic hydrolysates were analyzed. Table 2 shows the relative distribution of products against each major nucleosides.[16)] The values were obtained by dividing the peak areas by the respective molar extinction coefficients at 254 nm in the eluting buffer and by normalizing the data to 100% for each major nucleoside (see the Experimental section). Although the methylating conditions were vigorous, the distribution of the products agreed with

Table 2. Product distributions in the enzymatic hydrolysates of methylated yeast RNA[a,b)]

Compound	Buffer A[c)]		Buffer B[c)]	
	pH 7	pH 9	pH 7	pH 9
Ado (Ino)[d)]	85%	90%	93%	95%
m^{1}Ado	10	tr	tr	nd
m^{6}Ado[e)]	2	8	4	tr
Guo	70	50	85	83
m^{1}Guo	nd	25	nd	3
m^{6}Guo	nd	3	nd	nd
m^{7}Guo	13	tr	3	nd
Ring-opened m^{7}Guo	13	20	12	14
7-Methylguanine	4	2	tr	tr
Cyd	75	86	87	95
m^{3}Cyd	23	10	11	3
Urd	nc	nc	nc	nc
m^{3}Urd	tr	80	tr	11

a) Anion-exchange HPLC showed that the starting yeast RNA contained Ado, Guo, Cyd and Urd in the molar ratio of 0.95 : 1.37 : 0.84 : 1. b) Percentages are based on the amounts of products against the respective major nucleosides in the starting RNA. Tr, nd, and nc indicate "a trace yield," "a compound was not detected," and "a yield was not calculated" respectively. c) The reaction media; buffer A, KH_2PO_4-NaOH (0.03 M); buffer B, Tris-HCl (0.05 M). d) See Ref. 16. e) See Ref. 18.

the general order of the increasing reactivity of the alkylation sites of the nucleoside residues in RNA:[4,17] *e.g.* at pH 7, $m^7Guo > m^3Cyd > m^1Ado$, m^6Ado[18] > m^3Urd, and at pH 9, $m^3Urd > m^1Guo > m^3Cyd > m^1Ado$, m^6Ado. It was found that the methylation of RNA in the phosphate buffer occurred more smoothly than the methylation in the tris buffer. Possibly, tris(hydroxymethyl)aminomethane (tris) in the buffer scavenged trimethyl phosphate by reacting the methylating agent at a rate faster than RNA. It is also noteworthy that the extent of the formation of m^6Guo, which may be an adequate measure of the mutagenic activity of the methylating agents,[3] was very small when trimethyl phosphate was used.

In conclusion, a variety of methylated nucleosides can be analyzed rapidly and easily by the HPLC method. ODS-silica gel and cation-exchange columns are especially useful for the study of methylated RNA.

Experimental

HPLC was run by means of a Toyo-Soda 803 liquid chromatograph with a 254-nm UV flow-cell detector and a Milton Roy model 396/2396 piston pump (Riviera Beach, Florida). All the measurements were carried out at the ambient temperature.

An ODS-silica gel column (stainless steel, 0.4 cm × 30 cm, LS-410-ODS), a cation-exchange column (stainless steel, 0.4 cm × 30 cm, IEX-510-SP), and an anion-exchange column (stainless steel, 0.4 cm × 30 cm, IEX-260) were purchased from the Toyo-Soda Co., Shinnanyo-shi, Hiroshima.

The most frequently employed solvent systems were as follows: triethylamine–acetic acid–water–acetonitrile (0.3–0.3–100–2 v/v), an ammonium formate buffer (0.05 mol dm^{-3} with respect to the HCO_2^- concentration, pH 4.2), and a potassium phosphate buffer (0.03 mol dm^{-3} with respect to the $H_2PO_4^-$ concentration, pH 4.5, 3.9, and 2.9).

The major nucleosides (Ado, Guo, Cyd, Urd, and Ino) were commercially available. The methylated nucleosides (m^1Ado, m^6Ado, m^1Guo, m^6Guo, m^7Guo, the imidazole ring-opened m^7Guo, m^1Ino, m^3Cyd, and m^3Urd) and 7-methylguanine were prepared in previous experiments[17] or according to the literature.[15] The yeast RNA was obtained from the Sigma (U.S.A.) Chemical Co. (lot R6750). The ribonuclease (bovine pancrease) was from Miles Laboratory (U.S.A.) (code 36-511, batch 228). The phosphodiesterase (P-6877, type II) and RNAse T_2 (lot 57c-9510) were obtained from the Sigma (U.S.A.) Chemical Co. The alkaline phosphatase (36—482) was purchased from Miles-Seravac (Cape Town, South Africa).

Methylation of Yeast RNA. RNA (6 mg) was dissolved in a KH_2PO_4–NaOH buffer (1.5 ml, pH 7.0 or 9.0, 0.05 mol dm^{-3} with respect to the $H_2PO_4^-$ concentration) or in a Tris-buffer (1.5 ml, pH 7.0 or 9.0, 0.05 mol dm^{-3}). The solution was mixed with trimethyl phosphate (0.2 g, 1.7 mmol) and kept at 37 or 55 °C for 12 h. The homogeneous solution was then concentrated under −10 °C to give a residue, which was subsequently washed with ether and dissolved in water (0.8 ml). Ethanol was poured into the solution until a cloudy, turbid solution appeared. Sometimes a few drops of sodium acetate (3 mol dm^{-3}) were added to the solution in order to make the precipitation complete. After repeating the precipitation procedure thrice, the precipitate was dried and subjected to an enzymatic hydrolysis, which was carried out in a manner similar to the method previously reported.[6]

Quantitative Analysis of the Enzymatic Hydrolysate. The hydrolysate was dissolved in 2 ml of water, and then 10—20 μl of the solution was injected into the chromatograph. The sample peaks of the HPLC chart were cut and weighed. They were then divided by the respective molar extinction coefficient at 254 nm in the eluting buffer in order to obtain the molar ratios of the methylated nucleosides against the respective major nucleosides. The yields of the products were calculated from the ratio; they are shown in Table 2.

Since the imidazole ring-opened m^7Guo showed a complex elution pattern, its content (%) in the mixture of products was estimated by means of the following equation: 100—[yields (%) of m^7Guo (cation-exchange column), of 7-methylguanine (cation-exchange column), of m^1Guo (ODS-silica gel column), of m^6Guo (ODS-silica gel column), and of unreacted Guo (ODS-silica gel column)].

The yield of m^3Urd could not be determined by the aforementioned method because neither the ODS-silica gel column nor the cation-exchange column gave an isolated peak for Urd. The yield of m^3Urd was, therefore, obtained by means of this equation: 100·a/the amount of Urd in the starting RNA, where a is the amount of m^3Urd in the hydrolysate. This last quantity was determined as follows. The ODS-silica gel HPLC was run before and after the addition of a known amount of m^3Urd to the hydrolysate; a = the added amount of m^3Urd × (the original area of m^3Urd/the increased area of m^3Urd).

References

1) The packing is octadecylsilylated porous silica gel particles.

2) R. H. Hall, "The Modified Nucleosides in Nucleic Acids," Columbia University Press, New York (1971); J. A. McClosky and S. Nishimura, *Acc. Chem. Res.*, **10**, 403 (1977).

3) Y. Furuichi, M. Morgan, S. Shatkin, and A. J. Shatkin, *Pro. Natl. Acd. Sci., U.S.A.*, **72**, 742 (1975).

4) B. Singer, in "Progress in Nucleic Acid Research and Molecular Biology," ed by W. E. Cohn, Academic Press, New York (1975), Vol. 15, p. 219.

5) J. D. Mandell and A. D. Hershey, *Anal. Biochem.*, **1**, 66 (1960); H. Feldman and H. Falter, *Eur. J. Biochem.*, **18**, 573 (1971); J. L. Nichols and B. G. Lane, *Can. J. Biochem.*, **46**, 1487 (1968); R. H. Hall, *Biochemistry*, **3**, 876 (1964).

6) P. D. Lawley and S. A. Shah, *Biochem. J.*, **128**, 117 (1972).

7) B. Singer, *Nature*, **264**, 333 (1976).

8) R. A. Hartwick and P. R. Brown, *J. Chromatogr.*, **126**, 679 (1976).

9) J. Bockcek, *Anal. Biochem.*, **94**, 237 (1979).

10) H. Breter, G. Seibert, and R. K. Zahn, *J. Chromatogr.*, **140**, 251 (1977).

11) R. P. Singhal and W. E. Cohn, *Anal. Biochem.*, **45**, 585 (1972).

12) M. Uziel, C. K. Koh, and W. E. Cohn, *Anal. Biochem.*, **25**, 77 (1968).

13) Abbreviations used are: Ado: adenosine; Guo: guanosine; Ino: inosine; Cyd: cytidine; Urd: Uridine; m^1Ado: 1-methyladenosine; m^6Guo: O^6-methylguanosine; m^3Cyd: 3-methylcytidine. Similar connotations are used for the other methylated nucleosides.

14) The imidazole ring of m^7Guo is opened easily under alkaline conditions. The reaction may give the various compounds through the following postulated pathway.

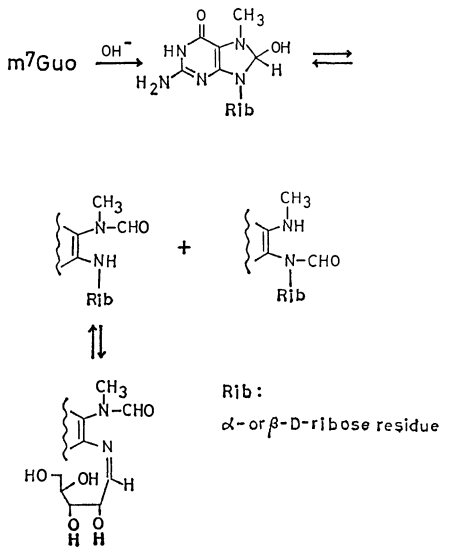

15) L. B. Townsend and R. K. Robins, *J. Am. Chem. Soc.*, **85**, 242 (1963); J. A. Haines, C. B. Reese, and L. Todd, *J. Chem. Soc.*, **1962**, 5281.

16) Since adenosine deaminase, which was present as an impurity in RNAse-T_2 and spleen phosphodiesterase, converted Ado substantially into Ino, the elution peak of Ado was always very small or was completely absent. The observed yield of Ino was, therefore, considered to be the yield of Ado.

17) K. Yamauchi and M. Kinoshita, *J. Chem. Soc., Perkin Trans. 1*, **1978**, 762; K. Yamauchi, T. Tanabe, and M. Kinoshita, *J. Org. Chem.*, **41**, 3691 (1976).

18) m^1Ado has been known to undergo a Dimroth rearrangement reaction to produce m^6Ado. Trimethyl phosphate does not methylate the 6-NH_2 of Ado. The combined extents of m^1Ado and m^6Ado may, therefore, be considered to represent the extent of methylation at the N-1 position of the adenosine residues in RNA.

19) T. Uchida and F. Egami, "Procedures in Nucleic Acid Research," ed by G. L. Cantoni and D. R. Davies, Harper and Row, New York (1966), p. 46.

Kinetic Study on the Reaction of (Arylthio)trimethylsilanes with Phenacyl Bromide Giving Aryl Phenacyl Sulfides and Bromotrimethylsilane

Seizi KOZUKA,* Tetsuji HIGASHINO, and Takuro KITAMURA

Department of Applied Chemistry, Faculty of Engineering, Osaka City University, Sugimotocho, Sumiyoshi-ku, Osaka 558

(Received August 23, 1980)

A kinetic study has been conducted on the reactions of (arylthio)trimethylsilanes with phenacyl bromide giving aryl phenacyl sulfides and bromotrimethylsilane. Remarkably large positive substituent effect ($\rho = +2.2$) and large negative entropy of activation were observed for the reaction. A mechanism involving 5-coordinated silicon intermediate prior to the rate-determining heterolysis of the Si–S bond has been suggested for the reaction based on the kinetic results.

Three different mechanisms are conceivable for the cleavage reaction of the group IVb–VIb bond by the reaction with haloalkane. Assuming the coordination ability of the IVb element, a 5-coordinated complex would be formed as an intermediate of the reaction (path a). On the other hand, a nucleophilic reaction by the attack of the VIb element is also a possible route for the reaction (path b). A mechanism involving four-centered transition state is the third possibility if the paths a and b occurred simultaneously (path c) although this mechanism for a bimolecular reaction of this type has recently been suspected by us.[1]

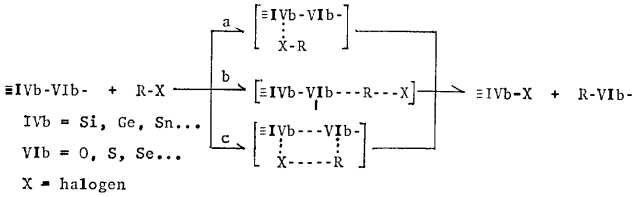

The reactions of (alkylthio and arylthio)trimethylstannanes with haloalkanes have been known to be the nucleophilic reaction (path b) based on detailed kinetic and stereochemical studies.[2] Namely the reaction obeys a second order rate equation, apparently negative ρ value (-1.40) of the substituent effect of the arylthio moiety, solvent effect on the rate of the reaction, relative reactivity of haloalkanes, and inversion of the alkyl group of the haloalkane by the reaction.

$$Me_3Sn\text{–}SPh + R\text{–}X \longrightarrow [Me_3Sn\text{–}S^{+}(Ph)\text{–}R\ X^{-}] \quad (I)$$
$$I \longrightarrow PhS\text{–}R + Me_3Sn\text{–}X$$

An analogous reaction of thiosilane with haloalkane has been known to give halosilane and sulfide which then further react with excess haloalkane giving trialkylsulfonium salt.[3,4] A silicon analogue of the sulfonium salt of the type I had once been reported as an isolable product in the reaction of (butylthio)trimethylsilane with an equimolar amount of iodomethane.[3b] If the silylsulfonium salt was actually an isolable product, it would be a definite evidence in support of a nucleophilic reaction of the sulfur atom. It has been found, however, to be an erroneous result.[4]

$$R_3Si\text{–}SR' + R''\text{–}X \longrightarrow R_3Si\text{–}X + R'\text{–}S\text{–}R''$$
$$R'\text{–}S\text{–}R'' + R'' \longrightarrow R'R''_2S^{+}X^{-}$$

Kinetic and stereochemical studies of this reaction would be of interest, since if the reaction proceeded by the same mechanism with that of the tin analogue,[2] stereochemistry of the silicon atom may clarify the final step of the reaction *i.e.*, the mechanism of the step leading to the product from the intermediate I. Thus, we have extended our study to the reaction of (arylthio)trimethylsilane with haloalkane in order to clarify the mechanism and to compare the aspects of the reaction with those of the reaction of the tin analogue.

Results and Discussion

Iodomethane was chosen as a typical haloalkane for the kinetic study of the reaction with (arylthio)-trimethylsilane. Although this reaction without the use of a solvent gave aryl methyl sulfide and iodotrimethylsilane on heating as analogously to the reaction of (alkylthio)silanes,[3,4] the reaction in a solvent was found to be sluggish even at high temperature and gave mainly unexpected product. Namely, hydrolysis by moisture or decomposition of the substrate giving hexamethyldisiloxane took place faster than the reaction with iodomethane when the reaction was carried out in such a nonpolar solvent as carbon tetrachloride at 120 °C. In a polar solvent, acetonitrile, the consumption of the thiosilane was found to be much faster than that in nonpolar solvent, the reaction gave a similar complex products. The reaction of the thiosilane with benzyl bromide was tried since this compound is more reactive than iodomethane toward tin analogue of the thiosilane *i.e.*, trimethyl-(phenylthio)stannane.[2] The main product derived from the reaction of benzyl bromide was bromotrimethylsilane but still accompanied with substantial amounts of the disiloxane although milder reaction conditions gave a better result.

$$Me_3SiSPh \xrightarrow{RX} Me_3SiX + RSPh$$
$$\xrightarrow{\text{hyd. or decompn.}} Me_3SiOSiMe_3$$

Kinetic study of the reaction was thus found to be difficult due to instability of the thiosilane and our attempts were failed to compare the kinetic and stereochemical results of the reaction with those of

the tin analogue by using the same haloalkanes. These results, however, reveal that the possibility of a kinetic study on the reaction of the thiosilane with more reactive haloalkane in a polar solvent under mild reaction conditions.

Phenacyl bromide was chosen as one of the most reactive haloalkane. The reaction of phenacyl bromide with an equivalent of trimethyl(phenylthio)silane was carried out at 60 °C in acetonitrile solution. Although the formation of the disiloxane was detected, even at the beginning of the reaction, the amount was found to increase little during the reaction until all the starting thiosilane was converted to the bromosilane (5h). The products of the reaction were bromotrimethylsilane, phenacyl phenyl sulfide, and small amounts of hexamethyldisiloxane and diphenyl disulfide. The volatile products were identified by GLC and NMR analyses and sulfides were characterized by isolation.

$$PhSSiMe_3 + PhCOCH_2Br \xrightarrow[\text{in } CH_3CN]{60\,^\circ C,\ 5\,h} Me_3SiBr + PhCOCH_2SPH + (Me_3Si)_2O + Ph_2S_2$$

75% 82% 10% 8%

The rate of the reaction of trimethyl(phenylthio)-silane with two equivalents of phenacyl bromide in acetonitrile was measured by monitoring ^1H NMR trimethyl signals of the thiosilane (δ 0.26 ppm) and bromotrimethylsilane (δ 0.57 ppm) at time intervals. A good second order rate constant was obtained with tolerable reproducibility ($\approx\pm10\%$). In order to confirm the first order dependency of the rate on the concentration of phenacyl bromide, the rate of the reaction was measured with different concentrations of phenacyl bromide. A clear first order dependency was observed. Thus, the reaction was found to be second order. Rates of the reactions of several (arylthio)trimethylsilanes were measured similarly. Rates were also measured at various temperatures to obtain activation parameters. These results are given in Table 1.

An unexpectedly large negative entropy of activation was observed for the reaction. A similar large negative value was observed for the reaction of thiostannane with haloalkane in a nonpolar solvent ($CHCl_3$) but it was shown to fall in a smaller negative value when the reaction was carried out in a polar solvent (PhCN).[2] By an analogy, a smaller negative entropy value was expected in the present study since a much polar solvent (CH_3CN) was used. Therefore, the value may suggest that the reaction of (arylthio)trimethylstannane with haloalkane differs from that of (arylthio)-trimethylsilane with phenacyl bromide in the mechanism.

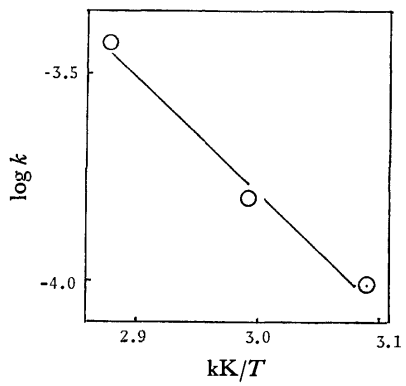

Fig. 1. Arrhenius plot of the rates of the reaction, $C_6H_5SSiMe_3 + C_6H_5COCH_2Br$ ($\gamma=0.984$).

Substituent effect also suggests that these two analogous reactions are quite different in their mechanisms. The results given in Table 1 are best correlated with σ constants giving a large positive ρ value (+2.2) with tolerable linearity as shown in Fig. 2. The deviation may be due to the instability of the thiosilanes.[5] The positive ρ value is consistent with a 5-coordination process and rules out the nucleophilic attack of the sulfur atom since the process would demand a negative ρ value as was observed for the reaction of the thiostannane with haloalkane.[2] The magnitude of the ρ value, however, appeared too large to be rationalized only by the formation of the 5-coordinated silicon intermediate.[6] A rate determining heterolysis of the Si–S bond of the coordinated intermediate would be involved in the reaction since

Table 1. Rate constant for the reaction of $X-C_6H_4SSiMe_3$ (0.56 mol dm^{-3}) with $PhCOCH_2Br$ in CH_3CN

Substituent X	Mol ratio $-CH_2Br/-SSi\equiv$	Temp °C	$10^5\,k$/dm^3 mol^{-1} s^{-1}	$\equiv SiOSi\equiv$[a] (%)	Remarks
H	1.20	51.5	6.09±0.37	—	
H	1.70	51.5	8.90±0.72	—	
H	2.16	51.5	9.68±0.10	3.5	54.0, −156[b]
H	3.72	51.5	16.7±1.1	—	
H	2.16	61.5	15.6±0.8	—	
H	2.16	75.0	37.2±3.7	6.8	
p-OCH_3	2.16	51.5	2.66±0.44	5.0	+2.2[c]
p-CH_3	2.16	51.5	9.23±0.60	13	
p-Cl	2.16	51.5	46.1±2.6	10	
p-Br	2.16	51.5	28.1±4.3	20	
m-Br	2.16	51.5	117±10	10	

a) The amount of hexamethyldisiloxane. b) ΔH^* and ΔS^* values in kJ mol^{-1} and J K mol^{-1}, respectively. c) ρ value against σ constant ($\gamma=0.966$).

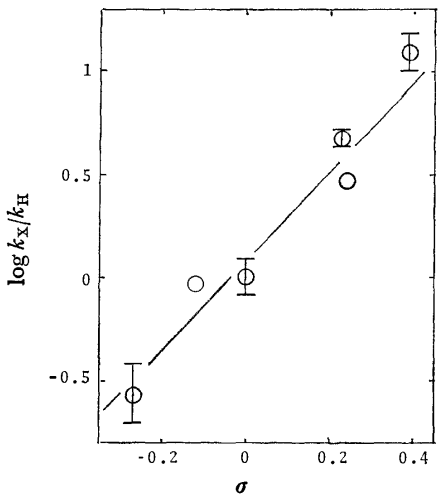

Fig. 2. Hammett plot of the rates of the reaction, $XC_6H_4SSiMe_3+C_6H_5COCH_2Br$ in CH_3CN at 51.5 °C.

the value appeared in almost comparable magnitude to that of dissociation constants of arenethiols (+2.58).[7] Thus, the most plausible mechanism for the reaction can be formulated as follows:

$$Me_3SiSAr + PhCOCH_2Br \rightleftharpoons \underset{\text{II}}{\left[\begin{matrix} Me_3Si^{\delta-}\text{–}Br^{+}\text{–}CH_2CPh \\ | \qquad\qquad \| \\ ArS \qquad\quad O \end{matrix}\right]}$$

$$\xrightarrow{\text{slow}} \underset{\text{III}}{\left[\begin{matrix} Me_3Si\text{–}Br^{+}\text{–}CH_2CPh \\ | \qquad\qquad \| \\ ArS^{-} \qquad\quad O \end{matrix}\right]} \xrightarrow{\text{fast}}$$

$$Me_3SiBr + ArSCH_2\overset{\overset{O}{\|}}{C}Ph.$$

The large positive ρ value observed in the present study would be rationalized in terms of the sum of those of the first and the second steps *i.e.*, the formation of II and the heterolysis of II giving III. The intermediate III would be a short lived tight ion pair which collapsed rapidly into the product since a large negative entropy of activation was observed in the present study even the reaction was carried out in a polar solvent. An ionic four-centered transition state (IV) leading to the product from II is an attractive alter-

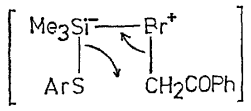

IV

native choice to account for the large negative entropy value since it has often been considered to suggest a cyclic transition state.[8] The large negative entropy value, however, could not be a definite evidence in support of a cyclic transition state since all the bimolecular reactions of this type which have been studied in detail, were found to proceed by non-cyclic process regardless of the large negative entropy values.[9]

The reaction of thiosilane with phenacyl bromide has thus appeared quite different in mechanism from that of thiostannane with haloalkane.[2] The reason for the difference is obscure at present but higher energy release by forming Si–X bond from Si–S bond (*ca.* 35 kcal/mol, X=Cl) than that of tin (23 kcal/mol, X=Cl)[10] may be one of the important factors to control the course of the reaction. The high reactivity of phenacyl bromide seems to play no important role to control the course of the reaction since the opposite substituent effects were also found for the reactions of benzoyl chloride with (arylthio)trimethylstannanes ($\rho=-1.6$)[11] and with (arylthio)trimethylsilanes ($\rho=+2.50$).[12]

Experimental

Materials. The (arylthio)trimethylsilanes were prepared by the same procedure described previously.[6] Phenacyl bromide was recrystallized from hexane–chloroform before use. Solvents were dried and distilled.

The Reaction of Trimethyl(phenylthio)silane with Iodomethane or Benzyl Bromide. The thiosilane (55 mg, 0.30 mmol) and iodomethane (426 mg, 3.0 mmol) were dissolved in carbon tetrachloride (total 5 cm^3). The solution was divided and sealed in glass tubes each containing *ca.* 0.5 cm^3. The tubes were heated in a constant temperature bath (120 °C) and subjected to NMR analysis at time intervals. After heating for 1 h, only a small amount of hexamethyldisiloxane (δ 0.07 ppm, 8%) was detected as the product. The formation of iodotrimethylsilane (δ 0.55 ppm) was detected after heating for 17 h (5%) accompanied with a large amount of the disiloxane (35%). The disiloxane would be formed by hydrolysis of the starting thiosilane and the product,

$$MeSiSAr \text{ and } Me_3SiI \xrightarrow{\text{moisture}} Me_3SiOH$$

$$2\,Me_3SiOH \longrightarrow Me_3SiOSiMe_3 + H_2O$$

iodotrimethylsilane or oxidation of them. All the materials and the apparatus were dried carefully but the results were not improved significantly. A similar result was also found by the reaction carried out in a polar solvent of acetonitrile. The consumption of the thiosilane was found to be faster in this solvent (within 1 h) but the detected product was manily the disiloxane. In separate experiments, both trimethyl(phenylthio)silane and iodotrimethylsilane were found to give substantial amounts of hexamethyldisiloxane by heating at 120 °C in these solvents.

The reaction of trimethyl(phenylthio)silane (0.06 mol dm^{-3}) with benzyl bromide (0.6 mol dm^{-3}) in acetonitrile was carried out similarly. The solution was heated at 80 °C until the thiosilane was consumed giving a mixture of bromotrimethylsilane (60%) and hexamethyldisiloxane (40%).

The Reaction of Trimethyl(phenylthio)silane with Phenacyl Bromide. The thiosilane (1 g, 5.5 mmol) and phenacyl bromide (1.1 g, 5.5 mmol) in acetonitrile (10 cm^3) were heated at 60 °C for 5 h. Solvent and volatile components were distilled off. Bromotrimethylsilane (75%) and hexamethyldisiloxane (10%) were identified by GLC and NMR analyses of the distillate. Identifications were done by comparing the NMR spectra and the GLC retention times with those of the authentic samples. The residue was separated by chromatography (silica gel, hexane–chloroform). Phenacyl phenyl sulfide (82%) and diphenyl disulfide (8%) were isolated and characterized. Phenacyl phenyl sulfide; Found: C, 73.42, H. 5.30%. Calcd for $C_{14}H_{12}OS$: C, 73.65, H, 5.30%.

Kinetics. The procedure is essentially the same with

that employed for the reaction of (arylthio)trimethylsilanes with carboxylic acids.[5] Concentrations of the substrates are recorded in Table 1. Temperatures were calibrated by measuring chemical shift of 1,2-ethanediol.

References

1) S. Kozuka and T. Higashino, *Tetrahedron Lett.*, **21**, 2067 (1980).

2) S. Kozuka and S. Ohya, *J. Organomet. Chem.*, **149**, 161 (1978), *Bull. Chem. Soc. Jpn.*, **51**, 2651 (1978).

3) a) E. W. Abel, *J. Chem. Soc.*, **1960**, 4406; b) E. W. Abel, D. A. Armitage, and R. P. Bush, *J. Chem. Soc.*, **1964**, 2455.

4) K. A. Hooton and A. L. Allred, *Inorg. Chem.*, **4**, 671 (1965).

5) The amounts of the disiloxane formed by the reactions varied with different substituents as shown in Table 1 which may affect the observed rates.

6) S. Kozuka and T. Kitamura, *Bull. Chem. Soc. Jpn.*, **52**, 3384 (1979). In the base catalyzed reaction of $RCOOH+Me_3SiSAr \rightarrow Me_3SiOCOR+ArSH$ which involves formation of 5-coordinated silicon atom, a ρ value of $+0.78$ was observed.

7) F. G. Bordwell and H. M. Anderson, *J. Am. Chem. Soc.*, **75**, 6019 (1953).

8) See for example, G. L. Larson and Y. V. Fernandez, *J. Organomet. Chem.*, **86**, 193 (1975); J. Stutsky and H. Kwart, *J. Am. Chem. Soc.*, **95**, 8678 (1973); T. H. Chan and A. Melnyk, *ibid.*, **92**, 3718 (1970); M. Kosugi, P. Q. Hanh, M. Nakayama, and T. Migita, *Chem. Lett.*, **1978**, 927.

9) See Refs. 1, 2, 6, 11, 12, and S. Kozuka, T. Kitamura, N. Kobayashi, and K. Ogino, *Bull. Chem. Soc. Jpn.*, **52**, 1950 (1979).

10) a) J. C. Baldwin, M. F. Lappert, J. B. Pedlay, and J. S. Poland, *J. Chem. Soc., Dalton Trans.*, **1972**, 1943; b) A. I. Vogel, W. T. Cresswell, and J. Leicester, *J. Phys. Chem.*, **58**, 174 (1954).

11) S. Kozuka and I. Naribayashi, *Bull. Chem. Soc. Jpn.*, **52**, 3638 (1979).

12) The reaction of $Me_3SiSC_6H_4X$ with YC_6H_4COCl in tetrachloroethane at 34 °C giving Me_3SiCl and $YC_6H_4COSC_6H_4X$ was found to be second order with ρ values of $+2.50$ (for X, $\gamma=0.984$) and -0.87 (for Y, $\gamma=0.994$) which may suggest 5-coordination of silicon atom prior to the rate determining cleavage of the Si–S bond. S. Kozuka and I. Naribayashi, Unpublished.

Asymmetric Reduction of Aromatic Ketones with Reagents Prepared from $NaBH_4$ and $ZnCl_2$ in the Presence of 1,2 : 5,6-Di-*O*-isopropylidene-α-D-glucofuranose

Akira HIRAO,* Masaki OHWA, Shinichi ITSUNO, Hidenori MOCHIZUKI, Seiichi NAKAHARA, and Noboru YAMAZAKI

Department of Polymer Science, Tokyo Institute of Technology, Ohokayama, Meguro-ku, Tokyo 152

(Received August 29, 1980)

Asymmetric reduction of prochiral aromatic ketones using a freshly prepared complex derived from $NaBH_4$, 1/3 equiv of $ZnCl_2$, and 1,2:5,6-di-*O*-isopropylidene-α-D-glucofuranose (**1**) gives an excess of the corresponding (*S*)-alcohols in substantial optical yields (28—68%). The effects of the $NaBH_4/ZnCl_2$/**1** ratio, temperature, solvent, structure of various monosaccharide derivatives, and the metal cation of the reagent on the optical yields were examined.

Asymmetric reduction of carbonyl compounds has recently been achieved by use of metal hydrides modified by chiral compounds such as chiral diols,[1] amines,[2] and α-pinene.[3,4] The hydrides would be of use for the synthesis of enantiomerically pure molecules of biological interest.

However, only a few reports have been made on the application of sodium borohydride($NaBH_4$) to the same type of asymmetric reduction, the reagent being found to be less effective with ketones,[5-8] though $NaBH_4$ is a mild and highly selective reducing agent.

It was found that aromatic ketones are asymmetrically reduced by $NaBH_4$ in the presence of monosaccharide derivatives, attempts for selectivity not being quite successful.[9] Stereoselectivities have been greatly enhanced by addition of Lewis acids. We reported on a test of modified reagents derived from $NaBH_4$ and Lewis acids such as zinc chloride and aluminium chloride in the presence of 1,2:5,6-di-*O*-isopropylidene-α-D-glucofuranose (**1**) for the asymmetric reduction of aromatic ketones.[10]

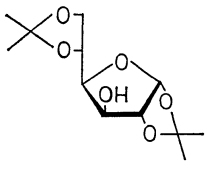

1

The results show that reaction of $NaBH_4$ with zinc chloride ($ZnCl_2$) affords a reagent, presumably a zinc borohydride or the related borohydride species, which give higher stereoselectivities than those achieved with $NaBH_4$ alone.

This paper describes a detailed study of asymmetric reduction of prochiral ketones with the reagents prepared from $NaBH_4$ and $ZnCl_2$ in the presence of **1** to establish the optimum conditions for maximum stereoselectivity. The species responsible for the maximum asymmetric induction (68%) has been discussed.

Results and Discussion

*Asymmetric Reduction of Ketones with the Reagents Derived from $NaBH_4$ and $ZnCl_2$ in the Presence of **1**.* Addition of 0.5 molar equiv of $ZnCl_2$ to the suspended $NaBH_4$ in tetrahydrofuran (THF) gave rise to quantitative precipitation of NaCl (1 mol) and the formation of soluble borohydride species in the solution. Subsequent addition of 2 equiv of monosaccharide **1** (R*OH) caused evolution of 2.0 mol of hydrogen, 2.0 equiv of hydride remaining in the reducing agents in the solution. No further hydrogen uptake took place after 24 h. The reaction of $NaBH_4$ with $ZnCl_2$ and subsequent addition of **1** seems to proceed according to the equation:

$$NaBH_4 + 1/2\,ZnCl_2 \rightleftarrows 1/2\,Zn(BH_4)_2 + NaCl\downarrow \quad (1)$$

$$1/2\,Zn(BH_4)_2 + 2\,R^*OH \longrightarrow 1/2\,Zn(BH_2(OR^*)_2)_2 + 2H_2\uparrow \quad (2)$$

Asymmetric reduction of propiophenone was carried out with suspension of $NaBH_4$ in THF to which $ZnCl_2$ in varying amounts and a fixed quantity (2 equiv to $NaBH_4$) of **1** had been added. The results are summarized in Table 1. We see that the stereoselectivity increases to a maximum and then decreases with addition of $ZnCl_2$. The reagent formed by adding 1/3 mol of $ZnCl_2$ per mole of $NaBH_4$ gives optimum induction; maximum selectivity as high as 68% was obtained. It was found that all the 1-phenyl-1-propanols produced with the reagents derived from $NaBH_4$ and $ZnCl_2$ have the (*S*)-configuration, while

Table 1. Effect of the ratio of $[ZnCl_2]/[NaBH_4]$ on optical yield in the presence of **1** in THF at 30 °C

Ratio $[ZnCl_2]/[NaBH_4]$	Produced alcohol			
	Chemical yield/%	$[\alpha]_D^{20}$	Optical yield/%	Configuration
0	100	−8.32°	18	*R*
0.2	100	−16.74°	36	*S*
0.25	100	−18.42°	39	*S*
0.26	100	−20.25°	42	*S*
0.28	100	−25.96°	55	*S*
0.30	100	−26.05°	55	*S*
0.33	100	−32.12°	68	*S*
0.4	98	−27.65°	59	*S*
0.5	100	−21.77°	46	*S*
1.0	100	−4.71°	10	*S*
1.1	100	−3.39°	7	*S*

a) Based on $[\alpha]_D^{20}$ +47.03° reported by H. Kwart and D. P. Hoster, *J. Org. Chem.*, **32**, 1867 (1967).

Table 2. Effect of the ratio of [1]/[$NaBH_4$+1/3 $ZnCl_2$] on optical yield in the asymmetric reduction of propiophenone in THF at 30 °C

Ratio	Produced alcohol			
[1]/[$NaBH_4$+1/3 $ZnCl_2$]	Chemical yield/%	$[\alpha]_D^{20}$	Optical yield/%	Configuration
0.5	100	−11.21°	24	*S*
1.0	100	−19.33°	41	*S*
2.0	100	−32.12°	68	*S*
3.0	80	−8.95°	19	*S*
4.0	0	—	—	—

the reduction with $NaBH_4$ alone gives the same alcohol of the (*R*)-configuration in 18% of an optical yield.

The effect of the amount of **1** to the $NaBH_4$–1/3 $ZnCl_2$ reagent on optical yield was examined (Table 2). Optical yield increased with the increase in the ratio of **1** to the reagent based on $NaBH_4$. The maximum selectivity could be obtained at a *ca.* 2 molar ratio. A marked fall in selectivity took place by addition of 3 molar equiv of **1**. This is curious since the resulting monohydride (**b**) would be in a more steric and chiral environment than the corresponding dihydride (**a**):

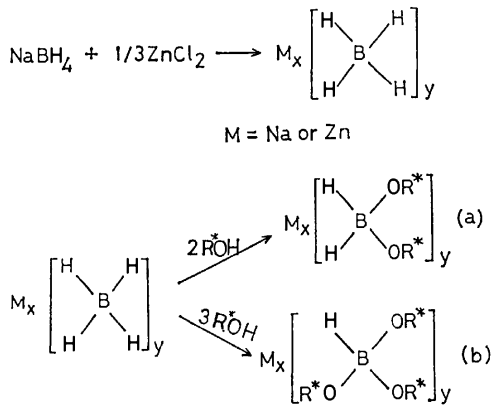

Further addition of **1** (4 equiv) might remove all hydrides on the reagent giving tetrasubstituted alkoxyborate complex which can not react further. Addition of 4 equiv of **1** evolved 4.0 mol of hydrogen, giving rise to incomplete reduction of propiophenone. The stoichiometric quantities of $NaBH_4$, $ZnCl_2$, and **1** were found to be optimum at 1,/1/3,/ and 2.0, respectively.

We next examined the dependency of selectivity on chemical yield with the complex from $NaBH_4$, 1/3 equiv of $ZnCl_2$, and 2 equiv of **1** and found that selectivity is constant until less than one equiv of propiophenone to the reagent was used (Table 3). However, a significant decrease in the optical yield was observed when 1.5 equiv of ketone was used. This suggests that of two available hydrides on the complex (**a**) as described above, the first hydride would be more effective for the asymmetric induction.

Optical yields vary with solvent, THF being the best in stereoselectivity (Table 4).

Table 3. The effect of [propiophenone]/[$NaBH_4$+1/3$ZnCl_2$] on optical yield in the asymmetric reduction of propiophenone in THF at 30 °C

Ratio	Produced alcohol			
[propiophenone]/[$NaBH_4$+1/3 $ZnCl_2$]	Chemical yield/%	$[\alpha]_D^{20}$	Optical yield/%	Configuration
0.3	100	−29.63°	63	*S*
0.5	100	−29.16°	62	*S*
0.8	100	−32.12°	68	*S*
1.0	100	−32.08°	68	*S*
1.5	100	−13.54°	29	*S*

Table 4. Solvent effct on optical yield in the asymmetric reduction of propiophenone with a reagent prepared from $NaBH_4$, 1/3 equiv of $ZnCl_2$, and 2 equiv of **1** at 30 °C

Solvent	Produced alcohol			
	Chemical yield/%	$[\alpha]_D^{20}$	Optical yield/%	Configuration
THF	100	−32.12°	68	*S*
Diethyl ether	100	−22.48°	48	*S*
Benzene	100	−14.48°	31	*S*

Table 5. Temperature effect on optical yield in the asymmetric reduction of propiophenone in THF

Temperature °C	Produced alcohol			
	Chemical yield/%	$[\alpha]_D^{20}$	Optical yield/%	Configuration
50	99	−23.50°	50	*S*
30	100	−32.12°	68	*S*
0	93	−29.30°	62	*S*
−30	0	—	—	—

The temperature effect on asymmetric reduction of propiophenone appeared not to be critical in the range 0—50 °C (Table 5). Rise in temperature from 0 °C to 50 °C caused decrease in optical yield to some extent. No reduction took place at −30 °C even after 108 h.

The complex from $NaBH_4$, 1/3 equiv of $ZnCl_2$, and 2 equiv of **1**, reduced a variety of aromatic ketones in excellent chemical yields with substantial enantiomeric excesses (⩾50%) except for the case of isopropyl phenyl ketone. The same complex also reduced an alkyl ketone such as isobutyl methyl ketone with moderate selectivity. The six ketones were reduced with $NaBH_4$ in the presence of **1** (Table 6). It is apparent from a comparison of the results that the complex system is superior to the original system with use of $NaBH_4$ and **1**. In each case with the complex the (*S*)-configuration of the alcohols produced was opposite that of the alcohols obtained by $NaBH_4$ alone in which (*R*) isomer predominates.

In order to determine the structural effect of various

TABLE 6. ASYMMETRIC REDUCTION OF VARIOUS KETONES WITH THE COMPLEX PREPARED FROM $NaBH_4$, 1/3 $ZnCl_2$, AND 2 EQUIV OF **1** IN THF AT 30 °C

Ketones	Produced alcohol			
	Chemical yield/%	$[\alpha]_D^{20}$	Optical yield/%	Configuration
$C_6H_5COCH_3$	100	−26.25°	50[a] (3)[b]	*S* (*R*)[b]
$C_6H_5COC_2H_5$	100	−32.12°	68[c] (18)	*S* (*R*)
$C_6H_5COC_3H_7$	100	−25.29°	58[d] (14)	*S* (*R*)
$C_6H_5COC_3H_7$-*i*	98	−13.36°	28[e] (9)	*S* (*R*)
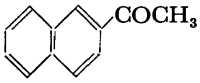	100	−28.49°	68[f] (20)	*S* (*R*)
$CH_3COC_4H_9$-*i*	99	+7.60°	37[g] (3)	*S* (*R*)

a) Based on $[\alpha]_D$ +52.5° (CH_2Cl_2) reported by U. Nagai and T. Shishido, *Tetrahedron*, **21**, 1701 (1965). b) Values in parentheses obtained by asymmetric reduction with $NaBH_4$ plus **1** in THF. c) Based on $[\alpha]_D^{20}$ +47.03° (Acetone) reported by H. Kwart and D. P. Hoster, *J. Org. Chem.*, **32**, 1867 (1967). d) Based on $[\alpha]_D$ +43.6° (C_6H_6) reported by S. Yamaguchi and H. S. Mosher, *J. Org. Chem.*, **38**, 1870 (1973). e) Based on $[\alpha]_D$ +47.7° (Diethyl ether) reported by P. A. Levene and L. A. Mikeska, *J. Biol. Chem.*, **70**, 355 (1926). f) Based on $[\alpha]_D$ −41.9° (Ethanol) reported by T. A. Collyer and J. Kenyon, *J. Chem. Soc.*, **1940**, 676. g) Based on $[\alpha]_D$ +20.54 (neat) reported by J. Kenyon and H. E. Strauss, *J. Chem. Soc.*, **1949**, 2153.

TABLE 7. ASYMMETRIC REDUCTION OF PROPIOPHENONE WITH A REAGENT FROM $NaBH_4$ AND 1/3 EQUIV OF $ZnCl_2$ IN THF 30 °C IN THE PRESENCE OF VARIOUS MONOSACCHARIDE DERIVATIVES (VALUES IN PARENTHESES WERE OBTAINED IN THE ASYMMETRIC REDUCTION WITH $NaBH_4$ PLUS **1**, **2**, **3**, **4**, **5**, OR **6** IN THF

Monosaccharid derivative	Produced alcohol			
	Chemical yield/%	$[\alpha]_D^{20}$	Optical yield/%	Configuration
1	100	−32.12°	68(18)	*S* (*R*)
2	97	−4.23°	9(25)	*S* (*R*)
3	100	+4.71°	10(13)	*R* (*S*)
4	94	−11.90°	25(7)	*S* (*S*)
5	100	+5.22°	11(6)	*R* (*S*)
6	100	−7.52°	16(0)	*S* (—)

monosaccharide derivatives on the reaction, we have examined the asymmetric reduction of propiophenone with the complexes prepared from $NaBH_4$, 1/3 equiv of $ZnCl_2$, and 2 equiv of **2**, **3**, **4**, **5**, or 2/3 equiv of **6** (2 equiv for OH moiety) in THF at 30 °C. The reactions resulted in complete reduction in all cases. The enantiomeric excess from each reduction is given in Table 7. Selectivity was generally low as compared with that obtained by the complex from **1**. The order of asymmetric induction by the complexes from **1** to **6** is not the same as that by $NaBH_4$. An increase in the stereoselectivity of $NaBH_4$ by adding 1/3 equiv of $ZnCl_2$ occurred with **1**, but it is not as

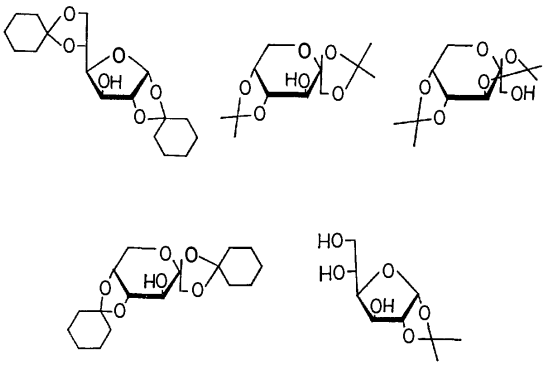

TABLE 8. ASYMMETRIC REDUCTION OF PROPIOPHENONE WITH REAGENTS FROM VARIOUS METAL BOROHYDRIDES AND 1/3 EQUIV OF $ZnCl_2$ IN THE PRESENCE OF **1** IN THF AT 30 °C (VALUES IN PARENTHESES WERE OBTAINED BY THE ASYMMETRIC REDUCTION WITH $LiBH_4$, $NaBH_4$, KBH_4, $RbBH_4$, OR $CsBH_4$ PLUS **1** IN THF AT 30 °C)

Reagents	Produced alcohol			
	Chemical yield/%	$[\alpha]_D^{20}$	Optical yield/%	Configuration
$LiBH_4$+1/3 $ZnCl_2$	100	0	0(0)	—(—)
$NaBH_4$+1/3 ZnCl	100	−32.12°	68(18)	*S* (*R*)
KBH_4+1/3 $ZnCl_2$	100	−17.12°	36(5)	*S* (*R*)
$RbBH_4$+1/3 $ZnCl_2$	100	−25.02°	53(—)[a]	*S* (—)
$CsBH_4$+1/3 $ZnCl_2$	70	−20.69°	44(—)[a]	*S* (—)

a) Chemical yields in both cases were less than 10% Optical rotations could not be measured.

pronounced as with other monosaccharides, **2**—**6**.

Four additional modified reagents were prepared from lithium, potassium, rubidium, or caesium borohydrides and 1/3 equiv of $ZnCl_2$ and were applied to the asymmetric reduction of propiophenone with subsequent addition of 2 equiv of **1** in THF at 30 °C. The results are summarized in Table 8. We see that the reagents from sodium, potassium, rubidium, and caesium borohydrides and 1/3 equiv of $ZnCl_2$ have emerged as more effective asymmetric reducing agents than the corresponding metal borohydrides and propiophenone can be reduced with these reagents in good chemical and optical yields, giving product mixtures in which the (*S*)-alcohol configuration predominates. Neither $LiBH_4$–1/3 $ZnCl_2$ nor $LiBH_4$ showed asymmetric induction, although the reducing yields were quantitative, the order of the influence of the metal cation on selectivity being Na>Rb>Cs≃K≫Li. The cause of the effect is not clear so far.

The rates of reduction by these reagents were much greater than those by the corresponding metal borohydrides except for the case when the metal was lithium: chemical yields: 100% with $NaBH_4$–1/3 $ZnCl_2$ *vs.* 20% with $NaBH_4$ for 2 h; 100% with KBH_4–1/3 $ZnCl_2$ *vs.* 25% with KBH_4 for 24 h; 100% with $RbBH_4$–1/3 $ZnCl_2$ *vs.* 10% with $RbBH_4$ for 72 h; 70% with $CsBH_4$–1/3 $ZnCl_2$ *vs.* 5% with $CsBH_4$ for 72 h. This can be, at least, attributed to the great increase in solubility of the metal borohydrides caused by the

addition of $ZnCl_2$. The order of reduction rate by the reagent, $LiBH_4$–1/3 $ZnCl_2$ > $NaBH_4$–1/3 $ZnCl_2$ > KBH_4–1/3 $ZnCl_2$ > $RbBH_4$–1/3 $ZnCl_2$ > $CsBH_4$–1/3 $ZnCl_2$, is in line with the order of the reducing strength of the metal borohydrides, $LiBH_4$ > $NaBH_4$ > KBH_4 > $RbBH_4$ > $CsBH_4$.[11]

Examination of the Reaction Species from $NaBH_4$ and $ZnCl_2$ in the Presence of **1**. The complex prepared from $NaBH_4$ and 1/3 equiv of $ZnCl_2$ with further addition of 2 equiv of **1** reduced propiophenone with the highest optical yield (68%). The complex responsible for the asymmetric induction was examined.

$ZnCl_2$ (7 mmol) in THF was added to a suspension of 21 mmol of $NaBH_4$ in THF at 30 °C. A solid was always present during the course of reaction. The resulting slurry was stirred at 30 °C for 3 h and then filtered. A very small amount of the starting zinc compound but no active hydride species was present in the solid product. From the result of analysis this seems to be sodium chloride, yield of which is nearly quantitative based on initial sodium amount. The filtrate contained *ca.* 100% of the initial amounts of zinc and the active hydrides. The analysis gave a Na:Zn: hydride (B-H): Cl of 1.0:1.0:12.3:0, indicating a physical mixture of $NaBH_4$ and $Zn(BH_4)_2$ at 1:1 molar ratio or a double hydride complex of $NaZn(BH_4)_3$. The reaction may be represented as follows.

$$NaBH_4 + 1/3\ ZnCl_2 \longrightarrow 1/3\ NaBH_4 + 1/3\ Zn(BH_4)_2 + 2/3\ NaCl\downarrow \quad (1)$$

$$NaBH_4 + 1/3\ ZnCl_2 \longrightarrow 1/3\ NaZn(BH_4)_3 + 2/3\ NaCl\downarrow \quad (2)$$

If the reaction of $NaBH_4$ and $ZnCl_2$ gives a physical mixture of $NaBH_4$ and $Zn(BH_4)_2$ (Eq. 1), the reaction might afford precipitates of $NaBH_4$ and NaCl, leaving $Zn(BH_4)_2$ in solution, since $NaBH_4$ is sparingly soluble in THF[12] and $Zn(BH_4)_2$ is soluble in THF. However, the reaction actually gave only a "soluble borohydride species" and a precipitate of sodium chloride. Thus, the product is not a physical mixture of the two simple borohydrides, but may be a soluble double borohydride complex, $NaZn(BH_4)_3$ (Eq. 2).

The double borohydride complex, first prepared by Nöth and his coworkers in 1971,[13] has been characterized by the ^{11}B-NMR, IR-spectra, and elemental analysis. The BH_4 groups in the reagent are bonded *via* double hydrogen bridges to the central Zn atom. The structure is as follows.

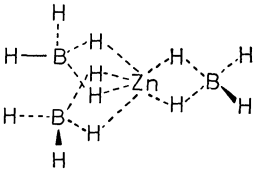

Further addition of 2 equiv of **1** evolved 2.2 moles of hydrogen, 1.8 equiv of hydrogen remaining in the complex. The reaction of the reagent with **1** seems to take place as follows.

$$NaBH_4 + 1/3\ ZnCl_2 \longrightarrow 1/3\ NaZn(BH_4)_3 + 2/3\ NaCl\downarrow$$

$$\downarrow 2\ R^*OH$$

$$1/3\ NaZn(BH_2(OR^*)_2)_3 + 2\ H_2\uparrow \quad (3)$$

The complex formed was soluble in THF and reduction with it was homogeneous, in contrast to $NaBH_4$ as reducing agent which was sparingly soluble in THF and gave reduction which was heterogeneous, at least in part.

Additional evidence for a homogeneous reduction was given when a suspension prepared from $NaBH_4$, 1/3 equiv of $ZnCl_2$, and 2 equiv of **1** was filtered under N_2 atomsphere. Addition of propiophenone to this clear filtrate resulted in the same asymmetric reduction obtained with the originally prepared complex.

Apart from the asymmetric induction, a comparison of the reagent from $NaBH_4$ and 1/3 equiv of $ZnCl_2$ with conventional hydridic reducing agents such as $NaBH_4$ demonstrates the potential utility of the reagent in organic reactions. (1) The reagent has a selectivity for functional groups similar to that of $NaBH_4$ but acts as a THF soluble analogue (*ca.* 4.5 g/100 mL at 25 °C) of $NaBH_4$ allowing selective reduction of carbonyl compounds in THF. Aldehydes and ketones are reduced in THF with much higher rates than those with $NaBH_4$ in the same solvent. For example, propiophenone was reduced to the corresponding alcohol quantitatively over a 2 h reaction period with the reagent in THF at 30 °C, whereas less than 20% of the alcohol was obtained with $NaBH_4$ under the same conditions. (2) The reagent can be easily modified in a stepwise fashion by various alcohols, *i.e.* even highly hindered alcohols such as **1**. No similar modification has been proposed for sodium borohydride. The highly hindered reagents thus formed indicate the possibility of developing a superior reducing agent with a high stereochemical selectivity.

Experimental

All reactions were carried out under an atmosphere of nitrogen. Tetrahydrofuran, diethyl ether, and benzene were heated under reflux over sodium metal and distilled from lithium aluminium hydride in a nitrogen atmosphere. Acetophenone, propiophenone, phenyl propyl ketone, and isopropyl phenyl ketone were dried and distilled over calcium hydride. Methyl 2-naphthyl ketone was purified by recrystallization. Sodium borohydride was purified by recrystallization from 2,5,8-trioxanonane. Zinc chloride was purified by sublimation and dried at 100 °C. The monosaccharide derivatives, 1,2:5,6-di-*O*-isopropylidene-α-D-glucofuranose **1**, 1,2:5,6-di-*O*-cyclohexylidene-α-D-glucofuranose **2**, 1,2:4,5-di-*O*-isopropylidene-D-fructopyranose **3**, 2,3:4,5-di-*O*-isopropylidene-D-fructopyranose **4**, 1,2:4,5-di-*O*-cyclohexylidene-β-D-fructopyranose **5**, and 1,2-*O*-isopropylidene-D-glucofranose **6** were prepared according to the methods reported.[14–17] All the substances were stored under a nitrogen atmosphere prior to use. GLPC analyses were performed on a Shimadzu GC-6A instrument using a Silicone SE-30 prepared column. NMR spectra were measured on a Hitachi R-22, 90 MHz spectrometer. Optical rotations were taken on a Zeiss visual polarimeter with reading to ±0.02° using a 1 dm cell. IR spectra were measured with a JASCO IR-G instrument for nujol mulls. Na analysis by flame photometry was performed on a Hitachi 170-30 instrument. Hydrogen evolution was measured by Brown's method.[18] Zinc was determined by EDTA titration, halogens (chlorine) by Volhard procedure.

General Procedure for Asymmetric Reduction of Propiophenone with $NaBH_4$–$ZnCl_2$ Reagent in the Presence of **1** *in THF.* All experiments were carried out under a nitrogen atmosphere, transfer being made with a syringe through rubber septums. A typical experiment is as follows. THF suspension of $ZnCl_2$ (3 mmol) was added to a THF suspension of $NaBH_4$ (9 mmol) at 30 °C. After stirring for 3 h at 30 °C, THF solution of **1** (18 mmol) was added. On addition of **1**, hydrogen gas evolved slowly. After stirring at 30 °C for 24 h, hydrogen gas evolution was completed, propiopheone (7.2 mmol) then being added dropwise. The resulting mixture was decomposed by addition of 2 mol/l hydrochloric acid. The hydrolyzed mixture was filtered, the organic solvents being removed by evaporation under reduced pressure. The resulting aqueous layer was stirred for 1 h in order to decompose **1** completely. The aqueous mixture was extracted with three 10 mL portions of diethyl ether and the extract washed with saturated NaCl solution (2×10 mL). The etheral layer was dried over $MgSO_4$, and concentrated to give a crude product which was analyzed by GLPC. This was further purified by distillation under reduced pressure. The optical rotation was measured for this purified sample. Absolute configuration and optical yield were calculated from known values.

A number of other asymmetric reductions using different reagents such as ketones and sugar derivatives were performed under conditions similar to those described above.

Reaction of $NaBH_4$ with $ZnCl_2$. THF suspension of $ZnCl_2$ (10 mmol) was added to a suspension of $NaBH_4$ (30 mmol) at 30 °C. The resulting slurry was stirred at 30 °C for 3 h. The solid was separated by filtration under a nitrogen atmosphere and dried at room temperature *in vacuo*. The filtrate contained 33% and 100% of initial sodium and zinc concentrations, respectively. The solid product was found to be sodium chloride by analysis. The filtrate showed Na:Zn:hydridic hydrogen in the ratio 1:1.00:12.3, analyzed by flame photometry, EDTA titration, and hydrogen evolution measurement, but no chloride.

References

1) a) R. Noyori, I. Tomino, and Y. Tanimoto, *J. Am. Chem. Soc.*, **101**, 3129 (1979); b) R. Noyori, I. Tomino, and M. Nishizawa, *ibid.*, **101**, 5843 (1979).

2) a) Mukaiyama, M. Asami, J. Hanna, and S. Kobayashi, *Chem. Lett.*, **1977**, 783; b) T. Mukaiyama, K. Soai, T. Sato, H. Shimizu, and K. Suzuki, *J. Am. Chem. Soc.*, **101**, 1455 (1979); c) J. P. Vigneron and V. Bloy, *Tetrahedron Lett.*, **1979**, 2683; d) N. Cohen, R. J. Lopresti, C. Neukom, and G. Saucy, *J. Org. Chem.*, **45**, 582 (1980).

3) M. M. Midland, S. Greer, A. Tramontano, and S. A. Zderic, *J. Am. Chem. Soc.*, **101**, 2352 (1979); b) M. M. Midland, D. C. McDowell, R. L. Hatch, and A. Tramontano, *ibid.*, **102**, 867 (1980).

4) S. Krishnamurthy, F. Vogel, and H. C. Brown, *J. Org. Chem.*, **42**, 2534 (1977).

5) J. P. Masśe and E. R. Parayre, *J. Chem. Soc., Chem. Commun.*, **1976**, 371.

6) S. Colonna and R. Fornasier, *J. Chem. Soc., Perkin Trans. 1*, **1978**, 371.

7) T. Sugimoto, Y. Matsumura, S. Tanimoto, and M. Okano, *J. Chem. Soc., Chem. Commun.*, **1978**, 926.

8) Y. Shida, N. Ando, Y. Yamamoto, J. Oda, and Y. Inoue, *Agric. Biol. Chem.*, **43**, 1979 (1797).

9) A. Hirao, H. Mochizuki, S. Nakahama, and N. Yamazaki, *J. Org. Chem.*, **44**, 1720 (1979).

10) A. Hirao, S. Nakahama, H. Mochizuki, S. Itsuno, M. Ohwa, and N. Yamazaki, *J. Chem. Soc., Chem. Commun.*, **1979**, 807.

In the communication, we used $[\alpha]_{D\ max}^{20}$ +34.8° (in diethyl ether) as maximum rotation of 1-phenyl-1-propanol which was quoted in *J. Chem. Soc., Perkin Trans. 1*, **1978**, 371. However, the value was found to be erroneous, the true value being $[\alpha]_{D\ max}$ 52±1° (in diethyl ether). Revision of the data for 1-phenyl-1-propanol is being made. During this study, the optical rotations of 1-phenyl-1-propanol were measured in acetone and the optical yields calculated by the observed and known maximum rotations reported by H. Kwart and D. P. Hoster, *J. Org. Chem.*, **32**, 1867 (1967). The optical yields thus obtained were found to agree reasonably with those obtained in neat, ethanol, and chloroform.

11) A. J. Porker, *Quarterly Reviews*, **9**, 196 (1955).

12) H. C. Brown and S. Krishnamurthy, *Tetrahedron*, **35**, 567 (1979).

13) H. Nöth, E. Wiberg, and L. P. Winter, *Z. Anorg. Allg. Chem.*, **386**, 73 (1971).

14) R. L. Whistler and M. L. Wolfrom, "Method in Carbohydrate Chemistry," Academic Press Inc., New York and London (1963), Vol. 2, p. 320.

15) R. C. Hockett, R. E. Miller, and A. Scattergood, *J. Am. Chem. Soc.*, **71**, 3072 (1949).

16) R. F. Brady, Jr., *Carbohydr. Res.*, **15**, 35 (1970).

17) K. James, A. R. Tatchell, and P. K. Ray, *J. Chem. Soc., C*, **1967**, 2681.

18) "Organic Syntheses *via* Boranes," ed by H. C. Brown, John Wiley and Sons, New York (1975), p. 214.

The Cycloaddition of Nitrilimines with 1,2-Dibenzoylethylenes

Tatsuo OIDA,† Tomio SHIMIZU, Yoshiyuki HAYASHI,* and Kazuhiro TERAMURA

Department of Dyeing, Faculty of Industrial Arts, Kyoto Technical University, Matsugasaki, Kyoto 606

(Received September 29, 1980)

The cycloaddition of nitrilimines with 1,2-dibenzoylethylenes gave an unexpected 1,3-diaryl-4-benzoylpyrazole and benzoic acid, along with an expected cycloadduct, 1,3-diaryl-4,5-dibenzoyl-2-pyrazoline, and its dehydrogenated product, 1,3-diaryl-4,5-dibenzoylpyrazole. The elimination of the benzoyl group from the pyrazoline followed by dehydrogenation was shown to be the course of the unusual reaction.

The 1,3-dipolar cycloaddition of diarylnitrilimines with olefins is a versatile method for the stereoselective and regioselective synthesis of 2-pyrazolines or pyrazoles.[1-4] Diarylnitrilimines for the cycloaddition with dipolarophiles are usually prepared *in situ* by the dehydrochlorination of hydrazonoyl chlorides with triethylamine[4] and by the other method.[5,6] 1,2-Dibenzoylethylenes, with particular reference to their geometrical isomerism, have been intensively investigated by Lutz and his collaborator;[7] the ethylenes are good dipolarophiles for the investigation of the stereochemistry of the cycloaddition.[8]

This paper will report that the cycloaddition of nitrilimines with 1,2-dibenzoylethylenes gave 4-benzoylpyrazoles in high yields, along with the expected products. For example, the reaction of *cis*-1,2-dibenzoylethylene with *N*-(*p*-nitrophenyl)-*C*-phenylnitrilimine gave the unexpected 4-benzoyl-1-(*p*-nitrophenyl)-3-phenylpyrazole as the sole isolable product in a 48% yield, with the elimination of a benzoic acid, probably from the 4,5-dibenzoyl-2-pyrazoline. There is no precedent for the oxidative elimination of benzoic acid from 4,5-dibenzoyl-2-pyrazoline. We now wish to propose a scheme in which the nucleophilic attack of water on the 5-carbonyl carbon of the pyrazoline followed by the elimination of benzoic acid yielded the 4-benzoylpyrazoline, which then eliminated hydrogen of afford the unexpected pyrazole.

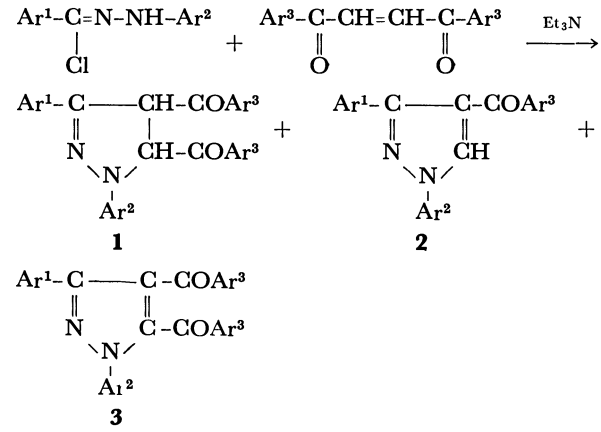

Scheme 1.

TABLE 1. THE REACTION OF DIARYLNITRILIMINES WITH 1,2-DIBENZOYLETHYLENES[a]

Nitrilimine		Dibenzoylethylene	Products yield/%		
Ar^1	Ar^2	$A^3=C_6H_5$	**1**	**2**	**3**
C_6H_5	*p*-$NO_2C_6H_4$	*trans*	21	47	10
C_6H_5	*p*-$NO_2C_6H_4$	*cis*	—	48	trace
p-Tolyl	*p*-Tolyl	*trans*	—	91	—

a) The reaction was carried out by Procedure A (see Experimental).

Results and Discussion

The cycloaddition between *trans*-1,2-dibenzoylethylenes and diarylnitrilimines prepared from hydrazonoyl chlorides in the presence of an excess of triethylamine was carried out in benzene at 80 °C for 5 h. The reaction products from the reaction mixture were shown to be *trans*-1,3-diaryl-4,5-dibenzoyl-2-pyrazolines (**1**), 1,3-diaryl-4,5-dibenzoylpyrazoles (**3**), and unexpected 1,3-diaryl-4-benzoylpyrazoles (**2**) (Scheme 1, Table 1. See Tables 2—4 for the notation of Ar^1, Ar^2, and Ar^3).

It is well-known that the reaction of nitrilimines with *cis*- and *trans*-olefins gives 2-pyrazolines stereospecifically in high yields.[4] With some *cis*-olefins in the presence of a base, however, two possible *cis*- and *trans*-pyrazolines can be formed by the base-catalyzed isomerization of the *cis*-product to the *trans*.[8,9] The pyrazole (**2a**) was isolated in a 48% yield from the reaction mixture of *N*-(*p*-nitrophenyl)-*C*-phenylnitrilimine and *cis*-1,2-dibenzoylethylene, while neither *cis*- nor *trans*-pyrazoline (*cis*- or *trans*-**1a**) was detected. The expected *cis*-pyrazoline (*cis*-**1a**) may be directly decomposed to **2a**, because some of the *trans*-pyrazoline (*trans*-**1a**) would remain in the reaction mixture under the conditions if the base-catalyzed isomerization product, *trans*-pyrazoline (*trans*-**1a**) were an intermediate to **2a**.

The NMR spectroscopy is a convenient method for establishing the stereochemistry of the adduct (**1**), since the coupling constants between 4- and 5-protons indicate whether the adduct is *trans* (J=6 Hz) or *cis* (J=12 Hz),[10] although some exceptions are known.[11] Thus, the *trans* structure of the expected 1,3-dipolar cycloadducts, (**1**) was confirmed on the basis of elemental analyses and NMR ($J_{4,5}$=6 Hz) and IR spectra.

2-Pyrazolines can be easily aromatized by autoxidation or thermal dehydrogenation, even in the absence of oxygen, or by some reagents such as a hydrogenation

† Present address: Institute for Chemical Research, Kyoto Universty, Uji, Kyoto 611.

catalyst, although little is known about these mechanisms[4,12] and only a small amount of hydrogen was identified.[18] The pyrazoles (**3**) were shown to be products dehydrogenated from **1** by the following experiment: the treatment of **1a** in a refluxing toluene solution with a suspension of active alumina gave **3a** in a 54% yield.

The structure of the pyrazole (**2b**) was established by elemental analysis ($C_{23}H_{20}N_2O$), NMR (two tolyl methyl at δ 2.34, H-5 at δ 8.19) and IR ($\nu_{C=O}$ 1635 cm^{-1}) spectra, and comparison with an authentic sample described below. Enamine is a regioselective dipolarophile,[13] and the reaction of nitrilimines with 3-dimethylamino-1-phenylpropen-1-one gave unstable intermediate pyrazolines, which eliminated dimethylamine to afford pyrazoles (**2**).[14,15] The regioselective cycloaddition of nitrilimines with ethynyl phenyl ketone[2,16,17] and phenyl vinyl ketone[13] gave pyrazoles (**4**) and pyrazolines (**5**) respectively. The alkaline–potassium hexacyanoferrate(III) oxidation of **5** also gave pyrazole (**4**), a regioisomer of the pyrazole (**2a**)[12] (Scheme 2). We could not find any trace amount of **4** in the reaction mixture of the *N*-(*p*-nitrophenyl)-*C*-phenylnitrilimine with dibenzoylethylenes.

If the reaction of the nitrilimines with *trans*-dibenzoylethylene was carried out at room temperature under nitrogen by the careful exclution of moisture and work-up below 30 °C the expected 1,3-dipolar cycloadducts **1** were isolated in high yields (Table 2). The isolated pure 4,5-dibenzoyl-2-pyrazolines (**1**) are

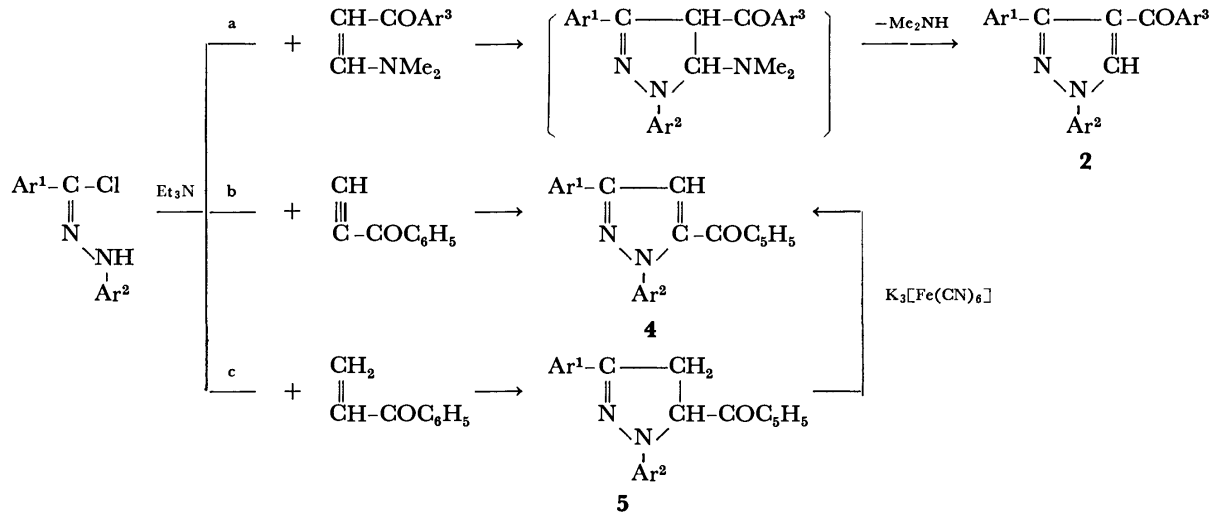

Scheme 2.

Table 2. Preparation of 2-pyrazoline (**1**)[a]

	Ar^1	Ar^2	Ar^3	Yield[c] %	Mp °C	IR (KBr) $\nu_{C=O}$/cm^{-1}	NMR($CDCl_3$) δ/ppm 4-H	5-H	$J_{4,5}$/Hz
1a	C_6H_5	*p*-$NO_2C_6H_4$	C_6H_5	77	160—162	1700 1675	5.38	5.97	6
1c	C_6H_5	*p*-$NO_2C_6H_4$	*p*-Tolyl	70	188—198	1699 1676	5.29	5.86	6
1d	C_6H_5	*p*-$NO_2C_6H_4$	*p*-ClC_6H_4	84	185—194	1708 1682	5.29	5.82	6
1e	C_6H_5	*p*-$NO_2C_6H_4$	Mesityl	74	210—220	1713 1709	4.99	5.92	3
1f	C_6H_5	C_6H_5	C_6H_5	58	201—202	1695 1681	5.26	5.75	7
1g	C_6H_5	C_6H_5	*p*-Tolyl	19[b]	178—183	1695 1680	5.23	5.72	7
1h	C_6H_5	*p*-Tolyl	C_6H_5	27[b]	161—166	1691 1685	5.26	5.72	7
1i	*p*-Tolyl	*p*-Tolyl	Mesityl	81	202—204	1708	4.89	5.67	3
1j	C_6H_5	*p*-ClC_6H_4	C_6H_5	75	160—165	1698 1680	5.26	5.73	6
1k	C_6H_5	*p*-ClC_6H_4	*p*-Tolyl	38	190—197	1693 1684	5.24	5.69	7
1l	*p*-$NO_2C_6H_4$	C_6H_5	C_6H_5	3[b]	147—150	1699 1680	5.24	5.89	6

a) The preparation was carried out by Procedure B (Experimental). b) Some of the pyrazolines (**1**) were decomposed to **2** or intractable compounds under the conditions. c) Isolated yields shown were not optimized.

Table 3. Decomposition of **1** to **2**

	Ar^1	Ar^2	Ar^3	Yield/%			Pyrazole **2**		
				2	Recovered **1**	Ar^3COOH	Mp/°C	IR (KBr) $\nu_{C=O}/cm^{-1}$	NMR ($CDCl_3$) δ 5-H/ppm
2a	C_6H_5	*p*-$NO_2C_6H_4$	C_6H_5	65	0	60	213—214	1645	8.39
2b[a]	*p*-Tolyl	*p*-Tolyl	C_6H_5				130—131	1635	8.19
2c	C_6H_5	*p*-$NO_2C_6H_4$	*p*-Tolyl	65	0	60	198—200	1636	8.32
2d	C_6H_5	*p*-$NO_2C_6H_4$	*p*-ClC_6H_4	55	0	50	188—190	1635	8.40
2e	C_6H_5	*p*-$NO_2C_6H_4$	Mesityl	75	0	65	180—183	1667	8.09
2f	C_6H_5	C_6H_5	C_6H_5	30	1	20	138—141	1635	8.24
2g	C_6H_5	C_6H_5	*p*-Tolyl	50	10	—	151—155	1640	8.24
2i	C_6H_5	*p*-Tolyl	C_6H_5	40	55	—	149—151	1639	8.21
2f	*p*-Tolyl	*p*-Tolyl	Mesityl	55	40	30	152—165	1648	7.90
2j	C_6H_5	*p*-ClC_6H_4	C_6H_5	10	60	—	171—172	1630	8.20
2k	C_6H_5	*p*-ClC_6H_4	*p*-Tolyl	2	98	—	183—188	1640	8.20
2l	*p*-$NO_2C_6H_5$	C_6H_5	C_6H_5	60	0	—	171—172	1643	8.30

a) Pure **1c** could not be isolated.

thermally stable up to about 150 °C. However, the pyrolysis of **1** about 150 °C or the treatment of **1** with a base (and moisture) at about 80 °C gave **2** with appreciable rate.

To our knowledge, no pyrolysis of 4- or 5- (or 4,5-di-)benzoylpyrazolines which eliminates a benzoyl group to pyrazoles has yet been reported. The cycloadducts of the dibenzoylethylenes with nitrones[8a] and diazomethane[8b] are rather thermally stable. The pyrolysis of the pyrazolines (**1**) at 180 °C really gave the pyrazoles **2**) and benzoic acid. We tried to decompose several *trans*-2-pyrazolines (**1**) to **2** (3—75% yields) at 200 °C for 10 min (Table 3), although the reaction conditions used were not strictly the same.

One can easily postulate the thermal elimination of benzaldehyde from **1** followed by the autoxidation of the benzaldehyde to produce the benzoic acid. However, all attempts to detect benzaldehyde, for example, by VPC, NMR, IR, and MS (the MS of **1a** was superimposable with that of an equimolar mixture of the **2a**, pyrazole, and benzoic acid), failed except for the one case to be described below. The careful exclusion of oxygen and moisture from the pyrolysis system under nitrogen decreased the yield of benzoic acid down to 35% along with a small amount of benzaldehyde (up to 10% yield), while the only decomposition products observed were the pyrazoles (**2**) and benzoic acid under usual conditions under nitrogen without strict drying over P_2O_5.

Benzaldehyde has been shown to react easily with aniline (or butylamine) to yield *N*-benzylideneaniline (or *N*-benzylidenebutylamine). No formation of any benzylideneamines in the pyrolysis products of **1a** in aniline (or butylamine) ruled out the formation of benzaldehyde as an intermediate. On the other hand, *N*-butylbenzamide (53% yield) and **2a** (62% yield) were isolated from the reaction mixture of **1a** in butylamine at 80 °C for 5 h, while benzoic acid is stable under the conditions. Furthermore, moisture and base enhanced the decomposition of **1** to **2**. The rate ratio of the decomposition of wet **1a** to that of dry **1a** was about 2. The decomposition of **1** to **2** in the presence of a small amount of water and triethyamine gave the pyrazole (**2**) in excellent yields (for example, **2a** in an 86% yield from **1a**) than the results shown in Table 3. Pyrazoline and pyrazole have some basic character; thus, the decomposition of **1** to **2** may be promoted by self-catalysis. Taking the results in butylamine into consideration, the acceleration of the pyrolysis rate by water can be explained if we assume that a reasonable first step involved the initial nucleophilic attack of water on 5-carbonyl carbon followed by the cleavage of the carbon-carbon bond to give 4-benzoylpyrazoline (**6**) (Scheme 3). Several attempts to prepare an authentic specimen of the intermediate, **6**, or to isolate it from the reaction mixture were fruitless; therefore, **6** may be thermally unstable and may undergo dehydrogenation to **2**. However, only a trace amount of hydrogen was detected in the pyrolysis products of **1a** by VPC (activated charcoal 5 m at 50 °C, carrier gas argon) and so far the fate of the hydrogen can not be identified.

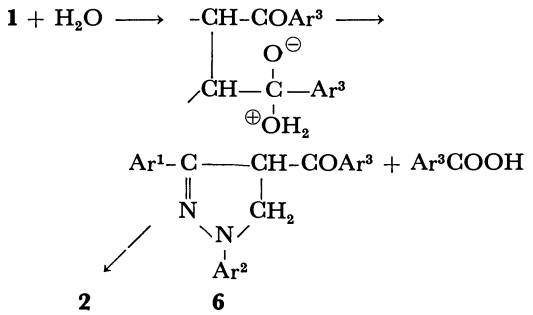

Scheme 3.

Importance of two benzoyl groups at both 4- and 5-positions for the facile decomposition of **1** to **2** was shown by comparison with a series of 2-pyrazolines, where only the 5-position has a benzoyl group (Scheme 4). None of the compounds (**7a**—**c**) has a tendency to decompose thermally up to 250 °C under conditions where the pyrolysis of **1** occurs very easily. We have so far been able to find any definite explanations of the importance of the two benzoyl groups

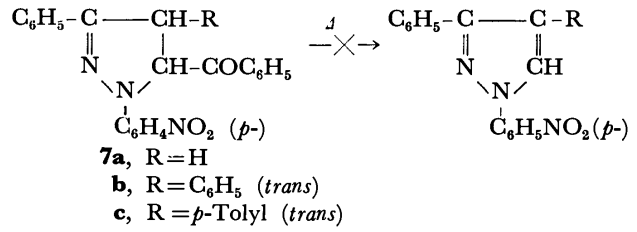

Scheme 4.

on **1** in the facile transformation of **1** into **2**. One possible explanation is that the carbonyl-carbonyl interactions between the two benzoyl groups, along with steric hindrance, would facilitate the reactivity of the carbonyl carbon toward nucleophiles.

Experimental

All the melting points are uncorrected. The IR spectra were obtained on a Hitachi 215A Infrared Spectrophotometer. The ^{1}H-NMR spectra were measured of a Varian T-60A instrument in $CDCl_3$ unless otherwise stated, with TMS as an internal standerd. The column chromatography was carried over silica gel eluted with $CHCl_3$. All the new compounds reported here gave satisfactory elemental analyses.

Materials. The *N*-arylarenehydrazonoyl chlorides were prepared by the method of Huisgen *et al.*[4,9] The *trans*- and *cis*-1,2-dibenzoylethylenes were prepared by the method of Lutz et al.[7] The phenyl vinyl ketone and ethynyl phenyl ketone are commercially available (Nakarai Chem. Co.) and were used without further purification.

Reactions of Diarylnitrilimines with 1,2-Dibenzoylethylenes. General Procedure A: *N*-(*p*-Nitrophenyl)benzohydrazonoyl chloride (2.6 g, 9.5 mmol) as a precursor of the *N*-(*p*-nitrophenyl)-*C*-phenylnitrilimine was added, in small portions to a stirred solution of *trans*-1,2-dibenzoylethylene (2.3 g, 9.5 mmol) and triethylamine (2 ml) in benzene (50 ml) at 80 °C over a period of 30 min. The mixture was then stirred at 80 °C for 5 h. The precipitated triethylamine hydrochloride was filtered off, and the filtrate was evaporated *in vacuo*. The residue was crystallized from benzene to give the 2-pyrazoline (*trans*-**1a**; 0.96 g, 21%). The filtrate from the crystallization was chromatographed to give the pyrazole **2a** (1.6 g, 47%) and **3a** (0.45 g, 10%). The results are shown in Table 1. **1a**. Found: C, 73.48; H, 4.59; N, 8.58%. Calcd for $C_{29}H_{21}N_3O_4$: C, 73.25; H, 4.45; N, 8.84%. **2a**. Found: C, 71.89; H, 4.23; N, 11.11%. Calcd for $C_{22}H_{15}N_3O_3$: C, 71.53; H, 4.09; N, 11.38%. **3a**. Found: C, 73.47; H, 4.22; N, 8.91%. Calcd for $C_{29}H_{19}N_3O_4$: C, 73.56; H, 4.05; N, 8.88%.

General Procedure B: A solution of *N*-(*p*-nitrophenyl)benzohydrazonoyl chloride (1.1 g 4.0 mmol), *trans*-1,2-dibenzoylethylene (0.95 g, 4.0 mmol), and triethylamine (0.7 ml) in dry benzene (50 ml) was stirred at room temperature under nitrogen for 2 d. The triethylamine hydrochloride thus precipitated was filtered off, and the filtrate was evaporated *in vacuo* at below 30 °C. The residue was triturated with cold benzene to give the 2-pyrazoline (*trans*-**1a**, 1.5 g, 77%). **1** were recrystallized from DMF–H_2O without heating. The results are shown in Table 2.

Decomposition of 2-Pyrazolines (1). General Procedure: **1a** (0.57 g, 1.2 mmol) was heated in a sublimation apparatus at 200 °C for 10 min under reduced pressure (*ca.* 30 mmHg). Benzoic acid was thus isolated (0.088 g, 60%) as a sublimate. The residue was chromatographed to give **2a** (0.29 g, 65%) (and the recovered **1**). The results are shown in Table 3.

Detection of Benzaldehyde in the Pyrolysis products of 1a.

a) By NMR: **1a** was decomposed at 180 °C for 10 min in an NMR sample tube under N_2. The peak of benzaldehyde (δ 9.9, -CHO) was not detected, but the peak of benzoic acid (δ 12.7, -OH) was detected.

b) By MS: The strong peak of benzoic acid (m/e=122) appeared, while that of benzaldehyde (m/e=106) appeared very weak in the mass spectrum of **1a**.

c) By IR: A KBr pellet containing **1a** was heated at 180 °C for 10 min under N_2. The characteristic absorption of benzaldehyde (ν=2770 cm^{-1}) was not detected.

d) By VPC: When **1a** was analyzed by VPC (injection temperature 200—250 °C), only a trace amount of benzaldehyde was detected.

e) Decomposition of 1a after Thorough Drying: **1a** (0.81 g, 1.7 mmol) was dried over P_2O_5 under reduced pressure (2 mmHg) for 2 d; then the **1a** was decomposed at 200 °C for 10 min under 2 mmHg in a sealed vessel to give the sublimated benzoic acid (0.072 g, 35%) and the benzaldehyde (*ca.* 0.02 g, less then 10%). The residue was crystallized from $CHCl_3$–EtOH to give **2a** (0.33 g, 53%).

Decomposition of 1a in Aniline. A solution of **1a** (0.22 g, 0.46 mmol) and hydroquinone (0.1 g) in aniline (5 ml, distilled over KOH) was refluxed for 10 min under N_2. The reaction mixture was then poured into aq $NaHCO_3$ and extracted with benzene. The benzene layer was washed with aq $NaHCO_3$ several times. The water layer was separated, acidified with aq HCl, and extracted with ether. The ether was evaporated to give the benzoic acid (0.028 g, 50%). The benzene layer was washed with aq HCl several times and evaporated *in vacuo*. The residue was crystallized from $CHCl_3$–EtOH to give **2a** (0.14 g, 65%). Neither benzylideneaniline nor *N*-phenylbenzamide was detected in the reaction products by TLC.

Decomposition of 1a in butylamine. A solution of **1a** (0.52 g, 1.1 mmol) in butylamine (50 ml, distilled over CaH_2) was refluxed for 5 h under N_2. After the amine was evaporated under nitrogen and reduced pressure, the residue was distilled to give *N*-butylbenzamide (140—170 °C/0.1 mmHg, 0.10 g, 53%). The residue of the distillation was crystallized from $CHCl_3$–EtOH to give **2a** (0.23 g, 62%). Neither benzoic acid nor *N*-benzylidenebutylamine was detected in the reaction products by TLC.

Preparation of Pyrazole (2) from Enamine (Scheme 2a). General Procedure: A solution of *N*-(*p*-nitrophenyl)benzohy-

Table 4. Pyrazole (**3**)

	Ar^1	Ar^2	Ar^3	Yield / %	Mp / °C	IR (KBr) $\nu_{C=O}$/cm^{-1}
3a	C_6H_5	*p*-$NO_2C_6H_4$	C_6H_5	54	137—139	1671
3c	C_6H_5	*p*-$NO_2C_6H_4$	*p*-Tolyl	51	143—148	1665
3e	C_6H_5	*p*-$NO_2C_6H_4$	Mesityl	38	150—155	1641
3f	C_6H_5	C_6H_5	C_6H_5	48	135—136	1668

drazonoyl chloride (1.4 g, 5.1 mmol), 3-dimethylamino-1-phenyl-2-propen-1-one (0.90 g, 5.2 mmol), and triethylamine (2 ml) in benzene (30 ml) was refluxed for 6 h. After a usual work-up, **2a** was recrystallized from $CHCl_3$–EtOH or DMF–H_2O in about a 30% yield.

Preparation of Pyrazole (3) from Pyrazoline (1). General Procedure: A solution of **1a** (0.44 g, 0.95 mmol) in toluene (50 ml) was refluxed with neutral aluminum oxide (5 g) until the solution was discolored (for about 5 h). The mixture was then filtered, and the filtrate was evaporated. The residue was crystallized from EtOH to give **3a** (0.23 g, 54%), which was then recrystallized from EtOH. The results are shown in Table 4.

Preparation of 2-Pyrazoline (7). General Procedure: A solution of *N*-(*p*-nitrophenyl)benzohydrazonoyl chloride (1.0 g, 3.7 mmol), phenyl vinyl ketone (0.57 g, 4.3 mmol), and triethylamine (2 ml) was stirred at room temperature for 2 d to give **7a** in a 88% yield; mp 242 °C (from EtOH). IR (KBr): 1698 cm^{-1} (C=O); NMR (DMSO-d_6) δ: 3.41 (dd, J=6 and 18 Hz, 1H, H-4), 4.17 (dd, J=12 and 18 Hz, 1H, H-4), 6.42 (dd, J=6 and 12 Hz, 1H, H-5). **7b** from *trans*-1,3-diphenyl-2-propen-1-one, 60% yield; mp 134—141 °C (from EtOH). IR (KBr): 1694 cm^{-1} (C=O); NMR ($CDCl_3$) δ: 4.66 (d, J=4 Hz, 1H, H-4), 5.71 (d, J=4 Hz, 1H, H-5). **7c** from *trans*-1-phenyl-3-*p*-tolyl-2-propen-1-one, 53% yield; mp 204—205 °C (from EtOH). IR (KBr): 1684 cm^{-1} (C=O); NMR ($CDCl_3$) δ: 4.61 (d, J=4 Hz, 1H, H-4), 5.67 (d, J=4 Hz, 1H, H-5).

Preparation of 5-Benzoyl-1-(p-nitrophenyl)-3-phenylpyrazole (4). Method A (Scheme 2b): A solution of *N*-(*p*-nitrophenyl)-benzohydrazonoyl chloride (0.69 g, 2.5 mmol), ethynyl phenyl ketone (0.33 g, 2.5 mmol), and triethylamine (1 ml) in benzene (50 ml) was stirred at room temperature for 20 h. After a usual work-up, the pyrazole was isolated in less than a 10% yield.

Method B (Scheme 2c): A solution of **7a** (0.26 g, 0.70 mmol) in EtOH (20 ml) was added to a solution of K_3-[Fe(CN)$_6$] (0.53 g, 1.6 mmol), and KOH (0.2 g) in aqueous EtOH (50 ml) at room temperature. The mixture was then stirred at room temperature for 10 h, poured into 200 ml of water, and extracted with benzene. The benzene layer was washed with water several times and concentrated. The residue was crystallized from EtOH to give the pyrazole (**4**) in a 28% yield; mp 164 °C (from EtOH). IR (KBr): 1670 cm^{-1} (C=O); NMR ($CDCl_3$); δ: 7.13 (s, 1H, 4-H). Found: C, 71.30; H, 4.04; N, 11.33%. Calcd for $C_{22}H_{15}N_3O_3$: C, 71.53; H, 4.09; N, 11.38%.

We would like to thank Professor Dr. Masaya Okano and Associate Professor Dr. Shigeo Tanimoto of Kyoto University for their valuable advice.

References

1) R. Huisgen, *Angew. Chem. Int. Ed. Engl.*, **2**, 565 (1963).
2) R. Huisgen, *Angew. Chem. Int. Ed. Engl.*, **2**, 633 (1963).
3) R. Huisgen, *J. Org. Chem.*, **41**, 403 (1976).
4) R. Huisgen, M. Seidel, G. Wallbillich, and H. Knupfer, *Tetrahedron*, **17**, 3 (1962).
5) R. Huisgen, J. Sauer, and M. Seidel, *Chem. Ber.*, **94**, 2503 (1961).
6) W. A. F. Gladstone, J. B. Aylward, and R. O. C, Norman, *J. Chem. Soc., C*, **1969**, 2583.
7) R. E. Lutz and J. C. Gillespie, Jr., *J. Am. Chem. Soc.*, **72**, 344, 2002, 5058 (1950).
8) a) K. Tada, T. Yamada, and F. Toda, *Bull. Chem. Soc. Jpn.*, **51**, 1839 (1978). b) L. I. Smith and K. L. Howard, *J. Am. Chem. Soc.*, **65**, 159 (1943).
9) R. Huisgen, H. Knupfer, R. Sustmann, G. Wallbillich, and V. Weberndorfer, *Chem. Ber.*, **100**, 1580 (1967).
10) R. Sustmann, R. Huisgen, and H. Huber, *Chem. Ber.*, **100**, 1802 (1967).
11) R. G. Micetich, *Can. J. Chem.*, **40**, 3753 (1970).
12) R. Fusco and P. D. Croce, *Tetrahedron Lett.*, **1970**, 3061.
13) M. E. Munk and Y. K. Kim, *J. Am. Chem. Soc.*, **86**, 2213 (1964).
14) D. Pocar, L. M. Ross, and R. Stradi, *Synthesis*, **10**, 684 (1976).
15) H. Bredereck and G. Simchen, *Chem. Ber.*, **97**, 3397 (1964).
16) a) P. Rutan and C. E. May, *J. Am. Chem. Soc.*, **69**, 2018 (1947). b) I. Iwai, Y. Okajima, and T. Konotsune, *Yakugaku Zasshi*, **78**, 505 (1958).
17) K. N. Houk, J. Sims, C. R. Watts, and C. J. Luskus, *J. Am. Chem. Soc.*, **95**, 7301 (1973).
18) a) E. Buchner and L. Perkel, *Ber.*, **36**, 3774 (1903). b) R. C. Elderfield, *Heterocyclic Compounds*, **5**, 108 (1957).

The Reaction of 2-Ethoxy-1,3-dithiolane with Carbonyl Compounds

Shigeo Jo,* Shigeo Tanimoto,* Tatsuo Oida, and Masaya Okano
Institute for Chemical Research, Kyoto University, Uji, Kyoto 611

(Received October 4, 1980)

The reaction of 2-ethoxy-1,3-dithiolane with carbonyl compounds such as aldehydes and ketones was investigated. The reaction proceeded smoothly in the presence of the $HgCl_2$-catalyst to afford 2-substituted and 2,2-disubstituted 1,3-dithiolanes. The reaction also offers an interesting alternative to the previously reported methods of synthesizing 1,3-dithiolanes which involve the acid-catalyzed reaction of carbonyl compounds with 1,2-ethanedithiol.

Although the chemistry of 1,3-dithiolanes has been extensively studied, together with that of 1,3-dithianes,[1] little is known about the 2-alkoxy derivatives of these compounds, which have been described as five-membered cyclic orthodithioformates. This is mostly because the derivatives are sensitive to acidic reagents, especially to such inorganic acids as hydrochloric and sulfuric acids. For example, the addition of a trace amount of concd hydrochloric acid to 2-ethoxy-1,3-dithiolane resulted in an exothermic reaction leading to 2,2'-[1,2-ethanediylbis(thio)]bis-1,3-dithiolane.[2] A recent report[3] from this laboratory has described a new method for the introduction of the 1,3-dithiolan-2-yl group into some active methylene compounds. The reaction using 2-ethoxy-1,3-dithiolane proceeded smoothly without a solvent under the catalytic action of a metal halide, such as $ZnCl_2$ or $FeCl_3$, and 1,3-dithiolan-2-yl derivatives of the active methylene compounds could be isolated in moderately good yields. As a broadening of the synthetic scope of 2-ethoxy-1,3-dithiolane, we had chosen to react it with such carbonyl compounds as aldehydes and ketones. To date there has been no information on any reaction between one of the so-called cyclic orthodithioformates and carbonyl compounds.

Results and Discussion

It has been observed that the reaction of 2-ethoxy-1,3-dithiolane with aldehydes or ketones proceeds smoothly in the presence of a Lewis-acid catalyst to afford either 2-substituted or 2,2-disubstituted 1,3-dithiolane respectively. Thus, the successful utilization of the readily available 2-ethoxy-1,3-dithiolane in the synthetic reaction has been demonstrated. The first attempt was directed toward establishing the most effective Lewis-acid catalyst in the reaction. When 2-ethoxy-1,3-dithiolane was allowed to react with acetone in dichloromethane at room temperature for 16 h, in the presence of a Lewis-acid catalyst, the major product was 2,2-dimethyl-1,3-dithiolane (**1a**), accompanied by a comparatively small amount of 1-(1,3-dithiolan-2-yl)-2-propanone (**2a**). The results of the reaction with some different Lewis-acid catalysts are

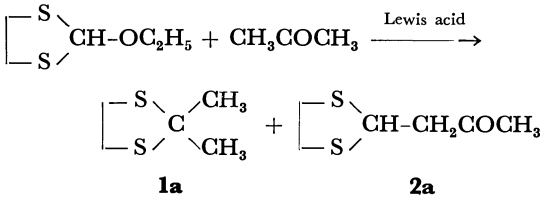

1a **2a**

Table 1. Reaction of 2-ethoxy-1,3-dithiolane with acetone in the peesence of several different Lewis-acid catalysts

Run[a]	Catalyst (mmol)	Yield/%[b]	
		1a	**2a**[c]
1	$HgCl_2$(6)	60	0
2	$ZnCl_2$(30)	44	17
3	$BF_3 \cdot Et_2O$(15)	52	12
4	$FeCl_3$(6)	60	3
5	$AlCl_3$(6)	45	21

a) In all the reaction runs, 30 mmol of 2-ethoxy-1,3-dithiolane, 30 mmol of acetone, and 40—50 ml of dichloromethane were employed. Reaction conditions: room temperature, 16 h. b) Determined by gas-chromatographic analysis. c) Bp 100—101 °C/2 Torr (lit,[4] 143—145 °C/10 Torr), ^{1}H-NMR, δ (ppm from TMS, in $CDCl_3$), 4.77 (t, 1H, CH), 3.20 (s, 4H, SCH_2CH_2S), 3.00 (d, 2H, CH_2), 2.13 (s, 3H, CH_3). Found: C, 44.20; H, 5.99%. Calcd for $C_6H_{10}OS_2$: C, 44.41; H, 6.21%.

shown in Table 1.

As is evident from Table 1, the reaction using $HgCl_2$ as the catalyst resulted in the formation of **1a** in a 60% yield, while no **2a** was produced. Thus, we have studied the $HgCl_2$-catalyzed reaction of 2-ethoxy-1,3-dithiolane with a number of different aldehydes and ketones in the hope that the desired 2-substituted and 2,2-disubstituted 1,3-dithiolanes (**1**) could be exclusively made by the reaction with $HgCl_2$. The results are summarized in Table 2.

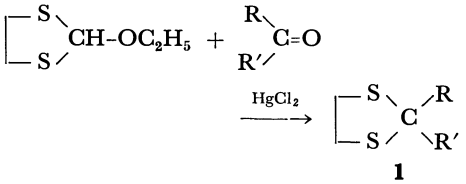

1

a R=CH_3, R'=CH_3
b R=n-C_3H_7, R'=H
c R=C_6H_5, R'=CH_3
d R=C_6H_5, R'=H
e R=p-ClC_6H_4, R'=H
f R=p-$CH_3OC_6H_4$, R'=H
g R=p-$NO_2C_6H_4$, R'=H
h R=p-$(CH_3)_2NC_6H_4$, R'=H
i R=p-$CHOC_6H_4$, R'=H
j R=C_6H_5CH=CH, R'=H
k R=CH_3CH=CH, R'=H
l 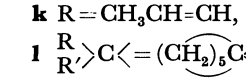

Table 2. Reaction of 2-ethoxy-1,3-dithiolane with aldehydes or ketones(RCOR') under the catalytic action of $HgCl_2$

Run	R	R'	Products	
			Abbreviation	Yield/%[a]
1[b]	CH_3	CH_3	**1a**	78
2[b]	n-C_3H_7	H	**1b**	82
3[b]	C_6H_5	CH_3	**1c**	64
4[b]	C_6H_5	H	**1d**	82
5[b]	p-ClC_6H_4	H	**1e**	87
6[b]	p-$CH_3OC_6H_4$	H	**1f**	79
7[c]	p-$NO_2C_6H_4$	H	**1g**	91
8[b]	p-$(CH_3)_2NC_6H_4$	H	**1h**	52
9[c]	p-$CHOC_6H_4$	H	**1i**	27
10[c]	C_6H_5CH=CH	H	**1j**	89
11[c]	CH_3CH=CH	H	**1k**	56
12[c]	-$(CH_2)_5$-		**1l**	91

a) All yields refer to isolated products. Some starting 2-ethoxy-1,3-dithiolane was recovered in all runs. b) Carried out without any solvent. c) Carried out in a dichloromethane solvent.

As was originally anticipated, 2-substituted or 2,2-disubstituted 1,3-dithiolane (**1**), which is well known as a carbonyl-protective group,[5] was the sole product in the $HgCl_2$-catalyzed reaction. It was recognized by thin-layer chromatography that, even in the run involving a low yield of the product, the residue consists of the starting materials containing a small amount of an indefinite by-product. It should also be noted that the procedure is simple to carry out and applicable to a wide range of aldehydes and ketones.

It is obvious that an exclusive C–S bond fission occurred in the $HgCl_2$-catalyzed reaction of 2-ethoxy-1,3-dithiolane. Therefore, the first necessary step in the reaction would seem to be the coordination of $HgCl_2$ with one of the S atoms of the ring. Thus, a mechanism for the reaction was proposed involving, first, the formation of a resonance-stabilized sulfocarbonium ion, which would then combine with carbonyl carbon.

This seems probable on the basis of the information on the symbiotic effect on the HSAB principle presented by Pearson and Songstad.[6] In previous work on the reduction of 1,3-oxathiolanes with a mixture of $LiAlH_4$ and $AlCl_3$ in ether solution, Leggetter and

Table 3. Physical properties and analytical data of 2-substituted and 2,2-disubstituted 1,3-dithiolanes (**1**)

Compound	Mp (°C) or Bp (°C/Torr)	^{1}H-NMR δ(ppm from TMS, in $CDCl_3$)	Found (Calcd) (%)		
			C	H	N
1a[a]	68—71/28	3.32(s, 4H, SCH_2CH_2S), 1.77(s, 6H, CH_3)	44.36	7.66	
	Lit,[10] 171/760		(44.73)	(7.51)	
1b[a]	109—110/26	4.40(t, 1H, CH), 3.18(s, 4H, SCH_2CH_2S), 2.0—1.2(m, 4H, CH_2CH_2), 1.1—0.8(m, 3H, CH_3)	48.80	8.21	
			(48.60)	(8.16)	
1c[a]	116—121/2	7.7—7.1(m, 5H, ArH), 3.36(broad s, 4H, SCH_2-CH_2S), 2.09(s, 3H, CH_3)	61.66	6.25	
	Lit,[11] 131/3		(61.18)	(6.16)	
1d[a]	176—177/20	7.6—7.1(m, 5H, ArH), 5.60(s, 1H, CH), 3.7—3.0(m, 4H, SCH_2CH_2S)	59.15	5.31	
	Lit,[10] mp 29 °C		(59.30)	(5.53)	
1e[b]	59—60	7.5—7.1(m, 4H, ArH), 5.53(s, 1H, CH), 3.5—3.2(m, 4H, SCH_2CH_2S)	49.64	4.48	
	Lit,[12] 62		(49.87)	(4.18)	
1f[c]	60—61	7.5—7.3(m, 2H, ArH), 6.9—6.7(m, 2H, ArH), 5.61(s, 1H, CH), 3.78(s, 3H, OCH_3), 3.7—3.2 (m, 4H, SCH_2CH_2S)	56.38	5.74	
	Lit,[10] 64—65		(56.57)	(5.70)	
1g[b]	67—69	8.3—8.1(m, 2H, ArH), 7.7—7.5(m, 2H, ArH), 5.67(s, 1H, CH), 3.7—3.2(m, 4H, SCH_2CH_2S)	47.35	4.06	6.29
			(47.56)	(3.99)	(6.16)
1h[d]	100—101	7.5—7.3(m, 2H, ArH), 6.7—6.5(m, 2H, ArH), 5.62(s, 1H, CH), 3.5—3.1(m, 4H, SCH_2CH_2S), 2.90(s, 6H, CH_3)	58.89	6.82	5.97
	Lit,[13] 105		(58.62)	(6.71)	(6.22)
1i[e]	148—152/3	10.00(s, 1H, CHO), 7.9—7.6(m, 4H, ArH), 5.64(s, 1H, CH), 3.6—3.3(m, 4H, SCH_2CH_2S)	56.95	4.95	
			(57.11)	(4.79)	
1j[b]	59—59.5	7.30(m, 5H, ArH), 6.53(d, 1H, ArCH), 6.14(dd, 1H, CH-<S/S>), 5.18(d, 1H, CH), 3.28(broad s, 4H, SCH_2CH_2S)	63.35	5.78	
			(63.42)	(5.81)	
1k[a]	60—61/2	5.7—5.2(m, 2H, CH=CH), 5.1—4.9(m, 1H, CH), 3.23(broad s, 4H, SCH_2CH_2S), 1.66(d, 3H, CH_3)	49.22	7.12	
			(49.27)	(6.89)	
1l[a]	147—148/30	3.27(s, 4H, SCH_2CH_2S), 2.1—1.2[m, 10H, $(CH_2)_5$]	55.04	8.26	
	Lit,[14] 114—115/6		(55.12)	(8.09)	

a) Purified by distillation. b) Purified by recrystallization (ethanol). c) Purified by recrystallization (hexane). d) Purified by both column chromatography and recrystallization (ethanol). e) Purified by both colume chromatography and distillation.

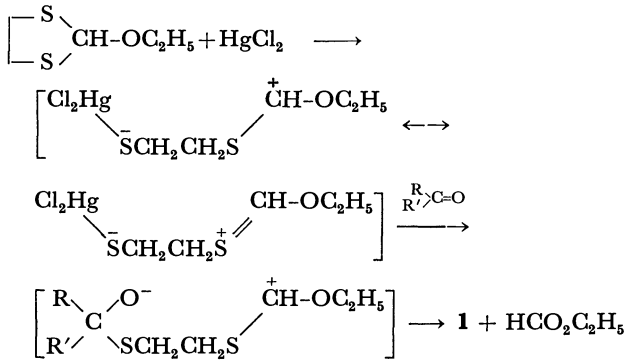

Brown[7] have found that the C–O, but not the C–S, bond is ruptured. This result suggests that the coordination of $AlCl_3$ with the O-atom is more favorable than the similar coordination of $AlCl_3$ with the S-atom. The formation of **2a** in the reaction of 2-ethoxy-1,3-dithiolane with acetone, using $AlCl_3$ as the catalyst, may be explained by a mechanism which involves the initial loss of the exocyclic ethoxyl group to give the 1,3-dithiolan-2-ium ion, and its subsequent attack on acetone. A similar coordination with the O-atom of 2-ethoxy-1,3-dithiolane leading to **2a** occurred in the end, but to a lesser extent, when $ZnCl_2$, $BF_3 \cdot Et_2O$, or $FeCl_3$ was used instead of the $AlCl_3$ catalyst. However, the major product formed in the reaction using these Lewis-acid catalysts is not **2a**, but **1a**, suggesting that the C–S bond fission in the starting 2-ethoxy-1,3-dithiolane is predominant. Because the only available evidence is that listed in Table 1, we are presently unable to establish a reasonable pathway to afford **1a** when these Lewis-acid catalysts are used. At least, as to the reaction with $AlCl_3$, which has a poor coordination ability with the S atom, **1a** might also be formed by another path involving the coordination[8] of $AlCl_3$ with acetone in the initial step of the reaction.

Such compounds as 2-substituted and 2,2-disubstituted 1,3-dithiolanes (**1**) can serve as protected aldehydes and ketones. They are commonly prepared by the acid-catalyzed reaction of carbonyl compounds with 1,2-ethanedithiol.[9] The present reaction offers an interesting alternative, because the protected carbonyl compounds are formed easily and under non-acidic conditions by the reaction of 2-ethoxy-1,3-dithiolane with carbonyl compounds.

Experimental

Preparation of 2-Substituted and 2,2-Disubstituted 1,3-Dithiolanes (1). General Procedure: To a mixture of 2-ethoxy-1,3-dithiolane (30 mmol) and an aldehyde (or ketone) (30 mmol) in dichloromethane (40—50 ml), was added $HgCl_2$ (6 mmol) at 0—5 °C. In some cases (Runs 1, 2, 3, 4, 5, 6, and 8) the dichloromethane solvent was omitted. The mixture was brought to room temperature, stirred for 24 h, and then poured into a mixture of ice water and ether. The ethereal layer was separated, and then it was combined with a dichloromethane extract of the aqueous phase. The organic layer was washed repeatedly with dilute aqueous $NaHCO_3$, and then with water, and dried ($MgSO_4$), a subsequent evaporation of the solvents gave a residue which was further purified by distillation, recrystallization or column chromatography on silica gel, using ether as the eluent.

References

1) D. S. Breslow and H. Skolnik, "The Chemistry of Heterocyclic Compounds. Multi-Sulfur and Sulfur and Oxygen Five- and Six-Membered Heterocycles (Part I)," Interscience, New York (1966), pp. 204 and 407.
2) S. Tanimoto, T. Miyake, and M. Okano, *Bull. Inst. Chem. Res., Kyoto Univ.*, **55**, 276 (1977).
3) S. Tanimoto, Y. Matsumura, T. Sugimoto, and M. Okano, *Bull. Chem. Soc. Jpn.*, **51**, 665 (1978).
4) N. K. Kochetkov, E. E. Nifant'ev, and V. N. Kulakov, *Dokl. Akad. Nauk SSSR*, **125**, 327 (1959); *Chem. Abstr.*, **53**, 19873 (1959).
5) E. J. Corey and D. J. Beames, *J. Am. Chem. Soc.*, **95**, 5829 (1973).
6) R. G. Pearson and J. Songstad, *J. Am. Chem. Soc.*, **89**, 1827 (1967).
7) B. E. Leggetter and R. K. Brown, *Can. J. Chem.*, **41**, 2671 (1963).
8) C. A. Mackenzie and J. H. Stocker, *J. Org. Chem.*, **20**, 1695 (1955).
9) H. Hauptmann, *J. Am. Chem. Soc.*, **69**, 562 (1947).
10) H. Fasbender, *Ber.*, **21**, 1476 (1888).
11) E. E. Reid and A. Jelinek, *J. Org. Chem.*, **15**, 448 (1950).
12) R. H. Jones, G. E. Lukes, and J. T. Bashour, U. S. Patent 2701253; *Chem. Abstr.*, **50**, 1086 (1956).
13) R. Wizinger and D. Duerr, *Helv. Chim. Acta*, **46**, 2167 (1963).
14) H. Hauptmann and M. M. Campos, *J. Am. Chem. Soc.*, **72**, 1405 (1950).

  Bull. Chem. Soc. Jpn., 54, 1437—1442 (1981)

Polarographic Studies on Oxygen Transport by Human Hemoglobin in Buffer Solutions

Katsumi HAYASHI and Masanosuke TAKAGI*

Department of Agricultural Chemistry, College of Agriculture, University of Osaka Prefecture, Sakai, Osaka 591

(Received October 11, 1980)

Oxygen transport by human hemoglobin (Hb) to an electrode surface with hypo-oxygen partial pressure has been studied by the polarographic technique. The oxygen reduction current in Hb solution open to the atmosphere increased linearly with Hb concentration up to *ca.* 2 mM (1 M=1 mol dm^{-3}) heme. The current was ascribed to free and Hb bound oxygen. The increase in current with Hb concentration was attributed to the increasing oxygen supply to the electrode from oxygen bound Hb (oxyhemoglobin;oxyHb). Changes in temperature and pH largely affected the current, corresponding to the change in dissociation rate of oxygen from oxyHb. The relation between the current due to oxyHb and the apparent first order rate constant of the dissociation (k) measured by the stopped-flow method implies two different rate-determining steps of oxygen transport by Hb. When k exceeded *ca.* 60 s^{-1}, the limiting step altered from the dissociation of oxygen to the diffusion of Hb molecules. It is concluded that the oxygen transport by Hb on physiological conditions is controlled by the diffusion of Hb. The diffusion coefficient of Hb in 20 mM heme as found in erythrocytes was estimated to be 5.8×10^{-8} cm^2 s^{-1} at 25 °C and pH 7.4.

For better understanding of the oxygen transporting capacity of erythrocytes, it is important to clarify rate-determining factors of uptake or release of oxygen by erythrocytes. Hartridge and Roughton[1] reported that the observed half-time of the oxygen uptake by erythrocytes was 40 times greater than that by free hemoglobin (Hb) in a rapid mixing continuous flow apparatus. Since then, investigators[2-4] have suggested that the behavior of oxygen in Hb solution, particularly in concentrated solutions corresponding to those in erythrocytes, should be investigated. The mechanisms of the association of oxygen with Hb and also the dissociation, were extensively studied by static or kinetic methods.[5-8] However, few quantitative studies have been carried out on the oxygen transport by Hb, further by erythrocytes to the region with hypo-oxygen partial pressure, *viz.* the transport phenomena involving diffusion process. Spectrophotometric methods which have been used for studying various problems of oxygen binding to Hb, do not seem very effective for the transport phenomena.

Scholander,[9] and Wittenberg[10-12] proposed the idea of "facilitated oxygen diffusion" for describing the oxygen transport by Hb in solution. They measured the flux of oxygen passing through a millipore filter holding Hb by gas-liquid chromatography and suggested that the rate-determining factor is the translational diffusion of Hb molecules. Wyman[13] gave the theoretical explanation for the facilitated diffusion. However, the conditions for the clear demonstration of the diffusion-controlled oxygen transport have not so far been established.

We tried an electrochemical method for covering the shortcomings of the previous investigations. In our method, an electrode, to which an appropriate potential is applied, works as a model of biological surface on which oxygen is consumed immediately on its arrival, that is, the electrode generates a region with hypo-oxygen partial pressure. The diffusion of oxyhemoglobin (oxyHb) to the electrode surface may result in the dissociation of oxygen from oxyHb and the electrochemical reduction of the oxygen. The oxygen reduction current due to oxyHb (I_{Hb}) corresponds to the rate of oxygen transport by Hb to the electrode surface. Thus, by analyzing the current, it is possible to clarify the rate-determining factor of oxygen transport in Hb solution. The electrochemical method is also applicable to a relatively concentrated solution corresponding to that in erythrocytes, since the result obtained by the electrochemical method is not restricted by the concentration of Hb in the system. The optical measurements can not be applied to a solution of high concentration of Hb, without any modification of the conventional method.

In this study, we have applied the d.c.-polarographic method with a dropping mercury electrode to Hb solution. The rate-determining steps of oxygen transport to the electrode surface by Hb are discussed as regards the behavior of the reduction current of oxygen in Hb solution.

Experimental

Materials. Human Hb was prepared from fresh blood of donors. Erythrocytes were washed four times with 0.9% sodium chloride and hemolyzed by addition of an equal volume of distilled water and 0.4 volume of toluene and by vigorous shaking for 3 min. A clear Hb solution was obtained by centrifuging the mixture at 12000 rpm for 10 min. The resulting Hb solution was dialyzed for 20 h with renewal of a large volume of distilled water several times followed by centrifuging at 12000 rpm for 30 min. All the operations were carried out at 4 °C. The Hb concentration was measured with a Hitachi 323 recording spectrophotometer in term of the absorbance of oxyHb at 576 nm. Concentrated Hb solutions were obtained by centrifugal filtration through Amicon CF 25 membrane cones (Amicon Co., Lexington Mass.). Methemoglobin (metHb) was prepared by adding a slight excess of potassium ferricyanide to the dialyzed oxyHb and was again dialyzed for 20 h with renewal of a large volume of distilled water several times. Experiments were performed within a week from the completion of preparation. Reagents of analytical grade were used.

Polarographic Measurements. Polarograms were record-

ed with a Yanagimoto Polarograph Model PA 101. The dropping mercury electrode had the following characteristics: $m=1.91$ mg s^{-1}, $t=5.87$ s at open circuit in distilled water with 60 cm height of mercury reservoir. Saturated calomel electrode (SCE) was used as a reference electrode. All measurements were carried out in test solutions thermostated and under the oxygen partial pressure equilibrated with open atmosphere.

Kinetic Measurements. Over-all first order rate constants of oxygen dissociation from oxyHb were measured with a Yanagimoto SPU-1S stopped-flow spectrophotometer with a memoriscope. The light path of the cell was 10 mm. The dissociation of oxygen from oxyHb was forced by mixing Hb solution equilibrated with atmospheric oxygen with a sodium dithionite solution. The time course was followed by measuring absorbance at 576 nm. In most cases, the concentrations of Hb and dithionite after mixing were 50 μM (1 M=1 mol dm^{-3}) heme and 30 mM, respectively. The dithionite solution was freshly prepared for each run of experiments.

Results and Discussion

Oxygen Reduction Current in Hb Solution. Oxygen gives two reduction waves at dropping mercury electrode in supporting electrolyte solutions, corresponding to the following equations.[14]

$$O_2 + 2e + 2H^+ \longrightarrow H_2O_2 \quad (1)$$

$$H_2O_2 + 2e + 2H^+ \longrightarrow 2H_2O \quad (2)$$

The reduction current increased largely with addition of the Hb in electrolyte solution open to the atmosphere (Fig. 1). The increase of the current gives rise to a wave newly appearing between the lst and 2nd waves. This may be due to the catalytic reduction of O_2 to H_2O involving the dismutation of H_2O_2 to O_2 and H_2O by some catalase or peroxidase action of Hb itself or a trace amount of a contaminant having a catalytic activity,[15,16] at this potential, at which only the reduction (1) is expected electrochemically. The catalytic activities can not alter the value of the total reduction current of O_2 to H_2O (at -1.45 to -1.50 V *vs.* SCE), unless the total oxygen supply to the electrode changes. On addition of metHb which has no oxygen binding capacity, the total reduction current of oxygen was practically constant, though a catalytic phenomenon similar to that of Hb was observed. Thus, the increase of the total current (I) can be attributed to the reduction of oxygen transported by Hb, since the concentration of free oxygen in Hb solution should be constant, equilibrated with atmospheric oxygen. Considering the oxygen transport by Hb to the electrode with the above observations, we can utilize the potential at which the 2nd wave reaches its limiting current, *i.e.* from -1.45 to -1.50 V *vs.* SCE. The following description deals with the 4 electron transfer current of oxygen.

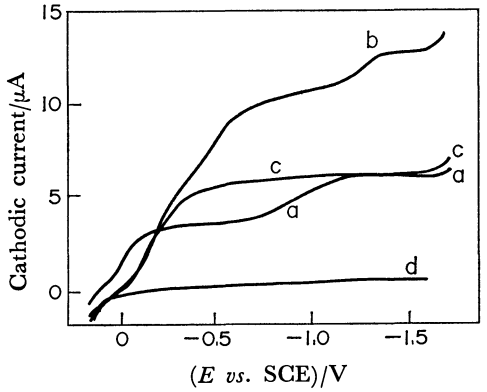

Fig. 1. Polarograms of oxygen reduction waves in electrolyte solutions open to the atmosphere.
a: Phosphate buffer (0.1 M, pH 7.4), b: a+Hb (2.3 mM heme), c: a+metHb (2.0 mM heme), d: b without oxygen. 25 °C.

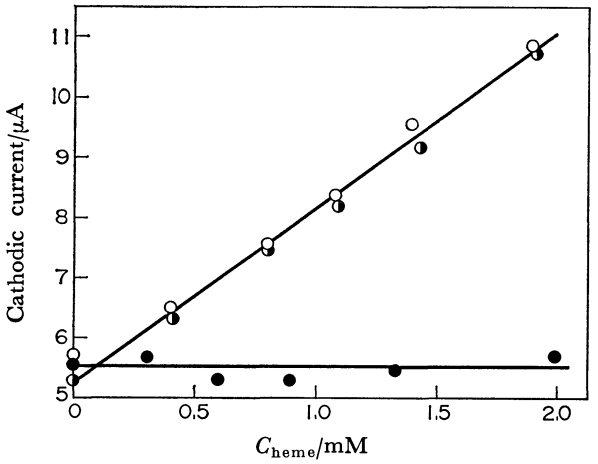

Fig. 2. Dependence of the reduction current of oxygen on the concentration of Hb without removing organic phosphates (○), stripped Hb (◐) and metHb (●) in phosphate buffer (0.1 M, pH 7.4) open to the atmosphere at 25 °C.

The dependence of I on the concentration of Hb is shown in Fig. 2. I is seen to increase linearly with Hb concentration. No appreciable difference between Hb prepared for the present study and stripped Hb prepared according to Benesch *et al.*,[17] could be observed. Thus, the subsequent experiments were carried out without removing organic phosphates from the Hb preparation. Since the current in metHb solution was almost constant, the increase of I in Hb solution might be due to the increasing supply of oxygen to the electrode by Hb. It seems that a flux of oxygen in Hb solution consists of the contributions from both free and Hb bound oxygen.[9-13] The current I might consist of the reduction currents of both:

$$I = I_{O_2} + I_{Hb}, \quad (3)$$

where I_{O_2} is diffusion current of free oxygen, and I_{Hb} the oxygen reduction current due to oxyHb. From Ilkovic equation,[18,19] we have

$$I_{O_2} = \kappa D_{O_2}^{1/2} C_{O_2}, \quad (4)$$

where $\kappa=607$ $nm^{2/3}$ $t^{1/6}$ with $n=4$, D_{O_2} and C_{O_2} being the diffusion coefficient and the concentration of free oxygen in the solution equilibrated with the atmospheric oxygen, respectively. In relatively dilute Hb solution, D_{O_2} and I_{O_2} might be nearly equal to those in the medium without Hb ($^*D_{O_2}$ and $^*I_{O_2}$, respectively). They can be regarded as constant under given conditions. The increase of I is due to only the increase of I_{Hb}, being directly proportional to the

concentration of Hb presented in heme (C_{heme}). Thus, I_{Hb} can be written as

$$I_{Hb} = \alpha C_{heme} Y, \quad (5)$$

where Y is fractional oxygen saturation of Hb. Under the present conditions we might put Y=1, since Hb solutions are equilibrated with the atmospheric oxygen partial pressure. α is a factor characterized by the rate-determining step of oxygen transport by Hb.

We can postulate two steps for α, (a) the diffusion process of Hb molecules bound oxygen to the electrode and (b) the oxygen dissociation from oxyHb in the vicinity of the electrode with hypo-oxygen partial pressure. When (a) is predominant, α might be proportional to the diffusion coefficient of Hb (D_{Hb}) and I_{Hb} might be the diffusion-controlled current. In (b) where the rate constant of oxygen dissociation (k) is included in α, I_{Hb} might be the kinetic current.[20,21] It seems that the alteration of the rate-determining step is practically caused by change in the rate of dissociation, since the D_{Hb} value does not change a great deal with temperature of pH, as compared with the dissociation step.

For the sake of confirmation we examined the effect of temperature and pH on I_{Hb}, since the oxygen dissociation rate is strongly dependent on the above two factors,[22,23] in contrast to the rate of oxygen combination with Hb which is little affected.[22]

Effects of Temperature and pH on I_{Hb}. Figure 3 shows the linear relationship between I_{Hb} (Eq. 3) and C_{heme} at various temperatures open to the atmospheric oxygen. The slope of the curve, I_{Hb}/C_{heme} *i.e.* α (Eq. 5) increases with temperature. The plot of α (slope of the curve, Fig. 3) against temperature indicates that α depends on the oxygen dissociation rate which changes with temperature (Fig. 4-a). The relation between the reciprocal temperature and logarithms of α obtained is shown in Fig. 4-b. When the rate-determining step of I_{Hb} is single, a straight line should be obtained. However, a bending curve with two different slopes was obtained indicating that I_{Hb} is controlled by at least two different steps. The apparent activation energy of each step was found to be 83.7 and 29.7 K J mol^{-1} for the lower and higher temperature ranges, respectively. Since the value of the former is in line with that of oxygen dissociation reported by Gibson[23] and Dalziel and O'Brien,[24] and our Arrhenius plot of stopped-flow data also gave 79.1 K J mol^{-1} as the activation energy, one of these steps might be oxygen dissociation, which turns to another step at the inflection point on the curve *i.e.* about 22 °C (at pH 7.4).

The change in pH also resulted in the variation in α (Fig. 5). The pattern of the variation is similar to that of the Bohr effect[25] which reflects the change in the dissociation rate of oxygen from oxyHb, and gives a symmetrical curve with pK'=7.0, when k is plotted against pH.[24] The change in I_{Hb} with pH can be ascribed to that in the rate of dissociation of oxygen from oxyHb. In order to clarify the rate-determining step for I_{Hb}, effects of temperature and pH were examined on the basis of the dissociation rate of oxygen at various temperatures or pH.

Figure 6 shows the relation between α and k obtained by the stopped-flow method, carried out by

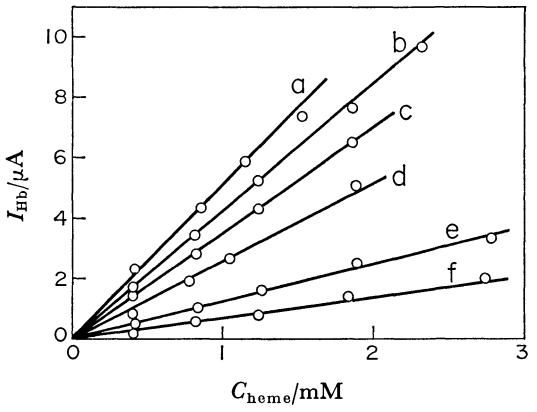

Fig. 3. Relation between I_{Hb} and relatively low concentration of Hb at various temperatures open to the atmosphere.
a: 40 °C, b: 35 °C, c: 30 °C, d: 25 °C, e: 15 °C, f: 12.5 °C. Other conditions are the same as in Fig. 2. I_{Hb} was obtained by subtracting $*I_{O_2}$ from I.

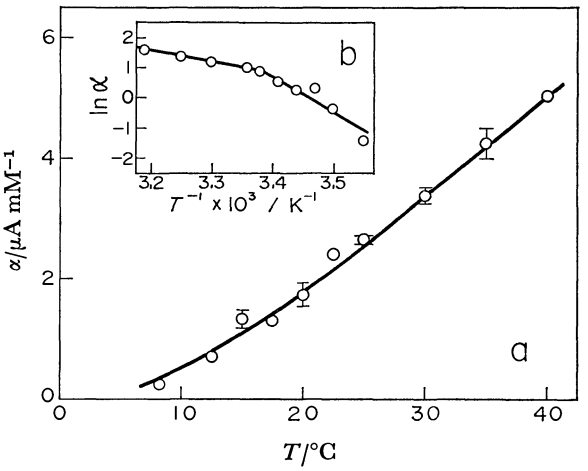

Fig. 4. Effect of temperature on α (a) and plots of logarithms of α against the reciprocal temperature (b).
α is I_{Hb}/C_{heme} or $(I-*I_{O_2})/C_{heme}$, and was obtained as the slope of the curve in Fig. 3.

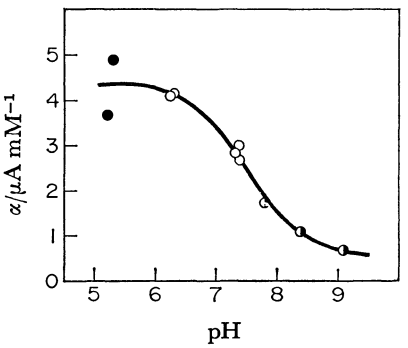

Fig. 5. Effect of pH on α.
○: 0.1 M phosphate buffer, ◑: 0.1 M tris–HCl buffer, ●: 0.1 M acetate buffer. Other conditions are the same as in Fig. 2.

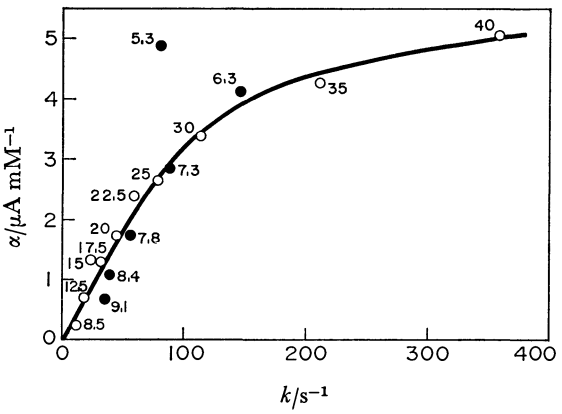

Fig. 6. Plot of α against apparent first order rate constant of oxygen dissociation from oxyHb (k). ○: Temperature effect at pH 7.4 (see Fig. 4-a), ●: pH effect at 25 °C (see Fig. 5). Numbers with experimental points are temperature (°C) (○) or pH (●) at which α and k were measured by polarography and by stopped-flow method, respectively.

TABLE 1. DIFFUSION COEFFICIENTS OF Hb(D_{Hb}) OBTAINED POLAROGRAPHICALLY AND APPARENT FRST ORDER RATE CONSTANTS OF OXYGEN DISSOCIATION FROM oxyHb (k) OBTAINED BY STOPPED-FLOW METHOD

k/s^{-1} (T/°C, pH)[a]	$D_{Hb}/10^{-7}$ cm² s⁻¹
78.4 (25, 7.4[b])	2.8
81.6 (25, 5.3[c])	9.4
114.0 (30, 7.4[b])	4.4
148.4 (25, 6.3[b])	7.0
209.1 (35, 7.4[b])	6.2
357.8 (40, 7.4[b])	7.6

a) Conditions for kinetic measurements. b) 0.1 M phosphate buffer. c) 0.1 M acetate buffer.
Values of k (Fig. 6) are given in increasing order, irrespective of experimental conditions. D_{Hb} is the value corrected for 25 °C, though each actual measurement was carried out at the temperature for the corresponding k measurement.

changing temperature at a fixed pH or changing pH at a constant temperature. A satisfactory coincidence could be obtained for the results of two series of different kinds of experiments. The curve obtained implies two rate-determining factors for oxygen transport by Hb to the electrode surface. At relatively small k values, where I_{Hb} is proportional to k, the rate-determining step is the dissociation of oxygen. When k value exceeds *ca.* 60 s^{-1}, where I_{Hb} is not appreciably affected by k, the dissociation is no longer rate-determining, and is replaced by the diffusion of Hb to the electrode. This can be supported by the following observation: current I is almost a diffusion current in the range beyond the k around 60 s^{-1}, while it obviously contains characteristics of kinetic current[20,21] up to the k value. This is in line with the idea of Wittenberg[11] and Wyman[13] who treated the oxygen transport by Hb in terms of translational diffusion of Hb and the oxygen dissociation from oxyHb. A slight increase in α with k in the diffusion-controlled region can be understood as due to the increase in D_{Hb} with temperature. The diffusion-controlled transport of oxygen should be confirmed by comparing the D_{Hb} value estimated from I_{Hb} with the published data.

In the diffusion-controlled region, D_{Hb} is involved in α. I_{Hb} can be expressed from Ilkovic equation,[18,19] by

$$I_{Hb} = \kappa D_{Hb}^{1/2} C_{heme}. \quad (6)$$

I_{O_2} can not be measured directly, but it can be estimated by

$$I_{O_2} = (D_{O_2}/{}^*D_{O_2})^{1/2} {}^*I_{O_2}, \quad (7)$$

where ${}^*I_{O_2}$ is I measured in the medium without Hb, and is given by

$${}^*I_{O_2} = \kappa {}^*D_{O_2}^{1/2} C_{O_2}. \quad (8)$$

Combining Eqs. 3, 6, 7, and 8, we obtain

$$I/{}^*I_{O_2} = (D_{O_2}/{}^*D_{O_2})^{1/2} + C_{O_2}^{-1}(D_{Hb}/{}^*D_{O_2})^{1/2} C_{heme}. \quad (9)$$

The value D_{Hb} at a given concentration can be estimated by means of the equation, substituting D_{O_2} value for given Hb concentration and other measured values. In practice, the value D_{Hb} in relatively dilute concentration range was obtained using α obtained experimentally for diffusion-controlled region under the assumption of $D_{O_2} = {}^*D_{O_2}$†. The value D_{Hb} obtained experimentally agrees with the reported values $6-7\times10^{-7}$ cm² s^{-1}, irrespective of the increase of k with either temperature or with pH (Table 1). The result might support the validity of the assumption that the rate-determining step for I_{Hb} changes from the dissociation of oxygen to the diffusion of Hb with increase in k.

A relatively large deviation of the experimental point at pH 5.3 and 25 °C in acetate buffer from the curve drawn through other experimental points (Fig. 6) can be explained by the contribution of an apparent increase of D_{Hb} with the dissociation of tetramer to dimer or further monomer of Hb (Table 1), since such dissociation was observed more readily in acetate buffer than in other buffer at pH 5.3.[28,29]

Under the physiological conditions (pH 7.4, 37 °C), the oxygen transport by Hb is restricted by the diffusion rate of Hb molecules (Fig. 6). It is of interest to examine whether the relation (Fig. 6) is also applicable to a relatively concentrated solution of Hb. Figure 7 shows the relation between k and α at 18 mM heme of Hb concentration. A similar relation to that in Fig. 6 was obtained, the same k values being used,

† Equation 9 is simplified as
$$I/{}^*I_{O_2} = 1 + C_{O_2}^{-1}(D_{Hb}/{}^*D_{O_2})^{1/2} C_{heme}.$$
Further modification gives
$$C_{O_2}(I - {}^*I_{O_2})/(C_{heme}\,{}^*I_{O_2}) = (D_{Hb}/{}^*D_{O_2})^{1/2}.$$
Since $(I - {}^*I_{O_2})/C_{heme}$ is α (Fig. 4), we have
$$\alpha C_{O_2}/{}^*I_{O_2} = (D_{Hb}/{}^*D_{O_2})^{1/2}.$$
Thus
$$D_{Hb} = {}^*D_{O_2}(\alpha C_{O_2}/{}^*I_{O_2})^2.$$
The value 2.0×10^{-5} cm² s^{-1} was used for ${}^*D_{O_2}$ at 25 °C in the present study, since similar values were reported for various electrolyte solutions at 20—25 °C.[26,27] The C_{O_2} value was taken from International Critical Tables. ${}^*I_{O_2}$ was obtained experimentally.

since the oxygen affinity of Hb is little affected by the variation of Hb concentration.[30] The observation enables us to consider that the behavior of oxygen in a relatively concentrated solution of Hb such as in erythrocytes is also restricted by the diffusion of Hb and not by the dissociation of oxygen from oxyHb.

In the following we examine the behavior of oxygen in concentrated solution of Hb corresponding to that in erythrocytes in term of D_{Hb}, since the value D_{Hb} in various concentrations can be calculated by Eq. 9, when I is diffusion-controlled.

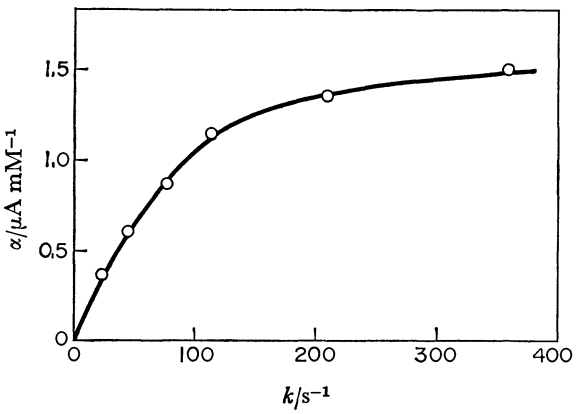

Fig. 7. Relation between apparent first order rate constant of oxygen dissociation from oxyHb (k) and α in a relatively concentrated Hb solution.
Hb concentration: 18 mM heme. α was obtained from the measurements at various temperatures at pH 7.4. The k values are the same as in Fig. 6. Other conditions are the same as in Fig. 2.

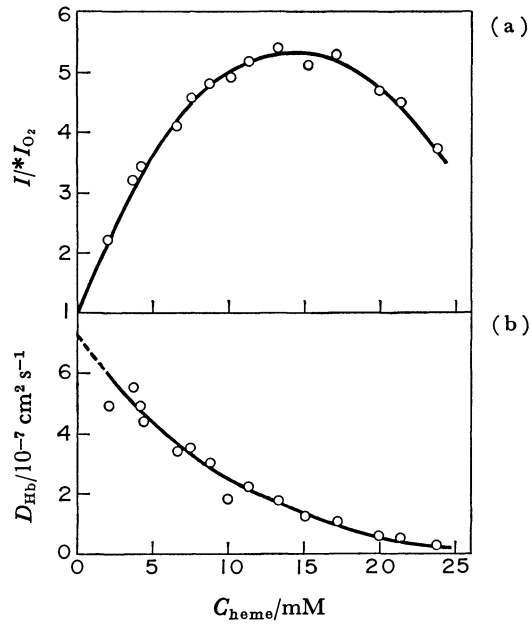

Fig. 8. Hb concentration dependence of $I/{}^*I_{O_2}$ (a), and diffusion coefficient of Hb (D_{Hb}) (b), in a relatively wide concentration range. D_{Hb} values were calculated by using Eq. 8 with $C_{O_2}=0.26$ mM and ${}^*D_{O_2}=2.0\times10^{-5}$ cm^2 s^{-1}. See the text for detail of estimation of D_{Hb}. Other conditions are the same as in Fig. 2.

D_{Hb} *in Concentrated Solution of Hb.* Figure 8-a shows the relation between $I/{}^*I_{O_2}$ and C_{heme} over a wide concentration range at pH 7.4 and 25 °C. The linear current increase with C_{heme} (Fig. 2 or 3) was observed only up to *ca.* 2 mM of C_{heme}, beyond which the current increase, whose maximum was around 14 mM, was lowered. This can not be attributed to the change in oxygen affinity of Hb, but to the decrease of D_{Hb} due to the increase of viscosity of the solution with C_{heme}. A similar observation has been reported by Wittenberg[11] by means of millipore filter method. However, no estimation was given on D_{Hb} in various concentration of Hb necessary for the demonstration of the diffusion-controlled oxygen transport. We can calculate D_{Hb} by substituting the $I/{}^*I_{O_2}$ value (Fig. 8-a) into Eq. 9, since we can expect diffusion current for oxygen reduction. In a relatively concentrated solution of Hb, D_{O_2} can not be identical with ${}^*D_{O_2}$. Hence, we employed the D_{O_2} value used by Roughton,[2] who estimated it in Hb solution, by comparison with D of nitrogen in a similar Hb solution. The relation between D_{Hb} obtained and C_{heme} in the present experiments is shown in Fig. 8-b. The increase of C_{heme} gave rise to a large decrease in D_{Hb}. The intercept on the ordinate of the curve passing through points experimentally obtained gave *ca.* 7×10^{-7} cm^2 s^{-1}, corresponding to the value known as D_{Hb} in dilute solution. In 20 mM Hb solution, *viz.*, equivalent concentration in erythrocytes, D_{Hb} is *ca.* 5.8×10^{-8} cm^2 s^{-1}. This is in agreement with 6.4×10^{-8} cm^2 s^{-1} obtained by Kreuzer.[31] The fact that the D_{Hb} obtained is 300 times smaller than ${}^*D_{O_2}$, suggests that oxygen in erythrocytes can move only with about one-three hundredth mobility of oxygen outside erythrocytes.

References

1) H. Hartridge and F. J. W. Roughton, *J. Phys. (London)*, **62**, 232 (1927).
2) F. J. W. Roughton, *Prog. Biophys. Biophysical Chem.*, **9**, 55 (1959).
3) F. J. W. Roughton, *Proc. R. Soc. London, Ser. B*, **111**, 1 (1932).
4) J. T. Coin and J. S. Olson, *J. Biol. Chem.*, **254**, 1178 (1979).
5) M. F. Perutz, *Nature*, **228**, 726 (1970).
6) J. M. Baldwin, *Prog. Biophys. Molec. Biol.*, **29**, 225 (1975).
7) E. Antonini and M. Brunori, "Hemoglobin and Myoglobin in Their Reaction with Ligands," North Holland, London (1971), pp. 235—260.
8) Q. H. Gibson, *J. Biol. Chem.*, **245**, 3285 (1970).
9) P. F. Scholander, *Science*, **131**, 585 (1960).
10) J. B. Wittenberg, *Nature*, **199**, 816 (1963).
11) J. B. Wittenberg, *J. Biol. Chem.*, **241**, 104 (1966).
12) J. B. Wittenberg, F. J. Berbersen, C. A. Appleby, and G. L. Turner, *J. Biol. Chem.*, **249**, 4057 (1974).
13) J. Wyman, *J. Biol. Chem.*, **241**, 115 (1966).
14) I. M. Kolthoff and J. J. Lingnane, "Polarography," Interscience Publishers, New York (1952), Vol. 2, p. 552.
15) J. Heyrovsky and J. Kůta, "Principles of Polarography," Acad. Press, New York (1966), p. 392.
16) M. R. Tarasevich and A. Bogdanovskaya, *Bioelectrochem. Bioenerg.*, **2**, 69 (1975).

17) R. Benesch, R. E. Benesch, and C. I. Yu, *Proc. Nat. Acad. Sci. U.S.A.*, **59**, 526 (1968).
18) D. Ilković, *Collect. Czech. Chem. Commun.*, **6**, 498 (1934).
19) D. Ilković, *J. Chim. Phys.*, **35**, 129 (1938).
20) J. Koutecky, *Collect. Czech. Chem. Commun.*, **18**, 597 (1953).
21) H. Matsuda and Y. Ayabe, *Bull. Chem. Soc. Jpn.*, **28**, 422 (1955).
22) E. Antonini and M. Brunori, "Hemoglobin and Myoglobin in Their Reaction with Ligands," North Holland, London (1971), p. 255.
23) Q. H. Gibson, *Prog. Biophys. Biophysical Chem.*, **9**, 1 (1959).
24) K. Dalziel and J. R. P. O'Brien, *Biochem. J.* **78**, 236 (1961).
25) E. Antonini, J. Wyman, M. Brunori, C. Fronticelli, E. Bucci, and A. Rossi Fanelli, *J. Biol. Chem.*, **240**, 1096 (1965).
26) V. S. Griffiths and M. I. Jackman, *Talanta*, **9**, 205 (1962).
27) S. L. Phillips, *Anal. Chem.*, **38**, 1714 (1966).
28) E. Chiancone and G. A. Gilbert, *J. Biol. Chem.*, **240**, 3866 (1965).
29) A. Rossi Fanelli, E. Antonini, and A. Caputo, *Adv. Protein Chem.*, **19**, 73 (1964).
30) C. Bruer and W. Moll, *J. Gen. Physiol.*, **72**, 765 (1978).
31) F. Kreuzer, *Respir. Physiol.*, **9**, 1 (1970).

Selective Oxidation of Unsymmetrical Thiosulfinic S-Esters to the Corresponding Thiosulfonic S-Esters with $NaIO_4$[1]

Toshikazu TAKATA, Yong Hae KIM,[2] and Shigeru OAE*
Department of Chemistry, The University of Tsukuba, Sakura, Ibaraki 305

(Received October 17, 1980)

Unsymmetrical thiosulfinic S-esters were oxidized with sodium metaperiodate in aqueous media to the corresponding unsymmetrical thiosulfonic S-esters nearly quantitatively. The oxidation was accelerated by addition of a catalytic amount of inorganic and organic acids or halogen. Sulfinic esters were produced competitively along with the thiosulfonic S-esters in the oxidation of thiosulfinic S-esters in aqueous alcohol. However, unsymmetrical disulfides were not oxidized selectively to the corresponding unsymmetrical thiosulfonic S-esters but a mixture of both symmetrical and unsymmetrical thiosulfonic S-esters was obtained.

We have recently reported that oxidations of unsymmetrical thiosulfinic S-esters with peroxy acid[3] or dinitrogen tetraoxide[4] afforded the corresponding symmetrical thiosulfonic S-esters which were undoubtedly derived by the cleavage of sulfur-sulfur bond. A few previous studies[3,5] on the oxidations of thiosulfinic S-esters with some peroxy acids or peroxides revealed that none of these oxidations resulted in the selective oxidation of unsymmetrical thiosulfinic S-ester to the corresponding unsymmetrical thiosulfonic S-ester with no apparent cleavage of sulfur-sulfur bond. The oxidation of linear unsymmetrical thiosulfinic S-ester generally afforded both symmetrical and unsymmetrical thiosulfonic S-esters (Eq. 1). Only the oxidation of a six-membered cyclic thiosulfinic S-ester with peroxy acid was found to proceed without any apparent cleavage of sulfur-sulfur linkage to afford two unsymmetrical thiosulfonic S-esters in good yields.[6a]

$$\mathrm{RSSR'} \xrightarrow{[O]} \mathrm{RS(O)SR'} + \mathrm{RSS(O)R'} + \mathrm{RS(O)SR} + \mathrm{R'S(O)SR'} \quad (1)$$

In attempts to detect imaginary "α-disulfoxide (RS(O)S(O)R')" which is considered to be formed initially in the oxidation of thiosulfinic S-ester but too unstable to be observed, Barnard[5a] and Kice *et al.*[5c] have carried out the oxidation of unsymmetrical thiosulfinic S-esters and obtained a mixture of thiosulfonic S-esters, resulting from the initial oxidation, subsequent cleavage of the disulfide linkage, and the recombination.

However, surprisingly, when sodium metaperiodate ($NaIO_4$) was used as an oxidant, many unsymmetrical thiosulfinic S-esters were found to be oxidized selectively to the corresponding unsymmetrical thiosulfonic S-esters in aqueous media such as dioxane–water under mild conditions, with no apparent cleavage of sulfur-sulfur bond. This paper describes this new selective oxidation in detail.

Results and Discussion

$NaIO_4$ Oxidation. When an unsymmetrical thiosulfinic S-ester **1** was treated with an equimolar amount of sodium metaperiodate, only one product, *i. e.* the corresponding unsymmetrical thiosulfonic S-ester **2**, was found to be obtained. The reaction was also found to be accelerated by addition of a catalytic amount of inorganic or organic acid as well as iodine. Selected results are listed in Table 1.

$$\mathrm{R\text{-}S(O)\text{-}S\text{-}R'} \xrightarrow[\text{aqueous solvent, r.t., Cat.}]{NaIO_4} \mathrm{R\text{-}S(O)_2\text{-}S\text{-}R'} \quad (2)$$

1 → **2** ≈100%

1a	R=Ph, R'=Ph	**1f**	R=Et, R'=Ph
1b	R=Ph, R'=*p*-Tol	**1g**	R=Ph, R'=Pr
1c	R=*p*-Tol, R'=Ph	**1h**	R=Me, R'= 
1d	R=Ph, R'=Me	**1i**	*p*-Tol, R'=Me
1e	R=Me, R'=Ph	**1j**	*p*-ClC_6H_4, R'=Me

Following is a typical run. A solution of $NaIO_4$ (1.2 mmol) in water (2.0 ml) was added into a dioxane solution (3.5 ml) containing thiosulfinic S-ester (**1**, 1.0 mmol) at room temperature. To the resulting mixture a small amount of a catalyst (*e. g.* concd HCl, 1 or 2 drop) was added. After stirring the mixture for *ca.* 30 min at the room temperature or until the solution turned to dark brown, the highly pure unsymmetrical thiosulfonic S-ester **2** was obtained nearly quantitatively by extraction of the reaction mixture. The product generally showed only one component on GC, LC, TLC, or NMR. The yield of the product was determined by isolation through column chromatography or GC. New products were identified by comparing their IR and NMR spectra with those of authentic samples prepared by a known method[7] which is the condensation of sulfinic acids and sulfenyl chlorides in the presence of a tertiary amine. The starting thiosulfinic S-ester **1** were prepared by the condensation of the corresponding sulfinyl chlorides and thiols in the presence of pyridine in carbon tetrachloride at a temperature lower than 0 °C, according to the method of Backer *et al.*[8] The purification of **1** was carried out by recrystallization or column chromatography, while the identification was performed by several spectra and elemental analysis, as described in "Experimental Section."

As shown in Table 1, thiosulfinic S-esters of various types were oxidized to the corresponding thiosulfonic S-esters without cleavage of sulfur-sulfur linkage. Electrophilic catalysts highly accelerated the reaction while the reaction usually had a long induction period without any catalyst. Yields of the unsymmetrical thiosulfonic S-esters were nearly quantitative regardless

TABLE 1. SELECTIVE OXIDATION OF UNSYMMETRICAL THIOSULFINIC *S*-ESTER WITH $NaIO_4$ AT 20 °C

Substrate	Solvent	Catalyst	Time/h	Yield of products/%	
1a	dioxane	no	26.0	**2a**	quant.[a]
1b	CH_3CN	concd HCl	<1.0	**2b**	quant.[a]
1c	CH_3CN	I_2	0.5	**2c**	quant.[a]
1d	dioxane	dioxane	<2.0	**2d**	quant.[a]
1e	dioxane	dioxane	8.0	**2e**	98[b]
1f	dioxane	concd HCl	1.0	**2f**	90[b]
1g	dioxane	dioxane	1.0	**2g**	85[b]
1h	dioxane	concd HCl	0.5	**2h**	90[c]
1i	CD_3COOD[d]	no	0.5	**2i**	quant.[a]
1j	CD_3COOD[d]	no	0.5	**2j**	quant.[a]

a) No other product was observed in GC and NMR. b) Isolated yield. c) The yield was determined by GC and NMR. d) The reaction was carried out in NMR sample tube; substrate: 0.1 mmol.

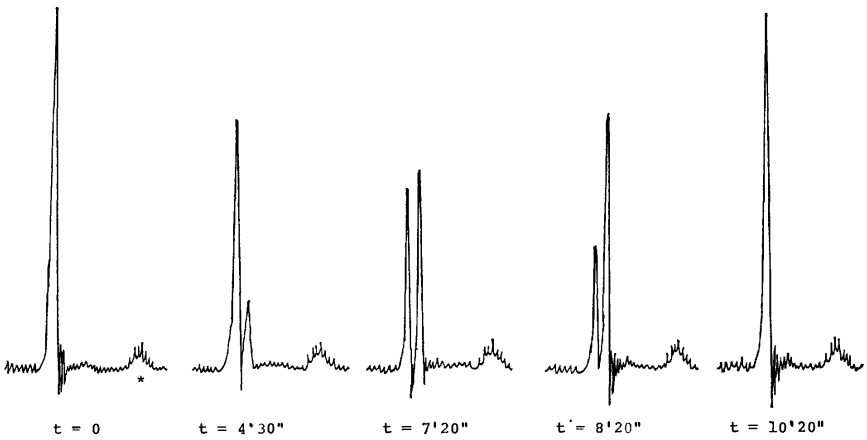

* Signals due to undeuterized proton of acetic acid-d_4.

Fig. 1. Spectral change in NMR spectra in the oxidation of **1j** with $NaIO_4$.

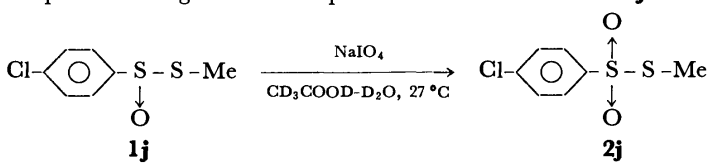

1j **2j**

of the substituent.

No detectable intermediate was observed in the NMR study of the oxidation of thiosulfinic *S*-ester **1j** with $NaIO_4$ in CD_3COOD–D_2O as shown in the following Fig. 1. Methyl signal at 2.33 ppm (from external TMS) of **1j** gradually changed to the signal at 2.26 ppm which is identical to that of **2j**. No other peak of methyl group was observed in the NMR spectra throughout the reaction. An interesting relationship found between the two unusual chemical shifts of **1** and **2** in which the chemical shift of **1j** is lower than that of **2j**, has been re-confirmed.[9]

Effects of Catalyst and Solvent. The oxidation was found to be accelerated by addition of a catalytic amount of organic or inorganic acid or halogen. While weaker acids such as acetic and formic acids than trifluoroacetic acid (pK_a 1.0) did show little catalytic ability, the oxidation was accelerated in acetic acid as solvent even without catalyst. Catalysts effective in the oxidation are the following: CF_3COOH, H_2SO_4, HIO_4, $HClO_4$, HCl, I_2, and Br_2, as shown partially in Table 2. The catalytic activity of iodine found in this reaction was already noticed in the oxidation of cyclic disulfide to the corresponding thiosulfonic *S*-ester with KIO_4 by Field and Kim.[10] Solvents used were dioxane, acetonitrile, and acetone, all of which can mix freely with water. Acetic acid was effective not only as a solvent but also as a catalyst and hence the best system for the oxidation. Alcohols were not effective because the competitive reaction of **1** with the alcohols took place, as described later.

If no catalyst was used, the reaction occurred suddenly with coloring by iodine derived from $NaIO_4$ after a long induction period (5—10 h) and finished within 1 h as in the case with catalyst, due mainly to the catalytic action of iodine accumulated. Figure 2 indicates the rate of disappearance of **1c** in the oxidation with $NaIO_4$ as monitored by LC. Appearance of color of iodine was in accordance with the initiation of the reaction. The reaction is presumed to be an auto-catalyzed reaction with iodine formed since iodine increases as the reaction proceeds.

Table 2. Effects of catalyst and solvent (20 °C)

Substrate	Solvent	Catalyst	Time/h	Yield of products/%[a]	
1d	dioxane	no	6.0	**2d**	92
1d	CH_3CN	no	5.0	**2d**	92
1d	acetone	no	27.0	—	—[b]
1c	CH_3CN	HCOOH	6.0	**2c**	90
1d	dioxane	CH_3COOH	6.0	**2d**	90
1d	acetone	I_2	3.0	**2d**	quant.[c]
1d	dioxane	concd HCl	1.0	**2d**	93
1d	dioxane	CH_3COOH	2.0	**2d**	quant.[c]
1d	CH_3COOH	no	0.5	**2d**	95[d]
1c	CH_3CN	Br_2	0.5	**2c**	95[e]
1c	CH_3CN	H_2SO_4	1.0	**2c**	quant.[c,e]
1c	CH_3CN	HIO_4	1.0	**2c**	quant.[c,e]
1c	CH_3CN	CH_3CN	1.0	**2c**	quant.[c,e]

a) The yield was determined by GC and NMR. b) Starting material was recovered. c) No other product was observed in GC and NMR. d) Solvent ratio: $CH_3COOH/H_2O=7/4$ (v/v). e) The yield was determined by LC.

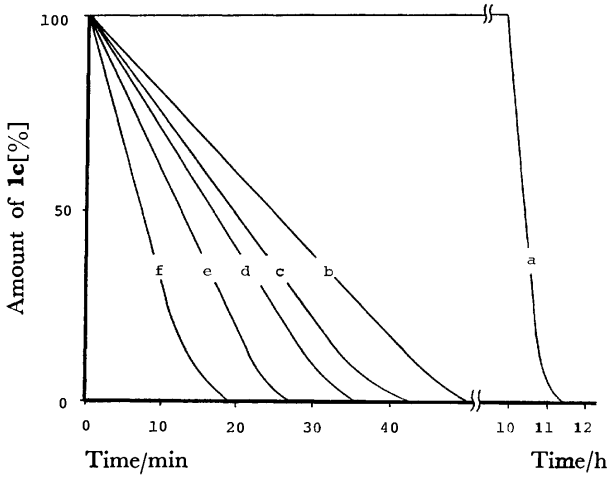

Fig. 2. Oxidation of thiosulfinic *S*-ester **1c** with $NaIO_4$ either with or without catalyst.
a: Reaction at 17 °C without catalyst, b: reaction at 0—4 °C with iodine as a catalyst, c: reaction at 20 °C with HIO_4, d: reaction at 20 °C with H_2SO_4, e: reaction at 20 °C with $HClO_4$, f: reaction at 20 °C with iodine or bromine.

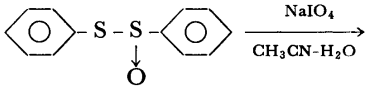

1c

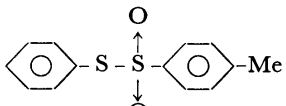

2c

Reaction in Aqueous Alcohol. The oxidation of **1d** with $NaIO_4$ in aqueous alcohol resulted in the competitive formation of the sulfinic ester of the alcohol along with that of the usual oxidation product of thiosulfonic *S*-ester **2d** (Eq. 3). When three different alcohols of varying bulkiness, *i.e.* ethanol, isopropyl alcohol and *t*-butyl alcohol were used as solvents, the amount of the sulfinic ester **3** produced was found

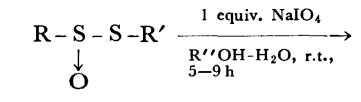

1

1d (R=Ph, R'=Me), R''=Et
R''=*i*-Pr,
R''=*t*-Bu

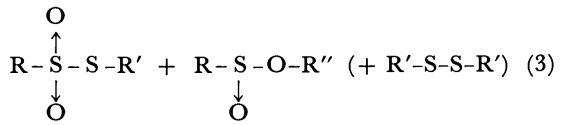

(3)

2 **3** **4**

42% (44)* 39% (47)*
67% 27%
82% 7%

* Reaction catalyzed by concd HCl within 1 h.

to decrease in the following order: ethanol>isopropyl alcohol>*t*-butyl alcohol, which is the order of bulkiness as well as the nucleophilicity of the alcohols used. The distribution of products changed little in the acid-catalyzed reaction (parentheses). Sulfinic esters (**3**) were not oxidized at all under these conditions. GC analysis confirmed that the symmetrical disulfide is derived only from the sulfenyl part. The disulfide was considered to be produced from the thiol formed during the reaction involving nucleophilic attack of alcohol to **1**. The thiol thus formed should be oxidized immediately to the corresponding disulfide under the conditions.

Reaction of Disulfide with $NaIO_4$. When an unsymmetrical disulfide, methyl phenyl disulfide **5**, was treated with two molar amount of $NaIO_4$ under the same conditions, the following two symmetrical thiosulfonic *S*-esters (**6** and **7**) were obtained as major products which are undoubtedly derived by the cleavage of sulfur-sulfur bond, along with $PhSSO_2Me$ (**8**) (Eq. 4). By direct observation of NMR spectral change in the reaction of **5** with 2 equiv. $NaIO_4$ in CD_3COOD-D_2O at 27 °C, the cleavage of sulfur-sulfur bond was found to occur at the beginning of the reaction and is competitive with the oxidation

$$\underset{\mathbf{5}}{\text{Ph-S-S-Me}} \xrightarrow[\text{dioxane-}H_2O,\ \text{r.t.}]{\text{2 equiv. } NaIO_4} \underset{\mathbf{6}\ 27\%}{PhSSO_2Ph} + \underset{\mathbf{7}\ 25\%}{MeSSO_2Me} + \underset{\mathbf{8}\ 31\%}{PhSSO_2Me} \quad (4)$$

of sulfur atom, since all the methyl signals of dimethyl disulfide and the starting disulfide and those attached to sulfinyl and sulfonyl groups were observed simultaneously during the reaction. Meanwhile, oxidation of a mixture of diphenyl disulfide and dimethyl disulfide with $NaIO_4$ under the same conditions as in the above NMR study, also afforded an unsymmetrical and two symmetrical thiosulfonic *S*-esters (Eq. 5).

$$\left.\begin{matrix}\text{PhSSPh}\ \ \mathbf{9}\\ \text{MeSSMe}\ \ \mathbf{10}\end{matrix}\right\} \xrightarrow[\substack{CD_3COOD\text{-}D_2O\\ 27\,^\circ C\ (NMR)}]{\text{4 equiv. } NaIO_4} \underset{\mathbf{8}}{PhSSO_2Me} + \underset{\mathbf{7}}{MeSSO_2Me} (+ \underset{\mathbf{6}}{PhSSO_2Ph}) \quad (5)$$

Thus, any unsymmetrical thiosulfinic *S*-ester can be selectively oxidized to the corresponding unsymmetrical thiosulfonic *S*-ester nearly quantitatively in this oxidation with $NaIO_4$.

Obviously the oxidation of thiosulfinic *S*-ester with $NaIO_4$ is entirely different from that with peracetic acid which proceeds *via* formation of "α-disulfoxide,"[3] which is so unstable to collapse immediately yielding the corresponding four symmetrical and unsymmetrical thiosulfonic *S*-esters by the cleavage of sulfur-sulfur bond. In fact, in order to confirm the difference, the oxidations of 3-methyl-1,2-dithiane 1-oxide, a six-membered unsymmetrical thiosulfinic *S*-ester, were carried out with both $NaIO_4$ and peroxy acid, and the clear difference between products of two oxidations was confirmed.[6] This new selective oxidation of thiosulfinic *S*-ester with $NaIO_4$ appears to proceed by the nucleophilic attack of the periodate on the sulfinyl sulfur atom to form the corresponding thiosulfonic *S*-ester.

Experimental

General. Chemicals were of reagent grade unless otherwise specified. All melting points were measured by Yanaco instrument and were uncorrected. IR spectra were taken on a Hitachi 215 spectrophotometer. NMR spectra of the compounds were taken with a Hitachi Perkin-Elmer R-20 spectrometer in $CDCl_3$ using TMS as an internal standard. Mass spectra were taken with a Hitachi RMU-6MG mass spectrometer. Shimadzu GC-6A instrument was used for gas chromatography using N_2 gas as a carrier gas. High pressure liquid chromatography was carried out with Yanaco L-1030 instrument using methanol as an eluent. Elemental analyses were carried out by the Chemical Analysis Center at this university.

Preparation of Thiosulfinic S-*Ester.* Both symmetrical and unsymmetrical thiosulfinic *S*-esters were prepared by the method reported by Backer and Kloosterziel[8] with rather little modification. Namely, addition of a thiol into a distilled sulfinyl chloride in CCl_4 under cooling at a temperature lower than 0 °C gave thiosulfinic *S*-ester (85—90%). The thiosulfinic *S*-ester was identified by comparing melting point with that reported previously, IR spectrum, and NMR spectrum, and elemental analysis.

S-*Phenyl Benzenethiosulfinate* **1a**: Pale yellow crystals; mp 69—70 °C (lit,[11] 69—70 °C); IR ($CHCl_3$, cm^{-1}) 3055, 1577, 1475, 1093, and 1060 (S=O).

S-p-*Tolyl Benzenethiosulfinate* **1b**: Pale yellow crystals; mp 70—71 °C (lit,[11] 68 °C); IR ($CHCl_3$, cm^{-1}) 3050, 1590, 1470, 1095, and 1055 (S=O).

S-*Phenyl* p-*Toluenethiosulfinate* **1c**: Pale yellow crystals; mp 82 °C (lit,[11] 83—84 °C); IR ($CHCl_3$, cm^{-1}) 3050, 1590, 1470, 1095, and 1065 (S=O).

S-*Methyl Benzenethiosulfinate* **1d**: Colorless crystals; mp 26—28 °C; IR (neat, cm^{-1}) 3050, 2975, 2900, 1570, 1470, 1095, and 1060 (S=O) (lit,[12] 1104 (in CCl_4)).

S-*Phenyl Methanethiosulfinate* **1e**: Colorless oil; IR (neat, cm^{-1}) 3050, 2980, 2900, 1570, 1470, and 1090 (S=O), (lit,[12] 1101 (in CCl_4)).

S-*Phenyl Ethanethiosulfinate* **1f**: Pale yellow oil; IR (neat, cm^{-1}) 3050, 1575, 1473, 1440, and 1085 (S=O); NMR ($CDCl_3$, δ) 1.41 (3H, t, $-CH_3$, J=7.5 Hz), 3.10 (2H, q, $-CH_2-$, J=7.5 Hz), 7.20—7.73 (5H, m, arom.). Found: C, 51.53; H, 5.50%. Calcd for $C_8H_{10}OS_2$: C, 51.58; H, 5.41%.

S-*Propyl Benzenethiosulfinate* **1g**: Colorless oil; IR (neat, cm^{-1}) 3050, 2950, 1575, 1470, 1090, and 1060 (S=O); NMR ($CDCl_3$, δ) 1.03 (6H, t, $-CH_3$, J=7.5 Hz), 1.80 (2H, m, $-C\underline{H}_2-CH_3$), 3.09 (1H, t, $-S-CH_2-$, H_A or H_B, J=6.0 Hz), 3.12 (1H, t, H_A or H_B, J=7.4 Hz), 7.33—7.75 (5H, m, arom.). Found: C, 54.08; H, 5.98%. Calcd for $C_9H_{12}OS_2$: C, 53.96; H, 6.03%.

S-*Cyclohexyl Methanethiosulfinate* **1h**: Colorless oil; IR (neat, cm^{-1}) 2970, 2905, 2840, 1440, and 1080 (S=O); NMR ($CDCl_3$, δ) 1.05—2.35 (10H, m, ring protons), 2.95 (3H, s, $-CH_3$), 3.28 (1H, broad s, $-S-CH\langle$). Found: C, 47.15; H, 7.85%. Calcd for $C_7H_{14}OS_2$: C, 47.15; H, 7.91%.

S-*Methyl* p-*Toluenethiosulfinate* **1i**: Pale yellow oil; IR (neat, cm^{-1}) 3000, 2900, 1590, 1490, 1085, and 1062 (S=O); NMR ($CDCl_3$, δ) 2.38 (3H, s, Ar–$C\underline{H}_3$), 2.52 (3H, s, $-S-CH_3$), 7.23 (2H, d, arom., J=8.3 Hz), 7.54 (2H, d, arom., J=8.3 Hz). Found: C, 51.60; H, 5.35%. Calcd for $C_8H_{10}OS_2$: C, 51.58; H, 5.41%.

S-*Methyl* p-*Chlorobenzenethiosulfinate* **1j**: Colorless oil; IR (neat, cm^{-1}) 3070, 2970, 1573, 1470, and 1080 (S=O); NMR ($CDCl_3$, δ) 2.53 (3H, s, $-CH_3$), 7.41 (2H, d, arom., J=8.9 Hz), 7.63 (2H, d, arom., J=8.9 Hz). Found: C, 41.03; H, 3.19%. Calcd for $C_7H_7ClOS_2$: C, 40.67; H, 3.41%.

Oxidation of Thiosulfinic S-*Ester* **1** *with* $NaIO_4$. All the reactions were carried out at room temperature (*ca.* 20 °C).

To a stirred solution of thiosulfinic *S*-ester (**1**, 1.0 mmol) in organic solvent (acetone, acetonitrile, or dioxane, 3.5 ml) a solution of sodium metaperiodate ($NaIO_4$, 1.2 mmol) in 2.0 ml of water was added. A small amount of one of catalysts (H_2SO_4, HCl, HIO_4, CF_3COOH, I_2, or Br_2, one or two drop(s) of liquid catalyst, or 3—10 mg of solid catalyst) was added to the mixture. Within 1.0 h the solution turned to light yellow and gradually changed to dark brown. The solution became usually homogeneous but sometimes remained heterogeneous. After disappearance of the starting material was confirmed by TLC, the reaction mixture was poured into water and extracted three times with chloroform (*ca.* 100 ml) and then organic layer was washed with an aqueous sodium thiosulfate solution (sat. 10 ml) and water. When chloroform was removed *in vacuo* after drying the organic layer with $MgSO_4$, the residue was highly pure thiosulfonic *S*-ester. Usually GC, LC, and NMR spectra showed only one component. Products were identified by comparing their IR and NMR spectra with those of authentic samples prepared by another method and the structures

of new compounds were confirmed by elemental analyses besides IR and NMR spectra.

If no catalyst was used, the oxidation was very slow and had a long induction period (*ca.* 5—10 h). However, the reaction after the long induction period was nearly as fast as the reaction with catalyst and completed within 1.0 h after the start of the reaction.

When acetic acid was used as a solvent, the oxidation proceeded as fast as the reaction with catalyst, although the catalytic amount of acetic acid did not accelerated the oxidation. In order to remove acetic acid from organic extract, the solution was washed with $NaHCO_3$ solution before washing with a sodium thiosulfate solution.

The reaction in alcohol as solvent was performed as in the above-mentioned oxidation procedure. The whole feature of the reaction was similar to the ordinary oxidation and the reaction was also accelerated by addition of catalyst. However, the distribution of products, *i. e.* thiosulfonic *S*-ester (**2**) and sulfinate (**3**), was affected rather little. Yields of both **2** and **3** were easily determined by measuring NMR spectra of the reaction mixture. The structures of the sulfinates obtained as side products were identified by comparison of their IR (S=O) and NMR spectra[13] with those of authentic samples which were prepared by the reaction of sulfinyl chloride and excess alcohol according to the known method.[14]

The reaction of disulfide with $NaIO_4$ was carried out using acetic acid as a solvent. The reaction procedure was also the same as the usual oxidation method mentioned above. The amount of $NaIO_4$ used was two equivalent to disulfide. After the disappearance of unsymmetrical disulfide **5** or the mixture of symmetrical disulfides **9** and **10** was confirmed, the usual work-up gave a mixture of both symmetrical and unsymmetrical thiosulfonic *S*-esters which were identified by comparing their retention times in GC charts and chemical shifts of methyl groups in NMR spectra with those of authentic samples.

S-*Phenyl Benzenethiosulfonate* **2a**: Pink crystals; mp 44—45 °C (lit,[15] 44—45 °C); IR (KBr, cm^{-1}) 3050, 1578, 1471, 1440, 1325, and 1310 (SO_2), 1147 (S=O); MS (70 eV) *m/e* 250 (M^+, 39%), 125 (M^+-PhSO, 100%).

S-p-*Tolyl Benzenethiosulfonate* **2b**: Colorless crystal; mp 52 °C (lit,[15] 54 °C); IR ($CHCl_3$, cm^{-1}) 3030, 1598, 1450, and 1330 (SO_2), 1145 (S=O); MS (70 eV) *m/e* 264 (M^+, 39%), 139 (M^+-PhSO, 100%).

S-*Phenyl* p-*Toluenethiosulfonate* **2c**: Colorless crystals; mp 78—80 °C (lit,[15] 78 °C); IR ($CHCl_3$, cm^{-1}) 3025, 1597, 1443, 1335 (SO_2), 1145 (S=O); MS (70 eV) *m/e* 264 (M^+, 68%), 155 (M^+-PhS, 100%).

S-*Methyl Benzenethiosulfonate* **2d**: Colorless oil; IR (neat, cm^{-1}) 3050, 3000, 2920, 1580, 1475, 1445, 1330, and 1302 (SO_2), 1142 (S=O); NMR ($CDCl_3$, δ) 2.48 (3H, s, $-CH_3$), 7.21—8.08 (5H, m, arom.). Found: C, 44.92; H, 4.18%. Calcd for $C_7H_8O_2S_2$: C, 44.66; H, 4.28%.

S-*Phenyl Methanethiosulfonate* **2e**: Colorless crystals; mp 85—86.5 °C, IR (KBr, cm^{-1}) 3050, 3000, 2905, 1565, 1465, and 1310 (SO_2), 1130 (S=O); NMR ($CDCl_3$, δ) 3.12 (3H, s, $-CH_3$), 7.30—7.83 (5H, m, arom.). Found: C, 44.87; H, 4.25%. Calcd for $C_7H_8O_2S_2$: C, 44.66; H, 4.28%.

S-*Phenyl Ethanethiosulfonate* **2f**: Colorless crystals; mp 52 °C (lit,[16] 50—52 °C); IR ($CHCl_3$, cm^{-1}) 3055, 2975, 2930, 1575, 1472, and 1326 (SO_2), 1128 (S=O); NMR ($CDCl_3$, δ) 1.41 (3H, t, $-CH_3$, J=7.4 Hz), 3.16 (2H, q, $-CH_2-$, J=7.4 Hz), 7.18—7.75 (5H, m, arom.).

S-*Propyl Benzenethiosulfonate* **2g**: Colorless oil; IR (neat, cm^{-1}) 3065, 2970, 2930, 2875, 1580, 1330, and (SO_2), 1150 (S=O); NMR ($CDCl_3$, δ) 0.90 (3H, t, $-CH_3$, J=6.6 Hz), 1.62 (2H, m, $-CH_2-CH_3$), 2.97 (2H, t, $-S-CH_2-$, J=6.4 Hz), 7.26—8.00 (5H, m, arom.). Found: C, 49.69; H, 5.38%. Calcd for $C_9H_{12}O_2S_2$: C, 49.97; H, 5.59%.

S-*Cyclohexyl Methanethiosulfonate* **2h**: Colorless oil; IR (neat, cm^{-1}) 2925, 2850, and 1321 (SO_2), 1132 (S=O); NMR ($CDCl_3$, δ) 1.10—2.35 (10H, m, ring protons), 3.32 (3H, s, $-CH_3$), 3.48 (1H, broad s, $-CH<$). Found: C, 43.10; H, 7.31%. Calcd for $C_7H_{14}O_2S_2$: C, 43.27; H, 7.26%.

S-*Methyl* p-*Toluenethiosulfonate* **2i**: Colorless crystals; mp 59—61 °C; IR ($CHCl_3$, cm^{-1}) 3050, 2915, 1592, 1493, 1335, and 1305 (SO_2), 1142 (S=O); NMR ($CD_3COOD-D_2O$ (3:1), δ, external TMS) 2.13 (3H, s, $Ar-CH_3$), 2.21 (3H, s, $-S-CH_3$), 7.08 (2H, d, arom.), 7.48 (2H, d, arom.). Found: C, 47.80; H, 4.99%. Calcd for $C_7H_{10}O_2S_2$: C, 47.50; H, 4.98%.

S-*Methyl* p-*Chlorobenzenethiosulfonate* **2j**: Colorless crystals; mp 35—37 °C; IR ($CHCl_3$, cm^{-1}) 3080, 3020, 2920, 1578, 1475, and 1335 (SO_2), 1145 (S=O); NMR ($CD_3COOD-D_2O$ (3:1), δ, external TMS) 2.32 (3H, s, $-CH_3$), 7.40 (2H, d, arom.), 7.70 (2H, d, arom.). Found: C, 38.01; H, 3.15%. Calcd for $C_7H_7ClO_2S_2$: C, 37.75; H, 3.16%.

References

1) Y. H. Kim, T. Takata, and S. Oae, *Tetrahedron Lett.*, **21**, 2305 (1980).

2) Address correspondence to Department of Chemistry, The Korea Advanced Institute of Science, P. O. Box 150, Chongyangni, Seoul, Korea.

3) S. Oae, Y. H. Kim, T. Takata, and D. Fukushima, *Tetrahedron Lett.*, **1977**, 1195.

4) S. Oae, D. Fukushima, and Y. H. Kim, *Chem. Lett.*, **1978**, 279.

5) a) D. Barnard and E. J. Percy, *Chem. Ind. (London)*, **1960**, 1332; b) U. Marangeli, G. Modena, and P. E. Todesco, *Gazz. Chim. Ital.*, **90**, 681 (1960); c) M. M. Chau and J. L. Kice, *J. Am. Chem. Soc.*, **98**, 7711 (1976); d) B. C. Gilbert, B. Gill, and M. J. Ramsden, *Chem. Ind. (London)*, **1979**, 283.

6) a) S. Oae and T. Takata, *Tetrahedron Lett.*, **21**, 3213 (1980); b) N. Isenberg and H. F. Herbrandson, *Int. J. Sulfur Chem.*, **A1**, 179 (1971).

7) C. J. M. Stirling, *J. Chem. Soc.*, **1957**, 3579.

8) H. J. Backer and H. Kloosterziel, *Recl. Trav. Chim. Pays-Bas*, **73**, 129 (1954).

9) T. Takata, Y. H. Kim, and S. Oae, *Tetrahedron Lett.*, **1978**, 4303.

10) L. Field and Y. H. Kim, *J. Org. Chem.*, **37**, 2710 (1972).

11) S. Oae, Y. Yoshikawa, and W. Tagaki, *Bull. Chem. Soc. Jpn.*, **42**, 2899 (1969).

12) G. Ghesetti and G. Modena, *Spectrochim. Acta*, **19**, 1809 (1963).

13) J. W. Wilt and W. J. Wagner, *Chem. Ind. (London)*, **1964**, 1389.

14) H. F. Herbrandson and K. T. Dickerson, Jr., *J. Am. Chem. Soc.*, **81**, 4120 (1959).

15) S. Oae, R. Nomura, Y. Yoshikawa, and W. Tagaki, *Bull. Chem. Soc. Jpn.*, **42**, 2903 (1969).

16) A. K. Bhattacharya and A. G. Hortman, *J. Org. Chem.*, **43**, 2728 (1978).

Synthesis of (+)-11-Hydroxyabieta-2,8,11,13-tetraen-1-one

Takashi MATSUMOTO,* Sachihiko IMAI, and Shuhei YUKI

Department of Chemistry, Faculty of Science, Hiroshima University, Higashisenda-machi, Naka-ku, Hiroshima 730

(Received October 21, 1980)

Treatment of methyl (+)-11-oxo-13β-abieta-8-en-18-oate with copper(II) bromide and lithium bromide afforded the corresponding phenol derivative, which was methylated to methyl 11-methoxyabieta-8,11,13-trien-18-oate (**7**). The same compound was also prepared from methyl (+)-7,11-dioxo-13β-abieta-8-en-18-oate *via* methyl 11-hydroxy-7-oxoabieta-8,11,13-trien-18-oate, its methyl ether, and methyl 11-methoxyabieta-6,8,11,13-tetraen-18-oate. The Grignard reaction of **7** with phenylmagnesium bromide followed by treatment with lead tetraacetate and subsequent oxidation with selenium dioxide afforded 11-methoxy-19-norabieta-4(18),8,11,13-tetraen-3α-ol (**12**), which was converted to 11-methoxy-19-norabieta-8,11,13-trien-3-one (**20**) by catalytic hydrogenation, Jones oxidation, and isomerization. The compound **20** was also obtained by Birch reduction of 11-methoxy-19-norabieta-4,8,11,13-tetraen-3-one prepared from **12** *via* 11-methoxy-19-norabieta-4,8,11,13-tetraen-3α-ol. Subsequently, the compound **20** was transformed to 11-methoxyabieta-1,8,11,13-tetraen-3-one (**27**) by a series of reactions: acetalization, demethylation, hydrolysis, acetylation, bromination, dehydrobromination, and methylation. Finally, the compound **27** was converted to the title compound, (+)-11-hydroxyabieta-2,8,11,13-tetraen-1-one (**1**), by oxidation with alkaline hydrogen peroxide, heating with hydrazine hydrate, Jones oxidation, and demethylation. Although the synthetic (+)-**1** was shown to be different from natural shonanol, the spectral analyses of the synthetic structural isomers showed the structure of shonanol to be 12-hydroxyabieta-2,8,11,13-tetraen-1-one.

Shonanol is a tricyclic diterpene phenol isolated from *Libocedrus formosana* by Lin and Liu.[1] On the basis of spectroscopic studies, they deduced the structure of shonanol to be 12-hydroxytotara-1,8,11,13-tetraen-3-one (I). This structure is unique among the naturally-occurring tricyclic diterpenes, in that it contains an α,β-unsaturated carbonyl group in the A ring and a hydroxyl group at the position meta to an isopropyl group in the C ring. To make the structural confirmation, (±)-I had been synthesized in our laboratory.[2] However, the synthetic (±)-I had been shown to be different from natural shonanol by spectral comparison. Further studies[3] on the syntheses of (±)-12-hydroxytotara-2,8,11,13-tetraen-1-one (II), (±)-14-hydroxy-12-isopropylpodocarpa-1,8,11,13-tetraen-3-one (III), and (±)-14-hydroxy-12-isopropylpodocarpa-2,8,11,13-tetraen-1-one (IV) led to the same result, whereas the chemical shifts of vinyl protons in the NMR spectra of these synthetic I—IV suggested that shonanol (δ 5.91 and 6.47 ppm) must have a Δ^2-1-oxo moiety (δ 5.95, 5.90 and 6.53, 6.48 ppm in those of II and IV) rather than the proposed Δ^1-3-oxo one (δ 5.99, 5.94, and 7.54, 7.55 ppm in those of I and III) in the A ring of the tricyclic skeleton. In this study, (+)-11-hydroxyabieta-2,8,11,13-tetraen-1-one (**1**) possessing a hydroxyl group at the position meta to an isopropyl group was synthesized starting from methyl (+)-11-oxo-13β-abieta-8-en-18-oate (**2**)[4] and methyl (+)-7,11-dioxo-13β-abieta-8-en-18-oate (**3**),[4] to allow a comparison of the physical and spectral data with those of natural shonanol.

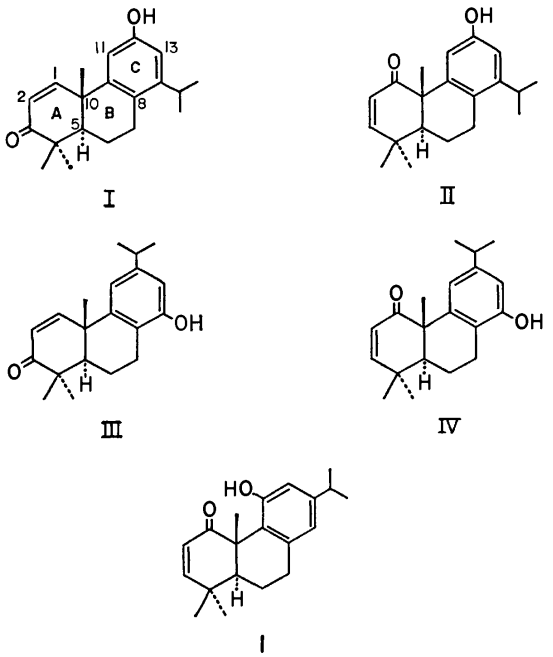

The 11-oxo compound (**2**) was refluxed with copper(II) bromide and lithium bromide in acetonitrile[5] to give methyl 11-hydroxyabieta-8,11,13-trien-18-oate (**4**) and a small amount of methyl 11-hydroxyabieta-6,8,11,13-tetraen-18-oate (**5**), which was also prepared from the 7,11-dioxo compound **3** by the following route. Similar treatment of **3** with copper(II) bromide and lithium bromide, followed by heating at 100 °C with lithium carbonate and lithium chloride in *N,N*-dimethylformamide and then at 45 °C with zinc in acetic acid, produced methyl 11-hydroxy-7-oxoabieta-8,11,13-trien-18-oate (**6**). This 7-oxo compound **6** was reduced with sodium borohydride in methanol and the resulting alcohol was immediately dehydrated with *p*-toluenesulfonic acid monohydrate in refluxing benzene to give **5**, which was easily converted to **4** by catalytic hydrogenation over PtO_2. **4** and **6** were each methylated at 35—40 °C with methyl iodide and sodium hydride in *N,N*-dimethylformamide under a stream of nitrogen to give the corresponding methyl ether, **7**[6] and **8**.[6,7] The compound **7** was also obtained by catalytic hydrogenation of methyl 11-methoxyabieta-6,8,11,13-tetraen-18-oate (**9**), which was prepared by reduction of **8** with sodium borohydride, followed by dehydration with *p*-toluenesulfonic acid monohydrate. The Grignard reaction of **7** with phen-

ylmagnesium bromide at 100—110 °C afforded a *gem*-diphenyl alcohol (**10**), which was treated with lead tetraacetate and calcium carbonate in refluxing benzene to give a mixture of Δ^3-, Δ^4-, and $\Delta^{4(18)}$-19-nor compounds (**11**) in a ratio of *ca.* 1:1:8. The mixture was oxidized at room temperature with selenium dioxide and *t*-butyl hydroperoxide in dichloromethane in the presence of salicylic acid[8] or with selenium dioxide in refluxing aqueous ethanol to yield 11-methoxy-19-norabieta-4(18),8,11,13-tetraen-3α-ol (**12**). The α-configuration of the hydroxyl group at the C-3 position in **12** was supported by a signal at δ 4.14 ppm with half-height width of 5 Hz in the NMR spectrum, suggesting the presence of an equatorial β hydrogen. The 3α-ol (**12**) was isomerized at 100 °C with lithium in ethylenediamine under a stream of nitrogen to 11-methoxy-19-norabieta-4,8,11,13-tetraen-3α-ol (**13**), which was immediately oxidized with Jones reagent to 11-methoxy-19-norabieta-4,8,11,13-tetraen-3-one (**14**). Methylation of this conjugated ketone **14** with methyl iodide and potassium *t*-pentyl oxide in refluxing benzene under a stream of nitrogen gave the corresponding 4,4-dimethyl ketone (**15**), which was reduced with lithium aluminium hydride in ether to give 11-methoxyabieta-5,8,11,13-tetraen-3β-ol (**16**). The stereochemistry of the hydroxyl group in **16**, which was expected to be β-configuration from previously published results,[2,3,9,10] was confirmed by conversion to the corresponding acetate (**17**), whose NMR spectrum showed a double doublet signal at δ 4.44 ppm (J=6.5 and 9 Hz), suggesting the presence of an α hydrogen at the C-3 position. The 3β-ol **16** was so unstable that it was gradually transformed to a naphthalene derivative (**18**). The structure of **18** was also supported by its NMR spectrum. Since catalytic hydrogenation of C-5 double bond in **16** proved to be more difficult than expected, this synthetic route was discontinued. Thus, another synthetic route was attempted.

Catalytic hydrogenation of **12** in ethanol over Raney Ni, followed by oxidation with Jones reagent, gave 11-methoxy-18-norabieta-8,11,13-trien-3-one (**19**) and its 19-nor isomer (**20**) in a ratio of 69:2. The former **19** was easily isomerized with sodium methoxide in refluxing methanol to the thermodynamically-stable latter **20** in an almost quantitative yield. The stable

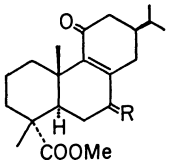

2 R=H_2
3 R=O

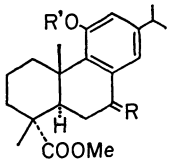

4 R=H_2, R'=H
6 R=O, R'=H
7 R=H_2, R'=Me
8 R=O, R'=Me

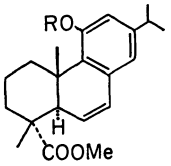

5 R=H
9 R=Me

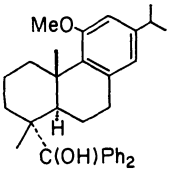

10

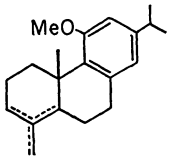

11

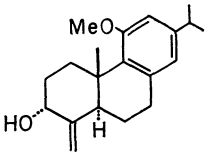

12

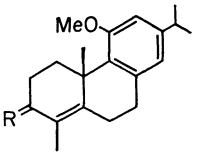

13 R=α-OH, β-H
14 R=O

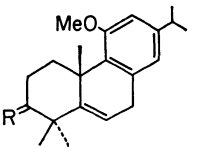

15 R=O
16 R=α-H, β-OH
17 R=α-H, β-OAc

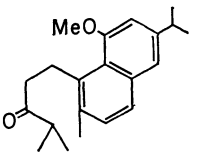

18

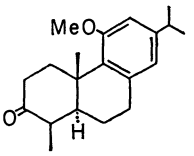

19

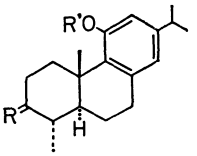

20 R=O, R'=Me
21 R=  , R'=Me
22 R=, R'=H
23 R=O, R'=H
24 R=O, R'=Ac

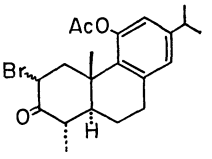

25

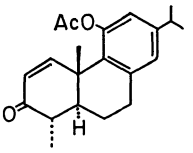

26

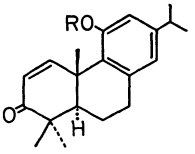

27 R=Me
28 R=H

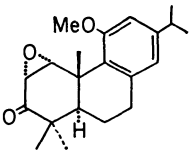

29

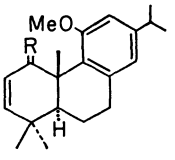

30 R=α-OH, β-H
31 R=O

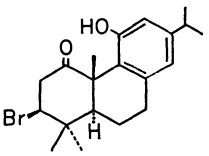

32

isomer **20** was also obtained by Birch reduction of **14** with lithium in liquid ammonia and tetrahydrofuran. Acetalization of **20** with ethylene glycol in the presence of *p*-toluenesulfonic acid monohydrate in refluxing benzene, followed by demethylation of the crude acetal (**21**) with sodium ethanethiolate in refluxing *N,N*-dimethylformamide, yielded a phenol derivative (**22**). This compound, without purification, was converted to 11-acetoxy-19-norabieta-8,11,13-trien-3-one (**24**) by hydrolysis with hydrochloric acid in acetone and subsequent acetylation of the resulting ketone (**23**) with acetic anhydride in pyridine. Bromination[11] of **24** in chloroform with bromine in carbon tetrachloride at 0 °C, followed by dehydrobromination of the crude 2-bromo derivative (**25**) with lithium carbonate and lithium bromide in *N,N*-dimethylformamide at 120—125 °C, afforded an α,β-unsaturated ketone (**26**) which was converted to 11-methoxyabieta-1,8,11,13-tetraen-3-one (**27**) by refluxing with methyl iodide and potassium *t*-pentyl oxide in benzene under a stream of nitrogen. Demethylation of **27** with sodium ethanethiolate in refluxing *N,N*-dimethylformamide produced 11-hydroxyabieta-1,8,11,13-tetraen-3-one (**28**), whose physical and spectral data were different from those of natural shonanol. Subsequently, 1,3-carbonyl transposition[3,12] of the α,β-unsaturated carbonyl group in **27** was carried out as follows. Oxidation of **27** with alkaline hydrogen peroxide in methanol at −10 °C, followed by treatment of the resulting epoxy ketone (**29**)[13] with hydrazine hydrate in refluxing methanol containing a small amount of acetic acid, led to 11-methoxyabieta-2,8,11,13-tetraen-1α-ol (**30**), which was immediately oxidized at 0 °C with Jones reagent to afford 11-methoxyabieta-2,8,11,13-tetraen-1-one (**31**). The 1-oxo compound **31** was finally demethylated at 0 °C with boron tribromide in dichloromethane to give the title compound, 11-hydroxyabieta-2,8,11,13-tetraen-1-one (**1**), and 3β-bromo-11-hydroxyabieta-8,11,13-trien-1-one (**32**) in a ratio of *ca.* 1:1. Dehydrobromination of **32** with lithium carbonate and lithium bromide in *N,N*-dimethylformamide at 120—125 °C produced **1** in an almost quantitative yield. The structure of **32** was supported by the NMR spectrum, which showed signals at δ 2.91 (1H, dd, J=12 and 4.5 Hz) and 3.60 ppm (1H, dd, J=13 and 12 Hz) due to the methylene protons at the C-2 position, and at δ 4.04 ppm (1H, dd, J=13 and 4.5 Hz) due to the methine proton at the C-3 position. The physical and spectral data of the synthetic **1** were also different from those of natural shonanol.

Another structural isomer possessing a hydroxyl group at the position meta to an isopropyl group is 13-hydroxy-11-isopropylpodocarpa-2,8,11,13-tetraen-1-one (V), whose isopropyl group should be sterically hindered by a methyl group at the C-10 position and a carbonyl group at the C-1 position. Therefore, the chemical shifts and coupling pattern of the isopropyl group in V might be expected to be different from those of sempervirol (VI) or ferruginol (VII), which possess an isopropyl group at the less hindered C-12 or C-13 position. However, since the reported chemical shifts of two methyl groups (6H, d, δ 1.15—1.20 ppm) and a methine proton (1H, hept, δ 3.03—3.30 ppm) of the isopropyl group in shonanol were very similar to those[14] in VI (δ 1.19 and 3.10 ppm) or VII (δ 1.19 and 3.09 ppm), the possibility of V could also be ruled out. In the NMR spectrum of natural shonanol, Lin and Liu[1] assigned two singlet signals at δ 6.67 (2H) and 7.30 ppm (1H) to two aromatic protons and a hydroxyl proton, respectively. However, we favored an alternative assignment, in which the signal at δ 6.67 ppm was due to an aromatic proton and a hydroxyl proton and that at δ 7.30 ppm was due to another aromatic proton, because II and IV showed a signal at δ 7.21 ppm[3] corresponding to an aromatic proton at the C-11 position. Consideration of these NMR spectral data suggested that shonanol is either 13-hydroxy-12-isopropyl or a 12-hydroxy-13-isopropyl derivative. Moreover, it is known[14] that VI shows a singlet signal at δ 6.18 ppm due to an aromatic proton at the C-14 position, while VII shows the corresponding signal at δ 6.68 ppm.

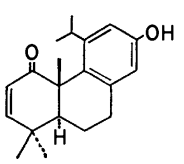

V

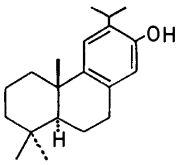

VI

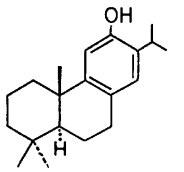

VII

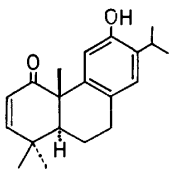

VIII

From these NMR analyses we now propose the structure of shonanol to be 12-hydroxyabieta-2,8,11,13-tetraen-1-one (VIII).

Experimental

All melting points are uncorrected. The IR and optical rotations were measured in chloroform. The NMR spectra (90 MHz) were taken in carbon tetrachloride on a Hitachi Model R-22 NMR spectrometer using tetramethylsilane as an internal standard, unless otherwise stated. The chemical shifts are presented in terms of δ values; s: singlet, bs: broad singlet, d: doublet, bd: broad doublet, dd: double doublet, t: triplet, m: multiplet. Column chromatography was performed using Merck silica gel (0.063 mm).

Methyl 11-Hydroxy-7-oxoabieta-8,11,13-trien-18-oate (6). A mixture of methyl 7,11-dioxo-13β-abieta-8-en-18-oate (**3**: 3.46 g)[4] (mp 87—89.5 °C, $[\alpha]_D$ +78°), copper(II) bromide (4.24 g), and lithium bromide (0.82 g) in freshly distilled acetonitrile (170 ml) was refluxed for 5 h and then evaporated *in vacuo*. After the addition of a mixture of ether and brine, the reaction mixture was extracted with ether. The ether extract was washed with brine, dried over sodium sulfate, and evaporated to give a brown oil (4.00 g).

A mixture of the brown oil (4.00 g), lithium carbonate (3.70 g), and lithium chloride (3.40 g) in *N,N*-dimethyl-

formamide (200 ml) was heated at 100 °C for 8 h in a stream of nitrogen. After cooling, the mixture was diluted with ether, acidified with dilute sulfuric acid, and then extracted with ether. The ether extract was washed successively with aqueous sodium thiosulfate and brine, dried over sodium sulfate, and evaporated to give a dark brown oil (3.81 g).

A mixture of the dark brown oil (3.81 g) and zinc dust (15.2 g) in acetic acid (95 ml) was stirred at 45 °C for 4 h. The reaction mixture was filtered and the filtrate was diluted with water, neutralized with sodium hydrogencarbonate, and extracted with ether. The ether extract was washed with brine, dried over sodium sulfate, and evaporated. The residue (3.58 g) was purified by column chromatography on silica gel (380 g), using ether–benzene (5:95) as the eluent, to give **6** (2.50 g: 73%), which was recrystallized from ethanol; mp 154—155 °C, mp 180—181 °C after drying at 140—145 °C; $[\alpha]_D$ +38° (*c* 1.17); IR: 3600, 3330br, 1725, 1680, 1610, 1577 cm^{-1}; NMR (DMSO-d_6); 1.17 (6H, d, J=7 Hz, $-CH(C\underline{H}_3)_2$), 1.27 and 1.37 (each 3H and s, C_4–CH_3 and C_{10}–CH_3), 3.61 (3H, s, $-CO_2CH_3$), 6.92 (1H, d, J=2 Hz, C_{12}–H), 7.28 (1H, d, J=2 Hz, C_{14}–H). Found: C, 72.93; H, 8.20%. Calcd for $C_{21}H_{28}O_4$: C, 73.22; H, 8.19%.

Methyl 11-Hydroxyabieta-6,8,11,13-tetraen-18-oate (5). A mixture of **6** (1.03 g) and sodium borohydride (170 mg) in methanol (25 ml) was allowed to stand overnight at room temperature. After the addition of acetone (1.0 ml), the solvent was removed *in vacuo* and the residue was acidified with dilute hydrochloric acid. The mixture was then extracted with ether. The ether extract was washed with brine, dried over sodium sulfate, and evaporated to give a curde alcohol (1.07 g) as a pale brown solid.

A mixture of the crude alcohol (1.07 g) and *p*-toluenesulfonic acid monohydrate (20 mg) in benzene (100 ml) was refluxed for 2 h. After cooling, the mixture was diluted with ether, washed successively with aqueous sodium hydrogencarbonate and brine, dried over sodium sulfate, and then evaporated *in vacuo*. The residue was recrystallized from methanol to afford **5** (0.87 g: 89%); mp 173.5—175 °C; $[\alpha]_D$ −35° (*c* 1.93); IR: 3600, 3400br, 1720 cm^{-1}; NMR ($CDCl_3$): 1.18 and 1.39 (each 3H and s, C_4–CH_3 and C_{10}–CH_3), 1.21 (6H, d, J=7 Hz, $-CH(C\underline{H}_3)_2$), 3.03 (1H, t, J=3 Hz, C_5–H), 3.65 (3H, s, $-CO_2CH_3$), 4.86 (1H, bs, –OH, disappeared on deutration), 5.64 and 6.43 (each 1H, dd, and J=10 and 3 Hz, C_6–H and C_7–H), 6.40 and 6.49 (each 1H and bs, C_{12}–H and C_{14}–H). Found: C, 76.78; H, 8.80%. Calcd for $C_{21}H_{28}O_3$: C, 76.79; H, 8.59%. The mother liquor of recrystallization was evaporated *in vacuo* and the residue was chromatographed on silica gel (15 g), using benzene as the eluent, to give some additional **5** (0.11 g: 11%).

Methyl 11-Hydroxyabieta-8,11,13-trien-18-oate (4). a): A mixture of methyl 11-oxo-13β-abieta-8-en-18-oate (**2**: 9.49 g)[4] (mp 108—110 °C, $[\alpha]_D$ +104° (EtOH)), copper(II) bromide (11.50 g), and lithium bromide (2.23 g) in freshly distilled acetonitrile (470 ml) was refluxed for 5 h and then evaporated *in vacuo*. After the addition of a mixture of ether and brine, the mixture was extracted with ether. The ether extract was washed with brine, dried over sodium sulfate, and evaporated *in vacuo*. The residual solid (10.37 g) was recrystallized from ethanol to give **4** (5.30 g: mp 201—203 °C). A pure sample for analysis was obtained by repeated crystallization; mp 203—205 °C; $[\alpha]_D$ +77° (*c* 1.22); IR: 3600, 3370br, 1720, 1617, 1575 cm^{-1}; NMR ($CDCl_3$): 1.19 (6H, d, J=7 Hz, $-CH(C\underline{H}_3)_2$), 1.29 and 1.35 (each 3H and s, C_4–CH_3 and C_{10}–CH_3), 3.14 (1H, bd, J=12.5 Hz, $C_{1\beta}$–H), 3.68 (3H, s, $-CO_2CH_3$), 4.82 (1H, s, –OH, disappeared on deutration), 6.32 and 6.51 (each 1H and bs, C_{12}–H and C_{14}–H). Found: C, 76.20; H, 9.16%. Calcd for $C_{21}H_{30}O_3$: C, 76.32; H, 9.15%. The mother liquor of recrystallization was evaporated *in vacuo* and the residue was chromatographed on silica gel (300 g), using benzene as the eluent, to give a colorless solid (**4**: 1.85 g) containing a small amount of **5**. Further elution with ether–benzene (1:99) afforded the recovered **2** (1.73 g: 18%).

b): A mixture of **5** (651 mg) and PtO_2 (100 mg) in ethanol (30 ml) was subjected to catalytic hydrogenation at room temperature. After the usual work-up, the crude product was recrystallized from ethanol to give **4** (600 mg: 90%), mp 201—203.5 °C, whose IR and NMR spectra were identical with those of the sample prepared in *a)*. The mother liquor of recrystallization was evaporated *in vacuo* and the residue was chromatographed on silica gel to give some additional **4** (61 mg: 9%).

Methyl 11-Methoxy-7-oxoabieta-8,11,13-trien-18-oate (8). A mixture of **6** (344 mg) and 50% sodium hydride (72 mg) in *N,N*-dimethylformamide (6.5 ml) was stirred at room temperature for 45 min under a stream of nitrogen. After the addition of methyl iodide (0.06 ml), the mixture was stirred at 35—40 °C for 3 h, cooled, and some additional methyl iodide (0.02 ml) was added. The mixture was further stirred at 35—40 °C for 5 h, poured into a mixture of ice and dilute hydrochloric acid, and extracted with ether. The ether extract was washed with brine, dried over sodium sulfate, and evaporated *in vacuo*. The residue was purified by column chromatography on silica gel (40 g), using ether–benzene (1:99) as the eluent, to give **8** (309 mg: 86%), which was recrystallized from hexane; mp 113—114 °C; $[\alpha]_D$ +60° (*c* 1.15); IR: 1727, 1680 cm^{-1}; NMR: ($CDCl_3$): 1.25 (6H, d, J=7 Hz, $-CH(C\underline{H}_3)_2$), 1.30 and 1.38 (each 3H and s, C_4–CH_3 and C_{10}–CH_3), 3.64 (3H, s, $-CO_2CH_3$), 3.82 (3H, s, C_{11}–OCH_3), 6.94 (1H, d, J=2 Hz, C_{12}–H), 7.59 (1H, d, J=2 Hz, C_{14}–H). Found: C, 73.44; H, 8.39%. Calcd for $C_{22}H_{30}O_4$: C, 73.71; H, 8.44%. The IR and NMR spectra of **8** were identical with those of an authentic sample.[7]

Methyl 11-Methoxyabieta-6,8,11,13-tetraen-18-oate (9). A solution of **8** (270 mg) and sodium borohydride (43 mg) in methanol (7.0 ml) was allowed to stand overnight at room temperature. The crude alcohol was then dehydrated with *p*-toluenesulfonic acid monohydrate in refluxing benzene, as described for the preparation of **5**. The crude product was chromatographed on silica gel (25 g), using hexane–benzene (1:1) as the eluent, to give **9** (244 mg: 95%); $[\alpha]_D$ −15° (*c* 1.45); IR: 1717 cm^{-1}; NMR: 1.10 and 1.33 (each 3H and s, C_4–CH_3 and C_{10}–CH_3), 1.21 (6H, d, J=7 Hz, $-CH(C\underline{H}_3)_2$), 2.89 (1H, t, J=3 Hz, C_5–H), 3.58 (3H, s, $-CO_2CH_3$), 3.73 (3H, s, C_{11}–OCH_3), 5.55 and 6.32 (each 1H, dd, J=10 and 3 Hz, C_6–H and C_7–H), 6.42 and 6.48 (each 1H, d, and J=2 Hz, C_{12}–H and C_{14}–H). Found: C, 77.45; H, 9.02%. Calcd for $C_{22}H_{30}O_3$: C, 77.15; H, 8.83%.

Methyl 11-Methoxyabieta-8,11,13-trien-18-oate (7). a): A mixture of **9** (190 mg) and PtO_2 (19 mg) in ethanol (20 ml) was submitted to catalytic hydrogenation at room temperature. After the usual work-up, the crude product was purified by column chromatography on silica gel (20 g), using hexane–benzene (1:1) as the eluent, to give **7**[6] (181 mg: 95%); $[\alpha]_D$ +89° (*c* 1.35); IR: 1718, 1610, 1568 cm^{-1}; NMR ($CDCl_3$): 1.22 (6H, d, J=7 Hz, $-CH(C\underline{H}_3)_2$), 1.27 and 1.31 (each 3H and s, C_4–CH_3 and C_{10}–CH_3), 3.65 (3H, s, $-CO_2CH_3$), 3.77 (3H, s, C_{11}–OCH_3), 6.50 (2H, bs, C_{12}–H and C_{14}–H). Found: C, 76.84; H, 9.50%. Calcd for $C_{22}H_{32}O_3$: C, 76.70; H, 9.36%.

b): A mixture of **4** (7.15 g) containing a small amount

of **5**, 50% sodium hydride (5.20 g), and *N,N*-dimethylformamide (200 ml) was methylated with methyl iodide (4.0 ml) as described for the preparation of **8**. The crude product was purified by column chromatography on silica gel (350 g), using hexane–benzene (1:1) as the eluent, to give **7** (3.98 g) and a mixture (2.42 g) of **7** and a small amount of **9**.

The above mixture (2.42 g) in ethanol (14 ml) was hydrogenated over PtO_2 and then purified by column chromatography to give **7** (2.14 g), whose IR and NMR spectra were identical with those of the sample prepared in *a)*.

Grignard Reaction of 7 with Phenylmagnesium Bromide. A solution of **7** (344 mg) in dry ether (3.4 ml) was added dropwise to a refluxing ethereal solution of phenylmagnesium bromide prepared from magnesium turnings (194 mg) and bromobenzene (1.26 g) in dry ether (3.4 ml). The mixture was further refluxed for 2 h and the ether was removed in a stream of nitrogen. The viscous residue was heated at 100—110 °C for 5 h, allowed to stand overnight at room temperature, carefully hydrolyzed with a mixture of ice and dilute sulfuric acid, and then extracted with ether. The ether extract was washed successively with aqueous sodium thiosulfate and brine, dried over sodium sulfate, and evaporated *in vacuo*. The residue was purified by column chromatography on silica gel (65 g), using hexane–benzene (1:1) as the eluent, to give a *gem*-diphenyl alcohol (**10**) (373 mg: 80%) as a colorless solid, which was recrystallized from methanol; mp 191.5—193 °C; $[\alpha]_D$ +101° (*c* 1.65); IR: 3580, 1610, 1568, 700 cm^{-1}; NMR: 1.15 (6H, d, J=7 Hz, $-CH(C\underline{H}_3)_2$), 1.28 and 1.30 (each 3H and s, C_4-CH_3 and $C_{10}-CH_3$), 2.34 (1H, s, –OH, disappeared on deutration), 3.69 (3H, s, $C_{11}-OCH_3$), 6.17 and 6.31 (each 1H and bs, $C_{12}-H$ and $C_{14}-H$), 6.9—7.9 (10H, m, 2-C_6H_5). Found: C, 84.84; H, 8.68%. Calcd for $C_{33}H_{40}O_2$: C, 84.57; H, 8.60%.

Fragmentation of 10 with Lead Tetraacetate. A mixture of lead tetraacetate (1.06 g) and calcium carbonate (1.20 g) in dry benzene (60 ml) was refluxed for 5 min. To this mixture was added a solution of **10** (937 mg) in dry benzene (30 ml). The mixture was refluxed for 8 h, cooled, and then filtered. The filtrate was diluted with ether and the solution was washed successively with aqueous potassium iodide, aqueous sodium thiosulfate, aqueous sodium hydrogencarbonate, and brine. After drying over sodium sulfate, the solution was evaporated *in vacuo* and the residue was chromatographed on silica gel (100 g), using hexane–benzene (95:5) as the eluent, to give a mixture of Δ^3-, Δ^4-, and $\Delta^{4(18)}$-19-nor isomers (**11**) (508 mg: 89%). The NMR spectrum of the mixture indicated that it was composed of approximately 10% of Δ^3- (δ 5.34 ppm, C_3-H), 10% of Δ^4- (δ 1.42 ppm, $C_{10}-CH_3$), and 80% of $\Delta^{4(18)}$-19-nor compound (δ 4.48 and 4.74 ppm, $CH_2=\overset{|}{C}-$). Found: C, 84.74; H, 10.18%. Calcd for $C_{20}H_{28}O$: C, 84.45; H, 9.92%. The above olefinic mixture (**11**) was recrystallized from methanol to afford the pure $\Delta^{4(18)}$-19-nor compound; mp 81—82 °C; $[\alpha]_D$ +242° (*c* 1.23); NMR: 1.17 (3H, s, $C_{10}-CH_3$), 1.21 (6H, d, J=7 Hz, $-CH(C\underline{H}_3)_2$), 3.01 (1H, bd, J=12 Hz, $C_{1\beta}-H$), 3.75 (3H, s, $C_{11}-OCH_3$), 4.48 and 4.74 (each 1H, bs, and $W_{1/2}$=4 Hz, $CH_2=\overset{|}{C}-$), 6.39 (2H, bs, $C_{12}-H$ and $C_{14}-H$). Found: C, 84.32; H, 10.15%. Calcd for $C_{20}H_{28}O$: C, 84.45; H, 9.92%.

11-Methoxy-19-norabieta-4(18),8,11,13-tetraen-3α-ol (12).

a): The olefinic mixture (**11**: 142 mg) was added to a stirred mixture of 70% *t*-butyl hydroperoxide (0.26 ml), selenium dioxide (1 mg), and salicylic acid (7 mg) in dichloromethane (0.3 ml). The mixture was further stirred at room temperature for 28 h, diluted with benzene (5.0 ml), and then evaporated. The residue was dissolved in ether and the ether solution was washed successively with aqueous potassium hydroxide and brine. After the solution had been evaporated *in vacuo*, the residue was dissolved in cold acetic acid (1.0 ml) and dimethyl sulfide (0.25 ml) was added slowly with stirring and cooling in a water bath. The mixture was then stirred at room temperature for 3 h, neutralized with aqueous potassium carbonate at 0—5 °C, and extracted with ether. The ether extract was washed with brine, dried over sodium sulfate, and evaporated *in vacuo*. The residue was purified by column chromatography on silica gel (17 g), using ether–benzene (1:99) as the eluent, to give **12** (95 mg: 63%), which was recrystallized from hexane; mp 68—69.5 °C; $[\alpha]_D$ +186° (*c* 2.59); IR: 3600, 3420br, 1648, 1610, 1568 cm^{-1}; NMR: 1.01 (3H, s, $C_{10}-CH_3$), 1.21 (6H, d, J=7 Hz, $-CH(C\underline{H}_3)_2$), 1.92 (1H, bs, –OH, disappeared on deutration), 3.73 (3H, s, $C_{11}-OCH_3$), 4.14 (1H, bs, $W_{1/2}$=5 Hz, C_3-H), 4.55 and 4.90 (each 1H and bs, $CH_2=\overset{|}{C}-$), 6.39 (2H, bs, $C_{12}-H$ and $C_{14}-H$). Found: C, 80.20; H, 9.56%. Calcd for $C_{20}H_{28}O_2$: C, 79.95; H, 9.39%.

b): A solution of selenium dioxide (566 mg) in ethanol (29 ml) and water (0.08 ml) was added dropwise to a stirred solution of the olefinic mixture (**11**: 2.88 g) in ethanol (29 ml) at room temperature over a 20 min period. The mixture was further stirred at room temperature for 30 min, refluxed for 8 h, cooled, and then filtered. The filtrate was diluted with ether and the ether solution was washed with brine, dried over sodium sulfate, and evaporated *in vacuo*. The residue was purified by column chromatography on silica gel (320 g), using ether–benzene (1:99) as the eluent, to give **12** (1.68 g: 55%) as a pale brown solid, whose IR and NMR spectra were identical with those of the sample prepared in *a)*.

11-Methoxy-19-norabieta-4,8,11,13-tetraen-3-one (14). A solution of **12** (1.01 g) in ethylenediamine (70 ml) was added to lithium (1.18 g) in ethylenediamine (70 ml). The mixture was heated at 100 °C for 1 h under a stream of nitrogen, poured into brine, and extracted with ether. The ether extract was washed with brine, dried over sodium sulfate, and evaporated to give a crude 11-methoxy-19-norabieta-4,8,11,13-tetraen-3α-ol (**13**) as an oil (1.00 g); NMR (60 MHz): 1.22 (6H, d, J=7 Hz, $-CH(C\underline{H}_3)_2$), 1.38 (3H, s, $C_{10}-CH_3$), 1.74 (3H, s, C_4-CH_3), 3.65 (1H, bs, $W_{1/2}$=6 Hz, C_3-H), 3.76 (3H, s, $C_{11}-OCH_3$), 6.42 (2H, bs, $C_{12}-H$ and $C_{14}-H$).

A solution of the crude **13** (1.00 g) in acetone (60 ml) was oxidized with Jones reagent (2.5 M: 3.37 ml) at 0 °C for 30 min. After the usual work-up, the crude product was purified by column chromatography on silica gel (50 g), using ether–benzene (1:99) as the eluent, to give **14** (830 mg: 83%) as an oil; $[\alpha]_D$ +362° (*c* 1.71); IR: 1650, 1613, 1570 cm^{-1}; NMR: 1.22 (6H, d, J=7 Hz, $-CH(C\underline{H}_3)_2$), 1.61 (3H, s, $C_{10}-CH_3$), 1.78 (3H, s, C_4-CH_3), 3.80 (3H, s, $C_{11}-OCH_3$), 6.44 and 6.48 (each 1H and bs, $C_{12}-H$ and $C_{14}-H$). Found: C, 80.25; H, 8.96%. Calcd for $C_{20}H_{26}O_2$: C, 80.49; H, 8.78%.

11-Methoxyabieta-5,8,11,13-tetraen-3-one (15). A solution of potassium *t*-pentyl oxide in *t*-pentyl alcohol prepared from potassium (141 mg) and *t*-pentyl alcohol (7.8 ml) was evaporated to dryness and the residual potassium *t*-pentyl oxide was suspended in dry benzene (7.0 ml). After a solution of **14** (596 mg) in dry benzene (18 ml) had been added over a 10 min period under a stream of nitrogen, the stirred mixture was refluxed for 30 min, cooled, and a solution of methyl iodide (0.37 ml) in dry benzene (5.0

ml) was added. The stirred mixture was further refluxed for 2 h, poured into dilute hydrochloric acid, and extracted with ether. The ether extract was washed successively with aqueous sodium thiosulfate and brine, dried over sodium sulfate, and evaporated *in vacuo*. The residue was purified by column chromatography on silica gel (60 g), using benzene as the eluent, to give **15** (447 mg: 72%) as a colorless solid; IR: 1700, 1612, 1573 cm^{-1}; NMR: 1.22 (6H, d, J=7 Hz, $-CH(C\underline{H}_3)_2$), 1.25 (6H, s) and 1.28 (3H, s) ($-\dot{C}(CH_3)_2$ and $C_{10}-CH_3$), 3.36 (2H, bd, J=4 Hz, $=CHC\underline{H}_2-$), 3.80 (3H, s, $C_{11}-OCH_3$), 5.67 (1H, t, J=4 Hz, C_6–H), 6.46 (2H, bs, C_{12}–H and C_{14}–H). The compound (**15**) was labile and it was immediately subjected to the next reaction.

*11-Methoxyabieta-5,8,11,13-tetraen-3β-ol (**16**).* A solution of **15** (99 mg) in dry ether (4.0 ml) was added to a stirred suspension of lithium aluminium hydride (24.3 mg) in dry ether (1.5 ml). The mixture was refluxed for 1.5 h, poured into a mixture of ice and dilute hydrochloric acid, and extracted with ether. The ether extract was washed with brine, dried over sodium sulfate, and evaporated *in vacuo*. The residue was chromatographed on silica gel (10 g), using ether–benzene (1:99) as the eluent, to give **16** (70 mg: 70%) as an oil; IR: 3610, 3400br, 1610, 1572 cm^{-1}; NMR: 1.13, 1.18, and 1.41 (each 3H and s, $-\dot{C}(CH_3)_2$ and $C_{10}-CH_3$), 1.21 (6H, d, J=7 Hz, $-CH(C\underline{H}_3)_2$), *ca.* 3.1 (2H, m, $C_{1\beta}$–H and C_3–H), 3.28 (2H, bd, J=4 Hz, $=CHC\underline{H}_2-$), 3.75 (3H, s, $C_{11}-OCH_3$), 5.78 (1H, t, J=4 Hz, C_6–H), 6.42 (2H, bs, C_{12}–H and C_{14}–H).

The compound (**16**) was labile and it gradually transformed into a naphthalene derivative (**18**); IR: 1705, 1627, 1572 cm^{-1}; NMR: 1.06 and 1.30 (each 6H, d, and J=7 Hz, 2-$CH(C\underline{H}_3)_2$), 2.38 (3H, s, $-CH_3$), 3.82 (3H, s, $-OCH_3$), 6.57 (1H, d, J=2 Hz), 7.01 (1H, d, J=2 Hz,) 7.05 (1H, d, J=8 Hz), and 7.30 (1H, d, J=8 Hz) (aromatic protons). Found: C, 80.76; H, 9.24%. Calcd for $C_{21}H_{28}O_2$: C, 80.73; H, 9.03%.

*3β-Acetoxy-11-methoxyabieta-5,8,11,13-tetraene (**17**).* A mixture of **16** (107 mg) and acetic anhydride (0.5 ml) in pyridine (0.5 ml) was allowed to stand overnight at room temperature. After the usual work-up, the crude product was chromatographed on silica gel (10 g). Elution with benzene gave **17** (77 mg), which was recrystallized from hexane; mp 122—122.5 °C; $[\alpha]_D$ +24° (*c* 0.37); IR: 1725, 1614, 1577 cm^{-1}; NMR: 1.11, 1.22, and 1.44 (each 3H and s, $-\dot{C}(CH_3)_2$ and $C_{10}-CH_3$), 1.21 (6H, d, J=7 Hz, $-CH(C\underline{H}_3)_2$), 1.98 (3H, s, $-OCOCH_3$), 3.30 (2H, bd, J=4 Hz, $=CHC\underline{H}_2-$), 3.78 (3H, s, $C_{11}-OCH_3$), 4.44 (1H, dd, J=9 and 6.5 Hz, C_3–H), 5.84 (1H, t, J=4 Hz, C_6–H), 6.42 and 6.44 (each 1H and bs, C_{12}–H and C_{14}–H). Found: C, 77.30; H, 9.19%. Calcd for $C_{23}H_{32}O_3$: C, 77.49; H, 9.05%.

*11-Methoxy-18-norabieta-8,11,13-trien-3-one (**19**) and 11-Methoxy-19-norabieta-8,11,13-trien-3-one (**20**).* *a)*: A solution of **12** (365 mg) in ethanol (8.0 ml) was hydrogenated using Raney Ni (W-2: 750 mg) at room temperature in an atmosphere of hydrogen. The crude dihydro compound, without purification, was oxidized with Jones reagent (2.5 M: 1.2 ml) in acetone (20 ml) at 0 °C for 30 min. After the usual work-up, the crude product was purified by column chromatography on silica gel (40 g), using ether–benzene (0.5:99.5) as the eluent, to give **20** (9 mg: 2%) as an oil. Further elution gave **19** (250 mg: 69%) as an oil; $[\alpha]_D$ +188° (*c* 2.07); IR: 1700, 1610, 1570 cm^{-1}; NMR: 1.16 (3H, d, J=7.5 Hz, C_4-CH_3), 1.21 (6H, d, J=7 Hz, $-CH(C\underline{H}_3)_2$), 1.24 (3H, s, $C_{10}-CH_3$), 3.77 (3H, s, $C_{11}-OCH_3$), 6.42 (2H, bs, C_{12}–H and C_{14}–H). Found: C, 80.05; H, 9.65%. Calcd for $C_{20}H_{28}O_2$: C, 79.95; H, 9.39%.

b): A mixture of **19** (172 mg) and sodium methoxide (154 mg) in methanol (10 ml) was refluxed for 1 h, poured into dilute hydrochloric acid, and extracted with ether. The ether extract was washed with brine, dried over sodium sulfate, and evaporated *in vacuo*. The residue was chromatographed on silica gel (15 g), using ether–benzene (1:99) as the eluent, to give **20** (168 mg: 98%) as an oil; $[\alpha]_D$ +138° (*c* 0.665); IR: 1698, 1610, 1570 cm^{-1}; NMR: 1.05 (3H, d, J=7 Hz, C_4-CH_3), 1.21 (6H, d, J=7 Hz, $-CH(C\underline{H}_3)_2$), 1.36 (3H, s, $C_{10}-CH_3$), 3.77 (3H, s, $C_{11}-OCH_3$), 6.42 (2H, bs, C_{12}–H and C_{14}–H). Found: C, 80.09; H, 9.39%. Calcd for $C_{20}H_{28}O_2$: C, 79.95; H, 9.39%.

c): A solution of **14** (121 mg) in tetrahydrofuran (2.5 ml) was added to a solution of lithium (28 mg) in liquid ammonia (12 ml) at −33 °C. The mixture was stirred at this temperature for 1 h, and ammonium chloride (321 mg) was added. After removal of the ammonia, the residue was diluted with water and extracted with ether. The ether extract was washed with brine, dried over sodium sulfate, and evaporated *in vacuo*. The residue was chromatographed on silica gel (12 g), using ether–benzene (0.5: 99.5) as the eluent, to give **20** (60 mg: 48%) as an oil; its IR and NMR spectra were identical with those of the sample prepared in *a)* and *b)*.

*11-Acetoxy-19-norabieta-8,11,13-trien-3-one (**24**).* A mixture of **20** (170 mg), ethylene glycol (0.32 ml), and *p*-toluenesulfonic acid monohydrate (17 mg) in benzene (15 ml) was refluxed for 4 h. The mixture was cooled, diluted with ether, and then washed successively with aqueous sodium hydrogencarbonate and brine. After drying over sodium sulfate, the solution was evaporated *in vacuo* to give a crude acetal (**21**) as an oil.

A solution of the above crude acetal (**21**) in *N*,*N*-dimethylformamide (10 ml) was added to sodium ethanethiolate prepared from sodium (92 mg) and ethanethiol (2.0 ml). The stirred mixture was refluxed for 2.5 h under a stream of nitrogen, cooled, poured into dilute hydrochloric acid, and extracted with ether. The ether extract was washed with brine, dried over sodium sulfate, and evaporated to give a crude phenol (**22**) as an oil.

A solution of the above crude phenol (**22**) in acetone (15 ml) was stirred with dilute hydrochloric acid (6 M: 2.0 ml) at room temperature for 1 h. The mixture was diluted with ether, washed with brine, and dried over sodium sulfate. Evaporation of the solution gave a crude keto phenol (**23**) as an oil, which was then acetylated with acetic anhydride (1.0 ml) in pyridine (1.0 ml) at room temperature for *ca.* 15 h. After the usual work-up, the crude product was purified by column chromatography on silica gel (20 g). Elution with ether–benzene (3:97) afforded **24** (173 mg: 92%), which was recrystallized from hexane; mp 105—106 °C; $[\alpha]_D$ +141° (*c* 1.37); IR: 1750, 1705, 1620, 1567 cm^{-1}; NMR: 1.07 (3H, d, J=6.5 Hz, C_4-CH_3), 1.22 (6H, d, J=7 Hz, $-CH(C\underline{H}_3)_2$), 1.31 (3H, s, $C_{10}-CH_3$), 2.23 (3H, s, $-OCOCH_3$), 6.53 and 6.71 (each 1H, d, and J=2 Hz, C_{12}–H and C_{14}–H). Found: C, 76.65; H, 8.70%. Calcd for $C_{21}H_{28}O_3$: C, 76.79; H, 8.59%.

*11-Acetoxy-19-norabieta-1,8,11,13-tetraen-3-one (**26**).* A solution of bromine (1 M: 1.25 ml) in carbon tetrachloride was added at 0 °C to a stirred solution of **24** (373 mg) in chloroform (13 ml). The mixture was further stirred at this temperature for 45 min, diluted with ether, and the ether solution was washed successively with aqueous sodium thiosulfate and brine. Evaporation of the dried solution gave a crude 2-bromo derivative (**25**) as an oil.

A stirred mixture of the crude 2-bromo compound (**25**), lithium carbonate (211 mg), and lithium bromide (158 mg)

in *N,N*-dimethylformamide (15 ml) was heated at 120—125 °C for 75 min under a stream of nitrogen. The mixture was cooled, poured into dilute sulfuric acid, and extracted with ether. The ether extract was washed with brine, dried over sodium sulfate, and evaporated *in vacuo*. The residue was purified by column chromatography on silica gel (40 g). Elution with ether–benzene (2:98) afforded **26** (205 mg: 55%) as an oil; $[\alpha]_D$ +199° (*c* 2.05); IR: 1760, 1670, 1620, 1570 cm^{-1}; NMR: 1.19 (3H, d, J=6.5 Hz, C_4–CH_3), 1.22 (6H, d, J=7 Hz, –CH($C\underline{H}_3$)$_2$), 1.34 (3H, s, C_{10}–CH_3), 2.27 (3H, s, –OCOCH_3), 5.77 (1H, d, J=10 Hz, C_2–H), 6.65 and 6.76 (each 1H, bd, and J=2 Hz, C_{12}–H and C_{14}–H), 7.78 (1H, d, J=10 Hz, C_1–H). Found: C, 77.07; H, 8.01%. Calcd for $C_{21}H_{26}O_3$: C, 77.27; H, 8.03%.

11-Methoxyabieta-1,8,11,13-tetraen-3-one (27). A solution of **26** (129 mg) in dry benzene (5.0 ml) was added to a stirred suspension of potassium *t*-pentyl oxide (prepared from potassium (139 mg) and *t*-pentyl alcohol (3.0 ml) in dry benzene (3.0 ml) over a 5 min period under a stream of nitrogen. The mixture was gently refluxed for 30 min, cooled, and a solution of methyl iodide (0.15 ml) in dry benzene (1.0 ml) was added. The mixture was refluxed for 2 h, cooled, and some additional solution of methyl iodide (0.15 ml) in dry benzene (1.0 ml) was added. The mixture was further refluxed for 2 h, cooled, poured into water, and extracted with ether. The ether extract was washed with brine, dried over sodium sulfate, and evaporated *in vacuo*. The crude product was chromatographed on silica gel (20 g). Elution with ether–benzene (1:99) gave **27** (84 mg: 68%), which was recrystallized from methanol; mp 84.5—85 °C; $[\alpha]_D$ +206° (*c* 0.670); IR: 1660, 1612, 1577 cm^{-1}; NMR: 1.11, 1.16, and 1.43 (each 3H and s, –$\underset{|}{C}(CH_3)_2$ and C_{10}–CH_3), 1.21 (6H, d, J=7 Hz, –CH($C\underline{H}_3$)$_2$), 3.86 (3H, s, C_{11}–OCH_3), 5.77 (1H, d, J=10 Hz, C_2–H), 6.49 (2H, bs, C_{12}–H and C_{14}–H), 7.96 (1H, d, J=10 Hz, C_1–H). Found: C, 80.71; H, 9.18%. Calcd for $C_{21}H_{28}O_2$: C, 80.73; H, 9.03%.

11-Hydroxyabieta-1,8,11,13-tetraen-3-one (28). A stirred mixture of **27** (28 mg) and sodium ethanethiolate (prepared from sodium (21 mg) and ethanethiol (1.5 ml)) in *N,N*-dimethylformamide (3.0 ml) was refluxed for 3 h under a stream of nitrogen. The mixture was cooled, poured into dilute hydrochloric acid, and extracted with ether. The ether extract was washed with brine, dried over sodium sulfate, and evaporated *in vacuo*. The residue was purified by column chromatography on silica gel (5.0 g), using ether–benzene (3:97) as the eluent, to give **28** (16 mg: 60%), which was recrystallized from methanol; mp 199—200 °C; $[\alpha]_D$ +190° (*c* 0.075); IR: 3580, 3280br, 1655, 1610, 1572 cm^{-1}; UV (λ_{max}^{EtOH}): 225 nm (ε 18900), 283 (2490); NMR ($CDCl_3$): 1.22 (6H, d, J=7 Hz, –CH($C\underline{H}_3$)$_2$), 1.22, 1.25, and 1.53 (each 3H and s, –$\underset{|}{C}(CH_3)_2$ and C_{10}–CH_3), 5.53 (1H, bs, –OH, disappeared on deutration), 5.96 (1H, d, J=10.5 Hz, C_2–H), 6.45 (1H, bd, J=2 Hz) and 6.59 (1H, bs) (C_{12}–H and C_{14}–H), 8.34 (1H, d, J=10.5 Hz, C_1–H). Found: C, 80.26; H, 8.98%. Calcd for $C_{20}H_{26}O_2$: C, 80.49; H, 8.78%.

11-Methoxyabieta-2,8,11,13-tetraen-1-one (31). A solution of **27** (35 mg) in methanol (10.5 ml) was cooled to −10 °C under a stream of nitrogen; then 30% hydrogen peroxide (0.064 ml) was added, followed by 5% aqueous sodium hydroxide (0.5 ml). The mixture was stirred at −12—−8 °C for 4.5 h, poured into dilute hydrochloric acid, and extracted with ether. The ether extract was washed with brine, dried over sodium sulfate, and evaporated to give an epoxy ketone (**29**) as an oil (37 mg). Without purification, this was immediately submitted to the next reaction.

A mixture of the crude **29** (37 mg), hydrazine hydrate (0.17 ml), acetic acid (0.04 ml), and methanol (3.7 ml) was refluxed for 13.5 h under a stream of nitrogen. After the methanol had been evaporated *in vacuo*, the residue was extracted with ether. The ether extract was washed successively with aqueous sodium hydrogencarbonate and brine, dried over sodium sulfate, and then evaporated to give a crude 1α-ol (**30**: 37 mg). The crude **30** (37 mg) was oxidized with Jones reagent (2.5 M: 0.112 ml) at 0 °C for 15 min. After the usual work-up, the crude product was purified by column chromatography on silica gel (5.0 g). Elution with benzene gave **31** (15 mg: 43%) as an oil; $[\alpha]_D$ +266° (*c* 1.02); IR: 1695, 1618, 1580 cm^{-1}; NMR: 1.13, 1.19, and 1.60 (each 3H and s, –$\underset{|}{C}(CH_3)_2$ and C_{10}–CH_3), 1.24 (6H, d, J=7 Hz, –CH($C\underline{H}_3$)$_2$), 3.73 (3H, s, C_{11}–OCH_3), 5.77 and 6.16 (each 1H, d, and J=10 Hz, C_2–H and C_3–H), 6.43 and 6.54 (each 1H and bs, C_{12}–H and C_{14}–H). Found: C, 80.55; H, 9.19%. Calcd for $C_{21}H_{28}O_2$: C, 80.73; H, 9.03%.

Demethylation of 31. A solution of **31** (10.0 mg) and boron tribromide (0.015 ml) in dichloromethane (0.50 ml) was stirred at 0 °C for 30 min, poured into a mixture of ice and water, and extracted with ether. The ether extract was washed with brine, dried over sodium sulfate, and evaporated *in vacuo*. The residue was purified by column chromatography on silica gel (5.0 g), using benzene as the eluent, to give 11-hydroxyabieta-2,8,11,13-tetraen-1-one (**1**) (4.7 mg: 49%) as an oil; $[\alpha]_D$ +470° (*c* 0.35); IR: 3200br, 1657, 1615, 1567 cm^{-1}; UV (λ_{max}^{EtOH}): 222.5 nm (ε 15500), 281.5 (2220); NMR: 1.21 (6H, d, J=7 Hz, –CH($C\underline{H}_3$)$_2$), 1.22 (6H, s, –$\underset{|}{C}(CH_3)_2$), 1.58 (3H, s, C_{10}–CH_3), 5.88 and 6.56 (each 1H, d, and J=10 Hz, C_2–H and C_3–H), 6.37 and 6.60 (each 1H and bs, C_{12}–H and C_{14}–H). Found: C, 80.28; H, 8.93%. Calcd for $C_{20}H_{26}O_2$: C, 80.49; H, 8.78%.

Further elution with benzene gave 3β-bromo-11-hydroxyabieta-8,11,13-trien-1-one (**32**) (6.0 mg: 50%) as an oil; IR: 3320br, 1690 cm^{-1}; NMR: 1.18 (6H, d, J=7 Hz, –CH($C\underline{H}_3$)$_2$), 1.22 and 1.24 (each 3H and s, –$\underset{|}{C}(CH_3)_2$), 1.64 (3H, s, C_{10}–CH_3), 2.91 (1H, dd, J=12 and 4.5 Hz, $C_{2\alpha}$–H), 3.60 (1H, dd, J=13 and 12 Hz, $C_{2\beta}$–H), 4.04 (1H, dd, J=13 and 4.5 Hz, $C_{3\alpha}$–H), 5.63 (1H, bs, –OH), 6.41 and 6.52 (each 1H and bs, C_{12}–H and C_{14}–H).

A mixture of **32** (6.0 mg), lithium carbonate (8.0 mg), and lithium bromide (6.0 mg) in *N,N*-dimethylformamide (1.0 ml) was heated at 120—125 °C for 3 h under a stream of nitrogen. After the same work-up as described for the preparation of **26**, the crude product was chromatographed on silica gel (5.0 g). Elution with benzene gave a colorless oil (4.9 mg: 96%), whose IR and NMR spectra were identical with those of **1**.

The authors are grateful to Arakawa Chemical Co. Ltd. for the generous gift of (+)-13β-abieta-8-en-18-oic acid.

References

1) Y. T. Lin and K. T. Liu, *J. Chinese Chem. Soc. Taiwan*, **12**, 51 (1965).

2) T. Matsumoto, I. Tanaka, T. Ohno, and K. Fukui, *Chem. Lett.*, **1973**, 321.

3) T. Matsumoto, T. Ohno, H. Fujita, and K. Fukui, *Chem. Lett.*, **1973**, 1117.

4) W. Herz and J. J. Schmid, *J. Org. Chem.*, **34**, 3464

(1969); the compounds, **2** and **3**, were also obtained by Collins oxidation of methyl (+)-13β-abieta-8-en-18-oate in our laboratory (unpublished data).

5) D. Bondon, Y. Pietrasanta, and B. Pucci, *Tetrahedron Lett.*, **1977**, 821.

6) Y. Ohtsuka and A. Tahara, *Chem. Pharm. Bull.*, **21**, 653 (1973).

7) T. Matsumoto, S. Imai, M. Aizawa, H. Kitagawa, and K. Fukui, *Chem. Lett.*, **1972**, 581.

8) M. A. Umbreit and K. B. Sharpless, *J. Am. Chem. Soc.*, **99**, 5526 (1977).

9) T. Matsumoto, S. Usui, H. Kawashima, and M. Mitsuki, *Bull. Chem. Soc. Jpn.*, **54**, 581 (1981).

10) M. Fetizon and G. Moreau, *Bull. Soc. Chim. Fr.*, **1965**, 3479.

11) A direct bromination of **20** gave a large amount of unexpected compounds possessing a bromine atom in the aromatic C ring.

12) H. W. Whitlock, Jr., P. B. Reichardt, and F. M. Silver, *J. Am. Chem. Soc.*, **93**, 485 (1971).

13) It is well known that epoxidation occurs preferentially from the less hindered α face of the molecule.[3,4,12]

14) T. Matsumoto and S. Usui, *Bull. Chem. Soc. Jpn.*, **52**, 212 (1979).

Intramolecular Cyclization of Nerol and the Related Attack of (*Z*)-Allylic Alcohol Moiety on the Terminal Olefin Linkage as Induced by $TiCl_4$-PhNHMe Complex. Synthesis of Nezukone

Akira Itoh, Tadashi Saito, Koichiro Oshima,* and Hitosi Nozaki

Department of Industrial Chemistry, Faculty of Engineering, Kyoto University, Yoshida, Sakyo-ku, Kyoto 606

(Received November 10, 1980)

Nerol was cyclized to terpinyl chloride or bromide in the presence of TiX_4–PhNHMe (1:1) complex (I, X= Cl, Br) in dichloromethane at −23 °C, geraniol being converted into geranyl halide by simple halogenation. Terminally modified derivatives $YCH_2C(Me)=CHCH_2CH_2CMe=CHCH_2OH$ (Y=$SiMe_3$, $SnBu_3$) of (2*Z*,6*E*) configuration were cyclized by treatment with I to afford limonene in high yields and 100% selectivity. Cyclization of (2*Z*) isomers of $CH_2=CR-CH_2CH_2CMe=CHCH_2OH$ (R=H, Me, Cl) produced seven-membered carbocyclic products in fair yields. The novel procedure has been utilized in the synthesis of nezukone from (2*E*)-3-isopropyl-2,6-heptadien-1-ol involving five steps.

The reaction of diethyl neryl phosphate with organoaluminium reagents R_2AlX (X=OR, NHR, *etc.*) has led to the stereospecific synthesis of limonene and similar cyclic terpenes.[1] The smooth cyclization is ascribed to the combined Lewis acid-base character of the reagents.[2] We wish to report on the cyclization technique of this type which is more efficient and much simpler.[3]

Addition of *N*-methylaniline (1.0 mmol) to a solution of TiX_4 (X=Cl or Br, 1.0 mmol) in dichloromethane at 0 °C gave a complex.[4] Both the chloride and bromide complexes reacted smoothly at −23 °C with nerol itself,[5] providing terpinyl halides **1a** and **1b**, respectively, in fair yields. In contrast to the previous organoaluminium reactions[1] or acid catalyzed solvolytic reactions,[6] formal carbocation is thus stabilized by halide ion-uptake rather than by proton-loss.[7]

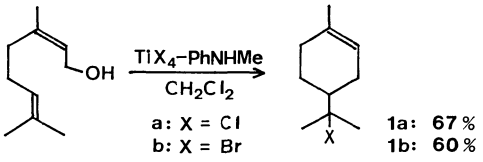

Analogous treatment of geraniol with TiX_4–PhNHMe complex gave the corresponding geranyl halides in good yields. The drastic alteration in the course of the reaction demonstrates that the steric integrity of the allylic double bond is strictly preserved in a possible intermediate, allylic carbocation.[2] The results are similar to those obtained in the reactions of diethyl neryl phosphate or diethyl geranyl phosphate with organoaluminium reagents R_2AlX or R_3Al.[1a,1b] The TiX_4–PhNHMe complex provides an efficient method for the transformation of allylic alcohols into allylic halides as shown below.[8]

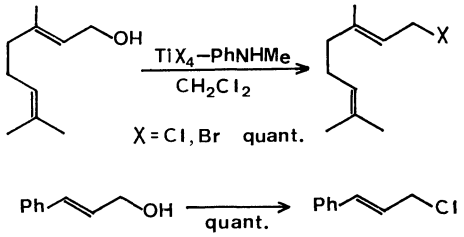

Reaction of nerol with $TiCl_4$ alone afforded a complex mixture not containing terpinyl chloride. It is apparent that the 1:1 complex behaves differently. The 1:1 molar ratio of $TiCl_4$ and PhNHMe gave the best result.[9] Several amines were examined for the reaction of nerol with $TiCl_4$–amine complex with reaction conditions and yield of terpinyl chloride as follows: *N*-methylaniline, 20 min at −23 °C, 67%; 2,2,6,6-tetramethylpiperidine, 20 min at −23 °C, 65%; triethylamine, 1 h at 25 °C, 52%; 1,4-diazabicyclo-[2.2.2]octane, 12 h at 25 °C, 40%; diethylamine, 20 min at −23 °C, 32%; α-methylbenzylamine, 20 min at −23 °C, 28%; pyridine, 3 h at 25 °C, 0%. Several other metal chlorides similar to $TiCl_4$ were also examined. A complex VCl_4–PhNHMe gave **1a** in 50% yield and $AlCl_3$–PhNHMe (38%) was found to be marginal. Halides such as $ZrCl_4$, WCl_6, and $SnCl_4$ gave no sign of cyclized products with or without an amine.

The halides **1a** and **1b** are slowly decomposed on treatment with silica gel in dichloromethane at room temperature to give a complex mixture of hydrocarbons mainly consisting of limonene and terpinolene. Selective synthesis of limonene was achieved in the following way.[10] Treatment of **2a** and **2b** with $TiCl_4$–PhNHMe complex resulted in the exclusive formation of limonene ascribed to the expected selective elimination of $SiMe_3$ or $SnBu_3$ groups from terpinyl carbocation.[11] This method is superior to the previously

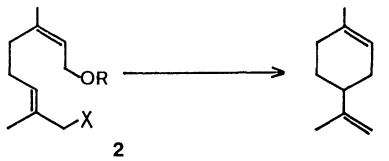

	X	R	Reagent	Yield of **3**/%
2a	$SiMe_3$	H	$TiCl_4$-PhNHMe/CH_2Cl_2	79
2a′	$SiMe_3$	$COCH_3$	$MeAl(OCOCF_3)_2$/hexane	29[a]
2b	$SnBu_3$	H	$TiCl_4$-PhNHMe/CH_2Cl_2	73
2b′	$SnBu_3$	$COCH_3$	$MeAl(OCOCF_3)_2$/hexane	51

a) Polymeric products were obtained.

Table 1. Seven-membered ring formation by means of TiX_4–PhNHMe complexes

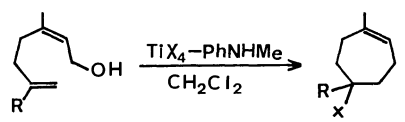

R	X	Y/%
H	Cl	65
H	Br	56
Me	Cl	66
Cl	Cl	18[a]

a) The corresponding allylic chloride was obtained in a 54% yield.

reported one[1c] using organoaluminium reagent $MeAl(OCOCF_3)_2$ as far as cyclization yields are concerned.

Treatment of (*Z*)-allylic alcohols $CH_2{=}CR{-}CH_2CH_2{-}CMe{=}CHCH_2OH$ (R=H, Me, Cl) with the complex $TiCl_4$–PhNHMe gave seven-membered ring products carrying X on the R-substituted carbon. The novel route to cycloheptenes gives satisfactory yields (Table 1). The (*E*)-alcohols produce the corresponding allylic halides as in the geraniol case.

The present method has provided us with a simple route to troponoid derivatives, which has been exemplified by the synthesis of nezukone. The transformation of allylic alcohol **4** into the cycloheptenyl chloride **5** was easily performed in 60% yield by means of $TiCl_4$–PhNHMe complex. None of the conceivable S_N2 type reactions worked at all with the C–Cl bond of **5**, which was always recovered intact.[12] The difficulty was solved by trapping the Grignard reagent derived from **5** with Bu_3SnCl and successive oxidation by Still's method,[13] which provided cycloheptenone **6** (65%). Nezukone was obtained by simple bromination-debromination procedure (60%).[14]

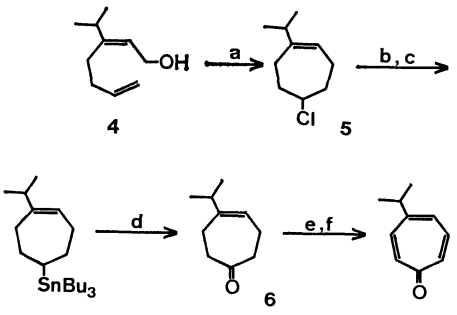

a, $TiCl_4$–PhNHMe ; b, Mg ; c, Bu_3SnCl

d, $CrO_3 \cdot 2py$; e, $(NH)_3 \cdot HBr_3$

f, LiCl–DMF

Experimental

Infrared spectra were determined on a Shimadzu IR 27-G spectrometer, mass spectra on a Hitachi RMU 6-L machine, GLPC analyses on a Yanagimoto GCG 550-F, and NMR spectra on a JEOL C-60H or Varian EM 390H spectrometer. The chemical shifts are given in δ in ppm with TMS as an internal standard. Splitting patterns are denoted by s, singlet; d, doublet; t, triplet; q, quartet; m, multiplet. Microanalysis was carried out at the Elemental Analyses Center of Kyoto University. All the experiments were carried out under an atmosphere of dry argon. Tetrahydrofuran was dried by distillation from sodium-benzophenone. Thin and thick layer plates were made of E. Merck PF-254, and preparative columns silica gel E. Merck Art. 7734.

Reaction between Nerol and $TiCl_4$–PhNHMe Complex. A solution of titanium tetrachloride in dichloromethane (1.0 M, 4.5 ml) was added to a solution of *N*-methylaniline (0.48 g, 4.5 mmol) in dichloromethane (5 ml) at 0 °C. No evolution of HCl took place. After 20 min, the resulting dark red solution was cooled to −23 °C, treated with nerol (0.46 g, 3.0 mmol), and allowed to stand at −23 °C for 1 h. Water and ether were added and the organic layer was washed with 1 M HCl, saturated aqueous solution of sodium hydrogencarbonate, and brine, dried, and concentrated. Purification by pre-cooled column chromatography on silica gel afforded terpinyl chloride **1a** (0.29 g, 57% yield) as a colorless oil: bp 108—109 °C (15 Torr, 1 Torr= 133.322 Pa); IR (neat) 2930, 1438, 1385, 1368, 1118 cm^{-1}; NMR (CCl_4) δ 1.50 (s, 3H), 1.55 (s, 3H), 1.63—2.20 (m, 10H), 5.33 (m, 1H); MS *m/e* (%) 174 (3), 172 (10), 136 (47), 121 (61), 95 (59), 93 (100). Found: C, 69.33; H, 10.14%. Calcd for $C_{10}H_{17}Cl$: C. 69.55; H, 9.92%.

Similarly, the reaction between nerol and $TiBr_4$–PhNHMe complex afforded terpinyl bromide **1b** (60% yiled): IR (neat) 2950, 1460, 1375, 1358, 1100 cm^{-1}; NMR (CCl_4) δ 1.50—1.80 (m, 3H), 1.63 (s, 3H), 1.71 (s, 3H), 1.77 (s, 3H), 1.90—2.10 (m, 4H), 5.28 (m, 1H); MS *m/e* (%) 218 (6), 216 (6), 186 (12), 137 (45), 136 (32), 121 (32), 95 (38), 93 (52), 81 (100).

(2Z)-3-Methyl-2,6-heptadien-1-ol and (2Z)-3,6-Dimethyl-2,6-heptadien-1-ol. These compounds were obtained according to a procedure similar to that for the preparation of (2*Z*)-6-chloro-3-methyl-2,6-heptadien-1-ol (**7**). Separation of *E* and *Z* isomers was performed prior to aluminium hydride reduction.

5-Chloro-1-methylcycloheptene: Bp 90 °C (20 Torr); IR (neat) 2950, 1450, 1235, 820 cm^{-1}; NMR (CCl_4) δ 1.70—2.50 (m, 11H), 4.17 (m, 1H), 5.50 (m, 1H); MS *m/e* (%) 146 (10), 144 (27), 109 (33), 95 (33), 93 (100), 91 (27). Found: C, 66.42; H, 9.35%. Calcd for $C_8H_{13}Cl$: C, 66.43; H, 9.06%.

5-Chloro-1,5-dimethylcycloheptene: Bp 96—97 °C (21 Torr); IR (neat) 2940, 1440, 1365, 1190, 1070, 770 cm^{-1}; NMR (CCl_4) δ 1.60 (s, 3H), 1.70 (s, 3H), 1.65—2.63 (m, 8H), 5.47 (m, 1H); MS *m/e* (%) 160 (12), 158 (29), 123 (30), 122 (30), 107 (84), 94 (63), 93 (100). Found: *m/e* 158.0874. Calcd for $C_9H_{15}Cl$: M, 158.0863.

(2Z)-6-Chloro-3-methyl-2,6-heptadien-1-ol (7). A solution of methyl acetoacetate (7.5 ml, 70 mmol) in THF (250 ml) was successively treated with sodium hydride (70 mmol) and butyllithium (1.8 M solution in hexane, 40 ml, 72 mmol) at 0 °C.[15] A solution of 2,3-dichloropropene (5.5 ml, 60 mmol) in THF (20 ml) was added to the resulting orange solution at −78 °C. After 3 h at −78 °C and 30 min at 0 °C, the mixture was poured into water and extracted with ethyl acetate. The crude product was dissolved in aqueous sodium hydroxide solution (0.9 M, 200 ml) and heated at reflux for 70 min. Extractive work-up (ether) gave essentially pure 5-chloro-5-hexen-2-one (6.4 g, 49 mmol) in 81% yield. Treatment of the hexenone (2.9 g, 22 mmol) with lithiated ethyl trimethylsilylacetate[16] (20 mmol, pre-

pared *in situ* from lithium dicyclohexylamide and ethyl trimethylsilylacetate) in THF (125 ml) at −78 °C for 30 min and at 25 °C for 30 min gave an *E* and *Z* mixture of ethyl 6-chloro-3-methyl-2,6-heptadienoate (**8**) in nearly quantitative yield. Pure samples of *E* and *Z* isomer were obtained by preparative TLC (hexane:ether=2:1) and the stereochemistry was assingned by the examination of their NMR spectra in CCl_4.

E-Isomer: δ 1.25 (t, J=6.9 Hz, 3H), 2.14 (s, 3H), 2.43 (bs, 4H), 4.06 (q, J=6.9 Hz, 2H), 5.12 (s, 2H), 5.60 (s, 1H).

Z-Isomer: δ 1.25 (t, J=6.9 Hz, 3H), 1.91 (s, 3H), 2.56 (m, 2H), 2.83 (m, 2H), 4.06 (q, J=6.9 Hz, 2H), 5.12 (s, 2H), 5.60 (s, 1H).

A solution of **8** (4.4 g, 22 mmol, mixture of stereoisomers) in ether (25 ml) was added to a mixture of lithium aluminium hydride (2.1 g, 55 mmol) and aluminium chloride (1.9 g, 14 mmol) in ether (200 ml) at 0 °C and the mixture was stirred for 80 min. Purification by silica gel column chromatography (hexane: ether=2:1) gave the title compound **7** (1.7 g, 11 mmol) in 48% yield along with the *E* isomer (0.86 g, 5.4 mmol, 24% yield). The (*Z*) compound (**7**): bp 118 °C (bath temp, 21 Torr); IR (neat) 3326, 1660, 1632, 878 cm^{-1}; NMR (CCl_4) δ 1.74 (s, 3H), 2.36 (bs, 5H), 4.03 (d, J=6.6 Hz, 2H), 5.11 (s, 2H), 5.41 (t, J=6.6 Hz, 1H); MS *m/e* (%) 144 (2), 142 (6), 129 (26), 107 (41), 91 (52), 84 (58), 79 (47), 71 (100). Found: C, 59.68; H, 8.10%. Calcd for $C_8H_{13}ClO$: C, 59.81; H, 8.16%.

E-Isomer of **7**: NMR (CCl_4) δ 1.69 (s, 3H), 2.19—2.57 (m, 4H), 4.03 (q, J=6.6 Hz, 2H), 5.17 (s, 2H), 5.45 (t, J=6.6 Hz, 1H).

5,5-Dichloro-1-methylcycloheptene. The compound was obtained in 18% yield by treatment of **7** with $TiCl_4$–PhNHMe complex: bp 60 °C (bath temp, 1 Torr); IR (neat) 2950, 1445, 1190, 1025, 980, 940, 835, 755, 700 cm^{-1}; NMR (CCl_4) δ 1.70 (s, 3H), 2.10—2.50 (m, 8H), 5.50 (t, J=6.0 Hz, 1H); MS *m/e* (%) 182 (2), 180 (10), 178 (15), 119 (20), 117 (25), 107 (100). Found: C, 53.36; H, 6.97%. Calcd for $C_8H_{12}Cl_2$: C, 53.65; H, 6.75%.

(2Z)-1,6-Dichloro-3-methyl-2,6-heptadiene: IR (neat) 1662, 1632, 1254, 883 cm^{-1}; NMR (CCl_4) δ 1.81 (s, 3H), 2.45 (bs, 4H), 4.03 (d, J=7.8 Hz, 2H), 5.19 (s, 2H), 5.53 (t, J=7.8 Hz, 1H); MS *m/e* (%) 182 (0.3), 180 (2), 178 (3), 142 (7), 107 (41), 91 (99), 79 (57), 77 (100).

Reaction between Geraniol and $TiCl_4$–PhNHMe Complex. A solution of geraniol (0.31 g, 2.0 mmol) in dichloromethane (2 ml) was added to the $TiCl_4$–PhNHMe complex derived from $TiCl_4$ (2.2 mmol) and PhNHMe (2.2 mmol) in dichloromethane (5 ml) at −23 °C. After 1 h, the mixture was diluted with hexane and washed with water and brine. Essentially pure geranyl chloride (NMR analysis) was obtained in quantitative yield after removal of the solvent.

*(2Z,6E)-3,7-Dimethyl-8-trimethylsilyl-2,6-octadien-1-ol (**2a**).* Treatment of (2*E*,6*Z*)-8-acetoxyl-1-bromo-2,6-dimethyl-2,6-octadiene **9**[17] (1.3 g, 4.6 mmol) with sodium benzenethiolate (13.5 mmol) in methanol (20 ml) at 65 °C for 2 h gave (2*Z*,6*E*)-3,7-dimethyl-8-phenylthio-2,6-octadien-1-ol quantitatively. The sulfide (1.0 g, 4.0 mmol) was dissolved in THF (18 ml) and successively treated with butyllithium (1.7 M solution in hexane, 2.8 ml, 4.8 mmol) and *s*-butyllithium (0.85 M solution in hexane, 5.6 ml, 4.8 mmol) at −78 °C. After 15 min, chlorotrimethylsilane (1.5 ml, 12 mmol) was added and the mixture was stirred for 45 min at −78 °C and for 15 min at 25 °C. Hydrochloric acid (1.0 M, 4.0 ml) was added and the mixture was stirred for an additional 30 min at 25 °C. The crude trimethylsilylated sulfide was added to a solution of lithium (0.16 g, 23 mg-atoms) in ethylamine (5 ml) at −70 °C. After 40 min, ether and methanol were added and the mixture was poured into ice–water. Purification by silica gel column chromatography afforded **2a** (0.49 g, 2.2 mmol, 55% yield based on the sulfide) as a colorless oil: bp 122 °C (bath temp, 0.5 Torr); IR (neat) 3350, 1665, 1252, 995 cm^{-1}; NMR (CCl_4) δ 0.00 (s, 9H), 1.41 (s, 2H), 1.54 (s, 3H), 1.66 (s, 3H), 2.00 (m, 4H), 3.95 (d, J=7.2 Hz, 2H), 4.91 (m, 1H), 5.35 (t, J=7.2 Hz, 1H); MS *m/e* (%) 147 (4), 143 (3), 141 (4), 134 (3), 121 (5), 105 (3), 75 (27), 73 (100). Found: C, 69.03; H, 11.51%. Calcd for $C_{13}H_{26}OSi$: C, 68.96; H, 11.57%.

*(2Z,6E)-3,7-Dimethyl-8-tributylstannyl-2,6-octadien-1-ol (**2b**).* A solution of butyllithium in hexane (1.5 M, 6.0 ml, 9.0 mmol) was added to a solution of hexabutyldistannane (5.0 ml, 9.8 mmol) in THF (30 ml) at −23 °C.[18] After 15 min, the resulting reddish yellow solution was cooled to −78 °C and treated with the bromide **9** (0.63 g, 2.3 mmol) dissolved in THF (2 ml). After 20 min at −78 °C and 20 min at 0 °C, the mixture was poured into water and extracted with ether. Purification by pre-cooled silica gel column chromatography (hexane: ether=2:1) gave **2b** (0.28 g, 27% yield) as a colorless oil: IR (neat) 3340, 1650, 1364, 1001 cm^{-1}; NMR (CCl_4) δ 0.77—0.95 (m, 15H), 1.08—1.60 (m, 15H), 1.54 (s, 3H), 1.71 (s, 3H), 2.02 (m, 4H), 3.95 (d, J=7.2 Hz, 2H), 4.87 (m, 1H), 5.35 (t, J=7.2 Hz, 1H); MS *m/e* (%) 365 (5), 363 (50), 361 (25), 360 (9), 359 (19), 358 (8), 357 (12), 69 (100).

*Reaction between **2a** and $TiCl_4$–PhNHMe Complex.* A solution of **2a** (0.20 g, 0.88 mmol) in dichloromethane (2 ml) was treated with the $TiCl_4$–PhNHMe complex (1.3 mmol) in dichloromethane (5 ml) at −23 °C. After 1 h, 1-dodecene (internal standard, 84 mg) was added and the mixture was worked up in the usual way. The yield of limonene (77%) was determined by GLPC analysis (Apiezone L 5% and KOH 1% on Chromosorb WMW dmcs, 2 m, 85 °C). Reaction between **2b** and the $TiCl_4$–PhNHMe complex was similarly performed (−23 °C, 2 h), the yield being determined by GLPC.

*Reaction between the Acetate of **2a** and Methylaluminium Bis(trifluoroacetate).* A solution of the acetate of **2a** (0.25 g, 0.94 mmol) in hexane (1 ml) was added to methylaluminium bis(trifluoroacetate)[11] (1.9 mmol, prepared *in situ*) in hexane (2 ml) and the mixture was stirred at 25 °C for 17 h. The yield (28%) was determined by GLPC. The reaction between the acetate of **2b** and the aluminium reagent was similarly performed (25 °C, 21 h).

*(2Z)-3-Isopropyl-2,6-heptadien-1-ol (**4**).* Allylation of 3-methyl-2-butanone dimethylhydrazone and subsequent hydrolysis[19] afforded 2-methyl-6-hepten-3-one in 51% yield based on the hydrazone. The allylic alcohol **4** was obtained from this ketone in the usual way.

*5-Chloro-1-isopropylcycloheptene (**5**).* A solution of **4** (0.80 g, 5.3 mmol) in dichloromethane (3.5 ml) was added to the $TiCl_4$–PhNHMe complex (8.0 mmol) in dichloromethane (15 ml) at 0 °C. After 15 min at 0 °C and 10 min at 25 °C, the mixture was worked up. The crude product was subjected to silica gel column chromatography to give **5** (0.55 g, 3.2 mmol) in 60% yield as a colorless oil: bp 120 °C (bath temp, 10 Torr); IR (neat) 1650, 1245, 830, 790, 735 cm^{-1}; NMR (CCl_4) δ 0.93 (d, J=7.0 Hz, 6H), 1.5—2.6 (m, 9H), 4.10 (m, 1H), 5.53 (t, J=6.3 Hz, 1H). Found: C, 69.77; H, 9.70%. Calcd for $C_{10}H_{17}Cl$: C, 69.55; H, 9.92%.

*4-Isopropyl-4-cycloheptenone (**6**).* A mixture of the chloride **5** (1.0 g, 6.0 mmol), granular magnesium (0.43 g, 18 mg-atoms), and ether (8.5 ml) was refluxed for 20 min, a solution of tributylstannyl chloride (3.3 g, 10 mmol) in

ether (3 ml) being added. After 20 min at reflux, the mixture was poured into saturated aqueous ammonium chloride and extracted with ether. The crude product was dissolved in dichloromethane (25 ml) and added to a mixture of pyridine (19 ml, 0.24 mol) and chromium(VI) oxide (12 g, 0.12 mol) in dichloromethane (300 ml). After 12 h at 25 °C, the mixture was filtered through a pad of Celite 545, the filtrate being washed with 5% sodium hydroxide solution (three times), 1 M HCl (three times), and brine. Purification by silica gel column chromatography gave **6** (0.60 g, 3.9 mmol, 65% yield based on the chloride **5**): bp 80 °C (bath temp, 3 Torr); IR (neat) 1705, 1660, 1460, 1260 cm^{-1}; NMR (CCl_4) δ 1.00 (d, J=7.0 Hz, 6H), 2.0—2.6 (m, 9H), 5.57 (t, J=5.7 Hz, 1H); MS *m/e* (%) 152 (M^+, 94), 137 (34), 124 (28), 119 (27), 110 (36), 109 (76), 95 (100). Found: *m/e* 152.1189. Calcd for $C_{10}H_{16}O$: M, 152.1200.

Nezukone. Pyrrolidone hydrotribromide (0.20 g, 0.40 mmol) was added to a solution of the cycloheptenone **6** (20 mg, 0.13 mmol) in THF (5 ml) and the mixture was stirred in the dark at 25 °C for 24 h. The solvent was removed under reduced pressure and the residue was diluted with water (25 ml) and chloroform (10 ml). The aqueous layer was extracted with chloroform (10 ml, four times). The crude product was dissolved in DMF (5 ml) and the solution heated at 150 °C for 1 h in the presence of anhydrous lithium chloride (0.10 g). Water was added and the product was extracted with chloroform. Purification by preparative TLC (benzene: ether=2:1) gave nezukone (12 mg, 0.08 mmol) in 62% yield whose spectral characteristics (IR, NMR, MS) were identical with those reported.[20]

Financial support by the Ministry of Education, Science and Culture, Japanese Government, (Grant-in-Aid No. 403022 and No. 375472) is acknowledged.

References

1) a) Y. Kitagawa, S. Hashimoto, S. Iemura, H. Yamamoto, and H. Nozaki, *J. Am. Chem. Soc.*, **98**, 5030 (1976); b) S. Hashimoto, Y. Kitagawa, S. Iemura, H. Yamamoto, and H. Nozaki, *Tetrahedron Lett.*, **1976**, 2615; c) S. Hashimoto, A. Itoh, Y. Kitagawa, H. Yamamoto, and H. Nozaki, *J. Am. Chem. Soc.*, **99**, 4192 (1977); d) H. Yamamoto and H. Nozaki, *Angew. Chem. Int. Ed. Engl.*, **17**, 169 (1978).

2) K. Oshima and H. Nozaki, *Yuki Gosei Kagaku Kyokai Shi*, **38**, 450 (1980).

3) Preliminary account of this work has appeared: T. Saito, A. Itoh, K. Oshima, and H. Nozaki, *Tetrahedron Lett.*, **1979**, 3519.

4) V. H. Burger and H. J. Neese, *Z. Anorg. Allg. Chem.*, **365**, 243 (1969).

5) Treatment of acetate or diethyl phosphate of nerol with these reagents afforded terpinyl halide in 46—56% yield.

6) C. A. Bunton, O. Cori, D. Hachey, and J-P. Leresche, *J. Org. Chem.*, **44**, 3238 (1979).

7) a) W. S. Johnson, *Angew. Chem. Int. Ed. Engl.*, **15**, 13 (1976); b) T. Kobayashi, S. Kumazawa, T. Kato, and Y. Kitahara, *Chem. Lett.*, **1975**, 301.

8) R. M. Magid, *Tetrahedron*, **36**, 1924 (1980).

9) In an attempt to find the suitable molar ratio between $TiCl_4$ and PhNHMe, we studied the reaction of nerol with a variety of complexes derived from different molar ratios. The yields of terpinyl chloride were 67% ($TiCl_4$: PhNHMe= 1: 1), 20% (1: 2), and 0% (1: 3 and 1: 4).

10) Another solution of this problem on the termination of the cationic cyclization was provided by the use of bulky O-base in the R_2AlOAr system. See Ref. 1d.

11) a) Allylsilanes for termination: I. Fleming and A. Pearce, *J. Chem. Soc., Chem. Commun.*, **1976**, 182; T. K. Sarkar and N. H. Anderson, *Tetrahedron Lett.*, **1978**, 3513; b) Silylacetylenes: K. Utimoto, M. Tanaka, M. Kitai, and H. Nozaki, *ibid.*, **1978**, 2301; W. S. Johnson, T. M. Yarnell, R. F. Myers, and D. R. Morton, *ibid.*, **1978**, 2549; c) Silyl enol ethers: See Ref. 1c.

12) The failure of all the S_N2 type reactions attempted is ascribed to the opposed π bond. See S. J. Rhoads, J. M. Watson, and J. G. Kambouris, *J. Am. Chem. Soc.*, **100**, 5151 (1978).

13) W. C. Still, *J. Am. Chem. Soc.*, **99**, 4836 (1977).

14) H. Takaya, Y. Hayakawa, S. Makino, and R. Noyori, *J. Am. Chem. Soc.*, **100**, 1778 (1978).

15) S. N. Huckin and L. Weiler, *J. Am. Chem. Soc.*, **96**, 1082 (1974).

16) K. Shimoji, H. Taguchi, K. Oshima, H. Yamamoto, and H. Nozaki, *J. Am. Chem. Soc.*, **96**, 1620 (1974).

17) P. A. Grieco, *J. Chem. Soc., Chem. Commun.*, **1972**, 486.

18) W. C. Still, *J. Am. Chem. Soc.*, **100**, 1481 (1978).

19) E. J. Corey and D. Enders, *Chem. Ber*, **111**, 1337 (1978).

20) "Spectral Atlas of Terpenes and the Related Compounds," ed by Y. Yukawa and S. Ito, Hirokawa Publishing Co. Inc., Tokyo (1973), p. 156.

Tellurium-catalyzed Carbonylation of Amines with Carbon Monoxide[1)]

Nobuaki KAMBE, Kiyoshi KONDO, Hideo ISHII, and Noboru SONODA*

Department of Petroleum Chemistry, Faculty of Engineering, Osaka University, Suita, Osaka 565

(Received November 10, 1980)

Carbonylation of amines with carbon monoxide was catalyzed by tellurium to produce corresponding urea derivatives, formamides, and molecular hydrogen. The urea formation proceeds according to the equation; $2RNH_2+CO \rightarrow (RNH)_2CO+H_2$. The successful achievement of the catalytic formation of urea derivatives would be due to the thermal instability of hydrogen telluride which decomposes to generate elemental tellurium and hydrogen. The formation of formamides and hydrogen was found to be suppressed by the addition of nitrobenzene which did not affect the urea formation. Effects of the reaction time, temperature, pressure of carbon monoxide, and additives on this carbonylation reaction are discussed.

Carbonylation of amines with carbon monoxide to produce urea derivatives by the use of S,[2)] Se,[3)] $Fe(CO)_5$,[4)] AgOAc,[5)] and inorganic oxidizing agents[6)] has been known to proceed as stoichiometric reaction. On the other hand, in order to carry out this carbonylation catalytically many studies have been done to show the effectiveness of Se,[3)] transition metals, and their complexes of Hg,[7)] Mn,[8)] Fe,[9)], Co,[10)] Ni,[11)] Rh,[12)] Pd,[13)] W,[14)] Pt.[15)]

The reaction of primary amines with carbon monoxide in the presence of sulfur gave corresponding urea derivatives and hydrogen sulfide[2)] (Reaction 1).

$$2\,RNH_2 + CO + S \longrightarrow (RNH)_2CO + H_2S \qquad (1)$$

This reaction gave moderate yields of ureas based on sulfur used, and it required high temperature and high pressure of carbon monoxide.

In contrast to the above sulfur dependent reaction, under mild reaction conditions selenium[3)] catalyzed the carbonylation of various amines with carbon monoxide and oxygen to afford quantitative yields of urea derivatives with high selectivity (Reaction 2). This

$$2\,RR'NH + CO + \frac{1}{2}O_2 \xrightarrow[\text{r. t., 1 atm}]{\text{Se}} (RR'N)_2CO + H_2O \qquad (2)$$

reaction was shown to consist of the carbonylation reaction (Reaction 3), and the oxidative regeneration of the catalyst (Reaction 4).

$$2\,RR'NH + CO + Se \longrightarrow (RR'N)_2CO + H_2Se \qquad (3)$$

$$H_2Se + \frac{1}{2}O_2 \longrightarrow Se + H_2O \qquad (4)$$

In the periodic table, tellurium belongs to the same VIa group as oxygen, sulfur, and selenium. The present paper describes the novel carbonylation of amines with carbon monoxide catalyzed by elemental tellurium. The tellurium-catalyzed carbonylation is shown characteristically in the simplest mode to form the equimolar amounts of ureas and molecular hydrogen (Reaction 5). In this reaction, the formation

$$2\,RNH_2 + CO \xrightarrow{\text{Te}} (RNH)_2CO + H_2 \qquad (5)$$

of formamide derivatives was found to occur (Reaction 6).

$$RNH_2 + CO \longrightarrow RNHCHO \qquad (6)$$

Results and Discussion

General Reactions. Butylamine, octylamine, cyclohexylamine, and benzylamine were examined for this carbonylation reaction. The results are shown in Table 1. The equimolar amounts of ureas and molecular hydrogen were obtained (Reaction 5). Un-

Table 1. Tellurium-catalyzed carbonylation[a)] of amines with CO

Run	Amine (100 mmol)	Te (mmol)	Time h	Urea (mmol)	H_2 (mmol)	Formamide (mmol)
1	*n*-$BuNH_2$	1	10	7.6	7.1	10.0
2	*n*-$BuNH_2$	1	10	7.7	7.4	15.3
3	*n*-$BuNH_2$	1	10	7.4	7.0	12.5
4	*n*-$BuNH_2$	1	10	7.8	7.2	17.3
5	*n*-$BuNH_2$	0.05	10	2.9	2.9	1.3
6	*n*-$BuNH_2$	1	72	22.0	21.0	51.8
7	*n*-$BuNH_2$	0	10	0.01	0.04	0.3
8	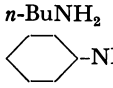 -NH_2	1	10	4.1	3.3	7.2
9	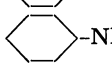 -NH_2[b)]	1	72	12.1	12.2	37.1
10	*n*-$OctNH_2$	1	10	2.3	1.9	1.0
11	*n*-$OctNH_2$[c)]	1	72	10.0	d)	24.8
12	$PhCH_2NH_2$	1	10	4.7	5.0	1.1

a) Temp: 140 °C, CO: 30 kg/cm². b) Cyclohexylamine: 85.1 mmol (10 ml). c) Octylamine: 60.2 mmol (10 ml).
d) Not determined.

less otherwise noted, 1 mmol of tellurium was always used, and thus the yields of products (in mmol) correspond to the turnover numbers. For all amines, the carbonylation reaction proceeded catalytically. The turnover number for the urea formation in Run 5 in Table 1, for example, corresponded to 5.8 per hour.

The reaction of butylamine with carbon monoxide in the presence of tellurium catalyst was carried out four times under the identical reaction conditions. The reproducibility of the formation of 1,3-dibutylurea and hydrogen was satisfactory (Runs 1—4). The reproducibility using octylamine and cyclohexylamine was also confirmed fairly good by duplicated experiments. In regard to the reproducibility of formamide formation, the yields varied much more than those of the urea derivatives and hydrogen.

In the reaction performed for 72 h, almost all butylamine was consumed to give urea and formamide derivatives (Run 6). The mass balance in the carbonylation of octylamine was confirmed nearly 100% (Run 11).

Dialkylamines such as diethylamine and dimethylamine failed to react resulting in the recovery of the starting materials. Ammonia and aniline were also unreactive under similar conditions.

Effects of Temperature and CO Pressure. The yields of 1,3-dibutylurea increased as the temperature was elevated, whereas plots of the yields of hydrogen and *N*-butylformamide showed the maxima around at 160 °C (Fig. 1). The temperature higher than 100 °C was required for the effective performance of the catalytic reaction. The change of the reaction temperature caused the similar effects both on the hydrogen formation and the formamide formation. This fact seemed very suggestive. That is, in both reactions the same species would play important roles; which was hydrogen telluride we tentatively considered.

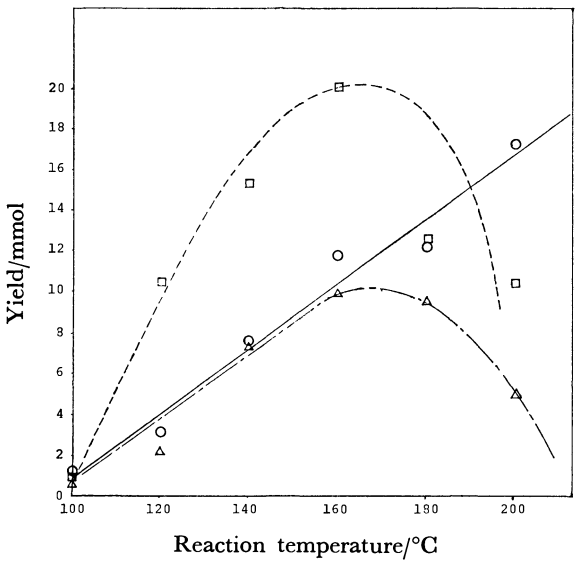

Fig. 1. Effect of temperature on tellurium-catalyzed carbonylation of amines with carbon monoxide. Tellurium: 1 mmol, butylamine: 100 mmol, carbon monoxide: 30 kg/cm², time: 10 h. —○—: 1,3-Dibutylurea, —△—: hydrogen, —□—: *N*-butylformamide.

The higher pressure of carbon monoxide was advantageous for all the formation of 1,3-dibutylurea, hydrogen, and *N*-butylformamide (Fig. 2). But it should be noted that the formamide formation was more sensitive to the pressure than the others.

Effects of Additives. We have reported that nitrobenzene was reduced with hydrogen telluride generated *in situ* from aluminum telluride and water.[16] Evidently, the addition of nitrobenzene to the present tellurium-catalyzed carbonylation system gave aniline in good yield, resulting in the drastic suppression of the formation of hydrogen and *N*-butylformamide (Run 2 in Table 2). The value of the reaction constant, ρ, of the Hammett equation for the concurrent reduction of nitrobenzenes in the tellurium-catalyzed carbonylation system was obtained as +0.8. These results might suggest the presence of hydrogen telluride in this carbonylation. The reaction would proceed as shown in Scheme 1.

Comparison of the Catalyses by Se and Te in the Urea Formation Reaction. We have reported[3] that carbonylation reaction of amines in the presence of selenium afforded stoichiometric amounts of urea derivatives and hydrogen selenide (Reaction 3). By use of selenium under the typical reaction conditions at 140 °C for 10 h, the carbonylation was carried out in a glass

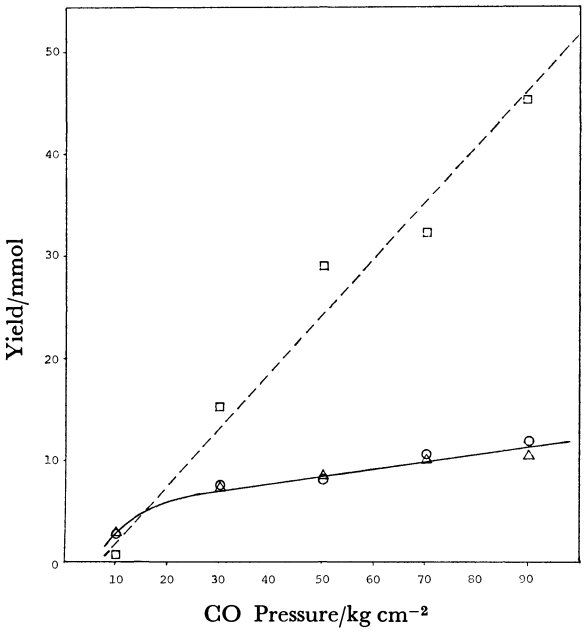

Fig. 2. Effect of CO pressure on tellurium-catalyzed carbonylation of amines with carbon monoxide. Tellurium: 1 mmol, butylamine: 100 mmol, temperature: 140 °C, time: 10 h. —○—: 1,3-Dibutylurea, —△—: hydrogen, —□—: *N*-butylformamide.

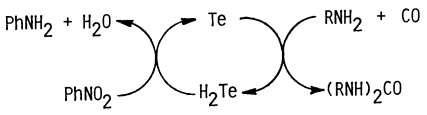

Scheme 1. Tellurium-catalyzed carbonylation of amines with carbon monoxide in the presence of nitrobenzene.

TABLE 2. CONTROLLED EXPERIMENTS[a]

Run	Te (mmol)	Additive (mmol)	Time h	Urea (mmol)	H_2 (mmol)	Formamide (mmol)	$PhNH_2$ (mmol)
1	1	—	72	22.0	21.0	51.8	—
2[b]	1	$PhNO_2$: 10	72	15.9	1.3	2.0	9.0
3	1	—	10	7.6	7.1	10.1	—
4	1	Se : 1	10	19.1	14.5	28.7	—
5	0	Se : 1	10	1.2	0.8	10.6	—

a) *n*-$BuNH_2$: 100 mmol (10 ml), Temp: 140 °C, CO: 30 kg/cm². b) Unreacted nitrobenzene was not detected after the reaction.

tube inserted in an autoclave. This reaction gave the stoichiometric amount of 1,3-dibutylurea to the used selenium with little formation of hydrogen. When this inserted glass tube was not used, more than equimolar amount of urea to selenium catalyst was produced (Run 5 in Table 2). This result would be attributed to the wall effect of the autoclave. In the tellurium-catalyzed carbonylation, no wall effect was observed on the contrary. These results show the similarity and the difference in the catalyses by selenium and tellurium; both non-transition metal elements, selenium and tellurium, catalyze the carbonylation of amines with carbon monoxide, where the former requires suitable oxidizing agents such as oxygen to give water, while the latter does not with the production of hydrogen. With regard to the reaction conditions, the selenium-catalyzed urea synthesis was achieved under much milder conditions than the other.

A Plausible Reaction Path. At present, we don't have enough evidence to propose the precise reaction mechanism. But some of the results mentioned above may help us to describe the plausible carbonylation path by tellurium catalyst, referring to the accumulated knowledge on selenium catalyzed carbonylation. From a close analogy to the selenium chemistry,[3] tellurium catalyzed urea formation (Reaction 5) would be best explained by the assumption that it consists of two reactions: one, the stoichiometric reaction of amines, carbon monoxide, and tellurium to produce ureas and hydrogen telluride (Reaction 7); the other, the dehydrogenative decomposition of hydrogen telluride to molecular hydrogen and activated tellurium (Reaction 8). The assumption of the intermediacy of hydrogen telluride in this reaction does not contradict the following evidences. i) Pure hydrogen telluride was prepared by the reaction of aluminum telluride and water. Thus prepared hydrogen telluride was found to decompose quite readily to its components, molecular hydrogen and tellurium (Reaction 8). This may be due to the weak bond energy between hydrogen and tellurium reported as 64 kcal/mol.[17] Therefore hydrogen telluride may well be the precursor of hydrogen and tellurium catalyst. ii) The equimolar formation of ureas and hydrogen should be well accounted for by the Reaction 5. iii) The formylation of nitrogen-hydrogen bond with carbon monoxide was also mentioned in the catalysis by the triethylammonium salt of hydrogen selenide at elevated temperature under CO pressure similar to the present reaction conditions.[18] The formation of formamides was observed in the tellurium catalyst system (see Table 1 and Reaction 6). These results might be also due to the catalysis of hydrogen telluride. iv) There was found a similar tendency in the temperature effects on the yields of hydrogen and formamides (Fig. 1). The same species, which we suppose is hydrogen telluride, might be responsible for it. v) The addition of nitrobenzene into the tellurium catalyzed carbonylation system gave important results as mentioned already; a) no effect on the urea formation, b) the drastic suppression on the formation of molecular hydrogen and formamides, c) the production of aniline, as the reduced form of nitrobenzene.

$$2\,RNH_2 + CO + Te \longrightarrow (RNH_2)CO + H_2Te \quad (7)$$

$$H_2Te \longrightarrow H_2 + Te \quad (8)$$

In conclusion a probable reaction path could be represented as shown in Scheme 2.

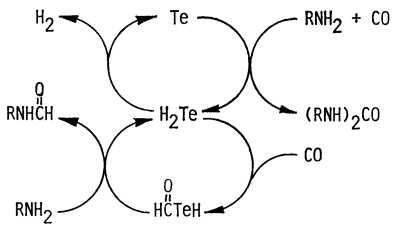

Scheme 2. A plausible reaction path for the tellurium-catalyzed carbonylation of amines with carbon monoxide.

The intermediacy of tellurol formic acid, $HC(=O)TeH$,[19] in the formamide formation reaction is still a subject to be solved.

Experimental

Instruments. Melting points were measured with a Yanagimoto Micro Melting Point apparatus. IR spectra were taken with a Shimadzu IR-400. NMR spectra (60 MHz) were recorded on a Hitachi R-24 B. Mass spectra were recorded on a Hitachi mass spectrometer, Model RMU-6E. Analytical gas chromatography was performed with a Shimadzu 3BT with thermal conductivity detector, Shimadzu 3BF and GC-6A both with flame ionization detector.

Apparatus. All carbonylations were carried out using 50 ml stainless steel autoclaves (SUS-304) purchased from Taiatsu Glass Kogyo. In order to eliminate the wall effect, the reaction was carried out in a glass tube inserted in the

autoclave.

Materials. Butylamine, cyclohexylamine, octylamine, and benzylamine were purchased from Nakarai Kagaku, and purified by distillation from KOH just before use. Tellurium lump (99.999%) was obtained from Wako Junyaku. Tellurium was powdered by use of agate mortar and pestle and stored under dry nitrogen in the absence of light. The reactive gray tellurium had to be used within a few weeks, since it gradually turned black becoming inactive for the carbonylation under similar conditions. Carbon monoxide (99.99%) was purchased from Neriki Gas in a cylinder and used without any purification. CO pressure mentioned in this paper refers to that at room temperature.

Product Analysis. The analysis of the gas phase after the reaction was performed with a Shimadzu 3BT gas chromatograph using a 3.3 m × 3 mm stainless steel column packed with 30—60 mesh molecular sieves 5A and nitrogen effluent gas at 150 °C of the oven temperature. The analytical error of hydrogen was less than 2%. 1,3-Dibutylurea was analyzed on a Shimadzu GC-6A using a 70 cm × 3 mm glass column packed with 3% DEGS on acid-washed, base-treated, DMCS-treated, 80—100 mesh Shimalite W at 150 °C of the oven temperature, and diethyl phthalate was used as an internal standard. Formamides, nitrobenzenes, and anilines were analyzed using a 3.3 m × 3 mm stainless steel column packed with 25% PEG-20M on acid-washed, 60—80 mesh Shimalite W at 200 °C of the oven temperature, and dodecane was used as an internal standard. 1,3-Dicyclohexylurea, 1,3-dioctylurea, and 1,3-dibenzylurea were obtained after the removal of unreacted amines and formed formamides from the reaction mixtures under reduced pressure. Identifications were made based on spectroscopic data (IR, NMR, and Mass measurements). Melting points were in good agreement with those[20] of authentic samples.

Carbonylation of Butylamine (Run 1 Table 1). In the autoclave were placed tellurium (1 mmol, 128 mg), butylamine (100 mmol, 10 ml), and a magnetic stirring bar. The autoclave was flushed with carbon monoxide three times and charged at 30 kg/cm². The autoclave was sunk in an oil bath maintained at 140 °C, and the reaction was conducted for 10 h with magnetic stirring. After the reaction, the autoclave was immediately cooled to room temperature with cold water. Then the resulting gas was collected in a gas sampler. The VPC analysis of the gas revealed to contain 7.1 mmol of molecular hydrogen. The reaction mixture was transferred into a 100 ml flask and was allowed to contact with air for 30 min with magnetic stirring in order to precipitate tellurium. Products were obtained after the removal of deposited tellurium followed by the evaporation of the unreacted butylamine. From GLPC analyses, 1,3-dibutylurea and *N*-butylformamide were found to be produced in the yields of 7.6 mmol and 10.1 mmol, respectively. 1,3-Dibutylurea was recrystallized from hexane.

Carbonylation of Octylamine (Run 11 in Table 1). Similarly, the carbonylation of octylamine (60.2 mmol, 10 ml) was carried out. 1,3-Dioctylurea was produced as crystals (2.48 g, 10.0 mmol). *N*-Octylformamide (114—120 °C/4 mmHg, 3.90 g, 24.8 mmol) and unreacted octylamine (54—57 °C/10 mmHg, 1.68 g 13.0 mmol) were obtained after fractionation.

Carbonylation of Butylamine by Te in the Presence of Nitrobenzene. In the autoclave tellurium (1 mmol, 128 mg), butylamine (100 mmol, 10 ml), and nitrobenzene (10 mmol, 123 mg) were placed with a magnetic stirring bar. The autoclave was then flushed with carbon monoxide three times and charged at 30 kg/cm². The reaction was conducted at 140 °C for 72 h with vigorous stirring. After the reaction, resulting gas was analyzed by VPC, and 1.3 mmol of hydrogen was found to be formed. GLPC analyses of the reaction mixture, after the removal of tellurium, showed the formation of 15.9 mmol of 1,3-dibutylurea and 2.0 mmol of *N*-butylformamide. Neither 1-butyl-3-phenylurea nor 1,3-diphenylurea was detected.

Competitive Reduction of Nitrobenzene and p-*Nitrotoluene in This Carbonylation System.* The autoclave was charged with tellurium (1 mmol, 128 mg), butylamine (100 mmol, 10 ml), nitrobenzene (5 mmol, 615 mg), *p*-nitrotoluene (5 mmol, 685 mg), and carbon monoxide (30 kg/cm²). After the reaction at 140 °C for 72 h, deposited tellurium was removed by filtration. GLPC analyses of the filtrate revealed that 2.48 mmol of aniline and 1.81 mmol of *p*-toluidine were formed.

Carbonylation of Butylamine by Selenium Using a Glass Tube. Into a glass tube inserted in the autoclave were placed selenium (1 mmol, 79 mg), butylamine (100 mmol, 10 ml), and a magnetic stirring bar. The apparatus was charged with carbon monoxide at 30 kg/cm². After the reaction at 140 °C for 10 h, the resulting gas was collected in a gas sampler, and little amount of hydrogen was detected by VPC analysis. The resulting mixture was transferred into a 100 ml flask and the oxidation with air at room temperature for 1 h precipitated selenium. Products were obtained by the removal of selenium followed by the evaporation of the solvent. GLPC analyses of the products showed the formation of 1.0 mmol of 1,3-dibutylurea and 1.5 mmol of *N*-butylformamide.

Generation of Pure Hydrogen Telluride. In a 100 ml three-necked glass vessel equipped with a 10 ml dropping funnel, a stopper, and a connection tube to a trapping vessel maintained at −196 °C, was placed powdered aluminum telluride (29 g, 66 mmol) under nitrogen atmosphere. All the apparatus was covered with aluminum foil to eliminate the effect of light. Then, 10 ml of water was dropped very slowly into the reaction vessel over a period of 1 h. The reaction was exothermic, so the reaction vessel should be cooled with ice. Hydrogen telluride was trapped at −196 °C as a white solid. When warmed to −78 °C, hydrogen telluride began to decompose. As the temperature was slowly elevated, hydrogen telluride decomposed below its melting point of −51 °C and gray tellurium remained.

The present work was partially supported by a Grant-in-Aid for Developmental Scientific Research (No. 485215) and by a Grant-in-Aid for Encouragement of Young Scientist (No. 575561) from the Ministry of Education, Science and Culture.

References

1) N. Kambe, K. Kondo, H. Ishii, S. Murai, and N. Sonoda, *Angew. Chem. Int. Ed. Engl.*, **18**, 547 (1979).

2) R. A. Franz and F. Applegath, *J. Org. Chem.* **26**, 3304 (1961); R. A. Franz, F. Applegath, F. V. Morriss, and F. Baiocchi, *ibid.*, **26**, 3306 (1961); R. A. Franz, F. Applegath, F. V. Morriss, F. Baiocchi, and C. Bolze, *ibid.*, **26**, 3309 (1961).

3) N. Sonoda, T. Yasuhara, K. Kondo, T. Ikeda, and S. Tsutsumi, *J. Am. Chem. Soc.*, **93**, 6433 (1971); K. Kondo, N. Sonoda, and S. Tsutsumi, *J. Chem. Soc., Chem. Commun.*, **1972**, 307; K. Kondo, N. Sonoda, K. Yoshida, M. Koishi, and S. Tsutsumi, *Chem. Lett.*, **1972**, 401; K. Kondo, K. Murata, N. Miyoshi, S. Murai, and N. Sonoda, *Synthesis*, **1979**, 735.

4) H. Behrens and H. Wakamatsu, *Z. Anorg. Allg. Chem.*, **320**, 30 (1963); *Chem. Abstr.*, **58**, 9870 (1963).

5) T. Tsuda, Y. Isegawa, and T. Saegusa, *J. Org. Chem.*, **37**, 2670 (1972).

6) B. K. Nefedov, V. A. Petukhov, N. S. Sergeeva, and Ya. T. Eidus, *Izv. Akad. Nauk SSSR, Ser. Khim.*, **1976**, 1541; *Chem. Abstr.*, **85**, 123292 (1976).

7) J. Tsuji and N. Iwamoto, Japan Patent 6904096; *Chem. Abstr.*, **71**, 12792 (1969); B. R. Nefedov, N. S. Sergeeva, Ya. T. Eidus, *Izv. Akad. Nauk SSSR, Ser. Khim.*, **1973**, 807; *Chem. Abstr.*, **79**, 31813 (1973).

8) B. D. Dombek and R. J. Angelici, *J. Organomet. Chem.*, **134**, 203 (1977); F. Calderazzo, *Inorg. Chem.* **4**, 293 (1965).

9) B. K. Nefedov and Ya. T. Eidus, *Izv. Akad. Nauk SSSR, Ser. Khim.*, **1976**, 1782; *Chem. Abstr.*, **86**, 16056 (1977); German Patent 1170396; *Chem. Abstr.*, **61**, 2979 (1964); H. J. Sampson, Jr., U. S. Patent 2589289; *Chem. Abstr.*, **46**, 11234 (1952).

10) A. Rosenthal, *Can. J. Chem.*, **40**, 1718 (1962).

11) Ya. Yu. Aliev, I. B. Romanova, and L. Kh. Freidlin, *Uzb. Khim. Zh.*, **5**, 54 (1961); *Chem. Abstr.*, **57**, 8413 (1962); Ya. Yu. Aliev and I. B. Romanova, *Neftekhim., Akad. Nauk Turkm., SSR*, **1963**, 204; *Chem. Abstr.*, **61**, 6913 (1964).

12) J. J. Byerley, G. L. Rempel, and N. Takebe, *J. Chem. Soc., Chem. Commun.*, **1971**, 1482; D. Durand and C. Lassau, *Tetrahedron Lett.*, **1969**, 2329; T. Yamahara, S. Takamatsu, and K. Hirose, Japan Kokai 72 34341; *Chem. Abstr.*, **78**, 43087 (1973); C. Lassau, Y. Chauvin, and G. Lefebvro, Ger. Offen 1902560; *Chem. Abstr.*, **72**, 21358 (1970).

13) H. A. Dieck, R. M. Laine, and R. F. Heck, *J. Org. Chem.*, **40**, 2819 (1975); J. Tsuji and N. Iwamoto, *J. Chem. Soc., Chem. Commun.*, **1966**, 380.

14) German Patent 1158494; *Chem. Abstr.*, **61**, 11900 (1964); German Patent 1163311; *Chem. Abstr.*, **60**, 15744 (1964); J. A. Patterson and H. V. Atwell, U. S. Patent 2993931; *Chem. Abstr.*, **56**, 1392 (1962).

15) V. I. Kucheryavyi, D. M. Gorlovskii, L. N. Al'tshuler, G. N. Zinov'ev, A. B. Karlik, and N. A. Klopina, USSR, 371210; *Chem. Abstr.*, **79**, 18161 (1973).

16) N. Kambe, K. Kondo, and N. Sonoda, *Angew. Chem. Int. Ed. Engl.*, **19**, 1009 (1980).

17) M. Schmidt, W. Siebert, and K. W. Bagnall, "The Chemistry of Sulphur, Selenium, Tellurium, and Polonium," Pergamon Press, New York (1973), p. 954.

18) K. Kondo, N. Sonoda, and H. Sakurai, *J. Chem. Soc., Chem. Commun.*, **1973**, 853.

19) In the triethylammonium salt of hydrogen selenide ($Et_3N \cdot H_2Se$) catalyzed formylation of aromatic amines under similar reaction conditions as present ones, the intermediacy of selenol formic acid, $HC(=O)SeH$, was considered; see Ref. 18.

20) S. R. Sandler and W. Karo, "Organic Functional Group Preparations," Academic Press, New York (1971), Vol. II, p. 150.

Reactivities of Stable Rotamers. VI. Manifestation of Differential Reactivities of the Methyls in a *t*-Butyl Group in Radical Halogenations[1,2]

Shigetaka Seki, Tsutou Morinaga, Hiromi Kikuchi, Tsutomu Mitsuhashi, Gaku Yamamoto, and Michinori Ōki*

Department of Chemistry, Faculty of Science, The University of Tokyo, Hongo, Bunkyo-ku, Tokyo 113

(Received November 22, 1980)

The methyls in a *t*-butyl group are shown to exhibit different reactivities in radical halogenations, if rotation about a $(CH_3)_3C$–CXY_2 bond is frozen. Barriers to rotation of halogenated 9-*t*-butyl-1,2,3,4-tetrachlorotriptycenes are obtained as ΔH^* *ca.* 32 kcal/mol. The cause of the selectivity in chlorination with sulfuryl chloride was discussed by obtaining reactivity data with a variety of compounds and halogenating reagents. It is concluded that the neighboring group participation of the peri-halo substituent is responsible for the observed selectivity.

Reactivities of rotamers drew attention of some investigators. Curtin and Hammett[3] discussed the problem from the product ratio and Winstein and Holness[4] from the reaction rates, when the reaction and the equilibration of rotamers are represented by Eq. 1.

$$A_1 \xleftarrow{k_{21}} A_2 \underset{k_{32}}{\overset{k_{23}}{\rightleftharpoons}} A_3 \xrightarrow{k_{34}} A_4 \qquad (1)$$

Eliel and Ro discussed the matter from the similar stand point[5] and Zefirov *et al.* elaborated further.[6] Although the scheme was mathematically treated by Seeman and Farone,[7] the solution gives some ambiguities because the rate constants, k_{21} and k_{34}, are both arbitrary. As far as the reactivity of a single rotamer is not known, this arbitrariness is always involved in the discussion. Winstein and Holness used a diastereomeric pair of 4-*t*-butylcyclohexyl derivatives as models of rotamers.[4] It may be assumed that a remote *t*-butyl group should not affect the reaction rate to a large extent. The assumption will succeed, if we are discussing the rule of thumb, but will fail in discussion with quantitative aspects. Therefore, in understanding the reactivities of rotamers, which are so often present in nonrigid organic molecules, the knowledge on the reactivities of respective rotamers is absolutely necessary.

Since we have been able to isolate stable rotamers of triptycene and 9-arylfluorene derivatives,[8] we have felt that comparison of the reactivities will produce useful information about those of rapidly exchanging systems. Furthermore, the merit of using these systems instead of using 1-substituted 4-*t*-butylcyclohexanes is the possibility of introducing a wide variety of substituents. Under these expectations, we decided to launch a project of studying the reactivities of triptycene and 9-arylfluorene systems.

As the beginning of the study in the triptycene system, we focussed our attention to the reactivities of the methyls in a *t*-butyl group. Chemically idential ligands in a group of local C_{3v} symmetry, such as the methyls in a *t*-butyl group, are usually treated nondistinguishable in organic chemistry, because they are usually interchanged rapidly on the laboratory time scale by rotation. However, if the rotation of a *t*-butyl group is frozen on the laboratory time scale, three methyls in a molecule of $(CH_3)_3C$–$CXYZ$ type are all diastereomeric. In a molecule of $(CH_3)_3C$–CXY_2 type, two methyls are enantiotopic and another is diastereotopic with any of the enantiotopic pair of methyls. In principle, the diastereomeric and diastereotopic methyls should show different reactivities if the rotation is frozen. This paper reports the manifestation of the differential reactivities of the diastereotopic methyls in 9-*t*-butyl-1,2,3,4-tetrachlorotriptycene (**1**) and related compounds in radical halogenation reactions.

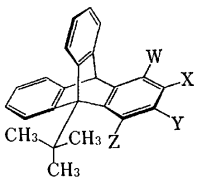

(**1**): W=X=Y=Z=Cl
(**2**): W=X=Y=Z=Br
(**3**): W=Z=H, X=Y=Cl
(**4**): W=X=Y=H, Z=Cl
(**5**): W=X=Y=Z=H

Experimental

Spectral Measurement. ^{1}H NMR spectra were obtained on a Hitachi R-20B spectrometer operating at 60 MHz or a Varian EM 390 spectrometer operating at 90 MHz.

9-t-Butyl-1,2,3,4-tetrachlorotriptycene (1). (a): To a suspension of hexachlorobenzene (5.7 g or 20 mmol) in 350 mL of dry ether was added a hexane solution of butyllithium (20 mmol) under a dry nitrogen atmosphere below −30 °C. To the mixture, which was stirred for 2 h at −30——20 °C, was added 2.34 g (10 mmol) of crystalline 9-*t*-butylanthracene[9] and the whole was heated under reflux for 3 h. Lithium chloride was filtered off and the filtrate was evaporated. Chromatography of the residue on alumina, using hexane–benzene (10:1) as an eluent, gave 3.3 g (72%) of the desired compound, mp 283.5—284.5 °C. Found: C, 64.07; H, 4.03; Cl, 31.83%. Calcd for $C_{24}H_{18}Cl_4$: C, 64.31; H, 4.05; Cl, 31.64%. ^{1}H NMR ($CDCl_3$, δ): 2.20 (3H, s), 2.31 (6H, s), 6.09 (1H, s), 6.90—7.15 (4H, m), 7.30—7.45 (2H, m), 7.82—8.15 (2H, m).

(b): To a boiling mixture of 1.0 g (4.3 mmol) of 9-*t*-butylanthracene and 1 mL of isopentyl nitrite in 50 mL of dichloromethane was added a solution of 2.5 g (5.0 mmol) of tetrachloroanthranilic acid[10] in 20 mL of acetone over a period of 2 h. Additional 1.0 mL of isopentyl nitrite was added in 2 portions with intervals of 30 min. The mixture was heated for further 30 min and evaporated. Chromatography of the residue on alumina with 10:1 hexane–benzene as an eluent afforded 700 mg (36%) of the desired compound.

9-t-Butyltriptycene (5), mp 241—241.5 °C, was prepared similarly from 9-*t*-butylanthracene and anthranilic acid in 76% yield. Found: C, 93.07; H, 7.24%. Calcd for $C_{24}H_{22}$: C, 92.86; H, 7.14%. ^{1}H NMR ($CDCl_3$, δ): 2.06 (9H,

s), 5.23 (1H, s), 6.85—7.10 (6H, m), 7.27—7.48 (3H, m), 7.70—8.93 (3H, m).

1,2,3,4-Tetrabromo-9-t-butyltriptycene (2), mp 287—288 °C, was similarly prepared from 9-*t*-butylanthracene and tetrabromoanthranilic acid[11] in 8% yield. Found: C, 46.23; H, 2.83; Br, 50.78%. Calcd for $C_{24}H_{18}Br_4$: C, 46.05; H, 2.90; Br, 51.06%. ^{1}H NMR ($CDCl_3$, δ): 1.98 (3H, s), 2.46 (6H, s), 6.22 (1H, s), 6.97—7.20 (4H, m), 7.37—7.58 (2H, m), 7.92—8.15 (2H, m).

9-t-Butyl-2,3-dichlorotriptycene (3), mp 184.5—185.5 °C, was similarly prepared from 9-*t*-butylanthracene and 4,5-dichloroanthranilic acid[12] in 39.7% yield. Found: C, 76.28; H, 4.77; Cl, 19.20%. Calcd for $C_{24}H_{20}Cl_2$: C, 75.99; H, 5.31; Cl, 18.69%. ^{1}H NMR ($CDCl_3$, δ): 1.99 (9H, s), 5.05 (1H, s), 6.65—7.03 (4H, m), 7.03—7.35 (2H, m), 7.39 (1H, s), 7.78 (1H, s), 7.46—7.90 (2H, m).

Reaction between 9-t-Butylanthracene and Lithiated m-Dichlorobenzene. To a solution of 3.54 g (24.1 mmol) of *m*-dichlorobenzene in dry ether was added 25.6 mmol of butyllithium in hexane at −40 °C in 40 min and the mixture was stirred for 1 h. 9-*t*-Butylanthracene (15.2 mmol) was added and the temperature was allowed to rise. After the mixture was refluxed for 2 h, it was treated as usual and the product was separated by careful chromatography. The following compounds were obtained (given by the order of elution from an alumina column by hexane).

9-t-Butyl-4-chlorotriptycene: Mp 273 °C, yield 21%. Found: C, 83.76; H, 6.08; Cl, 10.40%. Calcd for $C_{24}H_{21}Cl$: C, 83.58; H, 6.14; Cl, 10.28%. ^{1}H NMR (CCl_4, δ): 2.06 (3H, s), 2.08 (6H, s), 5.76 (1H, s), 6.7—7.1 (6H, m), 7.1—7.5 (2H, m), 7.5—7.8 (3H, m).

9-t-Butyl-2(and/or 3)-chlorotriptycene: Mp 258—268 °C, yield 11%. ^{1}H NMR (CCl_4, δ): 2.07 (9H, s), 5.43 (1H, s), 6.7—7.1 (3H, m), 7.1—7.4 (2H, m), 7.4—7.9 (6H, m).

9-t-Butyl-1-chlorotriptycene (4): Mp 260.0—260.5 °C, yield 47%. Found: C, 83.54; H, 6.50; Cl, 10.96%. Calcd for $C_{24}H_{21}Cl$: C, 83.58; H, 6.14; Cl, 10.28%. ^{1}H NMR (CCl_4, δ): 2.03 (3H, s), 2.29 (6H, s), 5.05 (1H, s), 6.6—7.05 (6H, m), 7.05—7.4 (3H, m), 7.6—8.0 (2H, m).

The assignment of the structures bases on the NMR spectral data and the consideration that the lithiation of *m*-dichlorobenzene should be preferred in 2-position. Namely, 3-chlorobenzyne should be the main intermediate in this reaction to lead to 1-chloro- and 4-chlorotriptycene derivatives. Of these major products, the chemical shift difference between the methyls of the *t*-butyl group should be larger in the 1-chloro derivative than in the 4-chloro derivative.

Chlorination of 9-t-Butyl-1,2,3,4-tetrachlorotriptycene (1) with Sulfuryl Chloride. A solution of 200 mg (0.45 mmol) of **1** and 1.2 mL (14 mmol) of sulfuryl chloride in 20 mL of chlorobenzene containing 10 mg of dibenzoyl peroxide was heated under reflux for 1 h. The solvent was evaporated and the residue was subjected to dry-column chromatography on silica gel, using hexane–dichloromethane (20:1) as an eluent, to give fractions containing the starting material (R_f 0.4), a $\pm sc$-*ap* mixture of monochlorinated compounds (R_f 0.3), *ap* isomer of dichlorinated compound (R_f 0.25), and $\pm sc$ isomer of the dichlorinated compound (R_f 0.2). The yields were 5, 28, 27, and 26%, respectively in a typical run. These compounds were purified by recrystallization from tetrahydrofuran–ethanol.

1,2,3,4-Tetrachloro-9-(2-chloro-1,1-dimethylethyl)triptycene. It was not possible to obtain pure isomers by chromatography on silica gel. Chromatography on alumina partially decomposed the $\pm sc$ form and the *ap* fraction afforded pure *ap* form, mp 251.5—252.5 °C, on recrystallization from chloroform–ethanol. Found: C, 60.02; H, 3.41; Cl, 36.89%. Calcd for $C_{24}H_{17}Cl_5$: C, 59.72; H, 3.55; Cl, 36.73%. ^{1}H NMR ($CDCl_3$, δ): 2.42 (6H, s), 4.58 (2H, s), 6.12 (1H, s), 7.00—7.21 (4H, m), 7.35—7.63 (2H, m), 7.77—8.13 (2H, m).

By subtracting the NMR signals of the *ap* form, the following ^{1}H NMR data ($CDCl_3$, δ) were obtained for the $\pm sc$ form: 2.14 (3H, s), 2.33 (3H, s), 4.97 (2H, br. s), 6.12 (1H, s), 7.00—7.21 (4H, m), 7.35—7.63 (2H, m), 7.77—8.13 (2H, m).

1,2,3,4-Tetrachloro-9-(2-chloro-1-chloromethyl-1-methylethyl)-triptycene. *ap* form, mp 210.5—211.5 °C. Found: C, 55.51; H, 2.97; Cl, 40.89%. Calcd for $C_{24}H_{16}Cl_6$: C, 55.75; H, 3.12; Cl, 41.14%. ^{1}H NMR ($CDCl_3$, 60 MHz, δ): 2.19 (3H, s), 5.01 (4H, q, $\Delta\delta_{AB}$=50.0 Hz, J_{AB}=12.4 Hz), 6.12 (1H, s), 7.03—7.22 (4H, m), 7.35—7.63 (2H, m), 7.82—8.17 (2H, m).

$\pm sc$ form, mp 221.0—221.5 °C. Found: C, 55.87; H, 2.97; Cl, 41.43%. Calcd for $C_{24}H_{16}Cl_6$: C, 55.75; H, 3.12; Cl, 41.14%. ^{1}H NMR ($CDCl_3$, 60 MHz, δ): 2.48 (3H, s), 4.65 (2H, q, $\Delta\delta_{AB}$=12.2 Hz, J_{AB}=12.4 Hz), 5.00 (2H, q, $\Delta\delta_{AB}$=15.2 Hz, J_{AB}=12.2 Hz), 6.12 (1H, s), 7.03—7.22 (4H, m), 7.35—7.63 (2H, m), 7.76—8.03 (2H, m).

Chlorination of Other 9-t-Butyltriptycenes with Sulfuryl Chloride. The reaction was carried out similarly and the following results were obtained.

(a): Chlorination of 9-*t*-butyl-1-chlorotriptycene (**4**) gave a mixture of *ap* and $\pm sc$ forms of monochlorinated compounds, of which separation was tedious. However, assignment of the structure and determination of the ratio of the products were straightforward because the ^{1}H NMR spectroscopic features of the rotamers were similar with others. The following ^{1}H NMR data (CCl_4, 60 MHz, δ) were obtained. *ap*: 2.37 (6H, s), 4.55 (2H, s). $\pm sc$: 2.13 (3H, br. s), 2.28 (3H, s), 4.97 (2H, q, $\Delta\delta_{AB}$=16.6 Hz, J_{AB}=11.9 Hz).

(b): Chlorination of 9-*t*-butyl-2,3-dichlorotriptycene (**3**) gave a 1:2 mixture of *ap* and $\pm sc$ forms. Chromatography of the product showed some enrichment of the respective forms but the final separation was not possible. The following ^{1}H NMR data were obtained at 60 MHz. *ap* (CCl_4, δ): 2.12 (6H, s). *ap* (C_6D_6, δ): 1.82 (6H, s). $\pm sc$ (CCl_4, δ): 2.12 (6H, s), 4.65 (2H, q, $\Delta\delta_{AB}$=14 Hz, J_{AB}=12 Hz). $\pm sc$ (C_6D_6, δ): 1.92 (3H, s), 1.85 (3H, s).

(c): Chlorination of 9-*t*-butyltriptycene (**5**) afforded a mixture of the starting material, 9-(2-chloro-1,1-dimethylethyl)triptycene and a dichlorinated compound in a 9:70:21 ratio. The mixture was chromatographed on a TLC plate using hexane–benzene (20:1) as a developing solvent. The chromatography afforded a mixture of *ca.* 10:1 monochlorinated compound and the starting material. Recrystallization of the mixture from acetone–hexane yielded pure 9-(2-chloro-1,1-dimethylethyl)triptycene, mp 201—202 °C. Found: C, 83.54; H, 5.88; Cl, 10.63%. Calcd for $C_{24}H_{21}Cl$: C, 83.58; H, 6.14; Cl, 10.28%. ^{1}H NMR ($CDCl_3$, δ): 2.15 (6H, s), 4.70 (2H, s), 5.22 (1H, s), 6.85—7.10 (6H, m), 7.25—7.48 (3H, m), 7.56—7.80 (3H, m). The following ^{1}H NMR data at 60 MHz were obtained for 9-(2-chloro-1-chloromethyl-1-methylethyl)triptycene from the spectrum of a mixture of mono- and dichlorinated compounds ($CDCl_3$, δ): 2.27 (3H, s), 4.71 (4H, q, $\Delta\delta_{AB}$=15.7 Hz, J_{AB}=12.2 Hz), 5.22 (1H, s).

(d): Chlorination of 9-*t*-butyl-1,2,3,4-tetrabromotriptycene (**2**) afforded a mixture of various products. It was not possible to isolate the desired product.

Bromination of 9-t-butyl-1,2,3,4-tetrachlorotriptycene (1). A solution of 100 mg (0.22 mmol) of the triptycene and 160 mg (1.0 mmol) of bromine in 50 mL of carbon tetra-

chloride was irradiated with tungsten lamps at room temperature. The reaction mixture was worked up as usual and the products were submitted to dry-column chromatography on silica gel or TLC. Elution with 20:1 hexane–dichloromethane afforded a mixture of *ap*- and ±*sc*-9-(2-bromo-1,1-dimethylethyl)-1,2,3,4-tetrachlorotriptycene (R_f 0.3), *ap*-9-(2-bromo-1-bromomethyl-1-methylethyl)-1,2,3,4-tetrachlorotriptycene (R_f 0.2), and the ±*sc* isomer (R_f 0.15) of the latter. The ±*sc* form of the monobrominated compound was concentrated up to 90% (as judged by ^{1}H NMR spectra) by the chromatography and the following ^{1}H NMR data ($CDCl_3$, δ) were obtained for the two forms. *ap*: 2.40 (6H, s), 4.53 (2H, s), 6.10 (1H, s), 6.95—7.16 (4H, m), 7.35—7.60 (2H, m), 7.80—8.15 (2H, m). ±*sc*: 2.14 (3H, s), 2.36 (3H, s), 4.93 (2H, br. s), 6.10 (1H, s), 6.95—7.16 (4H, m), 7.36—7.60 (2H, m), 7.80—8.15 (2H, m). Elemental analyses of the 10:1 mixture, mp 168—169 °C, gave the following data: C, 54.51; H, 3.08; Br, 15.02; Cl, 26.65%. Calcd for $C_{24}H_{17}BrCl_4$: C, 54.69; H, 3.25; Br, 15.16; Cl, 26.90%.

The following ^{1}H NMR data were obtained for the dibrominated compounds ($CDCl_3$, 60 MHz, δ). *ap*: 2.23 (3H, s), 4.97 (4H, q, $\Delta\delta_{AB}$=43.0 Hz, J_{AB}=11.9 Hz), 6.12 (1H, s), 7.02—7.23 (4H, m), 7.36—7.60 (2H, m), 7.85—8.10 (2H, m). ±*sc*: 2.53 (3H, s), 4.58 (2H, q, $\Delta\delta_{AB}$=14.1 Hz, J_{AB}=11.9 Hz), 4.96 (2H, q, $\Delta\delta_{AB}$=14.0 Hz, J_{AB}=12.0 Hz), 6.11 (1H, s), 7.02—7.23 (4H, m), 7.36—7.60 (2H, m), 7.75—7.99 (2H, m).

Bromination of 9-*t*-butyltriptycene afforded *9-(2-bromo-1,1-dimethylethyl)triptycene*, mp 212—213 °C. Found: C, 74.24; H, 5.34; Br, 20.88%. Calcd for $C_{24}H_{21}Br$: C, 74.04; H, 5.44; Br, 20.52%. ^{1}H NMR ($CDCl_3$, δ): 2.18 (6H, s) 4.67 (2H, s), 5.23 (1H, s), 6.83—7.10 (6H, m), 7.27—7.48 (3H, m), 7.55—7.90 (3H, m).

Bromination with Bromine-N-Bromosuccinimide. This reaction was carried out similarly with the photobromination except that the equimolar *N*-bromosuccinimide to bromine was added. The reaction was faster than that in the absence of *N*-bromosuccinimide but the products were the same as the photobromination.

Bromination of 9-*t*-butyl-1,2,3,4-tetrabromotriptycene with bromine–*N*-bromosuccinimide gave a *ca.* 10:1 mixture of ±*sc* and *ap* forms of a monobrominated compound of which separation was not possible. The compound was very labile, being decomposed even in chromatography on Florisil, and decomposed on standing at room temperature. The following ^{1}H NMR data ($CDCl_3$, 60 MHz, δ) were obtained. *ap*: 2.51 (6H, s), 4.48 (2H, s), 6.22 (1H, s). ±*sc*: 2.08 (3H, s), 2.48 (3H, s), 5.03 (2H, q, $\Delta\delta_{AB}$=15.0 Hz, J_{AB}=11.1 Hz), 6.22 (1H, s).

Photochlorination was carried out by irradiating a solution of 50 mg of a substrate in 50 mL of carbon tetrachloride containing 0.1 mmol of chlorine by tungsten lamps for 10—15 min. The products were identical with those obtained by chlorination with sulfuryl chloride.

Competitive Halogenation. It was carried out using the same conditions as described in the foregoing paragraphs except that equimolar amounts of *t*-butyltriptycene and a halotriptycene were dissolved in carbon tetrachloride or chlorobenzene. Analyses of the products were performed by ^{1}H NMR spectra.

Determination of the Rotational Barrier. (a): A solution was prepared by dissolving 50 mg of 9-(2-chloro-1,1-dimethylethyl)triptycene (±*sc*/*ap*=*ca.* 3) in 0.5 mL of 1-chloronaphthalene. The solution was placed in an NMR sample tube and the tube was sealed after purging the air by nitrogen. The tube was immersed in a boiling solvent bath and the ±*sc*/*ap* ratio was checked by ^{1}H NMR spectra at appropriate intervals. The solvents (boiling points) used for the study were naphthalene (218.5 °C), nitrobenzene (208.0 °C), ethylene glycol (197.0 °C), and *trans*-decalin (187.0 °C). The data were treated as the first order reversible reaction: consideration of Eqs. 2 and 3 gave rate constants given in Table 1.

Table 1. Rate constants for the exchange between and equilibrium constants of ±*sc* and *ap* isomers of 1,2,3,4-tetrachloro-9-(2-chloro-1,1-dimethylethyl)triptycene

T/°C	$k_{sc\rightarrow ap}/10^{-4}\,s^{-1}$	K(±*sc*/*ap*)
218.5	2.39	0.96
208.0	1.27	0.96
197.0	0.589	0.96
187.0	0.259	0.96

Table 2. Rate constants for the exchange between and equilibrium constants of ±*sc* and *ap* isomers of 1,2,3,4-tetrachloro-9-(2-chloro-1-chloromethyl-1-methylethyl)triptycene

T/°C	$k_{sc\rightarrow ap}/10^{-4}\,s^{-1}$	K(±*sc*/*ap*)
218.5	2.20	1.84
208.0	0.939	1.80
197.0	0.434	1.80
187.0	0.202	1.80

$$K = \frac{2\,k_{ap\rightarrow sc}}{k_{sc\rightarrow ap}} \tag{2}$$

$$\log\left[1-\left(1+\frac{1}{K}\right)\frac{x}{a}\right] = -\frac{k}{2.303}\left(1+\frac{1}{K}\right)t, \tag{3}$$

where a and x are the molar concentrations at time 0 and t, respectively. From the results shown in Table 1, the Eyring plot produced $\Delta H^*_{sc\rightarrow ap}$=32±5 kcal/mol (1 cal=4.18 J) and ΔS^*=−10±13 e. u. $\Delta H^*_{ap\rightarrow sc}$ and ΔS^* were obtained as 32±5 kcal/mol and −12±13 e. u., respectively. The compound tended to decompose at high temperatures on prolonged heating. This seems to cause errors to some extent.

(b): Similarly the rates of isomerization of 9-(2-chloro-1-chloromethyl-1-methylethyl)-1,2,3,4-tetrachlorotriptycene were determined and the data shown in Table 2 were obtained. These data produced $\Delta H^*_{ap\rightarrow sc}$ 31±0 kcal/mol and ΔS^* −13±0 e. u., respectively. We may have to admit errors as large as those for the monochlorinated compound, although the errors in the least squares treatment were small. Decomposition of the substrate on prolonged heating occurred to some extent.

Results and Discussion

Assignment of the Stereochemistry of the Halogenation Products. The assignment is straightforward because, if it is an *ap* isomer of the monohalogenated compound, the signal due to two methyl groups appears as a singlet and the methylene protons give a singlet as well, as can be seen from the Newman projections. In contrast, ±*sc* forms give two signals for the methyl protons and an AB quartet for the methylene protons, if it is a monohalogenated compound. Sim-

ilarly, in dihalogenated compounds, *ap* forms give a set of AB quartet because the methylene protons are diastereotopic, whereas the $\pm sc$ 2 sets of AB quartet for the methylene protons.

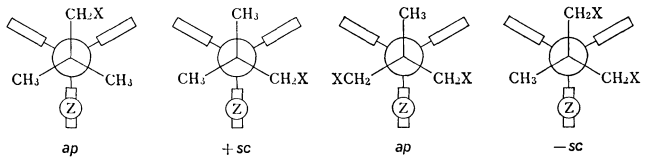

monohalogenated dihalogenated

Barriers to Rotation and Population Ratios. From the enthalpies and entropies of activation for rotation, we can calculate the life times of the respective rotamers at a given temperature. At the highest temperature, boiling point of chlorobenzene, we have used, it takes about two weeks for effecting the conversion of 5% of one conformer to another, the amount being considered as the error limit for detection of the change by integration of the NMR spectra. Thus we may neglect the isomerization, since the reaction is over within 1 h. Although not determined, other rotamers must also be stable since even 9-(2-phenyl-1,1-dimethylethyl)-2,3-dichlorotriptycene, a model for compound **2**, has a high barrier to rotation.[12] This assures that we are directly observing the reactivities of respective methyls by comparing the product ratios.

Population ratios of the rotamers are also interesting. At the equilibrium, the population ratio of 9-(2-chloro-1,1-dimethylethyl)-1,2,3,4-tetrachlorotriptycene is very close to unity. Since the statistical value must be $\pm sc/ap=2.0$, the $\pm sc$ form is disfavored to some extent. Probably the steric factor dominates. In contrast, 9-(2-chloro-1-chloromethyl-1-methylethyl)-1,2,3,4-tetrachlorotriptycene gives $\pm sc/ap$ values of *ca.* 1.80 which are very close to the statistical value. This is probably caused by the fact that at least one chloromethyl group always flanks the peri-chloro group irrespective of the conformation.

Comparison of the Reactivities of Methyl Groups. The following results are the mean values of 3—5 runs. Reproducibility of the results was good.

At the outset, we looked at the reactivities of methyls in 9-*t*-butyl-1,2,3,4-tetrachlorotriptycene (**1**) with sulfuryl chloride. The $\pm sc/ap$ ratio was 3.2 ± 0.2. Since there are two $\pm sc$ methyls and one *ap* methyl, the relative reactivity of the $\pm sc$ methyl is 1.6 if we take the *ap* methyl as a standard. The formation ratio $ap/\pm sc$ of dichlorinated product is in conformity with this relative reactivity also: if we assume the relative reactivities of 1.6 and 1.0 for the remaining $\pm sc$ and *ap* methyls in the monochlorinated compounds, the calculated ratio of $ap/\pm sc$ for the dichlorinated compounds is 0.8, which is in good agreement with the observed. The difference in reactivity must be caused by the presence of the peri-chloro group, because chlorination of 9-*t*-butyl-2,3-dichlorotriptycene gave a 2:1 mixture of $\pm sc$ and *ap* isomers.

Two reasons may be considered for the apparent enhancement of the reactivity of the $\pm sc$ methyls. Since the molecular structure of 9-*t*-butyl-1,2,3,4-tetrachlorotriptycene (**1**) studied by X-ray crystallography[13] reveals that the peri-chloro and the *t*-butyl groups are tilted away from each other, the *ap* methyl may be pushed into the triptycene skeleton to make it less exposed to the external attack of radicals. Or else, the peri-chloro group may stabilize the transition state for abstraction of hydrogen by radicals. Although the extent of neighboring participation of the chloro group in radical reactions is not large, yet it definitely exists.[14] In order to establish the cause for the selectivity, we took advantage of three techniques: changing halogenation reagents to examine the change in selectivity, changing the peri-substituent to change the extent of neighboring group participation, and competitive halogenation between 9-*t*-butyltriptycene (**5**) and a halogen-substituted 9-*t*-butyltriptycene.

Table 3. Effects of the halogenating reagent on the $\pm sc/ap$ ratios of 9-(2-halo-1,1-dimethylethyl)-1,2,3,4-tetrachlorotriptycenes

Reagent	$1/2(\pm sc/ap)$
SO_2Cl_2	1.6 ± 0.1
Cl_2	1.0 ± 0.05
Br_2	3.1 ± 0.06
Br_2–NBS	1.5 ± 0.1

The effects of changing the halogenation reagent on the $\pm sc/ap$ ratio are summarized in Table 3. The rate determining step in radical halogenations is the hydrogen abstraction.[15] Chlorination with sulfuryl chloride is known to be a little more selective than that with chlorine.[15,16] The product ratio in the chlorination with chlorine indicates that the $\pm sc$ and *ap* forms are formed almost statistically. If the steric reason had dominated, even chlorine would have given some selectivity, because the *ap* methyl should be protected sterically. Thus the results favor the chloro-participation. The neighboring group participation is further supported by the fact that bromination with bromine gives a very large $\pm sc/ap$ ratio, since the bromination is known to proceed with high selectivity.[17] The large $\pm sc/ap$ ratio suggests lowering the energy of the transition state because of the chloro-participation. If it were the steric reasons that preferred the $\pm sc$ form in the SO_2Cl_2-chlorination, the ratio should not have changed to a large extent. *N*-Bromosuccinimide is often used to trap hydrogen bromide in photobromination of hydrocarbons.[16] Usually *N*-bromosuccinimide is assumed to not participate in the halogenation reaction but in trapping hydrogen bromide. However, the present results suggest that succinimido radicals participate in hydrogen abstraction because the selectivity is inferior to the photobromination in the absence of *N*-bromosuccinimide. Skell reported recently that succinimido radicals sometimes participate in hydrogen abstraction,[18] and this is another example of such a kind. It is also interesting to note that sulfuryl chloride does give selectivity to some extent, although Russel observed that the difference in selectivity between chlorine and sulfuryl chloride chlorinations vanished in aromatic solvents and suggested that a complex be-

tween the aromatic molecule and the chlorine atom was a true attacking species.[19] It seems that chlorosulfonyl radicals participate in hydrogen abstraction in this case.

Now that the bromo group is known to give better assistance in radical formation,[17] if we introduce a bromo substituent in the peri-position, the reactivity of the $\pm sc$ methyls should be enhanced. In fact, the $\pm sc/ap$ ratio of 9-(2-bromo-1,1-dimethylethyl)-1,2,3,4-tetrabromotriptycene rose to >10 in bromine–*N*-bromosuccinimide bromination. Thus the results support again that the enhancement of the reactivity of the $\pm sc$ methyls must be attributed to the neighboring group participation of the peri-substituent.

The results of competitive halogenations are given in Table 4. The $\pm sc/ap$ ratios observed in the individual halogenations of the respective compounds were reproduced in these reactions. The results suggest that, while the reactivities of the *ap* methyls are uniformly suppressed to some extent, those of the $\pm sc$ methyls vary widely: while chlorination gives generally smaller values than unity, bromination gives larger values than that. It is especially noteworthy that the 1,2,3,4-tetrabromo compound (**2**) gives a value as high as 4. This is again the indication that the participation of the peri-substituent is important.

The less reactivity of the tetrachloro compound (**1**) in chlorination is confusing if one simply assumes the neighboring group participation. This phenomenon together with the suppressed reactivity of the *ap* methyls in all halogenations may be attributed to the inductive effect: since the halogenating radicals are known to be electron-demanding,[20] the tetrachloro substituents on a benzeno bridge should suppress the reactivity. We have had such an experience in bromination of 9-allyl-1,2,3,4-tetrachlorotriptycene.[21]

To give further support to this discussion, we have carried out halogenations of 9-*t*-butyl-1-chlorotriptycene (**4**) which should give less electron-withdrawing effect than the tetrahalo compounds. The results are given in Table 5, where $\pm sc/ap$ ratios are taken from the reactions carried out individually. Apparently the reactivity of the *ap* methyl is raised relative to the tetrahalo compounds. The results suggest that the inductive effect is important. It is also interesting to note that the $\pm sc/ap$ ratios are raised relative to the tetrachloro compound (**1**) except the chlorination with chlorine. Probably the higher electron-donating ability of the monochlorobenzeno bridge than the tetrachlorobenzo moiety[22] is responsible for the phenomenon.

Table 4. Relative reactivities of methyls in *t*-butyltriptycenes relative to one of the methyls in 9-*t*-butyltriptycene

Halogenating reagent	Substituents	Relative reactivities	
		$\pm sc$	*ap*
SO_2Cl_2	1,2,3,4-Cl_4	0.95±0.05	0.60±0.03
Cl_2	1,2,3,4-Cl_4	0.84±0.02	0.83±0.05
Br_2	1,2,3,4-Cl_4	2.78±0.3	0.89±0.04
Br_2-NBS	1,2,3,4-Cl_4	1.16±0.08	0.82±0.04
Br_2-NBS	1,2,3,4-Br_4	4.1±0.8	0.8±0.2

Table 5. $\pm sc/ap$ ratios and relative reactivities of methyls in 9-*t*-butyl-1-chlorotriptycene relative to one of the methyls in 9-*t*-butyltriptycene

Halogenation reagent	$\pm sc/ap$	Relative reactivities	
		$\pm sc$	*ap*
Cl_2	2.1±0.1	0.94±0.03	0.92±0.03
Br_2	7.8±0.3	4.2±0.2	1.05±0.02
SO_2Cl_2	3.80±0.04	—	—

This work was supported by a grant from Toray Science Foundation to which our thanks are due.

References

1) Preceding paper: S. Murata, S. Kanno, Y. Tanabe, M. Nakamura, and M. Ōki, *Angew. Chem. Int. Ed. Engl.*, in press.
2) A preliminary note has been published: T. Morinaga, S. Seki, H. Kikuchi, G. Yamamoto, and M. Ōki, *J. Am. Chem. Soc.*, **102**, 1173 (1980).
3) D. Y. Curtin and L. P. Hammett, "Physical Organic Chemistry," 2nd ed, McGraw Hill, New York (1970), pp. 119—120.
4) S. Winstein and N. J. Holness, *J. Am. Chem. Soc.*, **77**, 5562 (1955).
5) E. L. Eliel and R. S. Ro, *Chem. Ind. (London)*, **1956**, 251.
6) N. S. Zefirov, *Tetrahedron*, **33**, 2719 (1977); N. S. Zefirov and V. A. Palyulin, *Zh. Org. Khim.*, **15**, 1098 (1979).
7) J. I. Seeman and W. A. Farone, *J. Org. Chem.*, **43**, 1854 (1978); J. I. Seeman, E. B. Sanders, and W. A. Farone, *Tetrahedron*, **36**, 1173 (1980).
8) M. Ōki, *Angew. Chem. Int. Ed. Engl.*, **15**, 87 (1976).
9) R. C. Parish and L. M. Stock, *J. Org. Chem.*, **31**, 4265 (1966).
10) V. Villiger and L. Blangey, *Ber.*, **42**, 3549 (1909).
11) H. Heaney, K. G. Mason, and J. M. Stechley, *J. Chem. Soc.*, **1971**, 567.
12) G. Yamamoto and M. Ōki, *Bull. Chem. Soc. Jpn.*, **48**, 3686 (1975).
13) M. Mikami, K. Toriumi, M. Konno, and Y. Saito, *Acta Crystallogr., Sect. B*, **31**, 2474 (1975).
14) C. R. Everly, F. F. Schweisberg, and T. G. Traynham., *J. Am. Chem. Soc.*, **100**, 1200 (1978).
15) M. L. Poutsma, "Halogenation," in "Free Radicals" ed by J. K. Kochi, John Wiley & Sons, New York (1973), Vol. 2 pp. 159—229.
16) J. M. Tedder, *Quart. Rev. (London)*, **14**, 336 (1960).
17) P. S. Skell and K. J. Shea, "Bridged Free Radicals," in "Free Radicals" ed by J. K. Kochi, John Wiley & Sons, New York (1973), Vol. 2, pp. 809—852.
18) P. S. Skell, *Acc. Chem. Res.*, **11**, 381 (1978).
19) G. A. Russel, *J. Am. Chem. Soc.*, **80**, 5002 (1958). Incidentally, chlorination of 9-*t*-butyl-1,2,3,4-tetrachlorotriptycene with sulfuryl chloride in carbon tetrachloride yielded $\pm sc/ap$ ratio of 2.90 which is not significantly different from that obtained with the chlorobenzene solution.
20) For example, see C. S. Walling and B. Miller, *J. Am. Chem. Soc.*, **79**, 4181 (1957).
21) S. Hatakeyama, T. Mitsuhashi, and M. Ōki, *Bull. Chem. Soc. Jpn.*, **53**, 731 (1980).
22) Ionization potentials of chlorobenzene and 1,2,3,4-tetrachlorobenzene have been measured: D. G. Streets and G. P. Ceasar, *Mol. Phys.*, **26**, 1037 (1973).

Esterification of Carboxylic Acids by Alcohols with 2-Chloro-1,3,5-trinitrobenzene as Condensing Agent[1)]

Seiji TAKIMOTO,[2)] Junji INANAGA, Tsutomu KATSUKI, and Masaru YAMAGUCHI*
Department of Chemistry, Faculty of Science, Kyushu University, Higashi-ku, Fukuoka 812
(Received November 28, 1980)

When mixtures of carboxylic acids or their sodium salts and alcohols were treated with 2-chloro-1,3,5-trinitrobenzene in the presence of pyridine under mild conditions, the corresponding carboxylic esters were formed. The yields and the rates of the ester formation depended on the types of the acids and the alcohols used.

Though the high reactivity of 2,4,6-trinitrophenyl carboxylates (**2**) in substitution reactions has been well recognized,[3)] the applications of these active esters to synthetic reactions are not many because few good methods for the general preparation of **2** under mild conditions are known.[4)] The kinetic parameters for the formation of chloride ion in the aqueous methanolic solutions of 2-chloro-1,3,5-trinitrobenzene (**1**) and sodium carboxylates,[5)] indicate that **1** reacts with carboxylates fairly rapidly and that the intermediate thus formed, in situ, may be used for the synthetic reactions. Wittmann utilized **1** in this way for the preparation of phosphoric acid esters[6)] and recently Inomate *et al.* 2-fluoro-1,3,5-trinitrobenzene (FTNB) for the preparation of *N*-phenyl amides, carboxylic esters, and thiocarboxylic *S*-esters.[7)] Several studies on the use of other polynitrohalobenzenes are also known.[8)] The present paper describes that **1** is particularly useful for the synthesis of esters of aromatic and aliphatic carboxylic acids.

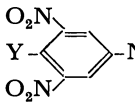

1 Y=Cl
2 Y=OCOR
3 Y=OH

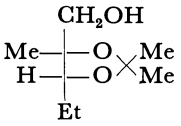

6

$$\mathbf{1} + 2R^1COOH(Na) \xrightarrow[\text{benzene}]{Et_3N} R^1COOCOR^1 + \mathbf{3}$$

4

$$\mathbf{1} + R^1COOH(Na) + R^2OH \xrightarrow{C_5H_5N} R^1COOR^2 + \mathbf{3}$$

5

Results and Discussion

Preliminarily, mixtures of sodium carboxylates and 2-butanol were treated with **1** at room temperature in ether, benzene, dichloromethane, acetonitrile, dimethyl sulfoxide, or hexamethylphosphoric triamide. In all cases, the formation of *s*-butyl carboxylates was observed but the esters were always contaminated with varied amounts of acid anhydrides. Alternatively, when **1**, carboxylic acids, and triethylamine were mixed in a 0.5:1:1 molar ratio under the absense of alcohols, acid anhydrides (**4**) were formed in good yields, as exemplified in Table 1.

On the other hand, however, when carboxylic acids or their sodium salts, alcohols, and **1** were mixed in pyridine used as the solvent, the corresponding esters (**5**) were formed in good yields, except for the esterification of carboxylic acids not branched at the α-carbon atom, where the use of a limited amount of pyridine in dichloromethane was preferable. Other bases such as triethylamine or 1,8-diazabicyclo[5.4.0]-undec-7-ene did not give the good yield and the products were contaminated with deep red substance. 4-Dimethylaminopyridine, known as an excellent acyl transfer reagent,[9)] was not effective and even retarded the reaction. In agreement with the trend in the nucleophilic aromatic substitution, the corresponding iodo- or bromotrinitrobenzene was less reactive than **1** and 2,4-dinitrochlorobenzene was almost useless.

The mechanism of this esterification is not clear at present. Inomata *et al.* described that the esteri-

Table 1. Formation of acid anhydrides

Acid	Base	Solvent	Reaction time/min	Products (Yield/%)
$(CH_3)_2CHCOOH$	Et_3N	Benzene	30	$[(CH_3)_2CHCO]_2O$[a)] (96)
$(CH_3)_3CCOOH$	Et_3N	Benzene	60	$[(CH_3)_3CCO]_2O$[a)] (98)
$CH_3CHCH_2CHCH_3$[b)] (COOH, COOH)	Et_3N	Benzene	5	$CH_3CHCH_2CHCH_3$ (CO-O-CO)[a),c)] (99)
2,3,6-$(CH_3)_3C_6H_2CO_2Na$		Pyridine	30	[2,3,6-$(CH_3)_3C_6H_2CO]_2O$[d)] (90)

a) The identity and the yield of the products were determined by GLPC by comparing with the authentic specimens. b) *meso*-2,4-Dimethylglutaric acid (1 mmol) was used per 1 mmol of **1** and 1 mmol of Et_3N. c) No *dl*-anhydride was detected. d) Isolated yield. Mp 100.5—101.5 °C. Found: C, 77.16; H, 7.08%. Calcd for $C_{20}H_{22}O_3$: C, 77.39; H, 7.14%.

fication using FTNB proceeds through the acyl fluorides as the intermediates which undergo the nucleophilic attack.[7b] On the other hand, in the esterification using **1** the main reaction seems to proceed through the acid anhydrides presumably formed from the other more reactive intermediates, the active esters (**2**) and/or acyl chlorides, by the attack of carboxylate anions remaining in the mixture. However, the direct attack of alcohols on **2** or on acyl chlorides are also considered to participate to a varied extent. For example, the formation of *t*-butyl pivalate (entry 7, Table 3) can not be explained by the anhydride route alone because the reaction between 2-methyl-2-propanol and pivalic anhydride in pyridine is extremely slow.[10] The difference between the two reagents, **1** and FTNB, in the esterification reaction can be easily understood when we consider the fact that fluorine atom attached to aromatic nucleous is much more reactive than chlorine atom in nucleophilic aromatic substitution, but that the acyl fluorides are, in turn, comparatively sluggish in nucleophilic displacements. In fact, the esterifications with FTNB are much slower than those with **1**.[11]

Aromatic Acids. Common aromatic acids were smoothly esterified in pyridine by the procedure exemplified in experimental part (Method A). They are summarized in Table 2. The esterification of 2,3,6-trimethylbenzoic acid by secondary or tertiary alcohol was difficult and a considerable amount of the acid anhydride was formed (entry 14 and 15, Table 2). An alcohol (**6**)[12] having an acid-sensitive acetal group could also be benzoylated in good yield.

Aliphatic Acids Branched at the α-Carbon Atom. The esters of primary, secondary, and tertiary alcohols were prepared by the same procedure as used in the above aromatic acid esters. The results are summarized in Table 3. Sterically crowded *t*-butyl pivalate was formed only in poor yield and a large amount of pivalic anhydride was detected. In order to examine the stability of the epimerizable α-carbon atom during the reaction, methyl hydrogen *meso*-2,4-dimethylglutarate was esterified with 2-methyl-2-propanol (entry 9, Table 3). The ester was obtained in good yield but the product was partly epimerized (*dl*:*meso*=1:10). On the other hand, the ester of secondary alcohol was obtained without any epimerization (entry 8, Table 3), presumably because of the rapidness of the reaction.

Aliphatic Acid Not Branched at the α-Carbon Atom. When aliphatic carboxylic acids which do not bear alkyl substituents on the carbon atom α to the carboxyl group, were esterified by the same procedure as described above (Method A), the products were contaminated by reddish brown substance and by some unchanged **1**. The yield of the esters was accordingly not satisfactory (50—60%). Various modifications were made to improve the yield, and the best result was obtained by conducting the reaction in dichloromethane using a limited amount of pyridine as catalyst (2—3 mole equiv. per 1 mole of **1**; Method B).[13] This procedure required much longer reaction time and the rate of esterification decreased in the order of primary alcohols>secondary alcohols>tertiary alcohols. They are summarized in Table 4.

Phenol Esters. The present method was not suitable for the preparation of phenol esters because of the concomitant formation of phenyl 2,4,6-trinitrophenyl ether (Table 5). Alternatively, the same ether

Table 2. Esterification of aromatic carboxylic acids

	Acid (2 mmol)	Alcohol (2.4 mmol)	Reaction time/h	Yield of esters/%
1	$C_6H_5CO_2H$	2-Butanol	3	93[a]
2	$C_6H_5CO_2Na$	2-Butanol	3	98[b]
3	$C_6H_5CO_2Na$	2-Methyl-2-propanol	18	85[a]
4	$4\text{-}NO_2C_6H_4CO_2H$	Ethanol	2	91[c]
5	$4\text{-}NO_2C_6H_4CO_2H$	Benzyl alcohol	2	97[c]
6	$4\text{-}NO_2C_6H_4CO_2H$	2-Propanol	3	93[c]
7	$4\text{-}NO_2C_6H_4CO_2H$	2-Methyl-2-propanol	3	88[c]
8	$4\text{-}NO_2C_6H_4CO_2Na$	2-Methyl-2-propanol	3	93[c]
9	$3,5\text{-}(NO_2)_2C_6H_3CO_2H$	2-Propanol	3	98[c]
10	$3,5\text{-}(NO_2)_2C_6H_3CO_2H$	2-Methyl-2-propanol	3	97[c]
11	$3,5\text{-}(NO_2)_2C_6H_3CO_2Na$	2-Methyl-2-propanol	3	90[c]
12	$2,3,6\text{-}(CH_3)_3C_6H_2CO_2H$	Benzyl alcohol	6	92[a]
13	$2,3,6\text{-}(CH_3)_3C_6H_2CO_2Na$	Methanol	1	96[b,d]
14	$2,3,6\text{-}(CH_3)_3C_6H_2CO_2Na$	2-Propanol	24	30[e,f] (37% Anhydride)
15	$2,3,6\text{-}(CH_3)_3C_6H_2CO_2Na$	2-Methyl-2-propanol	24	6[f] (44% Anhydride)

a) Isolated yield of once distilled product. b) Yield was determined by GLPC by comparison with authentic sample. c) Yield of crude ester. All these crude crystals melted within one degrees of melting points reported in the literature. d) A new compound. Bp 90 °C (bath)/2666 Pa. Found: C, 73.84; H, 7.85%. Calcd for $C_{11}H_{14}O_2$: C, 74.13; H, 7.92%. e) The authentic sample was prepared from the sodium salt of the acid and isopropyl bromide in HMPA. f) A mixture of ester and anhydride was obtained after preparative TLC. Yield was calculated from NMR data.

Table 3. Esterification of aliphatic acids branched at α-carbon atom

Acid (2 mmol)	Alcohol (2.4 mmol)	Reaction time/h	Isolated yield of esters/%
$CH_3(CH_2)_2CHCO_2H$ (CH₃ branch)	Benzyl alcohol	2	95[a]
	Cyclohexanol	3	95
	2-Methyl-2-propanol	3	74
$CH_3(CH_2)_2CHCO_2Na$ (CH₃ branch)	2-Methyl-2-propanol	3	69
$(CH_3)_3CCO_2H$	Benzyl alcohol	3	95
	Cyclohexanol	3	73(85[b])
	2-Methyl-2-propanol	32	30[b] (60% Anhydride)
$CH_3CHCH_2CHCH_3$[c] (COOH, $COOCH_3$)	2-Propanol	10 min	83[d]
	2-Methyl-2-propanol	3	79[e]

a) A new compound. Bp 85 °C (bath)/5599 Pa. Found: C, 75.56; H, 8.80%. Calcd for $C_{13}H_{18}O_2$: C, 75.69; H, 8.80%. b) Yield was determined by GLPC. c) Methyl hydrogen *meso*-2,4-dimethylglutarate. d) No *dl*-ester was detected. e) The ratio of *meso*-: *dl*-ester was 10 : 1 (GLPC).

Table 4. Esterification of aliphatic acids not branched at α-carbon atom

Acid (1 mmol)	Alcohol (1.1 mmol)	Pyridine (mmol)	Reaction time/h	Isolated yield of esters/%
Propionic acid	Benzyl alcohol	2.1	20	96[a]
	Cyclohexanol	2.1	30	97[a]
	2-Methyl-2-propanol[b]	2.1	60	83
Valeric acid	Benzyl alcohol	3.5	15	87
	Cyclohexanol	3.5	25	94[a]
	2-Methyl-2-propanol[b]	3.5	50	84
Hexanoic acid	Benzyl alcohol	3.5	15	88
	Cyclohexanol	3.5	25	93

a) Yield was determined by GLPC. b) Two mmol of 2-methyl-2-propanol was added.

Table 5. Formation of phenol esters

Acid	Reaction[a] time/h	Yield/%[b] Ester	Yield/%[b] $2,4,6\text{-}(NO_2)_3\text{-}C_6H_2OC_6H_5$
$4\text{-}NO_2C_6H_4CO_2Na$	3	66	27
$CH_3(CH_2)_3CO_2H$	40	54	36

a) The salt or acid (1 mmol), phenol (1 mmol), and **1** (1 mmol) were mixed by method B. b) Yields were calculated from the NMR data of the mixture of two products obtained.

was obtained in 73% yield by mixing **1** and phenol in the presence of pyridine. Similar preparation of unsymmetrical diphenyl ethers has already been reported.[14]

Experimental

All reagents employed were dried by appropriate methods. Commercial 2-chloro-1,3,5-trinitrobenzene (**1**) was recrystallized from chloroform to a constant mp 81—82 °C. The whole procedures were carried out under the exclusion of moisture. The progresses of the reactions were followed by GLPC and the esters formed were identified by comparing their NMR spectra with those of the authentic specimens.

Acid Anhydrides (Table 1). A mixture of **1** (1 mmol, 245 mg), carboxylic acid (2 mmol), and triethylamine (2 mmol, 276 μl) in benzene (3 ml) was stirred at room temperature. The products were identified by the comparison of the retention time in GLPC with the authentic specimens, and the yields were determined by comparison with appropriate internal standards.

Esters of Aromatic Acids and Esters of Aliphatic Acids Branched at the α-Carbon Atom (Method A) (Tables 2 and 3). The typical example is as follows. **1** (2 mmol, 490 mg) was added to a stirred mixture of benzoic acid (2 mmol, 244 mg) and 2-butanol (2.4 mmol, 220 μl) in pyridine (2 ml). After stirring for 3 h, an 8% aqueous sodium hydrogencarbonate solution (20 ml), water (10 ml), and ether (20 ml) were added and the whole mixture was stirred until the precipitate of pyridine picrate dissolved in the aqueous layer. The ether layer was separated and combined with the second extract (ether, 20 ml). The ether extract was washed with water until the yellow color of the solution was removed, then twice with 2% aqueous hydrochloric acid (20 ml) and water, and dried with sodium sulfate. Distillation of the residue gave *s*-butyl benzoate in 93% yield.

Crystalline esters (entries 4—13, Table 2) were filtered after treating with sodium hydrogencarbonate solution and washed well with water. All these crude crystalline esters showed correct mp and NMR spectra without further purification.

dl-erythro-*2,3-Isopropylidenedioxy-2-methylpentyl Benzoate.* It was prepared by the method A by stirring the corresponding isopropylidenedioxy alcohol (**6**)[12] (1.05 mmol, 186 mg), sodium benzoate (1.05 mmol, 152 mg), and **1** (1.05 mmol,

260 mg) in pyridine (1 ml) at room temperature for 3 h in 86% yield. Mp 70.5—71 °C. Found: C, 69.05; H, 7.97%. Calcd for $C_{16}H_{22}O_4$: C, 69.04; H, 7.97%.

Esters of Aliphatic Acids Not Branched at the α-Carbon Atom (Method B) (Table 4). A typical example is as follows. Pyridine (2.1 mmol, 170 μl) was slowly added over a period of five minutes to a stirred mixture of propionic acid (1 mmol, 75.5 μl), benzyl alcohol (1.1 mmol, 114.4 μl), and **1** (1 mmol, 245 mg) in dichloromethane (2 ml). The mixture was stirred for 20 h at room temperature. The reaction mixture was worked up as described in method A, giving benzyl propionate in 96% yield.

Phenol Esters. Carboxylic acid, phenol, and **1** (1 mmol each) reacted according to the method B (3.5 mmol of pyridine). Results were shown in Table 5. In an experiment without the carboxylic acid (40 h), 2,4,6-trinitrophenyl phenyl ether was obtained in 73% yield.

This work was partially supported by a Grant-in-Aid for Scientific Research No. 443008 from the Ministry of Education, Science and Culture.

References

1) A preliminary report of this work was presented at the 33rd National Meeting of the Chemical Society of Japan, Fukuoka, October, 1975.

2) Present address: Department of Chemistry, Faculty of Science, Fukuoka University, Nanakuma, Nishi-ku, Fukuoka 814.

3) a) G. Olivier and S. C. J. Berger, *Recl. Trav. Chim. Pays-Bus*, **40**, 609 (1927); b) A. Kirkien-Konasiewicz and A. Maccoll, *J. Chem. Soc.*, **1964**, 1267.

4) For example: From **1** and sodium carboxylate in refluxing xylene [Y. Yamashita and T. Shimamura, *Kogyo Kagaku Zasshi*, **60**, 432 (1957)]; from picric acid and acid anhydrides (Ref. 3b); from picric acid and acid chlorides [A. Hantzsch, *Chem. Ber.*, **39**, 1084 (1906); A. Laurent and C. Gerhardt, *Justus Liebigs Ann. Chem.*, **75**, 77 (1850)].

5) T. R. Mohanty and P. L. Nayak, *J. Chem. Soc., Perkin Trans. 2*, **1975**, 242.

6) R. Wittmann, *Chem. Ber.*, **96**, 2116 (1963).

7) a) H. Kotake, K. Inomata, H. Kinoshita, K. Tanabe, and O. Miyano, *Chem. Lett.*, **1977**, 647; b) K. Inomata, H. Kinoshita, H. Fukuda, K. Tanabe, and H. Kotake, *Bull. Chem. Soc. Jpn.*, **51**, 1866 (1978).

8) For example: 1-Chloro-2,4-dinitrobenzene for the preparation of carboxylic anhydrides [G. G. Yakobson, *Zhur. Vsesoyuz. Khim. Obshchestva in D. I. Mendelleev*, **5**, 708 (1960)]; 1-fluoro-2,4-dinitrobenzene for the preparation of phosphoric acid ester [R. Wittmann, *Chem. Ber.*, **96**, 771 (1963)]; polynitrohalobenzenes for the formation of *N*-phenyl amides (Ref. 7).

9) G. Höfle and W. Steglich, *Synthesis*, **1972**, 619; G. Höfle, W. Steglich, and H. Vorbrüggen, *Angew. Chem. Int. Ed. Engl.*, **17**, 569 (1978).

10) For example, a mixture of pivalic anhydride (1 mmol) and 2-methyl-2-propanol (1 mmol) in pyridine (2 ml) gave the ester only in 10% yield at room temperature after 10 d.

11) For example, FTNB method gave benzyl pivalate in 27—42% yield by refluxing in acetonitrile for 92 h,[7b] while the present method gave the same ester in 95% yield in 3 h at room temperature (entry 5, Table 3).

12) J. Inanaga, A. Takeda, N. Okukado, and M. Yamaguchi, *Mem. Fac. Sci., Kyushu Univ., C*, **9**, 293 (1975).

13) It has been known that **1** and an equimolar amount of pyridine gives 2,4,6-trinitrophenylpyridinium chloride [M. Busch and W. Kögel, *J. Prakt. Chem.*, **84**, 507 (1911)]. The salt could also be used as the condensing agent in place of **1** in the present esterification. But when a large excess of pyridine is present, the salt also gradually changes into a dark red substance. The nature of the substance is not known at present.

14) E. T. Borrows, J. C. Clayton, B. A. Hems, and A. G. Long, *J. Chem. Soc.*, **1949**, Spl. 190; G. A. Neville and R. Y. Moir, *Can. J. Chem.*, **47**, 2787 (1969).

Synthesis and Properties of Bridgehead-substituted Bicyclo[*n*.2.2] Bridgehead Alkenes

Yasuo SAKAI,* Shingo TOYOTANI, Masaru OHTANI, Masaharu MATSUMOTO, Yoshito TOBE, and Yoshinobu ODAIRA

Department of Petroleum Chemistry, Faculty of Engineering, Osaka University, Suita, Osaka 565

(Received November 28, 1980)

The bridgehead-substituted bicyclo[*n*.2.2] bridgehead alkenes (**1b—3b**) (**1**, $n=4$; **2**, $n=5$; **3**, $n=6$; **b**, R=OAc) were synthesized based on the oxidative decarboxylation of [*n*.2.2]propellanecarboxylic acids with lead tetraacetate. The parent alkene (**1a—3a**) (**a**, R=H) and other bridgehead-substituted derivatives (**1c—3c** and **1d—3d**) (**c**, R=OH; **d**, R=Cl) were prepared from **1b—3b**. The examination of the ^{13}C NMR chemical shifts of **1a—c**, **2a—c**, and **3a—c** indicates the presence of electronic interaction between the bridgehead double bond (C_γ) and the opposite bridgehead carbon (C_α), being the homoallylic position of the double bond. From the product study and the kinetic results of the solvolysis of the bridgehead chlorides **1d—3d**, it is indicated that the homoallylic participation of the strained bridgehead double bond to the carbonium ion center located at the opposite bridgehead position operates in the solvolysis of **1d** and **2d**. It may be, therefore, concluded that highly strained bridgehead alkenes, especially, bicyclo[4.2.2]decene system, show remarkable homoallylic type α,γ-interaction both in the ground state and in the transition state (carbonium ion).

There has been considerable interest in the chemistry of strained bridgehead olefins, especially with regard to the development of new efficient methods providing an entry to the highly strained molecules and the examination of specific physical properties and chemical reactivities associated with the distortion imposed on the double bond.[1] In a continuation of the study on the transformation of readily available [*n*.3.2]propellanones into other important carbocyclic ring systems,[2] we have recently developed a synthetic entry to the bicyclo[*n*.2.2]bridgehead alkenes (**1b—3b**) having an acetoxyl group at the opposite bridgehead position based on the oxidative decarboxylation of [*n*.2.2]propellanecarboxylic acids (**4a—6a**) with lead tetraacetate.[3a] In this connection, we wish to report here on the synthesis of bicyclo[*n*.2.2] bridgehead alkenes (**1a—3a**) and the bridgehead-substituted derivatives (**1c—3c**) and (**1d—3d**) from **1b—3b**, on the physical properties, that is, ^{13}C NMR spectra of **1a—3a**, **1b—3b**, and **1c—3c**, and on the chemical reactivities in the solvolysis of the bridgehead chlorides **1d—3d**.[3]

Although the ^{13}C NMR spectra of conformationally rigid polycarbocyclic compounds possessing bridgehead substituents have been extensively studied,[4] little is known concerning those of highly strained bridgehead olefins.[5] It is, therefore, of particular interest to examine the ^{13}C NMR chemical shifts of a series of the bridgehead-substituted bridgehead alkenes **1a—c**, **2a—c**, **3a—c** in connection with the effect of both oxygen substituents at the bridgehead position and the ring size (*n*) on the chemical shifts. The examination of the chemical shifts of **1a—c**, **2a—c**, and **3a—c** obviously indicated the presence of electronic interaction between the bridgehead double bond and the opposite bridgehead carbon, being the homoallylic position of the double bond. These results prompted us to investigate the homoallylic interaction between the bridgehead double bond and the carbonium ion center located at the opposite bridgehead position in the solvolysis of the bridgehead chlorides **1d—3d**.[6] As a result, the product study and the kinetic results of the solvolysis demonstrated the presence of the

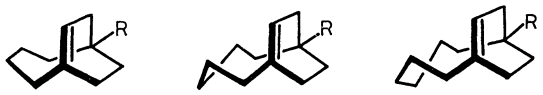

1a—d **2a—d** **3a—d**

a, R=H; **b**, R=OAc; **c**, R=OH; **d**, R=Cl

homoallylic participation of the strained double bond to the carbonium ion center, especially in the case of the most strained bicyclo[4.2.2]decene system (**1**).

Results and Discussion

Synthesis. The entry into the bridgehead-substituted bicyclo[*n*.2.2] bridgehead alkene systems was based on the oxidative decarboxylation of [*n*.2.2]-propellanecarboxylic acids **4a—6a** with lead tetraacetate, which were prepared from [*n*.3.2]propellanones[7] by the ring contraction involving the photochemical Wolff rearrangement. The reaction of **4a—6a** with lead tetraacetate was carried out in the presence of pyridine in benzene solution at 80 °C for 1 h. The [6.2.2]propellane **6a** gave the intended allylcarbinyl type bicyclic acetate **3b**, having a bridgehead double bond, in 81% yield. In the case of the [5.2.2]propellane **5a**, the cyclopropylcarbinyl type tricyclic acetate (**8b**), however, was obtained as the major product in 60% yield along with 13% of the desired bridgehead olefin **2b** and small amounts (3%) of [5.2.2]propellene (**10**). Moreover, the [4.2.2]propellane **4a** afforded the tricyclic acetate (**7b**) exclusively in 68% yield together with 5% of [4.2.2]propellene (**9**), but the intended olefin **1b** was not produced at all. These products may be derived from the rearrangement of the initially formed cyclobutyl cation to allylcarbinyl and/or cyclopropylcarbinyl ones. In order to transform the tricyclic acetates **7b** and **8b** into the corresponding bridgehead alkenes **1b** and **2b**, we first examined the

9 **10**

vapor phase thermolysis of **7b** and **8b** at 350 °C under nitrogen stream. Although the thermolysis proceeded in high efficiency to give **1b** and **2b**, this process seems to be not suited for large-scale preparation of **1b** and **2b**. We next tried, therefore, the acid catalyzed rearrangement of **7b** and **8b**. After many trials, it appeared that simple treatment of **7b** and **8b** with acetic acid was the best way for this purpose. The bridgehead alcohols **1c**—**3c** were prepared by the lithium aluminum hydride reduction of **1b**—**3b**, and the bridgehead chlorides **1d**—**3d**, being the substrates required for solvolysis experiments, were derived from the reaction of **1c**—**3c** with thionyl chloride or phosphoryl chloride. The preparation of the unsubstituted hydrocarbons **1a**—**3a** was not straightforward. Thus **1a** was prepared by the elimination of acetic acid by means of the vapor phase thermolysis of the saturated acetate (**11b**) (76%) or by the dehydration through treating the saturated alcohol (**11c**) with thionyl chloride/pyridine (74%), which were derived by the diimide reduction of **1b** and **1c**, respectively.[8] Although the similar reduction of **2c** afforded **12c**, those of **2b**, **3b**, and **3c**, however, were unsuccessful.[9,10] The bridgehead alkene **2a** was prepared, therefore, by the dehydration of **12c** (80%) or by the thermolysis of **12b** (82%) which was obtained by the acetylation of **12c** using 4-dimethylaminopyridine/acetic anhydride.[11] On the other hand, **3a** was prepared by the reduction of the chloride **3d** with lithium/*t*-butyl alcohol in 67% yield. All the synthetic scheme is summarized in Scheme 1.

^{13}C NMR Spectra. The ^{13}C NMR chemical shifts for the bridgehead-substituted bridgehead alkenes **1a**—**c**, **2a**—**c**, and **3a**—**c** are listed in Table 1. Though it was impossible to assign all the carbons, α carbon, olefinic γ carbon, and olefinic δ carbon (Fig. 1) were unequivocally assigned on the basis of

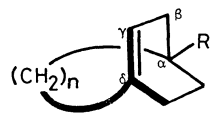

Fig. 1.

the multiplicities of the off-resonance decoupled spectra. Therefore, the discussion should be focused on the chemical shifts of the above three carbons. The substituent effects in each ring system, *i.e.*, the chemical shift differences between the alkenes having same ring system and different bridgehead substituents taking the hydrocarbons **1a**—**3a** as standard, are listed in Table 2, and the ring size effects, *i.e.*, the chemical shift differences between the alkenes having same substituent and different ring systems taking bicyclo[6.2.2]-dodecene systems **3a**—**3c** as standard, are in Table 3. As shown in Table 2, the magnitude of the substituent effects on each carbon is in the order α effects> γ effects>δ effects, as might be expected from the distance from the substituents to each carbon. The magnitude of α substituent effects, which are directly related to the electronegativity of oxygen, as well as the small degree of δ effects observed for **1b**—**c**, **2b**—**c**, and **3b**—**c** are in accord with the cases of other bridgehead substituted alkanes.[4] However, by contrast to the small downfield shifts for γ carbons in the bridgehead substituted alkanes,[4] the remarkable upfield shift was observed for the γ carbons in the present bridgehead alkenes. Thus, for example, the γ carbon resonances of **1b** and **1c** appeared 4.99 and 3.98 ppm higher field than that of **1a**. As can be seen in Table 3, most of α, γ, and δ carbons of **1a**—**c** and **2a**—**c**, except for γ carbons of **2a**—**c**, were deshielded compared with those of **3a**—**c**, which indicated the increase of steric strain with decrease in the ring size (n).

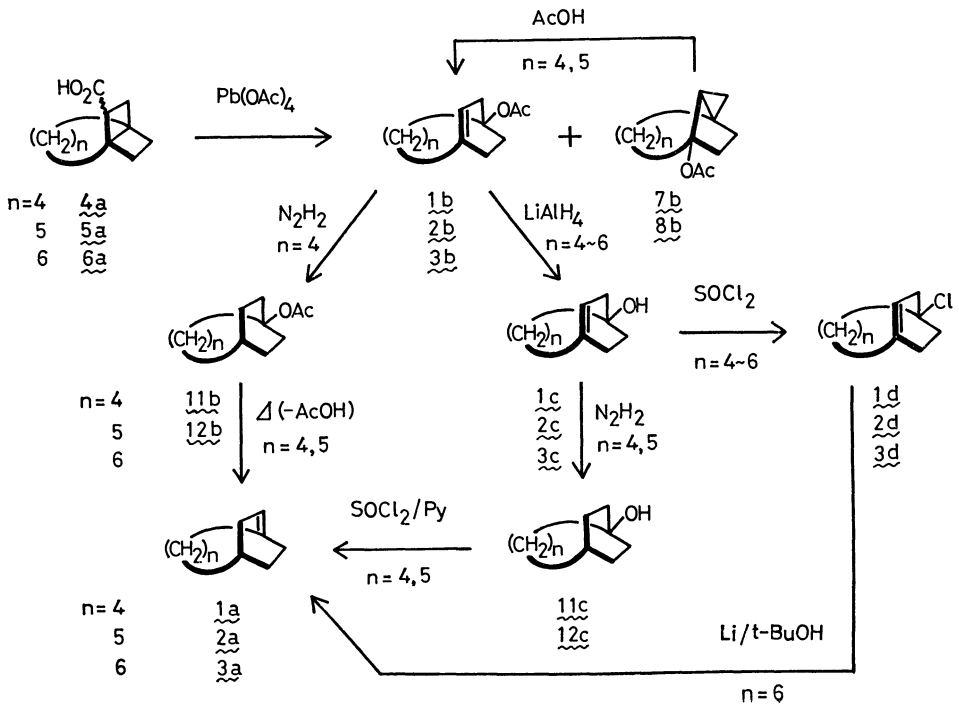

Scheme 1.

Table 1. ^{13}C NMR Chemical shifts of bicyclo[n.2.2] bridgehead alkenes **1a—c**, **2a—c**, and **3a—c**[a)]

Compd	R	C_α	C_γ	C_δ	Other carbons
1a	H	36.51	126.86	141.97	38.70, 35.37, 32.89, 29.48, 28.87, 27.74, 26.84
1b	OAc	88.70	121.87	143.00	170.70, 40.02, 37.09 (2C), 32.24, 30.14, 27.50, 25.49, 22.65
1c	OH	79.02	122.88	141.76	44.83, 40.77, 38.05, 35.94, 27.74, 26.92, 26.19
2a	H	30.82	122.80	138.92	37.20, 36.02, 33.58, 28.63, 28.43, 27.09, 24.69, 24.16
2b	OAc	86.60	119.72	140.71	170.60, 42.47, 37.33, 36.55, 30.24, 29.40, 27.99, 27.64, 24.85, 22.70
2c	OH	75.13	120.77	139.81	46.29, 41.34, 36.47, 33.14, 29.28, 28.26, 27.13, 25.75
3a	H	30.33	124.06	138.23	38.38, 35.90, 29.89, 29.16, 27.61 (2C), 27.49, 24.89 (2C)
3b	OAc	86.06	120.55	138.60	170.60, 39.34, 37.33 (2C), 35.76, 32.39, 28.03 (2C), 25.73 (2C), 22.80
3c	OH	73.78	121.46	138.27	44.55, 38.74, 37.40 (2C), 35.57, 28.87, 27.41 (2C), 26.35

a) Measured at −11—−14 °C in $CDCl_3$ solution and the shifts are in ppm with respect to internal Me_4Si.

Table 2. Substituent effects on the ^{13}C NMR chemical shifts for bicyclo[n.2.2] bridgehead alkenes[a)]

Compd	Substituent	C_α	C_γ	C_δ
1b[b)]	OAc	52.19	−4.99	1.03
1c[b)]	OH	42.51	−3.98	−0.21
2b[c)]	OAc	55.78	−3.08	1.79
2c[c)]	OH	44.31	−2.03	0.89
3b[d)]	OAc	55.77	−3.51	0.37
3c[d)]	OH	43.45	−2.60	0.04

a) Positive shifts are to lower field and negative shifts are to higher field. b) Relative to **1a**. c) Relative to **2a**. d) Relative to **3a**.

Table 3. Ring size effects on the ^{13}C NMR chemical shifts for bicyclo[n.2.2] bridgehead alkenes[a)]

Compd	Substituent	C_α	C_γ	C_δ
1a	H	6.18	2.80	3.64
1b	OAc	2.64	1.32	4.40
1c	OH	5.24	1·42	3.49
2a	H	0.49	−1.26	0.69
2b	OAc	0.54	−0.83	2.11
2c	OH	1.35	−0.69	1.54

a) Values refer to the differences between the chemical shifts of a given compound and those of **3a—3c** having the same bridgehead substituent. Positive shifts are to lower field and negative shifts are to higher field.

The most significant feature in the ^{13}C NMR spectra of the bicyclo[n.2.2] bridgehead alkenes is the remarkable shielding γ effects observed in **1b—c**, **2b—c**, and **3b—c**. The γ anti shielding effects is well known for some alicyclic systems and several possible mechanisms have been posturated for interpretation of the effect such as electrostatic field effect,[12)] back-lobe interaction of sp^3 orbitals on C_γ with that of C_α-hetero atom bond,[13)] and α,γ-hyperconjugative type interaction of free-electron pairs on hetero atom.[14)] The present γ effect may also be accounted by one or more

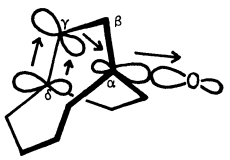

Fig. 2.

of the above explanations, because the molecular framework of the bridgehead alkenes are considerably deformed so that C_α and C_γ are in close proximity compared with unstrained saturated bicyclic systems. However, in view of the solvolysis behavior of the bridgehead chlorides **1d** and **2d** described later, we think it more attractive to ascribe the present γ effect to the interaction of the back-lobe of sp^3 orbital of C_α-oxygen bond with C_γ p orbital of the distorted bridgehead double bond, as shown in Fig. 2. Moreover, inspection of molecular models suggests that, in agreement with the observed effects, such interaction may be most pronounced in bicyclo[4.2.2]decene system (**1**) because of favorable geometry of the two orbitals for the interaction.

*Solvolysis of the Bridgehead Chlorides **1d—3d**.* From the standpoint of facility in the identification of the solvolysis products, the hydrolysis of the bridgehead chlorides **1d—3d** was attempted, because the expected hydrolysis products, that is, the bridgehead alcohols **1c—3c** and **7c—8c** should be readily available. The product study of the solvolysis of **1d—3d** was, therefore, carried out in 80% (v/v) acetone–water containing 2,6-lutidine buffer. Whereas the solvolysis of **3d** gave only the unrearranged alcohol **3c**, **1d** afforded the rearranged cyclopropylcarbinyl type alcohol **7c** as a sole product, and, in addition, **2d** gave 87% of the rearranged alcohol **8c** and 13% of the unrearranged one **2c**. The solvolysis rates of **1d—3d** were determined in ethanol solvent, because, unfortunately,

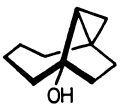

7c

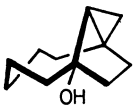

8c

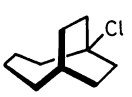

11d

Table 4. Kinetic data for the ethanolysis of the bridgehead chlorides **1d—3d** and **11d**

Chloride	Temp[a] °C	k[b] s^{-1}	k_{rel}	ΔH^* kcal mol^{-1}	ΔS^* eu
1d	25.0	1.52×10^{-4}	214	23.9	−1.8
	20.0	7.50×10^{-5}			
2d	33.0	1.96×10^{-4}			
	25.0	7.44×10^{-5}	105	21.4	−5.9
3d	33.0	3.00×10^{-5}			
	25.0	1.07×10^{-5}	15.1	22.8	−5.0
11d	55.0	4.27×10^{-5}			
	40.0	6.07×10^{-6}		25.9	+4.5
	25.0[c]	7.10×10^{-7}	1.0		

a) ±0.1 °C. b) The deviations are within 6%. c) Extrapolated value.

Table 5. Spectral and analytical data for the bridgehead alkenes **1a—3a**, **1b—3b**, **1c—3c**, and **1d—3d** and the cyclopropylcarbinyl type tricyclic compounds **7b**, **8b**, **7c**, and **8c**

Compd	IR $\tilde{\nu}$/cm^{-1}	MS (m/e)	^{1}H NMR[a] δ/ppm	Found (Calcd) C (%)	H (%)
1a[b,c]	3030, 1640	136 (M^+)	1.00—2.60 (m, 15H), 5.68 (t, J=7 Hz, 1H)		
2a[d]	3030, 1640	150 (M^+)	1.00—2.80 (m, 17H), 5.46—5.65 (m, 1H)	87.71 (87.92)	12.00 (12.08)
3a[e]	3030, 1640	164 (M^+)	0.90—2.60 (m, 19H), 5.66 (broad d, J=7 Hz, 1H)	87.73 (87.40)	12.27 (12.15)
1b[f]	3040, 1710, 1220	194 (M^+, trace), 134 (M^+−AcOH)	1.35—2.80 (m, 17H, s at 1.88), 5.32—5.56 (m, 1H)	74.55 (74.19)	9.54 (9.34)
2b[g]	3040, 1710, 1225	208 (M^+, trace), 148 (M^+−AcOH)	1.05—2.60 (m, 19H, s at 1.75), 5.36 (broad d, J=8 Hz, 1H)	75.08 (74.96)	9.68 (9.74)
3b[h]	3040, 1710, 1230	222 (M^+, trace), 162 (M^+−AcOH)	1.15—2.80 (m, 21H, s at 1.71), 5.32 (broad d, J=8 Hz, 1H)	75.20 (75.63)	9.93 (9.97)
1c[i]	3350, 3030, 1065, 1030	152 (M^+)	1.00—2.65 (m, 15H), 5.32—5.56 (m, 1H)	78.82 (78.89)	10.76 (10.59)
2c[i]	3350, 3030, 1060, 1020	166 (M^+)	1.05—2.70 (m, 17H), 5.48 (broad d, J=7 Hz, 1H)	79.21 (79.46)	10.78 (10.92)
3c[j]	3350, 3030, 1010	180 (M^+, trace), 162 (M^+-H_2O)	0.90—2.70 (m, 19H), 5.48 (broad d, J=6 Hz, 1H)	79.63 (79.94)	11.10 (11.18)
1d[k]	3030, 870, 730	170 (M^+)	0.95—2.80 (m, 14H), 5.25—5.40 (m, 1H)	70.53 (70.37)	8.89 (8.86)
2d[l]	3030, 870, 730	184 (M^+)	0.80—2.90 (m, 16H), 5.25 (broad d, J=8 Hz, 1H)	71.64 (71.52)	9.26 (9.28)
3d[m]	3030, 880, 730	198 (M^+)	0.90—2.80 (m, 18H), 5.26 (broad d, J=8 Hz, 1H)	72.94 (72.52)	9.64 (9.64)
7b	3050, 1720, 1230	194 (M^+, trace), 134 (M^+−AcOH)	0.92 (d, J=6 Hz, 2H), 1.13—2.60 (m, 16H, s at 1.74)	74.01 (74.19)	9.42 (9.34)
8b	3050, 1720, 1235	208 (M^+, trace), 148 (M^+−AcOH)	0.36—0.72 (m, 2H), 1.05—2.60 (m, 18H, s at 1.76)	74.77 (74.96)	9.86 (9.68)
7c[n]	3350, 3050, 1100, 1030	152 (M^+)	0.62 (t, J=7 Hz, 1H), 0.95 (d, J=7 Hz, 1H), 1.05—2.60 (m, 14H)	78.53 (78.89)	10.60 (10.59)
8c[o]	3350, 3050, 1070, 1020	166 (M^+)	0.41 (2d, J=8 Hz, 4 Hz, 1H), 0.60 (t, J=4 Hz, 1H), 1.05—2.40 (m, 16H)	79.13 (79.46)	11.13 (10.92)

a) ^{1}H NMR spectra of **1a—3a** were measured in $CDCl_3$ solutions and those of the other compounds were in C_6D_6 solutions. b) Since **1a** was highly sensitive to oxygen, correct analytical data could not be obtained. c) Mp 33—35 °C. d) Mp 30—32 °C. e) Bp 50—60 °C (bath temp)/20 mmHg. f) Bp 75—78 °C/0.5 mmHg. g) Bp 80—83 °C/0.2 mmHg. h) Bp 85—87 °C/0.3 mmHg. i) Semisolid. j) Mp 84—85 °C. k) Bp 55—65 °C (bath temp)/1 mmHg; ^{13}C NMR ($CDCl_3$) δ 141.46 (s), 123.31 (d), 76.73 (s), 46.55 (t), 41.64 (t), 38.23 (t), 36.40 (t), 28.97 (t), 27.24 (t), 26.79 (t). l) Bp 75—85 °C (bath temp)/2 mmHg; ^{13}C NMR ($CDCl_3$) δ 139.53 (s), 121.25 (d), 75.37 (s), 47.67 (t), 43.82 (t), 36.34 (t), 35.21 (t), 29.44 (t), 28.79 (t), 26.80 (t), 26.44 (t). m) Bp 102—105 °C/4 mmHg; ^{13}C NMR ($CDCl_3$) δ 138.07 (s), 122.27 (d), 75.49 (s), 46.50 (t, 2C), 37.36 (t, 3C), 28.55 (t), 27.13 (t), 26.92 (t, 2C). n) Mp 87—89 °C. o) Mp 90—92 °C.

the hydrolysis rates of **1d—3d** were too rapid to measure.[15] The rates of ethanolysis of **1d—3d** buffered with 10% (v/v) of 2,6-lutidine were listed in Table 4.[16] For comparison, the ethanolysis rates of the saturated chloride (**11d**) were also determined. As shown in Table 4, **1d** was most reactive and was solvolyzed at a rate 214 times faster than the corresponding saturated chloride **11d**. The solvolysis rate of **2d** was about a half of that of **1d** but was still considerably greater than those of **3d** and **11d**. The product study and the kinetic results indicate clearly the presence of the homoallylic participation of the strained bridgehead double bond to the carbonium ion center located at the opposite bridgehead position in bicyclo[4.2.2]decene and bicyclo[5.2.2]undecene systems, although it may be conceivable that relief of large strain in the ground state of **1d** and **2d** may partially contribute to the observed rate enhancement. Examination of molecular models suggests that, in analogy with the case of the ^{13}C NMR study, more favorable geometry, both in distance and in orientation, can be attained for the homoallylic interaction between the vacant p orbital at the bridgehead position and the p orbital of the distorted bridgehead double bond with decrease in the size (n) of the bicyclo[n.2.2] framework. Thus, it may be concluded that the highly strained bridgehead alkenes, especially bicyclo[4.2.2]-decene system, show remarkable homoallylic type α,γ-interaction both in the ground state and in the transition state (carbonium ion).

Experimental

All the melting and boiling points are uncorrected. IR spectra were recorded on a JASCO IR-G spectrometer. Mass spectra were taken by using a Hitachi RMU-6E spectrometer. ^1H NMR spectra were obtained on a JEOL JNM-PS-100 spectrometer and ^{13}C NMR spectra were on a JEOL JNM-FX-60S spectrometer. Analytical GLC was carried out on a Hitachi 163 gas chromatograph (10% FFAP or 5% SE-30 column) and preparative GLC separation was undertaken on a Varian Aerograph 920 gas chromatograph. The spectral and analytical data for the bridgehead alkenes **1a—3a**, **1b—3b**, **1c—3c**, and **1d—3d** and those for the cyclopropylcarbinyl type tricyclic compounds **7b**, **8b**, **7c**, and **8c** were listed in Table 5.

Preparation of [n.*2.2*]*Propellanecarboxylic Acids* ***4a—6a***. The ring contraction of [n.3.2]propellanones[7] were carried out by the usual procedure involving the photochemical Wolff rearrangement.[17] Namely, the condensation of [n.3.2]propellanones with ethyl formate using sodium hydride in ether[18] gave the corresponding hydroxymethylene derivatives (IR 1670, 1600, 1520, 1180 cm^{-1}) in 80—87% yields and subsequent diazo transfer with tosyl azide[19] gave the corresponding diazo ketones (IR 2050, 1650 cm^{-1}) in quantitative yield. The crude diazo ketones were dissolved in methanol and the solutions were irradiated in a Pyrex vessel with a 500 W high pressure mercury lamp for 16—20 h. The solvent was removed under reduced pressure and the residue distilled to afford the methyl esters (**4b—6b**) of [n.2.2]propellanecarboxylic acids **4a—6a** in 65—85% yields. GLC analysis showed that **4b—6b** were the mixtures of epimers in about 1:2 ratio. **4b**: bp 103—105 °C/10 mmHg; IR 1720, 1165 cm^{-1}; MS m/e 194 (M^+); ^1H NMR (CCl_4) δ 1.00—2.72 (m, 14H), 3.04, 3.16 (t, J=8 Hz, 1H), 3.58 (s, 3H). Found: C, 74.17; H, 9.43%. Calcd for $C_{12}H_{18}O_2$: C, 74.19; H, 9.34%. **5b**: bp 110—112 °C/5 mmHg; IR 1720, 1165 cm^{-1}; MS m/e 208 (M^+); ^1H NMR (CCl_4) δ 1.10—2.55 (m, 16H), 3.02, 3.04 (t, J=8 Hz, 1H), 3.59 (s, 3H). Found: C, 74.77; H, 9.79%. Calcd for $C_{13}H_{20}O_2$: C, 74.96; H, 9.68%. **6b**: bp 124—128 °C/8 mmHg; IR 1720, 1165 cm^{-1}; MS m/e 222 (M^+); ^1H NMR (CCl_4) δ 1.10—2.56 (m, 18H), 3.08 (t, J=8 Hz, 1H), 3.60 (s, 3H). Found: C, 75.35; H, 10.11%. Calcd for $C_{14}H_{22}O_2$: C, 75.63; H, 9.97%.

The solutions of the esters **4b—6b** and 2 equiv. of potassium hydroxide in methanol were heated at reflux for 3 h. The solvent was concentrated and the residue was diluted with water and washed with ether. The aqueous layer was acidified with 6 mol dm^{-3} hydrochloric acid and extracted with ether. Evaporation of the ether gave **4a—6a** (92—93% yield) as colorless viscous oil which solidified on standing. IR 3500—2500, 1690, 1220 cm^{-1}. The treatment of **4a—6a** with ethereal diazomethane gave **4b—6b** having the similar ratio of epimers to that of the original ester mixtures.[20]

Oxidative Decarboxylation of ***4a—6a*** *with Lead Tetraacetate.* The solution of **4a—6a**, 1.1 equiv. of lead tetraacetate, and 0.6 equiv. of pyridine in benzene was heated under nitrogen at 80 °C for 1 h. After filtration, the solution was washed successively with dilute hydrochloric acid, sodium hydrogencarbonate solution, and water and then dried over anhydrous sodium sulfate (Na_2SO_4). After evaporation of the solvent, the products were analyzed by GLC and the yields determined: **4a**; **7b** (68%), **9** (5%). **5a**; **2b** (13%), **8b** (60%), **10** (3%). **6a**; **3b** (81%). The products were separated by preparative GLC. **9**: IR 3030 cm^{-1}; MS m/e 134 (M^+); ^1H NMR (CCl_4) δ 1.20—2.00 (m, 12H), 6.17 (s, 2H). Found: C, 89.20; H, 10.64%. Calcd for $C_{10}H_{14}$: C, 89.49; H, 10.51%. **10**: IR 3030 cm^{-1}; MS m/e 148 (M^+); ^1H NMR (CCl_4) δ 1.10—2.20 (m, 14H), 6.14 (s, 2H). Found: C, 89.06; H, 10.92%. Calcd for $C_{11}H_{16}$: C, 89.12; H, 10.88%.

Preparation of ***1b*** *and* ***2b*** *by the Rearrangement of* ***7b*** *and* ***8b*** *in Acetic Acid.* The solution of **7b** and **8b** in acetic acid was stirred under nitrogen at room temperature for 5 and 22 h, respectively, and the progress of the reaction was monitored by GLC. The solution was cooled with ice and carefully neutralized with aqueous sodium hydroxide solution and extracted with ether. The ether extract was washed with water and dried over Na_2SO_4. Evaporation of the solvent followed by distillation afforded **1b** and **2b** in 90 and 97% yields, respectively. Analytical sample of **1b** was obtained by preparative GLC.

Preparation of the Bridgehead Alcohols ***1c—3c*** *and* ***7c—8c*** *by Lithium Aluminum Hydride Reduction of* ***1b—3b*** *and* ***7b—8b***. The solution of the acetates **1b—3b** and **7b—8b** in ether was added dropwise to the suspension of lithium aluminum hydride (1 equiv.) in the same solvent and the mixture was stirred at room temperature for 1 h. Water was added dropwise followed by dilute hydrochloric acid. The organic layer was separated and washed with sodium hydrogencarbonate solution and water and then dried (Na_2SO_4). Evaporation of the solvent gave the alcohols **1c—3c** and **7c—8c** in 68—80% yields which were purified by preparative GLC.

Preparation of the Bridgehead Chlorides ***1d—3d***. To the solution of **1c—3c** and 5 equiv. of pyridine in benzene was added 2 equiv. of thionyl chloride (phosphoryl chloride was used in the case of **1c**) and the solution was stirred at room temperature for 2 h. Water was added carefully and the organic layer was washed with dilute hydrochloric acid,

sodium hydrogencarbonate solution, and water. After drying over Na_2SO_4, the solvent was evaporated to give **1d—3d** as light brown oil (45—87% yields). Pure samples of **1d—3d** were obtained by preparative GLC.

*Preparation of **11b**, **11c**, and **12c** by the Diimide Reduction of **1b**, **1c**, and **2c**.* The solution of **1b**, **1c**, and **2c**, 20 equiv. of 90% hydrazine hydrate, and 0.1 equiv. of copper (II) sulfate in ethanol was stirred at room temperature while air was bubbled through a syringe. The course of the reaction was monitored by GLC and the reaction times required for completion were within 1 h for **1b** and **1c** and 20 h for **2c**. However, the similar reaction of **2b**, **3b**, and **3c** was unsuccessful.[10] The solution was diluted with water and extracted with ether. The ether extract was washed with water and dried (Na_2SO_4). After evaporation of the solvent, the products were purified by passing through a silica-gel column. Yields of the isolated products were 71—79%. **11b**: IR 1720, 1255, 1230 cm^{-1}; MS *m/e* 136 (M^+-AcOH); ^1H NMR (CCl_4) δ 1.32—2.40 (m, s at 1.84). Found: C, 73.45; H, 10.37%. Calcd for $C_{12}H_{20}O_2$: C, 73.43; H, 10.27%. **11c**: mp 73—74 °C; IR 3350, 1020 cm^{-1}; MS *m/e* 154 (M^+, trace), 136 (M^+-H_2O); ^1H NMR (CCl_4) δ 1.40—2.30 (m). Found: C, 77.49; H, 11.86%. Calcd for $C_{10}H_{18}O$: C, 77.86; H, 11.76%. **12c**: mp 79—80 °C; IR 3350, 1060, 1050 cm^{-1}; MS *m/e* 150 (M^+-H_2O); ^1H NMR (CCl_4) δ 1.35—2.30 (m). Found: C, 78.50; H, 11.63%. Calcd for $C_{11}H_{20}O$: C, 78.51; H, 11.98%.

*Preparation of **12b**.* To the solution of 80 mg of **12c** and 120 mg of 4-dimethylaminopyridine in 2 ml of dichloromethane was added with stirring the solution of 100 mg of acetic anhydride in 0.5 ml of dichloromethane and the solution was stirred at room temperature for 6 h. The solution was diluted with ether and washed successively with dilute hydrochloric acid, sodium hydrogencarbonate solution, and water and dried over Na_2SO_4. Evaporation of the solvent gave **12b** as a clear oil (80% yield). IR 1720, 1240 cm^{-1}; MS *m/e* 150 (M^+-AcOH); ^1H NMR (CCl_4) δ 1.10—2.40 (m, s at 1.84).[22]

*Preparation of the Alkenes **1a** and **2a**.* *(a) By the Vapor Phase Thermolysis of **11b** and **12b**:* The 3% solution of **11b** and **12b** in hexane was passed through a Pyrex column which was heated at 350 °C under nitrogen stream (15 ml/min) and the end of the column was connected to a trap containing powdered potassium carbonate cooled at −78 °C. The trapped solution was filtered and concentrated to give **1a** and **2a** as semisolid in 76—82% yields.

*(b) By the Dehydration of **11c** and **12c**:* The treatment of **11c** and **12c** with thionyl chloride/pyridine in the similar manner to the chlorination of **2c** and **3c** afforded **1a** and **2a** in 74—80% yields.

*Preparation of the Alkene **3a**.* The solution of 900 mg of **3d** and 3.3 g of *t*-butyl alcohol in 30 ml of tetrahydrofuran was heated at reflux with stirring and to this solution was added portionwise 315 mg of lithium cut in small pieces. The mixture was heated for 3 h and then poured into water. The organic layer was separated and the aqueous layer was extracted with ether. The combined extracts was washed with saturated sodium chloride solution and dried over Na_2SO_4. Evaporation of the solvent followed by distillation gave **3a** as a colorless oil in 67% yield.

*Preparation of the Bridgehead Chloride **11d**.* 138 mg of the alcohol **11c** was added portionwise to 1.0 g of thionyl chloride and the solution was stirred at room temperature for 1 h. Crashed ice was added followed by water and the mixture was extracted with ether. The extract was washed with sodium hydrogencarbonate solution and water and dried over Na_2SO_4. After evaporation of the solvent, **11d** was purified by sublimation (70 °C/20 mmHg): mp 70—71 °C; IR 850 cm^{-1}; MS *m/e* 172 (M^+, trace), 137 (M^+-HCl); ^1H NMR (CCl_4) δ 1.15—2.60 (m). Found: C, 69.94; H, 9.96%. Calcd for $C_{10}H_{17}Cl$: C, 70.14; H, 9.96%.

*Kinetic Measurements of the Ethanolysis of **1d—3d** and **11d**.* The solution (0.1 M) of the chlorides and the internal standard (octadecane or nonadecane) in ethanol containing 10% (v/v) of 2,6-lutidine was set in a constant temperature bath and at appropriate intervals aliquots were removed by a syringe and the decrease of the chlorides was determined by GLC. The products of the ethanolysis were isolated by preparative GLC and the ^1H NMR spectra of them were taken. **1d** gave a single ether which showed a multiplet (2H) at δ 0.52—0.98, a triplet at δ 1.21, and a quartet (2H) at δ 3.48 ppm. **2d** gave two ethers in a ratio of 3:1; the former exhibited a multiplet (2H) at δ 0.37—0.88, a triplet at δ 1.24, and a quartet (2H) at δ 3.52 ppm, and the latter a triplet at δ 1.11, a quartet (2H) at δ 3.28, and a multiplet (1H) at δ 5.36—5.52 ppm. **3d** afforded a single ether which showed a triplet at δ 1.15, a quartet (2H) at δ 3.31, and a broad doublet (1H) at δ 5.54 ppm.

*Preparative Hydrolysis of **1d—3d**.* The solution of **1d—3d** in 80% aqueous acetone containing 5 equiv. of 2,6-lutidine was stand at room temperature over night. The solvent was concentrated and extracted with ether. The products were identified by the comparison in GLC retention times and IR spectra with those of the authentic samples: **1d**; **7c** (96%). **2d**; **8c** (80%), **2c** (12%). **3d**; **3c** (99%).

References

1) For reviews: a) G. Köbrich, *Angew. Chem., Int. Ed. Engl.*, **12**, 464 (1973); b) G. L. Buchanan, *Chem. Soc. Rev.*, **3**, 41 (1974); c) R. Keese, *Angew. Chem., Int. Ed. Engl.*, **14**, 528 (1975); d) A. Greenberg and J. F. Liebman, "Strained Organic Molecules," Academic Press, New York (1978), pp. 117—133; e) K. J. Shea, *Tetrahedron*, **36**, 1683 (1980).

2) a) Y. Tobe, K. Kakiuchi, Y. Kawakami, Y. Sakai, K. Kimura, and Y. Odaira, *Chem. Lett.*, **1978**, 1027; b) Y. Tobe, Y. Hayauchi, Y. Sakai, and Y. Odaira, *J. Org. Chem.*, **45**, 637 (1980); c) K. Kakiuchi, Y. Tobe, and Y. Odaira, *ibid.*, **45**, 729 (1980); d) Y. Tobe, K. Terashima, Y. Sakai, and Y. Odaira, *J. Am. Chem. Soc.*, in press.

3) Preliminary reports in this series: a) Y. Sakai, S. Toyotani, Y. Tobe, and Y. Odaira, *Tetrahedron Lett.*, **1979**, 3855; b) Y. Sakai, Y. Tobe, and Y. Odaira, *Chem. Lett.*, **1980**, 691; c) Y. Sakai, M. Ohtani, Y. Tobe, and Y. Odaira, *Tetrahedron Lett.*, **1980**, 5025.

4) a) G. E. Maciel and H. C. Dorn, *J. Am. Chem. Soc.*, **93**, 1268 (1971); b) T. Pehk, E. Lippma, V. V. Sevostjanova, M. M. Krayuschkin, and A. I. Tarasova, *Org. Magn. Resonance*, **3**, 783 (1971); c) D. G. Morris and A. M. Murray, *J. Chem. Soc., Perkin Trans. 2*, **1975**, 734; d) G. S. Poindexter and P. J. Kropp, *J. Org. Chem.*, **41**, 1215 (1976); e) W. Kitching, W. Adcock, T. C. Khor, and D. Doddrell, *ibid.*, **41**, 2055 (1976).

5) K. B. Becker, *Helv. Chim. Acta*, **60**, 81 (1977).

6) There has been reported only one example of the homoallylic participation of strained bridgehead double bond: P. G. Gassman G. M. Lein and R. Yamaguchi, *Tetrahedron Lett.*, **1976**, 3113.

7) a) Y. Tobe, K. Kimura, and Y. Odaira, *J. Org. Chem.*, **44**, 639 (1979); b) Y. Tobe, A. Doi, K. Kimura, and Y. Odaira, *Bull. Chem. Soc. Jpn.*, **52**, 639 (1979).

8) The structure of the alkenes **1a** and **2a** prepared by the elimination of the respective bridgehead substituents was confirmed by the conversion into cyclooctanone and

cyclononanone derivatives through the ozonolysis: Y. Sakai, Y. Tobe, and Y. Odaira, unpublished results.

9) The catalytic hydrogenation of **1b—3b** and **1c—3c** at atmospheric pressure of hydrogen using Pd/C or PtO_2 catalyst was also unfruitful.

10) The reason for this distinct substituent effect found in the diimide reduction of **2b** and **2c** is not clear at present.

11) a) W. Steglich and G. Höfle, *Angew. Chem., Int. Ed. Engl.*, **8**, 981 (1969); b) G. Höfle and W. Steglich, *Synthesis*, **1972**, 619.

12) a) J. G. Batchlor, J. H. Prestgard, R. J. Cushley, and S. R. Lipsky, *J. Am. Chem. Soc.*, **95**, 6358 (1973); b) D. D. Giannini, P. A. Kollman, N. S. Bhacca, and M. E. Wolff, *ibid.*, **96**, 5462 (1974).

13) J. B. Grutzner, M. Jautelat, J. B. Dence, R. A. Smith, and J. D. Roberts, *J. Am. Chem. Soc.*, **92**, 7107 (1970).

14) E. L. Eliel, W. F. Bailey, L. D. Kopp, R. L. Willer, D. M. Grant, R. Bertrand, K. A. Christensen, D. K. Dalling, M. W. Duch, E. Wenkert, F. M. Schell, and D. W. Cochran, *J. Am. Chem. Soc.*, **97**, 322 (1975).

15) It was deduced that the products of the ethanolysis were similar to those of the hydrolysis in acetone-water based on the ^1H NMR analysis of the ethanolysis products (see Experimental).

16) Since the bridgehead chlorides, especially **1d**, were unstable in acidic media, the ethanolysis rate measurements were carried out in the presence of large excess of 2,6-lutidine. Considerable rate decrease was observed for the ethanolysis in this solvent system compared with that in ethanol solvent. For example, the ethanolysis rates of **11d** in ethanol solvent were about five times of those in the lutidine containing solvent; $k_{40\,^\circ C}=3.05\times10^{-5}$, $k_{55\,^\circ C}=2.00\times10^{-4}\ s^{-1}$.

17) J. Meinwald and J. K. Crandall, *J. Am. Chem. Soc.*, **88**, 1292 (1966), and references cited therein.

18) C. Ainsworth, *Org. Synth.*, Coll. Vol. 4, 536 (1963).

19) M. Regitz, J. Rüter, and A. Liedhegener, *Org. Synth.*, **51**, 86 (1971).

20) **4a—6a** thus prepared were mixtures of exo and endo epimers, however, the mixtures were used without separation for the lead tetraacetate oxidation, because it has been well known that the primary process of the reaction is the formation of alkyl radical species followed by further oxidation to classical cation intermediates[21] and, therefore, the stereochemistry of the acids may be disregarded in the present case.

21) R. A. Scheldon and J. K. Kochi, *Org. React.*, **19**, 279 (1972).

22) Correct analytical data were not obtained for this compound because of facile elimination of acetic acid during purification by preparative GLC.

  Bull. Chem. Soc. Jpn., 54, 1481—1491 (1981)

Chemistry of Dienyl Anions. IV. Geometry of Pentadienyl Anions in Solution and in the Solid State Determined by Regioselective Trimethylsilylation and NMR

Hajime YASUDA, Michihide YAMAUCHI, Yasuo OHNUMA, and Akira NAKAMURA*

Department of Macromolecular Science, Faculty of Science, Osaka University, Toyonaka, Osaka 560

(Received December 4, 1980)

The configurational analysis of a series of alkyl substituted pentadienyl anions in THF was examined by trimethylsilylation and from the variable temperature ^{1}H- and ^{13}C-NMR spectra. Potassium pentadienide, -2-methylpentadienide or -2,4-dimethylpentadienide produced preferentially (*Z*)-2,4-pentadienyltrimethylsilane or its methyl substituted analogues to indicate that these compounds have the "U"-shaped structure in solution. By contrast, trimethylsilylation of potassium pentadienide and -2-methylpentadienide in the crystalline state produced the (*E*)- and the (*E*),(*Z*)-isomers, respectively, suggesting that the geometry is drastically changed to the "W"- or "S"-shaped by the medium effect. The W-shaped structure of potassium 3-methylpentadienide in THF and in the solid state is exceptional. Geometry of trapped products of potassium cycloheptadienide and -cyclooctadienide is also (*Z*) but the silylation occurred on the central carbon in contrast to the terminal silylation seen for the open-chain pentadienides. Geometry of these dienyl anions determined by NMR below −30 °C was consistent with the result obtained from trimethylsilylation. Superficial conflict between MINDO/3 prediction and the experimental evidence was reasonably reconciled by considering contact ion pairs for potassium pentadienide in THF and more strongly-solvated ion pairs for the lithium analogues.

A study of structures and configurational stabilities of a series of pentadienyl anions is of particular importance since such carbanions are crucial intermediates for base-catalyzed equilibration[1] of diolefins and are valuable organometallic reagents for syntheses.[2] Several theoretical studies on the geometry of open-chain pentadienyl anions are now available. Extended Hückel calculations by Hoffmann and Olofson[3] and CNDO/2 by Bushby *et al.*[4] predict that the horseshoe-like "U"-shaped anion should be preferred over the zigzag-like "W"- or sickle-like "S"-shaped anions. However, Dewar *et al.*[5] recently reported on the basis of MINDO/3 and MNDO calculations that the W-shaped structure is more stable than the U- or S-shaped structure by 2.5—15.5 kJ/mol for pentadienyl, 3-methyl- or 1,3-dimethylhexadienyl anions. Dewar's prediction is in accord with the experimental evidence obtained by NMR which indicates that lithium pentadienide,[6] hexadienide[7] and 2-methylpentadienide in THF, and potassium pentadienide[8] and hexadienide[9] in liquid ammonia exist preferentially as W-shaped anions. However, Schlosser *et al.* recently reported evidence for the U-shaped structure for the first time in the cases of potassium 2-methyl- and 2,4-dimethylpentadienide in THF based on the geometry of 2,4-pentadien-1-ol chemically derived from the anions.[10] Such predominance of the U-shaped structure has also been confirmed by us independently for the parent potassium pentadienide in THF from the hydrolysis data.[11]

This paper is concerned with 1) the regioselective trimethylsilylation of a series of potassium pentadienide in THF to determine the geometry of the pentadienyl moiety to confirm Dewar's MO prediction and the geometry suggested by Schlosser *et al.*, 2) the direct measurement of the geometry in solution by variable temperature ^{1}H- and ^{13}C-NMR, and 3) the medium (solution *vs.* the solid state) and counter-cation dependence of the geometry of a series of pentadienyl anions. All the experiments were conducted with use of isolated crystalline pentadienyl anions.

Results and Discussion

Chemical Trapping in Solution and in the Solid State. Trimethylsilylation of pentadienyl anions with an equimolar amount of chlorotrimethylsilane can be accomplished with extreme regioselectivity as has been shown in the trimethylsilylation of some nucleophiles.[12] Potassium pentadienide **1**, rubidium pentadienide **2**, and caesium pentadienide **3** in THF at 20 °C gave (*Z*)-2,4-pentadienyltrimethylsilane in 88, 90, and 92% regioselectivity in 95—98% yield and at −40 °C in 96—98% regioselectivity as evidenced by high resolution GC, ^{1}H-NMR (Table 1), IR, MS, and the analytical data (Table 5 in experimental section). Such high regioselectivity has also been found in the protolysis of **1** at 5 °C giving 92—95% of (*Z*)-1,3-pentadiene.[11] No product derived from the electrophilic attack on the central atom is formed in either case. In contrast, lithium pentadienide **4** in THF gave the (*E*)-isomer exclusively (98% yield) at −40 °C. The *Z*/*E* ratio for **1**—**3** (98:2) was determined with a high resolution gas chromatograph equipped with a 45 m capillary column. The resulting products are thermally stable and no isomerization of (*Z*)- to (*E*)-2,4-pentadienyltrimethylsilane or of the (*E*)- to the (*Z*)-isomer occurred by heating to 80 °C for 1 h in THF. The thermal stability permits the isolation of the respective pure isomers (Fig. 1) by distillation or with preparative GC. Sodium pentadienide gave a 7:3 mixture of (*Z*)- and (*E*)-isomers at 30 °C and a 6:4 mixture at −20 °C. Thus, the geometry of trapped products was successfully controlled by changing the counter cation.

If above anions are present as a single torsional isomer and trimethylsilylation occurs equally at both termini (C_1 and C_5), it would yield just one pair of products as shown in Schemes 1 and 2. Based on this postulate, the above results are readily explained

TABLE 1. ^{1}H-NMR CHEMICAL SHIFTS(δ-VALUES) AND COUPLING CONSTANTS(Hz) FOR PENTADIENYLTRIMETHYLSILANES IN $CDCl_3$ AT 30 °C[a)]

Entry	Anion	Products	C_1-H(J_{12})	C_2-H(J_{23})	C_3-H(J_{34})	C_4-H	C_5-H(J_{45})	
Si-1	**1**	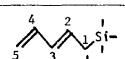	1.48 (d, 7.8)	5.63 (d of t, 15.2)	5.73 (d of d, 10.0)	6.25 (d of d of d)	4.93(trans, 16.2) 4.79(cis, 10.1)	−0.09 (CH_3-Si)
Si-2	**1**	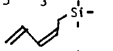	1.61 (d, 8.6)	5.47 (d of d, 10.4)	5.91 (d of d, 10.3)	6.54 (d of d of d)	5.08(trans, 16.2) 4.95(cis, 10.4)	−0.04 (CH_3-Si)
Si-3	**5**	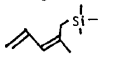	1.67(S)	—	5.75 (d, 10.8)	6.42 (d of d of d)	4.95(trans, 16.5) 4.84(cis, 10.4)	0.00(CH_3-Si) 1.74(CH_3)
Si-4	**5**	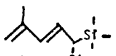	1.51 (d, 7.6)	5.61 (d of t, 15.0)	5.98 (d)	—	4.87(gem, 1.8) 4.80	−0.03(CH_3-Si) 1.80(CH_3)
Si-5	**5**	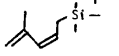	1.71 (d, 8.8)	5.40 (d of t, 11.3)	5.74 (d)	—	4.87 4.84	−0.01(CH_3-Si) 1.86(CH_3)
Si-6	**6**	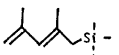	1.79(S)	—	5.50(S)	—	4.80 4.70	1.71(CH_3) 1.79(CH_3)
Si-7	**7**	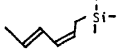	1.57 (d, 8.8)	5.30 (d of t, 9.8)	5.82 (d of d, 10.2)	6.17 (d of d)	5.59 (d of q, 14.5)	1.72(CH_3, 7.0) −0.05(CH_3-Si)
Si-8	**8**	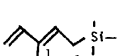	1.56 (d, 8.6)	5.53 (t, 8.6)		6.34 (d of d)	4.96(trans, 16.9) 4.79(cis, 10.7)	−0.02(CH_3-Si) 1.66(CH_3)
Si-9	**9**		5.66 (d of t, 11.1)	5.45 (d of d, 5.8)	2.50 (t)	5.45 (d of d)	5.67 (d of t, 11.7)	0.03(CH_3-Si) 2.22(J_{18}=3.8, CH_2)
Si-10	**10**		5.19 (d of t, 11.4)	5.67 (d of d, 4.1)	2.28 (d of d)	5.67 (d of d, 11.4)	5.19 (d of t)	0.00(CH_2-Si) 1.21(J_{18}=6.5, CH_2) 2.37(J_{78}=8.1, CH_2)
			5.48 (d of t, 10.8)	5.77(d)	—	5.05 (d, 5.0)	2.10(m)	1.49(CH_2) 0.06(CH_3-Si)
			2.08(m)	6.14 (d, 7.0)	6.00 (d, 7.0)	2.15(m)	2.08(m)	1.44(CH_2) 0.18(CH_3-Si)

a) $CHCl_3$ was used as an internal standard(assuming to be 7.20 ppm downfield from TMS).

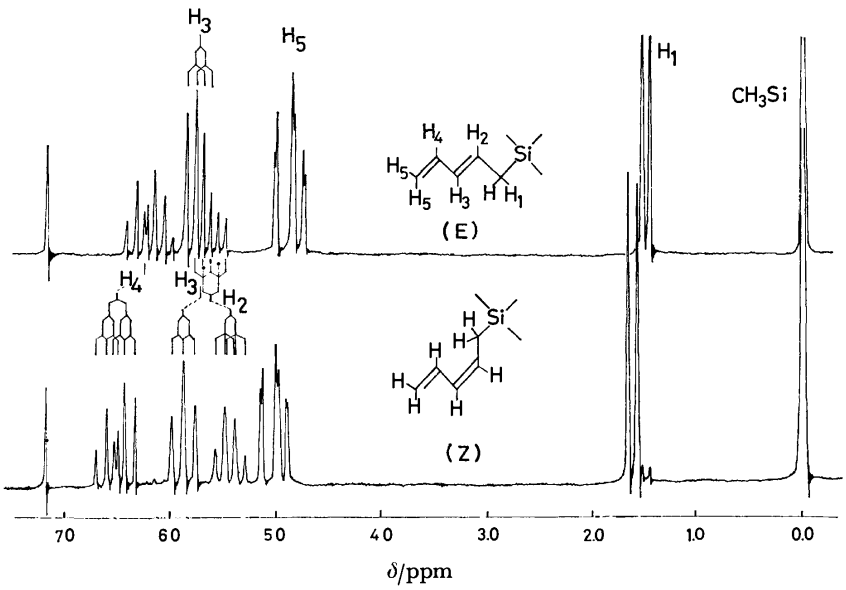

Fig. 1. ^{1}H-NMR spectra (100 MHz, in $CDCl_3$) of (*Z*)- and (*E*)-2,4-pentadienyltrimethylsilane prepared from **1** in THF and in the solid state.

by regarding the U-shaped structure for **1**—**3** in solution and the W-shaped structure for **4**. The S-shaped anion should produce a *Z*/*E* mixture. To rationalize this assumption, the chemical trapping of an unsymmetrical pentadienyl anion, potassium 2-methylpentadienide **5**, was examined in THF at −20 °C using pure single crystals of **5**. Indeed, a 11:9 mixture of (*Z*)-4-methyl-2,4-pentadienyltrimethylsilane and (*Z*)-2-methyl-2,4-pentadienyltrimethylsilane was obtained to indicate the presence of a single torsional isomer with the U-shaped structure. The configuration of the former was determined from the proton-proton coupling constant (described later) observed in the ^{1}H-NMR spectrum (100 MHz) and by the measurement of NOE for the latter. This behavior corresponds well to dimethoxyboration-oxidation sequence of **5** in THF at −78 °C reported by Schlosser which gave (*Z*)-4-methyl-2,4-pentadien-1-ol (41%) and (*Z*)-2-methyl-2,4-pentadien-1-ol (22%) implying the U-shaped structure in THF.[10a)] If the anion **5** assumes the *endo-S*-, *exo-S*-, or W-structure, (*E*)-2-methyl- or (*E*)-4-methyl-2,4-pentadienyltrimethylsilane should be accompanied. Ex-

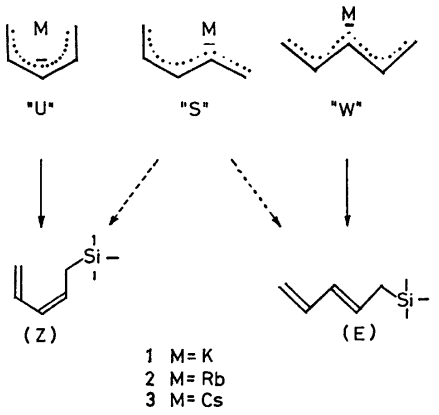

Scheme 1.

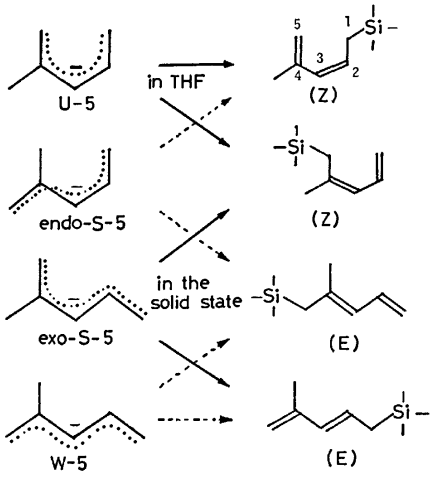

Scheme 2.

change of the counter cation to lithium changed the geometry of the product; *i.e.*, successive treatment of 2-methyl-1,4-pentadiene with *s*-butyllithium in THF, fluorodimethoxyborane and alkaline hydrogen peroxide has been reported to produce both 4-methyl- and 2-methyl-2,4-pentadien-1-ol.[13] The formation of (*E*)-isomer favored over (*Z*)-isomer consistent with the trimethylsilylation of **4**. Based on these facts, one can conclude the structure of **1**, **2**, **3**, and **5** in solution to be the U-shaped and **4** to be the W-shaped structure in solution. The S-shape may be, thus, excluded for **1**—**5**.

A drastic change in geometry of the trapped products was found when the medium was changed from solution to the solid state. The solubility of **1** in THF at 40 °C is 135 g/dm^3 and that of **2** and **3** is lower than that. Hence the addition of excess pentane or octane (10 ml) to the saturated THF solution (1 ml) at 40 °C brought about quantitative precipitation of **1**—**3** (90%) by cooling to −40 °C. Trimethylsilylation of the resulting suspension of **1**, **2**, and **3** in pentane

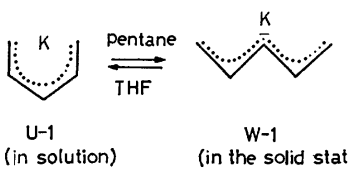

surprisingly produced (*E*)-2,4-pentadienyltrimethylsilane exclusively (98% GC yield) in 84, 90, and 92% regioselectivity at 0 °C and in 93—95% regioselectivity (~95% yield) at −70 °C in sharp contrast to the reaction in solution which gave the (*Z*)-isomer. THF-free pentadienyl anions of **1** and **2**, which were prepared by heating crystals to 80 °C *in vacuo*,[11a] are sparingly soluble in hydrocarbons and showed an extreme regioselectivity in silylation (99% in pentane at 0 °C). Lithium compound **4** or its TMEDA complex **4'** suspended in pentane at 0 °C also produced the (*E*)-isomer exclusively (97%) in line with the reaction in solution. No medium effect was observed for the lithium analogue. These results clearly indicate the W-shaped structure for **1**—**4** and **4'** in the crystalline state but the S-shape can not be ruled out distinctly from this experiment. Dialkoxyboration-oxidation of **1** in hexane (in the solid state reaction) also produced (*E*)-pentadien-1-ol exclusively,[10b] whereas it was recently found to give (*Z*)-isomer in good yield by reaction in THF solution in agreement with our result.[15c] Thus, the frequently experienced poor reproducibility on the (*Z*)/(*E*)-ratio has now solved by introducing the concept of the medium effect.

The similar medium effect was found also for **5**, which gave (*E*)-4-methyl-2,4-pentadienyltrimethylsilane (48%), (*Z*)-4-methyl-2,4-pentadienyltrimethylsilane (12%), and (*Z*)-2-methyl-2,4-pentadienyltrimethylsilane (40%) in the solid state reaction in pentane (THF coordinated to **5** was removed previously at 80 °C *in vacuo*). No contamination of (*E*)-2-methyl-2,4-pentadienyltrimethylsilane was detected in each isolated products. This shows that **5** has predominantly the *exo*-S-shaped structure in the crystalline state. The *exo*-S/U-ratio is calculated to be 78/22 if the U-**5** species in the solid state is postulated to give (*Z*)-4-methyl- and (*Z*)-2-methyl-2,4-pentadienyltrimethylsilane in 11/9 ratio as was observed in trimethylsilylation in solution. Protolysis of **5** with water producing a *ca.* 1:1 mixture of (*Z*)-2-methyl- and 4-methylpentadiene in both media[11] gave little information on the configuration.

The steric repulsion between the two methyl groups on the 2,4-dimethylpentadienyl anions will lead to the U- or S-shaped structure since planar W-form is sterically hindered for this anion. Indeed, (*Z*)-2,4-dimethyl-2,4-pentadienyltrimethylsilane was identified as the almost exclusive product (97% regioselectivity, 96% yield) from potassium 2,4-dimethylpentadienide **6** both in solution and in the solid state suggesting the presence of the U-shaped single torsional isomer. The geometry was determined by the NOE experiment. The U-shaped structure have recently been confirmed also by Schlosser *et al.* by dialkoxyboration-oxidation of **6** in THF which results in the exclusive production of (*Z*)-2,4-dimethylpentadien-1-ol.[10]

The trapped product of potassium hexadienide **7** also comprises one isomer, (2*Z*,4*E*)-2,4-hexadienyltrimethylsilane (92%) independent of the medium (solution and the solid state) and hexadiene precursor [1,3-hexadiene, 1,4-hexadiene, (*E*,*E*)-2,4-hexadiene and (*E*,*Z*)-2,4-hexadiene]. This result suggests the con-

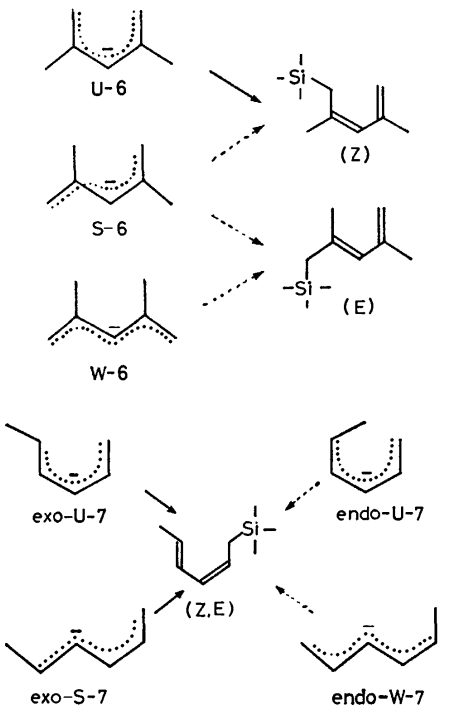

figuration of **7** to be either *exo*-U- or *exo*-S-shaped or their mixture. The value of the proton-proton coupling constant of J_{45}, 14.5 Hz, observed in ^{1}H-NMR (described later) evidently excludes the endo-W-form which had been considered for lithium derivative[7] or **7** in liquid ammonia.[9] The planar *endo*-U-shape seems implausible for steric reasons. The most striking feature of this reaction lies in the predominant attack of chlorotrimethylsilane on the primary carbon end (at C_1). Electrophilic attack on the secondary carbon (C_5 attached to CH_3 group) which should give 1-methyl-2,4-pentadienyltrimethylsilane was absent. This regioselectivity is valuable for organic syntheses[33a] and an insect pheromone was recently prepared utilizing this type of reagent.[14]

The geometry of 3-alkylpentadienyl anions seems exceptional. For example, potassium 3-methylpentadienide **8** in solution and in the solid state gave (*E*)-3-methylpentadienyltrimethylsilane (in 92—95% regioselectivity) by trimethylsilylation and (*E*)-3-methyl-1,3-pentadiene exclusively (97—99%) by hydrolysis in THF at −30 °C. Their structures were confirmed by the lack of NOE and the reaction with maleic anhydride.[11] Thus, only **8** gave the (*E*)-isomer contrary to the behavior of other open-chain dienyl anions (**1**—**3**, **5**—**7**) in solution. The difference in geometry may be correlated to the strong preference of allylic potassium for the endo configuration over the exo configuration.[15]

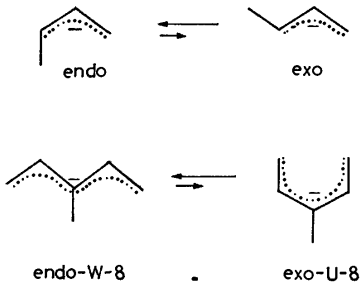

The mode of reaction of pentadienyl anions in a cyclic skeleton, *e.g.*, cycloheptadienyl or cyclooctadienyl anions, is known to be different from that of linear pentadienyl anions.[11,16] The former showed a clear predominance of the electrophilic attack on the central carbon while the latter underwent attack on the terminal carbons reflecting higher charge on C_3-atom as confirmed by the ^{1}H-NMR (described later). Trimethylsilylation of potassium cycloheptadienide **9** in solution occurred only at the central carbon as expected and pure (*Z*,*Z*)-2,6-cycloheptadienyltrimethylsilane was obtained in high yield (99%). Potassium cyclooctadienide **10** behaved similarly to **9** but the isomerization of (*Z*,*Z*)-2,7-cyclooctadienyltrimethylsilane into (*Z*,*Z*)-1,7-cyclooctadienyl derivative was rapid in THF at 40 °C presumably due to the base catalysis. Isomerization of isolated (*Z*,*Z*)-2,7-cyclooctadienyltrimethylsilane to (*Z*)-bicyclo[3.3.0]-oct-3-en-2-yltrimethylsilane by electrocyclization[17] was also observed by heating to 200 °C in a column of gas chromatograph (typical percent conversion, 30—40%).

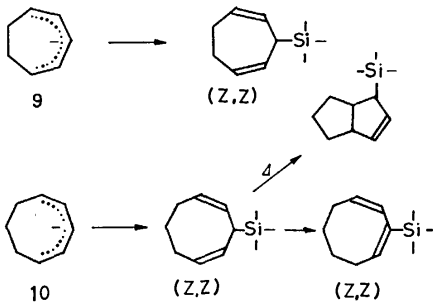

Determination of geometry of **1** in liquid ammonia by trimethylsilylation was unsuccessful due to the predominant production of 1,1,1,3,3,3-hexamethyldisilazane. To confirm the geometry of pentadienyldimethoxyborane, which was postulated by Schlosser *et al.* as the intermediate in dialkoxyboration-oxidation of **1**, we attempted its isolation by distillation but the borane compounds were thermally too unstable to permit the isolation and were converted to polymeric substances above 0 °C.

Direct Measurement of the Geometry in Solution by ^{1}H-NMR. The variable ^{1}H-NMR spectra (Table 2) were measured in THF-d_8 to obtain direct evidence for the configuration of above-mentioned anions and to confirm the geometry determined by the regioselective trimethylsilylation and hydrolysis. Lithium pentadienide **4** and its TMEDA complex, which were obtained by direct metalation of 1,4-pentadiene with metallic Li[11] or butyllithium[7] in THF, are fluxional at room temperature but the rotation around the C_1–C_2(C_4–C_5) and C_2–C_3(C_3–C_4) bonds was frozen by lowering the temperature below −70 °C (Fig. 2). The proton-proton coupling constant of J_{23}(J_{34}), 11.9—12.0 Hz observed for **4** (THF complex) and the TMEDA complex at −90 °C is essentialy the same as that reported by Bates *et al.*[6] indicating the presence of the W-shaped single torsional isomer. The coupling constant for allylic lithium compounds

TABLE 2. ^{1}H-NMR CHEMICAL SHIFTS(δ-VALUES) AND COUPLING CONSTANTS(Hz) OF POTASSIUM PENTADIENIDES IN THF-d_8 AT -40 °C AND RELATED COMPOUNDS[a]

	Geometry	Counter cation	C_1-H(J_{12})	C_2-H(J_{23})	C_3-H(J_{34})	C_4-H	C_5-H(J_{45})	Others
1		K	3.47(trans, 16.1) 3.55(cis, 10.6)	6.23 (d of d of d, 8.7)	3.55(t)	—	—	
2		Rb	3.40(trans, 16.4) 3.58(cis, 10.5)	6.15 (d of d of d, 8.7)	3.50(t)	—	—	
3		Cs	3.38(trans, 16.4) 3.59(cis, 10.5)	6.12 (d of d of d, 8.7)	3.50(t)	—	—	
4		Li	3.04(trans, 15.5) 2.68(cis, 9.1)	6.13 (d of d of d, 11.5)	4.35(t)	—	—	
1		K[b]	3.01(trans, 15.1) 2.58(cis, 9.0)	6.13 (d of d of d, 11.5)	4.35(t)	—	—	
5		K	3.39(gem, 3.0) 3.26(gem, 3.0)	—	3.59 (d, 9.0)	6.18 (d of d of d)	3.53(trans, 17.1) 3.50(cis, 11.1)	1.92(CH_3)
6		K	3.32(d, gem, 2.6)	—	3.46 (q, J_{13}=1.3)	—	3.54 (d, gem, 1.9)	1.96(CH_3) 1.98(CH_3)
7		K	3.39(d, 15.2) 3.26(d, 10.0)	6.21 (d of d of d, 8.6)	3.41 (d of d, 8.3)	6.05 (d of d)	4.13 (d of q, 8.7)	1.93 (d, 6.2, CH_3)
7		K[b]	3.01(trans, 15.1) 2.45(cis, 10.0)	6.09 (d of d of d, 11.5)	4.07 (d, 11.5)	5.84 (d of d)	3.07 (d of q, 8.7)	1.58 (d, CH_3)
8		K	2.90(trans, 15.8) 2.87(cis, 10.0)	6.20 (d of d)	—	—	—	1.57 (s, CH_3)
9		K	3.90(d of t, 9.2)	5.86(d of d, 7.8)	3.39(t)	—	—	2.53 (m, CH_2)
9		K[b]	3.51(d of t, 9.4)	5.67(d of d, 7.8)	3.14(t)	—	—	2.53 (m, CH_2)
10		K	3.10(d of q, 8.9)	5.87(d of d, 7.2)	2.64(t)	—	—	3.10(m, CH_2) 1.11(q, 6.0)
10		K[b]	2.61(d of q, 9.3)	5.65(d of d, 7.0)	2.33(t)	—	—	3.11(m, 7.8) 2.15(m, 5.9)

a) In ppm downfield from external TMS in THF-d_8(calibrated using the downfield THF peak, assumed to be 3.75 ppm). Data were collected at 100 MHz from the decoupled spectra. b) Data in liquid ammonia by Kloosterziel *et al.* (Refs. 8, 9, and 20).

is known to be 6.5—7.5 Hz for cis-inner bond,[16] 11.5—12.0 Hz for trans-inner bond, 9—10 Hz for cis-outer bond, and 16—17 Hz for trans-outer bonds. The values increased by exchanging the cation to potassium; cis-inner bond 8.3—9.1 Hz,[18] trans-inner bond 13 Hz,[18] cis-outer bond 9—10 Hz, and trans-outer bond 16—17 Hz. The increased value may be due to the increased C_1–C_2–C_3 angle derived from the electrostatic effect of the larger ionic radius of potassium.

Based on these data, the geometry of a series of potassium dienides was analyzed. The NMR signals of the protons on C_1(C_5) and C_3 of parent anion **1** heavily overlapped with each other and therefore the correct coupling constant was measured utilizing potassium 1,1,5,5-tetradeuterated pentadienide[2b] in THF-d_8 (Fig. 3). The value of J_{23} was found for the first time to be 9.1 Hz at 60 °C and was frozen out to give 8.7 Hz below -30 °C. This value clearly shows the cis-relationship of the two protons on the C_2–C_3 and C_3–C_4 bonds. The geometry of **1** in ethereal solution was thus shown to be U-shaped in accord with the chemical trapping experiment. The rotation around the outer bonds, C_1–C_2(C_4–C_5), is very slow even at 60 °C as evidenced by the coupling constant, J_{12}(trans)=15.9 Hz, J_{12}(cis)=10.0 Hz. The values are 16.1 and 9.9 Hz at -30 °C. The high barrier for rotation around the C_1–C_2 (estimated to be >25 kcal/mol by Schlosser[10c]) and C_2–C_3 bonds may account for the small temperature dependence of the coupling constant variation ΔJ_{12} (0.2 Hz) and ΔJ_{23} (0.4 Hz). Such high rotational barriers have recently been reported also for allylic potassium compounds.[18] The behavior of rubidium and caesium derivatives is similar to **1** but their coupling constants at 38 °C are a little smaller; J_{23}=8.9 Hz for **2** and 8.7 Hz for **3**. Therefore the rotational barrier around the C_2–C_3 bond in the pentadienyl anion was estimated to increase with the ionic radius of the alkali counter ion, Li<Na$\ll$K<Rb$\simeq$Cs in line with the order observed for allylic anion system,[19] though the line-shape analysis is required to obtain the exact value, ΔG. The spectra of **1** obtained from (*Z*)-, (*E*)-1,3-pentadiene or 1,4-pentadiene were the same with each other irrespective of the geometry of starting dienes.

Potassium hexadienide **7** was prepared from (*E*,*E*)-2,4-hexadiene, (*E*)-1,4-hexadiene, (*E*)-1,3-hexadiene and/or (*Z*)-1,3-hexadiene. All of these were heated to 70 °C for 30 min. The ^{1}H-NMR spectra of resulting anions **7** were the same independent of the geometry of the starting dienes and show the presence of two isomers in every cases; *exo*-U-shaped and presumably *exo*-S-shaped anions in 4:1 ratio. The predominant species was readily assigned to be *exo*-U-shaped from the chemical shift and the coupling constant obtained from the decoupled spectra (Table 2). The proton signals of minor species was too weak to make an assignment. However, the extreme stereoselec-

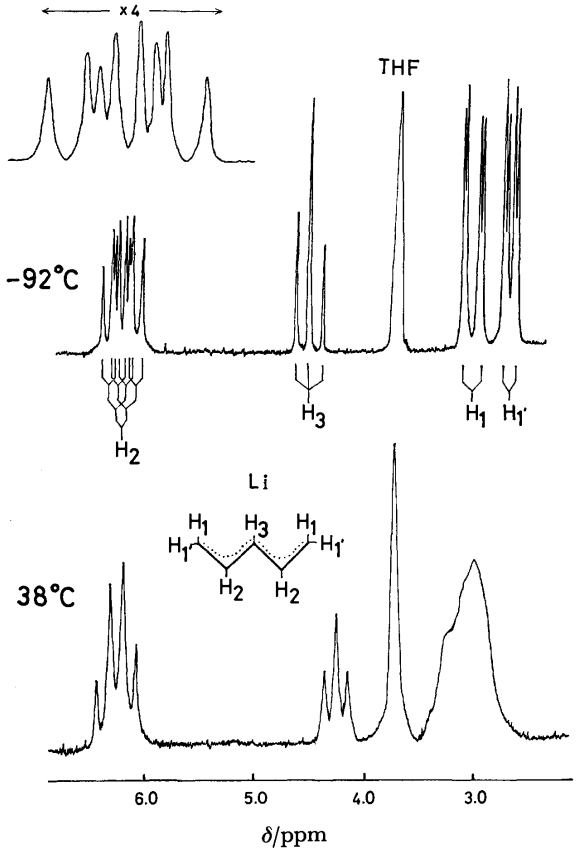

Fig. 2. Variable temperature ^{1}H-NMR spectra (100 MHz) of lithium pentadienide **4** in THF-d_8.

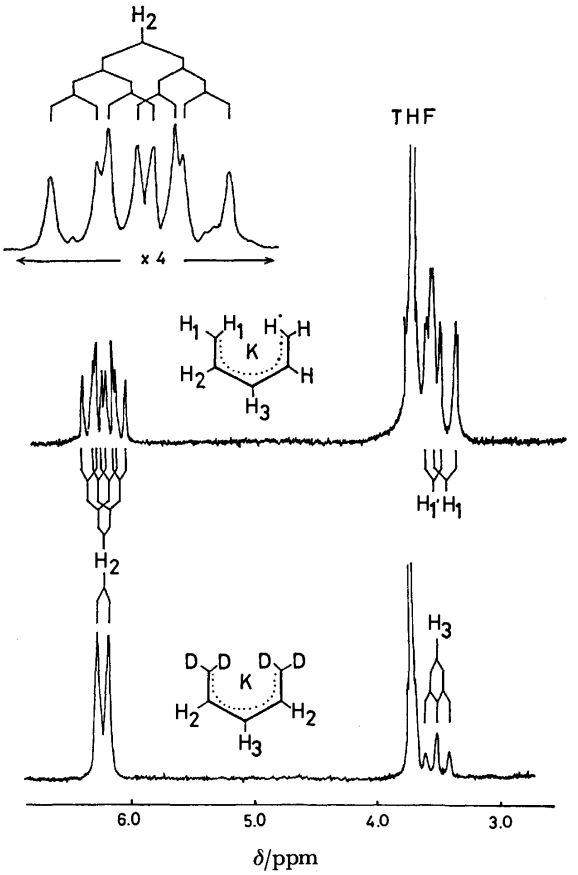

Fig. 3. ^{1}H-NMR spectra (100 MHz) of potassium pentadienide **1** and potassium 1,1,5,5-tetradeuterated pentadienide in THF-d_8 at −60 °C.

tivity observed in trapped products strongly suggests the presence of the *exo*-S-shaped anion as the minor species because only this isomer (except for the above *exo*-U) can provide (*Z,E*)-2,4-hexadienyltrimethylsilane. The ^{1}H-NMR spectrum of 2-methylpentadienyl anion **5** gave only partial information on the geometry. That is, J_{34} is 8.7 Hz below −30 °C. This value suggests the U- or *endo*-S-shaped structure for **5** and excludes the W- and *exo*-S-shape. However, we can reasonably suggest the U-shaped structure for **5** because of the result of chemical trapping experiments.

The chemical trapping of potassium 2,4-dimethylpentadienide **6** clearly shows the presence of the U-shaped single torsinal isomer in solution. However, the chemical shift difference was observed between the two terminal proton signals in ^{1}H-NMR below 10 °C (Fig. 4). The double doublet assigned to H-3 is caused by the H_1–H_3 coupling and H_5–H_3 coupling, not the CH_3–H_3 coupling, as evidenced from the decoupled spectrum. Supposition of the S-shaped structure which may explain the NMR data is in conflict with chemical trapping data. Hence, the deformed out-of-plane U-shaped or the following helicene-like U-shaped structure[15c] is suggested by Schlosser for

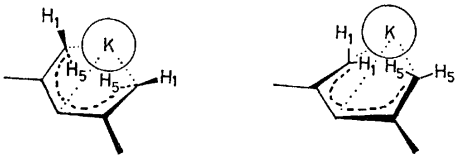

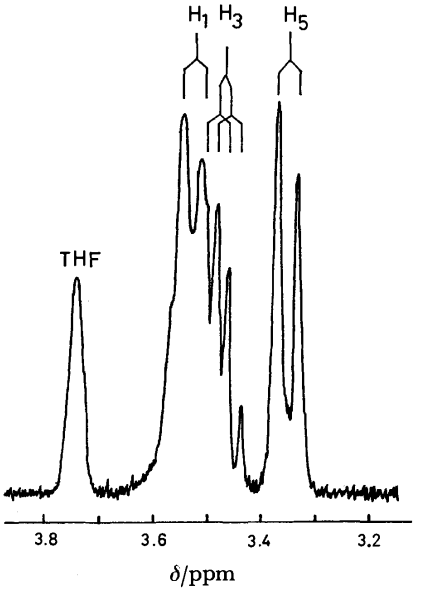

Fig. 4. ^{1}H-NMR spectra (100 MHz) of potassium 2,4-dimethylpentadienide **6** in THF-d_8 at −40 °C.

this observation, although they are indistinguishable by ^{1}H-NMR or chemical trapping experiments. The spectra simulation with a high resolution spectrometer will be required for further discussions.

The ^{1}H-NMR spectrum of **8** also gave little infor-

mation on the geometry but the presence of the single torsional isomer with the W-shaped structure is proposed based on the excellent stereospecificity observed in trimethylsilylation and hydrolysis in addition to the chemical shift values. The proton-proton coupling for the outer bonds (C_1–C_2 and C_4–C_5) is frozen below −30 °C and the spectral pattern was unchanged within 2 Hz on lowering the temperature to −90 °C. The ^{13}C-NMR spectral data at −40 °C (Table 3) also supports the presence of **8** as the single torsional isomer, W- or U-shaped anion. If rapid 1,3-rearrangement occurs exceeding the NMR time scale, a mixture of the (*Z*)- and the (*E*)-isomer should be formed chemically contrary to the fact. Thus, the extreme preference of the endo-W form is considered for **8**.

The coupling constants observed for **9** and **10** in THF-d_8 are essentially the same as those in liquid ammonia reported by Kloosterziel.[20] The plane defined by C_2–C_3–C_4 should never be coplanar to the plane made by C_1–C_2–C_4 or C_2–C_4–C_5 to relieve the ring strain.[21] Therefore, the decreased coupling constant of $J_{2,3}$ (6.8—7.0 Hz) for **9** and **10** compared to the value of $J_{2,3}$ (8.3—9.1 Hz) for open-chain dienylpotassium compounds may be rationalized in terms of the deviation of dihedral angle H_2–C_2–C_3–H_3 from zero to *ca.* 20° calculated by the Karplus equation. The smaller δ-values of H_3 of **9** and **10** as compared with that of **1**—**8** of the open-chain structure might be ascribed to both a larger electron-repelling effect of the CH_2 group bound to pentadienide termini and a larger torsion around the C_2–C_3 (and C_3–C_4) bond

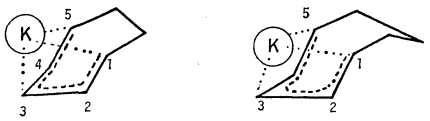

of **9** and **10** as Kloosterziel already suggested.[20]

Configurational Studies on Potassium Pentadienides by ^{13}C-NMR. ^{13}C-NMR chemical shifts provide the best measure of the electron density in many delocalized carbanions[22] and have been successfully employed to distinguish the geometry of the isomers considered for some lithium pentadienides.[5,23] ^{13}C-NMR parameters will be useful for configurational analysis of the present potassium derivatives since their rotational barriers around terminal- and inner-bonds is higher than those for lithium derivatives as mentioned above. The spectra of **1**—**3**, **6**, **8**—**10** (Table 3) clearly shows the presence of a single torsional isomer with a symmetric structure, U- or W-form, because the chemical shift value of C-1 or C-2 are equal to that of C-5 or C-4, respectively. The W-shaped structure can be ruled out from the chemical trapping experiments and the ^{1}H-NMR spectral data. The chemical shift of C-1 of **6** is equal to that of C-5 and hence the deformed out-of-plane U-shaped structure seems more probable than the helicene-like U-shaped one. In the case of **7**, two species were detected in agreement with ^{1}H-NMR measurement and the major species is assigned to the *exo*-U-shaped anion.

It is noteworthy that sodium pentadienide show a simple averaged NMR spectrum with three signals assignable to $C_1(C_5)$, $C_2(C_4)$, and C_3 (half-width of the signal is 1.1 ppm) at 20—50 °C but those were split into several peaks (the half-width, 0.2 ppm) by lowering the temperature below −40 °C. One of the best explanation for this is to consider the presence of a 4:1 mixture of S- and U-shaped anions at −40 °C, because this ratio is consistent to the *Z*/*E* ratio (42/58) of 1,3-pentadiene obtained by hydrolysis of sodium pentadienide in THF at −40 °C.

On the basis of the chemical shift data, one can conclude that the electron density on C-3 of potassium

Table 3. ^{13}C-NMR chemical shifts of potassium pentadienides and related compounds in tetrahydrofuran-d_8 at −40 °C[a]

Dienyl anions	C-1	C-2	C-3	C-4	C-5	Others
1 (K)	79.2	137.8	79.6	137.8	79.2	
2 (Rb)	80.5	138.7	80.8	138.7	80.5	
3 (Cs)	81.9	139.6	82.6	139.6	81.9	
(Na) 20 °C	77.7	138.0	77.7	138.0	77.7	
−40 °C	77.4	137.7	77.8	142.3	77.8	
			78.4			
4 (Li)[c]	66.2	143.8	86.9	143.8	66.2	
5 (K)	76.9	144.6	80.6	136.5	80.3	28.6(CH_3)
6 (K)	77.4	144.5	83.4	144.5	77.4	28.8(CH_3)
7 (K)[b]	77.8	144.4	85.4	141.4	95.4	27.1(CH_3)
7′ (Li)[c]	56.7	143.6	81.4	137.3	85.7	
8 (K)	68.7	143.2	85.6	143.2	68.7	12.3(CH_3)
8′ (Li)[d]	64.2	146.9	92.1	146.9	64.2	10.2
9 (K)	95.3	133.9	76.2	133.9	95.3	37.2(C-6, C-7)
9′ (Li)[d]	98.9	134.5	71.3	134.5	98.9	35.6(C-6, C-7)
10 (K)	90.8	138.6	70.7	139.1	90.8	16.5(C-7)
						29.3(C-6, C-8)

a) In ppm downfield from external TMS in THF-d_8(calibrated using the high-field THF peak, assumed to be 25.8 ppm). Peak assignments were made in part from an off-resonance decoupled spectrum. b) Major species (*exo*-U). c) Data of W. T. Ford *et al.*(Ref. 7). d) Data of R. B. Bates *et al.*(Ref. 16).

pentadienides (**1**, **5**, **6**, **9**, and **10**) is close to or higher than those on C-1 and C-5, while higher electron density lies on C-1 and C-5 for lithium derivatives (**4**, **8'**). That is, the latter has stronger sp^3 character on the terminal carbons than the former in THF.

Electronic Spectral Studies on Pentadienyl Anions. Acyclic and cyclic potassium pentadienides (except 3-alkylpentadienyl anions) have, thus, been revealed to assume the "U"-shaped structure in THF. The remaining problems to be solved are why potassium pentadienide **1** in liquid ammonia and lithium pentadienide **4** in THF assume the "W"-shape whereas **1** in THF assumes the "U"-shape. The geometry of potassium hexadienide **7** in liquid ammonia and lithium hexadienide (*exo*-W) is also different from **7** in THF (*exo*-U).

One of the key factors controlling the geometry is the solvation. It is generally accepted that organolithium compounds having carbanion with extensive charge delocalization exist as solvent-separated ion pairs in THF as evidenced by the strong bathochromic shift (24—44 nm) of the absorption maximum in polar solvents.[23-27] The sodium and higher analogues exist as contact ion pairs even in the polar solvents (the absorption maximum appears at shorter wavelength compared to that of the solvent-separated lithium compounds). Similar red shifts are also known for sodium naphthalenide and sodium benzophenone ketyl.[28] However, such cation dependence is observable only when the anion species have extensive π-electron systems; *e.g.*, diphenyl- and triphenylmethyl anions,[23] 1,1-diphenylhexyllithium,[24] diphenyl- and triphenylallylic anions,[25] 9-fluorenyl and the substituted fluorenyl anions.[26] The electronic spectra of organoalkali compounds without extensive negative charge delocalization are less sensitive to solvent polarity as was found for benzylic-,[22] allylic metals,[23] mono- or dianions of polystyrene, polybutadiene and polyisoprene.[29] Kinetic studies are sometimes more useful for these systems to detect the solvent-separated ion pairs.[30] Higher negative charge delocalization seems possible on the pentadienyl moiety compared to the allylic moiety mentioned above. If the π-electron system existing in pentadienyl group is sufficient for the extensive charge delocalization, lithium pentadienide **4** should show the bathochromic shift. The absorption maxima for **1**—**4** and the sodium analogue in THF (Table 4), indeed, appeared at longer wavelength than that of allylic anions (310—320 nm in THF and benzene).[31] However, the absorption maximum of **4** was observed at shorter wavelength than that of **1**—**3**, in line with the spectra of solvent less-sensitive allylic systems in which the wavelength for the absorption maxima increased with an increase of the radius of counter cations. The absorption maximum (355 nm) for **4** in hexane at 20 °C is nearly equal to that in THF. Therefore, the π-electron system existing in the pentadienyl group is concluded to be insufficient to compose the stable solvent-separated ion pairs. Other methods are required to evaluate the solvent-affinity by THF.

Table 4. Electronic absorption spectral data for **1**—**4** in THF

Dienyl anions	λ_{max}/nm (ε)
4 (Li)	358 (5400)
(Na)[a]	365 (5700)
1 (K)	376 (6200)
2 (Rb)	377 (6000)
3 (Cs)	379 (5800)

a) Sodium pentadienide. All the spectra were measured at 20 °C.

Effect of Solvent-affinity on the Geometry of Pentadienyl Anions. To estimate the approximate strength of the solvation by THF to pentadienyl metals, the ease in dissociation of THF was examined on heating the respective 1:1 THF complexes[11] *in vacuo*. The Rb and Cs complexes readily release the THF molecule (>90%) on heating the crystals at 60 °C/1 mm Hg† for 15 min, K complex at 80 °C/1 mmHg for 30 min (80% of THF was released as evidenced by GC of the hydrolyzate of octane suspension) while lithium and sodium complexes give off no THF even heating them at 120 °C/0.1 mmHg for 2 h. The weak interaction of THF to **1**, **2**, and **3** was also confirmed by washing the crystals of *ca.* 1:1 THF complexes of **1**—**3** (1 g) in excess of pentane (40 ml) four times at 30 °C, which resulted in the release of 70, 90, and 93% of THF, respectively. Lithium derivative **4** gives off no THF again and sodium derivative 10—20% of THF under the same conditions. This behavior clearly indicates that the solvent-affinity increases as size of the cation decreases, Li>Na$\gg$K>Rb$\simeq$Cs. Therefore, we can reasonably explain the solution structure of lithium pentadienide by strongly-solvated ion pairs and potassium and higher alkali metal analogues by contact ion pairs. This inference was also supported by ^{1}H-NMR of **1**—**3** which show the significant low-field shift of the $C_1(C_5)$-proton signals by 0.4—0.9 ppm and high-field shift of C_3-proton by 0.8 ppm compared to the corresponding signals of lithium derivative **4** in THF. A similar high-field shifts (0.18 ppm) of the terminal proton signals caused by the solvation is known for lithium 1,3-diphenylpropenide.[25] The anion **1** in liquid ammonia should also exist as strongly solvated or solvent-separated ion pairs because its ^{1}H-NMR data (chemical shifts and coupling constants, see Table 2) correspond well to that of **4** in THF. Thus, combination of chemical trapping, NMR data and the solvent-affinity will lead to the very important conclusion; *i.e.*, pentadienyl anions which exist as strongly-solvated ion pairs assume the "W"-shaped structure consistent to the MNDO prediction,[5] whereas potassium and the higher alkali metal pentadienides, which will exist as contact ion pairs, favor the "U"-shaped structure. Geometry of the pentadienyl anion in the solid state is probably controlled by the mode of packing in the crystal lattice rather than the solvation effect. The lattice energy would cancel the small difference in net stabilization energy calculated for the three geometries. The X-ray analysis of **1** and **2** with good single crystals confirmed absence of the solvation and the presence of THF molecule at the interstitial po-

† 1 mm Hg$\approx$133.322 Pa.

sition but the intensity data were insufficient to warrant definite conclusion on the geometry in the crystalline state.[32]

In contrast to pentadienyl anion, bis(2,4-pentadienyl)metal compounds of Be, Mg, and Zn prefer the (*E*)- over the (*Z*)-structure.[2] This behavior is ascribable to their fluxional properties which permit the rearrangement of (*Z*)- to thermally more stable (*E*)-configuration by 1,3- or 1,5-shift. The facile control of the geometry by changing the medium or exchanging the cation will be valuable for organic synthesis. For example, the Lewis acid catalyzed regioselective addition of carbonyl compounds to 2,4-pentadienyltrimethylsilane has been recently reported.[33] The reaction of 2,4-pentadienyltrimethylsilane with lithium amide is also useful for introduction of substituents to the pentadienyl group.[34]

Experimental

Potassium pentadienide used at the present work were prepared by the procedure previously reported.[11] Metallic rubidium (99.9% purity) and caesium (99.9%) used for the direct metalation of 1,3-dienes were purchased from Mitsuwa Pure Chem. Tetrahydrofuran-d_8 (99%, Merck Co.) and chloroform-d_1 (99.8%, Merck Co.) were dried over Na/K alloy and calcium hydride, respectively, and distilled before use. Starting dienes were purchased from Aldrich Chemicals or prepared using the reactions previously described.[2,11] Potassium pentadienide-1,1,5,5-d_4 was prepared starting from 1,4-pentadiene-1,1,5,5-d_4.[2b] GC analysis was made with a Hitachi Model 163 gas chromatograph using a capillary column (45 m) OV-1, CW-45, or HB-2000 and the separation of the reaction products was done with a Varian-Aerograph Model 700 gas chromatograph using a column (4 m) packed with Silicone DC-550. ^{1}H- and ^{13}C-NMR spectra were recorded on a Varian XL-100 instrument with a VFT-100-620L pulse Fourier transform accessory with the use of a sealed tube. NOE was measured using the tube sealed at 10^{-1} mmHg at 63 K after the solution was degassed (15—20% of NOE was observed in $CDCl_3$ and 20—25% in acetone-d_6). IR spectra were recorded on a Hitachi EPI-2 spectrometer. The absorption spectra were run on a JASCO Model UVIDEC-5A spectrometer. Elemental analysis for trimethylsilyl derivatives were carried out using a capillary with a Yanagimoto Model MT-2-CHN analyzer. The mass spectrum was recorded on a JEOL JNS-01SG-2 spectrometer. All the procedures were carried out in an argon atmosphere using the high vacuum technique.

Trimethylsilylation of Pentadienyl Anions in THF. A typical experiment is as follows. To a THF solution (100 ml) of **1** (0.5 g, 4.7 mmol) in a Schlenk tube was added dropwise a THF solution (5 ml) of chlorotrimethylsilane (0.6 ml, 4.9 mmol) over a 30 min period under the magnetic

Table 5. IR, MS, and analytical data for pentadienyltrimethylsilane

Entry	IR(Neat) $\tilde{\nu}$/cm^{-1} C=C	CH=CH	C-Si	Mass[a] (Relative intensity)	Found(%) C	H	Calcd(%) C	H
Si-1	1638	995, 897, 797	1246, 1149, 852, 839	140(M, 15), 141(M+1, 4), 142(M+2, 1)	68.58	11.50	68.49	11.48
Si-2	1641	1000, 892	1246, 1152, 850, 839	140(M, 19), 14(M+1, 11), 142(M+2, 4)	68.50	11.49	68.49	11.42
Si-3	1639	988, 896	1246, 1152, 862, 836	154(M, 25), 155(M+1, 4), 156(M+2, 2)	70.03	11.58	70.04	11.76
Si-4	1638	1036, 962	1245, 1150, 860, 835	154(M, 12), 155(M+1, 6), 156(M+2, 3)	70.04	11.76	70.04	11.76
Si-5	1636	1000, 987, 944	1245, 1150, 860, 837, 756, 702	154(M, 14), 155(M+1, 5), 156(M+2, 1)	70.00	11.61	70.04	11.76
Si-6	1638	1016, 882	1256, 1164, 866, 839	168(M, 20), 169(M+1, 4), 170(M+2, 1)	71.13	11.90	71.34	11.99
Si-7	1646	978, 942, 816	1245, 1149, 899, 758, 705	154(M, 17), 155(M+1, 7), 156(M+2, 5)	69.93	11.42	70.04	11.76
Si-8	1636	1082, 989, 885	1257, 1245, 1149, 855, 840, 760	154(M, 18), 155(M+1, 2), 156(M+2, 1)	70.03	11.58	70.04	11.76
Si-9	1644	896, 791, 751	1205, 837	166(M, 10), 167(M+1, 7), 168(M+2, 1)	71.87	10.92	72.21	10.91
Si-10	1640	909, 882, 756	1248, 842	180(M, 15), 181(M+1, 8), 182(M+2, 2)	73.20	11.10	73.25	11.18

a) Relative intensity assuming the fragment of $(CH_3)_3Si$ as 100. Spectrum was recorded at 70 eV.

stirring at −40 °C). A rapid addition of chlorotrimethylsilane should be avoided or it causes the production of 3-trimethylsilyl-1,4-pentadiene in <20% yield. The solution changes from orange to colorless near the equivalence point precipitating the salt. The mixture was stirred at −40 °C for 30 min and then at 0 °C for 1 h. After condensing the solution to 10 ml by evaporation, pentane (20 ml) was added for the complete precipitation of the salt. The resulting salt was separated by centrifugation with the use of a two-necked glass tube fitted with rubber stoppers protected with a plastic cover. The precipitate was washed with two portions of pentane (20 ml) for extraction of the products. After the removal of pentane and THF from the combined solution by evaporation, the remaining (*Z*)-pentadienyltrimethylsilane was separated by distillation (143 °C/760 mmHg. GC yield 98% and isolated yield 70—75%). A series of trimethylsilylated compounds was isolated in the similar manner. Trimethylsilylated products from **5**, **6**, and **9** were distilled at 45 °C/6 mmHg, 55 °C/4 mmHg and 75 °C/0.5 mmHg, respectively. When the product comprises isomers, they were separated into the respective isomers with a preparative GC. The geometries and structures of the isolated isomers were analyzed by ^{1}H-NMR (Table 1) and IR, MS, and the elemental analysis (Table 5).

Trimethylsilylation of Pentadienyl Anions in the Solid State. Solubility of potassium pentadienide **1** for THF is relatively small; 135 g/dm^3 at 40 °C, 27 g/dm^3 at 0 °C and that of rubidium and caesium derivatives, **2** and **3**, at 40 °C are 10.5 and 18.5 g/dm^3, respectively. Lithium and sodium derivatives are freely soluble in THF at 0 °C. The addition of pentane or octane (40 ml) to the THF solution (5 ml) of **1**, **2**, and **3** (7.5 mmol for **1**) saturated at 60 °C resulted in the quantitative precipitation (90—92%) of the crystals by cooling the mixture below −40 °C. To the resulting suspension of **1**, **2** or **3** (7.5 mmol) was added dropwise chlorotrimethylsilane (1 ml, 7.7 mmol) in pentane (5 ml) at −70 °C for undergoing the solid state reaction. After continuing the vigorous magnetic stirring for 1 h, the salt was removed by centrifugation at room temperature and trimethylsilylated compounds were isolated by distillation. A typical isolated yield, 85% (GC Yield, 99%). The regioselectivity in reactions of **1**, **2**, and **3** to give the (*E*)-isomer was 93, 95, and 95% respectively. THF-free pentadienyl anions **1**—**3** which were prepared by heating their THF complexes at 80 °C/0.1 mmHg for 40 min were completely insoluble in pentane, benzene or diethyl ether. To a suspension of THF-free compounds **1**—**3** (10 mmol) in pentane (40 ml) was added at −40 °C chlorotrimethylsilane (1.3 ml, 11 mmol) dissolved in pentane (5 ml). The mixture was stirred for 2 h at 0 °C. Thus, (*E*)-2,4-pentadienyltrimethylsilane was produced quantitatively (GC Yield, >98%) and was isolated by distillation (Yield, 90%, regioselectivity, 99%). Great care is necessary in handling the THF-free pentadienyl anions because of their flammability in the air. THF complexes of sodium- and lithium pentadienide **4** were also insoluble in pentane below −40 °C and the solid state reactions were carried out in the same procedure as described for **1**—**3**. The regioselectivity in trimethylsilylation of a series of pentadienyl anions in solution and in the solid state, the (*Z*)/(*E*) ratio of the major products and total yields were summarized in Table 6.

TABLE 6. RESULTS OF TRIMETHYLSILYLATION OF PENTADIENYL ANIONS IN SOLUTION[a] AND IN THE SOLID STATE[b]

Anions	Trimethylsilylation at $C_1(C_5)$/%	Trimethylsilylation at C_3/%	(*Z*)/(*E*) ratio of the products	Total yield/%[c]
1	98	2	94/6	97
1[b]	99	1	1/99	95
2	97	3	98/2	98
2[b]	99	1	7/93	92
3	98	2	98/2	95
3[b]	97	3	4/96	92
4	100	0	1/99	98
4[b]	95	5	5/95	98
5	99	1	99/1	90
5[b]	98	2	52/48	92
6	97	3	95/5	96
6[b]	95	5	92/8	92
7	99	1	96/4[d]	90
8	93	7	5/95[e]	99
9	2	98	99/1	99
10	3	97	99/1	71

a) The reaction of pentadienyl anions(4.5 mmol) in THF(100 ml) with $(CH_3)_3SiCl$ was carried out at −40 °C. b) Trimethylsilylation of THF-free pentadienyl anions(10 mmol) was done in pentane(30 ml) at 0 °C. c) GC yield. d) Ratio of (2*Z*,4*E*)-isomer to other isomers. e) Ratio of (*Z*)-isomer to other isomers.

We are grateful to Prof. M. Schlosser, Universite de Lausanne, and Prof. D. E. Bergbreiter, Texas A & M University for their valuable discussions. The financial support of this work by the Kurata Science Foundation is gratefully acknowledged.

References

1) a) R. B. Bates, R. H. Carninghan, and C. E. Staples, *J. Am. Chem. Soc.*, **85**, 3031 (1963); b) J. Klein, S. Glily, and D. Kost, *J. Org. Chem.*, **35**, 1281 (1970).

2) a) H. Yasuda, M. Yamauchi, A. Nakamura, T. Sei, Y. Kai, N. Yasuoka, and N. Kasai, *Bull. Chem. Soc. Jpn.*, **53**, 1089 (1980); b) H. Yasuda, Y. Ohnuma, A. Nakamura, Y. Kai, N. Yasuoka, and N. Kasai, *Bull. Chem. Soc. Jpn.*, **53**, 1101 (1980).

3) R. Hoffmann and R. A. Olofson, *J. Am. Chem. Soc.*, **88**, 943 (1966).

4) R. J. Bushby and A. S. Patterson, *J. Organomet. Chem.*, **132**, 163 (1977); see also A. Bongini, G. Cainelli, G. Cardillo, P. Palmieri, and A. Umani-Ronchi, *J. Organomet. Chem.*, **92**, C1 (1975).

5) M. J. S. Dewar, M. A. Fox, and D. J. Nelson, *J. Organomet. Chem.*, **185**, 157 (1980).

6) a) R. B. Bates, D. W. Gosselink, and J. A. Kaczynski, *Tetrahedron Lett.*, **1967**, 205; b) R. B. Bates, S. Brenner, W. H. Deines, D. A. McCombs, and D. E. Potter, *J. Am. Chem. Soc.*, **92**, 6354 (1970); c) S. Brenner and J. Klein, *Isr. J. Chem.*, **7**, 735 (1969).

7) W. T. Ford and M. Newcomb, *J. Am. Chem. Soc.*, **96**, 309 (1974).

8) G. J. Heiszwolf and H. Kloosterziel, *Recl. Trav. Chim. Pays-Bas*, **86**, 807 (1967).

9) a) H. Kloosterziel and J. A. A. vanDrunen, *Recl. Trav. Chim. Pays-Bas*, **88**, 1377 (1969); **89**, 270 (1970).

10) a) M. Schlosser and G. Rauchschwalbe, *J. Am. Chem. Soc.*, **100**, 3258 (1978); b) J. Hartmann, R. Muthukrishnan and M. Schlosser, *Helv. Chim. Acta*, **57**, 2261 (1974); c) G. Rauchschwalbe and M. Schlosser, unpublished.

11) a) H. Yasuda, Y. Ohnuma, M. Yamauchi, H. Tani, and A. Nakamura, *Bull. Chem. Soc. Jpn.*, **52**, 2036 (1979); b) For a preliminary report, see H. Yasuda, T. Narita, and H. Tani, *Tetrahedron Lett.*, **1973**, 2443.
12) J. M. Reuter, A. Shinba, R. G. Salomon, *J. Org. Chem.*, **43**, 2438 (1978); R. J. P. Corriu, J. Masse, and D. Samate, *J. Organomet. Chem.*, **93**, 71 (1975); H. J. Reich, *J. Org. Chem.*, **40**, 2570 (1975); A. Hosomi and H. Sakurai, *Tetrahedron Lett.*, **1978**, 2589.
13) M. Schlosser and J. Hartmann, *Angew. Chem. Int. Ed. Engl.*, **12**, 439 (1973).
14) 2,4-Decadien-1-ol was prepared, H. Bosshardt and M. Schlosser, *Helv. Chim. Acta.*, to be published; 8,10-Dodecadien-1-ol was obtained from bis(hexadienyl)magnesium prepared from **7**, H. Yasuda, K. Sugi, and A. Nakamura, unpublished work; see also K. Mori, *Tetrahedron*, **30**, 3807 (1974).
15) a) M. Schlosser and J. Hartmann, *J. Am. Chem. Soc.*, **98**, 4674 (1976); b) M. Schlosser, J. Hartmann, and V. David, *Helv. Chim. Acta*, **57**, 1567 (1974); c) M. Schlosser, private communication.
16) R. B. Bates, S. Brenner, C. M. Cole, E. W. Davidson, G. D. Forsythe, D. A. McCombs, and A. S. Roth, *J. Am. Chem. Soc.*, **95**, 926 (1973).
17) R. B. Bates and D. A. McCombs, *Tetrahedron Lett.*, **1969**, 977; W. Gausing and G. Wilke, *Angew. Chem. Int. Ed. Engl.*, **17**, 371 (1978).
18) T. B. Thompson and W. T. Ford, *J. Am. Chem. Soc.*, **101**, 5459 (1979).
19) V. R. Sandel, S. V. McKinley, and H. H. Freedman, *J. Am. Chem. Soc.*, **90**, 495 (1968).
20) H. Kloosterziel and J. A. A. vanDrunen *Recl. Trav. Chim. Pays-Bas*, **89**, 368 (1970).
21) F. Zuccarello, G. Buenmi, and G. Favini, *J. Mol. Struct.*, **18**, 295 (1973); N. L. Allinger, J. F. Viskocil. Jr, U. Burkert, and Y. Yuh, *Tetrahedron*, **32**, 33 (1976); F. A. L. Anet and I. Yavari, *Tetrahedron Lett.*, **1975**, 1567.
22) G. A. Olah and R. D. Porter, *J. Am. Chem. Soc.*, **93**, 6877 (1971).
23) R. Waack and M. A. Doran, *J. Phys. Chem.*, **67**, 148 (1962).
24) R. Waack, M. A. Doran, and P. E. Stevenson, *J. Am. Chem. Soc.*, **88**, 2109 (1966).
25) J. W. Burley and R. N. Young, *J. Chem. Soc., B*, **1971**, 1018; *J. Chem. Soc., Perkin Trans. 2*, **1972**, 835, 1006, and 1843.
26) L. L. Chan and J. Smid, *J. Am. Chem. Soc.*, **90**, 4654 (1968).
27) T. E. Hogen-Esch and J. Smid, *J. Am. Chem. Soc.*, **88**, 307 (1966).
28) D. G. Powell and E. Warhurst, *Trans Faraday Soc.*, **58**, 953 (1962); J. F. Garst, D. Walmsley, C. Hewitt, W. R. Richards, and E. R. Zabolothy, *J. Am. Chem. Soc.*, **86**, 412 (1964); N. Hirota and S. I. Weissman, *ibid.*, **86**, 2538 (1963).
29) S. Bywater, A. F. Johnson, and D. J. Worsfold, *Can. J. Chem.*, **42**, 1255 (1964).
30) D. N. Bhattacharyya, L. L. Lee, J. Smid, and M. Szwarc, *J. Phys. Chem.*, **69**, 608, 612 (1965).
31) P. West, J. I. Purmort, and S. V. McKinley, *J. Am. Chem. Soc.*, **90**, 797 (1968).
32) H. Yasuda, A. Nakamura, Y. Kai, and N. Kasai, unpublished work.
33) a) A. Hosomi, M. Saito, and H. Sakurai, *Tetrahedron Lett.*, **1980**, 3783; b) D. Seyferth and J. Pornet, *J. Org. Chem.*, **45**, 1721 (1980).
34) W. Oppolozer, S. Burford, and F. Marazza, *Helv. Chim. Acta.*, **63**, 555 (1980).

The Use of Grignard Reagents in the Synthesis of Carbohydrates. III.[1] The One-way Anomerization of Methyl Glycofuranosides and the Opening of Their Furanose Rings

Masajiro KAWANA,* Hiroyoshi KUZUHARA, and Sakae EMOTO
The Institute of Physical and Chemical Research, Wako, Saitama 351

(Received October 14, 1980)

The anomerization of methyl glycofuranoside derivatives with methylmagnesium iodide or *t*-butylmagnesium bromide occurred in a one-way manner. For example, methyl 5-*O*-benzyl-β-D-ribofuranoside (**3β**) was converted into the corresponding α-anomer (**3α**) in a 95% yield when a mixture of **3β** and *t*-butylmagnesium bromide in benzene–ether was heated at about 75 °C to remove the ether; the reverse reaction (from **3α** to **3β**) did not proceed. The reaction of **3β** with methylmagnesium iodide gave open-chain products (33%), besides **3α** (30%). Twenty kinds of anomers were tested, and the mechanisms of the reactions were discussed. The cleavage of a benzyl- or trityl-protecting group with the Grignard reagent was also observed during the reaction.

Glycosidic linkages and furanose rings of methyl glycofuranosides are generally stable under neutral or mild alkaline reaction conditions, whereas, in the presence of an acid, these furanosides are hydrolyzed, anomerized, or converted into the corresponding pyranosides, depending upon the conditions used.[2] In this paper we would like to report the first example of the anomerization and furanose-ring opening of methyl glycofuranosides using Grignard reagents; two preliminary reports of this work have been published.[3]

Mallory *et al.*[4] have reported that the cyclic acetal protecting groups in steroids were cleaved by Grignard reagents. Recently, Fischer and Horton[5] and also two of the present authors have found similar reactions in the carbohydrate field. For example,[1a] when methyl 5,6-*O*-cyclohexylidene-3-deoxy-2-*C*-methyl-β-D-*arabino*-hexofuranoside (**1a-β**) was treated with 4 molar equiv. of methylmagnesium iodide (MeMgI) in a benzene–ether solution under reflux for 3 h, the 5,6-*O*-cyclohexylidene ring of **1a-β** was cleaved and the methyl group was introduced to form the corresponding 6-*O*-(1-methylcyclohexyl) derivative (**2a-β**) in a 73% yield (Fig. 1). We applied this reaction to the corresponding C-2 epimer (**1b-β**) to obtain an expected 6-*O*-(1-methylcyclohexyl) derivative (**2b-β**), besides two additional products which had relatively large values of the specific rotations with a positive sign. This suggested that these two compounds had α-D-glycoside structures. On the basis of a comparison of their spectroscopic data with those for authentic samples, the one was identified as methyl 5,6-*O*-cyclohexylidene-3-deoxy-2-*C*-methyl-α-D-*ribo*-hexofuranoside (**1α**),[6] while the other was found to be the corresponding 6-*O*-(1-methylcyclohexyl) derivative (**2α**).[1a] The latter could also be obtained by the treatment of **1α** with MeMgI. These results clearly indicated that the stereocontrolled anomerization occurred under strong conditions with the Grignard reagent.

In order to clarify the scope and mechanism of this new anomerization, simple sugar derivatives, methyl mono-, di-, or tri-*O*-benzylated α- and β-D-pentofuranosides, were subjected to similar Grignard anomerizations. The preparations of the starting materials will be described in the Experimental section. The anomeric configurations of pairs of the new methyl α- and β-D-pentofuranosides were determined by the comparison of their coupling constants[7] of anomeric protons (Table 2) and of their optical rotations[8] (Table 4).

Results

The results are summarized in Table 1.

The Reaction of Methyl D-*Ribofuranoside Derivatives.* When methyl 5-*O*-benzyl-β-D-ribofuranoside (**3β**) was treated with 5 molar equiv. of MeMgI in a benzene–ether solution under forcing conditions,[1a] in which the ether was distilled out from the reaction mixture, an expected α-anomer (**3α**) was obtained in a 30% yield, along with a 7:3 diastereomeric mixture of open-chain products (**4**) in a 33% yield (Fig. 2). As the reaction went on, undissolved materials were deposited in a solution rich in benzene, and the reaction mixture became heterogeneous. Under similar conditions, **3α** gave neither **3β** nor **4**. Therefore,

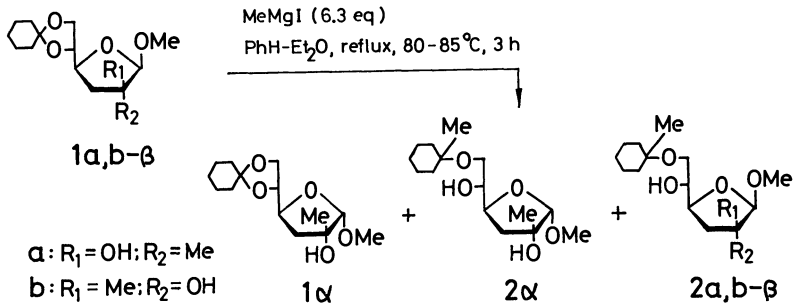

Fig. 1. The acetal ring-opening reaction and stereocontrolled anomerization of branched-chain deoxy sugars.

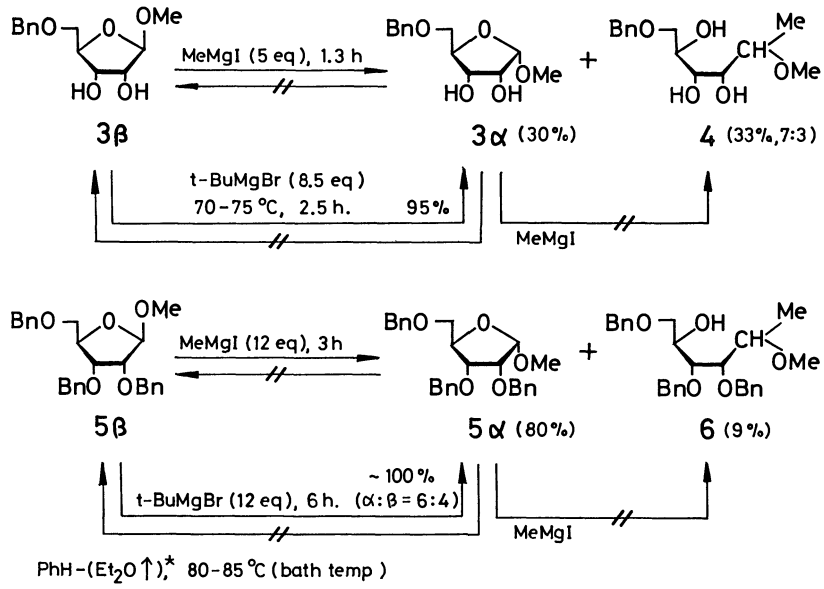

* The ether was allowed to evaporate.

Fig. 2. The reaction of methyl D-ribofuranoside derivatives with Grignard reagents.

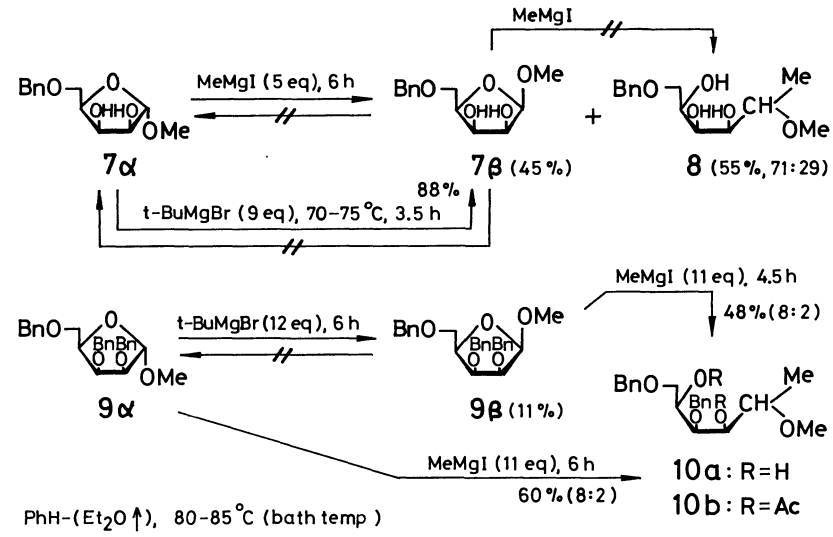

Fig. 3. The reaction of methyl D-lyxofuranoside derivatives with Griganrd reagents.

the anomerization took place in a one-way manner.

In order to obtain **3α** exclusively in the present reaction, we attempted to use *t*-butylmagnesium bromide (*t*-BuMgBr) instead of MeMgI, because the former reagent was sterically bulky, so that the formation of the open-chain products would be prevented. As expected, the reaction of **3β** with *t*-BuMgBr proceeded smoothly to give **3α** (95%) as the sole product, although it also contained a trace of the starting material, judging from TLC analyses and ^{1}H NMR spectroscopy.

Similarly, methyl 2,3,5-tri-*O*-benzyl-β-D-ribofuranoside (**5β**) reacted with MeMgI to give the corresponding α-anomer (**5α**, 80%) and open-chain products (**6**, 9%). The reverse reaction (from **5α** to **5β**) did not proceed. It should be noted here that, although the anomerization with MeMgI took place slower on the perbenzylated anomer (**5β**) than on the monobenzylated one (**3β**), the yield of **5α** was much better than that of **3α**. Some explanations for these phenomena will be presented later on. When *t*-BuMgBr was used in this reaction in place of MeMgI, the anomerization occurred very slowly and many precipitates were deposited during the reaction; after 6 h, we could not detect any anomers in the organic phase. The usual work-up gave a 6:4 mixture of **5α** and **5β**. Under the same reaction conditions, **5α** did not anomerize.

The Reaction of Methyl D-*Lyxofuranosides.* The behavior of MeMgI upon methyl 5-*O*-benzyl-α- and β-D-lyxofuranosides (**7α** and **7β**) was almost the same as that on the corresponding ribose derivatives (Fig. 3). Thus, **7α** was converted into **7β** by the use of MeMgI (yield, 45%) and *t*-BuMgBr (yield, 88%); the reaction with the former reagent also gave open-chain products (**8**, 55%). On the other hand, **7β**

did not react with these reagents under conditions similar to those used for the conversion of **7α**. However, the reaction of methyl 2,3,5-tri-*O*-benzyl-α-D-lyxofuranoside (**9α**) with MeMgI provided a 8:2 diastereomeric mixture of open-chain products (**10a**, 60%) as the main products; here the benzyloxy group originally attached to the C-2 position of **9α** was lacking. Starting from **9β**, we also obtained **10a** (48%) in the same diastereomeric ratio as that from **9α**.

When *t*-BuMgBr was used instead of MeMgI, only an 11% conversion of **9α** to **9β** was accomplished; many precipitates were deposited during this reaction, and no anomers survived in the organic phase after 6 h. The reverse reaction (from **9β** to **9α**) did not proceed under the same reaction conditions.

The Reaction of Methyl D-*Xylofuranosides.* The anomerization of methyl 5-*O*-benzyl-β-D-xylofuranoside (**11β**) with MeMgI occurred in a one-way manner to give an inseparable mixture of the anomers (**11α** and **11β**, *ca.* 19%, 1:1) and open-chain products (**12a**), which were isolated as their acetates (**12b**, 37%) (Fig. 4). With *t*-BuMgBr, only a small percentage of the **11β** was converted into **11α**.

When a 3,5-di-*O*-benzylated derivative (**13β**) was treated with MeMgI, the reaction smoothly proceeded in a one-way manner to provide the corresponding α-anomer (**13α**, 16%) and open-chain products (**14**, 38%). Similarly, *t*-BuMgBr was effective for the conversion of **13β** to **13α** (37%). However, in this case, we also obtained an unexpected crystalline ketone (**15a**) in a 52% yield. This compound was further converted into its acetate (**15b**). The structures of both compounds were tentatively assigned as depicted in Fig. 4.

The behavior of MeMgI or *t*-BuMgBr upon methyl-perbenzylated xylofuranosides (**16α** and **16β**) was somewhat different from that for **11** and **13** (Fig. 5). Thus, **16β** reacted with MeMgI to afford a 6:4 diastereomeric mixture of open-chain products (**17**, 19%), but 63% of the starting β-anomer was recovered. On the other hand, **16α** was easily converted into the corresponding β-anomer (**16β**, 32%), along with **17** (54%, 83:17), the main diastereomer being identical with that from **16β**. Both anomers reacted with *t*-BuMgBr to afford an anomeric mixture.

The Reaction of Methyl D-*Arabinofuranosides.* Only

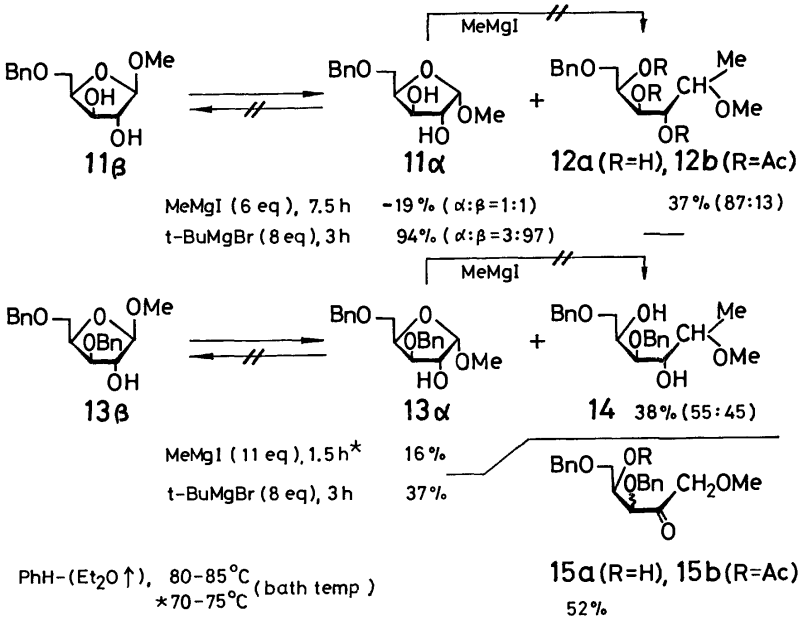

Fig. 4. The reaction of methyl D-xylofuranoside derivatives with Grignard reagents.

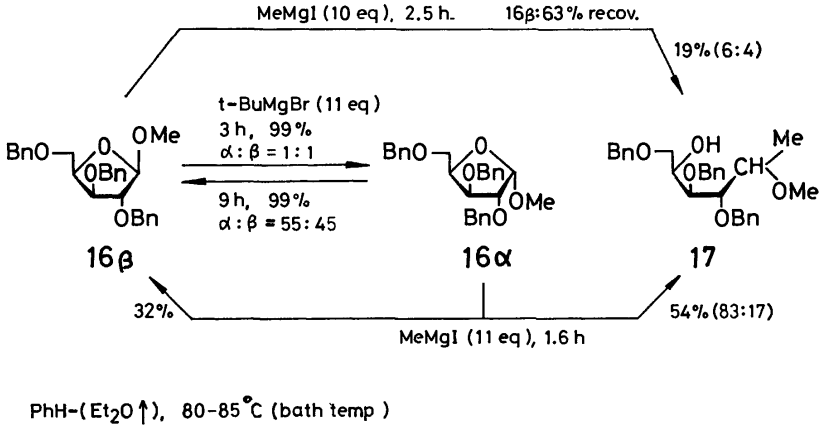

Fig. 5. The reaction of methyl 2,3,5-tri-*O*-benzyl-D-xylofuranosides with Grignard reagents.

perbenzylated anomers, methyl 2,3,5-tri-*O*-benzyl-α- and β-D-arabinofuranosides (**18α** and **18β**), were examined (Fig. 6). Upon treatment with MeMgI, both anomers were converted into a diastereomeric mixture of open-chain products (**19a** and **19b**), which were subsequently separated by silica-gel column chromatography. The selectivity of these reactions was higher on **18β** than on **18α**. The anomerization was also observed by means of TLC analyses, but neither anomer accumulated because of its consumption in the ring-opening reaction. Both anomers were anomerized with *t*-BuMgBr to give an anomeric mixture, the results being similar to those for the anomerization of **16**.

The Reaction of Other Methyl D-*Ribofuranosides.* Methyl 5-*O*-trityl-β-D-ribofuranoside (**20a-β**) also reacted with *t*-BuMgBr to produce the corresponding α-anomer (**20a-α**) in a 57% yield (Fig. 7). Since the trityl group was labile under the present Grignard reaction conditions, some of this group was removed from the α-anomer which had been formed during the reaction.

Similarly, methyl 5-deoxy-β-D-ribofuranoside (**20b-β**) was found to be converted into the corresponding α-anomer (**20b-α**) in a 59% yield; this yield was improved to 94% when a small amount of *t*-butyl alcohol was added to a Grignard solution prior to the addition of **20b-β**.[9]

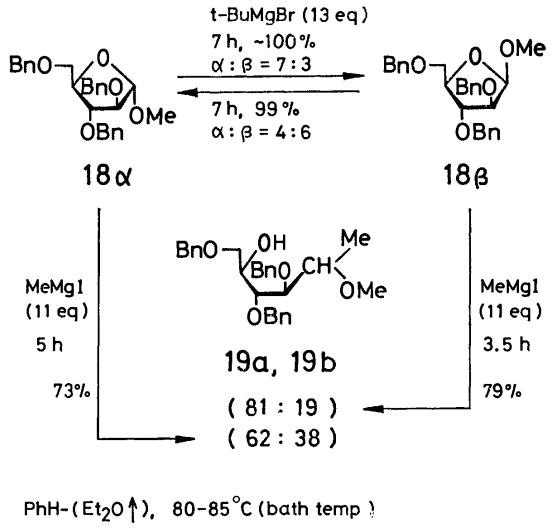

Fig. 6. The reaction of methyl 2,3,5-tri-*O*-benzyl-D-arabinofuranosides with Grignard reagents.

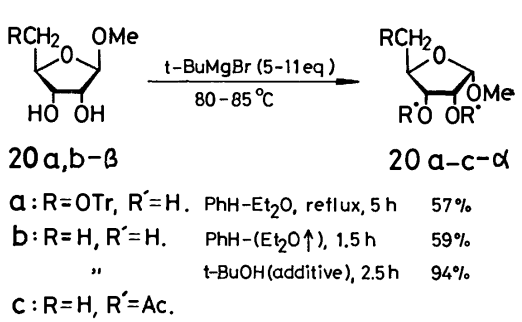

Fig. 7. The reaction of methyl 5-*O*-trityl- and 5-deoxy-β-D-ribofuranosides with *t*-BuMgBr.

Discussion

The formation of the 7:3 diastereomeric open-chain products, **4**, from **3β** suggested that the anomerization of this anomer proceeded through the opening of the furanose ring. A possible mechanism of the reactions for the ribose series is illustrated in Fig. 8. The magnesium atom of the Grignard reagnet is coordinated with the ring oxygen of the furanoside (**A** or **B**),[1a,10] resulting in a weakening of the C_1–O bond of the furan ring. Furthermore, either the oxygen at C-5 or the methoxyl one may participate in this coordination.[1a] When a large amount of the ether is distilled out from the reaction mixture, the complexation of the sugar with the Grignard reagent comes to be more favorable.[4] The cleavage of the C_1–O bond is thus accelerated to form an open-chain intermediate (**C**), which reacts with a methyl anion of MeMgI to yield the diastereomeric products (**D**). When the sterically bulky *t*-BuMgBr is used, the Grignard addition to **C** is prevented, presumably because for a steric reason. It is not clear whether or not there is another pathway to form **D** by the direct attack of MeMgI on the anomeric carbon of **A** or **B**.

The ring closure of **C** gives either the α- or β-anomer, although the presence of a **C**→**A** or **B** path has not been proved in this case. However, once the α-anomer (**E**) is produced, it may attain a high stability, probably by the appropriate coordination of the oxygens of the sugar to the Grignard reagent. At the end of the anomerization reaction, we observed many undissolved materials in the reaction mixture; the Grignard complex of the α-anomer precipitated out more easily than that of the respective β-anomer. The α-anomers, **3α** and **5α**, did not react with either MeMgI or *t*-BuMgBr, but were recovered. Therefore, the anomerization of **3β** and **5β** occurs in a one-way manner, the *trans*-1,2-anomers being preferably transformed into the respective *cis*-1,2-anomers. In a preliminary report,[3a] the selective ring closure of **C** to **E** has been proposed, but the present mechanism, based on these experimental results, dose not necessarily involve this selectivity. Recently, a catalytic anomerization of alkyl per-*O*-benzyl-β-D-glucopyranosides with titanium tetrachloride has been found by Morishima *et al.*,[11] who have also proposed a ring-opening, reclosure mechanism for the anomerization.

The perbenzylated anomer (**5β**) gave a better yield for the anomerization with MeMgI than the monobenzylated one (**3β**). This finding can be explained as follows. We have postulated the presence of a complex (**C'** in Fig. 8) as an intermediate for the reaction of **5β** with MeMgI. Ohrui *et al.*[12] have reported the base-catalyzed epimerization of *C*-glycosides (Fig. 9); for example, 2,3,-*O*-isopropylidene-5-*O*-trityl-β-D-ribofuranosylacetonitrile is epimerized to the corresponding α-*C*-glycoside via an open-chain intermediate (**F**), the latter epimer being thermodynamically more stable than the former one. They have also pointed out that the presence of one five-membered ring such as an isopropylidene group in **F** strongly favors the formation of a second, fused five-membered

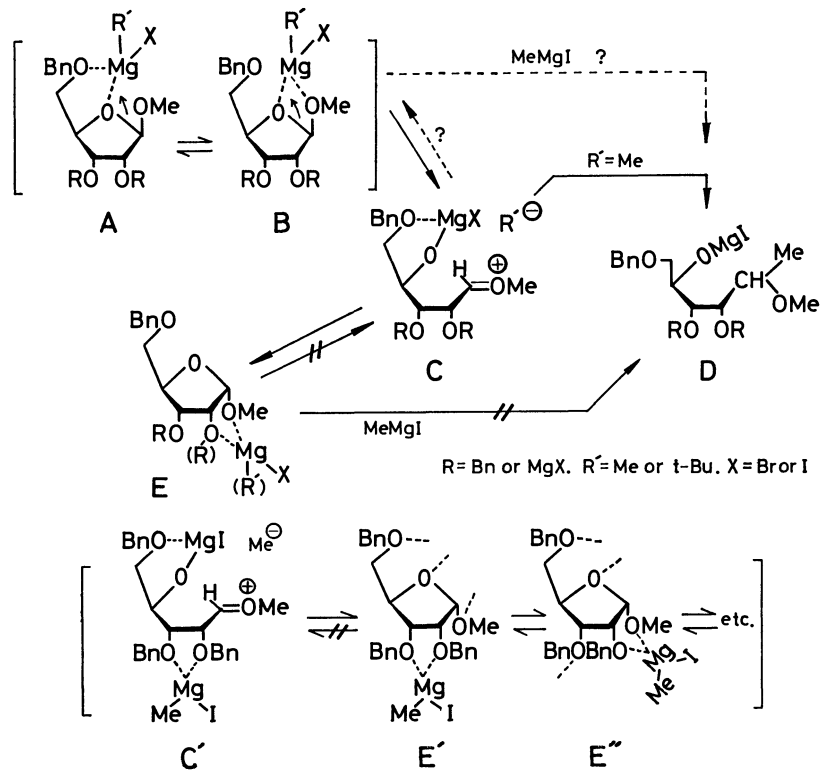

Fig. 8. The possible mechanisms of the one-way anomerization and of the formation of open-chain products.

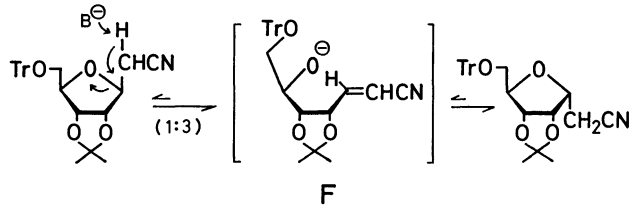

Fig. 9. The base-catalyzed epimerization of a *C*-glycoside reported by Ohrui *et al.*

ring.[12a] The two intermediates, **C'** and **F**, are quite similar in shape. Therefore, it seems likely that the structure of **C'** also fits a cyclization, resulting in the preferred formation of complexes (**E'**, **E''**,..*etc.*). On the other hand, it is rather difficult for **3β** to form an intermediate similar to **C'**.

The equilibrium between **3α** and **3β** in a boiling methanolic solution in the presence of an acid was found to be largely on the side of **3β** in a ratio of 20:80. Similarly, in the case of **5**, the ratio of **5α** to **5β** was 15:85. Therefore, the present one-way anomerization is a "contrathermodynamic" interconversion[13] of more stable isomers into less stable ones.

The reaction of all the lyxose and xylose derivatives except **16** resulted in the one-way anomerization and/or the formation of the open-chain products according to a mechanism similar to that for the ribose series. However, the extent of the one-way anomerization depended on the structure of the starting furanoside and on the reagent. For example, the reactions of **5β**, **9α**, and **11β** with *t*-BuMgBr proceeded very slowly and were incomplete; many precipitates appeared during these reactions.

The perbenzylated xylose derivative (**16α**), which had a *cis*-1,2 relationship, was predominantly transformed, with MeMgI, into the *trans*-1,2-anomer (**16β**), while it was apparent that the latter anomer did not anomerize. The direction of this transformation is in contrast with that for the other furanosides, but this phenomenon can be explained in terms of the difference in reaction rates. The reaction of **16α** with MeMgI is much faster than that of **16β**. In this reaction, **16β** may also anomerize to **16α** (we could observe the presence of a trace of **16α** on a TLC plate), but the latter anomer is consumed rapidly to form the former one and **17**. Both anomers, **16** and **18**, could be anomerized with *t*-BuMgBr. However, before the equilibrium of the anomerization was reached, these anomers had been precipitated out from the reaction mixture.

When the one-way anomerization did not occur, no, or only a small amount of, precipitates were observed at the early stage of the reaction, except that the reaction of **16α** with *t*-BuMgBr gave many precipitates like gels after a few minutes. There may be a relationship between the reactivity and the solubility of the Grignard complex of the sugar.

The newly formed chiral centers in the open-chain products have not been determined in the present work. In the case of the formation of the open-chain products from **16** and **18**, the *cis*-1,2-anomers showed a higher selectivity than did the *trans*-1,2-anomers; the reaction rates for the former anomers were also faster than those for the latter. These results suggest that the reactions involve the pathways of the direct attack of MeMgI on the anomeric carbons of **16α**

Table 1. The reactions of the sugar derivatives with the Grignard reagents

Starting material (mg, mmol)	Reagent (mmol)	[RMgX]/[Sugar]	Solvent PhH-Et_2O[a] ml	Reaction Temp[b]	Time h	Products[c] or recovered material (mg)	Yield/%	Chromatography[d]
1b-β (170, 0.63)	MeMgI (4)	6	5—5	H[e]	3	**1b-α** (10) 6; **2b-α** (68) 38; **2b-β** (32) 18		A (9:1)
2b-β (41, 0.14)	MeMgI (4)	29	14—5	H[e]	6	**2b-α** (13)	33	A (7:3)
3α (207, 0.81)	MeMgI (8)	10	15—10	H	2	**3α** (187)	90	D
3α (211, 0.83)	*t*-BuMgBr (8)	10	15—10	L	2.5	**3α** (200)	95	D
3β (250, 0.98)	MeMgI (5)	5	15—10	H	1.3	**3α** (74) 30; **4** (65) 33 (7:3)		A (1:1)
3β (238, 0.94)	*t*-BuMgBr (8)	9	15—10	L	2.5	**3α** (225)	95[f]	D
5α (150, 0.34)	MeMgI (6)	18	15—10	H	6	**5α** (150)	100[g]	D
5α (215, 0.49)	*t*-BuMgBr (6)	12	15—10	H	6	**5α** (208)	97[g]	D
5β (226, 0.52)	MeMgI (6)	12	15—10	H	3	**5α** (180) 80; **6** (20) 9[h]		A (7:3)
5β (215, 0.49)	*t*-BuMgBr (6)	12	15—10	H	6	**5α**+**5β** (6:4) (214)	99.5	D
7α (254, 1.0)	MeMgI (5)	5	15—10	H	6	**7β** (115) 45; **8** (105) 55[i] (71:29)		B (99:1)
7α (220, 0.87)	*t*-BuMgBr (8)	9	15—10	L	3.5	**7β** (194)	88	D
7β (120, 0.47)	MeMgI (2.5)	5	7—5	H	6	**7β** (118)	98	D
7β (123, 0.48)	*t*-BuMgBr (5.5)	11	7—7	L	3.5	**7β** (123)	100	D
9α (240, 0.55)	MeMgI (6)	11	15—10	H	6	**10a** (8:2)[j] (120)	60	A (6:4)
9α (220, 0.51)	*t*-BuMgBr (6)	12	15—10	H	6	**9α** (194) 88; **9β** (25) 11		A (95:5)
9β (250, 0.57)	MeMgI (6)	11	15—10	H	4.5	**10a** (8:2)[j] (100)	48	A (7:3)
9β (220, 0.51)	*t*-BuMgBr (6)	12	15—10	H	6	**9β** (213)	97	D
11α (230, 0.91)	MeMgI (6)	7	18—10	H	6.5	**11α** (222)	97	D
11α (240, 0.94)	*t*-BuMgBr (8)	8	15—10	H	3	**11α** (233)	97	D
11β (470, 1.85)	MeMgI (12)	6	25—20	H	7.5	**11α**+**11β**+**12a** (α:β=1:1) (387)[k]		D
11β (250, 0.98)	*t*-BuMgBr (8)	8	15—10	H	3	**11α**+**11β** (3:97) (234)[g]	94	D
13α (180, 0.52)	MeMgI (6)	12	15—10	L	3	**13α** (104)	58[l]	A (9:1)
13α (220, 0.64)	*t*-BuMgBr (5)	8	12—8	H	3	**13α** (225)	102	D
13β (195, 0.57)	MeMgI (6)	11	15—10	L	1.5	**13α** (32) 16; **14** (77) 38 (55:45)		A (95:5)
13β (515, 1.5)	*t*-BuMgBr (12)	8	25—20	H	3	**13α** (188) 37; **15a** (270) 52		A (7:3)
16α (245, 0.56)	MeMgI (6)	11	15—10	H	1.6	**16β** (78) 32; **17** (138) 54 (83:17)[m]		C (1:1)
16α (250, 0.57)	*t*-BuMgBr (6)	11	15—10	H	9	**16α**+**16β** (55:45) (248)	99	D
16β (260, 0.6)	MeMgI (6)	10	15—10	H	2.5	**16β** (163) 63; **17** (50) 19 (6:4)[m]		C (6:4)
16β (250, 0.57)	*t*-BuMgBr (6)	11	15—10	H	3	**16α**+**16β** (1:1) (248)	99	D
18α (240, 0.55)	MeMgI (6)	11	15—10	H	5	**19a** (112) 45; **19b** (70) 28		C (7:3)
18α (210, 0.48)	*t*-BuMgBr (6)	13	15—10	H	7	**18α**+**18β** (7:3) (213)	101	D
18β (230, 0.53)	MeMgI (6)	11	15—10	H	3.5	**19a** (153) 64; **19b** (35) 15		C (1:1)

TABLE 1. (Continued)

Starting material (mg, mmol)	Reagent (mmol)	[RMgX]/[Sugar]	Solvent PhH-Et_2O[a] ml	Reaction Temp[b]	Reaction Time h	Products[c] or recovered material (mg)	Yield/%	Chromatography[d]
18β (220, 0.51)	*t*-BuMgBr (6)	12	15—10	H	7	**18α**+**18β** (217) (4:6)	99	D
20a-β (325, 0.8)	*t*-BuMgBr (6.4)	8	10—10	H[e]	5	**20a-α** (185)	57[n]	B (99:1)
20b-β (170, 1.1)	*t*-BuMgBr (6)	5	15—10	H	1.5	**20b-α** (100)	59[o]	B (99:1)
20b-β (170, 1.1)[p]	*t*-BuMgBr (12)	11	20—20	H	2.5	**20b-α** (160)	94	B (99:1)

a) During the reaction, the ether was allowed to evaporate from the reaction mixture. b) H: 80—85 °C (bath temperature). L: 70—75 °C (bath temperature). c) The ratios of the diastereomers or anomers were estimated by ^{1}H NMR spectroscopy and TLC analyses. d) Each product was isolated by chromatography on a silica-gel column with the following solvent systems: A, benzene-ethyl acetate; B, chloroform-methanol; C, hexane-ether. D: The crude products were identified by ^{1}H NMR spectroscopy and TLC analyses. e) A reaction mixture was refluxed in a flask equipped with a condenser. f) Contained a trace amount of **3β**. g) Contained a small amount of by-products. h) Diastereomerically almost pure. i) A main diastereomer was crystallized. j) The ^{1}H NMR spectrum of the **10a** prepared from **9α** was identical with that prepared from **9β**. This product (**10a**) was characterized as its acetate (**10b**). k) **11α,β**:**12a**=4:6. The product (**12a**) was isolated as its diastereomeric acetate (**12b**, 87:13); see Experimental. l) A large amount of the starting material was decomposed under these conditions. m) The ^{1}H NMR spectrum of the main isomer obtained from **16α** was identical with that of the major isomer prepared from **16β**. n) Some of the trityl groups in **20a-α** were deblocked. o) An unknown by-product (10 mg) was isolated; see Ref. 9. p) Before the addition of **20b-β**, a solution of *t*-butyl alcohol (170 mg, 2.3 mmol) in dry benzene (1 ml) was added to a Grignard solution.

and **18β**, besides the pathways via common intermediates similar to **C** in Fig. 8. It seems likely that the *cis*-1,2 structure is desirable for the direct attack, presumably because of steric reasons, thus giving a high selectivity.

The crystalline ketone, **15a**, was the only open-chain product produced by the use of *t*-BuMgBr. The formation of this product results from the elimination of a proton on the carbon adjacent to the C–OMe group of an intermediate similar to **C** in Fig. 8, followed by the ketonization of the resulting enol in the work-up step. Although the configuration of the benzyloxy group next to the keto function of **15a** had not been determined, this compound was proved to be diastereomerically pure, judging from ^{1}H NMR spectroscopy and TLC analyses.

The present anomerization reaction was found to be applicable to 5-*O*-trityl- and 5-deoxy-ribose derivatives (**20a-β** and **20b-β**). Under the Grignard reaction conditions, however, some of the trityl groups of **20a-α** were removed. Debenzylation was also observed during the formation of **10a**. These findings suggest the posibility that the trityl and benzyl protecting groups in sugars may be selectively deblocked under appropriate reaction conditions with the Grignard reagents.

Experimental

The melting points were determined with a Yamato capillary-melting point apparatus and are uncorrected. The IR spectra were recorded on a Shimadzu IR-27 instrument. The ^{1}H NMR spectra were recorded on a Varian HA-100D apparatus, with tetramethylsilane as the internal standard. The optical rotations were measured on a Perkin-Elmer Model 241MC polarimeter.

Merck silica gel GF_{254} was used for the TLC, and the compounds were detected by heating after spraying them with a methanol-sulfuric acid-*p*-methoxybenzaldehyde (85:15:5, v/v) mixture. Merck silica gel 60 (0.063—0.29 mm) was utilized for the column chromatography. The elemental analyses were performed by this Institute.

The ^{1}H NMR spectral data of the compounds are listed in Tables 2 and 3, while their physical properties and the results of their elemental analyses are summarized in Table 4.

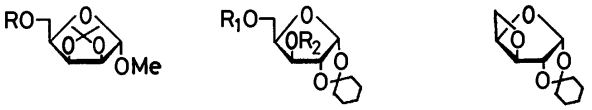

21: R = H
22: R = Bn

23: R_1 = Ts : R_2 = H
25: R_1 = Bn; R_2 = H
26: R_1, R_2 = Bn

24

Materials. In order to obtain new methyl pentofuranosides, the following sugar derivatives were prepared by the conventional methods. The oxidation of methyl 2,3-*O*-isopropylidene-α-D-mannofuranoside[14] with sodium metaperiodate, followed by reduction with sodium borohydride, gave methyl 2,3-*O*-isopropylidene-α-D-lyxofuranoside (**21**), which was then treated with sodium hydride-benzyl chloride to yield methyl 5-*O*-benzyl-2,3-*O*-isopropylidene-α-D-lyxofuranoside (**22**). The deprotection of **22** with an acid afforded **7α**. Starting from 1,2-*O*-cyclohexylidene-α-D-xylofuranose,[15] the corresponding 5-*O*-tosyl (**23**) and 3,5-di-*O*-benzyl (**26**) derivatives were prepared. An anhydro compound (**24**) was synthesized by the reaction of **23** with sodium methoxide. The treatment of **24** with sodium benzylate yielded 5-*O*-benzyl-1,2-*O*-cyclohexylidene-α-D-xylofuranose (**25**), which was then converted into an anomeric mixture of **11** by methanolysis. Similarly, an anomeric mixture of **13** was obtained from **26**.

General Procedure for the Anomerization and Ring-opening Reactions. Some of the reaction conditions and the results are summarized in Table 1. A solution of a Grignard reagent in ether was prepared from magnesium and an alkyl halide in a three-necked flask, and was then diluted with dry benzene. A solution of a sugar derivative (*ca.* 0.7 mmol) in dry benzene (2—3 ml) was added to the stirred Grignard

Table 2. The ^{1}H NMR spectral data of the sugar derivatives in $CDCl_3$

Compound	Anomeric proton δ	Other protons δ
2b-β[a]	4.37 (1H, s)	1.0—2.0 (12H, m, CH_2 of cyclohexane ring and H-3,3′), 1.06 and 1.19 (6H, s, C-CH_3×2), 3.1—3.5 (3H, m), 3.32 (3H, s, OCH_3), 4.09 (1H, m, H-4), 4.32 (1H, d, J=5.3 Hz, OH), 4.72 (1H, s, OH).
3α	4.93 (1H, d, J=4.1 Hz)	3.47 (3H, s, CH_3), 3.59 (2H, d, J=4.0 Hz, H-5,5′), 3.80—4.24 (3H, m), 4.55 (2H, s, CH_2Ph), 7.29 (5H, s, phenyl protons).
3β	4.80 (1H, s)	3.30 (3H, s, CH_3), 3.59 (2H, d, J=4.6 Hz, H-5,5′), 3.90—4.26 (3H, m), 4.57 (2H, s, CH_2Ph), 7.30 (5H, s, phenyl protons).
5α	4.86 (1H, br d, J=4 Hz)	3.38 (2H, m, H-5,5′), 3.44 (3H, s, CH_3), 3.70—3.96 (2H, m), 4.16—4.36 (1H, m), 4.44 (2H, s, CH_2Ph), 4.60 (4H, m, CH_2Ph×2), 7.0—7.6 (15H, m, phenyl protons).
5β	4.89 (1H, s)	3.28 (3H, s, CH_3), 3.5 (2H, m, H-5,5′), 3.8, 4.0, and 4.3 (3H, m), 4.48 (2H, d, J=3.2 Hz, CH_2Ph), 4.54 and 4.62 (4H, s, CH_2Ph×2), 7.1—7.4 (15H, m, phenyl protons).
7α	4.79 (1H, s)	2.97 (1H, d, J=9.2 Hz, OH), 3.32 (3H, s, CH_3), 3.59—4.01 (3H, m, 4.2 (1H, m), 4.5 (1H, m), 4.59 (2H, s, CH_2Ph), 7.29 (5H, s, phenyl protons).
7β	4.79 (1H, d, J=4.4 Hz)	2.92 (1H, br d, J=8 Hz, OH), 3.07 (1H, br d, J=10 Hz, OH), 3.37 (3H, s, CH_3), 3.54—3.90 (2H, m, H-5,5′), 3.90—4.30 (3H, m), 4.57 (2H, s, CH_2Ph), 4.29 (5H, s, phenyl protons).
9α	5.00 (1H, d, J=2.4 Hz)	3.35 (3H, s, CH_3), 3.75 (2H, m, H-5,5′), 3.88 (1H, m), 4.11—4.47 (2H, m), 4.47—4.77 (6H, m, CH_2Ph×3), 7.23 and 7.26 (15H, s, phenyl protons).
9β	4.81 (1H, d, J=4.8 Hz)	3.41 (3H, s, CH_3), 3.57—3.89 (3H, m), 3.98—4.29 (2H, m), 4.48—4.89 (6H, m, CH_2Ph×3), 7.26 and 7.28 (15H, s, phenyl protons).
11α	4.94 (1H, d, J=4.6 Hz)	3.44 (3H, s, CH_3), 3.74 (2H, m, H-5,5′), 3.96—4.40 (3H, m), 4.55 (2H, s, CH_2Ph), 7.27 (5H, s, phenyl protons).
11β	4.81 (1H, s)	3.33 (3H, s, CH_3), 3.51—3.93 (2H, m, H-5,5′), 3.93—4.20 (2H, m), 4.35—4.57 (1H, m), 4.58 (2H, s, CH_2Ph), 7.29 (5H, s, phenyl protons).
13α	4.95 (1H, d, J=4.6 Hz)	2.74 (1H, d, J=7.2 Hz, OH), 3.44 (3H, s, CH_3), 3.66 (2H, m, H-5,5′), 3.98 (1H, m), 4.14—4.48 (2H, m), 4.50—4.79 (4H, m, CH_2Ph×2), 7.1—7.5 (10H, m, phenyl protons).
13β	4.76 (1H, d, J=2.0 Hz)	2.36 (1H, d, J=5.0 Hz, OH), 3.36 (3H, s, CH_3), 3.7 (2H, m, H-5,5′), 3.9 (1H, m), 4.2 (1H, m), 4.4 (1H, m), 4.54 (4H, m, CH_2Ph×2), 7.1—7.4 (10H, m, phenyl protons).
16α	4.72 (1H, d, J=4.0 Hz)	3.38 (3H, s, CH_3), 3.44—3.82 (2H, m, H-5,5′), 4.0 (1H, m), 4.20—4.46 (2H, m), 4.46—4.72 (6H, m, CH_2Ph×3), 7.1—7.4 (15H, m, phenyl protons).
16β	4.89 (1H, d, J=1.3 Hz)	3.38 (3H, s, CH_3), 3.68—3.82 (2H, m, H-5,5′), 3.92—4.12 (2H, m), 4.34—4.46 (1H, m), 4.46—4.70 (6H, m, CH_2Ph×3), 7.1—7.5 (15H, m, phenyl protons).
18α	4.93 (1H, br s)	3.37 (3H, s, CH_3), 3.60 (2H, d, J=4.7 Hz, H-5,5′), 3.80—4.08 (2H, m), 4.08—4.33 (1H, m), 4.33—4.65 (6H, m, CH_2Ph×3), 7.22 and 7.26 (15H, s, phenyl protons).
18β	4.72 (1H, br d, J=4 Hz)	3.30 (3H, s, CH_3), 3.44—3.66 (2H, m, H-5,5′), 3.96—4.26 (3H, m), 4.53 (2H, s, CH_2Ph), 4.60 (4H, s, CH_2Ph×2), 7.24, 7.26, and 7.28 (15H, s, phenyl protons).
20a-α	4.97 (1H, d, J=4.0 Hz)	2.53 (1H, d, J=8.0 Hz, OH), 2.88 (1H, d, J=9.4 Hz, OH), 3.03—3.43 (2H, q, H-5,5′), 3.46 (3H, s, CH_3), 3.83—4.37 (3H, m), 7.1—7.5 (15H, m, phenyl protons).

TABLE 2. (Continued)

Compound	Anomeric proton δ	Other protons δ
20a-β	4.82 (1H, s)	2.31 (1H, br d, J=6 Hz, OH), 2.60 (1H, br d, J=4 Hz, OH), 3.28 (2H, m, H-5,5′), 3.30 (3H, s, CH_3), 3.9—4.32 (3H, m). 7.1—7.6 (15H, m, phenyl protons).
20b-α	4.88 (1H, d, J=4.4 Hz)	1.28 (3H, d, J=6.4 Hz, C-CH_3), 3.13 (1H, br d, J=8 Hz, OH), 3.32 (1H, br d, J=9 Hz, OH), 3.44 (3H, s, OCH_3), 3.5—3.7 (1H, m), 3.9—4.2 (2H, m).
20b-β	4.78 (1H, s)	1.35 (3H, d, J=6.0 Hz, C-CH_3), 3.36 (3H, s, OCH_3), 3.7 (2H, br s, OH×2), 3.9—4.1 (3H, m).
20c-α	4.75—5.10[b]	1.36 (3H, d, J=6.6 Hz, C-CH_3), 2.10 (6H, s, acetyl protons), 3.41 (3H, s, OCH_3), 4.16 (1H, dd, J=6.6, 4.3 Hz, H-4), 4.75—5.10 (3H, m, H-1,2, and 3).
21	4.91 (1H, s, H-1)	1.30 and 1.45 (6H, s, isopropylidene protons), 2.65 (1H, t, J=6.6 Hz, OH), 3.32 (3H, s, OCH_3), 3.8—4.2 (3H, m), 4.56 (1H, d, J=6.4 Hz, H-2), 4.76 (1H, dd, J=6.4, 3.6 Hz, H-3).
22	4.90 (1H, s, H-1)	1.29 and 1.42 (6H, s, isopropylidene protons), 3.32 (3H, s, OCH_3), 3.58—3.94 (2H, m), 4.04—4.26 (1H, m), 4.44—4.78 (4H, m), 7.2—7.4 (5H, m, phenyl protons).
23	5.84 (1H, d, J=3.6 Hz)	1.2—2.0 (10H, cyclohexylidene protons), 2.42 (3H, s, CH_3), 2.54 (1H, d, J=5.6 Hz, OH), 4.1—4.4 (4H, m), 4.46 (1H, d, J=3.6 Hz, H-2), 7.75 and 7.31 (4H, ABq, J=8.8 Hz, phenyl protons).
24	6.26 (1H, d, J=3.6 Hz)	1.2—1.9 (10H, m, cyclohexylidene protons), 4.24 (1H, dd, J=7.4, 2.0 Hz, H-5), 4.72 (1H, dd, J=7.4, 4.4 Hz, H-5′), 4.72 (1H, d, J=3.6 Hz, H-2), 5.08 (1H, dt, J=4.0, 2.0 Hz, H-4), 5.20 (1H, d, J=4.4 Hz, H-3).
25	5.96 (1H, d, J=3.8 Hz)	1.2—1.8 (10H, m, cyclohexylidene protons), 3.45 (1H, d, J=3.4 Hz, OH), 3.91 (2H, d, J=4.0 Hz, H-5,5′), 4.10—4.40 (2H, m), 4.49 (1H, d, J=3.8 Hz, H-2), 4.60 (2H, d, J=2 Hz, CH_2Ph), 7.29 (5H, s, phenyl protons).
26	5.91 (1H, d, J=4.0 Hz)	1.2—1.8 (10H, m, cyclohexylidene protons), 3.75 (2H, d, J=6.0 Hz, H-5,5′), 3.97 (1H, d, J=3.2 Hz), 4.3—4.7 (6H, m), 7.24 and 7.26 (10H, s, phenyl protons).

a) Measured in DMSO-d_6. b) Did not resolve.

solution in the flask without a refluxing condenser[3b] at room temperature under an atmosphere of dry nitrogen, and the mixture was heated at a given temperature for a given period to remove the ether. After cooling, aqueous ammonium chloride was added; the mixture was then extracted with ether. The extract was washed with water, dried ($MgSO_4$), and concentrated. The crude products were purified by silica gel column chromatography with a given solvent system.

*Methyl 5-O-Benzyl-α-D-ribofuranoside (**3α**) and Its β-Anomer (**3β**).* The method of Tener and Khorana[16] was modified. To a solution of methyl 5-*O*-benzyl-2,3-*O*-isopropylidene-β-D-ribofuranoside[16] (970 mg, 3.3 mmol) in methanol (20 ml) and water (4 ml), we added concd sulfuric acid (0.2 ml) after which the mixture was heated at 75—80 °C (bath temperature) for 1.5 h with stirring. After cooling, the acid was neutralized with calcium hydroxide (500 mg). The undissolved materials were filtered through a Celite pad and washed with methanol. The combined filtrate and washings were concentrated. The residue was chromatographed on a silica-gel column with chloroform–methanol (98:2) to give **3α** (160 mg, 19%) and **3β** (550 mg, 66%).

*Methyl 2,3,5-Tri-O-benzyl-α-D-ribofuranoside (**5α**) and Its β-Anomer (**5β**).*[17] To a stirred solution of **3α** (350 mg, 1.4 mmol) in dry benzene (5 ml) and *N,N*-dimethylformamide (2 ml) we added sodium hydride (*ca.* 60% in oil, 300 mg) at room temperature under an atmosphere of dry nitrogen. After 5 min, benzyl chloride (0.6 ml) was added, and the mixture was heated at 75—80 °C (bath temperature) for 30 min. After cooling, methanol was carefully added to decompose the excess sodium hydride. The mixture was then extracted with ether, and the extract was washed with water, dried ($MgSO_4$), and concentrated. The residue was chromatographed on a silica-gel column with benzene–ethyl acetate (95:5) to give **5α** (510 mg, 85%).

A solution of **3β** (460 mg, 1.8 mmol) in dry benzene (25 ml) and *N,N*-dimethylformamide (5 ml) was treated with sodium hydride (*ca.* 60% in oil, 850 mg) and benzyl chloride (0.8 ml) under conditions similar to those described above to give, after chromatography, **5β** in a quantitative yield.

*Methyl 5-O-Benzyl-α-D-lyxofuranoside (**7α**).* The method of Shunk *et al.*[18] was slightly modified. To a solution of **22** (4.0 g, 13.6 mmol) in methanol (75 ml), we added a solution of concd sulfuric acid (0.35 ml) in water (30 ml). The mixture was refluxed at 85—90 °C (bath temperature) for 5 h. After cooling, calcium hydroxide (2 g) was added.

Table 3. The ^{1}H NMR spectral data of the open-chain products

Compound[a)]	δ (in $CDCl_3$)
4	1.21 and 1.24 (3H, d, J=6.0 Hz, 7:3, C-CH_3), 3.35 (3H, s, OCH_3), 3.4—4.0 (6H, m), 4.55 (2H, s, CH_2Ph), 7.30 (5H, s, phenyl protons).
6	1.19 (3H, br d, J=5.8 Hz, C-CH_3), 3.15 (1H, br d, J=3 Hz, OH), 3.32 (3H, s, OCH_3), 3.5—3.8 (5H, m), 4.04 (1H, br s), 4.50 (2H, s, CH_2Ph), 4.59 (2H, d, J=2 Hz, CH_2Ph), 4.65 (2H, s, CH_2Ph), 7.23 and 7.26 (15H, s, phenyl protons).
8[b)]	1.19 (3H, d, J=6.4 Hz, C-CH_3), 3.00, 3.15, and 3.22 (3H, d, J=4.7, 5.6, 5.2 Hz, OH×3), 3.32 (3H, s, OCH_3), 3.38—3.88 (5H, m), 4.10 (1H, m), 4.54 (2H, s, CH_2Ph), 7.28 (5H, s, phenyl protons).
10a	1.13 and 1.16 (3H, d, J=6.4 Hz, 8:2, C-CH_3), 2.7—3.2 (2H, br m, OH×2), 3.25 (3H, s, OCH_3), 3.3—3.7 (4H, m), 3.9 (1H, m), 4.1 (1H, m), 4.35—4.70 (4H, m, CH_2Ph×2), 3.22 and 3.24 (10H, s, phenyl protons).
10b[c)]	1.09 (3H, d, J=6.4 Hz, C-CH_3), 2.00, 2.02, and 2.06 (6H, s, acetyl protons), 3.30 (3H, s, OCH_3), 3.46—3.80 (3H, m, -CH(OMe)- and CH_2OBn), 2.89 and 4.17 (1H, dd, J=7.5, 3.8 Hz, J=9.8, 2 Hz, 75:25, -CH(OBn)-), 4.46 and 4.48 (2H, s, 25:75, CH_2Ph), 4.60 (2H, s, CH_2Ph), 4.96—5.38 (2H, m, -CH(OAc)-×2), 7.24 (10H, s, phenyl protons).
12b[d)]	1.11 (3H, d, J=6.0 Hz, C-CH_3), 2.03, 2.04, and 2.06 (9H, s, acetyl protons), 3.26 (3H, s, OCH_3), 3.40 (2H, m), 3.55 (2H, d, J=5.0 Hz, CH_2Ph), 4.50 (2H, s, CH_2Ph), 5.04—5.26 (2H, m), 5.57 (1H, m), 7.28 (5H, s, phenyl protons).
14	1.10 and 1.20 (3H, d, J=6.0 Hz, 45:55, C-CH_3), 2.9 (2H, br m, OH×2), 3.26 and 3.32 (3H, s, 45:55, OCH_3), 3.3—3.7 (4H, m), 3.8—4.2 (2H, m), 4.49 (2H, d, J=2.0 Hz, CH_2Ph), 4.65 (2H, s, CH_2Ph), 7.26 (10H, s, phenyl protons).
15a	3.0 (1H, br s, OH), 3.33 (3H, s, OCH_3), 3.4—3.6 (2H, m, CH_2OBn), 4.0—4.2 (2H, m), 4.26 (2H, d, J=2.0 Hz, CH_2Ph), 4.46 and 4.61 (2H, ABq, J=12.0 Hz, $COCH_2$), 4.47 (2H, s, CH_2Ph), 7.26 (10H, s, phenyl protons).
15b	2.01 (3H, s, acetyl protons), 3.32 (3H, s, OCH_3), 3.63 (2H, d, J=6.4 Hz, CH_2OBn), 4.17 (2H, d, J=2.0 Hz, CH_2Ph), 4.34 (1H, d, J=4.0 Hz, -CH(OBn)-), 4.48 (2H, s, CH_2Ph), 4.3—4.9 (2H, m, $COCH_2$), 5.40 (1H, dt, J=6.4, 4.0 Hz, -CH(OAc)-), 7.26 and 7.27 (10H, s, phenyl protons).
17[e)]	1.16 and 1.26 (3H, d, J=6.0 Hz, 83:17, C-CH_3), 2.89 (1H, d, J=6.0 Hz, OH), 3.30 (3H, s, OCH_3), 3.40—3.70 (4H, m), 3.76—4.08 (2H, m), 4.42—4.82 (6H, m, CH_2Ph×3), 7.22, 7.24, and 7.25 (15H, s, phenyl protons).
19a	1.10 (3H, d, J=6.0 Hz, C-CH_3), 3.22 (1H, br m, OH), 3.32 (3H, s, OCH_3), 3.44—3.86 (5H, m), 4.0 (1H, br s), 4.53 (4H, s, CH_2Ph×2), 4.67 (2H, s, CH_2Ph), 7.22, 7.26, and 7.28 (15H, s, phenyl protons).
19b	1.25 (3H, d, J=6.0 Hz, C-CH_3), 2.73 (1H, br d, J=6 Hz, OH), 3.24 (3H, s, OCH_3), 3.44—4.10 (6H, m), 4.48 (2H, s, CH_2Ph), 4.55 (2H, d, J=2 Hz, CH_2Ph), 4.67 (2H, s, CH_2Ph), 7.22, 7.25, and 7.26 (15H, s, phenyl protons).

a) The values of the diastereomeric ratios for the open-chain products refer to Table 1. b) A crystalline isomer. c) Decoupling experiments showed that one proton (δ 5.26) on the carbon bearing an acetoxyl group coupled with a proton (δ 3.75) on the carbon bearing the methyl and methoxyl groups. d) The major isomer. e) A diastereomeric mixture from **16α**.

The undissolved materials were filtered through a Celite pad and washed with methanol. The combined filtrate and washings were concentrated to dryness. The residue was dissolved in methanol (100 ml), and concd sulfuric acid (0.7 ml) was added. The mixture was then refluxed at 80 °C (bath temperature) for 1 h. The acid was neutralized with calcium hydroxide (3 g). The work-up gave a syrupy product, which was chromatographed on a silica-gel column with benzene–ethyl acetate (7:3) to provide **7α** (2.1 g, 61%).

Methyl 5-O-Benzyl-β-D-lyxofuranoside (7β). A solution of **7α** (220 mg, 0.78 mmol) in dry benzene (2 ml) was added to a solution of *t*-BuMgBr (7.9 mmol) in dry benzene (15 ml) and ether (10 ml) at room temperature with stirring under an atmosphere of dry nitrogen. The mixture was heated at 70—75 °C for 3.5 h to remove the ether. The usual work-up gave a crystalline product (**7β**, 194 mg, 88%). Its TLC and ^{1}H NMR spectral analyses showed that the product was almost pure. Recrystallization from benzene–hexane afforded an analytically pure sample.

Methyl 2,3,5-Tri-O-benzyl-α-D-lyxofuranoside (9α) and Its β-Anomer (9β). To a stirred solution of **7α** (590 mg, 2.3 mmol) in dry benzene (10 ml) and *N,N*-dimethylformamide (4 ml) we added sodium hydride (*ca.* 60% in oil, 600 mg) at 0—5 °C (bath temperature) under an atmosphere of dry nitrogen, after which the mixture was stirred at room temperature for 30 min. Benzyl chloride (0.8 ml) was then added, and the mixture was heated at 75—80 °C (bath

temperature) for 30 min. A work-up similar to that used for the synthesis of **5α** gave a syrup, which was chromatographed on a silica-gel column with benzene–ethyl acetate (95:5) to afford **9α** in a quantitative yield.

The sugar derivative (**7β**, 280 mg, 1.1 mmol) was treated in a manner similar to that described above to yield **9β** (365 mg, 76%).

*Acetylation of the Open-chain Products (**10α**).* Acetic anhydride (0.4 ml) was added to a cold (0—5 °C) solution of **10a** (116 mg, 0.32 mmol) in dry pyridine (2 ml), after which the mixture was allowed to stand at room temperature overnight. The usual work-up gave a syrup, which was chromatographed on a silica-gel column with benzene–ethyl acetate (96:4) to afford **10b** (130 mg, 91%). IR (neat): 1735 (C=O) cm^{-1}. The ^1H NMR spectrum of **10b** showed that it consisted of a 75:25 diastereomeric mixture.

*Methyl 5-O-Benzyl-α-D-xylofuranoside (**11α**) and Its β-Anomer (**11β**).* A mixture of **25** (1.5 g, 4.7 mmol) and concd sulfuric acid (0.2 ml) in methanol (40 ml) was heated at 65 °C (bath temperature) for 3 h with stirring. After cooling, calcium hydroxide (2 g) was added and the mixture was vigorously stirred. The undissolved material were filtered through a Celite pad and washed with methanol. The combined filtrate and washings were concentrated, and the residue was chromatographed on a silica-gel column with chloroform–methanol (99:1) to give **11α** (350 mg, 29%) and **11β** (580 mg, 49%).

*Acetylation of the Open-chain Products (**12α**).* The sugar derivative (**11β**, 470 mg, 1.85 mmol) was treated with MeMgI according to the conditions described in Table 1 and according to the general procedure for the anomerization to yield a syrupy mixture, which consisted mainly of **11α**, **11β**, and **12a** in a ratio of 1:1:8, judging from the ^1H NMR spectroscopy. This mixture (340 mg) was dissolved in dry pyridine (5 ml). To this solution we then added acetic anhydride (2 ml) at 0—5 °C (bath temperature), after which the mixture was allowed to stand at room temperature overnight. The excess acetic anhydride was decomposed by iced water, and the mixture was extracted with ether. The extract was washed with water, dried ($MgSO_4$), and concentrated. The pyridine was removed by co-evaporation with xylene. The residue was chromatographed on a silica-gel column with hexane–ether (6:4) to give an anomeric mixture of methyl 2,3-di-*O*-acetyl-5-*O*-benzyl-D-xylofuranoside (120 mg, 19% based on the starting material), and **12b** (239 mg, 37% based on the starting material). IR (neat): 1735 (C=O) cm^{-1}.

*Methyl 3,5-Di-O-benzyl-α-D-xylofuranoside (**13α**) and Its β-Anomer (**13β**).* To a stirred suspension of **26** (2.3 g, 5.6 mmol) in methanol (80 ml) we added concd sulfuric acid (0.25 ml), after which the mixture was heated at 60—65 °C (bath temperature) for 6 h. After cooling, calcium hydroxide (2.5 g) was added. After the mixture had been vigorously stirred, the undissolved materials were filtered through a Celite pad and washed with methanol. The combined filtrate and washings were concentrated, and the residue was chromatographed on a silica-gel column with benzene–ethyl acetate (9:1) to give **13α** (930 mg, 48%) and **13β** (1.0 g, 52%).

*Acetylation of the Open-chain Product (**15α**).* A mixture of **15a** (200 mg, 0.58 mmol) and acetic anhydride (0.8 ml) in dry pyridine (3 ml) was stirred at room temperature for 4 h. The usual work-up gave a syrup, which was chromatographed on a silica-gel column with benzene–ethyl acetate (8:2) to give **15b** (188 mg, 84%). IR (neat): 1735 (C=O) cm^{-1}.

*Methyl 2,3,5-Tri-O-benzyl-α-D-xylofuranoside (**16α**) and Its β-Anomer (**16β**).* *From Methyl D-Xylofuranoside*: Sodium hydride (*ca.* 60% in oil, 3.0 g) was added to a stirred solution of methyl D-xylofuranoside[19] (3.2 g, 19.5 mmol) in dry benzene (60 ml) and *N,N*-dimethylformamide (35 ml) at 0—5 °C (bath temperature) under an atmosphere of dry nitrogen, after which the mixture was stirred for 10 min. Benzyl chloride (10 ml) was added, and the mixture was then heated at 75—80 °C (bath temperature) for 2 h. A work-up similar to that described in the synthesis of **5α** gave a syrup, which was chromatographed on a silica-gel column with hexane–ether (7:3) to afford **16β** (2.8 g, 33%) and **16α** (2.3 g, 27%).

*From **13α***: A solution of **13α** (80 mg, 0.23 mmol) in dry benzene (1 ml) and *N,N*-dimethylformamide (0.4 ml) was treated with sodium hydride (*ca.* 60% in oil, 60 mg) and benzyl chloride (0.1 ml), in a manner similar to that described for the synthesis of **16α** from methyl D-xylofuranoside, to give pure **16α** (55 mg, 54%) after chromatography. The physical properties of this product was identical with those of the sample prepared from methyl D-xylofuranoside.

*Methyl 2,3,5-Tri-O-benzyl-α-D-arabinofuranoside (**18α**) and Its β-Anomer (**18β**).* To a stirred solution of methyl D-arabinofuranoside[19] (1.6 g, 0.01 mol) in dry benzene (40 ml) and *N,N*-dimethylformamide (20 ml) we added sodium hydride (*ca.* 60% in oil, 1.8 g) at 0—5 °C (bath temperature) under an atmosphere of dry nitrogen. After the mixture had been stirred at this temperature for 5 min, benzyl chloride (5 ml) was added. The mixture was stirred at room temperature for 30 min and then heated at 75—80 °C for 1 h. After cooling, the mixture was treated in a manner similar to that described for the synthesis of **5α** to give a syrup, which was subsequently chromatographed on a silica-gel column with hexane–ether (8:2) to afford **18α** (1.8 g, 42%) and **18β** (1.1 g, 26%).

*Methyl 5-O-Trityl-α-D-ribofuranoside (**20a-α**) and Its β-Anomer (**20a-β**).* The method of Leonard *et al.*[20] was modified. To a cold (0—5 °C) solution of methyl D-ribofuranoside[21] (5.5 g, 34 mmol) in dry pyridine (70 ml) we added trityl chloride (15 g, 54 mmol), after which the mixture was stirred at room temperature for 2 d. After cooling, iced water was added and the mixture was extracted with ether. The extract was washed with water, dried ($MgSO_4$), and concentrated. The pyridine was removed by co-evaporation with xylene. The residue was chromatographed on a silica-gel column with chloroform–methanol (99:1) to give **20a-α** (1.8 g, 13%) and **20a-β** (9.4 g, 69%).

*Methyl 5-Deoxy-α-D-ribofuranoside (**20b-α**) and Its β-Anomer (**20b-β**).* The method of Shunk *et al.*[18,22] was modified. A solution of methyl 5-deoxy-2,3-*O*-isopropylidene-β-D-ribofuranoside[23] (1.7 g, 9 mmol) in a mixture of methanol (10 ml) and aqueous sulfuric acid (0.2 mol dm^{-3}, 4 ml) was refluxed at 85—90 °C (bath temperature) for 85 min. After cooling, the acid was neutralized with calcium hydroxide. The undissolved materials were filtered through a Celite pad and washed with methanol. The combined filtrate and washings were concentrated to give a syrup, which was subsequently chromatographed on a silica-gel column with chloroform–methanol (95:5) to afford **20b-α** (240 mg, 18%) and **20b-β** (780 mg, 58%).

*Methyl 2,3-Di-O-acetyl-5-deoxy-α-D-ribofuranoside (**20c-α**).* To a solution of **20b-α** (60 mg, 0.41 mmol) in dry pyridine (2 ml) we added acetic anhydride (0.4 ml), after which the mixture was allowed to stand at room temperature overnight. The usual work-up gave a syrup, which was chromatographed on a silica-gel column with benzene–ethyl acetate (85:15) to give **20c-α** (85 mg, 90%). IR (neat): 1740 (C=O) cm^{-1}.

TABLE 4. THE PHYSICAL PROPERTIES AND ELEMENTAL ANALYSES OF THE SUGAR DERIVATIYES AND OPEN-CHAIN PRODUCTS

Compound[a]	Mp/°C	$[\alpha]_D$ (c, $CHCl_3$)	Temp/°C	Formula	Found (%) C	Found (%) H	Calcd (%) C	Calcd (%) H
2b-β	syrup	−75.4° (0.7)	22	$C_{15}H_{28}O_5$	62.39	9.82	62.47	9.79
3α	syrup	+96.5° (0.9)	21	$C_{13}H_{18}O_5$	61.43	7.16	61.40	7.14
3β	syrup	−49.6° (1.5)	21	$C_{13}H_{18}O_5$	61.23	7.10	61.40	7.14
4[b]	syrup	+15.4° (1.4)	23	$C_{14}H_{22}O_5$	62.28	8.15	62.20	8.20
5α	syrup	+77.6° (1.4)	24	$C_{27}H_{30}O_5$	74.45	6.92	74.63	6.96
5β[c]	syrup	+25.8° (1.2)	21	$C_{27}H_{30}O_5$	74.74	6.96	74.63	6.96
6	syrup	+23.6° (0.8)	22	$C_{28}H_{34}O_5$	74.83	7.64	74.64	7.61
7α	syrup	+110° (1.2)	18	$C_{13}H_{18}O_5$	61.32	7.15	61.40	7.14
7β	103—104	−78.0° (1.0)	18	$C_{13}H_{18}O_5$	61.43	7.13	61.40	7.14
8	70.0—71.5[d]	−3.8° (1.0)	22	$C_{14}H_{22}O_5$	62.30	8.20	62.20	8.20
9α	syrup	+17.0° (1.5)	24	$C_{27}H_{30}O_5$	74.39	6.90	74.63	6.96
9β	syrup	−49.1° (1.2)	26	$C_{27}H_{30}O_5$	74.38	6.92	74.63	6.96
10b	syrup	+15.3° (1.4)	28	$C_{25}H_{32}O_7$	67.70	7.28	67.55	7.26
11α	64—65[e]	+118° (1.1)	22	$C_{13}H_{18}O_5$	61.23	7.19	61.40	7.14
11β	syrup	−60.5° (1.1)	20	$C_{13}H_{18}O_5$	61.23	7.06	61.40	7.14
12b[b]	syrup	−26.3° (1.1)	25	$C_{20}H_{28}O_8$	60.61	7.01	60.59	7.12
13α	syrup	+69.8° (1.4)	22	$C_{20}H_{24}O_5$	69.55	7.03	69.75	7.02
13β	syrup	−43.2° (1.3)	23	$C_{20}H_{24}O_5$	69.58	7.07	69.75	7.02
15a[f]	79—80[d]	−41.6° (1.0)	20	$C_{20}H_{24}O_5$	69.74	6.87	69.75	7.02
15b	syrup	−5.0° (1.1)	23	$C_{22}H_{26}O_6$	68.36	6.63	68.38	6.78
16α	syrup	+63.8° (1.3)	23	$C_{27}H_{30}O_5$	74.53	6.91	74.63	6.96
16β	syrup	−22.7° (1.4)	24	$C_{27}H_{30}O_5$	74.64	6.96	74.63	6.96
17[g]	syrup	−22.7° (1.0)	27	$C_{28}H_{34}O_5$	74.62	7.70	74.64	7.61
18α	syrup	+46.0° (1.4)	24	$C_{27}H_{30}O_5$	74.63	6.95	74.63	6.96
18β	syrup	−43.6° (1.0)	20	$C_{27}H_{30}O_5$	74.37	7.02	74.63	6.96
19a	syrup	+21.9° (1.0)	25	$C_{28}H_{34}O_5$	74.46	7.63	74.64	7.61
19b	syrup	+19.8° (1.0)	26	$C_{28}H_{34}O_5$	74.54	7.62	74.64	7.61
20a-α	104—105[d]	+82.7° (1.0)	21	$C_{25}H_{26}O_5$	73.98	6.45	73.86	6.45
20a-β[h]	glass	−26.1° (1.2)	19	$C_{25}H_{26}O_5$	74.03	6.25	73.86	6.45
20b-α	syrup	+150° (0.1)	22	$C_6H_{12}O_4$	48.26[i]	7.92	48.64	8.16
20b-β[j]	40—42[k]	−93.6° (0.9)	26	$C_6H_{12}O_6$	48.65	8.18	48.64	8.16
20c-α	syrup	+142° (0.6)	21	$C_{10}H_{16}O_6$	51.72	6.80	51.72	6.94
21	syrup	+72.3° (1.1)	18	$C_9H_{16}O_5$	52.66	7.68	52.93	7.90
22	syrup	+31.5° (1.0)	18	$C_{16}H_{22}O_5$	65.11	7.28	65.29	7.53
23	118—119	−8.6° (1.1)	24	$C_{18}H_{24}O_7S$[l]	56.19	6.24	56.23	6.29
24	syrup	+17.2° (1.2)	26	$C_{11}H_{16}O_4$	62.10	7.53	62.25	7.60
25	76—77	+6.9° (1.0)	22	$C_{18}H_{24}O_5$	67.56	7.53	67.48	7.55
26	90—91	−39.6° (1.0)	21	$C_{25}H_{30}O_5$	73.36	7.39	73.14	7.37

a) The values of the diastereomeric ratios for the open-chain products refer to Table 1. b) The major isomer. c) See Ref. 17. d) Recrystallized from benzene-hexane. e) Crystallized on standing. f) IR (KBr): 3510 (OH), 1728 (C=O) cm^{-1}. g) A 83:17 diastereomeric mixture from **16α**. h) See Ref. 20. i) The experimental error was 0.38%. This compound, which was volatile and hygroscopic, was further characterized as its acetate (**20c-α**). j) See Refs. 18 and 22. k) Crystallized on standing; hygroscopic. l) S: Found; 8.33%. Calcd; 8.34%.

Methyl 2,3-O-Isopropylidene-α-D-lyxofuranoside (21). A solution of sodium metaperiodate (20 g) in water (150 ml) was stirred into a solution of methyl 2,3-*O*-isopropylidene-α-D-mannofuranoside[14] (10 g, 43 mmol) in dioxane (250 ml) and water (20 ml) at room temperature. After the mixture had been stirred for 2 h, it was extracted with ether (750 ml) and the extract was washed with water. Sodium borohydride (3 g) was added to the extract. The mixture was stirred at room temperature for 1.5 h; then it was washed with water and dried ($MgSO_4$). The evaporation of the solvent gave a syrup, which was chromatographed on a silica-gel column with benzene–ethyl acetate (8:2) to afford **21** (3.6 g, 41%).

Methyl 5-O-Benzyl-2,3-O-isopropylidene-α-D-lyxofuranoside (22). To a solution of **21** (3 g, 15 mmol) in dry benzene (50 ml) and *N,N*-dimethylformamide (8 ml) we added sodium hydride (*ca.* 60% in oil, 900 mg) at room temperature under an atmosphere of dry nitrogen, after which the mixture was stirred for 1 h. Benzyl chloride (2.6 ml) was added, and the mixture was stirred at room temperature overnight. A work-up similar to that described for the synthesis of **5α** gave a syrup, which was chromatographed on a silica-gel column with benzene–ethyl acetate (95:5) to provide **22** (4.0 g, 93%).

1,2-O-Cyclohexylidene-5-O-tosyl-α-D-xylofuranose (23). Tosyl chloride (1.42 g, 5.1 mmol) was added to a stirred solution of 1,2-*O*-cyclohexylidene-α-D-xylofuranose[15] (1.15 g, 5 mmol) in dry pyridine (9 ml) at 0—5 °C (bath temperature). The mixture was stirred at this temperature for 1 h and then at room temperature for another 1.5 h. The

usual work-up gave a solid, which was chromatographed on a silica-gel column with benzene–ethyl acetate (9:1) to afford crystalline **23** (1.59 g, 83%). An analytically pure sample was obtained by recrystallization from ether–hexane. IR (KBr): 3440 (OH), 1365 (S=O), 1176 (S=O) cm^{-1}.

*3,5-Anhydro-1,2-O-cyclohexylidene-α-D-xylofuranose (**24**).* This compound was prepared according to the method used for the synthesis of the corresponding isopropylidene derivative reported by Levene *et al.*[24] To a solution of sodium methoxide (65 mmol) in methanol (50 ml) we added **23** (5.0 g, 13 mmol) at 0—5 °C (bath temperature), after which the mixture was stirred at room temperature for 17 h. After cooling, iced water was added, and the mixture was extracted with ether. The extract was washed with water, dried ($MgSO_4$), and concentrated to give a syrup, which was subsequently chromatographed on a silica-gel column with benzene–ethyl acetate (95:5) to afford **24** (2.6 g, 94%).

*5-O-Benzyl-1,2-O-cyclohexylidene-α-D-xylofuranose (**25**).* The method of Kuzuhara and Emoto[25] was modified. A mixture of sodium (2 g) and benzyl alcohol (30 ml) was stirred at room temperature until the exothermic reaction had finished; the mixture was then heated at 120—125 °C (bath temperature) for 4 h. After the mixture had been cooled to room temperature, **24** (2.5 g, 12 mmol) was added. The mixture was heated at 120—125 °C (bath temperature) for 3 h. After cooling, iced water was added, and the mixture was extracted with ether, dried ($MgSO_4$), and concentrated. The benzyl alcohol was removed by co-evaporation with xylene. The resulting syrup was chromatographed on a silica-gel column with benzene–ethyl acetate (95:5) to give **25** (3.1 g, 82%).

*3,5-Di-O-benzyl-1,2-O-cyclohexylidene-α-D-xylofuranose (**26**).* To a stirred solution of 1,2-*O*-cyclohexylidene-α-D-xylofuranose[15] (2.3 g, 0.01 mol) in dry benzene (40 ml) and *N,N*-dimethylformamide (5 ml) we added sodium hydride (*ca.* 60% in oil, 1.1 g) at 0—5 °C (bath temperature) under an atmosphere of dry nitrogen, after which the stirring was continued for 30 min. Benzyl chloride (3.2 ml) was then added, and the mixture was heated at 70 °C (bath temperature) for 4 h and subsequently treated in a manner similar to that described for the synthesis of **5α** to give **26** as a syrup, which was then crystallized from benzene–hexane: 3.7 g (90%).

*Anomerization of **3β** and **5β** with an Acid.* A mixture of **3β** (75 mg) and concd sulfuric acid (30 mg) in methanol (5 ml) was refluxed at 80—85 °C (bath temperature) for 6 h. Aliquots were analyzed by ^1H NMR spectroscopy after the usual work-up. An equilibrium was reached within 3 h, the ratio of **3α** to **3β** being 20:80.

In a similar way, a mixture of **5β** (99 mg) and concd sulfuric acid (30 mg) in methanol (4 ml) was treated for 24 h. An equilibrium was reached within 6 h (**5α**:**5β**= 15:85).

We wish to thank Dr. Haruo Homma and his staff for the elemental analyses, and Dr. Jun Uzawa and Mrs. Tamiko Chijimatsu for measuring the NMR spectra. We are also grateful to Dr. Hiroshi Ohrui for his valuable discussion.

References

1) a) Part II: M. Kawana and S. Emoto, *Bull. Chem. Soc. Jpn.*, **53**, 230 (1980); b) Portions of this work have been reported at the 9th International Symposium of Carbohydrate Chemistry, London, April 1978, Abstr. p. 111; the 38th National Meeting of the Chemical Society of Japan, Nagoya, Oct. 1978, Abstr. II, p. 438, and the 3rd Symposium of Carbohydrates, Tokyo, Aug. 1980, Abstr. p. 72.

2) J. W. Green, "Advances in Carbohydrate Chemistry," ed by M. L. Wolfrom and R. S. Tipson, Academic Press, New York (1966), Vol. 21, p. 95; W. G. Overend, "The Carbohydrates," ed by W. Pigman and D. Horton, Academic Press, New York (1972), Vol. 1A, p. 279.

3) a) M. Kawana and S. Emoto, *Tetrahedron Lett.*, **1978**, 1561; b) M. Kawana, *Jpn. J. Antibiot.*, **32**, Suppl., S-136 (1979).

4) R. A. Mallory, S. Rovinski, F. Kohen, and I. Scheer, *J. Org. Chem.*, **32**, 1417 (1976).

5) J.-C. Fischer and D. Horton, *Carbohydr. Res.*, **59**, 477 (1977).

6) M. Kawana and S. Emoto, *Tetrahedron Lett.*, **1975**, 3395; M. Kawana and S. Emoto, *Bull. Chem. Soc. Jpn.*, **53**, 222 (1980).

7) We have observed the coupling constants ($J_{1,2}$) of 0—2.5 and 4—5 Hz for the *trans*- and *cis*-1,2-anomers respectively; B. Capon and D. Thacker, *Proc. Chem. Soc.*, **1964**, 369.

8) In an α,β-pair of the anomers, the one which showed the more dextrorotatory value was identified as the α-anomer; C. S. Hudson, *J. Am. Chem. Soc.*, **31**, 66 (1909); C. S. Hudson, "Advances in Carbohydrate Chemistry," ed by W. W. Pigman and M. L. Wolfrom, Academic Press, New York (1948), Vol. 3, p. 1; S. J. Angyal, *Carbohydr. Res.*, **77**, 37 (1979).

9) We have obtained a small amount (10 mg) of an unknown by-product, the ^1H NMR spectrum (in $CDCl_3$) of which showed the presence of a *t*-butoxyl group (δ 1.28), but the absence of a methoxyl one. The addition of *t*-butyl alcohol precluded the formation of this by-product. The reason for this effect remains to be understood.

10) M. L. Wolfrom and S. Hanessian, *J. Org. Chem.*, **27**, 1800 (1962).

11) N. Morishima, S. Koto, and S. Zen, *Chem. Lett.*, **1979**, 749.

12) a) H. Ohrui, G. H. Jones, J. G. Moffatt, M. L. Maddox, A. T. Christensen, and S. K. Byram, *J. Am. Chem. Soc.*, **97**, 4602 (1975); b) H. Ohrui and S. Emoto, *J. Org. Chem.*, **42**, 1951 (1977).

13) E. L. Eliel, A. A. Hartmann, and A. G. Abatjoglou, *J. Am. Chem. Soc.*, **96**, 1807 (1974); C. R. Graham, G. Scholes, and M. Brookhart, *ibid.*, **99**, 1180 (1977).

14) M. H. Randall, *Carbohydr. Res.*, **11**, 173 (1969).

15) K. Heyns and J. Lenz, *Chem. Ber.*, **94**, 348 (1961).

16) G. M. Tener and H. G. Khorana, *J. Am. Chem. Soc.*, **79**, 437 (1957).

17) This compound has been prepared by Barker and Fletcher starting from methyl β-D-ribofuranoside (see Ref. 21), but they have not obtained an analytically pure sample.

18) C. H. Shunk, J. B. Lavigne, and K. Folkers, *J. Am. Chem. Soc.*, **77**, 2210 (1955).

19) I. Augestad and E. Berner, *Acta Chem. Scand.*, **8**, 251 (1954).

20) N. J. Leonard, F. C. Sciavolino, and V. Nair, *J. Org. Chem.*, **33**, 3169 (1968); They have prepared **20a-β**, but have not obtained an analytically pure sample.

21) R. Barker and H. G. Fletcher, Jr., *J. Org. Chem.*, **26**, 4605 (1961).

22) They have not obtained an anomerically pure sample of **20b-β** (see Ref. 18).

23) L. M. Lerner, *J. Org. Chem.*, **43**, 161 (1978).

24) P. A. Levene and A. L. Raymond, *J. Biol. Chem.*, **102**, 331 (1933).

25) H. Kuzuhara and S. Emoto, *Agric. Biol. Chem.*, **28**, 900 (1964).

  Bull. Chem. Soc. Jpn., 54, 1505—1510 (1981)

Catalysis by Alkaline Earth Metal Oxides. III. X-Ray Photoelectron Spectroscopic Study of Catalytically Active MgO, CaO, and BaO Surfaces

Yasunobu INOUE* and Iwao YASUMORI

Department of Chemistry, Tokyo Institute of Technology, Ookayama, Meguro-ku, Tokyo 152

(Received May 24, 1980)

X-Ray photoelectron spectroscopy was used to reveal the surface states of MgO, CaO, and BaO oxides, which are catalytically active for ethylene hydrogenation. The catalytic activity of CaO exposed to H_2O changed with an increase in the temperature of evacuation in a way similar to that of $Ca(OH)_2$ decomposed by heat treatment. The photoelectron spectrum of CaO evacuated at 1223 K showed a peak of O 1s at 529.6 eV, while those of Ca $2p_{3/2}$ were at 346.3 eV and Ca $2p_{1/2}$ at 349.8 eV. The adsorption of H_2O at room temperature gave rise to an additional peak of O 1s at 532.4 eV and one of Ca $2p_{3/2}$ at 348.6 eV, which were attributed to a Ca–O–H structure. With an increase in the temperature of evacuation from 553 to 1053 K, at which the catalytic activity attained a maximum, the latter O 1s peak shifted to the lower binding-energy side by 0.4 eV, and the corresponding Ca 2p peak became broader. These spectral variations were ascribable to the formation of O^- species. Evacuation above 1273 K destroyed both the catalytic activity and characteristic peaks. BaO provided three O 1s peaks, at 528.5, 530.6, and 532.1 eV, after evacuation at 1373 K; these peaks were assigned to lattice oxygen of the oxide, O^-, and OH^- species respectively. The Ba 4d spectra showed correspondingly superposed peaks. The XPS peak due to O^- was observed only when BaO was evacuated at temperatures high enough to generate the catalytic activity. Such spectral features were less pronounced in the case of MgO. The structural analysis of CaO showed that the coordinatively unsaturated cations also play a role in the catalytic hydrogenation. On the basis of these findings, it was concluded that a combined structure of O^- and the cations is responsible for the hydrogenation activity.

It has been recently established that alkaline earth metal oxides became catalytically active for the hydrogenation of olefins and dienes when the oxides are subjected to heat treatment *in vacuo* within definite ranges of temperature;[1] in the case of olefin hydrogenations, the temperature ranges for activation were 1200—1400 K for MgO, 850—1200 K for CaO and 1200—1400 K for BaO. In our previous studies,[2,3] the mechanism of ethylene hydrogenation on such thermally activated CaO[2] and MgO[3] was analyzed on the basis of the detailed kinetics as well as the deuterium distributions in the reaction with D_2. In view of the similarities in the kinetic behavior of the reactions on the two oxides, we predicted the presence of active sites possessing common features in their structures and nature.

The surface states of alkaline earth metal oxides, especially MgO, and their changes upon the adsorption of electron-donor or acceptor molecules have been extensively studied by means of ESR and IR techniques,[4] but the information so far accumulated is not necessarily definitive in elucidating the catalytic behavior of the oxides described above. Thus, the present study was undertaken in order to characterize the surface states of catalytically active MgO, CaO, and BaO oxides by X-ray photoelectron spectroscopy (XPS), which is capable of revealing the electronic state of metals and oxides. A few experiments using XPS have so far been done on alkaline earth metal oxides in connection with their catalytic properties.[5] The most interesting aspect of the catalytic behavior of these metal oxides is that the activity is lost by heat treatment at temperatures higher than the activation range, but can be recovered by exposing the oxides to water vapor and by then re-evacuating at temperatures in the activation range. Since these phenomena well reflect the characteristics of the active sites present on the oxides, it is important to investigate the changes in the surface states of the oxides with H_2O-adsorption and subsequent evacuation at various temperatures. The present work was mainly concentrated on CaO because its catalytic properties were well clarified in a previous study.[2] Scanning-electron microscopic observation and X-ray diffraction were also employed for the structure analysis.

Experimental

The X-ray photoelectron spectra were recorded at room temperature on a Hewlett-Packard 5950A ESCA spectrometer, using monochromatic Al $K\alpha$ exciting radiation. The magnesium, calcium, and barium oxides were prepared from the respective hydroxides. The magnesium and calcium hydroxides of an extra pure grade were the same as those used in the previous kinetic studies.[2,3] Barium hydroxide and barium oxide of an extra pure grade were purchased from Wako Chemical Ind. and the Rare Metallic Co. respectively. The hydroxides, after being pressed into discs and placed on a recessed quartz plate, were transferred into the preparation chamber of the spectrometer and subsequently subjected to *in situ* decomposition into the respective oxides and then to prolonged evacuation at various temperatures up to 1400 K in a vacuum below 3×10^{-7} Torr (1 Torr=133.3 Pa). For H_2O adsorption, the vapor was admitted to the preparation chamber through a leak valve. The samples were heated with a halogen infrared lamp, Osram 25, which had been placed inside the chamber at a distance of 2.5 cm from the sample surface. The irradiation permitted a rapid and fine control of heating over a wide temperature range, 400—1400 K. The temperature of the smaple surface was monitored by means of a calibrated Pt–Pt/13%Rh thermocouple which was brought into contact with the samples on the occasion of measurement. The experimental conditions of the heat treatment were analogous to those used previously in the kinetic studies.[2,3]

The shift of X-ray photoelectron peaks caused by the

positive charging of the surface was compensated for, or at least minimized, by showering electron beams from a "flood gun." The electric current and accelerating voltage of the beam were adjusted in the ranges of 0.1—0.5 mA and 0—4 eV so as to yield peaks with the narrowest full width at half maximum(fwhm) as optimum. The C 1s level of a trace of contaminant carbons, 285.0 eV, was taken as a reference. During XPS measurements, the background pressure was maintained below 2×10^{-9} Torr. For X-ray diffraction and scanning-electron microscopic observation, the calcium hydroxide was decomposed and subjected to heat treatment *in vacuo* at various temperatures. The pretreated samples were stored *in vacuo* in a quartz vessel until just before measurement. The procedures and apparatus used for the measurement of the catalytic activity of the oxides were the same as those reported previously.[2,3]

Results

Figure 1 compares the variations in the catalytic activity of MgO,[1] CaO,[2] and BaO[1] for olefin hydrogenations when the oxides were subjected to heat treatment *in vacuo* at various temperatures. These oxides possess different temperature ranges for the generation of the activity. The figure also shows the effect of pretreatment upon the recovery of the catalytic activity of CaO, which was almost completely deactivated by evacuation at 1273 K. The subsequent evacuation of the oxide at 1073 K had no effect at all. However, when the oxide was exposed to water vapor at room temperature to such a extent that its surface was nearly covered by a monolayer, followed by evacuation at high temperatures, the activity was regained at around 800 K and attained a maximum at around 1073 K. It should be noted that the H_2O-exposed oxide exhibits a similar pattern of the catalytic activity *vs.* the evacuation temperature, although the highest activity at 273 K was about a half of the original level, 3.6×10^{18} molecules m^{-2} min^{-1}.

Calcium Oxide. Figures 2 and 3 show the X-ray photoelectron spectra in the O 1s and Ca 2p regions respectively for CaO subjected to various treatments. The spectra of CaO evacuated at 1223 K gave a single peak of the O 1s, A, at 529.6 eV and a pair of Ca $2p_{3/2}$ and $2p_{1/2}$ peaks, A, at 346.3 and 349.8 eV respectively (Spectrum 6 in Figs. 2 and 3). The subsequent adsorption of H_2O on the oxide surface at room temperature produced a new O 1s peak, B, with a larger fwhm value of 3.0 eV at around 532.4 eV, in addition to the original A peak, the fwhm of which was 1.9 eV. In the Ca 2p region, the adsorption of H_2O gave rise to three peaks, the central one of which was apparently derived from a superposition of two peaks; the substraction of the original A peak from the superposed spectrum provided a pair of new peaks, B, *i.e.*, Ca $2p_{3/2}$ at 348.6 and $2p_{1/2}$ at 352.0 eV, which were similar in fwhm to those of $Ca(OH)_2$, 2.0 eV. Upon the evacuation of the catalyst at 553 K for 30 min, the intensity of the higher-binding-energy side of the O 1s B peak diminished; from the difference between Spectra 1 and 2, this was regarded as reflecting the disappearance of the B_h peak, whereas the Ca 2p spectra remained almost unchanged. The evacua-

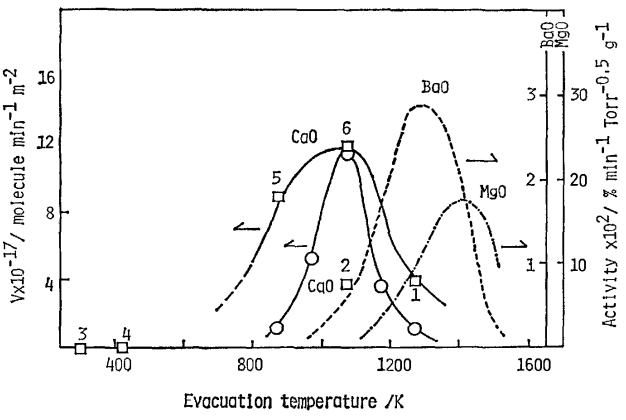

Fig. 1. Catalytic activities *vs.* evacuation temperature.
Squares and full line: ethylene hydrogenation on CaO exposed to H_2O and then evacuated. Reaction temperature=273 K. The numbers denote the experimental sequence; CaO was first evacuated at 1273 K (No. 1), then at 1073 K (No. 2), and exposed to H_2O at room temperature (No. 3) followed by evacuation (from No. 4 to 6).
Circles and full line: ethylene hydrogenation on CaO prepared by the decomposition of $Ca(OH)_2$. Reaction temperature=573 K. See Ref. 2. The rate of the hydrogenation at 273 K on this 1073 K-evacuated CaO was 3.6×10^{18} molecules m^{-2} min^{-1}.
Doubly dashed line: ethylene hydrogenation on MgO. See Ref. 1.
Simple dashed line: 1-butene hydrogenation on BaO. See Ref. 1.

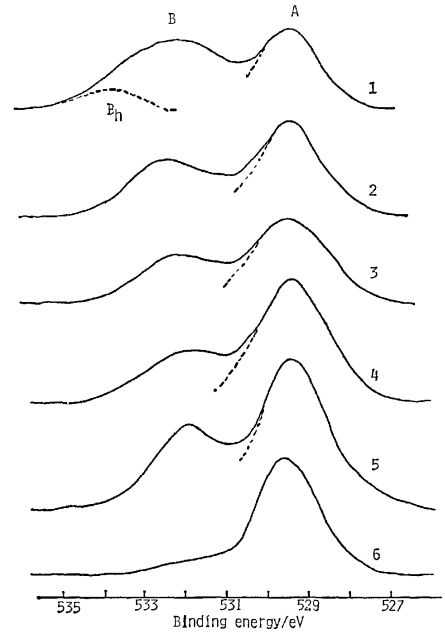

Fig. 2. X-Ray photoelectron spectra in the O 1s region of CaO.
1: After being evacuated at 1223 K for 30 min, CaO was exposed to 5 Torr of H_2O at room temperature and evacuated at the same temperature, 2: evacuated at 553 K for 30 min, 3: evacuated at 883 K for 30 min, 4: evacuated at 1053 K for 30 min, 5: $Ca(OH)_2$ was decomposed and evacuated at 1063 K for 30 min, 6: evacuated at 1223 K for 30 min.

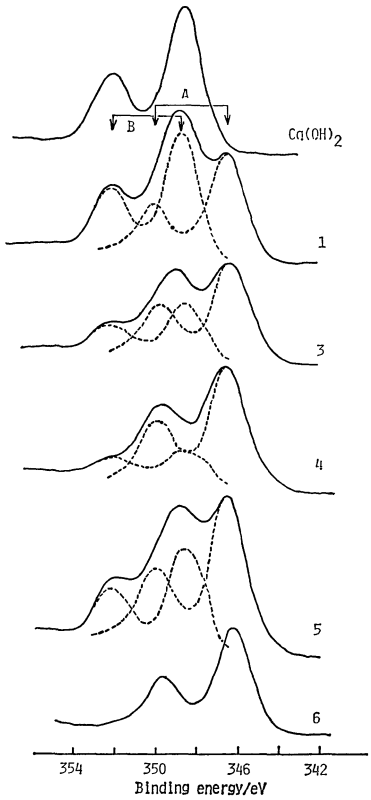

Fig. 3. X-Ray photoelectron spectra in the Ca 2p region. The pretreatments of CaO with respect to spectrum 1 to 6 are the same as those described in Fig. 2 except for the absence of a spectrum corresponding to No. 2.

tion of the sample at 883 K for 30 min, caused significant changes in both O 1s and Ca 2p spectra; the A peak of O 1s became broader by 0.4 eV, and the position of the O 1s-B peak shifted by 0.3 eV to the lower-binding-energy side. In the Ca 2p region, the substraction of the A peak from the observed spectra gave a pair of peaks, the fwhm values of which were broader by 0.2 eV than those of $Ca(OH)_2$ (Spectrum 3 in Fig. 3). Further evacuation at 1053 K considerably enhanced the intensity of the O 1s-A peak, decreasing its fwhm value by 0.2 eV. The B peak of Ca 2p became broader. For evacuation at 1273 K, these characteristic structures in the O 1s and Ca 2p regions vanished, and Spectra 6 in Figs. 2 and 3 were regained. In another experiment in which $Ca(OH)_2$ was decomposed *in vacuo* at various temperatures up to 1273 K, the spectral features of the activated CaO were quite similar to those of the above-mentioned CaO (cf. Spectra 5 in Figs. 2 and 3).

The X-ray diffraction of CaO showed that the relative intensities of lines from such index plane as (111), (220), and (200) remained nearly unchanged on heating *in vacuo* from 873 to 1073 K, but evacuation at 1273 K caused a considerable enhancement of the diffraction intensity from the (111) plane, compared to that from the (220) and (200) planes. Scanning-electron microscopic observation also indicated the preferential growth of particles, probably related to the (111) orientation, upon pretreatment at 1273 K.

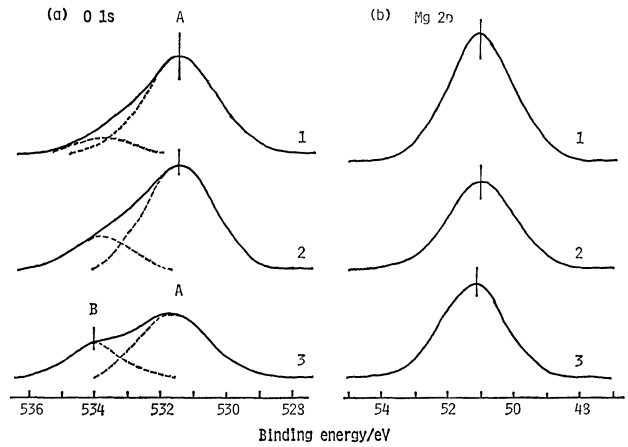

Fig. 4. X-Ray photoelectron spectra in the O 1s (a) and Mg 2p (b) regions of MgO. 1: $Mg(OH)_2$ was evacuated at 1373 K for 30 min, 2: exposed to 5 Torr of H_2O at room temperature for 30 min and evacuated at the same temperature, 3: $Mg(OH)_2$ was evacuated at 873 K for 30 min.

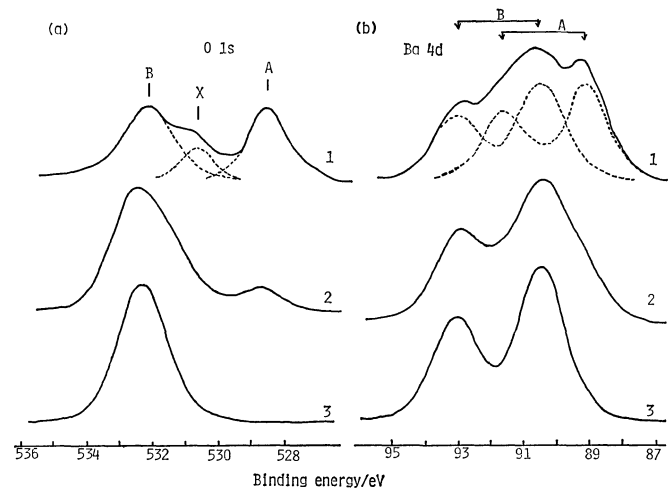

Fig. 5. X-Ray photoelectron spectra in the O 1s (a) and Ba 4d (b) regions of BaO. 1: evacuated at 1373 K for 40 min; the observed peak was roughly deconvoluted by assuming that the intensity ratio of the A to B peak in the Ba 4d line was the same as that in the O 1s line, 2: exposed to 3 Torr of H_2O at room temperature and evacuated at 853 K for 40 min, 3: exposed to air for a long time.

Magnesium Oxide. Figure 4 shows the X-ray photoelectron spectra of MgO pretreated in various ways. The heat treatment of $Mg(OH)_2$ *in vacuo* at 873 K gave rise to two peaks in the O 1s region, *i.e.*, A at 531.6 and B at 534.0 eV. Further treatment at 1373 K caused an appreciable development of the A peak at 531.4 eV and changed the B peak to a small one appearing at around 533.7 eV. The exposure of the oxide to 4 Torr of H_2O at room temperature for 30 min resulted in the appearance of a broad peak at almost the same position as that of the B peak, but its intensity was low. The temperature of H_2O adsorption was raised to 373 K, but no drastic development of the peak occurred. With the Mg 2p photo-

electron peak, no appreciable change was observed upon such treatment except for the broadening of the peak upon the H_2O adsorption.

Barium Oxide. Figure 5 shows the O 1s and Ba 4d spectra of BaO evacuated at 1373 K for 40 min. In the O 1s region, there existed three peaks, *i.e.*, A at 528.5 eV, X at 530.6 eV, and B at 532.1 eV. The corresponding Ba 4d spectra also consisted of superposed peaks. The adsorption of H_2O on the oxide at room temperature and the following evacuation at 853 K led to a drastic decrease in the intensity of the A peak and the development of a broad B peak at 532.4 eV in the O 1s region. With the Ba 4d spectra, the corresponding peaks due to $4d_{5/2}$ and $4d_{3/2}$ were still broad, but the doublets were considerably separated. For comparison, the figure also involves the spectra of BaO exposed to air at room temperature; the O 1s level gave a single peak at 532.3 eV, whereas the Ba 4d levels showed well-separated peaks of Ba $4d_{5/2}$ at 90.5 eV and $4d_{3/2}$ at 93.0 eV. These spectra were substantially identical with those of $Ba(OH)_2$.

Table 1 summarizes the values of the binding energies and fwhm of the photoelectron peaks described above.

Discussion

The adsorption of H_2O on the three oxides and subsequent evacuation caused similar variations in their X-ray photoelectron spectra. Deane *et al.* studied the adsorption of H_2O at room temperature on MgO by IR spectroscopy and classified the produced surface species into several kinds of groups,[6] such as

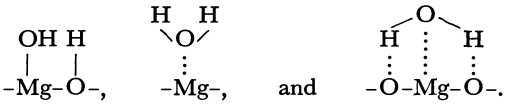

Similar situations are likely to hold for the other alkaline earth metal oxides. In Spectrum 1 in Fig. 2, the close similarities in the binding energy and fwhm to those of anhydrated CaO permit us to assign the A peak of O 1s to the lattice oxygen of the oxide. The broad B peak is evidently composed of more than one kind of peak and is attributable to the oxygen atoms in the hydroxyl groups and adsorbed water, by analogy with the above-mentioned IR results, since these species are substantially associated with a common unit structure, Ca–O–H, but with slightly different binding energies in their O 1s levels. The peak on the higher-binding-energy side of the B peak is attributable to the oxygen of the adsorbed water, because the value of the binding energy was close to that of condensed water (534—535 eV); the peak readily disappeared upon heat treatment at temperatures as low as 553 K. In the Ca 2p region, the three peaks were well resolved into the Ca 2p peaks due to CaO and $Ca(OH)_2$; the A peak is evidently to be assigned to the Ca ion of the oxide, whereas the B

TABLE 1. BINDING ENERGIES AND FWHM

Catalysts	Pretreatment	Peaks	O 1s		Cations	
			B. E./eV	fwhm/eV	B. E./eV	fwhm/eV
					Mg 2p	
MgO	Evac. at 1373 K	A	531.4±0.1	2.5	51.0±0.1	2.2
		B	533.7±0.2	1.9		
	Exposed to H_2O and evac. at r. t.	A	531.4±0.1	2.5	51.0±0.1	2.4
		B	533.8±0.2	2.2		
	Decomp. of $Mg(OH)_2$ and evac. at 873 K	A	531.6±0.1$_5$	2.5	51.1±0.1	2.2
		B	534.0±0.1$_5$	1.9		
					Ca $2p_{3/2}$	
CaO	Exposed to H_2O and evac. at r. t.	A	529.5±0.1	1.8	346.4±0.1	1.9
		B	532.4±0.1$_5$	3.0	348.6±0.1$_5$	2.0
		(as B_h)	533.8±0.2	1.9		
	Evac. at 553 K	A	529.5±0.1	1.8	346.6±0.1	1.9
		B	532.5±0.1$_5$	2.3	348.8±0.1$_5$	2.0
	Evac. at 883 K	A	529.6±0.1	2.2	346.3±0.1	1.9
		B, X	532.2±0.1$_5$	≈2.2	348.5±0.1$_5$	2.2
	Evac. at 1053 K	A	529.4±0.1	2.0	346.5±0.1	1.9
		B, X	532.1±0.1$_5$	≈2.0	348.6±0.2	≈2.3
	Decomp. of $Ca(OH)_2$ and evac. at 1063 K	A	529.5±0.1	2.0	346.5±0.1	1.9
		B, X	532.1±0.1$_5$	≈2.0	348.5±0.1$_5$	2.2
	Evac. at 1223 K	A	529.6±0.1	1.8	346.3±0.1	1.9
					Ba $4d_{5/2}$	
BaO	Evac. at 1373 K	A	528.5±0.1	1.4	≈89.2	1.6
		X	530.6±0.1$_5$	1.2		
		B	532.1±0.1	1.8	≈90.6	
	Exposed to H_2O at r. t. and evac. at 853 K	A	528.7±0.2	1.3		
		B	532.4±0.1	≈2.3	≈90.5	
	Exposed to air	B	532.3±0.1	1.8	90.5±0.1	1.8

C 1s=285.0 eV as reference.

peak was considered to combine with hydroxyl groups (and presumably involves Ca ions combining with adsorbed water). The intensity of the i peak, I_i, was evaluated from each peak area and the I_A/I_B ratios were calculated to be 0.7 ± 0.1 for the O 1s peak and 0.8 ± 0.1 for Ca 2p peak. From these intensity ratios and the escape depth of the electrons ejected, the thickness of the hydroxide layer was estimated to correspond to several monolayers.

The most significant changes caused by evacuation at 883 K were the broadening of the O 1s-A and Ca 2p-B peaks and the shift of the O 1s-B peak toward the lower-binding-energy side. The findings that these characteristic variations proceeded further upon evacuation at temperatures up to 1073 K, while the heat treatment at 1273 K destroyed the resulting spectral fine structures, strongly suggest that a new oxygen species is formed on the surface treated in this definite range of temperature, *viz.*, 900—1073 K.

The O 1s A and B peaks which were observed after the evacuation of $Mg(OH)_2$ at 873 K were assinged to oxygen of the oxide and hydroxides respectively. The separation between the two peaks, 2.4 eV, was consistent with the value, 2.5 eV, obtained by Fuggle *et al.* in the case of H_2O[7a] or O_2[7b] adsorbed on evaporated magnesium films. Upon evacuation at 1373 K, the A peak developed whereas the B peak changed to a small one and merged into the tail of the main A peak. The spectral features of the produced oxygen species were not so clear as in the case of CaO, but it is not unreasonable to ex ect that these variations in the O 1s peak upon heating are correlated with the process of the catalytic activation.

The most striking features of BaO treated at 1373 K, which gives a maximum activity for 1-butene hydrogenation,[1] were clearly observed in the O 1s region where three oxygen peaks appeared; from a comparison with Spectra 2 and 3, the A and B peaks were assigned to oxygen of the oxide and hydroxides respectively, whereas the X peak was assigned to a new oxygen species. As for the cation, the corresponding Ba 4d photoelectron spectra provided superposed peaks similar to those observed in the Ca 2p region of the activated CaO. An additional peak due to anhydrated BaO was not obtained under the present heating conditions; the superposed peaks were analyzed by substracting the peaks of hydrated BaO (Fig. 5b, 3). This procedure gave rise to a pair peak which shifted by 1.4 eV to the lower-binding-energy side and was assigned to anhydrated BaO. Since neither broadening nor shoulder peaks were appreciably observed, the resulting peak appears to be insensitive to the influence of the newly-produced oxygen species.

It should be noted that there existed a similarity in the photoelectron spectra of these oxides when they were subjected to the heat treatment by which their catalytic activities were generated, in spite of the difference in the optimum temperature for activation. A recent mass-spectrometric analysis of gases evolved during the thermal decomposition of $Mg(OH)_2$ showed that hydrogen and water molecules are released in the temperature range, 570—970 K, and oxygen atoms above 770 K.[8] The following processes were proposed to occur:

$$2\,OH^- \rightarrow O^-\cdots O^- + H_2 \text{ and } 2\,OH^- \rightarrow O^{2-} + H_2O$$

at a lower temperature, and:

$$OH^- \rightarrow O^- + 1/2\,H_2 \text{ and } 2\,O^- \rightarrow O^{2-} + O$$

at a higher temperature. The formation of O^- species on CaO[9] and MgO[10] upon heat treatment *in vacuo* was also confirmed by ESR studies. The change in surface structures due to this process is not clearly reflected in the XPS spectra of MgO, probably because of the low concentration of the species formed. This view is in line with the fact that the density of O^- species was estimated to be less than $1\times10^{17}\,m^{-2}$ from the quantitative analysis of the hydrogen evolved.[8] The processes described above are likely to take place on CaO and BaO to a greater extent, since the formation of peroxide is more favored in both oxides. Accordingly, the broadening of the O 1s-A peak of CaO after evacuation at 883 K seems to result from a contribution of the surface O^{2-} species thus formed, the binding energy of which is probably not far from that of lattice oxygen. The variation in the OH-band intensity of $Ca(OH)_2$ with an increase in the evacuation temperature showed that most of the OH groups were removed by evacuation up to 773 K, but still remained as isolated OH groups even after evacuation at 1173 K.[11] By taking the charge distribuitons into account, the B peak of O 1s appears to be derived from the O^- species and the residual OH^- groups. The splitting in energy between O^{2-} and O^- levels is not clear in the present case, but falls within the range of 1.9—2.2 eV, as was also observed in the adsorption of oxygen on NiO and Cu_2O surfaces.[12] The broadening of the Ca 2p-B peak by evacuation at temperatures between 883 and 1053 K appears to be brought about as a result of the partial conversion of OH^- species to O^- (and surface O^{2-}) species; it is likely that the broadening of the B peak toward the lower-binding-energy side is due to a contribution from the Ca ions, which combine with these oxygen species in place of the hydroxyl group, since the binding energies of O 1s were in this order; $O^{2-}<O^-<OH^-$ and since the Ca 2p level was lower in CaO than in $Ca(OH)_2$.

A similar consideration of the activated BaO leads to the conclusion that the O 1s X peak is associated with the O^- species. This assignment is supported by the results of the XPS study of H_2O adsorbed on the Fe surface;[13] the O 1s peak at 530 eV was assigned to the chemisorbed oxygen, $O^{\delta-}$, and the peak at 532 eV to the $OH^{\delta-}$ species. The findings described above for the oxides evidently show that the conditions necessary for the catalytic activation are also effective in producing the common oxygen species, which are coordinatively unsaturated O^- and O^{2-}. The O^- species appears to be more responsible for the catalysis as a part of the active sites for the hydrogenation, since the density of the surface O^{2-} was attenuated with an increase in the catalytic activity of CaO, as is shown in the narrowing of the O 1s-A peak upon evacuation at temperatures from 883 to 1053 K, and since the active BaO surface provided

exclusively the X peak associated with the O^- species. Besides, there is evidence that the species is able to contribute to the H_2-D_2 equilibration reaction.[14]

As was shown in a previous study,[2] evacuation following the calcination of $Ca(OH)_2$ in air gave rise to a low catalytic activity. This implies that the cations in specific positions also play an important role in the catalytic hydrogenation, because the UV reflectance spectra revealed that the sintering of CaO in O_2 at 1073 K preferentially decreased the intensities of the lower frequency bands which relate to ions with lower coordinations, indicating the preferential destruction of high-index faces and local imperfections.[15] The X-ray diffraction and electron microscopic results for the decomposition of $Ca(OH)_2$ demonstrated that the CaO produced by evacuation at temperatures between 873 and 1073 K was still in a crystallographically transient state, retaining many cations with a lower coordination, *e.g.*, those located at edges and corners, but it changed to an oxide with a well-developed (111) orientation upon heat treatment above 1273 K. These findings give support to the above view. Furthermore, the contribution of incompletely coordinated cations or oxygen-deficient sites of CaO to the exchange reaction of butene with D_2 has been pointed out.[16] Therefore, the consolidation of these findings leads to the conclusion that the active sites of the oxides are composed of the O^- species adjacent to the specific cations. This model apparently explains the fact that the fraction of the active sites was as small as 0.5% of the total surface ions.[2]

Evidence for the adsorption of H_2 and C_2H_4 on these sites was shown in the ESR study; the ESR signal of oxygen adsorbed on MgO and CaO was remarkably enhanced by the pre-exposure of MgO to H_2, C_2H_4, or CO[17] and by that of CaO to H_2,[9] and it was concluded that such effects were due to the adsorption of these reducing molecules on the coordinatively unsaturated ions. These considerations, as well as the above-mentioned conclusion as to the structure of the active sites, confirm the following pathway of ethylene hydrogenation, which was previously proposed on the basis of the kinetic results:[2]

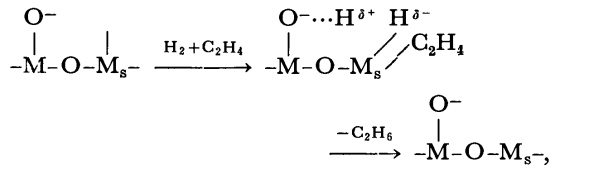

where M_s denotes a metal cation with a lower coordination on such specific sites as edges or corners. It appears likely that this structure of the isolated active sites produces heterolytically split hydrogen, thus leading to the formation of a π-allyl carbanion proposed as an intermediate in the 1,3-butadiene hydrogenation on MgO.[18] A comparison of the intensities of the O 1s peaks attributable to O^- shows that its concentration relative to lattice oxygen becomes higher in the order of: BaO>CaO>MgO. The above-mentioned structure of the active sites predicts that the catalytic activity also increases in this order, provided that the contribution of M_s is similar in the three oxides. This prediction is in line with the observed results.[1] An XPS study by Vinek *et al.* revealed that the hydroxide layer on MgO catalysts is enhanced with the storage time, causing a change in selectivity from the dehydrogenation of buta-2-ol to dehydration.[5] We have at present no evidence confirming the contribution of the OH groups to the hydrogenation; further study of their role is needed.

The authors are indebted to K. Kasama for his assistance in measuring the catalytic activity of CaO.

References

1) H. Hattori, Y. Tanaka, and K. Tanabe, *Chem. Lett.*, **1975**, 659; Y. Tanaka, H. Hattori, and K. Tanabe, *ibid.*, **1976**, 37.
2) K. Kasama, Y. Inoue, and I. Yasumori, *Bull. Chem. Soc., Jpn.*, **53**, 1842 (1980).
3) M. Tezuka, Y. Inoue, and I. Yasumori, in press.
4) H. Knozinger, *Adv. Catal.*, **25**, 184 (1976).
5) H. Vinek, J. Latzel, H. Noller, and M. Ebel, *J. Chem. Soc., Faraday Trans.*, **1978**, 2092.
6) M. Deana, D. L. Griffiths, I. A. Lewis, J. A. Winter, and A. J. Tench, *J. Chem. Soc., Faraday Trans. 1*, **71**, 1005 (1975).
7) a) J. C. Fuggle, L. M. Watson, and D. J. Fabian, *Surf. Sci.*, **49**, 61 (1975); b) J. C. Fuggle, *ibid.*, **69**, 581 (1977).
8) R. Martens, H. Gentsch, and F. Freund, *J. Catal.*, **44**, 366 (1976).
9) D. Cordischi, V. Indovina, and M. Occhiuzzi, *J. Chem. Soc., Faraday Trans. 1*, **74**, 883 (1978).
10) E. G. Derouane and V. Indovina, *Chem. Phys. Lett.*, **14**, 455 (1972).
11) T. Iizuka, H. Hattori, Y. Ono, J. Sohma, and K. Tanabe, *J. Catal.*, **22**, 131 (1971).
12) T. Robert, M. Bartel, and G. Offergeld, *Surf. Sci.*, **33**, 123 (1972).
13) M. W. Roberts and P. R. Wood, *J. Electron Spectrosc. Relat. Phenom.*, **11**, 431 (1977).
14) M. Boudart, A. Delbouille, E. G. Derouane, V. Indovina, and A. B. Walters, *J. Am. Chem. Soc.*, **94**, 6622 (1972).
15) A. Zecchina, M. G. Lofthouse, and F. S. Stone, *J. Chem. Soc. Faraday Trans. 1*, **71** 1476 (1975).
16) H. Hattori and A. Satoh *J. Catal.*, **45** 32 (1976).
17) V. Indovina and D. Cordisch *Chem. Phys. Lett.*, **43**, 485 (1976).
18) H. Hattori, Y. Tanaka, and K. Tanabe, *J. Am. Chem. Soc.*, **98**, 4652 (1976).

  Bull. Chem. Soc. Jpn., 54, 1511—1516 (1981)

The Magnetic Circular Dichroism of the Conjugated *O*- and *S*-Heterocycles

Nobuko IGARASHI, Akio TAJIRI, and Masahiro HATANO*

Chemical Research Institute of Non-aqueous Solutions, Tohoku University, Sendai 980

(Received September 20, 1980)

The MCD spectra of the monobenzo and dibenzo derivatives of thiophene and furan are reported; especially in dibenzofuran, two electronic origins are revealed in its lowest energy absorption band. The quantum-mechanical calculations of the transition energies and the Faraday parameters elucidate the experimental data to a fair extent, suggesting similarities in the electronic structures of the lower-lying excited states of furan and thiophen derivatives.

The oxygen (sulfur) atom is incorporated into a conjugated system so as to form ether (thioether) or ketone (thioketone). Sulfur heterocycles of the former type have attracted the attention of many authors because of their characteristic chemical and physical properties.

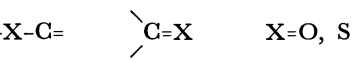

Johnstone *et al.*[1] have measured the UV and photoelectron spectra of molecules containing several sulfur atoms located in the five-membered ring part of the structure, and have tried to elucidate the observed spectra within the framework of semi-empirical SCF–MO–CI calculations, retaining both the one-center and two-center core integral terms as variable parameters. They have found reasonable values which reproduce the observed electronic spectra. The photoelectron spectra of planar sulfur heterocycles, such as benzothiophene, thienothiophene, and benzothiadiazole have been reported by Clark *et al.*[2] The ionization potentials calculated by the extended Hückel and the PPP method, without 3d atomic orbitals in the basis set, give good agreement with the experimental data; this suggests that sulfur 3d-orbital participation must be very small. The singlet-singlet absorption spectra of six-membered heterocyclic compounds were studied by the use of the PPP method in order to make spectroscopic assignments in the UV region.[3]

The UV spectra of thiophenes seem to have thus far been discussed in conjunction with those of furans, leading to a similarity and correspondence between their electronic transitions. Recently, however, Bree *et al.*[4] have measured the single-crystal absorption spectra of dibenzofuran and shown that the lowest absorption band, which seems to correspond to that of dibenzothiophene, consists of two electronic transitions; one is polarized along the short axis, and the other, along the long axis. Although this point has been further investigated by Tanaka,[5] the vibrational structure has complicated the resolution of the band into its two electronic components.

On the other hand, the magnetic circular dichroism (MCD) technique[6] has been recognized to be a powerful tool for investigating the electronic structures of molecules and their ions in their ground and excited states.[7] In addition, the MCD technique often reveals hidden transitions or resolves heavily overlapping bands into their components. However, although simple organic compounds and their ions have been extensively studied,[8] the MCD technique has not been applied to organic sulfur compounds except for thiophene.[9,10] Håkansson and Nordén[9,10] have demonstrated the existence of two transitions with opposite MCD in the UV-spectral region of thiophene.

In this paper, the electronic structures of thiophene, furan, and their benzo derivatives are investigated from the viewpoint of MCD spectroscopy. On the basis of the UV and MCD spectral data and the results of the PPP calculation, the electronic states of these compounds will be discussed.

Experimental

The thiophene, furan, benzo[*b*]thiophene, benzofuran, dibenzothiophene, and dibenzofuran were purified by repeated distillation or sublimation after recrystallization. Cyclohexane, ethanol, and heptane were used as solvents; all were of a spectral grade.

The MCD spectra were measured with a JASCO J-500C recording spectropolarimeter using an electromagnet, while the UV spectra were recorded on a HITACHI EPS-3T recording spectrophotometer. The magnetic-field strength was calibrated with freshly prepared potassium hexacyanoferrate(III) and was 1.169T.

The observed spectrum was resolved into its components according to the curve-fitting procedure assuming a Gaussian function. The error in estimating the area under the curve was less than ±5%. The experimental oscillator strengths, f, and Faraday B terms, B, were extracted according to the following equations:

$$f = 4.3792\times10^{-9}\times\tilde{\nu}_0\times\int\frac{\varepsilon(\tilde{\nu})}{\tilde{\nu}}d\tilde{\nu}, \quad (1)$$

$$B = \frac{1}{33.5294}\times\int\frac{[\theta]_M(\tilde{\nu})}{\tilde{\nu}}d\tilde{\nu}, \quad (2)$$

where f and B were expressed in units of cgs and (debye)$^2\beta$/cm^{-1} (β=Bohr magneton) respectively.

Theoretical Calculations

The excitation energies, the oscillator strengths, and the Faraday B values of the furans and thiophenes have been calculated within the framework of the PPP approximation,[11] including configuration interaction (CI) among the 28 singly excited configurations. The one-center core and repulsion integrals have been evaluated from the valence-state ionization potentials and electron affinities using the table of Hinze and Jaffé.[12] For the sulfur atom, the one-center core and repulsion integrals are −16.27 eV and 10.78 eV respectively. The two-center core and repulsion integrals have been evaluated by the use of the Wolfsberg-Helmholz[13] and Nishimoto-Mataga[14] equations respectively. The proportionality constant, κ, in the

Wolfsberg-Helmholz equation has been chosen to be 0.7602 so as to reproduce the observed extrema of the MCD spectra of thiophene.

In the absence of degeneracy, a quantum mechanical expression for the Faraday B value associated with an electronic transition a←0 is:

$$B_{0a} = \frac{1}{3} Im \left\{ \sum_{b \neq 0} \frac{\hat{\mu}_{b0}}{\nu_{b0}} \cdot \hat{m}_{0a} \times \hat{m}_{ab} + \sum_{b \neq a} \frac{\hat{\mu}_{ab}}{\nu_{ab}} \cdot \hat{m}_{0a} \times \hat{m}_{b0} \right\}, \quad (3)$$

where $\hat{\mu}_{ij}$ and $\hat{m}_{ij}$ represent the off-diagonal matrix elements of the magnetic- and electric-moment operators respectively, whereas *Im* stands for taking the imaginary part of the bracketed expression of the above equation. The denominator ν_{ij} is the energy difference between the i and j states. The atomic orbitals used in the calculation are the Slater AO's χ, with which the basis set, χ^{λ}, in the PPP procedure is expanded in terms of the overlap integral, S, according to this equation:[15]

$$\chi^{\lambda} = \chi S^{-1/2}. \quad (4)$$

The molecular geometries of furan and thiophene were taken from microwave results,[16,17] and those of dibenzofuran and dibenzothiophene, from the X-ray diffraction data.[18,19] In benzofuran and benzo[*b*]-thiophene, the nuclear arrangements were assumed to be those of furan and thiophene for the five-membered ring, while the bondlengths in the six-membered ring were taken to be equal, 1.40 Å.

Results and Discussion

The UV and MCD spectra of furans and thiophenes are reproduced in Figs. 1—5. In each figure, the full line shows the observed spectrum, while the broken lines stand for the curves after the curve-fitting procedure.

Thiophene and Furan. In the spectral region corresponding to the lowest energy-absorption band of thiophene, there have been observed two MCD bands; one is negative at a higher energy, while the other is positive, as is shown in Fig. 1. It is clear that there are at least two π-π^* electronic origins in this region, as has already been pointed out by Håkansson and Nordén.[9,10] In their calculation, based on the PPP method, these two oppositely directed MCD bands have nearly equal transition energies and Faraday B values which are too large to reproduce the experimental values. This comes from the small energy gap between the lowest two excited states predicted in their calculation. On the contrary, it should be noted that the experimental B values are larger for the higher-energy band than for the lower-energy band, even though cancellation is taken into account.

In Table 1 the theoretical results for thiophene are summarized and listed along with the experimental data. The lowest energy transition is predicted to be B_2←A_1, with its transition moment directed along the long axis, while the second is A_1←A_1, with its transition moment directed along the short axis. The theoretical oscillator strengths and Faraday B values seem to reproduce well the relative magnitudes of the experimental data. Especially the splitting of the first and second excited states is calculated to be 3500 cm^{-1}, in fairly good agreement with the observed

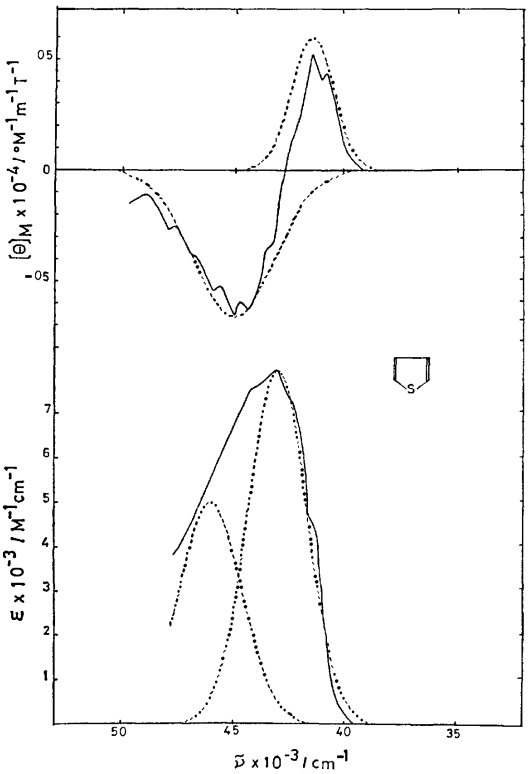

Fig. 1. The MCD (upper) and absorption (lower) spectra of thiophene in cyclohexane at room temperature.

TABLE 1. THE OBSERVED AND CALCULATED SINGLET-SINGLET π-π^* TRANSITION ENERGIES, $\bar{\nu}$, OSCILLATOR STRENGTHS, f, AND FARADAY PARAMETERS, B, FOR THIOPHENE AND FURAN

Molecule	Calculated				Observed			
	$\bar{\nu} \times 10^{-3}$ / cm^{-1}	f	$B \times 10^5$ / β Debye^2 cm	Transition symmetry	$\bar{\nu}^{UV} \times 10^{-3}$ / cm^{-1}	f	$\bar{\nu}^{MCD} \times 10^{-3}$ / cm^{-1}	$B \times 10^5$ / β Debye^2 cm
Thiophene[a]	42.6	0.433	−20.37	B_2←A_1	43.0	0.115	41.5	−101.6
	46.1	0.002	28.00	A_1←A_1	46.0	0.066	45.0	199.4
Furan[b]	41.7	0.299	4.86	B_2←A_1	48.5	0.300	47.0	30.0
	45.8	0.000	1.38	A_1←A_1				

a) The experimental values after curve analysis. b) The experimental values from B. Nordén, R. Håkansson, P. B. Pedersen, and E. W. Thulstrup, *Chem. Phys.*, **33**, 355 (1978).

value, 3000 cm^{-1}.

Nordén *et al.* observed a negative MCD band at 47000 cm^{-1} and also an onset of the positive MCD band in the energy region higher than 50000 cm^{-1} for the broad absorption spectrum of furan, which suggests that there are two electronic transitions.[10]

Our calculated results for furan are included in Table 1. In the lower-energy region two π-π^* transitions assigned to $B_2 \leftarrow A_1$ and $A_1 \leftarrow A_1$ are predicted. The sign of the *B* value associated with the first transition is positive, in agreement with the experimental results. As for the excitation energies, however, the theoretical values are in disagreement with the experimental values.

Benzo[b]thiophene and Benzofuran. The UV and MCD spectra of benzo[*b*]thiophene are illustrated in Fig. 2. In the highest energy region, two negative peaks are observed at *ca.* 44000 cm^{-1} and *ca.* 46000 cm^{-1} in the MCD spectrum. It seems to be interesting to consider whether they are due to the vibrational structure or to different electronic origins. We ascribed these bands to the latter, because the PPP method calculation indicates that there are two π-π^* electronic transitions in this energy region. Accordingly, the MCD and UV spectra are resolved into four components, assuming Gaussian functions. Then, corresponding to four absorption bands of benzo[b]thiophene, four MCD bands are observed; their signs are all negative except that of the lowest energy band, at 34500 cm^{-1}.

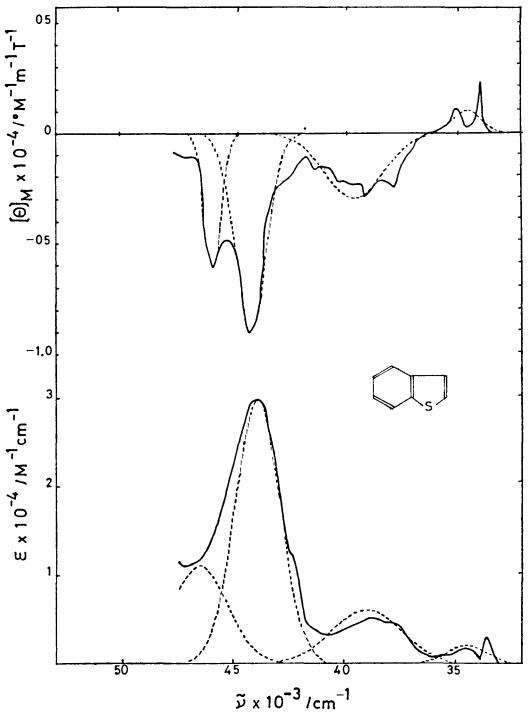

Fig. 2. The MCD (upper) and absorption (lower) spectra of benzo[b]thiophene in ethanol at room temperature.

The theoretical results for benzo[b]thiophene are listed in Table 2, along with the experimental data. Calculation gives the transition energies at 33000, 38600, 45300, and 47200 cm^{-1}, in good agreement with the observed values of 34500, 39000, 43900, and 46500 cm^{-1} respectively. Benzo[*b*]thiophene belongs to the point group C_s, and these four transitions are assigned to A′←A′ polarized on the molecular plane. The predicted *B* values seem to agree well with the extracted values both in sign and magnitude. Unfortunately, however, the calculation gives a negative *B* value associated with the fourth transition, while the experiment gives a positive value. The further inclusion of the CI neglected in this calculation may improve this disagreement.

As is shown in Fig. 3, the UV and MCD bands are blue-shifted in benzofuran. Only two bands are observed for benzofuran in the UV region, although there are four bands for benzo[*b*]thiophene. These two bands, however, in the lower-energy region are similar to those of benzo[*b*]thiophene with respect to the spectral-band shape and the absorption coefficient. At energies higher than 46000 cm^{-1}, a strong absorption band with a negative MCD is observed. As a result, it is expected that the MCD sign sequence of benzofuran is +, −, −, which is the same as that of benzo[*b*]thiophene, and benzofuran seems to show a band system similar to that of benzo[*b*]thiophene in the whole UV spectral region.

The calculation predicts that benzofuran has positive and negative MCD bands for the first and the second transitions respectively. The absolute values of the Faraday B term and the oscillator strength associated

Table 2. The observed and calculated singlet-singlet π-π^* transition energies, $\tilde{\nu}$, oscillator strengths, *f*, and Faraday parameters, *B*, for benzo[*b*]thiophene and benzofuran

Molecule	Calculated				Observed			
	$\tilde{\nu} \times 10^{-3}$ / cm^{-1}	*f*	$B \times 10^5$ / β Debye^2 cm	Transition symmetry	$\tilde{\nu}^{UV} \times 10^{-3}$ / cm^{-1}	*f*	$\tilde{\nu}^{MCD} \times 10^{-3}$ / cm^{-1}	$B \times 10^5$ / β Debye^2 cm
Benzothiophene	33.0	0.001	−20.22	A′←A′	34.5	0.019	34.5	−12.9
	38.6	0.565	85.91	A′←A′	39.0	0.103	39.5	76.5
	45.3	0.501	81.59	A′←A′	43.9	0.330	44.2	107.7
	47.2	0.130	−92.14	A′←A′	46.5	0.098	45.9	38.0
Benzofuran	32.8	0.001	−11.90	A′←A′	36.6	0.020	37.0	−71.8
	38.6	0.474	66.52	A′←A′	41.5	0.193	41.6	188.5
	44.9	0.374	71.61	A′←A′	—	—	—	(positive)
	47.2	0.041	22.47	A′←A′	—	—	—	

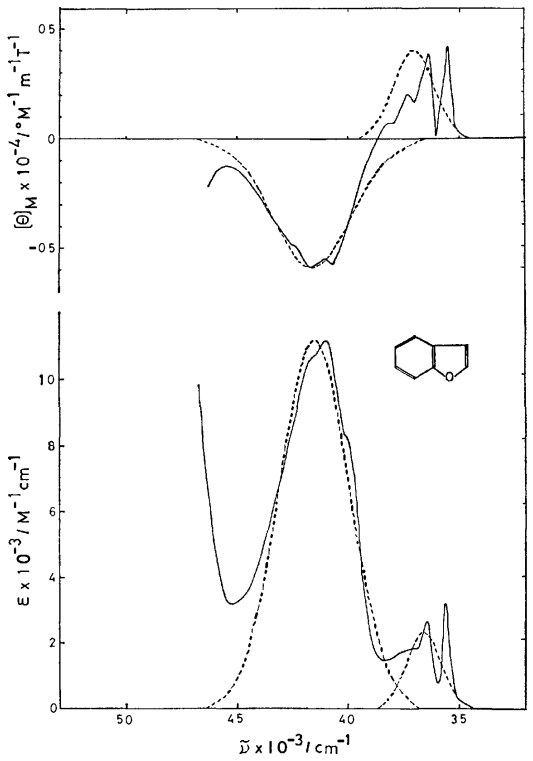

Fig. 3. The MCD (upper) and absorption (lower) spectra of benzofuran in ethanol at room temperature.

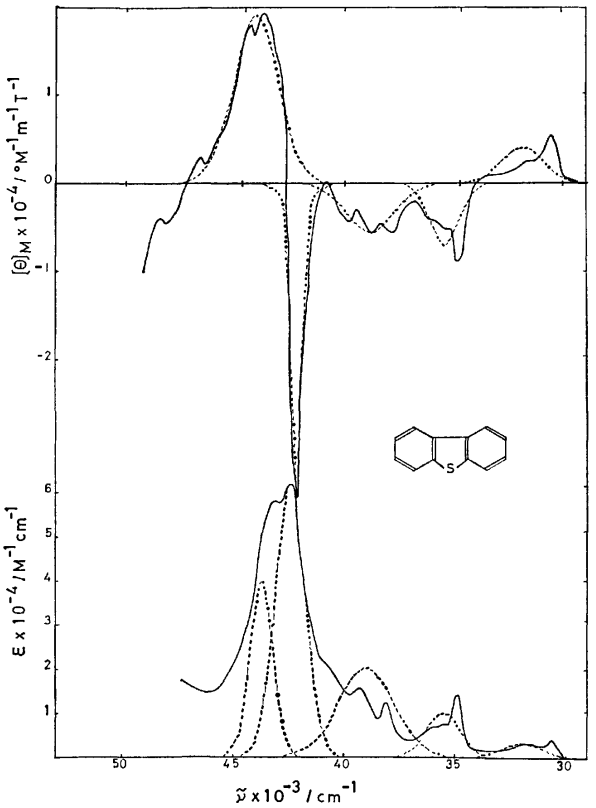

Fig. 4. The MCD (upper) and absorption (lower) spectra of dibenzothiophene in heptane at room temperature.

with the first transition are smaller than those associated with the second one, which is in good agreement with the experimental values. For the second and the third transitions, it is found that the relative magnitude of the theoretical values for benzofuran is similar to that for benzo[*b*]thiophene. The calculation seems to show the similarity between benzofuran and benzo[*b*]thiophene, as does the experiment.

Dibenzothiophene and Dibenzofuran. Figure 4 shows the observed and resolved spectra for dibenzothiophene. The MCD spectrum is considered to consist of five main bands, with extrema at 32000, 35500, 38800, 42100, and 44000 cm^{-1}. Accordingly, the observed UV spectrum is resolved into three components in the spectral range of 37000—46000 cm^{-1}, so as to give five absorption bands as a whole. In both the UV and MCD spectra the lowest energy band is assumed to be single.

The UV and MCD spectra of dibenzofuran are reproduced in Fig. 5. Apart from the blue-shifts of the bands, the observed UV spectrum of dibenzofuran seems to have the same profile as that of dibenzothiophene, provided that a shoulder at 43700 cm^{-1} in Fig. 5 corresponds to the third absorption band in dibenzothiophene.

On the other hand, the MCD spectrum of dibenzofuran shows a complicated band system different from that of dibenzothiophene; especially in the lowest energy absorption region, the MCD spectrum shows a fine structure with an alternating sign. These positive and negative MCD bands may be ascribed to either electronic or vibrational origins. In general, prominent sign-alternation is observed in the MCD

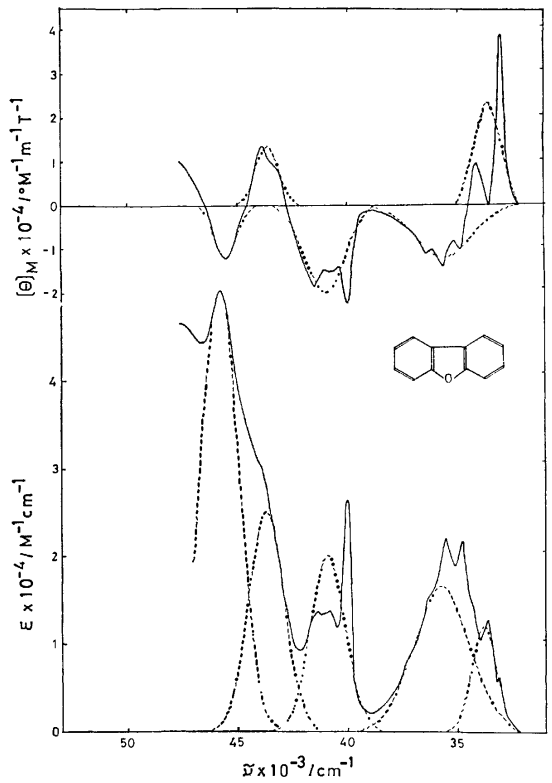

Fig. 5. The MCD (upper) and absorption (lower) spectra of dibenzofuran in cyclohexane at room temperature.

Table 3. The observed and calculated singlet-singlet π-π^* transition energies, $\bar{\nu}$, oscillator strength, f, and Faraday parameters, B, for dibenzothiophene and dibenzofuran

Molecule	Calculated				Observed			
	$\bar{\nu}\times10^{-3}$ / cm^{-1}	f	$B\times10^5$ / β Debye^2 cm	Transition symmetry	$\bar{\nu}^{UV}\times10^{-3}$ / cm^{-1}	f	$\bar{\nu}^{MCD}\times10^{-3}$ / cm^{-1}	$B\times10^5$ / β Debye^2 cm
Dibenzo-thiophene	32.6	0.001	−79.60	$A_1\leftarrow A_1$	32.0	0.031	32.0	−87.8
	34.1	0.040	6.60	$B_2\leftarrow A_1$				
	35.9	0.749	170.68	$B_2\leftarrow A_1$	35.5	0.084	35.5	95.6
	45.7	0.066	35.61	$A_1\leftarrow A_1$	39.0	0.280	38.8	112.5
	46.7	0.673	1588.92	$B_2\leftarrow A_1$	42.4	0.463	42.1	163.4
	46.9	1.111	−1444.46	$A_1\leftarrow A_1$	43.7	0.222	44.0	−321.2
Dibenzofuran	33.6	0.000	−18.70	$A_1\leftarrow A_1$	33.8	0.073	33.6	−298.9
	34.5	0.004	−3.93	$B_2\leftarrow A_1$	35.7	0.231	35.6	321.4
	38.5	0.683	104.84	$B_2\leftarrow A_1$	40.9	0.172	41.0	320.7
	45.8	0.080	54.72	$A_1\leftarrow A_1$	43.7	0.220	43.6	−116.8
	46.7	0.689	261.23	$B_2\leftarrow A_1$	45.8	0.441	45.5	101.8
	47.0	0.470	22.21	$B_2\leftarrow A_1$	47.2[a]	—	—	—

a) "UV Atlas of Organic Compounds," Verlag Chemie, Weinheim, Butterworths, London (1967).

spectra for symmetry-forbidden but vibronically-allowed transitions, such as the $B_{2u}\leftarrow A_{1g}$ transition of benzene.[20] In order to examine the existence of symmetry-forbidden transitions, the INDO/S calculations[21] were carried out for dibenzofuran. However, neither n-π^*, σ-π^* nor π-σ^* electronic transitions were predicted in the energy region lower than 40000 cm^{-1}. The possibilities of the electronic origins due to n-π^*, σ-π^*, and π-σ^* transitions, and, in turn, the possibility of the vibrational origin, seem to be quite small. The positive and negative MCD bands in the lowest energy region are ascribed to two π-π^* electronic transitions. Considering this in conjunction with the positive onset of the MCD spectrum in the highest energy region, dibenzofuran can be said to show a band system consisting of six main bands (see the resolved UV and MCD spectrum in Fig. 5).

The PPP method predicts two π-π^* electronic transitions in the lowest energy region for dibenzofuran. The $A_1\leftarrow A_1$ and $B_2\leftarrow A_1$ transitions are encountered at 33600 cm^{-1} and 35600 cm^{-1}; they are assigned to the first and second MCD bands at 33800 cm^{-1} and 35700 cm^{-1} respectively. The calculation gives the same results as for the single-crystal absorption spectra with regard to the polarization of these transitions.[4,5] For the remaining four transitions, the assignments are given in Table 3.

The theoretical results for dibenzothiophene are summarized and listed in Table 3, which shows that two π-π^* transitions are predicted in the lowest energy region; one is at 32600 cm^{-1} and the other, at 34100 cm^{-1}. For comparison, a schematic diagram of the states for dibenzothiophene and dibenzofuran is given in Fig. 6. A very close similarity is found for the predominant configuration which contributes to the excited state in question. In conclusion, six π-π^* electronic transitions are theoretically predicted in the UV spectral region of dibenzothiophene.

It seems reasonable to consider that there exists a similarity between dibenzofuran and dibenzothiophene as to the π-π^* electronic transitions, because

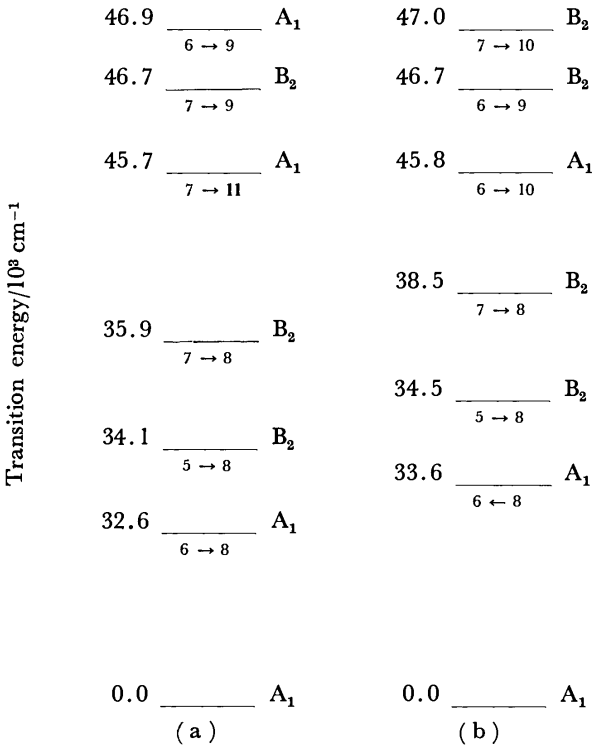

Fig. 6. The calculated lower lying excited states in dibenzothiophene(a) and dibenzofuran(b). The numbers under the bars stand for the main singly excited configuration contributing to the CI state.

both the molecules are iso-π-electronic; nevertheless, the observed UV and MCD spectra of the former consist of six main bands while those of the latter consist of five main bands.

Accordingly, it appears that there is one more transition in the lowest spectral region of dibenzothiophene as well as of dibenzofuran. This may be partially verified by the PPP calculation, which predicts two closely separated π-π^* transitions in dibenzothiophene. One of the two transitions in dibenzothio-

phene, however, is considered to be so weak as not to be observed or as to be hidden by the neighbouring transition, which was difficult to resolve even in the present MCD work.

Concluding Remarks

The lowest absorption band of dibenzofuran is confirmed, by the analysis of the MCD spectra and the PPP calculation, to be a super position of the two π-π^* electronic transitions, which is consistent with the results of the single-crystal experiments by Bree *et al.*[4] and Tanaka.[5] For dibenzothiophene, the lowest absorption band is expected to consist of two transitions, although the present work was not successful in resolving these transitions.

References

1) R. A. W. Johnstone and S. D. Ward, *Tetrahedron*, **25**, 5485 (1969); R. A. W. Johnstone and F. A. Mellon, *J. Chem. Soc., Faraday Trans. 2*, **1973**, 1155.

2) P. A. Clark, R. Gleiter, and E. Heilbronner, *Tetrahedron*, **29**, 3085 (1973).

3) J. Fabian, A. Mehlhorn, and R. Zahradnik, *J, Phys. Chem.*, **72**, 3975 (1968).

4) A. Bree, V. V. B. Vilkos, and R. Zwarich, *J. Mol. Spectrosc.*, **48**, 135 (1973).

5) M. Tanaka, *Bull. Chem. Soc. Jpn.*, **49**, 3382 (1976).

6) A. D. Buckingham and P. J. Stephens, *Ann. Rev. Phys. Chem.*, **17**, 399 (1966); P. N. Schatz and A. J. McCaffery, *Quart. Rev.*, **23**, 552 (1969); D. Caldwell, J. M. Thorne, and H. Eyring, *Ann. Rev. Phys. Chem.*, **22**, 259 (1971); P. J. Stephens, *J. Chem. Phys.*, **52**, 3489 (1970).

7) P. J. Stephens, P. N. Schatz, A. B. Ritchie, and A. J. McCaffery, *J. Chem. Phys.*, **48**, 132 (1968); P. J. Zandstra, D. J. Scholtens, and R. E. Koning, *J. Chem. Phys.*, **57**, 3821 (1972).

8) P. J. Stephens, W. Suetake, and P. N. Schatz. *J. Chem. Phys.*, **44**, 4592 (1966); A. Kaito, M. Hatano, and A. Tajiri, *J. Am. Chem. Soc.*, **99**, 524 (1977); P. E. Koning and P. J. Zandstra, *Chem. Phys.*, **20**, 53 (1977).

9) R. Håkansson, B. Nordén, and E. W. Thulstrup, *Chem. Phys. Lett.*, **50**, 305 (1977).

10) B. Nordén, R. Håkansson, P. B. Pedersen, and E. W. Thulstrup, *Chem. Phys.*, **33**, 355 (1978).

11) R. Pariser and R. G. Paar, *J. Chem. Phys.*, **21**, 466 (1953); *ibid.*, **21**, 767 (1953); J. A. Pople, *Trans. Faraday Soc.*, **49**, 1375 (1953).

12) J. Hinze and H. H. Jaffé, *J. Am. Chem. Soc.*, **84**, 540 (1962).

13) M. Wolfsberg and L. Helmholz, *J. Chem. Phys.*, **20**, 837 (1952).

14) N. Mataga and K. Nishimoto, *Z. Phys. Chem. N. F.*, **12**, 355 (1957).

15) P. O. Löwdin, *Chem. Phys.*, **18**, 365 (1950).

16) B. Bak, D. Christensen, L. Hansen-Nygaard, and J. Rastrup-Andersen, *J. Mol. Spectrosc.*, **7**, 58 (1961).

17) B. Bak, L. Hansen, and L. Rastrup-Andersen, *Discuss. Faraday*, **19**, 30 (1955).

18) R. M. Schaffrin and J. Trotter, *J. Chem. Soc., A*, **1970**, 1561.

19) A. Banerjee, *Acta Crystallogr., Sect. B*, **29**, 2070 (1973).

20) D. J. Shieh, S. H. Lin, and H. Eyring, *Proc. Natl. Acad. Sci. U.S.A.*, **69**, 2000 (1972); I. N. Douglas, R. Grinter, and A. J. Thomson, *Mol. Phys.*, **26**, 1257 (1973); S. D. Allen, M. G. Mason, O. Schnepp, and P. J. Stephens, *Chem. Phys. Lett.*, **30**, 140 (1975).

21) A. Kaito and M. Hatano, *Bull. Chem. Soc. Jpn.*, **53**, 1864 (1980).

Singlet-excitation Migration in Pure Liquid Methyl- and Ethylnaphthalenes

Takeshi Ohno* and Shunji Kato

College of General Education, Osaka University, Toyonaka, Osaka 560

(Received September 24, 1980)

The fluorescence quenching of solvent molecules and solute molecules was studied in the alkylnaphthalene solvents. The singlet-excited states of the solvent molecules were quenched by 1,4-bis(trichloromethyl)benzene with the rate parameter of 2.8×10^{10} mol^{-1} dm^3 s^{-1} at 45 °C. This rate parameter is twelve times as great as that of the solute, dibenz[*a,c*]anthracene, in the solvent, 1-methylnaphthalene. The diffusion constant of the excitation migration of the solvent molecule is calculated to be larger (0.35×10^{-4} cm^2 s^{-1} at 45 °C) than that (0.03×10^{-4} cm^2 s^{-1}) of the solute. The temperature coefficient (22 kJ/mol) of the excitation migration is too small to explain the migration mechanism on the hypothesis of the "successive association-dissociation reaction of excimer" proposed by Birks. The presence of a short-range exciton in the liquid is likely.

Since pure liquid aromatic hydrocarbons do not have such long-range periodicity as molecular crystals, it seems difficult to predict, from the point of view of exciton diffusion, the migration rate of the electronic-excitation energy in the molecular liquids,[1] while Lipsky and Burton suggested exciton diffusion in toluene.[2]

The solvent-solvent excitation migration in the liquid scintillator of toluene–2,5-diphenyloxazole has been attributed to multipole-multipole resonance interaction between the solvent molecules, which have been considered to be free from any kind of aggregation.[1]

However, since the singlet-excited states of many aromatic hydrocarbons form excimers which may be shallow traps and/or excitons with the shortest possible length, the role of the excimer in the excitation migration can not be neglected. Birks *et al.*[3] proposed that a sequence of the rapid association and dissociation of an excimer in the singlet-excited state brought about the solvent-solvent excitation migration. Though the excimer dissociation process (detrapping) should be the rate determing step of the excitation migration according to their mechanism, it has not yet been examined.

In this work, the singlet-excitation migration rates of several liquid naphthalenes are examined in the range from 5 to 75 °C. Two mechanisms of the excitation migration, exciton diffusion and the rapid association and dissociation of the excimer will be discussed.

Experimental

Materials. The 1-methylnaphthalene(1-MN, mp: −34 °C) was purified through a 30-cm column of Al_2O_3 followed by distillation using a Widmer column under reduced pressure. The 2-methylnaphthalene(2-MN, mp: 35.2 °C) was purified by two different methods. The purified sample(A) was obtained by three recystallizations from methanol and by subsequent simple distillation under reduced pressure. The other sample(B) was obtained by distillation using a 30-cm Widmer column in place of the simple distillation under reduced pressure. G. R. grade 1-ethylnaphthalene(1-EN, mp: −3.7 °C) and 2-ethylnaphthalene(2-EN, mp: −7.4 °C) were used without further purification.

The dibenz[*a,c*]anthracene(DBA) and pyrene were recrystallized three times from an ethanol solution, followed by sublimation. The 1,4-bis(trichloromethyl)benzene-(TCB), benzophenone, and CBr_4 were purified by two times recrystallizations from an ethanol solution, and *p*-phenylenediamine, from a benzene solution. After the CCl_4 had been refluxed with NaOH, washed with water, and dried by $CaCl_2$, it was distilled. G. R. grade diphenylamine was used without further purification.

Measurements. Quenching constant(K_{SV}): The intensities of the fluorescence were measured by using a Hitachi MPF-2A spectrofluorometer. In the measurement of the emission intensity from a sample of a high optical density such as neat liquids, a triangular cell was used so that we could see a small illuminated part of the sample cell. In order to exclude any error in the measurement, a slit was inserted between the cell and the condenser lens for emission. A N_2-substituted sample in the cell was set in a small thermostat (0—80 °C, ±0.5 °C).

The lifetime of the fluorescence was measured by means of laser excitation. One of the lasers was a compact, high-power N_2-laser with a Blumlein circuit (10 kV, pressure of N_2: 40 mmHg (1 mmHg=133.3 Pa), 2 mJ), which consists of two stainless steel electrodes (3 mmϕ) 20 mm apart, barium titanate capacitors (Taiyo Yuden, 750×14 pF, 25 kV), and a triggered spark gap. The other one was a compact, low-power N_2-laser (10 kV, 10 μJ) containg a coaxial cable as a capacitor.[4] The high-power laser was used for almost allthe samples. The dibenz[*a,c*]anthracene solution was excited by the dye laser (0.02 mol dm^{-3} 2,5-diphenyloxazole benzene solution, 368 nm). The fluorescence decay was recorded by using a Tektronix oscilloscope 475 and Fuji X-ray film or Kodak Recording Film 2475. As for 2-EN with the shortest life the low-power laser was used while a Tektronix sampling scope 661, and Yokogawa 3083 X-Y recorder were used for the detection.

Results and Discussion

Determination of the Molar Enthalpy of Excimer Formation. Each fluorescence spectrum from 280 K to 350 K of liquid naphthalene derivatives consists of a monomer band and an excimer band. At temperatures close to the melting point of the naphthalenes, the strong excimer emission with a peak at 400 nm is the most evident (see Fig. 1). As the temperature is raised, however, the monomer emission without a fine structure becomes stronger than the excimer emission. This situation is very similar to the spectral changes in 1-MN and 2-MN reported by Stevens and Dickinson.[5]

Because both the excimer-formation rate (k_{DM}[M]: 3.5×10^{11} s^{-1}) and the excimer-dissociation rate (k_{MD}: 10^8 s^{-1})[6] are more rapid than the decay rate (k_d: 1.8×10^7 s^{-1}) in the case of 1-MN, an equilibrium between the monomer and the excimer in the excited singlet state exists. The monomer-excimer equilibrium

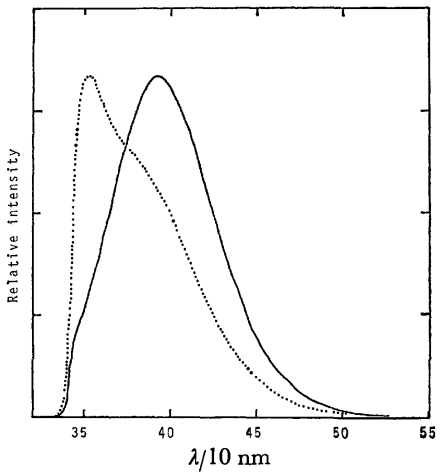

Fig. 1. Fluorescence spectra of liquid 1-MN on excitation at 316 nm.
Solid line: 12 °C, dotted line: 75 °C. The maximum intensity of fluorescence is normalized.

in the excited state is supported by the fact that the Stern-Volmer quenching constant (K_{SV}) obtained by using the excimer band is the same as that obtained by using the monomer band. Further, it is assumed that the intensity of the monomer band (or the excimer band) is proportional to the product of the excited-monomer (or the excimer) concentration and the radiative-rate parameter of the excited monomer (or the excimer), k_{FM} (or k_{FD}). From their dependence on the temperature, one can obtain the molar enthalpy of the excimer formation (ΔH) by using Eq. 1;

$$\ln\frac{I_{352}}{I_{440}} = \ln\frac{\alpha k_{FM}}{k_{FD}[M]} - \frac{\Delta S}{R} + \frac{\Delta H}{RT} \quad (1)$$

where I_{352} and I_{440} are the intensity of the monomer emission measured at 352 nm and that of the excimer measured at 440 nm respectively; α, the apparatus constant; [M], the concentration of the ground-state naphthalene, and ΔS, the molar entropy of the excimer formation. Plotting the left term of Eq. 1 against reciprocal of the temperature (see Fig. 2) gives a linear relation with the slope of $\Delta H/R$ in all cases; the values are shown in Table 1.

The values of ΔH for 1-MN and 2-MN seem similar to the reported values in the ethanol solution,[6] and the ΔH value for 1-EN is close to the value measured by Christophorou and Carter in the neat liquid,[7] though smaller values have been reported in a diluted heptane solution.[8]

Determination of Excitation-migration Coefficient. When the fluorescence of DBA or pyrene is quenched by an adequate quencher in liquid naphthalenes, the quenching-reaction-rate parameter is given by Eq. 2, according to Birks,[3] where N_0 is Avogadro's number; p, the quenching probability; R_{AQ}, the interaction distance, and D_A and D_Q, the diffusion coefficients of DBA (or pyrene) and the quencher respectively;

$$k_q = p4\times10^3 N_0(D_A+D_Q)R_{AQ}. \quad (2)$$

When the solvent fluorescence is quenched by the quencher, a term based on the excitation migration is added to Eq. 2, as Eq. 3 shows;

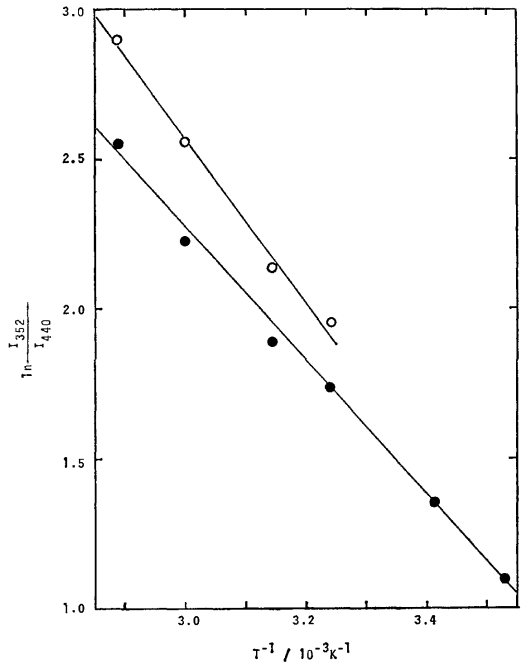

Fig. 2. Temperature dependence of the equilibrium between the excited species of the monomer and the dimer for 1-MN and 2-MN.
●: 1-MN, ○: 2-MN.

Table 1. The molar enthalpy of excimer formation

Fluorescer	Solvent	ΔH/kJ mol^{-1}	Reference
1-MN	Heptane	−29	5
	Ethanol	−20	6
	1-MN	−19	This work
2-MN	Heptane	−29	5
	Ethanol	−21	6
	2-MN	−19	This work
1-EN	1-EN	−26	7
	1-EN	−24	This work
2-EN	2-EN	−20	This work

$$k_q' = p4\times10^3 N_0(D_N+D_Q+\Lambda)R_{NQ} \quad (3)$$

where D_N and Λ are the diffusion coefficients of the solvent naphthalene and the excitation-migration coefficient of the solvent respectively.

Assuming (i) the values of R_{AQ} and R_{NQ} to be the same, and (ii) the values of D_A and D_N to be the same, one can obtain the value of Λ from the difference between the values of k_q and k_q' when an efficient quencher is chosen ($p=1$). The values of k_q and k_q' are calculated in the usual manner from the Stern-Volmer quenching constant and the fluorescence-decay-rate parameter(k_d).

A Stern-Volmer plot is linear in all cases using TCB as a quencher (see Fig. 3). The slopes (the quenching constants in Table 4) become a little steeper as the temperature is increased. While p-phenylenediamine quenches the fluorescence of 2-MN with the same efficiency as TCB, diphenylamine, CCl_4, and benzophenone are inefficient quenchers and the quenching constants are a little smaller (see Table 2).

The values of K_{SV} are sensitive to impurities in the

samples. The carefully purified samples, 2-MN(B), have larger K_{SV} values than 2-MN(A). In the case of 1-MN, the quenching constants obtained by the use of TCB as a quencher are dependent on the temperature in a way similar to those in the case of 2-MN (see Table 3). For 1-EN and 2-EN, TCB is used as a quencher; the measured quenching constants are listed in Tables 5 and 6.

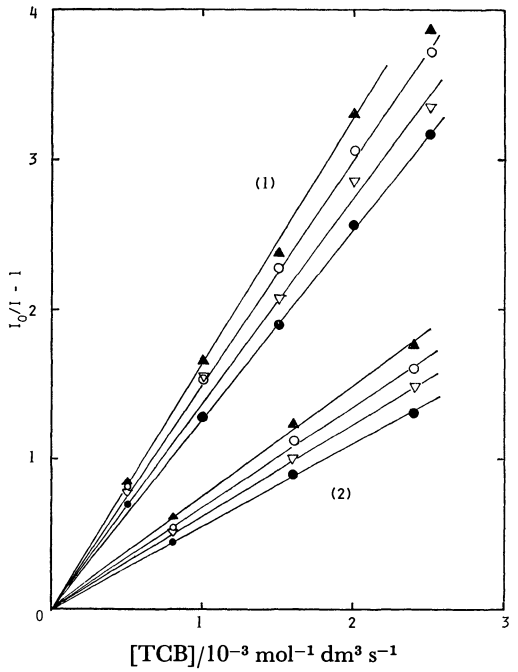

Fig. 3. Stern-Volmer plot for the fluorescence quenching of liquid 2-MN by TCB(1) and diphenylamine(2). ●: 36 °C, ▽: 45 °C, ○: 60 °C, and ▲: 70 °C.

In order to ascertain the product of the molecular diffusion constant (D_A+D_Q) and the interaction distance (R_{AQ}), the quenching constants for one solute in the several liquid naphthalenes are necessary at the same temperatures. DBA was used as a solute for 1-MN and 2-MN, and pyrene, for 1-EN and 2-EN. The values of K_{SV} are shown in Tables 3,4,5, and 6.

Determination of the Fluorescence-decay-rate Parameter. The sampling method and single-pulse method gave the same value of the first-order decay-rate parameter(k_d). As the temperature rises, k_d increases in all cases (see the fourth column of Tables 3,4,5, and 6). The value of k_d is sensitive to impurities in the sample, as is K_{SV}. The fluorescence lifetime of 2-MN(A) is 1/3 as long as that of 2-MN(B). All the k_d values measured are very close to or smaller than those previously reported: 1.7×10^7 s^{-1} for 1-MN at 20 °C, 5×10^7 s^{-1} for 2-MN at 40 °C,[9] and 2.5×10^7 s^{-1} for 1-EN at 20 °C.[8]

k_q, k_q', D, and A. Both quenching-rate parameters for the solute (k_q) and the naphthalenes (k_q') in the liquid naphthalenes are calculated from K_{SV} and k_d. The values shown in the fifth column of Tables 3—6 are based on the K_{SV}, using TCB as a quencher; which give the largest values of K_{SV}. The k_q values are in the order of 10^9 mol^{-1} dm^3 s^{-1} in all cases and are assumed to be diffusion-controlled. This is supported by the fact that they are similar to those (2×10^9 mol^{-1} dm^3 s^{-1}) for the triplet-excited state of DBA in liquid 1-MN,[10] which were obtained by using the most efficient quencher of ferrocene.[11]

Assuming $R_{AQ}=1$ nm and $p=1$ for the pair of TCB

Table 2. Quenching constants of fluorescence in neat methylnaphthalene using various quenchers (36 °C)

Fluorescer	Quencher	K_{SV}	$k_d/10^7$ s^{-1}	$k_q'/10^{10}$ mol^{-1} dm^3 s^{-1}
2-MN(A)	TCB	460	4.6	2.1
	CCl_4	370		1.8
2-MN(B)	TCB	1300	1.42	1.8
	Diphenylamine	560		0.77
	p-Phenylenediamine	1300		1.8
	Benzophenone	950		1.4

Table 3. Rate parameters and quenching constants in 1-MN

Fluorescer	T/°C	K_{SV}	$k_d/10^7$ s^{-1}	$k_q(k_q')/10^{10}$ mol^{-1} dm^3 s^{-1}	$D_A+D_Q/10^{-6}$ cm^2 s^{-1}	$A/10^{-6}$ cm^2 s^{-1}
1-MN	12	570	1.8	1.0		12
DBA		50	2.0	0.10	1.3	
1-MN	20	730	1.9	1.4		16
DBA		57	2.3	0.13	1.7	
1-MN	32	1000	2.1	2.1		24
DBA		75	2.3	0.17	2.2	
1-MN	45	1200	2.4	2.8		35
DBA		91	2.5	0.23	3.0	
1-MN	60	1400	3.0	4.1		49
DBA		110	2.7	0.29	3.8	
1-MN	75	1600	3.2	5.1		63
DBA		130	2.7	0.34	4.4	

Table 4. Rate parameters and quenching constants in 2-MN

Fluorescer	T / °C	K_{SV}	k_d / 10^7 s^{-1}	$k_q(k_q')$ / 10^{10} mol^{-1} dm^3 s^{-1}	D_A+D_Q / 10^{-6} cm^2 s^{-1}	Λ / 10^{-6} cm^2 s^{-1}
2-MN(A)		460	4.6	2.1		25
2-MN(B)	36	1300	1.4	1.8		21
DBA		73	2.7	0.19	2.6	
2-MN(A)		420	5.6	2.4		28
2-MN(B)	45	1400	1.7	2.3		28
DBA		84	2.9	0.24	3.2	
2-MN(A)		390	7.4	2.9		34
2-MN(B)	60	1500	2.1	3.1		37
DBA		100	3.0	0.31	4.0	
2-MN(A)		390	9.2	3.6		44
2-MN(B)	75	1600	2.4	3.8		47
DBA		100	2.9	0.29	3.9	

Table 5. Rate parameters and quenchching constants in 1-EN

Fluorescer	T / °C	K_{SV}	k_d / 10^7 s^{-1}	$k_q(k_q')$ / 10^{10} mol^{-1} dm^3 s^{-1}	D_A+D_Q / 10^{-6} cm^2 s^{-1}	Λ / 10^{-6} cm^2 s^{-1}
1-EN	15	520	1.8	0.93		10
Pyrene		260	0.52	0.14	1.8	
1-EN	25	580	2.0	1.2		13
Pyrene		320	0.53	0.17	2.2	
1-EN	40	680	2.5	1.7		19
Pyrene		390	0.57	0.22	2.9	
1-EN	55	750	2.9	2.2		25
Pyrene		480	0.62	0.30	3.9	
1-EN	70	820	3.2	2.6		30
Pyrene		590	0.64	0.38	5.0	

Table 6. Rate parameters and quenching constants in 2-EN

Fluorescer	T / °C	K_{SV}	k_d / 10^7 s^{-1}	$k_q(k_q')$ / 10^{10} mol^{-1} dm^3 s^{-1}	D_A+D_Q / 10^{-6} cm^2 s^{-1}	Λ / 10^{-6} cm^2 s^{-1}
2-EN	5	380	1.7	0.67		6.3
Pyrene		260	0.75	0.20	2.6	
2-EN	15	420	2.5	1.0		10
Pyrene		320	0.76	0.24	3.2	
2-EN	25	460	3.0	1.4		14
Pyrene		380	0.77	0.29	3.8	
2-EN	40	500	3.4	1.7		18
Pyrene		460	0.78	0.36	4.8	
2-EN	55	540	4.1	2.2		23
Pyrene		540	0.92	0.49	6.5	
2-EN	70	540	5.0	2.7		27
Pyrene		620	1.1	0.65	8.6	

and DBA at 45 °C, the values of D_A+D_Q are calculated, by using Eq. 1, to be 3×10^{-6} cm^2 s^{-1}. On the same assumption, the values of $D_N+D_Q+\Lambda$ are calculated to be 32×10^{-6} cm^2 s^{-1}. Therefore, it is concluded that Λ is 29×10^{-6} cm^2 s^{-1}, or about 19 times as great as the molecular diffusion constant in liquid 2-MN. This procedure also gives the Λ values in the other cases; they are shown in the last column of Tables 3—6. Though the better-purified sample, 2-MN(B), has a longer fluorescence lifetime than that of 2-MN(A), the Λ values are quite close to those of 2-MN(A). It can be expected that the calculated Λ values for the unpurified samples, 1-EN and 2-EN, will be close to the real values.

These present values of Λ are similar to those obtained in liquid benzene and alkylbenzenes, in which the molecular diffusion constants are of the same order as Λ,[3] so that a difference between the unknown diffusion constant of benzene in the singlet-excited state and that of some solute seems to result in a relatively larger error in the calculation of Λ. It is also noted that Λ is one-fifth as great as that (10^{-4} cm^2 s^{-1}) in the molecular crystal of naphthalene.[13] Eastman, Smutny, and Coppinger reported a little larger value (4.5×10^{10} mol^{-1} dm^3 s^{-1}) of the k_q' of 1-EN by using an aromatic quencher, such as sub-

stituted *p*-quinone, benzophenone, *p*-nitrophenol, and *p*-nitrosophenol.[12] However, it is very difficult to extract the contribution of the excitation migration from them because the Förster-type energy transfer between 1-EN and the quencher must increase the value of k'_q.

The Λ gradually increases with the temperature, as does D. Plotting $\log \Lambda$ against the reciprocal of the temperature, we obtain a curved line, as Figs. 4 and 5 show. Taking the best-fitting straight line through these points, an excitation-migration activation energy of about 17—22 kJ/mol is obtained.

Effect of Dilution on the Value of k'_q. The dilution of 1-MN with hydrogenated naphthalene (*cis*-decaline) makes the quenching reaction parameter smaller. Figure 6 shows the change in the rate parameter with the mole fraction of 1-MN at 20 °C. It should be noted that the rate-parameter increases in the very concentrated region, where some of the nearest neighbours are naphthalene itself. Because a collisional singlet-excitation transfer reaction is very efficient, the dilution effect suggests a collapse of the large molecular assembly responsible for excitation migration with dilution. This will be discussed further in the next section.

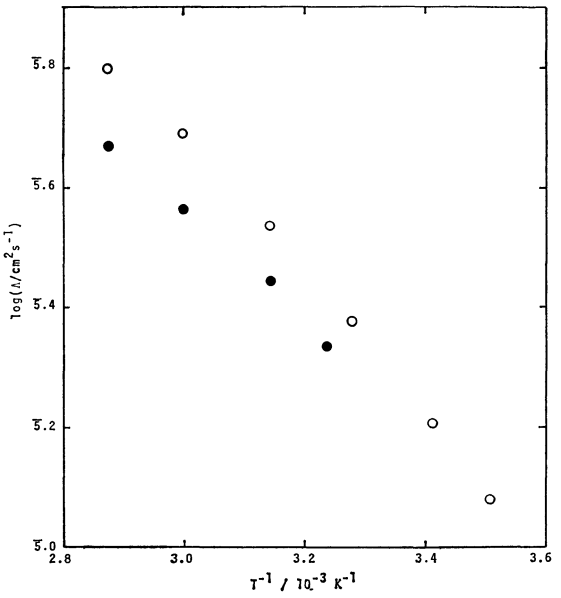

Fig. 4. Temperature dependence of the excitation migration in 1-MN and 2-MN.
○: 1-MN, ●: 2-MN.

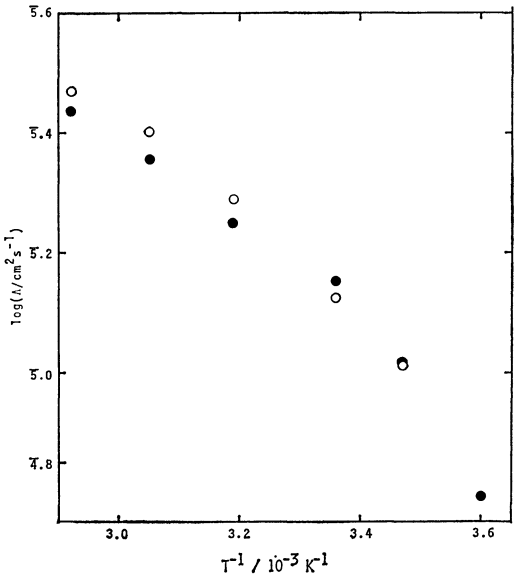

Fig. 5. Temperature dependence of the excitation migration in 1-EN and 2-EN.
○: 1-EN, ●: 2-EN.

Mechanism of Excitation Migration. With respect to the singlet-excitation migration in neat alkylbenzene, two mechanisms of excitation-migration have been proposed; the "association-dissociation reaction of an excimer"[3] and "exciton motion."[2] The "association-dissociation reaction of an excimer"—The formation of an excimer between the excited-singlet state of Molecule A and the neighbouring molecule, B, is followed by its dissociation, resulting in a 50% probability of Molecule B being in the monomer-excited state. The rapidty of the association-dissociation may create a large excitation-migration without any molecular displacement. In this case, Λ is described by Eq. 4[3], where β is the root-mean-square displacement of excitation, and K_e, the equilibrium constant of excimer formation:

$$\Lambda = \beta^2 \frac{k_{DM}[M]}{6(1+K_e[M])} \tag{4}$$

$$\approx \beta^2 \frac{k_{DM}}{6K_e} = (\beta^2/6)\exp(-\Delta E_{MD}/RT). \tag{5}$$

If the product of K_e and [M] is much larger than unity, Eq. 4 can be approximated to Eq. 5. Because K_e is 5.2—20.5 mol^{-1} dm^3 [6] and [M] is about 7 mol dm^{-3} for 1-MN and 2-MN, the value of Λ can be estimated by Eq. 5 and rewritten using the activation energy of the excimer-dissociation process (ΔE_{MD}).

"Exciton motion"—In neat liquid, there is a kind of singlet-exciton assumed whose length is shorter than that of the molecular crystal because (i) a periodicity in the radial and orientational distributions has been

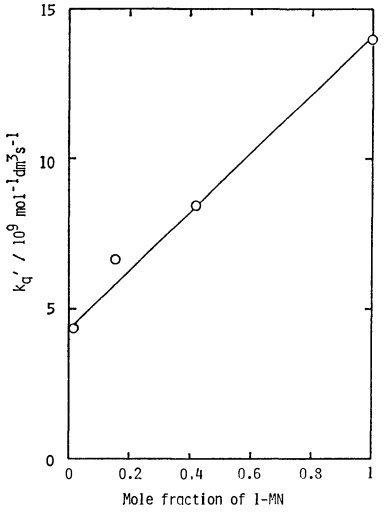

Fig. 6. Change of rate parameter for the fluorescence quenching of 1-MN diluted by *cis*-decaline at 20 °C. The quencher is TCB.

TABLE 7. ACTIVATION ENERGIES OF EXCITATION MIGRATION

Liquid	E_{ex} kJ mol^{-1}	ΔH kJ mol^{-1}	$\Delta E'_{MD}$ kJ mol^{-1}	$\Delta H'$ [a] kJ mol^{-1}
1-MN	22	−19	32	−20
2-MN	18	−19	33	−21
1-EN	17	−24	—	—
2-EN	16	−20	—	—

a) These values were obtained for the ethanol solution by B. K. Selinger (Ref. 6).

recognized for liquid benzene;[14,15] (ii) the absorption spectrum of liquid benzene has a crystal field K-band like that of crystal benzene;[15] and (iii) the band shifts of liquid benzene and 1-EN in the higher-energy region from those of the diluted solution have been explained in terms of excitonic interaction, as have those of the crystal sample.[16,17] Therefore, the excitation energy in neat liquid migrates through the small exciton, while the length of the exciton is shorter than that for the molecular crystal. Though the monomer-excited state is reproduced from a trap of the excimer with a certain temperature, the periodical structure of the liquid is destroyed by thermal motion, so that the excitation migration may not increase monotonically with the temperature. The migration constant of excitation is described by Eq. 6:

$$\Lambda = \Lambda_0(T) \exp\frac{-\Delta E_{MD}}{RT}, \quad (6)$$

where $\Lambda_0(T)$ is intrinsic to the exciton and is as dependent on the temperature as is the length of the exciton.

An experimentally determined value of the activation energy of the migration process is useful for the diagnosis of the migration mechanism. Since a curved line is drawn between log Λ and the reciprocal of the temperature, and since the activation energy gets a little smaller in the higher-temperature region, "exciton motion" is the more reasonable mechanism. It is based on the inference that the migration rate is dependent on both the detrapping and the intrisic exciton length, the latter of which gets smaller with a rise in the temperature. The values of the apparent activation energies are smaller than those of the excimer dissociation process ($\Delta E'_{MD}$) reported in the case of a diluted ethanol solution, as Table 7 shows. Even when taking account of the difference between ΔH in the pure liquid and $\Delta H'$ in the ethanol solution, ΔE_{MD} is considered to be approximately equal to $\Delta E'_{MD}-(\Delta H'-\Delta H)$, whose values are 31 kJ/mol in the cases of both 1-MN and 2-MN, higher than the observed values.

The smaller activation energy may be caused by a decrease in the intrinsic exciton length with a rise in the temperature. However, the collapse of such a liquid exciton at higher temperatures allows excitation transfer through the association-dissociation reaction mechanism at higher temperatures.

It seems that the dilution effect on excitation migration can be understood on the bases of the exciton mechanism. It is reasonable that the gradual increase in k'_q with the mole fraction of 1-MN comes from a concurrent increase in its exciton length. Alternatively, the "association-dissociation reaction of the excimer" mechanism predicts that the value of k'_q will be independent of the concentration of 1-MN for a concentrated solution (0.2 mol dm^{-3}) because of rapid excimer formation.

We wish to thank Dr. T. Okada for permission to use the low-power N_2-laser and the detection system.

References

1) R. Voltz, *Rad. Res. Rev.*, **1**, 301 (1968).
2) S. Lipsky and M. Burton, *J. Chem. Phys.*, **31**, 1221 (1959).
3) J. B. Birks and J. C. Conte, *Proc. Roy. Soc. London, Ser. A*, **303**, 85 (1968).
4) T. Okada, T. Fujita, and N. Mataga, *Z. Phys. Chem. N. F.* **101**, 57 (1976).
5) B. Stevens and T. Dickinson, *J. Chem. Soc.*, **1963**, 5492.
6) B. K. Selinger, *Aust. J. Chem.*, **19**, 825 (1966).
7) L. G. Christophorou and J. G. Carter, *Nature*, **209**, 678 (1966).
8) J. B. Aladekomo and J. B. Birks, *Proc. Roy. Soc. London, Ser. A*, **284** 551 (1965).
9) N. Mataga, M. Tomura, and H. Nishimura, *Mol. Phys.*, **9**, 367 (1965).
10) T. Ohno and S. Kato, unpublished work.
11) M. Kikuchi, K. Kikuchi, and H. Kokubun, *Bull. Chem. Soc. Jpn.*, **47**, 1331 (1974).
12) J. W. Eastman, E. J. Smutny, and G. M. Coppinger, *J. Chem. Phys.*, **53**, 4346 (1970).
13) H. C. Wolf, *Adv. Atom. Mol. Phys.*, **3**, 119 (1967).
14) J. Z. Fischer, "Statistical Theory of Liquids," The Univ. of Chicago Press, Chicago (1964).
15) A. H. Narten, *J. Chem. Phys.*, **48**, 1630 (1968).
16) T. Inagaki, *J. Chem. Phys.*, **57**, 2526 (1972).
17) R. A. MacRae, M. W. Williams, and E. T. Arakawa, *J. Chem. Phys.*, **61**, 861 (1974).

An *Ab Initio* Calculation of the Electronic Structure of the $[Co(CN_6)]^{3-}$ Ion

Mitsuru SANO, Yasuyo HATANO,† Hiroshi KASHIWAGI,†† and Hideo YAMATERA*

Department of Chemistry, Faculty of Science, Nagoya University, Chikusa-ku, Nagoya 464

† *Nagoya University Computation Center, Nagoya University, Chikusa-ku, Nagoya 464*

†† *Institute for Molecular Science, Myodaiji, Okazaki 444*

(Received August 14, 1980)

Ab initio LCAO MO SCF calculations were carried out on $[Co(CN)_6]^{3-}$. The character of the wave-functions was discussed in terms of the orbital-mixing rule. The radial distribution of electron density obtained from molecular orbital (MO) calculation was compared with that obtained from X-ray experiments. On the ionization from a metal d-orbital, a significant electronic relaxation was shown to occur, which makes Koopmans' theorem invalid. The calculated excitation energies without a configuration interaction showed a qualitative correspondence with the absorption spectrum.

The electronic structure of the hexacyanocobaltate (III) ion, $[Co(CN)_6]^{3-}$, is of interest from both experimental and theoretical points of view, because this ion is the simplest of the typical symmetrical complexes in which the back-donation of electrons from the metal $d\pi$ to the ligand $p\pi$ orbitals possibly takes place.[1] This complex has been the subject of extensive experimental studies in relation to the electronic structures in the ground and excited states; these studies have included studies of the absorption,[2] infrared (IR),[3,4] Raman,[5] photoelectron,[6,7] and NMR[8,9] spectra, and X-ray analysis.[10,11] A comprehensive review of the chemistry of cyano complexes has been published.[12]

Recently, a precise X-ray crystallographic study of hexamminecobalt(III) hexacyanocobaltate(III) has been made by Iwata and Saito,[13] who have shown the deformation of electron density distribution and calculated the electronic charge on the cobalt atom to be 26.8 ± 0.3 for the cyano complex. Previous theoretical calculations were done for the electronic state of this compound by Kida *et al.*[14] and by Alexander and Gray[2] using the Wolfsberg-Helmholz approach. The energy-level scheme for the octahedral cyanide complexes given by the latter authors have shown the following orbital energy sequence:

$$\sigma(CN^-) < \pi(CN^-) < \sigma(CN^-) < d\pi.$$

The cobalt charge was estimated to be $+0.18$ by Kida *et al.* and $+0.41$ by Alexander and Gray. The aim of the present work is to investigate the cobalt-ligand interaction, the mechanism of π back-donation, and the validity of the application of the Hartree-Fock method to transition-metal complexes. Results are reported for the ground, excited, and ionized states of $[Co(CN)_6]^{3-}$.

Computational Method

The present calculation is of the LCAO MO SCF type, using a basis set of Gaussian functions. The basis set for Co was chosen as follows. The primitive GTF (Gaussian-type function) set, [12s, 6p, 4d], which had been optimized for the ^4F state of the neutral Co atom,[15] was modified by replacing the two most diffuse s functions by tighter functions with the exponents of 0.26 and 0.10 and by adding two supplementary p functions with the same exponents. The resulting [12s, 8p, 4d] functions were contracted to [8s, 6p, 2d]. For C and N, [9s, 5p] sets[16] were contracted to [4s, 2p]. Thus, 348 GTF's were contracted to 158 GTO's (Gaussian-type orbitals). The ion was assumed to be octahedral, and the interatomic distances were taken as:[13]

$$Co\text{-}C = 1.894\,\text{Å}, \qquad C\text{-}N = 1.157\,\text{Å}$$

The calculations were carried out by using a program package called JAMOL2 written by Kashiwagi *et al.*[17] In order to make the integral calculations more tractable, an integral approximation scheme based on semi-orthogonalized orbitals[18,19] was utilized; the threshold value for the degree of overlap was set at 0.0007.

Open-shell calculations for the ionized and excited states have been performed in the restricted Hartree-Fock formalism as given by Roothaan.[20] The corresponding vector coupling coefficients for the various states were calculated according to the reference.[21] The electron-density map was prepared by using the program written by Sano and Miyoshi.[22]

Results and Discussion

The results for the orbital energies and populations of the ground state of the $[Co(CN)_6]^{3-}$ ion have been reported in previous papers.[23–25]

The Electron Density Associated with the Ground States of $[Co(CN)_6]^{3-}$ and CN^-. The charge distribution of the cyanide ion will first be discussed in order to give a basis for the discussion of the electronic structure of the complex. The cyanide ion is isoelectronic with N_2 and CO, and the molecular orbitals of CN^- can be expected to be similar to those of CO. The calculated wave-function contours for the valence shell of the CN^- ion are shown in Fig. 1.[26]

The CN^- 3σ MO consists of the nitrogen 2s and carbon 2s orbitals. The high amplitude in the region midway between the atoms is indicative of substantial σ bonding. In the 4σ MO, a node appears near the nitrogen nucleus; this shows that the nitrogen 2p orbital makes a significant contribution. This MO is derived from the nitrogen sp-hybrid orbital mixed with the predominantly 2s orbital of carbon, and it has approximately the character of the nitrogen lone-pair orbital. The 1π MO shows a higher density at the more electronegative nitrogen. The highest occupied MO (HOMO), 5σ, is strongly polarized towards carbon. This MO is mostly a carbon sp-

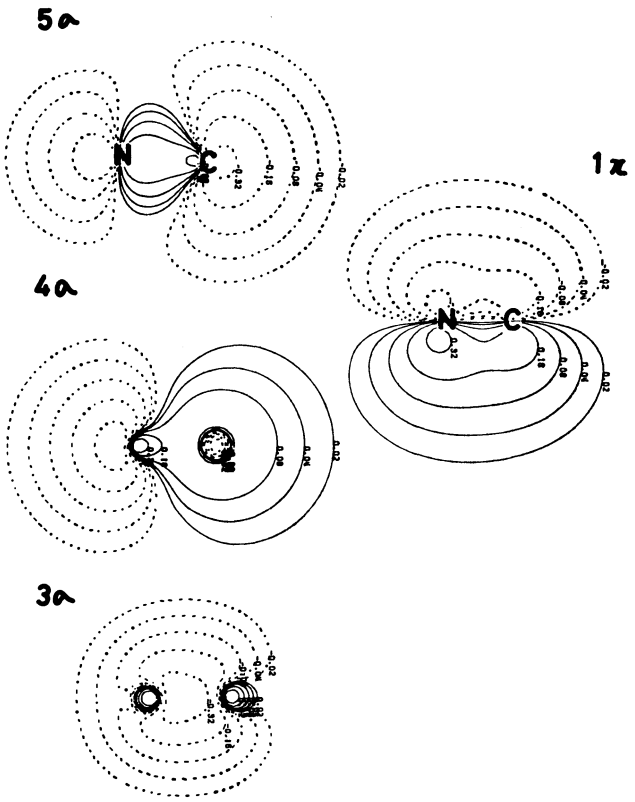

Fig. 1. The wave-function contours for valence shell MO's of the free CN^- ion. The first solid and dotted contours show ± 0.02, respectively, and neighboring contours differ by a factor of two.

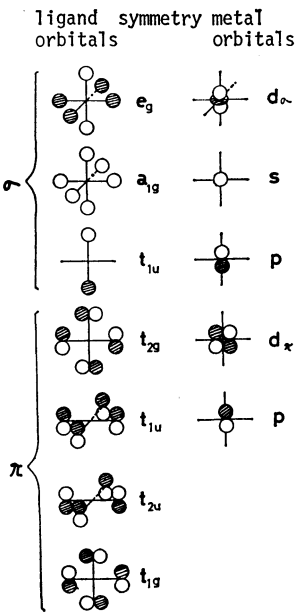

Fig. 2. Octahedral symmetry-adapted combinations of ligand orbitals (left), and the metal-atom orbitals with which they may interact (right). Only one orbital or orbital combination is shown from each degenerate set.

TABLE 1. THE ORBITAL MIXING RULE[27,28]

Case	Energy level	Perturbed |a'> orbital
(a)	$\varepsilon_b > \varepsilon_a$, $\varepsilon_c > \varepsilon_a$	$\|a> + \|b> + \|c>$
(b)	$\varepsilon_b < \varepsilon_a$, $\varepsilon_c > \varepsilon_a$	$\|a> - \|b> + \|c>$
(c)	$\varepsilon_b > \varepsilon_a$, $\varepsilon_c < \varepsilon_a$	$\|a> - \|b> - \|c>$

hybrid lone-pair orbital, slightly mixed with the nitrogen p orbital. These MO features explain why the cyanide ion is coordinated to the metal ion not at the nitrogen end, but at the carbon end. The 5σ MO, HOMO of the free CN^- ion, is primarily of the carbon lone-pair, and thus the theory predicts that the coordination of the cyanide ion to the cobalt ion will occur at the carbon end.

The symmetry-allowed interaction between $(CN^-)_6$ and Co^{3+} orbitals in $[Co(CN)_6]^{3-}$ is shown in Fig. 2. Selected wave-function contours for $[Co(CN)_6]^{3-}$ are shown in Fig. 3. In the formation of $[Co(CN)_6]^{3-}$, the σ-type metal 4s (a_{1g}), $3d\sigma$ (e_g), and $4p\sigma$ (t_{1u}) orbitals interact with the CN^- 4σ and 5σ orbitals, while the π-type metal $3d\pi$ (t_{2g}) and $4p\pi$ (t_{1u}) orbitals interact with the CN^- 1π and 2π orbitals. According to the orbital-mixing rule presented by Inagaki *et al.*,[27,28] the interaction of the |a> and |b> orbitals of one system with the |c> orbital of another system will result in a perturbed |a'> orbital consisting of the three orbitals with the signs given in Table 1.

This orbital-mixing rule will now be applied to the interactions between the $Co\sigma$ and the CN^- 4σ and 5σ orbitals and between the $Co\pi$ and the CN^- 1π and 2π orbitals. The σ interaction system will be considered first. The order of orbital energies in the σ system is $4\sigma < 5\sigma < Co\sigma$. The new orbital of the lowest energy resulting from the interaction of $Co\sigma$ with 4σ and 5σ is of the $4\sigma + 5\sigma + Co\sigma$ type (Case (a)), and the second lowest, of the $5\sigma - 4\sigma +$ $Co\sigma$ type (Case (b)). The $7a_{1g}$, $6t_{1u}$, and $4e_g$ MO's correspond to the MO's of the $4\sigma + 5\sigma + Co\sigma$ type. The amplitude of the carbon lone-pair increases through the in-phase mixing of 5σ into 4σ, while the amplitude decreases at the nitrogen atom. The ligand parts of $6t_{1u}$ and $4e_g$ are very similar to CN^- 4σ because of the small mixing of CN^- 5σ. In the $7a_{1g}$, however, CN^- 4σ is appreciably modified by CN^- 5σ. The $8a_{1g}$, $5e_g$ and $7t_{1u}$ MO's correspond to the $5\sigma - 4\sigma + Co\sigma$ type. This linear combination of 5σ and 4σ with the opposite sign means that the amplitudes are more or less compensated for at the carbon atom and intensified at the nitrogen atom. In the π interaction system, the energies of the orbitals of the t_{2g} symmetry are in the order: Co $d\pi$ < CN^- 1π < CN^- 2π. The 1π MO is bonding, and the 2π MO is antibonding, with respect to C–N. The $1t_{2g}$ MO consists mainly of Co $d\pi$. The $2t_{2g}$ MO of the $1\pi - 2\pi - d\pi$ type results from the 1π ligand orbital through mixing with Co $d\pi$ and 2π orbitals according to the orbital-mixing rule (Case (c) of Table 1). The $2t_{2g}$ MO in Fig. 3 has a node between the cobalt and carbon nuclei. This shows that the $2t_{2g}$ MO consists of a minus combination of $d\pi$ and the dominant CN^- 1π. According to the orbital-mixing rule, the combination of CN^- 2π with $d\pi$ in the $2t_{2g}$ MO is bonding; however, the extent of the mixing of CN^- 2π is small because of its high energy in com-

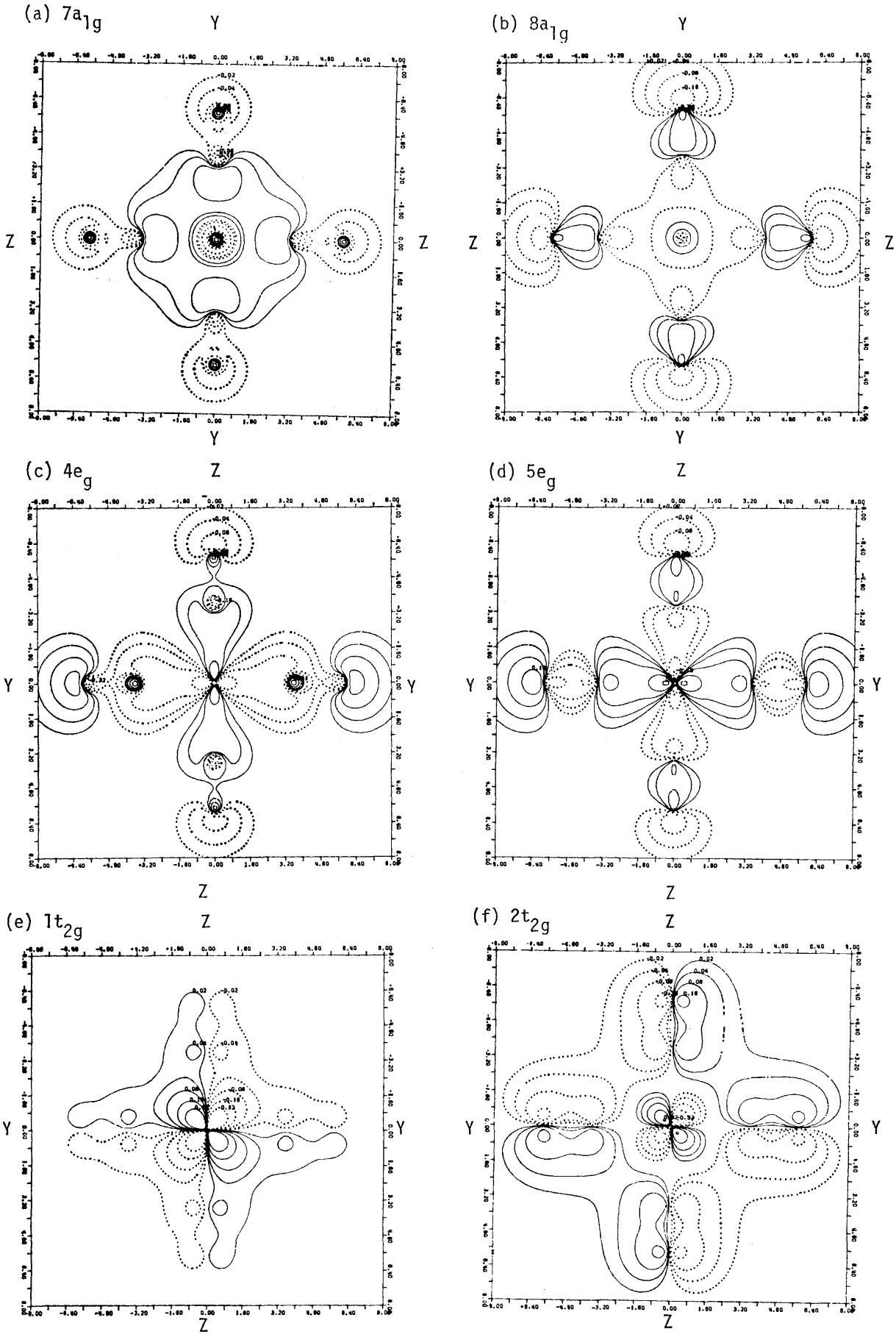
(a) $7a_{1g}$
Y
Z
Z
Y
(b) $8a_{1g}$
Y
Z
Z
Y
(c) $4e_g$
Z
Y
Y
Z
(d) $5e_g$
Z
Y
Y
Z
(e) $1t_{2g}$
Z
Y
Y
Z
(f) $2t_{2g}$
Z
Y
Y
Z

Fig. 3.

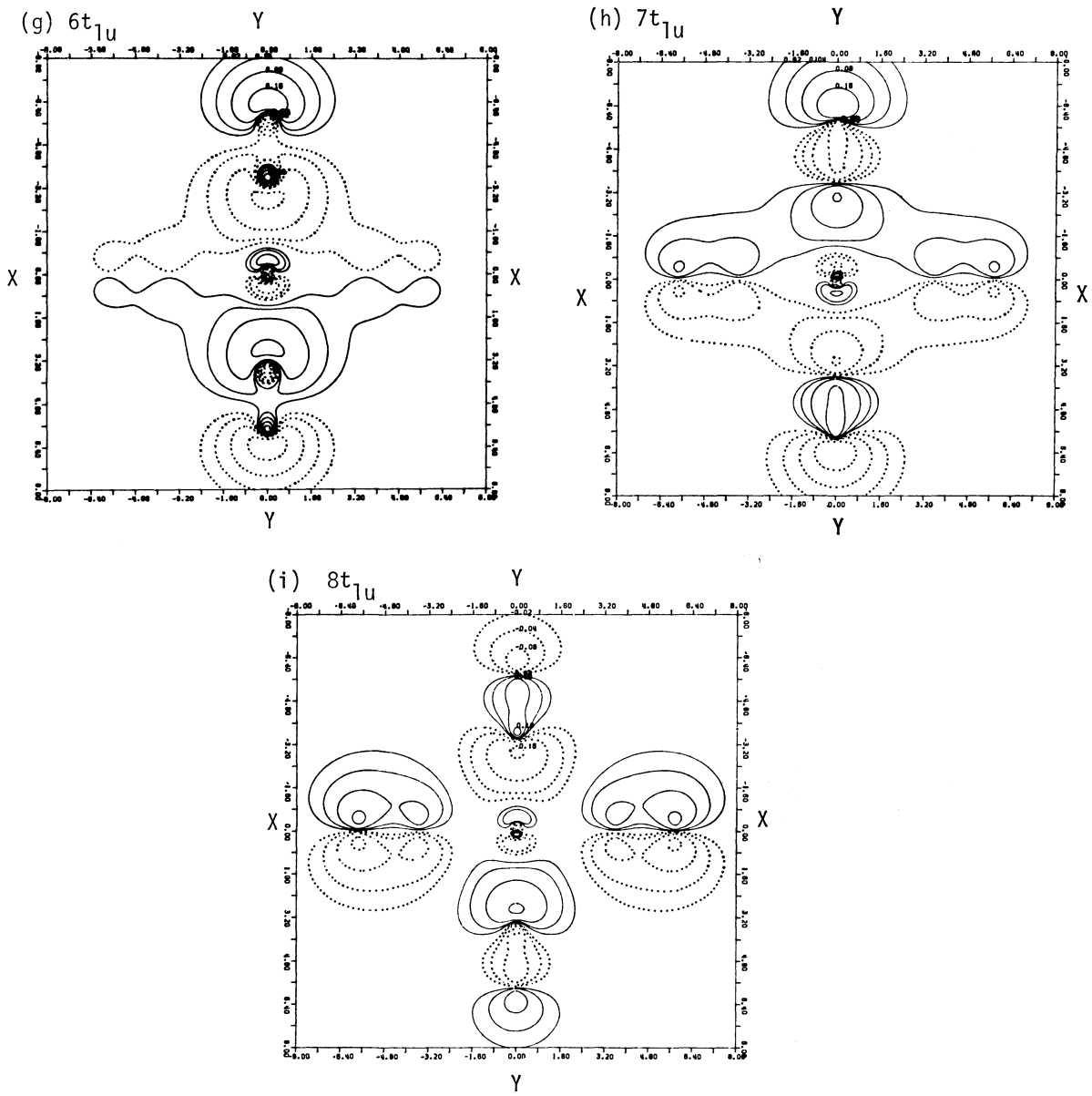

Fig. 3. Selected wave-function contours for valence shell MO's of $[Co(CN)_6]^{3-}$ on the plane containing Co and four CN^-. Each set of contours is drawn in a frame of 16 a.u.×16 a.u. (1 a.u.=0.529 Å= 52.9 pm). The Co atom is located at the center of the frame, and four C and four N atoms at the distances of 3.58 and 5.77 a.u. from the center, respectively. The first solid and dotted contours show ±0.02, respectively, and neighboring contours differ by a factor of two.

parison with CN^- 1π. This interaction scheme of cobalt cyanide is different from that of $d\pi$-π^* assumed by Alexander and Gray.[2] A small contribution of π back-donation still exist in $[Co(CN)_6]^{3-}$.

Figure 4 shows the map of the electron-density difference between $[Co(CN)_6]^{3-}$ and $Co^{3+}(d\pi^6)$ plus six free CN^- ions. The electron density for Co^{3+} was calculated like that of the t_{2g}^6 electron configuration in octahedral symmetry. The C–N bond length for the free CN^- was assumed to be the same as that in the complex. The CN^- ions were placed along three axes (x, y, z, −x, −y, −z) with the same geometry as in $[Co(CN)_6]^{3-}$. The solid and broken lines denote, respectively, an increase and a decrease in the electron density upon complexation. As can be seen from the increased electron density around the cobalt atom and the decreased density around the ligands, the electron flows from the ligands into cobalt. The positive region corresponding to the cobalt σ orbitals represents an increased electron density attributable to σ donation from the ligands. The decreased electron density in the $d\pi$ orbital indicates π back-donation. The increase in the cobalt charge accompanied by σ donation is larger than the decrease accompanied by π back-donation; thus, the positive charge of the cobalt atom is decreased. The orbital populations ($3d\sigma$, 1.040; 4s, 0.242; 4p, 0.667; and $3d\pi$, 5.885) obtained from the Mulliken population analysis of the semi-double-zeta basis set are consistent with the map. The electron density in the cyanide ligand decreases in the vicinity of the carbon nucleus, increases in the outer region of the carbon atom, and

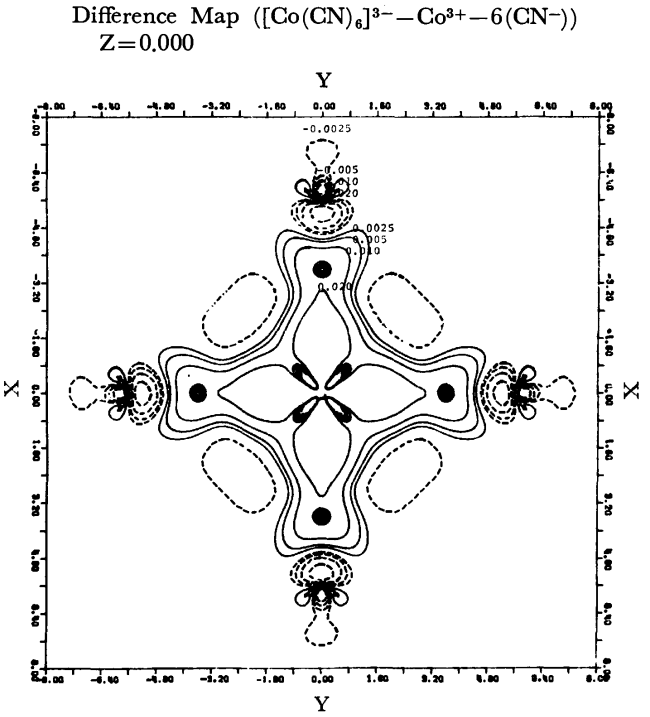

Fig. 4. The electron density difference between $[Co(CN)_6]^{3-}$ and Co^{3+} (with $d\pi^6$ configuration) plus six free CN^- ions. The first solid and dotted contours show ± 0.0025 e(a.u.)$^{-3}$, respectively, and neighboring contours differ by a factor of two.

decreases around the nitrogen nucleus. This shows that the cyanide ion is polarized by the positive charge of cobalt and that, in the carbon atom, the 2s population is decreased and the 2p population is increased. In effect, the nitrogen atom donates an electron density to the cobalt atom through the carbon atom; only slight π back-donation takes place from cobalt to nitrogen.

Comparison with X-Ray Results. In this section, the results of our calculation will be compared with those of the precise X-ray crystallographic study performed by Iwata and Saito,[13] who obtained 26.8 ± 0.3 e as the positive charge on the cobalt atom by directly integrating the electron density of the cobalt atom. They also showed the asphericity of the distribution of Co 3d electrons by difference Fourier synthesis.

The results of the present calculation are shown in Fig. 5, in which the radial distribution of the electron density around the central cobalt nucleus and the integrated number of electrons are plotted against the radius of the sphere, r. It is shown that the calculated radial electron density has a minimum value at 0.95 Å from the cobalt nucleus and that the number of electrons contained in a sphere of the 0.95 Å radius is 24.7. Both of these values are considerably lower than the corresponding experimental values of 1.22 Å and 26.8 ± 0.3. However, the integration of the electron density up to 1.22 Å gives 26.7 electrons, in good agreement with the experimental results. A fine structure which has not been reported by Iwata and Saito is observed: a minimum at 0.3 Å and a

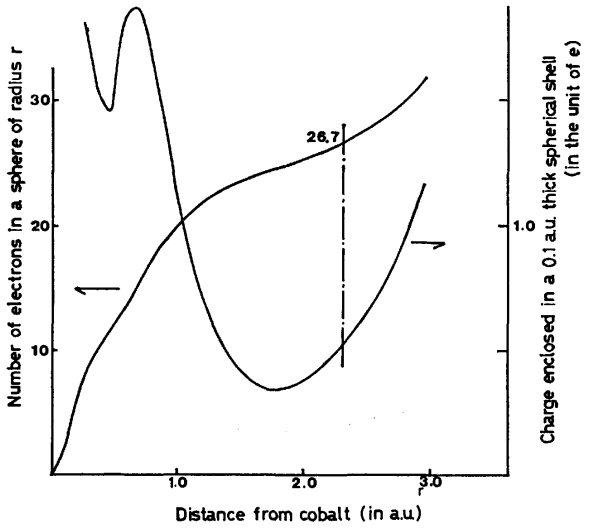

Fig. 5. The radial distribution and integrated number of electrons around the central cobalt atom.

maximum at 0.4 Å from the cobalt nucleus. Thermal vibrations in the experimental system may blur the fine structure and make the effective radii of orbitals greater than those for the frozen system assumed in the calculation.

Orbital Energies and Ionization Potentials. The sequence of orbital energies for the $[Co(CN)_6]^{3-}$ ion has already been reported.[23] The important finding was that the ordering:

$$\sigma(CN^-) < 3d\pi < \sigma(CN^-) < \pi(CN^-)$$

is different from that:

$$\sigma(CN^-) < \pi(CN^-) < 3d\pi$$

which has usually been assumed.

According to Koopmans' theorem,[29] the ionization potential (I.P.) associated with the removal of one electron from a given orbital of a closed-shell system is equal to the corresponding orbital energy with the sign inverted. Veillard and Demuynck[30] reported that Koopmans' theorem is not always valid and that it is not possible to rely on Koopmans' theorem to establish the spectral sequence. The most consistent way to compute ionization potentials is to calculate and compare two total energies at the same level of approximation for the molecule with N electrons and the ion with $N-1$ electrons. This is called the ΔSCF method. The ΔSCF calculation has been carried out in the following way. The energies of the electronic state with a hole in a given orbital and of the ground state are independently calculated in the SCF procedure; then the difference between them gives the ionization potential. The calculation has been carried out for the electronic states resulting from the removal of an electron from the orbitals, $8a_{1g}$, $5e_g$, $1t_{1g}$, $1t_{2g}$, $8t_{1u}$, and $1t_{2u}$. The geometry in these electronic states has been kept the same as that of the N-electron state; hence, the computed ionization energies may be compared with the vertical I.P.

The ΔSCF results are given in Table 2, together with the orbital energies in the ground state, $^1A_{1g}$.

TABLE 2. COMPUTED IONIZATION ENERGIES OF $[Co(CN)_6]^{3-}$

Species	Orbital from which an electron is removed	State	Energy[a]	Computed I.P.[b]	Koopmans' I. P.
$[Co(CN)_6]^{3-}$		$^1A_{1g}$	−1934.402		
$[Co(CN)_6]^{2-}$	$8t_{1u}$	$^2T_{1u}$	−1934.379	0.023	0.029
	$1t_{1g}$	$^2T_{1g}$	−1934.378	0.024	0.035
	$1t_{2u}$	$^2T_{2u}$	−1934.361	0.041	0.052
	$5e_g$	^2E_g	−1934.336	0.066	0.103
	$8a_{1g}$	$^2A_{1g}$	−1934.280	0.122	0.133
	$1t_{2g}$	$^2T_{2g}$	−1934.472	−0.070	0.250

a) Values in a.u. b) I.P. computed as the difference in the energy values for the ionized and ground states. (For the negative value, see the text and Ref. 31.)

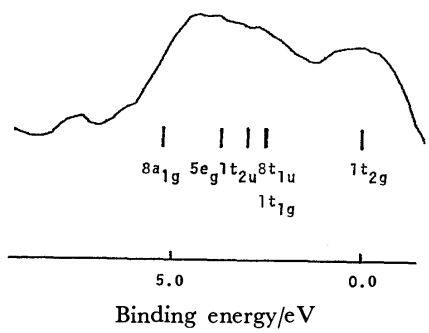

Fig. 6. Valence shell XPS and ΔSCF orbital energies.

The ΔSCF orbital energies decreased in the order:

$$3d\pi(1t_{2g}) > \pi(CN^-) > \sigma(CN^-)$$

which is similar to those in previous reports.[2,14] The computed I.P. corresponding to the removal of one electron from the $1t_{2g}(d\pi)$ orbital is negative; that is, the $[Co(CN)_6]^{2-}$ ion in its $^2T_{2g}$ state is shown to be more stable than the $[Co(CN)_6]^{3-}$ ion in its ground state, $^1A_{1g}$. However, $[Co(CN)_6]^{3-}$ is stable in actual systems, since the trinegative ion is stabilized to a greater extent than the dinegative ions by the electrostatic interaction with surrounding cations.[31] The experimental and calculated ionization potentials are compared in Fig. 6, in which the energy of the $d\pi$ orbital is taken as the reference in the comparison of the calculated I.P. with the X-ray photoelectron spectrum. The computed values show a good correspondence with the spectrum. This may support a previously proposed assignment for the valence-level peaks of XPS.[6,7] Koopmans' theorem may be valid when the electronic relaxation upon ionization and the change in correlation energy between the initial and the ionized states are sufficiently small to be ignored. The following discussion will attempt to clarify the importance of the electronic relaxation upon the ionization of a d-orbital electron. Figure 7 shows a map of the electron-density difference between the $8a_{1g}$ (located dominantly in the ligands) hole state and the $^1A_{1g}$ ground state, while Fig. 8 is a similar difference map for the $1t_{2g}$ (dominantly metal $d\pi$) hole state and the ground state. In these maps, the solid and broken lines denote, respectively, decreased and increased electron density upon ionization. The density map of $8a_{1g}$ MO is shown in Fig. 9; it resembles the difference map for the $8a_{1g}$ hole state (Fig. 7).

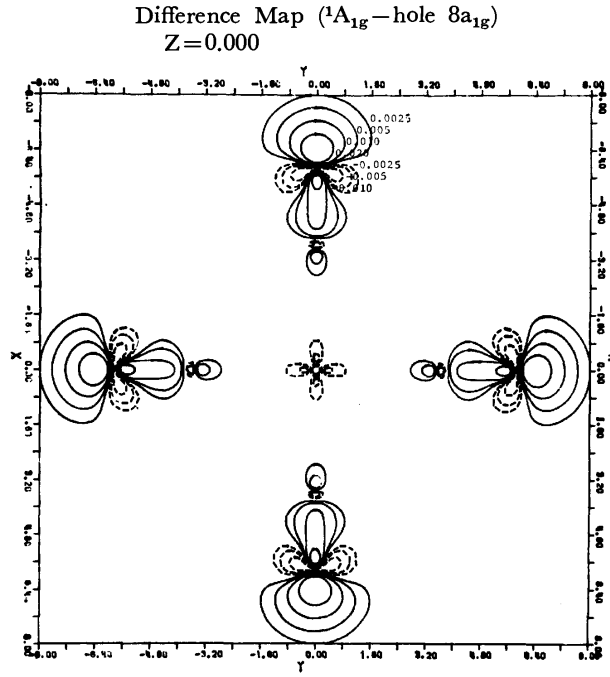

Fig. 7. The electron density difference between the $^1A_{1g}$ ground state and the $8a_{1g}$ hole state. The first contours show ± 0.0025 e(a.u.)$^{-3}$, neighboring contours differing by a factor of two. The positive and negative values represented by the solid and dotted curves correspond to decrease and increase in electron density upon the ionization, respectively.

This means that ionization from the $8a_{1g}$ orbital is accompanied by only a slight relaxation. Thus, Koopmans' theorem is valid for $8a_{1g}$ MO, which is essentially a ligand orbital. The map of the $1t_{2g}$ MO function (Fig. 3-e) is significantly different from the map of the difference between $^1A_{1g}$ and $^2T_{2g}$ states (Fig. 8). The latter shows that a decrease in $3d\pi$ electron density is accompanied by an increase in the $3d\sigma$ density, indicating an extensive relaxation upon ionization. The situation is more clearly demonstrated by Table 3, which shows the orbital population differences between the ground and ionized states on the semi-double-zeta basis set. The positive value shows an increase, and the negative value, a decrease, in the electron population caused by ionization. The Mulliken orbital populations for $8a_{1g}$ and $1t_{2g}$ are also given for the sake of comparison. It should be

TABLE 3. CHANGE IN ORBITAL POPULATION UPON IONIZATION

		$^2A_{1g}-{}^1A_{1g}$ Population change	($8a_{1g}$ MO Population)	$^2T_{2g}-{}^1A_{1g}$ Population change	($1t_{2g}$ MO Population)
Cobalt	3dσ	0.014		0.705	
	3dπ	0.001		−0.920	(0.894)
	4s	−0.020	(0.020)	0.056	
	4p	0.005		0.153	
Atomic charge		0.000		0.007	
Carbon	2s	−0.116	(0.050)	−0.646	
	2pσ	−0.220	(0.127)	−0.340	
	2pπ	−0.074		0.817	(0.092)
Atomic charge		−0.410		−0.169	
Nitrogen	2s	0.028	(0.231)	0.298	
	2pσ	−0.676	(0.572)	−0.217	
	2pπ	0.058		−0.919	(0.014)
Atomic charge		−0.590		−0.838	

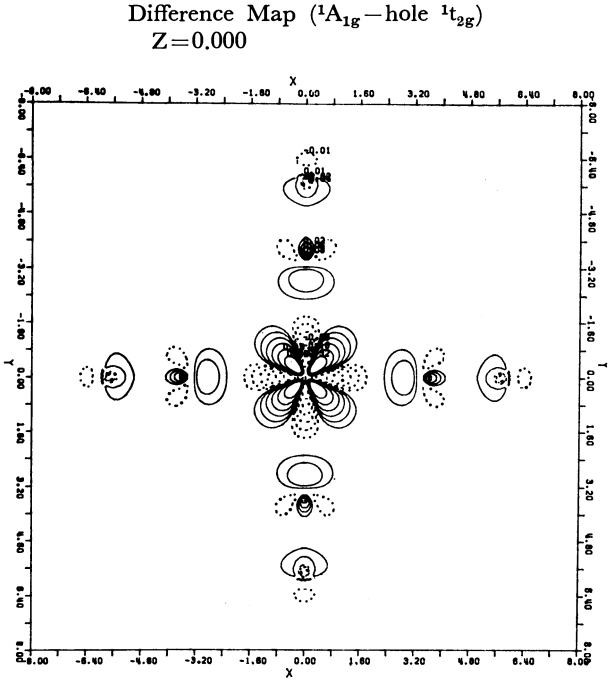

Fig. 8. The electron density difference between the $^1A_{1g}$ ground state and the $1t_{2g}$ hole state. The first contours show ±0.01 e(a.u.)$^{-3}$, neighboring contours differing by a factor of two. See also the caption to Fig. 7.

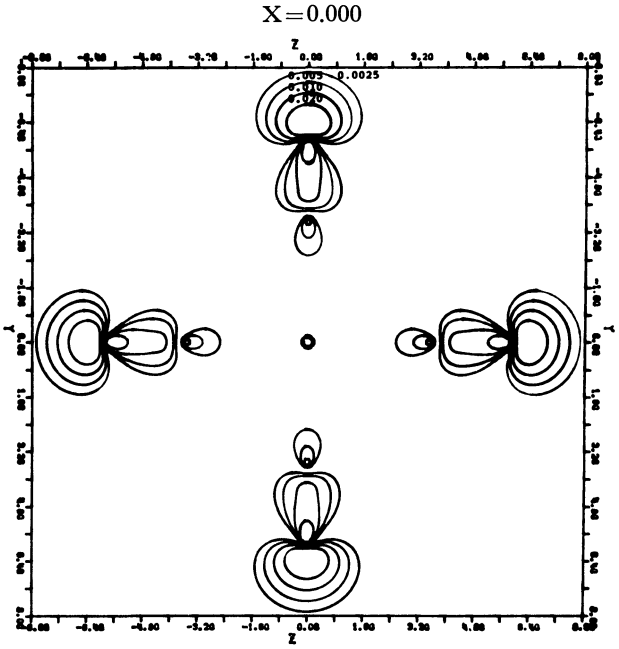

Fig. 9. The electron density map for $8a_{1g}$ MO. The first contour shows 0.0025 e(a.u.)$^{-3}$, neighboring contours differing by a factor of two.

noted that the Co atomic charge is scarcely changed by $8a_{1g}$ ionization or even by the ionization of the $1t_{2g}$ electron, which is dominantly the Co 3dπ electron. The $1t_{2g}$ ionization in effect removes an electron from the nitrogen atoms, not from the cobalt atom. This orbital relaxation explains why the low-lying $1t_{2g}$ electron is most easily ionized and why Koopmans' theorem becomes invalid.

The Excited States of the d-d Transition. In this section we will present some results relative to the excited states resulting from d-d transitions. As found in many other studies of transition metal complexes,[30,32] the excitation energy is not merely the difference between the energies of the occupied and virtual orbitals in the ground state. A rigorous way to calculate the transition energy is to achieve separately energy minimization for the ground and excited states and to equate the difference in their energies with the transition energy, E_{ij}:

$$E_{ij} = E_j - E_i,$$

where the subscripts i and j refer to the ground and excited states respectively. Restricted Hartree-Fock-type calculations have been performed on the two lowest triplet and the two lowest singlet excited states derived from d-d transitions, as is shown in Table 4. All the calculations were performed on the full octahedral space group. The ordering of the excited levels is in good agreement with that predicted by ligand-field theory with empirical parameters.[33] However,

TABLE 4. TOTAL ENERGIES AND RELATIVE ENERGIES OF VARIOUS *d*-STATES

State	Configration	Total energy/a.u.	Relative energy/eV
$^1A_{1g}$	t_{2g}^6	−1934.4016	0.0
$^3T_{1g}$	$t_{2g}^5e_g^1$	−1934.3325	1.88
$^3T_{2g}$	$t_{2g}^5e_g^1$	−1934.2928	2.96
$^1T_{1g}$	$t_{2g}^5e_g^1$	−1934.2745	3.46 (3.97)[a]
$^1T_{2g}$	$t_{2g}^5e_g^1$	−1934.2478	4.19 (4.77)[a]

a) In the parentheses the experimental values are shown.

the energies calculated for the $^1T_{1g}$ and $^1T_{2g}$ states are smaller than the spectroscopic data[2] by about 0.5 eV. Although the Hartree-Foock calculations without configuration interactions gave a qualitative correspondence with the spectrum, a more elaborate treatment is necessary for a quantitative agreement.

Conclusions

The electronic structure of the $[Co(CN)_6]^{3-}$ ion has been investigated by the LCAO MO SCF method, using a double-zeta basis set of Gaussian orbitals. The following results were obtained;

(1) The interaction of cobalt and cyanide ions can be satisfactorily explained in terms of the orbital-mixing rule.

(2) The σ donation from cyanide to cobalt is the dominant interaction, while the π back-donation is weak in $[Co(CN)_6]^{3-}$.

(3) Koopmans' theorem holds approximately for the ligand orbitals, but not for the metal 3d orbitals.

(4) An extensive electronic relaxation occurs during the ionization from a metal d orbital.

(5) The calculated value for the number of electrons around the cobalt atom is in good agreement with the experimental values.

(6) The d-d transition energies obtained by the Hartree-Fock calculation show a qualitative correspondence with the spectrum.

The work was partly supported by the Joint Studies Program (1979—1980) of the Institute for Molecular Science. The computations reported in this paper have been carried out on FACOM 230-75 computers of the Nagoya University Computation Center and the Hokkaido University Computing Center, while the calculation of the electron-density map has been carried out on the HITAC M-180 computer of the Institute for Molecular Science.

References

1) F. A. Cotton and G. Wilkinson, "Advanced Inorganic Chemistry," 3rd ed, John Wiley & Sons, New York (1972), p. 605.

2) J. J. Alexander and H. B. Gray, *J. Am. Chem. Soc.*, **90**, 4260 (1968).

3) K. Nakamoto, "Infrared and Raman Spectra of Inorganic and Coordination Compounds," 3rd ed, John Wiley & Sons, New York (1978).

4) L. H. Jones and B. I. Swanson, *Acc. Chem. Res.*, **9**, 128 (1976).

5) W. P. Griffith and G. T. Turner, *J. Chem. Soc.*, **1970**, 858.

6) A. Calabrese and R. G. Hayes, *J. Am. Chem. Soc.*, **96**, 5054 (1974).

7) N. G. Vannerberg, *Chem. Scripta*, **9**, 122 (1976).

8) M. Hirota, Y. Koike, H. Ishizuka, A. Yamasaki, and S. Fujiwara, *Chem. Lett.*, **1973**, 853.

9) J. J. Pesek and W. R. Mason, *Inorg. Chem.*, **18**, 924 (1979).

10) R. R. Ryan and B. I. Swanson, *Inorg. Chem.*, **13**, 1681 (1974).

11) S. Jagner, *Acta Chem. Scand.*, **A29**, 255 (1975).

12) A. G. Sharpe, "The Chemistry of Cyano Complexes of the Transition Metals," Academic Press, London (1976).

13) M. Iwata and Y. Saito, *Acta Crystallogr., Sect. B*, **29**, 822 (1973).

14) S. Kida, J. Fujita, K. Nakamoto, and R. Tsuchida, *Bull. Chem. Soc. Jpn.*, **31**, 79 (1958).

15) B. Roos, A. Veillard, and G. Vinot, *Theoret. Chim. Acta*, **20**, 1 (1971).

16) T. H. Dunning, Jr., *J. Chem. Phys.*, **53**, 2823 (1970).

17) H. Kashiwagi, T. Takada, E. Miyoshi, and S. Obara, "Program JAMOL2," Program Library, Hokkaido University Computing Center.

18) H. Kashiwagi, *Int. J. Quantum Chem.*, **10**, 135 (1976).

19) H. Kashiwagi and F. Sasaki, *Int. J. Quantum Chem.*, **S7**, 545 (1973).

20) C. C. J. Roothaan, *Rev. Mod. Phys.*, **32**, 179 (1960).

21) H. Kamimura, S. Sugano, and Y. Tanabe, "Ligand Field Theory and Its Applications," 4th ed, Shokabo, Tokyo (1975).

22) M. Sano and E. Miyoshi, Program Library, Institute for Molecular Science Computing Center.

23) M. Sano, Y. Hatano, and H. Yamatera, *Chem. Phys. Lett.*, **60**, 257 (1979).

24) M. Sano, Y. Hatano, and H. Yamatera, *Chem. Lett.*, **1979**, 789.

25) Reference may also be made to a paper to be published in *Bull. Chem. Soc. Jpn.*, **54** (M. Sano, H. Adachi, and H. Yamatera) in which the results of discrete variational Xα calculations are described on $[Co(CN)_6]^{3-}$ and other hexacyano complexes, together with the free cyanide ion.

26) Wave-function contours are here preferred to the numerical orbital populations given in Ref. 23, since the latter may be artifacts to some extent (Ref. 24). See also Ref. 25.

27) S. Inagaki and K. Fukui, *Chem. Lett.*, **1974**, 509.

28) S. Inagaki, H. Fujimoto, and K. Fukui, *J. Am. Chem. Soc.*, **98**, 4054 (1976).

29) T. Koopmans, *Physica*, **1**, 104 (1933).

30) A. Veillard and J. Demuynck, "Application of Electronic Structure Theory," ed by H. F. Schaefer, III, Plenum Press, New York (1977), p. 187.

31) The situation is analogous to the case of the oxide ion; the O^{2-} ion is stable in the crystals of metal oxides in spite of the fact that reaction, $O^{2-} \rightarrow O^- + e$, is exothermic, or that the ionization potential of O^{2-} is negative.

32) H. Johansen and U. Wahlgren, *Mol. Phys.*, **33**, 651 (1977).

33) C. K. Jørgensen, *Adv. Chem. Phys.*, **5**, 33 (1963).

  Bull. Chem. Soc. Jpn., 54, 1531—1537 (1981)

The CD Spectra of Carbonato Complexes of the $[Co(CO_3)(O,O)(N)_2]^-$ and $[Co(CO_3)(N)_4]^+$ Types and Related Diaqua Complexes[1)]

Kenshi Tsuji, Shuhei Fujinami, and Muraji Shibata*

Department of Chemistry, Faculty of Science, Kanazawa University, Kanazawa 920

(Received August 16, 1980)

Five carbonato complexes, $[Co(CO_3)(ox)(tn)]^-$, *cis*-$[Co(CO_3)(ox)(py)_2]^-$, *cis*·*cis*-$[Co(CO_3)(NH_3)_2(py)_2]^+$, *cis*-$[Co(CO_3)(en)(py)_2]^+$, *cis*-$[Co(CO_3)(NH_3)_2(bpy)]^+$, and two related complexes, *cis*-$[Co(ox)(NH_3)_2(en)]^+$ and *cis*-$[Co(mal)(NH_3)_2(en)]^+$, have been prepared and resolved. The solution CD spectra of these resolved complexes and those of diaqua complexes derived from the carbonato complexes have been measured. The CD spectral comparison in the first absorption band (T_{1g}-band) region has suggested a relation in the sign of the Cotton peak between each of the carbonato complexes and the corresponding diaqua complex. Based on this relation, the assignments of the absolute configurations for the present complexes have been established.

It is known[2,3)] that the CD spectra of $(-)_{589}[Co(CO_3)(ox)(en)]^-$ and $(+)_{546}[Co(CO_3)(en)_2]^+$ exhibit a (+) Cotton peak in the first absorption band (T_{1g}-band) region, while the spectra for $(+)_{589}[Co(ox)(en)(H_2O)_2]^+$ and $(+)_{546}[Co(en)_2(H_2O)_2]^{3+}$, which are derived from the above carbonato complexes by acid-hydrolysis, show two peaks, (−) and (+), in the T_{1g}-band region. The absolute configurations of these carbonato complexes have been assigned to *Λ* based on a suggestion[2,3)] that the observed (+) peak is due to the $A_{1g}\rightarrow E_g$ (D_{4h}) transition component, while the absolute configurations of the corresponding diaqua complexes are also assigned to *Λ* based on the fact that acid-hydrolysis proceeds with retention of configuration. However, the (−) peak for $(+)_{589}[Co(ox)(en)(H_2O)_2]^+$ with CoN_2O_4 chromophore and the (+) peak for $(+)_{546}[Co(en)_2(H_2O)_2]^{3+}$ with CoN_4O_2 chromophore seem to be assignable to the $A_{1g}\rightarrow E_g$ transition component, when the ligand-field strengths of N and O are considered. In comparison of the CD signs due to the $A_{1g}\rightarrow E_g$ transition component, the sign of the $(-)_{589}$ carbonato complex is opposite to that of the $(+)_{589}$ diaqua complex, while the sign of the $(+)_{546}$ carbonato complex is the same as that of the $(+)_{546}$ diaqua complex. These different results come from the above-mentioned assignments of Cotton peaks, suggesting that the assignments are inconsistent.

In this work, the preparation and resolution of some new complexes of the $[Co(CO_3)(O,O)(N)_2]^-$ and $[Co(CO_3)(N)_4]^+$ types have been carried out. Optically active diaqua complexes have been also derived from the resolved carbonato complexes by acid-hydrolysis. In addition, this work has been extended to derive optically active oxalato complexes from the resolved carbonato complexes by a substitution reaction. The CD spectra of these active complexes have been measured and compared.

Experimental

Synthesis and Resolution. *a)* cis-*Diamminecarbonatoethylenediaminecobalt(III) Chloride Monohydrate*, cis-$[Co(CO_3)(NH_3)_2(en)]Cl\cdot H_2O$: This complex had been prepared by Bailar and Peppard,[4)] but we found another convenient method: to a solution of *cis*-$K[Co(CO_3)_2(en)]\cdot H_2O$ (35 g, 0.1 mol, in 150 cm³ H_2O) were added concd aqueous ammonia (14 cm³, 0.2 mol) and ammonium chloride (5.35 g, 0.1 mol); the mixture was then stirred at 50 °C until a red solution was obtained. The resulting solution, once filtered, was charged on a column containing Dowex 50W-X8 resin in Na^+ form (100—200 mesh, 7×8 cm). When the elution was carried out with a 0.15 M (1 M=1 mol/dm³) NaCl aqueous solution, one red band descended. The effluent was concentrated to a small volume under reduced pressure; after being filtered once, the filtrate was kept in a refrigerator overnight. The deposited crystals were recrystallized from warm water. The yield was about 10 g. Found: C, 13.34; H, 6.12; N, 20.71%. Calcd for $[Co(CO_3)(NH_3)_2(C_2H_8N_2)]Cl\cdot H_2O$: C, 13.52; H, 6.00; N, 21.02%.

Though Hawkins *et al.* had resolved this complex using $[Co(SO_3)_2(NH_3)_2(R\text{-pn})]^-$ as the resolving agent,[5)] we resolved it with $(-)_{546}[Co(ox)_2(en)]^-$: the racemate (2 g, 0.008 mol) was dissolved in warm water (5 cm³, *ca.* 35 °C), and $(-)_{546}Na[Co(ox)_2(en)]$ (1.3 g, 0.004 mol) was added to the solution. On cooling the whole solution in an ice-bath, a less soluble diastereoisomer containing the $(+)_{589}$ carbonato complex deposited. Recrystallization from water was repeated three times. The final yield was about 0.5 g. Found: C, 19.02; H, 4.86; N, 14.13%. Calcd for $[Co(CO_3)(NH_3)_2(C_2H_8N_2)][Co(C_2O_4)_2(C_2H_8N_2)]\cdot 2.5H_2O$: C, 18.92; H, 5.08; N, 14.72%.

b) cis-*Diammine(2,2′-bipyridine)carbonatocobalt(III) Chloride Dihydrate*, cis-$[Co(CO_3)(NH_3)_2(bpy)]Cl\cdot 2H_2O$: A solution of 2,2′-bipyridine (7.8 g, 0.05 mol) in 20 cm³ CH_3OH was mixed with a solution of *cis*-$K[Co(CO_3)_2(NH_3)_2]\cdot H_2O$ (12.5 g, 0.05 mol) in 20 cm³ H_2O, and perchloric acid (30%) was then added dropwise to the mixture until the pH reached 5.5, with stirring in an ice-bath. After filtering off potassium perchlorate which precipitated, the filtrate was stirred at room temperature overnight. The resulting solution, filtered once, was poured into a column containing Dowex 50W-X8 in Na^+ form (100—200 mesh, 5×20 cm). Upon elution with a 0.2 M NaCl solution, only one red band descended. The eluate was concentrated to a small volume (*ca.* 20 cm³). After removal of the sodium chloride by filtration, the filtrate was kept in a refrigerator to precipitate powdery crystals. The crystals were recrystallized from a minimum amount of warm water (*ca.* 30 °C). The yield was about 1.5 g. Found: C, 37.39; H, 4.08; N, 15.35%. Calcd for $[Co(CO_3)(NH_3)_2(C_{10}H_8N_2)]Cl\cdot 2H_2O$: C, 37.36; H, 4.24; N, 15.84%.

The $(+)_{546}Na[Co(edta)]$ complex (1.2 g, 0.0029 mol) was dissolved in a warm solution of the above racemate (2 g, 0.0058 mol, in 10 cm³ H_2O). When the mixture was cooled in an ice-bath and the sides of the vessel were scratched with a glass rod, one diastereoisomeric salt of the $(+)_{589}$ carbonato complex precipitated. The recrystallization was repeated four times from water. The final yield was about

0.5 g. Found: C, 36.64; H, 4.16; N, 11.68%. Calcd for $[Co(CO_3)(NH_3)_2(C_{10}H_8N_2)][Co(C_{10}H_{12}N_2O_8)]\cdot 2H_2O$: C, 36.41; H, 4.33; N, 12.14%.

c) cis·cis-*Diamminecarbonatobis(pyridine)cobalt(III) Chloride Monohydrate*, cis·cis-$[Co(CO_3)(NH_3)_2(py)_2]Cl\cdot 2H_2O$: An appropriate amount of 60% $HClO_4$ was added dropwise to a mixture of $K[Co(CO_3)_2(NH_3)_2]\cdot H_2O$ (10 g, 0.036 mol, in 20 cm³ H_2O) and pyridine (6 cm³, 0.072 mol) in an ice-bath in order to adjust the pH to 5.5. After filtration, the filtrate was stirred at room temperature for some time. Some pink crystals deposited. A solution of the crude product was poured into a column of Dowex 50W-X8 resin in Na^+ form. The effluent obtained by elution with a 0.3 M NaCl was concentrated to a small volume (*ca.* 10 cm³). When the solution was kept in a refrigerator, red crystals deposited. These were recrystallized from warm water (*ca.* 35 °C). The yield was about 1.0 g. Found: C, 36.07; H, 4.93; N, 15.55%. Calcd for $[Co(CO_3)(C_5H_5N)_2(NH_3)_2]\text{-}Cl\cdot H_2O$: C, 36.23; H, 4.98; N, 15.36%.

Into a solution of this racemate (3.3 g, 0.009 mol, in 10 cm³ H_2O) was poured a resolving agent, $(-)_{546}Na[Co(ox)_2\text{-}(en)]\cdot H_2O$ (1.2 g, 0.0038 mol), with stirring. The less soluble diastereoisomer containing the $(-)_{589}$-isomer of the carbonato complex crystallized out when the solution was allowed to stand in an ice-bath. This was recrystallized from water. The final yield was about 0.3 g. Found: C, 31.37; H, 4.67; N, 12.82%. Calcd for $[Co(CO_3)(NH_3)_2\text{-}(C_5H_5N)_2][Co(C_2O_4)_2(C_2H_8N_2)]\cdot 2.5H_2O$: C, 31.35; H, 4.49; N, 12.90%.

d) cis-*Carbonatoethylenediaminebis(pyridine)cobalt(III) Chloride Monohydrate*, cis-$[Co(CO_3)(py)_2(en)]Cl\cdot H_2O$: This complex was prepared in the same way as described in c) except for the use of $K[Co(CO_3)_2(en)]\cdot H_2O$ (10 g, 0.034 mol, in 20 cm³ H_2O). The reacted solution, filtered once, was chromatographed on a column of Dowex 50W-X8 resin in Na^+ form (100—200 mesh, 5×25 cm) using 0.1 M NaCl as the eluting solution. Two bands colored pink and red descended. The eluate of the red band was collected in a fraction, and concentrated to a small volume (*ca.* 10 cm³). After filtration, the filtrate was kept in a refrigerator (*ca.* 4 h). The crude precipitates thus obtained were recrystallized from warm water. The yield was about 2 g. Found: C, 39.72; H, 5.02; N, 14.01%. Calcd for $[Co(CO_3)\text{-}(C_2H_8N_2)(C_5H_5N)_2]Cl\cdot H_2O$: C, 39.95; H, 5.12; N, 14.24%.

$(-)_{546}Na[Co(ox)_2(en)]\cdot H_2O$ (1.6 g, 0.005 mol) was dissolved in a hot solution of the racemate (3.9 g, 0.01 mol, in 10 cm³ H_2O), followed by addition of ethanol (*ca.* 2 cm³). The mixture was cooled in an ice-bath and the sides of the vessel were scratched with a glass rod, whereupon the diastereoisomeric salt of the $(-)_{589}$ carbonato complex deposited. The salt was collected and recrystallized four times from warm water (*ca.* 35 °C). The final yield was about 0.7 g. Found: C, 34.24; H, 4.40; N, 12.52%. Calcd for $[Co(CO_3)\text{-}(C_2H_8N_2)(C_5H_5N)_2][Co(C_2O_4)_2(C_2H_8N_2)]\cdot 2H_2O$: C, 34.16; H, 4.52; N, 12.57%.

e) *Sodium Carbonatooxalatotrimethylenediaminecobaltate(III)*, *Na[Co(CO₃)(ox)(tn)]*: Trimethylenediamine (7.4 g, 0.1 mol) and oxalic acid (12.6 g, 0.1 mol) were mixed with stirring in an ice-bath, and then ethanol was added until trimethylenediammonium oxalate deposited. This product (6.7 g, 0.05 mol) was added to a green solution of $[Co(CO_3)_3]^{3-}$ ($Co(NO_3)_2\cdot 6H_2O$ 15 g, 0.05 mol scale). The mixture was stirred at 45 °C until the color of the solution became blue-violet, and then the resulting solution was concentrated to a small volume under reduced pressure. After filtration, the filtrate was chromatographed using a column containing Dowex 1X-8 resin in Cl^- form (5× 20 cm) and 0.1 M NaCl as the eluent; one blue-violet band came out. The eluate was concentrated to a small volume under reduced pressure, and after being filtered once, was kept in a refrigerator (*ca.* 1 h). The crude product thus obtained was recrystallized from warm water. The yield was about 3 g. Found: C, 23.52; H, 3.20; N, 9.03%. Calcd for $Na[Co(CO_3)(C_2O_4)(C_3H_{10}N_2)]$: C, 23.68; H, 3.29; N, 9.21%.

A mixture of the racemate (2 g, 0.006 mol) and $(-)_{589}\text{-}[Co(ox)(en)_2](C_2H_3O_2)$ (0.9 g, 0.003 mol) in water (10 cm³) was cooled in an ice-bath. Immediately a less soluble diastereoisomeric salt of the $(-)_{589}$ carbonato complex deposited. The recrystallization was repeated five times from water. The final yield was about 0.4 g. Found: C, 24.10; H, 5.09; N, 13.40%. Calcd for $[Co(C_2O_4)(C_2H_8N_2)_2][Co\text{-}(CO_3)(C_2O_4)(C_3H_{10}N_2)]\cdot 3H_2O$: C, 23.93; H, 5.32; N, 13.95%.

f) cis-*Bis(ethylenediamine)dinitrocobalt(III)* cis-*Carbonatooxalatobis(pyridine)cobaltate(III) Dihydrate*, cis-$[Co(NO_2)_2(en)_2]\text{-}$cis-$[Co(CO_3)(ox)(py)_2]\cdot 2H_2O$: To a concentrated solution of *cis*-$[Co(CO_3)(ox)(py)_2]^-$, which was prepared by the literature method[6] ($Co(NO_3)_2\cdot 6H_2O$, 15 g scale, 0.05 mol), was added *cis*-$[Co(NO_2)_2(en)_2](C_2H_3O_2)$ (8.25 g, 0.025 mol). The mixture was kept in a refrigerator until a less soluble salt deposited; this was then recrystallized from warm water. Found: C, 30.33; H, 4.34; N, 16.24%. Calcd for $[Co(NO_2)_2(C_2H_8N_2)_2][Co(CO_3)(C_2O_4)(C_5H_5N)_2]\cdot 2H_2O$: C, 30.36; H, 4.46; N, 16.67%.

The resolving agent $(-)_{589}[Co(NO_2)_2(en)_2]I$ (1 g, 0.0025 mol) was converted into the acetate with silver acetate (0.4 g, 0.0025 mol). The compound, $[Co(NO_2)_2(en)_2][Co(CO_3)\text{-}(ox)(py)_2]\cdot 2H_2O$ (3 g, 0.005 mol), was dissolved in water (30 cm³) and converted into sodium salt by passing the solution through a column of Dowex 50W-X8 resin in Na^+ form. After the column had been rinsed thoroughly with water, the whole effluent was concentrated to a small volume (*ca.* 10 cm³). The concentrate was added to the solution of the above resolving agent. When the mixed solution was kept in a refrigerator, the precipitates obtained soon were optically inactive, and subsequently the desired diastereoisomer containing the $(+)_{589}$ carbonato complex was obtained. The yield was about 0.05 g. Found: C, 30.33; H, 4.34; N, 16.24%. Calcd for $[Co(NO_2)_2(C_2H_8N_2)_2]\text{-}[Co(CO_3)(C_2O_4)(C_5H_5N)_2]\cdot 2H_2O$: C, 30.36; H, 4.46; N, 16.67%.

g) cis-*Diammineethylenediamineoxalatocobalt(III) Chloride Monohydrate*, cis-$[Co(ox)(NH_3)_2(en)]Cl\cdot H_2O$: The preparation of this complex from trans(NH_3)-$[Co(Cl)_2(NH_3)_2(en)]Cl$ has been reported.[4] In our work, *cis*-$[Co(CO_3)(NH_3)_2(en)]Cl\cdot H_2O$ was used as the starting material. To a mixture of *cis*-$[Co(CO_3)(NH_3)_2(en)]Cl\cdot H_2O$ (10 g, 0.04 mol) and $K_2C_2O_4\cdot H_2O$ (7 g, 0.04 mol) in water (20 cm³), was added a solution of $H_2C_2O_4\cdot 2H_2O$ (5 g, 0.04 mol, in 10 cm³ H_2O) dropwise in an ice-bath. The solution was further stirred at 40 °C for 3 h. After filtering the solution, the filtrate was charged on a column containing Dowex 50W-X8 resin Na^+ form (4×20 cm). By elution with a 0.1 M NaCl solution, one band descended. The effluent was concentrated to a small volume, and this concentrated solution was filtered and then kept in a refrigerator. The red crystals which deposited were recrystallized from warm water (*ca.* 35 °C). The yield was about 7 g. Found: C, 16.26; H, 5.48; N, 19.15%. Calcd for $[Co(C_2O_4)(NH_3)_2(C_2H_8N_2)]Cl\cdot H_2O$: C, 16.30; H, 5.43; N, 19.02%.

The $[Co(ox)(NH_3)_2(en)]Cl\cdot H_2O$ complex (2 g, 0.007 mol) was converted to the acetate with silver acetate (1.2 g, 0.007 mol). On adding $(-)_{546}Na[Co(ox)_2(en)]\cdot H_2O$ (1.12 g,

0.0035 mol) to a solution of the acetate in 20 cm^3 water, a less soluble diastereoisomer containing the $(+)_{589}$ isomer of the cation separated out. The salt was recrystallized five times from warm water (*ca.* 35 °C). The final yield was about 0.4 g. Found: C, 21.49; H, 4.39; N, 14.86%. Calcd for $[Co(C_2O_4)(NH_3)_2(C_2H_8N_2)][Co(C_2O_4)_2(C_2H_8N_2)]\cdot H_2O$: C, 21.66; H, 4.34; N, 15.16%.

h) cis-Diammineethylenediaminemalonatocobalt(III) Chloride 0.5-Hydrate, cis-$[Co(mal)(NH_3)_2(en)]Cl\cdot 0.5H_2O$: An aqueous solution of *cis*-$[Co(CO_3)(NH_3)_2(en)]Cl\cdot H_2O$ (10 g, 0.004 mol, in 20 cm^3 H_2O) was treated in the same way as described in g) except for the use of potassium malonate (7 g, 0.04 mol) and malonic acid (4 g, 0.04 mol). The yield was about 4 g. Found: C, 20.16; H, 5.75; N, 19.07%. Calcd for $[Co(C_3H_2O_4)(NH_3)_2(C_2H_8N_2)]Cl\cdot 0.5H_2O$: C, 20.04; H, 5.67; N, 18.70%.

This complex was resolved by column chromatography: a solution of the racemic chloride complex was charged on a column containing Dowex 50W-X8 resin in Na^+ form (2×40 cm). Elution with a 0.1 M $K_2[Sb_2(d\text{-tart})_2]$ aqueous solution resulted in a partial resolution. The specific rotation of the later effluent was positive at 589 nm.

Derivation from Optically Active Complex *a)* $(+)_{546}[Co(ox)(en)_2]^+$: The compound, $(+)_{546}[Co(CO_3)(en)_2](+)_{546}[Co(ox)_2(en)]$ was dissolved in water and converted into the chloride by passing the solution through a column (5×2 cm) of Dowex 1-X8 resin in Cl^- form. After being washed with water, the whole effluent was concentrated to a small volume. To the concentrated solution was added a solution of $H_2C_2O_4\cdot 2H_2O$ dropwise in an ice-bath, and then the solution was stirred at 40 °C for 3 h. The resulting solution was charged on a column of Dowex 50W-X8 resin in Na^+ form. The elution was carried out with a 0.1 M NaCl solution, whereby one band descended. The absorption and CD spectral data of this effluent were identical with those of $(+)_{546}[Co(ox)(en)_2]^+$.[3]

b) $(+)_{589}[Co(ox)(NH_3)_2(en)]^+$: This complex was prepared in the same way as described in a) except for the use of $(+)_{589}[Co(CO_3)(NH_3)_2(en)]^+$ instead of $(+)_{546}[Co(CO_3)(en)_2]Cl$. The effluent showed the same absorption and CD spectra as those of $(+)_{589}[Co(ox)(NH_3)_2(en)]^+$.

c) $(-)_{546}[Co(ox)_2(en)]^-$: A solution of $H_2C_2O_4\cdot 2H_2O$ was added to a solution of $(-)_{589}[Co(CO_3)(ox)(en)]^-$ little by little with stirring in an ice-bath. After the resulting solution was stirred at 50 °C for a while, the solution was chromatographed on a column of Dowex 1-X8 resin in Cl^- form using a 0.1 M NaCl solution. Only one band descended. The absorption and CD spectra of this effluent was identical to those of $(-)_{546}[Co(ox)_2(en)]^-$.

Measurement. The absorption spectra in aqueous solution were recorded with a Hitachi 323 recording spectrophotometer. In the case of the *cis*-$[Co(CO_3)(ox)(py)_2]^-$ complex, the spectrum was measured with a solution passed through a cation exchange resin in Na^+ form in order to remove the counter ion, $[Co(NO_2)_2(en)_2]^+$. For the CD spectral measurements, a JASCO J-40CS automatic recording spectropolarimeter with a JASCO Model J-DPZ data processor was used; a JASCO Model DIP-SL automatic polarimeter was used for optical rotation measurements. In both cases, samples were converted into the same cations and anions as those of the corresponding racemates by means of ion-exchange techniques.

The absorption and CD spectra of the diaqua complex species were measured with solutions of the carbonato complexes acidified with 10% $HClO_4$. The absorption and CD spectra of the acidified solutions were reformed into the spectra of the parent carbonato complexes when potassium hydrogencarbonate was added to the acidified solutions. This result suggests that the acid hydrolyses proceed with retention of the configurations.

Results and Discussion

CD Spectra. The absorption spectra of the new complexes are shown in Figs. 1 and 2. The CD spectra for the complexes of the types $[Co(O,O)_2(N)_2]^-$, $[Co(O,O)(N)_4]^+$, $[Co(O,O)(N)_2(H_2O)_2]^+$, and $[Co(N)_4(H_2O)_2]^{3+}$ ($O,O=CO_3^{2-}$, ox^{2-}, and mal^{2-}; $(N)_2=2NH_3$, 2py, en, tn, and bpy) are shown in Figs. 3—7, while the numerical data are summarized in Tables 1 and 2. We are interested in the comparison of the CD spectra in the T_{1g}-band region; hereafter, only the spectra observed in the region are discussed.

The CD spectra of $(+)_{546}[Co(CO_3)(en)_2]^+$, $(+)_{589}$-

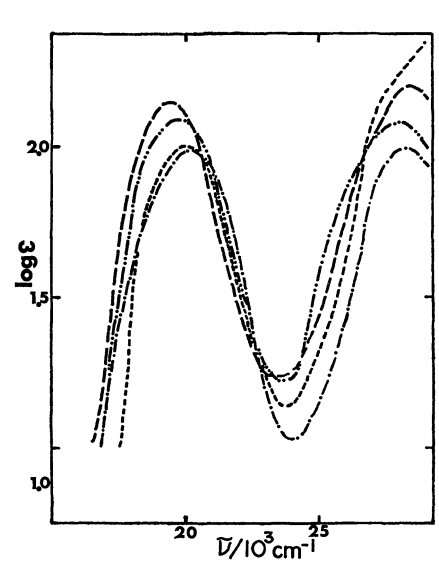

Fig. 1. Absorption spectra of
— — — $[Co(CO_3)(NH_3)_2(py)_2]^+$, —·— $[Co(CO_3)(en)(py)_2]^+$, —·— $[Co(mal)(NH_3)_2(en)]^+$, and ---- $[Co(CO_3)(NH_3)_2(bpy)]^+$.

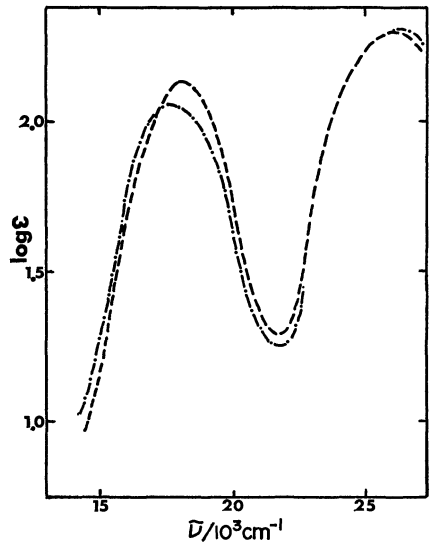

Fig. 2. Absorption spectra of
— — — $[Co(CO_3)(ox)(py)_2]^-$ and —·— $[Co(CO_3)(ox)(tn)]^-$.

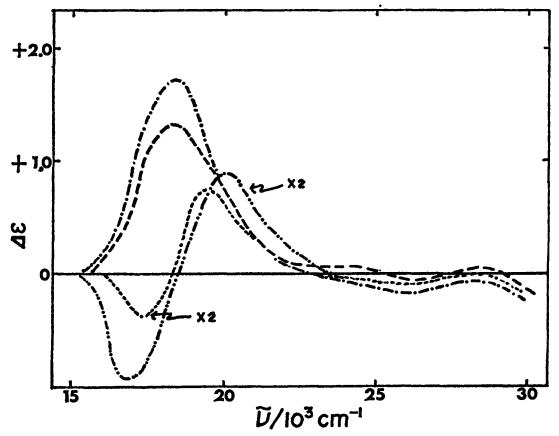

Fig. 3. CD spectra of
— — — $(+)_{589}[Co(CO_3)(ox)(tn)]^-$, —·— $(+)_{589}[Co(ox)(tn)(H_2O)_2]^+$, —·— $(+)_{589}[Co(CO_3)(ox)(py)_2]^-$, and ---- $(+)_{589}[Co(ox)(py)_2(H_2O)_2]^+$.

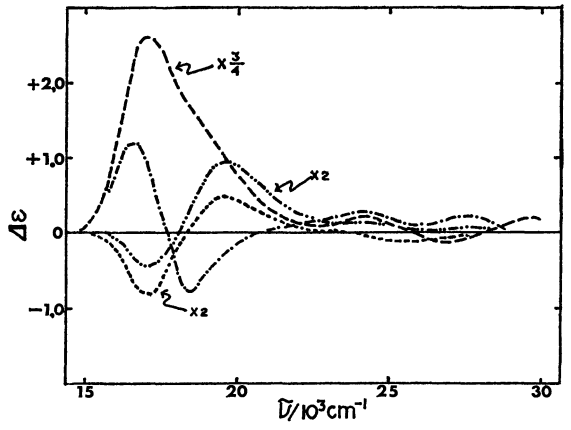

Fig. 4. CD spectra of
— — — $(-)_{589}[Co(CO_3)(ox)(en)]^-$, —··— $(+)_{589}[Co(ox)(en)(H_2O)_2]^+$, —·— $(-)_{589}[Co(CO_3)(mal)(NH_3)_2]^-$, and ---- $(+)_{589}[Co(mal)(NH_3)_2(H_2O)_2]^+$.

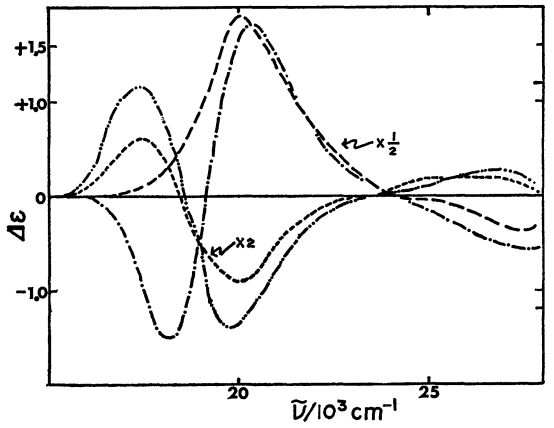

Fig. 5. CD spectra of
—·— $(-)_{589}[Co(CO_3)(NH_3)_2(py)_2]^+$, ----$(-)_{589}[Co(NH_3)_2(py)_2(H_2O)_2]^{3+}$, — — — $(+)_{589}[Co(CO_3)(en)(py)_2]^+$, and —··— $(-)_{589}[Co(en)(py)_2(H_2O)_2]^{3+}$.

$[Co(CO_3)(NH_3)_2(en)]^+$ and $(+)_{589}[Co(CO_3)(NH_3)_2(bpy)]^+$ show one (+) peak. On the other hand, the CD spectra of the diaqua complexes derived from

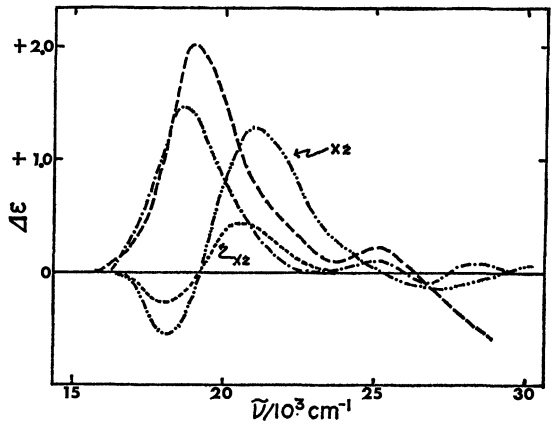

Fig. 6. CD spectra of
— — — $(+)_{589}[Co(CO_3)(NH_3)_2(bpy)]^+$, —·— $(+)_{589}[Co(NH_3)_2(bpy)(H_2O)_2]^{3+}$, —·— $(+)_{589}[Co(CO_3)(NH_3)_2(en)]^+$, and ---- $(-)_{589}[Co(NH_3)_2(en)(H_2O)_2]^{3+}$.

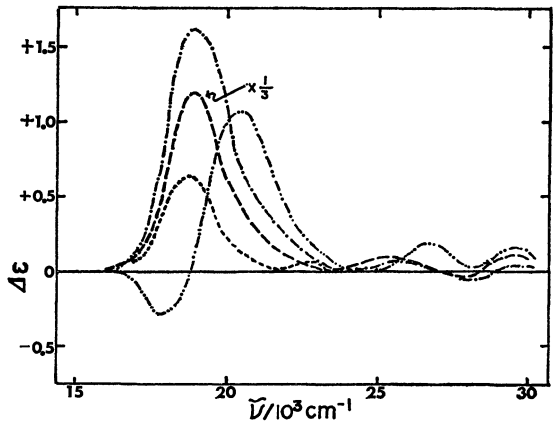

Fig. 7. CD spectra of
— — — $(+)_{546}[Co(CO_3)(en)_2]^+$, —··— $(+)_{546}[Co(en)_2(H_2O)_2]^{3+}$, —·— $(+)_{589}[Co(ox)(NH_3)_2(en)]^+$, and ---- $(+)_{589}[Co(mal)(NH_3)_2(en)]^+$.

the above carbonato complexes show (−) and (+) peaks from the lower frequncy side. The CD spectrum of $(-)_{589}[Co(CO_3)(NH_3)_2(py)_2]^+$ shows (−) and (+) peaks from the lower frequency side and the (+) peak is dominant. The CD spectrum of $(+)_{589}[Co(CO_3)(en)(py)_2]^+$ shows one (+) peak. The CD spectra of the diaqua complexes, $(-)_{589}[Co(NH_3)_2(py)_2(H_2O)_2]^{3+}$ and $(-)_{589}[Co(en)(py)_2(H_2O)_2]^{3+}$, derived from the above bis(pyridine) complexes by the acid hydrolyses show (+) and (−) peaks from the lower frequency side. The CD spectra of the carbonato complexes suggest that the above five carbonato complexes have the same absolute configuration. On the other hand, the CD spectra of the diaqua complexes suggest that the absolute configurations of the first three carbonato complexes are opposite to those of the last two carbonato complexes, since the acid hydrolyses proceed with retention of the configurations. Thus, the relative configurations based on the CD spectra of the carbonato complexes don't agree with those based on the CD spectra of the corresponding diaqua complexes in the bis(pyridine) complexes.

The CD spectra of $(-)_{589}[Co(CO_3)(ox)(en)]^+$,

Table 1. Spectral data

Complex	Absorption $\tilde{\nu}_{max}$[a] (log ε)	CD $\tilde{\nu}_{max}$[a] ($\Delta\varepsilon$)
$(-)_{589}[Co(CO_3)(ox)(en)]^-$ [b]	18.1(2.16)	17.2(+3.43)
	25.6(2.25)	23.9(+0.33)
		25.9(−0.07)
		28.3(+0.21)
$(+)_{589}[Co(ox)(en)(H_2O)_2]^+$ [b]	18.1(1.94)	17.3(−0.47)
		19.7(+0.99)
	26.2(2.06)	23.8(+0.16)
		27.9(+0.18)
$(+)_{589}[Co(CO_3)(ox)(tn)]^-$	17.8(2.08)	18.3(+1.27)
	25.8(2.29)	23.8(+0.09)
		25.8(−0.06)
$(+)_{589}[Co(ox)(tn)(H_2O)_2]^+$	18.2(1.84)	16.8(−0.43)
		19.3(+0.52)
	26.2(2.14)	26.0(−0.01)
		31.3(−0.02)
$(+)_{589}[Co(CO_3)(ox)(py)_2]^-$	18.0(2.14)	18.4(+0.87)
	25.6(2.28)	25.9(−0.10)
$(+)_{589}[Co(ox)(py)_2(H_2O)_2]^+$	18.3(1.91)	17.5(−0.19)
		19.4(+0.40)
	25.5(2.14)	26.0(−0.10)
$(-)_{589}[Co(CO_3)(mal)(NH_3)_2]^-$ [b]	17.8(2.00)	16.5(+1.21)
		18.4(−0.81)
	25.7(2.14)	23.9(+0.28)
		27.2(+0.26)
$(+)_{589}[Co(mal)(NH_3)_2(H_2O)_2]^+$ [b]	18.3(1.72)	17.0(−0.42)
		19.4(+0.49)
	26.4(1.89)	26.1(−0.04)
$(+)_{589}[Co(CO_3)(ox)(NH_3)_2]^-$ [c]	17.7(2.09)	17.3(+1.74)
	25.7(2.18)	23.6(+0.22)
		25.8(−0.11)
		28.3(+0.09)
$(+)_{589}[Co(ox)(NH_3)_2(H_2O)_2]^+$ [c]	18.2(1.84)	16.60(−0.76)
		19.37(+0.58)
	26.2(2.02)	

a) ν_{max} values in 10^3 cm^{-1}. b) Spectral data are in Ref. 2. c) Spectral data are in Ref. 10.

Table 2. Spectral data

Complex	Absorption $\tilde{\nu}_{max}$[a] (log ε)	CD $\tilde{\nu}_{max}$[a] ($\Delta\varepsilon$)
$(+)_{589}[Co(CO_3)(NH_3)_2(en)]^+$	19.4(2.08)	18.8(+1.53)
	27.9(2.08)	25.5(+1.30)
		27.4(−0.05)
		30.1(+0.11)
$(+)_{589}[Co(NH_3)_2(en)(H_2O)_2]^{3+}$	20.1(1.97)	18.1(−0.17)
		20.6(+0.22)
	27.9(1.96)	25.3(+0.01)
$(+)_{546}[Co(CO_3)(en)_2]^+$ [b]	19.4(2.16)	18.7(+3.70)
	27.7(2.12)	25.6(+0.27)
		27.5(−0.10)
		29.1(+0.15)
$(+)_{546}[Co(en)_2(H_2O)_2]^{3+}$ [b]	20.2(1.92)	17.9(−0.3)
		20.6(+1.05)
	27.7(1.82)	26.5(+0.20)
		29.4(+0.15)
$(+)_{589}[Co(CO_3)(NH_3)_2(bpy)]^+$	19.5(2.07)	19.0(+2.03)
		25.3(+0.25)
		29.2(−0.66)
$(+)_{589}[Co(NH_3)_2(bpy)_2(H_2O)_2]^{3+}$	20.1(1.82)	18.2(−0.29)
		21.1(+0.66)
		26.5(−0.05)
		28.8(+0.11)
$(-)_{589}[Co(CO_3)(NH_3)_2(py)_2]^+$	19.4(2.06)	18.1(−0.59)
		20.3(+0.92)
	27.6(2.07)	27.8(−0.28)
$(-)_{589}[Co(NH_3)_2(py)_2(H_2O)_2]^{3+}$	19.7(1.83)	17.4(+0.15)
		19.8(−0.22)
	28.3(1.83)	26.5(+0.05)
$(+)_{589}[Co(CO_3)(en)(py)_2]^+$	19.5(2.09)	20.0(+1.87)
	27.6(2.09)	27.4(−0.36)
$(-)_{589}[Co(en)(py)_2(H_2O)_2]^{3+}$	20.1(1.92)	17.4(+0.59)
		19.8(−0.72)
	27.8(1.92)	25.7(+0.08)
$(+)_{589}[Co(ox)(NH_3)_2(en)]^+$	19.8(2.03)	19.1(+1.65)
	28.1(2.17)	25.5(+0.13)
		27.5(−0.04)
		29.7(+0.06)
$(+)_{589}[Co(mal)(NH_3)_2(en)]^+$	19.9(1.99)	18.3(+0.66)
		22.2(+0.07)
	28.1(1.99)	25.6(+0.03)
		27.2(−0.02)
		29.5(+0.14)

a) $\tilde{\nu}_{max}$ values in 10^3 cm^{-1}. b) Spectral data are in Ref. 3.

$(+)_{589}[Co(CO_3)(ox)(NH_3)_2]^-$,[2] $(+)_{589}[Co(CO_3)(ox)(tn)]^-$ and $(+)_{589}[Co(CO_3)(ox)(py)_2]^-$ have all one (+) peak, and those of the diaqua complexes derived from the above carbonato complexes have (−) and (+) peaks from the lower frequency side. The CD spectrum of $(-)_{589}[Co(CO_3)(mal)(NH_3)_2]^-$ [2] shows (+) and (−) peaks, in which the (+) peak at the lower frequency side is dominant. The CD spectrum of $(-)_{589}[Co(mal)(NH_3)_2(H_2O)_2]^+$ derived from the above malonato complex shows (−) and (+) peaks from the lower frequency side. The CD spectra of these carbonato complexes suggest that the above five carbonato complexes have the same absolute configuration. The CD spectra of the corresponding diaqua complexes also suggest that the above five carbonato complexes have the same absolute configuration.

Assignment of Transition Component. In order to understand the various CD patterns in the T_{1g}-band region for a series of the $[Co(O,O)_2(N)]^-$-type complexes, Muramoto *et al.* attempted to analyze the observed patterns into Gaussian curves.[2] In this analysis, the CD curve was resolved into two components of opposite sign. The results showed that every pattern was a curve which resulted from the mutual cancellation of a component at a lower frequency and a component at a higher frequency, and that the component at the lower frequency never changed its CD sign due to the mutual cancellation. With the $[Co(O,O)_2(N)_2]^-$-type complexes, since the $A_{1g}\rightarrow A_{2g}$ (D_{4h}) transition lies at a higher frequency than the $A_{1g}\rightarrow E_g$ transition, the CD peak at the lower

frequency is assigned to the component corresponding to the latter transition (*i.e.* E_g component). From this assignment, the dominant peak in the spectrum of a $[Co(CO_3)(O,O)(N)_2]^-$-type complex is assignable to the E_g component. Since the CD spectrum of a $[Co(O,O)(N)_2(H_2O)_2]^+$-type complex shows two Cotton peaks with opposite sign, the peak at a lower frequency is assignable to the E_g component. From these assignments, the Cotton peak of the $A_{1g}\rightarrow E_g$ transition component for a $[Co(CO_3)(O,O)(N)_2]^-$-type complex has the opposite sign to that for the corresponding diaqua complex.

The CD spectrum of $(-)_{589}[Co(CO_3)(NH_3)_2(py)_2]^+$ and that of $(-)_{589}[Co(NH_3)_2(py)_2(H_2O)_2]^{3+}$ show (−) and (+) peaks and (+) and (−) peaks, respectively. Since the $A_{1g}\rightarrow E_g$ transition lies at a higher frequency than the $A_{1g}\rightarrow A_{2g}$ one in the case of the $[Co(O)_2(N)_4]^+$-type complexes, the (−) peak of the former complex and the (+) peak of the latter complex are both assignable to the $A_{1g}\rightarrow A_{2g}$ transition component (*i.e.* A_{2g} component).

The CD spectra of $(+)_{589}[Co(mal)(NH_3)_2(en)]^+$ and $(+)_{589}[Co(mal)(en)_2]^+$ [7] show two peaks of the same sign. On the other hand, the CD spectrum of $(-)_{589}[Co(ox)_2(NH_3)_2]^-$ [2] shows also (+) and (+) peaks and the dominant peak lies at the lower frequency side in the T_{1g}-band region. In the Gaussian analysis, the CD spectrum of $(-)_{589}[Co(ox)_2(NH_3)_2]^-$ was resolved into a (+) component at a lower frequency and a (−) component at a higher frequency. Since the major peaks for the above malonato complexs with CoN_4O_2 chromophore lie at a lower frequency than the minor peaks, if the observed CD spectra are resultant curves from the mutual cancellation of two components, which have opposite signs and correspond to the $A_{1g}\rightarrow A_{2g}$ and $A_{1g}\rightarrow E_g$ transitions, the two CD peaks of both malonato complexes are residues of the peak corresponding to the A_{2g} component.

A comparison of the CD spectra of $(+)_{546}[Co(CO_3)(en)_2]^+$, $(+)_{546}[Co(ox)(en)_2]^+$,[7] and $(+)_{589}[Co(mal)(en)_2]^+$ shows that the intensities of their dominant Cotton peaks decrease in the order of the carbonato, oxalato, and malonato complexes. Since the (+) Cotton peak of $(+)_{589}[Co(mal)(en)_2]^+$ has been assigned to the A_{2g} component, this change can be explained by considering that the intensity of the E_g component, which has a negative sign, increases according to the change in the O,O ligands. Therefore, the dominant CD peak of $(+)_{546}[Co(CO_3)(en)_2]^+$ is also assigned to the A_{2g} component.

Since the CD spectra of $(+)_{589}[Co(CO_3)(NH_3)_2(en)]^+$, $(+)_{589}[Co(ox)(NH_3)_2(en)]^+$ and $(+)_{589}[Co(mal)(NH_3)_2(en)]^+$ have the same CD patterns as those of $(+)_{546}[Co(CO_3)(en)_2]^+$, $(+)_{546}[Co(ox)(en)_2]^+$ and $(+)_{589}[Co(mal)(en)_2]^+$, respectively, the dominant peaks of these diammine-type complexes can be assigned to the A_{2g} component. On the other hand, since the CD spectra of $(+)_{546}[Co(en)_2(H_2O)_2]^{3+}$ and $(+)_{589}[Co(NH_3)_2(en)(H_2O)_2]^{3+}$ show (−) and (+) peaks from the lower frequency side, the Cotton peak at the lower frequency side in the T_{1g}-band region for $(+)_{546}[Co(en)_2(H_2O)_2]^{3+}$ or $(+)_{589}[Co(NH_3)_2(en)(H_2O)_2]^{3+}$ is also assignable to the A_{2g} component.

From these discussions, it may be concluded that the dominant Cotton peaks for the $[Co(O,O)(N)_4]^+$-type complexes are not always assignable to the E_g component and that the sign of the Cotton peak corresponding to the $A_{1g}\rightarrow A_{2g}$ for a complex of the $[Co(CO_3)(N)_4]^+$-type is opposite to that for the $[Co(N)_4(H_2O)_2]^{3+}$ complex derived from the acid-hydrolysis of the carbonato complex.

Since the CD spectrum of $(+)_{589}[Co(CO_3)(en)(py)_2]^+$ shows one (+) peak in the T_{1g}-band region and that of the corresponding diaqua complex shows (+) and (−) peaks from the lower frequency side, the (+) peak for $(+)_{589}$ carbonato complex can be assigned to the E_g component from the above conclusion. On the other hand, since the CD spectrum of $(+)_{589}[Co(CO_3)(NH_3)_2(bpy)]^+$ shows one (+) peak and that of the corresponding diaqua complex shows (−) and (+) peaks form the lower frequency side, the (+) peak for the $(+)_{589}$ carbonato complex is assignable to the A_{2g} component.

These assignments are supported by comparison of extrema of the dominant Cotton peaks with the corresponding absorption maxima. As given in Table 2, the extrema of the dominant peaks for the $[Co(CO_3)(NH_3)_2(bpy)]^+$, $[Co(O,O)(en)_2]^+$ and $[Co(O,O)(NH_3)_2(en)]^+$ complexes shift to lower frequencies compared with the corresponding absorption maxima, and the extremum for the $[Co(CO_3)(en)(py)_2]^+$ complex to a higher frequency than its absorption maximum. In the case of the $[Co(O,O)(N)_4]^+$-type complexes, the mutual cancellation of the two components, which have opposite sign and correspond to the $A_{1g}\rightarrow A_{2g}$ and $A_{1g}\rightarrow E_g$ transitions, would tend to shift the observed extremum for the former component to lower energies than the absorption maximum. On this basis, the dominant peaks of the $[Co(CO_3)(NH_3)_2(bpy)]^+$, $[Co(O,O)(en)_2]^+$, and $[Co(O,O)(NH_3)_2(en)]^+$ complexes are assignable to the A_{2g} component, and the dominant peak of the $[Co(CO_3)(en)(py)_2]^+$ complex to the E_g component.

Absolute Configuration. The (+) peak of $(+)_{546}[Co(ox)(en)_2]^+$ is assignable to the A_{2g} component and the absolute configuration has been known as Λ.[8] Since the (+) peaks of $(+)_{546}[Co(CO_3)(en)_2]^+$, $(+)_{589}[Co(CO_3)(NH_3)_2(en)]^+$, $(+)_{589}[Co(CO_3)(NH_3)_2(bpy)]^+$, $(+)_{589}[Co(ox)(NH_3)_2(en)]^+$, $(+)_{589}[Co(mal)(en)_2]^+$ and $(+)_{589}[Co(mal)(NH_3)_2(en)]^+$ are assignable to the A_{2g} component, the absolute configurations of the above six complexes are assignable to Λ. The facts that $(+)_{546}[Co(ox)(en)_2]^+$ and $(+)_{589}[Co(ox)(NH_3)_2(en)]^+$ are derived from $(+)_{546}[Co(CO_3)(en)_2]^+$ and $(+)_{589}[Co(CO_3)(NH_3)_2(en)]^+$ support the above assignments. Since the (+) peaks of $(+)_{589}[Co(CO_3)(en)(py)_2]^+$ and $(-)_{589}[Co(CO_3)(NH_3)_2(py)_2]^+$ are assignable to the E_g component, the $(+)_{589}$ complex has a Δ configuration and the $(-)_{589}$ one a S configuration, which is equivalent to a Δ configuration for the bis(chelate) complex. There is a question about the assignment of the absolute configurations of these pyridine complexes, because the dominant peak for the pyridine complexes arises from the E_g component, and that for other

complexes, which contain no pyridine, from the A_{2g} component. Such a difference makes it possible that the relationship between the sign of the Cotton peak and the absolute configuration differs between a $[Co(N)_4(O)_2]$-type complex containing pyridine and that containing no pyridine ligand.

Of the $[Co(O,O)_2(N)_2]^-$-type complexes, $(-)_{546}[Co(ox)_2(en)]^-$ has been known to have a *Λ* configuration.[9] Since the (+) peak for this complex is assigned to the E_g component, the peak corresponding to the E_g component for this type of complex in *Λ* configuration may have (+) sign. The (+) peak of $(-)_{589}[Co(CO_3)(ox)(en)]^-$ is assigned to the E_g component. Therefore, the absolute configuration of this $(-)_{589}$ complex is assignable to *Λ*. The fact that $(-)_{546}[Co(ox)_2(en)]^-$ is derived from $(-)_{589}[Co(CO_3)(ox)(en)]^-$ supports the above assignment. In the same way, since the (+) peaks of $(+)_{589}[Co(CO_3)(ox)(tn)]^-$ and $(+)_{589}[Co(CO_3)(ox)(py)_2]^-$ are both assigned to the E_g component, the absolute configurations of these two complexes are also assignable to *Λ*.

References

1) Presented in part at the 29th Symposium on Coordination Chemistry, Hamamatsu, October 1, 1979.
2) S. Muramoto, K. Kawase, and M. Shibata, *Bull. Chem. Soc. Jpn.*, **51**, 3505 (1978).
3) A. J. McCaffery, S. F. Mason, and B. J. Norman, *J. Chem. Soc.*, **1965**, 5094.
4) K. Kobayashi and M. Shibata, *Bull. Chem. Soc. Jpn.*, **48**, 2561 (1975).
5) C. J. Hawkins, J. A. Stark, and C. L. Wong, *Aust. J. Chem.*, **25**, 273 (1972).
6) Y. Ida, S. Fujinami, and M. Shibata, *Bull. Chem. Soc. Jpn.*, **50**, 2665 (1977).
7) W. T. Jordan, B. J. Brennan, L. R. Froebe, and B. E. Douglas, *Inorg. Chem.*, **12** 1827 (1973).
8) T. Aoki, K. Matsumoto, S. Ooi, and H. Kuroya, *Bull. Chem. Soc. Jpn.*, **46**, 159 (1973).
9) B. E. Douglas, R. A. Haines, and J. G. Brushmiller, *Inorg. Chem.*, **2**, 1194 (1963).
10) Y. Enomoto, T. Ito, and M. Shibata, *Chem. Lett.*, **1974**, 423.

Structural Study of Optical Resolution. IX. The Crystal Structure of $(-)_{589}$-Tris(biguanide)cobalt(III) Chloride *d*-Tartrate Pentahydrate

Toshiji TADA, Yoshihiko KUSHI, and Hayami YONEDA*

Department of Chemistry, Faculty of Science, Hiroshima University, Higashi-senda-machi, Naka-ku, Hiroshima 730

(Received September 11, 1980)

The crystal structure of the less-soluble diastereomeric salt, $(-)_{589}$-[Co(Hbg)$_3$]Cl(*d*-tart)·5H$_2$O, has been determined by X-ray analysis (R=0.056, 1277 reflections). The crystals are orthorhombic, with the space group of C222, Z=4, a=24.846(5), b=12.970(2), and c=8.645(2) Å. The main features of the crystal structure are as follows: (1) The complex cation and Cl$^-$ anion are arranged alternately along the b-axis to form an infinite spiral chain. The distances between N(Hbg) and Cl are 3.452 and 3.376 Å. (2) The tartrate ions exist as a dimeric unit whose structure closely resembles that of [Sb$_2$(d-tart)$_2$]$^{2-}$. Through the center of this dimeric unit pass three mutually orthogonal twofold axes. (3) There are short contacts between the Hbg ligands and the tartrate ions along the twofold axis of the complex; N(A2)···OT3 2.862, N(B2)···OT2 3.116, N(B3)···OT2 2.754, and N(B4)···OT1 2.963 Å. On the basis of these features, the chiral discrimination mechanism is discussed.

In the previous papers of this series,[1-3] the crystal structures of the diastereomeric salts composed of *Λ*-[M(en)$_3$]$^{3+}$ and *d*-tartrate ions (*d*-C$_4$H$_4$O$_6^{2-}$, abbreviated as *d*-tart), $(+)_{589}$-[Co(en)$_3$]Br(*d*-tart)·5H$_2$O,[1] Li{$(+)_{589}$-[Cr(en)$_3$]}(*d*-tart)$_2$·3H$_2$O,[2] and H{$(+)_{589}$-[Co(en)$_3$]}(*d*-tart)$_2$·3H$_2$O,[3] were determined. In all these crystals there exists a unique face-to-face ion-pair between the complex and *d*-tart; four carbon atoms of *d*-tart make a plane which is perpendicular to the threefold axis of the complex, and four oxygen atoms of *d*-tart are projecting toward the complex and facing the triangular face formed by three NH$_2$ groups of the complex. From these observations, we assumed that such a one-to-one ion-pair formation plays a dominant role in the chiral discrimination.[3] Our presumption was strongly supported by chromatographic separation of enantiomers using the *d*-tart solution as the eluent. The complete separation of the enantiomers was accomplished not only for [Co(en)$_3$]$^{3+}$,[4] but also for many octahedral complexes with three NH$_2$ groups in their triangular face,[5,6] including electrically neutral fac-[Co(*β*-alaninato)$_3$].[7] Consistently with the chromatographic results, the ion-association constant of *d*-tart proved to be greater for the *Λ* complex than for the *Δ* complex.[8-12]

On the other hand, it was reported that tris(biguanide)cobalt(III), [Co(Hbg)$_3$]$^{3+}$ (C$_2$H$_7$N$_5$, abbr. Hbg) could be separated into enantiomers *via* a diastereomeric salt containing both chloride and *d*-tart anions.[13] Here, it is interesting to note that the less-soluble diastereomeric salt has the [Co(Hbg)$_3$]Cl(*d*-tart)·5H$_2$O composition, which is quite analogous to that of [Co(en)$_3$]Br(*d*-tart)·5H$_2$O. Moreover, in both cases, the *Λ* complex forms the less-soluble diastereomeric salt with *d*-tart. The crystal structure of the optically active chloride salt, $(+)_{589}$-[Co(Hbg)$_3$]Cl$_3$·H$_2$O, has been determined by Snow;[14] in it biguanide ligands form almost planar chelate rings. The N–H bonds in the Hbg ligand are presumed to be different in nature from those in the ethylenediamine ligand. Thus, the chiral discrimination by *d*-tart in the [Co(Hbg)$_3$]$^{3+}$ complex is expected to be different from that in the [Co(en)$_3$]$^{3+}$ complex. We also attempted to determine the crystal structure of the less-soluble diastereomeric salt, $(-)_{589}$-[Co(Hbg)$_3$]Cl(*d*-tart)·5H$_2$O, in order to obtain the mode of chiral discrimination effected by the *d*-tart.

Experimental

Preparation of Compound. Biguanide sulfate and [Co(Hbg)$_3$]Cl$_3$ were prepared by the method given in the literature.[15,16] The less-soluble diastereomeric salt, $(-)_{589}$-[Co(Hbg)$_3$]Cl(*d*-tart)·5H$_2$O, was prepared by the procedure of Ray and Dutt.[13] The crystals thus obtained are thin, brownish orange plates. The optical purity of the crystals was checked by the CD measurement ($\Delta\varepsilon_{510}=-3.52$ and $\Delta\varepsilon_{452}=+4.76$).[17] Found: C, 19.15; H, 4.94; N, 33.33%. Calcd for $(-)_{589}$-[Co(Hbg)$_3$]Cl(*d*-tart)·5H$_2$O (4H$_2$O): C, 18.89 (19.44); H, 5.55 (5.38); N, 33.04 (34.01)%.

Crystallographic-data Collection. The unit-cell dimensions and crystal symmetry were initially checked from Weissenberg photographs taken with Ni $K\alpha$ radiation (λ=1.6591 Å). The results indicated an orthorhombic mmm Laue Symmetry. The systematic absence of *hkl* reflections when $h+k=2n+1$ suggested the following possible space groups: C222, Cmm2 (Cm2m), and Cmmm. Since the sample is optically active, the space group C222 was chosen; the later success of the structure determination confirmed the wisdom of this selection.

The intensities and cell dimensions were measured on a Rigaku AFC-5 automated four-circle diffractometer with Mo $K\alpha_1$ radiation (λ=0.70926 Å) monochromated by a graphite plate. The crystal size used was 0.39×0.19×0.08 mm. The unit-cell dimensions were refined by a least-squares treatment of the setting of 22 reflections. The crystal data were as follows: orthorhombic, space group C222, a=24.846(5), b=12.970(2), c=8.645(2) Å, D_m=1.51 g cm^{-3} (by flotation in a chloroform–bromoform mixture), Z=4, and D_c=1.52 g cm^{-3}. The intensity data were collected in the ω-2θ scan mode up to 2θ=55° with the scan rate of 16°/min (50 kV, 170 mA). The ω scan range was $(1.0+0.45\tan\theta)$°. Of the 1443 unique observed reflections, 1277 reflections with $|F_o| \geq 3\sigma(F_o)$ were used for the structure determination. Corrections for the absorption effect were neglected (μ(Mo $K\alpha$)=7.83 cm^{-1}).

Determination and Refinement of Crystal Structure

Since the number of formula units per unit-cell is four and the space group is C222, the central cobalt

atom, one nitrogen atom of the $[Co(Hbg)_3]^{3+}$ cation, and the Cl^- anion should lie on a twofold axis. The position of the Co atom was determined from a three-dimensional Patterson map. Subsequent electron density maps calculated with the phase of the Co atom revealed the positions of the remaining non-hydrogen atoms. Several cycles of the block-diagonal least-squares refinement reduced the R value (defined as $\Sigma||F_o|-|F_c||/\Sigma|F_o|$) to 0.070. At this stage, all the hydrogen atoms were located from a difference Fourier map. The final refinement including these H atoms with isotropic temperature factors converged the R value to 0.056. The final difference map showed no peaks higher than 0.4 electron/Å^3, and the highest peak (*ca.* 0.4 electron/Å^3) remained around the OW2 water molecule.

In the refinement, the quantity minimized was $w(|F_o|-k|F_c|)^2$. The weighting scheme used was $w=(\sigma_{cs}^2+a|F_o|+b|F_o|^2)^{-1}$, where σ_{cs} is the standard deviation obtained from the counting statistics for each reflection; the values of a and b were 0.2 and 0.0009 respectively. All the atomic scattering factors, with corrections for the anomalous dispersion of Co and Cl, were taken from the International Tables for X-Ray Crystallography, Vol. IV.[18]

All the computations were carried out by a HITAC 8700 computer at the Hiroshima University Information Processing Center. The computer programs used were FOUR-MMM[19] and HBLS-IV, with a slight modification.[20] An ORTEP drawing was carried out by the use of a computer system, XTL, in a Syntex R3 automated four-circle diffractometer.[21] The final atomic parameters are listed in Table 1. The anisotropic thermal parameters and complete lists of the $|F_o|$ and $|F_c|$ values have been preserved by the Chemical Society of Japan (Document No. 8121).

Results and Discussion

The projections of the crystal structure along the c- and b-axes are shown in Figs. 1 and 2 respectively. The thermal ellipsoids in these figures are illustrated with a 50% probability. The crystallographic twofold axes of the space group C222 pass through the complex, *d*-tart, Cl^-, and three kinds of water molecules (OW1, OW2, and OW3).

Cation Geometry. The bond distances and angles for the complex cation are listed in Table 2. These values are in good agreement with those reported in previous works.[14,22] However, there is a small but siginificant difference in geometry between the present results and those for $(+)_{589}$-$[Co(Hbg)_3]Cl_3\cdot H_2O$.[14] In both crystals, the planarity of biguanide itself is nearly kept, but that of the chelate ring as a whole (including the metal atom) is lost. The dihedral angles between the plane of the biguanide ligand and the plane of Co and two donor nitrogen atoms are 6.9, 6.0, and 12.8° for the $(+)_{589}$-$[Co(Hbg)_3]Cl_3\cdot H_2O$. The mean value is 8.6°.

In contrast, in the present crystal, a crystallographic twofold axis passes through the chelate ring A along the direction Co···N(A3), and the dihedral angle is only 3.0°. The chelate ring A is approximately planar, as is shown in Table 3. On the other hand, the planarity of the chelate ring B is definitely broken (Table 3). The corresponding dihedral angle is 16.4°. This fairly large difference between their dihedral angles suggests that the *d*-tart interacts more strongly

Table 1. Positional and thermal Parameters for $(-)_{589}$-$[Co(Hbg)_3]Cl(d\text{-tart})\cdot 5H_2O$

Atom	x	y	z	B_{eq}/Å^2	Atom	x	y	z	B_{eq}/Å^2
Co	0.29836(5)	0.5	0.5	1.92	OW3	0.3715(6)	0.5	0.0	9.92
Cl	0.25	0.25	0.0924(4)	3.79	OW4	0.4438(3)	0.3392(6)	0.0269(9)	5.06
N(A1)	0.2435(2)	0.4281(5)	0.3886(8)	2.39	H(NA1)	0.255(5)	0.381(10)	0.331(14)	4.29
N(A2)	0.1591(3)	0.3666(7)	0.3240(11)	3.87	H(NA21)	0.132(3)	0.380(6)	0.344(10)	1.04
N(A3)	0.1671(3)	0.5	0.5	3.26	H(NA22)	0.178(4)	0.322(8)	0.250(12)	1.88
N(B1)	0.3526(2)	0.4265(5)	0.3884(7)	2.11	H(NA3)	0.133(6)	0.5	0.5	4.14
N(B2)	0.4322(3)	0.3323(6)	0.3687(9)	3.29	H(NB1)	0.354(4)	0.442(8)	0.296(14)	2.76
N(B3)	0.3823(3)	0.3231(5)	0.5891(8)	2.57	H(NB21)	0.452(4)	0.279(9)	0.415(14)	3.71
N(B4)	0.3356(3)	0.2580(7)	0.7950(9)	3.87	H(NB22)	0.428(4)	0.326(9)	0.288(14)	3.11
N(B5)	0.2997(3)	0.3933(5)	0.6551(8)	2.35	H(NB3)	0.408(4)	0.275(9)	0.632(13)	3.09
C(A1)	0.1922(3)	0.4315(6)	0.4020(10)	2.58	H(NB41)	0.310(4)	0.264(8)	0.872(12)	2.60
C(B1)	0.3870(3)	0.3639(6)	0.4436(10)	2.44	H(NB42)	0.358(4)	0.249(10)	0.827(14)	3.37
C(B2)	0.3370(3)	0.3285(6)	0.6819(9)	2.30	H(NB5)	0.270(4)	0.390(10)	0.714(15)	4.22
CT1	0.0338(3)	0.6337(6)	0.2373(10)	2.45	H(CT2)	−0.033(4)	0.568(8)	0.119(14)	2.85
CT2	−0.0125(3)	0.5550(6)	0.2241(9)	2.13	H(OT3)	−0.032(4)	0.612(8)	0.391(13)	2.35
OT1	0.0652(2)	0.6422(5)	0.1273(7)	3.16	H(OW1)	0.109(6)	0.573(11)	0.002(32)	9.01
OT2	0.0352(3)	0.6848(5)	0.3626(7)	3.51	H(OW2)	0.249(6)	0.430(10)	0.033(18)	6.02
OT3	−0.0500(2)	0.5645(4)	0.3473(7)	2.47	H(OW3)	0.382(3)	0.524(7)	0.069(11)	1.93
OW1	0.1440(5)	0.5	0.0	7.66	H(OW41)	0.453(3)	0.380(9)	−0.045(15)	3.92
OW2	0.2606(6)	0.5	0.0	9.60	H(OW42)	0.451(4)	0.276(9)	0.002(24)	5.03

$B_{eq}=(8/3)\pi^2(U_{11}+U_{22}+U_{33})$. The anisotropic thermal parameters bave been preserved by the Chemical Society of Japan.

with the Hbg B ligand than with the Hbg A ligand. Indeed, the atoms in the chelate ring B and the α-hydroxy carboxylate moiety of *d*-tart lie on nearly the same plane, as is shown in Fig. 3.

Anion Geometry. A crystallographic twofold axis passes through the middle point of *d*-tart. The bond distances and angles for *d*-tart are listed in Table 2. These values coincide with those reported in previous works.[23] The five non-hydrogen atoms of each α-hydroxy carboxylate moiety lie approximately on a plane, as is shown in Fig. 3. The dihedral agnle between the planes of two moieties is 50.8°. This value is within the range of hitherto reported values, which show a wide variation in many crystals: *ca.* 50—75° (av. 66°) for $[Sb_2(d\text{-tart})_n(l\text{-tart})_{2-n}]^{2-}$ ($n=1$ or 2) and analogous compounds, and *ca.* 44—89° (av. 54°) for *d*- and *l*-tartrates.[24]

In addition, a unique dimeric structure of two *d*-tart anions is formed in the present crystal. The structure of this dimeric unit and that of $[Sb_2(d\text{-tart})_2]^{2-}$ [25] are compared in Fig. 4. Three mutually orthogonal crystallographic twofold axes pass through the center of this dimeric unit ($x=0$, $y=1/2$, $z=1/2$). The structure of this dimeric unit closely resembles that of $[Sb_2(d\text{-tart})_2]^{2-}$ if two Sb atoms are left out of consideration. However, the distances between the two hydroxyl oxygen atoms, 3.13 and 3.63 Å, in the dimeric unit differ from the corresponding distances, 3.69 and 3.08 Å, in $[Sb_2(d\text{-tart})_2]^{2-}$, as is shown by

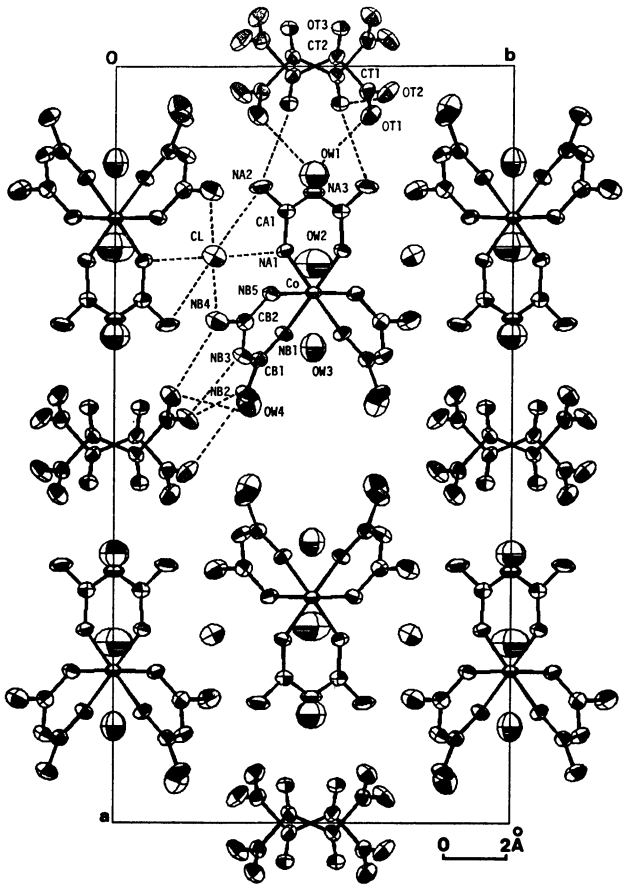

Fig. 1. An ORTEP drawing of the contents of the unit cell viewed down the c-axis with the numbering scheme. Possible hydrogen bonds are indicated by broken lines. All atoms are drawn with 50% probability ellipsoids. Hydrogen atoms are omitted for clarity.

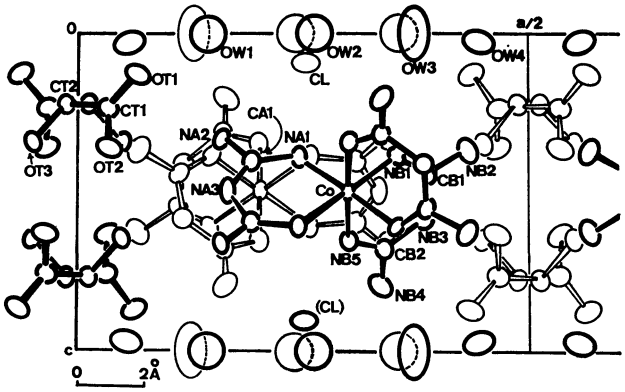

Fig. 2. A perspective drawing of the contents of the unit cell viewed down the b-axis with the numbering scheme.

TABLE 2. BOND DISTANCES AND ANGLES (e.s.d.'s IN PARENTHESES) FOR $(-)_{589}$-$[Co(Hbg)_3]Cl(d\text{-tart})\cdot 5H_2O$

(a) Bond distances *l*/Å

Co-N(A1)	1.911(7)	N(B5)-C(B2)	1.273(10)	C(A1)-N(A2)	1.355(13)	CT1-OT1	1.235(11)
Co-N(B1)	1.913(7)	C(A1)-N(A3)	1.378(12)	C(B1)-N(B2)	1.358(11)	CT1-OT2	1.271(11)
Co-N(B5)	1.927(7)	C(B1)-N(B3)	1.369(11)	C(B2)-N(B4)	1.339(12)	CT2-OT3	1.420(10)
N(A1)-C(A1)	1.282(11)	C(B2)-N(B3)	1.384(11)	CT1-CT2	1.542(12)	CT2-CT2^{i}	1.555(16)
N(B1)-C(B1)	1.272(10)						

(b) Bond angles ϕ/°

N(A1)-Co-N(A1)^{ii}	89.1(3)	N(A1)-C(A1)-N(A3)	121.9(8)	N(B3)-C(B2)-N(B4)	114.3(8)
N(B1)-Co-N(B5)	88.9(3)	N(B1)-C(B1)-N(B3)	122.2(8)	OT1-CT1-OT2	126.3(8)
Co-N(A1)-C(A1)	130.3(6)	N(B5)-C(B2)-N(B3)	121.3(7)	OT1-CT1-CT2	118.3(8)
Co-N(B1)-C(B1)	127.1(6)	C(A1)-N(A3)-C(A1)^{ii}	126.1(8)	OT2-CT1-CT2	115.4(7)
Co-N(B5)-C(B2)	127.9(6)	C(B1)-N(B3)-C(B2)	125.7(7)	CT1-CT2-OT3	112.1(6)
N(A1)-C(A1)-N(A2)	122.5(9)	N(A3)-C(A1)-N(A2)	115.6(8)	CT1-CT2-CT2^{i}	108.0(7)
N(B1)-C(B1)-N(B2)	124.7(8)	N(B3)-C(B1)-N(B2)	113.1(7)	OT3-CT2-CT2^{i}	110.0(6)
N(B5)-C(B2)-N(B4)	124.4(8)				

Roman numerals as superscripts refer to the following equivalent positions, relative to the reference atom at x, y, z: i $(-x, 1-y, z)$, ii $(x, 1-y, 1-z)$.

the asterisk in Fig. 4. The central C–C bonds of the two *d*-tart anions in the $[Sb_2(d\text{-tart})_2]^{2-}$ are nearly parallel, but those in the dimeric unit are not parallel.

Crystal-packing Mode. The crystal-packing modes viewed down along the c- and b-axes are shown in Figs. 1 and 2 respectively. The intermolecular distances and angles are summarized in Table 4.

The complex cation and Cl anion are arranged alternately along the b-axis, as is shown in Fig. 1.

Table 3. Distances of atoms from least-squares planes in Ångstroms

(a) Complex				(b) Tartrate	
Ring A		Ring B			
Co	−0.013	Co	−0.140	CT1	0.015
N(A1)	−0.072	N(B1)	0.213	CT2	0.080
N(A2)	0.077	N(B2)	−0.017	OT1	−0.047
N(A3)	0.008	N(B3)	−0.206	OT2	0.016
N(A2)^{II}	−0.059	N(B4)	0.098	OT3	−0.061
N(A1)^{II}	0.064	N(B5)	0.066		
C(A1)	−0.009	C(B1)	0.019		
C(A1)^{II}	0.017	C(B2)	−0.024		

Plane equations. Each plane is represented by $lx'+my'+nz'+p=0$ with respect to the orthogonal axes, where x', y', and z' are coordinates in Å.

l	−0.00628	−0.56310	0.54287
m	−0.68237	−0.65314	−0.72340
n	0.73098	−0.50629	0.42660
p	1.29976	10.45853	4.62939

Angles between planes (rings): A and B, 94.5°; A and B^{II}, 95.1°; B and B^{II}, 66.2°.

Roman numerals as superscripts refer to the following equivalent positions, relative to the reference atom at x, y, z: ii (x, 1−y, 1−z).

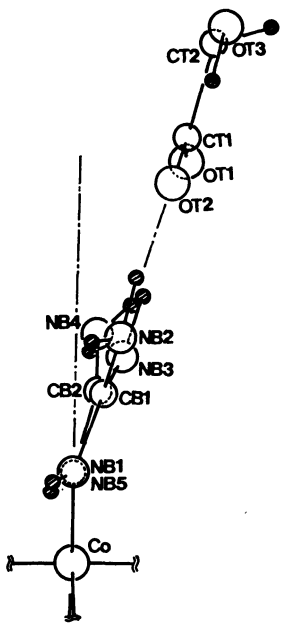

Fig. 3. Projecting of Hbg(B) ligand and α-hydroxycarboxylate moiety of *d*-tartrate viewed down the direction of N(B1)···N(B5).

Short contacts are formed between the N atoms of the Hbg A ligand and the Cl^- anion. The arrangement of the complex cation, $(-)_{589}$-$[Co(Hbg)_3]^{3+}$, and Cl^- can be regarded as an infinite spiral chain along the twofold screw, which is parallel to the b-axis through the ($x=1/4$, $z=1/2$) position, as is clearly shown in Fig. 2. Figure 5 shows the schematic illustration of the present crystal structure. If the complex cation and the Cl^- anion are linked alternately, as is shown by arrows in Fig. 5, the spiral is left-handed. Here, it should be noted that such a spiral arrangement of the complex cation, $(+)_{589}$-$[Co(Hbg)_3]^{3+}$, and the Cl^- anion is also found in the crystal structure of $(+)_{589}$-$[Co(Hbg)_3]Cl_3\cdot H_2O$,[14] but the spiral is the opposite, that is, right-handed.

There are short contacts between the Hbg ligands and the dimeric unit $(d\text{-tart})_2^{4-}$, as is shown in Table 4. It is worth noting that, while the hydroxyl oxygen atom of the *d*-tart forms a short contact with the Hbg

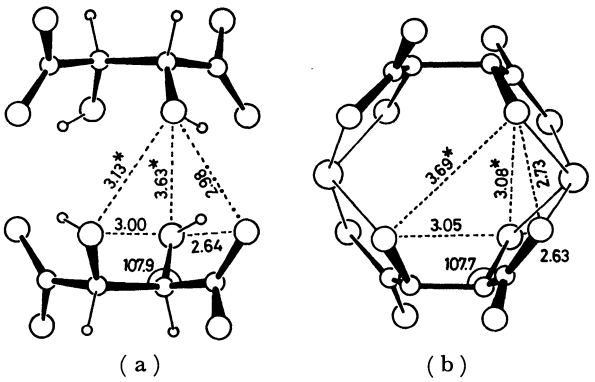

Fig. 4. (a) Structure of the $(d\text{-tart})_2^{4-}$ dimeric unit. (b) Structure of $[Sb_2(d\text{-tart})_2]^{2-}$. Short contacts are indicated by broken lines and their values are in Å.

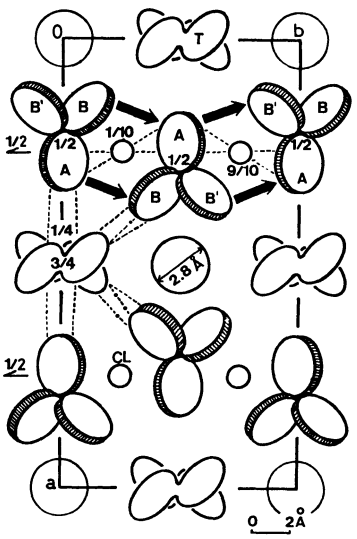

Fig. 5. A schematic drawing of the crystal structure viewed down the c-axis. A, B, and B′ are biguanide ligands. T and CL mean *d*-tartrate and chloride anions respectively. The numerals represent the fractional z-coordinates for the center of each molecule. Big open circles indicated empty channels. Water molecules are omitted for clarity.

TABLE 4. SELECTED INTERMOLECULAR DISTANCES AND ANGLES

D-H···A	D···A l/Å	H···A l/Å	D-H···A ϕ/°
N(A1)-H(NA1)···Cl	3.452(8)	2.68(13)	156(16)
N(A2)-H(NA22)···Cl	3.376(10)	2.44(10)	160(8)
N(A2)-H(NA21)···OT3^{i}	2.862(12)	2.17(8)	166(9)
N(B2)-H(NB21)···OT2^{iii}	3.116(11)	2.30(12)	145(10)
N(B2)-H(NB21)···OT2^{iv}	3.197(11)	2.44(12)	137(10)
N(B3)-H(NB3)···OT2^{iii}	2.754(10)	1.83(12)	159(11)
N(B4)-H(NB41)···Cl^{v}	3.338(9)	2.41(11)	169(9)
N(B4)-H(NB42)···OT1^{iii}	2.963(11)	2.38(13)	151(14)
OT1···OT3^{i}	3.309(9)	—	—
OT2···OT2^{vi}	2.951(14)	—	—
OT2···OT3^{i}	3.258(9)	—	—
OT3^{vii}-H(OT3)···OT2	2.977(9)	2.33(12)	133(10)
OT3···OT3^{i}	2.996(12)	—	—
OT3···OT3^{ii}	3.126(12)	—	—
OW1-H(OW1)···OT1	2.905(15)	1.78(28)	142(20)
OW1···OW2	2.898(19)	—	—
OW2-H(OW2)···Cl	3.350(14)	2.11(21)	151(19)
OW2···OW3	2.754(20)	—	—
OW3-H(OW3)^{viii}···OW4	2.763(16)	2.48(10)	105(9)
OW4-H(OW42)···OT1^{vii}	2.890(11)	2.11(21)	151(19)
OW4···OW4^{ix}	2·833(16)	—	—

Roman numerals as superscripts refer to the following equivalent positions, relative to the reference atom at x, y, z:
i ($-x$, $1-y$, z), ii (x, $1-y$, $1-z$), iii ($1/2-x$, $-1/2+y$, $1-z$),
iv ($1/2+x$, $-1/2+y$, z), v (x, y, $1+z$), vi ($-x$, y, $1-z$),
vii ($1/2-x$, $-1/2+y$, $-z$), viii (x, $1-y$, $-z$), ix ($1-x$, y, $-z$).
D, Hydrogen donor; A, Hydrogen acceptor.

A ligand, the carboxylate oxygen atoms of the *d*-tart form short contacts with the Hbg B ligand. All short contacts are formed along the twofold axes of the complex.

The positions of the water molecules are also shown in Fig. 2. There are four kinds of crystallographically independent water molecules. Three of them, OW1, OW2, and OW3, lie on a twofold axis parallel to the a-axis at the ($y=1/2$, $z=0$) position. The fourth water molecule, OW4, occupies the general position, but its z-coordinate ($z=0.0269$) is nearly equal to zero. Therefore, all the water molecules form a sheet on the ab plane at $z=0$.

The most remarkable feature of the present crystal is that a large empty channel with a diameter of *ca.* 2.8 Å passes through the ($x=1/2$, $y=1/2$) position along the c-axis, as is shown in Fig. 5. The size of the diameter is estimated from the van der Waals radii of the N(B2) and OW4 atoms[26] which surround this channel. The overall crystal-packing mode is highly symmetrical in comparison with those of the diastereomeric salts of $[Co(en)_3]^{3+}$–*d*-tart systems.

Chiral Discrimination Mode. As has been descrived above, there is no one-to-one intimate ion-pair of the complex cation and *d*-tart anion in the present crystal. This is a remarkable difference as compared with the case of the corresponding $(+)_{589}$-$[Co(en)_3]Br(d\text{-tart})\cdot 5H_2O$ crystal,[1] in which a unique one-to-one ion-pair, called "face-to-face" close contact, has been found. It has been proposed, on the basis of the CD change on the addition of *d*-tart, that *d*-tart probably discriminates the Λ- and Δ-forms of $[Co(en)_3]^{3+}$ through the formation of such a unique face-to-face close contact.[27]

An attempt was then made to see if any change in the CD spectrum of the optically active $[Co(Hbg)_3]^{3+}$ in solution is observed upon the addition of *d*-tart. No appreciable change was detected.[28] Another attempt was also made to see if the CD spectrum was induced for the racemic complex salt by the addition of *d*-tart, but no CD spectrum was observed. We also tried to separate the racemic $[Co(Hbg)_3]^{3+}$ ions into enantiomers through an SP-Sephadex ion-exchange column, using the *d*-tart solution as the eluent, but no separation was achieved. These facts suggest that the individual *d*-tart ion can not discriminate the chirality of the individual $[Co(Hbg)_3]^{3+}$ complex ion.

Therefore, it should be considered that the crystal-packing mode as a whole is responsible for the chiral discrimination in the present $[Co(Hbg)_3]^{3+}$–*d*-tart system. Figure 5 shows the schematic illustration of the left-handed spiral chain $\{\Lambda\text{-}[Co(Hbg)_3]Cl\}_\infty$. A similar but right-handed spiral chain is also found in the crystal of $(+)_{589}$-$[Co(Hbg)_3]Cl_3\cdot H_2O$. Therefore, it is reasonable to presume that $[Co(Hbg)_3]^{3+}$ ions have a strong tendency toward the formation of an infinite spiral chain in the presence of Cl^- ions. The questions are why such spiral chains of the same chirality come together to form a crystal, and why the crystal is less-soluble in the present case. In relation to those points, it must be noted that a layer

is formed on the ab plane, linked by hydrogen bonds between $\{\Lambda\text{-}[Co(Hbg)_3]Cl\}_\infty$ and $(d\text{-tart})_2^{4-}$, as is shown in Figs. 2 and 5. Between these layers, a sheet composed of water molecules is stacked along the c-axis; this prevents a strong interaction between these layers along the c-axis. Therefore, it can be considered that a strong interaction is present only in a layer structure of $\{\Lambda\text{-}[Co(Hbg)_3]Cl\}_\infty$ and $(d\text{-tart})_2^{4-}$ on the ab plane. The strong interaction in this layer is probably attributable to the hydrogen bonding. If the absolute configuration of the complex changes from Λ to Δ, the spiral chain would change from left-handed to right-handed, and a discrepancy would take place on the N–H···O hydrogen bonding between the right-handed spiral chains, $\{\Lambda\text{-}[Co(Hbg)_3]Cl\}_\infty$, and the dimeric unit, $(d\text{-tart})_2^{4-}$, so that a reasonable crystal packing could not be formed in this layer. In other words, the *d*-tart is locked by the left-handed spiral chains, $\{\Lambda\text{-}[Co(Hbg)_3]Cl\}_\infty$, formed along the b-axis. Therefore, it seems that the discrimination of optical isomers in this crystal originates in the formation of such a "lock-in-column" structure through the strong hydrogen-bond network on the ab plane. The crystal structures of several less-soluble diastereomeric salts, $(+)_{589}$-$[Ni(bpy)_3]_2Cl_2(d\text{-tart})\cdot nH_2O$,[29] $(+)_{589}$-$[Ru(bpy)_3]_2Cl_2(d\text{-tart})\cdot nH_2O$,[30] Λ-$[Co(bpy)_3]d\text{-tart}\cdot nH_2O$,[30] and $(+)_{589}$-$[Co(tame)_2]Cl(d\text{-tart})\cdot 5.4H_2O$,[31] have been determined. In these crystals, the dimeric unit of *d*-tart anions is not found. Thus, it is probable that, between the $\{\Lambda\text{-}[Co(Hbg)_3]Cl\}_\infty$ spiral chain and *d*-tart anions, there is a stereospecific interaction which stabilizes the dimeric unit of *d*-tart anions, and the formation of the dimeric unit, $(d\text{-tart})_2^{4-}$, plays a dominant part in the optical resolution of $[Co(Hbg)_3]^{3+}$, using *d*-tart as a resolving agent *via* the diastereomeric salt.

We wish to thank the Hiroshima University Information Processing Center for its generous allocation of computer time and wish to acknowledge a Grant-in-Aid for Scientific Research from the Ministry of Education.

References

1) Y. Kushi, M. Kuramoto, and H. Yoneda, *Chem. Lett.*, **1976**, 135.
2) Y. Kushi, M. Kuramoto, and H. Yoneda, *Chem. Lett.*, **1976**, 339.
3) T. Tada, Y. Kushi, and H. Yoneda, *Chem. Lett.*, **1977**, 379.
4) Y. Yoshikawa and K. Yamasaki, *Inorg. Nucl. Chem. Lett.*, **6**, 523 (1970).
5) M. Kojima, H. Takayanagi, and J. Fujita, *Bull. Chem. Soc. Jpn.*, **50**, 1891 (1977).
6) H. Yoneda, *J. Liquid Chromatogr.*, **2**, 1157 (1979).
7) H. Yoneda and T. Yoshizawa, *Chem. Lett.*, **1976**, 707.
8) K. Ogino and U. Saito, *Bull. Chem. Soc. Jpn.*, **40**, 826 (1967).
9) B. Norden, *Acta Chem. Scand.*, **26**, 111 (1972).
10) H. Yoneda, K. Miyoshi, S. Suzuki, and T. Taura, *Bull. Chem. Soc. Jpn.*, **47**, 1661 (1974).
11) H. Yoneda and T. Taura, *Chem. Lett.*, **1977**, 63.
12) T. Taura, H. Tamada, and H. Yoneda, *Inorg. Chem.*, **17**, 3127 (1978).
13) P. Ray and N. K. Dutt, *J. Indian Chem. Soc.*, **18**, 289 (1941).
14) M. R. Snow, *Acta Crystallogr., Sect. B*, **30**, 1850 (1974).
15) D. Karipides and W. C. Fernelius, *Inorg. Synth.*, Vol. VII, 56 (1963).
16) P. Ray and N. K. Dutt, *J. Indian Chem. Soc.*, **16**, 621 (1939).
17) K. Igi, T. Yasui, J. Hidaka, and Y. Shimura, *Bull. Chem. Soc. Jpn.*, **44**, 426 (1971).
18) "International Tables for X-Ray Crystallography," Kynoch Press, Birmingham (1974), Vol. IV, pp. 72—79, 149.
19) Y. Kushi, unpublished work.
20) T. Ashida, "The Universal Crystallographic Computation Program System," ed by T. Sakurai, The Crystallographic Society of Japan (1967).
21) C. K. Johnson, ORTEP, Report ORNL-3794, Oak Ridge National Laboratory, Oak Ridge, Tennessee, U. S. A., 1965.
22) W. C. Moucharafieh, P. G. Eller, J. A. Bertrand, and D. J. Royer, *Inorg. Chem.*, **17**, 1220 (1978).
23) For example, J. M. Bijvoet, A. F. Peerdeman, and A. J. van Bommel, *Nature*, **168**, 271 (1951); R. Sadanaga, *Acta Crystallogr.*, **3**, 416 (1950); S. Perez, *ibid., Sect. B*, **33**, 1083 (1977).
24) R. E. Tapscott, *Coordin. Chem. Rev.*, **4**, 323 (1969).
25) A. Miyanaga, Y. Kushi, and H. Yoneda, Presented at the 41st National Meeting of the Chemical Society of Japan, Osaka, March 1980, Abstr. I, 3L02.
26) L. Pauling, "The Nature of The Chemical Bond," 3rd ed, Cornell University Press, Ithaca (1960), p. 260.
27) M. Fujita and H. Yamatera, *Bull. Chem. Soc. Jpn.*, **49**, 1301 (1976).
28) The CD change of $[Co(Hbg)_3]^{3+}$ reported by G. R. Brubaker and L. E. Webb (*J. Am. Chem. Soc.*, **91**, 7199 (1969)) upon the addition of PO_4^{3-} is attributed to the deprotonation of the complex in a basic solution, leading to neutral $[Co(bg)_3]$[17] rather than to the stereoselective association of the complex with PO_4^{3-} along its C_3 axis.
29) A. Wada, C. Katayama, and J. Tanaka, *Acta Crystallogr., Sect. B*, **32**, 3194 (1976).
30) T. Tada, Y. Kushi, and H. Yoneda, Presented at the 30th Annual Meeting on Coordination Chemistry of Japan, Tokyo, October 1980, Abstr. No. 2C03.
31) R. J. Geue and M. R. Snow, *Inorg. Chem.*, **16**, 231 (1977).

  Bull. Chem. Soc. Jpn., 54, 1544—1547 (1981)

Spectrophotometric Determination of Iron(III) with *N,N'*-Bis(2-hydroxybenzyl)ethylenediamine-*N,N'*-diacetic Acid

Tetsuo KATSUYAMA* and Toshihiko KUMAI

Department of Basic Technology, Faculty of Engineering, Yamagata University, Yonezawa, Yamagata 992

(Received September 26, 1980)

N,N'-Bis(2-hydroxybenzyl)ethylenediamine-*N,N'*-diacetic acid (hbed) reacts with iron(III) to form a red complex having an absorption maximum at 485 nm. The iron(III) complex is so stable that the maximum absorbance of the solution is constant over the pH range from 2.5 to 13.2 and a large excess of reagent is not necessary. Beer's law is obeyed up to 1.6×10^{-4} mol dm^{-3} (9 μg cm^{-3}) of iron(III). The molar absorption coefficient is 3.95×10^{3} l cm^{-1} mol^{-1}, and the relative standard deviation for determination of 3.5 μg cm^{-3} of iron was 0.29%. The molar ratio of iron(III) to hbed was found to be 1:1. The effect of 32 diverse ions was examined; only colored aqua metal ions interfere. The present method was applied to the determination of iron in aluminium alloys.

Spectrophotometric determination of iron(III) has been extensively studied by many authors.[1-9] In these studies, the method[6-8] using the reagent ethylenediamine-*N,N'*-di(2-hydroxyphenylacetic acid) (eddha) is peculiar: the reagent reacts with iron(III) to form a very stable complex (stability constant *ca.* 10^{34}); hence the color development is maximal over a wide pH range, and a large excess of the reagent is not necessary in the determination. These features are desirable in spectrophotometric determinations.

The reagent *N,N'*-bis(2-hydroxybenzyl)ethylenediamine-*N,N'*-diacetic acid (hbed) gives a red color with iron(III) through the formation of a very stable complex whose stability constant is *ca.* 10^{40}. The constant is the highest of those of iron(III) complexes. Further, the constant is particularly large among metal–hbed complexes. So, in this study, hbed has been examined for the spectrophotometric determination of iron(III). The present method gives accurate results for iron(III) ranging from 1×10^{-5} to 16×10^{-5} M (1 M=1 mol dm^{-3}) (0.6—9 μg cm^{-3}), and has high selectivity.

Experimental

Reagents. *hbed Solution*: Material hbed·2HCl·2H$_2$O was prepared by the literature method.[10] Found: C, 48.75; H, 5.92; N, 5.65; Cl, 14.11%. Calcd for $C_{20}H_{24}N_2O_6\cdot2HCl\cdot2H_2O$: C, 48.30; H, 6.04; N, 5.64; Cl, 14.25%.

A 1×10^{-3} M hbed solution was prepared by dissolving a weighed amount of the prepared reagent in water.[11]

Iron(III) Solution: A 0.01 M iron(III) solution was prepared by dissolving guaranteed reagent grade iron(III) nitrate in 0.02 M nitric acid. The solution was standardized by edta titration using Variamine Blue B as indicator. This solution was diluted with 0.02 M nitric acid as required.

Iron(II) Solution: A 0.01 M iron(II) solution was prepared by dissolving GR grade iron(II) sulfate in 0.02 M nitric acid. The solution was standardized by the following procedure. Hydrogen peroxide was first added to the iron(II) solution. After the iron(II) was oxidized to iron(III), the excess hydrogen peroxide was expelled completely by warming the solution. Then the solution was titrated with edta, using Variamine Blue B as indicator.

Water: The ion-exchanged water was distilled with an allquartz distillation apparatus.

Apparatus. Absorbance and absorption spectra were measured with a Hitachi Perkin Elmer 139 spectrophotometer using 10 mm quartz cells. The pH values were measured with a Toa Electronics Model HM-15A digital pH-meter.

Standard Procedure. A sample solution containing up to 4 μmol (230 μg) of iron(III) is taken into a 50 cm^3 Erlenmeyer flask. Then 6 cm^3 of 1×10^{-3} M hbed, 1 cm^3 of 1 M acetic acid, and 2.5 cm^3 of 1 M sodium acetate are added. After being kept for about three minutes in a boiling water bath, the solution is cooled with running water. Next, the solution is transferred to a 25 cm^3 volumetric flask, and diluted to the mark with water (final pH: 5.1). The absorbance of the solution is measured at 485 nm against water.

Results and Discussion

Absorption Spectra. The red solution of Fe(III)–hbed complex had an absorption maximum at 485 nm. The reagent solution did not absorb light in the visible region.

Effect of pH. The pH of the Fe(III)–hbed complex solution was altered by the addition of nitric acid, acetic acid, acetic acid–sodium acetate, mannitol–boric acid–sodium borate, or sodium borate–sodium hydroxide buffer system. The absorbance of the solution at 485 nm remained constant over a wide pH range 2.5—13.2, as is shown in Fig. 1.

Stability of the Color. The color reaction of hbed with iron(III) seemed to take place rapidly, but the absorbance of the resultant colored solution increased very slowly. However, when the resultant solution was heated in a boiling water bath for about a few

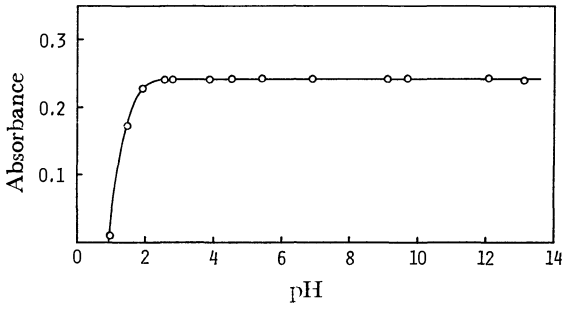

Fig. 1. Effect of pH on formation of Fe(III)–hbed complex.
Fe(III): 6.29×10^{-5} M (3.51 μg cm^{-3}), hbed: 1.03×10^{-4} M, wavelength 485 nm, reference: water, I= 0.1 M.

minutes, the maximum color development was obtained. The color, once developed, was very stable; the absorbance remained constant over a period of 72 h, and the absorbance was not affected by the measurement temperature (10—35 °C). Further, the reagent solution itself was stable; the concentration was unchanged for at least 40 d.

Effect of hbed Concentration. A constant absorbance was obtained over a [hbed]/[Fe(III)] ratio range 1.0—6.0. This fact shows that a large excess of reagent is not needed for full color development.

Effects of the Amount of Buffer Solution and Ionic Strength. A buffer solution was prepared by mixing 1 M acetic acid solution with 1 M sodium acetate solution in 1:2.5 ratio. The addition of from 1 to 10 cm^3 of the buffer solution (for 1.5 μmol of iron(III) in 25 cm^3 solution) had no effect on the color intensity of the iron(III) complex. The effect of ionic strength was also examined. The color intensity of the iron(III) complex did not change in ionic strengths from 0.1 to 0.4 M.

Calibration Curve. The calibration curve under the conditions described in the standard procedure was linear at least up to 1.6×10^{-4} M (9 μg cm^{-3}) of iron(III). The molar absorption coefficient of Fe(III)–hbed complex was 3.95×10^3 l mol^{-1} cm^{-1}, and the Sandell sensitivity for the absorbance of 0.001 was 1.41×10^{-2} μg cm^{-2}. The relative standard deviation of the absorbance was 0.29% for 6.3×10^{-5} M (3.5 μg cm^{-3}) of iron(III) (12 determinations).

Effect of Diverse Ions. The effect of diverse ions was investigated, as is shown in Table 1. It was seen that a large excess of colored metal ions interfered to some extent, and other metal ions did not interfere even if they were present at a concentration of 2000 times that of iron(III). The interferences from the metal ions such as chromium(III), cobalt(II), nickel(II), and uranyl(II) are considered to be attributed to the absorption of light by the colored aqua metal ions, since positive error occurs.

Composition of the Complex. The results obtained by the molar ratio study are shown in Fig. 2. It is seen that iron(III) forms a 1:1 complex with hbed. The same results were also obtained by the continuous variation method.

Determination of Iron(II). It seemed that hbed reacted with iron(II) and the Fe(II)–hbed complex formed was oxidized instantly to the red complex Fe(III)–hbed. Thus, the determination of iron(II) was run by use of the present method. The results of the three repeated determinations for 1.54 μmol/25 cm^3 of iron(II) were 1.53, 1.54, and 1.53 μmol/25 cm^3; iron(II) could be determined without addition of any oxidizing agent. Consequently, the total iron content, iron(II) and iron(III), is determined by the present method.

Determination of Iron in an Aluminium Alloy. Aluminium alloys were furnished by the National Bureau of Standards. 85b wrought: Fe, 0.24; Cu, 3.99; Si, 0.18; Mn, 0.61; Ni, 0.084; Cr, 0.21; Ti, 0.022; Pb, 0.021; Mg, 1.49; Zn, 0.03%. 87a Al-Si: Fe, 0.61; Cu, 0.30; Si, 6.24; Mn, 0.26; Ni, 0.57; Cr, 0.11; Ti, 0.18; Pb, 0.10; Mg, 0.37; Zn, 0.16%.

Table 1. Effect of diverse ions on the determination of iron(III)

Ion	Added as	Amount added to 25 cm^3	Iron(III) found in 25 cm^3
		μmol	μmol
K^+	KCl	3000	1.51
Li^+	$LiNO_3$	3000	1.51
Na^+	$NaNO_3$	3000	1.51
NH_4^+	NH_4Cl	3000	1.51
Rb^+	$RbNO_3$	3000	1.52
Tl^+	$TlNO_3$	3000	1.51
Ba^{2+}	$Ba(NO_3)_2$	3000	1.51
Be^{2+}	$Be(NO_3)_2\cdot3H_2O$	3000	1.53
Ca^{2+}	$Ca(NO_3)_2\cdot4H_2O$	3000	1.52
Cd^{2+}	$Cd(NO_3)_2\cdot4H_2O$	3000	1.51
Co^{2+}	$Co(NO_3)_2\cdot6H_2O$	20	1.54
Cu^{2+}	$Cu(NO_3)_2\cdot3H_2O$	750	1.43[20]
		300	1.51
Mg^{2+}	$Mg(NO_3)_2\cdot6H_2O$	3000	1.51
Mn^{2+}	$Mn(NO_3)_2\cdot nH_2O$	3000	1.55
		750	1.53
Ni^{2+}	$Ni(NO_3)_2\cdot6H_2O$	750	1.53
Pb^{2+}	$Pb(NO_3)_2$	3000	1.52
Sr^{2+}	$Sr(NO_3)_2$	3000	1.50
UO_2^{2+}	$UO_2(NO_3)_2\cdot6H_2$	30	1.55
		15	1.52
Zn^{2+}	$Zn(NO_3)_2\cdot6H_2O$	3000	1.52
Al^{3+}	$K_2Al_2(SO_4)_4\cdot24H_2O$	3000[a]	1.50
Ce^{3+}	$Ce(NO_3)_3\cdot6H_2O$	3000	1.52
Cr^{3+}	$Cr(NO_3)_3\cdot9H_2O$	20	1.58
		5	1.53
La^{3+}	$La(NO_3)_3\cdot6H_2O$	3000	1.51
Cl^-	NaCl	3000	1.51
ClO_4^-	$NaClO_4$	3000	1.52
F^-	NaF	3000	1.52
NO_2^-	$NaNO_2$	3000	1.52
NO_3^-	$NaNO_3$	3000	1.51
SCN^-	NH_4SCN	3000	1.52
SO_4^{2-}	$Na_2SO_4\cdot10H_2O$	3000	1.51
Citrate	$C_6H_8O_7\cdot H_2O$	1300	1.50
Phosphate	$NaH_2PO_4\cdot2H_2O$	3000	1.52

Iron(III) taken: 1.52 μmol(84.9 μg) in 25 cm^3 solution.
a) The pH was adjusted to 3.2.

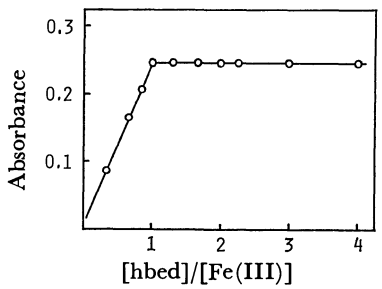

Fig. 2. Molar ratio plot at 485 nm.
Fe(III): 6.29×10^{-5} M, reference: water, pH=5.5, I=0.1 M.

A weighed amount of the alloy (85b wrought: 0.5 g, 87a Al–Si: 1.2 g) was taken in a 50 cm^3 Erlenmeyer flask, and concentrated hydrochloric acid

TABLE 2. ANALYTICAL RESULTS OF IRON IN ALUMINUM ALLOYS

Sample	Certified (%)	Found (%)
NBS 85, Wrought	0.24	0.23 0.24 0.24
NBS 87a, Al-Si	0.61	0.61 0.61 0.61

was added drop by drop. After the dissolving was complete, a small amount of concentrated nitric acid was added and the solution was boiled gently for several minutes. Next, the solution was transferred to a 100 cm^3 volumetric flask and diluted to the mark with water. Then, 3 cm^3 of the solution prepared was used for determination of iron. In the determination, the pH was adjusted to 3.2. The analyses were run three times, starting from the weighing of the sample. As shown in Table 2, satisfactory results were obtained.

Conditional Stability Constants. The stability constants for the hbed complexes of iron(III), copper(II), nickel(II), manganese(II), cadmium(II), lead(II), magnesium(II), calcium(II), cobalt(II), and zinc(II) are known.[10] Thus, the conditional stability constants[12] ($K_{M'L'(ML)'}$) for the hbed complexes were calculated from Eq. 1[13] with the aid of an electronic computer (OKITAC 50).

$$K_{M'L'(ML)'} = \frac{[(ML)']}{[M'][L']} = \frac{\alpha_{ML(H)}}{\alpha_{M(OH)}\alpha_{L(H)}} K_{ML}, \quad (1)$$

where

$$\alpha_{M(OH)} = 1 + \sum_{m=1}^{m} \beta_{M(OH)_m}[OH^-]^m,$$

$$\alpha_{L(H)} = 1 + \sum_{n=1}^{n} \beta_{H_nL}[H^+]^n,$$

$$\alpha_{ML(H)} = 1 + \sum_{i=1}^{i} \beta_{MH_iL}[H^+]^i.$$

Here, K_{ML} refers to the stability constant of the complex ML, $\beta_{M(OH)_m}$ and β_{H_nL} are the over-all stability constant of the metal complex with hydroxide ion and the over-all protonation constant of the ligand, respectively, and β_{MH_iL} is the over-all protolytic stability constant of the acid complex MH_iL $\left(\prod_{i=1}^{i} \frac{[MH_iL]}{[MH_{i-1}L][H^+]}\right)$. The formation of an acid complex with known constant was taken into consideration. In Fig. 3, the conditional constants calculated at various pH values are plotted. Figure 3 shows that the value of the conditional constant of Fe(III)–hbed complex is considerably higher than those of the hbed complexes of other metals.

Conditional stability constants of metal–eddha complexes were also calculated from the stability constants[14,15] of the related complexes, and compared with those of the metal–hbed complexes. The conditional constant of Fe(III)–hbed complex is higher than that of Fe(III)–eddha complex, as shown in Fig. 3. For other metals, however, the consitional

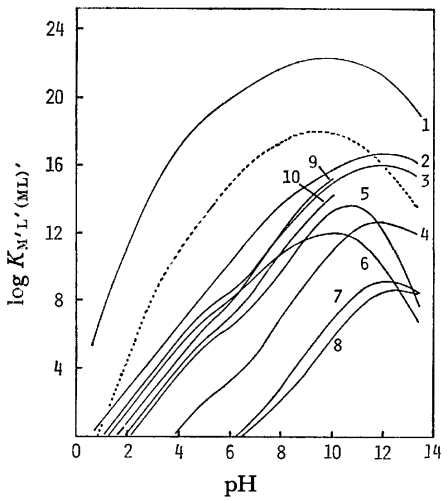

Fig. 3. Conditional stability constants, $K_{M'L'(ML)'}$, of various metal–hbed complexes as functions of pH. Metal: 1, Fe(III); 2, Cu(II); 3, Ni(II); 4, Mn(II); 5, Cd(II); 6, Pb(II); 7, Mg(II); 8, Ca(II); 9, Co(II); 10, Zn(II). The dotted line shows the conditional stability constant of Fe(III)–eddha complex.

constant of the hbed complex is similar in magnitude to that of eddha complex. Consequently, it may be seen that reagent hbed is superior to reagent eddha in the determination of iron(III).

Characteristics of the Present Method. The present method has high selectively without masking agents (Table 1). This is attributable to the following reasons: (1) the stability constant of Fe(III)–hbed complex is particularly large among those of metal–hbed complexes; (2) the absorption spectrum of Fe(III)–hbed complex in the visible region differs from those of other metal–hbed complexes, whose spectra are similar in shape and magnitude to those of aqua metal ions. The precision is relatively high (relative standard deviation: 0.29%); this seems to be attributable to the high stability of the developed color. On the other hand, the sensitivity is small. In selectivity the present reagent hbed is superior to other reagents, *e.g.*, eddha,[6] 5-sulfosalicylic acid,[16] tiron,[17] edta,[18] and salicylic acid,[19] whose sensitivities are also small.

References

1) "Zikken Kagaku Koza," 3rd ed, ed by the Chemical Society of Japan, Maruzen, Tokyo (1966), Vol. 15, Part II, p. 268.
2) "Shin Zikken Kagaku Koza," ed by the Chemical Society of Japan, Maruzen, Tokyo (1976), Vol. 9, Part I, p. 331.
3) "Bunseki Kagaku Binran," 2nd ed, ed by the Japan Society for Analytical Chemistry, Maruzen, Tokyo (1971), p. 102.
4) "Muki Oyo Hishoku Bunseki," Kyoritsu Shuppan, Tokyo (1974), Vol. 2, p. 323.
5) T. Takeuchi and Y. Shijo, *Bunseki Kagaku*, **14**, 930 (1965).
6) A. L. Underwood, *Anal. Chem.*, **30**, 44 (1958).
7) A. L. Underwood, *Anal. Chim. Acta*, **20**, 228 (1959).
8) G. V. Johnson and R. A. Young, *Anal. Chem.*, **40**, 354 (1968).

9) J. Ueda, *Bull. Chem. Soc. Jpn.*, **51**, 773 (1978).
10) F. L'Eplattenier, I. Murase, and A. E. Martell, *J. Am. Chem. Soc.*, **89**, 837 (1967).
11) The material prepared is slightly soluble in water. A 2×10^{-3} M solution may be prepared at room temperature. The velocity of dissolution is very slow. However, the velocity is accelerated by the addition of sodium hydroxide.
12) A. Ringbom, "Complexation in Analytical Chemistry," Interscience Publishers Inc., New York (1963), p. 35.
13) The formation of a basic complex was not taken into consideration since the formation constants of basic hbed complexes are not known.
14) A. E. Frost, H. H. Freedman, S. J. Westerback, and A. E. Martell, *J. Am. Chem. Soc.*, **80**, 530 (1958).
15) G. Anderegg and F. L'Eplattenier, *Helv. Chim. Acta*, **47**, 1067 (1964).
16) M. Kennard and C. R. Johnson, *Proc. Trans. Texas Acad. Sci.*, **27**, 45 (1944).
17) J. H. Yoe, *Ind. Eng. Chem., Anal. Ed.*, **16**, 111 (1964).
18) H. J. Cluley and E. J. Newman, *Analyst*, **88**, 3 (1963).
19) R. O. Scott, *Analyst*, **66**, 142 (1941).
20) The negative error can be attributed to the formation of a Cu(II)–hbed complex (with dissociation of Fe(III)–hbed complex) since the stability constant of the Cu(II)–hbed complex is high.

Wet Oxidation of Water-soluble Polymers

Sei-ichiro IMAMURA,* Yoshiaki TONOMURA, Nariyoshi KAWABATA, and Takane KITAO**

Department of Chemistry, Kyoto Institute of Technology, Matsugasaki, Sakyo-ku, Kyoto 606
***School of Regional Planning, Toyohashi University of Technology, Tenpaku-cho, Toyohashi 440*

(Received September 19, 1980)

Wet oxidation of various water-soluble polymers was carried out with particular attention given to the reactivity of polyethylene glycol. Polymers with high molecular weight were more reactive than their low molecular weight analogues or monomer models. It is suggested that the high reactivity of the polymers can be attributed to the ease of an intramolecular hydrogen abstraction in the propagation step of oxidation. Bio-degradability of the polymers was highly improved by wet oxidation. Wet oxidation is especially effective for the treatment of waste water containing water-soluble polymers.

Wet oxidation of organic compounds is carried out under a high pressure of air and at an elevated temperature between 100 °C and a critical temperature of water, 372 °C. This method has been successfully applied to the treatment of various sludges,[1,2] waste water from organic chemicals manufacturing process,[3] and pulp and paper mill waste matters.[4] Under appropriate conditions, organic pollutants can be completely removed. However, the severe reaction conditions require higher running and installation costs than other processes, and practical application of this method is limited.

The reaction mechanism of the process has not been clarified as yet. Mitigation of the conditions is desirable by the development of effective catalysts or improvement of the process of the operation.[5] Previously investigation was carried out on the wet oxidation of various low molecular weight organic compounds including dyes and amides.[6-8] The reactivity of these compounds is correlated with the carbon content in a molecule. Compounds with higher carbon content seem to lose carbon monoxide or carbon dioxide more easily in the course of their degradation to refractory lower carboxylic acids, giving rise to faster decrease in total organic carbon. If this reactivity-carbon content relationship can be applied to the wet oxidation of polymers, the reactivity of homologous polymers would be independent of their molecular weight.

We have investigated the wet oxidation of water-soluble polymers with an emphasis on polyethylene glycol. Water-soluble polymers are widely used as water treatment agents, food additives, antifreeze, and in cosmetics. Their discharge into environment might cause serious water pollution because some of them are inert to biological degradation and accumulate in the environment.[9] Their complete removal is difficult when ordinary physicochemical treatment such as adsorption or reverse osmosis is carried out. Improvement of the bio-degradability of the polymers by the treatment has also been examined.

Experimental

Material. Commercial reagents were used without further purification. Polyethylene glycol (PEG), polypropylene glycol (PPG), poly(vinyl alcohol) (PVA), polyacrylamide (PAM), pol(acrylic acid) (PAA), carboxymethylcellulose (CMC), 2-hydroxyethylcellulose (HEC), and methylcellulose (MC) were used as the water-soluble polymers. Their molecular weights, except for PEG and PPG, were determined from the corresponding molecular weight-viscosity relationship.[10] The results are given in Table 1.

TABLE 1. MOLECULAR WEIGHT OF POLYMERS

Polymer	Molecular weight
PEG-200	190—210
PEG-400	380—420
PEG-1000	950—1050
PEG-2000	1800—2200
PEG-4000	3000—3700
PEG-6000	7800—9000
PEG-20000	24900
PPG	1000
PVA	21500
PAM	485000
PAA	38000
CMC	17500
HEC	82600
MC	58200

Apparatus and Procedure. Deionized water, nitrogen (0.98 MPa), and Oxygen (1.96 MPa) were placed in the reaction vessel, a 1—1 autoclave equipped with a sample injector and a valve for sampling. The vessel was heated with an electric furnace. A polymer solution was injected through the injector under pressure, the solution being stirred magnetically. It was confirmed that the reactions were not controlled by the diffusion of oxygen into the liquid phase. At appropriate time intervals, an aliquot of the solution was withdrawn through a cooling jacket and subjected to analysis.

The reactivity of polymers was determined on the basis of the decrease in total organic carbon during the course of reaction.

Analysis. Total organic carbon (TOC) analysis was carried out with a Sumitomo Model GCT-12N TOC analyzer and gas chromatographic (GPC) analysis with a Shimadzu GC-6A gas chromatograph equipped with a flame ionization detector using nitrogen as the carrier gas. Polyester FF 10% on Neosorb NFH, 3 mm × 2 m, was used for the GPC analysis of ethylene glycol (EG), diethylene glycol (DEG), triethylene glycol (TEG) and formaldehyde, and chromosorb 101, 3 mm × 2 m, for ethanol and propionamide. Ion chromatographic analysis was performed on a Dionex Model 10 ion chromatograph using an anion separating column and 2.5×10^{-3} mol dm^{-3} Na_2CO_3 plus 3.0×10^{-3}

mol dm^{-3} $NaHCO_3$ as an eluent. Proton NMR spectra were taken on a Varian Model T-60A spectrometer using tetramethylsilane as a standard and deuteriochloroform as solvent, and infrared spectra on a Hitachi Model 215 grating spectrophotometer. Molecular weight of PEG was determined on a Toyo Soda Model HLC-802 UR gel permiation chromatograph using commercial PEG samples as standard.

Results and Discussion

Effect of Molecular Weight on the Wet Oxidation of PEG. Figure 1 shows the time courses of the TOC decrease in the wet oxidation of PEG-20000 at various temperature. The temperature dependency is remarkable as in the oxidation of benzyl alcohol reported previously.[6] The rate of the reaction was found to be independent of the oxygen pressure above 0.98 MPa.

The reactivity of PEG depends upon the molecular weight (Fig. 2). Ethylene glycol does not react under the conditions, but the reactivity of PEG increases with an increase in molecular weight. Although there is a maximum in the rate of TOC decrease at a molecular weight around 2000, PEG with higher molecular weight is more reactive as compared with its low molecular weight analogues. Thus, successive reaction was carried out with PEG-200 and PEG-20000.

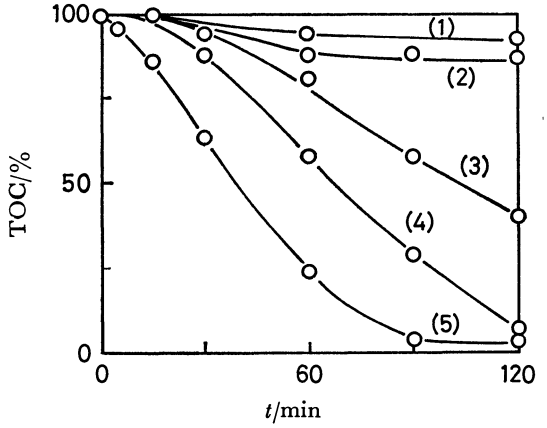

Fig. 1. Wet oxidation of PEG-20000. Effect of temperature.
$[PEG]_0$=5000 ppm, $P(O_2)$=1.96 PMa. (1): 160 °C, (2): 180 °C, (3): 200 °C, (4): 210 °C, (5) 220 °C.

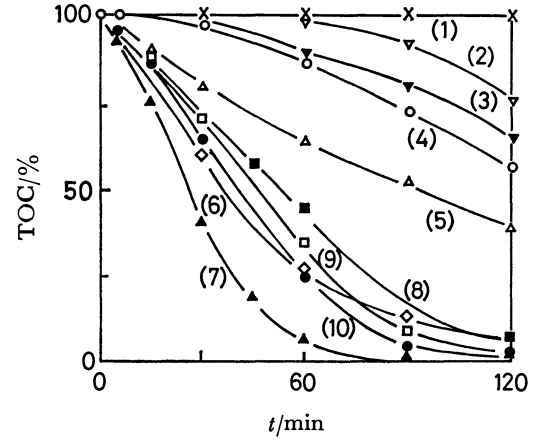

Fig. 2. Wet oxidation of PEG. Effect of molecular weight.
$[TOC]_0$=2500 ppm, $P(O_2)$=1.96 MPa, 220 °C.
(1): EG, (2): DEG, (3): TEG, (4): PEG-200, (5): PEG-400, (6): PEG-1000, (7): PEG-2000, (8): PEG-4000 (9): PEG-6000, (10): PEG-20000.

Accumulation of Acids during the Course of Reaction. Figure 3 shows the changes in pH and acid accumulation during the course of wet oxidation of PEG-200 and PEG-20000. The pH decreases at the initial stage of the reaction, recovering gradually. In the case of PEG-20000, the change in pH is more rapid as compared with PEG-200. The amount of acid increases at an early stage of the reaction, then decreasing. Both accumulation and decrease of acids were faster with PEG-20000 than with PEG-200, which can be explained in terms of the difference in molecular weight. Acids formed from PEG-20000 should have higher molecular weight than those from PEG-200, and should be more reactive. The molecular weight determined in the course of oxidation of PEG-20000 was *ca.* 600 after 5 min, and *ca.* 300 even after 30 min.

Product Analysis. Gas chromatographic analysis of the reaction mixture of the wet oxidation of PEG-200 and PEG-20000 showed formation of formaldehyde, EG, DEG, and TEG during the course of oxidation. The amount of these products, shown as functions of the reaction time in Figs. 4 and 5, increased with the progress of reaction in the case of PEG-200. Oxidation of PEG-20000 gave a large

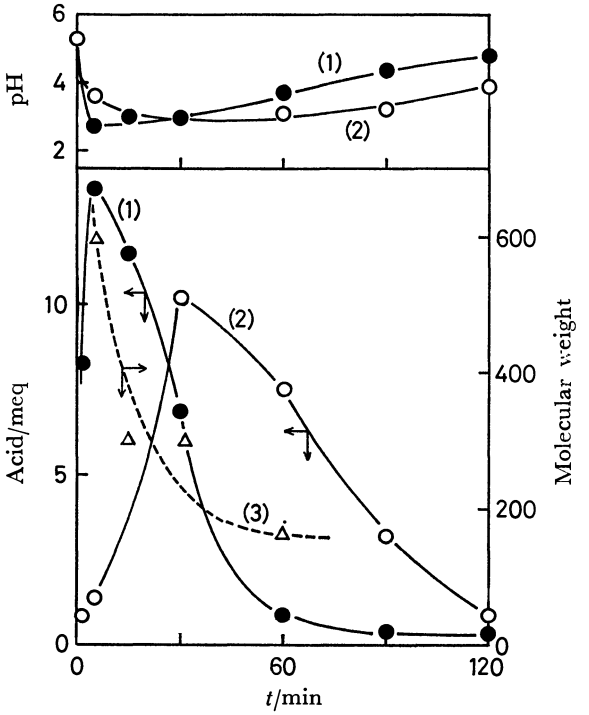

Fig. 3. pH change and acid accumulation during the wet oxidation of PEG-200 and PEG-20000.
$[TOC]_0$=500 ppm, $P(O_2)$=0.98 MPa, 220 °C. (1): PEG-20000, (2): PEG-200, (3): Molecular weight of oxidized PEG-20000.

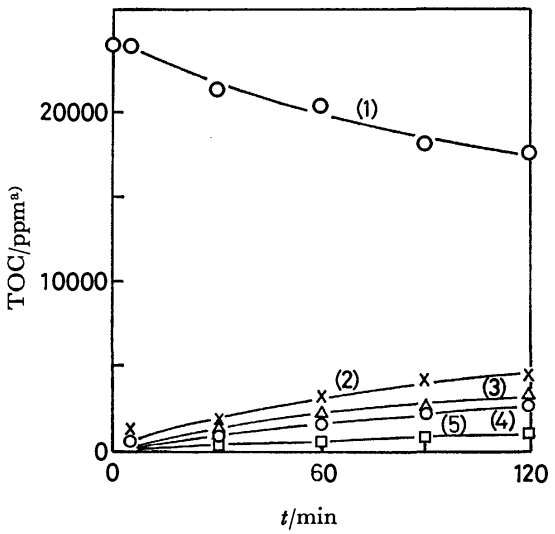

Fig. 4. Accumulation of EG, DEG, TEG, and formaldehyde during the wet oxidation of PEG-200.
$P(O_2)=1.96$ MPa, 220 °C. (1): Decrease of TOC, (2): TEG, (3): EG, (4): DEG, (5): Formaldehyde.
a) Accumulation of EG, DEG, TEG, and formaldehyde is expressed by TOC contained in these compounds.

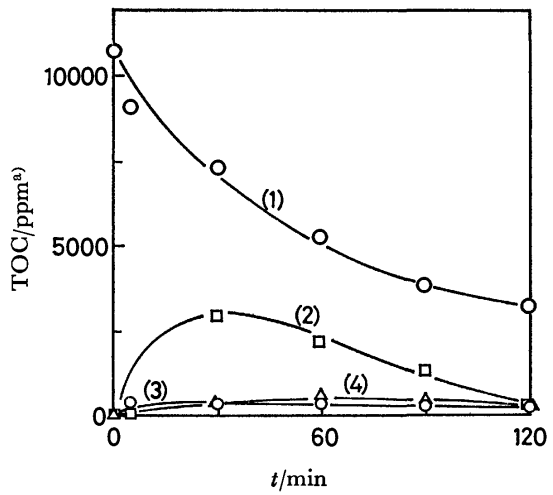

Fig. 5. Accumulation of EG, DEG, and formaldehyde during the wet oxidation of PEG-20000.
$P(O_2)=1.96$ MPa, 220 °C. (1): Decrease of TOC, (2): Formaldehyde, (3): EG, (4): DEG.
a) Accumulation of EG, DEG, and formaldehyde is expressed by TOC contained in these compounds.

amount of formaldehyde at an early stage of the reaction, decreasing with the progress of reaction. Only trace amount of EG and DEG were detected in this case.

Ion chromatographic analysis of the reaction mixture in the oxidation of PEG-20000 showed the formation of formic acid and acetic acid. Proton NMR spectra of the oxidation products of PEG-20000 showed unresolved signals at δ 4.4—4.7 and 3.6. A signal observed at δ 8.1 was assigned to formyl protons. The results indicate the formation of formic acid and/or formic esters. Infrared spectra of these products indicate the presence of carboxylic acids.

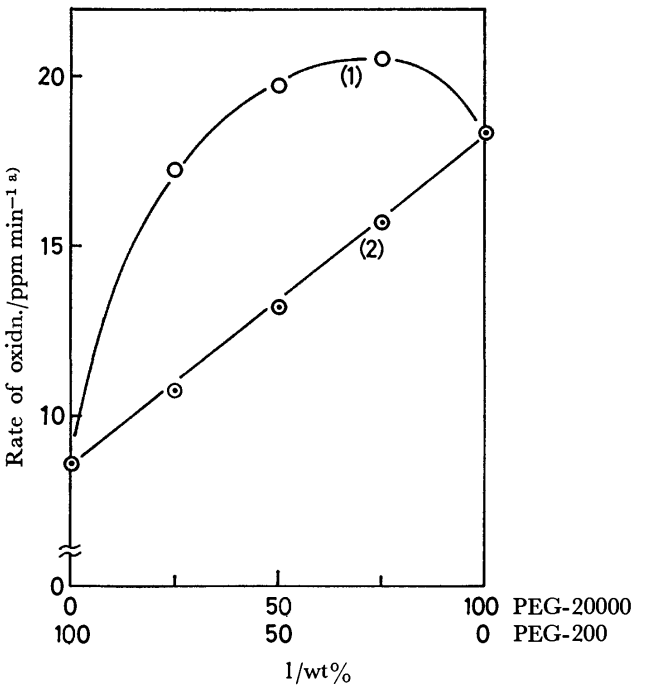

Fig. 6. Co-oxidation of PEG-200 and PEG-20000.
$P(O_2)=1.96$ MPa, Total $[TOC]_0=2500$ ppm, 220 °C. (1): obsd, (2): calcd.
a) The rate was calculated from TOC decrease.

Co-oxidation of PEG-200 with PEG-20000. First, the effect of the concentration of the polymers on the rate of oxidation was examined. The curves of TOC decrease show an induction period (Fig. 2), the rate of oxidation being expressed by the mean velocity of TOC decrease at the reaction time of 60 min. The apparent reaction orders with respect to TOC were found to be 1.0 and 0.75 for PEG-20000 and PEG-200 respectively.

Figure 6 shows the dependence of the rate of oxidation on the ratio of the concentrations of PEG-200 and PEG-20000. The calculated line was obtained by taking the reaction order into consideration. The experimental data lie far above this line, suggesting that the reaction proceeds in a radical mechanism, where active species produced from PEG-20000 attack PEG-200. Co-oxidation of reactive compounds with less reactive reactants would thus be useful in practical waste water treatment. The apparent activation energy for the oxidation of PEG-20000 was 97.9 kJ/mol in the temperature range 180—220 °C.

Mechanism of Product Formation in Wet Oxidation of PEG. The following scheme is proposed for an explanation of the formation of the identified products. A radical mechanism seems to support the result. Goglev and Neiman reported that the thermal oxidation of PEG proceeds in a radical mechanism in which the first step is the formation of hydroperoxide of PEG.[11] The first step would be the formation of a hydroperoxide A, which undergoes thermal decomposition to produce an alkoxyl radical B and a hydroxyl radical. The hydroxyl radical is highly reactive and would give rise to further degradation of PEG.

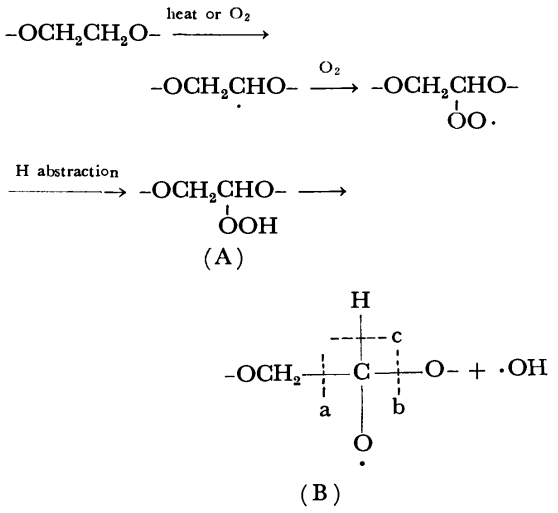

Hydrogen atom fragmentation at bond c or hydrogen abstraction of the intermediate B might lead to the formation of an alcohol or an ester, although they were not characterized.

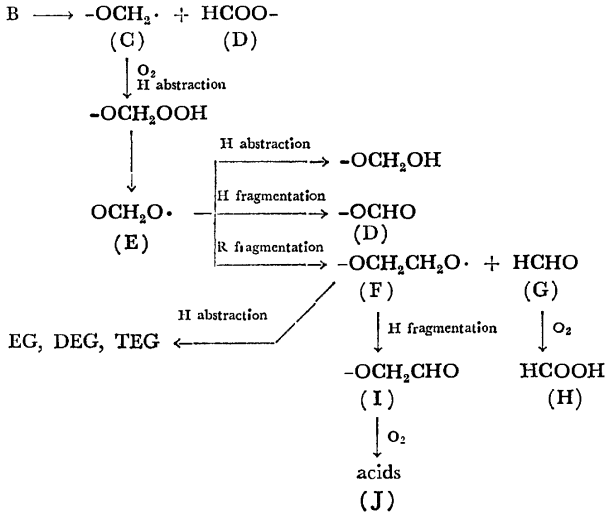

Fragementation at bond a of the radical B might produce formic ester D. The radical C is converted into an alkoxyl radical E, which undergoes an alkoxyl radical fragmentation (R fragmentation) to give another alkoxyl radical F and formaldehyde G. The latter might undergo further oxidation to produce formic acid H. Alkoxyl radical F would give EG, DEG, or TEG by hydrogen abstraction. Radical F might also produce aldehyde I, from which carboxylic acid J would be formed.

Fragmentation at bond b of the radical B can explain the formation of aldehyde and alkoxyl radical; their behaviour would be the same as discussed above.

$$B \longrightarrow -OCH_2CHO + \cdot OCH_2CH_2O-$$

Consideration on the Effect of Molecular Weight on the Reactivity of PEG. The reactivity of a hydrocarbon in the autoxidation depends upon the rate of the propagation step.

$$ROO\cdot + RH \longrightarrow ROOH + R\cdot$$

This step generally occurs intermolecularly, although intramolecular reaction is also possible. Intramolecular hydrogen abstraction *via* cyclic intermediate occurs easily in the oxidation of acyclic ethers.[11,12] It is assumed that intramolecular process plays an important role when the concentration of PEG is low. Ease of cyclization depends upon the stability of the ring formed and on the activation entropy of cyclization. In the lactone formation from hydroxy acid, five to seven membered rings are easily produced, rings with more than fourteen atoms being also possible.[13] In the oxidation of PEG, cyclic transition state with five, six, and more than fourteen membered rings including peroxy oxygen atoms seems favorable. However, in the oxidation of PEG with a low molecular weight, *e.g.* PEG-200, intramolecular hydrogen abstraction would be difficult after several chain scissions. On the other hand, PEG with a high molecular weight holds a long chain during the course of oxidation (Fig. 3) and would undergo further intramolecular reaction.

Although the above explanation is possible for the effect of molecular weight on the wet oxidation of PEG, it does not necessarily follow that the higher the molecular weight, the higher the reactivity. A maximum in the reactivity was observed for PEG with a molecular weight *ca.* 2000, further increase in molecular weight showing little effect (Fig. 2). This suggests that the propagation step is a competition between intra- and intermolecular hydrogen abstraction as Goglev and Neiman indicated.[11] Intermolecular reaction should decrease with the increase in the molecular weight of PEG as a result of the reduced rate in the diffusion of the molecule.

Wet Oxidation of Other Polymers. Reactivity of other polymers in the wet oxidation was also investigated. In the case of CMC, HEC, and MC, viscosity of the aqueous solution of these polymers was very high, making the use of the sample injector impossible. Thus, reactions were carried out by heating a sample solution under a nitrogen atmosphere followed by injecting oxygen into the vessel. Viscosity and pH of the solution decreased during the course of pre-heating, indicating that thermal degradation occurred during this period. As shown in Fig. 7, all polymers were equally or even more reactive than PEG-20000. The reactivities of PVA, PPG, PAM, and PAA and their respective monomer models, ethanol, 1,2-propanediol, propionamide, and propionic acid were compared (Figs. 8 and 9), the sample injector being used. The reactivity of PVA was high, but TOC decrease in the oxidation of ethanol was slow, the amount of residual TOC being in line with the residual amount of ethanol determined by gas chromatography. Propionamide gradually decomposed, but TOC remained unchanged. On the other hand, PAM oxidized rapidly. Similar results were observed for PPG and PAA.

The results indicate that the polymers are reactive to a greater extent than the corresponding low molecular weight analogues due to a significant polymer effect, and that wet oxidation is particularly effective for the treatment of these water-soluble polymers. The reactivity-carbon content relationship, observed in the

oxidation of low molecular weight compounds, is not applicable to the wet oxidation of polymers.

Improvement of Bio-degradability of Polymers. Synthetic polymers are generally inert to biological treatment. Although PEG can be degraded by some microorganism, the rate of degradation is low.[9]

We have examined the improvement of bio-degradability of the polymers by wet oxidation. The results are given in Table 2. The bio-degradability is expressed by $(BOD_5/COD_{Cr})\times 100$ of the sample solution. Although all the polymers examined were inert to biological degradation, their bio-degradability was remarkably improved by wet oxidation. Treatment for only 5 min considerably improved the reactivity. After 2 h of oxidation, complete reactivity in the biological treatment was attained with PEG-1000 and PEG-2000. The effects of atmosphere and temperature of wet oxidation on the improvement of the bio-degradability of PEG-20000 are given in Table 3. Although degradation of the polymer chain occurs under a nitrogen atmosphere, scarcely any improvement in bio-degradability was observed. Incorporation of oxygen atoms into the reactant is inevitable. The bio-degradability was considerably improved by the wet oxidation at 160 °C, although there

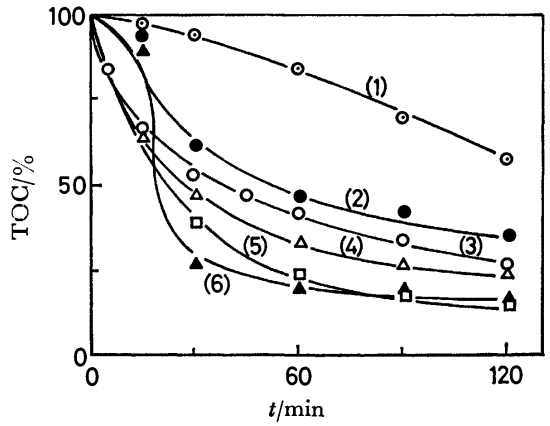

Fig. 7. Wet oxidation of water-soluble polymers.
$P(O_2)=2.94$ MPa, $[Polymer]_0=5000$ ppm, 220 °C.
(1): PEG-200, (2): PEG-20000, (3): PVA, (4): MC, (5): PAA, (6): PAM.

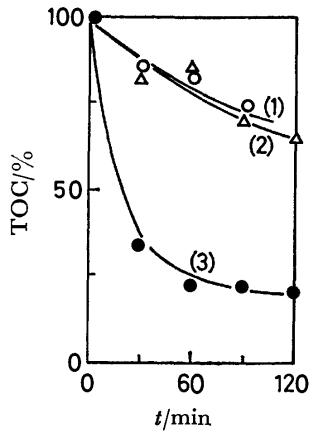

Fig. 8. Wet oxidation of PVA and ethanol.
$P(O_2)=1.96$ MPa, $[TOC]_0=2500$ ppm, 220 °C.
(1) Ethanol, (2) Ethanol determined by gas chromatograph and expressed by the TOC content, (3) PVA.

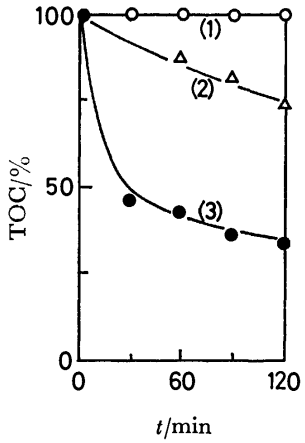

Fig. 9. Wet oxidation of PAM and propionamide.
$P(O_2)=0.98$ MPa, $[TOC]_0=500$ ppm, 220 °C.
(1): Propionamide, (2): Propionamide determined by gas chromatograph and expressed by the TOC content, (3): PAM.

TABLE 2. BIODEGRABILITY OF POLYMERS[a]

Polymer	Reaction time/min		
	0	5	120
EG —[b]	76.0	—	—
PEG-200	4.0	23.0	49.0
PEG-400	0.2	36.0	65.0
PEG-1000	0	51.0	100
PEG-2000	2.0	50.0	100
PEG-4000	2.0	73.0	80.0
PEG-6000	6.0	57.0	91.0
PEG-20000	0.4	61.0	64.0
PVA —	1.0	17.0	86.0
PPG —[c]	1.3	33.0	58.0
Ethanol	63.0	—	—
PAM	1.0	15.0	53.0
PAA —	1.5	47.0	46.0

a) Expressed by $(BOD_5/COD_{Cr})\times 100$. b) Reaction conditions shown in Fig. 3. c) Reaction conditions: [Reactant] = 1000 ppm, $P(O_2)=0.98$ MPa, 220 °C.

TABLE 3. BIO-DEGRADABILITY OF PEG-20000.[a] EFFECTS OF TEMPERATURE AND ATMOSPHERE IN THE TREATMENT OF PEG-20000

Reaction time / min	220 °C N_2[b]	220 °C N_2–O_2[c]	200 °C N_2–O_2[c]	180 °C N_2–O_2[c]	160 °C N_2–O_2[c]	100 °C N_2–O_2[c]
5	6.0	61.0	23.0	43.0	41.0	1.7
120	8.0	64.0	38.0	62.0	61.0	30.0

a) Expressed by $(BOD_5/COD_{Cr})\times 100$. b) $P(N_2)=1.96$ MPa. c) $P(O_2)=1.96$ MPa.

was scarcely any decrease in TOC. Moreover, the oxidation at as low as 100 °C was still effective when sufficient reaction time as 2 h was employed. This shows that wet oxidation under mild conditions is sufficient for the improvement of bio-degradability. Thus wet oxidation is an effective pre-treatment for the biological purification of waste water containing those water-soluble polymers.

We thank Dr. J. Yoshida and Dr. S. Kojiya, Kyoto Institute of Technology, for their helpful advice and discussions.

References

1) L. E. Sommers, *J. Water Pollut. Control. Fed.*, **49**, 2219 (1971).
2) G. H. Teletzke, W. B. Gitchel, D. G. Diddams, and C. A. Hoffman, *J. Water Pollut. Control. Fed.*, **39**, 994 (1967).
3) Y. Tagashira, H. Takagi, and K. Inagaki, Japan Kokai 75106862 (1975); *Chem. Abstr.*, **84**, 79359q (1976).
4) G. H. Teletzke, *Chem. Eng. Prog.*, **60**, 33 (1964).
5) N. Kawasaki, *Kogyo Kagaku Zasshi*, **67**, 1554 (1964).
6) S. I. Imamura, Y. Tonomura, M. Terada, and T. Kitao, *Water Purification and Liquid Wastes Treatment*, **20**, 317 (1979).
7) S. I. Imamura, J. Shimai, and T. Kitao, *Water Purification and Liquid Wastes Treatment*, **21**, 109 (1980).
8) S. I. Imamura, M. Fukuhara, and T. Kitao, *Nippon Kagaku Kaishi*, **1980**, 270.
9) G. K. Watson and N. Jones, *Water Res.*, **11**, 95 (1977).
10) "Polymer Handbook," 2nd ed, ed by J. Brandrup and E. H. Immergut, John Wiley & Sons. Inc., New York (1975), Chap. IV.
11) R. S. Goglev and M. B. Neiman, *Vysokomol. Soedin., Ser. A*, **9**, 2083 (1967).
12) J. A. Howard and K. U. Ingold, *Can. J. Chem.*, **48**, 873 (1970).
13) M. Sisido, *Makromolecules*, **4**, 737 (1971).

Peroxomonophosphoric Acid Oxidation. V.[1] A Kinetic and Mechanistic Study of Oxidation of Aminobenzoic Acids in Acid Medium. Double Bell Shaped pH Rate Profile

Ganesh Prasad PANIGRAHI* and Abhina Kumar PANDA
Department of Chemistry, Berhampur University, Berhampur 760007, India
(Received April 28, 1980)

Anthranilic acid and *p*-aminobenzoic acid were oxidized with peroxomonophosphoric acid in aqueous acid medium to the corresponding azoxy derivatives. Suitable rate laws for the double bell shaped pH rate profile were derived and rationalized on the basis of protonation of the amino group and ionization of the carboxyl group. The mechanism of oxidation involves the nucleophilic attack of nitrogen on the electrophilic peroxo oxygen. The reactivity of different peroxomonophosphoric acid species has been estimated.

Reports have been given on the oxidation of 3-aminopyridine,[1] dimethyl sulfide,[2] dimethyl sulfoxide,[3] and benzaldehyde[4] by peroxomonophosphoric acid (PMPA). In the oxidation of sulfide, the sulfur functions as a nucleophile. While the dimethyl sulfoxide oxidation presents dualistic behavior, sulfur acts as a nucleophile in the acid medium, becoming an electrophile in alkaline medium. It is of interest to see whether amines which are good nucleophiles act by a mechanism similar to that of sulfides. There seems to be no kinetic and mechanistic study on the oxidation of aromatic amines except for a preliminary work by Boyland and Manson[5] who screened a number of amines towards their reactivity to PMPA to see whether they involve oxidative phosphorylation. Recently, Ogata and co-workers[6] studied the oxidation of *N,N*-dimethylaniline to *N,N*-dimethylaniline *N*-oxide and determined the relative reactivity of the various species of PMPA. We felt it necessary to extend the kinetic studies to aromatic amines such as anthranilic acid (OAB) and *p*-aminobenzoic acid (PAB). We wish to report some of the salient kinetic features of the reaction.

Experimental

All the chemicals were of analytical grade. Conductivity water was used in the preparation of the solutions and as a reaction medium. PMPA was prepared by acid hydrolysis of $K_4P_2O_8$.[7] The concentration was checked frequently by iodometry, the self-decomposition being negligible in the pH region examined. The acidity was adjusted by adding appropriate amounts of perchloric acid or standard buffers[8] and measured with a Systronics digital pH-meter 335. Sodium perchlorate was used for adjusting the ionic strength. Whenever necessary sodium perchlorate was generated by neutralizing the perchloric acid with carbonate free sodium hydroxide. Both the aminobenzoic acids were purified by recrystallization from water, their melting points (OAB-144 °C, PAB-191 °C) agreeing with those in literature (OAB-145 °C, PAB-192 °C). The kinetics was followed by measuring the rate of disappearance of PMPA, the estimation of which was made by iodometry in an acetic acid–acetate buffer of pH 4—5 with a drop of ammonium molybdate solution.[4] The rate constants were computed by the usual method and were found in duplicate runs to be reproducible within ±5%. Computations were carried out with a DCM minicomputer Microsystem 1121. The IR absorption spectra were recorded on a Perkin Elmer 137 spectrophotometer.

Product Study. PMPA=0.04 mol dm^{-3} (50 ml) and anthranilic acid 0.008 mol dm^{-3} (50 ml) were mixed at pH 1.3 and 45 °C and kept for 48 h. The product azoxybenzene-2,2′-dicarboxylic acid was extracted with diethyl ether (dark brown solid, yield 75%), checked for its purity by TLC and identified by its mp 225 °C (uncorrected) and IR (Nujol): 1690(s) (ArCOOH) and 1290(s) (N=N→O) cm^{-1}. Under similar conditions the product azoxybenzene-4,4′-dicarboxylic acid isolated from *p*-aminobenzoic acid (a yellow solid, yield 80%) was identified by its mp 238 °C (uncorrected) and IR (Nujol): 1710(s) (ArCOOH) and 1300(s) (N=N→O) cm^{-1}.

Results

The kinetics of oxidation of OAB and PAB by PMPA in aqueous medium was investigated at 308 K. The rate data for both OAB and PAB suggest second order kinetics at constant acidity, the rate law being

$$V = k'[\text{Aminobenzoic acid}]_t[\text{PMPA}]_t, \quad (1)$$

where subscript t stands for total concentration and k' the observed second order rate constant.

Effect of Acidity. The kinetics was investigated over the pH range 0—7. The rate data are summarized in Table 1. The plots of log k' *vs.* pH (Figs. 1 and 2) have two bell shaped regions, 0—3 and 3—7. This indicates participation of different species of PMPA resulting from dissociation (Eqs. 4 and 16) as well as different aminobenzoic acid species either resulting from protonation of the amino group or dissociation of the carboxyl group (Eqs. 3 and 15).

It appears that the rate law has to include complex H^+ dependence for each of the pH regions. It is possible to write the rate law in a general form as

$$V = k'[\text{substrate}]_t[\text{PMPA}]_t[H^+]^n, \quad (2)$$

where $-1<n<+1$.

Effect of Added Substances. At pH 1 ionic strength has little influence on the rate. A marginal influence is observed at pH 4.17 (Table 1). The reaction rate was found to be insensitive to the addition of radical trapping agents such as acrylamide. No influence was observed on rate by variation of solvents such as acetic acid.

Temperature Variation. Activation parameters have been evaluated from the linear Arrhenius plots of log k' *vs.* T^{-1} by measuring the rates of oxidation at four temperatures in the range 308—323 K (Table 2).

TABLE 1. SECOND ORDER RATE CONSTANTS FOR THE OXIDATION OF AMINOBENZOIC ACIDS BY PMPA SPECIES AT 308 K, $\mu=0.4$ mol dm^{-3} IN AQUEOUS MEDIUM AT VARIOUS pH

Substrate	pH	[Substrate] $\times 10^3$ / mol dm^{-3}	[PMPA] $\times 10^4$ / mol dm^{-3}	$k' \times 10^2$ / dm^3 mol^{-1} s^{-1}
Anthranilic acid	1.0	5.15	4.10	5.44
	1.0	2.65	4.62	5.51
	1.0	6.50	4.76	5.48
	1.0	9.70	3.67	5.14
	1.0	3.70	4.31	5.87
	1.0	3.65	8.94	5.01
	1.0	3.60	16.35	5.01
	1.0	3.65	4.37	5.81[a]
	1.0	3.74	4.01	5.56[b]
	1.0	3.70	4.01	5.18[c]
	1.0	3.66	4.06	5.20[d]
	1.0	3.64	4.49	5.03[e]
	6.67	3.81	3.55	1.66[f]
	0.3	3.66	5.36	3.60
	0.6	3.75	5.26	4.98
	0.83	3.65	3.69	5.41
	1.3	3.75	4.37	6.37
	1.7	3.57	4.17	5.60
	2.0	3.678	5.254	4.75
	2.24	3.63	4.17	3.73
	3.33	3.85	3.89	3.75
	3.73	3.69	4.69	4.17
	4.13	3.55	3.68	4.51
	4.17	3.62	4.08	3.86[g]
	4.17	3.62	4.18	4.98[h]
	4.85	3.68	4.51	5.84
	5.32	3.68	5.56	4.30
	5.59	3.68	4.82	3.82
	6.21	3.68	4.05	1.89
	6.65	3.59	2.82	1.76
Anthranilic acid	6.96	3.85	4.41	1.28
	7.20	3.75	4.91	1.15
	1.0	3.73	4.15	9.59[i]
	1.0	3.73	4.45	13.50[j]
	1.0	3.73	3.84	21.12[k]
	4.85	3.64	3.27	8.69[i]
	4.85	3.64	2.96	13.36[j]
	4.85	3.64	4.25	16.19[k]
p-Amino-benzoic acid	0.0	3.87	3.83	1.01
	0.12	3.81	3.54	1.12
	0.3	3.78	4.25	1.61
	0.52	3.78	3.49	2.18
	0.7	3.78	4.54	2.88
	1.0	3.54	4.27	6.81[i]
	1.0	3.54	4.67	11.40[j]
	1.0	3.54	5.37	17.23[k]
	1.0	3.79	4.32	5.43[l]
	1.0	3.70	3.86	4.83[m]
	1.0	3.70	4.53	5.41[n]
	1.0	3.85	3.52	5.14
	0.89	3.65	4.35	4.40
	1.36	3.81	3.26	4.22
	2.85	4.03	4.21	3.14
	3.39	4.03	4.08	2.99
	3.93	3.71	4.71	3.36
	4.50	3.71	4.19	3.98
	5.31	3.71	3.62	5.46
	5.87	4.03	3.41	2.97
	6.43	3.85	3.89	1.66
	7.03	3.85	3.48	1.09

a) $\mu=0.65$ mol dm^{-3}. b) $\mu=0.15$ mol dm^{-3}. c) 10% AcOH. d) 30% AcOH. e) Acrylamide, 3.1×10^{-3} mol dm^{-3}. f) Acrylamide 3.25×10^{-3} mol dm^{-3}. g) $\mu=0.15$ mol dm^{-3}. h) $\mu=0.8$ mol dm^{-3}. i) At 313 K. j) At 318 K. k) At 323 K. l) $\mu=0.6$ mol dm^{-3}. m) 20% AcOH. n) 40% AcOH.

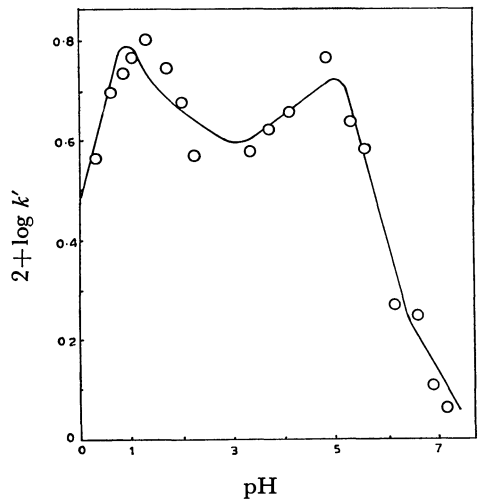

Fig. 1. Plots of log k' *vs.* pH (pH range 0 to 7) for OAB, ⊙ experimental points, — theoretical line obtained from Eq. 14 for pH 0 to 3 and Eq. 25 for pH 3 to 7.

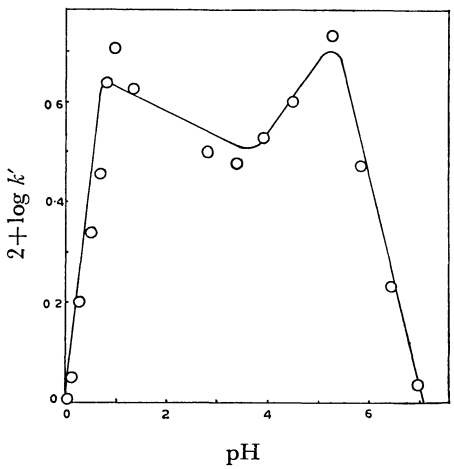

Fig. 2. Plots of log k' *vs.* pH (pH range 0 to 7) for PAB. ⊙ experimental points, — theoretical line obtained from Eq. 14 for pH 0 to 3 and Eq. 25 for pH 3 to 7.

TABLE 2. VALUES OF $\Delta H^{\ddagger}$ AND $\Delta S^{\ddagger}$ FOR THE OXIDATION OF AMINOBENZOIC ACIDS IN WATER AND $\mu=0.4$ mol dm^{-3} CALCULATED AT 308 K

pH	Substrate	$\Delta H^{\ddagger}$ / kJ mol^{-1}	$\Delta S^{\ddagger}$ / J K^{-1} mol^{-1}
1.0	OAB	66.6	−52.4
4.85	OAB	55.2	−89.2
1.0	PAB	66.0	−55.6

Discussion

In view of the rate-pH profile the following equilibria seem to be likely in the pH region 0—1.

$$BH^+ \overset{K_H}{\rightleftharpoons} B + H^+ \quad (3)$$

where B stands for aminobenzoic acid and BH^+ for N-protonated aminobenzoic acid.

$$H_3PO_5 \overset{K_1}{\rightleftharpoons} H_2PO_5^- + H^+ \quad (4)$$

The magnitude of $K_1(=8.0\times10^{-2})$ suggests that the peracid exists in a neutral form[9] as H_3PO_5 below pH 1. Similarly the protonation equilibria for the aminobenzoic acids suggest that it may exist both as BH^+ and B in the pH range 0—1. The inverse first order acid dependence in the region indicates the participation of free aminobenzoic acid but not the protonated species. The step may involve reaction between the neutral species of the substrate molecule and H_3PO_5 only.

The steps of the reaction below pH 1 may be as follows.

$$BH^+ \overset{K_H}{\rightleftharpoons} B + H^+ \quad (5)$$

and

$$B + H_3PO_5 \overset{k_1}{\longrightarrow} \text{Products.} \quad (6)$$

The total concentration of the base can be expressed as

$$[B]_t = [B] + [BH^+].$$

Hence

$$[B]_t = [B] + \frac{[B][H^+]}{K_H}$$

or

$$[B]_t = [B]\{1+[H^+]/K_H\} = \frac{B(K_H+[H^+])}{K_H}$$

or

$$[B] = \frac{[B]_t K_H}{(K_H+[H^+])}. \quad (7)$$

Hence the rate is expressed by

$$V = k_1[B][H_3PO_5]_t \quad (8)$$

$$= k_1\frac{K_H}{K_H+[H^+]}[B]_t[H_3PO_5]_t$$

$$= k'[B]_t[H_3PO_5]_t, \quad (9)$$

where

$$k' = \frac{k_1K_H}{K_H+[H^+]}, \quad (10)$$

which can be rearranged to

$$\frac{1}{k'} = \frac{1}{k_1} + \frac{[H^+]}{k_1K_H}. \quad (11)$$

Plot of $1/k'$ *vs.* $[H^+]$ was found to be linear (corr. coeff= 0.988 and 0.99) in both cases, confirming the rate law. The plot gives K_H values of 0.53 and 0.16 and value of $k_1=0.071$ and 0.054 dm^3 mol^{-1} s^{-1} for OAB and PAB, respectively.

In order to interpret the bell shaped nature of log k' *vs.* pH plot in the pH region 0—3, it seems necessary to consider the dissociation of both protonated OAB and PAB and that of H_3PO_5 to $H_2PO_5^-$ as well.

The other species of peracid, *viz.* HPO_5^{2-} and PO_5^{3-}, are not relevant in the pH region under consideration since the second and third dissociation constants of PMPA are of the order of 10^{-6} and 10^{-13}, respectively.[9] The probable steps of the reaction might be as follows.

$$BH^+ \overset{K_H}{\rightleftharpoons} B + H^+ \quad (5)$$

$$B + H_3PO_5 \overset{k_1}{\longrightarrow} \text{Products} \quad (6)$$

$$B + H_2PO_5^- \overset{k_2}{\longrightarrow} \text{Products} \quad (12)$$

which lead to the rate expression,

$$-\frac{d[PMPA]_t}{dt} = \frac{k_1K_H[H^+]+k_2K_1K_H}{K_1K_H+(K_1+K_H)[H^+]+[H^+]^2}[B]_t[PMPA]_t$$

$$= k'[B]_t[PMPA]_t, \quad (13)$$

where

$$k' = \frac{k_1K_H[H^+]+k_2K_1K_H}{K_1K_H+(K_1+K_H)[H^+]+[H^+]^2}. \quad (14)$$

A least-squares solution of Eq. 14 was attempted using the reported value of K_1. The K_H value obtained kinetically from $1/k'$ *vs.* $[H^+]$ plot (Eq. 11) in the region of pH 0—1 was used. k_1 and k_2 values are estimated from Eq. 14, the results being summarized in Table 3. These values are in line with the order of reactivity between peracid species[6] ($H_3PO_5>H_2PO_5^-$). In order to check the validity of the rate law, the computed k_1 and k_2 values were employed to calculate the pH-log k' profile (Figs. 1 and 2). Agreement between the experimental points and theoretical line is satisfactory.

TABLE 3. RATE CONSTANTS OF DIFFERENT PMPA SPECIES IN dm^3 mol^{-1} s$^{-1}\times10^2$

Substrate	k_1	k_2	k_3	$\left(k_4\frac{K_a}{K_2}+k_5\right)$	k_6
OAB	8.1	4.1	4.02	24.7	1.20
PAB	6.3	3.5	2.83	23.5	0.88

k_1 values from the composite rate law (Eq. 13) compare well with those obtained from the k'^{-1} *vs.* $[H^+]$ plot in the pH region 0—1 where the neutral species of PMPA alone was assumed to be effective. Indifference of rate to added salt at pH 1 can also be rationalized by the steps postulated above.

To account for the pH dependence of rate in the pH region 3—7, it is reasonable to assume that both the substrate as well as PMPA species are dissociated and all species resulting from dissociation are involved in controlling the rate.

$$B \overset{K_a}{\rightleftharpoons} B^- + H^+ \quad (15)$$

$$H_2PO_5^- \overset{K_2}{\rightleftharpoons} HPO_5^{2-} + H^+, \quad K_2 = 4.2\times10^{-6}, \quad (16)$$

where B has the same meaning as before and B^- is

$NH_2C_6H_4COO^-$.

In the pH region under discussion, the major oxidant species[9] are $H_2PO_5^-$ and HPO_5^{2-}. The total PMPA concentration $[PMPA]_t$ can therefore be assumed to consist of $H_2PO_5^-$ and HPO_5^{2-}. Similarly, total substrate concentration $[B]_t$ can be assumed to be due to B and B^-:

$$[B]_t = [B] + [B^-] \quad (17)$$

and

$$[PMPA]_t = [H_2PO_5^-] + [HPO_5^{2-}]. \quad (18)$$

In view of the overall second order dependence at constant pH, the steps of the reaction in the pH region may be described as

$$B + H_2PO_5^- \xrightarrow{k_3} \text{Products} \quad (19)$$

$$B^- + H_2PO_5^- \xrightarrow{k_4} \text{Products} \quad (20)$$

$$B + HPO_5^{2-} \xrightarrow{k_5} \text{Products} \quad (21)$$

$$B^- + HPO_5^{2-} \xrightarrow{k_6} \text{Products}. \quad (22)$$

These steps also explain the marginal salt effect on the rate at pH 4.17 (Table 1). From Eqs. 19—22, the rate law can be written as

$$-\frac{d[PMPA]_t}{dt} = k_3[B][H_2PO_5^-] + k_4[B^-][H_2PO_5^-] + k_5[B][HPO_5^{2-}] + k_6[B^-][HPO_5^{2-}]. \quad (23)$$

Equation 23 can be rearranged to give the rate expression

$$-\frac{d[PMPA]_t}{dt} = \frac{k_3[H^+]^2 + \left(k_4\frac{K_a}{K_2} + k_5\right)K_2[H^+] + k_6K_aK_2}{(K_a + [H^+])(K_2 + [H^+])} \times [PMPA]_t[B]_t = k'[PMPA]_t[B]_t, \quad (24)$$

where

$$k' = \frac{k_3[H^+]^2 + \left(k_4\frac{K_a}{K_2} + k_5\right)K_2[H^+] + k_6K_aK_2}{(K_a + [H^+])(K_2 + [H^+])}. \quad (25)$$

Using the reported values[10] of K_a for OAB or PAB, the least-squares solution of Eq. 24 yields values of k_3, $\left(k_4\frac{K_a}{K_2} + k_5\right)$ and k_6 (Table 3). Substituting these least square values of k_3, $\left(k_4\frac{K_a}{K_2} + k_5\right)$ and k_6 in Eq. 25, log k'-pH profile was calculated (Figs. 1 and 2). The agreement between the experimental points and the theoretical line (Figs. 1 and 2) justifies the rate law.

The values of k_3, $\left(k_4 \cdot \frac{K_a}{K_2} + k\right)$ and k_6 suggest minimum reactivity for the reaction with HPO_5^{2-} species compared with $H_2PO_5^-$ which is in agreement with the decreasing electrophilicity of HPO_5^{2-} over $H_2PO_5^-$. We see fair agreement between k_3 (reaction between B and $H_2PO_5^-$ in the pH range 3—7) and k_2 (reaction between B and $H_2PO_5^-$ in the pH range 0—3) for both the substrates. This is in favour of the rate laws postulated to account for the rate variation over the entire pH range.

Mechanism. Polar mechanisms in peroxide reactions have been advanced on the basis[11] of a) bimolecular kinetics, b) negative entropy of activation, and c) insensitivity to radical trapping agents.

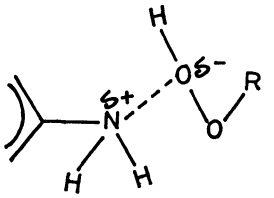

The present reactions confirm the above requirements and most probably involve polar transition states as shown in the following.

where $R = H_2PO_3$, HPO_3^-, or PO_3^{2-}.

Another question of importance is the nature of the peroxide attack, electrophilic *vs.* nucleophilic as dual character having been observed earlier[12,13] depending on the electronic environment. The species of PMPA namely H_3PO_5, $H_2PO_5^-$, HPO_5^{2-}, and PO_5^{3-} are in the decreasing order of electrophilicity. The fact that these aminobenzoic acids are not oxidized above pH 7 is strong evidence that the nucleophilic PMPA species are ineffective and the reaction essentially involves nucleophilic attack by the unprotonated amine on the electrophilic peroxo oxygen of the PMPA species. The rate should decrease with increase in pH.

The decrease in rate with increase in pH was not monotonic; there are two rate maxima-pH profiles, one at pH≈1, and the other at pH≈5, near the pK_a of the aminobenzoic acid. The rate maximum at pH 1 presents a situation where the concentration of the free base becomes maximum, the estimated K_H value being≈0.53. The amine is about 80% unprotonated at pH 1. The statistical distribution of H_3PO_5 and $H_2PO_5^-$ is 55 and 45% respectively. Even when the more electrophilic H_3PO_5 predominates at still lower pH, there is a marked decrease in rate because of the decrease in the unprotonated amine.

The second rate maximum around pH≈5 is unusual and the fact that this occurs near the pK_a of the carboxylic acid dissociation is of interest. The mesomeric effect taking place in the undissociated acid seems to cause a reduced nucleophilicity of nitrogen in I. In II, the carboxylate anion opposes the conjugation of amine lone pair and thus most probably increases the nucleophilicity of nitrogen.

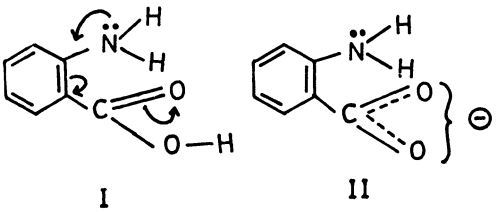

I II

The formation of azoxybenzene-2,2′-dicarboxylic acid from anthranilic acid is of interest. The abnormal course of oxidation was recognized in the oxidation of 3-aminopyridine by H_2O_2/fuming H_2SO_4,[14] Caro's acid,[15] and PMPA.[1] Anthranilic acid is oxidized to the phenylhydroxylamine derivative in the rate limiting step and its oxidation to the nitroso derivative is fast as in the case of aniline, the rate of oxidation of aniline to phenylhydroxylamine being about five times lower than that of the oxidation of phenylhydroxylamine to

nitrosobenzene.[16] The formation of azoxybenzene-2,2′-dicarboxylic acid involves the rapid condensation[17] between the nitroso and phenylhydroxylamine derivatives which are the reactive intermediates.

The authors wish to thank Drs. S. N. Mahapatro and R. K. Panda of this department for helpful discussions and Mr. B. Dash for product study. Financial assistance from C.S.I.R. by way of award of fellowship to A.K.P. is gratefully acknowledged.

References

1) S. N. Mahapatro, G. P. Panigrahi, and A. K. Panda, *Curr. Sci. (India)*, **49**, 227 (1980).
2) G. P. Panigrahi and R. S. Panda, *Bull. Chem. Soc. Jpn.*, **53**, 2366 (1980).
3) G. P. Panigrahi and R. S. Panda, *Int. J. Chem. Kinet.*, **12**, 491 (1980).
4) G. P. Panigrahi and R. S. Panda, *Bull. Chem. Soc. Jpn.*, **52**, 3084 (1979).
5) E. Boyland and D. Manson, *J. Chem. Soc.*, **1957**, 4689.
6) Y. Ogata K. Tomizawa, and T. Ikeda, *J. Org. Chem.*, **44**, 352 (1979).
7) F. Secco and M. Venturini, *J. Chem. Soc., Dalton Trans.*, **1976**, 1410.
8) N. A. Lange, "Handbook of Chemistry," McGraw-Hill, New York (1967), p. 971.
9) C. J. Battaglia and J. O. Edwards, *Inorg. Chem.*, **4**, 552 (1965).
10) A. I. Vogel, "A Textbook of Quantitative Inorganic Analysis," E. L. B. S. London (1971), p. 1167.
11) E. J. Behrman and J. O. Edwards, "Progress in Physical Organic Chemistry," ed by A. Streitwieser and R. W. Taft, Interscience, New York (1967), Vol. 4, p. 95.
12) C. A. Bunton, "Peroxide Reaction Mechanisms," ed by J. O. Edwards, Interscience, New York (1962), pp. 11—28.
13) J. O. Edwards, "Inorganic Reaction Mechanisms," Benjamin, New York (1964), Chap. 5.
14) J. L. Hartman and R. H. Wiley, *J. Am. Chem. Soc.*, **73**, 494 (1951).
15) C. S. Giam and A. E. Hauck, *Synth. Commun.*, **8**, 109 (1978).
16) E. J. Behrman and J. O. Edwards, "Progress in Physical Organic Chemistry," ed by A. Streitwieser and R. W. Taft, Interscience, New York (1967), p. 111.
17) Y. Ogata, M. Tsuchida, and Y. Takagi, *J. Am. Chem. Soc.*, **79**, 3397 (1957).

NOTES

Bull. Chem. Soc. Jpn., 54, 1559—1560 (1981)

Monophotonic Ionization Mechanism of *N,N,N',N'*-Tetramethyl-1,6-pyrenediamine in Acetonitrile Solution

Takashi Nogami,* Toshio Mizuhara, Naoki Kobayashi, Masaaki Aoki, Takao Akashi, Yasuhiko Shirota, Hiroshi Mikawa, and Minoru Sumitani**

Department of Applied Chemistry, Faculty of Engineering, Osaka University, Yamadakami, Suita, Osaka 565

***Institute for Molecular Science, Myodaiji, Okazaki 444*

(Received July 7, 1980)

Synopsis. Monophotonic ionization of *N,N,N',N'*-tetramethyl-1,6-pyrenediamine (TMPDA) in acetonitrile was studied by means of ns laser photolysis and transient photocurrent measurement. The time dependences of the absorption of TMPDA cation radical and of the photocurrent were different. Photoionization thus occurs through an ion-pair state.

Photoionization of *N,N,N',N'*-tetramethyl-*p*-phenylenediamine (TMPD) in organic solvent has been extensively studied in order to clarify the primary process of the photoionization.[1] These studies showed that biphotonic ionization occurs through excited singlet and triplet states as the intermediates in non- or less-polar solvents. On the other hand, monophotonic ionization was observed in polar solvents such as acetonitrile.[2] However, the mechanism of the monophotonic ionization in such a solvent as acetonitrile has not yet been clarified. The difficulty encountered in the photolysis of TMPD in organic solvent is that the triplet-triplet (T-T) absorption of TMPD and the absorption of TMPD cation radical are observed in the same wavelength region, which makes kinetic treatment difficult.[1] We noticed that *N,N,N',N'*-tetramethyl-1,6-pyrenediamine (TMPDA) has a low ionization potential compared to TMPD,[3] and that the absorptions of the T-T transition and of the TMPDA cation radical are well separated. In order to clarify the mechanism of the monophotonic ionization, we studied the photoionization of TMPDA in acetonitrile by ns laser photolysis and transient photocurrent measurements.

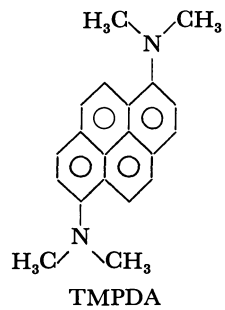

TMPDA

Experimental

TMPDA was synthesized according to the reported procedure.[4] Acetonitrile was distilled four times in the presence of phosphorus pentoxide, followed by distillation in the presence of potassium carbonate. It was finally distilled without any additives. In the case of ns photolysis, we used a nitrogen laser (peak power of 400 kW and pulse width of 5 ns) as an excitation light source, and a Xe-flash lamp (3CP-3, EG & G Co., Ltd) as a monitor light. In the transient photocurrent measurements, we also used the nitrogen laser as an excitation light source. The sample cell has two stainless steel electrodes (1.45 cm×0.95 cm) with a spacing of 0.8 cm: 110 V was applied between them. Special care was taken not to irradiate the electrodes. A load resistance of 1 kΩ was used: this results in the time constant of 0.4 μs. The sample solution was always degassed several times by a freeze-pump-thaw method.

Results and Discussion

Figure 1 (a) shows the change of the electronic absorption spectra of the acetonitrile solution of TMPDA after N_2 laser excitation ([TMPDA]=3.5×10^{-4} mol/l). We can assign the absorption bands at 510 and 560 nm as the T-T absorption and that at 595 nm as the TMPDA cation radical.[5] The absorption band longer than 600 nm is probably due to the solvated electron.[6] Figure 1 (b) shows the change of the absorption of $TMPDA^+$ at 590 nm with time in the ns time range. Although we could not measure

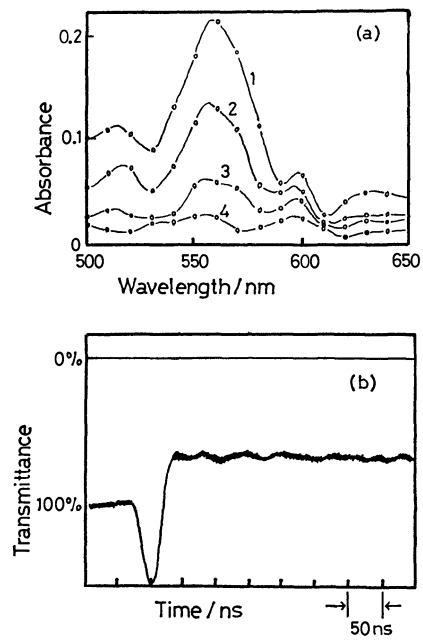

Fig. 1. (a) Time dependence of the absorption spectra of TMPDA in acetonitrile after N_2 laser excitation. 1, 0.4 μs; 2, 3 μs; 3, 10 μs; 4, 18 μs. (b) The change of the absorption of $TMPDA^+$ at 590 nm with time.

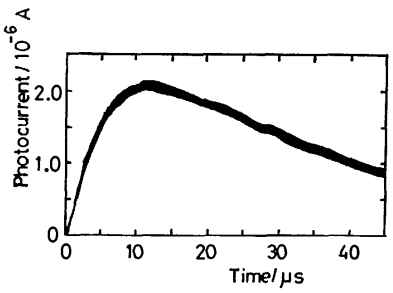

Fig. 2. Transient photocurrent of TMPDA in acetonitrile after N_2 laser excitation at 20 °C.

the absorption spectra of $TMPDA^+$ during the initial 50 ns after the laser pulse excitation because of the interference of the fluorescence of TMPDA, we assume that a TMPDA cation radical be produced immediately after the laser excitation. Figure 2 shows the transient photocurrent of the acetonitrile solution of TMPDA excited by the nitrogen laser at 20 °C ([TMPDA] $= 1.4 \times 10^{-4}$ mol/l). The curve showed gradual increase of the photocurrent during the initial 10 μs, and then the gradual decay of the current.[7] The plot of the peak photocurrent against the laser light intensity showed a linear relation, thus verifying the one-photon ionization of the present system.[8] In order to see whether photoionization occurs through the triplet state or not, we did the photocurrent measurement using a POPOP dye laser[10] ($\lambda_{max} = 418$ nm) as an excitation light source and anthracene as a triplet quencher of TMPDA.[11] The photocurrent measurement of the mixture of the acetonitrile solution of TMPDA and anthracene ([TMPDA] $= 1.04 \times 10^{-4}$ mol/l, [anthracene] $= 1.04 \times 10^{-3}$ mol/l) showed no obvious reduction of the photocurrent. On the other hand, the flash photolysis in the same system showed complete quenching of the T-T absorption. Thus, photoionization does not occur through the lowest triplet state of TMPDA.

If the electron were ejected directly by the laser pulse excitation in the one-photon ionization, the time-dependence of the absorption of $TMPDA^+$ and photocurrent should coincide. Figures 1 and 2 clearly show that this is not the case in the present system. The observed difference between the absorption and current may be ascribed to a cationic transient, which gives no current but shows an absorption similar to that of $TMPDA^+$. This transient seems to be an ion-pair of $TMPDA^+$ and an electron ($TMPDA^+e^-$). The ion-pair is produced by the laser pulse excitation

$$TMPDA \xrightarrow{h\nu} TMPDA^* \xrightarrow{\text{fast}} \underset{\text{ion-pair}}{TMPDA^+e^-} \xrightarrow{\Delta} TMPDA^+ + e^-$$

(probably through the singlet excited state) and dissociates thermally into free ions or recombines to give neutral TMPDA. One may ask whether an ion-pair can exist as long as 10 μs. It is noteworthy that the absorption of the solvated electron is observed for about 10 μs after the laser pulse excitation (Fig. 1 (a)). One possibility is that the TMPDA cation radical and a solvated electron form an ion-pair.

We are grateful to Dr. Masaaki Yokoyama, Faculty of Engineering, Osaka University, for constructing the nitrogen laser.

References

1) For example, J. T. Richards and J. K. Thomson, *Trans. Faraday Soc.*, **66**, 621 (1970); Y. Nakato, N. Yamamoto, and H. Tsubomura, *Bull. Chem. Soc. Jpn.*, **40**, 2480 (1967).

2) T. Imura, N. Yamamoto, H. Tsubomura, and K. Kawabe, *Bull. Chem. Soc. Jpn.*, **44**, 3185 (1971).

3) The half-wave oxidation potentials of TMPDA and TMPD are 0.49 and 0.1 V (*vs.* SCE), respectively (see Ref. 4).

4) H. Vollman, H. Becker, M. Correll, and H. Streek, *Ann.*, **531**, 1 (1937); A. Zweig, A. H. Maurer, and B. G. Roberts, *J. Org. Chem.*, **32**, 1322 (1967); TMPDA was purified by column chromatography (silica gel) using benzene as an eluent, and purified finally by two vacuum sublimations.

5) The 510 and 560 nm bands are assigned as the T-T absorption because of the following reasons. These bands decay exponentially with a life time of 11 μs, and they disappear completely by the addition of the triplet quencher, anthracene. The 595 nm band is assigned as the TMPDA cation radical because of the following reason. The same absorption spectrum is obtained by the one-electron oxidation of TMPDA with ferric nitrate, and by thermal ionic dissociation reaction of TMPDA with chloranil in acetonitrile.

6) A. Singh, H. D. Gesser, and A. R. Scott, *Chem. Phys. Lett.*, **2**, 271 (1968).

7) Similar curves are also obtained at 11, 30, and 40 °C.

8) When we compare the dependence of the photocurrent with the excitation laser intensity, we must consider the saturation effect. This effect is significant when the value *EH* exceeds 1 (see Ref. 9). Here *E* and *H* denote the absorption cross section of the molecule and photon number per unit area. In the present experimental condition, the maximum value of *EH* is 0.05. Thus, we need not worry about the saturation effect.

9) U. Lachish, A. Schafferman, and G. Stein, *J. Chem. Phys.*, **64**, 4205 (1976).

10) A dioxane solution of 1,4-bis(5-phenyl-2-oxazolyl)-benzene was excited by N_2 laser light to obtain the POPOP dye laser light.

11) The lowest singlet (S_1) and triplet (T_1) states o TMPDA and anthracene are as follows. TMPDA: S_1 2.91 eV, T_1 1.97 eV (estimated from the phosphorescence spectrum); anthracene: S_1 3.31 eV, T_1 1.85 eV.

Anomalous Solvatochromism of Charge-transfer Absorption Bands

Jun-ichi AIHARA

Department of Chemistry, Faculty of Science, Hokkaido University, Sapporo 060

(Received May 15, 1980)

Synopsis. When n-donor solvents are employed, charge-tansfer absorption bands become broader on the low-energy side, the absorption peaks shifting toward the high-energy side. This type of solvatochromism has an analogy with that of the n-π^* transitions.

Despite continued interest in the charge-transfer (CT) complexes in the solution phase, various aspects of the electronic spectra remain unclarified.[1-3] As Offen and Abidi pointed out,[1] no current theory of solvatochromism can be applied assuredly to the CT absorption bands. In order to solve the problem, the absorption spectra of weak CT complexes were reexamined in various solvents. It was found that the CT absorption band changes with solvent. An attempt was made to interpret this phenomenon in terms of specific solvation.

In general, unsubstituted aromatic hydrocarbons are suitable as donor components for the study of solvent effects on binary CT complexes. Bulky substituents of the donor molecule suppress solvatochromism to some extent.[4] Naphthalene and tetracyanoethylene (TCNE) best illustrate the donor-acceptor pair for the present purpose. Figure 1 shows the electronic absorption spectra of the naphthalene–TCNE complex in four solvents. The first two absorption bands appear in the visible region, and have been assigned to the CT transitions from naphthalene to TCNE.[5] These CT bands are usually asymmetric in appearance.[6]

The peak of the first CT band moves in a wide range when the solvent is changed. There is an absorption peak at 17670 cm^{-1} in carbon disulfide while it shifts to 19800 cm^{-1} in acetonitrile. The difference in energy amounts to 2100 cm^{-1}. The peaks in the 1,2-dichloroethane and bromoethane solutions are located halfway at 18170 and 18940 cm^{-1}, respectively. Despite such a large displacement of the peak position, the absorption edge remains in almost the same position, light absorption beginning at *ca.* 14500 cm^{-1} in each solution. All solutions of the complex do not exhibit the absorption edge here; in solvents, such as hexane, cyclohexane, ethyl acetate, and methanol, the absorption edge shifts to *ca.* 15500 cm^{-1}. However, such a displacement of the edge is small as compared with that of the absorption peak. The first absorption peaks are located at 18980 cm^{-1} in hexane, at 18520 cm^{-1} in cyclohexane, at 20200 cm^{-1} in ethyl acetate, and at 20530 cm^{-1} in methanol. Consequently, broadening of the entire absorption band occurs as the peak position is displaced to the higher-energy side.

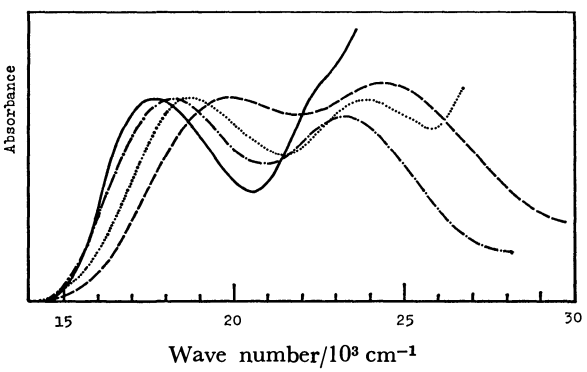

Fig. 1. Absorption spectra of the naphthalene–TCNE complex in carbon disulfide (——), 1,2-dichloroethane (—·—), bromethane (·····), and acetonitrile (– – –).

When hydrocarbon solvents, such as hexane and cyclohexane, are used, the absorption peak apparently follows the dielectric theory of solvatochromism.[2,7] However, most other solvents affect the CT band in quite a different manner. Even when a solvent has a large dielectric constant, it often gives rise to a large blue shift of the CT absorption band.[1-3] If we consider that a weak CT complex has a larger dipole moment in the excited state than in the ground state,[5] this is obviously inconsistent with the theory of solvatochromism described in terms of the refractive index and the dielectric constant of the solvent.[8] It is evident that the solvent dependence of the CT absorption band cannot be applied to the determination of the dipole moment of the excited-state complex by means of the dielectric theory.[9]

The absorption edge is closely related to the 0–0 vibronic level of the electronic transition. The first absorption band of the naphthalene–TCNE complex in the gas phase begins at 16900 cm^{-1} with a peak at 21100 cm^{-1}.[2] The edge shifts to the low-energy side by 2400 cm^{-1} when the complex is dissolved in the solvents given in Fig. 1; this indicates that both the 0-0 and higher vibronic levels move to the red in these solvents. The solvent shift caused by the dielectric effect, if any, should thus be evaluated as an energy shift of a certain (*i.e.*, fixed) vibronic level.

In principle, the absorption peak is related to the Franck-Condon (*i.e.*, vertical) transition. The shift of the CT absorption maximum along with the deformation of the band shape is determined mainly by the variation of the Franck-Condon transition level. It is evident that the first band maximum of the naphthalene–TCNE complex does not always represent a fixed vibronic level (Fig. 1). It is likely that the 0-1 vibronic level is the strongest in saturated-hydrocarbon solvents.[10] However, it seems that the higher vibronic levels are more intense in the other solvents although they are blurred. A plausible vibrational mode taking part in the first CT band of the naphthalene–TCNE complex is an intramolecular vibration with a frequency of about 1300 cm^{-1} in the excited state. The frequency was estimated from the fine structure in the CT bands of the saturated-hydrocarbon solutions.[10]

The systematic study so far carried out on weak CT complexes has enabled us to distinguish n-donor

solvents from other ones. Nagy *et al.* found that the n-donor solvents markedly shift the CT absorption band to the blue, and that the electron-donating power of the solvent is primarily responsible for the anomalous blue shift.[3] In line with this, the present observation revealed that the broadening of the CT band is conspicuous in such n-donor solvents as acetonitrile, ethyl acetate, and methanol. Therefore, it seems that the variation of the Franck-Condon envelope is substantially due to the coordination of n-donor-solvent molecules to the CT complex in the ground state.[3]

For example, acetonitrile is highly polar, and the molecular dynamics is highly anisotropic in the neat liquid.[11] An antiparallel arrangement seems to be the most probable orientational arrangement in acetonitrile. The acetonitrile molecules would, likewise, tend to be coordinated selectively to TCNE, since the C≡N bond moment of TCNE (3.6 D)[12] is comparable to the overall dipole moment of acetonitrile (3.92 D),[13] and acetonitrile has a large n-donor ability.[3,14] This suggests that the variation of the Franck-Condon envelope can be induced essentially by the solvation of the acceptor part (*i.e.*, TCNE). Thus, the vibrational mode which contributes to the first CT band of the naphthalene–TCNE complex might be ascribed to TCNE.

The above explanation is in line with that of McConnell[15,16] given to the blue shift of the n-π^* transitions, in which he states that the blue shift originates from the solvent molecules orienting themselves around the solute molecule to fit in with the ground-state charge distribution of the solute molecule. On excitation, if the charge distribution of the solute changes drastically (as in the case of n-π^* transitions and CT transitions alike), the solvent molecules would not have the position and orientation to bind most strongly with the excited-state charge distribution. This would give rise to the blue-shift phenomenon, since (relative to a saturated-hydrocarbon solvent) an n-donor solvent would give a greater solvation energy for the ground state of the solute than for the excited state. The resulting absorption peak would become much higher in energy than the relaxed excited state. This would give rise to the broadening of the absorption band on the low-energy side.

In conclusion, the anomalous blue shift, accompanied by band broadening, is commonly observed in the absorption spectra of weak CT complexes in solution. This blue-shift phenomenon seems to have caused great confusion in the analysis of solvent shifts.[1-3,9]

References

1) H. W. Offen and M. S. F. A. Abidi, *J. Chem. Phys.*, **44**, 4642 (1966).
2) J. Aihara, M. Tsuda, and H. Inokuchi, *Bull. Chem. Soc. Jpn.*, **42**, 1824 (1969).
3) O. B. Nagy, J. B. Nagy, and A. Bruylants, *J. Chem. Soc., Perkin Trans. 2*, **1972**, 968.
4) See, *e.g.*, J. Aihara, M. Tsuda, and H. Inokuchi, *Bull. Chem. Soc. Jpn.*, **43**, 3067 (1970).
5) T. Ohta, H. Kuroda, and T. L. Kunii, *Theor. Chim. Acta*, **19**, 167 (1970).
6) G. Briegreb and J. Czekalla, *Z. Phys. Chem. (Frankfurt am Main)*, **24**, 37 (1960).
7) E. M. Voigt, *J. Phys. Chem.*, **70**, 598 (1966).
8) Y. Ooshika, *J. Phys. Soc. Jpn.*, **9**, 594 (1954); E. G. McRae, *J. Phys. Chem.*, **61**, 562 (1957).
9) J. Czekalla and K. O. Meyer, *Z. Phys. Chem. (Frankfurt am Main)*, **27**, 185 (1961); C. N. R. Rao and P. C. Dwivedi, *J. Chem. Phys.*, **59**, 1555 (1973).
10) J. Aihara, *Bull. Chem. Soc. Jpn.*, **44**, 1174 (1971).
11) R. Hilbert, H. Langer, and H. Versmold, *Mol. Phys.*, **38**, 2107 (1979), and references cited therein.
12) R. J. W. Le Fèvre, D. V. Radford, and P. J. Stiles, *J. Chem. Soc., B*, **1968**, 1297.
13) "Handbook of Chemistry and Physics," 52nd ed., ed by R. C. Weast, The Chemical Rubber Co., Cleveland, Ohio (1971).
14) T. Kagiya, Y. Sumida, and T. Inoue, *Bull. Chem. Soc. Jpn.*, **41**, 767 (1968).
15) H. McConnell, *J. Chem. Phys.*, **20**, 700 (1952).
16) G. J. Brealey and M. Kasha, *J. Am. Chem. Soc.*, **77**, 4462 (1955).

The Separation of Solutes with Different Diffusion-coefficients by Two-layer Convection

Katsuyoshi KAMAKURA

Department of Industrial Chemistry, Toyama Technical College, Hongo-cho, Toyama 930-11

(Received July 18, 1980)

Synopsis. When a two-layer system which consists of water (upper layer) and an aqueous solution (lower layer) is heated from one side and cooled from the opposite side, a convection starts in each layer. The empirical formula for mass transfer between the convections was studied for a system of water containing a mixture of solutes; the flux of a solute in the mixture was found to be proportional to the square root of the diffusion coefficient of the solute. Therefore, solutes with different diffusion-coefficients can be separated by two-layer convection.

When a two-layer system which consists of water (upper layer) and an aqueous solution (lower layer) is heated from one side and cooled from the opposite side, a convection starts in each layer. We have already studied the system of a solution of one solute and have presented an empirical formula for mass transfer between convections.[1] From this formula, the flux of a solute in a mixture of solutes can be presumed, under certain conditions, to be proportional to the square root of the diffusion coefficient of the solute. Therefore, the separation of solutes may be done by the two-layer convection for a mixture of solutes. The purpose of this investigation is to discuss the possibility of the separation of solutes by this method.

Theoretical

In a previous paper[1] the empirical formula of mass transfer was presented for the two-layer convection in the case of a solution of one solute. Then, the flux, W_A, of a solute, A, was expressed by

$$W_A = a_1(\Delta\rho_1 - \Delta\rho_0)D^{0.5}(\Delta c_I/\Delta\rho_2). \quad (1)$$

Here, a_1 is the mass-transfer coefficient; $\Delta\rho_1$, the density difference between the liquid on the heated wall and that on the cooled wall; $\Delta\rho_0$, a constant; D, the diffusion coefficient of a solute; and Δc_I and $\Delta\rho_2$, the concentration difference and the density difference respectively between the solution of the upper layer and that of the lower layer.

In this paper we will discuss the mass transfer in the case of a mixture of two solutes. If the temperatures of cooling and heating are constant, $(\Delta\rho_1 - \Delta\rho_0)$ is approximately constant for a solution of different solutes. Then, the flux, W_x, of a solute, x, in a mixture may be expressed as follows:

$$W_x = a_2 D_x^{0.5}(\Delta c_x/\Delta\rho_2), \quad (2)$$

where a_2 is the mass transfer coefficient. The D_x[2] and the Δc_x are the values for a solute, x, while the $\Delta\rho_2$ is the density difference between the solutions. The $\Delta c_I/\Delta\rho_2$ was constant for the system of a solution of one solute. For that of two solutes, the $\Delta c_x/\Delta\rho_2$ will also be constant if the ratio of the amounts of solutes in a layer is constant while the two-layer convection is occurring, or if the amount of a solute, x, is very much larger than that of the other solute. Generally, the $\Delta c_x/\Delta\rho_2$ will be roughly constant for a small change of $\Delta\rho_2$. The ratio, W_x/W_y, of the fluxes of the two solutes is, then, expressed as follows:

$$W_x/W_y = (D_x D_y)^{0.5}(\Delta c_x/\Delta c_y). \quad (3)$$

When the Δc_x is equal to Δc_y, the W_x/W_y is expressed as follows:

$$W_x/W_y = (D_x/D_y)^{0.5}. \quad (4)$$

Experimental

The materials and apparatus used in this study were similar to those described in a previous paper.[1] The nitrates were used for the system of a solution of two electrolytes, while the chlorides were used for the other system (electrolyte-organic compound). The soluble starch was obtained from the Wako Pure Chem. Co. and was used without further purification. The temperatures of the heating and cooling water were 30 and 20 °C respectively, and the flow speed of those waters was 1.6 $dm^3\ min^{-1}$. The concentration of the electrolyte was determined by atomic absorption spectrometry, while that of the organic compound was determined by colorimetry as reported by Dubois *et al.*[3] The samples (30—50 mm^3) for the determination of the solute concentration were taken out from the solution in the middle of the upper layer.

Results and Discussion

We examined the system of a solution of two solutes (mass ratio; 1:1) in order to separate the solutes, and investigated the relation between W_x/W_y and $(D_x/D_y)^{0.5}$. Figure 1 shows a case in which the concentrations in the lower layer are low, while the

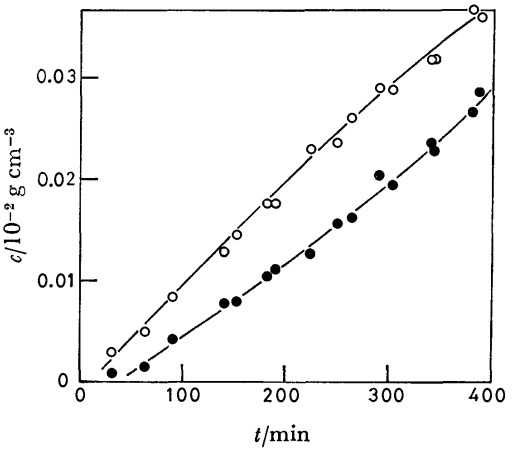

Fig. 1. Variation of concns in upper layer.
○: K^+, ●: Cu^{2+}.
Concns in lower layer at the start of convections; K^+: 0.1×10^{-2} g cm^{-3}, Cu^{2+}: 0.1×10^{-2} g cm^{-3}.

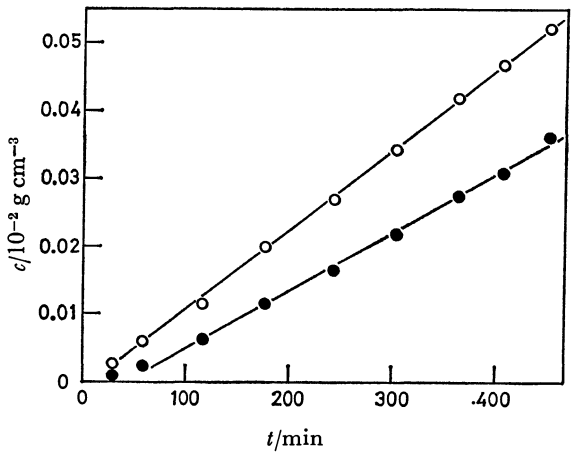

Fig. 2. Variation of concns in upper layer.
○: K^+, ●: Cu^{2+}.
Concns in lower layer at the start of convections; K^+: 0.25×10^{-2} g cm^{-3}, Cu^{2+}: 0.25×10^{-2} g cm^{-3}.

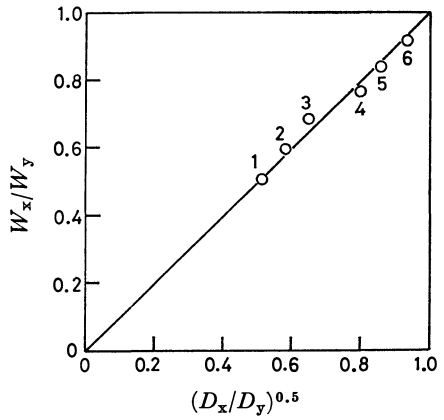

Fig. 3. Relation between W_x/W_y and $(D_x/D_y)^{0.5}$.
1: Sucrose–KCl, 2: D-glucose–KCl, 3: D-glucose–NaCl, 4: Cu^{2+}–K^+, 5: Pb^{2+}–K^+, 6: Cu^{2+}–Pb^{2+}.

relation between the concentration in the upper layer and the time is nonlinear. Figure 2 shows a case in which the concentrations in the lower layer are high and the relation is linear. If the relation is linear, the W_x or W_y can easily be evaluated. Therefore, subsequent experiments were carried out on the systems with the high concentrations.

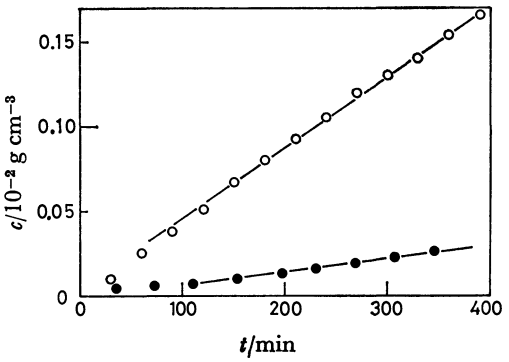

Fig. 4. Variation of concns in upper layer.
○: KCl, ●: starch.
Concns in lower layer at the start of convections; KCl: 1×10^{-2} g cm^{-3}, starch: 1×10^{-2} g cm^{-3}.

As Fig. 3 shows, W_x/W_y is equal to $(D_x/D_y)^{0.5}$.[2] Therefore, Eq. 4 seems to be proper and the separation of solutes is possible.

Figure 4 is the plot for the system of a solution containing an electrolyte (low molecular weight) and a starch. The electrolyte mainly moves from the lower layer to the upper layer. Nevertheless, the starch gradually moves to the upper layer. The diffusion coefficient of the starch was calculated by means of Eq. 4 from the two slopes for each solute. The value thus obtained, 0.72×10^{-6} cm^2/s, agreed with the order of the data (0.8×10^{-6} cm^2/s) in the literature.[4]

In view of the above results, we conclude that the separation of solutes is possible by this method.

References

1) K. Kamakura, *Bull. Chem. Soc. Jpn.*, **52**, 2175 (1979).
2) The diffusion coefficients (D_x or D_y) used in this paper were the values at an infinite dilution for a solution of one solute; the values of the electrolytes were calculated by means of the equation of Nernst-Hartley; those of sucrose and D-glucose were 0.523×10^{-5} and 0.673×10^{-5} cm^2 s^{-1} respectively.
3) M. Dubois, K. A. Gilles, J. K. Hamilton, P. A. Rebers, and F. Smith, *Anal. Chem.*, **28**, 350 (1956).
4) "International Critical Tables," Mcgraw-Hill (1929), Vol. 5, p. 71; for example, the diffusion coefficient of starch (powder-like) in a 1.25% solution at 20 °C is 0.8×10^{-6} cm^2 s^{-1}.

Spin Densities in the Radical Anion of 3,3′-Bipyridine

Hideo FUJITA* and Yasuo DEGUCHI

Department of Chemistry, College of Liberal Arts and Sciences, Kyoto University, Kyoto 606

(Received September 1, 1980)

Synopsis. The ESR spectrum of the radical anion of 3,3′-bipyridine has been measured. The hfs constants agree with the calculated values based on the spin densities using the McLachlan method.

Although the ESR spectra of the radical anion of 2,2′-[1-4] and 4,4′-bipyridines[5-7] are known, the radical anion of 3,3′-bipyridine has not been investigated by ESR tecniques. Therefore, it is of interest to measure the ESR spectrum of the radical anion of 3,3′-bipyridine in order to compare the spin distribution of this radical anion with those of 2,2′- and 4,4′-bipyridine. We wish to report here an ESR study of the radical anion of 3,3′-bipyridine.

The radical anion was generated by the reduction of 3,3′-bipyridine, which had been prepared from 3,3′-bipyridine-2,2′-dicarboxylic acids by the method of Smith,[8] with potassium metal in 1,2-dimethoxyethane (DME). This solution was investigated by ESR spectroscopy in the temperature range from 85 to −85 °C.

The intense well-resolved ESR spectrum measured at 80 °C of the radical anion of 3,3′-bipyridine is shown in Fig. 1a (g=2.0024). Figure 1a consists of hyperfine splitting (hfs) constants due to the equivalent protons, a_H=0.626, 0.582, and 0.115 mT and the nitrogens, a_N=0.094 mT (see Table 1). Using these parameters, the computer-simulated spectrum shown in Fig. 1b was obtained; it agreed well with the observed spectrum. On the other hand, we could not obtain the well-resolved ESR spectra at temperature lower than room temperature. Probably, this is due to the overlap of the hfs constants, because these spectra have a slight different values from the above hfs constants. In consequence, we can not yet analyze these spectra.

In order to assign the hfs constants, we have carried out MO calculations.[9] The results are summarised, together with the observed hfs constants, in Table 1. The most interesting features are the approximately equal and large hfs constants of the γ- and ε-protons, and the hfs constant of the α-protons, which is smaller than the simulated linewidth, 0.007 mT.

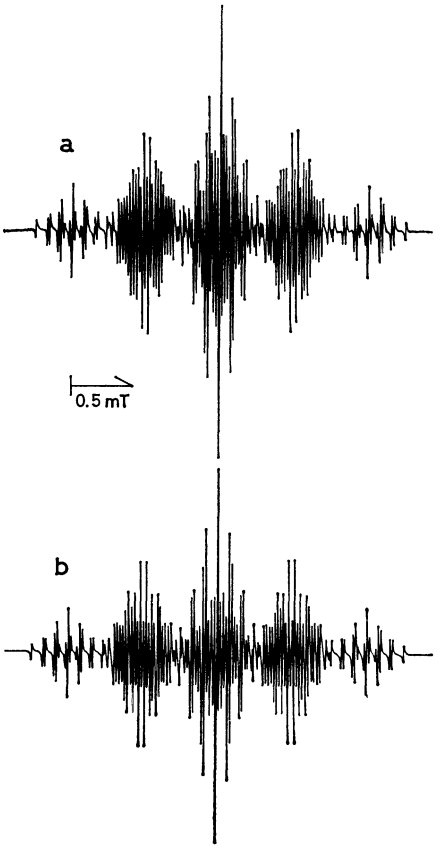

Fig. 1. (a) The observed ESR spectrum of the radical anion of 3,3′-bipyridine: solvent, DME; counterion, K^+; at 80 °C. (b) The spectrum simulated by means of the hfs constants listed in Table 1: lineshape, Lorentzian; linewidth, 0.007 mT.

TABLE 1. THE hfs CONSTANTS OF THE RADICAL ANION OF 3,3′-BIPYRIDINE AND ITS CALCULATED SPIN DENSITIES

Position	Calculated spin density		Calculated hfs const[c]	Observed hfs const[d]
	HMO[a]	McLachlan[b]	mT	mT
α	0.012	−0.006	0.016	•••
β(N)	0.055	0.038	0.093	0.094
γ	0.181	0.226	0.632	0.626
δ	0.002	−0.040	0.112	0.115
ε	0.157	0.193	0.540	0.582
ζ	0.093	0.089	···	—

a) Parameters, h_N=0.7 and k_{CN}=k_{CC}=1.0. b) Parameter, λ=0.8. c) Obtained by the use of this equation; a_x=$Q_x\rho$, with Q_N=|2.45| and Q_H=|2.8| mT, and using the calculated McLachlan-spin densities. d) Potassium-counterion in DME at 80 °C.

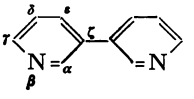

TABLE 2. THE hfs CONSTANTS OF THE RADICAL ANIONS OF BIPHENYL, BIPYRIDINES, AND BIPYRIMIDINE

Radical anion	hfs constants/mT				
	$a_{H\alpha}$	$\alpha_{H\beta}$	$a_{H\gamma}$	$a_{H\delta}$	$a_{H\varepsilon}$
Biphenyl[a]	0.266	0.041	0.531	0.041	0.266
4,4′-Bipyridine[b]	0.235	0.043	0.364[e]	0.043	0.235
2,2′-Bipyridine[c]	0.258[e]	0.057	0.470	0.120	0.106
2,2′-Bipyrimidine[d]	0.141[e]	0.015	0.498	0.015	0.141[e]

a), b), c), and d) Values reported in Refs. 10, 6, 4, and 11. e) These are the hfs constants of the nitrogen atoms.

We can recognize the suitability of the assignments for the hfs constants (see Table 1) of the radical anion of 3,3′-bipyridine, which are compared with the hfs constants of various radical anions of biphenyl,[10] 2,2′- and 4,4′-bipyridines,[4,6] and 2,2′-bipyrimidine[11] in Table 2. That is, the hfs constant of the nitrogens for the radical anion of 3,3′-bipyridine is a usual value, while the $a_{H_\alpha} \simeq 0$ and $a_{H_\epsilon} = 0.582$ mT values are unsual in comparison with the hfs constants of other bipyridines. However, the hfs constants agree well with the MO calculated values, as is shown in Table 1. Therefore, as an example to facilitate comparison with the a_{H_α} and $a_{H_\epsilon} = 0.235$ mT of the radical anion of biaxial symmetric 4,4′-bipyridine,[6] the computed average value of the hfs constant for the radical anion of 3,3′-bipyridine is about 0.29 mT and is normal. All thing considered, each of the three radical anions of bipyridine isomers has a proper hfs constant and a different MO calculated spin-density distribution[3,6] because each molecule containing two nitrogen atoms has a different space-coordination.[12,13] In conclusion, we have found that the ESR spectrum of the radical anion of 3,3′-bipyridine consists of the hfs constants shown in Table 1, and the spin densities calculated using the McLachlan method[9] satisfy the experimental values.

References

1) A. Zahlan, F. W. Heinecken, M. Bruin, and F. Bruin, *J. Chem. Phys.*, **37**, 683 (1962).
2) W. L. Reynolds, *J. Phys. Chem.*, **67**, 2866 (1963).
3) J. dos Santos-Veiga, W. L. Reynolds, and J. R. Bolton, *J. Chem. Phys.*, **44**, 2214 (1966).
4) T. Takeshita and N. Hirota, *J. Am. Chem. Soc.*, **93**, 6421 (1971).
5) R. L. Ward, *J. Am. Chem. Soc.*, **83**, 3623 (1961).
6) A. Carrington and J. dos Santos-Veiga, *Mol. Phys.*, **5**, 21 (1962).
7) A. Staško, A. Tkáč, L. Malík, V. Adamčík, and M. Hronec, *Chem. Zvesti*, **32**, 294 (1978).
8) C. R. Smith, *J. Am. Chem. Soc.*, **52**, 397 (1930).
9) A. D. McLachlan, *Mol. Phys.*, **3**, 233 (1960).
10) H. Nishiguchi, Y. Nakai, K. Nakamura, K. Ishizu, Y. Deguchi, and H. Takaki, *J. Chem. Phys.*, **40** 241 (1964).
11) D. E. Geske and G. R. Padmanabhan, *J. Am. Chem. Soc.*, **87**, 1651 (1965).
12) V. Galasso, G. D. Alti, and A. Bigotto, *Tetrahedron*, **27**, 991 (1971).
13) V. Bolotin and A. Bolotin, *Liet. Fiz. Rinkinys*, **19**, 195 (1979).

Structure of the Complex of Neodymium Nitrate with Pentaethylene Glycol

Yoshiyuki HIRASHIMA,* Koji KANETSUKI, Jiro SHIOKAWA, and Nobuo TANAKA**

Department of Applied Chemistry, Faculty of Engineering, Osaka University, Yamada-kami, Suita, Osaka 565

***Institute for Protein Research, Osaka University, Yamada-kami, Suita, Osaka 565*

(Received September 12, 1980)

Synopsis. Crystals of the complex, $Nd(NO_3)_3$–$HO(CH_2CH_2O)_5H$, are monoclinic. The Nd atom is coordinated by ten oxygen atoms, four from two bidentate nitrate ions and six from a pentaethylene glycol. The pentaethylene glycol forms a ring-like structure similar to that of crown compounds.

The preparation of the solid complexes of lanthanoid ions with macrocyclic polyethers was reported,[1-4] some structures being determined by X-ray crystallography.[5-7] It was found that some noncyclic polyethers form solid complexes with lanthanoid nitrates, their stability appearing to decrease with increasing atomic number of the lanthanoid in contrast to the lanthanoid complexes of most ligands.[8] This behavior is similar to that of the complexes of 18-crown-6,[9] and might be related to the structures of the complexes. X-Ray diffraction studies were carried out on the structure of the complex of pentaethylene glycol (denoted by EO5) with neodymium nitrate, the results of which are given in this report.

Crystals suitable for X-ray study were obtained by adding a dilute ethyl acetate solution of neodymium nitrate to an ethyl acetate solution of EO5 and then standing the resulting solution for crystal deposit.

Crystal data: $Nd(NO_3)_3\cdot(C_{10}H_{22}O_6)$, F.W.=568.5, monoclinic, space group $P2_1/n$, a=8.220(2) Å, b=15.072(3) Å, c=17.089(4) Å, β=110.80(2)°, V=1979.2(6) Å^3, D_{calcd}=1.91 g cm^{-3} for Z=4, D_{obsd}=1.90 g cm^{-3}, μ(Mo $K\alpha$)=27.2 cm^{-1}.

A crystal was sealed in a 1 mm diam. glass capillary because of its deliquescence. Intensity data were collected with a Rigaku automated four-circle diffractometer using β-filtered Mo $K\alpha$ radiation. The 2θ-ω scan technique was employed with a scan speed 4°/min on 2θ. A scan range of 1.4° plus θ-dependent dispersion term was used. A total of 4189 reflections were obtained. Net intensities of 1354 reflections were observed as zero. Lorentz and polarization corrections, but no absorption correction, were made.

The structure was solved by the heavy atom method, the atomic parameters except for the hydrogen atoms being refined by the block diagonal least squares method.[10] The weighting scheme applied was as follows, w=1 if $|F_o|>2.5$; w=0.3 if $|F_o|<2.5$. After several cycles of the calculation with anisotropic temperature factors, the R factor was converged to 0.11.

Figure 1 shows the structure of the complex $Nd(NO_3)_3\cdot HO(CH_2CH_2O)_5H$. The bond lengths and bond angles are given in Table 1.†

† The complete F_o-F_c data and the table of atomic parameters are deposited as Document No. 8122 at the Chemical Society of Japan.

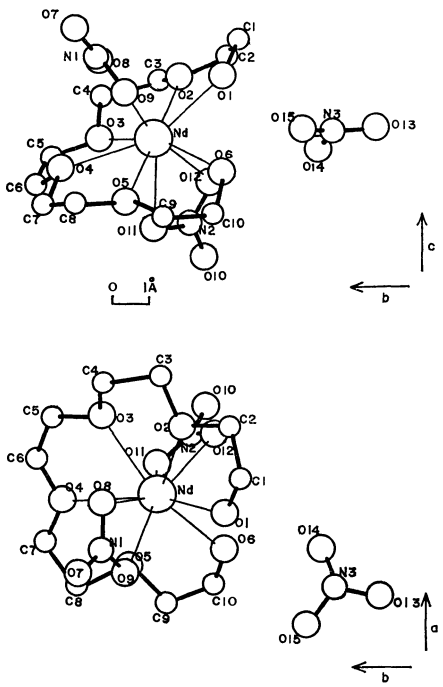

Fig. 1. Structure of $Nd(NO_3)_3\cdot EO5$.
Top: Projection along [001]. Bottom: Projection onto [001].

The Nd atom is coordinated by ten oxygen atoms, four from two nitrate ions and six from a pentaethylene glycol (EO5). The coordination polyhedron is similar to that based on bicapped-dodecahedron,[11] though it is irregular. The pentaethylene glycol acts as a hexadentate ligand forming a ring-like structure with its oxygen atoms. The ring-like structure is similar to the structure of so-called crown compounds. The six oxygen atoms of EO5 are not quite coplanar, their shifts from the mean plane being in the range 0.03—0.83 Å. The Nd atom is located near the center of the hexagon of the oxygen atoms of EO5. The angles of O_i–Nd–O_{i+1} (i=1—5) are close to 60° (60—63°), while the angle of O_1–Nd–O_6 is 67° a little higher than the others. This can be attributed to the large shifts of the two terminal oxygen atoms from the mean plane (0.64 and 0.83 Å). Above and below this mean plane two nitrate ions coordinate to a Nd atom as a bidentate ligands. The angle of N_1–Nd–N_2 is 169°, the bi-capped units being slightly distorted from the ideal form. A third nitrate ion does not coordinate to a Nd atom (the nearest Nd–O distance: 4.6 Å).

The average Nd–O bond length is 2.54 Å, which is between the bond lengths of La–O and Tb–O (2.6

TABLE 1. BOND LENGTHS(l/Å) AND ANGLES(θ/°) IN THE $Nd(NO_3)_3 \cdot EO5$ COMPLEX

Nd-O bond		N-O bond		C-C or C-O bond		C-C-O or C-O-C angle		O-N-O angle	
Nd-O(1)	2.49(1)	N(1)-O(7)	1.21(2)	C(1)-C(2)	1.46(5)	O(1)-C(1)-C(2)	113(3)	O(7)-N(1)-O(8)	123(2)
Nd-O(2)	2.55(2)	N(1)-O(8)	1.23(2)	C(3)-C(4)	1.57(4)	C(1)-C(2)-O(2)	108(3)	O(7)-N(1)-O(9)	121(2)
Nd-O(3)	2.58(2)	N(1)-O(9)	1.28(2)	C(5)-C(6)	1.36(6)	O(2)-C(3)-C(4)	105(2)	O(8)-N(1)-O(9)	116(2)
Nd-O(4)	2.62(2)	N(2)-O(10)	1.20(3)	C(7)-C(8)	1.38(5)	C(3)-C(4)-O(3)	108(2)	O(10)-N(2)-O(11)	123(2)
Nd-O(5)	2.62(2)	N(2)-O(11)	1.23(2)	C(9)-C(10)	1.43(4)	O(3)-C(5)-C(6)	118(4)	O(10)-N(2)-O(12)	122(2)
Nd-O(6)	2.48(2)	N(2)-O(12)	1.26(2)			C(5)-C(6)-O(4)	114(4)	O(11)-N(2)-O(12)	115(2)
Nd-O(8)	2.55(2)	N(3)-O(13)	1.23(3)	O(1)-C(1)	1.41(4)	O(4)-C(7)-C(8)	114(3)	O(13)-N(3)-O(14)	123(2)
Nd-O(9)	2.47(1)	N(3)-O(14)	1.22(3)	C(2)-O(2)	1.36(4)	C(7)-C(8)-O(5)	109(3)	O(13)-N(3)-O(15)	117(2)
Nd-O(11)	2.52(2)	N(3)-O(15)	1.25(3)	O(2)-C(3)	1.48(4)	O(5)-C(9)-C(10)	114(3)	O(14)-N(3)-O(15)	121(2)
Nd-O(12)	2.52(2)			C(4)-O(3)	1.41(4)	C(9)-C(10)-O(6)	114(2)		
				O(3)-C(5)	1.38(5)				
				C(6)-O(4)	1.35(5)	C(2)-O(2)-C(3)	114(2)		
				O(4)-C(7)	1.45(4)	C(4)-O(3)-C(5)	109(2)		
				C(8)-O(5)	1.41(4)	C(6)-O(4)-C(7)	109(3)		
				O(5)-C(9)	1.43(4)	C(8)-O(5)-C(9)	116(2)		
				C(10)-O(6)	1.43(3)				

TABLE 2. TORSION ANGLES(ϕ/°) IN THE PENTAETHYLENE GLYCOL

O(1)-C(1)-C(2)-O(2)	47	C(1)-C(2)-O(2)-C(3)	160	C(2)-O(2)-C(3)-C(4)	−172
O(2)-C(3)-C(4)-O(3)	−51	C(3)-C(4)-O(3)-C(5)	−170	C(4)-O(3)-C(5)-C(6)	−154
O(3)-C(5)-C(6)-O(4)	27	C(5)-C(6)-O(4)-C(7)	−174	C(6)-O(4)-C(7)-C(8)	165
O(4)-C(7)-C(8)-O(5)	−43	C(7)-C(8)-O(5)-C(9)	−160	C(8)-O(5)-C(9)-C(10)	−179
O(5)-C(9)-C(10)-O(6)	33				

and 2.47 Å, respectively) reported for bis(bipyridyl)-trinitratolanthanoids which are decacoordinate complexes.[11,12] The sequence of the bond lengths is reasonable in view of the expected contraction in radius for the lanthanoid series.

The tortion angles in EO5 are given in Table 2. The conformation around the CH_2–CH_2 bonds are all nearly gauche, while those around the CH_2–O bonds are all approximately trans. The conformation for CH_2–CH_2–O–CH_2–CH_2–O–CH_2 is GTT$\bar{G}$TT, which was reported by Iwamoto[13] to be the most stable conformation, where T, G, $\bar{G}$ denote trans, gauche, and minus gauche, respectively. Some of the angles around the CH_2–CH_2 bonds are considerably lower than 60°. The deviation can be attributed to the deformation of the EO5 molecule from the ideal form in order to maintain the Nd–O distances at suitable lengths for coordination.

References

1) R. B. King and P. R. Heckley, *J. Am. Chem. Soc.*, **96**, 3118 (1974).
2) M. Ciampolini and N. Nardi, *Inorg. Chim. Acta*, **32**, L9 (1979).
3) A. Cassol, A. Seminaro, and G. De Paoli, *Inorg. Nucl. Chem. Lett.*, **9**, 1163 (1973).
4) J.-C. G. Bünzli and D. Wessner, *Helv. Chim. Acta*, **61**, 1454 (1978).
5) M. E. Harman, F. A. Hart, M. B. Hursthouse, G. P. Moss, and P. R. Raithby, *J. Chem. Soc., Chem. Commun.*, **1976**, 396.
6) M. Ciampolini, P. Dapporto, and N. Nardi, *J. Chem. Soc., Dalton Trans.*, **1979**, 974.
7) J.-C. G. Bünzli, B. Klein, and D. Wessner, *Inorg. Chim. Acta*, **44**, L147 (1980).
8) Y. Hirashima and J. Shiokawa, *Chem. Lett.*, **1979**, 463.
9) R. M. Izatt, J. D. Lamb, and J. J. Christensen, *J. Am. Chem. Soc.*, **99**, 8344 (1977).
10) T. Ashida, "The Universal Crystallographic Computing System-Osaka," The computation Center, Osaka University (1973), p. 55.
11) A. R. Al-Karaghouli and J. S. Wood, *Inorg. Chem.*, **11**, 2293 (1972).
12) D. S. Moss and S. P. Sinha, *Z. Phys. Chem.*, **63**, 391 (1969).
13) R. Iwamoto, *Bull. Chem. Soc. Jpn.*, **46**, 1144 (1973).

The Methylation of Ribonucleosides by Trimethyl Phosphate or Dimethyl Sulfate in the Presence of Boric Acid

Yorisato HISANAGA, Toshizumi TANABE, Kiyoshi YAMAUCHI,* and Masayoshi KINOSHITA

Department of Applied Chemistry, Osaka City University, Sumiyoshi-ku, Osaka 558

(Received June 13, 1980)

Synopsis. Uridine, inosine, adenosine, and thymidine were methylated selectively at the base moieties by the use of trimethyl phosphate or dimethyl sulfate in the presence of boric acid. A suppressing effect of boric acid on the methylation of the ribose-hydroxyl groups was discussed briefly.

Alkylation reactions of nucleosides have been carried out in various ways in the search for useful physiological activity of the products.[1,2] The study has been also stimulated by the discovery of a variety of alkylated nucleosides from RNA.[3] The direct alkylation of nucleosides, however, frequently provides a mixture of mono- and multialkylated nucleosides, giving a desired product in a small yield.

In this paper we wish to report the selective methylation of ribonucleosides at the base moieties by the use of trimethyl phosphate (TMP) and dimethyl sulfate (DMS) in the presence of boric acid.

The reactions were carried out by stirring mixtures of a nucleoside, TMP or DMS, and boric acid at pH>12 and at 25 or 50 °C. The reaction sizes and results are summarized in Table 1. It was found generally that methylation at the base moieties of nucleosides was hardly affected at all by boric acid, whereas methylation on hydroxyl groups of the ribose moieties (*O'*-methylation) was suppressed with an increase in the amount of boric acid, the effect reaching its maximum when the amount of boric acid used was approximately equivalent to that of the nucleosides. For instance, the treatment of uridine with TMP in the absence of boric acid produced 3-methyl-, 3,$O^{2'}$-dimethyl-, and 3,$O^{3'}$-dimethyluridines in 51, 25, and 10% yields respectively; by contrast, the reaction in the presence of the acid afforded 3-methyluridine in a 78% yield and the dimethyluridines in combined yields of only 9% (Run 1 of the Table 1). Although DMS was more reactive than TMP, methylation by DMS gave results similar to those obtained with TMP.

The selective methylation at the base moieties of ribonucleosides is attributable to the decreased *O'*-methylation by boric acid. Possibly, the ribose hydroxyl groups were deactivated by complex formation with the acid (Fig. 1). A similar complex formation has been suggested in the phosphorylation of ribonucleosides,[4] the acylation of carbohydrates,[5] *etc.*[6] The NMR spectra of mixtures of ribonucleosides and boric acid also indicated a complex structure. Thus, the addition of the acid to an aqueous solution of a nucleoside considerably shifted the absorption signals of the ribose-protons, especially 2'-H and 3'-H. Figure 2 shows the NMR spectra of the ribose moiety of uridine as an example.

After the reactions, the boric acid was removed easily as the methyl ester from the reaction mixtures by coevaporation with anhydrous methanol.

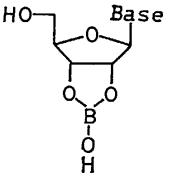

Fig. 1.

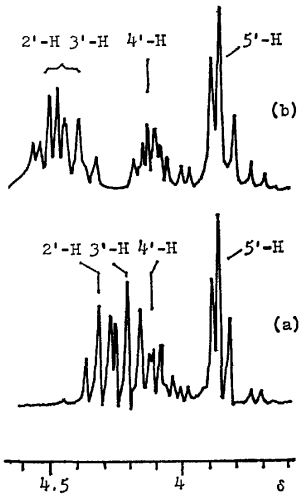

Fig. 2. ^{1}H-NMR (100 MHz) spectra of the ribose moiety of uridine (0.25 mol/l): (a) in the absence of boric acid: (b) in the presence of the acid (0.25 mol/l).
Solvent: D_2O, temperature: 25 °C, pH: *ca.* 12, spectrometer: JEOL PS 100. 3-(Trimethylsilyl)propionic acid-d^4 sodium salt was used as the internal standard.

Experimental

General Methylation Procedure. The reaction sizes and conditions are described in Table 1. A mixture of a nucleoside, a methylating agent, and boric acid in water was heated at 25 or 50 °C and at pH>12. The pH value of the solution was maintained by the occasional addition of 1 mol dm^{-3} sodium hydroxide. The progress of the methylation reactions was checked by silica-gel thin-layer chromatography (TLC) using the solvents employed previously.[2,7]

The reaction mixture was concentrated and washed with benzene or diethyl ether to remove the methylating agent unreacted. Anhydrous methanol was then added to the residue, and the solution was concentrated under reduced pressure. This coevaporation procedure was repeated several times to remove the boric acid completely. The resulting reaction mixtures were placed in a silica-gel column (Merck, 7734, 100—200 mesh) using the solvents indicated in Footnote c of Table 1. The yields and mp's of the prin-

Table 1. Methylation of various nucleosides in the presence of boric acid[a)]

Nucleoside	Methylating agent[b)]	Temp °C	Time h	Products[c)]	UV-Yield/%[d)]	
					$B(OH)_3$	None
Uridine(U)	TMP	50	24	3-Methyl-U[e)]	78(68)	51
				3,$O^{2'(3')}$-Dimethyl-U	9	35
U	DMS	25	1	3-Methyl-U	87(65)	43
				3,$O^{2'(3')}$-Dimethyl-U	10	49
Thymidine(dT)	TMP	50	3	3-Methyl-dT[f)]	90(58)	88
Inosine(I)	TMP	50	6	1-Methyl-I[e)]	91(36)	50
				1,$O^{2'(3')}$-Dimethyl-I	4	40
I	DMS	25	1	1-Methyl-I	90	65
				1,$O^{2'(3')}$-Dimethyl-I	8	33
Adenosine(A)	TMP	50	24	N^6-Methyl-A	20	trace
				$O^{2'(3')}$-Methyl-A	8	38
				N^6,$O^{2'(3')}$-Dimethyl-A	7	24

a) Reaction size: nucleoside-TMP(DMS)-boric acid-water=1.0 mmol-36(3) mmol-1.0 mmol-4 ml. See also the Experimental section. b) TMP: trimethyl phosphate. DMS: dimethyl sulfate. c) Mixtures of chloroform and methanol were used for the column chromatography: 10—1(v/v) for 3-methyluridine and 3-methylthymidine; 17—3(v/v) for 1-methylinosine. The yield ratios of $O^{2'}$-methylated nucleosides to $O^{3'}$-methylated nucleosides were 2.5—3.5, according to the NMR spectra of the reaction mixtures. d) The yields in parentheses were based on the amounts of products isolated. e) Mp: 3-methyluridine, 116—118 °C (from ethyl acetate); 1-methylinosine, 207—208 °C (from ethanol-methanol). J. Zemlicka (*Collect. Czech. Chem. Commun.*, **35**, 3572 (1970)) reports mp of 115—116 °C and 209—210 °C respectively. f) Mp 134—134.5 °C (from water). H. T. Miles, *J. Am. Chem. Soc.*, **79**, 2565 (1957) reports a mp of 128.5—132 °C.

cipal products are shown in the table.

The NMR and UV spectra of the isolated products agreed with the assigned structures. The unisolable products were identified by a comparison of the mobilities in TLC and the UV spectra of the aqueous extracts of the spots in TLC with those of authentic samples[2)] or literature values.

References

1) "Nucleic Acid Chemistry," ed by L. B. Towensend and R. S. Tipson, John Wiley and Sons, New York (1978), Parts 1 and 2.

2) K. Yamauchi and M. Kinoshita, *J. Chem. Soc., Perkin Trans. 1*, **1978**, 762, and the references cited therein.

3) J. A. McCloskey and S. Nishimura, *Acc. Chem. Res.*, **10**, 403 (1977); Y. Furuichi and K. Miura, *Nature*, **253**, 374 (1975).

4) M. Ikehara, E. Ohtsuka, and Y. Kodama, *Chem. Pharm. Bull. (Tokyo)*, **12**, 145 (1964).

5) J. M. J. Frechet, L. J. Nuyens, and E. Seymour, *J. Am. Chem. Soc.*, **101**, 432 (1979).

6) S. L. Johnson and K. W. Smith, *Biochemistry*, **15**, 553 (1976); A. M. Yurkevich, L. S. Vershavskaya, I. I. Kolodkina, and N. A. Preobrazhenskii, *Zh. Obshch. Khim.*, **37**, 2002 (1967).

7) K. Yamauchi, T. Tanabe, and M. Kinoshita, *J. Org. Chem.*, **41**, 3691 (1976).

Photolysis of Sodium Arenesulfonates in Alkaline Dimethyl Sulfoxide Solutions[1,2]

Nobutaka Suzuki,* Kinya Ito, and Yasuji Izawa
Chemistry Department, Faculty of Engineering, Mie University, Tsu, Mie 514
(Received April 21, 1980)

Synopsis. Photolysis of arenesulfonates in alkaline DMSO under air gave the corresponding desulfonation products, arenes, presumably *via* the π-π^* excited triplet state.

With respect to the relationship between the photochemical behavior and electronic configuration (n-π^* or π-π^*) of the excited states of the arenesulfonates, a report was given on a new photoelimination of SO_2 (desulfonylation) of sodium 9-anthracene-, 1-naphthalene-, and mesitylene-sulfonates (**1a—b** and **1g**) *via* n-π^* excited states, along with photoelimination of SO_3 (desulfonation) *via* π-π^* excited states.[2] This seems to be the first example of the photodesulfonylation of sulfonic acids. Ogata *et al.*[3] reported on a photochemical reaction of benzenesulfonic acid in an aqueous alkaline solution, giving benzene (16%) and biphenyl (1%) and assumed to involve an initial radical fission of C–S bond giving Ph· and $\cdot SO_3H$ radicals. In this report we describe the photolysis of arenesulfonates (**1a—f**) in alkaline DMSO to give the corresponding arenes (**2**) by desulfonation almost as the sole product, presumably *via* the π-π^* excited state.

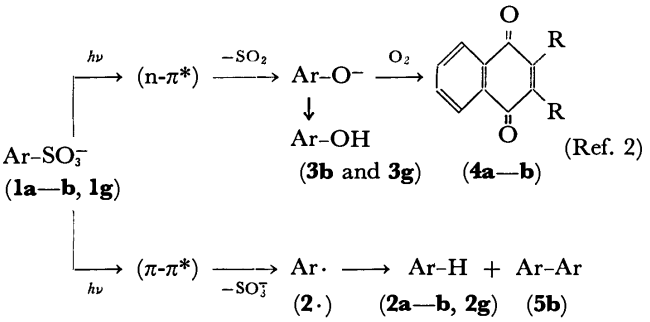

a: Ar=g-Anthryl, **b**: Ar=1-Naphthyl, **g**: Ar=Mesityl

Solutions of the sulfonic acids (**1a—f**: *ca.* 5 mmol/l) in DMSO with aqueous 1 mol/l NaOH were irradiated with a low-pressure mercury lamp (30W) in quartz cells at tap-water temperature. The photoreactions were monitored by GLC. The results are summarized in Table 1. It was found that the photolysis of **1d—f** gives the parent hydrocarbons (**2**), photodesulfonation products, whereas **1a—c** yielded traces of a quinone (**4a**), or 1- or 2-naphthol (**3b** or **3c**) besides the parent hydrocarbons (**2a—b**) as main products. The results significantly differ from those obtained by the experiments in aqueous medium. In aqueous solutions, photodesulfonylation was distinctly

$$\underset{\textbf{1a—f}}{Ar\text{-}SO_3^-} \xrightarrow[DMSO/H_2O]{h\nu} (\pi\text{-}\pi^*) \longrightarrow \underset{\textbf{2a—f}}{Ar\text{-}H}$$

a: Ar=9-anthryl; **b**: Ar=1-naphthyl;
c: Ar=2-naphthyl; **d**: Ar=*o*-tolyl;
e: Ar=*p*-tolyl; and **f**: Ar=phenyl

observed for **1a—b**.[2]

DMSO accelerates reactions of anions in contrast with the reduced activity of hydrogen-bonded anions in protic solvents of comparative dielectric constants.[4] A (π-π^*) excited state is more ionic than an appropriate (n-π^*) excited state considered to be biradical. Hence, in DMSO, preference of the desulfonation ($-SO_3$) to the desulfonylation ($-SO_2$) can be expected.

Steric effect of the sulfonyl group on the peri H atom(s) (**1a—b**) or the *o*-methyl group (**1d**) can be expected for the present reactions by the analogy of a similar photoelimination of 9-nitro- and 9-carboxy-anthracene (**6** and **7**),[5] whose nitro and carboxyl functional groups are not coplanar, not being able to resonate with aromatic rings[5] due to the steric hindrance with the peri H atoms. In contrast to **6** and **7**, the sulfonyl group is tetrahedral and the hindrance with the peri H atoms would not inhibit the coplanarity between one of the three S–O bonds and the aromatic nucleus as shown in formula **8**.

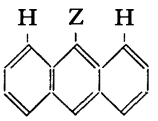

6: Z=NO_2
7: Z=CO_2H

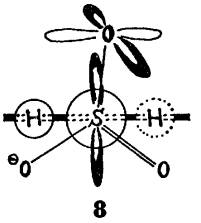

8

The data showing absence or presence of a trace of desulfonylation, obtained by changing the arene moieties attached to the sulfonyl groups for the purpose of differentiating the effect of peri H atom on the sulfonyl groups (*i.e.*, **1a**, **1b**, **1d**, and **1f**: also **1c** and **1e** were employed) supported the above interpretation on the steric effect.

It seems that the arene moieties determine the electronic configurations (n-π^* or π-π^*) of the S_1 and T_1 excited states of the arenesulfonates and also the reaction course. In contrast to the results in aqueous solution where desulfonylation and desulfonation of **1a** proceed *via* T_1 (n-π^*) and T_2 (π-π^*), respectively,[2] quenching experiments of **1a—c** in DMSO with 1,3-pentadiene on the fluorescence (not quenched), desulfonation (quenched), and desulfonylation (not quenched) revealed that desulfonation occurs *via* T and not S_1, and that desulfonylation might proceed *via* S_1 in DMSO. The results could be explained if the desulfonation and desulfonylation in DMSO proceed *via* T_1 (π-π^*) and S_1 (n-π^*), respectively. The relative stability of n-π^* and π-π^* excited states of **1a** might be inverted in water and in DMSO. Stern-Volmer plots of the other sulfonates with 1,3-pentadiene to the reaction products suggest that the desulfonation proceeds *via* T_1 excited states. Large viscosity of DMSO might cause relatively small rates of diffusion

of 1,3-pentadiene, and no quenching of the fluorescence and desulfonylation. Measurement of viscosity of DMSO, however, eliminated the possibility, the observed diffusion constant, $k_{dif.}$ being 3.80×10^9 l/mol, which is in the range of that of the other organic solvents ($k^{25}_{dif.}=10^9$—10^{10}).[6]

Experimental

Fluorescence and phosphorescence spectra were recorded on a Hitachi MPF-2A spectrometer and GLC on a Yanagimoto Yanaco G-1800F gas chromatograph.

Materials. Sodium anthracene-9-sulfonate (**1a**) was prepared according to the method worked out by Yura and Oda.[7] Commercial sodium naphthalene-1- and -2-, *o*- and *p*-toluene-, and benzene-sulfonates (**1b**—**1f**), and commercial authenitic samples (**2a**—**f**, **3b**—**f**, **4a**—**b**, **4f**, and **5b**) were used. DMSO was distilled *in vacuo* from CaH_2. 1,3-Pentadiene was distilled before use in quenching experiments.

General Method for Photolyses of 1a—f. A solution of compound **1** (*ca.* 5 mmol/l) in DMSO (3 ml) and aqueous 1 mol/l NaOH (100 μl) was irradiated with a low pressure mercury lamp (30 W, Eikosha; P1L-30) in a quartz cell (ϕ 10 mm) at tap-water temperature (*ca.* 15 °C). The reaction was monitored at intervals by GLC. The product(s) was identified and the yields were determined by comparison with the corresponding authentic sample(s) on GLC (Table 1). GLC were afforded on 10% Silicone SE-GE-31 on Diasolid L (60—80 mesh) for **1a**, **1d**—**e**, and **1f**, and on Apiezon L on Diasolid L, 2.2 m for **1b**—**c**.

Solvent Effect of 1 on Fluorescence and Phosphorescence Spectra. The 0-0 bands of fluorescence and phosphorescence spectra of **1a**—**f** were measured in various solvents at 77 K in a quartz cell. The results showed the electronic configurations (π-π^* or n-π^*) of the S_1 and T_1 excited states of **1a**—**f** to be n-π^* for S_1 and π-π^* for T_1.

Table 1. Photolysis of Ar-SO_3Na (**1a**—**f**) in DMSO

1	Concn / mmol l^{-1}	Irrad. time / min	Yield/%[a] Ar-H (2)	Ar-OH (3)	Quinone (4)
1a	5.0	50	60	n.d.[b]	1.8
	5.0	60			2.1
	[2.9	180	54	n.d.	36.8][c]
	[5.0	180	27.9	n.d.	13.2][c]
1b	5.1	50	3.0	n.d.	n.d.
	5.1	900	16.5	trace	n.d.
1c	5.3	50	6.7	n.d.	n.d.
	5.3	60	8.4	trace	n.d.
1d	5.0	50	3.3	n.d.	n.d.
	5.0	1820	50.0	n.d.	n.d.
1e	5.0	50	2.9	n.d.	n.d.
	5.0	1820	45.0	n.d.	n.d.
1f	5.0	50	6.7	n.d.	n.d.
	5.0	360	50.0	n.d.	n.d.

a) Yields based on the starting material used. b) Not detected. c) Photolysis in aqueous solution (Ref. 2).

Quenching with 1,3-Pentadiene. (a) Quenching on fluorescence of **1** in DMSO (5.0 mmol/l) with various concentrations of 1,3-pentadiene (1.3, 2.9, 5.2, 10.3, and 20.7 mmol/l) was observed by means of the MPF-2A spectrometer at 25 °C. (b) Quenching on the products of desulfonation and/or desulfonylation from **1** in DMSO (5.0 mmol/l) with various concentrations of 1,3-pentadiene in air was observed by GLC. The $k_q\tau$ values were calculated from the slopes of the Stern-Volmer plots.[8] The fluorescence and desulfonylation of **1a**—**c** were not quenched, while desulfonation of **1a**—**c** was quenched, the $k_q\tau$ values being 2.6×10, 7.4×10, and 5.8×10, respectively.

Viscosity of DMSO. The viscosity of DMSO used was calculated from the equation

$$\eta_{DMSO} = \eta_{H_2O}\cdot(\rho_{DMSO}\cdot t_{DMSO})/(\rho_{H_2O}\cdot t_{H_2O})$$
$$= 8.004^{9)}\times1.1014^{10)}\times122.3/(0.9956756^{9)}\times61.0)$$
$$= 17.751 \text{ (mpoise)},$$

the values of $t^{30°}_{H_2O}$ and $t^{30°}_{DMSO}$ being measured with an Ostwald viscometer. From the results the diffusion constant $k_{dif.}$ in DMSO was estimated by

$$k_{dif.} = 8RT/3000\eta \text{ (l/mol s)} = 3.80\times10^9 \text{ (l/mol s)},^{11)}$$

where

$$R = 8.314\times10^7 \text{ erg K}^{-1}\text{ mol}^{-1}.$$

References

1) Preliminary communication: N. Suzuki, K. Ito, A. Inoue, and Y. Izawa, *Chem. Ind. (London)*, **1977**, 399.

2) Photochemistry of Sulfonyl Compounds. 8. 7: Y. Izawa, N. Suzuki, A. Inoue, K. Ito, and T. Ito, *J. Org. Chem.*, **44**, 4581 (1979), and references cited therein.

3) Y. Ogata, K. Takagi, and S. Yamada, *Bull. Chem. Soc. Jpn.*, **50**, 2205 (1977).

4) L. F. Fieser and M. Fieser, "Reagents for Org. Synth.," Wiley, New York, N. Y. (1967), Vol. 1, p. 296.

5) a) O. L. Chapman, D. C. Heckert, J. W. Reasoner, and S. P. Thachaberry, *J. Am. Chem. Soc.*, **88**, 5550 (1966); b) A. W. Bradshaw and O. L. Chapman, *ibid.*, **89**, 2372 (1967); c) R. Hunt and S. T. Reid, *J. Chem. Soc., Perkin Trans. 1*, **1972**, 2527.

6) N. J. Turro, "Modern Molecular Photochemistry," Benjamin/Cummings, Menlo Park, California (1978), p. 314.

7) S. Yura and R. Oda, *Kogyo Kagaku Zasshi*, **44**, 731 (1941); (*Chem. Abstr.*, **42**, 6792i (1948)).

8) Ref. 6, p. 246.

9) Natl. Res. Council, U. S. A., "Intern. Critical Tables of Numerical Data, Phys., Chem., and Technol.," McGraw-Hill, New York, N. Y., Vol. 5, p. 10 and Vol. 3, p. 24.

10) J. A. Riddick and W. B. Bunger, "Org. Solvents," Wiley, New York, N. Y. (1970), p. 466.

11) An upper limit to the magnitude of the bimolecular quenching constant k_q of $k_q\tau$ calculated from the slope of Stern-Volmer plots is usually set by the rate of diffusion ($k_{dif.}$) of the excited state and quencher (1,3-pentadiene) into a solvent cage; see Ref. 6, p. 260.

A New Route to Vitispiranes

Tetsuya KATO* and Hisao KONDO

Basic Research Laboratories, Toray Industries, Inc., Tebiro, Kamakura 248

(Received April 26, 1980)

Synopsis. Diastereoisomeric vitispiranes have been synthesized from 2,6,6-trimethyl-1-(3-oxo-1-butenyl)-1,3-cyclohexadiene by five-step reactions including photooxygenation.

Vitispirane, an odoriferous C_{13} spiro-ether, was initially found in the aroma volatiles of grape juice (vine sp. *Vitis vinifera*), as well as in table and fortified wines and in distilled spirits.[1] Recently Ohloff *et al.* have also isolated vitispirane from the volatiles of a vanilla extract and have shown the presence of (2*RS*,5*RS*)- and (2*RS*,5*SR*)-vitispiranes (**1** and **2**) in the vanilla extract; their relative configurations were established by stereoselective synthesis.[2] In relation to our own interest in devising simplified approaches to the synthesis of ionone-related flavorants, we have developed an alternative synthesis of vitispiranes (**1** and **2**) from an easily accessible dehydroionone **3**.[3] Our synthetic route is outlined in the following scheme.

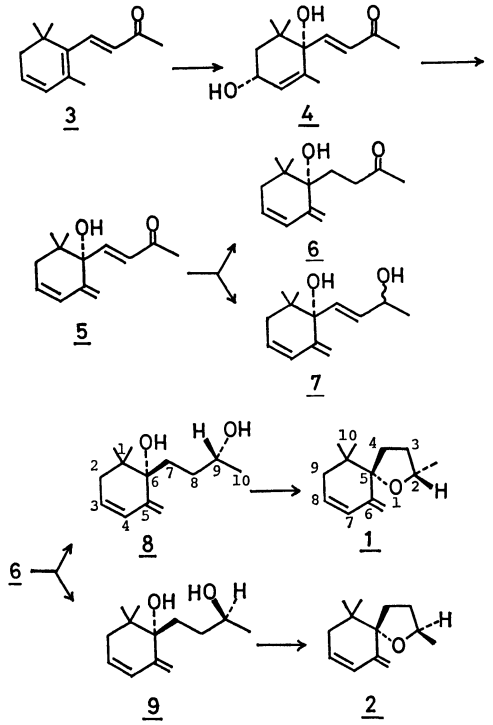

The photosensitized oxygenation of the dehydroionone **3**,[4] followed by the reduction of the resulting peroxide with thiourea,[5] provided the *cis*-diol **4**.[6] The subsequent treatment of **4** with dimethyl sulfoxide[7] at 140 °C for 8 h afforded the crystalline triene ketone **5** in a 47% yield. The conjugate reduction of the α,β-unsaturated ketone of **5** with $LiAlH(OMe)_3$–CuBr[8] in tetrahydrofuran at −20 °C provided the diene ketone **6** in a 48% yield. Although a high selectivity for 1,4-addition was reported by Semmelhack *et al.* with a variety of cyclic and acyclic α,β-unsaturated ketones,[8] the formation of a 1,2-adduct **7** in a moderate yield was also observed in the reduction of **5**. When the reagent prepared from $LiAlH_4$–CuI[9] was employed, the 1,2-adduct **7** was obtained as the major product.

The reduction of **6** with sodium borohydride in ethanol gave the diastereoisomeric diene diols, **8** and **9**, in a ratio of *ca.* 7:1. The pure **8** was obtained by the recrystallization of the mixture. The diene diol **8** was stereospecifically cyclized[10] to (2*RS*,5*RS*)-vitispirane **1** by heating with *p*-toluenesulfonyl chloride in pyridine, the relative configurations at C-6 and C-9 of **8** being established as (6*RS*,9*SR*). The filtrate fraction was chromatographed to afford a mixture containing **8** and **9** in a ratio of *ca.* 1:1. The ^{1}H-NMR spectrum of this mixture is practically identical with that of the pure **8** except for a pair of singlets at 5.18 and 5.20 ppm due to one of the *exo*-methylene protons of **8** and **9** respectively. The treatment of this mixture with *p*-toluenesulfonyl chloride afforded (2*RS*,5*RS*)- and (2*RS*,5*SR*)-vitispiranes (**1** and **2**) in a ratio of *ca* 1:1.

Experimental

The melting points are uncorrected. The following spectrometers were used: IR, Hitachi 215; NMR, Varian XL-100 or JOEL FX-100 (tetramethylsilane as the internal standard); mass spectra, JEOL D-300. The thin-layer chromatography (TLC) was performed on 0.25 mm precoated silica gel PF_{254} (Merck). Silica gel (70—230 mesh, Merck) was used for the column chromatography.

cis-2,6,6-Trimethyl-1-(3-oxo-1-butenyl)-2-cyclohexene-1,4-diol (4). A solution of dehydroionone **3** (3.00 g, 15.8 mmol, purity 85%) and Rose Bengal (30 mg) in methanol (50 ml) was irradiated externally with a high-pressure mercury vapor lamp (Toshiba HT-400PL) in a water-cooled (0—5 °C) apparatus, while oxygen was being bubbled through the solution (*ca.* 30 ml/min). The reaction was essentially complete after 25 min. After the addition of thiourea (1.37 g, 18.0 mmol), the mixture was stirred at 25 °C for 7 h. After the subsequent removal of the solvent, the residue was chromatographed (benzene–ethyl acetate, 1:1) on silica gel to give the *cis*-diol **4** (0.80 g, 28%). **4**: IR (neat) 3400, 1672, 1620, 1098, 1015, 988 cm^{-1}; NMR ($CDCl_3$) δ 0.97 (s, 3H), 0.99 (s, 3H), 1.65 (t, J=2 Hz, 3H), 1.60—2.16 (m, 4H), 2.88 (s, 3H), 4.25 (m, 1H), 5.65 (m, 1H), 6.43 (d, J=16 Hz, 1H), 6.74 (d, J=16 Hz, 1H): MS, *m/e* 224 (M^+), 191, 150, 108, 43. Found: *m/e* 224.1418. Calcd for $C_{13}H_{20}O_3$: M, 224.1412.

6,6-Dimethyl-2-methylene-1-(3-oxo-1-butenyl)-3-cyclohexen-1-ol (5). A solution of the *cis*-diol **4** (1.50 g, 6.70 mmol) in dimethyl sulfoxide (6.5 g) was heated at 140 °C for 8 h. The reaction mixture was then cooled, poured into water, and extracted with ethyl acetate. The ethyl acetate extracts were washed with water and dried over anhydrous sodium sulfate. After the removal of the solvent, the residue was chromatographed (benzene– ethyl acetate, 7:1) on silica gel to give the triene ketone **5** (0.65 g, 47%). **5**: mp 81—82 °C; IR (Nujol) 3490, 1785, 1682, 1655, 1595, 1140, 995, 978, 892 cm^{-1}; NMR ($CDCl_3$) δ 0.92 (s, 3H), 0.96 (s, 3H), 1.69 (s, 1H), 2.06—2.20 (m, 2H), 2.25 (s, 3H), 5.02 (s, 1H), 5.16 (s, 1H), 5.62—5.86 (m, 1H), 6.08—6.26

(m, 1H), 6.43 (d, J=16 Hz, 1H), 6.89 (d, J=16 Hz, 1H); MS, *m/e* 206 (M^+), 191, 163, 121, 43. Found: *m/e* 206.1270. Calcd for $C_{13}H_{18}O_2$: M, 206.1305.

*6,6-Dimethyl-2-methylene-1-(3-oxobutyl)-3-cyclohexen-1-ol (**6**).* A solution of lithium trimethoxyaluminium hydride in tetrahydrofuran (0.659 mol/l, 60.7 ml, 40.0 mmol) was added, drop by drop, to a suspension of copper(I) bromide (2.86 g, 20.0 mmol) in tetrahydrofuran (15 ml) at −20 to −10 °C. After 30 min, the resulting dark brown suspension was cooled to −20 °C. A solution of the triene ketone **5** (1.03 g, 5.00 mmol) in tetrahydrofuran (10 ml) was added (*ca.* 5 min). The mixture was then stirred at −20 °C for 50 min, poured into cold water, and extracted with ethyl acetate. The ethyl acetate extracts were washed with water and dried over anhydrous sodium sulfate. After the removal of the solvent, the residue was chromatographed (hexane–ethyl acetate, 5:4) on silica gel to give the diene ketone **6** (490 mg, 48%) and the triene diol **7** (499 mg, 49%). **6**: mp 60—62 °C; IR (Nujol) 3320, 3025, 1782, 1715 (weak), 1642, 1600, 1106, 1042, 892 cm^{-1}; NMR ($CDCl_3$) δ 0.8—1.2 (m, 6H, with two s at 0.88 and 1.06), 1.4—2.6 (m, 10H, with a d at 1.62 and a s at 2.14), 4.80—5.16 (m, 2H), 5.32—5.68 (m, 1H), 5.90—6.12 (m, 1H); MS *m/e* 208 (M^+), 190, 185, 150, 131, 99, 43. Found: *m/e* 208.1458. Calcd for $C_{13}H_{20}O_2$: M, 208.1461.

*1-(3-Hydroxybutyl)-6,6-dimethyl-2-methylene-3-cyclohexen-1-ols (**8** and **9**).* A solution of the diene ketone **6** (439 mg, 2.11 mmol) and sodium borohydride (300 mg, 7.93 mmol) in ethanol (15 ml) was stirred at 25 °C for 1 h. The reaction mixture was then poured into water and extracted with ethyl acetate. The ethyl acetate extracts were washed with water and dried over anhydrous sodium sulfate. After the removal of the solvent, the crystalline residue was recrystallized from hexane–ethyl acetate to yield **8** (179 mg). The filtrate was concentrated and crystallized again from hexane–ethyl acetate to yield **8** (90 mg). The filtrate was concentrated and chromatographed (hexane–ethyl acetate, 2:5) on silica gel to give a mixture containing **8** and **9** in a ratio *ca.* 1:1 (91 mg). The total yield of **8** and **9** was 81%. **8**: mp 141—142 °C; IR (Nujol) 3300, 3020, 1780, 1640, 1598, 1048, 988, 890 cm^{-1}; NMR ($CDCl_3$) δ 0.88 (s, 3H), 1.06 (s, 3H), 1.16 (d, J=6 Hz, 3H), 1.26—2.46 (m, 8H), 3.56—3.92 (m, 1H), 5.04 (s, 1H), 5.02 (s, 1H), 5.50—5.72 (m, 1H), 6.00—6.18 (m, 1H); MS, *m/e* 210 (M^+), 192 177, 126, 43. Found: *m/e* 210.1672. Calcd for $C_{13}H_{22}O_2$: M, 210.1620.

*Vitispiranes (**1** and **2**).* To a solution of the diene diol **8** (1.007 g, 4.79 mmol) in pyridine (13 ml), was added *p*-toluenesulfonyl chloride (1.57 g, 8.24 mmol). The mixture was then stirred at 0 °C for 18 h, heated at 80 °C for 4 h, and cooled to 0 °C. After the addition of water (6 ml), the mixture was stirred at 0 °C for 1 h, poured into water, and extracted with ether–pentane. The organic layers were washed with water and dried over anhydrous sodium sulfate. After the removal of the solvent, the residue was distilled (oil bath 100 °C/1 Torr) to give (2*RS*,5*RS*)-vitispirane **1** (812 mg, 88%). The mixture of **8** and **9** from the previous experiment, upon treatment under the same conditions, afforded (2*RS*,5*RS*)- and (2*RS*,5*SR*)-vitispiranes (**1** and **2**) in a ratio of *ca.* 1:1. The IR, NMR, and mass spectral data of **1** and **2** were identical with those of authentic samples.[2]

References

1) R. F. Simpson, C. R. Strauss, and P. J. Williams, *Chem. Ind. (London)*, **1977**, 663.

2) K. H. Schulte-Elte, F. Gautschi, W. Reinold, A. Hauser, P. Fankfauser, J. Limacher, and G. Ohloff, *Helv. Chim. Acta*, **61**, 1125 (1978).

3) J. A. Findlay and W. D. MacKay, *Can. J. Chem.*, **49**, 2369 (1971).

4) M. M. Canet, J. C. Mani, J. P. Dalle, and J. L. Olivé, *Bull. Soc. Chim. Fr.*, **1966**, 3874.

5) K. H. Schulte-Elte, M. Gadola, and G. Ohloff, *Helv. Chim. Acta*, **56**, 2028 (1973).

6) M. Koreeda, G. Weiss, and K. Nakanishi, *J. Am. Chem. Soc.*, **95**, 239, (1973).

7) V. J. Traynelis, W. L. Hergenrother, J. R. Livingston, and J. A. Valicenti, *J. Org. Chem.*, **27**, 2377 (1962); V. J. Traynelis, W. L. Hergenrother, H. T. Hansen, and J. A. Valicenti, *ibid.*, **29**, 123 (1964); V. J. Traynelis and W. L. Hergenrother, *ibid.*, **29**, 221 (1964).

8) M. F. Semmelhack, R. D. Stauffer, and A. Yamashita, *J. Org. Chem.*, **42**, 3180 (1977).

9) E. C. Ashby and J. J. Lin, *Tetrahedron Lett.*, **1975**, 4453.

10) G. Weiss, M. Koreeda, and K. Nakanishi, *J. Chem. Soc., Chem. Commun.*, **1973**, 565.

Synthesis and Reactions of Perylenecarboxylic Acid Derivatives. X. Synthesis of *N*-Alkyl-3,4-perylenedicarboximide

Yukinori NAGAO* and Takahisa MISONO

Department of Industrial Chemistry, Faculty of Science and Technology, Science University of Tokyo, Yamazaki, Noda 278

(Received August 14, 1980)

Synopsis. *N*-Alkyl-3,4-perylenedicarboximides (alkyl=methyl, ethyl, propyl, butyl, isobutyl, pentyl, hexyl, and octyl) were prepared by the decarboxylation of *N*-alkyl-3,4:9,10-perylenetetracarboxylic monoanhydride monoimides (same alkyls) in potassium hydroxide solution.

In a previous publication we reported that the 3,4-perylenedicarboximide was sulfonated, and that the *N*-substituted perylene-3,4-dicarboximides could be prepared from the sulfonic acid *via* sulfoperylene-3,4-dicarboxylic anhydride and *N*-substituted sulfoperylene-3,4-dicarboximide.[1] This method may be applicable to many kinds of *N*-substituted perylene-3,4-dicarboximide preparations, but it includes too many reaction steps. 3,4-Perylenedicarboximide was prepared by decarboxylation of 3,4:9,10-perylenetetracarboxylic monoanhydride monoimide in potassium hydroxide solution.[2] The present work was undertaken to apply the decarboxylation to *N*-substituted 3,4:9,10-perylenetetracarboxylic monoanhydride monoimides to prepare *N*-alkyl-3,4-perylenedicarboximide(**2a**—**h**) (alkyl=**a**, methyl; **b**, ethyl; **c**, propyl; **d**, butyl; **e**, isobutyl; **f**, pentyl; **g**, hexyl; **h**, octyl) from *N*-alkyl-3,4:9,10-perylenetetracarboxylic monoanhydride monoimide[3,4] (**1a**—**h**) (same alkyls).

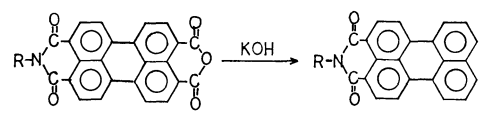

1a—h **2a—h**

R=**a**, methyl; **b**, ethyl; **c**, propyl; **d**, butyl; **e**, isobutyl; **f**, pentyl; **g**, hexyl; **h**, octyl.

Results and Discussion

The *N*-alkyl-3,4-perylenedicarboximides(**2a**—**h**) prepared by the decarboxylation of *N*-alkyl-3,4:9,10-perylenetetracarboxylic monoanhydride monoimides (**1a**—**h**) in potassium hydroxide solution are listed in Table 1. Their structures were confirmed by elemental analyses, absorption spectra, and IR and MS spectra. These are given in Table 2. All compounds could be prepared in 60—80% yield. The raw products of **2a**—**h** were given in good yields. The differences of yield are due to the difficulties of recrystallization from solvent.

All λ_{max} in the visible spectra of sulfuric acid solutions are 612—614 nm, and no different λ_{max} values due to alkyl group were found. All IR spectra indicate $\nu_{C=O}$ of imide on 1637—1647 cm^{-1} and 1680—1687 cm^{-1}, and no different $\nu_{C=O}$ due to alkyl group were found either. Mass spectra show the corresponding molecular ion peak. Table 3 shows the color, tinting strength, and light-fastness obtained by a similar method in previous work.[4] Colors were all reddish, and the colors of **2b**,**2c**,**2e**, and **2f** were very clear. Tinting strengths of **2b**,**2e**, and **2f** were high, and that of **2a** was the lowest. Light-fastness of *N*-butyl compound (**2d**) was the highest and *N*-pentyl compound(**2f**) was the lowest.

Table 1. Reaction conditions for the preparation of 3,4-perylenedicarboximide(**2a**—**h**)
Reaction temp: 220—230 °C; Time: 18 h.

1a—**h**(g)		12% KOH(ml)	Yield of **2a**—**h**/%	
1a	5.0	100	**2a**	74
1b	6.0	120	**2b**	62
1c	6.1	123	**2c**	64
1d	10.0	200	**2d**	67
1e	5.0	100	**2e**	71
1f	5.0	100	**2f**	81
1g	5.0	100	**2g**	70
1h	5.0	100	**2h**	76

Experimental

Material. **1a**—**h** were prepared by the previous methods.[3,4]

Preparation of 2a—h. For example, **2a** was prepared as follows. **1a** (5.0 g) and 12% potassium hydroxide solution (100 ml) were heated in an autoclave at 220—230 °C for 18 h with stirring. The cooled reaction mixture was filtered, and the precipitate was washed with water and dried to yield 3.7 g (89%) of crude reddish brown powder of **2a**. The crude **2a** was recrystallized from nitrobenzene–methanol to obtain 3.0 g (74%) of **2a** (mp>300 °C). **2b**—**h** were prepared with the same treatment under the conditions given in Table 1. The obtained crude yield of **2b**—**h** was: **2b**, 89%; **2c**, 81%; **2d**, 88%; **2e**, 77%; **2f**, 85%; **2g**, 90%; **2h**, 90%. The crude **2b**—**h** were recrystallized from benzene–methanol: **2b**, **2c**, **2d**, and acetic anhydride–methanol: **2e**, **2f**, **2g**, **2h**, respectively. The yields of **2b**—**h** were: **2b**, 62% (mp 292 °C); **2c**, 64% (mp 250 °C); **2d**, 67% (mp 267 °C); **2e**, 71% (mp 293 °C); **2f**, 81% (mp 249 °C); **2g**, 70% (mp 206 °C); **2h**, 76% (mp 190 °C).

Measurement. Mass spectra were recorded on a Hitachi RMU-7M mass spectrometer. Visible spectra were measured using a Hitachi 124 spectrometer for solutions in concd sulfuric acid (95.0%), and IR spectra on a Nippon Bunko IR-E spectrometer.

The prepared pigment (1.00 g) and 20.0 g of sodium sulfate were milled with a lab mill for 5 h. The mixture was added to water to remove sodium sulfate and then filtered. The residue was dried under vacuum at room temperature. The sample (100 mg), titanium dioxide (2.0 g), and boiled oil (1.2 ml) were mixed by a muller for three hundred revolutions. The mixture was painted on paper, then the tests were carried by the previous methods.[5]

Table 2. Analytical and spectral data for 3,4-perylenedicarboximide (**2a—h**)

2a—h R		Found (Calcd)% C	H	N	$\lambda_{max}^{H_2SO_4}$/nm	IR(KBr) $\nu_{C=O}$/cm^{-1} Imide		MS(*m/e*) (M^+)
2a	CH_3	81.18	3.68	4.36	612	1647	1687	335
		(82.37	3.87	4.18)				
2b	CH_2CH_3	81.97	4.06	4.17	613	1639	1680	349
		(82.54	4.30	4.01)				
2c	$(CH_2)_2CH_3$	81.17	4.45	4.01	613	1642	1682	363
		(82.64	4.68	3.86)				
2d	$(CH_2)_3CH_3$	82.87	4.98	4.04	614	1641	1680	377
		(82.74	5.07	3.71)				
2e	$CH_2CH(CH_3)_2$	83.12	5.06	3.81	614	1637	1684	377
		(82.74	5.07	3.71)				
2f	$(CH_2)_4CH_3$	82.76	5.30	3.64	612	1642	1683	391
		(82.84	5.41	3.58)				
2g	$(CH_2)_5CH_3$	82.65	5.57	3.48	615	1645	1680	405
		(82.94	5.72	3.45)				
2h	$(CH_2)_7CH_3$	83.31	6.29	3.25	615	1645	1680	433
		(83.11	6.28	3.23)				

Table 3. Properties of 3,4-perylenedicarboximide (**2a—f**)

2a—f R	Color	Tinting strength[a] *T*/%	Light-fastness[b] h
2a CH_3	Reddish violet	29	80
2b CH_2CH_3	Orange	62	100
2c $(CH_2)_2CH_3$	Reddish violet	58	100
2d $(CH_2)_3CH_3$	Reddish violet	37	140
2e $CH_2CH(CH_3)_2$	Orange	60	40
2f $(CH_2)_4CH_3$	Orange	63	30

a) *T*: Reflactance maxima(750 nm) − minima.
b) Exposure time before beginning to fade.

References

1) Y. Nagao and T. Misono, *Shikizai Kyokai Shi*, **49**, 29 (1976).
2) W. Neugebauer (I. G. Farbenind.), *D. R. P.*, 486491 (1929).
3) Y. Nagao, Y. Tanabe, and T. Misono, *Nippon Kagaku Kaishi*, **1979**, 528.
4) Y. Nagao and T. Misono, *Bull. Chem. Soc. Jpn.* in press.
5) Y. Nagao and T. Misono, *Bull. Chem. Soc. Jpn.*, in press.

1,3-Dioxolane Bearing Perfume and Herbicide Aldehyde Residues

Hiroyoshi KAMOGAWA,* Yuichiro HARAMOTO, Terumi NAKAZAWA, Harumitsu SUGIURA, and Masato NANASAWA

Department of Applied Chemistry, Yamanashi University, Takeda 4, Kofu 400

(Received October 17, 1980)

Synopsis. 4-Methacryloyloxymethyl-1,3-dioxolanes substituted at the 2 position with perfume and herbicide aldehyde residues were synthesized either by acetalization or by transacetalization involving 2,3-dihydroxypropyl methacrylate. The effect of the 2-substituent of the dioxolane ring on the rate of hydrolysis was remarkable.

In the course of studies to synthesize polymerizable acetals bearing various functions capable of being released by hydrolysis, those from perfume and vitamin alcohols have been reported.[1,2] In the meantime, polyurethanes containing the acetal linkage in the principal chain[3] and polyamide attached with acetal side chains,[4] both containing a herbicide function, have also been reported.

In this note, we wish to report on novel acetals containing the 1,3-dioxolane unit composed of the perfume or herbicide aldehyde and 2,3-dihydroxypropyl methacrylate residues.

Acetals **3a—g** were synthesized by the acid-catalyzed acetalization of **1** and **2a—g** (Eq. 1), where R represents a perfume or herbicide residue in Table 1.

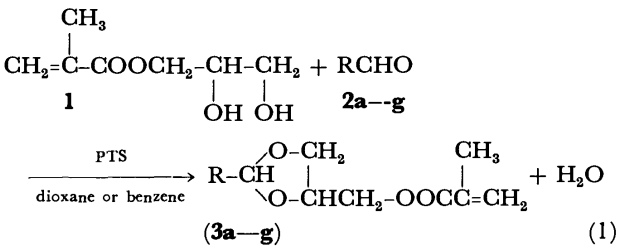

(1)

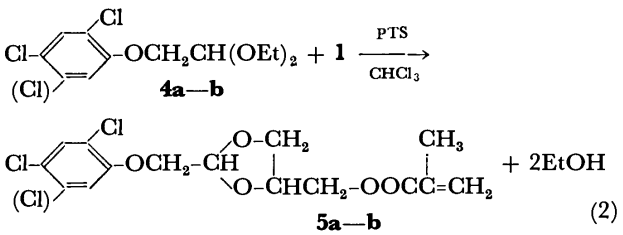

(2)

4a, **5a**: 2,4-Dichloro; **4b**, **5b**: 2,4,5-Trichloro

Diethyl acetals (**4a—b**) were also employed to conduct the *p*-toluenesulfonic acid (PTS)-catalyzed transacetalization as indicated in Eq. 2. A Soxhlet extractor, the thimble of which contained 4A or 5A molecular sieves for the removal of the ethanol produced, was employed in this case. Although the repetition of column chromatography decreased the yields of isolated products (9 and 11% for **5a** and **5b**, respectively), acetal conversions, calculated from the ^{1}H-NMR data for crude product **5a**, were 47 and 59% with 4A and 5A molecular sieves, respectively, on the basis of the starting **4a**, indicating advantage of the latter molecular sieves with larger micropores. The conversion for **5b** was 55% with 5A molecular sieves, also a much higher value than the yield (11%) of the purified product.

TABLE 1. ACETALS SYNTHESIZED ACCORDING TO Eq. 1

Abbreviation		Acetalization: Yield of 3a—g/%[a]	Acetalization: Solvent	Acetalization: Means of dehydration
2a, 3a		28	Dioxane	3A molecular sieves
2b, 3b		39	Dioxane	3A molecular sieves
2c, 3c		23	Dioxane	3A molecular sieves
2d, 3d		25	Dioxane	3A molecular sieves
2e, 3e		21	Dioxane	3A molecular sieves
2f, 3f		8	Benzene	Dean-Stark trap
2g, 3g		10	Benzene	Dean-Stark trap

a) Values for purified products.

TABLE 2. HYDROLYTIC RELEASE OF FUNCTIONAL ALDEHYDES FROM ACETALS

Acetals	Aldehyde released in: 2 h	Aldehyde released in: 24 h, %
3a	44	—
3d	Trace	—
3f	25	77
3g	27	—
5a	9	—

Novel 1,3-dioxolanes thus synthesized were subjected to acid hydrolysis, as exemplified in Table 2. The results indicate that the kind of 2-substituent of the dioxolane ring, *i.e.*, aldehyde residue, exerts a remarkable influence on the rate of hydrolysis: acetal **3a** bearing *p*-methoxyphenyl group as R which stabilizes the intermediate carbocation produced during the hydrolysis provides the highest rate, whereas, for **3d** and **5a** with aliphatic R, rates are much lower

than that for **3a** and even considerably lower than those for **3f** and **3g** with essentially the same release components as that in **5a**. This fact indicates that the release rate of the functional portion can be controlled here over a wide range by choosing the group neighboring to the C-2 atom of the 1,3-dioxolane ring.

Experimental

2,3-Dihydroxypropyl Methacrylate (**1**). A mixture of glycidyl methacrylate (14.2 g, 100 mmol), 4-*t*-butylcatechol (0.1 g), H_2SO_4 (concd, 0.2 ml), and water (100 ml) was stirred vigorously at room temperature for 24 h. The resulting clear solution was neutralized with an anion-exchange

resin (Diaion SA-10A) and freeze-dried to leave a liquid, which was distilled under reduced pressure to afford pure **1** as a colorless liquid (bp 115—120 °C/1.0 mmHg) in 60—70% yield. Found: C, 52.41; H, 7.74%. Calcd for $C_7H_{10}O_3$: C, 52.49; H, 7.55%. IR(CCl_4) 3500, 1720 cm^{-1}; NMR (D_2O) δ 2.0 (s, 3H, CH_3), 3.5—4.5 (m, 5 H, $-CH_2-CHCH_2$), 5.7 (s, 1H, $CH_2=$), 6.2 (s, 1H, $CH_2=$) ppm.

*2-(p-Methoxyphenyl)-4-methacryloyloxymethyl-1,3-dioxolane (**3a**).* A solution of **1** (1.3 g, 8.1 mmol), *p*-anisaldehyde (**2a**; 1.1 g, 8.1 mmol), PTS (0.3 g), and phenothiazine (0.05 g) in dioxane (50 ml) was stirred at room temperature for 24 h under nitrogen in the presence of 3A molecular sieves. The reaction mixture was diluted with chloroform and neutralized with aq $NaHCO_3$ by shaking. The organic layer was dried over anhyd. Na_2SO_4 and evaporated *in vacuo* to leave an oil, which was chromatographed on alumina (Wako, 300 mesh, neutral). Methanol elution provided an oily product. Found: C, 64.26; H, 7.01%. Calcd for $C_{15}H_{18}O_5$: C, 64.73; H, 6.52%. IR ($CHCl_3$) 1710 cm^{-1}; NMR (CCl_4) δ 1.9 (s, 3H, CH_3), 3.3—4.5 (m, 5H, $-CH_2-CHCH_2$), 3.7 (s, 3H, OCH_3), 5.1—5.8 (m, 1H, acetal CH), 5.6 (s, 1H, $CH_2=$), 6.1 (s, 1H, $CH_2=$), 6.6—7.4 (m, 4H, ArH) ppm; Mass (*m/e*) 278 (M^+).

Products **3b**, **3c**, **3d**, and **3e**, each oily compound, were synthesized in the same manner.

*2-(3,4-Methylenedioxyphenyl)-4-methacryloyloxymethyl-1,3-dioxolane (**3b**).* Found: C, 61.24; H, 5.92%. Calcd for $C_{15}H_{16}O_6$: C, 61.64; H 5.52%. IR (CCl_4) 1710 cm^{-1}; NMR (CCl_4) δ 1.9 (s, 3H), 3.4—4.5 (m, 5H), 5.1—5.8 (m, 1H), 5.5 (s, 1H), 5.9 (s, 2H), 6.0 (s, 1H), 6.5—6.9 (m, 3H) ppm; Mass (*m/e*) 292 (M^+).

*2-Styryl-4-methacryloyloxymethyl-1,3-dioxolane (**3c**).* Found: C, 69.65; H, 7.02%. Calcd for $C_{16}H_{18}O_4$: C, 70.05; H, 6.61%. IR ($CHCl_3$) 1710 cm^{-1}; NMR (CCl_4) δ 1.9 (s, 3H), 3.3—4.3 (m, 5H), 4.8—5.3 (b, 1H), 5.5 (s, 1H), 6.1 (s, 1H), 6.6—6.8 (d, 2H), 7.0—7.4 (s, 5H) ppm; Mass (*m/e*) 274 (M^+).

*2-(2,6-Dimethyl-5-heptenyl)-4-methacryloyloxymethyl-1,3-dioxolane (**3d**).* Found: C, 68.65; H, 8.67%. Calcd for $C_{17}H_{28}O_4$: C, 68.89; H, 8.86%. IR (CCl_4) 1720 cm^{-1}; NMR (CCl_4) δ 0.8—2.4 (m, 19H), 3.1—4.5 (m, 5H), 4.7—5.5 (m, 2H), 5.6 (s, 1H), 6.2 (s, 1H) ppm.

*2-(2,6-Dimethyl-1,5-heptadienyl)-4-methacryloyloxymethyl-1,3-dioxolane (**3e**).* Found: C, 69.75; H, 8.48%. Calcd for $C_{17}H_{26}O_4$: C, 69.35; H, 8.90%. IR (CCl_4) 1730 cm^{-1}; NMR (CCl_4) δ 0.8—3.0 (m, 16H), 3.1—4.2 (m, 5H), 4.5—6.1 (m, 3H), 5.5 (s, 1H) 6.0 (s, 1H) ppm.

*2-(2,6-Dichlorophenyl)-4-methacryloyloxymethyl-1,3-dioxolane (**3f**).* A mixture of **1** (1.6 g, 10 mmol), 2,6-dichlorobenzaldehyde (**2f**; 1.7 g, 10 mmol), hydroquinone (0.5 g), PTS (0.5 g), and benzene (100 ml) was refluxed for 2 h with a Dean-Stark trap fitted. The reaction mixture was washed with 5% aq K_2CO_3 (200 ml) and dried over anhyd. Na_2SO_4, followed by evaporation *in vacuo*. Silica gel (Wakogel C-300) column chromatography conducted on the crude product afforded pure **3f** as a viscous colorless oil (benzene eluate). Found: C, 52.61; H, 4.50%. Calcd for $C_{14}H_{14}O_4Cl_2$: C, 53.02; H, 4.45%. IR ($CHCl_3$) 1720 cm^{-1}; NMR ($CDCl_3$) δ 2.0 (s, 3H, CH_3), 3.8—4.9 (m, 5H, $-CH_2-CHCH_2$), 5.7 (s, 1H, $CH_2=$), 6.2 (s, 1H, $CH_2=$), 6.3, 6.6, 6.7 (t, 1H, acetal CH), 7.2—7.5 (t, 3H, ArH) ppm; Mass (*m/e*) 317 (M^+).

*2-(2,4-Dichlorophenyl)-4-methacryloyloxymethyl-1,3-dioxolane (**3g**).* A viscous oil [hexane–benzene (1:4 v/v) eluate]. Found: C, 52.83; H, 4.41%. Calcd for $C_{14}H_{14}O_4Cl_2$: C, 53.02; H, 4.45%. IR ($CHCl_3$) 1720 cm^{-1}; NMR ($CDCl_3$) δ 2.0 (s, 3H), 3.8—4.9 (m, 5H), 5.6 (s, 1H), 6.2 (s, 1H), 5.9, 6.2, 6.3 (t, 1H), 7.2—7.9 (m, 3H) ppm; Mass(*m/e*) 317 (M^+).

*(2,4-Dichlorophenoxy)acetaldehyde Diethyl Acetal (**4a**).* A solution of 2,4-dichlorophenol (16 g, 0.1 mmol) and potassium hydroxide (8 g) in methanol (100 ml) was evaporated *in vacuo* at 50—60 °C almost to dryness. The residue was dissolved in DMF (100 ml) and equimolar bromoacetaldehyde diethyl acetal (0.1 mol) was added, followed by stirring at 100 °C for 5 h under nitrogen. The reaction mixture was poured into excess aq $NaHCO_3$ (500 ml) and the oil thus separated was extracted with ether (200 ml). The ether extract was washed first with dil aq NaOH, then with water, dried over anhyd. Na_2SO_4, and concentrated *in vacuo*, followed by distillation under reduced pressure to afford **4a** as a light yellow oil (bp 121—122 °C/0.1 mmHg) in 33% yield. Found: C, 51.82; H, 5.70%. Calcd for $C_{12}H_{16}O_3Cl_2$: C, 51.79; H, 5.75%. NMR ($CDCl_3$) δ 1.2 (t, 6H, $2CH_3$), 3.2—4.2 (m, 6H, $3CH_2$), 4.8 (q, 1H, CH), 6.7—7.5 (m, 3H, ArH) ppm; Mass (*m/e*) 278 (M^+).

*(2,4,5-Trichlorophenoxy)acetaldehyde Diethyl Acetal (**4b**).* A light yellow oil of bp 135—137 °C/0.1 mmHg (30% yield). Found: C, 46.02; H, 4.94%. Calcd for $C_{12}H_{15}O_3Cl_3$: C, 46.15; H, 4.81%. NMR ($CDCl_3$) δ 1.3 (t, 6H), 3.5—4.2 (m, 6H), 4.9 (q, 1H), 7.3 (d, 2H) ppm; Mass (*m/e*) 312 (M^+).

*2-(2,4-Dichlorophenoxymethyl)-4-methacryloyloxymethyl-1,3-dioxolane (**5a**).* In a Soxhlet flask were placed **4a** (3.1 g, 10 mmol), **1** (3.2 g, 20 mmol), PTS (0.1 g), hydroquione (0.1 g), and chloroform (100 ml). The flask, fitted with a thimble containing 4A or 5A molecular sieves, was heated with stirring to reflux for 7 h. The reaction mixture was diluted with chloroform (50 ml), washed with aq Na_2CO_3, dried over anhyd. Na_2SO_4, and evaporated *in vacuo* to leave the crude product, which was chromatographed on silica gel (Wakogel C-300) to afford a viscous oil in 9% yield [benzene–ether (1:4 v/v) eluate]. Found: C, 51.94; H, 4.85%. Calcd for $C_{15}H_{16}O_5Cl_2$: C, 52.02; H, 4.62%. IR (CCl_4) 1720 cm^{-1}; NMR ($CDCl_3$+DMSO-d_6) δ 1.9 (s, 3H, CH_3), 3.1—4.3 (m, 7H, $3CH_2$+CH), 4.5—5.2 (b, 1H, acetal CH), 5.5 (s, 1H, $CH_2=$), 6.1 (s, 1H, $CH_2=$), 6.5—7.4 (m, 3H, ArH) ppm.

*2-(2,4,5-Trichlorophenoxymethyl)-4-methacryloyloxymethyl-1,3-dioxolane (**5b**).* A light yellow viscous oil [benzene–ether (4:1 v/v) eluate; 11% yield]. Found: C, 46.67; H, 4.12%. Calcd for $C_{15}H_{15}O_5Cl_3$: C, 47.18; H, 3.94%. IR (CCl_4) 1730 cm^{-1}; NMR ($CDCl_3$) δ 2.0 (s, 3H), 3.5—4.3 (m, 7H), 4.6—5.2 (b, 1H), 5.6 (s, 1H), 6.2 (s, 1H), 6.6—7.5 (m, 2H) ppm; Mass (*m/e*) 381 (M^+).

Hydrolysis of the Acetals Synthesized. A solution of an acetal (1 mmol), PTS (0.05 g), and 4-*t*-butylcatechol (0.01 g) in THF–water (2:1 v/v; 30 ml) was let stand at 20 °C for 2 h. The solution was neutralized with solid Na_2CO_3, filtered, and evaporated *in vacuo*. The residue was extracted with $CHCl_3$– aq $NaHCO_3$. The organic layer was dried over anhyd. Na_2SO_4 and evaporated *in vacuo* to dryness. The relative strength of either the aldehyde signal produced or the remaining acetal CH in the ^{1}H-NMR ($CDCl_3$) was determined for the residue to calculate the value of % hydrolysis. Time of hydrolysis was also prolonged to 24 h.

References

1) H. Kamogawa, S. Okabe, and M. Nanasawa, *Bull. Chem. Soc. Jpn.*, **49**, 1917 (1976).
2) H. Kamogawa, Y. Haramoto, and M. Nanasawa, *Bull. Chem. Soc. Jpn.*, **52**, 846 (1979).
3) E. Schact, G. Desmarets, and T. St. Pierre, *Makromol. Chem.*, **179**, 543 (1978).
4) E. Schacht, G. Desmarets, and Y. Bogaert, *Makromol. Chem.*, **179**, 837 (1978).

N-Trifluoroacetylimidazoles as a Reagent for Converting Aldoximes into Nitriles under Mild Conditions

Takashi KEUMI,* Takayoshi YAMAMOTO, Hiroshi SAGA, and Hidehiko KITAJIMA

Department of Fiber and Color Chemistry, Faculty of Engineering, Fukui University, Bunkyo, Fukui 910

(Received October 29, 1980)

Synopsis. It was found that *N*-trifluoroacetylimidazole was an excellent reagent for the intramolecular dehydration of aldoximes to give nitriles uner mold conditions.

There are only a few examples of the use of *N*-trifluoroacetylimidazole (TFAI) as an organic synthetic reagent, though it seems to have a great potential. Thus far, it has only been used as trifluoroacetylating agent of amines or alcohols[1] and as condensation agent of amino acids with *p*-nitrophenol.[2] We have previously shown that TFAI is useful for the condensation of carboxylic acids with aromatic hydrocarbons to give aromatic ketones.[3] In this paper, we wish to report that TFAI is also an excellent reagent for the intramolecular dehydration of aldoximes (**1**) to give nitriles (**4**).

Many methods are known for converting **1** into **4**, but some of them have disadvantages, such as needing vigorous reaction conditions or tedious work-up procedures, having unsatisfactory yields, or needing unusual reagents.[4-6] For example, recently reported trifluoroacetic anhydride is very useful as the reagent;[4] however, it requires at least two equivalents of a base to catalyze the reaction and to remove the acid generated.

TFAI converted **1** into **4** under practically neutral and mild conditions without any additives. The reac-

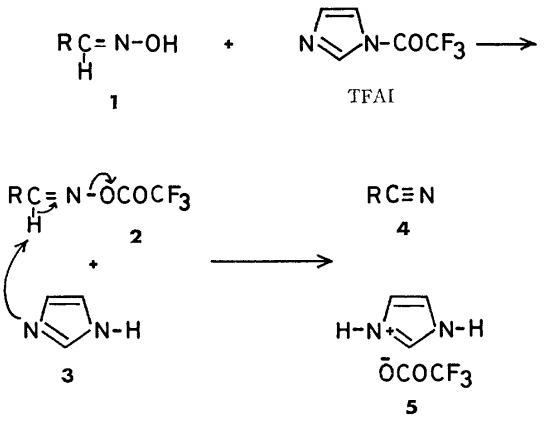

TABLE 1. NITRILES OBTAINED FROM ALDOXIMES BY TREATMENT WITH *N*-TRIFLUOROACETYLIMIDAZOLE

	R of **4**	Reaction time/h	Yield[a] of **4**/%	Bp/°C or [Mp/°C] Found	Bp/°C or [Mp/°C] Reported	IR(ν/cm^{-1})	^{1}H-NMR(δ/ppm, CCl_4)
4a	Propyl	2[c]	99[b]	117—119	117[8]	2220, 1450, 1060	0.9—1.3(m, 3H), 1.5—1.9(m, 2H), 2.2—2.4(m, 2H)
4b	Pentyl	2[c]	90	160	164[8]	2220, 1460, 1070	0.7—1.0(m, 3H), 1.2—1.9(m, 6H), 2.2—2.4(m, 2H)
4c	Hexyl	2	96	200	200.4[8]	2220, 1460, 1170	0.7—1.0(m, 3H), 1.1—1.7(m, 10H), 2.3—2.6(m, 2H)
4d	1-Ethylpentyl	2	95	187—190	98—100[9] (50 Torr)	2210, 1460, 1170	0.7—1.1(m, 6H), 1.2—1.8(m, 8H), 2.4—2.8(m, 1H)
4e	1-Propenyl	3.5	77	118—122	122[8]	2210, 1645, 1436	1.8—2.0(m, 3H), 5.3—5.6(m, 1H), 6.4—6.9(m, 1H)
4f	Phenyl	3.5	92	190	191[7]	2220, 1600, 1490	7.2—7.7(m, 5H)
4g	*p*-Chlorophenyl	3.5	94	[90—91]	[94—96][7]	2210, 1590, 1480	7.3—7.8(m, 4H)
4h	*o*-Chlorophenyl	3.5	97	[45—46]	[43—44][10]	2210, 1583, 1465	7.3—7.8(m, 4H)
4i	*m*-Nitrophenyl	3.5	91	[113—114]	[117—118][11]	2210, 1530, 1355	7.7—8.0(m, 1H), 8.3(d, 1H, J=8 Hz), 8.54(d, 1H, J=8 Hz), 8.73(s, 1H)
4j	*p*-Tolyl	3.5	81	215—217	217.6[8]	2220, 1610, 1175	2.39(s, 3H), 7.23(d, 2H, J=8 Hz), 7.44(d, 2H, J=8 Hz)
4k	Styryl	3.5	95	254—255	253—255[12]	2210, 1615, 970	5.80(d, 1H, J=16 Hz), 7.25(d, 1H, J=16 Hz), 7.33(m, 5H)
4l	2-Furyl	3.5	81	146—150	146—148[8]	2220, 1465, 1225	6.5—6.6(m, 1H), 7.1—7.2(m, 1H), 7.55—7.65(m, 1H)

a) The isolated yield of **4**. b) Obtained by GLC. c) Ether was used as the solvent for this reaction. In the other reactions, THF was used as the solvent.

tion is carried out by heating a solution of **1** and TFAI (in a molar ratio of 1:1.1) in ether or tetrahydrofuran under reflux for 2—3.5 h. The results are summarized in Table 1. A wide variety of **1** substances, from the aliphatic or aromatic to the olefinic, are dehydrated by TFAI to give the corresponding **4** substances in satisfactory yields.

The dehydration of **1** is generally considered to proceed by means of a base-promoted bimolecular mechanism.[4] TFAI has a powerful trifluoroacetylating ability; in addition, as a result of the trifluoroacetylation, the reagent generates imidazole (**3**), which can act as a base. Therefore, in the above reaction it seems that the trifluoroacetylation of **1** by TFAI takes place first to give *O*-trifluoroacetyl aldoxime (**2**) and **3**, followed by the elimination of trifluoroacetic acid by the **3** thus yielded to afford **4** and imidazolium trifluoroacetate (**5**). Thus, the reaction system should be kept constantly neutral during the reaction. Further, conveniently, the by-product, **5**, can be easily removed from the product, **4**, by filtration, because it is hardly soluble in cold ether and tetrahydrofuran. TFAI is familiar in the field of the peptides chemistry[2] and is commercially available. Consequently, TFAI seems to be an efficient reagent for converting **1** into **4**.

Experimental

Materials and Measurements. TFAI was prepared from imidazole and trifluoroacetic anhydride accoridng to the procedure described in the literature.[1] The aldoximes were prepared by a general method. The solvents used for the reactions were dried and distillated over lithium aluminium hydride. The IR spectra were recorded on a Hitachi EPI-S2 Model spectrophotometer. The NMR spectra were measured as carbon tetrachloride solutions at 100 MHz with a JEOL Model PS-100 spectrometer, using tetramethylsilane as the internal standard.

General Procedure. A typical procedure will be described for the preparation of benzonitrile (**4f**): To a solution of benzaldehyde oxime (0.500 g, 4.1 mmol) in dried tetrahydrofuran (6 ml), TFAI (0.745 g, 4.5 mmol) in tetrahydrofuran (4 ml) was added, after which the mixture was heated under reflux for 3 h. After cooling, the resultant precipitates of imidazolium trifluoroacetate were removed off by filtration and washed with ether (about 30 ml). The combined filtrate was washed with water (about 30 ml×2) and dried over anhydrous sodium sulfate. The solvent was then evaporated to obtain **4f** (0.400 g, 94%). Bp 190 °C (lit,[7] Bp 191 °C).

References

1) H. A. Staab, G. Walther, and W. Rohl, *Chem. Ber.*, **95**, 2073 (1962).
2) H. D. Low, *J. Chem. Soc.*, **1965**, 3897.
3) T. Keumi, H. Saga, and H. Kitajima, *Bull. Chem. Soc. Jpn.* **53**, 638 (1980).
4) A. Carotti and F. Campagna, *Synthesis*, **1979**, 56.
5) G. A. Olah and T. Keumi, *Synthesis*, **1979**, 112.
6) G. Sosnovsky, J. A. Krog, and S. G. Umhoefer, *Synthesis*, **1979**, 722, and the references cited therein.
7) "Handbook of Chemistry & Physics," 57th ed, ed by R. C. Weast and M. J. Astle, Chemical Rubber Co., Cleveland, Ohio (1976).
8) "Handbook of Chemistry," 11th ed, ed by J. A. Dean, McGraw-Hill Co., New York (1973).
9) P. A. Levene and M. Kuna, *J. Biol. Chem.*, **140**, 259 (1941).
10) A. Korczynski and B. Fandrich, *C. R. Acad. Sci.*, **183**, 421 (1926); *Chem. Abstr.*, **14**, 2919 (1920).
11) "Dictionary of Organic Compounds," 4th ed, Eyre and Spottiswoode Publishers, London (1965).
12) T. L. Ho, *Synthesis*, **1975**, 401.

Thermal Rearrangement of *N*-(Substituted allyl)-1-naphthylamines

Seisaku INADA* and Ryu-ichiro KURATA

Department of Chemical Engineering, Faculty of Engineering, Tokyo Institute of Technology, Ohokayama, Meguro-ku, Tokyo 152

(Received November 14, 1980)

Synopsis. The title reaction was examined and the results were compared with those of the thermal reaction of the corresponding *N*-tosyl derivatives.

In the previous papers,[1] we have reported the *amido*-Claisen rearrangement of *N*-tosyl and *N*-mesyl derivatives of aromatic *N*-allylamines which proceeds almost quantitatively in *N*,*N*-dialkylaniline solvent containing a small amount of triphenylphosphine. In the course of our studies, it was found that the thermal reaction of *N*-(substituted allyl)-*N*-tosyl-1-naphthylamines (**1f—h**) forms para-rearranged products (**3d—f**) as well as ortho-rearranged ones (**2g**, **2h**) respectively, when the allyl group contains substituents in γ-position.[2] So we were interested to confirm whether the thermal reaction of the corresponding *N*-(substituted allyl)-1-naphthylamines was accompanied by the para-rearrangement. About *N*-allyl-1- (**1a**) and 2-naphthylamine themselves, Marcinkiewicz *et al.* reported the formation of ortho rearranged product as sole one,[3] which have formed the only successful example of the aromatic *amino*-Claisen rearrangement.

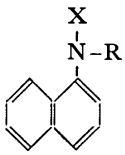

1a: X=H, R=$CH_2CH{=}CH_2$
1b: X=H, R=$CH_2C(CH_3){=}CH_2$
1c: X=H, R=$CH_2CH{=}CHCH_3$
1d: X=H, R=$CH_2CH{=}C(CH_3)_2$
1e: X=H, R=$CH_2CH{=}CHC_6H_5$
1f: X=Ts, R=$CH_2CH{=}CHCH_3$
1g: X=Ts, R=$CH_2CH{=}C(CH_3)_2$
1h: X=Ts, R=$CH_2CH{=}CHC_6H_5$

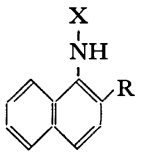

2a: X=H, R=$CH_2CH{=}CH_2$
2b: X=H, R=$CH_2C(CH_3){=}CH_2$
2c: X=H, R=$CH(CH_3)CH{=}CH_2$
2d: X=H, R=$CH(C_6H_5)CH{=}CH_2$
2e: X=H, R=$CH_2CH{=}CHC_6H_5$
2f: X=H, R=H
2g: X=Ts, R=$CH(CH_3)CH{=}CH_2$
2h: X=Ts, R=$CH(C_6H_5)CH{=}CH_2$

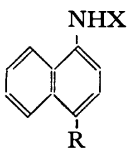

3a: X=H, R=$CH_2CH{=}CHCH_3$
3b: X=H, R=$CH_2CH{=}C(CH_3)_2$
3c: X=H, R=$CH_2CH{=}CHC_6H_5$
3d: X=Ts, R=$CH_2CH{=}CHCH_3$
3e: X=Ts, R=$CH_2CH{=}C(CH_3)_2$
3f: X=Ts, R=$CH_2CH{=}CHC_6H_5$

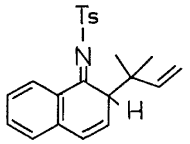

4

The amines (**1a—1e**) neat were heated at 260±0.3 °C under nitrogen. In general, the thermal reaction of these amines gave complicated products, together with some amount of tarry matters.[4] The reaction mixtures from **1a—1e** were converted to the ones of *N*-tosylamines by treating them with tosyl chloride in pyridine immediately after the reaction and analyzed according to the method previously described. The results are shown in Table.

The main products were the ortho rearranged ones throughout the reactions except for **1d** from which the deallylated product **2f** was formed as the only confirmable one. The formation of para-rearranged products was not observed except **3c** formed from **1e**.[5] It may be reasonably considered that **3c** should be formed partially at least *via* a dissociation-recombination process, since the formation of **2e** involving a sterically retained cinnamyl group in ortho position was also observed. In general, the ortho-rearrangement apparently proceeds *via* a [3,3]-sigmatropic reaction as denoted by the examples of the amines containing an asymmetrically-substituted allyl group (**1c**, **1e**). The results accorded with what we deduced about the para-rearrangement in the corresponding *amido*-Claisen rearrangement; a steric repulsion between a tosyl group and α-substituents in an inverted allyl group which is involved in the intermediate such as **4** formed by the first [3,3]-shift promotes the second one to para rearranged products.

Experimental

IR spectra were determined on a Shimadzu IR-27G spectrometer and NMR spectra on a Hitachi R-24 spectrometer; chemical shifts are given in δ with TMS as an internal standard. *N*-(Substituted allyl)-1-naphthylamines were obtained in excellent yields by the corresponding *N*-allylations of *N*-trifluoroacetyl-1-naphthylamine and the subsequent hydrolysis.

N-*(Substituted allyl)*-N-*trifluoroacetyl-1-naphthylamines.* To a stirred mixture of *N*-trifluoroacetyl-1-naphthylamine[6] (80 g, 0.33 mol) and K_2CO_3 (46.2 g, 0.33 mol) in DMF (100 ml) was added the corresponding allyl bromide (0.40 mol) at room temperature. Then the mixture was stirred for 2 h at 60 °C. The usual work up gave the following *N*-(substituted allyl) derivatives in 88—99% yields.

Table 1. Thermal rearrangement of *N*-(substituted allyl)-1-naphthylamines (260 °C, neat)

Starting material	React. time/h	Recovered (%)	Products (%)			
1a	1.1	58.0	**2a**: 30.4	**2f**: 3.2		
	2	40.8	40.9	3.3		
	3	30.0	54.5	5.1		
1b	1.1	65.4	**2b**: 21.8	**2f**: 2.2		
	2	47.0	31.9	4.4		
	3	32.7	43.5	6.4		
1c	1.1	63.8	**2c**: 17.7	**3a**: —[a]	**2f**: 5.1	
	2	48.1	28.7	—	6.9	
	3	35.4	36.4	—	6.3	
1d	1	61.9	**3b**: —[a]	**2f**: 7.8		
	2	55.7	—	9.3		
	3	46.9	—	11.5		
1e	1	47.9	**2d**: 30.8	**2e**: 8.7	**3c**: 1.6	**2f**: 4.7
	2	28.4	37.7	14.0	2.1	7.5
	3	14.9	34.1	15.5	2.2	9.5

a) The formation was not observed. See Ref. 5.

N-*Allyl Derivative*: Mp 45.5—46 °C. IR (KBr): 1690, 1210, 1180, 1150 cm^{-1}. Found: C, 64.70; H, 4.41; N, 4.91%. Calcd for $C_{15}H_{12}F_3NO$: C, 64.51; H, 4.33; N, 5.02%.

N-*(β-Methylallyl) Derivative*: Mp 61.5—62 °C. IR (KBr): 1690, 1210, 1190, 1145 cm^{-1}. Found: C, 65.38; H, 4.77; N, 4.54%. Calcd for $C_{16}H_{14}F_3NO$: C, 65.52; H, 4.81; N, 4.78%.

N-*(γ-Methylallyl) Derivative*: Mp 54.5—55.5 °C. IR (KBr): 1690, 1210, 1190, 1145, 965 cm^{-1}. Found: C, 65.49; H, 4.63; N, 4.66%. Calcd for $C_{16}H_{14}F_3NO$: C, 65.52; H, 4.81; N, 4.78%

N-*(γ,γ-Dimethylallyl) Derivative*: Bp 119.5—121 °C (1 mmHg). IR (neat): 1690, 1210, 1170, 1150 cm^{-1}. Found: C, 66.71; H, 5.03; N, 4.65%. Calcd for $C_{17}H_{16}F_3NO$: C, 66.44; H, 5.25; N, 4.56%.

N-*(γ-Phenylallyl) Derivative*: Mp 88.5—89.5 °C. IR (KBr): 1690, 1210, 1185, 1155, 975 cm^{-1}. Found: C, 71.14; H, 4.78; N, 4.07%. Calcd for $C_{21}H_{16}F_3NO$: C, 70.98; H, 4.54; N, 3.94%.

N-*(Substituted allyl)-1-naphthylamines (**1a—1e**)*. A solution of the trifluoracetamide (0.125 mol) in water–ethanol (1:3, 400 ml) containing NaOH (8.0 g) was refluxed for 10 min. The usual work up gave the hydrolyzed products in 80—99% yields. The melting points and IR spectra of the *N*-tosylated amines corresponded to those of the authentic samples.

1a: Bp 120—120.5 °C (2 mmHg). Mp of HCl salt, 229.5—231 °C (lit,[3] mp 229—230 °C).

1b: Bp 104.2—104.8 °C (2 mmHg). IR (neat): 3475, 1655, 890 cm^{-1}. NMR (CCl_4): 1.69 (s, 3H, β-CH_3), 3.58 (broad s, 2H, α-H), 4.89 (broad d, J=7 Hz, 2H, γ-H). Found: C, 85.10; H, 7.48; N, 6.97%. Calcd for $C_{14}H_{15}N$: C, 85.24; H, 7.66; N, 7.10%.

1c: Bp 131—131.5 °C (0.8 mmHg). IR (neat): 3450, 1675, 965 cm^{-1}. NMR (CCl_4): 1.60 (broad d, J=4 Hz, 3H, γ-CH_3), 3.53—3.65 (m, 2H, α-H), 5.48—5.65 (m, 2H, β- and γ-H). Found: C, 85.44; H, 7.79; N, 7.10%. Calcd for $C_{14}H_{15}N$: C, 85.24; H, 7.66; N, 7.10%.

1d: Bp 147—148 °C (2 mmHg). IR (neat): 3450, 1665 cm^{-1}. NMR (CCl_4): 1.63 and 1.69 (s, 3H, γ-CH_3, resp.), 3.67 (broad d, J=6 Hz, 2H, α-H), 5.35 (broad t, J=7 Hz, 1H, β-H). Found: C, 85.41; H, 8.36; N, 6.75%. Calcd for $C_{15}H_{17}N$: C, 85.26; H, 8.11; N, 6.63%.

1e: Mp 83—83.5 °C. IR (KBr): 3475, 1660, 970 cm^{-1}. NMR ($CDCl_3$): 3.76 (broad d, J=5 Hz, 2H, α-H), 5.89—6.46 (m, 2H, β- and γ-H). Found: C, 88.22; H, 6.89; N, 5.51%. Calcd for $C_{19}H_{17}N$: C, 87.99; H, 6.61; N, 5.40%.

*Thermal Rearrangement of **1a—1e***. A test-tube containing *N*-(substituted allyl)-1-naphthylamines (2—3 g) under nitrogen was immersed for an appropriate period of time in an oil bath, the temperature of which was maintained at 260.0±0.3 °C. The chilled reaction mixture was dissolved in pyridine (25 ml) and tosyl chloride (1.2 equivalents to **1**) was added. The whole solution was stirred at 60—70 °C for 6 h and poured into diluted hydrochloric acid (1:3). The resulting precipitate was filtered, washed with diluted hydrochloric acid and water, and dried. The samples thus obtained were analyzed by the method described previously.[2]

References

1) S. Inada, S. Hirabayashi, K. Taguchi, and M. Okazaki, *Nippon Kagaku Kaishi*, **1978**, 86 and other articles cited therein.

2) For example, when a solution of **1f** (1.00 g) in *N,N*-dibutylaniline (15 ml) containing a small amount of PPh_3 (0.1 g) was heated under nitrogen at 245 °C for 1.2 h, the ortho-rearranged product **2g** and the para-rearranged product **3d** were obtained in 63.0 and 26.8% yields, respectively. S. Inada, R. Kurata, T. Ishida, T. Uda, and M. Okazaki, *Nippon Kagaku Kaishi*, **1978**, 723.

3) S. Marcinkiewicz, J. Green, and P. Mamalis, *Tetrahedron*, **14**, 208 (1961).

4) For example, 6 spots were at least observed on TLC as the reaction products from **1a**.

5) The authentic samples of **3a**, **3b**, and **3c** which might be expected to form had been prepared in the form of their *N*-tosyl derivatives from the *amido*-Claisen rearrangement mentioned above and the possibility of their existence in the reaction mixture was examined on TLC and HLC.

6) M. Pailer and W. J. Hübsch, *Monat. Chem.*, **97**, 1553 (1966).

Substituent Effect on the N-H Stretching Absorptions of 2-(Substituted anilino)pyridines

Minoru HIROTA* and Kunio KOBAYASHI

Department of Applied Chemistry, Faculty of Engineering, Yokohama National University, Hodogaya-ku, Yokohama 240

(Received November 21, 1980)

Synopsis. The N-H stretching frequencies of the title compounds were determined precisely. These amines have two absorption bands in the N-H stretching region owing to the existence of the rotational isomers. Their frequencies were plotted against the Hammett σ-constants of the substituents, giving a negative ρ-value. The results gave support to the planar (sp^2) conformation of the *exo*-cyclic nitrogen atom.

The substituent effect on the N-H stretching (ν_{NH}) frequencies have been reported for anilines,[1,2] *N*-methylanilines,[1] anilides,[3] and diphenylamines.[4] In these investigations, the frequencies were plotted against the Hammett σ or similar substituent parameters standing for their electronic effect. The results are rather contradictory giving ρ-values of different signs depending on the substituent (R) on the nitrogen atom (Table 1).

TABLE 1. SUBSTITUENT(X) EFFECT ON THE ν_{NH} FREQUENCIES OF VARIOUS *N*-SUBSTITUTED(R) ANILINES XC_6H_4NHR

R	Sign of ρ	Ref.
H	+	1, 2
CH_3	+	1
$COCH_3$	−	3
C_6H_5	borderline	4
2-C_5H_4N	−	this work
Cf. XC_6H_4OH	−	5

In our previous report, the contradiction was interpreted by assuming the participation of the two competing factors of the opposite direction. The electron attracting nature of a substituent would decrease the electron density on the amino nitrogen atom, causing the increase in the s-character of its N-H bonding orbital. The increase in the s-character, in turn, shortens and strengthens the N-H bond, giving rise to a high frequency shift of the ν_{NH} absorption. Alternatively, the decrease in electron density of the amino nitrogen atom weakens the N-H bond when the change in the hybridization is absent.

On the other hand, 2-anilinopyridines have been shown to have two absorption bands in the ν_{NH} region. They were assigned to the two planar rotational isomers I and II.[6] An alternative assignment of these two bands to the amino and the imino tautomers (I and III, respectively) were excluded by the spectroscopic evidences.[7,8]

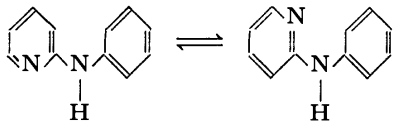

(I) (II)

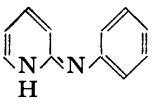

(III)

In this report, the hybridization of the *exo*-cyclic nitrogen atom will be discussed from the substituent effect on the ν_{NH} bands of 2-anilinopyridines.

Experimental

Infrared spectra were recorded with a Hitachi 225 infrared spectrophotometer. The frequencies were calibrated by the absorption bands of gaseous water at 3447.09 and 3442.41 cm^{-1} in order to keep the accuracy of the location of the band maxima within 0.2 cm^{-1}. The anilinopyridines were prepared by the usual procedures.

Results and Discussion

The frequencies and the intensities of the ν_{NH} bands are given in Table 2. The absorption bands were tentatively assigned to the rotamers I and II, respectively, according to the conclusion in our previous report.[6] The ν_{NH} frequencies, as well as the intensity ratios of the two bands, were plotted against the Hammett σ-constants.[9] In case when the substituent is mesomerically electron-attracting (+M), the σ^--constant is used instead. The ν_{NH} frequencies of both rotamers tend to decrease as the increase of σ-values, showing negative ρ-values. A negative ρ-value has been observed with a series of substituted benzamides,[3] of which nitrogen atoms have been proved to be sp^2-hybridized from other evidences. The results suggest that the *exo*-cyclic nitrogen atom in 2-anilinopyridine is sp^2 hybridized. Since the 2-pyridyl group in these

TABLE 2. THE ν_{NH} ABSORPTIONS OF 2-(SUBSTITUTED ANILINO)PYRIDINES

Substituent	ν_I / cm^{-1}	ε_I / l mol^{-1} cm^{-1}	ν_{II} / cm^{-1}	ε_{II} / l mol^{-1} cm^{-1}
4-NO_2	3412.4	97	3441.3	144
3-NO_2	3416.0	69	3445.3	97
4-$COOCH_3$	3416.1	89	3443.5	70
3-Br	3416.8	95	3446.1	73
3-Cl	3417.6	85	3446.2	67
4-Br	3417.7	91	3446.9	72
4-Cl	3417.8	86	3446.7	66
3-OCH_3	3418.6	90	3447.1	41
H	3418.9	92	3446.0	47
3-CH_3	3418.6	92	3447.2	40
4-CH_3	3419.6	102	3447.7	44
4-OCH_3	3419.1	94	3448.0	34

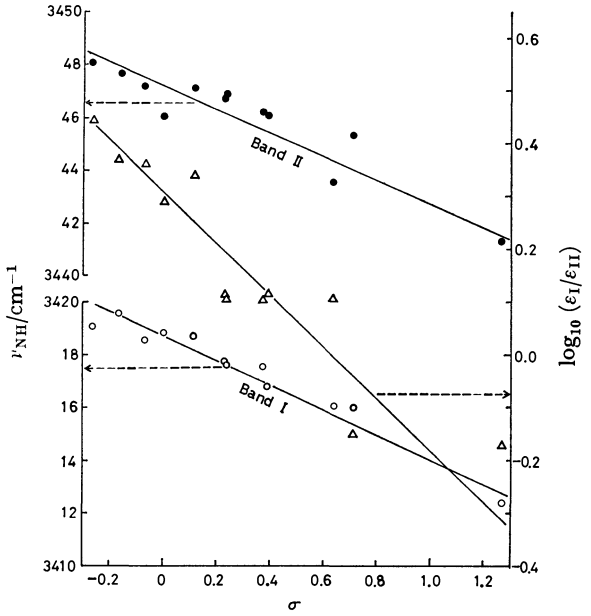

Fig. 1. The ν_{NH} and $\log_{10}(\varepsilon_I/\varepsilon_{II})$ *vs.* σ plot for 2-(substituted anilino)pyridines.

amines is more electronegative than the phenyl groups in diphenylamines which shows the borderline ρ-alue,[4] the negative ρ-values are reasonable.

The $\varepsilon_I/\varepsilon_{II}$ ratios are also correlated with the σ-constants, the rotamer I (giving rise to the lower ν_{NH} band) becoming less favorable than the rotamer II when the substituent is electron-attracting. The results can be explained as follows. In the rotamer I, a weak attractive interaction[10] keeps the N–H···N system nearly coplanar. As a result, the anilinopyridine molecule is twisted around the C_{Ph}–N bond because of the steric hindrance between 3- and 2′ (or 6′)-hydrogen atoms. On the other hand, the *exo*-cyclic nitrogen atom and the phenyl group can be coplanar in the rotamer II. In the latter case, the phenyl group with an electron-attracting substituent is stabilized by conjugating with the planarly attached amino group. Hence, the rotamer II is more favorable than the rotamer I when the substituent is electron-attracting.

References

1) P. J. Kruger and H. W. Thompson, *Proc. R. Soc. London, A*, **243**, 143 (1957).
2) P. J. Kruger, *Can. J. Chem.*, **40**, 2300 (1962).
3) H. W. Thompson and D. A. Jameson, *Spectrochim. Acta*, **13**, 236 (1958).
4) M. Kasai, M. Hirota, Y. Hamada, and H. Matsuoka, *Tetrahedron*, **29**, 267 (1973).
5) L. L. Ingraham, J. Corse, G. F. Bailey, and F. Stitt, *J. Am. Chem. Soc.*, **74**, 2297 (1952).
6) T. Mizuno, M. Hirota, Y. Hamada, and Y. Ito, *Tetrahedron*, **27**, 6011 (1971).
7) Y. Takahashi, S. Otsuka, H. Masuda, M. Hirota, Y. Ito, and Y. Hamada, *Bull. Chem. Soc. Jpn.*, **49**, 2770 (1976).
8) M. Hirota, T. Sekiya, A. Hishikura, H. Endo, Y. Hamada, and Y. Ito, *Bull. Chem. Soc. Jpn.*, **53**, 717 (1980).
9) H. H. Jaffe, *Chem. Revs.*, **53**, 191 (1953).
10) The low ν_{NH} frequency in the rotamer I suggests the participation of a weak hydrogen bond-like interaction, the N–H bond being weakened considerably by this interaction. However, the predominant force might be of dipolar nature.

A Selective Monodehydration of C_{4-14}-α,ω-Alkanediols with Stearic and/or Palmitic Acids

Tohr YAMANAKA* and TAKASHI IMAI

Central Research Laboratory of Takasago Perfumery Co., Ltd., Kamata, Ohta-ku, Tokyo 144

(Received November 26, 1980)

Synopsis. The formation of monoesters of the C_{4-14}-α,ω-alkanediol(**1**) with stearic and/or palmitic acids and the consecutive pyrolysis of the monoesters to an ω-alken-1-ol(**2**) were effected at 320—350 °C under 260—760 mmHg** in a backmix flow reactor of a constant volume equipped with a fractionating column, through which the unchanged **1** was partially recycled. The selectivity in the preparations of **2**(C_6, C_{10}, and C_{14}) was greater than 79%.

We found a useful synthetic method to prepare a C_{4-14}-ω-alken-1-ol(**2**) from the corresponding α,ω-alkanediol(**1**). Acid catalyzed dehydrations of an

$$\underset{\mathbf{1}}{HOCH_2(CH_2)_nCH_2OH} \longrightarrow \underset{\mathbf{2}}{CH_2{=}CH(CH_2)_{n-1}CH_2OH} + H_2O \quad (1)$$

alkanol to form the corresponding alkene are generally accompanied by migration of the double bond and the intermolecular and/or the intramolecular ether formations.[1] These reactions can not be applied to **1** in the substantial yield, without the formations of alkadienes, the double bond-isomers of **2**, and the polyethers.

The vapor phase pyrolysis of acetates at 300—600 °C is known to be effective for the preparation of alkenes from the corresponding alkanols without migration of the double bond.[2] Preparation of any ω-alken-1-ol *via* the esters of alkanediols has not been reported. The selective preparation of the monoacetate of **1** without accompanying the formation of the diacetate will be difficult. We used high boiling saturated fatty acids **3** *i.e.*, palmitic acid, stearic acid, or the mixture of them so that the ester formation (Eq. 2) and the subsequent pyrolysis (Eq. 3) to give the ω-alken-1-ols might be induced concurrently at 320—350 °C. These steps were operated by means

$$\mathbf{1} + \underset{\mathbf{3}}{RCOOH} \longrightarrow RCOOCH_2(CH_2)_nCH_2OH + H_2O \quad (2)$$

$$RCOOCH_2(CH_2)_nCH_2OH \longrightarrow \mathbf{3} + \mathbf{2} \quad (3)$$

of a backmix[3] flow reactor of a constant volume of a liquid phase. While H_2O and **2** are being taken out through the rectification column, **1** is continuously supplied to the reactor. Compound **3** initially introduced into the reactor steadily functions like a catalyst throughout the operation period.

Experimental

A mixture of 24.3 g of stearic acid and 30.9 g of palmitic acid, and 61.5 g of 1,10-decanediol(purity 98.2 wt%) were placed in a 200-ml flask equipped with a 20 mmϕ × 200 mm-Vigreux fractionating column of *ca.* three theoretical plates connected with a reflux condenser, and refluxed at 330—350 °C, under 700 mmHg.** The temperature at the top of the column initially indicated 295 °C and gradually lowered to 265 °C. Then the effluent vapor was started to be taken out from the column at a rate of 10 g/h. Concurrently, 1,10-decanediol was started to be fed to the flask at the same rate. The temperature of the effluent vapor was maintained by regulating the temperature in the flask between 330 and 350 °C as well as by regulating the feed rate. From 1500 g of 1,10-decanediol, 126 g of the H_2O layer and 1372 g of the oily part were obtained as the distillate.

Table 1. IR and NMR data for ω-alken-1-ols(**2**)

2 IR(neat) ν_{max}/cm^{-1}	NMR(20% in CCl_4 solution) δ
n=2 915, 990, 1643, 3070	4.85—6.09(ABX, 3H, C<u>H</u>$_2$=C<u>H</u>-), 3.56 (t, J=6 Hz, 2H, -CH$_2$-C<u>H</u>$_2$OH), 2.44(t, d, J=6 Hz, 2H, =CH-C<u>H</u>$_2$-CH$_2$OH), 3.29(s, 1H, -CH$_2$O<u>H</u>)
n=4 910, 995, 1643, 3070	4.75—6.07(ABX, 3H, C<u>H</u>$_2$=C<u>H</u>-), 3.48 (t, J=7 Hz, 2H, -CH$_2$-C<u>H</u>$_2$OH), 2.05 (t, d, J=7 Hz, 2H, =CH-C<u>H</u>$_2$-CH$_2$-), 1.48(m, 4H, -CH$_2$(C<u>H</u>$_2$)$_{n-2}$-CH$_2$-), 3.58 (s, 1H, CH$_2$O<u>H</u>)
n=8 910, 995, 1643, 3070	4.74—6.04(ABX, 3H, C<u>H</u>$_2$=C<u>H</u>-), 3.45 (t, J=6 Hz, 2H, -CH$_2$-C<u>H</u>$_2$OH), 2.02 (t, d, J=6 Hz, 2H, =CH-C<u>H</u>$_2$-CH$_2$-), 1.28(b, s, 12H, -CH$_2$-(C<u>H</u>$_2$)$_{n-2}$-CH$_2$-), 4.23(s, 1H, CH$_2$O<u>H</u>)
n=12 910, 995, 1643, 3060	4.74—6.05(ABX, 3H, C<u>H</u>$_2$=C<u>H</u>-), 3.46 (t, J=6 Hz, 2H, -CH$_2$-C<u>H</u>$_2$OH), 2.01 (t, d, J=6 Hz, 2H, =CH-C<u>H</u>$_2$-CH$_2$-), 1.27(b, s, 20H, -CH$_2$-(C<u>H</u>$_2$)$_{n-2}$-CH$_2$-), 4.13(s, 1H, CH$_2$O<u>H</u>)

The oily part was analyzed by gas chromatography using a Shimadzu GC 6A apparatus on a 2 mmϕ × 3 m column packed with 5 wt% of FFAP on Chromosorb W, AW-DMCS (80—100 mesh). The column temperature was elevated from 100 to 230 °C by 10 °C/min, N_2 was used as the carrier at 50 ml/min, and the injection temperature was 280 °C.

The oily part was fractionated by a further distillation. The main fraction of 869 g was identified to be 9-decen-1-ol; IR and NMR data are shown in Table 1. Each fraction was characterized by its boiling point and the main components were distinguished by their retention times in its gas chromatogram by comparison with those of the corresponding authentic samples.

In the same way as above, we prepared 3-buten-1-ol, 5-hexen-1-ol, and 13-tetradecen-1-ol from the corresponding 1,4-butanediol(purity 96.9 wt%), 1,6-hexanediol (99.0 wt%), and 1,14-tetradecanediol(81.3 wt%) in the presence of

**1 mmHg≈133.3 Pa.

Table 2. Results of continuous dehydrations

1	$n=2$	$n=4$	$n=8$	$n=12$
(**1**/**3**)[a]	0.8	0.8	1.7	1.7
Temperature/°C				
reactor	330—345	330—350	330—350	330—340
effluent vapor	170	204—215	265	235—240
Pressure/mmHg**	760	760	700	260
Operation time/h	32	24	150	19
Distillate composition[b]				
H_2O	0.58[f]	0.85	0.81	0.64
2	0.36	0.64	0.73	0.49
tetrahydrofuran	0.06[f]	—	—	—
double bond-isomers of **2**	0.13	0.05	0.07	—
alkadienes	(0.06[g])	0.12	0.01	0.05
1(unreacted)	0.37	0.19	0.18	0.46
Bp of **2**/°C(mmHg**)[c]	102(760)	74(28)	74(1)	120—122(2.5)
Selectivity/%[d]	57	79	89	91
Yield of **2**/%[e]	50	71	80	83

a) Starting mole ratio of **1** to **3**. b) Each content shows the ratio to 1 mol of **1** continuously supplied; a corrected value for the purity of a starting material. c) All boiling points are uncorrected. d) $100\times\{$(content of **2**)/(1.0−content of **1**)$\}$ in the distillate. e) $100\times\{\mathbf{2}_{\text{isolated}}/(\mathbf{1}_{\text{fed}}-\mathbf{1}_{\text{recovered}})\}$ after the fractionation. f) Prior to the fractional distillation, tetrahydrofuran containing H_2O was separated from the oily part. g) No butadiene was found. This value denotes twice the amount of dimers of butadiene.

palmitic acid.

Results and Discussion

Results are shown in Tables 1 and 2. By means of increasing the mole ratio **1**/**3** in the reactions of C_6- and C_{10}-alkanediol, the formation of the by-products such as double bond isomers of ω-alken-1-ol and the alkadienes were suppressed, although the conversions of **1** were decreased. However, the ratio should be reduced to the range 0.8—1.0 in order to maintain the reaction temperature at 320—350 °C in the reactions of 1,4-butanediol and 1,6-hexanediol, because boiling points of them were 230 and 250 °C respectively at an ordinary pressure. On the whole, the decrease of the carbon number of the alkanediol increased the difficulty in the application of this reaction.

In the case of 1,4-butanediol, the selectivity was exceptionally low. There tetrahydrofuran was formed as the smaller part of the by-products. However, it should be noticed that this result stands in contrast to the fact that tetrahydrofuran was a primary product in the dehydration of 1,4-butanediol catalyzed by HCl.[4]

ω-Alken-1-ols thus produced are important in perfumery; *e.g.*, 1-decen-1-ol has been used as the component of a rosy odor and 5-hexen-1-ol has a verdurous odor.

References

1) R. Askani, "Methoden der Organischen Chemie," ed by Eugen Müller, BdV/1b, Georg Thieme Verlag, Stuttgart (1972), p. 45.
2) M. Hanack and W. Kraus, p. 105 of Ref. 1.
3) O. Levenspiel, "Chemical Reaction Engineering," John Wiley and Sons, Inc., New York, London (1964), p. 99.
4) B. G. Hudson and R. Barker, *J. Org. Chem.*, **32**, 3650 (1967).

Regiospecific Synthesis of 3-Alkylfurans and 3-Alkylthiophenes *via* Organoboranes

Itaru Akimoto, Masahiro Sano, and Akira Suzuki*

Department of Applied Chemistry, Faculty of Engineering, Hokkaido University, Sapporo 060

(Received November 5, 1980)

Synopsis. The reaction of bromine or iodine with ate-complexes obtained from trialkylboranes and 3-lithiofuran or 3-lithiothiophene gives the corresponding 3-alkylfurans or 3-alkylthiophenes in good yields, respectively.

Heterocyclic compounds with one hetero atom have been recognized to be useful precursors and reagents for the syntheses of functionalized organic compounds.[1] Many synthetic procedures of such heterocycles through the alkylation of heterocyclic nuclei have been recently reported.[2-9] Especially, novel syntheses by the aromatic substitution *via* organoboranes readily obtainable from olefins are being watched with interest.[5-9] In connection with the synthesis, we reported that the reaction of iodine with ate-complexes prepared from trialkylboranes and 2-lithiofuran,[8] 2-lithiothiophene[9] or 1-methyl-2-lithiopyrrole[9] gave regiospecifically the corresponding 2-alkyl heterocycles in good yields (Scheme 1). One may wonder if the reaction is applicable for the preparation of 3-alkyl heterocycles from organoboranes and the corresponding 3-lithio derivatives. On the other hand, it was reported that there was a large difference of chemical properties between C_2 and C_3 atoms of furans and thiophenes.[10]

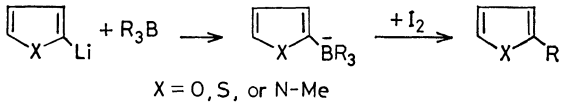

Scheme 1.

For instance, in the reaction of butyllithium with 3-bromobenzo[*b*]thiophene,[11] the following carboxylation even at −70 °C gives a mixture of 3-bromobenzo[*b*]thiophene-2-carboxylic acid, benzo[*b*]thiophene-2-carboxylic acid, benzo[*b*]thiophene-3-carboxylic acid, 3-bromobenzo[*b*]thiophene and benzo[*b*]thiophene, indicating that the reaction gives not only the straightforward metal-halogen exchange product but also 3-lithio derivatives as the intermediates. In the course of our studies on the aromatic substitution of heterocycles *via* organoboranes, we attempted the reaction of iodine or bromine with the ate-complexes prepared from trialkylboranes, butyllithium and 3-bromofuran or 3-bromothiophene, and found that the reaction proceeds smoothly without any difficulty to give regiospecifically the corresponding 3-alkylfurans or 3-alkylthiophenes in good yields. The results of reactions with representative trialkylboranes are summarized in Table 1.

In the present reaction, trialkylboranes with bulky alkyl groups such as isobutyl, *s*-butyl, and cyclopentyl seem to give high yields of corresponding 3-alkyl heterocycles. One of the possible procedures for the synthesis of such 3-substituted heterocycles may involve the reaction of 3-lithio derivatives with alkyl halides. Our experiment on the reaction of propyl bromide with 3-lithiothiophene formed from 3-bromothiophene and butyllithium, gave only a trace amount of 3-propylthiophene. Moreover, the synthesis of 3-*s*-alkyl heterocycles by the same method should be hopeless, because secondary alkyl halides readily undergo competitive elimination reactions.[12] On the other hand, the present reaction is free of this limitation. Secondary groups appear to be introduced more readily than primary groups, as indicated in Table 1. In the case of 3-alkylthiophene synthesis, bromine was found to be more effective as the electrophile than iodine.

Table 1. Synthesis of 3-alkylfurans or 3-alkylthiophenes by the reaction of ate-complexes (**2a** or **2b**) with iodine or bromine

Heterocycle	Organoborane R_3B, R	Alkyllithium (Solvent)	Halogen	Products[a] (Yield[b]/%)
3-Bromofuran	Butyl	BuLi (Et_2O)	I_2	3-Butylfuran (66)
	Butyl	MeLi (THF)		3-Butylfuran (47)
	Isobutyl	BuLi (Et_2O)		3-Isobutylfuran (61)
	Isobutyl	MeLi (THF)		3-Isobutylfuran (61)
	s-Butyl	BuLi (Et_2O)		3-*s*-Butylfuran (91)
	s-Butyl	MeLi (THF)		3-*s*-Butylfuran (85)
	s-Butyl	*t*-BuLi (THF)		3-*s*-Butylfuran (68)
	Cyclopentyl	BuLi (Et_2O)		3-Cyclopentylfuran (76)
	Hexyl	BuLi (Et_2O)		3-Hexylfuran (67)
3-Bromothiophene	Butyl	BuLi (Et_2O)	Br_2	3-Butylthiophene (64)
	Butyl	BuLi (Et_2O)	I_2	3-Butylthiophene (11)
	Isobutyl	BuLi (Et_2O)	Br_2	3-Isobutylthiophene (66)
	Isobutyl	BuLi (Et_2O)	I_2	3-Isobutylthiophene (9)
	s-Butyl	BuLi (Et_2O)	Br_2	3-*s*-Butylthiophene (75)
	s-Butyl	BuLi (Et_2O)	I_2	3-*s*-Butylthiophene (77)
	Cyclopentyl	BuLi (Et_2O)	Br_2	3-Cyclopentylthiophene (81)
	Cyclopentyl	BuLi (Et_2O)	I_2	3-Cyclopentylthiophene (29)
	Hexyl	BuLi (Et_2O)	Br_2	3-Hexylthiophene (54)
	Hexyl	BuLi (Et_2O)	I_2	3-Hexylthiophene (11)

a) All products were either compared with authentic samples or exhibited analytical data and spectra in accodance with the assigned structures. b) Based on the organoborane used and determined by VPC.

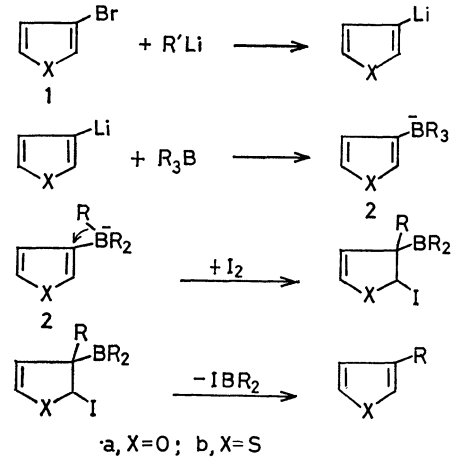

Scheme 2.

The reaction mechanism, although not explored in detail, could be considered to proceed through the following pathway (Scheme 2).

Experimental

Materials. All the chemicals and solvents were purified by distillation before use. Trialkylboranes were prepared by the usual procedure.[13] 3-Bromofuran was prepared by the Nazarova's method.[14]

The IR and NMR spectra were taken on a Hitachi-Perkin-Elmer Model 125 spectrophotometer and Hitachi R-22 spectrometer at 90 MHz using tetramethylsilane as an internal standard.

General Procedure. A representative procedure for the preparation of 3-*s*-butylfuran is as follows. A dry 50 ml round-bottomed flask equipped with a condenser, a septum inlet and a magnetic stirring bar was flushed with nitrogen. In the flask was placed 3-bromofuran (3 mmol, 0.27 ml) and anhydrous ether (5 ml) under nitrogen gas. Then butyllithium (3 mmol, 1.54 ml of a 1.95 M solution in ether) was added dropwise at −78 °C to form 3-lithiofuran.[15] The mixture was stirred for 30 min. After metallation was complete, tri-*s*-butylborane (3 mmol, 1.5 ml of a 2 M solution in THF) was added to the mixture at −78 °C, followed by stirring for 30 min. The solution was allowed to warm to 0 °C and then stirred again for 30 min. Finally, a solution of iodine (3 mmol, 0.726 g in 10 ml of ether) was fed in at −78 °C. The reaction mixture was allowed again to warm to room temperature and stirred for 2 h. In order to remove the residual organoborane, the mixture was treated with 3 M aqueous sodium hydroxide (2 ml), followed by a dropwise addition of 30% hydrogen peroxide (1 ml). The product thus obtained was extracted three times with ether and the combined organic layer was dried over magnesium sulfate. VPC analysis (15% Silicone DC-550 on Uniport B, 120 °C) indicated that 2.73 mmol (91%, based on tri-*s*-butylborane) of 3-*s*-butylfuran had been obtained. An analytically pure material was obtained by preparative VPC (15% Silicone DC-550 on Uniport B, 3 m) with Varian Autoprep Model-2800.

Identification of the Products. *3-Butylfuran*: n_D^{20} 1.4705. Found: C, 77.02: H, 9.85%. Calcd for $C_8H_{12}O$: C, 77.37; H, 9.74%. Mass; *m/e*=124 (M^+). IR(neat); 3150, 1520, 885, 780 cm^{-1}. NMR(CCl_4): δ, 0.95 (3H, t, J=7.0 Hz), 1.50 (4H, m), 2.42 (2H, t, J=7.0 Hz), 6.20—7.30 (3H, m).

3-Isobutylfuran: n_D^{20} 1.4580. Found: C, 77.26; H, 9.68%. Calcd for $C_8H_{12}O$: C, 77.37; H, 9.74%. Mass; *m/e*=124 (M^+). IR(neat); 3150, 1515, 885, 780 cm^{-1}. NMR(CCl_4); δ, 0.95 (6H, d, J=6.0 Hz), 1.90 (1H, m), 2.34 (2H, d, J=7.0 Hz), 6.20—7.30 (3H, m).

3-s-Butylfuran: n_D^{20} 1.4595. Found: C, 77.14; H, 9.86%. Calcd for $C_8H_{12}O$: C, 77.37; H, 9.74%. Mass; *m/e*=124 (M^+). IR(neat); 3150, 1515, 885, 785 cm^{-1}. NMR(CCl_4); δ, 0.95 (3H, t, J=7.0 Hz), 1.20 (3H, d, J=7.0 Hz), 1.57 (2H, m), 2.58 (1H, m), 6.25—7.30 (3H, m).

3-Cyclopentylfuran: n_D^{20} 1.4660. Found: C, 79.19; H, 8.71%. Calcd for $C_9H_{12}O$: C, 79.37; H, 8.88%. Mass; *m/e*=136 (M^+). IR(neat); 3150, 1510, 885, 780 cm^{-1}. NMR(CCl_4); δ, 1.35—2.18 (8H, m), 2.87 (1H, m), 6.22—7.30 (3H, m).

3-Hexylfuran: n_D^{20} 1.4820. Found: C, 78.73; H, 10.61%. Calcd for $C_{10}H_{16}O$: C, 78.89; H, 10.59%. Mass; *m/e*=152 (M^+). IR(neat); 3150, 1515, 885, 780 cm^{-1}. NMR(CCl_4); δ, 0.90 (3H, t, J=6.0 Hz), 1.17—1.78 (8H, m), 2.30 (2H, t, J=7.0 Hz), 6.20—7.30 (3H, m).

3-Butylthiophene: n_D^{20} 1.5680. Found: C, 68.45; H, 8.70%. Calcd for $C_8H_{12}S$: C, 68.51; H, 8.51%. Mass; *m/e*=140 (M^+). IR(neat); 3120, 1460, 850, 680 cm^{-1}. NMR(CCl_4); δ, 0.90 (3H, t, J=7.0 Hz), 1.30—1.72 (4H, m), 2.63 (2H, t, J=7.0 Hz), 6.80—7.22 (3H, m).

3-Isobutylthiophene: n_D^{20} 1.5475. Found: C, 68.38; H, 8.37%. Calcd for $C_8H_{12}S$: C, 68.51; H, 8.51%. Mass; *m/e*=140 (M^+). IR(neat); 3120, 1465, 855, 690 cm^{-1}. NMR(CCl_4); δ, 0.93 (6H, d, J=6.0 Hz), 1.93 (1H, m), 2.52 (2H, d, J=7.0 Hz), 6.80—7.25 (3H, m).

3-s-Butylthiophene: n_D^{20} 1.5490. Found: C, 68.66; H, 8.72%. Calcd for $C_8H_{12}S$; C, 68.51; H, 8.51%. Mass; *m/e*=140 (M^+). IR(neat); 3120, 1460, 850, 680 cm^{-1}. NMR(CCl_4); δ, 0.83 (3H, t, J=6.0 Hz), 1.22 (3H, d, J=7.0 Hz), 1.57 (2H, m), 2.73 (1H, m), 6.80—7.25 (3H, m).

3-Cyclopentylthiophene: n_D^{20} 1.5642. Found: C, 70.84; H 7.90%. Calcd for $C_9H_{12}S$: C, 71.00; H, 7.94%. Mass; *m/e*=152 (M^+). IR(neat); 3120, 1450, 860, 680 cm^{-1}. NMR(CCl_4); δ, 1.47—2.23 (8H, m), 3.05 (1H, m), 6.80—7.25 (3H, m).

3-Hexylthiophene: n_D^{20} 1.5790. Found: C, 71.43; H, 9.48%. Calcd for $C_{10}H_{16}S$: C, 71.36; H, 9.60%. Mass; *m/e*=168 (M^+). IR(neat); 3120, 1460, 855, 680 cm^{-1}. NMR(CCl_4); δ, 0.90 (3H, t, J=6.0 Hz), 1.15—1.78 (8H, m), 2.63 (2H, t, J=7.0 Hz), 6.80—7.25 (3H, m).

References

1) For a recent review, see A. I. Meyers, "Heterocycles in Organic Synthesis," John-Wiley & Sons, New York (1974).

2) V. Ramanathan and R. Levine, *J. Org. Chem.*, **27**, 1667 (1962).

3) Y. Kojima, S. Wakita, and N. Kato, *Tetrahedron Lett.*, **1979**, 4577.

4) A. Minato, K. Tamao, T. Hayashi, K. Suzuki, and M. Kumada, *Tetrahedron Lett.*, **1980**, 845.

5) A. B. Levy, *J. Org. Chem.*, **43**, 4684 (1978).

6) E. R. Marinelli and A. B. Levy, *Tetrahedron Lett.*, **1979**, 2313.

7) A. B. Levy, *Tetrahedron Lett.*, **1979**, 4021.

8) I. Akimoto and A. Suzuki, *Synthesis*, **1979**, 146.

9) T. Sotoyama, S. Hara, and A. Suzuki, *Bull. Chem. Soc. Jpn.*, **52**, 1865 (1979).

10) For example, see D. S. Sappenfield and M. Kreevoy, *Tetrahedron*, **19**, Suppl. 2, 157 (1963).

11) R. P. Dickinson and B. Iddon, *J. Chem. Soc., C*, **1971**, 3447.

12) B. J. Wakefield, "The Chemistry of Organolithium Compounds," Pergamon, Oxford (1976), p. 144.

13) H. C. Brown, "Organic Synthesis *via* Boranes," John-Wiley & Sons, New York (1975).

14) Z. N. Nazarova, Yu. A. Babaev, and L. G. Umanskaya, *Khim. Geterotsikl. Soedin.*, 17 (1969); *Chem. Abstr.*, **70**, 106411v (1969).

15) Y. Fukuyama, Y. Kawashima, T. Miwa, and T. Tokoroyama, *Synthesis*, **1974**, 443.

Transmission of Low-energy Electrons through Thin-films of Benzene and Hexane at 80 K

Kenzo HIRAOKA* and Masaji NARA
Faculty of Engineering, Yamanashi University, Takeda-4, Kofu 400
(Received May 6, 1980)

Transmission spectra of low-energy electrons (0—15 eV) for 10—100 Å films of benzene and hexane have been measured at 80 K. Resonances are clearly indicated by electron current I_t transmitted through the dielectric as a function of the incident electron energy V_1, displayed as dI_t/dV_1 *vs.* V_t. When the film thickness of hexane was increased, the height of the first peak (due to injection of electrons in the film) decreased drastically and a second peak appeared and grew strongly. From the energy of the second peak, the bulk electron affinity ($-V_0$) of thin film was estimated. The V_0 values for hexane and octane are 0.9 and 1.0 eV, respectively.

The excitation of gas-phase molecules by electron impact has often been studied by a variety of techniques ranging from low-energy threshold excitation[1,2] to energy loss spectroscopy,[3-5] using both high- and medium-energy electrons. Threshold excitation techniques of Schulz[1] and Compton *et al.*[2] are similar in that the yields of low-energy electrons produced by resonant electron impact processes are measured either by the trapped electron method or by the SF_6 scavenger technique.[2]

Applications of electron impact techniques to thin organic films have previously been restricted to the measurements of energy loss spectra of high-energy electrons transmitted through thin films of polymers.[6,7] Since the optical selection rules are relaxed for excitation by low-energy electrons,[8] it is not possible to extrapolate results from energy loss spectra involving high-energy electrons to processes involving low-energy electrons.

Recently, Hiraoka and Hamill[9-14] and Sanche[15,16] reported a simple method for measuring the electronic levels of molecules supported as ultrathin films on a metal surface at 77 K.[9-14] The film was bombarded by a beam of low-energy electrons, and the current transmitted through the film(I_t) was measured as a function of the incident electron energy(V_i). This method was found particularly useful for detecting optically forbidden electronic transitions.

A similar apparatus was constructed. The main objective of this work is to relate the energy dependence of the transmission features to specific interactions occuring in films of benzene and hexane.

Experimental

A schematic diagram of a prototype spectrometer housed in a stainless steel high-vacuum system (ULVAC, EBD-50M) maintained at $\lesssim 2\times10^{-7}$ Pa appears in Fig. 1. An electron gun used is a commercial TV gun (The Japan Lamp Industrial Co., LTD.) consisted of an einzel lense and an indirectly heated oxide-coated cathode. The gun is mounted in a grounded stainless steel cylinder. The angle of incidence of the electron beam to a metal target is normal.

A schematic diagram of the spectrometer system used for the measurement of electrons transmitted through thin solid films is shown in Fig. 2. Differentiation of the transmitted current I_t with respect to the incident electron energy V_1 is accomplished electronically by superimposing a small a.c. voltage (0.3 V peak-to-peak at 78 Hz) on the base cathode voltage and synchronously detecting the resulting a.c. signal

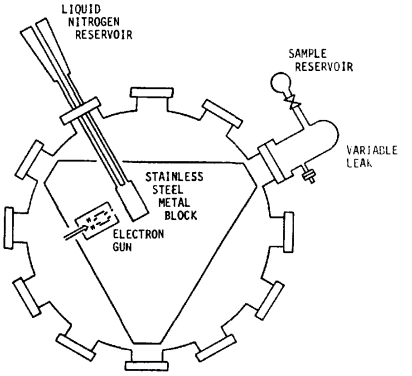

Fig. 1. Schematic diagram of the spectrometer.

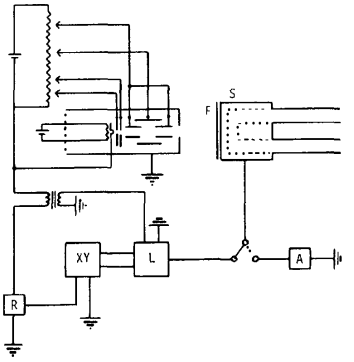

Fig. 2. Schematic arrangement of the apparatus used for measuring the electron current transmitted through the dielectric film F to the stainless steel support S at ≈80 K. Other components include a lock-in amplifier L, a ramp function generator R, a recorder XY, and an electrometer A.

at the target with a lock-in amplifier (NF Circuit Design Block Co., LTD. model LI-573). An X-Y recorder plot of the magnitude of the a.c. signal *vs.* the the cathode potential provides the transmission spectrum, dI_t/dV_1 *vs.* V_1.

The sample was deposited as a thin film on the stainless steel block (face 3.6×2.0 cm^2) cooled by circulating liquid nitrogen. The temperature of the metal block was measured by an iron-constantan thermocouple which was spot-welded on the metal block. A sample was admitted to the vacuum chamber through a variable leak valve. The film thickness was estimated by establishing a given partial pressure of a sample vapor in the vacuum chamber for a specific time, assuming a sticking probability of unity. The pressure gauge, which reads the ion current of an ion pump, was calibrated

for nitrogen. Because almost all of organic compounds have larger ionization cross sections than nitrogen, the reading of the pressure gauge must be higher than the actual pressure of an introduced organic compound at the ion pump. However, the position of the pressure gauge was far from the metal block, and the effective pressure at the metal block could be higher than the pressure at the ion pump. Thus the value of the film thickness given in this work should be considered as only a roughly estimated one. The film thickness was changed by changing the deposition time with the constant vapor pressure at 10^{-5} Pa. It has not been known whether films are crystalline or amorphous, but the randomness in the solid was suggested for benzene film at 77 K.[17]

In the previous works,[9-14,17] the incident electron current of 10^{-9}—10^{-8} A with a beam spot of $\approx$1 mm in diameter was used, where it was found that the condensed films of organic compounds were very sensitive to electron bombardment. The spectrum dI_t/dV_i *vs.* V_i for the bare metal block often showed apparent difference before and after the measurement of an aromatic sample, indicating that a metal surface was contaminated by the radiolytic products. The metal block had to be cleaned every time after the measurement of an aromatic sample. Saturated molecules gave less radiolytic products than aromatic compounds under the same experimental conditions.

In this experiment, the incident electron current of $\leq 2\times 10^{-9}$ A with a larger beam spot was used in order to reduce the radiation damage of a film. The diameter of the aperture for electrons in the end wall of the cylinder was 5 mm. The size of the beam spot could be roughly estimated by observing weak blue luminescence from thin-film benzene bombarded by electrons with the energy of 15—20 eV. The observed faint luminous lobe was about 13 mm in diameter. Thus the current density should be at most 2×10^{-9} A/cm^2. Matsushige and Hamill measured the yields of decomposition products from multilayer films of cyclohexane and hexane caused by low-energy electron irradiation.[18] They found the G values† to be $\approx$0.5 for electron energies of 10—20 eV. With decomposition yields of this magnitude, a monolayer of the hydrocarbons could be decomposed in 100 h under the conditions of our study. The spectrum for bare metal block did not change under repeated measurements for aliphatic and aromatic compounds, in agreement with the results of Matsushige and Hamill.[18]

Results and Discussion

Benzene. The transmission spectra dI_t/dV_i *vs.* V_i for benzene are shown in Fig. 3. The film thickness was changed from 2 to 10 L.†† The spectrum of the metal block is also shown in the Figure, which was measured before the organic sample was deposited. The temperature of the metal block was $\approx$80 K.

The spectra of benzene are in excellent agreement with the result obtained by Hiraoka and Hamill,[10] indicating a good reproducibility of the present method. In Fig. 3 are also shown the trapped electron spectrum[19] and the energy loss spectrum of 300 eV electrons[20] for comparison. These spectra serve to establish the energy

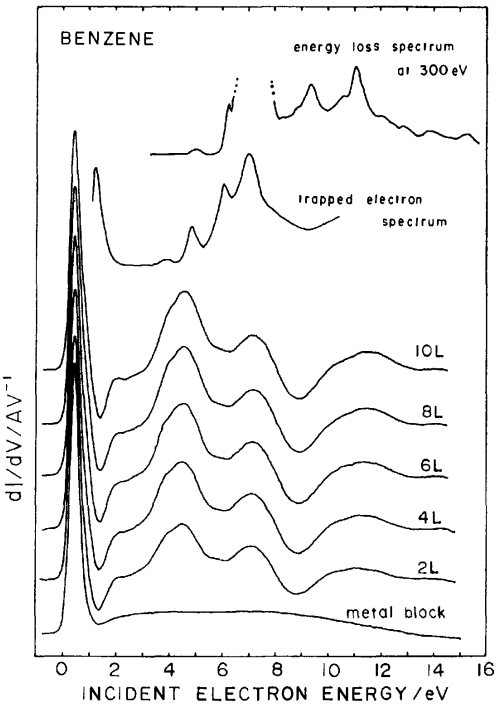

Fig. 3. The dependence of dI_t/dV_i *vs.* V_i for metal block and benzene. The film thickness was changed from 2 to 10 L. The trapped electron spectrum[19] and the energy loss spectrum of 300 eV electrons[20] are also shown for comparison.

shift of the spectrum dI_t/dV_i *vs.* V_i. The best fit locates the zero of the incident electron energy at the onset of the first peak.

The strong bands appear in the spectrum dI_t/dV_i *vs.* V_i at 3.9 and 4.6 eV in Fig. 3 which correspond to energies lost by exciting benzene to the $^3B_{1u}$ and $^1B_{2u}$ states, respectively. These optically forbidden transition bands are even larger than the optically allowed $^1E_{1u}\leftarrow{}^1A_{1g}$ transition band at 7 eV, indicating the major advantage of the electron impact over the photon spectroscopy for its ability to induce optically forbidden transitions.

Another weak events are also observed as a shoulder of the first peak and two small peaks in the range 1.5—3.0 eV. Although the shoulder peak corresponds approximately to the peak at 1 eV in the trapped electron spectrum which is due to the transient negative ion formation, the relative intensity of the shoulder peak is much smaller than the peak at 1 eV in the trapped electron spectrum, and the assignment of this peak would not be so straightforward. The origins of events in the range 1.5—3.0 eV were not well understood either. A further investigation for the detailed analysis of the spectra is now in progress.

It is evident from Fig. 3 that the 2 L film is thick enough to give a characteristic transmission spectrum of benzene and the spectra of thicker films did not show any marked dependence on the film thickness up to 10 L. This suggests that the interaction of low-energy electrons with only a few monolayers from the surface of benzene film gives the characteristic transmission spectrum. In addition, the onset of the first peak and the positions

† The *G* value refers to the number of molecules of a product formed on irradiation per 100 eV of energy absorbed.

†† The amount of the gas admitted in the vaccum chamber is expressed in Langmuir units (1 L$=1\times 10^{-6}$ Torr s). When the sticking probability is unity, the surface will be covered by approximately one monolayer with 1 L gas admission.

of peaks in transmission spectra appear at almost the same energies with increasing the film-thickness from 2 to 10 L. This indicates that the charging of electrons in the film is negligible for the present experimental conditions.

Since the first peak of the spectrum for the metal block describes a crude electron energy distribution function with the high-energy tail at the onset, the detailed examination of the change of the first peak after the dielectric film is deposited on the metal surface would be helpful for understanding the interaction of low-energy electrons (0—2 eV) with dielectrics. As shown in Fig. 3, there is almost no difference in shape (height and half-width) between the first peak for the metal block and those for benzene for 2—10 L. It is noteworthy that the acceptance coefficients for electrons at low energies are nearly the same for benzene and the stainless steel metal block. Only the difference is the appearance of a small shoulder peak at $\approx$1 eV and the sharp negative peak at $\approx$1.3 eV in the benzene spectra which are not observed for the stainless steel metal block.

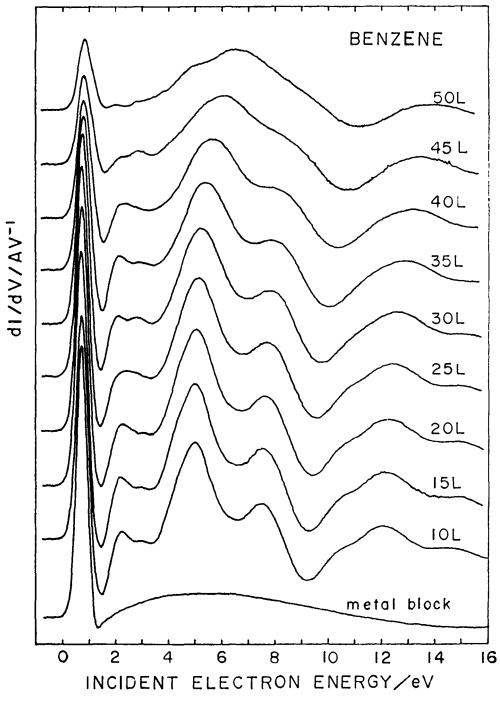

Fig. 4. The dependence of dI_t/dV_1 *vs.* V_1 for benzene. The film thickness was changed from 10 to 50 L.

In Fig. 4 is shown the change of spectra when the film thickness was increased from 10 to 50 L. The height of the first peak decreases only gradually with increasing the film thickness. The peaks of the spectra show only very small positive shifts with increasing the film thickness up to 25 L. Above 30 L, the positive shifts become more evident possibly due to the charging of the film.

Hexane. The transmission spectra are shown in Fig. 5. The film thickness was changed from 2 to 30 L. The zero of the energy scale is arbitrary. Contrary to the spectra of benzene, the first peak decreases drastically and the second peak at $\approx$1.4 eV grows strongly as the

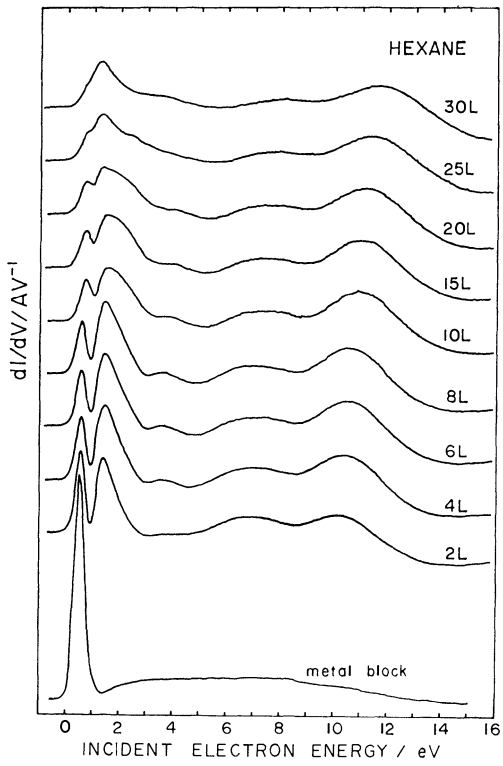

Fig. 5. The dependence of dI_t/dV_1 *vs.* V_1 for metal block and hexane. The film thickness was changed from 2 to 30 L.

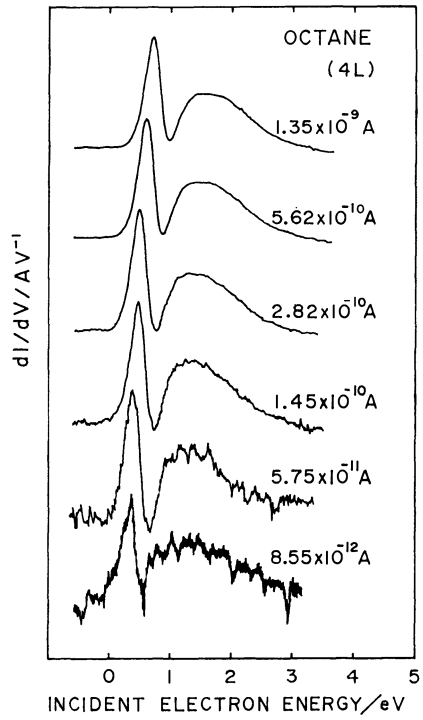

Fig. 6. Spectra of octane in the energy range 0—3 eV with the incident electron current changed from 8.55×10^{-12} to 1.33×10^{-9} A.

film thickness is increased. At 30 L, the first peak shows up as only a small shoulder peak of the second peak. Such a marked change of the spectra with an

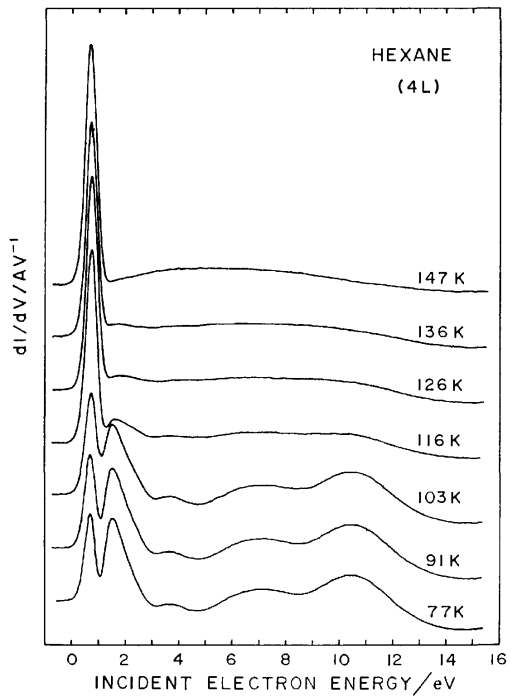

Fig. 7. Temperature programmed spectra following the adsorption of hexane on the stainless steel metal block at 77 K. The heating rate is 10 K/min.

increase of the film-thickness was also observed for octane (Fig. 6), but not for benzene and other aromatic compounds. These characteristic low-energy events of hexane may be related to the interaction of electrons with the bulk of the solid film, *i.e.*, the cluster of molecules.

Figure 7 shows spectra of the temperature dependence following the adsorption of hexane (4 L) on the metal block at 77 K. The heating rate is 10 K/min. As the temperature is increased, the intensity of first peak increases gradually with an expense of the second peak. The spectrum at 147 K coincides with that of the metal block, indicating that all samples are desorbed from the metal block at this temperature. The observed rapid desorption suggests the weak adsorption of hexane on the stainless steel substrate. Madey and Yates observed two peaks at 150—175 K and 277 K in the temperature programmed desorption spectra following the adsorption of cyclohexane on Ru(001) at 80 K.[21] They concluded that the state at 150—175 K is due to a condensed multilayer and that at 227 K is due to C_6H_{12} adsorbed in the first monolayer in contact with the Ru(001) substrate. In Fig. 7, the rapid change of spectra is observed from 77 to 126 K, but the spectra at 126 and 136 K are almost exactly the same, suggesting that these spectra are those for the monolayer of hexane on the metal substrate. The multilayer should be exhausted in this temperature range because the vapor pressure of hexane at 126 and 136 K are about 1×10^{-4} and 1×10^{-3} Pa, respectively. The second peak of spectra for 126 and 136 K is still observed but it shows the positive shift by 0.3—0.4 eV with respect to the peak of multilayer films. The coverage of hexane monolayer at these temperatures could not be estimated under the present experimental conditions.

Bulk Electron Affinity. As shown in Figs. 3 and 5, the low-energy events of benzene are very different from those of hexane in the range 0.5—2.0 eV. In the case of benzene, the first peak does not show a marked film-thickness dependence and a sharp negative peak is observed at $\approx$1.3 eV. On the contrary, a rapid decrease of the first peak accompanied by a strong growth of the second peak is observed for hexane as the film-thickness is increased. These experimental results suggest the existence of the positive energy barrier in hexane thin film and the negative one in benzene thin film for the injection of electrons from the vacuum into the film. If the positive energy barrier for hexane is due to the temporal charging of the film, the spectra should be dependent on the amount of the incident electron current at least to some extent. Figure 6 shows the spectra of octane in the energy range 0—3 eV with the incident electron current changed from 8.55×10^{-12} to 1.35×10^{-9} A. It is apparent from the Figure that the shape of the spectra does not change with an increase of the incident electron current more than two orders of magnitude. Thus the energy barrier for the incident electrons can not be attributed to the one generated by charging in the film. We would like to conclude that energy barrier is an intrinsic one for each compound, *i.e.*, the bulk electron affinity.

In Fig. 6, the gradual positive shifts of the spectra are observed with the increase of the incident electron current. This is *not* due to the charging of the film. When the film thickness is $\leq$10 L, the spectra of organic compounds generally do not show any observable peak shifts under repeated and prolonged irradiation of the electron beam of $\approx10^{-9}$ A. The shifts observed in Fig. 6 is a manifestation of the positive shifts of the current-voltage characteristic curve of the electron gun. The positive shift is always observed when the voltage of the draw-out electrode in front of the cathode is increased in order to get more electron current.

For an electron of energy E in the condensed medium, the Schrödinger equation is

$$\left[-\frac{\hbar^2}{2m}\nabla^2+V\right]\Psi=E\Psi, \tag{1}$$

where V is the one-electron potential exerted by the unperturbed medium. When the potential V is periodic from one sphere to another and spherically symmetric inside the sphere, only one radial equation needs to be solved, so that the ground state eigenvalue E of Eq. 1 can be uniquely defined. Springett *et al.*[22] calculated the energy levels of an excess electron in multiatom system by using a Wigner-Seitz model to obtain a spherically symmetric potential. In the Wigner-Seitz model each atom is replaced by a sphere of radius r_s given by

$$r_s=\left(\frac{3}{4\pi n}\right)^{1/3}, \tag{2}$$

where n is the number density. The wave function ψ is smooth inside r_s, and V is the pseudopotential approximated as ∞ for $r<\bar{a}$ and U_p for $r>\bar{a}$. This pseudopotential excludes the excess electron from the hard core radius $\bar{a}$ of the atom. U_p is the polarization potential from the atom inside and the atoms outside r_s which is approxi-

mated by

$$U_p = \frac{-3\alpha e^2}{2r_s^4}\left[\frac{8}{7}+\left(1+\frac{8}{3}\pi\alpha n\right)^{-1}\right], \quad (3)$$

where α is the isotropic polarizability. Then, Eq. 1 may be solved to yield

$$E = U_0 + \frac{\hbar^2 k_0}{2m} = U_0 + T_0, \quad (4)$$

where the electron wave vector k_0 is obtained from the Wigner-Seitz boundary condition $(d\psi/dr)_{r=r_s}=0$, which gives the equation

$$\tan k_0 (r_s-\bar{a}) = k_0 r_s, \quad (5)$$

and T_0 is the zero point energy which arises because the excess electron is excluded from the hard core region of radius in each Wigner-Seitz sphere. The lowest energy eigenvalue E of Eq. 1 is the ground state energy of an excess electron in the medium (V_0), *i.e.*, an energy required for injection of an electron from the vacuum into the medium. The bulk electron affinity of the medium corresponds to $-V_0$.

The positive bulk electron affinity may be assigned for benzene film. When the bulk electron affinity of the film is positive, the energy level of an excess electron (V_0) in the film is lower than that of the vacuum. In such a case, the electrons see the "negative" energy barrier when they enter the film from the vacuum, and the injection peak of electrons (the first peak) should not be very different from that of the bare metal block, in good agreement with the experiment. On the other hand, the excess electron in the film see the "positive" energy barrier for escaping into the vacuum. For a spherically-asymmetric distribution of elastically scattered electrons in a film, with a negative V_0, the quantum mechanical reflection coefficient at the film-vacuum interface may be given by $R=\{|V_0|/(|V_0|+E_i)\}^{1/2}$, where E_i is the energy of electrons.[16] According to this theory, the backscattered current will show an increase as the energy of incident electrons increases because it is easier for injected electrons in the film to overcome the positive energy barrier ($-V_0$) and escape the film into the vacuum at higher incident electron energy (E_i), *i.e.*, the effective reflection coefficient at the film-vacuum interface will decrease with an increase of the energy of electrons. This might explain the observed negative peak at $\approx$1.3 eV in the benzene spectrum.

The low-energy events observed for hexane and octane can be explained reasonably if the negative bulk electron affinity is assigned for these compounds. Figure 8 shows the schematic potential distribution along the axis of the spectrometer and the spectrum, dI_t/dV_i *vs.* V_i, for a film whose bulk electron affinity is negative ($0<V_0$). Because of the positive energy barrier of the film for the incident electrons, the injection peak of electrons (the first peak) should be much smaller than that of the metal block, and the transmitted electron current should show a sharp increase as a second peak in the spectrum, dI_t/dV_i *vs.* V_i, when the energy of the incident electrons exceeds the positive energy barrier, in all good agreement with the experimental results.

If the observed low-energy events are manifested by the bulk electron affinity of the films, it might be

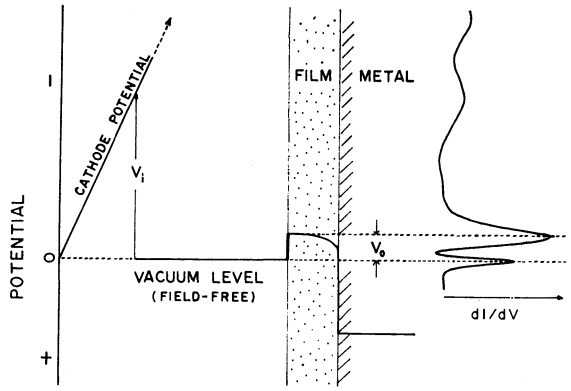

Fig. 8. The schematic diagram of the potential distribution along the axis of the spectrometer. The space between the electron gun and the metal block is field-free. The bulk electron affinity of the film shown in the figure is negative. The spectrum of hexane, dI_t/dV_i *vs.* V_i, is shown along the potential axis in the right part of the figure. V_i is the accelerating voltage. V_0 represents the ground state energy of excess-electrons in the film. The value of the bulk electron affinity corresponds to $-V_0$.

possible to estimate the bulk electron affinities from the spectra dI_t/dV_i *vs.* V_i. The spectrum is a convolution of the current-voltage characteristics of an electron gun $I(V)$, and the energy dependent acceptance coefficient of electrons for the film $F(V)$. $F(V)$ may be affected by many factors such as the bulk electron affinity, the density and the structure of the film, density of trapping sites and the distribution of the well-depth of trapping sites, *etc.* Because so many factors are involved in the low-energy events of the spectra, it would be difficult to determine the bulk electron affinity unequivocally. Here the bulk electron affinity ($-V_0$) is tentatively estimated by the energy difference of the first peak for the metal block and the second peak of the spectra for hexane and octane, which are -0.9 and -1.0 eV, respectively.

The positive bulk electron affinity could be estimated by the amount of the positive shift of the spectrum if the reference peak is available for the determination of the energy scale. For benzene, the horizontal axis of Fig. 3 is the energy for the trapped electron spectrum[19] and the energy loss spectrum of 300 eV electrons.[20] With this scale, the energy of the transmission spectrum is increased by 0.3 eV to establish a coincidence between structures present in these spectra. Thus the bulk electron affinity of benzene film could be estimated as about 0.3 eV (V_0 is -0.3 eV).

For solid hydrocarbons, no direct experimental V_0 determinations have been reported so far. Jortner's calculations[22,23] give nearly equivalent V_0 values for solid and liquid argon. On the other hand, recent experiments by Noda *et al.* have shown that V_0 increases with decreasing temperature in liquid ethane.[24] Recently Grand and Bernas[25,26] measured V_0 for solid hydrocarbons indirectly by measuring the ionization potential of a solute in various polar and nonpolar rigid solvents. Their indirectly measured V_0 for rigid hexane is 0.98 eV, in good agreement with our value (0.9 eV).

The Springett, Jortner and Cohen model for calculat-

ing V_0 (Eq. 4) was originally developed for rare gas liquids[22] but has been applied to hydrocarbons.[24,27] For liquid hexane, U_0 and T_0 can be calculated as -2.4 and 1.77 eV, respectively, and thus V_0 is -0.63 eV. The experimental value of V_0 in liquid hexane by photoelectric work function measurements is 0.04 eV,[28] which is much smaller than the value in rigid hexane. Grand and Bernas[26] also found that the 77 K V_0 values appear significantly greater than the ones measured at 298 K (liquid) by 0.7—1.0 eV.

The author would like to thank Professor W. H. Hamill of the University of Notre Dame for his encouragement and Professors E. Hayashi and K. Sakai and Mr. S. Takeuchi of Yamanashi University for valuable discussions. The financial supports of the Grant-in-Aid for Scientific Research from the Ministry of Education, Science and Culture (No. 354135, 1978) and of 1978 RCA Research Grant are gratefully acknowledged.

References

1) G. J. Schulz, *J. Chem. Phys.*, **33**, 1661 (1960).
2) R. N. Compton, R. H. Huebner, P. W. Reinhardt, and L. B. Christophorou, *J. Chem. Phys.*, **48**, 901 (1968).
3) C. R. Bowman and W. D. Miller, *J. Chem. Phys.*, **42**, 681 (1965).
4) E. N. Lassettre, A. Skerbele, and M. A. Dillon, *J. Chem. Phys.*, **49**, 2382, 5042 (1968).
5) J. P. Doering and A. J. Williams, Jr., *J. Chem. Phys.*, **47**, 4180 (1967).
6) N. Swanson and C. J. Powell, *J. Chem. Phys.*, **39**, 630 (1963).
7) A. M. Rauth and J. A. Simpson, *Radiat. Res.*, **22**, 643 (1964).
8) H. S. W. Massey and E. H. S. Burhop, "Electronic and Ion Impact Phenomenon," Oxford University Press, London (1952), pp. 141—146.
9) K. Hiraoka and W. H. Hamill, *J. Chem. Phys.*, **56**, 3185 (1972).
10) K. Hiraoka and W. H. Hamill, *J. Chem. Phys.*, **57**, 3870 (1972).
11) K. Hiraoka and W. H. Hamill, *J. Chem. Phys.*, **57**, 3881 (1972).
12) K. Hiraoka and W. H. Hamill, *J. Chem. Phys.*, **57**, 4058 (1972).
13) K. Hiraoka and W. H. Hamill, *J. Chem. Phys.*, **58**, 3686 (1973).
14) K. Hiraoka and W. H. Hamill, *J. Chem. Phys.*, **59**, 5749 (1973).
15) L. Sanche, *Chem. Phys. Lett.*, **65**, 61 (1979).
16) L. Sanche, *J. Chem. Phys.*, **71**, 4860 (1979).
17) K. Hiraoka and W. H. Hamill, *J. Phys. Chem.*, **77**, 1616 (1973).
18) T. Matsushige and W. H. Hamill, *J. Phys. Chem.*, **76**, 1255 (1972).
19) H. H. Brongersma, J. A. v. d. Hart, and L. J. Oosterhoff, "Proceedings of Nobel Symposium," Wiley Interscience, New York (1968), Vol. 5, p. 211.
20) A. Skerbele and E. N. Lassettre, *J. Chem. Phys.*, **42**, 395 (1965).
21) T. E. Madey and J. T. Yates, Jr., *Surf. Sci.*, **76**, 397 (1978).
22) B. E. Springett, J. Jortner, and M. H. Cohen, *J. Chem. Phys.*, **48**, 2720 (1968).
23) B. Raz and J. Jortner, *Chem. Phys. Lett.*, **4**, 155 (1969).
24) S. Noda, L. Kevan, and K. Fueki, *J. Phys. Chem.*, **79**, 2866 (1975).
25) A. Bernas, J. Blais, M. Gauthier, and D. Grand, *Chem. Phys. Lett.*, **30**, 383 (1975).
26) D. Grand and A. Bernas, *J. Phys. Chem.*, **81**, 1209 (1977).
27) K. Fueki, D. F. Feng, and L. Kevan, *Chem. Phys. Lett.*, **13**, 616 (1972).
28) R. A. Holroyd and M. Allen, *J. Chem. Phys.*, **54**, 5014 (1971).

  Bull. Chem. Soc. Jpn., 54, 1595—1599 (1981)

The Adsorption of Basic α-Amino Acids in an Aqueous Solution by Titanium(IV) Oxide

Susumu Okazaki,* Teruaki Aoki, and Koichi Tani

Department of Industrial Chemistry, Faculty of Engineering, Ibaraki University, Hitachi 316

(Received June 5, 1980)

TiO_2 showed a pronounced activity in the adsorption of basic α-amino acids, such as L-lysine and L-arginine, in an aqueous solution. The adsorptive activity of TiO_2 containing sulfate ions was lower than that of the sulfate ion-free TiO_2, and it was suppressed by phosphate ions. The pH of the aqueous solution hardly affected the adsorption, while the heat-treatment of TiO_2 above 500 °C noticeably lowered the adsorption. The Langmuir equation was applicable to the adsorption of L-lysine, showing that the amount of saturated adsorption was about 0.7 mmol/g TiO_2 heat-treated at 500 °C. The heat of adsorption of L-lysine, as determined from the adsorption isotherms at 10, 30, and 50 °C, was 2257 J/mol. A linear relationship was observed between the amount of L-lysine adsorbed and that of the surface OH groups.

The removal of excess α-amino acids in the blood is required for the treatment of certain kidney diseases.[1] The use of activated carbon has been an important removal method. Ito[2] has observed a marked adsorption of the basic amino acids, such as lysine, histidine, and arginine, by animal charcoals, and Wunderly[3] has obtained adsorption isotherms for phenylalanine, leucine, serine, and aspartic acid on animal and sugar charcoals. However, a systematic investigation of the adsorption of amino acids on Darco G-60 lignite charcoal by Cherdelin *et al.*[4] indicated that activated carbon was not effective for the adsorption of all kinds of α-amino acid, for the absence of the aromatic group in amino acids decreased the adsorption. Aliphatic amino acids, having a high solubility in water, can be expected to be better adsorbed by an adsorbent which is more polar than activated carbon.

In recent years, TiO_2 and its hydrate have been extensively used as catalysis,[5] catalyst-carriers,[6] and ion-exchangers.[7] They have also been observed to be excellent adsorbents for uranium in sea water.[8] However, no studies dealing with the adsorptions of α-amino acids by TiO_2 have been reported. The use of TiO_2 as an adsorbent for α-amino acids is, though, a matter of considerable interest because of its extremely low solubility in water, its nontoxicity, and its amphoteric nature.

In this paper, we wish to report our results concerning the activity of TiO_2 in the adsorption of basic α-amino acids in aqueous solutions. The adsorptive activities of alumina and activated carbon for α-amino acids were also examined for reference.

Experimental

Preparation of the Samples. Two TiO_2 samples were prepared: one by the hydrolysis of titanium tetraisoproxide (Wako Chemical Co.) at room temperature (designated as S-1), and the other, by the hydrolysis of titanium oxide sulfate (Nakarai Chemical Co.) at the temperature of boiling water (designated as S-2). After repeated washings and decantations, both samples were dried in air at 120 °C for 10 h. Although the complete removal of the sulfate ion was confirmed by the use of a $BaCl_2$ aqueous solution, S-2 contained a considerable amount of bound sulfate ion (for example, 0.5 mmol/g after heat-treatment at 400 °C). Therefore, in most experiments, S-1 was employed. Only in experiments relating to the effects of the heat-treatment temperature was S-2 used.

The alumina was prepared by the hydrolysis of aluminum isopropoxide (Wako Chemical Co.), followed by washing with water and drying at 120 °C. The activated carbons used were the commercial products of the Kureha Chemical Co. (MU and MU-E).

The various amino acids used in this study were commercial reagents of a special grade prepared by the Kokusan Kagaku Co.

Determination of the Amount of Surface OH Groups. The amount of surface OH groups was determined by a modification of Boehm's method.[9] The amount of OH on S-1 sample, which was heat-treated at 500 °C, was 0.7 mmol/g TiO_2.

Method of Adsorption. One or 2 g of the adsorbent were added to 50 or 200 ml of an amino solution of 400 or 200 mg dm^{-3}, and then the mixture was continuously shaken for 3 h at 30 °C using a shaker. Prior to the adsorption, the TiO_2 and Al_2O_3 were ground so as to pass through a 150-mesh sieve and then fabricated to granules of a 14—20 mesh size under a pressure of 40 MPa. The solutions were buffured at pH 7.3 by using KH_2PO_4 and Na_2HPO_4. To ascertain the effect of pH, KH_2PO_4/Na_2HPO_4 ratio was adjusted to give the solution pH values of 5.2 and 8.3. On the other hand, to find the effect of the phosphate-ion concentration on the adsorption, its concentration was adjusted to 0.025, 0.050, and 0.083 mol dm^{-3}. The adsorption isotherm was determined in deionized water, since phosphate ions affected the adsorption of amino acid.

Analysis. The analysis of the amino acids was carried out by using a Total Carbon Detector (Toshiba-Beckmann Co., Type 915) or the ninhydrin method.[10]

Results and Discussion

Comparisons of Adsorptive Activities of Adsorbents for Amino Acids. The results obtained for the adsorption of various types of α-amino acid are listed in Table 1. The adsorptive activities of other metal oxides, such as ZrO_2, MgO, and SiO_2, were also examined, but their activities appeared to be considerably less than that of TiO_2.

As is shown in Table 1, TiO_2 exhibited the highest activity for the adsorption of all the basic amino acids except L-tryptophan. Its activity for the neutral or acidic α-amino acids was far less than those of activated carbons. The high activities of TiO_2 in the adsorption of L-lysine·HCl and L-ornithine·HCl may be due to the high degree of hydrolysis of these salts in solution.

Effects of Phosphate Ion and pH on Adsorption. A

Table 1. Effect of acid-base property of amino acid on adsorption

Adsorbate	Degree of adsorption/%[a]			
			Activated carbon	
	Al_2O_3[b]	S-1[b]	MU-LE	MU-L
Neutral				
Glysine	18.5	22.9	24.4	23.3
L-Alanine	22.2	21.5	25.0	16.5
L-Valine	12.9	16.9	50.6	46.0
α-Amino-isobutyric acid	0	0	18.1	15.8
DL-Leucine	0	0	84.1	79.5
L-Isoleucine	20.6	0	81.6	84.8
Acidic				
DL-Glutamic acid	0	0	20.8	22.6
DL-Aspartic acid	0	0	18.1	12.2
Basic				
L-Lysine	12.0	83.4	20.5	15.1
L-Arginine	1.8	72.6	73.5	71.1
L-Histidine	8.6	86.2	92.2	94.3
L-Tryptophan	7.8	18.1	100	99.5
Salt				
L-Lysine·HCl	1.1	73.4	24.9	20.7
L-Citrulline·HCl	0	11.9	83.9	80.4
L-Ornithine·HCl	15.3	87.1	26.1	14.2

a) Adsorption temperature: 30 °C; time: 3 h; initial concentration of amino acid: 400 mg/l; phosphate buffer: pH 7.3 (0.033 mol/l). b) Heat-treated at 150 °C for 3 h immediately before use.

considerable change in the pH of the solutions was observed during the course of adsorption. The adsorption experiments in phosphate buffer solutions were carried out at pH values close to that of the blood. However, since the phosphate ion is adsorbed on TiO_2,[11] the effect of the phosphate ion on the adsorption of amino acid was examined, together with the effect of the pH of the solutions. L-Lysine was selected as representative of aliphatic and basic α-amino acids because of the ease of analyzing.

As is shown in Fig. 1, both the rate of adsorption and the amount of L-lysine adsorbed at the equilibrium were reduced by the presence of the phosphate ion. In

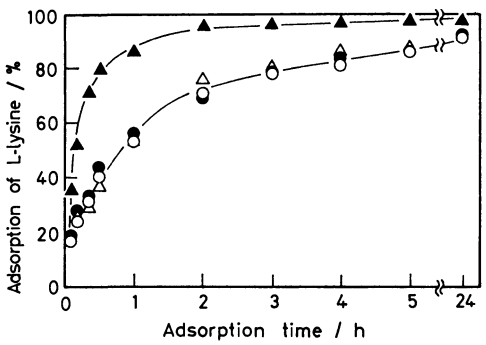

Fig. 1. Effect of pH on adsorption.
L-Lysine (20 mg) and S-1 (2 g) were added to 50 ml of the solntions buffered at pH 5.2 (○), 7.3 (●), and 8.3 (△). ▲ Denotes the result of the adsorption carried out in deionized water.

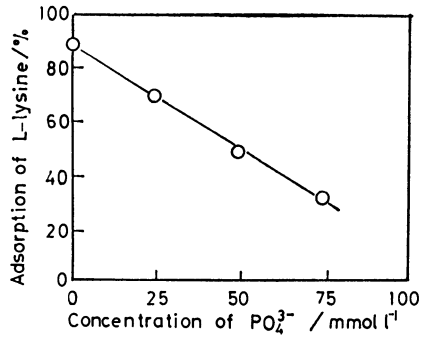

Fig. 2. Effect of concentration of phosphate ion on adsorption. S-1 (1 g) was added to 50 ml of the solution buffered at pH 7.3, and the adsorption was carried out 5 h. Other conditions were the same as those in Fig. 1.

the absence of the phosphate ion, the pH of the solution dropped from the initial value of 9.7 to 7.4 after 24 h. However, the effect of the pH on the adsorption of the amino acid was slight in the pH range of 5.2—8.3 when the concentration of phosphate ion was kept constant. The amount of L-lysine adsorbed at the equilibrium decreased linearly with the increase in the phosphate concentration as is shown in Fig. 2. This fact suggests that the α-amino acid and the phosphate would be adsorbed on identical sites. Thus, it appeared that the adsorption of the α-amino acids proceeded in competition with the phosphate ion. However, a preferential adsorption of the amino acid on TiO_2 was observed at higher phosphate concentrations (0.0033 mol dm^{-3}) and at dilute amino acid concentrations (0.0027 mol dm^{-3}).

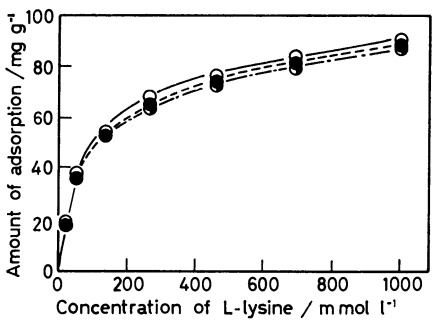

Fig. 3. Adsorption isotherm of L-lysine in deionized water. Adsorption were carried out for 70 h at 10 °C (○), 30 °C (●), and 50 °C (◑). Other conditions were the same as those Fig. 2.

Adsorption Isotherms in Deionized Water. Figure 3 shows the adsorption of L-lysine at 10, 30, and 50 °C. The effect of the temperature on the adsorption was slight. As is shown in Fig. 4, a linear relation was obtained between the logarithm of the equilibrium constant of adsorption, K_c, and $1/T$. Here, the equilibrium constant was calculated by dividing the amount of the amino acid adsorbed by that in the solution at the equilibrium (*i.e.*, about 1000 mg dm^{-3}). At this concentration, the surface of TiO_2 appeared to be saturated almost completely with the amino acid at

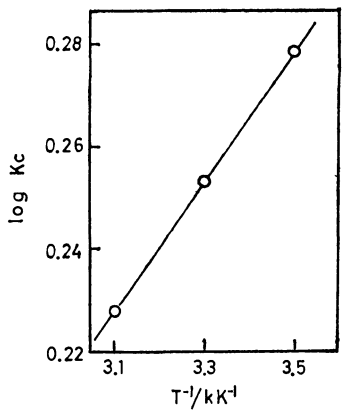

Fig. 4. Linear relationship between $1/T$ and log K_c.
K_c denotes the equilibrium constant of adsorption of L-lysine.

these temperatures. The heat of adsorption, H_a, was calculated to be 2257 J/mol by using the van't Hoff equation; this value indicates a weak interaction of the amino acid with the TiO_2 surface.

The linear relation between the concentration of L-lysine and the value of the concentration divided by the amount of adsorption at the equilibrium (Fig. 5) indicates that the Langmuir adsorption equation is applicable. The values of the monomolecular adsorption, V_m, were calculated to be 0.70 (at 10 °C), 0.67 (at 30 °C), and 0.65 (at 50 °C) mmol/g from the reciprocal of the slope, namely, $\Delta C/\Delta(C/V)$, shown in Fig. 5.

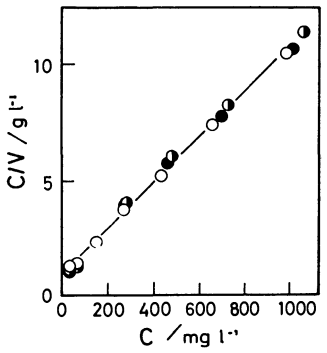

Fig. 5. Application of Langmuir equation to the adsorption shown in Fig. 3.

Effects of Heat-treatment Temperature of TiO_2 and the Amount of Surface OH Groups on the Adsorptive Activity. Figure 6 shows the effects of the heat-treatment temperature of S-1 and S-2 on the adsorption of L-lysine. The adsorptive activity of S-1 showed a maximum at 150 °C, which is close to the dehydration temperature (160 °C) of titanium hydroxide or $TiO_2 \cdot H_2O$.[12] Almost all the adsorptive activity was lost upon heat-treatment at 700 °C, which is the temperature of the conversion from anatase to rutile.[12]

The adsorptive activity of S-2, which contains sulfate ions, also decreased with the increase in the heat-treatment temperature. However, the adsorptive activity of S-2 was less than that of S-1, and it was lost

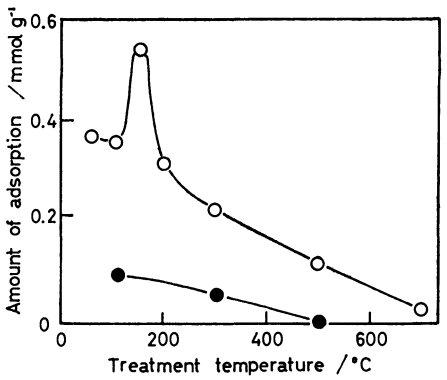

Fig. 6. Effect of heat-treatment temperature of TiO_2 on adsorption.
One gram of S-1 (○) or S-2 (●) was added to 50 ml of the buffered solution containing 2000 mg of L-lysine per litter, and the adsorption were carried out for 50 h at 30 °C.

upon heat-treatment at 500 °C. Since it has been established that TiO_2 containing sulfate ions has acid sites,[13] the adsorptive activity of TiO_2 toward α-amino acid is not related merely to the surface acidity. If the sulfate ions in TiO_2 diffuse to the surface at higher temperature and are lost as SO_3 at about 600 °C,[14] the surface of S-2 treated at temperatures near 600 °C may be covered by sulfate ions, which are then decomposed to SO_3 at slightly higher temperatures (about 600 °C). These sulfate ions on the TiO_2 surface possibly depress the adsorptive ability due to Ti^{4+} ions, O^{2-} ions, and/or OH groups on the surface, resulting in the observed decrease in the adsorptive activity. Since it is known that the Brönsted acid sites due to OH groups on the TiO_2 surface are able to interact with NH_3 and pyridine,[15] the OH groups may react also with amino acids through the interaction with lone-pair electrons of the N atom. The amount of surface OH groups was determined, therefore, to find the correlation between OH and the adsorptive activity.

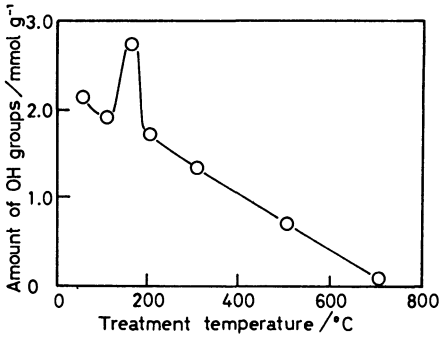

Fig. 7. Effect of heat-treatment temperature of TiO_2 on the amount of surface OH groups.

Figure 7 shows that the amount of surface OH groups was at its maximum when the sample was heat-treated at 150 °C, as was the activity of adsorption (Fig. 6). The linear relation between the amount of adsorption and the amount of surface OH groups shown in Fig. 8 indicates that the adsorptive activity of TiO_2 is largely dependent on the amount of surface OH

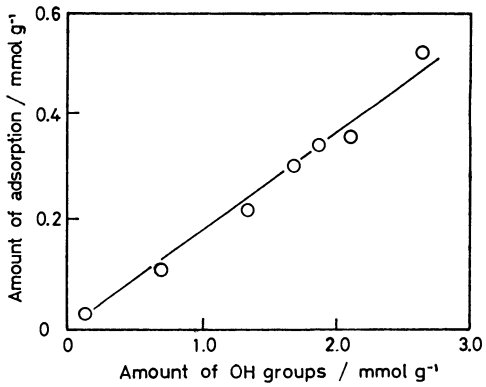

Fig. 8. Amount of L-lysine adsorbed *vs.* amount of surface OH groups for S-1.

groups. The amount of monomolecular adsorption of amino acid on TiO_2 was calculated as 0.65—0.70 mmol/g TiO_2 in the preceding section. This value almost coincides with the amount of surface OH groups on TiO_2 treated at 500 °C; the amount is shown to be 0.72 mmol/g TiO_2 in Fig. 7. This fact further supports the view that the adsorptive activity depends on the surface OH groups.

According to Kobayashi *et al.*,[11] TiO_2 heat-treated at 160 °C showed a maximum activity for the adsorption of phosphate ions. This temperature (160 °C) almost coincides with that at which the amount of OH was at its maximum, suggesting that the phosphate ions also may be adsorbed on the surface OH groups. The suppression of the adsorption of L-lysine by phosphate ions is possibly due to the competition between the phosphate ions and the amino acid for the interaction with surface OH groups.

Table 2. Comparison of adsorptions of various amino acids

Adsorbate	Degree of adsorption/%[a]			
	Al_2O_3[b]	S-1[b]	Activated carbon	
			MU-LE	MU-L
α-Aminoisobutyric acid	1.4	10.9	21.8	22.9
DL-α-Aminobutyric acid	0	15.7	32.1	33.2
γ-Aminobutyric acid	8.7	38.2	26.8	29.1
L-Lysil-L-lysine·2HCl	5.3	7.9	45.3	47.9

a) The adsorptions were carried out in deionized water. Adsorption temperature: 30 °C; time: 5 h; initial concentration of amino acid: 400 mg/l. b) Heat-treated at 150°C for 3h immediately before use.

Effect of Structure of Amino Acid on the Adsorption. In order to obtain some structural interpretation of the adsorption, the adsorption of three kinds of amino butyric acid were carried out under the same conditions. Table 2 shows the results, including also those of the dimer of L-lysine. γ-Amino acid is preferably adsorbed over α-amino acid, indicating that the end position is more favored for the interaction than is the α-position. The difference in the activity for the interaction between the α and γ position may be ascribed, at least in part, to steric factors. Also, the fact that the iso-type isomer and the dimer were adsorbed by less butyric acid than normal would seem to support this explanation.

Table 3. Acid-base parameters of some basic amino acids in an aqueous solution[16]

Amino acid	pK_{a1}	pK_{a2}	pK_{a3}	pH_I
Lysine	2.18	8.95 (α-Amino)	10.53 (ε-Amino)	9.74
Arginine	2.17	9.04 (α-Amino)	12.48 (Guanigino)	10.76
Histidine	1.82	6.00 (Imidazol)	9.17	7.58
Tryptophane	2.38	9.39		5.88

Behavior of Lysine on the TiO_2 Surface. In aqueous solutions, most amino acid molecules take one of these forms, NH_3^+RCOOH, $NH_3^+RCOO^-$, or NH_2RCOO^-, depending on the pH of the solution. The dissociation constants of the carboxyl group (pK_{a1}) and amino groups (pK_{a2}, pK_{a3}) in various basic amino acids listed in Table 3, together with the isoelectric points (pH_I). The pH_I values show that lysine and arginine should exist as cations in the pH range (5.2—8.3) of this study. For example, lysine should exist in the form of R^+, as is shown below.

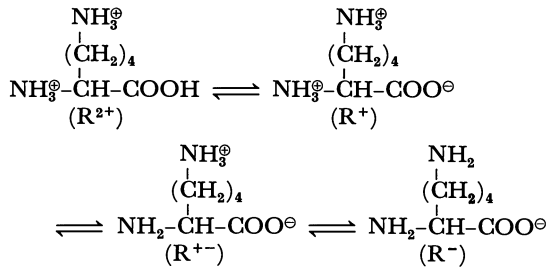

As is generally known, basic amino acids, which exist as cations in a neutral solutions, are selectively adsorbed by weakly acidic ion-exchange resins.[17] Accordingly, TiO_2 may show a high adsorptive activity for lysine and arginine, for the surface OH groups on TiO_2 show weak Brönsted acidity.[5] On the other hand, Al_2O_3, which has only Lewis acidity,[18] did not show a high adsorptive activity for the basic amino acids.

The fact that γ-aminobutyric acid was preferably adsorbed over a α-type isomer (Table 2) suggests that the activity of ω-NH_3^+ is higher than that of α-NH_3^+. Thus, the adsorption of lysine on TiO_2 is considered to proceed as follows:

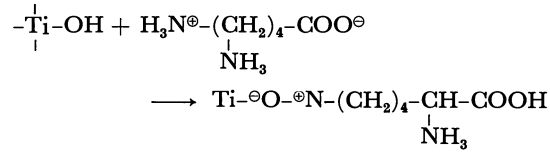

The authors wish to thank the Tokyo Laboratory of the Kureha Chemical Co. for the supply and analysis of some amino acids; they are also grateful to Mr. Atsumu Nishimura for helpful discussions of the experimental results.

References

1) K. Sanjo *et al.*, *Jinko Jinzo*, **5**, 231 (1976).
2) T. Ito, *J. Agric. Chem. Soc.*, **12**, 204 (1936).
3) K. Wunderly, *Helv. Chim. Acta*, **17**, 523 (1934).
4) V. H. Cheldelin and R. J. Williams, *J. Am. Chem. Soc.*, **64**, 1513 (1942).
5) S. Okazaki, "Kinzoku-sankabutsu To Fukugo-sankabutsu," ed by K. Tanabe, T. Seiyama, and K. Fueki, Kodansha, Tokyo (1978), p. 102.
6) S. Okazaki, *Kagakukogyo*, **22**, 56 (1978).
7) V. V. Pekrek, *Talanta*, **19**, 219 (1972); C. H. Wirguin and A. A. Yaron, *J. Appl. Chem.*, **15**, 445 (1965).
8) N. J. Keen, *Chem. Ind.*, **1977**, 579; N. Ogata, *Nippon Kaisui Gakkaishi*, **30**, 3 (1976).
9) H. P. Boehm, *Angew. Chem.*, **78**, 617 (1966).
10) N. Takahashi, "Seikagaku Jikken Koza," ed by Nippon Seikagakukai, Tokyokagakudojin, Tokyo (1978), Vol 1 (II), p. 69.
11) E. Kobayashi, M. Sugai, and M. Higuchi, *Nippon Kagaku Kaishi*, **1979**, 39.
12) J. Barksdale, "Titanium, Its Occurence, Chemistry, and Technology," The Ronald Press. Co., New York (1966), p. 71.
13) A. Kurosaki and S. Okazaki, *Nippon Kagaku Kaishi*, **1976**, 1816; K. Morishige, H. Hattori, and K. Tanabe, *Bull. Chem. Soc. Jpn.*, **48**, 3088 (1975).
14) T. Chinone and S. Okazaki, *Nippon Kagaku Kaishi*, **1978**, 1327.
15) G. D. Parfitt, J. Rambotham, and C. H. Rochester, *Trans. Faraday Soc.*, **67**, 841 (1971); **67**, 1500 (1971).
16) H. R. Mahler and E. H. Cordes, translated by F. Egami *et al.*, "Basic Biological Chemistry," Tokyokakudojin, Tokyo (1973), p. 43.
17) K. Satake, "Tanpakushitsu," Asakurashoten, Tokyo (1975), p. 25.
18) H. Pines and W. O. Haag, *J. Am. Chem. Soc.*, **82**, 2471 (1960); E. P. Parry, *J. Catal.*, **2**, 371 (1963).

The Equilibrium and the Vibrational Spectra of the *t*-Butylamine-Chloroform System

Isao KANESAKA,* Mitsue IZUMI, Misaki MITSUISHI, and Kiyoyasu KAWAI
Faculty of Science, Toyama University, Gofuku, Toyama 930
(Received June 17, 1980)

The thermodynamic constants, $\Delta H°$ and $\Delta S°$, of the *t*-butylamine (TBA)–chloroform-*d* system in carbon tetrachloride are obtained from the analysis of the Raman intensities observed in the C–D stretching region of chloroform-*d*, while the $\Delta H°$ on the associated species of $TBA \cdot CDCl_3$ and $(TBA)_2 \cdot CDCl_3$ are evaluated to be −14.2 and −22.6 kJ/mol respectively. The IR or Raman spectrum of a solid sample, adjusted by the rapid cooling of a gaseous or liquid one respectively, with the TBA: chloroform ratio of ≈1 is compared with that of TBA in the gaseous, liquid, or solid state; it is confirmed, on the basis of the assignments of the observed frequencies, that the solid sample consists almost entirely of the associated species of $TBA \cdot CHCl_3$. Only one associated species of $(TBA)_2 \cdot CHCl_3$ is also obtained by the crystallization of the gaseous sample with the molar ratio of 2.0. The NH_2 group vibrations in $TBA \cdot CHCl_3$ or $(TBA)_2 \cdot CHCl_3$ are related intimately in their frequencies and band shapes to those in gaseous or solid TBA respectively.

t-Butylamine (TBA) associates itself[1] and forms a weak hydrogen bond with chloroform. On account of those properties of TBA, we are interested in the thermodynamic properties of the present system. Here, we try to evaluate the thermodynamic constants, $\Delta H°$ and $\Delta S°$, by means of an analysis of the Raman intensities of the C–D stretching region of the system, using carbon tetrachloride as a solvent; hereafter, we will denote an associated species $(TBA)_m \cdot (CHCl_3)_n$ as a m : n species.

There are many studies of the vibrational spectra of self-associated species in the solid state by using the matrix-isolation technique, but no spectrum of a solid composed of two kinds of molecules capable of the formation of a weak hydrogen bond has yet been reported, as far as we know. We report here, on the basis of assignments of the vibrational spectra, that the solid sample made by the rapid cooling of a liquid or gaseous sample with a TBA : chloroform ratio of ≈1 or ≈2 consists almost entirely of the 1 : 1 or 2 : 1 species respectively. Although partial information on the structure or the bonding of associated species is obtained from the vibrational spectra of an equilibrium system in the liquid state, it is, of course, apparent that more definite information is obtained from those of a solid consisting of the associated species.

We here assign the IR and Raman spectra of the 1 : 1 species and the IR spectrum of the 2 : 1 species, by referring to those of the related compounds $(CX_3)_3CY$, where X refers to H or D, and Y to OH,[2] CN,[3] or halogen,[4-6] and compare the NH_2 group vibrations of the two species with those of gaseous or solid TBA.

Experimental

TBA or carbon tetrachloride was purified by distillation after drying with anhydrous calcium oxide or calcium chloride respectively. Chloroform was also purified by distillation after removing the ethanol, while commercially obtained chloroform-*d* was used as it was. The liquid Raman samples were adjusted *in vacuo*, so the molarity was determined by assuming that $n=PV/RT$ and by the volumetry of a liquid sample adjusted at 233 K by Hg; the molarities of TBA and chloroform-*d* in the carbon tetrachloride solution were, respectively, for three samples: (i) 3.72 and 1.93, (ii) 2.87 and 2.73, and (iii) 1.99 and 3.83. The Raman spectra were observed in the range from 223 to 244 K by adjusting them within±0.5 K by the use of ethanol and liquid nitrogen.

The solid IR sample was obtained by the deposit of a gaseous sample with a molar ratio of $R=P_{TBA}/P_{CHCl_3}$ on a KRS-5 plate cooled at 77 K in a cryostat; the spectrum was then observed without any annealing. The solid Raman sample was obtained by the rapid cooling of a liquid sample with an adequate *R*, and the Raman spectrum was observed at 113±2 K. The IR or Raman spectrum of solid TBA was also observed in the same way.

The IR spectrum was observed by using a JASCO-IRA spectrometer in the range of 4000—330 cm^{-1}, and the Raman one, by using a JASCO-R800 spectrometer and a 514.5 nm line of the Ar^+ ion laser with the power of 200 mW. The observed frequencies were calibrated by those of a polystyrene film or indene for the IR or Raman spectrum respectively; they are believed to be accurate within±2 cm^{-1}.

The Equilibrium of the TBA-Chloroform-*d* System in Carbon Tetrachloride

The polarized Raman spectrum of the C–D stretching region of Sample (i) at 223 K is given in Fig. 1, together with the one analyzed by two Foight functions[7,8] by means of the least-squares method. The higher and lower frequency components in Fig. 1 are assinged to the C–D stretching mode of the $CDCl_3$ monomer (hereafter,

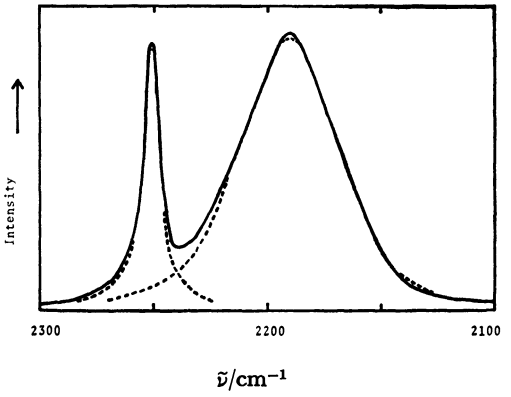

Fig. 1. The observed Raman spectrum (solid line) of the C–D stretching region of Sample (i) at 223 K. Two Foight functions analyzed are given by the broken lines.

$CDCl_3$) and the associated species respectively. The peak shift $\Delta\nu_{C-D}$ obtained from the analyzed band origins is 61.5—57.0 cm^{-1} in the order of the increase in temperature for Sample (ii). The observed relative intensity, $I_{R,O}$, is defined by S_{mn}/S_M, where S_{mn} and S_M are the band areas obtained from the parameters of the Foight functions for the associated species and $CDCl_3$ respectively; it is summarized in Table 1, where $I_{R,O}$ is found to be distributed over the sufficiently wide region of 5.69—0.73.

Under the assumption that some associated species give the lower frequency band, we analyze $I_{R,O}$ as follows: The equilibrium constant is defined by:

$$K_{mn} = \frac{C_{mn}}{C_t^m C_M^n}, \quad (1)$$

where C_t, C_M, and C_{mn} are the molarities of TBA, $CDCl_3$, and the m : n species respectively in the equilibrium state. K_{mn} relates to $\Delta H°$ and $\Delta S°$ as follows:

$$\ln K_{nm} = -\Delta H°_{mn}/RT + \Delta S°_{mn}/R. \quad (2)$$

The molarity of each species in the equilibrium state in the presence of some associated species is determined by using an iterative Newton method.[9] The calculated relative intensity, $I_{R,C}$, is defined by:

$$I_{R,C} = \sum \beta_{mn} C_{mn}/C_M, \quad (3)$$

where β_{mn} is the intensity ratio of each m : n species to $CDCl_3$, and the summation is carried out for all the associated species with chloroform.

The values of $\Delta H°$, $\Delta S°$, and β are adjusted by the least-squares method on the assumption that these parameters are constant in the range of temperature and concentration used here. The results obtained by taking K_{11} and K_{21} into consideration are given in Table 1. If only K_{11} is used, $I_{R,C}$ disagrees as a whole with $I_{R,O}$. The results obtained using K_{11}, K_{21}, and K_{20} are not better than those in Table 1. The NH_2 proton chemical shift of TBA[1] in cyclohexane at 24.5 °C has been analyzed by using only K_{30}, whose value is 2.3. An attempt to take K_{30} into consideration results, however, in less convergence. Since there should be small amounts of the species other than the 1 : 1 and 2 : 1 species under such high molarities of TBA and chloroform as are used here, the disagreement of about 5% found between $I_{R,O}$ and $I_{R,C}$ may, thus, be caused by not taking them into account.

Table 1. The observed and calculated relative intensities

Sample	T/K	$I_{R,O}$	$I_{R,C}$
(i)	244	3.72	3.56
	238	3.92	4.06
	233	4.47	4.47
	229	4.99	4.91
	223	5.69	5.62
(ii)	244	1.41	1.50
	238	1.52	1.62
	233	1.56	1.70
	229	1.66	1.79
	223	1.80	1.91
(iii)	244	0.73	0.69
	238	0.75	0.72
	233	0.78	0.75
	229	0.82	0.77
	223	0.85	0.80

Table 2. The values obtained for $\Delta H°$, $\Delta S°$, and β

$\Delta H°_{11}$	−14.2
$\Delta S°_{11}$	−58.5
$\Delta H°_{21}$	−22.6
$\Delta S°_{21}$	−90.3
β_{11}	1.78
β_{21}	0.62

$\Delta H°_{mn}$/kJ mol^{-1}, $\Delta S°_{mn}$/J K^{-1} mol^{-1}

The adjusted values for the parameters are given in Table 2, where $\Delta H°_{11}$ is −14.2 kJ/mol, larger than the −17.0[10] or −19[11] kJ/mol reported for the 1 : 1 species of triethylamine with chloroform. $\Delta\nu_{C-D}$ observed here is smaller than the 79 cm^{-1} [11] reported for the 1 : 1 species of triethylamine with chloroform. These facts reflect well the basicities of the two amines. $\Delta H°_{21}$ suggests that $\Delta H°_{20}$ is about −8.4 kJ/mol if the dimer has such an open-chain structure as is found in the 2 : 1 species to be shown later. The values of β indicate that the intensity of the C–D stretching in the 1 : 1 or 2 : 1 species is, respectively, stronger or weaker than that in $CDCl_3$. This means that the intensity depends on the spatial structures of the associated species; the C–D stretching frequencies of these species are nearly the same as those treated here.

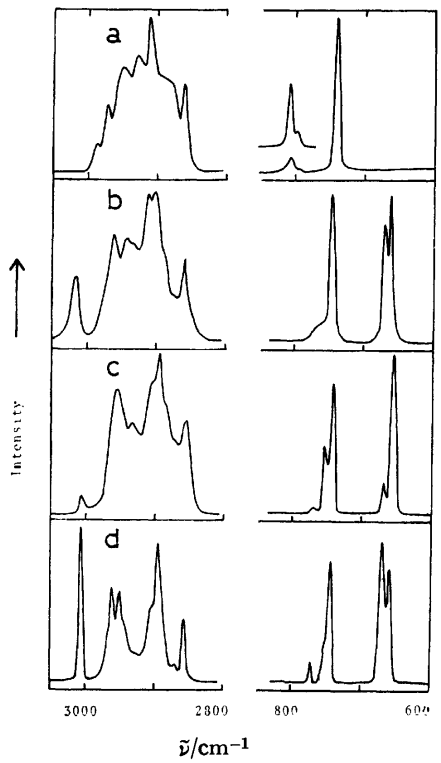

Fig. 2. The Raman spectra of the C–H and CCl_3 stretching regions of TBA and the TBA–chloroform system. (a) Gaseous TBA, (b) the liquid sample with R=0.66 at 212 K, (c) the solid sample with R=0.97 at 113 K, and (d) the solid sample with R=0.50 at 113 K.

The Vibrational Assignment of the 1 : 1 Species

The Confirmation of the 1 : 1 Species in $R \approx 1$. In Fig. 2 the Raman spectra of the C–H and CCl_3 stretching regions of the TBA–chloroform system in the solid and liquid states are compared with those of TBA in the gaseous state. By a comparison of Fig. 2-c (R=0.97) with 2-a (gas) or the spectrum of solid chloroform,[12-14] the weak bands at 3008 and 667 cm^{-1} in Fig. 2-c are assigned to the C–H stretching mode and the CCl_3 symmetric stretching mode of excess chloroform respectively (hereafter, H* denotes the hydrogen atom of chloroform), and the strong bands at 2895 and 657 cm^{-1}, to those of chloroform in the associated species. This assignment for excess chloroform is further confirmed by comparing the spectra in Fig. 2-c with those in Fig. 2-d (R=0.50), where the bands at 3005 and 669 cm^{-1} are relatively intensified. Similarly, by an examination of the Raman bands in the 1200—1280 cm^{-1} region, the two weak bands at 1211 and 1202 cm^{-1} observed for the sample with R=0.50 are assigned to the C–H* bending of excess chloroform, and the band near 1277 cm^{-1} observed for the samples with R=0.97 and 0.50, to that of chloroform in the associated species. The fact that bands due to excess chloroform are weak in the sample with R=0.97 is, thus, explained by the relation of $0.97TBA+CHCl_3 \rightarrow 0.97TBA \cdot CHCl_3 + 0.03CHCl_3$, with reference made also to the fact that there is no appearance of the bands characteristic of the 2 : 1 species, which will be discussed later. Thus, the solid sample with R=0.97 is found to consist mostly of the 1 : 1 species.

Most of the bands observed in the IR spectrum for the solid sample with R=1.03 are nearly consistent in their frequencies with those in the Raman spectrum with R=0.97, as is shown in Table 3, which indicates that the solid IR sample also consists mostly of the 1 : 1 species. Thus, the bands observed in both spectra for the solid samples with $R \approx 1$ are to be assigned on the basis of the 1 : 1 species, except for several weak ones regarded as other species.

The Band Due to Chloroform. From the assignment of the bands due to chloroform described above and given in Table 3, it is found that the C–H* stretching mode shifts to frequencies lower by 113 cm^{-1} than that of the isolated molecule, and the C–H* bending mode to ones higher by about 70 cm^{-1}, while, of the vibrations of the CCl_3 group, only the CCl_3 symmetric stretching mode shifts lower by about 10 cm^{-1}. These shifts can be explained reasonably by the interaction of chloroform with TBA through the hydrogen atom of the former with the nitrogen atom of the latter. Of the degenerate vibrations of chloroform in the 1 : 1 species, only the C–H* bending splits into two bands, whose separation is 13 cm^{-1}. On the other hand, the observed site splittings of excess chloroform in R=0.50 are nearly the same as the respective ones of solid chloroform.[12,13]

The Bands Due to the NH_2 Group. If chloroform interacts with TBA in the way described above, one can expect that the spectral features on TBA in the 1 : 1 species will differ from those on solid TBA, especial-

TABLE 3. THE OBSERVED FREQUENCIES ($\tilde{\nu}$/cm^{-1}) AND THEIR ASSIGNMENTS OF THE 1 : 1 SPECIES

Raman (R=0.97)	IR (R=1.03)	Assign.
3351 m	3358 w	NH_2 sym. str.
	3326 vw	D
3287 s		NH_2 sym. str.
	3244 w	D
	3168 w	D
3008 w		C–H* str.[a]
2955 vs	2955 s	CH_3 asym. str., 2 E
2936 m	2937 sh	CH_3 asym. str., A_1
2905 sh		CH_3 sym. str., A_1
2895 vs	2898 s	C–H* str.
2880 sh 2865 sh	2866 m	CH_3 sym. str., E
2854 s		1447×2=2894
2771 m		1392+1371=2763
2704 m		1392+1323=2715
	2510 m	1271×2=2542
1589 w	1585 s	NH_2 bend.
	1563 m	1245+320=1565
1472 w	1470 s	CH_3 asym. bend., E
1460 m	1460 m	CH_3 asym. bend., E
1451 w		CH_3 asym. bend., A_2
1447 m		CH_3 asym. bend., A_1
	1392 m	CH_3 sym. bend., A_1
	1371 s 1366 s	CH_3 sym. bend., E
1323 m	1318 m	C–N str.
1292 w		945+345=1290
1277 m	1284 m 1271 m	C–H* bend.
1248 m 1222 m	1245 s 1221 s	CC_3 asym. str., E
1203 sh		C–H* bend.[a]
	1127 w	D
1112 w	1110 w-m	NH_2 twis.
1043 w	1040 s	CH_3 asym. rock., E
999 w	1000 w	CH_3 asym. rock., A_2
	964 w	D
945 m	946 s	CH_3 sym. rock., A_1
927 m 915 m	918 w	CH_3 sym. rock., E
902 w		458×2=916
893 m	894 vs	NH_2 wag.
	873 sh	D
776 vw		CCl_3 asym. str.[a]
755 w	754 vs	CCl_3 asym. str.
744 s		CC_3 sym. str., A_1
667 w		CCl_3 sym. str.[a]
657 vs	662 s	CCl_3 sym. str.
	482 b,w	D
458 m	459 s	CCN bend., E
	410 b,w	D
366 s	369 s	CCl_3 sym. bend.
345 m	346 w	CC_3 asym. bend., E
320 w		NH_2 tors.
261 s		CCl_3 asym. bend.
114 w		
85 sh		
65 s		N···H str.
52 sh		
33 w		

a) Excess chloroform.

ly in the regions characteristic of the NH_2 group. The strong and medium Raman bands at 3287 and 3351 cm^{-1} are assigned to the NH_2 symmetric and asymmetric stretching modes respectively. They are the frequencies characteristic of the non-hydrogen bonded NH_2 group and are in a frequency region lower by 28 cm^{-1} than those of gaseous TBA.

The weak Raman band at 1589 cm^{-1} and the medium one at 893 cm^{-1} have their IR counterparts at 1589 and 894 cm^{-1} respectively; the former is assigned to the NH_2 bending mode, and the latter, to the wagging mode. In Fig. 2-a, the band at 811 cm^{-1}, which is a highly polarized one without any rotational structures,[15] is assigned to the NH_2 wagging mode, and the weak one at 799 cm^{-1}, to a combination band, 345+458=803 cm^{-1}. The weak Raman band at 1112 cm^{-1} in Table 3, whose IR counterpart is at 1110 cm^{-1}, is probably to be assigned to the NH_2 twisting mode rather than to be regarded as a combination band, because this band is considerably influenced by circumstances; it shifts to higher frequencies in solid TBA or the 2 : 1 species, as is shown in Table 4, though the NH_2 twisting mode of methylamine[16] or hydroxylamine[17] has been estimated from *ab initio* calculations to be about 1250 cm^{-1}. The NH_2 torsion of gaseous TBA has been assigned to the strong IR band at 245 cm^{-1}.[18] For the 1 : 1 species, there is no Raman band in this region, but a weak one at 320 cm^{-1}, which is not attributable to any of the skeletal bending modes. We assign this band to the NH_2 torsion of the 1 : 1 species. The NH_2-group frequencies thus assigned to the 1 : 1 species are summarized in Table 4, along with those for TBA and the 2 : 1 species.

Table 4. The vibrational frequencies ($\bar{\nu}$/cm^{-1}) observed for the NH_2 group of TBA in several states

	Gas		1:1 Species		Solid		2 : 1 Species
	IR	Raman	IR	Raman	IR	Raman	IR
Stretching		3379	3358	3351	3333	3333	3328
	3319	3315		3287	3253	3249	3248
					3165	3163	3168
Bending	1624	1629	1585	1589	1612	1608	1609
					1602		1584
Twisting	1111	1106	1110	1112	1127	1131	1130
							1109
Wagging	814	811	894	893	966	964	963
					894	894	877
Torsion	245[a]			320	480	482	498
					404	404	415
					396		
					339		

a) From Ref. 18.

The Bands Due to CH_3 Groups. By referring to the theoretical[19,20] and experimental[2,3] studies of the P-R separation, some typical bands observed with P-R separations of about 23 and 20 cm^{-1} for TBA can be regarded as the parallel and perpendicular ones respectively. These separations indicate that TBA has a slightly asymmetric oblate top, as would be expected for this molecule.

The vibrational modes of the methyl groups of the 1 : 1 species can be approximately interpreted as referring to the normal modes of such molecules with three methyl groups as trimethylacetonitrile[3] or $[(CH_3)_3AlCl]^-$.[21]

The medium band at 2936 cm^{-1} (Fig. 2-c) corresponds to the medium band at 2945 cm^{-1} (Fig. 2-b), which is a polarized band, and the very strong band at 2955 cm^{-1} (Fig. 2-c) splits into two sharp bands, at 2961 and 2951 cm^{-1} (Fig. 2-d). The former is assigned to the CH_3 asymmetric stretching mode (A_1), and the latter, to the CH_3 asymmetric stretching modes (E) accidentally degenerated from two more bands. There is no Raman band in the CH_3 symmetric bending region of the 1 : 1 species, but there are three IR bands whose spectral features correspond well to those of the IR-nitrogen-matrix spectrum of *t*-butyl alcohol.[2] The assignment of the bands due to the CH_3 rocking can be confirmed by examining the spectra for gaseous TBA in Fig. 3, where the IR or Raman band at 941 cm^{-1}

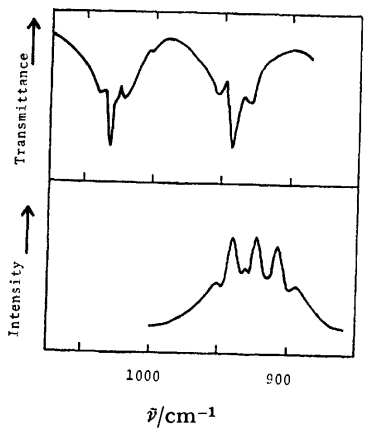

Fig. 3. The IR (upper) and Raman (lower) spectra of the CH_3 rocking region of gaseous TBA.

has a parallel-type envelope or a sharp Q branch respectively and is assigned to the symmetric rocking mode (A_1). This assignment correlates well with that in *t*-butyl alcohol[2] or trimethylacetonitrile,[3] but not to that in *t*-butyl chloride.[4] The A_1 mode of *t*-butyl chloride has been assigned to the band at 1155 cm^{-1} on the basis of the normal coordinate analysis; it is noticeably higher than those of the three related compounds. This fact may be explained in terms of the vibrational coupling between the CH_3-rocking and the C-X-stretching mode (X=Cl, NH_2, OH, or CN).

The Band Due to the Skeleton of TBA and the Lattice Modes. The CC_3 symmetric stretching mode is assigned to the strong Raman band at 744 cm^{-1}, and the CC_3 asymmetric ones, to two medium Raman bands at 1222 and 1248 cm^{-1}. The C–N stretching mode is assigned to the Raman band at 1323 cm^{-1}, which is a polarized band in liquid TBA. These stretching frequencies correlate well with those in *t*-butyl alcohol[2] or trimethylacetonitrile,[3] but not with those in *t*-butyl chloride.[4] The CC_3 asymmetric deformation and CCN bending

vibrations are assigned to two medium Raman bands, at 345 and 458 cm^{-1} respectively, by comparing them with the IR or Raman bands in gaseous TBA; two bands with strong rotational structures[15] are observed at 351 and 450 cm^{-1} in the Raman spectrum, and also two band with a perpendicular-type envelope at 347 and 447 cm^{-1} in the IR one.

A weak Raman band is observed at 428 or 429 cm^{-1} in liquid or solid TBA respectively; it may be assigned to the CC_3 symmetric bending mode. However, we could observe no band in this region of either the IR or Raman spectrum in the 1 : 1 species.

There are five Raman bands in the region of lattice vibrations of the 1 : 1 species. The strong band at 65 cm^{-1} can reasonably be assigned to the hydrogen-bonded N···H stretching mode, because there is no band in that region of solid TBA and chloroform.[12,13] The IR bands denoted by D in Table 3 are attributably to the species with excess TBA.

The 2 : 1 Species

One can expect, by analogy with the previous section, that the solid sample with $R \approx 2$ consists mainly of the 2 : 1 species. The IR spectrum of the solid sample with $R=2.0$ is given for the stretching, wagging, and torsion regions of the NH_2 group in Fig. 4, in which the stretching region has nearly the same spectral features as those observed for solid TBA in Fig. 5. A sharp band at about 3330 cm^{-1} in Fig. 4 or 5 lies almost in the middle of the two NH_2 stretching frequencies of the 1 : 1 species; it is assigned to the non-hydrogen-bonded N–H stretching mode. The other two bands have band shapes characteristic of the hydrogen-bonded stretching modes. We assign them to the two components of the Fermi resonance of the hydrogen-bonded N–H stretching mode, with an overtone of the NH_2 bending mode, and propose that solid TBA has a polymeric chain structure consisting of bridged TBA, which has both hydrogen-bonded and non-hydrogen-bonded N–H groups, and that the 2 : 1 species has bridged and terminal TBA, b-TBA, and t-TBA, such as:

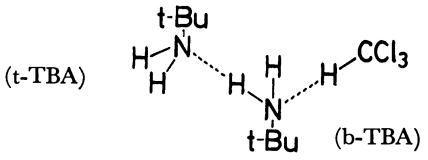

The IR bands due to the NH_2 stretching modes of t-TBA are still expected to be as weak as those of TBA in the gaseous state or the 1 : 1 species.

A strong band at 877 cm^{-1} is assigned to the NH_2 wagging mode, which is observed at 894 cm^{-1} for the 1 : 1 species. From this fact, it is concluded that this sample consists almost entirely of the 2 : 1 species as expected.

There are some bands characteristic of the 2 : 1 species, including the band mentioned above. Two bands, at 1609(b) and 1584(t), 1130(b) and 1109(t), or 963(b) and 877(t) cm^{-1}, are assigned to the bending, twisting or wagging modes respectively of the NH_2 groups, while the bands indicated by b in parentheses can be attributed to b-TBA, and those by t, to t-TBA, with reference to the bands observed for solid TBA or the 1 : 1 species. Of the two bands at 498 and 415 cm^{-1}, the former is assigned to the NH_2 torsion of b-TBA, while the latter may be a component of the Fermi resonance of the NH_2 torsion of b-TBA with the other mode, because this frequency is too high to be assigned to the NH_2 torsion of t-TBA as against 320 cm^{-1} in the 1 : 1 species. The two C–N stretching modes are at 1332 and 1316 cm^{-1}.

From the fact that the frequencies due to chloroform of the 2 : 1 species are nearly in accord with those of the 1 : 1 species, the basicity of an open-chain dimeric TBA is found to be almost equal to that of the monomeric one. The TBA in the present study is classified into non-bridged and bridged types. The wagging mode in non-bridged TBA shifts to the higher-frequency region in the order of gaseous TBA, the 2 : 1 species, and the 1 : 1 species; a similar shift can be expected for the torsion, though it is not observed for the 2 : 1 species. On the other hand, the NH_2-group frequencies of bridged-TBA of the 2 : 1 species correlate well with those of solid TBA.

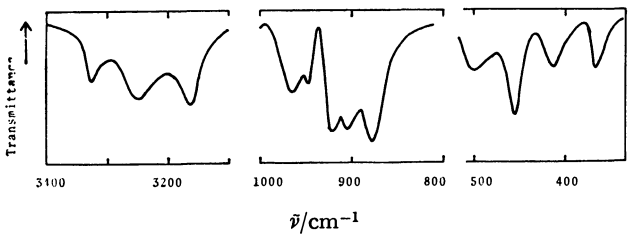

Fig. 4. The IR spectrum of the NH_2 stretching, wagging, and torsional regions of the solid sample with $R=2.0$ at 77 K.

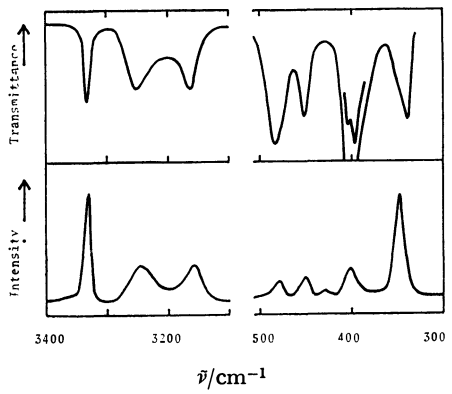

Fig. 5. The IR (upper) and Raman (lower) spectra of the NH_2 stretching and torsional regions of solid TBA at 77 and 113 K respectively.

References

1) J. C. Schug and W. M. Chang, *J. Phys. Chem.*, **75**, 938 (1971).

2) J. Korppi-Tommola, *Spectrochim. Acta, Part A*, **34**, 1077 (1978).

3) K. Kumar, *Spectrochim. Acta, Part A*, **28**, 459 (1972).

4) J. C. Evans and G. Y.-S. Lo, *J. Am. Chem. Soc.*, **88**, 2118 (1966).
5) C. Tanaka, *Nippon Kagaku Zasshi*, **83**, 398 (1962).
6) D. E. Mann, N. Acquista, and D. R. Lide, *J. Mol. Spectrosc.*, **2**, 575 (1958).
7) I. F. Kielkopf, *J. Opt. Soc. Am.*, **63**, 987 (1973).
8) K. Kanamori, M. Mihara, and K. Kawai, *Bull. Chem. Soc. Jpn.*, **52**, 2205 (1979).
9) H. Sugeta, private communication.
10) K. F. Wong and S. Ng, *J. Chem. Soc. Faraday Trans. 2.* **71**, 622 (1975).
11) F. L. Slejko, R. S. Drago, and D. G. Brown, *J. Am. Chem. Soc.*, **94**, 9210 (1972).
12) H. F. Shurvell, *J. Chem. Phys.*, **58**, 5807 (1973).
13) M. Ito, *J. Chem. Phys.*, **40**, 3128 (1964).
14) A. Kimoto and H. Yamada, *Bull. Chem. Soc. Jpn.*, **40**, 243 (1967).
15) G. Herzberg, "Infrared and Raman Spectra of Polyatomic Molecules," Van Nostrand, Princeton (1945).
16) P. Pulay and F. Torok, *J. Mol. Structure*, **29**, 239 (1975).
17) Y. Hamada, M. Tsuboi, and H. Umeyama, *Bull. Chem. Soc. Jpn.*, **53**, 48 (1980).
18) M. Tsuboi, A. Y. Hirakawa, and K. Tamagake, *Nippon Kagaku Zasshi*, **89**, 821 (1968).
19) T. Ueda and T. Shimanouchi, *J. Mol. Spectrosc.*, **28**, 350 (1968).
20) W. A. S. Paul and G. Dijkstra, *Spectrochim. Acta, Part A*, **23**, 2861 (1967).
21) I. Kanesaka, M. Shinoda, and K. Kawai, *Spectrochim. Acta, Part A*, **26**, 2345 (1970).

High Resolution Proton Nuclear Magnetic Resonance Studies of Solute Molecules in the Poly(vinylalcohol) Gel Medium

Shizuo FUJIWARA,† Ryo FUJIKURA, Takashi OGINO, Michiko TANAKA, and Yoji ARATA*

Department of Chemistry, Faculty of Science, The University of Tokyo, Hongo, Bunkyo-ku, Tokyo 113

(Received July 7, 1980)

It was shown that a pair of spectra is observed for each solute in the medium of poly(vinylalcohol) gels swollen in water. Each of the spectra was assigned as originating from the solute in the PVA gel itself and that in the bulk solution surrounding the gel. It was concluded that the chemical shift difference is primarily explained in terms of the difference in the volume susceptibility of the PVA gel and the bulk solution. It was observed in the case of nicotinamide adenine dinucleotide (NAD) that the chemical shift differences are different for different functional groups. We suggest that this observation reflects a contribution from intermolecular interaction between PVA gel and the NAD molecule.

In a previous work from this laboratory we have shown that in poly(vinylalcohol) (PVA) gels rotational diffusion of nitroxide radicals is strongly dependent upon the pore size of the gels.[1] In order to characterize in detail the PVA gel as a medium we have measured ^{1}H NMR spectra of a various kinds of solute molecules. The present paper reports an analysis of ^{1}H NMR spectra which are given by solute molecules in the PVA gels. Interactions between solute molecules and the PVA gel will briefly be described using nicotinamide adenine dinucleotide (NAD) which is flexible in shape and is expected to exhibit a pH dependent interaction with the PVA gel.

Experimental

PVA Gels. When an aqueous solution of PVA is irradiated with γ-rays at sufficient dose, the polymer molecules interlink each other, and insoluble gels are formed. It is known that a degradation process rather than cross-linking occurs predominantly when PVA solution is subject to ionizing radiation. When it is irradiated in the presence of water, however, a cross-linking type of reaction occurs, and a gel is formed in the following manner.[2] Upon γ-ray irradiation, water molecules are turned into free radicals, which react with the protons of PVA. This reaction occurs above the critical concentration; the gel formation does not occur below the critical concentration even upon prolongated irradiation. The critical concentration is approximately 0.36 g/100 ml for PVA with an initial degree of polymerization of 1740.[2] The gel prepared by a total dose of irradiation below 1×10^6 rads was like a paste. When the total dose was above that level, a rubber-like substance was formed; the gels formed with higher doses of irradiation were of higher density and more elastic. The gels sometimes contain small bubbles, which are mainly H_2 gas developed during the gel formation. The gel was usually colorless, sometimes pale yellow. It is chemically stable. It is stable even when it is heated with boiled water in an autoclave at 150 °C for one hour, and retains its original shape on boiling in 0.1 M HCl solution or in 0.1 M NaOH solution at 100 °C for 3 h.[2] When it was dried, it shrinked remarkably and turned into a hard colorless or pale yellow substance. When the dried gel is immersed in water, it is swollen back and the original color and shape were restored. However, the color was changed into yellow or light brown when it was swollen in alkaline solution (pH>11) or in DMSO. In the gel form, the size of the average diameter of the holes in the network can be calculated using

$$\langle l \rangle = 2.5 \times \left(\frac{5.1 \times 10^8 \pm 1.37 \times 10^8 \times C}{R} \right),$$

where R is the amount of the total dose in Rads and C is the concentration of PVA (g/100 ml).[2] It should be noted that the diameter is represented by a distribution function and that $\langle l \rangle$ does not represent any definite size of the hole. It should rather be, therefore, regarded as only one of the variables which describe the density of the gel. We also defined C_{GEL}, which is the gel concentration

$$C_{GEL} = \frac{w_{DRY}}{w_{ORIG}},$$

where W_{ORIG} is the weight of the original gel and W_{DRY} is that of the dried gel.

Preparation of PVA Gel. PVA, with an average degree of polymerization of 2000, was purchased from Wako Pure Chemicals. Twenty grams of the PVA powder were suspended in 1 L water and stirred while heating until dissolved. Then the solution was stirred another 10 h to be homogenized. Glass tubes filled with the aqueous solution were fixed on a brass stand and were irradiated by γ-ray. The γ-irradiation was performed using three different furnaces A, B, and C at Japan Atomic Energy Institute, Tokai, Japan Atomic institute, Takasaki and institute for Atomic Energy, The University of Tokyo, respectively. Because the gel contracts during formation. as mentioned above, the diameter of glass cylinder must be chosen according to the total dose of irradiation fitting the prepared gel to a 5 mm OD NMR sample tube.

Although all of the glass tubes and the aqueous solution became brown after the irradiation, the gels remained colorless. The gels were washed with distilled water several times, immersed in distilled water and left there overnight to exchange the colored water in the gels for distilled water. Then a 3—4 cm cylinder was cut out from the prepared gel and dried at 50—60 °C *in vacuo* for 20 h. If the temperature is above 70 °C, dried gels become yellow. The dried gel was soaked in sample solutions in 5-mm OD NMR tubes and kept at least for one night at room temperature. Then they swelled back to their original size. The time, which is necessary for PVA gels to be swollen back to the original size, depends strongly on temperature and solvent. In aqueous solution, it took a few hours in hot water, 10 h at 23 °C, 3 d at 10 °C, more than a week in the refrigerator and about a week in DMSO at room temperature. Although the gels which were irradiated using furnaces A and B were homogeneous for NMR measurements, the gels prepared using furnaces C were not suitable for NMR. They often tore to small pieces. Even when they did not, they contained a number of bubbles. In the case of furnace C, homogeneous gels finally could not be

† Present address: Department of Chemistry, Faculty of Science, Chiba University, Chiba 260.

prepared at any PVA concentration, any degree of polymerization and any dose rate examined. Degassing before irradiation also did not work. A possible reason for the difference between the gels prepared using furnaces A and B and that by furnace C is a difference in the temperature at which irradiation was made. In the case C, the temperature was at 30—50 °C, whereas in the cases of A and B the temperature was maintained at 10—30 °C. Therefore, it may be concluded that the temperature below 30 °C is a necessary condition for obtaining homogeneous gels that are suitable for NMR measurements.

Reagents. NAD was purchased from Kojin (Lot No. 2113) and used without further purification. All other chemicals were of reagent grade.

NMR Measurements. The concentration of NAD was 10—100 mM. The pH was adjusted by DCl or NaOD. All pH values reported are uncorrected meter readings of D_2O solution made with an electrode standardized by using H_2O buffers. PVA gels were prepared by 30 MRads irradiation and C_{GEL}=23.7%. A 3-cm cylinder was cut out from the prepared gels and dried *in vacuo*. The dried gels were immersed in 5-mm OD NMR tubes and kept at least one night at room temperature until they were swollen back to their original size. When the pH was above 8, NAD decomposed within 10 h, and the color of the solution turned into brown. NMR spectra were obtained at 100 MHz with a JEOL PS-100 spectrometer in the correlation mode.[3] Typically 100 transients (409.6 Hz/3.0 s) were accumulated to improve the signal to noise ratio. A Bruker HXS-360 spectrometer was used to apply the magnetic field to the direction which is perpendicular to that in the case of a conventional electromagnet. All chemical shifts are given in ppm relative to internal DSS. The probe temperature was 29 °C.

Results and Discussion

An NAD–PVA gel system gives a spectrum as shown in Fig. 1. Beside a broad signal of the methylene protons of the PVA molecule, all the signals consist of doublets; in each pair, the signal at lower field is broader than that at higher field. For the assignment of each of these signals, a small amount of Fe^{3+} ion was added from the top of the gel in an NMR tube. After addition of Fe^{3+}, each higher field signal instantaneously broadened and became unobservable. In contrast to this, the lower field signals started to show some broadening only after several hours. This result indicates that the signals at higher field arise from the molecules in the solution surrounding the PVA gel (Hereafter the solution will be referred to as the *surrounding solution*) and that the signals at lower field arise from those in the PVA gel.

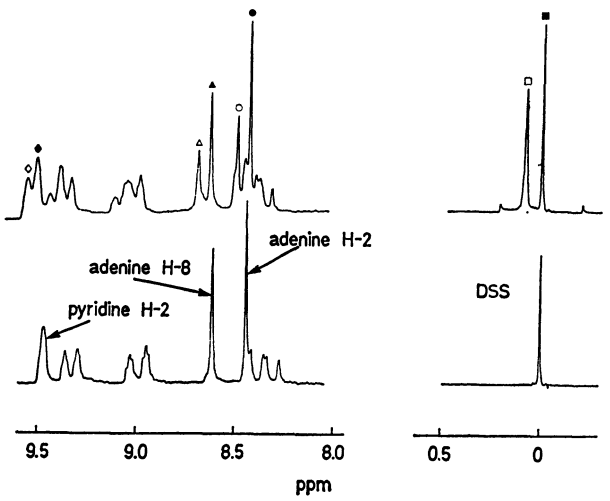

Fig. 1. 100 MHz ^1H NMR spectrum of NAD. The upper and lower spectra correspond to NAD in the PVA gel medium and aqueous solution, respectively. Open and closed symbols indicate signals due to the solutes in the PVA gel and in the surrounding solution, respectively.

Hereafter, the chemical shift for a signal due to the solutes in the PVA gel relative to the corresponding signal of that in the surrounding solution will be simply referred to as a *chemical shift difference*.

It was conformed that with an NMR spectrometer using a superconducting magnet signals due to solutes in PVA gel appear at higher field relative to those of the surrounding solution. The direction of the magnetic field of a superconducting magnet is perpendicular to that of a conventional magnet. It may be concluded, therefore, that the chemical shift difference is primarily due to the difference in the volume susceptibility of the PVA gel and the surrounding solution.[4]

It was observed that the chemical shift differences for each doublet were clearly different. This fact suggests that, in addition to the volume susceptibility effect, a contribution to the observed shift due to an intermolecular interaction between PVA gel and solutes exists at least to some extent. The chemical shift difference ($\Delta\delta$) will be written as

$$\Delta\delta = \Delta\delta_0 + \Delta\delta_1, \quad (1)$$

where $\Delta\delta_0$ is the chemical shift difference which would be given only by the difference in the volume susceptibility of two media, $\Delta\chi_v$, and $\Delta\delta_1$ is the deviation of the observed chemical shift difference from $\Delta\delta_0$.

Two independent methods can be used to estimate $\Delta\delta_0$ and $\Delta\delta_1$. The magnetic field H_n experienced by a nucleus may be given by[5]

$$H_n = H_0 + h_1 + h_2 + h_3 + h_4, \quad (2)$$

where H_0 is the applied external magnetic field; h_1 is dependent upon the shape of the sample tube and the bulk susceptibility of the sample and the sample tube. h_2 is the contribution due to magnetization external to the Lorentz sphere, *i.e.*,

$$h_2 = \frac{4}{3}\pi\chi_v H_0, \quad (3)$$

where χ_v is the volume susceptibility of the molecule. In the case of spherical samples, the contribution $(h_1 + h_2)$ is given for a conventional electromagnet (4) and a superconducting magnet (5), respectively, by [4]

$$h_1 + h_2 = +\frac{2}{3}\pi\chi_v H_0, \quad (4)$$

$$h_1 + h_2 = -\frac{4}{3}\pi\chi_v H_0. \quad (5)$$

h_3 is an intermolecular interaction effect, and h_4 is the intramolecular chemical shift in an isolated molecule. From Eqs. 4 and 5 the observed chemical shift differences $\Delta\delta_{obs}$ for an electromagnet and a superconducting magnet, respectively, are given by

$$\Delta\delta_{obsd} = \frac{2}{3}\pi\Delta\chi + \Delta\delta_1 \quad (6)$$

$$\Delta\delta_{obsd} = -\frac{4}{3}\pi\Delta\chi + \Delta\delta_1, \quad (7)$$

where $\Delta\chi = \chi_v^{in} - \chi_v^{out}$ is the difference in the bulk susceptibility between in and outside the PVA gel and $\Delta\delta_1$ is the chemical shift induced by the intermolecular interactions. Equations 6 and 7 can be solved simultaneously to give $\Delta\chi$ and $\Delta\delta_1$.

Alternatively, $\Delta\chi$ and $\Delta\delta_1$ can be evaluated by using only one kind of magnet.[5] In this case we assume a mathematically idealized system, *i.e.*, one regards the PVA gel and sample tube as an infinitely long perfect coaxial cylinder. In the absence of sample spinning, the observed NMR spectrum gives two maxima. The separation of the maxima ($\Delta\nu$ (Hz)) is a linear function of the difference in the volume susceptibility of both media which is given by[5]

$$\Delta\chi = 4\pi\nu_0\Delta\chi(a/r)^2, \quad (8)$$

where r is the radius of inner boundary of the tube, a is that of the PVA gel and ν_0 is a fixed radiofrequency (100 MHz in the present case). With sample spinning, the NMR spectrum of the surrounding solution collapses to a single line. Figure 2 is a spectrum of H_2O in the PVA gel. Spectra A and B are obtained without and with spinning, respectively. The difference in volume susceptibility of a sample can be obtained from this separation. The shape of signals were found to depend strongly on the mapping of heterogeneity in the magnetic field due to imperfections in the PVA gel system. If measurements are carefully performed in the same manner, the values of $\Delta\chi$ obtained in this way become quite reproducible within 0.005 ppm.

In Fig. 3, the chemical shift differences are shown for H_2O, DSS, and glycylglycylglycylglycine(Gly_4) as a function of C_{GEL}. In the case of DSS, $\Delta\delta$ was in excellent agreement with $\Delta\delta_0$ throughout the entire range of C_{GEL} examined. $\Delta\delta$ of DSS depends slightly upon temperature. As the temperature rose, $\Delta\delta_0$ increased; the slope of $\Delta\delta_0/(1/T)$ was quite similar for any sample and for any pH. This fact suggests that $\Delta\delta_0$ depends on temperature but not on pH.

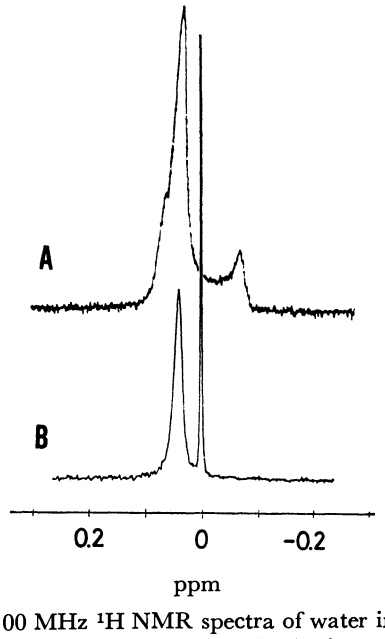

Fig. 2. 100 MHz ^1H NMR spectra of water in the PVA gel system. A and B are obtained without and with spinning, respectively.

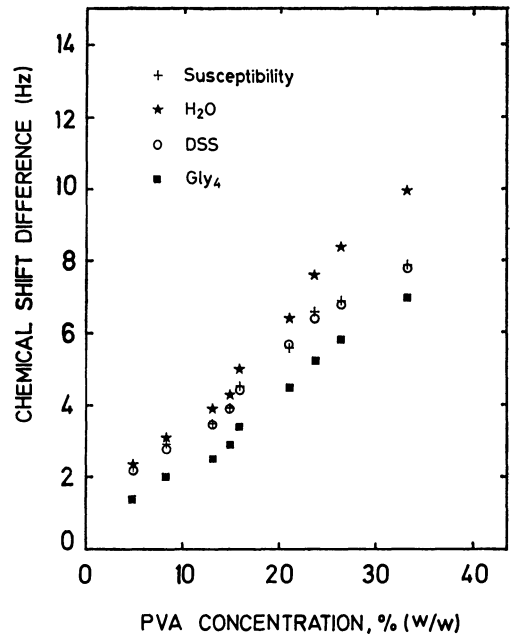

Fig. 3. Chemical shift differences for H_2O, DSS, and Gly_4 *versus* PVA concentration C_{GEL}.

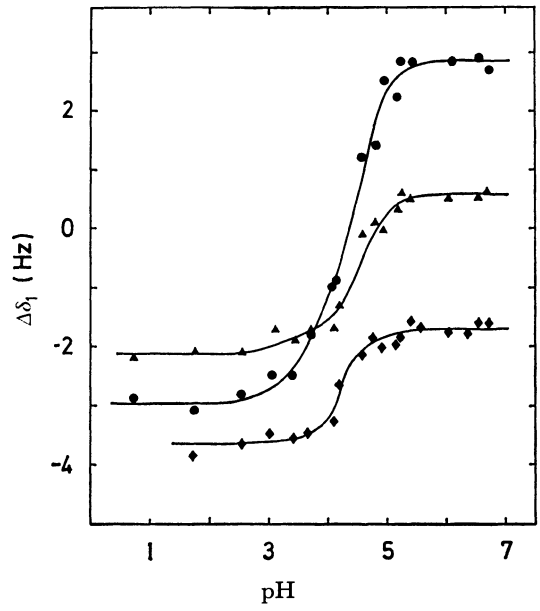

Fig. 4. Titration curves of $\Delta\delta_1$ of NAD.
●: Adenine H-2, ▲: adenine H-8, ◆: pyridine H-2.

As Fig. 4 shows, $\Delta\delta_1$ of the three protons of NAD are dependent upon pH. Each curve gives a quite similar pK_a of approximately 4. The chemical shifts of the adenine signals presumably reflect protonation of *N*-1 at pK_a 3.8.[6] This result may be interpreted in terms of an intermolecular interaction between NAD and PVA gel.

We are grateful to Prof. Michael Rode for his helpful comments and discussion.

References

1) T. Watanabe, T. Yahagi, and S. Fujiwara, *J. Am. Chem. Soc.*, **102**, 5187 (1980).
2) A. Danno, *J. Phys. Soc. Jpn.*, **13**, 722 (1958).
3) a) Y. Arata and H. Ozawa, *J. Magn. Reson.*, **21**, 67 (1976); b) Y. Arata, H. Ozawa, T. Ogino, and S. Fujiwara, *Pure Appl. Chem.*, **50**, 1274 (1978).
4) D. H. Live and S. I. Chan, *Anal. Chem.*, **42**, 791 (1970).
5) J. R. Zimmerman and M. R. Foster, *J. Phys. Chem.*, **61**, 282 (1957).
6) O. Jardetzky and N. G. Wade-Jardetzky, *J. Biol. Chem.*, **241**, 85 (1966).

The Thermal and Hydrothermal Behavior of Silica-adsorbed Magnesium Hydroxide

Haruto MURAISHI

Department of Chemistry, Fukuoka University of Education, Munakata-cho, Fukuoka 811-41

(Received July 14, 1980)

Silica-adsorbed $Mg(OH)_2$ was treated thermally and hydrothermally. The resulting change in the adsorption layer was followed, and the effects of the adsorbed silica on the change in the bulk ($Mg(OH)_2$, MgO) were examined. (1) Thermal treatment: The dehydration temperature of $Mg(OH)_2$ increased with an increase in the amount of silica adsorbed, and it was higher by 25 °C for $Mg(OH)_2$ adsorbing silica above 0.4 mmol/g than for pure $Mg(OH)_2$. The amorphous silicate of the adsorption layer on the $Mg(OH)_2$ surface was transformed into forsterite (Mg_2SiO_4) and chain or sheet-like silicate over the temperature range of 870—1100 °C, and the presence of the silica inhibited the sintering and crystallite growth of the MgO grains. At 1400 °C, these products were all transformed into forsterite, and the presence of the silica had little effect on the crystallite growth. (2) Hydrothermal treatment: Below 360 °C, the amorphous silicate on the surface crystallized as serpentine ($Mg_3Si_2O_5(OH)_4$), and the crystallite growth of $Mg(OH)_2$ was inhibited. Above 420 °C, on the other hand, the silicate was transformed into forsterite through serpentine-like silicate, and the crystallite growth of $Mg(OH)_2$ was promoted. The change in the crystallite size of the bulk by the treatment was interpreted mainly in terms of the behavior of the silicate on the surface.

Our previous works[1,2] have shown that soluble silica was chemisorbed at temperatures under 100 °C, forming –Mg–O–Si– bonds on the $Mg(OH)_2$ surface, and that the resulting surface had properties like magnesium silicate gels, *e.g.*, a relatively large amount of acidity and adsorptive properties for Methylene Blue and Methyl Red. The behavior of the silica-adsorbed $Mg(OH)_2$ upon the thermal and hydrothermal treatment is interesting from the viewpoint of the process of the formation of ceramics and the mechanism of producing magnesium silicate minerals.

In this work, the transformation of the magnesium silicate on the $Mg(OH)_2$ surface by thermal and hydrothermal treatment was observed. In addition, the effects of adsorbed silica were investigated on: (1) the dehydration temperature of $Mg(OH)_2$, (2) the crystallite growth of the dehydration product, MgO, upon the thermal treatment, and (3) the crystallite growth of the $Mg(OH)_2$ upon the hydrothermal treatment.

In some of the earlier works the effect of impurities on the dehydration temperature of $Mg(OH)_2$[3,4] and the effects of the addition of foreign materials on the sintering of MgO[5–8] have been investigated. However, there has been no investigation placing emphasis on the behavior of the silicate.

Experimental

Samples. The silica-adsorbed $Mg(OH)_2$ used as the starting material was prepared in a previously reported way.[2] The silica gel used for chromatography (Wako Pure Chemicals) was dissolved in hot water, and then the silica solution was adjusted to a concentration of about 100 ppm. $Mg(OH)_2$ powder (Kanto Kagaku) was suspended in this solution and was allowed to adsorb the soluble silica while being stirred at 500 rpm at 80 °C. The amount of silica adsorbed was determined by the decrease in the silica concentration in the solution. The silica concentration was determined colorimetrically by the usual molibdate yellow method. The aqueous silica was soluble in monomeric unit form, $Si(OH)_4$, since the value of the silica concentration did not vary when the solution was treated with a 0.1 mol/l NaOH solution. The non-adsorbed $Mg(OH)_2$ which was used as a reference standerd was immersed in distilled water at 80 °C for 8 h before use in order to have the same history as the silica-adsorbed $Mg(OH)_2$. Its surface area was about 30 m^2/g.

Experimental Procedures and Apparatus. The thermal treatment were carried out by the use of an electric furnace in the air at 430 °C for 4 h, 870 °C for 3 h, 1000 °C for 2 h, 1200 °C for 1 h, and 1400 °C for 1 h respectively. The hydrothermal treatment was carried out using a modified Morey-type autoclave with a fill ratio of water of 50% and a heating rate up to a fixed temperature of 75 °C/h.

The dehydration temperatures of the samples was measured by differential thermal analysis (DTA). The DTA was carried out using a Rigaku 8002 Thermal Analyser with a thermobalance. The sample (about 10 mg) was packed in a platinium dish, while the same weight of Al_2O_3 was packed in a reference dish; the heating rate was 10 °C/min.

The crystallite size of MgO and $Mg(OH)_2$ obtained was determined by the X-ray line-broadening method,[9] using diffraction peaks from the (110) and the (0001) planes respectively. The aspect of the samples was observed by means of an Hitachi S-430 scanning electron microscope (SEM). The samples submitted to treatment were examined by IR spectroscopy and X-ray diffractometry. The IR spectra were observed by the KBr tablet method; the tablet was made up of 2 mg of the sample and 150 mg of KBr. A Hitachi EPI-G IR Spectrometer and a Rigaku XGC-20 X-ray Diffractometer were used for the measurement.

The specific surface area of the sample was determined by applying the BET method to the nitrogen-adsorption data obtained at the temperature of liquid nitrogen, assuming the cross-sectional area of a nitrogen molecule to be 16.2 $Å^2$.

Results and Discussion

Part 1. Thermal Behavior

The Effect of Adsorbed Silica on the Dehydration of $Mg(OH)_2$. Figure 1 shows DTA and TG curves for pure $Mg(OH)_2$ and a typical silica-adsorbed $Mg(OH)_2$. The position of the endothermic peaks shows that the dehydration of the latter takes place at a higher temperature than that of the former. In addition to the rise of the dehydration temperature, the DTA curve for the silica-adsorbed sample had a small exothermic peak at about 850 °C which was assigned to the reaction of MgO with silica. Both the TG curves

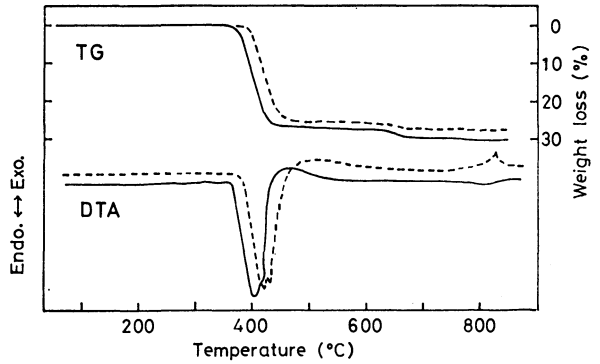

Fig. 1. TG and DTA curves for pure $Mg(OH)_2$ (——) and silica-adsorbed $Mg(OH)_2$ (------).

gradually declined with an increase in the temperature after the dehydration occurred at about 400 °C. Such a phenomenon has often been observed in various hydroxides and minerals containing water; it can be attributed to residual essential water or OH groups.

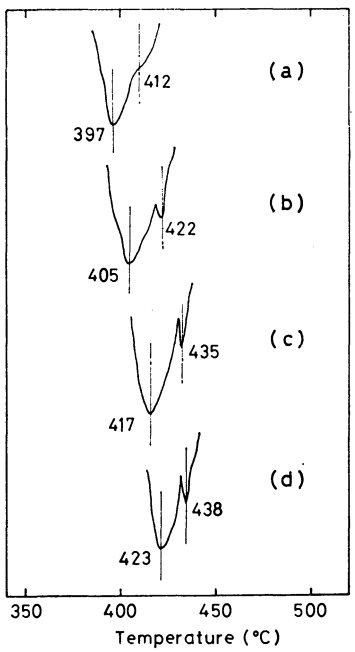

Fig. 2. DTA curves for pure $Mg(OH)_2$ and $Mg(OH)_2$ with various amount of adsorbed silica. Amount of adsorbed silica (mmol/g): (a), Non adsorption; (b), 0.097; (c), 0.34; (d), 1.26.

Figure 2 shows the change in the position and shape of the endothermic peak with a variation in the amount of silica adsorbed. The dehydration temperature increased with the increase in the amount of silica adsorbed, and the shape of the endothermic peak apparently varied from singlet to doublet for these silica-adsorbed $Mg(OH)_2$. This peak separation suggests that the two-step dehydration of $Mg(OH)_2$ was induced by the adsorption of silica. Weber and Rustum Roy[10] have observed a two-step dehydration of $Mg(OH)_2$ and presumed it to result from the formation of an intermediate phase in the dehydration process. Ball and Taylor[11] asserted the formation of an intermediate phase with a spinel-like structure (*e.g.*, $(MgO)_3 \cdot H_2O$) resulting from cation migration during dehydration. In this study, the intermediate phase was not observed by means of X-ray diffractometry. This bimordal DTA curve, therefore, is not ascribed to the structure change, but it indicates that the dehydration process following the release of the resulting H_2O from the $Mg(OH)_2$ particle is surely affected by the adsorbed silica.

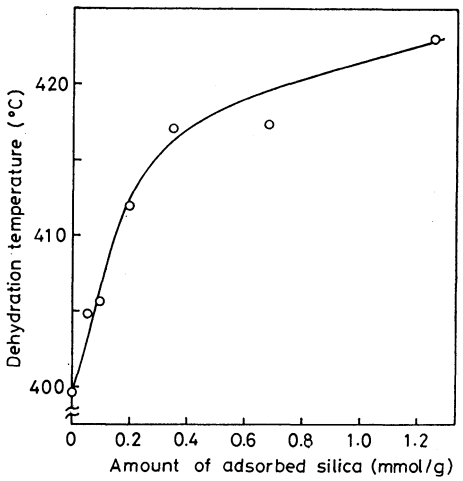

Fig. 3. Effect of amount of adsorbed silica on dehydration temperature of $Mg(OH)_2$.

Figure 3 shows the relation between the amount of silica adsorbed and the dehydration temperature. The dehydration temperature rose greatly with the increase in the amount of silica up to about 0.4 mmol/g, although above this amount it rose only slightly. The $Mg(OH)_2$ particles used were observed microscopically to be disk-like crystals with a well-developed (0001) plane. Consequently, it may be said that the crystal consists only of an approximate (0001) plane with respect to the estimate of its surface area. The number of Mg atoms exposed on the surface can, therefore, be calculated from the specific surface area and the array of Mg atoms on the (0001) plane.[12] On the other hand, it can reasonably be considered from the structure of the (0001) plane that two silica molecules combine with three Mg atoms on the surface of $Mg(OH)_2$. Thus, the amount of silica adsorbed required to form a monolayer on 1 g of the used $Mg(OH)_2$ is calculated to be 0.34 mmol/g. This amount corresponds to the quantity of about 0.4 mmol g^{-1} observed as a characteristic amount in the relation between the dehydration temperature and the amount of silica adsorbed. In other words, it can be said that the dehydration temperature of silica-adsorbed $Mg(OH)_2$ rose appreciably until the surface was completely covered with a monolayer of silicate, while it rose only slightly when the surface had an excess of silica. The rise in the dehydration temperature may be accounted for as follows. The dehydration of $Mg(OH)_2$ has been interpreted as an inhomogeneous mechanism in which the reaction takes place through the two steps of nucleus formation and growth.[13] The nucleus formation is known to be mainly initiated at such sites as grain boundaries or defects on the surface (*i.e.*, step, kink, and pit).[14] Since these sites are also atcive in the adsorption of silica, some of them are occupied by the

silica molecules in the case of silica-adsorbed $Mg(OH)_2$. The decrease in the active sites forces a delay in the rate of nucleus formation. In addition, the grain surface covered with the silica obstructs the release of the H_2O molecules formed by the decomposition. This effect may be compared with the rise in the decomposition temperature of $Mg(OH)_2$ due to an increase in the water-vapor pressure.[15]

The Change in Surface Products. In a previous study,[2] it has been found that the silica-adsorbed $Mg(OH)_2$ has surface properties and a structure similar to those of magnesium silicate gel. In addition, when magnesium silicate gels were calcined above 870 °C, forsterite (Mg_2SiO_4) and a small amount of enstatite ($MgSiO_3$) were produced in the case of a SiO_2/MgO ratio below 1, while mainly enstatite was produced in the case of a ratio above 1. Since the silica-adsorbed samples have a large excess of MgO, the silicate layer on the surface is presumed to be transformed into forsterite by thermal treatment.

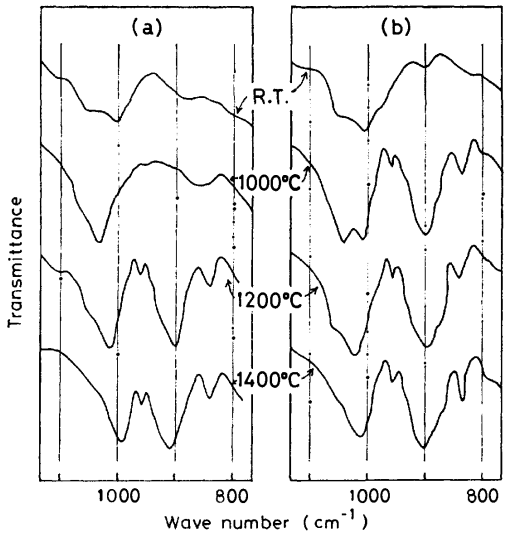

Fig. 4. The changes of IR spectra of silica-adsorbed $Mg(OH)_2$ by thermal treatment. Amount of adsorbed silica (mmol/g): (a), 0.19; (b), 1.26.

Figure 4 shows the change in the IR spectra by thermal treatment for $Mg(OH)_2$ with a different amount of the silica. It was found from the IR spectra that, when the samples were heated at 1000 °C, forsterite, which is composed of nesosilicates, was formed. In addition to the absorption spectrum for forsterite, some additional bands were observed in the region from 1000 to 1100 cm^{-1}. It is known that nesosilicates with a three-dimensional structure of single SiO_4^{4-} usually exhibit their absorption in the region of 800—1000 cm^{-1},[16] while chain silicates (*i.e.*, enstatite) or sheet silicates (*i.e.*, talc ($Mg_3Si_4O_{10}(OH)_2$)) do so in the region of 1000—1100 cm^{-1}. In order to examine the route of the appearance of the additional bands in the region of 1000—1100 cm^{-1}, the following procedure was carried out. The silica-adsorbed samples heated above 1000 °C were treated with a 5% NH_4Cl solution until the bulk MgO had been removed completely. This treatment is based on the fact that an amorphous material consisting of a –Mg–O–Si– bond, forsterite, and enstatite is insoluble in a NH_4Cl solution, but MgO is soluble.[17] The residue in the solution was filtered and dried. The residue was identified by IR spectroscopy and X-ray diffractometry. When the spectrum for the residue is compared with that for the parent sample, the absorption pattern in the region of 800—1000 cm^{-1} which was assigned to forsterite did not change; the slight absorption peaks in the region of 1000—1100 cm^{-1}, however, changed to larger, broad absorption bands ranging from 1010 to 1090 cm^{-1}. On the other hand, the X-ray diffraction pattern of the residue was assigned to forsterite and an amorphous material. Therefore, it is reasonable to assume that the additional bands are due to an amorphous material, which is an incomplete chain or sheet-like silicate.

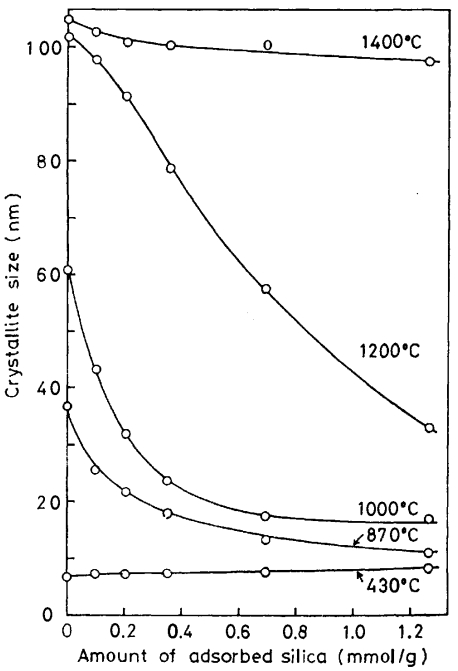

Fig. 5. Effect of amount of adsorbed silica on crystallite size of bulk MgO at various treatment temperatures.

The Effect of Adsorbed Silica on the Crystallite Growth of the Dehydration Product MgO. Figure 5 shows the crystallite size of MgO at various treatment temperatures. The crystallite size of MgO was not influenced by the adsorbed silica at a little above the dehydration temperature of $Mg(OH)_2$, but over the temperature range of 870 to 1200 °C it became smaller with an increase in the amount of silica adsorbed. At a temperature of 1400 °C, at which sintering evidently begins,[18] it became independent of the adsorbed silica.

Moreover, the thermal changes in pure $Mg(OH)_2$ and silica-adsorbed $Mg(OH)_2$ were observed comparatively by the use of the SEM. As may be seen from the photographs in Fig. 6, there was no difference between pure $Mg(OH)_2$ and silica-adsorbed $Mg(OH)_2$ before heat treatment (Figs. 6(a) and 6(d)). After the treatment at 1000 and 1400 °C, the apparent grain of MgO from pure $Mg(OH)_2$ grew; it was much larger than

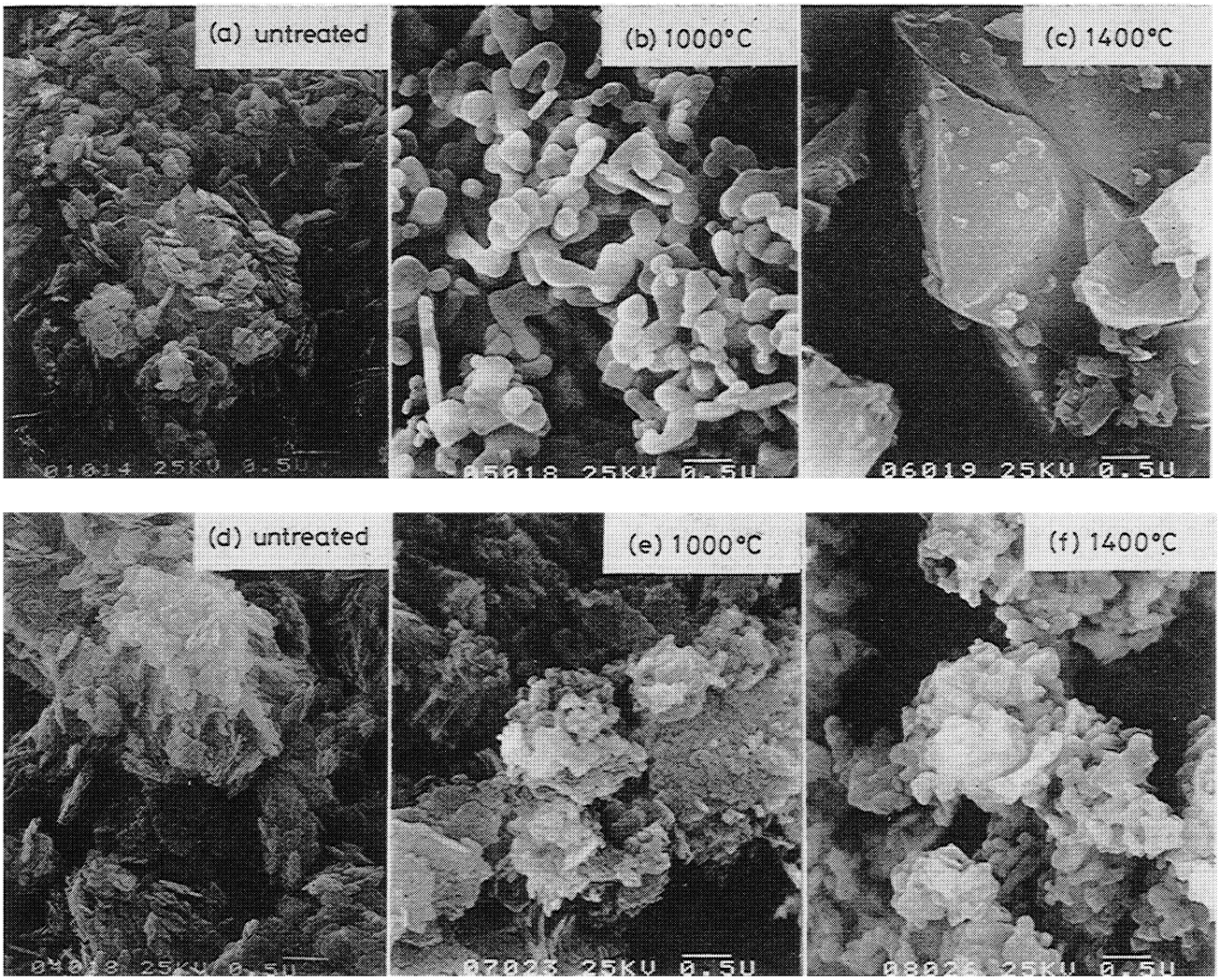

Fig. 6. SEM microphotographs of the samples treated thermally at 1000 and 1400 °C. (a), (b), (c): Non-adsorbed $Mg(OH)_2$. (d), (e), (f): Silica-adsorbed $Mg(OH)_2$.

the crystallite measured by the X-ray method. Therefore, the apparent grain seems to be an aggregate of crystallites formed by their sintering. On the other hand, the size of MgO from silica-adsorbed $Mg(OH)_2$ (amount of silica adsorbed; 1.26 mmol/g) was relatively similar to the crystallite size, as is shown in Fig. 5.

From these results, the thermal behavior of $Mg(OH)_2$ and MgO can be explained as follows. An untreated pure $Mg(OH)_2$ powder was observed by means of the SEM as a layered aggregate of disk-like grains 20 to 50 nm thick in the direction of the c-axis. The thickness of a single grain observed was in good agreement with the crystallite size as measured by the use of the X-ray line broadening method. Therefore, the single grain observed seems to be a single crystal of $Mg(OH)_2$. The dehydration product of the aggregate is also considered to be an aggregate of single crystals keeping the same crystallographic orientation with each other, since the dehydration of $Mg(OH)_2$ is a topotactic reaction.[11,19] The rise in the temperature leads to a grain growth resulting from the disappearance of the grain boundary upon the sintering of these single crystals. This grain growth may be limited to the size of the aggregate consisting of single grains with the same crystallographic orientation. The presence of a silicate layer on the grain surface will result in lowering the motion of the grain boundary because of its hindrance to the surface diffusion and the grain boundary diffusion. This hindrance will depress the grain growth and the formation of a polycrystal by sintering. At temperatures above 1300 °C (the so-called Tamman temperature of MgO (melting point, 2800 °C)), atoms or ions on the surface and in the bulk MgO are easy to diffuse. In addition, the silicate layer has been transformed into a forsterite crystal with a three-dimensional construction. It is, therefore, considered that the grain growth of the silica-adsorbed samples is not distinguishable from that of pure sample, since the silicate can no longer inhibit the motion of the grain boundary.

Part 2. Hydrothermal Behavior

The Change in the Surface Product. The silica-adsorbed $Mg(OH)_2$ indicated the IR absorption spectra of magnesium silicate gels-like material to be as has been described in the previous paper.[2] The hydrothermal treatment at 250 °C for 72 h changed them into absorption bands near 960, 1010, and 1080 cm^{-1}, which are

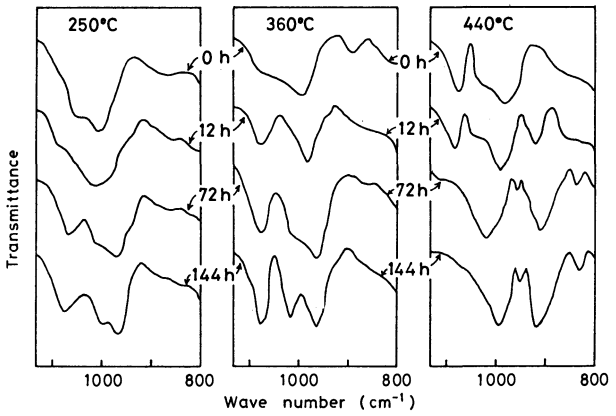

Fig. 7. IR spectra of silica-adsorbed $Mg(OH)_2$ treated hydrothermally at 250—440 °C for 0—144 h.

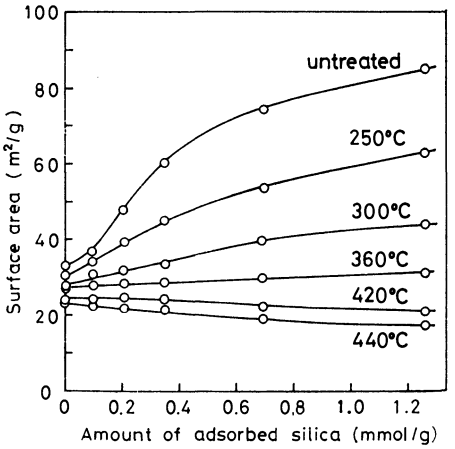

Fig. 8. The change of surface area by hydrothermal treatment for 72 h.

assigned to a compound having the sheet silicate group. The absorption bands became sharp upon treatment at 360 °C for 144 h. The results are shown in Fig. 7. On the basis of the data proposed by Brindley *et al.*[20] and the spectrum of serpentine synthesized in our laboratory, these IR spectra were assigned to serpentine. Above 420 °C, a serpentine-like spectrum was observed in the beginning of the treatment, but it was transformed into the absorption spectra of forsterite, which was characterized by four absorption peaks in the 800—1000 cm^{-1} region, upon subsequent treatment. The surface products obtained below 360 °C were easily isolated by dissolving the bulk $Mg(OH)_2$ with a 5% NH_4Cl solution or a dilute acid solution. The isolated silicate was identified by the use of X-ray diffractometry and IR spectroscopy. The IR spectra of surface products were hardly changed by isolation; therefore, the serpentine-like spectra are attributable to a poor crystalline serpentine.

The phase diagram of the SiO_2–MgO–H_2O system described by Bowen *et al.*[21] shows that, under relatively low water-vapor pressures, serpentine is stable below 380 °C, while above that point forsterite is stable. The phase boundary of the serpentine and forsterite formed hydrothermally from the silica-adsorbed $Mg(OH)_2$ was comparable to the phase boundary presented by Bowen *et al.* Talc was not formed, even if the ratio of the silica molecules and Mg^{2+} ions in the surface layer had the stoichiometric relationship of talc. It was found that the kind of magnesium silicate produced by hydrothermal treatment does not depend upon the composition of the silicate layer on the surface, but upon the composition of the sum of the silicate layer and the bulk.

The Change in the Surface Area. The effects of the amount of silica adsorbed and the treatment temperature on the surface area of silica-adsorbed $Mg(OH)_2$ are shown in Fig. 8. As has been described in the previous paper,[2] the chemisorption of soluble silica on the surface of $Mg(OH)_2$ led to an increase in the surface area; the increase was attributed to the formation of micro pores on the surface (see the "Untreated" curve in Fig. 8). The surface area was more or less decreased by hydrothermal treatment over the temperature range from 250 to 440 °C. It was found, from the measurement of the N_2-adsorption isotherms of the samples and the t-plots[22] derived from this isotherm, that the decrease in the surface area by the treatment is mainly attributable to the disappearance of the micro pores. However, on treatment above 420 °C, the surface area of the silica-adsorbed samples became smaller than that of the non-adsorbed sample. This reduction in the surface area cannot be interpreted only in terms of the disappearance of the micro pores. It will be discussed in the following section.

The Growth of the Crystallite of $Mg(OH)_2$. The change in the crystallite size of the bulk $Mg(OH)_2$ by the treatment was followed as a function of the time at various temperatures. The crystallite size of pure $Mg(OH)_2$ was not appreciably affected by the treatment, while that of silica-adsorbed $Mg(OH)_2$ was dependent on the treatment temperature. The growth of the crystallite of silica-adsorbed $Mg(OH)_2$ did not proceed below 300 °C, but above 360 °C it proceeded with the treatment time. Moreover, the crystallite

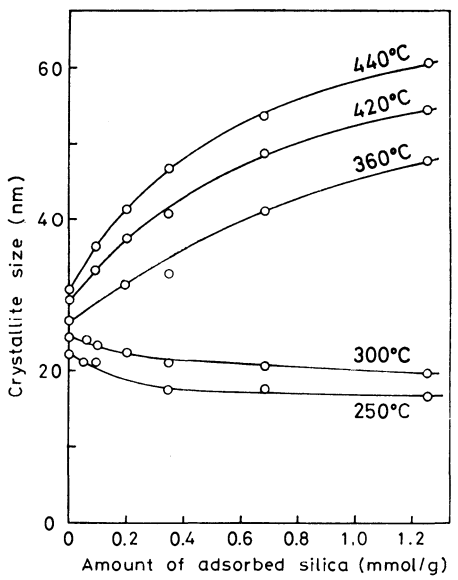

Fig. 9. Effect of amount of adsorbed silica on crystallite size of bulk $Mg(OH)_2$ at various treatment temperature for 72 h.

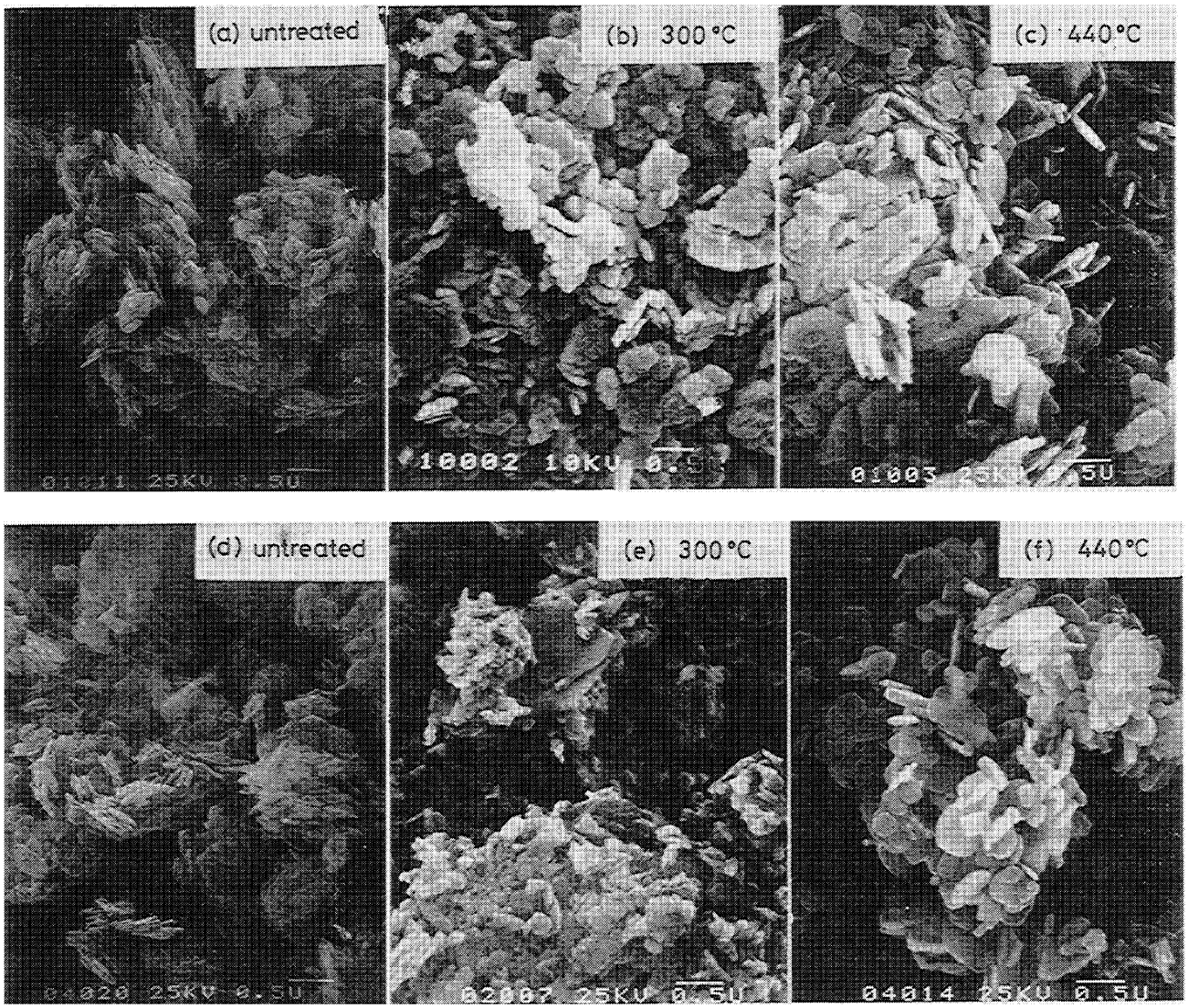

Fig. 10. SEM microphotographs of the samples treated hydrothermally at 300 and 440 °C.
(a), (b), (c): Non-adsorbed $Mg(OH)_2$. (d), (e), (f): Silica-adsorbed $Mg(OH)_2$.

growth at various temperatures was investigated with respect to the effects of the amount of adsorbed silica, as is shown in Fig. 9. The crystallite size at a temperature below 300 °C decreased with an increase in the amount of silica adsorbed, while above 360 °C, on the contrary, the size increased with the amount of silica adsorbed. In other words, the adsorbed silica contributes to inhibiting the growth of the crystallite of $Mg(OH)_2$ up to 300 °C, while above 360 °C it serves to promote it.

The non-adsorbed and the silica-adsorbed $Mg(OH)_2$ treated at various temperatures were observed comparatively by the use of the SEM. The microphotographs are shown in Fig. 10. As may be seen from the photographs, the grain of non-adsorbed $Mg(OH)_2$ did not grow throughout the treatment from 250 to 440 °C, while the grain of silica-adsorbed $Mg(OH)_2$ grew in thickness at the temperature of 440 °C. This increase in grain size corresponds to the change in the crystallite size of $Mg(OH)_2$ shown in Fig. 10, and also to the change in the surface area shown in Fig. 8. Therefore, the grain is considered to be a single crystal.

These phenomena may be explained as follows. The surface of the $Mg(OH)_2$ grain will still be covered by the silicate layer under treatment at temperatures below 300 °C. It was found, from the determination of the Mg^{2+} ion in the hydrothermal solutions, that the presence of the silicate layer tends to decrease the rates of the dissolution and solubility of $Mg(OH)_2$. This decrease seems to have resulted in the slower crystal growth of $Mg(OH)_2$, since its growth is considered to be a solution growth based on the dissolution and recrystallization of $Mg(OH)_2$. However, at temperatures above 360 °C, the silicate layer changed into a crystalline silicate (serpentine or forsterite), with a three-dimensional growth. The silicate may exist in the isolated state, and so may no longer coat the surface of $Mg(OH)_2$ grain. In order to confirm whether or not the characteristic crystal growth of silica-adsorbed $Mg(OH)_2$ is due to the presence of the isolated silicate, a mixture of pure $Mg(OH)_2$ and a synthesized serpentine (or forsterite) was treated hydrothermally above 360 °C. It was found that the $Mg(OH)_2$ crystal hardly grows at all under these conditions. Therefore, the growth is

not due to the presence of the silicate crystal, but the process of the crystallization of the silicate layer makes some contribution to the growth. Unfortunately, it is difficult to make this phenomenon clearer using our limited experimental procedure.

The author would like to express his hearty thanks to Professor Shigeo Kitahara for his valuable guidance and for his critical reading of this manuscript. The present work was partially supported by a Grant-in-Aid for Scientific Research No. 474205 from the Ministry of Education, Science and Culture.

References

1) S. Kitahara and H. Muraishi, *Nippon Kagaku Kaishi*, **1978**, 555.
2) H. Muraishi and S. Kitahara, *Nippon Kagaku Kaishi*, **1978**, 1457.
3) J. W. Nelson and I. B. Cutlur, *J. Am. Ceram. Soc.*, **41**, 406 (1958).
4) K. Hamano, K. Yoshino, and H. Togashi, *J. Ceram. Assoc. Jpn.*, **74**, 14 (1966).
5) G. K. Layden and M. C. McQuarrie, *J. Am. Ceram. Soc.*, **42**, 89 (1959).
6) H. J. S. Kriek, W. F. Ford, and J. White, *Trans. Brit. Ceram. Soc.*, **58**, 1 (1959).
7) M. H. Leipold, *J. Am. Ceram. Soc.*, **49**, 498 (1966).
8) K. Hamano, K. Yoshino, and H. Togashi, *J. Ceram. Assoc. Jpn.*, **74**, 312 (1966).
9) F. W. Jones, *Proc. Phys. Soc. (London)*, *A*, **166**, 16 (1938).
10) J. N. Weber and R. Roy, *Am. J. Sci.*, **263**, 668 (1965).
11) M. C. Ball and H. F. W. Taylor, *Mineral. Mag.*, **32**, 754 (1961).
12) L. G. Berry and B. Mason, "Mineralogy," W. H. Freeman, San Francisco (1961), p. 381.
13) S. J. Gregg and R. I. Razouk, *J. Chem. Soc.*, **1949**, S 36.
14) "Chemistry of the Solid States," ed by W. E. Garner, Butterworths, London (1955), p. 221.
15) G. W. Brindley, J. H. Sharp, J. H. Patterson, and B. N. Narahari, *Am. Mineral.*, **52**, 201 (1967); F. Toussaint, J. J. Fripiat, and M. C. Gaetuche, *J. Phys. Chem.*, **67**, 26 (1963).
16) J. A. Gadsden, "Infrared Spectra of Minerals and Related Inorganic Compounds," Butterworth, London (1975), p. 29.
17) S. F. Hulbelt and G. Lane, *Trans. Brit. Ceram. Soc.*, **67**, 391 (1968).
18) D. T. Livey, B. M. Wanklyn, M. Hewitt, and P. Murray, *Trans. Brit. Ceram. Soc.*, **56**, 217 (1957).
19) J. F. Goodman, *Proc. R. Soc. London, Ser. A*, **247**, 346 (1958);
20) G. W. Brindley and J. Zussman, *Am. Mineral.*, **44**, 1057 (1959).
21) N. L. Bowen and O. F. Tuttle, *Bull. Geol. Soc. Am.*, **60**, 439 (1949).
22) B. C. Lippens, B. G. Linsen, and J. H. de Boer, *J. Catal.*, **3**, 32 (1964); J. H. de Bore, B. C. Lippens, B. G. Linsen, J. C. P. Broekhoff, A. van den Heuvel, and Th. J. Osinga, *J. Colloid Interface Sci.*, **21**, 405 (1966).

The Crystal and Molecular Structure of the Photodimer of Biphenylene

Akio Furusaki,* Nobuhiro Hashiba, Takeshi Matsumoto, Tomoji Aotsuka, and Shinya Nishida

Department of Chemistry, Faculty of Science, Hokkaido University, Sapporo 060

(Received August 25, 1980)

The molecular structure of the photodimer of biphenylene has been determined by X-ray crystal analysis. The crystals are triclinic, with eight molecules in a unit cell with dimensions of $a=15.061$, $b=17.687$, $c=13.091$ Å, $\alpha=108.91$, $\beta=98.52$, and $\gamma=89.71°$; the space group is $P\bar{1}$. 6625 unique intensity data were collected on a four-circle diffractometer with LiF-monochromated Cu $K\alpha$ radiation. The structure was solved by the symbolic-addition method using 8 symbols, and refined by the block-diagonal least-squares method. The final R value was 0.101. The molecular structure thus obtained corresponds to *syn*-13,14 : 15,16-dibenzotricyclo[6.4.2.$2^{2,7}$]hexadeca-1,3,5,7,9,11,13,15-octaene. Of the four crystallographically-independent molecules, two have approximately the C_{2v} symmetry, while the remaining two are somewhat deformed, their symmetry being nearly C_2. The molecules are held together mainly by van der Waals interactions.

In 1968, Goldman and Ruden reported that, on ultraviolet irradiation, biphenylene (**1**) in refluxing hexane affords a dimer to which they assigned the **2** structure.[1] However, an X-ray study of the octahydrodimer[2] showed that this photodimer might correspond to **3**, not **2**. In order to determine the structure unambiguously, we have now undertaken an X-ray crystal analysis of the photodimer itself.

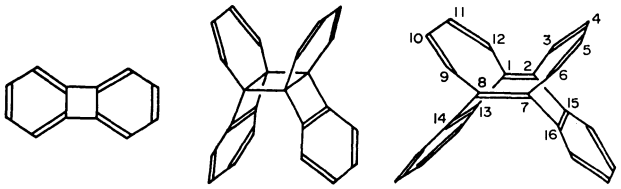

1 **2** **3**

Experimental

The biphenylene dimer (mp 257—267 °C (dec) (lit,[1] mp 255—265 °C (dec))) was prepared by the reported method.[1] The size of the sample used for the X-ray measurement was about $0.5\times0.5\times0.25$ mm^3. The crystal data are summarized in Table 1. The cell dimensions and reflection intensities were measured on a Rigaku four-circle diffractometer using Cu $K\alpha$ radiation ($\lambda=1.5418$ Å) monochromated with an LiF crystal. The intensity measurement was made by the θ-2θ continuous-scan technique at a 2θ scan rate of 2° min^{-1}; the background was measured for 20—30 s at each end of the scan range. Three standard reflections, measured at intervals of every 62 reflections, showed no significant decrease in intensity during the course of data collection. The intensities were corrected for the Lorentz and polarization factors, but not for the absorption or the extinction effect. In the range of 2θ values up to 140°, 6625 unique structure factor magnitudes above the $3\sigma(F)$ level were selected for the structure determination.

Table 1. The crystal data

$C_{24}H_{16}$	M.W. 304.39
Triclinic	
Space group	$P\bar{1}$
Cell dimensions	$a=15.061(3)$Å
	$b=17.687(4)$Å
	$c=13.091(4)$Å
	$\alpha=108.91(3)°$
	$\beta=98.52(3)°$
	$\gamma=89.71(3)°$
V	3259.2 Å^3
Z	8
D_x	1.241 g cm^{-3}
μ(Cu $K\alpha$)	4.98 cm^{-1}

Structure Determination

The structure was solved by the symbolic-addition method.[3] The space group was assumed to be $P\bar{1}$; this choice was later confirmed by a successful refinement. Of the phases of the 1016 reflections with $|E|$ values above 1.70, 408 were expressed in terms of 8 symbols. Since one of the 2^8 possible combinations of the symbol values led to a phase set showing a low R_K value of 0.240 ($R_K=\sum||E_o|-k|E_c||/\sum|E_o|$) and a nonzero q value[4] of 0.368 ($q=1-\sum_h|E_h|(|\sum_k E_kE_{h-k}|/\sum_k|E_kE_{h-k}|)/\sum_h|E_h|$), this phase set was further extended by the use of 1827 $|E|$ values above 1.40; the R_k and q values thus became 0.288 and 0.496 respectively. An E-map based on 1632 phases afforded two superimposed molecular arrangements which were related to each other by the center of symmetry, and each of which might be taken as centrosymmetric. These molecular arrangements could be easily resolved from a consideration of the molecular packing.

The structure thus obtained was refined by the block-diagonal-matrix least-squares method. After all the 64 hydrogen atoms had been located in a difference Fourier map, a further least-squares refinement was done including the hydrogen atoms with isotropic temperature factors. The weighting scheme used was as follows: $w=1/\{\sigma(F)^2\exp(AX^2+BY^2+CXY+DX+EY)\}$, where $X=|F_o|$ and $Y=\sin\theta/\lambda$. The A, B, C, D, and E coefficients are constants which were determined from the $(\Delta F)^2$ values; $A=0.2254\times10^{-4}$, $B=8.219$, $C=0.05559$, $D=-0.01387$, and $E=-7.770$. The final R value was 0.101. The final atomic parameters are listed in Table 2. The tables of the anisotropic temperature factors and hydrogen parameters, and those of the observed and calculated structure factors, are kept at the Chemical Society of Japan (Document No. 8126).

The calculations were performed on a FACOM 230-75 computer at the Hokkaido University Computing

Table 2. The final atomic parameters and estimated standard deviations
The coordinates are multiplied by 10^4.

Atom	x	y	z	B_{eq}[a)]/Å^2	Atom	x	y	z	B_{eq}[a)]/Å^2
C(A1)	− 870(4)	2142(3)	1241(5)	5.14	C(C1)	5937(4)	2930(3)	1602(5)	4.59
C(A2)	− 625(4)	2940(3)	1821(6)	5.30	C(C2)	6750(4)	3017(4)	2259(6)	5.37
C(A3)	− 579(4)	3227(3)	2917(6)	4.84	C(C3)	6787(4)	3300(3)	3374(6)	5.32
C(A4)	− 761(4)	2734(3)	3503(5)	4.17	C(C4)	6009(4)	3481(3)	3829(5)	4.42
C(A4a)	−1022(4)	1938(3)	2948(5)	3.65	C(C4a)	5191(3)	3366(3)	3178(5)	3.44
C(A5)	−1290(4)	1332(3)	3460(5)	3.60	C(C5)	4308(3)	3529(3)	3587(4)	3.40
C(A6)	− 738(3)	788(3)	3577(4)	3.33	C(C6)	3752(3)	2921(3)	3490(5)	3.60
C(A6a)	162(4)	749(3)	3213(5)	3.78	C(C6a)	4008(3)	2069(3)	2976(5)	3.56
C(A7)	968(4)	984(3)	3880(5)	4.38	C(C7)	4257(4)	1556(3)	3582(5)	4.77
C(A8)	1755(4)	965(3)	3464(6)	5.39	C(C8)	4457(4)	765(4)	2994(6)	6.05
C(A9)	1723(4)	687(3)	2330(6)	5.66	C(C9)	4382(4)	513(3)	1896(6)	6.01
C(A10)	924(4)	427(3)	1660(5)	4.90	C(C10)	4130(4)	1016(3)	1281(5)	4.52
C(A10a)	131(4)	460(3)	2062(5)	3.78	C(C10a)	3956(3)	1808(3)	1856(5)	3.44
C(A11)	− 791(4)	214(3)	1420(5)	3.78	C(C11)	3651(3)	2412(3)	1309(5)	3.60
C(A12)	−1355(4)	754(3)	1302(5)	4.32	C(C12)	4223(4)	3019(3)	1409(5)	3.60
C(A12a)	−1055(4)	1629(3)	1818(5)	4.03	C(C12a)	5141(3)	3085(3)	2026(5)	3.70
C(A13)	−2346(4)	591(3)	927(6)	5.36	C(C13)	3908(4)	3764(3)	1148(5)	4.30
C(A14)	−2986(4)	771(4)	1546(6)	6.27	C(C14)	3786(4)	4469(3)	1917(6)	5.58
C(A15)	−2963(4)	1103(3)	2730(6)	5.45	C(C15)	3851(4)	4733(3)	3089(6)	5.06
C(A16)	−2280(4)	1312(3)	3534(6)	5.08	C(C16)	4024(4)	4366(3)	3817(5)	4.24
C(A17)	−1005(4)	71(3)	3864(5)	4.05	C(C17)	2774(4)	3006(3)	3598(5)	4.71
C(A18)	−1171(4)	− 663(3)	3118(5)	4.44	C(C18)	2092(4)	2832(3)	2814(6)	5.38
C(A19)	−1198(4)	− 973(3)	1957(6)	4.94	C(C19)	2038(4)	2557(4)	1611(6)	5.83
C(A20)	−1071(4)	− 648(3)	1188(5)	4.72	C(C20)	2662(4)	2401(3)	960(5)	4.85
C(B1)	− 552(4)	5174(3)	8480(5)	4.81	C(D1)	5526(4)	−1497(3)	1498(5)	4.73
C(B2)	−1305(4)	5345(3)	7885(6)	5.72	C(D2)	6293(4)	−1044(3)	2104(6)	5.13
C(B3)	−1471(4)	5055(4)	6778(6)	5.46	C(D3)	6452(4)	− 810(3)	3206(6)	5.15
C(B4)	− 862(4)	4556(3)	6210(5)	4.36	C(D4)	5830(4)	−1029(3)	3771(5)	4.60
C(B4a)	− 105(3)	4364(3)	6790(5)	3.41	C(D4a)	5068(3)	−1487(3)	3183(5)	3.39
C(B5)	634(3)	3881(3)	6281(5)	3.28	C(D5)	4334(4)	−1736(3)	3681(5)	3.60
C(B6)	798(3)	3170(3)	6400(4)	2.98	C(D6)	4178(3)	−2508(3)	3574(5)	3.56
C(B6a)	236(3)	2797(3)	6954(4)	2.86	C(D6a)	4752(3)	−3149(3)	2983(5)	3.36
C(B7)	− 384(3)	2162(3)	6419(5)	3.82	C(D7)	5365(4)	−3543(3)	3495(5)	4.27
C(B8)	− 870(4)	1848(3)	7026(6)	5.02	C(D8)	5838(4)	−4141(4)	2857(6)	5.56
C(B9)	− 752(4)	2151(4)	8122(6)	5.26	C(D9)	5692(4)	−4362(3)	1743(6)	5.50
C(B10)	− 122(4)	2778(3)	8679(5)	4.62	C(D10)	5072(4)	−3981(3)	1222(5)	4.62
C(B10a)	352(3)	3116(3)	8104(5)	3.29	C(D10a)	4597(3)	−3362(3)	1853(5)	3.34
C(B11)	1069(3)	3759(3)	8579(4)	3.42	C(D11)	3881(4)	−2917(3)	1394(5)	3.85
C(B12)	949(4)	4478(3)	8467(5)	3.58	C(D12)	4019(4)	−2149(3)	1488(5)	3.88
C(B12a)	74(4)	4674(3)	7927(5)	3.65	C(D12a)	4909(3)	−1717(3)	2046(5)	3.63
C(B13)	1732(4)	5053(3)	8609(6)	5.50	C(D13)	3265(4)	−1631(3)	1327(6)	5.32
C(B14)	2056(4)	5223(3)	7824(6)	5.65	C(D14)	2931(4)	−1095(3)	2134(6)	5.62
C(B15)	1860(4)	4926(3)	6644(6)	5.34	C(D15)	3107(4)	− 852(3)	3312(6)	5.50
C(B16)	1292(4)	4347(3)	5941(6)	4.82	C(D16)	3659(4)	−1106(3)	4004(5)	4.91
C(B17)	1679(4)	2788(3)	6192(5)	4.14	C(D17)	3316(4)	−2800(3)	3772(6)	4.88
C(B18)	2340(4)	2730(3)	6960(6)	4.85	C(D18)	2643(4)	−3214(3)	2994(6)	6.04
C(B19)	2467(4)	3017(3)	8146(6)	5.22	C(D19)	2500(4)	−3444(3)	1820(6)	5.90
C(B20)	1970(4)	3474(3)	8870(5)	5.14	C(D20)	2965(4)	−3313(3)	1129(6)	5.63

a) $B_{eq}=8\pi^2(u_1^2+u_2^2+u_3^2)/3$, where u_i is the root-mean-square deviation in the i-th principal axis of the thermal ellipsoid.

Center, using our own programs. The atomic scattering factors were taken from the International Tables.[5)]

Results and Discussion

The molecular framework thus obtained is shown in Fig. 1. The bond distances and angles are listed in Table 3, while the torsion angles are given in Fig. 2. From these results, it is concluded that the biphenylene dimer has the **3** structure. As may be seen in Fig. 2, of the four crystallographically-independent molecules, the A and C molecules have approximately the C_{2v} symmetry, while the B and D molecules are somewhat deformed, their symmetry being nearly C_2. The mean

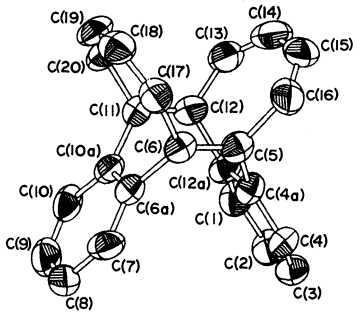

Fig. 1. A perspective view of the A molecule, and the numbering system of atoms. Carbon atoms are represented as thermal ellipsoids enclosing 50% probabilities. For the sake of clarity, hydrogen atoms are omitted.

values of the equivalent bond distances and angles for the four molecules are given in the last column of Table 3, the C_{2v} symmetry being assumed for all these molecules.

The mean lengths for the C(4a)–C(5) and C(5)–C(16) bonds, 1.499 and 1.500 Å, show that there is no appreciable conjugation between the C(5)=C(6) double bond and the benzene ring or the C(13)=C(14)–C(15)=C(16) diene part.[6] This can be explained by the fact that the mean magnitudes for the C(12a)–C(4a)–C(5)–C(6) and C(6)–C(5)–C(16)–C(15) torsion angles are 74 and 101° respectively. On the other hand, the mean length for C(14)–C(15), 1.450 Å, indicates that the C(13)=C(14) and C(15)=C(16) double bonds are thoroughly conjugated.

The central cyclooctatetraene ring takes a tub form. The bridging by the conjugated diene systems causes a close approach between the C(5)=C(6) and C(11)=C(12) double bonds; the average distance between the midpoints of these bonds is 2.67 Å, while the corresponding average for the C(4a)–C(12a) and C(6a)–C(10a) bonds is 2.85 Å. Because of this approach, the C(5)–C(4a)–C(12a) bond angle is somewhat shrunk, its mean value being 115.2°. The conjugated diene system further brings about a remarkable out-of-plane bending deformation[7] of the C(5)=C(6) and C(11)=C(12)

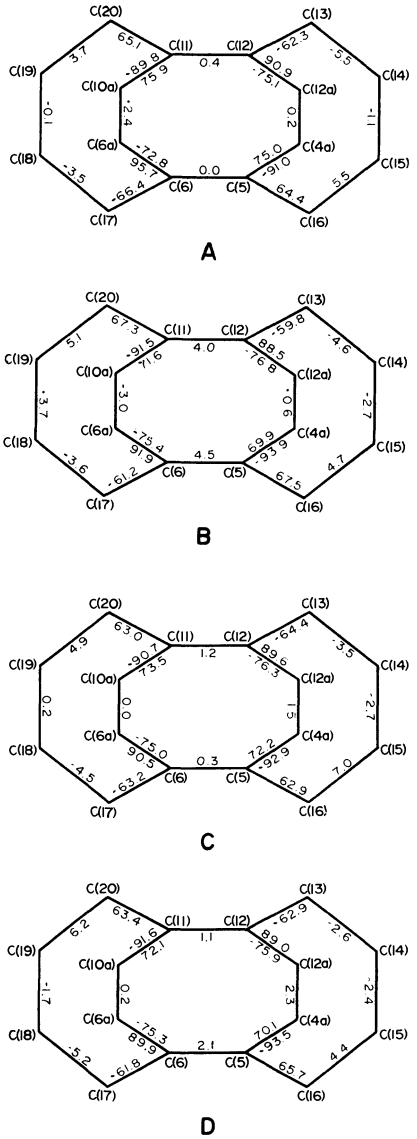

Fig. 2. The torsion angles (ϕ/°) for the tricyclo [6.4.-2.2^{2,7}]hexadeca-1,3,5,7,9,11,13,15-octaene skeletons. Only the torsion angles relevant to atoms which form the same ring are given in the ring.

Table 3. The bond distances (l/Å) and angles (ϕ/°), with their standard deviations
The standard deviations given in parentheses refer to the last decimal position.

	Mol. A	Mol. B	Mol. C	Mol. D	Mean[a]
C(1)-C(2)	1.391(7)	1.369(9)	1.366(8)	1.391(7)	
C(3)-C(4)	1.387(10)	1.394(8)	1.381(9)	1.402(10)	
C(7)-C(8)	1.371(9)	1.391(10)	1.416(8)	1.386(8)	
C(9)-C(10)	1.364(8)	1.393(8)	1.399(10)	1.376(9)	1.386(5)
C(1)-C(12a)	1.408(10)	1.405(8)	1.384(8)	1.382(9)	
C(4)-C(4a)	1.387(7)	1.378(8)	1.366(7)	1.383(7)	
C(6a)-C(7)	1.366(7)	1.390(6)	1.404(10)	1.379(8)	
C(10)-C(10a)	1.368(9)	1.373(10)	1.402(7)	1.406(7)	1.386(4)
C(2)-C(3)	1.349(10)	1.355(10)	1.373(10)	1.351(10)	
C(8)-C(9)	1.398(11)	1.344(10)	1.347(11)	1.364(11)	1.360(7)
C(4a)-C(12a)	1.394(8)	1.394(8)	1.417(8)	1.393(8)	
C(6a)-C(10a)	1.419(8)	1.411(8)	1.377(8)	1.385(8)	1.399(5)
C(4a)-C(5)	1.521(9)	1.501(7)	1.497(8)	1.498(9)	
C(6)-C(6a)	1.496(8)	1.474(8)	1.512(7)	1.500(7)	
C(10a)-C(11)	1.499(7)	1.485(7)	1.504(9)	1.500(8)	

Table 3. (Continued)

	Mol. A	Mol. B	Mol. C	Mol. D	Mean[a)]
C(12)-C(12a)	1.515(7)	1.494(8)	1.479(7)	1.508(7)	1.499(3)
C(5)-C(6)	1.300(8)	1.334(8)	1.328(8)	1.343(8)	
C(11)-C(12)	1.306(8)	1.334(8)	1.340(8)	1.336(8)	1.328(6)
C(5)-C(16)	1.510(8)	1.495(9)	1.486(7)	1.506(8)	
C(6)-C(17)	1.506(9)	1.506(7)	1.503(8)	1.488(9)	
C(11)-C(20)	1.505(8)	1.485(8)	1.490(8)	1.493(8)	
C(12)-C(13)	1.499(8)	1.512(8)	1.522(9)	1.489(8)	1.500(3)
C(13)-C(14)	1.323(10)	1.316(11)	1.357(8)	1.331(9)	
C(15)-C(16)	1.316(8)	1.339(7)	1.312(10)	1.322(10)	
C(17)-C(18)	1.345(7)	1.335(9)	1.299(8)	1.349(8)	
C(19)-C(20)	1.346(11)	1.349(9)	1.329(10)	1.299(11)	1.329(4)
C(14)-C(15)	1.464(11)	1.446(10)	1.440(11)	1.443(11)	
C(18)-C(19)	1.434(9)	1.451(10)	1.480(11)	1.440(11)	1.450(5)
C(2)-C(1)-C(12a)	118.9(6)	118.9(6)	121.9(6)	118.7(6)	
C(3)-C(4)-C(4a)	119.3(6)	119.0(6)	120.6(6)	119.1(6)	
C(6a)-C(7)-C(8)	121.5(6)	119.6(5)	117.2(6)	118.6(6)	
C(9)-C(10)-C(10a)	121.8(6)	120.0(6)	117.1(6)	119.0(6)	119.5(4)
C(1)-C(2)-C(3)	121.0(7)	122.7(6)	119.3(6)	122.1(7)	
C(2)-C(3)-C(4)	121.2(5)	119.5(6)	120.5(5)	119.7(5)	
C(7)-C(8)-C(9)	118.7(5)	121.1(5)	121.1(7)	121.8(6)	
C(8)-C(9)-C(10)	120.1(6)	120.4(7)	122.3(5)	120.2(6)	120.7(3)
C(4)-C(4a)-C(12a)	120.1(6)	121.5(5)	119.7(5)	120.6(6)	
C(7)-C(6a)-C(10a)	119.8(6)	119.0(5)	121.0(5)	120.6(5)	
C(6a)-C(10a)-C(10)	118.0(5)	119.8(4)	121.2(6)	119.9(5)	
C(1)-C(12a)-C(4a)	119.5(5)	118.4(5)	118.0(5)	119.8(5)	119.8(3)
C(4)-C(4a)-C(5)	125.9(5)	124.5(5)	124.9(5)	124.6(5)	
C(6)-C(6a)-C(7)	125.9(5)	124.4(5)	123.0(5)	123.9(5)	
C(10)-C(10a)-C(11)	127.3(5)	126.2(5)	123.4(5)	124.7(5)	
C(1)-C(12a)-C(12)	125.1(5)	124.6(5)	127.3(6)	123.6(5)	125.0(3)
C(5)-C(4a)-C(12a)	114.0(4)	113.8(5)	115.5(4)	114.7(4)	
C(6)-C(6a)-C(10a)	114.3(4)	116.5(4)	115.9(5)	115.5(5)	
C(6a)-C(10a)-C(11)	114.7(5)	113.8(5)	115.3(4)	115.4(4)	
C(4a)-C(12a)-C(12)	115.3(6)	116.9(5)	114.7(5)	116.4(5)	115.2(2)
C(4a)-C(5)-C(6)	119.8(5)	120.3(6)	119.5(4)	121.3(5)	
C(5)-C(6)-C(6a)	120.9(6)	122.6(5)	120.4(5)	121.2(5)	
C(10a)-C(11)-C(12)	120.4(5)	120.5(5)	118.5(5)	121.1(5)	
C(11)-C(12)-C(12a)	118.7(5)	121.2(5)	120.9(6)	120.3(5)	120.5(3)
C(4a)-C(5)-C(16)	113.3(5)	114.2(5)	115.5(5)	113.4(5)	
C(6a)-C(6)-C(17)	114.5(4)	115.4(5)	114.2(4)	115.1(4)	
C(10a)-C(11)-C(20)	114.7(5)	114.4(5)	115.0(5)	114.2(5)	
C(12a)-C(12)-C(13)	115.3(5)	115.4(5)	115.6(4)	115.7(4)	114.7(2)
C(6)-C(5)-C(16)	125.2(6)	123.4(5)	123.2(5)	123.1(5)	
C(5)-C(6)-C(17)	123.5(5)	120.8(5)	123.7(5)	122.0(5)	
C(12)-C(11)-C(20)	123.2(5)	122.9(5)	124.4(5)	122.6(5)	
C(11)-C(12)-C(13)	124.4(5)	121.7(5)	121.9(5)	122.1(5)	123.0(3)
C(12)-C(13)-C(14)	126.7(6)	126.3(5)	123.9(6)	124.5(6)	
C(5)-C(16)-C(15)	128.3(7)	123.8(7)	125.3(5)	124.8(6)	
C(6)-C(17)-C(18)	122.8(6)	125.5(6)	127.3(6)	125.8(7)	
C(11)-C(20)-C(19)	124.5(5)	124.9(6)	126.4(6)	126.3(6)	125.4(3)
C(13)-C(14)-C(15)	132.6(6)	134.2(5)	134.3(7)	134.8(6)	
C(14)-C(15)-C(16)	130.8(6)	132.5(7)	133.0(5)	132.9(6)	
C(17)-C(18)-C(19)	133.6(7)	133.3(5)	131.8(6)	132.8(7)	
C(18)-C(19)-C(20)	134.4(5)	132.5(6)	132.6(5)	132.9(5)	133.1(3)
C-H[b)]	1.04(1)				
C-C-H(Benzene)[b)]	120(1)				
C=C-H (Octaene)[b)]	119(1)				
C-C-H (Octaene)[b)]	112(1)				

a) The mean value calculated for the four molecules on the assumption that they all have the C_{2v} symmetry. The standard deviation was estimated from the formula: $\sigma^2=\Sigma(x_i-\bar{x})^2/n(n-1)$. b) The mean value for the four molecules.

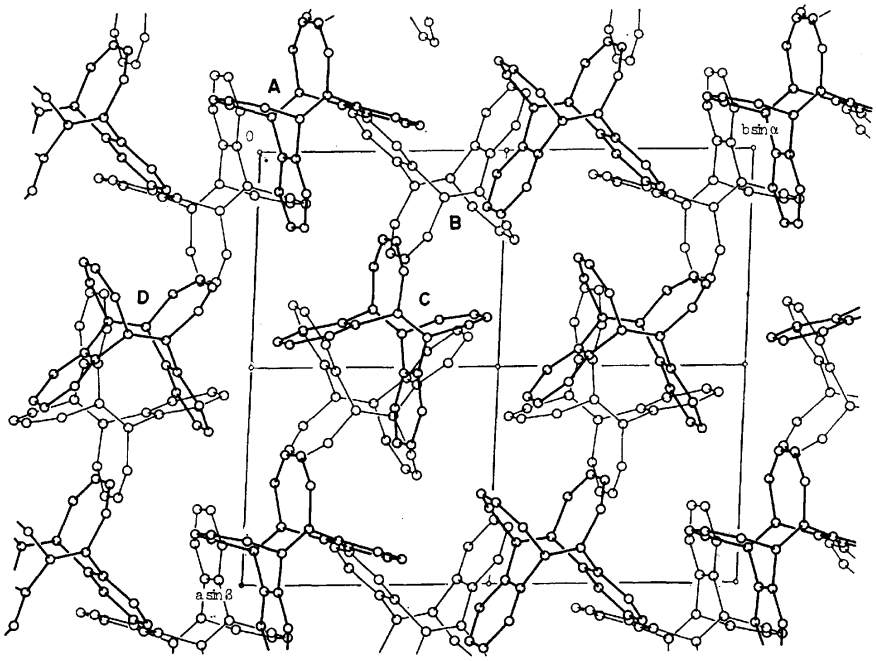

Fig. 3. The crystal structure viewed along the c axis.

TABLE 4. THE PROJECTIONS (ϕ/°) OF THE BOND ANGLES ALONG THE C(5)=C(6) OR C(11)=C(12) BOND

	A	B	C	D
(1) Along C(5)=C(6)				
C(4a)–C(5)–C(16)	164.2	162.2	163.9	161.9
C(6a)–C(6)–C(17)	167.5	166.6	164.0	164.3
(2) Along C(11)=C(12)				
C(10a)–C(11)–C(20)	164.4	161.6	162.6	162.3
C(12a)–C(12)–C(13)	164.6	164.4	165.1	163.9

ethylenic groups (see Table 4); the average for the projected angle of C(4a)–C(5)–C(16) along the C(5)=C(6) double bond is 164°.

On the other hand, the restricted approach between the C(5)=C(6) and C(11)=C(12) double bonds results in an enlargement of the C(12)–C(13)=C(14) and C(13)=C(14)–C(15) bond angles; the averages for these bond angles are 125.4 and 133.1° respectively. Such a way of deformation of the two bond angles can be reproduced by the following simple calculation. If one assumes that the C(12)–C(13)=C(14)–C(15)=C(16)–C(5) moiety has the C_{2v} symmetry, the C(5)···C(12) distance, l, is expressed by:

$$l = l_1 - 2l_2 \cos\theta_1 + 2l_3 \cos(\theta_1+\theta_2), \quad (1)$$

where l_1, l_2, and l_3 are the C(14)–C(15), C(13)=C(14), and C(12)–C(13) distances respectively, and where θ_1 and θ_2 are the C(13)=C(14)–C(15) and C(12)–C(13)=C(14) angles respectively. If, as a first approximation, the change in the bond distortion of the C(5) and C(12) terminal atoms is neglected, the variable part of the strain energy due to the bond-angle deformation, ΔE, is given by:

$$\Delta E = k\{(\theta_1-\theta_0)^2 + (\theta_2-\theta_0)^2\}, \quad (2)$$

where k is the force constant for the deformation of the C=C–C bond angle and where θ_0 is the strainless C=C–C bond angle, for which 120° is assumed in the present calculation. When the average observed values of 1.450, 1.329, 1.500, and 2.675 Å are used for l_1, l_2, l_3, and l respectively, ΔE is minimized at $\theta_1=132°$ and $\theta_2=127°$ under the conditions of Eq. 1. These θ_1 and θ_2 values are in good agreement with their respective observed values. For $\theta_1=\theta_2=120°$, $(\partial l/\partial\theta_1)$ is greater than $(\partial l/\partial\theta_2)$ by a factor of 1.886, while $(\partial\Delta E/\partial\theta_1)$ is equal to $(\partial\Delta E/\partial\theta_2)$; that is, the enlargement of θ_1 can separate the C(5) and C(12) atoms more effectively than that of θ_2. This explains why, in both the observed and calculated geometries, θ_1 is greater than θ_2.

In all four molecules, the C(14) and C(15) atoms deviate slightly from the least-squares plane for the C(5), C(12), C(13), and C(16) atoms onto the side of the benzene ring (C(1), C(2), C(3), C(4), C(4a), and C(12a)); the average for the dihedral angle between this plane and the least-squares plane of the C(13)=C(14)–C(15)=C(16) part is 3.9°.

The crystal structure viewed along the c axis is shown in Fig. 3. The orientations of the four independent molecules are somewhat different from one another. All the intermolecular contacts correspond to the normal van der Waals interactions.

References

1) N. L. Goldman and R. A. Ruden, *Tetrahedron Lett.*, **1968**, 3951.

2) E. L. Passer, Ph. D. Thesis, Fordham University, New York, U.S.A., 1976.

3) J. Karle and I. L. Karle, *Acta Crystallogr.*, **21**, 849 (1966).

4) W. Hoppe, J. Gassmann, and K. Zechmeister, "Crystallographic Computing," ed by F. R. Ahmed, Munksgaard, Copenhagen (1970), p. 26.

5) "International Tables for X-Ray Crystallography," The Kynoch Press, Birmingham (1974), Vol. IV.

6) "Interatomic Distances, Supplement," ed by L. E. Sutton, The Chemical Society, London (1965).

7) P. Ganis and J. D. Dunitz, *Helv. Chim. Acta*, **50**, 2379 (1967).

The Crystal and Molecular Structure of Grayanotoxin XIX. A New Minor Diterpene from *Leucothoe Grayana Max.*

Akio FURUSAKI,* Shinsei GASA, Ryūzō IKEDA, Takeshi MATSUMOTO, Noritake YASUOKA,† and Yoshiki MATSUURA†

Department of Chemistry, Faculty of Science, Hokkaido University, Sapporo 060
†Institute for Protein Research, Osaka University, Suita, Osaka 565

(Received September 30, 1980)

The molecular structure of grayanotoxin XIX, $C_{20}H_{30}O_3$, has been determined by means of X-ray crystal analysis. The crystals are triclinic, with two molecules in a unit cell with dimensions of $a=10.406$, $b=10.648$, $c=8.003$ Å, $\alpha=90.00$, $\beta=94.25$, and $\gamma=102.76°$; the space group is P1. 2671 unique intensity data were collected on a four-circle diffractometer with Ni-filtered Cu $K\alpha$ radiation. The structure was elucidated by the Monte Carlo direct method, using the 50 strongest reflections as the starting set. The block-diagonal least-squares refinement reduced the R value to 0.038. The structure obtained corresponds to 14-deoxygrayanotoxin VII. The two independent molecules exist in different conformations: one has a half-chair A-ring, and the other, an envelope A-ring. In both molecules, the B-ring takes a conformation intermediate between the chair and twist-chair forms, and the C-ring adopts a boat conformation. The crystal consists of infinite hydrogen-bonded molecular chains along the c axis.

A number of diterpenoids, such as grayanotoxins,[1,2] leucothols,[3] and grayathols,[4] have thus far been isolated from *Leucothoe grayana Max.* In this paper, we wish to report on the X-ray structure determination and molecular geometry of grayanotoxin (hereafter G) XIX, a new minor constituent from the same plant.

Experimental

Isolation of G XIX. Grayathol A was crystallized from a diethyl ether solution of the unknown-compound-containing fraction (81 mg)[5] obtained from the crude extract of *Leucothoe grayana Max.* The chromatography of the filtrate on silica gel (1 g) afforded G XIX (21 mg) in a 5×10^{-7} % yield from dried leaves; mp 132—133 °C (recrystallized from diethyl ether), $[\alpha]_D$ −12° (*c* 1, MeOH); IR (Nujol) 3496, 3370^{sh}, 1658, 1637 cm^{-1}; ^{1}H-NMR ($CDCl_3$) 1.05, 1.29 (each 3H, s), 1.69 (3H, d, $J=2$ Hz), 3.00 (1H, q, $J_{AX+BX}=8+11$ Hz), 3.60 (1H, q, $J_{AX+BX}=2+7$ Hz), 3.73 (1H, q, $J_{AX+BX}=4+11$ Hz), 4.91, 5.04 (each 1H, s), 5.18 (1H, bs); MS *m/e* 318 (M^+). Found: C, 74.91; H, 9.37%. Calcd for $C_{20}H_{30}O_3$: C, 75.43; H, 9.50%. The ^{1}H-NMR spectrum was recorded on a Hitachi R-20B spectrometer, using TMS as the internal reference. The chemical shifts are given on the δ scale (s=singlet, d=doublet, q=quartet, bs=broad singlet). The IR spectrum was obtained on a JASCO Model IR-S spectrophotometer.

X-Ray Measurement. A colorless single crystal cut into a cube with an edge of about 0.3 mm was used. The crystal data are summarized in Table 1. The cell dimensions and reflection intensities were measured on a Rigaku four-circle diffractometer with Ni-filtered Cu $K\alpha$ radiation (40 kV, 60 mA, $\lambda=1.5418$ Å). The θ-2θ continuous-scan technique was applied at a θ scan rate of 8° min^{-1}; the background was measured for 5 s at each end of the scan range. Three standard reflections, measured at intervals of every 60 reflections, showed no significant decrease in intensity during the course of data collection. The intensities were corrected for the Lorentz and polarization factors, but not for the absorption or the extinction effect. In the range of 2θ values up to 125°, 2671 unique structure factor amplitudes above the $\sigma(F)$ level were selected for the structure determination.

Table 1. The crystal data

$C_{20}H_{30}O_3$	M.W.=318.46
Crystal system	Triclinic
Space group	P1
Cell dimensions	$a=10.406(2)$ Å
	$b=10.648(2)$ Å
	$c=8.003(2)$ Å
	$\alpha=90.00(7)°$
	$\beta=94.25(3)°$
	$\gamma=102.76(2)°$
V	862.4 Å^3
Z	2
D_x	1.226 g cm^{-3}
μ(Cu $K\alpha$)	5.99 cm^{-1}

Structure Determination

The structure was elucidated by the Monte Carlo direct method,[6] using the 50 strongest reflections as the starting set. In order to extend the tentative phase set derived from successively-generated random numbers, 10 cycles of the tangent procedure were performed by the use of 556 $|E|$ values above 1.30. Since the 208th phase set gave a low R_K value of 0.296 ($R_K=\sum||E_o|-k|E_c||/\sum|E_o|$) and a moderate q value of 0.424 ($q=\sum_h|E_h|(|\sum_k|E_kE_{h-k}|\exp\{2\pi i(\phi_k+\phi_{h-k})\}|/\sum_k|E_kE_{h-k}|)/\sum_h|E_h|$), 6 additional cycles of the tangent procedure were carried out using 604 $|E|$ values above 1.25; the R_k and q values were 0.299 and 0.356 respectively. An E-map based on 560 phases afforded all the 46 non-hydrogen atoms.

The structure thus obtained was refined by the block-diagonal-matrix least-squares method, first with isotropic and then with anisotropic temperature factors. After 57 of the 60 independent hydrogen atoms had been located in a difference Fourier map, further least-squares refinement including these hydrogen atoms with isotropic temperature factors was carried out. The weighting scheme used was as follows: $w=1/\{\sigma(F)^2\exp(AX^2+BY^2+CXY+DX+EY)\}$, where $X=|F_o|$ and $Y=\sin\theta/\lambda$. The A, B, C, D, and E coefficients are constants which were determined from the $(\Delta F)^2$ values. In this manner, the R value reached 0.038. The final atomic parameters are listed in Table 2. The table of

TABLE 2. THE FINAL ATOMIC PARAMETERS AND ESTIMATED STANDARD DEVIATIONS

The coordinates of the non-hydrogen and hydrogen atoms are multiplied by 10^4 and 10^3 respectively.

(1) The non-hydrogen atoms.

Atom	x	y	z	B_{eq}[a)]/Å^2	Atom	x	y	z	B_{eq}/Å^2
O(A1)	6513(3)	8506(3)	4043(3)	5.38	O(B1)	312(2)	−1847(2)	−1978(3)	3.64
O(A2)	7452(2)	7991(2)	7370(3)	3.44	O(B2)	−969(2)	−1332(2)	1468(3)	3.24
O(A3)	6259(3)	8460(2)	10241(3)	3.61	O(B3)	222(3)	−1821(2)	4400(3)	4.19
C(A1)	5728(3)	6037(3)	6592(3)	2.41	C(B1)	518(3)	675(3)	1025(3)	2.47
C(A2)	5412(4)	6322(3)	4732(4)	3.59	C(B2)	563(4)	326(3)	− 825(4)	3.56
C(A3)	5323(3)	7732(3)	4631(4)	3.24	C(B3)	1121(3)	− 894(3)	− 887(4)	3.02
C(A4)	5177(4)	8142(3)	6454(4)	3.59	C(B4)	1321(3)	−1307(3)	973(4)	3.14
C(A5)	6092(3)	7378(3)	7489(4)	2.64	C(B5)	360(3)	− 648(3)	1895(4)	2.63
C(A6)	5905(3)	7235(3)	9367(4)	2.79	C(B6)	590(3)	− 526(3)	3808(4)	2.81
C(A7)	6672(3)	6310(3)	10232(4)	2.91	C(B7)	−187(3)	329(3)	4618(4)	2.80
C(A8)	6083(3)	4854(3)	10021(4)	2.56	C(B8)	335(3)	1793(3)	4529(3)	2.40
C(A9)	6442(3)	4263(3)	8378(4)	2.75	C(B9)	−180(3)	2370(3)	2876(4)	2.52
C(A10)	6708(3)	5194(3)	6949(4)	2.73	C(B10)	−498(3)	1452(3)	1381(3)	2.41
C(A11)	5362(4)	3074(3)	7769(4)	3.55	C(B11)	828(4)	3606(3)	2369(4)	3.33
C(A12)	4627(4)	2228(3)	9106(4)	3.78	C(B12)	1598(4)	4469(3)	3800(4)	3.69
C(A13)	4465(3)	3025(3)	10674(4)	3.18	C(B13)	1932(3)	3686(3)	5342(4)	3.03
C(A14)	4587(3)	4434(3)	10200(4)	2.80	C(B14)	1847(3)	2281(3)	4834(4)	2.84
C(A15)	6583(3)	4129(3)	11475(4)	3.00	C(B15)	− 104(3)	2491(3)	5980(4)	2.83
C(A16)	5672(3)	3108(3)	11874(4)	3.19	C(B16)	812(3)	3530(3)	6483(4)	3.01
C(A17)	5777(4)	2110(4)	13161(5)	4.36	C(B17)	785(4)	4493(4)	7821(5)	4.28
C(A18)	5610(6)	9613(4)	6719(5)	6.51	C(B18)	1026(5)	−2776(4)	1121(4)	4.87
C(A19)	3724(4)	7670(5)	6797(5)	5.42	C(B19)	2770(4)	− 749(4)	1584(5)	4.31
C(A20)	7734(4)	5243(4)	6060(5)	4.31	C(B20)	−1595(3)	1400(3)	406(4)	3.44

a) $B_{eq}=8\pi^2\ (u_1^2+u_2^2+u_3^2)/3$, where u_i is the root-mean-square deviation in the i-th principal axis of the thermal ellipsoid.

(2) The hydrogen atoms.

Atom[a)]	x	y	z	B/Å^2	Atom	x	y	z	B/Å^2
H(OA1)	635(5)	847(5)	303(7)	8.8(14)	H(OB3)	33(4)	−185(4)	549(5)	5.5(9)
H(OA2)	753(4)	812(4)	641(5)	4.9(9)	H(B1)	138(4)	115(3)	146(4)	4.2(8)
H(OA3)	717(5)	863(5)	1047(6)	8.1(13)	H(B2a)	104(4)	99(4)	− 124(5)	5.0(9)
H(A1)	492(3)	562(3)	705(3)	2.2(6)	H(B2b)	− 42(4)	6(3)	− 131(4)	4.1(8)
H(A2a)	440(5)	563(4)	439(6)	6.7(11)	H(B3)	198(3)	− 76(3)	− 142(4)	3.3(7)
H(A2b)	613(5)	622(4)	412(6)	6.1(10)	H(B6)	154(3)	− 18(3)	408(4)	3.0(7)
H(A3)	451(3)	782(3)	392(4)	4.0(8)	H(B7a)	− 14(4)	17(3)	581(5)	4.0(8)
H(A6)	484(3)	694(3)	951(4)	3.7(7)	H(B7b)	−114(3)	13(3)	436(4)	3.8(8)
H(A7a)	672(3)	651(3)	1143(4)	3.2(7)	H(B9)	−101(3)	259(3)	310(4)	2.5(6)
H(A7b)	762(3)	649(3)	986(4)	2.8(6)	H(B11a)	148(3)	324(3)	165(4)	3.2(7)
H(A9)	727(3)	403(3)	864(4)	2.8(6)	H(B11b)	29(4)	415(4)	159(5)	4.3(8)
H(A11a)	470(4)	340(3)	710(5)	4.2(8)	H(B12a)	252(5)	491(5)	345(6)	7.5(12)
H(A11b)	578(3)	260(3)	712(4)	4.1(8)	H(B12b)	107(4)	512(4)	420(5)	4.5(9)
H(A12a)	371(4)	181(4)	866(5)	5.4(10)	H(B13)	271(3)	399(3)	582(4)	3.6(7)
H(A12b)	507(4)	153(4)	945(5)	5.1(9)	H(B14a)	230(3)	217(3)	390(4)	3.6(7)
H(A13)	361(4)	261(4)	1126(5)	5.5(9)	H(B14b)	217(3)	177(3)	579(4)	2.6(6)
H(A14a)	403(3)	453(3)	920(4)	3.5(7)	H(B15)	−100(4)	213(4)	644(5)	4.5(8)
H(A14b)	435(3)	497(3)	1111(4)	3.2(7)	H(B17a)	3(4)	420(4)	852(5)	4.7(9)
H(A15)	759(4)	430(4)	1194(5)	4.7(9)	H(B17b)	89(5)	542(5)	733(7)	9.5(15)
H(A17a)	667(4)	227(4)	1376(5)	5.6(10)	H(B17c)	156(4)	455(4)	861(5)	6.1(10)
H(A17b)	577(4)	128(4)	1261(6)	6.7(11)	H(B18a)	116(4)	−302(4)	225(5)	5.4(9)
H(A17c)	519(5)	212(5)	1402(6)	8.2(13)	H(B18b)	164(5)	−313(5)	39(6)	7.0(12)
H(A19a)	311(5)	808(4)	603(6)	6.8(11)	H(B18c)	7(4)	−320(4)	73(5)	5.3(9)
H(A19b)	338(4)	782(4)	787(6)	6.6(11)	H(B19a)	339(5)	−115(4)	92(6)	7.0(12)
H(A19c)	344(5)	679(5)	653(6)	8.4(13)	H(B19b)	298(4)	−105(4)	280(5)	6.3(11)
H(A20a)	832(4)	475(4)	630(5)	5.9(10)	H(B19c)	311(5)	24(5)	153(7)	8.1(13)
H(A20b)	796(4)	585(4)	509(5)	5.0(9)	H(B20a)	−226(4)	197(4)	65(5)	4.7(8)
H(OB1)	− 48(5)	−200(5)	−165(6)	7.1(12)	H(B20b)	−179(3)	93(3)	−73(4)	3.7(7)
H(OB2)	−109(3)	−192(4)	221(4)	4.2(8)					

a) The hydrogen atoms are denoted by the number of the non-hydrogen atom to which they are attached, suffixed by a, b, or c where necessary.

the anisotropic thermal parameters and that of the observed and calculated structure factors are kept at the Chemical Society of Japan (Document No. 8128).

The calculations were performed on an ACOS 700 computer at the Institute for Protein Research, Osaka University, and on a FACOM 230-75 computer at the Hokkaido University Computing Center. The atomic scattering factors were taken from the International Tables.[7]

Results and Discussion

Molecular Structure. The skeletons of the two independent G XIX molecules, **A** and **B**, are illustrated in Fig. 1. The bond distances and angles and the torsion angles are given in Table 3 and Fig. 2 respectively. From these results, it is concluded that G XIX has the **1** structure.

The five-membered A-ring in the **A** molecule takes a half-chair form with an approximate two-fold rotation axis through the C(A2) atom, while that in the **B**

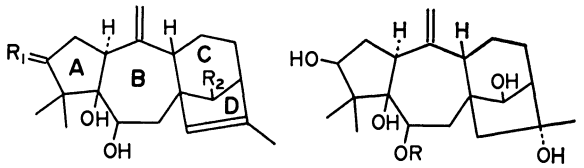

1 (GXIX): $R_1 = <^{OH}_{H}$ $R_2 = H$ 3 (GII): R = H

2 (GXVIII): $R_1 = O$ $R_2 = OH$ 4 (GXVI): R = Ac

Table 3. The bond distances (l/Å) and angles (ϕ/°), with their standard deviations

The standard deviations given in parentheses refer to the last decimal position.

(1) The bond distances.

	Mol. A	Mol. B		Mol. A	Mol. B
C(1)–C(2)	1.545(4)	1.533(4)	C(7)–C(8)	1.540(4)	1.537(4)
C(1)–C(5)	1.555(4)	1.552(4)	C(8)–C(9)	1.562(4)	1.567(4)
C(1)–C(10)	1.512(5)	1.521(5)	C(8)–C(14)	1.539(4)	1.545(4)
C(2)–C(3)	1.527(5)	1.538(5)	C(8)–C(15)	1.519(4)	1.529(4)
C(3)–C(4)	1.551(5)	1.565(4)	C(9)–C(10)	1.515(4)	1.515(4)
C(3)–O(1)	1.439(4)	1.419(4)	C(9)–C(11)	1.547(4)	1.564(4)
C(4)–C(5)	1.575(5)	1.567(5)	C(10)–C(20)	1.318(5)	1.324(4)
C(4)–C(18)	1.541(5)	1.532(5)	C(11)–C(12)	1.535(5)	1.528(4)
C(4)–C(19)	1.529(6)	1.536(5)	C(12)–C(13)	1.555(5)	1.550(5)
C(5)–C(6)	1.534(4)	1.533(4)	C(13)–C(14)	1.528(5)	1.532(5)
C(5)–O(2)	1.432(4)	1.430(4)	C(13)–C(16)	1.510(5)	1.514(5)
C(6)–C(7)	1.533(5)	1.519(5)	C(15)–C(16)	1.331(4)	1.331(4)
C(6)–O(3)	1.440(4)	1.437(4)	C(16)–C(17)	1.496(5)	1.489(5)

(2) The bond angles.

	Mol. A	Mol. B		Mol. A	Mol. B
C(2)–C(1)–C(5)	105.0(2)	103.0(2)	C(7)–C(8)–C(9)	113.4(2)	112.5(2)
C(2)–C(1)–C(10)	116.6(3)	115.1(3)	C(7)–C(8)–C(14)	115.4(3)	116.0(3)
C(5)–C(1)–C(10)	115.2(2)	116.0(2)	C(7)–C(8)–C(15)	110.4(2)	111.1(2)
C(1)–C(2)–C(3)	107.5(3)	107.5(3)	C(9)–C(8)–C(14)	110.0(2)	110.2(2)
C(2)–C(3)–C(4)	105.2(3)	106.2(3)	C(9)–C(8)–C(15)	107.0(3)	106.6(3)
C(2)–C(3)–O(1)	110.6(3)	111.4(3)	C(14)–C(8)–C(15)	99.4(2)	99.3(2)
C(4)–C(3)–O(1)	109.5(3)	115.5(2)	C(8)–C(9)–C(10)	115.0(3)	115.1(3)
C(3)–C(4)–C(5)	101.7(3)	103.0(3)	C(8)–C(9)–C(11)	111.1(3)	111.1(2)
C(3)–C(4)–C(18)	111.8(3)	111.4(3)	C(10)–C(9)–C(11)	109.2(2)	108.3(2)
C(3)–C(4)–C(19)	107.3(3)	107.6(3)	C(1)–C(10)–C(9)	116.5(3)	117.2(2)
C(5)–C(4)–C(18)	113.4(3)	114.0(3)	C(1)–C(10)–C(20)	122.5(3)	123.0(3)
C(5)–C(4)–C(19)	111.8(3)	111.4(3)	C(9)–C(10)–C(20)	121.0(3)	119.7(3)
C(18)–C(4)–C(19)	110.4(4)	109.3(3)	C(9)–C(11)–C(12)	117.6(3)	116.7(3)
C(1)–C(5)–C(4)	102.1(2)	102.8(2)	C(11)–C(12)–C(13)	112.2(3)	112.3(3)
C(1)–C(5)–C(6)	110.4(2)	113.0(2)	C(12)–C(13)–C(14)	109.4(3)	110.5(3)
C(1)–C(5)–O(2)	111.8(3)	106.4(2)	C(12)–C(13)–C(16)	108.2(3)	108.4(3)
C(4)–C(5)–C(6)	116.8(3)	116.5(3)	C(14)–C(13)–C(16)	101.6(2)	100.9(2)
C(4)–C(5)–O(2)	110.1(2)	108.8(2)	C(8)–C(14)–C(13)	100.8(3)	100.6(3)
C(6)–C(5)–O(2)	105.9(2)	108.8(2)	C(8)–C(15)–C(16)	111.8(3)	111.4(3)
C(5)–C(6)–C(7)	113.6(3)	114.7(3)	C(13)–C(16)–C(15)	108.1(3)	108.4(3)
C(5)–C(6)–O(3)	111.7(2)	105.1(2)	C(13)–C(16)–C(17)	122.7(3)	122.1(3)
C(7)–C(6)–O(3)	108.9(2)	110.4(3)	C(15)–C(16)–C(17)	129.0(3)	129.3(3)
C(6)–C(7)–C(8)	117.8(2)	117.4(3)			

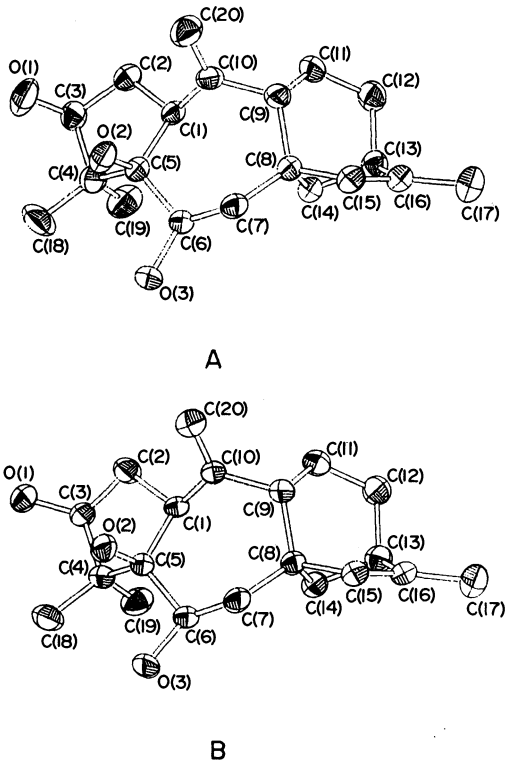

Fig. 1. Perspective views of the A and B molecules. Each non-hydrogen atom is represented as a thermal ellipsoid enclosing a 50% probability.

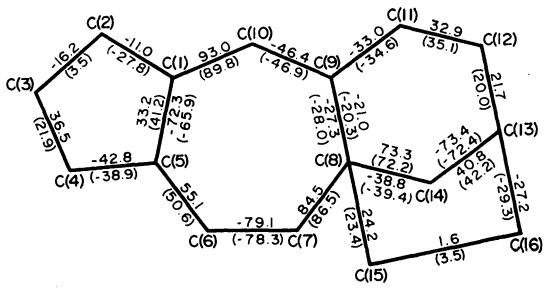

Fig. 2. The torsion angles (ϕ/°) of the A-, B-, C-, and D-rings. Only the torsion angles relevant to atoms which form the same ring are given in the ring. The values for the B molecule are given in parentheses.

molecule has an envelope form with an approximate mirror plane through the C(B5) atom. Although the former conformation permits the formation of the intramolecular hydrogen bond, O(2)–H···O(1) (see Table 4), the latter is unfavorable for this hydrogen bonding, the O(B1)···O(B2) distance being 3.248(3) Å. Consequently, the O(B2)H hydroxyl group forms a considerably bent hydrogen bond with the O(B3) atom of the same molecule; the O(B2)–H···O(B3) angle is 121°. Since, in the G XVIII (**2**) molecule[8] having almost the same ring conformation as the **B** molecule, the O(2)H hydroxyl group donates its proton to the exocyclic double bond, C(10)=C(20), the present O(B2)–H···O(B3) interaction will be nearly as weak as the O–H···π hydrogen bonding.[9] The O(1)–C(3)–C(4)–C(18) torsion angles in the **A** and **B** molecules are 38.9 and 20.4° respectively; the resulting difference in torsional strain results in a difference of 6.0° between the O(1)–C(3)–C(4) bond angles in the two molecules.

As is found also in other grayanotoxins, **2**—**4**,[8,10,11] the C(4)–C(5) bonds in the **A** and **B** molecules are somewhat lengthened. This bond lengthening is probably due to the steric repulsions between the C(18)H_3 and O(2)H groups and between the C(19)H_3 and C(6)H groups: C(A18)···O(A2), 2.871(7); C(A19)···C(A6), 3.061(6); C(B18)···O(B2), 2.872(6); C(B19)···C(B6), 3.034(5) Å. These steric repulsions further result in a distortion of the C(4)–C(18) and C(4)–C(19) bonds; the C(5)–C(4)–C(18) and C(5)–C(4)–C(19) bond angles are larger than the C(3)–C(4)–C(18) and C(3)–C(4)–C(19) bond angles by 1.6 and 4.5° respectively for the **A** molecule, and by 2.6 and 3.8° respectively for the **B** molecule.

In both molecules, the seven-membered B-rings adopt conformations intermediate between the chair form

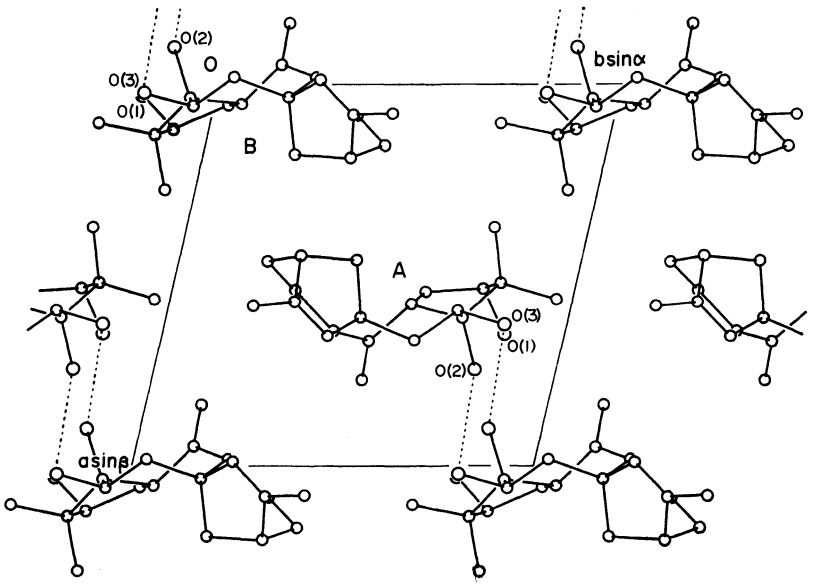

Fig. 3. The crystal structure viewed along the c axis.

characterized by the mirror plane through the C(5) atom and the twist-chair form characterized by the two-fold rotation axis through the C(9) atom. The corresponding torsion angles of these two B-rings are in good agreement with each other except for the three bonds associated with the A-ring atoms. If the present B-rings are considered to be of the chair form, the interaction between axial groups at the C(7) and C(10) atoms corresponds to the severe 3a-3'a repulsion in the chair cycloheptane.[12] However, since the C(10) atom forms a double bond with the C(20), the conformations of these B-rings are free from the 3a-3'a repulsion; hence, they are probably more stable than the B-ring conformations in G II[10] and XVI.[11]

The six-membered C-rings in both **A** and **B** molecules take boat conformations similar to that of the C-ring in G XVIII.[8] On the other hand, it has been found that, in all of the G I,[13] II, and XVI molecules where the C(15)–C(16) bond is a single bond, the C-rings possess the chair conformation. These facts suggest that the C-ring conformation depends largely on the nature of the C(15)–C(16) bond. Force-field calculations[14] for 6-methylbicyclo[3.2.1]octane and 6-methylbicyclo[3.2.1]oct-6-ene showed that, if the influence of the B-ring is neglected, the transformation of the C(15)–C(16) single bond into the double bond can reduce the chair-boat enthalpy difference of the C-ring by 1.8 kcal/mol, but that it cannot reverse the relative stabilities of the two C-ring conformations.[8] Accordingly, in order fully to understand the conformational behavior of the C-ring, the force-field calculations including the B-ring are now in progress.

Table 4. The hydrogen bonds, X–H···Y

	X	Y	X···Y l/Å	H···Y l/Å	X–H···Y ϕ/°
(1)	Intramolecular				
	O(A2)	O(A1)	2.863(4)	2.19(4)	145(4)
	O(B2)	O(B3)	2.676(3)	2.13(3)	121(3)
(2)	Intermolecular				
	O(A1)	O(A3)[a)]	3.034(3)	2.23(6)	171(5)
	O(A3)	O(B2)[b)]	2.938(4)	2.03(5)	165(5)
	O(B1)	O(A2)[c)]	2.950(3)	2.24(5)	140(4)
	O(B3)	O(B1)[d)]	2.894(3)	2.03(4)	171(4)

The symmetry codes are as follows: a) $x, y, -1+z$; b) $1+x, 1+y, 1+z$; c) $-1+x, -1+y, -1+z$; d) $x, y, 1+z$.

Crystal Structure. The crystal structure viewed along the c axis is shown in Fig. 3. The details of hydrogen bonding are given in Table 4. The **A** and **B** molecules are connected by the O(A3)–H···O(B2) and O(B1)–H···O(A2) hydrogen bonds, forming a dimer. These hydrogen-bonded dimers are further held together by the intermolecular hydrogen bonds, O(A1)–H···O(A3) and O(B3)–H···O(B1), to form a double molecular chain. The present crystal consists of such infinite hydrogen-bonded molecular chains along the c axis.

References

1) S. Miyajima and S. Takei, *J. Agric. Chem. Jpn.*, **10**, 1093 (1934); H. Kakisawa, M. Kurono, S. Takahashi, and Y. Hirata, *ibid.*, **1961**, 59; J. Iwasa and Y. Nakamura, *Tetrahedron Lett.*, **1969**, 3937; H. Hikino, M. Ogura, T. Ohta, and T. Takemoto, *Chem. Pharm. Bull.*, **18**, 1072 (1970).

2) T. Okuno, N. Hamanaka, H. Miyakoshi, and T. Matsumoto, *Tetrahedron*, **26**, 4765 (1970); N. Hamanaka, H. Miyakoshi, A. Furusaki, and T. Matsumoto, *Chem. Lett.*, **1972**, 779; S. Gasa, R. Ikeda, N. Hamanaka, and T. Matsumoto, *Bull. Chem. Soc. Jpn.*, **49**, 835 (1976).

3) A. Furusaki, N. Hamanaka, H. Miyakoshi, and T. Matsumoto, *Chem. Lett.*, **1972**, 783; **1972**, 787.

4) A. Furusaki, S. Gasa, N. Hamanaka, R. Ikeda, and T. Matsumoto, *Chem. Lett.*, **1979**, 665.

5) The fraction consisting of "unknown compounds" described in the Experimental section of the last paper in Ref. 2).

6) A. Furusaki, *Acta Crystallogr., Sect. A*, **35**, 220 (1979).

7) "International Tables for X-Ray Crystallography," The Kynoch Press, Birmingham (1974), Vol. IV.

8) A. Furusaki, S. Gasa, R. Ikeda, T. Matsumoto, N. Yasuoka, and Y. Matsuura, unpublished.

9) A. T. McPhail, G. A. Sim, A. J. Frey, and H. Ott, *J. Chem. Soc., B*, **1966**, 377; A. D. U. Hardy and D. D. MacNicol, *J. Chem. Soc., Perkin Trans. 2*, **1976**, 1140.

10) A. Furusaki, N. Hamanaka, and T. Matsumoto, *Bull. Chem. Soc. Jpn.*, **53**, 1956 (1980).

11) A. Furusaki, S. Gasa, R. Ikeda, and T. Matsumoto, unpublished.

12) J. B. Hendrickson, *J. Am. Chem. Soc.*, **83**, 4537 (1961).

13) P. Narayanan, M. Rohl, K. Zechmeister, and W. Hoppe, *Tetrahedron Lett.*, **1970**, 3943.

14) N. L. Allinger, J. T. Sprague, and J. Liljefors, *J. Am. Chem. Soc.*, **96**, 5100 (1974); D. H. Wertz and N. L. Allinger, *Tetrahedron*, **30**, 1579 (1974).

  Bull. Chem. Soc. Jpn., 54, 1627—1631 (1981)

The Characteristic Behavior of Recoil Tritium Atom in Solid Neopentane at 77 K. The Application of a Hot Zone Model

Yasuyuki Aratono, Enzo Tachikawa, Tetsuo Miyazaki,*,† Masayuki Sakurai,† and Kenji Fueki†

Division of Chemistry, Japan Atomic Energy Research Institute, Tokai-Mura, Ibaraki 319-11

†*Department of Synthetic Chemistry, Faculty of Engineering, Nagoya University, Chikusa-ku, Nagoya 464*

(Received October 21, 1980)

The behavior of recoil tririum atoms in solid neopentane containing a small amount of alkane has been studied at 77 K by means of ESR spectroscopy and radio-gas chromatography. Though it was reported that the H (or D) atoms produced in the radiolysis and photolysis of solid neopentane react selectively with the solute alkane, the T atoms neither diffuse into the matrix at 77 K nor react selectively with the solute alkane. Most of the recoil T atoms react in their own track. The results are explained by a hot-zone model. The radius and the duration time of the hot zone are estimated to be ≈60 Å and ≈10^{-10} s respectively.

Tritium-technology in fusion reactors requires the elucidation of the behavior of hot tritium atoms in solid materials, which involve the integrity of the constructing materials as well as a tritium inventory. So far many studies have been undertaken on the hot tritium reaction in the gas phase, and the fundamental reaction modes have well been established,[1] but many fewer studies have been reported for the solid phase. In the condensed phases, there exist two important factors controlling the final product-distributions. One is the rapid collisional stabilization of excited primary products, and the other is a cage effect. The latter effect, due to the confinements of both radicals and a thermalized atom, constitutes one of the central interests in the condensed phases. However, it has been verified experimentally that the cage effect is much less important in the hot tritium atom because of its small size and because of the high probability of diffusing out from the cage wall.[2] For example, the change from the high-pressure gas phase to the liquid leaves the H substitution reaction by T in 1,2-dichloro-1,2-difluoroethane almost unaffected.[3] Furthermore, the increase in the yield of c-C_4H_7T, found in the phase change of deuterated cyclobutane from gas to a liquid or to a solid was well interpreted by the rapid collisional stabilization of excited c-$C_4D_7T^*$ molecules in the condensed phase.[4]

Recently, the behavior of H (or D) atoms, produced by the photolysis of hydrogen iodide or by the γ-radiolysis of alkane, have been studied in the solid alkane at 77 K.[5] When hydrogen atoms with an initial kinetic energy of 2—3 eV are produced in solid neopentane containing a small amount of alkane at 77 K, they migrate through the solid matrix and abstract hydrogen atoms selectively from the solute alkane. The selective hydrogen-atom abstraction has the following characteristic features: (1) The ratio of the rate constant for the hydrogen atom abstraction from the solute to that from the solvent ($k_{solute}/k_{solvent}$) is 700 for neopentane–alkane mixtures at 77 K. (2) The selective hydrogen-atom-abstraction reaction by H or D atoms in the neopentane-alkane mixtures at 77 K becomes more favored with a decrease in the initial energy of the H or D atoms. (3) The selective hydrogen atom abstraction is suppressed above a certain temperature (140 K). (4) The selective hydrogen-atom abstraction is effectively caused by both H and D atoms: there exists no definite isotope effect between them. Thus, it can be expected that the T atom in the energy range of the photolysis and the radiolysis also reacts selectively with solute alkanes at 77 K if the T atom migrates through the matrix at that temperature.

The recoil tritium atoms produced by the $^6Li(n,\alpha)T$ reaction have an initial energy of 2.7 MeV. After the consequences of collisional energy losses, they enter the reaction-energy range and react there. However, certain fractions of them continue to escape reactions and finally become thermalized T atoms. In the cooling processes down to thermalization, the T atoms must pass through the energy range of 2—3 eV, which is equal to the initial energies of the hydrogen atoms formed in the photolysis. The effects of scavengers, such as O_2 and Br_2, on the recoil T-atom reaction in CH_4,[6] C_2H_6,[7] and i-C_4H_{10}[1a] systems indicated that 30—40% of the total recoil T atoms are thermalized in the gas phase.

The question raised here is whether or not such T atoms can migrate through the solid alkane at 77 K, as the hydrogen atoms formed in the photolysis can. Here, in order to solve this problem, the reactions of T atoms were studied in neopentane–alkane mixtures. Although the preliminary experiments[8] provided no evidence for the selective H abstraction reaction of recoil T atoms, the failure in the observation might have been because the sample temperature was raised during the neutron irradiations. In the present experiments, the sample temperature during the irradiation was checked through the ESR measurements of radicals formed concomitantly. The results obtained were analyzed by comparison with the characteristic features of the behavior of the H (or D) atoms formed in the photolysis and radiolysis.

Experimental

The LiF, used as the target for $^6Li(n,\alpha)T$, was purchased from the Johnson Mathey Chemicals. The mass-spectroscopic analysis showed that the $^6Li/^7Li$ ratio in the LiF is 0.04. The neopentane and propane were more than 99.9 mol % and 99.7 mol % respectively in purity. At least 95% of the isobutane-2-d_1 (i-C_4H_9D) was correctly labeled with the deuterium at the tetriary position. The 2-methyl-d_3-propane-1,1,1,3,3,3-d_6 (i-C_4D_9H), supplied by Merck Sharp and Dohm, Canada, Ltd., has a listed isotopic purity of 98 mol %.

In order to make solid neopentane–alkane–LiF mixtures, the liquid mixtures were immersed rapidly in liquid nitrogen.

H atoms, produced by the radiolysis of neopentane, react effectively with the alkane solute to form alkyl radicals. The yields of the alkyl radicals increase with an increase in the concentration of the solute alkane.[5c] Thus, most of the alkane solute may be dissolved uniformly in the neopentane matrix at 77 K. A part of the LiF may be dissolved in the neopentane matrix, while the rest is precipitated in the solvent. Thus, T atoms may be produced from the dissolved LiF as well as the precipitated LiF.

The reagents were sealed into a quartz cell. The sealed cell was inserted into a polyethylene capsule packed with powered dry ice. Subsequently, the capsule was immersed in liquid N_2 until it reached an equilibrium and was then immediately irradiated in the pneumatic tube of the JRR-4 reactor of the Japan Atomic Energy Research Institute. The neutron flux and the dose rate of γ-rays from the reactor were 3×10^{13} n cm^{-2} s^{-1} and 2×10^{8} rad h^{-1} respectively.[9] At the end of the irradiation, some capsules were immersed in liquid N_2 to make them ready for the subsequent ESR measurements.

The free radicals of the irradiated samples were measured at 77 K with a JEOL-PE3X ESR spectrometer at a microwave power level of 0.2 mW, which did not result in a saturation of the signals of the alkyl radicals. The tritiated products were analyzed by means of radio-gas chromatography. A 5-m ferric oxide γ-alumina column at 77 K was used for the separation of HT and DT, and a 3-m Parapak Q column at 380 K, for the organic products. The two columns were combined by means of a double-column technique,[10] in which a whole sample can be injected at a time.

Results and Discussion

ESR Spectra of Irradiated Sample. Figure 1a shows the ESR spectrum of a *neo*-C_5H_{12}–*i*-C_4H_9D(2 mol %)–LiF mixture irradiated at 77 K in the reactor. The spectrum of eight lines, indicated by arrows (↓), is ascribed to the *t*-C_4H_9 radical.[11] The spectrum of three broad lines, indicated by arrows (⇩), is ascribed to the *neo*-C_5H_{11} radical.[11] The unsymmetrical spectrum, indicated by arrows (⇣), is due to a color center of irradiated quartz. Figure 1b shows the ESR spectrum of a *neo*-C_5H_{12}–*i*-C_4H_9D(2 mol %) mixture γ-irradiated at 77 K with Co-60. The spectrum consists of spectra of *neo*-C_5H_{11} and *t*-C_4H_9 radicals. The amount of the *t*-C_4H_9 radical is about 30% of the total radical yield. Similarly, C_3H_7 or *t*-C_4D_9 radicals are remarkably produced in the γ-radiolysis of *neo*-C_5H_{12} containing C_3H_8(2 mol %) or *i*-C_4D_9H(2 mol %) at 77 K.

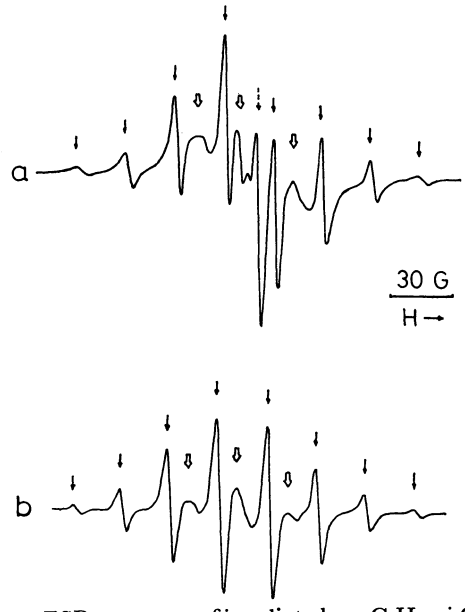

Fig. 1a. ESR spectrum of irradiated *neo*-C_5H_{12}–*i*-C_4H_9D-(2 mol %)–LiF mixture at 77 K with a reactor for 15 s at a dose of 0.8 Mrad. b. ESR spectrum of irradiated *neo*-C_5H_{12}–*i*-C_4H_9D(2 mol %) mixture at 77 K with γ-rays of Co-60 at a dose of 0.1 Mrad.

A comparison of Fig. 1a with Fig. 1b makes it obvious that the neutron-irradiation of the *neo*-C_5H_{12}–*i*-C_4H_9D-(2 mol %)–LiF mixture gives approximately the same ESR spectra of *neo*-C_5H_{11} and *t*-C_4H_9 radicals as in the γ-irradiation. This is reasonable since, during the neutron-irradiation in the reactor, the sample is also exposed to a high dose of γ-rays. The chemical damage caused by the recoil T and ^{3}He atoms amounts to only 1—2% of that caused by γ-rays.

According to the previous studies,[5] the *t*-C_4H_9 radicals are produced by the selective hydrogen-atom-abstraction reaction by H atoms produced from the radiolysis of neopentane (Reactions 1 and 2):

$$\textit{neo}\text{-}C_5H_{12} \rightsquigarrow \textit{neo}\text{-}C_5H_{11} + H \quad (1)$$

$$H + \textit{i}\text{-}C_4H_9D \longrightarrow HD + \textit{t}\text{-}C_4H_9. \quad (2)$$

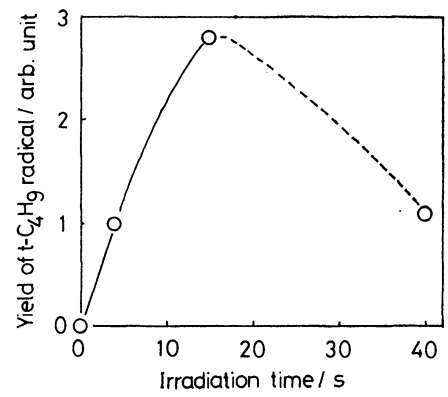

Fig. 2. Yield of *t*-C_4H_9 radical in the irradiation of *neo*-C_5H_{12}–*i*-C_4H_9D(2 mol %)–LiF mixture with a reactor against irradiation time.

Figure 2 shows the effect of the irradiation time in the reactor on the amount of the *t*-C_4H_9 radical produced in the irradiated *neo*-C_5H_{12}–*i*-C_4H_9D(2 mol %)–LiF mixture. The amount of the *t*-C_4H_9 radical increases almost linearly up to an irradiation time of 15 s, while the amount decreases drastically at 40 s. In the case of an irradiation time of 40 s, most of the *t*-C_4H_9 radicals may disappear as a result of the elevation of the temperature of the sample during the irradiation.[12] Thus, a sample temperature of near 77 K is assured within the irradiation time of 15 s, during which time the selective hydrogen-atom-abstraction reaction by T atoms can proceed. Therefore, the irradiation of the samples in the reactor was restricted to within 15 s.

Recoil T Atoms in Neopentane–Alkane Mixtures at 77 K. Table 1 shows the yields of tritiated products in the neopentane–alkane mixtures at 77 K. The DT/HT ratio in the *neo*-C_5H_{12}–*i*-C_4H_9D(2 mol %) system is only

TABLE 1. YIELDS OF TRITIATED PRODUCTS OF THE RECOIL TRITIUM REACTION IN NEOPENTANE AT 77 K

Sample[a]	Irradiation time / s	Relative yield/% HT	DT	CH_3T	RT[b]	P[c]	*neo*-$C_5H_{11}T$	DT/HT
neo-C_5H_{12}–*i*-C_4H_9D(2)	40	42	1	14	2	4	37	0.020
neo-C_5H_{12}–*i*-C_4H_9D(2)	15	37	2	16	2	4	39	0.055
neo-C_5H_{12}–*i*-C_4H_9D(2)	4	37	2	—	—	—	—	0.056
neo-C_5H_{12}–*i*-C_4D_9H(2)	15	38	1	15	3	4	39	0.029
neo-C_5H_{12}–C_3H_8(2)	15	40		14	2	6	38	
neo-C_5H_{12}–*i*-C_4H_{10}(2)–DI(0.5)	15	45	1	14	3	—	37	0.022
neo-C_5H_{12}	15	36		15		7	42	

a) The unit of concentration in mol% is shown in parentheses. LiF (0.05 g/l g of solvent) is added to all the samples. The yields at the irradiation time of 15 s are the mean values of three or four runs, and the errors are about 10%. b) RT represents a tritiated solute, such as *i*-C_4H_9T, *i*-C_4D_9T, or C_3H_7T. c) P may be *i*-C_4H_7T. d) Since not all the tritiated products were analyzed in this sample, it is assumed that the yield of hydrogen (HT+DT) is equal to that of *neo*-C_5H_{12}–*i*-C_4H_9D(2 mol%) at the irradiation time of 15 s.

0.055 for the irradiation time of 15 s.

Now, we will try to estimate the DT/HT ratio from the previously accepted mechanisms. Though the recoil T atoms have an initial energy of 2.7 MeV, a part of them may continue to lose energy through a series of collisional deactivations to the energy range of the H (or D) atoms produced by the photolysis. The scavenger study showed that about one-third of the total recoil T atoms are deactivated.[1a,6,7] If the deactivated T atoms (T_t)[13] behave in a manner similar to that of H (or D) atoms in the photolysis, they should migrate through the *neo*-C_5H_{12}–*i*-C_4H_9D mixture and react selectively with the isobutane solute (Reaction 3):[5]

$$T_t + CH_3\text{–}\underset{\displaystyle D}{\overset{\displaystyle CH_3}{\underset{|}{\overset{|}{C}}}}\text{–}CH_3 \longrightarrow DT + CH_3\text{–}\overset{\displaystyle CH_3}{\underset{\displaystyle \cdot}{\overset{|}{C}}}\text{–}CH_3 \qquad (3)$$

Furthermore, the possibility of the occurrence of Reactions 4 and 5 can be dismissed on the basis of the following results of H-atom reactions in the photolysis:

$$T_t + CH_3\text{–}\underset{\displaystyle D}{\overset{\displaystyle CH_3}{\underset{|}{\overset{|}{C}}}}\text{–}CH_3 \longrightarrow HT + CH_3\text{–}\overset{\displaystyle CH_3}{\underset{\displaystyle D}{\overset{|}{C}}}\text{–}CH_2\cdot \qquad (4)$$

$$\searrow \quad CH_3T + C_3H_6D\cdot \qquad (5)$$

When H atoms are produced by the photolysis of HI in the *neo*-C_5H_{12}–*i*-C_4H_9D mixtures at 77 K, only *t*-C_4H_9 radicals are produced by Reaction 3.[5b] The isobutyl or propyl radicals, which should be formed in Reactions 4 and 5, were not observed by ESR spectroscopy in the reaction of H atoms with *i*-C_4H_9D at 77 K. Thus, most of the T_t atoms can be expected to react with *i*-C_4H_9D to form DT by means of Reaction 3.

The amounts of hot T atoms with a high energy (T_h) are about 60—70% of the total-recoil T-atom reactions in alkanes.[1a,6,7] These T atoms react with alkane by means of abstraction, replacement, and fragmentation reactions. Since the ratio of the D atom to the H atom in the *neo*-C_5H_{12}–*i*-C_4H_9D(2 mol %) mixture is only 0.002, the hot T_h atoms in the abstraction reaction react virtually with the H atom to form HT by means of Reaction 6:

$$\underset{(i\text{-}C_4H_9D)}{T_h + \textit{neo}\text{-}C_5H_{12}} \longrightarrow HT + \underset{(C_4H_8D)}{C_5H_{11}\cdot} \qquad (6)$$

Thus, the maximun yield of HT is less than 60—70% of the total tritiated products. The T_t atoms, the amounts of which are about 40—30% of the total recoil T atoms, form DT by means of Reaction 3.

Therefore, the ratio of DT to HT can be expected to be higher than 0.4:

$$\frac{DT}{HT} = \frac{40 - 30\%}{\leqq 60 - 70\%} \geqq 0.4. \qquad (7)$$

The expected ratio (DT/HT) dose not coincide at all with the experimental value (0.055) in Table 1. The quite low value of the experimental DT yield indicates that most of the T_t atoms neither diffuse into the neopentane matrix at 77 K nor abstract D atoms selectively from *i*-C_4H_9D.

Hot-zone Model for Recoil-T-atom Reactions. If the thermalization process of recoil-T atoms in the solid phase is approximately the same as that in the gas phase, the question arises of why the thermalized recoil T_t atoms do not diffuse into the neopentane matrix at 77 K. The hot-zone model, proposed previously by Seitz *et al.*,[14] Harbottle *et al.*,[15] and others,[16] gives a hypothetical explanation for this question. The ratios of the rate constants ($k_{i\text{-}C_4H_9D}/k_{neo\text{-}C_5H_{12}}$) for hydrogen-atom

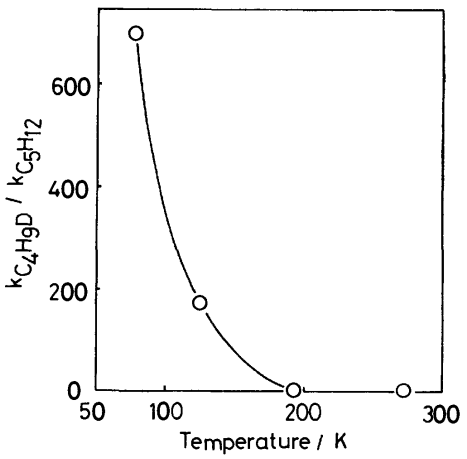

Fig. 3. Temperature effect of rate constants($k_{solute}/k_{solvent}$) for hydrogen atom abstraction by hydrogen atom produced by the UV-photolysis of *neo*-C_5H_{12}–*i*-C_4H_9D(2 mol %)–HI(0.5 mol %) mixture. The values are estimated from the results of previous papers.[5b,5d]

abstraction by H atoms in the photolysis of *neo*-C_5H_{12}–*i*-C_4H_9D-HI mixtures were determined previously,[5b,5d] and they are summarized in Fig. 3. The ratio of the rate constants, which represents the selectivity of the abstraction reaction, decreases drastically with an increase in the temperature. The selective hydrogen-atom-abstraction reaction in a neopentane matrix is suppressed at temperatures higher than 140 K, which is the transition point of solid neopentane.

A recoil-T-atom produces a "track," *i.e.* "continuous spurs," around its trajectory. If the temperature of the track is much higher than 77 K and the T atom reacts in its track, the T_t atom does not abstract a D atom selectively from solute *i*-C_4H_9D, but it may react with solvent *neo*-C_5H_{12} and free radicals in the track.

We can estimate the size of a hot zone from the negative temperature effect on the selective hydrogen-atom-abstraction reaction. A cylindrical hot-zone model is used for a high-LET track produced by a recoil T atom. The excess temperature distribution (T_{ex}) in space (r) and time (t) is given for this geometry by:

$$T_{ex} = T_0(1+4\delta t/r_0^2)^{-1} \exp[-r^2/(r_0^2+4\delta t)], \quad (8)$$

where T_0 is the initial temperature excess on the track axis and where r is the distance from it.[17] The quantity r_0 denotes the size parameter of the track cylinder, where 0.56 r_0 corresponds to the mean radius of the track. If S denotes the energy loss per unit length, then T_0 is given by the equation $T_0=S/(\pi\rho c\, r_0^2)$, where ρ and c are the density and the specific heat of the solid. Equation 8 is, in principle, the same as that proposed by Seitz *et al.*[14] except that the size of the initial track is considered according to the method of Mozumder.[17] The quantity δ, called the thermal diffusivity, equals $\kappa/\rho c$, where κ denotes the heat conductivity.

Recently the experimental and theoretical results on the stopping powers and path lengths of hydrogen and helium have been summarized by Ziegler.[18] The path lengths of the D atom and the ^{4}He atom with 1 keV through carbon are 160 Å and 100 Å respectively. It is assumed here that the length of the T atom with 1 keV through hydrocarbon is 130 Å. Thus, the average stopping power (S) is 7.7 eV Å^{-1}. The heat conductivity (κ), the specific heat (c), and the density (ρ) of solid neopentane at 77 K are 1.4×10^{-3} J s^{-1} cm^{-1} deg^{-1},[19] 0.80 J g^{-1} deg^{-1},[20] and 0.72 g cm^{-3} respectively. According to the experimental and theoretical studies of radiation chemistry, the radii of the track produced by β-rays are about 15 Å in water[17] and 25 Å in methanol[21] respectively. Thus, two values of 20 and 40 Å are tentatively taken here for the size parameters of the track (r_0). Since the selective hydrogen-atom-abstraction reaction in the *neo*-C_5H_{12}–*i*-C_4H_9D mixture is suppressed at 140 K (*cf.* Fig. 3), the lower limit of the temperature of the hot zone is assumed to be 140 K. Then, $T_{ex}=140-77=63$ K. If the excess temperature (T_{ex}) at the boundary of the hot zone is 63 K, the radius (r) of the hot zone can be calculated by Eq. 8 as a function of the duration time (t).

Figure 4 shows the size of the hot zone. The maximum radius and the duration time of the hot zone are found to be $\approx$60 Å and $\approx10^{-10}$ s respectively, both of which values are roughly independent of the initial size

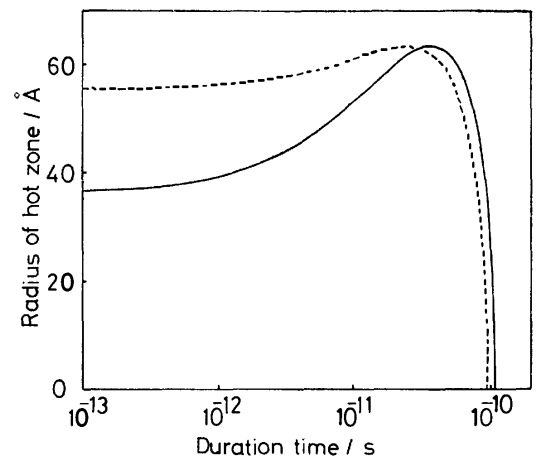

Fig. 4. Time dependence of hot zone produced by recoil T atom in solid neopentane.
——, A size parameter (r_0) of a track is 20 Å.
·····, A size parameter (r_0) of a track is 40 Å.

parameter (r_0) of the track. The radius increases with an increase in the duration time from 10^{-13} s to 3×10^{-11} s, and then decreases drastically at 10^{-10} s. The increase in the radius is caused by the diffusion of the initial energy deposited by a recoil T atom. The subsequent drastic decrease in the radius is due to the cooling of the hot zone. Most of the recoil T atoms may react in this hot zone within $\approx10^{-10}$ s, while only a few of them diffuse out of the zone.

Amount of T Atoms Leaking out of the Hot Zone. Though most of the recoil T atoms react in the hot zone, some of them may diffuse out of the zone. Now, we will attempt to estimate the upper limit of T_t atoms which may leak out of the zone. Table 1 shows the volatile tritiated products in the neopentane system. As no polymeric products are produced in a butane system,[2] most of the activity in the neopentane system may also appear in a volatile form. Thus, the yields in Table 1 represent roughly the overall reaction products.

The most possible reaction of the T_t atoms which diffuse out of the hot zone is a selective hydrogen-atom-abstraction reaction with the alkane solute in the neopentane matrix at 77 K. For example, the T_t atom reacts with *i*-C_4H_9D in the *neo*-C_5H_{12}–*i*-C_4H_9D(2 mol %) mixture to form DT (Reaction 3). The DT yield, however, amounts to only 2% of the total tritiated products.

There is a possibility that T_t atoms may migrate through the matrix and recombine with trapped radicals produced by the radiolysis of the sample. In order to examine this possibility, the reaction of T atoms has been studied in the *neo*-C_5H_{12}–C_3H_8(2 mol %) system. The ESR measurements of this mixture, after it has been γ-irradiated at 77 K, verified the production of a large amount of C_3H_7 radicals. If the C_3H_7 radicals are also produced by reactor-irradiation, the T_t atoms would recombine with the trapped C_3H_7 radicals.

$$T_t + C_3H_7 \longrightarrow C_3H_7T. \quad (9)$$

The yield of C_3H_7T is only 2% of the total tritiated products (*cf.* Table 1). Since C_3H_7T may also be formed by the substitution reaction of hot T atoms with

C_3H_8, the amount of T atoms which recombine with the trapped C_3H_7 radicals is much less than 2%.

There is also the additional possibility that the T_t atoms react with the trapped radicals by means of a disproportionation reaction. The disproportionation reaction between an H atom and a butyl radical occurs at such a low temperature as 90 K.[22] The ESR measurement of the γ-irradiated *neo*-C_5H_{12}–*i*-C_4D_9H(2 mol %) mixture shows the predominant formation of C_4D_9 radicals. It is expected that the C_4D_9 radicals are also produced by the reactor-irradiation. If the T_t atoms migrate through the *neo*-C_5H_{12}–*i*-C_4D_9H mixtures at 77 K and react with the trapped C_4D_9 radicals by means of the disproportionation reaction, DT should be formed by Reaction 10:

$$T_t + C_4D_9 \longrightarrow DT + C_4D_8. \quad (10)$$

Table 1 shows that the yield of DT is only 1% of the total tritiated products.

The effect of a radical scavenger, such as DI, has also been studied in the *neo*-C_5H_{12}–*i*-C_4H_{10}–DI mixtures at 77 K. It is expected that the T_t atoms may react with DI, with the resultant formation of DT:

$$T_t + DI \longrightarrow DT + I. \quad (11)$$

Table 1 shows that the yield of DT is only 1% of the total tritiated yield. This result also indicates that the amount of the diffusively mobile T atoms may be quite small.

The authors wish to thank Prof. Noriaki Ito of Nagoya University for his fruitful discussion. The authors wish also to thank Dr. Shigeo Tsujimura of the Japan Atomic Energy Research Institute for his encouragement throughout the work and Dr. Yasuo Ito of the University of Tokyo for his helpful advice concerning the ESR measurement. This work was done under the Collaboration Program between Japan Atomic Energy Research Institute and Nagoya University. It was supported by a Grant-in-Aid for Scientific Research from the Ministry of Education, Science and Culture.

References

1) a) R. Wolfgang, *Progress Reaction Kinetics*, **3**, 97 (1965); b) F. S. Rowland, "MTP Int. Review of Science," *Phys. Chem. Ser.*, **9**, 109 (1972); c) D. S. Urch, "MTP Int. Review of Science," *Inorg. Chem. Ser.*, One, **8**, 149 (1972).

2) M. Menzinger and R. Wolfgang, *J. Phys. Chem.*, **72**, 1789 (1968).

3) H. J. Machulla and G. Stöcklin, *J. Phys. Chem.*, **78**, 658 (1974).

4) A. Hosaka and F. S. Rowland, *J. Phys. Chem.*, **75**, 3781 (1971).

5) a) T. Wakayama, T. Miyazaki, K. Fueki, and Z. Kuri, *J. Phys. Chem.*, **77**, 2365 (1973); b) T. Miyazaki and T. Hirayama, *J. Phys. Chem.*, **79**, 566 (1975); c) T. Miyazaki, K. Kinugawa, and J. Kasugai, *Radiat. Phys. Chem.*, **10**, 155 (1977); d) T. Miyazaki, J. Kasugai, M. Wada, and K. Kinugawa, *Bull. Chem. Soc. Jpn.*, **51**, 1676 (1978); e) T. Miyazaki, S. M. L. Guedes, and K. Fueki, *ibid.*, **53**, 1813 (1980). Other related papers are cited therein.

6) D. See and R. Wolfgang, *J. Chem. Phys.*, **47**, 143 (1967).

7) a) D. S. Urch and M. J. Welch, *Trans. Faraday Soc.*, **62**, 388 (1966); b) R. T. K. Baker and R. Wolfgang, *ibid.*, **65**, 1153 (1969).

8) Y. Aratono, E. Tachikawa, and T. Miyazaki, *Radiat. Phys. Chem.*, **13**, 115 (1970).

9) Y. Aratono and E. Tachikawa, *J. Inorg. Nucl. Chem.*, **39**, 555 (1977).

10) E. Tachikawa, Ph. D. Thesis 1967, University of California. First, hydrogen and other products were separated by the use of a cooling trap. HT and DT were analyzed by the use of the first column of ferric oxide γ-alumina. Then, the other products were analyzed by the use of the second column of parapak Q.

11) R. W. Fessenden and R. H. Schuler, *J. Chem. Phys.*, **39**, 2147 (1963).

12) Since the irradiation time of the previous study (Ref. 8) was 60 s, the temperature of the sample was not kept at 77 K during irradiation.

13) T_t means a T atom equal to, or less than, the epithermal energy.

14) F. Seitz and J. S. Koehler, "Solid State Physics," ed by F. Seitz and D. Turnbull, Academic Press, New York, N. Y. (1956), Vol. 2.

15) G. Harbottle and N. Sutin, *J. Phys. Chem.*, **62**, 1344 (1958).

16) G. Harbottle, "Chemical Effects of Nuclear Transformations in Inorganic Systems," ed by G. Harbottle and A. G. Maddock, North-Holland Publ. Co., Amsterdam (1979), Chap. 3, The related papers are cited therein.

17) A. Mozumder, "Advances in Radiation Chemistry," ed by Burton and J. L. Magee, Wiley-Interscience, New York (1969), Vol. 1, p. 1.

18) J. F. Ziegler, "Stopping Powers and Ranges in All Elements," Pergamon Press, New York (1977), Vols. 3 and 4.

19) "Handbook of Chemistry and Physics," ed by R. C. Weast, CRC Press, Cleveland, (1976).

20) H. Enokido, T. Shinoda, and Y. Mashiko, *Bull. Chem. Soc. Jpn.*, **42**, 84 (1969).

21) R. I. Samoilova, A. M. Raitsimring, and Yu. D. Tsvetkov, *Radiat. Phys. Chem.*, **15**, 553 (1980).

22) R. Klein, M. D. Scheer, and R. Kelley, *J. Phys. Chem.*, **68**, 598 (1964).

Brillouin Scattering Study of Clathrate Hydrate Formation in Acetone-Water Solution

Tadashi KATO, Masako YUDASAKA, and Tsunetake FUJIYAMA*
Institute for Molecular Science, Myodaiji, Okazaki 444
(Received October 28, 1980)

Light scattering spectra have been observed for binary solutions of acetone and water at 24, 34, and 44 °C in the concentration range of $0 \leq x_{AC} \leq 0.25$, where x_{AC} is the mole fraction of acetone. The hypersonic velocities and the adiabatic compressibilities at 4.5 GHz were obtained from the observed values of Brillouin shifts. The observed concentration and temperature dependencies of the adiabatic compressibility were interpreted by assuming the existence of clathrate hydrate-like local structures in the solutions. The adiabatic compressibilities for binary solutions of *t*-butyl alcohol (TBA) and water were used as reference data. A comparison is made between the local structure formed in the acetone–water solution and that in the TBA–water solution.

Molecules such as tetrahydrofuran, *t*-butyl alcohol (TBA), and acetone are known to form solid clathrate hydrates.[1,2] Recently, Iwasaki *et al.* have observed the concentration and temperature dependencies of the mean-square concentration fluctuations for the binary solutions of TBA–water by means of light scattering.[3] In their study, the existence of local structures of the type $(H_2O)_l$TBA ($l \simeq 20$) has been suggested. The results of the X-ray diffraction analyses for the structure of solid clathrate hydrate have contributed to the following picture for the mixing state of the TBA–water mixtures. In the concentration range of $0 < x_{TBA} < 0.05$, a TBA molecule forms a polyhedron which is surrounded by water molecules; the polyhedra are dispersed in water (x_{TBA} is the mole fraction of TBA). In the concentration range of $0.05 < x_{TBA} < 0.15$, aggregates of several polyhedra are dispersed in TBA. At $x_{TBA} \simeq 0.05$, the number of molecules which take part in the clathrate hydrate formation becomes a maximum.

We believe that the above picture can be applied to the other aqueous solutions of non-electrolytes which are known to form solid clathrate hydrates. In the present study, the mixing state for the acetone–water system will be discussed through the observation of hypersonic velocity obtained from the Brillouin scattering measurements. Hypersonic velocity affords information about the structuring of a solution. For the TBA–water system, Stone *et al.* have shown that the hypersonic velocity takes a maximum value at $x_{TBA} \simeq 0.05$.[4] As the number of molecules which take part in the clathrate hydrate formation becomes maximum at this concentration for the TBA–water system, the characteristic concentration dependence of the hypersonic velocity seems to originate from the formation of the local structure of the type suggested by Iwasaki *et al.* An acetone molecule also forms a solid clathrate hydrate at about −35 °C.[5] We will interpret the concentration dependence of the hypersonic velocity or the adiabatic compressibility of the acetone–water solution based on the assumption that clathrate hydrate-like local structures exist in the solution. The mean-square concentration fluctuations could not be obtained accurately for the present system because the Rayleigh intensity arising from the concentration fluctuation is not so strong as that arising from the entropy fluctuation.

Experimental

The light scattering spectrometer used in the present study was designed and constructed in our laboratoly. Figure 1 shows the schematic diagram of the spectrometer. The light source is a He–Ne laser (NEC GLG 5800) which produces 50 mW power at 632.8 nm. The laser beam is irradiated on a sample cell made of quartz. The scattered light at 90° is directed into a piezoelectrically driven Fabry-Perot interferometer (Burleigh RC 110). After being passed through the interferomer, the light is focussed by a telemeter lens into a pinhole. The central spot of the interferometer ring system is then detected by a photomultiplier (HTV R-649). The photomultiplier signal is amplified, discriminated, and then put into a multichannel analyzer (Camberra Series 30) by which the spectra are averaged over many times. A stabilization system (Burleigh DAS 10, RC 43) was used for the elimination of the axial drift of the interferometer cavity and for maintaining the parallelism of the etalon. The free spectral range was 0.625 cm^{-1} and the finesse was about 20.

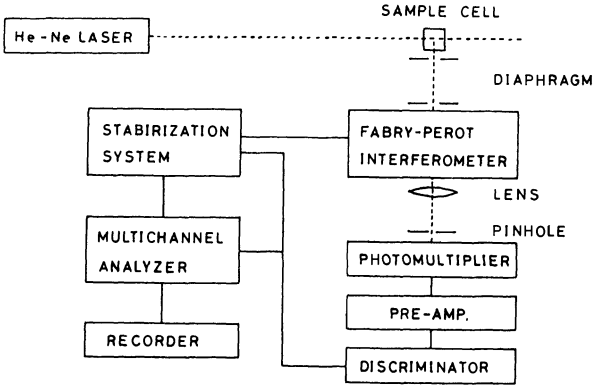

Fig. 1. Block diagram of the light scattering spectrometer.

Acetone was purchased from Wako Pure Chemical Industries, Ltd., and used after distillations. Water was distilled after being passed through an ion exchange resin. The binary mixtures of acetone–water were made dust-free by the use of Millipore filter FG with a pore size of 0.2 μm. The temperature of the sample was controlled by a high temperature cell. A temperature constancy of ±0.5 °C was obtained with the apparatus. The light scattering spectra were observed at 24, 34, and 44 °C. The refractive index of the sample was measured by means of an Atago Abbe refractometer; the results are shown in Table 1.

Table 1. Values of refractive indices (n) and densities (ρ) used for the calculations of v_S and κ_S

x_{AC}	n			ρ[a)]		
	24 °C	34 °C	44 °C	24 °C	34 °C	44 °C
0	1.3326	1.3314	1.3299	0.9972	0.9940	0.9905
0.0200	1.3368	1.3355	1.3338	0.9890	0.9854	0.9810
0.0346	1.3400	1.3362	1.3365	0.9832	0.9790	0.9740
0.0493	1.3427	1.3407	1.3388	0.9760	0.9730	0.9678
0.0600	1.3450	1.3430	1.3407	0.9734	0.9680	0.9620
0.0793	1.3476	1.3452	1.3432	0.9675	0.9613	0.9555
0.0966	1.3497	1.3478	1.3448	0.9618	0.9555	0.9488
0.1256	1.3530	1.4505	1.3475	0.9525	0.9452	0.9378
0.1480	1.3555	1.3522	1.3495	0.9448	0.9372	0.9293
0.2002	1.3584	1.3551	1.3518	0.9291	0.9203	0.9110
0.2490	1.3612	1.3573	1.3538	0.9145	0.9041	0.8950

a) Ref. 9.

Results and Discussion

Hypersonic Velocity and Adiabatic Compressibility. The sound velocity, v_S, and the adiabatic compressibility, κ_S, at 4.56 GHz were obtained from the observed Brillouin shifts, $\Delta\nu$, by the relations[6)]

$$v_S = \frac{c\lambda_0}{2n\sin(\theta/2)}$$

and

$$\kappa_S = (v_S^2\rho)^{-1},$$

where c is the velocity of light, λ_0 the wavelength of the incident light in a vacuum, n the reftactive index of the sample, θ the scattering angle, and ρ the density.[9)] In Figs. 2 and 3, the observed v_S and κ_S are plotted against the mole fraction of acetone, x_{AC}, for different temperatures. It is seen from these figures that v_S (or κ_S) takes a maximum (or minimum) value at $x_{AC}\simeq 0.1$ for 24 °C and $x_{AC}\simeq 0.05$ for 44 °C. These results suggest that some sort of long-range structures are formed in the binary solution of acetone–water, especially in the concentration range around $x_{AC}=0.1$.

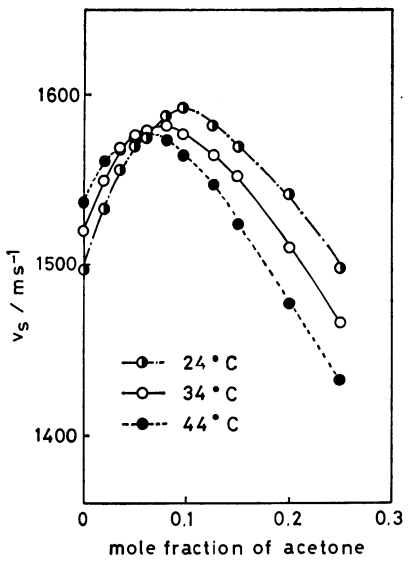

Fig. 2. Concentration dependence of hypersonic velocity for acetone–water system at 24, 34, and 44 °C.

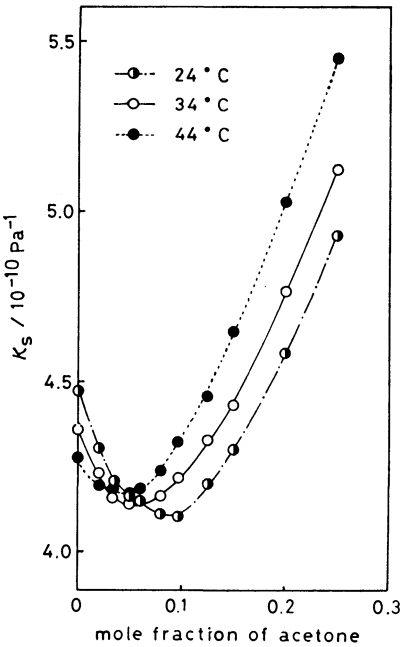

Fig. 3. Concentration dependence of adiabatic compressibility for acetone–water system at 24, 34, and 44 °C.

Mixing State of Acetone–Water Solution. X-Ray diffraction analysis has shown that an acetone molecule forms a solid clathrate hydrate with several water molecules at about −35 °C.[5)] The chatacterstic concentration dependence of v_S or κ_S may arise from the clathrate hydrate-like local structure formation in the solution. If the composition of such a structure is of the type $A(H_2O)_l$ where A is acetone, κ_S is expected to take a minimum value at $x_{AC}=1/(l+1)$, because the number of the molecules which do not take part in the clathrate formation becomes minimum at $x_{AC}=1/(l+1)$. Figs. 2 and 3 show that the number ratio of water molecules to acetone molecules in the local structure (we will call this ratio R, from now on) is about 10 at 24 °C and about 20 at 44 °C.

It has been established that water molecules in a solid clathrate hydrate form polyhedra, each of which encages a guest molecule.[1,2)] More than 24 water molecules are necessary to form a polyhedron which can encage a molecule as large as an acetone molecule. In the case of a solid hydrate, however, several polyhedra share one of their faces (we will call this "association of polyhedra") and, therefore, R can become less than 24. For example, R is 7⅔ or 5¾ for "structure I" and 17 for "Structure II."[1,2)] As R obtained from the observed κ_S is 10 at 24 °C, it may be concluded that polyhedra associate to some extent in the solution at this temperature.

If the concentration of acetone is very low, however, association of polyhedra cannot be expected. Therefore, R may be 24 or more. As the concentration increases, it is expected that the polyhedra begin to associate with each other near $x_{AC}\simeq 0.04$ because almost all the water molecules form polyhedra at this concentration. The slowing down of the gradient change of κ_S near

$x_{AC} \simeq 0.05$ at 24 °C may reflect this situation.

In the concentration range of $0.05 < x_{AC} < 0.1$, κ_s continues to decrease with the increase of x_{AC}. This fact suggests the growth of the local structures with the increase of the concentration. With the increase of x_{AC} up to 0.1, the association degree of the polyhedra increases and, therefore, R decreases down to 10. Since an acetone molecule is known to form a solid clathrate hydrate of the Structure II ($R=17$), at least 17 water molecules are thought to be necessary to form a stable local structure of a clathrate hydrate type. Therefore, the local structure formed at $x_{AC} \simeq 0.1$ ($R=10$) may be more unstable than the local structure formed at $x_{AC} \simeq 0.05$ ($R=20$). In fact, κ_s increases as the temperature increases near $x_{AC} \simeq 0.1$, while κ_s is almost independent of the temperature near $x_{AC} \simeq 0.05$.

In the concentration range of $x_{AC} > 0.1$, κ_s increases rapidly with the increase of the concentration. This suggests that the number of acetone molecules which are not encaged by water molecules increases with the increase of x_{AC}. Thus, it can be imagined that the associated polyhedra begin to be separated by acetone molecules at $x_{AC} \simeq 0.1$.

Burton has measured the ultrasonic velocity at 1 MHz for the acetone–water solution at 27 °C and found that v_s takes a maximum value at $x_{AC} \simeq 0.05$.[7] However, our results at 4.5 GHz show that v_s takes a maximum value at $x_{AC} \simeq 0.1$ at room temperature. This difference is considered to come from the fact that the life-time of the local structure, τ, is dependent of concentration. τ at $x_{AC} \simeq 0.1$ may be much shorter than the period of the ultrasonic wave, but may be longer than that of the hypersonic one. On the other hand, τ at $x_{AC} \simeq 0.05$ may be longer than the period of the ultrasonic wave.

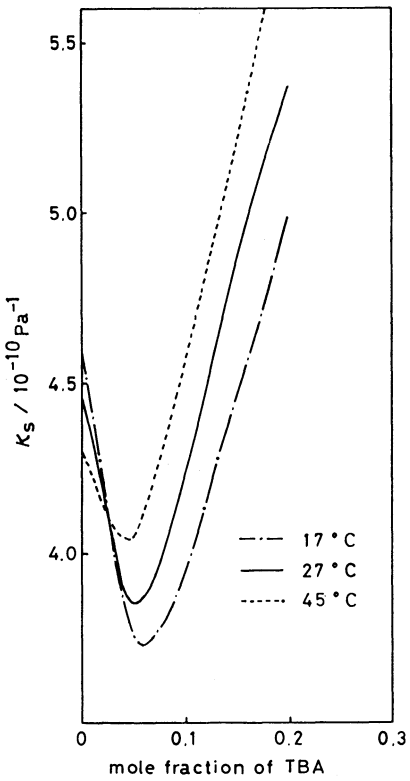

Fig. 4. Concentration dependence of adiabatic compressibility for *t*-butyl alcohol (TBA)–water system at 17, 27, and 45 °C calculated from the hypersonic velocity data of Stone *et al.*[4]

Comparison with TBA–Water System. Stone *et al.* have measured the hypersonic velocity for the TBA–water system at 6 GHz. Figure 4 shows the adiabatic compressibility for the system calculated from their sound velocity data. It is seen from the figure that κ_s takes a minimum value at x_{TBA} is about 0.06 (at 17 °C), 0.05 (at 27 °C), or 0.045 (at 45 °C). These data can be reduced to the R values of 16 (at 17 °C), 19 (at 27 °C), and 21 (at 45 °C). Iwasaki *et al.* have obtained the R values of 17 ± 2 at 17 °C and 21 ± 2 at 65 °C from the analyses of the concentration dependence of the concentration fluctuation.[3] The R value at 17 °C obtained from the adiabatic compressibility is in agreement with that obtained from concentration fluctuation at the same temperature. Moreover, those R values obtained from the measurements of the adiabatic compressibility and the concentration fluctuation have similar temperature dependences. These facts confirm the R values obtained for the acetone–water system in our present study. The R value for the acetone–water system at room temperature is smaller than that for the TBA–water system. This difference seems to come from the difference between acetone and TBA in the size of the hydrophobic group of the molecule. The number of molecules which can encage an acetone molecule may be smaller than that for a TBA molecule.[8]

Figures 3 and 4 also show that the minimum values of κ_s for the acetone system are larger than those for the TBA system. This difference may also originate from the difference in hydrophobicity between acetone and TBA. The more hydrophobic a solute molecule is, the more stabilization energy is required for dissolution. Thus, the hydrate-like structure for the TBA system becomes more stiff than that for the acetone system.

The authors wish to express their sincere thanks to Mr. Nobuyuki Ito for his helpful advice on the construction of the light scattering spectrometer.

References

1) D. W. Davidson, "Water," ed by F. Franks, Plenum Press, New York-London (1973), Vol. 2, Chap. 3.
2) D. N. Glew, H. D. Mak, and N. S. Rath, "Hydrogen-bonded Solvent Systems," ed by A. K. Convington and P, Jones, Taylor and Francis, London (1968), p. 195.
3) K. Iwasaki and T. Fujiyama, *J. Phys. Chem.*, **81**, 1098 (1977); **83**, 463 (1979).
4) J. Stone and R. E. Pontinen, *J. Chem. Phys.*, **47**, 2407 (1967).
5) A. S. Quist and H. S. Frank, *J. Phys. Chem.*, **65**, 560 (1961).
6) See for example, I. L. Fabelinskii, "Molecular Scattering of Light," Plenum Press, New York (1968).
7) C. J. Burton, *J. Acoust. Soc. Am.*, **20**, 186 (1947).
8) The molar volume of acetone and TBA are 74 and 94 cm^3 mol^{-1} at 20 °C, respectively.
9) The values of ρ were obtained from: Landort-Börnstein, "Physicalishe-Chemishe Tabellen," II Band, 1 Teil, Springer Verlag (1971).

  Bull. Chem. Soc. Jpn., 54, 1635—1639 (1981)

Elementary Patterns in Protein-Nucleic Acid Interactions. II.† Crystal Structure of 3-(Adenin-9-yl)propionamide

Midori TAKIMOTO,* Akio TAKENAKA, and Yoshio SASADA

Laboratory of Chemistry for Natural Products, Tokyo Institute of Technology, Nagatsuta, Midori-ku, Yokohama 227

(Received November 8, 1980)

In order to study adenine-amide interactions, 3-(adenin-9-yl)propionamide has been synthesized and its crystal structure examined. The crystals are monoclinic, the space group being $P2_1/a$, with unit-cell dimensions of $a=25.668$ (1), $b=8.025$ (1), $c=4.684$ (1) Å, $\beta=103.54$ (1)°, and $Z=4$. The adenine bases are linked along the two-fold screw axis through the hydrogen bonds, N(6)H···N(1) and N(6)H···N(7). The amide group is hydrogen-bonded to N(3) of adjacent adenine moiety, the distance NH···N(3) being 3.055 Å. The model fitting by computer graphics indicates that this binding scheme could be an elementary interaction pattern between the amide group in protein and adenine in the minor groove of double helical DNA.

Studies have been carried out on elementary patterns in protein-nucleic acid interactions using model crystals with the anticipation that their specificity might arise from the interaction between purine-pyrimidine bases and amino acid residues supported sterically and electronically by their three-dimensional structures. Several elementary patterns due to hydrogen bonds have been found in the following combinations: cytosine-carboxyl,[1-4] adenine-indole,[5,6] and adenine-carboxyl group.[7]

Attempts were made to extend the study to the adenine-glutamine or asparagine system. These amino acids contain an amide group in the side chain and significance of their interaction with nucleic acid base was proposed.[8,9] In order to examine the intermolecular hydrogen bonds between adenine and amide moieties, we have synthesized a new compound, 3-(adenin-9-yl)-propionamide and examined its crystal structure.

Experimental and Structure Determination

3-(Adenin-9-yl)propionic acid, synthesized from adenine and β-propiolactone by the method of Kondo *et al.*,[10] was converted into ester in CH_3OH solution saturated with HCl and then into amide in NH_3/CH_3OH. The amide formation was confirmed by elemental analysis and IR spectrum (δ_{N-H} 1600 cm^{-1}, amide group). By slow evaporation, prism crystals were obtained from water-methanol (1 : 1) solution at room temperature. Oscillation and Weissenberg photographs showed the space group to be $P2_1/a$. Density was measured by flotation in a mixture of cyclohexane and carbon tetrachloride. A crystal, $0.3\times0.5\times0.1$ mm in size, was mounted on a Rigaku automated four-circle diffractometer. Nickel-filtered Cu $K\alpha$ radiation ($\lambda=1.54178$ Å) was used. The accurate unit-cell dimensions were determined by least-squares calculation with 2θ values of 40 high-angle reflexions.

TABLE 1. CRYSTAL DATA

3-(Adenin-9-yl)propionamide	
$C_8H_{10}N_6O$	
Space group: $P2_1/a$	
$a=25.668(1)$ Å	$U=938.1(1)$ Å^3
$b=8.025(1)$ Å	$Z=4$
$c=4.684(1)$ Å	$D_x=1.46$ g cm^{-3}
$\beta=103.54(1)°$	$D_m=1.46$ g cm^{-3}

† Part I of this series is Ref. 5.

Crystallographic data are summarized in Table 1.

Intensity data were collected on the diffractometer by means of $\omega/2\theta$ scanning ($8°<2\theta<115°$), the scan speed being 4° (in 2θ) min^{-1} and scan width 0.9° (in ω) plus α_1-α_2 divergence. Five reference reflexions monitored periodically showed no significant intensity deterioration. Corrections were made for Lorentz and polarization factors, but not for absorption effects. A total of 1280 independent reflexions were obtained, 175 of which had no net intensities: the observational threshold value, F_{11m}, was 1.69. The standard deviations were estimated

TABLE 2. FRACTIONAL COORDINATES AND ISOTROPIC TEMPERATURE FACTORS

The B values with ⟨ ⟩ are the equivalent isotropic temperature factors calculated from anisotropic thermal parameters using the equation $B=8\pi^2\Sigma(U_1+U_2+U_3)/3$, where U_1, U_2, and U_3 are the principal components of mean square displacement matrix $\boldsymbol{U}$. Values in ⟨ ⟩ are anisotropicity defined by $(\Sigma(B-8\pi^2U_i)^2/3)^{1/2}$. The e.s.d.'s in ( ) refer to last decimal places.

Atom	x	y	z	B/Å^2
N(1)	0.28388(9)	0.5192(3)	0.7473(5)	3.3⟨9⟩
C(2)	0.3200(1)	0.5599(4)	0.5953(7)	3.7⟨8⟩
N(3)	0.35669(9)	0.4652(3)	0.5157(5)	3.3⟨8⟩
C(4)	0.3535(1)	0.3075(3)	0.6099(6)	2.9⟨6⟩
C(5)	0.3181(1)	0.2456(3)	0.7663(6)	2.8⟨5⟩
C(6)	0.2819(1)	0.3597(3)	0.8375(6)	2.9⟨6⟩
N(6)	0.2453(1)	0.3221(3)	0.9881(6)	3.6⟨18⟩
N(7)	0.32743(9)	0.0772(2)	0.8253(5)	3.3⟨13⟩
C(8)	0.3675(1)	0.0420(4)	0.7041(7)	3.7⟨11⟩
N(9)	0.38475(9)	0.1751(3)	0.5681(5)	3.2⟨9⟩
C(11)	0.4332(1)	0.1864(4)	0.4528(7)	3.5⟨13⟩
C(12)	0.4794(1)	0.2404(6)	0.6945(7)	4.5⟨26⟩
C(13)	0.5297(1)	0.2860(4)	0.5952(6)	3.6⟨11⟩
N(13)	0.5689(1)	0.3501(4)	0.7988(6)	4.4⟨23⟩
O(13)	0.53325(8)	0.2627(3)	0.3422(4)	5.9⟨42⟩
H(2)	0.319(1)	0.681(3)	0.533(5)	1.0(6)
H(6A)	0.224(1)	0.403(4)	1.023(7)	3.1(9)
H(6B)	0.244(1)	0.223(3)	1.068(6)	1.6(8)
H(8)	0.384(1)	−0.062(3)	0.704(5)	0.8(6)
H(11A)	0.424(1)	0.269(3)	0.283(5)	1.0(6)
H(11B)	0.437(1)	0.071(4)	0.372(6)	2.9(8)
H(12A)	0.489(1)	0.150(4)	0.840(8)	5.8(2)
H(12B)	0.470(1)	0.338(4)	0.801(7)	4.9(1)
H(13A)	0.597(1)	0.397(3)	0.751(6)	2.1(8)
H(13B)	0.565(1)	0.365(4)	0.987(6)	3.3(9)

by the equation $\sigma^2(F_o)=\sigma_p^2(F_o)+qF_o^2$, where $\sigma_p(F_o)$ was evaluated by counting statistics and q (6.8×10^{-6}) was derived from the variations of the monitored reflexions.[11]

The structure was solved by the symbolic addition procedure, the parameters being refined by the block-diagonal leasts-quares method. The quantity minimized was $\sum w(|F_o|-|F_o|)^2$, where $w=1/(\sigma^2(F_o))$. All the hydrogen atoms, found on a difference map, were included. The zero-reflexions, for which $|F_c|>F_{lim}$, were included in the least-squares calculation by assuming $F_o=F_{lim}$ and $w=w(F_{lim})$, The final R value was 0.049 for 1170 reflexions with $F_o\geq3\sigma(F_o)$; the maximum shift of parameters in the last cycle was 0.02σ for C, N, and O, and 0.1σ for H. Atomic scattering factors were taken from "International Tables for X-Ray Crystallography".[12] Atomic parameters are given in Table 2, and the observed and calculated structure factors in Table 3.[13]

Results and Discussion

Molecular Structure. Bond distances and angles are shown in Fig. 1. Bond angles involving hydrogen atoms are given in Table 4, and the least-squares planes of adenine and amide moieties in Table 5. Figure 2 shows a stereoscopic view of the 3-(adenin-9-yl)-propionamide molecule. The bond lengths and angles of the adenine ring are in good agreement with those found in 9-methyladenine[14] and other related compounds.[15] The adenine moiety is planar with maximum shift of 0.009 Å for C(5) and C(8) from the least-squares plane.

The dimensions of the amide group is similar to those in L-asparagine monohydrate (neutron study),[16] and L-glutamine (neutron study).[17] Small differences might be related to the strengths of the hydrogen bondings. A comparison of the dimensions of amide group is given in Table 6.

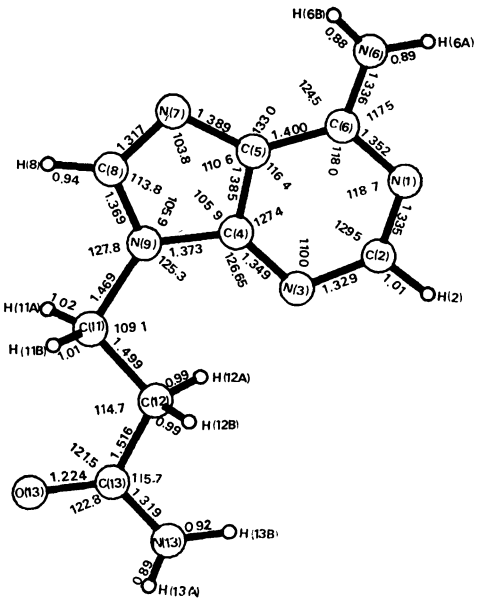

Fig. 1. Atomic numbering of 3-(adenin-9-yl)propionamide with bond lengths (l/Å) and angles (ϕ/°). E.s.d.'s are 0.006 Å and 0.3° for C, N, and O atoms, and 0.04 Å for H atoms. Bond angles involving H atoms are given in Table 4.

TABLE 4. BOND ANGLES (ϕ) INVOLVING HYDROGEN ATOMS OF 3-(ADENIN-9-YL) PROPIONAMIDE

	ϕ/°
N(1)–C(2)–H(2)	115(2)
N(3)–C(2)–H(2)	116(2)
C(6)–N(6)–H(6A)	118(2)
C(6)–N(6)–H(6B)	122(2)
H(6A)–N(6)–H(6B)	120(3)
N(7)–C(8)–H(8)	127(2)
N(9)–C(8)–H(8)	120(2)
N(9)–C(11)–H(11B)	105(2)
N(9)–C(11)–H(11A)	106(2)
N(11A)–C(11)–H(11B)	109(2)
C(12)–C(11)–H(11B)	114(2)
C(12)–C(11)–H(11A)	113(2)
C(11)–C(12)–H(12A)	109(2)
C(11)–C(12)–H(12B)	112(2)
C(13)–C(12)–H(12A)	107(2)
C(13)–C(12)–H(12B)	107(2)
H(12A)–C(12)–H(12B)	107(3)
C(13)–N(13)–H(13A)	121(2)
C(13)–N(13)–H(13B)	121(2)
H(13A)–N(13)–H(13B)	117(3)

TABLE 5. LEAST-SQUARES PLANES AND DEVIATIONS OF ATOMS FROM THE PLANES

X, Y, and Z are in Å along a^*, b, and c, respectively.

Plane 1 (ethyl chain)

$0.264(1)X-0.9538(9)Y+0.143(5)Z=1.31(2)$

Plane 2 (adenine plane)

$0.6557(5)X+0.2236(7)Y+0.7212(5)Z=10.243(2)$

Plane 3 (amide group)

$0.365(2)X-0.9164(8)Y+0.165(2)Z=2.65(3)$

Deviations (l/Å)

Plane 1		Plane 2		Plane 3	
N(9)*	−0.060	N(1)*	0.005	C(12)*	0.001
C(11)*	0.053	C(2)*	−0.001	C(13)*	−0.003
C(12)*	0.067	N(3)*	0.002	N(13)*	0.001
C(13)*	−0.060	C(4)*	−0.002	O(13)*	0.001
N(13)	−0.190	C(5)*	−0.009	C(11)	−0.163
O(13)	−0.031	C(6)*	−0.0		
		N(7)*	−0.001		
		C(8)*	−0.009		
		N(9)*	−0.001		
		N(6)	0.001		
		C(11)	0.209		

* Atoms included in the calculations of the least-squares plane.

The ethyl chain linking the adenine ring with the amide group is nearly planar within 0.067 Å. The torsion angles of N(9)–C(11)–C(12)–C(13) and C(11)–C(12)–C(13)–N(13) are −170.0(3)° and 173.3(3)°, respectively.

Crystal Structure. The crystal structure viewed down the c axis is shown in Fig. 3. Hydrogen bond lengths and angles are given in Table 7. Adenine moieties are arranged so as to form ribbons along the

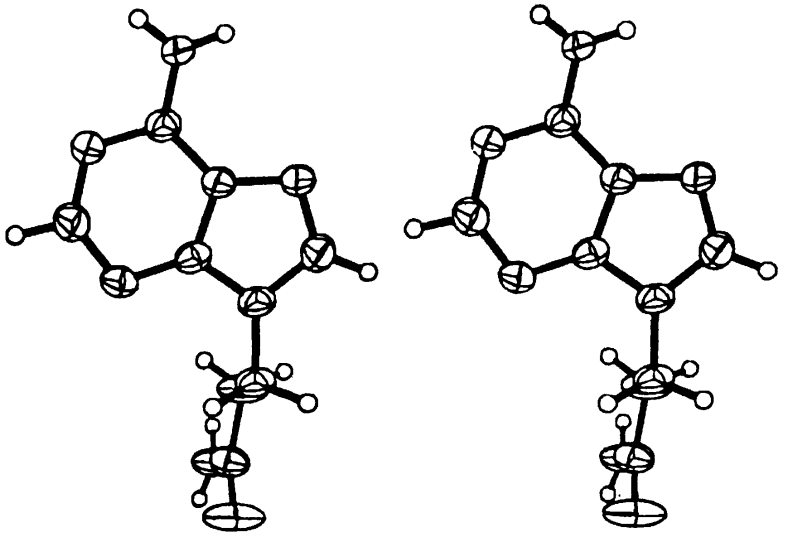

Fig. 2. Stereoview of 3-(adenin-9-yl)propionamide with 50% probability ellipsoids for the non-hydrogen atoms.

Table 6. Dimensions of the amide groups(l/Å)

	3-(Adenin-9-yl) propionamide	L-Asparagine[16] monohydrate	L-Glutamine[17]
C=O	1.224(4)	1.251(8)	1.228(3)
C–N	1.319(4)	1.352(6)	1.332(2)
C–C	1.516(6)	1.513(7)	1.509(2)

two-fold screw axis through the hydrogen bonds, N(6)H···N(1) and N(6)H···N(7). The arrangement is the same as that found in 3-(adenin-9-yl)propionic acid[7] and 5′-*O*-acetyladenosine.[18]

The amino group in amide is hydrogen-bonded to N(3) of the adenine moiety in the molecule related by inversion. The same kind of hydrogen bonding is found in 3-(adenin-9-yl)tryptamide crystal, in which the secondary amide of the peptide bond is a donor of hydrogen bond to N(3) of adenine moiety.

In the present crystal, the N(13)H···N(3) hydrogen bond links adenine ribbons in an anti-parallel mode to each other to form a sheet. The molecular sheet resembles that found in the 3-(adenin-9-yl)propionic acid crystal, though in the latter the linkage is the O–H···N(3) hydrogen bond, the adenine ribbons being parallel to each other.

The remaining hydrogen atom of the amide group participates in the hydrogen bond N(13)H···O(13) between the amide groups to link the molecular sheets (Fig. 4).

Table 7. Hydrogen bond distances and angles of 3-(adenin-9-yl)propionamide
Standard deviations are given in parentheses.

Distances	l/Å		
N(6)···N(7)^{c}	3.033(4)	C(6)–N(1)^{d}···H(6B)	125.4(9)
H(6A)···N(7)^{c}	2.15(3)	C(2)–N(1)^{d}···N(6)	107.7(2)
N(6)···N(1)^{d}	2.905(4)	C(2)–N(1)^{d}···H(6B)	112.5(9)
H(6B)···N(1)^{d}	2.06(3)	N(13)–H(13A)···N(3)^{b}	158(3)
N(13)···N(3)^{b}	3.055(4)	N(13)···N(3)–C(4)^{b}	134.9(2)
H(13A)···N(3)^{b}	2.21(3)	H(13A)···N(3)–C(4)^{b}	137.5(8)
N(13)···O(13)^{a}	2.983(4)	N(13)···N(3)–C(2)^{b}	115.0(2)
H(13B)···O(13)^{a}	2.18(3)	H(13A)···N(3)–C(2)^{b}	112.4(8)
Angles	ϕ/°	N(3)^{b}···N(13)···O(13)^{a}	151.3(1)
N(6)–H(6A)···N(7)	170(3)	O(13)^{a}···N(13)–C(13)	101.0(2)
N(6)···N(7)–C(8)^{c}	125.1(2)	C(13)–N(13)···N(3)^{b}	107.4(2)
H(6A)···N(7)–C(8)^{c}	127.1(9)	C(13)–O(13)^{a}···N(13)	153.8(2)
N(6)···N(7)–C(5)^{c}	128.7(2)	N(13)–H(13B)···O(13)^{a}	146(3)
H(6A)···N(7)–C(5)^{c}	127.5(9)	H(13B)···O(13)–C(13)^{a}	143.9(1)
C(6)–N(6)···N(7)^{c}	123.8(2)	Symmetry codes	
N(7)^{c}···N(6)···N(1)^{d}	101.8(1)	(a) $x, y, 1+z$	
N(1)^{d}···N(6)–C(6)	134.3(2)	(b) $1-x, 1-y, 1-z$	
N(6)–H(6B)···N(1)^{d}	161(3)	(c) $1/2-x, 1/2+y, 2-z$	
C(6)–N(1)^{d}···N(6)	128.8(2)	(d) $1/2-x, -1/2+y, 2-z$	

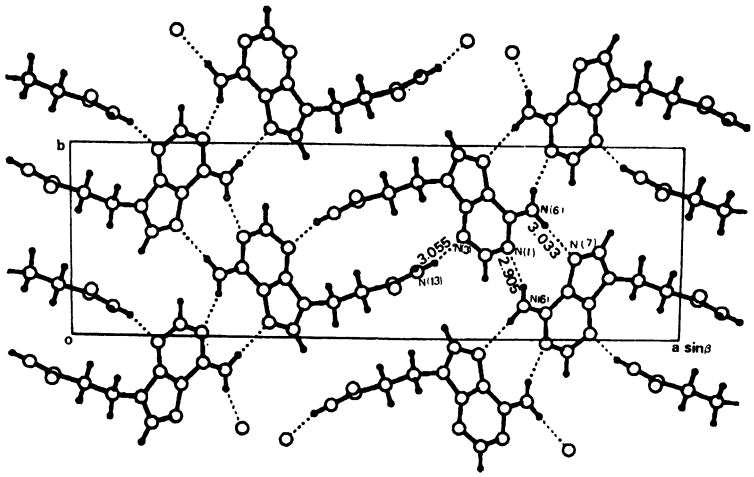

Fig. 3. Crystal structure of 3-(adenin-9-yl)propionamide projected along the c axis.

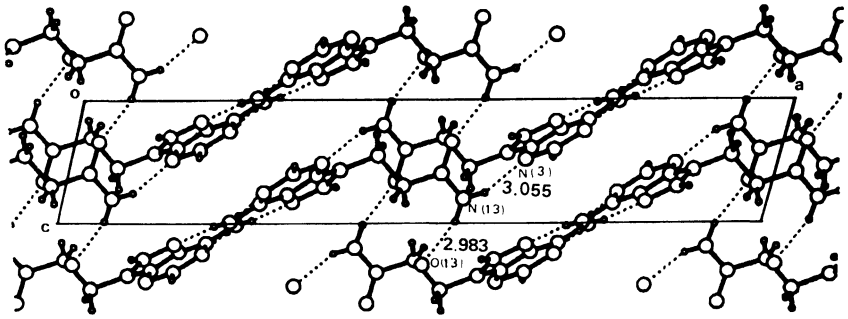

Fig. 4. Crystal structure of 3-(adenin-9-yl)propionamide projected along the b axis.

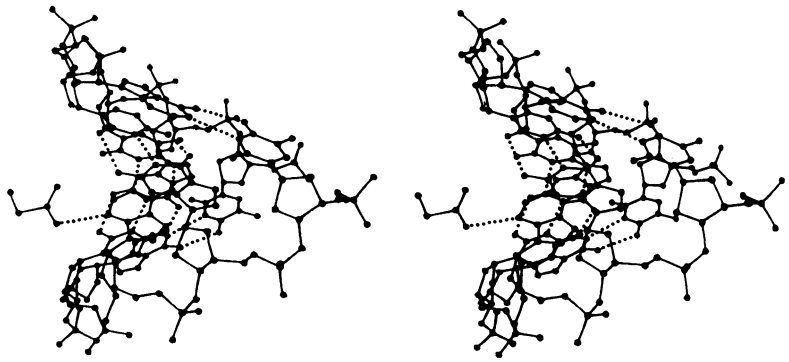

Fig. 5. Fitting model between amide group of the side chain of protein and adenine moiety paired with thymine residue in the minor groove of double helical DNA. (Conformation A)

Elementary Pattern of Interaction between Adenine and Amide Group. In order to see if the binding mode between adenine N(3) and amide group N(13) is an elementary pattern of protein–nucleic acid interactions, we have tried to fit the binding geometry into a minor groove of the double helical DNA by an interactive computer graphics; atomic coordinates of DNA were taken from the work of Arnott and Hukins.[19]

In DNA (A form), the amide side chain of amino acid fitting into adenine N(3) with the observed binding geometry (Table 8)[3] is free from any steric hindrance as shown in Fig. 5. However, the groove is not very large and the rotation of the amide group about the N(13)H···N(3) hydrogen bond (60°) gives rise to a close contact between O(13) and the ribose ring of the neighbouring nucleotide.

On the other hand, in DNA (B form) with a much narrower minor groove the amide side chain fitting into adenine N(3) gives rise to an abnormal contact between N(13) and oxygen atom of the ribose ring of the neighbouring nucleotide. Even after considerable adjustments of torsional angles and bond angles a close contact of 2.5 Å still remains. Conformational change of DNA should be introduced.

TABLE 8. BINDING PARAMETERS BETWEEN ADENINE AND AMIDE GROUP IN Fig. 5

Interaction bond distance			
l_{kl}/Å			3.055
Bond angle			
θ_{jkl}/°			115
θ_{klm}/°			107
Torsion angle[a)]			
ϕ_{ijkl}/°			176
ϕ_{jklm}/°			275
ϕ_{klmn}/°			203
Atoms in adenine		Atoms in amide group	
i	N(1)	l	N(13)
j	C(2)	m	C(13)
k	N(3)	n	C(12)

a) Values for the molecules related by inversion.

Figures 1, 3, 4, and 5 were drawn by TSD : XTAL and TSD: MODL,[20] computer-graphics interactive modelling programmes for NOVA 3 computer. The present work was supported in part by a Grant-in-Aid for Scientific Research from the Ministry of Education, Science and Culture.

References

1) M. Ohki, A. Takenaka, H. Shimanouchi, and Y. Sasada, *Bull. Chem. Soc. Jpn.*, **48**, 848 (1975).
2) C. Tamura, T. Hata, S. Sato, and N. Sakurai, *Bull. Chem. Soc. Jpn.*, **45**, 3254 (1972).
3) A. Takenaka, M. Ohki, and Y. Sasada, *Bull. Chem. Soc. Jpn.*, **53**, 2724 (1980).
4) T. Hata, M. Yoshioka, S. Sato, and C. Tamura, *Acta Crystallogr., Sect. B*, **31**, 312 (1975).
5) M. Ohki, A. Takenaka, H. Shimanouchi, and Y. Sasada, *Bull. Chem. Soc. Jpn.*, **50**, 2573 (1977).
6) M. Ohki, A. Takenaka, H. Shimanouchi, and Y. Sasada, *Acta Crystallogr., Sect. B*, **33**, 2954 (1977).
7) A. Takenaka and Y. Sasada, 38th National Meeting of the Chemical Society of Japan, Nagoya, October 1978, Abstr., p. 1004.
8) N. C. Seeman, J. M. Rosenberg, F. L. Suddath, J. J. P. Kim, and A. Rich, *J. Mol. Biol.*, **104**, 109 (1976).
9) G. Lancelot and C. Héléne, *Nucleic Acids Res.*, **16**, 1063 (1979).
10) K. Kondo, M. Miyata, and K. Takemoto, *Bull. Chem. Soc. Jpn.*, **44**, 2554 (1971).
11) L. E. McCandlish and G. H. Staut, *Acta Crystallogr., Sect. A*, **31**, 245 (1975).
12) "International Tables for X-Ray Crystallography," Kynoch Press, Birmingham (1974), Vol. IV, p. 71.
13) Table 3 is deposited as Document No. 8130, at the Office of the Bulletin of the Chemical Society of Japan.
14) T. J. Kistenmacher and M. Rossi, *Acta Crystallogr., Sect. B*, **33**, 253 (1977).
15) D. Voet and A. Rich, *Prog. Nucl. Acids. Res. Molec. Biol.*, **10**, 183 (1970).
16) J. J. Verbist, M. S. Lehmann, T. F. Koetzle, and W. C. Hamilton, *Acta Crystallogr., Sect. B*, **28**, 3006 (1972).
17) T. F. Koetzle, M. N. Frey, M. S. Lehmann, and W. C. Hamilton, *Acta Crystallogr., Sect. B*, **28**, 1571 (1973).
18) T. Koizumi, Y. Ohashi, and Y. Sasada, Annual Meeting of the Crystallographic Society of Japan, Nagoya, November, 1979, Abstr., p. 1B-13.
19) S. Arnott and D. W. L. Hukins, *Biochem. Biophys. Res. Commun.*, **47**, 1504 (1972).
20) A. Takenaka and Y. Sasada, *J. Cryst. Soc. Jpn.*, **22**, 214 (1980).

Energy Conversion and Storage in Solid-state Photogalvanic Cells

Hiroshi HADA,* Kazuchiyo TAKAOKA, Masahiko SAIKAWA, and Yoshiro YONEZAWA
Department of Industrial Chemistry, Faculty of Engineering, Kyoto University, Yoshida, Sakyo-ku, Kyoto 606
(Received November 22, 1980)

The solid-state photogalvanic cells involving photochemically deposited metals as active materials are presented. As these cells have many excellent features as compared with usual photogalvanic cells in which both the cathodic and anodic materials are dissolved in solution, they will promise a novel storage system for the conversion of solar energy to electrical energy. A typical two-compartment cell: TiO_2, aqueous $Ce(SO_4)_2$–$Ce_2(SO_4)_3$||aqueous $AgNO_3$, Pt could be charged by the irradiation of 300—400 nm light on TiO_2. The deposited silver on a platinum black storage electrode has almost the same electrochemical properties as the silver metal electrode and is capable of recharging after a nearly complete discharge.

Although good efficiencies in solar energy conversion have been achieved with solid-state devices, especially with a *pn*-junction solar cell, energy conversion of light in electrochemical cells based on the photovoltaic effect at the semiconductor-liquid interface has still attracted considerable attention.[1,2] Fujishima and Honda have shown that water photolysis occurs in a photoelectrochemical cell using TiO_2 as a photosensitive electrode, together with taking out the electrical energy through an external load (photoelectrolysis cell).[3] When a suitable redox couple is dissolved in the electrolyte solution, the chemistry occurring in the cell having a n-type semiconductor electrode can be represented by the two half-cell reactions: oxidation of the reduced form at the photoelectrode and reduction of the oxidized form at the dark electrode, respectively. Light energy is thus converted to electrical energy with no net chemical changes in the whole cell (photovoltaic cell).[4] Since Becquerel first discovered the photogalvanic effect,[5] a number of papers on the subject appeared in the scientific literature.[6–8] However, the energy conversion efficiency in the conventional photogalvanic cells which make use of the photochemically generated species in an electrolyte solution as active materials is not so high due mostly to wasteful recombination reactions. The photoelectrolysis cell of Fujishima and Honda can produce hydrogen and oxygen from water, which are both useful active materials of the fuel cell. On the practical aspect, it seems to be most convenient to store the light energy as solid-state active materials at the electrode surface. We want to call such cells as solid-state photogalvanic cell in a sense that light energy is stored in solid state and *in situ* before taking out electrical energy at any time. We expect that these cells will show more excellent properties of the conversion and storage of light energy than the conventional photogalvanic cells because of their relatively compact size and ease to prevent wasteful reactions of active materials. There have been only few reports on such cells until now. Zaromb *et al.* proposed the cyclic photogalvanic silver halide cells: Pt, Ag–AgX, aqueous FeX_3–FeX_2, Pt (X=Cl, Br).[9] Recently, Hodes *et al.* have investigated the photoelectrochemical storage cell: CdSe; S/S^{2-} couple, Ag_2S–Ag.[10]

We have investigated the photoreduction of Ag^+ at the surface of either ZnO or TiO_2 by means of 365 nm light which belongs to the fundamental absorption band of them and observed that the quantum yield of the reaction is about 10^{-1} and that general feature of the reaction is elucidable by a local cell model.[11] While ZnO suffers irreversible decomposition by positive holes in the course of the reaction, TiO_2 is fairly stable and decomposes water into oxygen. Therefore, the photochemical reaction at TiO_2 surface may be regarded as conversion of light energy to the chemical energies represented by Ag^+/Ag couple (0.80 V *vs.* NHE) and $O_2,H^+/H_2O$ couple (1.23 V at pH=1). If we construct a photocell so as to separate the photochemical reaction at TiO_2 surface; an anodic reaction at TiO_2 photoelectrode (O_2 evolution) and a cathodic reaction (Ag deposition) at a storage electrode, we can indeed store the light energy *in situ* as active materials of the galvanic cell ready to convert to electrical energy any time. Cyclic discharge and photoelectrochemical recharging of the cell are easily accessible by switching the TiO_2 electrode to an inert counter electrode and *vice versa*. One of the merits of this cell is a decreased internal resistance as the electrodes are not made of non-metallic materials such as AgX and Ag_2S which were used by Zaromb *et al.* and Hodes *et al.*, respectively. If we make use of anion specific membrane to separate the solutions of two half cells, we can employ various combinations of cathodic and anodic materials. The present study is aimed at a preliminary examination of the possibility of various solid-state photogalvanic cells by using TiO_2 as a photoelectrode.

Experimental

TiO_2 film electrode was prepared by heating a plate of titanium in a fire of town gas at about 1600 K for 300 s according to Fujishima *et al.*[12] Titanium oxide of *ca.* 2 μm in thickness and more than 10 cm^2 area could be easily formed on titanium metal. Photoelectrochemical behavior of the oxide film electrode was somewhat inferior to TiO_2 single crystal electrode. The maximum photocurrent of the former electrode in UV-region was less than the latter one. An experimental cell is schematically indicated in Fig. 1. A storage electrode (A) and a counter electrode(C) are both made of platinum black disc. Anion specific membrane ACH-45T (Tokuyama Soda Co. Ltd.) separated the solutions of two half cells. A TiO_2 electrode (P) was connected with A-electrode directly or through an external load under photoelectrochemical charging, and then exchanged to C-electrode on discharge by two switch terminals. The electrolyte solution in the compartment of P- and C-electrodes consisted of aqueous solutions of KNO_3 plus HNO_3, Ce^{4+}/Ce^{3+} couple, or Fe^{3+}/Fe^{2+} couple.

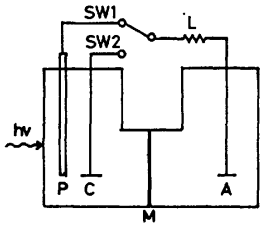

Fig. 1. Schematic representation of the solid-state photogalvanic cell with three electrodes.
P: TiO_2 electrode, A: Pt–Pt electrode (5.5 cm^2), C: Pt–Pt electrode (1.0 cm^2), M: Anion specific membrane, L: External load composed of variable resistance box, SW1, SW2: switches.

That in the A-electrode compartment ordinarily comprised KNO_3 plus either Ag^+ or Cu^{2+}. When we examined an applicability of AgCl/Ag, Cl^- couples as a storage electrode, AgCl electrode of *ca.* 0.1 cm^2 area was prepared according to Zaromb *et al.*[9] All potentials given in this paper are measured *versus* a normal hydrogen electrode (NHE).

As the light source, a high pressure 500-W mercury lamp (Ushio Denki Co. Ltd.) was used in combination with an interference filter UV-D2 (Toshiba Co. Ltd.) and water filter to select 300—400 nm light. The number of photons incident on the cell was 1.9×10^{17} cm^{-2} s^{-1} according to the trioxalatoferrate(III) actinometry.[13] Photoelectrochemical charging was achieved by irradiating on about 3 cm^2 area of TiO_2 electrode through the electrolyte solution. The photocurrent was measured by the voltage across a resistance box, which was recorded on an electrometer TR-84M (Takeda Riken Co. Ltd.) or a recorder EPR-100A (Toa Electronics Co. Ltd.). The current-voltage characteristics of the cells before and after charging were determined in a similar manner at 298 K in the darkness. The amounts of electricity passed through the circuit on the photoelectrochemical charging and discharge were obtained by the integration of the current monitored continuously as the voltage across a constant resistance. The amount of silver atoms deposited on a storage electrode was determined with an aid of a Jarrel-Ash AA-780 atomic absorption spectrophotometer. The optical density measurement of the solutions containing Ce^{4+}/Ce^{3+} couple has been carried out by using a MPS-5000 spectrophotometer (Shimadzu Seisakusho Co. Ltd.). All solutions were prepared from reagent grade chemicals purchased from Nakarai Chemicals Co. Ltd.

Results

Possibility of Solid-state Photogalvanic Cell. We have searched for a possibility of several combination of active materials which can be charged photoelectrochemically. With a reference of our former study on the photoreduction of Ag^+ at the semiconductor surface,[11] we at first examined the solid-state photogalvanic cell involving oxygen and silver as active materials: TiO_2, $HNO_3||Ag^+$, Pt (cell I). The electrolyte solutions comprised 1 M HNO_3 plus 1 M KNO_3 for a compartment of TiO_2 electrode and 1 M $AgNO_3$ plus 1 M KNO_3 for a compartment of the storage electrode, respectively. Figure 2 shows the curve of photocurrent against photovoltage in light. Photocurrent flowed from a storage electrode to TiO_2 electrode. The net electrochemical reactions will be as follows:

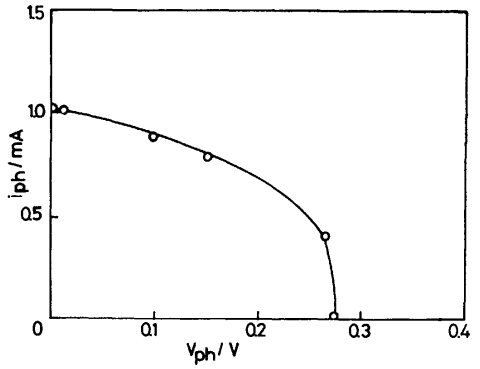

Fig. 2. Curve of photocurrent, i_{ph}, against photovoltage, V_{ph}, for the TiO_2 photocell: TiO_2, $HNO_3||Ag^+$, Pt.

$$TiO_2 + h\nu \longrightarrow e^- + p^+ \quad (1)$$

$$Ag^+ + e^- \longrightarrow Ag \quad (2)$$

$$2H_2O + 4p^+ \longrightarrow 4H^+ + O_2, \quad (3)$$

where e^- and p^+ denote an electron and positive hole, respectively. The photocurrent under a short-circuit condition was *ca.* 1 mA, which corresponds to an apparent quantum efficiency of about 1% (The number of electrons passed per s divided by the number of incident photons for 300—400 nm region per s). The open-circuit photovoltage was about 0.28 V. After illuminating the cell for 7200 s (the electricity flowed was 7.2 C), the discharge current from the counter electrode to the storage electrode was measured. The current-voltage curve of this cell was compared with that of a reference cell having a silver metal electrode of nearly equal surface area (Fig. 3). Except for some-

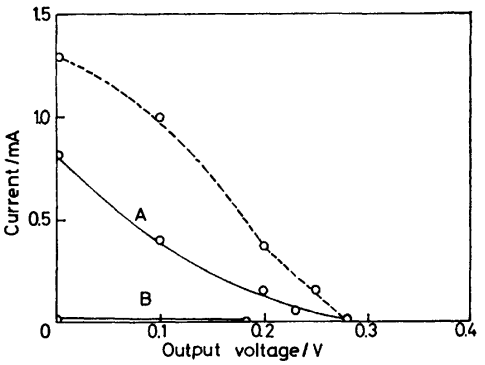

Fig. 3. The current-voltage characteristics for cells; Pt, $HNO_3||Ag^+$, Pt, ○—○, and Pt, $HNO_3||Ag^+$, Ag, ○···○. A: After charging, B: after nearly complete discharge.

what smaller short-circuit current, the current-voltage characteristics of the photogalvanic cell is not so inferior to the reference cell. Furthermore, we could hardly take out electrical energy from the cell either before the charging or after a nearly complete discharge. Therefore, we confirmed that this cell can be photoelectrochemically charged and that the contribution of a different hydrogen ion concentrations in the two cell compartments will be negligible.

In order to employ an active material more positive than O_2,H^+/H_2O couple, we next examined a photo-

galvanic cell: TiO_2, Ce^{4+}/Ce^{3+} couple ||Ag^+, Pt (cell II). The electrolyte solutions comprised 5×10^{-2} M $Ce_2(SO_4)_3$, 0.1 M $Ce(SO_4)_2$ plus 1 M HNO_3 for a compartment of P-electrode and 0.1 M $AgNO_3$ plus 1 M KNO_3 for A-electrode, respectively. The current flowed from a storage electrode to TiO_2 on irradiation. Silver atom was deposited at platinum black according to Eq. 2. Positive hole at the TiO_2 can oxidize Ce^{3+} according to Frank and Bard.[14] After illuminating the cell for 3600 s

$$Ce^{3+} + p^+ \longrightarrow Ce^{4+} \quad (4)$$

(2.6 C), the current-voltage curve of the cell was measured and compared with that of a reference cell having the same silver electrode as mentioned before (Fig. 4). Two cells show almost the same features. The open-circuit voltage nearly coincides with a difference of the standard electrode potentials of Ag^+/Ag and Ce^{4+}/Ce^{3+} (1.61 V) couples.

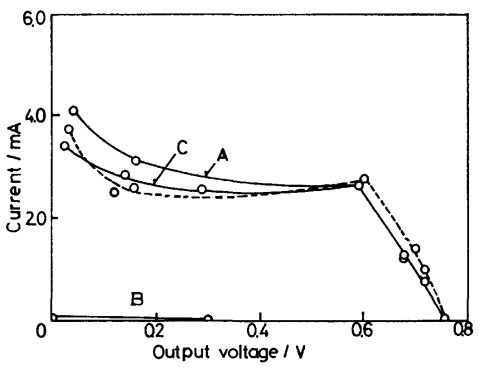

Fig. 4. The current-voltage characteristics for cells; Pt, Ce^{4+}/Ce^{3+} couple||Ag^+, Pt, ○—○, and Pt, Ce^{4+}/Ce^{3+} couple||Ag^+, Ag, ○···○.
A: After charging, B: after nearly complete discharge, C: after recharging.

With an aim to employ an active material more negative than Ag^+/Ag couple, we constructed a cell: TiO_2, Fe^{3+}/Fe^{2+} couple ||Cu^{2+}, Pt (cell III). Electrolyte solutions comprised 1.0×10^{-2} M $FeSO_4$ plus 1.09 M KNO_3 for P-electrode and 2.5×10^{-2} M $CuSO_4$ plus 1.1 M KNO_3 for A-electrode, respectively. This cell was capable of photoelectrochemical charging in agreement with an induction from the former work of Wrighton *et al.*[15] We charged the cell for 6600 s (2.3 C)

$$Cu^{2+} + 2e^- \longrightarrow Cu \quad (5)$$

$$Fe^{2+} + p^+ \longrightarrow Fe^{3+} \quad (6)$$

and then measured the current-voltage curve. Figure 5 gives a comparison of a deposited copper electrode with copper metal electrode of 2.2 cm^2 area. The current-voltage curves of the two cells resembled each other but the open-circuit voltage of them was somewhat smaller than the difference of the standard electrode potentials of Cu^{2+}/Cu (0.34 V) and Fe^{3+}/Fe^{2+} (0.77 V) couples.

We finally intended to employ a AgCl/Ag,Cl^- couple (0.22 V) and constructed a cell: TiO_2, Fe^{3+}/Fe^{2+} couple ||KCl, AgCl,Pt (cell IV) with a reference of the former study of Zaromb *et al.*[9] The electrolyte solutions contained 1.0×10^{-2} M $FeCl_2$ plus 0.2 M KCl for P-electrode and only 0.2 M KCl for A-electrode, respectively. Irradiation of TiO_2 extended the photocurrent to induce cathodic decomposition of AgCl:

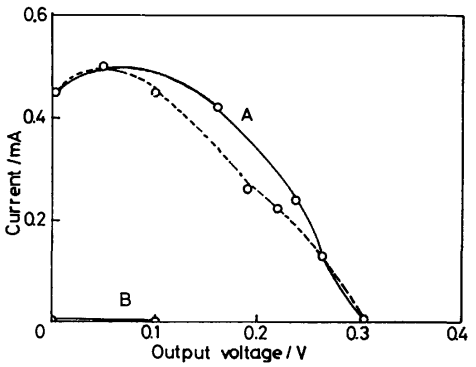

Fig. 5. The current-voltage characteristics for cells; Pt, Fe^{3+}/Fe^{2+} couple||Cu^{2+}, Pt, ○—○, and Pt, Fe^{3+}/Fe^{2+} couple||Cu^{2+}, Cu, ○···○.
A: After charging, B: after nearly complete discharge.

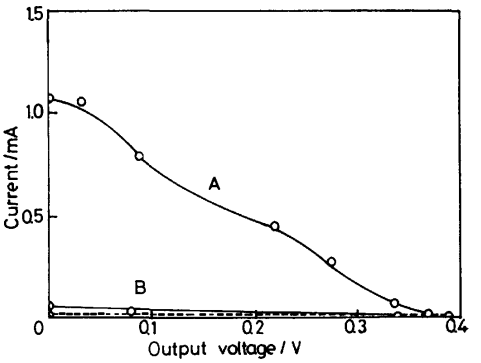

Fig. 6. The current-voltage characteristics for cells; Pt, Fe^{3+}/Fe^{2+} couple||KCl, AgCl, Pt, ○—○, and Pt, Fe^{3+}/Fe^{2+} couple||KCl, Ag/AgCl, ○···○.
A: After charging, B: after nearly complete discharge.

$$AgCl + e^- \longrightarrow Ag + Cl^- \quad (7)$$

accompanied with reaction (6). After illumination for 4200 s (0.21 C), we measured the current-voltage characteristics. Figure 6 gives a comparison of the Ag/AgCl electrode established in this manner with a commercial Ag/AgCl reference electrode HS-305D (Toa Electronics Co. Ltd.). The current-voltage curve of the former cell seems to be superior to the latter, although a direct comparison of the discharge current may be difficult because of a different surface area of them.

Energy Storage in the Cell II Using Ce^{4+}/Ce^{3+} Redox Couple. In order to obtain a most convincing proof of the true photoelectrochemical charging with a typical photogalvanic cell, we illuminated the cell II for varying irradiation time over a 110 Ω resistance. The electrolyte solution of the compartment of A-electrode was the same as in Fig. 4 throughout this item. That of a TiO_2 compartment contained 5×10^{-3} M $Ce_2(SO_4)_3$, 0.6 M HNO_3 plus 0.5 M KNO_3. The magnitude of silver atom deposited at the A-electrode was compared with the net charge stored which was determined by integrating the total photocurrent on irradiation (Fig. 7). A linear plot obtained is in agreement with the charging reaction of Eq. 2. It is observed that the greater part

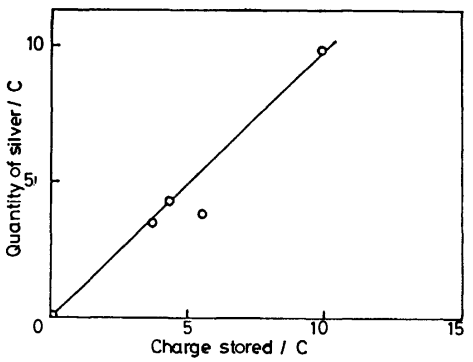

Fig. 7. Relation between the net charge stored in and the quantity of silver deposited on a Pt–Pt electrode for a cell: Pt, Ce^{4+}/Ce^{3+} couple||Ag^+, Pt.

of the photocurrent was consumed for the silver reduction at the A-electrode, because a slope of the straight line in this Figure is 0.94. The apparent quantum efficiency of silver deposition was about 1%. The power efficiency of this cell for 300—400 nm light was roughly estimated from the product of the apparent quantum efficiency of charging current and the ratio of energy level difference of Ag^+/Ag and Ce^{4+}/Ce^{3+} couples (0.81 eV) to the band-gap energy of TiO_2 (3.05 eV). It was about 0.3%. We next tried to detect an increase of Ce^{4+} in the TiO_2 compartment. The concentration of Ce^{4+} was determined spectrophotometrically by measuring the optical density at 375 nm corresponding to the absorption tail of this ion. The solutions in the cell were the same as those in Fig. 7. Ce^{4+} initially increased with time and then reached some stationary value after a prolonged irradiation. For example, the amount of oxidized Ce^{3+} corresponded initially to 98% of the net charge at 3.7 C charging but only to 22% after 10 C charging.

The relation between the charge stored on illumination and withdrawn in the darkness was examined by using two electrolyte solutions in the TiO_2 compartment, either the same as in Fig. 4 or 2.5×10^{-3} M $Ce_2(SO_4)_3$, 0.6 M HNO_3 plus 0.5 M KNO_3. It is observed that although a discharge current over a 1 kΩ resistance had initially a constant value of *ca.* 0.7 mA, it then successively decreased without stirring of a Ce^{4+}/Ce^{3+} half cell by a suitable stirrer. Such tendency was more evident for the cell containing smaller initial concentration of this couple. Figure 8 gives a plot between the net charge stored and withdrawn determined by integrating the total current before an above-mentioned fall-off region of the discharge current. From the slope, it is found that *ca.* 18% of the charge stored could be withdrawn as a nearly constant discharge current from cell A even without stirring. Furthermore, even from cell B which had smaller initial Ce^{4+}/Ce^{3+} concentration than cell A, up to 78% of the charge stored could be extracted only with a stirring by a magnetic stirrer.

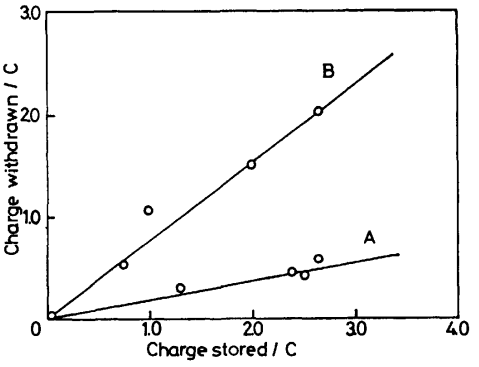

Fig. 8. Dependence of the net charge withdrawn on the charge stored in the two different Pt, Ce^{4+}/Ce^{3+} couple|| Ag^+, Pt cells.
A: 5×10^{-2} M $Ce_2(SO_4)_3$+0.1 M $Ce(SO_4)_2$ without stirring, B: 2.5×10^{-3} M $Ce_2(SO_4)_3$ with stirring.

We finally confirmed that the cell with the same electrolyte solution as in Fig. 4 could be recharged by many times after nearly complete discharge. A typical result is included in the same Figure.

Discussion

Photoelectrochemical charging of the solid-state photogalvanic cells having a TiO_2 photoelectrode was achieved with four different storage modes. According to an energetic consideration, it seems to be promising at sight to employ a combination of active materials: those which have as negative electrode potentials as the conduction-band edge and those which have as positive electrode potentials as the valence-band edge of the surface of the photoelectrode. In this respect, Ag^+/Ag–Ce^{4+}/Ce^{3+} combination is superior to Ag^+/Ag–O_2,H^+/H_2O one. Moreover, Cu^{2+}/Cu–Fe^{3+}/Fe^{2+} and AgCl/Ag,Cl^-–Fe^{3+}/Fe^{2+} combinations may also treasure up some possibilities. However, H_2 evolution at the cathode and O_2 evolution at the anode during photoelectrochemical charging strongly limit the choice of arbitrary redox couples in aqueous solution. A decreased charging current, as expected from a local cell consideration, may give an additional criterion for the choice.

So far as our experiments, solid-state photogalvanic cell of type II seems to be most excellent with regard to the short-circuit current and open-circuit voltage. Moreover, almost all the photocurrent could be stored as deposited silver. In the darkness, an active material Ce^{4+} could be stored over a long time at the open-circuit condition, because thermal reduction of Ce^{4+} by water is rather slow at room temperature.[16] In this respect, Ce^{4+}/Ce^{3+} couple seems to be superior to, say, Co^{3+}/Co^{2+} one, as Co^{3+} is reduced by water in the darkness.[17] Indeed, there are several problems to be solved with this cell. The power efficiency of the cell seems to be not so large at present. However, it will be due mostly to the reduced quantum efficiency of anodic photocurrent of TiO_2 film electrode employed here. So that, we may expect a considerable improvement if we operate a refined electrode under an optimum condition. Appearance of a stationary concentration of Ce^{4+} with irradiation time suggests an existence of competition processes of the formation and disappearance of this ion. It may be due at least in part to both the bulk photochemical reactions of Ce^{4+} and Ce^{3+} even in 300—400 nm region[18,19] and to the filter effect of

incident light on TiO_2 by Ce^{4+}. The effect of stirring of Ce^{3+},Ce^{4+}/Pt half cell in Fig. 8 suggests that discharge current will be limited by some reasons at this part of the photogalvanic cell. To overcome these difficulties, several efforts are undertaken at present.

In the silver halide cell of Zaromb *et al.*,[9] the energy of light absorbed by, say, AgCl was converted to the chemical energy by the following reaction:

$$AgCl + Fe^{2+} \longrightarrow Ag + Cl^- + Fe^{3+}. \quad (8)$$

A serious drawback of this cell was that it could operate satisfactorily only in light because there exist several self-discharge reactions in the darkness. With regard to this, cell IV may be an extension of their cell.

Though TiO_2 electrode is photochemically stable, spectral response of it is mostly in the ultraviolet. With regard to this point, the photoelectrochemical storage cell of Hodes *et al.*[10] using CdSe photoelectrode seems to be superior to ours. However, as CdSe suffers the irreversible decomposition reaction unless operated in the alkaline solution containing a suitable redox couple such as S/S^{2-}, the choice of active materials stable in alkaline solution will inevitably be reduced in consequence. Apart from an application of some other photoelectrode having smaller band-gap energy, the design of the solid-state photogalvanic cells which are capable of *in situ* storage of both anodic and cathodic materials is under way.

References

1) "Semiconductor Liquid Junction Solar Cells," ed by A. Heller Electrochemical Society, Princeton, New Jersey (1977).
2) A. Nozik, *Ann. Rev. Phys. Chem.*, **29**, 189—222 (1978).
3) A. Fujishima and K. Honda, *Nature*, **238**, 37 (1972).
4) H. Gerischer, *J. Electroanal. Chem. Interfacial Electrochem.*, **58**, 263 (1975).
5) E. Becquerel, *C. R. Acad. Sci.*, **9**, 561 (1839).
6) E. Rabinowitch ,*J. Chem. Phys.*, **8**, 551, 560 (1940).
7) A. W. Copeland, O. D. Black, and A. B. Garrett, *Chem. Rev.*, **31**, 117 (1942).
8) T. Sakata, Y. Suda, J. Tanaka, and H. Tsubomura, *J. Phys. Chem.*, **81**, 537 (1977); Y. Suda, Y. Shimoura, T. Sakata, and H. Tsubomura, *ibid.*, **82**, 268 (1978); H. Tsubomura, Y. Shimoura, and S. Fujiwara, *ibid.*, **83**, 2103 (1979).
9) S. Zaromb, M. E. Lasser, and F. Kalhammer, *J. Electrochem. Soc.*, **108**, 42 (1961).
10) G. Hodes, J. Manassen, and D. Cahen, *Nature*, **261**, 403 (1976); J. Manassen, G. Hodes, and D. Cahen, *J. Electrochem. Soc.*, **124**, 532 (1977).
11) H. Hada, H. Tanemura, and Y. Yonezawa, *Bull. Chem. Soc. Jpn.*, **51**, 3154 (1978).
12) A. Fujishima, K. Kohayakawa, and K. Honda, *J. Electrochem. Soc.*, **122**, 1487 (1975).
13) C. G. Hatchard and C. A. Parker, *Proc. R. Soc. London, Ser. A*, **235**, 518 (1956).
14) S. N. Frank and A. J. Bard, *J. Am. Chem. Soc.*, **99**, 4667 (1977).
15) M. S. Wrighton, P. T. Wolczanski, and A. B. Ellis, *J. Solid State Chem.*, **22**, 17 (1977).
16) D. Grant, *J. Inorg. Nucl. Chem.*, **26**, 337 (1964).
17) M. E. Gerstner, *J. Electrochem. Soc.*, **126**, 944 (1979).
18) L. J. Heidt and A. F. Mcmillan, *Science*, **117**, 75 (1953); *J. Am. Chem. Soc.*, **76**, 2135 (1954).
19) R. J. Marcus, *Science*, **123**, 399 (1956).

Use of Propagators in the Hückel Model. II. Propagators in Terms of Trigonometrical Functions

Shigeyuki Aono,* Takayuki Ohmae, and Kiyoshi Nishikawa

Department of Chemistry, Faculty of Science, Kanazawa University, Marunouchi, Kanazawa 920

(Received November 22, 1980)

The propagators of the chain molecules with and without the bond alternation are expressed in terms of trigonometrical functions. These expressions are convenient to practical manipulations. For exercises, the total energy, charge density and bond order are calculated.

In the previous paper,[1] we have developed a propagator theory for the Hückel model or in the tight-binding approximation. Useful methods to obtain the propagators of general networks have been presented, and propagators have been finally expressed as polynomials in terms of the energy parameter z. This analytical form being convincing from the theoretical viewpoints, is not so convenient for various application. As has been done in the simple examples of I, the actual calculations always need the contour integrals around the poles. If we use the polynomial expressions for propagators, it is difficult for us to find poles except the simplest cases. Therefore we give the compact analytical forms to the propagators in terms of trigonometrical functions. Then we calculate the charge density, bond order and total energy of the systems under consideration. Mathematical tools are almost due to the Coulson's old paper,[2] which is not so far in spirit from the present modern treatment.

Propagators of Linear Chain Molecules with Equal Bond Distance

In this section, the propagator of the linear chain molecule with same atoms and with equal bond length is investigated. The transfer integral between the nearest sites is scaled to be unity and if necessary it will be recovered by the dimensional analysis. The linear chain molecule with n sites are numbered as Fig. 1. The propagator of this system has been given in I as

$$G_n(0)^{-1} = z - \cfrac{1}{z - \cfrac{1}{z - \cfrac{1}{z - \cfrac{1}{\vdots}}}} = z + \frac{-1}{z} + \frac{-1}{z} + \frac{-1}{z} + \cdots, \tag{1}$$

where $G_n(0)$ is the (0,0) matrix element of the Green's function operator of this chain.

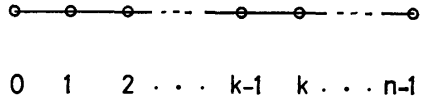

Fig. 1. Linear chain molecule.

The continued fraction more general than Eq. 1

$$S_n = b_0 + \frac{a_1}{b_1} + \frac{a_2}{b_2} + \cdots + \frac{a_{n-1}}{b_{n-1}} \tag{2}$$

is expressed as[3]

$$S_n = A_{n-1}/B_{n-1}. \tag{3}$$

Here A_k and B_k satisfy the recurrance formula

$$\begin{pmatrix} A_k \\ B_k \end{pmatrix} = \begin{pmatrix} A_{k-1} & A_{k-2} \\ B_{k-1} & B_{k-2} \end{pmatrix} \begin{pmatrix} b_k \\ a_k \end{pmatrix} \tag{4}$$

with

$$\begin{pmatrix} A_{-1} \\ A_0 \end{pmatrix} = \begin{pmatrix} 1 \\ b_0 \end{pmatrix}, \quad \begin{pmatrix} B_{-1} \\ B_0 \end{pmatrix} = \begin{pmatrix} 0 \\ 1 \end{pmatrix}. \tag{5}$$

In our case, b_k and a_k in Eq. 2 are simply

$$\begin{aligned} b_0 &= b_1 = b_2 = \cdots = z, \\ a_1 &= a_2 = a_3 = \cdots = -1, \end{aligned} \tag{6}$$

and then

$$\begin{aligned} A_k &= zA_{k-1} - A_{k-2}, \\ B_k &= zB_{k-1} - B_{k-2}, \end{aligned} \tag{7}$$

with the initial conditions

$$\begin{aligned} A_0 &= z, \quad A_1 = z^2 - 1, \\ B_0 &= 1, \quad B_1 = z. \end{aligned} \tag{8}$$

We have a theorem: If it holds that

$$S_k = bS_{k-1} + aS_{k-2}, \ (S_1 \text{ and } S_2 \text{ are given}) \tag{9}$$

the polynomial defined by

$$S(x) \equiv 1 + S_1x + S_2x^2 + \cdots \tag{10}$$

is calculated as

$$S(x) = \frac{1}{1-(bx+ax^2)}\{1+(S_1-b)x+(S_2-bS_1-a)x^2\}. \tag{11}$$

The proof is very easy and omitted.

Applying this theorem to A_k and B_k, we can find

$$\begin{aligned} A(x) &= 1 + A_0x + A_1x^2 + \cdots = \sum_{n=0}^{\infty} A_{n-1}x^n \\ &= \frac{1}{1-zx+x^2} = \sum_{n=0}^{\infty} \frac{\sin(n+1)\theta}{\sin\theta} x^n, \end{aligned} \tag{12}$$

$$z = 2\cos\theta \tag{13}$$

and

$$\begin{aligned} B(x) &= 1 + B_1x + B_2x^2 + \cdots = \sum_{n=0}^{\infty} B_nx^n \\ &= \frac{1}{1-zx+x^2} = \sum_{n=0}^{\infty} \frac{\sin(n+1)\theta}{\sin\theta} x^n. \end{aligned} \tag{14}$$

From Eq. 12 and Eq. 14 we can obtain

$$\begin{aligned} A_{k-1} &= \sin(k+1)\theta/\sin\theta \\ B_{k-1} &= \sin k\theta/\sin\theta \end{aligned} \tag{15}$$

and

$$G_n^{-1}(0) = A_{n-1}/B_{n-1} = \sin(n+1)\theta/\sin n\theta. \tag{16}$$

It should be mentioned that the replacement of Eq. 13 is safely permitted, because any site of this chain is

connected only to two nearest neighbors, and the value of z does not exceed 2.

The next problem is to obtain any diagonal element of the propagator, $G_n(k)$. If we employ a method composing the propagator,[1] it yields that

$$G_n^{-1}(k) = G_{n-k}^{-1}(0) - G_k(0) \tag{17a}$$

$$= \frac{\sin(n+1)\theta \sin\theta}{\sin(n-k)\theta \sin(k+1)\theta}. \tag{17b}$$

The relation (17a) is nothing but the Dyson equation in the site representation.

The off-diagonal element of propagator, $G_n(k,k+l)$ is expressed as

$$G_n(k,k+l) = G_n(k)G_n(k+1,[k]) \cdots G_n(k+l[k+l-1])$$
$$= G_n(k)G_{n-k-1}(0) \cdots G_{n-k-l}(0), \tag{18}$$

where $G_n(p[q])$ is the p-th diagonal element, when the q-th site is omitted. Note that the transfer integral is scaled to be unity. Using Eq. 17b in Eq. 18, we can easily obtain

$$G_n(k,k+l) = \frac{\sin(n-k-l)\theta \sin(k+1)\theta}{\sin(n+1)\theta \sin\theta}. \tag{19}$$

We now turn to evaluation of the charge density, bond order and total energy.

The charge density at k-th site is written as

$$q_n(k) = \frac{1}{2\pi i}\int_C dz G_n(k;z), \tag{20}$$

where integration is carried out along the so-called Coulson contour shown in Fig. 2a. In evaluating Eq. 20, we want to use the expression (17b) for G_n. Then we have to examine how the contour and poles are mapped onto the θ-plane by the relation (13). Let

$$z = x + iy, \quad \theta = \varphi + i\psi, \tag{21}$$

so that

$$x + iy = 2(\cos\varphi \cosh\psi - i \sin\varphi \sinh\psi). \tag{22}$$

The results obtained are displayed by Fig. 2b. The corresponding positions on the contours between two are indicated by ①. How the poles are mapped is also explained in the figure caption in the case of the six members ring. We note first of all that while the contour turns round once in the z-plane, it goes round twice in the θ-plane, so that we need the additional multiplicative factor, 1/2. Second, every pole in the z-plane splits into two except ones of values $\theta=0$ and π. However we need not worry about this behavior since the pole strength at any pole correctly produces the result.

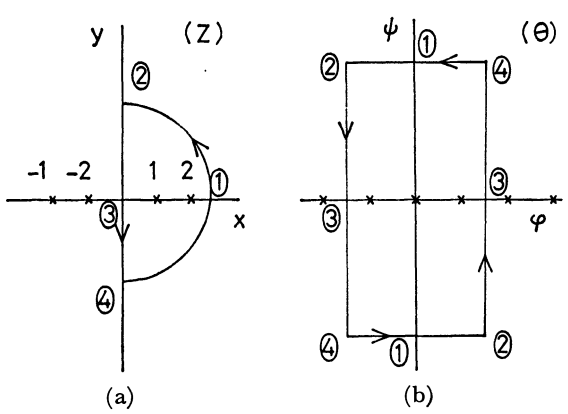

Fig. 2. (a) Contour in z-plane; Poles are those of the six member ring. (b) Contour in θ-plane; Poles are transfered as $2\to 0$; $1\to\pi/3$, $-\pi/3$; $-1\to 2\pi/3$, $-2\pi/3$; $-2\to\pi$.

Using Eq. 17b and Eq. 20, we obtain

$$q_n(k) = \frac{-1}{2\pi i}\int_C d\theta \frac{\sin(n-k)\theta \sin(k+1)\theta}{\sin(n+1)\theta}, \tag{23}$$

where poles are

$$\theta_r = \pi r/(n+1), \quad r = \pm 1, \pm 2, \cdots, \pm n. \tag{24}$$

Hereafter we confine ourselves to the simplest case of the so-called half-filled band, *i.e.*, the levels with $|n| \leq n/2$ being occupied. The contour integral in Eq. 23 yields (the spin factor, 2 is included)

$$q_n(k) = -2\sum_{r=-n/2}^{n/2} \frac{\sin(n-k)\theta_r \sin(k+1)\theta_r}{(n+1)\cos(n+1)\theta_r}$$
$$= \frac{n}{n+1} - \frac{2}{n+1}\sum_{r=1}^{n/2}(-1)^r \cos\left(\frac{n-2k-1}{n+1}\right)\pi r$$
$$= 1. \tag{25}$$

Here we have used the relation

$$\sum_{r=1}^{k}(-1)^{r-1}\cos xr$$
$$= \frac{1}{2} + (-1)^r \cos\frac{(k+1)}{2}x/2 \cos\frac{x}{2} \tag{26}$$

and see that in the second term of Eq. 25, the terms except with $r=1$ vanish. Note that $q_n(k)$ is independent of k.

The bond order, $q_n(k,k+1)$ is given by Eq. 19 as

$$q_n(k,k+l) = \frac{1}{2\pi i}\int_C dz G_n(k,k+l;z)$$
$$= \frac{-1}{2\pi i}\int_C d\theta \frac{\sin(k+1)\theta \sin(n-k-l)\theta}{\sin(n+1)\theta}. \tag{27}$$

In the similar way but a little tedious calculations lead to

$$q_n(k,k+l) = \frac{1}{n+1}\left\{\frac{\sin l\pi/2}{\sin l\pi/2(n+1)} - \frac{\sin(2k+l+2)\pi/2}{\sin(2k+l+2)\pi/2(n+1)}\right\}. \tag{28a}$$

If we here put

$$k = S-1, \quad k+l = t-1,$$

the above becomes

$$q_n(s-1,t-1) = \frac{1}{n+1}\left\{\frac{\sin(t-s)\pi/2}{\sin(t-s)\pi/2(n+1)} - \frac{\sin(t+s)\pi/2}{\sin(t+s)\pi/2(n+1)}\right\} \tag{28b}$$

as usual. From this expression, we can clearly conclude that $q_n(s-l, t-l)$ vanishes for the cases that $(t-s)$ is even, *i.e.*, between the starred atoms, or between the unstarred atoms.

The total energy of the present system, E is

$$E_n = \mathrm{Tr}\frac{1}{2\pi i}\int_C dz\, z\mathbf{G}_n(z) \tag{29}$$
$$= \sum_{k=0}^{n-1}\frac{-1}{\pi i}\int_C d\theta \frac{\cos\theta \sin(n-k)\theta \sin(k+1)\theta}{\sin(n+1)\theta}$$

$$= 4\sum_{r=1}^{n/2}\cos\theta_r$$

$$= 2\sum_{r=1}^{n/2} z(\theta_r). \tag{30}$$

In obtaining this result, we have made the k-summation at the beginning, using the relations,

$$\sum_{k=1}^{n}\sin xk = \sin\frac{(n+1)x}{2}\sin\frac{nx}{2}\Big/\sin\frac{x}{2}$$

$$\sum_{k=1}^{n}\cos xk = \cos\frac{(n+1)x}{2}\sin\frac{nx}{2}\Big/\sin\frac{x}{2}. \tag{31}$$

Propagator of Ring Molecule with Equal Bond Distance

We shall obtain the propagator of the ring molecule shown in Fig. 3. For simplicity, the number of atoms, n is assumed to be $4m+2$, $m=1,2,\cdots$ Employing the method[1] to build up the ring propagator from the chain propagator, we get

$$\begin{aligned} R_n^{-1}(0) &= G_1^{-1}(0) - G_n(1[0]) - G_n(1,n[0]) \\ &\quad - G_n(n[0]) - G_n(n,1[0]) \\ &= G_1^{-1}(0) - 2G_{n-1}(0) - 2G_{n-1}(0,n-2) \\ &= \frac{\sin 2\theta}{\sin\theta} - 2\left\{\frac{\sin(n-1)\theta}{\sin n\theta} + \frac{\sin\theta}{\sin n\theta}\right\} \\ &= -\frac{2\sin(n\theta/2)\sin\theta}{\cos(n\theta/2)}. \end{aligned} \tag{32}$$

The poles of R_n are

$$\theta_r = \frac{2\pi r}{n},\ r = 0,\ \pm 1,\ \cdots,\ \pm\left(\frac{n}{2}-1\right),\ \frac{n}{2} \tag{33}$$

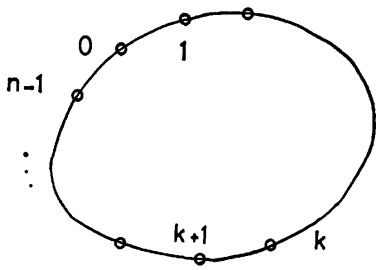

Fig. 3. Ring molecule.

Now we calculate the charge density, bond order and total energy for the case of the half-filled band. The charge density at any site is given by

$$\begin{aligned} q_n^R(0) &= \frac{1}{2\pi i}\int_C dz\, R_n(0;z) \\ &= \frac{1}{4\pi i}\int_C d\theta\,\frac{\cos(n\theta/2)}{\sin(n\theta/2)}. \end{aligned} \tag{34}$$

The integration along the contour shown in Fig. 2b is easily carried out as

$$q_n^R(0) = \frac{2}{n}\sum_{\text{Poles}} 1 = 1, \tag{35}$$

where the fact has been used that the number of poles corresponding occupied levels, *i.e.*$|\theta_r|<\pi/2$ is $n/2$. The spin summation is also done.

In order to estimate the bond order, $q_n(0,k)$, we need the off-diagonal element of the ring propagator, which is

$$\begin{aligned} R_n(0,k) &= R_n(0)R_n(1,k[0]) + R_n(0)R_n(n-1,k[0]) \\ &= R_n(0)G_{n-1}(0,k) + R_n(0)G_{n-1}(0,n-k-1), \end{aligned} \tag{36}$$

where the first and second terms correspond to the clockwise and anticlockwise propagations in Fig. 3, respectively. Using Eq. 32 and Eq. 19 in Eq. 36, we get

$$R_n(0,k) = \frac{-1}{4\sin^2\dfrac{n\theta}{2}\sin\theta}\{\sin(n-k)\theta + \sin k\theta\}. \tag{37}$$

Thus a little tedious but straightforward calculations yield

$$\begin{aligned} q_n^R(0,k) &= \frac{1}{4\pi i}\int_C d\theta\,\frac{1}{2\sin^2\dfrac{n\theta}{2}}\{\sin(n-k)\theta + \sin k\theta\} \\ &= \frac{2}{n^2}\{(n-k)+k\}\frac{\sin k\pi/2}{\sin k\pi/n} \\ &= \frac{2}{n}\frac{\sin k\pi/2}{\sin k\pi/n}, \end{aligned} \tag{38}$$

where, in the second line, the first and second terms are contributions from the clockwise and anticlockwise pathes, respectively. The final result clearly shows that in the alternant hydrocarbons the bond order vanishes between the starred atoms or between the unstarred atoms, *i.e.*, k is even. In the case of $k=1$,

$$q_n^R(0,1) = \frac{2}{n}\operatorname{cosec}\frac{\pi}{n}. \tag{39}$$

The total energy is given as

$$\begin{aligned} E &= \mathrm{Tr}\,\frac{1}{2\pi i}\int_C dz\, z\mathbf{R}_n(z) \\ &= n\frac{1}{4\pi i}\int_C d\theta\,\frac{\cos\theta\sin n\theta}{\sin^2(n\theta/2)} \\ &= 4\operatorname{cosec}\frac{\pi}{n}. \end{aligned} \tag{40}$$

Linear Chains with Bond Alternation

Linear polyenes actually show the bond alternation. If we consider phenomena concerning with linear polyene, it is natural to start with systems with the bond alternation. In this sense, it seems instructive to investigate the propagators for these molecules. Those which we are now considering are shown in Fig. 4.

The propagator of the chain molecule and chain radical are denoted G_{2n} and F_{2n+1}, respectively, where

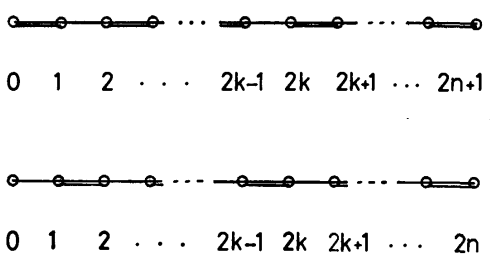

Fig. 4. Chain molecule $C_{2n}H_{2n+2}$ and chain radical $C_{2n+1}H_{2n+3}$.

indices give the number of the carbon atoms. The resonance integrals corresponding to the double and single bonds are written as β^* and β.

As has been done in Eq. 1, $G_{2n}(0)$ is given as

$$G_{2n}^{-1}(0) = z - \cfrac{\beta^{*2}}{z - \cfrac{\beta^2}{z - \cfrac{\beta^{*2}}{\ddots}}}$$

$$= z + \frac{-\beta^{*2}}{z} + \frac{-\beta^2}{z} + \cdots . \tag{41}$$

If we divide both sides by $\sqrt{\beta\beta^*}$, it yields that

$$\bar{G}_{2n}^{-1}(0) = \bar{z} + \frac{-\gamma}{\bar{z}} + \frac{-\gamma^{-1}}{\bar{z}} + \cdots , \tag{42}$$

where

$$\gamma = \beta^*/\beta , \tag{43}$$

and

$$\bar{G}_{2n} = G_{2n}/\sqrt{\beta\beta^*}, \quad \bar{z} = z/\sqrt{\beta\beta^*}. \tag{44}$$

Hereafter the dimensionless $\bar{G}_{2n}$ and $\bar{z}$ are rewritten as G_{2n} and z. Namely, instead of Eq. 42

$$G_{2n}^{-1}(0) = z + \frac{-\gamma}{z} + \frac{-\gamma^{-1}}{z} + \cdots . \tag{45}$$

Similarly, for the radical

$$F_{2n+1}^{-1}(0) = z + \frac{-\gamma^{-1}}{z} + \frac{-\gamma}{z} + \cdots . \tag{46}$$

If we write $G_k^{-1}(0)$ and $F_k^{-1}(0)$ as

$$G_k^{-1}(0) = \frac{A_{k-1}^*}{B_{k-1}^*}, \quad F_{k+1}^{-1}(0) = \frac{A_k}{B_k}. \tag{47}$$

The same treatments as has been done from Eq. 2 to Eq. 7 yield,

$$\begin{aligned}
A_0^* &= z \\
A_1^* &= z^2 - \gamma \\
A_2^* &= z^3 - z(\gamma+\gamma^{-1}) \\
A_3^* &= z^4 - z^2(2\gamma+\gamma^{-1}) + \gamma^2 \\
A_4^* &= z^5 - 2z^3(\gamma+\gamma^{-1}) + z(\gamma^2+1+\gamma^{-2}) \\
A_5^* &= z^6 - z^4(3\gamma+\gamma^{-1}) + z^2(3\gamma^2+\gamma^{-2}) - \gamma^3 \\
&\vdots
\end{aligned} \tag{48a}$$

$$\begin{aligned}
B_0^* &= 1 \\
B_1^* &= z \\
B_2^* &= z^2 - \gamma^{-1} \\
B_3^* &= z^3 - z(\gamma+\gamma^{-1}) \\
B_4^* &= z^4 - z^2(\gamma+2\gamma^{-1}) + \gamma^{-2} \\
B_5^* &= z^5 - 2z^3(\gamma+\gamma^{-1}) + z(\gamma^2+1+\gamma^{-2}) \\
&\vdots
\end{aligned} \tag{48b}$$

In the above interchanging γ and γ^{-1}, we can obtain the similar expressions for A_k and B_k,

$$\begin{aligned}
A_k &= A_k^*(\gamma \leftrightarrow \gamma^{-1}) \\
B_k &= B_k^*(\gamma \leftrightarrow \gamma^{-1}).
\end{aligned} \tag{49}$$

Also we can observe

$$\begin{aligned}
A_k &= B_{k+1}^* \\
B_k &= A_{k-1}^*.
\end{aligned} \tag{50}$$

From relations, Eqs. 48 and 49, we can immediately obtain the recurrance formulae:

$$\begin{aligned}
A_k^* &= zA_{k-1} - \gamma A_{k-2}^* \\
A_k &= zA_{k-1}^* - \gamma^{-1}A_{k-2}
\end{aligned} \tag{51}$$

and

$$\begin{aligned}
B_k^* &= zB_{k-1} - \gamma^{-1}B_{k-2}^* \\
B_k &= zB_{k-1}^* - \gamma B_{k-2}.
\end{aligned} \tag{52}$$

If we eliminate A in Eq. 51, we obtain

$$A_k^* + A_{k-2}^*(\gamma+\gamma^{-1}-z^2) + A_{k-4}^* = 0. \tag{53}$$

Entirely same relations hold for A_k, B_k^*, and B_k.

Now we can use the theorem given by Eq. 9 and Eq. 11. Let

$$A^*(x) = 1 + A_1^*x + A_2^*x^2 + \cdots + A_{2n-1}^*x^n + \cdots \tag{54}$$

and put

$$b = z^2 - \gamma - \gamma^{-1}, \quad a = -1 \tag{55}$$

in Eq. 9, it yields that

$$A^*(x) = \frac{1+\gamma^{-1}x}{1-(z^2-\gamma-\gamma^{-1})\,x + x^2}. \tag{56}$$

Here we put

$$z^2 = \gamma + \gamma^{-1} + 2\cos\theta \tag{57}$$

and obtain

$$\begin{aligned}
A^*(x) &= \sum_{n=0}^{\infty} \frac{\sin(n+1)\theta}{\sin\theta} x^n (1+\gamma^{-1}x) \\
&= \sum_{n=0}^{\infty} \left\{ \frac{\sin(n+1)\theta}{\sin\theta} + \gamma^{-1}\frac{\sin n\theta}{\sin\theta} \right\} x^n.
\end{aligned} \tag{58}$$

Combining this and Eq. 54, we get

$$A_{2n-1}^* = \left\{ \frac{\sin(n+1)\theta}{\sin\theta} + \gamma^{-1}\frac{\sin n\theta}{\sin\theta} \right\}. \tag{59a}$$

Similar analysis for B_{2n-1}^* enables us to get

$$B_{2n-1}^* = z\frac{\sin n\theta}{\sin\theta}. \tag{59b}$$

Remembering relations in Eq. 50, we obtain

$$A_{2n} = B_{2n+1}^* = z\frac{\sin(n+1)\theta}{\sin\theta}, \tag{60a}$$

$$B_{2n} = A_{2n-1}^* = \frac{\sin(n+1)\theta}{\sin\theta} + \gamma^{-1}\frac{\sin n\theta}{\sin\theta}. \tag{60b}$$

Consequently, the propagators of systems shown in Fig. 4 are

$$G_{2n}^{-1}(0) = \{\sin(n+1)\theta + \gamma^{-1}\sin n\theta\}/z\sin n\theta, \tag{61}$$

$$F_{2n+1}^{-1}(0) = z\sin(n+1)\theta/\{\sin(n+1)\theta + \gamma^{-1}\sin n\theta\}. \tag{62}$$

It is noted that once $G_{2n}^{-1}(0)$ is given, we can immediately obtain $F_{2n+1}^{-1}(0)$ by the following relation

$$F_{2n+1}^{-1}(0) = F_1^{-1}(0) - \gamma^{-1}G_{2n}(0), \tag{63}$$

and *vice versa*. Note that $F_1^{-1}(0) = z$.

Some Properties of Linear Chains with Bond Alternation

Since we have written the propagators of linear chains with bond alternation in the previous section, we now move to get some physical properties by use of them. The poles of propagators give the single particle energies: for example in the case of the chain with $2n$ members the relation

$$\sin(n+1)\theta_r + \gamma^{-1}\sin\theta_r = 0, \tag{64}$$

determines the single particle energies. The roots of Eq. 64 cannot be obtained easily, but if γ is not so far from unity, the solution has been approximately

obtained as[2,4]

$$\theta_r = \frac{2\pi r}{2n+1} - \frac{1}{2n+1}(1-\gamma^{-1}) + \tan\frac{\pi r}{2n+1}, \quad r=1,2,\cdots,2n, \tag{65}$$

where the first term stands for the case with equal bond distance, and the second for the correction in this case.

For further steps, we need the expressions of $G_{2n}(2k)$, $G_{2n}(2k+1)$, $F_{2n+1}(2k)$ and $F_{2n+1}(2k-1)$. For example, $G_{2n}(2k)$ is given as (see Fig. 4)

$$G_{2n}^{-1}(2k) = G_{2(n-k)}^{-1}(0) - \gamma^{-1} G_{2k}(0). \tag{66}$$

From this and similar equations for others, we obtain

$$G_{2n}^{-1}(2k) = \frac{\sin\theta\{\sin(n+1)\theta+\gamma^{-1}\sin n\theta\}}{z\sin(n-k)\theta\{\sin(k+1)\theta+\gamma^{-1}\sin k\theta\}}, \tag{67a}$$

$$G_{2n}^{-1}(2k-1) = \frac{\sin\theta\{\sin(n+1)\theta+\gamma^{-1}\sin n\theta\}}{z\sin k\theta\{\sin(n-k+1)\theta+\gamma^{-1}\sin(n-k)\theta\}}, \tag{67b}$$

$$F_{2n+1}^{-1}(2k) = \frac{z\sin(n+1)\theta\sin\theta}{\{\sin(k+1)\theta+\gamma\sin k\theta\}\{\sin(n-k+1)\theta+\gamma^{-1}\sin(n-k)\theta\}}, \tag{68a}$$

$$F_{2n+1}^{-1}(2k-1) = \frac{\sin(n+1)\theta\sin\theta}{z\sin(n-k+1)\theta\sin k\theta}, \tag{68b}$$

where $z=z(\theta)$ is shown in Eq. 57.

The Total Energy of the 2n *Chain.* This is given by

$$E_{2n} = \mathrm{Tr}\frac{1}{2\pi i}\int_C dz\, zG_{2n}(z) = 2\sum_{k=1}^{n-1}\frac{-1}{4\pi i}\int_C d\theta\frac{z\sin(n-k)\theta\{\sin(k+1)\theta+\gamma^{-1}\sin k\theta\}}{\sin(n+1)\theta+\gamma^{-1}\sin n\theta}. \tag{69}$$

The integration contour in this case is the same as Fig. 2b, if the two points $\pi/2$ and $-\pi/2$ are replaced by π and $-\pi$, respectively. Also note that the integration in Eq. 69 includes the spin sum. The summation with respect to k is made and then followed by the contour integration:

$$E_{2n} = 2\sum_{r=-n}^{n} \frac{z(\theta_r)\left[\frac{n}{2}\{\cos(n+1)\theta_r+\gamma^{-1}\cos n\theta_r\}-\frac{1}{2}\frac{\sin n\theta_r}{\sin\theta_r}\{1+\gamma^{-1}\cos\theta_r\}\right]}{(n+1)\cos(n+1)\theta_r+\gamma^{-1}\cos n\theta_r}. \tag{70}$$

Then using the relation (64), we can get

$$E_{2n} = \sum_{r=-n}^{n} z(\theta_r) = 2\sum_{r=1}^{n} z(\theta_r), \tag{71}$$

namely, we find the usual description that the levels with $r=1\sim n$ are doubly occupied. For numerical estimation, Eq. 65 should be invoked.

In the case of the $2n$ chain, we have been unable to give the simple and compact expressions for the poles of the propagator, which enable us difficult to carry out the contour integration. Therefore in the following we confine ourselves to treat the $2n+1$ chain, or radicals.

*The Charge Density at the (*2k−1*)-th Site of the* 2n+1 *Chain.* This is given simply by

$$q_{2n+1}(2k-1) = \frac{1}{2\pi i}\int_C dz\, F_{2n+1}(2k-1;z) = \frac{-1}{4\pi i}\int_C d\theta\frac{\sin(n-k+1)\theta\sin k\theta}{\sin(n+1)\theta}, \tag{72}$$

where poles are

$$\theta_r = \pi r/(n+1), \tag{73}$$

and those with $r=\pm1,\pm2,\cdots,\pm n$ are doubly occupied and $r=\pm(n+1)$ are singly occupied. In the course of the contour integration, we can observe that the contribution from the terms with $r=\pm(n+1)$ vanishes, and that from others exactly gives

$$q_{2n+1}(2k-1) = 1, \tag{74}$$

which is independent of k. Here we have also used the relation (26).

It is naturally expected to be

$$q_{2n+1}(2k) = 1, \tag{75}$$

but the proof seems tedious because of the rather complicated expression of Eq. 68a, and the z^2 term which appears in the denominator of the contour integrand. Briefly speaking, our proof is as follows: we separate the numerator into two parts, the first with z^2 as a common factor and the second not. We can show the contribution from the second to the integration vanishes. Concerning the first, the integration is carried out as well as in the case of $q_{2n+1}(2k-1)$, and yields the result (75). We expect a simpler proof.

The Bond Orders of the 2n+1 *Chain.* We investigate the bond order between the sites $2k-1$ and $2k$, which concerns with the double bond as indicated in Fig. 4. This is given by

$$q_{2n+1}(2k-1,2k) = \frac{1}{2\pi i}\int_C dz\, F_{2n+1}(2k-1,2k;z), \tag{76}$$

in which

$$F_{2n+1}(2k-1,2k) = F_{2n+1}(2k)\gamma^{-1/2}G_{2(n-k)}(0) = \frac{\sin k\theta\{\gamma^{1/2}\sin(n-k+1)\theta+\gamma^{-1/2}\sin(n-k)\theta\}}{\sin\theta\sin(n+1)\theta}. \tag{77}$$

Accordingly it follows that

$$q_{2n+1}(2k-1,2k) = \frac{-1}{4\pi i}\int_C \frac{d\theta}{z(\theta)}\frac{\sin k\theta\{\gamma^{1/2}\sin(n-k+1)\theta+\gamma^{-1/2}\sin(n-k)\theta\}}{\sin(n+1)\theta}. \tag{78}$$

Since the term, $z(\theta)$ is regular at the poles,

$$\theta_r=\pi r/(n+1),\ r=1,2,\cdots,(n+1). \tag{79}$$

The integration is easily carried out to yield,

$$q_{2n+1}(2k-1,2k) = \frac{2}{n+1}\sum_{r=1}^{n}\frac{\sin k\theta_r}{z(\theta_r)}\{\gamma^{1/2}\sin\theta_r+\gamma^{-1/2}\sin(k+1)\theta_r\}. \tag{80}$$

The similar result is also obtained for $q_{2n+1}(2k,2k+1)$ which concerns with the single bond:

$$q_{2n+1}(2k,2k+1) = \frac{2}{n+1}\sum_{r=1}^{n}\frac{\sin(k+1)\theta_r}{z(\theta_r)}\{\gamma^{1/2}\sin k\theta_r+\gamma^{-1/2}\sin(k+1)\theta_r\}. \tag{81}$$

In deriving these, we ignore the cut arisings from $z(\theta)=0$. If one worrys about this, the partial integration with respect to z should be done at the beginning. This

procedure moves $z(\theta)$ from the denominator to the numerator. Then tedious but straightforward calculations leads to the same results. For the case of $\gamma=1$, namely, with the equal bond length, it is simple task to get

$$q_{2n+1}(r, r+1) = \frac{1}{n+1}\left\{\cot\frac{\pi}{2n+2}+(-1)^{r-1}\cot\frac{(2r+1)\pi}{2n+2}\right\} \quad (85)^{5)}$$

from Eq. 80 or Eq. 81.

Concluding Remarks

We have presented some expressions for propagators of the chain molecules in the Hückel approximations. One may say that in deriving the physical quantity, *e.g.*, the charge density, the usual quantum chemical method is much simpler. However we can expect that in the future application, the propagator approach enables us to treat many problems in a quite general aspects and provide powerful devices to quantum chemical problems.

References

1) S. Aono and K. Nishikawa, *Bull. Chem. Soc. Jpn.*, **53**, 3418 (1980). This is referred to as I hereafter.

2) C. A. Coulson, *Proc. R. Soc. London. Ser. A*, **164**, 383 (1938).

3) "Handbook of Mathematical Functions," ed by M. Abramowitz and I. A. Stegun, Dover Publications (1970), p. 19.

4) J. E. Lennard-Jones, *Proc. R. Soc. London, Ser. A*, **158**, 280 (1937).

5) C. A. Coulson *et al.*, "Dictionary of π-Electron Calculations," Pergamon press (1965).

  Bull. Chem. Soc. Jpn., 54, 1651—1657 (1981)

Dynamic Properties of the Phosphorescent Triplet State of 9*H*-Thioxanthen-9-one (Thioxanthone) from Optically Detected Magnetic Resonance Spectroscopy

Kazuhiko SUGA and Minoru KINOSHITA*

The Institute for Solid State Physics, The University of Tokyo, Roppongi, Minato-ku, Tokyo 106

(Received December 10, 1980)

A variety of optically detected magnetic resonance (ODMR) experiments have been performed on the lowest excited triplet state of 9*H*-thioxanthen-9-one at 1.4 K. The absorption and phosphorescence excitation spectra were also measured to supplement the ODMR studies. The results were analyzed to determine the mechanisms responsible for the radiative decay and intersystem crossing processes. The z sublevel has large activity in vibronic bands due to non-totally symmetric vibrations. The intensity mainly comes from mechanisms involving vibronic coupling between $^1n,\pi^*$ and $^1\pi,\pi^*$ states. The y sublevel is selectively affected by the introduction of the sulfur atom, because of the increased importance of spin orbit coupling with $^1\sigma',\pi^*$ state which is largely localized on the thioether group.

Detailed information about the magnetic and spectroscopic properties of the lowest triplet states of aromatic carbonyls[1-13] has been accumulated in recent years, particularly by means of optically detected magnetic resonance (ODMR) spectroscopy. In the case of aromatic carbonyls having the lowest triplet states of π,π^* type, these properties have been shown to vary markedly depending on the molecular structure, the nature of environments, and the energy separations between the $^3\pi,\pi^*$ state and $^3n,\pi^*$ state (ΔE_{TT}) or the $^1n,\pi^*$ state (ΔE_{ST}). However, in the case of 9*H*-xanthen-9-one (we shall use the popular name, xanthone, hereafter) where ΔE_{TT} is rather large and the carbonyl group is rigidly held to the planar π-electron system, Chakrabarti and Hirota[17] have shown that the radiative and non-radiative properties are very different from those found in other carbonyls such as benzaldehydes and acetophenones.

The aims of the present paper are to study dynamic properties of the lowest triplet state of 9*H*-thioxanthen-9-one (we shall use the popular name, thioxanthone, hereafter) in comparison with those of xanthone[14-19] and to elucidate the mechanism of dynamical processes of the state.

Experimental

Xanthone, thioxanthone, and bis(4-bromophenyl) ether (DDE) were purified by recrystallization followed by extensive zone refining under vacuum. Hexane, heptane, and octane of spectroscopic grade (Tokyo Kasei Co., Ltd.) were used without further purification. Crystals were grown by the Bridgman method from the melts.

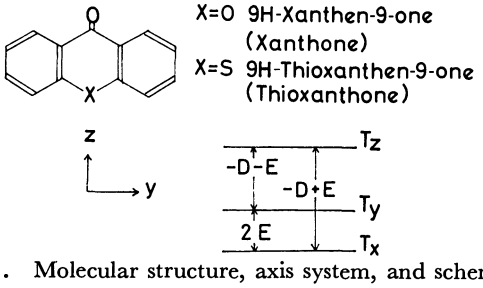

Fig. 1. Molecular structure, axis system, and scheme of zero field splitting.

The experimental set up for optical and magnetic resonance spectroscopic experiments was essentially the same as that reported previously.[20,21] The absorption spectra were measured on solutions in 1 cm path quartz cells by a Hitachi type 556 spectrophotometer at room temperature.

The molecular structures of xanthone and thioxanthone are shown in Fig. 1 together with the axis system used in this study and the zero-field(zf) splitting pattern which will be described below.

Results

Absorption Spectra. Figure 2 shows the absorption spectrum of thioxanthone observed in hexane at room temperature in comparison with that of xanthone. The intensity of the whole spectrum of thioxanthone is approximately halved as compared with that of xanthone, and each band shifts by about 3000 cm^{-1} to the red, showing that the excited π,π^* states lower their energy by sulfur substitution.

Phosphorescence Excitation Spectra. The phosphor-

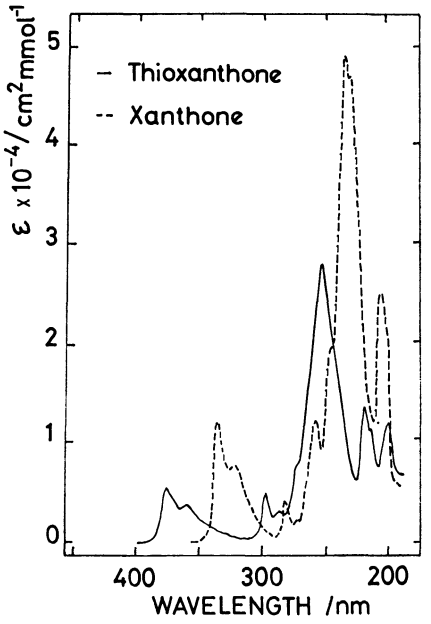

Fig. 2. The absorption spectra of thioxanthone (——) and xanthone (- - - -) in hexane at room temperature.

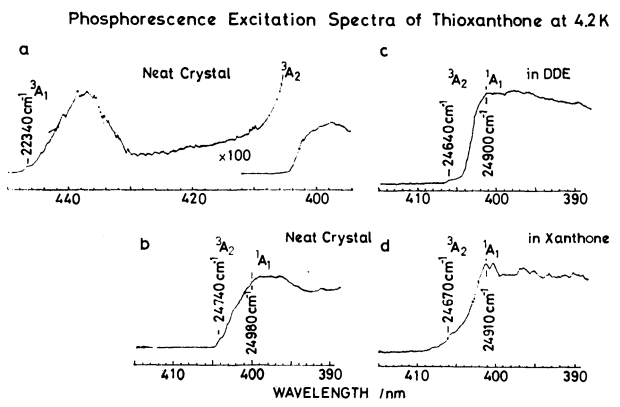

Fig. 3. The phosphorescence excitation spectra of thioxanthone at 4.2 K.
a) and b) neat crystal, c) in DDE, and d) in xanthone.

escence excitation spectra of thioxanthone in several host crystals are shown in Fig. 3. The excitation spectrum of the thioxanthone neat crystal starts at 22340 cm^{-1}, which is about 60 cm^{-1} higher than that of the origin of the phosphorescence spectrum. This indicates that the phosphorescence of the neat crystal, to be discussed below, originates from traps. There are a strong absorption band at 24980 cm^{-1} and a shoulder at about 24740 cm^{-1}. In the DDE and xanthone host crystals, the absorption at 22340 cm^{-1} is not observable, but other two absorption bands are clear.[22] The absorption at 24980 cm^{-1} is assigned to the $^1A_1(\pi,\pi^*)\leftarrow S_0$ absorption by considering the position of the first band in Fig. 2 and the excitation spectrum in heptane shown in Fig. 4. The absorptions starting at 24740 and 22340 cm^{-1} are assigned to the transitions of $^3A_2(n,\pi^*)\leftarrow S_0$ and $^3A_1(\pi,\pi^*)\leftarrow S_0$, respectively.

The excitation spectra of thioxanthone obtained in normal alkanes are complicated because of superposition of the spectra coming from multiple sites. The spectra coming from the sites are separated by using site selective monitoring technique. As an example, the spectra of the two major sites in heptane are shown in Fig. 4. The site higher in energy is referred to as site I, and the site lower as site II.

The phosphorescence excitation spectrum obtained in hexane is also shown in Fig. 5. Table 1 compares

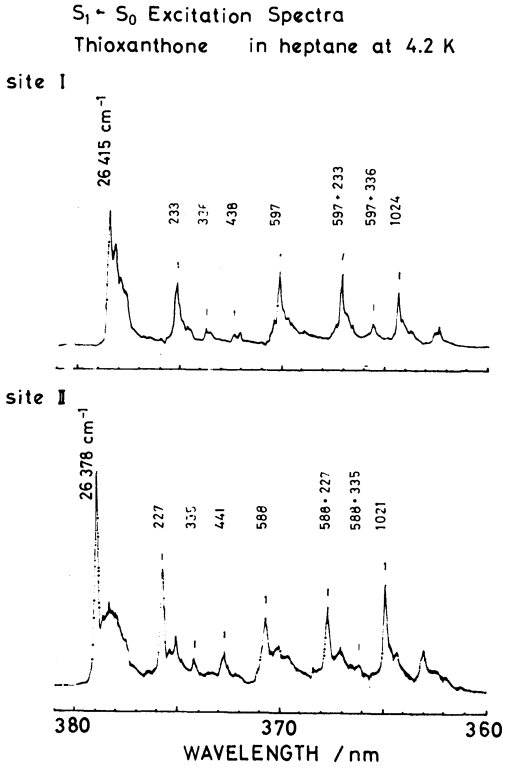

Fig. 4. The single site excitation spectra of thioxanthone in heptane at 4.2 K.
Site I (upper) and site II (lower).

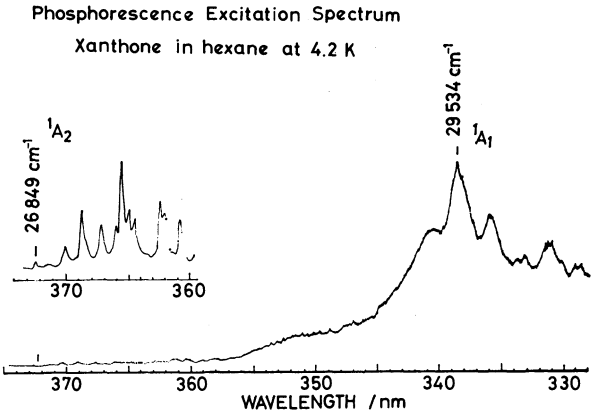

Fig. 5. The phosphorescence excitation spectrum of xanthone in hexane at 4.2 K.

TABLE 1. THE ENERGY LEVELS OF LOWER LYING EXCITED STATES AND THE ENERGY SEPARATIONS BETWEEN $^3\pi,\pi^*$ AND $^3n,\pi^*$ STATES (ΔE_{TT}) AND BETWEEN $^3\pi,\pi^*$ AND $^1n,\pi^*$ STATES (ΔE_{ST}) (IN UNITS OF cm^{-1})

	Thioxanthone				Xanthone	
	in neat crystal	in DDE	in xanthone	in hexane	in neat crystal	in hexane
$^3\pi,\pi^*$ (A_1)	22 340	22 270[a]	22 280[a]	23 215[a]	25 228	25 723[a]
$^3n,\pi^*$ (A_2)	24 740	24 640	24 670		26 689	
$^1n,\pi^*$ (A_2)					27 750	26 848
$^1\pi,\pi^*$ (A_1)	24 980	24 900	24 910	26 437		29 534
ΔE_{TT}	2400	2360	2390		1461	very small
ΔE_{ST}	>2640	>2630	>2630	>3222	>2522	1125

a) Obtained from the phosphorescence spectra. Others were determined from the phosphorescence excitation spectra.

the locations of the lower lying excited states of xanthone and thioxanthone determined from the excitation spectra. The energy levels for xanthone are essentially identical with those reported.[14,17] Most results for thioxanthone are new.

ODMR Experiments. Two strong MIDP signals at 3.088 and 1.098 GHz were observed for the emission of the traps in the thioxanthone neat crystal. Third zf transition at about 1.99 GHz could be observed by monitoring the emission at the 0,0 band. In view of the results of the other $^3\pi,\pi^*$ aromatic carbonyls so far studied,[1-9] the ordering of the sublevels is reasonably assigned as $T_z > T_y > T_x$ in energy. The x sublevel is the slowest decaying one. This assignment will be verified further by the unique behavior of the middle sublevel. Therefore, the zf transitions at 3.088 and 1.098 GHz are assigned as the $T_z \leftrightarrow T_x$ and $T_y \leftrightarrow T_x$ transitions, respectively. The ODMR transitions of thioxanthone observed in the DDE and xanthone host crystals are also assigned in a like manner. It is worthy to note that in the case of these three crystal systems, the total decay rates of the y and z sublevels are almost similar and large.

In the case of thioxanthone in hexane, on the other hand, only two positive PMDR signals were observed at 1.179 and 1.373 GHz. The third transition could be observed only slightly by the MIDP method at about 2.6 GHz. Since there is a strong likelihood that the x sublevel is the slowest decaying one, the signal at 1.179 GHz is attributed to the $T_y \leftrightarrow T_x$ transition and the signal at 1.373 GHz to $T_y \leftrightarrow T_z$. Two different sets of the zf ODMR transitions were observed for thioxanthone in heptane. The site selective experiment leads to the conclusion that site I is associated with the transitions at 1.186 and 1.376 GHz, and site II at 1.176 and 1.373 GHz.

The two sets of the ODMR signals corresponding to two distinct emitting species were observed for xanthone in the DDE host. The properties of these emitting species in the DDE host are very similar to those of the two traps observed in the xanthone neat crystal.[17]

The total decay rates k_i, relative steady state populations N_i^0, and relative populating rates P_i of the spin sublevels (i=x, y, z) were measured by the MIDP method. The relative radiative decay rates k_i^r were obtained for the 0,0 and vibronic bands at 0—670 cm^{-1}. The results are summarized in Table 2.

Phosphorescence and Sublevel Emission Spectra. The phosphorescence spectra of thioxanthone in alkanes were obtained under steady state excitation conditions. The spectrum obtained in hexane is shown in Fig. 6 in comparison with that of xanthone. The latter is resolved much better than the spectrum in the literature.[18] Unlike in hexane, where only one major site is evident, the phosphorescence spectra in heptane and octane appear as no less than two-site emission.

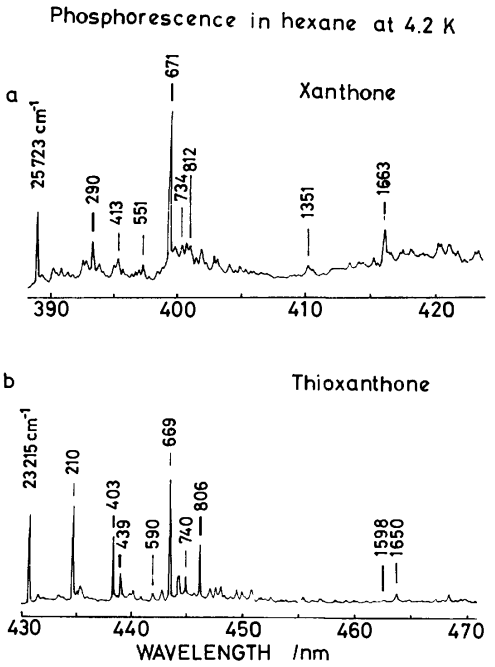

Fig. 6. The phosphorescence spectra in hexane at 4.2 K. a) Xanthone and b) thioxanthone.

Table 2. The kinetic and magnetic properties of the spin sublevels of $^3\pi, \pi^*$ states of xanthone and thioxanthone

	Thioxanthone						Xanthone	
	traps in crystal	in DDE	in xanthone	in hexane	in heptane Site I	in heptane Site II	in DDE Site I	in DDE Site II
$\|D\|/cm^{-1}$	0.0847	0.0825	0.0853	0.0655	0.0657	0.0654	0.1352	0.1111
$\|E\|/cm^{-1}$	0.0183	0.0185	0.0177	0.0197	0.0197	0.0196	0.0181	0.0188
k_z/s^{-1}	10.5	9.8	10.2	1.28	1.51	1.56	12.0	15.0
k_y/s^{-1}	12.1	10.5	9.4	9.9	8.2	9.5	1.70	1.42
k_z/s^{-1}	0.26	0.31	0.31	0.78	1.23	1.23	0.77	0.50
$P_z/\%$	51	54	57	23	33	31		
$P_y/\%$	47	43	40	59	43	49		
$P_x/\%$	2	3	3	18	24	20		
k_z^r/k_y^r 0[a]	0.06	0.10	0.11	0.13	0.02	0.06	1.2	1
670[b]	0.70	1.10	1.13	0.38	0.15	0.22	5.5	8.3
k_x^r/k_y^r 0[a]	0.01	0.01	0.01	0.08	0.03	0.04		
670[b]	0.02	0.04	0.05	0.24	0.11	0.16	0.20	0.31

a) Ratio obtained at the 0—0 band. b) Ratio obtained at the 0—670 cm^{-1} band.

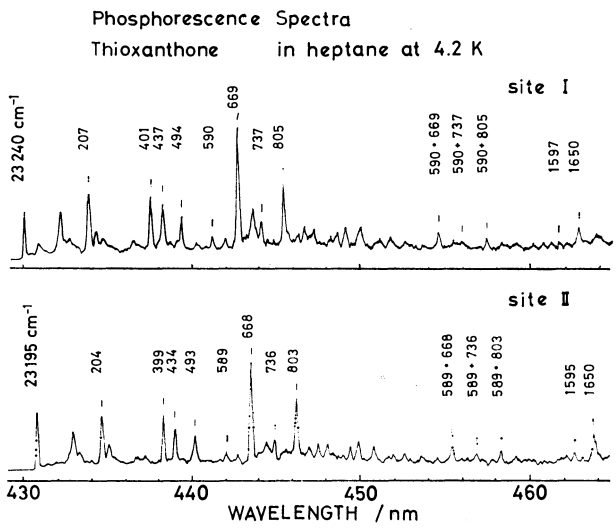

Fig. 7. The single site phosphorescence spectra of thioxanthone in heptane at 4.2 K.
Site I (upper) and site II (lower).

As an example, the emission spectra of sites I and II in heptane obtained by using the site selective excitation technique are shown in Fig. 7.

Much clear information can be obtained through separated sublevel emission spectra measured by means of the MIDP spectrum method reported previously.[20] Figure 8 shows the sublevel emission spectra of thioxanthone in hexane. Vibrational analysis of the spectrum is made by reference to the vibrational data for the compounds with related structure.[26-28] The vibronic bands found at 0—1650 and 0—1598 cm^{-1} are due to the C=O and C=C stretching modes of a_1 symmetry, respectively. The band at 0—590 cm^{-1} is also due to the totally symmetric mode, the combinations of which with the other modes have a certain intensity in the phosphorescence spectrum.

By considering the intensity behavior, the rest of bands of a considerable intensity may be attributed to the non-totally symmetric modes. The vibrations such as 670 and 810 cm^{-1} are considered as the same

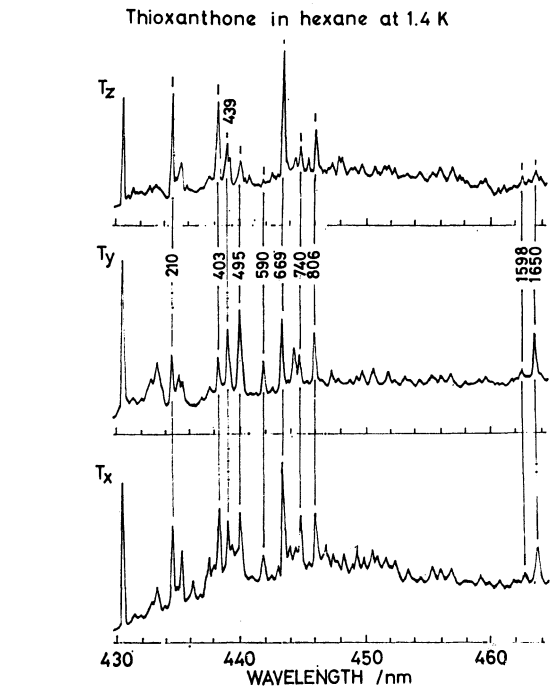

Fig. 8. The sublevel phosphorescence spectra of thioxanthone in hexane at 1.4 K.

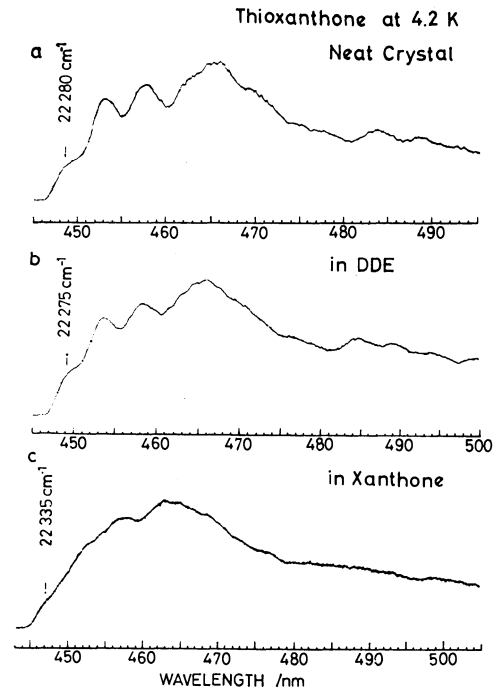

Fig. 9. The phosphorescence spectra at 4.2 K.
a) Thioxanthone traps in the neat crystal, b) thioxanthone in DDE, and c) in xanthone.

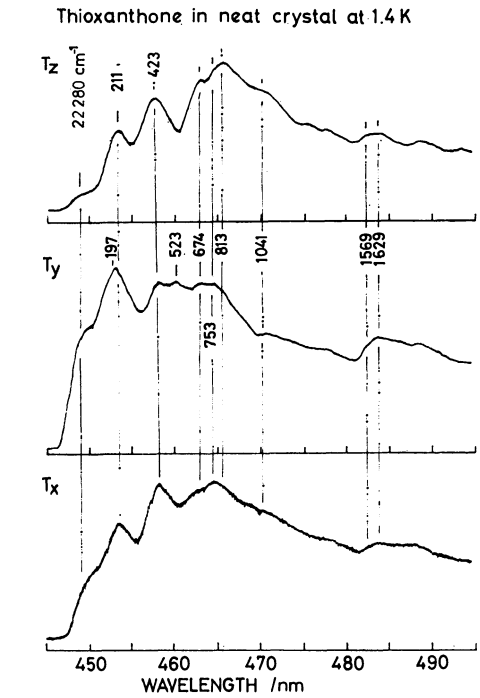

Fig. 10. The sublevel phosphorescence spectra of thioxanthone traps in the neat crystal at 1.4 K.

vibrations appearing in the spectrum of xanthone. In view of the infrared activity,[28] these vibrations are surely assigned to the out of plane vibrations of b_1 symmetry in the case of xanthone. The vibrational modes such as 430 and 720 cm^{-1}, more intense in the y sublevel spectrum than z, may be considered also as the out of plane vibrations probably of a_2 symmetry.

The phosphorescence spectra of thioxanthone also obtained in various crystals are shown in Fig. 9. The sublevel emission spectra obtained for traps in the neat crystal are shown in Fig. 10. The vibrational modes of 211, 423, 674, and 813 cm^{-1}, corresponding to frequencies 210, 403, 669, and 813 cm^{-1} observed in hexane, also appear in the z sublevel spectrum.

The phosphorescence spectra of xanthone are measured in alkanes and in the DDE host crystal. Although the spectra in heptane and octane appear as multi-site emission, the vibrational feature is very similar to that in hexane, shown in Fig. 6. As in the case of the xanthone neat crystal,[17] the phosphorescence spectrum in DDE appears to consist of the superposition of the spectra with different origins, one at 25023 cm^{-1} and the other at 24890 cm^{-1}.

Discussion

Total Decay Rate and Zero Field Splitting. The decay rate of the y sublevel, $k_y=12.1\ s^{-1}$, for traps in the thioxanthone neat crystal is larger by a factor of about six than that for traps in the xanthone neat crystal.[17] Such a remarkable change in the decay rate of the y sublevel must be due to the heavier nucleus S instead of O. In fact, the effective one electron spin orbit coupling constant for the 3p electrons of a S atom is expected to be much larger than that for the 2p electrons of an O atom.[25] Accordingly, the mixing with a $^1B_1(\sigma',\pi^*)$ state which is largely localized on the ether or thioether group may play a considerable role in determining k_y's of both compounds in addition to the mixing with the $^1B_1(\sigma,\pi^*)$ state, largely localized on the carbonyl group. This conclusion may be supported by the fact that the value of k_y of xanthone is considerably larger than the decay rates due to the mixing with $^1\sigma,\pi^*$ state commonly found in other systems such as quinoxaline[23] and naphthalene.[24] Furthermore, the above consideration confirms the assignment of the middle sublevel to y and verifies the zf splitting pattern of Fig. 1.

In the systems of thioxanthone traps in the neat, DDE, and xanthone crystals, the decay rates of the x sublevel are considerably smaller as compared with those of substituted benzaldehydes.[1,7,8] This seems to indicate that neither the $^3n,\pi^*$ admixture into the lowest $^3\pi,\pi^*$ state *via* vibronic coupling nor the deviation from the planarity contributes to k_x. A similar conclusion has been obtained for xanthone in crystalline hosts.[17] In the systems of thioxanthone in alkanes, however, relatively large values of k_x are obtained. The reason for this is not clear at present, but a possible contribution from spin-lattice relaxation is not completely eliminated in the alkane systems.

In xanthone it was shown that spin orbit mixing with $^1n,\pi^*$ state is mainly responsible for the decay from the z sublevel, because rather large ΔE_{TT} is unfavorable for mixing with $^3n,\pi^*$ state.[17] This is also true for thioxanthone. Both ΔE_{TT} and ΔE_{ST} become large by introduction of sulfur instead of oxygen. However, the decrease in k_z observed in the thioxanthone neat crystal is not so large as that expected from the increase in ΔE_{TT} and rather seems to reflect the increase in ΔE_{ST}. Therefore, rather small difference in k_z between xanthone and thioxanthone observed in the neat crystals seems to confirm the above inference.

It is notable that the total decay rates of the z sublevel of thioxanthone in alkanes are much smaller than those obtained in the crystal systems, clearly indicating that the mixing with $^1n,\pi^*$ state is reduced largely in hexane. This may be a consequence of larger value of ΔE_{ST} and/or smaller value of spin orbit matrix element, $G=\langle\pi,\pi^*|H_{SO}|n,\pi^*\rangle$, than in crystal system.

The $|D|$ values of thioxanthone traps in the neat crystal and in the DDE and xanthone hosts are small compared with that of xanthone.[17] By assuming that the value of the spin orbit coupling matrix element, G, is similar to that estimated for a series of benzaldehydes; $G^2=90\ cm^{-2}$,[5,8] the difference in the spin orbit contribution to D of xanthone and thioxanthone is predicted to be about 0.037 cm^{-1}. This value seems to be in agreement with the observed difference in D. Thus, the change in the spin orbit contribution is responsible, at least partly, for the change in D. Further reduction in $|D|$ observed when the environment is changed to alkanes suggests that the energy difference, ΔE_{TT}, becomes much larger in these matrices.

Intersystem Crossing. There is a distinct difference in the populating rates between the systems of thioxanthone in alkanes and in the other host crystals. Since the lowest excited triplet and singlet states of thioxanthone are π,π^* states of A_1 orbital symmetry, all the three sublevels require vibronic spin orbit mechanisms, when the intersystem crossing is assumed to proceed directly from S_1 to T_1. However, if the $T_2(n,\pi^*)$ state lies lower than S_1, it is necessary to consider an indirect process, namely $S_1\rightarrow T_2\rightarrow T_1$, which may make a contribution toward populating of the z sublevel.

In the case of thioxanthone traps in the neat crystal and in the DDE and xanthone hosts, the populating pattern of the sublevels is characterized by high selectivity for the y and z sublevels, relative to the x sublevel. In these host crystals, the $T_2(n,\pi^*)$ state is located lower than S_1. The high selectivity for the z sublevel, therefore, indicates clearly that the indirect process plays a role in the populating process of the z sublevel.

In the case of thioxanthone in hexane and heptane, on the other hand, ΔE_{TT} is much larger than in the DDE and xanthone host crystals, as described in the preceding section. As a result, the T_2 and S_1 states are expected to interchange position. If this is the case, the significant decrease in the relative populating rate of the z sublevel on going from in the host crystals to in alkanes is surely ascribed to the vanishment of the indirect process and also to the decrease of the vibronic interaction between the n,π^* and π,π^* states in singlet and/or triplet manifolds resulting from the increase of the energy separations.

As discussed in the preceding section, there is a good reason to expect that the mixing between the $^3A_1$ and $^1B_1(\sigma',\pi^*)$ states is effective. In addition, there is also evidence for considerably large b_1 vibration band activity in the y sublevel emission (Table 2). Thus, the large activity of the y sublevel with respect to the intersystem crossing process can be interpreted as a consequence of, for the main, large spin orbit coupling terms between the $^3A_1$ and $^1B_1(\sigma',\pi^*)$ states and also vibronic coupling matrix element between the $^1A_1$ and $^1B_1$ states.

Radiative Processes. Radiative Decay from the z Sublevel: The mechanisms governing the radiative decay from the z sublevel of $^3\pi,\pi^*$ aromatic carbonyls so far studied[7,8,10-13] may be classified as follows.

(1) Direct spin orbit mixing with the $^1n,\pi^*$ state

$$T_z(^3\pi,\pi^*) \leftarrow H_{so} \rightarrow {}^1n,\pi^*$$

(2) Direct configurational mixing with the $^3n,\pi^*$ state

$$T_z(^3\pi,\pi^*) \leftarrow H_{el} \rightarrow T_z(^3n,\pi^*) \leftarrow H_{so} \rightarrow {}^1\pi,\pi^*$$

(3) Herzberg-Teller type vibronic spin orbit mixing

(a) $T_z(^3\pi,\pi^*) \leftarrow H_v \rightarrow T_z(^3n,\pi^*) \leftarrow H_{so} \rightarrow {}^1\pi,\pi^*$

(b) $T_z(^3\pi,\pi^*) \leftarrow H_{so} \rightarrow {}^1n,\pi^* \leftarrow H_v \rightarrow {}^1\pi,\pi^*$

It has been shown that the relative importance of these is much dependent on the systems chosen.

In xanthone, Chakrabarti and Hirota[17] have shown that mechanisms (1), (2), and (3a) are not main ones and that only mechanism (3b) may be considered to be important for the emission of the z sublevel. A similar conclusion holds commonly for thioxanthone, but some more detailed information can be obtained by comparing the results with those of xanthone.

Mechanism (1) is important rather than mechanism (2) in the 0,0 band emission from the z sublevel. This inference can be derived from the facts that the relative intensity of the 0,0 band in the z sublevel emission is insensitive to the change in ΔE_{TT} from 1461 cm^{-1} for xanthone to 2400 cm^{-1} for thioxanthone and that the z sublevel emits only weakly at the 0,0 band even in the system of xanthone in hexane where ΔE_{TT} is relatively small.

With respect to xanthone, Chakrabarti and Hirota have suggested, on the basis of the phosphorescence polarization data by Pownall and Huber,[14] that such strong bands as found at 0—670 cm^{-1} likely gain intensity by the following mechanism.[17]

$$T_z(^3\pi,\pi^*) \leftarrow H_{so} \rightarrow {}^1n,\pi^*(A_2) \leftarrow H_v(b_1) \rightarrow {}^1\pi,\pi^*(B_2)$$

As mentioned above, the out of plane vibrational modes such as 670 and 810 cm^{-1} of thioxanthone can be assigned to the vibrations of b_1 symmetry. The observation that these vibrations appear strongly in the z sublevel spectra of thioxanthone seems to give a good proof of the validity of the mechanism suggested by Chakrabarti and Hirota.

The a_2 vibrational modes such as 430 and 730 cm^{-1} appear only weakly in the z sublevel spectrum of thioxanthone. These vibrations are still of quite low intensity in the case of xanthone where ΔE_{TT} is much smaller than that of thioxanthone. This indicates that also the vibronic bands involving the a_2 vibrations should gain intensity by mechanism (3b) rather than (3a).

Radiative Decay from the y Sublevel: In the case of $^3\pi,\pi^*$ aromatic carbonyls, the y sublevel emission was ascribed to the direct mixing with the $^1\sigma,\pi^*$ state, largely localized on the carbonyl group[7,12]

$$T_y(^3\pi,\pi^*) \leftarrow H_{so} \rightarrow {}^1\sigma,\pi^*(B_1).$$

The y sublevel emission of xanthone has also been explained with this mechanism.[17]

In xanthone, however, the ether group participates in the π-conjugation. It is therefore necessary to consider the importance of one center terms on the O atom of the ether group in spin orbit coupling matrix element in addition to the above mechanism. The y sublevel is expected to couple with $^1B_1(\sigma',\pi^*)$, where σ' orbital has a large contribution from in-plane non-bonding orbital of sp^2 hybrid type in the ether group. Since the effective one electron spin orbit coupling constant for sulfur is much larger than for oxygen,[25] the contribution of the mixing with $^1B_1(\sigma',\pi^*)$ state is more important in thioxanthone than in xanthone. In fact, there is evidence that the radiative activity of the y sublevel increases dramatically in going from xanthone to thioxanthone as given in Table 2. In addition, the vibronic bands involving non-totally symmetric vibrations appear with some intensity in the y sublevel spectrum. It is likely that the vibronic interaction in singlet manifolds involving the $^1B_1(\sigma',\pi^*)$ and $^1\pi,\pi^*$ states is the main source for the emission in these bands, rather than the vibronic interaction in triplet manifolds.

The authors wish to thank Prof. Saburo Nagakura of the University of Tokyo and Prof. Nobuyuki Nishi of Institute for Molecular Science for their valuable discussions. The present work was in part supported by a Grant-in-Aid for Scientific Research from the Ministry of Education, Science and Culture (Nos. 334026, 410401).

References

1) A. H. Nishimura and J. S. Vincent, *Chem. Phys. Lett.*, **13**, 89 (1972).
2) A. H. Nishimura and D. S. Tinti, *Chem. Phys. Lett.*, **13**, 278 (1972).
3) T. H. Cheng and N. Hirota, *J. Chem. Phys.*, **50**, 5019 (1972).
4) C. R. Jones, D. R. Kearns, and A. H. Maki, *J. Chem. Phys.*, **50**, 873 (1973).
5) H. Hayashi and S. Nagakura, *Mol. Phys.*, **24**, 801 (1972); **27**, 969 (1974).
6) M. A. Souto, P. J. Wagner, and M. A. El-Sayed, *Chem. Phys.*, **6**, 193 (1974).
7) T. H. Cheng and N. Hirota, *Mol. Phys.*, **27**, 281 (1974).
8) E. T. Harrigan and N. Hirota, *Mol. Phys.*, **31**, 663, 681 (1976).
9) S. J. Sheng and M. A. El-Sayed, *Chem. Phys.*, **20**, 61 (1977).
10) T. Takemura and H. Baba, *Bull. Chem. Soc. Jpn.*, **44**, 2756 (1969).
11) W. A. Case and D. R. Kearns, *J. Chem. Phys.*, **52**, 2175 (1970).
12) Y. Tanimoto, H. Kobayashi, S. Nagakura, and T.

Azumi, *Chem. Phys. Lett.*, **16**, 10 (1972).
13) C. R. Jones, D. R. Kearns, and R. M. Wing, *J. Chem. Phys.*, **58**, 1370 (1973).
14) H. J. Pownall and J. R. Huber, *J. Am. Chem. Soc.*, **93**, 6429 (1971).
15) H. J. Pownall and I. Granoth, *J. Phys. Chem.*, **80**, 508 (1976).
16) H. J. Pownall and W. W. Mantulin, *Mol. Phys.*, **31**, 1393 (1976).
17) A. Chakrabarti and N. Hirota, *J. Phys. Chem.*, **80**, 2966 (1976).
18) R. E. Connors and P. S. Walsh, *Chem. Phys. Lett.*, **52**, 436 (1977).
19) T. Terada, M. Koyanagi, and Y. Kanda, *Chem. Phys. Lett.*, **80**, 508 (1980).
20) N. Nishi and M. Kinoshita, *Bull. Chem. Soc. Jpn.*, **49**, 1221 (1977).
21) E. Kanezaki, N. Nishi, and M. Kinoshita, *Bull. Chem. Soc. Jpn.*, **52**, 2836 (1979).
22) The $T_1 \leftarrow S_0$ absorptions of the host crystals are hidden in the strong absorption bands starting at about 24900 cm^{-1}.
23) J. Schmidt, D. A. Antheunis, and J. H. van der Waals, *Mol. Phys.*, **22**. 1 (1971).
24) D. A. Antheunis. J. Schmidt, and J. H. van der Waals, *Mol. Phys.*, **27**, 1571 (1974).
25) M. Blume and R. E. Watson, *Proc. R. Soc. London, Ser. A*, **270**, 127 (1962); **271**, 565 (1963).
26) T. L. Brown, *Spectrochim. Acta*, **18**, 1067 (1962).
27) E. D. Bergman and S. Pinchas, *J. Chem. Phys.*, **49**, 517 (1966).
28) F. M. Abdel-Kerin and H. A. Shoeb, *Z. Phys. Chem. (Leipzig)*, **251**, 209 (1972).

A New Method for Conformational Analysis by Photoelectron Spectroscopy with Application to Alkyl-substituted Styrenes

Tsunetoshi KOBAYASHI,*,†,†† Tatsuo ARAI,††† Hirochika SAKURAGI,†††
Katsumi TOKUMARU,*,††† and Chikatoshi UTSUNOMIYA†

†*The Institute of Physical and Chemical Research, Wako, Saitama 351*
††*The Institute for Solid State Physics, The University of Tokyo, Roppongi, Minato-ku, Tokyo 106*
†††*Department of Chemistry, The University of Tsukuba, Sakura-mura, Ibaraki 305*

(Received December 10, 1980)

A new method for molecular conformational analysis using photoelectron spectral data was developed and applied to alkyl-substituted styrenes as an example. The dihedral angle between the phenyl ring and the olefinic group planes, θ, in each molecule is evaluated by comparing the observed difference between the first and the third vertical ionization energies, $\Delta E_{iv}^{1,3}$, with the empirically estimated $\Delta E_{iv}^{1,3}$ *vs.* θ curve, the alkyl substituent effect being taken into account by the first order perturbation theory. The new method gives reasonable results consistent qualitatively with those given by other former methods.

As a part of our program to investigate the steric hindrance effect on molecular photoelectron spectra and the application of photoelectron spectroscopy to molecular conformational analysis,[1] in this paper a new method for conformational analysis by photoelectron spectroscopy is presented and applied to some β-alkylstyrenes and related compounds as an example.

The simplest method for molecular conformational analysis by photoelectron spectroscopy is at present that by Maier and Turner.[2] They estimated empirically the dihedral angles in molecules by the composite molecule type consideration on the HMO level taking into account the interaction between two group orbitals only, that is, in their method the conjugative interaction of these two group orbitals with other group orbitals are completely neglected throughout the calculations. The new method presented in this paper is devised to be applicable even to the cases where this type of interaction is not negligible.

The relations between the molecular conformations and photoelectron spectra of some styrenes have formerly been studied by us[1c] and Maier and Turner.[2b] During the course of our photochemical study of β-alkylstyrenes[3] it was found that the accurate conformational data of these molecules useful for the interpretation of photochemistry are still completely lacking. This is the reason why alkylstyrenes are revisited here.

Experimental

Measurements. The photoelectron spectra were recorded with the He I resonance line as the excitation source in the same way as described formerly.[1c]

Materials. *cis*-β-Methylstyrene[4] and *cis*-β-ethylstyrene[4] were obtained by hydrogenation of 1-phenylpropyne and 1-phenylbutyne, respectively, on Pd/C in ethyl alcohol and purified by column chromatography. *trans*-β-Methylstyrene[4] and *trans*-β-ethylstyrene[4] were prepared by dehydration of the alcohols obtained through the reaction of acetaldehyde and benzaldehyde, respectively, with the appropriate Grignard reagents. A mixture of *cis*- and *trans*-β-*t*-butylstyrene was synthesized according to Ref. 5 and the *cis*- and *trans*-isomer were isolated by column chromatography. The purities of the samples were checked by gas chromatography and their molecular structures were identified by NMR spectroscopy. These styrenes were distilled under reduced pressure just before use.

Computational

The CNDO/S[6] calculations of styrene, *s-trans*-butadiene, and naphthalene were carried out with a FACOM 230-75 computer at the Institute of Physical and Chemical Research. All the necessary atomic integrals and parameters were taken from or estimated according to Ref. 6.

The structural parameters of *s-trans*-butadiene and naphthalene were taken from Ref. 7 and those of styrene were assumed as follows:

The C=C and the C–H bond lengths of the phenyl group were assumed to be 1.397 Å and 1.084 Å, respectively, on the basis of the data for benzene.[7] The C=C, the C–H bond lengths of the vinyl group, and the C–C bond length between the phenyl and the vinyl groups were assumed to be 1.337 Å, 1.08 Å, and 1.483 Å, respectively, by consulting the data for *s-trans*-butadiene.[7] All the C–C–C and the C–C–H bond angles were assumed to be 120°.

Results and Discussion

Photoelectron Spectra. The photoelectron spectra of *cis*- and *trans*-β-methyl-, ethyl-, and *t*-butylstyrene measured in this study are shown in Figs. 1, 2, and 3. The vertical ionization energies of the lower energy bands of these compounds obtained from the spectra are summarized in Table 1 with those of the related compounds.

The first three bands of β-methyl-, β-ethylstyrenes, or *trans*-β-*t*-butylstyrene are well separated from one another, their vertical ionization energies being rather close to those of styrene, and are safely correlated with the first three bands of styrene,[1c] from the top respectively. The first and the third bands of styrene,[1c] respectively, correspond to the ionizations from the two molecular orbitals approximately expressed as the anti-bonding and the bonding types of combinations of the benzene ring $e_{1g}(S)$-like group orbital with the vinyl group occupied π orbital. Here $e_{1g}(S)$ denotes one of the doubly degenerate e_{1g} π orbitals of benzene, and is symmetrical with respect to the mirror plane passing the 1- and the 4-position and perpendicular to the benzene ring. On the other hand, the second

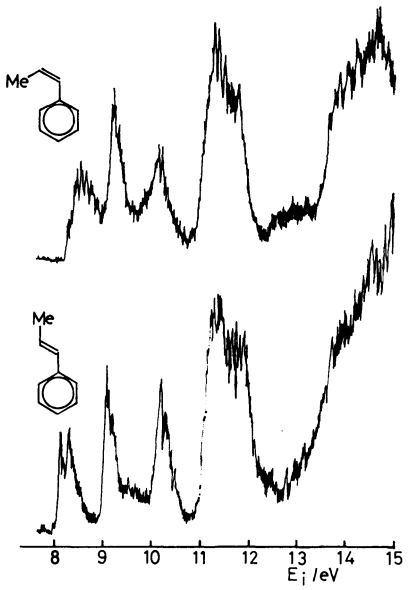

Fig. 1. Photoelectron spectra of *cis*-β-methylstyrene and *trans*-β-methylstyrene.

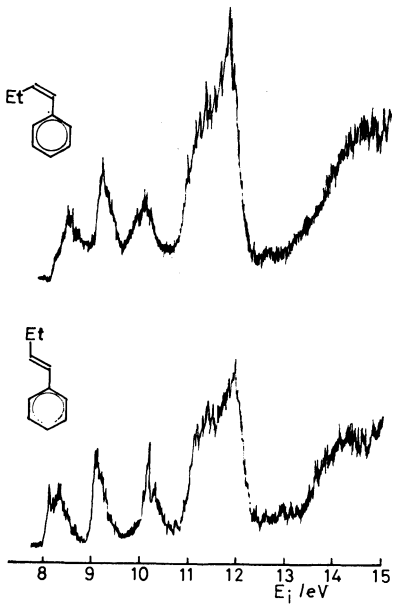

Fig. 2. Photoelectron spectra of *cis*-β-ethylstyrene and *trans*-β-ethylstyrene.

band corresponds to the ionization from the orbital composed almost completely of the benzene ring e_{1g}(A)-like orbital. Here e_{1g}(A) denotes the other e_{1g} orbital of benzene which is antisymmetrical with respect to the mirror plane mentioned above. The ionization energies of and the splitting between the first and the third bands of styrene are, therefore, quite sensitive to the dihedral angle, θ, between the vinyl group and the benzene ring planes, while the second ionization energy is almost indifferent to the change in θ because of its completely localized nature on the benzene ring as visualized in Fig. 4 of Ref. 1c.

In the case of *cis*-β-*t*-butylstyrene the second and the third bands are evidently highly overlapping with each other, and it is quite natural to consider that this has been caused by the heavy steric hindrance effect of the bulky *t*-butyl group. But one should be careful in the point that the electronic effect of *t*-butyl group is also contributing to the lower ionization energy shift of the third band of *cis*-β-*t*-butylstyrene when compared to styrene. Similar care is more or less important for the other bands and for the other alkyl-substituted styrenes also.

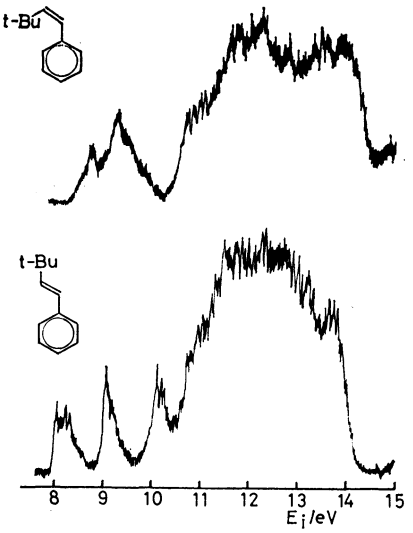

Fig. 3. Photoelectron spectra of *cis*-β-*t*-butylstyrene and *trans*-β-*t*-butylstyrene.

Table 1. Vertical ionization energies, E_{iv}, of styrenes and related compounds

Compound	E_{iv}/eV			
	Band 1	2	3	4
Styrene[a]	8.49	9.27	10.55	11.52
2-Methylstyrene[a]	8.53	8.99	10.37	11.22
3-Methylstyrene[a]	8.37	8.98	10.34	11.27
4-Methylstyrene[a]	8.20	9.11	10.24	11.29
α-Methylstyrene[a]	8.52	9.18	10.12	11.26
cis-β-Methylstyrene	8.48	9.18	10.26	11.30
trans-β-Methylstyrene	8.34	9.09	10.25	11.46
cis-β-Ethylstyrene	8.54	9.16	10.02	11.24
trans-β-Ethylstyrene	8.30	9.09	10.19	11.37
cis-β-*t*-Butylstyrene	8.85	9.27	9.5[c]	10.91
trans-β-*t*-Butylstyrene	8.18	9.05	10.10	11.02
2,4-Dimethylstyrene[a]	8.22	8.80	10.11	11.06
2,6-Dimethylstyrene[a]	8.48	8.62	10.04	11.04
Propylene[b]	9.744			
Ethylbenzene[a]	8.78	9.27		

a) Ref. 1c. b) Ref. 8. c) This value is the approximate one because of the heavy overlapping between the second and the third bands of *cis*-β-*t*-butylstyrene.

In the following we use the observed differences between the first and the third vertical ionization energies of alkyl-substituted styrenes, $\Delta E_{iv}^{1,3}$, for the estimation of the dihedral angles, taking into account the electronic effect of the alkyl groups.

Conformational Analysis by Photoelectron Spectroscopy. The calculational steps of the new method for conformational analysis by photoelectron spectroscopy are described in the following.

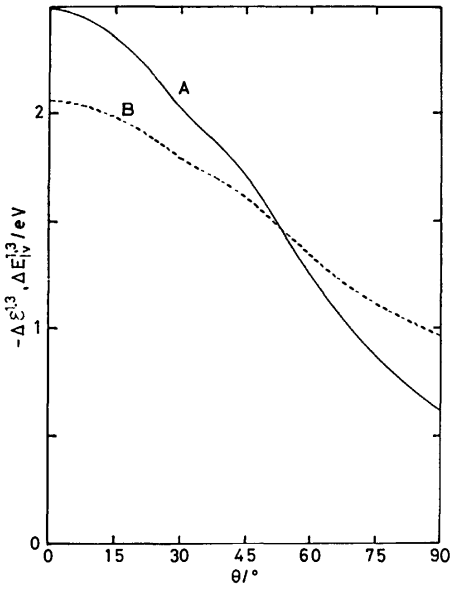

Fig. 4. Twist angle, θ, dependence of calculated orbital energy difference between the highest and the third highest occupied π orbitals for styrene, $\Delta\varepsilon^{1,3}$, (curve A) and that of difference between the first and the third vertical ionization energies of styrene, $\Delta E_{iv}^{1,3}$, estimated using curve A and formula (1) (curve B).

At first SCFMO calculations including all valence electrons are carried out for various twist angles of the parent compound. In this study we carried out CNDO/S[6] calculations of styrene itself for the twist angle from 0° to 90° at the intervals of 15°.

The calculated energy difference between the highest and the third highest occupied π orbitals of styrene, $\Delta\varepsilon^{1,3}$, is plotted against θ. Thus we get the $\Delta\varepsilon(\theta)^{1,3}$ *vs.* θ curve (curve A in Fig. 4).

In most cases this type of curve deviates more or less from the corresponding $\Delta E_{iv}(\theta)^{1,3}$ *vs.* θ curve. To estimate the realistic $\Delta E_{iv}(\theta)^{1,3}$ *vs.* θ curve, in this paper we transform curve A in Fig. 4 by the following simple formula:

$$\Delta E_{iv}(\theta)^{1,3} = a\Delta\varepsilon(\theta)^{1,3} + b \qquad (1)$$

Here a and b are constants and are evaluated by using the experimental $\Delta E_{iv}^{1,3}$ of styrene as $\Delta E_{iv}(0°)^{1,3}$ and the difference between the first ionization energies of propene[8] and ethylbenzene[1c] as $\Delta E_{iv}(90°)^{1,3}$. Styrene itself is planar in the ground state according to the Raman spectral study.[9] The a and b values thus evaluated are −0.586 and 0.603 eV, respectively. Now we get curve B in Fig. 4.

The $\Delta E_{iv}(\theta)^{1,3}$ *vs.* θ curve obtained above takes into account effectively the effect of the interactions of the two molecular orbitals under consideration with other orbitals. This curve B is expected to simulate rather well the real $\Delta E_{iv}(\theta)^{1,3}$ *vs.* θ curve, especially in the small θ region because styrene, which is known to be planar in the ground state as mentioned before, was used as the reference compound for $\theta=0°$.

By the way, the following equation can simulate well curve B in Fig. 4 if we adopt the same $\Delta E_{iv}(0°)^{1,3}$ and $\Delta E_{iv}(90°)^{1,3}$ values as in the case of formula (1):

$$\Delta E_{iv}(\theta)^{1,3} = \sqrt{\{\Delta E_{iv}(90°)^{1,3}\}^2 + [\{\Delta E_{iv}(0°)^{1,3}\}^2 - \{\Delta E_{iv}(90°)^{1,3}\}^2]\cos^2\theta} \qquad (2)$$

This equation can easily be derived by the composite molecule type consideration on the HMO level taking into account the interaction between two group orbitals only. This means that in the case of styrene the two-orbital model is not bad approximation.

Returning to the main story, for the conformational analysis of alkyl-substituted styrenes, we must correct curve B by taking into account the alkyl substituent electronic effect. This effect on the ionization energies can be estimated by the following formula according to the first order perturbation theory:[10,11]

$$-\Delta E_{ivj} = g\{\sum_{\alpha} C_{j\alpha}^2 + m\sum_{\beta} C_{j\beta}^2\} + h \qquad (3)$$

Here ΔE_{ivj} denotes the j-th vertical ionization energy change caused by alkyl substitution, C_{jk} the pπ atomic orbital coefficient of the atom k in the j-th molecular orbital, being calculated by the CNDO/S method in this study, α the alkyl-substituted carbon atom(s) and β the carbon atom(s) adjacent to the atom α. The parameter m is a kind of damping factor and is put equal to 1/3 by consulting the result in Ref. 10. Though the g and h values for methyl and t-butyl groups have already been given in Ref. 11, we reevaluated these parameter values by the least square method using the recent ionization energy data with those for ethyl group.

The compounds and the vertical ionization energy data used for the evaluation of g and h are as follows:

For methyl group, the first ionization energies of ethylene,[8] its methyl,[8] *cis*- and *trans*-1,2-dimethyl derivatives,[8] *s-trans*-butadiene,[12] its 1-methyl[12] and 1,4-dimethyl derivatives,[12] benzene,[13] toluene,[1d] and *m*-xylene.[1d]

For ethyl group, the first ionization energies of ethylene,[8] its ethyl derivative,[8] *s-trans*-butadiene,[12] its 4-ethyl derivative,[12] benzene,[13] ethylbenzene,[1c] and the first three ionization energies of naphthalene, 8.15, 8.88, 10.00 eV,[10] those of 1-ethylnaphthalene, 7.91, 8.72, 9.68 eV, and those of 2-ethylnaphthalene, 7.94, 8.63, 9.83 eV.

For t-butyl group, the first ionization energies of ethylene,[8] its t-butyl derivative,[8] propylene,[8] its *cis*- and *trans*-t-butyl derivatives,[8] three isomers of di-t-butylethylenes,[8] benzene,[13] and the first two ionization energies of t-butylbenzene.[11]

The g and h values with the mean square errors, and the mean square error for ΔE_{ivj} thus obtained are for methyl group, $1.04^0\pm0.04^2$ eV, $-0.00^7\pm0.03^1$ eV, $\pm0.06^4$ eV; for ethyl group, $1.30^0\pm0.03^1$ eV, $0.00^3\pm0.00^8$ eV, $\pm0.02^3$ eV; for t-butyl group, $1.33^8\pm0.04^6$ eV, $0.00^2\pm0.03^5$ eV, $\pm0.08^4$ eV, respectively.

Thus we can estimate the $\Delta E_{iv}(\theta)^{1,3}$ *vs.* θ curve for each alkyl-substituted styrene by correcting curve B in Fig. 4 for alkyl substituent effect by applying formula (3) to the highest and the third highest occupied π orbitals of styrene. For example, we get the curve shown in Fig. 5 in the case of 2-methylstyrene.

Now it is quite easy to estimate the twist angle θ. By comparing the observed $\Delta E_{iv}^{1,3}$ value of 2-methylstyrene, for example, with the curve shown in Fig. 5

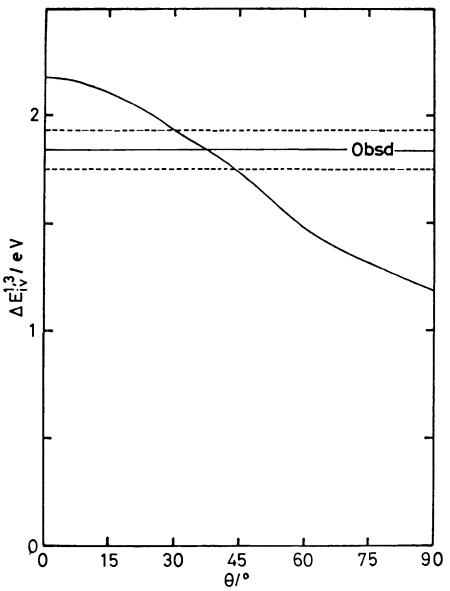

Fig. 5. Estimated twist angle, θ, dependence of difference between the first and the third vertical ionization energies of 2-methylstyrene, $\Delta E_{iv}^{1,3}$ with observed $\Delta E_{iv}^{1,3}$. Broken lines denote the mean square error.

TABLE 2. DIHEDRAL ANGLES, θ, IN STYRENES

Compound	θ/° UPS: This work	UPS: M.-T.[a]	UVS: S.[b]	UVS: B.-S.[c]
2-Methylstyrene	$38\pm{}^{7}_{8}$	22	31	28
3-Methylstyrene	$18\pm{}^{9}_{18}$			
4-Methylstyrene	$11\pm{}^{12}_{11}$		(0)[d]	
α-Methylstyrene	29±6	38	33	
cis-β-Methylstyrene	22±6		35.2	
trans-β-Methylstyrene	$12\pm{}^{7}_{12}$	(0)	(0)	
cis-β-Ethylstyrene	$38\pm{}^{1}_{2}$			
trans-β-Ethylstyrene	12±4			
cis-β-*t*-Butylstyrene	72[e]			
trans-β-*t*-Butylstyrene	$8\pm{}^{14}_{8}$			
2,4-Dimethylstyrene	41±8		30.7	
2,6-Dimethylstyrene	$68\pm{}^{12}_{10}$	55	54	

a) Ref. 2b. b) Ref. 14. c) Ref. 15. d) The values in the parentheses are the assumed ones. e) This value is the approximate one. See footnote c) for Table 1.

the twist angle θ of 2-methylstyrene is estimated to be $38°\pm{}^{7°}_{8°}$. The error limits for θ were approximately estimated from the mean square error for ΔE_{ivj} multiplied by $\sqrt{2}$. The dihedral angles of the other molecules were also estimated in the same way and are summarized in Table 2.

In the case of 3-methyl-, 4-methyl-, *trans*-β-methyl-, and *trans*-β-*t*-butylstyrene, the error ranges for θ include 0° as shown in Table 2, and in the case of *trans*-β-ethylstyrene the lower error limit is not so far from 0°. These results are reasonable because *trans*-β-alkyl substitution can not be considered to cause any steric hindrance effect upon the benzene ring parts in these cases. These reasonable results support the validity of the method developed here.

The θ value for *cis*-β-ethylstyrene given in Table 2 is slightly larger than that for *cis*-β-methylstyrene, and that for *cis*-β-*t*-butylstyrene is far larger than that for *cis*-β-ethylstyrene. These tendencies are also reasonable.

Suzuki[14] estimated the twist angles of some styrenes from the UV absorption band energies in solution by the HMO level consideration. Braude and Sondheimer[15] estimated the angles from the UV absorption spectral intensities on the assumption of $\varepsilon/\varepsilon_0=\cos^2\theta$ where ε and ε_0 are the molar absorptivity of the conjugation band of the alkylstyrene in question and that of the corresponding planar reference system, respectively. Maier and Turner[2b] estimated the twist angles for 2-methyl-, α-methyl-, and 2,6-dimethylstyrene by the two-orbital model consideration on the HMO level mentioned before. The twist angles of some styrenes estimated by these authors are also summarized in Table 2. The general tendency of the calculated twist angles in this paper seems to correspond roughly to those by the other methods mentioned above.

To our regret there are at present no accurate data on the conformations for these alkyl-substituted styrenes as yet. The θ values predicted here may be useful as guiding data until accurate conformational data become available.

References

1) a) T. Kobayashi and S. Nagakura, *Chem. Lett.*, **1972**, 903; b) T. Kobayashi and S. Nagakura, *ibid.*, **1972**, 1013; c) T. Kobayashi, K. Yokota, and S. Nagakura, *J. Electron Spectrosc. Relat. Phenom.*, **2**, 449 (1973); d) T. Kobayashi and S. Nagakura, *Bull. Chem. Soc. Jpn.*, **47**, 2563 (1974); e) T. Kobayashi, K. Yokota, and S. Nagakura, *ibid.*, **48**, 412 (1975); f) R. Nakagaki, T. Kobayashi, and S. Nagakura, *ibid.*, **53**, 901 (1980); g) R. Akaba, K. Tokumaru, T. Kobayashi, and C. Utsunomiya, *ibid.*, **53**, 2002 (1980) and see also, R. Akaba, K. Tokumaru, and T. Kobayashi, *ibid.*, **53**, 1993 (1980).

2) a) J. P. Maier and D. W. Turner, *Faraday Discuss. Chem. Soc.*, No. 54, 149 (1972); b) J. P. Maier and D. W. Turner, *J. Chem. Soc., Faraday Trans. 2*, **69**, 196 (1973); c) J. P. Maier and D. W. Turner, *ibid.*, **69**, 521 (1973).

3) T. Arai, H. Sakuragi, and K. Tokumaru, *Chem. Lett.*, **1980**, 261.

4) K. Yasufuku, S. Hirose, S. Nozakura, and S. Murahashi, *Bull. Chem. Soc. Jpn.*, **42**, 2605 (1969).

5) H. Kristinsson and G. W. Griffin, *J. Am. Chem. Soc.*, **88**, 378 (1966).

6) R. L. Ellis, G. Kuehnlenz, and H. H. Jaffé, *Theor. Chim. Acta*, **26**, 131 (1972).

7) "Tables of Interatomic Distances and Configuration in Molecules and Ions," Sp. Pub. No. 18, ed. by L. E. Sutton, The Chemical Society, London (1965).

8) P. Masclet, D. Grosjean, G. Mouvier, and J. Dubois, *J. Electron Spectrosc. Relat. Phenom.*, **2**, 225 (1973).

9) L. A. Carreira and T. G. Towns, *J. Chem. Phys.*, **63**, 5283 (1975).

10) F. Brogli, E. Heilbronner, and T. Kobayashi, *Helv. Chim. Acta*, **55**, 274 (1972).

11) E. Heilbronner, V. Hornung, F. H. Pinkerton, and S. F. Thames, *Helv. Chim. Acta*, **55**, 289 (1972).

12) G. Bieri, F. Brogli, E. Heilbronner, and J. P. Maier, *Helv. Chim. Acta*, **60**, 2213 (1977).

13) C. R. Brundle, M. B. Robin, and N. A. Kuebler, *J. Am. Chem. Soc.*, **94**, 1466 (1972).

14) H. Suzuki, *Bull. Chem. Soc. Jpn.*, **33**, 619 (1960).

15) E. A. Braude and F. Sondheimer, *J. Chem. Soc.*, **1955**, 3773.

Raman Scattering and Phase Transition of Ammonium Nitrates

Kenji AKIYAMA,† Yoshiyuki MORIOKA, and Ichiro NAKAGAWA*
Department of Chemistry, Faculty of Science, Tohoku University, Aoba, Aramaki, Sendai 980
(Received December 15, 1980)

Polarized Raman spectra of single crystals are observed for the room-temperature phase NH_4NO_3(IV). The spectra in the low-frequency lattice vibration region as well as in the internal vibration region are well interpreted based on D_{2h}^{13} structure. Raman spectra of powdered samples are measured at various temperatures covering whole phases NH_4NO_3 I—V. A characteristic feature of Raman spectrum is clarified for each phase. An abrupt spectral change occurs in the phase transition, indicating a first order transition. The splitting of A_g and B_{1g} components of ν_3 (asymmetric stretching mode of NO_3^- ion) in NH_4NO_3 is quite large, due to the strong interionic interaction between NH_4^+ and NO_3^- ions.

In our previous paper we discussed the lattice vibrations and phase transitions of KNO_3 and $NaNO_3$ crystals.[1] In relation to the study on a series of alkali nitrates, the investigation on NH_4NO_3 is significant, from the viewpoint of the behavior of NO_3^- ion in the crystal as well as that of NH_4^+ ion. There have been several reports on the phase transition of NH_4NO_3 and it has been shown that the phase transition at high temperature is caused by the order-disorder on the rotational motion of NO_3^- ion and the following crystalline modifications exist:[2-5]

Phase I	cubic	169°C—126°C
Phase II	tetragonal	126°C— 80°C
Phase III	orthorhombic	80°C— 32°C
Phase IV	orthorhombic	32°C——18°C
Phase V	tetragonal	below −18°C

Tang and Torrie measured polycrystalline Raman spectra from room temperature down to 11 K and discussed IV⇌V phase transition.[6] James *et al.* also discussed IV⇌V phase transition as well as III⇌IV phase transition,[7] based on their Raman data measured in the temperature range 210 K—320 K. Iqbal seemed to suggest the existence of an additional phase VII,[8] for which no evidence was found by Tang and Torrie.[6] The study on the high-temperature phases by Raman measurement was made by Österlund and Rosen,[5] whose spectra seem however insufficient. Théorêt and Sandorfy measured the infrared spectra of solid crystalline films in the temperature range 169 °C——190 °C and obtained four different spectra corresponding to the I, II, IV, and VII phases.[9] In all of these studies polycrystalline samples were used for the spectral measurement and thus a definite assignment of the observed bands to the symmetry species could not be done by the polarization measurement.

We attempted a thorough spectroscopic study at various temperatures covering whole phases and clarified a characteristic feature of Raman spectrum in the low-frequency lattice vibration region for each phase. Polarized Raman spectra of single crystals were measured for the room temperature phase IV to give a characterization of the lattice vibrations. A supplementary far infrared transmission measurement was also made. We present here these results and specify how the successive phase transitions in NH_4NO_3 are reflected on the vibrational spectra.

† Present address: Shin-Etsu Handotai Co., Ltd., Isobe, Annaka, Gunma 379-01.

Experimental

Single crystals of NH_4NO_3 were grown by slow evaporation of saturated aqueous solution at room temperature. Needle-like crystals of ≈5 mm length along a-axis of NH_4NO_3(IV) were obtained.

Raman spectra were recorded with a JRS 400 T triple monochromator using a standard 90° scattering configuration. The 514.5 nm line from Ar ion laser (Lexel, model 95) was used for excitation. For the measurement of polarized spectra, the natural shaped crystals were used without any polishing. At the transition temperatures these crystals cracked, probably due to the change in crystal structure, and therefore in the measurement for the high and low-temperature phases the powdered samples were employed.

Far infrared spectra were measured by a Hitachi 070 far infrared interferometer.

Crystal Structure and Factor Group Analysis

The room temperature phase IV is orthorhombic with the space group D_{2h}^{13} and two formula units per unit cell ($z=2$). The phase III is also orthorhombic but it has four formula units per unit cell and its space group is D_{2h}^{16}. The structures of these phases III and IV are sketched in Fig. 1. The low-temperature phase V is non-centric tetragonal with the space group C_4^3 and $z=8$. The high-temperature phase II is also tetragonal with the space group C_{4v}^2 and $z=2$. The phase I has a CsCl-type structure with $z=1$ in a cubic unit cell. The results of factor group analysis based on the space groups mentioned above are summarized in

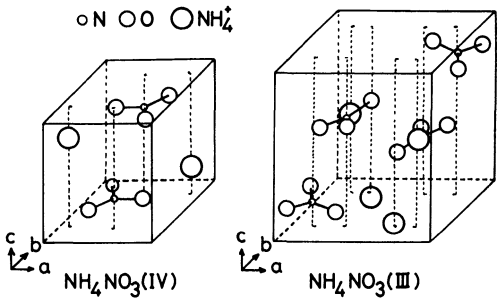

Fig. 1. Structures of NH_4NO_3(IV) and (III) crystals.

TABLE 1. FACTOR GROUP ANALYSIS FOR NH_4NO_3 CRYSTALS[a)]

NH_4NO_3(V) ($T<-18$ °C) C_4^3 $z=8$									
C_4^3	N_t	N_a	N_o	$N_{tr.}$	$N_{ro.}$[b)]	$N_{in.}(NO_3^-)$	$N_{in.}(NH_4^+)$		Activity
A	52	1	51	9	10(5)	12	20	c	$\alpha_{aa}+\alpha_{bb}$, α_{cc} (IR) (R)
B	52	0	52	10	10(5)	12	20		$\alpha_{aa}-\alpha_{bb}$, α_{ab} (R)
E	56	1	55	13	14(7)	12	16	(a,b)	(α_{bc}, α_{ca}) (IR) (R)
NH_4NO_3(IV) (-18 °C$<T<$32 °C) D_{2h}^{13} $z=2$									
D_{2h}^{13}	N_t	N_a	N_o	$N_{tr.}$	$N_{ro.}$[b)]	$N_{in.}(NO_3^-)$	$N_{in.}(NH_4^+)$		Activity
A_g	9	0	9	2	0	3	4		α_{aa}, α_{bb}, α_{cc} (R)
B_{1g}	8	0	8	2	2(1)	2	2		α_{ab} (R)
B_{2g}	7	0	7	2	2(1)	1	2		α_{ac} (R)
B_{3g}	3	0	3	0	2(1)	0	1		α_{bc} (R)
A_u	3	0	3	0	2(1)	0	1		
B_{1u}	7	1	6	1	2(1)	1	2		c (IR)
B_{2u}	8	1	7	1	2(1)	2	2		b (IR)
B_{3u}	9	1	8	1	0	3	4		a (IR)
NH_4NO_3(III) (32 °C$<T<$80 °C) D_{2h}^{16} $z=4$									
D_{2h}^{16}	N_t	N_a	N_o	$N_{tr.}$	$N_{ro.}$[b)]	$N_{in.}(NO_3^-)$	$N_{in.}(NH_4^+)$		Activity
A_g	16	0	16	4	2(1)	4	6		α_{aa}, α_{bb}, α_{cc} (R)
B_{1g}	11	0	11	2	4(2)	2	3		α_{ab} (R)
B_{2g}	16	0	16	4	2(1)	4	6		α_{ac} (R)
B_{3g}	11	0	11	2	4(2)	2	3		α_{bc} (R)
A_u	11	0	11	2	4(2)	2	3		
B_{1u}	16	1	15	3	2(1)	4	6		c (IR)
B_{2u}	11	1	10	1	4(2)	2	3		b (IR)
B_{3u}	16	1	15	3	2(1)	4	6		a (IR)
NH_4NO_3(II) (80 °C$<T<$126 °C) C_{4v}^5 $z=2$									
C_{4v}^5	N_t	N_a	N_o	$N_{tr.}$	$N_{ro.}$	$N_{in.}(NO_3^-)$			Activity
A_1	5	1	4	1	0	3		c	$\alpha_{aa}+\alpha_{bb}$, α_{cc} (IR) (R)
A_2	2	0	2	1	1	0			
B_1	4	0	4	1	0	3			$\alpha_{aa}-\alpha_{bb}$ (R)
B_2	1	0	1	0	1	0			α_{ac} (R)
E	9	1	8	3	2	3		(a,b)	(α_{bc},α_{ca}) (IR) (R)

a) N_t; total freedom, N_a; acoustic modes, N_o; optical active modes, $N_{tr.}$; translational lattice modes, N_{ro}; rotational lattice modes, $N_{in.}$ (NO_3^-); internal modes of NO_3^-, $N_{in.}$ (NH_4^+); internal modes of NH_4^+, (R); Raman active modes. (*IR*); infrared active modes. b) Values in parentheses denote the rotational freedom of NH_4^+ ions.

Table 1. No Raman active mode exists for the structure of the phase I.

Results and Discussion

Low frequency Lattice Vibration. In this region we may expect primarily the rotational and translational lattice modes of NO_3^- ion. The rotational modes of NH_4^+ ion are expected in the region higher than 300 cm^{-1}.[10] The polarized Raman spectra below 300 cm^{-1} at room temperature are shown in Fig. 2, which arise from the phase IV. The observed frequencies and assignments to the symmetry species based on D_{2h}^{13} structure are listed in Table 2. In the spectra of powdered sample shown in Fig. 3, three bands around 90 cm^{-1}, 140 cm^{-1}, and 170 cm^{-1} are observed at 29 °C, which correspond to the three intense bands at 85 cm^{-1} (B_{2g}), 139 cm^{-1} (B_{2g}), and 170 cm^{-1} (B_{3g}), respectively, observed in the polarized spectra. On referring to Table 1, the 170 cm^{-1} band (B_{3g}) is unambiguously

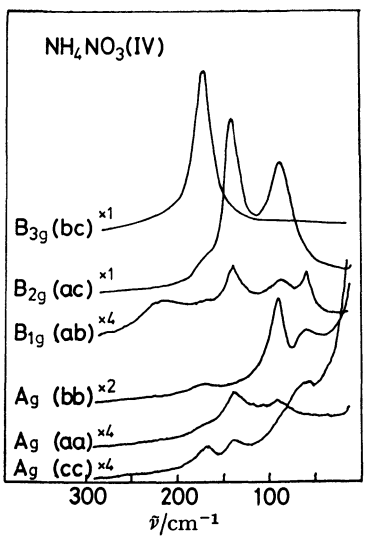

Fig. 2. Polarized Raman spectra of NH_4NO_3(IV) crystal in the low-frequancy lattice vibration region.

Table 2. Observed frequencies in cm^{-1} of NH_4NO_3[a)]

NH_4NO_3(V) IR (77 K)	NH_4NO_3(V) R (77 K)	NH_4NO_3(V) R[b)] (11 K)		NH_4NO_3(IV) IR	NH_4NO_3(IV) R (room temperature)		NH_4NO_3(III) R (32 °C)		NH_4NO_3(II) R (81 °C)
43	48	49	$T(NO_3^-)$		58(B_{1g})	$T_b(NO_3^-)$			≈ 60
65	61	62					58(B_{2g})	$T_{ac}(NO_3^-)$	
69	73	75			60(A_g)	$T_a(NO_3^-)$			
78	85	84					68(A_g)	$T_{ac}(NO_3^-)$	
89		87			85(B_{2g})	$T_c(NO_3^-)$			
102	98	96					100(A_g)	$R_b(NO_3^-)$	
104		98			90(A_g)	$T_a(NO_3^-)$			≈120
	110	112	$R(NO_3^-)$						
119	135	135			139(B_{2g})	$R_b(NO_3^-)$	128(B_{1g}, B_{3g})	$R_a(NO_3^-)$	
140	138	140							
160	161	162			170(B_{3g})	$R_a(NO_3^-)$			
190	189	185							
		191							
	201	203	$T(NH_4^+)$						
		207		≈200	220(B_{1g})	$T_c(NH_4^+)$			
≈240	230	231							
		245							
	709	726	ν_4	717	715(A_g, B_{1g})	ν_4	715	ν_4	710
	728						717		722
				830		ν_2			
	1057		ν_1	1046	1043(A_g)	ν_1	1050	ν_1	1050
	1288	1321	ν_3	≈1350	1289(A_g)	ν_3	1320	ν_3	
	1389	1406			1415(B_{1g})		≈1355		
	1415		ν_4'	1450	1418(A_g)	ν_4'	≈1410	ν_4'	
					1461(B_{1g})				
	1419	1427	ν_3						
	1447	1451							
	1458								

a) T and R denote translational and rotational lattice modes, respectively. ν_1—ν_4: internal modes of NO_3^- ion. ν_4': internal mode of NH_4^+ ion. b) Observed values by Tang and Torrie.[6)]

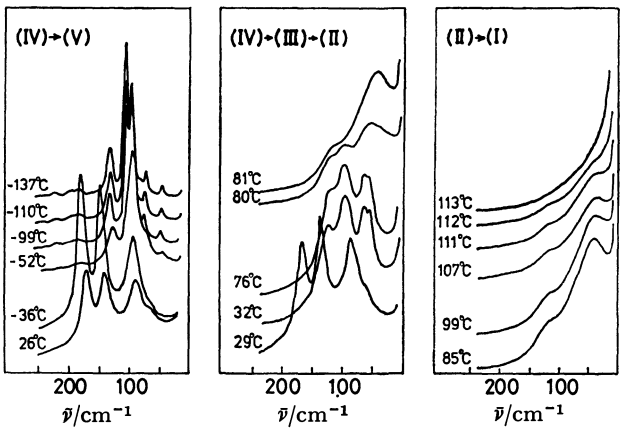

Fig. 3. Raman spectra of powdered samples at various temperatures in the low-frequency region.

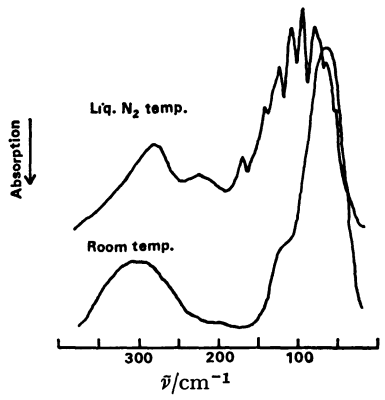

Fig. 4. Far infrared transmission spectrum of NH_4NO_3-(IV) (Nujol mull). This spectrum is recorded by the single-beam operation. The low transmissivity around 0 and 400 cm^{-1} is due to the efficiency of the beam-splitter.

assigned to the rotational lattice mode of NO_3^- ion about a-axis, while the 85 cm^{-1} (B_{2g}) and 139 cm^{-1} (B_{2g}) bands are assigned to the translational mode along c-axis and the rotational mode about b-axis, which are more or less coupled with each other. The B_{1g} rotational lattice mode about c-axis might be very weak since the polarizability does not change singnificantly for the rotation about an axis perpendicular to the NO_3 plane.

Other four weak bands 58 cm^{-1} (B_{1g}), 60 cm^{-1} (A_g), 90 cm^{-1} (A_g), and 220 cm^{-1} (B_{1g}) observed in the polarized spectra are assigned to the translational lattice modes. Among them the 220 cm^{-1} (B_{1g}) band is associated with the NH_4^+ translational mode, since in the Raman spectrum of KNO_3 no band is observed

around 200 cm^{-1}. Furthermore in the far infrared transmission spectrum shown in Fig. 4 a broad band around 200 cm^{-1} is observed, which also exists in the far infrared spectrum of NH_4Cl.

The Raman spectra at various temperatures in Fig. 3 reveal an abrupt spectral change in the phase transition as expected for a first order transition. This can be seen more clearly in the frequency change with temperature shown in Fig. 5.

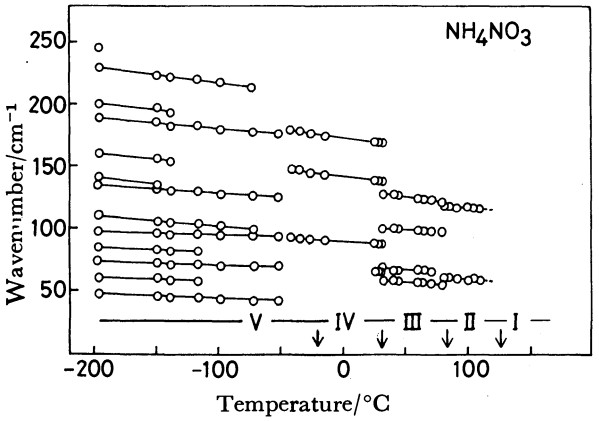

Fig. 5. Temperature dependence of Raman frequencies in NH_4NO_3.

First we discuss the spectra of high-temperature phases. Österlund and Rosen showed in their Raman spectra the phase III was not observed but the phase IV was converted directly to the phase II at 50 °C.[5] In our measurement the spectrum at 81 °C in Fig. 3(b) is considered to arise from the phase II. However, in the temperature range 32 °C—80 °C we have the spectrum which is different from those of both phase II and IV and this corresponds to the spectrum of phase III. The spectrum of phase III is also confirmed by the single crystal spectrum of NH_4NO_3–KNO_3 mixed crystal which takes the same structure as NH_4NO_3-(III).[11]

In the spectrum of phase II two bands are observed. As the temperature is raised these bands shift to lower frequency and show no anomalous behavior as the II→I transition is approached. Actually at 113 °C no band is observed. In the phase I, NO_3^-, and NH_4^+ groups are freely rotating and are described to have a spherical symmetry, resulting in the CsCl-type structure of NH_4NO_3(I). No Raman band is observed as expected from this structure.

Next we discuss the spectra of the low-temperature phase V. As seen in Figs. 3 and 5, an abrupt spectral change corresponding to the phase transition IV⇌V is observed around −50 °C, which is lower than the generally accepted temperature −18 °C. Probably a supercooling state is produced. The cooling rate in our measurement is ≈0.5 K/min. Our measurement is made down to 77 K but no evidence is found for another low-temperature phase VII. Our result at 77 K is in agreement with that at 11 K by Tang and Torrie,[6] who also could not find phase VII.

Table 2 summarizes the observed frequencies in various phases.

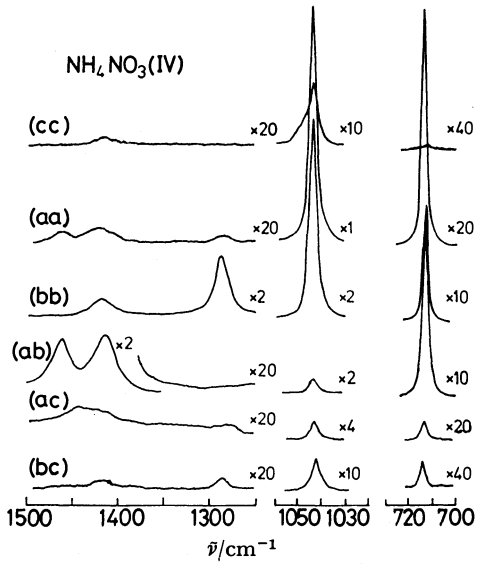

Fig. 6. Polarized Raman spectra of NH_4NO_3(IV) crystal in the internal vibration region.

Internal Vibrations of NO_3^- and NH_4^+ Ions. The polarized Raman spectra in the internal vibration region at room temperature are shown in Fig. 6, which can be interpreted based on D_{2h}[13] crystal symmetry. The correlation between the D_{3h} (NO_3^- free ion) and the D_{2h}[13] (NH_4NO_3 crystal) is as follows:

	$D_{3h}(NO_3^-$ ion)	C_{2v}(site sym.)	$D_{2h}^{13}(NH_4NO_3)$
A_1'	ν_1(≈1050 cm^{-1})	A_1	A_g+B_{3u}
A_2''	ν_2(≈ 830 cm^{-1})	B_2	$B_{2g}+B_{1u}$
E'	ν_3(≈1350 cm^{-1})	A_1	A_g+B_{3u}
	ν_4(≈ 720 cm^{-1})	B_1	$B_{1g}+B_{2u}$

As for NH_4^+ ion the following correlation exists:

	$T_d(NH_4^+$ ion)	C_{2v}(site sym.)	$D_{2h}^{13}(NH_4NO_3)$
A_1	ν_1'	A_1	A_g+B_{3u}
E	ν_2'	A_1	A_g+B_{3u}
		A_2	$B_{3g}+A_u$
F_2	ν_3'	A_1	A_g+B_{3u}
		B_1	$B_{1g}+B_{2u}$
	ν_4'(≈1450 cm^{-1})	B_2	$B_{2g}+B_{1u}$

In the spectra of Fig. 6, the 1043 cm^{-1} band (ν_1 : A_g) and the 715 cm^{-1} band (ν_4 : A_g) are observed as expected from the correlation diagram. The 715 cm^{-1} band is also observed in the (ab) scattering configuration, which corresponds to the $\nu_4(B_{1g})$.

In the region 1250 cm^{-1}—1500 cm^{-1}, the ν_3 of NO_3^- ion and ν_4' of NH_4^+ ion are expected. On referring to the correlation diagram, the 1289 cm^{-1} and 1418 cm^{-1} bands observed in the (bb) configuration are assigned to the $\nu_3(A_g)$ and $\nu_4'(A_g)$ respectively, and the 1415 cm^{-1} and 1461 cm^{-1} bands observed in the (ab) configuration are assigned to the $\nu_3(B_{1g})$ and $\nu_4'(B_{1g})$ respectively.

The splitting of the A_g and B_{1g} components of the ν_3 (asymmetric stretching mode of NO_3^- ion) in NH_4NO_3-(IV) is 126 cm^{-1}, which seems abnormally large

compared with $\approx 10\ cm^{-1}$ in KNO_3(II). In NH_4NO_3-(III) this splitting is $\approx 35\ cm^{-1}$ (see Table 2). In the NH_4NO_3–KNO_3 mixed crystals $(NH_4)_xK_{1-x}NO_3$ which will be discussed in the following paper, the ν_3 splitting is $\approx 40\ cm^{-1}$. The large splitting of ν_3 may be caused by the strong interionic interaction between NH_4^+ and NO_3^- ions. The neutron diffraction measurement by Choi *et al.* showed that in NH_4NO_3(IV) the hydrogen bond is formed between the hydrogen in NH_4^+ ion and one of the oxygens in NO_3^- ion.[12] This kind of hydrogen bond also exists in NH_4NO_3(V), which gives rise to the large splitting of ν_3 in the low-temperature phase V as observed by Tong and Torrie.[6] A crystallographic study suggests that the phase transition III⇌IV is related to the hydrogen bonding, which is reflected on the splitting of ν_3. James *et al.* suggested that the bands at $1289\ cm^{-1}$ and $1415\ cm^{-1}$ are the transverse and longitudinal components of ν_3 and the structure of phase IV is non-centric due to the observation of such a polar mode in the Raman spectrum.[7] However, their interpretation is highly unlikely since as seen in Fig. 6 polarized Raman spectra of single crystals for various scattering configurations do not reveal any TO/LO character and they can be interpreted based on D_{2h}^{13} structure as mentioned before.

In conclusion, the structural change can be sensitively probed by studying the Raman active lattice modes in the low-frequency region. An abrupt spectral change occurs in the phase transition, indicating a first order transition. The spectra of single crystals for the room-temperature phase IV, in the low-frequency region as well as in the internal vibration region, are reasonably interpreted based on D_{2h}^{13} structure.

A part of this investigation was supported by a grant of Yamada Science Foundation.

References

1) K. Akiyama, Y. Morioka, and I. Nakagawa, *J. Phys. Soc. Jpn.*, **48**, 898 (1980).
2) M. Nagatani, T. Seiyama, M. Sakiyama, H. Suga, and S. Seki, *Bull. Chem. Soc. Jpn.*, **40**, 1833 (1967).
3) R. N. Brown and A. C. Mclaren, *Proc. R. Soc. London, Ser. A*, **266**, 329 (1962).
4) S. B. Hendricks, E. Posnjak, and F. C. Kracek, *J. Am. Chem. Soc.*, **54**, 2766 (1932).
5) K. Österlund and H. J. Rosen, *Solid State Commun.*, **15**, 1355 (1974).
6) M. C. Tang and B. H. Torrie, *J. Phys. Chem. Solids*, **39**, 845 (1977).
7) D. W. James, M. T. Carrick, and W. H. Leong, *Chem. Phys. Lett.*, **28**, 117 (1974).
8) Z. Iqbal, *Chem. Phys. Lett.*, **40**, 41 (1976).
9) A. Théorêt and C. Sandorfy, *Can. J. Chem.*, **42**, 57 (1964).
10) J. R. Durig and D. J. Antion, *J. Chem. Phys.*, **51**, 3639 (1969).
11) J. R. Holden and C. W. Dickinson, *J. Phys. Chem.*, **79**, 249 (1975).
12) C. S. Choi, J. E. Mapes, and E. Prince, *Acta Crystallogr., Sect. B*, **28**, 1357 (1972).

  Bull. Chem. Soc. Jpn., 54, 1667—1670 (1981)

Raman Scattering and Phase Transition of NH_4NO_3-KNO_3 Mixed Crystals

Kenji Akiyama,† Yoshiyuki Morioka, and Ichiro Nakagawa*

Department of Chemistry, Faculty of Science, Tohoku University, Aoba, Aramaki, Sendai 980

(Received December 15, 1980)

NH_4NO_3–KNO_3 mixed crystals, $(NH_4)_xK_{1-x}NO_3$ (x=0.88, 0.75, and 0.61), are prepared by evaporation of aqueous solutions of ammonium nitrate and potassium nitrate. Polarized Raman spectra of single crystals of mixed crystals are observed at room temperature and are interpreted based on the NH_4NO_3(III) type D_{2h}^{16} structure. Raman spectra of powdered samples are examined at various temperatures and it is shown that the NH_4NO_3-(IV) type phase which is a room-temperature phase of NH_4NO_3 is not realized in the mixed crystals. In $(NH_4)_{0.88}K_{0.12}NO_3$, NH_4NO_3(III) type is converted to NH_4NO_3(V) type around −120 °C. In the spectra of high-temperature phase of mixed crystals, only one broad band in the region 100 cm^{-1}—120 cm^{-1} is observed, which corresponds to KNO_3(I) or KNO_3(III) type structure.

In alkali nitrates, Rb and Cs salts, where the ionic radii of the cations are larger than that of K^+ ion, take the CsCl type structure at high temperatures as in NH_4NO_3, while Li and Na salts consisting of smaller cations take the distorted NaCl type structure. KNO_3 is ferroelectric in its phase III, which has not been known in other univalent nitrates. The ionic radius of NH_4^+ ion is slightly larger than that of K^+ ion, and the effect of the substitution of NH_4^+ ion for K^+ ion and the phase transition of NH_4NO_3–KNO_3 mixed crystals have been studied in relation to ferroelectricity.[1-4] It is considered that at high temperatures mixed crystals take the KNO_3(III) type structure, which is ferroelectric, as well as KNO_3(I) type, from the study on the temperature dependence of the lattice constant.[2,3] An X-ray crystallographic study showed that the room-temperature structure of mixed crystals is the NH_4NO_3-(III) type.[5] As for the low-temperature structure no crystallographic study has been reported.

On these backgrounds we attempted spectroscopic studies on the phase transition of NH_4NO_3–KNO_3 mixed crystals. In the preceding paper we studied Raman scattering and phase transition of NH_4NO_3 and clarified a characteristic spectral feature for each phase.[6] In the present investigation Raman spectra of single crystals of NH_4NO_3–KNO_3 mixed crystals at room temperature are studied and the structural changes at high temperatures are examined spectroscopically. Furthermore an elaborate measurement of temperature dependence of Raman spectra at low temperatures is made to find whether an abrupt spectral change associated with the phase transition exists, since so far no study has been done as to the phase transition at low temperatures.

Another objective of this study is to make a definite vibrational assignment of NH_4NO_3(III) for which single crystal spectra could not be obtained, by using the results of NH_4NO_3–KNO_3 mixed crystals of NH_4NO_3(III) type structure.

Experimental

$(NH_4)_xK_{1-x}NO_3$ mixed crystals were prepared by evaporation of aqueous solutions of ammonium nitrate and potassium nitrate of appropriate molar ratio in a desiccator at room temperature. The initial crops in each solution which precipitate in microcrystalline form were removed from this solution and subsequently single crystals began to grow. Thus uniform solid solutions of NH_4NO_3 and KNO_3 were obtained. All these crystals grew as a long needle whose axis coincides with the b-axis of the NH_4NO_3(III) type crystal. It was confirmed from the X-ray powder diffraction measurement that these mixed crystals have the same structure as that of NH_4NO_3(III). The molar ratio of mixed crystals was determined by chemical analysis.

In the preparation of $(NH_4)_xK_{1-x}NO_3$ mixed crystals by evaporation of aqueous solutions, the molar ratio (x) of NH_4NO_3 amounts to the value in the range $0.96>x>0.60$ for the produced crystals. The mixed crystals with the x value in the range $0.60>x>0.04$ are not produced from aqueous solutions at room temperature. (It is reported that the crystal with $x<0.04$ is isomorphous with KNO_3 (II)[1,5]).

We prepared the following three kinds of mixed crystals:

Molar ratio of NH_4NO_3 in aqueous solution	Molar ratio of NH_4NO_3 in mixed crystal
0.9	0.88
0.8	0.75
0.7	0.61

Spectral measurements were performed in the procedure described in the preceding paper.[6]

Results and Discussion

Temperature Dependence of Raman Spectra of Polycrystalline Samples. Figure 1 shows the Raman spectra of powdered samples of $(NH_4)_xK_{1-x}NO_3$ mixed crystals (x=0.88, 0.75, and 0.61) at room temperature, compared with those of NH_4NO_3 at 32°C, which corresponds to the spectrum of NH_4NO_3(III) as discussed in the preceding paper.[6] The spectra of the above three kinds of mixed crystals are similar to that of NH_4NO_3-(III), confirming the crystallographic conclusion that $(NH_4)_xK_{1-x}NO_3$ ($x>0.6$) at room temperature takes the NH_4NO_3(III) type structure with the space group D_{2h}^{16} (z=4).[5] Raman frequencies of $(NH_4)_{0.88}K_{0.12}NO_3$ at various temperatures in the process of cooling and heating from room temperature are shown in Fig. 2.

In the low-temperature spectra, a phase transition is found around −120 °C for $(NH_4)_{0.88}K_{0.12}NO_3$, while for the other two kinds of mixed crystals no sudden change in the spectra is found. Figure 3 shows the

† Present address: Shin-Etsu Handotai Co., Ltd., Isobe, Annaka, Gunma 379-01.

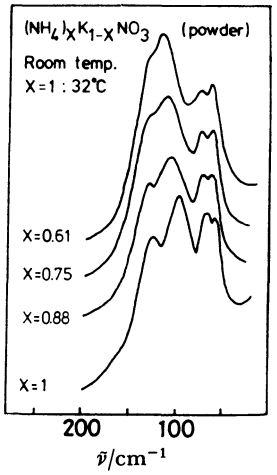

Fig. 1. Raman spectra of powdered samples of $(NH_4)_x$-$K_{1-x}NO_3$ mixed crystals at room temperature. For NH_4NO_3 ($x=1$) the spectrum at 32 °C is given.

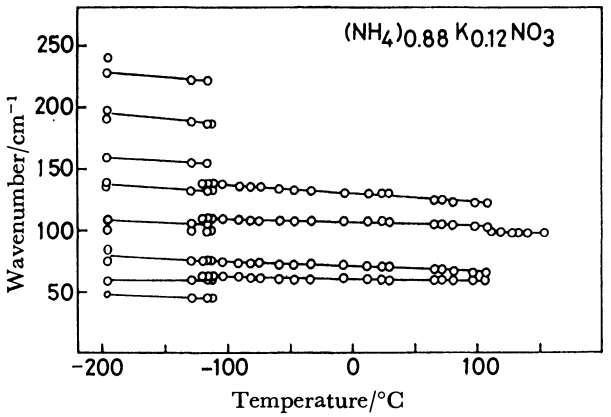

Fig. 2. Raman frequencies at various temperatures for $(NH_4)_{0.88}K_{0.12}NO_3$ mixed crystal.

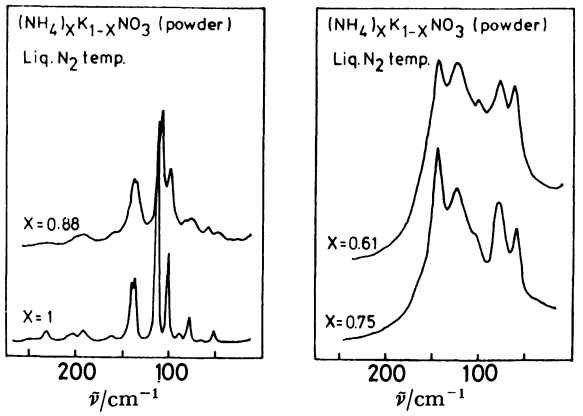

Fig. 3. Raman spectra of powdered samples of $(NH_4)_x$-$K_{1-x}NO_3$ mixed crystals at liquid-N_2 temperature.

Raman spectra at liquid-N_2 temperature. From Fig. 3(a), it is shown that the low-temperature phase of $(NH_4)_{0.88}K_{0.12}NO_3$ takes the NH_4NO_3(V) type structure (low-temperature phase of NH_4NO_3). It should be noted that in this mixed crystal NH_4NO_3(III) type→ NH_4NO_3(V) type phase transition occurs without passing through NH_4NO_3(IV) type structure unlike NH_4NO_3 crystal. As seen in Fig. 3(b), for the mixed crystals with $x=0.75$ and $x=0.61$, the room-temperature structure of NH_4NO_3(III) type is still retained at liquid-N_2 temperature. However, it might be possible that a supercooling state is produced in these mixed crystals.

Next we see the spectra of high-temperature phase. It is generally accepted that the following phase transitions exist in the mixed crystals at high temperature:[3]

$$NH_4NO_3(III)\ \text{type} \underset{75°C—115°C}{\overset{105°C—125°C}{\rightleftharpoons}}$$

$$KNO_3(III)\ \text{type} \underset{\approx 120°C}{\overset{\approx 130°C}{\rightleftharpoons}} KNO_3(I)\ \text{type}$$

The spectra of high-temperature phase are shown in Fig. 4. In the high-temperature spectra, only one broad band with the peak around 100 cm^{-1}—120 cm^{-1} is observed, which is assigned to the NO_3^- ion rotational lattice mode of C_{3v}^5 ($z=1$) or D_{3d}^5 ($z=1$) structure. KNO_3(I) type⇌KNO_3(III) type phase transition is not revealed in the spectra markedly.

Polarized Raman Spectra of Single Crystals. Figure 5 shows polarized Raman spectra of single crystals for $(NH_4)_xK_{1-x}NO_3$ mixed crystals at room-temperature in the low-frequency lattice vibration region. As the ratio of NH_4NO_3 decreases, the observed bands shift

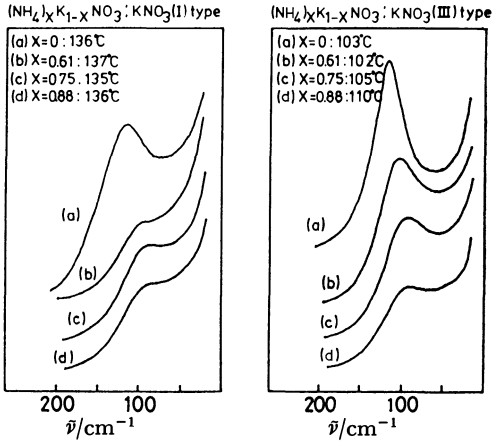

Fig. 4. Spectra of high-temperature phase of $(NH_4)_x$-$K_{1-x}NO_3$ mixed crystals.

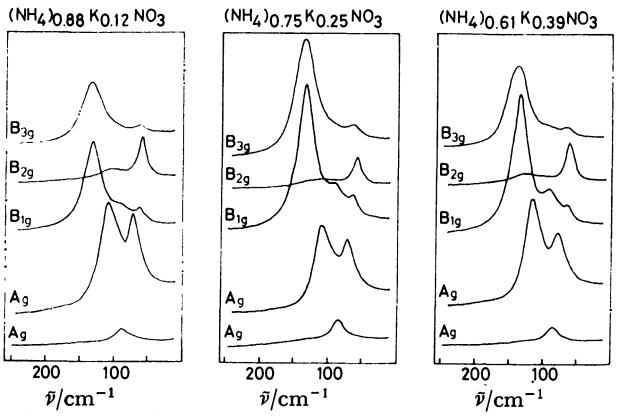

Fig. 5. Polarized Raman spectra of single crystals of $(NH_4)_xK_{1-x}NO_3$ mixed crystals (Low-frequency region).

Table 1. Observed raman frequencies in cm^{-1} of $(NH_4)_xK_{1-x}NO_3$[a)]

$x=1$[b)]	$x=0.88$	$x=0.75$	$x=0.61$	Assignment based on D_{2h}[13]	
58	59	60	63	(B_{2g}) $T_{ac}(NO_3^-)$	
	63	64	65	(B_{1g}) T_b (NO_3^-)	
	65	66	65	(B_{3g}) T_b (NO_3^-)	
68	71	73	76	(A_g) $T_{ac}(NO_3^-)$	
	88	88	88	(A_g) $T_{ac}(NO_3^-)$	
	93	93	93	(B_{1g}) T_b (NO_3^-)	
100	105	109	115	(A_g) R_b (NO_3^-)	
128	131	133	135	(B_{1g}) R_a (NO_3^-)	
	135	136	139	(B_{3g}) R_a (NO_3^-)	
715	714	714	714	(B_{1g}, B_{3g})	ν_4
717	719	719	719	(A_g)	ν_4
	830	830	830	(A_g)	ν_2
1050	1048	1048	1048	(A_g)	ν_1
1320	1320	1325	1330	(B_{3g})	ν_3
	1330	1330	1335	(A_g)	ν_3
1355	1354	1356	1360	(B_{1g})	ν_3
	1360	1365	1373	(B_{2g})	ν_3
1410	1418	1422	1425	(A_g)	ν_4'

a) T and R denote translational and rotational lattice modes, respectively. ν_1—ν_4: internal modes of NO_3^- ion. ν_4': internal mode of NH_4^+ ion. b) Powdered sample at 32 °C.

to the higher frequency, which reflects the crystallographic result that the lattice constants become smaller. Table 1 summarizes the vibrational frequencies together with the mode assignments.

In NH_4NO_3(IV) crystal reported in the preceding paper, it was found that the lattice mode about a-axis of NO_3^- ion (R_a) is observed as a single band while that about b-axis (R_b) is accompanied by a band due to the translational lattice mode which is coupled with the rotational mode and strengthens its intensity. In the NH_4NO_3(III) type crystal a similar feature is seen, but somewhat in an approximate description. One of the oxygen atoms (O_1) in NO_3^- ion is located in the mirror plane in NH_4NO_3(III) crystal (refer to Fig. 1 of the preceding paper[6]). Although NO_1 is not exactly parallel to the a-axis of crystal, we designate approximately the rotational mode about the NO_1-axis, R_a, and that about the axis perpendicular to the NO_1-axis and in the NO_3^- plane, R_b. In the NH_4NO_3(III) type D_{2h}^{16} structure, R_a belongs to the B_{1g} and B_{3g} species and R_b to the A_g and B_{2g} species. As seen in Fig. 5, in the spectrum of the a scattering configuration (A_g), two strong bands are observed, while in the spectra of the ab (B_{1g}) and bc (B_{3g}) configurations one strong band is observed with a very weak band around 60 cm^{-1}. The spectral feature revealed in NH_4NO_3(IV) crystal and $(NH_4)_xK_{1-x}NO_3$ crystal of the NH_4NO_3(III) type, that the rotational lattice mode about a-axis is observed as a single band while that about b-axis coupled with the translational mode as two bands, is characteristic of the orthorhombic structure. In the crystals possessing C_3-axis perpendicular to NO_3^- plane, such as KNO_3(I), KNO_3(III), and $NaNO_3$(I) types, the rotational modes about a- and b-axes are degenerate

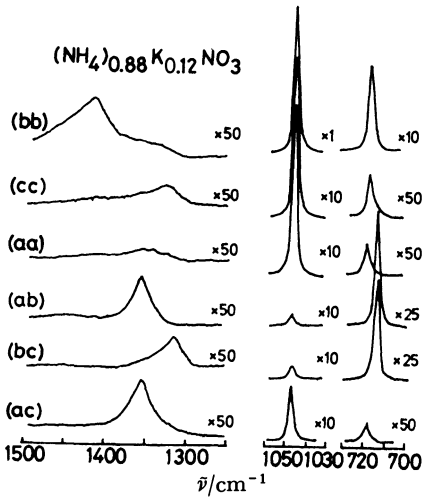

Fig. 6. Polarized Raman spectra of single crystals of $(NH_4)_{0.88}K_{0.12}NO_3$ mixed crystal (Internal vibration region).

and a single band corresponding to E_g species is observed, as seen in the high-temperature phase of mixed crystal.

Next we discuss briefly the polarized Raman spectra in the internal vibration region in Fig. 6. Based on the spectra of six kinds of scattering configurations, the observed bands are assigned straightforwardly to the symmetry species of D_{2h}^{16} factor group as shown in Table 1. The splitting of ν_3 (NO_3 asymmetric stretching mode) in mixed crystals is within $\approx$40 cm^{-1}, comparable with 35 cm^{-1} in NH_4NO_3(III), which indicates that in the NH_4NO_3(III) type structure no strong hydrogen bond is formed between NH_4^+ and NO_3^- ions unlike in the case of NH_4NO_3(IV) and NH_4NO_3(V) type structures.

To sum up, polarized Raman spectra of single crystals of mixed crystals at room temperature are interpreted based on the NH_4NO_3(III) type D_{2h}^{16} structure. In NH_4NO_3(III) itself single crystal spectra could not be obtained due to the crack of crystals at phase transition NH_4NO_3 IV→III. Therefore it is significant that a vibrational assignment of the spectra of powdered sample for NH_4NO_3(III) can be done on comparing with the single crystal spectra of mixed crystals at room temperature. The NH_4NO_3(IV) type phase which is a room-temperature phase of NH_4NO_3 is not realized in the mixed crystals. In some mixed crystals, the NH_4NO_3(III) type is converted directly to the NH_4NO_3-(V) type around −120 °C, without passing through the NH_4NO_3(IV) type. At high temperatures, only one broad band in the region 100 cm^{-1}—120 cm^{-1} is observed, which corresponds to KNO_3(I) or KNO_3(III) type structure.

The authors wish to express their sincere thanks to Prof. Takei, The Research Institute for Iron, Steel and Other Metals, Tohoku University, for permitting us to use X-ray diffractometer.

A part of this study is supported by a grant of Yamada Science Foundation.

References

1) T. Yanagi and S. Sawada, *J. Phys. Soc. Jpn.*, **18**, 1228 (1963).
2) T. Yanagi, *J. Phys. Soc. Jpn.*, **20**, 1351 (1965).
3) U. Kawabe, T. Yanagi, and S. Sawada, *J. Phys. Soc. Jpn.*, **20**, 2059 (1965).
4) E. Janecke, H. Hamacher, and E. Rahlfs, *Z. Anorg. Allg. Chem.*, **206**, 357 (1932).
5) J. R. Holden and C. W. Dickinson, *J. Phys. Chem.*, **79**, 249 (1975).
6) K. Akiyama, Y. Morioka, and I. Nakagawa, *Bull. Chem. Soc. Jpn.*, **54**, 1662 (1981).

Mechanism of the Current Doubling Effect. I. The ZnO Photoanode in Aqueous Solution of Sodium Formate

Akira FUJISHIMA,* Tamihiko KATO,† Etsuro MAEKAWA,† and Kenichi HONDA

Department of Synthetic Chemistry, Faculty of Engineering, The University of Tokyo, Hongo, Bunkyo-ku, Tokyo 113

†*Department of Industrial Chemistry, Nagoya Institute of Technology, Gokiso, Showa-ku, Nagoya 466*

(Received December 18, 1980)

Current doubling mechanism of the photoanodic reaction of sodium formate at the ZnO electrode is re-examined. Quantitative analysis of the reaction products revealed that ZnO electrode corroded during the current doubling reaction, which has not been previously reported. However, zinc ions were formed with about 50% of current efficiency. Carbon dioxide, instead of oxygen, was formed during the reaction. These experimental observations strongly suggested mechanism proposed by earlier workers were incorrect. A new mechanism is proposed.

The anodic photoreaction of a ZnO electrode in an inert electrolyte solution is known[1,2] as a dissolution reaction ($ZnO+2p^+ \rightarrow Zn^{2+}+1/2O_2$), in which the current efficiencies of Zn^{2+} dissolution and oxygen evolution are each 100%.

However, when formic acid, aldehydes or alcohols are added to the electrolyte solution, Morrison *et al.*[3-6] found that the anodic photocurrent of a ZnO single crystal doubled, and they proposed a current doubling mechanism. Subsequently, similar effects were reported on other semiconductor electrodes. Gerischer *et al.* observed[7,8] current doubling behavior on a single crystal CdS electrode when aldehydes or alcohols were added to the electrolyte. Tamura *et al.*[9,10] found that the photooxidation current for a TiO_2 single crystal electrode increased with the addition of alcohols. Bard *et al.*[11-15] studied the oxidation of acetate ions, both on an irradiated TiO_2 electrode and on TiO_2 powders, and they named the reaction the Photo-Kolbe Reaction. Using irradiated p-type GaP electrode, Memming showed[16,17] that $S_2O_8^{2-}$, H_2O_2, or *p*-benzoquinone were current-doubling agents under cathodic polarization.

According to the mechanism proposed by Morrison *et al.*,[3-6] holes formed by photoirradiation of an n-type semiconductor react with a current doubling agent R to give R^+, which then donates an electron to the conduction band and becomes R^{2+}. In this case, the dissolution reaction of ZnO is suppressed.

However, our preliminary study[18] with the ZnO electrode shows that while typical current doubling agents such as formate ion or ethyl alcohol made the photoanodic current increase, oxygen evolution could not be observed and zinc ions were detected in the electrolyte solution after photoelectrolysis. The quantity of zinc ions dissolved was almost equivalent to the quantity of holes flowing to the ZnO surface. These facts indicate that the current doubling effect may not always follow Morrison's mechanism.

In this paper we re-examine the mechanism of current doubling. Using a polycrystalline ZnO electrode and $HCOO^-$ as the current doubling agent, we present quantitative data on the magnitude of photocurrent, the amount of zinc ions dissolved, and the amount of oxygen and CO_2 formed.

Experimental

Polycrystalline ZnO Electrode. A polycrystalline ZnO pellet was made by pressing the powder (reagent grade) with a pressure of 0.5 t/cm^2 and then heating it for 3 h at 1300 °C in air.[19] Its diameter was 17 mm and the thickness about 2 mm. After an ohmic contact was made with an In–Ga alloy, a lead wire was connected with Silver Epoxy, and then all surfaces except one were covered with an epoxy resin.

Electrochemical Reaction on Illuminated Polycrystalline ZnO Electrode. Current-potential and photocurrent-time behavior of the ZnO electrode were measured with a potentiostat (Nikko Keisoku NPG 301), with a saturated calomel electrode as the reference electrode and platinum as the counter electrode. Irradiation was carried out with the light from a 500 W high pressure mercury lamp with a quartz lens and a filter (Toshiba Kasei UVD2) to pass wavelengths around 360±30 nm. The electrolyte contained Na_2SO_4 or KNO_3, and HCOONa was employed as a current doubling agent. A potassium nitrate agar salt bridge separated the cell compartments containing the ZnO and the Pt electrodes. All chemicals. were reagent grade. The experimental setup is shown in Fig. 1.

To elucidate the reaction mechanism, quantitative analyses of the products (Zn^{2+}, O_2, H_2O_2, and CO_2), which could be predicted by the photoanodic reactions on the ZnO electrode, were carried out, as follows: Zn^{2+} ions, which were formed as the result of photoanodic reaction of ZnO electrode, were quantitatively analysed photometrically[20] using the absorp-

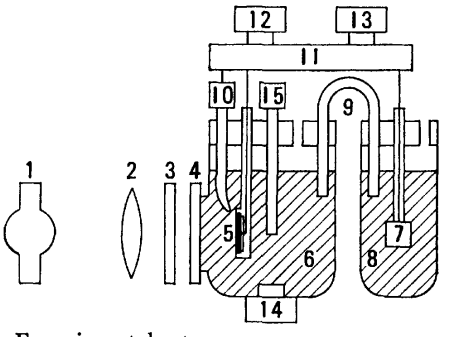

Fig. 1. Experimental setup.
1: 500W high pressure Hg lamp, 2: lens, 3: filter, 4: optical window, 5: sintered ZnO electrode, 6: electrolyte, 7: Pt electrode, 8: electrolyte, 9: salt bridge, 10: SCE, 11: potentiostat, 12: potential sweeper, 13: recorder, 14: stirrer, 15: O_2 detector.

tion peak (λ=570 nm) of complex between Zn^{2+} and Xylenol Orange at pH 6.0. The amount of dissolved oxygen was measured with an oxygen meter (Ishikawa Seisakusho DG) and a gas-chromatography (Ohkura Denki). The amount of CO_2 formed after photoelectrolysis was determined by making the electrolyte solution pH 12 with highly purified NaOH, then adding an aqueous $BaCl_2$ solution, and finally weighing the $BaCO_3$. For this measurement we used KNO_3 as the electrolyte. Hydrogen peroxide was quantitatively analyzed with permanganate.[21]

Results

The current-potential curves obtained using a polycrystalline ZnO electrode were almost the same as those obtained previously using a single crystal ZnO, as shown in Fig. 2. With addition of formate ions to the supporting electrolyte solution, a saturated photoanodic current increased.

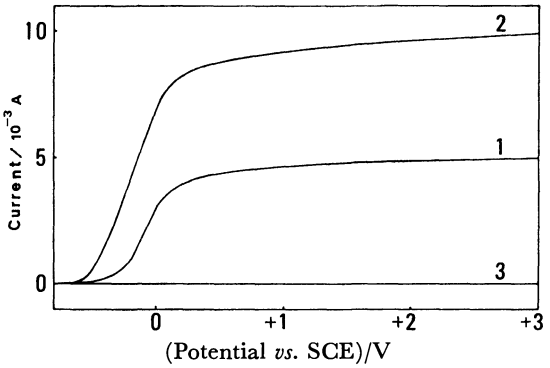

Fig. 2. The current-potential curves of a polycrystalline photoanode.
1: 0.4 M KNO_3, 2: 0.4 M HCOONa+0.4 M KNO_3 (1 M=1 mol dm^{-3}), 3: in dark.

Table 1 shows the results of photocurrent densities, current efficiencies of Zn^{2+}, oxygen, H_2O_2, and CO_2 formation. With addition of HCOONa, photocurrent increased up to almost twice. However, the amounts of dissolved Zn^{2+} were almost the same, that was, the current efficiencies of dissolution of Zn^{2+} were the half. Figure 3 shows amounts of dissolved Zn^{2+} and current efficiencies of Zn^{2+} against time. At any irradiation time current efficiencies were almost the half. This indicates that Zn^{2+} ions were dissolved in the equivalent

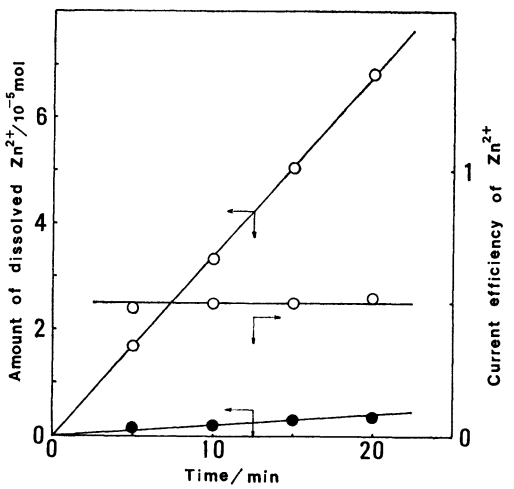

Fig. 3. Amounts of dissolved Zn^{2+} and current efficiency of Zn^{2+} against time.
Electrolyte solution: 0.4 M HCOONa +0.4 M KNO_3, ●: in dark, ○: under irradiation (density of photocurrent: 17.5 mA cm^{-2}).

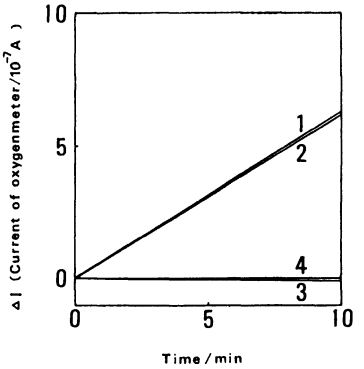

Fig. 4. Detection of oxygen.
1: ZnO photoanode (+1.0 V vs. SCE) in 0.4 M KNO_3 (i=4.1 mA), 2: Pt anode (oxygen evolution reaction) in 0.4 M KNO_3 (i=4.1 mA), 3: ZnO photoanode (+1.0 V vs. SCE) in 0.4 M HCOONa+0.4 M KNO_3 (i=7.8 mA), 4: without electrolysis (blank test; i=0)
ΔI is in proportion to the dissolved oxygen.

quantity of the numbers of the holes formed in the valence band by the light excitation. It means that under irradiation of the constant intensity of light, the rates of dissolution of Zn^{2+} were almost the same with

Table 1. Quantitative analyses of products on a polycrystalline ZnO photoanode

Reactants	Photocurrent density / mA cm^{-2}	The amount of Zn^{2+} ions dissolved in 150 ml anolyte for 10 min / 10^{-5} M	Current efficiencies				
			Zn_2^+	O_2[a] (1)	O_2[a] (2)	H_2O_2	CO_2
	4.62	2.91	1.03	1.02	0.91	0.0	0.00
0.01 M HCOONa	5.94	2.44	0.67		0.67		0.37
0.1 M HCOONa	8.78	2.69	0.50	0.00	0.00	0.0	0.51
0.4 M HCOONa	9.14	2.79	0.50	0.00	0.00		0.55
0.4 M NaI	3.42	0.00	0.00	0.00	0.00		0.00

Supporting electrolyte: 0.4 M KNO_3, Applied potential: + 1.0 V vs. SCE, Irradiation wavelength: 360±30 nm.
a) (1): By the oxygen meter, (2): by gas chromatography.

and without the presence of HCOONa, even photocurrent increased with it. On the other hand, with addition of concentrated HCOONa increase of oxygen was not observed, as shown in Table 1. The results of the quantitative analysis of dissolved oxygen versus time are shown in Fig. 4. The quantity of oxygen produced versus time upon irradiating the ZnO in 0.4 M KNO_3 and with a photocurrent $i=4.1\times10^{-3}$ A/cm^2 is shown in Curve 1. About the same oxygen versus time relationship was obtained without irradiation by substituting the ZnO electrode with a Pt electrode and with an oxidation current of 4.1×10^{-3} A/cm^2 (Curve 2). The latter conditions correspond to electrolysis of water. With the addition of HCOONa the photocurrent increased, and at a high enough concentration ($>10^{-2}$ M) the photocurrent was almost double the value obtained with the inert electrolyte alone. This addition of HCOONa decreased the rate of oxygen during photolysis to essentially zero as shown in Curve 3. Finally, a blank run was made without electrolysis but with irradiation of the ZnO electrode in an electrolyte, with or without HCOONa, and the results show essentially a zero oxygen evolution rate (Curve 4).

Formation of H_2O_2, which was reported by Hauffe and Range[22] during the photooxidation of ZnO electrode, was not detected with and without HCOONa, as shown in Table 1.

The amount of the formation of CO_2 was almost the half compared with the charge flowed, but nearly close to that calculated by the charge based on the increased part of photocurrent in the presence of HCOONa.

As shown in the last column in Table 1, we analyzed the products when iodide ions were added to the electrolyte solution. The photocurrent decreased to less than the value only in the supporting electrolyte, because iodine formed absorbed light quanta. Both current efficiencies of Zn^{2+} dissolved and CO_2 formation became to zero, and also increase of O_2 dissolved was not detected. The behavior can easily be understood[6] that holes formed in the valence band reacted preferentially with I^- ions, resulting in suppression of dissolution ZnO.

Discussion

According to Morrison's current doubling mechanism,[3-6] the holes formed by irradiation of a semiconductor react with $HCOO^-$, to give $H^\cdot$ and CO_2;

$$HCOO^- + p^+ \longrightarrow H^\cdot + CO_2. \quad (1)$$

The $H^\cdot$ formed as an intermediate donates an electron to the conduction band:

$$H^\cdot \longrightarrow H^+ + e^-. \quad (2)$$

Therefore, the net current doubling reaction is

$$HCOO^- + p^+ \longrightarrow H^+ + CO_2 + e^-. \quad (3)$$

Recently, Harbour and Hair,[23] using the spin trapping technique, detected $COO^\cdot$ as an intermediate of the photocatalytic reaction occurring on ZnO powder irradiated in an aqueous solution containing formate or oxalate ions. They proposed a new mechanism in which $COO^\cdot$ donated an electron to the conduction band as follows,

$$HCOO^- + p^+ \longrightarrow H^+ + COO^\cdot \quad (4)$$

$$COO^\cdot \longrightarrow CO_2 + e^-. \quad (5)$$

In this case the net reaction is the same as Eq. 3.

The above mechanisms assume that ZnO is not photooxidized to Zn^{2+}. However, the results in Table 1 show that we observed Zn^{2+} in the electrolyte solution after photoirradiation when the photocurrents was increased, even in the presence of $HCOO^-$. When $HCOO^-$ was present, the current efficiency of Zn^{2+} formation was about 0.5, but the current efficiency would be almost 1.0 if we used the same value of photocurrent observed without $HCOO^-$ addition.

Can we explain these facts from the Morrison's mechanism? One possibility is that the H^+ formed by Eq. 3 reacts chemically with the ZnO,

$$ZnO + 2H^+ \longrightarrow Zn^{2+}(aq) + H_2O. \quad (6)$$

However, it may be very difficult for H^+ formed on the ZnO surface to attack the ZnO lattice. In an alternative and more probable mechanism, an intermediate oxygen species, O*, which is assumed to be one of the intermediates of the simple dissolution reaction of ZnO, reacts with $HCOO^-$ to produce an active $\cdot COO^-$ radical;

$$ZnO + 2p^+ \longrightarrow Zn^{2+} + O^* \quad (7)$$

$$O^* + 2HCOO^- \longrightarrow 2COO^\cdot + H_2O. \quad (8)$$

Then, $COO^\cdot$ can donate an electron to the conduction band, as in Eq. 5,

$$2COO^\cdot \longrightarrow 2CO_2 + 2e^-. \quad (9)$$

By combining Eqs. 7, 8, and 9 we obtain the net reaction,

$$ZnO + 2p^+ + 2HCOO^- \longrightarrow Zn^{2+} + H_2O + 2CO_2 + 2e^-. \quad (10)$$

The experimental results shown in Table 1, *e.g.* the current efficiencies of the products Zn^{2+}, O_2, and CO_2, can be explained if Eq. 10 is valid for the current doubling effect. For example, with HCOONa present in solution, the current efficiencies for Zn^{2+} and CO_2 are observed to be almost 0.5, in accordance with the stoichiometry of Eq. 10.

Conclusion

Mechanism of current doubling reaction of formate ion was re-examined by using a polycrystalline ZnO photoanode. From the quantitative analyses of the products of the current doubling reaction, a new mechanism is proposed;

$$ZnO + 2p^+ + 2HCOO^- \longrightarrow Zn^{2+} + H_2O + 2CO_2 + 2e^-.$$

The ZnO electrode corrodes during the current doubling reaction.

References

1) H. Gerischer, *J. Electrochem. Soc.*, **113**, 1174 (1966).
2) A. Fujishima and K. Honda, *Denki Kagaku*, **40**, 33 (1972).
3) S. R. Morrison and T. Freund, *J. Chem. Phys.*, **47**, 1543 (1967).
4) S. R. Morrison and T. Freund, *Electrochim. Acta*, **13**,

1343 (1968).
5) W. P. Gomes, T. Freund, and S. R. Morrison, *J. Electrochem. Soc.*, **115**, 818 (1968).
6) W. P. Gomes, T. Freund, and S. R. Morrison, *Surf. Sci.*, **13**, 201 (1968).
7) H. Gerischer, *Surface Sci.*, **14**, 97 (1969).
8) H. Gerischer and H. Rosler, *Chem. Ing. Tech.*, **42**, 176 (1970).
9) M. Miyake, H. Yoneyama, and H. Tamura, *Chem. Lett.*, **1976**, 635.
10) M. Miyake, H. Yoneyama, and H. Tamura, *Denki Kagaku*, **45**, 411 (1977).
11) B. Kraeutler and A. J. Bard, *J. Am. Chem. Soc.*, **99**, 7729 (1977).
12) B. Kraeutler and A. J. Bard, *J. Am. Chem. Soc.*, **100**, 2239 (1978).
13) B. Kraeutler and A. J. Bard, *J. Am. Chem. Soc.*, **100**, 4317 (1978).
14) B. Kreaeutler, C. D. Jaeger, and A. J. Bard, *J. Am. Chem. Soc.*, **100**, 4903 (1978).
15) B. Kraeutler and A. J. Bard, *J. Am. Chem. Soc.*, **100**, 5985 (1978).
16) R. Memming, *J. Electrochem. Soc.*, **116**, 785 (1968).
17) R. Memming and F. Möllers, *Ber. Bunsenges. Phys. Chem.*, **76**, 609 (1972).
18) A. Fujishima, Dissetation, University of Tokyo, (1971).
19) M. Matsumura, Y. Nomura, and H. Tsubomura, *Bull. Chem. Soc. Jpn.*, **52**, 1559 (1979).
20) "Kagakubinran," ed by. The Chemical Society of Japan, Maruzen, Tokyo (1975), p. 1538.
21) JIS K 1463-1971.
22) K. Hauffe and J. Range, *Ber. Bunsenges. Phys. Chem.*, **71**, 690 (1967).
23) J. R. Harbour and M. L. Hair, *J. Phys. Chem.*, **83**, 652 (1979).

Temperature Dependence of Thermal Positive Ion Production through Dissociation of Polyatomic Molecules

Hiroyuki KAWANO,* Yoshiaki HIDAKA, and Masao SUGA

Department of Chemistry, Faculty of Science, Ehime University, 2-5, Bunkyo-cho, Matsuyama 790

(Received August 6, 1980)

The production of a thermal positive ion (M^+) from a polyatomic molecule (MX) incident upon a heated metal surface is investigated theoretically as a function of surface temperature (T). The quantitative expression of the ion emission current (i^+) of M^+ at a constant incident flux (N) of MX is found to change according to the condition whether the work function (ϕ) of the surface is higher or lower than the first ionization energy (I) of M and also to the degree of dissociation (γ) of MX on the surface. Namely,

(1) When $\phi - I > 0$,

$$i^+ \approx \begin{cases} K_1 \text{ for } \gamma \approx 1. \\ K_2\, T^{-1/4} \exp\left[\dfrac{\phi - I - D}{2\,R\,T}\right] \text{ for } \gamma \ll 1. \end{cases}$$

(2) When $\phi - I < 0$,

$$i^+ \approx \begin{cases} K_3 \exp\left[\dfrac{\phi - I}{R\,T}\right] \text{ for } \gamma \approx 1. \\ K_4\, T^{-1/4} \exp\left[\dfrac{\phi - I - D/2}{R\,T}\right] \text{ for } \gamma \ll 1. \end{cases}$$

Here D is the bond dissociation energy of MX and K's are virtually independent of T. In any other cases i^+ cannot be expressed in such a simple form. The particular temperature regions corresponding to $\gamma \approx 1$ or $\gamma \ll 1$ are evaluated for given sets of N, D, I, and ϕ.

When a beam of an atom (M) with a small value of the first ionization energy (I(M)) is impinged upon a positively biased metal surface at a high temperature, a positive ion (M^+) is emitted after attaining the following equilibrium on the surface.

$$M \rightleftharpoons M^+ + e^-. \tag{1}$$

This phenomenon is usually called thermal positive ion emission or positive surface ionization, and has long been investigated both experimentally and theoretically by great many workers. Nowadays, in consequence, it is generally accepted that the ionization coefficient (α^+(M)) of M is described by Saha-Langmuir's equation.[1,2]

$$\alpha^+(M) \equiv \frac{n(M^+)}{n(M)} = \frac{w^+}{w^0} \exp\left[\frac{\phi - I(M)}{R\,T}\right]. \tag{2}$$

Here $n(M^+)$ and $n(M)$ are the numbers of M^+ and M emitted per unit time from unit surface area, respectively, w^+/w^0 the statistical weight ratio of M^+ to M, ϕ the work function of the surface, R the gas constant, and T the absolute temperature of the surface. The enthalpy change (ΔH_1) due to the surface reaction ($M \rightarrow M^+ + e^-$) is equal to $-(\phi - I(M))$, which is naturally included in Eq. 2. The ionization efficiency is usually given by

$$\beta^+(M) \equiv \frac{n(M^+)}{N(M)} = \sigma(M) \frac{n(M^+)}{n(M) + n(M^+)}$$

$$= \sigma(M) \frac{\alpha^+(M)}{1 + \alpha^+(M)}, \tag{3}$$

where N(M) and σ(M) are the incident flux per unit time per unit surface area and the accommodation coefficient of M, respectively.

The ion current collected with a Faraday cage is generally expressed by

$$i^+(M) = e\,S\,\eta(M^+)\,N(M)\,\beta^+(M). \tag{4}$$

Here e, S, and $\eta(M^+)$ are the elementary electric charge, the area of the ionizing surface, and the collection efficiency of M^+, respectively. Substitution of Eqs. 3 and 2 in Eq. 4 yields

$$i^+(M) \approx \begin{cases} C_1 \text{ for } \alpha^+(M) \gg 1. & (5) \\ C_1 \left[1 + \dfrac{w^0}{w^+} \exp\left[\dfrac{\Delta H_1}{R\,T}\right]\right]^{-1} \text{ for neither} \\ \quad \alpha^+(M) \gg 1 \text{ nor } \alpha^+(M) \ll 1. & (6) \\ C_1 \dfrac{w^+}{w^0} \exp\left[\dfrac{-\Delta H_1}{R\,T}\right] \text{ for } \alpha^+(M) \ll 1. & (7) \end{cases}$$

Here C_1 is given by

$$C_1 \equiv e\,S\,\eta(M^+)\,\sigma(M)\,N(M). \tag{8}$$

Clearly the quantitative expression of i^+(M) changes according to the value of α^+(M), and it is ΔH_1, of course, that is included in the Boltzmann factor governing the thermal positive ion production from the incident atom M. When $\alpha^+(M) \gg 1$, however, i^+(M) is virtually independent of both ΔH_1 and T, as shown by Eq. 5. When α^+(M) is neither much larger nor much smaller than unity, Eq. 6 indicates that the slope of an emission plot ($\log i^+(M)$ *vs.* $1/T$) is not constant. On the other hand, such a plot as is based on Eq. 7 yields a straight line, the gradient (G) of which is equal to $-(0.434/R)\,\Delta H_1$. Only when $\alpha^+(M) \ll 1$, therefore, it is possible to determine I(M)[3-5] or ϕ[6-9] from G.

Such emission of the positive ion M^+ is observed also when a beam of a molecule (MX) including the same element M impinges upon the surface. In the case of this molecular beam incidence, however, M^+ is emitted after attaining Equilibria (9) and (1) on the ionizing surface, and the ion production processes are more complicated than those in the case of the atomic beam incidence described above.

$$MX \rightleftharpoons M + X. \tag{9}$$

The enthalpy change (ΔH_2) due to the surface reaction

($MX \rightarrow M^+ + X + e^-$) is equal to $-(\phi - I(M) - D(MX))$, where $D(MX)$ is the bond dissociation energy of MX. The temperature dependence of the collected ion current ($i^+(MX)$) of M^+ thus produced from MX has long been investigated experimentally by many workers.[1,2] The theoretical investigation of the dependence, however, has not yet fully been made, and a quantitative expression of $i^+(MX)$ as a function of T seems not to be derived theoretically or empirically by any workers. Consequently, the quantitative relation between $i^+(MX)$ and ΔH_2 also seems to be left unknown, in contrast to the case of the atomic beam incidence described above. From analogy with Eqs. 6 and 7, it may possibly be inferred that none other than ΔH_2 can be included in the Boltzmann factor governing the production of M^+ from MX. The validity of this inference, however, should be checked rigorously on the basis of thermochemistry. Previously one of the present authors made a theoretical study of thermal negative ion production from incident molecules.[10,11] A theoretical model developed in the previous work may probably be useful for solving the above problems, too.

From the viewpoints described above, the present authors have applied the theoretical model to the thermal positive ion production from polyatomic molecules. In consequence, they have found that $i^+(MX)$ is expressed as a function of T by seven different equations according to the ionization coefficient and to the degree of dissociation of MX, and also that the Boltzmann factors in some of the equations include ΔH_1, $\Delta H_2/2$, or $(\Delta H_1 + \Delta H_2)/2$, as opposed to the above inference that ΔH_2 alone is included.

This paper describes the theoretical investigation leading to the above findings and also illustrates an application of the present theory to several sample–surface systems.

Theoretical

Expression of the Ionization Coefficient. In a similar way as in the previous work,[10,11] let us consider an isothermal airtight metal vessel, inside of which Equilibria (9) and (1) exist. If the density of the charged particles is so small that the space-charge effect may be neglected, then Eqs. 10—12 are derived from thermochemical considerations.

$$\frac{P(M)\,P(X)}{P(MX)} = \frac{f(M)\,f(X)}{f(MX)} \exp\left[\frac{-D(MX)}{R\,T}\right]. \quad (10)$$

$$\frac{P(M^+)\,P(e^-)}{P(M)} = \frac{f(M^+)f(e^-)}{f(M)} \exp\left[\frac{-I(M)}{R\,T}\right]. \quad (11)$$

$$P(e^-) = f(e^-) \exp\left[\frac{-\phi}{R\,T}\right]. \quad (12)$$

Here $P(Y)$ and $f(Y)$ are the equilibrium vapor pressure and the partition function, respectively, of the particle Y, and ϕ is the work function of the surface of the vessel.

The flux of Y evaporating per unit time from a unit area of the surface is given by

$$J(Y) = \frac{N_A P(Y)}{\{2\pi M(Y)\,R\,T\}^{1/2}}, \quad (13)$$

where N_A and $M(Y)$ are Avogadro's number and the molecular (or atomic) weight of Y, respectively. In surface ionization, however, free evaporation occurs in a vacuum. Strictly speaking, therefore, $P(Y)$ should be corrected with a factor of the evaporation coefficient ($\varepsilon(Y)$).[12] Consequently, the flux of Y emitted from an ionizing surface is

$$n(Y) = \varepsilon(Y)\,J(Y). \quad (14)$$

From Eqs. 10—14 we obtain Eqs. 15—17.

$$\frac{n(M)\,n(X)}{n(MX)} = \frac{N_A \rho(MX)}{\{2\pi\mu R\,T\}^{1/2}} \exp\left[\frac{\Delta S^\circ(MX)}{R}\right] \times \exp\left[\frac{-D(MX)}{R\,T}\right]. \quad (15)$$

$$\alpha^+(MX) \equiv \frac{n(M^+)}{n(M)} = C_2 \exp\left[\frac{\phi - I(M)}{R\,T}\right]. \quad (16)$$

$$C_2 \equiv \rho(M) \exp\left[\frac{\Delta S^\circ(M)}{R}\right]. \quad (17)$$

Here $\Delta S^\circ(MX)$ and $\Delta S^\circ(M)$ are the standard entropy changes due to the dissociation and the positive ion production, respectively; and $\rho(MX)$, $\rho(M)$, and μ are given by $\varepsilon(M)\,\varepsilon(X)/\varepsilon(MX)$, $\varepsilon(M^+)/\varepsilon(M)$, and $M(M) \times M(X)/M(MX)$, respectively. Essentially C_2 is equal to w^+/w^0 because Eq. 2 is derived on the implicit assumption $\rho(M)=1$. If the flux of MX or M impinging separately upon the same ionizing surface is so small that ϕ may be regarded essentially constant without being affected by adsorption of MX or M, then the ionization coefficient $\alpha^+(MX)$ given by Eq. 16 is equal to $\alpha^+(M)$ by Eq. 2.

Under such a steady-state condition that all of the particles evaporate from the ionizing surface immediately after attaining Equilibria (9) and (1) on the surface, the following relations hold.

$$n(M) + n(M^+) = n(X) = \sigma(MX)\,\gamma(MX)\,N(MX). \quad (18)$$

$$n(MX) = \{1-\gamma(MX)\}\,\sigma(MX)\,N(MX). \quad (19)$$

Here $\sigma(MX)$ is the accommodation coefficient of MX incident upon the ionizing surface, and represents the fraction of the MX molecules attaining Equilibria (9) and (1) on the surface. Namely,

$$\sigma(MX) \equiv \frac{n(MX) + n(M) + n(M^+)}{N(MX)}. \quad (20)$$

The ionization efficiency is given by

$$\beta^+(MX) \equiv \frac{n(M^+)}{N(MX)} = \sigma(MX)\,\gamma(MX)\,\frac{\alpha^+(MX)}{1+\alpha^+(MX)}. \quad (21)$$

Eqs. 16 and 18 yield

$$n(M) = \frac{\sigma(MX)\,\gamma(MX)\,N(MX)}{1+\alpha^+(MX)}. \quad (22)$$

By substituting Eqs. 18, 19, and 22 in Eq. 15, we obtain

$$\frac{\gamma(MX)^2}{1-\gamma(MX)} = \{1+\alpha^+(MX)\}\,B, \quad (23)$$

or

$$\gamma(MX) = \frac{\{1+\alpha^+(MX)\}B}{2} \times \left[\left\{1 + \frac{4}{\{1+\alpha^+(MX)\}B}\right\}^{1/2} - 1\right]. \quad (24)$$

Here

$$\begin{cases} B \equiv b\ T^{-1/2} \exp\left[\dfrac{-D(\mathrm{MX})}{R\ T}\right]. & (25) \\ b \equiv \dfrac{N_{\mathrm{A}}\ \rho(\mathrm{MX})}{\sigma(\mathrm{MX})\ N(\mathrm{MX})\{2\pi\mu R\}^{1/2}} \exp\left[\dfrac{\Delta S^{\circ}(\mathrm{MX})}{R}\right]. & (26) \end{cases}$$

Again, it should be noted that Eq. 2 is based upon simplifying assumptions such as $\rho(\mathrm{M})=1$ and $\sigma(\mathrm{M})=1$ but is nevertheless approved widely as a quantitative expression of $\alpha^{+}(\mathrm{M})$ in usual surface ionization, where the electric field drawing out M^{+} from the surface is so weak that Schottky effect may be neglected. When potassium halide molecules impinge upon a rhenium surface, for example, $\beta^{+}(\mathrm{KX})$ is virtually unity in the range 1200—1900 K.[13] This result may give evidence that both $\sigma(\mathrm{KX})$ and $\rho(\mathrm{KX})$ are essentially unity in the above cases. In addition, cesium chloride molecules are completely accommodated on both iridium and carburized iridium surfaces.[14]

Judging from the experimental results described just above, it may be reasonable at least with alkali halide molecules to regard that both $\sigma(\mathrm{MX})$ and $\rho(\mathrm{MX})$ are virtually unity in usual surface ionization. In a narrow temperature range usually covered in positive surface ionization, therefore, b given by Eq. 26 may be regarded essentially constant for a constant value of $N(\mathrm{MX})$.

Expression of the Ion Emission Current. The ion current collected with a Faraday cage is expressed by Eq. 27, which is derived from Eq. 21.

$$\begin{aligned} i^{+}(\mathrm{MX}) &= e\,S\,\eta(\mathrm{M}^{+})\ N(\mathrm{MX})\ \beta^{+}(\mathrm{MX}) \\ &= C_3\,\gamma(\mathrm{MX})\,\frac{\alpha^{+}(\mathrm{MX})}{1+\alpha^{+}(\mathrm{MX})}, \end{aligned} \quad (27)$$

where C_3 is

$$C_3 \equiv e\,S\,\eta(\mathrm{M}^{+})\ \sigma(\mathrm{MX})\ N(\mathrm{MX}). \quad (28)$$

Since C_3 may be regarded constant for a fixed value of $N(\mathrm{MX})$, it is essentially upon $\gamma(\mathrm{MX})$ and $\alpha^{+}(\mathrm{MX})$ that $i^{+}(\mathrm{MX})$ depends. First, therefore, Eq. 27 will be treated as a function of $\gamma(\mathrm{MX})$.

(A) Equation 24 indicates that $\gamma(\mathrm{MX})\approx 1$ when $\{1+\alpha^{+}(\mathrm{MX})\}B \gg 4$. In this case Eq. 27 becomes

$$i^{+}(\mathrm{MX}) \approx C_3\,\frac{\alpha^{+}(\mathrm{MX})}{1+\alpha^{+}(\mathrm{MX})}. \quad (29)$$

In usual surface ionization the measurement of $i^{+}(\mathrm{MX})$ is accompanied with an error of about $\pm 5\%$, and hence a prerequisite for Eq. 29 may be written down

$$\gamma(\mathrm{MX}) \gtrsim 0.95 \text{ or } \{1+\alpha^{+}(\mathrm{MX})\}\,B \gtrsim 18. \quad (30)$$

(B) When $\gamma(\mathrm{MX}) \ll 1$, Eq. 23 reduces to

$$\gamma(\mathrm{MX}) \approx [\{1+\alpha^{+}(\mathrm{MX})\}\,B]^{1/2}. \quad (31)$$

Substitution of Eq. 31 in Eq. 27 yields

$$i^{+}(\mathrm{MX}) \approx C_3\,B^{1/2}\,\frac{\alpha^{+}(\mathrm{MX})}{\{1+\alpha^{+}(\mathrm{MX})\}^{1/2}}. \quad (32)$$

Consideration of the experimental error mentioned above leads to the conclusion that a prerequisite for Eq. 32 may be set up

$$\gamma(\mathrm{MX}) \approx [\{1+\alpha^{+}(\mathrm{MX})\}\,B]^{1/2} \lesssim 0.098. \quad (33)$$

(C) When $\gamma(\mathrm{MX})$ is intermediate, namely,

$$0.95 > \gamma(\mathrm{MX}) > 0.098 \text{ or}$$
$$18 > \{1+\alpha^{+}(\mathrm{MX})\}\,B > 0.0095, \quad (34)$$

$i^{+}(\mathrm{MX})$ cannot be approximated adequately in such a simple form as in Eq. 29 or 32. In this case, $i^{+}(\mathrm{MX})$ is expressed in a complex form by Eq. 35, which is obtained by substituting Eqs. 16 and 24 in Eq. 27.

$$i^{+}(\mathrm{MX}) = C_4 T^{-1/2}\,\mathrm{F}(T) \exp\left[\frac{\phi - I(\mathrm{M}) - D(\mathrm{MX})}{R\ T}\right]. \quad (35)$$

Here

$$\begin{cases} C_4 \equiv \dfrac{e\,S\,\eta(\mathrm{M}^{+})\ N_{\mathrm{A}}\,\rho(\mathrm{M})\ \rho(\mathrm{MX})}{2\{2\pi\ \mu\ R\}^{1/2}} \\ \qquad \times \exp\left[\dfrac{\Delta S^{\circ}(\mathrm{M}) + \Delta S^{\circ}(\mathrm{MX})}{R}\right], & (36) \\ \mathrm{F}(T) \equiv \left[1 + \dfrac{4}{\{1+\alpha^{+}(\mathrm{MX})\}\,B}\right]^{1/2} - 1. & (37) \end{cases}$$

It should be noted that Eq. 35 holds not approximately but exactly for any values of $\gamma(\mathrm{MX})$ and $\alpha^{+}(\mathrm{MX})$.

Consideration of the Ionization Coefficient. Secondly, let us treat $i^{+}(\mathrm{MX})$ as a function of $\alpha^{+}(\mathrm{MX})$.

(A) Equation 16 indicates that $\alpha^{+}(\mathrm{MX})$ is much larger than unity when $\phi - I(\mathrm{M}) \gtrsim 10$ kcal mol^{-1}. Because $R\ T$ is less than about 3 kcal mol^{-1} in a temperature range (1100—1800 K) usually covered in positive surface ionization, and also because C_2 is about 1/2 for alkali metal or its salt, which is the most typical sample material in positive surface ionization. Under the above condition we obtain Eqs. 38 and 39 from Eqs. 29 and 32, respectively, while no simple equation other than Eq. 35 holds for the intermediate values of $\gamma(\mathrm{MX})$.

$$i^{+}(\mathrm{MX}) \approx \begin{cases} C_3 \text{ for } \gamma(\mathrm{MX}) \gtrsim 0.95. & (38) \\ C_4\ T^{-1/2}\,\mathrm{F}(T) \exp\left[\dfrac{\phi - I(\mathrm{M}) - D(\mathrm{MX})}{R\ T}\right] \\ \quad \text{for } 0.95 > \gamma(\mathrm{MX}) > 0.098. & (35) \\ C_5\ T^{-1/4} \exp\left[\dfrac{\phi - I(\mathrm{M}) - D(\mathrm{MX})}{2\ R\ T}\right] \\ \quad \text{for } \gamma(\mathrm{MX}) \lesssim 0.098. & (39) \end{cases}$$

Here C_5 is

$$C_5 \equiv \frac{e\,S\,\eta(\mathrm{M}^{+})\,\{N_{\mathrm{A}}\,\sigma(\mathrm{MX})\ N(\mathrm{MX})\ \rho(\mathrm{M})\ \rho(\mathrm{MX})\}^{1/2}}{\{2\ \pi\ \mu\ R\}^{1/4}} \times \exp\left[\frac{\Delta S^{\circ}(\mathrm{M}) + \Delta S^{\circ}(\mathrm{MX})}{2\ R}\right]. \quad (40)$$

(B) Under the condition that $\phi - I(\mathrm{M}) \lesssim -10$ kcal mol^{-1}, $\alpha^{+}(\mathrm{MX})$ in the usual temperature range is negligibly small compared with unity, and hence Eqs. 41 and 42 are obtained from Eqs. 29 and 32, respectively. Similarly as in the case (A) described just above, it is only Eq. 35 that holds for the intermediate values of $\gamma(\mathrm{MX})$.

$$i^{+}(\mathrm{MX}) \approx \begin{cases} C_6 \exp\left[\dfrac{\phi - I(\mathrm{M})}{R\ T}\right] \text{ for } \gamma(\mathrm{MX}) \gtrsim 0.95. & (41) \\ C_4\ T^{-1/2}\,\mathrm{F}(T) \exp\left[\dfrac{\phi - I(\mathrm{M}) - D(\mathrm{MX})}{R\ T}\right] \\ \quad \text{for } 0.95 > \gamma(\mathrm{MX}) > 0.098. & (35) \\ C_7\ T^{-1/4} \exp\left[\dfrac{\phi - I(\mathrm{M}) - D(\mathrm{MX})/2}{R\ T}\right] \\ \quad \text{for } \gamma(\mathrm{MX}) \lesssim 0.098. & (42) \end{cases}$$

Here C_6 and C_7 are given by Eqs. 43 and 44, respectively.

$$C_6 \equiv e\,S\,\eta(\mathrm{M}^{+})\ \sigma(\mathrm{MX})\ N(\mathrm{MX})\ \rho(\mathrm{M}) \exp\left[\frac{\Delta S^{\circ}(\mathrm{M})}{R}\right]. \quad (43)$$

$$C_7 \equiv \frac{e S \eta(M^+) \rho(M) \{N_A \rho(MX) \sigma(MX) N(MX)\}^{1/2}}{\{2 \pi \mu R\}^{1/4}} \times \exp\left[\frac{\Delta S^\circ(M) + \Delta S^\circ(MX)/2}{R}\right]. \quad (44)$$

(C) When $|\phi - I(M)| < 10$ kcal mol^{-1}, the condition that neither $\alpha^+(MX) \gg 1$ nor $\alpha^+(MX) \ll 1$ holds in the usual temperature range so long as the allowable error due to approximation is restricted to less than about $\pm 5\%$. In this case, $i^+(MX)$ is expressed as follows:

$$i^+(MX) \approx \begin{cases} C_6\, G(T) \exp\left[\dfrac{\phi - I(M)}{R\,T}\right] \\ \quad \text{for } \gamma(MX) \gtrsim 0.95. \quad (45) \\ C_4\, T^{-1/2}\, F(T) \exp\left[\dfrac{\phi - I(M) - D(MX)}{R\,T}\right] \\ \quad \text{for } 0.95 > \gamma(MX) > 0.098. \quad (35) \\ C_7\, T^{-1/4}\, G(T)^{1/2} \exp\left[\dfrac{\phi - I(M) - D(MX)/2}{R\,T}\right] \\ \quad \text{for } \gamma(MX) \lesssim 0.098. \quad (46) \end{cases}$$

Here $G(T)$ is given by

$$G(T) \equiv \left[1 + C_2 \exp\left[\frac{\phi - I(M)}{R\,T}\right]\right]^{-1}. \quad (47)$$

Equations 45 and 46 are derived from Eqs. 29 and 32, respectively. So long as $|\phi - I(M)| < 10$ kcal mol^{-1}, therefore, $i^+(MX)$ cannot be expressed in such a simple form as in Eq. 38, 39, 41, or 42.

Evaluation of the Degree of Dissociation. For the reasons described just below Eq. 26, the factors $\sigma(MX)$, $\rho(M)$, and $\rho(MX)$ may be assumed to be unity, and hence Eqs. 48—50 may be obtained from Eqs. 23—26.

$$\frac{\gamma(MX)^2}{1 - \gamma(MX)} \approx \frac{2.67 \times 10^{25}}{N(MX)\{\mu T\}^{1/2}} \times \exp\left[\frac{\Delta S^\circ(MX)}{R}\right] \exp\left[\frac{-D(MX)}{R\,T}\right] \times \begin{cases} 1 \text{ for } \alpha^+(MX) \ll 1. \quad (48) \\ \left\{1 + \exp\left[\dfrac{\Delta S^\circ(M)}{R}\right] \exp\left[\dfrac{\phi - I(M)}{R\,T}\right]\right\} \\ \quad \text{for neither } \alpha^+(MX) \ll 1 \text{ nor } \alpha^+(MX) \gg 1. \quad (49) \\ \exp\left[\dfrac{\Delta S^\circ(M)}{R}\right] \exp\left[\dfrac{\phi - I(M)}{R\,T}\right] \text{ for } \alpha^+(MX) \gg 1. \quad (50) \end{cases}$$

Here the first figure on the right hand side includes the factor 1.013×10^6, which is necessary because the entropy changes refer to a standard gaseous state for $P(Y) = 1$ atm. At $\alpha^+(MX) \gg 1$, $\gamma(MX)$ depends strongly upon ϕ in contrast to the other cases, as may be easily understood from Eqs. 48—50. Obviously Eq. 50 is $\exp[\{\phi - I(M) + \Delta S^\circ(M)\, T\}/R\, T]$ times as large as Eq. 48, thereby indicating that the dissociation of MX is promoted at $\alpha^+(MX) \gg 1$. In a high temperature range where $\gamma(MX)$ is close to unity, of course, $\gamma(MX)$ is virtually independent of the factors such as $N(MX)$, $D(MX)$, $I(M)$, and ϕ included in Eqs. 48—50, as will be illustrated below (see Fig. 1).

To take concrete examples, let us consider that a beam of NaF strikes single crystal surfaces of Mo(100), W(100), W(110), and Ir(111), the work functions of which are

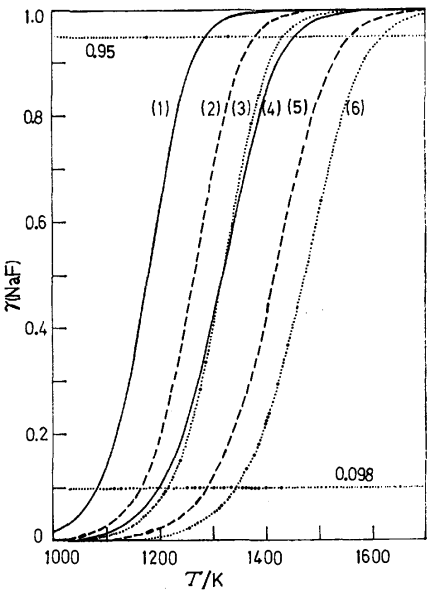

Fig. 1. Temperature dependence of the degree of dissociation of NaF on several surfaces.
Curves (1), (2), and (3); $N(NaF) = 10^{10}$ molecules cm^{-2} s^{-1} on the surfaces of Ir(111), W(110), and W(100) or Mo(100), respectively. Curves (4), (5), and (6); $N(NaF) = 10^{12}$ molecules cm^{-2} s^{-1} on the surfaces of Ir(111), W(110), and W(100) or Mo(100), respectively.

TABLE 1. THE BOUNDARY TEMPERATURES ($T_{0.098}$ AND $T_{0.95}$) CORRESPONDING TO $\gamma(NaF) = 0.098$ AND 0.95, RESPECTIVELY, UNDER VARIOUS EXPERIMENTAL CONDITIONS.

Surface	ϕ / kcal mol^{-1}	$\alpha^+(NaF)$[a]	Eq.[b]	$N(NaF)$ / molecules cm^{-2} s^{-1}	Curve in Fig. 1	$T_{0.098}$ / K	$T_{0.95}$ / K
Mo(100)	100	1×10^{-4}—3×10^{-3}	48	10^{10}	(3)	1220	1430
				10^{12}	(6)	1340	1620
W(100)	105	1×10^{-3}—1×10^{-2}	48	10^{10}	(3)	1220	1430
				10^{12}	(6)	1340	1620
W(110)	124	7.8—2.7	49	10^{10}	(2)	1170	1380
				10^{12}	(5)	1290	1560
Ir(111)	132	300—25	50	10^{10}	(1)	1080	1280
				10^{12}	(4)	1200	1450

a) The values of $\alpha^+(NaF)$ calculated for 1100—1800 K by using Eq. 16. b) The equation employed to evaluate the boundary temperatures.

100,[15] 105,[15] 124,[16] and 132[17] kcal mol^{-1}, respectively. Since I(Na) is 118 kcal mol^{-1}, it is concluded from Eq. 16 in the usual temperature range (1100—1800 K) that α^+(NaF)$\ll$1 for both Mo(100) and W(100), that α^+(NaF)$\gg$1 for Ir(111), and that α^+(NaF) is intermediate for W(110). The values of γ(NaF) at various temperatures are calculated with the above surfaces by using Eqs. 48—50. The thermochemical data for $\Delta S°$(Na), $\Delta S°$(NaF), and D(NaF) are cited from Refs. 18 and 19. The results thus obtained for γ(NaF) are shown in Fig. 1. The boundary temperatures ($T_{0.098}$ and $T_{0.95}$) corresponding to γ(NaF)=0.098 and 0.95, respectively, at N(NaF)=10^{10} or 10^{12} molecules cm^{-2} s^{-1} may be read off in Fig. 1. The temperatures thus evaluated are summarized in Table 1, which shows that both $T_{0.098}$ and $T_{0.95}$ depend upon N(NaF) and also upon α^+(NaF) unless α^+(NaF) is much smaller than unity. The three temperature regions ($T\lesssim T_{0.098}$, $T_{0.098}<T<T_{0.95}$, and $T\gtrsim T_{0.95}$) are hereafter referred to as T_L, T_M, and T_H, respectively. As may be seen in Fig. 1, γ(NaF) at $T\gtrsim$1700 K is essentially constant at about unity without depending upon both N(NaF) and the nature (ϕ) of the ionizing surface employed. In the temperature range below about 1600 K, however, γ(NaF) at N(NaF)=constant depends upon ϕ unless α^+(NaF)$\ll$1, as already stated above.

Therefore, the following results (A)—(C) are obtained when the present theory as to molecular beam surface ionization is applied to the above sample-surface systems at N(NaF)=10^{12} molecules cm^{-2} s^{-1}.

(A) For the NaF-Ir(111) system where α^+(NaF)$\gg$1,

$$i^+(\mathrm{NaF})\approx\begin{cases} C_3 \text{ at } T_H\gtrsim 1450 \text{ K.} & (38)\\ C_4\,T^{-1/2}\,F(T)\exp\left[\dfrac{-\Delta H_2}{RT}\right] & \\ \quad \text{at } 1450>T_M>1200 \text{ K.} & (35)\\ C_5\,T^{-1/4}\exp\left[\dfrac{-\Delta H_2}{2RT}\right] \text{ at } T_L\lesssim 1200 \text{ K.} & (39)\end{cases}$$

(B) For the NaF-Mo(100) or NaF-W(100) system where α^+(NaF)$\ll$1,

$$i^+(\mathrm{NaF})\approx\begin{cases} C_6\exp\left[\dfrac{-\Delta H_1}{RT}\right] \text{ at } T_H\gtrsim 1620 \text{ K.} & (41)\\ C_4\,T^{-1/2}\,F(T)\exp\left[\dfrac{-\Delta H_2}{RT}\right] & \\ \quad \text{at } 1620>T_M>1340 \text{ K.} & (35)\\ C_7\,T^{-1/4}\exp\left[\dfrac{-\Delta H_1-\Delta H_2}{2RT}\right] & \\ \quad \text{at } T_L\lesssim 1340 \text{ K.} & (42)\end{cases}$$

(C) For the NaF-W(110) system where neither α^+(NaF)$\gg$1 nor α^+(NaF)$\ll$1,

$$i^+(\mathrm{NaF})\approx\begin{cases} C_6\,G(T)\exp\left[\dfrac{-\Delta H_1}{RT}\right] \text{ at } T_H\gtrsim 1560 \text{ K.} & (45)\\ C_4\,T^{-1/2}\,F(T)\exp\left[\dfrac{-\Delta H_2}{RT}\right] & \\ \quad \text{at } 1560>T_M>1290 \text{ K.} & (35)\\ C_7\,T^{-1/4}\,G(T)^{1/2}\exp\left[\dfrac{-\Delta H_1-\Delta H_2}{2RT}\right] & \\ \quad \text{at } T_L\lesssim 1290 \text{ K.} & (46)\end{cases}$$

Characteristics of the Emission Plots. All of the factors C_1—C_7 in the above equations are virtually independent of T because, σ, ρ, and $\Delta S°$ may be regarded constant in a narrow temperature range usually covered in positive surface ionization and also because N is usually kept constant throughout the course of a run. On the other hand, both $F(T)$ and $G(T)$ depend upon T. The characteristics of an emission plot ($\log i^+$(M) *vs.* $1/T$) for atomic beam surface ionization is already outlined below Eq. 8. Similarly those for molecular beam surface ionization will be summarized in this section.

Equation 35 indicates that an emission plot of $\log[i^+(\mathrm{MX})\,T^{1/2}]$ *vs.* $1/T$ does not yield a straight line in the region T_M, irrespectively of the value of α^+(MX). Also when α^+(MX) is neither much smaller nor much larger than unity, no straight line is obtained in any temperature range if $\log i^+$(MX) or $\log[i^+(\mathrm{MX})\,T^{1/4}]$ is plotted against $1/T$, as may readily be understood from Eq. 45 or 46. In the case of α^+(MX)$\ll$1, on the other hand, the emission plots ($\log i^+$(MX) *vs.* $1/T$ and $\log[i^+(\mathrm{MX})\,T^{1/4}]$ *vs.* $1/T$) owing to Eqs. 41 and 42, respectively, yield straight lines except in T_M so long as ϕ is constant in the temperature range covered in a run. The gradients of the plots are equal to $-(0.434/R)\times\Delta H_1$ and $-(0.434/R)(\Delta H_1+\Delta H_2)/2$ in the ranges T_H and T_L, respectively. Similarly the gradients in the case α^+(MX)$\gg$1 are constant for a constant value of ϕ and are equal to null and $-(0.434/R)\,\Delta H_2/2$ in T_H and T_L, as may be proved from Eqs. 38 and 39, respectively. In any case, therefore, the gradient of an emission plot ($\log[i^+(\mathrm{MX})\,T^n]$ *vs.* $1/T$ where n=0, 1/4, or 1/2) is never equal to $-(0.434/R)\,\Delta H_2$ in any temperature range. If $\log[i^+(\mathrm{MX})\,T^{1/2}/F(T)]$ instead of $\log[i^+(\mathrm{MX})\times T^{1/2}]$ is plotted against $1/T$, on the other hand, a straight line is obtained even in T_M when ϕ is constant, and its gradient is equal to $-(0.434/R)\,\Delta H_2$, as may readily be concluded from Eq. 35. In a similar way, straight lines with a different slope are obtained in T_H and T_L if $\log[i^+(\mathrm{MX})/G(T)]$ and $\log[i^+(\mathrm{MX})\,T^{1/4}/G(T)^{1/2}]$ are plotted against $1/T$ according to Eqs. 45 and 46, respectively. For making the plots, however, the accurate values of N(MX), ΔH_2, $\Delta S°$(MX), and $\Delta S°$(M) and of ΔH_1 and $\Delta S°$(M) are required to evaluate $F(T)$ and $G(T)$, respectively.

These characteristics of the above various emission plots should be taken into consideration when an experiment of molecular beam surface ionization is made to confirm the present theory or to determine ϕ, I(M), or D(MX).

Experimental Confirmation of the Present Theory. In this section the conclusions derived theoretically in this work will be compared with experimental results obtained by other workers in order to verify the present theory.

When α^+(MX) is much larger than unity and also γ(MX) is essentially unity, β^+(MX) defined by Eq. 21 is virtually unity and hence i^+(MX) is independent of T, just as concluded by Eq. 38. This conclusion may be supported strongly by the experimental result that i^+(MX) is essentially constant in a high temperature region when a molecular beam of alkali halide (KCl,

KBr, KI, or CsCl) impinges upon a surface of Re[13] or Pt.[20]

In the cases other than both $\alpha^+(MX)\gg1$ and $\gamma(MX)\approx1$, the characteristics of the plots described in the preceding section may afford a quite simple method to experimentally confirm the present theory. Namely, the gradient determined experimentally under a certain condition (*e.g.*, $\alpha^+(MX)\gg1$ and $\gamma(MX)\ll1$) may be expected virtually equal to the value (*e.g.*, $-(0.434/R)\,\Delta H_2/2$) predicted by the corresponding theoretical conclusion (*e.g.*, Eq. 39).

When atomic and molecular beams including a common alkali element (Li, Na, or K) impinges separately upon the same polycrystalline surface (Re, Ir, or Pt), the temperature dependence of $i^+(MX)$ shows a strong resemblance to that of $i^+(M)$ in a region above a certain temperature (T_C).[20-22] A similar result is obtained with potassium halide–tungsten systems.[23] These results may suggest with the region that (a) $\gamma(MX)$ is approximately unity, (b) the temperature dependence of both $i^+(MX)$ and $i^+(M)$ is governed by the common Boltzmann factor including ΔH_1, and hence (c) $i^+(MX)$ is expressed by Eq. 41 or 45 at $T\gtrsim T_C$. Below T_C, on the other hand, a large difference in temperature dependence appears between $i^+(MX)$ and $i^+(M)$, and this difference is concluded to arise from incomplete dissociation of MX.[21,22] Unfortunately the experimental data reported in Refs. 20—23 are not available enough to obtain a definite answer to the question whether the gradient of the emission plot such as $\log[i^+(MX)\ T^{1/2}/F(T)]$ *vs.* $1/T$ or $\log[i^+(MX)\ T^{1/4}]$ *vs.* $1/T$ is equal to that predicted by the present theory. Firstly because the accurate value of ϕ below T_C is unknown, and secondly because the quantitative relation between $i^+(MX)$ and T in each run is not described in detail but is shown roughly in a figure where a relative value of $i^+(MX)$ is plotted against T. In addition, the comparison of T_C with $T_{0.95}$ is not useful for confirming experimentally the present theory because there is no evidence that the value of ϕ in the ranges both above and below T_C is constant and also identical between the atomic and molecular beam surface ionizations. The workers[20-23] have neither employed single crystal surfaces nor tried to plot $\log[i^+(MX)\ T^n]$ against $1/T$ for each of the sample–surface systems under study. Accordingly, they seem to have eliminated the possibility of finding the following consequences (a)—(c); when ϕ remains unchanged in the whole temperature range investigated in a run, (a) the plot shows a line having constant, inconstant, and constant gradients in the high, middle, and low temperature regions (T_H, T_M, and T_L), respectively, and hence (b) the quantitative expression of $i^+(MX)$ changes according to the condition $\gamma(MX)\gtrsim0.95$, $0.95>\gamma(MX)>0.098$, or $\gamma(MX)\lesssim0.098$, and also (c) the boundary temperatures ($T_{0.95}$ and $T_{0.098}$) depend largely upon $D(MX)$ and $N(MX)$ in the case $\alpha^+(MX)\ll1$ but strongly upon ΔH_2 and $N(MX)$ in the case $\alpha^+(MX)\gg1$.

It should be emphasized that a clean surface of single crystal is homogeneous with respect to ϕ and that the value of ϕ effective for thermal positive ion emission is equal to that for thermal electron emission, in contrast to a polycrystalline surface.[8,12,17,24] Therefore, the possible dependence of ϕ upon T during sample beam incidence upon the single crystal surface under study may be checked definitely by monitoring electron emission current soon after and/or before running positive surface ionization. In other words, the value of ϕ or its change may be determined from a Richardson plot without depending upon any datum obtainable from a Saha-Langmuir plot. This merit of single crystal over polycrystal may be quite helpful for confirming experimentally the theoretical predictions made in this work.

In conclusion, none of the published experimental data that are known to the present authors is available for confirming sufficiently the present theory as to the temperature dependence of $i^+(MX)$ especially in the region $T<T_{0.95}$.

Conclusions

The theoretical investigation described above may be summarized as follows:

(1) In usual positive surface ionization where $N(MX)$ is kept constant during the study of temperature dependence, the quantitative expression of $i^+(MX)$ varies according to the values of both $\gamma(MX)$ and $\alpha^+(MX)$, and hence to the temperature region T_L, T_M, or T_H.

(2) When $\alpha^+(MX)\gg1$ and also $\gamma(MX)\ll1$, $i^+(MX)$ is a function of both $T^{-1/4}$ and the Boltzmann factor, the numerator of which is not $-\Delta H_2$ but $-\Delta H_2/2$. Consequently, the gradient of an emission plot ($\log[i^+(MX)\ T^{1/4}]$ *vs.* $1/T$) in the region T_L is equal to $(0.434/R)\{\phi - I(M) - D(MX)\}/2$.

(3) In such a high temperature region that $\gamma(MX)$ may be estimated to be essentially unity, it is not ΔH_2 but ΔH_1 that is included in the Boltzmann factor governing the production of M^+ from MX, and hence temperature dependence of $i^+(MX)$ is essentially the same to that of $i^+(M)$ when ϕ is virtually identical between the atomic and molecular beam surface ionizations under study.

(4) When both $\alpha^+(MX)\ll1$ and $\gamma(MX)\ll1$, $i^+(MX)$ is proportional to both $T^{-1/4}$ and the Boltzmann factor, the numerator of which is neither $-\Delta H_1$ nor $-\Delta H_2$ but is $-(\Delta H_1+\Delta H_2)/2$. In consequence, the gradient of a plot ($\log[i^+(MX)\ T^{1/4}]$ *vs.* $1/T$) is equal to $(0.434/R)\times\{\phi - I(M) - D(MX)/2\}$.

(5) When neither $\gamma(MX)\approx1$ nor $\gamma(MX)\ll1$, $i^+(MX)$ cannot be expressed by a simple equation, and a plot ($\log[i^+(MX)\ T^{1/2}]$ *vs.* $1/T$) does not show a straight line in the region T_M even if $\alpha^+(MX)\gg1$ or $\alpha^+(MX)\ll1$.

(6) When neither $\alpha^+(MX)\gg1$ nor $\alpha^+(MX)\ll1$, $i^+(MX)$ is not expressed in a simple form, and hence the gradient of a plot ($\log[i^+(MX)\ T^n]$ *vs.* $1/T$ where $n=0$, 1/2, or 1/4) is not constant in any temperature region (T_H, T_M, or T_L).

(7) Under any condition the gradient of a plot ($\log[i^+(MX)\ T^n]$ *vs.* $1/T$) is never equal to $-(0.434/R)\times\Delta H_2$.

(8) Under the condition that (a) $\alpha^+(MX)\gg1$ and

$\gamma(MX) \ll 1$, (b) $\alpha^+(MX) \ll 1$ and $\gamma(MX) \approx 1$, or (c) $\alpha^+(MX) \ll 1$ and $\gamma(MX) \ll 1$, either ϕ or $I(M)$ can be determined from the gradient (G) of a plot ($\log[i^+(MX) \times T^n]$ *vs.* $1/T$) while such a determination in atomic beam surface ionization is available only at $\alpha^+(M) \ll 1$. Determination of $D(MX)$ from G, however, can be made under the condition (a) or (c) alone.

(9) For $\alpha^+(MX) \ll 1$, $\gamma(MX)$ is essentially independent of the value of $\alpha^+(MX)$. In any other cases, however, $\gamma(MX)$ increases with increase in $\alpha^+(MX)$.

To the best of the present authors' knowledge, neither theoretical nor experimental investigation arriving at the above conclusions (1)—(9) except (3) has yet been carried out.

The present work was supported by a Grant-in-Aid for Scientific Research No. 364150 from the Ministry of Education, Science and Culture.

References

1) N. I. Ionov, "Progress in Surface Science," ed by S. G. Davison, Pergamon Press, Oxford (1972), Vol. 1, Part 3, pp. 237—354.
2) M. Kaminsky, "Atomic and Ionic Impact Phenomena on Metal Surfaces," Springer-Verlarg, Berlin (1965), pp. 98—141.
3) J. M. Zinkiewicz, *Ann. Univ. Mariae Curie-Sklodowska, Sec. AA*, **23**, 135 (1968).
4) N. I. Ionov and M. A. Mittsev, *Zh. Eksp. Teor. Fiz.*, **38**, 1350 (1960).
5) S. D. Dey and S. B. Karmohapatro, *J. Phys. Soc. Jpn.*, **22**, 682 (1967).
6) M. D. Scheer and J. Fine, *J. Chem. Phys.*, **50**, 4343 (1969).
7) M. A. Mittsev and N. I. Ionov, *Zh. Tekh. Fiz.*, **37**, 2229 (1967).
8) É. Ya. Zandberg and A. Ya. Tontegode, *Zh. Tekh. Fiz.*, **35**, 325 (1965).
9) F. L. Reynolds, *Surf. Sci.*, **14**, 327 (1969).
10) H. Kawano, *Shinkū*, **22**, 346 (1979).
11) H. Kawano, "Advances in Mass Spectrometry," ed by A. Quayle, Heyden and Son, London (1980), Vol. 8A, pp. 255—261. Erratum; the figure 0.05 with respect to γ should be read 0.098.
12) H. Kawano, *Shitsuryō Bunseki*, **26**, 147 (1978).
13) A. Persky, E. F. Greene, and A. Kuppermann, *J. Chem. Phys.*, **49**, 2347 (1968).
14) É. Ya. Zandberg, A. Ya. Tontegode, and F. K. Yusifov, *Fiz. Tverd. Tela*, **12**, 1740 (1970).
15) É. F. Chaikovskii, L. G. Mel'nik, and G. M. Pyatigorskii *Zh. Tekh. Fiz.*, **40**, 225 (1970).
16) F. L. Reynolds, *J. Chem. Phys.*, **39**, 1107 (1963).
17) É. Ya. Zandberg and A. Ya. Tontegode, *Fiz. Tverd. Tela*, **12**, 1124 (1970).
18) D. R. Stull and H. Prophet, "JANAF Thermochemical Tables," 2nd ed, National Bureau of Standards, Washington (1971).
19) V. I. Vedeneyev, L. V. Gurvich, V. N. Kondrat'yev, V. A. Medvedev, and Ye. L. Frankevich, "Bond Energies, Ionization Potentials, and Electron Affinities," Edward Arnold, London (1966).
20) É. Ya. Zandberg and A. Ya. Tontegode, *Zh. Tekh. Fiz.*, **38**, 763 (1968).
21) É. Ya. Zandberg and A. Ya. Tontegode, *Zh. Tekh. Fiz.*, **35**, 1115 (1965).
22) É. Ya. Zandberg and A. Ya. Tontegode, *Zh. Tekh. Fiz.*, **37**, 2101 (1967).
23) N. I. Ionov, *Zh. Tekh. Fiz.*, **26**, 2200 (1956).
24) H. Kawano, *Shinkū*, **23**, 1 (1980).

Electrochemical Fixation of Molecular Nitrogen on p-Type Gallium Phosphide Photocathode

Masashi KOIZUMI, Hiroshi YONEYAMA,* and Hideo TAMURA

Department of Applied Chemistry, Faculty of Engineering, Osaka University, Yamadakami, Suita, Osaka 565

(Received September 11, 1980)

Electrochemical fixation of molecular nitrogen to ammonia and hydrazine at p-type GaP photocathodes was studied in nonaqueous electrolytes containing either one of titanium tetraisopropoxide, titanium trichloride, vanadium trichloride, or chromium trichloride and a trace amount of water. Positive evidences for the nitrogen fixation were obtained in these electrolytes, but the current efficiency was quite low, and usually less than 1%. It is suggested from the present study that there are a variety of choices of electrolyte systems for the nitrogen fixation.

The fixation of molecular nitrogen to ammonia and hydrazine under mild ambient conditions has been an important subject in chemical research fields. The most intensive studies have been done on nitrogen fixation *via* nitrogen complexes, which are summarized in a recent review.[1]

The fixation of N_2 by a photoelectrochemical process was reported in 1978 by Dickson and Nozik,[2] who used an electrolyte system reported by Van Tamelen and his coworkers,[3-5] *i.e.*, titanium tetraisopropoxide in 1,2-dimethoxyethane(glyme) which was originated from previous studies on nitrogen fixation *via* nitrogen metallo-organic complexes.[3] An essential component of the electrolyte is judged to be titanium tetraisopropoxide which can bind and ionize N_2 when reduced to a divalent species in the course of the electrolysis. Electrochemical fixation of N_2 was also reported to be possible if N_2 is subjected to a silent discharge prior to bubbling into aqueous electrolytes of sulfuric acid or potassium hydroxide,[6] but this approach should be excluded from nitrogen fixation under mild conditions.

It is known from redox potentials of $Ti^{3+/4+}$ and $Ti^{2+/0}$ in aqueous solutions[7] that Ti(II) is a strong reducing agent. The Ti(II) species originated from titanium tetraisopropoxide in glyme must also have a high reducing power. The idea has then developed that from an electrochemical point of view the chemical species having a reducing power comparable to that of the Ti(II) species may work effectively to fix N_2. We tested Cr(II), V(II) as well as Ti(II), and found that nitrogen fixation is possible on illuminated p-type GaP cathodes with assistance of these reducing agents. Although obtained current efficiencies for the nitrogen fixation were very low, the results obtained in the present study suggested that there are a variety of choices of solvent–electrolyte systems to fix N_2 by the photoelectrochemical process.

Experimental

1,2-Dimethoxyethane (glyme), propyrene carbonate (PC), methanol, acetonitrile, and *N,N*-dimethylformide (DMF) were chosen as the solvent of electrolytes into which $AlCl_3$ as an indifferent electrolyte and either one of the redox agents, $Ti[OCH(CH_3)_2]_4$, $TiCl_3$, VCl_3, or $CrCl_3$ were dissolved. In the case $CrCl_3$, $CrCl_2$ was also dissolved in a small amount to raise its solubility. We arbitrarily chose the concentration of the redox agent to be 10 mmol per 50 ml of the solvent. However, the solubility was often found to be too low to satisfy this standard, necessitating the use of a much lower concentration. The solubility of $AlCl_3$ was also often too low in the presence of the redox agents of the chloride form to dissolve 15 mmol to 50 ml of the redox solutions. Among the solvents used, PC, with which major experiments of the present study were carried out, was purified first by passing through molecular sieve 3A columns, then by twice distillation under 5—10 mmHg (1 mmHg=133.332 Pa). Methanol and acetonitrile were distilled before use. The other solvents were used without purification of commercially available reagent grade chemicals.

An Al plate and a p-type GaP wafer were used as an anode and a cathode, respectively. The preparation of the GaP cathode, the area of which was *ca.* 0.5 cm^2, was already reported.[8] The electrolytic cell made of quartz was equipped with a water cooled jacket, gas inlet and outlet. The electrode was set in a sealed cell with a silicone rubber stopper which positioned *ca.* 2 cm above the electrolyte. An electrolyte bridge was inserted into the electrolytic cell through the stopper from an air-tight another cell which was filled with the same electrolyte. An electrical connection between the latter cell and an SCE reference was made by using a salt bridge. By placing the one more cell between the electrolytic cell and the reference electrode, probable contamination from the reference electrode was believed to decrease.

All the insertion points of the stopper were sealed with silicone rubber cement to keep the cell assembly air-tight. N_2 was bubbled into the electrolyte after purification with a flow rate of *ca.* 5 ml/min. The purification was done by successively passing N_2 through an alkaline pyrogallol solution, sulfuric acid, water, a column packed with $CaCl_2$ and a column packed with silica gel. Prior to flowing into the electrolyte, the nitrogen gas was pre-saturated with the same solvent as used in the electrolyte. The effluent gas from the cell was passed through a 0.05 mmol dm^{-3} H_2SO_4 trap before exiting to atmospheres. Light from an 1 kW xenon lamp was focused to a diameter of *ca.* 15 mm by using a glass lenz, by which light of wavelengths longer than 350 nm struck on the electrolytic cell. The intensity of the beam was *ca.* 2 W, as determined by a power meter (Coherent Radiation, model 201), and water at room temperatures was flowed through the water-cooled jacket to prevent evaporation of the electrolyte.

Ammonia was analyzed by the method of Kruse and Mellon.[9] Both the electrolyte and the acid trap was analyzed. For this purpose, the electrolyte was protonated with 20 ml of 0.05 mol dm^{-3} H_2SO_4 under air-tight conditions. A known portion of the solution was subjected to distillation in a micro-Kjeldahl apparatus after adding 10 ml of 30% NaOH to the acidified solution. The ammonia in the distillates was collected in 0.05 mol dm^{-3} H_2SO_4, and its amount was determined. The solution in the acid trap was also subjected to the almost same distillation. Hydrazine was determined for the protonated electrolyte solutions. By adding 30% NaOH

to the acidified solution, metal salts in the solution precipitated. After the filtration, the hydrazine in the filtrate was determined with *p*-dimethylaminobenzaldehyde.[10]

The current efficiency η for the formation of NH_3 and N_2H_4 was determined by using Eq. 1;

$$\eta = \frac{\text{Moles of } NH_3(N_2H_4) \text{ produced}}{\dfrac{\text{Coulombs consumed in the electrolysis}}{69480 \times 3\,(4)}}. \quad (1)$$

Results and Discussion

Ammonia Production in Glyme Containing Three Different Redox Agents. In order to investigate whether or not the combination of glyme and titanium tetraisopropoxide is essential as the electrolyte solution to fix N_2 to NH_3, glyme solutions containing $TiCl_3$ and VCl_3 were tested. Current-potential curves of the Al anode and the p-type GaP cathode are shown in Fig. 1, from which it is shown that the onset potential of the anode was negative of that of the illuminated cathode, indicating that photoelectrochemical cells can be constructed. The principal anodic reaction is the dissolution of Al, and the oxidation of the reduced form of the redox electrolyte, which is produced at the illuminated cathode as its main reaction, must be superposed on the dissolution reaction of the anode. The main reaction at the individual electrode is then given by Eqs. 2 and 3;

$$\text{Al anode: } Al = Al^{3+} + 3e^- \quad (2)$$

$$\text{p-type Gap cathode: } 3Ox + 3e^- = 3R \quad (3)$$

where Ox and R represent an oxidant and a reductant of a redox couple, respectively. When the photoelectrochemical cell was operated under short-circuited conditions, the initial photocurrent usually decreased with illumination time, suggesting that the electrode potential of the p-type GaP cathode varied under the short-circuited conditions. In order to eliminate ambiguities introduced by such a nonsteady behavior of photocurrents, experiments were carried out under potentiostatic control.

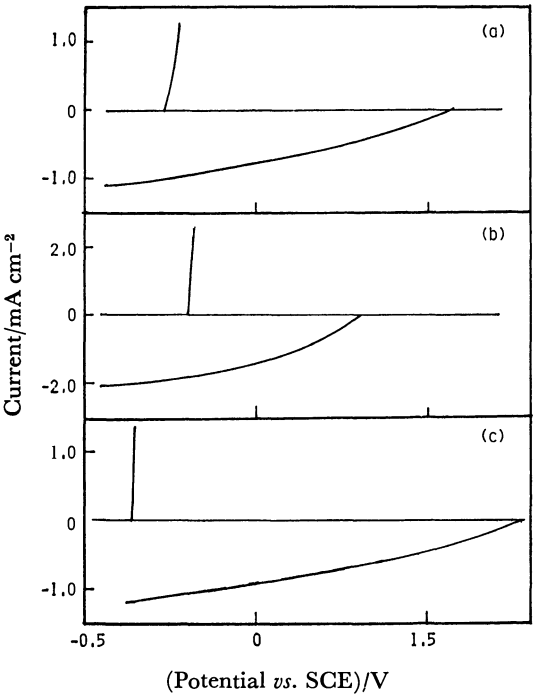

Fig. 1. Current-potential curves for photoelectrochemical cells using an Al anode and a p-type GaP cathode in three kinds of glyme solutions. Electrolyte; (a): 0.5 mol dm^{-3} $Ti[OCH(CH_3)_2]_4$ and 0.75 mol dm^{-3} $AlCl_3$, (b): 0.2 mol dm^{-3} $TiCl_3$ and 0.3 mol dm^{-3} $AlCl_3$, and (c): 0.07 mol dm^{-3} VCl_3 and 0.06 mol dm^{-3} $AlCl_3$.

Table 1 shows results obtained in glyme solutions. In the first row of the table, the results for titanium tetraisopropoxide are given. This electrolyte was already used by Dickson and Nozik.[2] The results for $TiCl_3$ and VCl_3 electrolytes are shown in the second and third rows, from which it is known that ammonia is produced in these electrolytes with a rate almost comparable to that in the titanium tetraisopropoxide electrolyte. Since there is no doubt concerning nitrogen fixation with the electrolyte of glyme–titanium tetraisopropoxide,[2] the glyme–$TiCl_3$ and glyme–VCl_3 electrolytes must also be effective for nitrogen fixation, even though the produced amount was very tiny.

The current efficiency for the formation of ammonia was quite low for all the glyme solutions used. A large fraction of the charge given in the table must have been consumed to reduce the oxidizing agents of the redox couples, *i.e.*, Ti(III) to Ti(II) for $TiCl_3$, V(III) to V(II) for VCl_3, and Ti(IV) to Ti(II) *via* Ti(III) for titanium tetraisopropoxide. If a Pt cathode was used instead of the p-type GaP, no fixation of N_2 was found to occur, as shown in the fourth row of Table 1, suggesting that photosensitization seems to be important for nitrogen fixation.

Nitrogen Fixation Using a Variety of Redox Solutions. In order to catch information on whether or not glyme is essential as the solvent of electrolytes, $TiCl_3$ solutions in different media were tested. As the media, aqueous 0.05 mol dm^{-3} H_2SO_4, methanol and PC were chosen. Results obtained for these electrolytes are shown from the second to fourth rows of Table 2. In the case of the aqueous electrolyte, the hydrogen evolution preferen-

Table 1. Fixation of N_2 at p-type GaP cathode in glyme containing redox agents

Redox species	Its concn M[a]	$AlCl_3$ (M)	Onset potential *vs.* SCE V		Electrolysis potential *vs.* SCE V	Charge C	NH_3 produced mol	Current eff. %
			Anode	Cathode				
$Ti[OCH(CH_3)_2]_4$	0.5	0.75	−0.27	0.59	−0.2	45.5	0.80	0.51
$TiCl_3$	0.2	0.3	−0.3	0.3	−0.3	62.8	1.98	0.91
VCl_3	0.07	0.06	−0.36	0.8	−0.3	60.4	0.97	0.46
VCl_3[b]	0.07	0.06	−0.8	−0.1	−0.3	60.6	0	0

a) 1 M=1 mol dm^{-3}. b) A Pt cathode was used intead of the p-type GaP.

TABLE 2. FIXATION OF N_2 ON p-TYPE GaP CATHODE IN SEVERAL REDOX SOLUTIONS

Electrolyte: Medium (50 ml)	Redox species	Its amount / mmol	$AlCl_3$ (mmol)	Onset potential *vs.* SCE / V: Anode	Onset potential *vs.* SCE / V: Cathode	Electrolysis potential *vs.* SCE / V	Charge / C	Amount fixed / μmol: NH_3	Amount fixed / μmol: N_2H_4	Current eff. / %: NH_3	Current eff. / %: N_2H_4
Glyme	$TiCl_3$	10	15	−0.3	0.3	−0.3	62.8	1.98	u.d.	0.91	u.d.
0.05 M H_2SO_4	$TiCl_3$	25	37.5	−1.0	0	−0.3	71.3	0.0	u.d.	0	u.d.
Methanol	$TiCl_3$	10	15	−1.16	0.24	−0.5	14.9	0.20	u.d.	0.39	u.d.
PC	$TiCl_3$	3	4.5	−0.3	0.4	−0.3	44.5	0.45	0.16	0.29	0.13
PC	VCl_3	5	7.5	−0.25	0.5	−0.2	77.7	0.26	u.d.	0.10	u.d.
PC	$CrCl_3$+ $CrCl_2$	10 1	15	−0.3	0.5	−0.3	26.8	0.24	0.08	0.26	0.12
DMF[a)]	$CrCl_3$+ $CrCl_2$	5 0.5	7.5	−1.0	0.0	−0.5	54.0	0.19	0.0	0.034	0.0
CH_3CN[a)]	VCl_3	*ca.* 8 (saturated)	*ca.* 8	−0.43	0.62	−0.5	7.2	0.14	u.d.	0.19	u.d.

a) Only NH_3 and N_2H_4 trapped in a 0.05 mol dm^{-3} H_2SO_4 trap were determined.

tially took place, as judged from occurring no color change of the electrolyte, resulting in no nitrogen fixation. On the other hand, methanol and PC solutions containing $TiCl_3$ were found to be effective for nitrogen fixation, although the current efficiencies of these electrolytes were very low. In these electrolytes, the color of electrolytes which are characteristics of dissolved Ti(III) were gradually changed in the course of electrolysis. Then, the suggestion was given that the divalent state of the redox agents is necessary for nitrogen fixation to occur. When analyses of hydrazine were made for a $TiCl_3$–PC solution, a positive result for its formation was obtained, as shown in Table 2. It is known from positive results on nitrogen fixation in glyme, methanol and PC solutions that the nature of the solvent does not play a primarily important role in determining whether or not nitrogen fixation takes place.

The results mentioned above give the suggestion that there are a variety of choices for combinations of solvents and electrolytes to fix N_2 in photoelectrochemical processes at p-type GaP cathodes. In order to have experimental evidences for this, additional experiments were performed. Results obtained are summarized from the fifth to eighth rows of Table 2. In the cases of DMF and acetonitrile solutions, it was found that these solvents brought about errors in the determined amounts of NH_3 in the distillates due to contribution of nitrogen originated from the solvent molecules. By this reason, the results for these solutions were obtained only for the acid trap. It is noticed from the obtained results that nitrogen fixation is possible in all the nonaqueous electrolytes tested.

Effects of the Concentration of Electrolyte on Nitrogen Fixation. The current efficiency for the formation of ammonia was investigated as a function of the electrolyte concentration. PC was chosen as the solvent and $TiCl_3$ and $AlCl_3$ as the electrolytes. The molar ratio of $TiCl_3$ to $AlCl_3$ was arbitarily fixed to 2/3. The electrolysis was conducted for 2 d at potentials almost equal to those obtained under short-circuited conditions of the photoelectrochemical cells, which were influenced by the electrolyte concentration as suggested in the captions of Fig. 2. Figure 2 shows the current efficiency for ammonia production (the ordinate in the left hand side) and photocurrents obtained in the initial stage of the electrolysis (the ordinate in the right hand side) as a function of the electrolyte concentration. The magnitude of the cathodic photocurrent in the initial stage of electrolysis was affected by the electrolyte concentration. The current value decreased gradually from those shown in this figure with polarization time probably due to some change in surface conditions of the electrode, as already mentioned. Nevertheless, Fig. 2 gives a strong suggestion that the current efficiency for ammonia production increases with decreasing the cathodic photocurrent.

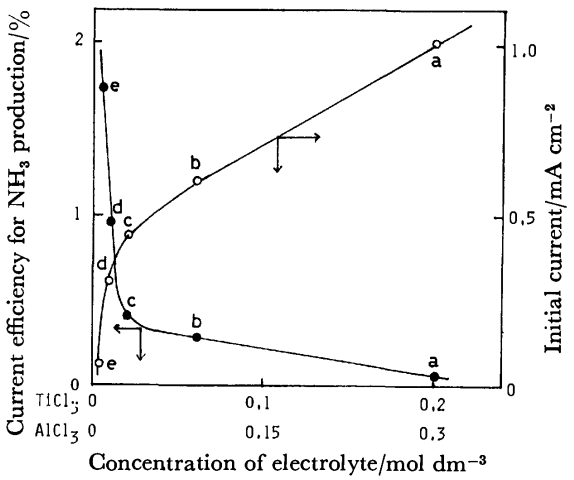

Fig. 2. Effects of the electrolyte concentration in PC solutions on the current efficiency for NH_3 production and initial photocurrent at the p-type GaP cathode at potentials close to those obtained under short-circuited conditions. The potential (V *vs.* SCE); a: −0.3 V, b: −0.3 V, c: −0.2 V, d: −0.2 V, and e: −0.5 V.

Such a dependency of the current efficiency for ammonia production on the magnitude of cathodic photocurrent will be obtained if either one of the following conditions is fulfilled. (1) N_2 is easily reduced but its solubility is so low that the rate of N_2 reduction is determined by mass transport control of N_2. Since the photocurrent is increased with an increase in the electrolyte concentration due to high reducibility of the redox agents, the current efficiency is decreased with

increasing the electrolyte concentration. (2) The concentration of N_2 in the electrolyte is relatively high, but the amount of reducible N_2, which may be bound to the reduced form of the redox agents, is quite low so that the supply of the reducible N_2 to the electrode is limited. In this case, the current efficiency depends on the electrolyte concentration as in the case (1). (3) The rate of the electrochemical reduction of N_2 is quite low and hence almost fixed at a fixed polarization potential regardless of the electrolyte concentration. Since the photocurrent is increased with increasing the electrolyte concentration, the current efficiency decreases in the electrolyte concentration.

No one will believe that the first case is valid. It is well known that nitrogen molecuoes are very stable. Furthermore, it was ascertained that the concentration of dissolved N_2 in the electrolyte was in a range of that usually chosen in kinetic studies of electroactive species. For example, a gas chromatographic analysis of N_2-saturated PC, which was carried out by using a molecular sieve 5A column at 180 °C, showed that the solubility of N_2 is 5.6 mmol dm^{-3}. Such a solubility will be high enough to give an photocurrent of an order of mA cm^{-2} if N_2 were easily reduced, as judged from the reduction of oxygen in aqueous solution which has a comparable solubility, *i.e.*, *ca.* 12 mmol dm^{-3}. As a result, if the case (1) is valid, a much larger current efficiency should be obtained.

As already shown above, V(II), Ti(II), and Cr(II) can assist the reduction of N_2 at illuminated GaP cathodes. This seems to imply that there is some interaction of N_2 with the reduced form of the redox agents. However, the interaction will not be so high as to destroy the N–N bond in a nitrogen molecule, because if the bond breaking would occur, no photosensitization at the GaP cathode would be required for nitrogen fixation. In order to investigate whether or not the case (2) is the most important rate controlling factor, experiments were carried out in electrolytes containing a relatively high amount of the reducing agents. The amount of N_2 bound to the reduced form of the redox agents, if any, must be proportional to the concentration of the reducing agent. If the case (2) is valid, therefore, the current efficiency will be high for an electrolyte rich in the reductant. The experiments were carried out in $AlCl_3$–PC solutions into which either $TiCl_3$ or VCl_3 was dissolved, and the solutions were pre-electrolyzed by using an Al anode and a Pt or an illuminated p-type GaP cathode to prepare Ti(II) or V(II) in the solutions. When the GaP cathode was used, the pre-electrolysis was conducted under Ar atmospheres. By the pre-electrolysis, the electrolytes changed their color, indicating that the reduced form of the redox agents became rich. At this stage, the p-type GaP cathode was polarized under illumination in the prepared electrolytes into which N_2 was continuously bubbled. Results obtained in these experiments are shown in Table 3. According to this table, the current efficiency for production of ammonia was not increased by the pre-electrolysis of the electrolytes, suggesting that the concentration of N_2 bound to the reductant, if any, does not affect significantly on the reduction of N_2. It follows then that the case (3) seems to be most probable as the rate controlling factor for the electrochemical reduction of N_2.

Effects of Water as an Impurity in the Electrolyte on the Production of Ammonia. As a proton source of the ammonia formation, attention was focused to water dissolved in the electrolytes. It was shown by the Karl-Fischer titration method that $TiCl_3$–PC solutions contained 0.29 mg of water for 1 ml of 0.02 mol dm^{-3} $TiCl_3$ and 0.20 mg for the same volume of 0.01 mol dm^{-3} $TiCl_3$. These contents correspond to the water concentration of 0.016 and 0.011 mol dm^{-3}, respectively. If 1 ml of water was intentionally added to 50 ml of the solution, the water concentration increased to 1.1 mol dm^{-3}. According to results obtained by using these aquated PC solutions, the current efficiency was found to be influenced by the water content and was high for solutions of high concentrations, as Table 4 shows. However, it was found that by adding water to PC solutions, the chloride salts in the electrolyte were hydrolyzed, giving rise to precipitates. As a result, the conductivity of solutions decreased. By this reason, more negative potentials were chosen for the electrolysis of the intentionally aquated solutions. Nevertheless, the initial current for the electrolysis was still small compared to that obtained for solutions of no intentional water. As already shown in Fig. 2, the current efficiency for nitrogen fixation was increased by decreasing the current density for electrolysis. Therefore, the enhancement of the current efficiency by introducing water into PC solutions may be ascribable at least in part to the decreasing effect of the current density. Although a simple conclusion may not be drawn from the results given in Table 4, it will be of no doubt that a trace amount of water in the electrolyte can act as a proton source for nitrogen fixation.

Table 3. Fixation of N_2 in electrolytes containing relatively high amount of reducing agents[a)]

Redox species	Its amount / mmol	$AlCl_3$ (mmol)	Preelectrolysis[b)] Potential *vs.* SCE / V	Preelectrolysis[b)] Charge / C	Electrolysis Potential *vs.* SCE / V	Electrolysis Charge / C	NH_3 (μmol)	Current eff. / %
VCl_3	5	7.5	−0.2 (GaP)	19.4	−0.2	4.85	0.12	0.60
$TiCl_3$	1	10	−1.0 (Pt)	172	−0.3	37.8	0.13	0.10
VCl_3	1	5	−0.4 (Pt)	100.5	−0.4	2.36	0.05	0.59

a) The solvent of all the electrolytes was PC. b) The pre-electrolysis was carried out by using an Al anode and a Pt or an illuminated p-type GaP cathode. In the case of the GaP cathode, the pre-electrolysis was conducted under Ar atmospheres.

Table 4. Effects of water on ammonia production at p-type GaP cathode in PC solutions

$TiCl_3$ (M)	$AlCl_3$ (M)	H_2O (M)	Onset potential *vs.* SCE / V: Anode	Onset potential *vs.* SCE / V: Cathode	Electrolysis potential *vs.* SCE / V	Initial current / μA cm^{-2}	Charge / C	Amounts of NH_3 produced / μmol	Current eff. / %
0.02	0.03	0.016	−0.27	0.45	−0.2	430	17.9	0.24	0.39
0.02	0.03	1.1	−0.8	0.4	−0.5	200	14.3	0.27	0.55
0.01	0.015	0.011	−0.2	0.8	−0.2	300	4.6	0.15	0.94
0.01	0.015	1.1	−0.77	0.3	−0.7	110	3.72	0.19	1.48

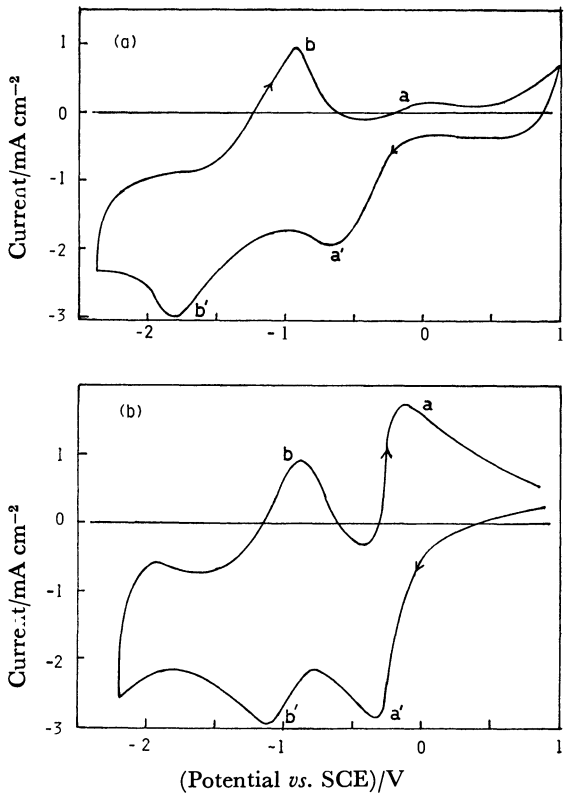

Fig. 3. Voltammograms at a Pt electrode at 0.2 V/s for two kinds of redox electrolytes. (a): PC containing 0.1 mol dm^{-3} VCl_3 and 0.5 mol dm^{-3} $LiClO_4$, (b): PC containing 0.05 mol dm^{-3} $TiCl_3$ and 0.05 mol dm^{-3} $LiClO_4$. The couple of waves a and a' are related to the redox reaction of M(III)/M(II), and those of b and b' to the reaction of M(II)/M(0).

Peak Potentials of Redox Agents. Qualitative information on the reducing power of the redox agents used were compared by measuring peak potentials of voltammograms for the redox reactions at a Pt electrode. The electrolytes used contained not $AlCl_3$ but $LiClO_4$ as an indifferent electrolyte, being different from those used in the experiments of nitrogen fixation. If $AlCl_3$ was used, obtained voltammograms were ill-defined compared to those obtained in $LiClO_4$. By using $LiClO_4$ as the indifferent electrolyte, the obtained results may not directly be applicable to the electrolyte systems used for the experiments of nitrogen fixation, but qualitative information is believed to be still useful.

Two examples of voltammograms are shown in Figs. 3(a) and (b), which were obtained in VCl_3–PC and $TiCl_3$–PC solutions, respectively. The waves a and a' in these figures are connected to the redox reactions between the trivalent and divalent states, b' to the deposition of the metal ions of the divalent state, and b to the re-oxidation of the depositied metal to give dissolution. The voltammograms were also obtained for other electrolytes used in the experiments for nitrogen fixation at 0.2 V/s, and obtained results of peak potentials for individual redox reaction are collected in Table 5.

According to the obtained results, the separation between E_{pc} and E_{pa} is larger than that expected theoretically for a reversible system, which is 0.057 V,[12] suggesting that the value of the peak potentials are varied by the sweep rate chosen for all the electrolytes given in this table. Therefore, rigid comparison of the peak potentials with each other will be of no significance. However, if one assumes that the redox potentials will be obtained as average values of E_{pc} and E_{pa}, it becomes then possible to compare these values with

Table 5. Peak potentials of voltammograms for redox reactions used for nitrogen fixation experiments

Solvent	Redox agent	Its concn / M	(Peak potentials *vs.* SCE)/V[a)]: M(III)/M(II) E_{pc}	M(III)/M(II) E_{pa}	M(II)/M(0) E_{pc}	M(II)/M(0) E_{pa}
Glyme	$Ti[OCH(CH_3)_2]_4$	0.1	−0.65	−0.3	−1.5	−0.93
Glyme	$TiCl_3$	0.1	−0.65	0.05	n.d.[b)]	n.d.
CH_3OH	$TiCl_3$	0.1	−0.5	−0.08	n.d.	n.d.
PC	$TiCl_3$	0.05	−0.3	−0.1	−1.1	−0.8
Glyme	VCl_3	0.1	−0.7	−0.1	−1.45	−1.05
PC	VCl_3	0.1	−0.65	0	−1.8	−0.94
PC	$CrCl_3$	0.02	−0.45	−0.4	−1.4	n.d.

a) The electrolytes contained 0.5 mol dm^{-3} $LiClO_4$ except for glyme–$TiCl_3$ and glyme–VCl_3 where its concentration was 0.3 mol dm^{-3}. Sweep rate: 0.2 V/s. b) Not determined due to no appearence of the peak in the voltammogram. The cathodic current increased monotonically with increasing cathodic polarization in these cases.

one another. By such comparisons, it can be roughly said that the redox potential of Ti(III)/Ti(II) are not greately different among the kind of solvents chosen and that the reducing power of vanadium and chromium ions are also comparable to that of titanium ions. This observation seems to give a basis on the finding that nitrogen fixation occurs with almost the same degree in all the redox electrolytes given in Table 5.

Conclusion. It has been revealed from the present study that nitrogen fixation occurs when the following conditions are fulfilled. (1) Titanium, vanadium and chromium ions are in the divalent state. (2) The electrolytes contain a trace amount of water as an proton source. (3) The cathode can photosensitize the reduction reaction. The fact that the redox agent of a high reducing power is essential for nitrogen fixation seems to suggest that there is some interaction between the redox agent and nitrogen molecules before nitrogen is reduced, as already discussed above. Then the following schemes are evolved as the most probable path for nitrogen fixation.

$$M(III)(solv)_n \xrightarrow{+e^-} M(II)(solv)_n$$

$$M(II)(solv)_n \xrightarrow{+N_2} M(II)(solv)_n\cdots N_2$$

$$M(II)(solv)_n\cdots N_2 + 6H_2O \xrightarrow[\text{photosensitization}]{+6e^-,\ -6OH^-} M(II)(solv)_n + 2NH_3$$

where $M(III)(solv)_n$ and $M(II)(solv)_n$ represent solvated redox agents having trivalent and divalent states, respectively. The experimental results obtained in the present study were rather scattered, as noticed from comparison of the current efficiency for a variety of redox agents, but the scatters are believed to have been brought about partly by different experimental conditions such as different electrolyte and water concentrations and partly by errors in determination of the amounts of ammonia and hydrazine due to very small amounts of production of these substances. If these are taken into consideration, the results obtained in the present study will be much enough to suggest that there are a variety of choices of electrolyte systems for nitrogen fixation at illuminated p-type GaP cathodes.

The present study was supported by Grant-in-Aid for Scientific Research Nos. 412212 and 505008 from the Ministry of Education, Science and Culture.

References

1) J. Chatt, J. R. Dilworth, and R. L. Richards, *Chem. Rev.*, **78**, 589 (1978).
2) C. R. Dickson and A. J. Nozik, *J. Am. Chem. Soc.*, **100**, 8007 (1978).
3) E. E. Van Tamelen, *Acc. Chem. Res.*, **3**, 361 (1970).
4) E. E. Van Tamelen and D. A. Seeley, *J. Am. Chem. Soc.*, **91**, 5194 (1968).
5) E. E. Van Tamelen and B. J. Akermark, *J. Am. Chem. Soc.*, **90**, 4492 (1968).
6) K. Sasaki, T. Kihara, and H. Shiba, *J. Chem. Soc. Jpn.*, **89**, 1201 (1968).
7) M. Pourbaix, "Atlas of Electrochemical Equilibria in Aqueous Solutions," Pergamon Press, Oxford (1966), p. 214.
8) H. Yoneyama, S. Mayumi, and H. Tamura, *J. Electrochem. Soc.*, **125**, 68 (1978).
9) J. M. Kruse and M. G. Mellon, *Anal. Chem.*, **25**, 1188 (1953).
10) G. W. Watt and J. D. Chrisp, *Anal. Chem.*, **24**, 2006 (1952).
11) K. J. Vetter, "Elektrochemische Kinetik," Springer-Verlag, Berlin (1961), pp. 357—410.
12) D. D. Macdonalds, "Transient Techniques in Electrochemistry," Plenum Press, New York (1977), p. 185.

  Bull. Chem. Soc. Jpn., 54, 1688—1692 (1981) [Vol. 54, No. 6

Studies on Electrode Processes of Stabilized Zirconia Cell System by Complex Impedance Method

Jun SASAKI,* Junichiro MIZUSAKI, Shigeru YAMAUCHI, and Kazuo FUEKI

Department of Industrial Chemistry, Faculty of Engineering, The University of Tokyo, Hongo, Bunkyo-ku, Tokyo 113

(Received November 20, 1980)

Three kinds of materials, Pt, Ag, and $La_{0.5}Sr_{0.5}CoO_3$, were applied to stabilized zirconia as electrodes and the electrode behavior was investigated by means of the complex impedance method. The impedance arc due to the electrode/stabilized zirconia interface was always depressed semi-circles. Impedance behavior was strongly dependent on the electrode materials. Assuming that the impedance arc could be interpreted by a parallel *R-C* circuit, the interface resistance R_i and the interface capacitance C_i were determined. The apparent activation energy determined from the slope of the plots of log R_i *vs.* $1/T$ was nearly the same for the same electrode material. (Ag electrode: 92 kJ/mol and Pt electrode: 201 kJ/mol). The oxygen pressure dependence of C_i and R_i was also investigated. Although C_i was virtually independent of the oxygen partial pressure P_{O_2}, R_i was proportional to $P_{O_2}^{-2/3}$ for Ag electrodes and $P_{O_2}^{-1/4}$ for Pt electrodes. The rate-determining step was supposed to be the dissociation of oxygen molecules into atoms for Ag electrodes, and the dissociation of oxygen molecules or one of the subsequent steps for Pt electrodes.

The complex impedance method has been widely used to study the solid state cell systems.[1-8] This method provides an important tool for separating the impedance due to interfacial phenomena from that due to bulk properties of solid state cells.

So far, a lot of works have been carried out by this method to investigate the polarization processes at the stabilized zirconia/electrode interface.[1-7] However, results by different investigators were often inconsistent. This would be partly due to the scarcity of experimental evidence on the relationship between the interface behavior and electrode materials.

The purpose of the present study is to elucidate the influences of the nature of electrode materials on the polarization process by the complex impedance method.

Experimental

The electrolyte used in the experiments was 8 m/o yttria-stabilized zirconia disks supplied by Toray Industries, Inc. The diameter of the sample was 10 mm. Three different thickness, 1, 5, and 10 mm, were used in order to separate bulk properties from the interfacial ones of the stabilized zirconia cell. Both faces of stabilized zirconia disk were polished with No. 2000 emery paper and rinsed with alkaline cleaning solution.

The electrodes were prepared in various ways. Three kinds of electrode materials, Pt, Ag, and $La_{0.5}Sr_{0.5}CoO_3$ were applied to both faces of stabilized zirconia disks. The methods of preparation are listed in Table 1. Sputtered electrodes were prepared by means of RF sputtering (1500 V, 5×10^{-2} Torr† argon, 10—180 min) from a nominally pure foil of Pt or Ag. Evaporation was carried out by means of the electron beam melting furnace. Pt electrodes from H_2PtCl_6 were obtained by repeated application of H_2PtCl_6 aqueous solution subsequently followed by firing to drive off H_2O and Cl_2 gas. Pastes with glass flux were commercial materials from Tanaka-Matthey (Pt paste: 760A, Ag paste: FSP-306). Platinum paste without glass flux were prepared using Pt powder and an organic suspending medium. $La_{0.5}Sr_{0.5}CoO_3$ was prepared by mixing $La_2(CO_3)_3$, $SrCO_3$ and $CoCO_3$, and firing the mixture at 1100 °C for 8 h. $La_{0.5}Sr_{0.5}CoO_3$ thus obtained was then ground into powder and mixed with organic suspending medium. Then the paste of $La_{0.5}Sr_{0.5}CoO_3$ was applied on both faces of stabilized zirconia. Platinum gauze (200 mesh-cm^{-1}) connected with a Pt lead wire was dipped into the $La_{0.5}Sr_{0.5}CoO_3$ paste. Then, the paste was dried and fired at 1200 °C for 12 h. As current collectors, Ag gauze was used for Ag electrodes and Pt gauze for other electrodes. The gauze was pressed to electrodes by two very porous alumina disks to make sure the good contact.

Table 1. Electrode materials and method of preparation

Electrode material	Method of preparation
Platinum	Sputtering
	Evaporation
	Decomposition of H_2PtCl_6
	Paste with glass flux
	Paste without glass flux
Silver	Paste with glass flux
	Sputtering
$La_{0.5}Sr_{0.5}CoO_3$	Paste without glass flux

Measurements were made in the temperature ranges, 500—900 °C for the cells with Pt electrodes, 350—800 °C for those with Ag electrodes and 400—1200 °C for those with $La_{0.5}Sr_{0.5}CoO_3$ electrodes.

The complex impedance measurements were performed over the frequency range of 20 kHz to 5 Hz by means of a phase sensitive detector (Complex Impedance Meter 7010, Toho Technical Research Co.). In the frequency range from 1 Hz to 0.001 Hz Lissajous figure method was used. In this method the sine wave voltage was applied to the combination of the cell and a standard resistance in series by a sine wave generator (WAVETEK Model 184). The input and output signals were displayed simultaniously on an X-Y recorder, and the impedance of the cell was determined from the dimensions of Lissajous figures. The oxygen partial pressure (1—10^{-4} atm) was controlled by mixing oxygen and pure argon gas.

Results and Discussion

Effects of Electrode Materials on Interface Impedance.

Pt Electrode: Figure 1 gives the impedance plots of the specimens with various types of Pt electrodes measured

† 1 Torr = 133.322 Pa.

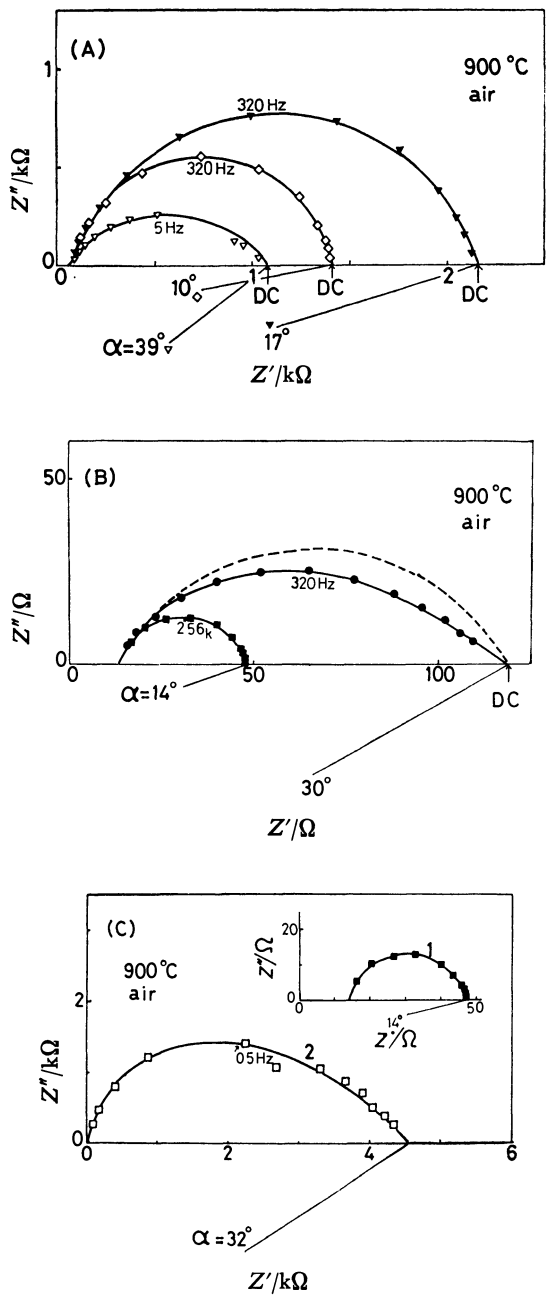

Fig. 1. Impedance plots of the cell with Pt electrodes. (A): ▼; evaporated Pt, ◇; sputtered Pt, ▽; Pt from H_2PtCl_6. (B): ●; Pt paste with glass flux, ■; Pt paste without glass flux. (C): Pt paste without glass flux, ■; before annealing at 1300 °C for 72 h, □; after annealing at 1300 °C for 72 h.

in air. Stabilized zirconia disks used were 5 mm in thickness. The semi-circular arc corresponds to the impedance at the electrode/stabilized zirconia interface. Figure 1(A) shows the impedance plots of specimens with Pt electrodes from evaporation, sputtering or decomposition of H_2PtCl_6. The centers of semi-circles are not on the real axis. Therefore, the results cannot be fully interpreted by an equivalent circuit of a parallel *R-C* combination. The depression angle α represents the deviation of the center of circle from the real axis. Two intercepts of the arc with the real axis give the resistivity of the equivalent circuit of the interface impedance.[1,2,10] The difference R_i between these intercepts is the sum of the interface resistances at cathode and anode. In the present study, the voltage applied to the electrode was kept below 10 mV in order to avoid non-linearity between the current and the overvoltage, and the polarization resistances at both electrodes are therefore supposed to be equal.

Figure 1(B) gives the impedance plots of specimens with Pt paste electrodes with or without glass flux. It is evident that glass flux depresses the impedance arc, especially in the right side of arc, which means that the curvature of arc in the low frequency region is smaller than that in the high frequency region.

Figure 1 (C) shows the effects of the annealing on the impedance plots for the specimen with Pt paste electrode without glass flux. Platinum paste without glass flux was applied on the faces of stabilized zirconia and fired at 900 °C for 3 h and then at 1300 °C for 72 h. Curves 1 and 2 in the figure were impedance arcs measured before and after the annealing at 1300 °C respectively. It is apparent from the figure that the long period annealing has resulted in a noticeable increase in interface resistance and a depression of semi-circle. This may be due to the decrease in the three phase boundary (lines where the electrode, electrolyte and gas phase meet) and the decrease in the interconnected gas channels in the Pt electrode. So far, the depression of impedance arc has been accounted for by the contribution of Warburg impedance.[2] The decrease in the volume of open pores in electrode accompanies the decrease in diffusion flux of gaseous species. Accordingly, the contribution of Warburg impedance to the interface impedance increases. Likewise, the addition of glass flux is supposed to decrease the diffusion flux and to cause the increase in the depression angle.

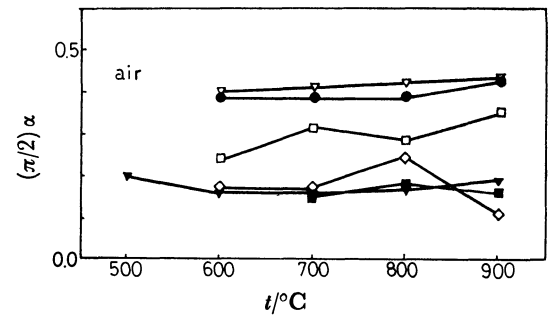

Fig. 2. Temperature dependence of α.
▽: Pt from H_2PtCl_6, ●: Pt paste with glass flux, □: Pt paste without glass flux annealed at 1300 °C for 72 h, ◇: sputtered Pt, ▼: evaporated Pt, ■: Pt paste without glass flux.

Figure 2 shows the depression angle α against temperature for various types of Pt electrodes in air. The electrodes with relatively thin films, for example the sputtered or evaporated electrodes, seem to have somewhat small depression angle. But in the case of Pt paste electrodes with glass flux, correlation was not observed between the electrode thickness and the depression angle.

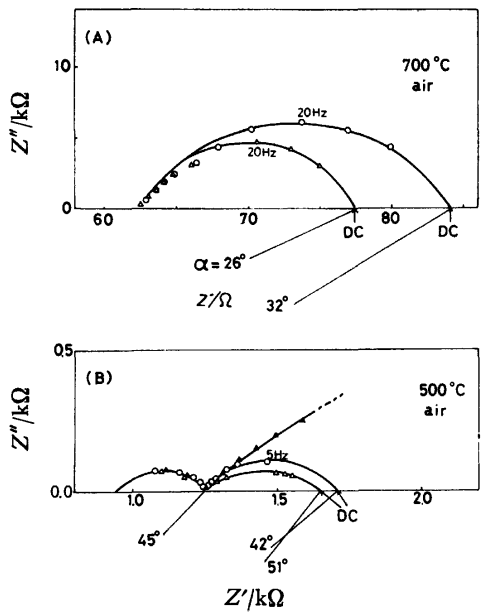

Fig. 3. Impedance plots of the cell with Ag and $La_{0.5}Sr_{0.5}CoO_3$ electrodes.
○: Ag paste with glass flux, △: sputtered Ag, ▲: $La_{0.5}Sr_{0.5}CoO_3$.

Ag Electrode: Figure 3 shows the impedance plots of the cells with Ag electrodes and $La_{0.5}Sr_{0.5}CoO_3$ electrode measured in air. Stabilized zirconia disks used were 5 mm in thickness. Although only one arc was observed at high temperature (above 550 °C), below 550 °C the second arc appeared in the high frequency region for both Ag and $La_{0.5}Sr_{0.5}CoO_3$ electrodes. Impedance measurements on specimens with different thickness of electrolyte showed that the high frequency dispersion is dependent on the electrolyte thickness but independent of the method of preparation of Ag electrodes. Accordingly, the arc of high frequency region would corresponds to the impedance of grain boundary.[1-8]

The arc in the low frequency region would corresponds to the interface impedance. Silver electrodes prepared from Ag paste with glass flux gave a more depressed arc in the low frequency region than the sputtered one at temperatures below 500 °C. In the case of Ag and $La_{0.5}Sr_{0.5}CoO_3$ electrodes, the interface resistance R_i is given from the two intercepts of impedance arc with the real axis in the low frequency region.

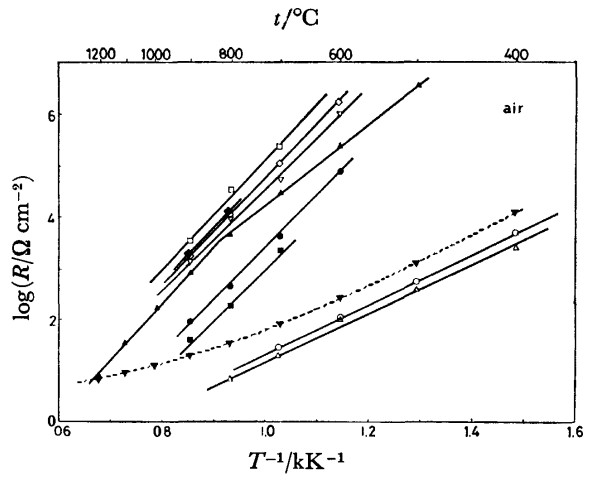

Fig. 4. Plots of log R_i *vs.* $1/T$.
□: Pt paste without glass flux annealed at 1300 °C for 72 h, ◇: sputtered Pt, ◆: evaporated Pt, ▽: Pt from H_2PtCl_6, ▲: $La_{0.5}Sr_{0.5}CoO_3$, ●: Pt paste with glass flux, ■: Pt paste without glass flux, ○: Ag paste with glass flux, △: sputtered Ag.

Figure 4 shows the plots of log R_i against $1/T$ for various kinds of electrodes. The broken line indicates the bulk resistance of stabilized zirconia measured in this study. Since the grain boundary impedance is negligible above 550 °C, the bulk resistance is determined from the intercept of the impedance arc with the real axis at high frequency region. When the grain boundary impedance arc appears below 550 °C, the bulk resistance is determined from the extrapolation to high frequency in the grain boundary region.[2] As can be seen from the figure, Ag electrodes have relatively low interface resistance. $La_{0.5}Sr_{0.5}CoO_3$ is a mixed conductor which has high ionic conductivity as well as high electronic conductivity.[9] So, it is expected that oxygen dissolves into the oxide electrode and is ionized at the electrode/electrolyte interface. This means that the reaction area is much larger than that of three phase boundary. But, the experimental results did not show any evidence of low interface resistance.

From Fig. 4, it is evident that the same metal has nearly the same activation energy. This fact suggests that the rate-determining step of the electrode processes is the same for the same metal in a temperature range studied. It was found that the activation energy for Pt electrodes is about 201 kJ/mol and that for Ag electrodes is about 92 kJ/mol.

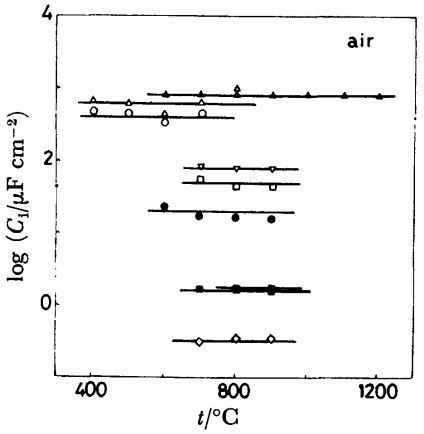

Fig. 5. Temperature dependence of log C_i.
▲: $La_{0.5}Sr_{0.5}CoO_3$, △: sputtered Ag, ○: Ag paste with glass flux, ▽: Pt from H_2PtCl_6, □: Pt paste without glass flux annealed at 1300 °C for 72 h, ●: Pt paste with glass flux, ▼: evaporated Pt, ■: Pt paste without glass flux, ◇: sputtered Pt.

Figure 5 shows log C_i against temperature for various kinds of electrode materials, where C_i is the interface capacitance calculated from the impedance plots assuming that the interface impedance is approximated by *R-C* parallel circuit. It is obvious that the interface capacitance is independent of the temperature and strongly dependent on the preparation of electrode.

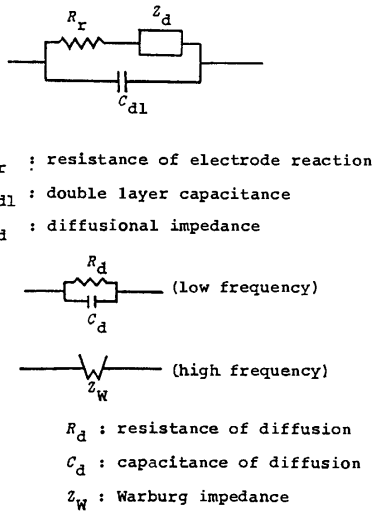

Fig. 6. Equivalent circuit of interface impedance.

Sputtered or evaporated Pt electrodes show small capacitance. Since C_i is considered to be proportional to the contact area at the electrode material/electrolyte interface, the small capacitance would be explained as the low contact area.

Equivalent Circuit and Oxygen Pressure Dependence of the Interface Impedance. As shown in Figs. 1 and 3, the impedance arcs for various kinds of electrodes are depressed. Therefore they cannot be accounted for by a parallel R-C combination.

According to Franklin,[10] when the gas diffusion in pores of electrode is slow, the equivalent circuit is as shown in Fig. 6. In this equivalent circuit, Z_d expresses the impedance due to diffusional process of gaseous oxygen in pores, which is approximated by Warburg impedance in the high frequency region and by a parallel R_d-C_d circuit in the low frequency region. Accordingly, the interface resistance is represented by the sum of the diffusional resistance R_d and the electrode reaction resistance R_r. Therefore, the higher one of R_d and R_r determines the interface resistance. Since R_d is proportional to $1/P_{O_2}$ and C_d is proportional to P_{O_2}, the P_{O_2} dependence of the impedance plots elucidate the contribution of R_d and C_d.

Figure 7 gives the change in the impedance plots with oxygen pressure for specimens with Pt electrode from H_2PtCl_6 and sputtered Ag electrode. The interface resistance R_i increases as the P_{O_2} decreases. However, the capacitance obtained by assuming the parallel R-C circuit was found to be independent of the P_{O_2} as shown in Fig. 8. Probably, the capacitance would correspond to the double layer capacitance in Fig. 6.

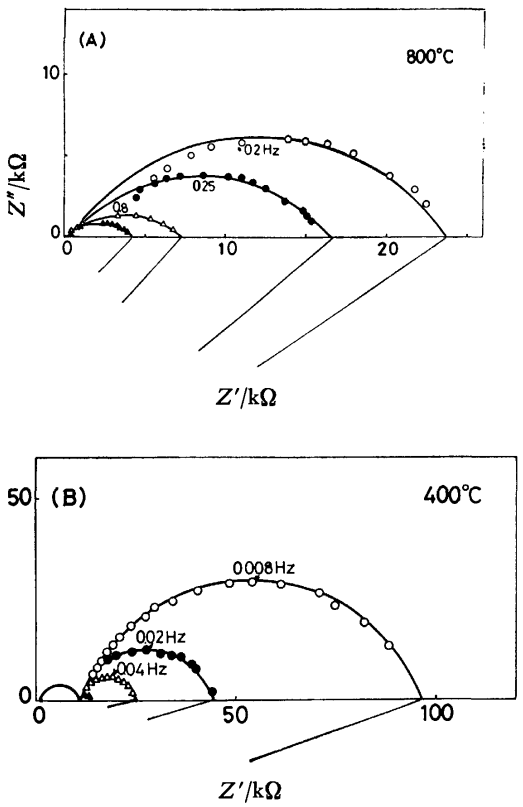

Fig. 7. P_{O_2} dependence of impedance plot.
(A): Pt from H_2PtCl_6. P_{O_2}/atm ▲; 1.0, △; 2.0×10^{-1}, ●; 1.1×10^{-2}, ○; 8.5×10^{-4}. (B): sputtered Ag P_{O_2}/atm ▲; 3.0×10^{-2}, △; 1.1×10^{-2}, ●; 2.1×10^{-3}, ○; 6.5×10^{-4}.

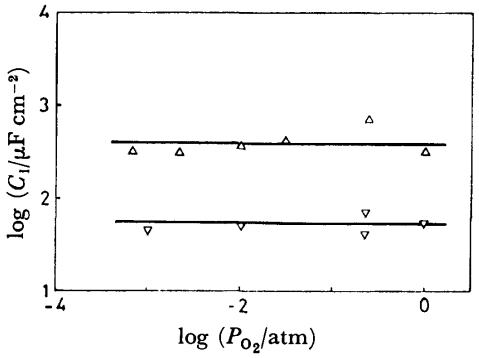

Fig. 8. P_{O_2} dependence of log C_i.
△: Sputtered Ag (400 °C), ▽: Pt from H_2PtCl_6 (800 °C).

Figure 9 (A) shows the P_{O_2} dependence of the interface resistance of Pt electrodes. The interface resistance is proportional to $P_{O_2}^{-1/4}$, irrespective of electrode preparation. Bauerle's[1] results on sputtered Pt electrodes show a tendency of saturation with the increase in P_{O_2}.

Figure 9 (B) shows the same plot for the sputtered Ag electrode. The interface resistance is proportional to $P_{O_2}^{-2/3}$.

From the results shown in Fig. 9, under low overvoltages the interface resistance of both Pt and Ag electrode is attributed to the resistance of electrode reaction R_r in Fig. 6.

Electrode Reaction. As indicated in the preceding section, the interface impedance can be approximated by the parallel R_r(resistance of electrode reaction)-C_{dl} (double layer capacitance) circuit in spite of the depression of the impedance arcs. Unlike C_{dl}, R_r was found to be sensitive to temperature and oxygen pressure. One may consider $1/R_r$ to be a measure of the rate of over-all electrode reaction. The over-all electrode reaction consists of several elementary steps given in Table 2. The value of n in the form of $1/R_r \propto P_{O_2}^n$,

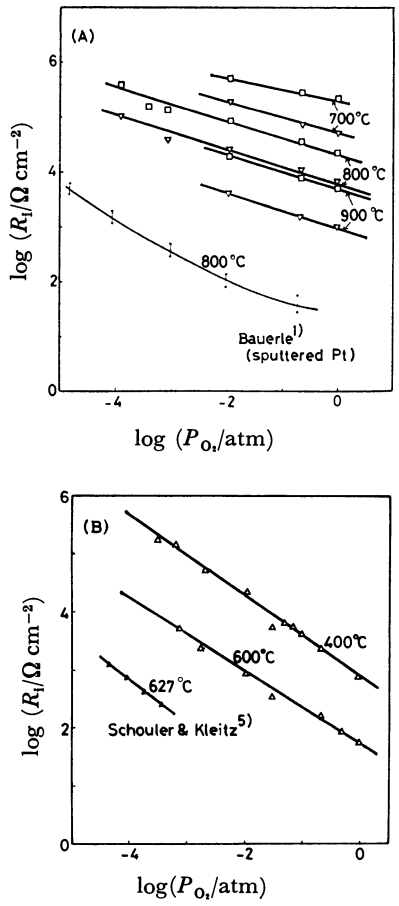

Fig. 9. P_{O_2} dependence of log R_i.
(A): □; Pt paste without glass flux annealed at 1300 °C for 72 h, ▽; Pt from H_2PtCl_6. (B): Sputtered Ag.

characteristic of each rate-determining step is also given in Table 2. If step (I) is rate-determining, $1/R_r$ should be proportional to P_{O_2} ($n=1$). From the results obtained in this work, $1/R_r$ is not proportional to P_{O_2}. So, this adsorption process is considered to be not rate-determining. When the step (II) is rate-determining and the adsorption of oxygen obeys Langmuir isotherm, n is supposed to take values from 1 to 0. Similarly, n would take values from 1/2 to 0, when step (III) or (IV) is rate-determining. Results of the present work indicate that n is 2/3 for Ag electrodes. Moreover, Buttner and his co-investigators[11)] have found that

TABLE 2. ELEMENTARY REACTION STEPS AND THE VALUE OF n, CHARACTERISTIC OF RATE-DETERMINING STEP

	Elementary step	n in $1/R_r \propto P_{O_2}^n$
I	$O_2(g) \rightleftarrows O_2$ (ad)	1
II	O_2(ad) $\rightleftarrows$ 2O (ad)	1—0
III	Surface diffusion of O(ad)	1/2—0
IV	O(ad)+2e $\rightleftarrows$ O^{2-}	1/2—0

oxygen is strongly adsorbed on the surface of Ag. From these results, the rate-determining step of the electrode processes on Ag electrodes is supposed to be the dissociation of adsorbed oxygen molecules into atoms.

For Pt electrodes, n was found to be 1/4. According to Fryburg and Petrus,[12)] at temperatures and oxygen pressure studied, the surface of Pt would be completely covered with a tightly bound monolayer of oxygen atoms. So, we could assume the weakly adsorbed molecular oxygen. If the adsorption is Langmuir type, the rate-determining step would be the dissociation of oxygen molecules into atoms or either one of the subsequent steps.

References

1) J. E. Bauerle, *J. Phys. Chem. Solids*, **30**, 2657 (1969).
2) Y. Suzuki and T. Takahashi, *Denki Kagaku*, **39**, 406 (1971).
3) E. Schouler, M. Kleitz, and C. Deportes, *J. Chim. Phys.*, **70**, 923 (1973).
4) E. Schouler, G. Giroud, and M. Kleitz, *J. Chim. Phys.*, **70**, 1309 (1973).
5) E. Schouler and M. Kleitz, *J. Electroanal. Chem. Interfacial Electrochem.*, **64**, 135 (1975).
6) N. Matsui, *Surf. Sci.*, **86**, 353 (1979).
7) P. Fabry, E. Schouler, and M. Kleitz, *Electrochim. Acta*, **23**, 539 (1978).
8) S. H. Chu and M. A. Seitz, *J. Solid State Chem.*, **23**, 297 (1978).
9) H. Obayashi and T. Kudo, "Application of Solid Electrolytes," ed by T. Takahashi and A. Kozawa, JEC Press, Ohio, U.S.A. (1980), p. 106.
10) A. D. Franklin, *J. Am. Ceram. Soc.*, **58**, 465 (1975).
11) F. H. Buttner, E. R. Funk, and H. Udin, *J. Phys. Chem.*, **56**, 657 (1952).
12) G. C. Fryburg and H. M. Petrus, *J. Electrochem. Soc.*, **108**, 496 (1961).

The IR Spectra of $Cs_xV_2O_5$ ($x=0-0.66$)

Yoshiya KERA*

Department of Chemistry, Faculty of Science, Osaka University, Toyonaka, Osaka 560

(Received February 23, 1980)

The IR spectra of Cs-vanadates (C=[Cs]/[V]=0—0.332) were recorded in the 650—1200 cm^{-1} region. In the V_2O_5, which had cautiously been purified, the V=O stretching band was found at 1022 cm^{-1}, and the V–O–V stretching band, at 815 cm^{-1}. Upon the addition of Cs, sharp new bands began to appear at 965 cm^{-1} at C=0.0042 and also at 1000 cm^{-1} at C=0.0120, and a shift in the 815-cm^{-1} band was found. Finally, at C=0.332 the original 1022-cm^{-1} band was replaced by the 965 and 1000 cm^{-1} bands, the intensity ratio (I_{965}/I_{1000}) of which was 2.0. The X-ray diffraction pattern of the last sample was in agreement with that of CsV_3O_8. The IR and the X-ray results suggest that the CsV_3O_8 phase appears at around C=0.004. Based on the band shifts of 1022→965 and 1000 cm^{-1}, the force constant and the bond strength of V=O in CsV_3O_8 were discussed. With respect to the band shift in the 815-cm^{-1} region with the increase in the Cs content, the corretion of $\Delta\bar{\nu}$ to $C^{1/3}$ is shown in $C<0.020$.

V_2O_5 has a layer structure and has large channels along the b- and c-axes,[1-3] through which oxygen ions can be easily taken into and/or out of the lattice.[4] The property of the vanadium oxide as a catalyst has been discussed in relation to such a structural feature and behaviour of the oxygen ion.[4-8] V_2O_5 can also take many kinds of metal ion into the channels to form "vanadium bronzes;" the physico-chemical properties vary delicately and complicatedly depending upon the kind and the concentration of metal ions.[9] Recently, a big change was found in the catalytic properties of V_2O_5 when a commercial V_2O_5 (guaranteed grade) was cautiously purified.[10] This finding forces us to think that it is very important to control a small amount of impurities for a clear study of the catalytic activity and the catalytic property of vanadium oxide.

Now a series of studies of the effects of alkali metal-addition (Li–Cs) on the physico-chemical and the catalytic properties in V_2O_5 has been started. Upon the addition of Cs, the largest effects were found on the catalytic activity leading to ethanol decomposition and on the band shift in the V–O–V stretching in the IR spectrum.[11] These results could easily be expected because the Cs atom has the lowest ionization potential and the largest ionic radius of the alkali metals. However, the details of the structural change of V_2O_5 upon alkali-metal addition have not yet been made clear. In the present paper, the changes in the V=O and the V–O–V bonding properties in the original V_2O_5 lattice upon the addition of Cs are examined in especial detail. The IR spectra of the Cs–vanadates, the Cs content of which was controlled over a wide range, were measured for the purpose.

Experimental

The Cs–vanadates were prepared from Cs_2CO_3 (guaranteed grade) and NH_4VO_3 which had been purified cautiously[12] by the following procedures. The NH_4VO_3 was immersed into a aq. soln. of Cs_2CO_3, dried at 120° C, and calcined in air at 600 °C for 16—20 h. The Cs-contents of the samples are summarized in Table 1. The Cs-5 sample was prepared by grinding Cs-1 and Cs-7 well in an agate mortar, followed by heat treatment at 623 °C for 12 h and then by fusing at 700 °C for 6 h. The Cs-6 sample was prepared by grinding Cs-1 and Cs-7 well followed by heat treatment at 610 °C for 24 h; it was then fused at 623 °C for 12 h.

TABLE 1. Cs-CONTENT OF Cs-VANADATES

Sample	Cs-content([Cs]/[V])
Pure-V_2O_5	0.0000
Cs-1	0.0013
Cs-2	0.0042
Cs-3	0.0120
Cs-4	0.0203
Cs-5	0.100
Cs-6	0.168
Cs-7	0.332

The IR spectra of the Cs–vanadates were recorded in the frequency range from 650 to 1200 cm^{-1} by the normal KBr-disk method. The IR spectrometer used was JASCO, Model DS-402 G. The X-ray powder diffraction was checked on five samples: pure-V_2O_5 and Cs-4—Cs-7. The X-ray diffractmeter used was Rigaku Denki, Model 2001; Cu $K\alpha$-radiation (at 35 kV) and an Ni-filter were used.

Results

The IR spectra of the pure-V_2O_5 and the Cs–vanadates are shown in Fig. 1. In the spectrum of the pure-V_2O_5[8,13] a sharp band assigned to the V=O stretching vibration and a broad band assigned to V–O–V stretching are seen at 1022 and 815 cm^{-1} respectively (Fig. 1-a). The spectrum changes with the increase in the Cs–content (C=[Cs]/[V]): with C=0.0042 a new sharp band begins to appear at 965 cm^{-1} (Fig. 1-c) and with C=0.0203, one also appears at 1000 cm^{-1} (Fig. 1-e). In the samples with contents higher than C=0.0203, the bands at 965 and 1000 cm^{-1} were intensified with the Cs-content without any change in the frequencies. With C=0.332, finally, the original band at 1022 cm^{-1} disappeared and was completely replaced by the bands at 965 and 1000 cm^{-1} (Fig. 1-h).

On the other hand, the broad band at 815 cm^{-1} became broader and shifted toward the low frequencies from C=0.0013 to 0.0203 with the addition of Cs ions. In the samples with contents higher than C=0.100, the band split further into two peaks. With C=0.332,

* Present address: Department of Applied Chemistry, Faculty of Science and Engineering, Kinki University, Higashi-Osaka, Osaka 577.

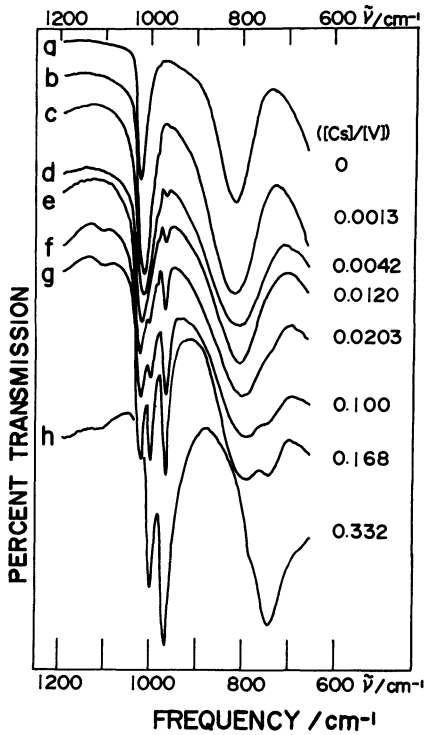

Fig. 1. IR spectra of $Cs_xV_2O_5$ (x=0—0.664), recorded in the frequency range of 1200—650 cm^{-1}. Spectrum a shows IR spectrum of the original V_2O_5, which was cautiously purified:[12] the bands at 1022 and 815 cm^{-1} have been assigned to the V=O and the V–O–V stretching, respectively.[8] The frequencies of the bands in the spectra b—h are summarized in Table 2.

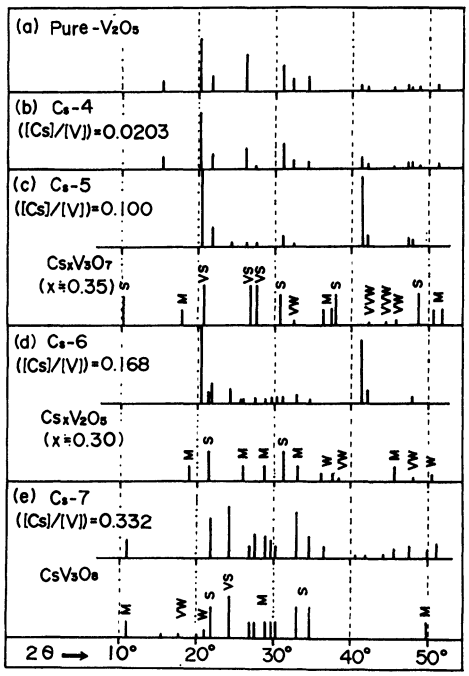

Fig. 2. The X-ray powder diffraction patterns of the pure-V_2O_5 and $Cs_xV_2O_5$ (x=0—0.664). For comparison the X-ray powder patterns of Cs–vanadates, already reported,[14–16] were added in Figs. 2-c, d, and e. In Cs-4 the patterns is almost agreement with that of the pure-V_2O_5 except for a little difference in the relative intensities. In Cs-7 the main lines of the pattern is agreement with that of Cs–hexavanadate. In Cs-5 and Cs-6 the very strong lines were seen at 20.4 and 41.2°, which have not been reported yet.

finally, the band at 815 cm^{-1} seems to be replaced by the bands at 742 and 780 cm^{-1}. The frequencies of all the bands in the spectra shown in Fig. 1 are summarized in the third column of Table 2.

The X-ray diffraction patterns of the pure-V_2O_5 and the Cs-4—Cs-7 samples are shown in Figs. 2-a—e. The pattern of Cs-4 (at C=0.0203) is almost the same as that of the pure-V_2O_5,[3] except for a very weak line appearing at 27.4° and a small change in the intensities between the corresponding peaks (Figs. 2-a and b). Strong lines appear at 20.3 and 41.3° in the diffraction patterns of Cs-5 and Cs-6. Both samples were prepared by mixing pure-V_2O_5 with Cs-7, followed by fusing and recrystallizing. Thus, the "preferred orientation" toward the (010) plane may be expected in the samples. The lines at 20.3 and 41.3° shifted just a little bit from those at 20.2 and 41.2°, which are ascribed to the diffraction from the (010) and the (020) planes respectively in pure-V_2O_5. These shifts might be caused by the formation of a non-stoichiometric phase of $Cs_xV_2O_5$ (x: too small).

In Cs-5, besides the lines at 20.3 and 41.3°, the very weak lines at 21.7, 26.2, 31.0, 32.4, and 47.3° correspond to the diffraction from pure-V_2O_5. The weak lines at

TABLE 2. THE FREQUENCIES OF THE V=O AND THE V–O–V STRETCHING BANDS IN THE IR-SPECTRA OF PURE-V_2O_5 AND Cs-VANADATES, AND THE BAND SHIFT ($\Delta\tilde{\nu}$) OF THE V–O–V STRETCHING UPON Cs-ADDITION

Samples	Cs-content ([Cs]/[V])	Frequencies/cm^{-1}					$\Delta\tilde{\nu}$/cm^{-1}
		V=O stretching			V–O–V stretching		
Pure-V_2O_5	0	1022	—	—	815		0
Cs-1	0.0013	1017	—	—	818		—3
Cs-2	0.0042	1017	—	966	808		7
Cs-3	0.0120	1020	—	965	806		9
Cs-4	0.0203	1023	1000	965	797		18
Cs-4	0.0203	1021	1001	965	803		12
Cs-5	0.100	1022	1000	965	795	750	—
Cs-6	0.168	1020	999	965	790	743	—
Cs-7	0.332	—	1000	965	780	742	—

27.5 and 24.2° correspond well to the strong lines in Cs-7, which are ascribed to the diffractions from the (021) and the (210) planes in CsV_3O_8 respectively. However, no lines accord with the diffraction from $Cs_xV_3O_7$ (x: 0.35), given for comparison in Fig. 2. Thus, Cs-5 may be regarded as a composite phase of V_2O_5 and CsV_3O_8 or $Cs_xV_2O_5$ (x: too small) and CsV_3O_8. In Cs-6, the lines other than those at 20.3 and 41.3° which correspond to the diffraction from V_2O_5, appear at 21.7, 31.0, and 47.8°. The lines at 24.1, 27.4, 32.8, and 34.5° accord with the main lines of Cs-7. However, unknown lines appear at 25.5 and 25.8° in this samples, although they are very weak. No lines correspond to the diffraction from $Cs_xV_2O_5$ (x=0.3), given also for comparison in Fig. 2-d. This evidence suggests the formation of a new phase other than a mixed phase of V_2O_5 and CsV_3O_8 or $Cs_xV_2O_5$ (x: too small) and CsV_3O_8.

Finally, it is noteworthy that the diffraction at 27.5° was found in Cs-4 (at C=0.020), which is ascribed to the diffraction from the (021) plane in CsV_3O_8. This suggests that CsV_3O_8 phase can be already formed in such a low concentration as C=0.020 with Cs-addition to pure-V_2O_5.

The main lines of the diffraction in Cs-7 are completely in agreement with the pattern of CsV_3O_8, but none of the minor lines correspond to that of the Cs–vanadates reported hitherto. Thus, the Cs-7 sample consists of the Cs–trivanadate (CsV_3O_8), accompanied by a small quantity of an unknown compound.

Discussion

The V=O Stretching Bands. The peak intensities of the bands at 1022, 1000, and 965 cm^{-1} (I_{1022}, I_{1000}, and I_{965}) were estimated by drawing a base line smoothly under the bands in the spectra of Fig. 1. The intensities of the bands and the intensities normarized by the use of I_t ($I_{1022}+I_{1000}+I_{965}$) are summarized in Table 3.

Table 3. Intensity changes in the V=O stretching bands upon Cs-addition

Samples	C	I_{1022}	I_{1000}	I_{965}	$\frac{I_{1022}}{I_t}$	$\frac{I_{1000}}{I_t}$	$\frac{I_{965}}{I_t}$
Cs-2	0.0042	0.639	—	0.037	0.946	—	0.054
Cs-3	0.0120	0.397	—	0.042	0.904	—	0.096
Cs-4	0.0203	0.487	0.054	0.136	0.719	0.080	0.201
		0.549	0.059	0.103	0.772	0.083	0.145
Cs-5	0.100	0.492	0.124	0.301	0.536	0.135	0.328
Cs-6	0.168	0.677	0.405	0.672	0.386	0.231	0.383
Cs-7	0.332	0	0.514	1.095	0	0.319	0.681

The normalized intensities are plotted against the Cs-content in Fig. 3. The (I_{965}/I_t) and (I_{1000}/I_t) grow linearly with the Cs-content, but the ratio of I_{965} to I_{1000} remains constant at about 2 in the range of C= 0.020—0.332. When the curves of (I_{965}/I_t) and (I_{1000}/I_t) *vs.* C are extrapolated to C=0, they cut the vertical axis while keeping the ratio constant at about 2. On the other hand, at contents lower than C=0.020, the curve of (I_{965}/I_t) *vs.* C cuts the point of origin. Figure 3

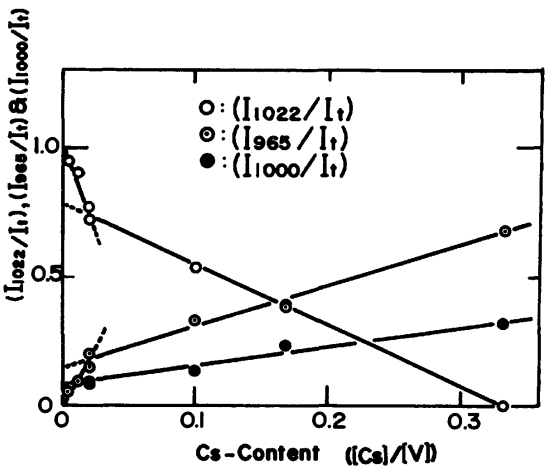

Fig. 3. The changes in the intensities of the original band at 1022 and the new bands at 1000 and 965 cm^{-1} with the increase in the Cs-content. In the Cs-content higher than C=0.020 the ratio of (I_{965}/I_t) to (I_{1000}/I_t) is kept constant at about 2.0.

indicates that the fashion of the Cs-insertion in the range of C=0—0.012 differs from that in C=0.020—0.332.

According to the X-ray analysis described above, Cs-5 and Cs-6 were regarded as mixtures of V_2O_5 and CsV_3O_8, while the CsV_3O_8 phase seems to co-exist with the V_2O_5 phase in Cs-4. That is, the CsV_3O_8-content in the V_2O_5 increases with the Cs-addition in the range of C=0.020—0.332, until finally the unified CsV_3O_8 is formed at C=0.332. The X-ray results correspond completely to the IR results that the intensities of the bands at 1000 and 965 cm^{-1} increase linearly with the Cs-content without any changes in the frequencies. Therefore, the bands at 1000 and 965 cm^{-1} can be ascribed to the characteristic bands of CsV_3O_8.

The results of the X-ray analysis by Walterson *et al.*[14,15] showed that the Cs ion occupies one kind of site in $Cs_xV_3O_7$ ($x\simeq0.35$), but in $Cs_xV_2O_5$ ($x\simeq0.3$) it occupies two kinds of sites, the ratio of which is 2 : 1. Evans *et al.*[17] also showed, in CsV_3O_8, two kinds of Cs-occupation, the ratio of which was 2 : 1. The ratio of the Cs-occupation corresponds well to the intensity ratio of the bands at 965 and at 1000 cm^{-1} (I_{965}/I_{1000}) in the samples of Cs-4—Cs-7. Thus, the bands at 965 and 1000 cm^{-1} could be ascribed to the stretching bands of V=O groups, affected by the nearest-neighbored Cs ions, which are placed in two kinds of sites.

An application of the Bond-Strength-Bond-Length-Parameters of Brown an Shannon to the band shifts from 1022 to 1000 and to 965 cm^{-1} will now be tried. The bond strength, S, is defined as Eq. 1;

$$S = S_0(R/R_0)^{-N}. \quad (1)$$

The bond strength is evaluated as S=1.848 for the V=O bond in pure-V_2O_5 by the use of the values in Table 3 of Ref. 18 : S_0=1.25, R_0=1.700, and N=4.8. The V=O bond length, R, was regarded as 1.567 Å, which is the average of the values given by Ketelaar,[1] Byström,[2] and Bachmann.[3] The bond strength, S, is assumed to be proportional to the force constant, k. Thus, the IR-frequency, f, is proportional to $S^{1/2}$

because the $f=(k/\mu)^{1/2}$ relation, holds, where μ denotes a reduced mass. From the isotope shift of the V=O stretching band with the replacement of ^{16}O for ^{18}O, the reduced mass for the band has been regarded exactly as 16.[18] This means that the oxygen ion bonds to a large body with an infinite mass. For this reason, the V=O stretching mode is prevented from the interuption of the other modes, thus giving a very sharp band. The same situation could remain in the V=O groups of such Cs–vanadates as Cs-3—Cs-7 because the bands at 965 and 1000 cm^{-1} of the samples are also very sharp, as is the original band at 1022 cm^{-1}.

The changes in the bond strength and the subsequent changes in the V=O bond length with the Cs-addition, therefore, can be estimated exactly from the band shifts from 1022 to 1000 and 965 cm^{-1} based on the relation, $f \propto S^{1/2}$. For the shift from 1022 to 1000 cm^{-1},

$$(1000/1022) = \{S(1000)/1.848\}^{1/2},$$

where the 1.848 value is $S(1022)$, which was evaluated above for the V=O bond in pure-V_2O_5; thus, the bond strength corresponding to the band at 1000 cm^{-1}, $S(1000)$, became 1.769. For the shift from 1022 to 965 cm^{-1},

$$(965/1022) = \{S(965)/1.848\}^{1/2}.$$

Thus, the bond strength corresponding to the band at 965 cm^{-1}, $S(965)$, became 1.648. By substituting the values of $S(1000)$ and $S(965)$ into Eq. 1, the V=O bond lengths corresponding to the bands at 1000 and 965 cm^{-1}, $R(1000)$ and $R(965)$, were estimated as 1.581 and 1.605 Å respectively. These values are consistent with the V=O bond distances in the CsV_3O_8, 1.575 and 1.624 Å, as deduced from X-ray analysis by Evans *et al.*[17] This agreement confirms that, in CsV_3O_8, the V=O stretching band is subjected to shifts from 1022 to 1000 and 965 cm^{-1} by the Cs ions in two different sites.

Recently, Blasse[19] found a linear correlation between the Ti–O symmetric stretching frequencies in titanates of several metals and the bond strength, P, as estimated by Pauling's Electrostatic Valence Rule. The linear correlation means that the bond strength, P, is proportional to the square root of the force constant, because the $P \propto f=(k/\mu)^{1/2}$ relation holds. Under the assumption of $f \propto S$ according to Blasse, the bond lengths of the V=O are estimated as 1.574 and 1.586 Å by a procedure similar to that described above. The values are less consistent with those in CsV_3O_8 than those estimated above under the assumption of $f \propto S^{1/2}$. From a physical analogy, the bond strength seems to correspond directly to the force constant itself rather than the square root of the force constant. In Fig. 1 in Ref. 19 by Blasse, the plots of $P^{1/2}$ against f seem, in fact, to give a better linearity than that of P against f.

The crystal structure of the Cs–vanadates (C= 0.100—0.50) has been determined by X-ray diffraction;[14–17,20,21] the V=O bond length has also been estimated. The bond length expands linearly with the Cs-content, as is indicated by the open circles in Fig. 4. The bond lengths estimated above at C=0.332 are shown by the closed circles. They are located near the linear line.

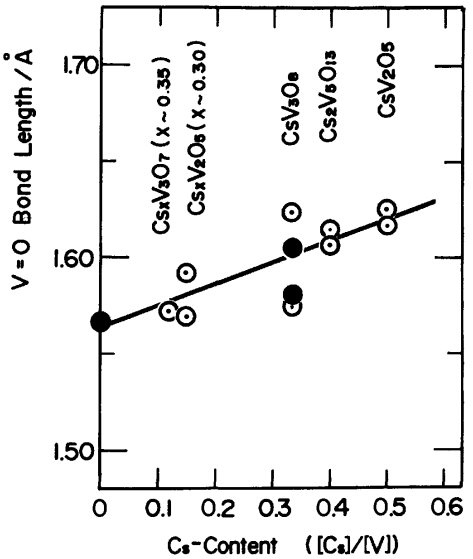

Fig. 4. The expansion of the V=O bond with the Cs-addition to V_2O_5. The open circles indicate the V=O bond lengths for the Cs–vanadates: $Cs_xV_3O_7$ ($x \approx 0.35$),[14] $Cs_xV_2O_5$ ($x \approx 0.3$),[16] CsV_3O_8,[17] $Cs_2V_5O_{13}$,[20] and CsV_2O_5,[21] which have been determined by the X-ray analysis. The closed circles at C=0.332 indicates the V=O bond lengths, estimated by the application of the Bond-Strength-Bond-Length parameters by Brown and Sahnnon to the band shifts from 1022 to 1000 and to 965 cm^{-1}. The closed circle at C=0 indicates the reference for the estimation of the V=O bond length mentioned above and the values (1.567 Å) is the average of the values determined by Ketelaar,[1] Byström *et al.*,[2] and Backmann *et al.*[3]

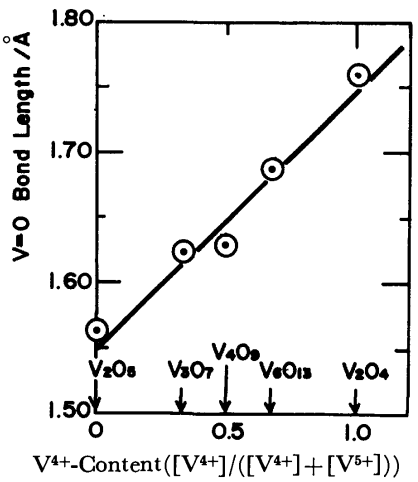

Fig. 5. The expansion of the V=O bond with the reduction of V_2O_5. In V_2O_5 the average of the values by Ketelaar,[1] Byström *et al.*,[2] and Backmann *et al.*,[3] and in V_2O_4 the value by Anderson[25] were given. In the intermediate phases, V_3O_7,[22] V_4O_9,[23] and V_6O_{13},[24] the V^{4+}-content was evaluated under the assumption that the V-ions take a mixed valency of V^{4+} and V^{5+}. In the phases there are two or three kinds of the V=O group and thus the averages of the V=O bond length were given.

Therefore, it is confirmed that Cs-ions occupy two kinds of sites, which are close to the V=O groups in

the CsV_3O_8 crystalline lattice, and that the bond strengths of the V=O groups are weakened by the Cs ions inserted; thus, the stretching frequency decreases from 1022 to 1000 cm^{-1} and to 965 cm^{-1}.

With the reduction in V_2O_5, the VO_6 polyhedral unit changes in symmetry from a distorted trigonal bipyramid toward an octahedron.[12] The V=O bond expands linearly with the reduction, as is shown in Fig. 5; the expansion in the V=O bond is accompanied by a decrease in the valence state of the vanadium ion and then by a change in the symmetry around the vanadium ion. In other words, the bond expansion is caused by the formation of the V^{4+} ion, that is, V^{4+}=O. The curve of the V=O bond length *vs.* the V^{4+}-content in Fig. 5 corresponds well to that of the V=O bond length *vs.* the Cs-content in Fig. 4. The complete transfer of electrons from alkali metals such as Li and Na to vanadium ions has, in fact, been observed in alkali-vanadates by NMR and ESR spectrometry.[26] With Cs–vanadates, electron transfer could occur more favorably because Cs atom has the lowest ionization potential of all the alkali metals. Therefore, it can be concluded that the expansion in the V=O bond by the Cs-addition is caused not only by its steric effect, but also by the electron transfer from Cs to the vanadium ion to form the V^{4+}=O group.

The V–O–V Stretching Bands. With respect to the V–O–V stretching vibration in pure-V_2O_5, the original band itself was too broad. The band broadened further and also shifted toward the low frequencies upon the Cs-addition. The band shifts from 815 cm^{-1}, $\Delta\tilde{\nu}$, are summarized in the last column of Table 2. In the three samples of C=0.100—0.332, in which the band is split into two peaks, the band shift could not be estimated. The plot of $\Delta\tilde{\nu}$ *vs.* C is shown in Fig. 6-a. In the range of C=0—0.020, there is a good correlation between the band shift, $\Delta\tilde{\nu}$, and the cubic root of the Cs-content, $C^{1/3}$, as is shown in Fig. 6-b.

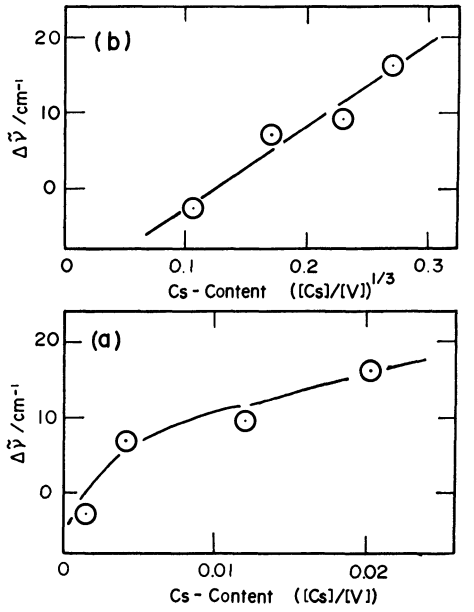

Fig. 6. The band shift of the V–O–V stretching ($\Delta\tilde{\nu}$) with the Cs-content (C) in the region of C=0—0.020; a) the plot of $\Delta\tilde{\nu}$ *vs.* C, b) the plot of $\Delta\tilde{\nu}$ *vs.* $C^{1/3}$.

In samples of Cs-4—Cs-6, the phases of V_2O_5 or $Cs_xV_2O_5$ and CsV_3O_8 co-exist, as was clearly shown above in the discussion of the V=O stretching band. In Cs-3 (C=0.012) the characteristic bands of CsV_3O_8 appear at 965 and 1000 cm^{-1}. In Cs-2 (C=0.0042), the 965 cm^{-1} band appeared, but the 1000 cm^{-1} band did not appear; it might have been masked under the steep part of the 1022 cm^{-1} band of pure-V_2O_5. If so, CsV_3O_8 would already be formed in such a low concentration as C=0.0042. In such a situation, the broadening and the shifts in the 815 cm^{-1} band might arise for the mixing of the 815 cm^{-1} by V_2O_5 with the 780 and the 742 cm^{-1} by CsV_3O_8 even though it is very weak. Furthermore, the intensities of the 780 and the 742 cm^{-1} bands grow relatively with the increase in the Cs-content; thus, the band shifts may be expected to become larger.

In fact, the region where the non-stoichiometric phase of $Cs_xV_2O_5$ (x=too small) can exist stably and the Cs-content, at which the CsV_3O_8 phase begins to appear, can not be exactly determined in the present paper. Therefore, even in the region of C=0—0.020, where the linear correlation of $\Delta\tilde{\nu}$ to $C^{1/3}$ holds as is shown in Fig. 6-b, the x in the $Cs_xV_2O_5$ could not be simply regarded as varying with the changes in the Cs-content. The physical meanings of the correlation can not be discussed further.

The author wishes to express his appreciation to Mr. Shinichi Ishikawa and Mr. Tetuo Yamamoto for their measurements of the IR spectra, and to Professor Keiji Kuwata for his continued interest in this work and for his valuable suggestions.

References

1) J. A. A. Ketelaar, *Z. Kristallogr.*, **95**, 9 (1936).
2) A. Byström, K. A. Wilhelmi, and O. Brotzen, *Acta Chem. Scand.*, **4**, 1119 (1950).
3) H. G. Bachmann, F. R. Ahmed, and W. H. Barnes, *Z. Kristallogr.*, **115**, 110 (1961).
4) E. Gillis, *C. R. Acad. Sci.*, **258**, 4765 (1964).
5) G. L. Simard, J. F. Steger, R. J. Arnott, and L. A. Siegel, *Ind. Eng. Chem.*, **47**, 1424 (1955).
6) E. R. S. Winter, *Adv. Catal.*, **10**, 196 (1958); G. K. Boreskov, *ibid.*, **15**, 285 (1964).
7) T. Toda, K. Kosuge, and S. Kachi, *Nippon Kagaku Zasshi*, **87**, 1311 (1966).
8) Y. Kera and K. Hirota, *J. Phys. Chem.*, **73**, 3973 (1969); Y. Kera, S. Teratani, and K. Hirota, *Bull. Chem. Soc. Jpn.*, **40**, 2458 (1967).
9) For instance, P. Hagenmuller, "Chem. Extend. Defects in Non-Metal. Solids," Amsterdam (1970), pp. 91—108; *Prog. Solid State Chem.*, **5**, 71 (1971); M. Nygren, *Chem. Commun. Univ. Stockholm*, No. 11 (1973); T. Horlin, *ibid.*, No. 6 (1977); K. Waltersson, *ibid.*, No. 7 (1976).
10) Y. Kera, *Bull. Chem. Soc. Jpn.* **52**, 888 (1979); **50**, 2841 (1977).
11) Y. Kera, unpublished.
12) Y. Kera and K. Kuwata, *Bull. Chem. Soc. Jpn.*, **52**, 1268 (1979).
13) L. D. Frederickson, Jr., and D. M. Hansen, *Anal. Chem.*, **35**, 818 (1963).
14) K. Waltersson and B. Forslund, *Acta Crystallogr., Sect.*

B, **33**, 775 (1977).
15) A. D. Kelmers, *J. Inorg. Nucl. Chem.*, **21**, 45 (1961).
16) K. Waltersson and B. Forslund, *Acta Crystallogr., Sect. B*, **33**, 780 (1977).
17) H. T. Evans, Jr., and S. Block, *Inorg. Chem.*, **5**, 1808 (1966).
18) I. D. Brown and R. D. Shannon, *Acta Crystallogr., Sect. A*, **29**, 266 (1973).
19) G. Blasse, *J. Solid State Chem.*, **20**, 217 (1977).
20) K. Walterson and B. Forslund, *Acta Crystallogr., Sect. B*, **33**, 784, (1977).
21) K. Walterson and B. Forslund, *Acta Crystallogr., Sect. B*, **33**, 789 (1977).
22) K. Waltersson, B. Forslund, and K. A. Wilhelmi, *Acta Crystallogr., Sect. B*, **30**, 2644 (1974).
23) K. A. Wilhelmi and K. Waltersson, *Acta Chem. Scand.*, **24**, 3409 (1970).
24) K. A. Wilhelmi, K. Waltersson, and L. Kihlborg, *Acta Chem. Scand.*, **25**, 2675 (1971).
25) G. Andersson, *Acta Chem. Scand.*, **10**, 623 (1956).
26) For instance, J. Gendel, R. M. Cotts, and M. J. Sienko, *J. Chem. Phys.*, **37**, 220 (1962); R. N. Pletnev, V. K. Kapustkin, and V. L. Volkov, *Sov. Phys.-Solid State*, **15**, 1700 (1974).

Kinetic Studies of the Oxidation Reactions of *o*-, *m*-, and *p*-Benzenediols with Tris(1,10-phenanthroline)iron(III). An Estimation of the Redox Potentials of the Organic Radicals by Application of the Marcus Theory

Masaru KIMURA,* Shinichi YAMABE,† and Tsutomu MINATO††

Department of Chemistry, Nara Women's University, Nara 630

†*Department of Chemistry, Nara University of Education, Nara 630*

††*Department of Chemistry, The University of British Columbia, Vancouver, B.C., Canada V6T 1Y6*

(Received September 11, 1980)

Kinetic studies of the oxidation of *o*-, *m*-, and *p*-benzenediols (H_2A) by tris(1,10-phenanthroline)iron(III) were made in dilute perchloric acid solution at an ionic strength of 1.0 mol dm^{-3} at four temperatures between 10 and 30 °C. The second-order rate constants (k_0) which follow the observed rate law of $-d[Fe(phen)_3^{3+}]/dt = k_0[Fe(phen)_3^{3+}][H_2A]$ were determined under varied conditions. The order of the rate constants was *m*-<*o*-<*p*-benzenediols, with the ratio being approximately $1 : 10^3 : 10^4$. By the application of the Marcus theory to the kinetic parameters obtained, the standard redox potentials of the dihydroxyphenyl radicals (H_2A^+) were estimated in 0.11 mol dm^{-3} perchloric acid solution to be 1.41, 1.10, and 0.97 V for *m*-, *o*-, and *p*-benzenediols, respectively. The energies of the highest occupied molecular orbitals for the H_2A molecules (ε_{HOMO}) were calculated to be −0.4468, −0.4332, and −0.4224 a.u. for *m*-, *o*-, and *p*-benzenediols, respectively. The differences of the total electronic energies between H_2A^+ and H_2A molecules (ΔE_T) were calculated to be 0.4183, 0.4033, and 0.3957 a.u. for *m*-, *o*-, and *p*-benzenediols, respectively. Thus, the standard redox potentials of the free-radicals estimated are found to be well correlated with the HOMO energies and also with the differences of the total electronic energies between the cation radicals and the parent molecules.

The application of the Marcus theory[1] to kinetics of the reactions involving organic and inorganic substrates has given satisfactory results in the explanation of the observed kinetic parameters. An application of Marcus theory to the investigation of the kinetic data in the outer-sphere electron transfer reactions allows an estimation of the redox potentials of the unstable free-radicals of organic molecules.[2,3] The present paper demonstrates the kinetics of the outer-sphere electron transfer reactions of *o*-, *m*-, and *p*-benzenediols with tris(1,10-phenanthroline)iron(III), and explains the estimation of the standard redox potentials of those free-radicals by means of the application of Marcus theory to the kinetic parameters obtained. We calculated the energy of the highest occupied molecular orbitals (HOMO) of each benzenediol and the difference in the total electronic energy between the cation radical and the parent molecule, by using CNDO/2 MO.[5] The correlation between the theoretically calculated energies and the standard redox potentials estimated by the application of Marcus theory to the kinetic parameters is discussed in the present paper.

Experimental

Chemicals. Reagent-grade *o*-, *m*-, and *p*-benzenediols from Wako Pure Chemical Co. Inc., were used without further purification. The solution of each reagent was prepared just before use. Tris(1,10-phenanthroline)iron(III) perchlorate was prepared by oxidizing tris(1,10-phenanthroline)iron(II) with lead(IV) dioxide in dilute sulfuric acid solution; after removal of lead(IV) dioxide and lead(II) sulfate, the perchlorate salt of the tris(1,10-phenanthroline)-iron(III) was precipitated by the addition of sodium perchlorate solution. The solid obtained was recrystallized from aqueous perchlorate solution. A stock solution of tris(1,10-phenanthroline)iron(III) was prepared by dissolving the perchlorate salt in 70% (v/v) perchloric acid. The stock solution of the blue solution having an absorption maximum at 600 nm was very stable in perchloric acid and no appreciable decomposition occurred for at least 3 months at room temperature in the dark. Sodium perchlorate, used for adjusting ionic strength, was recrystallized twice from aqueous solution. Deionized water was distilled with and without addition of some permanganate in a glass still.

Kinetic Measurements. The kinetic experiments were carried out with a Union Stopped Flow Spectrophotometer RA-401 by following the increase of the absorbance at 510 nm due to the tris(1,10-phenanthroline)iron(II) of a reaction product. The concentrations of *m*-benzenediol were kept at least 10-fold larger than those of tris(1,10-phenanthroline)iron-(III) in order to ensure pseudo-first-order conditions. In most of the reactions of *o*- and *p*-benzenediols with tris(1,10-phenanthroline)iron(III), second-order conditions were adopted because these reactions were extremely fast under the conditions of excess benzenediols with respect to tris(1,10-phenanthroline)iron(III). The rate constants were evaluated by treating an average-kinetic curve for 10 runs, the Stopped-Flow apparatus being equipped with a micro-computer system for memorizing and averaging the multiple runs. The acidity was kept constant at 0.055, 0.11, or 1.0 mol dm^{-3} in perchloric acid. The ionic strength was adjusted to be 1.0 mol dm^{-3} by the addition of sodium perchlorate solution. The temperature (with ±0.1 °C) of the cell housing was regulated by circulating the thermostated water.

Results

Stoichiometry. By the titration of 2.6×10^{-5} mol dm^{-3} tris(1,10-phenanthroline)iron(III) with *o*- or *p*-benzenediol monitoring the absorbance at 510 nm due to tris(1,10-phenanthroline)iron(II), the stoichiometry was determined to be 2 : 1 for $[Fe(phen)_3^{3+}]$: [bezenediol]. Thus, the stoichiometric equation is written as Eq. 1:

$$2\,Fe(phen)_3^{3+} + H_2A \longrightarrow 2\,Fe(phen)_3^{2+} + A + 2H^+, \quad (1)$$

where H_2A indicates a benzenediol and A, a quinone. The stoichiometry for the reaction between *m*-benzenediol and tris(1,10-phenanthroline)iron(III) was not determined by the titrimetric method due to the slow reaction. A large excess of *m*-benzenediol was necessary for the reaction to proceed completely.

Kinetics of Reaction. The kinetic runs were carried out in the acid solutions so that the acid dissociation of benzenediols could be completely neglected.[4] For the reactions of *o*- and *p*-benzenediols with tris(1,10-phenanthroline)iron(III), when pseudo-first-order conditions were adopted, plots of ln $(A_\infty - A_t)$ *vs.* t were linear for at least 80% of a whole reaction. Moreover, when the reaction was started at a second-order condition of $[Fe(phen)_3^{3+}] = 2[H_2A]$, plots of $1/(A_\infty - A_t)$ *vs.* t were also linear for at least 60% of a whole reaction. This confirms the first-order dependence of each reactant and the stoichiometry given in Eq. 1. Thus, the following empirical rate law can be written:

$$-d[Fe(phen)_3^{3+}]/dt = k_0[Fe(phen)_3^{3+}][H_2A], \quad (2)$$

where k_0 is the observed second-order rate constant. In case of the reaction between *m*-benzenediol and tris(1,10-phenanthroline)iron(III), plots of ln $(A_\infty - A_t)$ *vs.* t were linear for the initial periods of about 20% of a whole reaction and gradually deviated from the straight line under a pseudo-first-order condition. Thus, the rate constants in this case were evaluated by using the initial slope. The second-order rate constants obtained were, within the experimental error, constant irrespective of the reactants over the wide ranges of 5.0×10^{-5} to 5.0×10^{-2} mol dm^{-3} *m*-benzenediol and of 1.2×10^{-6} to 2.0×10^{-5} mol dm^{-3} tris(1,10-phenanthroline)iron(III). However, when tris(1,10-phenanthroline)iron(II) was added to the reaction solution before starting the reaction, the rate of reaction decreased according to the amounts of tris(1,10-phenanthroline)iron(II) added. Unless the amounts of tris(1,10-phenanthroline)iron(II) exceeded about 10% of the tris(1,10-phenanthroline)-iron(III) concentrations, the rate constants obtained from the initial slope of ln $(A_\infty - A_t)$ *vs.* t were not influenced.

Temperature Dependence. The observed second-order rate constants k_0 at varied temperatures were determined under given conditions. The forward rate constants k_1 in Reaction 3 (and Eq. 5) are tabulated in

TABLE 1. TEMPERATURE DEPENDENCE OF THE RATE CONSTANTS AT AN IONIC STRENGTH OF 1.0 mol dm^{-3}

Temp °C	*m*-Benzenediol[a] $10^{-3}k_1$ / dm^3 mol^{-1} s^{-1}	*o*-Benzenediol[b] $10^{-6}k_1$ / dm^3 mol^{-1} s^{-1}	*p*-Benzenediol[c] $10^{-7}k_1$ / dm^3 mol^{-1} s^{-1}
10			12.0[d]
			9.5[e]
			6.3[f]
15	6.9[d]	9.3[d]	13.9[d]
	4.5[e]	8.7[e]	11.6[e]
	0.7[f]	6.5[f]	7.2[f]
20	10.3[d]	11.6[d]	16.4[d]
	6.0[e]	10.6[e]	12.8[e]
	1.1[f]	7.0[f] 8.2[f]	8.2[f]
25	13.4[d]	15.0[d]	17.3[d]
	8.8[e]	13.2[e]	15.0[e]
	1.0[f]	9.2[f]	10.2[f]
30	18[d]	17.7[d]	
	11.0[e]	16.2[e]	
	2.6[f]	10.9[f]	

a) The initial concentrations of *m*-benzenediol and tris(1,10-phenanthroline)iron(III) were 2.0×10^{-3} and 7.0×10^{-6} mol dm^{-3}, respectively. b) and c) The initial concentrations of benzenediols and tris (1,10-phenanthroline)iron (III) were 7.0×10^{-6} and 1.4×10^{-5} mol dm^{-3}, respectively. d), e), and f) indicate the results in 0.055, 0.11, and 1.0 mol dm^{-3} perchloric acid, respectively.

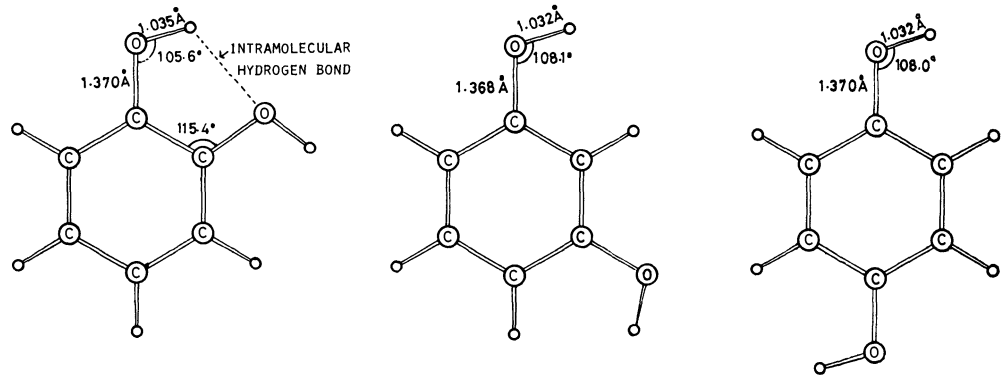

ortho	*meta*	*para*
−0.4332 a.u.	−0.4468 a.u.	−0.4224 a.u.
0.4033 a.u.	0.4183 a.u.	0.3957 a.u.

Fig. 1. The structures of the benzenediols calculated by the CNDO/2 MO, and the values of ε_{HOMO} (negative values in the above) and ΔE_T (positive values in the below). The small empty circle denotes the hydrogen atom. The C–C distance of 1.40 Å and the C–H length of 1.08 Å in the benzene are common to the three molecules. The structure of the cation (H_2A^+) is assumed to be the same as that of the neutral molecule (H_2A). The energy unit is a.u., where 1 a.u. = 2625.7 kJ mol^{-1}. The larger ε_{HOMO} in the absolue and the larger ΔE_T correspond to the more difficult oxidation.

Table 2. Kinetic parameters for the oxidation of *m*-, *o*-, and *p*-benzenediols by tris (1,10-phenanthroline)iron(III), and the estimated redox potentials (E°)[a]

Benzenediols	$\Delta H^{\neq}$ [b] / kJ mol^{-1}	$\Delta S^{\neq}$ [c] / J K^{-1} mol^{-1}	ΔG^{*}_{12} / kJ mol^{-1}	ΔG°_{12} / kJ mol^{-1}	E° / V
m-	42[d]	−28[d]	39.2[d]	31.8[d]	1.39[d]
	41[e]	−32[e]	40.4[e]	33.5[e]	1.41[e] 1.39[e,g]
	57[f]	10[f]	45.0[f]	39.8[f]	1.47[f]
o-	29[d]	−10[d]	22.0[d]	3.52[d]	1.10[d]
	28[e]	−15[e]	22.1[e]	3.71[e]	1.10[e] 1.07[e,g]
	23[f]	−35[f]	23.0[f]	5.42[f]	1.12[f]
p-	15[d]	−36[d]	15.7[d]	−9.57[d]	0.96[d]
	19[e]	−25[e]	16.2[e]	−8.44[e]	0.97[e] 0.94[e,g]
	19[f]	−28[f]	17.3[f]	−6.02[f]	1.00[f]

a) $r_1=4.0\times10^{-10}$ m for benzenediols; $r_2=7.0\times10^{-10}$ m for $Fe(phen)_3^{3+/2+}$; $\lambda_{12}=80.8$ kJ mol^{-1}; the potentials estimated for the reaction $H_2A^+ + e^- \rightleftarrows H_2A$; the error of E° is ±0.01 V. b) The error is $\pm$ 1 kJ mol^{-1}. c) The error is ±4 J K^{-1} mol^{-1}. d), e), and f) indicate the results in 0.055, 0.11, and 1.0 mol dm^{-3} perchloric acid at an ionic strength of 1.0 mol dm^{-3}. g) Evaluated by using $\Delta G^{*}_{11}=23$ and $\Delta G^{*}_{22}=20$ kJ mol^{-1} (see Text).

Table 1, where the observed rate constants k_0 are equal to $2k_1$ (*v. i.*).

Calculation of ε_{HOMO} *and* ΔE_T. To evaluate the oxidation potential theoretically, a CNDO/2 MO[5] calculation was made for *o*-, *m*-, and *p*-benzenediols and the corresponding dihydroxyphenyl radicals. The following two energies may be compared to the redox potentials determined experimentally. One is the energy level of the highest occupied molecular orbital of the neutral species (ε_{HOMO}). This gives the ionization potential of benzenediols of H_2A species. The other is ΔE_T, the difference of the total electronic energies between the neutral molecule and its cation radical of H_2A^+. The ΔE_T corresponds to the energy required to cause $H_2A \rightarrow H_2A^+ + e^-$, and is described as $\Delta E_T = E_T(H_2A^+) - E_T(H_2A)$. The value of E_T of the radical was computed by using the UHF MO. For the calculation of ε_{HOMO} and E_T, the geometries of the molecules were determined through the optimization of the functional group (-OH part). The structure of the benzene ring was fixed throughout this work. The geometries determined in this way are exhibited in Fig. 1, together with the pictures of ε_{HOMO} and ΔE_T.

Discussion

Tris(1,10-phenanthroline)iron(III) is an one-electron oxidizing agent. Thus, the non-complementary oxidation reactions are expected to occur through two successive one-electron transfer reactions, as follows:

$$H_2A + Fe(phen)_3^{3+} \underset{k_{-1}}{\overset{k_1}{\rightleftharpoons}} H_2A^+ + Fe(phen)_3^{2+}, \quad (3)$$

$$H_2A^+ + Fe(phen)_3^{3+} \xrightarrow{k_2} Fe(phen)_3^{2+} + 2H^+ + A. \quad (4)$$

Assuming the steady state conditions for the concentrations of H_2A^+ species, the following rate equation can be derived:

$$-d[Fe(phen)_3^{3+}]/dt = \left\{1 + \frac{k_2[Fe(phen)_3^{3+}]}{k_{-1}[Fe(phen)_3^{2+}] + k_2[Fe(phen)_3^{3+}]}\right\} \times k_1[H_2A][Fe(phen)_3^{3+}]. \quad (5)$$

When the condition of $k_2[Fe(phen)_3^{3+}] \gg k_{-1}[Fe(phen)_3^{2+}]$ is satisfied, Eq. 5 can be represented by the empirical rate law of Eq. 2 with relationship of $k_0=2k_1$. These conditions were fulfilled for the reactions of *o*- and *p*-benzenediols with tris(1,10-phenanthroline)iron(III) for at least 80% of a whole reaction, and for the reactions of *m*-benzenediol with tris(1,10-phenanthroline)iron(III) for about 20% of a whole reaction. In the reaction of *m*-benzenediol, the rate of reaction decreased with increasing the ratios of $[Fe(phen)_3^{2+}]_i/[Fe(phen)_3^{3+}]_i$, and the value of k_{-1}/k_2 was approximately 0.7. According to the Marcus theory[1] for the outer-sphere electron transfer reaction, the excess free energy of activation for a cross reaction (ΔG^{*}_{12}) varies with the standard free energy change (ΔG°_{12}) for the redox step, as shown in Eqs. 6 and 7:

$$\Delta G^{*}_{12} = \omega_{12} + \lambda_{12}(1+\Delta G^{\circ}_{12}/\lambda_{12})^2/4, \quad (6)$$

$$\lambda_{12} = 2(\Delta G^{*}_{11} - \omega_{11} + \Delta G^{*}_{22} - \omega_{22}), \quad (7)$$

where ΔG^{*}_{11} and ΔG^{*}_{22} are the activation free energies for the self-exchange electron-transfer reactions, and ω_{11} and ω_{22} represent the work terms involved in the same reactions; ω_{12} is the work term required to bring the reactants onto the activated complex. The work terms can be evaluated from Eq. 8:

$$\omega_{ij} = \frac{Z_1 Z_2 e^2}{D_s r_{ij}} \exp[-\kappa r_{ij}], \quad (8)$$

where Z_1 and Z_2 are the formal charges of reactants, e is the electron charge, D_s is the static dielectric constant, r_{ij} is the distance of the closest approach of the reactants in the activated complex, and κ is the reciprocal Debye radius. According to the Marcus theory,[1] the parameter λ_{12} is equal to $\lambda_o+\lambda_i$, where λ_o is the solvent reorientation term and λ_i is the contribution term from the inner-sphere change in bond lengths and angles in the molecules. When λ_i is negligible, then λ_{12} is set to be λ_0, which is represented as Eq. 9:

$$\lambda_0 = \left(\frac{1}{2r_1} + \frac{1}{2r_2} - \frac{1}{r_{12}}\right)\left(\frac{1}{n^2} - \frac{1}{D_s}\right)(\Delta e)^2, \quad (9)$$

where r_1 and r_2 are the radii of the reactants, r_{12} is the distance between the reacting centers in the activated state and can be approximately set as (r_1+r_2), n is the

refractive index of the medium, D_s the static dielectric constant, and Δe the charge transferred. By assuming $r_1=4.0\times10^{-10}$ m for *o*-, *m*-, and *p*-benzenediols[6,7] and $r_2=7.0\times10^{-10}$ m for tris(1,10-phenanthroline)iron(III),[8] $n=1.342$,[9] and $D_s=78.5$,[10] the value of λ_0 is calculated to be 80.8 kJ mol^{-1}. The work terms for the forward reaction of Eq. 3 are evaluated to be zero for ω_{12} and ω_{11}, and 0.08 kJ mol^{-1} for ω_{22} at an ionic strength of 1.0 mol dm^{-3} at 25 °C. The activation free energy ΔG^*_{12} is described as follows:

$$k_{12} = Z \exp\left[-\Delta G^*_{12}/RT\right], \qquad (10)$$

where Z is the collision frequency in solution and is usually taken as 10^{11} at 25 °C. Thus, the ΔG^*_{12} for the forward reaction of Eq. 3 are determined by using the data in Table 1. By using the parameters obtained, the value of ΔG°_{12} can be evaluated by Eq. 6. The ΔG°_{12} allows the estimation of the standard redox potentials of the cation radicals of *o*-, *m*-, and *p*-benzenediols. By using $E^\circ(\mathrm{Fe(phen)_3^{3+/2+}})=1.06$ V,[11] the values of the standard reduction potentials of the cation radicals were estimated; these are shown in Table 2. The potentials of the radicals could be estimated without knowledge of the contributions of ΔG^*_{11}, ΔG^*_{22}, ω_{11}, and ω_{22}. The rate constant for the self-exchange reaction of tris(1,10-phenanthroline)iron(III) and -(II) has been reported to be larger than 3×10^7 dm^3 mol^{-1} s^{-1} at 25 °C.[12] Meisel[13] has reported that the observed self-exchange rate constants for a series of reactions between the organic radicals and the parent molecules fall in the range of 1×10^7 to 1×10^9 dm^3 mol^{-1} s^{-1}. If we adopt the values of 3×10^7 dm^3 mol^{-1} s^{-1} for k_{22} of $\mathrm{Fe(phen)_3^{3+/2+}}$ and 1×10^7 dm^3 mol^{-1} s^{-1} for k_{11} of $\mathrm{H_2A^+/H_2A}$, the activation free energies of ΔG^*_{22} and ΔG^*_{11} are evaluated to be 20 and 23 kJ mol^{-1} for $\mathrm{Fe(phen)_3^{3+/2+}}$ and $\mathrm{H_2A^+/H_2A}$ from Eq. 10, respectively.[14] This leads to the value of 86 kJ mol^{-1} for λ_{12}. Therefore, we can determine the values of $E^\circ(\mathrm{H_2A^+/H_2A})$ to be 1.39, 1.07, and 0.94 V in 0.11 mol dm^{-3} perchloric acid solution for *m*-, *o*-, and *p*-benzenediols, respectively. These values are in good agreement with the corresponding ones which are estimated without using ΔG^*_{11} and ΔG^*_{22} and neglecting λ_i (refer to Table 2). The values of $E^\circ(\mathrm{H_2A^+/H_2A})$ increased slightly with increasing acidity in *m*- and *p*-benzenediols. This may indicate some contributions of Reaction 11, which involves a simultaneous transfer of an electron and a proton:

$$\mathrm{HA^\cdot + H^+ + e^- \rightleftharpoons H_2A.} \qquad (11)$$

The Marcus theory[1] holds for a reaction which occurs adiabaticly by the outer-sphere electron transfer reaction, and thus, the activation entropy is expected to be close to zero. Although the collision frequency (Z) is generally assumed to be 10^{11} dm^3 mol^{-1} s^{-1} in solution, the pre-exponential factor deviates sometimes from the value, indicating some contribution of a non-adiabatic reaction. The activation enthalpy and entropy ΔH^* and ΔS^* can be determined by assuming $\kappa=1$ in Eyring's absolute rate equation:

$$k = \kappa \frac{kT}{h} \exp\left[\Delta S^*/R\right] \exp\left[-\Delta H^*/RT\right], \qquad (12)$$

where κ is the probability of the electron-transfer within the activated complex. The values of ΔH^* and ΔS^* were estimated by assuming $\kappa=1$; they are listed in Table 2 together with the other parameters.

It is of interest to interpret theoretically the order of the redox potentials of *o*-, *m*-, and *p*-benzenediols and to compare them to those estimated experimentally. Since the environment effect such as the solvent effect on the potentials is expected to be almost the same among these isomers, the differences of the genuine electronic properties must be related to the order of the redox potentials. According to the results in Fig. 1, both ε_{HOMO} and ΔE_T indicate that the ease for the oxidation is in the order of *m*-<*o*-<*p*-. This trend is well correlated with that obtained experimentally by the application of Marcus theory to the kinetic parameters. The order of these potentials is ascribed to the positional difference of the O–H group. To apply the orbital interaction scheme to this analysis, benzenediol is regarded as a system of phenol and O–H group. In this respect, the HOMO of benzenediols is mainly composed of the highest occupied MO of phenol (*homo*) and the p_π atomic orbital on the oxygen of the O–H group. Thus, ε_{HOMO} is determined by the extent of this orbital interaction. Examining the shape of *homo* in

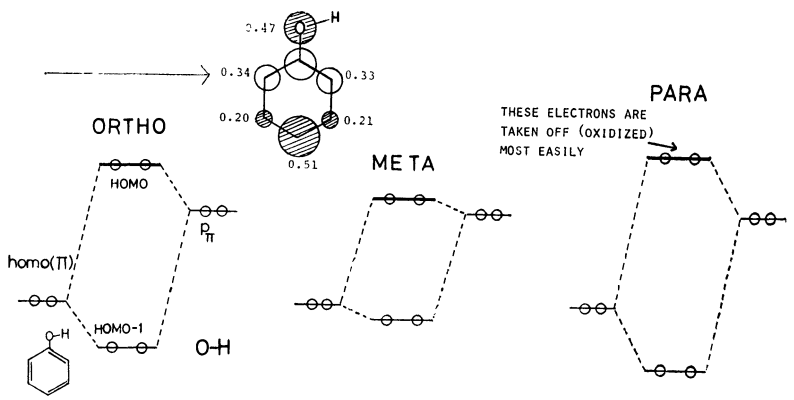

Fig. 2. Schematic sketch of the orbital interaction between homo of phenol and the pπ atomic orbital of the O–H group. The HOMO levels of benzenediols (ε_{HOMO}) are determined by the extent of this orbital interaction. The degree of the interaction is ascribed to the coefficient attached to the atomic orbital of homo, the coefficient being shown by the absolute value in this figure.

Fig. 2, one may find that the *para* position has the largest coefficient (0.51), the *ortho* is of the second (0.33 or 0.34) and the *meta* is of the smallest one (0.21 or 0.20). Since the position with the large coefficient undergoes the large extent of the orbital interaction (the bigger energy splitting in Fig. 2), the order of the coefficients should be reflected in that of ε_{HOMO}. This prediction is confirmed by the comparison of the values of ε_{HOMO} in Fig. 1. Thus, the order of the ease of oxidation may be interpreted in terms of the orbital interaction and the origin of the difference of ε_{HOMO} is basically the same as the *ortho, para orientation* for the nucleophilic substitution onto the benzene ring of phenol.

This work was partly supported by a Grant-in-Aid for Scientific Research B (No. 447039) from the Ministry of Education, Science and Culture.

References

1) R. A. Marcus, *J. Phys. Chem.*, **72**, 891 (1968).
2) E. Pelizzetti and E. Mentasti, *Z. Phys. Chem.*, **105**, 21 (1977).
3) E. Pelizzetti, E. Mentasti, and E. Pramauro, *Inorg. Chem.*, **17**, 1181 (1978).
4) "Stability Constants of Metal-Ion Complexes," ed by L.G. Sillén and E. Martell, Chem. Soc. Special Publication No. 25, 1971, pp. 400 and 403: pK_1 9.30, pK_2 11.06 for *m*-H_2A; pK_1 9.45, pK_2 12.8 for *o*-H_2A; not given for *p*-H_2A.
5) J. A. Pople and D. L. Beveridge, "Approximate Molecular Orbital Theory," McGraw-Hill, New York (1970).
6) Using the equation $4\pi r^3/3=M/(\rho N)$ where N is Avogadro's number, ρ the density, and M the molecular weight, a value of $r=3.4\times10^{-10}$ m can be obtained for a series of benzenediols (Refs. 2 and 7). A value 4×10^{-10} m is adopted as r in the present paper.
7) M. E. Peover, *Electrochim. Acta*, **13**, 1083 (1968).
8) J. E. Dickens, F. Basolo, and H. M. Neumann, *J. Am. Chem. Soc.*, **79**, 1289 (1957).
9) "Chemical Handbook (Kagaku-Binran)," *ed by* the Chemical Society of Japan, Maruzen (1969), p. 1113. The value in aqueous solution of 1 mol dm^{-3} potassium nitrate at 17.5 °C.
10) G. Åkerlöf, *J. Am. Chem. Soc.*, **54**, 4126 (1932); The value at 25 °C.
11) N. Sutin and B. M. Gordon, *J. Am. Chem. Soc.*, **83**, 70 (1961).
12) D. W. Larsen and A. C. Wahl, *J. Chem. Phys.*, **43**, 3765 (1965).
13) D. Meisel, *Chem. Phys. Lett.*, **34**, 263 (1975).
14) The values of ΔG^*_{11} and ΔG^*_{22} were estimated by using the equation: $k=10^{11}\ exp\ [-\Delta G^*/RT]$ at 25 °C.

Kinetics and Equilibrium of the Reaction between Bis(trifluoroacetylacetonato)palladium(II) and Tri-*o*-tolylphosphine

Shinichi MATSUMOTO and Shinichi KAWAGUCHI*

Department of Chemistry, Faculty of Science, Osaka City University, Sumiyoshi-ku, Osaka 558

(Received October 2, 1980)

Tri-*o*-tolylphosphine reacts with bis(trifluoroacetylacetonato)palladium(II), $Pd(tfac)_2$, to convert one of the chelating ligands into the unidentate state, resulting in $Pd(tfac)(tfac\text{-}O)P(o\text{-tolyl})_3$. The reaction was studied by a spectrophotometric method. The equilibrium constant was determined at several temperatures, K being 1.38×10^3, 4.35×10^3 dm^3 mol^{-1} and more than 10^9 dm^3 mol^{-1} in benzene, dichloromethane, and methanol, respectively, at 25 °C. In the presence of excess phosphine, the reaction proceeds as a pseudo first order reaction to attain equilibrium. The forward and reverse rate constants, k_1 and k_{-1}, were obtained as 0.172 dm^3 mol^{-1} s^{-1} and 1.22×10^{-4} s^{-1} in benzene and 2.28 dm^3 mol^{-1} s^{-1} and 4.9×10^{-4} s^{-1} in dichloromethane at 25 °C, respectively. In methanol the forward rate was measured under irreversible pseudo first order conditions and conforms with the usual two term rate law, $k_{obsd}/s^{-1}=2\times10^{-3}+56.6[P(o\text{-tolyl})_3]$. The remarkable dependence of K and k_1 on the nature of solvent is related to the hydrogen bonding interaction between the carbonyl group of the coordinated tfac anion and a solvent molecule.

The kinetic study in a previous paper[1] of the reactions between bis(acetylacetonato)palladium(II) and alkylamines (L) to afford the mixed-ligand cationic complexes of the $[Pd(acac)L_2](acac)$ type revealed that $Pd(acac)(acac\text{-}C^3)L$ is not an intermediate in this reaction but is formed *via* the above outer-sphere complex.** A complex such as $Pd(acac)(acac\text{-}O)L$ containing an *O*-unidentate acetylacetonate anion is then supposed to be involved as an intermediate in the reaction pathway, although it is not sufficiently accumulated to be detected spectrophotometrically.

Mercury(II)[2,3] and silicon(IV)[4,5] complexes containing an oxygen-bonded β-diketonate anion as a unidentate ligand have been reported. Recently the reactions of bis(acetylacetonato)platinum(II) with triethylphosphine[6] at low temperature (<-10 °C) and with piperidine[7] at 70 °C were found to give the $Pt(acac\text{-}O)_2L_2$ complexes. Similarly the reaction of dimethyl(acetylacetonato)gold(III) with tricyclohexylphosphine[8] and reactions of bis(trifluoroacetylacetonato)-platinum(II) and -palladium(II) with tri-*o*-tolylphosphine[9] also gave the *O*-bonded β-diketonato complexes. The present paper reports on the kinetic and equilibrium studies of the reaction between bis(trifluoroacetylacetonato)palladium(II) and tri-*o*-tolylphosphine.

Experimental

Materials. Tri-*o*-tolylphosphine was recrystallized from ethanol and stored under nitrogen. Methanol and benzene were dried with Linde Molecular Sieves 3A and 4A, respectively, and distilled before use. Dichloromethane was stored over sodium carbonate, dried with Linde Molecular Sieve 4A, and distilled. Water contents of these solvents were determined with an MCI digital water microanalyzer CA-01 to be $3—4\times10^{-3}$ mol dm^{-3} for methanol and $1—2\times10^{-3}$ mol dm^{-3} for benzene and dichloromethane.

Bis(trifluoroacetylacetonato)palladium(II), $Pd(tfac)_2$, was prepared according to Okeya *et al.*[10] by reacting sodium hexachlorodipalladate(II) with trifluoroacetylacetone in methanol containing sodium carbonate. Found: C, 29.13; H, 1.94%. Calcd for $C_{10}H_8O_4F_6Pd$: C, 29.11; H, 1.95%.

Trifluoroacetylacetonato(trifluoroacetylacetonato-*O*) (tri-*o*-tolylphosphine)palladium(II), $Pd(tfac)(tfac\text{-}O)P(o\text{-tolyl})_3$, was also prepared by the method of Okeya *et al.*[9] A solution in benzene (20 cm^3) of $Pd(tfac)_2$ (0.602 g, 1.46 mmol) and $P(o\text{-tolyl})_3$ (0.456 g, 1.50 mmol) was stirred for 1 h and then concentrated to *ca.* 3 cm^3 by evaporation under reduced pressure. Petroleum ether (bp *ca.* 40 °C) was added dropwise to the concentrate to deposit an orange precipitate in an 85% yield, which was recrystallized from benzene–petroleum ether. Found: C, 52.07; H, 4.11%. Calcd for $C_{31}H_{29}O_4PF_6Pd$: C, 51.92; H, 4.08%.

Measurements. For the kinetic and equilibrium studies, absorbance at 380 nm was used which involves negligible contribution by uncoordinated $P(o\text{-tolyl})_3$. In benzene and dichloromethane, $Pd(tfac)_2$ ($8—24\times10^{-5}$ mol dm^{-3}) was allowed to react with excess $P(o\text{-tolyl})_3$ ($8—21\times10^{-4}$ mol dm^{-3}) and the pseudo first order rate to attain the equilibrium was determined. In methanol, the equilibrium shifts further to right and a large excess of the phosphine ($1—4\times10^{-3}$ mol dm^{-3}) was used to measure the irreversible first order rate. The reverse reaction of $Pd(tfac)(tfac\text{-}O)P(o\text{-tolyl})_3$ in benzene to produce $Pd(tfac)_2$ was also followed spectrophotometrically, and the first order rate constant was obtained by analyzing the initial stage of reaction. Spectral measurements were carried out with a Hitachi EPS-3T recording spectrophotometer and a Union stopped-flow rapid-scan spectrophotometer RA-1300.

Results and Discussion

Equilibria of the Reaction. When a mixture of $Pd(tfac)_2$ and $P(o\text{-tolyl})_3$ was stirred in benzene or dichloromethane for 24 h, the following reaction attained equilibrium. Concentrations of both the palladium(II) complexes were calculated from their absorption spectra shown in Fig. 1. Values of the equilibrium constant K thus obtained in both solvents

$$Pd(tfac)_2 + P(o\text{-tolyl})_3 \underset{k_{-1}}{\overset{k_1}{\rightleftharpoons}} Pd(tfac)(tfac\text{-}O)P(o\text{-tolyl})_3,\ K \qquad (1)$$

** In this paper, acac and tfac represent the acetylacetonate and trifluoroacetylacetonate anions, respectively, chelating a metal ion through two oxygen atoms, while acac-*O*, tfac-*O*, and acac-C^3 refer to the oxygen-bonded and central-carbon-bonded states, respectively.

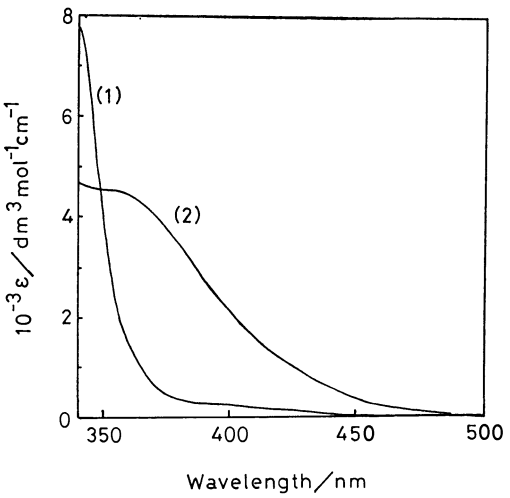

Fig. 1. Absorption spectra of $Pd(tfac)_2$ (curve 1) and Pd(tfac) (tfac-*O*) $P(o\text{-tolyl})_3$ (curve 2) in benzene.

Table 1. Equilibrium constants of the reaction between $Pd(tfac)_2$ and $P(o\text{-tolyl})_3$ (Eq. 1)

Solvent	Temp / K	$10^{-3}K$ / dm^3 mol^{-1}	$\Delta H°$ / kJ mol^{-1}	$\Delta S°$ / J K^{-1} mol^{-1}
C_6H_6	318	0.680		
	308	0.958		
	298	1.38	−27.4±0.2	−32.0±0.6
	288	2.00		
CH_2Cl_2	298	4.35	−41.2±2.1	−68.7±7.1
	293	5.33		
	288	7.28		
	283	10.4		

at several temperatures are listed in Table 1. The plot of ln K against $1/T$ gave good straight lines (Fig. 2), from which the thermodynamic parameters were calculated and included in Table 1. Similar experiments in methanol were not successful for determining the equilibrium constant because of its too large value. Conversely, a methanol solution of Pd(tfac)(tfac-*O*)$P(o\text{-tolyl})_3$ was kept in a 5-cm cell and degree of the phosphine dissociation was determined. In this way the value of K in methanol at 25 °C was estimated to be larger than 10^9 dm^3 mol^{-1}.

As is seen in Table 1, reaction (1) is exothermic and the K value depends remarkably on the nature of solvent, increasing in the sequence, benzene<dichloromethane≪methanol. The dangling carbonyl group of the unidentate tfac ligand might be stabilized by interaction with the hydrogen-bonding solvent. Even in the presence of a large excess of the phosphine, however, the product complex shows no sign of further substitution, whereas tricyclohexylphosphine (PCy_3) reacts with $Pd(tfac)_2$ to afford not only Pd(tfac)(tfac-*O*)-PCy_3 but also $[Pd(tfac)(PCy_3)_2](tfac)$.[9] The large steric requirement of $P(o\text{-tolyl})_3$ seems to make the bisphosphine complex thermodynamically unfavorable.

Kinetics of the Reaction in Benzene and Dichloromethane. When $Pd(tfac)_2$ reacts with $P(o\text{-tolyl})_3$ in benzene or dichloromethane, absorption spectrum of the solution changes with time, exhibiting an isosbestic point at 348 nm, to reach a final spectrum corresponding to an equilibrium mixture of the two complexes. The plot of $\ln(A_t - A_\infty)$ against time gave a straight line covering

Table 2. The pseudo first order rate constant for equilibrium attainment of reaction(1) at 25 °C

Solvent	10^4[Complex] / mol dm^{-3}	10^3[Phosphine] / mol dm^{-3}	$10^3 k_{obsd}$ / s^{-1}
C_6H_6	1.360	0.8140	0.262
		1.161	0.320
		1.380	0.363
		1.715	0.415
		2.105	0.485
CH_2Cl_2	2.176	0.8610	2.44
		1.151	3.12
	1.978	1.435	3.75
		1.628	4.20
		1.805	5.59
CH_3OH	1.954	1.557	90.6
		1.984	116
		2.536	146
	2.356	2.602	148
		3.569	206

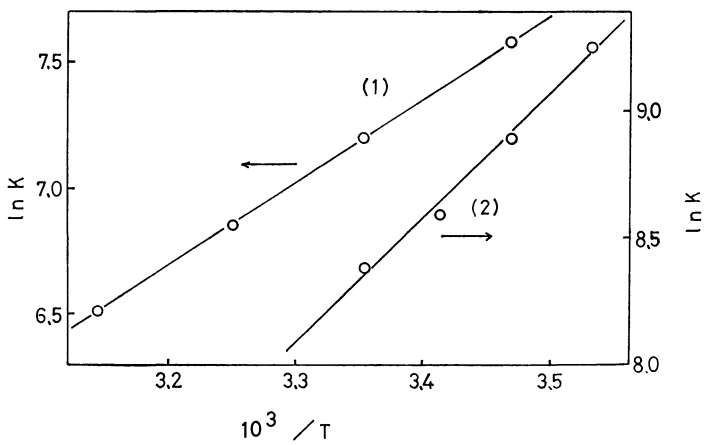

Fig. 2. Plot of ln K for reaction (1) in benzene (line 1) and dichloromethane (line 2) against $1/T$.

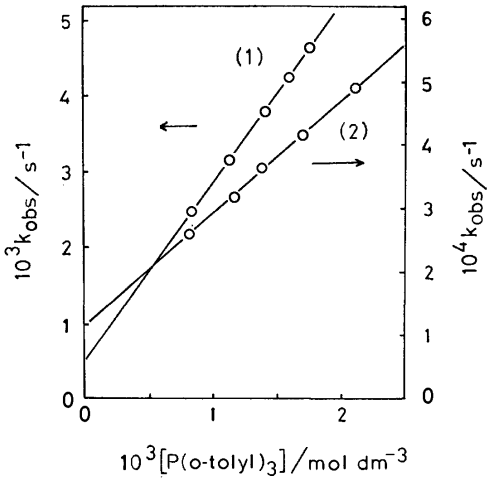

Fig. 3. Plot of the pseudo first order rate constant for the equilibrium attainment of reaction (1) in dichloromethane (line 1) and benzene (line 2) at 25 °C against the concentration of $P(o\text{-tolyl})_3$.

absorbances of the solution at 380 nm at time t and equilibrium, respectively. Thus the rate of reaction is expressed by Eq. 2 and the pseudo first order rate constant k_{obsd} increases with the concentration of $P(o\text{-tolyl})_3$ (Table 2).

$$\text{rate} = k_{obsd}[Pd(tfac)_2] \quad (2)$$

The plots of k_{obsd} against concentration of the phosphine give straight lines (Fig. 3) in line with the equation

$$k_{obsd} = k_1[P(o\text{-tolyl})_3] + k_{-1}. \quad (3)$$

TABLE 3. FORWARD AND REVERSE RATE CONSTANTS FOR REACTION (1) AT 25 °C

Solvent	$10^3 k_0/s^{-1}$	$k_1/dm^3\ mol^{-1}\ s^{-1}$	$10^4 k_{-1}/s^{-1}$
C_6H_6		0.172±0.002	1.22±0.02
CH_2Cl_2		2.28 ±0.01	4.9±0.2
CH_3OH	2±1	56.6 ±0.6	

more than three half-lives. Here A_t and A_∞ represent The forward and reverse rate constants, k_1 and k_{-1} obtained from the slope and intercept of the straight line, respectively, are given in Table 3. Both the forward and the reverse reactions are faster in dichloromethane than in benzene. The values of $K=k_1/k_{-1}$ calculated from these rate constants in benzene and dichloromethane are 1410 and 4650 $dm^3\ mol^{-1}$, respectively, at 25 °C, showing satisfactory coincidence with those obtained from the equilibrium measurements (Table 1).

When a solution of Pd(tfac)(tfac-*O*)$P(o\text{-tolyl})_3$ in benzene (*ca.* 10^{-4} mol dm^{-3}) is left to stand, the phosphine molecule is expelled from the coordination sphere to produce $Pd(tfac)_2$. The reaction attains equilibrium after decomposition of *ca.* 90% of the mixed-ligand complex (Fig. 4). Values of the first order rate constant k_{-1} obtained by analyzing the early stage of the reaction at a few temperatures are given in Table 4. The k_1 values at each temperature were calculated by combining the value of k_{-1} with that of K. The values of k_1 and k_{-1} at 25 °C thus obtained coincide with those

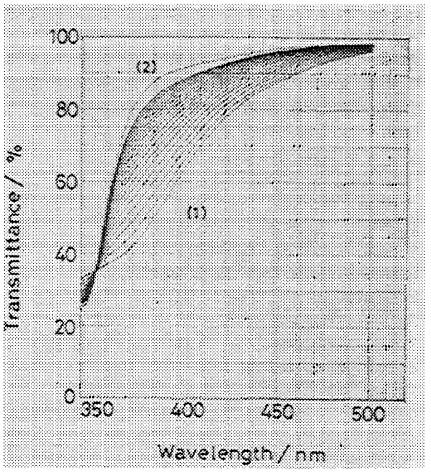

Fig. 4. Change with time of the absorption spectrum of a solution of Pd(tfac)(tfac-*O*)$P(o\text{-tolyl})_3$ in benzene at 25 °C, curves 1 and 2 representing the spectra 5 min and 24 h after commencement of the reaction, respectively. The initial concentration of the starting complex was 1.360×10^{-4} mol dm^{-1}.

TABLE 4. THE RATE CONSTANTS AND ACTIVATION PARAMETERS IN BENZENE

Temp / K	$10\,k_1$ / $dm^3\ mol^{-1}\ s^{-1}$	$10^4\,k_{-1}$ / s^{-1}
298	1.71[a]	1.24±0.01[b]
	1.72±0.02[c]	1.22±0.02[c]
308	1.94[a]	2.03±0.02[b]
318	2.60[a]	3.82±0.04[b]
ΔH^*/kJ mol^{-1}	14±3	42±3
ΔS^*/J K^{-1} mol^{-1}	−210±10	−180±10

a) Calculated by combining the values of k_{-1} and K at each temperature. b) Determined directly by following the reverse reaction of (1). c) Determined by following the equilibrium attainment of (1).

determined under the reversible reaction conditions. The activation parameters related to k_1 and k_{-1} in benzene were obtained from the Eyring plot and are included in Table 4. The data used for calculations are insufficient to allow detailed discussion, but the small values of ΔH^* associated with k_1 accords with the fast rate of reaction (1), ΔS^* being largely negative as is expected for the associative mechanism. Even ΔS^* for the reverse k_{-1} reaction is largely negative and might be related with the intramolecular nucleophilic attack of the dangling trifluoroacetyl group on the central metal atom. The differences between the kinetic parameters, $\Delta(\Delta H^*)$ and $\Delta(\Delta S^*)$, for the forward and reverse processes of reaction (1) coincide with $\Delta H°$ and $\Delta S°$ determined by equilibrium studies.

Kinetics of the Reaction in Methanol. The reaction in methanol was carried out under the irreversible pseudo first order conditions employing a large excess of $P(o\text{-tolyl})_3$. The plot of k_{obsd} thus obtained (Table 2) against the concentration of $P(o\text{-tolyl})_3$ gives a straight line (Fig. 5). The intercept of the straight line can not be the reverse rate contrary to the case for the reaction in benzene and dichloromethane (Fig. 3), since the

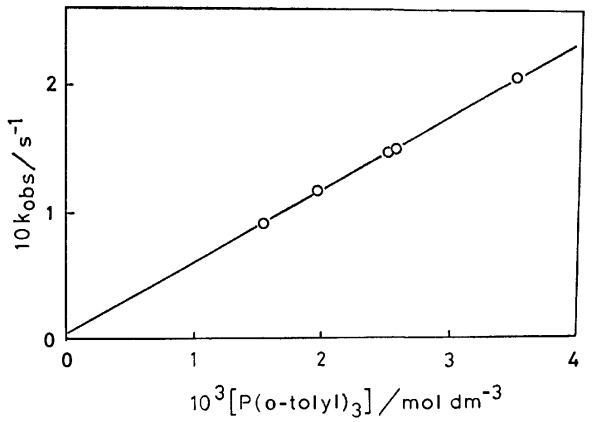

Fig. 5. Plot of the pseudo first order rate constant for the forward reaction of (1) in methanol at 25 °C against the concentration of $P(o\text{-tolyl})_3$.

equilibrium constant in methanol was estimated to be greater than 10^9 dm^3 mol^{-1}. The rate thus follows the two term rate law:

$$k_{obsd} = k_0 + k_1[P(o\text{-tolyl})_3]. \quad (4)$$

This type of rate equation is widely applicable to the ligand substitution reactions of square planar complexes,[11] the first term being attributed to the nucleophilic attack of a solvent molecule on the complex. In the case of Fig. 3, the intercept was entirely ascribed to the reverse rate, giving a consistent value of equilibrium constant. Thus the solvent path is not involved in the forward reaction in benzene and dichloromethane, but contributes a little to the reaction in methanol which has higher coordination ability.

The rate constant k_1 for the reagent path also depends remarkably on the nature of solvent, decreasing in the sequence $CH_3OH \gg CH_2Cl_2 > C_6H_6$ (Table 3). The ratio of rates in methanol and benzene, 330 : 1, is larger than that (180 : 1) observed for the reaction of $Pd(acac)_2$ with dipropylamine.[1] Such a solvent effect might be related to the difference in hydrogen-bonding ability. A solvent molecule might interact with a carbonyl group of the coordinated tfac anion, enhancing the one bond cleavage of the chelated ligand. Of the three kinds of solvents, methanol has the highest tendency of hydrogen bonding and dichloromethane possesses weak hydrogen donating ability.[12]

The change of spectrum during the course of reaction (1) in each solvent shows a distinct isosbestic point, indicating that the five-coordinate intermediate is not accumulated enough to be detected spectrophotometrically. Bis(hexafluoroacetylacetonato)palladium(II) reacts with $P(o\text{-tolyl})_3$ to afford $Pd(hfac)_2P(o\text{-tolyl})_3$, which was confirmed by X-ray analysis to have a squarepyramid structure with the phosphine at a basal position.[13] On the other hand, $Pd(acac)_2$ does not react with $P(o\text{-tolyl})_3$ at all.[9] The three related Pd-(β-dik)$_2$ complexes show substantially different tendency of reaction with $P(o\text{-tolyl})_3$.

The starting complex $Pd(tfac)_2$ was reported to have the *trans* configuration in solid but exist as a mixture of *cis* and *trans* (1 : 3) in C_6D_6.[10] As to the structure of the reaction product, there exist the following two possibilities and the ^1H NMR spectrum in $CDCl_3$ showed that the isomer ratio *cis*(Me, L)/*trans*(Me, L) in equilibrium is 1/5.[9]

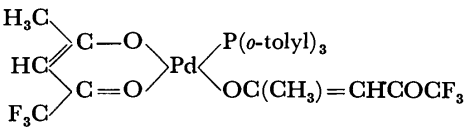

cis(Me, L)

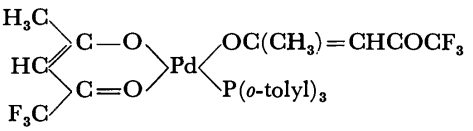

trans(Me, L)

This work was partly supported by Grant-in-Aid for Scientific Research No. 243014 from the Ministry of Education, Science and Culture. A scholarship given to S. M. by the Suntory Institute for Bioorganic Research is acknowledged.

References

1) S. Matsumoto and S. Kawaguchi, *Bull. Chem. Soc. Jpn.*, **53**, 1577 (1980).
2) G. S. Hammond, D. C. Nonhebel, and C.-H. S. Wu, *Inorg. Chem.*, **2**, 73 (1963); D. C. Nonhebel, *J. Chem. Soc.*, **1963**, 738.
3) R. H. Fish, *J. Am. Chem. Soc.*, **96**, 6664 (1974).
4) R. West, *J. Am. Chem. Soc.*, **80**, 3246 (1958).
5) J. J. Howe and T. J. Pinnavaia, *J. Am. Chem. Soc.*, **91**, 5378 (1969); T. J. Pinnavaia, W. T. Collins, and J. J. Howe, *ibid.*, **92**, 4544 (1970); T. J. Pinnavaia and J. A. McClarin, *ibid.*, **96**, 3012 (1974).
6) T. Ito, T. Kiriyama, and A. Yamamoto, *Chem. Lett.*, **1976**, 835.
7) S. Okeya, F. Egawa, Y. Nakamura, and S. Kawaguchi, *Inorg. Chim. Acta*, **30**, L319 (1978).
8) S. Komiya and J. K. Kochi, *J. Am. Chem. Soc.*, **99**, 3695 (1977).
9) S. Okeya, Y. Nakamura, and S. Kawaguchi, 25th Symposium Organomet. Chem. Jpn., Oct., 1978, Osaka, Abstr. p. 35.
10) S. Okeya, S. Ooi, K. Matsumoto, Y. Nakamura, and S. Kawaguchi, *Bull. Chem. Soc. Jpn.*, Submitted for publication.
11) F. Basolo and R. G. Pearson, "Mechanism of Inorganic Reactions," 2nd ed, Wiley, New York (1967), Chap. 5.
12) R. W. Taft and M. J. Kamlet, *J. Am. Chem. Soc.*, **98**, 2886 (1976).
13) S. Okeya, T. Miyamoto, Y. Nakamura, S. Ooi, and S. Kawaguchi, *Inorg. Chim. Acta*, **45**, L147 (1980).

Reaction Process between Zinc Oxide and Sulfur Dioxide in the Presence of Carbon

Akimasa YAJIMA, Ryoko MATSUZAKI, and Yuzo SAEKI*

Research Laboratory of Resources Utilization, Tokyo Institute of Technology, 4259, Nagatsuta-cho, Midori-ku, Yokohama 227

(Received October 21, 1980)

The reaction products obtained by heating a mixture of ZnO and carbon in a SO_2 stream at various temperatures were examined. The possible reactions during the above process were also examined. When a mixture of ZnO and carbon was heated in a SO_2 stream, the formation of ZnS was observed above 600 °C. At 800 °C, all the ZnO used was converted to ZnS. Sulfur was also obtained outside the heating zone, and its amount increased markedly above *ca.* 750 °C. The ZnS formed was a mixture of α-ZnS and β-ZnS regardless of the reaction temperature. The process of formation of ZnS can be represented as follows: the reaction between carbon and SO_2 occurs at first to form sulfur. Above *ca.* 600 °C, the reaction between ZnO and the sulfur occurs to form ZnS. In addition to these reactions, the reduction of ZnO with carbon occurs slightly to form zinc, which then reacts with sulfur to form ZnS.

The chemical process for synthesizing metal sulfides from the oxides using sulfur dioxide(SO_2) as a sulfidizing agent is not only interesting from the viewpoint of the synthesis itself, but also important for the development of SO_2 utilization. In this work, the reaction process between zinc oxide (ZnO) and SO_2 in the presence of carbon was examined in order to understand the above chemical process.

Regarding the reaction between ZnO and SO_2 in the presence of carbon, little information has been available apart from the work of Pechkovskii,[1] who reports that zinc sulfide (ZnS) is formed at 650—800 °C by heating a mixture of ZnO and carbon in a SO_2 stream and that 91.8% of the charged ZnO is sulfidized at 800 °C by using a 4 : 1 mixture of carbon and ZnO (molar ratio). The formation process of ZnS and the modification of ZnS formed have not been described.

In this work, the reaction products between ZnO and SO_2 in the presence of carbon at various temperatures were examined. The reactions between ZnO and carbon, between ZnO and gaseous sulfur in a SO_2 stream, and between zinc and gaseous sulfur in a SO_2 stream were also examined in order to elucidate the reaction process between ZnO and SO_2 in the presence of carbon.

Experimental

The ZnO used was prepared by the thermal decomposition of tetrazinc monocarbonate hexahydroxide monohydrate ($Zn_4CO_3(OH)_6 \cdot H_2O$), which was prepared by adding ammonium carbonate solution to zinc nitrate solution, at 600 °C.[2] The carbon was prepared by the thermal decomposition of the guaranteed reagent D-glucose. The above materials were used as powders under 150 mesh. Zinc (guaranteed reagent, sandy form) was used after washing with acetone and with dilute hydrochloric acid. Gaseous SO_2 was dried by passing it through concd H_2SO_4 and over P_2O_5.

A mixture of ZnO and carbon at a specified ratio in a quartz boat (length: 72 mm, width: 16 mm, depth: 9 mm) was placed in a transparent quartz reaction tube (inner diameter: 28 mm, length: 1000 mm). Gaseous SO_2 was then introduced into the reaction tube. The sample part was positioned in the middle of a tubular electric furnace (heating length: 300 mm) maintained at a specified temperature for 1 h. The temperature of the sample part was controlled within ±2 °C. After heating, the sample was held at 100 °C for 1 h in an argon stream in order to release the adsorbed SO_2 on unreacted carbon.[3] The reactions between ZnO and carbon in an argon stream, between ZnO and gaseous sulfur in a SO_2 stream, and between zinc and gaseous sulfur in a SO_2 stream were examined in a similar manner.

The X-ray analysis of the sample was performed with an X-ray powder diffractometer equipped with a proportional counter using Ni filtered Cu radiation.

Results and Discussion

Reaction Products between ZnO and SO_2 in the Presence of Carbon. Prior to the examination of the reaction products between ZnO and SO_2 in the presence of carbon, the thermogravimetry of ZnO in a SO_2 stream was carried out in the temperature range up to 900 °C. The sample of ZnO (0.3 g) was heated at a rate of 2.5 °C/min and the flow-rate of SO_2 was maintained at 50 cm³/min. The sensitivity of the quartz helix used was approximately 72 mm/g. No weight change was observed, and the sample after the heating was found by X-ray analysis[4] to be unreacted ZnO. These results indicate that ZnO does not react with SO_2.

The products obtained by heating a mixture of 2.00 g of ZnO and 1.20 g of carbon at various temperatures for 1 h in a SO_2 stream at a flow-rate of 100 cm³/min were examined. The results are shown in Table 1, together with the weight changes in the samples. The

Table 1. Products obtained by heating a mixture of ZnO and carbon in a SO_2 stream at various temperatures

Temp /°C	Weight change/%	Sample in the boat	Amount of sulfur obtained outside the heating zone/g
550	+ 0.1	ZnO	Trace
600	+ 1.5	ZnO>>ZnS[α>β]	Trace
650	+ 2.1	ZnO>>ZnS[α>β]	<0.01
700	+ 2.7	ZnO>ZnS[α>β]	<0.01
750	− 3.0	ZnS[α>β]>ZnO	0.24
800	−24.9	ZnS[α>β]	1.59

Note; α=α-ZnS, β=β-ZnS.

sample in the boat was identified by X-ray analysis.[4-6] The modification of the ZnS formed is represented in the brackets.

The formation of ZnS was observed above 600 °C, and no unreacted ZnO was observed at 800 °C. Sulfur was obtained outside the heating zone throughout the temperature range in this experiment, and the amount of sulfur markedly increased above *ca.* 750 °C. The sample weight also markedly decreased above *ca.* 750 °C. The slight increase in the sample weight at 550 °C was due to the adsorption of the sulfur formed by the reaction on the unreacted carbon.[3]

The ZnS formed was a mixture of α-ZnS (high-temperature form, hexagonal) and β-ZnS (low-temperature form, cubic) at all temperatures.

Chemical analysis of the sample in the boat at 800 °C showed that the atomic ratio of zinc to sulfur[3] to be 1.0_0. From this result, it is confirmed that all the ZnO used was sulfidized at 800 °C.

Reaction Process between ZnO and SO_2 in the Presence of Carbon. To elucidate the reaction process between ZnO and SO_2 in the presence of carbon, the following experiments were carried out under conditions similar to those described in the preceding paragraph.

Reaction between ZnO and Carbon: The experimental results obtained by heating a mixture of ZnO (2.00 g) and carbon (1.20 g) in an argon stream (100 cm^3/min) for 1 h at various temperatures are shown in Table 2.

Table 2. Experimental results for the reaction between ZnO and carbon in an argon stream

Temp /°C	Weight loss/%	Amount of Zn obtained outside the heating zone/g	Conversion of ZnO to Zn/%
600	0.1	Detectable	Not calculated
650	0.2	0.001	<0.1
700	0.3	0.003	0.2
800	1.1	0.021	1.3

The samples after heating at all the temperatures were found to be unreacted ZnO by X-ray analysis. Zinc deposited outside the heating zone above 600 °C was dissolved in dilute nitric acid, and was determined by chelatometric titration.[7] The percentages of ZnO converted to zinc were calculated from the amounts of the zinc deposited.

These results indicate that a slight reduction of ZnO with carbon to zinc occurs above *ca.* 600 °C under the conditions in this experiment.

Reaction between ZnO and Sulfur in a SO_2 Stream: As seen from Table 1, when the mixture of ZnO and carbon was heated in a SO_2 stream, sulfur was formed. The reaction between carbon and SO_2 occurs even at 350 °C to form sulfur. This reaction proceeds markedly above *ca.* 700 °C, as reported by the present authors.[3] Therefore, the reaction between ZnO and sulfur was examined in a SO_2 stream.

ZnO (2.00 g) was heated in a stream of SO_2 containing a specified amount of gaseous sulfur at various temperatures for 1 h. The gaseous sulfur was formed by heating liquid sulfur and was carried by a stream of SO_2 (100 cm^3/min). Based on the experimental results for the reaction between carbon and SO_2, reported by the present authors,[3] the amounts of sulfur introduced at various temperatures were controlled to be 0.01 g for the experiments below 550 °C, 0.03 g at 600 °C, 0.25 g at 700 °C, and 1.90 g at 800 °C, since the experimental conditions (the amount of carbon, the flow-rate of SO_2, *etc.*) in this work were identical to those for the experiment on the reaction between carbon and SO_2. The results are shown in Table 3. The percentages of ZnO converted to ZnS shown in Table 3 were calculated from the weight gains in the samples.

Table 3. Products obtained by heating ZnO in a stream of SO_2 containing gaseous sulfur

Temp /°C	Sample in the boat	Conversion of ZnO to ZnS/%
550	ZnO	—
600	ZnO>>ZnS[α>β]	2
700	ZnO>ZnS[α>β]	12
800	ZnS[α>β]>ZnO	74

These results and the fact that ZnO does not react with SO_2 as described above show that the reaction between ZnO and sulfur proceeds above *ca.* 600 °C to form ZnS under the conditions in this experiment. The ZnS formed was a mixture of α-ZnS and β-ZnS, similar to the ZnS obtained by the reaction between ZnO and SO_2 in the presence of carbon as described above.

Reaction between Zinc and Sulfur in a SO_2 Stream: As mentioned in the previous paragraph, on heating ZnO and carbon, ZnO was slightly reduced with carbon to form zinc above *ca.* 600 °C. It has been briefly reported in the early literature[8] that zinc powder vigorously reacts with sulfur in a SO_2 atmosphere. But no details of the reaction were given.

The products obtained by heating zinc (1.00 g) at various temperatures for 1 h in a stream of SO_2 (100 cm^3/min) containing a specified amount of sulfur were examined. The amounts of sulfur introduced were controlled so as to be the same as those in the experiment on the reaction between ZnO and sulfur in a SO_2 stream described above. The experimental results are shown in Table 4.

Table 4. Products obtained by heating zinc in a stream of SO_2 containing gaseous sulfur

Temp /°C	Sample in the boat	Conversion of Zn to ZnS/%
350	Zn	—
400	Zn>>ZnS[β]	<1
500	Zn>>ZnS[β]	1
600	Zn > ZnS[β]	2
700	Zn > ZnS[β]	3
800	Zn > ZnS[β]	6

These results show that on heating zinc in a stream of SO_2 containing gaseous sulfur, the reaction between zinc and sulfur proceeds above *ca.* 400 °C to form β-ZnS.

Although there has been a report[9] which describes that ZnO, ZnS, $ZnSO_4$, and $ZnSO_4 \cdot ZnO$ are formed on heating zinc and SO_2 in a sealed tube at 500—800 °C, the formation of these compounds except ZnS is not observed in this experiment.

From the above-mentioned experimental results, the reaction process between ZnO and SO_2 in the presence of carbon can be represented as follows: On heating a mixture of ZnO and carbon in a SO_2 stream, the reaction between carbon and SO_2 occurs at first to form sulfur. Above *ca.* 600 °C, the reaction between ZnO and the sulfur occurs to form ZnS. In addition to these reactions, the reduction of ZnO with carbon occurs slightly to form zinc, which then reacts with sulfur to form ZnS.

It has been reported that the $\beta \rightleftharpoons \alpha$ transition temperature of ZnS is 1020 °C.[10] The temperature range in this work was below the transition temperature, and β-ZnS was only formed by the reaction between zinc and sulfur in a SO_2 stream, as shown in Table 4. While, the ZnS formed by heating the mixture of ZnO and carbon in a SO_2 stream was found to be a mixture of α-ZnS and β-ZnS, as shown in Table 1. The percentages of α-ZnS and β-ZnS were calculated to be α-ZnS 75% and β-ZnS 25% at 700 °C, and α-ZnS 70% and β-ZnS 30% at 750 and 800 °C, by the method reported by Bansagi *et al.* (the reproducibility: *ca.* ±2.5%).[11] Also, the ZnS formed by the reaction between ZnO and sulfur in a SO_2 stream was found to be a mixture of α-ZnS and β-ZnS, as shown in Table 3. And the percentages of α-ZnS and β-ZnS were calculated to be α-ZnS 70% and β-ZnS 30% at 700 and 800 °C.

The variation of the modification of ZnS, formed by heating the mixture of ZnO and carbon in a SO_2 stream or by the reaction between ZnO and gaseous sulfur in a SO_2 stream, with the reaction time (0.5—3 h) was examined. The ZnS formed by both processes was a mixture of α-ZnS and β-ZnS, and the wide variation in the percentages of α-ZnS and β-ZnS with the reaction time was not observed.

Regarding the formation of α-ZnS in the temperature range at which β-ZnS is stable, it has been reported that when ZnO having the wurtzite (α-ZnS) structure is present in ZnS, the metastable growth of α-ZnS can be promoted below the $\beta \rightleftharpoons \alpha$ transition temperature,[12] and that on heating β-ZnS mixed with a small amount of ZnO[12] or CdS,[13] both having the wurtzite structure, a part of the β-ZnS is transformed into α-ZnS even below the $\beta \rightleftharpoons \alpha$ transition temperature. Considering the above reports, the formation of a mixture of α-ZnS and β-ZnS observed in this work is due to the presence of ZnO during the formation of ZnS.

The present work was partially supported by a Grant-in-Aid for Scientific Research No. 555306 from the Ministry of Education, Science and Culture.

References

1) V. V. Pechkovskii, *J. Appl. Chem. USSR*, **30**, 873 (1957).
2) "Mukikagobutsu No Gosei [I], Shin-Zikkenkagaku-Koza 8," ed by the Chemical Society of Japan, Maruzen, Tokyo (1976), p. 308.
3) H. Araki, Y. H. Ryoo, M. Eguchi, R. Matsuzaki, and Y. Saeki, *Bull. Chem. Soc. Jpn.*, **53**, 2271 (1980).
4) ASTM X-Ray Powder Data File, 5-664.
5) ASTM X-Ray Powder Data File, 5-492.
6) ASTM X-Ray Powder Data File, 5-566.
7) W. Biedermann and G. Schwarzenbach, *Chimia(Switz)*, **2**, 56 (1948).
8) R. Coustal and F. Prevet, *C. R. Acad. Sci.*, **188**, 703 (1929).
9) E. I. Danilova and G. S. Frents, *Izv. Akad. Nauk. SSSR, Otdel. Tekh. Nauk*, **1955** (11), 25.
10) O. Kubaschewski, E. Ll. Evans, and C. B. Alcock, "Metallurgical Thermochemistry," 4th ed, Pergamon Press, Oxford (1967), p. 362.
11) T. Bansagi, E. A. Secco, O. K. Srivastava, and R. R. Martin, *Can. J. Chem.*, **46**, 2881 (1968).
12) B. J. Skinner and P. B. Barton, Jr., *Am. Mineral.*, **45**, 612 (1960).
13) M. Sakaguchi, M. Ohta, M. Satoh, and T. Hirabayashi, *J. Electrochem. Soc.*, **124**, 550 (1977).

The σ-Bonded Palladium(II) Complexes of 2-Aryl-4,4-dimethyl-2-oxazolines

Takeo Izumi, Hiroyuki Watabe, and Akira Kasahara*

Department of Applied Chemistry, Faculty of Engineering, Yamagata University, Yonezawa 992

(Received October 27, 1980)

Reactions of 2-phenyl-4,4-dimethyl-2-oxazoline with lithium tetrachloropalladate(II) and palladium(II) acetate give dichlorobis(2-phenyl-4,4-dimethyl-2-oxazoline,3-*N*)palladium(II) and a cyclopalladated binuclear complex, di-μ-acetato-bis[2-(4′,4′-dimethyl-2′-oxazolinyl)phenyl,1-*C*,3′-*N*]dipalladium(II), respectively. The latter complex is readily converted by a metathetical reaction with lithium chloride into its chloro-bridged analogue. The chloro-bridged complex reacts with triphenylphosphine to give the corresponding mononuclear σ-bonding palladium complex. All the complexes prepared in this study were characterized by means of IR and NMR spectroscopies.

Following the first report of the intramolecular cyclopalladation of azobenzene and *N*,*N*-dimethylbenzylamine,[1] there has been considerable interest in the intramolecular cyclometalation of nitrogen, phosphorus, and sulfur donor ligands by transition metals.[2] The cyclometalation reaction of 2-aryloxazolines with butyllithium proceeds regiospecifically and nearly quantitatively to the formation of an ortho-lithiation product.[3,4] One might, therefore, expect 2-aryloxazolines to undergo cyclopalladation. In this paper, we wish to report on the intramolecular cyclopalladation reaction of 2-phenyl-4,4-dimethyl-2-oxazoline (**1**) and 2-(3,4-dimethoxyphenyl)-4,4-dimethyl-2-oxazoline (**2**) in the formation of acetato-bridged binuclear complexes.

Results and Discussion

In the presence of sodium acetate, the reaction of **1** with lithium tetrachloropalladate(II) in methanol at room temperature gave dichloro-bis(2-phenyl-4,4-dimethyl-2-oxazoline)palladium(II) (**3**), which has no palladium-carbon σ-bonding. The NMR spectrum could not be measured because of the low solubility of **3** in all common solvents. However, the structure of **3** was consistent with the results of the elemental analysis and the IR spectrum of the compound. The IR bands of the aromatic ring C–H out-of-plane deformation vibrations suggest the modes of ring substitution.[5] The bands of the starting material **1** are observed at 745 and 695 cm^{-1}, corresponding to five adjacent ring hydrogens. The bands of complex **3** are observed at 750 and 690 cm^{-1}. This indicates the presence of monosubstituted benzene ring. Furthermore, complex **3** also shows ν(Pd–Cl) at 350 cm^{-1}, the position characteristic of *trans*-$[PdCl_2L_2]$,[6] and ν(C=N) was shifted to lower frequencies (1630 cm^{-1}) compared with **1** (ν(C=N)= 1650 cm^{-1}). Judging from these results, complex **3** contains two moles of **1** as ligands coordinated only with

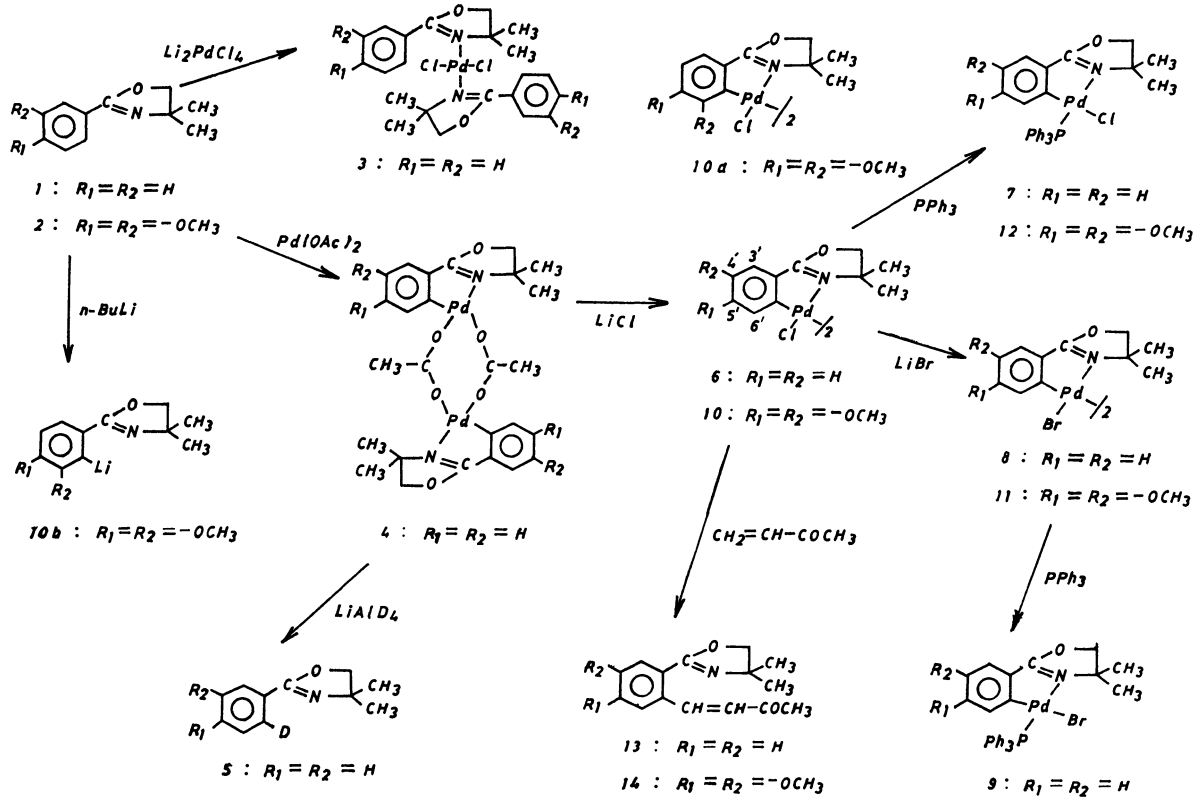

Fig. 1.

a nitrogen donor site, but does not contain a cyclopalladation moiety, and may have a trans-configuration with **1** as a N-donor.

On the other hand, the reaction of **1** with equimolar quantities of palladium(II) acetate in acetic acid at reflux produced the desired σ-bonded palladium complex (**4**), whose IR spectrum exhibited two strong absorption bands due to bridging acetato ligand at 1570 and 1410 cm^{-1}.[7] Moreover, the IR spectrum in **4** exhibits a band about 725 cm^{-1} which is characteristic of ortho-disubstituted benzene ring. The lithium aluminum hydride reduction of **4** gave **1**, whose mass spectrum was identical with that of an authentic sample, while the lithium aluminum deuteride reduction of **4** gave 2-(phenyl-2-*d*)-4,4-dimethyl-2-oxazoline (**5**). On the basis of elementary analysis and the characterization of the derivatives from **4**, the complex was assigned to a binuclear cyclopalladated complex, di-μ-acetato-bis[2-(4′,4′-dimethyl-2′-oxazolinyl)phenyl, 1-*C*, 3′-*N*]-dipalladium(II). It is noteworthy that even in the presence of acetate ion, **1** reacted with tetrachloropalladate(II) ion to give only the addition product **3** and with palladium(II) acetate to produce the cyclopalladated complex **4**, similar to the case of 1-ethyl-2-phenylimidazole.[8] The NMR spectrum of **4** was also in good agreement with the proposed structure, and the methyl resonance of bridging acetato ligand showed a sharp singlet at δ 2.22 together with two weak resonances at 2.15 and 2.28 ppm. These resonances were ascribed to two geometrical isomers, as shown in Fig. 2;[9] the former was due to two magnetically equivalent methyl protons in an ab-hg type and the latter were due to non-equivalent methyl protons in an ab-gh type (the isomer ratio ab-hg : ab-gh=4 : 1, approximately).

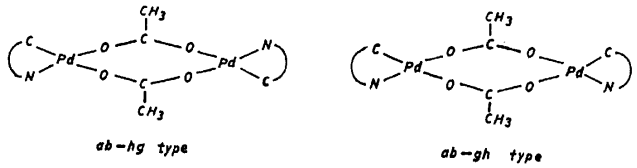

(C, N) =2-[4′,4′-Dimethyl-2′-oxazolinyl]phenyl,1-*C*, 3′-*N*-

Fig. 2. Geometrical isomers of **4**.

The complex **4** was smoothly converted by metathetical reaction with lithium chloride in acetone into its chloro-bridged analogue, di-μ-chloro-bis[2-(4′,4′-dimethyl-2′-oxazolinyl)phenyl,1-*C*,3′-*N*]dipalladium(II) (**6**). The IR spectrum in **6** exhibits a band at 730 cm^{-1} which can be assigned to the C–H deformation mode of an ortho-disubstituted benzene derivative. In the far-IR spectrum of **6**, there are two bridged Pd–Cl stretching absorptions at 270 and 245 cm^{-1}. The NMR spectrum of the complex was also in agreement with the proposed structure. The singlet at 1.51 ppm corresponds to the methyl group, the singlet at 4.36 ppm corresponds to the methylene group, and a typical ABCD system at 6.86—7.56 ppm corresponds to the *o*-phenyl group in 2-(4,4-dimethyl-2-oxazolin-2-yl)phenyl moiety. The 4′- or 5′-H was observed at δ 6.98 (2H) and 7.31 ppm (2H) as a double triplet due to coupling with other ring protons. The 6′-H and 3′-H appeared at 6.86 (2H) and 7.56 ppm (2H) as a double doublet due to coupling with 4′- and 5′-H, respectively. The coupling constants were $3'J_{HH}=7.0$ Hz and $4'J_{HH}=1.5$ Hz. Moreover, the complex **6** underwent a typical bridge-splitting reaction with triphenylphosphine to give a monomeric triphenylphosphine derivative (**7**). These results indicate unambiguously that the complex **4** has the cyclopalladated structure of **1**. In the far-IR spectrum of **7**, a band at 295 cm^{-1} was assigned as the ν(Pd–Cl) frequency, by comparison with the corresponding bromo derivative (**9**) which was derived from the bromo-bridged complex (**8**). Crociani *et al.* reported that the ν(Pd–Cl) frequencies trans to an aromatic nitrogen atom and an ary-carbon one fell in the range of 353—321 and 299—280 cm^{-1}, respectively.[10] The chloride ligands in **7**, therefore, are located trans to a carbon donor.

On the other hand, the reaction of **2** with equimolar amounts of palladium(II) acetate in acetic acid at reflux, followed by treatment with lithium chloride, gave di-μ-chloro-bis[2-(4′,4′-dimethyl-2′-oxazolinyl)-4,5-dimethoxyphenyl, 1-*C*, 3′-*N*]dipalladium(II) (**10**). The IR spectrum in the complex **10** exhibits a band near 860 cm^{-1} which is characteristic of 1,2,4,5-tetrasubstituted benzene ring. In addition, the NMR spectrum in the region of aromatic absorption displays two singlets at 6.73 and 6.98 ppm. The infrared frequencies and the coupling constants in the NMR spectrum are all in agreement with the proposed structure **10** rather than with $\mathbf{10}_a$. Meyers and Mihelich[4] had reported that ortho-lithiation of **2** with butyllithium led to the formation of 1,2,3,4-tetrasubstituted phenyllithium derivative ($\mathbf{10}_b$). It is noteworthy that **2** reacted with palladium(II) acetate to produce the 1,2,4,5-tetrasubstituted benzene derivative (**10**). The complex **10** also shows a quite low ν(Pd–Cl) frequency at 240 cm^{-1}; this band disappears on metathesis with lithium bromide, and yields the bromo analogue product (**11**). Furthermore, the complex **10** underwent the typical bridge-splitting reaction with triphenylphosphine to afford **12**.

The reactions of cyclopalladation products from σ-aryl-nitrogen derivatives with numerous reagents have been reported.[2] In the presence of triethylamine, complexes **6** and **10** reacted with methyl vinyl ketone in toluene at 100 °C, leading to the formation of 1-(2-acetylvinyl)-2-(4,4-dimethyl-2-oxazolin-2-yl)benzene (**13**) and 1-(2-acetylvinyl)-2-(4,4-dimethyl-2-oxazolin-2-yl)-4,5-dimethoxybenzene (**14**), respectively.

Experimental

Materials. All the melting points are uncorrected. 2-Phenyl-4,4-dimethyl-2-oxazoline (**1**) and 2-(3,4-dimethoxyphenyl)-4,4-dimethyl-2-oxazoline (**2**) were prepared according to the method described by A. I. Meyers *et al.*[11]

Measurements. The IR spectra were measured on KBr disks (4000—650 cm^{-1}) and nujol mulls mounted on thin polyethene windows (700—200 cm^{-1}) with Hitachi 215 and EPI-L spectrometers. The NMR spectra were determined in $CDCl_3$ with a Hitachi R-22 spectrometer (90 MHz), using TMS as the internal standard (δ, ppm). The mass spectra were obtained on a Hitachi RMU-6M mass spectrometer, using a direct insertion probe at an ionization energy of 70 eV.

The molecular weight was determined in $CHCl_3$ with a Hitachi 115 vapor pressure osmometer.

Dichlorobis(2-phenyl-4,4-dimethyl-2-oxazoline)palladium(II) (3). A solution of **1** (2.0 g, 11.4 mmol) in 50 cm³ of methanol was added to a solution of lithium tetrachloropalladate (II) (1.31 g, 5 mmol) in 50 cm³ of methanol at room temperature for 15 h. The yellow precipitate which formed immediately was filtered and washed with several portions of methanol. The solid (2.3 g, 88% yield based on Li_2PdCl_4) was insoluble in all common solvents: mp 245—248 °C (dec). IR: 1630 (coordinated C=N), 750, 690 (monosubstituted benzene ring), and 350 cm^{-1} (ν Pd–Cl). Found: C, 49.75; H, 4.79; N, 5.16%. Calcd for $C_{22}H_{26}Cl_2N_2O_2Pd$: C, 49.97; H, 4.95:; N, 5.29%.

Di-μ-acetato-bis[2-(4',4'-dimethyl-2'-oxazolinyl)phenyl, 1-C, 3'-N]dipalladium(II) (4). To a solution of palladium(II) acetate (1.3 g, 5.7 mmol) in acetic acid (30 cm³) was added **1** (1.0 g, 5.1 mmol) in acetic acid (30 cm³) at room temperature. After refluxing for 1.5 h, the resulting mixture was diluted with water and extracted with chloroform. The chloroform extracts were concentrated and chromatographed on silica gel. A yellow band eluted by chloroform was collected and the solvent was evaporated. Recrystallization from benzene gave 0.8 g of **4** as yellow crystals: yield 46% based on **1**, mp 135—137 °C (dec). IR: 1625 (coordinated C=N), 1570, 1410 (bridging acetate), and 720 cm^{-1} (*o*-disubstituted benzene ring). NMR: δ 1.55 (s, 12H, CH_3–C), 2.15, 2.22, and 2.28 (each s, 6H, CH_3 of acetato group), 4.38 (s, 4H, $-CH_2-$), 6.96—7.55 ppm (m, 8H, Ar–H). Found: C, 45.74; H, 4.34; N, 3.97%; mol wt (in $CHCl_3$), 665. Calcd for $C_{26}H_{30}N_2O_6Pd_2$: C, 45.82; H, 4.43; N, 4.12%; mol wt 679.

Reduction of 4 with Lithium Aluminium Hydride. Lithium aluminium hydride (0.02 g, 0.5 mmol) in anhydrous ether (50 cm³) was slowly added to a suspended solution of **4** (0.66 g, 1 mmol) in anhydrous ether (100 cm³). The resulting black mixture was stirred at room temperature for 6 h; then water (10 cm³) was added with cooling. The ether layer was washed with water and dried over anhydrous $MgSO_4$. After removal of the solvent, **1** was obtained as a pale yellow oil and the IR, NMR, and MS spectra were identical with those of the authentic sample.[12] IR: 1650 cm^{-1} (C=N). NMR: δ 1.24 (s, 6H, CH_3–), 3.95 (s, 2H, $-CH_2-$), 7.31 (m, 3H, Ar–H), and 7.89 ppm (m, 2H, Ar–H). MS: 175 (M^+). Calcd for $C_{11}H_{13}NO$: M, 175.

Reduction of 4 with Lithium Aluminium Deuteride. The reduction of **4** (0.66 g) in anhydrous ether with lithium aluminium deuteride (0.02 g) was carried out as in the preceding experiment; this gave a pale yellow oily product which can be identified as 2-(phenyl-2-d)-4,4-dimethyl-2-oxazoline (**5**) on the basis on the following evidence: IR: 1650 cm^{-1} (C=N). NMR: δ 1.24 (s, 6H, CH_3–), 3.95 (s, 2H, $-CH_2-$), 7.31 (m, 3H, Ar–H). 7.89 ppm (m 1H, Ar–H). Found: C, 74.31; H, 7.94; N, 7.88%; M^+, 176. Calcd for $C_{11}H_{12}DNO$: C, 74.40; H, 7.99; N, 7.94%; M, 176.

Di-μ-chloro-bis[2-(4',4'-dimethyl-2'-oxazolinyl)phenyl, 1-C, 3'-N]dipalladium(II) (6). A mixture of lithium chloride (0.10 g, 2.4 mmol) and **4** (0.78 g, 1.16 mmol) in acetone (50 cm³) was stirred at room temperature for 10 h. The evaporation of the solvent gave a pale yellow solid, which was washed with water and diethyl ether. The solid was purified by passing through a short silica gel column with chloroform, and 0.72 g of **6** was obtained as pale yellow crystals; yield 98% based on **4**, mp 175—178 °C (dec.) IR: 1620 (coordinated C=N), 730 (*o*-disubstituted benzene ring), 270, and 245 cm^{-1} (bridged Pd–Cl). NMR: δ 1.51 (s, 12H, CH_3–), 4.36 (s, 4H, $-CH_2-$), 6.86 (d-d, 2H, 6'-H), 6.98 (d-t, 2H, 4'- or 5'-H), 7.31 (d-t, 2H, 5'- or 4'-H), and 7.56 ppm (d-d, 2H, 3'-H). Found: C, 41.69; H, 3.73; N, 4.27%; mol wt (in $CHCl_3$), 624. Calcd for $C_{22}H_{24}Cl_2N_2O_2Pd_2$: C, 41.80; H, 3.82; N, 4.43%; M, 632.

Reaction of 6 with Triphenylphosphine. Triphenylphosphine (0.24 g, 0.92 mmol) was added to a suspension of **6** (0.29 g, 0.46 mmol) in 30 cm³ of benzene. A clear solution formed immediately; this was concentrated after stirring for 10 h at room temperature. The evaporation of the solvent gave a pale yellow solid, which was purified by passing through a silica gel column with chloroform. 0.52 g of chloro-[2-(4',4'-dimethyl-2'-oxazolinyl)phenyl, 1-*C*, 3'-*N*](triphenylphosphine)palladium(II) (**7**) was obtained as pale yellow crystals: yield 98%, mp 181—183 °C (dec). IR: 1630 (coordinated C=N), 740 (*o*-disubstituted benzene ring), 750, 690 (mono-substituted benzene ring), and 295 cm^{-1} (terminal Pd–Cl). NMR: δ 1.67 (s, 6H, CH_3–), 4.34 (s, 2H, $-CH_2-$), 6.72—7.11 (m, 4H, Ar–H), and 7.24—7.75 ppm (m, 15H, Ar–H). Found: C, 60.11; H, 4.57; N, 2.33%; mol wt (in $CHCl_3$), 565. Calcd for $C_{29}H_{27}ClNOPPd$: C, 60.22; H, 4.70; N, 2.42%; M, 578.

Di-μ-bromo-bis[2-(4',4'-dimethyl-2'-oxazolinyl)phenyl, 1-C, 3'-N]dipalladium(II) (8). The complex **6** (0.2 g) suspended in acetone (50 cm³) was treated with lithium bromide (0.2 g), and the mixture was warmed at reflux for 6 h. The resulting orange red solution was evaporated to dryness under reduced pressure. After silica gel column chromatography with chloroform, recrystallization from benzene–hexane gave pale yellow crystals of **8**; yield 60% based on **6**, mp 186—188 °C (dec). IR: 1620 (coordinated C=N) and 730 cm^{-1} (*o*-disubstituted benzene ring). NMR: δ 1.52 (s, 12H, CH_3–), 4.36 (s, 4H, $-CH_2-$), and 6.90—7.54 ppm (m, 8H, Ar–H). Found: C, 36.89; H, 3.31; N, 3.85%; mol wt (in $CHCl_3$), 695. Calcd for $C_{22}H_{24}Br_2N_2O_2Pd_2$: C, 37.05; H, 3.39; N, 3.92%; M, 713.

Bromo[2-(4',4'-dimethyl-2'-oxazolinyl)phenyl, 1-C, 3'-N](triphenylphosphine)palladium(II) (9). The reaction of **8** with triphenylphosphine was carried out in the same way as described for **7**, and pale yellow crystals of **9**, mp 198—200 °C (dec), were produced in 57% yield. IR: 1625 (coordinated C=N), 740 (*o*-disubstituted benzene ring), 750, and 690 cm^{-1} (mono-substituted benzene ring). NMR: δ 1.67 (s, 6H, $-CH_3$), 4.35 (s, 2H, $-CH_2-$), 6.75—7.13 (m, 4H, Ar–H), and 7.26—7.73 ppm (m, 15H, Ar–H). Found: C, 55.81; H, 4.30; N, 2.17%; mol wt (in $CHCl_3$), 615. Calcd for $C_{29}H_{27}BrNOPPd$: C, 55.92; H, 4.36; N, 2.24; M, 622.

Di-μ-chloro-bis[2-(4',4'-dimethyl-2'-oxazolinyl)-4,5-dimethoxyphenyl, 1-C, 3'-N]dipalladium(II) (10). To a solution of palladium(II) acetate (1.23 g, 5.5 mmol) in acetic acid (20 cm³) was added the compound **2** (1.15 g, 5.0 mmol) in acetic acid (15 cm³) at room temperature. After refluxing for 1 h, the resulting mixture was treated with an aqueous solution of lithium chloride (5.0 g) in water (20 cm³) for 10 h at room temperature. The reaction mixture was diluted with water and extracted with several portions of chloroform. The combined extracts were washed with water, dried over anhydrous $MgSO_4$, concentrated, and chromatographed on silica gel. The product **10** (0.90 g, 45% yield based on **2**) was obtained as pale yellow crystals from benzene–hexane: mp 245—248 °C (dec). IR: 1620 (coordinated C=N), 860 (1,2,4,5-tetra-substituted benzene ring), 270, and 240 cm^{-1} (bridged Pd–Cl). NMR: δ 1.62 (s, 12H, $-CH_3$), 3.82 (s, 6H, $-OCH_3$), 3.91 (s, 6H, $-OCH_3$), 4.37 (s, 4H, $-CH_2-$), 6.73 (s, 2H, Ar–H), and 6.98 ppm (s, 2H, Ar–H), Found: C, 41.44; H, 4.21; N, 3.63%; mol wt (in $CHCl_3$), 746. Calcd for $C_{26}H_{32}Cl_2N_2O_6Pd_2$: C, 41.51; H, 4.28; N, 3.72%; M, 752.

Di-μ-bromo-bis[2-(4',4'-dimethyl-2'-oxazolinyl)-4,5-dimethoxyphenyl, 1-C, 3'-N]dipalladium(II) (11). The reaction of **10** with lithium bromide in acetone was carried out in the same way as described for **8**, and pale yellow crystals of **11**, mp

242—245 °C (dec), were produced in 65% yield. IR: 1620 (coordinated C=N) and 860 cm^{-1} (1,2,3,5-tetra-substituted benzene ring). NMR: δ 1.64 (s, 12H, $-CH_3$), 3.82 (s, 6H, $-OCH_3$), 3.93 (s, 6H, $-OCH_3$), 4.38 (s, 4H, $-CH_2-$), 6.75 (s, 2H, Ar–H), and 6.99 ppm (s, 2H, Ar–H), Found: C, 37.06; H, 3.77; N, 3.28%; mol (in $CHCl_3$), 810. Calcd for $C_{26}H_{32}Br_2N_2O_6Pd_2$: C, 37.12; H, 3.83; N, 3.33%; M, 821.

Chloro[2-(4',4'-dimethyl-2'-oxazolinyl)-4,5-dimethoxyphenyl, 1-C, 3'-N](triphenylphosphine)palladium(II) (12). The reaction of **10** with triphenylphosphine was carried out in the same way as described for **7**, and pale yellow crystals of **12** were obtained; mp 225—227 °C (dec). IR: 1620 (coordinated C=N), 860 (1,2,4,5-tetrasubstituted benzene ring), 750, 690 (monosubstituted benzene ring), and 290 cm^{-1} (terminal Pd–Cl). NMR: δ 1.65 (s, 6H, $-CH_3$), 3.80 (s, 3H, $-OCH_3$), 3.89 (s, 3H, $-OCH_3$), 4.36 (s, 2H, $-CH_2-$), 6.75 (s, 1H, Ar–H), 7.01 (s, 1H, Ar–H), and 7.25—7.73 ppm (m, 15H, Ar–H). Found: C, 58.19; H, 4.81; N, 2.05%; mol wt (in $CHCl_3$) 626. Calcd for $C_{31}H_{31}ClNO_3PPd$: C, 58.32; H, 4.89; N, 2.19; M, 638.

Reaction of 6 with Methyl Vinyl Ketone. In a closed vessel, a mixture of the complex **6** (1.26 g, 2 mmol) and methyl vinyl ketone (6 mmol) and triethylamine (0.60 g, 6 mmol) in toluene (50 cm^3) was stirred for 5 h at 80 °C under a nitrogen atomsphere. The reaction mixture was cooled and filtered to remove precipitated palladium, and the filtrate was evaporated *in vacuo*. The residue was dissolved in ether, which had been washed with water and dried over anhydrous $MgSO_4$. After removal of the solvent, purification of the crude product by column chromatography (silica gel–hexane) gave 1-(2-acetylvinyl)-2-(4,4-dimethyl-2-oxazolin-2-yl)benzene (**13**), a pale yellow oil, in 45% yield based on **6**. IR (oil film): 1680 (C=O), 1650 (C=N), 1620 and 950 cm^{-1} (trans –CH=CH–). NMR: δ 1.33 (s, 9H, $-CH_3$), 4.10 (s, 2H, $-CH_2-$), 6.94—7.40 (m, 5H, Ar–H+–C=CH–CO–), and 7.55 ppm (d, 1H, –CH=C–CO–). Found: C, 74.96; H, 6.91; N, 5.70%; M^+, 243. Calcd for $C_{15}H_{17}NO_2$: C, 75.05; H, 7.04; N, 5.76%; M, 243.

Reaction of 10 with Methyl Vinyl Ketone. The reaction of **10** with methyl vinyl ketone was carried out in the same way as above, and 1-(2-acetylvinyl)2-(4,4-dimethyl-2-oxazolin-2-yl)-4,5-dimethoxybenzene (**14**), a pale yellow oil, was obtained in 38% yield. IR (oil film): 1675 (–C=O), 1650 (–C=N), 1620, and 950 cm^{-1} (trans –CH=CH–). NMR: δ 1.31 (s, 9H, $-CH_3$), 3.89 (s, 3H, $-OCH_3$), 3.91 (s, 3H, $-OCH_3$), 4.07 (s, 2H, $-CH_2-$), 6.85 (d, 1H, –C=CH–CO–), 7.27 (s, 1H, Ar–H), 7.47 (s, 1H, Ar–H), and 7.53 ppm (d, 1H, –CH=C–CO–). Found: C, 67.19; H, 6.88; N, 4.53; M^+, 303 Calcd for $C_{17}H_{21}NO_4$: C, 67.31; H, 6.98; N, 4.62%; M, 303.

References

1) A. C. Cope and R. W. Siekman, *J. Am. Chem. Soc.*, **87**, 3272 (1965).
2) I. Omae, *Chem. Rev.*, **79**, 287 (1979).
3) H. W. Gschwend and A. Hamdan, *J. Org. Chem.*, **40**, 2008 (1975).
4) A. I. Meyers and E. D. Mihelich, *J. Org. Chem.*, **40**, 3158 (1975).
5) L. J. Bellamy, "The Infrared Spectra of Complex Molecules," 2nd ed, Methuen, London (1966), p. 75.
6) J. R. Ferraro, "Low Frequency Vibrations of Inorganic and Coordination Compounds," Plenum Press, New York (1971), p. 111.
7) H. Onoue and I. Moritani, *J. Organomet. Chem.*, **43**, 431 (1972).
8) K. Hiraki, Y. Fuchita, H. Nakaya, and S, Takakura, *Bull. Chem. Soc. Jpn.*, **52**, 2531 (1979).
9) A. J. Deeming and I. P. Rothwell, *J. Chem. Soc., Chem. Commun.*, **1978**, 344.
10) B. Croiani, T. Boschi, R. Pietropaolo, and U. Belluo, *J. Chem. Soc., A*, **1970**, 531.
11) A. I. Meyers, D. L. Temple, D. Haldikewych, and E. D. Mihelich, *J. Org. Chem.*, **39**, 2787 (1974).
12) P. Allen and J. Ginos, *J. Org. Chem.*, **28**, 2759 (1963).

Catalytic Polarographic Wave of Fe(II) in Neutral Thiocyanate Solutions at Dropping Mercury Electrode

Sadayuki HIMENO* and Atsuyoshi SAITO

Department of Chemistry, College of General Education, Kobe University, Nada-ku, Kobe 657

(Received October 27, 1980)

The electrochemical behavior of Fe(II) in neutral thiocyanate solutions has been investigated at a dropping mercury electrode (DME). It was found that Fe(II) in neutral thiocyanate solutions gave a catalytic polarographic wave at potentials prior to the main Fe(II) reduction wave. The mechanism of the catalytic process involves the chemical reduction of thiocyanate ions with $Fe(OH)_{2,aq}$ at the electrode surface. Controlled potential electrolysis suggests that the reduction of thiocyanate ions proceeds with the formation of sulfide and cyanide ions. Sulfide ions produced at the electrode surface can react with Fe(II) diffusing to the electrode to form FeS. The discharge of this is responsible for the catalytic current, while cyanide ions have no essential role in the catalytic process. The effects of surface active substances and iodate ions on the catalytic wave are also discussed.

A number of papers have been devoted to the study of the electrode reactions of the iron group metal ions occurring in thiocyanate solutions.[1-4] Electrode reactions of these systems at a mercury electrode are quite complex, due to the low solubility of these metals in mercury.[5-8]

In the electroreduction of Ni(II) or Co(II) from thiocyanate solutions, catalytic polarographic currents are observed at DME. There are, however, conflicting ideas concerning the origin of the catalytic wave. Itabashi *et al.* proposed a mechanism involving the cyclic regeneration of Ni(II) or Co(II) by the oxidation of electrodeposited metals with thiocyanate ions.[9-11] On the other hand, Krogulec *et al.* explained the catalytic current of the Ni(II)–thiocyanate system in terms of the discharge of hydrogen ions on metallic nickel.[12] However, there seems to be agreement that, with Ni(II) or Co(II) present, the reduction of thiocyanate ions proceeds with the formation of sulfide and cyanide ions at the mercury surface.

The formation of sulfide ions was also observed during the electroreduction of Co(II) in thiosulfate solutions.[13] According to Baranski and Galus,[14] the reduction of transition metal ions in solutions containing sulfur-containing organic compounds resulted in the formation of sulfide ions at the mercury surface.

Stojek and Kublik investigated the process of the reduction and reoxidation of Fe(II) in neutral thiocyanate solutions at a stationary mercury electrode.[15] During the course of the investigation, they observed a small prewave preceding the usual Fe(II) reduction wave. However, they have given no detailed discussion about the reaction mechanism.

In the present paper we report the characteristics of the catalytic current of Fe(II) in neutral thiocyanate solutions. A possible explanation for the catalytic process is proposed.

Experimental

Apparatus. All polarographic measurements were performed with a Princeton Applied Research polarographic analyzer, model 174, and were recorded with a Riken Denshi X-Y recorder, model D-8CP. The controlled potential electrolysis was carried out with a Yanagimoto potentiostat, model V-8. The working electrode for the controlled potential electrolysis was a mercury pool with a surface area of approximately 7 cm^2. Potentials were measured against a saturated calomel electrode (SCE) with the use of a Kikusui Electronics digital voltmeter, model 156-A. The dropping mercury electrode (DME) had a flow rate of 1.95 mg s^{-1} and a drop time of 4.32 s in a 0.1 M KCl solution with an open circuit. The pH of the solutions was measured with a Hitachi-Horiba pH meter, model M-7. Dissolved oxygen was removed from the solution with nitrogen. The cell was immersed in a water bath maintained at (25±0.1) °C.

Reagents. All chemicals were of analytical reagent grade and were used without further purification. All solutions were prepared from redistilled water.

Results

Prewave of Fe(II)–Thiocyanate System. A d. c. polarogram of 1.0 mM† Fe(II) in 0.1 M NaSCN (pH 5.5) is shown in curve a of Fig. 1. A prewave appears at about 0.2 V more positive than the main Fe(II) reduction wave. The current of the prewave was independent of the height of the mercury reservoir, indicating that the electrode process was kinetically controlled.

The relationship between the catalytic wave height and pH of the solution is shown in curve a of Fig. 2. The catalytic wave was obtained in the pH range 4.8—8.2 under the above conditions. By buffering the solution, however, the catalytic wave disappeared completely without any surfactant. With an Fe(II) concentration of 1 mM, the catalytic wave first increased with thiocyanate concentration up to 0.1 M and then decreased above this thiocyanate concentration.

Effect of Iodate Ions on the Catalytic Wave. With iodate ions present, there appeared an increase of the catalytic current in unbuffered thiocyanate solutions. The reduction of iodate ions proceeds as follows:

$$IO_3^- + 3H_2O + 6e = I^- + 6OH^-$$

The iodate reduction process was a source of hydroxide ions, and buffering of the solution caused the catalytic wave to disappear under these conditions.

The effect of iodate concentration on the catalytic current is shown in Fig. 3. For iodate concentrations

† 1 M=1 mol dm^{-3}.

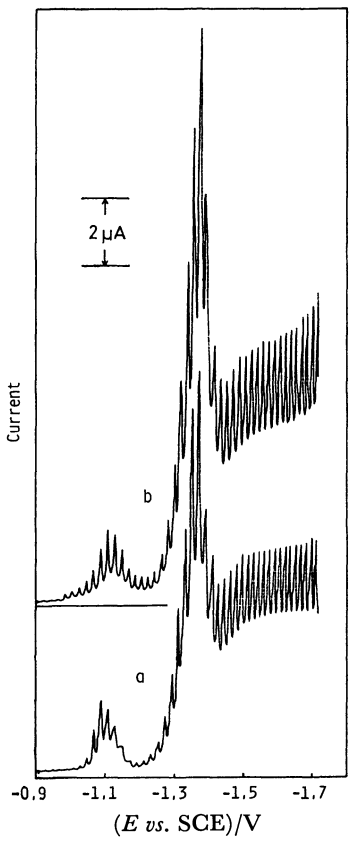

Fig. 1. D. c. polarograms of 1.0 mM Fe(II) in (a) 0.1 M NaSCN (pH 5.5), (b) 0.1 M acetate buffer (pH 5.9) containing 0.2 mM Na_2S.

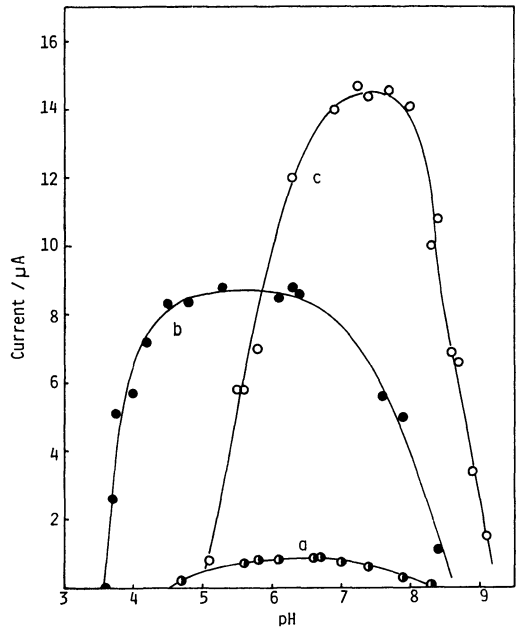

Fig. 2. Relationship between pH and catalytic current of 1.0 mM Fe(II) in (a) 0.1 M NaSCN, (b) solution (a) with 0.01% decylamine, (c) solution (a) with barbital buffer and 0.01% decylamine.

exceeding 0.04 mM, the catalytic current obtained in a 0.5 M NaSCN solution became practically equal to that obtained in a 0.1 M NaSCN solution. The result in

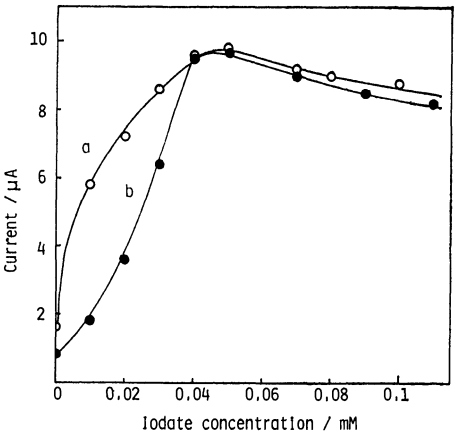

Fig. 3. Catalytic currents of 1.0 mM Fe(II) as a function of iodate concentration in (a) 0.1 M NaSCN (pH 5.6), (b) 0.5 M NaSCN (pH 6.1).

Fig. 3 suggests that the increase in pH in the vicinity of the electrode leads to the increase of the rate of the catalytic reaction.

Effect of Surfactant on the Catalytic Wave. The catalytic wave was practically unaffected by the presence of an anionic surfactant such as sodium dodecyl sulfate. However, the presence of a cationic surfactant like decylamine resulted in the appearance of the catalytic wave even in buffered solutions, and caused the current increase in unbuffered media.

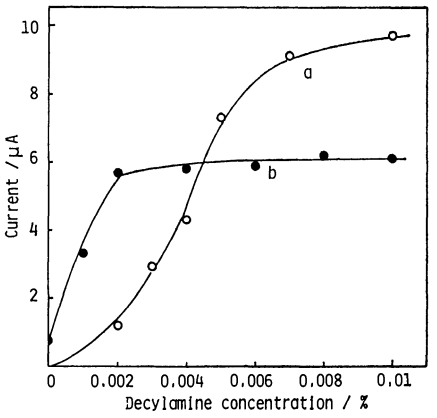

Fig. 4. Catalytic currents of 1.0 mM Fe(II) as a function of decylamine amount in (a) 0.1 M acetate buffer and 0.1 M NaSCN (pH 5.9), (b) 0.1 M NaSCN (pH 6.0).

The effect of the amount of decylamine on the catalytic current is given in Fig. 4. In the solution containing 0.1 M acetate buffer and 0.1 M NaSCN, the current increased gradually on increasing the amount of decylamine up to 0.01%, while it reached a limiting value when 0.002% decylamine was present in the 0.1 M NaSCN solution. Hence, most of the following experiments were carried out in a solution containing 0.01% decylamine.

In the presence of 0.01% decylamine, the catalytic wave was observed in the pH range of 3.6—8.5 and 5.1—9.1 in unbuffered and barbital buffer solutions, respectively (curves b and c in Fig. 2).

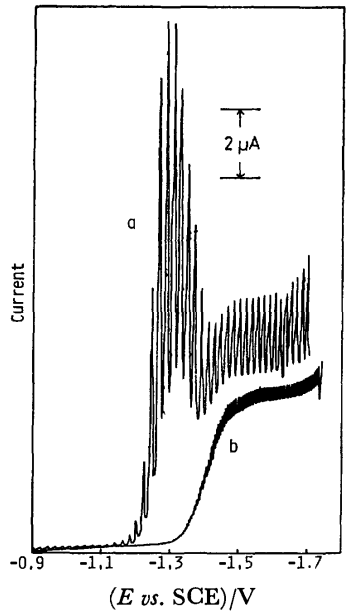

Fig. 5. D. c. polarograms of 1.0 mM Fe(II) in 0.1 M acetate buffer (pH 5.9), 0.1 M NaSCN and 0.01% decylamine with (a) natural drop, (b) a drop time of 0.5 s.

Figure 5 shows d. c. polarograms of 1.0 mM Fe(II) in the solution containing 0.1 M acetate buffer (pH 5.9), 0.1 M NaSCN, and 0.01% decylamine, using natural drop and forced drop (t=0.5 s) methods. No catalytic wave was observed with a drop time of 0.5 s. It is well known that catalytic and kinetic currents can be minimized or eliminated with rapid DME.[16,17] From comparison of a with b in Fig. 5, it follows that the catalytic wave was obtained at potentials before the reduction of aquairon(II) ions reached its limiting plateau. This result clearly shows that the catalytic reaction takes place under the conditions where aquairon(II) ions exist at the electrode surface.

Effect of Thiocyanate and Fe(II) Concentrations on the Catalytic Wave. Figure 6 presents the relationship between the catalytic current and thiocyanate concentrations. In buffered solutions, the catalytic current increased with thiocyanate concentrations up to 0.1 M. Above this concentration, the current went through a maximum and then decreased. In unbuffered solutions, however, the current increased over the thiocyanate concentration range studied.

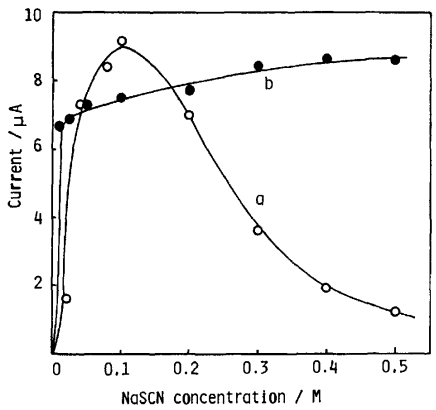

Fig. 6. Catalytic currents of 1.0 mM Fe(II) as a function of thiocyanate concentration in (a) 0.1 M acetate buffer (pH 5.9), (b) 0.1 M $NaClO_4$ (pH 6.0). Each solution contains 0.01% decylamine.

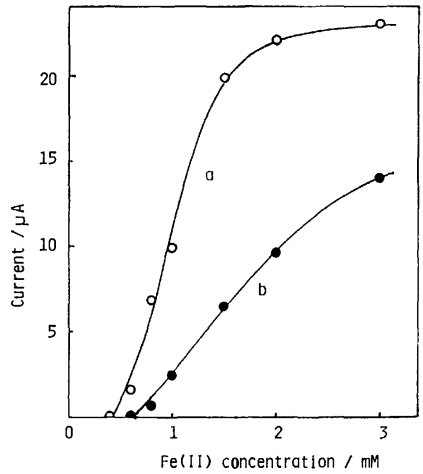

Fig. 7. Catalytic currents as a function of Fe(II) concentration in 0.1 M acetate buffer (pH 5.9) and 0.01% decylamine containing (a) 0.1 M NaSCN, (b) 0.5 M NaSCN.

Figure 7 shows the catalytic currents as a function of Fe(II) concentration. As can be seen, the wave height was dependent on Fe(II) concentration, although it was not a linear function.

D.c. Polarography of Fe(II) in an Acetate Buffer Containing Na_2S. To identify the Fe(II) species responsible for the catalytic current, d. c. polarograms of Fe(II) in neutral solutions containing sodium sulfide were also recorded. As an example, curve b in Fig. 1 shows a d. c. polarogram of 1.0 mM Fe(II) in 0.1 M acetate buffer (pH 5.9) containing 0.2 mM Na_2S. There appeared a prewave preceding the main Fe(II) reduction wave. The kinetic character of the prewave was verified by its dependence of the height of the mercury reservoir. Both catalytic waves of Fe(II) obtained in thiocyanate and sulfide solutions are very similar in appearance in d. c. polarography, suggesting that the same species of Fe(II) is responsible for the catalytic currents. In this case, however, an addition of decylamine had no effect on the catalytic current.

In cyclic voltammetry at a hanging mercury drop electrode (HMDE), Itabashi recently found a similar prewave of Fe(II) in unbuffered perchlorate solutions containing Na_2S; he ascribed the prewave to the reduction of FeS.[18]

Pulse Polarography for an Anodic Scan. Normal pulse polarograms for anodic scans of 1.0 mM Fe(II) in 0.1 M NaSCN (pH 6.0) are shown in Fig. 8. When the initial potential was set at −1.5 V, no oxidation current of iron was obtained, as shown in curve a. However, when the initial potential was chosen at a potential where the catalytic wave appeared (at −1.15 V), an oxidation current was observed with a half-wave potential of −0.53 V.

On the basis of cyclic voltammetry, Stojek and Kublik

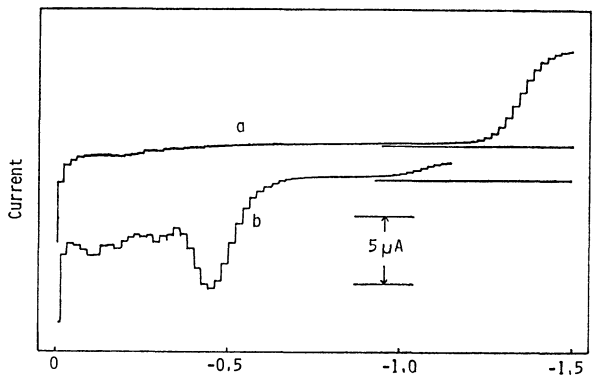

Fig. 8. Normal pulse polarograms for anodic scans of 1.0 mM Fe(II) in 0.1 M NaSCN (pH 6.0). Initial potential, (a) −1.50 V, (b) −1.15 V. Drop time, 2 s.

suggested that metallic iron electrodeposited at potentials of the catalytic wave stayed on the mercury surface, while iron deposited in the main reduction wave penetrated into the electrode.[15] The result obtained by pulse polarography seems to be in line with their observations and shows that, in the potential region of the catalytic wave, Fe(II) is reduced to metal which stays on the electrode surface.

Controlled Potential Electrolysis. For the purpose of elucidating the reaction mechanism, controlled potential electrolysis experiments were carried out with 25 ml of a 2.0 mM Fe(II) solution in 0.5 M NaSCN (pH 5.3) containing 0.01% decylamine at a potential of −1.25 V. After the solution was carefully deoxygenated, the electrode potential was held at −0.9 V to remove any remaining traces of oxygen dissolved in the solution. The pH of the solution increased during the electrolysis and the precipitation of Fe(II) as the hydroxide was observed. This result is in accord with the work of Stojek and Kublik, who explained this behavior in terms of the decomposition of water on an electrodeposited metallic iron. Hence, the following experiments were performed in acetate buffer solutions.

Electrolysis was carried out with a 25 ml solution containing 2.0 mM Fe(II), 0.1 M acetate buffer (pH 5.9), 0.5 M NaSCN, and 0.01% decylamine at −1.25 V. During the course of the electrolysis, gas evolution was observed on the mercury surface. The gas was introduced into a 0.25 M NaOH solution and was analyzed by d. c. polarography. The polarogram obtained showed a single anodic wave with a half-wave potential of −0.36 V, which corresponded to that of cyanide ions. A black solid was obtained on the mercury surface after the progress of the electrolysis. After the black solid was washed carefully with distilled water, it was dissolved in a 5 M H_2SO_4 solution. Bubbles of gas were observed. The polarographic analysis revealed the presence of sulfide ions in the solutions. The sulfuric acid solution was treated with thiocyanate ions and the solution turned red on the addition of hydrogen peroxide. This result indicates that the black solid is FeS.

The electrolysis of 1.0 mM Fe(II) in a 0.1 M acetate buffer (pH 5.9) containing 0.8 mM Na_2S was also performed at a potential of −1.20 V. There appeared a black solid on the mercury surface. Analysis of the black compound according to the procedure mentioned above showed the presence of FeS, suggesting that the prewave was due to the reduction of FeS.

Discussion

The catalytic current can not be ascribed to the formation of Fe(II)–thiocyanate complexes, since Fe(II) and thiocyanate ions form only a weak complex, $FeSCN^+$,[19] and the increase of thiocyanate concentrations is not necessarily related to the increase of the catalytic current. As shown in Fig. 7, on the other hand, the catalytic current is closely related to the Fe(II) concentration.

Wells and Salam investigated the hydrolysis of Fe(II) in perchlorate media.[20] According to them, $Fe(OH)^+$ exists in equilibrium with Fe^{2+} at about pH 3. Above pH 4, the predominant species is $Fe(OH)_{2,aq}$, which is converted slowly to a hydrated dimer. Since such polymerization reactions are known to be slow,[21] we can assume that the predominant species of Fe(II) in the pH range where the catalytic wave appears is $Fe(OH)_{2,aq}$ which has a much stronger reducing ability than Fe^{2+}.[22]

Controlled potential electrolysis shows that thiocyanate ions are reduced to sulfide and cyanide ions in the presence of Fe(II). The formation of these ions by the reduction of thiocyanate ions has also been observed in the solution of either Ni(II) or Co(II).[4,9-12] Taking account of the resemblance of the catalytic wave of Fe(II) in thiocyanate solutions to that in sulfide media, we can ascribe the current to the discharge of FeS formed at the electrode surface. In an attempt to check the effect of cyanide ions on the catalytic reaction, sodium cyanide was added to the thiocyanate-free Fe(II) solution. The presence of cyanide ions only caused the decrease of the main Fe(II) reduction wave and no contribution of Fe(II)–cyanide complexes in the catalytic process could be observed.

Wroblowa *et al.* observed that the adsorption of thiocyanate ions on the mercury electrode occurred in the potential region of the catalytic wave.[23]

On the basis of these observations, the reaction mechanism of the Fe(II)–thiocyanate system can be written as the following sequence of reactions:

$$SCN^-_{bulk} \longrightarrow SCN^-_{ads}$$

$$2Fe(OH)_{2,aq} + SCN^-_{ads} + 2OH^- \longrightarrow 2Fe(OH)_3 + CN^- + S^{2-}$$

$$Fe^{2+} + S^{2-} \longrightarrow FeS \xrightarrow{2e} Fe(0)_{metal} + S^{2-}.$$

The fact that the catalytic current is greatly enhanced by the presence of iodate ions can be accounted for by the increase of $Fe(OH)_{2,aq}$ in the vicinity of the electrode. In the absence of iodate ions, hydroxide ions produced by the decomposition of water on the metallic iron are available for the formation of $Fe(OH)_{2,aq}$ at the electrode surface. As shown in Fig. 2, therefore, no catalytic wave may be observed in buffered media below pH 5. However, we cannot fully explain why we can obtain greater catalytic currents in buffered media

than in unbuffered media.

As long as the electrode potential is more positive than the main Fe(II) reduction potentials, aquairon(II) ions are continuously supplied at the electrode surface and can react with hydroxide ions and sulfide ions. At the limiting plateau of the main Fe(II) reduction wave, on the other hand, the formation of either $Fe(OH)_{2,aq}$ or FeS becomes impossible because of the direct reduction of aquairon(II) ions to the metal. As shown in Figs. 1 and 5, therefore, no catalytic current is observed in the limiting region of the main Fe(II) reduction wave.

It is possible to assume that, in the potential region of the catalytic wave, $FeSCN^+$ adsorbs on the electrode surface, and in the adsorbed state it stimulates the catalytic reaction. On the basis of this adsorption process, however, we cannot explain the effect of the surfactants on the catalytic wave. Thus we excluded the participation of this process in the overall electrode reaction.

The effect of decylamine on the catalytic current may be attributed to the formation of a bridge between thiocyanate ions, the positively charged surfactant, and the negatively charged mercury surface. The adsorption of thiocyanate ions onto the mercury surface may thus take place more easily.

The present investigation was partially supported by a Grant-in-Aid for Scientific Research No. 554170 from the Ministry of Education, Science and Culture.

References

1) S. P. Perone and W. F. Gutknecht, *Anal. Chem.*, **39**, 892 (1967).
2) T. Hurlen and E. Eriksrud, *J. Electroanal. Chem.*, **54**, 331 (1974).
3) E. Eriksrud, *J. Electroanal. Chem.*, **54**, 341 (1974).
4) L. Janiszewska and Z. Galus, *Chem. Anal. (Warsaw)*, **17**, 691 (1972).
5) M. Fleischmann, J. A. Harrison, and H. R. Thisk, *Trans. Faraday Soc.*, **61**, 2742 (1965).
6) A. Baranski and Z. Galus, *J. Electroanal. Chem.*, **46**, 289 (1973).
7) T. Hurlen, E. Eriksrud, and S. Jorgensen, *J. Electroanal. Chem.*, **43**, 339 (1973).
8) E. Eriksrud and T. Hurlen, *J. Electroanal. Chem.*, **36**, 311 (1972).
9) E. Itabashi and S. Ikeda, *J. Electroanal. Chem.*, **27**, 243 (1970).
10) E. Itabashi, *J. Electroanal. Chem.*, **60**, 285 (1975).
11) E. Itabashi and M. Tan, *J. Electroanal. Chem.*, **60**, 299 (1975).
12) T. Krogulec, A. Baranski, and Z. Galus, *J. Electroanal. Chem.*, **57**, 63 (1974).
13) E. Itabashi, *J. Electroanal. Chem.*, **91**, 339 (1978).
14) A. Baranski and Z. Galus, *J. Electroanal. Chem.*, **75**, 613 (1977).
15) Z. Stojek and Z. Kublik, *J. Electroanal. Chem.*, **70**, 317 (1976).
16) R. E. Cover and J. G. Connery, *Anal. Chem.*, **41**, 918 (1969).
17) D. R. Canterford, A. S. Buchanan, and A. M. Bond, *Anal. Chem.*, **45**, 1327 (1973).
18) E. Itabashi, *J. Electroanal. Chem.*, **101**, 113 (1979).
19) A. E. Martell and L. G. Sillen, "Stability Constants of Metal-ion Complexes," The Chemical Society, London (1964), p. 119.
20) C. F. Wells and M. A. Salam, *J. Chem. Soc.*, **1968**, 24.
21) L. G. Sillen, *Quart. Rev.*, **13**, 146 (1959).
22) W. M. Latimer, "Oxidation Potentials," Prentice-Hall, New York (1952), p. 220.
23) H. Wroblowa, Z. Kovac, and J. O'M. Bockris, *Trans. Faraday Soc.*, **61**, 1523 (1965).

Preparation and Properties of Monoalkylnickel(II) Complexes $NiR(NR^1R^2)L_2$ Having Imido, Imidazolato, or Methyl Phenylcarbamato-*N* Ligand

Takakazu YAMAMOTO,* Teiji KOHARA, and Akio YAMAMOTO*

Research Laboratory of Resources Utilization, Tokyo Institute of Technology, 4259 Nagatsuta, Midori-ku, Yokohama 227

(Received November 26, 1980)

Reactions of dialkylnickel(II) complexes NiR_2L_2 **1** ($R=CH_3$, C_2H_5; $L=1/2$ bpy(2,2'-bipyridine), 1/2 dpe (1,2-bis(diphenylphosphino)ethane), PEt_3) with compounds having acidic N–H bonds (succinimide, phthalimide, diacetamide, pyromellitimide (1,2 : 4,5-benzenebis(dicarboximide)), imidazole) gave corresponding monoalkylnickel(II) complexes having Ni–N bond formulated as $NiR(NR^1R^2)L_2$. A reaction of $NiMe_2(PEt_3)_2$ with CH_3OH and phenyl isocyanate gives $NiMe(N(Ph)COOMe)(PEt_3)_2$. The IR, NMR, and visible spectroscopic studies of the complexes indicate that the electronegativity of Ni is enhanced by the replacement of one of the two R groups in **1** with the NR^1R^2 ligand. NMR spectra of complexes of a type $NiMe(NR^1R^2)(PEt_3)_2$ show that they have *trans*-configurations. Thermolyses of the monoalkylnickel(II) complexes start at temperatures higher by 80—100 °C than those of **1**, liberating RH, R–R, and olefin R(–H). Exposure of monoethylnickel(II) complexes to air releases ethylene as the main gaseous product. Reactions of the complexes of a type NiR(phthalimido)L_2 with R'X ($R'=C_6H_5$, $C_6H_5CH_2$) and C_6H_5COCl produce *N*-alkyl- or *N*-arylphthalimide and ketone C_6H_5COR, respectively.

Although a number of compounds having metal-nitrogen (M–N) covalent bonds have been prepared with various transition metals such as Ti, V, and Mo,[1,2] only a few reports[3–5] have appeared on the preparation of compounds having Ni–N covalent bonds. We previously reported in preliminary form the preparation and some chemical properties of monoalkylnickel(II) complexes with a succinimido or phthalimido ligand by reactions of dialkylnickel(II) complexes with the imides:[6]

$$NiR_2L_2 + HN(COR^1)_2 \longrightarrow RNi[N(COR^1)_2]L_2 + RH. \quad (1)$$

We have expanded the work by using other several active N–H compounds such as pyromellitimide (1,2 : 4,5-benzenebis(dicarboximide)) and imidazole to obtain the corresponding monoalkylnickel(II) complexes with the covalent Ni–N bond.

This paper deals with details of the preparation, characterization, spectroscopic data, and chemical properties of the monoalkylnickel(II) complexes with succinimido, phthalimido, or the other *N*-ligands. In connection with the preparation of the monoalkylnickel-(II) complexes having the *N*-anionic ligands, we also report the preparation of a monoalkylnickel(II) complex with a methyl phenylcarbamato-*N* ligand by treating $NiMe_2(PEt_3)_2$ with CH_3OH and Ph–N=C=O.

Results and Discussion

Preparation of Complexes. Dialkylnickel(II) complexes, NiR_2L_2 ($R=CH_3$, C_2H_5; $L=1/2$ bpy (2,2'-bipyridine), PEt_3, 1/2 dpe (1,2-bis(diphenylphosphino)-ethane)), react smoothly at room temperature with imides including succinimide ($pK_a=9.6$[7,8]), phthalimide ($pK_a=9.9$[8]), diacetamide, and pyromellitimide to give monoalkylnickel(II) complexes with covalent Ni–N bonds in medium to high yields (52—94%) with evolution of 1 mol of RH per NiR_2L_2:

$$NiR_2L_2 + HN(COR^1)_2 \longrightarrow L_2Ni(R)[N(COR^1)_2] + RH. \quad (1)$$

1

1a: $NiMe_2(bpy)$
1b: $NiEt_2(bpy)$
1c: $NiMe_2(PEt_3)_2$
1d: $NiMe_2(dpe)$

2—11

NiMe(suc)(bpy) **2**
NiMe(pht)(bpy) **3**
NiEt(suc)(bpy) **4**
NiEt(pht)(bpy) **5**
trans-NiMe(suc)$(PEt_3)_2$ **6**
trans-NiMe(pht)$(PEt_3)_2$ **7**
NiMe(suc)(dpe) **8**
NiMe(pht)(dpe) **9**
trans-NiMe[$N(COCH_3)_2$]$(PEt_3)_2$ **10**

trans, trans-$NiMe(PEt_3)_2$–N(CO)$_2$C$_6$H$_2$(CO)$_2$N–$NiMe(PEt_3)_2$ **11**

suc = Succinimido. pht = Phthalimido.
Me = Methyl. Et = Ethyl.

Addition of excess imides afforded the same products and further replacement of the R ligand in NiR-$[N(COR^1)_2]L_2$ by the $-N(COR^1)_2$ ligand did not proceed. A reaction of **1c** with *N*-phenylbenzamide also led to liberation of 1 mol of CH_4 per **1c** with formation of a pale brown complex whose IR spectrum suggests the formation of a complex of a type $NiR(NR^1R^2)L_2$. However, isolation of the complex was not feasible.

The reaction expressed by Eq. 1 generally proceeds more rapidly with **1c** than with the other dialkylnickel-(II) complexes with bidentate ligands (see Table 1). NMR spectroscopic studies of **1c** indicate that the PEt_3 ligand in **1c** rapidly exchanges with free PEt_3, partly liberated from **1c** into solution, presumably through a dissociative mechanism involving formation of a three coordinate intermediate. The formation of the three coordinate species in solution seems to account for the high reactivities of **1c** toward the imides.

Employment of compounds with less acidic N–H bonds such as benzimide (pK_a=13—14[8]), diphenylamine (pK_a=23[7]), and methyl phenylcarbamate did not lead to the formation of $NiR(NR^1R^2)L_2$, but addition of imidazole with a pK_a value of 14.5[8] leads to the formation of a polymeric monoalkylnickel(II) complex:

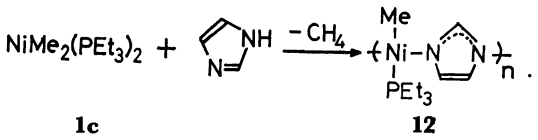

1c **12** (2)

It is known that the N–H bond in imidazole ring has high reactivities toward metals such as Hg,[10] Cu,[3] and Ni[3] to form complexes of a type $M(C_3H_3N_2)_mX_n$, in spite of its weak acidity.

Although methyl phenylcarbamate did not react with NiR_2L_2 to give a complex with the –N(Ph)COOMe ligand, the complex with the –N(Ph)COOMe ligand can be prepared through a different reaction pathway:

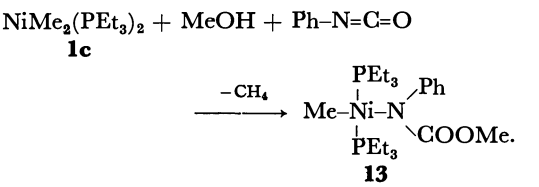

1c **13** (3)

The reaction most probably proceeds through insertion of phenyl isocyanate into a Ni–O bond in an intermediate species, $NiMe(OCH_3)(PEt_3)_2$:

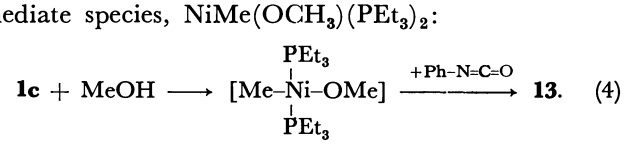

(4)

Several examples of insertion of isocyanates into metal-alkoxy bonds to form the M–N compounds are known.[11,12]

Table 1 shows preparative conditions, yields, melting points, and analytical data of the complexes **2**—**13**.

The bpy-coordinated complexes are reddish brown and PEt_3 or dpe-coordinated complexes are yellow or yellowish. The complexes with the bidentate neutral ligand (bpy, dpe) have moderate stabilities to air in solid, whereas those with the PEt_3 ligand are very sensitive to air even in the solid state. All of the complexes are very sensitive to air in solutions.

Characterization of the Complexes. IR, NMR, and visible spectroscopic data are summarized in Table 2.

IR Spectra: The ν(C=O) bands of succinimide (1700 cm^{-1}), phthalimide (1755 cm^{-1}), diacetamide (1965 cm^{-1}), and pyromellitimide (1700 cm^{-1}) are shifted to lower frequencies by 50—130 cm^{-1} on complex formation, and the shift is accounted for by asumming electron migration from Ni to the imido ligands. The magnitudes of the shifts are comparable to those observed with Pd,[13] Pt,[13] and Cu[14] imido complexes which have

Table 1. Preparative conditions, yields, and analytical data of complexes **2**—**13**

Complex[a]	Preparative conditions: NiR_2L_2 mmol	Temp °C	Solv. ml	Time h	Yield %	Color[b]	Mp[c] °C	Found (Calcd) (%): C	H	N	R/Ni[d]	Imi/Ni[d]	Mw
NiMe (suc)(bpy) **2**	0.37	r.t.	THF (2)	24	89	r.b.	190 (dec)	55.4 (55.4)	4.5 (4.6)	12.8 (12.8)			
NiMe (pht)(bpy) **3**	2.1	r.t.	THF (4)	24	87	r.b.	230 (dec)	60.1 (60.7)	3.8 (4.0)	11.0 (11.2)	0.93	0.99	
NiEt (suc)(bpy) **4**	1.3	r.t.	THF (4)	24	79	r.b.	175 (dec)	56.2 (56.2)	4.8 (5.0)	12.2 (12.3)	0.94	0.92	
NiEt (pht)(bpy) **5**	0.97	r.t.	THF (4)	24	87	r.b.	190 (dec)	60.7 (61.6)	4.2 (4.4)	10.4 (10.8)			
trans-NiMe(suc)-$(PEt_3)_2$ **6**	3.3	r.t.	Ether (6)	0.5	94	y.b.	76—77	49.3 (50.0)	9.7 (9.1)	3.5 (3.4)			352 (408)
trans-NiMe(pht) $(PEt_3)_2$ **7**	0.37	r.t.	Ether (2)	0.5	82	y.	158 (dec)	55.5 (55.3)	8.5 (8.2)	3.0 (3.1)	0.93	0.99	
NiMe(suc)(dpe) **8**	1.1	r.t.	THF (4)	24	79	y.	220 (dec)	65.2 (65.3)	5.5 (5.5)	2.6 (2.5)			
NiMe(pht)(dpe) **9**	1.0	r.t.	THF (4)	24	74	y.	200 (dec)	68.9 (68.0)	5.0 (5.1)	2.3 (2.3)			
trans-NiMe[N-$(COMe)_2$]$(PEt_3)_2$ **10**	1.8	r.t.	Ether (5)	0.5	52	y.	67—68	—[e]	—[e]	—[e]			
trans, *trans*-Ni_2Me_2-$(PEt_3)_4[C_6H_2(CO)_4$-$N_2]$ **11**	2.3	r.t.	Ether (10)	3	80	Orange	195 (dec)	51.1 (51.8)	8.4 (8.2)	3.5 (3.4)			
$[NiMe(NC_3H_3N)$-$(PEt_3)]_n$**12**	0.71	r.t.	Ether (5)	0.2	97	y.	175 (dec)	46.4 (46.4)	8.3 (8.2)	10.2 (10.8)	0.95		
NiMe(N(Ph)-COOMe)$(PEt_3)_2$ **13**	1.0	0 °C	Ether (3)	18	55	y.		55.0 (54.8)	9.1 (9.0)	3.0 (3.0)			

a) suc=succinimido. pht=phthalimido. b) r.b.=reddish brown. y.b.=yellowish brown. y.=yellow. c) dec=decomposed. d) Moles of RH and imide per Ni liberated on acidolysis of the complex. e) Micro analysis of **10** was not feasible since it is very sensitive to air, thus **10** was identified by NMR spectroscopy.

TABLE 2. SPECTRAL DATA OF COMPLEXES **2**—**13**

Complex	IR[a] $\tilde{\nu}$/cm^{-1}	^{1}H-NMR δ/ppm[b] Ni–R	Ni–NR^{1}R^2	L	^{31}P{^{1}H}-NMR[c] δ/ppm	Visible λ/nm
2	1630* 1235 765	−0.08 (3H, s)	2.64 (4H, s)	7.4 (2H, m) 7.8—8.2 (5H, m) 8.36(1H, d, 6 Hz)		498 (THF) 479 (CH_2Cl_2)
3	1655* 1600 725	0.00 (3H, s)	7.2—8.4 (12H) (Overlapped to each other)			
4	1620* 1610* 1230	0.61(3H, t, 7 Hz, CH_3) 0.90(2H, q, 7 Hz, CH_2)	2.64(4H, s)	7.4 (2H, m) 7.9 (5H, m) 8.35 (1H, d, 6 Hz)		512 (THF) 530 (Toluene) 495 (CH_2Cl_2)
5	1620* 1350 1230	0.63(3H, t, 6 Hz, CH_3) 0.96(2H, q, 6 Hz, CH_2)	7.2—8.4 (12H) (Overlapped to each other)			492 (CH_2Cl_2)
6	1650* 1300 725	−0.74(3H, t, 10 Hz, CH_3)	2.24(4H, s)	0.9—1.5(30H, m)		
7	1620* 1340 1220	−0.30 (3H, t, 10 Hz, CH_3)	7.04 (2H, m) 7.73 (2H, m)	0.8—1.6(30H, m)	36.1	
8	1610* 1350 1240	−0.03 (3H, dd, 7 Hz and 5 Hz)	2.17 (4H, s)	2.12(4H, d, 17 Hz, CH_2) 7.5 (12H, *m,p*-CH_5) 7.8 (8H, m)		
9	1650* 1375 1305	0.06 (3H, dd, 7 Hz and 5 Hz)	7.2—8.2 (24H) (Overlapped to each other)	2.14 (4H, d, 17 Hz, CH_2)		
10	1640* 1600* 1305	−0.78 (3H, s)	2.57 (6H, s)	0.8—1.1 (30H, m)		
		−1.06 (3H, t, 10 Hz)[d]	2.42 (6H, s)	1.0—1.6 (30H, m)[d]		
11	1645* 1380 1295	−0.88 (3H, t, 10 Hz)	7.50 (1H, s)	e)		
12	1080 1035 740	Not measurable due to poor solubilities in solvents.				
13	1650* 1330 760	−0.88 (3H, t, 9 Hz)	3.80 (3H, s, CH_3) 6.98 (1H, t, 8 Hz, *p*-C_6H_5) 7.43 (2H, t, 8 Hz, *m*-C_6H_5) 9.12 (2H, d, 8 Hz, *o*-C_6H_5)	0.92 (qui, 7 Hz) 1.24 (m) 30H	31.3	

a) Strongest three peaks are given. The absorption peaks with an asterisk are assigned to ν(C=O). b) Measured at r.t. s=singlet, d=doublet, t=triplet, q=quartet, qui=quintet. Solvent: CD_2Cl_2 for **2**, **3**, **4**, **5**, **8**, and **9**; C_6D_6 for **6**, **7**, **10**, and **13**; THF-d_8 for **11**. c) From external H_3PO_4 (downfield positive). d) In acetone-d_6 at −60 °C. e) Signals of the PEt_3 ligand are overlapped with signals of impurities of THF-d_8.

covalent M–N bonds. The covalency of the Ni–N bonds in **2**—**9** is supported by negligible electric conductivities (Λ=0.17−0.80 S cm^2) of CH_2Cl_2 solutions of the complexes. The possibility that one of the two N–H bonds in pyromellitimide remains intact is excluded not only on the basis of the analytical data given in Table 1 but also by the absence of ν(N–H) bands in the IR spectrum.

The IR spectrum of **12** resembles those of polymeric Hg(II)[10] and Tl(III)[15] complexes with the imidazolato ligand, showing bands characteristic of the imidazole ring at 1480 and 1080 cm^{-1} and no band associated with an NH group. The insolubility of **12** in common organic solvents suggests a polymeric structure which has been proposed for the Hg(II) and Tl(III) complexes:

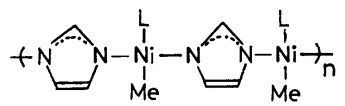

Coordination of only one PEt_3 ligand to Ni in **12** is consistent with the polymeric structure.

The IR spectrum of **13** shows a similar pattern to that of methyl phenylcarbamate except for the N–H region, showing ν(C=O) and ν(C–O) bands at 1650 and 1330 cm^{-1}, respectively, and no ν(N–H) band. The IR data together with NMR data given in Table 1 support the formation of **13**.

NMR Spectra: Patterns of ^{1}H-NMR spectra of complexes **2**—**11** and **13** are consistent with the formulation of the complexes as given in Table 1. The CH_3 signals of **2**, **3**, **6**—**11**, and **13** appear at normal positions

where CH_3 signals of methylnickel(II) complexes appear.[4,16,17] ^1H-NMR spectra of **4** and **5** show CH_2 signals of the ethyl ligand at lower field than CH_3 signals, in contrast to the NMR spectrum of $NiEt_2(bpy)$ **1b** which shows the CH_2 signal (δ 0.8 ppm) at higher field than the CH_3 signal (δ 1.1 ppm).[17] Since it is known[18] that the chemical shift difference between the CH_2 and CH_3 signals ($\Delta=\delta_{CH_2}-\delta_{CH_3}$) increases linearly with the increase in the electronegativity of the atom to which the ethyl group is attached, the appearance of the CH_2 signal at the lower magnetic field can be taken as an indication of an increase in electronegativity of nickel through replacement of the Et ligand of **1b** by the electron-withdrawing imido ligand.

As described above the PEt_3 ligand of $NiMe_2(PEt_3)_2$ **1c** rapidly exchanges at room temperature with free PEt_3 in solutions partly liberated from **1c** and therefore the ^{31}P–^1H coupling is not observable for the Ni–CH_3 signal of **1c**, whereas the Ni–CH_3 signals of **6**, **7**, **11**, and **13** clearly show the ^{31}P–^1H coupling, indicating that the PEt_3 ligand in the complexes is bonded to Ni on NMR time scale. The difference in the dynamic behavior between **1c** and complexes of the type $NiR(NR^1R^2)(PEt_3)_2$ is accounted for by the increase in the electronegativity of nickel through the replacement of the Me ligand by the NR^1R^2 ligand, since electron-donating ligands such as PEt_3 are expected to bond to the central atom more strongly when the electronegativity of the central atom increases. Triplet patterns of the Ni–CH_3 signals in the $NiR(NR^1R^2)L_2$-type complexes indicate not only that the complexes have a trans configuration but also that the complexes have monomeric structures, since if the complexes have multi-nuclear structures, the coupling patterns will become more complex. For **6** the monomeric structure has been established by cryoscopic measurement of the molecular weight (Table 1).

The methylene protons of the succinimido ligand in *cis*-complexes **2**, **4**, and **8** appear as a sharp singlet, indicating that the four hydrogens in the succinimido ligand are magnetically equivalent either due to rapid rotation of the imido ligand around the Ni–N bond or due to accidental coincidence of chemical shifts. The CH_2-signal of **4** appears as a sharp singlet even at -30 °C.

Each of $^{31}P\{^1H\}$-NMR spectra of **7** and **13** shows only one sharp signal and this also supports that the two PEt_3 ligands bonds tightly to Ni occupying the trans position to each other.

Visible Spectra: Solutions of the monoalkylnickel(II) complexes with the bpy ligand have very strong ($\varepsilon \fallingdotseq 3\times10^3$) adsorption bands at about 500 nm, which are assignable to Ni→bpy CT-bands. The dialkyl complexes **1a** and **1b**, show the Ni→bpy CT-bands of lowest transition energy at about 650 nm. The blue shift of the CT-band from 650 nm to 500 nm on the replacement of the Et ligand by the imido ligand is associated with the lowering of the highest occupied level of Ni due to the electron-withdrawing imido ligand.[21]

Chemical Properties. Thermolysis, Acidolysis, and Degradation in Air: Complexes $NiR(NR^1R^2)L_2$ have remarkably high thermal stabilities as shown in Table 1. Their thermolyses start at temperatures by 80—100 °C higher than those of the starting dialkylnickel(II) complexes NiR_2L_2.[17a,19,20] For example, **3** begins to decompose at 230 °C, the temperature being one of the highest decomposition temperatures among dialkyl- and monoalkylnickel(II) complexes reported to date.[4] Even if the alkyl group has β-hydrogens as in **4** and **5**, the complexes is thermally stable up to 175 and 190 °C, respectively.

In cases of Ni–bpy complexes the starting dimethyl- and diethylnickel(II) complexes decomposes mainly through unimolecular reductive elimination process,[21]

$$NiR_2(bpy) \longrightarrow R\text{-}R. \quad (5)$$
$$R = Me, Et$$

The marked enhancement of the thermal stability by the replacement of one of the ethyl ligands by the imido ligand may be attributed to the lack of the low energy intramolecular reductive elimination pathway with NiR(imido)(bpy). Thermolyses of **2** and **3** give C_2H_6 as the main product (Table 3), suggesting a bimolecular process in the thermolyses. Thermolyses of **4** and **5** afford disproportionation products, C_2H_4 and C_2H_6, which are considered to be formed through a β-elimination process,

$$NiEt(imido)(bpy) \longrightarrow [NiH(imido)(bpy)] + C_2H_4. \quad (6)$$
$$[\mathbf{14}]$$
$$\downarrow + NiEt(imido)(bpy)$$
$$C_2H_6$$

Mechanisms involving coupling between metal hydrides and metal alkyls have been proposed for thermolyses of a few transition alkylmetals.[22] Evolution of CH_4 and C_2H_4 as main products together with some ethane (Table 3) in the thermolysis of a mixture of **2** and **4** (*ca.* 1 : 1) supports the β-elimination mechanism shown above and suggests further that the hydride intermediate [**14**] reacts with the methyl **2** and the ethyl complex **4** to form methane and ethane. In thermolysis of com-

$$[\mathbf{14}] \begin{cases} \xrightarrow{\mathbf{2}} CH_4 \\ \xrightarrow[\mathbf{4}]{} C_2H_6 \end{cases} \quad (7)$$

Table 3. Products of thermolysis of $NiR(imido)(bpy)$[a]

Complex	Gaseous products (mol/Ni)			ΣR/Ni[b]
	CH_4	C_2H_6	C_2H_4	
R=Methyl				
2	0.19	0.35	—	0.89
3	0.09	0.39	Trace	0.87
R=Ethyl				
4	—	0.40	0.53	0.93
5	—	0.24	0.36	0.60
2 (0.16 mmol) + **4** (0.19 mmol)	0.11 mmol	0.07 mmol	0.14 mmol	

a) At 220—230 °C, in solid in a vacuum. b) $\Sigma R = CH_4+2(C_2H_6+C_2H_4)$ for methyl complexes, $=C_2H_6+C_2H_4$ for ethyl complexes.

TABLE 4. PRODUCTS OF THE REACTIONS OF NiR(imido)L_2 WITH ORGANIC HALIDES (R'X AND R'COX)[a]

No	Complex	Organic halide	Temp °C	Time h	Products (%-yield/Ni) R'-Imide	R-R'	Others
1	**3**	$C_6H_5CH_2Br$[b]	100	1	83	74	
2	**4**	$C_6H_5CH_2Br$[b]	50—60	6	51	51	C_2H_4 (6)
3	**6**	$C_6H_5CH_2Br$[b]	30	0.8	29	66	Bibenzyl (26)
4	**7**	C_6H_5Br[b]	120	1	95	30	
					RCOR'		
6	**7**	C_6H_5COCl[c]	r.t.	12	71		

a) 0.2—0.4 mmol of the complex was used. b) In *N,N*-dimethylacetamide (1 ml). c) In THF (0.5 ml).

plexes containing the PEt_3 ligand, the amount of C_2H_4 evolved sometimes exceeded 1 mol/Ni. The evolution of excess C_2H_4 seems to be due to thermal degradation of the PEt_3 ligand on Ni. Evolution of more than 1 mol of C_2H_4 per Ni was observed also in the thermolysis of complexes with the dpe ligand.

As described above complexes **2**—**13** do not react with excess HNR^1R^2, although a complex having a composition of Ni(phthalimido)$_2$(bpy) is known.[5] The poor reactivities of the monoalkylnickel complexes seem to be attributable to decrease in nucleophilicity of nickel or the Ni-bound alkyl group by bonding of the electron-withdrawing NR^1R^2 ligand. Treatment of the monoalkylnickel(II) complexes with stronger acids such as CH_3COOH, HCl, and H_2SO_4, however, leads to acidolysis of the Ni–R bond to liberate RH quantitatively (Table 1). Imides are also released from complexes of a type NiR(imido)L_2 on the acidolysis by dry HCl.

Complexes **2**—**13** are decomposed on exposure to air as described above. In cases of the ethylnickel complexes, **4** and **5**, they generate C_2H_4 as the main gaseous product on exposure to dry air,

e.g., **4**(solid) + dry air
$$\longrightarrow C_2H_4(40\%/Ni) + C_2H_6(\text{trace}). \quad (8)$$

The fact suggests that β-hydrogen elimination process is promoted by interaction of the complex with dioxygen or by direct interaction of β-hydrogens with oxygen. IR spectrum of the residue shows strong ν(O–H) absorption band, implying the presence of an Ni–OH or Ni–OOH bond in the residual substance.

Reactions with Organic Halides: Reactions of complexes NiR(imido)L_2 with alkyl or aryl halides R'X give *N*-alkyl or -aryl imides with formation of alkanes R–R' (Table 4). Relative reactivities of Ni–N and Ni–R bonds toward R'X varies with the complex and R'X employed. For example, the Ni–CH_3 bond in **6** reacts smoothly with $C_6H_5CH_2Br$ to liberate ethylbenzene in a 66% yield, whereas only 29% of the imido ligand is alkylated. An opposite trend is observed for the reaction of **7** with C_6H_5Br, whereas both the Ni–C and Ni–N bonds in **3** are reactive toward $C_6H_5CH_2Br$. Occurrence of the reaction of **7** with C_6H_5Br to liberate *N*-phenyl phthalimide stands in contrast to the known poor reactivity of potassium phthalimide against aryl halides in Gabriel synthesis of amines, and the reaction may be applied to prepare arylamines from phthalimide and aryl halides. A reaction of **7** with C_6H_5COCl affords ketone $CH_3COC_6H_5$ in 71% yield, accompanied by decarbonylation from C_6H_5COCl to afford benzene and biphenyl. A similar reaction of **9** also affords the same ketone with a lower yield (18%/Ni).

Reactions of NiR(imido)(bpy) with dihalomethanes afford RCH_2CH_2R, RCH_2R, RCH_3, and olefin R(–H)=CH_2 (*e.g.*, propylene from ethyl complexes) besides normal degradation products (R–R, RH, and R(–H)).[23] The formation of the unusual products can be accounted for by assuming insertion of CH_2 carbene formed from CH_2X_2 into the Ni–R bonds.

Reactions with Unsaturated Compounds: Complexes of the type NiR(imido)L_2 (**2**, **4**, **7**, **8**) initiate polymerization of acrylonitrile to yield polyacrylonitrile in high yields (>70%). Attempts to yield a copolymer from butadiene and acrylonitrile were not successful and only homopolymers of acrylonitrile were obtained. Methyl methacrylate is polymerized by **4** to give syndiotactic poly(methyl methacrylate) (Bovey's σ value[24]=0.17) in a 35% yield. Vinyl monomers with less electron-withdrawing substituents such as styrene and vinyl acetate were not polymerized by NiR(imido)L_2. The trend is similar to the polymerization of vinyl monomers initiated by isolated transition metal alkyls and hydrides.[25] Acetylene was trimerized by **7** to benzene and propionaldehyde was dimerized to EtCH=CMeCHO by **2**.

Experimental

General and Materials. All reactions were carried out under nitrogen or argon or in vacuum by using Schlenk type tubes. Complexes **1a**—**1d** were prepared according to literature.[17,19,21] The compounds with N–H bonds were used as purchased from Tokyo Kasei Co. Ltd. Solvents were dried over Na wires or CaH_2, distilled under N_2, and stored under an atmosphere of N_2.

Analyses and Spectroscopic Measurements. Microanalysis of C, H, and N was performed by Mr. T. Saito in our laboratory with a Yanagimoto CHN Autocorder Type MT-2. The melting point was measured in a sealed glass capillary. Amounts of gases evolved during reactions or thremolysis were measured with a Toepler pump and analyzed by GLC using a Shimadzu GC-3BT gas chromatograph. Identification and quantitative analysis of organic compounds were carried out by NMR spectroscopy and GLC.

IR and NMR spectra were recorded on a Hitachi Model 295 infrared spectrophotometer and a JEOL JNM-PS-100 spectrometer, respectively. Visible spectra were obtained by using a Hitachi Model 200-20 spectrophotometer. Electric conductivities of the CH_2Cl_2 solutions of complexes were measured by a Toa Model CM-5B conduct meter.

Preparation of Complexes. NiMe(suc)(bpy) 2 and NiMe(pht)(bpy) 3: THF (2 cm³) was added to a mixture of **1a** (91 mg, 0.37 mmol) and succinimide (38 mg, 0.38 mmol). Stirring the solution for 1 d at room temperature gave a reddish brown precipitate, which was recrystallized from CH_2Cl_2–hexane to give 109 mg (89%) of **2**. Evolution of CH_4 (0.94 mol/Ni) was observed during the reaction.

A similar reaction of **1a** (500 mg, 2.1 mmol) with phthalimide (300 mg, 2.1 mmol) in THF (4 cm³) and recrystallization from CH_2Cl_2–hexane yielded 670 mg (87%) of **3**.

NiEt(suc)(bpy) 4 and Other Complexes with suc or pht Ligand 5—9: THF (4 cm³) was added to a mixture of **1b** (350 mg, 1.3 mmol) and succinimide (130 mg, 1.3 mmol). Stirring the solution at room temperature for 1 d gave a reddish brown precipitate with evolution of C_2H_6 (0.92 mol/Ni). The reddish brown precipitate was recrystallized from CH_2Cl_2–hexane to yield 344 mg (79%) of **4**.

The other complexes were prepared in similar manners under conditions listed in Table 1. Solvents for recrystallization were diethyl ether for **6** and **7** and a mixture of CH_2Cl_2 and hexane for **5**, **8**, and **9**.

trans-*NiMe(diacetamido)*$(PEt_3)_2$ *10*: Diethyl ether (5 cm³) was added to a mixture of **1c** (580 mg, 1.8 mmol)and diacetamide (180 mg, 1.8 mmol) at −10 °C. On warming the solution to room temperature, a smooth reaction occurred with vigorous evolution of CH_4. A red solution was obtained after 30 min and cooling the solution to Dry Ice temperature gave 520 mg of yellow crystals. Recrystallization from diethyl ether gave 270 mg (52%) of **10**.

trans, trans-Ni_2Me_2*(pyromellitimido)*$(PEt_3)_2$ *11*: Diethyl ether (10 cm³) was added to a mixture of **1c** (740 mg, 2.3 mmol) and pyromellitic diimide (240 mg, 1.2 mmol) at −20 °C and then the mixture was warmed to room temperature. Stirring the mixture for 3 h at room temperature afforded a yellow precipitate, which was collected by filtration and recrystallized from THF to yield 760 mg (80%) of **11**.

$[NiMe(imidozolato)(PEt_3)]_n$ *12*: Diethyl ether (5 cm³) was added to a mixture of **1c** (230 mg, 0.71 mmol) and imidazole (49 mg, 0.72 mmol). Stirring the solution at room temperature caused precipitation of a yellow solid with evolution of CH_4. The precipitate was washed thoroughly with diethyl ether, THF, and toluene to yield 170 mg (93%) of **12**. The complex was insoluble in diethyl ether, benzene, toluene, THF, ethyl alcohol, acetone, and *N,N*-dimethylformamide.

NiMe(methyl phenylcarbamato-N*)*$(PEt_3)_2$ *13*: A diethyl ether (3 cm³) solution of **1c** (330 mg, 1.0 mmol) was solidified by cooling to −196 °C and then phenyl isocyanate (0.11 cm³, 1.0 mmol) and methyl alcohol (0.041 cm³, 1.0 mmol) were added by microsyringe at −196 °C. The mixture was warmed to 0 °C and the solution was stirred for 18 h at the temperature to give a homogeneous yellow solution. Evolution of CH_4 (0.86 mmol) during the reaction was observed. Cooling the yellow solution to −78 °C afforded yellow crystals, which were separated by filtration and recrystallized from diethyl ether to yield 260 mg (55%) of **13**.

Thermolysis, Acidolysis, and Degradation in Air. A Schlenk type tube containing 44 mg (0.13 mmol) of **2** was connected to a vacuum line and evacuated. The tube was immersed in an oil bath and the temperature of the oil bath was raised to 210 °C. After 2 h, evolution of 0.025 mmol (0.19/Ni) of CH_4 and 0.048 mmol (0.35/Ni) of C_2H_6 was observed. Thermolyses of other complexes were carried out in similar manners.

A Schlenk type tube containing a diethyl ether (0.5 cm³) solution of **3** (30 mg, 0.080 mmol) was connected to a vacuum line and evacuated. Dry HCl (excess) was introduced to the vessel and the mixture was stirred for 1 d at room temperature to obtained 0.074 mmol of CH_4 and 0.080 mmol of phthalimide. Acidolyses of other complexes were carried similarly.

A Schlenk type tube (25 cm³) containing **4** (120 mg, 0.35 mmol) was evacuated, and then dry air (1 atm) was introduced. After 11 h a brown powder (120 mg) was obtained with evolution of 0.14 mmol of C_2H_4. IR spectrum of the brown powder showed strong ν(O–H) and ν(C=O) bands at 3400 and 1590 cm^{-1}, respectively. Elemental analysis of the brown powder roughly agrees with a composition of Ni(OOH)–(succinimido)(bpy) (Found: C, 46.7; H, 3.9; N, 11.2%. Calcd: C, 48.6; H, 3.8; N, 12.1%). A reaction of **4** with dry air in diethyl ether and those of **5** in solid and in solution afforded similar results.

Reactions with Organic Halides. Benzyl bromide (0.063 cm³, 0.53 mmol) was added to a *N,N*-dimethylacetamide solution of **3** (79 mg, 0.21 mmol). Stirring the solution at 100 °C for 1 h gave a green precipitate with formation of *N*-benzylphthalimide (0.17 mmol, 83%/Ni). Reactions of the Ni–phthalimido complexes with benzyl bromide or bromobenzene were carried out similarly under conditions listed in Table 4.

Benzoyl chloride (0.059 cm³. 0.51 mmol) was added to a THF (0.5 cm³) solution of **7** (46 mg, 0.10 mmol). Stirring the solution for 12 h at room temperature produced 0.071 mmol of acetophenone, 0.031 mmol of benzene, and 0.008 mmol of of biphenyl.

Reactions with Unsaturated Compounds. Acrylonitrile (3.3 g) was added to a vessel containing **2** (33 mg) by trap-to-trap distillation in a vacuum. Almost all of acrylonitrile was polymerized on standing the mixture for 40 min at room temperature. After 2 h the polymer was dissolved in *N,N*-dimethylformamide and precipitated by pouring the solution into HCl–methyl alcohol to yield 2.5 g (74%) of polyacrylonitrile. Other polymerizations were carried out similarly.

Acetylene (500 cm³, 1 atm) was introduced into a vessel containing a THF (1 cm³) solution of **7** (24 mg, 0.052 mmol). Stirring the solution for 30 min at room temperature gave a black precipitate. After 2 d formation of benzene (0.72 mmol) was observed.

Propionaldehyde (3.0 g, 51 mmol) was added to a vessel containing **2** (76 mg, 0.23 mmol). Stirring the solution for 12 h at room temperature gave a viscous pale green solution, in which 0.65 g (6.6 mmol) of $EtCH{=}C(CH_3)CHO$ was contained as determined by GLC.

References

1) G. W. A. Fowles, *Prog. Inorg. Chem.*, **6**, 1 (1964).
2) D. C. Bradley, *Adv. Inorg. Chem. Radiochem.*, **15**, 259 (1972).
3) J. E. Bauman, Jr. and J. C. Wang, *Inorg. Chem.*, **3**, 268 (1964).
4) P. W. Jolly and G. Wilke, "The Organic Chemistry of Nickel," Academic Press, New York (1974), Vol. I pp. 213, 347, 350.
5) P. Shukla, M. P. Khare, and L. N. Srivastava, *Z. Anorg. Allg. Chem.*, **333**, 165 (1964).
6) T. Kohara, T. Yamamoto, and A. Yamamoto, *J. Organomet. Chem.*, **154**, C37 (1978).
7) J. B. Hendrickson, D. J. Cram, and G. S. Hammond "Organic Chemistry," McGraw-Hill, New York (1970).
8) J. A. Dean, "Lange Handbook of Chemistry," 11th ed, McGaw-Hill, New York (1973).
9) H. Walba and R. W. Isensee, *J. Org. Chem.*, **21**, 702 (1956).
10) P. Brooks and N. Davidson, *J. Am. Chem. Soc.*, **82**, 2118

(1960).
11) A. J. Bloodworth and A. G. Davies, *J. Chem. Soc.*, **1965**, 5238.
12) T. Yamamoto, M. Kubota, and A. Yamamoto, *Bull. Chem. Soc. Jpn.*, **53**, 680 (1980).
13) D. M. Roundhill, *J. Chem. Soc., Chem. Commun.*, **1969**, 567; D. M. Roundhill, *Inorg. Chem.*, **9**, 254 (1970).
14) T. Yamamoto, Y. Ehara, M. Kubota, and A. Yamamoto, *Bull. Chem. Soc. Jpn.*, **53**, 1299 (1980).
15) A. G. Lee, *J. Chem. Soc., A*, **1971**, 880.
16) A. Yamamoto, T. Yamamoto, T. Saruyama, and Y. Nakamura, *J. Am. Chem. Soc.*, **95**, 4073 (1973).
17) a) T. Saito, Y. Uchida, A. Misono, K. Morifuji, A. Yamamoto, and S. Ikeda, *J. Am. Chem. Soc.*, **88**, 5198 (1966); b) T. Yamamoto, Y. Nakamura, and A. Yamamoto, *Bull. Chem. Soc. Jpn.*, **49**, 191 (1976).
18) P. T. Narasimhan and M. T. Rogers, *J. Am. Chem. Soc.*, **82**, 5983 (1960).
19) T. Kohara, T. Yamamoto, and A. Yamamoto, *J. Organomet. Chem.*, **192**, 265 (1980).
20) A. Yamamoto, T. Yamamoto, M. Takamatsu, T. Saruyama, and Y. Nakamura, "Chemistry of Alkylnickel Complexes, Preparation and Properties of Alkylnickel with Tertiary Phosphine Ligands," Organotransitionmetal Chem., Plenum Publishing Co. (1975) p. 281.
21) T. Yamamoto, A. Yamamoto, and S. Ikeda, *J. Am. Chem. Soc.*, **93**, 3350 (1971).
22) A. Miyashita, T. Yamamoto, and A. Yamamoto, *Bull. Chem. Soc. Jpn.*, **50**, 1109 (1977); G. M. Whitesides, E. J. Panek, and E. R. Stedronsky, *J. Am. Chem. Soc.*, **94**, 232 (1972).
23) T. Yamamoto, *J. Chem. Soc., Chem. Commun.*, **1978**, 1003.
24) F. A. Bovey, "Polymer Conformation and Configuration," Academic Press, New York (1969).
25) A. Yamamoto, *Ann. N. Y. Acad. Sci.*, **239**, 60 (1974); A. Yamamoto and S. Ikeda, "Progress in Polymer Science Japan," Kodansha, Tokyo (1972), Vol. 3; A. Yamamoto and T. Yamamoto, *Macromol. Rev.*, **13**, 161 (1978).

Oxidized Rubredoxin Models. Iron(III) Complexes of Z-Cys-Ala-Ala-Cys-OMe and Z-Ala-Cys-OMe

Norikazu UEYAMA, Michio NAKATA, and Akira NAKAMURA*

Department of Macromolecular Science, Faculty of Science, Osaka University, Toyonaka, Osaka 560

(Received November 29, 1980)

Oxidized rubredoxin models using Fe(III) ion and cysteine-containing peptide as Z-Cys-Ala-Ala-Cys-OMe were synthesized in solution and characterized by the absorption, CD, MCD, and EPR spectra. The Fe(III)/Z-Cys-Ala-Ala-Cys-OMe complex exhibits similar CD spectra as well as absorption, MCD, EPR spectra to native oxidized rubredoxin. Thus, the model complex has a similar electronic configuration and core structure to that of native protein. From the comparison with the result of Fe(III)/Z-Ala-Cys-OMe complex, the tetrapeptide complex probably has a relatively stable chelate structure with the hairpin turn conformation of the tetrapeptide.

Iron-sulfur proteins play important roles in biological electron-transfer and oxygenation reactions.[1,2] These proteins have two major classes. One is a rubredoxin type, $[Fe(SR)_4]^{-,2-}$ (SR denotes cysteine thiolate), which has one or two independent active sites per molecule. Its active site is constructed by one iron atom with four cysteine thiolate groups but without inorganic sulfide. The X-ray crystallographic studies on oxidized rubredoxin from *Clostridium pasteurianum* revealed that the iron atom is coordinated by the four cysteine thiolates with distorted tetrahedral geometry.[3] The other is ferredoxin type, which has also one or two active sites per molecule. Each active site consists of two or four iron atoms with the same number of inorganic sulfide (S^{2-}) to form $[Fe_2S^*_2(SR)_4]^{n-}$(n=2 or 3) or $[Fe_4S^*_4(SR)_4]^{n-}$(n=1, 2, or 3) cluster, respectively (S* denotes inorganic sulfide), and each cluster is coordinated by four cysteine thiolates. Very recently the existence of new type ferredoxin, [3Fe3S*], was suggested.[4]

It is interesting that amino acid sequence, -Cys-A-B-Cys-, exists at the metal binding site of many iron-sulfur proteins. In such cases, it is supposed that conformational restriction due to the steric effects caused by side chains of the two amino acid residues, A and B, interposed between the two cysteine residues may contribute to the stabilities of chelate rings, the determination of the geometries around the metal ion, and the revelation of the enzymatic activities. Although many model studies for iron-sulfur proteins have been reported,[5-10] the roles of the protein or chelating units as ligands in controlling metal ion activities still remain ambiguous. It is presumed that the model studies by the use of peptide complexes possessing partial amino acid sequences of native metalloenzymes give significant informations about the roles of proteins. The preparation of cysteine-containing peptide-iron complexes so far investigated,[6,8,10] however, has employed sequencial oligopeptides such as $\{Gly-Cys-Gly\}_n$ which possess no sterical restriction by the side chains of two amino acids interposed between two terminal cysteine residues. For example, Rydon *et al.*[8] reported the rubredoxin-like complex formation between Fe(III) and $Ac\{Gly-Cys-Gly\}_nNH_2$ (n=1—4) but these complexes were very unstable to result in the oxidation of thiols by Fe(III) ion under strictly unaerobic conditions whereas native rubredoxin is stable under such conditions. Denatured rubredoxin[11,12] in 80 or 90% aqueous dimethyl sulfoxide (DMSO) exhibits a similar absorption spectra to that of native protein and it is stable under unaerobic conditions. These informations indicate that the stability of $[Fe(SR)_4]^-$ chromophore is dependent on the amino acid sequence of the active site as well as the whole protein environment. In native rubredoxin,[1] two well-separated tetrapeptide units at the binding site, Cys(6)-Thr-Val-Cys(9) and Cys(39)-Pro-Leu-Cys(42) for *C. pasteurianum* rubredoxin, should take specific conformations by interactions of side chains of the two amino acid residues interposed between two terminal cysteine residues, of course with the aid of the other peptide sequence, to form a stable chelate complex and to prevent the oxidation of thiols by Fe(III) ion. In view of importance of identity of amino acid residues in native metalloenzymes, these simple models such as Rydon's models are not sufficient in discussion of the role of amino acids in the structures and functions of iron-sulfur proteins. Thus we took the tetrapeptide such as Z-Cys-Ala-Ala-Cys-OMe in order to establish basic informations about the points mentioned above.

In this report, we describe the formation of $[Fe(SR)_4]^-$ moiety with cysteine-containing peptides. In particular, spectroscopic properties of Fe(III)/Z-Cys-Ala-Ala-Cys-OMe complex are discussed on the basis of its relevance to rubredoxin.

Experimental

Peptide Syntheses. The syntheses of peptides were carried out by mixed anhydride method using isobutyl chloroformate as a coupling reagent by stepwise elongation from C-terminus and cysteine thiolate group was protected by acetamidomethyl group. The detail will be reported separately. The SH-free peptides, Z-Ala-Cys-OMe and Z-Cys-Ala-Ala-Cys-OMe, were prepared by the reaction of the corresponding S-blocked peptides with Hg(II) and H_2S.

Complex Formation. All operations were carried out under argon atmosphere. Dimethyl sulfoxide and triethylamine were degassed and distilled before use. Iron(III) chloride hexahydrate was of commercial grade.

The metal salt and 4 molar equivalents of SH-groups based on the cysteine contents of cysteine-containing peptide were dissolved in DMSO. The addition of an equimolar amount of triethylamine for one SH-group to the solution gave a deep red-violet solution. The color faded gradually in the absence of air, especially for Fe(III)/Z-Ala-Cys-OMe complex.

Physical Measurements. Absorption and circular dichroism (CD) spectra were measured on a JASCO UVIDEC-5A and a JASCO J-40 spectrometer, respectively. Magnetic circular dichroism (MCD) spectra were measured on a JASCO J-20 spectrometer equipped with an electromagnet in field strength of 1.5 T and corrected for the zero-field circular dichroism. Electron paramagnetic resonance (EPR) spectra were recorded on a JEOL JESFE 1X with 100 kHz magnetic field modulation using Mn(II) as *g*-marker ($g=1.981$). Absorption, CD, and MCD spectra were recorded at room temperature whereas EPR spectra at 77 K. The values of ε, $\Delta\varepsilon$, and $\Delta\varepsilon_M$ were based on the molar concentration of Fe(III).

Results and Discussion

Addition of triethylamine to a DMSO solution of cysteine-containing peptide and iron(III) chloride gave a deep red-violet solution. The resulting Fe(III) complex of cysteine-containing peptide were characterized with absorption, CD, MCD, and EPR spectra in solution. Figures 1 and 2 show the absorption and CD spectra of Fe(III)/peptide complex, respectively, together with those of native oxidized rubredoxin from *C. pasteurianum*[13,14] for comparison. The CD spectrum of native rubredoxin[14] was converted from wave-number-linear scale in the original paper to wavelength-linear scale and was reproduced in Fig. 2. The CD spectra of other rubredoxins from different organisms show similar spectral pattern to *C. pasteurianum* rubredoxin.[15]

The Fe(III)/Cys-containing peptide complexes showed absorption maxima at 355 and 495 nm, which are typical for the oxidized rubredoxin. These spectral

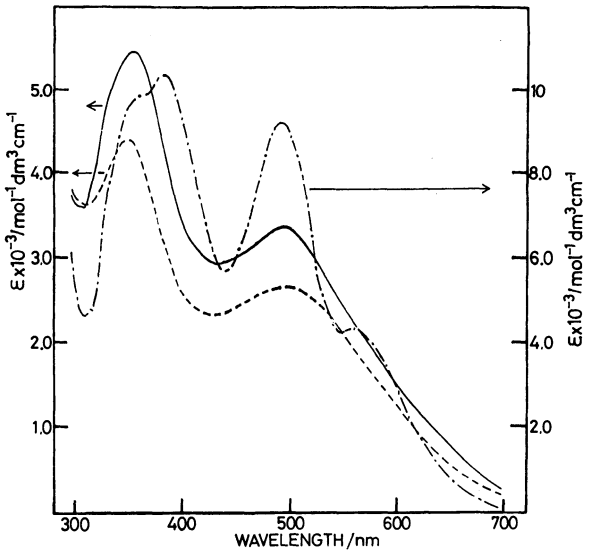

Fig. 1. Absorption spectra of Fe(III)/Cys-containing peptide complexes.
——: Fe(III)/Z–Cys–Ala–Ala–Cys–OMe complex in DMSO, ------: Fe(III)/Z–Ala–Cys–OMe complex in DMSO, -·-·-: oxidized rubredoxin (*C. pasterurianum*) in Tris buffer. The spectrum of the native protein (W. A. Lovenberg and B. E. Sobel, *Proc. Natl. Acad. Sci. U.S.A.*, **54**, 193 (1965)) was inserted together with our spectra for comparison.

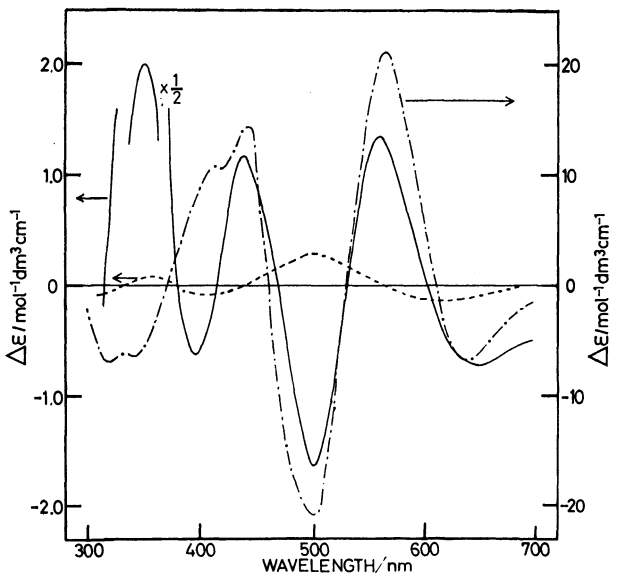

Fig. 2. CD spectra of Fe(III)/Cys-containing peptide complexes.
——: Fe(III)/Z–Cys–Ala–Ala–Cys–OMe complex in DMSO, ------: Fe(III)/Z–Ala–Cys–OMe complex in DMSO, -·-·-: oxidized rubredoxin (*C. pasteurianum*) in Tris buffer. The spectrum of the native protein (W. A. Eaton and W. Lovenberg, "Iron-Sulfur Proteins," ed by W. Lovenberg, Academic Press, New York and London (1973), Vol. II) was converted to wavelength-linear scale and was inserted together with our spectra for comparison.

patterns disappeared gradually due to the oxidation of thiols by the Fe(III) ion. Rydon *et al.*[8] reported that the rubredoxin-like spectra of Fe(III)/Ac{Gly–Cys–Gly}$_n$NH$_2$ ($n=1$—4) complex disappeared rapidly and after 5 min no typical spectra were observed in visible region under strictly unaerobic conditions. In our study, Fe(III)/Z–Ala–Cys–OMe complex was more unstable toward the autoxidation of thiols than Fe(III)/Z–Cys–Ala–Ala–Cys–OMe. The half-life times of absorbance at 495 nm of Fe(III)/peptide complexes were about 22 and 10 min for the Z–Cys–Ala–Ala–Cys–OMe complex and the Z–Ala–Cys–OMe complex, respectively.

The EPR spectra at 77 K showed signals at $g=4.0$ and 4.2 for Fe(III)/Z–Cys–Ala–Ala–Cys–OMe complex and Fe(III)/Z–Ala–Cys–OMe complex, respectively, whereas oxidized rubredoxin at $g=4.3$.[1] It is clear that these peptide complexes have high-spin d^5 Fe(III) structure under an approximately tetrahedral environment surrounded by four cysteine thiolates identical with the core structure of the active site of oxidized rubredoxin.

The MCD spectra also supported the conclusion but there was a little difference between dipeptide and tetrapeptide complex. The MCD spectrum of oxidized rubredoxin in the visible region has two dispersion type bands with crossover points at 382 and 495 nm, and a positive and negative bell-shaped bands at 565 and 357 nm, respectively.[14] Both dispersion type bands were assigned to the Faraday *A* terms, while the bell-shaped bands were assigned to the Faraday *B* terms.[14]

Hatano *et al.*[9] investigated the MCD spectra of Fe(III) complexes of various simple dithiols such as 1,2-ethanedithiol, 1,4-butanedithiol, 1,6-hexanedithiol, and *o*-xylene-α,α'-dithiol. They reported that Fe(III)/1,6-hexanedithiol complex has very similar MCD spectral pattern to that of oxidized rubredoxin and, consequently, a similar core structure, whereas Fe(III)/1,2-ethanedithiol complex has very different spectral pattern from that of oxidized rubredoxin. The complex of 1,2-ethanedithiol was reported to exhibit no dispersion type band at around 490 nm but a positive bell-shaped band at 590 nm ascribed to the Faraday *B* terms, and this indicates that this complex had a binuclear form, $[Fe(SCH_2CH_2S)_2]_2^{2-}$, with five sulfur atoms coordinated to each Fe(III) ion, and its geometry was distorted trigonal bipyramidal around the high-spin Fe(III) ion with coupling interaction between iron atoms confirmed with X-ray crystallographic study.[16]

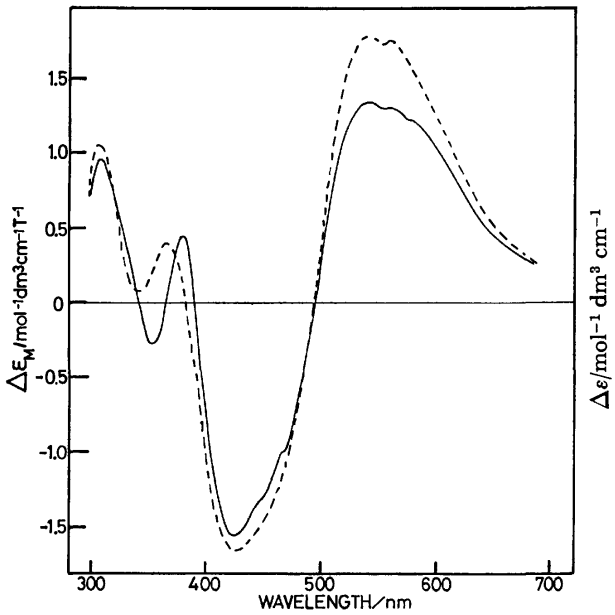

Fig. 3. MCD spectra of Fe(III)/Cys-containing peptide complexes.
——: Fe(III)/Z-Cys-Ala-Ala-Cys-OMe complex in DMSO, ------: Fe(III)/Z-Ala-Cys-OMe complex in DMSO.

Figure 3 shows the MCD spectra of the Fe(III)/peptide complexes. The MCD spectra of the di- and the tetrapeptide complexes in 400—700 nm region have similar spectral pattern. The dispersion type bands with crossover points at around 380 and 490 nm were assigned to the Faraday *A* terms and the positive bell-shaped band at around 540 nm to the Faraday *B* term tentatively. In the shorter wavelength below 400 nm, however, the complex of Fe(III)/Z-Cys-Ala-Ala-Cys-OMe had a negative bell-shaped band at 355 nm which was assignable to the Faraday *B* term. Similar MCD was observed for oxidized rubredoxin. On the other hand, Fe(III)/Z-Ala-Cys-OMe had a positive MCD band. Such difference has also been reported between Fe(III)/1,6-hexanedithiol and Fe(III)/1,4-butanedithiol or *o*-xylene-α,α'-dithiol complexes by Hatano *et al.*[9] They suggested that the MCD spectra of the dithiol Fe(III) complexes at around 350 nm reflect the chelate ring size.

In our case, the potential difference between Z-Cys-Ala-Ala-Cys-OMe and Z-Ala-Cys-OMe, affects the geometry of $[FeS_4]$ core (S denotes cysteinyl sulfur atom). The fact that Z-Cys-Ala-Ala-Cys-OMe can coordinate to Fe(III) ion as a chelating dithiolate ligand should be considered. The Fe(III)/peptide complexes have monomeric $[FeS_4]$ core structure as inferred from the MCD measurements and the core structure of Fe(III)/Z-Cys-Ala-Ala-Cys-OMe complex thus resembles to that of oxidized rubredoxin more closely than Fe(III)/Z-Ala-Cys-OMe complex.

Although the absorption, MCD, and EPR spectra of Fe(III)/peptide complexes did not show so large differences between the dipeptide and the tetrapeptide complexes, the CD spectra exhibited very different spectral pattern between them (Fig. 2). The CD spectrum of Fe(III)/Z-Cys-Ala-Ala-Cys-OMe complex was very similar to that of oxidized rubredoxin in visible region while the intensity was *ca.* 1/10. For oxidized rubredoxin the transitions at 565 and 494 nm have been assigned by MO treatments to the charge transfer transitions from occupied ligand π-orbitals to Fe d-orbitals.[17] The similarity in the CD spectra between oxidized rubredoxin and Fe(III)/Z-Cys-Ala-Ala-Cys-OMe complex in these transitions suggests that not only geometry of the $[FeS_4]$ core but also the major parts of the orientations of Fe–S–C_β (C_β denotes cysteine β carbon) groups resembles each other. The differences in the CD patterns and the CD strength between Fe(III)/Z-Cys-Ala-Ala-Cys-OMe and Fe(III)/Z-Ala-Cys-OMe complexes suggest that the $[FeS_4]$ core is formed for the dipeptide complex similar to the tetrapeptide complex but the orientations of the Fe–S–C_β groups largely differ from the tetrapeptide complex because the CD spectra are generally very sensitive to both the identity of asymmetric ligands and their orientations relative to the metal.

Bair *et al.*[18] studied the electronic properties of the active site of rubredoxin by *ab initio* methods. They used $[Fe(SH)_4]^{-/2-}$ as a model complex for the rubredoxin active site and examined several different sets of S–Fe–S–H dihedral angles. They found that energy separation of the d-d transitions is sensitive to the dihedral angle of the S–H bonds, and that the orientations of the S lone pairs pointing toward Fe ion, which are strongly influenced by the positions of the S–H bonds, directly affect the splitting energies of the Fe d-orbitals and thus play important roles in determining the redox properties of the Fe site. So it is expected that the tetrapeptide complex has different redox properties and also catalytic activities from the dipeptide complex.

We have studied Pd(II)/Z-Cys-Ala-Ala-Cys-OMe complex and revealed that the tetrapeptide coordinates to Pd(II) at two cysteine thiolate groups as a *cis*-chelate ligand from the conformational analyses of the peptide using ^{1}H-NMR spectra.[19] Other related di-cysteine peptides that we have also examined, Z-Cys-Ala-Cys-OMe, Z-Cys-Val-Val-Cys-OMe, and Z-Cys-Gly-Pro-Cys-OMe, were not able to take such stable chelate structure. These results allow us to conclude

that the tetrapeptide, Z–Cys–Ala–Ala–Cys–OMe, prefers a folded structure like a hairpin turn to form a stable *S,S-cis*-chelate Pd(II) structure which has rigid square planar geometry. Stability of such chelate structures should be influenced by the identity and sequence of amino acids intervening the two terminal cysteine residues. It is reasonable to think that the conformational restriction toward chelate ligand caused by tetrahedral metal ion as Fe(III) is looser than by square planar metal ion as Pd(II). Thus, a macro ring chelate structure probably exists for Fe(III)/Z–Cys–Ala–Ala–Cys–OMe system although direct evidences such as X-ray structure are lacking.

In conclusion, the CD spectrum as well as the absorption, MCD, and EPR spectra of Fe(III)/Z–Cys–Ala–Ala–Cys–OMe complex is similar to those of oxidized rubredoxin. The tetrapeptide complex has the mononuclear $[Fe(S\text{–}C_\beta)_4]^-$ structure similar to the rubredoxin active site and probably has the chelate structure although the amino acid sequence is different from the native protein except for two terminal cysteines. The tetrapeptide complex was more stable than the dipeptide complex. This is interesting in connection with the fact that mononuclear Fe(III) complex with monodentate thiolate ligand such as benzenethiolate anion has not been isolated whereas corresponding bidentate chelate complex, $[Fe(o\text{-xylene-}\alpha,\alpha'\text{-dithiolate})_2]^-$, is isolated.[7] Conceivably, Z–Cys–Ala–Ala–Cys–OMe chelated to Fe(III) ion takes a relatively stable conformation by the interaction between side chains of the alanyl residues to resist the oxidation of thiols. It is presumed that a tetrapeptide unit such as Cys–Gly–Gly–Cys lacking such interaction takes more flexible conformation and consequently the stability of the complex will decrease even if a chelate structure exists.

The roles of amino acid residues intervening the two terminal cysteine residues on the geometry and stability of active site of native enzyme is now being investigated using oligopeptides having the same sequence as the native enzyme active site.

The authors wish to express their thanks to Assistant Professor Mikiharu Kamachi of Osaka University for measuring the EPR spectra and Professor Yoichi Shimura, Osaka University, for his kindly offering the MCD equipment.

References

1) W. H. Orme-Johnson, *Annu. Rev. Biochem.*, **42**, 159 (1973).
2) "Iron-Sulfur Proteins," ed by W. Lovenberg, Academic Press, New York and London (1973, 1977), Vols. I—III.
3) K. D. Watenpaugh, L. C. Sieker, and L. H. Jensen, *J. Mol. Biol.*, **131**, 509 (1979).
4) M. H. Emptage, T. A. Kent, B. H. Huynh, J. Rawlings, W. H. Orme-Johnson, and E. Münck, *J. Biol. Chem.*, **255**, 1793 (1980); C. D. Stout, D. Ghosh, V. Pattabhi, and A. H. Robbins, *ibid.*, **255**, 1797 (1980).
5) Y. Sugiura, M. Kunishima, and H. Tanaka, *Biochem. Biophys. Res. Commun.*, **48**, 1400 (1972).
6) J. R. Anglin and A. Davison, *Inorg. Chem.*, **14**, 234 (1975).
7) R. H. Holm and J. A. Ibers, "Iron-Sulfur Proteins," (1977), Vol. III, Chap. 7.
8) G. Christou, B. Ridge, and N. H. Rydon, *J. Chem. Soc., Chem. Commun.*, **1977**, 908.
9) T. Muraoka, T. Nozawa, and M. Hatano, *Bioinorg. Chem.*, **8**, 45 (1978).
10) R. J. Burt, B. Ridge, and H. N. Rydon, *J. Chem. Soc., Dalton Trans.*, **1980**, 1228.
11) R. W. Lane, J. A. Ibers, R. B. Frankel, G. L. Papaefthymiou, and R. H. Holm, *J. Am. Chem. Soc.*, **99**, 84 (1977).
12) G. Christou, B. Ridge, and H. N. Rydon, *J. Chem. Soc., Chem. Commun.*, **1979**, 20.
13) W. Lovenberg and B. E. Sobel, *Proc. Natl. Acad. Sci. U.S.A.*, **54**, 193 (1965).
14) W. A. Eaton and W. Lovenberg, "Iron-Sulfur Proteins," ed by W. Lovenberg, Academic Press, New York and London (1973), Vol. II, Chap. 3.
15) N. M. Atherton, K. Garbett, R. D. Gillard, R. Mason, S. J. Mayhew, J. L. Peel, and J. A. Stangroom, *Nature*, **212**, 590 (1966); D. J. Newman and J. R. Postagate, *Eur. J. Biochem.*, **7**, 45 (1968); K. K. Rao, M. C. W. Evans, R. Cammeck, D. O. Hall, C. L. Thompson, P. J. Jackson, and C. E. Johnson, *Biochem. J.*, **129**, 1063 (1972).
16) T. H. Herskovitz, B. V. Depamphilis, W. O. Gillum, and R. H. Holm, *Inorg, Chem.*, **14**, 1426 (1975).
17) R. A. Bair and W. A. Goddard, III, *J. Am. Chem. Soc.*, **100**, 5669 (1978).
18) R. A. Bair and W. A. Goddard, III, *J. Am. Chem. Soc.*, **99**, 3505 (1977).
19) N. Ueyama, M. Nakata, and A. Nakamura, "Peptide Chemistry," ed by H. Yonehara, Proc. 17th Symp. Peptide Chem., 1979, Protein Research Foundation, Osaka (1980), p. 145.

  Bull. Chem. Soc. Jpn., 54, 1731—1735 (1981)

Reaction of Dimeric Copper(II) Acetate with Pyridine and Quinoline Bases in Dioxane

Kazuo HASEGAWA,† Noriyuki NAKASUKA, and Motoharu TANAKA*

Laboratory of Analytical Chemistry, Faculty of Science, Nagoya University, Chikusa-ku, Nagoya 464

(Received December 15, 1980)

Copper(II) acetate reacts with pyridine and quinoline bases in dioxane giving rise to adduct compounds, which were characterized by UV and EPR techniques. The reaction is formulated as follows:

$$Cu_2(OAc)_4 + L \overset{K_{21}}{\rightleftharpoons} Cu_2(OAc)_4L,$$

where L denotes a free base and K_{21} is an adduct formation constant. Values of K_{21} range from 12 for quinoline or 2-picoline to 146 $mol^{-1}\,dm^{-3}$ for 4-ethylpyridine. A linear free energy relationship is observed between the adduct formation and the protonation of bases in water except for sterically crowded bases.

Considerable interest has been shown in synthesis and physical properties of copper(II) carboxylates and of their adduct compounds with Lewis bases.[1-3] Usually copper(II) carboxylates and their adducts with pyridine bases have absorption maxima at about 370 nm, and the effective magnetic moments of these compounds are less than the spin-only value at room temperature. This has been taken as an indication of a dimeric structure, which is well established by X-ray diffraction studies for copper(II) acetate monohydrate[4] and its pyridine adducts in a solid state.[5]

Copper(II) carboxylate retains the dimeric structure also in solvents with weak solvating power and low dielectric constant, such as ethanol,[6,7] dioxane,[7,8] acetic acid,[9] benzene,[8,10] and chloroform.[10] On the other hand it dissociates into monomers in strongly solvating solvents such as water and pyridine. The latter solvent, having strong coordinating ability, breaks the dimeric structure despite a rather low dielectric constant ($\varepsilon=12$). At any rate dielectric properties may play an important role in the dissociation of the dimer.[11] Few quantitative investigations have, however, been carried out on reactions of these compounds in solution,[10-12] as compared with a number of works on their physical properties in a solid state.[1-3]

In this paper we report the reaction of copper(II) acetate with pyridine and quinoline bases in dioxane ($\varepsilon=2.2$).

Experimental

Reagents. *Dioxane*: Anhydrous tin(II) chloride was added to dioxane (G. R., Wako Pure Chemical Ind. Ltd.) to remove peroxides and the solution was distilled after refluxing for about 10 h. The distillate was then refluxed over sodium for about 10 h, followed by distillation. The water content of the dioxane thus purified was found to be 3.2×10^{-3} to 2.1×10^{-2} M†† by the Karl-Fischer method.

Copper(II) Acetate Solution in Dioxane: G. R. anhydrous copper(II) acetate (Wako Pure Chemical Ind. Ltd.) was washed with dioxane several times before use. The solution was standardized complexiметrically with 4-(2-thiazolylazo)-resorcinol as an indicator.[13]

Pyridine and Quinoline Bases: All bases were distilled under atmospheric or reduced pressure over sodium or potassium hydroxide.

Measurements. All measurements were made at 25±1 °C unless otherwise noted.

Absorbance was measured on a Union Giken spectrophotometer Model SM-401 (absorption curve) or on a Carl Zeiss spectrophotometer Model PMQ II (at 650 nm).

Electron paramagnetic resonance spectra were obtained with a JEOL ES-SCXA X-band spectrometer.

Results and Discussion

An apparent molar extinction coefficient remained constant at 650 nm for a solution containing copper(II) acetate alone over the concentration range from 3.7×10^{-4} to 4.6×10^{-3} M ($\varepsilon_0=220\pm5$ $M^{-1}\,cm^{-1}$†††). This indicates retention of the dimeric structure. Absorption spectra are shown in Fig. 1 for a copper(II) acetate–pyridine system, and similar ones are observed for the other bases employed. Addition of a base gives rise to a considerable change in absorption in the visible region, in contrast to virtual invariance of the shoulder discernible at about 370 nm. Since all the bases used in the present study do not absorb in these regions, this spectral behavior may be accounted for by coordination of the base to an apical position of a copper(II) dimer without dissociation into monomers.[10]

This argument is substantiated by the fact that the red shift of the band I in solution corresponds well to that in a solid state on addition of pyridine,[8] which is summarized in Table 1.

Presence of isosbestic points in Fig. 1 suggests only

Table 1. Absorption maxima of pyridine adducts

species[a]	Band I[b]	Band II[b]	State	Ref.
$Cu_2(OAc)_4$	682	370	Solid[c]	d)
$Cu_2(OAc)_4L$	718	370	Solid[c]	d)
$Cu_2(OAc)_4L$	680	370	Solid[e]	f)
$Cu_2(OAc)_4$	662	373	In dioxane	d)
$Cu_2(OAc)_4$	665	370	In dioxane	g)
$Cu_2(OAc)_4L$	708	375	In dioxane	d)

a) L represents pyridine. b) The wavelength expressed in nm. c) Nujol mull. d) The present work. e) Reflectance spectra. f) 8b. g) 8a.

† Present address: Nalco-Hakuto Chemical Co. Central Research Laboratory, Betsumei, Yokkaichi 510.

†† Throughout this paper: 1 M=1 mol dm^{-3}.

††† Extinction coefficients and molarities are both based on formula weights.

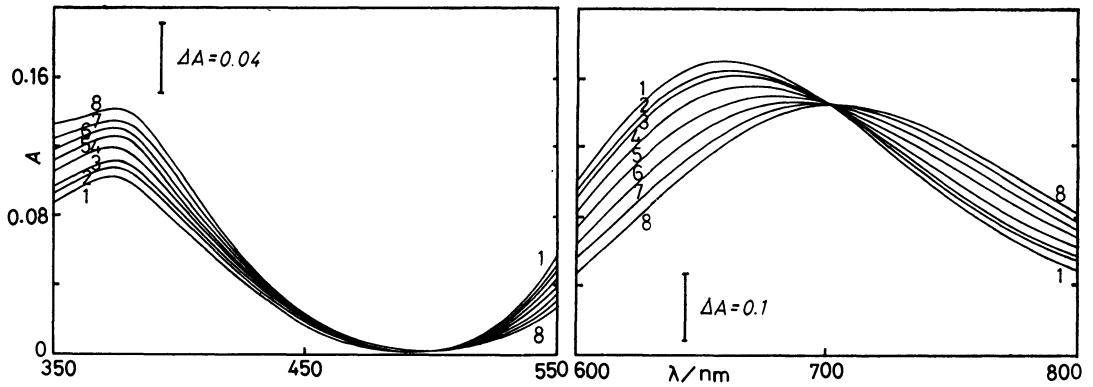

Fig. 1. Absorption spectra of the solutions of copper(II) acetate and pyridine.
$C_{Cu}=1.993\times10^{-3}$ M. $C_L/C_{Cu}=$(1) 0, (2) 0.614, (3) 2.47, (4) 6.16, (5) 8.65, (6) 10.5, (7) 14.8, (8) 24.7.
The figure at right is diminished in scale on the abscissa by a factor of 2.5.

one chemical equilibrium between a base and the dimeric acetate. Therefore the main reaction may be formulated as follows:

$$Cu_2(OAc)_4 + nL \overset{K_{2n}}{\rightleftharpoons} Cu_2(OAc)_4L_n, \quad (1)$$

where L denotes a free base and K_{2n} is the constant for the equilibrium (1). Unless the base concentration is considerably high, a 1 : 1 complex will predominate ($n=1$). Let D and DL stand for $Cu_2(OAc)_4$ and $Cu_2(OAc)_4L$ respectively, then consideration of stoichiometric relations gives the following expressions:

$$A = 2\varepsilon_0[D] + 2\varepsilon_{21}[DL] \quad (2)$$

$$A_0 = \varepsilon_0 C_{Cu} \quad (3)$$

$$C_{Cu} = 2[D] + 2[DL] \quad (4)$$

$$C_L = [L] + [DL], \quad (5)$$

where A and A_0 are the absorbances at 650 nm in the presence and in the absence of a base, ε_0 and ε_{21} the molar extinction coefficients of D and DL. C_{Cu} and C_L represent the total concentrations of copper and a base, respectively.

Combination of these equations leads to:

$$\frac{C_{Cu}C_L}{A-A_0} = \frac{1}{\varepsilon_{21}-\varepsilon_0}\left[C_L+\frac{C_M}{2}-\frac{A-A_0}{2(\varepsilon_{21}-\varepsilon_0)}\right] + \frac{1}{K_{21}(\varepsilon_{21}-\varepsilon_0)}. \quad (6)$$

Plots of the left-hand side against $[C_L+C_M/2-(A-A_0)/2(\varepsilon_{21}-\varepsilon_0)]$ yielded a family of straight lines as was expected, with ε_{21} roughly chosen. A better extinction coefficient ε_{21} and an adduct formation constant K_{21} were obtained from the gradient and the intercept of the straight line (Fig. 2).

Formation of the 1 : 1 adduct DL was confirmed in a more general fashion.

An apparent molar extinction coefficient may be expressed in the following way:

$$\varepsilon = \frac{A}{C_M} = \frac{\varepsilon_0+\varepsilon_{2n}K_{2n}[L]^n}{1+K_{2n}[L]^n}. \quad (7)$$

Transformation of Eq. 7 gives

$$\log(\varepsilon_0-\varepsilon) = \log(\varepsilon_0-\varepsilon_{2n}) + \log\left(\frac{K_{2n}[L]^n}{1+K_{2n}[L]^n}\right). \quad (8)$$

A plot of $\log(\varepsilon_0-\varepsilon)$ against $\log[L]$ may be compared

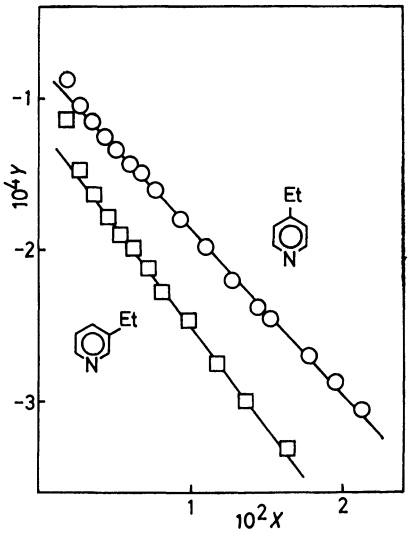

Fig. 2. Linear plot for change in absorbance at 650 nm.
$y=C_{Cu}C_L/(A-A_0)$, $x=C_L+C_M/2-(A-A_0)/2(\varepsilon_{21}-\varepsilon_0)$. See Eq. 6.
○: 4-Ethylpyridine, $C_{Cu}=2.44_7\times10^{-3}$ M, □: 3-ethylpyridine, $C_{Cu}=2.14_8\times10^{-3}$ M.

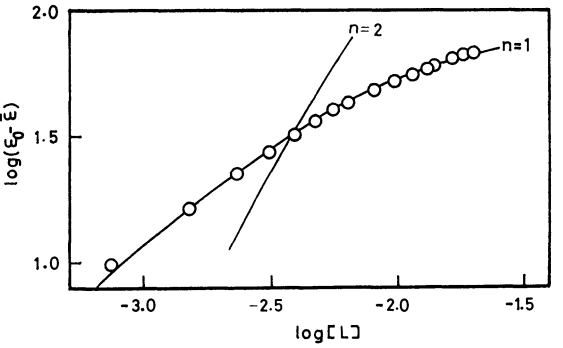

Fig. 3. Curve-fitting of change in absorbance at 650 nm for 4-ethylpyridine (Eq. 9).
[L] was refined with the computer and $C_{Cu}=2.44_7\times10^{-3}$ M.

with a family of normalized curves with different parameter n, that is $y=\log[p^n/(1+p^n)]$ as a function of $x=\log p$. As is evident from Fig. 3, the best fit curve is obtained when $n=1$, and the values of ε_{21} and K_{21} were

TABLE 2. ADDUCT FORMATION CONSTANTS

Base	K_{21}/M^{-1}	$\varepsilon_{21}/M^{-1}\,cm^{-1}$ e)	pK_a
Pyridine	83±9	136±5	5.19a)
2-Picoline	12±6	116±3	5.95a)
3-Picoline	98±21	131±4	5.66a)
4-Picoline	114±13	138±4	6.00a)
2,4-Lutidine	25±6	126±4	6.74a)
3,5-Lutidine	132±9	129±4	6.09a)
3,4-Lutidine	137±22	127±3	6.47a)
2,6-Lutidine	f)		6.71a)
3-Ethylpyridine	97±13	139±5	5.70b)
4-Ethylpyridine	146±6	134±4	6.02b)
Collidine	f)		7.59c)
Quinoline	12±1	144±3	4.93d)
Isoquinoline	73±1	135±4	5.46d)

Protonation constants pK_a refer to 25 °C and $\mu=0$ M unless otherwise noted.
a) H.-H. Perkampus and G. Prescher, *Ber. Bunsenges. Phys. Chem.*, **72**, 429 (1968). b) H.C. Brown and X. R. Mihm, *J. Am. Chem. Soc.*, **77**, 1723 (1955). c) H. C. Brown, D. Gintis, and H. Podall, *J. Am. Chem. Soc.*, **78**, 5375 (1956). d) A. Albert and J. N. Phillips, *J. Chem. Soc.*, **1956**, 1294. e) At 650 nm. f) Too small to evaluate.

determined by the curve-fitting method.

These values were further refined by the least squares method with an electronic computer FACOM 230-75 at Computation Center of Nagoya University. The final results are summarized in Table 2.

The experimental data were also treated by plotting graphically the spectral change at 650 nm as well as by refining with the computer, dissociation of the dimer being assumed as the main reaction. Then the predominant reaction might be written as follows:

$$Cu_2(OAc)_4 + 2nL \overset{K_{1n}}{\rightleftharpoons} 2Cu(OAc)_2L_n. \quad (9)$$

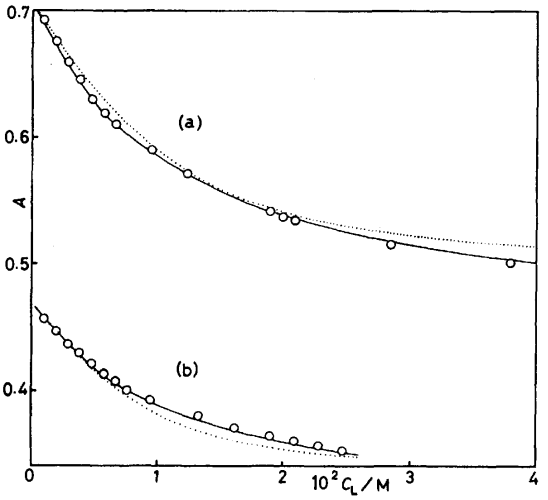

Fig. 4. Change in absorbance at 650 nm with the concentration of 3-ethylpyridine.
a) $C_{Cu}=3.22_1\times10^{-3}$ M. b) $C_{Cu}=2.14_8\times10^{-3}$ M.
○ refers to the experimental value. ——: Calculated curve assuming DL alone, ……: calculated curve assuming ML alone. It was drawn with tentative values of $K'_{11}=78.8\ M^{-1}$ and $\varepsilon'_{11}=156\ M^{-1}\,cm^{-1}$ (see text).

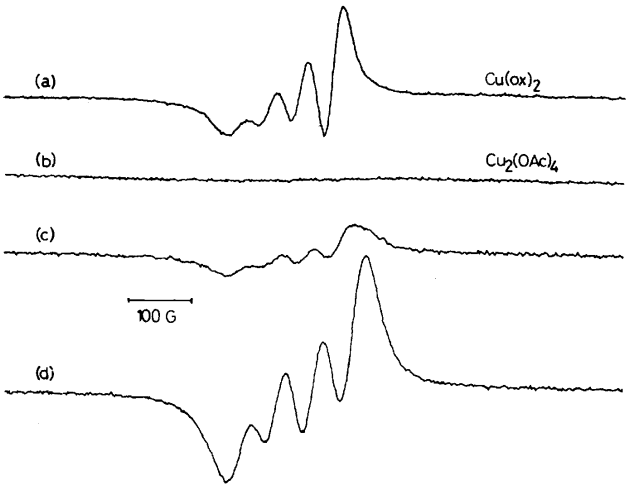

Fig. 5. EPR spectra of dioxane solutions at room temperature (about 20 °C).
a): Copper(II) 8-quinolinolate ($C_{Cu}=6.10\times10^{-5}$ M), b): $C_{py}=0$ M, c): $C_{py}=2.62\times10^{-2}$ M, d) $C_{py}=2.47_2\times10^{-1}$ M.
The concentration was $2.39_2\times10^{-3}$ M in copper(II) acetate except for a).

The assumption of a monomer formation alone results in a systematic deviation of the calculated curves from the experimental data for 3-ethylpyridine as shown in Fig. 4. The dotted lines are drawn with tentative values of K'_{11} and ε'_{11}[14] that gave the best fit to the data on assuming only the Eq. 9. In the case of pyridine, however, the dissociation reaction also accounts for the spectral change satisfactorily when $n=1$.

This finding prompted us to an electron paramagnetic resonance study. A solution containing copper(II) acetate alone did not exhibit any EPR spectra other than ones characteristic of the dimeric structure, while typical copper(II) spectra began to appear on addition of pyridine at concentrations higher than those used in the UV study (Fig. 5). Analysis of spin concentration was carried out for a monomeric form by double integration of the spectra.[15] Copper(II) 8-quinolinolate in dioxane was selected as a standard, since the shape of EPR spectra is similar to those of monomeric copper(II) acetate. Table 3 indicates that the monomeric concentration [ML] thus determined experimentally is much lower than the value of [ML]', which was tentatively estimated with $K'_{11}=11.3\ M^{-1}$ (*cf.* Eq. 9).

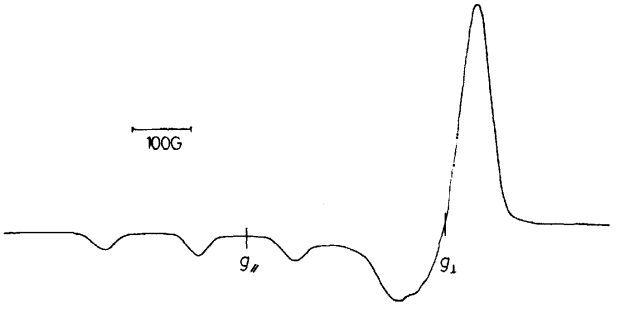

Fig. 6. EPR spectra of copper(II) acetate monopyridine adduct in dioxane at 99.3 K.
$C_{py}=2.47_2\times10^{-1}$ M and $C_{Cu}=2\times10^{-3}$ M.

Table 3. Comparison of monomeric and dimeric species [a)]

No.	10 C_L/M	10^3[ML]′/M[b)]	10^4[ML]/M	10^3[DL]/M	[L]/M	log (K_{11}/M^{-1})
1	0.131	1.05	0.24	0.609	0.0125	−2.20
2	0.262	1.62	0.35	0.811	0.0254	−2.31
3	0.524	2.09	0.71	0.969	0.0514	−2.08
4	0.786	2.24	1.00	1.035	0.0775	−1.99
5	1.236	2.33	1.13	1.089	0.1225	−2.10
6	2.472	2.38	1.69	1.140	0.2461	−2.07

a) L, ML, and DL denote pyridine, $Cu(OAc)_2L$, and $Cu_2(OAc)_4L$, respectively. The concentration of copper(II) acetate was maintained at $2.39_2 \times 10^{-3}$ M. b) [ML]′ was calculated using a tentative value of K'_{22}= 11.3 M^{-1} (see text).

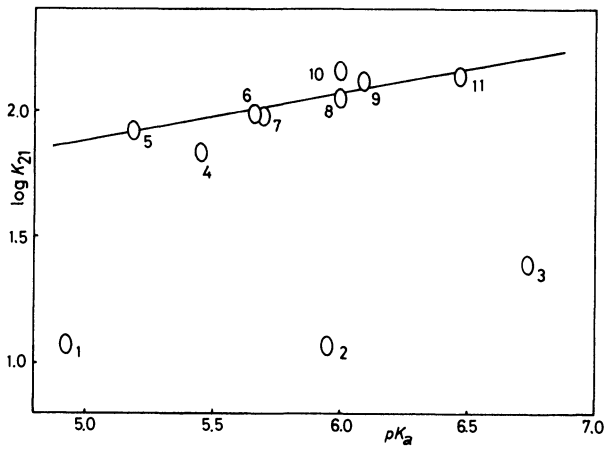

Fig. 7. Linear free energy relationship between the addition of bases to dimeric copper acetate and the protonation of bases.
1): Quinoline, 2): 2-picoline, 3): 2,4-lutidine, 4): isoquinoline, 5): pyridine, 6): 3-picoline, 7): 3-ethylpyridine, 8): 4-picoline, 9): 3,5-lutidine, 10): 4-ethylpyridine, 11): 3,4-lutidine.

In brief, monomeric species appear appreciably only when a base concentration becomes much higher. The last column in Table 3 shows experimental quotients $K_{11}=[ML]^2/[D][L]^2$, which are roughly constant (log $K_{11}=-2.1\pm0.1$).

The EPR spectra at room temperature (about 20 °C) gave merely an average value of g, which was determined as $\bar{g}=2.142$ from Fig. 5. Therefore spectra were also measured at 99.3 K for a dioxane solution, and $g_\perp=2.063$ and $g_{//}=2.309$ were obtained (Fig. 6). These values give $g=2.148$ in a fair accord with the above value found at room temperature, and are compared with the values $g_x=2.065$, $g_y=2.070$, and $g_z=2.362$ for the crystal of $Cu_2(OAc)_4Py_2$.[16] Distortion from the O_h symmetry with an elongation along the z axis is expected in the monomeric $Cu(OAc)_2Py$, because $g_{//}>g_\perp>2$.[17]

For most bases the formation constant of the 1 : 1 adduct log K_{21} increases linearly with pK_a of a base as illustrated in Fig. 7. Among the pyridine bases examined, however, 2-picoline and 2,4-lutidine have abnormally low formation constants, possibly because of the steric hindrance of 2-methyl group. More crowded 2,6-lutidine and collidine hardly react with copper(II) acetate. The steric effect of an adjacent benzene ring is also observed with quinoline.

Similar relations are also observed in other systems, such as copper(II)–β-diketone,[18–20] oxovanadium(IV)–β-diketone,[21] and 2,3-butanedionebis(benzoylhydrazonato)nickel(II)[22] complexes with pyridine or quinoline bases. A linear free energy relationship is also found between the adduct formation constant for copper(II) acetate (log K_{21}) and that for bis(acetylacetonato)oxovanadium(IV) (log K_x) with pyridine or quinoline bases. Linearity holds, however, for all bases including the sterically crowded ones, as shown in Fig. 8.

Contrary to exclusive formation of a 1 : 2 adduct DL_2 in a solid state, a 1 : 1 species DL predominates in

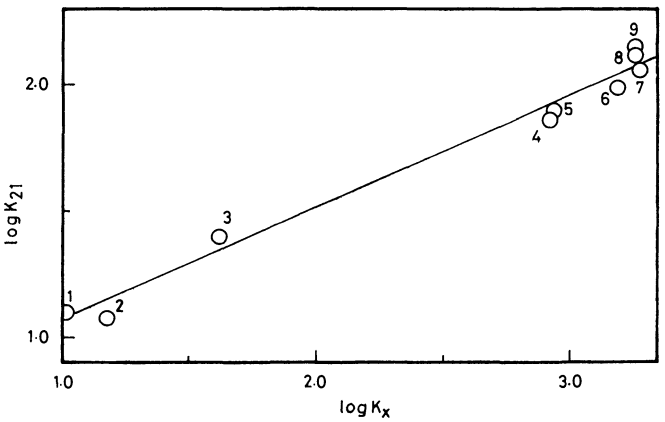

Fig. 8. Linear free energy relationship for the addition reactions of bases.
K_{21} refers to dimeric copper(II) acetate and K_x to bis(acetylacetonato)oxovanadium(IV).
1): 2-Picoline, 2): quinoline, 3): 2,4-lutidine, 4): isoquinoline, 5): pyridine, 6): 3-picoline, 7): 4-picoline, 8): 3,5-lutidine, 9): 4-ethylpyridine.

dioxane. This is rather unusual when compared with the reactions in other solvents. In anhydrous acetic acid, for example, copper acetate dissociates into monomer at early stage on addition of lithium acetate[9] and pyridine,[23] with rapid dissappearance of the shoulder at 370 nm. Extraction of copper(II) with an aliphatic long chain carboxylic acid also revealed existence of a monomer ML as well as a dimer DL in the presence of pyridine in benzene.[12]

Adduct formation may be interpreted in terms of substitution of a solvent molecule, bound to an apical site of the dimeric copper(II), by a base which has stronger coordination power than dioxane.

The authors are greatly indebted to Dr. W. Mori, Osaka University, for helpful discussions in interpreting the EPR data, and also to Mr. T. Seto, Nagoya University, for performing the EPR measurement. This research was financially supported by a Grant-in-Aid for Scientific Research No. 347029 from the Ministry of Education, Science and Culture (Japan).

References

1) M. Kato, H. B. Jonassen, and J. C. Fanning, *Chem. Rev.*, **64**, 99 (1964).

2) J. Catterick and P. Thornton, "Structures and Physical Properties of Polynuclear Carboxylates," in "Advances in Inorganic Chemistry and Radiochemistry," ed by H. J. Emeléus and A. G. Sharpe, Academic Press (1977), Vol. 20, pp. 291—362.

3) R. J. Doedens, "Structure and Metal-Metal Interactions in Copper(II) Carboxylate Complexes," in "Progress in Inorganic Chemistry," ed by S. J. Lippard, John Wiley & Sons, New York (1976), Vol. 21, pp. 209—231.

4) J. N. van Niekerk and F. R. L. Schoening, *Acta Crystallogr.*, **6**, 227 (1953).

5) a) G. A. Barclay and C. H. L. Kennard, *J. Chem. Soc.*, **1961**, 5244; b) F. Hanic, D. Štempelová, and K. Hanicová, *Acta Crystallogr.*, **17**, 633 (1964).

6) S. Yamada, H. Nakamura, and R. Tsuchida, *Bull. Chem. Soc. Jpn.*, **30**, 953 (1957).

7) M. Kondo and M. Kubo, *J. Phys. Chem.*, **62**, 468 (1958).

8) a) R. L. Martin and A. Whitley, *J. Chem. Soc.*. **1958**, 1394; b) L. Dubicki and R. L. Martin, *Inorg. Chem.*, **5**, 2203 (1966).

9) K. Sawada, H. Ohtaki, and M. Tanaka, *J. Inorg. Nucl. Chem.*, **34**, 625 (1972).

10) D. P. Graddon, *J. Inorg. Nucl. Chem.*, **17**, 222 (1961).

11) H. Grasdalen and I. Svare, *Acta Chem. Scand.*, **25**, 1089 (1971); H. Grasdalen, *ibid.*, **25**, 1103 (1971).

12) K. Hirose, N. Matsumoto, and M. Tanaka, *J. Inorg. Nucl. Chem.*, **39**, 2261 (1977).

13) H. Wada and G. Nakagawa, *Jpn. Analyst*, **14**, 28 (1965).

14) The prime was affixed to emphasize a hypothetical nature of the reaction (9).

15) R. S. Alger, "Electron Paramagnetic Resonance," Interscience, New York (1968). (Translation into Japanese by T. Isobe *et al.* Yoshioka-shoten (1973), p. 224).

16) F. E. Mabbs, J. K. Porter, and W. R. Smail, *J. Inorg. Nucl. Chem.*, **36**, 819 (1974).

17) B. A. Goodman and J. B. Raynor, "Electron Spin Resonance of Transition Metal Complexes," in "Advances in Inorganic Chemistry and Radiochemistry," ed by H. J. Emeléus and A. G. Sharpe, Academic Press (1970), Vol. 13, pp. 135—362.

18) T. Shigematsu, M. Tabushi, M. Matsui, and M. Munakata, *Bull. Chem. Soc. Jpn.*, **41**, 2656 (1968); T. Shigematsu, M. Matsui, Y. Sasaki, and M. Sakurada, *ibid.*, **49**, 2325 (1976); Y. Sasaki, M. Sakurada, M. Matsui, and T. Shigematsu, *ibid.*, **52**, 2295 (1979).

19) D. P. Graddon and E. C. Watton, *J. Inorg. Nucl. Chem.*, **21**, 49 (1961).

20) K. Ueda, *Bull. Chem. Soc. Jpn.*, **51**, 805 (1978).

21) E. Kwiatkowski and J. Trojanowski, *J. Inorg. Nucl. Chem.*, **38**, 131 (1976).

22) L. Sacconi, G. Lombardo, and P. Paoletti, *J. Inorg. Nucl. Chem.*, **8**, 217 (1958).

23) K. Hasegawa, unpublished results.

Syntheses and Characterizations of μ-Dicarboxylato-bis[pentaamminecobalt(III)] Complexes

Hiroshi OGINO,* Keiichi TSUKAHARA,† Yoshiyuki MORIOKA, and Nobuyuki TANAKA

Department of Chemistry, Faculty of Science, Tohoku University, Aoba, Aramaki, Sendai 980

(Received December 22, 1980)

Five new complexes, $[(NH_3)_5Co(dicarboxylate)Co(NH_3)_5]X_4$ (dicarboxylate=oxalate, succinate, pimelate, fumarate, and maleate; $X=ClO_4^-$ or Cl^-), were synthesized by the reactions of $[Co(hydrogen\ dicarboxylate)(NH_3)_5](ClO_4)_2$ with $[Co(NH_3)_5(H_2O)](ClO_4)_3$ and characterized by chromatographic behavior and electronic and NMR techniques. When maleate was used as the dicarboxylate, the formation of $[(NH_3)_5Co(fumarate)Co(NH_3)_5]^{4+}$ as well as $[(NH_3)_5Co(maleate)Co(NH_3)_5]^{4+}$ was observed. The IR and Raman spectra of $[(NH_3)_5Co(oxalate)Co(NH_3)_5]^{4+}$ indicate that the symmetry of the oxalate ion in the complex may be approximated by D_{2h}.

The syntheses of a series of μ-dicarboxylato-bis[pentaamminecobalt(III)] complexes were reported by Duff,[1] where malonic, glutaric, adipic, malic, phthalic, citraconic, and itaconic acids were used as the μ-bridging ligands. However, the synthetic procedure of Duff is time consuming, that is, it takes a week or more. Our attempt to prepare μ-malonato-bis[pentaamminecobalt(III)] complex using Duff's procedure failed. Furthermore, synthesis of the simplest complex of this series, $[(NH_3)_5Co(O_2CCO_2)Co(NH_3)_5]X_4$, has not been reported.

This paper reports the syntheses and characterizations of the bis[pentaamminecobalt(III)] complexes containing μ-oxalate, malonate, succinate, pimelate, fumarate, and maleate ligands.[2] Some observations on the products of the reaction of $[Co(Hdic)(NH_3)_5]^{2+}$ with $[Co(NH_3)_5(H_2O)]^{3+}$ are also described.

Experimental

Materials. The complexes $[Co(NH_3)_5(H_2O)](ClO_4)_3$ and $[Co(Hox)(NH_3)_5](ClO_4)_2$ were prepared by the published methods.[3,4] The other complexes containing Hdic, $[Co(Hdic)(NH_3)_5](ClO_4)_2$, were prepared by the published method with slight modifications:[5,6] The H_2dic (0.2 mol) was dissolved into 200 cm^3 of water containing NaOH (0.2 mol). After the addition of $[Co(NH_3)_5(H_2O)](ClO_4)_3$ (0.02 mol), the temperature of the solution was kept at 70—75 °C for 3 h, and then the solution was cooled, and diluted to 3 dm^3 with water. The solution was poured into an SP-Sephadex C-25 column (4.5 cm × 35 cm). The desired species was eluted out with a 0.1 M $NaClO_4$ solution of pH 2—3 adjusted with $HClO_4$ (1 M=1 mol dm^{-3}).[7] Small amounts of $[Co(NH_3)_5(H_2O)]^{3+}$ and $[(NH_3)_5Co(dic)Co(NH_3)_5]^{4+}$ (yield=2—3%) remained in the column. The eluate was evaporated to a small volume with a rotary evaporator whereupon red crystals of $[Co(Hdic)(NH_3)_5](ClO_4)_2$ were obtained; yield 80—90%.

Syntheses of μ-Dicarboxylato-bis[pentaamminecobalt(III)] Perchlorates. The complex $[Co(Hdic)(NH_3)_5](ClO_4)_2$ (0.01 mol) was dissolved into 150 cm^3 of water. The pH of the solution was adjusted to 4 with $NaHCO_3$. To this solution was added 0.01 mol of $[Co(NH_3)_5(H_2O)](ClO_4)_3$. The solution was kept at 70—75 °C for 2—3 h and then cooled to room temperature. After diluting the solution to 1.5 dm^3 with water, the pH was adjusted to 3 with $HClO_4$. This was poured into the SP-Sephadex C-25 column. The adsorbed species were eluted with $NaClO_4$ solutions of pH 2—3 adjusted with $HClO_4$. Major species on the column were identified as $[Co(Hdic)(NH_3)_5]^{2+}$,[7] $[Co(NH_3)_5(H_2O)]^{3+}$, and $[(NH_3)_5Co(dic)Co(NH_3)_5]^{4+}$. Detailed product distribution will be given in Results and Discussion. The $[(NH_3)_5Co(dic)Co(NH_3)_5]^{4+}$ was eluted with a 0.4 M $NaClO_4$ solution,[9] after the species less charged than 4+ had been eluted out. The eluate was evaporated to a small volume with a rotary evaporator whereupon red crystals of the perchlorate salt were obtained. The recrystallizations were made from water. The chloride salt of $[(NH_3)_5Co(ox)Co(NH_3)_5]^{4+}$ was obtained when 0.4 M KCl solution was used in place of the 0.4 M $NaClO_4$ eluant.

The analytical data for the complexes are given in Table 1.

Apparatus. Electronic spectra of the complexes in aqueous solutions were recorded on a Union-Giken SM-401 spectrophotometer. ^1H-NMR spectra (in D_2O containing 0.1 M D_2SO_4, with sodium 2,2-dimethyl-2-silapentane-5-sulfonate as the internal standard) were obtained by the use of a Varian A 60 spectrometer and a JEOL MH-100 spectrometer. ^{13}C-NMR spectra were recorded on a Varian XL-200 at a frequency of 50 MHz (D_2O lock) in the proton noise decoupled mode. The solubility of the perchlorate salts of

Table 1. Analytical data of the complexes

Compound	Found(Calcd)(%)		
	C	H	N
$[Co(Hpim)(NH_3)_5](ClO_4)_2$	16.58(16.74)	5.43(5.23)	14.05(13.95)
$[(NH_3)_5Co(ox)Co(NH_3)_5](ClO_4)_4$	3.01(3.10)	4.01(3.91)	17.93(18.10)
$[(NH_3)_5Co(ox)Co(NH_3)_5]Cl_4$	4.51(4.63)	6.11(5.84)	26.87(27.04)
$[(NH_3)_5Co(malo)Co(NH_3)_5](ClO_4)_4\cdot 2H_2O$	4.50(4.37)	4.23(4.41)	17.06(17.00)
$[(NH_3)_5Co(suc)Co(NH_3)_5](ClO_4)_4$	6.26(5.99)	4.46(4.28)	17.62(17.47)
$[(NH_3)_5Co\ (fum)\ Co(NH_3)_5]\ (ClO_4)_4\cdot 0.5H_2O$	6.11(5.94)	4.20(4.12)	17.23(17.31)
$[(NH_3)_5Co(male)Co(NH_3)_5](ClO_4)_4\cdot 2H_2O$	5.89(5.75)	4.25(4.35)	16.78(16.76)
$[(NH_3)_5Co(pim)Co(NH_3)_5](ClO_4)_4\cdot 3H_2O$	9.71(9.36)	4.82(5.17)	15.19(15.60)

† Present address: Department of Chemistry, Faculty of Science, Shimane University, Nishikawatsucho, Matsue 690.

Table 2. Numerical data for the electronic spectra of the complexes prepared in this work and related complexes

Compound	Medium	λ_{max}/nm(ε/M^{-1} cm^{-1})[a]	Ref.
$[(NH_3)_5Co(ox)Co(NH_3)_5](ClO_4)_4$	H_2O	505(156), 344sh(240), 274sh(4690), 220sh(23700)	This work
$[Co(Hox)(NH_3)_5](ClO_4)_2$	pH<2.5	505(73.0)	10
	pH 7.5	505(76.0)	
$[(NH_3)_5Co(malo)Co(NH_3)_5](ClO_4)_4\cdot 2H_2O$	H_2O	505(174), 352(135), 228(24900)	This work
$[Co(Hmalo)(NH_3)_5](ClO_4)_2$	0.05 M $HClO_4$	505(74.9), 350(58.2)	11
$[(NH_3)_5Co(suc)Co(NH_3)_5](ClO_4)_4$	H_2O	505(158), 353(120), 227(24400)	This work
$[Co(Hsuc)(NH_3)_5](ClO_4)_2$	0.05 M $HClO_4$	505(68.2), 355(54.8)	11
$[(NH_3)_5Co(fum)Co(NH_3)_5](ClO_4)_4\cdot 0.5H_2O$	H_2O	504(170), 351(142), 232(36700)	This work
$[Co(Hfum)(NH_3)_5](ClO_4)_2$	pH 1—10	502(75.3), 351(61.8)	12
$[(NH_3)_5Co(male)Co(NH_3)_5](ClO_4)_4\cdot 2H_2O$	H_2O	505(160), 353(131), 229(25800)	This work
$[Co(Hmale)(NH_3)_5](ClO_4)_2$	H_2O	502.5(76.8), 351(66.5)	13
$[(NH_3)_5Co(pim)Co(NH_3)_5](ClO_4)_4\cdot 3H_2O$	H_2O	504(152), 353(122), 229(23600)	This work
$[Co(Hpim)(NH_3)_5](ClO_4)_2$	0.1 M $HClO_4$	505(76.3), 355(60.9)	

a) sh=Shoulder.

the μ-dicarboxylato complexes into D_2O was found to be too low for the measurement of the NMR spectra. These complexes converted to the chloride salts with the aid of Dowex 1 X-4 resin in the chloride form, because the chlorides were found to be much more soluble than the perchlorates. The IR spectra (KBr disks) were recorded on a Hitachi EPI-S2 spectrometer. Raman spectra of $[(NH_3)_5Co(ox)Co(NH_3)_5](ClO_4)_4$ were recorded on a JEOL JRS-400T spectrometer. The 488 nm line of an Ar-ion laser (150 and 250 mW of power) was used as a light source. The spectra were measured in the solid state with KBr as a support. The rotating sample technique was employed to avoid decomposition.

Results and Discussion

Formulation of the Complexes. The analytical results of the $[(NH_3)_5Co(dic)Co(NH_3)_5]X_4$ shown in Table 1 are compatible with the assigned formulation. The positions of the absorption maxima due to the d-d transitions are characteristic for the $[CoN_5O]$ chromophores (Table 2) and the molar absorption coefficients (ε/M^{-1} cm^{-1}) are approximately 2 times larger than those of the corresponding $[Co(Hdic)(NH_3)_5]^{2+}$ complexes. The dimeric complex ions showed flow rates on a Sephadex column such that the ions must be the 4+ charged species.[14]

The ^{1}H-NMR spectra of $[(NH_3)_5Co(dic)Co(NH_3)_5]^{4+}$ showed only two NH_3 peaks at 2.90—2.94 ppm (6H) and 3.86—3.93 ppm (24H) (Table 3). This result also supports the μ-dicarboxylato-bis[pentaamminecobalt(III)] formulation, because the two peaks can be assigned to *trans*-NH_3 and *cis*-NH_3 to the μ-dicarboxylate ion, respectively, on the basis of the assignment reported for the spectra of $[CoX(NH_3)_5]^{n+}$ complexes.[15,16] The ^{1}H-NMR spectra of $[Co(Hmale)(NH_3)_5]^{2+}$ and $[Co(Hfum)(NH_3)_5]^{2+}$ showed AB splitting patterns due to the presence of CH=CH protons. Chemical shifts (coupling constants) were 6.10 and 6.43 ppm (J_{H-H}= 12.0 Hz) for the Hmale complex and 6.53 and 6.75 ppm (J_{H-H}=16.0 Hz) for the Hfum complex. In the spectra of $[(NH_3)_5Co(male)Co(NH_3)_5]^{4+}$ and $[(NH_3)_5Co(fum)Co(NH_3)_5]^{4+}$, each complex showed a singlet signal for the CH=CH protons which is compatible with the assigned formulation.

Table 3. Numerical data for the ^{1}H-NMR spectra of $[(NH_3)_5Co(dic)Co(NH_3)_5]^{4+}$ complexes

dic	Chemical shift δ/ppm		
	trans-NH_3	*cis*-NH_3	C–H_n
ox	2.93	3.93	—
malo	2.90	3.90	3.33(CH_2)
suc	2.90	3.86	2.46(CH_2CH_2)
pim	2.92	3.89	2.19, 2.26, 2.34 triplet (CH_2COO) 1.12—1.64 multiplet ($CH_2CH_2CH_2$)
fum	2.94	3.92	6.45 (CH=CH)
male	2.94	3.92	6.11 (CH=CH)

Table 4. Numerical data for the ^{13}C-NMR spectra of $[(NH_3)_5Co(dic)Co(NH_3)_5]^{4+}$ complexes[a]

dic	ox	malo	suc	pim	fum	male
$O_2\underline{C}$–	165.8	181.3	186.8	188.5	178.3	179.3
$O_2C\underline{C}$–	—	49.1	34.5	38.7	135.2	130.4
$O_2CC\underline{C}$–	—	—	—	25.8	—	—
$O_2CCC\underline{C}$–	—	—	—	29.0	—	—

a) Dioxane (δ=67.4 ppm *vs.* tetramethylsilane) was used as the internal standard. Chemical shifts were referenced to tetramethyl silane, downfield shifts having positive values.

As expected from the symmetric nature of the complexes, the ^{13}C-NMR spectra showed only one signal for the μ-ox complex, two signals for the μ-malo, μ-suc, μ-fum, and μ-male complexes, and four signals for the μ-pim complex (Table 4).

Product Distribution of the Reaction of $[Co(Hdic)(NH_3)_5](ClO_4)_2$ with $[Co(NH_3)_5(H_2O)](ClO_4)_3$. Figure 1 shows a chromatogram for the solution produced in the reaction between $[Co(Hox)(NH_3)_5]^{2+}$ and $[Co(NH_3)_5(H_2O)]^{3+}$. The distribution of the species formed in the reaction of $[Co(Hdic)(NH_3)_5](ClO_4)_2$ with $[Co(NH_3)_5$-

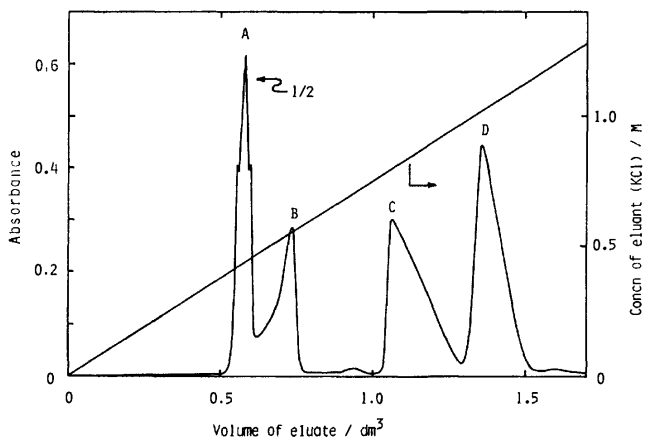

Fig. 1. Chromatogram for the solution produced in the reaction between $[Co(Hox)(NH_3)_5](ClO_4)_2$ and $[Co(NH_3)_5(H_2O)](ClO_4)_3$. The bands A, B, C, and D correspond to $[Co(ox)(NH_3)_5]^+$, $[Co(Hox)(NH_3)_5]^{2+}$, $[Co(NH_3)_5(H_2O)]^{3+}$, and $[(NH_3)_5Co(ox)Co(NH_3)_5]^{4+}$, respectively. The preparative scale was one-fourth of that given in Experimental. Heating time of the mixture was 4 h. The chromatography was made with an SP-Sephadex C-25 column ($\phi 2.6 \times 40$ cm). The pH of the eluant was asjusted to 3 with HCl. Absorbance was measured at 505 nm with a flow-cell of 0.5 cm optical length.

$(H_2O)](ClO_4)_3$ was determined semi-quantitatively. The results are shown in Table 5. In the case of ox, malo, male, or pim system, a small amount of a violet species was detected at the lowest band. The species could be eluted out very easily with a 0.1 M $NaClO_4$ solution and hence the charge of the species was considered to be 1+. For the ox and malo systems, the species were characterized as chelated complexes $[Co(dic)(NH_3)_4]^+$ from a comparison of the electronic spectra with published data.[17,18]

In most systems, the amounts of $[Co(Hdic)(NH_3)_5]^{2+}$ which remained unreacted were less than those of $[Co(NH_3)_5(H_2O)]^{3+}$ unreacted. This suggests the simultaneous occurrence of the dimerization reaction with $[Co(NH_3)_5(H_2O)]^{3+}$ and the aquation reaction of the $[Co(Hdic)(NH_3)_5]^{2+}$.

The ^1H-NMR spectra of the starting material pentaamminemaleatocobalt(III) complex did not show a detectable amount of pentaamminefumaratocobalt(III) complex (<2%). However, the formation of $[(NH_3)_5Co(fum)Co(NH_3)_5]^{4+}$ was observed in the male system. Therefore, the μ-fum complex is thought to be formed by the isomerization of $[(NH_3)_5Co(male)Co(NH_3)_5]^{4+}$.

IR and Raman Spectra. IR spectra of all the dimeric complexes show intense bands in the regions of 1300—1400 cm^{-1} and 1600—1650 cm^{-1}, which can be assigned to the CO stretching vibrations, though these bands are obscured by the overlap of the NH_3 deformation vibrations.[19] The deuterated μ-ox complex exhibits three CO stretching absorptions, *i.e.*, at 1625 (strong), 1435 (weak), and 1302 cm^{-1} (strong). Table 6 shows the IR and Raman spectral data of $[(NH_3)_5Co(ox)Co(NH_3)_5](ClO_4)_4$ and related compounds. The IR spectral pattern of $[(NH_3)_5Co(ox)Co(NH_3)_5]^{4+}$ is quite similar to that of free $C_2O_4^{2-}$ whose symmetry is known to be D_{2h} and hence the symmetry of the oxalate ion in the complex may be approximated by D_{2h}. A strong Raman band at 1438 cm^{-1} can be assigned to vibration of a_g mode. A weak IR band at 1435 cm^{-1} may be also assigned to the vibration of a_g mode which appears by the lowering of symmetry in a crystal.

The complexes $[(NH_3)_5Cr(ox)Cr(NH_3)_5]^{4+}$ and $[(NH_3)_5Co(ox)Co(NH_3)_4(H_2O)]^{4+}$ have been prepared

Table 5. Product distribution of the reaction of $[Co(Hdic)(NH_3)_5]^{2+}$ with $[Co(NH_3)_5(H_2O)]^{3+}$ [a]

Order of elution	Complex	Dicarboxylate[b]							Concn of eluant
		ox	ox[c]	malo	suc	fum[d]	male	pim	
1	$[Co(dic)(NH_3)_4]^+$	3	—[e]	1.5	0	0	tr[f]	tr[f,g]	0.1 M $NaClO_4$
2	$[Co(Hdic)(NH_3)_5]^{2+}$	87	72	32	80	73	87	—[e]	0.1—0.2 M $NaClO_4$
3	$[Co(NH_3)_5(H_2O)]^{3+}$	90	70	120	90	76	96	—[e]	0.3 M $NaClO_4$
4	$[(NH_3)_5Co(dic)Co(NH_3)_5]^{4+}$	10	24	12	15	20	2[h] / 4[i]	8	0.4 M $NaClO_4$[q]
≥5	Complexes which were not characterized	tr[j]	tr[j]	0.44[k,l] 0.7[k,m] 0.4[k,p]	tr(pink) tr(pink)	tr(violet) tr[n]	tr(pink)	—[e]	0.5—1 M $NaClO_4$[r]

a) The reaction conditions are the same as those given in Experimental, unless otherwise indicated. b) The numerical values given in this table denote the yields(%) which were calculated by means of the following relation: yield=(mol of the indicated species) × 100/(mol of $[Co(Hdic)(NH_3)_5](ClO_4)_2$ (=mol of $[Co(NH_3)_5(H_2O)](ClO_4)_3$) used as the starting material). Symbol "tr" denotes a trace amount. c) The reaction conditions are given in Fig. 1. The gradient elution was made with KCl solution. d) Two species (trace amounts) were found between fractions $[Co(Hfum)(NH_3)_5]^{2+}$ and $[Co(NH_3)_5(H_2O)]^{3+}$ (λ_{max}=524 and 357 nm) and between fractions $[Co(NH_3)_5(H_2O)]^{3+}$ and $[(NH_3)_5Co(fum)Co(NH_3)_5]^{4+}$ (λ_{max}=506 and 532 nm). e) Not determined. f) The species is assigned tentatively to the chelated complex $[Co(dic)(NH_3)_4]^+$. g) λ_{max}=515 nm. h) The yield of $[(NH_3)_5Co(fum)Co(NH_3)_5]^{4+}$. i) The yield of $[(NH_3)_5Co(male)Co(NH_3)_5]^{4+}$. j) λ_{max}=505 and 345 nm. k) The yield was calculated on the assumption that the species is a monomer. l) λ_{max}=508 and 353 nm. m) λ_{max}=509 and 353 nm. n) λ_{max}=512 and 354 nm. p) λ_{max}=504 and 350 nm. q) For fum system, 1.0 M CH_3CO_2H–1.0M CH_3CO_2Na buffer solution was used. r) For fum system, 1 M HCl was used.

Table 6. Numerical data for the IR and Raman bands of oxalate ions in various compounds[a)]

Free $C_2O_4^{2-}$ [b)]		$[(NH_3)_5Co(ox)Co(NH_3)_5]^{4+}$		$[(NH_3)_5Cr(ox)Cr(NH_3)_5]^{4+}$ [c)]	$[(NH_3)_5Co(ox)Co(NH_3)_4(H_2O)]^{4+}$ [d)]
IR	Raman	IR[e)]	Raman	IR	IR
	1664 s (b_{1g})			1705 s	1721 ms, 1701 s
1627 s (b_{2u})		1625 s		1620 m, 1680 s	1629 vs, 1670 ms
	1450 s, 1485 s (a_g)	1435 w	1438 s	1395 s,	1430 s, 1439 vs
1338 s (b_{3u})		1302 s		1240 s	1250 m, 1276 ms

a) vs=Very strong; s=strong; m=moderate; w=weak. Numerical values are wave numbers/cm^{-1}. b) From Ref. 20. c) From Ref. 21. d) From Ref. 22. e) Deuterated sample.

and characterized in two laboratories.[21,22] The IR spectral patterns of these complexes are quite different from that of $[(NH_3)_5Co(ox)Co(NH_3)_5]^{4+}$. The symmetry of the oxalate ion in $[(NH_3)_5Cr(ox)Cr(NH_3)_5]^{4+}$ has been assigned to C_{2v}[21] and that in $[(NH_3)_5Co(ox)Co(NH_3)_4(H_2O)]^{4+}$, to C_{2v} or C_2.[23]

References

1) J. C. Duff, *J. Chem. Soc.*, **123**, 560 (1923).

2) Abbreviations used in this paper are as follows: dic=dicarboxylate; ox=$O_2CCO_2^{2-}$; malo=$O_2CCH_2CO_2^{2-}$; suc=$O_2CCH_2CH_2CO_2^{2-}$; pim=$O_2C(CH_2)_5CO_2^{2-}$; fum=*trans*-$O_2CCH{=}CHCO_2^{2-}$; male=*cis*-$O_2CCH{=}CHCO_2^{2-}$.

3) A. Werner, *Ber. Dtsch. Chem. Ges.*, **40**, 4104 (1907).

4) P. Saffir and H. Taube, *J. Am. Chem. Soc.*, **82**, 13 (1960).

5) K. K. Sebera and H. Taube, *J. Am. Chem. Soc.*, **83**, 1785 (1961).

6) E. S. Gould and H. Taube, *J. Am. Chem. Soc.*, **86**, 1318 (1964).

7) Under the present experimental conditions, the pentaaminecobalt(III)–ox complex shows two bands on the Sephadex column (see Fig. 1). This may arise from the fact that $[Co(Hox)(NH_3)_5]^{2+}$ is rather strongly acidic ($pK_a=2.06$)[8] and the complex is present as the equilibrium mixture of $[Co(Hox)(NH_3)_5]^{2+}$ and its conjugate base form, $[Co(ox)(NH_3)_5]^{+}$. Restricted supply of acid during the elution prevents interconversion between these two forms.

8) C. Andrade and H. Taube, *Inorg. Chem.*, **5**, 1087 (1966).

9) For the elution of $[(NH_3)_5Co(fum)Co(NH_3)_5]^{4+}$, 1 M CH_3CO_2H–1 M CH_3CO_2Na buffer solution was used to avoid crystallization of the perchlorate salt in the column. When a small amount of $HClO_4$ was added to the eluate which was then evaporated, the desired perchlorate salt was obtained.

10) R. van Eldik and G. M. Harris, *Inorg. Chem.*, **14**, 10 (1975).

11) A. C. Dash and R. K. Nanda, *J. Inorg. Nucl. Chem.*, **38**, 119 (1976).

12) J. K. Hurst and H. Taube, *J. Am. Chem. Soc.*, **90**, 1178 (1968).

13) E. S. Gould, *J. Am. Chem. Soc.*, **88**, 2983 (1966).

14) H. Ogino and J. Fujita, *Bull. Chem. Soc. Jpn.*, **48**, 1836 (1975).

15) W. L. Jolly, A. D. Harris, and T. S. Briggs, *Inorg. Chem.*, **4**, 1604 (1965).

16) H. Yoneda and Y. Nakashima, *Bull. Chem. Soc. Jpn.*, **47**, 669 (1974).

17) J. Fujita and Y. Shimura, *Bull. Chem. Soc. Jpn.*, **36**, 1281 (1963).

18) J. D. Edwards, Y. Sulfab, and A. G. Sykes, *Inorg. Chem.*, **14**, 1474 (1975).

19) K. Nakamoto, "Infrared Spectra of Inorganic and Coordination Compounds," Wiley, New York, N. Y. (1963).

20) H. Murata and K. Kawai, *J. Chem. Phys.*, **25**, 589 (1956).

21) J. Casabo, J. M. Coronas, and J. Ribas, *Inorg. Chim. Acta*, **11**, 149 (1974).

22) K. L. Scott, K. Wieghardt, and A. G. Sykes, *Inorg. Chem.*, **12**, 655 (1973).

Electron-transfer Reaction from Sodium Benzenethiolate to Acceptors Assisted by Photo-excited Tris(2,2′-bipyridine)ruthenium(II)

Tokuji MIYASHITA and Minoru MATSUDA*

Chemical Research Institute of Non-aqueous Solutions, Tohoku University, Katahira 2-1-1, Sendai 980

(Received May 12, 1980)

The photo-excited tris(2,2′-bipyridine)ruthenium(II) ($Ru(bpy)_3^{2+*}$) was effectively quenched by sodium benzenethiolate in acetonitrile (Stern-Volmer constant=4860 $dm^3\ mol^{-1}$). The flash photolysis of a solution containing $Ru(bpy)_3^{2+}$ and benzenethiolate (excitation wavelength (λ)>480 nm) produced transient species absorbing *ca.* 510 nm; this species was identified as $Ru(bpy)_3^{+}$ and decayed with first-order kinetics with $k=3.0\ s^{-1}$. This slow decay of $Ru(bpy)_3^{+}$ implies that the back-electron-transfer reaction was suppressed. The decay of $Ru(bpy)_3^{+}$ was accelerated by the addition of water, suggesting the possibility of the reaction between $Ru(bpy)_3^{+}$ and water, though no H_2 was detected. The steady irradiation of a solution containing $Ru(bpy)_3^{2+}$, benzenethiolate, and an electron-acceptor produced the radical anion of the added acceptor, which was detected with ESR spectroscopy.

Recently there has been considerable interest in photo-induced electron-transfer reactions in a solution containing $Ru(bpy)_3^{2+}$ from the viewpoint of solar energy conversion.[1-6] $Ru(bpy)_3^{3+}$ and $Ru(bpy)_3^{+}$ generated by the electron-transfer quenching of photo-excited tris(2,2′-bipyridine)ruthenium ($Ru(bpy)_3^{2+*}$) (Eqs. 1 and 2) are thermodynamically capable of

$$Ru(bpy)_3^{2+*} + Q \rightleftharpoons Ru(bpy)_3^{3+} + Q^{-} \quad (1)$$

$$Ru(bpy)_3^{2+*} + Q \rightleftharpoons Ru(bpy)_3^{+} + Q^{+} \quad (2)$$

oxidizing water to O_2 and of reducing water to H_2, respectively. However, the practical utility of these

$$Ru(bpy)_3^{2+} + e^{-} \rightleftharpoons Ru(bpy)_3^{+} \qquad E_{1/2} = -1.33\ V^{7)}$$

$$Ru(bpy)_3^{3+} + e^{-} \rightleftharpoons Ru(bpy)_3^{2+} \qquad E_{1/2} = +1.29\ V^{8)}$$

reactions is limited by the energy-wasting back-electron-transfer of Eqs. 1 and 2.[8-10] One approach to suppressing the back-electron-transfer reaction is to remove the quenching products by rapid irreversible reactions coupled with quenching processes.

We have found that the life-time of $Ru(bpy)_3^{+}$ can be elongated when benzenethiolate is used as the electron-donor for the quenching of $Ru(bpy)_3^{2+*}$. The thiyl radical formed in the electron-transfer from benzenethiolate to $Ru(bpy)_3^{2+*}$ can disappear upon rapid dimerization into disulfide,[11] which has a high redox (more negative) potential,[12] leading to the result that the back-electron-transfer can be suppressed. This paper reports the photo-induced reduction of $Ru(bpy)_3^{2+}$ in the presence of sodium benzenethiolate and the electron-transfer reaction from the $Ru(bpy)_3^{+}$ generated to some organic electron-acceptors.

Results and Discussion

The quenching experiments of the luminescence of $Ru(bpy)_3^{2+*}$ by sodium benzenethiolate were carried out in a highly degassed acetonitrile solution. The emission maximum of $Ru(bpy)_3^{2+*}$ was not shifted by the addition of benzenethiolate, and only the intensity of emission (I) decreased. The plot of I_0/I *vs.* the concentration of benzenethiolate (Stern-Volmer plot) is shown in Fig. 1. The Stern-Volmer quenching constant, $K_{sv}=4860\ dm^3\ mol^{-1}$, was obtained from the slope in Fig. 1. The quenching-rate constant (k_q) was calculated to be $5.7\times10^9\ dm^3\ mol^{-1}\ s^{-1}$ from the Stern-Volmer constant,

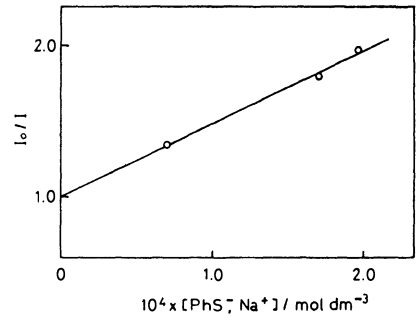

Fig. 1. Stern-Volmer plots for the quenching of the $Ru(bpy)_3^{2+*}$ luminescence (610 nm) by sodium benzenethiolate in acetonitrile. [$Ru(bpy)_3^{2+}=1.4\times10^{-5}$ mol dm^{-3}, excitation at 450 nm.

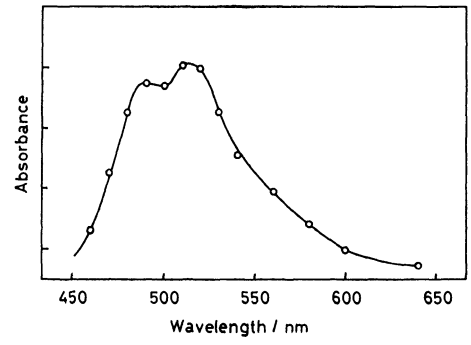

Fig. 2. Transient absorption spectrum in flash photolysis of acetonitrile solution containing $Ru(bpy)_3^{2+}$ (1×10^{-5} mol dm^{-3}) and sodium benzenethiolate (1×10^{-4} mol dm^{-3}).

assuming that the rate constant for the natural deactivation of $Ru(bpy)_3^{2+*}$ (k_0) is $1.18\times10^6\ s^{-1}$ in acetonitrile.[13]

The flash photolysis of acetonitrile solutions containing $Ru(bpy)_3^{2+}$ ($1—4\times10^{-5}$ mol dm^{-3}) and benzenethiolate ($1—5\times10^{-4}$ mol dm^{-3}) gave the transient absorption spectrum shown in Fig. 2, which was assigned to $Ru(bpy)_3^{+}$. Similar spectra have been reported in pulse-radiolysis,[14] laser-photolysis,[15] and electrochemical studies.[7] The absorbance of transient species at a given wavelength was not changed on repetitive flashing (up to 20 flashes were tested). The photoanation reaction of $Ru(bpy)_3^{2+}$ by thiocyanate has been reported,

although the quantum yield is low.[16] Our above results concerning repetitive flashing and both the absorption and emission spectra showed that such a photoanation reaction did not occur. The transient species decayed with first-order kinetics and had a long life-time ($\tau=1/k=333$ ms). These results imply that the back-electron-transfer reaction was effectively suppressed, because the decay of $Ru(bpy)_3^+$ by the back-electron-transfer reaction should obey second-order, equal-concentration kinetics.[13] When Eu(II) or aromatic amine was used as a quencher, the decays of $Ru(bpy)_3^+$ obeyed second-order kinetics, and the rate constants were 2.7×10^7 for Eu(II)[17] and 10^7—10^{10} $dm^3\ mol^{-1}\ s^{-1}$ for amines.[13] Whitten *et al.*[18] have found the very long-lived $Ru(bpy)_3^+$, which was generated by the quenching of $Ru(bpy)_3^{2+*}$ with triethylamine in dry acetonitrile. Since the triethylamine cation radical formed in the quenching as a counterpart of $Ru(bpy)_3^+$ was removed by an irreversible reaction with a solvent (CH_3CN), the back-electron-transfer reaction was almost entirely avoided. The irreversible reactions and their products were complex, whereas the irreversible product in our system was diphenyl disulfide, which could reproduce benzenethiolate (see below).

The results obtained here can be explained by a mechanism (Eqs. 3—6) in which the $Ru(bpy)_3^+$ formed in the reductive quenching of $Ru(bpy)_3^{2+*}$ (Eq. 4) may transfer an electron to disulfide, not to thiyl radicals (back-electron-transfer reaction), which dimerize each other to disulfide with $k_d=10^9$ $dm^3\ mol^{-1}\ s^{-1}$ (Eq. 5):[11]

$$Ru(bpy)_3^{2+} \underset{k_0}{\overset{h\nu}{\rightleftharpoons}} Ru(bpy)_3^{2+*} \quad (3)$$

$$Ru(bpy)_3^{2+*} + PhS^- \xrightarrow{k_q} Ru(bpy)_3^+ + PhS\cdot \quad (4)$$

$$PhS\cdot + PhS\cdot \xrightarrow{k_d} PhSSPh \quad (5)$$

$$Ru(bpy)_3^+ + PhSSPh \xrightarrow{k_{et}} Ru(bpy)_3^{2+} + PhS^- + PhS\cdot \quad (6)$$

The pseudo-first-order rate constant for the decay of $Ru(bpy)_3^+$ varied upon an added concentration of diphenyl disulfide (Fig. 3), showing the occurrence of an electron-transfer reaction, as is shown in Eq. 6. The rate constant (k_{et}) for the electron-transfer reaction

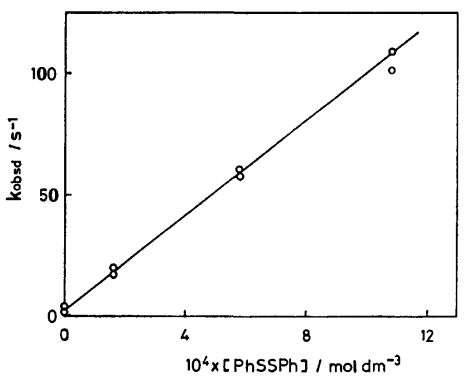

Fig. 3. Dependence of first-order rate constants for the decay of $Ru(bpy)_3^+$ (510 nm) on the concentration of added diphenyl disulfide.

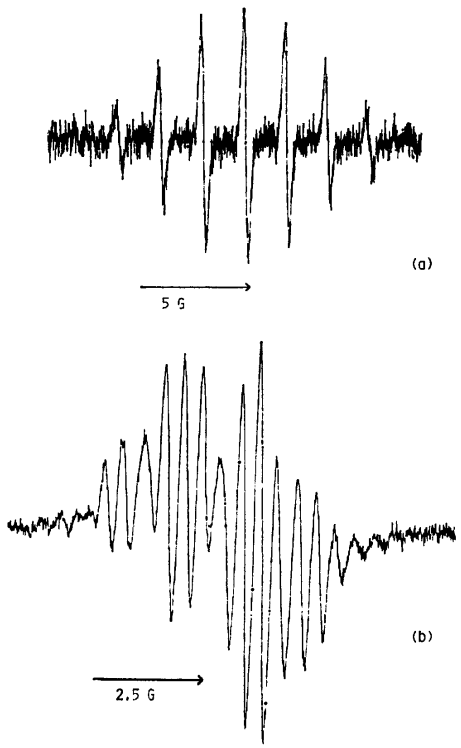

Fig. 4. ESR spectra of duroquinone radical anion (a) and benzil radical anion (b) in acetonitrile.

Table 1. Photo-induced electron-transfer from sodium benzenethiolate in the presence of $Ru(bpy)_3^{2+}$ in acetonitrile

Acceptor(X)	$E_{1/2}$/V[a]	Formation of X^-
Duroquinone	−0.69[23]	Yes, $a_H=1.88$ G (Septet)
Acenaphthene-quinone	−0.96	Yes, $g=2.0045$(Multiplet)
Benzil	−1.21	Yes, $g=2.0048$(Multiplet)[24]
9-Fluorenone	−1.26	Very small
Azobenzene	−1.36	No

a) *vs.* SCE and used $(n\text{-}C_4H_9)_4NClO_4$ as a supporting electrolyte in acetonitrile.

was found to be 9.6×10^4 $dm^3\ mol^{-1}\ s^{-1}$. This slow electron-transfer reaction is due to the high redox potential of diphenyl disulfide ($E_{peak}=-1.6$ V *vs.* 10^{-3} mol dm^{-3} Ag^+/Ag).[12]

The steady irradiation (wavelengths longer than 510 nm) of an acetonitrile solution containing $Ru(bpy)_3^{2+}$, benzenethiolate, and an electron-acceptor produced the radical anion of the added acceptor, which was detected with ESR spectroscopy (Table 1) (*e.g.*, the ESR spectra of duroquinone and benzil radical anions are shown in Fig. 4). As can be seen from Table 1, acceptors with a potential more positive than the $E_{1/2}$ of the $Ru(bpy)_3^{2+}/Ru(bpy)_3^+$ couple ($E_{1/2}=-1.33$ V *vs.* SCE) were reduced to radical anions. The irradiation in the absence of either $Ru(bpy)_3^{2+}$ or benzenethiolate produced no acceptor's radical anion, and the mixing of $Ru(bpy)_3^{2+}$, benzenethiolate, and acceptor in the dark produced no radical anion, either. The results suggest the following electron-transfer cycle:

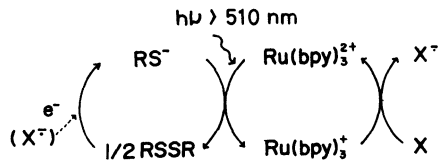

where X is an electron-acceptor. Benzenethiolate could be reproduced with the reduction of disulfide.[19] The RS^-/RSSR redox couple is known to be biologically important in an electron-transport system in ferredoxin or other iron-sulfur proteins.[20]

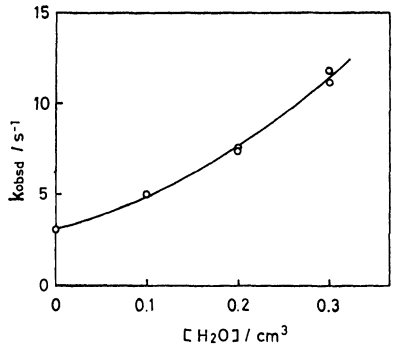

Fig. 5. Effect of added water on the rate constants for the decay of $Ru(bpy)_3^+$ (510 nm); total volume was 10 cm^3.

Although the decay of $Ru(bpy)_3^+$ was accelerated by the addition of water (Fig. 5), the formation of H_2 could not be detected.[21] Meyer *et al.*[6] have reported that there was no production of H_2 in the reaction of water with $Ru(bpy)_3^+$, whereas the reaction with $Ru(bpy)_3^0$ could produce H_2. This has been explained by the difference in two-electron reducing capability between $Ru(bpy)_3^+$ and $Ru(bpy)_3^0$:

$$Ru(bpy)_3^+ \rightleftharpoons Ru(bpy)_3^{3+} + 2e^- \qquad E = 0.00 \text{ V } vs. \text{ NHE}$$

$$Ru(bpy)_3^0 \rightleftharpoons Ru(bpy)_3^{2+} + 2e^- \qquad E = -1.42 \text{ V } vs. \text{ NHE}.$$

Although our system could not succeed in the formation of H_2, the electron-transport cycle described above shows the possibility of applying this system to other reduction reactions. An experiment for the application to the photo-galvanic cell of this system using the $Ru(bpy)_3^+/Ru(bpy)_3^{2+}$ couple is also undertaken.

Experimental

$Ru(bpy)_3Cl_26H_2O$ was synthesized according to published procedures.[22] Commercially available (reagent-grade) acceptors (duroquinone, acenaphthenequinone, benzil, 9-fluorenone, and azobenzene) were recrystallized twice from ethanol and sublimed under high vacuum (about 10^{-3} Pa). The preparation of sodium benzenethiolate was described previously.[19] The concentration of benzenethiolate in acetonitrile was determined from the absorbance at 298 nm ($\varepsilon = 1.8 \times 10^4$ dm^3 mol^{-1} cm^{-1}). The solutions for the experiments of the flash photolysis, the quenching, and the ESR measurement were prepared by a high-vacuum-line technique.[19] The prepared sodium benzenethiolate solution was introduced through a breakseal to a solution containing $Ru(bpy)_3^{2+}$ and acceptor which had been degassed by the freeze-thaw-cycle method.

The quenching experiment of $Ru(bpy)_3^{2+*}$ by benzenethiolate was carried out with a Shimadzu RF 501 fluorescence spectrophotometer. The FSR measurements were carried out with a Varian E-4 ESR spectrometer. The steady irradiation for the photo-ESR study was obtained using a 500-W xenon lamp. The light shorter than 510 nm was cut off with a filter (Toshiba L-51).

The flash apparatus delivered a flash with an energy of 98 J and a half-peak duration of 10 μs from xenon lamps. The filter was used to cut off flash light shorter than 480 nm.

References

1) V. Balzani, L. Maggi, M. F. Manfrin, F. Bolletta, and G. S. Laurence, *Coord. Chem. Rev.*, **15**, 321 (1975).
2) C. Creutz and N. Sutin, *Proc. Natl. Acad. Sci. U.S.A.*, **72**, 2858 (1975).
3) J. N. Demas and J. W. Addington, *J. Am. Chem. Soc.*, **98**, 5800 (1976).
4) K. Kalyanasundaram, J. Kimi, and M. Grätzel, *Helv. Chim. Acta*, **61**, 2720 (1978).
5) G. M. Brown, B. S. Brunschwig, C. Creutz, J. F. Endicott, and N. Sutin, *J. Am. Chem. Soc.*, **101**, 1298 (1979).
6) H. D. Abruna, A. Y. Teng, G. J. Samuels, and T. J. Meyer, *J. Am. Chem. Soc.*, **101**, 6745 (1979).
7) N. E. Tokel-Takvoryan, R. E. Hemingway, and A. J. Bard, *J. Am. Chem. Soc.*, **95**, 6582 (1973).
8) C. R. Bock, T. J. Meyer, and D. G. Whitten, *J. Am. Chem. Soc.*, **97**, 2909 (1975).
9) R. C. Young, T. J. Meyer, and D. G. Whitten, *J. Am. Chem. Soc.*, **98**, 286 (1976).
10) C. R. Bock, T. J. Meyer, and D. G. Whitten, *J. Am. Chem. Soc.*, **96**, 4710 (1974).
11) T. Miyashita, M. Iino, and M. Matsuda, *Bull. Chem. Soc. Jpn.*, **50**, 317 (1977).
12) R. E. Dessy, P. M. Weissman, and R. L. Pohl, *J. Am. Chem. Soc.*, **88**, 5117 (1966).
13) C. P. Anderson, D. J. Salmon, T. J. Meyer, and R. C. Young, *J. Am. Chem. Soc.*, **99**, 1980 (1977).
14) J. H. Baxendale and M. Fiti, *J. Chem. Soc., Dalton Trans.*, **1972**, 1995.
15) M. Maestri and M. Grätzel, *Ber. Bunsenges. Phys. Chem.*, **81**, 504 (1977).
16) P. E. Hoggard and G. B. Porter, *J. Am. Chem. Soc.*, **100**, 1457 (1978).
17) C. Creutz and N. Sutin, *J. Am. Chem. Soc.*, **98**, 6384 (1976).
18) P. J. Delaine, J. T. Lee, H. W. Sprintschnik, H. Abruna, T. J. Meyer, and D. G. Whitten, *J. Am. Chem. Soc.*, **99**, 7094 (1977).
19) T. Miyashita, T. Aoki, and M. Matsuda, *Bull. Chem. Soc. Jpn.*, **49**, 231 (1976).
20) P. C. Jocelyn, "Biochemistry of the SH Group," Academic Press, London (1972).
21) H_2 analysis was carried out by gas chromatography (molecular sieve 5A column; 40 °C; carrier gas, N_2).
22) I. Fujita and H. Kobayashi, *Ber. Bunsenges. Phys. Chem.*, **76**, 115 (1972); R. A. Palmer and T. S. Piper, *Inorg. Chem.*, **5**, 864 (1966).
23) B. R. Eggins and J. Q. Chambers, *J. Chem. Soc., Chem. Commun.*, **1969**, 232.
24) Y. Ohnishi and A. Ohno, *Chem. Lett.*, **1976**, 697.

Synthetic Studies of Rifamycins. III.[1] The Partial Synthesis of Rifamycin Ansa-chain Compounds from Their Degradation Products†

Masaya NAKATA, Toshiya SAKAI, Kuniaki TATSUTA, and Mitsuhiro KINOSHITA*

Department of Applied Chemistry, Faculty of Engineering, Keio University, Hiyoshi, Kohoku-ku, Yokohama 223

(Received July 29, 1980)

The ansa-chain compound methyl [methyl 2,4,6,8,10,11,12,13,14-nonadeoxy-4,6,8,10,14-penta-*C*-methyl-3-*O*-methyl-L-*manno*-β-D-*galacto*-(11*E*,13*Z*)-11,13-pentadecadienopyranosid]uronate (**1a**) and its (*R*)-2-bromo derivative, **1b**, were transformed into the corresponding 7,9-diacetate **3a** and **3b** or the 7,9-acetonide **7a** and **7b**. The ozonolysis of **3a** or **3b** gave methyl 7,9-di-*O*-acetyl-2,4,6,8,10-pentadeoxy-4,6,8,10-tetra-*C*-methyl-3-*O*-methyl-L-*manno*-β-D-*galacto*-undecodialdopyranoside-(1,5) (**4a**) or its (*R*)-2-bromo derivative (**4b**) respectively. The Wittig condensation of **4b** with (methoxycarbonylmethylene)triphenylphosphorane, followed by debromination with tributylstannane, afforded methyl [methyl-7,9-di-*O*-acetyl-2,4,6,8,10,11,12-heptadeoxy-4,6,8,10-tetra-*C*-methyl-3-*O*-methyl-L-*manno*-β-D-*galacto*-(*E*)-11-tridecenopyranosid]uronate (**6a**). The diisobutylaluminium hydride reduction of **6a**, followed by acetonation, gave methyl 2,4,6,8,10,11,12-heptadeoxy-7,9-*O*-isopropylidene-4,6,8,10-tetra-*C*-methyl-3-*O*-methyl-L-*manno*-β-D-*galacto*-(*E*)-11-tridecenopyranoside-(1,5) (**10a**). The allylic alcohol, **10a**, was converted into the allylic bromide, **12a**, which then yielded the triphenylphosphonium bromide, **13a**. The Wittig condensation of the reactive ylide generated from **13a** with methyl pyruvate afforded a 4 : 5 mixture of **7a** and its 13*E*-isomer. The partial synthesis of **1a** was accomplished by the selective hydrolysis of the **7a** isolated from the mixture.

The ansa-chain compound **1a**,[2] corresponding to the 25-deacetylated ansa-bridge portion, **2**, of rifamycin B, O, S, and SV, has recently been obtained *via* its (*R*)-2-bromo derivative, **1b**, itself produced by the novel degradation of 25-deacetylrifampicin. During the course of our studies of the synthesis of **1a**,[1] a degradation-reconstruction program of **1a** and **1b** has been under-

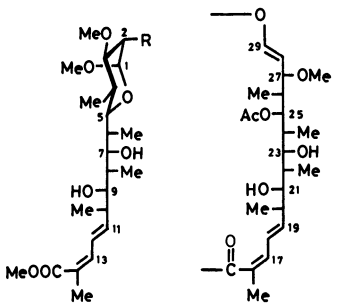

1a R=H **1b** R=Br **2**

taken to secure materials for establishing the structure of the synthetic intermediate, **4a** or **6a**, and to survey the practical methods for the construction of **1a** starting with **4a** or **6a**. This paper will describe the partial degradation of **1a** or **1b** to their synthetic intermediates, **4a**, **4b**, **8a**, and **8b**, and the partial synthesis of **1a** or **1b** from the degradation products *via* the intermediates, **6a**, **9a** or **9b**, and **10a** or **10b**, by Wittig reaction.

The acetylation of **1a** with acetic anhydride in pyridine afforded a mixture of the diacetate, **3a** (15%), and its 13*E*-isomer, **3'a** (22%), and a mixture of the monoacetate of **1a** (20%) and its 13*E*-isomer (18%). The structures of the isomeric products were confirmed by the ^{1}H-NMR data. On the contrary, the acetylation of **1b** with acetic anhydride and 4-dimethylaminopyridine (DMAP) in ethyl acetate gave the diacetate, **3b**, as the sole product in a 90% yield.[3] Both **1a** and **1b** were smoothly acetonated with 2,2-dimethoxypropane (DMP) in acetone containing a small amount of sulfuric acid to afford the 7,9-acetonides, **7a** and **7b**, in 99% and 76% yields respectively. Although it is unclear why the bromine atom situated far from the unsaturated system of the molecule of **1b** prevents its 13 *Z*-geometry from geometrical isomerization during acetylation, the unsaturated system of a free ansa-chain compound such as **1a** seems to be less stable than that of the intact ansa-chain in rifamycins.

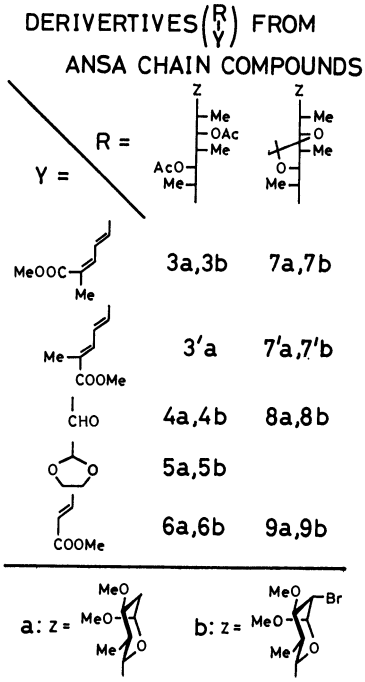

The ozonolysis of a mixture of **3a** and **3'a** with ozone and dimethyl sulfide in dichloromethane[4] gave the aldehyde, **4a**, in a 77% yield: this is a strategic intermediate in the synthesis of **1a**. The direct treatment of **4a** with ethylene glycol and *p*-toluenesulfonic acid in

† Presented at the ACS/CSJ Chemical Congress, Honolulu, Hawaii, April 6, 1979; Organic Abstract No. 481.

acetonitrile failed, however, to afford the ethylene acetal, **5a**, because of the simultaneous hydrolysis of the cyclic methyl acetal moiety of **4a**, and so the following alternative process was necessary. The ozonolysis of **3b**, followed by the treatment of the resulting aldehyde, **4b**, with ethylene glycol, gave the crystalline ethylene acetal, **5b**, in a 53% yield; on selective hydrolysis with 70% trifluoroacetic acid (TFA), this then provided **4b** in a quantitative yield. The debromination of **5b** with tributylstannane afforded plates of **5a** in a 64% yield after recrystallization. Attempts to obtain **4a** by the selective hydrolysis of the ethylene acetal group of **5a** were all unsuccessful. From these results, it was found that **5a** was not a synthetic precursor suitable for **4a**, while **5b** was a useful precursor for **4b**. The useful derivative, **6a**,[5] was obtained in a 95% yield by the debromination of **6b**, which had itself prepared by the Wittig condensation of **4b** with (methoxycarbonylmethylene)triphenylphosphorane in an 84% yield. The ozonolysis of **7a** or **7b**, followed by the Wittig condensation of the resulting aldehyde, **8a** or **8b** with the phosphorane, gave **9a** or **9b** in an 88 or 70% yield respectively.

We examined the possibility of the formation of **7a** *via* the allylic alcohol, **10a**, from **6a** or **9a**. At the same time, the transformation of **9b** into **7b** *via* **10b** was also examined, taking into account the fact that **7b** might be more stable than **7a** in the geometrical isomerization of an unsaturated system. The treatment of **6a** with diisobutylaluminium hydride (DIBAL) in toluene led to the corresponding triol, which, without purification, was acetonated with DMP in DMF containing *p*-toluenesulfonic acid to afford **10a** in a 73% yield. The reduction of **9a** or **9b** with DIBAL in toluene gave **10a** or **10b** in a 70 or 96% yield respectively. At first, the

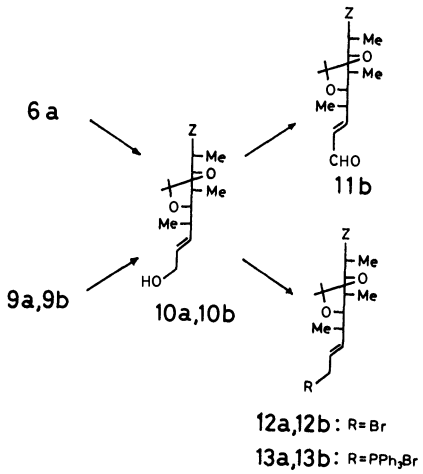

condensation of the phosphonate anion generated from dimethyl [1-(methoxycarbonyl)ethyl]phosphonate (**14**) with the α,β-unsaturated aldehyde, **11b**, which had been obtained in a 62% yield by the oxidation of **10b** with chromium trioxide in hexamethylphosphoric triamide (HMPA),[6] was examined. The reaction was carried out in THF at −75——60 °C to afford, predominantly, the undesired 11*E*,13*E*-isomer **7'b** in an 83% yield, accompanied by a small amount of **7b** (1.5%) [Reaction 1]. The structure of **7'b** was confirmed by the ^{1}H-NMR data. This reaction was highly stereoselective, and similar results have been reported in a recent paper;[7] therefore, it was conclusively disadvantageous for the formation of the desired 11*E*,13*Z*-isomer **7b**.

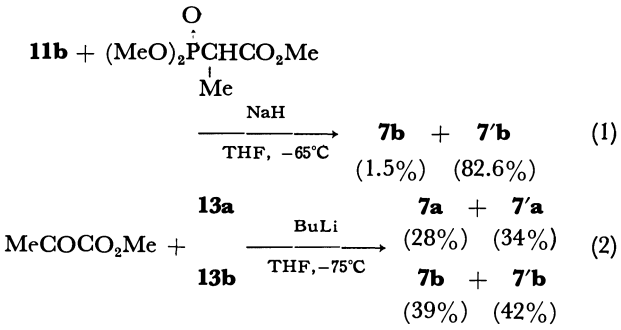

House and Rasmusson[8] reported that the Wittig condensation of [1-(methoxycarbonyl)ethylidene]triphenylphosphorane with acetaldehyde gave a 27.6 : 1 mixture of methyl tiglate and methyl angelate, while the reaction of ethylidenetriphenylphosphorane and methyl pyruvate provided a 2.13 : 1 mixture of tiglate and angelate. As the second approach to **7a** or **7b**, we condensed methyl pyruvate with the reactive ylide formed from a triphenylphosphonium salt, such as **13a** or **13b**. The allylic alcohol, **10a** or **10b**, was then transformed into the corresponding allylic bromide, **12a** (79%) or **12b** (90%), by treatment with mesyl chloride and a mixture of triethylamine, lithium bromide, and dichloromethane.[9] The reaction of **12a** or **12b** with triphenylphosphine in benzene afforded **13a** or **13b** in a quantitative yield. The phosphonium bromide, **13a** or **13b**, was treated with butyllithium in THF at −75 °C and then allowed to react with methyl pyruvate at the same temperature to give a 4 : 5 mixture of **7a** and **7'a** or an 1 : 1 mixture of **7b** and **7'b** in a 62 or 81% yield respectively (Reaction 2). The desired condensation product, **7a** (28%) or **7b** (39%), was separated from the isomer, **7'a** or **7'b**, by alumina-column chromatography or by preparative layer chromatography (PLC) on silica gel, which was identical with the aforesaid corresponding sample. The structure of isomeric product, **7'a**, was confirmed by the ^{1}H-NMR data.

A recent publication[10] described a new stereospecific process for the conversion of an aldehyde to a 5-substituted (2*Z*,4*E*)-2-methyl-2,4-pentadienoic acid *via* the lactone of 5-substituted 5-hydroxy-2-methyl-2-pentenoic acid. This reaction process, reported after our work had been completed, is undoubtedly better than our five-step process starting with **4a**, provided that the new process is applicable to **4a** for the synthesis of **1a**. Although Reaction 2 seems to be almost non-stereoselective, it is noteworthy that the reaction yielded a significant amount of (*Z*)-olefins compared with Reaction 1. Furthermore, when the Wittig reaction (2) is carried out by an intramolecular version[11] for the purpose of the construction of the medium ring of unsaturated lactone or the macrocyclic lactam ring of rifamycins, it may be expected that the tendency to form the desired (*Z*)-olefin is strengthened, because the formation of the intermediate betaine with the erythro configuration,[12] the precursor of (*Z*)-olefin, might be kinetically

more favored in the intramolecular cyclization of the lactone or the lactam than in the intermolecular reaction.

The last step of the synthesis of **1a** was the selective deacetonation of **7a**, which was effected with 50% difluoroacetic acid (DFA) at 0 °C to afford **1a** in an 80% yield. The treatment of **7b** with 90% TFA at 0 °C gave **1b**, which could then be converted into **1a** by debromination.[2)]

Experimental

The melting points were determined on a micro hot-stage Yanaco MP-83 and are uncorrected. The specific rotations were measured with a Carl Zeiss photoelectric polarimeter. The ^{1}H-NMR spectra were determined in $CDCl_3$ with either a Varian A60 or EM-390 spectrometer, using TMS as the internal standard. The TLC was performed on Merck TLC plates, 60F-254 0.25 mm. The PLC was carried out on precoated PLC plates (20×20×0.5 mm) of Merck Kieselgel 60F-254. The column chromatography was performed on silica gel, Wakogel C-200. In general, evaporation was conducted under reduced pressure below 30 °C.

*Methyl [Methyl 7,9-Di-*O*-acetyl-2,4,6,8,10,11,12,13,14-nona-deoxy-4,6,8,10,14-penta-*C*-methyl-3-*O*-methyl-*L*-manno-β-*D*-galacto(11E, 13Z)-11,13-pentadecadienopyranosid]uronate (3a) and 13E-Isomer (3'a).* A mixture of **1a** (253 mg, 0.590 mmol), acetic anhydride (1.35 ml, 14.3 mmol), and dry pyridine (2.5 ml) was allowed to stand at 40 °C for 6 d. The mixture was then poured into ice water and extracted with ether. The ether layer was washed with water and a saturated aqueous NaCl solution, dried, and evaporated. The residue was chromatcgraphed on silica gel (30 g) with 10: 1 benzene–acetone to afford the following four fractions: **3a**, 45 mg (15%); R_f 0.37 (8: 1 benzene–acetone); mp 132—133 °C (ether); $[\alpha]_D^{29}$ +30° (*c* 1.0, MeOH); UV_{max} (EtOH) 262 nm (ε 23100); IR (KBr) 1732, 1710, 1641, and 1607 cm^{-1}; ^{1}H-NMR δ=0.8—1.1 (12H, m, 4, 6, 8, and 10-Me), 1.94 (6H, broad s, 14-Me and OAc), 2.01 (3H, s, OAc), 3.32 and 3.34 (each 3H, each s, OMe×2), 3.76 (3H, s, COOMe), 4.7—5.2 (3H, m, H-1,7, and 9),5.68 (1H, dd, H-11, $J_{10,11}$= 8.9 Hz, $J_{11,12}$=15.0 Hz), 6.32 (1H, m, H-13, $J_{12,13}$=11.0 Hz, $J_{13,Me}$=1.9 Hz), and 7.08 (1H, dd, H-12) [Found: C, 63.16; H, 8.52%. Calcd for $C_{27}H_{44}O_9$: C, 63.26; H, 8.65%]; **3'a**, 68 mg (22%); R_f 0.33; mp 146—147 °C (acetone); $[\alpha]_D^{31}$ −33° (*c* 0.9, MeOH); UV_{max} (EtOH) 263 nm (ε 26600); IR (KBr) 1732, 1703, and 1641 cm^{-1}; ^{1}H-NMR δ=0.8—1.1 (12H, m, 4, 6, 8, and 10-Me), 1.94 (6H, broad s, 14-Me and OAc), 2.01 (3H, s, OAc), 3.32 and 3.34 (each 3H, each s, OMe×2), 3.73 (3H, s, COOMe), 4.7—5.2 (3H, m, H-1,7, and 9), 5.91 (1H, dd, H-11, $J_{10,11}$=8.2 Hz, $J_{11,12}$=14.8 Hz), 6.34(1H, dd, H-12, $J_{12,13}$=10.4 Hz), and 7.10 (1H, m, H-13, $J_{13,Me}$=1.5 Hz) [Found: C, 63.08; H, 8.44%. Calcd for $C_{27}H_{44}O_9$: C, 63.26; H, 8.65%]; monoacetate of **1a**, 54 mg (20%); R_f 0.24; ^{1}H-NMR δ=1.96 (3H, s, 7 or 9-OAc), 5.74 (1H, dd, H-11, $J_{11,12}$=15 Hz, $J_{10,11}$=9.0 Hz), 6.34 (1H, dd, H-13, $J_{12,13}$=11.0 Hz), and 7.09 (1H, dd, H-12), and monoacetate of 13*E*-isomer of **1a**, 49 mg (18%); R_f 0.21; ^{1}H-NMR δ=1.96 (3H, s, 7 or 9-OAc), 5.91 (1H, dd, H-11, $J_{11,12}$= 14.7 Hz, $J_{10,11}$=8.0 Hz), 6.34 (1H, dd, H-12, $J_{12,13}$=10.0 Hz), and 7.11 (1H, dd, H-13, $J_{13,Me}$=1.0 Hz).

(R)-2-Bromo Deivative (3b). A mixture of **1b** (199 mg, 0.393 mmol), acetic anhydride (0.371 ml, 3.93 mmol), DMAP (106 mg, 0.864 mmol), and ethyl acetate (2 ml) was stirred at 45 °C for 24 h. The mixture was then diluted with ethyl acetate (18 ml) and washed with saturated aqueous $KHSO_4$, $NaHCO_3$, and NaCl solutions successively, dried, and evaporated. The residual brown syrup (270 mg) was chromatographed on silica gel (23 g) with 8: 1 benzene–ethyl acetate to afford **3b** (210 mg, 90%) as a colorless syrup: $[\alpha]_D^{29}$ +16° (*c* 0.77, MeOH); UV_{max} (EtOH) 264 nm (ε 21300); IR (CCl_4) 1737, 1641, and 1605 cm^{-1}, ^{1}H-NMR δ=0.88—1.08 (12H, m, 4, 6, 8, and 10-Me), 1.93 (6H, s, 14-Me and OAc), 2.00 (3H, s, OAc), 3.16 (1H, dd, H-3, $J_{2,3}$=3.0 Hz, $J_{3,4}$=10.0 Hz), 3.35 (6H, s, OMe×2), 3.74 (3H, s, COOMe), 4.28 (1H, dd, H-2, $J_{1,2}$=1.5 Hz), 4.8—5.1 (3H, m, H-1,7, and 9), 5.64 (1H, dd, H-11, $J_{10,11}$=9.0 Hz, $J_{11,12}$=15.1 Hz). 6.30 (1H, m, H-13, $J_{12,13}$=10.7 Hz, $J_{13,Me}$=1 Hz), and 7.07 (1H, dd, H-12).

Found: C, 54.53; H, 7.18; Br, 13.27%. Calcd for $C_{27}H_{43}O_9Br$: C, 54.82; H, 7.33; Br, 13.51%.

*Methyl 7,9-Di-*O*-acetyl-2,4,6,8,10-pentadeoxy-4,6,8,10-tetra-*C*-methyl-3-*O*-methyl-*L*-manno-β-*D*-galacto-undecodialdopyranoside-(1,5) (4a).* A mixture of **3a** and **3'a** (74 mg, 0.144 mmol) was dissolved in dry dichloromethane (3.68 ml), and then the mixture was cooled to −75 °C. Ozonolyzed oxygen gas (475 ml) containing 0.287 mmol of ozone was passed through the solution at the rate of 23.8 ml/min. To the resulting solution was added dimethyl sulfide (0.105 ml, 1.44 mmol) at the same temperature. The mixture was gradually warmed to room temperature over the period of 3 h and then washed with water and a saturated aqueous NaCl solution, dried, and evaporated. The residual syrup was chromatographed on silica gel (3 g) with 8: 1 benzene–acetone to give **4a** (46 mg, 77%) as a pale yellow syrup: ^{1}H-NMR δ=0.85—1.15 (12H, m, 4,6,8, and 10-Me), 2.02 and 2.04 (each 3H, oach s, OAc×2), 3.32 and 3.37 (each 3H, each s, OMe×2), 4.8—5.5 (3H, m, H-1,7, and 9), and 9.50 (1H, d, H-11, $J_{10,11}$=3.3 Hz).

(R)-2-Bromo Derivative (4b) and Its 11-Ethylene Acetal (5b). A sample (163 mg) of **3b** was ozonolyzed by the procedure described in the preparation of **4a** and then worked-up to afford the crude aldehyde, **4b**, as a syrup. A mixture of the crude **4b** (137 mg), ethylene glycol (0.153 ml), anhydrous *p*-toluenesulfonic acid (4.8 mg), and dry acetonitrile (1.4 ml) was stirred at room temperature for 0.5 h. The reaction mixture was then poured into ice-cooled water containing $NaHCO_3$ (2.3 mg) and extracted with chloroform. The extract was washed with a saturated aqueous NaCl solution, dried, and evaporated. The residual syrup (218 mg) was chromatographed on silica gel (20 g) with 4 : 1 benzene–ethyl acetate to give **5b** (78 mg, 53%) as a colorless solid. Recrystallization from 1 : 1 acetone–hexane afforded needles of **5b**: mp 142—143 °C; $[\alpha]_D^{30}$ −47° (*c* 0.96, MeOH); IR (KBr) 1737 cm^{-1}; ^{1}H-NMR δ=0.92, 0.95, 0.98, and 1.00 (each 3H, each d, 4,6,8, and 10-Me, *J*=7 Hz), 2.02 (6H, s, OAc×2), 3.17 (1H, dd, H-3, $J_{2,3}$=3.5 Hz, $J_{3,4}$=9.9 Hz), 3.37 (6H, s, OMe×2), 3.7—4.0 (4H, m, $-OCH_2CH_2O-$), 4.35 (1H, dd, H-2, $J_{1,2}$=1.6 Hz), 4.73 (1H, d, H-11, $J_{10,11}$=3.4 Hz), 4.92 (1H, d, H-1), and 5.0—5.4 (2H, m, H-7 and 9).

Found: C, 51.30; H, 7.16; Br, 14.71%. Calcd for $C_{23}H_{39}O_9Br$: C, 51.21; H, 7.29; Br, 14.81%.

A sample (65 mg) of **5b** was dissolved in 70 (v/v)% aqueous TFA (0.65 ml) and allowed to stand at 0—2 °C for 20 h. The reaction mixture was then poured into cold chloroform and neutralized with solid $NaHCO_3$. The organic layer thus separated was washed with water and a saturated aqueous NaCl solution, dried, and evaproated to give a practically pure sample of **4b** (60 mg, 100%); ^{1}H-NMR δ=0.94, 0.99, 1.02, and 1.10 (each 3H, each d, 4,6,8, and 10-Me, *J*=6.5 and 7.0 Hz), 2.01 and 2.03 (each 3H, each s, OAc×2), 3.17 (1H, dd, H-3, $J_{2,3}$=3.4 Hz, $J_{3,4}$=10.1 Hz), 3.37 (6H, s, OMe×2), 4.34 (1H, dd, H-2, $J_{1,2}$=1.5 Hz), 4.91 (1H, d, H-1), 4.9—5.2 (1H, m, H-7 or H-9), 5.39 (1H, dd, H-7 or

H-9, J=2.0 and 9.4 Hz), and 9.56 (1H, d, H-11, $J_{10,11}$=3.2 Hz).

11-Ethylene Acetal (5a). To a solution of **5b** (81 mg, 0.150 mmol) in dry benzene (2.0 ml) was added tributylstannane (0.048 ml, 0.180 mmol) and α,α'-azobisisobutylonitrile (AIBN) (4.9 mg, 0.03 mmol). The mixture was then stirred at 60 °C for 6 h under argon. The reaction mixture was evaporated, and the residue (198 mg) was chromatographed on silica gel (10 g) with 3: 1 benzene–ethyl acetate to afford **5a** (44 mg, 64%) as a colorless solid. Recrystallization from 1: 2 acetone–hexane gave colorless plates: mp 113—114 °C; $[\alpha]_D^{20}$ −85° (*c* 1.0, MeOH); IR (KBr) 1731 cm^{-1}; ^{1}H-NMR δ=0.86−1.08 (12H, m, 4, 6, 8, and 10-Me), 1.2—1.7 (1H, m, H-2ax), 2.05 (6H, s, OAc×2), 3.35 and 3.37 (each 3H, each s, OMe×2), 3.8—4.0 (4H, m, $-OCH_2CH_2O-$), 4.76 (1H, d, H-11, $J_{10,11}$=3.5 Hz), and 4.7—5.4 (3H, m, H-1,7, and 9).

Found: C, 59.74; H, 8.57%. Calcd for $C_{23}H_{40}O_9$: C, 59.98; H, 8.75%.

Methyl [Methyl 7,9-Di-O-acetyl-2-bromo-2,4,6,8,10,11,12-heptadeoxy-4,6,8,10-tetra-C-methyl-3-O-methyl-L-glycero-L-talo-β-L-manno-(E)-11-tridecenopyranosid]uronate (6b). To a solution of the crude sample of **4b** (60 mg) in dry benzene (1.2 ml) was added (methoxycarbonylmethylene)triphenylphosphorane (61 mg, 0.182 mmol). The mixture was refluxed for 3 h under argon and then evaporated. The residual syrup was chromatographed on silica gel (7 g) with 6: 1 benzene–ethyl acetate to afford **6b** (56 mg, 84%) as a colorless solid. Recrystallization from ether gave needles of **6b**: 131—133 °C; $[\alpha]_D^{22}$ −34° (*c* 0.88, MeOH); IR (KBr) 1731 and 1662 cm^{-1}: ^{1}H-NMR δ=0.91−1.12 (12H, m, 4,6,8, and 10-Me), 2.00—2.04 (each 3H, each s, OAc×2), 3.20 (1H, dd, H-3, $J_{2,3}$=3.3 Hz, $J_{3,4}$=10.5 Hz), 3.40 (6H, s, OMe×2), 3.75 (3H, s, COOMe), 4.38 (1H, dd, H-2, $J_{1,2}$=1.1 Hz), 4.96—5.20 (3H, m, H-1,7, and 9), 5.83 (1H, d, H-12, $J_{11,12}$=15.6 Hz), and 6.83 (1H, dd, H-11, $J_{10,11}$=9.0 Hz).

Found: C, 52.50; H, 7.13; Br, 14.38%. Calcd for $C_{24}H_{39}O_9Br$: C, 52.27; H, 7.13; Br, 14.49%.

Methyl [Methyl 7,9-Di-O-acetyl-2,4,6,8,10,11,12-heptadeoxy-4,6,8,10-tetra-C-methyl-3-O-methyl-L-manno-β-D-galacto-(E)-11-tridecenopyranosid]uronate (6a). A solution of **6b** (137 mg, 0.248 mmol), tributylstannane (0.080 ml, 0.298 mmol), and AIBN (8 mg, 0.05 mmol) in dry benzene (2.7 ml) was stirred under argon at 60 °C for 3 h, and then the solvent was removed. The residue (300 mg) was chromatographed on silica gel (12 g) with 3: 1 benzene–ethyl acetate to give **6a** (111 mg, 95%) as colorless crystals. Recrystallization from hexane afforded colorless needles: mp 100—101 °C; $[\alpha]_D^{17}$ −61° (*c* 1.22, MeOH); IR (KBr) 1728 and 1653 cm^{-1}; ^{1}H-NMR δ=0.8−1.1 (12H, m, 4, 6, 8, and 10-Me), 1.41 (1H, ddd, H-2ax, $J_{2ax,2eq}$=11.0 Hz, $J_{2ax,3}$=9.0 Hz, $J_{1,2ax}$=3.6 Hz), 2.00 and 2.04 (each 3H, each s, OAc×2), 3.35 and 3.37 (each 3H, each s, OMe×2), 3.76 (3H, s, COOMe), 4.75—5.25 (3H, m, H-1,7, and 9), 5.84 (1H, d, H-12, $J_{11,12}$=16.0 Hz), and 6.86 (1H, dd, H-11, $J_{10,11}$=8.9 Hz).

Found: C, 60.94; H, 8.37%. Calcd for $C_{24}H_{40}O_9$: C, 61.00; H, 8.53%.

Methyl [Methyl 2,4,6,8,10,11,12,13,14-Nonadeoxy-7,9-O-isopropylidene-4,6,8,10,14-penta-C-methyl-3-O-methyl-L-manno-β-D-galacto-(11E,13Z)-11,13-pentadecadienopyranosid]uronate (7a). To a stirred solution of **1a** (538 mg, 1.26 mmol) and DMP (0.308 ml, 2.52 mmol) in dry acetone (11 ml), was added a 0.1% H_2SO_4 solution in acetone (0.54 ml) under ice-cooling. After standing at 0 °C for 3 h, the mixture was neutralized with solid $NaHCO_3$. The insoluble material was filtered and washed with acetone. The filtrate and washings were combined and evaporated. The residual brown syrup (698 mg) was chromatographed on silica gel (22 g) with 10: 1 benzene–ethyl acetate to afford **7a** (583 mg, 99%) as a syrup: $[\alpha]_D^{25}$ −20° (*c* 0.75, MeOH); UV_{max} (EtOH) 266 nm (ε 11400); IR (CCl_4) 1705 and 1631 cm^{-1}; ^{1}H-NMR δ=0.8—1.1 (12H, m, 4,6,8, and 10-Me), 1.27 and 1.30 (each 3H, each s, CMe_2), 1.95 (3H, d, 14-Me, $J_{13,Me}$=1.0 Hz), 3.23 (1H, m, H-3, $J_{3,4}$=10.0 Hz), 3.35 (6H, s, OMe×2), 3.76 (3H, s, COOMe), 4.82 (1H, dd, H-1, $J_{1,2ax}$=3.2 Hz, $J_{1,2eq}$=1.4 Hz), 5.98 (1H, dd, H-11, $J_{10,11}$=6.0 Hz, $J_{11,12}$=15.0 Hz), 6.40 (1H, dd, H-13, $J_{12,13}$=11.0 Hz), and 7.16 (1H, dd, H-12).

Found: C, 66.61; H, 9.29%. Calcd for $C_{26}H_{44}O_7$: C, 66.64; H, 9.46%.

(R)-2-Bromo Derivative of 7a (7b). A sample (205 mg) of **1b** was acetonated by the procedure described in the preparation of **7a** and then worked-up. The crude syrup (281 mg) of **7b** was chromatographed on silica gel (22 g) with 17: 1 benzene–ethyl acetate to afford a pure sample (168 mg, 76%) of **7b** as a syrup: $[\alpha]_D^{27}$ +4° (*c* 0.70, MeOH); UV_{max} (EtOH) 267 nm (ε 23000); IR (CCl_4) 1709, 1640, and 1601 cm^{-1}; ^{1}H-NMR δ=0.88−1.04 (12H, m, 4,6,8, and 10-Me), 1.27 and 1.30 (each 3H, each s, CMe_2), 1.96 (3H, s with a little long-range coupling with H-13, 14-Me), 3.20 (1H, dd, H-3, $J_{3,4}$=7.5 Hz, $J_{2,3}$=3.1 Hz), 3.38 (6H, s, OMe×2), 3.76 (3H, s, COOMe), 4.39 (1H, dd, H-2, $J_{1,2}$=1.5 Hz), 4.97 (1H, d, H-1), 5.98 (1H, dd, H-11, $J_{10,11}$=7.0 Hz, $J_{11,12}$=15.4 Hz), 6.40 (1H, dd, H-13, $J_{12,13}$=11.0 Hz), and 7.17 (1H, dd, H-12).

Found: C, 57.32; H, 7.84; Br, 14.37%. Calcd for $C_{26}H_{43}O_7Br$: C, 57.04; H, 7.92; Br, 14.59%.

Methyl [Methyl 2,4,6,8,10,11,12-Heptadeoxy-7,9-O-isopropylidene-4,6,8,10-tetra-C-methyl-3-O-methyl-L-manno-β-D-galacto-(E)-11-tridecenopyranosid]uronate (9a). Ozonized oxygen gas containing 1.11 mmol of ozone was passed slowly through a solution of **7a** (260 mg, 0.555 mmol) in dry dichloromethane (13 ml) at −75 °C. To the resulting solution was added dimethyl sulfide (0.1 ml, 5.55 mmol) at the same temperature. The mixture was gradually warmed to room temperature, washed with water and a saturated aqueous NaCl solution, dried, and evaporated. The resulting crude aldehyde **8a** (207 mg) was dissolved in dry benzene (4 ml). To this was added (methoxycarbonylmethylene)triphenylphosphorane (225 mg, 0.675 mmol), and the mixture was refluxed for 4 h under argon. After the removal of the solvent, the residual syrup was chromatographed on silica gel (20 g) with 4 : 1 benzene–ether to afford **9a** (209 mg, 89%) as a colorless syrup: $[\alpha]_D^{27}$ −35° (*c* 0.71, $CHCl_3$); IR (CCl_4) 1713 and 1625 cm^{-1}: ^{1}H-NMR δ=0.8−1.0 (12H, m, 4,6,8, and 10-Me), 1.26 and 1.30 (each 3H, each s, CMe_2), 3.37 (6H, s, OMe×2), 3.74 (3H, s, COOMe), 4.8−4.9 (1H, m, H-1), 5.85 (1H, d, H-12, $J_{11,12}$=15.6 Hz), and 7.04 (1H, dd, H-11, $J_{10,11}$=7.2 Hz).

Found: C, 64.56; H, 9.26%. Calcd for $C_{23}H_{40}O_7$: C, 64.46; H, 9.41%.

(R)-2-Bromo Derivative of 9a (9b). A sample (168 mg) of **7b** was ozonolyzed by the procedure described in preparation of **9a** to afford a crude aldehyde, **8b** (138 mg). A solution of this sample of **8b** (138 mg) and (methoxycarbonylmethylene)triphenylphosphorane (204 mg) in dry benzene (2.9 ml) was refluxed for 5 h under argon. The reaction mixture was then evaporated, and the residue was chromatographed on silica gel (20 g) with 15: 1 benzene–ethyl acetate to give **9b** (109 mg, 70%) as a colorless syrup: $[\alpha]_D^{25}$ −12° (*c* 0.64, MeOH); IR (CCl_4) 1728 and 1658 cm^{-1}; ^{1}H-NMR δ=0.88−1.05 (12H, m, 4,6,8, and 10-Me), 1.27 and 1.30 (each 3H, each s, CMe_2), 3.38 (6H, s, OMe×2), 3.37 (3H, s, COOMe), 4.37 (1H, dd, H-2, $J_{2,3}$=3.2 Hz, $J_{1,2}$=1.5 Hz), 4.97 (1H, d, H-1), 5.83 (1H, dd, H-12, $J_{11,12}$=15.9 Hz, $J_{10,12}$=1.0 Hz), and 7.01 (1H, dd, H-11, $J_{10,11}$=7.3 Hz).

Found: C, 54.22; H, 7.64; Br, 15.47%. Calcd for $C_{23}H_{39}$-

O_7Br: C, 54.44; H, 7.75; Br, 15.75%.

*Methyl 2,4,6,8,10,11,12-Heptadeoxy-7,9-O-isopropylidene-4,6,8,10-tetra-C-methyl-3-O-methyl-*L*-manno-β-*D*-galacto-(E)-11-tridecenopyranoside-(1,5) (**10a**).* *(A)*: A 27.5 (W/W)% DIBAL in hexane (0.460 ml, 0.803 mmol) was added dropwise to a stirred cooled solution (−75 °C) of **9a** (172 mg, 0.401 mmol) in dry toluene (17.2 ml). Once the addition of the DIBAL was complete, the reaction mixture was stirred at −75 °C for 30 min. It was then warmed to 0 °C, and to this mixture 50% aqueous acetic acid (0.08 ml) and ethyl acetate (4 ml) were added successively. The resulting insoluble matter was filtered through Celite and washed with ethyl acetate. The combined filtrate and washings were evaporated. The residual syrup (180 mg) was chromatographed on silica gel (8 g) with 2 : 1 benzene–ethyl acetate to afford **10a** (112 mg, 70%) as a colorless syrup: $[\alpha]_D^{25}$ −30° (*c* 1.16, $CHCl_3$); ^{1}H-NMR δ=0.8−1.0 (12H, m, 4,6,8, and 10-Me), 1.29 and 1.33 (each 3H, each s, CMe_2), 2.23 (1H, ddd, H-2eq, $J_{2eq,2ax}$ =13.1 Hz, $J_{2eq,3}$=4.7 Hz, $J_{1,2eq}$=1.6 Hz), 3.40 (6H, s, OMe×2), 4.0—4.2 (2H, m, H-13×2), 4.86 (1H, dd, H-1, $J_{1,2ax}$=4.0 Hz), and 5.7—5.8 (2H, m, H-11 and 12).

Found: C, 66.22; H, 9.87%. Calcd for $C_{22}H_{40}O_6$: C, 65.97; H, 10.07%.

(B): To a stirred solution of **6a** (75 mg, 0.158 mmol) in dry toluene (3.7 ml) was added dropwise 27.5% DIBAL in hexane (0.040 ml, 0.07 mmol) at −75 °C. After being stirred at the same temperature for 10 min, the reaction mixture was warmed to 0 °C and treated with a 50% aqueous acetic acid (0.079 ml) and ethyl acetate (1 ml). After the removal of the resulting insoluble matter by filtration, the filtrate was evaporated to give a colorless syrup (52 mg, 92%) of the triol. A mixture of the crude triol (52 mg), DMP (0.036 ml, 0.29 mmol), and dry DMF (0.52 ml) was stirred at room temperature for 5 h. The mixture was then neutralized with triethylamine and evaporated. The residue was chromatographed on silica gel (5 g) with 2 : 1 benzene–ethyl acetate to afford **10a** (43 mg, 73%).

*(R)-2-Bromo Derivative of **10a** (**10b**).* A solution of **9b** (96 mg, 0.189 mmol) in dry toluene (9.6 ml) was treated with a 27.5% DIBAL in hexane (0.215 ml, 0.378 mmol) at −75 °C for 10 min and then worked-up by the procedure described in the preparation of **10a** from **9a**. The crude syrup of **10b** (108 mg) thus obtained was chromatographed on silica gel (10 g) with 3: 1 benzene–ethyl acetate to afford a colorless syrup of **10b** (87 mg, 96%): $[\alpha]_D^{22}$ −7° (*c* 1.40, MeOH); ^{1}H-NMR δ=0.89−1.03 (12H, m, 4,6,8, and 10-Me), 1.27 and 1.31 (each 3H, each s, CMe_2), 3.20 (1H, dd, H-3, $J_{3,4}$=7.1 Hz, $J_{2,3}$=3.1 Hz), 3.39 (6H, s, OMe×2), 4.0—4.2 (2H, m, H-13×2), 4.39 (1H, dd, H-2, $J_{1,2}$=1.5 Hz), 4.98 (1H, d, H-1), and 5.65—5.79 (2H, m, H-11 and 12).

Found: C, 54.89; H, 7.98; Br, 16.38%. Calcd for $C_{22}H_{39}O_6Br$: C, 55.11; H, 8.20; Br, 16.67%.

*Methyl 2-Bromo-2,4,6,8,10,11,12-heptadeoxy-7,9-O-isopropylidene-4,6,8,10-tetra-C-methyl-3-O-methyl-*L*-glycero-*L*-talo-β-*L*-manno-(E)-11-tridecenodialdopyranoside-(1,5) (**11b**).* A mixture of chromium trioxide (71 mg, 0.716 mmol) and dry HMPA (0.21 ml) was stirred at room temperature for 2.5 h, and a solution of **10b** (172 mg, 0.358 mmol) in HMPA (0.34 ml) was then added. Stirring was continued for 1 week at room temperature, after which the mixture was poured into ice water and extracted with ether. The ether layer was washed successively with a 5% aqueous NaOH solution, water, and a saturated aqueous NaCl solution, dried, and evaporated. The residue was chromatographed on silica gel (8.3 g) with 10 : 1 benzene–ethyl acetate to give **11b** (106 mg, 62%) as a colorless crystal. Recrystallization from ether–petroleum ether afforded colorless needles of **11b**: mp 129—130 °C; $[\alpha]_D^{25}$ −10° (*c* 0.96, MeOH); IR (KBr) 1689 and 1634 cm^{-1}; ^{1}H-NMR δ=0.94, 0.98, 1.01, and 1.05 (each 3H, each d, 4,6,8, and 10-Me, J=6—7 Hz), 1.27 and 1.32 (each 3H, each s, CMe_2), 3.23 (1H, dd, H-3, $J_{2,3}$=3.1 Hz, $J_{3,4}$=9.9 Hz), 3.39 (6H, s, OMe×2), 4.40 (1H, dd, H-2, $J_{1,2}$=1.6 Hz), 4.98 (1H, d, H-1), 6.14 (1H, ddd, H-12, $J_{11,12}$=15.9 Hz, $J_{12,13}$=7.7 Hz, $J_{10,12}$=1.0 Hz), 6.96 (1H, dd, H-11, $J_{10,11}$=6.5 Hz), and 9.53 (1H, d, H-13).

Found: C, 55.38; H, 7.64; Br, 16.50%. Calcd for $C_{22}H_{37}O_6Br$: C, 55.35; H, 7.81; Br, 16.74%. On column chromatography, unchanged **10b** (37 mg, 22%) was recovered.

*13E-Isomer of **7b** (**7'b**); Condensation of **11b** with **14**.* To an ice-cooled suspension of NaH (3.6 mg, 0.082 mmol; 55% dispersion in mineral oil) in dry THF (0.27 ml), **14**[13] (15 mg, 0.074 mmol) was added, and the mixture was stirred at room temperature for 1 h. It was then cooled to −75 °C, and a solution of **11b** (29.6 mg, 0.062 mmol) in dry THF (0.3 ml) was added. Stirring was continued at −60——65 °C for 1 h. The reaction mixture was then poured into ice water and extracted with ether. The extract was washed with a saturated aqueous NaCl solution, dried, and evaporated. The residue was preparatively thin-layer chromatographed on Merck Kieselgel 60-F_{254} (0.5 mm) with 25 : 1 and 30 : 1 benzene–ethyl acetate (two passes), to afford **7b** (0.5 mg, 1.5%) and **7'b** (28 mg, 83%): $[\alpha]_D^{20}$ 0° (*c* 0.78, MeOH); UV_{max} (EtOH) 266 nm (ε 28800); IR (CCl_4) 1711 and 1641 cm^{-1}; ^{1}H-NMR δ=0.88−1.05 (12H, m, 4,6,8, and 10-Me), 1.27 and 1.30 (each 3H, each s, CMe_2), 1.94 (3H, d, 14-Me, $J_{13,Me}$=1.0 Hz), 3.20 (1H, dd, H-3, $J_{3,4}$=7.1 Hz, $J_{2,3}$=3.0 Hz), 3.38 (6H, s, OMe×2), 3.77 (3H, s, COOMe), 4.38 (1H, dd, H-2, $J_{1,2}$=1.6 Hz), 4.97 (1H, d, H-1), 6.03 (1H, dd, H-11, $J_{11,12}$= 15.0 Hz, $J_{10,11}$=6.0 Hz), 6.42 (1H, dd, H-12, $J_{12,13}$=10.0 Hz), and 7.19 (1H, dd, H-13).

Found: C, 57.37; H, 7.97; Br, 14.26%. Calcd for $C_{26}H_{43}O_7Br$: C, 57.04; H, 7.92; Br, 14.59%.

*Allylic Bromide (**12a**) and Triphenylphosphonium Salt (**13a**).* Triethylamine (0.05 ml, 0.315 mmol) and lithium bromide (20 mg, 0.23 mmol) were added to a solution of **10a** (83 mg, 0.21 mmol) in dichloromethane (1.6 ml), and then the new mixture was cooled at 0 °C. To this cooled suspenion, mesyl chloride (0.02 ml, 0.24 mmol) was added under stirring. Stirring was continued at 0 °C for 1 h at room temperature for 12 h. The reaction mixture was then diluted with acetone, and the precipitates were filtered off using Celite and washed with ethyl acetate. The filtrate and washings were combined and evaporated to afford a yellow syrup. The syrup was chromatographed on silica gel (Kieselgel 60, 8 g) with 9: 1 hexane–ethyl acetate to give **12a** (77 mg, 80%) as a colorless crystalline solid: ^{1}H-NMR δ=0.8−1.0 (12H, m, 4, 6, 8, and 10-Me), 1.28 and 1.32 (each 3H, each s, CMe_2), 3.36 (6H, s, OMe×2), 3.9—4.0 (2H, doublet like, H-13 and 13'), 4.85 (1H, m, H-1), and 5.7—5.9 (2H, m, H-11 and 12). A solution of **12a** (30 mg, 0.06 mmol) and triphenylphosphine (17 mg, 0.065 mmol) in dry ether (0.3 ml) was stirred under argon at 30 °C for 2 d. The resulting solid was separated from ether by decantation and triturated with ether to afford a colorless powder of **13a** (46.5 mg, 100%); IR (KBr) 1430, 1110, 1000, 730, and 710 cm^{-1}.

*Allylic Bromide (**12b**) and Triphenylphosphonium Salt (**13b**).* By the procedure described in the preparation of **12a**, a sample (91 mg) of **10b** was converted into a crude bromide, **12b**, which was then purified by column chromatography, using Kieselgel 60 (10 g) with 50: 1 benzene–ethyl acetate, to afford a practically pure sample of **12b** (93 mg, 90%) as colorless needles: mp 126—127 °C; ^{1}H-NMR δ=0.97 (doublet like, 12H, 4, 6, 8, and 10-Me), 1.27 and 1.31 (each 3H, each s, CMe_2), 3.20 (1H, dd, H-3, $J_{2,3}$=3.5 Hz, $J_{3,4}$=6.6 Hz), 3.40 (6H, s,

OMe×2), 4.40 (1H, dd, H-2, $J_{1,2}$=1.6 Hz), 4.99 (1H, d, H-1), and 5.69—5.87 (2H, m, H-11 and 12). A solution of **12b** (92 mg, 0.17 mmol) and triphenylphosphine (89 mg, 0.339 mmol) in dry benzene (0.28 ml) was stirred under arogn at 55 °C for 5 d. After the subsequent removal of the solvent by evaporation, the resulting solid was washed with hexane by trituration to afford a colorless powder of **13b** (136 mg, 100%): IR (KBr) 1440, 1118, 998, and 724 cm^{-1}.

Wittig Condensation of Methyl Pyruvate with Triphenylphosphorane Generated from ***13a*** *or* ***13b***. *(A)*: A 1.6 M butyllithium in hexane (0.027 ml, 0.043 mmol) was added, under argon, to a stirred, cooled solution (−75 °C) of **13a** (46.5 mg, 0.064 mmol) in dry THF (0.5 ml). After the solution had been stirred at −75 °C for 1 h, to the deep red solution was added a solution of methyl pyruvate (4.4 mg, 0.043 mmol) in dry THF (0.1 ml). Stirring was continued at −75 °C for 0.5 h, and then it was evaporated. Ether was added to the residual syrup, and the precipitates were filtered off and washed with ether. The combined filtrate and washings were then evaporated to afford a yellow syrup (40.3 mg). The crude product was purified by PLC with 10 : 1 benzene–ethyl acetate to give a mixture of **7a** and its 13*E*-isomer, **7'a** (11.9 mg). The mixture was chromatographed on alumina (Woelm grade I, 1 g) with 3: 1 benzene–chloroform to afford **7a** [R_f 0.51 (2: 1 hexane–ether, two passes)] as a colorless syrup [4 mg (28%)] and **7'a** [R_f 0.49 (2: 1 hexane–ether, two passes)], also as a colorless syrup [5 mg (34%)]: $[\alpha]_D^{30}$ −9° (*c* 1.29, MeOH); UV_{max} (EtOH) 266 nm (ε 35700); IR (CCl_4) 1709 and 1641 cm^{-1}; ^{1}H-NMR δ=0.85—1.05 (12H, m, 4, 6, 8, and 10-Me), 1.27 and 1.31 (each 3H, each s, CMe_2), 1.95 (3H, d, 14-Me, $J_{13,Me}$=1.5 Hz), 3.34 (6H, s, OMe×2), 3.75 (3H, s, COOMe), 4.81 (1H, dd, H-1, $J_{1,2ax}$=3.5 Hz, $J_{1,2eq}$=1.5 Hz), 6.4 (1H, dd, H-11, $J_{11,12}$=14.6 Hz, $J_{10,11}$=6.2 Hz), 6.40 (1H, dd, H-12, $J_{12,13}$=10.0 Hz), and 7.17 (1H, dd, H-13).

Found: C, 66.37; H, 9.45%. Calcd for $C_{26}H_{44}O_7$: C, 66.64; H, 9.46%.

(B): A 1.6 M butyllithium in hexane (0.089 ml) was added, under argon, to a stirred, cooled solution (−75 °C) of **13b** (77 mg) in dry THF (0.77 ml). After the mixture had been stirred at −75 °C for 15 min, methyl pyruvate (19 mg) was added to the deep-red solution. The solution immediately turned pale yellow. It was then poured into ice-cooled water, and the mixture was extracted with chloroform. The extract was washed with a saturated aqueous NaCl solution, dried, and evaporated. The residue (116 mg) was preparatively thin-layer chromatographed on two PLC plates (in two passes) with 25: 1 and 30: 1 benzene–ethyl acetate to afford **7b** [R_f 0.47 (15: 1 benzener–ethyl acetate)] as a pale yellow viscous syrup [21 mg (40%)] and **7'b** [R_f 0.42 (15: 1 benzene–ethyl acetate)] also as a pale yellow viscous syrup [22 mg (42%)]; these two substances were found by ^{1}H-NMR analysis and TLC to be identical with the corresponding authentic samples.

Methyl [*Methyl 2,4,6,8,10,11,12,13,14-Nonadeoxy-4,6,8,10,14-penta-*C*-methyl-*3*-O-methyl-*L*-manno-β-*D*-galacto (11*E*, 13*Z*)-11,13-pentadecadienopyranosid*]*uronate (**1a**)*. A sample of **7a** (15 mg) was dissolved in 50 (v/v)% aqueous DFA (0.15 ml), after which the mixture was stand at 0 °C for 25 min. The solution was then neutralized with solid $NaHCO_3$ and extracted with ether. The extract was washed with a saturated aqueous NaCl solution, dried, and evaporated. Chromatographic purification using silica gel (1 g) with 3: 2 benzene–ethyl acetate afforded **1a** (11 mg, 80%) as a colorless syrup; this syrup was identical with the authentic sample.

(R)-2-Bromo Derivative of ***1a*** *(****1b****)*. A solution of **7b** (27 mg) in 90 (v/v) % TFA (0.27 ml) was kept at 0 °C for 15 min. The subsequent removal of the solvent, followed by column chromatography on silica gel (2.5 g) with 3: 1 benzene–ethyl acetate, gave a pale yellow syrup of **1b** (25 mg, 100%), whose ^{1}H-NMR, IR, and UV spectra were identical with those of the authentic sample.

We wish to thank Mr. Saburo Nakada for carrying out the microanalyses and the Daiichi Seiyaku Co., Ltd., for the kind supply of rifampicin. The authors are also grateful to the Institute of Microbial Chemistry for its financial support.

References

1) Part II: M. Nakata, Y. Ikeyama, H. Takao, and M. Kinoshita, *Bull. Chem. Soc. Jpn.*, **53**, 3252 (1980).
2) M. Kinoshita, K. Tatsuta, and M. Nakata, *J. Antibiot.*, **31**, 630 (1978).
3) The acetylation of **1b** with acetic anhydride in pyridine also gave **3b** in a 94% yield after it had been kept at 45 °C for 7 d.
4) J. J. Pappas, W. P. Keaveney, E. Gancher, and M. Berger, *Tetrahedron Lett.*, **1966**, 4273.
5) The **6a** could be derived directly from the synthetic sample of **4a** in a good yield; see the following paper.
6) G. Cardillo, M. Orena, and S. Sandri, *Synthesis*, **1976**, 394.
7) A. I. Meyers, K. Tomioka, D. M. Roland, and D. Comins, *Tetrahedron Lett.*, **1978**, 1375; E, J, Corey, L. O. Weigel, D. Floyd, and M. G. Bock, *J. Am. Chem. Soc.*, **100**, 2916 (1978).
8) H. O. House and G. H. Rasmusson, *J. Org. Chem.*, **26**, 4278 (1961).
9) R. K. Crossland and K. L. Servis, *J. Org. Chem.*, **35**, 3195 (1970); D. A. Evans, C. E. Sacks, R. A. Whitney, and N. G. Mandel, *Tetrahedron Lett.*, **1978**, 727; E. W. Collington and A. I. Meyers, *J. Org. Chem.*, **36**, 3044 (1971).
10) E. J. Corey and G. Schmidt, *Tetrahedron Lett.*, **1979**, 2317.
11) K. B. Becker, *Helv. Chim. Acta*, **60**, 68 (1977), and the references cited therein.
12) M. Schlosser, *Topics in Stereochemistry*, **5**, 1 (1970).
13) The reagent **14** [bp 110—115 °C (10 mmHg)] was prepared according to the procedure used for the preparation of diethyl [1-(ethoxycarbonyl)ethyl]phosphonate described by Wadsworth: W. S. Wadsworth, Jr., *Org. React.*, **25**, 142 (1977).

The Reaction of Acetophenones with Manganese(III) Acetate

Kazu KUROSAWA* and Katsutoshi YAMAGUCHI

Department of Chemistry, Faculty of Science, Kumamoto University, Kurokami 2-39-1, Kumamoto 860

(Received August 12, 1980)

The reaction of 4′-methoxyacetophenone with manganese(III) acetate in the presence of ammonium chloride yielded 2-chloro-4′-methoxyacetophenone (**2a**) and 2,2-dichloro-4′-methoxyacetophenone (**3a**). The reaction of **2a** with these reagents gave **3a**, 4′-methoxy-2,2,2-trichloroacetophenone, and 1,4-bis(4-methoxyphenyl)-2,2,3,3-tetrachloro-1,4-butanedione (**8a**). The reactions of **2a** and 2-bromoacetophenone with manganese(III) acetate yielded the corresponding 2,3-dihalo-1,4-diphenyl-1,4-butanediones, 1,4-diphenyl-2-halo-2-butene-1,4-diones, 2,3-dihalo-2-butene-1,4-diones, 2,2-dibromoacetophenone, and **8a**. The reaction pathways are discussed.

It has been reported that the reaction of acetophenone with oxygen in the presence of manganese(III) acetate in butyric acid gave benzoic acid.[1] The reactions of aliphatic and cyclic ketones with manganese(III) acetate have also been reported to give α-acetoxy ketones as the major product when the reaction was conducted under nitrogen.[2] The reactions of ketones with manganese(III) acetate in the presence of olefins have been reported by many investigators.[2-6] It seems that the chloride ion, in place of olefins, oxygen and acetate ion, will react with the benzoylmethyl radical formed from acetophenone. The acetophenone derivatives examined are 4′-methoxyacetophenone (**1a**) and 2-chloro-4′-methoxyacetophenone (**2a**). The reactions were carried out in boiling acetic acid. The structure of the reaction products were determined by means of the study of their IR, NMR, and mass spectra, by elemental analyses, and by comparison with authentic samples.

When **1a** was oxidized with manganese(III) acetate–ammonium chloride in acetic acid containing acetic anhydride, 2-chloro-4′-methoxyacetophenone (**2a**) and 2,2-dichloro-4′-methoxyacetophenone (**3a**) were obtained (Table 1, Entries 2—9), in contrast to the reaction in the absence of ammonium chloride (Entry 1), which gave 2-acetoxy-4′-methoxyacetophenone (**2b**) and *p*-anisic acid (**4a**). The yields of **2a** were first increased and then decreased with the increase in the oxidant, while the yields of **3a** were increased (Entries 2, 4, and 8). The total yields decreased with a higher molar ratio of the oxidant to the substrate, because of the formation of a number of undefined products. It was also found that acetic anhydride added to the reaction mixture effected the yield of **3a** more than that of **2a** (Entries 3, 4, 5, and 6), although no rational explanation could be given. Lithium chloride and hydrochloric acid were also employed as chloride-ion sources; the results are shown in the table (Entries 10 and 11). It could be assumed that the reaction is initiated by the formation of the benzoylmethyl radical[1] (Ia in Scheme 1), which captures the chloride ion in the presence of manganese(III) acetate, but this is the least possible because it is difficult for the three species to get together at one time. It seems reasonable to

$$ArCOCH_2^{\cdot} + Cl^- + Mn(III) \longrightarrow ArCOCH_2Cl + Mn(II)$$

assume that the chloride ion either forms a complex

Table 1. The reactions of 4′-methoxyacetophenone (**1a**) and 2-chloro-4′- methoxyacetophenone (**2a**) with manganese (III) acetate in the presence of ammonium chloride in acetic acid containing acetic anhydride at the reflux temperature

Entry	Substrate	Reaction conditions: Molar ratio of substrate: oxidant : Ac_2O	Reaction conditions: Time / min	Products (yield/%)[a] **2a**	**2b**	**3a**	**4a**	**5a**	**8a**	Recovered substrate / %
1	**1a**	1 : 2 : 0[b]	60		24		22			40
2	**1a**	1 : 2 : 8	12	33		7				49
3	**1a**	1 : 3 : 6	17	34		26				39
4	**1a**	1 : 3 : 12	15	38		21				28
5	**1a**	1 : 3 : 24	10	40		14				30
6	**1a**	1 : 3 : 48	7	25		2				52
7	**1a**	1 : 4 : 8	22	16		29				25
8	**1a**	1 : 4 : 16	20	22		45				14
9	**1a**	1 : 4 : 32	15	16		28				40
10	**1a**	1 : 3 : 12[c]	12	16		22				20
11	**1a**	1 : 3 : 40[d]	10	15		18				25
12	**2a**[8]	1 : 2 : 4	11	—		47				57
13	**2a**	1 : 3 : 6	21	—		41		10	4	13

a) The yields are based on the amount of the substrate used. b) The reaction was carried out in the absence of ammonium chloride. c) Lithium chloride (20 mmol) was used in place of ammonium chloride. d) 12 M Hydrochloric acid (9 mmol) was used in place of ammonium chloride.

TABLE 2. THE REACTIONS OF 2-HALOACETOPHENONES (**2a** AND **2c**) AND 2,2-DIHALOACETOPHENONES (**3a** AND **3c**) WITH MANGANESE(III) ACETATE IN ACETIC ACID AT THE REFLUX TEMPERATURE

Entry	Substrate	Reaction conditions: Molar ratio of substrate : oxidant : Ac_2O	Reaction conditions: Time / min	Products (yield/%): 3	4	8	9	10	11	Recovered substrate / %
1	**2a**	1 : 2 : 0	95	0	10	8	9	40	5	0
2	**2c**	1 : 1 : 0	14	9	0	0	12	8	0	31
3	**2c**	1 : 2 : 0	45	8	0	0	8	23	8	0
4	**2c**	1 : 2 : 8	25	4	0	0	6	20	3	2
5	**2c**+**3c**[b]	1 : 2 : 0	60	—	0	0	1	12	21	5,[c] 12[d]
6	**3a**[9]	1 : 1 : 0	65	—	0	37	0	0	0	25

a) The yields are based on the amount of the substrate used. b) A mixture of 1 mmol each. c) The recovery of **2c**. d) The recovery of **3c**.

with manganese(III) acetate such as $[Mn(OAc)_3Cl]^-$ or replaces some of the acetate ions to form $Mn(OAc)_{3-n}Cl_n$, which then reacts with Ia. In fact, the visible spectrum of manganese(III) acetate in acetic acid showed a maximum at 470 nm (ε 288) which was shifted to 530 nm (shoulder, ε 439) by the addition of lithium chloride. It has been reported that a similar shift was caused by the addition of potassium acetate.[7] **2a** can be further chlorinated in the same way to **3a** and **5a** (Table 1, Entries 12 and 13, and Scheme 1).

The reaction of **1a** with chlorine in acetic acid gave 3′-chloro-4′-methoxyacetophenone (**6**) and 2,3′-dichloro-4′-methoxyacetophenone (**7**), along with **2a**. The absence of the nuclear chlorinated compounds among the manganese(III) acetate–ammonium chloride oxidation products from **1a** eliminated the pathway in which the chloride ion is oxidized to chlorine, with the latter then reacting with **1a** to give **2a** and **3a**. Other nucleophiles, such as methanol and benzoic acid, failed to react with **1a**, and **2b** was obtained in poor yields (10 and 6% respectively). When ammonium bromide was used, bromine was liberated.

When 2-chloro-4′-methoxyacetophenone (**2a**) was treated with manganese(III) acetate–ammonium chloride, 1,4-bis(4-methoxyphenyl)-2,2,3,3-tetrachlorobutanedione (**8a**) was obtained, together with **3a** and 4′-methoxy-2,2,2-trichloroacetophenone (**5a**) (Entry 13). **8a** can be formed by the dimerization of the benzoyldichloromethyl radical (IIIa), which is derived from **3a** by the action of manganese(III) acetate. This led us to examine the reactions of **2a** and 2-bromoacetophenone (**2c**) with manganese(III) acetate.

When 2-bromoacetophenone (**2c**) was oxidized with manganese(III) acetate, 2,2-dibromoacetophenone (**3c**), 2,3-dibromo-1,4-diphenyl-1,4-butanedione (**9c**), 2-bromo-1,4-diphenyl-2-butene-1,4-dione (**10c**), and (*E*)-2,3-dibromo-1,4-diphenyl-2-butene-1,4-dione (**11c**) were obtained (Table 2). The yields of the reaction products depended on the molar ratio of the oxidant to the substrate (Entries 2 and 3) and were decreased by the presence of acetic anhydride, which shortened the reaction time considerably (Entry 4). In boiling acetic acid, **9c** was converted to **10c** with the loss of hydrogen bromide. The configurations of **9c** and **10c** could not be determined. When 1 : 1 mixture of **2c** and **3c** was oxidized with manganese(III) acetate, **11c** was obtained in an increased yield, at the expense of decreased yields of **9c** and **10c** (Entry 5). The reaction pathway may be explained as follows. The reaction of **2c** with manganese(III) acetate gives the benzoylbromomethyl radical (IIc), which dimerizes to **9c**. The dehydrobromination of **9c** yields **10c**. IIc, on the other hand, reacts with the hydrogen bromide now present in the reaction mixture to give **3c**. The benzoyldibromomethyl radical (IIIc), which is formed from **3c** by manganese(III) acetate, reacts with IIc to give IVc. The dehydrobromination of IVc gives **11c**. The reaction of 2-chloro-4′-methoxyacetophenone (**2a**) with manganese(III) acetate in acetic acid gave similar products except for the presence of **8a** and the absence of **3a** among the reaction products. The difference in the product distributions in Entry 11 of Table 1 and in Entry of Table 2 may be ascribed to the difference in the chloride-ion concentration. **3a** was converted to **8a** with manganese(III) acetate (Entry 6). These values are shown in Scheme 1.

It is thus concluded that the benzoylmethyl radical

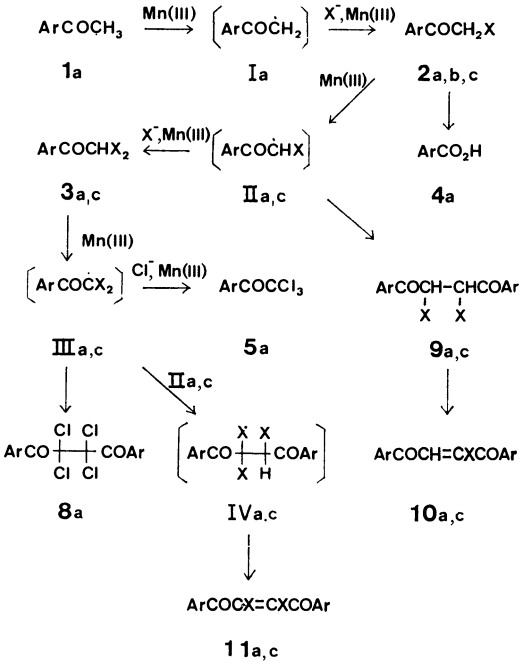

Scheme 1. **a**: Ar=4-methoxyphenyl, X=Cl; **b**: Ar=4-methoxyphenyl, X=OAc; **c**: Ar=phenyl, X=Br.

(Ia) and the benzoylhalomethyl radicals (IIa and IIc) derived from the corresponding acetophenone with manganese(III) acetate can react with the halide ion in the presence of manganese(III) acetate to give **2a**, **3a**, **3c**, and **5a**, and that the benzoylhalomethyl radicals (IIa, IIc, IIIa, and IIIc) tend to dimerize to form **8a**, **9a**, **9c**, **10a**, **10c**, **11a**, and **11c** in low halide-ion concentrations.

Experimental

All the ^{1}H NMR spectra were recorded with a Hitachi-Perkin-Elmer R 24 spectrometer, with tetramethylsilane as the internal reference. The IR spectra were taken for the chloroform solution on a JASCO grating spectrometer, while the UV spectra were recorded for the methanol solution with a Hitachi EPS-3T spectrophotometer. The mass spectra were recorded with a JMS-01 SG-2 instrument. The melting points were determined with a Yanagimoto micro-melting point apparatus and were not corrected.

Acetophenones. The 4′-methoxyacetophenone (**1a**) and 2-bromoacetophenone (**2c**) were commercial samples from Wako Pure Chemical Industries, Ltd. The 2-chloro-4′-methoxyacetophenone (**2a**)[8] and 2,2-dichloro-4′-methoxyacetophenone (**3a**)[9] were prepared by the standard procedure.

Oxidations of 4′-Methoxyacetophenone (1a) and 2-Chloro-4′-methoxyacetophenone (2a) with Manganese(III) Acetate–Ammonium Chloride. The general procedure for the oxidations of **1a** and **2a** with manganese(III) acetate–ammonium chloride was as follows. A mixture of **1a** (or **2a**) (2 mmol), manganese(III) acetate dihydrate,[10] acetic acid (20 ml), acetic anhyride and ammonium chloride (19 mmol) was heated under reflux for the time shown in Table 1. After the removal of the solvent *in vacuo*, 2 M hydroric acid (40 ml) was added to the reaction mixture and the mixture was extract with benzene (30 ml). The benzene solution was washed with aqueous sodium hydrogencarbonate and then evaporated *in vacuo*. The resulting liquid was chromatographed on TLC (Wakogel B10), with benzene or chloroform as the developing solvent. The yields are summarized in Table 1.

2-Chloro-4′-methoxyacetophenone (2a): Mp 100—102 °C (CCl_4) (lit,[8] mp 101—102 °C); IR 1700 and 1710 cm^{-1}; NMR ($CDCl_3$) δ=3.83 (3H, s, OCH_3), 4.58 (2H, s, $-CH_2-$), 6.95 (2H, m, $H_{(3')}$ and $H_{(5')}$), and 7.91 (2H, m, $H_{(2')}$ and $H_{(6')}$).

2,2-Dichloro-4′-methoxyacetophenone (3a): Mp 78—79 °C (CCl_4) (lit,[9] mp 74—75 °C); IR 1700 and 1718 cm^{-1}; NMR (CCl_4) δ=3.82 (3H, s, OCH_3), 6.43 (1H, s, >CH–), 6.79 (2H, m, $H_{(3')}$ and $H_{(5')}$), and 7.90 (2H, m, $H_{(2')}$ and $H_{(6')}$).

4′-Methoxy-2,2,2-trichloroacetophenone (5a): Liquid (lit,[11] mp 33—34.5 °C); IR 1720 cm^{-1}; NMR (CCl_4) δ=3.86 (3H, s, OCH_3), 6.87 (2H, m, $H_{(3')}$ and $H_{(5')}$), and 8.20 (2H, m, $H_{(2')}$ and $H_{(6')}$).

1,4-Bis(4-methoxyphenyl)-2,2,3,3-tetrachloro-1,4-butanedione (8a): Mp 145—146 °C (CCl_4); IR 1708 cm^{-1}; UV λ_{max} 229 (12000) and 304 nm (25900); NMR ($CDCl_3$) δ=3.84 (6H, s, 2×OCH_3), 6.89 (4H, m, $H_{(3')}$, $H_{(3'')}$, $H_{(5')}$, and $H_{(5'')}$), and 8.25 (4H, m, $H_{(2')}$, $H_{(2'')}$, $H_{(6')}$, and $H_{(6'')}$). Found: C, 49.33; H, 3.34%. Calcd for $C_{18}H_{14}Cl_4O_4$: C, 49.57; H, 3.24%.

Chlorination of 4′-Methoxyacetophenone (1a) with Chlorine in Acetic Acid. Through a solution of **1a** (1 g) in acetic acid (10 ml), chlorine gas was passed (The weight of the chlorine absorbed was 0.5 g), after which the solution was left at room temperature for 30 min. After the removal of the acetic acid *in vacuo*, the resulting mixture was chromatographed on TLC, with benzene as the developing solvent, giving unchanged **1a** (74 mg, 7%), 3′-chloro-4′-methoxyacetophenone (**6**) [237 mg, 19%, mp 73—74 °C (MeOH) (lit,[12] mp 71—73 °C)], **2a** (358 mg, 29%), and 2,3′-dichloro-4′-methoxyacetophenone (**7**) [207 mg, 14%, mp 89—90 °C (EtOH); IR 1700 cm^{-1}; NMR ($CDCl_3$) δ=3.96 (3H, s, OCH_3), 4.62 (2H, s, $-CH_2-$), 7.00 (1H, d, J=8.0 Hz, $H_{(5')}$), 7.75—8.05 (2H, m, $H_{(2')}$ and $H_{(6')}$). Found: C, 49.43; H, 3.79%. Calcd for $C_9H_8Cl_2O_2$: C, 49.34; H, 3.68%].

Oxidation of Acetophenones (1a, 2a, 2c, 3a, and 3c) with Manganese(III) Acetate. The general procedure for the oxidation of acetophenones was as follows. A mixture of an acetophenone (2 mmol), manganese(III) acetate dihydrate, and acetic acid (40 ml) was heated under reflux until the color of the manganese(III) ion disappeared. The reaction mixture was then worked-up in a manner similar to the above. The yields are summarized in Table 2.

Oxidation Products of 1a. *2-Acetoxy-4′-methoxyacetophenone (2b)*: Liquid (lit,[13] mp 58—59 °C; IR 1718 (C=O) and 1760 cm^{-1} (OAc); NMR (CCl_4) δ=2.08 (3H, s, OAc), 3.73 (3H, s, OCH_3), 5.07 (2H, s, $-CH_2-$), 6.78 (2H, m, $H_{(3')}$ and $H_{(5')}$), and 7.73 (2H, m, $H_{(2')}$ and $H_{(6')}$).

p-*Anisic Acid (4a)*: Mp 185 °C.

Oxidation Products of 2a. *1,4-Bis(4-methoxyphenyl)-2,3-dichloro-1,4-butanedione (9a)*: Mp 190—191 °C (dec) (CCl_4); IR 1696 cm^{-1} (C=O); UV λ_{max} (ε) 229 (16600) and 300 nm (35000); NMR ($CDCl_3$) δ=3.85 (6H, s, 2×OCH_3), 5.68 (2H, s, >CH–), 6.93 (4H, m, $H_{(3')}$, $H_{(3'')}$, $H_{(5')}$, and $H_{(5'')}$), and 8.00 (4H, m, $H_{(2')}$, $H_{(2'')}$, $H_{(6')}$, and $H_{(6'')}$). Found: C, 58.56; H, 4.45%. Calcd for $C_{18}H_{16}Cl_2O_4$: C, 58.87; H, 4.39%.

1,4-Bis(4-methoxyphenyl)-2-chloro-2-butene-1,4-dione (10a): Liquid; IR 1680 cm^{-1} (C=O); UV λ_{max} (ε) 227 (14600) and 305 nm (19900); NMR (CCl_4) δ=3.68 (s, OCH_3), 3.72 (s, OCH_3), 6.65—6.95 (m, $H_{(3')}$, $H_{(3'')}$, $H_{(5')}$, and $H_{(5'')}$), 7.12 (s, =CH–), 7.30 (s, =CH–), and 7.6—7.9 (m, $H_{(2')}$, $H_{(2'')}$, $H_{(6')}$, and $H_{(6'')}$). The presence of two singlets with nearly equal intensities at δ=7.12 and 7.30 indicated that this substance was a mixture of (*Z*)- and (*E*)-isomers in a 1 : 1 molar ratio. MS *m/e* 330 (M^+), 295 ($M^+ - Cl$), 223 ($M^+ - C_6H_4OCH_3$), 207, 195 ($M^+ - COC_6H_4OCH_3$), 135 ($CH_3OC_6H_4CO^+$), 107, and 92.

1,4-Bis(4-methoxyphenyl)-2,3-dichloro-2-butene-1,4-dione (11a): Mp 132.5—134 °C (CCl_4); IR 1680 cm^{-1} (C=O); UV λ_{max} (ε) 228_{sh} (15200) and 309 nm (25800); NMR (CCl_4) δ=3.78 (6H, s, 2×OCH_3), 6.80 (4H, $H_{(3')}$, $H_{(3'')}$, $H_{(5')}$, and $H_{(5'')}$), and 7.68 (4H, m, $H_{(2')}$, $H_{(2'')}$, $H_{(6')}$ and $O_{(6')}$: Found: C, 59.02; H, 3.62%. Calcd for $C_{18}H_{14}Cl_2O_4$: C, 59.20; H, 3.86%.

1,4-Bis(4-methoxyphenyl)-2,2,3,3-tetrachloro-1,4-butanedione (8a): Mp 145—146 °C.

Oxidation Products of 2c. *2,2-Dibromoacetophenone (3c)*: Liquid (lit,[14] mp 36—37 °C); IR 1695 and 1718 cm^{-1}; NMR (CCl_4) δ=6.55 (1H. s. >CH–), 7.2—7.7 (3H, m, $H_{(3')}$, $H_{(4')}$, and $H_{(5')}$), and 7.9—8.2 (2H, m, $H_{(2')}$ and $H_{(6')}$).

2,3-Dibromo-1,4-diphenyl-1,4-butanedione (9c): Mp 180—182 °C (dec) (CCl_4); IR 1710 cm^{-1} (C=O); UV λ_{max} (ε) 264 nm (24200); NMR ($CDCl_3$) δ=5.99 (2H, s, >CH–), 7.2—7.8 (6H, m, $H_{(3')}$, $H_{(3'')}$, $H_{(4')}$, $H_{(4'')}$, $H_{(5')}$, and $H_{(5'')}$), and 8.0—8.25 (4H, m, $H_{(2')}$, $H_{(2'')}$, $H_{(6')}$, and $H_{(6'')}$). Found: C, 48.20; H, 3.07%. Calcd for $C_{16}H_{12}Br_2O_2$: C, 48.52; H, 3.05%.

2-Bromo-1,4-diphenyl-2-butene-1,4-dione (10c): Liquid; IR 1690 cm^{-1} (C=O); UV λ_{max} (ε) 270 nm (20200); NMR (CCl_4) δ=7.2—7.7 (6H, m, $H_{(3')}$, $H_{(3'')}$, $H_{(4')}$ $H_{(4'')}$, $H_{(5')}$, and $H_{(5'')}$), 7.60 (1H, s, =CH–), and 7.7—8.0 (4H, m, $H_{(2')}$. $H_{(2'')}$, $H_{(6')}$, and $H_{(6'')}$); MS *m/e* 314 (M^+), 235 ($M^+ - Br$), 105 ($PhCO^+$), and 77 (Ph^+). **10c** could be a mixture of (*Z*)- and (*E*)-isomers.

(E)-2,3-Dibromo-1,4-diphenyl-2-butene-1,4-dione (11c): Mp 208—210 °C (CCl_4–light petroleum) (lit,[15,16] mp 213 °C);

IR 1685 cm^{-1} (C=O); UV λ_{max} (ε) 266 (16600) and 293 nm (shoulder) (6220); NMR (CCl_4) δ=7.2—7.7 (6H, m, $H_{(3')}$, $H_{(3'')}$, $H_{(4')}$, $H_{(4'')}$, $H_{(5')}$, and $H_{(5'')}$), and 7.7—7.95 (4H, m, $H_{(2')}$, $H_{(2'')}$, $H_{(6')}$, and $H_{(6'')}$). Found: C, 49.07; H, 2.66%. Calcd for $C_{16}H_{10}Br_2O_2$: C, 48.77; H, 2.56%. MS *m/e* 392 (M^+), 313 (M^+ −Br), 129 ($PhCOC{\equiv}C^+$), 105 ($PhCO^+$), and 77 (Ph^+).

Oxidation Products of a Mixture of ***2c*** *and* ***3c***.

*2,3-Dibromo-1,4-diphenyl-1,4-butanedione (****9c****)*: Mp 180—182 °C (dec).

*2-Bromo-1,4-diphenyl-2-butene-1,4-dione (****10c****)*: Liquid.

*(E)-2,3-Dibromo-1,4-diphenyl-2-butene-1,4-dione (****11c****)*: Mp 208—210 °C.

Oxidation Products of ***3a***. *1,4-Bis(4-methoxyphenyl)-2,2,3,3-tetrachloro-1,4-butanedione (****8a****)*: Mp 145—146 °C.

Dehydrobromination of ***9c***. A solution of **9c** (40 mg) in acetic acid (1 ml) was heated under reflux for 35 min. The reaction mixture was then worked-up as has been described previously, giving **10c** (18.5 mg, 45%) identical with the sample obtained by the reaction of **2c** with manganese(III) acetate dihydrate, and also unchanged **9c** (12 mg, 30%).

We wish to thank Professor J. F. W. McOmie of Bristol University, England, and Assistant Professor Fumiaki Kai of the Department of Chemistry, Kumamoto University, for their helpful discussions, and Mr. Shuichi Ueda at the Taiho Pharmaceutical Co., Tokushima, for his measurements of the mass spectra.

References

1) R. Van Helden and E. C. Kooyman, *Recl. Trav. Chim. Pays-Bas*, **80**, 57 (1961).
2) M. Okano and T. Aratani, *Bull. Chem. Soc. Jpn.*, **49**, 2811 (1976).
3) M. G. Vinogradov, S. P. Verenchikov, and C. I. Nikishin, *Izu. Akad. Nauk SSSR., Ser. Khim.*, **1971**, (1), 200; *Chem. Abstr.*, **75**, 5162 (1971).
4) E. I. Heiba and R. M. Dessau, *J. Am. Chem. Soc.*, **93**, 524 (1971).
5) E. I. Heiba and R. M. Dessau, *J. Am. Chem. Soc.*, **94**, 2888 (1972).
6) F. J. McQuillin and M. Wood, *J. Chem. Soc., Perkin Trans. 1*, **1976**, 1762.
7) E. I. Heiba, R. M. Dessau, and W. J. Koehl, Jr., *J. Am. Chem. Soc.*, **91**, 138 (1969).
8) F. Kunekell and F. Johanssen, *Ber.*, **30**, 1714 (1897).
9) F. Kunekell and F. Johanssen, *Ber.*, **31**, 169 (1898).
10) P. J. Andrulis, Jr., M. J. S. Dewar, R. Dietz, and R. L. Hunt, *J. Am. Chem. Soc.*, **88**, 5473 (1966).
11) J. Houben and W. Fischer, *Ber.*, **60**, 1759 (1927).
12) L. A. Dancanson, J. F. Grove, J. MacMillan, and T. P. C. Mulholland, *J. Chem. Soc.*, **1957**, 3555.
13) K. Kindler and L. Blaas, *Ber.*, **77**, 585 (1944).
14) H. Hunnius, *Ber.*, **10**, 2010 (1877).
15) J. B. Conant and R. E. Lutz, *J. Am. Chem. Soc.*, **47**, 881 (1925).
16) R. E. Lutz, *J. Am. Chem. Soc.*, **52**, 3405 (1930).

  Bull. Chem. Soc. Jpn., 54, 1761—1766 (1981)

Multiple Paths for Photo-alkylation and -alkoxylation of 3-Pyridinecarboxylic Ester in Alcohol. Simultaneous Contribution of Several Kinds of Excited States

Akira SUGIMORI,* Etsuo TOBITA, Yasuyuki KUMAGAI, and Gen P. SATÔ

Department of Chemistry, Faculty of Science and Technology, Sophia University, Kioi-cho 7-1, Chiyoda-ku, Tokyo 102

(Received August 27, 1980)

UV-irradiation of methyl 3-pyridinecarboxylate (**1**) in acidic alcoholic solutions brings about the alkoxylation and alkylation at the pyridine ring. Photoalkylation occurs in several paths: 1) alkylation initiated by the triplet π-π^* state, 2) alkylation initiated by the triplet n-π^* state of the carbonyl moiety of the ester group, 3) alkylation initiated by an exciplex between a free base form of **1** and a pyridinium form of **1**, and 4) alkylation promoted by chloride ions. Photoalkoxylation originates from a singlet excited state of **1**. In the photoreactions of **1** in strongly acidic methanolic solutions acidified with H_2SO_4, three kinds of excited states (two kinds of triplet states for alkylation and a singlet state for alkoxylation) contribute simultaneously.

Photochemical reactions of azaaromatic compounds with alcohols have been extensively investigated.[1] Previously we reported alkylation and alkoxylation in the photoreactions of pyridinecarboxylic acid derivatives.[2] Stermitz *et al.* explained the photoalkylation at α- and γ-positions of the pyridine ring according to the mechanism of hydrogen abstraction by excited protonated pyridines from alcohol, followed by the geminate radicals and dehydration.[3] Castellano *et al.* proposed a mechanism for photoalkylation *via* the monophotonic hydrogen abstraction by n-π^* state-pyridine in neutral alcoholic solutions, and *via* biphotonic electron transfer in alcoholic solutions acidified with HCl.[4] In the latter case they did not detect the formation of Cl atoms. We report here that the photoalkylation and photoalkoxylation of 3-pyridinecarboxylic ester in alcohol proceed in several different pathways.[5] The 3-pyridinecarboxylic ester–alcohol system is a very interesting system in which several excited states of the same multiplicity contribute simultaneously. β,γ-Unsaturated ketone is another system in which $^3(\pi$-$\pi^*)$ and ^{3}(n-π^*) contribute simultaneously.[6]

Results and Discussion

The UV-irradiation of methyl 3-pyridinecarboxylate (**1**) in alcohols in the presence of mineral acids brings about two types of substitution by the groups derived from the solvent alcohols: alkylation and alkoxylation. The substitution occurs at the α- and γ-positions of the pyridine ring. In the methanolic solutions acidified with sulfuric acid, two alkylation products (**2a** and **3a**) and two alkoxylation products (**4a** and **5a**) are formed by the irradiation with 254 nm light.

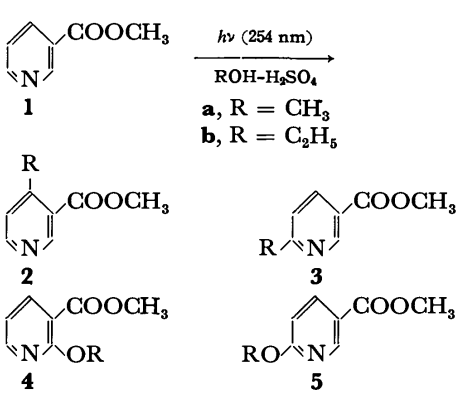

The yields of the products are linear with the irradiation time, as exemplified by the photoreaction under the conditions of $[\mathbf{1}]=1\times10^{-2}$ mol dm^{-3} and $[H_2SO_4]=5\times10^{-2}$ mol dm^{-3} (Fig. 1).

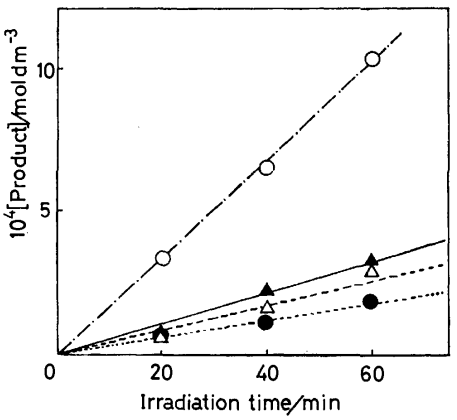

Fig. 1. Relation between the product yield and the irradiation time. Irradiated with 254 nm light in methanol.
$[\mathbf{1}]=1\times10^{-2}$ mol dm^{-3}; $[H_2SO_4]=5\times10^{-2}$ mol dm^{-3}.
---△---: **2a**, —▲—: **3a**, -·-○-·-: **4a**, ···●···: **5a**.

The photo-alkylation and -alkoxylation of 3-pyridinecarboxylic ester are dependent upon the reaction conditions: 1) the concentration of the substrate, 2) the mineral acid added, 3) the concentration of the added acid, 4) the nature of the solvent alcohol, and 5) additives.

Figure 2 shows the dependences of photoreactions on the concentrations of sulfuric acid at 1×10^{-3}, 3×10^{-3}, and 1×10^{-2} mol dm^{-3} concentrations of methyl 3-pyridinecarboxylate.

As is seen typically in Figs. 2—3, the acidity dependence of the photoreactions of **1** is complex, with photoalkylation and -alkoxylation competing. The region where photoalkylation is effective is divided into two parts.

In the higher acidity region (Region B), alkylation and alkoxylation are comparable. The peak of alkyla-

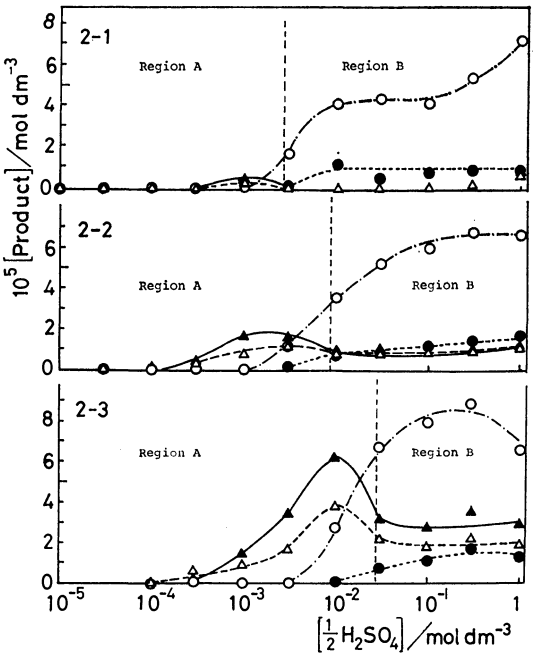

Fig. 2. Dependence of the photoreactions of **1** on the concentration of H_2SO_4 (irradiation time, 60 min).
2-1: $[\mathbf{1}]=1\times10^{-3}$ mol dm^{-3}, 2-2: $[\mathbf{1}]=3\times10^{-3}$ mol dm^{-3}, 2-3: $[\mathbf{1}]=1\times10^{-2}$ mol dm^{-3},
---△---: **2a**, —▲—: **3a**, -·-○-·-: **4a**, ···●···: **5a**.

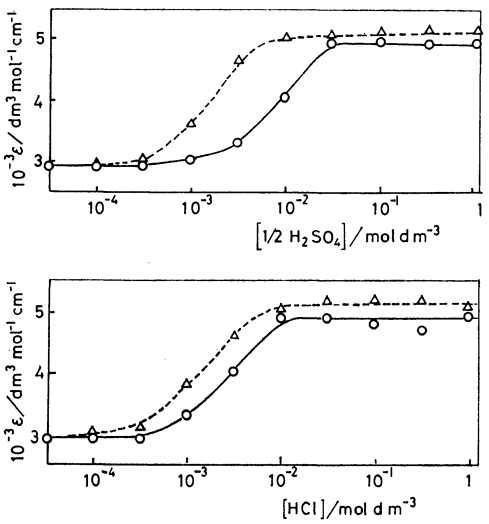

Fig. 3. Relation between the molar absorption coefficients of **1** and the concentration of mineral acids.
--△--: $[\mathbf{1}]=10^{-3}$ mol dm^{-3}, —○—: $[\mathbf{1}]=3\times10^{-3}$ mol dm^{-3}.

tion in the lower acidity region (Region A) moves depending on the concentration of the substrate (**1**). As the concentration of **1** becomes lower, the acid concentration which gives the peak becomes lower and the peak height goes down.

The acidity dependence of the molar absorption coefficient of **1** in methanol (Fig. 3) indicates that **1** exists in the pyridinium form in Region B. In Region A the pyridinium form and the free base-form of **1** coexist.

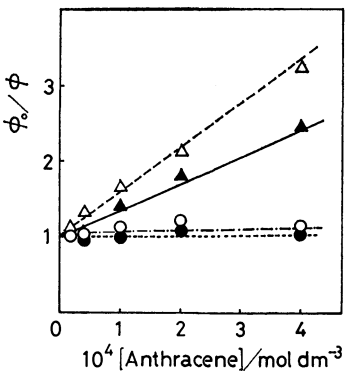

Fig. 4. Effect of anthracene on the photoreactions of **1**.
$[\mathbf{1}]=1\times10^{-2}$ mol dm^{-3}; $[H_2SO_4]=5\times10^{-2}$ mol dm^{-3},
--△--: **2a**. —▲—: **3a**, -·-○-·-: **4a**, ···●···: **5a**.

The excited states responsible for the photo-alkylation and -alkoxylation in the higher acidity region were assigned by the effects of additives, solvents, and temperature.

Figure 4 shows Stern-Volmer plots for the quenching by anthracene, a triplet quencher ($E_T=176$ kJ mol^{-1}). Because anthracene absorbs the light of 254 nm competitively with the substrate, the quantum yields are normalized on the basis of the light absorbed by the substrate by the following formula:

$$\phi_0/\phi = \mathrm{L/Y},$$

$$\mathrm{Y} = \frac{\text{Yield in the presence of quencher}}{\text{Yield in the absence of quencher}},$$

$$\mathrm{L} = \frac{\text{Light absorbed by the substrate}}{\text{Light absorbed by the substrate} + \text{Light absorbed by the quencher}}.$$

The Stern-Volmer plots indicate that the alkylation and the alkoxylation originate from triplet and singlet exited states, respectively. Furthermore, the different dependences of anthracene on the two alkylation reactions suggest that the product alkylated at α- and γ-positions originate from the triplet excited states of different character.

This view is supported by the temperature dependence of the photoreactions. Figure 5 is the plot of ln(relative

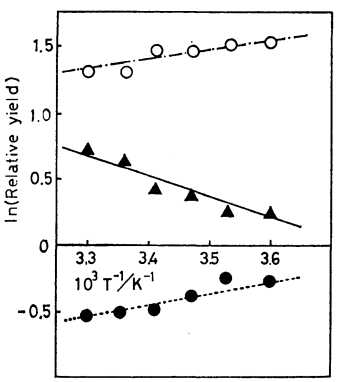

Fig. 5. Temperature dependence of photoreactions of **1**.
Relative yield=yield of product/yield of **2a**.
—▲—: **3a**, -·-○-·-: **4a**, ···●···: **5a**.

Table 1. Effects of additives on the photoalkylation and alkoxylation of **1**
[**1**] = 1×10^{-2} mol dm^{-3}; Irradiation time, 50 min.

Additive	[Additive] / mol dm^{-3}	$[H_2SO_4] = 5 \times 10^{-3}$ mol dm^{-3} 10^5 [Product]/mol dm^{-3}				$[H_2SO_4] = 5 \times 10^{-2}$ mol dm^{-3} 10^5[Product]/mol dm^{-3}			
		Alkylation		Alkoxylation		Alkylation		Alkoxylation	
		2a	**3a**	**4a**	**5a**	**2a**	**3a**	**4a**	**5a**
—	—	3.7	6.1	2.7	0.5	1.8	2.7	7.9	1.1
Benzene	10^{-1}	1.6	3.3	0.0	0.0	3.1	5.8	6.6	1.1
Naphthalene	10^{-2}	0.9	5.4	0.0	0.0	2.7	9.3	6.6	0.5
Anisole	10^{-2}	1.8	3.3	0.0	0.0	1.3	1.8	6.5	1.0
Oxygen						0.0	0.0	1.4	0.5

Table 2. Dependence of photoreactions of **1** on alcohol
[**1**] = 2×10^{-2} mol dm^{-3}.
[H_2SO_4] = 1.5×10^{-1} mol dm^{-3}.

Alcohol	Yield of product/%[a]			
	Alkylation		Alkoxylation	
	2	**3**	**4**	**5**
Methanol	7.1	9.5	8.8	3.8
Ethanol	0.0	31.6	2.0	0.7

a) Yields are based on the quantity of **1** consumed. Analysis was done by means of TLC and NMR.

yield) *vs.* the reciprocal of temperature; the slope of the plot gives the difference in the activation energies between a given reaction and the standard reaction (in this case the formation of **2a**).

The plots for the two alkoxylation reactions have the same temperature dependence, whereas the photoalkylations at α- and γ-positions differ in temperature dependence.

The effects of benzene, naphthalene, and anisole (Table 1) (small effects on the photoalkoxylation, large effects on the photoalkylation, and different effects on the two alkylation reactions) also support the view.

The results obtained in the irradiation in ethanol are compared with those in methanol (Table 2). The irradiation in ethanol depresses the alkoxylation, but the change in the ratio of the isomers is small. Alkylation becomes dominant and the product ethylated at the 6-position is selectively formed. The solvent effect indicates that the triplet states responsible for the alkylation at the 6-position and the 4-position are of n-π^* and π-π^* character, respectively.

As the photoreactions occur in acidic solutions, the n-π^* state should not be the excitation of the electrons at N atom, because the lone pair electrons are donated to a proton. However, the excitation of the lone pair electrons located at O atom of the ester C=O is possible. In the UV-irradiation of 2-pyridinecarboxylic ester in methanol, methylation occurs at the 5-position.[5] This indicates the participation of the excited C=O moiety in the alkylation. The hydrogen abstraction by the excited C=O of the ester group (or the electron transfer followed by the proton transfer) has been reported for some aromatic esters.[7] These facts suggest that the excitation of the ester C=O can contribute to the photoreactions of 3-pyridinecarboxylic ester. If the excitation of a non-bonding electron of C=O is taken into account, the alkylation at the 6-position can be explained as is shown in Scheme 1.

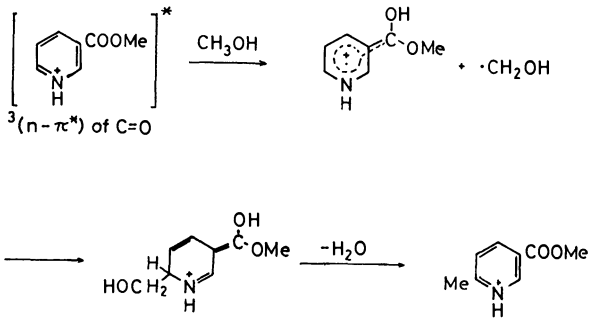

Scheme 1.

The alkylation at the 4-position can be explained by the reaction of π-π^* state through the mechanism proposed by Stermitz *et al.*[3]

The results of quenching, solvent effects, and temperature dependence show that the two alkoxylation products are due to the same excited state. Alkoxylation occurs presumably *via* the nucleophilic attack of alcohol to the polar, singlet excited-state substrate.

The fact that, in Region A, pyridinium and free base forms of **1** coexist suggest that the alkylation in Region A is brought about by the cooperation of the pyridinium and free base forms.

The effects of benzene, naphthalene, and anisole on the photoalkylation in Region A are different from those in Region B (Table 1). This also suggests that the mechanism for alkylation reactions in Regions A and B are different.

We propose two mechanisms for alkylation in Region A: *via* an excited complex between the excited pyridinium and the ground-state free base and *via* that between the excited free base and the ground-state pyridinium; these are shown in Scheme 2.

In the Scheme, Py and PyH^+ stand for the free base and pyridinium forms of 3-pyridinecarboxylic esters, respectively. K is the equilibrium constant and k's are the rate constants of the corresponding reactions, and ε_A and ε_B are the molar absorption coefficients of the pyridinium and free base forms of **1** at the wavelength

Mechanism A

$$Py + H^+ \overset{K}{\rightleftharpoons} PyH^+$$

$$PyH^+ \overset{h\nu,\ k_2}{\underset{k_{-2}}{\rightleftharpoons}} (PyH^+)^* \qquad k_2 = \frac{I\varepsilon_A[PyH^+]}{\varepsilon_A[PyH^+] + \varepsilon_B[Py]}$$

$$(PyH^+)^* + Py \xrightarrow{k_3} (PyHPy^+)^*$$

$$(PyHPy^+)^* \xrightarrow{k_4} PyH^+ + Py$$

$$(PyHPy^+)^* \xrightarrow{k_5} \longrightarrow \text{Alkylation product}$$

Mechanism B

$$Py + H^+ \overset{K}{\rightleftharpoons} PyH^+$$

$$Py \overset{h\nu,\ k_2'}{\underset{k'_{-2}}{\rightleftharpoons}} Py^* \qquad k_2' = \frac{I\varepsilon_B[Py]}{\varepsilon_A[PyH^+] + \varepsilon_B[Py]}$$

$$Py^* + PyH^+ \xrightarrow{k_3'} (PyHPy^+)^*$$

$$(PyHPy^+)^* \xrightarrow{k_4'} PyH^+ + Py$$

$$(PyHPy^+)^* \xrightarrow{k_5'} \longrightarrow \text{Alkylation product}$$

Scheme 2.

of the irradiating light (intensity, I).

The mechanisms A and B can explain a) the appearance of the peak for the alkylation at an acid concentration and b) the fact that the peak height (maximum quantum yield) increases with the increase in the substrate concentration.

According to mechanism A, the quantum yield of the product (ϕ) is:

$$\phi = \frac{k_3k_5}{k_4 + k_5} \frac{c}{k_{-2}(1+K[H^+]) + k_3c} \frac{K[H^+]}{K[H^+] + \varepsilon_B/\varepsilon_A},$$

where $c=[Py]+[PyH^+]$.

The quantum yield of the photoreaction reaches the maximum at $[H^+]_{max}$:

$$[H^+]_{max} = \frac{1}{K}\sqrt{\frac{\varepsilon_B k_3}{\varepsilon_A k_{-2}}\left(c + \frac{k_{-2}}{k_3}\right)}.$$

The maximum quantum yield, ϕ_{max}, at $[H^+]_{max}$ is

$$\phi_{max} = \frac{\dfrac{k_3c}{k_{-2}}}{\left\{2\sqrt{\dfrac{\varepsilon_B}{\varepsilon_A}\left(1+\dfrac{k_3c}{k_{-2}}\right)} + \left(1+\dfrac{\varepsilon_B}{\varepsilon_A}\right) + \dfrac{k_3c}{k_{-2}}\right\}\left(1+\dfrac{k_4}{k_5}\right)}.$$

The ϕ_{max} value thus obtained is 0 at $c=0$ and increases monotonously with c to reach the limiting value of $(1+k_4/k_5)^{-1}$. A similar conclusion can be deduced from mechanism B.

Mechanisms A and B can explain qualitatively the results shown in Fig. 2, where the vertical axis is expressed in the concentrations of the products formed after 60 minutes' irradiation. The values are proportional to the quantum yields for the products. No direct evidence for the participation of an excited complex is obtained, because methyl 3-pyridinecarboxylate is not fluorescent under any conditions. At present we have no experimental results from which we decide which mechanism actually operates.

Table 3. Effect of lithium chloride on the photoreaction of **1**. Irradiation time, 10 min.

[**1**] mol dm^{-3}	[HCl] mol dm^{-3}	[LiCl] mol dm^{-3}	[Alkylation product] 10^{-5} mol dm^{-3}		[Alkoxylation product] 10^{-5} mol dm^{-3}	
			2a	**3a**	**4a**	**5a**
1×10^{-3}	1×10^{-2}	—	1.8	2.2	3.7	0.5
1×10^{-3}	1×10^{-2}	1	3.4	4.5	0.9	—
1×10^{-2}	1×10^{-2}	—	11.8	17.3	5.2	0.3
1×10^{-2}	1×10^{-2}	1	14.4	20.4	—	—

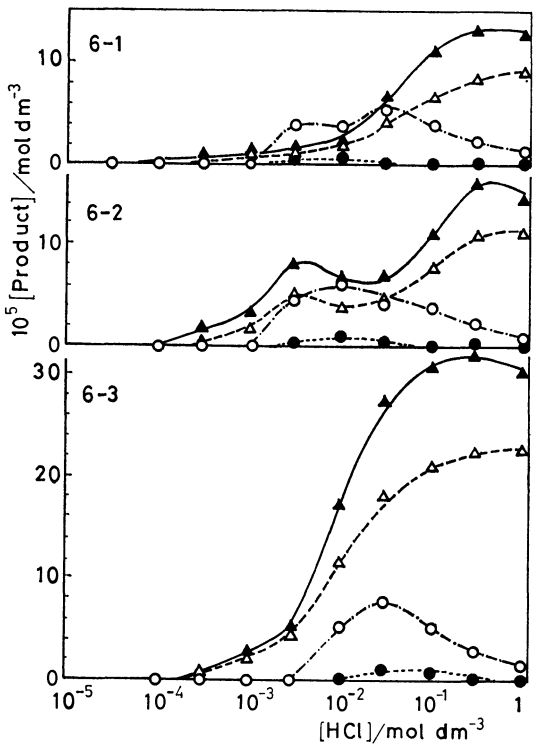

Fig. 6. Dependence of the photoreactions of **1** on the concentration of HCl (irradiation time, 60 min).
6-1: [**1**]$=1\times10^{-3}$ mol dm^{-3}, 6-2: [**1**]$=3\times10^{-3}$ mol dm^{-3}, 6-3: [**1**]$=1\times10^{-2}$ mol dm^{-3},
---△---: **2a**, —▲—: **3a**, -·-○-·-: **4a**, ···●···: **5a**.

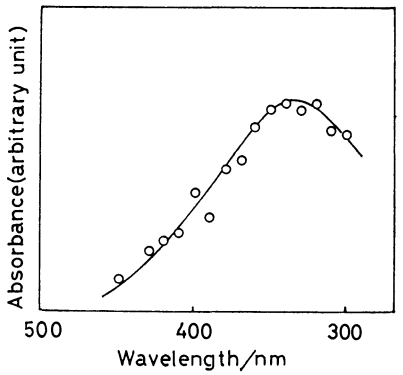

Fig. 7. Absorption spectrum in the flash photolysis of the 3-pyridinecarboxylic acid–HCl–H_2O system. Spectrum of 2 μs after the flash. [3-Pyridinecarboxylic acid]$=5\times10^{-4}$ mol dm^{-3}, [HCl]$=1$ mol dm^{-3}.

Dependences of the photoreactions on the concentration of hydrochloric acid are shown in Fig. 6. The presence of hydrochloric acid depresses the alkoxylation

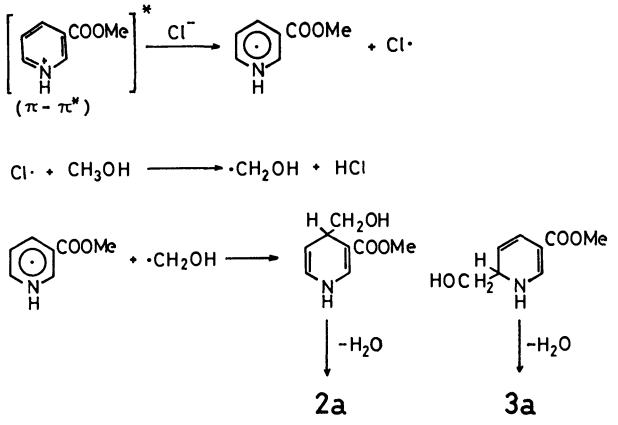

Scheme 3.

and instead promotes the alkylation. The inhibition of alkoxylation and the promotion of alkylation are remarkable in the higher concentration region of hydrochloric acid.

The promotion of alkylation by hydrochloric acid can be attributed to the participation of chloride ions; the addition of lithium chloride promotes the alkylation and depresses the alkoxylation (Table 3).

As the mechanism for the promotion of alkylation by chloride ions, two paths are conceivable: the acceleration of intersystem crossing by the external heavy atom effect and/or a reaction involving chloride ions. At present we can not conclude which mechanism operates. However, the results of the flash photolysis favor the latter mechanism.

In the microsecond flash photolysis of aqueous 3-pyridinecarboxylic acid acidified with hydrochloric acid (photolyzing light, emission from Ar; duration of a flash, 4 μs; energy of a flash, 10 J), a transient absorption was observed at $\lambda_{max}=340$ nm, which is similar to that of Cl_2^- reported by Anbar and Thomas.[8]

The promotion of alkylation by chloride ions thus can be explained by a mechanism *via* chlorine atoms formed in the electron transfer from chloride ions to the excited pyridinium, which should undergo electrophilic alkoxylation in the absence of chloride ions. The alkylation of 3-pyridinecarboxylic ester *via* chlorine atoms should proceed as in Scheme 3.

The photoreactions of 3-pyridinecarboxylic ester in the region of higher concentration of acids are summarized in Scheme 4.

Experimental

Materials. Commercial methyl 3-pyridinecraboxylate (GR grade reagent of Tokyo Kasei Co.) was purified by vacuum distillation. Mp, 36—37 °C. Anthracene (standard reagent for elemental analysis made by E. Merck Co.) was used for the quenching experiment.

UV-irradiation. Methanolic or ethanolic solutions containing methyl 3-pyridinecarboxylate (10^{-3} —10^{-2} mol dm^{-3}), sulfuric acid or hydrochloric acid (10^{-5}—1 mol dm^{-3}), and the additive in the quenching experiment were deaerated by bubbling nitrogen or argon for 30 min before irradiation. The solutions were irradiated with a low pressure mercury lamp in a merry-go-round type irradiation apparatus normally at 32 °C.

Isolation and Identification of Products. After the irradiation the solution was concentrated under reduced pressure. The solution was neutralized with sodium hydrogencarbonate and the products were extracted repeatedly with dichloromethane. The products were separated by means of thin-layer chromatography (plate, GF_{254} (Type 60) of E. Merck Co.; developing solvent, ethyl acetate–dichloromethane 1 : 1 v/v).

Methyl 2-methoxy-3-pyridinecarboxylate (**4a**), liquid (lit,[9] 28—29 °C), IR, 2980, 2950, 2850 (C-H), 1732 (ester C=O), 1270, 1130, 1082 (C-O-C), and 790 cm^{-1} (bending of C-H in the pyridine ring); NMR($CDCl_3$) $\delta=8.27$ (1H, dd, $J=5.1$ and 2.5 Hz, H at the 6-position), 8.09 (1H, dd, $J=7.9$ and 2.5 Hz, H at the 4-position), 6.92 (1H, q, $J=7.9$ and 5.1 Hz, H at the 5-position), 4.09 (3H, s, OCH_3), and 3.91 (3H, s, $COOCH_3$).

Methyl 6-methoxy-3-pyridinecarboxylate (**5a**) was identified by the accordance of its NMR spectra with those obtained by Deady *et al.*[10]

Methylation products (the products methylated at 4- and 6-positions) could not be isolated by means of TLC. Methyl 6-methyl-3-pyridinecarboxylate (**3a**), one of the methylation products, was identified by the accordance of NMR and GLC with those of the authentic sample synthesized by the method of Graf.[11] The other component in the mixture was identified NMR-spectroscopically. The following NMR spectra were ascribed to methyl 4-methyl-3-pyridinecarboxylate (**2a**). NMR($CDCl_3$) $\delta=9.10$ (1H, s, H at the 2-position), 8.52 (1H, d, $J=6.0$ Hz, H at the 6-position), 7.15 (1H (1H, d, $J=6.0$ Hz, H at the 5-position), 3.9 ($COOCH_3$), and 2.6 (CH_3).

The corresponding ethylation and ethoxylation products were identified by comparing their NMR and IR spectra with those of the corresponding methylation and methoxylation products.

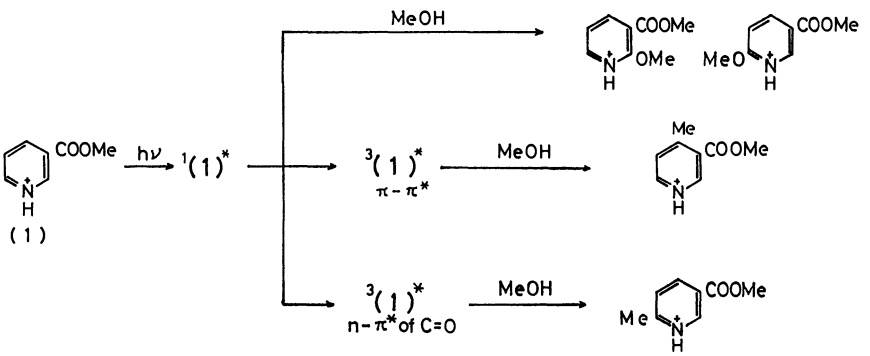

Scheme 4.

Determation of the Yields of Products. After the irradiation the reaction mixture was concentrated under reduced pressure and was neutralized with sodium hydrogencarbonate. The products were extracted with dichloromethane and were analyzed by means of GLC (column, 3 m column of PEG 20M (10%) on Celite 545; column temperature, 165 °C) with a Shimadzu gas-chromatograph Model GC-6A. The gas-chromatographic sensitivy of each compound was determined by using the solution of the known concentration. For **2a**, which could not be obtained in pure form, the same sensitivity as for **3a** was presumed.

Flash Photolysis. The experimental detail of the flash photolysis has been described elsewhere.[12)]

The authors wish to express their thanks to Dr. Horst Hermann and Mrs. Ch. Kuling of Institut für Strahlenchemie im Max-Planck-Institut für Kohlenforschung in West Germany for the measurement of flash photolysis and Professor L. W. Deady of La Trobe University in Australia for sending us the spectral data of pyridinecarboxylic acid derivatives.

References

1) D. G. Whitten, "Photoreduction and Photoaddition Reactions of Heterocyclic Compounds," in "Photochemistry of Heterocylic Compounds," ed by O. Buchardt, John Wiley and Sons, New York (1976), Chap. 8, pp. 524—573.

2) F. Takeuchi, T. Sugiyama, T. Fujimori, K. Seki, Y. Harada, and A. Sugimori, *Bull. Chem. Soc. Jpn.*, **47**, 1245 (1974); T. Sugiyama, T. Furihata, Y. Edamoto, R. Hasegawa, G. P. Satô, and A. Sugimori, *Tetrahedron Lett.*, **1974**, 4339.

3) F. R. Stermitz, C. C. Wei, and W. H. Huang, *J. Chem. Soc., Chem. Commun.*, **1968**, 482.

4) A. Castellano, J. P. Catteau, and A. Lablanche-Combier *Tetrahedron*, **31**, 2255 (1975).

5) Preliminary report, T. Sugiyama, E. Tobita, K. Takagi, M. Sato, Y. Kumagai, G. P. Satô, and A. Sugimori, *Chem. Lett.*, **1980**, 131.

6) M. J. Mirbach, A. Henne, and K. Schaffner, *J. Am. Chem. Soc.*, **100**, 7127 (1979).

7) K. Fukui, K. Senda, Y. Shigemitsu, and Y. Odaira, *J. Org. Chem.*, **37**, 3176 (1972).

8) M. Anbar and J. K. Thomas, *J. Phys. Chem.*, **68**, 3829 (1964).

9) E. Hardegger and E. Nickles, *Helv. Chim. Acta*, **39**, 505 (1956).

10) L. W. Deady, P. M. Harrison, and R. D. Topson, *Org. Magn. Reson.*, **7**, 41 (1975); L. W. Deady, private communication.

11) R. Graf, *J. Prakt. Chem.*, **133**, 19 (1933).

12) T. Akiyama, A. Sugimori, and H. Hermann, *Bull. Chem. Soc. Jpn.*, **46**, 1855 (1973).

  Bull. Chem. Soc. Jpn., 54, 1767—1772 (1981)

Cyclization of Isothiosemicarbazones. IV.[1] Synthesis of the [1,2,4]Triazolo[1,5-*c*]pyrimidine Ring System

Chiji YAMAZAKI

Department of Chemistry, School of Hygienic Sciences, Kitasato University, Kitasato, Sagamihara, Kanagawa 228

(Received October 29, 1980)

Condensation of isothiosemicarbazones with ethoxymethylenemalononitrile gave 2,3-dihydro[1,2,4]triazolo-[1,5-*c*]pyrimidines in moderate to high yields. The 2,3-dihydro compounds were readily oxidized in dimethyl sulfoxide to give the corresponding [1,2,4]triazolo[1,5-*c*]pyrimidines.

Isothiosemicarbazones (**1**) are polyfunctional nucleophiles for the reaction with α-halo carbonyl compounds leading to the formation of nitrogen-containing heterocycles.[1,2] The internal nitrogen (N-2) of **1** preferentially attacks the halogen-bearing carbon of the halo compound to displace the halide and is considered to be a softer nucleophilic center[3] than the terminal nitrogen (N-4). On the other hand, N-4 invariably becomes attached to the carbonyl carbon whether it is unsubstituted[2] or monosubstituted.[1] In the present work, an attempt was made to initiate the cyclization of **1** at N-4 by the reaction with ethoxymethylenemalononitrile (**2**) and to examine the formation of a six-membered heterocycle. If **1** reacts with **2** at N-4, 3,4-disubstituted isothiosemicarbazone (**3**) might initially be formed, undergoing intramolecular cycloaddition to give a 1-(alkylidene- or benzylideneamino)-5-cyano-6-imino-2-mercapto-1,6-dihydropyrimidine derivative (**4**) in a similar way to that for pyrimidine formation from *S*-alkylisothioureas.[4]

It was found that the reaction of **1** with **2** leads directly to the formation of 2,3-dihydro[1,2,4]triazolo-[1,5-*c*]pyrimidines (**5**) and that, when R^2 is hydrogen, the dihydro compound (**5**) easily undergoes oxidation to [1,2,4]triazolo[1,5-*c*]pyrimidines (**6**) (Scheme 1). Among many condensed pyrimidine derivatives, few examples are known for the preparation of [1,2,4]-triazolo[1,5-*c*]pyrimidines,[5] no reports having been published on a one-step synthesis of the bicyclic pyrimidines from an open-chain, flexible molecule. This paper deals with the preparation and structure of a new series of 2,5-disubstituted and 2,2,5-trisubstituted 8-cyano-2,3-dihydro[1,2,4]triazolo[1,5-*c*]pyrimidines (**5a—n**) and 2,5-disubstituted 8-cyano[1,2,4]triazolo-[1,5-*c*]pyrimidines (**6a—i**).

Results and Discussion

The reaction was performed by allowing a solution of **1** and **2** in a 1 : 1.15 molar ratio in benzene to stand at room temperature (Procedure A). Except for **5i** and **5n**, most of **5** crystallized out of the reaction mixture in a substantially pure form, yields depending in part on the reaction period. For example, **5a** was obtained in 97% yield after the reaction mixture had been left to stand for one week, but the yield decreased to 82 and 56% with the elapse of 18 and 3 h, respectively (Table 1). Prolonged periods of time, however, may cause discoloration of the product, analytically pure compounds being obtained within no more than 1 d. The reaction can also be performed by heating a mixture of **1** and **2** (1 : 1.15) at 95—100 °C in the absence of solvent (Procedure B). The melted mixture rapidly solidifies within a few minutes, giving **5** in 55—86% yields after

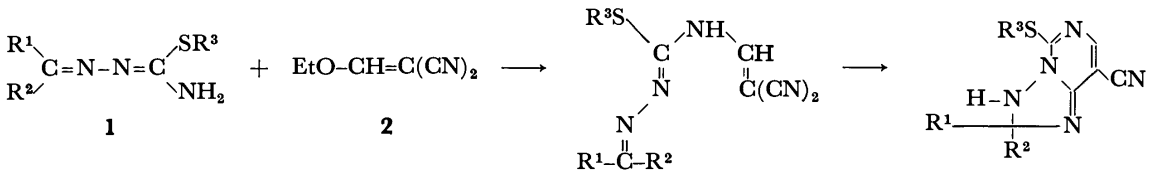

	R^1	R^2	R^3
a	C_6H_5	H	CH_3
b	*o*-ClC_6H_4	H	CH_3
c	*p*-ClC_6H_4	H	CH_3
d	2,6-$Cl_2C_6H_3$	H	CH_3
e	*o*-$CH_3OC_6H_4$	H	CH_3
f	*p*-$CH_3OC_6H_4$	H	CH_3
g	*p*-$CH_3OC_6H_4$	H	$CH_2CH_2CH_3$
h	*p*-$CH_3OC_6H_4$	H	$CH_2{=}CHCH_2$
i	2,6-$Cl_2C_6H_3$	H	$CH_2{=}CHCH_2$
j	C_6H_5	H	$C_6H_5CH_2$
k	CH_3	CH_3	CH_3
l	C_6H_5	CH_3	CH_3
m	*p*-ClC_6H_4	CH_3	CH_3
n	C_6H_5	C_6H_5	CH_3

Scheme 1. The reaction of isothiosemicarbazones with ethoxymethylenemalononitrile.

TABLE 1. 2,5-DI- AND 2,2,5-TRISUBSTITUTED 8-CYANO-2,3-DIHYDRO[1,2,4]TRIAZOLO[1,5-*c*]PYRIMIDINES

Compd No.	Yield/%	Procedure	Mp/°C	Formula	Found (Calcd) (%) C	H	N
5a	56—97	A	181—182(dec)[a]	$C_{13}H_{11}N_5S$	57.93 (57.98	4.19 4.12	26.33 26.01)
5b	76—82	A	162—175[b,c]	$C_{13}H_{10}ClN_5S$	51.38 (51.40	3.28 3.32	23.26 23.06)
5c	92	A	159—159.5[a]	$C_{13}H_{10}ClN_5S$	51.43 (51.40	3.30 3.32	23.23 23.06)
5d	86	B	191[d]	$C_{13}H_9Cl_2N_5S$	46.18 (46.17	2.65 2.68	20.98 20.71)
5e	86	A	162—163[b]	$C_{14}H_{13}N_5OS$	56.32 (56.18	4.29 4.38	23.58 23.40)
5f	64[e]—87	A	193—194[a,f]	$C_{14}H_{13}N_5OS$	56.16 (56.18	4.35 4.38	23.44 23.40)
5g	63—70	A	141—170[a,c]	$C_{16}H_{17}N_5OS$	58.73 (58.72	5.23 5.20	21.46 21.41)
5h	71—80	A	151[b]	$C_{16}H_{15}N_5OS$	59.04 (59.07	4.62 4.65	21.61 21.53)
5i	80	B	174—175[d]	$C_{15}H_{11}Cl_2N_5S$	49.48 (49.46	3.00 3.04	19.49 19.23)
5j	70	A,B	160.5—161.5[b]	$C_{19}H_{15}N_5S$	65.97 (66.07	4.53 4.38	20.51 20.28)
5k	77	g)	180.5—181.5[h]	$C_9H_{11}N_5S$	48.91 (48.86	4.99 5.01	31.74 31.66)
5l	70	i)	157(dec)[j]	$C_{14}H_{13}N_5S$	59.39 (59.35	4.66 4.63	24.99 24.72)
5m	60	A	176 (dec)[k]	$C_{16}H_{18}ClN_5OS$	52.83 (52.82	4.98 4.99	19.27 19.25)
5n	86	B	200.5—201.5(dec)[h]	$C_{19}H_{15}N_5S$	65.90 (66.07	4.37 4.38	20.39 20.28)

a) An analytically pure compound obtained without recrystallization. b) Light yellow needles from EtOH–MeCN (1 : 1). c) Homogeneous on TLC (Kieselgel 60 F_{254} plate, $CHCl_3$ containing 5% by volume of MeOH), partial oxidation during the course of melting point measurement presumably responsible for the wide melting range. d) Yellow prisms from EtOH–MeCN (1 : 1). e) MeCN used in place of benzene. f) Substantially converted into **6f** on recrystallizing from EtOH–MeCN (1 : 1). g) Refluxed in benzene for 30 min. h) Light yellow needles from 80% aqueous EtOH. i) Refluxed in EtOH for 30 min. j) An analytically pure compound obtained by drying *in vacuo* the initially formed product solvated with one molecule of EtOH. k) Yellow needles solvated with one molecule of EtOH.

TABLE 2. 2,5-DISUBSTITUTED 8-CYANO[1,2,4]TRIAZOLO[1,5-*c*]PYRIMIDINES

Compd No.	Yield/%	Method	Mp/°C	Formula	Found (Calcd) (%) C	H	N
6a	57	A	256[a]	$C_{13}H_9N_5S$	58.44 (58.42	3.42 3.39	26.46 26.21)
6b	50	B	226—226.5[a]	$C_{13}H_8ClN_5S$	51.70 (51.74	2.61 2.67	23.32 23.21)
6c	61	A	213—214[b]	$C_{13}H_8ClN_5S$	51.72 (51.74	2.71 2.67	23.31 23.21)
6d	82	B	261—262[c]	$C_{13}H_7Cl_2N_5S$	46.35 (46.49	2.13 2.10	21.03 20.83)
6e	50	A	192—193[b]	$C_{14}H_{11}N_5OS$	56.62 (56.55	3.60 3.73	23.72 23.56)
6f	53	A	238—239[d]	$C_{14}H_{11}N_5OS$	56.32 (56.55	3.64 3.73	23.88 23.56)
6g	50	B	191.5—192[e]	$C_{16}H_{15}N_5OS$	58.82 (59.07	4.62 4.65	21.42 21.53)
6i	56	C	140.5—142.5[f]	$C_{15}H_9Cl_2N_5S$	49.65 (49.73	2.58 2.50	19.19 19.34)

a) Colorless needles from EtOH–pyridine (1 : 1). b) Colorless needles from benzene–EtOH (1 : 1). c) Pale yellow needles from EtOH–pyridine (1 : 1). d) Pale yellow needles from EtOH–MeCN (1 : 1). e) Colorless needles from 80% EtOH. f) Colorless prisms from benzene–EtOH (1 : 1).

Table 3. Partial spectral data on 2,5-disubstituted and 2,2,5-trisubstituted 8-cyano-2,3-dihydro[1,2,4]triazolo[1,5-*c*]pyrimidines

Compd No.	IR (KBr) $\tilde{\nu}_{CN}/cm^{-1}$	Mass spectra, *m/e* (rel int)			^1H NMR spectra δ/ppm (from TMS in DMSO-d_6)				
		M^+	M^+-R^2	M^+-R^1	SCH_2	SCH_3	H-2(J/Hz)	H-3(J/Hz)	H-7
5b	2220	303(17)	302(28)	192(100)	—	2.50	6.52(9.3)	7.49(9.3)	8.05
5c	2220	303(30)	302(56)	192(100)	—	2.53	6.28(9.7)	7.30(9.7)	8.04
5e	2230	299(35)	298(100)	192(88)	—	2.53	6.42(9.1)	7.20(9.1)	8.06
5f	2225	299(55)	298(100)	192(69)	—	2.51	6.20(10.0)	7.08(10.0)	8.04
5g	2215	327(66)	326(100)	220(50)	3.13[a]	—	6.19(9.5)	7.07(9.5)	8.01
5h	2230	325(15)	324(37)[b]	218(34)	3.85[c]	—	6.20(9.8)	7.10(9.8)	8.04
5i	2220	263(9)	362(7)	218(100)	3.90[c]	—	7.15(9.4)	7.85(9.4)	8.13
5j	2215	345(15)	344(11)[d]	268(11)	4.49	—	6.27(9.5)	7.23(9.5)	8.10
5k	2225	221(10)	206(100)	—	—	2.50	—	6.47	8.00
5k-d_6[e]		227(6)	209(100)	—	—	2.50	—	6.46	7.97
5l	2210	283(5)	268(100)	206(41)	—	2.50	—	6.90	8.02
5l-d_3[f]		286(2)	268(100)	209(16)	—	2.51	—	6.90	8.02
5m	2220	317(4)	302(100)	206(42)	—	2.52	—	7.22	7.71
5n	2210	345(5)	268(100)	—	—	2.55	—	7.18	8.07

a) Triplet, J=6.9 Hz. b) Base peak allyl cation(*m/e* 41). c) Doublet, J=6.2 Hz. d) Base peak tropylium ion (*m/e* 91). e) $R^1=R^2=CD_3$. f) $R^2=CD_3$.

Table 4. Partial spectral data on 2,5-disubstituted 8-cyano[1,2,4]triazolo[1,5-*c*]pyrimidines

Compd No.	IR (KBr) $\tilde{\nu}_{CN}/cm^{-1}$	Mass spectra, *m/e* (rel int)			^1H NMR spectra δ/ppm (from TMS in CF_3COOD)		
		M^+	M^+-R^1CN	$R^1C\equiv\overset{+}{N}H(D)$	SCH_2	SCH_3	H-7
6c	2225	301(24)	164(69)	138(9)	—	3.01	9.00
6d	2240	335(83)	164(100)	172(24)	—	3.00	8.98
6e	2240	297(85)	164(49)	134(6)	—	3.01	9.07
6e-d_3[a]		300(61)	167(56)	135(9)	—	—	9.06
6f	2230	297(100)	164(21)	134(29)	—	3.01	9.03
6f-d_3[a]		300(100)	167(27)	135(27)	—	—	9.03
6g	2240	325(100)	192(6)	134(31)	3.64[b]	—	9.00

a) $R^3=CD_3$. b) Triplet, J=7.1 Hz.

washing with appropriate solvents. Procedure B was satisfactory for **1i** and **1n** from which no **5** was obtained by Procedure A. With ketone isothiosemicarbazones **1k** and **1l**, refluxing in benzene or EtOH gave good results. The reaction of aliphatic aldehyde isothiosemicarbazones (**1**: R^1=Et or *n*-Pr, R^2=H, R^3=Me or *p*-$ClC_6H_4CH_2$) with **2** under these conditions gave a complex mixture from which no expected product was isolated. Attempts to cyclize benzaldehyde 4-methyl- or 4-phenylthiosemicarbazone were unsuccessful with total recovery of the starting thiosemicarbazone.

In view of the high yields of hindered compounds (**5d**, **5i** and **5n**), no steric factor may be involved in the 2,3-dihydro-1,2,4-triazole ring formation. Although no intermediate has been detected on the NMR time-scale in the reaction carried out in C_6D_6, C_5D_5N or dimethyl-d_6 sulfoxide (DMSO-d_6), the reaction should proceed through a 3,4-disubstituted isothiosemicarbazone (**3**). In line with the proposed intermediacy, the reaction of **1a** with ethyl ethoxymethylenecyanoacetate gave the open-chain product **7**, the structure of which was established by elemental analysis and spectral data, particularly by the large coupling constant between N^4H and the methine proton (J=13.2 Hz).[6] If a

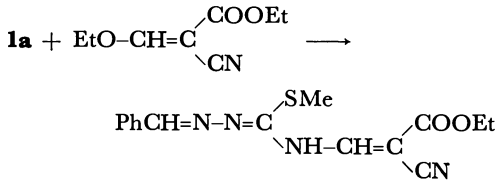

7

nucleophilic attack of N-2 in **3** on the cyano carbon had occurred, **4** would have been formed which might consecutively undergo intramolecular addition of the 6-imino group to the azomethine double bond at the 1-position giving **5**, although the ring closure of **4** to **5** is disfavored according to the rules proposed by Baldwin.[7] A mechanistic study on the ring formation is now being continued with related compounds including **7**.

Intramolecular hydrogen bonding between the N^4H and the carbonyl oxygen in **7** might stabilize the

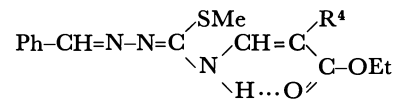

8: R^4=CN
9: R^4=COOEt

conformation **8** and prevent N-2 from approaching the cyano group. The resulting insusceptibility to cyclization makes it possible to isolate **7** at the open chain stage. In the infrared spectrum of **7**, N^4-H and the carbonyl stretching frequencies (νNH 3195 and νC=O 1690 cm^{-1}) observed at 4×10^{-3} mol dm^{-3} in carbon tetrachloride were comparable with those of **9** (νNH 3195 and νC=O 1697 cm^{-1}) obtained at the same concentration in carbon tetrachloride. The diester **9**, however, exhibited an additional carbonyl band at a higher frequency (νC=O 1730 cm^{-1}). This band can unambiguously be assigned to the free stretching vibration of the remaining ethoxycarbonyl group which is not involved in the internal bonding. The anomalously downfield resonance (lower than δ 12 ppm) of the N^4H protons of **7** and **9** in chloroform-*d* might also account for the hydrogen bond.[8]

Oxidation of **5** (R^2=H) to the corresponding [1,2,4]-triazolo[1,5-*c*]pyrimidines (**6**) was performed simply by leaving a solution of **5** in DMSO in an open vessel to stand at ambient temperature (Method A), a relatively insoluble **6** crystallizing out of the solution. In another procedure, the reaction between **1** and **2** was conducted in the absence of solvent, and the crude **5**, without isolation, was dissolved in DMSO to give **6** in moderate overall yields (Method B). The oxidation was also carried out with iron(III) chloride in aqueous acetic acid with poor yields of **6** (Method C), although **6i** was obtained only by this procedure in satisfactory purity. Some of **5** in which R^1 is unsubstituted or para-substituted phenyl group were particularly susceptible to oxidation and could not be recrystallized without contamination with the oxidized product.

The structures of the compounds **5** and **6** have been established on the basis of spectral measurements and elemental analyses. Partial spectral data are given in Tables 3 and 4 together with those for certain deuterated compounds. In mass spectrometry, molecular ions were obtained for all the compounds **5a**—**n**, with the intensity depending upon steric crowding at the 2-position (2—65%). Abundant ions M^+-R^1 and M^+-R^2 observed in the spectra of **5** characterized the 2,3-dihydro-1,2,4-triazole structure. The fragmentation pathways were confirmed by the mass spectra of deuterated compounds of **5a**, **5k**, and **5l**, in which R^2 is D, CD_3, and CD_3, respectively. The dehydrogenated compounds **6** showed a much more intense peak for M^+ ion than that of **5**, indicating their extended conjugation systems (24—100%). A characteristic fragment ion $R^1C{\equiv}\overset{+}{N}H$ (6—31%) observed in the spectra of **6** should be formed by hydrogen transfer from R^3 group to N-3 probably through a six-membered transition state as evidenced by the spectra of trideuterated compounds of **6b**, **6e**, and **6f** (R^3=CD_3), confirming the proposed arrangements of **5** and **6**. In NMR spectroscopy, two protons H-2 and H-3 on the dihydro-1,2,4-triazole ring of **5** (R^2=H) appear as two AB-type doublets with coupling constants of 9.1—10.0 Hz. The peak assignment is based on the observation that the upfield resonance collapses to a singlet while the downfield one disappears on addition of methanol-d_1. The spectrum of 2-deuterated **5a** (R^2=D) lacks the upfield resonance, exhibiting the H-3 proton as a singlet. The chemical shift values of the H-2 proton in **5** are *ca.* 2.0 ppm higher than those of the azomethine proton in the corresponding isothiosemicarbazones, reflecting rehybridization of the carbon atom (C-2) from sp^2 in **1** to sp^3 in **5**. The 2-methyl protons of **5k**—**m** (R^2=Me) resonate at 0.6—0.7 ppm higher than those of the corresponding **1k**—**m**, also indicating the rehybridization of C-2. In line with the rehybridization of C-2, the anisotropic deshielding (0.43 ppm in DMSO-d_6) of phenyl protons ortho to the azomethine double bond in **1a** disappears in **5a** which exhibits only a single signal for the phenyl protons at δ 7.36. The effect recommences in **6a** in which the ortho protons (H^o) of 2-phenyl group are deshielded by 0.49 ppm (trifluoroacetic acid-*d*) relative to the remaining aromatic protons ($H^{m,p}$) due to the resonance interaction with the heteroaromatic ring system.[9] Substantially constant values of the chemical shifts of H-7 proton in **5** or **6** when R^1–R^3 were widely changed in structure are in line with the assigned structures.

Experimental

General. Melting points were taken in open glass capillaries and are uncorrected. Infrared spectra were recorded on a Hitachi EPI-G2 or 260-30 spectrophotometer, and calibrated by comparison with a standard polystyrene film sample. Proton nuclear magnetic resonance spectra were obtained with a Hitachi R-24 spectrometer at 60 MHz. Unless otherwise stated, chemical shifts are given in parts per million (δ scale) downfield from internal tetramethylsilane (TMS). Solvents used are DMSO-d_6 for 2,3-dihydro-1,2,4-triazolo compounds (**5**) and trifluoroacetic acid-*d* for 1,2,4-triazolo compounds (**6**). The mass spectra (75 eV) were recorded on a JMS-D100 mass spectrometer. Ethoxymethylenemalononitrile (**2**) (Aldrich Chemical Co. Inc.) was used after removal of insoluble substances in benzene at room temperature.

Isothiosemicarbazones. The compounds **1a**—**n** were prepared by the method reported.[8] *S*-(Methyl-d_3)isothiosemicarbazones were obtained by using methyl-d_3 iodide in place of methyl iodide in the usual procedure. Other deuterated isothiosemicarbazones were similarly prepared from the corresponding deuterated carbonyl compounds, acetone-d_6 (CD_3COCD_3), acetophenone-α,α,α-d_3 ($C_6H_5COCD_3$), and benzaldehyde-*formyl-d* (C_6H_5CDO). New compounds are: 2,6-dichlorobenzaldehyde *S*-allylisothiosemicarbazone (**1i**): pale yellow prisms (from *i*-Pr_2O), mp 99—101 °C; NMR ($CDCl_3$) δ=3.76 (2H, dt, *J*=6.5 and 0.8 Hz, SCH_2), 5.5—6.3 (5H, m, CH_2=CH and NH_2), 7.06—7.45 (3H, m, aromatic), 8.62 (1H, s, CH=N). Found: C, 45.54; H, 3.79; N, 14.83%. Calcd for $C_{11}H_{11}Cl_2N_3S$: C, 45.84; H, 3.85; N, 14.58%. *p*-Chloroacetophenone *S*-methylisothiosemicarbazone (**1m**): colorless needles (from aqueous EtOH), mp 231 °C (HBr salt); NMR ($CDCl_3$) (free base): δ=2.38 (3H, s, CCH_3), 2.47 (3H, s, SCH_3), 5.41 (2H, bs, NH_2), 7.30 (2H, d, *J*=8.3 Hz, aromatic), 7.75 (2H, d, *J*=8.3 Hz, aromatic). Found: C, 37.30; H, 3.96; N, 13.30%. Calcd for $C_{10}H_{13}BrClN_3S$: C, 37.22; H, 4.06; N, 13.02%. Benzophenone *S*-methylisothiosemicarbazone (**1n**): colorless fine needles (from EtOH), mp 135.5—136 °C; NMR ($CDCl_3$) δ=2.20 (3H, s, SCH_3), 5.35 (2H, bs, NH_2), 7.35 (5H, s, aromatic), 7.21—7.73 (5H, m, aromatic). Found: C, 66.95; H, 5.57; N, 15.91%. Calcd for $C_{15}H_{15}N_3S$: C, 66.90; H, 5.61; N, 15.61%.

8-Cyano-2,3-dihydro-5-methylthio-2-phenyl[1,2,4]triazolo[1,5-c]-pyrimidine (5a) (A Typical Example of Procedure A). A solution

of **1a** (0.19 g, 1 mmol) and **2** (0.14 g, 1.15 mmol) in benzene (1 ml) was allowed to stand at room temperature. After *ca.* 30 min, yellow prisms began to separate and the reaction was allowed to proceed for 18 h. The crystals were collected by filtration, washed with benzene, and air-dried, giving 0.22 g (82%) of analytically pure **5a**; mp 181—182 °C (dec); IR (KBr) 2220 (CN) cm^{-1}; NMR δ=2.53 (3H, s, SCH_3), 6.26 (1H, d, J=9.7 Hz, H-2), 7.24 (1H, d, J=9.7 Hz, H-3), 7.36 (5H, s, aromatic), 8.04 (1H, s, H-7); MS, *m/e* (rel intensity), 269 (29) (M^+), 268 (56) ($M^+ - H$), 192 (100) ($M^+ - C_6H_5$).

The 2-deuterio compound of **5a** was similarly obtained from benzaldehyde-*formyl-d* *S*-methylisothiosemicarbazone [Ph-CD=N-N=C(SMe)NH_2] as yellow prisms, mp 181 °C (dec); NMR δ=2.51 (3H, s, SCH_3), 7.20 (1H, s, H-3), 7.34 (5H, s, aromatic), 8.03 (1H, s, H-7); MS, *m/e* (rel intensity), 270 (25) (M^+), 268 (40) ($M^+ - D$), 193 (100) ($M^+ - C_6H_5$).

8-Cyano-2-(2,6-dichlorophenyl)-2,3-dihydro-5-methylthio[1,2,4]-triazolo[1,5-c]pyrimidine(5d) (A Typical Example of Procedure B). A mixture of **1d** [hydriodide, mp 200—200.5 °C (dec)(lit,[10] mp 209—211 °C (dec)); Found: C, 27.88; H, 2.60; N, 11.00%. Calcd for $C_9H_{10}Cl_2IN_3S$: C, 27.71; H, 2.58; N, 10.77%] (0.26 g, 1 mmol) and **2** (0.14 g, 1.15 mmol) was heated on a boiling water bath to melt the solids. The liquid formed, still of low viscosity, was thoroughly agitated in order to confirm complete homogeneity. The mixture rapidly solidified within 30 s and heating was continued for 5 min to allow the by-product EtOH to evaporate. After cooling, the solid was triturated with acetone, collected by filtration, washed with acetone, and air-dried to give 0.29 g (86%) of **5d** as yellow crystalline powder, mp 175—178 °C. This was recrystallized from an EtOH–MeCN mixture (1 : 1 by volume) giving sparkling yellow prisms, mp 191 °C; IR (KBr) 2220 (CN) cm^{-1}; NMR δ=2.55 (3H, s, SCH_3), 7.14 (1H, d, J=9.7 Hz, H-2), 7.43 (3H, s, aromatic), 7.79 (1H, d, J=9.7 Hz, H-3), 8.09 (1H, s, H-7); MS *m/e* (rel intensity), 337 (8) (M^+), 336 (7) ($M^+ - H$), 192 (100) ($M^+ - C_6H_3Cl_2$).

When Procedure A was applied to the preparation of **5d**, a product, mp 189—190 °C, was obtained in 65% yield after standing for 6 h.

8-Cyano-5-methylthio-2-phenyl[1,2,4]triazolo[1,5-c]pyrimidine (6a) (A Typical Example of Method A; One-step Synthesis from Isothiosemicarbazones). A mixture of **1a** (0.1 g, 0.52 mmol) and **2** (0.07 g, 0.58 mmol) was heated in an open vessel on a boiling water bath with constant shaking, the ethanol formed being allowed to evaporate for 5 min. The resulting crystalline mass was dissolved still hot in DMSO (1 ml) and the solution was allowed to stand at room temperature for 1 d. The separated crystals were collected by filtration, washed with DMSO and water and then air-dried, giving analytically pure **6a** in 57% overall yield as colorless needles, mp 255.5—256 °C. Recrystallization from an EtOH–pyridine mixture (1 : 1 by volume) gave colorless needles, mp 256 °C; IR (KBr) 2220 (CN) cm^{-1}; NMR δ=3.00 (3H, s, SCH_3), 7.73 (3H, m, $H^{m,p}$ of phenyl), 8.22 (2H, m, H^o of phenyl), 9.02 (1H, s, H-7); MS, *m/e* (rel intensity), 267 (100) (M^+), 164 (85) ($M^+ - C_6H_5CN$), 104 (31) ($C_6H_5C{\equiv}\overset{+}{N}H$), 103 (27).

2-(o-Chlorophenyl)-8-cyano-5-methylthio[1,2,4]triazolo[1,5-c]pyrimidine (6b) (A Typical Example of Method B). A solution of **5b** (0.1 g) in DMSO (1 ml) was allowed to stand at room temperature for 1 d and separated crystals were collected by filtration, washed with DMSO and water and then air-dried, giving **6b** in 50% yield as colorless needles, mp 226—226.5 °C. Recrystallization from an EtOH–pyridine mixture (1 : 1 by volume) did not change the mp or appearance. IR (KBr) 2230 (CN) cm^{-1}; NMR δ=3.00 (3H, s, SCH_3), 7.50—8.07 (4H, m, aromatic), 9.04 (1H, s, H-7); MS, *m/e* (rel intensity), 301 (66) (M^+), 266 (53) ($M^+ - Cl$), 164 (24) ($M^+ - ClC_6H_4CN$), 138 (29) ($ClC_6H_4C{\equiv}\overset{+}{N}H$), 137 (100).

The 5-methylthio-d_3 compound of **6b** was obtained from the corresponding trideuterated **5b** by Method B as colorless needles, mp 225—226 °C; NMR δ=7.48—8.07 (4H, m, aromatic), 9.04 (1H, s, H-7); MS, *m/e* (rel intensity), 304 (100) (M^+), 269 (84) ($M^+ - Cl$), 167 (95) ($M^+ - ClC_6H_4CN$), 139 (33) ($ClC_6H_4C{\equiv}\overset{+}{N}D$).

5-Allylthio-8-cyano-2-(2,6-dichlorophenyl)[1,2,4]triazolo[1,5-c]-pyrimidine (6i) (Method C). To a solution of **5i** (0.09 g, 0.25 mmol) in AcOH (2 ml) was added 0.5 ml of a solution containing 1 mmol/ml of iron(III) chloride in 60% aqueous AcOH and the mixture was allowed to stand at room temperature with occasional agitation for 10 d. After being diluted with water, separated crystals (0.07 g), mp 127—140 °C, were recrystallized from a benzene–EtOH mixture (1: 1 by volume) to give 0.05 g (56%) of **6i** as colorless prisms, mp 140.5—142.5 °C; IR (KBr) 2230 (CN) cm^{-1}; NMR δ=4.26 (2H, d, J=6.6 Hz, SCH_2), 5.26—6.34 (3H, m, $CH{=}CH_2$), 7.55 (3H, s, aromatic), 8.95 (1H, s, H-7); MS, *m/e* (rel intensity), 361 (61) (M^+), 190 (80) ($M^+ - Cl_2C_6H_3CN$), 172 (25) ($Cl_2C_6H_3C{\equiv}\overset{+}{N}H$), 121 (100), 41 (77) (allyl cation).

Benzaldehyde 3-Methyl-4-[2-cyano-2-(ethoxycarbonyl)vinyl]isothiosemicarbazone (7). A mixture of **1a** (0.19 g, 1 mmol), ethyl ethoxymethylenecyanoacetate (0.19 g, 1.15 mmol), and benzene (0.5 ml) was heated at 70 °C for 1 h. On cooling, the separated solid was collected by filtration, washed with EtOH and air-dried, giving 0.27 g (84%) of **7** as pale yellow crystalline powder, mp 140—143 °C. Recrystallization twice from EtOH provided pale yellow needles, mp 145 °C; IR (CCl_4) 3195 (NH), 2220 (CN), 1690 (C=O) cm^{-1}; NMR ($CDCl_3$) δ=1.39 (3H, t, J=7.2 Hz, $CH_2C\underline{H}_3$), 2.60 (3H, s, SCH_3), 4.34 (2H, q, J=7.2 Hz, $C\underline{H}_2CH_3$), 7.43 (3H, m, $H^{m,p}$ of phenyl), 7.69 (1H, d, J=13.2 Hz, NH=C$\underline{H}$), 7.90 (2H, m, H^o of phenyl), 8.47 (1H, s, CH=N), 12.40 (1H, d, J=*ca.* 13 Hz, N$\underline{H}$-CH).

Found: C, 56.97; H, 5.09; N, 17.52%; M^+, 316. Calcd for $C_{15}H_{16}N_4O_2S$: C, 56.96; H, 5.10; N, 17.71%; M, 316.

Benzaldehyde 3-Methyl-4-[2,2-bis(ethoxycarbonyl)vinyl]isothiosemicarbazone (9). A mixture of **1a** (0.19 g, 1 mmol) and diethyl ethoxymethylenemalonate (0.22 g, 1 mmol) in benzene (0.5 ml) was refluxed for 4 h, the solvent being evaporated. Recrystallization of the crystalline residue from EtOH gave **9** as pale yellow prisms (0.27 g, 74%), mp 99—100 °C; NMR ($CDCl_3$) δ=1.31 (3H, t, J=7.0 Hz, $CH_2C\underline{H}_3$), 1.36 (3H, t, J=7.0 Hz, $CH_2C\underline{H}_3$), 2.60 (3H, s, SCH_3), 4.18 (2H, q, J=7.0 Hz, $C\underline{H}_2CH_3$), 4.29 (2H, q, J=7.0 Hz, $C\underline{H}_2CH_3$), 7.41 (3H,m, $H^{m,p}$ of phenyl), 7.88 (2H, m, H^o of phenyl), 8.22 (1H, d, J=13.3 Hz, C$\underline{H}$-NH), 8.42 (1H, s, CH=N), 12.28 (1H, d, J=13.3 Hz, CH-N$\underline{H}$).

Found: C, 56.11; H, 5.83; N, 11.67%; M^+, 363. Calcd for $C_{17}H_{21}N_3O_4S$: C, 56.19; H, 5.83; N, 11.57%; M, 363.

The author wishes to thank Miss Yoko Ishizuka for assistance in the preparation of compounds.

References

1) Part III: C. Yamazaki, *Bull. Chem. Soc. Jpn.*, **53**, 3289 (1980).

2) C. Yamazaki, *Bull. Chem. Soc. Jpn.*, **51**, 1846 (1978); *Tetrahedron Lett.*, **1978**, 1295.

3) Exclusive methylation on the internal nitrogen with methyl iodide has been observed for isothiosemicarbazones[8] and also for benzaldehyde amidinohydrazone [W. G. Finnegan, R. A. Henry, and G. B. L. Smith, *J. Am. Chem. Soc.*, **74**, 2981

(1952)].
4) S. G. Cottis and H. Tieckelmann, *J. Org. Chem.*, **26**, 79 (1961).
5) Y. Tamura, J. Kim, and M. Ikeda, *J. Heterocycl. Chem.*, **12**, 107 (1975).
6) K. Saito, I. Hori, M. Igarashi, and H. Midorikawa, *Bull. Chem. Soc. Jpn.*, **47**, 476 (1974).
7) J. E. Baldwin, *J. Chem. Soc., Chem. Commun.*, **1976**, 734; 736.
8) C. Yamazaki, *Can. J. Chem.*, **53**, 610 (1975).
9) L. A. Lee and J. W. Wheeler, *J. Org. Chem.*, **37**, 348 (1972); R. N. Butler, *Can. J. Chem.*, **51**, 2315 (1973); L. G. Tensmeyer and C. Ainsworth, *J. Org. Chem.*, **31**, 1878 (1966).
10) W. J. Houlihan and R. E. Manning, Ger. Offen. 1 902449 (1969); *Chem. Abstr.*, **71**, 123963q (1969).

  Bull. Chem. Soc. Jpn., 54, 1773—1776 (1981)

Nucleophilic Reactions of Hydrazido(2-) Complexes of Molybdenum and Tungsten with Succinyl Dichloride and Phenyl Isocyanate†

Kiyotaka Iwanami, Yasushi Mizobe, Tamotsu Takahashi, Teruyuki Kodama, Yasuzo Uchida, and Masanobu Hidai*

Department of Industrial Chemistry, Faculty of Engineering, University of Tokyo, Hongo, Bunkyo-ku, Tokyo 113

(Received November 12, 1980)

Nucleophilic attack of the $WNNH_2$ group in the hydrazido(2-) complex $[WF(NNH_2)(dpe)_2][BF_4]$ (dpe=$Ph_2PCH_2CH_2PPh_2$) on succinyl dichloride gives a novel ethanedioylhydrazido(2-) complex, $[WF(\overline{NNCOCH_2CH_2CO})(dpe)_2][BF_4]$. X-Ray structural analysis shows that the carbon, nitrogen, and oxygen atoms of the ethanedioylhydrazido(2-) ligand lie nearly in the same plane, indicating sp^2 character of the nitrogen atom bearing the two carbonyl groups. Phenyl isocyanate also undergoes nucleophilic attack by the hydrazido(2-) complex $[MBr(NNH_2)(dpe)_2]Br$ (M=Mo or W) to yield the phenylsemicarbazido(2-) type complex, $[MBr(NNHCONHPh)(dpe)_2]Br$. Treatment of the semicarbazido(2-) complex with triethylamine gives a new diazenido complex $[MBr(NNCONHPh)(dpe)_2]$.

Many hydrazido(2-) complexes containing the $MNNH_2$ moiety have been isolated by the reaction of dinitrogen complexes $[M(N_2)_2L_4]$ (M=Mo or W; L=phosphine) with acids.[1,2] These complexes are important intermediates in the reduction of ligating dinitrogen to both ammonia[3] and hydrazine.[4-6] The X-ray structural analyses of $[MoF(NNH_2)(dpe)_2][BF_4]$[2] and $[WCl(NNH_2)(dpe)_2][BPh_4]$[7] show that the M–N–N bond distances give a bond order greater than unity, the M–N bond distances being in line with considerable multiple bonding between the metal and nitrogen. This result is interpreted in terms of two resonance structures (i) and (ii). The basicity of the terminal nitrogen in

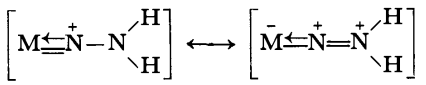

(i) (ii)

the $MNNH_2$ moiety is, thus, expected to be weaker than that of hydrazine and amines. However, hydrazido(2-) complexes, $[MF(NNH_2)(dpe)_2][BF_4]$ and $[MX(NNH_2)(PMe_2Ph)_3]$ (M=Mo or W; X=Cl or Br), have been found to undergo condensation with a variety of aldehydes and ketones in a similar way to that for hydrazines, giving diazoalkane complexes containing the M≡N–N=CRR′ moiety.[8-11] In this paper, we wish to describe other nucleophilic reactions of hydrazido(2-) complexes with succinyl dichloride and phenyl isocyanate.

Experimental

All reactions were carried out under pure nitrogen atmosphere. Solvents were purified by the usual methods, thoroughly dried, and distilled under nitrogen atmosphere. Commercial succinyl dichloride, phenyl isocyanate, triethylamine, and sodium tetraphenylborate were used without further purification. The complexes *trans*-$[Mo(N_2)_2(dpe)_2]$[1,12] *trans*-$[W(N_2)_2(dpe)_2]$,[1] $[WF(NNH_2)(dpe)_2][BF_4]$,[9] $[MBr(NNH_2)(dpe)_2]Br$ (M=Mo or W),[1] and $[WBr(NNH)(dpe)_2]$[1] were prepared by the methods reported. IR spectra were determined with a Hitachi 215 spectrometer, ^{1}H-NMR spectra of the complexes $[MBr(NNHCONHPh)(dpe)_2]Br$ (M=Mo or W) with a Hitachi R-600 FT-spectrometer because of low solubility, and spectra of the other complexes with a JEOL PS-100 spectrometer. Analytical data are given in Table 1.

$[WF(\overline{NNCOCH_2CH_2CO})(dpe)_2][BF_4]$. To a yellow solution of $[WF(NNH_2)(dpe)_2][BF_4]$ (255 mg, 0.228 mmol) in dichloromethane (7.5 ml) was added succinyl dichloride (0.21 ml, 8 mol equiv.) at room temperature, and the mixture was stirred for 20 h. The red solution obtained was concentrated under reduced pressure to about half its volume, hexane (10 ml) then being added to precipitate the pinkish red crude product (246 mg, 90%). The product was recrystallyzed from chloroform–hexane (3—8 ml) and then chloroform–ether (3—6 ml) to give pure crystals which were dried *in vacuo* (97 mg, 35%). Suitable crystals for X-ray analysis were selected.

$[MoBr(NNHCONHPh)(dpe)_2]$. To a brown suspension of $[MoBr(NNH_2)(dpe)_2]Br$ (322 mg, 0.315 mmol) in tetrahydrofuran (10 ml) was added phenyl isocyanate (0.28 ml, 8 mol equiv.), and the mixture was stirred at refluxing temperature for 10 h. The green supension obtained was filtered off and the residue was crystallyzed from dichloromethane–hexane (15—15 ml). Green crystals were filtered off, washed with hexane, and then dried *in vacuo* (171 mg, 45%).

$[WBr(NNHCONHPh)(dpe)_2]Br$. This complex was prepared by the same method as described above for molybdenum analogue. From 219 mg of $[WBr(NNH_2)(dpe)_2]Br$ was obtained 114 mg of $[WBr(NNHCONHPh)(dpe)_2]Br$ as red crystals in 47% yield.

$[MoBr(NNCONHPh)(dpe)_2]$. To a stirred green suspension of $[MoBr(NNHCONHPh)(dpe)_2]$ (49 mg, 0.041 mmol) in tetrahydrofuran (3 ml) was added triethylamine (5.7 μl, 1 mol equiv.) After 2 h, to the orange homogeneous solution obtained was added ether (6 ml), affording orange crystals of $[MoBr(NNCONHPh)(dpe)_2]$ which were filtered off, washed with ether and dried *in vacuo* (23 mg, 50%).

$[WBr(NNCONHPh)(dpe)_2]$. *1)*: From 216 mg of $[WBr(NNHCONHPh)(dpe)_2]Br$ was obtained 64 mg of $[WBr(NNCONHPh)(dpe)_2]$ as orange crystals in 32% yield by the same method as described above for the molybdenum analogue.

2): To a yellow suspension of $[WBr(NNH)(dpe)_2]$ (95 mg, 0.087 mmol) in tetrahydrofuran (5 ml) was added phenyl isocyanate (76 μl, 8 mol equiv.) and the mixture was stirred at refluxing temperature for 2 h. From the brown solution obtained, red crystals of $[WBr(NNCONHPh)(dpe)_2]$ were precipitated by addition of ether, which were filtered off,

† Preparation and Properties of Molybdenum and Tungsten Dinitrogen Complexes 15. For part 14 of this series, see M. Hidai, T. Takahashi, I. Yokotake, and Y. Uchida, *Chem. Lett.*, **1980**, 645.

Table 1. Analytical and spectroscopic data of the new complexes

Complex	Found (Calcd)(%) C	H	N	IR (cm^{-1})[a] ν(C=O)	ν(N–H)	δ(N–H)	^{1}H-NMR δ/ppm[b]
[WF(NNCOCH$_2$CH$_2$CO)(dpe)$_2$] [BF$_4$]	55.80 (56.12)	4.33 (4.37)	2.20 (2.34)	1720			2.0(s) COCH$_2$
[MoBr(NNHCONHPh) (dpe)$_2$]Br	58.68 (58.96)	4.67 (4.62)	3.41 (3.50)	1715	3170 2730[c]	1530	1.5(s) CONH 11.7(s) MNNH
[WBr(NNHCONHPh)(dpe)$_2$]Br	55.16 (54.94)	4.19 (4.31)	3.15 (3.26)	1710	3180 2800[c]	1540	1.5(s) CONH 10.5(s) MNNH
[WBr(NNDCONDPh)(dpe)$_2$]Br	—	—	—	1700	2300 2150	1360	—
[WBr(NNHCONHPh)(dpe)$_2$][BPh$_4$]	64.05 (65.20)	4.82 (4.94)	2.60 (2.75)	1690	3300[d] 3380[d]	1530	4.7(s) MNNH 5.2(s) CONH
[MoBr (NNCONHPh)(dpe)$_2$]·1/2THF[e]	62.47 (63.33)	5.23 (5.05)	3.60 (3.63)	1630	3380[d]	1510	5.6(s) CONH
[WBr(NNCONHPh)(dpe)$_2$]·ether[e]	58.67 (58.99)	4.69 (5.02)	3.28 (3.28)	1620	3400[d]	1510	5.7(s) CONH

a) KBr disk. b) In CD_2Cl_2, relative to $SiMe_4$. s=Singlet. c) Broad. d) Nujol mulls, very weak. e) Determined from ^{1}H-NMR spectra.

washed with ether and then dried *in vacuo* (8 mg, 7%).

[WBr(NNHCONHPh)(dpe)$_2$][BPh$_4$]. A solution of [WBr(NNHCONHPh)(dpe)$_2$]Br (280 mg, 0.217 mmol) in dichloromethane (18 ml) and a solution of sodium tetraphenylborate (297 mg, 4 mol equiv.) in dichloromethane–tetrahydrofuran (5—5 ml) were combined and stirred at room temperature. After 2 h, the reaction mixture was evaporated to dryness *in vacuo*, and the residue was extracted by dichloromethane (3 ml). Addition of hexane (5 ml) to the extract gave red crystalline solid of [WBr(NNHCONHPh)(dpe)$_2$]-[BPh$_4$], which was filtered off, washed with hexane, and then dried *in vacuo* (221 mg, 67%).

Results and Discussion

Dinitrogen complexes [M(N$_2$)$_2$(dpe)$_2$] and [M(N$_2$)-(RCN)(dpe)$_2$] (M=Mo or W; R=aryl) react with acyl or aroyl chlorides to give acyl- or aroyldiazenido complexes, [MCl(NNCOR')(dpe)$_2$] (R'=acyl or aroyl), which, on treatment with hydrochloric acid, are converted into acyl- or aroylhydrazido(2-) complexes, [MCl(NNHCOR')(dpe)$_2$]Cl.[13,14] The latter complexes are also obtained by nucleophilic reactions of the hydrazido(2−) complex [WCl(NNH$_2$)(dpe)$_2$]Cl with acyl halides.[15] We have found that the hydrazido (2−)complex [WF(NNH$_2$)(dpe)$_2$][BF$_4$] reacts smoothly with succinyl dichloride to give ethanedioylhydrazido (2−) complex as follows.

$$[WF(NNH_2)(dpe)_2][BF_4] \xrightarrow{ClCOCH_2CH_2COCl} [WF(NN\overset{O}{\overset{\|}{C}}-CH_2-CH_2-\overset{O}{\overset{\|}{C}}N)(dpe)_2][BF_4] + 2HCl$$

1

When an excess of succinyl dichloride was added to an orange solution of [WF(NNH$_2$)(dpe)$_2$][BF$_4$] at room temperature, a red solution was obtained after *ca.* 20 h, from which pink crystals of [WF(NNCOCH$_2$CH$_2$CO)-(dpe)$_2$][BF$_4$] (**1**) were isolated. When adipoyl dichloride and phthaloyl dichloride were used instead of succinyl dichloride, no analogous products were obtained, probably because of steric effects. Treatment of another complex, [WBr(NNH$_2$)(dpe)$_2$]Br, with succinyl dichloride did not proceed satisfactorily under the same conditions. The lower reactivity of the latter is caused by the lower nucleophilicity of the terminal nitrogen atom relative to that of [WF(NNH$_2$)(dpe)$_2$][BF$_4$], as estimated by the δ-value of the hydrazido protons in the ^{1}H-NMR spectra ([WBr(NNH$_2$)(dpe)$_2$]Br: 6.3 ppm;[1] [WF(NNH$_2$)(dpe)$_2$][BF$_4$]: 4.5 ppm[9]).

In the IR spectrum of **1**, a strong absorption band assignable to ν(C=O) was observed at 1720 cm^{-1}, higher by 25 cm^{-1} than that of succinimide. This shows that the carbonyl groups in complex **1** have no single bond character and the lone pair electrons on the terminal nitrogen atom do not flow over the carbonyl groups. Four succinyl protons appeared in the ^{1}H-NMR spectrum at 2.0 ppm as a singlet peak, indicating that four protons are completely equivalent.

X-Ray analysis was performed to determine the

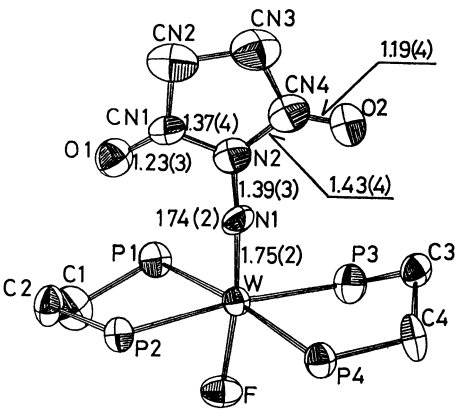

Fig. 1. Perspective view of [WF(NNCOCH$_2$CH$_2$CO)-(dpe)$_2$][BF$_4$]. The shapes of the atoms on this drawing represent 50% probability contours of thermal motions. The bond angles are as follows: W–N1–N2=174.16°, N1–N2–CN1=120.50°, N1–N2–CN4=125.85°, CN1–N2–CN4=113.64°, N2–CN1–O1=122.01°, CN2–CN1–O1=123.99°, CN2–CN1–N2=113.86°.

structure of ethanedioylhydrazido(2−) ligand. However, since a good crystal could not be obtained, the final residuals were R=0.109 and Rw=0.097 using block-diagonal least squares with anisotropic thermal factors for nonhydrogen atoms, and further refinement was no longer carried out.[16]

Analysis shows that this complex has an octahedral geometry with the ethanedioylhydrazido(2−) ligand and fluoride anion in a trans position (Fig. 1). The W–N–N linkage is essentially linear. From the result of angle summations around the terminal nitrogen and two carbonyl carbon atoms, it is concluded that two nitrogen, four carbon, and two oxygen atoms lie in the same plane. This indicates that the terminal nitrogen atom is predominantly sp^2 hybridized. Considering the fact that the lone pair electrons on the terminal nitrogen do not flow over the carbonyl groups, the canonical structures (iv), rather than structure (v), might take part in the formation of structure (iii) to some extent.

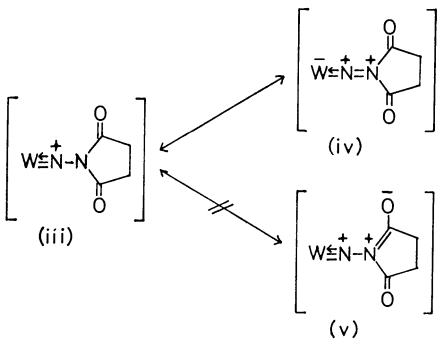

We have found that hydrazido(2−) complexes [MBr(NNH$_2$)(dpe)$_2$]Br (M=Mo or W) react with phenyl isocyanate to give the semicarbazido type complexes [MBr(NNHCONHPh)(dpe)$_2$]Br.

The reaction is understood as the nucleophilic addition of the terminal nitrogen in the hydrazido(2−) ligand to the electron-defficient carbon in phenyl isocyanate.

When the hydrazido(2−) complexes [MBr(NNH$_2$)(dpe)$_2$]Br suspended in tetrahydrofuran were treated with excess phenyl isocyanate at refluxing temperature for 10 h, the semicarbazido type complexes [MBr(NNHCONHPh)(dpe)$_2$]Br precipitated from the reaction mixture as a green (M=Mo) or red (M=W) solid. The complexes were obtained as pure crystals by crystallization from dichloromethane–hexane. In their IR spectra (Table 1), strong absorption bands characteristic of the amide group were observed (M=Mo: ν(C=O)=1715 cm^{-1}, δ(N–H)=1530 cm^{-1}; M=W: ν(C=O)=1710 cm^{-1}, δ(N–H)=1540 cm^{-1}). As regards the tungsten complex, frequencies assigned to ν(N–D) and δ(N–D) were observed on deuteration by D_2O. The shift to low frequency and the peak broadening of the N–H stretching bands are interpreted in terms of hydrogen bonding between the proton and bromide anion. This hydrogen bonding seems to be formed between the more electropositive hydrazido proton and bromide anion; the lower stretching band is due to the NH moiety in the NNH and the higher one to that in the amide group. The existence of hydrogen bonding is also supported by the result obtained from the ^{1}H-NMR spectra of these complexes (Table 1), that is, NNH protons were observed at 11.7 ppm for Mo and 10.5 ppm for W. The shift to a lower field from the usual NH region is due to the hydrogen bonding with bromide anion. Similar observations have been reported for [WHClBr(NNH$_2$)(PMe$_2$Ph)$_3$]Br[6] and [WBr(NNH$_2$)L(PMe$_2$Ph)$_3$]Br (L=N⟨⟩–Me *etc.*).[16] On the other hand, the amido protons appeared at relatively high field (M=Mo and W; 1.5 ppm) which may be explained by the shielding effect of the phenyl groups of dpe ligands. Analogous results have been found in the methyl protons of the complex, [WF{NN=C(CH$_3$)-CH$_2$COCH$_3$}(dpe)$_2$][BF$_4$]·THF[9] and [WBr{NN=C(CH$_3$)CH$_3$}(dpe)$_2$]Br.[18]

When the semicarbazido type complex [WBr(NNHCONHPh)(dpe)$_2$]Br was treated with excess sodium tetraphenylborate, anion exchange took place to afford the red complex [WBr(NNHCONHPh)(dpe)$_2$][BPh$_4$]. Since hydrogen bonding between NNH proton and the anion no longer exists in this complex, the NH stretching band in the IR spectrum and the NH resonance in the ^{1}H-NMR spectrum appear in the usual neutral NH region. The amido proton is observed at 5.2 ppm in the ^{1}H-NMR spectrum, lying in the common amido proton region. The cleavage of the hydrogen bonding might give rise to the conformational change, the amido proton being freed from the position shielded by the phenyl groups of dpe ligands. Spectroscopic data are summerized in Table 1.

The semicarbazido type complexes [MBr(NNHCONHPh)(dpe)$_2$]Br (M=Mo or W) easily react with a weak base such as triethylamine to afford the new diazenido complexes [MBr(NNCONHPh)(dpe)$_2$]. Strong absorption bands characteristic of the amide group were observed in the IR spectra, and amido protons appearing in the common amido region in the ^{1}H-NMR spectra. The relatively low ν(C=O) frequencies observed (M=Mo: 1630 cm^{-1}; M=W: 1620 cm^{-1}) as compared with the semicarbazido type complexes (M=Mo: 1715 cm^{-1}; M=W: 1710 cm^{-1}) can be explained by the large contribution of the structure (vii), which is formed by the electron flow from the metal to the carbonyl group.

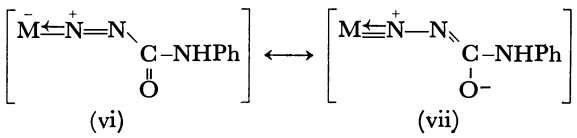

The combination of resonance structures has been proposed for the diazenido complex, [MoCl(NNCOPh)(dpe)$_2$].[14,19] Spectroscopic data of the new diazenido complexes are also given in Table 1.

This diazenido complex, [WBr(NNCONHPh)(dpe)$_2$], can also be prepared by way of another route. The diazenido complex, [WBr(NNH)(dpe)$_2$], obtained by the reaction of [WBr(NNH$_2$)(dpe)$_2$]Br with triethylamine, reacts with phenyl isocyanate to give the complex [WBr(NNCONHPh)(dpe)$_2$]. This shows that the terminal nitrogen atom of the NNH ligand also has considerable nucleophilicity.[20] These synthetic routes are summarized as follows.

$$\begin{array}{ccc} [MBr(NNH_2)(dpe)_2]Br & \xrightarrow{PhNCO} & [MBr(NNHCONHPh)(dpe)_2]Br \\ \downarrow NEt_3 & & \downarrow NEt_3 \\ [MBr(NNH)(dpe)_2] & \xrightarrow{PhNCO} & [MBr(NNCONHPh)(dpe)_2] \end{array}$$

As regards the nucleophilicity of the NNH ligand, Colquhoun has found that the NNH ligand in the complexes $[WX(NNH)(dpe)_2]$ (X=F or Br) undergoes nucleophilic attack to 2,4-dinitrobenzene to give the dinitrophenylhydrazido complexes or, by successive deprotonation, dinitrophenyldiazenido complexes.[21]

The authors are grateful to Dr. Takashi Tatsumi for recording FT-NMR and Mr. Masayuki Nishina for experimental assistance.

References

1) J. Chatt, A. J. Pearman, and R. L. Richards, *J. Chem. Soc., Dalton Trans.*, **1974**, 2074.
2) M. Hidai, T. Kodama, M. Sato, M. Harakawa, and Y. Uchida, *Inorg. Chem.*, **11**, 2694 (1976).
3) J. Chatt, A. J. Pearman, and R. L. Richards, *J. Chem. Soc., Dalton Trans.*, **1977**, 1852.
4) M. Hidai, Y. Mizobe, T. Takahashi, and Y. Uchida, *Chem. Lett.*, **1978**, 1187.
5) T. Takahashi, Y. Mizobe, M. Sato, Y. Uchida, and M. Hidai, *J. Am. Chem. Soc.*, **101**, 3405 (1979).
6) T. Takahashi, Y. Mizobe, M. Sato, Y. Uchida, and M. Hidai, *J. Am. Chem. Soc.*, **102**, 7461 (1980).
7) G. A. Heath, R. Mason, and K. M. Thomas, *J. Am. Chem. Soc.*, **96**, 259 (1974).
8) M. Hidai, Y. Mizobe, and Y. Uchida, *J. Am. Chem. Soc.*, **98**, 7824 (1976).
9) M. Hidai, Y. Mizobe, M. Sato, T. Kodama, and Y. Uchida, *J. Am. Chem. Soc.*, **100**, 5740 (1978).
10) P. C. Bevan, J. Chatt, M. Hidai, and G. J. Leigh, *J. Organomet. Chem.*, **160**, 165 (1978).
11) Y. Mizobe, Y. Uchida, and M. Hidai, *Bull. Chem. Soc. Jpn.*, **53**, 1781 (1980).
12) M. Hidai, K. Tominari, and Y. Uchida, *J. Chem. Soc., Chem. Commun.*, **1969**, 1392; *J. Am. Chem. Soc.*, **94**, 110 (1972).
13) J. Chatt, A. A. Diamantis, G. A. Heath, N. E. Hooper, and G. J. Leigh, *J. Chem. Soc., Dalton Trans.*, **1977**, 688 and references therein.
14) T. Tatsumi, M. Hidai, and Y. Uchida, *Inorg. Chem.*, **14**, 2530 (1975).
15) J. Chatt, R. A. Head, G. J. Leigh, and C. J. Pickett, *J. Chem. Soc., Dalton Trans.*, **1978**, 1638.
16) The complex crystallized in the monoclinic space groups $P2_1/n$ with cell dimensions $a=17.92(1)$ Å, $b=18.26(1)$ Å, $c=17.59(1)$ Å, and $\beta=110.56(3)°$. Diffraction data were collected on a Rigaku automatic four-circle diffractometer; 4639 reflections ($|F_o| \geqq 3\sigma|F_o|$) were used in the structure solution and refinement. The structure was solved by the heavy atom method. The programs used for this analysis were UNICS and X-ray system, all calculations being carried out with a HITAC 8700/8800 computer.
17) J. Chatt, A. J. Pearman, and R. L. Richards, *J. Chem. Soc., Dalton Trans.*, **1978**, 1766.
18) J. Chatt, R. A. Head, P. B. Hitchcock, W. Hussain, and G. J. Leigh, *J. Organomet. Chem*, **133**, Cl (1977).
19) M. Sato, T. Kodama, M. Hidai, and Y. Uchida, *J. Organomet. Chem.*, **152**., 239 (1978).
20) J. Chatt, A. J. Pearman, and R. L. Richards, *J. Chem. Soc., Dalton Trans.*, **1977**, 1852.
21) H. M. Colquhoun, *J. Chem. Research (S)*, **1979**, 325.

A Convenient Synthesis of Condensed Cyclopentane System. Annelation by Intramolecular 1,3-Dipolar Addition of Nitrones

Satoru TAKAHASHI, Takenori KUSUMI, Yoko SATO, Yoshinobu INOUYE, and Hiroshi KAKISAWA*

Department of Chemistry, The University of Tsukuba, Sakura-mura, Niihari-gun, Ibaraki 305

(Received November 22, 1980)

Intramolecular 1,3-dipolar addition reactions of nitrones were investigated. Four alkenyl nitrones were studied: 2-allyl-, 2-(3-butenyl)-, 2-(4-pentenyl)-, and 2-(9-decenyl)-*N*-methylcyclohexanimine *N*-oxides. Among these, 2-(3-butenyl)-*N*-methylcyclohexanimine *N*-oxide was found to cyclize most smoothly, giving a perhydroindene derivative as a single regio- and stereoisomer. A perhydroazulene derivative was obtained by cyclization of 2-(3-butenyl)-*N*-methylcycloheptanimine *N*-oxide.

1,3-Dipolar addition reactions are currently of interest in the synthesis of natural products. The reaction between nitrones and olefins is frequently applied for the synthesis of alkaloids.[1] Both intra-[2] and intermolecular[3] 1,3-dipolar reactions are used, depending on the target molecules. Usually nitrones react with olefins stereo- and regiospecifically,[4] giving versatile 1,3-dipolar adducts. When a nitrone reacts intramolecularly with an olefin group as in the following system, a new carbocyclic ring is formed along with an isoxazolidine ring.

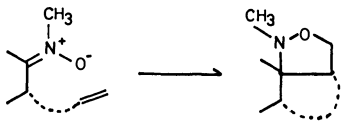

Fig. 1.

In order to develop a new annelation method, the authors studied the cyclization of the compounds **5**—**8**,[5] each of which has both a nitrone and an olefin group in the same molecule. These nitrones were easily prepared by treatment of the corresponding alkenylcyclohexanones **1**—**4** with *N*-methylhydroxylamine.

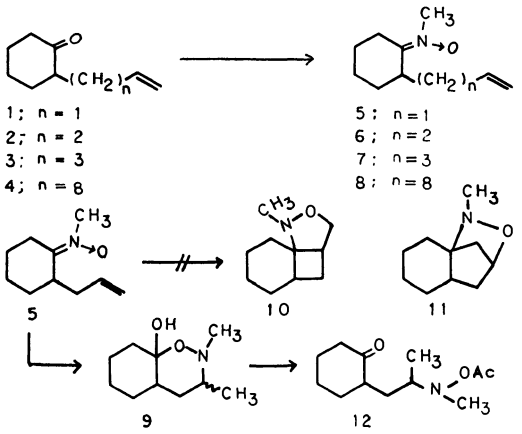

Fig. 2.

When the nitrone (**5**) having an allyl side chain was heated in refluxing benzene, it decomposed into a complex mixture, from which the expected cyclization products, **10** and **11**, could not be extracted. However, when **5** was allowed to stand at room temperature for one week, an unexpected oxazine (**9**) was obtained in 43% yield. The structure was assigned on the basis of spectroscopic data of **9** and its acetate (**12**), which was produced by the treatment of **9** with acetic anhydride in pyridine.

A possible mechanism for the formation of **9** is suggested by the equation in Fig. 3.

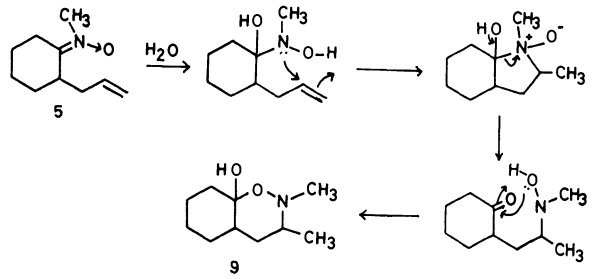

Fig. 3.

However, the nitrone (**6**), carrying a butenyl side chain, cyclized at room temperature to yield the expected cycloadduct (**13**) in a quantitative yield. In this case, neither the regioisomer (**16**) nor the oxazepine analog of **9** was formed; the reaction afforded a stereochemically single product.

Attempts to cleave the N–O bond with catalytic hydrogenation (on Pd/C or PtO_2) were unsucessful. Irradiation[6] of UV light (high pressure mercury lamp using a Pyrex filter) on a hexane solution of **18** in the presence of fluorenone gave rise to an oxazine (**21**) in 39% yield. The oxazine ring of **14** was cleaved with lithium aluminium hydride to give an amino alcohol (**15**). The N–O bond of **13** was cleaved more effectively with titanium(III) chloride, to yield the same compound (**15**).

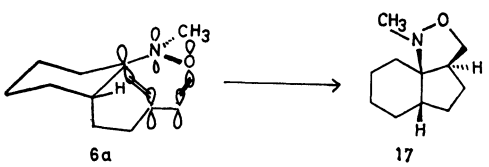

Fig. 4.

The stereochemistry of **13** was tentatively described as **17**; thus, the most favorable transition state leading to **13** seemed to be **6a**, because it permitted the maximum overlapping of the π orbitals of the nitrone and the side chain olefin groups.

Unlike **6**, the nitrone (**7**) resisted cyclization at room temperature for one week. However, when **6** was

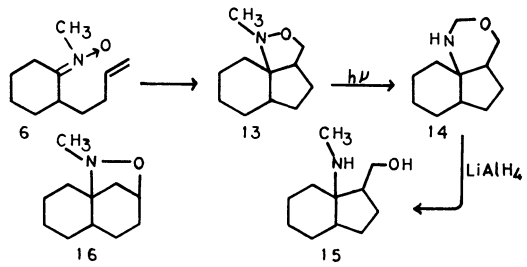

Fig. 5.

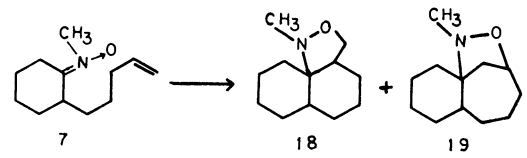

Fig. 6.

refluxed in benzene for 16 h, it gave rise to a 1 : 1 mixture of the intramolecular adducts, **18** and **19**. These adducts were separated by column chromatography.

The nitrone (**8**), which has a 9-decenyl side chain, gave no cyclized product. Thus, heating of **8** at 60 °C for 24 h resulted in the recovery of **8**, and heating at 120 °C for 1 h brought about decomposition.

From these results, a system bearing the 3-butenyl side chain such as in **6** was considered to be most suitable for annelation which would result in the formation of a cyclopentane ring. In order to confirm the utility of this annelation, we tried to synthesize a perhydroazulene system, which is a common skeleton of some sesquiterpenes.

A mixture of 2-(3-butenyl)cycloheptanone (**20**) and *N*-methylhydroxylamine in methanol was heated at reflux. The NMR of the reaction mixture showed a strong *N*-methyl signal (δ=3.67) due to the nitrone (**21**) after several hours. This signal gradually decreased, and it completely disappeared after 44 h; an intense *N*-methyl signal (δ=2.52) due to the cyclized product (**22**) remained. By simple purification, a perhydroazulene compound (**22**) was isolated in 84% yield as a single product.

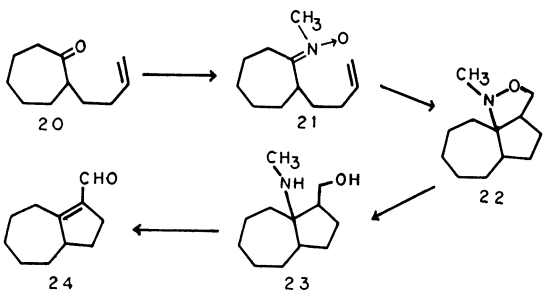

Fig. 7.

Although the N–O bond of substituted isoxazolidine or isoxazolidinium can be cleaved by reduction with zinc–acetic acid,[7] lithium aluminium hydride,[8] or catalytic hydrogenation,[9] these methods are not suitable for the compounds having easily reducible functions such as halogens, ketones, or esters. We found that the N–O bond of **22** can be cleaved by simple treatment with titanium(III) chloride in refluxing ethanol, affording an amino alcohol (**23**). Treatment of **23** with chromium trioxide–pyridine hydrochloride complex[10] effectively yielded **24**, Thus the nitrone-annelation would provide a new method for syntheses of hydroazulene derivatives.

Experimental

^{1}H-NMR spectra were recorded on a Hitachi H-60 instrument, TMS being used as an internal standard (ppm). IR spectra were taken on a Hitachi EPS-3T spectrometer. Mass spectra were obtained with a Hitachi RMU-6M spectrometer.

8a-Hydroxy-2,3-dimethyl-3,4,4a,5,6,7,8,8a-octahydro-2H-1,2-benzoxazine(9). To a solution of *N*-methylhydroxylamine hydrochloride (889 mg, 10.6 mmol) in 5 ml of methanol was added a solution of potassium hydroxide (664 mg, 11.5 mmol) in 3 ml of methanol, followed by the addition of allylcylohexanone (865 mg, 6.27 mmol). The mixture was stirred overnight, and diluted with ether. The precipitate was removed by filtration, and the filtrate was concentrated to give crude **5** (830 mg) as an oil; IR($CHCl_3$) 3300 (H_2O), 1640, 990, and 910 (–CH=CH_2), 1590 (nitrone) cm^{-1}; NMR ($CDCl_3$) δ=5.75 (1H, m), 5.00 (2H, m), 3.75 (3H, s, CH_3–N(→O)=), 2.5—0.8 (11H, m). The crude nitrone **5** (830 mg) was allowed to stand at room temperature for 7 d. The resulting oil was chromatographed on silica gel, giving allylcyclohexane (650 mg), the unchanged nitrone **5** (298 mg), and a mixture of the oxazine stereoisomers **9** (316 mg, 43% from allylcyclohexanone): bp 59 °C/0.3 Torr†; IR(film) 3450 (OH), 1015 (C–O) cm^{-1}; NMR($CDCl_3$) δ=4.28 (1H, s, OH), 2.60 (3H, s, N–CH_3), 2.50 (1H, m, CH_3–C<u>H</u>–N), 1.05 (3H/2, d, J=6.5 Hz, C<u>H</u>$_3$–CH–N), 0.97 (3H/2, d, J=6.5 Hz, isomeric C<u>H</u>$_3$–CH–N), 2.0—1.0 (12H, m); ^{13}C-NMR($CDCl_3$) 98.14(s), 61.69(d), 61.54(d), 43.70(d), 43.55(d), 42.88(q), 35.62(t), 35.47(t), 35.31(t), 35.14(t), 28.97(t), 28.81(t), 25.83(t), 25.70(t), 23.19(t), 23.04(t), 22.84(q), 19.03(q). Found: C, 64.49; H, 10.15; N, 7.25%. Calcd for $C_{10}H_{19}NO_2$: C, 64.83; H, 10.34; N, 7.56%.

By repeated chromatography of the diastereomeric mixture **9** (500 mg) using benzene–ethyl acetate (10 : 1) as an eluting solvent, one isomer of **9** was obtained as a colorless oil (45 mg): NMR($CDCl_3$) δ=2.60 (3H, s), 2.50 (1H, m), 1.05 (3H, d, J=6.5 Hz); ^{13}C-NMR($CDCl_3$) 98.21(s), 61.54(d), 43.54(d), 43.88(q), 35.46(t), 35.13(t), 28.80(t), 25.79(t), 23.04(t), 19.03(q).

2-[2-(N-Acetoxymethylamino)propyl]cyclohexanone(12). A solution of diastereomers(**9**) (73 mg, 0.40 mmol) in 2 ml of pyridine was treated with acetic anhydride (2 ml), and the mixture was allowed to stand overnight. After the usual work-up, the resulting oil (91 mg) was chromatographed on silica gel, giving **12** (66 mg, 73%) as an oil: IR($CHCl_3$) 1750 (AcO), 1700 (C=O) cm^{-1}; NMR($CDCl_3$) δ=3.05 (1H, m, CH–N), 2.72 (3H, s, CH_3–N), 2.02 (3H, s, AcO), 1.08 (3H, d, J=6.5 Hz), 2.5—1.0 (11H, m).

Hydrolysis of **12** with potassium hydroxide in methanol afforded a diastereomeric mixture **9** in a quantitative yield.

Attempt at Cyclization of 5. The nitrone **5** exhibited a strong absorption band at 3300 cm^{-1} in its IR spectrum due to water. The nitrone in this state was labile to heat; thus, vaccum distillation at 65 °C/0.15 Torr produced a distillate, which showed at least six spots in TLC. The NMR spectrum

† 1 Torr=133.322 Pa.

of the distillate showed no singlet at 3.73 ppm due to the *N*-methyl group of **5**. Similarly, a complex mixture was obtained when **5** was heated in refluxing benzene. By chromatography of the product, minor amounts of **9** and 2-allylcyclohexanone were isolated. However, the expected cyclization product, **10** or **11**, was not detected.

12-Methyl-11-ox-12-azatricyclo[7.3.0.0^{1,6}]dodecane(13). Treatment of 2-(3-butenyl)cyclohexanone **2** with *N*-methylhydroxylamine afforded crude nitrone **6**: IR(film) 3300 (H_2O), 1635, 990, 910 (-CH=CH_2), 1590 (nitrone) cm^{-1}; NMR($CDCl_3$) δ=4.10 (1H, t, J=8.0 Hz), H_A of O-CH_AH_B-CH_X), 3.48 (1H, dd, J=3.5, 8.0 Hz, H_B of O-CH_AH_B-CH_X), 2.63 (3H, s, CH_3-N), 2.7—1.0 (14H, m); MS (70 eV), *m/e* (rel intensity), 181 (M^+, 100), 138 (72), 135 (84), 127 (77). An analytical sample was obtained by short-path distillation: bp 98—103 °C/17 Torr. Found: C, 72.79; H, 10.45; N, 7.65%. Calcd for $C_{11}H_{19}NO$: C, 72.88; H, 10.56; N, 7.72%.

1-Methylamino-9-(hydroxymethyl)bicyclo[4.3.0]none (15). A solution of **13** (194 mg, 1.07 mmol) in 40 ml of hexane was irradiated for 18 h in the presence of fluorenone (23 mg, 0.13 mmol) with a high pressure mercury lamp (450 W) using a Pyrex filter. After removal of the hexane, the residue was chromatographed on silica gel. Elution with benzene gave fluorenone; further elution with benzene–ethyl acetate (3 : 1) gave **14** as an oil in a pure state (TLC). IR(film) 3300 (NH) cm^{-1}; NMR($CDCl_3$) δ=4.35 (2H, s, N-CH_2-O), 3.70 (2H, m, CH_2-O), 1.85 (1H, s, NH), 2.5—0.8 (14H, m). The oxazine **14** (49 mg, 0.27 mmol) was treated with lithium aluminium hydride (50 mg, 1.3 mmol) in 5 ml of tetrahydrofuran, and the mixture was stirred at room temperature overnight. The excess hydride was decomposed with water, 15% sodium hydroxide solution, and water, the precipitate being filtered. The filtrate was concentrated, and the residue was crystallized from ether, affording needles (33.8 mg, 68%): mp 188—190 °C; IR(KBr) 3325 (OH and NH); NMR($CDCl_3$) δ=3.78 (2H, br.s, NH and OH), 3.68 (2H, d, J= 5.0 Hz, CH_2-O), 2.42 (3H, s, CH_3-N), 2.3—1.0 (14H, m). An analytical sample was obtained by bulb-to-bulb distillation: bp 130 °C/2 Torr. Found: C, 72.23; H, 11.69; N, 7.30%. Calcd for $C_{11}H_{21}NO$: C, 72.08; H, 11.54; N, 7.64%.

13-Methyl-12-ox-13-azatricyclo[8.3.0.0^{1,6}]tridecane (18) and 12-Methyl-11-ox-12-azatricyclo[8.2.1.0^{1,6}]tridecane (19). The nitrone **7** was prepared from the pentenylcyclohexanone **3** by a method similar to that described above. A solution of the nitrone **7** (2.2 g, 11.3 mmol) in benzene (100 ml) was heated under refluxing in a nitrogen atmosphere for 16 h. The solvent was evaporated, and the residue (2.51 g) was chromatographed on silica gel. Elution with benzene–ethyl acetate (10 : 1) produced **19** (260 mg, 11.8%), a mixture of **19** and **18** (820 mg, 37.3%), and **18** (162 mg, 7.4%). Analytical samples were prepared by short-path distillation: **18**: 60 °C/2 Torr; NMR(C_6D_6) δ=3.98 (1H, dd, J=10.0, 7.0 Hz, CH_2-O), 3.47 (1H, dd, J=9.0, 7.0 Hz, CH_2-O), 2.43 (3H, s, CH_3-N). Found: C, 73.92; H, 10.95; N, 7.48%. Calcd for $C_{11}H_{21}NO$: C, 73.79; H, 10.83; N, 7.17%. **19**: 80 °C/2 Torr: NMR(C_6D_6) δ=4.45 (1H, m, CH-O), 2.43 (3H, s, CH_3-N), 1.96 (1H, dd, J=12.5, 8.5 Hz, CH_AH_B-CH-O), 1.65 (1H, dd, J=12.5, 2.5 Hz, CH_AH_B-CH-O). Found: C, 73.91; H, 10.92; N, 7.43%. Calcd for $C_{12}H_{21}NO$: C, 73.79; H, 10.83; N, 7.17%.

Attempt at Cyclization of the Nitrone 8. 2-(9-Decenyl)-cyclohexanone **8**; bp 112—125 °C/13 Torr, was prepared in 78% yield by treating the pyrrolidine enamine of cyclohexanone with 10-iodo-1-decene. The decenylcyclohexanone **8** (213 mg, 0.9 mmol) was dissolved in methanol (6 ml), and *N*-methylhydroxylamine hydrochloride (178 mg, 2.1 mmol) was added. The solution was treated with a solution of potassium hydroxide (171 mg, 3.1 mmol) in methanol (1 ml), and the reaction mixture was heated at refluxing temperature for 18 h. The mixture was diluted with ether, the precipitate was filtered, and the filtrate was concentrated to a brown oil (202 mg). The formation of the nitrone **8** was confirmed by the absence of the carbonyl absorption in the IR spectrum, and the appearance of a singlet at δ 3.75 (3H) due to *N*-methyl of the nitrone group in the NMR. The oil was heated in benzene at 60 °C for 24 h. The NMR spectrum of the product exhibited no signal at δ 3.75. Although the product was cautiously chromatographed on silica gel, no cyclization product could be isolated.

13-Methyl-12-ox-13-azatricyclo[8.3.0.0^{1,7}]tridecane (22). A solution of 2-(3-butenyl)cycloheptanone **20** (520 mg, 3.13 mmol), *N*-methylhydroxylamine hydrochloride (449 mg, 3.74 mmol), and potassium hydroxide (238 mg, 4.24 mmol) in methanol (20 ml) was heated at refluxing. After 4 h, a small portion of the reaction mixture was taken out. The NMR spectrum exhibited a singlet at δ 3.67 due to the *N*-methyl group of the nitrone **21**, together with a singlet at δ 2.52 due to the *N*-methyl group of the cyclization product **22**. The reaction mixture was heated for an additional 44 h, and diluted with ether. The precipitate was filtered and the filtrate was concentrated. The residual oil was distilled with a Kuhgel-Rohr apparatus, affording **22** (514 mg, 84% from **20**): NMR ($CDCl_3$) δ=3.82 (1H, t, J=8.0 Hz, O-CH_AH_B-CH_X), 3.23 (1H, dd, J=4.5, 8.0 Hz, O-CH_AH_B-CH_X), 2.52 (3H, s, CH_3-N). An analytical sample was obtained by short-path distillation: 140 °C/17 Torr. Found: C, 73.65; H. 10.92; N, 7.00%. Calcd for $C_{12}H_{21}NO$: C, 73.79; H, 10.83; N, 7.17%.

10-Hydroxymethyl-1-(methylamino)bicyclo[5.3.0]decane (23). To a solution of **22** (435 mg, 2.2 mmol) in ethanol (80 ml) was added 20% aqueous titanium(III) chloride solution (22 ml), and the mixture was allowed to reflux under an argon atmosphere overnight. The solvent was removed on a rotary evaporator, and the pH of the residual mixture was brought to 14 with a potassium hydroxide solution. The alkaline mixture was continuously extracted with ether for 24 h, and the ethereal extract was concentrated. The resultant oil was distilled with a Kuhgel-Rohr apparatus, giving **23** (302 mg, 89%) as a colorless oil: bp 170 °C/4 Torr; IR(film) 3300 cm^{-1}; NMR($CDCl_3$) δ=3.73 (2H, m, CH_2O), 3.08 (2H, s, NH and OH), 2.34 (3H, s, CH_3-N). Found: C, 72.75; H, 11.69; N, 6.81%. Calcd for $C_{12}H_{23}NO$: C, 73.04; H, 11.74; N, 7.09%.

Bicyclo[5.3.0]dec-1(10)-ene-10-carbaldehyde (24). A solution of the alcohol **23** (30 mg, 0.15 mmol) in dichloromethane (1.5 ml) was treated with chromium trioxide–pyridine hydrochloride complex (41 mg, 0.34 mmol), and the mixture was stirred at room temperature for 1 h. The mixture was diluted with ether, and water was added. The organic layer was separated, dried, and concentrated. After column chromatography of the residue on silica gel, a colorless oil **24** (12 mg, 52%) was obtained: IR(film) 2710, 1660 (CHO) cm^{-1}; NMR($CDCl_3$) δ=9.96 (HCO). High resolution mass spectrum: Found, M. W. 164.1185; Calcd for $C_{11}H_{16}O$, 164.1197.

References

1) T. Iwashita, M. Suzuki, T. Kusumi, and H. Kakisawa, *Chem. Lett.*, **1980**, 383; J. J. Tufariello and S. A. Ali, *J. Am. Chem. Soc.*, **101**, 7114 (1979), and the references cited therein.

2) For a recent review, see W. Oppolzzer, *Angew. Chem. Int. Ed. Engl.*, **16**, 10 (1977).

3) For a recent review, see D. S. C. Black, R. F. Crozier, and V. C. Davis, *Synthesis*, **1975**, 205.

4) R. Huisgen, *Angew. Chem.*, **75**, 604 (1963).

5) T. Kusumi, S. Takahashi, Y. Sato, and H. Kakisawa, *Heterocycles*, **10**, 257 (1978).
6) N. A. LeBel, T. A. Lajimess, and D. B. Ledlie, *J. Am. Chem. Soc.*, **80**, 3076 (1967).
7) J. J. Tufariello and E. J. Trybulski, *J. Org. Chem.*, **39**, 3378 (1974).
8) J. J. Tufariello and E. J. Trybulski, *J. Chem. Soc., Chem. Commum.*, **1973**, 720.
9) J. J. Tufariello and J. P. Tette, *J. Chem. Soc., Chem. Commum.*, **1971**, 469.
10) E. J. Corey and J. W. Suggs, *Tetrahedron Lett.*, **1975**, 2647.

  Bull. Chem. Soc. Jpn., 54, 1781—1786 (1981)

The Thermal Decomposition of *N,O*-Diacyl-*N*-*t*-butylhydroxylamines. II.[1] Thermal Rearrangement of *O*-Acyl-*N*-[2-(methylthio)-benzoyl]-*N*-*t*-butylhydroxylamines

Yuzuru Uchida,* Yusho Kobayashi, and Seizi Kozuka†

Department of Applied Chemistry, Osaka Institute of Technology, Asahi-ku, Osaka 535

†*Department of Applied Chemistry, Faculty of Engineering, Osaka City University, Sumiyoshi-ku, Osaka 558*

(Received December 22, 1980)

Several *O*-acyl-*N*-[2-(methylthio)benzoyl]-*N*-*t*-butylhydroxylamines (**1**) were prepared and their thermal decompositions were studied. The thermal decomposition of **1** at 200 °C in *o*-dichlorobenzene gave *N*-*t*-butyl-2-(acyloxymethylthio)benzamide (**4**), the carboxylic acid derived from the acyl part of **1**, and 2-*t*-butyl-1,2-benzothiazol-3(2*H*)-one as the main products, together with small amounts of 4*H*-3,1-benzoxathiin-4-one, *N*-*t*-butyl-2-(methylthio)benzamide, methyl ester of the carboxylic acid, and *N*-*t*-butylamide. The benzamide (**4**) was found to be an initial product of the thermolysis and the subsequent decomposition gave the carboxylic acid and other products. Pummerer type reaction, *via* acylaminosulfonium ion as the intermediate, was suggested for the thermal decomposition of **1** since similar products were also obtained by the Pummerer reaction of *N*-*t*-butyl-2-(methylsulfinyl)benzamide with acylating reagents.

N,O-Diacylhydroxylamines have been known to react with nucleophiles both at the carboxyl carbon atom and at the nitrogen atom depending on the nature of the nucleophiles. In general, nucleophiles such as amines,[2] sulfide,[3] alkoxide,[1,3] azide,[3] and cyanide ions[3] attack the carboxyl carbon atom of the *N,O*-diacylhydroxylamines. On the other hand, Ohta *et al.* have shown the substitution reaction at the nitrogen atom by the reaction of *O*-acetyl-*N*-benzoyl-*N*-(4-methoxyphenyl)hydroxylamine with phenols, pyrrole, and indoles.[4] In the previous paper, we have reported that *N,O*-diacyl-*N*-*t*-butylhydroxylamines were decomposed thermally to afford amides and carboxylic acids in good yields. A mechanism involving nucleophilic substitution at the nitrogen atom has been suggested for the thermolysis of the hydroxylamines.[1]

Meanwhile, formations of acylaminosulfonium salts by the nucleophilic substitution at the amide-nitrogen atom have been known for the reaction of *N*-haloamides with dialkyl sulfides.[5] In this connection, thermolysis of a *N,O*-diacylhydroxylamine bearing a nucleophilic group at an appropriate position would take place by a different way, that is, an intramolecular substitution. Thus, we have prepared several *N,O*-diacyl-*N*-*t*-butylhydroxylamines (**1**) and studied their thermal decompositions. An intramolecular substitution reaction at the nitrogen atom by the methylthio-sulfur atom has been found as was expected.

Results and Discussion

Preparation of O-*Acyl*-N-[*2-(methylthio)benzoyl*]-N-t-*butylhydroxylamines (1).* Several title hydroxylamines (**1**) were prepared by the acylation of *O*-acyl-*N*-*t*-butylhydroxylamines (**2**) or *N*-[2-(methylthio)-benzoyl]-*N*-*t*-butylhydroxylamine (**3**) with corresponding acyl chlorides in the presence of pyridine (Scheme 1). Syntheses of **1a** and **1b** were performed by the reactions of 2-(methylthio)benzoyl chloride with **2a** and **2b**, respectively, in good yields. By the reaction of **2c** and **2d**, **1c** and **1d**, however, were obtained, respectively, in only poor yields. Alternatively, **1a** was hydrolized giving **3** which was acylated by appropriate acyl chlorides giving **1c—e** in satisfactory yields. Yields, physical properties, and analyses of **1** are summarized in Table 1.

Thermal Decomposition of N,O-*Diacyl*-N-t-*butylhydroxylamine (1).* On heating at 200 °C for 25 h in *o*-dichlorobenzene, 78% of **1a** was decomposed to give *N*-*t*-butyl-2-(benzoyloxymethylthio)benzamide (**4a**), benzoic acid (**5a**), 2-*t*-butyl-1,2-benzothiazol-3(2*H*)-one (**6**), 4*H*-3,1-benzoxathiin-4-one (**7**), *N*-*t*-butyl-2-(methylthio)benzamide (**8**), methyl benzoate (**9a**), and *N*-*t*-butylbenzamide (**10a**). The yields of the products

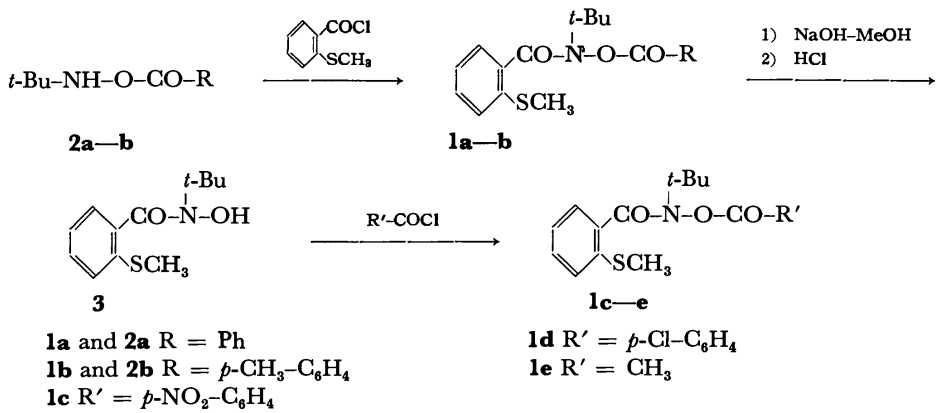

1a and **2a** R = Ph
1b and **2b** R = *p*-CH_3-C_6H_4
1c R′ = *p*-NO_2-C_6H_4
1d R′ = *p*-Cl-C_6H_4
1e R′ = CH_3

Scheme 1.

Table 1. Yields and physical properties of *O*-acyl-*N*-[2-(methylthio)-benzoyl]-*N*-*t*-butylhydroxylamines (**1a—e**)

Compd	Starting compd	Yield %	Mp(Bp) °C	IR (KBr) $\tilde{\nu}$(C=O)/cm^{-1}	Found (Calcd) (%) C	H	N
1a	**2a**	83	116.5—117.5	1760, 1640	66.37 (66.45)	5.98 (6.16)	4.02 (4.08)
1b	**2b**	69	70.5— 71.5	1750, 1650	67.27 (67.20)	6.43 (6.49)	3.75 (3.92)
1c	**3**	82	119.0—120.0	1760, 1670	58.58 (58.75)	5.13 (5.19)	7.30 (7.21)
1d	**3**	80	97.0— 98.0	1760, 1650	60.33 (60.39)	5.30 (5.34)	3.57 (3.71)
1e	**3**	86	(156—157/3 mmHg)††	1790, 1660	59.95 (59.76)	6.89 (6.81)	5.01 (4.98)

††Through this paper 1 mmHg=133.322 Pa.

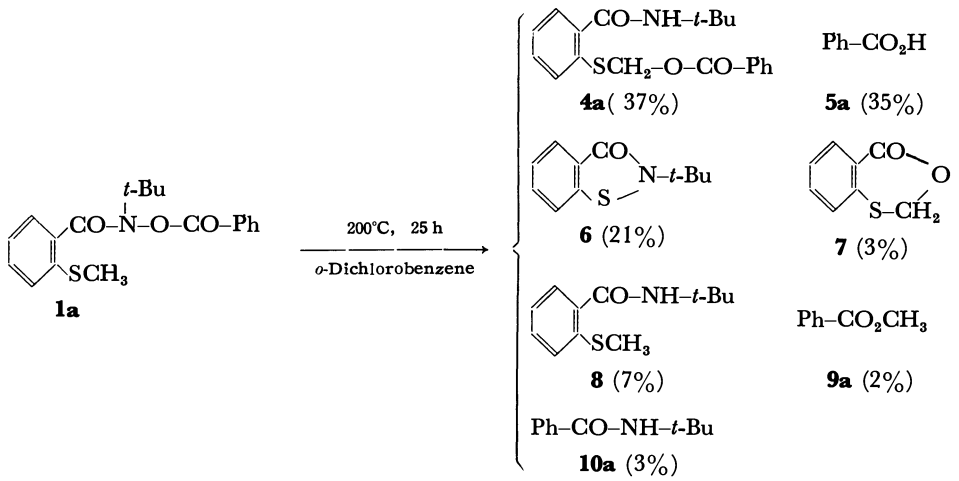

Scheme 2.

were estimated by means of GLC (Scheme 2).

The structures of the products were ascertained on the basis of the spectral and chemical evidences. The NMR spectrum of **4a** in carbon tetrachloride showed singlets at δ 1.38 (9H) and δ 5.57 (2H), broad singlet at δ 6.10 (1H), and multiplet at around δ 7.1—8.1 (9H). The characteristic amide and ester bands of **4a** were observed at 3290 (N–H), 1720 (ester C=O), 1630 (amide C=O), and 1540 cm^{-1} (N–H) in its IR spectrum. In addition, the structure of **4a** was confirmed by comparision these physical properties with those of an authentic sample prepared by the reaction of *N*-*t*-butyl-2-(methylsulfinyl)benzamide (**11**) with benzoic anhydride.

The NMR spectrum of **6** in carbon tetrachloride showed a singlet at δ 1.68 (9H) and aromatic proton signals at δ 7.3—8.0 (4H). The IR spectrum of **6** consisted with amide carbonyl absorption at 1650 cm^{-1}. The elemental analysis also did not conflict with the structure. The compound **6** was synthesized by a different route. Namely, the reaction of *N*-*t*-butyl-2-(methylsulfinyl)benzamide (**11**) with acetyl or thionyl chlorides gave **6** in good yields. The structure of **7** was confirmed by comparing physical properties with those of the authentic sample prepared by the method of Numata and Oae.[6]

Table 2. Thermal decomposition of *O*-acyl-*N*-[2-(methylthio)benzoyl]-*N*-*t*-butylhydroxylamines at 200 °C in *o*-dichlorobenzene (0.1 mol/dm^3)

Compd	Time h	Conversion %	Products yield/%[a] 4	5[b]	6	7	8	9	10
1a	25	78	37	35	21	3	7	2	3
1a	50	94	11	60	36	7	11	1	9
1b	25	67	30	14	30	2	4	1	2
1b	50	85	22	51	38	3	6	2	5
1c	7	100	50[c]	23	9	7	2	1	11
1d	25	96	44	43	26	7	7	2	4
1e	25	56	7	[d]	20	2	1	[d]	[d]
1e	50	70	6	[d]	28	5	7	[d]	[d]

a) Based on the starting **1**. Estimated by GLC. b) The amounts of the acid were estimated after methylation with diazomethane. c) Isolated yield. d) Not determined.

The rearranged products (**4b—e**) were obtained similarly together with **5**, **6**, **7**, **8**, **9**, and **10** by the thermal decompositions of **1b—e**. These results are summarized in Table 2. Physical properties and analyses of **4** are summarized in Table 3.

Inspection of the results given in Table 2 reveals that

Table 3. Physical properties of *N*-*t*-butyl-2-(acyloxymethylthio)benzamides

Compd	Mp °C	IR (KBr) $\tilde{\nu}$/cm^{-1} (N–H)	IR (KBr) (Ester C=O)	IR (KBr) (Amide C=O)	Found (Calcd) (%) C	H	N
4a	85.0— 86.0	3290	1720	1630	66.47 (66.45)	6.26 (6.16)	4.02 (4.08)
4b	91.0— 92.0	3300	1720	1640	67.05 (67.20)	6.44 (6.49)	4.00 (3.92)
4c	120.5—121.5	3310	1720	1640	58.94 (58.75)	5.19 (5.19)	7.24 (7.21)
4d	83.0— 84.0	3290	1720	1630	60.38 (60.39)	5.29 (5.34)	3.77 (3.71)
4e	69.5— 70.5	3350	1730	1660	60.00 (59.76)	6.95 (6.81)	5.01 (4.98)

the rates of the decompositions of **1** were affected by the substituent of the *O*-acyl group. Electron-withdrawing groups accelerated the reaction. Namely, the thermal decomposition of **1c** which has 4-nitrobenzoyl group, completed within 7 h on heating at 200 °C, while, 33 and 44% of the starting materials were recovered by the decompositions of **1b** and **1e**, respectively, under the same reaction conditions. The yields of **4** were found to be depressed by prolonged heating as shown in Table 2. In a control experiment, **4a** was found to be decomposed under the same reaction conditions (200 °C, 25 h) giving **5a**, **6**, **7**, **8**, and **10a** in 46, 6, 7, 10, and 5% yields, respectively, with 60% decomposition of the starting material. These results suggest a successive decomposition of **4** giving the products, **5**—**8** and **10**, for the decomposition of **1**, although the yield of **6** from **4** (6%) could not account for that from **1** (21%).

A probable mechanism leading to the rearranged product, **4**, from **1** would involve an intramolecular nucleophilic attack of sulfur atom on the nitrogen atom giving acylaminosulfonium salt, **12**, as the intermediate. The salt **12** would afford **4** by subsequent Pummerer rearrangement *via* ylid **13**. An alternative possible pathway leading to **4** from **12** may involve attack of the anion on the sulfur giving sulfonium salt **14** and proton migration would give the ylid **15**. Pummerer rearrangement of **15** may afford **4** as shown in Scheme 3. Direct formation of the sulfonium amide **14** by the attack of the sulfur on the ester oxygen of **1** seems to be unlikely by considering differences in leaving abilities of carboxylate and amide anions, and also in electronegativities of oxygen and nitrogen atoms. In fact, acceleration of the rate by the electron-withdrawing substituent on the *O*-acyl group is in accordance with the proposed mechanism involving the carbooxylate ion as the leaving group.

As mentioned above, another pathway would be required to account for the yield of **6**. This may be a demethylation reaction of the acylamisosulfonium ion (**12**) by a nucleophile. The formation of methyl ester (**9**) by the decomposition of **1** would support this prosess.

Pummerer Reactions of N-t-*Butyl-2-(methylsulfinyl)benzamide (11).* In order to prove the intermediacy of the acylaminosulfonium ion (**12**) for the thermolysis

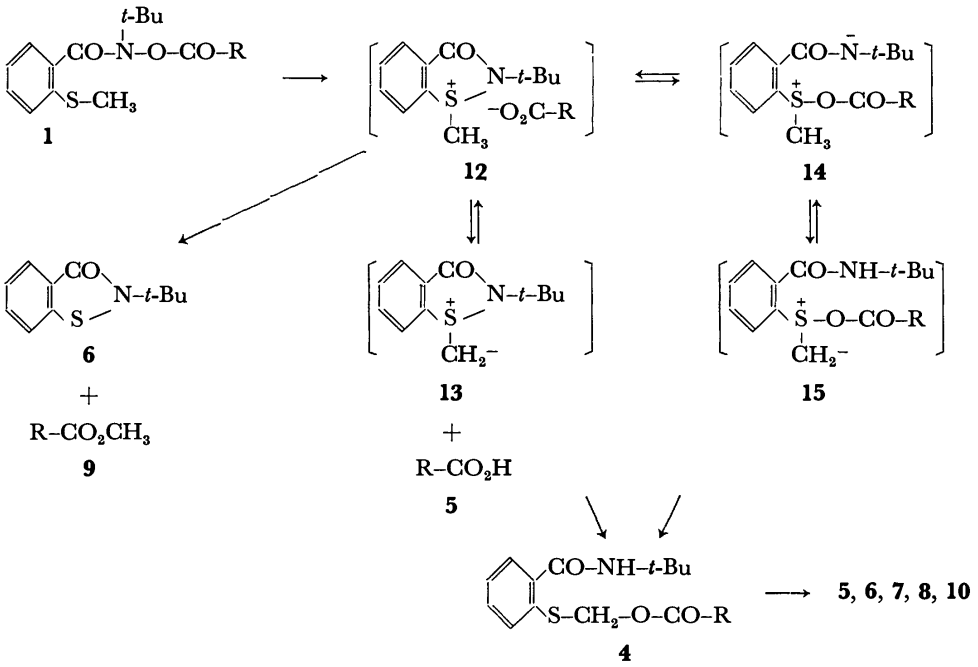

Scheme 3.

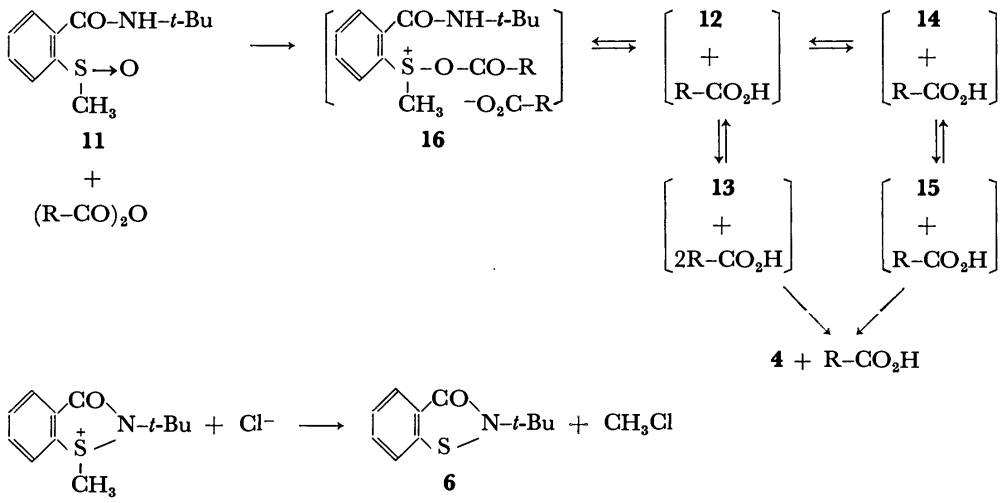

Scheme 4.

of **1**, Pummerer reaction of **11** with acylating reagents, such as benzoic anhydride, acetic anhydride, acetyl chloride, and thionyl chloride were examined. In Pummerer reaction of **11**, the acylaminosulfonium ion **12** and/or the sulfonium salt **14** would be the intermediate. The sulfoxide **11** was heated at 180 °C for 10 h with 1.2 equiv. of benzoic anhydride in *o*-dichlorobenzene. The product **4a** (55%) was obtained together with small amount of **6** as was expected. The reaction of **11** with acetic anhydride gave **4e** and **6** similarly. On the other hand, the reaction of **11** with acetyl chloride or thionyl chloride proceeded at room temperature affording **6** in good yields. When excess of thionyl chloride was added to carbon tetrachloride solution of **11**, the NMR signals of *t*-butyl protons (δ 1.47, s) and *S*-methyl protons (δ 2.73, s) disappeared and new signals appeared at δ 1.73 (s), 1.80 (s), 2.99 (s), and 3.70 (s). During the reaction, the intensities of the signals at δ 1.80 and 3.70 decreased and the signals at δ 1.73 and 2.99 increased. The down field shift to δ 1.80 and 3.70 of the *t*-butyl and *S*-methyl signals, respectively, would apparently due to a positive charge which in turn suggest the formation of acylaminosulfonium ion (**12**) as the intermediate. After about 20 min, the signals at δ 1.80 and 3.70 disappeared and the ratio of the intensities of the signals at δ 1.73 and 2.99 was about 3 : 1. These signals were assigned to be *t*-butyl protons of **6** and methyl protons of chloromethane, respectively.

The reaction of **11** with acylating reagents can be explained by the mechanism shown in Scheme 4. The sulfonium salt **16**, initially formed by the reaction of **11** with acylating reagents gives **12** and/or **14**,[7] then rearranges to **4** by Pummerer reaction.[8] In the reactions of **11** with acetyl and thionyl chlorides, the acylaminosulfonium ion (**12**) is attacked by chloride ion giving **6** and chloromethane. Thus, the intermediacy of the acylaminosulfonium ion (**12**) for the thermal decomposition of **1** has been confirmed by the Pummerer reaction of the corresponding sulfoxide.

Experimental

All the melting points and the bioling points are uncorrected. The IR spectra were recorded on a Shimazdu IR-430 infrared spectrometer. The NMR spectra were recorded on a Varian EM-360 spectrometer using TMS as the internal standard.

Preparation of O-*Acyl*-N-[*2-(methylthio)benzoyl*]-N-t-*butylhydroxylamines (1)*. *Typical Procedure (a)*: A solution of 2-(methylthio)benzoyl chloride (58.0 g, 300 mmol), *O*-benzoyl-*N*-*t*-butylhydroxylamine (58.0 g, 310 mmol),[1] and pyridine (25.0 g, 320 mmol) in dry benzene (200 cm^3) was stirred at 75 °C for 20 h. The reaction mixture was washed with aq NH_3, dil NaOH, dil HCl, and water, and then dried over Na_2SO_4. The solvent was evaporated *in vacuo*, and the residue was recrystallized from benzene giving **1a** (86.0 g, 83%).

By the reaction of *O*-(4-methylbenzoyl)-*N*-*t*-butylhydroxylamine[1] with 2-(methylthio)benzoyl chloride, **1b** was prepared similarly.

(b): A solution of *N*-[2-(methylthio)benzoyl]-*N*-*t*-butylhydroxylamine (**3**) (12.0 g, 50 mmol), 4-chlorobenzoyl chloride (10.5 g, 60 mmol), and pyridine (4.7 g, 59 mmol) in dry benzene (150 cm^3) was stirred at 75 °C for 20 h. The reaction mixture was washed with aq NH_3, dil NaOH, dil HCl, and water, and then dried over Na_2SO_4. The solvent was evaporated *in vacuo* and the residue was recrystallized from CH_2Cl_2–petroleum ether giving **1d** (15.2 g, 80%).

By the same procedure, **1c** and **1e** were prepared by the reaction of **3** with 4-nitrobenzoyl chloride and acetyl chloride, respectively. The yields and physical properties are summarized in Table 1.

Preparation of N-[*2-(Methylthio)benzoyl*]-N-t-*butylhydroxylamine (3)*. A solution of NaOH (10.0 g, 250 mmol) in water (40 cm^3) was added to a solution of **1a** (34.3 g, 100 mmol) in methanol (200 cm^3). The mixture was stirred at room temperature for 3 h. After evaporation of the solvent, the residue was dissolved in water (200 cm^3), washed with diethyl ether, and acidified with HCl. The separated crystals were extracted with CH_2Cl_2, and the organic layer was washed with aq $NaHCO_3$ and water, and then dried over Na_2SO_4. The solvent was evaporated and the residue was recrystallized from benzene to give **3** (19.7 g, 82%); mp 145.0—146.0 °C. Found: C, 60.36; H, 7.31; N, 5.78%. Calcd for $C_{12}H_{17}O_2S$: C, 60.22; H, 7.16; N, 5.85%. IR: (KBr) 3150 (O–H) and 1600 cm^{-1} (C=O). NMR: ($CDCl_3$, δ) 1.38 (9H, s), 2.48 (3H,

s), 7.1—7.4 (4H, m), and 8.33 (1H, s).

Thermal Decomposition of **1**. A solution of **1** in *o*-dichlorobenzene (0.1 mol/dm³, 10 cm³) was sealed in a degassed tube and then heated in a constant-temperature bath at 200 °C. The tube was opened and 60 mg of biphenyl was added to the reaction mixture as an internal standard. The mixture was subjected to GLC analysis. In order to estimate the yield of carboxylic acid, an excess of an diethyl ether solution of diazomethane was added to a portion of the sample, and the mixture was allowed to stand for 1 h. After the evaporation of the ether *in vacuo*, the reaction mixture was subjected to GLC analysis. The following five columns were used; a 45 cm column packed with Silicone GE SE-30 (5%) on Shimalite W to analyze **1a**, **1**, **1d**, **4a**, **4b**, and **4d**; a 1 m column packed with Silicone GE SE-30 (5%) on Shimalite W to analyze **1e**, **4e**, **6**, and **8**; a 2 m column packed with Apiezon Grease L (30%) on Cerite 545 to analyze **6**, **7**, **8**, **9b**, **10a**, **10c**, and **10d**; a 2 m column packed with Thermon 1000+H_3PO_4 (5+0.5%) on Chromosorb W to analyze **9c**, and a 5 m column packed with polyethylene glycol 20 M (25%) on Shimalite 101 to analyze **9a** and **9d**.

For the isolation of the products, the thermal decompositions of **1** were carried out in a large scale. Typical procedure was as follows: A solution of **1c** (2.000 g, 5.15 mmol) in *o*-dichlorobenzene (40 cm³) was sealed in a degassed tube and heated at 200 °C for 7 h. The reaction mixture was washed with aq Na_2CO_3 and water. The alkaline solution was acidified with HCl to give **5c** (65 mg, 8%). The organic layer was dried over Na_2SO_4 and the solvent was evaporated *in vacuo*. The residue was chromatographed on silica gel with CH_2Cl_2 to give crude **4c**, **6**, and **7**. The crude **4c** was purified by recrystallization from ethanol (820 mg, 41%). The crude **6** and **7** were purified by preparative GLC.

Thermal Decomposition of **4a**. A solution of **4a** (343.4 mg, 1 mmol) in *o*-dichlorobenzene (10 cm³) was sealed in a deassed tube and then heated in a constant-temperature bath at 200 °C for 25 h. Biphenyl (60 mg) was added to the reaction mixture as an internal standard. The mixture was subjected to GLC analysis.

Preparation of N-t-*Butyl-2-(methylthio)benzamide* (**8**). A solution of 2-(methylthio)benzoyl chloride (37.3 g, 200 mmol) in dry benzene (100 cm³) was added to a solution of *t*-butylamine (30.7 g, 420 mmol) in dry benzene (200 cm³) with stirring. The mixture was refluxed for 1 h, washed with dil HCl, aq $NaHCO_3$, and water, and then dried over Na_2SO_4. The benzene was evaporated, and the residue was recrystallized from benzene–petroleum ether giving **8** (38.1 g, 85%); mp 133.0—134.0 °C.

Preparation of N-t-*Butyl-2-(methylsulfinyl)benzamide* (**11**). A solution of sodium metaperiodate (21.4 g, 100 mmol) in water (80 cm³) was added to a solution of *N-t*-butyl-2-(methylthio)benzamide (**8**) (22.3 g, 100 mmol) in methanol (200 cm³). The mixture was stirred for 3 h at room temperature. The reaction mixture was filtered and the filtrate was condensed to dryness. Water (50 cm³) and CH_2Cl_2 (150 cm³) was added to the residue, and the organic layer was separated. The extract was dried over Na_2SO_4 and the solvent was evaporated. The residue was recrystallized from CH_2Cl_2–petroleum ether to give **11** (22.1 g, 92%); mp 150.0—151.0 °C. Found: C, 59.93; H, 7.34; N, 5.78%. Calcd for $C_{12}H_{17}NO_2S$: C, 60.22; H, 7.16; N, 5.85%. IR (KBr): 3250 (N–H) and 1640 cm⁻¹ (C=O). NMR: ($CDCl_3$, δ) 1.48 (9H, s), 2.86 (3H, s), 6.57 (1H, broad s), and 7.4—8.2 (4H, m).

Reaction of **11** *with Acid Anhydrides*. A mixture of **11** (2.4 g, 10 mmol) and benzoic anhydride (2.7 g, 12 mmol) in *o*-dichlorobenzene (20 cm³) was refluxed for 10 h. The solvent was removed *in vacuo*, and the residue was dissolved in diethyl ether (50 cm³), washed with aq NH_3, Na_2CO_3, and water. The ether was evaporated after being dried over Na_2SO_4 and the residue was chromatographed on silica gel with CH_2Cl_2 as the eluant to give a mixture of **4a** and **6**. The mixture was recrystallized from CH_2Cl_2–petroleum ether giving **4a** (1.9 g, 55%).

The reaction of **11** with acetic anhydride was carried out in the same manner as mentioned above giving **4e** (1.7 g, 60%).

Reaction of **11** *with Acetyl Chloride*. Acetyl chloride (0.9 g, 10 mmol) was added to a solution of **11** (2.4 g, 10 mmol) in CH_2Cl_2 (20 cm³). The mixture was allowed to stand over night at room temperature, washed with aq NH_3 and water, and dried over Na_2SO_4. The solvent was removed and the residue was distilled under reduced pressure to give **6** (1.6 g, 77%); bp 165—166 °C/2.5 mmHg (lit,[9] bp 142 °C/0.5 mmHg). The distillate was recrystallized from petroleum ether; mp 57.0—58.0 °C. Found: C, 63.66; H, 6.55; N, 6.66%. Calcd for $C_{11}H_{13}NOS$: C, 63.74; H, 6.32; N, 6.76%. IR (KBr): 1650 cm⁻¹ (C=O). NMR (CCl_4, δ): 1.67 (9H, s) and 7.2—8.0 (4H, m).

Reaction of **11** *with Thionyl Chloride*. Thionyl chloride (1.8 g, 15 mmol) was added to a solution of **11** (2.4 g, 10 mmol) in CH_2Cl_2 (20 cm³). The mixture was allowed to stand for 1 h at room temperature, washed with aq Na_2CO_3 and water, and then dried over Na_2SO_4. The solvent was removed and the residue was distilled under reduced pressure to give **6** (1.6 g, 77%).

Preparation of 2-(Methylsulfinyl)benzoic Acid. Sodium metaperiodate (25.7 g, 120 mmol) in water (80 cm³) was added to a solution of 2-(methylthio)benzoic acid (20.0 g, 119 mmol) in methanol (250 cm³). The mixture was stirred for 4.5 h at room temperature and filtered. The filtrate was condensed to dryness and the residue was recrystallized from methanol–water to give 2-(methylsulfinyl)benzoic acid (18.4 g, 84%); mp 170.0—171.0 °C (dec) [lit,[10] mp 172 °C (dec)].

Preparation of 4H-*3,1-Benzoxathiin-4-one* (**7**). A mixture of 2-(methylsulfinyl)benzoic acid (5.0 g, 27 mmol) and acetic anhydride (4.1 g, 40 mmol) was refluxed for 15 h. The excess acetic anhydride was removed by distillation. The residue was dissolved in diethyl ether and washed with aq $NaHCO_3$ and water. The solvent was removed after being dried over Na_2SO_4, and the residue was recrystallized from CCl_4–petroleum ether giving **7** (3.9 g, 87%); mp 47.0—48.0 °C (lit,[11] 47 °C). IR (KBr): 1720 cm⁻¹ (C=O). NMR (CCl_4, δ): 5.38 (2H, s), 7.1—7.5 (3H, m), and 8.0—8.3 (1H, m).

Preparation of N-t-*Butylbenzamide* (**10a**). A solution of benzoyl chloride (14.0 g, 100 mmol) in dry benzene (50 cm³) was added to a solution of *t*-butylamine (18.0 g, 246 mmol) in dry benzene (150 cm³) with stirring. The reaction mixture was refluxed for 1 h, washed with aq NH_3, dil HCl, aq Na_2CO_3, and water, and then dried over Na_2SO_4. The solvent was removed, and the residue was recrystallized from CH_2Cl_2–petroleum ether giving **10a** (17.2 g, 97%); mp 134.0—135.0 °C (lit,[12] mp 134.0—134.5 °C).

By the same procedures. **10b—d** were prepared by the reactions of *t*-butylamine and the corresponding acyl chlorides. **10b**: mp 115.5—116.5 °C. **10c**: mp 159.0—160.0 °C. **10d**: mp 137.0—138.0 °C.

References

1) Part I of this series: Y. Uchida, Y. Hashimoto, and S. Kozuka. *Bull. Chem. Soc. Jpn.*, **53**, 2309 (1980).

2) P. G. Sammes, *J. Chem. Soc.*, **1965**, 6608; D. Sarantakis, J. K. Sutherland, C. Tortorella, and V. Tortorella, *J. Chem. Soc., C*, **1968**, 72.

3) S. Oae and T. Sakurai, *Bull. Chem. Soc. Jpn.*, **48**, 1075

(1975).
4) T. Ohta, K. Shudo, and T. Okamoto, *Tetrahedron Lett.*, **1978**, 1983.
5) H. Kise, G. F. Whitfield, and D. Swern, *J. Org. Chem.*, **37**, 1121 (1972); P. G. Gassman and R. J. Balchunis, *Tetrahedron Lett.*, **1977**, 2235.
6) T. Numata and S. Oae, *Chem. Ind. (London)*, **1972**, 726.
7) T. E. Varkey, G. E. Whitfield, and D. Swern, *J. Org. Chem.*, **39**, 3365 (1974); A. K. Sharma, T. Ku, A. D. Dawson, and D. Swern, *J. Org. Chem.*, **40**, 2758 (1975).
8) H. Kise, G. F. whitfield, and D. Swern, *J. Org. Chem.*, **37**, 1125 (1972).
9) J. S. Morley, Brit. Patent 848139 (1960); *Chem. Abstr.*, **55**, 9430f (1961).
10) A. Kucsman, I. Kapovits, and B. Tanacs, *Tetrahedron*, **18**, 79 (1962).
11) W. G. Bentrude and J. C. Martin, *J. Am. Chem. Soc.*, **84**, 1561 (1962).
12) J. J. Ritter and P. P. Minieri, *J. Am. Chem. Soc.*, **70**, 4045 (1948).

  Bull. Chem. Soc. Jpn., 54, 1787—1792 (1981)

Catalysis by Mixed Oxide Perovskites. II. The Hydrogenolysis of C_3—C_5 Hydrocarbons on $LaCoO_3$

Kenji Ichimura, Yasunobu Inoue,* and Iwao Yasumori

Department of Chemistry, Tokyo Institute of Technology, Ookayama, Meguro-ku, Tokyo 152

(Received September 25, 1980)

The catalytic hydrogenolysis of C_3—C_5 alkanes on $LaCoO_3$ perovskite oxide was found to show a highly selective formation of methane in the temperature range of 350—620 K. The reaction order with respect to the hydrocarbon pressure was unity in every hydrogenolysis, whereas the hydrogen order increased from zero for propane to 1.0 for butane and isobutane and to 2.0 for pentane, isopentane, and neopentane. The activation energies of the reactions ranged from 120 for propane to 32 kJ mol^{-1} for butane. The reaction of propane or butane with D_2 on $LaCoO_3$ provided large fractions of methane [D_3] and [D_4], but a negligible amount of deuterium-exchanged alkanes. An equilibrium among the gaseous H_2, HD, and D_2 was reached. These hydrogenolyses are described by a mechanism involving the almost concurrent repture of all the carbon-carbon bonds in the alkanes by the attack of adsorbed hydrogen atoms, and were proposed to be catalyzed by a synergetic effect; the CO^{3+} ion is effective in breaking the C–C bond, whereas the La^{3+} and O^{2-} ions serve to supply hydrogen atoms to the decomposed species. The reaction of propene or butenes with hydrogen produced the corresponding alkanes and methane. The kinetic analyses showed that the fractions of methane produced consecutively *via* the alkanes amounted to 16% for propene and to more than 93% for butenes. The observed pressure dependence and deuterium distributions in the alkene hydrogenation were interpreted in terms of the associative mechanism. The correlation between the structures of the reactant molecules and of the active sites present on $LaCoO_3$ was briefly discussed.

In the first paper of this series,[1] we reported the noteworthy catalytic properties of $LaCoO_3$ for the hydrogenolysis of ethylene and ethane. This mixed oxide exhibited a stable and high catalytic activity and retained its original perovskite structure even after several runs in a reducing atmosphere. At reaction temperatures above 420 K, the ethylene hydrogenolysis to form methane was found to proceed in a consecutive way *via* ethane as a stable intermediate, accompanied by a minor side-reaction of the direct methane formation. The X-ray photoelectron spectroscopic studies emphasized the importance of the trivalent state of the cobalt ion in rupturing the C–C bond, and the active structures were proposed to be composed of the (110) plane.

The catalytic hydrogenolysis of C_3—C_{10} hydrocarbons has been extensively studied on transition-metal catalysts,[2-6] but no detailed kinetic analyses have yet been done well because of complexities in the product distributions and because of the fast deactivation of the metal catalysts during the hydrogenolysis. In view of the remarkable selectivity and stable activity of $LaCoO_3$, it is of interest to examine the hydrogenolysis of alkanes and alkenes with longer carbon or side-carbon chains. Furthermore, we can expect that the employment of a variety of reactant molecules with different stereochemical conformations might be useful in obtaining information on the structure and distributions of the active sites exposed at the perovskite surface. In the present work, therefore, we investigated the hydrogenolysis of propene, butenes, and a series of alkanes from propane to pentane isomers by performing detailed kinetic studies, which were supplemented by a tracer work using D_2.

Experimental

The preparation of the mixed oxide perovskite, $LaCoO_3$, was described in the previous paper.[1] This perovskite catalyst was activated by heating *in vacuo* in the temperature range of 600—800 K in order to obtain a constant catalytic activity; the activity was reproducible enough for more than ten successive hydrogenolysis runs of C_2—C_5 hydrocarbons, except for that of acetylene.

The reaction of hydrocarbons with hydrogen was studied in a closed circulating system at temperatures between 350 and 620 K in the pressure range of 5—30 Torr (1 Torr = 133.3 Pa) for hydrocarbons and in that of 50—150 Torr for hydrogen. The procedures of kinetic study and of the analysis of the deuterium-distributed reactant and products in the reaction with D_2 were much the same as those employed previously.[1]

Reactant gases such as hydrogen (99.98% in purity), deuterium (containing less than 0.4% HD), propene (99.9%), propane (99.9%), butenes (99.0%), and butane (99.7%) were purchased from the Takachiho Shoji Co. and were used without further purification. Pentane and isopentane of an extra pure grade, obtained from the Wako Chemical Co., and neopentane from the Tokyo Kasei Co., were distilled and then subjected to several freeze-evacuation-thaw cycles to remove gaseous impurities.

Results

Hydrogenolysis of Alkanes. In the temperature and pressure ranges employed here, the hydrogenolysis of C_3 to C_5, *i.e.*, propane, butane, isobutane, pentane, isopentane, and neopentane, on $LaCoO_3$ produced only methane as a product. Neither the corresponding alkenes nor the fragmented hydrocarbons were detected in the gas phase.. The rates of hydrocarbon consumption fell within the same order of magnitude, $0.5—1.5 \times 10^{13}$ molecule s^{-1} cm^{-2} at 573 K, irrespective of the alkanes, except for the case of butane, which gives a higher rate of 7×10^{13} molecule s^{-1} cm^{-2}. The kinetic analysis of the reaction showed that the reaction orders with respect to the hydrocarbon pressure, $P_{C_nH_{2n+1}}$, were unity for all the reactions. Figure 1 shows the dependence of the rate on the hydrogen pressure, P_{H_2}; the hydrogen orders increased with the number of carbon atoms involved in the reactant hydrocarbons and were found to be 0.0, 1.0, and 2.0 for the reactions of C_3H_8, C_4H_{10},

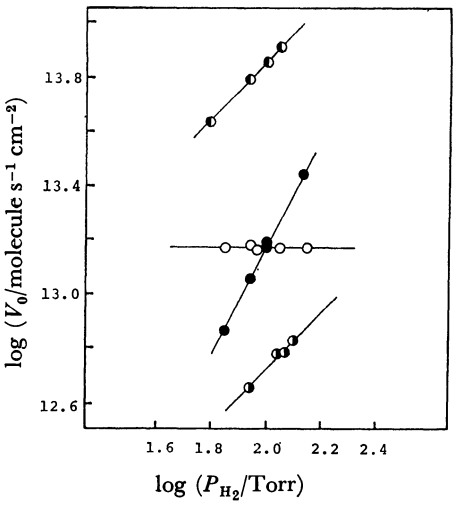

Fig. 1. Dependence of rate upon hydrogen pressure in the hydrogenolysis of C_3—C_5 alkanes.
○: C_3H_8, ◐: n-C_4H_{10}, ◑: i-C_4H_{10}, ●: n-C_5H_{12}, P_{HC}=10 Torr, Reaction temperature=573 K.

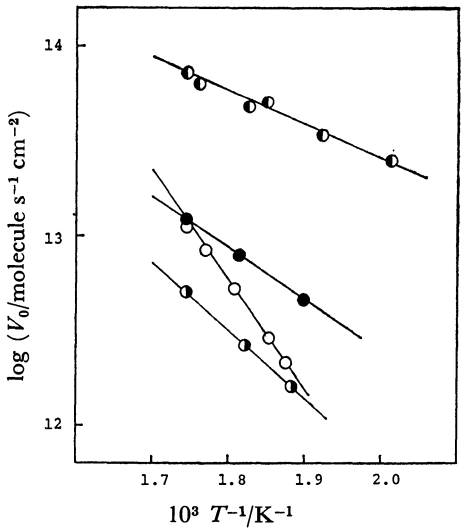

Fig. 2. Arrhenius plots of alkane hydrogenolysis.
○: C_3H_8, ◐: n-C_4H_{10}, ◑: i-C_4H_{10}, ●: n-C_5H_{12}, P_{HC}=11 Torr, P_{H_2}=100 Torr.

Table 1. Kinetic parameters in the hydrogenolysis of C_2 to C_5 alkanes on $LaCoO_3$

Reactions	Reaction order[a]		Activation energy[b]	Rate[c]
	m	n	kJ mol^{-1}	molecule s^{-1} cm^{-2}
$C_2H_6+H_2 \longrightarrow 2CH_4$	1.0	−0.5	35	1.0×10^{13}
$C_3H_8+2H_2 \longrightarrow 3CH_4$	1.0	0.0	120	1.5
n-$C_4H_{10}+3H_2 \longrightarrow 4CH_4$	1.0	1.0	32	7.2
i-$C_4C_{10}+3H_2 \longrightarrow 4CH_4$	1.0	1.0	71	0.5
n-$C_5H_{12}+4H_2 \longrightarrow 5CH_4$	1.0	2.0	55	1.5
i-$C_5H_{12}+4H_2 \longrightarrow 5CH_4$	1.0	2.0	38	1.0
$C(CH_3)_4+4H_2 \longrightarrow 5CH_4$	1.0	2.0	102	0.9

a) ±0.1, Rate=$k_e P^m_{C_nH_{2n+2}} P^n_{H_2}$ (573 K). b) ±3.
c) P_{H_2}=100 Torr, $P_{C_nH_{2n+2}}$=10 Torr. d) See Ref. 1

and C_5H_{12} respectively. The Arrhenius plots of the reaction are demonstrated in Fig. 2. The values of the activation energy and other kinetic parameters are summarized in Table 1, together with the previous results on ethane hydrogenolysis. It should be noted that the activation energy was remarkably high for propane and neopentane, but low for ethane, butane, pentane, and isopentane hydrogenolysis. An intermediate value was obtained for isobutane hydrogenolysis.

Table 2 shows the deuterium distributions in the reactant and products in the reaction of propane and butane with D_2 at 573 K and compares them with the results for ethane hydrogenolysis. A common distribution pattern was observed in these three reactions; at conversions of 16—23%, an equilibrium among H_2, HD, and D_2 in the gas phase is established. The formation of the deuterium-exchanged ethane, propane, and butane was negligibly small, whereas the product, methane, consisted mainly of [D_3] and [D_4] species.

Hydrogenolysis of Propene and Butenes. The reaction of propene with hydrogen at 573 K produced a considerable amount of methane, together with propane at the initial stage of reaction. This behavior contrasts with the predominantly consecutive formation of methane which was observed in the case of ethylene hydrogenolysis.

The reaction of 1-butene, *trans*-2-butene, or *cis*-2-butene with hydrogen at 573 K underwent rapid isomerization, followed by the formation of butane and then methane; the ratio of the produced butene isomers, R(*cis*-2-butene/*trans*-2-butene), R(*cis*-2-butene/1-butene), and R(*trans*-2-butene/1-butene), were determined to be 1.0, 1.8, and 1.8 respectively. These ratios remained almost unchanged until the disappearance of the reactant butene. Table 3 shows the deuterium distributions of the reactant and products in the deuterogenation of propene and 1-butene at 573 K. There existed common features in the distributions for both reactions;

Table 2. Deuterium distributions in the reaction of C_2—C_4 alkanes with D_2 at 573 K on $LaCoO_3$

Reaction		$C_2H_6+D_2$[a]			$C_3H_8+D_2$[b]			n-$C_4H_{10}+D_2$[c]		
Conversion/%		15			16			23		
Gases		C_2H_6	CH_4	H_2	C_3H_8	CH_4	H_2	C_4H_{10}	CH_4	H_2
Distributions	D_0	98	0	0.7	98	0	1	98	0	3
	D_1	1	0	14.7	2	0	17	2	2	27
	D_2	1	6	84.6		7	82		9	70
	D_3		21			20			34	
	D_4		73			73			55	

a) P_{D_2}=117 and $P_{C_2H_6}$=10 Torr. b) P_{D_2}=97 and $P_{C_3H_8}$=11 Torr. c) P_{D_2}=97 and $P_{C_4H_{10}}$=11 Torr.

TABLE 3. DEUTERIUM DISTRIBUTIONS IN THE REACTION OF PROPENE AND 1-BUTENE WITH D_2 AT 573 K ON $LaCoO_3$

Reaction		$C_3H_6+D_2$[a]				$1\text{-}C_4H_8+D_2$[b]					
Gases		C_3H_6	C_3H_8	CH_4	H_2	$1\text{-}C_4H_8$	*cis*-$2\text{-}C_4H_8$	*trans*-$2\text{-}C_4H_8$	$n\text{-}C_4H_{10}$	CH_4	H_2
Distributions	D_0	27	4	0	0.1	37.6	44.6	45.6	17.5	0	0.2
	D_1	31	30	3	5.4	37.0	35.9	36.7	35.0	0	8.4
	D_2	27	44	10	94.5	19.0	14.0	13.7	32.5	0	91.4
	D_3	13	19	19		5.3	4.5	3.7	12.5	12	
	D_4	2	3	68		1.1	1.3	0.5	2.5	88	
	D_5—D_8		0			0	0	0	0		

a) $P_{C_3H_6}=11$ and $P_{D_2}=96$ Torr; conversion=11%. b) $P_{1\text{-}C_4H_8}=11$ and $P_{D_2}=97$ Torr; conversion=71%.

the gaseous composition of H_2, HD, and D_2 nearly reached equilibrium. Propene and 1-butene used as reactants gave rise to wide distributions of deuterium ranging from $[D_0]$ to $[D_4]$. The products involved deuterium-exchanged propane and butane distributed from $[D_0]$ to $[D_4]$. The subsidiary isomerization of 1-butene during hydrogenolysis gave *cis*- and *trans*-2-butenes possessing almost the same distributions of deuterium. Methane contained highly-exchanged methane $[D_3]$ and $[D_4]$, in which the fraction of the latter species amounted to as much as 70—90% of the total methane.

In the reaction of acetylene with hydrogen, ethylene was the only product, and the catalytic activity was drastically decreased during the course of reaction. The initial rate was about one hundredth that of ethylene hydrogenation at 473 K.

Discussion

The features of the hydrogenolysis of propene and butenes on $LaCoO_3$ are similar to those of ethylene hydrogenolysis in that there existed no products other than methane and the corresponding alkanes (except for the butene isomers). Thus, the change in the gaseous compositions of the reactant and products as a function of the time was analyzed by the same procedure as was used in the previous study of the ethylene hydrogenolysis:[1]

$$\begin{array}{ccc} & C_nH_{2n} & \\ & \text{I}\swarrow H_2 \quad nH_2 \searrow \text{II} & \\ C_nH_{2n+2} & \xrightarrow[\text{III}]{(n-1)\,H_2} & n\,CH_4. \end{array} \qquad (1)$$

By assuming that the reaction order with respect to the partial pressure of respective hydrocarbons was unity, the following rate equation can be derived for the consumption of the alkene and alkane under the conditions of an excess of hydrogen:

$$\frac{dP_{C_nH_{2n}}}{dt} = -(k_1+k_2)\,P_{C_nH_{2n}} \qquad (2)$$

$$\frac{dP_{C_nH_{2n+2}}}{dt} = k_1P_{C_nH_{2n}} - k_3P_{C_nH_{2n+2}} \qquad (3)$$

$$\frac{dP_{CH_4}}{dt} = n(k_2P_{C_nH_{2n}}+k_3P_{C_nH_{2n+2}}), \qquad (4)$$

where k_i denotes the rate constant for Process i in Scheme (1). The values of k_i as parameters were determined by applying the non-linear least-squares method so as to give the curves best-fitting the experimental plots. For the reaction with propene, the determined values were $k_1=0.023$, $k_2=0.123$, and $k_3=0.167\ h^{-1}$ at 573 K ($P_{H_2}=100$ Torr), which indicates that the fraction of the direct hydrogenolysis *via* Process (II) is about 84%.

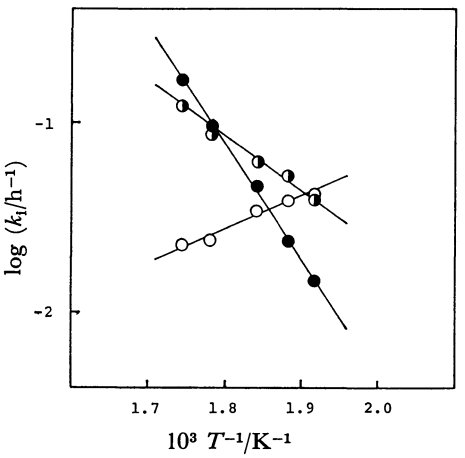

Fig. 3. Arrhenius plots of k_i.
○: k_1, ◑: k_2, ●: k_3.

Figure 3 shows the temperature dependence of k_i; the values of the activation energy, E_a, for Process (I), (II), and (III) were determined to be −33, 52, and 119 kJ mol^{-1} respectively. The analysis of the reaction with different initial hydrogen pressures provided the hydrogen order of unity for both Process (I) and (II) and of zero for Process (III). These results are summarized in Table 4. It should be noted that the rate, the activation energy, and the rate equation for Process (III) were in substantial agreement with the respective values in the propane hydrogenolysis (*cf.* Tables 1 and 4).

Since there was no marked difference in the observed rates of the hydrogenation of 1-butene, *trans*-2-butene, and *cis*-2-butene, the average of these rates could be employed as that of butene hydrogenation. The kinetic analysis gave the values of $k_1=0.040$, $k_2\approx0.003$, and $k_3=0.95\ h^{-1}$ at 573 K, indicating that the fraction of the direct formation of methane from butene was about 7%. As is demonstrated in Tables 1 and 4, there also exists a good agreement in the kinetic parameters and reaction rates between Process (III) and butane hydrogenolysis. These close coincidences give support to the analytical procedure employed here for

Table 4. Kinetic parameters in the hydrogenolysis of propene and butenes

Reaction	Path[a]	Rate[b] molecule s^{-1} cm^{-2}	Reaction order[c] m	Reaction order[c] n[d]	Activation energy[e] kJ mol^{-1}
$C_3H_6+H_2$	I	0.18×10^{13}	1	1.0	−33
	II	0.96×10^{13}	1	1.0	52
	III	1.3×10^{13}	1	0.0	119
$C_4H_8+H_2$	I	0.31×10^{13}	1	1.0	−33
	II	$\approx0.03\times10^{13}$	1	—	—
	III	7.4×10^{13}	1	1.0	32

a) See text. b) Under the standard conditions; reaction temp=573 K, $P^{\circ}_{H_2}=100$ Torr, $P^{\circ}_{C_nH_{2n}}=10$ Torr, and $P^{\circ}_{C_nH_{2n+2}}=10$ Torr. c) Rate$=k'_e P^m_{HC} P^n_{H_2}$. d) ±0.1. e) ±4.

the propene and butene hydrogenolysis.

The previous kinetic study of the ethylene hydrogenation[1] over $LaCoO_3$ revealed that the reaction proceeded mainly on the La and O ions *via* the associative mechanism and that, as the reaction temperature increased, the slow step varied from the dissociative adsorption of hydrogen to the hydrogenation of an ethyl radical. The reaction orders and the way of deuterium distribution in the present hydrogenation of propene and butene were quite similar to those observed in the ethylene hydrogenation in the high-temperature region. Thus, we can safely adopt the associative mechanism as well as the same active-site structure for both reactions, and the rate equation is given[1] by:

$$R_h=k_hK_sK_aK_h\,P_{C_nH_{2n}}\;P_{H_2}=k\,P_{C_nH_{2n}}\,P_{H_2}, \qquad (5)$$

in a simplified form, where k_h is the rate constant for the hydrogenation of the half-hydrogenated species. The constants, K_h, K_a, and K_s, denote, respectively, the equilibrium constants for the adsorption of hydrogen, the adsorption of alkenes, and the surface reaction between adsorbed alkenes and a hydrogen atom. This equation accords well with the experimental pressure dependence.

Alkane Hydrogenolysis. The hydrogenolysis of alkanes has thus far been mostly confined to those catalyzed by transition-metal catalysts;[2] these reactions are characterized by negative orders with respect to P_{H_2} and, generally, by a wide variety of products, coinsisting of fragmented hydrocarbons, except for the selective formation of methane in the case of Ni.[6,7] The proposed mechanism involves the dissociative adsorption of alkanes, liberating a hydrogen atom on the surface, followed by the step-by-step scission of carbon-carbon bonds. The most striking features in the present hydrogenolysis on $LaCoO_3$ are the high reaction order with respect to P_{H_2} and the formation of only methane as the product. Neither the other fragmented nor dehydrogenated hydrocarbons were produced in the gas phase. Therefore, it is evident that the catalysis by this perovskite is essentially different from those by the transition metals, and so the above-mentioned mechanism can not be applied to the present reaction system.

The deuterium distributions in the reaction of the alkanes with D_2 showed a common feature irrespective of the alkanes employed: large amounts of methane [D_3] and [D_4] were produced even at the initial stage of hydrogenolysis, whereas the fractions of the deuterium-exchanged alkanes were negligibly small. These results clearly indicate that the adsorption of alkanes is irreversible, but the surface species thus produced undergo a rapid hydrogen exchange. Another important finding is that the reaction order with respect to the alkane pressure was unity in all cases, but the hydrogen order increased with the number of carbon atoms in the alkanes, independently of their molecular structure (*i.e.*, 0.0, 1.0, and 2.0 for the hydrogenolyses of C_3H_8, C_4H_{10}, and C_5H_{12} respectively). The value of −0.5 obtained previously for the ethane hydrogenolysis is also in line with this tendency.[1] It should be noted that such a variation in the hydrogen order is not observed for the alkane hydrogenolysis on the transition-metal catalysts. These findings on the present hydrogenolysis indicate that the slowest elementary step involves not only the simultaneous rupture of the C–C bonds to produce monocarbon species, but also the attack of hydrogen atoms, the number of which is strongly related to that of the resulting monocarbon species.

A comparative study of hydrogenolysis by perovskite compounds, such as $LaAlO_3$, $LaFeO_3$, and $LaCoO_3$,[8] and by component oxides, such as La_2O_3 and Co_2O_3,[1] revealed that only $LaCoO_3$ and Co_2O_3 can accelerate the hydrogenolysis; this indicates that the cobalt ion plays an impotant role in breaking the C–C bond. The study also showed that La_2O_3 can effectively catalyze the H_2-D_2 equilibration reaction as well as ethylene hydrogenation, indicating the capability of adsorbing hydrogen dissociatively.[1] These findings lead to the consideration that the peculiar activity of $LaCoO_3$ arises from the synergetic effect of La, Co, and O ions; the Co ion is responsible for the C–C bond rupture, whereas the La and O ions contribute mainly as sites for supplying hydrogen atoms to the decomposed species. Furthermore, the application of X-ray photoelectron spectroscopy to the active and deactivated $LaCoO_3$ catalysts showed that the presence of a trivalent cobalt ion rather than a divalent one is essential for the activity.[1,8] Accordingly, we would like to propose the following mechanism as the most plausible pathway for the reaction of the C_3 to C_5 alkanes, which involves surface intermediates analogous to those suggested in the ethane hydrogenolysis:

$$H_2 \rightleftharpoons 2H(a) \qquad (6)$$

$$H_2 \rightleftharpoons 2H(a^*) \qquad (7)$$

$$C_nH_{2n+2} + 2(n-2)H(a) \longrightarrow 2CH_3(a^*) + (n-2)[H\cdots CH_2(a)\cdots H] \quad (8)$$

$$\left.\begin{array}{l} CH_3(a^*) \rightleftharpoons CH_2(a^*) + H(a) \\ [H\cdots CH_2(a)\cdots H] \rightleftharpoons CH_3(a) + H(a) \\ CH_3(a) \rightleftharpoons CH_2(a) + H(a) \end{array}\right\} \quad (9)$$

$$\left.\begin{array}{l} CH_3(a^*) + H(a) \longrightarrow CH_4 \\ [H\cdots CH_2(a)\cdots H] \longrightarrow CH_4 \end{array}\right\}, \quad (10)$$

where the symbols (a*) and (a) represent the adsorbed species on the Co^{3+} ion and those on the other sites respectively. The surface species, $[H\cdots CH_2(a)\cdots H]$, denotes a precursor of desorbing methane. The absence of deuterium-exchanged alkanes in the gas phase suggests that Step (8) is rate-determining, and the following rate equation is given to the hydrogenolysis by assuming that the requisite number of the site on the Co^{3+} ion is two for the selective adsorption of methyl groups in the alkane molecules:

$$R = k_8 P_{C_nH_{2n+2}} \theta_v^{*2} \theta_H^{2(n-2)}, \quad (11)$$

where θ_v^* denotes the fraction of the vacant Co^{3+} sites, and θ_H, the fractions of the La^{3+} and O^{2-} sites, occupied by hydrogen atoms. Provided that the fraction of the sites covered with hydrocarbon species is negligibly small, these fractions can be expressed, respectively, as;

$$\theta_v^* = 1/(1+\sqrt{K_h^* P_{H_2}}) \quad (12)$$

and

$$\theta_H = \sqrt{K_h P_{H_2}}/(1+\sqrt{K_h P_{H_2}}), \quad (13)$$

where K_h^* and K_h are equilibrium constants. After introducing Eqs. 12 and 13 into Eq. 11, the rate equation is written as;

$$R = k_8 K_h^{n-2} P_{C_nH_{2n+2}} P_{H_2}^{n-2}/(1+\sqrt{K_h^* P_{H_2}})^2 (1+\sqrt{K_h P_{H_2}})^{2(n-2)}. \quad (14)$$

Under the conditions of a strong hydrogen adsorption on the Co^{3+} sites, $1 \ll \sqrt{K_h^* P_{H_2}}$, and a weak adsorption on the other sites, $1 \gg \sqrt{K_h P_{H_2}}$, Eq. 14 is simplified to;

$$R = k_8 \frac{K_h^{n-2}}{K_h^*} P_{C_nH_{2n+2}} P_{H_2}^{n-3}. \quad (15)$$

For normal and side-chain alkanes with the three to five carbon atoms, the observed pressure dependences of the rate are well represented by Eq. 15. Step (8) might proceed rapidly in a consecutive way involving the step-by-step C–C bond scission, but it is regarded as being a simultaneous step, as far as the kinetics is concerned, and the surface intermediates produced are not desorbed in the gas phase. In the above-mentioned mechanism, the surface Co^{3+} ion favors the adsorption of the methyl group rather than the methylene group. This is not unexpected, since a similar selective adsorption occurred on the Cr^{3+} ion in α-Cr_2O_3.[9] The formation of highly deuterium-exchanged methane is ascribable to the rapid hydrogen exchange between monocarbon species, such as methyl and carbene, as is shown in Step (9). The presence of surface carbene as an intermediate is possible, since this species was recently, by means of ultraviolet photoelectron spectroscopy, confirmed in the adsorption of C_2H_2 on the Ni (110) surface.[10]

The formation of methane *via* the direct hydrogenolysis of propene was expressed by a rate equation of the first order with respect to both the hydrogen and propene pressures (Table 4); the hydrogen order was different from that observed in the case of propane hydrogenolysis. One possible interpretation for this pressure dependence might be given by assuming the same surface intermediates as those described in Step (8). This assumption leads to this pathway;

$$C_3H_6 + 4H(a) \longrightarrow 2CH_3(a^*) + [H\cdots CH_2(a)\cdots H]. \quad (16)$$

Thus, it follows that the insertion of a stoichiometry number, $n=4$, of hydrogen atoms into Eq. 15 provides the same rate equation as the observed one.

The alkane hydrogenolysis showed a variety of activation energies, as is demonstrated in Table 1; E_a is high for propane and neopentane, intermediate for isobutane, and low for pentane, butane, isopentane, and ethane. It is difficult at present to give a clear interpretation for this variation, especially the extremely high value for propane. One might argue that the C–C bond between methylene groups in alkanes dissociates more readily than that between methylene and methyl group and that, thus, the number of the CH_2 group in the respective alkanes would govern the activation energy of reaction. This view, however, is unlikely, because the energy difference between those bonds (13 kJ mol^{-1})[11] is too small to explain the large variation in E_a, and no correlation between them exists. The following consideration of the conformation of alkane molecules and the $LaCoO_3$ surface appears to be useful. In previous studies,[1,8] the (110) plane of $LaCoO_3$ was supposed to be active for the hydrogenolysis because of the high density of the exposed Co, La, and O ions. The distance between the adjacent surface Co ions is 5.42 Å. The carbon-atom chain of butane or higher alkanes is long and flexible enough to interact with two Co ions in a bridged form, as shown in Fig. 4. Although the La^{3+} and O^{2-} ions fail to adsorb alkanes dissociatively, both ions are likely to accommodate the methyl and carbene groups formed as a result of the bond rupture. Thus, such bridged adsorption makes the nearby La^{3+} and O^{2-} ions effective in supplying hydrogen atoms to the decomposed species, thus lowering the activation energy. On the other hand, propane and neopentane can hardly take the bridged configuration because of their smaller size and less flexible shape. The adsorption

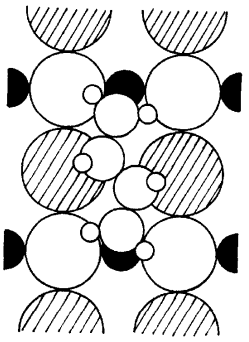

Fig. 4. Schematic representation of butane configuration on the (110) plane of $LaCoO_3$.
●: La^{3+}, ○: O^{2-}, ●: Co^{3+}, ○: carbon atom, ○: hydrogen atom.

of these molecules on a single Co ion results in a larger steric hindrance, which makes the activation energy higher. In this regard, the small E_a in the ethane hydrogenolysis is exceptional, but presumably due to a lesser extent of the steric hindrance. As for the propane hydrogenolysis, the extremely larger E_a seems to be related to the specificity in the propene hydrogenolysis; *i.e.*, the direct methanation of propene was remarkably favored, compared to those of the ethylene and butene hydrogenolyses. This consideration is certainly supported by the fact that the E_a of the direct methane formation from propene was as low as 52 kJ mol^{-1}.

In order to reveal the peculiar behavior of propene and propane in the hydrogenolysis reaction, further information on the adsorbed states of the hydrocarbons on $LaCoO_3$ is needed; a thermal-desorption study is now in progress.

References

1) K. Ichimura, Y. Inoue, and I. Yasumori, *Bull. Chem. Soc. Jpn.*, **53**, 3044 (1980).
2) J. H. Sinfelt, *Adv. Catal.*, **23**, 91 (1973); *Catal. Rev.*, **3**, 175 (1970).
3) J. R. Anderson and B. G. Baker, *Proc. R. Soc. London, Ser. A*, **271**, 402 (1963).
4) J. R. Anderson and N. R. Avery, *J. Catal.*, **2**, 542 (1963); **5**; 446 (1966).
5) K. Kochloefl and V. Bazant, *J. Catal.*, **10**, 140 (1968).
6) H. Matsumoto, Y. Saito, and Y. Yoneda, *J. Catal.*, **19**, 101 (1970).
7) C. G. Myers and G. W. Munns, Jr., *Ind. Eng. Chem.*, **50**, 1727 (1958).
8) K. Ichimura, Y. Inoue, I. Kojima, E. Miyazaki, and I. Yasumori, *Proc. Intern. Congr. Catal., 7th*, 1980, *B*, 1281 (1981).
9) G. Pass, A. B. Littlewood, and R. L. Burwell, Jr., *J. Am. Chem. Soc.*, **82**, 6281 (1960).
10) J. E. Demuth, *Surf. Sci.*, **93**, 127 (1980).
11) "Kagaku Binran," ed by the Chemical Society of Japan, Maruzen, Tokyo (1975), p. 977.

Conformational Change of Poly(L-lysine) by Sodium Octyl Sulfate as Studied by Stopped-flow Circular Dichroism Method

Kunio TAKEDA,* Akira IBA, and Keishiro SHIRAHAMA†

Department of Applied Chemistry, Faculty of Science, Okayama University of Science, Ridai-cho 1-1, Okayama 700
†Department of Chemistry, Faculty of Science and Engineering, Saga University, Saga 840

(Received October 27, 1980)

Circular dichroism (CD) studies were made on the conformational changes of poly(L-lysine) (PLL) induced by sodium octyl sulfate (SOS). The conformation of PLL has a negative double maximum characterizing the α-helix in $4.0—6.0\times10^{-3}$ mol/dm^3 SOS solutions. At a higher concentration of SOS, PLL takes the β-structure, the random coil remaining below it. These conformational changes were followed by measuring ellipticities at 192, 207, and 221 nm according to a CD stopped-flow method. The rate constant was *ca.* 2.7×10^{-1} s^{-1} for the coil-helix transition, the transition rate from coil to β-structure being high depending on SOS concentration. The β-structure was attained by adding a small amount of 1-octanol to the α-helical PLL in 5.0×10^{-3} mol/dm^3 SOS. The effect of the surfactant on the triphasic conformation changes is discussed in terms of hydrophobic environment.

Conformational changes of polypeptides and proteins have been extensively studied by circular dichroism (CD) measurements. Poly(L-lysine) (PLL) has been frequently selected as a typical substance because of its diversity in conformations.[1-3] Satake and Yang gave an evidence that PLL adopts β-structure in the presence of sodium alkyl sulfates which have longer hydrocarbon chains than 10 carbons. They obtained a distorted CD spectrum reminiscent of α-helix,[3] which should show a characteristic CD spectrum with a double negative maximum. It has not been clarified which conformation PLL takes in a SOS solution. This paper reports the SOS concentration dependence of PLL conformation as well as the kinetics of conformational changes studied by the CD stopped-flow method.

Experimental

The surfactant, SOS, was prepared from 1-octanol (purity: 99%, Aldrich Chemical Co.) by the method of Dreger *et al.*,[4] and recrystallized twice from 2-propanol and once from pure water. The critical micelle concentration of the surfactant was determined to be 148 mM (as concentration unit, 1 M= 1 mol/dm^3, is used) at 25 °C by means of electric conductivity in agreement with that reported.[5] The hydrobromide salt of PLL (degree of polymerization: 140, Sigma Chemical Co.) was converted into hydrochloride by dialysis against 0.1 M HCl and then water. The concentration of PLL was determined by colloid titration.[6,7]

Measurements of CD were carried out with a JASCO-J500A spectropolarimeter (Japan Spectroscopic Co.) equipped with a DP-501 data processor. The data processor was partially modified to follow rapid reactions. The sampling time required for 5 data points/nm on a chart in both X and Y directions was selected from 1.0×10^{-4} to 1.0×10^{-1} s for kinetic measurements. The stopped-flow measurements by CD detection were carried out with a rapid mixer (Union Giken Co.) and a specially designed observation cell whose lightpath length and incident area being 1.0 mm and 1.0 cm^2, respectively. The dead volume beyond the mixer was calculated to be 250 μl for the stopped-flow system. The stopped-flow system was driven by *ca.* 2.0 kg/cm^2 compressed air.

Results and Discussion

Figure 1 shows typical CD spectra of PLL in the absence and the presence of 5.0 mM SOS and the difference CD spectrum between them. The conformation of PLL in the SOS concentrations between 4.0 and 6.0 mM seems to be the α-helical structure characterized by a double negative maximum. Satake and Yang reported that the CD spectrum of poly(L-ornithine)(PLO)-sodium dodecyl sulfate (SDS) complex is characteristic of a helical conformation with a double negative maximum, but the PLO–SOS and PLL–SOS complexes display the CD spectrum with a negative maximum at 225 nm and a shoulder near 210 nm suggesting a helical conformation.[3] The CD spectrum of PLL–SOS complex closely resembles that of PLO-

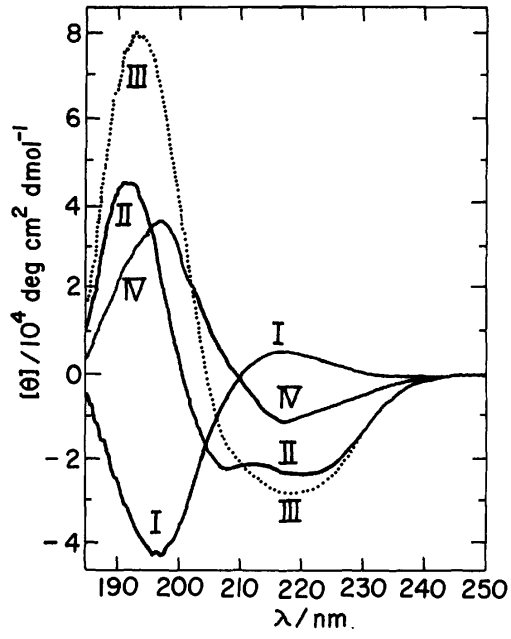

Fig. 1. Typical CD spectra of PLL solutions in the absence (curve I) and the presence (curve II) of 5.0 mM SOS and the difference CD spectrum between them (curve III) at 20 °C. Curve IV represents the CD spectrum of PLL in 7.5 mM SOS solution. The concentration of PLL was 2.8×10^{-4} M. The thickness of cell used was 1.0 mm. The time constant and the scanning speed of spectropolarimeter were 1.0 s and 20 nm/min, respectively. These spectra are averaged over 8 repetitions.

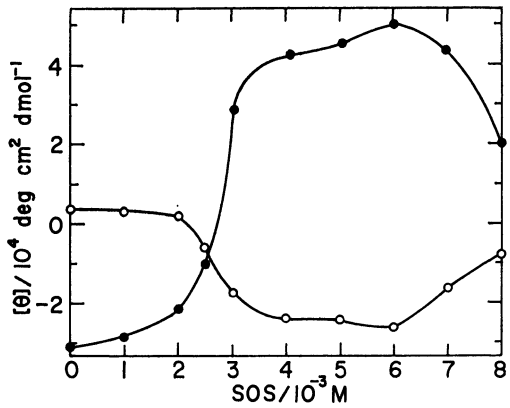

Fig. 2. Plots of $[\theta]_{192}$ (●) and $[\theta]_{221}$ (○) *vs.* concentration of SOS at 20 °C. These data were obtained from the measurements under the same experimental conditions as stated in Fig. 1.

SDS complex in their work. The magnitude of ellipticity of the PLL–SOS complex around 220 nm is considerably smaller than that of ordinary α-helical PLL.[1,2,8,9] It is not clear whether this is due to an environment effect of the bound surfactant ions on the rotational strength of the n-π* transition as pointed out by Grourke and Gibbs[10] and Satake and Yang,[3] or incomplete helix formation due to very low SOS concentration.

Figure 2 shows the dependence of residue ellipticities, $[\theta]_{192}$ and $[\theta]_{221}$ on SOS concentration. PLL is seen to be α-helical only in the range 4.0—6.0 mM SOS, taking disordered structure and β-structure below and above the SOS concentration range, respectively.

The conformational change of the PLL induced by

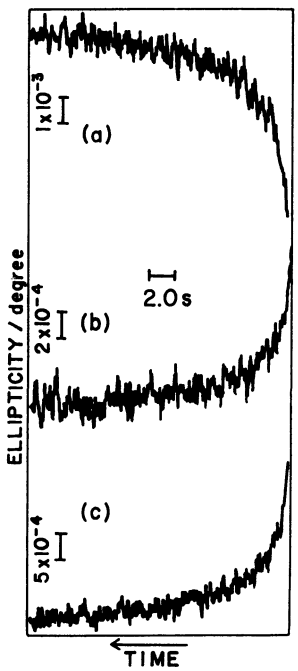

Fig. 3. Typical traces of ellipticity changes at 192 (a), 207 (b), and 221 nm (c) at 20 °C. The trace (a) is average of 32 repetitions and the traces (b) and (c) are averages of 8 repetitions. The final concentrations of PLL and SOS were 2.8×10^{-4} M and 6.0 mM, respectively.

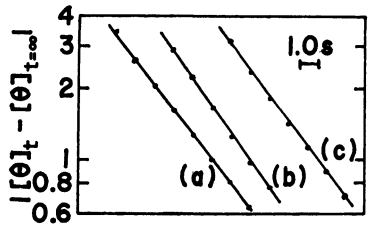

Fig. 4. Semilogarithmic first order plots for the approach to equilibrium on the three time courses in Fig. 3. The quantities representing $|[\theta]_t-[\theta]_{t=\infty}|$ are expressed in units in (a) 1×10^{-3}, (b) 2×10^{-3}, and (c) 5×10^{-4} degree, respectively, on the basis of best fit curve drawn on time course in each case.

SOS was followed by CD changes at 192 (wavelength at which the positive maximum appears in the difference CD spectrum directly obtained by use of a data processor; dotted curve III, Fig. 1), 207 and 221 nm (wavelengths at which the negative maximum appears in SOS solution, Fig. 1). Typical time courses are given in Fig. 3. As anticipated from the changes in the CD spectra (Fig. 1), the ellipticity at 192 nm changed from negative to positive, the negative ellipticities at 207 and 221 nm increasing with time. Although only half of the total ellipticity change with time near new equilibrium was observed at each wavelength due to the large dead volume of the stopped-flow system, the directions of the ellipticity changes with time at the three wavelengths were in line with the changes expected from the CD spectra (Fig. 1). This result and the identical rate constants calculated at three wavelengths led us to conclude that the observed process is the conformational change of PLL from the disordered structure to the α-helix, free from any possible artifacts which might be occasionally observed in stopped-flow measurements.[11] The forward rate constant for the conformational change from the coil to α-helix was determined by assuming that the conformational change of PLL is a first order reaction. The first order plot gives a linear relationship between $|[\theta]_t-[\theta]_{t=\infty}|$ and time, t (Fig. 4). The time courses at the three wavelengths approximately gave the same rate constant, k being almost independent of the SOS concentration between 4.0 and 6.0 mM (Fig. 5).

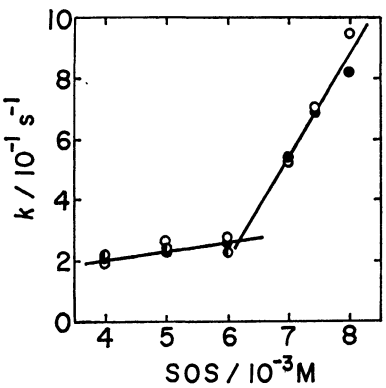

Fig. 5. Dependence of rate constant, k on SOS concentration at 20 °C. The rate constants were obtained from time courses at 192 (○), 207 (◐), and 221 nm (●). Final concentration of PLL was 2.8×10^{-4} M.

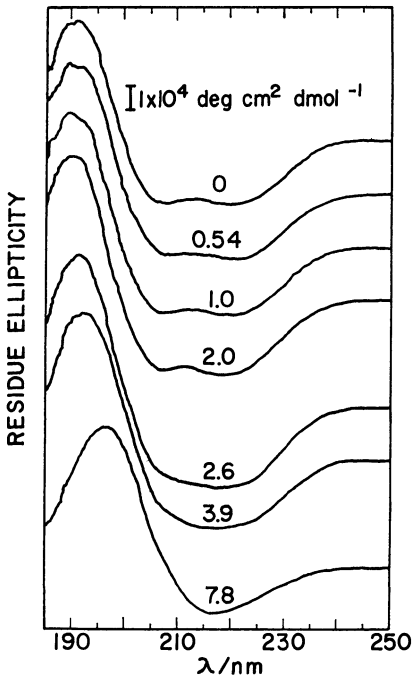

Fig. 6. Changes of CD spectrum of PLL in 5.0 mM SOS by addition of small amounts of 1-octanol at 20 °C. Numerical values in the figure denote concentrations of the 1-octanol in mM.

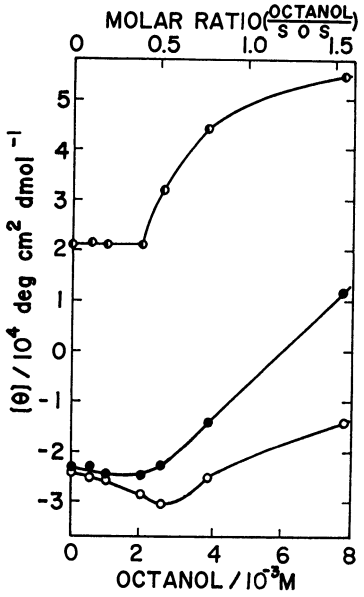

Fig. 7. Plots of $[\theta]_{197}$ (◐), $[\theta]_{207}$ (●), and $[\theta]_{221}$ (○) *vs.* concentration of 1-octanol and molar ratio of octanol/SOS at 20 °C. The concentration of SOS was 5.0 mM.

On the other hand, PLL adopts the β-structure above 7.0 mM SOS. Addition of a small amount of 1-octanol to α-helical PLL in 4.0—6.0 mM SOS caused the β-structure as shown in Fig. 6. The residue ellipticities at 197, 207, and 221 nm, $[\theta]_{197}$, $[\theta]_{207}$, and $[\theta]_{221}$ *vs.* 1-octanol and 1-octanol/SOS molar ratio plot is shown in Fig. 7. Above the octanol/SOS molar ratio=0.5, $[\theta]_{197}$, $[\theta]_{207}$, and $[\theta]_{221}$ gradually change with increase in the ratio of octanol/SOS. The PLL conformation is in a delicate balance between the coil, α-helix, and β-structure state. A slight change in circumstances may cause the interchange among the three states. Bound SOS neutralizes the charges on PLL, giving rise to ordered structures, especially α-helix at first. Increased degree of binding gives more hydrophobic atmosphere to the host polymer, the β-structure being enhanced. Addition of octanol also gives the α-helical PLL–SOS complex a more hydrophobic atmosphere, making it adopt the β-structure. The tendency that more hydrophobic environment favors β-structure is seen in Satake and Yang's study in which alkyl sulfates longer than SOS exclusively bring about the β-structure.[3] Alkyl sulfates bound to the charged sites on polymer would be in contact with each other more efficiently on the β-structure than the α-helix, since the alkyl sulfates are implanted radially on the α-helix, while they are oriented in the same direction on the β-structure. Such a difference in mutual contact is also reflected on a binding isotherm which is much steeper for the β-structured polypeptide than the α-helical one.[12]

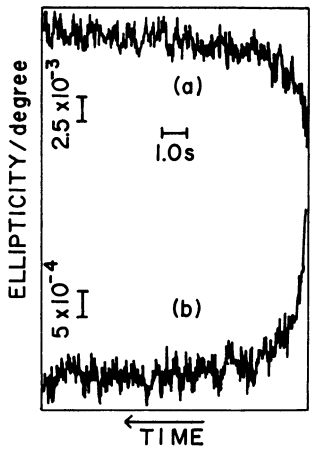

Fig. 8. Typical traces of ellipticity changes at 192 (a) and 221 nm (b) at 20 °C. The traces (a) and (b) are averages of 16 and 8 repetitions, respectively. The final concentrations of PLL and SOS were 2.8×10^{-4} M and 7.5 mM, respectively.

The ellipticity changes with time were observed above 7.0 mM SOS (Fig. 8). The change seems to be due to the conformational change of PLL from coil to β-structure, the rate constant sharply increasing with SOS concentration (Fig. 5).[13] There is no possibility that PLL passes through the α-helical state before attaining β-structure in the higher SOS concentration range, since no corresponding process was observed in such time courses as shown in Fig. 8. The disordered structure of PLL directly turned to the β-structure.

The octanol-induced conformational change of PLL was followed by the CD stopped-flow method. Typical time courses are shown in Fig. 9. The directions of the ellipticity changes in this case, as expected from a comparison of curve II with curve IV in Fig. 1, were reversed in contrast with those in the conformational change from the coil to α-helix or β-structure. Most of the total ellipticity change could be observed through-

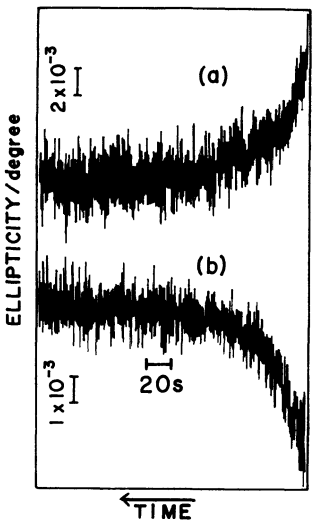

Fig. 9. Typical traces of ellipticity changes at 192 (a) and 221 nm (b) at 20 °C. This is the case of mixing PLL solution containing 5.0 mM SOS with a solution of 5.0 mM SOS containing slight amounts of 1-octanol. The final concentrations of the PLL and the octanol were 2.8×10^{-4} M and 7.8 mM, respectively. The traces (a) and (b) are averages of 8 and 2 repetitions, respectively.

out the time courses at these wavelengths, since the rate was one order of magnitude lower than those of the other two processes, the coil to α-helix or β-structure. The observed processes in Fig. 9 reflect the conformational change of PLL, from the α-helix to β-structure. The time courses at 192 and 221 nm gave an identical rate constant, 7.2×10^{-2} s^{-1} at 20 °C. Such a slow process would be responsible for destruction-reconstruction mechanism: α-helix is unfolded and then the highly ordered β-structure is constructed. The conformational change of PLL from coil to β-structure was also observed in mixing the PLL solution with 5.0 mM SOS solution containing 7.8 mM 1-octanol (both final concentrations). The observed time courses in this case also gave a similar rate constant, 5.5×10^{-1} s^{-1}, to those obtained in the conformational change from coil to β-structure in the presence of 7.0 mM SOS. The process may proceed without passing through α-helix, implying lack of destruction of α-helix.

The rate constants for three kinds of conformational changes of PLL in SOS solution seem to be low as compared with the reported values for conformational changes of polypeptides.[14] The difference is probably due to the characteristic situation in surfactant solutions as follows. The binding of SOS to PLL causes a discharge of the cationic groups of PLL, but the amount of bound SOS is not enough to discharge all of them. The surfactants are forced to move from the first binding sites to other vacant sites with the progress of conformational change of the polypeptide, since the bulky hydrophobic groups of surfactants should find minimal free energy in order to reconcile the structure formation with maximal contact between the hydrophobic groups of bound surfactants and the hydrophobic parts of the polypeptide. Such rearrangements of bound surfactants to the polypeptide require a much longer time in comparison with conformational change induced by proton which is more effective than the surfactant in reactivity and mobility because of its small size. The conformational change of polypeptide in the surfactant solution seems to occur accompanied by strong interaction.

References

1) G. Holzwarth and P. Doty, *J. Am. Chem. Soc.*, **87**, 218 (1965).
2) R. Townend, T. F. Kumosinski, S. N. Timasheff, G. D. Fasman, and B. Davidson, *Biochem. Biophys. Res. Commun.*, **23**, 163 (1966).
3) I. Satake and J. T. Yang, *Biochem. Biophys. Res. Commun.*, **54**, 930 (1973).
4) E. E. Dreger, G. I. Keim, and G. D. Miles, *Ind. Eng. Chem.*, **36**, 610 (1944).
5) P. Mukerjee and K. J. Mysels, "Critical Micelle Concentration of Aqueous Surfactant Solution," U. S. Government Printing Office, Washington D. C. (1971).
6) H. Terayama, *J. Polym. Sci.*, **8**, 243 (1952).
7) R. Senju, "Colloid Titration Method," (in Japanese), Nankoudo, Tokyo (1969).
8) N. Greenfield and G. D. Fasman, *Biochemistry*, **8**, 4108 (1969).
9) J. Y. Cassim and J. T. Yang, *Biopolymers*, **9**, 1475 (1970).
10) M. J. Grourke and J. H. Gibbs, *Biopolymers*, **10**, 795 (1971).
11) No ellipticity changes were observed in mixing the PLL solution with the other electrolyte solutions or solutions of lower SOS concentrations, indicating that the effect by heat of mixing is negligible.
12) I. Satake and J. T. Yang, *Biopolymers*, **15**, 2263 (1976).
13) The CD measurement itself was incapable above 9.0 mM SOS because of appearance of precipitate.
14) G. Schwarz, *J. Mol. Biol.*, **11**, 64 (1965).

Electronic Structures of Uracil and Its Anions

Hiroshi MORITA,*,† Józef S. KWIATKOWSKI,†† and Anna TEMPCZYK†††

The Institute for Solid State Physics, The University of Tokyo, Roppongi, Minato-ku, Tokyo 106

††*Institute of Physics, Nicholas Copernicus University, Toruń, Poland*

†††*Institute of Chemistry, University of Gdańsk, Gdańsk, Poland*

(Received November 22, 1980)

Electronic structures of uracil and its anions were theoretically investigated by a modified CNDO-CI method. Theoretical results were in good agreement with the observed spectra of uracil and of both the uracil-3-ide and uracil-1-ide anions, indicating that the second π-π^* band of uracil may tentatively be assigned to the 215 nm band observed in circular dichroism spectrum, and that the lowest singlet and triplet states of uracil are n-π^* and π-π^* states, respectively, in accord with the observed solvent dependence on emission properties. The first π-π^* band of uracil-1-ide anion was correctly predicted by the method at longer wavelengths than the corresponding band of uracil-3-ide anion. For the purpose of comparison, a modified INDO-CI, CNDO/S-CI, and a modified π-SCF-MO-CI methods were also applied to the molecules under consideration. The results were only partly successful in predicting the observed spectra.

Electronic structures and spectra of pyrimidinic nucleic acid bases and their model compounds have been studied extensively from experimental and theoretical points of view.[1,2] As for uracil and thymine, electronic spectra were predicted less satisfactorily by the semi-empirical calculations[1-7] compared with the results for other pyrimidinic bases.[1,2,8] This is partly because the σ-core charge in atomic valence state usually taken to be an integral number in π-electron approximation changes significantly in the actual molecule by redistribution of σ-electrons over the whole molecule,[9] and is partly related to the unestablished band assignment concerning the 215 nm band observed in circular dichroism (CD) spectrum of uridine.[10]

The ordering of the lowest n-π^* and π-π^* states is important in understanding the photophysical properties of nucleic acid bases. Fluorescence and phosphorescence lifetimes and quantum yields of uracil and thymine were found to be largely affected by a variety of solvents.[11] The experimental results strongly suggested that in aprotic solvents the lowest singlet state is of highly forbidden character.[11] Theoretical investigation of the lowest excited state is necessary in order to interpret the photophysical properties of uracil.

Studies on the electronic structure of anionic species are few.[1,4,9,12] In aqueous alkaline solution, uracil exists as a mixture of two monoanionic species (*i.e.*, uracil-3-ide and uracil-1-ide anions) of comparable amounts.[1] The electronic spectra of these monoanions differ from each other, particularly in the nearest ultraviolet (UV) region.[13,14] The relative positions of the first π-π^* band of the anions could not be predicted correctly by the CNDO/S calculation.[9]

Under these circumstances, in order to interpret satisfactorily the experimental results, the electronic structures of uracil and of its anions have been investigated by a modified CNDO-CI method[15] by employing new semiempirical parameters for C, N, and O atoms. The calculated results have been compared with the observed results and also with the theoretical ones calculated by CNDO/S-CI method,[16] a modified INDO-CI method,[17] and a modified π-SCF-MO-CI method[9,18] which considers the effect of σ-core charge in the π-electron approximation.

Theoretical

Modified CNDO-CI Method. A modified CNDO-CI (mCNDO-CI) method[15] was applied by evaluating the two-center Coulomb repulsion integrals by Nishimoto-Mataga approximation.[19] To choose the best semiempirical parameters, various sets of the bonding parameters (β^0's) and one-center Coulomb repulsion integrals (γ_{AA}'s) which consider several atomic valence states of C, N, and O atoms were tested in the preliminary calculations of benzene, pyridine, pyrrole, aniline, formaldehyde, and phenol. Considering the agreement with the observed orbital sequences[21-25] and transition energies,[26-30] the semiempirical parameters listed in Table 1 were finally employed in the present paper. In the course of the preliminary calculations, it was found that the adoption of the Nishimoto-Mataga equation instead of the Klopman's equation[20] results in an SCF procedure that often converges very slowly and sometimes practically does not converge at all. Taking the one-center Coulomb repulsion integrals of σ-AO's to be equal to those of π-AO's, as in the case of CNDO/S method,[16] is in some cases necessary and in others effective in improving convergence of the SCF procedure. The parameters for N atom were mainly

Table 1. One-center Coulomb repulsion integral (γ_{AA}/eV) and bonding parameter (β_A°/eV)) for H, C, N, and O atoms used in the modified CNDO-CI method

	H	C		N		O	
		σ-AO	π-AO	σ-AO	π-AO	σ-AO	π-AO
γ_{AA}	12.85	10.60	10.60	12.03	12.03	14.67	14.67
β_A°	−12.0	−16.8	−12.1	−23.2	−16.4	−31.4	−20.4

† Present address: Department of Image Science and Engineering, Faculty of Engineering, Chiba University, Chiba 260.

determined from the calculated result of pyridine. Somewhat different parameters for N atom are acceptable in pyrrole and aniline, but for simplicity of the following calculations the same set of the semi-empirical parameters were used for all the valence states of N atom.

The $(I+A)/2$ values needed for the evaluation of one-center core matrix elements,[15,31] $U_{\mu\mu}$, were taken to be the same as the original values[31] for C and N atoms, and for O atom to be 24.390 eV for the 2s AO and 8.111 eV for the $2p_x$, $2p_y$, and $2p_z$ AO's as in a previous paper.[15]

In the configuration interaction (CI) treatment, 40 singly excited π-π^* and σ-σ^* configurations, 23—25 singly excited π-σ^* configurations, and 20 singly excited n-π^* and σ-π^* configurations were taken into account.

Modified π-SCF-MO-CI (mPPP) Method. In order to avoid the problems which appear in the description of anionic forms of heterocyclic molecules within the original π-SCF-MO-CI (Pariser-Parr-Pople) method,[32,33] the modification in view of polarizable σ-core was introduced[9] in the evaluation of core integral, W_i, core potential, V_i, and resonance integrals, β_{ij}. The modified diagonal and off-diagonal elements[9,18,34] of the π-electron Hartree-Fock matrix are

$$F_{ii} = \left(1 + \kappa \frac{\delta Z_i}{Z_i}\right)[-I_i - (n_i - 1)\gamma_{ii}] + 1/2\, P_{ii}\gamma_{ii} + \sum_{j \neq i}\left[P_{jj} - \left(1 + \frac{\delta Z_j}{Z_j}\right) n_j\right]\gamma_{ji},$$

and

$$F_{ij} = \beta_{ij}\left[1 + 0.5\left(\frac{\delta Z_i}{Z_i} + \frac{\delta Z_j}{Z_j}\right)\right] - 1/2\, P_{ij}\gamma_{ij},$$

where Z_i is the formal core charge with integral number in the valence state of isolated atom, i, and δZ_i stands for the change of σ-charges introduced by redistribution of σ-electrons over the whole molecule. The symbol κ denotes the empirical "scaling" parameter which has been fixed[9] to be 0.85 in the present calculation.

A more precise expression for the diagonal element, F_{ii}, which includes penetration integrals shows that the expression for the one-center Coulomb integral for the difinite atom i (*i.e.*, from which a proton was removed) in the anionic species differs from that in the neutral species. The integral for atom i in the anion decreases mainly by the penetration integral between atom i and removed proton. For a series of hydroxy-pyridines,[34] the decrease of the integral for N atom was calculated to be of the order 2.7—3.1 eV. In the present calculation for the uracil anions, an average value of 3.0 eV was taken as the decrement of the integral for the N_3 or N_1 atom. This means that in the case of the anions, the ionization potential, I_i, for N_3 or N_1 atom was increased by 3.0 eV compared to the

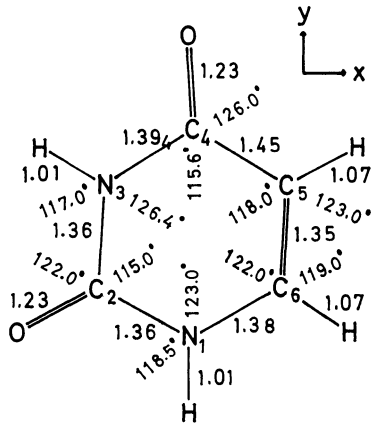

Fig. 1. Molecular structure of uracil, numbering of atoms, and coordinate system.

TABLE 2. SINGLET AND TRIPLET TRANSITION ENERGIES ($^1\Delta E$/eV AND $^3\Delta E$/eV) AND OSCILLATOR STRENGTHS (f) CALCULATED AND OBSERVED FOR URACIL

Assignment	mCNDO-CI			CNDO/S-CI		INDO-CI			mPPP		Obsd	
	$^1\Delta E$	$^3\Delta E$	f[a]	$^1\Delta E$	f	$^1\Delta E$	$^3\Delta E$	f	$^1\Delta E$	f	$^1\Delta E$	(f)
n-π^*		2.74	0.001 (z)	3.42		3.65	3.20	0.000_4				
n-π^*		3.62	0.000 (z)	4.09		4.37		0.000				
π-π^*	5.28	2.80	0.359 (y)	5.42	0.214	5.13	3.21	0.371	5.00	0.288	5.08[b]	4.79 (0.16)[c]
n-π^*		5.34	0.000_4(z)	6.19		6.52		0.000_4				
n-π^*		5.81	0.000_1(z)	6.81								
π-π^*	5.95	3.66	0.095 (xY)	6.34	0.048	5.88	4.25	0.199	5.78	0.221	5.77[d]	
π-π^*	6.17	4.01	0.176 (X$\bar{y}$)	6.54	0.108	6.29		0.379	5.92	0.385	6.05[b]	6.14 (0.26)[c]
π-π^*	6.59	5.72	0.283 (xY)	7.26	0.264	6.57		0.496	6.49	0.518	6.63[b]	6.85[c]
n-π^*		6.67	0.004 (z)									
π-σ^*		6.67	0.010 (z)	7.49								
σ-π^*		7.09	0.004 (z)									
π-σ^*		7.31	0.061 (z)									
π-π^*	7.38	6.64	0.007 (x)	7.49	0.057							
π-σ^*		7.60	0.013 (z)									

a) Oscillator strength is calculated for the singlet manifold. The direction of transition moment is shown in parentheses, x-, y-, and z-axes being taken as is shown in Fig. 1. When the transition moment has both x- and y-components, the larger one is designated by capital letter. x-Component with negative sign is designated as $\bar{x}$, and y-component, as $\bar{y}$. b) Observed value in the vapor phase; Ref. 39. c) Observed value in aqueous solution at pH=7; L. B. Clark and I. Tinoco, Jr., *J. Am. Chem. Soc.*, **87**, 11 (1965). d) Observed value in the CD spectrum of uridine; Ref. 10.

value of I_i for the neutral molecule. The two-center Coulomb repulsion integrals were evaluated by the Nishimoto-Mataga equation. The other semiempirical parameters adopted in the present mPPP method are the same as used previously.[35,36] In the CI treatment, all the singly excited configurations were taken into account.

Molecular Structure. Considering the results of X-ray crystal analysis[37] and of theoretical calculation,[38] molecular structure of uracil was assumed as is shown in Fig. 1. The molecular structures of uracil-3-ide and uracil-1-ide anions were assumed to be the same as the one of the neutral molecule, except that one proton bonded to N_3 and N_1 atoms, respectively, was removed.

Results and Discussion

The electronic structures of uracil calculated by mCNDO-CI, CNDO/S-CI, INDO-CI, and mPPP methods are presented in Table 2. Comparison of the result calculated by mCNDO-CI method with the observed spectrum in the vapor phase[39] and with the CD spectrum[10] strongly suggests that the first, third, and fourth π-π^* states predicted at 5.28, 6.17, and 6.59 eV, respectively, can be assigned to the 244 nm (5.08 eV), 205 nm (6.05 eV), and 187 nm (6.63 eV) bands in the vapor phase,[39] respectively. The weak second π-π^* band predicted at 5.95 eV may correspond to the 215 nm (5.77 eV) band in the CD spectrum.[10]

As tabulated in Table 2, INDO-CI and mPPP methods predict that the transition energies for π-π^* states agree semiquantitatively well with the result by mCNDO-CI method, but the transition intensity to the second π-π^* state is not weak. CNDO/S-CI method, on the other hand, predicts the second π-π^* band being weak, although the calculated transition energies for π-π^* states are high. The theoretical result presented by only one of the above three methods is not conclusive to support any assignments of the spectrum (see Ref. 1 for more detailed discussion of the excited states of uracil), bu they altogether suggest that the assignment based on mCNDO-CI method mentioned above is a plausible one for uracil.

Table 3. Occupied molecular orbital energies/eV calculated and observed for uracil

Assignment	Obsd[a]	Calcd[b]		
		mCNDO	CNDO/S[c]	INDO[d]
π_1	9.55	9.56	9.5_7	11.4_6
n_1	10.15	9.82	10.5_7	12.0_0
π_2	10.65	10.29	11.0_1	12.4_0
n_2	11.12	10.37	11.5_1	12.8_7
π_3	12.63	13.24	13.4_0	18.7_7

a) Vertical ionization potential (I_V) taken from HeI photoelectron spectrum; Ref. 41. b) Minus sign of the occupied orbital energy (ε) is omitted. From Koopmans' theorem, $I_V = -\varepsilon$ holds. c) Ref. 42. d) Ref. 41.

The ordering of the lowest π-π^* and n-π^* states is important to understand the photophysical properties of pyrimidine bases.[11] In mCNDO-CI method, calculated transition energies for n-π^*, σ-π^*, and π-σ^* states correspond to those of the triplet manifold.[15] Preliminary calculation of formaldehyde by mCNDO-CI method has shown that the calculated transition energy (2.31 eV) of the lowest n-π^* triplet state is $\approx$0.7 eV lower than the observed value (3.0 eV).[40] Considering this underestimation of transition energy of the n-π^* triplet state, nearly degenerate n-π^* and π-π^* triplet states of uracil predicted at $\approx$2.8 eV by mCNDO-CI method can be ordered as the π-π^* state being the lowest triplet in agreement with the suggestion by Becker *et al.*[11] The singlet-triplet separation of n-π^* state is expected to be $\approx$1 eV or less. In the singlet manifold, the n-π^* state is predicted to be lower than the first π-π^* state. This agrees with the prediction based on fluorescence lifetime measurement.[11]

In Table 3, the orbital energies calculated by mCNDO method are compared with the observed and theoretical values reported previously.[41,42] The predicted order of the occupied molecular orbitals, $\pi > n > \pi > n > \pi$, is in

Table 4. Singlet and triplet transition energies ($^1\Delta E$/eV and $^3\Delta E$/eV) and oscillator strengths (f) calculated and observed for uracil-3-ide anion

Assignment	mCNDO-CI			CNDO/S-CI		INDO-CI			mPPP		Obsd[b]	
	$^1\Delta E$	$^3\Delta E$	f[a]	$^1\Delta E$	f	$^1\Delta E$	$^3\Delta E$	f	$^1\Delta E$	f	$^1\Delta E$	f
n-π^*		2.39	0.000 (z)	3.24		3.28	3.14	0.000_3				
n-π^*		3.64	0.002 (z)	4.31		4.34		0.000				
n-π^*		3.82	0.000 (z)	4.45		4.79		0.000				
π-π^*	4.57	3.31	0.111 (xy)	4.19	0.032	4.30	3.18	0.102	4.72	0.025	4.68	0.15
n-π^*	4.80		0.001 (z)	5.41								
π-π^*	5.14	3.73	0.023 ($\bar{x}$Y)	5.24	0.013	4.82	3.79	0.020	5.33	0.395	$\approx$5.4[c]	
n-π^*	5.54		0.012 (z)	5.94								
π-π^*	5.80	2.84	0.728 (y)	6.06	0.637	6.05		1.218	5.38	0.454	>5.8	
n-π^*	6.29		0.004 (z)	6.40								
π-π^*	6.36	5.13	0.136 (Xy)	7.04	0.093	6.82		0.209	5.82	0.664		
π-σ^*	6.69		0.013 (z)									
σ-π^*	6.81		0.000_2(z)									
π-π^*	6.94	6.25	0.025 (x$\bar{y}$)									
σ-σ^*	7.06	6.91	0.016 (y)									

a) See footnote (a) in Table 2. b) Observed value for 1-methyluracil-3-ide anion; Ref. 13. c) Shoulder.

Table 5. Singlet and triplet transition energies ($^1\Delta E$/eV and $^3\Delta E$/eV) and oscillator strengths (f) calculated and observed for uracil-1-ide anion

Assignment	mCNDO-CI			CNDO/S-CI		INDO-CI			mPPP		Obsd[b]	
	$^1\Delta E$	$^3\Delta E$	f[a]	$^1\Delta E$	f	$^1\Delta E$	$^3\Delta E$	f	$^1\Delta E$	f	$^1\Delta E$	f
n-π^*		3.11	0.001 (z)	3.85		3.67	3.40	0.001				
n-π^*		3.48	0.000_4(z)	4.13		4.85		0.001				
n-π^*		4.00	0.003 (z)	4.44		5.45		0.001				
π-π^*	4.38	2.89	0.347 (xY)	4.31	0.220	4.50	2.88	0.431	4.41	0.366	4.39	0.17
π-π^*	5.59	3.52	0.246 (x)	5.74	0.172	5.62	3.88	0.352	5.52	0.278	5.69	0.17
n-π^*		5.68	0.003 (z)	6.39								
n-π^*		5.80	0.000 (z)	6.66								
π-π^*	6.15	5.21	0.044 (y)	6.75	0.002	6.28		0.220	5.93	0.175		
n-π^*		6.28	0.012 (z)	6.98								
π-σ^*		6.50	0.016 (z)									
π-π^*	6.65	4.39	0.030 (xy)	6.93	0.034	6.62		0.130	6.44	0.635		
n-π^*		6.81	0.001 (z)									
π-π^*	6.87	6.31	0.115 (xy)									
n-π^*		7.33	0.001 (z)									

a) See footnote (a) in Table 2. b) Observed value for 3-methyluracil-1-ide anion; Ref. 13.

good agreement with the result by photoelectron spectroscopy.[41,42]

The dipole moment of the ground state calculated by mCNDO method is 4.60 Debye,** in agreement with the observed value (4.16 Debye in dioxane).[43]

Tables 4 and 5 present the calculated results for uracil-3-ide and uracil-1-ide anions, respectively. As can be seen from the tables, the agreement between the observed[13,14] and predicted values for uracil-1-ide anion is satisfactory by all the methods presented here, but the spectrum of uracil-3-ide anion[13,14] can be predicted satisfactorily only by mCNDO-CI method. It is worth noting that the first π-π^* band of uracil-1-ide anion is correctly predicted at longer wavelengths than the corresponding band of uracil-3-ide anion only by mCNDO-CI and mPPP methods. CNDO/S-CI method as well as INDO-CI method failed to predict the first π-π^* band position of uracil-3-ide anion. Very recent calculation using CNDO/S-CI method[4] has predicted correctly the absorption band positions of both monoanions of uracil; however the authors have not described the details of the parametrization of the method.

This work was initiated during the stay of J.S.K. at the Institute for Solid State Physics, the University of Tokyo. J.S.K. wishes to thank the Japan Society for the Promotion of Sciences for support of his stay in Japan. This work was also supported in part by the Polish Academy of Sciences within the project 09.7. The authors wish to express their thanks to Professor Saburo Nagakura, the University of Tokyo, for valuable discussions, and to Dr. J. Lipiński, Technical University, Wrocław, Poland, for calculation of the spectra of uracil and its monoanions by means of his modified INDO-CI method.

References

1) J. S. Kwiatkowski and B. Pullman, *Adv. Heterocyclic Chem.*, **18**, 199 (1975).

2) C. Nagata, A. Imamura, and H. Fujita, *Adv. Biophys.*, **4**, 1 (1973).

3) W. Hug and I. Tinoco, Jr., *J. Am. Chem. Soc.*, **95**, 2803 (1973); **96**, 665 (1974).

4) F. A. Savin, Yu. V. Morozov, A. V. Borodavkin, V. O. Chekhov, E. I. Budowsky, and N. A. Simukova, *Int. J. Quantum Chem.*, **16**, 825 (1979).

5) M. Tanaka and S. Nagakura, *Theor. Chim. Acta*, **6**, 320 (1966).

6) A. Denis and A. Pullman, *Theor. Chim. Acta*, **7**, 110 (1967).

7) H. Ito and Y. J. I'haya, *Chem. Phys. Lett.*, **38**, 271 (1976).

8) H. Morita and S. Nagakura, *Theor. Chim. Acta*, **11**, 279 (1968).

9) J. S. Kwiatkowski and B. Lesyng, *Int. J. Quantum Chem., QBS*, **6**, 391 (1979).

10) D. W. Miles, M. J. Robins, R. K. Robins, M. W. Winkley, and H. Eyring, *J. Am. Chem. Soc.*, **91**, 824 (1969).

11) C. Salet, R. Bensasson, and R. S. Becker, *Photochem. Photobiol.*, **30**, 325 (1979); R. S. Becker and G. Kogan, *ibid.*, **31**, 5 (1980).

12) L. C. Snyder, R. G. Shulman, and D. B. Neumann, *J. Chem. Phys.*, **53**, 256 (1970).

13) D. Shugar and J. J. Fox, *Biochim. Biophys. Acta*, **9**, 199 (1952).

14) A. V. Borodavkin, E. I. Budowsky, Yu. V. Morozov, F. A. Savin, and N. A. Simukova, *Itogi Nauk. Tekh. Molekul. Biol.*, **14**, 1 (1977).

15) H. Morita, K. Fuke, and S. Nagakura, *Bull. Chem. Soc. Jpn.*, **49**, 922 (1976).

16) J. Del Bene and H. H. Jaffé, *J. Chem. Phys.*, **48**, 1807, 4050 (1968); **49**, 1221 (1968).

17) J. Lipiński, A. Nowek, and H. Chojnacki, *Acta Phys. Pol. A*, **53**, 169 (1978).

18) A. Tempczyk and J. S. Kwiatkowski, *Bull. Acad. Pol. Sci., Ser. Sci. Chim.*, **27**, 161 (1979).

19) K. Nishimoto and N. Mataga, *Z. Phys. Chem. (Frankfurt am Main)*, **12**, 335 (1957).

20) G. Klopman, *J. Am. Chem. Soc.*, **86**, 4550 (1964); **87**, 3300 (1965).

21) T. Kobayashi and S. Nagakura, *Chem. Lett.*, **1972**, 903; *J. Electron Spectrosc. Relat. Phenom.*, **7**, 187 (1975).

22) C. Utsunomiya, T. Kobayashi, and S. Nagakura,

** 1 Debye$=3.333\times10^{-30}$ C m.

Bull. Chem. Soc. Jpn., **51**, 3482 (1978).
23) P. J. Derrick, L. Åsbrink, O. Edqvist, B. Ö. Jonsson, and E. Lindholm, *Int. J. Mass Spectrom. Ion. Phys.*, **6**, 191 (1971).
24) T. Kobayashi and S. Nagakura, *Chem. Lett.*, **1972**, 1013; *Bull. Chem. Soc. Jpn.*, **47**, 2563 (1974).
25) D. W. Turner, C. Baker, A. D. Baker, and C. R. Brundle, "Molecular Photoelectron Spectroscopy," John Wiley & Sons, London (1970).
26) K. Kimura, H. Tsubomura, and S. Nagakura, *Bull. Chem. Soc. Jpn.*, **37**, 1336 (1964).
27) J. E. Perkin and K. K. Innes, *J. Mol. Spectrosc.*, **15**, 407 (1965).
28) W. C. Price and A. D. Walsh, *Proc. R. Soc. London, Ser. A*, **179**, 201 (1941).
29) K. Kimura and S. Nagakura, *Mol. Phys.*, **9**, 117 (1965).
30) A. D. Walsh, *Trans. Faraday Soc.*, **42**, 66 (1946).
31) J. A. Pople and G. A. Segal, *J. Chem. Phys.*, **44**, 3289 (1966).
32) R. Pariser and R. G. Parr. *J. Chem. Phys.*, **21**, 466, 767 (1953).
33) J. A. Pople, *Proc. Phys. Soc. London, Ser. A*, **68**, 81 (1955).
34) J. S. Kwiatkowski and A. Tempczyk, in preparation.
35) M. Berndt and J. S. Kwiatkowski, *Theor. Chim. Acta*, **17**, 35 (1970).
36) J. S. Kwiatkowski, *Acta Phys. Pol. A*, **39**, 695 (1971); *J. Mol. Struct.*, **10**, 245 (1971).
37) R. F. Stewart and L. H. Jensen, *Acta Crystallogr.*, **23**, 1102 (1967).
38) K. Morokuma, *Kagaku To Kogyo*, **32**, 749 (1979).
39) L. B. Clark, G. G. Peschel, and I. Tinoco, Jr., *J. Phys. Chem.*, **69**, 3615 (1965).
40) A. D. Cohen and C. Reid, *J. Chem. Phys.*, **24**, 85 (1956).
41) A. Padva, T. J. O'Donnell, and P. R. LeBreton, *Chem. Phys. Lett.*, **41**, 278 (1976).
42) D. Dougherty, K. Wittel, J. Meeks, and S. P. McGlynn, *J. Am. Chem. Soc.*, **98**, 3815 (1976).
43) I. Kulakowska, M. Geller, B. Lesyng, and K. L. Wierzchowski, *Biochim. Biophys. Acta*, **361**, 119 (1974).

The Structure of Liquid Water by Neutron Scattering

Norio Ohtomo,† Kazuo Tokiwano,† and Kiyoshi Arakawa*

Research Institute of Applied Electricity, Hokkaido University, Sapporo 060

†*Faculty of Engineering, Hokkaido University, Sapporo 060*

(Received January 9, 1981)

A comprehensive analysis of the structure of liquid water was performed by combining neutron and X-ray diffraction data. A formula expressing the structure factor of fluids composed of small molecular clusters was obtained and applied to the analysis. In the interpretation of the diffraction data, the tetrahedral pentamer model as an aggregate of the regular tetrahedral pentamers is considered to be the best structure model of liquid water from the excellent agreement between calculated structure factors and experimental data. Some critical discussions about other structure models were made.

Recent diffraction studies of liquid water have brought much valuable information on the structure of the liquid. Among them, the followings are distinguishable: X-ray diffraction studies by Narten and Levy[1] and Hajdu *et al.*,[2] electron diffraction studies by Kálmán *et al.*,[3] and neutron diffraction studies by Page and Powles,[4] Narten[5] and the authors.[6,7] However, the conclusions drawn from the diffraction results by these workers are found to be contradictory to each other. The most important reason for the circumstances is, of course, the "complexity" of the liquid structure of water and the lack of the reasonable general method of analysis for diffraction data by liquids. At the present stage of the development of studies in this field, the combined and comprehensive interpretation of diffraction results[8] is strongly required.

Concerning the X-ray studies, observed intensity data agree well with each other in the low Q range (<5 Å^{-1}), though, for large Q, marked discrepancies are found there, for example, between the data reported by Hajdu *et al.*[2] and that by Narten *et al.*[1,9] In addition, the proposed structure models in those papers are considered to have implausible aspects in several respects: Hajdu's model consists of a fundamentally anisotropic nearest neighbor arrangement of water molecules[10] and Narten's earlier model ("interstitial model") in 1967[9] has a "largely extended lattice structure."

With respect to the neutron studies, the observed structure factors are found to agree virtually with each other, taking the differences of the experimental method into consideration.[6,7] However, the conclusions on the structure model of water are largely inconsistent with each other.[4-6] The authors mentioned earlier the cause of the marked discrepancies.[6,7] It has turned out that Narten's "near-neighbor model" is physically unacceptable and also that Page and Powles' conclusion disproving all the structure models treated is too severe. We analyzed the neutron data using a "revised watery model," which is a modification of Page and Powles' "watery model." However, the agreement between calculated and experimental structure factors was still insufficient.[6,7]

Despite these incompatible results, it has become certain through those recent X-ray and neutron diffraction studies that the most dominant local environment of a water molecule within liquid water is nearly tetrahedral on the average. Furthermore, a large amount of information accumulated so far by various experimental[11] and theoretical studies[12-15] have also ascertained the fact. However, further knowledge on the nearest neighbor coordination shell remains quite undetermined. Concerning the nearest neighbor coordination number, for example, it has been believed to be slightly larger than 4 since the pioneering study by Morgan and Warren, while according to the recent study by Hajdu *et al.*, it is smaller than 4, though slightly.

The major reason for the existence of those contradictory circumstances stated here is supposed to be attributed to the inadequacy of the method of analysis as well as to the experimental difficulties. Thus, we have attempted to perform a combined analysis of the neutron and X-ray diffraction data from various sources including our own, and then to propose a structure model of liquid water. The main purpose of our present analysis is the direct confirmation of the basic structural entities by the combined interpretation of neutron and X-ray diffraction data through the presentation of a new method of analysis. Though the number of the nearest neighbor coordination is believed to be nearly equal to 4, it is not sure whether the average configuration of the nearest neighbor molecules is regular-tetrahedral or not. In another word, it is still a central problem whether the regular tetrahedral pentamer is the primary entity (of course, on the average) or not. This is the most important point as the object of debate with respect to the structure model of liquid water. The details of the present analysis are written in the following.

Neutron and X-Ray Diffraction Data

For the present purpose, we used the X-ray diffraction data of Narten *et al.*[1,9] and of Hajdu *et al.*[2] As to the neutron diffraction our own data was used.

Neutron Diffraction Data. In addition to the structure factor $S_m(Q)$ data in the low Q region (<10 Å^{-1}),[6,7] the factors in the higher Q region (<25 Å^{-1}) were obtained by LINAC-TOF neutron diffraction method.[16] Details of the experimental apparatus have been stated in the preceding papers together with the correction and calibration procedures.[6,7,16] The neutron structure factor $S_m(Q)$ over a wide range of Q (1—25 Å^{-1}) obtained by combining the low Q data with the higher Q data,[17] are shown in Fig. 1. The $S_m(Q)$ data in the low Q region, 1—8 Å^{-1}, agree well with those reported previously, though the slight differences of a main peak at 2 Å^{-1} and a broader

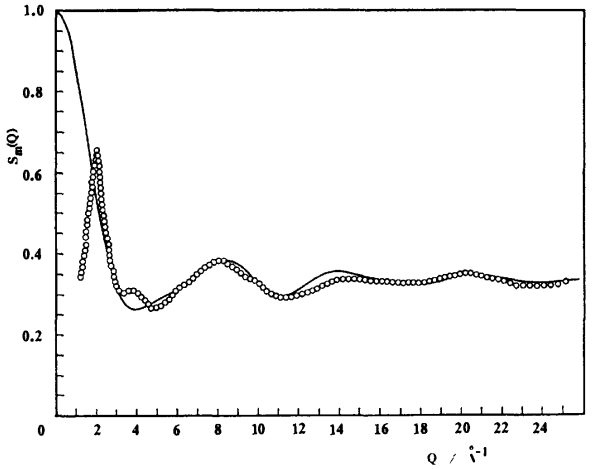

Fig. 1. Observed neutron structure factors $S_m(Q)$ for heavy water at room temperature (15 ± 1 °C), compared with the calculated intramolecular structure factor $S_m^{(1)}(Q)$.
○: $S_m(Q)$ observed ——: $S_m^{(1)}(Q)$ calculated (r_{OD}= 0.98 Å, r_{DD}=1.60 Å, and DOD angle=109.5°).

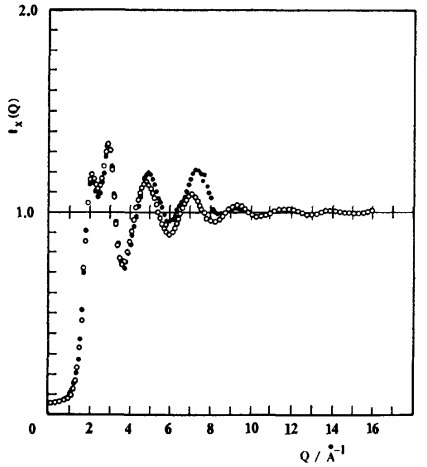

Fig. 2. Observed X-ray intensity function $I_x(Q)$.
○: $I_x(Q)$ by Narten *et al.* (20 °C),[1,9] ●: $I_x(Q)$ by Hajdu *et al.* (25 °C).[2]

peak at *ca.* 8 Å^{-1} are observed.[6,7] It is noticeable that the $S_m(Q)$ data for D_2O obtained by the authors at LINAC are found to agree virtually with Page and Powles' and Narten' data at reactor, taking the experimental uncertainities as well as the small difference in temperature into consideration. The reproducibility of the neutron data in the low Q region is thus confirmed with sufficient accuracy.

X-Ray Diffraction Data. Many X-ray diffraction data of liquid water have been reported. Among them, the data of Narten *et al.*[1,9] and those of Hajdu *et al.*[2] are available for the present purpose. "Molecular" modified intensity functions given in those papers are shown in Fig. 2. The two data are found in good agreement with each other in the low Q range, though marked discrepancies are observed in the higher Q range ($Q\gtrsim5$ Å^{-1}).

Theoretical Procedures of Analysis

Coherent Neutron Structure Factor. The coherent neutron scattering cross-section $(d\sigma/d\Omega)_{coh}$ is given in the static approximation by

$$\left(\frac{d\sigma}{d\Omega}\right)_{coh} = N_m\Sigma^2 S_m(Q), \quad (1)$$

where $\Sigma=\sum_n b_n$. Equation 1 defines the coherent neutron structure factor $S_m(Q)$ for molecular liquid.[4] N_m is the number of molecules in the sample and b_n the scattering length of nucleus n. $\sum$ is over all the nuclei in the molecule. $\vec{Q}(=\vec{k}_0-\vec{k}_s)$ is the scattering vector and $|\vec{Q}|=Q=(4\pi/\lambda)\sin\theta$, where $\vec{k}_0$ and $\vec{k}_s$ are the incident and scattered wave vectors, respectively.

In this study we attempt to determine the best structure model of water for the interpretation of its diffraction data. For that purpose, we will give here a general expression of $S_m(Q)$ for liquid which can be regarded as an aggregate of small clusters composed of molecules. The derivation of the $S_m(Q)$ is as in the following.

Structure Factor $S_m(Q)$ for Fluids Composed of Molecular Clusters. The coherent neutron structure factor $S_m(Q)$ in Eq. 1 is given in general by

$$S_m(Q) = N_m^{-1}\Sigma^{-2}\langle\sum_{i\neq j}\sum_{n_i,n_j} b_{n_i}b_{n_j}\exp(i\vec{Q}\cdot\vec{r}_{n_in_j})\rangle, \quad (2)$$

where i and j label molecules in a liquid and n_i denotes the n-th nucleus in the molecule i. $\vec{r}_{n_in_j}$ is the vector distance between the nuclei n_i and n_j, and b_{n_i} the scattering length of nucleus n_i. We sum over all the scatterers in the N_m molecules in the system.

Then, in the right hand side of Eq. 2, the separation of the contribution of atom-pair interactions within the clusters from the "inter-cluster" contribution is permitted in general, because a liquid can always be regarded virtually as an aggregate of small clusters of various sizes. We have

$$S_m(Q) = f_1^c(Q) + N_m^{-1}\Sigma^{-2}\langle\sum_{\alpha\neq\beta}\sum_{l_\alpha,l_\beta}\sum_{n_{l_\alpha},n_{l_\beta}} b_{n_{l_\alpha}}b_{n_{l_\beta}}\exp(i\vec{Q}\cdot\vec{r}_{n_{l_\alpha}n_{l_\beta}})\rangle \quad (3)$$

and

$$f_1^c(Q) = N_m^{-1}\Sigma^{-2}\langle\sum_{\alpha}\sum_{l_\alpha,l'_\alpha}\sum_{n_{l_\alpha},n_{l'_\alpha}} b_{n_{l_\alpha}}b_{n_{l'_\alpha}}\exp(i\vec{Q}\cdot\vec{r}_{n_{l_\alpha}n_{l'_\alpha}})\rangle, \quad (4)$$

where l and l′ label molecules within a given cluster, and l_α denotes the l-th molecule in the cluster α. The transformation of Eq. 2 to Eq. 3 is only mathematical and it should be noted that the two equations are physically identical.

Let us use $\vec{r}_{c_{l_\alpha}l_\beta}$ to denote the vector distance from the center of the molecule l_α to that of the molecule l_β. Since $\vec{r}_{n_{l_\alpha}n_{l_\beta}}=\vec{r}_{c_{l_\alpha}l_\beta}-\vec{r}_{cn_{l_\alpha}}+\vec{r}_{cn_{l_\beta}}$ where $\vec{r}_{cn_{l_\alpha}}$ is the vector distance from the center of the molecule l_α to its n-th nucleus within the cluster α, Eq. 3 is written as

$$S_m(Q) = f_1^c(Q) + N_m^{-1}\Sigma^{-2}\langle\sum_{\alpha\neq\beta}\sum_{l_\alpha,l_\beta}\exp(i\vec{Q}\cdot\vec{r}_{c_{l_\alpha}l_\beta}) \times\sum_{n_{l_\alpha},n_{l_\beta}} b_{n_{l_\alpha}}b_{n_{l_\beta}}\exp[i\vec{Q}\cdot(-\vec{r}_{cn_{l_\alpha}}+\vec{r}_{cn_{l_\beta}})]\rangle. \quad (5)$$

Equation 5 is quite general, and we now consider

the case of a system consisting of identical clusters, each of which is composed of N_c molecules. Further, we assume that $\vec{r}_{cn|\alpha}$, $\vec{r}_{cn|\beta}$, and $\vec{r}_{cl\alpha|l\beta}$ are all stasistically independent. That is, the molecules belonging to different clusters are assumed to be orientationally-uncorrelated. Then, Eq. 5 becomes

$$\begin{aligned} S_m(Q) &= f_I^c(Q) + N_m^{-1}\Sigma^{-2}\langle\sum_{\alpha\neq\beta}\sum_{l\alpha,l\beta}\exp(i\vec{Q}\cdot\vec{r}_{cl\alpha|l\beta})\rangle \\ &\times[\sum_n b_n\langle\exp(i\vec{Q}\cdot\vec{r}_{cn})\rangle]^2, \\ &= f_I^c(Q) + \Sigma^{-2}[\sum_n b_n\langle\exp(i\vec{Q}\cdot\vec{r}_{cn})\rangle]^2 N_m^{-1} \\ &\times[\langle\sum_{I\neq J}\exp(i\vec{Q}\cdot\vec{r}_{cIJ})\rangle \\ &-\frac{N_m}{N_c}\langle\sum_{I\neq I'}\exp(i\vec{Q}\cdot\vec{r}_{cII'})\rangle], \end{aligned} \tag{6}$$

where $\vec{r}_{cn}$ is the vector distance from the center of a molecule to its n-th nucleus.

Thus, we can write the $S_m(Q)$ as in the form,

$$S_m(Q) = f_I^c(Q) + f_{2U}(Q)[S_C(Q) - f_3(Q) - 1], \tag{7}$$

$$f_I^c(Q) = \Sigma^{-2}N_c^{-1}\langle\sum_{I,I'}\sum_{n_I,n_{I'}} b_{n_I}b_{n_{I'}}\exp(i\vec{Q}\cdot\vec{r}_{n_In_{I'}})\rangle, \tag{8}$$

$$f_{2U}(Q) = \Sigma^{-2}[\sum_n b_n\langle\exp(i\vec{Q}\cdot\vec{r}_{cn})\rangle]^2, \tag{9}$$

$$S_C(Q) = 1 + N_m^{-1}\langle\sum_{I\neq J}\exp(i\vec{Q}\cdot\vec{r}_{cIJ})\rangle, \tag{10}$$

and

$$f_3(Q) = N_c^{-1}\langle\sum_{I\neq I'}\exp(i\vec{Q}\cdot\vec{r}_{cII'})\rangle, \tag{11}$$

where $f_I^c(Q)$ is the contribution of atom-pairs within the cluster, $S_C(Q)$ the molecular-centers structure factor of the liquid, $f_3(Q)$ a factor resulting from the molecular-center pairs within the cluster, and $f_{2U}(Q)$ a factor resulting from the completely uncorrelated orientational configuration between molecules.

In the following of this section the formula for the analysis of diffraction data will be given according to the theoretical procedure described above to examine structure models of liquid water.

Regular Tetrahedral Pentamer Model. We will give here the $S_m(Q)$ for the regular tetrahedral pentamer model where the structural unit as the basic entity of liquid water is the regular tetrahedral pentamer. In the model water is considered to be an aggregate of the pentamers on the average which are packed to give the density of 1 g/cm³. The central oxygen atom in the pentamer is tetrahedrally surrounded by four oxygen atoms at the corners of a regular tetrahedron, each pair of the central and peripheral oxygens being connected by a straight hydrogen bond (Fig. 3).

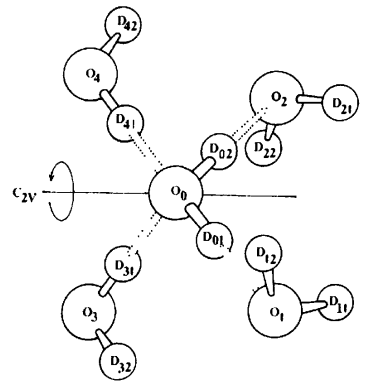

Fig. 3. The structure of the regular tetrahedral pentamer model with the C_{2v} symmetrical coordination. O_m indicates oxygen in the m-th molecule with the pentamer and D_{mn} the n-th deuteron in the m-th molecule. The dotted line denotes the hydrogen bond.

In this case, Eq. 7 becomes

$$S_m(Q) = S_m^p(Q) + f_{2U}(Q)[\{S_C(Q) - S_{m.p}^{(OO)}(Q)\} - 1], \tag{12}$$

where the intra-pentamer contribution $S_m^p(Q)(\equiv f_I^c(Q))$ is[18]

$$\begin{aligned} S_m^p(Q) &= S_m^{(1)}(Q) + 0.092S_{m.p}^{(OO)}(Q) + 0.422S_{m.p}^{(OD)}(Q) \\ &+ 0.486S_{m.p}^{(DD)}(Q), \end{aligned} \tag{13}$$

and

$$f_{2U}(Q) = \Sigma^{-2}[b_O + 2b_D Y_{OD}(Q)]^2. \tag{14}$$

$S_m^{(1)}(Q)$ is the intramolecular contribution and the $S_{m.p}^{(OO)}(Q)$ ($\equiv f_3(Q)$[19]), $S_{m.p}^{(OD)}(Q)$, and $S_{m.p}^{(DD)}(Q)$ are the intra-pentamer part of the contributions of the O–O, O–D, and D–D pairs, respectively. $Y_{nn'}(Q) = j_0(Qr_{nn'})\exp(-\gamma_{nn'}Q^2)$, where $j_0(\chi) = \sin\chi/\chi$, $r_{nn'}$ is the distance between the n-th and n'-th nuclei, and $2\gamma_{nn'}$ the mean-square variation to the distance $r_{nn'}$. Thus, we can calculate the $S_m(Q)$ by using Eq. 12. Each term in Eqs. 12 and 13 will be specified in the following.

The $S_m^{(1)}(Q)$ for heavy water molecules is

$$S_m^{(1)}(Q) = \Sigma^{-2}[b_O^2 + 2b_D^2 + 4b_O b_D Y_{OD}(Q) + 2b_D^2 Y_{DD}(Q)]. \tag{15}$$

For the regular tetrahedral pentamer model as shown in Fig. 3 the $S_{m.p}^{(OO)}(Q)$ becomes

$$S_{m.p}^{(OO)}(Q) = \frac{4}{5}[2Y_{OO}(Q) + 3Y_{O_1O_1}(Q)]. \tag{16}$$

In order to obtain the expression of the $S_{m.p}^{(OD)}(Q)$ and $S_{m.p}^{(DD)}(Q)$, we consider two extreme cases with respect to the orientation of the peripheral molecules within the pentamer: the one orientation where deuterium atoms of those molecules are located in the positions of the C_{2v} symmetry (Fig. 3) and the other orientation where the peripheral molecules are rotating freely around the axis on a straight line joining the central and peripheral oxygens.

Thus, for the C_{2v} symmetry cluster the contributions of the intra-pentamer O–D and D–D pairs, $S_{m.p}^{(OD)}(Q)$ and $S_{m.p}^{(DD)}(Q)$, become

$$\begin{aligned} S_{m.p}^{(OD)}(Q) &= \frac{1}{5}[2Y_{O_1D_{II}}(Q) + 3\{Y_{O_1D_{I}}(Q) + Y_{O_1D_{II}}(Q)\} \\ &+ 6\{Y_{O_ID_{II}}(Q) + Y_{O_ID_{II}}(Q)\}] \end{aligned} \tag{17}$$

and

$$\begin{aligned} S_{m.p}^{(DD)}(Q) = \frac{1}{5}\Big[&\frac{1}{2}\{Y_{D_{I}D_{II}}(Q) + Y_{D_{II}D_{II}}(Q)\} \\ &+ Y_{D_{I}D_{II}}(Q) + Y_{D_{II}D_{II}}(Q) + Y_{D_{II}D_{II}}(Q) \\ &+ 2\{Y_{D_{I}D_{II}}(Q) + Y_{D_{II}D_{II}}(Q)\} \\ &+ 4\{Y_{D_{I}D_{II}}(Q) + Y_{D_{II}D_{II}}(Q) + Y_{D_{II}D_{II}}(Q)\}\Big], \end{aligned} \tag{18}$$

respectively. For the model with freely rotating peripheral molecules, we assumed that the positions of six deuterons at a larger distance within the peripheral molecules are reduced approximately to the positions

of peripheral oxygens on the average. Then, the $S^{(OD)}_{m,p}(Q)$ and $S^{(DD)}_{m,p}(Q)$ can be written as

$$S^{(OD)}_{m,p}(Q) = \frac{1}{5}[2Y_{O,D_{II}}(Q)+3Y_{O,D_{II}}(Q)+6Y_{O,D_{II}}(Q) + 9Y_{O,O_{I}}(Q)] \quad (19)$$

and

$$S^{(DD)}_{m,p}(Q) = \frac{1}{10}[Y_{D_{I},D_{II}}(Q)+8Y_{O,D_{II}}(Q)+10Y_{O,D_{II}}(Q) + 3Y_{O,O_{I}}(Q)], \quad (20)$$

respectively.

Finally, for the $S_C(Q)$ required in the calculation of the inter-pentamer contribution (the second term in the right hand side of Eq. 12), we can use the observed X-ray intensity data assuming the molecular center to be at the oxygen nucleus.

Interpretation of Experimental Data

We calculated first the total neutron structure factor $S_m(Q)$ for the tetrahedral pentamer model using Eqs. 12—20, compared the calculated curves with the experimental data.

Calculation of the $S^p_m(Q)$. The intra-pentamer contribution $S^p_m(Q)$ (the first term of Eq. 12) was calculated by using Eq. 15 together with Eqs. 16—20, and the curves obtained at each stage of the calculations were compared with the corresponding experimental data.

The intramolecular contribution $S^{(1)}_m(Q)$ calculated by use of Eq. 15 are shown in Fig. 4 for four possible cases assumed for the intramolecular structure: (1) the intramolecular oxygen-to-deuteron distance $r_{OD}=0.96$ Å and the deuteron-to-deuteron distance $r_{DD}=1.52$ Å, corresponding to the molecule in the vapor when all the DOD angle is 104.5°, (2) $r_{OD}=1.01$ Å and $r_{DD}=1.65$ Å, corresponding to the molecule in heavy ice-I when all the DOD angle is 109.5°, (3) the earlier "revised watery model,"[6,7,16] and (4) the equally weighted average values, $r_{OD}=0.98$ Å and $r_{DD}=1.60$ Å, when all the DOD angle is taken to be 109.5°. The $S^{(1)}_m(Q)$ calculated for the case (3) is found to be quite identical with that for the case (4) over all range of Q. For the calculated curves (Fig. 4) in comparison with the observed data (Fig. 1), the best fit curve with observed $S_m(Q)$ for the larger Q region ($Q \gtrsim 6$ Å^{-1}) is obtained in the cases (3) and (4). The calculated $S^{(1)}_m(Q)$ curve for the case (4) is indicated in Fig. 1. Then, in the analysis of diffraction data in the following sections, we shall use the values of the case (4) for intramolecular parameters.

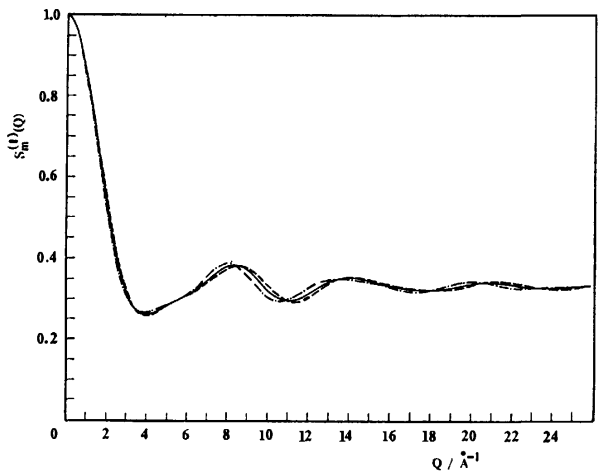

Fig. 4. Calculated intramolecular structure factor $S^{(1)}_m(Q)$ for heavy water.
——: $S^{(1)}_m(Q)$ for the averaged intramolecular parameters ($r_{OD}=0.98$ Å, $r_{DD}=1.60$ Å, and DOD angle=109.5°) and that for the revised watery model,[6,7] ($\varepsilon=0.0047$), ------: $S^{(1)}_m(Q)$ for the vapor molecule ($r_{OD}=0.96$ Å, $r_{DD}=1.52$ Å, and DOD angle=104.5°), ($\varepsilon=0.0057$), -·-·-: $S^{(1)}_m(Q)$ for the heavy ice-I molecule ($r_{OD}=1.01$ Å, $r_{DD}=1.65$ Å, and DOD angle=109.5°), ($\varepsilon=0.0061$). ε is a measure for indicating the deviations of $S^{(1)}_m(Q)$ from the experimental data, and it is expressed as[16]

$$\varepsilon = \{\sum_{i=1}^{N}[S_m(Q_i)_{obsd} - S^{(1)}_m(Q_i)^2]\}^{1/2}/\sum_{i=1}^{N}[S_m(Q_i)_{obsd}],$$

where N is the number of data points in the fitting range of Q, 8—25 Å^{-1}.

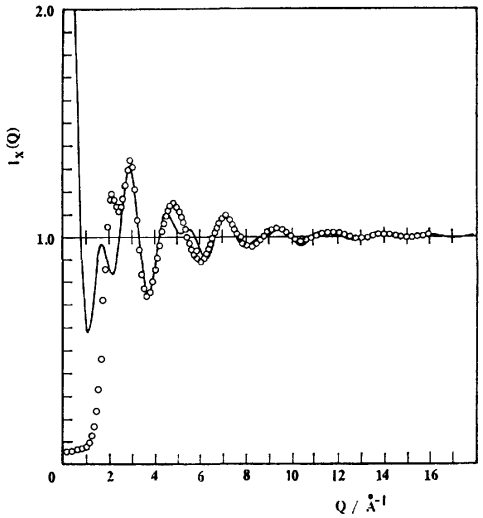

Fig. 5. The comparison between the calculated $[1+S^{(oo)}_{m,p}(Q)]$ and the observed X-ray intensity function $I_x(Q)$.
○: Observed $I_x(Q)$ by Narten *et al.*,[1,9] ——: calculated $[1+S^{(oo)}_{m,p}(Q)]$ for the regular tetrahedral pentamer model.

The $S^{(oo)}_{m,p}(Q)$ was calculated by using Eq. 16. The value of distance r_{oo} for the hydrogen-bonded O–D···O was taken to be 2.85 Å from various sources,[1,2,5,9,12,15,20,21] and the O-O-O angle was taken to be the tetrahedral angle (109.5°). The factor $S^{(oo)}_{m,p}(Q)$ is also known from X-ray diffraction. The X-ray diffraction pattern is almost completely determined by oxygen-oxygen pairs only. Then, the calculated values of $[1+S^{(oo)}_{m,p}(Q)]$ for the model proposed can be compared with the X-ray data. The function $[1+S^{(oo)}_{m,p}(Q)]$ calculated from Eq. 16 is shown in Fig. 5 together with the total experimental data. The calculated curve is in agreement with the data of Narten *et al.* on the whole, except for the deviation in the first peak at 2.1 Å^{-1} and that in the range of $Q=4.5$—6 Å^{-1}. The main contribution

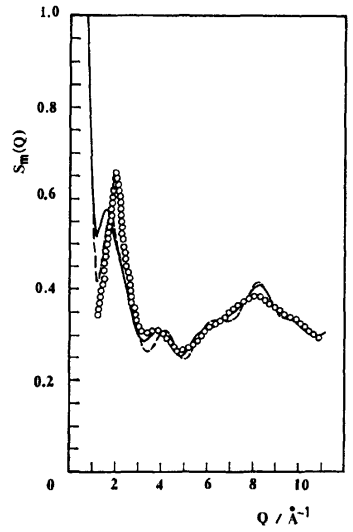

Fig. 6. The comparison between the calculated $S_m^P(Q)$ for the regular tetrahedral pentamer model and the observed neutron structure factor $S_m(Q)$.
○: Observed $S_m(Q)$, ——: calculated $S_m^P(Q)$ for the C_{2v} symmetry structure, ------: calculated $S_m^P(Q)$ for the freely rotating structure.

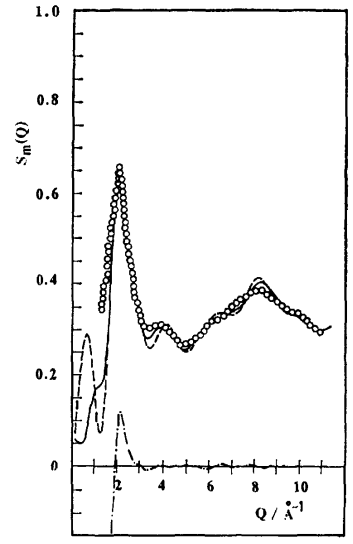

Fig. 7. The comparison between the calculated $S_m(Q)$ for the regular tetrahedral pentamer model and the observed neutron structure factor $S_m(Q)$.
○: Observed $S_m(Q)$, ——: calculated $S_m(Q)$ for the C_{2v} symmetry structure, ------: calculated $S_m(Q)$ for the freely rotating structure, -·-·-: $f_{2U}(Q)$-$[S_C(Q)-S_{m,p}^{(oo)}(Q)-1]$.

to the diffraction data at low Q region ($Q \lesssim 2$ Å^{-1}) comes from the long range interactions of molecules and so the contribution from the interaction pairs between pentamers is expected to recover the deviation of the first peak. Then, the result of the analysis of X-ray data suggests the essential effectiveness of the regular tetrahedral pentamer model.

In order to obtain the $S_m^P(Q)$, the calculation of $S_{m,p}^{(OD)}(Q)$ and $S_{m,p}^{(DD)}(Q)$ as the intra-pentamer contribution is required further, and we performed it for the C_{2v} symmetry model by using Eqs. 17 and 18, and also for the freely rotating model by using Eqs. 19 and 20. The $S_m^P(Q)$ thus obtained are shown in Fig. 6 together with the total experimental data. As clearly seen in Fig. 6, the curve for the freely rotating model is slightly deviated from that for the C_{2v} symmetry model, but, except for the first peak region ($Q \lesssim 3$ Å^{-1}) which is attributed to the long range (inter-pentamer) interactions of molecules, the agreement between the two calculated $S_m^P(Q)$ curves and the experimental data is essentially satisfactory. The comparison between the calculated $S_m^P(Q)$ and the observed total $S_m(Q)$ shows that the structure factor of liquid water is well-reproduced by the $S_m^P(Q)$ only except for the lower Q region ($Q \lesssim 3$ Å^{-1}), that is, $S_m(Q) \simeq S_m^P(Q)$ for $Q \gtrsim 3$ Å^{-1}.

Calculation of the Total Structure Factor $S_m(Q)$.
In the calculated values shown in Figs. 5 and 6 the contribution from the inter-pentamer atomic pairs (the second term in Eq. 12) is not contained. In order to estimate that contribution, we calculated the second term $f_{2U}(Q)[S_C(Q) - S_{m,p}^{(oo)}(Q) - 1]$ using Eqs. 14 and 16 for the $f_{2U}(Q)$ and $S_{m,p}^{(oo)}(Q)$ together with the observed X-ray intensity data for the $S_c(Q)$. Its values are shown in Fig. 7 as a dash-dot line. As seen in Fig. 7, the inter-cluster term contributes only in the lower Q region, $Q \lesssim 3$ Å^{-1}.

The total $S_m(Q)$ curves thus calculated as the sum of all terms described in the preceding items by using Eq. 12 together with Eqs. 13—20 for the two orientational arrangements (the C_{2v} symmetry model and the freely rotating model) are shown in Fig. 7 in comparison with the observed $S_m(Q)$. The agreements between the calculated curves and the scattering data are excellent on the whole, though the detailed shape of $S_m(Q)$ is less well-reproduced for the freely rotating model compared with the C_{2v} model. The result suggests that the extent of orientational correlation of liquid water lies between these two extremes.

We see that the behavior of the curve near 4 Å^{-1} is essential for the adequacy of the model as stated in Page and Powles' paper.[4] From this point of view, it is noticeable that the agreement with respect to the bump at *ca.* 4 Å^{-1} is achieved satisfactorily without any adjustable parameters. Especially, in addition to this agreement concerning the bump at *ca.* 4 Å^{-1}, the excellent agreement with respect to the first peak justifies the assumption that liquid water is composed of the aggregate of the regular tetrahedral pentamers on the average. Thus, we can conclude from the present result that the regular tetrahedral pentamer model is considered to be one of the best structure models of liquid water.

Discussion

Comparison with the Page and Powles' Analysis.[4]
Page and Powles' analysis of the neutron diffraction data of liquid heavy water has a marked feature in which the orientational correlation between molecules is separated from the positional one between molecular centers. This separation is exact when there is no orientational correlation for any intermolecular distances

(the completely uncorrelated orientation model), and then, the structure factor $S_m(Q)$ becomes

$$S_m(Q) = f_1(Q) + f_{2U}(Q)[S_C(Q) - 1], \quad (21)$$

where

$$f_1(Q) = \Sigma^{-2}\langle|\sum_n b_n \exp(i\vec{Q}\cdot\vec{r}_{cn})|^2\rangle. \quad (22)$$

$f_1(Q)$ is identical with $S^m_{(1)}(Q)$ in the present paper. On the other hand, Eq. 12 is rewritten as follows,

$$S_m(Q) = S^{(1)}_m(Q) + f_{2U}(Q)[S_C(Q) - 1] + [S^p_m(Q) - S^{(1)}_m(Q) - f_{2U}(Q)S^{(00)}_{m,p}(Q)]. \quad (23)$$

The third term in Eq. 23 clearly originates from the orientational correlation of molecules within the clusters (see Appendix).

From the comparison of Eq. 23 with Eq. 21, the feature of our present analysis can be understood. The most important point is the presence of additional terms in Eq. 23 resulting from the pentamer structure. The terms vanish for the completely-uncorrelated orientation model and then Eq. 23 reduces to Eq. 21.

In another extreme of Page and Powles' treatment, that is, for the completely-correlated orientation model (Eq. 7 in Ref. 4), the $S_m(Q)$ was expressed as

$$S_m(Q) = f_1(Q) + f_{2C}(Q)[S_C(Q) - 1]. \quad (24)$$

The orientational correlation between molecules was introduced through the replacement of $f_{2U}(Q)$ by $f_{2C}(Q)$. This is compared with the feature in our model that the third term in Eq. 23 expresses directly the correlated-orientation effect between molecules within clusters. Page and Powles' assumption of complete correlated orientation which is independent of the distance apart is, however, too severe in principle. In the analysis carried out by Page and Powles, they could not succeed to reproduce the bump at 4 Å^{-1} in the $S_m(Q)$ curve calculated, and they rejected all the model treated in their paper. The most important reason for their failure is considered to lie in their procedure of analysis.

Interstitial Model. We examine the "interstitial model," which consists of the regular tetrahedral pentamers and non-hydrogen-bonded monomers, where the positions of its monomer oxygens are restricted to the four triad axes of the regular tetrahedron formed by pentamer oxygens. Then, one tetrahedral pentamer plus N_i monomers ($N_i \lesssim 4$) is regarded as the basic structure unit of this model.

The X-ray intensity function $I^{in}_x(Q)$ which corresponds to $[1 + f_3(Q)]$ in Eq. 7 becomes

$$I^{in}_x(Q) = 1 + S^{(00)}_{m,p}(Q) + \frac{1}{(N_c + N_i)}[2(N_i - 1)Y_{O_iO_i}(Q) + 2N_i\{Y_{O_iO_c}(Q) + Y_{O_iO_c}(Q) + Y_{O_iO_c}(Q)\}], \quad [N_i = 1, 2, 3, \text{and } 4] \quad (25)$$

where N_c is the number of molecules within a cluster, being taken to be 5 for the pentamer. O_i denotes the oxygen atom of the interstitial molecules. The number of interstitial molecules N_i per pentamer is considered to be not larger than one practically.[11,22] Then, for the present purposes, it is sufficient for us to take into consideration the following two cases only: $N_i = 1$ and 2. The calculated $I^{in}_x(Q)$ curves are shown in Fig. 8 in comparison with the experimental data. The two

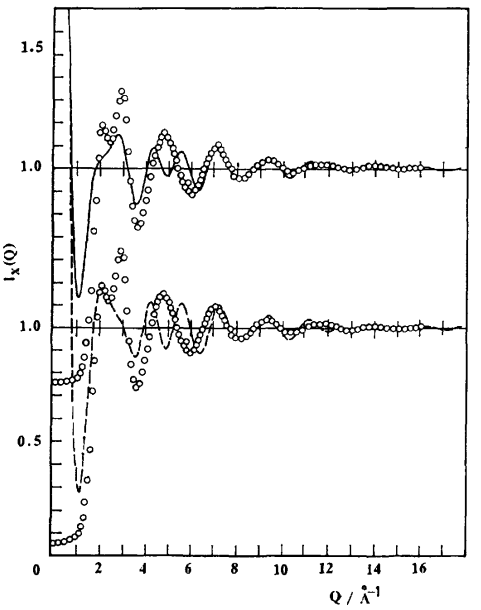

Fig. 8. The comparison between the calculated $I^{in}_x(Q)$ for the interstitial model with variation of the number of interstitial molecules N_i and the observed X-ray intensity function $I_x(Q)$.
○: Observed $I_x(Q)$ by Narten *et al.*,[1,9] ——: calculated $I^{in}_x(Q)$ ($N_i = 1$), ------: calculated $I^{in}_x(Q)$ ($N_i = 2$).

$I^{in}_x(Q)$ curves deviate appreciably from the experimental data, and thus, the interstitial model should be rejected.

Comment on Narten's Near-neighbor Model. The authors pointed out formerly that Narten's later model (the "near-neighbor model") was physically unacceptable despite its success in the calculation of $QS_m(Q)$ curves because several unplausible parameters were used.[6] Here, we discuss the defect of Narten's model in comparison with the present analysis.

Narten's near-neighbor model consists of a tetrahedral arrangement of molecules around a central molecule and a continuum region outside of the discrete near-neighbor structure.[5] In the calculation of $S_m(Q)$ by this model, the contribution of atomic pairs at various distances from a central molecule were summed up, where the molecule was taken as the origin. Accordingly, the contribution of the atomic pairs between the peripheral molecules within the discrete structure, for example, is not contained substantially in the calculation of the contribution of the discrete structure. In this respect, Narten's model differs from our tetrahedral model essentially. As the result, the curve calculated from the discrete structure only is found to deviate largely from the observed data. Thus, there appears an intensive contribution from the continuum region beyond a distance r_c taken as a measure of the extent of the discrete structure as described in his paper,[23,24] and the latter contribution is found to play a dominant role for the overall agreement between the calculated $S_m(Q)$ and the observed data by using r_c as a disposable parameter.

According to the same procedures as described in Narten's paper,[5,23] we calculated $S_m(Q)$ using quite identical parameters except for the value of r_c, its

magnitude being not specified in those papers.[5,23] As reported previously by the authors,[6] a practically complete fit of the calculated $S_m(Q)$ curve with the observed data was obtained for the assignment of $r_c=3$ Å. For values larger than 3 Å a good fit was not obtained. Thus, in the analysis using Narten's near-neighbor model, the fitness of the calculated curve with the observed data is influenced decisively by the assignment of the value r_c.[6,25] Narten stated later in his review[24] that "the contribution of longer distances can be estimated as arising from a uniform distance distribution starting at r_c, the radius of sphere of volume $(N+1)/\rho_0$, ρ_0 being the bulk density of liquid water. Using Eq. 7 (in his review; Ref. 24) and adjusting by least squares the distance r_0 and the mean-square variations in both r_0 and r_c, we find that a value of $N=4.4$ gives the best agreement with the experimental curves for water at all temperatures." According to this description the magnitude of r_c is given to be about 3 Å from the relation: $(N+1)/\rho_0=(4\pi/3)r_c^3$ using $N=4.4$. Considering from the size of the discrete structure, however, the magnitude of $r_c=3$ Å is clearly too small and physically unacceptable, of course.

Thus, from all the consideration described above Narten's model should be said to be implausible physically in spite of its successful appearance.

Concluding Remarks

A general expression of the neutron structure factor for liquid regarded as an aggregate of small molecular clusters was obtained. The equations derived are widely applicable to liquids for analyzing diffraction data under due assumptions. We applied it to water and obtained the following conclusions:

1) The regular tetrahedral pentamer model is the best as a structure model of water in interpreting neutron diffraction data combined with X-ray results,

2) The interstitial model composed of tetrahedral pentamers and unbonded monomers is rejected because of the large deviations of calculated curves from experimental data,

3) Narten's near-neighbor model can not be accepted, because it is impossible to obtain calculated structure factor fitted with experimental data without assigning unreasonable value to its main disposable parameter r_c,

4) Page and Powles' (completely-correlated) orientation model has turned out to bring a too severe restriction with respect to orientational correlation compared with the authors' model which is considered to be the main reason of the deviation of their calculated curves from experimental data.

Appendix

In the right hand side of Eq. 6, we can separate the intramolecular terms from the intermolecular contributions. Then, Eq. 6 becomes

$$S_m(Q)=f_1(Q)+f_{2U}(Q)[S_C(Q)-1]$$
$$+\Sigma^{-2}N_c^{-1}\{\langle\sum_{l\neq l'}\exp(\vec{r}_{cll'})\sum_{n_l,n_{l'}}b_{n_l}b_{n_{l'}}\exp[i\vec{Q}\cdot(\vec{r}_{cn_l}-\vec{r}_{cn_{l'}})]\rangle$$
$$-\langle\sum_{l\neq l'}\exp(i\vec{Q}\cdot\vec{r}_{cll'})\rangle[\sum_n b_n\langle\exp(i\vec{Q}\cdot\vec{r}_{cn})\rangle]^2\}.$$

The third term in Eq. 23 corresponds to the last term of this equation which means the orientational correlations of molecules within the clusters.

References

1) A. H. Narten and H. A. Levy, *J. Chem. Phys.*, **55**, 2263 (1971).
2) F. Hajdu, S. Lengyel, and G. Pálinkás, *J. Appl. Crystallogr.*, **9**, 134 (1976).
3) E. Kálmán, G. Pálinkás, and P. Kovács, *Mol. Phys.*, **34**, 505 (1977).
4) D. I. Page and J. G. Powles, *Mol. Phys.*, **21**, 901 (1971).
5) A. H. Narten, *J. Chem. Phys.*, **56**, 5681 (1972).
6) N. Ohtomo and K. Arakawa, *Bull. Chem. Soc. Jpn.*, **51**, 1649 (1978).
7) N. Ohtomo and K. Arakawa, *Bull. Chem. Soc. Jpn.*, **52**, 2755 (1979).
8) G. Pálinkás, E. Kálmán, and P. Kovács, *Mol. Phys.*, **34**, 525 (1977).
9) A. H. Narten, M. D. Danford, and H. A. Levy, *Discuss. Faraday Soc.*, **43**, 97 (1967); A. H. Narten, "X-Ray Diffraction Data on Liquid Water in the Temperature Range 4 °C—200 °C," ORNL-4578 (1970).
10) F. Hajdu, *Acta Chim. Acad. Sci. Hung.*, **93**, 371 (1977); **96**, 355 (1978).
11) "Water," ed by F. Franks, Plenum, New York (1972), Vol. 1.
12) A. Rahman and F. H. Stillinger, *J. Chem. Phys.*, **55**, 3336 (1971); F. H. Stillinger and A. Rahman, *ibid.*, **57**, 1281 (1972); **60**, 1545 (1974); **61**, 4973 (1974); A. Rahman and F. H. Stillinger, *J. Am. Chem. Soc.*, **95**, 7943 (1973); A. Rahman, F. H. Stillinger, and H. Lemberg, *J. Chem. Phys.*, **63**, 5223 (1975).
13) R. O. Watts, *Mol. Phys.*, **28**, 1069 (1974).
14) O. Weres and S. A. Rice, *J. Am. Chem. Soc.*, **94**, 8983 (1972).
15) K. Arakawa, K. Tokiwano, and K. Kojima, *Bull. Chem. Soc. Jpn.*, **50**, 65 (1977).
16) N. Ohtomo, K. Arakawa, M. Takeuchi, T. Yamaguchi, and H. Ohtaki, *Bull. Chem. Soc. Jpn.*, **54**, 1314 (1981).
17) N. Ohtomo and K. Arakawa, *Bull. Chem. Soc. Jpn.*, **53**, 1510 (1980).
18) G. Kostorz and S. W. Lovessey, "Treatise on Materials Science and Technology," Academic Press (1979), Vol. 15, pp. 5—8.
19) The $f_3(Q)$ in Eq. 7 is a factor resulting from the molecular-center pairs within the cluster, and then, for the present tetrahedral model for water we can take the $f_3(Q)$ for $S_{m,p}^{(\infty)}(Q)$ safely, by assuming the molecular-center to be at the oxygen nucleus.
20) T. R. Dyke and J. S. Muenter, *J. Chem. Phys.*, **60**, 2929 (1974).
21) L. L. Shipman and H. A. Scheraga, *J. Phys. Chem.*, **78**, 909 (1974).
22) K. Arakawa, *Kagaku No Ryoiki Zokan*, No. 106, 15 (1974); *Kagaku Sosetsu*, No. 11, 35 (1976).
23) A. H. Narten and H. A. Levy, *Science*, **165**, 447 (1969).
24) A. H. Narten, "Water," ed by F. Franks, Plenum, New York (1972), Vol. 1, Chap. 8.
25) G. Pálinkás, T. Radnai, and F. Hajdu, *Z. Naturforsch., Teil A*, **35**, 107 (1980).

Kinetic Studies of the Stripping of Bis(2,4-pentanedionato)beryllium in Various Liquid-Liquid Partition Systems

Hitoshi WATARAI and Nobuo SUZUKI*

Department of Chemistry, Faculty of Science, Tohoku University, Sendai 980

(Received August 8, 1980)

The rate constant, k_{st}, for the stripping of bis(2,4-pentanedionato)beryllium from inert solvents into water or a mixed solvent of water with a miscible organic solvent, such as ethylene glycol, methanol, acetonitrile, and pimethyl sulfoxide, was determined and discussed in connection with the dissociation rate constant, k_d, of the chelate in the aqueous phase and the liquid-liquid partition coefficient, P, of the chelate. The $k_{st}=k_d/(1+P)$ relationship was found to hold true in all systems studied. The solvent effect of the aqueous mixed solvents on k_d was discussed in terms of the transfer activity coefficient.

The solvent extraction technique is widely employed in analytical chemistry to separate or concentrate a metal ion in an aqueous phase by removing it into an organic phase. Kinetic studies of a solvent-extraction mechanism of metal ions have been carried out by many workers. The rate-determining step of a chelate extraction has, in many cases, been reported to be a chelate-formation process in an aqueous phase.[1] The importance of an interfacial reaction for chelate formation has recently been pointed out for the extraction of calcium with bis(2-ethylhexyl)hydrogenphosphate[2] and copper with *o*-hydroxybenzaldehyde oximes.[3] On the other hand, the process of removing a metal compound from an organic phase into an aqueous phase, say stripping, is also important for an effective separation between metal ions.[4] However, on the stripping rate and the mechanism of the metal chelate there is no detailed information at present.

In this study, the rate and mechanism of the stripping reaction of the β-diketonato complex have been investigated utilizing bis(2,4-pentanedionato)beryllium as an example of the β-diketonates; it was chosen because of its moderate substitution lability and its simple dissociation behavior.[5] The stripping rate of the metal ion is expected to be influenced by the partition coefficient of the metal chelate and the dissociation behavior of the chelate in the aqueous phase. Therefore, the solvent effect of an aqueous phase is particularly interesting. In this study, various mixed solvents were used for the strip solution, *i.e.*, water–ethylene glycol, water–methanol, water–acetonitrile, and water–dimethyl sulfoxide. The stripping mechanism and solvent effect were studied from the measurements of the stripping rate constant, the hydrolysis rate constant in the aqueous phase, and the partition coefficient of the chelate. The partition coefficient is not only a measure of the extractability of a chelate from a nonpolar phase into a polar phase, but also a measure of the solution free-energy difference of the chelate in given solvents. With this in view, the kinetic solvent effect of the mixed solvent on the stripping rate will be discussed by correlating the rate constant with the partition coefficient.

Experimental

Chemicals. Bis(2,4-pentanedionato)beryllium(II) (Dotite, G. R.) was purified by vacuum sublimation at 80 °C. Organic solvents of dodecane, heptane, carbon tetrachloride, ethylene glycol, methanol, acetonitrile, and dimethyl sulfoxide were purified by ordinary methods.[6] Reagent-grade perchloric acid was used without further purification. Sodium perchlorate commercially purchased was purified by recrystallization. Redistilled water was used throughout. The stock solution of the acid was standardized by sodium carbonate titration. The mixed solvent of water and organic solvent was prepared by weight. The ionic strength in the aqueous phase used was adjusted to 0.1 M (1 M=1 mol dm^{-3}) by the use of sodium perchlorate.

Kinetic Measurements. The stripping rates of beryllium were observed by means of an ordinary batch method, except for the experiment in the carbon tetrachloride/water system. An organic solution of $Be(acac)_2$ (10^{-4} M) was agitated with an aqueous phase. The shaking speed of the partition tube, which contained 5 ml for each phase, had to be as high as 430 tpm to establish a rapid mass transfer across the interface. Under these conditions, the observed stripping rate reflects purely the chemically rate-controlled process. In practice, a shaking rate of 460 tpm was adopted for all measurements. The stripping-rate constant was calculated from the absorbance decrease in the chelate in the organic phase. The absorbance change was observed intermittently at given shaking-time intervals. Although the absorption maximum of $Be(acac)_2$ in an inert solvent is at 293 nm, the absorbance change was observed at 310 nm to prevent any interference due to acetylacetone produced from the hydrolysis of the chelate. For the kinetic experiment in the carbon tetrachloride/water system, the continuous partition method, described previously in detail,[7] was applicable because of the large difference in the densities of the two phases. Fifty μl of 0.03 M $Be(acac)_2$ in carbon tetrachloride was spiked into the two-phase system which had been agitated in a continuous-partition vessel. The decrease in the absorbance of the complex in the organic phase, observed at 310 nm soon after the injection, was recorded as a function of the time. A first-order analysis of the results gave the stripping-rate constant. The sample preparation and the batch experiment were carried out in a thermostated room at 25±1 °C.

The rate of the acid hydrolysis of $Be(acac)_2$ in the aqueous phase was observed photometrically. The absorbance change at 310 nm was observed as a function of the time after the injection of 15 μl of a 0.01 M dioxane solution of $Be(acac)_2$ into 3 ml of an aqueous solution contained in an optical cell thermostated at 25±0.1 °C. The reproducibility of the rate constant thus determined is within ±5%.

Partition Experiment. The partition coefficient of $Be(acac)_2$ was determined by means of the kinetic method at 25±1 °C. A 5-ml portion of an organic solution of the chelate was agitated with an equal volume of the aqueous phase for a given period, and then the absorbance of the

organic phase was observed. From the absorbance change observed at four different periods at least, the absorbance at $t=0$ was estimated by extraporation and has then used to calculate the partition coefficient. All of the photometric measurements in this study was performed by means of a UVIDEC-2 or Hitachi 356 spectrophotometer.

Results

Stripping in Inert Solvent/Water Systems. Stripping-rate constant, k_{st}, in the carbon tetrachloride/water system is shown in Fig. 1 as a function of the hydrogen-ion concentration in the aqueous phase. The k_{st} is linearly proportional to $[H^+]$ in the concentration range from 0.001 M to 0.004 M. The observed rate constants for the acid hydrolysis of $Be(acac)_2$, shown in Fig. 2, are also linearly proportional to $[H^+]$ in the concentration range from 0.001 M to 0.012 M and coincide with those reported by Pearson and Moor.[5] The stripping data obtained in the three inert solvent/water systems are summarized in Table 1. The partition coefficients of $Be(acac)_2$ greatly depend on the solvents, and the stripping-rate constant appears to be proportional to the partition coefficient.

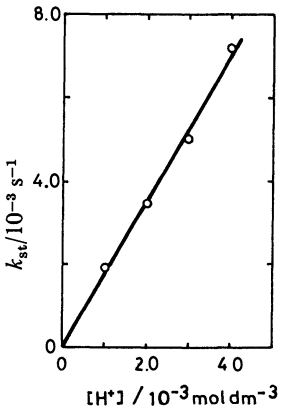

Fig. 1. Correlation between k_{st} and hydrogen ion concentration in aqueous phase. Organic phase: CCl_4.

Stripping in Dodecane/Water–Organic Solvent Mixture. The stripping-rate constants in the systems of dodecane/water–organic solvent mixtures at a constant hydrogen-ion concentration of 0.001 M are shown in Fig. 3.

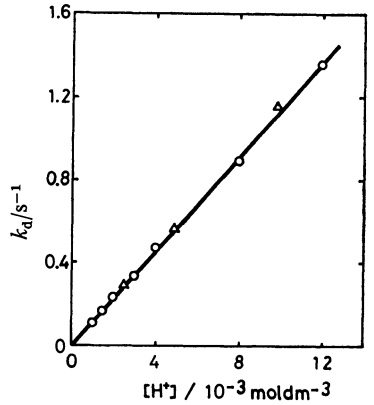

Fig. 2. Plot of k_d *vs.* hydrogen ion concentration for the acid hydrolysis of Be $(acac)_2$.
△: Pearson and Moore (1966), ○: this work.

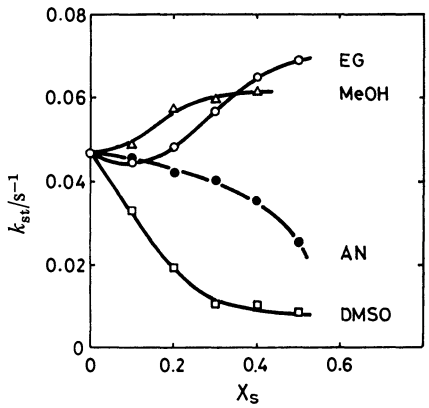

Fig. 3. Effect of aqueous mixed solvent on the stripping rate constant. $[H^+]=0.001$ M.

The stripping-rate constant is found to be greatly affected by the co-solvent. Remarkably, in system of the both H_2O–EG and H_2O–MeOH, the k_{st}'s increase with an increase in the mole fraction of the co-solvents. The rate constants for the solvolysis also greatly depend on the mixed solvent, as is shown in Fig. 4, where an increase of k_d in the H_2O–EG system is noticeable. In the mixed solvent systems also, the k_d raises with an increase in the hydrogen-ion concentration, as is shown in Fig. 5. The variation of the partition coefficient of $Be(acac)_2$ with the mole fraction of the co-solvent in

Table 1. The partition coefficients, P, the dissociation rate constants, k_d, and the stripping rate constants, k_{st}, of $Be(acac)_2$ at 25 °C

Organic solvent	Acid concentration/M[a]	P	k_d/s^{-1}	k_{st}/s^{-1}	$k_{st,calcd}/s^{-1}$[b]
Dodecane	0.0010	1.61	0.115	0.0471	0.044
	0.0020		0.220	0.0876	0.084
Heptane	0.0005	3.15	0.060	0.0145	0.015
	0.0010		0.115	0.0258	0.028
	0.0020		0.220	0.0535	0.053
Carbon tetrachloride	0.0010	70.8	0.115	0.00192	0.0016
	0.0020		0.220	0.00347	0.0030
	0.0030		0.337	0.00501	0.0047
	0.0040		0.478	0.00722	0.0067

a) $I=0.1$ M by $NaClO_4$. b) $k_{st,calcd}=k_d/(1+P)$.

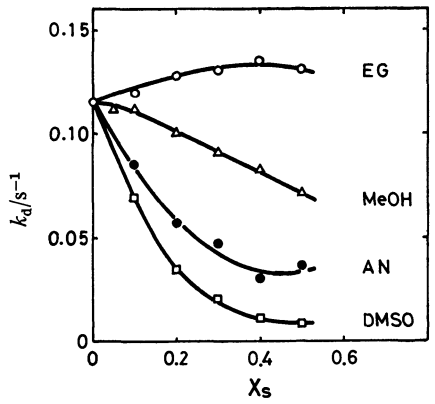

Fig. 4. Effect of aqueous mixed solvent on the rate constant of dissociation of Be $(acac)_2$. $[H^+]=0.001$ M. $I=0.1$ M by (H, Na) ClO_4.

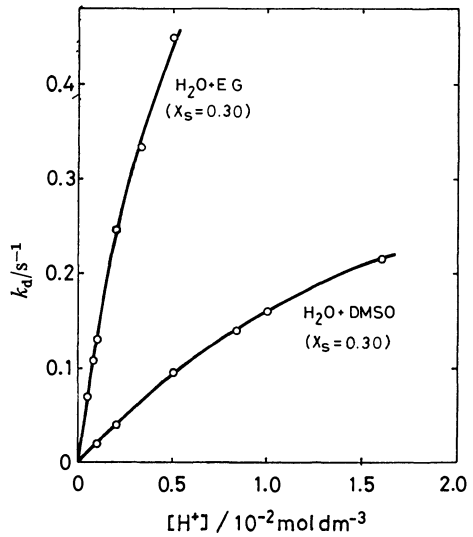

Fig. 5. Plot of k_d *vs.* hydrogen ion concentration.

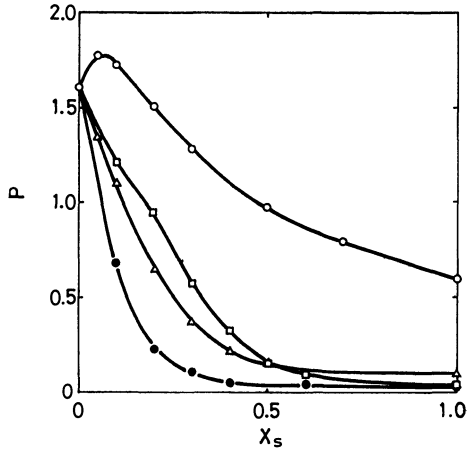

Fig. 6. Variation of partition coefficient of Be $(acac)_2$ with solvent composition.
Organic phase: dodecane. Aqueous phase: ○; H_2O–EG, □; H_2O–DMSO, △: H_2O–MeOH, ●; H_2O–AN.

the mixed-solvent phase is shown in Fig. 6. A maximum in the partition coefficient was observed in the dodecane/H_2O–EG system.

Discussion

Mechanism of the Stripping Reaction. As is shown in Figs. 1 and 2, both k_{st} and k_d depend on the hydrogen-ion concentration. The plot of k_{st} against k_d showed a simple linear relationship, $k_{st}=C\,k_d$, where C is a proportional constant. Therefore, we assumed the following scheme for the stripping reaction:

$$Be(acac)_{2,org} \rightleftharpoons Be(acac)_{2,aq} \quad (1)$$

$$Be(acac)_2 + H^+ \longrightarrow Be(acac)^+ + Hacac. \quad (2)$$

Processes 1 and 2 are represented by the partition coefficient, $P=[Be(acac)_2]_{org}/[Be(acac)_2]_{aq}$, and the dissociation rate constant, k_d, respectively. The rate equation for the stripping reaction:

$$-d[Be(acac)_2]_{org}/dt = k_{st}[Be(acac)_2]_{org} \quad (3)$$

gives the relation among k_{st}, k_d, and P:

$$k_{st} = k_d/(1+P). \quad (4)$$

Equation 4 strongly supports the proportionality between k_{st} and k_d observed experimentally. According to this equation, k_{st} was calculated and compared with the observed one. The results for the three solvent systems are listed in the last column of Table 1. The agreement between $k_{st,calcd}$ and k_{st} is satisfactory; this confirms the proposed scheme of Eqs. 1 and 2. For the mixed solvent systems also, the linear relationship between k_{st} and $k_d/(1+P)$ was confirmed, as is shown in Fig. 7, and the proposed mechanism was supported.

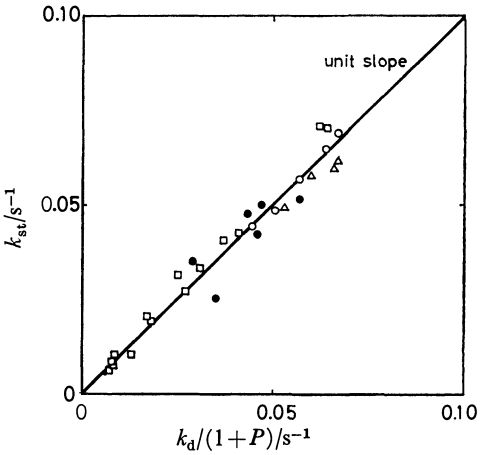

Fig. 7. Correlation between k_{st} and $k_d/(1+P)$.
Solid line represent an expected relation with unit slope.
Organic phase: dodecane. Aqueous phase: ○; H_2O–EG, □; H_2O–DMSO, △; H_2O–MeOH, ●: H_2O–AN.

Solvent Effect on the Acid Solvolysis. Equation 4 indicates that the solvent effect on the stripping rate is due to the effects on the dissociation rate and the partition equilibrium. The partition coefficient of $Be(acac)_2$ in the dodecane/aqueous mixed solvent system is related to the transfer-activity coefficient, y_s, of $Be(acac)_2$ from water to a mixed solvent by means of Equation 5:[8]

$$y_s = P/P_o, \quad (5)$$

where the subscript o denotes the reference value

observed in a pure-water system. On the other hand, the rate equation for the acid hydrolysis can be represented by the following equation under the conditions of a dilute acid concentration:

$$-\mathrm{d}[\mathrm{Be(acac)_2}]/\mathrm{d}t = k[\mathrm{H^+}][\mathrm{Be(acac)_2}], \quad (6)$$

where k is a constant in the equation of $k_d=k[H^+]$. In terms of the transfer-activity coefficient, the solvent effect on the dissociation rate can be represented by the next equation:[9]

$$k_d/k_{d,o} = y_s y_{H^+}/y_*, \quad (7)$$

where y_{H^+} and y_* are the transfer-activity coefficients from water to a mixed solvent of proton and the transition state. Equation 7 shows that the solvent effect of the mixed solvent on k_d can be represented by the three transfer-activity coefficients of y_s, y_{H^+}, and y_*. The substitution of Eq. 5 for y_s in Eq. 7 gives the next equation:

$$\log (y_*/y_{H^+}) = \log (P/P_o) - \log (k_d/k_{d,o}). \quad (8)$$

The values of $\log (y_*/y_{H^+})$ calculated from the above equation are plotted in Fig. 8 for the four mixed-

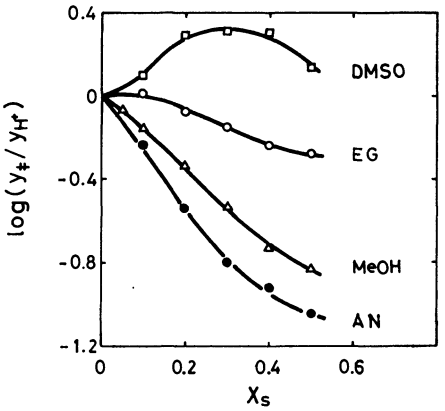

Fig. 8. Variation of $\log (y_*/y_{H^+})$ with solvent composition.

solvent systems. This figure shows that $\log (y_*/y_{H^+})$ decreases in the order of H_2O–DMSO>H_2O–EG>H_2O–MeOH>H_2O–AN in every solvent composition studied and that the value of the ratio of y_*/y_{H^+} is larger than unity for H_2O–DMSO and smaller than unity for the other systems. The large value of y_*/y_{H^+} observed in H_2O–DMSO system can be explained by the small value of y_{H^+} in the mixed solvent.[10] However, for the H_2O–EG and H_2O–MeOH systems, the reported order of y_{H^+}, *i.e.*, H_2O–EG>H_2O–MeOH,[11,12] is in disagreement with the order of $-\log (y_*/y_{H^+})$ in the two systems. This suggests that the solvent effect on y_{H^+} is not the only factor governing the solvent effect on the solvolysis of $Be(acac)_2$, the variation in y_* with the solvent composition being also an important factor. At the present stage, the evaluation of y_* is difficult because of the lack of reliable data for y_{H^+}. However, a test of the correlation between $\log (y_*/y_{H^+})$ and $\log y_s$ will be worthwhile in order to get a clue as to the solvent effect on the transition state. Figure 9 shows the linear proportionality of $\log (y_*/y_{H^+})$ to $\log y_s$ in the three systems except H_2O–DMSO, which shows a curved line with a

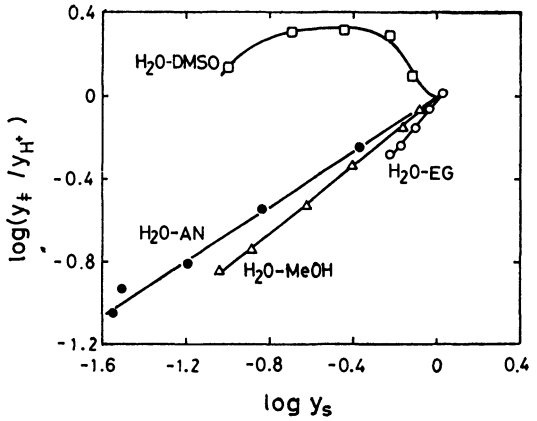

Fig. 9. Correlation between $\log (y_*/y_{H^+})$ and $\log y_s$.

maximum and a great difference from the others. Because the transition state in the acid hydrolysis can be expected to be a positively charged species, $\log y_*$ can be expected to include the two contributions to solute-solvent interaction, *i.e.*, ionic and nonionic interaction. The linear relationship, shown in Fig. 9, suggests that the ionic contributions to $\log y_*$ and $\log y_{H^+}$ may be compensated for each other and/or be proportionate to $\log y_s$ which is a measure of the nonionic interaction between $Be(acac)_2$ and a polar solvent. The great discrepancy in the plot in H_2O–DMSO suggests a strong proton affinity of the mixed solvent.[10]

The hydrogen-ion-concentration dependence of k_d in the H_2O–EG (X_s=0.30) and H_2O–DMSO (X_s=0.30) mixed solvents was discussed according to the general scheme proposed for the acid hydrolysis of acetylacetonates in an aqueous solution:[5]

$$\mathrm{Be(acac)_2} \underset{k_{-1}}{\overset{k_1}{\rightleftharpoons}} \mathrm{Be(acac)(acac')} \quad (9)$$

$$\mathrm{Be(acac)(acac')} + \mathrm{H^+} \overset{K_1}{\rightleftharpoons} \mathrm{Be(acac)(Hacac)^+} \quad (10)$$

$$\mathrm{Be(acac)(Hacac)^+} \overset{k_2}{\longrightarrow} \mathrm{Be(acac)^+ + Hacac}, \quad (11)$$

where (acac') denotes a half-bonded acetylacetone. This mechanism is represented by the next equation:

$$\frac{1}{k_d} = \frac{k_{-1}}{k_1 k_2 K_1}\frac{1}{[\mathrm{H^+}]} + \frac{1}{k_1}. \quad (12)$$

Following Eq. 12, the dissociation-rate constants in H_2O–EG and H_2O–DMSO systems, shown in Fig. 5, were analyzed. An intercept of the linear plot between k_d^{-1} and $[H^+]^{-1}$ gave the values of k_1; 0.75 s^{-1} for H_2O–DMSO (X_s=0.30) and 1.10 s^{-1} for H_2O–EG (X_s=0.30). Both of these values are smaller than the reported value in an aqueous solution, 6.5 s^{-1}.[5] The decreasing order of k_1 values: H_2O (P=1.61)>H_2O–EG (X_s=0.30) (P=1.28)>H_2O–DMSO (X_s=0.30) (P=0.58) corresponds to that in the partition coefficient. This indicates that the larger the solvation free energy of $Be(acac)_2$ in the mixed solvent, the slower the rate of the Be–O bond rupture.

In this study, the kinetic mechanism of the stripping of $Be(acac)_2$ was elucidated. For the purpose of practical separation using the stripping method, a solvent system with a smaller P value and a larger k_d value is promised

from the present results. A further investigation of the other metal chelates will provide insight into the solvent's role in the solvolysis of metal chelate and into the separation mechanism of metal ions in extraction chromatography.

References

1) T. Sekine and Y. Hasegawa, "Solvent Extraction Chemistry: Fundamentals and Applications," Mercel Dekker, New York, N. Y. (1977).
2) G. F. Vandegrift and E. P. Horwitz, *J. Inorg. Nucl. Chem.*, **39**, 1425 (1977).
3) J. S. Preston and Z. B. Luklineka, *J. Inorg. Nucl. Chem.*, **42**, 431 (1980).
4) D. S. Flett, *Chem. Ind, (London)*, **3**, 706 (1977).
5) R. G. Pearson and J. W. Moore, *Inorg. Chem.*, **5**, 1528 (1966).
6) A. Weissberger, E. S. Proskauer, J. A. Riddick, and E. E. Toops, Jr., "Technique of Organic Chemistry," Interscience, New York (1955), Vol. 7.
7) H. Watarai and N. Suzuki, *J. Inorg. Nucl. Chem.*, **43**, 761 (1981).
8) H. Watarai and N. Suzuki, *J. Inorg. Nucl. Chem.*, **38**, 1683 (1976).
9) B. G. Cox and P. T. McTigue, *Aust. J. Chem.*, **20**, 1815 (1967).
10) Von D. Geheb, N. F. Kasanskaja, and I. W. Beresin, *Chem., Ber.*, **76**, 160 (1972).
11) C. Kalidas, P. Sivaprasad, and U. V. Venkatram, *Z. Naturforsch., Teil A*, **32**, 791 (1977).
12) V. S. Rao and C. Kalidas, *Ind. J. Chem.*, **13**, 1303 (1975).

^{13}C NMR Spectra of Series of Bis(2,2′-bipyridine)cobalt(III) and Bis(1,10-phenanthroline)cobalt(III) Complexes

Shunji UTSUNO,* Yuzo YOSHIKAWA,** Akira TATEHATA, and Hideo YAMATERA**

Department of Chemistry, Faculty of Science, Shizuoka University, Oya, Shizuoka 422

***Department of Chemistry, Faculty of Science, Nagoya University, Chikusa-ku, Nagoya 464*

(Received September 3, 1980)

Twenty-eight cobalt(III) complexes of these types: $[Co(LL)_3]^{3+}$ and $[CoXX(LL)_2]^{n+}$ (LL=2,2′-bipyridine or 1,10-phenanthroline, and XX=$2CN^-$, $2NO_2^-$, ethylenediamine, $2NH_3$, glycinate ion, $2H_2O$, $C_2O_4^{2-}$, CO_3^{2-}, $2SCN^-$, $2N_3^-$, $2CH_3COO^-$, $2Cl^-$, or $2Br^-$), were prepared, and their ^{13}C NMR spectra were recorded. Most of the resonances in the complexes were assigned mainly by the technique of selective proton decoupling. In the bpy complexes, the chemical-shift difference between corresponding carbon atoms was the greatest in the C-6 and C-6′ pair. The phen complexes also gave parallel results. The main factor responsible for the chemical-shift differences of the C-6 and C-6′ pair is explained as resulting from the difference in σ-bonding ability between the pyridyl group and the ligand, X.

Recently the ^{13}C NMR technique has been widely used as a useful tool in investigating the structures of organic[1] and organometallic compounds.[2] The application of ^{13}C NMR to the study of transition-metal complexes is also increasing, but it has not yet been systematized. The spectra of ^{13}C NMR were reported for the complexes containing a quadridentate ligand (trimethylenediamine-*N,N′*-diacetate, ethylenediamine-*N,N′*-diacetate ion) and a bidentate ligand (2,2′-bipyridine, 1,10-phenanthroline, *etc.*) by Gailey *et al.*[3] and for the platinum complexes containing 2,2′-bipyridine and various diamines by Erickson *et al.*[4] However, there exists a partial disagreement between the two sets of assignments; *i.e.*, the assignments for the C-3 and C-5 carbons of 2,2′-bipyridine differ.

The present study was undertaken in order to ascertain the assignments of the ^{13}C NMR spectra of a series of bis-type cobalt(III) complexes, $[CoXX(LL)_2]^{n+}$, where LL=2,2′-bipyridine or 1,10-phenanthroline and where XX represents unidentate ligands or a bidentate ligand, and in order to find the relationship between the chemical shift and the nature of the second ligand, X.

Experimental

Materials. *Preparation of 2,2′-Bipyridine Complexes*: Most of the 2,2′-bipyridine complexes were prepared according to the literature, with a minor modification. The dichloro complex was prepared by the method of Vlcek.[5] The carbonato complex, $[Co(CO_3)(bpy)_2]^+$, was prepared by the reaction of $K_3[Co(CO_3)_3]$ with 2,2′-bipyridine; it was then used as the starting material for the preparation of diaqua, oxalato, and diacetato complexes.[6] The dinitro, dithiocyanato, and diazido complexes were prepared by Maki's method with the modification that *cis*-$[CoCl_2(bpy)_2]Cl$ or *cis*-$[Co(H_2O)_2(bpy)_2](ClO_4)_3$ was used as the starting material instead of the compound reported as "*trans*-$[CoCl_2(bpy)_2]Cl$".[7] Each crude complex was adsorbed on a small amount of SP-Sephadex C-25. Elution with 0.1 M (1 M=1 mol dm^{-3}) NaCl, followed by the evaporation of the eluent with a rotatory vacuum evaporator, gave each pure substance. The glycinato complex was prepared by the method of Murakami *et al.*[8] and subsequently purified by using a column of SP-Sephadex C-25, with 0.3 M NaCl as the eluent.

Ethylenediaminebis(2,2′-bipyridine)cobalt(III) Chloride, $[Co(en)(bpy)_2]Cl_3 \cdot 4H_2O$: The carbonato complex, $[Co(CO_3)(bpy)_2]Cl \cdot H_2O$, weighing 0.97 g (2 mmol), was dissolved in 4.2 cm^3 of 1 M HCl with heating at about 50 °C, and then 0.53 g (4 mmol) of ethylenediamine dihydrochloride, 0.15 cm^3 (2.3 mmol) of ethylenediamine, and 0.1 g of active charcoal were added. After it had stood overnight, the resulting yellow solution was filtered. The filtrate and washings were collected, and the cationic species were adsorbed at the top of a column of SP-Sephadex C-25 (120 cm long and 3 cm in diameter) and eluted with a solution of sodium pyrophosphate (pH=6.7). The first fraction was found to contain a mixture of $[Co(bpy)_3]^{3+}$ and $[Co(en)(bpy)_2]^{3+}$. They were separated on a column of SP-Sephadex C-25, using a 0.5 M NaCl solution as the eluent.

Found: C, 43.81; H, 5.17; N, 13.69; H_2O, 11.87%. Calcd for $C_{22}H_{32}N_6O_4Cl_3Co$: C, 43.33; H, 5.29; N, 13.78; H_2O, 11.82%. Absorption spectrum $\tilde{\nu}_{max}/cm^{-1}$ (log ε) 21600 (2.00).

cis-*Diamminebis(2,2′-bipyridine)cobalt(III) Perchlorate,* cis-$[Co(NH_3)_2(bpy)_2](ClO_4)_3 \cdot 2H_2O$: This complex was prepared and separated in a manner similar to that used in the preparation of the ethylenediamine complex.

Found: C, 32.49; H, 3.38; N, 11.34; H_2O, 4.86%. Calcd for $C_{20}H_{26}N_6O_{14}Cl_3Co$: C, 32.45; H, 3.54; N, 11.36; H_2O, 4.87%. Absorption spectrum $\tilde{\nu}_{max}/cm^{-1}$ (log ε) 21700 (1.82).

cis-*Dicyanobis(2,2′-bipyridine)cobalt(III) Chloride,* cis-$[Co(CN)_2(bpy)_2]Cl \cdot 4.5H_2O$: Into a solution of 1.38 g (2 mmol) of $[Co(bpy)_3]Cl_3 \cdot 3H_2O$ in 10 cm^3 of water, 0.1 g of active charcoal and 0.27 g (4.15 mmol) of KCN were stirred. Although the reaction seemed to take place within about five minutes, the solution was kept in a refrigerator overnight. It was then filtered to remove the charcoal, which was washed several times with hot water. The filtrate and washings were collected, and the cationic species in the solution were adsorbed on a small amount of SP-Sephadex C-25. The adsorbed species were eluted with 0.1 M hydrochloric acid, and the eluate was evaporated almost to dryness. The residue was washed with a small amount of cold water. It was then recrystallized from hot water and air-dried at room temperature.

Found: C, 48.77; H, 4.20; N, 15.74; H_2O, 14.91%. Calcd for $C_{22}H_{25}N_6O_{4.5}ClCo$: C, 48.95; H, 4.67; N, 15.57; H_2O, 15.02%. Absorption spectrum $\tilde{\nu}_{max}/cm^{-1}$ (log ε) 26000sh. (2.2).

cis-*Dibromobis(2,2′-bipyridine)cobalt(III) Perchlorate,* cis-$[CoBr_2(bpy)_2]ClO_4$: To a solution of 1.41 g (2 mmol) of $[Co(H_2O)_2(bpy)_2](ClO_4)_3$ in 1.5 cm^3 of water, 2 cm^3 of a 2 M KBr solution and 50 cm^3 of ethanol were added. After the mixture had stood overnight in a refrigerator, it was filtered and the filtrate was evaporated to dryness with a rotatory vacuum evaporator at a bath temperature of 60 °C. The

residue was redissolved in about 150 cm^3 of hot ethanol, and then, to the filtrate, an ethanol solution of $LiClO_4 \cdot 3H_2O$ was added to give the perchlorate crystals.

Found: C, 37.57; H, 2.19; N, 9.11%. Calcd for $C_{20}H_{16}N_4O_4Br_2ClCo$: C, 38.10; H, 2.56; N, 8.89%.

Preparation of 1,10-Phenanthroline Complexes: The complexes, $[Co(phen)_3]Cl_3 \cdot 4H_2O$,[9] $[Co(CN)_2(phen)_2]Cl \cdot 4H_2O$,[7] $[Co(H_2O)_2(phen)_2](NO_3)_3 \cdot 2H_2O$,[10] $[Co(SCN)_2(phen)_2]NCS$,[10] $[Co(CO_3)(phen)_2]Cl \cdot 5H_2O$,[11] and $[CoBr_2(phen)_2]Br \cdot 3H_2O$,[11] were prepared by the known methods. For the other complexes, the methods were essentially the same as those used for the preparation of the corresponding 2,2′-bipyridine complexes. The diammine complex was prepared by a method, which was different from that previously reported.[12]

cis-Diamminebis(1,10-phenanthroline)cobalt(III) Chloride, cis-$[Co(NH_3)_2(phen)_2]Cl_3 \cdot 3H_2O$: The complex, $[Co(NO_3)_2(phen)_2]NO_3$, was prepared by heating $[Co(H_2O)_2(phen)_2](NO_3)_3$ in an air bath at 110 °C for 4—5 h. The dinitrato complex, weighing 1.0 g, was added to 20 cm^3 of dimethyl sulfoxide, taking up sufficient ammonia gas. The resulting yellow solution was kept at room temperature for 2—3 h and then diluted with 30 cm^3 of water. The complex was adsorbed on a small amount of SP-Sephadex C-25 and eluted with 0.5 M HCl. The eluate was concentrated by evaporation, and then the chloride of the complex was precipitated by adding ethanol to the concentrated solution.

Found: C, 47.36; H, 4.26; N, 13.70; H_2O, 8.67%. Calcd for $C_{24}H_{28}N_6O_3Cl_3Co$: C, 46.96; H, 4.60; N, 13.69; H_2O, 8.80%. Absorption spectrum $\tilde{\nu}_{max}$/cm^{-1} (log ε) 21600 (1.87).

Identification of the Complexes. The complexes prepared were identified by comparing their electronic absorption spectra with those reported in the literature. The spectra of the dicyano and dibromo complexes were different from the reported ones; *i.e.*, the latter complex showed no maxima in the d-d band region, but only some undefined shoulders. The absorption maximum of the dicyano complex is given above. The elemental analyses were performed on dicyano, dibromo, and newly prepared compounds. The water contents were also determined by measuring the weight loss under the conditions of 100 °C and 20 mmHg.

It is well established that bis-type cobalt(III) complexes of 2,2′-bipyridine or 1,10-phenanthroline take only the *cis*-configuration because of the repulsion between the ligands. The *cis* configuration of all the present complexes was confirmed by the ^{13}C NMR spectra, as will be discussed later.

Physical Measurements. The electronic absorption spectra were measured using a Shimadzu MPS-50L spectrophotometer. The ^{13}C NMR spectra were measured at 15.04 MHz on a JEOL JNM-FX60 spectrometer equipped with a Fourier transform accessory under the condition of a noise-modulated proton decoupling. A sweep width of 2500 Hz, a pulse width of 9 μs (corresponding to the tipping angle of about 90°), and a pulse interval of 3 s were employed. The free-induction signal derived after each pulse was accumulated in a JEOL JEC-980A computer (8K). From approximately 500 up to 60000 accumulations were made for each spectrum. The ambient temperature was 35 °C. The solvents used were H_2O, $CHCl_3$, CH_3NO_2, CH_3OH, and a mixture of CH_3NO_2 and DMSO, and the concentrations of the samples were 0.3 M or lower depending on the solubilities. The spectra were obtained from samples contained in 10-mm-diameter tubes; D_2O in an inner coaxial tube 5-mm in diameter was used to provide a field-frequency lock signal. The external standard used was a dioxane–tetramethylsilane (TMS) mixture contained in a capillary (approximately 1-mm). Dioxane had a δ-value of 67.37 (downfield from TMS). All the chemical shifts are given relative to TMS, with a digital resolution of 0.6 Hz.

Selectively proton-decoupled ^{13}C NMR spectra were also measured for 2,2′-bipyridine (in $CDCl_3$), $[Co(bpy)_3]Cl_3$ (in D_2O), *cis*-$[CoCl_2(bpy)_2]Cl$ (in DMSO-d_6), and *cis*-$[Co(CN)_2(bpy)_2]Cl$ (in D_2O) in 5-mm-diameter tubes. Prior to each ^{13}C NMR measurement, the ^1H NMR spectrum of the same sample solution was recorded at 59.80 MHz. The internal standards used were TMS for the free ligand and sodium trimethylsilylpropanesulfonate (DSS) for the complexes.

In order to avoid the dissociation of the unidentate ligand and to obtain a sufficient solubility of the complex, nitromethane and dimethylsulfoxide were used as the solvent instead of water in some cases. The solvent effects on the ^{13}C NMR spectra of 2,2′-bipyridine complexes were measured for dicyano, dinitro, carbonato, diacetato, and tris-type complexes. In general, carbon resonance positions shifted to fields higher by 0.3—0.4 ppm for nitromethane solutions than for aqueous solutions. The greatest solvent effect was observed in the chemical-shift difference between the C-6 and C-6′ signals of the diacetato complex (1.07 ppm in the aqueous solution and 2.24 ppm in the nitromethane solution); the second largest was the C-6 and C-6′ pair of the carbonato complex (1.83 ppm in the aqueous solution and 2.62 ppm in the nitromethane solution). However, these large changes are exceptional. The solvent dependence of the chemical-shift differences is small in other resonances of these complexes and in all the resonances of the other complexes.

Results and Discussion

The ^{13}C NMR spectra with noise-modulated and selective proton decoupling are given in Fig. 1 for 2,2′-bipyridine dissolved in deuterated chloroform and for $[Co(bpy)_3]Cl_3 \cdot 3H_2O$ in deuterium oxide. The three signals appearing in the lower field in the proton-decoupled bipyridine spectrum were identified as those

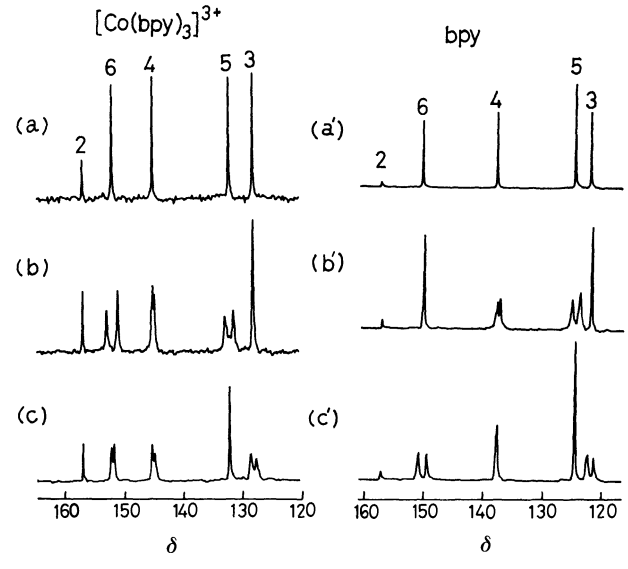

Fig. 1. Noise-modulated and selective proton-decoupled ^{13}C NMR spectra of $[Co(bpy)_3]Cl_3$ in D_2O and 2,2′-bipyridine in $CDCl_3$. (a) and (a′): Noise-modulated spectra, (b) and (b′): H-3 proton-decoupled spectra irradiated at 536 Hz from DSS and 501 Hz from TMS, respectively, (c) and (c′): H-5 proton-decoupled spectra irradiated at 475 Hz from DSS and 434 Hz from TMS, respectively.

of C-2, C-6, and C-4, in agreement with the literature.[3,4,13,14] The assignment of the C-4 signal was confirmed by comparing the spectral feature with that of 4,4′-dimethyl-2,2′-bipyridine (Fig. 2). The low intensity of the signal appearing at the lowest field is consistent with the absence of hydrogen atoms attached to C-2. The two signals appearing at the higher fields were identified as those of C-5 and C-3 in the order shown in Fig. 1 by measurement with selective proton decoupling (Figs. 1b, b′, c, and c′).

The assignments are consistent with those of Erickson *et al.*,[4] but different from those of Gailey *et al.*[3] in the C-3 and C-5 signals.

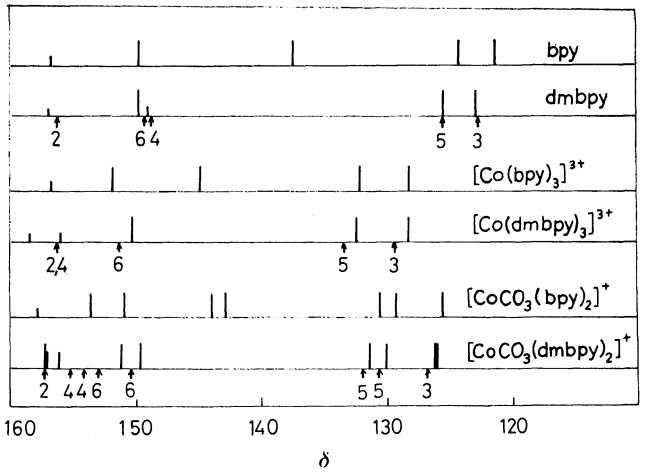

Fig. 2. Noise-modulated ^{13}C NMR spectra of 2,2′-bipyridine and 4,4′-dimethyl-2,2′-bipyridine (dmbpy) in $CHCl_3$, and their complexes in H_2O.

In Fig. 2, schematic comparisons of the ^{13}C NMR spectra are made between bipyridine and its 4,4′-dimethyl derivative, and also between their cobalt(III) complexes. The arrows under the spectra of the dimethyl derivative and its complexes show the positions of the signals predicted on the assumption that the methyl substitution at the 4 sites of bipyridine and its complexes would result in chemical-shift changes of the same magnitudes as those resulting from the corresponding substitution in pyridine.[1] The signals of the 4,4′-dimethyl derivative and its complexes appear near the predicted positions. Thus, each signal may be assigned as indicated by the nearby arrow.

The ^{13}C NMR spectra due to aromatic carbons of the $[CoXX(bpy)_2]^{n+}$-type complexes are listed in Fig. 3 in the order of the decreasing wavenumber of the first absorption band of the complex. As expected, each of the five resonance lines found in $[Co(bpy)_3]^{3+}$ splits into two in the $[CoXX(bpy)_2]^{n+}$-type complexes, except for the carbonato complex, in which the splitting was not detected in the C-2 and C-3 signals. The spectra of the 1,10-phenanthroline complexes also exhibit patterns similar to those of the bipyridine complexes. The assignment of the spectra of 1,10-phenanthroline and its complexes was made in a manner similar to the case of bipyridine, excepting that the C-5 and C-7 resonances of the complex can not be unambiguously differentiated.

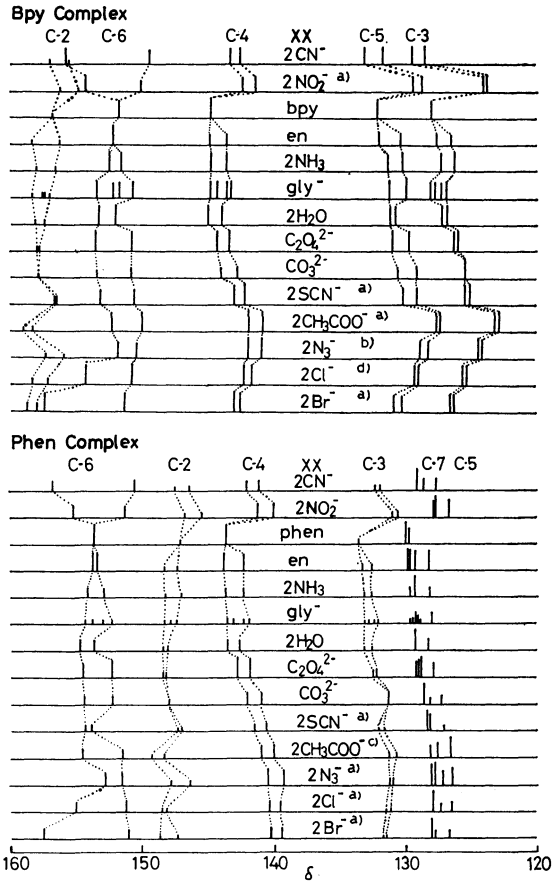

Fig. 3. Noise-modulated ^{13}C NMR spectra of cobalt(III) complexes of 2,2′-bipyridine and 1,10-phenanthroline in aqueous solutions.
a): Nitromethane solution, b): dimethyl sulfoxide solution, c): methanol solution, d): nitromethane-dimethyl sulfoxide (1 : 1) solution.

For the convenience of a ready comparison with bipyridine, the numbering system given below is here used for 1,10-phenanthroline:

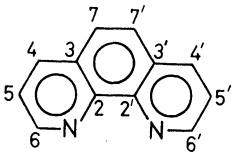

In both series of complexes, the magnitude of the splitting, *i.e.*, the chemical-shift difference between corresponding carbon atoms, is the largest between C-6 and C-6′.

It is well-known that diamagnetic shielding due to the ring current of the pyridyl group causes a drastic shift of proton resonances toward a higher field.[15] Therefore, in the present complexes, $[CoXX(bpy)_2]^{n+}$ and $[CoXX(phen)_2]^{n+}$, it can be expected that the H-6 proton lying above the plane of the pyridine ring of a neighboring ligand group resonates at the highest field, and the H-6′ proton lying near the expansion of the pyridine plane, at a lower field.

Taking these facts into account, the C-6 and C-6′ signals of the spectra of $[CoCl_2(bpy)_2]Cl$ and $[Co(CN)_2$-

$(bpy)_2]Cl$ were assigned by the selective proton-decoupling technique. When each complex was irradiated with the resonance frequency of the H-6 proton at the highest field, one of the ^{13}C signals at a lower field in the C-6 region split into two, while the other, at a higher field, remained unsplit; the latter is identified as a C-6 signal. This C-6 carbon nucleus is situated next to the nitrogen atom at the *trans* site of X in $[CoXX(bpy)_2]^{n+}$. Thus, for all complexes of the $[CoXX(LL)_2]^{n+}$ type (LL=bpy or phen), the resonances at the higher field may be assigned to C-6, and those at the lower field, to C-6′.

The chemical shifts of ^{13}C NMR were also measured of *N,N′*-bis(2-pyridylmethyl)ethylenediamine (penp) complexes, *cis*-α-$[CoXX(penp)]^{n+}$ (XX=2CN$^-$, en, $2NH_3$, $2H_2O$, $2N_3^-$, $2Cl^-$, and $2Br^-$), in which two pyridyl groups are located in positions *trans* to each other. The signal of the pyridyl C-6 of each complex of this series appeared near the C-6′ signal of the corresponding bis(bipyridine) complex.[16] This is consistent with the assignment given above for the C-6′ signal.

The difference between the C-6 and C-6′ chemical shifts in $[CoXX(LL)_2]^{n+}$ might be due to diamagnetic shielding, analogously to the cases of H-6 and H-6′. However, the observed shift differences are too large to be attributed to this effect only.

Recently, Nakashima *et al.*[17] gave a theoretical equation for use in calculating the chemical shift of a ligand proton under the influence of the paramagnetic anisotropy of the central cobalt(III) ion of a complex. The chemical-shift differences estimated for the present phenanthroline complexes after Nakashima *et al.*[17] are much smaller than the observed splittings; thus, the paramagnetic anisotropy of the cobalt(III) ion cannot be the main cause of the chemical-shift differences observed between the corresponding atoms of each ligand.

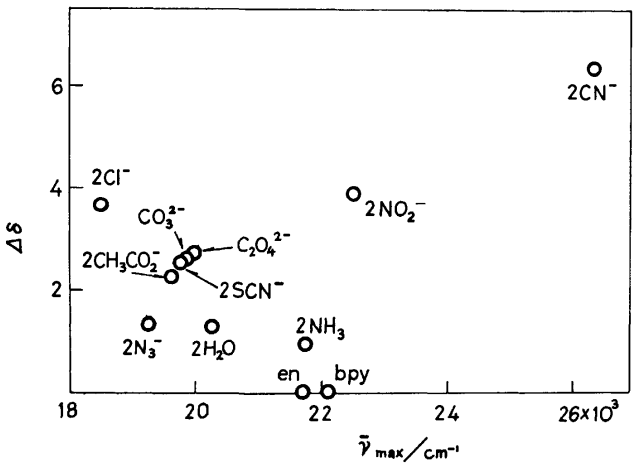

Fig. 4. A plot of the chemical-shift difference of C-6 and C-6′ carbons *vs.* the $\bar{\nu}_{max}$ value of the first absorption band of the complex, $[CoXX(bpy)_2]^{n+}$.

When the difference between the C-6 and C-6′ chemical shifts is plotted against the wavenumber of the first absorption band for each complex of the $[CoXX(LL)_2]^{n+}$ type (LL=bpy or phen), a roughly linear relationship can be observed (Fig. 4). The dinitro and dicyano complexes, however, greatly deviated from the linear relationship. This may be due to the strong π-interaction of NO_2^- and CN^-. Thus, the difference between the C-6 and C-6′ chemical shifts seems to be related to the σ-donating ability of the ligand, XX. For other carbon atoms, however, no simple relationship was observed between the chemical-shift difference and the ligand-field strength.

The present work was supported in part by a Grant-in-Aid for Scientific Research from the Ministry of Education, Science and Culture.

References

1) J. B. Stothers, "Carbon-13 NMR Spectroscopy," Academic Press, New York, N.Y. (1972); G. L. Nelson, "Carbon-13 Nuclear Magnetic Resonance for Organic Chemists," Wiley-Interscience, New York, N. Y. (1972).

2) For example, P. W. Hickmott, M.Cais, and A. Modiano "NMR Data on Organic-metal Carbonyl Complexes (1965—1971)," ed by E. F. Mooney, Annual Reports on NMR Spectroscopy, Academic Press, London (1977), Vol. 7.

3) K. D. Gailey, K. Igi, and B. E. Douglas, *Inorg. Chem.*, **14**, 2956 (1975); references to the ^{13}C NMR spectra of the complexes are cited therein.

4) L. E. Erickson, J. E. Sarneski, and C. N. Reilley, *Inorg. Chem.*, **14**, 3007 (1975).

5) A. A. Vlcek, *Inorg. Chem.*, **6**, 1425 (1967).

6) F. Aprile and F. Maspero, *Atti. Acad. Nazl. Lincei Rend., Classes Sci. Fis. Mat. Nat.*, **39**, 310 (1965).

7) N. Maki, *Bull. Chem. Soc. Jpn.*, **42**, 2275 (1969). See also J. G. Gibson, R. Raird, and E. D. MacKenzie, *J. Chem. Soc.*, **1969**, 2089.

8) M. Murakami, S. Seo, T. Matsusato, H. Itaya, and M. Sho, *Nippon Kagaku Zasshi*, **83**, 734 (1962).

9) L. S. Dollimore and R. G. Gillard, *J. Chem. Soc.*, **1973**, 933.

10) A. V. Ablov, *Zh. Neorg. Khim.*, **6**, 309 (1961); *Russ. J. Inorg. Chem.*, **6**, 157 (1961).

11) A. V. Ablov and D. M. Palade, *Zh. Neorg. Khim.*, **6**, 601 (1961); *Russ. J. Inorg. Chem.*, **6**, 306 (1961).

12) D. M. Palade, *Zh. Neorg. Khim.*, **12**, 987 (1967); *Chem. Abstr.*, **67**, 49960k (1967).

13) H. L. Retcofsky and R. A. Friedel, *J. Phys. Chem.*, **72**, 2619 (1968).

14) H. Rosenberger, M. Petig, K. Madeia, T. Pehk, and E. Lippmaa, *Org. Magn. Reson.*, **2**, 329 (1970).

15) H. Ito, J. Fujita, and T. Ito, *Bull. Chem. Soc., Jpn.*, **44**, 723 (1971).

16) S. Utsuno, K. Yamazaki, Y. Yoshikawa, and H. Yamatera, unpublished results.

17) Y. Nakashima, U. Sakaguchi, and H. Yoneda, *Bull. Chem. Soc. Jpn.*, **48**, 762 (1975).

The Aluminium Ion-assisted Aquation of $[CoF(NH_3)_5]^{2+}$

Masayasu IIDA,* Eiko KAI,** Kichisuke NISHIMOTO,** and Hideo YAMATERA***

Department of Chemistry, Faculty of Science, Nara Women's University, Nara 630

***Department of Chemistry, Faculty of Science, Osaka City University, Sumiyoshi-ku, Osaka 558*

****Department of Chemistry, Faculty of Science, Nagoya University, Chikusa-ku, Nagoya 464*

(Received September 25, 1980)

A kinetic study of the aluminium ion-assisted aquation of $CoF(NH_3)_5^{2+}$ was carried out. The pseudo-first-order rate constant obtained can be expressed as $k_{obsd}=k_{Al}[Al^{3+}]$, where $k_{Al}=(1.6\pm0.2)\times10^{-3}$ dm^3 mol^{-1} s^{-1} (I=2.0 mol dm^{-3}, 25 °C). The reaction rate is independent of the pH in the $(pH)_{obsd}<3.3$ range, in contrast with the pH-dependent rate for the $CrF(NH_3)_5^{2+}$–Al^{3+} system. The different behavior between $CoF(NH_3)_5^{2+}$ and $CrF(NH_3)_5^{2+}$ in aquation can be explained in terms of their electronic structures, as calculated on the basis of the CNDO/2 method.

There has been much interest in the reactions of the metal ion-assisted aquations of transition-metal complexes.[1] We ourselves have been studying this type of reaction from the point of view that this is a good and simple model to explain the mechanism of an inorganic reaction.[2,3]

In a previous paper, we reported the kinetics for the aluminium ion-assisted aquation of the pentaammine-fluorochromium(III) ion and attributed the pH dependency of the reaction rate to an easy protonation of $CrF(NH_3)_5^{2+}$.[3] The present paper is concerned with an aluminium ion-assisted aquation of $CoF(NH_3)_5^{2+}$, which showed a pH dependence entirely different from that of $CrF(NH_3)_5^{2+}$.

Different behavior has also been observed between $CrF(NH_3)_5^{2+}$ and $CoF(NH_3)_5^{2+}$ in their spontaneous aquation.[3,4] In order to understand the differences, the CNDO/2 calculation has been carried out on these complexes.

Experimental

Materials. Pentaamminefluorocobalt(III) nitrate was prepared according to the literature.[5] The nitrate was converted to perchlorate by the addition of $NaClO_4$. The purity of the crystals was confirmed by means of SP-Sephadex column chromatography with spectrophotometric detection. Found: Co, 15.80; N, 18.90; H, 3.93%. Calcd for $[CoF(NH_3)_5](ClO_4)_2$: Co, 16.28; N, 19.34; H, 4.17%.

The preparation of sodium perchlorate and aluminium perchlorate and the confirmation of their purity were carried out as previously described.[3]

The other chemicals used were guaranteed reagents from Wako Pure Chemicals Industries, Ltd.

Kinetic Procedure. Kinetic measurements were made in a manner similar to that previously described.[3] The concentration of the complex was controlled to 5.0×10^{-3} mol dm^{-3}. The absorbance changes were followed at 330 nm for all the sample solutions. The pseudo-first-order rate constants were determined by plotting $\ln(D_t-D_\infty)$ against the time, where D_t and D_∞ are the absorbances at the time t and at an infinite time respectivey.

pH Measurements. The procedure of pH measurements has been described previously.[3] We used this relation: $(pH)_{obsd}+\log[H^+]=-0.21$ for a 0.1 mol dm^{-3} $Al(ClO_4)_3$ solution. The pH of the sample solution was controlled by mixing a 0.2 mol dm^{-3} $Al(ClO_4)_3$ solution with a NaOH solution of an appropriate concentration.

^{19}F NMR Measurements. A JEOL FX 60Q spectrometer was used in the pulse Fourier transform mode at 56.26 MHz, with a deuterium lock to obtain the ^{19}F spectra. The water used in the sample solution was doubly distilled; it contained 5% by volume D_2O to provide a lock signal for the NMR spectrometer. The sample temperature was controlled to 30±1 °C, and the concentration of the complex was controlled to 0.05 mol dm^{-3}. All samples were examined in 5-mm tubes using $BF_3(C_2H_5)_2O$ as an external reference. The values of the chemical shifts obtained with reference to the external $BF_3(C_2H_5)_2O$ was converted to those with reference to F^- (in a neutral aqueous solution); the latter will be designated by δ below.

Calculations

In the present calculation, the standard values[6] are used for the CNDO/2 parameters associated with the H, N, and F atoms. The parameter values for the Co and Cr atoms, including those previously reported,[7] are summarized in Table 1. The geometries of the complexes are given by the experimental data:[8] 1.97 Å (Co–N), 1.87 Å (Co–F), 2.06 Å (Cr–N), 1.96 Å (Cr–F), and 1.01 Å (N–H).

Table 1. CNDO/2 parameters

		Cr	Co
$1/2(I_\mu+A_\mu)$/eV[a]	4s	3.909	4.17
	4p	0.876	1.16
	3d	4.822	5.839
$-\beta_\mu^\circ$/eV[b]	4s	15.70	17.10
	4p	3.52	4.76
	3d	23.00	28.00
ζ_μ[c]	4s, 4p	1.31	1.423[d]
	3d	2.48	2.83[d]

a) Clack's parameter.[6] I_μ: ionization potential. A_μ: electron affinity. b) β_μ°: bonding parameter. c) ζ_μ: orbital exponent. d) Zerner's parameter.[15]

Results and Discussion

Al^{3+}-assisted Aquation. The aquation of $CoF(NH_3)_5^{2+}$ yielding $CoOH_2(NH_3)_5^{3+}$ was promoted by aluminium ions. The spectrum of the sample solution changed with the time, showing isosbestic points at 360 and 506 nm, which indicates that no by-products were formed. Table 2 shows that the pseudo-first-order-rate constant obtained is approximately proportional to the aluminium-ion concentration, *i.e.*, $k_{obsd}=$

Table 2. Dependence of the rate constant on the concentration of the aluminium ion
(The ionic strength is controlled to 2.0 mol dm^{-3} by $NaClO_4$; at 25 °C, pH 2.5, and [complex]= 5.0×10^{-3} mol dm^{-3}.)

$[Al^{3+}]$ / mol dm^{-3}	k_{obsd}/s^{-1}	$\frac{k_{obsd}}{[Al^{3+}]}$/dm^3 mol^{-1} s^{-1}
0.030	4.54×10^{-5}	1.51×10^{-3}
0.050	7.59×10^{-5}	1.52×10^{-3}
0.10	1.57×10^{-4}	1.57×10^{-3}
0.15	2.46×10^{-4}	1.64×10^{-3}
0.20	3.58×10^{-4}	1.79×10^{-3}

$k_{Al}[Al^{3+}]$, where $k_{Al}=(1.6\pm0.2)\times10^{-3}$ dm^3 mol^{-1} s^{-1}. The small systematic variation in k_{Al} may result from the change in the perchlorate concentration (1.91—1.40 mol dm^{-3}) for the solutions of equal ionic strength. Considering the results of Swaddle and Jones[4] and of Chan,[9] we can write the total rate constant as:

$$k_{obsd} = k_0 + k_H[H^+] + k_{Al}[Al^{3+}],$$

where $k_0=3.3\times10^{-7}$ s^{-1} [4] (2.44×10^{-7} s^{-1} [9]), $k_H=5.2\times10^{-4}$ dm^3 mol^{-1} s^{-1} [9] at 35 °C and I=0.112—0.12 mol dm^{-3}. Under the present conditions, the first and second terms can be neglected in comparison with the third term.

The dependency of the reaction rate on the pH is shown in Fig. 1, together with the degree of hydrolysis of aluminium ions.[10] Previous results for the $CrF(NH_3)_5^{2+}$–Al^{3+} reaction are also depicted for comparison.

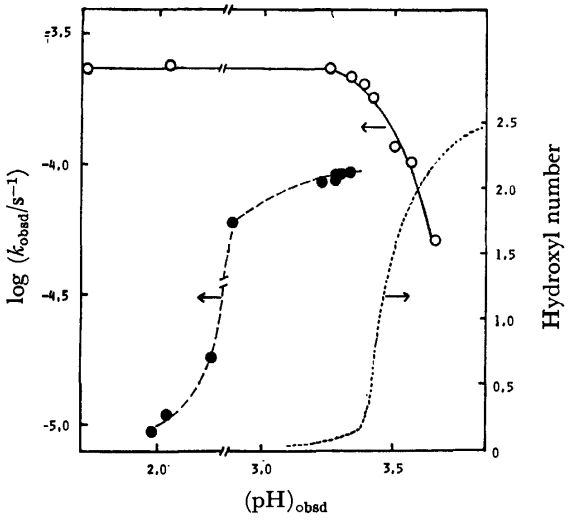

Fig. 1. pH dependence of the pseudo-first-order rate constants for $CoF(NH_3)_5^{2+}$–Al^{3+} system (—○—) and for $CrF(NH_3)_5^{2+}$–Al^{3+} system (---●---),[3] and the degree of hydrolysis of aluminium ions (------).[10] The hydroxyl number means the $[OH^-]/[Al^{3+}]$ ratio in hydrolysis products. Aveston (Ref. 10) gave the degree of the hydrolysis as a function of log[H$^+$], which is transformed to $(pH)_{obsd}$ (see pH measurements in the text). The experimental conditions for the reaction rates are: [complex]=5.0×10^{-3} mol dm^{-3}, $[Al(ClO_4)_3]$=0.10 mol dm^{-3}, and at 35 °C, and for the hydrolysis: $[Al(ClO_4)_3]$=0.10 mol dm^{-3}, at 25 °C.

A distinct difference exists in the reactivity between the chromium(III) and cobalt(III) complexes. The chromium(III) complex was considered to be easily protonated at the site of the fluoro ligand, and the complex is blocked from the approach of aluminium ions in the pH region lower than 3.0.[3] On the other hand, the present results show that the cobalt(III) complex is not so easily protonated as the chromium(III) complex and that the contribution of the protonated species to the reaction can be neglected even at a pH lower than 3.0. The reaction rate decreases with an increase of pH above $(pH)_{obsd}$=3.4, where a marked change occurs in the degree of hydrolysis of aluminium ions. According to Aveston[10] and Turner,[11] the formation of polycationic complexes begins to occur around this pH region, and their reactivity may be considerably smaller than that of Al^{3+} or $AlOH^{2+}$.

Table 3. Second-order rate constants at various temperatures
([complex]=5.0×10^{-3} mol dm^{-3}, $[Al^{3+}]$=0.10 mol dm^{-3}.)

t/°C	k_{Al}/dm^3 mol^{-1} s^{-1}
20	4.9×10^{-4}
25	1.2×10^{-3}
30	1.7×10^{-3}
35	2.6×10^{-3}
40	4.2×10^{-3}

Table 3 lists the rate constants at different temperatures; those rate constants give the values of ΔH^* and ΔS^* as 74 ± 5 kJ mol^{-1} and -72 ± 15 J mol^{-1} K^{-1} respectively. On the other hand, the activation parameters for the electron-transfer reaction, $CoF(NH_3)_5^{2+}+Fe^{2+}\rightarrow Co^{2+}+FeF^{2+}+5NH_3$, are $\Delta H^*=56$ kJ mol^{-1} and $\Delta S^*=-96$ J mol^{-1} K^{-1}.[12] The comparison of the ΔS^* values for the aquation and the reduction satisfies the general tendency that more stringent geometrical conditions have to be satisfied in the reduction.[13]

^{19}F NMR Study. The ^{19}F NMR signal of $CoF(NH_3)_5^{2+}$ cannot be detected even by 5000 scans for a 0.15 mol kg^{-1} solution of the complex. However, when an excess of aluminium ions was added to the solution of the cobalt(III) complex, a signal appeared which was assigned to the AlF^{2+} species (chemical shift $\delta=-36.1$ ppm from F$^-$).[14] As the reaction proceeds, the signal grows and approaches a constant height. This change corresponds to the formation of AlF^{2+} in the $CoF(NH_3)_5^{2+}+Al^{3+}\rightarrow CoOH_2(NH_3)_5^{3+}+AlF^{2+}$ reaction. When the aluminium-ion concentration was so low as to be compared with the $CoF(NH_3)_5^{2+}$ concentration ($[Al^{3+}]/[CoF(NH_3)_5^{2+}]<5$), an additional peak appeared. This peak had a chemical shift 0.65 ppm lower than that of the AlF^{2+} peak and was assigned to AlF_2^+.[14] All the kinetic studies were, therefore, carried out in the concentration range of $[Al^{3+}]/[CoF(NH_3)_5^{2+}]>5$, where the formation of by-products can be disregarded.

Electronic Effects on the Aquation of $CrF(NH_3)_5^{2+}$ and $CoF(NH_3)_5^{2+}$. In the spontaneous aquation of $CrF(NH_3)_5^{2+}$, the ammonia ligands are more easily displaced than the fluoro ligand, but the tendency

TABLE 4. THE CALCULATED BOND ORDERS ASSOCIATED WITH METAL-LIGAND BONDS

	$CrF(NH_3)_5^{2+}$		$CoF(NH_3)_5^{2+}$		$CrFH(NH_3)_5^{3+}$	
	Cr–F	Cr–N[a)]	Co–F	Co–N[a)]	Cr–F	Cr–N[a)]
σ-Donation						
4s-2s	0.238	0.260	0.235	0.258	0.217	0.267
4s-$2p_\sigma$	0.242	0.221	0.250	0.242	0.129	0.226
$4p_\sigma$-2s	0.357	0.340	0.360	0.351	0.334	0.350
$4p_\sigma$-$2p_\sigma$	0.384	0.318	0.417	0.355	0.213	0.338
$3d_\sigma$-2s	0.134	0.184	0.116	0.178	0.178	0.196
$3d_\sigma$-$2p_\sigma$	0.620	0.322	0.645	0.323	0.253	0.359
π-Donation						
$3d_\pi$-$2p_\pi$	0.101	—	0.0	—	0.061	—

a) The N atom here refers to the *cis*-N atom to F^-, because *cis*-$[CrF(OH_2)(NH_3)_4]^{2+}$ is the main product in the spontaneous aquation of $CrF(NH_3)_5^{2+}$ (Ref. 3).

is reversed in $CoF(NH_3)_5^{2+}$.[4,9] These results suggest that the Cr–F bond is stronger than the Cr–N bond, but Co–F is weaker than Co–N. The strength of the metal-ligand bond can be measured by the corresponding bond order. Table 4 lists the calculated bond orders of the complexes. The results show that the $3d_\pi$-$2p_\pi$ interaction strengthens the Cr–F bond, but makes no contribution to the Co–F bond, which explains the significantly greater stiffness of the Cr–F bond as compared with the Co–F bonds. On the other hand, the bond-order values show only a slight difference between Cr–N and Co–N. Therefore, it is possible that Cr–F is stronger than Cr–N, but Co–F is weaker than Co–N, although a simple comparison of bond orders cannot predict which is the stronger between bonds of different types, *i.e.*, between ionic M–F and ion-dipolar M–N.

As has been stated above, $CrF(NH_3)_5^{2+}$ is more easily protonated than $CoF(NH_3)_5^{2+}$. This can be explained by the greater value of the net negative charge of F in the chromium complex than in the cobalt analogue, as is shown in Table 5. The experimental results can also be explained qualitatively from the viewpoint of electronegativities; the less electronegative chromium forms a more ionic bond and the F linked to Cr should be more easily protonated than that bonded to Co. Therefore, the pH dependency of the aquation in the $CrF(NH_3)_5^{2+}$–Al^{3+} system can be well understood.

TABLE 5. THE CALCULATED NET CHARGES OF $CrF(NH_3)_5^{2+}$ AND $CoF(NH_3)_5^{2+}$

	M(Cr or Co)	*cis*-N	F
$CrF(NH_3)_5^{2+}$	+0.653	−0.202	−0.387
$CoF(NH_3)_5^{2+}$	+0.480	−0.183	−0.342

Table 4 also gives the results for the protonated complex, $CrFH(NH_3)_5^{3+}$, for the sake of comparison. Although it shows that the Cr–F bond is considerably weakened by the protonation, this is not well reflected in the experimental results shown in a previous paper:[3] the ammonia ligands in $CrF(NH_3)_5^{2+}$ are more easily removed than the fluoro ligand at pH 2, where most of the $CrF(NH_3)_5^{2+}$ should be protonated ($\log K_H = 3.0$).

References

1) R. G. Wilkins, "The Study of Kinetics and Mechanism of Reactions of Transition Metal Complexes," Allyn and Bacon, Boston (1974), p. 213.
2) M. Iida and H. Yamatera, *Bull. Chem. Soc. Jpn.*, **52**, 2290 (1979).
3) M. Iida and H. Yamatera, *Bull. Chem. Soc. Jpn.*, **54**, 441 (1981).
4) T. W. Swaddle and W. E. Jones, *Can. J. Chem.*, **48**, 1054 (1970).
5) F. Basolo and R. K. Murmann, *Inorg. Synth.*, **4**, 172 (1953).
6) D. W. Clack, N. S. Hush, and J. R. Yandle, *J. Chem. Phys.*, **57**, 3503 (1972).
7) E. Kai and K. Nishimoto, *Int. J. Quantum. Chem.*, **18**, 403 (1980).
8) Y. Kushi, 37th National Meeting of the Chemical Society of Japan, 2J28, Tokyo, April 1978; S. A. Goldfield and K. N. Raymond, *Inorg. Chem.*, **10**, 2604 (1971).
9) S. C. Chan, *J. Chem. Soc.*, **1964**, 2375.
10) J. Aveston, *J. Chem. Soc.*, **1965**, 4438.
11) R. C. Turner, *Can. J. Chem.*, **53**, 2811 (1975).
12) H. Diebler and H. Taube, *Inorg. Chem.*, **4**, 1029 (1965).
13) A. E. Ogard and H. Taube, *J. Am. Chem. Soc.*, **80**, 1084 (1958).
14) R. E. Connick and R. E. Poulson, *J. Phys. Chem.*, **79**, 5153 (1957).
15) M. Zerner and M. Gouterman, *Theor. Chim. Acta.*, **4**, 44 (1966).

Thermal Reactions of Metal Complexes under Quasi-isothermal and -isobaric Conditions. II.[1] Formation of Triamminetrihalogenochromium(III) Complexes *via* the Decomposition of Hexaammine, Pentaamminehalogeno, and *trans*-Tetraamminedihalogeno Complexes[2]

Hitoshi Ueno, Akira Uehara, and Ryokichi Tsuchiya*
Department of Chemistry, Faculty of Science, Kanazawa University, Kanazawa 920
(Received October 2, 1980)

The thermal decomposition of the following chromium(III) complexes was investigated in the solid phase by means of Q-derivatograph under quasi-isothermal and -isobaric conditions (Q-conditions) and D-derivatograph under dynamic conditions (D-conditions): $[Cr(NH_3)_6]X_3$, $[CrX(NH_3)_5]Y_2$, and *trans*-$[CrX_2(NH_3)_4]Y$, where X and Y are chloride and/or bromide ions. The complexes were finally converted into triamminetrihalogeno complexes $[CrBr_xCl_y(NH_3)_3]$ ($x+y=3$; x and $y=0$, 1, 2, or 3) under Q-conditions but decomposed in complicated ways under D-conditions. All the triamminetrihalogeno complexes thus obtained have *mer*-configuration with respect to the positions of the three halide ions.

Methods for preparing triamminetrihalogenochromium(III) complexes are usually based on the use of $[Cr(O_2)_2(NH_3)_3]$ in aqueous media[3] or that of thermal decomposition of ammine complexes in open systems.[4] However, the former is considerably troublesome while the latter has the disadvantage that thermal reactions in open systems do not always proceed uniformly to give pure products. The thermal reactions of metal complexes have been reported to proceed reproducibly and uniformly under quasi-isothermal and -isobaric conditions (Q-conditions),[1] and the intermediates and the final products in each reaction step can be obtained in remarkably pure constitution.[5]

This paper deals with the investigation of (1) the thermal decomposition of various amminechromium(III) complexes under Q-conditions as well as dynamic conditions (D-conditions)[1] and (2) the possibility of the formation of triamminetrihalogeno complexes.

The reactions in this work are classified as follows according to the final products: (A) Formation of $[CrCl_3(NH_3)_3]$ from $[Cr(NH_3)_6]Cl_3$, $[CrCl(NH_3)_5]Cl_2$, and *trans*-$[CrCl_2(NH_3)_4]Cl$; (B) formation of $[CrBr_3(NH_3)_3]$ from $[Cr(NH_3)_6]Br_3$ and $[CrBr(NH_3)_5]Br_2$; (C) formation of $[CrBrCl_2(NH_3)_3]$ from $[CrBr(NH_3)_5]Cl_2$, *trans*-$[CrCl_2(NH_3)_4]Br$, and *trans*-$[CrBrCl(NH_3)_4]Cl$; and (D) formation of $[CrBr_2Cl(NH_3)_3]$ from $[CrCl(NH_3)_5]Br_2$ and *trans*-$[CrBrCl(NH_3)_4]Br$.

Experimental

Preparation of Complexes. The complexes except for the mixed halogeno complexes were prepared according to known procedures.

$[Cr(NH_3)_6]Cl_3$ (I),[6] $[Cr(NH_3)_6]Br_3$ (II),[7] and $[CrCl(NH_3)_5]Cl_2$ (III)[8] were obtained by the methods reported.

$[CrCl(NH_3)_5]Br_2$ (IV) was prepared by adding NaBr to an aqueous solution of $[CrCl(NH_3)_5]Cl_2$ (III).

trans-$[CrCl_2(NH_3)_4]Cl$ (V) and *trans*-$[CrCl_2(NH_3)_4]Br$ (VI) were obtained by the acid cleavage of rhodochromic chloride $[(NH_3)_5Cr(OH)Cr(NH_3)_5]Cl_5$.[9]

$[CrBr(NH_3)_5]Br_2$ (VII) was prepared by the method of Linhard and Weigel.[10]

$[CrBr(NH_3)_5]Cl_2$ (VIII) was obtained by the addition of NH_4Cl to $[CrBr(NH_3)_5]Br_2$ (VII) in ice-cooled water.

trans-$[CrBrCl(NH_3)_4]Cl$ (IX) and *trans*-$[CrBrCl(NH_3)_4]Br$ (X): Chloroerythrochromic bromide $[(NH_3)_5Cr(OH)CrCl(NH_3)_4]Br_4$ prepared from the corresponding chloride[9] was added to a mixture of 60% $HClO_4$ and concd HBr (2: 1) in a loosely stoppered flask. The mixture was left to stand at room temperature for 2 h. The solid product was collected and washed with a small amount of 1 M $HClO_4$. Bright green *trans*-$[CrBrCl(NH_3)_4]ClO_4$ thus obtained was converted into *trans*-$[CrBrCl(NH_3)_4]Cl\cdot nH_2O$ and *trans*-$[CrBrCl(NH_3)_4]Br\cdot nH_2O$ with a saturated solution of NH_4Cl and concd HBr, respectively, and then collected and dried at 100 °C for 5 and 2 h to give the anhydrous chloride and bromide, respectively. Analytical data for the mixed halogeno complexes are given in Table 1.

Measurements. The thermal reactions were traced on MOM D- and Q-derivatographs.[1] Measurements by D-derivatograph were carried out in a constant flow of nitrogen at heating rate 1 °C min^{-1}. The electronic spectra were measured in powder state with a Hitachi EPU-2A spectrophotometer equipped with a standard Hitachi reflection attachment (Type R-3).

Table 1. Analytical data for starting complexes

Complex	H (%)		N (%)		Cr (%)	
	Found	Calcd	Found	Calcd	Found	Calcd
$[CrCl(NH_3)_5]Br_2$ (IV)	4.60	4.51	21.08	21.05	15.32	15.64
$[CrBr(NH_3)_5]Cl_2$ (VIII)	5.31	5.21	24.23	24.31	17.91	18.05
trans-$[CrCl_2(NH_3)_4]Br$ (VI)	4.47	4.43	20.66	20.66	18.97	19.18
trans-$[CrBrCl(NH_3)_4]Cl$ (IX)	4.63	4.43	20.43	20.66	19.22	19.18
trans-$[CrBrCl(NH_3)_4]Br$ (X)	3.85	3.80	17.83	17.75	16.26	16.48

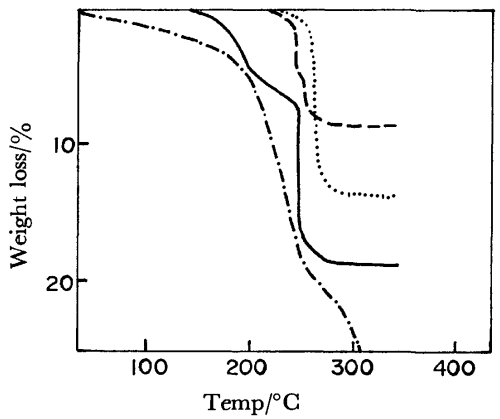

Fig. 1. Q-derivatograms of complexes I (——), III (·····), and V (– – –) together with D-derivatogram of complex I (—·—).

Results and Discussion

Formation of Triamminetrihalogeno Complexes. (A) Formation of $[CrCl_3(NH_3)_3]$ *from* $[Cr(NH_3)_6]Cl_3$ *(I),* $[CrCl(NH_3)_5]Cl_2$ *(III), and* trans-$[CrCl_2(NH_3)_4]Cl$ *(V).* Figure 1 shows the Q-derivatograms of complexes I, III, and V together with the D-derivatogram (TG curve only) of complex I. As seen from the D-derivatogram of complex I, a monotonous decrease takes place and no plateau is obtained in the TG curve, indicating that the complex decomposes gradually in a complicated manner with no formation of uniform products. Since this tendency was found in all the other complexes, their D-derivatograms are omitted in the following discussion.

On the other hand, the Q-derivatogram of complex I shows a gradual weight loss at 150—242 °C due to the evolution of 1 mol of ammonia (Found: 7.61%; Calcd: 6.52%), and then an abrupt weight loss takes place at 242 °C until a plateau is attained. The total weight loss is 18.69% approximately agreeing with that (19.58%) calculated for the formation of $[CrCl_3(NH_3)_3]$. The original yellow color turned green at this stage. The results suggest that complex I undergoes deammonation to be converted into $[CrCl_3(NH_3)_3]$ *via* $[CrCl(NH_3)_5]Cl_2$ without forming $[CrCl_2(NH_3)_4]Cl$.

The Q-derivatogram of complex III shows rapid evolution of 2 mol of ammonia in a narrow temperature range (250—260 °C), after which a clear plateau is obtained, the complex turning green from red. The net weight loss (13.77%) coincides with the value calculated for the formation of $[CrCl_3(NH_3)_3]$ (13.99%).

In the Q-derivatogram of complex V, a sharp change in weight takes place nearly isothermally (230—250 °C) until a distinct plateau appears. The weight loss in 7.73% which is close to that (7.50%) calculated for 1 mol of ammonia.

The analytical data for the triamminetrihalogeno complexes are summarized in Table 2. The observed and calculated values agree, indicating that $[CrCl_3(NH_3)_3]$ is obtained under Q-conditions irrespective of the starting complex.

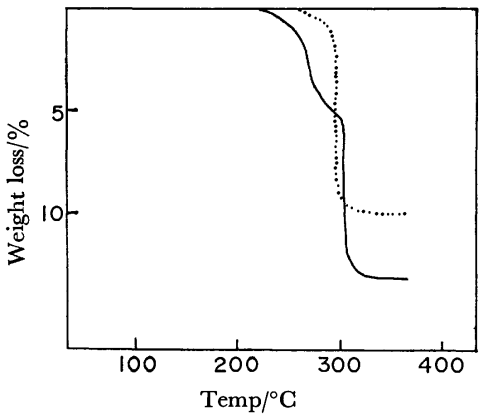

Fig. 2. Q-derivatograms of complexes II (——) and VII (·····).

Table 2. Analytical data for triamminetrihalogeno complexes produced

( ): Calcd

Triammine complex	Starting complex	H (%)	N (%)	Cr (%)
(A) *mer*-$[CrCl_3(NH_3)_3]$	$[Cr(NH_3)_6]Cl_3$	4.19 (4.29)	19.78 (20.04)	24.69 (24.82)
	$[CrCl(NH_3)_5]Cl_2$	4.24 (4.29)	20.01 (20.04)	24.84 (24.82)
	trans-$[CrCl_2(NH_3)_4]Cl$	4.30 (4.29)	19.61 (20.04)	25.02 (24.82)
(B) *mer*-$[CrBr_3(NH_3)_3]$	$[Cr(NH_3)_6]Br_3$	2.53 (2.62)	11.82 (12.24)	14.64 (15.16)
	$[CrBr(NH_3)_5]Br_2$	2.40 (2.62)	12.29 (12.24)	14.95 (15.16)
(C) *mer*-$[CrBrCl_2(NH_3)_3]$	$[CrBr(NH_3)_5]Cl_2$	3.50 (3.54)	16.40 (16.54)	20.50 (20.47)
	trans-$[CrCl_2(NH_3)_4]Br$	3.52 (3.54)	16.91 (16.54)	20.31 (20.47)
	trans-$[CrBrCl(NH_3)_4]Cl$	3.61 (3.54)	16.70 (16.54)	20.15 (20.47)
(D) *mer*-$[CrBr_2Cl(NH_3)_3]$	$[CrCl(NH_3)_5]Br_2$	2.99 (3.02)	14.61 (14.09)	17.66 (17.42)
	trans-$[CrBrCl(NH_3)_4]Br$	3.07 (3.02)	14.23 (14.09)	17.52 (17.42)

(B) Formation of $[CrBr_3(NH_3)_3]$ *from* $[Cr(NH_3)_6]Br_3$ *(II) and* $[CrBr(NH_3)_5]Br_2$ *(VII).* Figure 2 shows the Q-derivatograms of complexes II and VII. They give patterns similar to those of the foregoing chlorides I and III, respectively. The first gradual weight loss for complex II (250—303 °C) is due to the evolution of 1 mol of ammonia (Found: 4.95%; Calcd: 4.31%) and the second rapid weight loss is due to the evolution of 2 mol of ammonia. The TG curve then reaches a plateau. The overall weight loss (12.50%) agrees with that (12.94%) calculated for the formation of $[CrBr_3(NH_3)_3]$.

Complex VII gives only one rapid weight loss step corresponding to the liberation of 2 mol of ammonia (Found: 8.97%; Calcd: 9.02%). The formation of $[CrBr_2(NH_3)_4]Br$ was not detectable in the decomposition pathways of both the complexes.

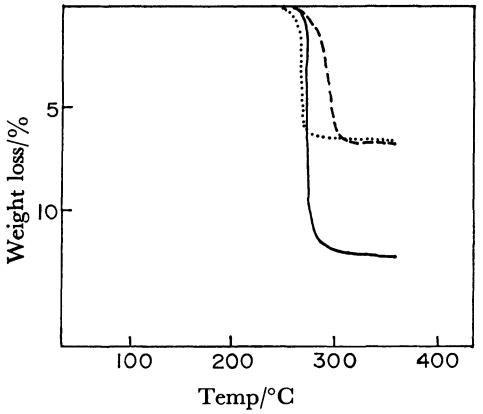

Fig. 3. Q-derivatograms of complexes VIII (——), VI (·····), and IX (---).

(C) Formation of $[CrBrCl_2(NH_3)_3]$ *from* $[CrBr(NH_3)_5]Cl_2$ *(VIII),* trans-$[CrCl_2(NH_3)_4]Br$ *(VI), and* trans-$[CrBrCl(NH_3)_4]Cl$ *(IX).* The Q-derivatograms of complexes VIII, VI, and IX are shown in Fig. 3. Complex VIII evolves 2 mol of ammonia nearly isothermally (275—285 °C), and complexes VI and IX, 2 mol of ammonia at 267—280 °C and 253—290 °C, respectively. The observed weight loss due to the evolution of ammonia is 11.62% (Calcd: 11.81%) for complex VIII, 6.26% (Calcd: 6.27%) for complex VI and 6.34% (Calcd: 6.27%) for complex IX. The analytical data indicate that all the final products have exactly the same composition as $[CrBrCl_2(NH_3)_3]$ (Table 2).

(D) Formation of $[CrBr_2Cl(NH_3)_3]$ *from* $[CrCl(NH_3)_5]Br_2$ *(IV) and* trans-$[CrBrCl(NH_3)_4]Br$ *(X).* We see from Fig. 4 that complexes IV and X evolve 2 mol (Found: 5.46%; Calcd: 5.39%) and 1 mol (Found: 10.26%; Calcd: 10.22%) of ammonia, respectively, at 270—290 °C to form $[CrBr_2Cl(NH_3)_3]$.

Configuration of Triamminetrihalogeno Complexes Obtained. Two configurations are possible for the triamminetrihalogeno complexes, facial and meridional with respect to the positions of the three halide ions (or three ammonia molecules). Such distinction in $[CrX_3N_3]$ chromophore (X denotes halide ion and N nitrogen atom) has been achieved from electronic spectral measurements.[4a,11] *fac*-Form has two bands, whereas *mer*-form has three in d-d transition region, a weak band due to the spin-forbidden transition ($^4A_{2g} \rightarrow {}^2E_g$) appearing in lower wavelength region ($\approx 13 \times 10^3$ cm^{-1}) being characteristic of *mer*-form.

Figures 5—8 show the electronic spectra of $[CrCl_3(NH_3)_3]$, $[CrBr_3(NH_3)_3]$, $[CrBrCl_2(NH_3)_3]$, and $[CrBr_2Cl(NH_3)_3]$. The triamminetrihalogeno complexes obtained from *trans*-dihalogeno complexes have the

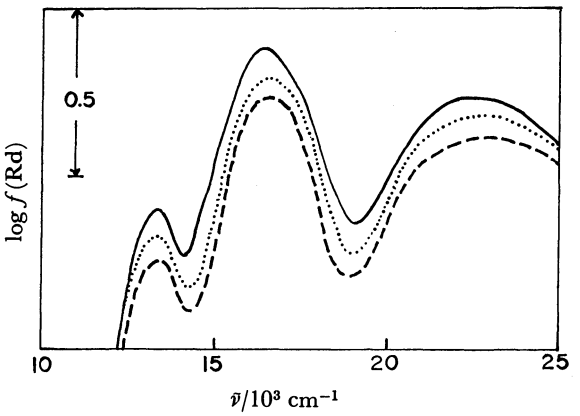

Fig. 5. Electronic spectra of $[CrCl_3(NH_3)_3]$ produced from complexes I (——), III (·····), and V (---).

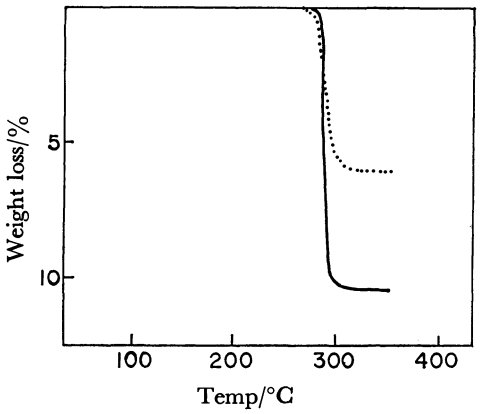

Fig. 4. Q-derivatograms of complexes IV (——) and X (·····).

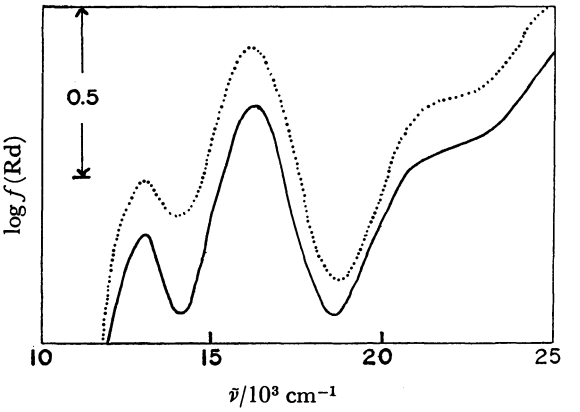

Fig. 6. Electronic spectra of $[CrBr_3(NH_3)_3]$ produced from complexes II (——) and VII (·····).

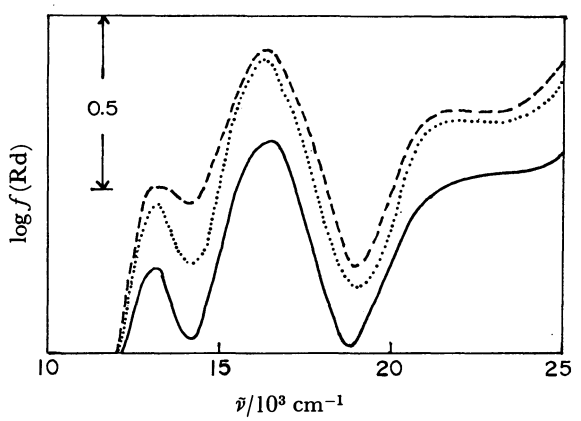

Fig. 7. Electronic spectra of $[CrBrCl_2(NH_3)_3]$ produced from complexes VIII (——), VI (·····), and IX (---).

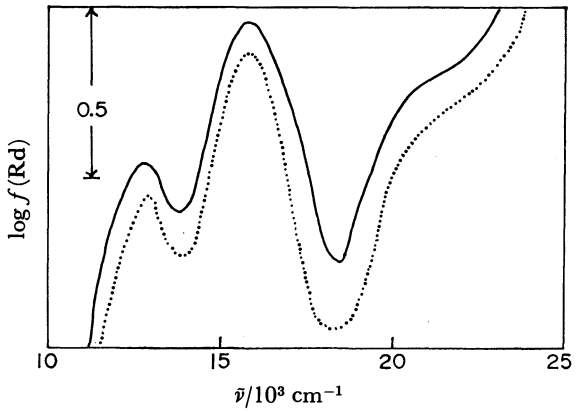

Fig. 8. Electronic spectra of $[CrBr_2Cl(NH_3)_3]$ produced from complexes IV (——) and X (·····).

possibility to take only *mer*-configuration. All the spectra have one weak and two strong bands, indicating that all the triamminetrihalogeno complexes are in *mer*-configuration.

Table 3. Absorption maxima for triamminetrihalogeno complexes

Complex	Maxima ($^4A_{2g} \rightarrow {}^2E_g$) $\tilde{\nu}$/cm^{-1}	Maxima ($^4A_{2g} \rightarrow {}^4T_{2g}$) $\tilde{\nu}$/cm^{-1}
mer-$[CrCl_3(NH_3)_3]$	13400	16700
mer-$[CrBrCl_2(NH_3)_3]$	13100	16200
mer-$[CrBr_2Cl(NH_3)_3]$	12900	16000
mer-$[CrBr_3(NH_3)_3]$	12800	15600

The absorption maxima due to $^4A_{2g} \rightarrow {}^2E_g$ and $^4A_{2g} \rightarrow {}^4T_{2g}$ transitions are given in Table 3. The absorption maxima due to $^4A_{2g} \rightarrow {}^4T_{2g}$ are shifted to the lower energy region according to spectrochemical series in the order $[CrCl_3(NH_3)_3] \rightarrow [CrBrCl_2(NH_3)_3] \rightarrow [CrBr_2Cl(NH_3)_3] \rightarrow [CrBr_3(NH_3)_3]$. Two structures are possible for *mer*-$[CrBrCl_2(NH_3)_3]$ and *mer*-$[CrBr_2Cl(NH_3)_3]$: *viz.*, *cis*-form and *trans*-form regarding chloride and bromide ions, but the question is still pending.

Summary of Thermal Reaction Pathways. The hexaammine complexes are converted into pentaamminehalogeno and then triamminetrihalogeno complexes without forming tetraamminedihalogeno complexes. The pentaamminehalogeno complexes undergo deammonation in one step to yield triamminetrihalogeno complexes, without forming tetraamminedihalogeno complexes. Why no tetraamminedihalogeno complexes can be produced in the reaction pathways of hexaammine and pentaammine complexes is easily understandable from a comparison of the formation temperature of triamminetrihalogeno complexes:

$[CrCl(NH_3)_5]Cl_2 \longrightarrow [CrCl_3(NH_3)_3]$ 250—270 °C

trans-$[CrCl_2(NH_3)_4]Cl \longrightarrow [CrCl_3(NH_3)_3]$ 230—250 °C

$[CrBr(NH_3)_5]Cl_2 \longrightarrow [CrBrCl_2(NH_3)_3]$ 275—285 °C

trans-$[CrBrCl(NH_3)_4]Cl \longrightarrow [CrBrCl_2(NH_3)_3]$ 253—273 °C

$[CrCl(NH_3)_5]Br_2 \longrightarrow [CrBr_2Cl(NH_3)_3]$ 290—300 °C

trans-$[CrBrCl(NH_3)_4]Br \longrightarrow [CrBr_2Cl(NH_3)_3]$ 270—290 °C.

The temperatures of the tetraamminedihalogeno complexes are lower than those of the corresponding pentaamminehalogeno complexes. Thus, even though the tetraamminedihalogeno complexes are produced in each reaction pathway, they are immediately decomposed, forming triamminetrihalogeno complexes.

The authors are grateful to Hungarian Optical Works and Kubota Trading Co. for the use of Q-derivatograph.

References

1) Part I: R. Tsuchiya, A. Uehara, and K. Kobayashi, *Bull. Chem. Soc. Jpn.*, **53**, 921 (1980).

2) Presented at the Symposium on Calorimetry and Thermal Analysis, Japan, Kanazawa, October 1979.

3) "Shin-Jikkenkagakukoza," ed by The Chemical Society of Japan, Maruzen, Tokyo (1977), Vol. 8, p. 1136; A. Werner, *Ber.*, **43**, 2290 (1910).

4) a) N. Tanaka and K. Nagase, *Bull. Chem. Soc. Jpn.*, **42**, 2854 (1969); b) N. D. Peschko and B. P. Block, *J. Inorg. Nucl. Chem.*, **15**, 71 (1960); c) W. W. Wendlandt and C. Y. Chou, *ibid.*, **26**, 943 (1964).

5) R. Tsuchiya and A. Uehara, *Netsusokutei*, **6**, 16 (1979).

6) E. L. Muetterties, *Inorg. Synth.*, **10**, 153 (1967).

7) F. Hein and H. Kraft, *Z. Anorg. Allg. Chem.*, **245**, 334 (1940).

8) H. Biltz and W. Biltz, "Laboratory Method of Inorganic Chemistry," 2nd ed, John Wiley and Sons (1928), p. 185.

9) a) D. W. Hoppenjans, J. B. Hund, and C. R. Gregoire, *Inorg. Chem.*, **7**, 2506 (1968); b) M. Linhard and M. Weigel, *Z. Anorg. Allg. Chem.*, **299**, 15 (1959).

10) M. Linhard and M. Weigel, *Z. Anorg. Allg. Chem.*, **265**, 49 (1951).

11) D. A. House, *Inorg. Nucl. Chem. Lett.*, **3**, 67 (1967).

  Bull. Chem. Soc. Jpn., 54, 1825—1829 (1981)

Binuclear Metal Complexes. XXXIX.[1] Synthesis and Properties of Binuclear Copper(II) Complexes with [2-(2-Pyridyl)ethylamino]-alkanols and [2-(2-Pyridyl)ethylthio]alkanols

Masaaki NAKAMURA, Masahiro MIKURIYA, Hisashi OKAWA,* and Sigeo KIDA

Department of Chemistry, Faculty of Science, Kyushu University 33, Hakozaki, Higashi-ku, Fukuoka 812

(Received January 31, 1981)

Di-μ-alkoxo-bridged binuclear copper(II) complexes, Cu(py-3-3-nno)X, Cu(py-3-2-nso)X, and Cu(py-3-3-nso)X (X=Cl, Br, ClO_4, NO_3, PF_6, BF_4), have been synthesized and characterized, where Hpy-3-3-nno, Hpy-3-2-nso, and Hpy-3-3-nso denote 3-[2-(2-pyridyl)ethylamino]-1-propanol, 2-[2-(2-pyridyl)ethylthio]ethanol, and 3-[2-(2-pyridyl)ethylthio]-1-propanol, respectively. It was found that 2-[2-(2-pyridyl)ethylamino]ethanol (Hpy-3-2-nno) cannot form di-μ-alkoxo-bridged binuclear copper(II) complexes owing to the high strain in the fused ring system. These complexes exhibited a band at 22000—27000 cm^{-1} characteristic of the di-μ-alkoxo-bridged structure, the bands for Cu(py-3-2-nso)X and Cu(py-3-3-nso)X being lower in frequency compared with those for Cu(py-3-3-nno)X. Antiferromagnetic interaction was stronger and reduction potential (Cu(II)-Cu(II)$\rightarrow$Cu(I)-Cu(I)) was higher for Cu(py-3-3-nso)X than those for Cu(py-3-3-nno)X. Cu(py-3-3-nso)Cl and Cu(py-3-2-nso)Br showed two reduction waves at about +0.15 and −0.4 V *vs.* SCE. These results were discussed in terms of the structure in solution on the basis of conductivity measurements.

Di-μ-alkoxo-bridged binuclear copper(II) complexes containing a thioether sulfur as a donor atom are of interest as models of Type III copper proteins. In the preceding papers of this series,[2-6] we have reported preparations and properties of di-μ-alkoxo-bridged binuclear copper(II) complexes with the nso- and sno-type ligands (Fig. 1). Substitution of thioether sulfur for aliphatic amino nitrogen resulted in 1) a red shift of the characteristic band of di-μ-alkoxo-bridged binuclear copper(II) complexes in the near ultraviolet region (this band being assigned to the $p_\pi(O)\rightarrow d_\sigma(Cu)$ charge transfer band[7-9]), 2) an enhancement in antiferromagnetic spin-exchange interaction between the two copper(II) ions, 3) a positive shift of the copper(II)$\rightarrow$copper(I) reduction potential, and 4) a strain relaxation in the fused ring system of the binuclear skeleton.

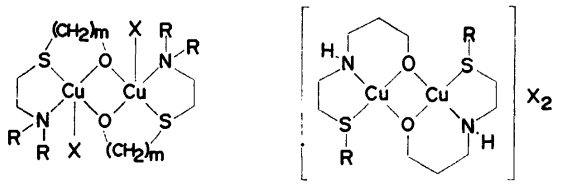

(a) (b)

Fig. 1. Complexes of (a) Cu(R-2-m-nso)X (m=2, 3) and (b) Cu(R-2-3-sno)X.

In order to further investigate the nature of binuclear copper(II) complexes with sulfur-containing ligands, new binuclear copper(II) complexes, Cu(py-3-m-nso)X (X=Cl, Br, ClO_4, NO_3, BF_4, PF_6; m=2, 3) (Fig. 2a), of 2-[2-(2-pyridyl)ethylthio]ethanol (abbreviated as Hpy-3-2-nso) and 3-[2-(2-pyridyl)ethylthio]-1-propanol (Hpy-3-3-nso) have been prepared and their spectral, magnetic, and electrochemical properties were compared with those of Cu(py-3-2-nno)X and Cu(py-3-3-nno)X (X=ClO_4, BF_4, PF_6), where Hpy-3-2-nno denotes 2-[2-(2-pyridyl)ethylamino]ethanol and Hpy-3-3-nno 3-[2-(2-pyridyl)ethylamino]-1-propanol (Fig. 2b).

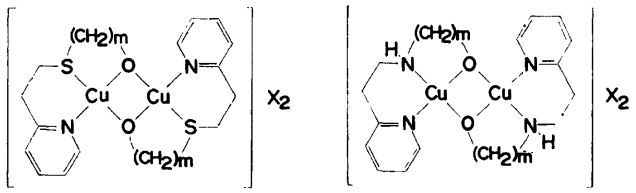

(a) (b)

Fig. 2. Complexes of (a) Cu(py-3-m-nso)X (m=2, 3) and (b) Cu(py-3-m-nno)X (m=2,3).

Another purpose of this study is to examine the effect of substitution of pyridine-nitrogen for alkyl amine group in binuclear copper(II) complexes of diaminoalcohols.

Experimental

Preparation of the Ligands. Hpy-3-2-nno and Hpy-3-3-nno were prepared by the reaction of 2-vinylpyridine with 2-aminoethanol and 3-amino-1-propanol, respectively.[10] Similarly, Hpy-3-2-nso and Hpy-3-3-nso were prepared by the addition of 2-mercaptoethanol and 3-mercapto-1-propanol to 2-vinylpyridine, respectively.

Preparation of the Complexes. Cu(py-3-3-nno)X (X=ClO_4, BF_4). The preparation was exemplified by Cu(py-3-3-nno)ClO_4. To a solution of Hpy-3-3-nno (0.5 mmol) in absolute ethanol (10 cm^3) was added a solution of copper(II) perchlorate hexahydrate (0.5 mmol) in absolute ethanol (20 cm^3). To this mixture was added triethylamine to precipitate a blue solid. It was collected by filtration and recrystallized from methanol.

Cu(py-3-3-nno)PF_6. A mixture of Cu(py-3-3-nno)-ClO_4 (0.5 mmol) and KPF_6 (0.5 mmol) in acetonitrile (20 cm^3) was stirred for 2 h at room temperature. The solvent was evaporated, and a remaining blue precipitate was collected by filtration and recrystallized from methanol twice to give deep blue needles.

Cu(py-3-2-nso)X and Cu(py-3-3-nso)X (X=ClO_4, Cl, Br, NO_3, BF_4). The compounds were prepared by a method similar to that for Cu(py-3-3-nno)ClO_4. They were recrystallized from methanol.

Cu(py-3-2-nso)PF_6 and Cu(py-3-3-nso)PF_6. These were prepared by the reaction of Cu(py-3-2-nso)ClO_4 and Cu(py-3-3-nso)ClO_4 with KPF_6 in acetonitrile, respectively.

TABLE 1. ELEMENTAL ANALYSES OF COMPLEXES

Complex	Found (%)			Calcd (%)		
	H	C	N	H	C	N
Cu(py-3-3-nno)ClO_4	4.39	34.90	8.14	4.42	35.10	8.18
Cu(py-3-3-nno)BF_4	4.61	36.42	8.49	4.59	36.44	8.50
Cu(py-3-3-nno)PF_6	4.02	30.99	7.29	3.90	30.98	7.22
Cu(py-3-3-nso)ClO_4	4.06	33.52	3.89	3.93	33.43	3.90
Cu(py-3-3-nso)PF_6	3.60	29.70	3.43	3.49	29.67	3.46
Cu(py-3-2-nso)Cl	4.40	38.22	4.90	4.30	38.43	4.98
Cu(py-3-2-nso)Br	3.77	32.81	4.21	3.71	33.19	4.30
Cu(py-3-2-nso)ClO_4	3.69	31.13	3.99	3.50	31.31	4.06
Cu(py-3-2-nso)$NO_3 \cdot 1/2CH_3OH$	4.48	34.78	8.62	4.36	35.24	8.65
Cu(py-3-2-nso)$BF_4 \cdot H_2O$	4.14	31.05	4.12	4.02	30.83	3.99
Cu(py-3-2-nso)$PF_6 \cdot 1/2H_2O$	3.49	27.01	3.52	3.28	27.04	3.50

Carbon, hydrogen, and nitrogen analyses were carried out at the Service Center of Elemental Analysis, Kyushu University. The results are given in Table 1.

Measurements. Infrared spectra were measured with a Hitachi grating infrared spectrophotometer Model 215 in the region 4000—650 cm^{-1} on a KBr disk and on a nujol mull. Electronic spectra were measured with a Shimadzu multipurpose spectrophotometer Model MPS-5000 in methanol solutions and on solid samples. Magnetic susceptibilities were measured by the Faraday method in the temperature range from liquid nitrogen temperature to room temperature. The apparatus was calibrated by the use of $[Ni(en)_3]S_2O_3$.[11] All the susceptibilities were corrected for the diamagnetism of the constituting atoms by the use of Pascal's constants.[12] Effective magnetic moments were calculated by the equation, $\mu_{eff}=2.828\sqrt{(\chi_A-N\alpha)T}$, where χ_A is the atomic magnetic susceptibility and $N\alpha$ is the temperature-independent paramagnetism. Normal pulse polarography (NPP) and differential pulse polarography (DPP) were measured with a Yanagimoto voltammetric analyzer Model P-1000 in *N,N*-dimethylformamide (DMF) containing 0.1 mol dm^{-3} tetraethylammonium perchlorate at room temperature using a three-electrode cell. The saturated calomel electrode (SCE) was used as a reference, which was connected to a sample solution through a salt bridge. A dropping mercury electrode was used as a working electrode. The counter electrode was platinum coil. Conductivity was measured with a Yanagimoto conductivity outfit Model MY-8 for methanol and *N,N*-dimethylformamide solution. The cell constants were determined by the use of NaCl and KBr.[13,14]

Results and Discussion

Among the binucleating ligands utilized in this study, Hpy-3-3-nno, Hpy-3-3-nso, and Hpy-3-2-nso formed di-μ-alkoxo-bridged binuclear copper(II) complexes. On the other hand, we were unsuccessful in isolating Cu(py-3-2-nno)X using Hpy-3-2-nno. The product obtained by the reaction of Hpy-3-2-nno and copper(II) halide was supposed to be $Cu(H_2NCH_2CH_2O)X$ (X=halogenide ion)[9] on the basis of elemental analyses and cryomagnetic properties, and this was confirmed by comparing the infrared spectrum of the product with that of the authentic sample obtained from 2-aminoethanol and a copper(II) halide. Thus, it is evident that Hpy-3-2-nno cleaved into 2-aminoethanol and 2-vinylpyridine in this reaction. The complex, Cu-

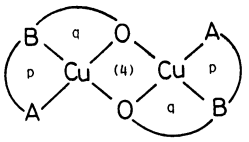

Fig. 3. Representation of the fused chelate-ring system, p-q-(4)-q-p, for binuclear complexes of alcoholic tridentate ligands.

(py-3-2-nno)X, should have a 6-5-(4)-5-6 fused ring system (Fig. 3) which is generally thought to be stable in the complexes with the fully saturated ligands, such as HR-3-2-nno.[7-9] However, the terminal six-membered chelate ring of Cu(py-3-2-nno)X must be small in size and may be comparable to the five-membered ring of a saturated ligand, because of short bond-distance in pyridine ring. So far, binuclear copper(II) complexes with a 5-5-(4)-5-5 fused ring system have not been obtained using diamino alcohols,[15-19] owing to a high strain in this system. A similar strain should exist in the 6-5-(4)-5-6 fused ring system of Cu(py-3-2-nno)X, and should be responsible for the cleavage of Hpy-3-2-nno and the formation of strain-free $Cu(H_2NCH_2CH_2O)X$.

On the other hand, we were successful in isolating Cu(py-3-2-nso)X, although it has the same 6-5-(4)-5-6 fused ring system as Cu(py-3-2-nno)X. It is to be noticed that the chelate ring system in Cu(py-3-2-nso)X contains a thioether group. Previously, we showed that the binuclear copper(II) complexes, Cu(R-2-2-nso)X (HR-2-2-nso=2-(2-dialkylaminoethylthio)ethanol), possessing a fully saturated 5-5-(4)-5-5 fused ring system can be isolated, because of a high flexibility in bond angle and large coordination bond distance of the thioether sulfur atom.[5] It is likely that a similar strain-releasing effect contributes to the formation of Cu(py-3-2-nso)X.

Since no band attributable to OH-stretching vibration was observed, the alcoholic oxygen should be deprotonated and coordinated to copper. The shift of the 990 cm^{-1} band of free pyridine to higher frequency showed the coordination of pyridine nitrogen. The bands due to ClO-stretching vibration in Cu(py-3-3-nno)ClO_4 and Cu(py-3-3-nso)ClO_4 were observed at 1070 cm^{-1}. Practically no splitting of the bands indicates

Table 2. Band maxima of electronic spectra of complexes ($\bar{\nu}/10^3$ cm^{-1})

Complex	Reflectance		Methanol solution (log ε)	
$Cu(py\text{-}3\text{-}3\text{-}nno)ClO_4$	25.6	16.7	26.7(3.06)	15.7(1.89)
$Cu(py\text{-}3\text{-}3\text{-}nno)BF_4$	26.5	16.7	26.5(3.14)	16.3(1.95)
$Cu(py\text{-}3\text{-}3\text{-}nno)PF_6$	26.5	17.2	26.7(3.13)	16.0(1.94)
$Cu(py\text{-}3\text{-}3\text{-}nso)ClO_4$	23.3	17.4	25.0(2.95)	16.4(1.97)
$Cu(py\text{-}3\text{-}3\text{-}nso)PF_6$	23.5	17.2	24.8(3.02)	16.3(2.05)
$Cu(py\text{-}3\text{-}2\text{-}nso)Cl$	22.2	14.5	25.3(2.99)	16.3(2.09)
$Cu(py\text{-}3\text{-}2\text{-}nso)Br$	21.7	14.2	24.8(3.03)	15.3(2.19)
$Cu(py\text{-}3\text{-}2\text{-}nso)ClO_4$	23.1	16.1	24.6(3.02)	15.4(2.07)
$Cu(py\text{-}3\text{-}2\text{-}nso)NO_3\cdot 1/2CH_3OH$	23.8	15.4	24.7(3.15)	15.5(2.20)
$Cu(py\text{-}3\text{-}2\text{-}nso)BF_4\cdot H_2O$	24.1	15.9	24.5(3.11)	15.6(2.45)
$Cu(py\text{-}3\text{-}2\text{-}nso)PF_6\cdot 1/2H_2O$	23.3	16.3	24.4(3.16)	15.6(2.24)

that the perchlorate ion is free from coordination.[20] On the other hand, the ClO-stretching vibration of $Cu(py\text{-}3\text{-}2\text{-}nso)ClO_4$ splits into three components at 1120, 1030, and 930 cm^{-1}. This indicates the coordination of the perchlorate ion to the copper(II).[20] The NO-stretching band of the nitrate ion in $Cu(py\text{-}3\text{-}2\text{-}nso)NO_3\cdot 1/2CH_3OH$ was observed at 1320 and 1380 cm^{-1}, suggesting non-coordination of the nitrate ion to the metal.[21]

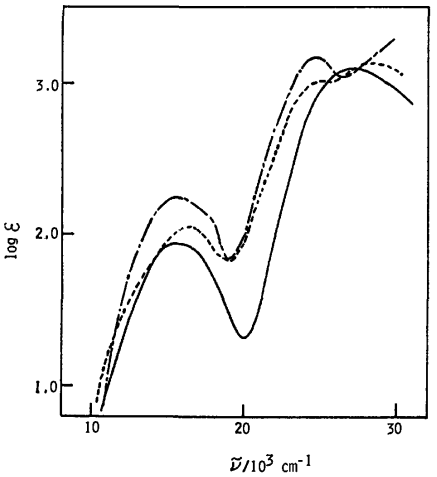

Fig. 4. Electronic absorption spectra of (——)Cu(py-3-3-nno)PF_6, (·····) Cu (py-3-3-nso)PF_6, and (-·-) Cu (py-3-2-nso) PF_6 in methanol.

Electronic spectra of the complexes were measured in methanol and *N,N*-dimethylformamide solutions and on powder samples. Results are given in Table 2. Typical examples of absorption spectra are shown in Fig. 4. Spectra in solution and in solid state resemble each other, indicating essentially the same structure in solid and in solution. The band in the 14000—17000 cm^{-1} region can be assigned to d-d transition band. The d-d band of Cu(py-3-2-nso)X is slightly lower in frequency compared with those of Cu(py-3-3-nso)X and Cu(py-3-3-nno)X in solid state. This suggests that the coordination geometry around the copper ion in Cu(py-3-2-nso)X is distorted from square plane. Among these complexes, the d-d band of Cu(py-3-2-nso)Cl and Cu(py-3-2-nso)Br is notably low in energy. Recently, we determined the crystal structure of $Cu(CH_3\text{-}2\text{-}2\text{-}nso)Br$ by the X-ray diffraction method.[5] The structure consists of alkoxo-bridged binuclear units, $Cu_2(CH_3\text{-}2\text{-}2\text{-}nso)_2Br_2$, where bromide ions coordinate to copper(II) ions and the coordination geometry around each copper ion is a distorted square pyramid. As already mentioned, the strain in the fused ring system of Cu(py-3-2-nso)X is similar to that of Cu(R-2-2-nso)X. Hence, it is likely that Cu(py-3-2-nso)X (X=Cl, Br) takes a distorted square pyramidal structure similar to that of $Cu(CH_3\text{-}2\text{-}2\text{-}nso)Br$. The band with a relatively large intensity (ε=1000—2000) in the 24000—27000 cm^{-1} region is known to be characteristic of the di-μ-alkoxo-bridged binuclear copper(II) structure. Kida *et al.* have assigned this band to the $p_\pi(O)\rightarrow d_\sigma(Cu)$ charge transfer transition.[7-9] This is observed around 26000 cm^{-1} in the case of Cu(py-3-3-nno)X, while the CT band for Cu(py-3-3-nso)X and Cu(py-3-2-nso)X appeared in the region 22000—25000 cm^{-1}. Therefore, the $p_\pi(O)\rightarrow d_\sigma(Cu)$ charge transfer band shifts by 3000—4000 cm^{-1} to lower frequency when one of the amine nitrogen is replaced by a thioether sulfur. The present result is in line with our previous findings that the thioether substitution for amino group causes a red-shift of the charge-transfer band in di-μ-alkoxo-bridged binuclear copper(II) complexes.

The magnetic susceptibilities were measured over the temperature range 80—300 K. The magnetic moments per copper atom are all subnormal at room temperature and decrease with lowering of temperature, indicating the existence of an antiferromagnetic spin-exchange interaction between a pair of copper(II) ions. The temperature dependences of magnetic susceptibility for $Cu(py\text{-}3\text{-}3\text{-}nso)ClO_4$ and $Cu(py\text{-}3\text{-}3\text{-}nno)BF_4$ are shown in Fig. 5 as examples. These magnetic behaviors can be interpreted in terms of the Bleaney-Bowers equation,[22]

$$\chi_A = \frac{Ng^2\beta^2}{3kT}\left[1+\frac{1}{3}\exp(-2J/kT)\right]^{-1} + N\alpha, \qquad (1)$$

where χ_A is susceptibility per copper atom and other symbols have their usual meanings. The $-2J$ (the energy separation between the spin-singlet ground state and the spin-triplet excited state) and $N\alpha$ values were obtained by the best-fit of the experimental susceptibilities to the Eq. 1, assuming g at 2.10. The results are given in Table 3. Table 3 also includes the effective magnetic moments of the complexes at room tempera-

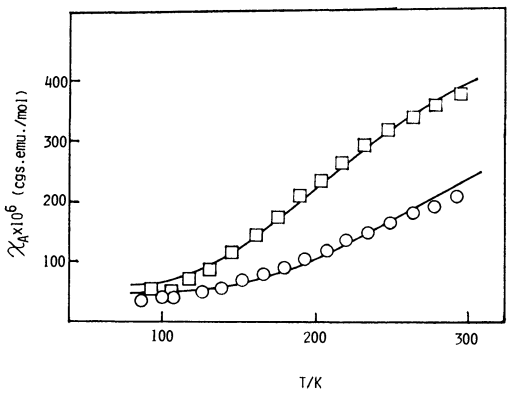

Fig. 5. Temperature-dependences of magnetic susceptibility of (○) Cu (py-3-3-nso) ClO_4 and (□) Cu (py-3-3-nno) BF_4.

TABLE 3. MAGNETIC DATA OF COMPLEXES

Complex	μ_{eff} [a] / BM	$-2J$ / cm^{-1}	$N\alpha \times 10^6$ / c.g.s. mol^{-1}
Cu(py-3-3-nno)ClO_4	0.88	510	60
Cu(py-3-3-nno)BF_4	0.87	540	60
Cu(py-3-3-nno)PF_6	0.67	700	40
Cu(py-3-3-nso)ClO_4	0.61	705	50
Cu(py-3-3-nso)PF_6	0.47	850	60
Cu(py-3-2-nso)Cl	1.63	170	90
Cu(py-3-2-nso)Br	1.48	225	60
Cu(py-3-2-nso)ClO_4	1.26	300	60
Cu(py-3-2-nso)$NO_3 \cdot 1/2CH_3OH$	0.83	550	60
Cu(py-3-2-nso)$BF_4 \cdot H_2O$	0.71	650	65
Cu(py-3-2-nso)$PF_6 \cdot 1/2H_2O$	0.48	850	60

a) Magnetic moment at room temperature.

ture. The $-2J$ values for Cu(py-3-3-nno)X (X=ClO_4, BF_4, PF_6) range from 510 to 700 cm^{-1}, which are comparable to the $-2J$ values for the binuclear copper(II) complexes with aliphatic diaminoalcohols.[9] Therefore, we can not detect any marked effect of pyridine nitrogen donation on antiferromagnetic spin-exchange interaction in di-μ-alkoxo-bridged binuclear copper(II) complexes. It is to be noted that the $-2J$ values of Cu(py-3-3-nso)X (750—850 cm^{-1}) are much larger than the values of Cu(py-3-3-nno)X. Thus, antiferromagnetic spin-exchange interaction betweem the two copper(II) ions becomes stronger upon substitution of the sulfur donor atom for the nitrogen donor atom. A similar trend was already noticed in Cu(R-2-3-nso)X and Cu(R-2-3-sno)X.[2-6] The $-2J$ values of Cu(py-3-2-nso)X seem to depend on X. Namely, the complexes containing Cl, Br, or ClO_4 ion have smaller $-2J$ values compared with other complexes containing NO_3, BF_4, or PF_6 ion. Since the infrared and electronic reflectance spectral data evidenced the coordination of the anion X, the complexes Cu(py-3-2-nso)X (X=Cl, Br, ClO_4) should have a five-coordinate structure whose

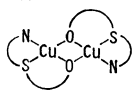

skeleton is much distorted from a coplane. Since spin-exchange interaction is known to be highly dependent on planarity around the metal, this distortion must be the main reason for the reduction in the exchange integral of Cu(py-3-2-nso)X (X=Cl, Br, ClO_4).

TABLE 4. HALF-WAVE POTENTIALS OF NORMAL PULSE (NPP) AND DIFFERENTIAL PULSE (DPP) POLAROGRAPHIES (V *vs.* SCE)

Complex	NPP	DPP	
Cu(py-3-3-nno)ClO_4	−0.40		−0.43
Cu(py-3-3-nno)BF_4	−0.40	−0.39	−0.42
Cu(py-3-3-nno)PF_6	−0.42	−0.40	−0.42
Cu(py-3-3-nso)ClO_4		−0.09	
Cu(py-3-3-nso)PF_6		−0.09	
Cu(py-3-2-nso)Cl		+0.16	−0.56
Cu(py-3-2-nso)Br		+0.11	−0.56
Cu(py-3-2-nso)ClO_4		−0.06	
Cu(py-3-2-nso)$NO_3 \cdot 1/2CH_3OH$		−0.09	
Cu(py-3-2-nso)$BF_4 \cdot H_2O$		−0.08	
Cu(py-3-2-nso)$PF_6 \cdot 1/2H_2O$		−0.09	

The results of normal pulse polarography (NPP) and differential pulse polarography (DPP) are listed in Table 4. The reduction from Cu(II)-Cu(II) to Cu(I)-Cu(I) for Cu(py-3-3-nno)X occured at −0.4 V *vs.* SCE. These reduction potentials are comparable to those of the binuclear complexes with the aliphatic diaminoalcohols.[4] Therefore, it seems that the reduction potential from Cu(II)-Cu(II) to Cu(I)-Cu(I) is little affected by substitution of aromatic amine nitrogen for aliphatic amine nitrogen. The reduction of Cu(py-3-3-nso)X (X=ClO_4, PF_6) at −0.10 V *vs.* SCE positively shifted by *ca.* 300 mV relative to reduction potentials of Cu(py-3-3-nno)X. As was already pointed out in the preceding paper,[4] the positive shift of the Cu(II)-Cu(II)→Cu(I)-Cu(I) reduction potential implies that the optical electronegativity[24] of copper(II) ion increases when a sulfur atom is introduced as a donating atom. Electrochemical property of Cu(py-3-2-nso)X (X=ClO_4, NO_3, BF_4, and PF_6) resembles that of Cu(py-3-3-nso)X, showing a two-electron reduction at about −0.10 V. On the other hand, Cu(py-3-2-nso)Cl and Cu(py-3-2-nso)Br showed two reduction waves at +0.2 and −0.60 V, and +0.10 and −0.40 V, respectively. These complexes bear a marked electrochemical resemblance to Cu(R-2-2-nso)X (X=Cl, Br),[4] which also showed two one-electron reductions at +0.15—+0.20 and −0.30——0.50 V *vs.* SCE. The controlled-potential electrolysis[4] showed that Cu(R-2-2-nso)X (X=Cl, Br) was reduced stepwise as Cu(II)-Cu(II)→Cu(II)-Cu(I)→Cu(I)-Cu(I). Accordingly, it is assumed that Cu(py-3-2-nso)Cl and Cu(py-3-2-nso)Br are also stepwise reduced. In order to clarify the reasons for the difference in electrochemical behaviors between the two groups of the binuclear complexes, *i.e.*, those undergoing two one-electron reductions and those undergoing one two-electron reduction, conductivities were measured in methanol and *N*,*N*-dimethylformamide. The results are shown in Table 5. The conductivities of Cu(py-3-2-nso)ClO_4 and Cu(py-3-2-nso)PF_6 clearly indicate that they are 1 : 2 electrolyte in the solutions.[23] Since two copper(II) ions in a molecule are equivalent in solution, we can reasonably understand

Table 5. Molar conductivity, Λ_M, of complexes at 10^{-3} mol dm^{-1} in methanol and *N,N*-dimethylformamide (Ω^{-1} cm^{-2} mol^{-1})

Complex	MeOH	DMF
$Cu(en)_2(ClO_4)_2$	204	146
Cu(py-3-2-nso)Cl	107	74
Cu(py-3-2-nso)Br	124	72
$Cu(py\text{-}3\text{-}2\text{-}nso)ClO_4$	195	
$Cu(py\text{-}3\text{-}2\text{-}nso)PF_6 \cdot 1/2H_2O$	198	

the one two-electron reduction of these complexes. On the other hand, the conductivities of Cu(py-3-2-nso)Cl and Cu(py-3-2-nso)Br are about one half of those of $Cu(py\text{-}3\text{-}2\text{-}nso)ClO_4$ and $Cu(py\text{-}3\text{-}2\text{-}nso)PF_6$, implying that they are 1 : 1 electrolyte in methanol and *N,N*-dimethylformamide. This suggests that these complexes exist as 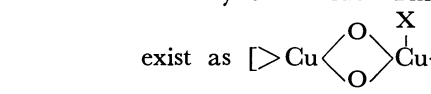 in solution, where two inequivalent copper(II) ions are reduced at different potentials. In general, copper(II) ions with a distorted coordination geometry have a high reduction potentials.[25] Therefore, it is likely that the reduction waves at +0.1—+0.2 V and −0.4—−0.6 V are due to the reduction of the five-coordinate copper(II) ion and the four-coordinate copper(II) ion, respectively. In relation to this result, conductivities of Cu(R-2-2-nso)X (X=Cl, Br) were also measured in *N,N*-dimethylformamide. The result again demonstrated the existence of 1 : 1 electrolyte in solution. Thus, we may conclude that Cu(py-3-2-nso)X (X=Cl, Br) as well as Cu(R-2-2-nso)X (X=Cl, Br) contains a five- and a four-coordinate copper(II) ions in solution, which are reduced at $\approx$+0.15 and $\approx$−0.5 V, respectively.

References

1) Part XXXVIII: T. Izumitani, H. Okawa, and S. Kida, *Chem. Lett.*, **1981**, 483.

2) M. Mikuriya, H. Okawa, and S. Kida, *Inorg. Chim. Acta*, **34**, 13 (1979).

3) M. Mikuriya, H. Okawa, and S. Kida, *Inorg. Chim. Acta*, **42**, 233 (1980).

4) M. Mikuriya, M. Aihara, Y. Nishi, H. Okawa, and S. Kida, *Chem. Lett.*, **1980**, 795.

5) M. Mikuriya, H. Okawa, and S. Kida, *Bull. Chem. Soc. Jpn.*, **53**, 2871 (1980).

6) M. Mikuriya, H. Okawa, and S. Kida, *Bull. Chem. Soc. Jpn.*, **53**, 3717 (1980).

7) Y. Ishimura, Y. Nonaka, Y. Nishida, and S. Kida, *Bull. Chem. Soc. Jpn.*, **46**, 3728 (1973).

8) Y. Nishida and S. Kida, *Chem. Lett.*, **1974**, 339.

9) Y. Nishida, F. Numata, and S. Kida, *Inorg. Chim. Acta*, **11**, 189 (1974).

10) R. G. Lacoste, and A. E. Martell, *Inorg. Chem.*, **3**, 881 (1964).

11) N. F. Curtis, *J. Chem. Soc.*, **1961**, 3147.

12) A. Earnshow, "Introduction to Magnetochemistry," Academic Press, London (1968), p. 4.

13) R. A. Robinson, R. H. Stokes, "Electrolyte Solutions," Butterworths, London (1965), Chap. 5.

14) D. P. Ames and P. G. Sears, *J. Phys. Chem.*, **5**, 16 (1955).

15) M. Kato, Y. Muto, H. B. Jonassen, K. Imai, and A. Harano, *Bull. Chem. Soc. Jpn.*, **41**, 1864 (1968).

16) A. Nakahara, I. Miyachi, and T. Kohno, *Bull. Chem. Soc. Jpn.*, **42**, 573 (1969).

17) K. Yamada and H. Ojima, *Nippon Kagaku Zasshi*, **91**, 457 (1970).

18) K. Nonoyama and H. Ojima, *Nippon Kagaku Zasshi*, **92**, 612 (1971).

19) H. Ojima and K. Yamada, *Z. Anorg. Allg. Chem.*, **379**, 322 (1970).

20) K. Nakamoto, "Infrared and Raman Spectra of Inorganic and Coordination Compounds," Wiley, New York (1978), pp. 242—247.

21) F. A. Miller and C. H. Wikins, *Anal. Chem.*, **24**, 1253 (1952).

22) B. Bleaney and K. D. Bowers, *Proc. R. Soc. London, Ser. A*, **214**, 451 (1952).

23) W. J. Geary, *Coord. Chem. Rev.*, **7**, 81 (1971).

24) C. K. Jørgensen, "Orbitals in Atomic and Molecules," Academic press (1962), pp. 80—100.

25) G. S. Patterson and R. H. Holm, *Bioinorg. Chem.*, **4**, 257 (1975).

Synthetic Approach toward Antibiotic Tunicamycins

Yoshimasa FUKUDA, Hiroaki SASAI, and Tetsuo SUAMI*

Deparment of Applied Chemistry, Faculty of Engineering, Keio University, Hiyoshi, Kohoku-ku, Yokohama 223

(Received October 8, 1980)

Higher-carbon carbohydrates, undecose, and dodecose derivatives have been synthesized by base-catalyzed addition between nitro sugar and sugar aldehydes. The addition reaction of 3,5-*O*-benzylidene-6,7-dideoxy-1,2-*O*-isopropylidene-7-nitro-α-D-*gluco*-heptofuranose (**3**) with 2,3 : 4,5-di-*O*-isopropylidene-D-arabinose yielded two isomeric dodecose derivatives. The analogous addition of **3** with 2,4-*O*-ethylidene-D-erythrose afforded an undecose derivative.

The nucleoside antibiotics tunicamycins exhibit broad-spectrum antitumor activity.[1] They have a unique common structure, consisting as they do of uracil, fatty acids, and an undecose derivative named tunicamine as the carbohydrate moiety, together with *N*-acetyl-D-glucosamine. The tunicamine is, in turn, bound to the uracil residue, designated as the tunicaminyl uracil[5] (Scheme 1).

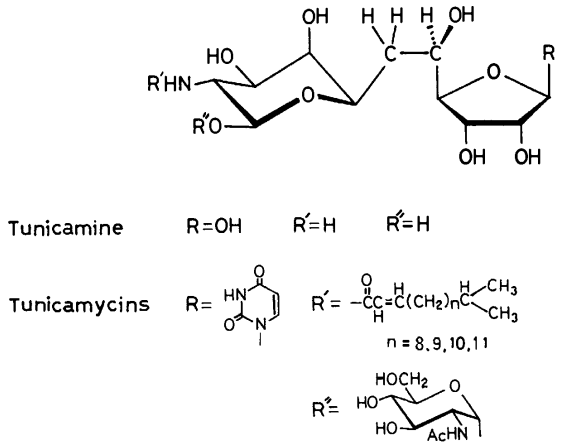

Scheme 1.

The higher-carbon carbohydrates, such as undecose and decose derivatives, have been found in other nucleoside antibiotics, anthelmycin (hikizimycin),[2,3] and sinefungin.[4]

Since carbon-chain elongation toward the higher-carbon carbohydrates has not been well established, a synthesis of tunicamine is an attractive challenging target for a carbohydrate chemist. In synthetic chemistry, several methods of preparing higher-carbon sugar have been described in the literature.[6–10] More recently, two undecose derivatives have been prepared by a method involving the condensation of galactose 6-phosphorane with two pentose aldehydes.[11] A hexadecose derivative has been synthesized by the oxidative dimerization of acetylenic sugar, followed by catalytic hydrogenation.[12]

As one of the methods of lengthening a carbon-chain in carbohydrates, the base-catalyzed addition of nitroalkanes with aldehyde has been applied;[13–16] such reactions have been widely used for ascensions of sugar chains.[17–19] However the reagents are restricted to low-molecular-weight nitro compounds, such as nitromethane,[20] nitroethane,[21] and nitroethanol.[22,23] Furthermore, neither the reaction of nitro sugar with aldehyde nor that of nitro sugar with sugar aldehyde has been described in the literature as a synthetic approach to a higher-carbon carbohydrate. Therefore, as a preliminary synthetic study toward the tunicamine, the possibility of the formation of higher-carbon sugar by the addition reaction between nitro sugar and sugar aldehyde has been explored. In the present article we wish to report the development of addition reactions for undecose and dodecose derivatives.

Results and Discussion

The addition of 3,5-*O*-benzylidene-6,7-dideoxy-1,2-*O*-isopropylidene-7-nitro-α-D-*gluco*-heptofuranose (**3**) to 2,3 : 4,5-di-*O*-isopropylidene-D-arabinose[24] (**4**) and 2,4-*O*-ethylidene-D-erythrose[25] (**9**) afforded dodecose (**5** and **6**) and an undecose derivative (**10**) respectively.

As a starting material, the readily accessible 3,5-*O*-benzylidene-1,2-*O*-isopropylidene-α-D-glucofuranose[26] (**1**) was used. The oxidation of **1** by the Pfitzner-Moffatt method[27,28] afforded 3,5-*O*-benzylidene-1,2-*O*-isopropylidene-α-D-*gluco*-1,6-dialdo-1,4-furanose, which was further converted to the 7-nitro compound (**2**) in a 61% yield by adding nitromethane in the presence of sodium methoxide in methanol.

The dehydration of **2** with acetic anhydride in chloroform, followed by hydrogenation with sodium borohydride, produced the 6-deoxy-7-nitro compound (**3**) in a 47% yield.

When **3** reacted with the arabinose derivative, **4**, in the presence of sodium methoxide, a mixture of two isomeric dodecose derivatives (**5** and **6**) was obtained in a 44% yield after chromatography. Attempts were made to isolate each compound, but only **6** was isolable as crystals. The structure of **6** was established by ^{1}H NMR and IR as 3,5-*O*-benzylidene-6,7-dideoxy-1,2 : 9,10 : 11,12-tri-*O*-isopropylidene-7-nitro-α-dodeco-1,4-furanose.

The catalytic hydrogenation of the mixture of **5** and **6** in ethyl acetate in the presence of Raney nickel afforded a crude mixture of reduction products. The subsequent *N*-acetylation of this mixture, followed by chromatography, produced two crystalline *N*-acetylaminodideoxydodecoses (**7** and **8**) in 51 and 24% yields respectively.

The structures of **7** and **8** were determined by means of the ^{1}H NMR and mass spectra. The ^{1}H NMR spectrum of **7** revealed 18 proton signals at δ 1.2—1.5 attributable to the three *O*-isopropylidene groups, and a sharp singlet of 3-protons at δ 1.85 attributable to the

acetamido group. The mass spectrum of **7** yielded the molecular ion peak [M^+] at *m/e* 593 and the fragmentation peak [M^+-15] at *m/e* 578. The ^1H NMR spectrum of **8** showed patterns of the signals similar to those observed for **7**. The mass spectrum of **8** gave the same ion peaks at *m/e* 593 and 578. Concerning the stereochemistry of the two newly introduced chiral centers on C-7 and 8 of the compounds, four diastereomers are theoretically possible, but these configurations have not yet been established.

An analogous addition reaction was carried out between **3** and **9** to give a mixture of the two products. Only the main component (**10**) was isolated as homogeneous crystals in a 32% yield by chromatography. The catalytic hydrogenation of **10** in the presence of Raney nickel, followed by *N*-acetylation, afforded the *N*-acetylaminodideoxyundecose (**11**).

It has been demonstrated by the present study that a higher-carbon carbohydrate is prepared by a base-catalyzed addition between a nitro sugar and a sugar aldehyde. The reaction proceeds quite smoothly and can be used as a general method for the synthesis of higher-carbon complex carbohydrates.

Experimental

General Methods. The melting points were taken in capillary tubes in a liquid bath and are uncorrected. Solutions were concentrated under reduced pressure below 50 °C. The IR spectra were measured with a Hitachi 225 spectrophotometer and are expressed in reciprocal centimeters. The ^1H NMR spectra were obtained on a Varian EM-360A (60 MHz) spectrometer. The chemical shifts are reported as δ values

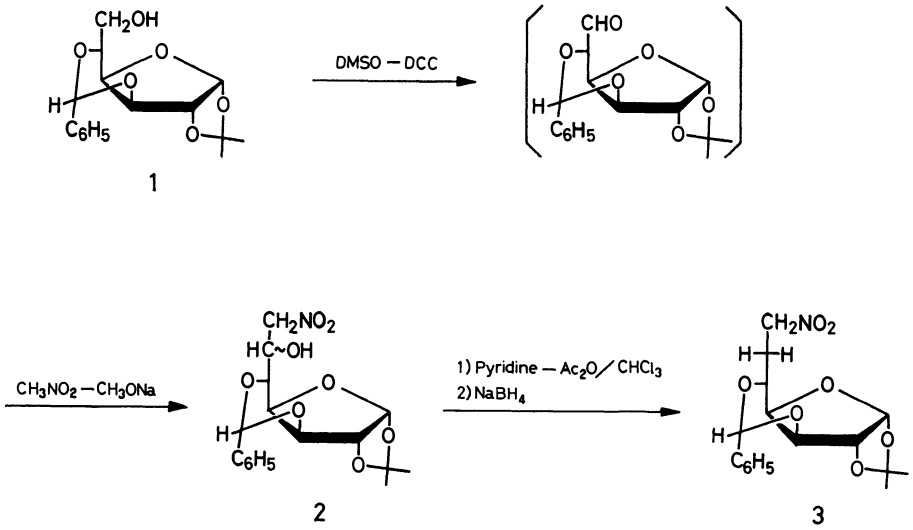

Scheme 2.

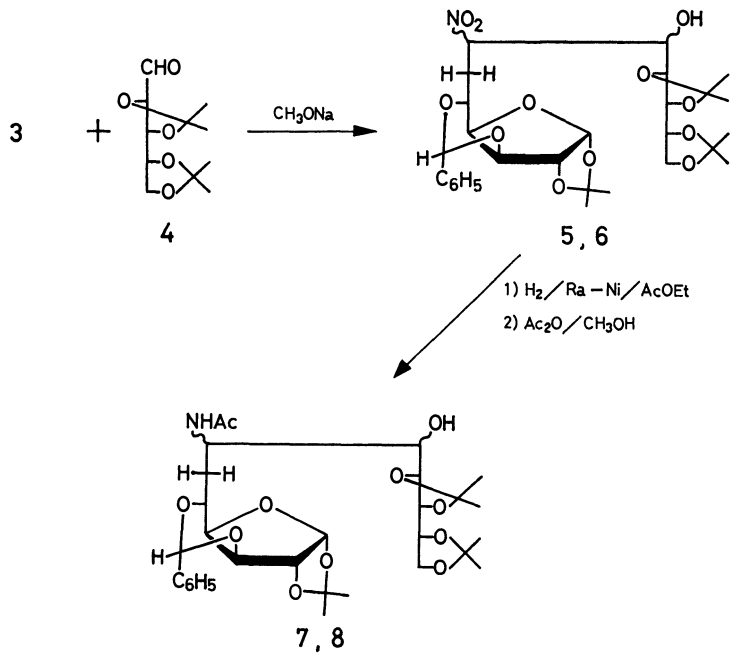

Scheme 3.

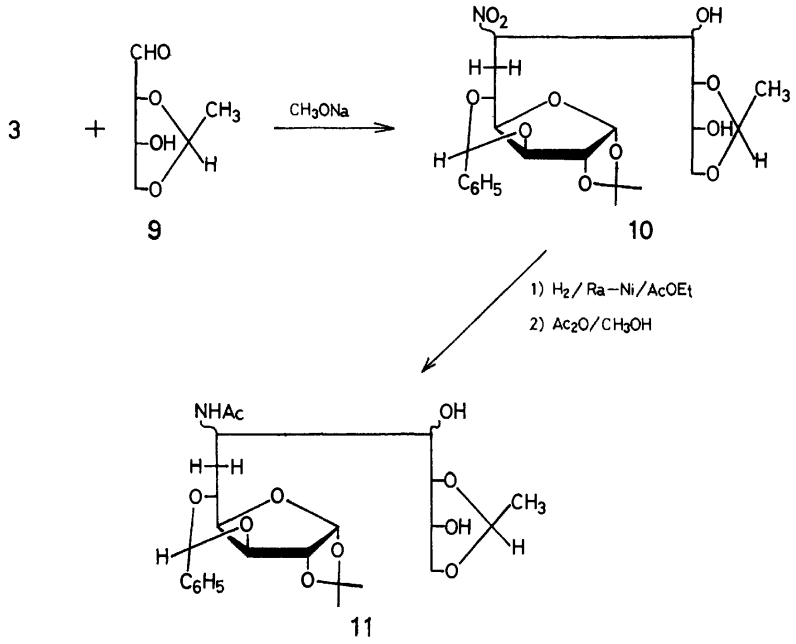

Scheme 4.

in parts per million relative to tetramethylsilane as an internal standard. The mass spectra were obtained with a Hitachi RMU-6MG spectrometer. The TLC was performed on precoated silica gel 60 F-254 plaques (Merck, Darmstadt; Art. 5715, 0.25 mm thickness). The silica-gel columns used for chromatography utilized Wako gel C-200 (Wako Pure Chemical Industries, Ltd.).

*3,5-O-Benzylidene-7-deoxy-*1,2-O-*isopropylidene-*7-*nitro-*α-DL-glycero-D-gluco-*hepto-*1,4-*furanose (2)*. Into a solution of 3,5-*O*-benzylidene-1,2-*O*-isopropylidene-α-D-glucofuranose[26] (**1**, 2.0 g) in benzene (8 ml) and dimethyl sulfoxide (16 ml) we stirred dichloroacetic acid (0.4 ml), dicyclohexylcarbodiimide (2.0 g), and pyridine (0.8 ml) under ice cooling. After the mixture was stirred for 5 h at an ambient temperature, a suspension of oxalic acid (2.0 g) in methanol (2.0 ml) was added to the solution. The mixture was then diluted with cold water (20 ml) and extracted with chloroform. The chloroform layer was washed with a $NaHCO_3$ solution and brine, dried over Na_2SO_4, and concentrated. To a solution of the residue in methanol (20 ml) we added nitromethane (6 ml) and 1 M methanolic sodium methoxide (6.5 ml). After standing 1 h, the solution was neutralized with Amberlite IR-120B (H^+) resin and concentrated. The resdiue was chromatographed on a silica-gel column using 1: 10 (v/v) 2-butanone–toluene; the product was then recrystallized from benzene–cyclohexane to give 1.45 g (61%) of **2**; mp 176.5—177.5 °C, $[\alpha]_D^{24}$ −58° (*c* 0.5, chloroform). IR(KBr) 3520 (OH), 1565, 1395 cm^{-1} (NO_2).

Found: C, 55.30; H, 5.74; N, 3.64%. Calcd for $C_{17}H_{21}NO_8$: C, 55.58; H, 5.76; N, 3.81%.

*3,5-O-Benzylidene-6,7-dideoxy-1,2-*O-*isopropylidene-7-nitro-*α-D-gluco-*hepto-1,4-furanose (3)*. Into a suspension of **2** (1.28 g) in chloroform (22 ml) we stirred acetic anhydride (1.56 ml) and pyridine (0.8 ml). After 5 h, the chloroform solution was washed with a $NaHCO_3$ solution, and cold water, dried over Na_2SO_4, and concentrated. $NaBH_4$ (0.8 g) was added to a solution of the residue in ethanol (30 ml). After 1 h, the solution was neutralized with Amberlite IR-120B (H^+) resin and concentrated. The residue was recrystallized from ethanol to give 614 mg (47%) of **3**; mp 154 °C, $[\alpha]_D^{24}$ +89° (*c* 1.0, chloroform). IR(KBr) 1555, 1387 cm^{-1} (NO_2).

Found: C, 58.07; H, 5.97; N, 3.93%. Calcd for $C_{17}H_{21}NO_7$: C, 58.11; H, 6.02; N, 3.99%.

*3,5-O-Benzylidene-6,7-dideoxy-1,2: 9,10: 11,12-tri-*O-*isopropylidene-7-nitro-*α-*dodeco-1,4-furanose (5 and 6)*. To a solution of **3** (0.5 g) and 2,3: 4,5-di-*O*-isopropylidene-D-arabinose[24] (**4**, 1.6 g) in methanol (4 ml) and tetrahydrofuran (3 ml) we added 1 M methanolic sodium methoxide (2 ml) under ice cooling. After 3 h at an ambient temperature, the solution was neutralized with Amberlite IR-120B(H^+) resin and concentrated below 30 °C. The residue was chromatographed on a silica-gel column using 20: 1 (v/v) chloroform–ethyl acetate. Fractions homogeneous on TLC (R_f 0.25) in 5: 1 (v/v) chloroform–ethyl acetate gave 75 mg of **6** as crystals; mp 149—150 °C, $[\alpha]_D^{23}$ +38.4° (*c* 0.55, methanol). IR(KBr) 3440 (OH), 1560, 1385 (NO_2), 760, 705 cm^{-1} (C_6H_5).

Found: C, 57.58; H, 6.58; N, 2.47%. Calcd for $C_{28}H_{39}NO_{12}$: C, 57.82; H, 6.76; N, 2.42%.

Compound **5** (R_f 0.34 on TLC) was not obtained as pure crystals. The total yield of the mixture of **5** and **6** was 44% (361 mg).

*7-Acetamido-3,5-*O-*benzylidene-6,7-dideoxy-1,2: 9,10: 11,12-tri-*O-*isopropylidene-*α-*dodeco-1,4-furanose (7 and 8)*. A solution of the mixture of **5** and **6** (75 mg) in ethyl acetate (5 ml) was hydrogenated in the presence of Raney nickel at an initial H_2 pressure of 2.7 kg/cm^2 for 18 h. The catalyst was then filtered off, and the filtrate was concentrated. The *N*-acetylation of the residue with acetic anhydride (0.3 ml) in methanol (3 ml) was followed by purification by column chromatography, using 1: 1 (v/v) chloroform–ethyl acetate, to give 39 mg (51%) of **7** and 18 mg (24%) of **8**.

7: Mp 126—127 °C, $[\alpha]_D^{23}$ +24.6° (*c* 0.3, methanol), R_f 0.29 on TLC in 1: 2 (v/v) chloroform–ethyl acetate. ^1H NMR ($CDCl_3$) δ 1.2—1.5 (m, 18, $3C(CH_3)_2$), 1.85 (s, 3, NAc), 5.84 (s, 1, benzylidene CH), 5.98 (d, 1, $J_{1,2}$=3 Hz, H-1); mass spectrum *m/e* 593 [M+], 578 [M+−15].

Found: C, 60.46; H, 7.27; N, 2.39%. Calcd for $C_{30}H_{43}NO_{11}$: C, 60.70; H, 7.30; N, 2.36%.

8: Mp 188—189.5 °C, $[\alpha]_D^{23}$ +60.8° (*c* 0.67, methanol)

R_f 0.18 on TLC in the same solvent. ^{1}H NMR ($CDCl_3$) δ 1.3—1.5 (m, 18, 3C(CH_3)$_2$), 1.96 (s, 3, NAc), 5.84 (s, 1, benzylidene CH), 6.00 (d, 1, $J_{1,2}$=3 Hz, H-1); mass spectrum *m/e* 593 [M$^+$], 578 [M$^+$−15].

Found: C, 60.46; H, 7.21; N, 2.37%. Calcd for $C_{30}H_{43}NO_{11}$: C, 60.70; H, 7.30; N, 2.36%.

*3,5-O-Benzylidene-6,7-dideoxy-9,11-O-ethylidene-1,2-O-isopropylidene-7-nitro-α-D-undeco-1,4-furanose (**10**).* Into a solution of **3** (368 mg) and 2,4-*O*-ethylidene-D-erythrose[25] (**9**, 300 mg) in tetrahydrofuran (3 ml) and methanol (2 ml) we stirred 1 M methanolic sodium methoxide (1.2 ml). After 3 h, the reaction solution was worked up analogously to the preparation of **5** and **6** to give 167 mg (32%) of **10** as crystals; mp 81—83 °C, $[\alpha]_D^{15}$ +33.4° (*c* 0.35, methanol). IR(KBr) 3430 (OH) 1555, 1380 cm^{-1} (NO_2), ^{1}H NMR($CDCl_3$) δ 1.33, 1.50 (2s, 6, C(CH_3)$_2$), 5.60 (s, 1, benzylidene CH), 6.00 (d, 1, $J_{1,2}$=3 Hz, H-1), 7.33 (broad s, 5, C_6H_5).

Found: C, 55.79; H, 6.30; N, 2.88%. Calcd for $C_{23}H_{31}NO_{11}$: C, 55.53; H, 6.28; N, 2.82%.

Two components were detectable on TLC in the crude product, but the other component was not obtained as a pure crystalline product.

*7-Acetamido-3,5-O-benzylidene-6,7-dideoxy-9,11-O-ethylidene-1,2-O-isopropylidene-α-D-undeco-1,4-furanose (**11**).* A solution of **10** (101 mg) in ethyl acetate (3 ml) was hydrogenated and subsequently worked up analogously to the preparation of **7** and **8** to give 48 mg (46%) of **11**; mp 85—86 °C, $[\alpha]_D^{14}$ +8.4° (*c* 0.5, methanol). IR(KBr) 3390 (OH), 1650 cm^{-1} (C=O). ^{1}H NMR ($CDCl_3$) δ 1.27 (d, 3, J=4.5 Hz, ethylidene CH_3), 1.33, 1.50 (2s, 6, C(CH_3)$_2$), 1.73 (s, 3, NAc), 5.62 (s, 1, benzylidene CH), 5.98 (d, 1, $J_{1,2}$=3 Hz, H-1), 7.37 (broad s, 5, C_6H_5).

Found: C, 59.06; H, 6.97; N, 2.97%. Calcd for $C_{25}H_{35}NO_{10}$: C, 58.93; H, 6.92; N, 2.74%.

The authors wish to thank Professor Gakuzo Tamura, Tokyo University, for his helpful suggestions. They also wish to express their appreciation to Mr. Mikio Munakata, Meiji Seika Kaisha, Ltd., for the mass spectral data, to Mr. Saburo Nakada for the elemental analyses, and to Mr. Hiderou Kitasato for some exploratory experiments related to the work descrived herein.

References

1) A. Takatsuki, K. Kawamura, M. Okina, Y. Kodama, T. Ito, and G. Tamura, *Agric. Biol. Chem.*, **41**, 2307 (1977).
2) R. L. Hamill and M. M. Hoehn, *J. Antibiot., Ser. A*, **17**, 100 (1964).
3) M. Vuilhorgne, S. Ennifar, B. P. Das, J. W. Paschal, R. Nagarajan, E. W. Hagman, and E. Wenkert, *J. Org. Chem.*, **42**, 3289 (1977).
4) R. Nagarajan, B. Chao, D. E. Dorman, S. M. Nash, J. L. Occolowitz, and A. Schabei, 17th International Conference on Antimicrobial Agents and Chemotherapy, New York, N.Y., (1977), Abstract 50.
5) T. Ito, Y. Kodama, K. Kawamura, K. Suzuki, A. Takatsuki, and G. Tamura, *Agric. Biol. Chem.*, **41**, 2303 (1977).
6) H. Paulsen, K. Roden, V. Sinnwell, and W. Koebernick, *Angew. Chem., Int. Ed. Engl.*, **15**, 439 (1976).
7) M. L. Wolfrom, W. W. Binkley, C. C. Spencer, and B. W. Lew, *J. Am. Chem. Soc.*, **73**, 3357 (1951).
8) R. B. Roy and W. S. Chilton, *J. Org. Chem.*, **36**, 3242 (1971).
9) V. I. Kornilov, L. D. Suong, and Y. A. Zhdanov, *J. Gen. Chem. USSR*, **41**, 202 (1971).
10) E. I. Stout, W. M. Doane, and V. C. Trinkus, *Carbohydr. Res.*, **50**, 282 (1976).
11) J. A. Secrist, III, and S. R. Wu, *J. Org. Chem.*, **44**, 1434 (1979).
12) D. Horton and J. Tsai, *Carbohydr. Res.*, **75**, 154 (1979).
13) L. Henry, *C. R. Acad. Sci.*, **120**, 1265 (1895).
14) H. B. Hass, *Ind. Eng. Chem.*, **35**, 1151 (1943).
15) G. A. Shvegheimer, N. F. Piatakov, and S. S. Novikov, *Usp. Khim.*, **28**, 484 (1959).
16) A. Pictet and A. Barbier, *Helv. Chim. Acta*, **4**, 924 (1921).
17) J. C. Sowden, *Adv. Carbohydr. Chem.*, **17**, 1 (1962).
18) S. M. Cantor, *Adv. Carbohydr. Chem.*, **20**, 1 (1965).
19) H. H. Baer, *Adv. Carbohydr. Chem. Biochem.*, **24**, 67 (1969).
20) T. Suami and S. Ogawa, *Bull. Chem. Soc. Jpn.*, **37**, 194 (1964).
21) G. B. Howarth, D. G. Lance, W. A. Szarek, and J. K. N. Jones, *Can. J. Chem.*, **47**, 75 (1969).
22) J. C. Sowden, *J. Am. Chem. Soc.*, **72**, 3325 (1950).
23) J. C. Sowden and D. R. Strobach, *J. Am. Chem. Soc.*, **80**, 2532 (1958).
24) L. F. Wiggins, *J. Chem. Soc.*, **1946**, 13.
25) R. Schaffer, *J. Am. Chem. Soc.*, **81**, 2838 (1959).
26) P. Brigl and H. Gruner, *Ber.*, **65**, 1428 (1932).
27) K. E. Pfitzner and J. G. Moffatt, *J. Am. Chem. Soc.*, **85**, 3027 (1963).
28) K. E. Pfitzner and J. G. Moffatt, *J. Am. Chem. Soc.*, **87**, 5661 (1965).

Structural Studies on the Cyclic Carbamate Derivatives of Kanamycin A

Yasushi TAKAGI, Chikara KOMURO, Tsutomu TSUCHIYA,* and Sumio UMEZAWA
Institute of Bioorganic Chemistry, 1614 Ida, Nakahara-ku, Kawasaki 211
(Received October 21, 1980)

Treatment of tetrakis(*N*-benzyloxycarbonyl)-6″-*O*-tritylkanamycin A with sodium hydride in *N*,*N*-dimethylformamide, followed by chromatography, afforded 4′,6′ : 3″,4″-, and 4′,6′ : 2″,3″-bis(cyclic carbamate) and 3″,4″- and 2″,3″-mono(cyclic carbamate) (**2**, **3**, and others). The structures of the position isomers **2** and **3** were determined by the NMR spectra at 500 MHz of their *N*-tosyl-*O*-acetyl derivatives.

Simultaneous protection of vicinal trans-equatorial amino and hydroxyl groups of amino sugars is very advantageous in aminoglucoside synthesis. For this purpose we previously reported an efficient and facile procedure[1,2] involving formation of a cyclic carbamate; this procedure has been widely applied. In this paper, we describe the separation and structural determination of the isomeric carbamate derivatives of kanamycin A as an example of the carbamate formation of complex aminoglycosides.

One method[2] for the preparation of cyclic carbamate is to treat an *N*-benzyloxycarbonyl derivative with sodium hydride in *N*,*N*-dimethylformamide (DMF). In the case of kanamycin A, 4′,6′ : 2″,3″-bis(cyclic carbamate) and/or 4′,6′ : 3″,4″-bis(cyclic carbamate) are expected to be formed by this treatment.

Tetrakis(*N*-benzyloxycarbonyl)kanamycin A[3] gave several products which could not be separated[4] by chromatographic separation in pure states owing to their low solubility in common organic solvents. Similar treatment of tetrakis(*N*-benzyloxycarbonyl)-4″,6″-*O*-cyclohexylidenekanamycin A[3] did not improve the purification. In order to enhance the solubility of the products, we introduced a trityl group and prepared tetrakis(*N*-benzyloxycarbonyl)-6″-*O*-tritylkanamycin A (**1**). This compound was soluble in most common organic solvents. Treatment of **1** with sodium hydride in DMF, followed by separation of the products by column chromatography, gave two isomers of mono- (**4**,**4′**; 10% in total) and di-carbamates (**2** and **3**, 62% in total in the ratio of about 5 : 2). All products isolated showed the absorption peak at 1760 cm^{-1}, indicating the presence of a five-membered cyclic carbamate.[1] NMR spectra and elemental analysis showed that **2** and **3** had two benzyloxycarbonyl groups and **4** and **4′** had three.

In order to determine the structures of **2** and **3**, several derivatives were prepared. When **2** or **3** was hydrolyzed with a limited amount of barium hydroxide, the cyclic carbamate rings were cleaved selectively to give the same product, 1,3-bis(*N*-benzyloxycarbonyl)-6″-*O*-tritylkanamycin A. Tosylation of the product gave a di-*N*-tosyl derivative (**5**). Acidic hydrolysis (with 8 M aqueous HCl–EtOH=1 : 1 at 100 °C) of **5** followed by detection by TLC of the hydrolyzates showed a single ninhydrinpositive spot for 2-deoxystreptamine, but no spots corresponding to 6-amino-6-deoxy- and 3-amino-3-deoxy-D-glucose or their glucosides were observed. This indicates the location of the tosyl groups of **5** at 6′- and 3″-amino groups; it is therefore clear that the same amino groups in **2** and **3** are protected by the cyclic carbamates. This result was further supported by another experiment. Catalytic hydrogenolysis of the benzyloxycarbonyl groups of **2** and **3**, followed by tosylation of the products, gave 1,3-di-*N*-tosyl derivatives (**7** and **11**). On cleavage of the cyclic carbamates followed by acidic hydrolysis, those derivatives gave 3-amino-3-deoxy- and 6-amino-6-deoxy-D-glucose (detected by TLC), a result which supports the structures of **7** and **11**.

The structures of the position isomers **2** and **3** were clarified by high-resolution NMR spectra of their tri-*O*-acetyl derivatives. Acetylation of **2** and **3** in the usual manner gave the tri-*O*-acetyl derivatives (**8** and **12**). In the NMR spectra of **12** at 200 MHz, H-2′ appeared as a quartet at δ 5.35, (J=3.5 and 10 Hz), and, H-3′ and H-4″ appeared as triplets at δ 6.27 (J=10 Hz) and 5.76 (J=9 Hz). The assignments were made from their shift and J values and suggested that the five-membered cyclic carbamate of **12** is formed between the 3″-amino and 2″-hydroxyl groups; therefore, **8** was deduced to have the 3″,4″-carbamate structure. These results were further verified by the NMR spectra at 500 MHz of **9** and **13**, which were obtained from **8** and **12** by catalytic hydrogenolysis followed by *N*-tosylation. In the NMR spectrum of **9**, H-2′ and H-2″ appeared as quartets at δ 5.30 and 5.51, respectively, and H-3′ appeared as a triplet at 5.80. In the NMR spectrum of **13**, H-2′ appeared as a quartet at δ 5.30 and H-3′ and H-4″ appeared as triplets at 6.04 and 5.69. These assignments were confirmed by the decoupling method. These results clearly showed that **9** and **13**, and consequently **2** and **3**, have the 3″,4″-*N*,*O*- and 3″,2″-*N*,*O*-carbonyl structure, respectively. It is noteworthy that the yield of the 3″,4″-*N*,*O*-carbonyl derivative (**2**, 38%) dominates over that of 3″,2″-derivative (**3**, 15%) in contrast to the results for the 3″,2″-*N*,*O*-carbonyl structure given by Kumar *et al.*[4] Debenzyloxycarbonyl derivatives (**10** and **14**) could not be obtained in pure state from **2** and **3**, but they will be usable as key intermediates for derivations of the 1- and 3-amino groups of kanamycin A.

Similarly, the minor products **4** and **4′** were determined to be monocarbamates. The mixture of **4** and **4′** was subjected to sequential mild alkaline hydrolysis and *N*-tosylation to afford 3″-*N*-tosyl derivative (**6**). Acid hydrolyzate of **6** showed, on TLC, two ninhydrin-positive spots of 2-deoxystreptamine and 6-amino-6-deoxy-D-glucose, suggesting that cyclic carbamate was formed at the 3″-amino group. When the mixture of **4** and **4′** was hydrogenated and then tosylated, two products (**15** and **16**) were obtained in a ratio of 2.4 : 1.

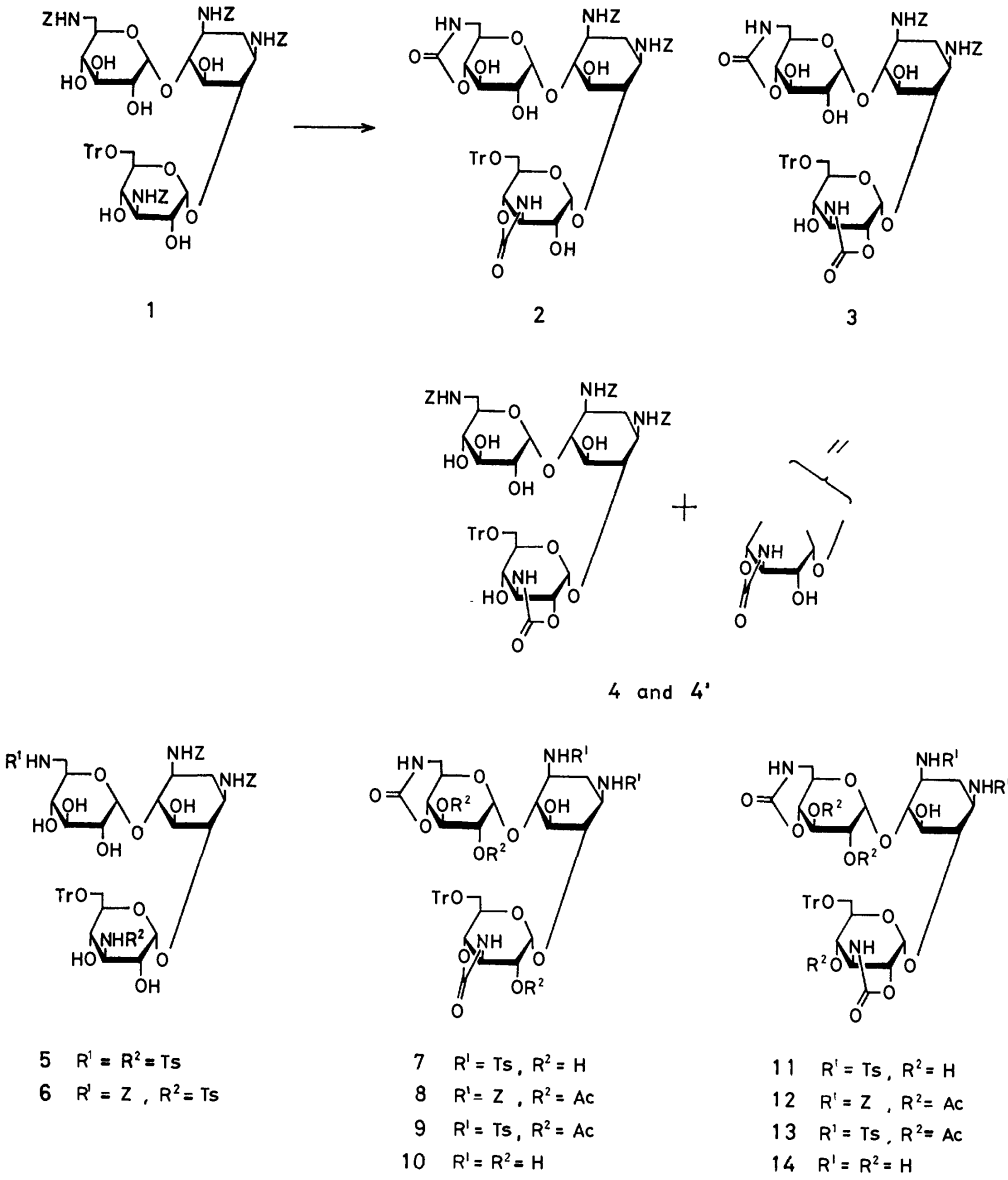

NMR spectra and elemental analysis of **15** and **16** showed that each has three tosyl groups. Decarbamation of **15** and **16** with barium hydroxide, followed by acidic hydrolysis, gave 3-amino-3-deoxy-D-glucose as the sole ninhydrin-positive product (checked by TLC), showing that **4** (and **4'**) is 3″,2″- or 3″,4″-cyclic carbamate. The position of the cyclic carbamate in **4** and **4'** remains unsolved.

Experimental

^{1}H-NMR spectra were recorded at 90, 200, and 500 MHz with Varian EM-390, Varian XL-200, and Bruker WM-500 spectrometers, respectively. TLC was performed on Wakogel B-5 and E. Merck silica gel with sulfuric acid spray for detection and on microcrystalline Avicel SF (Funakoshi Co.) with the spray of 0.5% ninhydrin in pyridine. In the latter case, the solvent system of 1-butanol–pyridine–water–acetic acid (6 : 4 : 3 : 1) was used as developer. For column chromatography, silica gel (Wakogel C-200) was used. On the description of reprecipitation, substance was dissolved in the first-cited solvent, and precipitated by adding the last-cited solvent.

*1,3,6′,3″-Tetrakis(*N*-benzyloxycarbonyl)-6″-*O*-tritylkanamycin A (**1**).* To a solution of tetrakis(*N*-benzyloxycarbonyl)-kanamycin A[3] (3.00 g) in dry pyridine (30 ml), trityl chloride (4.14 g, 2 mol equivalents for the starting material) was added and the solution was kept at room temperature for 18 h. The solution showed, on TLC with chloroform–ethanol (15 : 1), a major spot at R_f 0.3 (**1**). After addition of water (3 ml), the solution was poured into an ice-cold aqueous saturated sodium hydrogencarbonate (300 ml) with stirring. The mixture was extracted with chloroform (100 ml×4) and the chloroform solution was washed with aqueous sodium hydrogencarbonate and concentrated with several additions of toluene to give a pale yellow solid (6.76 g). The solid was chromatographed over silica gel with benzene as the developer to remove triphenylmethanol, then with ethyl acetate–chloroform (7 : 1) to elute **1**, 2.98 g (80%). The solid was reprecipitated from chloroform–hexane, $[\alpha]_D^{25}$ +64° (*c* 1, dioxane).

Found: C, 65.35; H, 5.96; N, 4.39%. Calcd for $C_{69}H_{74}N_4O_{19}$: C, 65.60; H, 5.90; N, 4.44%.

*Reaction of **1** with Sodium Hydride in DMF (Formation of **2**, **3**, **4**, and **4'**).* To an ice-cold solution of **1** (20.1 g) in dry

DMF (200 ml), 50% oily sodium hydride (5.02 g, 6.6 mol equivalents for **1**) was added under nitrogen atmosphere and the mixture was stirred at 5 °C for 13 h whereupon a slurry resulted. On TLC with chloroform–ethanol (7 : 1), the slurry showed four spots: R_f 0.36 (trace), 0.30 (**4**, minor), 0.24 (**3**, minor), and 0.21 (**2**, major). The slurry was poured into an ice-cold 1% acetic acid solution (1.6 l) and the mixture was extracted with chloroform (0.5 l×4). The chloroform solution was washed with aqueous sodium hydrogencarbonate and water, dried over sodium sulfate and concentrated with several additions of xylene to give a syrup, which was washed with ether. The resulting pale brown solid (16.9 g) was charged on a silica gel column and eluted with chloroform-ethanol (8 : 1). From the earlier fractions, a mixture of 1,3,6′-tris-(*N*-benzyloxycarbonyl)-3″,2″-*N*,*O*-carbonyl-6″-*O*-tritylkanamycin A (**4**) and its 3″,4″-*N*,*O*-carbonyl isomer (**4′**) were obtained, 1.79 g (10%). This mixture was reprecipitated from chloroform–ether, $[\alpha]_D^{25}$ +60° (*c* 1, dioxane); IR (KBr): 1760 (five-membered cyclic carbamate), 1700, 1520 cm^{-1}.

Found: C, 64.45; H, 5.77; N, 4.81%. Calcd for $C_{62}H_{66}N_4O_{18}$: C, 64.46; H, 5.76; N, 4.85%.

From the middle fractions, a solid of 1,3-bis(*N*-benzyloxycarbonyl)-6′,4′: 3″, 2″-di-*N*,*O*-carbonyl-6″-*O*-tritylkanamycin A (**3**), 2.56 g (15%), was obtained. Since the solid was slightly contaminated with **2**, **4**, and **4′**, it was purified by column chromatography and then reprecipitated from dioxane–water, $[\alpha]_D^{25}$ +46° (*c* 1, dioxane); IR (KBr): 1760 (five-membered cyclic carbamate), 1700, 1510 cm^{-1}.

Found: C, 62.21; H, 5.47; N, 5.15%. Calcd for $C_{55}H_{58}N_4O_{17}\cdot H_2O$: C, 62.02; H, 5.68; N, 5.26%.

From the last fractions, a solid of 1,3-bis(*N*-benzyloxycarbonyl)-6′,4′: 3″,4″-di-*N*,*O*-carbonyl-6″-*O*-tritylkanamycin A (**2**), 6.33 g (38%), was obtained. Since the solid was slightly contaminated with **3**, it was further purified by column chromatography and then reprecipitated from chloroform–ether, $[\alpha]_D^{25}$ +55° (*c* 1, dioxane); IR (KBr): 1760, 1700, 1510 cm^{-1}.

Found: C, 63.32; H, 5.71; N, 5.33%. Calcd for $C_{55}H_{58}N_4O_{17}$: C, 63.09; H, 5.58; N, 5.35%.

From the fractions between the middle and the last fractions, an additional mixture of **2** and **3** (1.50 g, 9%) was obtained.

*1,3-Bis(*N*-benzyloxycarbonyl)-6′,3″-di-*N*-tosyl-6″-*O*-tritylkanamycin A (**5**).* *a) From **2**:* To a solution of **2** (101 mg) in aqueous acetone (1 : 10, 5.5 ml), $Ba(OH)_2\cdot 8H_2O$ (37 mg) was added; the mixture was then stirred at 60 °C for 26 h. More $Ba(OH)_2\cdot 8H_2O$ (15 mg) was added and the mixture was stirred for an additional 3 h. The resultant mixture showed, on TLC with chloroform–methanol–8% ammonia (1 : 1 : 1, lower layer), spots of R_f 0.36 (trace), 0.22 (trace), 0.13 (major), and 0.05 (slight). After introduction of carbon dioxide, the mixture was filtered and the solid was washed thoroughly with dioxane. The filtrate and the washings were combined and concentrated to give a solid, 94 mg. To an ice-cold solution of the solid (94 mg) in aqueous dioxane (1 : 6, 2.5 ml), anhydrous sodium carbonate (24 mg) and tosyl chloride (42 mg) were added and the mixture was stirred at 5 °C for 15 h. On TLC with chloroform–ethanol (15 : 1), the mixture showed spots of R_f 0.39 (trace), 0.34 (trace), 0.20 (**5**, major), and 0.05 (slight). The mixture was poured into ice–water and the precipitate was filtered, washed with water and ether, and dried. The solid (94 mg) was chromatographed over silica gel with chloroform–ethanol (15 : 1). Concentration of the fractions containing only **5** gave a colorless solid, 42 mg (32%), $[\alpha]_D^{25}$ +60° (*c* 1, chloroform); IR (KBr): 1710, 1520, 1320 (ν_{as} SO_2), 1150(ν_s SO_2) cm^{-1}; ^{1}H-NMR (pyridine-d_5): δ 2.10 and 2.12 (each 3H s, CH_3 of Ts).

Found: C, 61.52; H, 5.77; N, 4.18; S, 4.98%. Calcd for $C_{67}H_{74}N_4O_{19}S_2$: C, 61.74; H, 5.72; N, 4.30; S, 4.92%.

*b) From **3**:* Compound **3** (58 mg) was treated as described above to give a solid of **5**, 23 mg (31%), $[\alpha]_D^{25}$ +63° (*c* 1, chloroform). The IR and ^{1}H-NMR spectra were superimposable with those of **5** obtained in *a)*.

*1,3,6′-Tris(*N*-benzyloxycarbonyl)-3″-*N*-tosyl-6″-*O*-tritylkanamycin A (**6**).* To an solution of a mixture of **4** and **4′** (99 mg) in aqueous dioxane (2 : 3, 5 ml), $Ba(OH)_2\cdot 8H_2O$ (28 mg) was added and the mixture was stirred at 60 °C for 14 h. The resultant mixture was then treated as described for **5** to give a colorless solid, 92 mg. The solid was then treated with tosyl chloride (19 mg) and anhydrous sodium carbonate (11 mg) as described for **5** to give a solid of **6**, 50 mg (46%), $[\alpha]_D^{25}$ +53° (*c* 0.8, chloroform); IR (KBr): 1710, 1520, 1320 (ν_{as} SO_2), 1150(ν_s SO_2) cm^{-1}; ^{1}H-NMR (pyridine-d_5): δ 2.11 (3H s, CH_3 of Ts).

Found: C, 63.37; H, 5.94; N, 4.16; S, 2.28%. Calcd for $C_{68}H_{74}N_4O_{19}S_1$: C, 63.64; H, 5.81; N, 4.37; S, 2.50%.

*6′,4′ : 3″,4″-Di-*N*,O-carbonyl-1,3-di-*N*-tosyl-6″-*O*-tritylkanamycin A (**7**).* To a solution of **2** (53 mg) in aqueous dioxane (1 : 5, 3 ml), 0.2 M aqueous hydrochloric acid was added until the pH became 4—5; the solution was then hydrogenated in the presence of palladium black at room temperature for 1.5 h. During the reaction, pH was maintained at 4—5 by occasional additions of diluted hydrochloric acid. Palladium black was removed by filtration. To the ice-cold filtrate, anhydrous sodium carbonate (20 mg) and tosyl chloride (22 mg) were added and the mixture was stirred at 5 °C for 15 h. The reaction mixture showed, on TLC with chloroform–ethanol (7 : 1), a major spot at R_f 0.2 (**7**). Concentration to a small volume followed by addition of water gave a solid, which was washed with water and ether, and dried. The solid (46 mg) was chromatographed over silica gel with the same solvent system to give **7**, 42 mg (76%), $[\alpha]_D^{25}$ −3° (*c* 1, dioxane); IR (KBr): 1760, 1700, 1330, 1160 cm^{-1}. The absorption peak for amide II (≈1510 cm^{-1}) disappeared; ^{1}H-NMR (pyridine-d_5): δ 2.31 (6H s, CH_3 of Ts).

Found: C, 58.33; H, 5.50; N, 4.88; S, 5.72%. Calcd for $C_{33}H_{58}N_4O_{17}S_2$: C, 58.55; H, 5.38; N, 5.15; S, 5.90%.

*2′,3′,2″-Tri-*O*-acetyl-1,3-bis(*N*-benzyloxycarbonyl)-6′,4′ : 3″,4″-di-*N*,O-carbonyl-6″-*O*-tritylkanamycin A (**8**).* To a solution of **2** (327 mg) in dry pyridine (6 ml), acetic anhydride (0.4 ml) was added and the solution was kept at room temperature for 25 h. The solution showed, on TLC with chloroform–ethanol (7 : 1), a single spot of **8** (R_f 0.43). After addition of water (0.4 ml), the solution was concentrated *in vacuo* and the chloroform solution of the concentrate was washed with aqueous potassium hydrogensulfate and water, dried (Na_2SO_4), and concentrated to give a colorless solid 332 mg (91%), $[\alpha]_D^{25}$ +80° (*c* 1, dioxane); ^{1}H-NMR (pyridine-d_5): δ 1.73, 2.00, 2.23 (each 3H s, Ac).

Found: C, 62.52; H, 5.60; N, 4.61%. Calcd for $C_{61}H_{64}N_4O_{20}$: C, 62.45; H, 5.50; N, 4.78%.

*2′,3′,2″-Tri-*O*-acetyl-6′,4′ : 3,″4″-di-*N*,O-carbonyl-1,3-di-*N*-tosyl-6″-*O*-tritylkanamycin A (**9**).* To a solution of **8** (228 mg) in aqueous dioxane (1 : 10, 11 ml), 1 M hydrochloridc acid was added until it became weakly acidic (pH≈4); the solution was then hydrogenated in the presence of palladium black for 2 h. During the reaction, pH was maintained at ≈4 by occasional additions of 1 M hydrochloric acid. The solution was filtered and water (3 ml) was added. To this solution, anhydrous sodium carbonate (70 mg) and tosyl chloride (91 mg) were added, and the mixture was treated as described for **7** to give a solid of **9** (after chromatography with chloroform–ethanol=15 : 1), 144 mg (61%), $[\alpha]_D^{25}$ +73° (*c* 1, dioxane); IR (KBr): 1760 (broad), 1330, 1160 cm^{-1}; ^{1}H-NMR (pyridine-d_5) (at 500 MHz): δ 1.61, 2.01, 2.28, 2.32,

2.38 (each 3H s, Ac and CH_3 of Ts), 3.31 (1H t, $J_{5',6'a}=J_{6'a,6'b}=10$ Hz, H-6'a), 3.41 (1H dd, $J_{5'',6''a}=6$ Hz, $J_{6''a,6''b}=10.5$ Hz, H-6''a), 3.49 (1H dd, $J_{5'',6''b}=3$ Hz, $J_{6''a,6''b}=10.5$ Hz, H-6''b), 3.76 (1H, ddd, $J_{6'b,NH}=4.5$ Hz, $J_{5',6'b}=6.5$ Hz, $J_{6'a,6'b}=10$ Hz, H-6'b), 4.34 (1H, t, $J_{3',4'}=J_{4',5'}=10$ Hz, H-4'), 4.96 (1H, dt, $J_{4',5'}=J_{5',6'a}=10$ Hz, $J_{5,6'b}=6.5$ Hz, H-5'), 5.300 (1H, m, H-5''), 5.51 (1H, dd, $J_{1'',2''}=3.5$ Hz, $J_{2'',3''}=10.5$ Hz, H-2''), 5.302 (1H, dd, $J_{1',2'}=4$ Hz, $J_{2',3'}=10$ Hz, H-2'), 5.80 (1H, t, $J_{2',3'}=J_{3',4'}=10$ Hz, H-3'), 6.33 (1H, d, $J_{1',2'}=4$ Hz, H-1'), 6.47 (1H, d, $J_{1'',2''}=3.5$ Hz, H-1''). The signals assignable to H-5'' cculd only be discerned after resolution enhancement.

Irradiation at δ 5.30 (H-2' and 5'') collapsed the quartet of H-6''a to a doublet, the quartet of H-6''b to a doublet, the triplet of H-3' to a doublet, and the doublet of H-1' to a singlet. Irradiation at δ 5.51 (H-2'') collapsed the doublet of H-1'' to a singlet. Irradiation at δ 6.33 (H-1') collapsed the quartet of H-2' to a doublet. Irradiation at δ 6.47 (H-1'') collapsed the quartet of H-2'' to a doublet.

Found: C, 58.02; H, 5.51; N, 4.35; S, 4.84%. Calcd for $C_{59}H_{64}N_4O_{20}S_2$: C, 58.41; H, 5.32; N, 4.62; S, 5.29%.

6',4': *3'',4''-Di*-N,O-*carbonyl-6''*-O-*tritylkanamycin A (**10**)*. Compound **2** (550 mg) dissolved in ethanol–acetic acid (97 : 3, 28 ml) was hydrogenated with palladium black as described before. Filtration followed by concentration gave a solid which was thoroughly washed with ether to give **10**, 366 mg. The solid was slightly contaminated with an impurity of R_f 0.39 (on TLC developed with the lower layer of chloroform–methanol–20% acetic acid=5 : 7 : 5; *cf* **10**, 0.33). IR (KBr): 1760 (five-membered cyclic carbamate), 1700 cm^{-1} (six-membered cyclic carbamate). No peak for amide II (near 1520 cm^{-1}).[4]

6',4' : *3'',2''-Di*-N, O-*carbonyl-1, 3-di*-N-*tosyl-6''*-O-*tritylkanamycin A (**11**)*. Compound **3** (55 mg) was hydrogenated and tosylated as described for **7**. The crude solid (46 mg, 81%) obtained was chromatographed over silica gel with chloroform–ethanol (7 : 1) to give pure **11**, 34 mg $[\alpha]_D^{25}$ −1° (*c* 1, dioxane); Ir (KBr): 1760, 1700, 1330, 1160 cm^{-1}; ^{1}H-NMR (pyridine-d_5): δ 2.30 (6H s, CH_3 of Ts).

Found: C, 58.84; H, 5.52; N, 5.05; S, 5.72%. Calcd for $C_{53}H_{58}N_4O_{17}S_2$: C, 58.55; H, 5.38; N, 5.15; S, 5.90%.

2',3',4''-Tri-O-*acetyl-1,3-bis(*N-*benzyloxycarbonyl)-6',4'* : *3'',2''-di*-N,O-*carbonyl-6''*-O-*tritylkanamycin A (**12**)*. Compound **3** (331 mg) was acetylated as described for **8** to give a solid of **12**, 344 mg (93%), $[\alpha]_D^{25}$ +87° (*c* 1, dioxane); ^{1}H-NMR (pyridine-d_5) (at 200 MHz): δ 1.60, 1.77, 1.99 (each 3H s, Ac), 5.35 (1H, dd, $J_{1',2'}=3.5$ Hz, $J_{2',3'}=10$ Hz H-2'), 5.43 (2H, AB q, $C_6H_5C\underline{H}_2OCO$, $J=12$ Hz), 5.53 (2H s, $C_6H_5C\underline{H}_2OCO$), 5.76 (1H, t, $J=9$ Hz, H-4''), 6.06 (1H, broad s, H-1''), 6.27 (1H t, $J=10$ Hz, H-3'), 6.31 (1H, d, $J=3.5$ Hz, H-1').

Found: C, 62.21, H, 5.52; N, 4.56%. Calcd for $C_{61}H_{64}N_4O_{20}$: C, 62.45; H, 5.50; N, 4.78%.

2',3',4''-Tri-O-*acetyl-6',4'* : *3'',2''-di*-N,O-*carbonyl-1,3-di*-N-*tosyl-6''*-O-*tritylkanamycin A (**13**)*. Compound **12** (246 mg) was hydrogenated and tosylated as described for **9**. The crude solid (183 mg, 72%) was chromatographed over silica gel with chloroform–ethanol (15 : 1) to give pure **13**, 173 mg (68%), $[\alpha]_D^{25}$ +66° (*c* 1, dioxane); IR (KBr): 1750 (broad), 1330, 1160 cm^{-1}; ^{1}H-NMR (pyridine-d_5) (at 500 MHz): δ 1.61, 1.78, 2.01 (each 3H, s, Ac); 2.32, 2.36 (each 3H, s, CH_3 of Ts), 3.13 (1H, dd, $J_{5'',6''a}=4$ Hz, $J_{6''a,6''b}=10.5$ Hz, H-6''a), 3.369 (1H, dd, $J_{5'',6''b}=2$ Hz, $J_{6''a,6''b}=10.5$ Hz, H-6''b), 3.374 (1H t, $J_{5',6'a}=J_{6'a,6'b}=10$ Hz, H-6'a), 4.41 (1H, t, $J_{3',4'}=J_{4',5'}=10$ Hz, H-4'), 4.86 (1H, ddd, $J_{5'',6''b}=2$ Hz, $J_{5'',6''a}=4$ Hz, $J_{4'',5''}=10$ Hz, H-5''), 5.22 (1H, dt, $J_{5',6'b}=6.5$ Hz, $J_{5',6'a}=J_{4',5'}=10$ Hz, H-5'), 5.30 (1H, dd, $J_{1',2'}=4$ Hz, $J_{2',3'}=10$ Hz, H-2'), 5.69 (1H, t, $J_{3'',4''}=J_{4'',5''}=10$ H-4''), 6.04 (1H, t, $J_{2',3'}=J_{3',4'}=10$ Hz, H-3'), 6.14 (1H, d, $J_{1',2'}=4$ Hz, H-1'), 6.49 (1H, d, $J_{1'',2''}=2$ Hz, H-1'').

Irradiation at δ 4.86 (H-5'') collapsed the quartet of H-6''a to a doublet, the quartet of H-6''b to a doublet, and the triplet of H-4'' to a doublet. Irradiation at δ 5.22 (H-5') collapsed the triplet of H-4' to a doublet. Irradiation at δ 5.30 (H-2') collapsed the triplet of H-3' to a doublet and the doublet of H-1' to a singlet. Irradiation at δ 5.69 (H-4'') collapsed the octet of H-5'' to a quartet.

Found: C, 58.13; H, 5.38; N, 4.35; S, 5.13%. Calcd for $C_{59}H_{64}N_4O_{20}S_2$: C, 58.41; H, 5.32; N, 4.62; S, 5.29%.

6',4': *3'',2''-Di*-N,O-*carbonyl-6''*-O-*tritylkanamycin A (**14**)*. Compound **3** (105 mg) was hydrogenated as described for **10** to give a solid **14** (75 mg). The solid was slightly contaminated with an impurity of R_f 0.39. (TLC with the lower layer of chloroform–methanol–20% acetic acid=5 : 7 : 5; *cf.* **14**, 0.33); IR (KBr): 1760, 1700 cm^{-1}. No peak for amide II was observed.

*3'',2''-(and 3'',4''-)*N,O-*Carbonyl-1,3,6'-tri*-N-*tosyl-6''*-O-*trityl-kanamycin A (A Mixture of **15** and **16**)*. A mixture of **4** and **4'** (526 mg) was hydrogenated and tosylated as described for **7**. The reaction mixture showed, on TLC with chloroform–ethanol (7 : 1), spots of R_f 0.46 (trace), 0.34 (**15**, major), and 0.23 (**16**, minor). Concentration gave a syrup, which was washed with water and ether, and dried to give a solid. It was chromatographed over silica gel with chloroform–ethanol (12 : 1) to give **15**, 234 mg (42%) and **16**, 97 mg (18%).

15: $[\alpha]_D^{25}$ +32° (*c* 1, dioxane); IR (KBr): 1760, 1320, 1160 cm^{-1}; ^{1}H-NMR (dioxane-d_8–D_2O=9 : 1): δ 2.43 (6H, s, CH_3 of Ts), 2.47 (3H, s, CH_3 of Ts).

Found: C, 58.02; H, 5.59; N, 4.41; S, 7.69%. Calcd for $C_{59}H_{66}O_{18}S_3$: C, 58.31; H, 5.47; N, 4.61; S, 7.91%.

16: $[\alpha]_D^{25}$ +16° (*c* 1, dioxane); IR (KBr): 1760, 1320, 1160 cm^{-1}; ^{1}H-NMR (dioxane-d_8–D_2O=9 : 1): δ 2.42 (3H, s, CH_3 of Ts), 2.49 (6H, s, CH_3 of Ts).

Found: C, 58.04; H, 5.71; N, 4.34; S, 7.61%.

The authors with to express their deep thanks to Prof. Hamao Umezawa of the Institute of Microbial Chemistry for his encouragement. We are also indebted to Analytica Corp. (Tokyo) and Bruker Messtechnik GmbH for measurements of 200 and 500 MHz NMR spectra, respectively.

References

1) S. Umezawa, Y. Takagi, and T. Tsuchiya, *Bull. Chem. Soc. Jpn.*, **44**, 1411 (1971).

2) D. Ikeda, T. Tsuchiya, S. Umezawa, and H. Umezawa, *J. Antibiot.*, **25**, 741 (1972).

3) T. Miyake, T. Tsuchiya, S. Umezawa, and H. Umezawa, *Bull. Chem. Soc. Jpn.*, **50**, 2362 (1977).

4) V. Kumar and W. A. Remers (*J. Med. Chem.*, **22**, 432 (1979)) reported the formation of 4',6': 2'',3''-bis (cyclic carbamate) by the same reaction with the same starting material. There was no clear discussion of possible formations of position isomers.

Syntheses of *N*-Substituted 3,3,4-Triaryl- and 3,3,4,4-Tetraphenyl-2-azetidinones

Kailash Nath MEHROTRA* and Surendra Bahadur SINGH
Department of Chemistry, Banaras Hindu University, Varanasi-221005, India
(Received June 28, 1980)

The reactions of 2-diazo-1,2-diphenylethanone with Schiff's bases Ar–CH=N–R gave new substituted 2-azetidinones together with 1,1′,4,4′-tetraphenyl-2,2′-azinodiethanone. 2-Diazo-1,2-diphenylethanone reacts with *N*-benzhydrylidene-*N*′-phenylurea to give 1-(phenylcarbamoyl)-3,3,4,4-tetraphenyl-2-azetidinone.

The cycloaddition of diphenylketene with anils is known to form 2-azetidinones.[1] Diphenylketene, in these cases, has been generated either thermally by dehydrohalogenation of suitable acid chlorides with tertiary bases[2] or photochemically from diazo ketone.[3] On the other hand, diphenylketene has been known to add on carbon-oxygen double bond in α,β-unsaturated ketones to give β-lactones.[4] We now report the cycloaddition of diphenylketene, generated *in situ* by thermal decomposition of 2-diazo-1,2-diphenylethanone (**1**), with Schiff's bases **2a—g** leading to *N*-alkyl-2-azetidinones **3a—g** in fair yields. The reaction of diphenylketene with *N*-benzhydrylidene-*N*′-phenylurea (**5**), having three reactive sites (C=N, C=O, and NH), has shown that C=N group is attacked by diphenylketene in preference to either C=O group or NH group. The products, **3a—g**, show extraordinary stability amongst β-lactams[5] towards common degradative reagents.

Results and Discussion

An equimolecular mixture of 2-diazo-1,2-diphenylethanone (**1**) and *N*-benzylideneisopropylamine (**2a**: Ar=C_6H_5, R=$CH(CH_3)_2$) was heated to reflux in dry benzene for 12 h under stream of nitrogen. The reaction product was separated by fractional crystallization from hexane–ethanol (1 : 1) and vacuum distillation; it consisted of 1,1′,4,4′-tetraphenyl-2,2′-azinodiethanone (**4**, 2%) and 1-isopropyl-3,3,4-triphenyl-2-azetidinone (**3a**, 85%). An authentic sample of product **4** was prepared according to method reported[6] for comparison (IR, NMR, and also melting point). The structural assignment of **3a** was made on the basis of its analytical and spectral data.

Similar treatment of Schiff's bases **2b—f** gave 2-azetidinones **3b—f**, identified on the basis of their analytical and spectral data, together with ketazine (**4**, 3—5%) in each case.

The racemic *N*-benzylidene-α-methylbenzylamine (**2g**) on similar treatment gave two products, a white crystalline solid **3g** (81%) and a yellow crystalline solid, identified as ketazine **4** (3%). The white crystalline solid, mp 94—95 °C, showed absorption band at 1740 (C=O, β-lactam[2]) cm^{-1} in IR spectrum. The NMR spectrum of product exhibited two doublets at δ 1.47 and 1.92, two quartets at δ 4.32 and 5.01 and one singlet at δ 5.02 which may be due to presence of two enantiomeric forms of product **3g**. This would be expected as the starting Schiff's base **2g** is racemic. The elemental analyses and spectral data agree with assigned structure, (±) 1-(α-methylbenzyl)-3,3,4-triphenyl-2-azetidinone (**3g**), to the product.

The products **3a—g** were found to be unaffected on treatment with ordinary alkali or acid, whereas, *N*-aryl-2-azetidinones reported earlier[5] have been known to undergo hydrolysis. The formation of products can be explained as in Scheme 1.

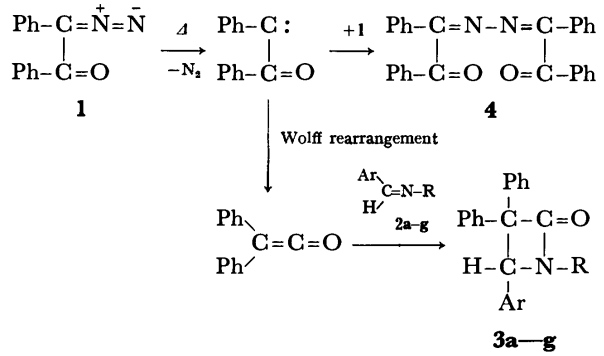

	Ar	R
3a	C_6H_5	$CH(CH_3)_2$
3b	C_6H_5	$CH(C_6H_5)_2$
3c	*p*-$CH_3OC_6H_4$	$CH(C_6H_5)_2$
3d	*p*-ClC_6H_4	$CH(C_6H_5)_2$
3e	*p*-$NO_2C_6H_4$	$CH(C_6H_5)_2$
3f	*p*-$(CH_3)_2NC_6H_4$	$CH(C_6H_5)_2$
3g	C_6H_5	$CH(CH_3)C_6H_5$

Scheme 1.

Thermal decomposition of **1** may lead to benzoylphenylcarbene which may combine with **1** to form ketazine **4**. The benzoylphenylcarbene has been known to undergo Wolff rearrangement to give diphenylketene[7] which on reaction with C=N bond of Schiff's bases **2a—g** may lead to 2-azetidinones **3a—g** through the collapse of a possible zwitterionic intermediate. A similar intermediate has been proposed in the reaction of diphenylketene and *N*-benzylideneaniline giving *N*-phenylimidate.[8]

When *N*-benzhydrylidene-*N*′-phenylurea (**5**) was allowed to react with **1**, in an analogous manner, a white crystalline solid (70%) was obtained. The substituted urea **5** contains three possible reactive sites *viz.* C=N, C=O, and NH groups. It is known that interaction of ketene with C=N, C=O, and NH groups leads to the formation of β-lactam,[8] β-lactone[9] (which on decarboxylation gives corresponding olefin) and acetyl derivative[10] of NH group, respectively. The presence of an absorption bands at 1760 cm^{-1}, characteristic of a β-lactam[11] and 1710 (C=O, CONH[11]) cm^{-1}, absence of an absorption band between 1700

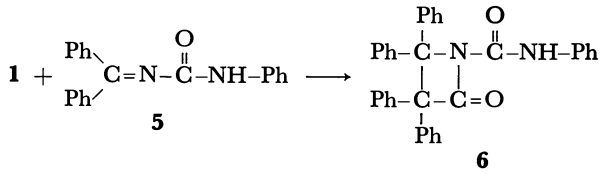

and 1600 cm^{-1} in IR spectrum and absence of a signal between δ 6—5 in NMR spectrum strongly support the assigned structure, 1-(phenylcarbamoyl)-3,3,4,4-tetraphenyl-2-azetidinone (**6**), to the product. It appears that diphenylketene adds exclusively on the C=N bond in preference to either C=O or NH bonds. The NH bond in an amide does not react with diphenylketene.[10]

Experimental

Melting points have been determined in capillaries on Büchi melting point apparatus and are uncorrected. The IR spectra were measured in Nujol mull on a Perkin-Elmer 720-spectrophotometer. The NMR spectra were recorded on Varian A-60 MHz spectrometer in $CCl_4/CDCl_3$ with TMS as an internal standard.

Materials. The aldehydes were obtained from BDH, India and 1,[12]-methylbenzylamine,[13] benzhydrylamine,[14] and *N*-benzhydrylidene-*N'*-phenylurea[15] were prepared according to reported methods.

Preparation of Schiff's Bases ***2a—g.*** *General Procedure*: The Schiff's bases **2a—g** were obtained by mixing equimolar amount of aldehyde and amine at room temperature. In all the cases, except **2a** where purification was done by vacuum distillation, the products were purified by fractional crystallization from ethanol. Yield: 80—85%.

Preparation of 2-Azetidinones ***3a—g.*** *General Procedure*: A mixture of 0.01 mol of **1** and 0.01 mol of a Schiff's base **2a—g** was heated to reflux in 80 ml of dry benzene (free from thiophene) for 12 h under stream of nitrogen. The reaction mixture was kept overnight. The solvent was removed on rotatory evaporator and residual matter was crystallised from ethanol to give 2-azetidinone **3a—g**. From the mother liquor 1,1',4,4'-tetraphenyl-2,2'-azinodiethanone (**4**, 2—5%), mp 202—303 °C (lit,[6] mp 202 °C) [UV (EtOH, nm): 255 and 315; IR (Nujol, cm^{-1}): 1680 (C=O) and 1601 (C=N-N=C); NMR ($CDCl_3$, δ ppm): 8.30—7.20 (m, H, aromatic protons). Found: C, 80.35; H, 5.12; N, 6.83%. Calcd for $C_{28}H_{20}N_2O_2$: C, 80.75; H, 4.84; N, 6.73%] was recovered by evaporation of solvent and recrystallization of residual matter from hexane–ethanol (1 : 1).

*1-Isopropyl-3,3,4-triphenyl-2-azetidinone (**3a**)* A yield of 85% obtained, bp 165/0.01 mmHg† (mp 102—103 °C). UV (EtOH, nm): 250, 255, and 260; IR (CCl_4, cm^{-1}): 1740 (C=O, β-lactam); NMR (CCl_4, δ ppm): 7.75—6.90 (m, 15H, aromatic protons); 5.31 (s, 1H, CH, ring); 3.81 (Sept, 1H, CH, isopropyl, J=7 Hz); 1.37 and 1.15 (a pair of doublets, 6H, CH_3, isopropyl, J=7 Hz). Found: C, 84.66; H, 6.72; N, 4.07%. Calcd for $C_{24}H_{23}NO$: C, 84.45; H, 6.74; N, 4.11%.

*1-Benzhydryl-3,3,4-triphenyl-2-azetidinone (**3b**).* A yield of 78% was obtained, mp 159—160 °C. UV (EtOH, nm): 250, 255, and 260; IR (Nujol, cm^{-1}): 1742 (C=O, β-lactam); NMR (CCl_4, δ ppm): 7.73—6.87 (m, 25H, aromatic protons); 5.61 (s, 1H, CH, benzhydryl); 5.45 (s, 1H, CH, ring). Found: C, 87.50; H, 5.64; N, 3.24%. Calcd for $C_{34}H_{27}NO$: C, 87.74; H, 5.80; N, 3.01%.

† 1 mmHg≈133.322 Pa.

*1-Benzhydryl-3,3-diphenyl-4-(p-methoxyphenyl)-2-azetidinone (**3c**).* A yield of 61% was obtained, mp 129—130 °C. UV (EtOH, nm): 260, 265, and 270; IR (Nujol, cm^{-1}): 1730 (C=O, β-lactam) and 1250 (C-O-C); NMR (CCl_4, δ ppm): 7.70—7.00 (m, 20H, aromatic protons); 6.80 and 6.65 (A_2B_2q, 4H, aromatic protons, J=8 Hz); 5.67 (s, 1H, CH, benzhydryl); 5.27 (s, 1H, CH, ring); 3.67 (s, 3H, CH, OCH_3). Found: C, 84.83; H, 5.74; N, 3.04%. Calcd for $C_{35}H_{29}NO_2$: C, 84.84; H, 5.85; N, 2.83%.

*1-Benzhydryl-3,3-diphenyl-4-(p-chlorophenyl)-2-azetidinone (**3d**).* A yield of 59% was obtained, mp 145—146 °C. UV (EtOH, nm): 250, 260, and 270; IR (Nujol, cm^{-1}): 1735 (C=O, β-lactam); NMR (CCl_4, δ ppm): 7.83—7.03 (m, 20H, aromatic protons); 6.97 and 6.71 (A_2B_2q, 4H, aromatic protons, J=9Hz); 5.65 (s, 1H, CH, benzhydryl); 5.27 (s, 1H, CH, ring). Found: C, 81.79; H, 5.34; N, 2.72%. Calcd for $C_{34}H_{26}NOCl$: C, 81.68; H, 5.20; N, 2.80%.

*1-Benzhydryl-3,3-diphenyl-4-(p-nitrophenyl)-2-azetidinone (**3e**).* A yield of 61% was obtained, mp 206—207 °C. UV (EtOH, nm): 278; IR (Nujol, cm^{-1}): 1735 (C-O, β-lactam), 1520 and 1350 (NO_2); NMR ($CDCl_3$, δ ppm): 8.05—7.00 (m, 24H, aromatic protons); 5.91 (s, 1H, CH, benzhydryl); 5.57 (s, 1H, CH, ring); Found: C, 79.80; H, 5.50; N, 5.45%. Calcd for $C_{34}H_{26}N_2O_3$: C, 80.00; H, 5.09; N, 5.49%.

*1-Benzhydryl-3,3-diphenyl-4-(p-dimethylaminophenyl)-2-azetidinone (**3f**).* A yield of 62% was obtained, mp 150—151 °C. UV (EtOH, nm); 265: IR (Nujol, cm^{-1}): 1730 (C=O, β-lactam); NMR (CCl_4, δ ppm): 7.70—7.00 (m, 20H, aromatic protons): 6.75 and 6.48 (A_2B_2q, 4H, aromatic protons, J=9 Hz); 5.51 (s, 1H, CH, benzhydryl); 5.17 (s, 1H, CH, ring); 2.82 (s, 6H, CH, $-N(CH_3)_2$). Found: C, 85.48; H, 6.54; N, 5.72%. Calcd for $C_{36}H_{32}N_2O$: C, 85.67; H, 6.29; N, 5.51%.

*1-(α-Methylbenzyl)-3,3,4-triphenyl-2-azetidinone (**3g**).* A yield of 81% was obtained, mp 94—95 °C. UV (EtOH, nm): 255, 260, and 265; IR (Nujol, cm^{-1}): 1740 (C=O, β-lactam); NMR (CCl_4, δ ppm): 7.67—6.90 (m, 20H, aromatic protons); 5.05 (s, 1H, CH, ring); 5.01 and 4.32 (a pair of quartets, 1H, CH, $CH(CH_3)C_6H_5$, J=7 Hz); 1.92 and 1.47 (a pair of doublets, 3H, CH, $CH(CH_3)C_6H_5$, J=7 Hz). Found: C, 85.90; H, 6.45; N, 3.32%. Calcd for $C_{29}H_{25}NO$: C, 86.35; H, 6.20; N, 3.47%.

Attempted Ring Opening of ***3a—g.*** A mixture containing 0.20 g of **3a**, 15 ml of 85% ethanol and 1 ml of concentrated hydrochloric acid was heated to reflux for 30 h. After the usual work up 0.18 g (90%) of starting material was recovered. Similar treatment of **3a—g** with either 40% aqueous alkali (potassium hydroxide or sodium hydroxide) or saturated ethanolic potassium hydroxide solution resulted in recovery of starting material almost quantitatively.

*Preparation of 1-(Phenylcarbamoyl)-3,3,4,4-tetraphenyl-2-azetidinone (**6**).* A mixture of 0.01 mol of **1** and 0.01 mol of **5** was heated to reflux in 80 ml of dry benzene (free from thiophene) for 8 h under stream of nitrogen. The reaction mixture was kept overnight. The solvent was removed on rotatory evaporator and residual matter was recrystallized from ethanol to give a white crystalline solid **6** (70%), mp 200—202 °C. UV (EtOH, nm): 235, 250, and 260; IR (Nujol, cm^{-1}): 3310 (NH), 1760 (C=O, β-lactam) and 1710 (C=O, CONH–); NMR ($CDCl_3$, δ ppm): 9.10 (b, 1H, NH, D_2O exchangeable); 7.83—7.05 (m, 25H, aromatic protons). Found: C, 82.77; H, 5.42; N, 6.01%. Calcd for $C_{34}H_{26}N_2O_2$: C, 82.59; H, 5.26; N, 5.68%.

We are thankful to Professor B. M. Shukla for providing the facilities and to C.S.I.R., New Delhi, for grant of a fellowship to SBS.

References

1) A. K. Mukerjee and R. C. Srivastava, *Synthesis*, **1973**, 327, and references cited therein.
2) A. K. Bose and I. Kugajevsky, *Tetrahedron*, **23**, 957 (1967).
3) W. Kirmse and L. Horner, *Chem. Ber.*, **89**, 2759 (1956).
4) H. Staudinger, *Chem. Ber.*, **41**, 1355 (1908).
5) H. T. Clarke, J. R. Johnson, and R. Robinson, "The Chemistry of Penicillin," Princeton University Press (1949), p. 945.
6) T. Curtius and R. Kastner, *J. Prakt. Chem.*, **83**, 215 (1911); *Chem. Abstr.*, **5**, 2649 (1911).
7) V. Franzen, *Justus Liebigs Ann. Chem.*, **614**, 31 (1958).
8) H. B. Kagan and J. L. Luche, *Tetrahedron Lett.*, **1968**, 3093.
9) L. L. Muller and J. Hamer, "1,2-Cycloaddition Reactions," Interscience Publ., New York (1967), p. 139.
10) W. Jugelt and D. Schmidt, *Tetrahedron*, **25**, 969 (1969).
11) G. Wittig and A. Hesse, *Justus Liebigs Ann. Chem.*, **1976**, 500.
12) C. D. Nenitzescu and E. Solomonica, *Org. Synth.*, Coll. Vol. II, 496 (1950).
13) A. W. Ingersoll, *Org. Synth.*, Coll. Vol. II, 503 (1950).
14) A. Michaelis, *Chem. Ber.*, **26**, 2169 (1893).
15) G. E. P. Smith, Jr., and F. W. Bergstrom, *J. Am. Chem. Soc.*, **56**, 2095 (1934).

  Bull. Chem. Soc. Jpn., 54, 1841—1843 (1981)

Synthesis of New Chiral Phase-transfer Catalysts and Their Application to Michael Additions

Stefano BANFI, Mauro CINQUINI, and Stefano COLONNA*

C.N.R. e Istituto di Chimica Industriale dell' Universita', Via C. Golgi 19, 20133 Milano, Italy

(Received July 30, 1980)

A series of chiral onium salts derived from (L)-(+)-methionine have been examined for the catalysis of Michael additions in phase-transfer conditions. The chemical yields are high, but no asymmetric induction was observed. Catalyst **6** represents the first example of an onium salt anchored to a polimeric matrix having a higher catalytic efficiency than its soluble counterpart.

In the last few years much interest has been aroused by stereoselective syntheses under phase-transfer conditions in the presence of chiral "onium salts" as catalysts.[1] The quaternary ammonium salts, usually derived from ephedra or cinchona alkaloids, must have a hydroxyl group in the β-position to the "onium" function in order for asymmetric induction and/or kinetic resolution[1,2] to be observed. In the search for new chiral phase-transfer catalysts, we have now prepared onium salts containing the SO group as an asymmetric centre. The behaviour of the sulfinyl group, compared to other chiral groups, is indeed particularly influenced by ligands very different from each other from a stereoelectronic point of view; an oxygen, a lone pair and two aryl or alkyl groups. This accounts for the high conformational preference of sulfoxides as well as the high stereoselectivity in reactions involving chiral or prochiral groups α or β to the sulfur moiety.[3]

For this reason we have investigated the behaviour of the chiral onium salts (**1**—**2**), derived from (L)-(+)-methionine, in a series of reactions carried out under phase-transfer conditions. These are the Michael additions of nitromethane to *trans*-chalcone and of thiophenol to 2-cyclohexen-1-one, [Reactions A and B respectively] and the addition of methyl vinyl ketone to methyl 1-oxoindan-2-carboxylate (Reaction C). For the sake of comparison the same reactions have been performed in homogeneous medium in the presence of catalytic amounts of catalysts **3** and **4**. The effect of the binding of the catalyst to a polymeric solid support [catalysts **5** and **6**] has also been examined.

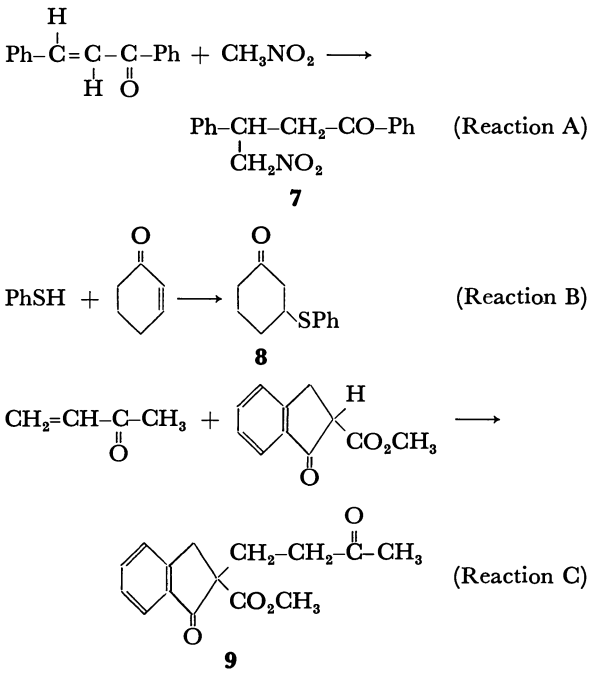

Results and Discussion

Synthesis of the Catalysts. All catalysts were prepared starting from commercial (L)-(+)-methionine (**10**), $[\alpha]_{546}^{20}$ +28.7°.

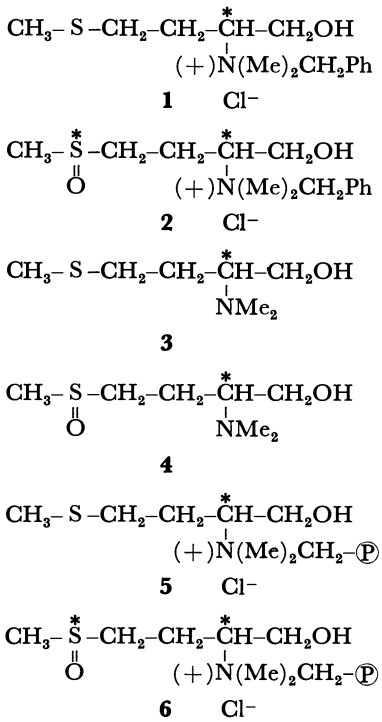

The onium salt **1** was prepared by methylation of (+)-**10**, followed by reduction to give the alcohol **3** and quaternarization of the latter with benzyl chloride (Scheme 1).

Similarly **2** was obtained by methylation of diastereomerically pure[4] (L)-methionine-*d*-*S*-oxide (**12**), followed by esterification with diazomethane to give **14**, which was reduced to the alcohol **4** with $LiAlH_4$ and quaternarizated to **2** with benzyl chloride (Scheme 2).

The catalysts **5** and **6** supported on a polymeric matrix were prepared by reaction of alcohols **3** and **4** with chloromethylated polystyrene in anhydrous DMF

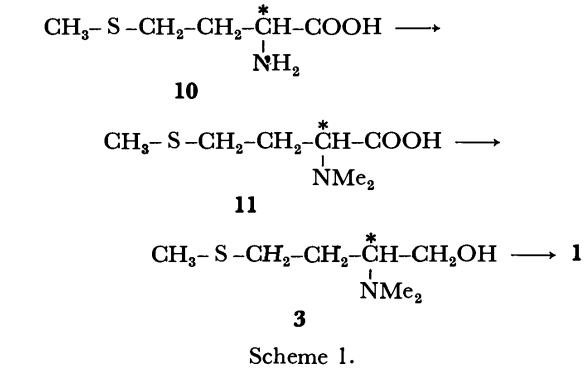

Scheme 1.

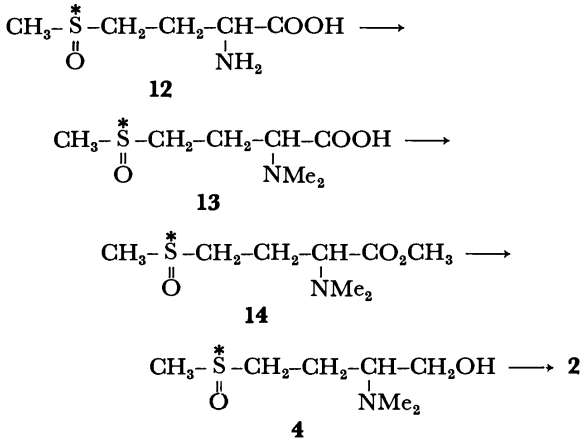

Scheme 2.

as solvent (see Experimental).

Michael Additions. The reactions with catalysts **1**, **2**, **5**, and **6**, were carried out at room temperature under solid-liquid phase-transfer conditions in toluene as solvent in the presence of an excess of solid KF. In the case of catalysts **3**, **4** the reactions were performed in the same solvent and in the absence of the inorganic salt.

The results collected in the Table show that conversion into the Michael adducts is more efficient under phase-transfer conditions with catalysts **1**, **2** than in homogeneous medium with catalysts **3** and **4**. The difference is particularly noticeable in the nitromethane addition to *trans*-chalcone; a reaction which occurs only in the presence of the onium salts and potassium fluoride. In homogeneous medium methioninol *S*-oxide (**4**) is a more efficient catalyst than the corresponding sulfide (**3**).

As far as soluble "onium" salts are concerned, catalyst **1** is more efficient than catalyst **2** in the nitromethane addition to *trans*-chalcone, whereas the latter is more efficient in the addition of thiophenol to 2-cyclohexen-1-one. Both **1** and **2** gave similar results in the Michael addition of methyl vinyl ketone to methyl 1-oxoindan-2-carboxylate. The same behaviour was observed with catalysts **5** and **6** supported on a polimeric matrix. It should also be pointed out that in Reactions A and B the yields obtained with catalyst **6** are equal or higher than those obtained with the corresponding soluble onium salts (**2**). To the best of our knowledge this is the first example of an onium salt supported on a polimeric matrix having a catalytic efficiency comparable to that of the corresponding soluble onium salt.[5,6]

Table 1. Michael additions at room temperature in the presence of chiral catalysts 1—6 in toluene as solvent

Catalyst	Yield/%		
	Reaction A[a]	Reaction B[b]	Reaction C[c]
(**3**)	0	40	45[d]
(**1**)	99	68	88[e]
(**5**)	75	93	85[d]
(**4**)	0	54	57[f]
(**2**)	35	87	86[d]
(**6**)	54	96	89[d]
(**15**)	50	80	99[g]

a) Nitromethane 75 mmol, *trans*-chalcone 5 mmol, catalyst 0.5 mmol, 3 d; KF 7.5 mmol in the case of "onium" catalysts. b) Thiophenol 5 mmol, 2-cyclohexen-1-one 6.25 mmol, catalyst 0.02 mmol, 4 h; KF 7.5 mmol in the case of "onium" catalysts. c) Methyl vinyl ketone 4 mmol, methyl 1-oxoindan-2-carboxylate 2 mmol, catalyst 0.025 mmol, KF 2.5 mmol in the case of "onium" catalysts. d) For 3 d. e) For 20 h. f) For 4 d. g) For 3 h.

The last relevant feature of the new phase-transfer catalysts **1** and **2** in comparison with the "classical" *N*-dodecyl-*N*-methyl-ephedrinium bromide (**15**),[1] is that they give higher conversions into the Michael adducts in Reactions A and B, but they are less active than **15** in the reaction of methyl vinyl ketone with methyl 1-oxoindan-2-carboxylate (Reaction C).[7] This suggests that among these catalysts there is selectivity, depending on the nature of the Michael donors and acceptors.

Finally the polymer supported catalysts **5** and **6**, as is normal for this type of reactions, are easily removed from the reaction mixture by a simple filtration and retain their catalytic efficiency after several reactions.[6] Although it was hoped that the optically active catalysts **1**—**6** might lead to asymmetric induction in the chiral Michael adducts, unfortunately all samples were obtained in a racemic form.[8] These results were particularly frustrating in the case of catalysts **2**, **6** in view of the known ability of the sulfinyl group to promote asymmetric induction.[3,9]

Experimental

General. Optical rotations were measured on a Perkin-Elmer 241 polarimeter. Infrared spectra were recorded on a Perkin-Elmer 377 spectrometer. ^1H and ^{13}C NMR spectra were recorded on a Varian HA 100 and/or a Varian A 390 instrument.

Materials. (L)-Methionine-*d*-*S*-oxide was prepared according to the literature; $[\alpha]_D^{20}$ +127° (*c* 1.15, 1 mol dm^{-3} HCl); lit,[4] $[\alpha]_D^{24}$ +131° (*c* 1.8, 1 mol dm^{-3} HCl). It has the (*S*,*S*) absolute configuration.[4] Methyl 1-oxoindan-2-carboxylate was obtained by literature methods.[10]

N,N-*Dimethyl-(*L*)-methionine.* (L)-(+)-Methionine (**10**) was methylated by reductive condensation with formaldehyde and hydrogen in the presence of palladized charcoal for 18 h

according to Bowman.[11] The product, obtained in 86% yield, had mp 186 °C, $[\alpha]_D^{20}$ +57.0° (*c* 1, H_2O) lit,[12] mp 187 °C, $[\alpha]_D^{20}$ +57.9° (H_2O).

N,N-*Dimethyl-(L)-methioninol.* Boron trifluoride etherate (12.2 mmol) was added dropwise under nitrogen at room temperature to a stirred suspension of sulfide **11** (10 mmol) and $NaBH_4$ (12.2 mmol) in anhydrous tetrahydrofuran (40 ml). The mixture was stirred for 15 h, then a second aliquot of boron trifluoride (12.2 mmol) and $NaBH_4$ (12.2 mmol) was added. The mixture was stirred for 48 h, then ethanol (10 ml) was added and the suspension was acidified to pH 1 with 3 mol dm^{-3} hydrochloric acid. The mixture was evaporated off *in vacuo*. Water (15 ml) was added to the residue.

The insoluble material was filtered off and NaOH was added to the solution up to pH 10. Extraction with diethyl ether and evaporation of the solvent afforded the title compound in 75% yield. It had n_D^{20} 1.4949, $[\alpha]_D^{20}$ +35.0° (*c* 1.1, CH_2Cl_2). Compound **3** had been previously obtained[13] by reduction of *N,N*-dimethyl methionine methyl ester with $LiAlH_4$.

Benzyldimethyl (3-Methylthio-1-hydroxymethylpropyl)ammonium Chloride. Compound **1** was obtained by reaction of **3** (2.75 mmol) with benzyl chloride (2.8 mmol) in ethanol (15 ml) at 50 °C for 24 h. After evaporation of the solvent under vacuum and treatment of the residue with pentane, compound **1** was obtained (67%), n_D^{21} 1.5605, $[\alpha]_D^{20}$ +26.9° (*c* 4.95, EtOH). Found: C, 58.00; H, 8.30; N, 4.83%. Calcd for $C_{14}H_{24}ClNOS$: C, 58.02; H, 8.35; N, 4.83%.

N,N-*Dimethyl-(L)-methionine*-d-S-*oxide.* Sulfoxide **12** was methylated as described above in the case of sulfide **10** with a 5 h reaction time. Compound **13** (81%) had mp 196—197 °C, $[\alpha]_D^{20}$ +141.0° (*c* 1.1, 1 mol dm^{-3} HCl). Found: C, 43.40; H, 7.78; N, 7.23%. Calcd for $C_7H_{15}NO_3S$: C, 43.50; H, 7.82; N, 7.25%.

N,N-*Dimethyl-(L)-methionine*-d-S-*oxide Methyl Ester.* Acid **13** (27 mmol) was dissolved in methanol (50 ml), cooled at 0 °C, and esterified with an ethereal solution of diazomethane. The usual work up afforded the crude ester which was purified by column cromatography (SiO_2, CH_2Cl_2/CH_3OH 9: 1). Compound **14** (80%) had mp 55—57 °C, $[\alpha]_D^{20}$ +20.9° (*c* 2.1, CH_2Cl_2). Found: C, 46.27; H, 8.25; N, 6.71%. Calcd for $C_8H_{17}NO_3S$: C, 46.35; H, 8.27; N, 6.76%.

N,N-*Dimethyl-(L)-methioninol*-d-S-*oxide.* Ester **14** (4 mmol) was added at 0 °C under nitrogen to a stirred suspension of $LiAlH_4$ (6 mmol) in anhydrous diethyl ether (40 ml). The mixture was stirred at room temperature for 6 h, monitoring the reaction by IR. Excess of hydride was destroyed and the mixture was evaporated off. The residue was extracted with dichloromethane and the organic layer evaporated off. The alcohol **4** (78%) had mp 58—61 °C, $[\alpha]_D^{20}$ +100.4° (*c* 1.04, CH_2Cl_2). Found: C, 46.70; H, 9.56; N, 7.75%. Calcd for $C_7H_{17}NO_2S$: C, 46.89; H, 9.56; N, 7.81%.

Benzyldimethyl (3-Methylsulfinyl-1-hydroxymethylpropyl)ammonium Chloride. Onium salt **2** was obtained by reaction of **4** with benzyl chloride with a 48 h reaction time as described above in the case of **1**. Compound **2**, a viscous oil, (66%) had $[\alpha]_D^{20}$ +51.1° (*c* 2.0, CH_3OH). Found: C, 55.02; H, 7.88; N, 4.60%. Calcd for $C_{14}H_{24}ClNO_2S$: C, 54.98; H, 7.91; N, 4.58%.

Poly(styrene-divynilbenzene) Onium Salts (5 and 6). Equimolecular amounts of commercial anion-exchange resin in the chloride form Biobeads S-X1 (Cl^-); exchange capacity 1.25 mequiv. Cl/g and sulfide **3** or sulfoxide **4** were heated at 60 °C under stirring in DMF as solvent (10 ml for 1 mmol of substrate) for 3 d.

The resin was filtered off, washed with absolute ethanol, water, 1 mol dm^{-3} HCl, water, absolute ethanol, and anhydrous diethyl ether. The exchange capacity of **5** and **6**, determined by Volhard's method, were 1.156 and 0.84 mequiv Cl/g, respectively.

Michael Additions. Michaels additions of nitromethane to *trans*-chalcone, of thiophenol to 2-cyclohexene-1-one, and of methylvinyl ketone to methyl 1-oxoindan-2-carboxylate in homogeneous and phase-tranfser conditions were carried on according to procedures described in the literature.[2a,14] Reactions with polymer supported catalysts **5** and **6** were performed as the corresponding reactions in the presence of soluble onium salt, except that at the end of the reaction the catalysts **5** and **6** were removed by simple filtration. Adducts **7—9** had physical and spectroscopic properties identical to those of reference samples prepared according to known procedures.[2a,14] Compounds **7**, **8**, and **9**, obtained by using **15** as catalyst had $[\alpha]_{578}^{21}$ −9.8° (*c* 2, CH_2Cl_2),[2a] $[\alpha]_{578}^{25}$ −2.0° (*c* 2, C_6H_6),[2a] and $[\alpha]_{578}^{25}$ −2.56° (*c* 2, C_6H_6); 3.3% e.e.[14]

References

1) a) S. Colonna and R. Fornasier, *J. Chem. Soc., Perkin Trans. 1*, **1978**, 317, and references therein; b) S. Julia, A. Ginebreda, and J. Guixer, *J. Chem. Soc., Chem. Commun.*, **1978**, 742; c) H. Wynberg and B. Greijdanus, *ibid.*, **1978**, 427.

2) a) S. Colonna, A. Re, and H. Wynberg, *J. Chem. Soc., Perkin Trans. 1*, **1981**, 547, and references therein; b) S. Julia, A. Ginebreda, J. Guixer, J. Masana, A. Tomas, and S. Colonna, *ibid.*, **1981**, 574.

3) F. Montanari, "Organic Sulphur Chemistry," ed by C. J. M. Stirling, Butterworths, London and Boston (1975).

4) B. W. Christensen and A. Kjaer, *J. Chem. Soc., Chem. Commun.*, **1965**, 225.

5) S. Colonna, R. Fornasier, and U. Pfeiffer, *J. Chem. Soc., Perkin Trans. 1*, **1978**, 8.

6) H. Molinari, F. Montanari, S. Quici, and P. Tundo, *J. Am. Chem. Soc.*, **101**, 3920 (1979).

7) The adducts obtained by using **15** as catalyst are optically active (see Experimental).

8) In ancillary experiments it was shown that also a diastereomeric mixture of sulfoxides **2** gave racemic Michael adducts.

9) Recently the absence of stereoselectivity in the micellar hydrolysis of *p*-nitrophenyl esters in the presence of optically active oxosulfonium salts has been reported: S. Jugé and G. Meyer, *Tetrahedron*, **36**, 959 (1980).

10) H. O. House and C. B. Hudson, *J. Org. Chem.*, **35**, 647 (1970).

11) R. E. Bowman and H. H. Stroud, *J. Chem. Soc.*, **1950**, 1342.

12) T. Suyama and S. Kanao, *J. Pharm. Soc. Jpn.*, **85**, 284 (1965).

13) A. Wacker, R. Selzer, D. Pfahl, and R. Schmitt, *Z. Naturforsch., Teil B*, **19**, 1083 (1964).

14) H. Wynberg and R. Helder, *Tetrahedron Lett.*, **1975**, 4057.

Synthesis of Oxazolidines, Thiazolidines, and 5,6,7,8-Tetrahydro-1*H*,3*H*-pyrrolo[1,2-*c*]oxazole (or thiazole)-1,3-diones from β-Hydroxy- or β-Mercapto-α-amino Acid Esters†

Mahmoud Zarif Amin BADR,* Morsy Mohamed ALY, Atiat Mohamed FAHMY, and Mansour Esmael Younis MANSOUR

Chemistry Department, Faculty of Science, Assiut University, Assiut, Egypt

(Received January 10, 1980)

2-Aryl-4-(ethoxycarbonyl)oxazolidines and thiazolidines (**1**) were prepared from the corresponding α-amino acid ethyl esters containing either hydroxyl or mercapto groups in the β-position by fusion with some aromatic aldehydes. Dehydrogenation of **1** with *N*-bromosuccinimide gave the corresponding oxazoles and thiazoles. The oxazolidines and thiazolidines gave Mannich bases on interaction with *p*-nitrobenzaldehyde and piperidine. Acetylation of **1** gave the corresponding *N*-acetylderivatives, which on fusion in the presence of anhydrous $ZnCl_2$ undergo cyclization, giving the corresponding bicyclic compounds, 5,6,7,8-tetrahydro-1*H*,3*H*-pyrrolo[1,2-*c*]-oxazole (or thiazole)-1,3-diones.

Fusion of the β-hydroxy and/or β-mercapto-α-amino acid ethyl esters (L-serine, 3-phenyl-DL-serine, L-threonine, or L-cysteine) with aromatic aldehydes such as benzaldehyde, *p*-anisaldehyde, *p*-chlorobenzaldehyde, and/or *p*-nitrobenzaldehyde gave the corresponding oxazolidines or thiazolidines **1** rather than azomethine derivatives (**2**).

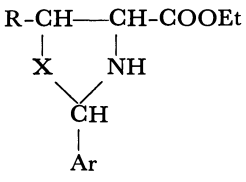

1

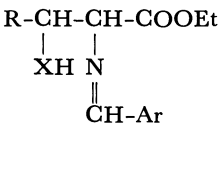

2

X=O or S;
R=H, CH_3 or C_6H_5;
Ar=C_6H_5, *p*-$CH_3OC_6H_4$, *p*-ClC_6H_4, *p*-$NO_2C_6H_4$, or *p*-BrC_6H_4.

Structure **1** is apparent by elemental analysis data, UV, and IR spectral data, the latter two reasonably agreeing with those of the comparable compounds.[1,2] The alternative structure **2** for the products is excluded by the absence of the NMR signal near δ 7.5 ascribable to azomethine.

The oxazolidines and/or thiazolidines (**1**) on treatment with acetyl bromide in glacial acetic acid afforded *N*-acetyl derivative (**3**) whose IR spectra showed an absorption band at 1570 cm^{-1} due to the amide group (>$NCOCH_3$) but no NH stretching vibration band. On treatment with piperidine and *p*-nitrobenzaldehyde (**1**) gave the corresponding Mannich base (**4**).

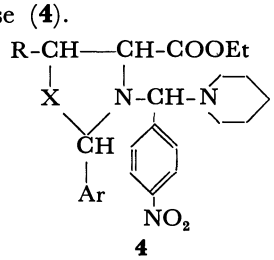

4

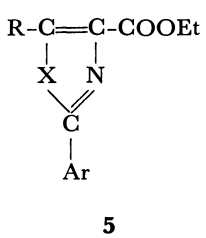

5

The oxazolidines and thiazolidines (**1**) were converted into the corresponding oxazoles and thiazoles (**5**) on dehydrogenation using *N*-bromosuccinimide in boiling carbon tetrachloride. The IR spectra of the oxazoles and thiazoles (**5**) showed no NH band but an apparent shift in the ester group was observed at 1735—1750 cm^{-1} due to conjugation with the double bond at C_4–C_5.[3] The C=N absorption band at 1590—1550 cm^{-1} is affected by substituents on aryl moiety at C_2; *p*-nitro group causes a decrease in wave number down to 30 cm^{-1}, whereas *p*-methoxyl group causes an increase up to *ca.* 10 cm^{-1}. In addition, characteristic absorptions of oxazole ring[4] were observed in the range 1190—1250 cm^{-1}.

N-Acetyloxazolidines and/or thiazolidines (**3**) undergo cyclization by fusion with anhydrous zinc chloride affording 5,6,7,8-tetrahydro-1*H*,3*H*-pyrrolo[1,2-*c*]oxazole (or thiazole)-1,3-dione (**6**) whose IR spectra showed no absorption of ($COCH_3$) group, but a broad band at 3300 cm^{-1} due to associated OH group, confirming the assumption that the bicyclic structure **6** exists in the enolic form rather than its diketonic tautomer (**7**). The cyclization reaction seems to proceed according to the following mechanism.

Experimental

All melting points are uncorrected. IR spectroscopic analysis was carried out on a Pye-Unicam IR spectrophotometer, Model SP 200 G, UV absorptions were measured on a Pye-Unicam UV spectrophotometer, Model SP 8000, using 95% ethanol as a solvent. NMR spectra were taken with a Varian T-60 instrument in deuterochloroform with tetramethylsilane as an internal standard.

Amino Acids Ethyl Esters. Prepared in more than 80% yield by the general method described by Fischer[5] and used without further purification in the preparation of the oxazolidines and/or thiazolidines.

Preparation of Oxazolidine and/or Thiazolidine Derivatives (1). The amino acid ethyl ester (0.01 mol) was heated with the appropriate aldehyde (0.011 mol) in an oil bath at 80—90 °C for 2 h. Extraction with ethyl acetate gave the corresponding 2-aryl-4-(ethoxycarbonyl)oxazolidines and/or thiazolidines (**1**) which was purified by column chromatography using 1×50 cm column of Davison 950 silica-gel, slurry packed with hexane and eluted with benzene–hexane (3:1 v/v). The results are given in Table 1.

Acetylation of Oxazolidines and Thiazolidines (3). Acetyl bromide (0.01 mol) was added to the oxazolidine or thia-

† Presented in part at the 7th International Congress of Heterocyclic Chemistry, University of South Florida, Tampa, Florida, U.S.A., August 1979.

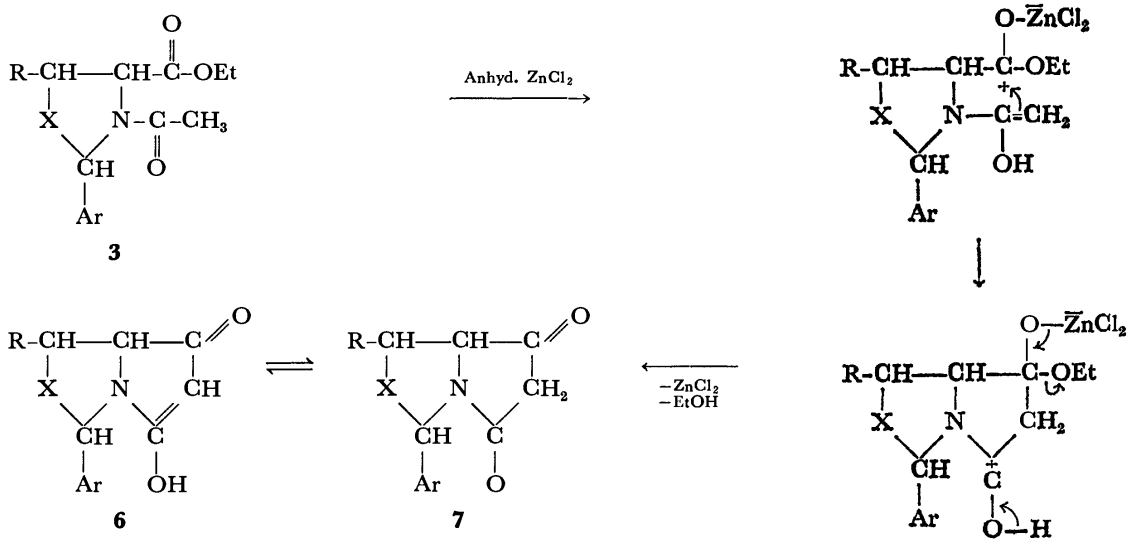

TABLE 1. 2-ARYL-4-(ETHOXYCARBONYL)OXAZOLIDINES OR THIAZOLIDINES

Compound No.	X	R	Ar	Yield %	n_D^{27}	ν(NH) cm^{-1}	ν(COOEt) cm^{-1}	Molecular formula	Analysis (Calcd/Found) % C	H	N
1a	O	H	C_6H_5	85.9	1.5522	3370	1720	$C_{12}H_{15}O_3N$	65.14	6.83	6.33
									65.08	6.80	6.35
1b	O	H	p-$CH_3OC_6H_4$	87	1.5522	3350	1730	$C_{13}H_{17}O_4N$	62.15	6.82	5.57
									62.12	6.78	5.58
1c	O	H	p-ClC_6H_4	86.2	1.5440	3360	1700	$C_{12}H_{14}O_3NCl$	56.36	5.48	5.48
									56.32	5.49	5.51
1d	O	H	p-$NO_2C_6H_4$	88.7	1.5605	3380	1730	$C_{12}H_{14}O_5N_2$	54.13	5.30	10.52
									54.08	5.28	10.56
1e	O	CH_3	C_6H_5	85	1.5210	3370	1740	$C_{13}H_{17}O_3N$	66.36	7.28	5.95
									66.36	7.26	5.95
1f	O	CH_3	p-$CH_3OC_6H_4$	86.7	1.5592	3300	1730	$C_{14}H_{19}O_4N$	63.38	7.22	5.28
									63.50	6.98	5.30
1g	O	CH_3	p-ClC_6H_4	89.27	1.5500	3320	1700	$C_{13}H_{16}O_3NCl$	57.88	5.94	5.19
									57.86	5.96	5.21
1h	O	CH_3	p-$NO_2C_6H_4$	94	1.5435	3300	1730	$C_{13}H_{16}O_5N_2$	55.71	5.75	10.00
									55.70	5.73	10.02
1i	O	C_6H_5	p-ClC_6H_4	98.1	1.5530	3320	1730	$C_{18}H_{19}O_3NCl$	64.96	5.71	4.21
									65.02	5.42	4.22
1j	S	H	C_6H_5	80.1	1.5532	3400	1740	$C_{12}H_{15}O_2NS$	60.76	6.37	5.90
									60.74	6.34	5.90
1k	S	H	p-$CH_3OC_6H_4$	82.3	1.5718	3400	1730	$C_{13}H_{17}O_3NS$	58.42	6.41	5.24
									58.40	6.38	5.26
1l	S	H	p-ClC_6H_4	81.5	1.5855	3420	1730	$C_{12}H_{14}O_2NClS$	53.04	5.16	5.16
									53.01	5.18	5.16
1m	S	H	p-BrC_6H_4	83.3	1.5528	3400	1730	$C_{12}H_{14}O_2NBrS$	45.57	4.43	4.43
									45.55	4.46	4.45
1n	S	H	p-$NO_2C_6H_4$	82.6	1.5608	3410	1735	$C_{12}H_{14}O_4N_2S$	51.06	5.00	9.93
									51.08	4.98	9.94

zolidine derivative (**1**) (0.01 mol) in glacial acetic acid (30 ml) and the solution was refluxed for 3 h. The reaction product was poured in cold dilute sodium hydrogencarbonate solution; the solid deposited were collected, washed with water and crystallized from ethanol to give the corresponding *N*-acetyl oxazolidines or thiazolidines (**3**). The results are given in Table 2.

Cyclization of N-*Acetyloxazolidines and Thiazolidines: Formation of 5,6,7,8-Tetrahydro-1*H,*3*H-*pyrrolo[1,2-c]oxazole-1,3-diones and Their Thiazole Analoges (7).* *N*-Acetyloxazolidine or thiazolidine (**3**) (0.01 mol) was fused with anhydrous zinc chloride (0.0125 mol) in an oil bath at 180 °C for 20 min.

Table 2. *N*-Acetyloxazolidines and thiazolidines

Compound No.	X	R	Ar	Yield %	Mp °C	ν(NCOCH$_3$) cm^{-1}	ν(COOEt) cm^{-1}	Molecular formula	N% Calcd	N% Found
3a	O	H	C_6H_5	72.2	170—172	1670	1747	$C_{14}H_{17}O_4N$	5.32	5.30
3b	O	H	*p*-$CH_3OC_6H_4$	75	167—169	1670	1750	$C_{15}H_{19}O_5N$	4.78	4.73
3c	O	H	*p*-ClC_6H_4	74.4	168—169	1670	1745	$C_{14}H_{16}O_4NCl$	4.71	4.53
3d	O	H	*p*-$NO_2C_6H_4$	75.6	165	1660	1750	$C_{14}H_{16}O_6N_2$	9.09	8.88
3e	S	H	*p*-ClC_6H_4	67.3	195	1650	1720	$C_{14}H_{16}O_3NClS$	4.47	4.50
3f	S	H	*p*-BrC_6H_4	64.2	120—122	1600	1750	$C_{14}H_{16}O_3NBrS$	3.91	3.87
3g	S	H	*p*-$NO_2C_6H_4$	67.9	205	1670	1740	$C_{14}H_{16}O_5N_2S$	8.64	8.62

Table 3. 5,6,7,8-Tetrahydro-1*H*,3*H*-pyrrolo[1,2-*c*]oxazole or thiazole-1,3-diones

Compound No.	X	R	Ar	Yield %	Mp °C	ν(C=O) cm^{-1}	ν(C=C) cm^{-1}	ν(OH) cm^{-1}	Molecular formula	Analysis (Calcd/Found) % C	H	N
7a	O	H	C_6H_5	78.3	320	1680	3010	3300	$C_{12}H_{11}O_3N$	66.35	5.10	6.45
										66.34	5.08	6.45
7b	O	H	*p*-$CH_3OC_6H_4$	80.3	245	1700	3020	3300	$C_{13}H_{13}O_4N$	63.15	5.30	5.67
										63.12	5.28	5.68
7c	O	CH_3	*p*-$CH_3OC_6H_4$	76	242	1700	3020	3300	$C_{14}H_{15}O_4N$	64.36	5.79	5.36
										64.34	5.76	5.35
7d	S	H	*p*-ClC_6H_4	78.2	220	1700	3020	3320	$C_{12}H_{10}O_2NClS$	53.83	3.79	5.23
										53.80	3.81	5.24

Table 4. Oxazole or thiazole derivatives

Compound No.	X	R	Ar	Yield %	Mp °C	ν(C=C) cm^{-1}	ν(C=N) cm^{-1}	Molecular formula	Analysis (Calcd/Found) % C	H	N
5a	O	H	C_6H_6	70.7	75	3030	1580	$C_{12}H_{11}O_3N$	66.35	5.10	6.45
									66.33	5.08	6.46
5b	O	H	*p*-$CH_3OC_6H_4$	73.5	105	3050	1590	$C_{13}H_{13}O_4N$	63.15	5.30	5.67
									63.14	5.28	5.67
5c	O	H	*p*-ClC_6H_4	74.7	98	3050	1590	$C_{12}H_{10}O_3NCl$	57.25	3.97	5.56
									57.22	3.98	5.55
5d	O	H	*p*-$NO_2C_6H_4$	76.4	125	3050	1550	$C_{12}H_{10}O_5N_2$	54.96	3.84	10.68
									54.92	3.84	10.66
5e	S	H	C_6H_5	72.9	116	3050	1580	$C_{12}H_{11}O_2NS$	61.80	4.75	6.01
									61.76	4.75	6.00
5f	S	H	*p*-$CH_3OC_6H_4$	72.2	95	3050	1595	$C_{13}H_{13}O_3NS$	59.31	4.94	5.32
									59.25	4.97	5.34
5g	S	H	*p*-$NO_2C_6H_4$	75.5	98—99	3040	1550	$C_{12}H_{10}O_4N_2S$	51.80	3.62	10.07
									51.74	3.61	10.06

Table 5. Mannich bases containing oxazolidine or thiazolidine moiety

Compound No.	X	R	Ar	Yield %	Mp °C	ν(NO$_2$) cm^{-1}	ν(COOEt) cm^{-1}	Molecular formula	N% Calcd	N% Found
4a	O	CH_3	*p*-$CH_3OC_6H_4$	72	142	1350, 1560	1750	$C_{26}H_{33}O_6H_3$	0.69	8.68
4b	O	H	*p*-ClC_6H_4	67	128	1370, 1570	1700	$C_{24}H_{28}O_5N_3Cl$	8.87	8.87
4c	S	H	C_6H_5	55.5	135	1300, 1500	1700	$C_{24}H_{29}O_4N_3S$	9.23	9.26

The mixture was treated with cold dilute hydrochloric acid, the solid formed being collected by filtration. Crystallization of the solid from dilute acetic acid gave 5,6,7,8-tetrahydro-1*H*,3*H*-pyrrolo[1,2-*c*]oxazole-1,3-diones or their thiazole analoges (**7**). The results are given in Table 3.

Dehydrogenation of Oxazolidine and Thiazolidine Derivatives by N-*Bromosuccinimide: Formation of Oxazole and Thiazole Derivatives (**5**).* *N*-Bromosuccinimide (0.02 mol) and benzoyl peroxide were added to the oxazolidine or thiazolidine derivative (0.01 mol) dissolved in carbon tetrachloride (100 ml) and the solution was refluxed for 6 h. The reaction product was filtered off in order to separate the succinimide and the filtrate was concentrated. The oxazole or thiazole derivatives (**5**) obtained were crystallized from petroleum ether (40—60 °C). The results are given in Table 4.

*Preparation of Mannich Bases (**4**).* A mixture of 2-aryl-4(ethoxycarbonyl)oxazolidine or thiazolidine (0.01 mol) *p*-nitrobenzaldehyde (0.01 mol) and piperidine (0.02 mol) in ethanol (50 ml) was refluxed for 6 h. The reaction product was poured onto ice, washed with petroleum ether (40—60 °C) several times and extracted with ether. The Mannich bases (**4**) were crystallized from dilute acetic acid. The results are given in Table 5.

References

1) Z. Badr, R. Bonnett, T. R. Emerson, and W. Klyne, *J. Chem. Soc.*, **1965**, 4503; Z. Badr, R. Bonnett, W. Klyne, R. L. Swan, and J. Wood, *ibid.*, **1965**, 2047.

2) E. D. Bergmann, *Chem. Rev.*, **53**, 309 (1953); F. Bergel and M. A. Peutherer, *J. Chem. Soc.*, **1964**, 3963.

3) J. R., Dyer, "Application of Absorption Spect," Prentice Hall Inter. Inc., London (1965), p. 43.

4) V. V. Somayajulu and N. V. Subba, *Curr. Sci. (India)*, **25**, 86 (1957).

5) E. Fischer, *Ber.*, **34**, 433 (1901).

Dielectric Relaxation Processes in Some Substituted Amides in Dilute Solutions

S. K. Saxena,† J. P. Shukla, and M. C. Saxena*
Physics Department Lucknow University, Lucknow, 226007, India
(Received May 16, 1980)

The dielectric measurements have been carried out in the microwave region (3.1 cm) over a range of temperatures on propionamide, *N*-methylpropionamide, *N*,*N*-dimethylpropionamide, and *N*-ethylacetamide. All the molecules except propionamide exhibit high value of distribution parameter. The dielectric dispersion, when resolved by Higasi, Koga, and Nakamura method gives two relaxation times $\tau(1)$ and $\tau(2)$ widely different from each other, suggesting the two separate processes occurring in the system. The enthalpies for different processes involved have been evaluated by the Eyring equations. The comparison with NMR data of enthalpy to $\Delta H_{\tau(1)}$, which is related to the process other than molecular, suggests that the rotation of $-NR_2$ group around the carbonyl carbon nitrogen bond is not feasible. The observed result indicates that this may be due to group inversion process. These results are in agreement with the earlier investigations of Saxena *et al.* on some substituted amides and of Phillips on *N*,*N*-dimethylamide using proton resonance spectra. The substituted amides in dilute solution of benzene exhibit some association with the benzene molecules.

Leader and Gromley[1] reported a remarkable variation in the dielectric constant in the amides and substituted amides. The high values of dielectric constant of monosubstituted amides were suggested to be due to their association as a chain polymerisation. Since his initial work, a series of investigations have been carried out by several workers.[2-10] Jordon *et al.*[11] recently confirmed Debye behaviour for formamide, Itoh *et al.*[12] for *N*-methylacetamide and Srivastava *et al.*[13] for dimethylformamide. Brown and Price[14] have ruled out the molecular flexibility in dimethylacetamide. Karamyan and Shakhparonov[15] confirmed a long frequency dispersion region for *N*-substituted amides with much smaller amplitude at mm wavelength. In order to study the possibility of molecular flexibility and to ascertain the thermodynamics of dipolar relaxation Misra *et al.*[16] recently made a study of *N*-methylformamide, *N*-methylacetamide, dimethylformamide, and dimethylacetamide in the dilute solution of benzene over a range of temperatures. The enthalpies of different relaxation processes observed suggest the possibility of molecular and group inversion processes in the above molecules. Due to interesting results observed in the case of *N*-substituted amides, a further study in this direction has been undertaken. The molecules chosen are propionamide, *N*-methylpropionamide, dimethylpropionamide, and *N*-ethylacetamide so that the effect of propionyl (CH_3CH_2-CO) group in different substituted amides could be studied. The possibility of molecular association as pointed out by other workers[8,10] has also been examined.

Experimental

The chemicals were of purest quality available and the physical properties were checked against literature values. The solvent used in the measurements was benzene (A. R. Grade) obtained from B. D. H., England and was distilled twice before use. The dielectric constant ε' and dielectric loss ε'' at X- band have been measured by the technique given by Dakin and Works.[17] The static dielectric constant ε_0 was measured by dipolmeter and dielectric constant at infinite frequencies ε_∞ was determined from the measured refractive indices of the system ($\varepsilon_\infty = n_D^2$). The slopes a_0, a', a'', and a_∞, the most probable relaxation time τ_{OH} and the distribution parameter 'α' have been evaluated using Higasi method.[18] The details of determining these parameters and the dipolemoments have been reported in our earlier paper.[19] The dielectric absorbtion has been further resolved by using Higasi *et al.* method[20] in terms of two seperate relaxation processes $\tau(1)$ and $\tau(2)$ where $\tau(2)$ stands for the molecular relaxation process and $\tau(1)$ is associated with the group process being an implicit function of τ_1, τ_2, and the weight factor C_2. The parameter $\tau(0)$ stands for the average relaxation time given by $[\tau(0) = \sqrt{\tau(1), \tau(2)}]$ and τ_0 is the average relaxation time (Cole-Cole method) as reported in the literature.[14] Eyring equations[21] have been utilised to evaluate the thermodynamical parameters. The enthalpies associated with different modes of relaxation have been evaluated by plotting the relaxation times against $1/T$. The dipolemoments calculated using Higasi method[18] have been compared with the literature values (Table 2).

Discussion

The distribution parameter 'α' has been found to be low in the case of propionamide but its value is sufficiently high in the case of other three *N*- substituted amides indicating the flexibility of all the three molecules under microwave field. The dielectric dispersion is further resolved by Higasi *et al.* method[20] in terms of molecular relaxation time $\tau(2)$ and the relaxation time associated with group relaxation time $\tau(1)$. The $\tau(1)$ (=23.7 ps) and $\tau(2)$ (=30.5 ps) are not widely different from one another in the case of propionamide. Thus a single Debye dispersion seems to occur for the above molecule. Further $\tau(2)$ and τ_{OH} calculated by Higasi method[18] are close to each other for propionamide, suggesting that the molecular process and the overlapped process are similar to one another in this molecule. The observed single Debye dispersion for this molecule is in agreement with the earlier results of Jordon *et al.*[11] on formamide.

The most probable relaxation time τ_{OH} at 297 K for *N*-methylpropionamide (=22.8 ps) and *N*-ethylacetamide (=26.2 ps) can be compared with our

† On leave from Department of Physics, D.B.S. College, Kanpur, India.

Table 1. Values of a_0, a', a'', a_∞ for the samples in benzene at different temperature using Higasi method[18]

Compound	T/K	a_0	a'	a''	a_∞
Propionamide	313	18.10	4.00	6.10	0.363
	321	21.00	6.15	8.00	0.606
	329	15.40	5.71	6.70	−0.289
N-Methylpropionamide	289	23.50	8.00	8.00	−1.18
	297	21.05	8.20	7.50	−0.53
	305	19.04	9.60	7.30	−0.33
	313	15.70	8.90	6.90	−0.31
N,*N*-Dimethylpropionamide	289	22.2	8.30	8.7	−1.00
	297	19.0	8.00	8.3	−0.68
	305	18.0	10.00	7.4	−0.18
	313	15.4	10.30	7.0	−0.25
N-Ethylacetamide	297	36.4	13.00	13.5	−0.72
	305	33.0	12.30	12.9	−0.71
	313	26.6	13.50	10.5	−0.43
	321	24.6	15.00	10.00	−0.25

Table 2. Relaxation times and dipolemoment using Higashi method[18] and corresponding activation parameters

Compound	T/K	α	τ_{OH}	μ / Debye	ΔF_ε / kJ mol^{-1}	ΔH_ε / kJ mol^{-1}	ΔS_ε / J mol^{-1} deg^{-1}	μ_{ilt} / Debye
Propionamide	313	0.08	37.8	3.56	(13.6—14.2)	22.5	(25.2—27.0)	3.47
	321	0.07	30.0					
	329	0.00	21.4					
N-Methylpropionamide	289	0.24	26.4	3.72	(10.6—12.2)	18.2	(20.0—24.3)	3.59
	297	0.22	22.8					
	305	0.18	15.8					
	313	0.09	13.6					
N,*N*-Dimethylpropionamide	289	0.17	21.8	4.0	(11.2—11.7)	14.2	(8.1— 9.6)	—
	297	0.14	19.2					
	305	0.12	14.2					
	313	0.02	11.5					
N-Ethylacetamide	297	0.19	26.2	5.0	(11.7—12.7)	19.1	(21.3—23.1)	—
	305	0.15	23.1					
	313	0.16	15.6					
	321	0.10	12.0					

Table 3. Relaxation times $\tau(1)$, $\tau(2)$, and $\tau(0)$ and enthalpy of activation $\Delta H_{\tau(1)}$, $\Delta H_{\tau(2)}$, and $\Delta H_{\tau(0)}$ using Higasi, Koga, and Nakamura method[20]

Compound	T/K	$\tau(1)$ / ps	$\tau(2)$ / ps	$\tau(0)$ / ps	$\Delta H_{\tau(1)}$ / kJ mol^{-1}	$\Delta H_{\tau(2)}$ / kJ mol^{-1}	$\Delta H_{\tau(0)}$ / kJ mol^{-1}
Propionamide	313	27.6	38.0	32.4	16.6	22.5	21.3
	321	23.7	30.5	26.9			
	329	18.4	23.7	20.9			
N-Methylpropionamide	289	14.3	31.8	21.3	—	21.3	13.7
	297	14.1	27.7	19.8			
	305	12.0	21.3	16.0			
	313	12.3	16.2	14.1			
N,*N*-Dimethylpropionamide	289	15.4	26.3	20.1	8.1	15.9	12.8
	297	15.7	21.8	18.5			
	305	12.7	17.8	15.0			
	313	11.4	12.0	11.7			
N-Ethylacetamide	297	16.2	29.6	21.9	10.9	21.3	15.3
	305	16.3	26.4	20.7			
	313	12.4	20.5	15.9			
	321	10.8	15.8	13.1			

previous results[16] on *N*-methylformamide (=17.8 ps) and *N*-methylacetamide (=18.0 ps). The observed results are supported by the earlier observations of Dannhauser and Johari[9] establishing that the relaxation times show specific dependence on the shape and size of alkyl group attached to the carbonyl or amino group. The τ_{OH} for dimethylpropionamide (=21.8 ps) can be compared with our earlier work[16] on dimethylformamide (=18.1 ps) and dimethylacetamide (=25.6 ps). The value is comparatively high as regards to τ_0 (6.0—8.4 ps) reported for dimethylacetamide by Brown and Price[14] in benzene at 293 K. The longer value of relaxation time seems to result from the association of disubstituted amide. The association in amides has been observed by many earlier workers.[8,10] Further, $\tau(1)$ and $\tau(2)$ are widely different for all the three *N*-substituted amides showing the non rigid behaviour of these molecules in the microwave region.

The enthalpies corresponding to $\tau(1)$, $\tau(2)$, $\tau(0)$, and τ_{OH} processes have been evaluated. $\Delta H_{\tau(1)}$ and $\Delta H_{\tau(2)}$ are widely different from each other except in case of propionamide, showing again the flexible nature of the molecules in the microwave field. $\Delta H_{\tau_{OH}}$ for *N*-ethylacetamide (=19.1 kJ mol^{-1}), *N*-methylpropionamide (=18.2 kJ mol^{-1}) are comparable with those *N*-methyl acetamide (=14.9 kJ mol^{-1}) and *N*-methyl formamide (=14.2 kJ mol^{-1}) observed in our earlier study.[16] Further $\Delta H_{\tau_{OH}}$ for dimethylpropionamide (=14.2 kJ mol^{-1}) can be compared with the values for dimethylformamide (=13.7 kJ mol^{-1}) and dimethylacetamide (=12.8 kJ mol^{-1}) reported in our previous work.[16] The enthalpies for $\Delta H_{\tau_{OH}}$ and $\Delta H_{\tau(2)}$ are almost equal, showing the probability of the molecular process being predominant. The enthalpy $\Delta H_{\tau(1)}$ for *N*-methylpropionamide could not be evaluated due to irregular variation of $\tau(1)$. However, the observed value of $\Delta H_{\tau(1)}$ for *N*-ethylacetamide and for dimethylpropionamide which represent a process other than molecular has been found to be small when compared with the enthalpy of activation for internal rotation of $-NR_2$ group (>40 kJ mol^{-1}), reported using NMR data.[22,23] Therefore, this value can not be assigned to the internal rotation of –NXR (where R=CH_3, C_2H_5, and X=H, CH_3). This, however, could be assigned to the group inversion process of R and X substituents from their respective position within the –NXR group. This is in agreement with our earlier investigations on *N*-substituted amide[16] and with the studies of Phillips[24] using proton resonance spectra of *N,N*-dimethylamides.

The dipolemoments of all the four molecules have been evaluated by Higasi method[18] and they agree well with the literature values[25-27] wherever available. The slightly higher value of dipolemoments may be due to the association and the interaction of benzene with, *N*-subsituted amide. The observed association is in agreement with the earlier studies of many workers[8,10] and such interactions in the dilute solution of benzene have been prodicted by Ellision and Mayer.[28]

The free energy of activation has been found to be almost of the same order in all the molecules and the entropy values of them have been found to be positive. These have been reported in Table 2.

Conclusion

All the amides studied including propionamide follow Debye behaviour. The propionamide has been found to behave as a rigid molecule. This is in agreement with the earlier work of Jordon *et al.*[11] on formamide.

It is observed that *N*-substituted amides give rise to a high value of the distribution parameter, indicating that the three systems exhibit flexible behaviour which is supported by two discrete relaxation times $\tau(1)$ and $\tau(2)$. There appears to be a possibility of group inversion in amides, which is in agreement with our previous work[16] and also with the studies of Phillips,[24] using proton resonance spectra of *N,N*-dimethylamide.

Also a close study of the molecular process shows that in *N*-substituted amides the relaxation time varies according to the shape and size of the alkyl group attached to the carbonyl or the amino group. This agrees well with the studies made by Dannhauser and Johari.[9] In almost all the cases investigated, the relaxation times associated with the molecular process and with the overlapped process have been found to be longer than the values expected for such species. The dipolemoments have been calculated and found to be slightly higher than the literature values. This indicates the possibility of association of the amide molecules with the solvent benzene. The higher value of dipolemoment in dilute solution of benzene has been reported in an earlier study by Worsham and Hobbs[8] in *N*-substituted amide.

One of us (SKS) is grateful to University Grant Commission, New Delhi, India for the award of fellowship and financial assistance.

References

1) G. R. Leader and J. F. Gromley, *J. Am. Chem. Soc.*, **73**, 5731 (1951).
2) J. W. Vaughan and P. G. Sears, *J. Phys. Chem.*, **62**, 183 (1958).
3) A. E. Lutskie and S. A. Mikhailenko, *Zh. Straukt. Khim.*, **4**, 350 (1960).
4) L. R. Dawson, J. W. Vaughan, M. E. Pruitt, and H. C. Eckstrom, *J. Phys. Chem.*, **66**, 2684 (1962); **67**, 278, 281 (1963).
5) R. Y. Lin and W. Dannhauser, *J. Phys. Chem.*, **67**, 1805 (1963).
6) G. P. Johari and P. N. Tewari, *J. Phys. Chem.*, **69**, 3167 (1967); **70**, 197 (1966).
7) O. P. Donner, G. F. Gordon, and K. W. Bunzel, *J. Phys. Chem.*, **68**, 2450 (1964).
8) J. E. Worsham and M. E. Hobbs, *J. Am. Chem. Soc.*, **76**, 206 (1954).
9) W. Dannhauser and G. P. Johari, *Can. J. Chem.*, **46**, 3143 (1968).
10) S. J. Bass, W. I. Nathan, R. M. Meighan, and R. H. Cole, *J. Phys. Chem.*, **68**, 509 (1964).
11) B. P. Jordon, R. J. Sheppard, and S. Szwarnowski, *J. Phys. D*, **11**, 695 (1978).

12) K. Itoh, H. Sato, H. Takshashi, and K. Higasi, *Bull. Chem. Soc. Jpn.*, **49**, 329 (1976).
13) G. P. Srivastava, P. C. Mathur, and K. N. Tripathi, *Ind. J. Pure Appl. Phys.*, **6**, 113, 561 (1968).
14) V. L. Brownsell and A. H. Price, *J. Phys. Chem.*, **74** 4004 (1970).
15) G. G. Karamyan, M. I. Shakhparonov deposited Doc. VINITI, 1098—76, 15 (1976) Russ, Avail VINITI.
16) C. K. Misra, J. P. Shukla, and M. C. Saxena, *Adv. Mol. Relax. Procs*, **15**, 181—192 (1979).
17) T. W. Dakin and C. N. Works, *J. Abb. Phys.*, **18**, 789 (1947).
18) K. Higasi, *Bull. Chem. Soc. Jpn.*, **39**, 2157 (1966).
19) S. K. Saxena, J. P. Shukla, and M. C. Saxena, *Bull. Chem. Soc. Jpn.*, **53**, 1732 (1980).
20) K. Higasi, Y. Koga, and M. Nakamura, *Bull. Chem. Soc. Jpn.*, **44**, 988 (1971).
21) S. Glasstone, K. J. Leider, and H. Eyring "The Theory of Rate Process," McGraw-Hill Book Co., New York (1941), p. 548.
22) L. W. Reeves, R. C. Sheddick, and K. N. Shaw, *Can. J. Chem.*, **49**, 3683 (1971).
23) A. G. Whittaker and S. Siegel, *J. Chem. Phys.*, 42, 3320 (1965).
24) W. D. Phillips, *J. Chem. Phys.*, **23**, 1363 (1955).
25) M. E. Hobbs and W. B. Bates, *J. Am. Chem. Soc.*, **74**, 746 (1952).
26) R. M. Meighan and R. H. Cole, *J. Phys. Chem.*, **68**, 503 (1964).
27) M. J. Aroney, R. J. W. Le Fevere, and A. N. Singh, *J. Chem. Soc.*, **1965**, 3179.
28) H. R. Ellision and B. W. Meyer, *J. Phys. Chem.*, **74**, 3861 (1970).

Kinetics and Mechanism of Hydrolysis of Ruheman's Purple in the Absence and Presence of Micelles in Aqueous Medium

Sudhir MALAVIYA and Sarvagya S. KATIYAR*

Department of Chemistry, Indian Institute of Technology, Kanpur-208016, India

(Received May 17, 1980)

The mechanism of acid hydrolysis of Ruheman's purple has been investigated and the effect of micelles on the rate has been examined. First order rate constant for the hydrolysis reaction decreases linearly with decreasing hydrogen ion concentration up to pH 3 and levels off thereafter with no reaction occurring above pH 7. Increasing ionic strength decreases the rate in accordance with the Bronsted-Christiansen equation. The salt effect in the dipole-dipole reaction is probably a reflection of the fast equilibrium steps involving ions preceding the rate-determining step. Solvents like ethylene glycol and dioxane have no effect, indicating that the rate-determining step of the reaction does not involve ionic species. A mechanism of the reaction has been proposed which is consistent with our observed results. In the presence of micelles the reaction rate was strongly inhibited by the cationic micelles of hexadecyltrimethylammonium bromide, whereas anionic micelles of sodium dodecyl sulfate showed a slight enhancement. The micellar data have been analyzed on the basis of available models.

The reaction of amines with ninhydrin yields a color product, Ruheman's purple sometimes erroneously referred to as "azine-bis-indandione. This reaction has immense biological and analytical significance as it serves as a model for several biochemical reactions that occur in the metabolism of deamination and transpeptidation[1,2] as well as it is involved in the most common method for the analysis of amino groups.[3,4] The course and mechanism of ninhydrin reaction has been extensively studied by Friedman and Williams[5] who investigated the effect of various parameters on the formation of Ruheman's purple. However, the mechanism of reverse reaction, namely the decolorization reaction, of Ruheman s purple in the presence of acids has not been investigated in detail. We have undertaken a systematic analysis of the kinetics and mechanism of decolorization reaction of Ruheman's purple in the hope that the data on the reverse reaction might provide insight into the ninhydrin reaction.

The reaction responsible for the hydrolytic instability was also studied in the presence of cationic micelles of hexadecyltrimethylammonium bromide (CTAB), sodium dodecyl sulfate (SDS), and poly(oxyethylene) (23) 1-dodecanol (Brij-35, Lauromacrogol). Micelles are known to affect the rates of reactions due to several factors by differential distribution of the substrates inside and outside the micelles and by perturbing the thermodynamic parameters of the reaction.[6] The interpretation of the mechanism of catalysis or inhibition of reaction rates by micelles has received considerable attention in view of the analogies drawn between the micellar and enzyme-catalysis. The rate of the present reaction is considerably inhibited in the presence of cationic micelles of CTAB. The data obtained have been analyzed quantitatively on the basis of available models.

Experimental

Ruheman's purple (RP) was prepared by the method of Ruheman.[11] The product was further purified by employing a method similar to that of Davidson.[12] The final product was obtained as ammonium salt. Sodium dodecyl sulfate obtained from Fisher Scientific Co. was recrystallized twice from 95% ethanol.[13] CTAB (extra pure, Sisco Research Laboratories) was crystallized twice with hot methanol–ether[13] before use. HCl and KCl of analytical grade(B.D.H.) were used without further purification. Organic solvents (analytical grade, B.D.H.) were further purified by the usual methods[14] before use.

The hydrolysis was studied using a Beckman DU spectrophotometer at the absorption maximum of RP (570 nm).

Results and Discussion

Reaction in the Absence of Micelles. First order rate constant for the reaction of RP in acidic medium was found to increase linearly with the increase in the hydrogen ion concentration (Fig. 1). Graphical analysis of the results gave the value of second order rate constant $k' = 0.94$ mol^{-1} dm^3 s^{-1}, comparable to that obtained earlier by Sattar and Chaturvedi[15] ($k' = 0.86$ mol^{-1} dm^3 s^{-1}). However, when the reaction was studied over the pH range 2—11, the initial

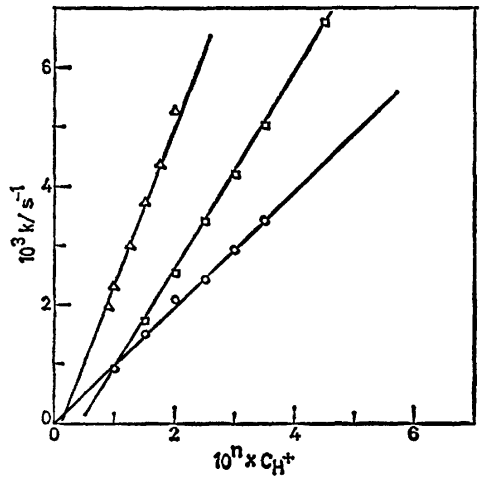

Fig. 1. Variation of first order rate constant with H^+ ion concentration in mol dm^{-3} for the hydrolysis of RP at 25 °C in acid medium in the presence and absence of surfactants. (○) Aqueous medium; (△) in presence of 2×10^{-3} mol dm^{-3} CTAB; (□) in presence of 0.01 mol dm^{-3} SDS. Value of n is 3 in presence of CTAB and 1 in the other two cases.

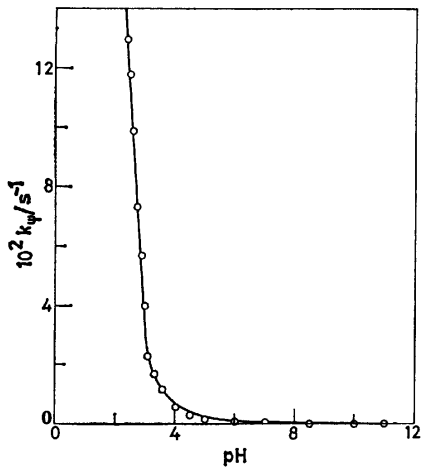

Fig. 2. Variation of first order rate constant with pH for the hydrolysis of RP at 25 °C at constant ionic strength (0.20).

Table 1. Effect of ionic strength on the reaction rate[a)]

μ	10^3 k/s^{-1}	μ	10^4 k/s^{-1}
0.003	3.258	0.523	1.503
0.023	2.802	0.603	1.517
0.043	2.123	0.763	1.401
0.083	2.111	0.843	1.381
0.263	1.746	0.923	1.259
0.363	1.631		
0.443	1.554		

a) Concentration of H^+ ion $=3\times10^{-3}$ mol dm^{-3}.

linear dependence of rate on pH faded at pH≈3. No hydrolysis of RP was observed at pH>7 (Fig. 2). This pattern of change in the rate with increase in pH differs from that observed by Cordes and Jencks[16] for the hydrolytic scission of >C=N- bond in schiff bases. They observed a rate maximum with the increase in pH followed by a pH region where the rate was unaffected by the increase in pH. In the reaction of RP no change in the reaction rate was observed with the change in RP concentration at fixed H^+ ion concentration. This shows that the reaction rate is independent of the initial RP concentration.

Dependence of the RP reaction on neutral salts added was investigated. Reaction rate was found to decrease with the increase in the ionic strength of the medium (Table 1) at constant H^+ ion concentration. Use of the following equation which is an approximation of Bronsted-Christiansen equation[17,18] gives the impression as if the reaction is taking place between two oppositely charged ions. However, despite

$$\log k' = \log k_o' + \frac{1.02 Z_A Z_B \sqrt{\mu}}{1+\sqrt{\mu}} \qquad \text{(i)}$$

the applicability of above equation, observed salt effect seems to be secondary salt effect, a purely thermodynamic effect, arising from the change in activity of the dissociable reactant species. It seems that the salt effect is a reflection of the equilibrium steps involving ions occurring prior to the rate determining step in the overall mechanism (*vide infra*).[19] The magnitude and direction of secondary salt effect on reaction rate depends on concentration terms that appear in the overall rate expression.

Table 2. Effect of solvents on the hydrolysis of RP in acid medium at 25 °C[a)]

Composition of solvent (v/v)	k'/mol^{-1} dm^3 s^{-1}		
	Acetone	Dioxane	Ethylene glycol
5%	0.85	0.84	0.91
10%	0.78	0.84	0.91
15%	0.72	0.84	0.92
20%	0.67	0.82	0.92
25%	0.65	0.84	0.92
30%	0.69	0.88	0.92
40%	—	—	0.90

a) Concentration of H^+ ion $=4\times10^{-3}$ mol dm^{-3}.

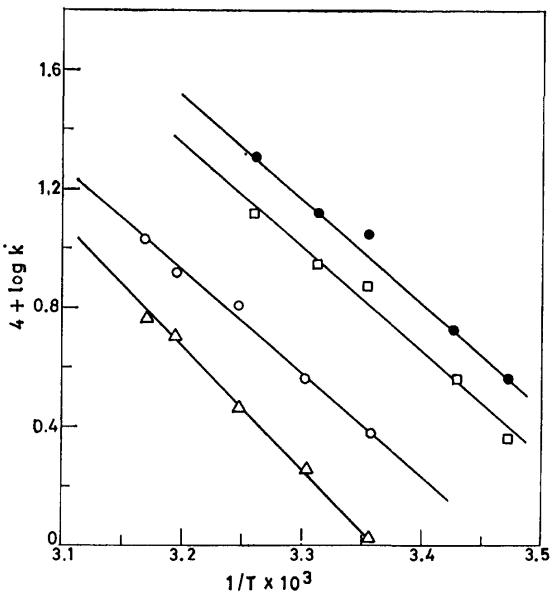

Fig. 3. Effect of temperature on the hydrolysis of RP. Plots of log k' *vs.* $1/T$. (○) μ=0.001; (△) μ=0.501; (□) 25% (v/v) acetone; (●) 36% (v/v) ethylene glycol.

The effect of solvents on the reaction rate was studied in the presence of 5—30% (v/v) of acetone, dioxane, and ethylene glycol in aqueous medium (Table 2). Reaction rate was found to be independent of increasing concentration of ethylene glycol and dioxane but a slight decrease was observed in the presence of acetone. The solvent effects give a positive indication that the rate determining step of the reaction involves no ionic species.

Effect of temperature on the reaction rate was studied in the range 288—320 K at ionic strength of 0.001 and 0.501. In order to examine the influence of temperature on the specific solvent effect, studies were carried out in 25% acetone and 36% (v/v) ethylene glycol, which have the same dielectric constant. The reaction rate was found to follow the Arrhenius equation (Eq. 2) under all the four experimental conditions (Fig. 3). Graphical analysis of

Table 3. Thermodynamic quantities of activation for the hydrolysis of RP at 25 °C

Thermodynamic quantity	Aqueous medium		Acetone 25% (v/v)	Ethylene glycol 36% (v/v)
	μ=0.001	μ=0.501		
E^*/kJ mol^{-1}	66.9	79.5	54.4	54.4
ΔG^*/kJ mol^{-1}	92.0	92.0	92.0	87.8
Z/mol^{-1} dm^3 s^{-1}	2.8×10^8	1.9×10^{10}	3.1×10^6	5.0×10^6
ΔS^*/J K^{-1} mol^{-1}	−87.8	−54.4	−125.5	−125.5
ΔH^*/kJ mol^{-1}	66.9	75.3	37.6	37.6

log k *versus* $1/T$ plot gave the value of activation energy E^* which was then used to calculate other activation parameters, ΔG^*, ΔS^*, ΔH^*, and Z, using Eqs. 3—5. The values of the parameters at 25 °C are

$$\log k' = \log Z - E^*/2.303RT \quad (2)$$

$$\Delta G^* = 2.303RT\left(\log\frac{RT}{Nh} - \log k'\right) \quad (3)$$

$$\Delta S^* = 2.303R\left(\log Z - \log\left(e\frac{RT}{Nh}\right)\right) \quad (4)$$

$$\Delta H^* = \Delta G^* + T\Delta S^* \quad (5)$$

given in Table 3. High negative entropy values −90.8 J K^{-1} mol^{-1} and −55.2 J K^{-1} mol^{-1} at μ=0.001 and 0.501, respectively, suggest bimolecular nature of the rate determining step.[20] Moreover, activation energies obtained for isodielectric mixture of 25% acetone (55.6 kJ mol^{-1}) and 36% ethylene glycol (54.8 kJ mol^{-1}) are similar, reflecting the fact that the decrease in rate observed in the presence of acetone is due to nonelectrostatic terms generally associated with the effect of solvent on the reaction rate.[21]

A tentative reaction mechanism for the hydrolysis of RP, proposed by Friedman and Williams,[5] is given in Scheme 1. No justification other than the product analysis has been given by these authors. Moreover, the proposed mechanism can not explain the observed deviation from the linear relationship observed at pH$\geqslant$4. Another objection to proposed mechanism is that RP is known to be strongly acidic (pK_a of RP is almost equal to that of H_2SO_4) p$K_a\leqslant0$,[5] hence, even in fairly strong acidic solution (pH$\approx$2) RP will remain in ionic form and no protonation can occur at the negatively charged oxygen. We propose a reaction mechanism (Scheme 2) which is consistent with our observed results. At relatively low pH, when concentration of H^+ ion is much higher than that of RP, attack of water on the zwitterionic species to give α-hydroxy amine intermediate [x] seems to be the rate determining step. This is supported by the high negative value of entropy (−87.8 J K^{-1} mol^{-1}) and also by the absence of any significant solvent effect. The observed salt effect, though unusual for a dipole-dipole reaction, is not unique for a reaction between two dipoles, where a fast equilibrium step preceeds the rate-limiting step. For example, Sinha and Katiyar[22] and others[23] has also observed a pronounced salt effect on the color-fading reaction of rosaniline. Though this reaction is ion-dipole reaction, it could be cited as an example because theoretically an ion-dipole reaction like a dipole-dipole reaction, should show no pronounced salt effect. Such

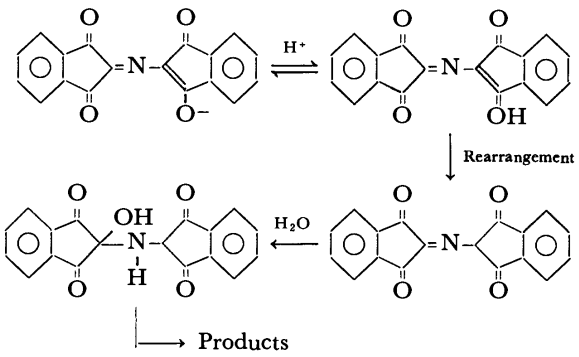

Scheme 1.

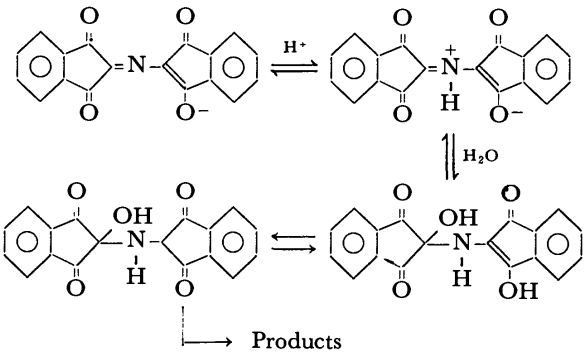

Scheme 2.

salt effects might be due to reflection of fast equilibrium steps involving ions, in the overall reaction mechanism as pointed out by Hine.[19] The observed deviation from the linear behavior at pH$\geqslant$4 can also be explained by the proposed mechanism. At higher pH, concentration of H^+ ion and RP become similar, and the rate of formation of zwitterion progressively decreases with the increase in pH. No reaction takes place at pH$\geqslant$7 because of absence of first protonation step.

Reaction in the Presence of Micelles. Change in absorption maximum from 570 nm to 579 nm was observed in the presence of 0.01 M CTAB. However, no such shift was detected in the presence of 0.02 M SDS or 0.01 M Brij-35. This indicates binding between RP and CTAB micelles. The reaction was studied at different surfactant concentrations keeping the hydrogen ion concentration constant in each case. An inhibition of reaction rate was observed in the presence of cationic surfactant (CTAB) whereas the reaction rate was slightly enhanced in the presence of anionic micelles of SDS. However, no definite trend of reaction rate emerged in the presence of nonionic surfactant of Brij-35 (Fig. 4). At fixed SDS or CTAB

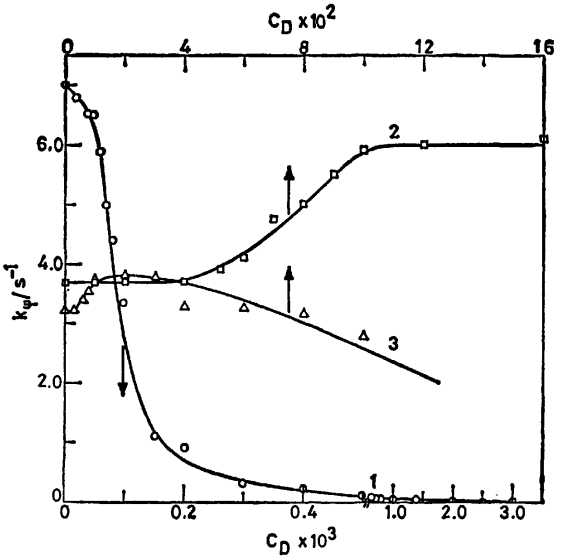

Fig. 4. Effect of surfactant concentration (mol dm^{-3}) on the reaction rate at 25 °C. (○) CTAB; (□) SDS; and (△) Brij-35.

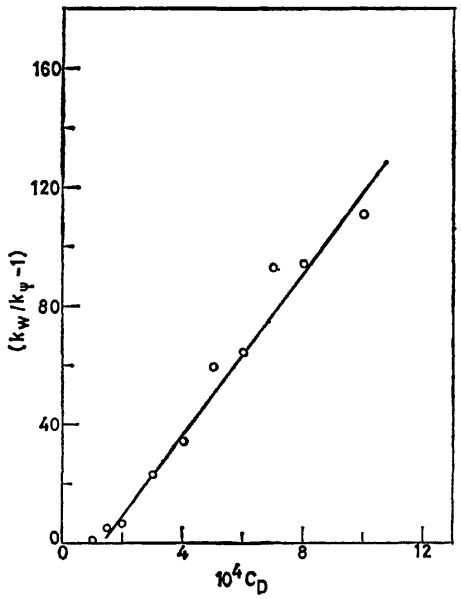

Fig. 5. Variation of $(k_w/k_\psi - 1)$ with the surfactant concentration (mol dm^{-3}) for the hydrolysis of RP at 25 °C in the presence of CTAB.

concentration, a linear increase in reaction rate was observed with increase in hydrogen ion concentration (Fig. 1).

Surfactant micelles provide an unusual medium which may affect the reaction rate in more than one way:[7-10,23] (a) a decrease in entropy of the reactants arising due to their binding on the micellar surface, *i.e.*, by virtue of relatively higher concentration of reactants in micellar phase in comparison to bulk phase, (b) a high degree of closeness attained by reactants in the micellar phase, and (c) relative stabilization or destabilization of substrate arising due to electrostatic and hydrophobic interaction between substrates and micelles. Moreover, in the hydrolysis of RP, the micelles may affect the first equilibrium step where proton gets associated with anion to give zwitterion or the subsequent rate determining attack of water molecule to form an α-hydroxy amine. It appears that in the presence of CTAB, because of favorable hydrophobic as well as electrostatic interactions the anionic imine gets bound with the surface of cationic micelle, shifting the protonation equilibrium towards the lefthand side, retarding the reaction rate. However, in the presence of SDS, hydrophobic forces oppose the electrostatic repulsion. However it seems that a fraction of anionic substrate does bind with the anionic micelles, where it is more prone to proton attack, and hence a slight acceleration in the reaction rate is observed. Thus the effect of micelles on the reaction is consistent with the mechanism we proposed.

Quantitative Treatment of the Micellar Data. Simple kinetic model proposed by Menger and Portnoy[24] (Scheme III) was applied to explain quantitatively

$$\begin{array}{ccc} D_n + S & \overset{K}{\rightleftharpoons} & D_n \cdot S \\ {\scriptstyle k_w}\downarrow & & \downarrow{\scriptstyle k_m} \\ \text{Products} & & \text{Products} \end{array}$$

Scheme 3.

the effect of cationic and anionic micelles on the reaction rate. This kinetic scheme provides the following rate equation:

$$\frac{k_\psi - k_w}{k_m - k_\psi} = \frac{K}{N}(C_D - \text{cmc}), \tag{7}$$

where k_ψ is the observed rate constant and k_w and k_m are the rate constants in aqueous and micellar pseudophases, respectively. K is the equilibrium constant for the association of substrate S with micelle D_n, N is the aggregation number and C_D is the stoichiometric surfactant concentration. This equation predicts a linear relationship between $\frac{k_\psi - k_w}{k_m - k_\psi}$ and C_D. However, for micellar inhibited reaction we can further assume that $k_m = 0$.[8] Hence, we obtain

$$\frac{k_w}{k_\psi} - 1 = \frac{K}{N}(C_D - \text{cmc}). \tag{8}$$

The results obtained in the presence of CTAB were analyzed using Eqs. 7 and 8. Slope of the straight line thus obtained (Fig. 5) gives the value of K/N, which was further utilized to calculate the fraction (α) of RP present in the micellar phase by means of

$$K/N = \frac{\alpha}{1-\alpha} \cdot \frac{1}{C_D - \text{cmc}}. \tag{9}$$

The values of K/N, cmc, and α for the acidic hydrolysis of RP in the presence of CTAB correspond to 1.36×10^4 mol^{-1} dm^3, 1.32×10^{-5} mol dm^{-3} and 99.27%, respectively. Since the effect on the reaction rate is very small, no quantitative analysis was carried out for the catalysis observed in the presence of SDS.

Recently, Piszkiewicz[25] has proposed a different kinetic scheme based on the observed sigmoidal dependence of rate constant on surfactant concentration. According to his model (Scheme 4) a substrate molecule combines with n detergent molecules to form a catalytic aggregate.

$$S + nD \underset{}{\overset{K_D}{\rightleftharpoons}} S\cdot D_n$$

$k_w \downarrow$ Products $k_m \downarrow$ Products

Scheme 4.

Mathematical formulation based on this scheme gives

$$\log\left(\frac{k_\psi - k_w}{k_m - k_\psi}\right) = n \log [D] - \log K_D, \quad (10)$$

which predicts a linear relationship between $\log (k_\psi - k_w)/(k_m - k_\psi)$ and $\log [D]$ with a slope equal to n. In this equation [D] is the total detergent concentration, K_D the dissociation constant of surfactant-substrate complex and n the index of cooperativity. This equation gives a set of parameters which have a different significance from that obtained from Menger and Portnoy's scheme,[24] *e.g.* at $\log (k_\psi - k_w)/(k_m - k_\psi) = 0$, $n \log [D] = \log K_D$. Also at $\log (k_\psi - k_w)/(k_m - k_\psi) = 0$, catalysis by the surfactant shows one-half of its maximum effect, the value of log [D] at this concentration being designated by $\log [D]_{50}$. Another parameter which can be used to compare the effect of micelles is the index of cooperativity '*n*'. Double log plot for the hydrolysis of RP in presence of CTAB is shown in Fig. 6. For the CTAB inhibited reaction, when k_m is assumed to be zero, the values of $\log [D]_{50}$ and *n* obtained from the plot correspond to −4.0 and 2.66 respectively.

Successful application of both the kinetic schemes to the hydrolysis of RP in the acid medium is not surprising. Though the two schemes are based on different assumptions, the final mathematical equations based on them are similar (Eqs. 7 and 10). However, the kinetic parameters associated with these equations have quite different significance. Piszkiewicz's model draws its strength from a model used for enzyme catalysed reactions showing positive homotropic interaction (also called positive cooperativity). Positive cooperativity is reflected in the value of *n*, the index of cooperativity. In the micellar systems, the value of *n* reflects the average number of surfactant molecules associated with each substrate molecule. Another useful parameter which we obtained by the application of Piszkiewicz's model is $\log [D]_{50}$, the concentration of surfactant where it shows half of its maximum effect. On the other hand the scheme of Menger and Portnoy[24] is based on the distribution of substrate into micellar and aqueous pseudophases and has been extensively applied to micelle catalysed and micelle inhibited reactions. It puts more emphasis on the interaction between the substrate and micellar aggregation, whereas Piszkiewicz's model gives prominence to interaction between substrate and surfactant molecule. Hence the simultaneous application of both models provides a better insight and understanding of micellar effects on the reaction rate.

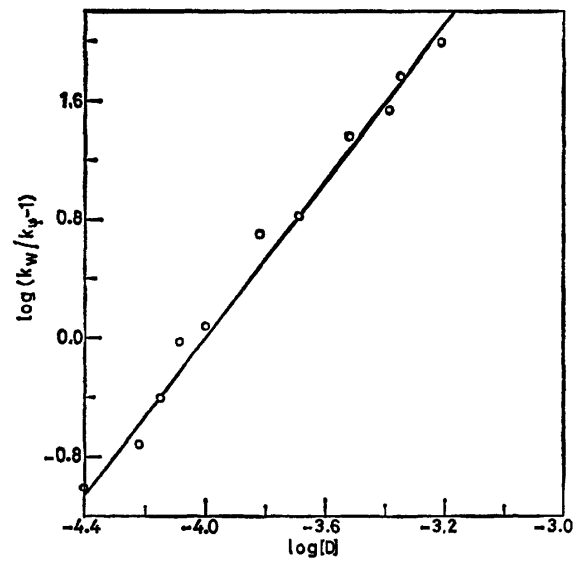

Fig. 6. Plot of $\log (k_w/k_\psi - 1)$ *vs.* log [D] for the hydrolysis of RP in the presence of CTAB.

References

1) G. C. Connel, G. H. Dixon, and C. S. Hanes, *Can. J. Biochem.*, **33**, 416 (1955).
2) G. D. Kayankar and E. E. Snell, *Nature (London)*, **180**, 1069 (1957).
3) D. J. McCaldin, *Chem. Rev.*, **60**, 39 (1960).
4) M. P. Lynch and K. L. Webb, *Comp. Biochem. Physiol. B*, **45**, 407 (1973).
5) M. Friedman and L. D. Williams, *Bioorg. Chem.*, **3**, 267 (1974).
6) See Refs. 7—10.
7) J. H. Fendler and E. J. Fendler, "Catalysis in Micellar and Macromolecular Systems," Academic Press, New York, N. Y. (1975).
8) C. A. Bunton, *Prog. Solid State Chem.*, **8**, 239 (1973).
9) E. H. Cordes and C. Gitler, *Prog. Bioorg. Chem.*, **2**, 1 (1973).
10) E. H. Cordes, "Reaction Kinetics in Micelles," Plenum Press, New York, N. Y. (1973).
11) S. Ruheman, *J. Chem. Soc.*, **99**, 1306 (1911).
12) D. Davidson, *J. Am. Chem. Soc.*, **58**, 1821 (1936).
13) E. F. J. Duynstee and E. Grunwald, *J. Am. Chem. Soc.*, **81**, 4540 (1959).
14) A. I. Vogel, "Textbook of Practical Org. Chem," Longmans, London (1956), pp. 163—178.
15) A. Sattar and R. K. Chaturvedi, *Naturwissenschaften*, **50**, 101 (1973).
16) E. H. Cordes and W. P. Jencks, *J. Am. Chem. Soc.*, **85**, 2843 (1963).
17) E. S. Amis and J. F. Hinton, "Solvent Effects on Chemical Phenomenon," Academic Press, New York, N. Y. (1966), p. 229.
18) A. Weller, *Prog. React. Kinet.*, **1**, 189 (1961).
19) H. Hine, "Physical Organic Chemistry," McGraw-Hill, New York, N. Y. (1962).
20) V. Gold, "Advances in Physical Organic Chemistry," Academic Press, New York, (1963).
21) See Ref. 17, Chap. 5.
22) S. K. Sinha and S. S. Katiyar, *Bull. Chem. Soc. Jpn.*, **50**, 507 (1977).
23) R. Cigen and L. G. Ekstrom, *Acta Chem. Scand.*, **17**, 1189, 2083, (1963).
24) F. M. Menger and C. E. Portnoy, *J. Am. Chem. Soc.*, **89**, 4698 (1967).
25) D. Piszkiewicz, *J. Am. Chem. Soc.*, **99**, 1550 (1977).

  Bull. Chem. Soc. Jpn., 54, 1857—1867 (1981)

Reductive Elimination of d^8-Organotransition Metal Complexes

Kazuyuki TATSUMI, Roald HOFFMANN,* Akio YAMAMOTO,** and John K. STILLE***

Department of Chemistry, Cornell University, Ithaca, New York 14853, U.S.A.

** *Research Laboratory of Resources Utilization, Tokyo Institute of Technology, Nagatsuta, Midori-ku, Yokohama 227*

*** *Department of Chemistry, Colorado State University, Fort Collins, Colorado 80523, U.S.A.*

(Received August 30, 1980)

A theoretical analysis of two aspects of the mechanism of reductive elimination is presented—how the choice of central metal and peripheral ligands affects the activation energy for reductive elimination from a four-coordinate $MR_2(PR_3)_2$ complex and how ligand asymmetry controls *cis-trans* rearrangements and elimination pathways proceeding through three-coordinate intermediates. The following conclusions emerge: (1) In the four-coordinate complex, the better the σ-donating capability of the leaving groups, the more facile the elimination; (2) Stronger donor ligands *trans* to the leaving groups will increase the barrier to elimination; (3) The reductive elimination barrier in four-coordinate complexes is controlled by the energy of an antisymmetric b_2 orbital, which in turn depends on the energy of the metal levels. The activation energy for such direct reductive elimination should be, and is, substantially lower for Ni than for Pt or Pd; (4) T-shaped *trans* $PdLR_2$, arising from dissociation of L in PdL_2R_2, will encounter a substantial barrier to polytopal rearrangement to *cis* $PdLR_2$, which in turn has an open channel for reductive elimination of R_2; (5) If the leaving groups are poor donors, *cis-trans* isomerization in the three-coordinate manifold should be easier than elimination.

The coupling of two alkyl moieties into an alkane, *e.g.* (1), is a reaction efficiently accomplished by a number of d^8 transition metal centers—Ni(II), Pd(II),

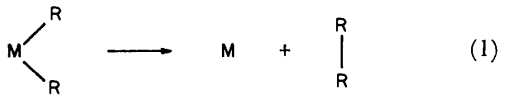

(1)

Pt(II), Au(III). But the simple form of the summary equation (1) for this process masks a multitude of mechanistic choices. Let us examine some of the possibilities in Scheme 1.

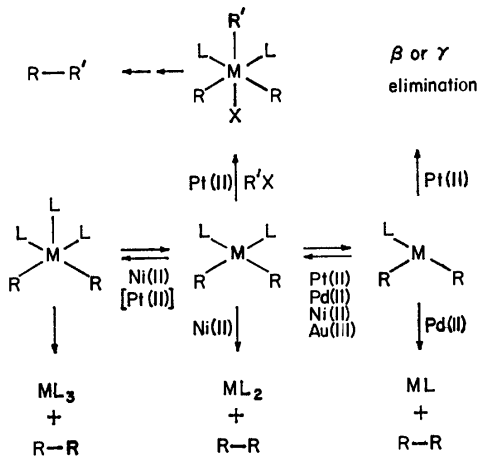

Scheme 1.

The most common starting point for these reactions is a preformed square-planar 16 electron, d^8 dialkyl (or tri-or tetraalkyl for Au(III)) complex which appears in the middle of the Scheme. The two other ligands, marked L, are typically phosphines. Depending on the size and electronic characteristics of the phosphine substituents one may observe associative or dissociative steps away from the four-coordinate complex. Both elementary processes have been clearly demonstrated in the Grubbs system, where M=Ni(II) and R_2 is a tetramethylene bridge.[1,2] Evidence is in fact in hand for the dissociative step in most such reactions.

The four-coordinate complex eliminates R–R cleanly and easily in the Ni(II) case only. For Pd(II) the work of the Yamamoto[3] and Stille[4] groups and for Au(III) of the Kochi group[5] has produced kinetic evidence for elimination from a three-coordinate intermediate. Pt(II) apparently does not eliminate R–R readily.[6] The Whitesides group[6a] has demonstrated β or γ elimination (where feasible) through a three-coordinate intermediate, while Puddephatt and coworkers[7] have found elimination reactions, but only after oxidative addition of an RX.

No stereochemical implications were meant to be drawn from Scheme 1. In fact the mechanistic possibilities are enriched by the range of equilibrium geometries and polytopal rearrangements available to the various intermediates. Some of the geometrical extremes are drawn in **1**—**9**. For the square-planar

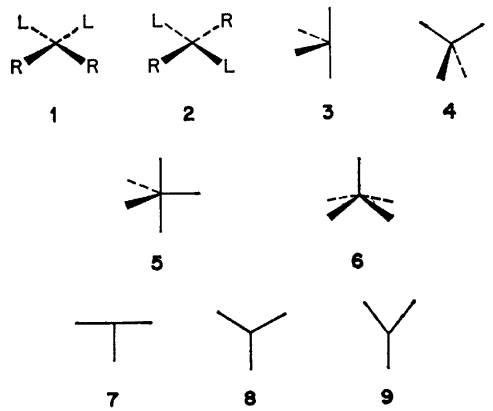

geometry one has available the *cis* and *trans* isomers **1** and **2**, and indeed the mechanism of elimination from either starting point has been studied. Some recent theoretical work[8] on the Grubbs system has focussed on another possible low-spin intermediate—the C_{2v} *cis*-octahedral fragment **3**. And at least for Ni(II) one has to worry about the tetrahedral, presumably high-spin,

alternative **4**. Even more geometrical isomers are available for a five-coordinate structure—here we remind ourselves only of the underlying geometries, the trigonal bipyramid **5** and the aquare pyramid **6**. For the three-coordinate geometry the idealized trigonal D_{3h} geometry **8** might seem to be the geometry of choice. But for reasons that are well understood,[5b] this most symmetrical structure is unlikely, and instead we must examine "T" and "Y"-shaped C_{2v} deformations, **7** and **9**. Mind you, these are only idealized geometrical extremes—the real molecules will certainly depart, to a variable degree, from these structures.

Our goal is a comprehensive theoretical understanding of this reaction type. Theoretical analyses of reductive elimination exist—the early and important work of Pearson[9] and of Braterman and Cross,[10] the more comprehensive and detailed approach of Åkermark and coworkers[11]—to mention some of the studies of this reaction. We ourselves have contributed an analysis of competitive elimination from three- and four-coordinate alternatives in the Au(III) system,[5b] and in work to be published still have investigated the nickellacyclopentane fragmenations.[8] All of these studies, those of others and ours as well, encounter one fundamental problem: *The reductive elimination is symmetry-allowed for many (not all) polytopal geometries of the three-, four-, and five-coordinate structures of Scheme 1. Why then does one metal choose one route, while a second metal opts for another?* We will try to give a partial answer to this question in this paper. We will also show how the electronic asymmetry of the ligand set controls the detailed mode of alkane elimination.

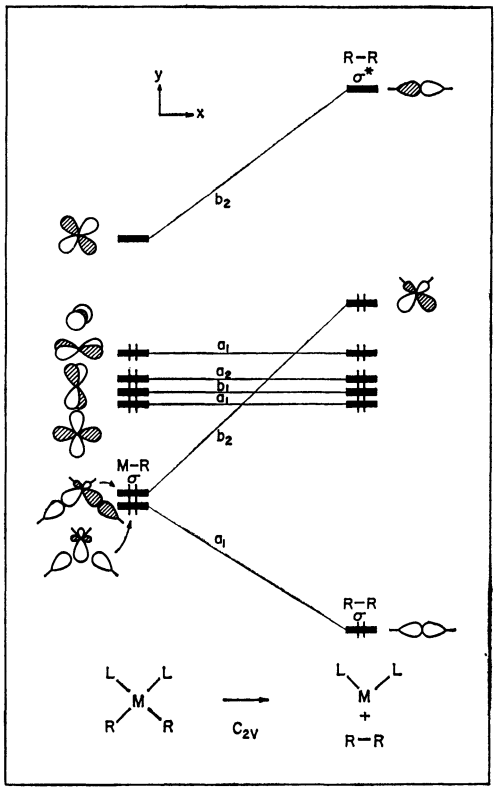

Fig. 1. Schematic correlation diagram for the elimination of R–R from a square-planar d^8 transition metal complex ML_2R_2. The reaction pathway maintains C_{2v} symmetry.

Reductive Elimination from *cis* Four-coordinate Complexes

The basic reaction, *cis* d^8 L_2MR_2 to d^{10} L_2M and R_2, is symmetry-allowed for a least motion C_{2v} departure.[8-11] A schematic correlation diagram to a bent ML_2 (the adjustment in making ML_2 linear is minor) is shown in Fig. 1. As usual these correlation diagrams abstract reality by proceeding from a semi-localized starting point in which only orbitals essential to the reaction are included.[12] Thus in the present case the orbitals in the diagram for L_2MR_2 are the five d-block orbitals of the metal and the two σ orbitals of the MR_2 unit. For ML_2+R_2 we have the R_2 σ and σ^* levels and the five metal d orbitals. The reality must be that these orbitals are not so simple and substantial mixing between the orbitals illustrated, as well as with others, not included in the figure, must occur. The purpose of these diagrams is to decide whether a level crossing does or does not occur—the actual details of the levels we will learn from a full calculation.

There is nevertheless one general feature of this allowed reaction that is evident from the figure and that we will return to later. This is the required evolution of one MR_2 bonding orbital, b_2 in symmetry,[13] into a primarily metal d orbital of the same symmetry, *i.e.* xy in a linear ML_2. This is indicated in **10**→**11**. Note

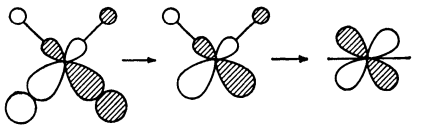

10 **11**

the loss of M–R bonding and electron transfer to the metal implied by this correlation. These will be important.

Our detailed analysis of the elimination reaction was carried out by means of extended Hückel calculations, with parameters specified in Appendix I. In several cases three degrees of freedom were studied, as illustrated in **12**: the angle between the leaving groups, φ; the separa-

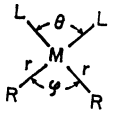

12

tion from the metal to these leaving R's, r; and the angle between the remaining. ligands, θ. As in our previous study of the Au(III) system[5b] we found that the essential features of the elimination were revealed in angular variations alone, *i.e.* changes of θ and φ at constant M–R separation. This is just as well, for the extended Hückel method is not good at representing correctly degrees of freedom in which distances are varied.

The ligands of course play a vital role in determining the feasibility of any reductive elimination. We carried out calculations with PH_3 and CH_3 ligands. These

led us to focus on the σ donor or acceptor strength of the ligands. Our interpretation was easiest made on a still simpler "hydride model." Here the ligands were simply hydrogen 1s functions with modified valence state ionization potentials. We called the two extremes A and D. A and D are hydrogen atoms, the 1s orbital energies of which are set to be -14.34 and -11.75 eV, respectively. The value -14.34 eV is the calculated orbital energy of a lone pair in PH_3 and -11.75 eV corresponds to that of a lone pair in CH_3^-. Thus A^- may be a model for PH_3 and D^- for CH_3^-. Or one can regard A as a poor donor ligand and D as a strong donor ligand.

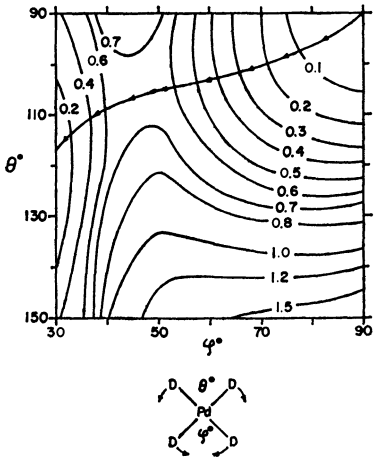

Fig. 2. Potential energy surface for variation of the two D–Pd–D angles, θ and φ, in planar PdD_4^{2-}. The energy contours are in electron volts relative to the square-planar geometry ($\theta=\varphi=90°$). A line with arrows indicates a reaction path corresponding to the elimination of D_2 from PdD_4^{2-}.

A potential energy surface in θ and φ for the elimination of D_2 from PdD_4^{2-} is illustrated in Fig. 2. The reaction path is shown by a line with arrows. In general the surface is quite analogous to that computed earlier by us for $Au(CH_3)_4^-$ [5b] $-\theta$ lags somewhat behind φ. Corresponding energy surfaces for the departure of A_2 and D_2 from PdA_2D_2 are illustrated in Fig. 3.

As these surfaces show, the reactions of these model compounds have a saddle point at around $\theta=100$—$110°$, $\varphi=40$—$50°$. When the two leaving ligands are gradually removed (r increased) at the point $\theta=110°$ $\varphi=30°$, no additional energy barrier was found. Thus each potential surface represents sufficiently well the reductive elimination reaction of a corresponding compound. The calculated activation energies for PdD_4^{2-}, $PdD_2A_2^{2-}$ (A leaving), and $PdA_2D_2^{2-}$ (D leaving) are 0.65, 2.7 (A_2 leaving), and 0.20 eV (D_2 leaving), respectively. We should not rely on these numbers in a quantitative sense, partly because we used the very simplified hypothetical hydride model (we will discuss this later), and partly because the calculational method is rather primitive. However the observed trends are quite suggestive. Here are two conclusions: (1) *The better the σ-donating capability of the leaving groups, the more readily the elimination reaction proceeds.* (2) *Stronger donor ligands which are* trans *to the leaving groups give a higher barrier for the elimination reaction.*

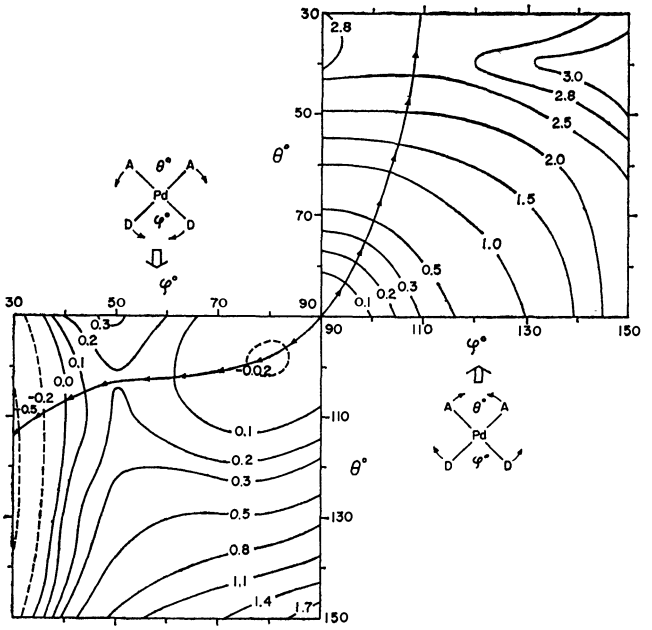

Fig. 3. Potential energy surface for variation of the two angles, θ (A–Pd–A) and φ (D–Pd–D), in planar $Pd-D_2A_2^{2-}$. The energy contours are in electron volts relative to the square-planar geometry ($\theta=\varphi=90°$). A line with arrows corresponds to reaction paths for D_2 elimination, lower left, and A_2 elimination, upper right.

The potential energy surface for $NiA_2D_2^{2-}$ is shown in Fig. 4, in which the leaving groups are the stronger donors D. Although this model compound is just the Ni analogue of $PdA_2D_2^{2-}$, the calculated potential surface of $NiA_2D_2^{2-}$ is quite different from that of $PdA_2D_2^{2-}$. While the elimination reaction of $PdA_2D_2^{2-}$ has a small but obvious energy barrier along the reaction coordinate, the reaction pathway of the Ni analogue is

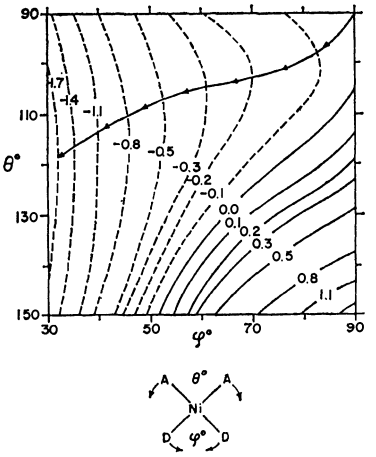

Fig. 4. Potential energy surface for variation of the two angles, θ(A–Ni–A) and φ(D–Ni–D), in planar $NiA_2-D_2^{2-}$. The energy values on the contours are in electron volts relative to the square-planar geometry ($\theta=\varphi=90°$). A line with arrows indicates a reaction path for D_2 elimination from $NiA_2D_2^{2}$.

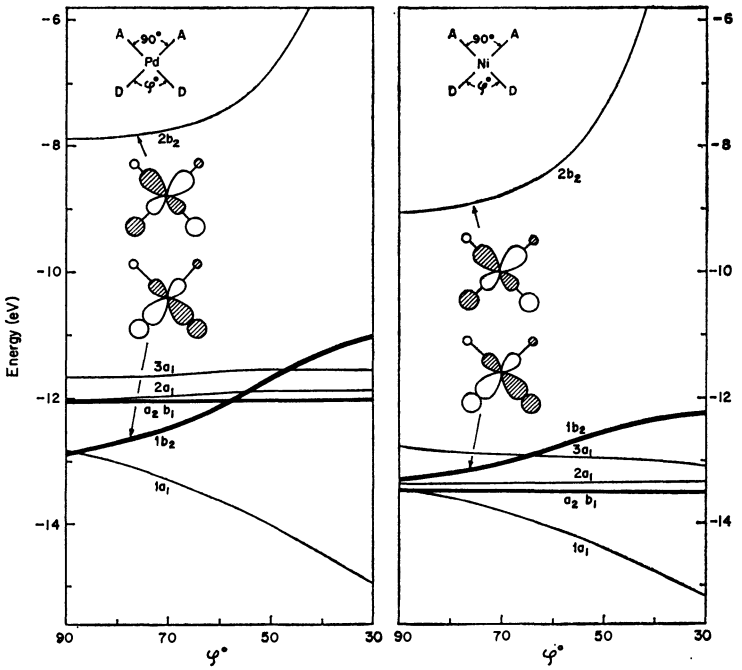

Fig. 5. Computed Walsh diagrams for $PdA_2D_2^{2-}$(left) and $NiA_2D_2^{2-}$(right), for decrease of the D–M–D angle φ. The A–M–A angle is kept at 90°. The $2b_2$ orbital is vacant.

merely downhill in energy and has no barrier.

Why is there such a different pattern for $PdA_2D_2^{2-}$ and $NiA_2D_2^{2-}$? The answer must lie, ultimately, in the Pd 4d *vs.* Ni 3d orbital energies. The effect is traced through Fig. 5, a set of Walsh diagrams. Each of the diagrams shows the variation of the important molecular orbital levels as a function of D–M–D (M=Pd or Ni) angle φ (90—30°), while A–M–A angle is kept at 90°. There are seven levels shown in Fig. 5. To make the correspondence to the schematic correlation diagram of Fig. 1 we can say that five of these seven levels are the d-block orbitals and two are M–D bonding orbitals. The reality is not so simple—there is extensive delocalization in some of the symmetry types. a_2 and b_1 are simple, pure metal yz and xz, unaffected by the elimination. $2a_1$ and $3a_1$ contain substantial d character, z^2 and x^2-y^2. But in fact they are part of a trio of a_1 orbitals which includes $1a_1$. We can think of these orbitals as derived from localized z^2, x^2-y^2 and the a_1 M–D σ bond combination. As the angle φ closes, one of the three a_1's goes down in energy and ends up as the σ bonding MO of D_2. Obviously the main stabilization which drives the elimination reaction is in these a_1 orbitals. However, the contribution to the total energy change of the three a_1 orbitals is quite similar in the Pd and Ni compounds. Thus the a_1 set does not differentiate between the two metals.

There are two b_2 orbitals in Fig. 5. We can think of them as bonding and antibonding M–D, A σ combinations, alternatively the higher orbital of the two could be thought of as that metal orbital, xy, which is destabilized by the square planar ligand field. Decreasing φ destabilizes both $1b_2$ and $2b_2$. The unoccupied $2b_2$ correlates to the eliminated D_2 σ^* level **13**, while the occupied $1b_2$ correlates to an MA_2 orbital which is nearly pure xy, **14**. The latter correlation was the one alluded to earlier, **10**→**11**.[14]

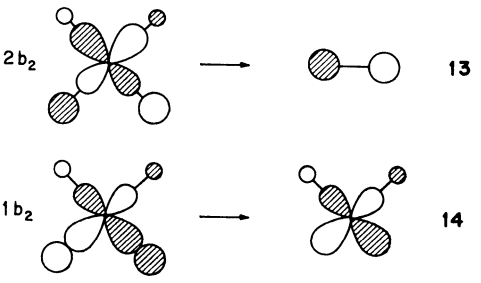

There is no level crossing for elimination of D_2 in either the Pd or the Ni case, confirming the simplified analysis of Fig. 1. The contrast between the potential energy surfaces for the two metals (Figs. 3 and 4) arises from the difference in slope of the $1b_2$ orbitals. As φ decreases $1b_2$ of $PdA_2D_2^{2-}$ is singificantly more pushed up than that of $NiA_2D_2^{2-}$, producing an energy barrier in the elimination of D_2 from the Pd compound.

The differential $1b_2$ destabilization may arise from two causes—decreasing M–D bonding and increasing D–D antibonding. Either way, it would be anticipated that if the D 1s orbital component in $1b_2$ is large, the destabilization of $1b_2$ will also be large. Indeed the calculated D 1s orbital contribution in $1b_2$ is 54% for Pd and 38% for Ni at $\varphi=90°$, which accords with the larger destabilization of the Pd $1b_2$ level.

There is another way of analyzing this effect. The $1b_2$ orbital of MA_2D_2 is constructed in **15** from the antisymmetric D_2 combinations interacting with a bent MA_2 fragment. This interaction carries in it a substantial fraction of the M–D bond energy. Since the resulting

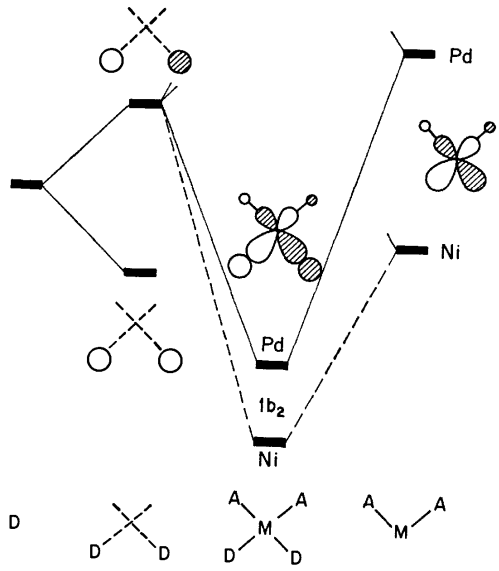

15

$1b_2$ level of $MA_2D_2^{2-}$ correlates to the b_2 of MA_2 in the D_2 elimination step, a greater energy difference between the $MA_2D_2^{2-}$ b_2 level and the MA_2^{2-} b_2 level would be associated with a greater activation energy for the reaction. The computed energy differences of the b_2 level are 2.1 eV for Pd and 1.3 eV for Ni. This is exactly what would be required to explain the different energy pattern of the Pd and Ni eliminations.

We have assigned the effect of the b_2 levels, but in fact it can be traced deeper. The b_2 level in the MA_2^{2-} fragment left behind is mainly a metal d orbital. It is higher for Pd than for Ni because the Pd and Ni d parameters are in that order. To probe this explanation we performed a numerical experiment in which D_2 was eliminated from a $MA_2D_2^{2-}$, where the M carried the Pd orbitals but with a variable 4d valence state ionization potential. The results shown on Fig. 6 clearly illustrate the dependence of the activation barrier on the metal d energy.

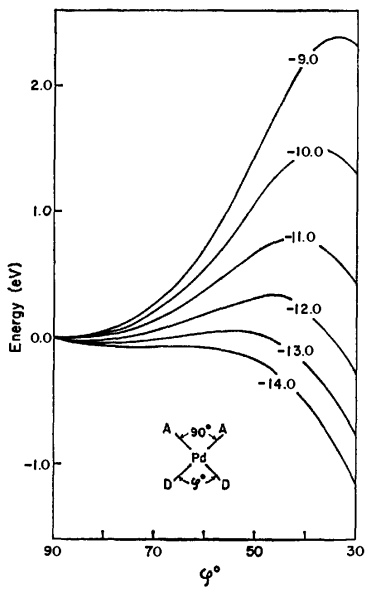

Fig. 6. The total energy of the hypothetical palladium complex $PdA_2D_2^{2-}$ as a function of the D–Pd–D angle φ. Potential curves for various choices of the "Pd" 4d ionization potential are superimposed, so that all curves are referred to an arbitrary zero of energy at $\varphi=90°$.

There is a temptation here to correlate the M–D bond strength, formed in part by this b_2 interaction, with increased activation energy to reductive elimination. Some thought about the matter, with the help of diagram **15**, shows that the relationship is not so simple. When the A_2M orbital is higher in energy than the antisymmetric combination of D orbitals, a more destabilized MA_2 b_2 would lead to a weaker M–D bond, while at the same time it would give a larger energy gap between b_2 levels of MA_2 and $MA_2D_2^{2-}$. The numerical experiment, varying M H_{ii}, that we described above, is useful in testing this supposition. Figure 7 shows how the Pd–D overlap population does not increase monotonically with higher Pd 4d energy, but peaks at the position of resonance with the D_2 antisymmetric combination. Thus, the energy gap is not always an index of the thermodynamic stability of an M–D bond, but it can be an index of the "kinetic" stability of $MA_2D_2^{2-}$ to reductive elimination.

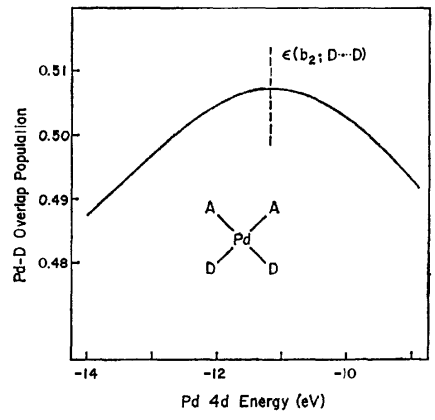

Fig. 7. Pd–D overlap population in the hypothetical palladium complex $PdA_2D_2^{2-}$ as a function of the valence state ionization potential of the Pd 4d level.

Our third conclusion: A lower positioning of the MA_2 b_2 orbital facilitates the reductive elimination of D_2. A lower MA_2 b_2 energy will be given by a lower metal d orbital energy.

While our major focus was the difference between Ni and Pd, we have also studied, albeit in abbreviated form, the Pt case. A model $PtA_2D_2^{2-}$ elimination surface gives a barrier slightly higher than in the Pd case. The Pt 5d parameters place it between Ni and Pd, but closer to Pd. The b_2 orbital is 50% on the D_2 ligands at $\varphi=90°$, a value again close to that computed for Pd. These theoretical findings are in accord with the experimental observation of difficult reductive elimination from Pt complexes.

Our next objective was to move from the model MA_2D_2 structures to more realistic models. To this end we examine reductive elimination of ethane from $Pd(PH_3)_2(CH_3)_2$, $Pd(CH_3)_4^{2-}$, and $Ni(PH_3)_2(CH_3)_2$. The essence of our orbital symmetry considerations for the hydride model system should and does carry over to those more complicated systems. Then our interest

lies in a rough theoretical estimate of the activation energies. In describing the elimination of ethane, we must consider the elongation of the Pd–C distance and the rocking motion of the methyl groups in addition to the variation of C–Pd–C angle φ and P–Pd–P angle θ. Full geometry optimization was beyond our means, so we constructed two hypothetical reation coordinates. In the first path, the P–M–P angle θ (see **16**) is fixed

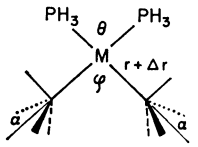

16

at 90°, while the C–Pd–C angle φ and the rocking angle α between the local three fold axis of the methyl group and the Pd–C bond extension were varied simultaneously (90—30° for φ, 0—60° for α). At the same time the Pd–C distance was stretched by Δr. The second reaction coordinate allowed θ to open from 90° to 150° while the above mentioned geometrical variations took place. We present the results for the second reaction path, the one which allows the $M(PH_3)_2$ remnant more freedom, in Fig. 8. The first reaction path differs only in destabilization of the product side.

It is clear from Fig. 8 that the calulated activation energies for ethane elimination are in the order $Pd(CH_3)_4^{2-}$>$Pd(PH_3)_2(CH_3)_2$>$Ni(PH_3)_2(CH_3)_2$. This trend accords with our previous conclusions (2) and (3) based on the hydride model calculations. Estimated activation energies (second, more complete reaction coordinate) are around 2.9, 1.7, and 0.6 eV for $Pd(CH_3)_4^{2-}$, $Pd(PH_3)_2(CH_3)_2$, and $Ni(PH_3)_2(CH_3)_2$ respectively. These numbers are all larger than the computed activation energies of the corresponding hydride models, PdD_4^{2-}, $PdD_2A_2^{2-}$, and $PdA_2D_2^{2-}$, probably because of the bulk of the CH_3 groups and/or Pd–CH_3 bond weakening necessitated by the rocking motion.

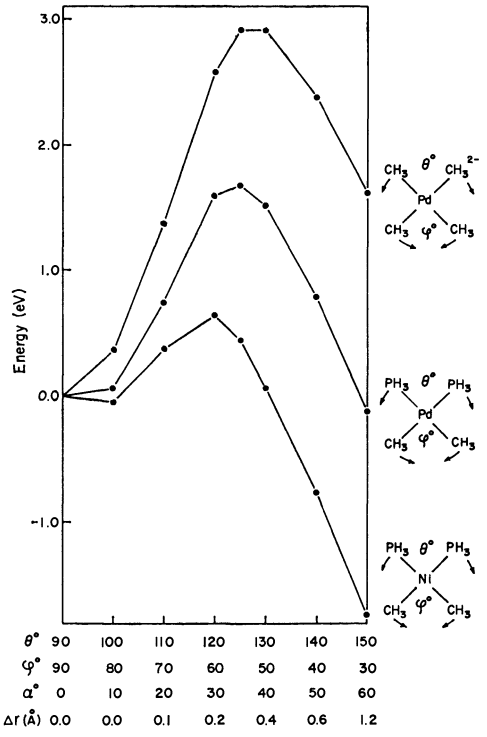

Fig. 8. Total energy changes along the hypothetical reaction path for elimination of ethane from $Pd(CH_3)_4^{2-}$, $Pd(PH_3)_2(CH_3)_2$, and $Ni(PH_3)_2(CH_3)_2$. In the reaction path the three angles and the M–C (of a leaving CH_3) distance, which are defined in **16**, are varied simultaneously. The reaction path is defined by the values or θ, φ, α, and r given at the bottom.

We have investigated briefly the possibility of direct elimination of R_2 from a *trans*-PdR_2L_2 system through a quasi-tetrahedral transition state. The energy required to achieve such a geometry is very high, and we think this reaction mode is unlikely, at least for Pd(II) or Pt(II).

Whether a given four-coordinate complex in Scheme 1 eliminates R_2 or chooses another path, possibly ligand dissociation, depends on the relative activation energies of the various processes. Unfortunately extended Hückel calculations are not reliable for such a comparison. Nevertheless we believe that our calculations on model compounds provide a theoretical framework for understanding why the Ni complexes eliminate alkanes from the four-coordinate geometry, whereas their Pd (and Pt) analogues do different things.

Reductive Elimination from Three-coordinate Complexes.

Kinetic studies of *cis* Pd(II)[4,3] dimethyls and Au(III) trimethyls[5] indicate that elimination is preceded by a dissociative step. The resulting MLR_2 intermediate is a representative of the intriguing d^8 ML_3 class of complexes. The geometrically attractive trigonal planar structure (**7**) for these molecules turns out to be Jahn-Teller unstable in the low-spin configuration. Distortions to T or Y shaped structures (**8** or **9**) ensue. The structure of the potential energy surface is summarized in **17**.[5b] Both T and Y shaped structures should be more stable than the trigonal geometry, but which alternative is the absolute minimum cannot be easily predicted. Whichever conformation is preferred, interconversion

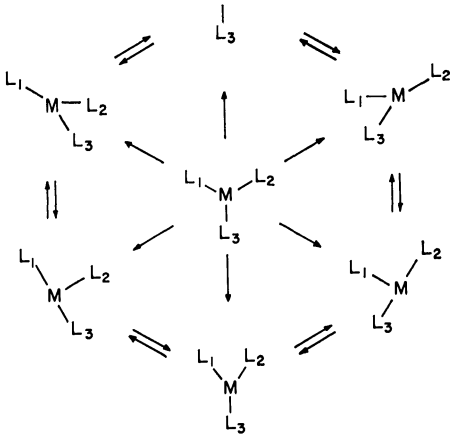

17

of isomeric C_{2v} equilibrium structures (if the ligands differ) is most unlikely to occur through the D_{3h} hill in the middle, but may proceed easily by sweeping through less symmetrical C_s waypoints along the periphery of the Jahn-Teller wheel. Direct structural evidence for deformation of d^8 ML_3 complexes is hard to come by because of the coordinative unsaturation of such 14 electron complexes. If ligand steric bulk is used to stabilize such complexes, one has to worry that the very same ligand property will also perturb the equilibrium geometry from its idealized form. One case where one can see a clear T deformation is for $Rh(PPh_3)_3^+$.[15]

What if the ligand set is substantially asymmetric, as in the $Pd(CH_3)_2(PR_3)_2$ decompositions studied by the Stille and Yamamoto groups? If phosphine dissociation occurs we are led to a three coordinate PdR_2PR_3 complex. The ligand isomerization scheme **17** simplifies to **18**. By symmetry the right-hand side of **18** is identical to the left. We will soon present a detailed analysis of this polytopal surface. For the moment let us assume that the scheme summarizes the experimental possibilities and see how it fits the available experimental data.

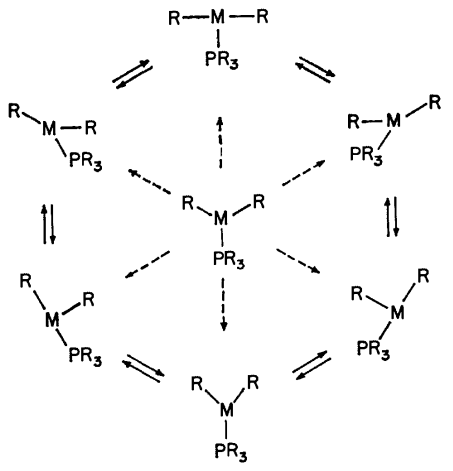

18

Least-motion departure of a phosphine from *cis* $Pd(CH_3)_2(PR_3)_2$ brings one into a T-shaped entry point in **18**, at 4 o'clock. It is easy to imagine a minor rearrangement to the Y-shapped conformer at 6 o'clock. This geometry is an obvious exit channel for elimination of R_2. Alternatively elimination could proceed directly from the T-shaped entry point.

Now consider the *trans* isomer of $Pd(CH_3)_2(PR_3)_2$. Departure of a phosphine leads one into **18** at 12 o'clock. Elimination from there is most unlikely. If the general features of the ML_3 surface were preserved one would nevertheless expect an easy transit around the Jahn-Teller wheel to 6 o'clock, the ethane exit channel. Apparently this does *not* happen. *trans* Dialkyl Pd complexes appear to be quite stable to simple reductive elimination, and instead often undergo β-elimination where that process is possible. Where reductive elimination occurs it is preceded by isomerization to the *cis* form, assisted either by polar, coordinating solvents,[4]

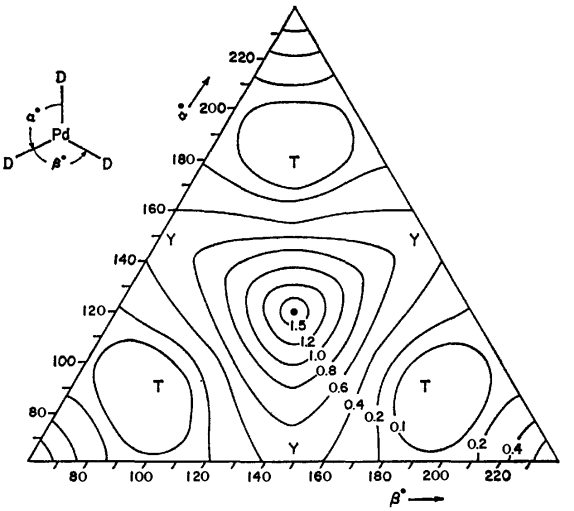

Fig. 9. Potential energy surface calculated for PdD_3^- varying the two D–Pd–D angles α and β. The energies of the contours are in electron volts relative to the T shape.

or by addition of the *cis* isomer, in an autocatalytic process.[3] Obviously the simple picture of unrestricted motion around the rim of **18** needs modification. We decided to investigate the effect of ligand electronic asymmetry on polytopal rearrangements in the three-coordinate manifold.

Again we first employ the hydride model, as we did for the four-coordinate complexes. Thus the d^8 molecules studied were PdD_3^-, $PdDA_2^-$, and $PdAD_2^-$. The characteristic features of the Jahn-Teller surface that we first delineated for $Au(CH_3)_3$ are preserved in the PdD_3^- surface (Fig. 9). A high hill of D_{3h} geometry is in the center surrounded by three descending ridges of Y-shaped geometry. Each of three equivalent T-shaped minima is in a round valley between the two ridges and has two open channels leading to reductive elimination. The activation energy for the elimination is about 0.1 eV, while the energy barrier for isomerization from one T-shape to another amounts to 0.4 eV.

The topology of the potential surface is explained by orbital diagram **19**. The half-filled e′ level immediate-

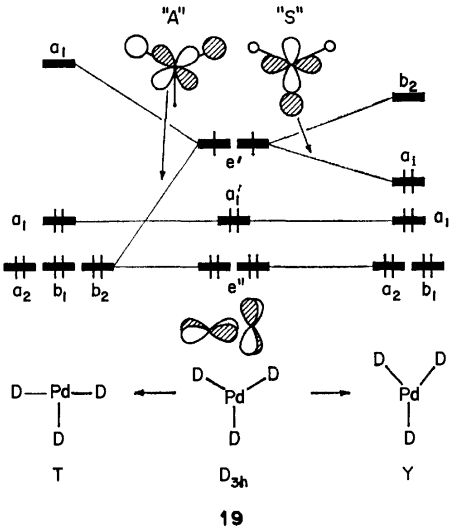

19

ly shows the Jahn-Teller instability of the D_{3h} geometry. When PdD_3^- is distorted to a T-shape, one of the e′ components, "A", is stabilized by decreasing Pd–D antibonding interaction and eventually becomes a pure Pd d orbital. On the other hand, the distortion to a Y-shape stabilizes another component, "S" of e′. But it is not by so much, because some Pd–D antibonding character still remains in the "S" component in the Y geometry. This is why the T-shape is more stable than the Y.

Potential surfaces for $PdAD_2^-$ and $PdDA_2^-$ are shown in Fig. 10. $PdAD_2^-$ will be a model for Pd-$(PR_3)(CH_3)_2$. In spite of the reduced symmetry, these surfaces maintain the basic electronic properties of the more symmetric PdD_3^-. The trigonal geometry is on a hill, and two kinds of approximate T-shapes are local minima.

Let us try to understand the relative stability of the T and Y shapes in these less symmetrical systems. We know from **19** that T is basically more stable than Y.

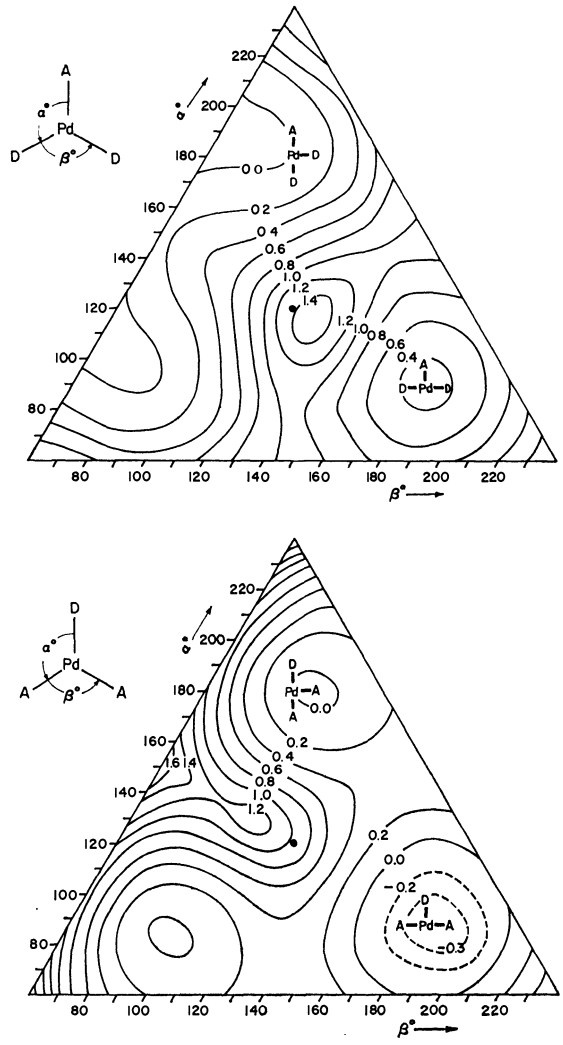

Fig. 10. Potential energy surfaces calculated for Pd-AD_2^-(top) and $PdDA_2^-$ (bottom), varying the two angles α(A–Pd–D) and β(D–Pd–D or A–Pd–A). The energies of the contours are in electron volts relative to the T shape in which one wing is occupied by D and another wing by A.

What is required is a procedure for evaluating substituent site preferences in T and Y. In the T form the occupied e′ component is "A" (see **19**) which has some ligand contribution on the wings of the T and so produces the charge distribution **20**. In the Y shape "S" is occupied, and that forces the charge imbalance shown in **21**. This is all relative to the trigonal form, where one can think of both orbitals equally occupied, by symmetry the same electron density on all ligands.

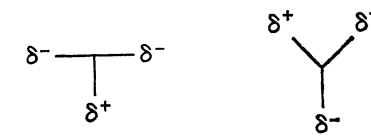

20 **21**

Now we reason that more *electronegative* substituents (poorer σ donors, better σ acceptors) will preferentially go where there is an excess of electron density.[16] The optimum substitution patterns that follow are presented in **22** and **23**. We can now summarize our qualitative

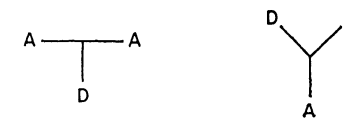

22 **23**

expectations for the relative stabilities of the asymmetric T and Y shapes, in Scheme 2. Beside some of the structures we place one or more arrows. Each indicates a stabilization, a solid arrow for the inherent greater stability of the T, a dashed arrow for fulfilling to a variable extent, the desired substitution pattern summarized in **22** or **23**. There is good qualitative agreement between Scheme 2 and the computed surfaces of Fig. 10.

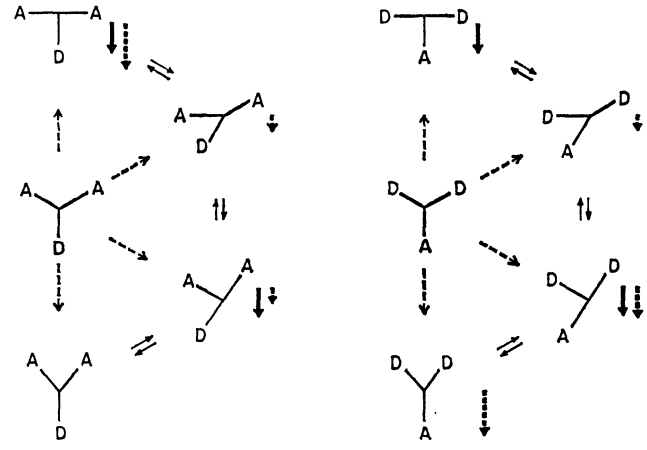

Scheme 2.

The triangular potential energy surfaces of Fig. 10 contain a great deal of interesting information. First note that reductive elimination of D_2 from **24** is just downhill in energy, while steep and high energy barriers

24 **25**

block the elimination of A_2 from **25**. The same trend was observed in reductive elimination from the four-coordinate system (conclusion (1))—*i.e.* a stronger σ-donor is a better leaving group. The similarity between the three- and four-coordinate systems can be traced in some detail, but the argument will not be presented here.

Another interesting consequence of the electronic asymmetry of A and D ligands to be seen from Fig. 10 is the creation of substantial energy barriers to a transit around the Jahn-Teller wheel. The activation energy for going from *trans*-$PdAD_2^-$ **26** to *cis*-$PdAD_2^-$, **27**, is

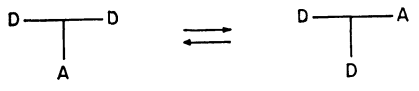

26 **27**

0.75 eV, and that for the reverse isomerization is 1.1 eV. Corresponding activation energies for $PdDA_2^-$ are 0.6 and 0.3 eV. Thus conclusion (4): *T-shaped* trans-$PdLR_2$, *which might be produced by liberating L from* trans-PdL_2R_2, *will encounter a substantial energy barrier to rearrangement of* cis-$PdLR_2$, *which has an open channel for reductive elimination of* R_2; *and* (5): *When the leaving groups are poor donors, A,* cis-trans *isomerization between two T-shaped geometries should be much easier than elimination of* A_2. *If R is a strong* σ *donor and L is a poor donor or an acceptor then the rearrangement from the* trans-*derived three-coordinate structure to the* cis-*derived one (motion from 12 o'clock to 4 in* ***18****) will not be facile.*

These are model calculations. They were supported by detailed examination of a surface for valence tautomerism in $Pd(PH_3)(CH_3)_2$, Fig. 11. P–Pd–C angles α and C–Pd–C angle β are varied. Note the presence of three T-shaped minima, and an activation energy of 0.5 eV for the *trans*→*cis* $Pd(PH_3)(CH_3)_2$ isomerization and 0.8 eV for the reverse reaction.[23] A hypothetical reaction coordinate for ethane elimination from T- and Y-shaped conformations was also studied, modelled after the first reaction coordinate of the four-coordinate complex, discussed above. The results of such a calculation are shown in Fig. 12. As one might have guessed from the surfaces in which only angles are varied, the elimination need not proceed directly from a Y-shaped locus. Instead one can start out from a T-geometry and pay no greater price in activation energy. The computed activation energy to ethane formation along this highly simplified reaction path is 1.1 eV. The general features of this $Pd(PH_3)(CH_3)_2$ calculation are in accord with the conclusions we reached on the hydride models.

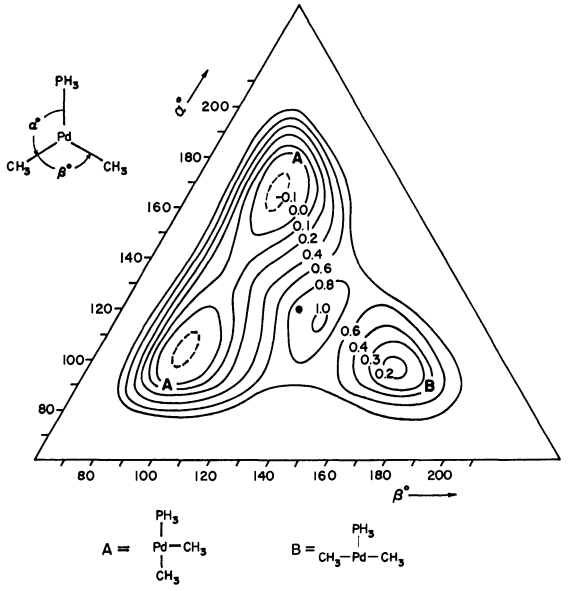

Fig. 11. Potential energy surface calculated for $Pd(PH_3)(CH_3)_2$ varying the two angles α(P–Pd–C) and β(C–Pd–C). The energies of the contours are in electron volts relative to the T shape defined by A below the triangle.

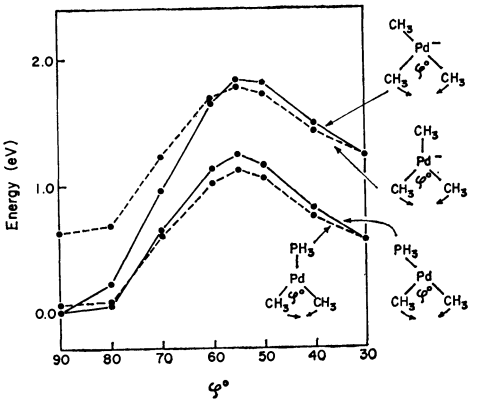

Fig. 12. Total energy changes along the hypothetical reaction path for the elimination of ethane from $Pd(CH_3)_3^-$ and $Pd(PH_3)(CH_3)_2$. The reaction path is the same one as that defined in Fig. 8, except that the angle θ is not included here. The solid lines are for the elimination reaction from the T shape while the dashed lines are for that from the Y shape.

Please return to Scheme 1, the starting point of our analysis. We have tried to elucidate but two aspects of the mechanism of reductive elimination—1. how changing the metal or the electronic properties of the ligands affects the activation energy for reductive elimination directly from the four-coordinate complex and 2. how ligand electronic asymmetry controls polytopal rearrangements, and thereby *cis-trans* isomerization and elimination, in the three-coordinate manifold. So much more remains to be understood.

We are grateful to J. Jorgensen for the drawings, to E. Stolz for the typing to the National Science Foundation for its support of this work through Research Grant CHE 7828048, and to the Exxon Education Foundation, some earlier work on $PtXY_2$ isomerizations had been carried out in our group by D. L. Thorn.

Appendix I

Our calculations are of the extended Hückel type[17] with a weighted H_{ij} approximation.[18] The Coulomb integrals and orbital exponents are listed in Table 1. The metal parameters were taken from the following sources: Exponents of Ni 3d orbitals were taken from the work of Richardson *et al.*,[19] while those of Pd 4d, 5s and 5p, and Pt 5d orbitals were from the Basch and Gray orbitals.[20] Other exponents are those given by previous work.[21] The H_{ii}'s for Pt[21] and Ni[22] are the same as those used previously. For Pd charge iterations were performed on *trans*-$Pd(CH_3)_2(PH_3)_2$ assuming a quadratic dependence of metal H_{ii}'s on charge.

TABLE 1. EXTENDED HUCKEL PARAMETERS USED IN THE CALCULATIONS

Parameters	H_{ii}/eV	Orbital exponent[a]
Ni 3d	−13.49	5.75(0.5798)+2.30(0.5782)
4s	−9.17	2.10
4p	−5.15	2.10
Pd 4d	−12.02	5.983(0.5535)+2.613(0.6701)
5s	−7.32	2.190
5p	−3.75	2.152
Pt 5d	−12.59	6.013(0.6334)+2.696(0.5513)
6s	−9.077	2.554
6p	−5.475	2.554
C 2s	−21.4	1.625
2p	−11.4	1.625
P 3s	−18.6	1.60
3p	−14.0	1.60
H 1s	−13.6	1.3
"D" 1s	−11.75	1.3
"A" 1s	−14.34	1.3

a) For the d functions a double zeta expansion was used. The expansion coefficients are given in parentheses.

Geometrical assumptions included the following: C–H 1.09, P–H 1.42, Ni–C 2.02, Ni–P 2.23, Pd–C 2.05, Pd–P 2.30, Ni–D(A) 1.60, Pd–D(A) 1.65, Pt–D(A) 1.75Å; PH_3 and CH_3 tetrahedral.

Appendix II

There is no unique way to define the coordinate system in the molecules under study. The "classical" choice for a four-coordinate complex, **28**, is tied to D_{4h} symmetry. It

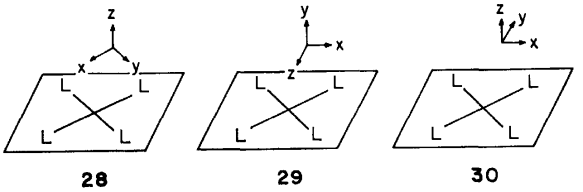

28 **29** **30**

makes the destabilized d orbital the familiar-sounding $d_{x^2-y^2}$. But the axis system of **28** is cumbersome if one wishes to study a reductive elimination that preserves C_{2v} symmetry, for the C_2 axis preserved is not one of the axes of **28**. Neither are d_{xz} and d_{yz} appropriate symmetry adapted linear combinations. **29** would be more appropriate, but it in turn loses the mnemonic connection to the classical square-planar crystal field. We choose to compromise, using **30**. This retains the z axis where the four-fold axis used to be, and allows the use of d_{xz} and d_{yz}. The price we pay is that the destabilized d orbital is d_{xy}, not $d_{x^2-y^2}$. And we have to use the non-standard character table, Table 2.

TABLE 2. C_{2v} CHARACTER TABLE USED IN THIS WORK

	E	$C_2(y)$	$\sigma(yz)$	$\sigma(xz)$
A_1	1	1	1	1
A_2	1	1	−1	−1
B_1	1	−1	1	−1
B_2	1	−1	−1	1

References

1) R. H. Grubbs, A. Miyashita, M. Liu, and P. Burk, *J. Am. Chem. Soc.*, **99**, 3863 (1977); **100**, 2418 (1978); R. H. Grubbs and A. Miyashita, *ibid.*, **100**, 1300, 7416, 7418 (1978).

2) The reductive elimination of NiR_2(dipyridyl) is accelerated by a presence of electronegative olefins, suggesting formation of five coordinated Ni complexes prior to the elimination steps; T. Yamamoto, A. Yamamoto, and S. Ikeda, *J. Am. Chem. Soc.*, **93**, 3350, 3360 (1971).

3) F. Ozawa, T. Ito, Y. Nakamura, and A. Yamamoto, *Bull. Chem. Soc. Jpn.*, see the preceding paper; F. Ozawa, T. Ito, and and A. Yamamoto, *J. Am. Chem. Soc.*, in press.

4) D. Milstein and J. K. Stille, *J. Am. Chem. Soc.*, **101**, 4981 (1979); A. Gillie and J. K. Stille, *ibid.*, **102**, 4933 (1980).

5) a) A. Tamaki, S. A. Magennis, and J. K. Kochi, *J. Am. Chem. Soc.*, **96**, 6140 (1974); A. Tamaki and J. K. Kochi, *J. Organomet. Chem.*, **40**, C81 (1972); **51**, C39 (1973). b) S. Komiya, T. A. Albright, R. Hoffmann, and J. K. Kochi, *J. Am. Chem. Soc.*, **98**, 7255 (1976); **99**, 8440 (1977).

6) a) G. M. Whitesides, J. F. Gaasch, and E. R. Stedronsky, *J. Am. Chem. Soc.*, **94**, 5258 (1972); J. X. McDermott, J. F. White, and G. M. Whitesides, *ibid.*, **98**, 6521 (1976); G. B. Young and G. M. Whitesides, *ibid.*, **100**, 5808 (1978). b) S. Komiya, A. Yamamoto, and T. Yamamoto, *Chem. Lett.*, **1978**, 1273. c) Pyrolyses of $PtL_2(R)_2$ (L=PPh_3 *etc.*, L_2=dppm, dppe, R=Ph, *p*-$CH_3C_6H_4$, and CH_3 *etc.*,) yield the reductive elimination products R–R at high temperature 150—260 °C. In this case β-hydrogen elimination cannot take place. Added phosphines enhance the reductive elimination. Five-coordinated complexes $PtL_3(R)_2$ are proposed as intermediates for the reaction; P. S. Braterman, R. J. Cross, and G. B. Young, *J. Chem. Soc., Dalton Trans.*, **1976**, 1306 and 1310; F. Glockling, T. McBride, and R. J. I. Pollock, *J. Chem. Soc., Chem. Commun.*, **1973**, 650; J. D. Ruddick and B. L. Shaw, *J. Chem. Soc., A*, **1969**, 2969.

7) M. P. Brown, R. J. Puddephatt, and C. E. Upton, *J. Organomet. Chem.*, **49**, C61 (1973); *J. Chem. Soc., Dalton Trans.*, **1974**, 2457.

8) R. J. McKinney, D. L. Thorn, R. Hoffmann, and A. Stockis, to be published.

9) R. G. Pearson, *Acc. Chem. Res.*, **4**, 152 (1971); *Pure Appl. Chem.*, **27**, 145 (1971); *Fortschr. Chem. Forsch.*, **41**, 75 (1973); "Symmetry Rules for Chemical Reactions," Wiley-Interscience, New York (1976), pp. 286, 405.

10) P. S. Braterman and R. J. Cross, *Chem. Soc. Rev.*, **2**, 271 (1973).

11) B. Åkermark and A. Ljungqvist, *J. Organomet. Chem.*, **182**, 59 (1979); B. Åkermark, H. Johansen, B. Roos, and U. Wahlgren, *J. Am. Chem. Soc.*, **101**, 5876 (1979).

12) R. B. Woodward and R. Hoffmann, *Angew. Chem.*, **81**, 797 (1969).

13) See Appendix II for a discussion of the coordinate systems.

14) The metal part of the b_2 orbital **14** (or **11**) is here

mainly d_{xy}. In our previous work on tetraalkyl gold the analogous orbital was mainly metal p_x. This is a consequence of the different metal parameters—in the Au(III) case the d orbitals were very low in energy and in metal-ligand interaction mainly metal s and p orbitals were used. In our present calculations the s and p orbitals are relatively high, and it is the metal d functions which interact most. The arguments carry through no matter which metal orbitals are involved.

15) Y. W. Yared, S. L. Miles, R. Bau, and C. A. Reed, *J. Am. Chem. Soc.*, **99**, 7076 (1977).

16) This type of argument has been successfully used by us before: R. Hoffmann, J. M. Howell, and E. L. Muetterties, *J. Am. Chem. Soc.*, **94**, 3047 (1972); A. R. Rossi and R. Hoffmann, *Inorg. Chem.*, **14**, 365 (1975); R. Hoffmann, J. M. Howell, and A. R. Rossi, *J. Am. Chem. Soc.*, **98**, 2484 (1976); R. Hoffmann, B. F. Beier, E. L. Muetterties, and A. R. Rossi, *Inorg. Chem.*, **16**, 511 (1977).

17) R. Hoffmann, *J. Chem. Phys.*, **39**, 1397 (1963); R. Hoffmann and W. N. Lipscomb, *ibid.*, **36**, 2179 (1962); **37**, 2872 (1962).

18) J. H. Ammeter, H.-B. Bürgi, J. C. Thibeault, and R. Hoffmann, *J. Am. Chem. Soc.*, **100**, 3686 (1978).

19) J. W. Richardson, R. R. Powell, and W. C. Nieuwpoort, *J. Chem. Phys.*, **38**, 796 (1963).

20) H. Basch, A. Viste, and H. B. Gray, *Theor. Chim. Acta*, **3**, 458 (1965).

21) R. H. Summerville and R. Hoffmann, *J. Am. Chem. Soc.*, **98**, 7240 (1976).

22) A charge iteration on the model porphyrin complex $Ni(NH_2)_4^{2-}$, K. Tatsumi and R. Hoffmann, to be published.

23) **Note added in proof**. A recent study, T. J. McCarthy, R. G. Nuzzo, and G. M. Whitesides, *J. Am. Chem. Soc.*, **103**, 1676 (1981) provides an excellent confirmation of our conclusions: Isotopic labeling and kinetics indicate that the two Pt-bound Et groups of a coordinatively unsaturated $Pt(PEt_3)$-Ft_2 intermediate lose hydrogen with approximately equal probability.

  Bull. Chem. Soc. Jpn., 54, 1868—1880 (1981) [Vol. 54, No. 6

Mechanisms of Thermal Decomposition of *trans*- and *cis*-Dialkylbis-(tertiary phosphine)palladium(II). Reductive Elimination and *trans* to *cis* Isomerization

Fumiyuki Ozawa, Takashi Ito,** Yoshiyuki Nakamura, and Akio Yamamoto*

Research Laboratory of Resources Utilization, Tokyo Institute of Technology, Nagatsuta, Midori-ku, Yokohama 227

(Received August 30, 1980)

Series of *trans*- and *cis*-dialkylpalladium(II) complexes having tertiary phosphine ligands (L) of various basicities and bulkiness have been prepared and their thermolysis and isomerization mechanisms in solution have been studied. Examination of the cause of selective formation of *cis*-dialkyl isomers by using alkyllithium revealed a new type of *trans* to *cis* isomerization promoted by the alkyllithium. A process involving the formation of a trialkylpalladate intermediate is proposed as a mechanism for the *trans* to *cis* isomerization. Evidence to support the mechanism has been obtained by experiments using $LiCD_3$. Thermolysis of *cis*-PdR_2L_2 has been demonstrated to proceed through a unimolecular process initiated by a rate-determining dissociation of L to produce a three-coordinate "*cis*-PdR_2L" which reductively eliminates the R groups. Addition of free ligand to the system containing *cis*-$PdMe_2L_2$ effectively blocks the reductive elimination pathway thus forcing the complex to be thermolyzed by a route involving liberation of methane. The second, novel type of *trans* to *cis* isomerization reaction proceeding *via* an intermolecular methyl transfer process has been discovered. As the crucial intermediate in the process a methyl-bridged complex formed between the partly dissociated three-coordinate species and undissociated complex has been postulated. Thermolysis of *trans*-$PdMe_2L_2$ has been found to proceed *via* initial isomerization to the *cis* form followed by reductive elimination. The *trans-cis* isomerization equilibrium greatly favors the *cis* form for complexes having phenyl-substituted phosphines. For the PEt_3-coordinated palladium dimethyl, however, an equilibrium *trans*/*cis* ratio of 1.2 is reached at 39 °C. Factors influencing the stability of the palladium alkyls having the tertiary phosphine ligand are discussed on the basis of the present results as well as comparison of the thermolysis behavior of *trans*-$PdEt_2L_2$ and other transition metal alkyls. The presence of an energy barrier between the dissociated T-shaped intermediates *trans*-$PdMe_2L$ and *cis*-$PdMe_2L$ has been assumed. A unimolecular reductive elimination pathway proceeding from the T-shaped *cis*-$PdMe_2L$ intermediate through a Y-shaped transition state consistently accounts for the thermolysis as well as isomerization behavior of the *trans*- and *cis*-$PdMe_2L_2$.

Despite the abundance of organic reactions promoted by palladium and its compounds,[1] the fundamental studies on the behavior of alkylpalladium compounds, which may be regarded as key compounds in the Pd-promoted reactions, are still scarce.[2,3] By studying the decomposition mechanisms of palladium alkyls having stabilizing ligands such as tertiary phosphines, one can expect to get important information concerning the factors controlling the cleavage of the Pd–C bond and the subsequent C–C coupling reactions of the alkylpalladium complexes coordinated with the stabilizing ligands. The recent study by Stille and co-workers contributed to unveil part of the decomposition mechanisms of dialkylpalladium complexes having tertiary phosphine ligands,[2] but obviously more studies are required for understanding fundamental properties of the palladium alkyls.

As continuation of our effort to clarify the behavior of various transition metal alkyls,[4] we have prepared series of *cis*- and *trans*-dialkylbis(tertiary phosphine)-palladium(II) and have studied the chemical properties of these complexes. Examination of the thermolysis mechanisms of these isolated *cis* and *trans* complexes provides us a rare opportunity to study the crucial roles of the tertiary phosphine ligands in enhancing the stability of transition metal alkyls, affecting the thermolysis pathways, and determining the configurations of these complexes. In the previous paper we confirmed that *trans*-PdR_2L_2 (R=Et, Pr^n, and Bu^n; L=various tertiary phosphines) is thermolyzed through clean β-elimination pathways, liberating 1 : 1 mixtures of alkane and alkene. The reactions were shown to proceed predominantly from undissociated four-coordinate

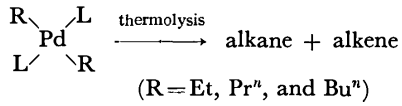

(R=Et, Pr^n, and Bu^n)

species.[5] It was noted that the presence of the free tertiary phosphine ligands had small effect in hindering the thermolysis, and we proposed a thermolysis mechanism involving distortion from the square-planar configuration to facilitate the β-hydrogen elimination.

In the present paper we report the results of our mechanistic studies on thermolysis of *cis*- and *trans*-$PdMe_2L_2$, and of *cis*-$PdEt_2L_2$ and on *trans-cis* isomerization of the dimethylpalladium complexes. In contrast to the minor inhibition effect of tertiary phosphine ligands on β-elimination reaction of *trans*-PdR_2L_2 (R=Et, Pr^n, Bu^n), a pronounced inhibition effect of tertiary phosphine ligands on reductive elimination of the alkyl groups from *cis*-PdR_2L_2 type complexes was revealed. Two new types of *trans-cis* isomerization reactions were discovered. The behavior of these palladium alkyls was found to have some similarities with that of AuR_3L type complexes[6] which liberate the coordinated tertiary phosphine ligand in order to initiate reductive elimina-

** Present address: Department of Materials Chemistry, Faculty of Engineering, Yokohama National University, Tokiwadai, Hodogaya-ku, Yokohama 240.

tion of the alkyl groups and isomerization between trialkylgold isomers having different alkyl groups.

Results and Discussion

Preparation of cis- *and* trans-*PdR_2L_2*. Employment of suitable synthetic methods has been found to lead to selective production of *cis*- and *trans*-PdR_2L_2. The *trans* isomers can be conveniently prepared by treating $Pd(acac)_2$ (acac=2,4-pentanedionato ligand) with $AlR_2(OEt)$ (R=Me, Et, Pr^n, Bu^n), or more preferably with $Al_2R_3(OEt)_3$, in the presence of tertiary phosphines (Method A, Eq. 1).[3,5] The *trans* isomers obtained by Method A are sometimes contaminated with *cis* isomers which may be removed by recrystallization. The *cis* isomers are prepared by alkylating $PdCl_2L_2$ with alkyllithium (Method B, Eq. 2).[7] For some complexes having basic tertiary phosphines such as PEt_3 where the preparation of a *cis* isomer by Method B is not suitable, a ligand exchange reaction of PEt_3 with another *cis* isomer provides an indirect route to selectively prepare the *cis* isomer (Method C, Eq. 3, Scheme 1).

Method A

$$Pd(acac)_2 + \text{excess } AlR_2(OEt) \text{ or } Al_2R_3(OEt)_3 + 2L \xrightarrow[-70 \text{ to } 0\,^\circ C]{Et_2O} \textit{trans}\text{-}PdR_2L_2 (+\textit{cis}\text{-}PdR_2L_2) \quad (1)$$

(I—V)

(R=Me, Et, Pr^n, Bu^n; L=PEt_3, PMe_2Ph, PEt_2Ph, $PMePh_2$, $PEtPh_2$)

Method B

$$PdCl_2L_2 + \text{excess LiR} \xrightarrow[0\,^\circ C \text{ to room temp}]{Et_2O} \textit{cis}\text{-}PdR_2L_2 \quad (2)$$

(**2**—**5**)

(R=Me, Et; L=PMe_2Ph, PEt_2Ph, $PMePh_2$, $PEtPh_2$)

Method C

$$\textit{cis}\text{-}PdMe_2(PMePh_2)_2 + PEt_3 \quad (\textbf{4a}) \xrightarrow[\text{room temp}]{Et_2O} \textit{cis}\text{-}PdMe_2(PEt_3)_2 \quad (3)$$

(**1a**)

Scheme 1.

Employment of the chelating diphenylphosphinoethane (dpe) ligand gives the *cis* isomers by the spatial constraint posed by the chelating ligand even by using Method A. The isolated dialkylpalladium complexes are listed in Table 1 with reference to the preparative methods. For differentiation of the isomers we use the Roman letters for describing the *trans* isomers and gothic Arabic numbers for representing the *cis* isomers.

Characterization of the complexes has been made on the basis of elemental analysis and IR and NMR spectroscopy. The characteristic IR and ^1H NMR data of the dimethyl- and diethylpalladium complexes are given in Table 2 (for further details of characterization, see Experimental part).

The trans-cis *Isomerization of $PdMe_2L_2$ Promoted by Alkyllithium.* Examination of the cause of the selective production of the *cis* and *trans* isomers by using different experimental methods led us to the discovery of a new type of isomerization reaction. The ethyl as well as the methyl complexes show similar behavior. Here we deal mainly with the *trans-cis* isomerization of the methyl complexes, since the isomerization of the ethyl complexes are essentially similar but complicated by their thermal instability.

Table 1. List of isolated PdR_2L_2

Compound				Method[a]
Configuration	R	L		
trans	Me	PEt_3	Ia	A
		PEt_2Ph	IIIa	A
		$PMePh_2$	IVa	A
		$PEtPh_2$	Va	A
	Et	PEt_3	Ib	A
		PMe_2Ph	IIb	A
		PEt_2Ph	IIIb	A
		$PMePh_2$	IVb	A
		$PEtPh_2$	Vb	A
	n-Pr	PEt_3	Ic	A
		PMe_2Ph	IIc	A
		$PMePh_2$	IVc	A
	n-Bu	PMe_2Ph	IId	A
cis	Me	PEt_3	**1a**	C
		PEt_2Ph	**3a**	B
		$PMePh_2$	**4a**	A, B
		$PEtPh_2$	**5a**	B
	Et	PMe_2Ph	**2b**	B
		PEt_2Ph	**3b**	B
	Me	dpe[b]	**6a**	A
	Et	dpe[b]	**6b**	A
	n-Pr	dpe[b]	**6c**	A

a) See Scheme 1. b) dpe=$Ph_2PCH_2CH_2PPh_2$.

The *trans*-$PdMe_2(PEt_2Ph)_2$ (IIIa) was found to isomerize readily to the *cis* isomer (**3a**) in high yield on treatment with two equivalents of LiMe in ether for 2 h at room temperature. The LiMe was removed by hydrolysis after the isomerization was complete. Treatment of the *trans* isomer (IIIa) with 1.5 equivalents of $AlMe_2(OEt)$ under similar conditions did not give any *cis* isomer and the unreacted IIIa was recovered. It was further established that treatment of *trans*-$Pd(CH_3)_2(PEt_2Ph)_2$ (IIIa) with an equimolar amount of $LiCD_3$ in ether at room temperature gave the *cis* isomer (**3a'**) containing the CD_3 group after removal of the methyllithium by hydrolysis. Thermolysis of **3a'** at 60 °C in toluene containing dimethyl maleate, the presence of which serves to cause the clean thermolysis of the dialkyl complexes (*vide infra* and Ref. 5), released CD_3CD_3, CH_3CD_3, and CH_3CH_3 in a molar ratio of 0.18; 0.48: 0.34. Methyl scrambling was also observed in the reaction of *cis*-$Pd(CH_3)_2(PEt_2Ph)_2$ with an

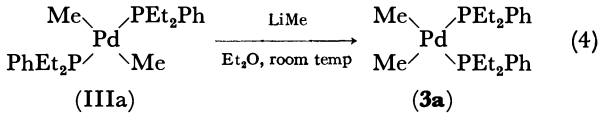

(IIIa) (**3a**) (4)

Table 2. IR[a] and ^{1}H NMR[b] data of PdR_2L_2 (R=Me, Et)

	Compound R	L		IR Data: Pd-R group δ(C-H)	IR Data: Pd-R group ν(Pd-C)	^{1}H NMR Data[c]: Pd-R -CH$_3$	Pd-R -CH$_2$-	P-R -CH$_3$	P-R -CH$_2$-
trans	Me	PEt_3	Ia	1130	455	−0.61(t)[d]	—	1.10(qui)[g]	1.75(m)
		PEt_2Ph	IIIa	1135	462	−0.55(t)[e]	—	1.17(qui)[g]	2.17(m)
		$PMePh_2$	IVa	1140	460	−0.91(t)[f]	—	1.92(t)[h]	—
		$PEtPh_2$	Va	1140	450	−0.82(t)[e]	—	1.13(qui)[g]	2.31(m)
	Et	PEt_3	Ib	1145, 1360	455	—[i]	0.33(q)[g]	1.12(qui)[g]	1.82(m)
		PMe_2Ph	IIb	1135, 1350	452	0.92(t)[g]	0.36(q)[g]	1.68(t)[h]	—
		PEt_2Ph	IIIb	1135, 1350	440	1.31(t)[g]	0.71(q)[g]	0.92(qui)[g]	1.92(m)
		$PMePh_2$	IVb	1140, 1355	455	0.41(t)[k]	0.05(q)[k]	1.99(t)[k]	—
		$PEtPh_2$	Vb	1140, 1355	455	0.55(t)[k]	0.17(q)[k]	1.23(qui)[k]	2.41(m)
cis	Me	PEt_3	**1a**	1120	465, 487	0.07(q)[j]	—	1.16(dt)[i]	1.79(m)
		PEt_2Ph	**3a**	1120	478, 505	0.17(q)[j]	—	1.04(dt)[i]	1.89(m)
		$PMePh_2$	**4a**	1125	475, 510	0.10(q)[j]	—	1.58(d)[e]	—
		$PEtPh_2$	**5a**	1123	470, 515	0.15(q)[j]	—	1.09(dt)[i]	1.81(m)
	Et	PMe_2Ph	**2b**[m]	1130, 1150, 1355	475, 490	1.20(br)[k]	1.02(br)[k]	1.38(d)[f]	—
		PEt_2Ph	**3b**[m]	1130, 1148, 1352	470, 505	1.15(t)[k]	0.99(br)[k]	0.88(dt)[k]	1.80(m)

a) KBr disc, in cm^{-1}. b) 100 MHz, chemical shifts are in δ values (ppm) with respect to Me_4Si as an external or internal standard (down field positive). Solvent: acetone-d_6 (Ia, IIIa, Ib, IIb, **1a**, **3a**, **4a**, **5a**, **2b**, **3b**); toluene-d_8 (IIIb); CD_2Cl_2 (IVa, Va, IVb, Vb). Temp (°C): 25 (Ia, IIIa, Ib, **1a**, **3a**, **4a**); −20 (IIb, IIIb, **5a**), −40 (IVa, Va, IVb, Vb, **2b**, **3b**). c) Multiplicity abbreviations are: d, doublet; t, triplet; q, quartet; qui, quintet; m, multiplet; dt, doublet of triplets. Coupling constants in Hz: d) 5.5. e) 5. f) 6. g) 8. h) 2. i) ^3J(HH)=7, ^3J(PH)=14. j) Abnormal quartet, see Ref. 3. k) Coupling constants are obscured due to broadening. e) Chemical shift is obscured due to the signals of P–C–CH$_3$ protons. m) Chemical shifts of these complex were determined by using ^{1}H{^{31}P} NMR.

equimolar amount of $LiCD_3$. Thermolysis of the isolated *cis*-$PdMe_2(PEt_2Ph)_2$ containing the CD_3 group librated CD_3CD_3, CD_3CH_3, and CH_3CH_3 in a molar ratio of 0.13: 0.40: 0.47. Since the calculated ratio of the deuterated and undeuterated ethanes expected on the assumption of random scrambling of the methyl groups in the 1: 1 mixture of the methylpalladium and the trideuterio methyllithium is 0.11: 0.45: 0.45, and the separate experiment has established that the thermolysis of **3a** proceeds *via* a unimolecular process as discussed later, the results indicate that complete intermolecular scrambling of the methyl groups takes place on treatment of the *trans*- or *cis*-$PdMe_2(PEt_2Ph)_2$ with methyllithium.

Based on these results, we propose the following isomerization mechanism, which accounts for the predominant formation of the *cis* isomers when alkyllithiums are employed as the alkylating agent for preparation of the palladium alkyls. In this scheme, approach of the methyl anion toward the square-planar complex, forming an ionic penta-coordinated species (**A**) from which the tertiary phosphine ligand is displaced to give a square-planar trimethylpalladate intermediate, (**B**) seems to be a reasonable assumption.[8] Ensuing coordination of the phosphine ligand to the square-planar intermediate would displace one of the methyl groups, reforming a square-planar dimethyl complex. If the displacement reaction by L dispels the methyl group situated at the *cis* position to the remaining L, the regenerated complex formed through the intermediate (**A'**) in Scheme 2 would have the *cis* configuration, whereas displacement of the methyl

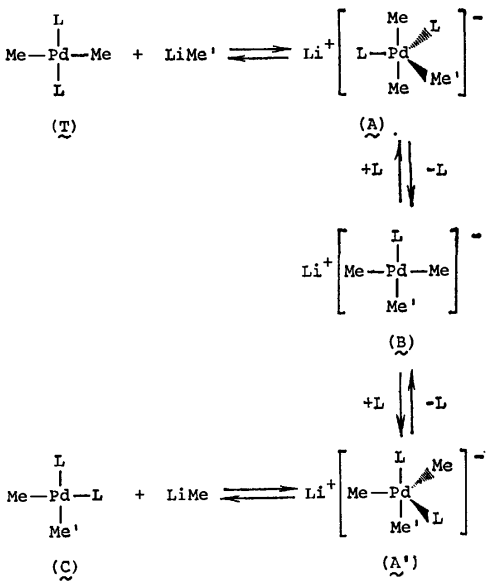

Scheme 2. Proposed mechanism for the *trans-cis* isomerization of $PdMe_2L_2$ promoted by methyllithium.

group (Me') *trans* to the remaining L in (**B**) would revert the square-planar intermediate back to the initial *trans* configuration. If one assumes that the *trans* effect of the methyl group in the intermediate (**B**) is greater than that of L, the preferential formation of the *cis* configuration may be reasonably explained. An alternative scheme involving a trigonal-bipyramid containing the phosphine ligands in axial positions as an

intermediate corresponding to (**A**) is also conceivable, although in that case pseudo rotation by a Berry mechanism should be invoked to account for the *trans-cis* isomerization and consequently the mechanism is less straightforward than the one proposed in Scheme 2. The proposed mechanism is reminiscent of the isomerization mechanism of $MCl_2(PR_3)_2$ (M=Pd, Pt) promoted by PR_3.[9] Although there has been no report on preparation of alkylpalladate type complexes, the assumption of the intermediate alkylpalladate does not seem unreasonable in view of the reported examples of the corresponding alkyl analogs of nickel, platinum, and gold.[10]

Table 3. Gases evolved on thermolysis of PdR_2L_2 (R=Me, Et)[a]

Run	Compound	Evolved gas ratio				Total[b] amounts
		R(-H)	RH	RR	Others	
1	*trans*-$PdMe_2(PEt_2Ph)_2$(IIIa)	—	0.04	0.96	c)	0.98
2	*trans*-$PdMe_2(PMePh_2)_2$(IVa)	—	0.08	0.92	c)	0.86
3	*trans*-$PdMe_2(PEtPh_2)_2$(Va)	—	0.05	0.95	c)	0.83
4	*cis*-$PdMe_2(PEt_2Ph)_2$(**3a**)	—	0.01	0.99	c)	0.96
5	*cis*-$PdMe_2(PMePh_2)_2$(**4a**)	—	0.04	0.96	c)	0.96
6	*cis*-$PdMe_2(PEtPh_2)_2$(**5a**)	—	0.01	0.99	c)	0.91
7	*cis*-$PdMe_2$(dpe)(**6a**)	—	0.02	0.98	c)	0.86
8	*trans*-$PdEt_2(PMe_2Ph)_2$(IIb)	0.49	0.51	—	—	0.95
9	*trans*-$PdEt_2(PEt_2Ph)_2$(IIIb)	0.49	0.49	0.02	—	1.03
10	*cis*-$PdEt_2(PMe_2Ph)_2$(**2b**)	trace	trace	1.00	—	0.94
11	*cis*-$PdEt_2(PEt_2Ph)_2$(**3b**)	trace	trace	1.00	—	0.85
12	*cis*-$PdEt_2$(dpe)(**6a**)	0.41	0.41	0.18	—	0.90

a) [Complex]≈0.05 mol/l. Solvent; benzene (Runs 1, 3, and 4); toluene (Runs 2 and 5—12). Additive; dmm (0.17 mol/l). Thermolysis temp (°C); 60 (Runs 1—7 and 12); 55 (Run 8); r.t. (Runs 9—11). b) Total amounts (mol/mol of complex)=[(1/2){R-(-H)+R(H)}+RR]/(complex). c) Evolution of a trace amount of C_2H_4 was observed.

Thermolysis Mechanism of PdR_2L_2. In the previous papers thermolysis of PdR_2L_2 in the solid state[3] and of *trans*-PdR_2L_2 (R=Et, Pr^n, Bu^n), in solution[5] has been reported. Having established procedures for selective synthesis of the *cis*- and *trans*-alkyls, we now examine the thermolysis behavior of these complexes in solutions. Table 3 summarizes the distribution of hydrocarbons produced in thermolysis of various palladium methyls and ethyls. For obtaining quantitative data regarding the thermolysis of palladium alkyls it is essential to carry out the thermolysis under conditions which allow the complete liberation of the alkyl groups and prevent the precipitation of palladium metal in the reaction system. Otherwise, accurate measurement of the amounts of the liberated hydrocarbon products is hindered and release of the tertiary phosphine by decomposition of the phosphine-coordinated palladium complexes prevents the thermolysis of the remaining palladium alkyls and may severely distort the thermolysis kinetics. As it has been proved quite useful in the thermolysis study of *trans*-PdR_2L_2,[5] addition of dimethyl maleate (dmm) into the system containing the palladium alkyl under investigation serves quite satisfactorily to trap the $L_2Pd(0)$ complexes displacing all of the olefin produced by β-elimination and prevents the undesirable side reactions which may liberate the tertiary phosphine ligand to affect the thermolysis course. It has been confirmed that addition of dmm did not alter the rate of thermolysis of the palladium alkyls. Table 3 indicates that thermolysis of *trans*- and *cis*-$PdMe_2L_2$ liberates cleanly almost all of the methyl groups as ethane accompanied by formation of a small amount of methane and a negligible amount of ethylene (Runs 1—7). When the *trans*- or

$$\underset{\text{(}trans\text{ and }cis\text{)}}{PdMe_2L_2} \xrightarrow[\text{dmm}]{\text{thermolysis}} Pd(dmm)L_2 + \underset{(>0.95)}{CH_3CH_3} + \underset{(<0.05)}{CH_4} + \underset{(\approx 0)}{CH_2CH_2} \quad (5)$$

cis-$PdMe_2L_2$ were thermolyzed in the presence of free tertiary phosphines, the thermolysis course releasing ethane was severely hindered, making methane the main thermolysis product, albeit in small quantities as shown in Table 4. Thermolysis of *cis*-$Pd(CD_3)_2(PMePh_2)_2$ in C_6D_6 at 60 °C in the presence of 0.25 mol/l of $PMePh_2$ liberated methane composed of 98% of CD_3H and 2% of CD_4. The results suggest that the hydrogen abstraction is taking place probably *via* a process involving an orthometallated intermediate when the *cis*-dimethyl complex is thermolyzed in the presence of free phosphine.

In contrast to the liberation of ethane and ethylene in a 1:1 ratio on thermolysis of *trans*-$PdEt_2(PMe_2Ph)_2$

Table 4. The effects of addition of *t*-phosphines on the thermolysis of $PdMe_2L_2$[a]

Run	Compound[b]	Additive[c] (mol/l)	$\frac{[PR_3]}{[Complex]}$	$\frac{CH_4}{C_2H_6}$
1	**4a**	dmm (0.052)	0	0
2	**4a**	$PMePh_2$(0.025)	0.5	39
3	**4a**	$PMePh_2$(0.050)	1.1	72
4	**4a**	$PMePh_2$(0.125)	2.8	231
5	**4a**	$PMePh_2$(0.250)	5.8	838
6	Va	dmm (0.052)	0	0
7	Va	$PEtPh_2$(0.047)	1.0	3.2
8	Va	$PEtPh_2$(0.117)	1.2	5.3
9	Va	$PEtPh_2$(0.140)	2.8	8.1
10	Va	$PEtPh_2$(0.234)	3.1	10.1

a) Total amounts of evolved gases were below 5% except for Runs 1 and 6. b) **4a**, *cis*-$PdMe_2(PMePh_2)_2$; Va, *trans*-$PdMe_2(PEtPh_2)_2$. c) dmm, dimethyl maleate.

(IIb) and *trans*-$PdEt_2(PEt_2Ph)_2$ (IIIb) (Runs 8 and 9 in Table 3 and Ref. 5), thermolysis of *cis*-$PdEt_2(PMe_2Ph)_2$ (**2a**) and *cis*-$PdEt_2(PEt_2Ph)_2$ (**3b**) in toluene containing dmm (Runs 10 and 11 in Table 3) gave almost quantitative amounts of butane, the reductive elimination product of the palladium diethyls. The dichotomy

$$\begin{array}{l} \mathrm{L\text{–}Pd(Et)\text{–}Et} \xrightarrow{\text{thermolysis}} \mathrm{Et\text{–}Et} \\ \quad \mathrm{L} \\ \quad (\mathrm{L}=\mathrm{PMe_2Ph},\ \mathrm{PEt_2Ph}) \\ \mathrm{L\text{–}Pd(Et)\text{–}L} \xrightarrow{\text{thermolysis}} \mathrm{C_2H_6} + \mathrm{C_2H_4} \\ \quad \mathrm{Et} \\ (\mathrm{L}=\mathrm{PMe_2Ph},\ \mathrm{PEt_3},\ \mathrm{PEt_2Ph},\ \mathrm{PMePh_2},\ \mathrm{PEtPh_2}) \end{array} \qquad (6)$$

of the thermolysis products of the palladium diethyls depending on the configuration of the isomer is intriguing. The fact that the reductive elimination of the *cis*-alkyls is hindered whereas the β-elimination pathway of the *trans*-alkyls is not hindered by addition of free phosphines suggests that the tertiary phosphine ligand is serving to stabilize the *cis*-dialkyls by blocking the route leading to the three-coordinate species, whereas the phosphine does not block the site for β-elimination of *trans*-$PdEt_2L_2$ to take place. The results are in conflict with the generally held view that the tertiary phosphine's role is merely to block the site for the β-elimination to take place.[11]

In contrast to the occurrence of reductive elimination of the ethyl groups from *cis*-$PdEt_2L_2$ having the monodentate phosphine ligands, the thermolysis of *cis*-$PdEt_2$(dpe) having the bidentate ligand (**6b**, Run 12 in Table 3) liberated ethane and ethylene together with butane, indicating that both β-elimination and reductive elimination pathways are operative. Thermolysis of *cis*-$PdMe_2$(dpe), however, gave ethane, the reductive elimination product. The reason for the different thermolysis behavior of **6b** is not clear.

The occurrence of the reductive elimination of ethyl groups from *cis*-$Pd(CH_2CD_3)_2(PMe_2Ph)_2$ without involvement of H–D scrambling in the deuterated ethyl groups was confirmed by examination of the ^1H NMR of the deuterated butane formed on thermolysis. It was revealed that the proton content in the methyl and methylene groups in the butane produced on thermolysis was 7 and 93% respectively.

Kinetic Study of Thermolysis of cis-$PdMe_2(PMePh_2)_2$ (**4a**). In order to obtain further information on the thermolysis mechanism of the *cis*-dialkyl isomers, the thermolysis of *cis*-$PdMe_2(PMePh_2)_2$ (**4a**) was followed by measuring the evolved amount of ethane produced on thermolysis of **4a** in diphenylmethane containing dmm. Complex **4a** was chosen because of the stability of the *cis* isomer concerning the isomerization to the *trans* isomer as well as the convenient temperature range where the thermolysis proceeds at reasonable rates for the kinetic measurement. The thermolysis is first order in the palladium dimethyl concentration up to the decomposition of 80—90% of the complex (Fig. 1). The thermolysis is severely hindered by addition of small amounts of free $PMePh_2$

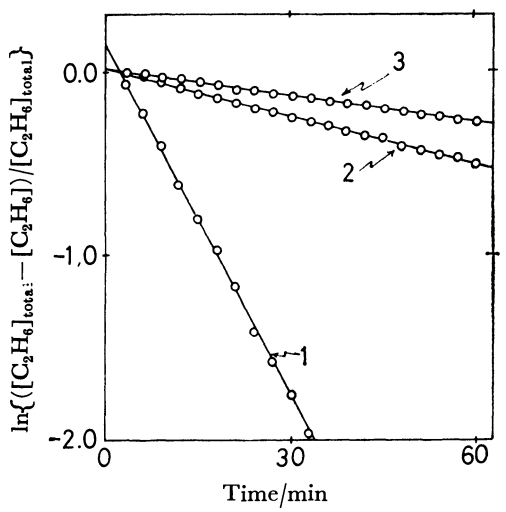

Fig. 1. Pseudo-first order plots for thermolysis of *cis*-$PdMe_2(PMePh_2)_2$ in Ph_2CH_2 containing 0.087 mol/l of dmm at 45.0 °C. [Complex]≈0.025 mol/l. Additive ($PMePh_2$, mol/l): 1) 0.00; 2) 1.25×10^{-3}; 3) 2.50×10^{-3}.

Table 5. The effects of addition of various ligands on thermolysis rates of *cis*-$PdMe_2(PMePh_2)_2$ (**4a**)

Run	Additive (mol/l)	$10^3\ k_{obsd}/s^{-1}$
1	dmm (0.087)	1.1
2	dmm (0.17)	1.1
3	dmm (0.35)	1.2
4	dmm (0.087) $PMePh_2$ (0.75×10^{-3})	0.21
5	dmm (0.087) $PMePh_2$ (1.25×10^{-3})	0.15
6	dmm (0.087) $PMePh_2$ (2.50×10^{-3})	0.08
7	dmm (0.087) Pyridine (0.15)	0.59
8	dmm (0.087) $AsPh_3$ (0.033)	0.37

a) [Complex]≈0.025 mol/l, at 45.0 °C, in Ph_2CH_2.

to the system. The pseudo-first-order rate constant k_{obsd} of thermolysis of **4a** under various experimental conditions are summarized in Table 5. As can be seen from Table 5 the thermolysis rate was not affected by the amount of dmm added to the system, whereas the addition of $PMePh_2$, pyridine, and $AsPh_3$ suppressed the thermolysis. The retardation effect of pyridine and $AsPh_3$ was smaller than that of $PMePh_2$. Plotting of the $1/k_{obsd}$ value *vs.* the concentration of $PMePh_2$ added to the system gave a straight line (Fig. 2). The results suggest that the thermolysis proceeds through a dissociative pathway involving the three-coordinate intermediate formed on partial dissociation of the phosphine ligand from *cis*-$PdMe_2(PMePh_2)_2$ as represented in Scheme 3. Assumptions of the ligand

$$\mathrm{L\text{–}Pd(Me)\text{–}Me} \underset{+\mathrm{L},\ k_{-1}}{\overset{-\mathrm{L},\ k_1}{\rightleftharpoons}} \left[\mathrm{Pd(Me)\text{–}Me}\right] \xrightarrow{k_2} \mathrm{C_2H_6}$$

Scheme 3. Theromlysis mechanism of *cis*-$PdMe_2L_2$ (L=$PMePh_2$).

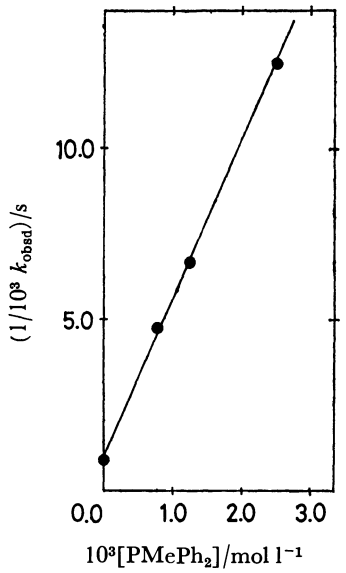

Fig. 2. Plots of $1/k_{obsd}$ *vs.* [$PMePh_2$] in thermolysis of *cis*-$PdMe_2(PMePh_2)_2$ (**4a**) in Ph_2CH_2 containing 0.087 mol/l of dmm at 45.0 °C. [**4a**]≈0.025 mol/l.

dissociation as the rate-determining process and of the steady-state approximation for the concentration of the three coordinate intermediate in Scheme 3 leads to the kinetic equations (7) and (8) which are in agreement with the experimental results as shown in Figs. 1 and 2.

$$-\frac{d[cis\text{-}PdMe_2L_2]}{dt} = \frac{k_1k_2}{k_{-1}[L]+k_2}[cis\text{-}PdMe_2L_2] \quad (7)$$

$$\frac{1}{k_{obsd}} = \frac{k_{-1}}{k_1k_2}[L] + \frac{1}{k_1} \quad (8)$$

Retardation effect of $AsPh_3$ and pyridine is also accommodated by the mechanism shown in Scheme 3. The corresponding *cis*-diethyl analog (**2b**) behaved similarly. An almost quantitative amount of butane was liberated on thermolysis of 0.077 mol/l of **2b** at 55 °C for 5 h in toluene containing dmm. The thermolysis was severely hindered in the presence of 0.17 mol/l of PMe_2Ph under otherwise the same conditions and only *ca.* 2% of butane per complex was released.

In order to see the effect of tertiary phosphine on the stability of the palladium dimethyls having various tertiary phosphine ligands, pseudo-first-order rate constant was measured for each complex in the absence of the added phosphine. The results summarized in Table 6 reflect both electronic and steric effects of the phosphine ligands on stability of the palladium dimethyls. Comparison of the thermolysis rate constants

Table 6. Thermolysis rates of *cis*-$PdMe_2L_2$[a]

L	θ/°[b]	pK_a[c]	$10^3\ k_{obsd}/s^{-1}$
PEt_3	132	8.65	0.42
PEt_2Ph	136	6.78	0.53
$PMePh_2$	136	4.65	1.1
$PEtPh_2$	140	4.91	2.0

a) [Complex]≈0.025 mol/l, at 45.0 °C, in Ph_2CH_2 containing 0.087 mol/l of dmm. b) See Ref. 20. c) See Ref. 21.

of **3a** and **4a** having the phosphine ligands of similar cone angles but different basicities indicate that the more basic ligand is more strongly attached to the methyl complex giving rise to a slower thermolysis rate. On the other hand, the $PEtPh_2$-coordinated complex (**5a**) having a larger cone angle than $PMePh_2$ but a similar basicity is thermolyzed at a higher rate than the $PMePh_2$-coordinated complex (**4a**) as a consequence of the steric bulkiness. The PPh_3-coordinated complex is more unstable than **5a** and the thermolysis rate measurement was not attempted. The PEt_3-coordinated complex is much more stable as expected from its high basicity and low steric bulkiness than the complexes coordinated by phenyl-substituted phosphines. Comparison of the thermolysis rate constant of the PEt_3-coordinated complex with thermolysis rate of other complexes, however, was not feasible because of the considerably high rate of the *cis-trans* isomerization occurring concurrently with the thermolysis (*vide infra*). The thermolysis of $PdMe_2$(dpe) (**6a**) at 80 °C in diphenylmethane was almost completely suppressed by addition of about 2 equivalents of dpe. Since the dpe ligand usually serves as a better coordinating ligand than the mono phosphines, the previously mentioned formation of ethane and ethylene and not of butane as the main thermolysis product of $PdEt_2$(dpe) (**6b**) may be partly due to reluctance of the partial dissociation of the dpe ligand from **6b**. Thermolysis without partial dissociation of the ligand may force the complex decomposed by another route. It is noteworthy that addition of the phosphine ligand in thermolysis of $NiMe_2$(dpe)[12] showed no inhibition effect, suggesting a difference in the thermolysis mechanisms of the nickel and palladium congeners.

The unimolecular thermolysis pathway of the *cis* palladium alkyls was further supported by examining the thermolysis product of a mixture of *cis*-$Pd(CH_3)_2(PMePh_2)_2$ (**4a**) and *cis*-$Pd(CD_3)_2(PMePh_2)_2$ in a molar ratio of 0.90: 1.00. The ethane formed on thermolysis of the mixture contained CD_3CD_3, CD_3CH_3, and CH_3CH_3 in a ratio of 0.47: 0.05: 0.48, indicating that scrambling of the methyl groups constitutes only a minor process in thermolysis of **4a**. Stille and coworkers have obtained evidence supporting the involvement of the methyl group in $PMePh_2$ in thermolysis of **4a**.[13] The formation of the minor amount of CD_3CH_3 may have arisen from such a process since thermolysis of *cis*-$Pd(CD_3)_2(PMePh_2)_2$ evolved about 5% of CH_3-CD_3 but the thermolysis result of the mixed CH_3- and CD_3-complexes clearly indicates intramolecular coupling of the *cis* dimethyl groups as the main process. Further support of the unimolecular process in thermolysis of *cis*-PdR_2L_2 was provided by the negligible formation of propane on thermolyses of mixtures of *cis*-$PdMe_2(PMePh_2)_2$ and *cis*-$PdEt_2(PMe_2Ph)_2$.

trans-cis *Isomerization of* $PdMe_2L_2$ *and Mechanism of Thermolysis of* trans-$PdMe_2L_2$. In contrast to the thermolysis behavior of *cis*-$PdMe_2L_2$ which is decomposed by a unimolecular reductive elimination mechanism, the thermolysis of *trans*-$PdMe_2L_2$ deviates from the first-order rate law and shows a marked acceleration in the thermolysis rate as the thermolysis proceeds.

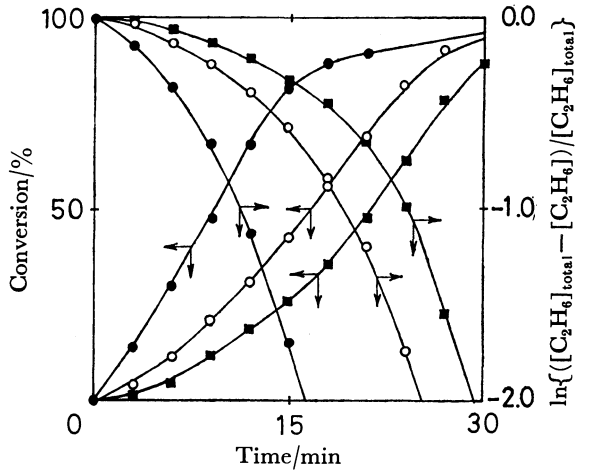

Fig. 3. Time-conversion curves and pseudo-first order plots for thermolysis of *trans*-$PdMe_2L_2$ in Ph_2CH_2 containing 0.087 mol/l of dmm at 62.0 °C. L=PEt_2Ph (IIIa, —■—), $PMePh_2$ (IVa, —○—), $PEtPh_2$ (Va, —●—).

Fig. 4. ^1H NMR spectral change of *trans* to *cis* isomerization of $PdMe_2(PMePh_2)_2$ in CD_2Cl_2 at 36.0 °C.

This indicates the presence of an autocatalytic thermolysis process. The typical time-conversion curves of thermolysis of *trans*-$PdMe_2L_2$ (IIIa, IVa, and Va) are shown in Fig. 3. Further examination of the thermolysis reactions of the *trans*-$PdMe_2L_2$ type complexes revealed the initial isomerization of the *trans* isomer to the *cis* isomer from which the reductive elimination proceeds. By selecting the proper complex and suitable reaction conditions the thermolysis of the palladium dimethyl can be kept minimal and the *trans-cis* isomerization can be conveniently observed. Figure 4 illustrates the typical change of the ^1H NMR spectrum of *trans*-$PdMe_2(PMePh_2)_2$ (IVa) to *cis*-$PdMe_2(PMePh_2)_2$ (**4a**) at 36 °C in CD_2Cl_2. The initial NMR spectrum shows the Pd–Me as well as the methyl signals of $PMePh_2$ as singlets, suggesting exchange between the phosphine ligand liberated from the *trans*-$PdMe_2(PMePh_2)_2$ and the phosphine ligand coordinated to palladium. The liberation and recoordination of the phosphine ligand is a reversible process at this stage, retaining the *trans* configuration since cooling of the solution gives a triplet pattern for the methyl signals of the methyl groups bonded to palladium in the *trans* form. When the solution is kept at 36 °C the signals due to the *trans* isomer decrease. This is accompanied by increase of the signals characteristic of the *cis* isomer. During the isomerization process no change of the chemical shifts of the signals due to the *trans* and *cis* isomers was observed. The isomerization was free of thermolysis up to the 80% conversion. Beyond that stage, formation of ethane in a minor amount was noticed, revealing the occurrence of a slow thermolysis.

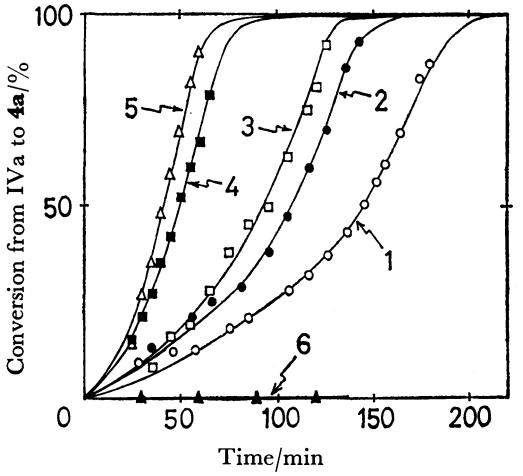

Fig. 5. Time-conversion curves of isomerization of *trans*-$PdMe_2(PMePh_2)_2$ (IVa) to *cis*-$PdMe_2(PMePh_2)_2$ (**4a**) in CD_2Cl_2 at 36.0 °C.

Initial concentration/mol l^{-1}

Run	IVa	Additive	
		4a	$PMePh_2$
1	0.067	0	0
2	0.107	0	0
3	0.064	0.027	0
4	0.069	0.059	0
5	0.071	0.114	0
6	0.090	0	0.050

For the $PMePh_2$-coordinated dimethylpalladium complex the equilibrium lies on the side of the *cis* form. Leaving the acetone-d_6 solution containing the *cis*-$PdMe_2(PMePh_2)_2$ (**4a**) at room temperature for one week led only to the slow decomposition of **4a** without any sign of *cis-trans* isomerization. With increasing replacement of the phenyl groups in the tertiary phosphine ligand by alkyl groups a noticeable effect on the *cis-trans* equilibrium becomes apparent. Although the equilibrium for the $PdMe_2(PMePh_2)_2$ type complex lies far on the side of the *cis* form in CD_2Cl_2 and in acetone-d_6, the PEt_3-coordinated dimethylpalladium complex undergoes *cis-trans* and *trans-cis* isomerization slowly reaching an equilibrium of *trans*/*cis*=1.2 after a few days at room temperature. For **3a** having the less basic and more bulky PEt_2Ph ligand than PEt_3, *cis-trans* isomerization was also observed with an quilibrium *trans*/*cis* ratio of 0.20 at room temperature in acetone-d_6. Apparently both steric and electric factors are involved to determine the *cis-trans* equilibrium, but the electronic factor may be dominant in influencing the equilibrium, as judged from the higher *trans* ratio at equilibrium of the PEt_2Ph-coordinated complex than that of the $PMePh_2$-coordinated complex, both phosphines having the same cone angle.

For the dimethylpalladium complex coordinated with $PMePh_2$, kinetic studies concerning the *trans* to *cis* isomerization have been made by pursuing the decrease of the Pd–Me signal in the ^1H NMR spectra of the *trans* form IVa measured in CD_2Cl_2 at 36.0 °C. This system is free from the reverse, *cis* to *trans* isomerization and the time-conversion curves, as reproduced in Fig. 5, shows a typical autocatalytic acceleration effect. The *trans-cis* isomerization rate is increased with increase of the initial concentration of the *trans* form IVa (Runs 1 and 2 in Fig. 5) and the rate is particularly enhanced on addition of the increasing amount of the *cis* form (**4a**) to the system (Runs 3, 4, and 5). The isomerization was markedly suppressed by adding free $PMePh_2$ to the system (Run 6).

Further examination of the *trans-cis* isomerization using the deuterated dimethylpalladium complex revealed scrambling of the methyl groups during the isomerization process. Examination of the thermolysis product liberated from *cis*-$PdMe_2(PMePh_2)_2$, derived by isomerization of *trans*-$Pd(CH_3)_2(PMePh_2)_2$ in CH_2Cl_2 at 30 °C for 2 h in the presence of an equilmolar amount of *cis*-$Pd(CD_3)_2(PMePh_2)_2$, revealed that the ratio of CD_3CD_3: CH_3CD_3: CH_3CH_3 in the evolved ethane was 0.29: 0.46: 0.25, indicating the complete scrambling of the methyl groups. Since it has been already

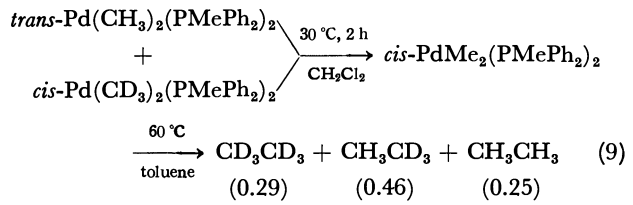

(9)

confirmed that the thermolysis of the mixture of *cis*-$Pd(CH_3)_2(PMePh_2)_2$ and *cis*-$Pd(CD_3)_2(PMePh_2)_2$ predominantly gives CD_3CD_3 and CH_3CH_3, the above result clearly indicates the involvement of an intermolecular process causing the exchange of the methyl groups. Since it has been established on the basis of ^1H NMR spectrum that *trans*-$PdMe_2(PMePh_2)_2$ is partly dissociated with retention of the "*trans*" configuration in solution without rapid transformation into the *cis* configuration, it is reasonable to assume the presence of an energy barrier between the three-coordinate species having the methyl groups at mutually *trans* positions (**T′** form in the following equations) and another three-coordinated species having the methyl groups at mutually *cis* positions (**C′**). Our next task is to find a reasonable mechanism which allows the complex led to the *cis* form with the assistance of the *cis*-$PdMe_2L_2$ or *trans*-$PdMe_2L_2$ with involvement of the methyl scrambling.

Since there is no precedent of the *trans-cis* isomerization proceeding by an intermolecular mechanism to our knowledge, examination of various isomerization models merits the consideration. In the first place, the intramolecular isomerization mechanism is excluded on the basis of the kinetic results and the intermolecular scrambling experiment. Secondly, inhibition of the isomerization by addition of free phosphine supports a mechanism involving the partial dissociation of the phosphine ligand from the square-planar complex with exclusion of other mechanisms involving association of non-dissociated four coordinate species. Thirdly, a bimolecular mechanism between two three-coordinated species formed by the ligand dissociation is unlikely on the ground of kinetic results. After exclusion of these other possible mechanisms we are left with the following mechanism to account for the isomerization of *trans*-$PdMe_2L_2$ promoted by *cis*-$PdMe'_2L_2$. As the inter-

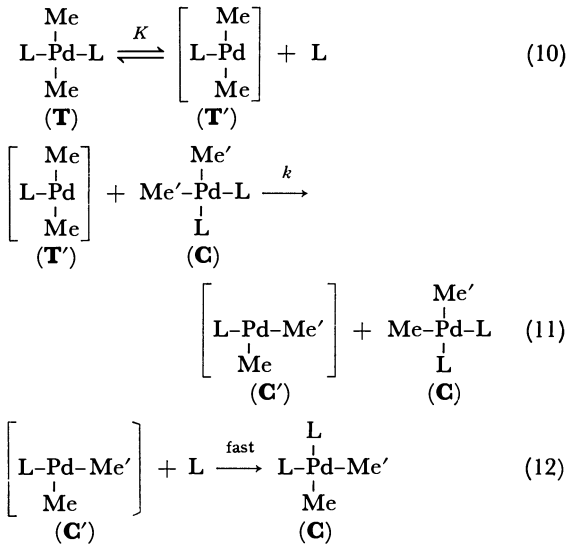

Scheme 4. Proposed mechanism for *trans-cis* isomerization of *trans*-$PdMe_2L_2$ promoted by *cis*-$PdMe_2L_2$.

mediate in the crucial intermolecular reaction (11) we postulate the formation of the following methyl bridged species, which on cleavage of the original methyl–palladium bonds may give the dissociated (**C′**) and undissociated *cis*-dimethyl (**C**) complexes. Rapid coordination of the free phosphine ligand to the unsaturat-

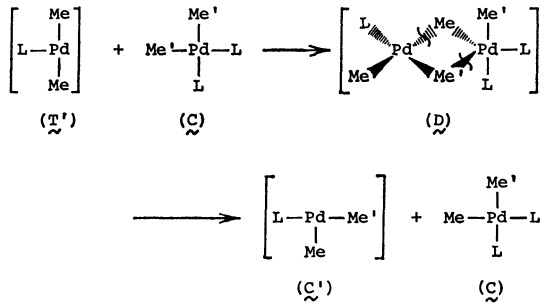

(13)

ed species (**C**′) completes the isomerization, giving the product *cis*-PdMeMe′L_2 (Eq. 12). Retention of the *cis* configuration of the added *cis* isomer after departure from the bridged species (**D**), in which a trigonal bipyramidal structure is assumed, is in agreement with the generally observed retention of configuration in the other isomerization reactions of square-planar transition metal complexes.[8] Since the methyl group has a greater *trans* effect than the tertiary phosphine, cleavage of the methyl group in the position *trans* to the terminal methyl group as shown in **D** is reasonable. The rapid coordination of the free phosphine to the split-out species (**C**′) leading to the square-planar *cis*-$PdMe_2L_2$ (Eq. 12) is a likely process in view of the absence of broadening of the ^1H NMR signal of the palladium bonded methyl groups in *cis*-$PdMe_2L_2$.

The *trans-cis* isomerization strongly favors the *cis* form for complexes having phosphines with the phenyl groups as discussed previously. For these cases assumption of Scheme 4, in which rapid equilibrium for Eq. 10, the rate determining step for Eq. 11 and the subsequent rapid trapping of the (**C**′) in Eq. 12 are involved, leads to the kinetic expression given by Eq. 14.

$$-\frac{d[\mathbf{T}]}{dt} = k[\mathbf{T}'][\mathbf{C}] \tag{14}$$

Since $[\mathbf{T}]_0+[\mathbf{C}]_0=[\mathrm{T}]+[\mathbf{C}]$, where $[\mathbf{T}]_0$ and $[\mathbf{C}]_0$ stand for the initial concentrations of the *trans* and *cis* isomers and [**T**] and [**C**] the concentrations of the isomers at time *t*, [**C**] may be expressed as

$$[\mathbf{C}] = [\mathbf{T}]_0 + [\mathbf{C}]_0 - [\mathbf{T}]. \tag{15}$$

From Eq. 10 it follows

$$K = [\mathbf{T}'][\mathrm{L}]/[\mathbf{T}] \quad \text{where } [\mathbf{T}'] = [\mathrm{L}] \text{ and}$$
$$[\mathbf{T}'] = \sqrt{K[\mathbf{T}]}. \tag{16}$$

From Eqs. 14, 15, and 16

$$-\frac{d[\mathbf{T}]}{dt} = k\sqrt{K}\sqrt{[\mathbf{T}]}([\mathbf{T}]_0+[\mathbf{C}]_0-[\mathbf{T}]) \tag{17}$$

$$\int_{[\mathbf{T}]_0}^{[\mathbf{T}]} \frac{d[\mathbf{T}]}{\sqrt{[\mathbf{T}]}([\mathbf{T}]_0+[\mathbf{C}]_0-[\mathbf{T}])} = -\int_0^t k\sqrt{K}\,dt. \tag{18}$$

From Eq. 18 the following equation is derived:

$$\ln\frac{(\sqrt{[\mathbf{T}]_0+[\mathbf{C}]_0}+\sqrt{[\mathbf{T}]})^2}{[\mathbf{C}]} = -k\sqrt{K}\sqrt{[\mathbf{T}]_0+[\mathbf{C}]_0}\cdot t + \ln\frac{(\sqrt{[\mathbf{T}]_0+[\mathbf{C}]_0}+\sqrt{[\mathbf{T}]_0})^2}{[\mathbf{C}]_0}. \tag{19}$$

Plots of $\ln(\sqrt{[\mathbf{T}]_0+[\mathbf{C}]_0}+\sqrt{[\mathbf{T}]})^2/[\mathbf{C}]$ *vs.* *t* as computed from the time-conversion curves shown in Fig. 5 are straight lines as shown in Fig. 6 up to about 60—

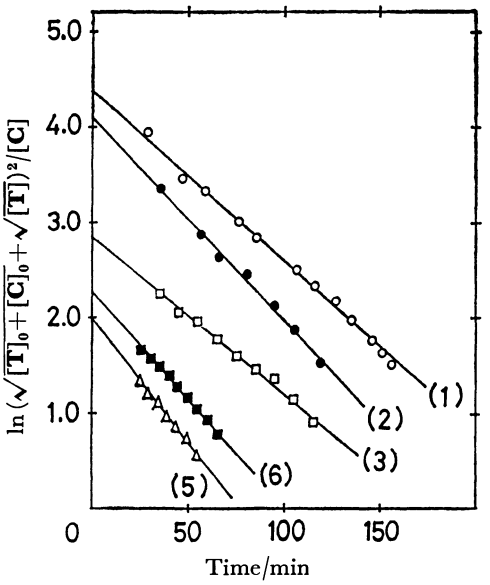

Fig. 6. Plots of $\ln(\sqrt{[\mathbf{T}]_0+[\mathbf{C}]_0}+\sqrt{[\mathbf{T}]})^2/[\mathbf{C}]$ *vs.* *t* in *trans* to *cis* isomerization of $PdMe_2(PMePh_2)_2$.

80% conversions. The values obtained by dividing the slopes of these lines in Fig. 6 by $-\sqrt{[\mathbf{T}]_0+[\mathbf{C}]_0}$ give a constant value $(1.0\pm0.1)\times10^{-3}$ s^{-1} $mol^{-1/2}$ $l^{-1/2}$ corresponding to $k\sqrt{k_1}$ in a reasonable agreement with each other value. Thus the isomerization of the *trans* isomer to the *cis* isomer catalyzed by the *cis* isomer can be explained by assuming the mechanism shown in Scheme 4, at least for the most part where the acceleration effect is observed.

The initial period of isomerization, however, where the *cis* isomer is not present, remains to be explained by the other mechanism than the one involving the *cis* isomer. If the slow isomerization of the three-coordinate **T**′ complex to **C**′ complex shown below is excluded

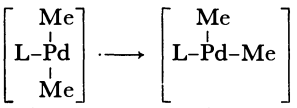

(19)

even in the initial period, the remaining reasonable mechanism to account for the isomerization in the initial period is the one assisted by the undissociated *trans* isomer itself. Experimentally it is difficult to get evidence to prove or disprove mechanisms given by Eq. 19 or Eq. 20 for the initial period where the isomerization rate is small. The acceleration effect observed by increasing the initial concentration of the

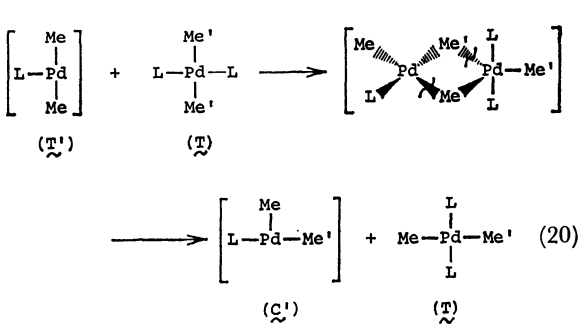

(20)

trans isomer suggests an intermolecular mechanism such as Eq. 20. The much enhanced acceleration of the isomerization by addition of the *cis* isomer (*e.g.* Run 3 in Fig. 5 in comparison with Run 2 in which the total concentration is higher than in Run 3) suggests that the reaction proceeds mainly by a mechanism involving acceleration by the *cis* isomer (*e.g.* Scheme 4). For the *cis* to *trans* isomerization, which was noticeable for the PEt_3-coordinated complex **1a** and to a lesser extent for the PEt_2Ph-coordinated complex **3a**, a mechanism following the reverse course of the *trans* to *cis* isomerization as expressed by Scheme 4 may be operative.

With the information concerning the *trans* to *cis* isomerization we are now in a situation to resume the discussion on the thermolysis behavior of the *trans* palladium dimethyls at elevated temperatures as shown in Fig. 3. As can been seen from the figure, the thermolysis rate is markedly accelerated as the reaction proceeds. These results combined with those on the thermolysis of *cis*-$PdMe_2L_2$ previously discussed suggest that the thermolysis of *trans*-$PdMe_2L_2$ proceeds after its isomerization to the (**C′**) type three-coordinate intermediate. This intermediate is also formed by partial dissociation of the ligand in thermolysis of *cis*-$PdMe_2L_2$ as shown in Scheme 5.

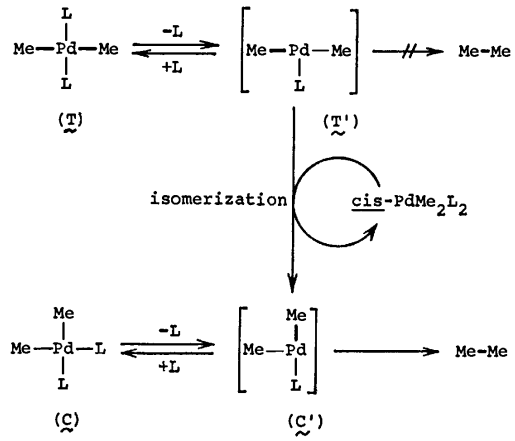

Scheme 5. Proposed mechanism of reductive elimination of methyl group from *trans*- and *cis*-$PdMe_2L_2$.

It is noteworthy that the three-coordinate "*cis*" type complex (**C′**) has a moderate stability without being immediately thermolyzed by a reductive elimination pathway. The results suggest intervention of another type of three-coordinate species connected with the transition state for the reductive elimination. A plausible candidate for the species formed by the rearrangement of configuration from the T-shaped species (**C′**) is a planar Y-shaped complex from which the alkyl groups are reductively eliminated. A similar intermediate has been invoked in explanation of the

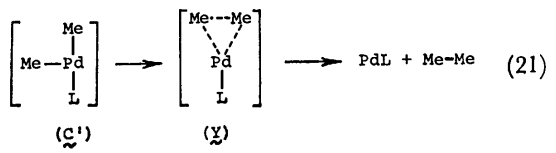

(21)

thermolysis and isomerization behavior of AuR_3L type complexes.[6]

It is intriguing to note the similarity between thermolysis mechanisms of the alkyl complexes of Group I transition metal, AuR_3L, and of Group VIII transition metal, $PdMe_2L_2$. Furthermore, comparison of the thermolysis behavior of PdR_2L_2 with that of NiR_2L_2 and PtR_2L_2 reveals the contrasting difference in thermolyses of these three, Group VIII dialkyls. Pertinent characteristics in thermolysis patterns of the three dialkyls are as follows. (1) Reductive elimination of $NiMe_2(bpy)$[14] and $NiMe_2(dpe)$[12] is not hindered by the presence of free ligand. This suggests that the reductive elimination from the four-coordinate species can proceed without ligand liberation in contrast to the striking inhibition effect of the phosphine ligand on thermolysis of *cis*-PdR_2L_2. (2) Thermolysis of *cis*-PtR_2L_2 by a β-hydrogen elimination pathway is severely hindered by addition of a free phosphine,[15] whereas the thermolysis of *trans*-$PdEt_2L_2$ proceeding also through a β-hydrogen elimination pathway is not hindered by the presence of the free phosphine.[5]

Attempting to clarify the difference in the thermolysis behavior of *cis*-$PdMe_2L_2$ and *cis*-$NiMe_2L_2$, Tatsumi and Hoffmann recently performed extended HMO calculations.[16] Their results explain most of the thermolysis behavior of *cis*-$PdMe_2L_2$ and *cis*-$NiMe_2L_2$ and suggest the presence of an energy barrier between the T-shaped "*trans*" form (**T′**) and "*cis*" form (**C′**). Their calculation indicates that a lower energy barrier is found for reductive elimination *via* the Y-shaped species rather than directly from the undissociated complex or from **C′** intermediate in the case of palladium dialkyls, whereas the reductive elimination from the undissociated $NiMe_2L_2$ complex may take place with a lower energy barrier than the case for *cis*-$PdMe_2L_2$.

On Factors Influencing the Stability of Palladium Alkyls.

In discussion of the factors influencing the stability of transition metal alkyls one of the most important information regarding the roles of the supporting ligands such as tertiary phosphines and organic nitrogen bases may be obtained by careful kinetic studies of the thermolysis mechanism of the isolated transition metal alkyls. It has been established in the previous report[5] that the tertiary phosphine ligand does not serve in blocking the β-hydrogen elimination pathway effectively in the thermolysis of *trans*-$PdEt_2L_2$ but rather the bulky ligands destabilize the Pd–Et bonds. The present study, however, indicates that thermolysis of the *cis*-dialkylpalladium complexes proceeding through a reductive elimination pathway can be severely hindered by the presence of free tertiary phosphines. In the thermolysis involving the ligand dissociation the nature of the ligands and that of the alkyl groups give mutual influence on the ease of cleavage of the Pd–PR_3 bond and Pd–alkyl bonds. Although the intrinsic bond strength of the Pd–Et bond may certainly differ from that of the Pd–Me bond, the principal factor in determining the stability of the phosphine-coordinated *cis*-palladium dialkyls, may be sought in the ease of release of the phosphine ligand. The ethyl group situated at the *trans* position to one of the phosphine ligands may

have greater *trans* labilizing effect than the methyl group in the rate-determining phosphine dissociating process. This would explain the greater stability of the dimethyl complexes than the corresponding diethyl complexes.

The results obtained in the present study as well as the previous one provide pertinent information not only about the factors concerning the stability of palladium alkyls but also regarding palladium-catalyzed reactions causing the C–C bond coupling. Although the actual catalyst systems, being constituted of a series of elementary steps, are much more complicated than the simple thermolysis of the isolated palladium dialkyls, part of the roles of the added ligands may be connected with the effect of the ligand on reductive elimination of dialkyls as discussed here.

Experimental

All manipulations were carried out under an atmosphere of nitrogen or argon, or *in vacuo*. Solvents were dried in the usual manner, distilled, and stored under a nitrogen atmosphere.

Infrared spectra were recorded on a Hitachi 295 spectrometer using KBr pellets. ^{1}H NMR spectra were measured on a JEOL PS-100, FX-100, and PMX-60 spectrometers. ^{1}H NMR signals are referred to Me_4Si as internal or external standard. Analysis of the gases evolved by the reactions was carried out by gas chromatography (Shimadzu GC-3BF) after collecting gases using a Toepler pump, by which the volumes of gases were also measured. Analysis of the gases dissolved in solution was also carried out by gas chromatography (Shimadzu GC-6A) after collecting the volatile matters in the reaction solution by a trap-to-trap distillation. Micro analyses (C and H) were carried by Mr. T. Saito of our laboratory using Yanagimoto CHN Autocorder Type MT-2. Analysis of the palladium content was performed by colorimetric method using 1-nitroso-2-naphthol as a color-producing reagent.[17] The complete ionization of the palladium in the complex was achieved by treating the sample with a hot aqua regia.

Triethylphosphine (Strem) was used as purchased. Dimethylphenylphosphine, diethylphenylphosphine, diphenylmethylphosphine, and diphenylethylphosphine were prepared by the reactions of $PPhCl_2$ and PPh_2Cl, respectively, with RMgX (R=Me, X=I; R=Et, X=Br). 1,2-Bis(diphenylphosphino)ethane (dpe) was prepared by the literature method starting from PPh_3.[18]

trans-$PdMe_2(PEt_3)_2$ (Ia), *cis*-$PdMe_2$(dpe) (**6a**), *cis*-$PdEt_2$(dpe) (**6b**), and *cis*-$PdPr^n_2$ (dpe) (**6c**) were prepared by the reactions of Pd(acac)$_2$, $AlR_2(OEt)$ (R=Me, Et, Pr^n), and tertiary phosphines according to the method described previously.[3] A series of *trans*-PdR_2L_2 (R=Et, L=PEt_3 (Ib), PMe_2Ph (IIb), PEt_2Ph (IIIb), $PMePh_2$ (IVb), $PEtPh_2$ (Vb); R=Pr^n, L=PEt_3 (Ic), PMe_2Ph (IIc), $PMePh_2$ (IVc); R=Bu^n, L=PMe_2Ph (IId)) were also prepared by the reactions of Pd(acac)$_2$, $AlR_2(OEt)$, and tertiary phosphines.[3,5]

Preparation of trans-*PdMe$_2$(PEt$_2$Ph)$_2$ (IIIa) (Method A).* To the heterogeneous red mixture of Pd(acac)$_2$ (2 g, 6.6 mmol), PEt_2Ph (3 ml, 17.1 mmol) and Et_2O (40 ml) cooled to −70 °C, a hexane solution of $AlMe_2(OEt)$ (5 ml, 19 mmol) was added dropwise. On raising the temperature of the mixture gradually, it became homogeneous at −30 °C. The solution was stirred for several hours at 0 °C. After concentrating the solution to *ca.* 10 ml, the solution was cooled to −70 °C overnight to yield a white precipitate of *trans*-$PdMe_2(PEt_2Ph)_2$ (IIIa), which was filtered, washed with a small amount of Et_2O at the same temperature and dried *in vacuo*. It was confirmed that the crude product of complex IIIa contained only *trans* isomer by means of IR spectroscopy. The product was recrystallized from acetone to yield white crystals of IIIa (1.5 g, 49%). Similarly obtained was *trans*-$PdMe_2(PEtPh_2)_2$ (Va) by using $PEtPh_2$ in place of PEt_2Ph. Complex Va was recrystallized from THF–CH_2Cl_2 (yield, 65%).

trans-$PdMe_2(PMePh_2)_2$ (IVa) was also prepared in a similar way from Pd(acac)$_2$, $PMePh_2$, and $AlMe_2(OEt)$. The crude complex first isolated from the reaction system, however, was a mixture of *trans* isomer (IVa) and *cis* isomer (**4a**). These two isomers were separated by extraction with acetone, in which the *cis* isomer is readily dissolved. The *trans* isomer (IVa) and the *cis* isomer (**4a**) were recrysrallized from THF–CH_2Cl_2 and acetone, respectively (yield; IVa, 14%; **4a**, 32%).

Characterization of these complexes was carried out by means of IR and ^{1}H NMR spectroscopy, and elemental analysis. Anal. (IIIa) Found: C, 56.3; H, 8.2%. Calcd for $C_{22}H_{36}P_2Pd$: C, 56.4; H, 7.7%. (IVa) Found: C, 62.1; H, 5.9%. Calcd for $C_{28}H_{32}P_2Pd$: C, 62.6; H, 6.0%. (Va) Found: C, 64.0; H, 6.5%. Calcd for $C_{30}H_{36}P_2Pd$: C, 63.8; H, 6.4%. (**4a**) Found: C, 63.2; H, 6.5%. Calcd for $C_{28}H_{32}P_2Pd$: C, 62.6; H, 6.0%.

Preparation of cis-*PdMe$_2$(PEt$_2$Ph)$_2$ (3a) (Method B).* To the heterogeneous yellow mixture of *trans*-$PdCl_2(PEt_2Ph)_2$ (3.5 g, 6.8 mmol) and Et_2O (40 ml) containing a small amount of PEt_2Ph (*ca.* 0.2 ml), Et_2O solution of MeLi (*ca.* 60 mmol) was added at −30 °C. The system was stirred at room temperature to give a heterogeneous pale yellow mixture containing a white precipitate of LiCl. Stirring was continued for 2 h. Evaporation (by pumping) of the ether phase, after hydrolysis at 0 °C, afforded a crude product of *cis*-$PdMe_2(PEt_2Ph)_2$ (**3a**) as confirmed by IR spectroscopy. The crude product was recrystallized from Et_2O to yield white crystals of **3a** (2.7 g, 85%). Similarly obtained by Method B was *cis*-$PdMe_2(PMePh_2)_2$ (**4a**) and *cis*-$PdMe_2(PEtPh_2)_2$ (**5a**). These complexes (**4a** and **5a**) were recrystallized from acetone (yield; **4a**, 48%; **5a**, 71%).

Characterization of **4a** was carried out by means of IR spectroscopy. Characterizations of **3a** and **5a** were carried out by means of IR and ^{1}H NMR spectroscopy, and elemental analysis. Anal. (**3a**) Found: C, 56.2; H, 8.0%. Calcd for $C_{22}H_{36}P_2Pd$: C, 56.4; H, 7.7%. (**5a**) Found: C, 63.5; H, 6.5%. Calcd for $C_{30}H_{36}P_2Pd$: C, 63.8; H, 6.4%.

Preparation of cis-*PdMe$_2$(PEt$_3$)$_2$ (1a) by the Ligand Exchange Reaction of* cis-*PdMe$_2$(PMePh$_2$)$_2$ (4a) with PEt$_3$ (Method C).* To a white heterogeneous mixture of *cis*-$PdMe_2(PMePh_2)_2$ (**4a**) (0.53 g, 0.99 mmol) and Et_2O (4 ml), PEt_3 (3.4 mmol) was added at room temperature to instantly yield a pale yellow clear solution. Evaporation of solvent by pumping afforded a pale yellow oil, which was washed with hexane at −70 °C to yield a white precipitate of *cis*-$PdMe_2(PEt_3)_2$ (**1a**). The product was filtered, washed with a small amount of Et_2O at −70 °C, and dried *in vacuo* (0.19 g, 52%). Characterization of **1a** was carried out by IR and ^{1}H NMR spectroscopy, and elemental analysis. Found: C, 45.7; H, 9.9%. Calcd for $C_{14}H_{36}P_2Pd$: C, 45.1; H, 9.7%.

Preparation of cis-*PdEt$_2$(PMe$_2$Ph)$_2$ (2b) (Method B).* To a Schlenk tube containing the mixture of $PdCl_2(PMe_2Ph)_2$ (1.6 g, 3.4 mmol) and EtLi (solid state) (0.28 g, 7.7 mmol) cooled at −70 °C, Et_2O (30 ml) containing a small amount of PMe_2Ph was added. On gradually raising the temperature the mixture became homogeneous at −20 °C. Stirring the solution at −20 °C for several hours yielded LiCl as a white precipitate, the amount of which increased gradually. After

concentration of the mixture to *ca.* 3 ml, hexane (30 ml) was added to the system at −10 °C. The solution was collected by filtration at the same temperature. Concentration of the filtrate to *ca.* 5 ml yielded a pale yellow precipitate, which was filtered, washed with a small amount of hexane at −70 °C and dried *in vacuo*. The product was recrystallized from cold Et_2O containing a small amount of PMe_2Ph to yield white crystals of *cis*-$PdEt_2(PMe_2Ph)_2$ (**2b**) (26%). Similarly obtained was *cis*-$PdEt_2(PEt_2Ph)_2$ (**3b**) by the use of $PdCl_2(PEt_2Ph)_2$ in place of $PdCl_2(PMe_2Ph)_2$ (13%). Since these complexes are too unstable for microanalysis, their characterization was carried out by means of IR and ^1H NMR spectroscopy, macroscopic analysis of Pd, and determination of the amount of ethane evolved on acidolysis with concd H_2SO_4. Anal. (**2b**) Found: Pd, 24.5%. Calcd for $C_{20}H_{32}P_2Pd$: Pd, 24.1%. (**3b**) Found: Pd, 21.1%. Calcd for $C_{24}H_{40}P_2Pd$: Pd, 21.4%. The amounts of ethane evolved by acidolysis with concd H_2SO_4 (mol/mol of complex): **2b**, 2.0; **3b**, 1.9.

Characterization of trans- *and* cis-*PdR_2L_2 by ^1H NMR and IR Spectroscopy (see also Table 2).* The ^1H NMR spectrum of *trans*-$PdMe_2L_2$ gives a triplet for the Pd–Me groups whereas that of *cis*-$PdMe_2L_2$ gives rise to a characteristic pattern of a distorted quartet ($A_3XX'A_3'$ pattern).[3] Other spectral patterns helping the assignment are a quintet pattern for the *trans* isomers and a doublet of triplets pattern for the *cis* isomers having tertiary phosphine ligands with ethyl group(s), and a triplet pattern for the *trans* isomers and a doublet for the *cis* isomers containing tertiary phosphine ligands with methyl group(s).

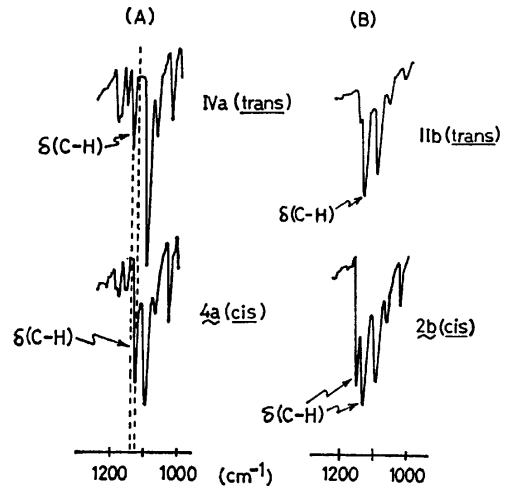

Fig. 7. Characteristic IR absorptions due to δ(C–H) of Pd–R groups of *trans*- and *cis*-PdR_2L_2 (KBr disc). (A) *trans*- and *cis*-$PdMe_2(PMePh_2)_2$. (B) *trans*- and *cis*-$PdEt_2(PMe_2Ph)_2$.

The IR spectra also serve in diagnosis of the isomers. The *trans* isomers show only one ν(Pd–C) band in the range of 455 to 462 cm^{-1} whereas the *cis* isomers give two ν(Pd–C) bands in the region of 465 to 515 cm^{-1}. Other characteristic bands helping to differentiate the *cis* and *trans* isomers are those arising from the C–H deformation of the Pd-bonded alkyl groups as shown in Fig. 7. The δ(C–H) vibration of the methylpalladium complexes gives a single absorption at 1120 cm^{-1} for the *cis* isomers and 1140 cm^{-1} for the *trans* isomers, whereas the δ(C–H) of the ethyl complexes gives two absorptions at 1130 and 1150 cm^{-1} for the *cis* isomers and a single band at 1140 cm^{-1} for the *trans* isomer. Since these absorptions are relatively unperturbed by the tertiary phosphine ligands, observation of these bands helps to determine the configuration of the isomers.

Mass Spectral Analysis of Deuterated Ethanes. Ethane produced by thermolysis was collected by using a Toepler pump through a dry ice–EtOH trap in order to avoid contamination by the solvent, and analyzed by mass spectrometer. To obtain accurate cracking patterns for each component, authentic samples of C_2D_6, CH_3CD_3, and C_2H_6 were prepared. CH_3CD_3 was prepared by the acidolysis of *trans*-$Pd(CH_2CD_3)_2(PMePh_2)_2$ (isotopic purity, 97%)[5] with concd H_2SO_4. CH_3CH_3 was used as purchased (Takachiho Chemical Industry). C_2D_6 was prepared by cracking *cis*-$Pd(CD_3)_2(PMePh_2)_2$ at 60 °C in toluene containing dmm. Since the deuterated ethane thus produced contains a small amount of CH_3CD_3, the true fragmentation pattern of CD_3CD_3 was obtained by subtracting the contribution of peaks due to CH_3CD_3 using the independently obtained fragmentation pattern of CH_3CD_3. The results of mass spectral analysis were reproducible within ±5%.

Reactions of trans-*$PdMe_2(PEt_2Ph)_2$ (IIIa) with MeLi and $AlMe_2(OEt)$.* To a homogeneous Et_2O solution (4 ml) of *trans*-$PdMe_2(PEt_2Ph)_2$ (IIIa) (0.25 g, 0.53 mmol), an ether solution of MeLi (1.1 mmol) was added by means of a syringe at room temperature and the system was stirred for 2 h at the same temperature. After hydrolysis at 0 °C, the solvent was evaporated from the solution to leave a white precipitate, which was washed with a small amount of Et_2O and dried *in vacuo* (0.23 g, 93%). The product was identified as *cis*-$PdMe_2(PEt_2Ph)_2$ (**3a**) on the basis of the IR and ^1H NMR spectroscopy.

On the other hand, the reaction of IIIa (0.098 g, 0.21 mmol) with $AlMe_2(OEt)$ (0.39 mmol) in Et_2O (2 ml at room temperature for 2 h yielded only *trans*-$PdMe_2(PEt_2Ph)_2$ (0.090 g, 92%) after concentration of the solution, washing with hexane at −70 °C, and drying *in vacuo*. Characterization of the product was carried out by IR spectroscopy.

Reactions of trans-*$PdMe_2(PEt_2Ph)_2$ (IIIa) and* cis-*$PdMe_2(PEt_2Ph)_2$ (3a) with CD_3Li.* To a homogeneous Et_2O (2 ml) solution of *trans*-$PdMe_2(PEt_2Ph)_2$ (IIIa) (0.16 g, 0.34 mmol), CD_3Li (isotopic purity, 99%) (0.37 mmol) was added by means of a syringe at room temperature. The system was stirred for 2 h at the same temperature. After hydrolysis at 0 °C, the solvent was removed by pumping to yield a white precipitate (0.14 g). The precipitate was identified as *cis*-$PdMe_2(PEt_2Ph)_2$ containing CD_3 groups on the basis of the IR spectrum (ν(C–D) (KBr disc)=2190, 2080, and 2030 cm^{-1}). Ethane evolved on thermolysis of the reaction product in toluene (2 ml) containing dmm (50 μl) at 60 °C was collected and analyzed by mass spectrometry, and the ratio of CD_3CD_3, CH_3CD_3, and CH_3CH_3 in the ethane was found to be 0.18: 0.48: 0.34.

On the other hand, the reaction of *cis*-$PdMe_2(PEt_2Ph)_2$ (**3a**) (0.15 g, 0.31 mmol) and CD_3Li (0.32 mmol) in ether (2 ml) at room temperature for 2 h also gave *cis*-$PdMe_2(PEt_2Ph)_2$ containing CD_3 groups as a white precipitate after hydrolysis at 0 °C (0.13 g). The ethane evolved on thermolysis of the reaction products in toluene (2 ml) containing dimethyl maleate (50 μl) at 60 °C was determined to be consisted of CD_3CD_3, CH_3CD_3, and CH_3CH_3 in a molar ratio of 0.13: 0.40: 0.47 as measured by mass spectrometry.

Preparation and Thermolysis Products of cis-*$Pd(CD_3)_2(PMePh_2)_2$.* *cis*-$Pd(CD_3)_2(PMePh_2)_2$ was prepared by the reaction of $PdCl_2(PMePh_2)_2$ and CD_3Li (isotopic purity, 99%) in a similar manner to the preparation of **4a** and was identified by means of IR and ^1H NMR spectroscopy: ν(C–D) (KBr disc) =2200, 2090, and 2040 cm^{-1}. In ^1H NMR

spectrum (100 MHz, in acetone-d_6, at room temperature), the complete absence of the signal due to Pd–CH_3 was confirmed.

It was confirmed by mass spectrometry that ethane evolved on thermolysis of *cis*-$Pd(CD_3)_2(PMePh_2)_2$ at 60 °C in toluene (2 ml) containing dmm (50 μl) consisted of CD_3CD_3 and CH_3CD_3 in a molar ratio of 0.95: 0.05.

Thermolysis of the mixture of *cis*-$Pd(CD_3)_2(PMePh_2)_2$ (0.061 g, 0.11 mmol) and *cis*-$Pd(CH_3)_2(PMePh_2)_2$ (0.067 g, 0.12 mmol) in toluene (2 ml) containing dmm (50 μl) at 60 °C gave CD_3CD_3, CH_3CD_3, and CH_3CH_3 in a molar ratio of 0.47: 0.05: 0.48.

Preparation and Thermolysis Products of cis-*Pd(CH_2CD_3)$_2$(PMe_2Ph)$_2$*.* CD_3CH_2Li was prepared by the reaction of CD_3CH_2Br (isotopic purity, 97%)[19] with Li in pentane. *cis*-$Pd(CH_2CD_3)_2(PMe_2Ph)_2$ was prepared by the reaction of $PdCl_2(PMe_2Ph)_2$ and CD_3CH_2Li in a similar manner to the preparation of **2b** and was characterized by means of IR and ^1H NMR spectroscopy: ν(C–D) (KBr disc)=2170, 2145, 2095, and 2040 cm^{-1}. In ^1H NMR spectrum (100 MHz, in acetone-d_6, at −40 °C), only a signal due to Pd–CH_2 was observed as broad $A_2XX'A'_2$ pattern.

Butane produced by thermolysis of *cis*-$Pd(CH_2CD_3)_2(PMe_2Ph)_2$ in toluene containing dmm at room temperature was collected by means of GLC after collecting the volatile materials in thermolysis solution by the trap-to-trap distillation. In ^1H NMR spectrum (100 MHz, in C_6D_6, at room temperature) of collected butane, the ratio of methyl and methylene protons was 7: 93.

Kinetic Studies of Thermolysis of $PdMe_2L_2$. A 30 ml Schlenk tube containing a Ph_2CH_2 solution (4 ml) of the complex (about 0.05 g) and the additive (dmm or tertiary phosphine) was sealed with a gas-tight rubber serum cap and evacuated. The Schlenk tube was placed in a thermostatted bath (HAAKE F2) controlled to ±0.5 °C. The rate constants for thermolysis of the complex were obtained by measureing the amount of ethane evolved with time. The amount of ethane was confirmed by means of GLC using ethylene as an internal standard.

Kinetic Studies of trans *to* cis *Isomerization of $PdMe_2(PMePh_2)_2$.* The appropriate amount of *trans*-$PdMe_2(PMePh_2)_2$ (IVa) and and *cis*-$PdMe_2(PMePh_2)_2$ (**4a**) or $PMePh_2$ were placed in a weighed NMR tube and the tube was connected to a vacuum line with a Teflon joint. After evacuation, CD_2Cl_2 was transferred by the trap-to-trap distillation. The amount of transferred CD_2Cl_2 was determined by weighing, and concentrations of the complexes and $PMePh_2$ were determined by measuring the weight of CD_2Cl_2 added. The sealed tube was placed in a thermostatted NMR probe (±1.0 °C). The amount of IVa on isomerization was determined by measuring the ratio of the area of Pd–Me signals of IVa and **4a**.

Reaction of trans-*Pd(CH_3)$_2$($PMePh_2$)$_2$ and* cis-*Pd(CD_3)$_2$($PMePh_2$)$_2$.* To a Schlenk tube containing *trans*-$Pd(CH_3)_2(PMePh_2)_2$ (IVa) (0.072 g, 0.13 mmol) and *cis*-$Pd(CD_3)_2(PMePh_2)_2$ (0.076 g, 0.14 mmol), CH_2Cl_2 (2 ml) was added by means of a syringe to yield a clear pale yellow solution. After stirring the system for 2 h at 30 °C, the solvent was removed by pumping to yield a white precipitate of *cis*-$PdMe_2(PMePh_2)_2$ containing CD_3 groups (0.14 g). Identification of the product was carried out by IR spectroscopy. Thermolysis of the reaction product in toluene (2 ml) containing dmm (50 μl) at 60 °C liberated CD_3CD_3, CH_3CD_3, and CH_3CH_3 in a molar ratio of 0.29: 0.46: 0.25.

This work was supported by a Grant-in-Aid for Scientific Research No. 555340 from the Ministry of Education, Science and Culture.

References

1) For example; P. M. Maitlis, "The Organic Chemistry of Palladium," Academic Press, New York (1971), Vols. 1 and 2; J. Tsuji, "Advances in Organometallic Chemistry," Academic Press, New York (1979), Vol. 17, p. 141; R. F. Heck, "Organotransition Metal Chemistry," Academic Press, New York (1974).

2) D. Milstein and J. K. Stille, *J. Am. Chem. Soc.*, **101**, 4981 (1979).

3) T. Ito, H. Tsuchiya, and A. Yamamoto, *Bull. Chem. Soc. Jpn.*, **50**, 1319 (1977).

4) A. Yamamoto and T. Yamamoto, a review paper in preparation.

5) F. Ozawa, T. Ito, and A. Yamamoto, *J. Am. Chem. Soc.*, **102**, 6457 (1980).

6) S. Komiya, T. A. Albright, R. Hoffmann, and J. K. Kochi, *J. Am. Chem. Soc.*, **98**, 7255 (1976).

7) G. Calvin and G. E. Coates, *J. Chem. Soc.*, **1960**, 2008.

8) F. Basolo and R. G. Pearson, "Mechanisms of Inorganic Reaction," 2nd ed, John Wiley and Sons Inc., New York (1967).

9) R. Romeo, P. Ugualiati, and V. Belluco, *J. Mol. Catal.*, **1**, 325 (1975/76), and references cited therein.

10) G. W. Rice and R. S. Tobias, *J. Am. Chem. Soc.*, **99**, 2141 (1977), and references cited therein.

11) W. Mowat, S. G. Yagupsky, N. J. Hill, M. Yagupsky, and G. Wilkinson, *J. Chem. Soc., Dalton Trans.*, **1972**, 533.

12) T. Kohara, T. Yamamoto, and A. Yamamoto, *J. Organomet. Chem.*, **192**, 265 (1980).

13) J. K. Stille, private communication.

14) T. Yamamoto, A. Yamamoto, and S. Ikeda, *J. Am. Chem. Soc.*, **93**, 3350 and 3360 (1971).

15) S. Komiya, T. Yamamoto, and A. Yamamoto, *Chem. Lett.*, **1978**, 1273; G. M. Whitesides, J. F. Gaasch, and E. R. Stedronsku, *J. Am. Chem. Soc.*, **94**, 5258 (1972); J. X. McDermott, J. F. White, and G. M. Whitesides, *ibid.*, **98**, 6521 (1976).

16) K. Tatsumi, R. Hoffmann, A. Yamamoto, and J. K. Stille, *Bull. Chem. Soc. Jpn.*, **54**, 0000 (1981).

17) K. L. Cheng, *Anal. Chem.*, **26**, 1894 (1954).

18) W. Hewertson and H. R. Watson, *J. Chem. Soc.*, **1962**, 1490.

19) T. Yamamoto, T. Saruyama, Y. Nakamura, and A. Yamamoto, *Bull. Chem. Soc. Jpn.*, **49**, 589 (1976).

20) C. A. Tolman, *Chem. Rev.*, **77**, 313 (1977).

21) G. M. Kosolapoff and L. Maier, "Organic Phosphorus Compounds," Wiley-Interscience, New York (1972), Vol. 1, p. 78.

22) **Note added in proof.** A related independent study to the present work dealing with the *trans-cis* isomerization and reductive elimination of ethane from $PdMe_2L_2$ was recently reported by Gillie and Stille.[22] Their results mostly agree with ours except for the *trans-cis* isomerization mechanism.

23) A. Gillie and J. K. Stille, *J. Am. Chem. Soc.*, **102**, 4933 (1980).

A Reinvestigation of the Crystal and Molecular Structure of the β-Form of 2,4,6-Trimethyl-1,3,5-Trithiane

Kiyotane SEKIDO,* Jun ITOH,† Teruo NOGUCHI,† and Sakutaro HIROKAWA

Department of Chemistry, The National Defense Academy, Hashirimizu, Yokosuka 239

†*Koa Oil Co., Ltd., Ōtemachi, Tokyo 100*

(Received April 28, 1980)

Synopsis. The crystal structure of the title compound has been reinvestgated and refined to a final R factor of 0.057 for 1286 independent reflections. The six-membered ring takes a chair-form. All the three methyl groups are in the equatorial position. The mean values are 1.818 Å and 1.513 Å for the S–C and C–C distances respectively, and 101.3° and 108.5° for the C–S–C and S–C–S angles respectively.

The structure analysis of β-TTA has been reported by Valle *et al.*[1] and by the present authors.[2] The intensity data used in these works were collected by the photographic method, however, so the molecular geometry obtained was not accurate. Recently, the structure analysis of α-TTA using three-dimensional intensities collected by the counter-technique was reported by the present authors.[3] The crystal structure of β-TTA was, therefore, reinvestigated for comparison with that of α-TTA.

Experimental

The single crystals of β-TTA used in the analysis were obtained by the slow evaporation of an acetone solution. They are transparent prisms elongated along a principal axis, having approximately square cross sections.

The cell constants were determined by the least-squares method using various sets of high-angle reflections on a diffractometer. The crystal data are as follows: $C_6H_{12}S_3$, $F.W.$ =180.4, orthorhombic, space group $P2_12_12_1$, a=13.437(13), b=4.740(5), c=14.688(15)Å, V=935.4(1.6)Å^3, D_m=1.274 g cm^{-3}, D_c=1.280 g cm^{-3}, μ(Mo K_α)=7.17 cm^{-1}.

A prismatic crystal of 0.3×0.5×0.8 mm was mounted on a four-circle diffractometer (Rigaku AFC-III) with Mo K_α from a graphite monochrometer, and the intensities were collected for the independent 1614 reflections within $2\theta<60°$, using the ω-2θ scan technique with a scanning speed of 4° min^{-1} in 2θ, while 324 reflections with $|F_o|< 3\sigma(F)$ were designated as unobserved. Corrections for background and the Lorentz-polarization factor were made, but corrections for the absorption or the extinction were omitted.

The atomic parameters determined in the previous work[2] were used as input into the block-diagonal least-squares program on a computer CDC-6600 in the Century Reserch Center Co., Tokyo. At the stage of R=0.096, the hydrogen atoms were located, assuming the tetrahedral angle for each carbon atom and a bond length of 1.09 Å for each C–H bond. Further refinements were made with block-diagonal least-squares using anisotropic thermal parameters for the non-hydrogen, and isotropic B values for the hydrogen, atoms. After six cycles, convergence was attained with R=0.057. The final coordinates and equivalent isotropic temperature factors for the non-hydrogen atoms are given in Table 1.**

TABLE 1. ATOMIC COORDINATES(×10^4) AND EQUIVALENT ISOTROPIC TEMPERATURE FACTORS

	x	y	z	B_{eq}/Å^2
S(1)	2237(2)	1602(5)	711(1)	5.34
S(2)	3937(1)	3904(4)	1863(1)	4.58
S(3)	2032(1)	1755(5)	2759(1)	4.94
C(4)	3573(6)	1789(17)	889(5)	4.92
C(5)	3379(5)	1995(16)	2813(5)	4.42
C(6)	1866(5)	−318(15)	1728(5)	4.75
C(7)	4070(7)	2988(25)	53(6)	7.20
C(8)	3663(7)	3549(21)	3675(5)	5.90
C(9)	775(6)	−1088(22)	1628(6)	6.13

Results and Discussion

The thermal vibration ellipsoids[4] scaled to a 50% probability, together with the atomic numbering, are shown in Fig. 1. The intramolecular interatomic distances and angles involving the non-hydrogen atoms are given in Table 2. The mean S–C length is 1.818 Å, the C–S–C angles are 100.2—102.6° (mean 101.3°), and the S–C–S angles are 112.3—114.1° (mean 113.5°). The mean values reported previously were: S–C, 1.814 Å; C–S–C, 98.9°; S–C–S, 114.7° in the unsubsituted 1,3,5-trithiane,[5] 1.818 Å, 101.89°, 113.09° in α-TTA.[3]

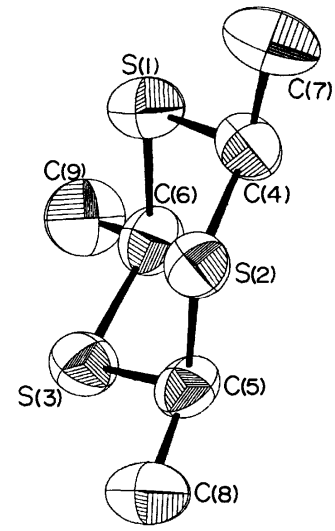

Fig. 1. The thermal vibration ellipsoids of non-hydrogen atoms drawn by ORTEP.[4]

The triangle formed by three sulfur atoms is regular, the averaged length being 3.040 Å (3.029 Å in α-TTA).

** The complete tables of the anisotropic thermal parameters, the F_o–F_c data, the least-squares planes, and the torsion angles are deposited as Document No. 8138 at the Office of the Editor of the Bulletin, the Chemical Society of Japan.

Table 2. Intramolecular interatomic distances(l) and angles ϕ involving the non-hydrogen atoms
Estimated standard deviations are given in parentheses.

	l/Å		ϕ/°
S(1) – C(4)	1.816(8)	C(6) – S(1) – C(4)	100.2(3)
S(2) – C(4)	1.815(8)	C(4) – S(2) – C(5)	102.6(3)
S(2) – C(5)	1.823(7)	C(5) – S(3) – C(6)	101.1(3)
S(3) – C(5)	1.816(7)	S(1) – C(4) – S(2)	114.0(4)
S(3) – C(6)	1.820(8)	S(2) – C(5) – S(3)	114.1(4)
S(1) – C(6)	1.818(8)	S(3) – C(6) – S(1)	112.3(3)
C(4) – C(7)	1.508(12)	S(1) – C(4) – C(7)	109.9(6)
C(5) – C(8)	1.514(10)	S(2) – C(4) – C(7)	108.3(6)
C(6) – C(9)	1.518(10)	S(2) – C(5) – C(8)	107.2(5)
S(1)···S(2)	3.045(3)	S(3) – C(5) – C(8)	108.5(5)
S(2)···S(3)	3.053(3)	S(3) – C(6) – C(9)	109.2(5)
S(3)···S(1)	3.022(3)	S(1) – C(6) – C(9)	107.8(5)
C(4)···C(5)	2.840(10)	S(1)···S(2)···S(3)	59.4(1)
C(5)···C(6)	2.807(10)	S(2)···S(3)···S(1)	60.2(1)
C(6)···C(4)	2.789(10)	S(3)···S(1)···S(2)	60.4(1)
S(1)···C(5)	3.452(7)	C(4)···C(5)···C(6)	59.2(3)
S(3)···C(4)	3.440(7)	C(6)···C(4)···C(5)	59.8(3)
S(2)···C(6)	3.434(7)	C(5)···C(6)···C(4)	61.0(3)

The other triangle formed by three ring-membered carbon atoms is also regular, with a length of 2.812 Å (2.833 Å in α-TTA).

The C–C bond distances are in the range of 1.508—1.518 Å, with a mean of 1.513 Å, shorter than the previously reported values (1.58 Å by Valle *et al.*[1] and 1.572 Å by the present authors[2]). However, it agrees with the lengths of C–C_{eq} (from a ring-membered carbon to a methyl carbon in the equatorial position) in α-TTA (1.514 and 1.524 Å). The S–C–C bond angles are in the range of 107.2—109.9°, with a mean of 108.5°, in accordance with the value of α-TTA (107.60°).

The conformation of the chair-form can clearly be seen from the alternative change of sign assigned to each torsion angle. The averaged value of the endocyclic torsion angles is 65.0° (in absolute values), showing a good agreement with the 64.9° in α-TTA. The calculated exocyclic torsion angles (174.4° as a mean in absolute values) show that all three methyl groups are co-ordinated in an equatorial. In α-TTA they are

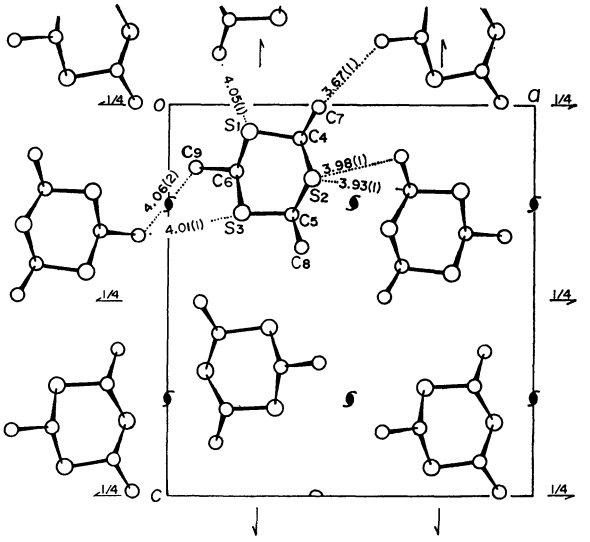

Fig. 2. The molecular packing viewed down **b**, showing all intermolecular distances (the non-hydrogen atoms) of less than 4.10 Å.

175.2° as a mean for the C···C_{eq}, and 68.3° for the C···C_{ax}, rotation.

The molecular packing, together with intermolecular interatomic distances less than 4.10 Å, are shown in Fig. 2. The shortest contact is 3.67 Å between C(7) and C(9) at $(1/2+x, 1/2-y, \bar{z})$. Since this is shorter than the van der Waals contact between two methyl groups, the rotations of the methyl groups may be hindered.

References

1) G. Valle, V. Busetti, and M. Mammi, *Acta Crystallogr., Sect. B*, **25**, 1631 (1969).

2) S. Hirokawa, K. Sekido, A. Suzuki, and T. Noguchi, *Memoirs of the Defense Academy, Jpn.*, XIV, No. 3, 89 (1974).

3) K. Sekido, H. Ono, T. Noguchi, and S. Hirokawa, *Bull. Chem. Soc. Jpn.*, **50**, 3149 (1977).

4) C. K. Johnson, *ORTEP*, ORNL-3794, Oak Ridge National Laboratory, Tennessee (1965).

5) G. Valle, V. Busetti, M. Mammi, and G. Carazzolov, *Acta Crystallogr., Sect. B*, **25**, 1432 (1969).

Enthalpies of Fusion of Intermediate Compounds, $KMgCl_3$, K_2MgCl_4, K_2BaCl_4, $KCaCl_3$, K_2SrCl_4, K_2LaCl_5, K_3PrCl_6, K_3NdCl_6, KGd_3Cl_{10}, and KDy_3Cl_{10}

Takeo HATTORI,* Kazuo IGARASHI, and Junichi MOCHINAGA

Department of Industrial Chemistry, Faculty of Engineering, Chiba University, Yayoi-cho, Chiba 260

(Received October 1, 1980)

Synopsis. The enthalpies of fusion were measured on the intermediate compounds of the binary systems of KCl and some other chlorides. These were compared with the values calculated using C_p of the component salts according to the additivity. The enthalpies of fusion measured were in good agreement with calculated in K_2LaCl_5 and K_2BaCl_4.

Some intermediate compounds have been known in such binary systems of KCl and some rare earth chlorides as of KCl and alkaline earth chlorides. Enthalpies and entropies of fusion of these compounds are thermodynamically valuable on obtaining theoretical understanding of phase diagrams of these binary or ternary molten chloride systems. In the present work, heats of fusion were measured using a differential scanning calorimeter (DSC) on some intermediate compounds of the binary systems of KCl and some other chlorides and were compared with values calculated using C_p (heat capacity at constant pressure) of component salts.

Experimental

Starting raw materials used were KCl, alkaline earth chlorides ($MgCl_2$, $CaCl_2$, $SrCl_2$, and $BaCl_2$), and rare earth chlorides ($LaCl_3$, $PrCl_3$, $NdCl_3$, $GdCl_3$, and $DyCl_3$). In these chlorides, KCl, $CaCl_2$, $SrCl_2$, and $BaCl_2$, were of reagent grade and separately demoistured by heating under the reduced pressure of about 10^{-3} Torr† at slightly below their melting points for 5—10 h. These were then heated to the molten states and after cooling, they were sealed in test tubes in Ar atmosphere till use.

On the other hand, $MgCl_2$ and rare earth chlorides which were prepared according to the similar procedure in the previous paper,[1] were sublimated to purify at about 1000 °C for 8—10 h under vacuum using the apparatus described elsewhere.[2]

The chlorides were weighed in the mole ratios 1-1, 2-1, and 3-1 corresponding to the compositions $KMgCl_3$, $KCaCl_3$, K_2MgCl_4, K_2BaCl_4, K_2SrCl_4, K_2LaCl_5, K_3PrCl_6, K_3NdCl_6, KGd_3Cl_{10}, and KDy_3Cl_{10}. All kinds of mixtures were weighed in a dry box with purified N_2 gas and heated in a quartz tube ($15^{\phi}\times 300^{mm}$) at about 50 °C lower than the melting point in an electric furnace under vacuum, and then raised temperature to melt in Ar atmosphere. After melting thoroughly, the mixtures were solidified in the inclined quartz tube and kept in sealed test tubes.

These samples were ground to 100—300 mesh in an agate mortar in a dry box with purified N_2 gas. Enthalpies of fusion of the samples were measured using DSC on about 20 mg in a platinum pan ($5^{\phi}\times 5^{mm}$) in Ar atmosphere of a flow rate of 50 ml/min at heating rate of 10 °C/min. The enthalpy was measured from the equation

$$\Delta H = KA/M,$$

where ΔH is an enthalpy of fusion per unit weight of a sample, M a weight of a sample, A an area of peak on a recording chart, and K an apparatus constant. As the apparatus constant K was dependent on temperature, it was determined on calibration curve about heat of transition of some NBS-ICTA** standard materials, that is Ag_2SO_4 (transition temp: 412 °C, heat of transition: 6.09 cal/g), K_2SO_4 (583 °C, 11.13 cal/g), and K_2CrO_4 (665 °C, 12.62 cal/g).

Results and Discussion

The results obtained were summarized in Table 1. Experimental enthalpies were measured from endothermic peaks of DSC curves. The calculated values were derived as follows.

Table 1. Experimental and calculated enthalpies of fusion of the intermediate compounds in binary component salts

End components Against KCl	Intermediate compounds (mp/K)	Enthalpies of fusion / kcal mol^{-1}	
		Exptl	Additive value
$MgCl_2$	K_2MgCl_4(688)	8.9	21.4
$MgCl_2$	$KMgCl_3$ (754)	7.9	15.7
$BaCl_2$	K_2BaCl_4(932)	16.4	15.8
$CaCl_2$	$KCaCl_3$(1021)	16.6	13.0
$SrCl_2$	K_2SrCl_4(865)	13.6	14.6
$LaCl_3$	K_2LaCl_5(902)	25.0	25.4
$PrCl_3$	K_3PrCl_6(938)	20.1	30.7
$NdCl_3$	K_3NdCl_6(961)	22.6	30.8
$GdCl_3$	KGd_3Cl_{10}(833)	13.5	
$DyCl_3$	KDy_3Cl_{10}(830)	19.9	

In each binary system, the heat capacities of the end component salts at their melting points were extrapolated to the melting point of the corresponding intermediate compound. The enthalpy values for the compound were estimated from those for the binary compounds by the relation

$$\Delta H_{C,T} = a\Delta H_{A,T} + b\Delta H_{B,T}, \quad (1)$$
$$(aA + bB \rightarrow A_aB_b = C)$$

where ΔH is heat of fusion and T the melting point of the compound C. And

$$\Delta H_{A,T} = \Delta H_{A,mp} + \int_{mp}^{T} \Delta C_p dT, \quad (2)$$

where, ΔC_p is represented by the relation in the reaction $A(s) = A(l)$,

$$\Delta C_p = C_p(l) - C_p(s). \quad (3)$$

The melting points, heats of fusion, and heat capacities

† 1 Torr = 133.322 Pa.

** NBS-ICTA: National Bureau of Standard-International Circular Thermal Analysis.

Table 2. Heat capacities (C_p), heats of fusion (L_f), and melting points of the substances used

Substance	Mp/°C	L_f/kcal mol^{-1}	$C_p = a + bT + cT^2$/cal deg^{-1}mol^{-1}			
			a	10^3 b	10^{-5} c	Temp range/K
KCl (s)	772	6.35±0.1	9.89	5.20	0.77	298—mp
KCl (l)			16.00	—	—	mp—1200
$MgCl_2$ (s)	714	10.3 ±0.3	18.90	1.42	−2.06	298—mp
$MgCl_2$ (l)			22.10	—	—	mp—1500
$BaCl_2$ (s)	962	4.0 ±0.1	26.61	—	—	1198—mp
$BaCl_2$ (l)			24.96	—	—	mp—1339
$CaCl_2$ (s)	772	6.8 ±0.1	17.18	3.04	−0.60	600—mp
$CaCl_2$ (l)			24.70	—	—	mp—1700
$SrCl_2$ (s)	873	3.8 ±0.2	18.2	2.44	—	298—mp
$SrCl_2$ (l)			26.2	—	—	
$LaCl_3$ (s)	855	13.0±0.2	22.4	9.4	—	
$LaCl_3$ (l)			32	—	—	
$PrCl_3$ (s)	786	12.1±0.2	21.8	8.4	—	
$PrCl_3$ (l)			32	—	—	
$NdCl_3$ (s)	760	12.0±0.2	22.8	7.4	—	
$NdCl_3$ (l)			31	—	—	
$GdCl_3$ (s)	609	9.6				
$DyCl_3$ (s)	654	7				

of the end component chlorides were shown in Table 2.[3-5]

In the systems of KCl–$LaCl_3$ and KCl–$BaCl_2$, the experimental enthalpies of the compounds of K_2LaCl_5 and K_2BaCl_4 were in good agreement with the calculated and value of K_2SrCl_4 were relatively good. These compounds were all 2 : 1 in mole ratio.

The deviation of the experimental enthalpies from the additivity were very small, especially in K_2LaCl_5 and the experimental were only 0.4 kcal/mol lower than the calculated.

Holm *et al.*[6] studied the binary system of KCl–$MgCl_2$ using a drop-calorimeter and reported that the melting points and enthalpies of fusion of the compounds were 705 K, 10.75 kcal/mol and 755 K, 10.33 kcal/mol in K_2MgCl_4 and $KMgCl_3$, respectively.

References

1) J. Mochinaga and K. Irisawa, *Bull. Chem. Soc. Jpn.*, **47**, 364 (1974).

2) J. Mochinaga and Y. Iwadate, *J. Fac. Eng. Chiba Univ.*, **30** [58], 213 (1979).

3) O. Kubaschewski, E. Li. Evans, and C. B. Alcock, "Metallurgical Thermochemistry," 4th ed (revised and enlarged), Pergamon Press (1967), p. 303 .

4) A. Glassner, AEC Report ANL-5750.

5) R. E. Thoma, "The Rare Earth Halides," in "Progress in the Science and Technology of the Rare Earths," ed by LeRoy Eyring, Pergamon Press (1966), p. 90.

6) J. L. Holm, B. J. Holm, B. Rinnan, and F. Grønvold, *J. Chem. Thermodyn.*, **1973**, 97.

Kinetics of the Hydrolysis of Zeolite 4A Surface by the Pressure-jump Relaxation Method

Tetsuya IKEDA, Minoru SASAKI, Raymond D. ASTUMIAN, and Tatsuya YASUNAGA*

Department of Chemistry, Faculty of Science, Hiroshima University, Higashisenda-machi, Naka-ku, Hiroshima 730

(Received December 2, 1980)

Synopsis. Single relaxation was found in the basic zeolite 4A suspension by the pressure-jump method. The relaxation phenomenon was attributed to the hydrolysis of the zeolite 4A surface and the kinetic parameters were obtained.

One important property of zeolite 4A is the existence of sodium ion in surface cage-like structures from where ion exchange with other cations such as Ca^{2+}, K^+, and NH_4^+ occurs.[1-3] It has been determined by surface electrical conductivity measurements and by infrared absorption spectra[4-6] that these cages are terminated by surface hydroxyl groups. In solid catalysis the cage of the zeolite plays an important role, giving rise to ion sieve effects, and thus the determination of the mechanism of the ion exchange, as well as that of the specific adsorption of ions into the cage, is of major importance in understanding the ion sieve action in the ion exchange of the zeolites. However, hydrolysis of the surface hydroxyls also occurs, varying the charge density on the framework of the zeolite, and so the dynamic behavior of these hydroxyls, which differs greatly from that of γ-alumina or titanium dioxide[7,8] must be clarified before the mechanism of ionic adsorption and exchange can be well understood. In this paper we present the results of pressure-jump relaxation experiments on the kinetics of zeolite 4A surface hydrolysis.

Experimental

Zeolite 4A ($Na_2O \cdot Al_2O_3 \cdot 2SiO_2 \cdot nH_2O$) was purchased from the Toyo Soda Co., and was purified as previously described.[8] X-Ray diffraction patterns before and after purification showed no change. Aqueous suspensions of zeolite 4A with NaOH were prepared under nitrogen atmosphere and the measurements were performed with particle concentration of 30 g/dm³ at 25 °C after equilibration for 1 d.

The pressure-jump apparatus used is the same one reported previously.[8] The time constant of the pressure-jump was within 80 μs.

Results and Discussion

Kinetic measurements were carried out by the pressure-jump method with conductivity detection on basic aqueous suspensions of zeolite 4A and a single relaxation process of decreasing conductivity with decreasing pressure on the order of s was observed only above the pH≃11.5. Figure 1 shows the concentration dependence of the reciprocal relaxation time, τ^{-1}, and it may be seen that τ^{-1} increases with increasing concentration of hydroxide ion. Since the sodium ion can enter into the cage of zeolite as mentioned above, one of plausible mechanisms of the relaxation phenomenon observed may be the base catalyzed adsorption-desorption process of the sodium ion. However, in the system to which tetramethylammonium hydroxide was added as the base in the same manner, where the tetramethylammonium ion can not enter into the cage,[9] the same relaxation phenomenon was observed. Therefore, it is clear that the relaxation observed is due to the interaction between the hydroxide ion and the active sites on the zeolite surface.

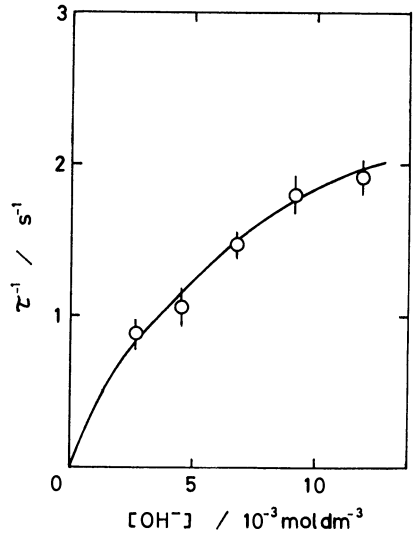

Fig. 1. Dependence of the reciprocal relaxation time on the equilibrium concentration of OH^- in the zeolite 4A–NaOH system at particle concentration of 30 g/dm³ and 25 °C.

In order to clarify the mechanism of the relaxation, the concentrations of the surface group, SOH, and the dissociated surface group, SO^-, existing on the zeolite

Table 1. Static and kinetic data in aqueous suspensions of zeolite 4A at 25 °C

$\frac{[OH^-]}{10^{-3}\ mol\ dm^{-3}}$	$\frac{[SOH]}{10^{-3}\ mol\ dm^{-3}}$	$\frac{[SO^-]}{10^{-2}\ mol\ dm^{-3}}$	$\frac{\tau^{-1}}{s^{-1}}$	$-pK$
2.63	3.1	1.54	0.88±0.10	3.28
4.57	2.2	1.63	1.06±0.13	3.21
6.76	1.1	1.74	1.47±0.09	3.37
9.12	1.0	1.75	1.80±0.13	3.28
11.8	0.8	1.77	1.91±0.12	3.27

surface were determined from the adsorption isotherm of hydroxide ion[10] and are listed in Table 1. For the hydrolysis of the hydroxyl group on the framework of the zeolite 4A surface in basic region, the following scheme can be written

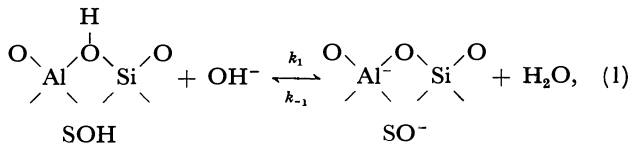

where k_1 and k_{-1} are the rate constants of the adsorption and the desorption of hydroxide ion, respectively. Henceforth, we use SOH and SO^- for the two surface species, as indicated above. In the present pH region, as can be seen from Table 1, the zeolite surface may be assumed to be fully occupied by the dissociated surface group, with the value of the equilibrium constant calculated from $K(=[SO^-]/[SOH][OH^-])$ being nearly constant. The constancy of the pK's supports the validity of the above assumption. Thus, in the determination of the mechanism we ignored the effect of the variable surface potential. Under the constant surface potential, the equation of τ^{-1} in the above scheme is given by

$$\tau^{-1} = k_1([SOH]+[OH^-]) + k'_{-1}, \quad (2)$$

with

$$k'_{-1} = k_{-1}[H_2O]. \quad (3)$$

The plot of τ^{-1} *vs.* the concentration term of Eq. 2 yields a straight line as shown in Fig. 2. The linearity of this plot confirms the plausibility of the mechanism assumed above. From the slope and the intercept of the line, the values $k_1=1.6\times10^2$ mol^{-1} dm^3 s^{-1} and $k'_{-1}=8.7\times10^{-2}$ s^{-1} respectively, were obtained and the value of negative log of the kinetic equilibrium constant, pK', was determined to be -3.26 from the ratio of the obtained rate constants.

The kinetic equilibrium constant is in good agreement with the static equilibrium constant obtained from the adsorption isotherm. Therefore, this fact also justifies the mechanism described above. Thus, we are led to the conclusion that the relaxation phenomenon observed

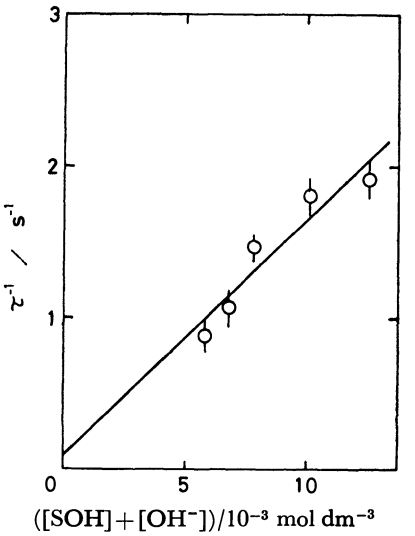

Fig. 2. The plot of τ^{-1} *vs.* the concentration term in Eq. 2.

can be attributed to the adsorption-desorption process of OH^-, *i.e.*, hydrolysis on the zeolite 4A surface.

References

1) D. W. Breck, "Zeolite Molecular Sieves," Wiley-Interscience, New York (1974).
2) H. S. Sherry and H. F. Walton, *J. Phys. Chem.*, **71**, 1457 (1967).
3) R. M. Barrer and J. Klinowski, *J. Chem. Soc., Faraday Trans. 1*, **68**, 1956 (1972).
4) G. T. Kerr, E. Dempsey, and R. J. Mikovsky, *J. Phys. Chem.*, **69**, 4050 (1965).
5) J. Uytterhoeven, L. G. Christner, and W. K. Hall, *J. Phys. Chem.*, **69**, 2117 (1965).
6) L. V. C. Rees and C. J. Williams, *Trans. Faraday Soc.*, **61**, 1481 (1965).
7) K. Hachiya, M. Ashida, M. Sasaki, M. Karasuda, and T. Yasunaga, *J. Phys. Chem.*, **84**, 2292 (1980).
8) K. Hachiya, M. Ashida, M. Sasaki, H. Kan, T. Inoue, and T. Yasunaga, *J. Phys. Chem.*, **83**, 1866 (1979).
9) R. M. Barrer and W. M. Meire, *Trans. Faraday Soc.*, **54**, 1074 (1958).
10) P. W. Shindler and H. Gamsjäger, *Kolloid Z. Z. Polym.*, **250**, 759 (1972).

The Spectrophotometric Determination of Zirconium(IV) by Solvent Extraction with Trioctylphosphine Oxide and Benzophenone

Yasumasa SHIGETOMI and Takehiro KOJIMA*

Department of Chemistry, Okayama College of Science, Ridai-cho, Okayama 700

(Received August 30, 1980)

Synopsis. The colorimetric determination of zirconium(IV) was investigated by means of liquid-liquid extraction, where zirconium in a nitric-acid solution was quantitatively extracted into molten TOPO–benzophenone at about 60 °C. The organic phase solidifies on cooling and is separated and dissolved in methanol. The addition of an ethanolic solution of 1-(2-pyridylazo)-2-naphthol to this solution yields as intense red colour.

Recently, spectrophotometric determination has again, because, with it one is able easily, come to be of interest to determine a number of metals without difficulty. However, one of the major problems is the lack of the specificities of any chromogenic agents except bathophenanthroline, 1,10-phenanthroline, *etc.* On the other hand, tributyl phosphate (TBP), tributylphosphine oxide (TBPO), and trioctylphosphine oxide (TOPO) are well known as selective extractants.[1-4] Also, solvent extraction by using naphthalene or benzophenone has the disadvantage that it must be carried out at a comparatively high temperature (70 °C), but it has the merit that metal ions can be extracted with less volume than when a liquid solvent is used, for, upon cooling, the organic phase separates out as a solid.[5-8]

In this investigation, we studied the selective spectrophotometric determination method of zirconium, combined with such a selective extraction and a conventional colour development.[9]

Experimental

Reagents and Apparatus. All the reagents were of an analytical grade. The standard zirconium(IV) solution was prepared by dissolving 0.2767 g of zirconium nitrate in ion-exchanged water and by then diluting the solution to 100 cm^3. Stock solutions of the other metal salts were prepared by dissolving salts in 0.1 mol dm^{-3} hydrochloric acid or nitric acid. The trioctylphosphine oxide (TOPO), tributylphosphine oxide (TBPO), tris(2-ethylhexyl)-phosphine oxide (TEHPO), and triphenylphosphine oxide (TPPO) were used without further purification. The absorbancy curves of the solution contained in a 1-cm matched-glass cell were measured with a Hitachi 101 spectrophometer.

Procedure. Transfer a solution containing 0—230 μg of zirconium into a 100-cm^3 Erlenmeyer flask with a tight-fitting stopper, and adjust the acidity of the solution to 2 mol dm^{-3} with nitric acid. Add 100 mg of TOPO and 300 mg of benzophenone. Heat the flask on a water bath at about 60 °C untile the TOPO phase melts completely, and then shake it vigorously for 2 min. Remove the flask from the bath, cool the molten extractant rapidly while stirring in cold water, and separate the resulting solidified extract in granular form from the aqueous solution by filtration. Wash the extract several times with water and transfer it to a 10-cm^3 volumetric flask containing 1 cm^3 of a 1-(2-pyridylazo)-2-naphthol (PAN) solution and 0.5 cm^3 of a triethanolamine solution. Dilute the solution to the mark with methanol. Shake well and measure the absorbance of the solution at 545 nm against a reagent blank.

Results and Discussion

Extraction with Various Extractants. The extraction was carried out through the procedures using TOPO, TBPO, TEHPO, and TPPO. TOPO and TBPO would seem to be suitable extractants. However, TBPO interferes with the colour development of zirconium with PAN. Therefore, we used TOPO as an extractant in the following experiments. Also, we simultaneously examined the effect of acidity on the extraction. Zirconium was extracted quantitatively from more than 2 mol dm^{-3} nitric acid. Its extractability from a hydrochloric-acid solution is not so much as that from a nitric-acid solution; for instance, the extraction percentage in a 2 mol dm^{-3} nitric-acid medium showed more than 99%, while that at hydrochloric acid reached only 55% at 50 °C, though it increases with an increase in the temperature and, at 80 °C, reaches 99%.

Effect of Amount of TOPO. The experiments were carried out at temperatures ranging from 50 to 90 °C in order to examine the relation between the amount of TOPO and the extraction percentage. It was found that the elevation of the extraction temperature causes the extractability to increase slightly, and that adding more than 100 mg of TOPO brings to about a quantitative extraction. Further, naphthalene and biphenyl were investigated as diluents instead of benzophenone; however, naphthalene is not sufficiently soluble in methanol, and so it interferes with the colour developing because of forming a opaque solution.

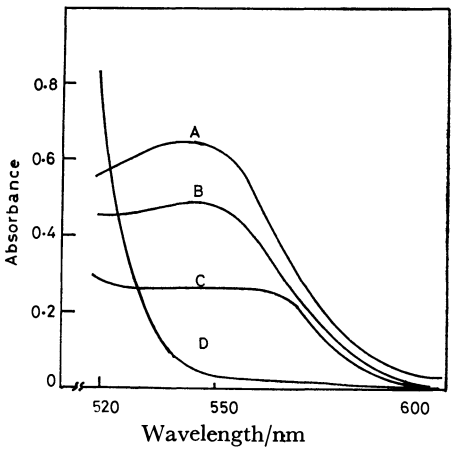

Fig. 1. Absorption curves.
A: 4.6 ppm Zr(IV) *vs.* reagent blank (TOPO), B: 4.6 ppm Zr(IV) *vs.* reagent blank (TBPO), C: 4.6 ppm Zr(IV) *vs.* reagent blank (TEHPO), D: reagent blank *vs.* ethanol, PAN: 1.0 cm^3, buffer: 0.5 cm^3.

Absorption Spectra. Figure 1 show the absorption spectra of the reagent blank and of the PAN–zirconium-(IV) complex in a benzophenone–methanol solution resulting from taking in 46 μg of zirconium through the above procedures. The magnitudes of the absorbance are in this order: TOPO, TBPO, and TEHPO; this order is compatible with that of the extraction percentage. However, no quantitative relation was observed between these values. For instance, the TBPO complex is as extractable as the TOPO one, but the absorbance of the former is only two-thirds that of the latter. We may suppose that TBPO complex is more stable than the TOPO complex; therfore, the exchange reaction does not proceed not so much as in the TOPO complex. Further, we examined how the absorbance varied as a function of the amount of triethanolamine or PAN added. The addition of 0.5 cm^3 of 10% triethanolamine as a buffer sufficed to develop the colour of the zirconium complex. Also, the colour intensity showed a plateau. Adding a large amount of a PAN solution causes the reagent blank to have a colour of a strong intensity. Therefore, the determination was carried out by adding 1 cm^3 of a 0.1% PAN solution to 10 cm^3 of a zirconium solution.

Choice of Solvent. Tests were made with verious solvents in dissolving mixtures of the complex and benzophenone. Such a mixture is soluble in many organic solvents, such as methanol, ethanol, *N,N'*-dimethylformamide, and acetone, but dissolving with cyclohexane, isobutyl methyl ketone, and chloroform formed an opaque solution. Furthermore, to these solutions are also added 1 cm^3 of a 0.1% PAN solution. The spectra observed are shown in Fig. 2. The absorbance is higher in methanol than in the others.

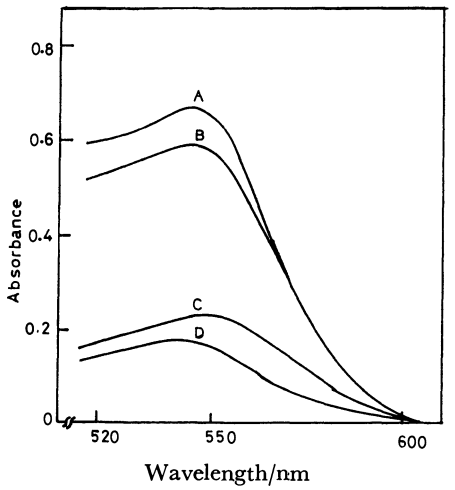

Fig. 2. Effect of the various solvents.
A: CH_3OH, B: C_2H_5OH, C: DMF, D: $(CH_3)_2CO$.
Conditions Zr(IV): 4.6 ppm, PAN: 1.0 cm^3, buffer: 0.5 cm^3, TOPO: 100 mg, benzophenone: 300 mg.

Effects of Diverse Ions. Possible interference was looked for by placing 46 μg of zirconium in 25 cm^3 of a 2 mol dm^{-3} nitric-acid solution. One milligram of the following cations gave no interference; Mg(II), Ca(II), Sr(II), Ba(II), Y(III), La(III), Ce(III), Nd(III), Cr(III), Mn(II), Cu(II), Zn(II), Al(III), Fe(III), V(V), Co(II), and Ni(II), but Sc(III) and U(VI) gave considerable positive interference. As has been mentioned above, the apparent molecular absorptivity, 1.24×10^4 cm^3 mol cm^{-1}, we obtained is not so large as that[10] obtained by combining with the colour development and the solvent extraction with dibutyl hydrogenphosphate. However, zirconium can be determined up to 10^{-5} mol dm^{-3}, as it can be easily concentrated two hundred times by means of the proposed extraction, though allowance must be made for large volumes by shaking for a longer times and by using larger amounts of the extractants.

References

1) Y. Marcus and A. S. Kertes, "Ion Exchange and Solvent Extraction of Metal Complexes," John Wiley and Sons, New York, N. Y. (1969), p. 650
2) J. C. White and W. J. Ross, NAS-NA 3102, 1961.
3) T. Ishimori, K. Kimura, T. Fujina, and H. Murata, *J. Atomic Energy Soc. Jpn.*, **4**, 41 (1962).
4) T. Ishimori, K. Watanabe, and E. Nakamura, *Bull. Chem. Soc. Jpn.*, **33**, 636 (1960).
5) M. Satake, Y. Matsumura, and T. Fujinaga, *Talanta*, **25**, 718 (1978).
6) T. Fujinaga, M. Satake, and T. Yonekubo, *Bull. Chem. Soc. Jpn.*, **46**, 2090 (1973).
7) T. Fujinaga, M. Satake and M. Shimizu, *Bunseki Kagaku*, **25**, 313 (1976).
8) Y. Shigetomi, T. Kojima, H. Kamba, and Y. Yamamoto, *Anal. Chim. Acta*, **116**, 199 (1980).
9) Y. Shigetomi, T. Kojima, and H. Kamba, *Talanta*, **27**, 1079 (1980).
10) R. F. Rolf, *Anal. Chem.*, **33**, 125 (1961).

Dual-wavelength Spectrophotometric Determination of Trace Amounts of Phosphate in the Presence of Large Amounts of Silicate Using Molybdenum Blue

Kousaburo OHASHI,* Toshie ENOMOTO, and Katsumi YAMAMOTO
Department of Chemistry, Faculty of Science, Ibaraki University, Mito 310
(Received September 2, 1980)

Synopsis. A method is described for the determination of trace amounts of phosphate in the presence of large amounts of silicate. It is based on the difference in the absorption spectra of molybdenum blues formed from phosphate and silicate using a dual-wavelength spectrophotometer. The difference in absorbances at 797.3 nm and 825.0 nm is proportional to phosphate concentration over the range 1.60×10^{-7} to 7.00×10^{-5} M (1 M=1 mol dm^{-3}).

The spectrophotometric determinations of phosphate based on the formations of molybdophosphoric acid and molybdenum blue have been widely used. Though many different applications of these methods have been proposed,[1] difficulties are often encountered when two or more ions which can form molybdenum blue are present simultaneously. Many studies on the separation of phosphate from silicate have been reported. Fujinaga *et al.*[2] studied a solvent extractive separation of phosphate from silicate based on the difference in the behavior of molybdophosphoric acid and molybdosilicic acid toward the mixed solvents of 1-butanol–cyclohexane–water and of 1-butanol–isobutyl methyl ketone–water. Recently, a kinetic method for the simultaneous determination of phosphate and silicate, based on the difference in the formation rate of molybdenum blue was reported.[3] This method needs a careful control of the conditions. The present authors have developed a method for the determination of trace amounts of phosphate in the presence of large amounts of silicate based on the difference in the absorption spectra of molybdenum blue formed from phosphate and silicate using a dual-wavelength spectrophotometer.

Experimental

Materials. Molybdenum(VI) solution (1.00×10^{-1} M) was prepared by dissolving 12.09 g of sodium molybdate dihydrate in 500 ml of redistilled water. Working solutions were prepared by dilution with redistilled water to the desired concentrations. Molybdenum(V) ($Mo_2O_4^{2+}$) perchlorate solution was prepared as reported in a previous paper.[4] The concentration of molybdenum(V) solution was determined spectrophotometrically using the molar extinction coefficient ($\varepsilon=103$) at 384 nm.[5] The stock solution of molybdenum(V) perchlorate was stored in a refrigerator. Before use the stock solution was diluted to each desired concentration. This molybdenum(V) solution was stable for at least two months. Phosphate solution was prepared from sodium dihydrogenphosphate dihydrate, and silicate solution by fusing pure silica with anhydrous sodium carbonate. All the other chemicals were of analytical grade.

Apparatus. A Hitachi 356 type dual-wavelength spectrophotometer was used for the measurements of difference in absorbances at two different wavelengths.[6]

General Procedure for the Determination of Phosphate. For each run, 2 ml of 1.0 M perchloric acid, 8 ml of 2.00×10^{-2} M molybdenum(VI), 6 ml of 1.60×10^{-2} M molybdenum(V) in 2.0 M perchloric acid, and 3 ml of 4.00×10^{-4} M phosphate and 5 ml of 3.34×10^{-3} M silicate solutions were pipetted into a 50-ml measuring flask. After dilution to 50 ml with redistilled water, the solution was thermostated for 20 min at 80 °C. Below 8.00×10^{-7} M phosphate, the thermostating time was 50 min at 80 °C. The difference in absorbances at 797.3 nm and 825.0 nm was measured by a dual-wavelength spectrophotometer; two wavelengths were chosen: 825.0 nm, which is the absorption maximum of the molybdenum blue from phosphate; and 797.3 nm, at which the molydenum blue from silicate gives the same molar extinction coefficient as that at 825.0 nm.

Results and Discussion

Absorption Spectra of Molybdenum Blue Formed from Phosphate and Silicate. The absorption spectra of the molybdenum blue formed from phosphate and silicate with a mixture of 1.80×10^{-3} M molybdenum(V) and 3.20×10^{-3} M molybdenum(VI) in 0.28 M perchloric acid are shown in Fig. 1; the spectrum was measured after the solution had been thermostated for 20 min at 80 °C. The absorption maximum of molybdenum blue from phosphate appears at 825 nm (curve (A)). Curve (B) is the absorption spectrum (λ_{max} 810 nm) of the molybdenum blue from silicate. The thermostating for 20 min at 80 °C provides complete formation of molybdenum blue from phosphate, but only a partial formation of molybdenum blue from silicate, because of the small rate of molybdenum blue formation. The effect of the perchloric-acid concentration on the formation of molybdenum blue from phosphate showed that the

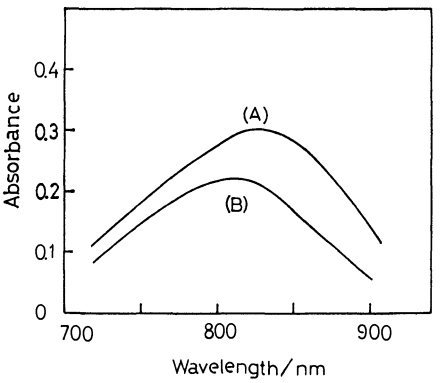

Fig. 1. The absorption spectra of molybdenum blues. (A): 1.60×10^{-5} M phosphate, (B): 2.00×10^{-4} M silicate (SiO^{2+}), both with 3.20×10^{-3} M Mo(VI), 1.80×10^{-3} M Mo(V), 0.28 M $HClO_4$. The absorption spectra (A) and (B) were measured after thermostating 20 min at 80 °C.

maximum absorbance was obtained in the range from 0.20 to 0.41 M with 2.90×10^{-5} M phosphate, 1.76×10^{-3} M molybdenum(V), and 3.20×10^{-3} M molybdenum(VI) by thermostating at 80 °C for 20 min. The rate of the formation of molybdenum blue from silicate decreases with the increase in the perchloric-acid concentration in the range from 0.25 to 5.0 M. For concentrations below 0.20 M perchloric acid, molybdenum(VI) reacts with molybdenum(V) to give isomolybdenum blue. In this work the perchloric-acid concentration of the reaction solution was adjusted to 0.28 M, and the reaction solution was thermostated for 20 min. Almost the same concentrations of molybdenum(V) and molybdenum(VI) as used previously for the determination of phosphate[4] were adopted for the determination of phosphate using a dual-wavelength spectrophotometer.

Calibration Curve. The calibration curve was obtained by the general procedure for the determination of phosphate. The calibration curve is linear in the phosphate range of 1.60×10^{-5} to 7.00×10^{-5} M (0—1.0 full scale), 1.80×10^{-6}—8.00×10^{-6} M (0—0.1 full scale), and 1.60×10^{-7}—8.0×10^{-7} M (0—0.01 full scale).

Table 1. Determinations of phosphate in the presence of 3.34×10^{-4} M silicate

PO_4^{3-} added/M	PO_4^{3-} found/M	Error/%
6.3×10^{-7}	5.8×10^{-7}	−9.2
2.4×10^{-6}	2.3×10^{-6}	−4.2
6.3×10^{-6}	6.6×10^{-6}	4.8
9.8×10^{-6}	9.7×10^{-6}	−1.0
3.0×10^{-5}	2.9×10^{-5}	−3.3

$[Mo(V)]=3.20\times10^{-3}$ M, $[Mo(V)]=1.80\times10^{-3}$ M, $[HClO_4]=0.28$ M.

Table 1 shows the results of the determination of phosphate in the presence of 3.34×10^{-4} M silicate.

Effect of Diverse Ions. The effect of diverse ions on the determinations of phosphate was previously examined in detail.[4] In the present work, these effects were not reexamined. Metal ions such as Mg^{2+}, Ca^{2+}, Mn^{2+}, Co^{2+}, Ni^{2+}, Zn^{2+}, Cd^{2+}, Pb^{2+}, Hg^{2+}, Fe^{3+}, Al^{3+}, Cr^{3+}, and UO_2^{2+} do not interfere with the determination of phosphate, in concentrations up to *ca.* 100 molar amounts. The presence of more than 500 molar amounts of Fe^{3+} can be tolerated by adding sodium hydrogensulfite solution. The presence of an equimolar amount of As(V) interferes somewhat with the determination of phosphate.

Determination of Phosphate in the Hinuma River. One liter of the sample was evaporated to 100 ml. A 10 ml of 1.6 M HNO_3 was added to the solution, and then the solution was evaporated to 20 ml on a sand bath. After neutralization with sodium hydroxide solution and dilution to 100 ml with redistilled water the solution was filtered. The phosphate concentration was determined by the general procedure. The phosphate concentration was found to be 7.0×10^{-6} M.

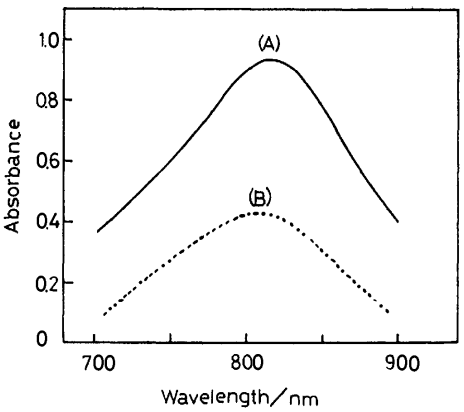

Fig. 2. The absorption spectra of molybdenum blue. (A): 12 ml of the 10-fold concentrated sample, conditions as for Fig. 1. (B): Absorption spectrum obtained by the subtraction of the spectrum of molybdenum blue obtained using the determined phosphate concentration from a curve (A).

Curve (A) in Fig. 2 is the absorption spectrum of the molybdenum blue formed by the general procedure for the color development of molybdenum blue. Curve (B) is the absorption spectrum obtained by subtraction of the absorption spectrum of the molybdenum blue prepared using the phosphate concentration determined from curve (A). The spectrum coincides with that of the molybdenum blue from silicate. A trace amount of phosphate in the Hinuma River, which contains large amounts of soluble silicate, was determined by the present method.

The method described here will be widely applicable to the determination of phosphate in samples containing silicate.

References

1) See, for example, "Colorimetric determination of nonmetals," 2nd ed, ed by D. F. Bolz and J. A. Howell, Wiley-Interscience, New York (1978).

2) T. Fujinaga, T. Hori, and Y. Kanda, *Bunseki Kagaku*, **27**, 395 (1978).

3) K. Ohashi, H. Kawaguchi, and K. Yamamoto, *Anal. Chim. Acta*, **111**, 301 (1979).

4) K. Ohashi, K. Yasu, C. Suzuki, and K. Yamamoto, *Bull. Chem. Soc. Jpn.*, **50**, 3202 (1977).

5) Y. Sasaki, R. S. Taylor, and A. G. Sykes, *J. Chem. Soc., Dalton Trans.*, **1975**, 396.

6) S. Shibata, M. Furukawa, and K. Goto, *Anal. Chim. Acta*, **46**, 271 (1969).

Phosphorylation with Pyrophosphoric Acid

Hachiro YAMAGUCHI,* Fumio OGURA, Tetsuo OTSUBO, and Yasuhiro IKEURA

Department of Applied Chemistry, Faculty of Engineering, Hiroshima University, Sendamachi, Naka-ku, Hiroshima 730

(Received October 27, 1980)

Synopsis. Dihydrogenphosphates of primary and secondary aliphatic alcohols as well as phenol were prepared by a very simple procedure with pyrophosphoric acid. *t*-Butyl and benzyl dihydrogenphosphates could be obtained by a slight modification of the reaction conditions. For the purpose of phosphorylation pyrophosphoric acid was more reactive than orthophosphoric acid.

Organic phosphoric acid esters play a very important role in many fields of organic and biological chemistry, and they are attractive objectives in synthetic organic chemistry. Various synthetic methods and reagents for phosphorylation have been used.[1] Pyrophosphoric acid (abbreviated below as PPA) as well as polyphosphoric acid has been used as a phosphorylating agent by many workers. To elucidate and utilize the presumed remarkable phosphorylating ability of PPA,[2] we also studied its reaction with various alcohols and phenol. Mere by mixing and warming with equimolar PPA, primary and secondary aliphatic alcohols as well as phenol afforded the dihydrogenphosphates, which were isolated as Ba salts and identified as anilinium salts (Table 1). The effect of temperature on the yield of phosphate was studied with reference to EtOH, and the highest yield was obtained at *ca.* 90 °C. Bisethylation became apparent above the temperature and the yield of diethyl ester gradually increased from 1.4% (80 °C) to 7.8% (140 °C). Orthophosphoric acid (100%) gave $EtOPO_3H_2$ in only 2.3% yield at 90 °C.[3] This result clearly indicated the higher reactivity of PPA than H_3PO_4. With regards to secondary alcohols, considerable dehydration occured at higher temperature to decrease the yield of $ROPO_3H_2$.[4] *t*-Butyl and benzyl alcohols did not give the desired phosphates by the simple procedure. But in the presence of CCl_3CN and 2 molar Et_3N, phosphorylation proceeded successfully to yield dihydrogenpyrophosphates, which were isolated as cyclohexylammonium salts and converted to anilinium hydrogenphosphates by ion exchange and concomitant hydrolysis (Table 1). The active phosphorylating agent was probably the imidoylpyrophosphate, which was formed from the PPA dianion and CCl_3CN and reacted with alcohols to give pyrophosphates and trichloroacetamide.[1b,6]

Experimental

Apparatus and Measurements. The melting points were

TABLE 1. PHYSICAL PROPERTIES OF THE ANILINIUM HYDROGENPHOSPHATE $ROPO_3H_2 \cdot C_6H_5NH_2$

R	Mp/°C	^{1}H-NMR, δ from DSS (in D_2O)	IR (cm^{-1}) ν (P=O)	ν(C–O–P)	δ (N–H) ν (N–H)
CH_3	166—167 (167—168)[a]	3.58(3H, d, J_{HP}=10 Hz, CH_3), 7.53 (5H, s, aromatic)	1240	1025 1055	2900 1505
CH_3CH_2	164—165 (164—166)[a]	1.26 (3H, t, J=7 Hz, CH_3), 3.93 (2H, ap. quin, J=7 Hz, J_{HP}=8 Hz, CH_2), 7.50 (5H, s, aromatic)	1220	1020 1045	2880 1495
$CH_3CH_2CH_2$	150—152 (137—139)[a]	0.90 (3H, t, J=7 Hz, CH_3), 1.62 (2H, ap. sex, J=7 Hz, CH_2), 3.83 (2H, ap quar, J=7 Hz, J_{HP}=8 Hz, CH_2–O), 7.50 (5H, s, aromatic)	1222	1030 1070	2870 1500
$CH_3(CH_2)_2CH_2$	144—148 (138—140)[a]	0.92 (3H, br, t, CH_3), 1.13—1.93 (4 H, m, CH_2), 3.85 (2H, ap. quar, J_{HP}=7 Hz, CH_2O)	1230	1030 1060	2890 1500
$HOCH_2CH_2$	127—128	3.53—4.20(4H, m, CH_2), 7.50 (5H, s, aromatic)	1245	1030 1090	2900 1500
$(CH_3)_2CH$	171 (160—162)[a]	1.25 (6H, d, J=6 Hz, CH_3), 4.20—4.53 (1H, m, J_{HP}=8 Hz, methine) 7.23—7.72 (5H, m, aromatic)	1230	1035	2960 1500
$C_2H_5\underset{\displaystyle CH_3}{\underset{\vert}{C}}H$	158—159	0.90 (3H, t, J=7 Hz, CH_3), 1.23 (3H, d, J=6 Hz, CH_3), 1.40—1.86 (2H m, CH_2), 3.93—4.72 (1H, m, methine), 7.16—7.77(5H, m, aromatic)	1235	1015	2870 1500
Cyclohexyl	166—168 (168—169)[a]	0.80—2.20 (10H, m, CH_2), 3.56—4.31 (1H, m, methine), 7.06—8.03 (5H, m, aromatic)	1215	1025 1060	2910 1500
Phenyl	169—170 (171—175)	6.92—7.45 (5H, m, aromatic) 7.47—7.92 (5H, m, aromatic)	1230	1040	2860 1495
$(CH_3)_3C$	139—143 dec	1.41 (9H, s, CH_3) 7.01—7.83 (5H, m, aromatic)	1250	1015 1075	2900 1505
Benzyl	151—154 dec[a,b]	4.93 (2H, d, J_{HP}=7.4 Hz, CH_2), 7.27—7.70 (10H, m, aromatic)	1225	1050	2860 1500

a) See Ref. 5. b) Corresponding dianilinium salt was reported, but we could not obtain it.

measured on a Yanagimoto MP-J3 apparatus and corrected. The IR spectra (KBr) were obtained on a JASCO IR-S spectrometer. The ^{1}H-NMR spectra were recorded on a JEOL PMX-60 spectrometer in D_2O using DSS as an internal standard, unless otherwise stated, and given in δ units.

Procedures and Results. Pyrophosphoric acid was prepared from 86% H_3PO_4 (199 g) and P_2O_5 (188 g) as colorless crystals (360.8 g, 97.3%).[7] The spectral data and melting points for all the anilinium hydrogenphosphates were summarized in Table 1. All the compounds described in this paper gave satisfactory elementary analyses. The equivalent weights of Ba salts determined by acid titration (Methyl Orange) were in good agreement with the calculated values. Dihydrogenphosphates of primary and secondary aliphatic alcohols and phenol were prepared by essentially the same procedure described below for the typical ethyl alcohol case.

Ethyl Dihydrogenphosphate: Ethanol (5.0 g, 108.5 mmol) was added dropwise to PPA (18.36 g, 103.2 mmol) with stirring. The mixture was warmed up to 90 °C and kept for 60 min. After cooling down and dilution with water (80 ml), the reaction mixture was neutralized with saturated aqueous $Ba(OH)_2$ (phenolphthalein) and the precipitated $Ba_3(PO_4)_2$ was filtered. Carbon dioxide was bubbled into the filtrate until the red color of indicator disappeared. Then the mixture was again filtered to remove $BaCO_3$ and concentrated under reduced pressure. The residue was triturated with EtOH to obtain $EtOPO_3Ba$ as colorless crystals (21.8 g, 76.9%). The Ba salt (3 g) was dissolved in water (200 ml) and treated with Na_2CO_3 (1.22 g). After removal of $BaCO_3$, the filtrate was subjected to ion exchange (Amberlite CG 120 H^+ form) to yield the free dihydrogenphosphate. The eluent was mixed with a slight excess aniline and concentrated under reduced pressure. The crude crystals (1.76 g) of anilinium ethyl hydrogenphosphate were washed and recrystallized with acetone. As an alternative and simple procedure, the salt could be prepared by treatment of $EtOPO_3Ba$ with equimolar anilinium sulfate in water. Anilinium diethyl phosphate; mp 72—75 °C; IR: 2860 (νNH_3), 1500 (δNH_3), 1200 (νP=O), 1050 (νP–O–C) cm^{-1}; ^{1}H-NMR ($CDCl_3$, TMS): 1.21 (t, J= 7 Hz, 6H, CH_3), 3.92 (ap. quin, J=7 Hz, J_{HP}=8 Hz, 4H, CH_2), 7.03—7.50 (m, 5H, aromatic), 9.36—9.83 (m, 3H, NH).

2-Hydroxyethyl Dihydrogenphosphate: Crude Ba salt (4.74 g), obtained as a mixture of mono-, bis-, and cyclic phosphates by the reaction (1 h) of $HOCH_2CH_2OH$ (2.23 g, 35.5 mmol) and PPA (6.24 g, 34.7 mmol) at 100 °C, was mixed with $Ba(OH)_2$ (3.43 g, 20 mmol) in water (150 ml) and heated to reflux for 30 min. After cooling down, the mixture was neutralized (phenolphthalein) with CO_2 and filtered to remove $BaCO_3$. The filtrate was concentrated under reduced pressure and the residue was triturated with methanol to crystallize the desired salt, $HOCH_2CH_2OPO_3Ba$ (4.92 g, 51.1%); cyclohexylammonium salt; mp 165—167 °C.[1c]

The Yields of Other Ba Salts were Shown Below with the Reaction Temperatures of Synthses: Methyl, 65 °C, 80.6%; propyl, 90 °C, 84.3%; butyl, 90 °C, 70.6%; isopropyl, 90 °C, 60.9%; *s*-butyl, 50 °C, 30.7% (60 °C, 10.5%; 90 °C, 0%); cyclohexyl, 80 °C, 49.5%; phenyl, 70 °C, 22.3%.

t-Butyl Dihydrogenphosphate: To the mixture of PPA (5.08 g, 28.5 mmol) and CCl_3CN, Et_3N (5.77 g, 57.1 mmol) was added. *t*-Butyl alcohol (8.44 g, 114.1 mmol) was added dropwise to this mixture and warmed at 35 °C for 60 min with stirring. The reaction mixture was poured into cyclohexylamine (20 g, 200 mmol) in acetone (200 ml) and stored in a freezer overnight. Light yellow precipitates obtained were washed with chilled acetone and recrystallized from EtOH (100 ml) containing cyclohexylamine (10 ml). By a usual ion exchange followed by neutralization with aniline, the salt was converted to the anilinium salt, which was recrystallized from acetone (0.78 g, 11.1%.) The crystals were identical with the authentic specimen synthesized.[6b]

Benzyl Dihydrogenphosphate: The mixture of PPA (5.15 g, 28.9 mmol), CCl_3CN (25.2 g, 175 mmol) and Et_3N (5.84 g, 57.8 mmol) was stirred for 60 min at room temperature. Benzyl alcohol (12.50 g, 115.7 mmol) was added to the mixture and heated to 75 °C for 2 h with stirring . The reaction mixture was poured into water and extracted with ether. The aqueous layer was mixed with cyclohexylamine (20 g, 200 mmol) and concentrated *in vacuo*. The residue was recrystallized from water (60 ml) to yield the bis(cyclohexylammonium) dibenzyl pyrophosphate. Vacuum concentration of the mother liquor afforded the cyclohexylammonium dibenzyl phosphate, which was recrystallized from acetone–H_2O (2 : 3 v/v). Both of the crystals were converted to the free acids by ion exchange and neutralized with aniline to yield dianilinium dibenzyl pyrophosphate (1.39 g, 8.8%, mp 151—153 °C; ^{1}H-NMR: 4.83—5.10 (m, 4H, CH_2), 7.20—7.68 (m, 20H, aromatic)) and anilinium dibenzyl phosphate (1.00 g, 9.3%, mp 115—117 °C; ^{1}H-NMR ($CDCl_3$, TMS): 5.78 (d, J_{HP}=7 Hz, 4H, CH_2), 6.93—7.42 (m, 15H, aromatic), 8.03—8.45 (m, 3H, NH_3)) respectively. The aqueous solution (160 ml) of free dibenzyl pyrophosphate (2.24 mmol) was refluxed for 2 h to obtain the benzyl dihydrogenphosphate, which was identified as anilinium salt (1.6 mmol).[5,6a]

The authors are grateful to Mr. Masayuki Watanabe for his assistance in purifying the anilinium benzyl hydrogenphosphate.

References

1) a) D. M. Brown, "Phosporylation," in "Advances in Organic Chemistry," ed by R. A. Raphael, E. C. Taylor, and H. Wynberg, Interscience, New York (1963), Vol. 3, pp. 75—157; b) F. Cramer, "Preparation of Esters, Amides, and Anhydrides of Phosphoric Acid," in "Newer Methods of Preparative Organic Chemistry," ed by W. Forest, Academic Press, New York (1964), Vol. 3, pp. 319—356; c) E. Cherbuliez "Organic Derivatives (Esters and Organic Anhydro Acid) of Phosphoric and Polyphosphoric Acids," in "Organic Phosphorus Compounds," ed by G. M. Kosolapoff and L. Maier, Wiely, New York (1973), Vol. 6, Chapt. 15, pp. 226—577; d) L. A. Slotin, *Synthesis*, **1977**, 737; e) T. Hata, *Kagaku No Ryoiki*, **33**, 832 (1979).

2) H. Yamaguchi and T. Nishi, *Nippon Kagaku Kaishi*, **1978**, 850.

3) W. Davis and W. C. J. Ross reported (*J. Chem. Soc.*, **1952**, 4296) that EtOH was heated under reflux for 6 d with metaphosphoric acid to obtain $EtOPO_3H_2$. But they did not give the yield.

4) Presence of olefinic hydrocarbons (at least three kinds) in the reaction products of *s*- and *t*-BuOH was detected by gas chromatography, ^{1}H-NMR, and IR spectra.

5) T. Obata and T. Mukaiyama, *J. Org. Chem.*, **32**, 1003 (1967).

6) a) F. Cramer and G. Weimann, *Chem. Ind.* (*London*), **1960**, 46; b) F. Cramer, W. Rittersdorf, and W. Böhm, *Ann.*, **654**, 180 (1962).

7) J. E. Malowan, *Inorg. Synth.*, Vol. III, 96 (1950).

Synthesis of 7-Halo-6*H*-benz[*cd*]azulen-6-ones

Shigeyasu KURODA,* Masaru SUGIMORI, Shinya KAWAHIGASHI, Nobuo MATUZAKI, Toshihiro NISHIYAMA, and Syuzi HIROOKA

Department of Industrial Chemistry, Faculty of Engineering, Toyama University, Takaoka, Toyama 933

(Received September 24, 1980)

Synopsis. 7-Bromo-6*H*-benz[*cd*]azulen-6-one, 7-Chloro-6*H*-benz[*cd*]azulen-6-one and its derivative were prepared in four steps starting from tetrahydroacenaphthene. Formation of the corresponding cations in strong acid is suggested on the basis of ^{1}H NMR and UV spectra.

6*H*-Benz[*cd*]azulen-6-one (**A**), one of the isomers of phenalenone (**B**),[1] was synthesized from acenaphthene,[2] but although its physical properties were reported no ^{1}H NMR spectral data were given on its cation. Because of the poor yield, chemical and biological properties have not been examined. We wish to report an alternative preparation of the title compounds in good yields, together with the ^{1}H NMR and UV spectra of their cations in strong acid.

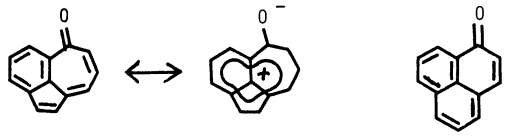

(A) (B)

The reaction of 2*a*,3,4,5-tetrahydroacenaphthen-5-one (**1**)[3] with triethyl orthoformate in the presence of a catalytic amount of *p*-toluenesulfonic acid gave enol ether (**2**) as colorless crystals. Dihalocyclopropanation[4] of **2** proceeded smoothly by using chloroform and bromoform in the presence of potassium *t*-butoxide in cyclohexane to give dihalocyclopropyl ethers (**3a**) and (**3b**) as colorless needles in 73% and 25% yields, respectively. Treatment of **3a** and **3b** with silver nitrate in aqueous methanol[5] afforded ring expanded halo enones (**4a**) and (**4b**) as colorless needles in 64% and 66% yields, respectively. Treatment of **4a** with *o*-chloranil in refluxing benzene gave a trace amount of the desired fully conjugated compound (**5a**) together with colorless crystals (**6**), presumably formed by cyclo-addition of the ene moiety of **4a** with *o*-chloranil.[6] Dehydrogenation of **4a** was achieved by using 2,3-dichloro-5,6-dicyano-*p*-benzoquinone (DDQ) in refluxing dioxane to give **5a** as reddish needles in 75% yield. Bromo compound **4b** also gave (**5b**) under the same reaction conditions. Dehydrogenation of **4a** with *N*-bromosuccinimide (NBS) afforded 2-bromo-7-chloro compound (**7**) as deep red needles in 58% yield. Its structure was assigned by comparison of ^{1}H NMR spectra with those of **5a**. The fact that the treatment of **5a** with NBS resulted only in the recovery of the starting material is significant as regards the mechanism of formation of **7**. The ^{1}H NMR and UV spectra of **5a**, **5b**, and **7** in strong acid such as concd sulfuric acid suggest the formation of cations **5a**′, **5b**′, and **7**′, respectively. The chemical shifts of **5a**, **5b**, and **7** in concd H_2SO_4 are about 0.6—1.6 ppm lower than those in $CDCl_3$ (Table 1). The UV spectra of these compounds in the acid show absorption maxima at around 550—600 nm, in a greater wavelength by *ca.* 200 nm than those in EtOH. These cations regenerated the original ketones quantitatively when diluted with a large amount of water.

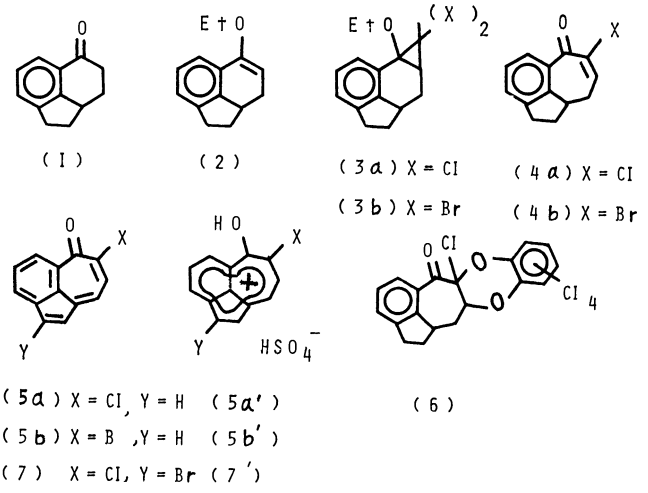

(1) (2) (3a) X = Cl (4a) X = Cl
(3b) X = Br (4b) X = Br
(5a) X = Cl, Y = H (5a′)
(5b) X = Br, Y = H (5b′)
(7) X = Cl, Y = Br (7′)
(6)

Experimental

Melting points and boiling points are uncorrected. Mass spectra were measured on a JEOL JMS-OISG-2 mass

TABLE 1. ^{1}H NMR DATA OF **5a**, **5a**′, **5b**, **5b**′, **7** AND **7**′

	δ/ppm (Multiplicity, *J*/Hz)							Δ_{ppm}
	H_1	H_2	H_3	H_4	H_5	H_8	H_9	
5a	6.40 (d, 5.6)	6.77 (d, 5.6)	7.37 (m)		8.05 (m)	7.59 (d, 8.8)	6.64 (d,8.8)	0.67—1.61
5a′	7.07 (d, 5.6)	7.50 (d, 5.6)	8.10 (m)		8.78 (m)	9.10 (d, 10.2)	8.25 (d, 10.2)	
5b	6.55 (d, 6.0)	6.97 (d, 6.0)	7.50 (m)		8.20 (m)	8.07 (d, 8.0)	6.70 (d, 8.0)	0.50—1.40
5b′	7.05 (d, 6.0)	7.55 (d, 6.0)	8.10 (m)		8.75 (d, 7.2)	9.35 (d, 9.6)	8.10 (m)	
7	6.82 (s)	—	7.28 (m)		8.00 (m)	7.66 (d, 10.0)	6.80 (d, 10.0)	0.78—1.64
7′	7.60 (s)	—	8.12 (m)		8.80 (d, 8.0)	9.30 (d, 10.0)	8.44 (d, 10.0)	

spectrometer, IR spectra on a JASCO IRA-1, UV spectra on a Hitachi EPS-3T spectrometer, and ^{1}H NMR on a JEOL JNM-MH-100 (100 MHz) and Hitachi R-24B (60 MHz) spectrometer in deuteriochloroform and concd sulfuric acid containing tetramethylsilane and dichloromethane as an internal standard, respectively.

2a,3-Dihydro-5-ethoxyacenaphthene (2). Triethyl orthoformate (72 ml, 0.44 mol) and *p*-toluenesulfonic acid (0.72 g) were added at 25 °C to a solution of ketone (**2**)[3] (28 g, 0.16 mol) in dry ethanol (540 ml). The mixture was stirred at room temperature for 12 h and then distilled under reduced pressure to give 33 g (98%) of enol ether (**2**); bp 110—112 °C/5 Torr, (1 Torr=133.322 Pa), which crystallized on standing. Recrystallization from ethanol gave colorless needles; mp 79—81 °C. IR (neat) 2950, 1630 cm^{-1}; ^{1}H NMR ($CDCl_3$) δ 7.85—7.20 (m, 4H), 4.70 (q, 2H, J=7.2 Hz), 3.52 (m, 4H), 2.40 (m, 1H), 1.45 (t, 3H, J=7.2 Hz), 1.52 (m, 1H); MS *m/e* 200 (M$^+$). Found: C, 83.93; H, 7.79%. Calcd for $C_{14}H_{16}O$: C, 83.96; H, 8.05%.

Dichlorocyclopropanation of 2. Potassium *t*-butoxide (20 g, 18 mmol) was added to a solution of 3.7 g (19 mmol) of **2** in 90 ml of dry cyclohexane, and the solution was cooled to 10 °C in an ice bath. Freshly distilled chloroform (50 g, 42 mmol) was then added to the solution over a period of 12 h. After addition of 100 ml of water, the mixture was extracted with chloroform and worked up in the usual way. The crude product was chromatographed on silica gel (hexane and benzene, 1 : 1) to give 4.8 g (73%) of **3a**, which was recrystallized from hexane to give colorless needles; mp 98—100 °C; IR (KBr) 3020, 2950, 1540 cm^{-1}; ^{1}H NMR ($CDCl_3$) δ 7.42 (m, 3H), 3.52 (q, 2H, J=7.2 Hz), 3.12 (m, 1H), 2.86 (m, 3H), 2.32 (m, 1H), 2.04 (m, 1H), 1.52 (m, 1H), 1.16 (t, 3H, J=7.2 Hz); MS *m/e* 284 (M$^+$). Found: C, 63.70; H, 5.79%. Calcd for $C_{15}H_{16}Cl_2O$: C, 63.62; H, 5.70%.

Dibromocyclopropanation of 2. The dibromo compound (**3b**) was prepared from **2** (6.0 g 30 mmol) by the same method as described above in 25% (2.6 g) yield. It was then recrystallized from hexane to give colorless needles; mp 101—102 °C; IR (KBr) 2960, 1460 cm^{-1}; ^{1}H NMR ($CDCl_3$) δ 7.08 (m, 3H), 3.40 (q, 2H, J=8 Hz), 3.04 (m, 1H), 2.76 (m, 3H), 2.24 (m, 1H), 1.44 (m, 1H), 1.14 (t, 3H, J=8 Hz); MS *m/e* 372 (M$^+$). Found: C, 48.13; H, 4.31%. Calcd for $C_{15}H_{16}Br_2O$: C, 48.42; H, 4.33%.

7-Chloro-1,2,6,9,9a-pentahydrobenz[cd]*azulen-6-one (4a).* A solution of silver nitrate (18 g, 116 mmol) in 530 ml of water was added to a solution of **3a** (7.3 g, 26 mmol) in 1.5 l of ethanol, and then the resulting solution was refluxed for 24 h. After being worked up in the usual way, the crude product was chromatographed on silica gel (benzene) to give 3.6 g (64%) of **4a** and 2.4 g (33%) of **3a**. A pure sample of **4a** was obtained by recrystallization from hexane as colorless needles; mp 66.2—68 °C; IR (KBr) 1640, 1610 cm^{-1}; ^{1}H NMR ($CDCl_3$) δ 7.78 (d, 1H, J=8 Hz), 7.14 (m, 3H), 3.52 (m, 1H), 2.29 (m, 2H), 2.44 (m, 3H), 1.72 (m, 1H); MS *m/e* 220, 218 (M$^+$). Found: C, 71.13; H, 5.15%. Calcd for $C_{13}H_{11}ClO$: C, 71.40; H, 5.07%.

7-Bromo-1,2,6,9,9a-pentahydrobenz[cd]*azulen-6-one (4b).* The bromo compound (**4b**) was obtained from **3b** (2.6 g) by the same method as described above in 66% (1.2 g) yield. It was then recrystallized from ethanol to give colorless needles; mp 87.5—89.5 °C; IR (KBr) 1640, 1610 cm^{-1}; ^{1}H NMR ($CDCl_3$) δ 7.80 (d, 1H, J=8 Hz), 7.32 (m, 3H), 3.52 (m, 1H), 2.88 (m, 2H), 2.40 (m, 3H), 1.66 (m, 1H); MS *m/e* 264, 262 (M$^+$). Found: C, 59.18; H, 3.94%. Calcd for $C_{13}H_{11}BrO$: C, 59.34; H, 4.21%.

*7-Chloro-6*H*-benz*[cd]*azulen-6-one (5a)* A solution of **4a** (1.5 g, 6.7 mmol) and DDQ (3.7 g, 16 mmol) in 50 ml of dry dioxane was refluxed for 30 h. The resulting solution was chromatographed on silica gel (benzene) to give 0.39 g (30%) of **5a** and 0.98 g (66%) of **4a**. The yield of **5a** was 75% accumulatively after repetation of the reaction three times with recovered **4a**. Recrystallization from ethanol gave red needles; mp 109—111 °C; IR (KBr) 1620, 1600, 745 cm^{-1}; UV (EtOH) nm (log ε) 240 (4.55), 283 (4.08), 335 (3.43), 385 (4.01); MS *m/e* 216, 214 (M$^+$). Found: C, 72.48; H, 3.18%. Calcd for $C_{13}H_7ClO$; C, 72.74; H, 3.29%.

5a': UV (concd H_2SO_4) nm (log ε) 251 (4.45), 284 (4.17), 292 (4.19), 332 (3.43), 348 (3.48), 402 (3.08), 422 (3.95), 590 (2.59).

*7-Bromo-6*H*-benz*[cd]*azulen-6-one (5b).* A solution of **4b** (0.81 g, 3.1 mmol) and DDQ (1.9 g, 8.2 mmol) in 28 ml of dry dioxane was refluxed for 12 h. The resulting solution was worked up by the same method as described above to give **5b** in 11% (0.09 g) yield and 0.02 g (3%) of recovered **4b**. Recrystallization from ethanol gave deep red needles; mp 123—124.5 °C; IR (KBr) 1610, 1600, 1590 cm^{-1}; UV (EtOH) nm (log ε) 236 (4.60), 275 (4.09), 280 (4.11), 337 (3.83), 385 (4.07); MS *m/e* 260, 258 (M$^+$). Found: C, 59.98; H, 3.00%. Calcd for $C_{13}H_7BrO$: C, 60.26; H, 2.72%.

5b': UV (concd H_2SO_4) nm (log ε) 245 (4.60), 270 (4.36), 291 (4.75), 330 (3.55), 364 (3.31), 408 (3.81), 418 (3.90), 427 (3.96), 450 (3.43), 470 (2.95), 560 (2.59).

*2-Bromo-7-chloro-6*H*-benz*[cd]*azulen-6-one (7).* A solution of 3.1 g (1.4 mmol) of **5a** and 5.0 g (2.8 mmol) of NBS in 45 ml of CCl_4 was refluxed for 3.5 h under irradiation with a 100-W tungsten lamp. The reaction mixture was cooled, filtered and chromatographed on silica gel (benzene) to afford 2.4 g (58%) of **7**, which was recrystallized from ethanol to give deep red needles; mp 171—174 °C; IR (KBr) 1610, 1590, 755 cm^{-1}; UV (EtOH) nm (log ε) 280 (4.19), 336 (3.90), 384 (4.12); MS *m/e* 294 (M$^+$). Found: C, 52.93; H, 1.81%. Calcd for $C_{13}H_6BrClO$: C, 53.19; H, 2.06%.

7': UV (concd H_2SO_4) nm (log ε) 244 (4.49), 269 (4.45), 287 (4.61), 327 (3.70), 360 (3.52), 540 (2.94).

Cycloadduct of 4a with o-Chloranil. A solution of 1.0 g (4.5 mmol) of **4a** and 2.7 g (11 mmol) of *o*-chloranil in 35 ml of dry dioxane was refluxed for 30 h. The solution was cooled, filtered and chromatographed on silica gel (benzene) to give 0.61 g (29%) of **6** and a trace amount of **5a**. Recrystallization from acetone gave colorless needles; mp 250 °C; IR (KBr) 1700 cm^{-1}; ^{1}H NMR (DMSO-d_6-TMS) δ 7.50—6.90 (m, 4H), 2.30—1.70 (m, 7H); MS *m/e* 468 (M$^+$). Found: C, 49.08; H, 2.45; Cl, 38.20%. Calcd for $C_{19}H_{11}Cl_5O$: C, 49.12; H, 2.45; Cl, 38.16%.

This research was supported by a Grant-in-Aid for Scientific Research No. 53232 from the Ministry of Education, Science and Culture.

References

1) D. H. Reid, *Quart. Rev.*, **19**, 274 (1965).
2) V. Boekelheide and C. D. Smith, *J. Am. Chem. Soc.*, **88**, 3950 (1966).
3) A. G. Anderson and R. H. Wade, *J. Am. Chem. Soc.*, **74**, 2274 (1952).
4) R. D. Miller and C. G. Gtierrez, *J. Org. Chem.*, **43**, 1569 (1978).
5) W. E. Parham, R. D. Soeder, J. R. Throckmorton, K. Kuncl, and R. M. Dodson, *J. Am. Chem. Soc.*, **87**, 321 (1965).
6) L. Horner and H. Merz, *Justus Liebigs Ann. Chem.*, **570**, 89 (1950).

α-Glucosylation of Phenols with Tetra-*O*-benzyl-α-D-glucose

Shinkiti Koto,* Naohiko Morishima, Mihoko Araki, Takuji Tsuchiya, and Shonosuke Zen

School of Pharmaceutical Sciences, Kitasato University, Shirokane, Minato-ku, Tokyo 108

(Received October 8, 1980)

Synopsis. An α-glucosylation of phenols with 2,3,4,6-tetra-*O*-benzyl-α-D-glucopyranose is described. This uses a mixture of *p*-nitrobenzenesulfonyl chloride, silver trifluoromethanesulfonate and triethylamine in dichloromethane in a two-stage treatment.

Continuing our study of glucosylation using 2,3,4,6-tetra-*O*-benzyl-α-D-glucopyranose (**1**),[1] we have found a novel α-glucosylation of phenols in two stages, as shown by Eq. 1. Although there have been several procedures reported for α-glucosylation of phenols,[2] the recommended one seems to give the product only in low yields.[3]

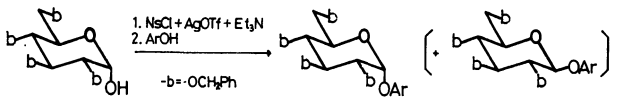

Eq. 1

When **1** was pre-treated with an equimolar mixture of *p*-nitrobenzenesulfonyl chloride, silver trifluoromethanesulfonate, and triethylamine in dichloromethane

Table 1. Results of glucosylation of 2-methylphenol[a]

Run	Reaction time/h[b]	Yield/%	
		α-Anomer	β-Anomer
23	0.1	21	7
24	0.5	42	14
2	3.0	47	16
25	5.0	46	17
26[c]	3.0	46	19
27[d]	3.0	14	17

a) The first stage was conducted at −10 °C for 0.5 h. b) Reaction time for the second stage. c) An excess amount (5.0 equiv.) of the phenol was used. d) An equimolar mixture of the phenol and triethylamine in dichloromethane was used.

Table 2. Yields and physical data of aryl tetra-*O*-benzyl-α-D-glucopyranosides

Run	Phenol	Code	Yield/%	Solv.[a]	Mp/°C[b]	$[\alpha]_D(c)$[c]	δ of C-1[d]/ppm
1	Phenol[e]	**2**	63[h]	HI	—	+82°(2.0)	95.4
2	2-Methylphenol[g]	**3**	47[i]	HC	69—70(n)	+84°(0.5)	96.1
3	2-Ethylphenol[g]	**4**	38	HC	55—56(n)	+78°(0.8)	95.9
4	2-Isopropylphenol[g]	**5**	44	HC	—	+73°(0.6)	96.1
5	2-*t*-Butylphenol[g]	**6**	28	HC	—	+71°(1.4)	95.0
6	2-Methoxyphenol[g]	**7**	50	BB	86—87(n)	+74°(0.6)	97.0
7	3-Methoxyphenol[g]	**8**	47	HC	—	+77°(0.7)	95.4
8	4-Methoxyphenol[f]	**9**	52	HC	—	+92°(1.0)	96.3
9	2-Ethoxyphenol[g]	**10**	35	BB	78—79(n)	+71°(0.4)	96.9
10	2-Fluorophenol[g]	**11**	43	BB	75—76(p)	+67°(0.3)	97.6
11	2-Phenylphenol[e]	**12**	48	BB	—	+58°(2.1)	96.5
12	3-(Methoxycarbonyl)phenol[f]	**13**	48	BB	87—88(n)	+95°(1.0)	95.5
13	4-(Methoxycarbonyl)phenol[f]	**14**	40	HC	—	+107°(1.0)	95.2
14	4-(Dodecyloxycarbonyl)phenol[f]	**15**	51	BB	—	+71°(0.8)	95.1
15	4-(Benzyloxycarbonyl)phenol[f]	**16**	45	BB	—	+83°(1.8)	95.2
16	4-(Phenoxycarbonyl)phenol[e]	**17**	46	HC	—	+102°(0.8)	95.8
17	3-Nitrophenol[e]	**18**	38	HC	—	+90°(0.8)	95.9
18	4-Nitrophenol[e]	**19**	32	BB	98—99(n)	+131°(0.4)	95.6
19	2,6-Dimethylphenol[e]	**20**	14[j]	HI	—	+46°(0.8)	99.5
20	2,6-Dimethoxyphenol[e]	**21**	30	BB	74—75(l)	+84°(1.4)	97.9
21	1-Naphthol[f]	**22**	50	HC	92—93(p)	+72°(0.8)	96.3
22	2-Naphthol[e]	**23**	66	HC	70—71(n)	+98°(1.3)	95.3

a) Solvent systems for chromatography: BB=benzene–butanone, HC=hexane–chloroform, HI=hexane–diisopropyl ether. b) n=Needles, p=prisms, l=leaves. c) At 20 °C in $CHCl_3$. d) In $CDCl_3$ with TMS. e) A supersaturated solution of the phenol in a small amount of the solvent was injected into the vessel. f) The phenol was added into the vessel during the short time the stopper was removed. g) The phenol was injected into the vessel. h) The β-anomer (**2β**), 21%: mp 84.5—86 °C; $[\alpha]_D$ −9° (*c* 1.0, $CHCl_3$); δ 101.6 (C-1) (Found: C, 77.70; H, 6.50 %). i) The β-anomer (**3β**), 16%: mp 106—107 °C; $[\alpha]_D$ −7° (*c* 0.7, $CHCl_3$); δ 101.2 (C-1) (Found: C, 77.70; H, 6.66%). j) The β-anomer (**20β**), 17%: mp 140—141 °C; $[\alpha]_D$ +25° (*c* 1.0, $CHCl_3$); δ 104.1 (C-1) (Found: C, 78.19; H, 6.86%)

Table 3. Analysis of aryl tetra-*O*-benzyl-α-D-glucopyranosides

Code	Mole formula	Found (%)		Calcd (%)	
		C	H	C	H
2	$C_{40}H_{40}O_6$	77.29	6.53	77.90	6.54
3	$C_{41}H_{42}O_6$	77.94	6.70	78.07	6.71
4	$C_{42}H_{44}O_6$	78.01	6.87	78.23	6.88
5	$C_{43}H_{46}O_6$	78.05	7.06	78.39	7.04
6	$C_{44}H_{48}O_6$	77.60	7.41	78.54	7.19
7	$C_{41}H_{42}O_7$	75.57	6.23	76.14	6.55
8	$C_{41}H_{42}O_7$	75.66	6.64	76.14	6.55
9	$C_{41}H_{42}O_7$	75.38	6.60	76.14	6.55
10	$C_{42}H_{44}O_7$	76.18	6.69	76.34	6.17
11	$C_{40}H_{39}FO_6$	75.42	6.18	75.69	6.19
12	$C_{46}H_{44}O_6$	79.50	6.64	79.74	6.40
13	$C_{42}H_{42}O_8$	74.71	6.21	74.76	6.27
14	$C_{42}H_{42}O_8$	74.15	6.40	74.76	6.27
15	$C_{53}H_{64}O_8$	76.59	7.75	76.78	7.78
16	$C_{48}H_{46}O_8$	76.34	6.39	76.78	6.17
17	$C_{47}H_{44}O_8$	76.06	6.32	76.61	6.02
18	$C_{40}H_{39}NO_8$	72.17	6.00	72.60	5.94
19	$C_{40}H_{39}NO_8$	72.33	6.24	72.60	5.94
20	$C_{42}H_{44}O_6$	77.43	7.06	78.23	6.88
21	$C_{42}H_{44}O_8$	74.46	6.75	74.53	6.55
22	$C_{44}H_{42}O_6$	79.18	6.25	79.25	6.35
23	$C_{44}H_{42}O_6$	79.07	6.30	79.25	6.35

at −10 °C[1a] and then reacted with phenol, we found that phenyl 2,3,4,6-tetra-*O*-benzyl-α-D-glucopyranoside (**2**) was formed predominantly. This is in contrast with the fact that a similar glucosylation of alkanol with **1** gave β-anomer preferentially.[1a,b] The ratio of anomers measured by ^{1}H NMR spectroscopy in the case of 2-methylphenol was constant throughout the reaction (Table 1). Various phenols were glucosylated with **1** in a similar way (Table 2). Except for 2,6-dimethylphenol, α-glucosides were formed prepondantly. But in the reaction of **1** with triethylammonium 2-methylphenolate, the β-glucoside was formed in a significant yield.

Our procedure is useful for preparing a compound such as 4-phenoxylcarbonylphenyl α-D-glucopyranoside (**25**), which was prepared through glucosylation of the phenol with **1** and subsequent catalytic hydrogenolysis to remove benzyl groups.

Experimental

Specific rotations were measured at 20 °C in a 1-dm cell. Column chromatography was carried out on silica gel (Kanto Kagaku). Silica gel (Merck, No. 7731) was used for TLC.

General Procedure for Glucosylation. To a mixture of **1** (270 mg, 0.5 mmol), *p*-nitrobenzenesulfonyl chloride (122 mg, 0.55 mmol), and silver trifluoromethanesulfonate (141 mg, 0.55 mmol) in dichloromethane (2.7 ml), triethylamine (77 μl, 0.55 mmol) was added at −10 °C. After stirring for 0.5 h, a phenol (0.65 mmol) was added to the mixture, which was then stirred for 3 h at 0 °C. After filtration the reaction mixture was chromatographed using appropriate solvent systems (Table 2) to give aryl 2,3,4,6-tetra-*O*-benzyl-α-D-glucopyranoside. Usually, the β-anomer was isolated as a by-product.

Anomeric Phenyl 2,3,4,6-Tetra-O-acetyl-α- and β-D-glucopyranosides ***24*** *and* ***24β***. An anomeric mixture (70 mg) of **2** and **2β** (Run 1) was hydrogenated in acetic acid (3 ml) containing water (1 ml), methanol (3 ml), and palladium black (80 mg, Wako) at 340 kPa, acetylated with acetic anhydride and pyridine, and then chromatographed using benzene containing butanone (gradient) to give first **24** (35 mg): mp 113—114 °C; $[\alpha]_D$ +165° (*c* 1, $CHCl_3$) [lit,[4] mp 115 °C; $[\alpha]_D^{20}$ +169.7° (*c* 2, $CHCl_3$)], and then **24β** (8 mg): mp 124.5—125.5 °C; $[\alpha]_D$ −21° (*c* 0.6, $CHCl_3$) lit,[4] mp 125—126 °C; $[\alpha]_D^{20}$ −22.5° (*c* 2, $CHCl_3$).

*4-(Phenoxycarbonyl)phenyl α-D-Glucopyranoside (****25****).* Compound **17** (60 mg, 0.8 mmol) was hydrogenated in acetic acid (3.7 ml) containing methanol (3.5 ml), water (1.2 ml), and palladium black (60 mg) at 340 kPa overnight, purified chromatographically using chloroform containing methanol (20%), and crystallized from ethanol to give **25** (26 mg, 84%): 155—157 °C; $[\alpha]_D$ +151° (*c* 0.7, MeOH). Found: C, 60.04; H, 5.38%. Calcd for $C_{19}H_{20}O_8$: C, 60.63; H, 5.36%.

Alternative Synthesis of ***2*** *and* ***2β***. A mixture of phenyl α-D-glucopyranoside (60 mg, 0.23 mmol), benzyl bromide (Tokyo Kasei 0.86 ml), barium oxide (1.08 g), and barium hydroxide octahydrate (0.42 g) in *N,N*-dimethylformamide (1.2 ml)[5] was stirred at 25 °C overnight, filtered, and evaporated *in vacuo*. The residue was chromatographed using benzene containing butanone (2%) to give **2** (53 mg, 56%), $[\alpha]_D$ +83° (*c* 3.0, $CHCl_3$).

Phenyl β-D-glucopyranoside[4] (0.54 g, 2.1 mmol) was converted in a similar way into **2β** (0.44 g, 34%): mp 83.5—85 °C; $[\alpha]_D$ −13° (*c* 0.4 EtOH), −12° (*c* 1.0, $CHCl_3$) [lit,[6] mp 82 °C; $[\alpha]_D^{18}$ −13.5° (EtOH)].

References

1) a) S. Koto, Y. Hamada, and S. Zen, *Chem. Lett.*, **1975**, 587; b) S. Koto, T. Sato, N. Morishima, and S. Zen, *Bull. Chem. Soc. Jpn.*, **53**, 1761 (1980); c) S. Koto, N. Morishima, and S. Zen, *Chem. Lett.*, **1976**, 1109; d) S. Koto, N. Morishima, and S. Zen, *Bull. Chem. Soc. Jpn.*, **52**, 784 (1979).

2) a) O. Westphal and H. Feier, *Chem. Ber.*, **89**, 582 (1956); b) A. N. Hall, S. Hollingshead, and H. N. Lydon, *J. Chem. Soc.*, **1961**, 4290.

3) W. E. Trevelyan, *Carbohydr. Res.*, **2**, 418 (1966).

4) E. M. Montgomery, N. K. Richtmyer, and C. S. Hudson, *J. Am. Chem. Soc.* **64**, 690 (1942).

5) S. Koto, T. Tsumura, Y. Kato, and S. Umezawa, *Bull. Chem. Soc. Jpn.*, **41**, 2765 (1968).

6) G. Grynkiewicz, *Pol. J. Chem.*, **53**, 1571 (1979).

A Convenient Preparation of Some *N*-Alkylcarbazoles and *N*-Alkylacridones

Hisao Nishi,* Hisao Kohno, and Toshihiro Kano

Department of Applied Chemistry, Faculty of Engineering, Saitama University, Shimo-Okubo, Urawa 338

(Received October 24, 1980)

Synopsis. *N*-Alkylation of aromatic compounds involving nitrogen heterocycles such as carbazole and acridone with alkyl halide in the presence of caustic solution and benzyl triethyl ammonium chloride (BTEAC) as a phase-transfer catalyst readily proceeded under mild conditions. These results show that this procedure is effective for the preparation of the title compounds in high yields.

A few investigations of *N*-alkylation of aromatic compounds involving nitrogen heterocycles with alkyl halide under phase-transfer catalytic conditions have been reported. Makosza,[1] for example, synthesized some *N*-alkylindoles and *N*-butylcarbazole by the use of phase-transfer catalysis in more than 80% yield under mild conditions. On the other hand, Kricka *et al.*[2] studied the synthesis of *N*-alkylcarbazoles, which were prepared by the reaction of carbazole, alkyl halide, and thallium(I) ethoxide under mild conditions.

Recently, Galy *et al.*[3] have reported the reaction of acridone with alkyl halide by the use of the phase-transfer catalysis under severe conditions (refluxing in toluene for 5 d). This procedure afforded a mixture of *N*-alkylacridones (41—65%) and *O*-alkyl-acridones.

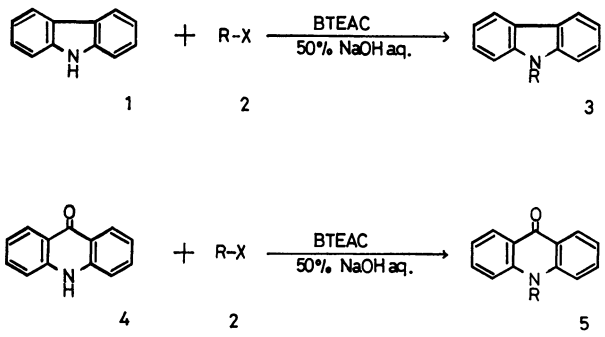

Scheme 1.

In the course of our synthetic studies of nitrogen heterocycles as intermediates of dyes and pigments, we have attempted to extend the phase-transfer catalytic reaction on *N*-alkylation of carbazole and acridone derivatives. We selectively obtained the desired *N*-alkyl compounds in high yields under milder conditions than those in Galy's procedure. *N*-Alkylation takes place as shown in Scheme 1.

The results are summarized in Table 1.

Experimental

The products were identified by the examinations of their melting points and N elemental analysis. Typical procedures are as follows:

*9-Methylcarbazole (**3a**).* To a mixture of 10.03 g (0.06 mol) of carbazole, 35 ml of aqueous 50% sodium hydroxide, 5 ml of benzene as a solvent and 410 mg (1.8 mmol) of BTEAC, a 5.6 ml (0.09 mol) of methyl iodide was added dropwise under stirring. It was continued at room temperature for 2 h. The reaction mixture was poured into hot water and left overnight at room temperature. The precipitated solid was collected, washed with water and dried. Recrystallizations from ethanol afforded 8.95 g of colorless plates (mp 88—89 °C) in the yield of 82.3%.

*10-Methylacridone (**5a**).* Methyl iodide (1.64 ml, 0.0263 mol) was added dropwise under stirring to a mixture of 3.42 g (0.0175 mol) of acridone, 13.5 ml of aqueous 50% sodium hydroxide, 13.6 ml of ethyl methyl ketone as a solvent, and 120 mg (0.527 mmol) of BTEAC, and was stirred at 55—60 °C for 3 h. The reaction mixture was poured into hot water, and separated solid worked up in the manner used for **3a**. Recrystallizations from ethanol provided 3.30 g of pale yellow needles (mp 200—201 °C) in the yield of 82.7%.

Table 1. Preparations of some *N*-alkylcarbazoles and *N*-alkylacridones

Compound No. [f,g]	RX	RX[a] / 1 or 4	Temp °C	Time [b] h	Products yield/% (Lit)	Mp/°C [c,d] (Lit)	Appearance
3a	CH_3I	1.50	r.t.	2	82.3(78)	88—89(87)	Colorless plates
3b	C_2H_5Br	1.50	r.t.	2	86.2(85)	67—68(67—68)	Colorless needles
3c	n-C_3H_7Br	1.25	55—60	1	81.0(72)	48—49(50)	Colorless needles
3d	n-C_4H_9Br	1.25	70—75	1	86.5(71)[e]	58—59(58)	Colorless needles
3e	$PhCH_2Cl$	1.25	70—75	1	92.0(97)	118—119(118—119)	Colorless needles
3f	$CH_2{=}CH_2CH_2Cl$	1.50	r.t.	2	74.3(67)	55—56(56)	Colorless plates
5a	CH_3I	1.50	55—60	3	82.7(45)	200—201(201)	Pale yellow needles
5b	C_2H_5Br	1.50	55—60	2	79.3(45)	158—160(158)	Yellow plates
5c	n-C_3H_7Br	1.50	65—70	2	75.1(43)	131—132(130)	Yellow prisms
5d	n-C_4H_9Br	1.50	70—75	1	80.0(65)	97—98(98)	Yellow needles
5e	$PhCH_2Cl$	1.20	70—75	1	75.7(63)	180—181(181)	Yellow needles

a) Molar ratio. b) r.t.: Room temperature. c, d) Carbazole: L. J. Kricka and A. Ledwith, *J. Chem. Soc., Perkin Trans. 1*, **1972**, 2292. Acridone: J. P. Galy and J. Barbe, *Synthesis*, **1979**, 944. e) Yield 84%, M. Makosza, *Rocz. Chem.*, **49**, 1203 (1975). f) Molar ratio of BTEAC and 1 or 4 is 0.03 : 1. g) Solvent is benzene in the case of carbazole and is ethyl methyl ketone in the case of acridone.

References

1) M. Makosza, *Rocz. Chem.*, **49**, 1203 (1975).
2) L. J. Kricka and A. Ledwith, *J. Chem. Soc., Perkin Trans. 1*, **1972**, 2292.
3) J. P. Galy and J. Barbe, *Synthesis*, **1979**, 944.

Homogeneous Hydrogenation of α,β-Unsaturated Ketones and Aldehydes Catalyzed by $Co_2(CO)_8$–Di(tertiary phosphine) Complexes

Kazuhisa MURATA* and Akio MATSUDA

National Chemical Laboratory for Industry, Tsukuba Research Center, Yatabe, Tsukuba, Ibaraki 305

(Received November 26, 1980)

Synopsis. The cobalt complexes modified by some di(tertiary phosphine)s as ligands were found to be much more active catalysts than $Co_2(CO)_8$ for the hydrogenation of α,β-unsaturated ketones and aldehydes under hydroformylation conditions.

When an α,β-unsaturated ketone or aldehyde is treated with a cobalt catalyst under hydroformylation conditions, the olefinic linkage is hydrogenated rather than hydroformylated.[1] However, since the rate of hydrogenation is much slower than that of hydroformylation, little attention has been paid to the cobalt-catalyzed hydrogenation.

Recently, we reported that complexes prepared *in situ* from $Co_2(CO)_8$ and various di(tertiary phosphine)s are more active catalysts for the homogeneous hydroformylation of methyl acrylate than $Co_2(CO)_8$.[2] We find that these cobalt complexes can be successfully used as catalysts effective for the hydrogenation of α,β-unsaturated ketones and aldehydes to give the corresponding saturated carbonyl compounds. We describe here the results of some of our studies on the hydrogenation under hydroformylation conditions.

$CH_2{=}C(R){-}COCH_3 \longrightarrow CH_3CH(R){-}COCH_3$

1 **2**

$CH_2{=}C(R){-}CHO \longrightarrow CH_3CH(R){-}CHO$

3 **4**

[a: R=H, b: R=CH_3]

The results are listed in Table 1, where the initial rate of the reaction was taken as a measure of the catalytic activity. The hydrogenation of 2-butenone (**1a**) preferentially occurred under the experimental conditions to give 2-butanone (**2a**) in high yield; the catalytic activity of $Co_2(CO)_8$-1,2-bis(diphenylphosphino)ethane(diphos) complex was *ca.* 30 times or above that of $Co_2(CO)_8$[3] (Compare Runs 3 and 6). The reaction can proceed even at a temperature as low as 50 °C (Run 7). $Co_2(CO)_8$–diphos system was effective for the hydrogenation of **1b**, **3a**, and **3b** (Runs

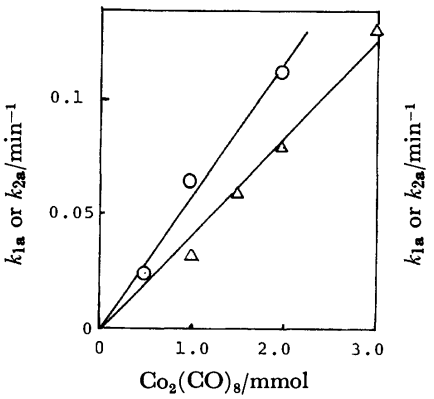

Fig. 1. Effect of catalyst concentration on k_{1a} or k_{2a}.
Diphos/$Co_2(CO)_8$=0.75 (const).
Toluene 50 ml, substrate 50 mmol, CO/H_2=1100 kg/cm^2 (const.), temp 110 °C.
—○—: **1a**, —△—: **2a**.

TABLE 1. HYDROGENATION OF α,β-UNSATURATED KETONES AND ALDEHYDES UNDER HYDROFORMYLATION CONDITIONS

Toluene (solvent) 50 ml, substrate 50 mmol, CO/H_2=1, total pressure 100 kg/cm^2 (const.), temp 120 °C.

Run No.	Substrate	Diphos/$Co_2(CO)_8$ (mmol/mmol)	Time / min	Initial rate[a] / mmol min^{-1}	k[b] / min^{-1}	Products (yield/%)[c]
1	**1a**	1.5/1.0	180	0.02	—	**2a**(1.1)
2	**1a**	1.0/1.0	40	1.0	—	**2a**(75)
3	**1a**	0.75/1.0	15	2.4	0.09	**2a**(80)
4	**1a**	0.5/1.0	15	2.2	—	**2a**(78)
5	**1a**	0.25/1.0	30	0.85	—	**2a**(65)
6	**1a**	0/1.0	240	0.07	—	**2a**(31)
7[d]	**1a**	2.0/4.0	500	—	—	**2a**(91)
8[d]	**1a**	0/4.0	500	—	—	**2a**(1.3)
9	**1b**	0.5/1.0	30	1.2	—	**2b**(80)
10	**1b**	0/1.0	225	0.12	—	**2b**(65)
11	**3a**	1.0/2.0	20	2.5	0.095	**4a**(74)
12	**3a**	0/2.0	180	0.15	—	**4a**(44)
13	**3b**	1.0/2.0	20	2.4	—	**4b**(82)
14	**3b**	0/2.0	120	0.26	—	**4b**(66)

a) See text. b) The "k" denotes the first order rate constant. c) Based on substrate initially introduced.
d) The reaction was carried out at 50 °C.

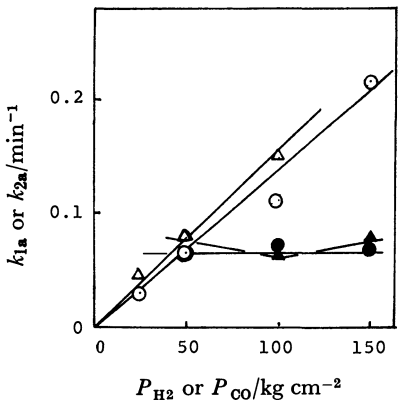

Fig. 2. Effect of partial pressure of hydrogen or CO. Toluene 50 ml, substrate 50 mmol, temp 110 °C, $Co_2(CO)_8$ 1 mmol (**1a**), 2 mmol (**2a**), diphos 0.75 mmol (**1a**), 1.5 mmol (**2a**).
—○—: **1a** (P_{CO}=50 kg/cm², const.), —△—: **2a** (P_{CO}=50 kg/cm², const.), —●—: **1a** (P_{H_2}=50 kg/cm², const.), —▲—: **2a** (P_{H_2}=50 kg/cm², const.).

9, 11, and 13).

In the hydroformylation of methyl acrylate, the maximum activity has been achieved when the molar ratio of diphos to $Co_2(CO)_8$ was *ca.* 0.5—0.75.[2] The results listed in Table 1 (Runs 1—6) are similar to this. The effect of phosphine structure on the activity was examined: the order of reactivity was in accordance with that of hydroformylation.[4]

Using **1a** and **2a**, kinetic behaviors were briefly examined. The rate of hydrogenation exhibits a first order dependence on the concentration of **1a** or **2a**, the rate constant k_{1a} or k_{2a} being calculated (See Table 1 (Runs 3 and 11)). Good Arrhenius plots of the constants provide the apparent activation energies of 12.3 kcal/mol with respect to k_{1a} and 9.1 kcal/mol to k_{2a} (temperature range: 90—120 °C).

As shown in Fig. 1, these constants increase with increase in $Co_2(CO)_8$ concentration. Also, plots of the constants *vs.* partial pressure of hydrogen reveal first order behaviors, while those *vs.* CO pressure give zero order (Fig. 2). These observations are identical with those described in the hydroformylation, with the exception of the CO pressure effect (Figs. 1, 2).

Experimental

Materials. Phosphines and toluene were obtained commercially and used with no further purifications. All α,β-unsaturated carbonyls were distilled prior to use.

Reaction Procedure. A catalyst solution containing $Co_2(CO)_8$ (1—4 mmol), phosphine (0.25—2 mmol), and substrate (50 mmol) in toluene (50 cm³) was placed in a stainless-steel autoclave (100 cm³), which was subsequently charged with a mixture of H_2 and CO (*ca.* 1/1 ratio).[5] The reaction was carried out at 120 °C under 100 kg/cm² of total pressure (const.) and aliquot samples were withdrawn from the vessel at several reaction times and analyzed by GLC (determination of the initial rate, Table 1).

Kinetic measurements were performed as follows. The hydrogenation system described above was brought to the desired reaction temp and the total pressure was kept constant during the reaction by supplying hydrogen from a 100 ml pressure storage vessel through a pressure regulator. The amount of hydrogen consumed was calculated from the pressure drop in the storage (Figs. 1 and 2).

References

1) R. W. Goetz and M. Orchin, *J. Org. Chem.*, **27**, 3698 (1962); R. W. Goetz and M. Orchin, *J. Am. Chem. Soc.*, **85**, 2782 (1963); H. Adkins and G. Krsek, *ibid.*, **71**, 3051 (1949).

2) K. Murata and A. Matsuda, *Bull. Chem. Soc. Jpn.*, **53**, 214 (1980).

3) It has been reported that in the absence of phosphine the hydrogenation is slow (See Table 1, Run 6), because a stable π-oxapropenyl complex (A) is formed.[1] Therefore, the phosphine ligand may play an important role in further hydrogenation of (A) to form the products, but there is no more evidence at the present time.

4) Diphos (2.2) > $Ph_2PC{\equiv}CPPh_2$ (1.5) > *cis*-$Ph_2PCH{=}CHPPh_2$ (1.0) > $PhP(CH_2CH_2PPh_2)_2$ (0.64) > $Ph_2P(CH_2)_3PPh_2$ (0.40) > $Ph_2PCH_2PPh_2$ (0.16) > $Ph_2P(CH_2)_2AsPh_2$ (0.14) > none (0.07) > PPh_3 (0.04) (numerical values refer to the initial rate in Table 1).

5) In the absence of CO, a perfect decomposition of $Co_2(CO)_8$ occurred.

Photolysis of Dispiro-substituted 3-Thioxo-1-cyclobutanones

Koji KIMURA,* Yoshihiro FUKUDA, Toshihiko NEGORO, and Yoshinobu ODAIRA

Department of Petroleum Chemistry, Faculty of Engineering, Osaka University, Suita, Osaka 565

(Received December 6, 1980)

Synopsis. Photolysis of dispiro-substituted 3-thioxo-1-cyclobutanones in dichloromethane or even in methanol gave rise to the photoisomerization to afford thiolactones preferentially.

As part of our studies on the photolysis of 1,3-cyclobutanediones, we previously reported[1] that three primary competing photochemical processes,[2] consisted in α-fission, β-fission (cycloelimination), and ring expansion (the formation of α-oxacarbene), were markedly affected by the ring size of spiro alicyclic groups substituted at the 2- and 4-positions of the diones. In this connection, our interest is focused on the effect of the ring size of 2,4-dispiro alicyclic substituents on the photochemical behavior of 3-thioxo-1-cyclobutanones, being similar in structure to 1,3-cyclobutanediones. However, little is known concerning the photochemistry of 3-thioxo-1-cyclobutanones except for only one report on the photooxygenation of 2,2,4,4-tetramethyl-3-thioxo-1-cyclobutanone to give the corresponding 1,3-cyclobutanedione.[3]

Accordingly, we wish to report in the first place on the alternative photochemical behavior of dispiro-substituted 3-thioxo-1-cyclobutanones, compared with that of the corresponding 1,3-cyclobutanediones. In addition, the effect of the ring size of 2,4-dispiro alicyclic substituents on the product-formation is mentioned.

When 12-thioxodispiro[4.1.4.1]dodecan-6-one (**1a**) was irradiated in dichloromethane in a degassed sealed Pyrex tube at −70 °C for 50 h,[4] photoisomerization took place to afford the unsaturated thiolactone (**3a**) almost quantitatively. Moreover, photolysis of **1a** under the similar conditions in methanol,[5] a good trapping agent of an α-oxacarbene intermediate, led to the formation of **3a** (26%) along with the ring-expanded acetal (**5a**, X=S, 38%) *via* an α-oxacarbene intermediate (**C**, X=S).[6] Since the most preferential photoprocess of cyclobutanones or cyclobutanediones in methanol is widely known to be the ring expansion *via* an α-oxacarbene intermediate,[2] it is very significant that the photoisomerization takes place appreciably even in methanol. In the similar irradiation of the dichloromethane solution of 14-thioxodispiro[5.1.5.1]-tetradecan-7-one (**1b**), the photoisomerization also proceeded predominantly. In this case, however, the formation of the unsaturated thiolactone (**3b**, 6%) was minor and, interestingly, the saturated thiolactone (**4b**, 46%) was obtained as the major product. Furthermore, photolysis of **1b** in methanol afforded **4b** (40%), accompanied by the ring-expanded acetal (**5b**, X=S, 23%). On the other hand, no formation of **3b** was observed.

The photolysis of **1a** and **1b** may be considered to proceed in the following scheme.

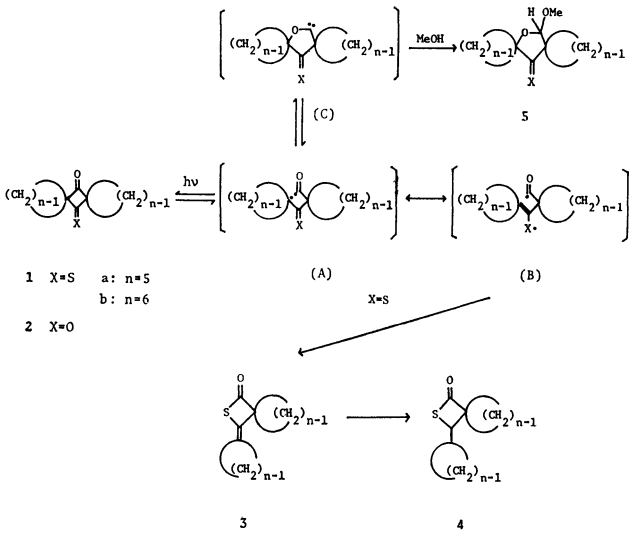

Scheme 1.

Unlike the case of the corresponding dispiro-1,3-cyclobutanediones (**2a** and **2b**), the preferential occurrence of photoisomerization in **1a** and **1b**, regardless of the ring size of spiro substituents and solvents, may be explained on the basis of the great differences in contribution between two canonical formula of the radical of allylic structures, (**6A′**) and (**6B′**), which are each part of 1,4-biradical intermediates, that is, the 1-acyl 4-cycloalkyl biradical (**A**, X=S) and the 1-acyl 4-thiyl biradical (**B**, X=S), derived from the initial α-fission of **1a** and **1b**.

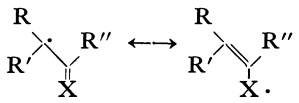

6 X=S (A′) (B′)
7 X=O

Of two canonical formula, (**6A′**) and (**6B′**), the contribution of (**6B′**) to the radical of allylic structure, in which the unpaired electron is localized on sulfur atom, is greater than that of (**6A′**), because radical stabilization energies[7,8] are strongly influenced by the electronegativity of the atom bearing the unpaired electron and the stabilization energies of a series of structually related oxygen, carbon, and sulfur centered radicals increase in this order. Consequently, it appears that (**B**, X=S) would form thiolactone (**3**) by ring closure. In the case of **7**, on the contrary, the contribution of (**A′**) is greater than that of (**B′**).[9,10] Therefore, in the case of 1,3-cyclobutanediones (**2**), no isomerized product was obtained. In conclusion, the difference in the electronegativities of sulfur and oxygen plays a key role in determining the reaction pathways after the photochemical α-fission.

In addition, it was found that the ring size of spiro alicyclic groups substituted at 2- and 4-positions affected the process of product-formation in a striking manner. In order to clarify the photochemical conversion of **3b**

into **4b**, **3b** was irradiated in dichloromethane or deuterodichloromethane under the similar conditions. As expected, the photochemical hydrogen abstraction of **3b** proceeded smoothly to give **4b**, and, moreover, the NMR spectrum of reaction product in dichloromethane showed the doublet peak (δ 2.92, 1H) assigned to the signal of the methine proton attached to the position α to the sulfur atom in **4b**, whereas, in the case of deuterodichloromethane, such peak was absent. Concerning the high reactivity of **3b** toward hydrogen abstraction, it is not clear at present, but we tentatively infer that the rotation around the double bond of **3b** in the excited state may be fairly restricted owing to the nonbonded interaction of hydrogens between the adjacent two cyclohexyl substituents, just like the photochemically excited triplet olefin.[11] Further study on the above photochemical hydrogen abstraction is now undertaken.

Experimental

Materials. 12-Thioxodispiro[4.1.4.1]dodecan-6-one (**1a**) and 14-thioxodispiro[5.1.5.1]tetradecan-7-one (**1b**) were prepared by the modification of the method of Krapcho.[12] **1a**, mp 35—36 °C; IR (KBr) 1780 cm^{-1}; NMR (CCl_4) δ 1.9 (m, 16H); Mass (*m/e*) 208 (M^+); UV (MeOH) λ_{max} 241 (ε, 7160), 326 (90), 513 (8), 527 nm (8); Found: C, 69.21; H, 7.71; S, 15.53%. Calcd for $C_{12}H_{16}OS$: C, 69.18; H, 7.74; S, 15.39%. **1b**, mp 113—114 °C (lit,[12] 113—115 °C); IR (KBr) 1765 cm^{-1}; UV (MeOH) λ_{max} 237 (ε, 8940), 326 (104), 514 nm (8).

General Irradiation Procedure. A solution of **1a** or **1b** (0.2 mol dm^{-3}) was irradiated in a degassed sealed Pyrex tube at −70 °C for 40—50 h. After the solvent was evaporated, the residue was chromatographed on silica gel and was subjected to purification by preparative GLC. The yields were determined by GLC analysis (10% FFAP).

Irradiation of 1a. *In CH_2Cl_2*: Preparative GLC afforded the isomeric product (**3a**) almost quantitatively. **3a**, IR (neat) 1770, 1675 cm^{-1}; NMR (CCl_4) δ 1.6—2.8 (m, 16H); Mass (*m/e*) 208 (M^+), 180; Found: C, 69.23; H, 7.69; S, 15.51%. Calcd for $C_{12}H_{16}OS$: C, 69.18; H, 7.74; S, 15.39%.

In MeOH: Analysis of the photolysate by GLC revealed the isomeric product (**3a**, 26%), the ring-expanded acetal (**5a**, 38%), and the unidentified product (16%). **5a**, IR (neat) 1180, 1085, 1015 cm^{-1}; NMR (CCl_4) δ 1.4—2.2 (b, 16H), 3.3 (s, 3H), 4.7 (s, 1H); Mass (*m/e*) 240 (M^+), 207, 180; Found: C, 65.16; H, 8.39; S, 13.34%. Calcd for $C_{13}H_{20}O_2S$: C, 64.96; H, 8.39; S, 13.42%.

Irradiation of 1b. *In CH_2Cl_2*: Analysis of the photolysate by GLC revealed the following products: the unsaturated thiolactone (**3b**, 6%), the saturated thiolactone (**4b**, 46%). **3b**, IR (neat) 1760, 1675 cm^{-1}; NMR (CCl_4) δ 1.4—1.8 (m, 20H); Mass (*m/e*) 236 (M^+), 208; UV (CH_2Cl_2) 268 nm (ε, 69); Found: C, 71.28; H, 8.39; S, 13.61%. Calcd for $C_{14}H_{20}OS$: C, 71.14; H, 8.53; S, 13.56%. **3b** was also confirmed by the comparison of the sample which was synthesized by the treatment of **1b** with sodium methoxide. **4b**, IR (neat) 1755 cm^{-1}; NMR (CCl_4) δ 1.1—1.8 (m, 21H), 2.9 (d, 1H); Mass (*m/e*) 238 (M^+), 210; Found: C, 70.44; H, 9.46; S, 13.23%. Calcd for $C_{14}H_{22}OS$: C, 70.54; H, 9.30; S, 13.45%. Irradiation of **3b** in CH_2Cl_2 at −70 °C for 2 h gave **4b**, on the other hand, reflux of **3b** in CH_2Cl_2 failed to form **4b**.

In MeOH: Saturated thiolactone (**4b**) and the ring-expanded acetal (**5b**) were obtained in 40% and 23% yields, respectively, along with trace of methyl cyclohexanecarboxylate. **5b**, IR (neat) 1230, 1130, 1100 cm^{-1}; NMR (CCl_4) δ 1.2—2.2 (m, 20H), 3.4 (s, 3H), 5.1 (s, 1H); Mass (*m/e*) 268 (M^+), 237, 208; Found: C, 67.29; H, 8.87; S, 11.58%. Calcd for $C_{15}H_{24}O_2S$: C, 67.12; H, 9.01; S, 11.95%.

Quantum Yield Measurement. The quantum yields for disappearance of **1a** and **1b** were measured according to the method of Jones[13] by employing a merry-go-round apparatus and valerophenone as the actinometer.[14]

References

1) a) K. Kimura, M. Takamura, A. Kunai, and Y. Odaira, *J. Chem. Soc., Chem. Commun.*, **1974**, 685; b) K. Kimura, S. Koshibe, M. Juro, Y. Fukuda, and Y. Odaira, *Bull. Chem. Soc. Jpn.*, **49**, 741 (1976). Photochemistry of dispiro-1,3-cyclobutanediones has also been reported; A. P. Krapcho and B. Abegaz, *J. Org. Chem.*, **39**, 2251 (1974).

2) P. Yates and R. O. Loutfy, *Acc. Chem. Res.*, **8**, 209 (1975), and references therein.

3) J. J. Worman, M. Shen, and P. C. Nichols, *Can. J. Chem.*, **50**, 3923 (1972).

4) Irradiation of **1a** or **1b** in the presence of oxygen gave rise to the corresponding 1,3-cyclobutanedione (**2a**) or (**2b**) and its further reaction products.

5) Quantum yield for disappearance of **1a** or **1b** in MeOH is 0.043 or 0.015, which is somewhat lower than that for 1,3-cyclobutanediones (**2a**, 0.10; **2b**, 0.07).

6) As an alternative path, an α-oxacarbene intermediate is formed directly from the electronic excited state but not *via* an 1-acyl 4-alkyl biradical intermediate; G. Quinkert, P. Jacobs, K. H. Kaiser, G. Wiech, and W.-D. Stohrer, *Angew. Chem. Int. Ed.*, **13**, 197, 198, 199, 200 (1974).

7) a) G. Griller and K. U. Ingold, *Acc. Chem. Res.*, **9**, 13 (1976); b) S. W. Benson, "Thermochemical Kinetics," Wiley, New York, N. Y. (1969); c) H. E. O'Neal and S. W. Benson, "Free Radicals," ed by J. K. Kochi, Wiley, New York, N. Y. (1973), Vol. II, Chap. 17.

8) From ESR studies, the existence of similar allylic radical, 1-propenylthiyl radical ($CH_3CH{=}CH\dot{S}$), has been reported; H. Nishimura and J. Mizutani, *J. Org. Chem.*, **40**, 1567 (1975).

9) D. Forrest and K. U. Ingold, *J. Am. Chem. Soc.*, **100**, 3868 (1978).

10) The contribution of the canonical formula having the unpaired electron on oxygen, **7B′**, has been calculated to be only 15%; D. M. Camaioni, H. F. Walter, J. E. Jordan, and D. W. Pratt, *J. Am. Chem. Soc.*, **95**, 7978 (1973).

11) a) P. J. Kropp, *J. Am. Chem. Soc.*, **89**, 3650 (1967); b) P. S. Engel and H. Ziffer, *Tetrahedron Lett.*, **1969**, 5181.

12) A. P. Krapcho, D. R. Rao, M. P. Silvon, and B. Abegaz, *J. Org. Chem.*, **36**, 3885 (1971).

13) G. Jones II and L. P. McDonnell, *J. Am. Chem. Soc.*, **98**, 6203 (1976).

14) P. J. Wagner, P. A. Kelso, and R. G. Zepp, *J. Am. Chem. Soc.*, **94**, 7480 (1972).

Optical Resolution of Heterohelicenes by High Performance Liquid Chromatography

Hiroko NAKAGAWA, Susumu OGASHIWA, Hisao TANAKA, Koh-ichi YAMADA, and Hiroshi KAWAZURA*

Faculty of Pharmaceutical Sciences, Josai University, Sakado, Saitama 350-02

(Received December 22, 1980)

Synopsis. Heterohelicenes up to 15 rings were resolved by high performance liquid chromatography (HPLC) on silica gel covalently linked with a chiral charge transfer complexing agent 2-(2,4,5,7-tetranitro-9-fluorenylideneamino-oxy)propionic acid(TAPA). The efficiency of resolution was discussed in terms of the helical structure of heterohelicenes.

In the course of our work on heterohelicenes, optical resolution was found to be necessary, since their chiroptical properties require isolation of the pure enantiomers. Mikes *et al.* reported the resolution of helicenes by HPLC on a short column containing chiral reagents which function as a selector,[1] and achieved resolution for carbohelicene series. However, they examined only a few heterohelicenes containing sulfur atoms in a molecule, separation between enantiomers being poor.

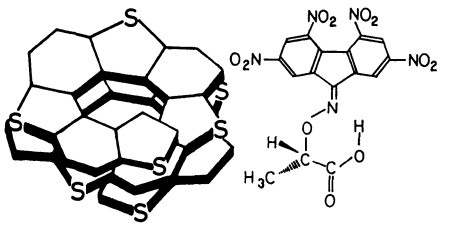

(P)-(+)-[15] (S)-(+)-TAPA

Fig. 1

We describe here a better resolution of heterohelicenes up to 15 rings consisting of alternant thiophene and benzene nucleus (Fig. 1) by HPLC with a chiral TAPA-bonded silica-gel column. TAPA is a chiral charge transfer (CT) complexing agent in which tetranitro-fluorenylidene moiety provides a strong binding power, oxypropionic acid moiety playing the chiral recognition for the electron donating heterohelicenes.

The chromatogram of [7] to [15] heterohelicenes (Fig. 2) was obtained by using a 30 cm silica-gel (5 μ)

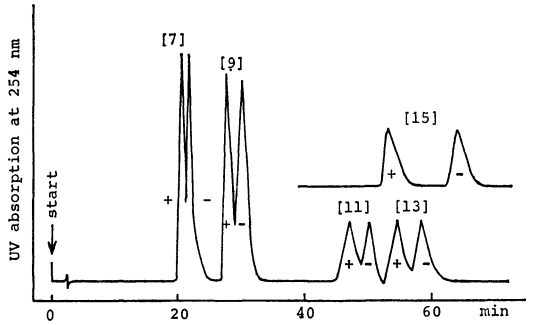

Fig. 2. Chromatogram of heterohelicenes. Column: 11% (*S*)-(+)-TAPA bonded on 5 μ silica gel, mobile phase: 50% dichloromethane–hexane.

Table 1. Resolution of heterohelicenes by HPLC using a (*S*)-(+)-TAPA-bonded silica-gel column

Heterohelicene	k'	$r^{a)}$	$[\alpha]_{500}^{23}$
[7]	5.97 6.42	1.076	2990 −2980
[9]	8.24 9.38	1.138	3760 −3700
[11]	16.88 18.09	1.072	4440 −4550
[13]	19.68 21.20	1.077	8170 −8290
[15]	19.15 23.02	1.202	b) b)

a) $r=k'_-/k'_+$, where k'_- is k' for a minus enantiomer and k'_+ for a plus enantiomer. b) Amount separated too small to measure $[\alpha]_{500}^{23}$.

column linked with 11% (*S*)-(+)-TAPA. The parameters for resolution are given together with the optical rotations of alternatives isolated by the preparative HPLC in Table 1. The capacity factor k' denoting the ratio of partition coefficients between stationary and mobile phase depends upon the strength of CT interaction of a selector with a selectand. Higher heterohelicene having more powerful electron donating ability gave a larger k' value. (*S*)-(+)-TAPA interacted more strongly with (*M*)-(−)-heterohelicene than with its antipode.

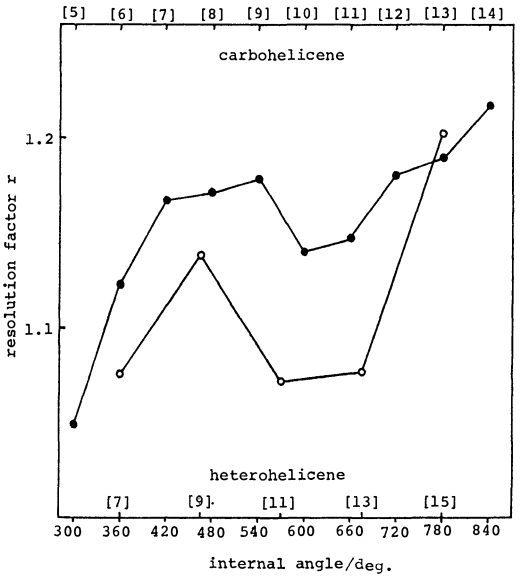

Fig. 3. Relationship between resolution factor and internal angle of helicenes. The data for carbohelicenes were quoted from the literature.[1]
○: Heterohelicene, ●: carbohelicene.

The absolute values of $[\alpha]_{500}^{23}$ for each antipode were almost the same, indicating that satisfactory separation was achieved. $[\alpha]_{500}^{23}$ increased abruptly with an increase in the number of rings.

Figure 3 shows the relationship of the resolution factor r against the internal angle evaluated by allocating 45° for a thiophene ring and 60° for a benzene ring.[2] The curve for heterohelicenes as well as that for carbohelicenes have no monotonically increasing slope with the progression of helix, but a concave in the range 540°—720° where separation is worse. The range of angle corresponds to a helix possessing 1—1.5 turns. This might be explained in terms of the steric repulsion of the methyl group attached to an asymmetric carbon atom of TAPA against the terminal ring of helicenes, in which a chiral recognition is effectuated. The steric repulsion should give a predominant influence on the r value, since this value refers to the difference in the diastereomeric interaction of TAPA with each enantiomer. On the other hand the k' values are mainly determined by the strength of CT interaction. [11] and [13] heterohelicene have a relatively large k', but small r value, as compared with those of [9] and [15] respectively. Thus, helicenes of the helical structure with 1.5—2 turns undergo a stronger CT interaction owing to the smaller repulsion, resulting in smaller chiral selection from TAPA.

Experimental

Materials. The synthesis of heterohelicenes has been reported.[3] Chiral (*R*)-(−)- and (*S*)-(+)-TAPA were prepared according to the method of Block and Newman.[4] Aminated silica gel (5 μ, Polygosil 60-5 NH_2, Macherey-Nagel Co.) was used as a fixer of TAPA. Silica gel covalently linked with chiral TAPA was prepared according to the method of Mikes.[1] A TAPA content in the silica gel was calculated from the nitrogen content obtained by elemental analysis.

Apparatus. HPLC system (Model 204, Waters assoc.), slurry packing apparatus (Model 124, Chemco), and columns (0.39 cm O. D. × 30 cm I. D. and 0.8 cm × 25 cm) were used. Optical rotations were measured on an automatic recording spectropolarimeter (Model J-20A. Japan Spectroscopic Co.).

This work was supported by Grant-in-Aid No. 447010 from the Ministry of Education, Science and Culture.

References

1) F. Mikes and G. Boshart, *J. Chromatogr.*, **149**, 455 (1978); F. Mikes, G. Boshart, and E. Gil-Av, *J. Chromatogr.*, **122**, 205 (1976); F. Mikes, G. Boshart, and E. Gil-Av, *J. Chem. Soc., Chem. Commun.*, **1976**, 99.

2) H. Wynberg, *Acc. Chem. Res.*, **4**, 65 (1971).

3) K. Yamada, S. Ogashiwa, H. Tanaka, H. Nakagawa, and H. Kawazura, *Chem. Lett.*, **1981**, 343.

4) P. Block and M. S. Newman, *Org. Synth.*, **48**, 120 (1968).

The Stability of the Supersaturation State in Optical Resolution by the Preferential Crystallization Procedure

Chikara HONGO,* Shigeki YAMADA, and Ichiro CHIBATA

Research Laboratory of Applied Biochemistry, Tanabe Seiyaku Co., Ltd., 16-89, Kashima-3-chome, Yodogawa-ku, Osaka 532

(Received May 28, 1980)

In the optical resolution process of DL-serine *m*-xylene-4-sulfonate dihydrate by the preferential crystallization procedure, the stability of the supersaturation state of the unseeded isomer was investigated in connection with the cooling conditions. The experiment was initiated with the model solution and was then extended to the actual resolution process. The metastable region of the unseeded isomer on a two-dimensional diagram with the supersaturation degree and cooling time could be divided into the first and the second metastable regions. The limits of the first and the second metastable regions were expressed by a supersaturation degree and by an area on the diagram respectively. Both limiting values were constant, independent of cooling speed and the lowest arrival temperature, if the conditions for the crystallizer, the initial concentration of the DL-form, the amount of the seed crystals, and the degree of stirring were fixed.

The advantages of the optical resolution of DL-amino acids by the preferential crystallization procedure have been well recognized, and many DL-amino acids have been resolved successfully by this procedure.[1-5] Although several requirements must be fulfilled to achieve the resolution by this procedure, it is most important that the racemic modification be crystallized as a racemic mixture and not as a racemic compound. The resolution is carried out in the following manner. The crystals of a desired isomer (for example, L-isomer) are seeded into a supersaturated solution of a racemic modification. Only the L-isomer crystallizes preferentially, and the crystallized L-isomer is separated in an appropriate manner from the mother liquor before the spontaneous crystallization of the unseeded D-isomer. During the preferential crystallization, the same amount of the D-isomer as that of the crystallized L-isomer remains in the liquid phase as a supersaturation state. After a certain time, however, the unseeded D-isomer also begins to crystallize spontaneously because of the limitation of the stability of the supersaturation state. The situation in this process is shown in Fig. 1.

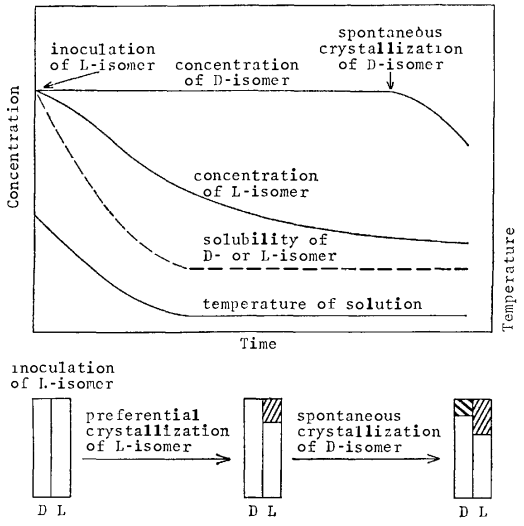

Fig. 1. Time course of optical resolution process by preferential crystallization procedure.

□: D- or L-Isomer in solution, ▨: crystals of L-isomer, ▨: crystals of D-isomer.

To avoid the crystallization of the unseeded D-isomer, and to crystallize only the desired L-isomer in an optically pure form, it is also important to know the limitations of the stability of the supersaturation state of the D-isomer, especially the starting time of the spontaneous crystallization of the unseeded D-isomer. Although a few non-quantitative descriptions of the stability of supersaturation in the preferential crystallization process have appeared,[6-8] no quantitative study of the prediction of the waiting time for the spontaneous crystallization of the unseeded isomer has yet been reported.

In our previous report on the optical resolution of DL-serine,[1] DL-serine *m*-xylene-4-sulfonate dihydrate (DL-Ser·mXS·$2H_2O$) was found to form a racemic mixture and to be easily resolved by the preferential crystallization procedure. In the present experiment, the stability of the supersaturation state of the unseeded isomer was investigated in order to predict the waiting time for the spontaneous crystallization of the unseeded isomer in this optical resolution process. Although the stability of the supersaturation state is influenced by various factors, it was examined under a variety of cooling conditions, *i.e.*, cooling speed and the lowest arrival temperature, which are the most important factors in industrial operations. The experiments were initiated with the model solution, assuming a situation of the resolution process, and then extended to the actual resolution process.

Materials and Methods

Materials. Optically active and racemic Ser·mXS·$2H_2O$ were prepared according to the previous report[1] and dried at 35 °C in a chamber with a relative humidity of 67%.

Apparatus and Cooling Methods. A 2*l*-cylindrical glass vessel with a jacket was employed as the crystallizer. Schematic drawings of the crystallizer and their dimensions are shown in Fig. 2. The solution was stirred at 210 rpm with poly(vinyl chloride)-paddle and cooled under the various cooling patterns shown in Fig. 3, which were achieved by using a Chino

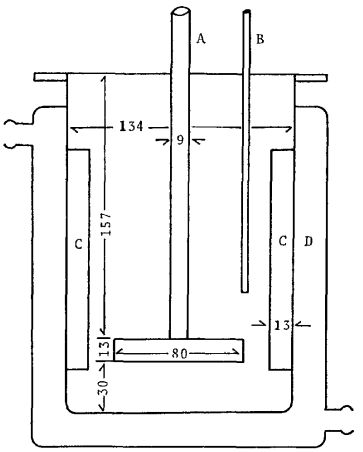

Fig. 2. Schematic drawings of the crystallizer and their dimensions (in millimeter).
A: Poly(vinyl chloride)-agitator, B: glass-thermistor (diameter, 6 mm), C: glass-baffle plate, D: jacket.

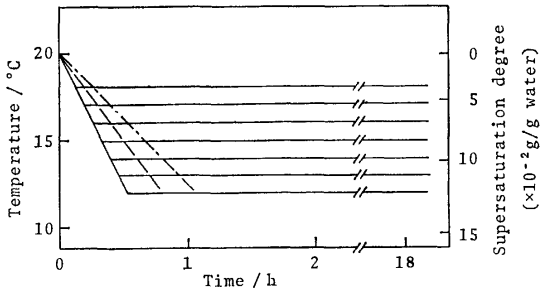

Fig. 3. Cooling patterns and supersaturation degree. The solution is saturated with D-Ser·mXS·$2H_2O$ at 20 °C (C_D=0.360 g/g water). Cooling speed is 1/4 °C per min (——), 1/6 °C per min (— — —), or 1/8 °C per min (———).

program setter, PMS-2, and a Chino electronic recording controller, ET-2p (Chino Works Ltd., Japan). The ranges of experimental variables for cooling were as follows: cooling speed, 1/4, 1/6, and 1/8 °C per min; the lowest arrival temperature, 12, 13, 14, 15, 16, 17, and 18 °C.

Analysis of Solution. The total concentration of D- and L-isomers in the sample solution, C_D+C_L [g/g(water)], was determined from the standard curve and the refractive index which was measured with a Karl Zeiss immersion refractometer, where C_D and C_L are the concentrations of D- and L-isomers [g/g(water)] respectively.

The concentration of the optical isomer (for example, D-isomer) existing in excess, C_D-C_L [g/g(water)], was obtained by the measurements of the rotation angle of the sample solution, its density, and the total concentration of D- and L-isomers according to the following calculation. The specific rotation of the D-isomer existing in excess in the solution is expressed as:

$$[\alpha]_D^{35} = 100 \times \frac{\alpha}{c}, \quad (1)$$

where α is the rotation angle and where c is the weight in grams of the D-isomer existing in excess per 100 ml of solution. c is expressed as:

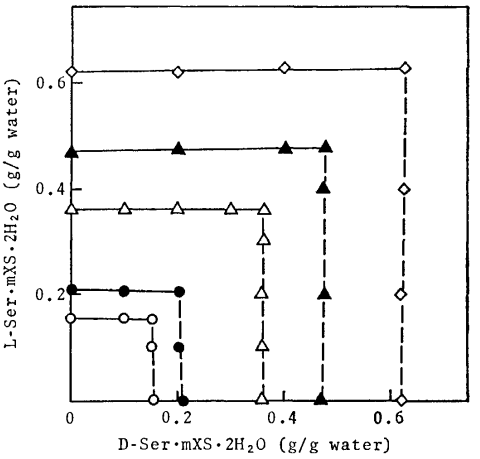

Fig. 4. Solubility of L- and D-Ser·mXS·$2H_2O$ in the coexisting system.
——: Solubility curve for L-isomer, — —: solubility curve for D-isomer, ○: at 5 °C, ●: at 10 °C, △: at 20 °C, ▲: at 25 °C, ◇: at 30 °C.

$$c = 100 \times \frac{C_D - C_L}{(1+C_D+C_L)/d}, \quad (2)$$

where d is the density of the solution.

The value of the specific rotation of D-Ser·mXS·$2H_2O$ was observed to be $[\alpha]_D^{35}=+5.787°$ under the conditions employed ($0.5<C_D+C_L<1.0$, $0<C_D-C_L<0.12$ g/g(water)). From Eqs. 1 and 2, C_D-C_L is expressed as:

$$C_D - C_L = \frac{\alpha(1+C_D+C_L)}{5.787\,d}. \quad (3)$$

From Eq. 3, C_D-C_L can be obtained by measuring the values of α, d, and C_D+C_L. The optical rotation was measured in a 1-dm tube at 35 °C with sodium light by means of a Perkin-Elmer 141 automatic polarimeter. The density was determined with a hydrometer.

The concentrations of the D- and L-isomers, C_D and C_L, were calculated from the values of C_D+C_L and C_D-C_L respectively.

Determination of Waiting Time. The waiting time for the spontaneous crystallization of the D-isomer was determined by measuring the concentration of the D-isomer, and the time when the concentration decreased by 0.002 [g/g(water)] was taken as the starting time of the spontaneous crystallization. Also, a sudden spontaneous crystallization could be determined by visual observation.

Results and Discussion

Solubility of L- and D-Ser·mXS·$2H_2O$ in the Coexisting System. Mixtures of L- and D-isomers in various proportions were dissolved in water at an elevated temperature and equilibrated at different temperatures. The concentrations of both the isomers in the equilibrium solution were determined. The equilibrium compositions of the coexisting system are shown in Fig. 4. The figure shows that: (i) the solubility of an optical isomer is little influenced by the concentration of the opposite isomer coexisting in the solu-

Table 1. Composition of model solution

Solution No.	I	II	III	IV
D-Ser·mXS·$2H_2O$ (g)	468	468	468	468
L-Ser·mXS·$2H_2O$ (g)	468	393	351	295
Water (g)	1300	1300	1300	1300
Ratio of L/D	1.00	0.84	0.75	0.63

Each solution was saturated with the D-isomer in the presence of various amounts of the L-isomer at 20 °C.

tion, (ii) the solubility of the racemic modification is nearly equal to the sum of the individual solubilities of both isomers, and (iii) the saturated solution of the racemic modification no longer dissolves an optical isomer. These properties show that DL-Ser·mXS·$2H_2O$ crystallized from water forms a typical racemic mixture and that there is no appreciable interaction between the two isomers on the respective solubilities. Therefore, the supersaturation degree for each optical isomer was expressed as C_D-C_S (for the D-isomer) or C_L-C_S (for the L-isomer) [g/g(water)], regardless of the concentration of the coexisting opposite isomer, where C_S [g/g(water)] is the solubility of the D- or L-isomers at a given temperature. From Fig. 4, the solubilities of optically active and racemic Ser·mXS·$2H_2O$ could be expressed as a function of the temperature, t, by following empirical formulas over a range from $t=5$ to 30 °C respectively:

$$\log C_S = 2.34 \times 10^{-2} t - 9.12 \times 10^{-1},$$

$$\log C_{SR} = 2.48 \times 10^{-2} t - 6.39 \times 10^{-1},$$

where C_{SR} [g/g(water)] is the solubility of DL-Ser·mXS·$2H_2O$.

Stability of Supersaturation in Model Solution. The First Metastable Region and Its Width, S_I: Assuming, in the resolution process of DL-Ser·mXS·$2H_2O$, that the L-isomer is preferentially crystallized, while the D-isomer remains in the initial concentration as a supersaturation state, the model solutions were prepared as is shown in Table 1. The mixtures of the D-isomer and the L-isomer in different proportions were dissolved by heating at 35 °C. The solutions were saturated at 20 °C with the D-isomer in the presence of various amount of the L-isomer. The solutions were cooled at various speeds (1/4, 1/6, and 1/8 °C per min) to given temperatures ranging from 12 °C to 18 °C, as is shown in Fig. 3, under a constant stirring speed; 0.2 g of D-Ser·mXS·$2H_2O$ (28—35 meshes) was added at 20 °C in the course of cooling. The addition of the crystals was preferable for the reproducibility of the waiting time. No significant decrease in the concentration of the D-isomer attributable to the growth of the added crystals was observed until the spontaneous crystallization of the supersaturated D-isomer took place. In other words, the first significant decrease in the concentration was mainly attributed to the spontaneous crystallization of the D-isomer. Under the above cooling conditions, the temperature of the solution was recorded and the waiting time for the D-isomer was determined. The range in the waiting times observed in these experiments was from 30 min to about 15 h. One example

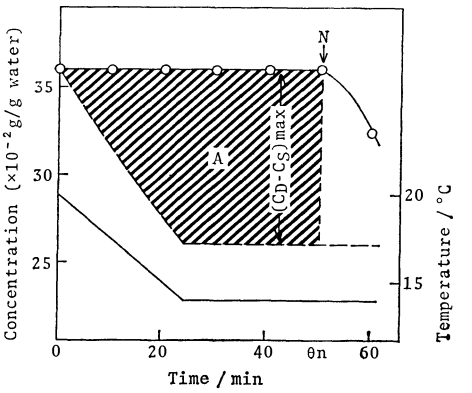

Fig. 5. Time course of supersaturation degree of D-isomer in model solution. The model solution I described in Table 1 was cooled at 1/4 °C per min to 14 °C and maintained at 14 °C
——: Temperature of solution, — — —: solubility of D-isomer (C_S) at the temperature of solution, —O— O—: concentration of D-isomer (C_D), N: the point occurring a large spontaneous crystallization, A: the area given by $A=\int_0^{\theta n}(C_D-C_S)d\theta$.

of the time course for model solution I is shown in Fig. 5, indicating that the supersaturation degree of the D-isomer, (C_D-C_S), increases with a decrease in the temperature and that a large spontaneous crystallization of the D-isomer begins suddenly at the point N (time θn, 50 min). This point, N, varied with the cooling speed and with the lowest arrival temperature. That is to say, it varied not only with the cooling speed, but also with the maximum supersaturation degree, $(C_D-C_S)_{max}$, depending on the lowest arrival temperature.

To obtain the relationship between the waiting time, θn, and the cooling conditions described above, a certain area, A, expressed as a shaded part in Fig. 5 was considered. The area may be expressed mathematically as follows:

$$A = \int_0^{\theta n}(C_D-C_S)\mathrm{d}\theta \quad [\mathrm{g\cdot min/g(water)}], \tag{4}$$

where θ is the time and where θn is the time when spontaneous crystallization is observed at point N. In this study, the A area was graphically eva.uated.

For each model solution shown in Table 1, the evaluation of A was carried out under various cooling conditions. The logarithm of A was plotted against $(C_D-C_S)_{max}$ on semilogarithmic graph paper. The results obtained when the cooling speed was 1/4 °C per min are shown in Fig. 6. In the case of any model solution, the log A decreased linearly with $(C_D-C_S)_{max}$, but the slope of the straight line changed at the point of $(C_D-C_S)_{max}=6.6\times10^{-2}$ [g/g(water)], expressed as S_I in Fig. 6. Furthermore, the figure shows that the value of A is markedly large when $(C_D-C_S)_{max}$ is lower than S_I. In this range, the spontaneous crystallization of the D-isomer did not occur for a longer time, and the supersaturation state was more stable than in the other range. Thus, the region where the supersaturation degree is within S_I was termed "the first metastable region".

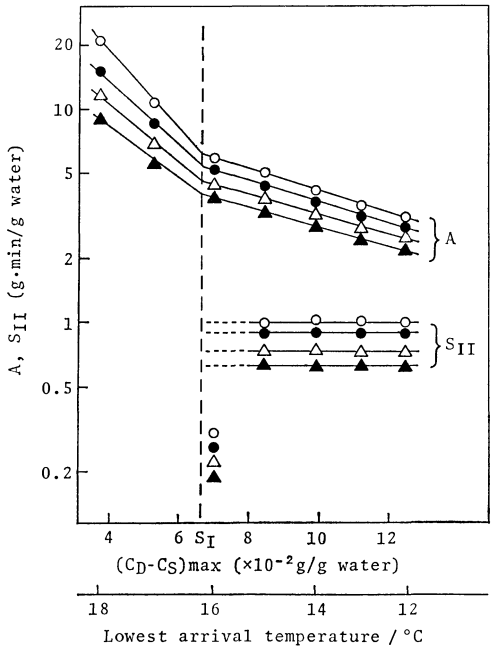

Fig. 6. Relationship among A, S_I, S_{II}, and $(C_D-C_S)_{max}$ in model solution. The solutions were cooled at 1/4 °C per min to given temperatures ranged from 12 °C to 18 °C.

$A=\int_0^{\theta n}(C_D-C_S)d\theta$, $S_{II}=\int_0^{\theta n}(C_D-C_S-S_I)d\theta$.

○: Model solution I ($C_L/C_D=1.00$), ●: model solution II ($C_L/C_D=0.84$), △: model solution III ($C_L/C_D=0.75$), ▲: model solution IV ($C_L/C_D=0.63$).

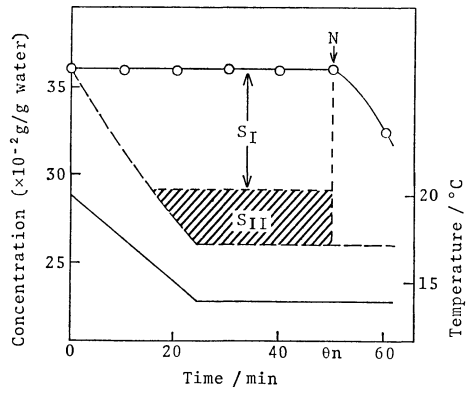

Fig. 7. Illustration of the first and the second metastable regions. The experiment was the same as that in Fig. 5. S_I represents the width of the first metastable region. S_{II} represents the area of the second metastable region.

The Second Metastable Region and Its Area, S_{II}: In the above experiments, the supersaturation was relatively unstable in the region where the supersaturation degree was higher than S_I. Then, an area, S_{II}, expressed as a shaded part in Fig. 7, was considered. This may be expressed mathematically as follows:

$$S_{II}=\int_0^{\theta n}(C_D-C_S-S_I)d\theta \quad [\text{g·min/g(water)}], \qquad (5)$$

where the integration is restricted to cases of $C_D-C_S \geqq S_I$.

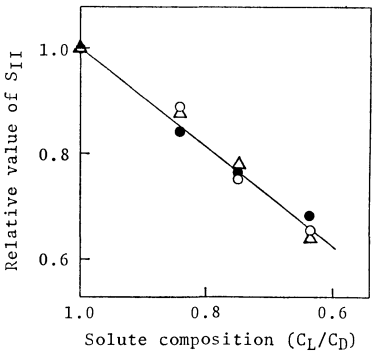

Fig. 8. Relationship between the value of S_{II} and C_L/C_D.
Cooling speed: ○; 1/4 °C/min, ●; 1/6 °C/min, △; 1/8 °C/min.

In this paper, the value of S_{II} was graphically evaluated. The logarithm of S_{II} is plotted against $(C_D-C_S)_{max}$ in Fig. 6. The figure indicates that the values of S_{II} for the solution with a constant ratio of C_L/C_D are constant independent of the maximum supersaturation degree, with the exception of the case when $(C_D-C_S)_{max}$ closely approaches S_I. However, these values decreased with a decrease in the ratio of C_L/C_D. The relationship between S_{II} and the ratio of C_L/C_D is shown in Fig. 8.

Also, in case where the cooling speed was 1/6 or 1/8 °C per min, the values of S_I and S_{II} themselves were the same as those at the cooling speed of 1/4 °C per min, as is shown in Fig. 8. Generally, it may be concluded that the values of S_I and S_{II} are constant, independent of the cooling speed and the lowest arrival temperature. Thus, the region shown as a shaded part in Fig. 7 was termed "the second metastable region," and its area was expressed as S_{II}.

Ting and McCabe[9] and also Tanimoto *et al.*[10] found that two points existed in the supersaturation region for magnesium sulfate or copper sulfate. One was the first supersaturation point, where new nuclei was first observed, while the other was the second supersaturation point, where a sudden increase in the rate of formation of new crystals was observed. The conception of the first and second metastable regions in the present paper seems to correspond to the conception proposed by them. In fact, at a supersaturation degree lower than S_I, the spontaneous crystallization did not occur for a long time. In the second metastable region, where the integral in Eq. 5 is within S_{II}, the spontaneous crystallization was rarely observed for a period sufficient to achieve the optical resolution by the preferential crystallization procedure. In the supersaturation region where the integral in Eq. 5 is beyond S_{II}, a large amount of crystals appeared suddenly and grew rapidly.

Stability of Supersaturation in Actual Resolution Process. A Correction of the S_{II} Value by the Ratio of the L-*Isomer to the* D-*Isomer*: The above experiments with the model solutions were carried out when the initial ratios of C_L/C_D were different, as is shown in Table 1, but the ratio in each individual solution was kept constant during the experiment. Under such conditions, the

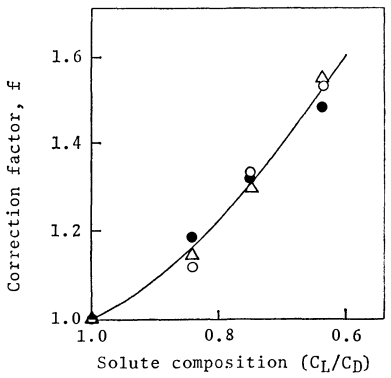

Fig. 9. Relationship between correction factor f and C_L/C_D.
Cooling speed: ○; 1/4 °C/min, ●; 1/6 °C/min, △; 1/8 °C/min.

value of S_{II} was found to be constant, independent of the cooling speed and the lowest arrival temperature. However, it decreased with a decrease in the initial ratio of C_L/C_D, as is shown in Fig. 8. On the other hand, in the actual resolution process, the ratio of C_L/C_D is the solution decreases gradually with the progress of the preferential crystallization of the L-isomer. Therefore, in order to estimate the value of S_{II} in the actual resolution process, the S_{II} shift resulting from the change in the ratio of C_L/C_D should be compensated for. From the data of Fig. 8 showing the relationship between S_{II} and C_L/C_D, the correction factor, f, was determined so that the values of $f_i \cdot S_{II,i}$ became constant:

$$f_i \cdot S_{II,i} = S_{II,1},$$

where f_i and $S_{II,i}$ are the values of f and S_{II} respectively when the ratio of C_L/C_D is i, and where $S_{II,1}$ is the value of S_{II} when the ratio of C_L/C_D is 1.00. The relationship between the correction factor, f, and the ratio of C_L/C_D is shown in Fig. 9. In order to extend the rule obtained on the model solutions to the actual resolution process, in which the ratio of C_L/C_D changes from moment to moment, the evaluation of the S_{II} value in the actual resolution process should be carried out by using the correction factor, f, and the S_{II} value in the actual resolution process should be expressed by the following equation:

$$S_{II} = \int_0^{\theta n} f(C_D - C_S - S_I)d\theta \quad [g \cdot min/g(water)], \qquad (6)$$

where the integration is restricted to cases of $C_D - C_S \geqq S_I$ and where f is a function of the ratio of C_L/C_D, which changes from moment to moment with the progress of the preferential crystallization of the L-isomer. In this paper, the S_{II} value may be graphically evaluated from the sum of the individual $f_i \cdot (C_D - C_S - S_I) \cdot \Delta\theta$ values between zero and θn by using the f_i shown in Fig. 9.

Supersolubility in Actual Resolution Process: According to the above manner, the values of S_{II} were determined in the actual resolution process, in which the L-isomer was preferentially crystallized from the supersaturated solution of DL-Ser·mXS·$2H_2O$ and the D-isomer remained in a supersaturated state.

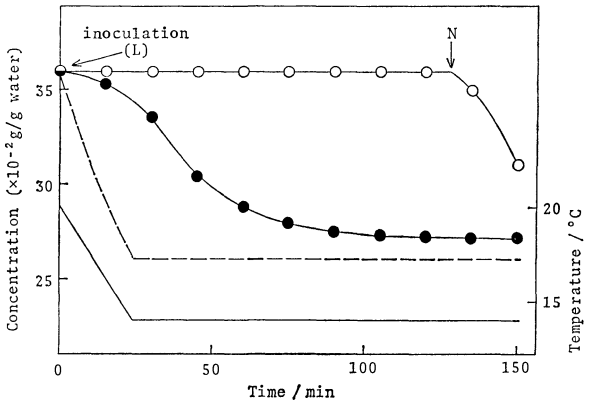

Fig.10. An example of time course of actual resolution process. The solution consisting of 936 g of DL-Ser·mXS·$2H_2O$ and 1300 g of water was seeded with 2 g of L-Ser·mXS·$2H_2O$ (100—200 meshes) at 20 °C, and was cooled at 1/4 °C per min to 14 °C. ——: Temperature of solution, — — —: solubility of D-isomer at the temperature of solution, —●—●—: concentration of L-isomer, —○—○—: concentration of D-isomer, N: the point occurring a large spontaneous crystallization.

A mixture of DL-Ser·mXS·$2H_2O$ (936 g) and water (1300 g) was dissolved by heating it at 35 °C for 1 h. The saturation temperature of each isomer in the solution was 20 °C. The solution was then seeded with 2.0 g of L-Ser·mXS·$2H_2O$ (100—200 meshes) at 20 °C and subsequently cooled at the cooling speed of 1/4 °C per min to a given temperature at a constant stirring speed. During the preferential crystallization of the L-isomer, the temperature was recorded and the concentration of each individual isomer was measured. In this case, a good reproducibility of the waiting time was obtained, though the crystals of the D-isomer were absent, because the crystals of the L-isomer were always present during the preferential crystallization of the L-isomer. The range of the waiting times observed in these experiments was from 30 min to about 15 h. One example of the time course of an actual resolution process is shown in Fig. 10. In the same manner as was described in connection with the model solution, the A area in Eq. 4 was graphically determined. The logarithm of A obtained under various cooling conditions was then plotted against the maximum supersaturation degree, $(C_D - C_S)_{max}$, on semilogarithmic graph paper. The results are shown in Fig. 11. The $\log A$ changed linearly with $(C_D - C_S)_{max}$, but the slope of the straight line was changed at the point of 6.6×10^{-2} [g/g(water)], which is shown as S_I in the figure. This result was similar to that obtained for the model solution.

In the region where the supersaturation degree was higher than 6.6×10^{-2} [g/g(water)], the value of S_{II} expressed by Eq. 6 was graphically evaluated in individual experiments. The values were then plotted against $(C_D - C_S)_{max}$ in Fig. 11, much as in the case of the model solution. The figure shows that the S_{II} values thus obtained were constant 4.49 [g·min/g (water)], independent of $(C_D - C_S)_{max}$, with the exception of the case where $(C_D - C_S)_{max}$ closely approached

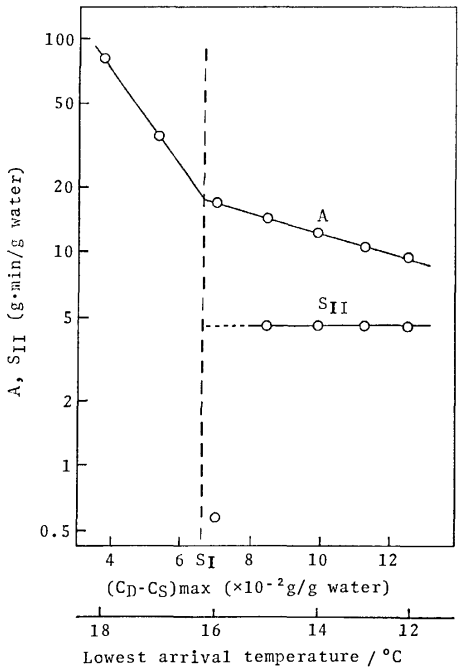

Fig. 11. Relationship among A, S_I, S_{II}, and $(C_D-C_S)_{max}$ in actual resolution process.

$$A=\int_0^{\theta n}(C_D-C_S)d\theta,\quad S_{II}=\int_0^{\theta n}f(C_D-C_S-S_I)d\theta.$$

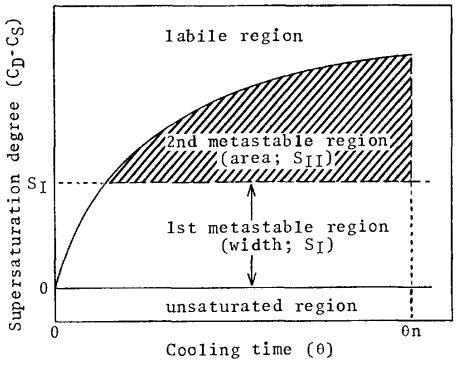

Fig.12. Time course of supersaturation degree of D-isomer and relationship between the first and the second metastable regions.
——: Increase in supersaturation degree of D-isomer due to cooling, θn: starting time of spontaneous crystallization of D-isomer. S_I and S_{II} are constant, independent of cooling speed and the lowest arrival temperature.

S_I. However, the value of S_{II} in the actual resolution process, 4.49 [g·min/g(water)], was different from that of the model solution, 1.00 [g·min/g(water)]. This discrepancy in the S_{II} value for the D-isomer is considered to arise from the following difference. In the case of the model solution, a small amount of crystals of the D-isomer was added to obtain the reproducibility. On the other hand, in the actual resolution process, the crystals of the D-isomer were absent, though the crystals of the L-isomer were present.

Consequently, the conception for the supersaturation state of the model solution was found to be applicable to the actual resolution process.

The results obtained in the actual resolution process of DL-Ser·mXS·$2H_2O$ can be summarized as follows; they are illustrated in Fig. 12.

(1) The metastable region on a two-dimensional diagram with the supersaturation degree of the unseeded D-isomer and cooling time could be divided in two regions, the first metastable region and the second metastable region.

(2) The first metastable region was the one where the supersaturation degree was lower than a constant value, $S_I=6.6\times10^{-2}$ [g/g(water)]. In this region, no spontaneous crystallization was observed for about 4 h or more.

(3) The second metastable region was the one where the supersaturation was stable for a certain time (within 4 h). This range was limited by the constant value of the integral in Eq. 6, $S_{II}=4.49$ [g·min/g(water)]. In other words, no spontaneous crystallization took place until the integrated area of the supersaturation degree as a function of the cooling time reached 4.49 [g·min/g(water)].

(4) The limiting values of both the first metastable region and the second metastable region were constant, independent of the cooling speed and the lowest arrival temperature.

Although the present work was carried out under fixed conditions with respect to type of crystallizer, the initial concentration of DL-form, the amount of seed crystals, and the degree of stirring, the metastable region of the unseeded isomer existing as a supersaturation state in the actual resolution process of DL-Ser·mXS·$2H_2O$ could be quantitatively defined. Then, the preferential crystallization should be achieved in the second metastable region. If the increase in supersaturation degree due to cooling the solution and the change in the ratio of the L- and D-isomers due to the preferential crystallization of L-isomer can be predicted, it is also possible to predict the waiting time for the spontaneous crystallization of the unseeded D-isomer. Our study of the prediction will be reported next.

References

1) S. Yamade, M. Yamamoto, and I. Chibata, *J. Org. Chem.*, **38**, 4408 (1973).
2) S. Yamada, M. Yamamoto, C. Hongo, and I. Chibata, *J. Agric. Food Chem.*, **23**, 653 (1975).
3) S. Yamada, C. Hongo, M. Yamamoto, and I. Chibata, *Agric. Biol. Chem.*, **40**, 1425 (1976).
4) C. Hongo, M. Shibazaki, S. Yamada, and I. Chibata, *J. Agric. Food Chem.*, **24**, 903 (1976).
5) S. Yamada, C. Hongo, and I. Chibata, *Agric. Biol. Chem.*, **42**, 1521 (1978).
6) Y. Sakata, T. Horikawa, and K. Takenouchi, *Agric. Biol. Chem.*, **27**, 518 (1963).
7) T. Watanabe, H. Kurokawa, T. Koga, Y. Kawauchi, and G. Noyori, *Kogyo Kagaku Zasshi*, **70**, 2170 (1967).
8) T. Akashi, *Nippon Kagaku Zasshi*, **83**, 421 (1962).
9) H. H. Ting and W. L. McCabe, *Ind. Eng. Chem.*, **26**, 1201 (1934).
10) A. Tanimoto, K. Ohta, H. Kakogi, and S. Fujita, *Kagaku Kogaku*, **26**, 1239 (1962).

  Bull. Chem. Soc. Jpn., 54, 1911—1913 (1981)

The Prediction of the Optical Resolution Process by the Use of the Preferential Crystallization Procedure

Chikara HONGO,* Shigeki YAMADA, and Ichiro CHIBATA

Research Laboratory of Applied Biochemistry, Tanabe Seiyaku Co., Ltd., 16-89, Kashima-3-chome, Yodogawa-ku, Osaka 532

(Received May 28, 1980)

In the optical resolution of DL-serine *m*-xylene-4-sulfonate dihydrate by the preferential crystallization procedure, the prediction of the resolution process was studied. The solution saturated with the DL-form at 20 °C was cooled under a programmed cooling pattern and was seeded with the L-isomer. The decrease in the concentration of the L-isomer during the process was predicted by a conventional calculation method. Then, the waiting time for the spontaneous crystallization of the D-isomer was predicted by using the limiting values of the first and the second metastable regions, which were discussed in a previous report. As a result, a good agreement was obtained between the predicted results and the experimental results.

In the previous report,[1] the waiting time for the spontaneous crystallization of the unseeded isomer was investigated in an attempt to perform successfully the optical resolution DL-serine *m*-xylene-4-sulfonate dihydrate (DL-Ser·mXS·$2H_2O$) by the preferential crystallization procedure. As a result, it was found that the spontaneous crystallization of the unseeded isomer did not occur until the value of S_{II} expressed by the equation of $S_{II}=\int_0^{\theta n} f(C_D-C_S-S_I)d\theta$ reached a constant value independent of the cooling speed and the lowest arrival temperature. Here, S_I and S_{II} are the limiting values of the first and the second metastable regions for the unseeded D-isomer respectively: C_D, the concentration of the D-isomer; C_S, the solubility of the D-isomer; f, the correction factor approximated by C_D/C_L; θ, the cooling time; and θn, the waiting time for the spontaneous crystallization of the unseeded D-isomer. Therefore, the waiting time for the spontaneous crystallization of the unseeded D-isomer might be predicted if the increase in the supersaturation degree due to cooling and the decrease in the concentration of the seeded L-isomer due to preferential crystallization were previously known.

In the present paper, the decrease in the concentration of the seeded L-isomer in the optical resolution process of DL-Ser·mXS·$2H_2O$ under given cooling conditions was predicted according to the usual methods.[2-4] Then, the waiting time for the unseeded D-isomer, θn, was predicted from the above equation by using the values of S_I and S_{II} determined in the previous report. As a result, a good agreement was obtained between the predicted results and the experimental results.

Materials and Methods

Materials, Apparatus, and Analytical Methods. The materials, experimental apparatus, analytical methods, expression of the supersaturation degree, and operation of the preferential crystallization procedure were described in the previous report.[1]

Cooling Methods. The solution for preferential crystallization was cooled under cooling patterns previously programmed. Two cooling patterns were used. One was cooled at the rate of 1/8 °C per min and maintained at 12.0 °C. The other was cooled at the rate of 1/2 °C per min and maintained at 14.5 °C.

Prediction of the Decrease in the Concentration of the Seeded L-Isomer, C_L. The crystal growth rate of the seeded L-isomer in the process of preferential crystallization can be expressed as the following general equation:[2-4]

$$-\frac{dC_L}{d\theta} = aK(C_L-C_S)^n, \quad (1)$$

where C_L is the concentration of the L-isomer; K, the overall crystal-growth coefficient; a, the surface area of the crystals; n, the crystal-growth rate order; and C_S, the solubility of the L-isomer as a function of the temperature, t. The value of a increases with the growth of the seed crystals. In this report, it was assumed that a increased in proportion to $(W/W_0)^{2/3}$,[2,3] namely:

$$a = (W/W_0)^{2/3}\cdot a_0, \quad (2)$$

where W_0 is the initial weight of the seed crystals, W is the weight of the crystals at time θ, and a_0 is the initial surface area corresponding to W_0.

Substituting Eq. 2 into Eq. 1 gives:

$$-\frac{dC_L}{d\theta} = \left(\frac{W}{W_0}\right)^{2/3}\cdot a_0K\cdot(C_L-C_S)^n. \quad (3)$$

Taking logarithms, Eq. 3 gives:

$$\log\left\{\left(-\frac{dC_L}{d\theta}\right)\Big/\left(\frac{W}{W_0}\right)^{2/3}\right\} = n\log(C_L-C_S) + \log a_0K. \quad (4)$$

Equation 4 means that the plot of $\log\{(-dC_L/d\theta)/(W/W_0)^{2/3}\}$ against $\log(C_L-C_S)$ is a straight line, and that the values of n and a_0K can be evaluated from the slope and the intercept of the straight line respectively. In order to determine the values of a_0K and n, the time course of the decrease in C_L was obtained under the following conditions. The supersaturated solution of DL-Ser·mXS·$2H_2O$ (936 g) and water (1300 g) was maintained at a constant temperature of 14.5 °C or 12.0 °C, seeded with 2 g of L-Ser·mXS·$2H_2O$ (100—200 meshes), and allowed to crystallize. From the slope of the tangent on the time course of the decrease in C_L, the value of $(-dC_L/d\theta)$ was determined. The value of W was calculated from the decrease of C_L. A plot of $\log\{(-dC_L/d\theta)/(W/W_0)^{2/3}\}$ against $\log(C_L-C_S)$ gave a straight line, as is shown in Fig. 1. Then, the values of n and a_0K could be

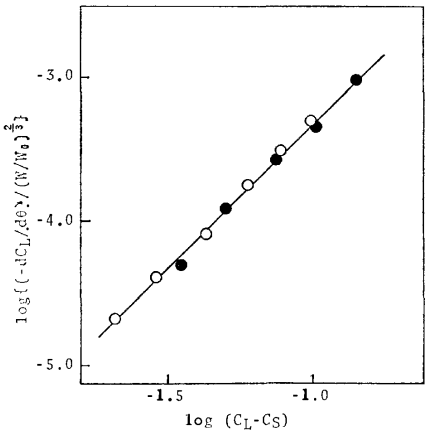

Fig. 1. Plots of $\log\{(-dC_L/d\theta)/(W/W_0)^{2/3}\}$ against $\log(C_L-C_S)$.
○: 14.5 °C, ●: 12.0 °C.

determined from the straight line; they were $n=2[-]$ and $a_0K=6.49\times10^{-2}$ [min^{-1}].

On the other hand, the relationship between C_S in Eq. 3 and t was already obtained in the previous report at the following empirical equation:

$$\log C_S = 2.34\times10^{-2}t - 9.12\times10^{-1}. \quad (5)$$

Since the solution is cooled under a programmed pattern, t is already given. Therefore, C_S is known.

Consequently, the decrease in C_L due to preferential crystallization can be predicted by means of calculations based on Eq. 3 on the assumption that the n and K obtained above are constant during the preferential crystallization procedure.

Prediction of Waiting Time for the Spontaneous Crystallization of the D-*Isomer, θn.* The previous report showed that the supersaturation state of the unseeded D-isomer in the actual resolution process on the solution saturated with DL-Ser·mXS·$2H_2O$ at 20 °C was stable until the value of S_{II} in Eq. 6 reached 4.49 [g·min/g(water)].

$$S_{II} = \int_0^{\theta n} f(C_D - C_S - S_I)d\theta, \quad (6)$$

where the integration is restricted to cases of $C_D-C_S \geqq S_I$; f is the correction factor against the change in the ratio of C_L/C_D, which may be empirically approximated by $f=C_D/C_L$, judging from the result of our previous report.

The values of S_I and S_{II} are known to be 6.6×10^{-2} [g/g(water)] and 4.49 [g·min/g(water)] respectively; C_D is the initial concentration until the spontaneous crystallization takes place, C_S is obtainable from Eq. 5, and f is also obtainable because C_L is obtained from Eq. 3. Therefore, the waiting time for the spontaneous crystallization of the D-isomer can be predicted by calculating θn from Eq. 6.

Results and Discussion

As an example, it was assumed that the optical resolution of DL-Ser·mXS·$2H_2O$ was carried out as follows. DL-Ser·mXS·$2H_2O$ (936 g) was dissolved in water (1300 g) by heating it at 35 °C for one hour in a 2l-cylindrical glass vessel. The solution was then

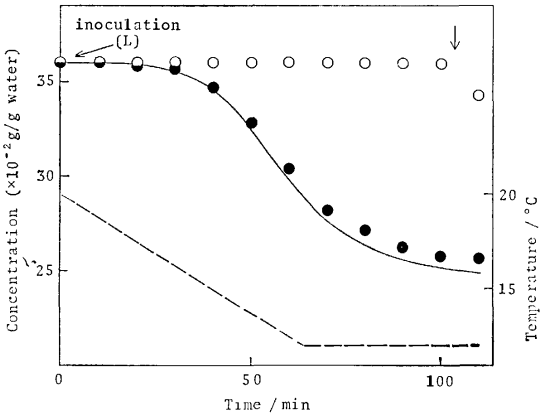

Fig. 2. Comparison between calculated results and experimental data in the optical resolution process of DL-Ser·mXS·$2H_2O$.
——: Calculated curve, ○, ●: experimental data of concentrations of D-isomer (○) and L-isomer (●), ↓: predicted point of spontaneous crystallization of D-isomer, — — —: temperature curve programmed so as to cool at the rate of 1/8 °C per min to 12 °C.

stirred at a constant speed (210 rpm), subsequently cooled at the rate of 1/8 °C per min, and thereafter maintained at 12.0 °C. Two grams of L-Ser·mXS·$2H_2O$ (100—200 meshes) was seeded at 20 °C in the course of cooling, and only the L-isomer was preferentially crystallized.

In order to calculate the decrease in the concentration of the L-isomer according to Eqs. 3 and 5, the numerical values of the constants in those equations were obtained as has been described in the section on Materials and Methods. The product of the overall crystal-growth coefficient and the surface area of the seed crystals, a_0K, was 6.49×10^{-2} [min^{-1}]; the crystal-growth rate order was $n=2$ [—].

Under the present experimental conditions, the initial values of C_L, C_D, and W were 0.360 [g/g (water)], 0.360 [g/g(water)], and 0.00154 [g/g(water)] respectively. Using these values and according to Eqs. 3 and 5, the decrease in C_L due to the preferential crystallization of the L-isomer under the programmed cooling pattern described above was calculated. The calculated result for the decrease of C_L is shown in Fig. 2.

To predict the waiting time for spontaneous crystallization, θn, the value of S_{II} was caluclated according to Eq. 6. The waiting time, θn, at which the value of S_{II} reached 4.49 [g·min/g(water)] was 104 [min]. That is, it was predicted that the spontaneous crystallization of the unseeded D-isomer would occur 104 min after the time of inoculation of the L-isomer, as is shown in Fig. 2.

On the other hand, the actual resolution was carried out under the same conditions as have been described in the above illustrative example. The experimental data are also plotted, together with the predicted results, in Fig. 2, indicating that these were in good agreement.

As another example, the prediction of the preferential crystallization process was carried out on the assumption that the solution was cooled at the rate

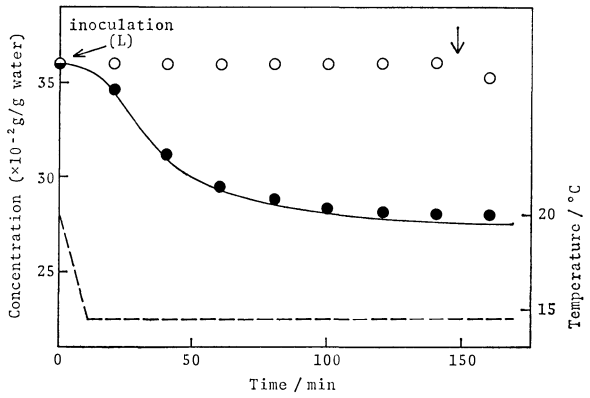

Fig. 3. Comparison between calculated results and experimental data in the optical resolution process of DL-Ser·mXS·$2H_2O$.
——: Calculated curve, ○, ●: experimental data of concentrations of D-isomer (○) and L-isomer (●), ↓ : predicted point of spontaneous crystallization of D-isomer, — — —: temperature curve programmed so as to cool at the rate of 1/2 °C per min to 14.5 °C.

of 1/2 °C per min and thereafter maintained at 14.5 °C. The results ($\theta n = 148$ [min]), predicted in the manner described above, and the experimental data are shown in Fig. 3, indicating that these were also in good agreement.

These results show that the our quantitative approach to ascertaining the limit of the metastable region in the preferential crystallization process is proper and that the waiting time for the spontaneous crystallization of the unseeded isomer can be successfully predicted. Although we did not study the optimization of the optical resolution process of DL-Ser·mXS·$2H_2O$, it seems to be possible to do so by the method presented here. It would also be interesting to learn whether such a prediction method can be applied for the optical resolution processes of other racemic mixtures.

References

1) C. Hongo, S. Yamada, and I. Chibata, *Bull. Chem. Soc. Jpn.*, **54**, 1905 (1981).
2) J. D. Jenkins, *J. Am. Chem. Soc.*, **47**, 903 (1925).
3) G. Amiard, *Experientia*, **15**, 38 (1959).
4) N. Mizoguchi, *Nippon Nogei Kagaku Kaishi*, **41**, 607 (1967).

Amination Kinetics of Chloromethylated Polystyrene Accompanied by Acceleration and Deceleration[1)]

Hiroshi KAWABE

The Institute of Physical and Chemical Research, Wako, Saitama 351

(Received August 30, 1980)

Procedures to evaluate rigorously the rate constants in the aminations of chloromethylated polystyrene which are accompanied by acceleration and deceleration have been developed. The calculated fractional conversions in the reaction of chloromethylated polystyrene with 2-amino-1-butanol in dioxane, accompanied by acceleration, and the reaction with triethylamine in dimethyl sulfoxide, accompanied by deceleration, are proved to be in good agreement with the observed ones. The activation parameters of these reactions, in addition to the kinetic data in *N,N*-dimethylformamide, support the conclusion that the acceleration and the deceleration are due to the formation of the hydrogen bond and to the electrostatic effect from the neighboring groups in the respective transition states.

The rate constants of the chemical reactions of ploymers with small molecules in homogeneous solutions sometimes increase or decrease during the reactions, as observed in the aminations of chloromethylated polystyrene (CMPS). Although the reaction of CMPS with 2-amino-1-butanol in *N,N*-dimethylformamide (DMF) and dimethyl sulfoxide (DMSO) follows the second-order kinetics, the rate constant increases during the reaction in dioxane.[2)] Such acceleration was also observed in the amination of CMPS with diethanolamine in dioxane and it was considered to be caused by the hydroxyl groups of the already-aminated neighbors in the macromolecule.[3)] Similar acceleration was reported by Drăgan *et al.*[4)] in the reaction of CMPS with 1-dimethylamino-3-propanol and 1-dimethylamino-2-propanol in dioxane and dimethylacetamide. Tsuchida and Irie[5)] observed the acceleration during the reaction of CMPS with γ-picolin in DMF.

On the other hand, the rate constant of the reaction of CMPS with butylamine decreases during the reaction in dioxane, though the reaction in DMF follows the second-order kinetics.[6,7)] Such deceleration was also observed in the reaction of CMPS with diethylamine in both dioxane and DMF and in the reaction with diethanolamine in both DMF and DMSO. The deceleration in these reactions was considered to due to the steric effect of the already-aminated neighboring groups.[3,8)]

The reaction kinetics in polymer solutions which deal with the deceleration was first proposed by Fouss *et al.*,[9)] who studied the quaternization of poly(4-vinylpyridine) with butyl bromide in sulfolane and propyrene carbonate. Since then, deceleration during the quaternization of poly(vinylpyridine) in sulfolane has been investigated kinetically by many investigators,[10-13)] who ascribed it to the steric hindrance or the electrostatic effect by the already-reacted groups in the polymer. But the quaternization of triethylamine with CMPS in DMF was reported to obey the ordinary second-order rate equation by Noda and Kagawa.[14)] Yet the deceleration in DMF was observed in the quaternization of poly(4-dimethylaminostyrene) with methyl iodide by Arcus and Hall[15)] and in the quaternization of poly(4-vinylpyridine) with benzyl chloride by Tsuchida and Irie;[5)] Kawabe and Yanagita[3)] observed also that the quaternization of poly[4-[bis(2-hydroxyethyl)aminomethyl]styrene] with methyl iodide decelerated in an aqueous DMF solution.

The aminations of CMPS accompanied by the deceleration were previously reported by Kawabe and Yanagita[3,6-8)] to conform to a modified second-order rate equation. Recently the present author has also found that the quaternization of triethylamine with CMPS in DMSO is accompanied by deceleration and that the reaction kinetics conforms to the modified rate equation. In the amination of CMPS with 2-amino-1-butanol, which is accompanied by acceleration, however, the conformity of the kinetic data to a similarly modified second-order rate equation was not so excellent, as reported previously.[2)] This reaction is re-examined and a procedure to evaluate the rate constants rigorously is described in this paper. The activation parameters of these reactions will be discussed in relation to their reaction mechanism.

Experimental

Materials. Chloromethylated polystyrenes (chlorine content: 21.4—22.8%, degree of chloromethylation: 0.89—0.97, mol wt: about 1×10^5) were prepared and purified by the procedures described in previous papers.[2,6)] (*R*)-2-Amino-1-butanol was prepared as reported previously.[2)] Triethylamine and solvents were of reagent grade and were distilled before use; they were proved to be pure by their refractive indices.

Kinetic Measurements. The procedures of the kinetic measurements in the amination of CMPS and benzyl chloride were the same as those described previously.[2,6)] The temperature of the reaction mixture was kept constant within ±0.1 K. The initial concentration of chloromethyl group was 0.04 mol dm^{-3}, that of 2-amino-1-butanol was 0.40—0.86 mol dm^{-3}, and that of triethylamine was 0.04 mol dm^{-3}.

Rate Equations

All the reactions of benzyl chloride with 2-amino-1-butanol and triethylamine conform to the second-order rate equation, Eq. 1. The reactions of CMPS with both amines in DMF also conform to Eq. 1:

$$kt = \frac{1}{a-b}\ln\frac{b(a-x)}{a(b-x)} = \frac{1}{a-b}\ln\frac{1-\alpha}{1-\beta} \equiv \bar{k}t, \qquad (1)$$

where a is the initial concentration of the amines; b, that of the chloromethyl groups; x, the concentra-

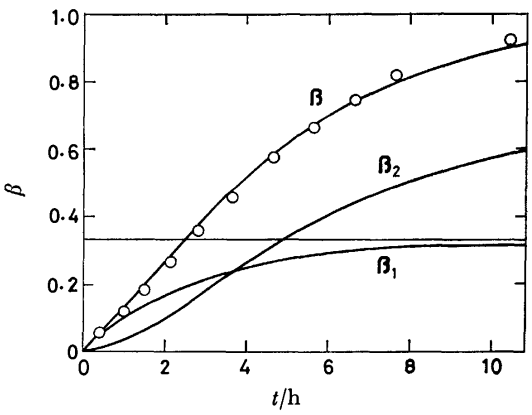

Fig. 1. Amination of CMPS with 2-amino-1-butanol in dioxane at 333.2 K.

tion of chloride ions at time t; and where $\alpha=x/a$ and $\beta=x/b$.

Amination of CMPS with 2-Amino-1-butanol in Dioxane. The second-order rate constant of the reaction of CMPS with 2-amino-1-butanol (k in Eq. 1) increases as the reaction proceeds, and k is a linear function of β:[2]

$$k = k_0(1+m\beta), \tag{2}$$

where k_0 and m are constants. On the basis of a model which represents the neighboring-group effect, β was expressed by Eq. 3 under the condition that a large excess of the amine is present ($a \gg b$):[2]

$$\beta = 1 - A' \exp(-3k_1at) - B' \exp(-k_2at), \tag{3}$$

$$k_1t = \frac{1}{D'a-b} \ln \frac{1-\alpha}{1-D'\beta} \equiv \overline{k_1t} \quad (\beta<1/3), \tag{4}$$

$$k_2t = \overline{kt} - C' \quad (\beta>1/3), \tag{5}$$

where $A'=(k_1-k_2)/(3k_1-k_2)$, $B'=2k_1/(3k_1-k_2)$, $D'=3-2k_2/k_1$, and $C'=\ln[(1-\chi'/a)/(1-\chi'/b)]/(a-b)-k_2\tau'$; τ' and χ' are the values of t and x when $x_1 \simeq b/3$. The k_2 value was obtained from the plot of $\overline{kt}$ against t by virtue of Eq. 5 within the range $\beta>1/3$, while k_1 was obtained on the basis of Eq. 4 by the use of the k_2 value and an approximate value of k_1 which was determined by Eq. 1 in the range $\beta<1/3$.

The over-all course of the reaction was expressed on the basis of Eq. 3 by the use of the k_1 and k_2 values thus obtained; however, the agreement between the calculated and observed values was not so excellent.[2] To explain this discrepancy, the following points need clarification: (i) evaluation of k_1 and k_2, (ii) conditions of the reaction, (iii) the character of the group interaction, and (iv) the model from which the rate equations are derived.

Let us first re-examine the estimation of the rate constants. Taking a glance at Fig. 1, where β is divided into $\beta_1(=x_1/b)$ and $\beta_2(=x_2/b)$ by Eq. 6, we realize that the over-all reaction rate is still controlled by k_1 in a range far beyond the β value of 1/3; β_1 is given by

$$\beta_1 = x_1/b = [1-\exp(-3k_1at)]/3. \tag{6}$$

This may arise owing to the facts that $k_2>k_1$, where k_1 and k_2 are the rate constants of the elementary reactions which are independent of the neighboring group and under the influence of it respectively, and that the elementary reaction characterized by k_1 takes place in a range where β is still larger than 1/3. The k_2 value obtained simply by means of Eq. 5 will have to be corrected in this case, since it does not represent the genuine k_2.

From Eq. 3, we obtain

$$\left.\begin{aligned} k_2t &= -\ln X'/a \equiv \overline{k_2t}, \\ X' &\equiv [(1-\beta)-A' \exp(-3k_1at)]/B'. \end{aligned}\right\} \tag{7}$$

The k_1 value used in the computation is first obtained from a linear plot of $\overline{k_1t}$ against t in a range of $\beta<1/3$ on the basis of Eq. 4. After repeating the computation according to Eq. 7, one may obtain finally a linear plot of $\overline{k_2t}$ against t, which starts from the origin and covers data in a whole range of β; the corrected value of k_2 is thus obtained from the slope of this line. The value of k_1 may further be corrected, if necessary, on the basis of the following equations, which are derived also from Eq. 3:

$$\left.\begin{aligned} k_1t &= -\ln Y'/3a \equiv \overline{k_1t}, \\ Y' &= [(1-\beta)-B' \exp(-k_2at)]/A'. \end{aligned}\right\} \tag{8}$$

After repeating the computation, the final plot of $\overline{k_1t}$ against t will be represented by a straight line which starts from the origin and covers the whole range of β. When neccesary, one may repeat the computations by means of Eqs. 7 and 8 until fixed values of k_1 and k_2 are obtained. In the following section of this paper, it is shown that, in the amination of CMPS with 2-amino-1-butanol, Eq. 7 yields a somewhat greater k_2 value than that determined on the basis of Eq. 5, though Eqs. 4 and 8 yield the same k_1 value.

Quaternization of Triethylamine with CMPS in DMSO. The present author has found that the second-order rate constant (k in Eq. 1) of the reaction of CMPS with triethylamine decreases with the progression of the reaction and that the kinetic data fit Eq. 9; the equation was derived previously on the assumption that the reactivity of a group present between two already-reacted neighboring groups decreases owing to neighboring-group interaction:[3]

$$\beta = 1 - A \exp(-2k_1at) - B \exp(-k_2at), \tag{9}$$

$$k_1t = \frac{1}{Da-b} \ln \frac{1-\alpha}{1-D\beta} \equiv \overline{k_1t} \quad (\beta<1/2), \tag{10}$$

$$k_2t = kt - C \quad (\beta>1/2), \tag{11}$$

where $A=(k_1-k_2)/(2k_1-k_2)$, $B=k_1(2k_1-k_2)$, $D=2-k_2/k_1$, and $C=[(1-\chi/a)/(1-\chi/b)]/(a-b)-k_2\tau$; τ and χ are the values of t and x when $x_1 \simeq b/2$. Not only the present quaternization reaction but also many amination reactions of CMPS accompanied by deceleration fit Eq. 9 with k_1 and k_2 values estimated by Eqs. 10 and 11.[3,6,8] This may be understood by referring to Fig. 4 (also refer to Fig. 9 in Ref. 6), where β of the reaction at 303 K is divided into β_1 and β_2 by virtue of the equation;

$$\beta_1 = [1-\exp(-2k_1at)]/2. \tag{12}$$

Since $k_1>k_2$ in these cases, k_1 is no longer an important kinetic parameter in a range beyond $\beta>1/2$. In cases

TABLE 1. KINETIC PARAMETERS IN THE AMINATION OF CMPS WITH 2-AMINO-1-BUTANOL IN DIOXANE[a)]

Temp / K	Rate constants $\times 10^5$/dm^3 mol^{-1} s^{-1}			
	k_0 (Eq. 2)	k_1 (Eq. 8)	k_2 (Eq. 5)	k_2 (Eq. 7)
313.2	0.933	0.960	2.20	2.72
323.2	1.87	1.88	4.62	5.38
333.2	3.50	3.77	8.02	10.8
343.2	6.30	6.32	15.5	18.2
E_a/kJ mol^{-1}	56.8±0.3	56.8±1.1	57.3±1.2	57.3±1.1
log A[b)]	4.45±0.05	4.46±0.18	4.90±0.19	4.99±0.17

a) a=0.86 mol dm^{-3}, b=0.043 mol dm^{-3}. b) A is expressed by dm^3 mol^{-1} s^{-1}.

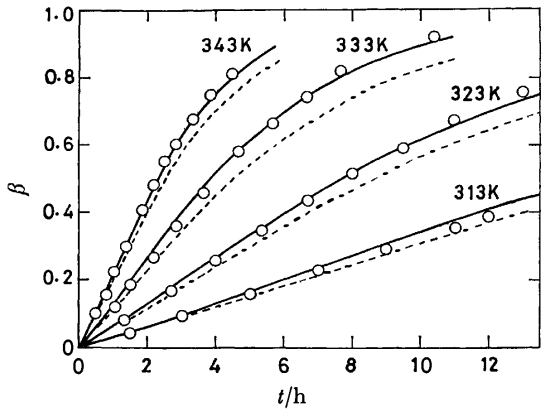

Fig. 2. Amination of CMPS with 2-amino-1-butanol in dioxane.

TABLE 2. RATE CONSTANTS IN THE AMINATION OF BENZYL CHLORIDE WITH 2-AMINO-1-BUTANOL IN DIOXANE[a)]

Temp / K	a / mol dm^{-3}	$k \times 10^5$ / dm^3 mol^{-1} s^{-1}
333.2	0.396	2.53
	0.656	3.00
	1.055	4.10
348.2	0.400	6.23
	0.656	7.17
	0.860	8.00
363.2	0.400	14.5
	0.656	15.8
	0.860	16.8

a) b=0.041—0.044 mol dm^{-3}.

where k_1/k_2 is not large, however, the agreement between observed and calculated values may not be so excellent. Rigorous treatment of this kinetics then requires the correction of k_2 and also k_1, if necessary, on the basis of the following equations which are derived from Eq. 9:

$$\left.\begin{aligned} k_2 t &= -\ln X/a \equiv \overline{k_2 t}, \\ X &\equiv [(1-\beta) - A\exp(-2k_1 at)]/B, \end{aligned}\right\} \quad (13)$$

$$\left.\begin{aligned} k_1 t &= -\ln Y/2a \equiv \overline{k_1 t}, \\ Y &\equiv [(1-\beta) - B\exp(-k_2 at)]/A. \end{aligned}\right\} \quad (14)$$

Results and Discussion

Amination Kinetics of CMPS and Benzyl Chloride with 2-Amino-1-butanol in Dioxane. The previously reported kinetic data of the amination of CMPS with 2-amino-1-butanol in dioxane (a=0.86 and b=0.043 mol dm^{-3})[2)] have been re-examined by the procedures described in the preceding section. The rate constants k_1 and k_2, evaluated on the basis of Eqs. 7 and 8, are listed in Table 1. Although the numerical values of k_1 thus obtained are the same as those obtained by means of Eq. 4 and also the same as the k_0 values obtained by Eq. 2, the k_2 values are a little greater than those obtained by Eq. 5. The plots of β against t represented by the solid lines in Fig. 2 are calculated on the basis of Eq. 3; they are in good agreement with the observed values represented by the circles. In the figure, the dotted lines are the previously reported ones, which were computed by using the k_2 values determined by means of Eq. 5. It may therefore be concluded that the disagreement between the calculated and observed values shown in the previous paper[2)] originated in the fact that the evaluation of the rate constants, especially k_2, was not accurate. This correction of k_2, nevertheless, does not cause any change in activation energy, E_a, though the frequency factor, A, for k_2 (Eq. 7) is a little greater than that for k_2 (Eq. 5).

The second problem we concern ourselves with is the effect of the reaction conditions, such as the initial concentration of 2-amino-1-butanol and the reaction temperature. Although the amination kinetics of benzyl chloride fits Eq. 1, k has been found to be dependent on the initial concentration of 2-amino-1-butanol, a, as shown in Table 2. The kinetic data in the amination of CMPS in various conditions have been treated on the basis of Eqs. 2, 4, 5, 7, and 8; the results are summarized in Table 3. The table shows that the k_0 values, which are equal to the k_1 values obtained on the basis of both Eq. 4 and Eq. 8, are also dependent on a, and that the k_2 values obtained by Eq. 5, which are almost equal to the k values extrapolated to β=1 according to Eq. 3, are independent of a. The agreement between the calculated and observed β values is better when the k_2 values obtained on the basis of Eq. 7, instead of Eq. 5, are used.

Tables 2 and 3 indicate that k of benzyl chloride is equal to k_0 of CMPS at the same a and that they increase a little with a, while k_2 of CMPS is independent

Table 3. Rate constants in the amination of CMPS with 2-amino-1-butanol in dioxane[a)]

Temp / K	a / mol dm^{-3}	m	Rate constants $\times 10^5$/dm^3 mol^{-1} s^{-1}		
			k_0 (Eq. 2)	k_2 (Eq. 5)	k_2 (Eq. 7)
333.2	0.400	1.77	2.68	7.52	10.8
	0.656	1.55	2.95	7.50	
	0.859	1.24	3.50	8.02	
348.2	0.400	1.89	6.42	18.8	25.1
	0.656	1.61	7.13	20.8	
	0.860	1.43	7.75	18.7	
363.2	0.400	1.83	14.5	41.0	56.7
	0.656	1.72	15.8	43.5	
	0.860	1.57	16.9	42.0	

a) b=0.040 mol dm^{-3}.

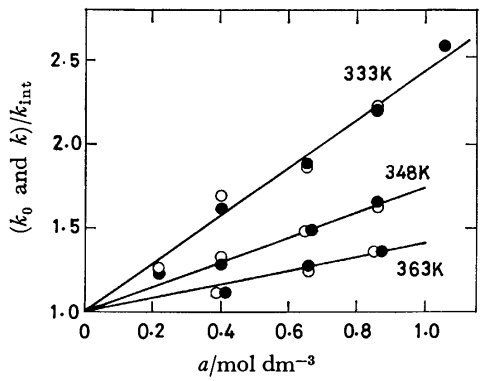

Fig. 3. Dependence of rate constants on a in the amination of CMPS (k_0, ○) and benzyl chloride (k, ●) with 2-amino-1-butanol in dioxane.

of a. Figure 3 shows that k and k_0 increase linearly with a according to the relation:

$$(k_0 \text{ and } k) = k_{int}(1+Ka), \quad (15)$$

where k_{int} and K are constants. The numerical values of k_{int} and K are listed in Table 4; E_a for k_{int} is greater than that for k_0 in Table 1. Consider that the hydroxyl group of 2-amino-1-butanol can form a hydrogen bond, in a non-polar solvent such as dioxane, with the chlorine of the chloromethyl group in the transition state to accelerate the reaction. Then an expression similar to Eq. 15 is easily derived according to the theory of transition states, on the assumption that two kinds of activation complexes coexist, the ordinary one and the hydrogen-bonded one. The physical meaning of the constants in Eq. 15 may thus be realized by considering that k_{int} corresponds to the intrinsic rate constant independent of the hydrogen bond and K is a measure of the force of the hydrogen bond.

The acceleration during the amination of CMPS may be explained by assuming that it is caused by the intramolecular hydrogen bond between the hydroxyl group of the already-aminated neignbor and the chlorine in the transition state. Provided that the intramolecular hydrogen bond is stronger than the intermolecular hydrogen bond, k_2 will be independent of a. The ratio, k_2/k_{int}, is also interpreted as a measure of the intramolecular hydrogen bond. Table 4 indicates that both K and k_2/k_{int} decrease

Table 4. Intrinsic rate constants in the amination of benzyl chloride and CMPS with 2-amino-1-butanol in dioxane

Temp / K	$k_{int}\times 10^5$ / dm^3 mol^{-1} s^{-1}	K / mol dm^{-3}	k_2/k_{int}
333.2	1.58	1.41	6.80
348.2	4.83	0.74	5.17
363.2	12.4	0.42	4.56
E_a/kJ mol^{-1}	69.1±1.0		
log $A^{a)}$	6.04±0.16		

a) A is expressed by dm^3 mol^{-1} s^{-1}.

Table 5. Kinetic parameters in the quaternization of triethylamine with CMPS and benzyl chloride in DMF

Temp / K	$k\times 10^5$/dm^3 mol^{-1} s^{-1}	
	CMPS	Benzyl chloride
303.2	3.58	2.07
318.2	9.22	5.38
333.2	22.0	13.4
E_a/kJ mol^{-1}	50.8±0.1	52.3±0.5
log $A^{a)}$	4.31±0.02	4.32±0.08

a) A is expressed by dm^3 mol^{-1} s^{-1}.

with the increase of temperature; this is not inconsistent with the assumption of the hydrogen bonds.

Quaternization Kinetics of Triethylamine with CMPS and Benzyl Chloride in DMF. In DMF, the quaternization of triethylamine with CMPS as well as with benzyl chloride fits to the ordinary second-order rate equation, Eq. 1. The results are shown in Table 5.

Quaternization Kinetics of Triethylamine with CMPS and Benzyl Chloride in DMSO. Although the quaternization of triethylamine with benzyl chloride fits Eq. 1, that with CMPS is accompanied by deceleration and its rate constants are computed on the basis of Eqs. 10, 11, and 13. The results are summarized in Table 6. Equation 13 gives slightly smaller values of k_2 than those obtained by Eq. 11. The plots of β against t calculated on the basis of Eq. 9, represented by the solid lines in Fig. 4, are in excellent agreement with the observed values represented by the circles.

TABLE 6. KINETIC PARAMETERS IN THE QUATERNIZATION OF TRIETHYLAMINE WITH CMPS AND BENZYL CHLORIDE IN DMSO

Temp / K	Rate constants $\times 10^4$/dm^3 mol^{-1} s^{-1}			
	k[a] (Eq. 1)	k_1 (Eq. 10)	k_2 (Eq. 11)	k_2 (Eq. 13)
303.2	1.01	1.83	1.05	0.853
318.2	2.60	4.47	2.35	2.21
333.2	5.87	9.87	5.95	5.18
E_a/kJ mol^{-1}	49.2±0.5	47.2±0.2	48.6±2.1	50.5±0.2
log A[b]	4.49±0.08	4.39±0.04	4.38±0.35	4.63±0.03

a) The rate constant of benzyl chloride. b) A is expressed by dm^3 mol^{-1} s^{-1}.

TABLE 7. ACTIVATION PARAMETERS AT 298.2 K[a]

Solvent	Amine	Chloride	ΔS^* / J K^{-1}	ΔH^* / kJ	ΔG^* / kJ
Dioxane	2-Amino-1-butanol	CMPS, k_1	−168±3	54.3	104.4
		k_2	−158±3	54.8	101.8
		k_{int}	−138±3	66.7	107.7
DMF	Triethylamine	BC[a]	−171±1	49.8	100.7
		CMPS	−171±0.3	48.4	99.3
DMSO	Triethylamine	BC[a]	−167±2	46.7	96.6
		CMPS, k_1	−169±1	44.7	95.1
		k_2	−165±1	48.0	97.1

a) BC: benzyl chloride.

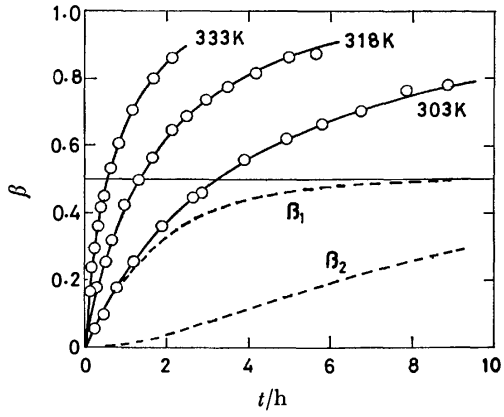

Fig. 4. Amination of CMPS with triethylamine in DMSO.

Activation Parameters. The activation parameters of the reactions are listed in Table 7. In dioxane the ΔG^* values for k_1 and k_2 are lower than that for k_{int} owing to their lower ΔH^* values; this fact supports the assumption that the hydroxyl group of 2-amino-1-butanol in the solution or the already-aminated neighbor in the polymer forms the inter- or intramolecular hydrogen bond with the chlorine of the chloromethyl group in the transition state. On the other hand, the lower ΔG^* value for k_2 than for k_1 is ascribed to the higher ΔS^* value; this suggests that the intramolecular hydrogen bond is formed in preference to the intermolecular one because the former is favorable with respect to entropy.

In the amination with 2-amino-1-butanol of a definite concentration, a, the ΔG^* values of both CMPS and benzyl chloride are the same, since k_0 (or k_1) of CMPS is equal to k of benzyl chloride, as shown in Fig. 3. In the quaternization of triethylamine in DMF, the ΔG^* of CMPS is lower than that of benzyl chloride owing to its lower ΔH^*; the same trend is noticed also in DMSO, when one compares the ΔG^* and ΔH^* values of benzyl chloride and CMPS (k_1).

The present work finds that the quaternization of triethylamine with CMPS in DMF conforms to the ordinary second-order rate equation, as was already reported by Noda and Kagawa,[14] whereas Arcus and Hall[15] found that the quaternization of poly(4-dimethylaminostyrene) with methyl iodide in DMF was accompanied by deceleration. They concluded that this deceleration was caused by the accumulation of positive charges on the polymer. Arcus and Hall[16] also noticed the reduction of rate during the quaternization of poly(4-vinylpyridine) with butyl bromide in sulfolane, as had been reported by Coleman and Fouss,[17] though they found that the reaction followed the second-order kinetics in DMF. It is interesting to note that the quaternization of poly(vinylpyridine) with butyl bromide and the quaternization of triethylamine with CMPS have the similar feature that they behave "normally" in DMF but "autodecelerate" in more polar solvents, such as DMSO and sulfolane.[18] In these cases, the deceleration may be explained by the electrostatic effect of the neighboring quaternary groups rather than by the steric obstruction by the neighbors. The more polar the solvent is, the more easy the ionization of quaternary ammonium chloride formed by the reac-

tion on the polymer may become. As the reaction proceeds, the formation of a positive activation complex may become more difficult owing to the electrostatic effect of the positive charges of the neighboring quaternary ammonium groups. Table 7 indicates that, in the quaternization of triethylamine in DMSO, the ΔG^{*} for k_2 is higher than that for k_1, owing to the higher ΔH^{*}.

Table 7 indicates also that ΔG^{*} values of the quaternization in DMSO are lower than those in DMF owing to the lower ΔH^{*} values. The same fact was also found in the amination of CMPS and benzyl chloride with 2-amino-1-butanol and diethanolamine.[7,21] This may be explained, as discussed in a previous paper,[1] by assuming that the positive activation complex is stabilized by solvation in dipolar aprotic solvents and that the solvated complex is more stable in DMSO than in DMF.

The author wishes to express his thanks to Dr. Masaya Yanagita for his valuable discussions. He is also grateful to Mr. Masaaki Kodera and Mr. Yukio Uesugi for their generous assistance in carrying out the measurements.

References

1) Group Interactions in Polyelectrolytes. XIII. For Part XII: H. Kawabe, *Bull. Chem. Soc. Jpn.*, **49**, 2043 (1976).
2) H. Kawabe and M. Yanagita, *Bull. Chem. Soc. Jpn.*, **44**, 896 (1971).
3) H. Kawabe, *Bull. Chem. Soc. Jpn.*, **47**, 2963 (1974).
4) S. Drăgan, I. Petrariu, and M. Dima, *J. Polym. Sci., Polym. Chem. Ed.*, **10**, 3077 (1972).
5) E. Tsuchida and S. Irie, *J. Polym. Sci., Polym. Cem. Ed.*, **11**, 789 (1973).
6) H. Kawabe and M. Yanagita, *Bull. Chem. Soc. Jpn.*, **41**, 1518 (1968).
7) H. Kawabe and M. Yanagita, *Bull. Chem. Soc. Jpn.*, **46**, 38 (1973).
8) H. Kawabe and M. Yanagita, *Bull. Chem. Soc. Jpn.*, **46**, 3627 (1973).
9) R. M. Fuoss, M. Watanabe, and B. D. Coleman, *J. Polym. Sci.*, **48**, 5 (1960).
10) C. B. Arends, *J. Chem. Phys.*, **39**, 1903 (1963).
11) J. Marcellet-Sauvage and C. Loucheux, *Makromol. Chem.*, **176**, 315 (1975).
12) E. A. Boucher and C. C. Mollett, *J. Polym. Sci., Polym. Phys. Ed.*, 15, 283 (1977).
13) E. A. Boucher, J. A. Groves, C. C. Mollett, and P. N. Fletcher, *J. Chem. Soc., Faraday Trans. 1*, **73**, 1629 (1977).
14) I. Noda and I. Kagawa, *Kogyo Kagaku Zassi.*, **66**, 857 (1963).
15) C. L. Arcus and W. A. Hall, *J. Chem. Soc.*, **1963**, 4199.
16) C. A. Arcus and W. A. Hall, *J. Chem. Soc.*, **1964**, 5995.
17) B. D. Coleman and R. M. Fuoss, *J. Am. Chem. Soc.*, **77**, 5472 (1955).
18) The electrostatic factor EF, defined as the product of ε (dielectric constant) and μ (dipole moment), of DMSO (209) is rather higher than that of DMF (140);[19] The EF value of sulforane is estimated to be 208 on the basis of published ε and μ data.[20]
19) M. R. J. Dack, "The Influence of Solvent on Chemical Reactivity" in "Techniques of Chemistry," ed by A. Weissberger, Wiley-Interscience, New York (1976), Vol. 8 ("Solution and Solubilities," ed by M. R. J. Dack), Part II, Chap. 11, p. 100.
20) J. A, Riddick and W. B. Bunger, "Organic Solvents," in "Technique of Chemistry," 3rd ed, ed by A. Weissberger, Wiley-Interscience, New York (1970), Vol. 2, p. 468.
21) H. Kawabe, *Bull. Chem. Soc. Jpn.*, **47**, 2936 (1974).

NQR Zeeman Study of Bis(triphenylphosphine)copper(I) Bromide

Tsutomu Okuda,* Morio Hiura, and Hisao Negita
Department of Chemistry, Faculty of Science, Hiroshima University, Naka-ku, Hiroshima 730
(Received November 4, 1980)

Zeeman effects of ^{63}Cu and ^{81}Br NQR spectra of bis(triphenylphosphine)copper(I) bromide, $CuBr(PPh_3)_2$, have been studied at room temperature. The asymmetry parameters and the quadrupole coupling constants (e^2Qq/h) have been found to be 0.113 and 64.58 MHz for ^{63}Cu and 0.518 and 105.91 MHz for ^{81}Br. The large asymmetry parameter of the ^{81}Br NQR line is caused by the π-bonding character of the copper-bromine bond. The bonding scheme between the copper and bromine atoms is discussed on the basis of the obtained directions of the electric field gradient axes.

A trigonal planar coordination is occasionally seen in copper(I) compounds, though it is rarely found in the other transition metal complexes. The X-ray analysis of $CuBr(PPh_3)_2 \cdot 0.5C_6H_6$ (PPh_3=triphenylphosphine) has shown that the $CuBr(PPh_3)_2$ molecule is monomeric and the coordination geometry about its copper atom is trigonal planar.[1] NQR (nuclear quadrupole resonance) is very useful for the study of bonding character in copper(I) halide compounds, since both copper and halogen atoms have nuclear quadrupole moments. The ^{63}Cu NQR frequency in $CuBr(PPh_3)_2 \cdot 0.5C_6H_6$ has been reported.[2]

In the present study, both the ^{63}Cu and ^{81}Br NQR lines were observed for two compounds, $CuBr(PPh_3)_2$ and $CuBr(PPh_3)_2 \cdot 0.5C_6H_6$. Furthermore, since ^{63}Cu and ^{81}Br both have a nuclear spin $I=3/2$, a Zeeman study of NQR was carried out to determine the nuclear quadrupole coupling constant e^2Qq_{zz}/h, the electric field gradient (efg) principal axes x, y, z, and asymmetry parameter $(q_{xx}-q_{yy})/q_{zz}$. These can be used to describe more explicitly the nature of the bonding.

Experimental

$CuBr(PPh_3)_2 \cdot 0.5C_6H_6$ was prepared according to the method described by Davis *et al.*[1] $CuBr(PPh_3)_2$ was obtained by recrystallization from the ethanol solution of $CuBr(PPh_3)_2 \cdot 0.5C_6H_6$. Found: C, 66.05; H, 4.38%. Calcd for $CuBrP_2C_{39}H_{33}$: C, 66.25; H, 4.56%. Found: C, 64.37; H, 4.66%. Calcd for $CuBrP_2C_{36}H_{30}$: C, 64.72; H, 4.54%. A single crystal of $CuBr(PPh_3)_2$ was obtained by the Bridgman-stockbarger method.

The NQR spectrometers used were super-regenerative oscillators employing a frequency modulation or a Zeeman modulation mode. The resonance lines due to four isotopes: ^{63}Cu, ^{65}Cu, ^{79}Br, and ^{81}Br were assigned on the basis of the known quadrupole moment ratios, $Q(^{63}Cu)/Q(^{65}Cu)=1.0806$ and $Q(^{79}Br)/Q(^{81}Br)=1.1974$. The Zeeman effect on the resonance line was examined by means of the zero-splitting cone method at room temperature with the magnetic field of about 2.5×10^{-2} T. The Zeeman-split signals were displayed on an oscilloscope. The magnetic field orientation for the zero-splitting was determined in polar coordinates (Φ, Θ), where Φ is the azimuthal angle and Θ is the polar angle.

Results and Discussion

The observed frequencies are listed in Table 1. The crystal structure for the benzene solvated compound $CuBr(PPh_3)_2 \cdot 0.5C_6H_6$ is available,[1] but that for unsolvated $CuBr(PPh_3)_2$ is not. From the small difference in both ^{63}Cu and ^{81}Br NQR frequencies, however, it is reasonable to consider that the molecular structure of the unsolvated crystal is essentially the same as that in the solvated crystal, that is, the individual $CuBr(PPh_3)_2$ molecules are monomeric and have the trigonal planar coordinations in the unsolvated crystal.

The zero-splitting patterns obtained for both the ^{63}Cu and ^{81}Br nuclei of $CuBr(PPh_3)_2$ are shown in Fig. 1. From these zero-splitting patterns the asymmetry parameters (η) and the directions of the efg axes were obtained. The quadrupole coupling constant e^2Qq_{zz}/h can be calculated by substituting the value of η in the following relation:

$$\nu = (e^2Qq_{zz}/2h)(1+\eta^2/3)^{1/2}. \quad (1)$$

The values of e^2Qq_{zz}/h derived in this way are listed in Table 1. For comparison, Table 1 includes the ^{63}Cu and ^{81}Br NQR frequencies of $(Bu_4N)CuBr_2$ (Bu=C_4H_9) reported by Bowmaker *et al.*[3] $(Bu_4N)CuBr_2$ has a linear dibromocuprate(I) ion, so that the asymmetry parameters of Cu and Br atoms are assumed

Table 1. ^{63}Cu and ^{81}Br NQR parameters for bis(triphenylphosphine)copper(I) bromide and dibromocuprate(I) compounds

Compound	Nucleus	Frequency/MHz		η	$\frac{e^2Qq/h}{\text{MHz}}$
		298 K	77 K		
$CuBr(PPh_3)_2$	^{63}Cu	32.36	33.93	0.113±0.005	64.58±0.02
	^{81}Br	55.28	56.63	0.519±0.003	105.91±0.02
$CuBr(PPh_3)_2 \cdot 0.5\,C_6H_6$	^{63}Cu	32.16	33.66		
	^{81}Br	52.88	55.53		
$(Bu_4N)CuBr_2$[a]	^{63}Cu	28.25	28.85	0[b]	56.50
	^{81}Br	60.35	62.6	0[b]	125.2

a) Ref. 3. b) The asymmetry parameter was assumed to be zero.

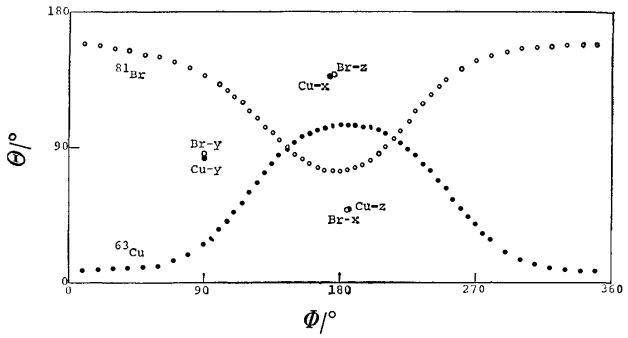

Fig. 1. The zero-splitting patterns of the ^{63}Cu and ^{81}Br NQR lines in $CuBr(PPh_3)_2$.

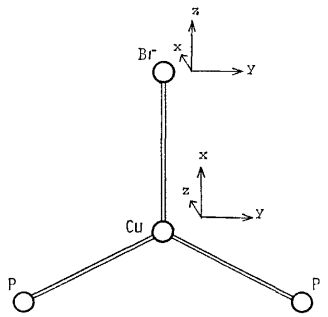

Fig. 2. The orientations of the efg principle axes for the copper and bromine atoms in the $CuBrP_2$ portion of the $CuBr(PPh_3)_2$ molecule.

to be zero.

One of the interesting features obtained from the Zeeman experiments is the large asymmetry parameter, 0.519, for the bromine atom. In this complex the bromine atom is considered to link to only one copper atom, as in the solvated compound. However, the obtained, asymmetry parameter is too large for a singly-bonded halogen atom. Accordingly, we can consider that the extraordinarily large asymmetry parameter results from the existence of the π-bond. Since the trigonal copper atom is considered to form sp^2-hybridized orbitals, the p_z orbital of copper is nonbonding, and can be used for π-bonding with ligands. In the previous NQR study and X-ray analysis of $Cu_2X_2(PPh_3)_3$ (X=Cl, Br, and I),[4,5] it was suggested that the p_π-p_π double bonding must occur in the bonds between copper and halogen atoms. In the present study, this suggestion has been confirmed by the large asymmetry parameter obtained for the bromine atom. The Zeeman study using a single crystal, furthermore, has revealed the relative orientations of the efg principal axes for both the ^{63}Cu and ^{81}Br atoms, *i.e.*, the efg x-, y-, and z-axes for the Br atom are along the z-, y-, and x-axes for the copper atom, respectively, as shown in Fig. 1. The z-axis of terminal halogen atom, in general, points along its bond direction. In the case of trigonal planar copper atoms it has become apparent from the Zeeman studies of $KCu(CN)_2$,[6] $Cu_2Cl_2(PPh_3)_3$, and $Cu_2I_2(PPh_3)_3$[4] that the efg z-axis of the three coordinated copper atom is perpendicular to the plane formed by three ligands. Therefore, both the y- and x-axes of the copper atom lie on the coordinate plane. On the basis of these results, the directions of the principal efg axes for both nuclei could be determined in a discrete molecule $CuBr(PPh_3)_2$, as shown in Fig. 2. The x-axis direction of the bromine atom is parallel to the z-axis direction of the copper atom, that is, it is perpendicular to the ligand plane. The y-axis direction of the bromine atom is normal to both its x-axis and its z-axis. This situation is similar to those of the trigonal planar species BBr_3 and BI_3,[7,8] which have p_π-p_π double bondings.

For the Cu–Br bond, one simple bonding model is proposed. The p_x, p_y, and p_z orbitals at the bromine atom are taken to be pointed toward the efg x-, y-, and z-axes, respectively. The p_z orbital forms a σ-bond with one of the sp^2-hybridized orbitals on the three-coordinated copper, and the p_x orbital can form a π-bond with the remaining p orbital on the copper atom. The p_y orbital is thought to have little interaction with the orbitals of the copper atom, so we can assume that the p_y orbital of the bromine atom does not take part in the Cu–Br bond formation. Then, e^2Qq_{zz}/h and the asymmetry parameter (η) are given by

$$e^2Qq_{zz}/e^2Qq_o = N_z - (N_x+N_y)/2, \quad (2)$$

$$\eta = 3(N_x-N_y)/2[N_z-(N_x+N_y)/2], \quad (3)$$

where e^2Qq_o/h is the quadrupole coupling constant for one 4p electron of the ^{81}Br, and N_x, N_y, and N_z denote the number of electrons in the p_x, p_y, and p_z orbitals of the bromine atom, respectively. Assuming $N_y=2$, the occupation numbers N_x and N_z are calculated, to be $N_x=1.943$ and $N_z=1.807$. This N_z value is compared with the ^{81}Br NQR data of the centrosymmetric $CuBr_2^-$ ion,[3] in which $N_z=1.812$ at 298 K, assuming that the bromine atom is singly bonded to the copper(I) atom ($N_x=N_y=2$).

Bersohn[9] has shown that the Townes and Dailey analysis of the halogen coupling constants leads to the following relationship between the fractional π-bonding character, Π, and the coupling constants

$$\Pi = (2/3)(e^2Qq_{zz}/e^2Qq_o)(\eta). \quad (4)$$

The partial π-bonding character calculated according to this equation is 5.7%. This value is significantly smaller than the π-bonding character of the trigonal planar BBr_3 and BI_3 molecules: 13.3% and 15.6% for the boron-bromine and boron-iodine bonds, respectively,[7,8] although the asymmetry parameter of $CuBr(PPh_3)_2$, $\eta=0.519$, is slightly larger than those of the boron trihalides, $\eta=0.45$ for BBr_3 and $\eta=0.456$ for BI_3.[7,8] Thus, the small π-bonding character of the Cu–Br bond results from the fact that the e^2Qq_{zz}/e^2Qq_o ratio of the bromine atom in $CuBr(PPh_3)_2$ is significantly smaller than those of BBr_3 and BI_3. Therefore, it is concluded that the ionic character of the copper-bromine bond is larger than those of the boron-bromine and boron-iodine bonds.

On the other hand, the Cu atom in $CuBr(PPh_3)_2$ has a larger value of e^2Qq_{zz}/h (64.58 MHz) than that of the three-coordinated copper atom in $Cu_2Br_2(PPh_3)_3$ (55.82 MHz at room temperature) in which the copper atom is linked by one triphenylphosphine and two bromine atoms. The e^2Qq_{zz}/h of an sp^2 hybridized

copper atom is considered to be caused by the 4p valence electron donated from three ligands. It is well known that a triphenylphosphine ligand is a better donor than halogen atoms. Therefore, the larger value of e^2Qq_{zz}/h found in $CuBr(PPh_3)_2$ is explained by the increase in the number of the coordinate phosphine ligands, from one to two. In addition, although the efg y-axis was nearly along the Cu–P bonding direction in the case of $Cu_2Br_2(PPh_3)_3$, the y-axis direction in $CuBr(PPh_3)_2$ is normal to the bisector of the P–Cu–P angle. This finding is consistent with the idea that the copper(I) atom receives more electrons from the triphenylphosphine ligand than the halogen atom.

References

1) P. H. Davis, R. L. Belford, and I. C. Paul, *Inorg. Chem.*, **12**, 213 (1973).
2) T. Okuda, M. Hiura, K. Yamada, and H. Negita, *Chem. Lett.*, **1977**, 367.
3) C. A. Bowmaker, L. D. Brockless, and R. Whiting, *Aust. J. Chem.*, **26**, 29 (1973).
4) H. Negita, M. Hiura, K. Yamada, and T. Okuda, *J. Mol. Struct.*, **18**, 205 (1980).
5) D. F. Lewis, S. J. Lippard, and P. S. Welcker, *J. Am. Chem. Soc.*, **92**, 3805 (1970).
6) G. L. McKown and J. D. Graybeal, *J. Chem. Phys.*, **44**, 610 (1966).
7) T. Chiba, *J. Phys. Soc. Jpn.*, **13**, 860 (1958).
8) W. G. Lauvita and W. S. Koski, *J. Am. Chem. Soc.*, **81**, 3179 (1959).
9) R. Bersohn, *J. Chem. Phys.*, **22**, 2078 (1954).

  Bull. Chem. Soc. Jpn., 54, 1923—1927 (1981)

ESR Spectra of Six-coordinate Cobalt(III) Tetraphenylporphyrin Cation Radicals Generated by Electrochemical Oxidation

Hiroaki OHYA-NISHIGUCHI,* Masahiro KHONO,† and Kiyoko YAMAMOTO††

Department of Chemistry, Faculty of Science, Kyoto University, Sakyo-ku, Kyoto 606

† *JEOL Ltd., Akishima, Tokyo 196*

†† *The Institute of Physical and Chemical Research, Wako, Saitama 351*

(Received November 19, 1980)

The ESR spectra of the paramagnetic species generated electrochemically from $\alpha,\beta,\gamma,\delta$-tetraphenylporphinatocobalt(II), [Co^{II}(tpp)], have been observed under the conditions of low-temperature, in chlorinated or non-chlorinated solvents, and in the presence of various supporting electrolytes. From the ESR parameters obtained, three different paramagnetic species, [Co^{III}(tpp)]$^{2+}$(X^-)$_2$, [Co^{III}(tpp)]$^{2+}$(Y^-)$_2$, and [Co^{III}(tpp)]$^{2+}$(X^-)(Y^-), have been confirmed. The ESR spectrum of thermally and optically accessible paramagnetic species in the solution of chlorotetraphenylporphinatocobalt(III) has been reproduced by the pertinent combination of solvent and supporting electrolyte, and well interpreted by assuming the formation of [Co^{III}(tpp)]$^{2+}$(Cl^-)$_2$. Arguing from a correlation between the hfcc of cobalt and nitrogen nuclei in this species, a spin-polarization mechanism is proposed to interpret the cobalt hfcc.

The application of electrochemical techniques to the study of biologically important metal-complexes has some advantages over the usual physico-chemical techniques: One is a selective formation of paramagnetic species by applying a pertinent potential comparable to the polarographic half-wave potential ($E_{1/2}$) of the compound under consideration, and another is a close correlation of the electrochemical reaction with the biological redox reactions.[1,2] On the other hand, the ESR measurements are very powerful for the detection of paramagnetic species.[2,3] It is quite natural, therefore, to combine these techniques for a more quantitative investigation of the metal-complexes.

One of the present authors (H.O.) recently developed a simple two-electrode cell using a helix for variable temperature ESR measurements which has several advantages over the commonly used electrolysis cell for ESR in obtaining the spectra of unstable radicals.[4] Using the cell, we have succeeded in obtaining ESR spectra from which the paramagnetic species oxidized electrochemically in the solution of [Co^{II}(tpp)] could be identified as a π-cation radical of six-coordinate [Co^{III}(tpp)]$^{2+}$ having two axial ligands.

It has been reported previously[5] that [Co^{III}(tpp)]$^+$(Cl^-) is a five-coordinate Co(III) complex of tpp which has a square-pyramidal structure with the chlorine atom at the apex. Subsequent ^{1}H FT-NMR[6] and ESR[7] studies have shown that this complex in chlorinated solvents changes partially into paramagnetic species by thermal and light activations. The formation of this species in the solutions occurs reversibly with small enthalpy difference. Such behavior of [Co^{III}(tpp)]$^+$(Cl^-) can be related to the enzymatic reactions of metalloporphyrins and their related compounds. In order to obtain a complete understanding about the behavior of [Co^{III}(tpp)]$^+$(Cl^-), it is necessary first to identify the paramagnetic species generated thermally in the solution of the complex. Secondly it is desirable to determine the molecular and electronic structures of this species.

In this paper we first describe the three kinds of spectra obtained by electrochemical oxidation of [Co^{II}(tpp)] and [Co^{III}(tpp)]$^+$(Cl^-) in chlorinated and non-chlorinated solvents, using various supporting electrolytes, and explain the results by an axial-ligand effect on the π-cation radical of [Co^{III}(tpp)]$^{2+}$. Secondly, the identification of the paramagnetic species formed thermally in the solution of [Co^{III}(tpp)]$^+$(Cl^-) is given. Thirdly, the molecular and electronic structures of the species are discussed based on the ESR parameters obtained experimentally.

Model compounds such as are treated here are sometimes amenable to a more detailed ESR investigation than the bilogical system itself. Therefore the definitive ESR characterization of the compound can provide a framework for understanding the spin states and the electronic structures of active sites of the biological system.

Experimental

[Co^{II}(tpp)], [Co^{III}(tpp)]$^+$(Cl^-), and pyridine-coordinated [Co^{III}(tpp)]$^+$(Cl^-), [Co^{III}(tpp)]$^+$(Cl^-)(py), were prepared using the methods described previously.[5,8] They were identified by elemental analysis and absorption spectra. Commercially available dichloromethane(DCM), 1,1,2,2-tetrachloroethane(TCE), and propionitrile(PCN) of special grade were dried with Woelm 200 neutral alumina. Tetrabutylammonium chloride(TBCl), tetrabutylammonium tetrafluoroborate(TBFB) of special grade for polarography were dried in vacuo before use. Electrochemical oxidation of 10^{-2} mol solution flushed with pure nitrogen gas after degassing by the freeze-thaw-pumping cycle was carried out inside the cavity, using the cell consisting of a helix and a gold wire going through the inside of the helix. The details of the cell construction were given previously.[4] It should be noted here that no reference electrode was used, in order to simplify the electrolysis apparatus. Alternatively, as an indicator of the electrochemical reactions we used the minimum voltage, V_a, applied between two electrodes, at which the ESR spectrum of the radicals generated during the electrolysis appears. The cyclic voltammogram of [Co^{II}(tpp)] was measured using a Hewlett-Packard 3310A function generator in conjunction with a Princeton Applied Research 173 Potentio-Galvanostat equipped with I/V convertor, Model 176. The ESR spectra were taken with a JEOL PE-3X spectrometer equipped with a temperature controller. The g-value of the Cr(III) ion in MgO used as the secondary standard for the determination of g-value was calibrated as 1.9800 ± 0.0001 by that of potassium ni-

trosylbis(sulfate) ($K_2(SO_3)_2NO$, 2.0057).

Results and Discussion

Oxidation of [Co^{II}(tpp)] and [Co^{III}(tpp)]$^+$(Cl$^-$). The cyclic voltammogram of [Co^{II}(tpp)] in benzonitrile with TBFB showed three one-electron reversible oxidation steps corresponding to $E_{1/2}$ *vs.* SCE. Here the

$$[Co^{II}(tpp)] \xrightarrow[(0.52\,V)]{0.45\,V} [Co^{III}(tpp)]^+ \xrightarrow[(1.19\,V)]{1.13\,V} [Co^{III}(tpp)]^{2+} \xrightarrow[(1.42\,V)]{1.41\,V} [Co^{III}(tpp)]^{3+}$$

Scheme 1.

values in parentheses are the data reported by Wolberg and Manassen.[9] The neutral species [Co^{II}(tpp)] (**1**) is paramagnetic, with spin 1/2 compatible with a square-planer $3d^7$ configuration, but can not be detected by ESR measurements in solution, because of its short spin-lattice relaxation time. The first and third oxidation products are expected to be diamagnetic species with the configurations $(3d)^6(a_{2u})^2$ and $(3d)^6(a_{2u})^0$, respectively; indeed, no ESR signal was observed. Therefore, only the second oxidation product, [Co^{III}(tpp)]$^{2+}$, takes part in the ESR spectrum.

[Co^{III}(tpp)]$^+$ (**2**) requires a counter ion with which a five-coordinate complex (**3**) is expected to be formed (see Scheme 2, Eq. 1). Because **3** is diamagnetic, we can not directly observe its formation by the ESR measurements; but we can presume the formation of **3**, because the five-coordinate complex formation after one electron oxidation of **1** was well established by X-ray diffraction of [Co^{III}(tpp)]$^+$(Cl$^-$) single crystal.[5] Further support for Eq. 1 is available in the complexes [M^{II}(tpp)]$^+$(X$^-$) (M=Mg and Zn).[10] Eq. 2 postulates an equilibrium between two five-coordinate complexes formed in the presence of two different anions in solution. If the association power of Y$^-$ is stronger than that of X$^-$, the equilibrium proceeds to the right hand side of Eq. 2. When species **3** is oxidized further at the voltages between

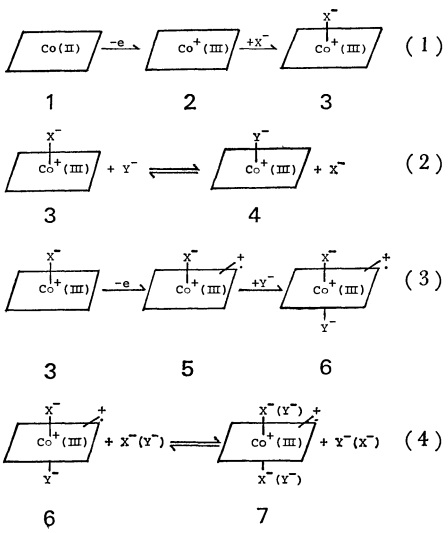

Scheme 2.

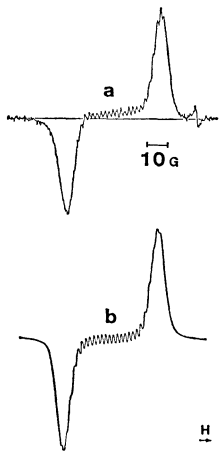

Fig. 1. The ESR spectrum of the paramagnetic species generated by electrochemical oxidation of [Co^{II}(tpp)] in PCN at −70 °C (a). Supporting electrolyte: TBFB. Simulation (b) assumes one cobalt a_{Co}= 6.00 G and four nitrogens a_N=1.85 G.

1.1 and 1.4 V SCE the first ligand oxidation proceeds (Eq. 3). In a manner similar to Eq. 1, the π-cation radical (**5**) produced is followed by the formation of a six-coordinate complex (**6**) with the anion Y$^-$. If X$^-$ (Y$^-$) exists sufficiently in excess, or the association power of X$^-$ (Y$^-$) is sufficiently stronger than that of Y$^-$ (X$^-$), the equilibrium of Eq. 4 proceeds to the right hand side. As the result of two one-electron oxidations of **1** or one-electron oxidations of **3** in various atmospheres, it is presumed that three different paramagnetic species: [Co^{III}(tpp)]$^{2+}$(X$^-$)$_2$, [Co^{III}(tpp)]$^{2+}$(X$^-$)(Y$^-$), and [Co^{III}(tpp)]$^{2+}$(Y$^-$)$_2$ are generated.

[Co^{III}(tpp)]$^{2+}$(X$^-$)$_2$(X=BF$_4$ and ClO$_4$). **1** was dissolved in chlorinated solvent, DCM or TCE, or non-chlorinated solvent, PCN, including a supporting electrolyte with a weak-ligand anion such as ClO_4^- or BF_4^-. After the temperature of the solution of PCN with BF_4^- was decreased to −70 °C, the voltage applied between the two electrodes was increased until the ESR signal could be observed on a recorder with the modulation amplitude of 4 G.** As the voltage reached V_a, corresponding to the second oxidation, an ESR signal (g=2.0034) with partially resolved hyperfine structure (hfs) appeared, as shown in Fig. 1a. V_a depended on the combination of solvent and supporting electrolyte:[4] For example, 2.5 V for PCN with BF_4^- or ClO_4^-, 1.7 V for DCM with BF_4^-, and 1.3 V for TCE with BF_4^-. When the temperature was increased to −50 °C, the spectrum showed appreciable broadning and coincided with that reported in the literature.[9] When DCM and TBPC(TBFB) were used as solvent and supporting electrolyte, respectively, the g-value and the hyperfine coupling constant(hfcc) of ^{59}Co of the spectrum were very similar (see Table 1). As the temperature of the solution was increased above −50 °C, a new signal superposed to the original one appeared. The g-value and the peak-to-peak width ΔH of this signal were

** 1 G=10^{-4} T.

Table 1. ESR parameters of $[Co^{III}(tpp)]^{2+}(X)(Y)$ at −70 °C

Axial ligands X	Axial ligands Y	Solvent	g (±0.0002)	$\Delta H^{a)}$ 10^{-4} T	hfcc/10^{-4} T Co	N	^{35}Cl
BF_4^-	BF_4^-	DCM	2.0024	39.6	5.3	—	—
ClO_4^-	ClO_4^-	DCM	2.0026	37.7	5.0	—	—
BF_4^-	BF_4^-	PCN	2.0034	44.6	6.0	1.85	—
ClO_4^-	ClO_4^-	PCN	2.0034	44.7	6.0	1.85	—
Cl^-	Cl^-	DCM	2.0028	80	10.3	2.8	2.2
		(DCM	2.0029	82)			
Cl^-	Cl^-	PCN	2.0035	85.5	11.0	2.6	2.2
Cl^-	Cl^-	TCE[b)]	2.0047	79.0	10.0	—	—
		(TCE	2.0048	77)			
BF_4^-	Cl^-	DCM	2.0052	49.0	6.6	—	—
py	Cl^-	DCM	2.0056	63.8	8.0		

a) Total peak-to-peak width including hfcc. b) Data at room temperature. The values in parentheses are the data of the paramagnetic species in the solution of $[Co^{III}(tpp)]^+(Cl^-)$.

2.0052 and 49 G, respectively. This paramagnetic species was identified as a mixed-ligand complex attached by one chlorine anion, as will be discussed later.

The small variations of the hfcc of cobalt and g-values in Table 1 can be attributed to the solvent and axial-ligand effect, as was extensively investigated in the ion-pairs of aromatic hydrocarbon anion radicals with counter ions.[11] The spectrum simulation of Fig. 1a was carried out using $a_{Co}=6.0$ G for one cobalt and $a_N=1.85$ G for four nitrogens (Fig. 1b), which led to the best fit to the experimental data. We note here that the Lorentzian line shape with the line-width of 3.5 G is used and the unresolved hfs due to eight equivalent protons of phenyl rings ($a_H=0.3$ G)[11] are included; the contribution of the protons attached to the meso-phenyl rings to the line-width is also taken into account. This procedure was useful in improving the spectrum simulation. The g-value and a_N of this paramagnetic species are very close to those of $[M^{II}(tpp)]^+$ (M=Mg, Zn, and Cd), as was already reviewed by Fajer and Davis.[10] Such a nice coincidence of these values indicates that the paramagnetic species generated by the oxidation of **1** is a π-cation radical similar to $[M^{II}(tpp)]^+$. Further, the value of a_N measured at temperatures below −60 °C guides us to the quantitative discussion of the spin distribution in the highes occupied molecular orbitals (HOMO) of the porphyrins.

$[Co^{III}(tpp)]^{2+}(Y^-)_2(Y=Cl)$. The ESR spectrum of the radical obtained by the electrochemical oxidation of **1** in DCM or PCN at 1.4 V, changing the anion of electrolyte from BF_4^-(ClO_4^-) to an intermediate-ligand, Cl^-, was somewhat different from those mentioned above. The most resolved spectrum measured at −70 °C is shown in Fig. 2 together with simulated ones. The spectra measured at temperatures above −50 °C agreed entirely with that of the paramagnetic species derived thermally from $[Co^{III}(tpp)]^+(Cl^-)$ in DCM.[7] In Fig. 2a, one can recognize hfs in addition to the hfs due to ^{59}Co, which could be resolved at temperatures below −60 °C. The hfcc were determined by comparing the observed spectrum with the simulated ones. Figures 2b and 2c were obtained using $a_{Co}=10.3$ G and $a_N=2.80$ G without and with the hfcc due to two chlorine atoms, respectively. In both cases the contribution of the unresolved proton hfcc ($a_H=0.3$ G) is taken into account. Figure 2c was obtained by the superposition of two simulation spectra, corresponding to the existence of two chlorine isotopes ($a_{^{35}Cl}=2.20$ G and $a_{^{37}Cl}=1.80$ G). Figure 2b is similar to the observed one, but the intensity sequences of the absorption lines and the tails of both wings of the spectrum do not coincide with the observed spectrum. The simulated spectrum, Fig. 2c, which includes the splittings due to two chlorine nuclei, coincided excellently with the observed one. The values of hfcc used for the simulations are listed in Table 1, with the measured

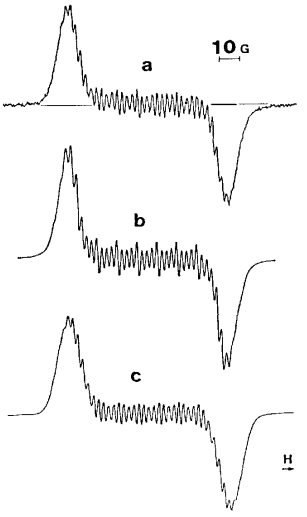

Fig. 2. The ESR spectrum of the paramagnetic species generated by electrochemical oxidation of $[Co^{II}(tpp)]$ in DCM at −70 °C (a). Supporting electrolyte: TBCl. Simulation (b) assumes one cobalt $a_{Co}=10.3$ G and four nitrogens $a_N=2.80$ G. Simulation (c) assumes one cobalt $a_{Co}=10.3$ G, four nitrogens $a_N=2.80$ G, and two chlorines $a_{^{35}Cl}=2.20$ G ($a_{^{37}Cl}=1.80$ G). Contribution of the isotope to the spectrum is included.

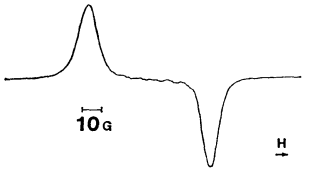

Fig. 3. The ESR spectrum of the paramagnetic species generated by electrochemical oxidation of $[Co^{III}(tpp)]^{2+}(Cl^-)(py)$ in DCM at −90 °C. Supporting electrolyte: TBCl.

g-values. The detection of the hfs due to two equivalent chlorines in addition to those due to ^{59}Co and ^{14}N reflects unequivocally the fact that two axial positions of **3** are occupied by chlorine anions. Thus the radical generated by the oxidation of **1** in DCM and PCN with Cl^- is identified as a π-cation radical of six-coordinate $[Co^{III}\ tpp)]^{2+}$, having two chlorine anions as axial ligands.

It was established in the metal complexes of meso-tetraphenylporphyrins[10] that meso-positions carry large spin density, whereas the nitrogen splittings (a_N= 1.2—1.9 G) show about 20% of the total spin with only limited variations in a_N. The nitrogen hfcc in $[Co^{III}(tpp)]^{2+}(Cl^-)_2$ is a little large compared with those of $[Co^{III}(tpp)]^{2+}(X^-)_2$(X=$BF_4$ and ClO_4) and of $[M^{II}(tpp)]^{+}$(M=Mg, Zn, and Cd), but it is reasonable to conclude that the unpaired electron is mostly localized in a_{2u} orbital of the porphyrin ligand. The metal hfcc of 10.3 G reflects only a small unpaired electron density, of the order of 0.01.[10] The large *g*-value and ^{59}Co hfcc of $[Co^{III}(tpp)]^{2+}(Cl^-)_2$, compared with those of $[Co^{III}(tpp)]^{2+}(X^-)_2$(X=$BF_4$ and ClO_4), may indicate that the chlorine ligation enhances the localization of spin density at nitrogens, which leads to the large spin polarization at the cobalt nuclei.

$[Co^{III}(tpp)]^{2+}(Cl^-)(Z)$ (Z=py and BF^-_4). The possible alternative species generated by the oxidation of **1** is the one in which different ligands are present in the two axial positions. Such a configuration of the ligands could first be visualized by the oxidation of pyridine-coordinated $[Co^{III}(tpp)]^{+}(Cl^-)$, in which one of the two ligand positions is strongly masked by a pyridine molecule. Figure 3 shows the spectrum of the paramagnetic species obtained by the oxidation of $[Co^{III}(tpp)]^{+}(Cl^-)(py)$ in DCM with Cl^- (V_a=2.0 V). The hfs due to ^{59}Co could only be resolved at temperatures below −50 °C (a_{Co}=8.0 G). The *g*-value, 2.0056, was appreciably larger than those described above.

The oxidation of $[Co^{III}(tpp)]^{+}(Cl^-)$ in DCM with BF_4^-, on the other hand, showed the spectrum due to the new radical species with *g*-value of 2.0052 and peak-to-peak width of 49 G, which was superimposed on that of $[Co^{III}(tpp)]^{2+}(Cl^-)_2$. It was found from the temperature variation of the spectrum that these two species are in equilibrium. Therefore, one can conclude that the new signal corresponds to the $[Co^{III}(tpp)]^{2+}(Cl^-)(BF_4^-)$, which shows larger *g*-value and smaller ^{59}Co hfcc, compared with those of $[Co^{III}(tpp)]^{2+}(Cl^-)_2$. We note here that this signal could also be observed when $[Co^{II}(tpp)]$ in DCM with BF_4^-, the condition without chlorine anion, was oxidized at temperatures above −50 °C. This means that the radical substracts the chlorine anion from the solvent used.

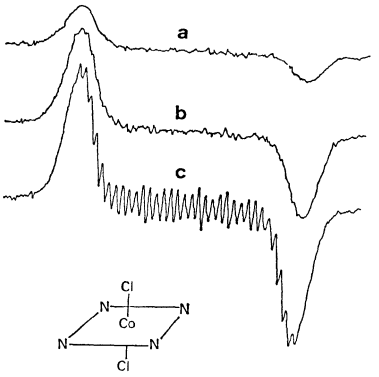

Fig. 4. Temperature dependence of the ESR spectrum of $[Co^{III}(tpp)]^{2+}(Cl^-)_2$ in DCM generated by electrochemical oxidation at −20, −35, and −70 °C (a, b, and c, respectively).

Consequently, $[Co^{III}(tpp)]^{2+}(X^-)_2$ (X=BF_4 and ClO_4) showed a nearly free *g*-value and small ^{59}Co hfcc of 5.0 to 6.0 G. The *g*-value of $[Co^{III}(tpp)]^{2+}(Cl^-)_2$ is also very close to the free *g*-values, but the hfcc of ^{59}Co is about twice as large as those of the former. The mixed-ligand complex can be characterized by a large *g*-value compared with those described above, although the value of the hfcc of ^{59}Co is in the middle.

π-Cation Radical of $[Co^{III}(tpp)]^{2+}$ Formed Thermally in the Solution of $[Co^{III}(tpp)]^{+}(Cl^-)$. The solution of $[Co^{III}(tpp)]^{+}(Cl^-)$ in chloroform, DCM, and TCE (10^{-3} mol dm^{-1}) showed an ESR spectrum at room temperature even in the presence of air.[7] The spectrum showed reversible temperature dependence, the enthalpy difference being about 4 kJ mol^{-1}. By comparing the spectrum in DCM with that of $[Co^{III}(tpp)]^{2+}(Cl^-)_2$ in DCM oxidized electrochemically at temperatures above −50 °C, as shown in Fig. 4, we could unequivocally identify the species as $[Co^{III}(tpp)]^{2+}(Cl^-)_2$. On the other hand, $[Co^{III}(tpp)]^{+}(Cl^-)$ in TCE exhibited the temperature dependent ESR spectra, which were nicely reproduced by the electrochemical oxidation of $[Co^{III}(tpp)]^{+}(Cl^-)$ in TCE with Cl^-. Comparison of the ESR parameters of this spectra with those listed in Table 1 leads to an equilibrium between two species

$$[Co^{III}(tpp)]^{2+}(Cl^-)_2 + S \rightleftharpoons [Co^{III}(tpp)]^{2+}(Cl^-)(S) + Cl^-. \quad (5)$$

S: Solvent molecule

The details of the experiments described here will be given separately.

The Electronic Configuration of $[Co^{III}(tpp)]^{2+}$. As was already pointed out, the observation of the hfs due to ^{35}Cl in addition to those due to ^{59}Co and ^{14}N led to the definite electronic structure and wave function of the radical. It was well established that the neutral species $[Co^{II}(tpp)]$ is paramagnetic with an effective electron spin 1/2 with a square-planer $3d^7$ configuration: $(3d_z)^4(3d_{xy})^2(3d_{z^2})^1$. The two-electron oxida-

tion product, on the other hand, showed definite free radical parameters which can be interpreted by a formal electronic configuration $(3d_\pi)^4(3d_{xy})^2(a_{2u})^1$: a_{2u} π-orbital has a spin distribution characterized by the appreciable localization (76%) at meso-carbon atoms, followed by 20% spin density at four nitrogen atoms. This spin distribution was experimentally confirmed by the observation of four nitrogen hfcc of 1.85 to 2.8 G in our case. The nearly free g-value of the radical tells us that 3d orbitals do not contribute to the HOMO of the radical. The almost isotropic hfcc due to ^{59}Co indicates that the configuration of the central metal-ion is mainly $(3d_\pi)^4(3d_{xy})^2$ and the contribution to the hfcc is almost due to the Fermi contact term polarized by the spin on the neighboring π-orbital of the ligand.

One can consider the following mechanism to interpret ^{59}Co hfcc: 1) The spin polarization of σ-electron in the Co–N bonds by the σ-electron spin density on the nitrogen nuclei produces a spin density at the cobalt nucleus: This is essentially an extension of McConnell relation[12] developed originally to interpret the proton hfcc in the fregment of C–H. It should be noted that in this case the spin density at the Co nucleus is of opposite sign to that of the spin density at the π-orbital of the N atoms. 2) The direct overlap of the Co atomic orbital with the π-orbital of the ligand induces a net plus spin density at the Co nucleus. The π-orbital of tpp on which the unpaired electron resides has a nodal plane which coincides with the tpp molecular plane. Therefore, it is necessary to deviate from this plane for the Co atom to have the direct overlap. Then one can describe the a_{Co} as

$$a_{Co} = Q^{Co}_{N-Co} \times \rho^{\pi}_{N} + \alpha, \quad (6)$$

where Q^{Co}_{N-Co} is a proportionality constant and α means a contribution from the direct overlap.

Figure 5 shows a correlation between a_{Co} and a_N listed in Table 1, in addition to those of other Co(III) porphyrins reported previously.[9,13,14] We assume here that the sign of a_{Co} of Co(III) meso-substituted porphyrin cation radicals is negative. The data points are not so many, but one can conclude that the a_{Co} is roughly expressed by a linear function of a_N, which results in a linear relationship between a_{Co} and ρ^{π}_{N}, because a_N is usually expressed as $a_N = Q^{\pi}_{N} \times \rho^{\pi}_{N} - \sum_i Q_{NC} \times \rho_{C_i}$ and $\rho_{C_i} \cong 0$ for the a_{2u} orbital of tpp. It is now difficult to explain quantitatively the variation of the a_{Co} depending on the axial ligands and solvent used, but we can regard its variety as the result of the spin-polarization mechanism in the clouds of the a_{2u} π-orbital of tpp, which changes according to the axial ligands and the solvent molecules.

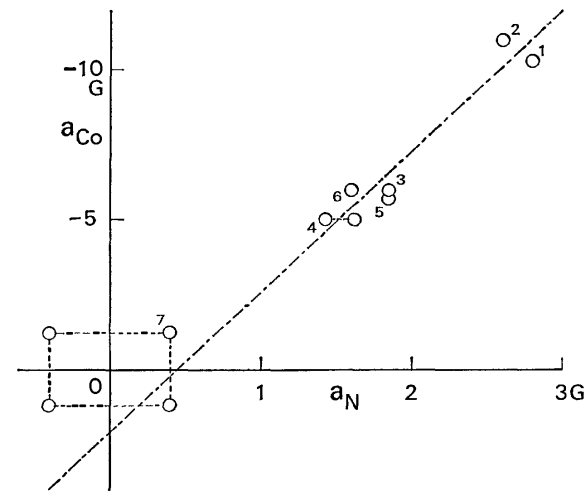

Fig. 5. A correlation between a_{Co} and a_N of some six-coordinate Co(III) porphyrin cation radicals; 1: $[Co^{III}(tpp)]^{2+}(Cl^-)_2$ (in DCM), 2: $[Co^{III}(tpp)]^{2+}(Cl^-)_2$ (in PCN), 3: $[Co^{III}(tpp)]^{2+}(BF_4^-)_2$ (in PCN), 4: $[Co^{III}(tpp)]^{2+}(ClO_4^-)_2$ (in DCM), 5: $[Co^{III}(tpp)]^{2+}(ClO_4^-)_2$ (in butyronitrile (BCN)) 6: $[Co^{III}((pr)_4p)]^{2+}(ClO_4^-)_2$ (in BCN), and 7: $[Co^{III}(oep)]^{2+}(ClO_4^-)_2$. For numbers 4, 5, 6, and 7, a_N of corresponding cation radicals of the Zn(II) complexes were used. Four points for number 7 correspond to the possibilities by the combination of the signs of a_{Co} and a_N.

References

1) See, for example, P. L. Dutton and D. G. Wilson, *Biochim. Biophys. Acta*, **346**, 165 (1974); D. G. Davis, "Electrochemistry of Porphyrins," in "The Porphyrins," ed by D. Dolphin, Academic Press, Inc., New York and London (1978), Vol. 5, p. 127.

2) A. J. Hoff, *Phys. Reports*, **54**, 76 (1979).

3) P. F. Knowles, D. Marsh, and H. W. Rattle, "Magnetic Resonance of Biomolecules," John Wiley & Sons Ltd., London (1976), p. 168.

4) H. Ohya-Nishiguchi, *Bull. Chem. Soc. Jpn.*, **52**, 2064 (1979).

5) T. Sakurai, K. Yamamoto, H. Naito, and N. Nakamoto, *Bull. Chem. Soc. Jpn.*, **49**, 3042 (1976).

6) K. Yamamoto, J. Uzawa, and T. Chijimatsu, *Chem. Lett.*, **1979**, 89.

7) K. Yamamoto, M. Khono, and H. Ohya-Nishiguchi, *Chem. Lett.*, **1981**, 255.

8) K. Yamamoto and S. Tonomura, *Sci. Papers Inst. Phys. Chem. Res.*, **58**, 122 (1964).

9) A. Wolberg and J. Manassen, *J. Am. Chem. Soc.*, **92**, 2982 (1970).

10) J. Fajer and M. S. Davis, "Electron Spin Resonance of Porphyrin π Cations and Anions," in "The Porphyrins," ed by D. Dorphin, Academic Press, Inc., New York and London (1979), Vol. 4, p. 197.

11) N. Hirota, "Magnetic Resonance," ed by C. A. McDowell, Butterworths, London and Boston, (1975), Phys. Chem. Series Two, Vol. 4, p. 85.

12) H. M. McConnell, *J. Chem. Phys.*, **24**, 764 (1956).

13) D. Dorphin, A Forman, D. C. Borg, J. Fajer, and R. H. Felton, *Proc. Natl. Acad. Sci. U.S.A.*, **68**, 614 (1971).

14) J. Fajer, D. C. Borg, A. Forman, A. D. Adler, and V. Varedi, *J. Am. Chem. Soc.*, **96**, 1238 (1974).

  Bull. Chem. Soc. Jpn., 54, 1928—1932 (1981)

Collision Induced Perturbations on the Long-lived Fluorescence of Pyrazine in S_1

Hisao IGARASHI and Koji KAYA*,†

Department of Chemistry, Faculty of Science, Tohoku University, Aza-Aoba, Aramaki, Sendai 980

(Received December 5, 1980)

Collision induced intersystem crossing (slow fluorescence quenching and phosphorescence induction) from selected vibronic levels of pyrazine in $S_1(n\pi^*, B_{3u})$ was investigated. It was found that slow fluorescence quenching rate at the zero point level exceeds the hard sphere collision rate several times and rapidly approaches it as the excitation energy is increased. On the other hand, phosphorescence induction rate was found to be nearly equal to the collision rate and to have little excitation energy dependence. These differences were discussed on the basis of the collision induced relaxation mechanisms.

In the past decade, the photophysical properties of the electronic excited states of polyatomic molecules in an isolated molecular condition have been studied extensively both from experimental and theoretical points of view and the concept of the intramolecular radiationless transition has been established. On the basis of the understanding of the unimolecular processes, the subsequent problem to be studied seems to be the collision induced intramolecular relaxations which are essentially important in understanding the photochemical reactions. Despite the importance of the collision induced processes, the theoretical interpretation does not seem to be successful yet. This comes from, (1) the lack of the accumulation of the experimental results which are worthwhile to be analyzed theoretically and, (2) the difficulty in dealing with the intermolecular interaction as the perturbation due to the collision.

Spectroscopic and dynamical properties of S_1 ($n\pi^*$, $^1B_{3u}$) pyrazine have been investigated thoroughly by many workers.[1-20] Individual vibronic levels of S_1 up to 1000 cm^{-1} from the 0-0 band have been assigned by the absorption,[1-7] SVL fluorescence[13,14] and pre-resonance Raman scattering works.[8-12] Under the collision free condition, the fluorescence of pyrazine from the S_1 state exhibits bi-exponential decay that is typical of the intermediate strong coupling molecule as reported by Lahmani *et al.*[16] In pyrazine, the short-lived component of the fluorescence has the lifetime shorter than 10^{-9} s and the long-lived one is of the order of 10^{-7} s.

When one looks at the effect of collision on the prompt fluorescence, one is able to study the vibrational relaxation within S_1 manifolds. The vibrational mode dependence of V-V transfer rate has been investigated by us on the selected vibronic levels of S_1 pyrazine.[21]

The long-lived fluorescence derives from the interaction of S_1 with the isoenergetic triplet ro-vibronic levels. The effect of the collision appears on the two optical phenomena, *i.e.*, (1) the quenching of the slow fluorescence and (2) the induction of the phosphorescence from T_1. In the present work, we have investigated the excitation energy dependences of the quenching rate of the slow fluorescence and the induction rate of the phosphorescence under the SVL excitation condition. The amount of the energy loss within the triplet manifolds by a collision has been also obtained under the assumption of the step-ladder relaxation model.

Experimental

As an exciting light source, the second harmonics of a tunable dye laser (Rh-640) pumped by a Molectron nitrogen laser (UV-22) was used. Either RDP or ADA was used as an SHG crystal. The emission intensity was measured by an HTV-R-562 photomultiplier averaged by a boxcar integrator (Brookdeal 9415 and 9425). In order to distinguish fluorescence from phosphorescence, a Nikon P-250 monochromator of 6 nm slit width with a fixed wavelength (345 nm for fluorescence or 390 nm for phosphorescence) was placed in front of the photomultiplier. Moreover, a delay time of the boxcar integrator was adjusted to get the best separation between them. As a collision partner, isopentane whose pressure extends from 0 to 20 Torr (1 Torr= 133.322 Pa.) was added to 2×10^{-2} Torr pyrazine. The gas pressure was measured by a Baratron 222A capacitance manometer. Pyrazine was purified by vacuum sublimations and spectral grade isopentane was used without further purification. The samples were degassed by the freeze-thaw cycles prior to the experiments.

By varying the excitation wavelength up to 1000 cm^{-1} above the 0-0 of S_1-S_0 absorption and the pressure of isopentane, wavelength and pressure dependences of the fluorescence and the phosphorescence were measured by the following procedures. As mentioned above, the fluorescence contains the prompt and slow components. The former component is affected only by adding high pressure gas exceeding 100 Torr. Still the latter one is sensitive to the trivial amount of a foreign gas and is quenched completely in the presence of 20 Torr isopentane. Then, the intensity of the long-lived fluorescence $I_{sf}(P)$ at the pressure P($P<20$ Torr) is given by

$$I_{sf}(P) = I_{345}(P) - I_{345}(P=20\ \text{Torr}).$$

Where $I_{345}(P)$ is the fluorescence intensity observed at 345 nm with the spectral slit width of 6 nm. The phosphorescence of pyrazine at the pressure P as denoted $I_{ph}(P)$ is dispersed around 390 nm and is overlapped with the fluorescence. By noting the fact that the phosphorescence is induced by collisions, the phosphorescence component is extracted from the total emission observed at 390 nm by the following correction.

$$I_{ph}(P) = I_{390}(P) - I_{345}(P) \times \frac{I_{390}(P=0)}{I_{345}(P=0)}$$

$I_{390}(P)$ is the total (phosphorescence and fluorescence) emis-

† Present address: Department of Chemistry, Faculty of Science and Technology, Keio University, Hiyoshi, Kohoku-ku, Yokohama 223.

sion intensity at 390 nm and $I_{345}(P)$ is the fluorescence intensity observed at 345 nm at the pressure P. The emission intensity at 390 nm extrapolated at zero pressure $I_{390}(P=0)$ contains only the fluorescence. Thus, the second term of the above equation gives the fluorescence component at 390 nm at the pressure P.

Results and Discussion

The observed fluorescence and phosphorescence intensities against the excitation wavelength and the foreign gas pressure inform us of three physical quantities of the collision induced relaxation. They are, the slow fluorescence quenching rate, the phosphorescence induction rate or the vibrational relaxation rate within the triplet levels and the energy removed per an effective collision. First, the kinetic scheme is given to describe the collision induced relaxation processes from S_1 pyrazine. Then, the experimental results will be discussed on the basis of the kinetic scheme.

The Kinetic Scheme. Temporal behavior of the excited state of an intermediate size molecule like pyrazine has been described quantum mechanically by Lahmani *et al.*[16] van der Werf *et al.*[23] have adopted a kinetic scheme to explain the electronic relaxation of biacetyl. In the present wotk, the kinetic description was used for the evaluation of the above mentioned physical quantities from the experimental data.

Bi-exponential dacay of an excited intermediate size molecule with strong S-T coupling is described by

$$1/\tau_{f1} \simeq \Delta_{ST}, \tag{1}$$

$$1/\tau_{f2} = \bar{\gamma}_n \simeq \bar{\gamma}_S/N + \gamma_T. \tag{2}$$

τ_{f1} and τ_{f2} are the lifetimes of the fast and slow fluorescence, respectively. Δ_{ST} stands for the coupling strength between a vibronic level of the singlet state and N triplet levels. Total decay widths of a S state and a T state are defined as γ and γ which are given as superpositions of individual decay channels by

$$\gamma_S = \Gamma_S + \Delta_{ST} + \gamma_{SS_0}, \tag{3}$$

$$\gamma_T = \Gamma_T + \gamma_{TS_0}. \tag{4}$$

Here Γ_S and Γ_T are the radiative widths of the S and T states, respectively. γ_{SS_0} and γ_{TS_0} indicate the nonradiative decay widths between S and S_0 and between T and S_0, respectively. γ_n represents the total decay width of $(N+1)$ quasistationary states which are formed by the interaction between a S state and N triplet states ($N \approx 10^3$). $\bar{X}$ implies the mean value of the physical quantity X. Because Δ_{ST} is much larger than γ_n, the influence of the collision appears mainly on the $\bar{\gamma}_n$ or γ_T values at relatively low pressure (<20 Torr). That is to say, the collisional perturbation affects only the long-lived fluorescence with a negligible influence on the prompt component as described by

$$\gamma_T(P) = \gamma_T(P=0) + k_q P, \tag{5}$$

where k_q is the quenching rate constant of the slow fluorescence and is obtained by the following Stern-Volmer relation.

$$I_{sf}(P=0)/I_{sf}(P) = 1 + A_f P \tag{6}$$

$$A_f = k_q \tau_{f2} \tag{7}$$

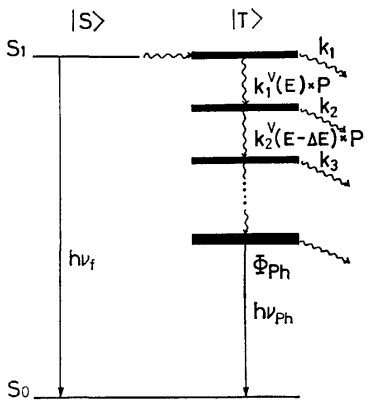

Fig. 1. Step-ladder scheme of vibrational relaxation within triplet manifolds. Symbols are defined in the text.

Here $I_{sf}(P)$ represents the intensity of the slow fluorescence at the pressure P.

It is already known that the phosphorescence of pyrazine is the induced one by collisions after the excitation of a S_1 vibronic level. The pressure dependence of the collision induced phosphorescence intensity informs us of the vibrational relaxation rate within the triplet manifolds and the amount of the removed energy per an effective collision by assuming the step-ladder relaxation model as illustrated in Fig. 1. In the figure, k_i represents the unimolecular decay constant from the triplet manifolds and k_i^v is the collision induced vibrational relaxation rate. ΔE stands for the removed energy by an effective collision. Then, the intensity of the collsion induced phosphorescence at the pressure P is given by

$$I_{ph}(P) = \Phi_{ph} \prod_{i=1}^{n} k_i^v P/(k_i + k_i^v P). \tag{8}$$

Here n is the number of the effective collisions to induce the phosphorescence. Φ_{ph} indicates the quantum yield of the phosphorescence. The reciprocal of the $I_{ph}(P)$ in Eq. 8 can be expanded in the form of the power series of P^{-1} up to the n-th order. k_i values

$$I_{ph}^{-1}(P) = C(1 + \alpha P^{-1} + \beta P^{-2} + \cdots) \tag{9}$$

$$\alpha = \sum_{i=1}^{n} k_i/k_i^v \tag{10}$$

$$\beta = \sum_{i<j} k_i k_j/k_i^v k_j^v \tag{11}$$

can be obtained experimentally only at the initial (i=1) and the final (i=n) level of the step-ladder relaxation from the known slow fluorescence and phosphorescence lifetimes, respectively. k_i for the intermediate step was estimated from the semilogarithmic plot of k_i against the excess energy from T_1. As will be discussed in the later section, the removed energy by a collision was found to be around 1200 cm^{-1}, k_i decreases rapidly as the vibrational relaxation proceeds to the lower step. On the other hand, k_i^v can be assumed to have no appreciable energy dependence as has been found in S_1 pyrazine.[21] Thus, the relation $k_i/k_i^v \gg k_{i+1}/k_{i+1}^v$ may hold for each step. Under these assumptions, Eqs. 10 and 11 can be approximated as

TABLE 1. THE RATE CONSTANTS OF SLOW FLUORESCENCE QUENCHING AND PHOSPHORESCENCE INDUCTION

Level	E / cm^{-1}	A_f a)	A_f b)	K_q / $10^7\ s^{-1}\ Torr^{-1}$	A_{ph} a)	A_{ph} b)	k_1^v / $10^7\ s^{-1}\ Torr^{-1}$
0	30876	18	10.5	6.2	3.3	0.95	1.14
10_a^1	31259	9	8.5	4.2	2.0	0.55	0.94
6_a^1	31459	7.5	3.5	3.5	1.7	0.5	0.79
10_a^2	31709	6.6	—	3.2	1.5	—	0.72
$6_a^1 10_a^1$	31821	3.4	2.6	1.8	1.4	0.4	0.72
6_a^2	32043	2.7	2.2	1.3	1.3	0.3	0.63

a) Our result using isopentane as a collision partner. b) Result using SF_6 as a collision partner by Lahmani *et al.* in Ref. 16.

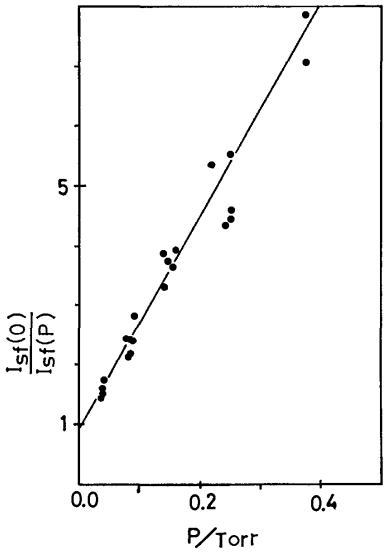

Fig. 2. Stern-Volmer plot of slow fluorescence intensity from the zero point level of S_1. P indicates isopentane pressure. The slope gives the A_f value in Eq. 7.

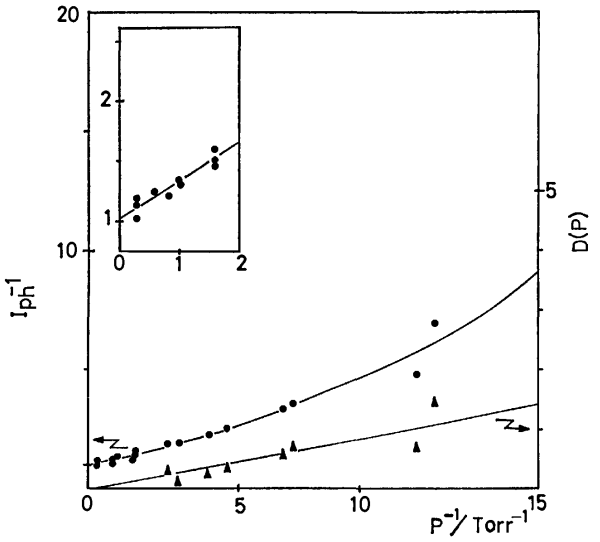

Fig. 3. Phosphorescence induction after the excitation in the zero point level of S_1. I_{ph}^{-1} is plotted against P^{-1} (—●—). The region of 0—2 $Torr^{-1}$ is expanded and its slope gives α value in Eq. 12. The deviation from the linearity is also plotted (—▲—) in the from of the function $D(P)=\{I_{ph}^{-1}-(1+\alpha P^{-1})\}^{1/2}$ and its slope ($\sqrt{\beta}$) gives β value in Eq. 13.

$$\alpha(E) = k_1(E)/k_1^v(E), \tag{12}$$

$$\beta(E) = k_1(E)k_2(E-\Delta E)/k_1^v(E)k_2^v(E-\Delta E) = \alpha(E)\alpha(E-\Delta E). \tag{13}$$

First, the reciprocal of the phosphorescence intensity is plotted against the inverse of the pressure. The linear slope and the deviation from the linearity give the values α and β. Because $1/k_1$ is the experimentally observed lifetime of the long-lived fluorescence from a selected vibronic level of S_1, the vibrational relaxation rate k_1^v can be evaluated from the α and the k_1 values. In the next step, α and β/α values are plotted against the excitation energy. The energy separation that gives the identical values of α and β/α corresponds to the removed energy ΔE per an effective collision.

The Slow Fluorescence Quenching Rate. By use of the Eqs. 6 and 7, the slow fluorescence quenching rates for the individual vibronic levels of S_1 pyrazine were evaluated on the basis of the observed slow fluorescence intensities $I_{sf}(0)$ and $I_{sf}(P)$. The result is illustrated in Fig. 2 taking the 0-0 band excitation as an example. k_q and A_f values for the individual levels are tabulated in Table 1. One notices easily that k_q values in the excitation around the 0-0 band exceed several times the hard sphere collision value ($\approx 10^7\ s^{-1}\ Torr^{-1}$). Moreover, the value decreases rapidly to reach the hard sphere collision one as the excitation energy is increased.

The Vibrational Relaxation Rate within the Triplet Levels. As the intensity of the slow fluorescence is decreased by collisions, the phosphorescence from T_1 is induced *via* the collision induced vibrational relaxation from the higher triplet levels. Thus, one can evaluate the vibrational relaxation rate from the pressure dependence of the phosphorescence induction. In Fig. 3, the reciprocal intensity of the phosphorescence is plotted against the inverse pressure taking the 0-0 band excitation as an example. The α value that contains the information of two body collision gives us the vibrational relaxation rate within the triplet manifolds. k_1^v values obtained from the α values for the individual vibronic levels of S_1 are of the order of the hard sphere collision rate as seen in Table 1. They do not exhibit appreciable variation as the excitation energy is increased, which is in contrast to k_q.

Discussion on the Slow Fluorescence Quenching and the Phosphorescence Induction Mechanisms. As seen in the

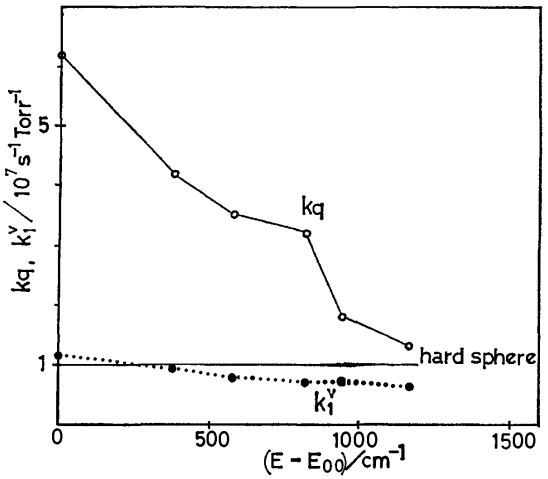

Fig. 4. Excitation energy dependence of the collision induced relaxation rate constant. Slow fluorescence quenching rate k_q(—○—) and phosphorescence induction rate k_1^v(···●···) are shown. The calculated hard sphere collision rate (——) is shown for comparison. The ordinate is the rate constant in 10^7 s^{-1} Torr^{-1} scale and the abscissa is the vibrational energy above the zero point level of S_1 in cm^{-1} unit.

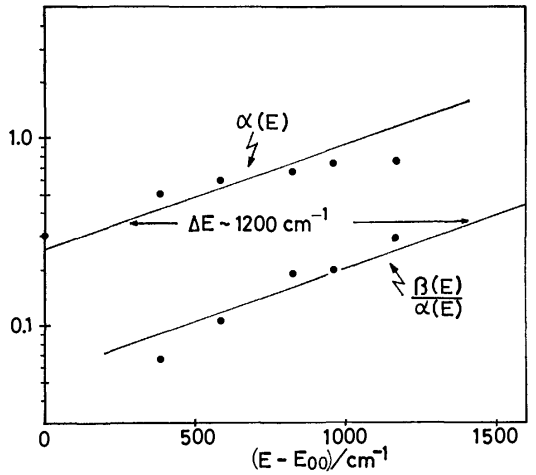

Fig. 5. Vibrational energy removed by an effective collision.

previous sections, the evaluated k_1^v's and k_q's differ greatly each other in their magnitudes and excitation energy dependences. This indicates that the quenching of the long-lived fluorescence and the induction of the thermally equilibrated T_1 phosphorescence are caused by different collision processes. As discussed already in the previous section, the slow fluorescence is quenched by the relaxation of the excited molecule from the interaction region of the width Δ_{ST} to the non-interacting one where there is no strong activity of emitting the radiation. Because Δ_{ST} is of the order of 10^{-2} cm^{-1},[16,17] even a single rotational relaxation is enough to cause the slow fluorescence quenching. This may explain the observed large value of k_q in contrast to k_1^v. It is also suggested that the optical experiment by the use of an ordinary optical cell at low pressure ($\approx 10^{-3}$ Torr) does not satisfy the isolated molecule condition and that the condition will be met only by a molecular beam. The results of the lifetime measurement of the slow fluorescence of pyrazine under the supersonic expanded beam condition will be published soon.[22]

In going from the lower to the higher energy side, k_q tends to the hard sphere collision value as seen in Fig. 4. Van der Werf *et al.* have found the similar behavior of k_q values in biacetyl and explained it in terms of the overlap of the emitting regions in the higher vibronic levles. However, in pyrazine the overlap cannot be expected in the region up to 1000 cm^{-1} above the 0-0 level of S_1 because each vibronic state in that region is well defined as viewed from the absorption and SVL fluorescence studies. Recently, rotational level dependence of the slow fluorescence has been reported by Baba *et al.*[18] Strong j dependence of the slow fluorescence intensity and decaying rate has been found in the supersonic beam which will be published elsewhere.[22] The excitation energy dependence of k_q values is now under investigation from that point of view.

The vibrational relaxation rate k_1^v within the triplet mainfolds of pyrazine has the value around the hard sphere collision one as seen in Fig. 4 and Table 1. They are as comparably large as the vibrational relaxation rate within S_1, which is seen in Table 1 of our previous paper.[21] In the figure and table, gradual decrease of k_1^v is seen as the excitation energy is increased, which is in conflict to the expectation that k_1^v may increase in the higher energy side due to the increase in the vibrational state density and the anharmonicity. It should be noted that k_1^v stands for the overall rate of the vibrational relaxation from the level i and contains the relaxation rates of various removed energy even though the effective energy loss ΔE has been evaluated to be 1200 cm^{-1}. The relaxation among the triplet levels both of which are located above the 0-0 of S_1 commences to occur increasingly as the excitation wavelength is increased from the 0-0 to the higher vibronic level of S_1. In that energy region, the non-radiative decay rate estimated from the slow fluorescence lifetime does not exhibit appreciable energy dependence. Thus it is suggested that the $k_1/k_1^v(i \geqq 2)$ terms make non-negligble contributions to α in addition to k_1/k_1^v in Eq. 12. This results into the apparent decrease of k_1^v in the higher vibronic level excitation.

The Removed Energy by an Effective Collision. In Fig. 5, α and β/α values are plotted against the excitation energy. From that figure, the amount of the energy loss per an effective collision was evaluated to be $\approx$1200 cm^{-1}. The value is qualitatively in agreement with those of biacetyl in the triplet levels[23] and *p*-difluorobenzene in S_1.[24] This gives us the qualitative picture of the relaxation that the excited pyrazine molecule undergoes 3 or 4 effective collisions before it reaches the phosphorescence emitting level of T_1. To confirm the picture, it seems necessary to find a hot phosphorescence from the higher vibronic level of T_1 pyrazine.

Comparison of the Present Results with Those by Lahmani et al. In the work by Lahmani *et al.*,[15,16] A_f and A_{ph} ($=1/\alpha$) values have been evaluated by using

SF_6 as the collision partner. As to the former value, the present result is in good agreement with their result. However, with regard to the A_{ph}, our value exceeds several times that by Lahmani *et al.* This comes from the fact that the collision partner in the present work is isopentane instead of SF_6. In other words the rotational relaxation (or the relaxation of the small energy loss) is insensitive to the shape of the collision partner because the long range interaction governs the relaxation, which is reflected in the large value of k_q. Still, because the vibrational relaxation rate is of the order of the hard sphere collision, the intermolecular coupling that induces the relaxation of the large energy loss of 1200 cm^{-1} is restricted to the shorter range one which is sensitive to the difference in the molecular shape.

Prof. Ito and Dr. Mikami are acknowledged for their stimulating discussion and suggestions.

References

1) M. Ito, R. Shimada, T. Kuraishi, and W. Mizushima, *J. Chem. Phys.*, **26**, 1508 (1957).
2) K. K. Innes, J. A. Merritt, W. C. Tincher, and S. G. Tilford, *Nature*, **187**, 500 (1960).
3) K. K. Innes, J. Simmons, and S. G. Tilford, *J. Mol. Spectrosc.*, **11**, 257 (1963).
4) K. K. Innes, J. P. Byrne, and I. G. Ross, *J. Mol. Spectrosc.*, **22**, 125 (1967).
5) I. Suzuka, N. Mikami, and M. Ito, *J. Mol. Spectrosc.*, **52**, 21 (1974).
6) E. F. Zalewski, D. S. McClure, and D. L. Narva, *J. Chem. Phys.*, **61**, 2964 (1974).
7) D. L. Narva and D. S. McClure, *Chem. Phys.*, **11**, 151 (1975).
8) M. Ito, I. Suzuka, Y. Udagawa, N. Mikami, and K. Kaya, *Chem. Phys. Lett.*, **16**, 211 (1972).
9) I. Suzuka, N. Mikami, Y. Udagawa, K. Kaya, and M. Ito, *J. Chem. Phys.*, **57**, 4500 (1972).
10) M. Ito and I. Suzuka, *Chem. Phys. Lett.*, **31**, 467 (1975).
11) A. H. Kalanter, E. S. Franzona, and K. K. Innes, *Chem. Phys. Lett.*, **17**, 335 (1972).
12) H. K. Hong and C. W. Jacobson, *J. Chem. Phys.*, **68**, 1170 (1978).
13) Y. Udagawa, M. Ito, and I. Suzuka, *Chem. Phys. Lett.*, **60**, 25 (1978).
14) Y. Udagawa, M. Ito, and I. Suzuka, *Chem. Phys.*, **46**, 237 (1980).
15) A. Frad, F. Lahmani, A. Tramer, and C. Tric, *Chem. Phys. Lett.*, **14**, 337 (1972).
16) A. Frad, F. Lahmani, A. Tramer, and C. Tric, *J. Chem. Phys.*, **60**, 4419 (1974).
17) R. Lopez-Delgado, A. Tramer, and I. H. Munro, *Chem. Phys.*, **5**, 72 (1974).
18) H. Baba, M. Fujita, and K. Uchida, *Chem. Phys. Lett.*, **73**, 425 (1980).
19) A. E. W. Knight and C. S. Parmenter, *Chem. Phys.*, **15**, 85 (1976).
20) K. Aizawa, H. Igarashi, and K. Kaya, *Chem. Phys.*, **23**, 273 (1977).
21) H. Igarashi and K. Kaya, *Chem. Lett.*, **1980**, 543.
22) H. Igarashi, N. Mikami, K. Kaya, and M. Ito, unpublished.
23) R. van der Werf and J. Kommandeur, *Chem. Phys.*, **16**, 125 (1976).
24) R. P. Steer, M. D. Swords, and D. Phillips, *Chem. Phys.*, **34**, 95 (1978).

  Bull. Chem. Soc. Jpn., 54, 1933—1938 (1981)

Chloride-35 NMR Studies of the Ion Pairing of the Chloride Ion in Water and Aqueous Acetone

Masako YUDASAKA,† Tadashi SUGAWARA, Hiizu IWAMURA, and Tsunetake FUJIYAMA*

Institute for Molecular Science, Myodaiji, Okazaki 444

† *Department of Chemistry, Faculty of Science, Tokyo Metropolitan University, Setagaya-ku, Tokyo 158*

(Received December 22, 1980)

The chloride–water mixture and the chloride–water–acetone mixtures were studied by measuring the ^{35}Cl NMR spectra. From the line-width analyses, it has been concluded that the line-widths of the chloride solutions are affected only by the nearest neighbours of the chloride ions, which makes it possible to study the interaction between the chloride ion and the solvent molecules microscopically. The problem concerning the ion pair formation in solutions was discussed. It has been shown that the observation of the concentration dependence of line-widths can be very powerful method for the detection of contact ion pairs formed in the solutions.

The behaviour of electrolytes in solution has multifold importance in solution chemistry. The change in the solution structures caused by the addition of electrolytes affords important clue for elucidating the structures of the solutions and the interaction between solvents and solutes. Many physicochemical and biological properties of electrolyte solutions can also be interpreted in terms of the equilibria between ionic species.

Conductivity measurements are the conventional and the most well-established means for investigating equilibria in ionic species. This method, however, is not of universal validity for elucidating various phenomena. Since the conductivity is a macroscopic property, it has limitations in elucidating the behaviour of electrolytes at the molecular level. Besides, theoretical formulae which describe the conductivity in an ionic solution are valid only in highly dilute concentrations ($c<10$ mmol dm^{-3}).

On the other hand, the recently developed multinuclear FT-NMR technique can be expected to give information on electrolyte solutions from a different point of view. First, the information obtained can be discussed at the microscopic level and should provide direct information about the first nearest neighbours. Secondly, information over a wide range of concentrations (from several mmol dm^{-3} to several mol dm^{-3}) is made available by this method of measurement. Thirdly, by selecting the nucleus to observe, one can get information about individual ions in the presence of many different ions. These characteristics give this method a great potentiality for investigating a complex mixture of ionic species, although the theoretical interpretation of data has not yet been fully established.

The relaxation time of a nucleus having a quadrupole moment, such as ^{35}Cl, ^{17}O, and ^{14}N, is controlled by the quadrupolar relaxation. If the rotation is much faster than the observing frequency ω, the line width can be expressed as:[1]

$$\Delta\nu = \frac{2\pi}{5}\left(1+\frac{\chi_a^2}{3}\right)\left(\frac{e^2qQ}{h}\right)^2\tau_c, \qquad (1)$$

where χ_a is the asymmetric parameter; e^2qQ, the quadrupole coupling constant; q, the electric field gradient at the nucleus; Q, the quadrupole moment; τ_c, the correlation time of a chloride ion, and h, Planck's constant. Ignoring the asymmetric factor ($0\leq\chi_a\leq 1$), the line-width is considered to be proportional to the product of the square of the quadrupole coupling constant and the rotational correlation time. Therefore, after an appropriate estimation of the rotational correlation time, the line-width should give information about the magnitude of the quadrupole coupling constant or about the electric field gradient, q, at the nucleus.

It is well known that a quadrupole coupling constant depends largely on the ionic character of the bond in question.[2] For instance, the values of the quadrupole coupling constants of KCl, TlCl, ICl, and BrCl are 0.04, 15.8, 82.5, and 103.6 MHz respectively, while the differences in the electronegativities of the atoms forming these bonds are 2.35, 1.75, 0.50, and 0.20 respectively. One can notice the clear tendency that the quadrupole coupling constant increases as the ionic character of the bond decreases. Thus, the line-width in ^{35}Cl NMR is a powerful tool for investigating the bond character involving chlorine atoms. In fact, the line-width is only about 10 Hz in aqueous sodium chloride, where chlorine exists as an ionic form, while it reaches as much as 14.5 kHz in carbon tetrachloride, where chlorine forms a covalent bond.

One of the intriguing applications utilizing this dramatic change of line-width is to see the environment of chloride ions in solution discussed above. Stengle *et al.* reported the line-widths of several perchlorates in various organic solvents, and they discussed the effect of solvents on the dissociation of ions.[3] Baldeschwieler *et al.* applied the line-broadening phenomena caused by the exchange of chloride ions between different environmental sites to the quantitative analysis of the active sites in the proteins.[4]

In the present study, we have examined the factors which affect the ^{35}Cl NMR line-widths of electrolyte solutions and attempted to analyze the line-widths quantitatively in terms of the equilibria of the ionic species.

Experimental

The acetone and all the electrolytes were commercially available in a guaranteed grade, and they were used without further purification. The water was distilled and passed through an ion-exchange resin.

The ^{35}Cl NMR spectra were recorded on a Varian FT80A spectrometer at 7.794 MHz. For a spectral width of 4000

Hz and an aquisition time of 0.1 s, 800 data points are available in the time-domain spectra. The Fourier number was kept at 16384. About 5×10^4 transients were accumulated to give a good S/N ratio for the 3%(w/w) solution of electrolytes. A weighting function was not applied to avoid the artificial broadening of the line-widths. The errors in measuring a half-line-width were estimated to be ±3%. The temperature variation was less than ±0.5 °C.

The viscosity was measured by means of a Tokyo Keiki VISCONIC ED. The errors in measuring the viscosity were ±0.005 cP.

Results and Discussion

Estimation of the Correlation Time of Rotational Motion. The half-line-width, $\Delta\nu$, of the ^{35}Cl NMR spectrum is expressed by Eq. 1. In order to get information only about the ion pairing of the chloride ions in an aqueous solution from the line-width measurements, τ_c should be estimated in advance. The value of τ_c is given by the following equation, using Stokes' formula:

$$\tau_c = V\eta/kT, \quad (2)$$

where V is the volume of a chloride ion; η, the viscosity; k the Boltzmann constant, and T, the temperature. We neglect the volume change of a chloride ion, although it may vary slightly as the concentration is changed.

In practice, we calculated a viscosity-corrected half-line-width, $\Delta\nu^\circ$, as follows using the measured half-line-width, $\Delta\nu$, and the viscosity, η:

$$\Delta\nu^\circ = \Delta\nu/(\eta/\eta_0), \quad (3)$$

where $\Delta\nu$ is the observed half-line-width; η is the viscosity, and η_0 is equal to 1cP (1P=0.1Pa s). Hereafter, we will use this newly defined half-line-width for the discussion of the behaviour of a line-width.

Concentration Dependence of the Line-widths in the Aqueous Tetraethylammonium Chloride and the Aqueous Potassium Chloride Systems. The concentration dependences of $\Delta\nu$ and $\Delta\nu^\circ$ in the aqueous tetraethylammonium chloride and the aqueous potassium chloride systems are shown in Figs. 1 and 2. The concentration dependences of η in both systems are shown in Fig. 3.

The Line-width in Dilute Solutions: We could measure the ^{35}Cl NMR spectra with a reasonable S/N ratio (>5) up to a solution of several mmol dm^{-3} in both systems. We found that the line-width is about 12 Hz in this highly dilute concentration range. Since the salts dissociate perfectly in this concentration range, we may conclude that the line-width of the "free ion" is *ca.* 12 Hz. Here, the "free ion" means the chloride ion being solvated only by water molecules and not interacting with cations.

The Line-width in the Concentrated Solutions: Let us consider the aqueous potassium chloride system first. Within the concentration range studied, potassium and chloride ions can exist partly as "solvent separated ion pairs." In 3.8 mol dm^{-3} aqueous potassium chloride solution, which is the most concentrated solution studied, the molar ratio of (potassium ion) : (chloride

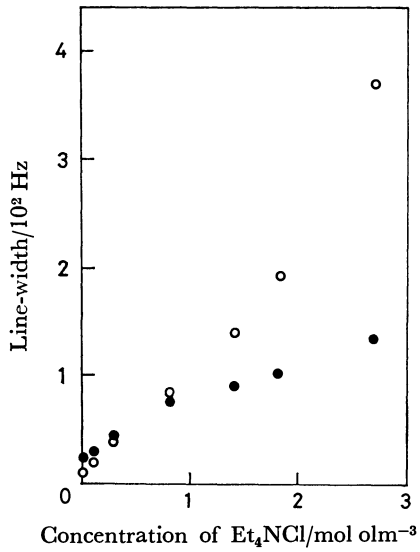

Fig. 1. Concentration dependence of the half-line-width in the aqueous tetraethylammonium chloride sysmtem at 30 °C.
(○): The observed value, (●): the viscosity corrected value (see Eq. 3 in the text).

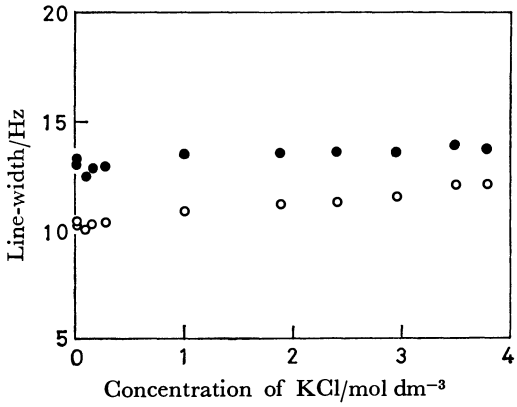

Fig. 2. Concentration dependence of the half-line-width of the aqueous potassium chloride system at 30 °C.
(○): The observed value, (●): the viscosity corrected value (see Eq. 3 in the text).

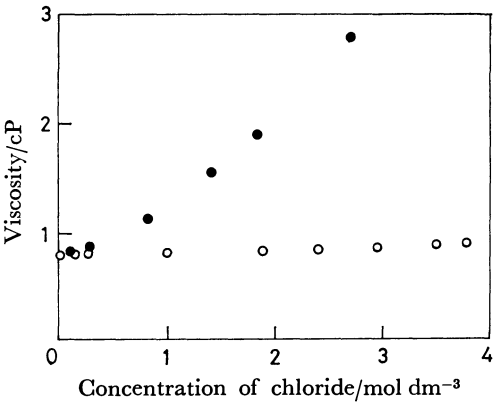

Fig. 3. Concentration dependence of the viscosity coefficient in the aqueous tetraethylammonim chloride system (●) and in the potassium chloride system (○) at 30 °C.

ion) : (water) is about 1:1:13. Therefore, each ion is surrounded by only six or seven molecules, and there are no excess free-water molecules left; that is, the ions are separated from each other by two layers of water molecules. One might think that this would increase the line-width to some extent. Nevertheless, the line-width remains *ca.* 12 Hz throughout the concentration range studied. Here, we may draw the important conclusion that the line-width of chloride ions in "solvent separated ion pairs" is also 12 Hz. In other words, the line-width of a chloride ion is not affected by the other cations which are separated from the ion in question by at least two layers of water molecules. That is, the line-width is determined only by the nearest neighbours of the chloride ions.[5]

Next we shall consider the behaviour of the line-width in the aqueous tetraethylammonium chloride system. As is shown in Fig. 1, the line-width varies remarkably with the change in the concentration, which is in good contrast to the concentration dependence of the line-width observed for the aqueous potassium chloride system (see Fig. 2). It is said that tetraethylammonium ions and chloride ions partly exist as "contact ion pairs" in aqueous solutions.[6] Taking this into account together with the above conclusion that the line-width is affected only by the nearest neighbours of chloride ions, we may conclude that the concentration dependence of the line-width in Fig. 1 originates from the formation of "contact ion pairs," in which the chloride ions associate directly with tetraethylammonium ions. It is easily recognized that the line-width is larger when a "contact ion pair" is formed because the electric field gradient at the nucleus must become larger, and this causes a rapid quadrupolar relaxation.

Quantitative Consideration of the Line-widths.[6] In highly dilute aqueous tetraethylammonium chloride solutions, the following equilibria may be realized:[7]

$$Et_4N^+ + Cl^-(H_2O)_n \underset{K_1}{\rightleftharpoons} Et_4N^+(H_2O)_nCl^- \underset{K_2}{\rightleftharpoons} Et_4N^+Cl^-(H_2O)_{n-1} + H_2O, \quad (4)$$

where K_1 and K_2 are the association constants defined as:

$$K_1 = [Et_4N^+(H_2O)_nCl^-]/[Et_4N^+][Cl^-(H_2O)_n],$$
$$K_2 = [Et_4N^+Cl^-(H_2O)_{n-1}][H_2O]/[Et_4N^+(H_2O)_nCl^-]. \quad (5)$$

According to the conclusion of the previous section, the line-width of the chloride ion in a "solvent separated ion pair," $Et_4N^+(H_2O)_nCl^-$, should be nearly equal to that of a "free chloride ion," which we will represent as $\Delta\nu_f$ from now on. On the other hand, the line-widths of "contact ion pairs," $Et_4N^+Cl^-(H_2O)_{n-1}$, which we express as $\Delta\nu_p$ here-after, should be much larger than $\Delta\nu_f$. The observed line-widths may, then, be expressed as:[8]

$$\Delta\nu = (1-\alpha)\Delta\nu_p + \alpha\Delta\nu_f \quad (6)$$

with

$$\alpha = ([Cl^-(H_2O)_n] + [Et_4N^+(H_2O)_nCl^-])/c_{Et_4NCl}, \quad (7)$$

where c_{Et_4NCl} is the concentration of tetraethylammonium chloride. In order to confirm that the behaviour of ion pairing of chloride ions can be known through the line-width measurements, we calculated $\Delta\nu_f$ and $\Delta\nu_p$ using Eqs. 6 and 7.

Table 1. The concentration dependence of conductivity in aqueous tetraethylammonium chloride at 25 °C

The data are cited from Landolt-Börnstein.

Concentration $10^4\,c$/mol dm^{-3}	Conductivity Λ/Ω^{-1} cm^2 mol^{-1} dm^3
0.1	109.14
0.5	108.93
0.7	108.84
1.0	108.69
2.0	108.28
5.0	107.43
10.0	106.53
6.919	106.7
11.76	106.0
12.09	105.8
17.33	105.4
26.94	104.4
34.74	103.8
44.79	103.0

Table 2. The parameter values used for the calculations of K_a and K_1

$\Lambda_0=109.1\ \Omega^{-1}$ cm^2 mol^{-1} dm^3	$a=8$ Å
$T=298.16$ K	$T=298.16$ K
$D=78.57$ Debye	$e=4.770\times10^{-10}$ esu.
$\eta=0.895$ cP	$D=78.3$ Debye
$a=8$ Å	
$e=4.770\times10^{-10}$ esu.	
$K_a=3.7$ mol^{-1} dm^3	$K_1=3.14$ mol^{-1} dm^3
	$K_2=9.8$ mol^{-1} dm^3

The equilibrium constants, K_1 and K_2, can be calculated by the use of the Matesich method.[7] First, the apparent association constant, K_a, is calculated from the conductivity data of Table 1 by the method of Fuoss and Krauss:[9]

$$K_a = c(\text{ion pairs})/(c_{R_4N^+})(c_{Cl^-(H_2O)_n})$$
$$= K_1(1+K_2/c_{H_2O}), \quad (8)$$

and K_1 is estimated by using the Fuoss-Eigen equation.[6] As a result, K_2 can be calculated by substituting the observed values of K_a and K_1 into Eq. 8. The equilibrium constants finally obtained, K_a, K_1, and K_2, and the parameters used in the calculation of K_a and K_1 are summarized in Table 2.

The line-widths in this system were measured under the same conditions as those used for the electric-conductivity measurements; that is, the temperature was kept at 25 °C, and the concentrations of the salts were smaller than, or nearly equal to, 10 mmol dm^{-3}. The viscosities of these solutions are 0.89 cP, which equals that of pure water at 25 °C.

The degree of dissociation, α, was calculated at six different concentrations (see Table 3), and the intrinsic line-widths, $\Delta\nu_p$ and $\Delta\nu_f$, were determined by the least-squares method using Eq. 6. The calculated values are; $\Delta\nu_p=546\pm195$ Hz[9] and $\Delta\nu_f=$

TABLE 3. THE CONCENTRATION DEPENDENCE OF THE LINE-WIDTHS IN AQUEOUS TETRAETHYLAMMONIUM CHLORIDE AT 25 °C

The observed viscosities are 0.089 cP in all solutions.

Concentration of Et_4N^+Cl/mol dm^{-3}	$\Delta\nu$/Hz	$\Delta\nu^\circ$/Hz
3.16	11.1	12.5
4.78	11.82	13.3
5.99	11.9	13.4
8.42	12.4	13.9
9.27	12.45	14.0
11.9	13.2	14.8

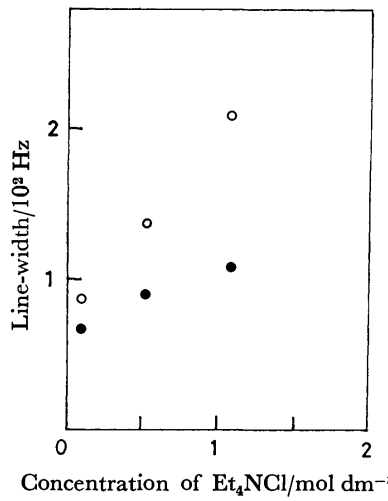

Fig. 4. Concentration dependence of the half-line-width of the tetraethylammonium chloride–aqueous acetone system at 30 °C (the mole fraction of acetone is 0.14).
(○): The observed value, (●): the viscosity corrected value (see Eq. 3 in the text).

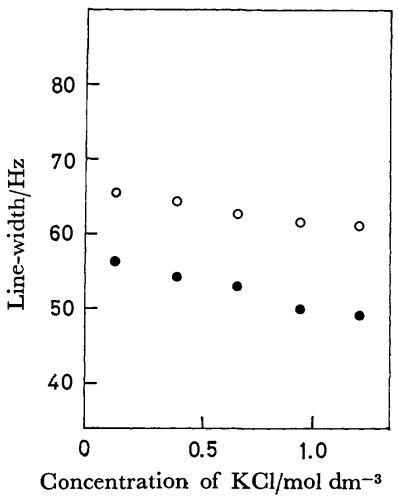

Fig. 5. Concentration dependence of the half-line-width of the potassium chloride–aqueous acetone system at 30 °C (the mole fraction of acetone is 0.14).
(○): The observed value, (●): the viscosity corrected value (see Eq. 3 in the text).

11.6±0.3 Hz. The obtained line-widths of "free ions" or "solvent separated ion pairs" are reasonably close to those estimated in the former sections; the line-width of "contact ion pairs" also seems to be reasonable, because the line-width is about 380 Hz in a pure acetone solution of tetraethylammonium chloride, in which the contribution of "contact ion pairs" is known to be significant ($\alpha \simeq 0.3$).

The above consideration confirm our approach and so we propose this line-width-measurement method as a convenient and straightforward method for judging whether or not chlorine ions form "contact ion pairs" in aqueous solutions.

Line-width in the Tetraethylammonium Chloride and Potassium Chloride in an Aqueous Acetone System. The concentration dependences of the line-widths in tetraethylammonium chloride and potassium chloride in the aqueous acetone systems were also observed: the results are shown in Figs. 4 and 5, where the mole fraction of acetone is fixed at 0.14.

We can point out from the concentration dependence of the line-width in the tetraethylammonium chloride system that "contact ion pairs" are also formed in this system, while the concentration-independent line-width in the potassium chloride system indicates that in this system, "contact ion pairs" do not contribute to any detectable extent.

Aside from this, we can point out two peculiar phenomena in Figs. 4 and 5. The observed values of the line-widths ($\simeq$60 Hz) in the potassium chloride system are larger than those in the aqueous solution, and the line-width of the tetraethylammonium chloride system in the very dilute solutions ($\simeq$70 Hz) is also larger than that in an aqueous solution (12 Hz).

To make clear the reason for these peculiar phenomena, we also measured the line-width by changing the fraction of acetone in an aqueous acetone solution. The results are shown in Figs. 6 and 7. The observed line-width becomes broader according to the increase in the fraction of acetone in both cases.

There are at least two possible explanations. One is that the acetone molecules enter the first coordination sphere of chloride ions to make the electric field gradients at the nuclei larger; the other is that acetone molecules break the structure of the first coordination sphere, which results in the breaking down of the spherical symmetry around the chloride ion. The MO calculations may shed light upon this problem, and so investigations along this line are now under way.

Line-width Broadening Due to Common-ion Effect. If our interpretation that the line-width broadening is caused by the existence of the "contact ion pair" in the equilibria is correct, the ^{35}Cl line-width should be broadened by adding other salts containing the common ion, that is, the tetraethylammonium ion, judging from the mass-law effect. Therefore, we measured the change in the ^{35}Cl line-width of tetraethylammonium chloride by adding tetraethylammonium bromide. One should notice that the added bromine has a dual effect on the ionic equilibria. That is, because of the mass-law effect, it makes the concentration of "paired species" larger on one band, while

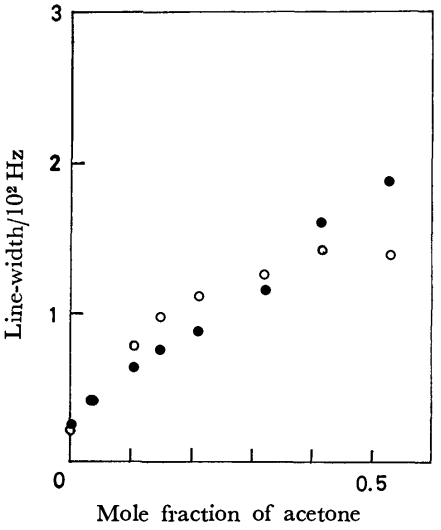

Fig. 6. Dependence of the half-line-width of the tetraethylammonium chloride–aqueous acetone system on the mole fraction of acetone at 30 °C (the concentration of tetraethylammonium chloride is 0.1 mol dm^{-3}). (○): The observed value, (●): the viscosity corrected value (see Eq. 3 in the text).

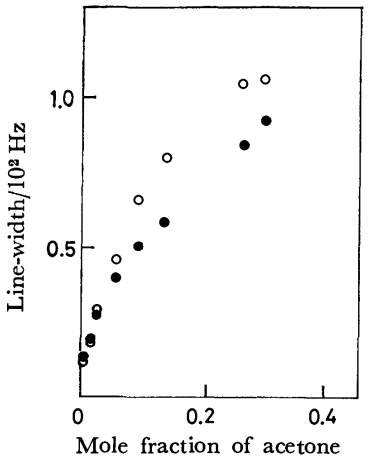

Fig. 7. Dependence of the half-line-width of the potassium chloride system on the mole fraction of acetone at 25 °C (the concentration of potassium chloride is 0.2 mol dm^{-3}).
(○): The observed value, (●): the viscosity corrected value (see Eq. 3 in the text).

on the other it makes "paired species" dissociate to "free ions" as a result of an increase in the ionic strength of the solution.

The results are shown in Fig. 8. A tendency for the line-width to increase is clearly recognized. This shows that the net effect of the added common ion in this case results in the increase in the concentration of "contact ion pairs," which in turn causes the line broadening in the ^{35}Cl NMR.

Summary. In summary, the line-widths of ^{35}Cl NMR spectra are found to reflect the circumstances of the first coordination sphere around chloride ions quite sensitively. The dependence of the line-widths on the concentration of ions can afford important information on "contact ion pair" formation. By ana-

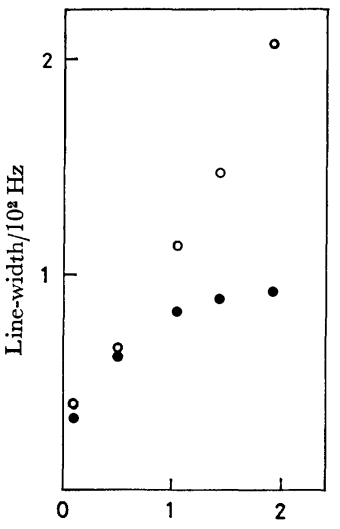

Fig. 8. Dependence of the half-line-width of the aqueous tetraethylammonium chloride system on the concentration of tetraethylammonium bromide.
(○): The observed value, (●): the viscosity corrected value (see Eq. 3 in the text).

lyzing the concentration dependence of line-widths in the dilute concentration range, we have proposed values of the intrinsic line-width of the "contact ion pair" ($\Delta\nu_p$=546±195 Hz) and that of "free ions" or "solvent separated ion pairs" ($\Delta\nu_f$=11.6±0.3 Hz).

This methodology may be found to be quite unique when it is compared with the conventional one based upon conductivity data. While the latter can distinguish "free ions" from "ion pairs," our present method distinguishes a "contact pair" from a "solvent separated" one.

The ^{35}Cl NMR method promises to afford fruitful information on solvation or ion pairing phenomena from the point of view of the microscopic aspects over the range from dilute to highly concentrated solutions.

References

1) J. A. Pople, W. G. Schneider, and H. J. Bernstein, "High Resolution Nuclear Magnetic Resonance," McGraw-Hill, New York, N. Y. (1959).

2) B. P. Daily and C. H. Townes, *J. Chem. Phys.*, **23**, 118 (1955).

3) H. A. Berman and T. R. Stengle, *J. Phys. Chem.*, **79**, 1001 (1975).

4) T. R. Stengle and J. D. Baldeschwieler, *J. Am. Chem. Soc.*, **89**, 3045 (1967); *Proc. Natl. Acad. Sci. U.S.A.*, **55**, 1021 (1966).

5) The effect of cations separated by one layer of water molecules can not be specified in this experiment. The broadening of the line-width might be caused by this kind of ion pair, namely, "solvent shared ion pairs," to some extent. If this is the case, the contribution of "solvent shared ion pairs" is included by "contact ion pairs" in the present study.

6) Hertz *et al.* reported that the line-width of the ^{81}Br NMR of inorganic salts, such as sodium bromide and rubidium bromide, was broadened by adding tetraethylammonium bromide and that the line-width of tetraethylammonium

bromide showed a concentration dependence. They interpreted those phenomena in terms of an electrostatic theory (see H. G. Hertz and M. Holz, *J. Phys. Chem.*, **78**, 1002 (1974)). The ^{81}Br NMR line-width of the bromide ion in an aqueous dilute solution is about 290 Hz (see T. R. Collins, Z. Starcuk, A. H. Burr, and E. J. Wells, *J. Am. Chem. Soc.*, **95**, 1469 (1973); this value is much larger than the corresponding value of the ^{35}Cl NMR line-width of chloride in a dilute aqueous solution. This difference becomes rather critical when measuring a very dilute solution. Apparently ^{35}Cl NMR has an advantage in this respect (see also H. Wennerstrom, B. Lindman, and S. Forsen, *J. Phys. Chem.*, **75**, 2936 (1971)).

7) S. M. A. Matesich, J. A. Nadas, and D. F. Evans, *J. Phys. Chem.*, **74**, 4568 (1970).

8) Since exchange among "free ions," "solvent separated ion pairs," and "contact ion pairs" is fast compared to the reciprocal of the line-width (<2 ms), the observed spectra are composite lines. Therefore, the line-width can be expressed as the average of the intrinsic line-widths of "free," "solvent separated," and "contact" ion pairs. In the present system, the conditions of the fast exchange and extreme motional narrowing conditions are realized (see A. G. Marshall, *J. Chem. Phys.*, **52**, 2527 (1970)).

9) R. M. Fuoss and C. A. Krauss, *J. Am. Chem. Soc.*, **55**, 1019 (1933).

10) Since $\Delta\nu_p$ was calculated from the data at very dilute concentrations, the errors are inevitably large. Substituting the value of the line-width for "free ions" ($\Delta\nu=12$ Hz) into Eq. 1, e^2qQ can be calculated to be 3 MHz, assuming $\tau_c=1$ ps. As for "contact ion-pairs" ($\Delta\nu=300$ Hz), e^2qQ becomes 15 MHz.

  Bull. Chem. Soc. Jpn., 54, 1939—1942 (1981)

Light Scattering Study of the 12-Hydroxyoctadecanoic Acid and Benzene Mixture in the Gel State

Nobuyuki Ito,† Masako Yudasaka,† and Tsunetake Fujiyama*

Institute for Molecular Science, Myodaiji, Okazaki 444

† *Department of Chemistry, Faculty of Science, Tokyo Metropolitan University, Setagaya-ku, Tokyo 158*

(Received December 22, 1980)

The structure of the 12-hydroxyoctadecanoic acid–benzene gel was studied by the use of the light scattering spectrometer. The scattering angular dependence of the scattering intensity and the time correlation function of the electric field were measured. It was found that the coarse mesh network and the fine mesh network coexist in this gel. The former was detected by the intensity measurement, while the latter was detected by intensity-fluctuation spectroscopy. The usefulness of the light scattering technique was emphasized.

A measurement of light scattered by the fluctuation of a dielectric constant is a preferred method for studying a molecular arrangement in a dimension of several hundred or several thousand angstroms. Gels are interesting objects to study by the light scattering method, as has been shown by the reports of Prins *et al.*[1] and Tanaka *et al.*[2] on the structure determination of the agarose or polyacrylamide gel.

In the present work, we study a gel made of 12-hydroxyoctadecanoic acid (12HOA hereafter) and benzene in order to examine the structure utilizing the features of the light scattering method. The 12HOA–benzene gel has already been studied in detail by Tachibana *et al.* using the X-ray diffraction method, circular dichroic spectroscopy, an electron microscope, and other methods.[3] According to their conclusions, the 12HOA molecules construct fiber-like crystallites in which 12HOA molecules are aligned to form a chiral smectic structure. These fiber-like crystallites enmeshing the gel may be thinner than 10—100 nm, as estimated from the observation of the dried gel (the solvent having been evaporated) under an electron microscope.

The purpose of the present study is to get direct information about the structure of network constructed by the fiber-like crystallites. Using the light scattering method, we can study the structure of the gel state without evaporating the solvent. We measured the angular dependence of the scattered light intensity and the time correlation function of the electric field of the scattered light. The light is scattered essentially by the crystallites in this gel.

Experimental

A schematic diagram of the light scattering spectrometer constructed in this laboratory is shown in Fig. 1. The light source is an argon-ion laser (Spectra-Physics Model 165-09). The scattering angle, θ, is varied by adjustable mirrors, M_1 and M_2, and is defined by two pinholes, P_1 and P_2, with a diameter of 1 mm. P_1 and P_2 are approximately 50 cm apart from each other. The incident light is focused into a sample cell ($12\times15\times16$ mm^3) made of fused quartz.

The photomultiplier tube, PM, has a S-20 response (Hamamatsu TV, R-374) and is operated at 840 V at room temperature. The photomultiplier, and the output power is integrated at a time constant of 1 s and is read out on an oscilloscope. The autocorrelation function of the photocurrent is observed by means of a 400-channel correlation and probability analyzer (KANOMAX, SAI 43A).

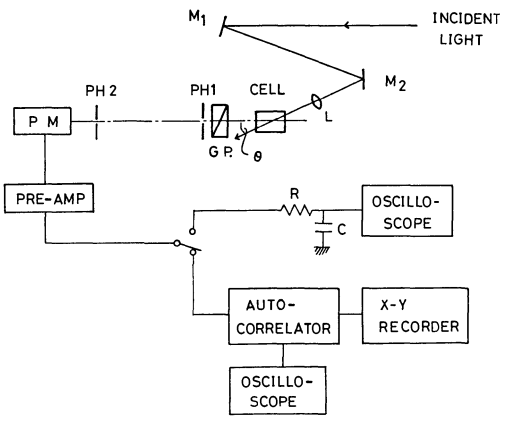

Fig. 1. The block diagram of the light-beating spectrometer.

All the measurements were performed at 24±1 °C. The power of the incident light was controlled within 60—15 mW by the use of ND filters in order to avoid any temperature elevation in the sample.

12HOA was purified from commercial products following the method described in the literature.[4] The purity was ascertained to be more than 99% by observing the presence of the methyl ester by gas chromatography. The concentration of 12HOA in this gel was about 33 mmol dm^{-3}.

12HOA was dissolved in benzene at 50 °C. Then, it was made dust-free by the use of a millipore filter FG of 0.1 μm pore size and was injected into the sample cell. This sample was cooled down from 50 °C to 24 °C with the cooling rate of 2 °C/h. Further, the sample was left for about one day at 24 °C. The gel finally obtained was an aggregate of spherulitical domains, as has been reported by Tachibana *et al.*[3] For the actual measurement, we used a gel whose spherulitical domains were larger several centimeters in diameter so that we could avoid the reflection effect at the boundaries of these domains. This gel was transparent to the human eye.

For the polarization measurements, Glan-Thompson prisms (1×1 cm^2 in section) were used to define the polarization direction of the light.

Results and Discussion

The power spectrum of the light scattered from the gel corresponds to the fluctuation of the dielectric constant in space and time, as expressed by these relations:[5]

$$I(\tilde{q},\ \omega) = \frac{1}{2\pi}\int \langle \tilde{E}_s(\tilde{q},\ t)\tilde{E}_s(\tilde{q},\ 0)\rangle e^{i\omega t}dt$$
$$= \frac{A}{2\pi}\int \left\{\int_V \langle \Delta\varepsilon_{si}(\tilde{r},\ t)\Delta\varepsilon_{si}(O,\ 0)e^{i\tilde{q}\cdot\tilde{r}}d^3r\, e^{i\omega t}dt\right.$$
$$= \frac{A}{2\pi}\int \gamma(\tilde{q},\ t)e^{i\omega t}dt, \quad (1)$$

with

$$\Delta\varepsilon_{si} = \tilde{n}_s\cdot\Delta\varepsilon\cdot\tilde{n}_i, \quad (2)$$

$$\gamma(\tilde{q},\ t) = \int_V \langle \Delta\varepsilon_{si}(\tilde{r},\ t)\Delta\varepsilon_{si}(O,\ 0)\rangle e^{i\tilde{q}\cdot\tilde{r}}\, d^3r, \quad (3)$$

and

$$A = k_s^4 E_0^2 V/16\pi^2 R^2 \varepsilon_0^2, \quad (4)$$

where $E_s(\tilde{q},t)$ is the electric field of the scattered light at time t and for a scattering vector, $\tilde{q}$, $\Delta\varepsilon_{si}$ the element of the dielectric-constat fluctuation tensor, $\Delta\varepsilon$; $\tilde{n}_s$ and $\tilde{n}_i$, the directions of the electric field of the scattering and incident light respectively; V, the scattering volume; $\tilde{k}_s$, the wave vector of the scattered light in the medium; E_0, the electric field of the i-component of the incident light; R, the distance between the scattering volume and the detector, and ε_0, the macroscopic dielectric constant; the suffixes i and s identify the polarization directions of the incident and scattered lights respectively.

Integrating Eq. 1 over the frequency, one gets:

$$I(\tilde{q}) = A\int_V \langle \Delta\varepsilon_{si}(\tilde{r})\Delta\varepsilon_{si}(O)\rangle e^{i\tilde{q}\cdot\tilde{r}}\, d^3r, \quad (5)$$

which shows that the integrated intensity of a Rayleigh line can afford information about the dielectric-constant fluctuation.

On the other hand, the photo-current correlation function, $\langle i(t)i(0)\rangle$, is related to the field correlation function by this formula:[5]

$$\langle i(t)i(0)\rangle \propto \langle |\boldsymbol{E}(\tilde{q},\ 0)|^2\rangle + |\langle \boldsymbol{E}(\tilde{q},\ t)\cdot\boldsymbol{E}(\tilde{q},\ 0)\rangle|^2 \quad (6)$$

so long as the optical field obeys Gaussian statistics. A comparison of Eqs. 1 and 6 leads to the conclusion that it is possible to obtain the square of the field correlation function experimentally, because we can observe the photocurrent correlation function with the use of our instrument, in which an analog correlator is installed.

Angular Dependence of the Intensity of the Scattered Light. We consider here only the intensity of the light scattered from the isotropic fluctuation of the dielectric constant, because the intensity of the depolarized component is only about 8% that of the polarized one in this gel. Although several kinds of fluctuations can cause the dielectric-constant fluctuation, the existence of the fiber-like crystallites of 12HOA has the decisive effect. Other fluctuations—for example, the thermally excited density fluctuation of a solvent and the density and orientation fluctuation of 12HOA in each crystalline, have negligibly small effects on the fluctuation of the dielectric constant.

If we expand the exponential term in the right-hand side of Eq. 5 and neglect the terms higher than cubic, we obtain these relations:

$$I(\tilde{q}) = A\int_V \langle \Delta\varepsilon(\tilde{r})\Delta\varepsilon(0)\rangle d^3r\left(1-\frac{1}{6}q^2R_c^2\right) \quad (7)$$

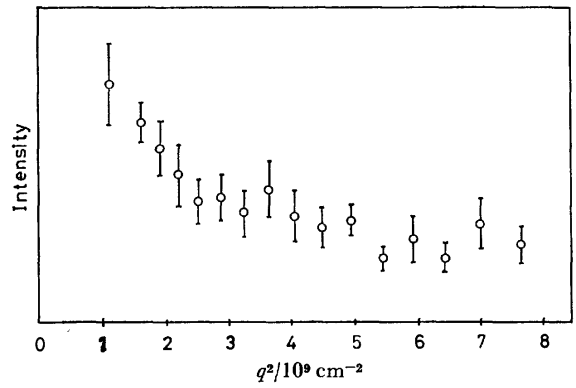

Fig. 2. The scattering intensity against q^2 for the 33 mmol dm^{-3} 12HOA–benzene gel at 24 °C.

with

$$R_c^2 = \int_V \langle \Delta\varepsilon(\tilde{r})\Delta\varepsilon(0)\rangle r^2 d^3r \Big/ \int_V \langle \Delta\varepsilon(\tilde{r})\Delta\varepsilon(0)\rangle d^3r. \quad (8)$$

R_c is called a correlation length of the fluctuation and corresponds to the mean size of the mesh of the gel network, made of 12HOA in the present system. R_c can be estimated by using Eq. 7 if we measure the intensity of the scattered light as a function of $\tilde{q}$.

The observed intensities are plotted against q^2 in Fig. 2. The scattered-light intensity is nearly constant in the range of $3.0\times10^9 < q^2 < 8.0\times10^9$ and then increases as q^2 increases in the range of $3.0\times10^9 > q^2$ (see Fig. 2). We have to put a large uncertainty in the final "correlation length" value because we could not measure $I(0) = A\int_V \langle \Delta\varepsilon(0)\Delta\varepsilon(\tilde{r})\rangle d^3r$ with sufficient accuracy. This arises from the existence of the stray light which is inevitable for small-angle measurements. In addition, the neglections of the higher-order terms of Eq. 7 can be a source of considerable uncertainty for the R_c value. However, it may be reasonable to conclude that the "correlation length of fluctuation" or the size of mesh in this gel is in the order of a few thousand angstroms.

Intensity Fluctuation Spectroscopy of the Scattered Light. The intensity fluctuation of the light scattered from the gel originates from various types of motions: (1) the relative motions between the solvent and the fiber-like crystallites which construct the gel network; (2) the relative motions of the 12HOA molecules in the crystallites, and (3) the relative motions of the solvent molecules. The correlation functions, $\gamma(\tilde{q},t)$, of the dielectric constant fluctuation caused by these relative motions can be expressed by this relation:[5]

$$\gamma(\tilde{q},\ t) \propto \exp(-q^2Dt), \quad (9)$$

where $\tilde{q}$ is the scattering vector and D is the parameter describing the rapidity of the motion, the dimension of which is $[L]^2/[T]$. In the case of the relative motion of Type (3), D is estimated from the thermal diffusivity of liquid benzene, to be in the order of 10^{-3} cm^2/s.[6] In the case of the relative motion of Type (2), D can be in the order of 10^{-6} cm^2/s, which is estimated from the elastic constant, K, and the

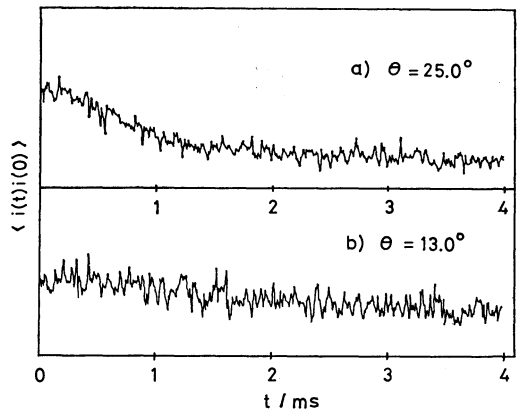

Fig. 3. The observed correlation function for the 33 mmol dm^{-3} 12HOA-benzene gel at 24 °C. The scattering angles are: a) 25° and b) 13°.

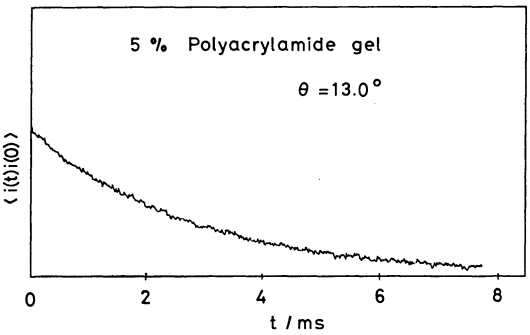

Fig. 4. The observed correlation function of the 5% w/w aqueous polyacrylamide gel at 24 °C with the scattering angle of 13°.

viscosity, η, for the ordinary smectic A-type liquid crystal through the relation: $D \simeq K/\eta$.[7] Furthermore, the scattered light strongly depolarized in this case, because this fluctuation is caused by the orientation of the mesophase molecules. On the other hand, the D-value for Type (1) has been known to be in the order of 10^{-7} cm^2/s, as estimated from the longitudinal compressional modulus, G, and the friction constant, f, observed for polyacrylamide gel through the relation: $D=G/f$.[2] Therefore, these three different modes can be observed separately if we adopt an appropriate experimental set-up for the actual measurement of the correlation function.

Figure 3 shows some typical examples of the actually observed current correlation function, which corresponds to the electrical field of the polarized component of the light scattered from the 12HOA-benzene gel. The correlation function of the depolarized component could not be observed in this case, because the intensity of the depolarized component was negligibly small in comparison with that of the correlation function in the aqueous polyacrylamide gel (5% w/w). One of the results is illustrated in Fig. 4. In the case of the aqueous polyacrylamide gel, we could observe the correlation function with a good reproducibity from any scattering volumes in the sample. From Eqs. 1, 6, and 9 it can be seen that the time-dependent part of the current correlation

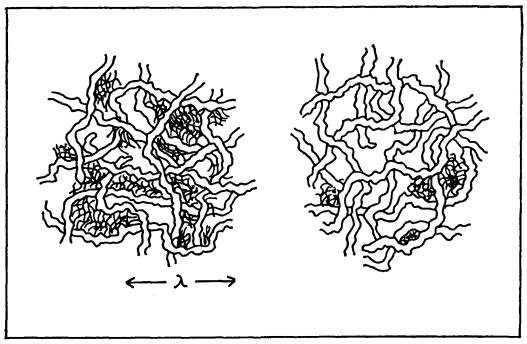

Fig. 5. The structure of the netweork constructed in the 12HOA-benzene gel (schematic). λ is several thousand Ångstroms which corresponds to the wavelength of the incident light.

function is related to the correlation function of the dielectric constant as:

$$\langle i(t)i(0)\rangle_t \propto \exp(-2q^2Dt). \quad (10)$$

The D-value was obtained for the polyacrylamide system as $(2.2\pm0.2)\times10^{-7}$ cm^2/s from the least-squares fitting to Eq. 9, which agrees well with the observation of Tanaka *et al.* ($D=(2.4\pm0.1)\times10^{-7}$ cm^2/s).

In the case of the 12HOA-benzene gel, D was obtained as $(0.97\pm0.24)\times10^{-7}$ cm^2/s. The relatively large uncertainty attached to the D-value arises from the poor S/N ratio of the observed correlation function. As the magnitude of D is as large as that of the polyacrylamide gel, we can conclude that the scattered light from the 12HOA-benzene gel reflects the relative motions of Type (1), that is, the relative motion between the solvent and the crystallites. The mesh of the network made from the crystallites should be much finer than the wavelength of the incident light. It must be emphasized that the correlation function was not always observed in the 12HOA-benzene gel; that is, the appearance of the correlation function was dependent on the position of the scattering volume. This may reflect the situation that the network with the fine mesh is not dispersed homogeneously in the sample, quite different the situation in the aqueous polyacrylamide gel.

Concluding Discussion. According to the results reported in the previous paragraphs, a network with rather complicated structures is formed in the 12HOA-benzene gel. The integrated intensity data and the current correlation function show that there are two kinds of networks in this gel. One is a network with a mesh of a few thousand angstroms (obtained from the intensity data), and the other is one with a much finer mesh (from the correlation function).

Tachibana *et al.* observed fiber-like crystallites whose thickness was 10—100 nm in the dried gel (the solvent being evaporated) under an electric microscope. The network with a mesh of a few thousand angstroms may be constructed from such fiber-like crystallites. As the thickness of the fiber-like crystallites is 10—100 nm, and as those crystallites contain no solvent,[3] the fiber might be very hard. Therefore, they cannot entangle themselves with each other densely, thus forming a rather coarse network. These fibers which

form the coarse network are linked together here and there by smaller networks with a fine mesh. These fine networks are dispersed inhomogeneously in the gel: that is, there might be some areas in which the fine networks are stretched densely and others in which the fine networks are not stretched. In Fig. 5 we visualize the structure of the network formed in the 12HOA–benzene gel schematically. The existence of the fine network has not been noticed before in the 12HOA–benzene gel. We believe the existence of this fine network is essential for the formation of the gel phase, because the solvent molecules can be trapped in this fine network much more easily than in the coarse network.

Incidentally, the present work has emphasized the importance of the light scattering study for the determination of complicated structures in materials, because we are able to choose appropriate regions of time and space for the measurements of the intensity and the correlation function of the electric field of the scattered light.

The authors of this report wish to express their thanks to Professor Taro Tachibana for suggesting to them this interesting system (12HOA).

References

1) K. L. Wun, G. T. Feke, and W. Prins, *Faraday Discuss. Chem. Soc.*, **57**, 146 (1974).
2) T. Tanaka, L. O. Hocker, and G. B. Benedek, *J. Chem. Phys.*, **59**, 5151 (1973).
3) T. Tachibana, T. Mori, and K. Hori, *Bull. Chem. Soc. Jpn.*, **53**, 1714 (1980).
4) T. Tachibana and H. Kambara, *Bull. Chem. Soc. Jpn.*, **42**, 3422 (1969).
5) B. J. Berne and R. Pecora, "Dynamic Light Scattering," Wiley-Interscience, New York (1976).
6) E. Gulari, R. J. Brown, and C. J. Pings, *AIChE J.*, **19**, 1196 (1973).
7) R. Ribbotta, D. Salin, and G. Durand, *Phys. Rev. Lett*, **32**, 6 (1974).

Encapsulation of Krypton with (K, M^{II})-A Zeolites

Keiji ITABASHI,† Tetsuo TAKAISHI, and Tatsuo OHGUSHI*

School of Materials Science, Toyohashi University of Technology, Toyohashi 440

† *Central Research Laboratories, Toyo Soda Manufacturing Co., Ltd., 4560, Tonda Shin-Nanyo, Yamaguchi 746*

(Received January 20, 1981)

The encapsulation of krypton is realized with zeolite A, having compositions $(K_{12-2x}M^{II}_x)$-A with $1.11 \leqq x \leqq 3.78$, at temperatures lower than 300 °C and a pressure of 3.7×10^6 Pa. This encapsulation condition is much milder than the usual one, 350 °C and 4.2×10^8 Pa, which is adopted in industry. Such lowerings of the encapsulation temperature and pressure are caused by bivalent cations introduced through ion-exchanges. The result is an experimental evidence to the existence of the ion-loosening effect proposed in preceding papers.

Zeolite A has, at the center of its unit cell cube, a large cavity which is nearly spherical with a diameter of 1.14 nm and can accomodate sorbed molecules. This cavity is surrounded by six 8-membered oxygen rings, which are on {100} faces of the cube and constitute windows to the cavity. In commercial molecular sieves 3A and 4A, all of these windows are blocked by potassium and sodium ions, respectively.[1] The molecular sieving characters of these zeolites are primarily determined by the size of the aperture of the partially-blocked windows. The effective size of the aperture, however, depends upon temperature. At higher temperatures, a situation is realized that larger molecules, which are not sorbed at lower temperatures, are able to be sorbed. If the temperature is lowered after the large molecule being sorbed at higher temperature, the windows are closed and the sorbed molecules are encapsulated.[2]

An example of the practical use of the encapsulation is that of radio-active ^{85}Kr into 3A zeolite, for commercial distributions. It is a large merit that a lead container, required as a radiation shield, becomes very small for such a compactly encapsulated ^{85}Kr. Usually, krypton is encapsulated into 3A at 350 °C and a pressure of 4.2×10^8 Pa.[3,4]

It is expected that the encapsulation temperature and pressure are lowered by the ion-loosening techniques presented in the preceding papers.[5,6] The techniques consist in increasing the temperature dependence of the window size by introducing bivalent cations onto 6-membered oxygen rings. In the present paper, results of the krypton encapsulation are reported, which prove the ion-loosening effect.

Experimental

The starting material was commercial sodium-A zeolite of powder form, manufactured by Toyo Soda Co. or Union Carbide Co. Sodium-A zeolite was treated at 80 °C with an 1 mol dm^{-3} aqueous solution of KCl, repeatedly, to obtain K_{12}-A. Resultant K_{12}-A was further treated with a solution containing KCl and $M^{II}Cl_2$, of 0.2 total normality, where M^{II} is Ca, Co, Mn, or Zn. The composition of the zeolite was determined by the usual chemical analysis and atomic absorption spectrometry. The zeolite used contained M^{II} ions less than 4 per unit cell.

The dehydration process of the zeolite was studied with a quartz spring balance. The weight of the sample decreased to 75% of the initial one after vacuum baking-out for 2 h at 300 °C. After this treatment, no change was observed in the crystallinity of the sample with X-ray diffraction techniques. This degree of the dehydration, we judged, is appropriate to the practical use of the zeolite as an adsorbent. In the following experiments, the sample zeolite was dehydrated at 300 °C for 2 h under vacuum.

The sample zeolite (3—5 g) was packed in a conventional autoclave(300 cm^3) and dehydrated. Then, krypton gas at a pressure of 3.7×10^6 Pa was introduced into the autoclave, held at 300 °C, and sorbed into the zeolite. After a waiting time of 60 min, the system was slowly cooled under the pressure, to room temperature, and then a residual gas of a high pressure was evacuated from the dead space in the autoclave. The amount of gas encapsulated in the zeolite was measured by a thermal desorption method. The autoclave was heated at a rate of about 1.3 °C min^{-1}, and the amount of evolved gas was caught, through a flexible stainless steel tube, into a messcylinder placed upside-down in a water-filled vessel.

Results

Figuers 1 and 2 show the amount of krypton decapsulated as a function of temperature. The total amount encapsulated, $V_{tot.}$, depended sharply upon the content of calcium in the zeolite as shown in Fig.

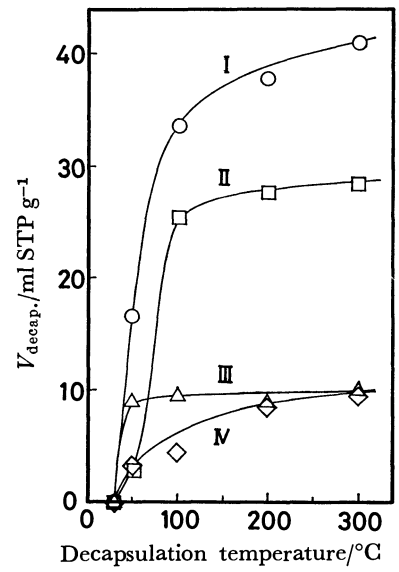

Fig. 1. Amount of Kr decapsulated as a function of temperature.
Curve I: $(K_{6.76}Ca_{2.62})$-A, Curve II: $(K_{7.84}Ca_{2.08})$-A, Curve III: Na_{12}-A, Curve IV: $(K_{5.81}Na_{6.19})$-A. Conditions of encapsulation: 300 °C, 3.7×10^6 Pa.

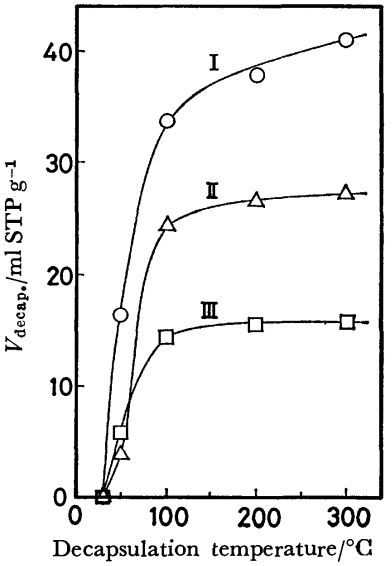

Fig. 2. Effect of encapsulation condition to the amount encapsulated with $(K_{6.76}Ca_{2.62})$-A.
Curve I: 300 °C, 3.7×10^6 Pa, Curve II: 150 °C 3.7×10^6 Pa, Curve III: 300 °C, 1.7×10^6 pa.

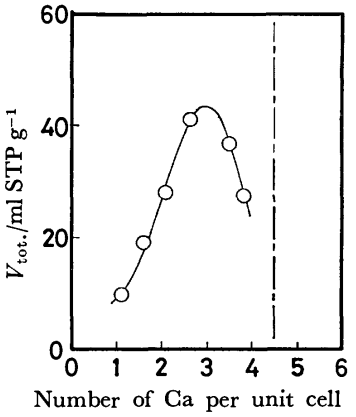

Fig. 3. Effect of calcium content to the total amount of encapsulation.

3. At a composition of 4.5 Ca per unit cell (represented by a chain line), the completely unblocked, say, open window starts to manifest itself.[7] Since krypton can freely pass through such an open window, V_{tot} should drastically decrease over this critical content. Experimentally, however, the value of $V_{tot.}$, starts to decrease when calcium content exceeds 3 per unit cell. To realize a maximum encapsulation, the content of calcium must be considerably smaller than 4.5 per unit cell.

Other bivalent cations, such as Co^{2+}, Mn^{2+}, and Zn^{2+}, have the effect as Ca^{2+}. Results are shown in Fig. 4.

Discussion

The diameter of krypton is slightly larger than that of the aperture in the K^+-blocked window. In order that a visiting krypton atom is sorbed into the large cavity, the blocking K^+ must be pushed aside to make

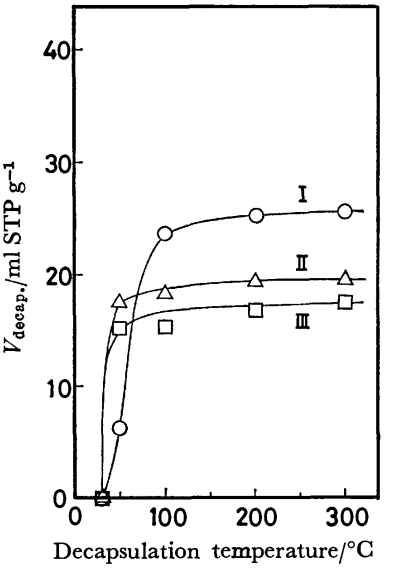

Fig. 4. Encapsulation with various kinds of (K, M^{II})-A zeolites.
Curve I: $(K_{7.08}Co_{2.46})$-A, Curve II: $(K_{6.52}Mn_{2.74})$-A, Curve III: $(K_{5.58}Zn_{3.21})$-A. Conditions of encapsulation: 300 °C, 3.7×10^6 Pa.

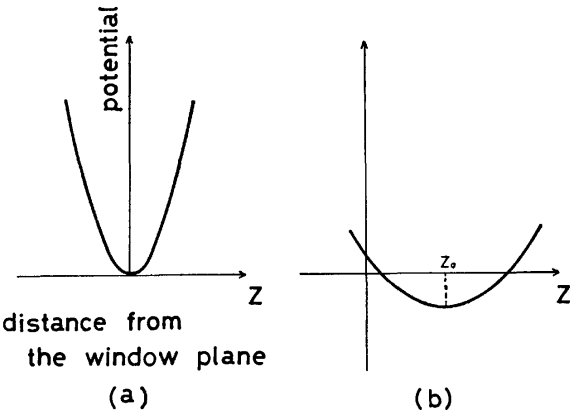

Fig. 5. Potential experienced by the window-blocking K^+.
(a) Potential in K_{12}-A zeolite. (b) Potential in (K,M^{II})-A zeolite.

a way for the visitor. In other words, an activation energy is required in krypton sorption. The magnitude of the activation energy is primarily determined by the potential experienced by the blocking K^+. The activation energy is large if the radius of curvature is small in the valley of the potential surface, while small if the radius is large. With this in view, we schematically represent the concerned potential forms for K_{12}-A and (K,M^{II})-A zeolites in Fig. 5. The abscissa, z, denotes the distance from the window plane, and z_o the position of the potential valley in (K,M^{II})-A. A permanent widening of the aperture results from a large value of z_o, while a temperature dependent one does from an increase in the radius of curvature. Such an aperture widening, due to bivalent cations, is named as an ion-loosening effect. The ion-loosening may increase with the increasing

content of M^{II}.[8] Thus, krypton can easily pass through K^+-blocked windows if the content of M^{II} exceeds 4 per unit cell, as shown in Fig. 3.

In the last place, let us discuss a problem of the storage of ^{85}Kr which is released in the reprocessing of nuclear fuel. The container tank must be air-tight and have a thick wall. (K,M^{II})-A zeolite cannot be used for such a purpose, since the zeolite will be destroyed by radiations from ^{85}Kr.†† However, it may be used as a transient storager. For instance, zeolites encapsulating ^{85}Kr are installed in an air-tight vessel of thin wall, and then vessel is concreted by cement before the zeolites are seriously damaged by the radiation. This packing process may considerably be economical than the usual direct containment with a thick vessel of corrosion-resistive metal.

†† Penzhorn and his coworkers are trying to encapsulate permanently.[9] In their case, zeolite A is structurally changed, and the situation is very different from ours.

The present paper was in part supported by a Grant-in-Aid for Research from the Ministry of Education, Science and Culture of the Japanese Goverment, Contract No. 443001.

References

1) D. W. Breck, "Zeolite Molecular Sieves," John Wiley & Sons, New York (1974), pp. 88, 89.
2) D. W. Breck, "Zeolite Molecular Sieves," John Wiley & Sons, New York (1974), p. 623.
3) D. W. Breck, *J. Chem. Educ.*, **41**, 678 (1964).
4) W. J. Sesny and L. H. Shaffer, U. S. Patent 3 316 691.
5) T. Takaishi, A. Yusa, Y. Kamei, and T. Ohgushi, *Bull. Chem. Soc. Jpn.*, **54**, 45 (1981).
6) T. Takaishi, K. Itabashi, and T. Ohgushi, *Recent Res. Rep. 5th Int. Conf. Zeolite*, (1980), in press.
7) T. Ohgushi, A. Yusa, and T. Takaishi, *J. Chem. Soc., Faraday Trans., 1*, **74**, 613 (1978).
8) N. V. Raghavan and K. Seff, *J. Phys. Chem.*, **80**, 2133 (1976).
9) R. D. Penzhorn, "Kernforschungszentrum Karlsruhe," Berlin (1977), p. 67.

Polarized Absorption and Reflection Spectra of the Single Crystals of 11,11,12,12-Tetracyano-2,6-naphthoquinodimethan (TNAP) Complexes

Kyuya YAKUSHI, Yoshiyuki SATO, Isao IKEMOTO,*,† and Haruo KURODA

Department of Chemistry, Faculty of Science, The University of Tokyo, Hongo, Bunkyo-yu, Tokyo 113

† *Research Center for Spectrochemistry, Faculty of Science, The University of Tokyo, Hongo, Bunkyo-ku, Tokyo 113*

(Received January 21, 1981)

The electronic absorption spectra of 2,6-bis(dicyanomethylene)-2,6-dihydronaphthalene (11,11,12,12-tetracyano-2,6-naphthoquinodimethan; TNAP) and its anion radical ($TNAP^-$) were studied. The absorption bands of the solution spectra of $TNAP^0$ and $TNAP^-$ were successfully assigned to the electronic transitions which were calculated by the use of molecular orbital method. The polarized absorption and reflection spectra were measured on the single crystals of Na·TNAP and (methyltriphenylphosphonium)$(TNAP)_2$ [(MTPP)$(TNAP)_2$]. The low-lying electronic excitations of these complexes are quite similar to those of the corresponding tetracyanoquinodimethan (TCNQ) salts.

The discovery of the low-dimensional metallic behavior of organic charge-transfer salts such as tetrathiafulvalene–tetracyanoquinodimethan (TTF–TCNQ)[1] strongly stimulated research concerning the physical properties of related organic charge-transfer salts and the synthesis of new organic electron donors and acceptors.

2,6-Bis(dicyanomethylene)-2,6-dihydronaphthalene (11,11,12,12-tetracyano-2,6-naphthoquinodimethan; TNAP) was synthesized by Diekmann *et al.* and shown to be a strong acceptor.[2] The simple salts of TNAP were found to have higher conductivities than the analogous TCNQ salts,[2] and HMTSF–TNAP (2,2′-bi[2,4-diselenabicyclo[3.3.0]octan-2-ylidene]–TNAP) was found to have very high electrical conductivity at room temperature.[3] For understanding the electronic behaviors of those TNAP complexes, it is necessary to accumulate the data concerning the electronic structures of TNAP complexes.

In the present study, we have investigated the polarized absorption and reflection spectra of the single crystals of the simple salt, Na·TNAP, and the complex salt, (methyltriphenylphosphonium)$(TNAP)_2$ [(MTPP)$(TNAP)_2$].

Experimental

TNAP was synthesized by the procedures described in the literature[2,4,5] and purified by recrystallization from an acetonitrile solution. The complexes, Na·TNAP and (MTPP)$(TNAP)_2$ were obtained according to the method described in the literature.[2,5]

Polarized absorption and reflection spectra were measured on very small single crystals by use of the microspectrophotometric apparatuses for the transmission and reflection spectroscopies. The details of those apparatuses and the procedure of measurement have been described elsewhere.[6,7] All spectra were obtained at room temperature.

Absorption spectra of solutions were measured using a Hitachi EPS-3 spectrometer.

Results and Discussion

Electronic Transitions of TNAP Molecule and $TNAP^-$ Ion. In order to interpret the crystal spectra of TNAP complexes, it is of essential significance to know the electronic transitions in TNAP molecule and $TNAP^-$ ion. In Fig. 1, we show the solution spectra of $TNAP^0$ and $TNAP^-$, obtained from acetonitrile solutions of TNAP and K·TNAP. The observed wave numbers, molar extinction coefficients, and oscillator strengths of absorption bands are listed in Table 1. To find out the assignments of the observed absorption bands, we carried out SCF-MO-CI calculations on the π electron systems of the molecule and ion of TNAP.[8] The results are also included in Table 1. The predicted transitions are indicated in Fig. 1, with the vertical lines, the length of which is proportional to the predicted oscillator strengths, the directions of transition moment being shown with an arrow.

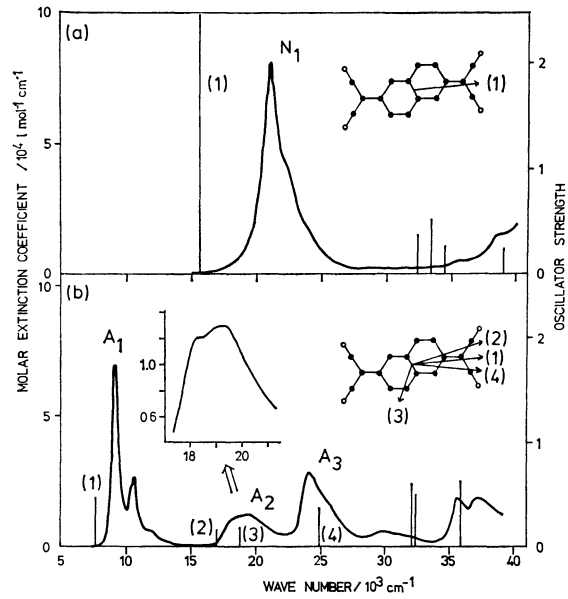

Fig. 1. The solution spectra of (a) TNAP molecule and (b) $TNAP^-$ ion in the acetonitrile solutions. The vertical lines represent the results of the SCF-MO-CI calculations. The arrows represent the directions of the transition moments.

In the solution spectrum of $TNAP^0$, there appears a strong absorption band at 21.1×10^3 cm^{-1} which is completely isolated from other weak absorption bands. The molecular orbital calculation predicted that the transition (1) had a strong oscillator strength (2.47) and was separated far from other transitions as shown in Fig. 1a. Therefore, the absorption band, N_1, is unambiguously assigned to the transition (1).

Table 1. Wave numbers, molar absorption coefficients, and oscillator strengths of local excitation bands of $TNAP^0$ and $TNAP^-$

	Obsd				Calcd			
	Transition	$\tilde{\nu}$[a] / 10^3 cm^{-1}	ε[b] / 1 mol^{-1} cm^{-1}	f[c]	Transition	$\tilde{\nu}$[d] / 10^3 cm^{-1}	f[e]	Dominant[f] configuration
$TNAP^0$	N_1	21.1	79600	0.94	(1)	16.6	0.82	$6a_u \leftarrow 5b_g$
$TNAP^-$	A_1	9.0	84400	0.38	(1)	7.7	0.16	$6a_u \leftarrow 5b_g$ and vibrational structures
		10.6	30400					
		11.8	7500					
	A_2	18.8	14200	0.18	(2)	17.0	0.12	$6b_g \leftarrow 6a_u$
		19.3	15000		(3)	18.8		$7b_g \leftarrow 6a_u$
	A_3	23.9	32800	0.32	(4)	25.0	0.12	$8b_g \leftarrow 6a_u$

a) Wave numbers. b) Molar absorption coefficients. c) Oscillator strengths. d) Wave numbers. e) Oscillator strengths which are divided by 3 in order to compare them with the experimentally obtained values from the solution spectrum. f) The dominant configuration of the wave functions of the ground states in $TNAP^0$ and $TNAP^-$ ion are represented as follows respectively;

$TNAP^0$: $\Psi_0 = (1a_u)^2(1b_g)^2(2a_u)^2(3a_u)^2(2b_g)^2(3b_g)^2(4b_g)^2(4a_u)^2(5a_u)^2(5b_g)^2(6a_u)^0$,

$TNAP^-$: $\Psi_0 = (1a_u)^2(1b_g)^2(2a_u)^2(3a_u)^2(2b_g)^2(3b_g)^2(4b_g)^2(4a_u)^2(5a_u)^2(5b_g)^2(6a_u)^1(6b_g)^0(7a_u)^0(7b_g)^0(8b_g)^0$.

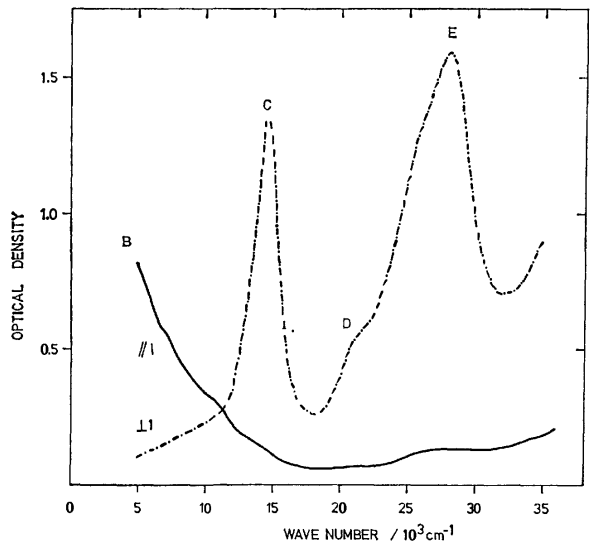

Fig. 2. Polarized absorption spectra of the single crystal of Na·TNAP.

The direction of the transition moment is almost parallel to the long axis of the molecule. The spectral features in this region are quite similar to those of $TCNQ^0$ except that the excitation energy of $TNAP^0$ is lower by about 3×10^3 cm^{-1} as compared with $TCNQ^0$.

The solution spectrum of $TNAP^-$ ion is more complicated than that of $TCNQ^-$ ion. We will denote the absorption bands as A_1, A_2, and A_3, respectively, in the order of increasing wave number, as shown in Fig. 1b. The structure of the band A_1 is similar to the vibrational structure of the absorption band of $TCNQ^-$ ion which has been assigned to the transition from the highest doubly occupied molecular orbital to the top-most singly-occupied molecular orbital. We can assign this band to the transition (1). The absorption band A_2 is broad and has a shoulder in the low wave number edge as shown in the inset of Fig. 1b. Probably it is composed of two electronic transitions. We will tentatively assign the band A_2 to the superimposition of the transitions (2) and (3). The band A_3 can be assigned to the transition (4) by comparing the observed energy and oscillator strength of this band with the calculated results.

Table 2. Wave numbers of absorption bands in the spectra of Na·TNAP

Absorption bands	$\tilde{\nu}$[a] / 10^3 cm^{-1}	Transition character
B	<5	CT: $(TNAP)^-(TNAP)^- \rightarrow (TNAP)^0(TNAP)^{2-}$
C	14.5	LE: A_1
D	21.0	LE: A_2
E	28.0	LE: A_3

a) Wave numbers.

Na·TNAP. Na·TNAP is expected to be a salt composed of Na^+ and $TNAP^-$. Light-green plate-like crystals of this complex can be obtained from the acetonitrile solution. Since the crystal structure has not been known, the absorption spectra of the crystal were observed with the light polarized parallel and perpendicular to the elongated axis (*//l* and *⊥l*) of the crystal. The observed spectra are shown in Fig. 2. The wave numbers of the observed bands are listed in Table 2. The *//l* spectrum exhibits a strong absorption band below 5×10^3 cm^{-1} (B). There is no absorption band in this region in *⊥l* spectrum. Thus the absorption band (B) is completely polarized in the direction of the *l*-axis which is likely to be the stacking axis of $TNAP^-$. We cannot expect any local excitation band associated with an intramolecular transition of $TNAP^-$ in this region. Thus the observed absorption band (B) must be the one arising from the charge transfer (CT) between $TNAP^-$ ions.

In the region above 9×10^3 cm^{-1}, the *//l* spectrum shows no absorption band although the *⊥l* spectrum

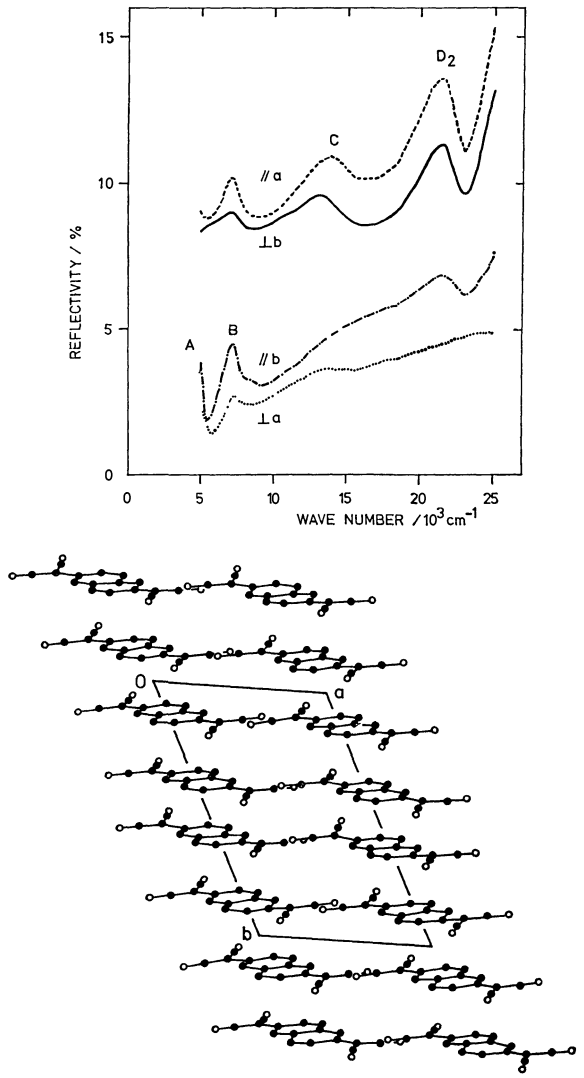

Fig. 3. Polarized reflection spectra of the single crystal of (MTPP)(TNAP)$_2$ measured on the (001) plane and the projection of TNAP molecules in the crystal onto (001) plane.

shows three absorption bands (C, D, and E). By comparing this $\perp l$ spectrum of Na·TNAP with the solution spectrum of TNAP$^-$, we can conclude that 14.5×10^3 (C), 21.0×10^3 (D), and 28.0×10^3 (E) cm^{-1} bands are the local-excitation bands corresponding to the 9—11.8×10^3 (A_1), 18.8—19.3×10^3 (A_2) and 23.9×10^3 (A_3) cm^{-1} bands in the solution spectrum of TNAP$^-$ ion, respectively. The relative intensity of the band D is very weak in comparison with the solution spectrum. It seems to be due to the difference of the direction of transition moment between the transition (2) and (3).

The local excitation bands C, D, and E are located at wave numbers higher by about 4—5×10^3 cm^{-1} as compared with the corresponding absorption bands of the solution spectrum of TNAP$^-$ ion. This is just the magnitude of the shift that is often found in the crystal where the intermolecular charge-transfer interaction is taking place between the constituent radical ions.[9]

(MTPP)(TNAP)$_2$. The crystal structure of this complex has been revealed by Sanz and Daly.[10] It is triclinic. In this crystal, TNAP molecules are arranged in groups of the four molecules which are almost parallel and equally spaced (3.30 Å) with each other. In other words, the crystal is composed of TNAP tetrads. The molecules between two consecutive tetrads are 3.46 Å apart. There is not significant difference in the molecular geometries of the four molecules in a tetrad.

The reflection spectra were measured on the (100) and (001) planes. On the (001) plane, the spectra were measured with the light polarizations, parallel to b and a axes (//b and //a) and perpendicular to b and a axes ($\perp$b and $\perp$a). On the (100) plane, the spectra were measured with the light polarizations parallel to b and c axes (//b and //c) and perpendicular to b and c axes ($\perp$b and $\perp$c). The observed reflection spectra are shown in Figs. 3 and 4 with the projections of TNAP molecules. The absorption spectra directly measured by the transmission method are shown in

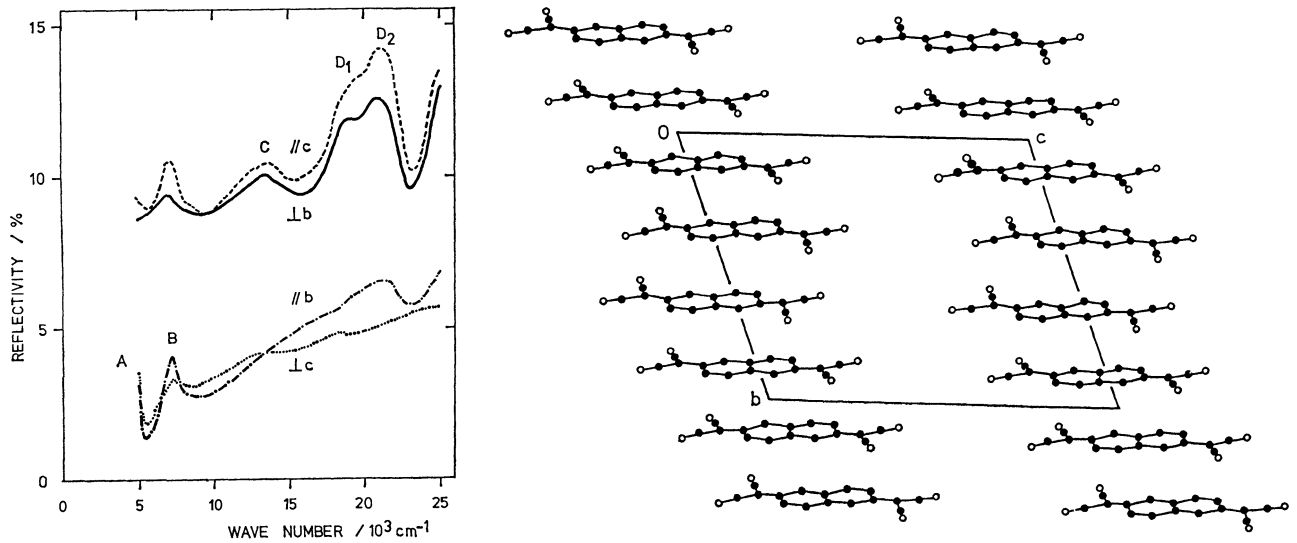

Fig. 4. Polarized reflection spectra of the single crystal of (MTPP)(TNAP)$_2$ measured on the (100) plane and the projection of TNAP molecules in the crystal onto (100) plane.

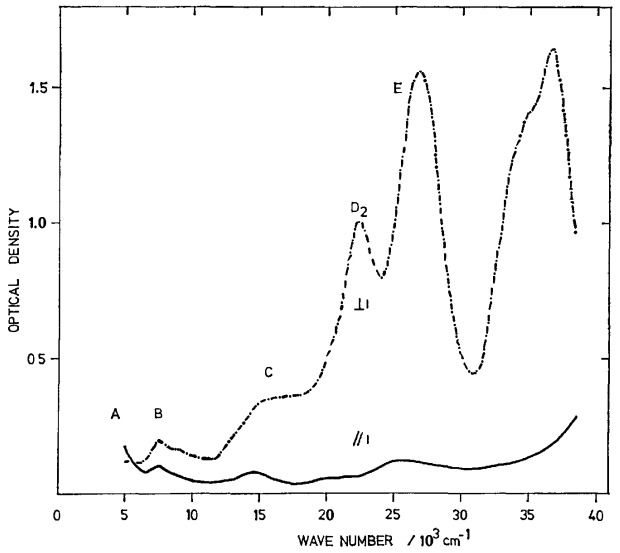

Fig. 5. Polarized absorption spectra of the single crystal of (MTPP)(TNAP)$_2$.

Fig. 5. Although we were not able to determine the observed crystallographic face directly, it is likely to be the (001) plane since it is in satisfactory agreement with the absorption spectra derived from the dispersion analysis of the reflection spectra obtained on the (001) crystal face. Therefore, we can consider that the spectra shown in Fig. 5 and the //a and ⊥a spectra. The wave numbers of the observed bands are listed in Table 3. The absorption spectra of this salt in the region lower than 17×10^3 cm^{-1} is quite similar to that of (MTPP)(TCNQ)$_2$ when we shift the spectrum of (MTPP)(TCNQ)$_2$ by about 3×10^3 cm^{-1} to higher wave number. The solution spectra of TNAP^0 and TNAP$^-$ are quite similar in nature with the spectra of TCNQ^0 and TCNQ$^-$, respectively, and the general feature of the crystal structure of (MTPP)(TNAP)$_2$ are almost the same as that of (MTPP)(TCNQ)$_2$. Therefore, we can interpret the electronic spectrum of (MTPP)(TNAP)$_2$ in analogy with that of (MTPP)-(TCNQ)$_2$. We have previously examined the temperature dependency of the reflection spectrum of (MTPP)(TCNQ)$_2$ and proposed an interpretation of the observed spectrum.[11] Using this result, we can assign the band A to the CT transition of the type TNAP^{0}TNAP$^-\rightarrow$TNAP$^-$TNAP^0, the band B mainly to the local excitation of TNAP$^-$ (A_1) and the band C to the CT transition from the second highest occupied molecular orbital of TNAP$^-$ to the lowest unoccupied molecular orbital of TNAP^0, which appears with an increased intensity by borrowing the intensity from the strong lowest transition of TNAP^0.

Let us examine the transition in the region about 20×10^3 cm^{-1}. The absorption spectrum measured on the (001) plane shows one absorption band in this region. The reflection spectra of the (001) crystal face also shows only one dispersion at the corresponding region. However, the c-polarized reflection spectra in the (100) crystal face shows that another dispersion (D_1) is superimposed on the dispersion D_2 as shown in Fig. 4. This result means that the direction of the transition moment of D_1 band is different from that of D_2 band. Since the direction of the transition moment of D_2 is almost parallel to those of C and E, D_1 must be attributable to the local excitation band associated with the transition (3) of TNAP$^-$, whose transition moment was predicted to be different from other transitions by the molecular orbital calculation as illustrated in Fig. 1b.

The absorption band E seems to correspond to the superimposition of the lowest transition of TNAP^0 and the transition (4) of TNAP$^-$.

Table 3. Wave numbers of absorption bands derived from the dispersion analysis of the reflection spectra of (MTPP)(TNAP)$_2$

Absorption bands	$\bar{\nu}$[a] / 10^3 cm^{-1}	Transition character
A	<5	(TNAP)^0(TNAP)$^-\rightarrow$ (TNAP)$^-$(TNAP)^0
B	7.2, 8.5(sh)	LE : mainly A_1
C	15.0	CT : See the text
D_1	18.5	LE : A_2 (transition (3))
D_2	21.0	LE : A_2 (transition (2))
E	27.0	LE : A_3 and N_1

a) Wave numbers.

References

1) L. B. Coleman, M. J. Cohen, D. J. Sandman, F. G. Yamagishi, A. F. Garito, and A. J. Heeger, *Solid State Commun.*, **12**, 1125 (1973); J. Ferraris, D. O. Cowan, V. Walatka, Jr., and J. H. Perstein, *J. Am. Chem. Soc.*, **95**, 948 (1973).

2) J. Diekmann, W. R. Hertler, and R. E. Benson, *J. Org. Chem.*, **28**, 2719 (1963).

3) K. Bechgaard, C. S. Jacobsen, and N. H. Andersen, *Solid State Commun.*, **25**, 875 (1978).

4) D. J. Sandman and A. F. Garito, *J. Org. Chem.*, **39**, 1165 (1974).

5) G. R. Johnson, M. G. Miles, and J. D. Wilson, *Mol. Cryst. Liq. Cryst.*, **33**, 67 (1976).

6) H. Kuroda, T. Kunii, S. Hiroma, and H. Akamatsu, *J. Mol. Spectrosc.*, **22**, 1 (1967).

7) K. Yakushi, M. Iguchi, and H. Kuroda, *Bull. Chem. Soc. Jpn.*, **52**, 3180 (1979).

8) For closed shell π-conjugated system, Pariser-Parr-Pople method was used with the semiempirical parameters determined by using Nishimoto-Mataga's formula for the two-center repulsion integrals and the Katagiri-Sandorfy's formula for two-center resonance integrals. For open shell π-conjugated system, the method of Longuet-Higgins and Pople was used with the semi-empirical parameters determined by using the Nishimoto-Mataga's formula for the two-center repulsion integrals and the Nishimoto-Forster's formula for the two-center resonance integrals.

9) T. Sugano, K. Yakushi, and H. Kuroda, *Bull. Chem. Soc. Jpn.*, **51**, 1041 (1978); J. Tanaka, M. Tanaka, T. Kawai, T. Takabe, and O. Maki, *Bull. Chem. Soc. Jpn.*, **49**, 2358 (1976); J. B. Torrance, B. A. Scott, B. Welber, F. B. Kaufman, and P. E. Seiden, *Phys. Rev. B*, **19**, 730 (1979).

10) F. Sanz and J. J. Daily, *J. Chem. Soc., Perkin Trans. 2*, **1975**, 1142.

11) K. Yakushi, M. Iguchi, G. Katagiri, T. Kusaka, T. Ohta, and H. Kuroda, *Bull. Chem. Soc. Jpn.*, **54**, 348 (1981).

TiO_2-supported Noble Metal Catalysts for the NO–CO and NO–CO–H_2O–H_2–O_2 Reactions

Ryuichi Nakamura, Shuichi Nakai, Kazuo Sugiyama, and Etsuro Echigoya*

Department of Chemical Engineering, Tokyo Institute of Technology, Ookayama, Meguro-ku, Tokyo 152

(Received March 8, 1980)

TiO_2-supported noble metal catalysts, such as Pt–, Pd–, and Rh–TiO_2, are much more active for the NO–CO reaction in the presence or absence of H_2O, H_2, and O_2 than the corresponding Al_2O_3– or other supported catalysts. They are effective even in an oxidative gas composition range for the NO–CO–(H_2O)–H_2–O_2 reaction, producing no NH_3 in the NO–CO–H_2O reaction. Comparison of the catalytic activity and properties of Pt–TiO_2 with those of other supported catalysts suggests that the higher activity of the TiO_2-supported catalysts could be attributed to their ability to activate NO molecules by the dissociative adsorption at lower temperatures.

The reduction of NO in automotive exhaust over supported Pt group catalysts has been extensively investigated by many workers, Al_2O_3 being commonly employed as the catalyst support.[1-3] However, few studies have been made on supports other than Al_2O_3 or Al_2O_3-based materials. As a result, no supports more effective for NO–CO reaction than Al_2O_3 are known. In the present investigation, a few types of TiO_2 were employed as a support for noble metals such as Pt, Rh, Pd, and Ru and their catalytic activities for the NO–CO reaction in the presence or absence of H_2O, H_2, and O_2 were determined and compared with those of the corresponding Al_2O_3-supported catalysts. Various supported Pt catalysts such as Pt–TiO_2, Pt–Al_2O_3, Pt–SiO_2, and Pt–SiO_2–Al_2O_3 were also employed, the catalytic activities and properties of the catalysts and supports being measured and compared with each other, and the role of the TiO_2 support in the catalytic activity was discussed.

Experimental

Catalyst Support. TiO_2(a) : TiO_2(anatase) was prepared by neutralization of HCl-acidic solution of $TiCl_4$ (Oosaka Titanium Co., Ltd., pH=0.1—0.2, 3.8 mol dm^{-3} $TiCl_4$) with ammonia water (1 mol dm^{-3}) up to a pH *ca.* 6, followed by washing of the precipitate obtained with water several times, drying at 393 K for 18 h, and calcination in air at 823 K for 4 h. TiO_2(a-s) : TiO_2(anatase) containing a very small amount of SO_4^{2-} was prepared from the $TiCl_4$ solution according to a procedure similar to that of Funaki and Saeki.[5] The resulting TiO_2 was calcined in the air at 823 K for 4 h. TiO_2(r-HSA) : TiO_2(rutile) with higher BET surface area as compared with the conventional rutile type TiO_2 was prepared from the $TiCl_4$-solution by evaporation followed by drying and air calcination. TiO_2(r-LSA) : TiO_2(rutile) with low BET surface area was prepared from TiO_2(a) by air calcination at 1273 K for 5 h. The BET surface area of TiO_2(a), TiO_2(a-s), TiO_2(r-HSA), and TiO_2(r-LSA) were 78, 73, 16, and 1 $m^2 g^{-1}$, respectively. $Al_2O_3(\gamma)$, SiO_2·Al_2O_3, SiO_2, MgO: These supports were prepared by the same procedure as reported[6]. Calcination was carried out in the air at 873 K for 4 h. The BET surface area of Al_2O_3, SiO_2, SiO_2·Al_2O_3, and MgO were 240, 150, 265, and 50 $m^2 g^{-1}$, respectively.

Catalyst. Supported noble metal catalysts (Tables 1—3) were prepared by impregnation of the support materials such as TiO_2(a), $Al_2O_3(\gamma)$ with a solution of $H_2PtCl_6 \cdot 6H_2O$, $RhCl_3 \cdot 3H_2O$, $RuCl_3 \cdot 3H_2O$, or $PdCl_2$, and subsequent evaporation and drying at 393 K for 18 h. Before the activity test, the catalysts were activated *in situ* by reduction with H_2 at 773 K for 1 h, followed by the purge of hydrogen in the reactor with oxygen-free dry helium at the same temperature for 1 h.

Reaction and Analysis. The reaction was carried out by use of the conventional flow system with a fixed bed of catalyst under gas compositions, NO(3*%), CO(3*%), H_2O(0*—6%), H_2(0*—6%), O_2(0*—6%), and He(balance*), where * denotes a standard gas composition. The flow rate of the reactant/helium gas mixture was kept at 100 cm^3 min^{-1}. The reaction temperature ranged from 423 to 673 K, being mostly fixed at 573 K. The composition of the product gas was determined by gas chromatography and mass spectrometry.

Measurement of Catalytic Properties. The structure of support materials was determined by an X-ray powder diffraction method. The BET surface areas of the supports or catalysts were measured by a high speed surface area analyzer (Shimadzu Micromeritics). The number of surface Pt atoms of the supported Pt catalysts was estimated by conventional H_2–O_2 pulse titration. Adsorption experiments for NO and CO were carried out in a gas adsorption heat analyzer (Tokyo Riko GAC-2) connected to a vacuum system equipped with mercury and oil manometers and a calibrated pirani vacuum gauge. Heat of adsorption and gas uptakes can be measured calorimetrically and volumetrically. Temperature programed desorption (TPD) experiments were carried out in a vacuum system equipped with a pirani gauge and a mass spectrometer under the following conditions. One gram of the sample was put in a quartz tube. After reduction of the sample with H_2 at 773 K for 1 h and subsequent outgassing at the same temperature for several hours (Activation Method I), NO was adsorbed to the sample at room temperature and 1.33×10^3 Pa, followed by evacuation at room temperature for 20 min. The temperature then rose *in vacuo* with a constant rate of 10 K min^{-1}. The total pressure response of the gas desorbed from the sample was measured with a pirani gauge, the composition of the gas being monitored periodically with a mass spectrometer. The following activation method (Activation Method II) was also employed. Before the NO-adsorption, the sample which had been activated by Activation method I was oxidized with O_2 at 773 K for 10 min, evacuated at the same temperature for 10 min, reduced with H_2 at 493 K for 15 min, followed by evacuation at 493 K for 5 min and then at 623 K for 20 min.

Results and Discussion

The catalytic activities of various supported Pt catalysts for the NO–CO reaction were measured and

Table 1. Catalytic activities and properties of supported Pt catalysts

Catalyst[a]	NO[b] conversion %	Turn over frequency[b,c] s^{-1}	Selctivity to N_2[b] %	BET area $m^2\,g^{-1}$	Surface Pt atoms[e] $10^{18}\,g^{-1}$	Gas adsorption[f] Uptakes[g] 10^{-5} mol g^{-1} NO	Uptakes[g] CO	Heats kcal mol^{-1} NO	Heats CO
Pt-TiO_2	100 (100)[d]	>2.75 (>2.75)	85 (85)	65	1.7	3.3 (2.5)	6.4 (1.2)	33 (29)	89 (70)
Pt-TiO_2 (*r*-LSA)	1	≈0.47	—	1	0.1	Small		—	
Pt-Al_2O_3(γ)	100[h] (85)[d,h]	>0.55 (≈0.45)[d]	57 (57)	240	8.9	6.6 (0)	4.2 (0)	46 (—)	27 (—)
Pt-SiO_2·Al_2O_3	16	0.17	46	270	4.4	3.8 (0.5)	1.5 (0)	10 (6)	29 (—)
Pt-SiO_2	9	0.21	39	150	2	3.1 (0.7)	0.5 (0)	9 (—)	55 (—)
Pt-MgO	10	≈1.1	68	50	0.2	1.1 (1.2)	0.1 (0)	21 (31)	— (—)

a) Pt 1 wt%. b) At 573 K, NO, CO: 3%, He: 94%, 100 $cm^3\,min^{-1}$, catalyst: 0.3 g. c) The values were roughly estimated by the relation: Turn over frequency (s^{-1}) = apprant rate of NO consumption (mol s^{-1})/surface Pt (mol), after 10 min. d) After 60 min. e) From an H_2–O_2 pulse titration method. f) At 298 K. g) The values in ( ) correspond to those for the supports themselves. h) The decrease in the catalytic activity is due to the formation of surface NCO species.

Table 2. Comparison of activities of TiO-supported metal catalysts with those of Al_2O_3-supported ones[a]

Support	Promoter	NO conversion/% 523 K	573 K	623 K
TiO_2	Rh	9	76	100
	Pd	25	30	45
	Pt	≈2	9	21
	Ru	≈0	≈1	10
Al_2O_3(γ)	Rh	≈1	50	100
	Pd	≈3	17	40
	Pt	0	6	10
	Ru	0	≈1	6

a) NO, CO, 3%, He 94% flow rate 100 $cm^3\,min^{-1}$, catalyst: 0.01 g(1 wt%).

compared with each other. Conversion of NO distinctly depends on the support materials and decreases in the following order in the reaction temperature range 423—623 K: Pt-TiO_2(a-s)[100*, 98**]>Pt-TiO_2(a)[100*, 96**]>Pt-TiO_2(r-HSA)[100*, 87**]>Pt-Al_2O_3(γ)[100*, 25**] > Pt-SiO_2·Al_2O_3[16*] > Pt-MgO[10*] > Pt-SiO_2[9*] > Pt-TiO_2(r-LSA)[≈1*] > Pt-Al_2O_3(α)[0*]. The numeral in [ ] represents the % conversion of NO, after 10 min from the start of reaction, at 523 K and at $W/F=3\times10^{-3}$ g min cm^{-3} (*) or at $W/F=4\times10^{-4}$ g min cm^{-3}(**). The selectivity to N_2 also depends on the support meterials (Table 1). TiO_2, even a rutile type, unless its surface area is extremely small, gives better results. Similar carrier-effects were obtained when Rh, Pd, and Ru were employed instead of Pt. The catalytic activities of the TiO_2-supported noble metal catalysts are compared with those of the Al_2O_3-supported ones in Table 2.

Table 3. Activities of Pt-Al_2O_3(γ), Pt-TiO_2(a), and Pd-TiO_2(a) catalysts for NO-CO-H_2O or NO-CO-H_2-O_2 reaction

Catalyst	Reaction	% Conversion of NO or (NO+NO_2)	% Yield of (N_2+N_2O)	% Yield of NH_3
Pt-Al_2O_3(γ)	A	72	52	20
Pt-TiO_2(a)	A	100	100	0
Pt-Al_2O_3(γ)	B	100[a] (35)[b,c]	35	0
Pt-TiO_2(a)	B	100[a] (49)[b]	49	0
Pd-TiO_2(a)	B	100[a] (67)[b]	67	0
Pd-TiO_2(a)	C	99[a] (75)[b]	75	0

Reaction conditions, temperature: 573 K, flow rate: 100 $cm^3\,min^{-1}$; A: NO, CO 3%, H_2O 1.7%, He 92.3%, $W/F=3\times10^{-3}$ g min cm^{-3}, after 150 min; B: NO, CO, O_2 3%, H_2 5%, He 86%, $W/F=1\times10^{-4}$ g min cm^{-3}, after 5 min; C: NO, CO 2%, H_2 3%, O_2 5%, He 88%, $W/F=2\times10^{-4}$ g min cm^{-3}. a) Conversion of NO including a non-catalytic reaction: $NO+(1/2)O_2\rightarrow NO_2$. b) Conversion of (NO+$NO_2$). c) The catalytic activity gradually decreased with increase in the time on stream.

TiO_2-supported noble metal catalysts show higher catalytic activity and selectivity to N_2. In addition they have the advantage of (a) producing very minor NH_3 in both NO-CO-H_2O and NO-CO-H_2O-H_2-O_2 reactions and (b) working effectively even in a rather oxidative gas composition range for the NO-CO-(H_2O)-H_2-O_2. Examples are given in Table 3. We see that Pt-TiO_2(a) gives no NH_3 when the NO-CO reaction is carried out in the presence of H_2O vapor. Pd-TiO_2, which has a significant catalytic activity for the NO-CO reaction even around 473 K, is a very active for the NO-CO-(H_2O)-H_2-O_2 reaction when the ratio of O_2 to H_2 is near 2, while Pt-Al_2O_3(γ), which is a conventional catalyst gives rise to high

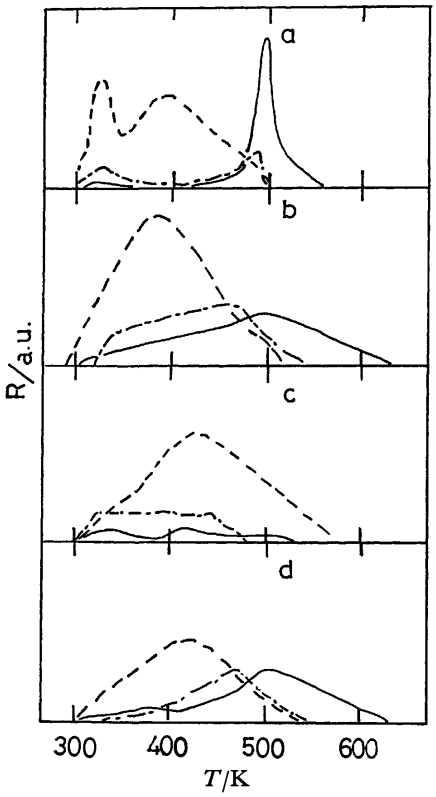

Fig. 1. TPD profiles for NO-preadsorbed catalysts and support.
a: Pt-$Al_2O_3(\gamma)$,* b: Pt-TiO_2(a),* c: TiO_2(a),* d: Pt-TiO_2(a),** T: Temperature, R: Response of desorbed gas.
NO was adsorbed at 293 K after Activation Method I(*) or after Activation Method II(**).
----: NO, ——: N_2, —·—·—: N_2O.

concentration of NH_3 in the NO-CO-H_2O reaction under the same conditions, not working effectively in such an O_2-rich region.

Some catalytic properties of the supported Pt catalysts are summarized in Table 1. The surface area of Pt depends on the support. Pt on TiO_2(a) is less dispersed than that $Al_2O_3(\gamma)$ or $SiO_2 \cdot Al_2O_3$. Baker *et al.*, who studied the particle size of Pt on the thin film of titanium oxide, aluminium oxide, *etc.* by means of electron microscopy have shown that the mean particle size of Pt in the Pt-titanium oxide (Ti_4O_7) sample reduced with H_2 below 825 K is almost the same as that of Pt in the Pt-aluminium oxide sample[4]. The disagreement of the relative dispersion of Pt may fall in the difference in the method of preparation.

Comparison of the catalytic activities with the BET surface area of the catalyst and with the number of Pt surface atoms (corresponding to the surface area of Pt metal particles dispersed over the supports) or roughly estimated turn over frequencies for the consumption of NO (Table 1) led us to the conclusion that the surface area of Pt as well as that of the catalyst is not always a dominant factor in the catalytic activity. In other words, the catalyst with larger BET area or Pt surface area does not necessarily exhibit higher activity although the low catalytic activity of Pt-TiO_2(r-LSA) might be attributed to the low surface area of Pt. Table 1 indicates that the highly active catalysts, Pt-$Al_2O_3(\gamma)$ and Pt-TiO_2(a), are characterized by their higher heat of a adsorption for NO and also by both high NO and CO uptakes, while the other less active catalysts lack either one or both of the terms. For example, the lower activity of Pt-SiO_2 and Pt-$SiO_2 \cdot Al_2O_3$ might be due to their poor ability to activate NO molecules compared with Pt-$Al_2O_3(\gamma)$ and Pt-TiO_2(a), since they have lower heat of adsorption for NO.

In order to clarify why Pt-TiO_2(a) is more active than Pt-$Al_2O_3(\gamma)$, in particular at lower temperatures, temperature programmed desorption (TPD) experiments with respect to the NO-preadsorbed Pt-$Al_2O_3(\gamma)$ and Pt-TiO_2(a) were carried out. The results are shown in Figs. 1a and 1b, respectively. For Pt-$Al_2O_3(\gamma)$, there is a relatively sharp desorption peak of N_2 around 503 K, which was formed from the NO molecules adsorbed on the catalyst. The result closely agrees with that reported by Unland who concluded that the dissociation of NO on Pt-$Al_2O_3(\gamma)$ occurs above 503 K.[6-8] On the contrary, the TPD spectrum for Pt-TiO_2(a), in our case, was found to differ from that for Pt-$Al_2O_3(\gamma)$, the spectrum being characterized by the following two points: (a) N_2-desorption occurs at lower temperatures around 373 K, indicating that NO molecules dessociate on Pt-TiO_2(a) at much lower temperature on Pt-$Al_2O_3(\gamma)$, and (b) the spectrum of N_2-desorption spreads over a wide temperature range. This might be due to the heterogeneity of the active site on the Pt-TiO_2(a) catalyst.

It should be noted that N_2 and N_2O are formed not only by the reaction between the adsorbed NO molecules and Pt but also by the reaction between those and the TiO_2(a) support, since the support is probably reduced to some extent during the course of activation with H_2 at 773 K and adsorbs NO molecules. In fact an EPR experiment showed the presence of Ti^{3+} in the TiO_2(a) support activated by Activation Method I. NO-preadsorbed TiO_2(a) gave a TPD spectrum consisting of N_2, N_2O, and NO (Fig. 1c). A comparison of Figs. 1b and 1c, however, suggests that both N_2 and N_2O are formed mostly by the reaction between the adsorbed NO molecules and Pt, especially above 423 K. A TPD experiment for a Pt-TiO_2(a) catalyst which had been previously activated by Activation Method II was carried out (Fig. 1d). An EPR experiment revealed that the concentration of Ti^{3+} in Pt-TiO_2(a) activated by Activation Method II is negligible-less than one tenth of that in the Pt-TiO_2(a) sample activated by Activation Method I. This indicates that Activation Method II gives an almost fully oxidized TiO_2(a) support. In fact a TPD experiment showed that nither N_2 nor N_2O is liberated from NO-preadsorbed TiO_2(a) previously activated by Activation Method II. On the contrary, the Pt surface area of the Pt-TiO_2(a) catalyst activated by Activation Method II was close to that of Pt-TiO_2(a) activated by Activation Method I. These results indicate that the Pt-TiO_2(a) catalyst activated by Activation Method II consists of almost completely reduced Pt and almost fully oxidized TiO_2(a). No reaction between NO and the fully oxidized TiO_2(a)

support can be expected, the formation of N_2 and N_2O shown in Fig. 1d being ascribed to the reaction between NO and Pt on the TiO_2(a) support.

IR studies on the surface NCO species formed on the catalysts during the course of NO–CO reaction showed that the NCO species is formed on TiO_2-supported catalysts at lower temperatures than on the corresponding Al_2O_3-supported catalyst. The NCO species, for example, was observed not on Pt–$Al_2O_3(\gamma)$ at 473 K but on Pt–TiO_2(a) at the same temperature. The result suggests that the dissociation of NO occurs on the TiO_2-supported ones, since the NCO seems to be produced by the reaction between a CO molecule and an adsorbed N atom formed by the dissociation of an adsorbed NO molecule.

The big difference in catalytic activity between Pt–TiO_2(a) and the other suppored Pt catalysts is not attributed to the difference of the surface area of Pt but to that of the NO-dissociation ability of the catalysts. The reason why the TiO_2-supported catalysts easily dissociated NO at lower temperature than the others is still unknown. However, an explanation is that the NO-dissociation ability might be due to the high concentrations of free electrons of the TiO_2 support or Ti^{3+} ions having thermally emissive electrons; probably, the back donation of one of these electrons into a π^* (antibonding) orbital of the adsorbed NO molecule through the dispersed Pt metal on TiO_2 weakens the N–O bond.

In conclusion, TiO_2, either anatase or rutile unless its surface area is extremely low, was found to be a most effective support for different noble metal catalysts in the NO–CO reaction even in the presence of H_2O, H_2, and O_2. The high catalytic activity of the TiO_2-supported catalyst could be attributed, at least, to its ability to activate NO molecules by dissociative adsorption at lower temperatures.

This work was supported by Grant-in-Aid for Special Project Research.

References

1) J. Wei, *Adv. Catal.*, **24**, 57 (1975).
2) E. Echigoya, *Kagaku*, **33**, 338 (1977).
3) R. L. Klimish, Preprints of Papers for the Japan-U.S.A. Seminar on Catalytic NO_x Reactions 2—4 November 1975 Susono, Japan.
4) R. T. K. Baker, E. B. Prestridge, and R. L. Garten, *J. Catal.*, **56**, 390 (1979).
5) K. Funaki and Y. Saeki, *Kogyo Kagaku Zasshi*, **59**, 1291, 1295 (1956).
6) R. Nakamura and E. Echigoya, *Bull. Jpn. Petrol. Inst.*, **14**, 187 (1972).
7) M. L. Unland, *J. Phys. Chem.*, **77**, 1952 (1973).
8) M. L. Unland, *J. Catal.*, **31**, 459 (1973).
9) H. Arai, *Hyomen*, **14**, 427 (1976).
10) S. Okazaki, "Kinzoku-sankabutsu To Fukugo-sankabutsu," ed by K. Tanabe, T. Seiyama, and K. Fueki, Kodan-sha, Tokyo (1978), p. 104.

The Structure of the Cyclodextrin Complex. X. Crystal Structure of α-Cyclodextrin–Benzaldehyde (1 : 1) Complex Hexahyderate

Kazuaki HARATA,* Kaneto UEKAMA,† Masaki OTAGIRI,†
Fumitoshi HIRAYAMA,† and Hisashi OGINO††

Research Institute for Polymers and Textiles, 1-1-4, Yatabe-Higashi, Tsukuba, Ibaraki 305

† *Faculty of Pharmaceutical Sciences, Kumamoto University, 5-1, Oe-honmachi, Kumamoto 862*

†† *Kaken Chemical Co., Ltd., Honkomagome, Bunkyo-ku, Tokyo 113*

(Received November 12, 1980)

The crystal structure of the α-cyclodextrin–benzaldehyde (1:1) complex hexahydrate, $C_{36}H_{60}O_{30}\cdot C_7H_6O\cdot 6H_2O$, was determined by the X-ray method. The crystal is monoclinic, the space group being $P2_1$ with $Z=2$. The cell dimensions are $a=7.932(1)$, $b=13.500(1)$, $c=24.704(2)$ Å, and $\beta=90.85(1)°$. The structure was solved by means of a Patterson map and a trial-and-error method combined with the rigid-body least-squares technique. Refinement was carried out by the block-diagonal least-squares method to the final R-value of 0.057 for 4565 reflections. α-Cyclodextrin molecules are stacked along the a axis in a head-to-tail fashion to form a channel-type structure. The α-cyclodextrin ring is tilted by an angle of 11.5° against the channel axis. Adjacent α-cyclodextrin molecules along the channel are linked by hydrogen bonds between the primary hydroxyl groups and the secondary hydroxyl groups, and O(2)···water···O(6) hydrogen-bond bridges. The guest benzaldehyde molecules are aligned inside the α-cyclodextrin column. The benzene ring is inserted into the α-cyclodextrin ring from the secondary hydroxyl side, while the carbonyl group is in the van der Waals contact with the primary hydroxyl side of the next α-cyclodextrin. The guest plane is nearly parallel to the channel axis, making an angle of 71.2° against the plane through six glycosidic oxygen atoms. Spaces between α-cyclodextrin columns are filled with water molecules. Many hydrogen bonds are observed among hydroxyl groups of α-cyclodextrin and water molecules, forming a hydrogen-bond network in the crystal.

Interaction of cyclodextrins with drugs has received considerable attention because the complexation may increase their solubility and chemical stability.[1] It was recently found that the photolysis and oxidation of benzaldehyde are significantly retarded by cyclodextrins,[2] several crystal structures of α-cyclodextrin complexes with benzene derivatives having been investigated by the X-ray method.[3–6] In this paper, the crystal structure of the benzaldehyde complex is discussed.

Experimental

α-Cyclodextrin and benzaldehyde in a 1:1 molar ratio were dissolved in degassed water at 80 °C. The solution was sealed under nitrogen and then cooled slowly to room temperature, colorless plate-like crystals being obtained. Experiments were carried out in the dark to avoid photolysis and oxidation of benzaldehyde. Measurements of lattice parameters and intensities were carried out on a Rigaku automatic four-circle diffractometer with graphite monochromated Cu $K\alpha$ radiation; 4565 independent reflections with $|F_o|>3\sigma(F)$ were collected up to 150° in 2θ by a θ-2θ scan technique. No corrections were made for absorption and extinction.

Crystal Data: $C_{36}H_{60}O_{30}\cdot C_7H_6O\cdot 6H_2O$, $F.W.=1187.1$, monoclinic, space group $P2_1$, $Z=2$, $a=7.932(1)$, $b=13.500(1)$, $c=24.704(2)$ Å, $\beta=90.85(1)°$, $V=2645.1$ Å^3, $D_x=1.490$, $D_m=1.495$ g·cm^{-3}.

Determination and Refinement of the Structure

The orientation of the α-cyclodextrin molecule in the crystal was easily deduced by inspection of a Patterson map. The position of the molecule was determined by the trial-and-error method. The positional and orientational parameters of each glucose residue were corrected by the rigid-body least-squares method. Benzaldehyde and water molecules were found on Fourier and difference-Fourier maps. A primary hydroxyl group (O(6,G1)) of α-cyclodextrin and a water molecule (W2) were statistically disordered. Their occupancy was estimated from an electron-density map, but the results were not refined. Seventy-three hydrogen atoms were found on a difference-Fourier map. The refinement of the structure was carried out by the block-diagonal least-squares method. The quantity minimized was $\Sigma w(|F_o|-|F_c|)^2$, with $w=1.0$ for all the reflections, the final R-value being 0.057. The atomic scattering factors were taken from "International Tables for X-Ray Crystallography."[7] The atomic coordinates are given in Table 1. Tables of anisotropic temperature factors of non-hydrogen atoms, atomic parameters of hydrogen atoms, observed and calculated structure factors, bond distances, angles, and conformation angles in α-cyclodextrin are kept at The Chemical Society of Japan (Document No. 8135).

Description of the Structure and Discussion

Outline of the Structure. The structure and numbering scheme of the complex are shown in Fig. 1, the atom numbering for α-cyclodextrin being the same as that used in the *m*-nitroaniline complex.[6] The α-cyclodextrin molecule is in the shape of a distorted hexagon, and is stacked along the a axis in the head-to-tail mode to form a typical channel-type structure (Fig. 2). The guest benzaldehyde molecule is linearly arranged in the channel, being fixed by the van der Waals force.

Table 1. Final atomic coordinates($\times 10^4$) and B_{eq}[a] (B/Å^2) of non-hydrogen atoms[b]

	x	y	z	B_{eq}/Å^2		x	y	z	B_{eq}/Å^2
C (1, G1)	−255 (8)	4863 (−)	1074 (2)	3.38	O (3, G4)	−755 (5)	11841 (4)	2788 (2)	3, 56
C (2, G1)	−1766 (7)	4418 (4)	1360 (2)	3.14	O (4, G4)	1591 (5)	10714 (3)	2212 (1)	2.78
C (3, G1)	−1781 (7)	4754 (5)	1943 (2)	2.88	O (5, G4)	3505 (4)	10793 (3)	3574 (2)	3.12
C (4, G1)	−99 (6)	4517 (4)	2227 (2)	2.64	O (6, G4)	5735 (5)	11444 (5)	2785 (2)	5.13
C (5, G1)	1313 (7)	5014 (5)	1908 (2)	3.26	C (1, G5)	1167 (7)	7134 (5)	4668 (2)	2.89
C (6, G1)	3057 (8)	4753 (7)	2131 (2)	4.74	C (2, G5)	−122 (7)	7898 (5)	4857 (2)	3.05
O (2, G1)	−3285 (5)	4696 (4)	1086 (2)	4.12	C (3, G5)	−202 (7)	8752 (4)	4458 (2)	2.67
O (3, G1)	−3088 (5)	4231 (4)	2220 (2)	3.82	C (4, G5)	1550 (6)	9178 (4)	4360 (2)	2.54
O (4, G1)	−195 (4)	4933 (3)	2753 (1)	2.66	C (5, G5)	2827 (7)	8356 (5)	4238 (2)	2.41
O (5, G1)	1248 (5)	4634 (4)	1360 (2)	3.70	C (6, G5)	4658 (8)	8698 (5)	4210 (1)	3.94
O (6A, G1)	3338 (12)	3665 (9)	2140 (6)	6.96	O (2, G5)	−1731 (5)	7402 (3)	4872 (2)	4.01
O (6B, G1)	4189 (11)	5503 (11)	1913 (5)	6.63	O (3, G5)	−1211 (5)	9556 (3)	4648 (2)	3.72
C (1, G2)	1222 (7)	8382 (5)	295 (2)	3.36	O (4, G5)	1363 (4)	9782 (3)	3885 (1)	2.61
C (2, G2)	−454 (7)	7997 (5)	61 (2)	3.23	O (5, G5)	2775 (5)	7601 (3)	4641 (2)	3.02
C (3, G2)	−1128 (7)	7177 (5)	417 (2)	3.32	O (6, G5)	5208 (5)	9167 (4)	4678 (2)	4.68
C (4, G2)	168 (7)	6399 (5)	558 (2)	3.13	C (1, G6)	192 (7)	4316 (4)	3198 (2)	2.72
C (5, G2)	1943 (7)	6829 (5)	696 (2)	3.07	C (2, G6)	−1178 (6)	4458 (4)	3623 (2)	2.73
C (6, G2)	3336 (8)	6072 (6)	636 (3)	4.40	C (3, G6)	−1101 (6)	5500 (5)	3845 (2)	2.86
O (2, G2)	−1594 (6)	8806 (4)	17 (2)	4.24	C (4, G6)	679 (6)	5762 (4)	4040 (2)	2.47
O (3, G2)	−2519 (6)	6741 (4)	126 (2)	5.00	C (5, G6)	1920 (6)	5573 (4)	3588 (2)	2.61
O (4, G2)	−496 (5)	5898 (3)	1025 (2)	3.12	C (6, G6)	3764 (6)	5759 (5)	3738 (2)	3.31
O (5, G2)	2375 (5)	7606 (3)	329 (2)	3.39	O (2, G6)	−2787 (5)	4272 (3)	3374 (2)	3.35
O (6, G2)	4852 (5)	6426 (4)	884 (2)	5.15	O (3, G6)	−2243 (4)	5560 (3)	4295 (2)	3.36
C (1, G3)	2173 (7)	11225 (5)	1754 (2)	3.24	O (4, G6)	631 (4)	6798 (3)	4157 (1)	2.36
C (2, G3)	696 (8)	11355 (5)	1355 (2)	4, 03	O (5, G6)	1807 (4)	4554 (3)	3423 (2)	2.81
C (3, G3)	72 (7)	10348 (5)	1161 (2)	3.58	O (6, G6)	4214 (5)	5188 (4)	4194 (2)	4.19
C (4, G3)	1526 (7)	9768 (4)	921 (2)	2.84	C (1, BA)	−3464 (10)	7678 (6)	2464 (2)	5.38
C (5, G3)	2996 (7)	9705 (5)	1326 (2)	3.22	C (2, BA)	−2535 (13)	7891 (9)	2950 (3)	8.36
C (6, G3)	4584 (8)	9247 (6)	1081 (3)	4.60	C (3, BA)	−812 (13)	8043 (7)	2923 (4)	9.79
O (2, G3)	−586 (6)	11928 (4)	1601 (2)	5.37	C (4, BA)	−96 (11)	8007 (9)	2436 (4)	7.51
O (3, G3)	−1186 (6)	10519 (4)	749 (2)	4.97	C (5, BA)	−961 (12)	7822 (8)	1974 (7)	6.97
O (4, G3)	890 (5)	8802 (3)	806 (1)	3.14	C (6, BA)	−2637 (10)	7628 (7)	1989 (3)	5.68
O (5, G3)	3478 (5)	10675 (3)	1502 (2)	3.37	C (7, BA)	−5337 (15)	7511 (12)	2433 (6)	11.53
O (6, G3)	4976 (7)	9725 (5)	588 (2)	6.43	O (1, BA)	−6114 (10)	7653 (10)	2872 (4)	14.26
C (1, G4)	2037 (7)	10752 (5)	3883 (2)	3.09	O (W1)	5591 (10)	2476 (7)	1885 (3)	10.14
C (2, G4)	676 (8)	11422 (5)	3636 (2)	3.34	O (W2A)	5162 (9)	8564 (6)	−364 (3)	4.33
C (3, G4)	344 (7)	11131 (4)	3046 (2)	2.87	O (W2B)	6029 (16)	8378 (10)	−873 (5)	5.16
C (4, G4)	1997 (6)	11116 (4)	2731 (2)	2.56	O (W3)	6020 (8)	11803 (5)	823 (3)	7.51
C (5, G4)	3287 (7)	10456 (5)	3019 (2)	3.04	O (W4)	6256 (6)	12450 (4)	3756 (2)	4.84
C (6, G4)	5028 (7)	10476 (6)	2774 (3)	4.46	O (W5)	5192 (14)	11258 (9)	4717 (4)	14.70
O (2, G4)	−826 (6)	11347 (4)	3946 (2)	4.29	O (W6)	6388 (8)	8179 (4)	5649 (2)	6.62

a) $B_{eq}=8\pi^2(U_1+U_2+U_3)/3$ where U_1, U_2, and U_3 are the principal components of U matrix. b) The occupancy factors for O(6A, G1), O(6B, G1), O(W2A), and O(W2B) are 0.5, 0.5, 0.6, and 0.4, respectively.

Conformation of α-Cyclodextrin. Average bond distances and angles in six glucose residues are shown in Fig. 3. The C–C bond distances are in the range 1.518—1.533 Å. The C(1)–C(2) and C(4)–C(5) bonds are somewhat longer than the C(2)–C(3) and C(3)–C(4) bonds. The anomeric C–O bonds (1.411 and 1.414 Å) are shorter than the other C–O bonds (1.421—1.437 Å). The C(3)–C(4)–O(4) and C(6)–C(5)–O(5) angles are relatively small, the C(4)–C(5)–C(6) angle (113.7°) being large. The same tendency has been observed in the uncomplexed α-cyclodextrin and in the α-cyclodextrin complexes with some other guests.[3,8] The larger C(4)–C(5)–C(6) angle may be ascribed to the repulsive interaction between the C(6) methylene group and the adjacent glucose residue. The C(4)–O(4)–C(1′) glycosidic oxygen angles are in the range 117.7—119.7° in good agreement with those of other α-cyclodextrin complexes.[3–6,8] Except for the G1 and G2 residues, the primary hydroxyl group is in the *gauche-gauche* conformation. The G2 residue has the hydroxyl group with the *gauche-trans* conformation, the primary hydroxyl group of the G1 residue being statistically disordered showing the *gauche-gauche* and *gauche-trans* conformations for O(6A,G1) and O(6B,G1), respectively (Fig. 1).

The hexagonal α-cyclodextrin ring is elliptically distorted owing to the inclusion of the planar molecule, as seen from the diagonal distances measured between

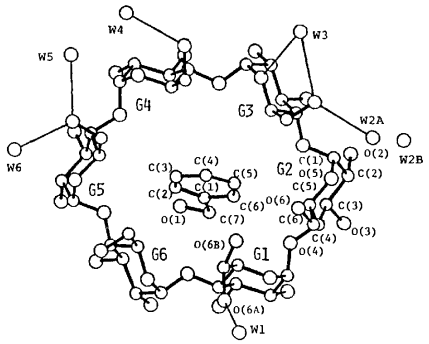

Fig. 1. Structure and numbering scheme of the α-cyclodextrin-benzaldehyde complex hexahydrate. The water molecules are shown by W1, W2A, W2B, W3, W4, W5, and W6, in which W2A and W2B denote the disordered W2 water. The disordered primary hydroxyl group of the G1 residue is denoted by O6A and O6B. Intermolecular contacts less than 3.1 Å are shown by thin lines.

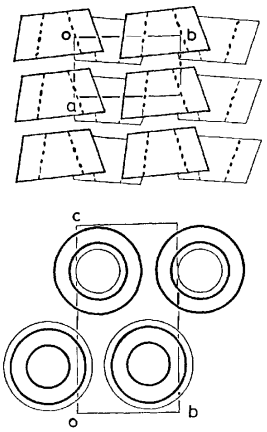

Fig. 2. Schematic drawings of the packing feature of α-cyclodextrin in the crystal.

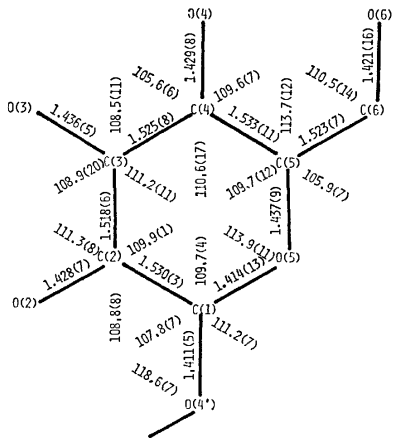

Fig. 3. Average bond distances (l/Å) and angles (ϕ/°) over six glucose residues. Standard deviations in parentheses were estimated according to the equation: $\sigma=[\sum_{i=1}^{6}(x_i-\bar{x})^2/5]^{1/2}$, where x_i referes to the bond distance or angle in the i-th glucose residue, and $\bar{x}$ is the average value.

TABLE 2. GEOMETRICAL DATA FOR α-CYCLODEXTRIN RING

I. O(4)···O(4) distances

Distance (l/Å)		Distance (l/Å)	
O(4, G1)···O(4, G2)	4.466	O(4, G5)···O(4, G6)	4.126
O(4, G1)···O(4, G6)	4.328	O(4, G1)···O(4, G4)	8.047
O(4, G2)···O(4, G3)	4.110	O(4, G2)···O(4, G5)	8.905
O(4, G3)···O(4, G4)	4.357	O(4, G3)···O(4, G6)	8.714
O(4, G4)···O(4, G5)	4.327		

II. Torsion-angle index (I), tilt-angle (II), glycosidic oxygen angle (III), and the angle made by the planes through O(4'), C(1), C(4), and O(4) (IV)

Residue	I(ϕ/°)	II(ϕ/°)	III(ϕ/°)	IV(ϕ/°)
G1	117	19.5	118.8	27.6(G1-G2)
G2	143	19.9	117.8	13.3(G2-G3)
G3	122	15.7	118.4	13.0(G3-G4)
G4	123	10.9	117.7	12.2(G4-G5)
G5	140	11.8	119.7	15.4(G5-G6)
G6	122	18.3	119.3	14.0(G6-G1)

TABLE 3. LEAST-SQUARES PLANES AND DEVIATIONS OF ATOMS FROM THE PLANE

The plane equation is of the $AX+BY+CZ=D$ from, where X, Y, and Z are the coordinates in Å unit along the a, b, and c* axis, respectively.

I. The plane through six O(4) atoms			
$0.980X-0.196Y-0.049Z=-1.878$			
G1	0.089	G4	0.013
G2	−0.192	G5	−0.120
G3	0.144	G6	0.066
II. Benzaldehyde			
$-0.140X+0.979Y-0.144Z=9.697$			
C1	−0.039	C5	0.047
C2	−0.034	C6	−0.028
C3	−0.015	C7	−0.040
C4	0.031	O1	0.078

the glycosidic oxygen atoms in Table 2. The conformation of each glucose residue is affected by such distortion. The distance between the adjacent glycosidic oxygen atoms is in the range 4.110—4.466 Å. The O(4)···O(4) distance is closely related to the conformation of pyranose ring characterized by the torsion-angle index.[3] The shorter O(4)···O(4) distance gives the large torsion-angle index. This is ascribed to the smaller conformation angles of C(2)–C(3)–C(4)–C(5) and C(3)–C(4)–C(5)–O(5) and the larger angles of O(5)–C(1)–C(2)–C(3) and C(5)–O(5)–C(1)–C(2).

A tilt-angle between the plane through six glycosidic oxygen atoms and the plane through O(4'), C(1), C(4), and O(4) atoms of each glucose residue was proposed as a convenient measure to describe the orientation of each glucose residue relative to the macro-cyclic ring.[9] In the benzaldehyde complex, the tilt-angles are in the range 10.9—19.9, the average value being 16.0°. These values are similar to those found in the *m*-nitroaniline complex,[6] but considerably larger than those of complexes with other aromatic

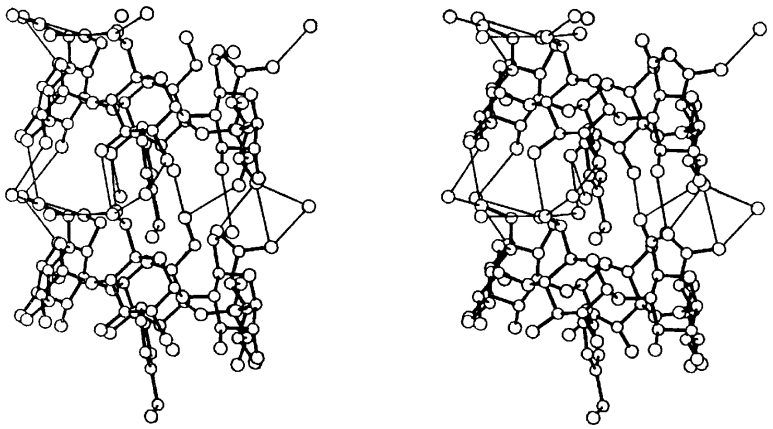

Fig. 4. A stereo-drawing of the packing feature of the complex with associated water molecules. Thin lines denote intermolecular contacts less than 3.1 Å.

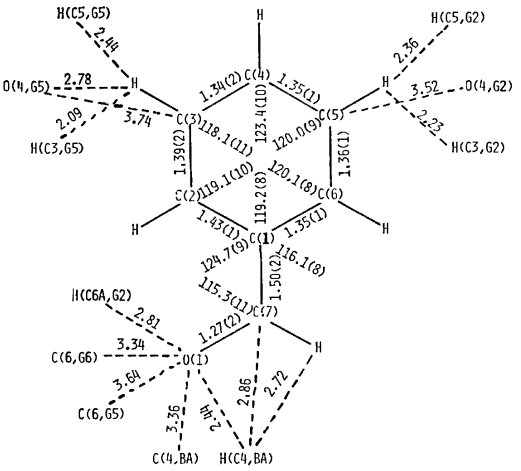

Fig. 5. Bond distances (l/Å) and angles (ϕ/°) in benzaldehyde and selected intermolecular distances (l/Å) between α-cyclodextrin and benzaldehyde. Estimated standard deviations in benzaldehyde are given in parentheses.

guests (average values of 10—12°).[9] Since the packing of α-cyclodextrin in the crystal is nearly the same in the complexes with *m*-nitroaniline and benzaldehyde, we propose another example to support the suggestion that the tilt-angle is largely determined by the packing of α-cyclodextrin in the crystal.

The O(2)···O(3) contact between the adjacent glucose residues is also important to interpret the α-cyclodextrin conformation. The greatest O(2)···O(3) distance is 3.695 Å observed between the G1 and G2 residues, while the other O(2)···O(3) distances are in the range 2.857—2.994 Å. We see from Table 2 that the C(4)–O(4)–C(1′) angle scarecely affects the O(2)···O(3) distance; the greatest O(2)···O(3) distance is observed between the most tilted residues, but the O(2,G2)···O(3,G3) distance is the smallest in spite of the large tilt of the G2 and G3 residues. The O(2)···O(3) distance is more sensitive to the angle made by two planes through O(4′), C(1), C(4), and O(4) of the corresponding glucose residues. The largest angle of 27.6° is found between the G1 and G2 residues, while the other values are in a relatively small region (12.2—15.4°) in accordance with the distribution of the O(2)···O(3) distances.

α-Cyclodextrin-Guest Interaction. Figure 5 shows bond distances and angles in benzaldehyde and intermolecular distances between α-cyclodextrin and benzaldehyde. There is no unusual value in bond distances and angles in benzaldehyde, the planarity of the molecule being fairly good (Table 3). The α-cyclodextrin ring includes about two-third of the benzene ring, while the carbonyl group protrudes from the secondary hydroxyl side and is inserted into the next α-cyclodextrin ring from the primary hydroxyl side (Fig. 4). The benzaldehyde molecule is tilted towards the G1 residue, making an angle of 71.2° against the O(4) plane. The value differs significantly from those found in the α-cyclodextrin complexes with benzene derivatives, in which the aromatic plane is nearly perpendicular to the O(4) plane.[3,5] In those complexes, the benzene ring is deeply inserted into the α-cyclodextrin ring. The benzaldehyde plane is nearly parallel to the C(3,G2)···C(3,G5) diagonal. The relatively short hydrogen···hydrogen contacts are observed between the benzene ring and the C(3) methine groups; H(C3,G5)···H(C3,BA) of 2.09 Å and H(C3,G2)···H(C5,BA) of 2.23 Å. Such a short intermolecular distance is also found between the benzaldehyde molecules; H(C4,BA)···O(1,BA) of 2.44 Å. It is noteworthy that the carbonyl group does not form a hydrogen bond with α-cyclodextrin, and the benzaldehyde molecule is fixed in the α-cyclodextrin ring by the van der Waals contact. In the α-cyclodextrin complexes with other aromatic guests, the guest molecule is hydrogen-bonded to the next α-cyclodextrin or adjacent water molecules. Although the inclusion geometry of the sodium benzenesulfonate complex is similar to the benzaldehyde complex, the sulfonato group of the guest is hydrogen-bonded to primary hydroxyl groups which are in the *gauche-trans* conformation.[4] In the benzaldehyde complex, the nearest primary hydroxyl group is in the *gauche-gauche* conformation, being oriented in the opposite direction. The carbonyl group is so deeply inserted into the α-cyclodextrin ring that it can not form a hydrogen bond with the primary hydroxyl group even when it is in the *gauche-trans* conformation.

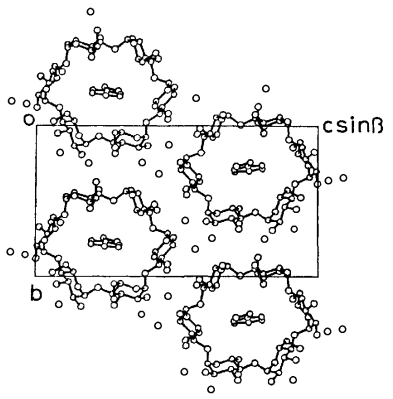

Fig. 6. Crystal structure viewed down the a axis.

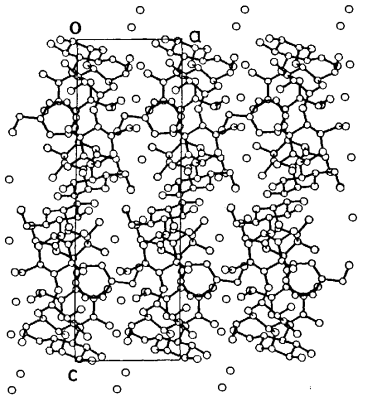

Fig. 7. Crystal structure viewed down the b axis.

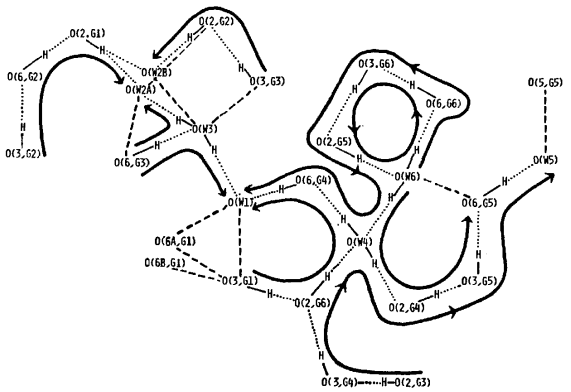

Fig. 8. A schematic drawing of the hydrogen-bond network in the crystal. Arrows indicate the direction of the O–H bond. Intermolecular O···O contacts less than 3.0 Å are shown by broken lines.

Molecular Packing and Hydrogen Bonds. Crystals of the α-cyclodextrin–benzaldehyde complex are built up of the stack of α-cyclodextrin molecules along the a axis to form endless columns. The projections of the crystal structure are shown in Figs. 6 and 7. The α-cyclodextrin molecule is nearly parallel to the a axis, being tilted by 11.5°. The guest benzaldehyde molecules are aligned inside the column with their planes parallel to the ac plane; the angle between these planes is 11.7°. The repetition unit along the column axis (7.932 Å) is almost the same as that of the *m*-nitroaniline complex (8.054 Å), but shorter by 0.3 Å than that of the sodium benzenesulfonate complex. Since the channel axis is perpendicular to the two-fold screw axis, the α-cyclodextrin molecule of the symmetry-related column is arranged up-side-down. These α-cyclodextrin columns are closely packed in the crystal, spaces between columns being filled with water molecules.

So far, no details of hydrogen-bond scheme have been described in the α-cyclodextrin complexes with the channel-type structure.[4,5] A number of hydrogen-bonding contacts were defined in the benzaldehyde complex since most of the hydrogen atoms were found. Five intramolecular hydrogen bonds are formed between the adjacent glucose residues: O(3,G1)–H···O(2,G6), O(3,G3)–H···O(2,G2), O(2,G3)–H···O(3,G4), O(2,G4)–H···O(3,G5), and O(3,G6)–H···O(2,G5). No hydrogen-bonding contact is observed between the G1 and G2 residues, but they are linked by the O(3,G2)–H···O(6,G2)–H···O(2,G1) hydrogen bonds. The adjacent α-cyclodextrin molecules along the channel are connected by the direct hydrogen bonds and hydrogen-bonding linkages involving water molecules. The G2, G4, G5, and G6

Table 4. Hydrogen-bond distances (*l*/Å) and angles (*φ*/°) and intermolecular distances (*l*/Å) less than 3.0 Å

Estimated standard deviations are in the ranges 0.006—0.008 Å for the distance, 0.06—0.10 Å for the distance involving the hydrogen atoms, and 1.0—4.0° for the O–H···O angle.

O	H	O		DISTANCES O–H	H···O	O···O	ANGLES O–H···O
O(2,G1)	–H(O2,G1)	O(W2A)	(e)	1.09	1.89	2.767	135
O(2,G1)	–H(O2,G1)	O(W2B)	(e)	1.09	1.85	2.855	152
O(3,G1)	–H(O3,G1)	O(2,G6)		0.99	1.88	2.857	168
O(2,G2)	–H(O2,G2)	O(W2A)	(b)	0.96	1.83	2.746	158
O(2,G2)	–H(O2,G2)	O(W2B)	(b)	0.96	2.03	2.933	157
O(3,G2)	–H(O3,G2)	O(6,G2)	(b)	0.78	2.08	2.855	174
O(6,G2)	–H(O6,G2)	O(2,G1)	(b)	1.08	1.86	2.804	144
O(2,G3)	–H(O2,G3)	O(3,G4)		0.96	2.01	2.939	169
O(3,G3)	–H(O3,G3)	O(2,G2)		0.86	2.23	2.950	141
O(6,G3)	–H(O6,G3)	O(W3)		0.91	2.29	2.825	111
O(2,G4)	–H(O2,G4)	O(3,G5)		1.05	1.94	2.994	176
O(3,G4)	–H(O3,G4)	O(6,G4)	(b)	1.08	1.91	2.836	142
O(6,G4)	–H(O6,G4)	O(W1)	(a)	1.05	1.63	2.623	157
O(2,G5)	–H(O2,G5)	O(W6)	(b)	1.10	1.64	2.663	154
O(3,G5)	–H(O3,G5)	O(6,G5)	(b)	0.81	2.11	2.891	162
O(6,G5)	–H(O6,G5)	O(W5)		1.04	2.29	2.825	111
O(2,G6)	–H(O2,G6)	O(W4)	(d)	1.02	1.74	2.747	169
O(3,G6)	–H(O3,G6)	O(2,G5)		1.10	1.82	2.891	165
O(6,G6)	–H(O6,G6)	O(3,G6)	(b)	0.92	1.96	2.862	169
O(W3)	–H(1,W3)	O(W1)	(c)	1.32	1.51	2.802	163
O(W3)	–H(2,W3)	O(W2A)	(g)	1.00	2.20	2.791	116
O(W4)	–H(1,W4)	O(2,G4)	(b)	0.94	1.87	2.789	165
O(W4)	–H(2,W4)	O(6,G4)		1.19	1.62	2.782	166
O(W6)	–H(1,W6)	O(6,G6)	(h)	0.78	2.20	2.783	132
O(W6)	–H(2,W6)	O(W4)	(f)	1.11	1.69	2.761	162
O(3,G1)		O(6A,G1)	(b)			2.940	
O(3,G1)		O(6B,G1)	(b)			2.854	
O(3,G1)		O(W1)	(b)			2.715	
O(6,G1)		O(W1)				2.490	
O(3,G3)		O(W3)	(b)			2.822	
O(6,G3)		O(W2A)				2.832	
O(5,G5)		O(W5)	(h)			2.885	
O(6,G5)		O(W6)				2.919	
O(W2B)		O(W3)	(g)			2.680	

Code	Symmetry operator		
None	x,	y,	z
a	x	1+y,	z
b	-1+x,	y,	z
c	x,	-1+y,	z
d	-1+x,	-1+y,	z
e	-x,	-1/2+y,	-z
f	1-x,	1/2+y,	1-z
g	1-x,	-1/2+y,	-z
h	1-x.	-1/2+y,	1-z

residues are linked by the O(3)···O(6) hydrogen bond. In the G2, G4, and G5 residues, the O(3) hydroxyl group donates the hydrogen atom, while the O(6) hydroxyl group acts as a donor in the G6 residue. Although no hydrogen atom of the O(6A,G1) and O(6B,G1) hydroxyl group was found, the intermolecular distance (Table 4) indicates that they are hydrogen-bonded to the O(3,G1) hydroxyl group of the adjacent α-cyclodextrin. The O(2) hydroxyl groups are also involved in the hydrogen bonds connecting the adjacent α-cyclodextrins. The O(6,G2) hydroxyl group donates the hydrogen atom to O(2,G1). O(2, G4) and O(6,G4) are linked through the O(2,G4)···H–O(W4)–H···O(6,G4) hydrogen-bond bridge.

Water molecules are located in two intermolecular spaces. W1, W2A, W2B, and W3 fill the space encircled by the G1, G2, and G3 residues. W2 is statistically disordered, occupying two positions. The water molecules are linked by the O(W1)···H–O(W3)–H···O(W2A) hydrogen-bond bridge. Although no hydrogen atoms of the W2B water molecule were found, the O(W3)···O(W2B) distance of 2.680 Å suggests a hydrogen-bond formation. W4, W5, and W6 occupy the space encircled by the G4, G5, and G6 residues. W4 and W6 are connected by the O(W6)–H···O(W4) hydrogen bond, W5 being isolated and only hydrogen-bonded to O(6,G5).

In the crystal, a hydrogen-bond network is constructed by circles and chains of hydrogen bonds (Fig. 8). The four-membered hydrogen-bond circle is formed by O(2,G5), O(3,G6), O(6,G6), and W6. O(2,G4), O(3,G5), O(6,G5), O(W6), and O(W4) form a five-membered ring, but the circle is not closed since the O(W6) and O(6,G5) forms no hydrogen bond in spite of a suitable distance of 2.919 Å. In the five-membered ring composed of O(3,G1), O(2,G6), O(W4), O(6,G4) and O(W1), the O(W1)–H bond should be oriented to O(3,G1) to close the circle.

The α-cyclodextrin packing in the present crystal resembles that in the *m*-nitroaniline complex, but their crystal property is quite different; the crystal of the *m*-nitroaniline complex easily breaks up in the air. This may be mainly due to the conformation of G1, G2, and G3 residues and water molecules hydrogen-bonded to them. The primary hydroxyl group of the G1 residue in the benzaldehyde complex is disordered and that of the G2 residue is in the *gauche-trans* conformation. On the other hand, in the *m*-nitroaniline complex, the primary hydroxyl groups of the G2 and G3 residues are disordered, and the *gauche-gauche* conformation is found in the G1 residue. Four water molecules in the *m*-nitroaniline complex are located in the same positions as those of W3, W4, W5, and W6 in the benzaldehyde complex, but the other two water molecules occupy different sites.

References

1) J. L. Lach and J. Cohen, *J. Pharm. Sci.*, **52**, 137 (1963); K. Uekama, F. Hirayama, K. Ikeda, and K. Inaba, *ibid.*, **66**, 706 (1977); K. Uekama, F. Hirayama, Y. Yamada, K. Inaba, and K. Ikeda, *ibid.*, **68**, 1059 (1979).

2) F. Hirayama, S. Narusawa, T. Irie, M. Otagiri, K. Uekama, K. Kawano, Y. Ohtani, and H. Ogino, 101th Annual Meeting of the Pharmaceutical Society of Japan, Kumamoto, April 1981, Abstr. No. 4Za 3-1.

3) K. Harata, *Bull. Chem. Soc. Jpn.*, **48**, 2409 (1975); **50**, 1416 (1977); *Carbohydr. Res.*, **48**, 265 (1976); W. Saenger, K. Beyer, and P. C. Manor, *Acta Crystallogr., Sect. B*, **32**, 120 (1976).

4) K. Harata, *Bull. Chem. Soc. Jpn.*, **49**, 2066 (1976).

5) K. Harata, H. Uedaira, and J. Tanaka, *Bull. Chem. Soc. Jpn.*, **51**, 1627 (1978).

6) K. Harata, *Bull. Chem. Soc. Jpn.*, **53**, 2782 (1980).

7) "International Tables for X-Ray Crystallography," Kynoch Press, Birmingham (1974), Vol. IV, pp. 72—75.

8) P. C. Manor and W. Saenger, *J. Am. Chem. Soc.*, **96**, 3630 (1972); B. Hingerty and W. Saenger, *ibid.*, **98**, 3357 (1976).

9) K. Harata, *Bull. Chem. Soc. Jpn.*, **52**, 2451 (1979).

Determination of Thermodynamic Properties of Gibbsite from Its Solubility Data in NaOH Solutions[1)]

Byong-Tae CHANG

Department of Chemistry, Faculty of Science, Korea University, Kodaira, Tokyo 187

(Received January 29, 1981)

A reasonable method for determination of thermodynamic properties of alumina hydrates from their solubility data in alkaline pH range was presented and applied to the solubility data of gibbsite in NaOH solutions with success. When $\log(K_s/a_w)$, where $K_s=m_H m_{Al}$ and a_w is the activity of water, was plotted against a Debye-Hückel function of the ionic strength I, $I^{1/2}/(1+B_t a_i I^{1/2})$, a linear relationship to moderately high ionic strengths was found over the range of temperatures from 40 to 110 °C, having the theoretical Debye-Hückel limiting slope and the intercept of $\log K_s^\circ$ at $I=0$. Assuming the same ionic size parameters, $a_1=a_2$, the solubility product (K_s°) of gibbsite was found to depend upon temperature up to 110 °C as follows: $\log K_s^\circ=-4064/T-1.54$ or $-4023/T-1.65$. At high ionic strengths above 1.0, $\log(K_s/a_w)$ showed positive deviations from the straight line, which may be attributed to the formation of complex ions, *e.g.*, $Al_2O(OH)_6^{2-}$, or the dehydration of $Al(OH)_4^-$ to $AlO(OH)_2^-$ and AlO_2^- ions.

The solubility of alumina hydrates such as gibbsite, boehmite, and diaspore in aqueous solutions is very important not only for alumina production by the alkaline or acid process, but also for quantitative understanding of aqueous geochemistry of aluminous minerals.[2-15)] Furthermore, the thermodynamics of Al-H_2O system is much useful in considering the corrosion and passivation of aluminium in water.[16)] A number of solubility data of gibbsite in alkaline solutions have been reported by many investigators.[2-13)] A purpose of most previous solubility studies is to determine precisely the standard thermodynamic properties of gibbsite and hydroxy-aluminium ions in aqueous solubtions. Unfortunately, these results do not agree well with each other; for example, as the ionic solubility product of gibbsite at 25 °C, Kittrick[6)] and May[10)] reported the values of 5.01×10^{-16} and 8.94×10^{-15}, respectively.

Russell, Edward and Taylor[2)] calculated an equilibrium constant (K_1) and its temperature dependancy from their solubility data of gibbsite in NaOH solutions from 40 to 170 °C, assuming that activity coefficients of OH^- and AlO_2^- ions are equal to each other, *i.e.*, $\gamma_{OH^-}=\gamma_{AlO_2^-}$;

$$Al(OH)_3(s) + OH^-(l) = AlO_2^-(l) + 2H_2O(l), \quad (1)$$

$$K_1 = C_{Al}a_w^2/C_{OH}, \quad (2)$$

$$\log K_1^\circ = -1605/T + 4.11, \quad (3)$$

where C_{Al} and C_{OH} are the equivalents per liter of aluminate and hydroxide ions, a_w is the activity of the water in the molar fraction unit, and K_1° is the value derived by extraporating K_1 to zero NaOH concentration at a given temperature. There are some doubtful problems in the Russell's method for determining K_1°; firstly, the differences in the ion size and interactions between the ions and water were neglected, assuming that the activity coefficients of AlO_2^- and OH^- ions are the same. Secondly, the values of a_w for NaOH solutions at 25 °C were used for sodium aluminate and hydroxide solutions at higher temperatures up to 170 °C without any correction. Finally the aluminate ion was expressed in the form of AlO_2^-.

The purpose of this work is to determine the thermodynamic properties of gibbsite in NaOH solution from its solubility data by a more reasonable method according to the Debye-Hückel theory.

Theoretical

According to various studies on the sodium aluminate and hydroxide solutions, the most probable structure of the aluminate ion is tetrahedral $Al(OH)_4^-$ ion at low aluminium concentrations, which, at higher concentrations, becomes dehydrated AlO_2^- ion.[17-19)] Therefore, it is reasonable to express the dissolution process of gibbsite as follows;

$$Al(OH)_3(s) + H_2O(l) = H^+(l) + Al(OH)_4^-, \quad (4)$$

$$K_s^\circ = a_H a_{Al}/a_w = K_s\cdot\gamma_1^2/a_w, \quad (5)$$

where $K_s=m_H m_{Al}$, $\gamma_1^2=\gamma_H\gamma_{Al}$, and m_i is the molality of species i. On the other hand, for the dissociation of water,

$$H_2O(l) = H^+(l) + OH^-(l), \quad (6)$$

$$K_w^\circ = a_H a_{OH}/a_w = K_w\gamma_2^2/a_w, \quad (7)$$

where $K_w=m_H m_{OH}$ and $\gamma_2^2=\gamma_H\gamma_{OH}$. From Eqs. 5 and 7 a general equation (8) for alumina trihydrates can be derived, introducing a new function, $f(I)$, of ionic strength (I).

$$f(I) = \log(m_{Al}/m_{OH}) + \log K_w^\circ = \log K_s^\circ + 2\log(\gamma_2/\gamma_1). \quad (8)$$

It should be noted that $f(I)$ is independent on the activity of water. Figure 1 gives relationships between $f(I)$ and I which were calculated from the solubility data of gibbsite reported by Russell *et al.*[2)] and K_w° values[20)] at a given temperature.

Using the extended Debye-Hückel equation with added terms, we can express the mean activity coefficient (γ_1) as follows;

$$\log\gamma_1 = -A_t I^{1/2}/(1+B_t a_i I^{1/2}) - c_i I - d_i I^2, \quad (9)$$

where A_t is the theoretical limiting Debye-Hückel slope, B_t a parameter depending upon temperature and dielectric constant of solvent, a_i an ion size parameter, and c_i and d_i are adjustable parameters. Substituting Eq. 9 into Eq. 8,

$$f(I) = \log K_s^\circ + 2A_t I^{1/2}[1/(1+B_t a_1 I^{1/2}) - 1/(1+B_t a_2 I^{1/2})] + CI + DI^2, \quad (10)$$

where $C=2(c_1-c_2)$ and $D=2(d_1-d_2)$. The problem is to decide the five parameters, K_s°, a_1, a_2, C, and

Table 1. Temperature dependency of K_s°, K_w°, C, and D

No.	t/°C	Case 1				Case 2		
		$\log K_s^\circ$	$C\times10^2$	$D\times10^3$	$\log K_r^\circ$	$\log K_s^\circ$	$C\times10^2$	$\log K_r^\circ$
1	40	−14.51	3.44	4.11	−0.97	−14.55	5.98	−1.01
2	60	−13.76	6.94	1.78	−0.74	−13.75	6.18	−0.74
3	70	−13.36	3.20	4.99	−0.57	−13.38	5.68	−0.59
4	80	−13.03	4.82	2.66	−0.44	−13.04	5.94	−0.45
5	90	−12.73	4.61	3.61	−0.32	−12.74	6.14	−0.33
6	100	−12.42	3.97	3.29	−0.18	−12.44	5.72	−0.19
7	110	−12.15	4.27	−0.57	−0.05	−12.22	6.80	−0.12
8	130	−11.77	5.24	5.68	0.08	−11.83	9.04	0.02
9	150	−11.54	11.18	−3.89	0.09	−11.51	9.24	0.12
10	170	−11.16	7.37	10.31	0.30	−11.26	13.71	0.20

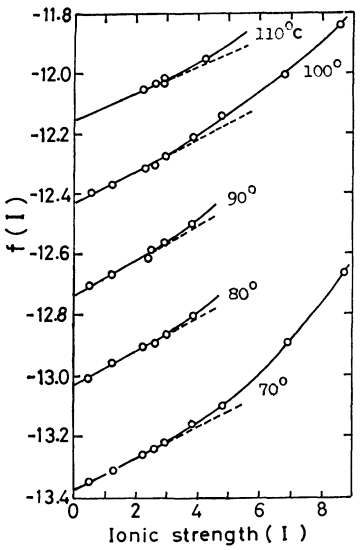

Fig. 1. Relationships between f(I) and ionic strength(I) according to Eq. 8.

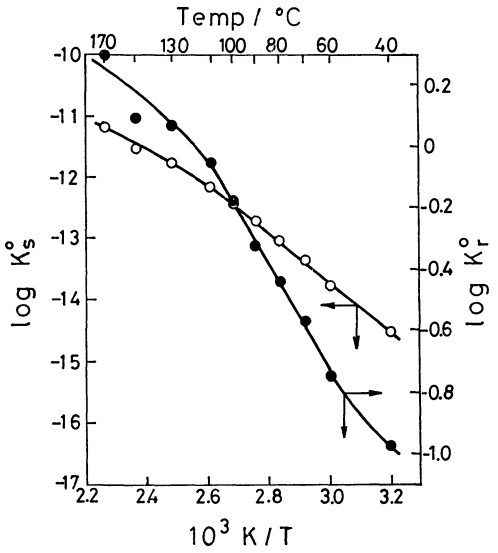

Fig. 2. Temperature dependencies of log K_s° and log K_r° from 40 to 170 °C for the case 1.

D to get the best statistical fit for the data given in Fig. 1.

Results and Discussion

Most of solubility measurements of gibbsite in alkaline solutions presented up to date were carried out at 25 °C. Lyapunov reported interesting results showing an effect of NaCl addition on the solubility of gibbsite at 60 and 95 °C, but the range of conditions of solubility measurements was limited.[11] The Russel's data seems to be the most useful solubility data of gibbsite in the range of higher temperature and NaOH concentrations. The method presented here, therefore, was applied mainly to the Russel's data.

The Case of the Same Ion Size Parameters. Assuming the same ion size parameters, *i.e.*, $a_1=a_2$, as did May[10] or Smith,[21] Eq. 10 can be simplified into a following equation:

$$f(I) = \log K_s^\circ + CI + DI^2 \quad \text{(Case 1)}. \tag{11}$$

Table 1 gives log K_s°, C, and D obtained by the least square calculations for Eq. 11. Furthermore, Fig. 1 shows good straight line relationship between f(I) and I in the range of low ionic strengths, that is,

$$f(I) = \log K_s^\circ + CI \quad \text{(Case 2)}. \tag{12}$$

Table 1 also gives the values of log K_s° and C for Eq. 12.

Figures 2 and 3 show temperature dependency of the ionic solubility product of gibbsite for the case 1 and 2, respectively. Good linear relationships between log K_s° and $1/T$ can be observed in the range of 40—110 °C.

$$\log K_s^\circ = -4064/T - 1.54 \quad \text{(Case 1)}, \tag{13}$$

$$\log K_s^\circ = -4032/T - 1.65 \quad \text{(Case 2)}. \tag{14}$$

According to Eqs. 13 and 14, the values of log K_s° at 25 °C become the same value of −15.18, which is very close to the value of −15.30 reported by Kittrick,[6] being considerably lower than the value of −14.05 presented by May.[10] Based on the ΔG_f° value of −1151.9 kJ/mol selected for gibbsite by Parks,[8] the standard Gibbs free energy of formation (ΔG_f°) for $Al(OH)_4^-$ ion is calculated to be −1302.5 kJ/mol. The heat of reaction of Eq. 4 was found to be 77.4 −77.8 kJ between 40 and 110 °C, and to have a tendency to decrease at temperature above 110 °C.

For the following reaction of gibbsite with OH^- ion,

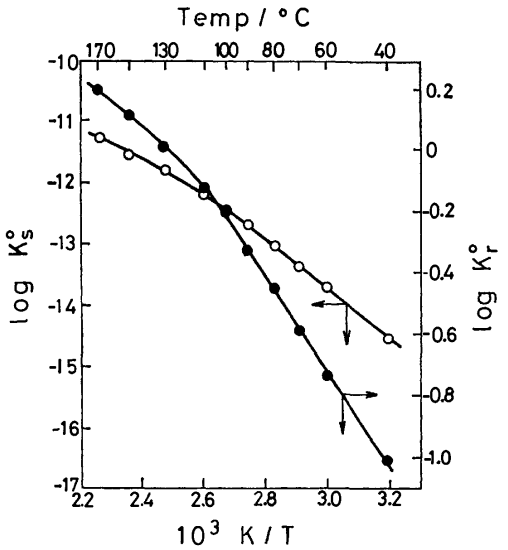

Fig. 3. Temperature dependencies of log K_s° and log K_r° from 40 to 170 °C for the case 2.

$$Al(OH)_3(s) + OH^-(l) = Al(OH)_4^-(l), \quad (15)$$

$$K_r^\circ = a_{Al}/a_{OH}, \quad (16)$$

using Eqs. 5 and 7, K_r° is given by

$$K_r^\circ = K_s^\circ/K_w^\circ. \quad (17)$$

Table 1, Figs. 2 and 3 also show the values of log K_r°, and its temperature dependency in the range from 40 to 110 °C is given as follows;

$$\log K_r^\circ = -1598/T + 4.10 \quad \text{(Case 1)}, \quad (18)$$

$$\log K_r^\circ = -1567/T + 3.98 \quad \text{(Case 2)}. \quad (19)$$

According to Eq. 18 or 19, the heat of reaction of Eq. 15 is 30.1—30.5 kJ.

The Case of Different Ion Size Parameters. In order to evaluate effects of the ion size parameters, a_1 and a_2, on log K_s°, we assumed conveniently $c_2=d_2=0$ for the dissociation of water. Then, from Eqs. 7 and 9.

$$\log (K_w/a_w) = \log K_w^\circ + 2A_tI^{1/2}/(1+B_ta_2I^{1/2}). \quad (20)$$

Using $K_s=m_Hm_{Al}=K_w(m_{Al}/m_{OH})$ and Eq. 20,

$$\log (K_s/a_w) = \log K_w^\circ + \log (m_{Al}/m_{OH}) + 2A_tI^{1/2}/(1+B_ta_2I^{1/2}). \quad (21)$$

At a given temperature, the value of log (K_s/a_w) depends upon the concentration ratio, (m_{Al}/m_{OH}), at equilibrium and the ion size parameter, a_2, for H^+ and OH^- ions. Figure 4 shows plots of log (K_s/a_w) and $I^{1/2}/(1+1.51I^{1/2})$ at 70 °C with a_1=4.5 Å and various values of a_2 from 3.5 to 6.0 Å. It is obvious from Fig. 4 that log (K_s/a_w) and slopes of curves increase with decrease in the a_2 value.

On the other hand, from Eqs. 5 and 9,

$$\log (K_s/a_w) = \log K_s^\circ + 2A_tI^{1/2}/(1+B_ta_1I^{1/2}) + 2c_1I + 2d_1I^2. \quad (22)$$

According to the Debye-Hückel theory, generally a plot of log (K_s/a_w) *vs.* $I^{1/2}/(1+B_ta_1I^{1/2})$ produces a straight line at low lonic strengths with the theoretical limiting slope, $2A_t$, and the intercept of log K_s° at I=0, and the last two terms becomes important only at higher ionic strengths. Figure 5 shows a plot of log (K_s/a_w) *vs.* $I^{1/2}/(1+B_ta_1I^{1/2})$ at 70, 80, 90, and 100 °C in the case of a_1=4.5 Å and a_2=5.0 Å.[24] Similarly, Fig. 6 shows a plot of log (K_s/a_w) *vs.* $I^{1/2}/(1+B_ta_1I^{1/2})$ at 60 °C, which were calculated from the Russell's data in NaOH solutions and the Lyapunov's data in both NaOH and (NaOH+NaCl) solutions. It is obvious from Figs. 5 and 6 that the straight line relationships hold at ionic strengths as high as 1.0, and that these slopes are very close to the theoretical values, $2A_t$, of 1.09, 1.11, 1.14, 1.16, and 1.19 at 60, 70, 80, 90, and 100 °C, respectively. The Lyapunov's data in NaOH and (NaOH+NaCl) solutions are able to be represented by the same curve as shown in Fig. 6, and gives log K_s°=−13.60 at I=0, which differs a little from a value of log K_s°=−13.73 for the Russell's data.

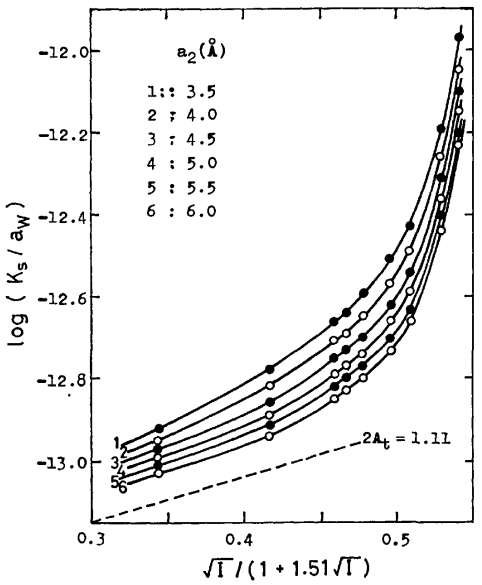

Fig. 4. Plots of $\log(K_s/a_w)$ *vs.* $I^{1/2}/(1+1.51I^{1/2})$ at various values of a_2 in the case of a_1=4.5 Å and 70 °C.

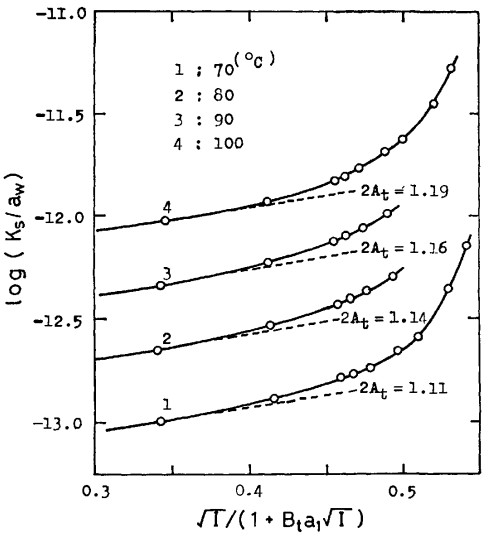

Fig. 5. Plots of $\log(K_s/a_w)$ *vs.* $I^{1/2}/(1+B_ta_1I^{1/2})$ at temperatures of 70, 80, 90, and 100 °C in the case of a_1= 4.5 Å and a_2=5.0 Å.

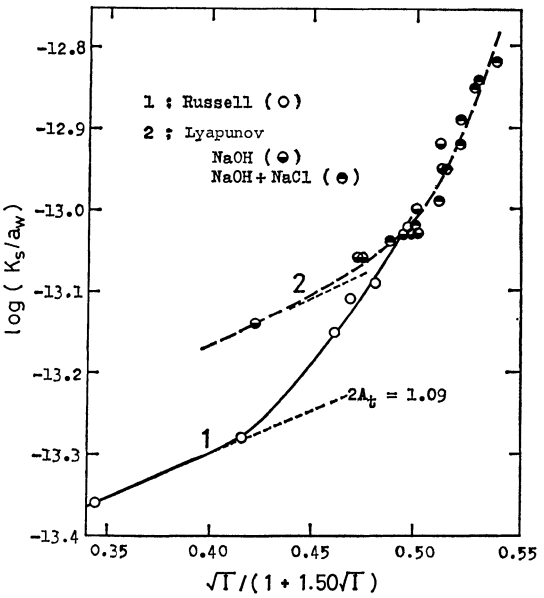

Fig. 6. Plots of $\log(K_s/a_w)$ *vs.* $I^{1/2}/(1+1.50I^{1/2})$ at 60 °C obtained from the Russell's data[2] and the Lyapnov's data[11] in the case of $a_1=4.5$ Å and $a_2=5.0$ Å.

At ionic strengths above 1.0, $\log(K_s/a_w)$ shows positive deviations from the straight line. Such positive deviation at high ionic strengths was also observed in $Ca(OH)_2$–$NaNO_3$–H_2O[22] or $NiSO_4$–$CoSO_4$–$(NH_4)_2SO_4$–H_2O[23] system, and was considered to be attributed to the formation of complexes. Moolnaar concluded from Infrared, Raman, and ^{23}Na and ^{27}Al NMR spectra of sodium aluminate solutions that at aluminium concentrations below 1.5 M, the tetrahedral $Al(OH)_4^-$ ions exist as the predominant aluminium-bearing species in the solution and that at aluminium concentrations of about 1.5 M and above, $Al(OH)_4^-$ condenses to form $Al_2O(OH)_6^{2-}$ ion.[19] In a detailed study of the saturated vapour pressures exerted by sodium hydroxide and aluminate solutions, Dibrov advanced evidence for the aluminate ion undergoing dehydration to the meta-aluminate ion AlO_2^- at high concentrations of 15% Na_2O and above:

$$Al(OH)_4^- \longrightarrow AlO(OH)_2^- + H_2O \longrightarrow AlO_2^- + 2H_2O. \quad (23)$$

From the above discussions it is reasonable to consider that the positive deviation from the straight line may be attributed to the formation of complex ion such as $Al_2O(OH)_6^{2-}$ and/or the dehydration of $Al(OH)_4^-$, leading to decrease in the activity coefficient of aluminate ion. This presents a striking contrast to increase in the activity coefficient designated by the salting-out effect.[20] The similar application of the method presented in this paper to alumina monohydrates is currently performed with success.

References

1) Thermodynamics of Al_2O_3–Na_2O–H_2O System. Part 2. Part 1: B.-T. Chang, L.-H. Pak, and Y.-S. Li, *Bull. Chem. Soc. Jpn.*, **52**, 1321 (1979).
2) A. S. Russell, J. D. Edwards, and C. S. Taylor, *J. Met.*, **7**, 1123 (1955).
3) K. Goto, *Nippon Kagaku Zasshi*, **81**, 349 (1960).
4) C. R. Frink and M. Peech, *Soil Sci. Soc. Am. J.*, **26**, 346 (1962).
5) K. H. Gayer, L. C. Thompson, and O. T. Zajicek, *Can. J. Chem.*, **36**, 1268 (1958).
6) J. A. Kittrick, *Soil Sci. Soc. Am. J.*, **30**, 595 (1966).
7) N. Dezlic, H. Bilinski, and R. H. H. Wolf, *J. Ionorg. Nucl. Chem.*, **33**, 791 (1971).
8) G. A. Parks, *Am. Mineral.*, **57**, 1163 (1972).
9) B. S. Hemingway and R. A. Robie, *Geochim. Cosmochim. Acta*, **41**, 1402 (1977); **42**, 1533 (1978).
10) H. M. May, P. A. Helke, and M. L. Jackson, *Geochim. Cosmochim. Acta*, **43**, 861 (1979).
11) A. N. Lyapunov, A. G. Khodakova, and Z. G. Galkina, *Tsvet. Metal.*, **37** (3), 48 (1964).
12) M. N. Smirnov, M. V. Mishanina, and V. A. Panasko, *Tsvetn. Met.*, **44** (5), 45 (1971).
13) J. A. Kittrick, *Soil Sci. Soc. Am. J.*, **44**, 139 (1980).
14) R. E. Mesmer and C. F. Baes, Jr., *Inorg. Chem.*, **10**, 2290 (1971).
15) S. S. Singh, *Soil Sci. Soc. Am. J.*, **38**, 415 (1974).
16) D. D. MacDonald and P. Butler, *Corros. Sci.*, **13**, 259 (1973).
17) I. A. Dibrov, G. Z. Mal'tsev, and V. P. Mashovets, *Zh. Prikl. Khim.*, **37**, 1920 (1964).
18) R. Glastonbury, *Chem. Ind. (London)*, 121 (1969).
19) R. J. Moolnaar, J. C. Evans, and L. D. McKeever, *J. Phys. Chem.*, **74**, 3629 (1970).
20) H. S. Harned and B. B. Owen, "The Physical Chemistry of Electrolytic Solutions," 3rd ed, Reinhold, New York (1958), pp. 508 and 645.
21) R. M. Smith and J. D. Hem, *U. S. Geol. Surv. Water Supply Paper* 1827-D (1972).
22) L. B. Yeatts and W. L. Marshall, *J. Phys. Chem.*, **71**, 2641 (1967).
23) H. Gesell and D. Neuschütz, *Z. Anorg. Allg. Chem.*, **354**, 172 (1967).
24) The values of $a_1=4.5$ Å and $a_2=5.0$ Å were selected in consideration of a difference in the ionic size of $Al(OH)_4^-$ and OH^-, that is, the ionic size of $Al(OH)_4^-$ may be equal to 2.2—2.4 Å,[18] which is smaller by *ca.* 1 Å than that of OH^-.

Quantitative Interpretation of Infrared Diffuse Reflectance Spectra over Whole Concentration Range

Tadashi HATTORI,* Kenji SHIRAI, Miki NIWA, and Yuichi MURAKAMI

Department of Synthetic Chemistry, Faculty of Engineering, Nagoya University, Furo-cho, Chikusa-ku, Nagoya 464

(Received August 18, 1980)

The infrared diffuse reflectance spectra of $CaCO_3$ dispersed in KBr and Si were measured over a wide concentration range. The relation between relative reflectance and concentration varies with dispersing medium. The relation follows the Kubelka-Munk (K-M) equation only in the low concentration region. The deviation in the high concentration region from the K-M equation changes with wavelength and dispersing medium. The results over the whole concentration range can be interpreted by means of a modified K-M equation in which the difference in the scattering coefficients between the sample and the dispersing medium is taken into account. The tendency of scattering coefficients of $CaCO_3$, KBr, and Si calculated by the modified Kubelka-Munk equation agrees with that of refractive indexes.

The diffuse reflectance spectroscopy is widely used in the ultraviolet and visible regions.[1] The infrared diffuse reflectance spectroscopy would also be useful, several equipments having been succesfully developed.[2,3] We have constructed an emissionless infrared diffuse reflectance spectrometer (EDR) for *in situ* determination of reacting species on catalyst surface at elevated temperature.[4] Several theories have been proposed for the quantitative interpretation of the diffuse reflectance spectra.[5,6] The Kubelka-Munk equation is most widely used for analysis, but it should be regarded as a limiting law which holds only in a low concentration range.[6] A convenient equation is desirable for quantitative analysis over a wide concentration range.

We would like to show that the infrared diffuse reflectance spectra over the whole concentration range can be interpreted by means of a modified K-M equation, and that the factor determinig the intensity of absorption band is not only the absorption coefficient but also the scattering coefficient of the sample in the high concentration region.

Experimental

Fine powder of commercial calcium carbonate was used without further purification. Potassium bromide crystals for spectroscopy (Japan Spectroscopic Co.) and silicone wafers (99.9999%, Shin-Etsu Chem. Co. Ltd.) were ground to fine powder and used as dispersing media. Mixtures of the sample and a dispersing medium with predescribed ratios were packed in a sample holder, and the spectra were measured with an emissionless infrared diffuse reflectance spectrometer (Japan Spectroscopic Co., EDR-31) at an ambient temperature and at 200 °C. The details of the spectrometer were reported.[4]

Results

Figure 1 shows typical diffuse reflectance spectra of mixture of $CaCO_3$ and KBr. The absorption bands at 873 and 711 cm^{-1} can be ascribed to characteristic vibrations of carbonate ion, and the band at 2520 cm^{-1} to a combination band.[7] Even when the concentration of $CaCO_3$ was as low as 0.19%, the absorption bands were conspicuous. The band intensities increase with increase in concentration, but the relation between band intensity and concentration differs with wavelength. The band intensity of 100% $CaCO_3$ at 2520 cm^{-1} was much greater than that of 10% $CaCO_3$; the difference in band intensity at 873 cm^{-1} was not so great. On the other hand, the difference in band intensity between 0.19% and 1% $CaCO_3$ samples was greater at 873 cm^{-1} than that at 2520 cm^{-1}. The relation between band intensity

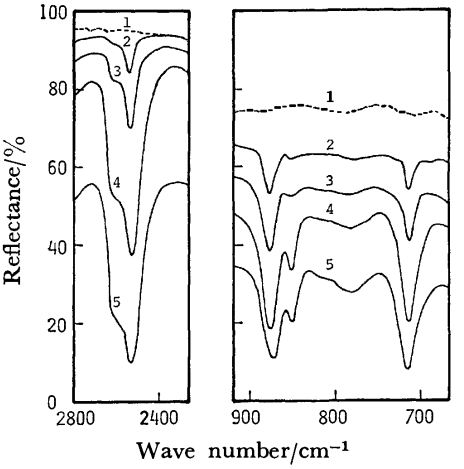

Fig. 1. IR diffuse reflectance spectra of $CaCO_3$ dispersed in KBr. Wt fraction of $CaCO_3$: (1) 0%, (2) 0.19%, (3) 1.0%, (4) 10%, and (5) 100%.

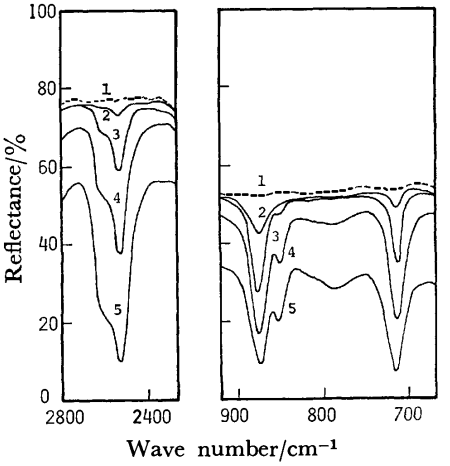

Fig. 2. IR diffuse reflectance spectra of $CaCO_3$ dispersed in Si. Wt fraction of $CaCO_3$: (1) 0%, (2) 1.0%, (3) 10%, (4) 40%, and (5) 100%.

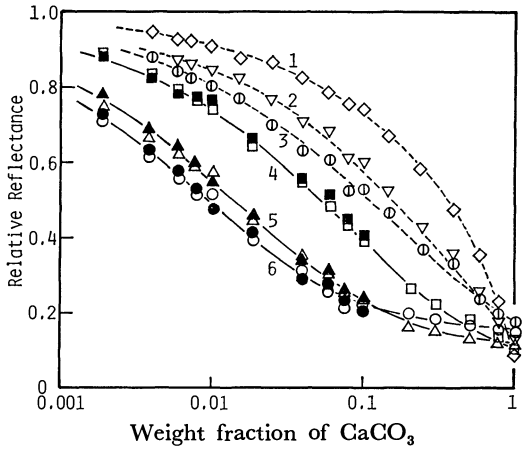

Fig. 3. Variation of relative reflectance with wt fraction of $CaCO_3$. Wavenumber and dispersing medium: (1) 2520 cm^{-1} in Si, (2) 711 cm^{-1} in Si, (3) 873 cm^{-1} in Si, (4) 2520 cm^{-1} in KBr, (5) 711 cm^{-1} in KBr, and (6) 873 cm^{-1} in KBr. Solid marks, at 200 °C; and empty marks, at ambient temp.

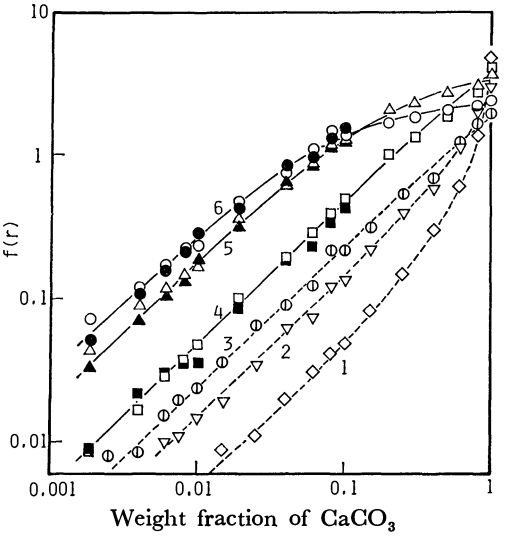

Fig. 4. Variation of K-M function with wt fraction of $CaCO_3$. For the symbols, see the legend of Fig. 3.

and concentration changes with dispersing medium. When Si was used as a dispersing medium, the band intensity changes a great deal with concentration in the high concentration region, as shown in Fig. 2. The difference in band intensity between 10% and 100% samples was much greater than that shown in Fig. 1. The band intensity does not change much with concentration in the low concentration region. The absorption bands of the 0.15% sample at 2520 and 711 cm^{-1} could not be observed.

The variation of band intensity with dispersing medium is shown in Fig. 3, in which the relative reflectance, defined as the ratio of reflectance at peak minimun to the reflectance of pure dispersing medium, is plotted against the weight fraction of $CaCO_3$ in a mixture of $CaCO_3$ and the dispersion medium. With increase in concentration the relative reflectance decreases remarkably in the low concentration region, when KBr is used as the disperison medium. In the case of Si, the relative reflectance decreases remarkably in a high concentration region. In both cases, the relative reflectance at 2520 cm^{-1} decreases in a higher concentration region as compared with that at 873 and 711 cm^{-1} (the results at ambient temperature ○, at 200 °C ●). Agreement between results indicates that the quantitative relation in the emissionless diffuse reflectance spectrometer does not change with temperature.

In the K-M theory, the reflectance is related to the absorption constant K and the scattering constant S of the mixture of the sample and dispersion medium:

$$f(R) = \frac{(1-R)^2}{2R} = \frac{K}{S}, \qquad (1)$$

where f(R) is the Kubelka-Munk function and R the absolute reflectance. In practice, the relative reflectance r defined as above is used in place of R. The following assumptions are usually made. The absorption constant K is equal to the product of the absorption coefficient ε_s and the concentration X of the sample, and the scattering constant S is equal to the scattering coefficient of the scattering medium σ_m. Thus, we have

$$f(r) = \frac{(1-r)^2}{2r} = \frac{\varepsilon_s X}{\sigma_m}. \qquad (2)$$

Figure 4 shows the relation between the logarithm of the K-M function and the logarithm of the sample concentration. In all cases, the plots give straight lines with the slope of unity only in the low concentration region. This is in line with the fact that the K-M equation is regarded as a limiting law which holds only in the low concentration region. The plots deviate from the straight lines in the high concentration region depending on the wavelength and dispersion medium.

Hecht[6] found that the reflectance in the ultraviolet and visible regions sometimes follows the Rozenberg equation, though a constant in the equation is too large to be physically interpreted. The results in the present study do not follow the Rozenberg equation, according to which the second derivarive of the reflectance with respect to the concentration should be positive. In the infrared diffuse reflectance spectra of $NaCO_3$, $NaNO_3$, and Na_2SO_4 dispersed in KI, Ishii *et al.*[2] found a linear relationship between the reflective absorbance and logarithm of the concentration in the low concentration region. The intensities of absorption bands at 711 and 873 cm^{-1} of $CaCO_3$ in KBr appeared to obey their relation in the low concentration region, but not the intensities of the other bands.

Discussion

In the K-M theory it is assumed that the absorption constants of a mixture of the sample and the dispersion medium is proportional to the concentration of the sample and the scattering constant is independent of concentration. However, both constants would depend on the concentrations of both sample

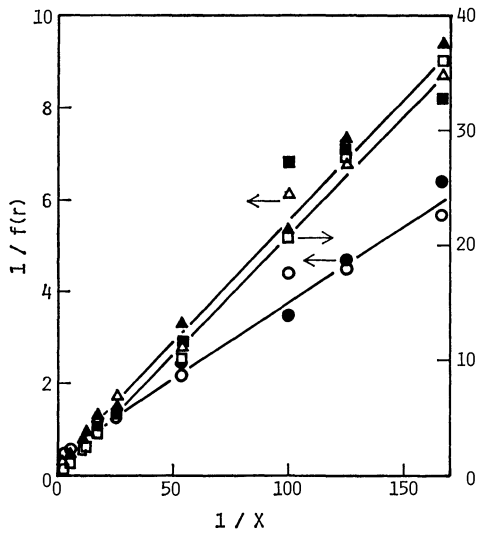

Fig. 5. Reciprocal plot of K-M function *vs.* wt fraction of $CaCO_3$ dispersed in KBr. (○,●) 873 cm^{-1}, (□,■) 2520 cm^{-1}, and (△,▲) 711 cm^{-1}.
Solid marks, at 200 °C; and empty marks, at ambient temp.

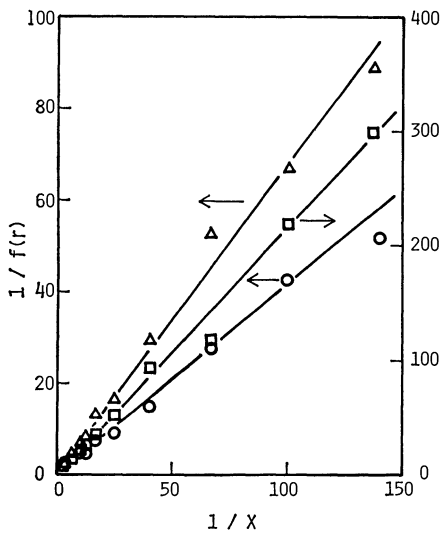

Fig. 6. Reciprocal plot of K-M function *vs.* wt fraction of $CaCO_3$ dispersed in Si. For the symbols, see the legend of Fig. 5.

and diepersion medium.[6,8] Thus, the K-M equation should be written as

$$f(r) = \frac{(1-r)^2}{2r} = \frac{\varepsilon_s X + \varepsilon_m(1-X)}{\sigma_s X + \sigma_m(1-X)}, \quad (3)$$

where σ_s and σ_m are the scattering coefficients and ε_s and ε_m the absorption coefficients of the sample and the dispersion medium, respectively. The absorption coefficient of the dispersion medium can be neglected, when the dispersion medium has no characteristic absorption. Thus we have

$$f(r) = \frac{(1-r)^2}{2r} = \frac{\gamma X}{1+(\delta-1)X}, \quad (4)$$

where δ is the ratio of the scattering coefficient of the sample to that of the dispersing medium, σ_s/σ_m, and γ is the ratio of the absorption coefficient of the sample to the scattering coefficient of the dispersion medium, ε_s/σ_m. Equation 4 indicates that the plot of the inverse K-M function against the inverse concentration would give a straight line.

$$\frac{1}{f(r)} = \frac{\delta-1}{\gamma} + \frac{1}{\gamma X} \quad (5)$$

Figures 5 and 6 show the relations between the inverse K-M function and the inverse weight fraction. We see that the plots give straight lines. Although the intercepts are not obvious, they can not be neglected; the scattering constant of the mixture changes with the concentration of sample.

The constants in Eq. 5 were calculated from the slopes and the intercepts (Figs. 5 and 6), and are given in Table 1. The curves (Fig. 4) calculated by substituting the constants into Eq. 4 agree with the experimental results over the whole concentration range. In the ratios of the scattering constant of KBr to that of Si (Table 1), two groups were calculated from the ratio of γ in the $CaCO_3$–Si mixture to that in the $CaCO_3$–KBr mixture and from the corresponding ratio of δ at each wavelength. The ratios thus obtained agree with each other, *i.e.*, $\sigma_{KBr}/\sigma_{Si}=0.086\pm 0.010$. The scattering coefficient varies with the refractive index, shape, size and the packing of the particles.[2,5] The refractive index of KBr is *ca.* 1.52 in the present wavelength region, and that of Si, *ca.* 3.42. The fact that the refractive index of KBr is smaller than that of Si is in line with the result that the scattering coefficient of KBr is smaller than that of Si. The effect of the shape and the size of particles also would be significant. The reflected light from the powder layer consists of the specularly reflected light at the surface of the powder layer as well as the diffusely reflected light.[9] The refractive index might have a predominant effect on the specular reflection and the shape and the size of powder on the diffuse reflection. The ratio of scattering coefficient of KBr to that of Si is fairly constant, but the ratio of the scattering coefficient of $CaCO_3$ to that of the dispersing medium varies with the wave length. This is in line with the fact that the refractive index of the substance which absorbs the light changes with wavelength in a complicated manner near the absorption band.[1]

In the K-M equation, the K-M function is proportional to the sample concentration (Eq. 2). Thus the Kubelka-Munk spectrum, or the plot of the K-M

Table 1. Ratio between absorption and scattering coefficients

Band position	711 cm^{-1}	873 cm^{-1}	2520 cm^{-1}
$\gamma(CaCO_3\text{-KBr})$[a]	9.5	15.0	2.40
$\delta(CaCO_3\text{-KBr})$[b]	6.0	13.5	1.30
$\gamma(CaCO_3\text{-Si})$	0.73	1.20	0.23
$\delta(CaCO_3\text{-Si})$	0.52	1.30	0.10
σ_{KBr}/σ_{Si}[c]	0.087	0.096	0.077
σ_{KBr}/σ_{Si}[d]	0.076	0.080	0.096

a) $\varepsilon_{CaCO_3}/\sigma_{KBr}$. b) $\sigma_{CaCO_3}/\sigma_{KBr}$. c) $\gamma(CaCO_3\text{-Si})/\gamma(CaCO_3\text{-KBr})$. d) $\delta(CaCO_3\text{-Si})/\delta(CaCO_3\text{-KBr})$.

function against wavenumber, would be the same as absorbance spectrum in transmission spectroscopy. Actually, however, discrepancy has been observed both in the ultra-violet and visible regions[6] and the infrared region.[3] Equation 4 indicates that the intensity of the absorption band in the diffuse reflectance spectrum also depends on the scattering coefficient of the sample, especially when the sample concentration is high. Since the scattering coefficient of the substance which absorbs the light appears to vary with the wavelength near the absorption band, the Kubelka-Munk spectrum is not always the same as the absorbance spectrum.

The modified K-M equation would also be useful in the ultraviolet and visible regions. The deviation of the K-M function from linearity appears to be greater in the ultraviolet and visible regions than in the infrared region. The variation of the scattering coefficient with the substance might be large in the ultraviolet and visible regions.

References

1) W. W. Wendtlandt and H. G. Hecht, "Reflectance Spectroscopy," Interscience, New York (1966).
2) E. Ishii, M. Mamiya, and T. Murakami, *Nippon Kagaku Kaishi*, **1972**, 353.
3) M. P. Fuller and P. R. Griffiths, *Anal. Chem.*, **50**, 1906 (1978), and references cited there.
4) M. Niwa, T. Hattori, M. Takahashi, K. Shirai, M. Watanabe, and Y. Murakami, *Anal. Chem.*, **51**, 46 (1979).
5) H. G. Hecht, *J. Res. Nat. Bur. Stand.*, **80A**, 567 (1976).
6) H. G. Hecht, *Anal. Chem.*, **48**, 1775 (1976).
7) F. A. Miller, G. L. Carlson, F. F. Bentley, and W. H. Jones, *Spectrochim. Acta*, **16**, 135 (1960).
8) D. R. Duncan, *J. Oil Colour Chem. Assoc.*, **45**, 300 (1962).
9) M. Mamiya, *Bunko Kenkyu*, **25**, 99 (1976).

The Rapid Determination of Sulfide, Thiosulfate, and Polysulfide in the Lixiviation Water of Blast-furnace Slag by Means of Argentimetric Potentiometric Titration

Hiromu SATAKE, Takeo HISANO, and Sanae IKEDA*

Department of Applied Chemistry, Faculty of Engineering, Tokushima University, Minamijosanjima-cho, Tokushima 770

(Received September 27, 1980)

Sulfide, thiosulfate, and polysulfide ions in their mixtures were determined potentiometrically with a silver-nitrate standard solution. These three species can be precisely determined from two titrations for each sample with the coefficient of variation of 0.3% at the concentration level of 5×10^{-4} M (1 M=1 mol dm^{-3}). One aliquot is titrated, after making the titrand acidic with an acetate buffer (pH=4), to get the end points of the sulfide and thiosulfate ions respectively, in the presence of free sulfur. The other is titrated, after the sulfitolysis of the sample solution, to show the end points of the sulfide and thiosulfate(the original thiosulfate plus the thiosulfate which is formed from polysulfide) ions in the presence of excess sulfite. The addition of calcium nitrate is effective in making the end points clear and accurate. This method was applied to determine these species in lixiviation water of blast-furnace slag.

Elemental sulfur dissolves in an alkaline solution of sulfide to form polysulfides:[1)]

$$xS + S^{2-} \longrightarrow S_{x+1}^{2-}. \quad (1)$$

In addition, sulfur[2)] reacts with alkali hydroxide to produce sulfide, polysulfide, and thiosulfate through the following equation:

$$(4+2x)S + 6OH^- \longrightarrow 2S_{x+1}^{2-} + S_2O_3^{2-} + 3H_2O. \quad (2)$$

Therefore, there are many cases which involve these three species together, *e.g.*, sulfide, thiosulfate, and polysulfide, in such solutions as the lixiviation water of blast-furnace slag.[3,13)]

One sulfur atom in each polysulfide ion is denoted as sulfide sulfur(S^{2-}), while the rest of the ion(S_x) is denoted as polysulfide sulfur (or dissolved sulfur).[11)]

Various methods, such as potentiometric,[4,5)] biamperometric,[6)] and iodometric methods,[2)] to determine S^{2-}, $S_2O_3^{2-}$, and S_x in a polysulfide solution have already been presented. Blasius and his co-workers[3,14)] determined sulfur compounds in the lixiviation water of blast-furnace slag by photometric and titrimetric methods. Most of these methods are, however, rather complicated and time-consuming because of the necessity of separation, masking, and several titrations. Papp and Havas[7)] determined these three species potentiometrically by using a sulfide-ion-selective electrode as the indicator; they added an excess amount of sulfite to the sample solution, and the resultant $S_2O_3^{2-}$, equivalent to the S_x, was titrated with a mercury(II) chloride solution. Although this method is simple and useful, there are some problems, such as water pollution due to waste mercury and the necessity of masking the excess sulfite ions with formaldehyde. It was previously reported[8,9)] that $S_2O_3^{2-}$ in the presence of large amounts of SO_3^{2-} could be titrated with the silver ion by utilizing the formation of thiosulfatoargentate or silver sulfide in an acidic solution without masking SO_3^{2-} with formaldehyde. Sulfide, $S_2O_3^{2-}$, and SO_3^{2-} could also be determined[10)] directly by the three successive argentimetric titrations of the same sample solution in the presence of calcium nitrate. Sulfide and S_x in a polysulfide solution could be determined[11)] after the cyanolysis of the polysulfide, but the end points were affected by the presence of $S_2O_3^{2-}$. In these investigations, silver–silver sulfide, silver–silver iodide, and silver-ion-selective electrodes were used.

The present paper reports a method of determining S^{2-}, S_x, and $S_2O_3^{2-}$ in a synthetic polysulfide solution and the lixiviation water of blast-furnace slag by argentimetric potentiometric titration with silver–silver sulfide, silver–silver iodide, and saturated-calomel electrodes. The advantage of this method is that the contents of these three species can be determined from two titrations for each sample. One aliquot is titrated, after making the titrand acidic with an acetate buffer (pH=4), to give the end points of S^{2-} and $S_2O_3^{2-}$ in the presence of elemental sulfur. The other is titrated, after the sulfitolysis of the sample solution, to give the end point of S^{2-} and that of $S_2O_3^{2-}$ plus S_x in the presence of sulfite:

$$S_{x+1}^{2-} \xrightarrow{H^+} HS^- + S_x, \quad (3)$$

$$S_{x+1}^{2-} + xSO_3^{2-} \longrightarrow S^{2-} + xS_2O_3^{2-}, \quad (4)$$

$$S_2O_3^{2-} + Ag^+ \longrightarrow Ag(S_2O_3)^-. \quad (5)$$

Experimental

Reagent and Apparatus. All the chemicals used were of a reagent grade. Oxygen-free redistilled water was used for the preparation of all solutions. The stock solution of polysulfide was prepared and stored by a method described previously.[11)] Working solutions were prepared by the further dilution of the stock solution.

An automatic recording potentiometric titrator, Hiranuma RAT-101, with a silver–silver sulfide or a silver–silver iodide electrode, together with a saturated calomel electrode, was used.

Procedure. *Assay of S^{2-} and $S_2O_3^{2-}$ in S_{x+1}^{2-}*: Place a definite amount of a sample solution in a titration cell containing 10 ml of oxygen-free water and a 1-cm-thick liquid-paraffin layer. Add, successively, 2 ml of 1 M calcium nitrate, acetic acid, or acetate buffer to adjust the pH to 4 and oxygen-free water to make the volume up to about 100 ml, which should then be gently poured against the wall of the cell so that air bubbles are not entrained. Titrate this solution potentiometrically with 0.1 M silver nitrate solution using a silver–silver sulfide indicator electrode until the titration curve shows a sudden change, which corresponds to the end point for S^{2-} (Fig. 1, 1-A). Then replace the

Table 1. Determination of sulfide and thiosulfate in polysulfide solutions

$[S^{2-}]$ / M	$[S^0]$ / mg	$[S_2O_3^{2-}]$ / M	Difference/%		Coefficient of variation/%	
			S^{2-} b)	$S_2O_3^{2-}$ c)	S^{2-}	$S_2O_3^{2-}$
5×10^{-4}	0.5	5×10^{-4}	+0.3	−0.5	0.3	0.3
5×10^{-4}	1.6	5×10^{-4}	−0.3	±0.0	0.3	0.3
5×10^{-4}	3.2	5×10^{-4}	+0.3	+0.9	0.1	0.3
5×10^{-4}	5.0	2.5×10^{-4}	+0.2	±0.0	0.1	0.5
5×10^{-5}	0.16	5×10^{-5}	+1.1	+1.9	0.3	0.7
5×10^{-4}	1.6	10^{-4}	−0.4	+0.3	0.2	0.2
5×10^{-4}	1.6	2.5×10^{-4}	−0.2	+0.7	0.1	0.5
5×10^{-4}	1.6	10^{-5} a)	+0.5	+5.8	0.1	3.7

Titrant: 0.1 M $AgNO_3$. Each value is the average of 4 titrations. a) Standard addition method. b) Compared with the mercury(II) chloride method.[7] c) Compared with the iodometric method.[2]

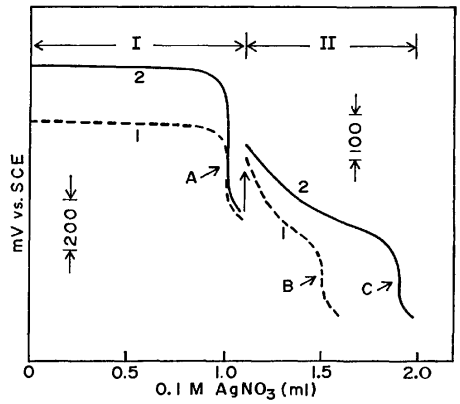

Fig. 1. Potentiometric titration curves for sulfide, polysulfide-sulfur, and thiosulfate in polysulfide solution.
Sample solution: 100 ml of 5×10^{-4} M Na_2S_{x+1} (S^0= 1.6 mg) and 5×10^{-4} M $Na_2S_2O_3$.
1: Without sulfitolysis. Titration medium: 10^{-2} M $Ca(NO_3)_2$ and 2×10^{-2} M acetate buffer (pH=4).
2: With sulfitolysis. Titration medium: 10^{-2} M $Ca(NO_3)_2$ and 0.1 M NH_3 up to the end point related to S^{2-}, then pH 1.5—3 (with 0.5 M H_2SO_4).
I: Ag-Ag_2S electrode, II: Ag-AgI electrode. A: S^{2-}, B: $S_2O_3^{2-}$, C: S^0.

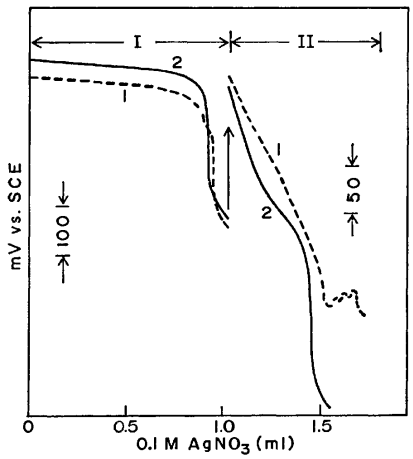

Fig. 2. Effect of calcium ion on the titration curves for sulfide and thiosulfate in polysulfide solution.
Sample solution: 100 ml of 5×10^{-4} M Na_2S_{x+1} (S^0= 1.6 mg), 5×10^{-4} M $Na_2S_2O_3$ and 2×10^{-2} M acetate buffer (pH=4).
1: Without $Ca(NO_3)_2$, 2: With 10^{-2} M $Ca(NO_3)_2$
I: Ag-Ag_2S electrode, II: Ag-AgI electrode.

indicator electrode by a silver-silver iodide and continue the titration until the end point for $S_2O_3^{2-}$ (Fig. 1, 1-B) is reached.

Assay of S^{2-} and S_x in S_{x+1}^{2-}: Add 10 ml of 0.5 M sodium sulfite and 30 ml of oxygen-free water to a sample solution which has been prepared in the manner described above. Heat this to about 50 °C and then allow it to stand for 3 min. Cool the solution below 15 °C. Add 10 ml of 1 M ammonia and 2 ml of 1 M calcium nitrate, and bring the total volume to about 100 ml with oxygen-free water. Titrate this solution with 0.1 M silver nitrate by using a silver-silver sulfide indicator electrode until the titration curve shows a sudden change for S^{2-} (Fig. 1, 2-A). Then adjust the pH to 1.5—3 with 0.5 M sulfuric acid and continue the titration until the end point for $S_2O_3^{2-}$ plus S_x is reached (Fig. 1, 2-C) by using a silver-silver iodide indicator electrode.

The S^{2-} (free sulfide plus the sulfide bound by polysulfide) content is obtained by the use of the end point(A). The original $S_2O_3^{2-}$ content is calculated from the difference between (A) and (B). The S_x content (measured as $S_2O_3^{2-}$) is estimated by (C) minus (B).

Results and Discussion

Determination of Sulfide, Thiosulfate, and Polysulfide-Sulfur in a Synthetic Polysulfide Solution. Figure 1 shows some typical titration curves. Acetate buffer (pH= 4) and calcium nitrate were added in order to isolate elemental sulfur and to get clear and accurate end points for S^{2-} and $S_2O_3^{2-}$. Calcium nitrate may be considered to have a coagulating action to the elemental sulfur isolated from the S_{x+1}^{2-} and silver sulfide produced during the titration. Figure 2 shows the effect of calcium nitrate on the titration of sulfide and thiosulfate ions in a polysulfide solution. The end point of $S_2O_3^{2-}$ was obtained by the formation of thiosulfatoargentate. The solution was protected from the evolution of hydrogen sulfide by covering it with a liquid-paraffin layer. Table 1 shows the results thus obtained from solutions with various concentrations. The S^{2-} and $S_2O_3^{2-}$ contents ranging from 10^{-4} to 5×10^{-4} M in the polysulfide solution could be determined with a good accuracy and reproducibility.

On the other hand, the S_x in polysulfide solution

TABLE 2. DETERMINATION OF SULFIDE, THIOSULFATE, AND POLYSULFIDE-SULFUR

$[S^{2-}]$ M	$[S^0]$ mg	$[S_2O_3^{2-}]$ M	Difference/%			Coefficient of variation/%		
			S^{2-} b,c)	S^0 c)	$S_2O_3^{2-}$ d)	S^{2-}	S^0	$S_2O_3^{2-}$
5×10^{-4}	0.5	5×10^{-4}	+1.1	+0.5	−0.5	0.1	0.5	0.3
5×10^{-4}	1.6	5×10^{-4}	+0.5	+0.2	±0.0	0.1	0.3	0.3
5×10^{-4}	3.2	5×10^{-4}	+0.3	−0.2	+0.9	0.1	0.3	0.3
5×10^{-4}	5.0	2.5×10^{-4}	+1.3	−2.6	±0.0	0.3	0.2	0.5
5×10^{-5}	0.16	5×10^{-5}	−1.1	+4.3	+1.9	0.6	0.5	0.7
5×10^{-4}	1.6	10^{-4}	+0.8	−1.3	+0.3	0.2	0.3	0.2
5×10^{-4}	1.6	2.5×10^{-4}	+0.1	+0.4	+0.7	0.2	0.4	0.5
5×10^{-4}	1.6	10^{-5} a)	+0.6	−1.1	+5.8	0.2	0.2	3.7

Titrant: 0.1 M $AgNO_3$. Each value is the average 4 titrations. a) Standard addition method. b) The result determined after sulfitolysis. c) Compared with the mercury(II) chloride method.[7] d) Compared with the iodometric method.[2]

TABLE 3. DETERMINATION OF SULFIDE, THIOSULFATE, AND POLYSULFIDE-SULFUR IN LIXIVIATION WATER OF BLAST-FURNACE SLAG

Sample	S^{2-} (mM)				S^0 (mM)				$S_2O_3^{2-}$ (mM)			
	I		II		I		II		I		II	
	Found[a]	C.V.[b]	Found[a]	C.V.[b]	Found[a]	C.V.[b]	Found[a]	C.V.[b]	Found[a]	C.V.[b]	Found[a]	C.V.[b]
A	2.00	0.2	1.99	0.4	3.91	0.7	3.92	0.6	8.09	0.4	8.07	0.3
B	1.35	0.5	1.30	0.6	3.36	0.9	3.44	0.5	8.27	0.3	8.27	0.3
C	2.93	0.5	2.87	0.4	3.06	0.7	3.14	0.5	8.10	0.3	8.32	0.4

I: Iodometric method[2,12]. II: Proposed method. a) Average of 4 titrations. b) Coefficient of variation. A sample solution was prepared by immersing 450 g of blast-furnace slag in 450 ml of demineralized water for 4 d.

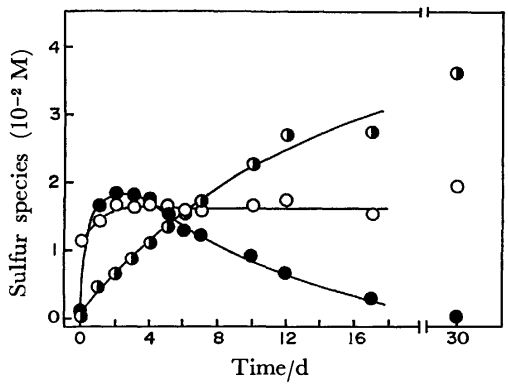

Fig. 3. Variation of sulfide, thiosulfate and polysulfide-sulfur in lixiviation water with the lapse of time.
Sample: Slag(700 g)+Demineralized water(300 ml).
Sample was placed in a dark room at 30 °C.
—◑—: S^{2-}, —○—: $S_2O_3^{2-}$, —●—: $S_x^{2-}(S^0)$.

was determined after converting it to $S_2O_3^{2-}$ through a reaction with SO_3^{2-}. An excess amount of SO_3^{2-} had no effect on the determination. The resulting solution was first titrated, after the addition of ammonia and calcium nitrate, to get the end point of S^{2-}, and then, after adjusting the titrand pH to 1.5—3, the titration was continued until the end point of $S_2O_3^{2-}$ (the original $S_2O_3^{2-}$ plus the $S_2O_3^{2-}$ produced from S_x) was attained. Any mixture containing each of the three species in various concentrations could be determined by the proposed method with a good accuracy and reproducibility, as is shown in Table 2. The analytical values for S_x in S_{x+1}^{2-} were identical to those determined by the mercury(II)–chloride method.[7]

The presence of sodium hydroxide, sodium carbonate, and sodium sulfate(the concentration of each being 2.5×10^{-2} M) did not disturb the determination.

Determination of Sulfide, Thiosulfate, and Polysulfide-Sulfur in Lixiviation Water of Blast-furnace Slag. The lixiviation waters were prepared by immersing 450-g portions of three different examples of blast-furnace slag (A, B, and C) in 450 ml of demineralized water for 4 d. Each lixiviation water was covered with a liquid-paraffin layer to prevent air oxidation. The contents of S^{2-}, $S_2O_3^{2-}$, and S_x in the lixiviation waters were then determined by the proposed method, and the values were compared with those obtained with other methods.[2,12] The results are shown in Table 3. When a 700-g portion of blast-furnace slag was immersed in 300 ml of water, the concentration variations of S^{2-}, $S_2O_3^{2-}$, and S_x in the lixiviation water with the lapse of time were as is shown in Fig. 3.

The present work was partially supported by a Grant-in-Aid for Scientific Research from the Ministry of Education, Science and Culture. The authors wish to express their thanks to Mr. Masaru Hiraiwa of the Fukuyama Works of Nippon Kokan Co., Ltd., for his kind offer of the blast-furnace slag.

References

1) K. Johnsen, *Norsk. Skogindnstri*, **20**, 91 (1966).
2) L. Legradi, *Analyst (London)*, **89**, 854 (1961).

3) E. Blasius and K. Ziegler, *Arch. Eisenhuettenwes.*, **44**, 669 (1973).
4) E. Bilberg, *Norsk. Skogindustri*, **13**, 307 (1959).
5) E. Bilberg and P. Landmark, *Norsk. Skogindustri*, **13**, 375 (1959).
6) S. A. Kiss, *Fresenius' Z. Anal. Chem.*, **188**, 341 (1962).
7) J. Papp and J. Havas, *Hung. Sci. Instru.*, **17**, 17 (1970).
8) S. Ikeda and H. Satake, *Bunseki Kagaku*, **25**, 544 (1976).
9) S. Ikeda and H. Satake, *Nippon Kagaku Kaishi*, **1977**, 1953.
10) S. Ikeda and H. Satake, *Chem. Lett.*, **1972**, 1191.
11) S. Ikeda, H. Satake, T. Hisano, and T. Terazawa, *Talanta*, **19**, 1650 (1972).
12) J. H. Karchmer, "The Analytical Chemistry of Sulfur and Its Compounds," Wiley-Interscience, New York, N. Y. (1970), Part 1, p. 349.
13) H. Kondo, M. Oguro, A. Nanbu, I. Tahara, Y. Watari, S. Isawa, A. Okazaki, K. Shigekiyo, and K. Murakami, *J. Shikoku Public Health Soc.*, **23**, 159 (1978).
14) E. Blasius, H. Wagner, and K. Ziegler, *Arch. Eisenhuettenwes.*, **42**, 473 (1971).

Chromatographic Behavior of Metalloporphyrins by Cellulose Thin-layer Chromatography

Yoshiaki ONOUE

Department of Chemistry, Faculty of Science and Technology, Kinki University, 3-4-1, Kowakae, Higashi-Osaka 577

(Received October 6, 1980)

Cellulose thin-layer chromatographic separation of chlorophyll a, b, and c, pheophytin a, b, and c, Zn(II)- and Cu(II)-complexes of protoporphyrin-IX dimethyl ester (PPDE) was studied by using a light petroleum–acetone developing solvent system. The hR_f values of metal–PPDE chelates were found to be virtually linearly related with the electronegativities-to-radius ratio (En/ri) of central-metal ions. The hR_f values of metalloporphyrins become progressively greater with increase in En/ri values of the central metal. This suggests that a dominant factor influencing the hR_f values of metal–porphyrins is the extent of electron transfer from the four nitrogens and/or the π-electron system of porphyrin to central metal.

Metalloporphyrins have been widely investigated because of their biological and chemical importance.[1,2] Recently porphyrins have also been used as a chelating agent for analysis of trace metals since free porphyrins and their metal chelate exhibit intense fluorescence and/or characteristic color.[3] Metal chelates could be further utilized for analysis by applying thin-layer chromatography (TLC). It is being widely used for the separation and purification of metalloporphyrins. In this paper, the chromatographic behavior of cobalt(II) and (III), nickel(II), copper(II), zinc(II), magnesium(II), and iron(III) complexes with PPDE, and magnesium(II) (=chlorophyll a), copper(II), and zinc(II) pheophytin a chelates on cellulose layer is described, considering the dominant factor controlling the mobility.

Experimental

Materials. Chlorophyll a and b: Pigments were extracted from spinach with a methanol–acetone (1:1, v/v) mixed solvent. After partial purification according to the dioxane method,[4] the complexes were separated by chromatography of the crude chlorophyll extract on a glucose column.

Chlorophyll c_1 and c_2: The compounds were isolated from Undaria pinnatifida and Sargassum racemosum, respectively, according to the Jeffrey method.[5]

Pheophytin a, b, c_1, and c_2: The compounds were prepared[6] from their original chlorophylls by shaking an ethereal solution of the chlorophyll with 13% hydrochloric acid (w/w) for 5 min.

Cu and Zn Pheophytin a: These were prepared by heating pheophytin a and five-fold excess of zinc and copper acetate in ethanol at 40 °C, for 10 min.

PPDE and Its Metal Chelates: The carboxyl side chain of protoporphyrin IX (Midori Jūji Co., Ltd.) was esterified[7] with methanol containing 5% (w/v) concentrated sulfuric acid at 0 °C. After esterification, the ester was crystallized from methanol–chloroform solution.

Metal Insertion: Cobalt, nickel, and magnesium PPDE were prepared by the *N,N*-dimethylformamide method as described by Adler *et al.*,[8] using metal chloride. After reaction in *N,N*-dimethylformamide, the crude product was crystallized by addition of water and cooling. Insertion of zinc, copper, and iron to PPDE was carried out by heating the porphyrin with a metal salt [zinc acetate, copper acetate, and iron(II) chloride] in chloroform–ethanol, 40 °C for 30 min. After heating, the metalloporphyrin was crystallized by removing chloroform in a stream of nitrogen.

Purification of Metal Chelates: Purification of Ni, Co, and Zn chelates was carried out on a calcium carbonate column with chloroform eluent. After evaporation of the eluate to a small volume, the metalloporphyrins were crystallized by addition of ethanol. Crude Mg–PPDE was chromatographed on a cellulose column with a light-petroleum: acetone (20:3, v/v) eluent. Crystallization of Mg-chelate from benzene–chloroform solvent was then repeated three times.

Stationary Phase. Thin-layer chromatography was performed with commercial cellulose plates (Merck precoated cellulose plate Art. 5716, 5×20 cm).

Chromatographic Procedure. One μl solution of samples (PPDE and its metal chelates; 0.04 μg/ml in chloroform, chlorophylls, and their derivatives; *ca.* 0.05 μg/ml in diethyl ester) was spotted with a 10 μl micro-syringe at a point 3 cm from the lower edge of TLC. After air-drying, the chromatograms were developed (10 cm/*ca.* 14 min) in thin-layer chambers lined with filter paper, in which the atmosphere had been equilibrated with developing solvent for 15 min before the plates were inserted. Light-petroleum: acetone (20:3, v/v) was chosen as a developing solvent, in view of results obtained for (1) light-petroleum (bp 50—80 °C):acetone (20:3, v/v), (2) light-petroleum:1-propanol (24:1, v/v), and (3) light-petroleum:chloroform (7:3, v/v). After developing, the chromatograms were air dried and examined in daylight and under ultraviolet light (365 nm).

Results

A typical chromatogram of PPDE and its metal chelates on cellulose plate is shown in Fig. 1. The hR_f values obtained for seventeen porphyrins derivatives are given in Table 1. Porphyrins with carboxyl side chain, pheophytin c and Ni-protoporphyrin IX *etc.*, did not move from the origin of chromatogram with a light-petroleum:acetone (20:3, v/v) solvent system. More polar solvent systems such as light-petroleum:acetone (7:3, v/v) and dimethylpyridine:water system[9] should be used in order to separate the above compounds. However, porphyrin derivatives with carboxyl side chain showed extensive tailing and were not separated from each other on the chromatogram in the more polar solvent systems.

Free porphyrins are readily esterified with a alcohol[7] or diazomethane,[10] the esters being hydrolysed without degradation. The esters are more lipophilic than the free porphyrins, as indicated by their solubility in organic solvents. The ester of protoporphyrin IX was

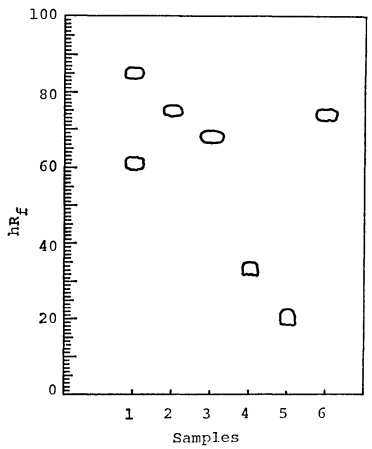

Fig. 1. Thin-layer chromatogram of PPDE and its metal chelates.
Solvent system; light petroleum:acetone=20:3, v/v. TLC; Merck precoated cellulose plate.
1: Co–PPDE, 2: Ni–PPDE, 3: Cu–PPDE, 4: Zn–PPDE, 5: Mg–PPDE, 6: PPDE.

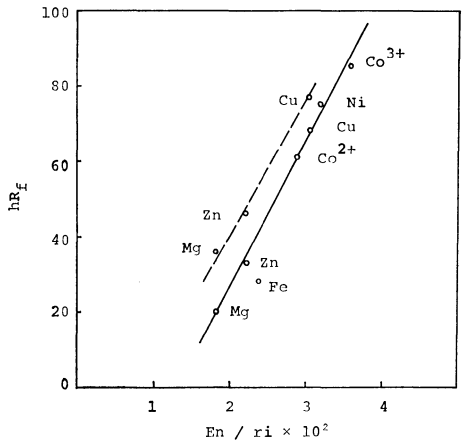

Fig. 2. Relationship between En/ri and TLC hR_f values of metalloporphyrins.
En: Pauling's electronegativity value, ri: Effective ionic radius, ——: Metal–PPDE chelate, ----: Metal–pheophytin-a chelate.

therefore used for the thin-layer chromatographic studies.

Since the hR_f values of the chromatogram were reproducible to about ±2 on repeated runs, porphyrins having hR_f values with a difference of over four were separated perfectly. Under ultraviolet light (365 nm) the separated spots exhibited either a characteristic, very intense red fluorescence (Zn, Mg–PPDE, and PPDE, chlorophylls, and their derivatives, except Cu–pheophytin a) or a dark one against the lighter background of the rest of the plate. The lower limits of detection were about 1 ng for the fluorescent substances, and 10 ng for non-fluorescent porphyrin metal complexes. As shown in Table 1, PPDE and Ni–PPDE were not separated completely, but they could be clearly distinguished by their different behavior under ultraviolet light (365 nm). The former (hR_f: 75) appeared as a black spot, the latter (hR_f: 74) showing red fluorescence.

Table 1. hR_f values and identification under ultraviolet light of porphyrins and their chelates

Compound	hR_f value[a)]	Identification[b)]
Pheophytin a	86	red-f
Pheophytin b	72	red-f
Pheophytin c	0	red-f
Protoporphyrin IX	0	red-f
Chlorophyll a	36	red-f
Chlorophyll b	21	red-f
Chlorophyll c	0	red-f
Cu–Pheophytin a	77	non-f
Zn–Pheophytin a	46	red-f
Protoporphyrin IX dimethyl ester	74	red-f
Co–Protoporphyrin IX dimethyl ester	85 61	non-f
Ni–Protoporphyrin IX dimethyl ester	75	non-f
Cu–Protoporphyrin IX dimethyl ester	68	non-f
Zn–Protoporphyrin IX dimethyl ester	33	red-f
Mg–Protoporphyrin IX dimethyl ester	20	red-f
Fe–Protoporphyrin IX dimethyl ester	28	non-f

a): Solvent system; light-petroleum: acetone (20 : 3, v/v). b): In ultraviolet light the separated zones exhibited either a red fluorescence or a dark one against the lighter background of the rest of the plate. TLC: Merck precoated cellulose plate (14 min/10 cm).

Co–PPDE has two varieties of hR_f values depending on the preservation time of the chloroform solution of Co–PPDE. The hR_f value of the freshly prepared solution of Co–PPDE was 85, but after being left to stand, it was 61, tailing being observed.

Discussion

The relationship between the individual metals of the porphyrin chelates and the hR_f values on cellulose TLC was studied. As shown in Fig. 2, the hR_f values of the metal chelates were proportional to the En/ri values of the central metals, where En is the Pauling electronegativity values[11] of the elements, irrespective of their oxidation state, and ri is the effective ionic radii cited from the recent compilation by Shannon and Prewitt.[12,13] Assuming that the En/ri value of the central atom is a measure of field strength, the extent of electric transfer from four nitrogens of porphyrin to central atom increased with increase in En/ri values. The charge transfer would make the metal atom nearly neutral, and the total positive charge of the central atom might be dispersed over the surrounding π-electron system of porphyrin.[14] The more delocalized bond between the metal and ligand of the chelates leads to less dipole-dipole interaction between the chelate to cellulose and higher solubility of the chelate in the developing solvent, and accordingly a larger hR_f value.

Co–PPDE shows two kinds of mobility (hR_f value). The hR_f values 61 and 85 could be assigned respectively to low(II) and high(III) oxidation state of cobalt ion for the following reasons. (1) The ionic radius of the cobalt in the two kinds of complexes is estimated to be 65 and 53 pm from the hR_f values 61 and 85, respectively. (2) Cobalt(II)–porphyrins are briefly oxidized to higher oxidation state(III) complex by air.[16] (3) The oxidation potentials of metalloporphyrins are Fe: −0.32, Co: +0.52, and Ni: +1.00.[17] Although the data could not be applied directly to this TLC condition, they indicate that the oxidation states of Co, Fe–porphyrins are easily changed by the change in the conditions. It should be expected that cobalt in the crystal of Co(II)–PPDE is air oxydized during storage, but reduced gradually in chloroform.

Fe–PPDE, which have a more sensitive oxidation-potential to the conditions than Co-porphyrin, moved more slowly than expected. The reason for the deviation from hR_f-En/ri relationship is not clear.

Conclusion

The mobility (hR_f values) of metalloporphyrin dimethyl esters on cellulose TLC is closely correlated to the En/ri values of central metal. The En/ri value determines the extent electron transfers from nitrogen to central metal, and it will be a dominant factor to control the mobility of metalloporphyrin. Thus the hR_f values of the metalloporphyrin dimethyl esters can be used for identification and also for metal determination of chelates with unknown central metal. These findings have prompted a study of chromatographic behavior of metalloporphyrin in non-aqueous developing solvent systems.

The author expresses his sincere thanks to Dr. Yasuharu Nishikawa and Dr. Keizō Hiraki, Faculty of Science and Technology, Kinki University, and Dr. Masayuki Tabushi, College of Medical Technology of Hirosaki University, for their advice and suggestions throughout the investigation.

References

1) Y. Niwa, H. Kobayashi, and T. Tsuchiya, *Inorg. Chem.*, **13**, 2891 (1974).
2) D. G. Davis and L. A. Truxillo, *Anal. Chim. Acta*, **64**, 55 (1973).
3) K. S. Hui, B. A. Davis, and A. A. Boulton, *J. Chromatogr.*, **115**, 581 (1975).
4) K. Iriyama, N. Ogura, and A. Takamiya, *J. Biochem.*, **76**, 901 (1974).
5) S. W. Jeffrey, *Biochim. Biophys. Acta*, **279**, 15 (1972).
6) P. H. Hynninen and N. Ellfolk, *Acta Chem. Scand.*, **27**, 1463 (1973).
7) J. E. Falk, "Porphyrins and Metalloporphyrins," K. M. Smith, Elsevier Publishing Co., New York, N. Y. (1975), p. 835.
8) A. D. Adler, F. R. Longo, F. Kampas, and J. Kim, *J. Inorg. Nucl. Chem.*, **32**, 2443 (1970).
9) J. E. Falk, *Biochem. Soc. Symp. (Cambrige, England)*, **12**, 17 (1954).
10) M. Blumer, *Anal. Chem.*, **28**, 1640 (1956).
11) A. L. All-red, *J. Inorg. Nucl. Chem.*, **17**, 215 (1961).
12) R. D. Shannon and C. T. Prewitt, *Acta Crystallogr.*, **1325**, 925 (1969).
13) H. Rieck and R. Hoppe, *Z. Anorg. Allg. Chem.*, **392**, 139 (1972).
14) M. B. Crute, *Acta Crystallogr.*, **12**, 24 (1959).
15) Ref. 7, p. 193.
16) J. F. Taylor, *J. Biol. Chem.*, **135**, 569 (1940).
17) A. Wolberg and J. Manassen, *J. Am. Chem. Soc.*, **92**, 2982 (1970).

  Bull. Chem. Soc. Jpn., 54, 1975—1977 (1981)

The Depth Profiling of Glass Surfaces by Mass Spectrometry Using Neutral-particle Bombardment

Akira Iino and Atsushi Mizuike*

Faculty of Engineering, Nagoya University, Chikusa-ku, Nagoya 464

(Received October 9, 1980)

Glass surfaces are bombarded by energetic neutral argon atoms or oxygen molecules, and the resulting sputtered ions are mass-analyzed. This technique has a higher depth resolution than conventional secondary-ion mass spectrometry. Quantitative depth-concentration profiles of sodium and potassium in the top layer of the surface (within several tens of nanometers of the surface) of Pyrex glass are obtained by the proposed technique.

Depth profiles of glass components, especially of univalent ions, in the glass surface layer are quite useful in studies of the physical chemistry of glass surfaces and glass technology. Recently, secondary-ion mass spectrometry (SIMS),[1-3] Auger electron spectrometry (AES) using ion beams for etching,[4] and ion-beam-induced radiation[5] have been applied to the depth profiling of glass surfaces. In the top layer of the surface (within several tens of nanometers of the glass surface), however, discrepancies[3-5] have been found among the profiles of the alkali ions obtained by these techniques. These facts suggest that all the techniques using ion bombardment are still qualitative in the top layer of the surface.

By the energetic ion or electron bombardment of glass, the surfaces become charged, and the resulting electric field may cause a migration of the univalent ions in the glass. Additionally, preferential sputtering, knock-on effects, and primary-ion implantation may be caused by ion bombardment within the top layer of the surface. These phenomena may distort the original depth-concentration profiles in glass and may change the secondary-ion yields, thus resulting in the discrepancies described above. McCaughan and Kushner[6] investigated the migration of sodium in thin silicon dioxide films on silicon by the radioactive-tracer technique. Neutral-particle bombardment gave less sodium migration than ion bombardment by at least four orders of magnitude, and less migration than ion bombardment with electron flooding (spraying) by at least two orders of magnitude. These results suggest that the migration of univalent ions in glass may be disregarded if mass spectrometry using neutral-particle bombardment[7] is used for depth profiling. Although the effects of preferential sputtering, knock-on effects, and primary-particle implantation cannot be reduced, it is shown in the present work that mass spectrometry using neutral-particle bombardment is more useful than conventional SIMS for obtaining quantitative depth-concentration profiles of sodium and potassium ions in the top layer of the surface of borosilicate glass.

Experimental

Apparatus. A Hitachi IMA-2 ion microanalyzer was modified for neutral-particle bombardment, as is shown in Fig. 1. The neutral-particle beam was obtained by removing ions by electrostatic deflection electrodes (515—530 V)[8] from the primary beam consisting of ions and neutral atoms or molecules probably produced by ion-neutral particle reactions and recombination. The spot diameters of the neutral atom or molecule beam were adjusted by means of apertures of 0.3, 0.5, 1, and 3 mm. The operating conditions of the microanalyzer are listed in Table 1. The ion intensities of boron, sodium, aluminium, silicon, and potassium were measured intermittently by means of manual magnetic scanning. For SIMS, electron flooding was started 10 s before the ion bombardment to eliminate the charge accumulation.

The depth of the craters formed on glass surfaces by sputtering was measured with a Mizojiri Kogaku Model II multiple-beam interferometer (Hg 546.1 nm, magnification

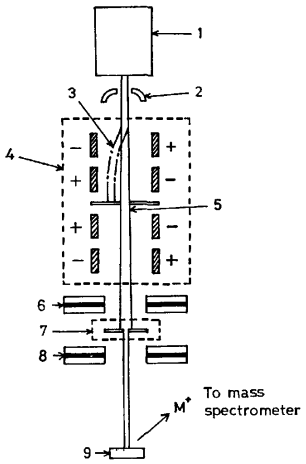

Fig. 1. Apparatus for mass spectrometry with neutral-particle bombardment. [::] indicates the parts attached to a Hitachi IMA-2 ion microanalyzer. 1: Primary-ion source, 2: accelerator electrode, 3: ion beam, 4: electrostatic deflection electrodes (4 pairs), 5: neutral-particle beam, 6: condenser lens, 7: aperture, 8: objective lens, 9: sample.

Table 1. Operating conditions

Bombarding particles and their energies		Bombarding-beam spot diameter	Sputtering rate
keV		mm	nm h^{-1}
Ar^0	4	1	5
	7	1	20
Ar^+	4	0.3	73
	7	0.3	160
O_2^0	7	1	12
O_2^+	7	0.3	110

Other conditions: source gas, 99.99% argon or 99.7% oxygen; primary-ion current, 50 nA; sample-chamber pressure, 3×10^{-5} Pa; secondary-ion accelerating voltage, 3 kV; electron-multiplier voltage, 2.5 kV.

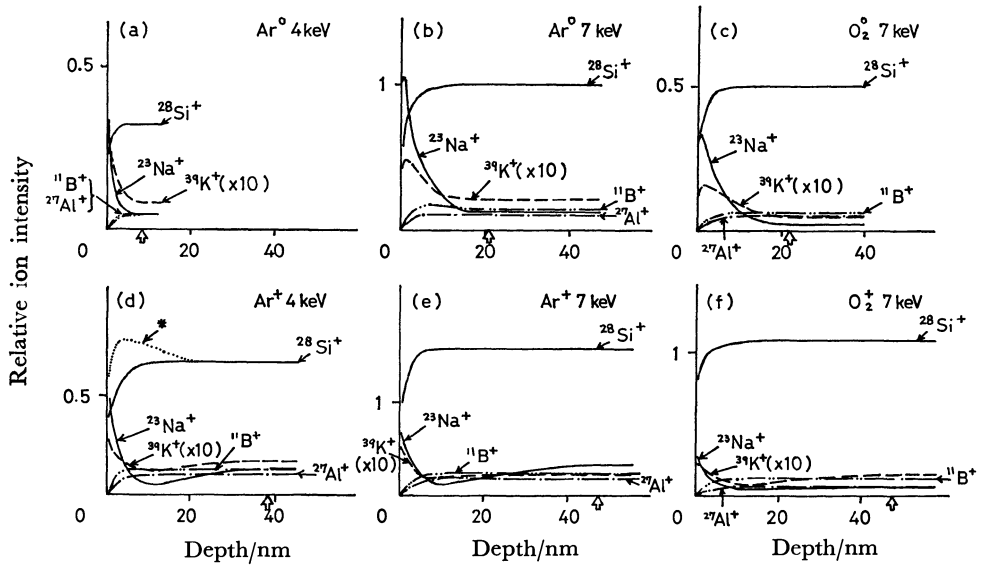

Fig. 2. Depth profiles of fracture-exposed surfaces of borosilicate glass R501.
*: A maximum peak sometimes appears. ⌂: Depth where the ion intensities reach steady values.

40X), with a maximum error of ±3 nm. An Olympus Model MF microscope (magnification 100—400X) with a Model MF-NIC Nomarski interference contrast attachment, and a Hitachi-Akashi Model MSM-2 scanning electron microscope (magnification 2000—10000X) were used for the observation of the glass surfaces.

Materials. Japanese standard-reference-material borosilicate glass R501 rods (79.9 SiO_2, 13.2 B_2O_3, 3.88 Na_2O, 2.17 Al_2O_3, 0.30 K_2O wt%, 6 mmϕ × 100 mm) were cut into *ca.* 8-mm lengths. The fracture-exposed surfaces were smooth under optical and electron microscopes. Pyrex glass sheets (81 SiO_2, 13 B_2O_3, 3.9 Na_2O, 2.2 Al_2O_3, 0.5 K_2O wt%, thickness; 1 mm) were annealed, etched *ca.* 1 μm with 1.4 M hydrofluoric acid-1.3 M sulfuric acid at 20±3 °C for 15 min, washed with water, and dried in a silica-gel desiccator.

Interdiffusion of Potassium and Sodium Ions. In a 50-ml silica glass beaker, 17.8 g of potassium nitrate and 6.4 g of sodium nitrate (70 KNO_3–30 $NaNO_3$ mol%) were melted and thoroughly mixed at 270±1 °C. A 30-mm-square piece of a Pyrex glass sheet was immersed in the molten salt to effect the interdiffusion of potassium and sodium ions in the glass. The piece was then withdrawn, cooled, washed in water, and dried in a silica-gel desiccator. After the interdiffusion no change was observed on the glass surfaces under optical and electron microscopes.

Results and Discussion

Bombardment by Neutral Atoms and Molecules. The fracture-exposed surfaces of borosilicate glass R501 were bombarded by the neutral atom (Ar^0), the neutral molecule (O_2^0), or the ion (Ar^+, O_2^+) beam, and the resulting sputtered ions were mass-analyzed. Figure 2 shows the depth profiles thus obtained. The concentrations of boron, sodium, aluminium, silicon, and potassium in the top layer of the fracture-exposed surfaces can be assumed to be constant.[9] The ion intensities of these elements, however, change with the increase in the depth in the top layer of the surface. The depth where the ion intensities reach steady values

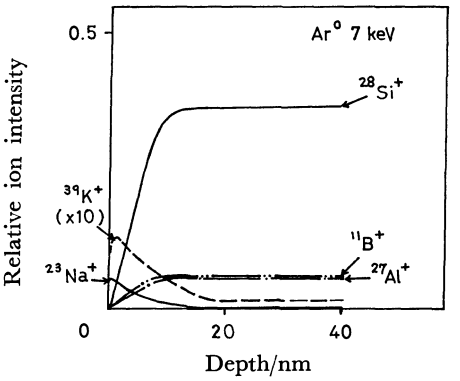

Fig. 3. Depth profiles of fracture-exposed surface of borosilicate glass R501 after electron flooding (1.5 keV, 25 μA) for 5 min.

is smaller in the neutral-atom or -molecule bombardment than in SIMS. This suggests a higher depth resolution in the former technique. In SIMS, primary ions with energies as low as 3 keV produced insufficient secondary ions for mass spectrometry, and lower primary-ion densities on the sample surface did not improve the depth resolution. Bombardment with neutral argon atoms is mainly used in the present work, because there is little difference in depth resolution between the argon-atom and the oxygen-molecule bombardment and because the sputtering rate is larger in the former.

In SIMS, in addition to ion bombardment, electron flooding may distort the depth profiles. The latter effects are shown in Fig. 3. Compared with Fig. 2(b), the ion intensities of sodium and potassium relative to silicon remarkably decreased upon electron flooding.

Calibration Graphs. To obtain quantitative depth-concentration profiles from the observed depth profiles in the top layer of the surface, calibration graphs were constructed by the use of the borosilicate

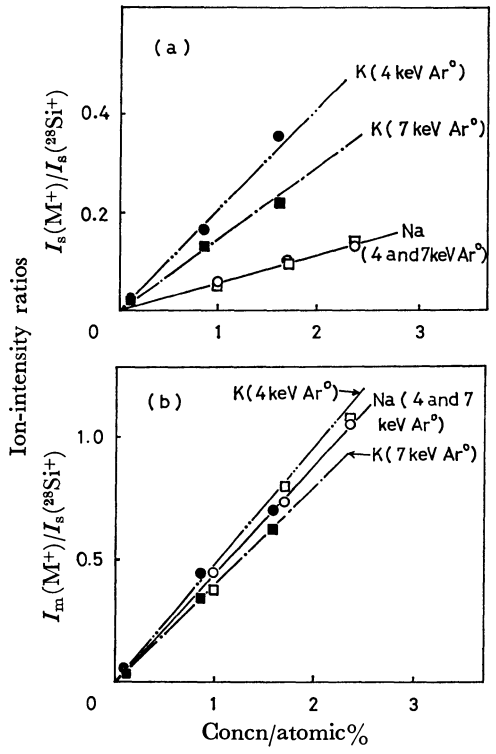

Fig. 4. Calibration graphs.
(a) For sodium and potassium concentrations at 10 nm (4 keV Ar^0) and 20—30 nm (7 keV Ar^0) from surfaces. (b) For surface sodium and potassium concentrations.

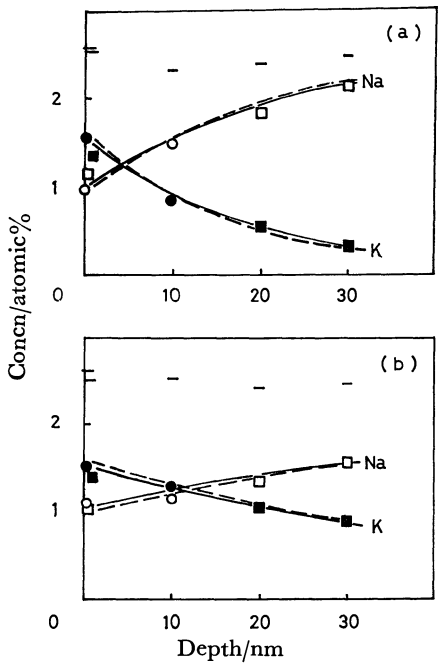

Fig. 5. Depth-concentration profiles after interdiffusion of potassium and sodium in Pyrex glass at 270 °C for (a) 1 min and (b) 7 min.
□■: 7 keV Ar^0, ○●: 4 keV Ar^0. Solid line: measured. Dashed line: calculated. —: Sum of K and Na (measured).

glass R501 and standard samples reported previously.[2] For obtaining sodium and potassium concentrations, at 10 and 20—30 nm from the surfaces, for 4 and 7 keV Ar^0 bombardments respectively, the steady values of the ion-intensity ratios, $I_s(^{23}Na^+)/I_s(^{28}Si^+)$ and $I_s(^{39}K^+)/I_s(^{28}Si^+)$, were plotted against the sodium and potassium concentrations {Fig. 4(a)}. For obtaining the sodium and potassium concentrations at the surfaces, the ratios of the maximum ion intensities of sodium and potassium to the steady values of the silicon-ion intensity, $I_m(^{23}Na^+)/I_s(^{28}Si^+)$ and $I_m(^{39}K^+)/I_s(^{28}Si^+)$, were plotted against the sodium and potassium concentrations {Fig. 4(b)}. All the calibration graphs were straight lines passing through the origin; the scattering of the points was less than ±10%. Also, no day-to-day variation in the calibration graphs was observed.

Depth-concentration Profiles. Figure 5 shows the quantitative depth-concentration profiles in the top layer of the surface of potassium-treated Pyrex glass sheets. The profiles obtained by the proposed technique (solid lines) are in good agreement with the calculated profiles (broken lines). The latter were calculated by using the interdiffusion coefficients reported previously[2] and the equilibrium surface concentrations of sodium and potassium as measured with a glass sheet immersed in a molten 70 KNO_3–30 $NaNO_3$ mol% bath at 270 °C for 1200 min.

References

1) A. Mizuike and A. Iino, *Bull. Chem. Soc. Jpn.*, **50**, 1469 (1977).
2) A. Iino, H. Nakamura, and A. Mizuike, *Nippon Kagaku Kaishi*, **1977**, 1324.
3) R. G. Gossink, H. A. M. de Grefte, and H. W. Werner, *J. Am. Ceram. Soc.*, **62**, 4 (1979).
4) C. G. Pantano, Jr., D. B. Dove, and G. Y. Onoda, Jr., *J. Vac. Sci. Technol.*, **13**, 414 (1976).
5) H. Bach, *Radiat. Eff.*, **28**, 215 (1976).
6) D. V. McCaughan and R. A. Kushner, "Characterization of Solid Surfaces," ed by P. F. Kane and G. B. Larrabee, Plenum Press, New York (1974), Chap. 22.
7) S. Scherrer and F. Naudin, "Proc. The XIth Intern. Cong. Glass," Prague, July (1977), Vol. III, p. 301.
8) H. Kobayashi, K. Suzuki, Y. Yanagisawa, and K. Yukawa, *Shitsuryo Bunseki*, **25**, 315 (1977).
9) J. H. Escard and D. J. Brion, *J. Am. Ceram. Soc.*, **58**, 296 (1975).

Reactions of the Bis(β-diketonato)palladium(II) Complexes with Various Nitrogen Bases

Seichi Okeya,* Hiroyuki Sazaki, Michiyo Ogita, Takako Takemoto, Yukio Onuki,† Yukio Nakamura,† B. K Mohapatra,†† and Shinichi Kawaguchi*,†

Faculty of Education, Wakayama University, Masago-cho, Wakayama 640

† *Faculty of Science, Osaka City University, Sumiyoshi-ku, Osaka 558*

(Received October 31, 1980)

Reactions of the bis(β-diketonato)palladium(II) complexes with various nitrogen bases (L) afforded [Pd(β-dik)L_2](β-dik), [PdL_4](β-dik)$_2$, or [Pd(β-dik)(β-dik-*C*)L] according to the natures of L and β-diketonate anions. Less basic ligands such as 1,1,1,5,5,5-hexafluoro- and 1,1,1-trifluoro-2,4-pentanedionates are readily removed by L to the outer sphere. Tendency of preferring the central-carbon-bonded state of the β-diketonate anion is related with the keto-favoring nature of its conjugate acid. Excess primary amines and pyridines can displace both of the β-diketonate ligands but secondary amines only one. These two types of compounds containing the 2,4-pentanedionate anion in the outer sphere undergo prompt deuteration of methine and amine protons by $CDCl_3$. Tribenzylamine and 2,6-diphenylpyridine react with bis(1,1,1,5,5,5-hexafluoro-2,4-pentanedionato)palladium(II) to afford orthometallated products.

β-Dicarbonyl compounds constitute a group of the most popular ligands and usually form the *O,O'*-chelate as a monoanion with almost all metal ions.[1] In recent years, reactions of the bis(β-diketonato)palladium(II) and -platinum(II) complexes with Lewis bases have been examined and found to give products involving the β-diketonate ligand of various bonding modes as shown in Fig. 1. Compounds **7** containing the central-carbon-bonded 2,4-pentanedionate anion (acac-C^3) were obtained by the reactions of [Pd(acac)$_2$] with bases such as pyridine, diethylamine, and triphenylphosphine,[2] but the kinetic and equilibrium studies of the reactions between [Pd(acac)$_2$] and alkylamines revealed that compounds **7** are produced *via* the outer-sphere complex **4**.[3] Primary amines give rise to **5**.[4] Complexes of type **6** were obtained by the reactions of [Pt(acac)$_2$] with piperidine[5] and triethylphosphine,[6] and the precursor complex of type **3** was isolated in the reaction of bis(1,1,1-trifluoro-2,4-pentanedionato)palladium(II), [Pd(tfac)$_2$], with tertiary phosphines.[7] The established examples of **2** are [M(hfac)$_2$L], where hfac stands for an *O,O'*-chelated 1,1,1,5,5,5-hexafluoro-2,4-pentanedionate anion and L=tri-*o*-tolylphosphine for M=Pd(II) and Pt(II), and L=tricyclohexylphosphine for M=Pt(II).[8] Complexes **8** have been reported for [Pd(etac-C^2)$_2$L$_2$] (L=py, 2-Me-py, $PhCH_2NH_2$, $BuNH_2$, and 1/2bpy)[9] and [Pt(acac-C^3)$_2$(py)$_2$],[10] where etac represents anion of 1-ethoxy-1,3-butanedione (ethyl acetoacetate).

In a previous paper we reported preparation and characterization of the palladium(II) and platinum(II) complexes of various β-dicarbonyl compounds.[11] The present paper is concerned with the reactions of [Pd(β-dik)$_2$] (**1**) with a number of nitrogen bases (L) which are listed in Table 1. Various combinations of L(**a**—**u**) and bis-chelates (**1A**—**1I**) as well as a mixed-ligand chelate [Pd(acac)(tfac)] (**1M**) were examined and especially the reactions of **1A**—**1D** were investigated in detail.

†† On leave from Ravenshow College, Cuttack-3 (Orissa), India.

Table 1. β-Diketonate and nitrogen-base ligands used

β-Diketonate anion	Abbr.	Symbol
2,4-Pentanedionate	acac	A
1-Phenyl-1,3-butanedionate	bzac	B
1,1,1-Trifluoro-2,4-pentanedionate	tfac	C
1,1,1,5,5,5-Hexafluoro-2,4-pentanedionate	hfac	D
3-Phenyl-2,4-pentanedionate	Ph-acac	E
1,3-Diphenyl-1,3-propanedionate	dbm	F
2,2,6,6-Tetramethyl-3,5-heptanedionate	dpm	G
1,1,1-Trifluoro-4-(2-thienyl)-2,4-butanedionate	tta	H
1-Ethoxy-1,3-butanedionate	etac	I

Base(L)	Symbol	Base(L)	Symbol
NH_3	a	Bz_3N	*l*
$MeNH_2$	b	py	m
$EtNH_2$	c	2-Me-py	n
n-$PrNH_2$	d	3-Me-py	o
$BzNH_2$	e	4-Me-py	p
½en	f	4-Me_2N-py	q
Me_2NH	g	2,6-Ph_2-py	r
Et_2NH	h	½bpy	s
pip	i	½(4,4'-Me_2-bpy)	t
BzNHMe	j	½(2,9-Me_2-phen)	u
Bz_2NH	k		

a) Bz: benzyl, pip: piperidine, bpy: 2,2'-bipyridine, phen: 1,10-phenanthroline.

Results and Discussion

Table 2 lists decomposition temperature and analytical data of complexes **4**, **5**, and **7** which were obtained by reactions of **1** either with neat liquid L or with L in appropriate solvents. The tendency of nitrogen bases to ligate palladium(II) is very strong and primary amines and pyridines displace both of the β-diketonate ligands to produce complexes **5**. It is difficult to isolate the intermediate products **4** in

TABLE 2. NEWLY PREPARED COMPLEXES, [Pd(β-dik)L_2](β-dik) (**4**), [PdL_4](β-dik)$_2$ (**5**), AND [Pd(β-dik)(β-dik-*C*)L] (**7**)

Compd	Dec temp °C	Found(Calcd)(%) C	H	N
4Ag[a]	≈r. t.	39.28(39.03)	7.37 (7.49)	6.48 (6.50)
4Ah	86—88	48.00(47.95)	8.15 (8.05)	6.29 (6.21)
4Ai[b]	54—56	48.84(48.73)	7.84 (7.77)	5.68 (5.68)
4Bi	89—91	60.26(60.15)	7.30 (6.73)	5.08 (4.68)
4Cg	*ca.* 75	33.86(33.45)	4.45 (4.41)	5.68 (5.57)
4Ch	*ca.* 64	38.51(38.68)	5.32 (5.41)	4.98 (5.01)
4Ci	*ca.* 130	41.39(41.21)	5.22 (5.19)	4.76 (4.81)
4Cj	*ca.* 133	47.73(47.68)	4.61 (4.62)	4.24 (4.28)
4Ck	106—108	56.52(56.55)	4.72 (4.75)	3.40 (3.47)
4Cs	*ca.* 122	42.01(42.23)	2.79 (2.84)	5.00 (4.93)
4Dg	g)	27.63(27.53)	2.68 (2.64)	4.66 (4.59)
4Di	105—115	34.79(34.77)	3.46 (3.50)	4.06 (4.06)
4Ds	*ca.* 160	35.52(35.30)	1.52 (1.49)	4.11 (4.14)
4Dt	140—145	37.56(37.49)	1.98 (2.00)	4.05 (3.98)
4Du	g)	39.51(39.55)	1.96 (1.94)	3.98 (3.84)
4Mb	*ca.* 92	33.99(34.26)	4.99 (5.03)	6.60 (6.66)
4Mh	*ca.* 85	42.78(42.82)	6.61 (6.59)	5.51 (5.55)
4Mi	135—137	44.55(45.42)	6.09 (6.29)	5.07 (5.30)
5Aa[a]	g)	29.87(29.39)	7.31 (7.40)	13.86(13.70)
5Ab[e]	<r. t.	35.40(39.21)	6.85 (7.99)	10.31(10.07)
5Ac[c]	≈r. t.	43.96(43.77)	8.63 (8.77)	11.27(11.34)
5Ad[f]	78—82	51.07(50.38)	9.75 (9.49)	9.69 (9.59)
5Ae	g)	62.23(62.25)	6.86 (6.87)	7.52 (7.64)
5Af[a]	g)	36.99(36.49)	7.18 (7.44)	12.53(12.16)
5Ba	120—123	48.02(48.34)	6.01 (6.09)	11.01(11.28)
5Bb	<r. t.	e)		
5Bc	≈r. t.	55.24(55.21)	7.67 (7.61)	9.32 (9.20)
5Bd	95—97	57.61(57.78)	8.06 (8.18)	8.23 (8.42)
5Be	124—126	67.68(67.24)	6.41 (6.35)	6.76 (6.54)
5Bf[a]	177—178	49.46(49.27)	6.27 (6.55)	9.56 (9.58)
5Ca	175—213	25.10(24.99)	4.14 (4.19)	11.61(11.66)
5Cb	g)	31.14(31.32)	5.28 (5.26)	10.48(10.44)
5Cc	93—95	36.46(36.46)	6.12 (6.12)	9.63 (9.45)
5Cd	150—153	40.63(40.71)	6.82 (6.83)	8.54 (8.63)
5Ce	129—130	54.31(54.26)	5.27 (5.27)	6.67 (6.66)
5Cf[b]	202—203	30.67(30.53)	4.71 (4.76)	10.50(10.17)
5Cm[d]	59—61	46.02(45.87)	4.37 (4.20)	7.16 (7.15)
5Da	125—127	19.34(19.23)	2.78 (2.90)	9.08 (8.97)
5Db	*ca.* 106	26.13(26.08)	3.50 (3.44)	8.86 (8.69)
5Dc	100—120	31.16(30.85)	4.32 (4.31)	8.02 (7.99)
5Dd	*ca.* 100	35.01(34.91)	5.11 (5.06)	7.42 (7.40)
5Dm	97—100 (subl)	43.23(43.05)	2.68 (2.65)	6.74 (6.69)
5Dt	164—166	46.13(45.94)	2.99 (2.95)	6.23 (6.30)
5Ed	150—152	58.75(58.91)	8.44 (8.43)	8.10 (8.09)
5Fd	g)	63.92(63.91)	7.52 (7.41)	6.85 (7.10)
5Gd	150—152	57.58(57.56)	10.67(10.52)	8.34 (7.90)
5Hm	115—125	49.90(49.98)	3.26 (3.26)	6.39 (6.48)
5Ho	g)	52.11(52.13)	3.92 (3.91)	6.10 (6.08)
5Hp	g)	51.88(52.13)	3.90 (3.91)	6.06 (6.08)
5If	g)	e)		
5Mb	g)	34.44(34.83)	6.65 (6.47)	11.74(11.60)
7Ag	*ca.* 80 (subl)	41.06(41.21)	6.07 (6.05)	3.91 (4.01)
7Be	134—136	60.61(60.51)	5.11 (5.08)	2.54 (2.61)

Table 2. (Continued)

Compd	Dec temp °C	Found(Calcd)(%) C	H	N
7Bi	148—149	58.14(58.43)	5.66(5.69)	2.80(2.73)
7Bm	120—130	59.08(59.13)	4.56(4.56)	2.91(2.76)
7Bn	130—131	60.00(59.84)	4.88(4.83)	2.80(2.68)
7Bq	166—169	58.82(58.86)	5.11(5.12)	5.13(5.08)
7Ci	127—129	36.27(36.20)	3.86(3.85)	2.83(2.81)

a) Dihydrate. b) Monohydrate. c) Hemihydrate. d) Trihydrate. e) The analysis is unsatisfactory because of instability. f) Hemietherate. g) Not determined.

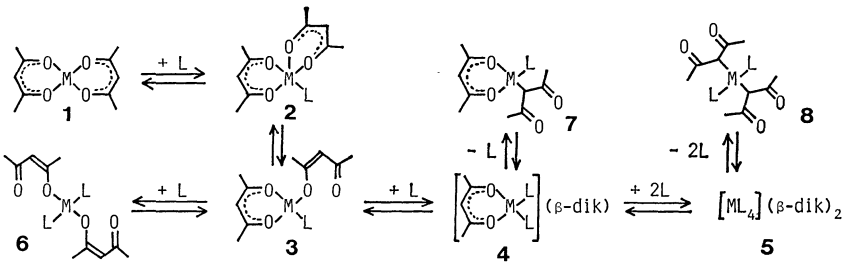

Fig. 1. The schematic sequence of reactions between the bis(β-diketonato)palladium(II) complexes and Lewis bases, L.

Table 3. Characteristic IR bands in Nujol of representative complexes

Compd	ν(NH)	ν(C=O)+ν(C=C)	Compd	ν(NH)	ν(C=O)+ν(C=C)
4Ah	3060 s	1604 vs, 1573 vs, 1543 s, 1517 vs	**5Ca**	3260 vs, 3120 s	1640 vs, 1512 s
			5Cd	3180 s, 3120 m	1638 vs, 1505 m
4Ai	3110 s	1609 vs, 1578 vs, 1525 vs, 1500 vs	**5Cm**		1635 vs, 1555 vs, 1505 s
			5Da	3340 m, 3160 s, br	1670 vs, 1590 vs, 1525 s
4Bi	3070 m	1604 vs, 1585 s, 1552 vs, 1510 vs	**5Dd**	3230 vs, 3150 s	1662 vs, 1630 s, 1524 m
			5Dt		1678 vs, 1530 vs, br
4Ci	3108 m	1636 vs, 1604 vs, 1575 m, 1524 s, 1504 m	**5Ed**	3170 vs, 3100 vs	1620 s, 1598 vs, 1560 vs, 1508 s
4Cs		1598 vs, 1542 vs, br	**5Fd**	3170 vs, 3085 vs	1601 s, 1590 vs, 1530 m, 1504 s
4Di	3170 vs	1679 vs, 1634 vs, 1604 s, 1553 vs, 1540 s	**5Gd**	3165 vs, 3100 vs	1601 vs, 1584 vs
4Ds		1681 vs, 1525 m	**5Hm**		1625 vs, 1573 s, 1506 vs
4Dt		1680 s, 1615 vs, br, 1563 vs, 1526 m, 1510 w	**5Mb**	3150 vs, br	1645 vs, 1605 vs, 1525 s, 1500 s
4Mb	3220 s, 3120 s	1649 vs, 1583 vs, 1566 vs, 1530 vs	**7Ad**	3250 s, 3180 m	1682 vs, 1640 s, 1575 vs, 1519 vs
4Mi	3110 m	1639 vs, 1602 w, 1573 s, 1546 s, 1520 s	**7Ai**	3130 w	1675 vs, 1628 w, 1570 vs, 1543 m, 1520 vs
5Aa	3180 vs, br	1609 vs, 1505 vs	**7Bi**	3130 m	1704 m, 1679 s, 1638 s, 1608 vs, 1572 s, 1523 vs
5Ad	3140 vs, 3080 s	1608 vs, 1500 vs			
5Ba	3230 vs, 3080 s	1600 vs, 1565 s, 1506 vs	**7Ci**	3150 w	1710 vs, 1660 m, 1604 vs, 1518 s
5Bd	3169 vs, 3103 s	1624 s, 1599 vs, 1572 s, 1508 s			

these cases except **4Mb**. On the other hand secondary amines can not form complexes of type **5** because of their steric requirement, but result in **4**.

Transformation of the *O,O'*-chelated 2,4-pentanedionate ligand (acac) to the central-carbon-bonded state was first found by Baba *et al.*[2] for the reactions of $[Pd(acac)_2]$ with bases in dichloromethane. The equilibrium study of the $[Pd(acac)_2]$–Et_2NH system showed that the equilibrium is almost completely shifted to **4** in methanol, but is favorable to **7** in dichloromethane.[3] Preparation of complexes **7** in the present study was therefore carried out mainly in dichloromethane.

X-Ray analysis of $[Cu(dmed)_2(hfac)_2]$ (dmed=*N,N*-dimethylethylenediamine)[12] and $[Cu(en)_2](acac)_2 \cdot 2H_2O$[13] revealed that the β-diketonate anions occupy the apical positions though the Cu–O distances (2.79 Å) are too long to be considered as the coordination bond in either case. On the contrary, the X-ray crystal structure of $[Pd(acac)(Et_2NH)_2](acac)$ (**4Ah**) determined by Kasai and his collaborators at −170 °C showed that the acac anion does not lie on the

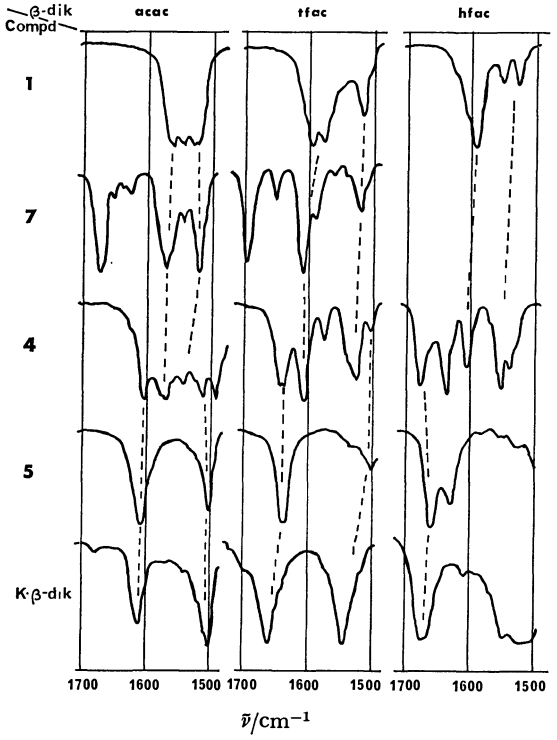

Fig. 2. IR spectra in Nujol of [Pd(β-dik)$_2$] (**1**), [Pd(β-dik)(β-dik-*C*^{3})(pip)] (**7**), [Pd(β-dik)(pip)$_2$](β-dik) (**4**), and [Pd(PrNH$_2$)$_4$](β-dik)$_2$ (**5**) together with those of K(β-dik) hydrate for comparison.

apical position, but stands aside of the coordination plane, forming hydrogen bonds with the ligated amine groups.[14] Compound **4Ah** is not stable at room temperature even in the solid state, but looses gradually the volatile amine ligand to convert into **7Ah**.

Infrared Spectra. Characteristic IR bands of some representative mixed-ligand complexes are listed in Table 3. The bands in the 1700—1500 cm^{-1} region which are assigned to the ν(C=O)+ν(C=C) vibrations are most useful for distinguishing the bonding mode of β-diketonate anions in metal complexes. Figure 2 exemplifies these IR bands for some acac, tfac, and hfac complexes. Substitution of the methyl group in acac with the electron-attracting trifluoromethyl group raises frequency of the ν(C=O) band in each type of complexes. Thus the highest-frequency band in this region is observed at 1595 and 1591 cm^{-1} for *trans*-[Pd(tfac)$_2$] (**1C**) and [Pd(hfac)$_2$] (**1D**), respectively, 30 cm^{-1} higher than 1563 cm^{-1} for [Pd(acac)$_2$] (**1A**). The central-carbon-bonded β-diketonate ligand in **7** has the keto structure,[2] and absorbs in the 1700—1650 cm^{-1} region. The absorption bands for the β-diketonate anions in the outer sphere appear in the frequency region lower than those for the carbon-bonded β-diketonate and higher than those for the chelated one. Thus the spectra of compounds **5** are quite similar to those of K(β-dik), although the spectra of **4** are more composite since the complexes contain β-diketonate anions in both the inner and outer spheres (Fig. 2).

In crystals of [Pd(acac)(Et$_2$NH)$_2$](acac) (**4Ah**), the C–O distance of the chelated acac anion is 1.277(5) Å, nearly the same as that in [Pd(acac)$_2$] (1.275(4) Å).[14] In accordance with this situation, the ν(C=O) frequency (1573 cm^{-1}) assignable to the former carbonyl bond is not so different from that (1563 cm^{-1}) for the latter. On the other hand the ν(C=O) frequency (1604 cm^{-1}) due to the acac anion in the outer sphere conforms with the shorter C–O distance (1.246(5) Å)[14] and is close to 1610 cm^{-1} of K(acac) hydrate in which the C–O distance is 1.25(2) Å.[15]

Secondary amines coordinated to palladium(II) in complexes **4** exhibit single ν(N–H) band in the 3180—3060 cm^{-1} region, whereas primary amines in complexes **5** and **4Mb** show two bands in the 3250—3030 cm^{-1} region.

^{1}H NMR Spectra. Table 4 lists the ^{1}H NMR data for complexes **5**. In the case of the platinum(II) complexes, for instance [Pt(py)$_4$](hfac)$_2$, absence of coupling to ^{195}Pt of ^{1}H, ^{13}C, and ^{19}F atoms in hfac confirms that the hfac anions are not coordinated to the metal ion but exist in the outer sphere as counter anions.[4] The β-diketonate anions involved in **5** exhibit only one set of ^{1}H signals, indicating that the two anions in each complex are environmentally equivalent. These data do not necessarily certify that they exist in the outer sphere. However, the methyl and methine protons of [Pd(NH$_3$)$_4$](tfac)$_2$ (**5Ca**) resonate at 2.22 and 5.38 ppm from internal DSS in D$_2$O (Table 4). The chemical shifts coincide with those of K(tfac), indicating that **5Ca** dissociates completely in D$_2$O. Proton signals from the ammine ligands were not observed because of rapid H-D exchange with D$_2$O.

In spite of their salt-like structures, most of complexes **4** and **5** are not soluble in water, but dissolve in organic solvents and the β-diketonate anions seem to be associated with the cation in solution. Thus, for instance, molecular weights determined in dichloromethane at 25 °C of **4Ch**, **4Ci**, and **5Dm** are 534, 551, and 811 in fair agreement with the calculated values 559, 583, and 837, respectively. The amine protons of complexes **4** and **5** resonate generally at substantially lower field than those of the corresponding neutral complexes **7**. The amine signal from **5Ad** for instance, is shifted downfield by 2.6 ppm compared with that from **7Ad** in C$_6$D$_6$. Similarly the amine protons of **4Ag**, **4Ai**, and **4Ci** resonate at lower field in C$_6$D$_6$ by 3.2, 3.2, and 3.4 ppm than the corresponding complexes **7**, respectively. Thus the hydrogen-bonding interaction between the coordinated amine and the β-diketonate anion in the outer sphere as revealed in crystals[14] persists in solution and is stronger in the case of compounds **4** than in **5**. The sequence of chemical shift (ppm) of the propylamine protons in CDCl$_3$, **5Bd**(5.8)>**5Ad**(5.6)>**5Cd**(5.3)>**5Dd**(4.9), reflects the relative strength of hydrogen bonding by the β-diketonate anions in accordance with the basicity sequence,[16] bzac~acac>tfac>hfac.

The methyl protons of β-diketonate anions in **5** resonate at about 0.3 ppm higher field than those in the corresponding parent bis-chelates,[11] reflecting the higher charge density in the former than in the latter. Complexes **5Ae**, **5Be**, and **5Ce** exhibit the methyl proton signals at extraordinarily high field. The phenyl ring of benzylamine in these complexes may exert the anisotropic shielding effect. It is strange that

Table 4. ^{1}H NMR data for complexes **5**, $[PdL_4](\beta\text{-dik})_2$[a]

Compd	Solvent[b]	β-dik			L[c]	
		Me	Ph or *t*-Bu	CH	NH_2	Other
5Ab	i	1.76		5.00[d]	5.4[d]	Me : 2.42 t, br[6]
5Ac	i	1.67		4.97[d]	5.5[d]	Et : 2.6 br, 1.13 t(7)
	ii	1.84		5.26	5.8	Et : 2.5_5 br, 1.27 t(7)
5Ad	i	1.71		5.02[d]	5.6[d]	Pr : 2.52 br, 1.60 m, 0.86 t(7)
	ii	1.90		5.37	6.0_1	Pr : 2.67 br, 1.8 m, 0.96 t(7)
	vi	1.68		5.0	5.6_0	Pr : 2.5_6 br, 1.5 m, 0.86 t(7)
5Ae	i	1.26		4.51[d]	6.5[d]	CH_2 : 3.7_0 br, Ph : 7.3 m
5Bb	ii	2.04	7.9m, 7.1m	6.02	6.0	Me : 2.11 t, br[7]
5Bc	i	1.88	7.7m, 7.1m	5.69[d]	5.8[d]	Et : 2.5_7 br, 1.11 t(7)
	ii	2.02	7.9m, 7.1m	5.97	6.0	Et : 2.4_7 br, 1.21 t(7)
5Bd	i	1.83	7.6m, 7.2m	5.64[d]	5.8[d]	Pr : 2.5 br, 1.5 m, 0.74 t(7)
	ii	2.09	8.0m, 7.2m	6.07	6.2_2	Pr : 2.6_5 br, 1.80 m, 0.82 t(7)
5Be	i	1.38	7.1m	5.17[d]	6.5[d]	CH_2 : 3.5_5 br, Ph : 7.1 m
5Ca	viii	2.22		5.38	d)	
5Cb	i	1.90		5.36[d]	5.0_5 d[d]	Me : 2.37 t[6]
	ii	1.75		5.55	5.1_8 d	Me : 2.04 t[6]
5Cc	i	1.82		5.39	5.2	Et : 2.6 br, 1.07 t(7)
	ii	1.73		5.70	5.4	Et : 2.4 br, 1.13 t(7)
5Cd	i	1.85		5.46	5.3	Pr : 2.5_4 br, 1.47 m, 0.85 t(7)
	ii	1.77		5.75	5.5	Pr : 2.5_3 br, 1.6_7 m, 0.88 t(7)
5Ce	i	1.32		4.61	5.9	CH_2 : 3.5_7 br, Ph : 7.1 m
	ii	1.32		4.86	6.0	CH_2 : 3.5_5 br, Ph : 7.2 m
	iii	1.35		4.69	6.0	CH_2 : 4.0 br, Ph : 7.2 m
5Cm	vii	2.47		5.97		e)
5Dd	i			5.92	4.9	Pr : 2.5_3 br, 1.4_5 m, 0.8_5 t(7)
5Dm	i			6.00		py : 9.81 dd(5 and 2), ≈7.6 m, ≈7.4 m
5Ed	i	1.49		Ph : 7.1 m	5.8	Pr : 2.6 br, 1.5 m, br, 0.94 t(7)
5Fd	i		7.7m, 7.1m	6.33[d]	6.0[d]	Pr : 2.5 br, 1.5 m, br, 0.63 t(7)
5Gd	i		1.00	5.33[d]	5.5[d]	Pr : 2.5 br, 1.4 br, 0.76 t(7)
5Hm	vii	thienyl protons[e]		4.70		e)
5Mb	i	1.78	-acac-	5.10	5.3	Me : 2.43 t[6]
		1.93	-tfac-	5.43		
5Mc	ii	1.82	-acac-	5.27	5.9	Et : 2.5 br, 1.20 t, br(7)
		1.75	-tfac-	5.70	5.3	

a) Chemical shifts in ppm from internal Me_4Si in various solvents except D_2O in which sodium 2,2-dimethyl-2-silapentane-5-sulfonate (DSS) was used as internal referrence. b) Solvent: i) $CDCl_3$, ii) C_6D_6, iii) $(CD_3)_2CO$, iv) $(CD_3)_2SO$, v) CD_3OD, vi) CD_2Cl_2, vii) py, viii) D_2O. c) Figures in parentheses and brackets give J(CH–CH) and J(CH–NH), respectively, in Hz. The NH_2-proton signals are usually broad. d) The H-D exchange reaction occurs with the solvent. e) Indiscernible due to overlapping with other signals.

compounds **5Cd** and **5Dd** give the molecular-weight values of 1330 and 1522, respectively, in dichloromethane at 25 °C which are equal to twice the calculated values. The molecular weight of **5Ad** also exceeds the value (665) calculated for monomer, depending substantially on concentration: 720—855 for 0.01—0.1 mol(monomer) dm^{-3}. The ^{19}F NMR spectrum (one signal at 77.7 ppm upfield from $CFCl_3$ in CH_2Cl_2) and the ^{13}C NMR data of **5Dd** which will be described later indicate that the two hfac anions are magnetically equivalent as was shown by the ^{1}H NMR spectrum. The dimeric structures of these compounds are very interesting and X-ray analysis of **5Dd** is now in progress.

Compounds **5Mb** and **5Mc** which were prepared by the reactions of [Pd(acac)(tfac)] (**1M**) with methylamine and ethylamine, respectively, exhibit two sets of methyl and methine signals assignable to the acac and tfac anions in the outer sphere. It is interesting that **5Mc** shows two amine-proton signals at 5.9 and 5.3 ppm in C_6D_6, presumably distinguishing the hydrogen-bonding with acac and tfac anions, although **5Mb** gives only one NH_2 signal in $CDCl_3$.

Table 5 lists the ^{1}H NMR data for complexes **4**. In accordance with the proposed structure, compounds **4A**, **4B**, **4C**, and **4M** exhibit two sets of proton signals from both β-diketonate anions in inner and outer spheres. The signal assignment was made by reference to data for the parent bis-chelates[11] and complexes **5** (Table 4). Results obtained for the related

TABLE 5. ^{1}H NMR DATA FOR COMPLEXES **4**, [Pd(β-dik)L$_2$](β-dik)[a)]

Compd	Solvent[b)]	β-dik(IS)		β-dik(OS)		L[c)]	
		CH_3	CH	CH_3	CH	NH	Other
4Ag	i	1.93	5.27[d)]	1.83	5.02[d)]	d)	Me : 2.40
	ii	1.51	4.87	2.05	5.38	7.7	Me : 2.31 br
	iii	2.03	5.53[d)]	1.75	4.98[d)]	7.4[d)]	Me : 2.42 br
4Ah	i	1.98	5.38[d)]	1.98	5.04[d)]	7.1[d)]	Et : 2.6 m, 1.53 t(7)
	ii	1.61	5.00	2.11	5.45	8.1_2	Et : 2.7 m, 1.52 t(7)
	iii	1.99	5.51	1.79	4.92[d)]	7.5[d)]	Et : 2.6 m, 1.49 t(7)
	iv	1.98	5.54	1.80	4.70	6.5_4	Et : *ca.* 2.5 m, 1.43 t(7)
	v	2.02	5.55[d)]	2.02	d)	d)	Et : 2.6 m, 1.53 t(7)
	vi	1.96	5.39	1.88	4.92	7.2_4	Et : 2.5 m, 1.49 t(7)
4Ai	i	1.92	5.22[d)]	1.83	5.03[d)]	7.0[d)]	pip[f)] : 3.2, 2.7, 1.4_5
	ii	1.60	4.95	2.12	5.47	7.8	pip[f)] : 3.7, 2.7, 1.3_7
4Bi	ii	1.75	5.68	2.21	6.12	e)	pip[f)] : 3.6, 2.7_5, 1.3_7
4Cg	i	2.14	5.86	1.96	5.45	7.1[d)]	Me : 2.43 d[$5._5$] and 2.40 d[$5._5$]
	ii	1.38	5.41	1.97	5.85	7.4	Me : 2.12 d[6]
	vi	2.15	5.80	1.91	5.32	6.9	Me : 2.41 d[6] and 2.37 d[6]
4Ch	i	2.13	5.78	1.99	5.40	7.1	Et : 2.5_5 m, 1.52 t($6._5$), and 1.49 t(6.5)
	ii	1.37	5.32	1.91	5.67	7.5	Et : 2.4 m, 1.35 t($6._5$)
4Ci	ii	1.42	5.42	1.99	5.89	7.4_6	pip[f)] : 3.3, 2.5, 1.25
4Cj	i	2.17	5.73	2.01	5.43	7.5	Me : 1.80 d[5] and 1.72 d[5] CH_2 : 3.5—3.1 m; Ph : 7.2_6 br
	ii	1.24	5.28	1.96	5.87	8.1	Me : 1.86 d[5] and 1.74 d[5] CH_2 : *ca.* 3.3 m; Ph : 7.4 m, 7.0 m
4Ck	i	2.12	5.73	1.82	5.50	7.8	CH_2 : 3.3 m; Ph : 7.23 m, 7.13 m
	ii	1.05	5.22	2.02	5.93	8.3	CH_2 : 3.5 m; Ph : 7.3 m
4Cs	i	2.47	6.14	2.25	5.44		bpy : 8.9—7.3 m
4Di	i		6.26		5.89	6.90	pip[f)] : 3.4 d, 2.8, 1.51
	ii		5.85		6.35	6.88	pip[f)] : 3.1 d, 2.3_2 q, 1.1
4Dt	i		6.08 br		6.08 br		bpy : $H^{3,3'}$ 9.14 br, $H^{5,5'}$ 7.4_6 d, br(6), $H^{6,6'}$ 8.0_8(6), $Me^{4,4'}$ 2.65
4Du	iii		5.96		e)		phen : $H^{3,8}$ 8.77 d(8), $H^{4,7}$ 7.80 d(8) $H^{5,6}$ 8.05, $Me^{2,9}$ 3.04
4Mb[g)]	i	1.93	5.43[d)]	2.41	5.37[d)]	5.3[d)]	Me : 2.41 d[$6._5$] and 2.23 d[$6._5$]
4Mh[g)]	i	1.96	5.35	2.07	5.31[d)]	6.5_5[d)]	Et : 2.6 m, 1.51 t(7)
	ii	1.55	4.85	1.95	5.67	7.1	Et : 2.5 m, 1.42 t(7)
4Mi[g)]	ii	1.59	4.94	2.02	5.95	7.2	pip[f)] : 3.4, 2.7, 1.3

a—e) Same as footnotes for Table 4. IS and OS abbreviate inner and outer spheres, respectively. f) Chemical shifts refer to $H^{2,6}$(equatorial), $H^{2,6}$(axial), and $H^{3,4,5}$(equatorial) in this sequence. Signals are all broad and those for $H^{3,4,5}$(axial) are indiscernible. g) The acac anion exists in IS and tfac in OS.

platinum(II) complexes such as [Pt(β-dik)(pip)$_2$](β-dik)[5)] were also helpful. Thus the methyl and methine protons resonating at higher field in $CDCl_3$ were assigned to the β-diketonate anion in the outer sphere.

It is noticed in Table 4 that the methyl and methine resonances from the acac (**5A**) and bzac (**5B**) compounds are shifted downfield by 0.14—0.26 ppm and 0.28—0.43 ppm, respectively, in C_6D_6 as compared with those in $CDCl_3$. In the case of the tfac compounds (**5C**), the methine protons are shifted in the same direction by 0.19—0.31 ppm but the methyl protons show slight upfield shifts by 0—0.15 ppm in C_6D_6. The same trend is observed for β-diketonate anions in the outer sphere of compounds **4** (Table 5). On the contrary, the methyl and methine resonances from the chelated β-diketonate ligands are shifted upfield by 0.32—0.42 ppm and 0.27—0.40 ppm for acac (**4A**) and by 0.57—0.93 and 0.45—0.51 ppm for tfac (**4C**), respectively.

Pinnavaia and Fay[17)] compared the methyl and methine chemical shifts for [M(acac)$_4$] and [M(tfac)$_4$] [M=Zr, Hf, Ce, and Th) as well as for free ligands in C_6D_6 with those in $CDCl_3$ and CCl_4. All signals were shifted upfield in C_6D_6; the methyl signals from enol tautomers of acacH and tfacH by 0.39 and 0.89 ppm, and the methine signals by 0.48 and 0.60 ppm, respectively. The metal chelates showed the same trend but the shifts were less pronounced. The authors ascribed the solvent effect to the diamagnetic anisotropy of the benzene ring and the especially large upfield shifts for the free ligands were supposed to result from a sandwiching of the planar enol molecules between the benzene molecules.

The present data are quite different from theirs, the upfield shifts for the chelated ligands being much pronounced and the effect on the counter anions being

Table 6. ^{1}H NMR data for complexes 7[a)]

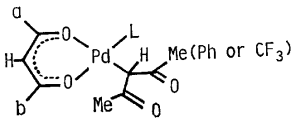

Compd	Solvent[b)]	[*cis*]/[*trans*]	Isomer[f)]	Chelated β-dik a	Chelated β-dik b	Chelated β-dik CH	*C*-Bonded β-dik Me	*C*-Bonded β-dik CH	L[c)] NH	L[c)] Other
7Ab	ii			1.71	1.75	5.08	2.17	4.56	3.4	Me : 2.02 t[7]
7Ad	ii			1.72	1.75	5.09	2.19	4.57	3.4	Pr : 2.4 m, 1.4 m, 0.73 t(7)
7Ae	ii			1.73	1.73	5.08	2.11	4.55	e)	CH_2 : 3.5 br
7Ag	i			1.91	1.92	5.25[d)]	2.16	4.47[d)]	3.9	Me : 2.25 d[6]
	ii			1.66	1.71	4.98	2.07	4.49	4.5	Me : 2.02 d[6]
7Ah	i			1.96	1.97	5.34[d)]	2.19	4.52[d)]	3.4	Et : 2.6 m, 1.32 t(7)
7Ai	ii			1.75	1.75	5.06	2.10	4.59	4.6	pip[g)] : 2.8—2.3, 1.2
7Ak	ii			1.67	1.81	5.06	1.81	4.32	5.1	CH_2 : 4.0 d, 3.4 d(AB quartet) Ph : 7.5 m, 7.0 m
7Be	i	1/1	*cis*	2.09	Ph	5.96	2.31	5.36	d)	CH_2 : 3.6 br
			trans	Ph	2.16	5.96	2.31	5.30		
	ii	1/1	*cis*	1.79	Ph	5.87	2.19	5.54	e)	CH_2 : 3.6 br
			trans	Ph	1.89	5.87	2.22	5.51		
7Bi	ii	6/7	*cis*	1.80	Ph	5.79	2.19	5.77	4.8	pip[g)] : 3.1—2.4, 1.2
			trans	Ph	1.97	5.79	2.23	5.74		
7Bm	i	3/2	*cis*	1.99	Ph	5.97	2.47	5.00		py : 8.6_6 m, $8._0$ m
			trans	Ph	2.12	5.95	2.38	5.17		
	ii	5/3	*cis*	1.69	Ph	5.90	2.83	5.23		py : 8.72 m, 6.5 m
			trans	Ph	1.87	5.85	2.64	5.39		
7Bn	i	3/2	*cis*	1.93 1.89	Ph	5.94 5.92	2.41 2.37	5.10 4.92		Me : 2.19
			trans	Ph	2.12 2.06	5.97 5.86	2.37 2.22	5.13 5.07		Me : 2.91, 2.75 py : 8.6 m, *ca.* 7.9 m
7Bq	i	5/3	*cis*	2.00	Ph	6.00	2.54	4.98		NMe_2 : 2.10
			trans	Ph	2.10	5.96	2.44	5.10		py : 8.16 d(7), 6.49 d(7)
7**Cg**	ii	3/4	*cis*	1.39		5.30	1.87	4.80	3.7	Me : 1.73 d[6]
			trans		1.46	5.30	1.92	4.76		Me : 1.72 d[6]
7Ch	ii	1/2	*cis*	1.44		5.43	1.94	4.85	3.5	CH_2 : 2.1 m, br{CH_3 : 1.03 t(7), CH_3 : 0.99 t(7)}
			trans		1.48	5.38	1.99	4.75		
7Ci	i	3/2	*cis*	2.14		5.81	2.34	4.94	3.5_4	pip[g)] : 2.78, 1.64
			trans		2.21	5.81	2.33	4.92		
	ii	3/2	*cis*	1.51		5.49	1.96	4.98	4.0_4	pip[g)] : 2.6, 1.1
			trans		1.52	5.51	1.92	5.01		
7Ck	ii	1/1	*cis*	1.43		5.43	1.53	4.65	e)	CH_2 : *ca.* 3.6 m
			trans		1.43	5.39	1.54	4.52		

a—e) Same as footnotes for Table 4. f) *cis* and *trans* mean *cis*(Me, L) and *trans*(Me, L), respectively. g) Chemical shifts refer to $H^{2,6}$ and $H^{3,4,5}$, respectively. Signals are all broad.

reversed. Benzene molecules may exert the diamagnetic anisotropic effect on the chelated β-diketonate ligand by sandwiching the coordination plane. The β-diketonate anion in the outer sphere is oblique to the coordination plane, forming hydrogen bonds with amine ligands.[14)] Thus the methyl and methine protons of the counter anion may experience the paramagnetic anisotropy of the benzene rings.

Since the tfac ligand is unsymmetric, two alkylamines in complexes **4C** are not environmentally equivalent. Thus two sets of the alkyl proton signals from the amine ligands are observed for **4Cg**, **4Ch**, and **4Cj**. In the reactions of [Pd(acac)(tfac)] (**1M**) with nitrogen bases, two types of products, [Pd(acac)L_2](tfac) and [Pd(tfac)L_2](acac) are conceivable. However ^{1}H NMR spectra indicate that the former type of products were obtained exclusively in each case (**4Mb**, **4Mh**, and **4Mi** in Table 5), reflecting the substantial difference in basicities of the acac and tfac anions.

Complex **4Dt** exhibits only one broad methine proton signal at 6.08 ppm in $CDCl_3$ at room temperature. The signal becomes sharper with increasing temperature probably by virtue of enhanced exchange between the two hfac anions in inner and outer spheres. The base L_2 (4,4'-Me_2-bpy) freed by reaction (1) may attack **4Dt** to give rise to **5Dt** in reaction (2).

$$[Pd(hfac)L_2](hfac) \rightleftharpoons [Pd(hfac)_2] + L_2 \quad (1)$$

$$[Pd(hfac)L_2](hfac) + L_2 \rightleftharpoons [PdL_4](hfac)_2 \quad (2)$$

Compound **5Dt** was isolated (Table 2) but its NMR spectrum is not determined because of poor solubility.

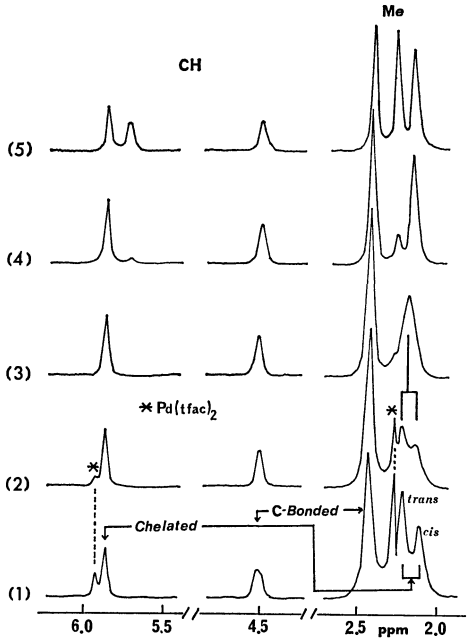

Fig. 3. ^{1}H NMR spectra of $CDCl_3$ solutions containing [Pd(tfac)$_2$] and various amounts of pyridine, the [pyridine]/[complex] molar ratio being 1.0(1), 1.5(2), 3.0(3), 6.0(4), and 11.0(5).

Averaging of the hfac anions in **4Dt** may be realized either by reaction (1) alone or by both of (1) and (2). A similar exchange of tfac anions in [Pd(tfac)(PPh$_3$)$_2$](tfac) was also noticed,[18] but the interrelation between the rate of exchange and the natures of β-diketonate and base ligands has not been studied.

The ^{1}H NMR data for complexes **7** are collected in Table 6. Spectra in $CDCl_3$ of the acac complexes **7A** are similar to those reported for analogous complexes containing triphenylphosphine, pyridine, diethylamine, and *N*-methylbenzylamine as L[2] except that the chemical-shift difference for the two methyl groups of the chelated acac ligand is quite small in the present complexes **7**. By reference to the previous work[2] the signal at the highest field in $CDCl_3$ was assigned to the methyl group (a) located at the position cis to L and the lower-field signal to the methyl group (b) trans to L. The 6H signal around 2 ppm is easily assigned to methyl protons of the carbon-bonded acac ligand, of which the methine proton resonates at higher field than that of the chelated acac ligand.[2]

Since the bzac and tfac ligands are unsymmetric, two geometrical isomers, *cis*(Me,L) and *trans*(Me,L) are conceivable for **7B** and **7C**. In fact proton signals from these complexes exhibit splitting. The higher-field one of the two methyl signals from the chelated β-dik was assigned to the *cis*(Me,L) isomer based on the above consideration and the equilibrium quotient *cis*(Me,L)/*trans*(Me,L) was determined as the signal area ratio. Complexes **7B** except **7Bi** showed a single set of proton signals assignable to *cis*(Me,L) immediately after dissolution, but new signals ascribable to *trans*(Me,L) grew with time at the expense of the *cis*(Me,L) signals to attain an equilibrium. The rate of geometrical isomerization depends on the nature of L, **7Bm** and **7Bn** attaining equilibrium within 3 and 30 min, respectively, but **7Be** requiring *ca.* 10 h.

The [*cis*]/[*trans*] equilibrium quotient is 1 for **7Be** containing benzylamine as L and is larger than 1 for **7Bm**, **7Bn**, and **7Bq** containing pyridines, while the *trans*(Me,L) isomer is slightly more favorable for the piperidine complex, **7Bi**. In the case of **7C**, the *trans*(Me,L) isomers are favorable except for **7Ci** and **7Ck**. Complexes **7I** containing nitrogen bases as L also favor the *trans*(Me,L) form.[9]

Attainment of the isomerization equilibrium is accelerated by a free ligand L. Figure 3 shows ^{1}H NMR spectra of solutions containing [Pd(tfac)$_2$] (**1C**) and various amounts of pyridine. The spectrum in the presence of an equimolar amount of pyridine shows attainment of equilibria (3) and (4). About 80% of

$$[Pd(tfac)_2] + py \rightleftharpoons [Pd(tfac)(tfac\text{-}C^3)py] \quad (3)$$
1C **7Cm**

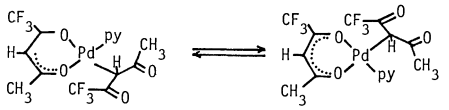

(4)

trans(Me,L)-**7Cm** *cis*(Me,L)-**7Cm**

1C is converted into **7Cm** and the *cis*(Me,L)/*trans*(Me,L) ratio is *ca.* 2/1. With increasing amount of pyridine, the methyl signals at 2.11 and 2.21 ppm become broader. When three times moles of pyridine is added, equilibrium (3) is almost completely shifted to right. The two methyl signals from the chelated tfac are also lost and instead a new signal is observed at 2.16 ppm, the chemical shift being close to the weighted mean of the values for two isomers. Thus the geometrical isomerization (exchange of the coordination sites) (Eq. 4) is assisted by free ligand and becomes fast on the NMR time scale at higher pyridine concentrations. Increased temperature also accelerates the isomerization, the *cis*- and *trans*(Me,L) signals in the presence of equimolar pyridine coalesce at higher temperatures.

Various mechanisms have been proposed for the cis-trans isomerization of square planar complexes.[19] The fact that the rapid isomerization occurs only in the presence of free pyridine does not accord with the dissociative mechanism *via* a three coordinate intermediate.[20] The double displacement mechanism[19] as is expressed by Eq. 5, where R represents the central-carbon-bonded β-diketonate ligand, is most widely accepted as the mechanism for the free-ligand catalyzed

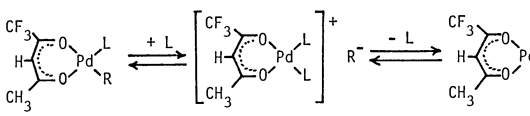

(5)

trans(Me,L)-**7Cm** **4Cm** *cis*(Me,L)-**7Cm**

isomerization. The reactions of [Pd(acac)$_2$] with alkylamines to produce complexes **7A** were also found to proceed *via* the outer-sphere complex **4A**, the acac anion in turn replacing L as a carbanion.[3] If this mechanism is operative in the present case, that is, if the geometrical isomerization occurs rapidly on the NMR time scale *via* the forward and reverse reactions (5), environment of the carbon-bonded tfac and that

Table 7. ^{13}C NMR data for some of complexes **5**, $[PdL_4](\beta\text{-dik})_2$[a]

Compd	Solvent	β-dik						L[b]		
		CH_3	CF_3	CH	$CH_3\underline{C}O$	$CF_3\underline{C}O$	$Ph\underline{C}O$	C^α	C^β	C^γ
5Ad	CD_2Cl_2	28.8 (123)		97.7 (152)	187.5			48.3 (138)	24.8 (*ca.* 128)	11.8 (123)
	C_6D_6	29.0 (123)		98.1 (151)	187.4			48.5 (135)	24.8	11.9 (124)
5Bd	C_6D_6	29.6 (125)		96.1 (152)	189.6		183.0[c]	48.5 (136)	24.9 (129)	12.0 (127)
5Cd	$CDCl_3$	29.5 (126)	119.2 q [289]	92.8 (158)	194.6	168.2 q [30]		47.9 (137)	24.2 (128)	11.3 (126)
5Dd	$CDCl_3$		117.6 q [290]	87.6 (163)		176.0 q [33]		47.9 (139)	24.3 (125)	10.9 (127)
5Dm	$CDCl_3$		118.7 q [292]	85.2 (159)		174.4 q [30]		152.3 (188)	126.5 (170)	139.4 (167)
[K]-tfac[d]	$CDCl_3$	29.8 (126)	120.2 q [291]	92.4 (153)	194.6	168.9 q [27]				
[K]-hfac[d]	$CDCl_3$		118.3 q [291]	84.6		173.7 q [31]				

a) Chemical shifts in ppm from internal Me_4Si. Figures in parentheses and brackets give J(C–H) and J(C–F) in Hz, respectively. b) Symbols for carbon atoms are given referred to nitrogen. c) Resonances for the phenyl carbons are: quaternary C 144.7, *o*-C 127.4 (*ca.* 158), *m*-C 127.8 (*ca.* 158), and *p*-C 129.1 (159) ppm(Hz). d) [K] denotes a potassium ion surrounded by 18-crown-6, $[K(18\text{-crown-6})]^+$.

of the tfac anion in the outer sphere should be averaged. As is seen in Fig. 3, new signals grew at 2.26 and 5.69 ppm when increasing amount of pyridine was added to **7Cm**. These signals are assigned to the methyl and methine protons of the tfac anions in the outer sphere of $[Pd(py)_4](tfac)_2$ (**5Cm**). Compound **4Cm** is not so stable as to be detected spectroscopically, but converted into **5Cm**. The discrepancy in the ^1H chemical shifts in this reaction mixture from those (2.47 and 5.97 ppm, respectively) for pure **5Cm** in pyridine (Table 4) may be ascribed to the difference in the solution media. Thus the signals from the tfac anions both carbon bonded and in the outer sphere are separate and sharp, indicating that the exchange between these two types of tfac anions is not fast on the NMR time scale, even though the *cis*(Me,L) and *trans*(Me,L) configurations are rapidly averaged. Therefore the consecutive displacement mechanism is not realized in this case.

As an alternative mechanism for the geometrical isomerization (Eq. 4), we propose a rapid coordination site exchange of the five-coordinate square-pyramid intermediate as is exemplified in Eq. 6 by moving the unidentate ligands. Of course twisting of the chelate ring may be involved as well. This mechanism was first proposed in order to rationalize the dynamic behaviors in solution of $[M(hfac)_2P(o\text{-tolyl})_3]$ (M=Pd and Pt).[8] The exchange between apical and equatorial positions will occur *via* a trignal-bipyramid intermediate more easily than the Ray-Dutt twist in octahedral complexes.[21] Averaging of environments in solution of both halves of the 1,10-phenanthroline molecule in $[PtCN(phen)_2]NO_3$, which has a similar square-pyramid structure with a cyanide ligand in the basal plane, was also explained by virtue of an analogous mechanism.[22]

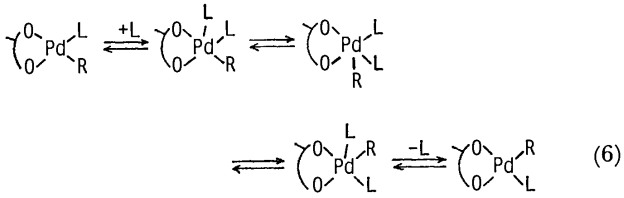

(6)

Complex **7Bn** containing 2-methylpyridine as L shows additional 1:1 splitting of each proton signal besides the splitting due to the geometrical isomerism (Table 6). This additional splitting is caused by hindered rotation of the bulky ligand around the Pd–N bond and the two sets of signals are assigned to the following two rotamers similar to those postulated for the central-carbon-bonded ester ligand in complexes **7I** containing 2-methylpyridine and 2,6-dimethylpyridine as L.[9] At higher temperatures, signals merge into one set for an equilibrium mixture of geometrical isomers.

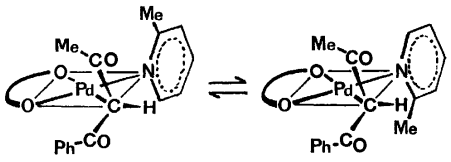

^{13}C NMR Spectra. Table 7 lists the ^{13}C NMR data for some of complexes **5** containing propylamine or pyridine as L together with the data for [K(18-crown-6)](tfac) and [K(18-crown-6)](hfac) for comparison. The chemical shift of each carbon atom of the tfac and hfac anions involved in **5** is close to that of free anions separated from the potassium ion by virtue of the crown ether. The methyl carbons in **5** and free anions resonate at lower fields than those in the parent bis-chelates (25.4, 28.2, and 26.8 ppm for **1A**, **1B**, and **1C**), and the trifluoromethyl carbons than those in **1D** (114.7 ppm).[11] On the other hand, the methine carbons are shifted to upfield as compared with those in the corresponding bis-chelates (101.6,

TABLE 8. ^{13}C NMR DATA FOR SOME OF COMPLEXES **4**, [Pd(β-dik)L_2](β-dik)[a)]

4Ah

Solvent	acac (IS)			acac (OS)			Et_2NH	
	CH_3	CH	CO	CH_3	CH	CO	CH_2	CH_3
$CDCl_3$	26.2 (128)	100.8 (159)	186.3	28.8 br (125)	c)	188.8 br	46.5 (136)	14.2 (125)
C_6D_6	26.0 (128)	100.8 (159)	186.3	29.7 (125)	97.4 (150)	186.5	46.5 (135)	14.0 (121)

4Ci in C_6D_6

	tfac					pip[b)]		
	CH_3	CF_3	CH	$CH_3\underline{C}O$	$CF_3\underline{C}O$	C^α	C^β	C^γ
IS	27.5 (129)	118.1 [284]	97.3 (164)	194.1	167.4 [33]	51.1 (140)	26.5 (128)	{24.1[d)] {24.0 (128)
OS	30.1 (125)	120.6 [290]	92.5 (157)	194.7	169.2 [29]			

4Di in $CDCl_3$

hfac (IS)			hfac (OS)			pip[b)]		
CF_3	CH	CO	CF_3	CH	CO	C^α	C^β	C^γ
116.5 [284]	92.7 (168)	175.4 [36]	118.1 [290]	86.3 (162)	175.5 [32]	51.8 (140)	26.4 (128)	23.7 (129)

4Dt in $CDCl_3$

hfac			4,4′-Me_2-bpy			
CF_3	CH	CO	C^2, C^4	C^3, C^5	C^6	CH_3
117.1 [287]	88.4 br	175.0 br [34]	157.3 156.2	128.0 127.9	145.6	21.8

a, b) Same as footnotes for Table. 7. c) Indiscernible. d) Splitting due to unsymmetry of the tfac ligand.

TABLE 9. ^{13}C NMR DATA FOR COMPLEXES **7Ah**, **7Bq**, AND **7Ci** IN $CDCl_3$[a)]

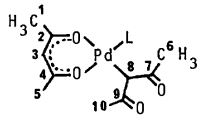

cis(Me,L)

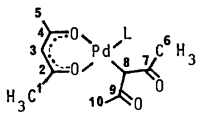

trans(Me,L)

Compd	Chelated acac				C-Bonded acac			L[b)]	
	C^1, C^5		C^2, C^4	C^3	C^6, C^{10}	C^7, C^9	C^8	C^α	C^β
7Ah	26.8, 27.0 (128) (128)		186.3, 186.6	100.2 (158)	31.2 (127)	202.4	48.7 (145)	46.0 (136)	14.0 (127)

Compd		Chelated β-dik[c)]					C-Bonded β-dik[c)]					L[b)]			
		C^1	C^2	C^3	C^4	C^5	C^6	C^7	C^8	C^9	C^{10}	C^α	C^β	C^γ	NCH_3
7Bq	*cis*	27.7	188.2	97.1	178.5	137.2	31.2	206.8	44.5	196.7	140.9	150.2	107.6	154.4	39.1
	trans	27.9	187.5	97.1	179.5	138.2	31.2	206.5	44.0	196.5	140.8	150.2	107.5	154.4	39.1
7Ci	*cis*	28.2 (128)	194.6	96.2 [≈2] (164)	167.9 [33]	117.8 [284]	31.4 (128)	200.3	42.0 (147)	183.3 [33]	116.5 [293]	50.6 (141)	27.9 (132)	23.8 (128)	
	trans	28.6 (129)	194.6	96.6 [≈2] (164)	167.4 [33]	117.4 [284]	31.4 (128)	200.4	41.1 (146)	183.6 [33]	116.5 [293]	50.3 (141)	27.8 (132)	23.8 (128)	

a, b) Same as footnotes for Table 7. c) The phenyl-ring carbons except the quaternary carbon resonate in the 127.0—130.8 ppm region.

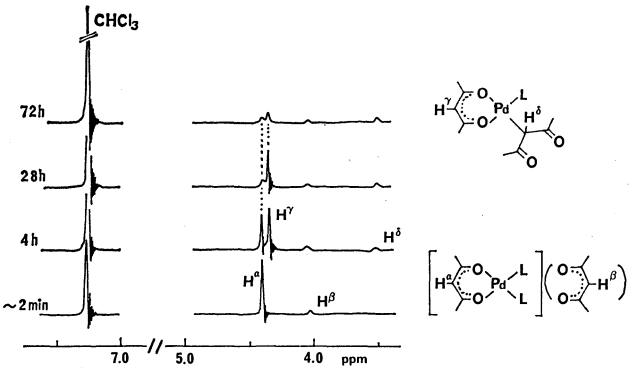

Fig. 4. Change with time of the methine proton signals from **4Ah** in $CDCl_3$ at room temperature.

98.5, 97.8, and 93.8 ppm for **1A**, **1B**, **1C**, and **1D**).[11] It should be noted that the values of ^1J(C–F) for compounds **5** and the free hfac anion (290—292 Hz) are larger and the ^2J(C–F) values (30—33 Hz) are smaller than 284 and 37 Hz, respectively, for [Pd(hfac)$_2$]. In contrast to the case of ^{1}H NMR spectra, ^{13}C resonances of β-diketonate anions in C_6D_6 make no appreciable difference from those in $CDCl_3$ and CD_2Cl_2.

Similar ^{13}C NMR data for some of compounds **4** are collected in Table 8. Each complex except **4Dt** exhibits two sets of ^{13}C signals assignable to β-diketonate anions in the inner and outer spheres. Based on the above criteria, the upfield methyl and trifluoromethyl signals and the downfield methine signal for each complex are assigned to the coordinated β-diketonate ion. It is noteworthy that the ^1J(C–H) values for methine carbons of the coordinated β-diketonate are 5—10 Hz larger than those for the anion in the outer sphere. In the case of **4Ci** and **4Di**, the ^1J(C–F) values for the tfac and hfac ions in the outer sphere are larger than those for the coordinated anions. Then the CF_3CO carbons with lower ^2J(C–F) values are ascribed to the anion in the outer sphere. Compound **4Dt** shows dynamic behavior. The environments of two hfac anions are averaged on the NMR time scale as was evidenced by the ^{1}H NMR signal for the methine proton. Both of the chemical shifts and the J(C–F) values are intermediate for those for hfac anions in inner and outer spheres. It is not certain why the ^{13}C signals from the acac anion in the outer sphere of **4Ah** are broad. Various solvents were examined but the signals were always broad except in C_6D_6.

The ^{13}C NMR spectrum of [Pd(acac)(acac-C^3)-(Et_2NH)] (**7Ah**) resembles that of [Pt(acac)(acac-C^3)-(py)] reported by Ito *et al.*[10] Spectra of **7Ah** were recorded in several solvents (Table 9) and no appreciable solvent effect is noticed. Compounds **7Bq** and **7Ci** exhibit two sets of the β-diketonate signals caused by the unsymmetry of the bzac ligand. According to the ^{1}H NMR information, a set of more intense signals was assigned to the *cis*(Me,L) isomer.

The H-D Exchange Reactions of Complexes 4 and 5 with $CDCl_3$.[23] When complexes **4A** are dissolved in $CDCl_3$, the proton signals due to NH_2 and CH of the acac anion in the outer sphere become smaller, and instead the $CHCl_3$ signal grows with time. The H-D exchange reaction attains equilibrium within several minutes in the case of **4Ag** and **4Ah**, and after about 13 min for **4Ai**. The reaction is also detected by ^{13}C NMR spectroscopy. Besides the H-D exchange, complexes **4A** change spontaneously to **7A**, attaining equilibria during several days. Figure 4 exemplifies the change with time of the methine proton signals from complex **4Ah**. The spectrum at 4 h after dissolution involves signals attributable to **7Ah**, of which the one due to the methine group of the carbon-bonded acac ligand is much weaker than the other from that of the chelated acac. This fact indicates that the carbon-bonded acac originated from the counter anion of **4Ah** in accordance with the previous kinetic evidence (Eq. 7).[3] Deuteration of the methine group

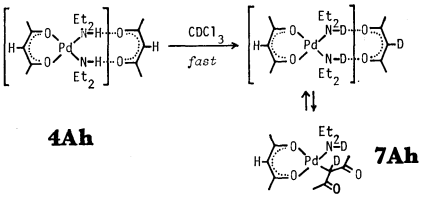

(7)

in the chelated acac anion is much slower, requiring about three days for completion. It may be accomplished by the exchange of acac anions in the inner and outer spheres as shown by Eq. 8.

$$[Pd(acac)(Et_2NH)_2](acac^*) \rightleftharpoons [Pd(acac)(acac^*)] + 2Et_2NH \rightleftharpoons [Pd(acac^*)(Et_2NH)_2](acac) \quad (8)$$

A similar reaction of **4Cg** with $CDCl_3$ is much slower, attaining equilibrium after about ten days. Transformation to **7Cg** does not occur. Because of the unsymmetric tfac chelate, two dimethylamine molecules exhibit two separate doublets at 2.40 and 2.43 ppm with J(NH–CH_3)=5.$_5$ Hz (Table 5), which are transformed to singlets on deuteration of the NH proton. Amine ligands in other **4C** complexes are not deuterated by $CDCl_3$. The hfac complex **4Di** does not react either.

Complexes **5** react with $CDCl_3$ in a similar manner but the rate is slower than **4**. Necessary time for equilibrium attainment is about three days, two days, several hours, and less than 1 h for **5Ab**, **5Ac**, **5Ad**, and **5Ae**, respectively. Transformation to **7A** also occurs at the same time. Compounds **5Bd** and **5Be** attain the exchange equilibria within 16 and several hours, respectively, accompanied by the reactions to **7B**. Complex **5Cb** requires more than twenty days for completion of the reaction. Complexes **5Cc**, **5Cd**, **5Ce**, and **5Dd** are neither deuterated, nor transformed to **7**.

Amine protons and the methine proton of the tfac anion in the outer sphere of **4Mb** and **4Mh** attain the H-D exchange equilibria within several hours, but deuteration of the methine group of the chelated acac ligand requires more than four days. Substitution of the chelated acac ligand by the tfac anion *via* the pathway analogous to Eq. 8 seems more difficult than

Table 10. ^{1}H NMR data for some **4C** and **5C** compounds in trifluoroacetic acid[a)]

Compd	Chelated tfac		L[b)]		tfacH	
	CH_3	CH	NH	Other	CH_3	CH
4Ch	2.26	6.14	3.7	Et : 2.8 m, 1.63 t(7), and 1.61 t(7)	2.35	6.25
4Cj	2.26	5.91	3.2	Me : 1.85 br; CH_2 : 3.6 br; Ph : 7.29	2.23	5.88
5Ca			2.90		2.27	5.98
5Ce			3.2	CH_2 : 3.51 br; Ph : 7.28	2.23	5.95
5Cf			4.13	CH_2 : 2.9 br	2.29	6.01
tfacH					2.29	6.00

a) Chemical shifts in ppm from internal DSS. b) The NH resonances are all broad. The figure in parenthesis is J(CH-CH) in Hz.

by the acac anion.

Deuteration of the coordinated amine and the β-diketonate anion in the outer sphere proceeds concurrently, and the rate seems to be greater for complexes containing stronger hydrogen bonds, since the reaction proceeds faster for **4** than for **5** and for more basic β-diketonate than for less basic anion. Kinetic study of deuteration by $CDCl_3$ of cationic palladium(II) alkylamine complexes containing various counter anions is now in progress and the following mechanism is tentatively proposed at present (Eq. 9).

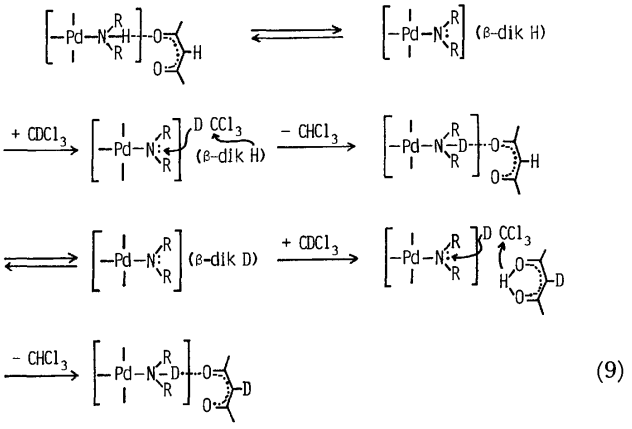

(9)

Chloroform can be regarded as an acid and detritiation of C^3HCl_3 in aqueous solution by hydroxide ion[24)] and amines[25)] has been investigated. Dehalogenation of chloroform by ethylenediamine was also presumed to be initiated by proton abstraction from chloroform by the diamine.[26)] Although solutions of alkylamines in $CDCl_3$ show no sign of H-D exchange, complexes **4**, **5** or their precursors [Pd(β-dik)$_2$] can catalyze the reaction.[23)] Proton transfer from the coordinated amine to the β-diketonate anion in the outer sphere is presumed to reach equilibrium quickly and the concerted reaction among the amide center, $CDCl_3$ and β-dikH may be the rate-determining step. The deuterated amine molecule will be readily substituted by amine in solution to accomplish the catalytic cycle.

Anion Exchange of Compounds 4 and 5. In order to test validity of the proposed mechanism (9) for deuteration of compounds **4** and **5** by $CDCl_3$, substitution of the β-diketonate ions in the outer sphere with other appropriate anions is desirable. As a preliminary trial some anion exchange reactions have been examined. Addition of silver nitrate to a solution of **5Cm** in pyridine resulted in [Pd(py)$_4$](NO$_3$)$_2$ in a 62% yield, and **4Ah** reacted with equimolar K(tfac) in aqueous solution to give **4Mh** in a 72% yield. Thus the β-diketonate ion in the outer sphere is easily replaced by other anions. Table 10 lists the ^{1}H NMR data for some **4C** and **5C** compounds in trifluoroacetic acid. The methyl and methine proton signals assignable to tfacH are observed, indicating that the tfac anion in the outer sphere was completely protonated by the acid. The exact chemical shifts of CH_3 and CH are more or less different from those of authentic tfacH, but the identity was confirmed in each case by addition of the authentic sample. On being left in trifluoroacetic acid for a long time, compound **5Ce** decomposed gradually to give rise to the benzylammonium ion.

Relative Stabilities in Various Bonding Modes of β-Diketonate Anions. The reactions of [Pd(β-dik)$_2$] (**1**) with excess nitrogen bases are exothermic and it depends on the natures of both the β-diketonate ligand and base employed which of compounds **4**, **5**, **7**, and **8** is produced preferentially. When the chelating ligand is the acetylacetonate or other β-diketonate of weaker basicity, primary and secondary amines afford **5** and **4**, respectively. Basicities of both types of amines are not so different and the steric requirement of secondary amines seems to make **5** unfavorable. Although 2,2′-bipyridine reacts with **1D** to afford solely **4Ds**, 4,4′-dimethyl-2,2′-bipyridine produces either of **4Dt** and **5Dt** depending on the mole ratio of the reactants. Increased basicity of the latter ligand might overcome the steric disadvantage of the bis(bpy)-complexes **5**.

Tertiary amines do not react with **1** probably because their bulkiness is both kinetically and thermodynamically unfavorable for the ligand substitution. Tribenzylamine did react with **1D** not to afford a ligand-substituted product but to produce an orthometallated complex **9D*l***. 2,6-Diphenylpyridine also gave a similar product **9Dr**. The ^{1}H and ^{13}C NMR assay revealed that the hfac anion worked as a proton acceptor to result in hfacH (Eq. 10). In recent years a great many articles have appeared concerning orthometallated compounds, or "organometallic intramolecular-coordination compounds."[27)] Thus the reaction of lithium tetrachloropalladate(II) with *N,N*-dimethylbenzylamine in methanol gave di-μ-chlorobis-

Table 11. Equilibrium constants[a] estimated by ^{1}H NMR spectroscopy in $CDCl_3$ and C_6D_6 at room temperature:

$4 \rightleftharpoons 7 + L$, $K_1 = [7]^2/[4]$; $5 \rightleftharpoons 7 + 3L$, $K_2 = [7]^4/[5]$

L	β-dik			
	acac	bzac	tfac	hfac
		K_1		
Me_2NH	>4 (2.6)		≈0 (1×10^{-2})	
Et_2NH	2.4 (≈0)		≈0 (≈0)	
pip	3.2 (0.2)	(3×10^{-2})	≈0 (≈0)	≈0
		K_2[b]		
$MeNH_2$	2×10^{-3}	(≪2×10^{-6})	<2×10^{-6} (≪7×10^{-7})	
$EtNH_2$	2×10^{-3} (9×10^{-7})	6×10^{-6} (≪8×10^{-7})	≈0 (≈0)	
n-$PrNH_2$	(1×10^{-8})		≈0 (≈0)	≈0 (≈0)
$BzNH_2$	1×10^{-2}		(2×10^{-6})	
py			≫8×10^{-2}	≈0

a) The figures in parentheses were determined in C_6D_6. The lower- and upper-limit values accompanied by the mark ≫ and ≪ were estimated by assuming concentration of the minor component as 1/10 of the initial concentration employed when it is detected but can not be determined quantitatively. The symbol ≈0 means that compound **7** can not be observed on the spectrum. b) The values of K_2 were tentatively calculated on the assumption that **5** exists as a monomer, although complexes of propylamine and presumably other alkylamines are dimeric in dichloromethane.

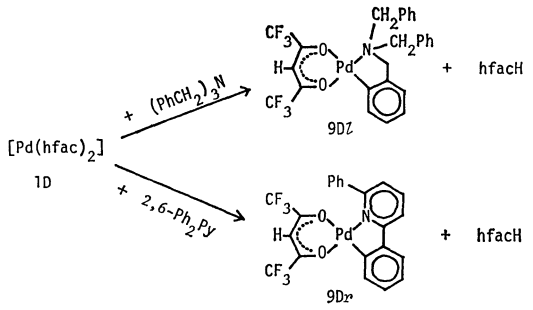

(10)

(*N*,*N*-dimethylbenzylamine-2*C*,*N*)dipalladium(II),[28] of which the bridge bond was cleaved by thallium(I) acetylacetonate to result in acetylacetonato(*N*,*N*-dimethylbenzylamine-2*C*,*N*)palladium(II)[29] analogous to **9D*l***. 2-Phenylpyridine also reacts with sodium tetrachloropalladate(II) to yield the chloro-bridged five-membered (*C*, *N*) chelate.[30] However, the reaction of [Pd(β-dik)$_2$] with a tertiary amine or a substituted pyridine to afford an orthometallated compound as expressed by Eq. 10 may be the first example. Furthermore it should be noted that triphenylphosphine can cleave the Pd–N coordination linkage in **9D*l*** to result in a phenylpalladium(II) complex **10D*l*** stable enough to be isolated (Eq. 11).

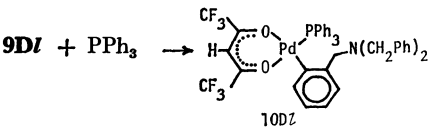

(11)

When a base reacts with complexes **1**, the β-diketonate ligand of weaker basicity is displaced more easily and the hfac and tfac ligands like to remove into the outer sphere. The acac ligand is also expelled from the coordination sphere by nitrogen bases, but the nature of solvent plays an important role in determining the most stable bonding mode. In polar solvents such as methanol compounds of type **4** and **5** are favorable, but dichloromethane stabilizes the carbon-bonded complexes.[3] The anion of ethyl acetoacetate is more basic than acac and complex **1I** readily reacts with pyridine to afford **8Im**,[9] while **1A** gives only **7Am** (Fig. 1). Thus the preference of bonding modes by β-dicarbonyl anions is related with the sequence of basicity as follows.

etac > acac ~ bzac > tfac > hfac

C-bonded——*O*,*O*′-chelate——Outer sphere

The relative tendency of β-dicarbonyl anions to form the central carbon bonding parallels with preference of the keto tautomer to enol. The percentage of enol in neat liquid at 33 °C was recorded as 8, 81, 97, and 100% for etacH, acacH, tfacH, and hfacH, respectively.[31] A β-dicarbonyl anion which prefers to accept a hydrogen ion at the central carbon atom rather than at an oxygen atom likes also to react with a metal ion as a carbanion. Ito and Yamamoto studied the reactions of [M(acac)(acac-*C*^{3})PPh_3] with several β-dikH and found that the keto-favoring β-dikH selectively replaces the carbon-bonded acac, while the enol-favoring β-dikH substitutes the chelated acac.[32]

Complexes **4**, **5**, and **8** gradually libcrate base to produce **7**. Table 11 lists the equilibrium constants estimated by the ^{1}H NMR spectroscopy and supports the above conclusion concerning the preference of bonding modes. Thus the stability of the outer-sphere complexes is in the sequence of hfac>tfac>bzac>acac and RNH_2>$BzNH_2$>py. The value (2.4) of K_1 for [Pd(acac)(Et_2NH)$_2$](acac) (**4Ah**) ⇄ **7Ah** + Et_2NH is not so different from the more accurate value (4.46) determined in dichloromethane at 25 °C by the spectrophotometric method.[3] When compounds **5** are converted to **7**, the reaction should proceed *via* **4**. However complexes **4** containing primary amines as L are usually unstable except **4Mb** and are not detected spectroscopically. Compound **4Mb**

as well as **4Mh** and **4Mi** is very stable in solution, showing no sign of transformation to **7**. The chelate-favoring acac and the outer sphere-favoring tfac may cooperate in stabilizing these compounds.

Experimental

Preparation of Compounds. The starting complexes, bis(β-diketonato)palladium(II) [Pd(β-dik)$_2$] (**1**) including [Pd(acac)(tfac)] (**1M**), were prepared by the methods described in a previous paper.[11] Methylamine, ethylamine, and dimethylamine were evolved by dissolving potassium or sodium hydroxide in aqueous solutions of these amines which are commercially available. Other amines, pyridines, and ammonia were purchased and used without purification. Most of the new compounds reported in this paper were prepared by one of the following two methods and the remaining compounds by other methods. (1) When the base is liquid at room temperature, compound **1** was dissolved or suspended in the neat liquid and the mixture was stirred. After reaction for appropriate time duration, the product was precipitated by cooling the solution, by adding another solvent such as diethyl ether, hexane, and petroleum ether to the reaction mixture, or by distilling away the excess base. (2) An appropriate amount of base was added to a solution of **1** in dichloromethane, benzene, or diethyl ether. The reaction mixture was worked up in a similar manner as above.

*[Pd(acac)(Me$_2$NH)$_2$](acac)·2H$_2$O (**4Ag**)*: Dimethylamine was distilled under nitrogen into a flask containing fine powder of [Pd(acac)$_2$] (**1A**) which was cooled with Dry Ice–methanol. The reaction mixture was then warmed to room temperature and stirred to result in a yellow solution. The amine was distilled away under reduced pressure to leave tiny yellow plates in a 90% yield.

*[Pd(acac)(Et$_2$NH)$_2$](acac) (**4Ah**)*: Pulverized **1A** (1.55 g, 5.09 mmol) was added to diethylamine (*ca.* 10 cm^3) and the mixture was warmed to result in a yellow solution, which was then cooled and kept at −5 °C in a refrigerator overnight to precipitate yellow columns. The product was filtered and washed several times with petroleum ether (boiling point<60 °C). The yield was 1.52 g (66%).

*[Pd(acac)(pip)$_2$](acac)·H$_2$O (**4Ai**)*: Complex **1A** (215 mg, 0.706 mmol) was dissolved in piperidine (*ca.* 0.8 cm^3) and diethyl ether (*ca.* 30 cm^3) was added to the solution. The solvent was then allowed to evaporate spontaneously to leave yellow needles on the wall of vessel. The product was gathered and washed with hexane. The yield was 156 mg (45%).

*[Pd(bzac)(pip)$_2$](bzac) (**4Bi**)*: Hexane was added to a solution of [Pd(bzac)$_2$] (**1B**, 59 mg, 0.14 mmol) in piperidine (0.9 cm^3) and the mixture was kept in a refrigerator to deposit yellow needles. The product was filtered and washed with a mixture of diethyl ether and petroleum ether (1:1 by volume). The yield was 77 mg (93%).

*[Pd(tfac)(Me$_2$NH)$_2$](tfac) (**4Cg**)*: In a similar manner as for **4Ag**, [Pd(tfac)$_2$] (**1C**, 300 mg, 0.727 mmol) was dissolved in dimethylamine. The amine was then distilled away to leave a yellow powder (331 mg) in a 91% yield.

*[Pd(tfac)(Et$_2$NH)$_2$](tfac) (**4Ch**)*: After **1C** (200 mg, 0.484 mmol) was dissolved in diethylamine, the excess amine was distilled away promptly under reduced pressure to leave a yellow crystalline solid (238 mg) in an 88% yield.

*[Pd(tfac)(pip)$_2$](tfac) (**4Ci**)*: Piperidine (*ca.* 0.2 cm^3) was added dropwise to a suspension of **1C** (413 mg, 1.00 mmol) in dichloromethane (0.5 cm^3) with stirring to result in a yellow solution. Hexane (20 cm^3) was added and the mixture was kept in a refrigerator overnight to deposit pale yellow plates (252 mg). The filtrate was concentrated and then cooled to precipitate another crop. The total yield was 392 mg (67%).

*[Pd(tfac)(BzNHMe)$_2$](tfac) (**4Cj**)*: A dichloromethane solution (2 cm^3) of *N*-methylbenzylamine (214 mg, 1.77 mmol) was added slowly to a solution of **1C** (511 mg, 1.24 mmol) in dichloromethane (5 cm^3) with stirring. After further addition of the amine (200 mg, 1.65 mmol), the solvent was allowed to evaporate spontaneously. Yellow crystals deposited on the wall of vessel were collected and washed with a mixture of diethyl ether and petroleum ether (1:1 by volume). The yield was 581 mg (72%).

*[Pd(tfac)(Bz$_2$NH)$_2$](tfac) (**4Ck**)*: Complex **1C** (100 mg, 0.242 mmol) was dissolved in hot dibenzylamine. Hexane was added to the solution to deposit a yellow precipitate, which was filtered and washed with hexane. The yield was 132 mg (67%).

*[Pd(tfac)(bpy)](tfac) (**4Cs**)*: A benzene solution (2 cm^3) of 2,2′-bipyridine (156 mg, 1.00 mmol) was added to a solution of **1C** (413 mg, 1.00 mmol) in benzene (10 cm^3) to precipitate a yellow crystalline solid immediately, which was filtered and washed with a mixture of benzene and hexane (1:1 by volume). The yield was 489 mg (86%).

*[Pd(hfac)(Me$_2$NH)$_2$](hfac) (**4Dg**)*: In a similar manner as the case of **4Ag**, [Pd(hfac)$_2$] (**1D**, 104 mg, 0.20 mmol) was dissolved in dimethylamine. On distilling away of the amine, white cubes and red oil were left, which were extracted with diethyl ether. The solvent was allowed to evaporate spontaneously to leave yellow plates of **4Dg** and a small amount of white columns. The yield of **4Dg** was 60 mg (49%). The latter was confirmed to be dimethylammonium 1,1,1,5,5,5-hexafluoro-2,4-pentanedionate. Found: C, 33.02; H, 3.58; N, 5.54%. Calcd for C$_7$H$_9$NO$_2$F$_6$: C, 33.21; H, 3.58; N, 5.53%. IR: ν(NH) 3150s, ν(C=O) 1680vs.

*[Pd(hfac)(pip)$_2$](hfac) (**4Di**)*: Piperidine (98 mg, 1.2 mmol) was added to a solution of **1D** (300 mg, 0.576 mmol) in diethyl ether (3 cm^3). The solvent was allowed to evaporate spontaneously to leave yellow cubes in a 97% yield (387 mg).

*[Pd(hfac)(bpy)](hfac) (**4Ds**)*: A solution of 2,2′-bipyridine (71 mg, 0.45 mmol) in diethyl ether (1 cm^3) was added to a solution of **1D** (103 mg, 0.198 mmol) in diethyl ether (1 cm^3) to deposit a pale yellow precipitate immediately, which was filtered and washed with diethyl ether. The yield was 124 mg (93%).

*[Pd(hfac)(4,4′-Me$_2$-bpy)](hfac) (**4Dt**)*: In a similar manner as above, **1D** (208 mg, 0.400 mmol) reacted with 4,4′-dimethyl-2,2′-bipyridine (74 mg, 0.47 mmol) in diethyl ether (2 cm^3) to precipitate yellow needles immediately. The yield was 259 mg (92%).

*[Pd(hfac)(2,9-Me$_2$-phen)](hfac) (**4Du**)*: White crystals of compound **4Du** were prepared in a similar way as above. The yield was about 30%.

*[Pd(acac)(MeNH$_2$)$_2$](tfac) (**4Mb**)*: Methylamine (19 mg, 0.61 mmol) was kept in a small glass-stoppered bottle cooled with dry ice-methanol. Dichloromethane (1 cm^3) was poured into this bottle quickly and the solution was added to a dichloromethane solution (1 cm^3) of **1M** (114 mg, 0.318 mmol). The mixture was kept at room temperature for 1 h. Then petroleum ether (1 cm^3) was added to the solution and solvents were allowed to evaporate spontaneously to leave yellow plates (76 mg) in a 57% yield.

*[Pd(acac)(Et$_2$NH)$_2$](tfac) (**4Mh**)*: Compound **4Mh** was prepared *via* three alternative routes. (1) Immediately after dissolution of [Pd(acac)(tfac)] (**1M**, 100 mg, 0.279

mmol) in diethylamine (2 cm³), excess amine was distilled away at room temperature under reduced pressure to leave a yellow powder (136 mg) in a 97% yield. Recrystallization from dichloromethane–hexane gave yellow plates (yield: 80 mg, 57%). (2) Aqueous solution of potassium 1,1,1-trifluoro-2,4-pentanedionate (16 mg, *ca.* 0.1 mmol) was added to a fresh solution of [Pd(acac)(Et_2NH)$_2$](acac) (**4Ah**, 44 mg, 0.098 mmol) in water (1 cm³) with stirring to separate out a yellow precipitate (36 mg) in a 72% yield. After being dried *in vacuo*, the crude product was recrystallized from dichloromethane–hexane to give yellow hexagonal plates. The yield was 25 mg (51%). (3) A methanol solution of equimolar amount of potassium 2,4-pentanedionate was added to an acetone solution of [Pd(tfac)-(Et_2NH)$_2$](tfac) (**4Ch**) and the mixture was stirred for *ca.* 10 min. The solvents were distilled away under reduced pressure and the residue was extracted with diethyl ether. Then the solvent was allowed to evaporate spontaneously to leave yellow needles of **4Mh**, but the yield was very low.

*[Pd(acac)(pip)$_2$](tfac) (**4Mi**)*: Small portions of hexane and diethyl ether were added to a solution of **1M** (100 mg, 0.279 mmol) in piperidine (0.1 cm³) and the mixture was cooled to precipitate yellow plates, which were filtered and washed with hexane. The yield was 52 mg (35%).

*[Pd(NH_3)$_4$](acac)$_2$·2H_2O (**5Aa**)*: Gaseous ammonia from a cylinder was bubbled into a solution of **1A** (254 mg, 0.834 mmol) in dichloromethane (10 cm³) for *ca.* 15 min to deposit white crystallites, which were filtered, washed with diethyl ether. The yield was 280 mg (83%).

*[Pd($MeNH_2$)$_4$](acac)$_2$ (**5Ab**)*: A suspension of **1A** (270 mg, 0.886 mmol) in several cm³ of methylamine was stirred to produce a white precipitate on reaction. After distillation of the amine, a white powder was washed with a small portion of hexane. The yield was 357 mg (94%). Compound **5Ab** is not stable but turns yellow gradually on decomposition at room temperature.

*[Pd($EtNH_2$)$_4$](acac)$_2$·1/2H_2O (**5Ac**)*: On addition of **1A** (232 mg, 0.762 mmol) to *ca.* 3 cm³ of ethylamine, a white precipitate appeared immediately. The excess amine was distilled away slowly at −5 °C to leave a pale yellow crystalline solid, which was washed with hexane. The yield was 360 mg (96%). Compound **5Ac** was alternatively obtained by addition of an aqueous solution of ethylamine drop by drop to a suspension of **1A** in acetone. It is more stable than **5Ab** but decomposes slowly at room temperature.

*[Pd($PrNH_2$)$_4$](acac)$_2$ (**5Ad**)*: When **1A** was added to propylamine with stirring, the reaction occurred exothermically to deposit a white precipitate. The excess amine was distilled away and the residue was washed with diethyl ether. The yield was quantitative and recrystallization from diethyl ether–hexane gave colorless transparent columns. Compound **5Ad** also decomposes slowly at room temperature.

*[Pd($BzNH_2$)$_4$](acac)$_2$ (**5Ae**)*: Benzylamine (1.6 cm³) was added drop by drop to a solution of **1A** (400 mg, 1.31 mmol) in dichloromethane (5 cm³) and the solution was stirred for a while. Petroleum ether (6 cm³) was added to it and the mixture was kept in a refrigerator for three days to deposit white plates (840 mg) in an 87% yield, which decompose slowly to a white powder at room temperature.

*[Pd(en)$_2$](acac)$_2$·2H_2O (**5Af**)*: Six times as many moles of ethylenediamine was added dropwise to a solution of **1A** (294 mg, 0.97 mmol) in dichloromethane (10 cm³) with stirring to deposit a white precipitate (414 mg) in a 93% yield. The method is similar to that used for preparation of [Cu(en)$_2$](acac)$_2$·2H_2O.[13]

*[Pd(NH_3)$_4$](bzac)$_2$ (**5Ba**)*: Gascous ammonia was passed through a solution of [Pd(bzac)$_2$] (**1B**, 155 mg, 0.362 mmol) in dichloromethane at 0 °C for 10 min to separate out a yellowish white precipitate. On washing with diethyl ether a white powder of **5Ba** (164 mg) was obtained in a 91% yield.

*[Pd($MeNH_2$)$_4$](bzac)$_2$ (**5Bb**), [Pd($EtNH_2$)$_4$](bzac)$_2$ (**5Bc**), and [Pd($PrNH_2$)$_4$](bzac)$_2$ (**5Bd**)*: These compounds were obtained in similar manners as for the corresponding 2,4-pentanedionates in 90, 97, and 89% yields, respectively. Each complex decomposes gradually at room temperature.

*[Pd($BzNH_2$)$_4$](bzac)$_2$ (**5Be**)*: Cold benzylamine was added dropwise onto a fine powder of **1B** (327 mg, 0.763 mmol) with stirring at 0 °C to produce a white precipitate immediately, which was filtered and washed with hexane. The yield was 587 mg (90%).

*[Pd(en)$_2$](bzac)$_2$·2H_2O (**5Bf**)*: Five drops of ethylenediamine was added to a solution of **1B** (112 mg, 0.261 mmol) in dichloromethane to deposit a white precipitate immediately, which was filtered and washed with diethyl ether. The yield was 123 mg (81%).

*[Pd(NH_3)$_4$](tfac)$_2$ (**5Ca**), [Pd($MeNH_2$)$_4$](tfac)$_2$ (**5Cb**), [Pd($EtNH_2$)$_4$](tfac)$_2$ (**5Cc**), [Pd($PrNH_2$)$_4$](tfac)$_2$ (**5Cd**), [Pd-($BzNH_2$)$_4$](tfac)$_2$ (**5Ce**), and [Pd(en)$_2$](tfac)$_2$ (**5Cf**)*: These compounds were prepared by similar methods as those for the corresponding 2,4-pentanedionates in 90—99% yields. Recrystallization of **5Cf** from water gave colorless transparent needles of monohydrate.

*[Pd(py)$_4$](tfac)$_2$·3H_2O (**5Cm**)*: Compound **1C** (100 mg, 0.242 mmol) was dissolved in pyridine (*ca.* 0.3 cm³) and the mixture was allowed to stand overnight at room temperature. Large colorless plates were separated and washed with hexane. The yield was 144 mg (76%).

*[Pd(NH_3)$_4$](hfac)$_2$ (**5Da**):, [Pd($MeNH_2$)$_4$](hfac)$_2$ (**5Db**), [Pd($EtNH_2$)$_4$](hfac)$_2$ (**5Dc**), and [Pd($PrNH_2$)$_4$](hfac)$_2$ (**5Dd**)*: These compounds were obtained in similar manners as for the corresponding 2,4-pentanedionates in 90—99% yields. Compounds **5Db**—**5Dd** were able to be recrystallized from dichloromethane–hexane.

*[Pd(py)$_4$](hfac)$_2$ (**5Dm**)*: Compound **1D** dissolved in a small amount of pyridine exothermically. Diethyl ether and hexane were added to the solution and the mixture was cooled to deposit colorless plates in an 80% yield.

*[Pd(4,4′-Me_2-bpy)$_2$](hfac)$_2$ (**5Dt**)*: Compound **1D** (208 mg, 0.400 mmol) reacted with 4,4′-dimethyl-2,2′-bipyridine (147 mg, 0.800 mmol) in diethyl ether (4 cm³). Yellow crystallites were filtered and washed with diethyl ether. The yield was 332 mg (93%).

*[Pd($PrNH_2$)$_4$](Ph-acac)$_2$ (**5Ed**), [Pd($PrNH_2$)$_4$](dbm)$_2$ (**5Fd**), and [Pd($PrNH_2$)$_4$](dpm)$_2$ (**5Gd**)*: These compounds were obtained in 35—50% yields by dissolving [Pd(Ph-acac)$_2$] (**1E**), [Pd(dbm)$_2$] (**1F**), and [Pd(dpm)$_2$] (**1G**), respectively, in propylamine and distilling away the excess amine at −5 °C. Each product was washed with hexane.

*[Pd(py)$_4$](tta)$_2$ (**5Hm**)*: [Pd(tta)$_2$] (**1H**, 250 mg, 0.455 mmol) was dissolved in a mixture of dichloromethane (3 cm³) and pyridine (2 cm³) by stirring at 50 °C. The resulting clear solution was kept in a refrigerator overnight to give light yellow crystals, which were recrystallized from dichloromethane–petroleum ether. The yield was 350 mg (90%).

*[Pd(3-Me-py)$_4$](tta)$_2$ (**5Ho**) and* [Pd(4-Me-py)$_4$](tta)$_2$ *(**5Hp**)*: Both compounds were obtained in a similar manner as above in more than 90% yields.

*[Pd(en)$_2$](etac)$_2$ (**5If**)*: Ethylenediamine (0.5 cm³) was mixed with pulverized [Pd(etac)$_2$]·1/2H_2O[9] (277 mg, 0.741 mmol). A white precipitate deposited immediately, which was washed with large volumes of diethyl ether and acetone,

successively, and dried *in vacuo*. A gray powder of **5If** (311 mg) was obtained in an 86% yield. The compound does not dissolve in organic solvents other than alcohols, but is readily soluble in water and methanol and the ester anion in the outer sphere is solvolyzed. Thus recrystallization from a mixture of methanol, diethyl ether, and petroleum ether (2:2:1 by volume) resulted in colorless crystals of [Pd(en)$_2$](meac)$_2$·H$_2$O, where meac stands for the anion of methyl acetoacetate. Found: C, 35.99; H, 6.70; N: 11.96%. Calcd for $C_{14}H_{32}N_4O_7Pd$: C, 35.41; H, 6.79; N, 11.80%.

[Pd(MeNH$_2$)$_4$](acac)(tfac) (**5Mb**): Compound **1M** (100 mg, 0.279 mmol) was dissolved in several cm^3 of methylamine to result in a colorless solution. The excess amine was distilled away to leave white crystals (130 mg) in a 96% yield.

[Pd(EtNH$_2$)$_4$](acac)(tfac) (**5Mc**): In a similar manner as above white needles of **5Mc** were obtained in a quantitative yield. Recrystallization from petroleum ether gave pale yellow columns.

Dimethylamine(2,4-pentanedionato)(2,4-pentanedionato-C^3)palladium(II), *[Pd(acac)(acac-C^3)(Me$_2$NH)]* (**7Ag**): Compound **1A** (121 mg, 0.397 mmol) reacted with slightly excess dimethylamine (23 mg, 0.51 mmol) in dichloromethane (1 cm^3). Spontaneous evaporation of the solvent left a yellow mass and yellow liquid, which were washed with hexane to afford a yellow powder of **7Ag** (131 mg) in a 94% yield.

[Pd(acac)(acac-C^3)(Et$_2$NH)] (**7Ah**): This compound was previously prepared by the reaction of **1A** with diethylamine,[2] and now derived from **4Ah** (60 mg) by leaving its aqueous solution at room temperature. Yellow needles precipitated were filtered and dried *in vacuo*. The yield of **7Ah** from **4Ah** was 61% (31 mg).

[Pd(acac)(acac-C^3)(pip)] (**7Ai**): The compound was obtained in an 81% yield in a similar manner as **7Ag**, and recrystallized from diethyl ether–hexane. Compounds **7Ab**, **7Ad**, **7Ae**, and **7Ak** were also prepared in a similar manner.

Benzylamine(1-phenyl-1,3-butanedionato)(1-phenyl-1,3-butanedionato-C^2)palladium(II), *[Pd(bzac)(bzac-C^2)(BzNH$_2$)]* (**7Be**): Compound **1B** (179 mg, 0.418 mmol) reacted with benzylamine (71 mg, 0.66 mmol) in dichloromethane (3 cm^3) and the solvent was evaporated spontaneously to leave a yellow crystalline solid contaminated with oil. The product was washed with diethyl ether and dried *in vacuo*. The yield of a yellow powder of **7Be** was 196 mg (88%). The product was a mixture of *cis*(Me,L) and *trans*(Me,L) isomers. When it was dissolved in dichloromethane and the solvent was evaporated spontaneously after addition of a small amount of methyl iodide, a yellow crystalline solid left and washed with diethyl ether was pure *cis*(Me,L). The role of methyl iodide is not clear which was used in order to examine the possibility of substituting the carbon-bonded ligand.

[Pd(bzac)(bzac-C^2)(pip)] (**7Bi**): After the reaction of **1B** (123 mg, 0.287 mmol) with benzylamine (37 mg, 0.44 mmol) in dichloromethane (2 cm^3), the solvent was allowed to evaporate spontaneously to leave orange oil. A mixture (2 cm^3) of diethyl ether and hexane (1:2 by volume) was added to the vessel and the mixture was stirred. A yellow precipitate appeared, which was filtered, washed with diethyl ether and dried *in vacuo*. The yield was 92 mg (63%).

[Pd(bzac)(bzac-C^2)(py)] (**7Bm**): Compound **1B** (200 mg, 0.467 mmol) was dissolved in a small amount of pyridine by heating. Hexane was added to the solution and the mixture was cooled to deposit yellow crystals, which were filtered and washed with hexane. Compound **7Bm** (225 mg) thus obtained in a 95% yield is composed of the *cis*-(Me,L) isomer alone.

[Pd(bzac)(bzac-C^2)(2-Me-py)] (**7Bn**): Complex **7Bm** (100 mg, 0.196 mmol) was dissolved in a small amount of 2-methylpyridine by heating. Hexane was added to the solution and the mixture was cooled to separate out yellow needles (86 mg) in an 84% yield, which contain only the *cis*(Me,L) isomer.

[Pd(bzac)(bzac-C^2)(4-Me$_2$N-py)] (**7Bq**): Compound **1B** (100 mg, 0.233 mmol) reacted with 4-dimethylaminopyridine (28 mg, 0.23 mmol) in dichloromethane (2 cm^3) at room temperature. After 3 h, hexane (1 cm^3) was added to the solution and the mixture was cooled to deposit yellow needles (105 mg) in an 82% yield.

[Pd(tfac)(tfac-C^3)(Me$_2$NH)] (**7Cg**): Complex **1C** (268 mg, 0.650 mmol) reacted with twice molar dimethylamine (67 mg) in dichloromethane and the solvent was vaporized spontaneously to leave yellow plates, which were filtered and washed with hexane. The yield was 279 mg (94%). *[Pd(tfac)(tfac-C^3)(Et$_2$NH)]* (**7Ch**), *[Pd(tfac)(tfac-C^3)(pip)]* (**7Ci**), and *[Pd(tfac)(tfac-C^3)(Bz$_2$NH)]* (**7Ck**) were similarly obtained as a yellow powder, yellow needles, and yellow crystallites in 50, 80, and 50% yields, respectively.

1,1,1,5,5,5-Hexafluoro-2,4-pentanedionato(tribenzylamine-2C,N)-palladium(II), *[Pd(hfac)(Bz$_3$N-2C,N)]* (**9Dl**): A mixture of **1D** (287 mg, 0.551 mmol) and tribenzylamine (316 mg, 1.10 mmol) were heated in toluene under reflux and the solvent was distilled away under reduced pressure to leave pale yellow needles. Recrystallization from dichloromethane–petroleum ether (1:1 by volume) gave **9Dl** (196 mg) in a 52% yield. Found: C, 51.98; H, 3.45; N, 2.37%; mol wt 574 in CH_2Cl_2. Calcd for $C_{26}H_{21}NO_2F_6Pd$: C, 52.06; H, 3.53; N, 2.34%; mol wt 600. Dec temp: 152—162 °C. IR in Nujol: ν(C=O)+ν(C=C), 1640vs, 1547s, 1515m cm^{-1}. ^{1}H NMR in $CDCl_3$, δ (ppm from internal Me_4Si): 3.97 (2H, s, 6CH$_2$); 3.9 and 4.3 (4H, AB-quartet, J=12 Hz,

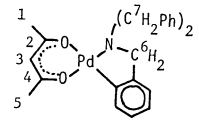

7CH$_2$); 5.94 (1H, s, 3CH); 7.0—7.8 (*ca.* 15H, m, Ph). ^{13}C NMR in $CDCl_3$, δ(ppm from internal Me_4Si): C^2 and C^4, 174.7q and 174.9q (J(C–F)=34 Hz); C^3, 89.9; C^6, 65.7; C^7, 64.8. Signals from C^1 and C^5 are not discernible because of overlapping with other signals.

(2,6-Diphenylpyridine-2C,N)(1,1,1,5,5,5-hexafluoro-2,4-pentanedionato)palladium(II), *[Pd(hfac)(2,6-Ph$_2$-py-2C,N)]* (**9Dr**): The change with time of ^{1}H NMR spectrum in a $CDCl_3$ solution containing complex **1D** and equimolar 2,6-diphenylpyridine showed that the reaction to form **9Dr** and hfacH was completed after 16 h at 25 °C. Diethyl ether was added to the solution and the mixture was cooled to deposit yellow crystals of **9Dr** in *ca.* 80% yield. Found: C, 48.36; H, 2.38; N, 2.56%. Calcd for $C_{23}H_{13}NO_2F_6Pd$: C, 48.60; H, 2.41; N, 2.58%. Dec temp: 201—203 °C. IR in Nujol: ν(C=O)+ν(C=C), 1632vs, 1550s.

[2-(Dibenzylaminomethyl)phenyl](1,1,1,5,5,5-hexafluoro-2,4-pentanedionato)(triphenylphosphine)palladium(II), *[Pd(hfac)(2-Bz$_2$NCH$_2$C$_6$H$_4$)(PPh$_3$)]* (**10Dl**): Complex **9Dl** (129 mg, 0.215 mmol) readily reacted with triphenylphosphine (56 mg, 0.214 mmol) in dichloromethane at room temperature. After concentration of the solution by evaporation under reduced pressure, haxane was added to the concentrate and the mixture was cooled to precipitate yellow crystals (61 mg) in a 33% yield. Found: C, 61.23; H, 4.18; N, 1.50%. Calcd for $C_{44}H_{36}NO_2F_6PPd$: C, 61.30; H, 4.21; N, 1.62%. Dec temp: 145—148 °C. IR in Nujol: ν(C=O)+ν(C=C), 1675vs, 1525vs cm^{-1}. ^{1}H NMR in $CDCl_3$, δ (ppm from

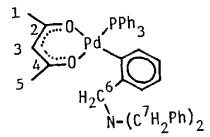

internal Me_4Si): 3.91 (4H, s, $7CH_2$); 4.10 (2H, s, $6CH_2$); 5.21 (1H, s, 3CH); 6.4—7.6 (*ca.* 30H, m, Ph). ^{13}C NMR in $CDCl_3$, δ (ppm from internal Me_4Si): C^1 and C^5, 117.6 q (J(C–F)=290 Hz): C^2 and C^4, 173.9 q (J(C–F)=32 Hz); C^3, 86.0; C^6, 63.3; C^7, 59.6.

*Reaction of $[Pd(py)_4](tfac)_2 \cdot 3H_2O$ (**5Cm**) with Silver Nitrate.* A solution of silver nitrate (48 mg, 0.28 mmol) in pyridine (0.3 cm^3) was added to a solution of complex **5Cm** (82 mg, 0.10 mmol) in pyridine (0.5 cm^3) to deposit a white precipitate immediately, which was filtered, washed with benzene, and dried *in vacuo*. The yield of $[Pd(py)_4](NO_3)_2$ was 35 mg (62%). It is not soluble in organic solvents, but dissolves in hot water and gives white needles on cooling. The compound coincides with the authentic sample which was prepared by the reaction among sodium tetrachloropalladate(II), silver nitrate, and pyridine. Found: C, 43.92; H, 3.68; N, 15.60%. Calcd for $C_{20}H_{20}N_6O_6Pd$: C, 43.93; H, 3.69; N, 15.37%. IR in Nujol: $\nu(NO_3)$, 1376vs, br, 1325vs, br. ^1H NMR in D_2O at 75 °C, δ (ppm from internal DSS): 8.77 (2H, d, J=5 Hz, H^2 and H^6), 8.0 (1H), m, H^4), 7.6 (2H, m, H^3 and H^5).

Measurements. IR spectra were recorded in Nujol on Hitachi EPI-S2 and 295 spectrophotometers. NMR spectra were measured with JEOL JNM-C60HL and JNM-MH 100 (for ^1H), FX60Q (for ^1H and ^{13}C), and PS-100 (for ^{19}F) spectrometers. The molecular weight was determined by vapor pressure osmometry with an instrument manufactured by Knauer in West Berline, West Germany.

We wish to thank Mr. Junichi Gohda for elemental analyses, and also Professor T. Tanaka and Dr. K. Kawakami of Osaka University for ^{19}F NMR measurements. B. K. M. thanks Japan Society for the Promotion of Science for the award of Fellowhsip. This work was partly supported by Grant-in-Aid for Scientific Research No. 243014 from the Ministry of Education, Science and Culture.

References

1) J. P. Fackler, Jr., *Progr. Inorg. Chem.*, **7**, 361 (1966).
2) S. Baba, T. Ogura, and S. Kawaguchi, *Bull. Chem. Soc. Jpn.*, **47**, 665 (1974); M. Horike, Y. Kai, N. Yasuoka, and N. Kasai, *J. Organomet. Chem.*, **72**, 441 (1974).
3) S. Matsumoto and S. Kawaguchi, *Bull. Chem. Soc. Jpn.*, **53**, 1577 (1980).
4) S. Okeya, Y. Onuki, Y. Nakamura, and S. Kawaguchi, *Chem. Lett.*, **1977**, 1305.
5) S. Okeya, F. Egawa, Y. Nakamura, and S. Kawaguchi, *Inorg. Chim. Acta*, **30**, L319 (1978); *Bull. Chem. Soc. Jpn.*, to be submitted.
6) T. Ito, T. Kiriyama, and A. Yamamoto, *Chem. Lett.*, **1976**, 835.
7) S. Okeya, Y. Nakamura, and S. Kawaguchi, 25th Symposium Organomet. Chem. Jpn., Oct., 1978, Abstr. p. 35.
8) S. Okeya, T. Miyamoto, S. Ooi, Y. Nakamura, and S. Kawaguchi, *Inorg. Chim. Acta*, **45**, L147 (1980).
9) S. Okeya and S. Kawaguchi, *Inorg. Chem.*, **16**, 1730 (1977).
10) T. Ito, T. Kiriyama, Y. Nakamura, and A. Yamamoto, *Bull. Chem. Soc. Jpn.*, **49**, 3257 (1976).
11) S. Okeya, S. Ooi, K. Matsumoto, Y. Nakamura, and S. Kawaguchi, *Bull. Chem. Soc. Jpn.*, **54**, 1085 (1981).
12) M. A. Bush and D. E. Fenton, *J. Chem. Soc., A*, **1971**, 2446.
13) T. Kurauchi, M. Matsui, Y. Nakamura, S. Ooi, S. Kawaguchi, and H. Kuroya, *Bull. Chem. Soc. Jpn.*, **47**, 3049 (1974).
14) S. Kotake, T. Sei, K. Miki, Y. Kai, N. Yasuoka, and N. Kasai, *Bull. Chem. Soc. Jpn.*, **53**, 10 (1980).
15) S. Shibata, S. Onuma, Y. Mastui, and S. Motegi, *Bull. Chem. Soc. Jpn.*, **48**, 2516 (1975).
16) The pK_a values of acacH and bzacH were reported to be 10.28 and 10.43, respectively, in dioxane–water (1:1 by volume) at 25 °C [J. L. Ault, H. J. Harries, and J. Burgess, *Inorg. Chim. Acta*, **25**, 65 (1977)]. Sekine *et al.* determined pK_a's of acacH, bzacH, tfacH, and hfacH in several solvent extraction systems. They are 8.99, 8.55, 6.09, and 4.34, respectively, at 25 °C and μ=1 mol dm^{-3} [T. Sekine, Y. Hasegawa, and N, Ihara, *J. Inorg. Nucl. Chem.*, **35**, 3968 (1973)].
17) T. J. Pinnavaia and R. C. Fay, *Inorg. Chem.*, **5**, 233 (1966).
18) S. Okeya *et al.*, to be published.
19) R. Favez, R. Roulet, A. A. Pinkerton, and D. Schwarzenbach, *Inorg. Chem.*, **19**, 1356 (1980); G. K. Anderson and R. J. Cross, *Chem. Soc. Rev.*, **9**, 185 (1980).
20) R. Romeo, D. Minniti, and S. Lanza, *Inorg. Chem.*, **18**, 2362 (1979).
21) J. J. Fortman and R. E. Sievers, *Coord. Chem. Rev.*, **6**, 331 (1971); N. Serpone and D. G. Bickley, *Progr. Inorg. Chem.*, **17**, 391 (1972).
22) O. Wernberg and A. Hazell, *J. Chem. Soc., Dalton Trans.*, **1980**, 973.
23) Preliminary communication: S. Okeya, Y. Nakamura, and S. Kawaguchi, *J. Chem. Soc., Chem. Commun.*, **1977**, 914.
24) Z. Margolin and F. A. Long, *J. Am. Chem. Soc.*, **95**, 2757 (1973).
25) D. B. Dahlberg, A. J. Kresge, and A. C. Lin, *J. Chem. Soc., Chem. Commun.*, **1976**, 35.
26) D. F. Martin, *J. Inorg. Nucl. Chem.*, **37**, 1941 (1975).
27) I. Omae, *Chem. Rev.*, **79**, 287 (1979); J. Dehand and M. Pfeffer, *Coord. Chem. Rev.*, **18**, 327 (1976).
28) A. C. Cope and E. C. Friedrich, *J. Am. Chem. Soc.*, **90**, 909 (1968).
29) B. E. Reichert and B. O. West, *J. Organomet. Chem.*, **71**, 291 (1974).
30) A. Kasahara, *Bull. Chem. Soc. Jpn.*, **41**, 1272 (1968).
31) J. L. Burdett and M. T. Rogers, *J. Am. Chem. Soc.*, **86**, 2105 (1964).
32) T. Ito and A. Yamamoto, *J. Organomet. Chem.*, **174**, 237 (1979).

Paramagnetic Cobalt(III) Complexes with Organic Ligands. VI. An X-Ray Photoelectron Spectroscopic Study

Yoshihisa YAMAMOTO, Masayasu MORI,*,† and Hidetaka KONNO††

Faculty of Pharmaceutical Science, Higashi Nippon Gakuen University, Ishikari-Tobetsu, Hokkaido 061-02

† *Faculty of Science, Osaka City University, Sumiyoshi-ku, Osaka 558*

†† *Faculty of Engineering, Hokkaido University, Sapporo 060*

(Received December 3, 1980)

Paramagnetic tetraammine-5-nitrosalicylato cobalt complex, paramagnetic μ-hyperoxo-dicobalt complexes and related diamagnetic compounds have been studied by X-ray photoelectron spectroscopy. In all these compounds, the binding energies of Co 2p electrons and their spin-orbit separation were those of usual Co(III) complexes. In the spectrum of paramagnetic tetraammine-5-nitrosalicylatocobalt salt, satellites appeared near the Co 2p peaks showing certain spin density at the cobalt atoms. At the same time, the C 1s spectrum showed that considerable portion of carbon atoms has high binding energy suggesting delocalization of electron hole over the organic ligand. The O 1s peaks in μ-hyperoxo complexes were *ca.* 0.6 eV higher than those in μ-peroxo complexes. Deconvolution of the O 1s peak in the μ-OOH complex gave OH, =O–, and H_2O peaks at the 1:1:1 ratio, supporting the μ-OOH formulation.

Previous papers[1–5] described the preparation and properties of a series of deep green ammine 5-nitrosalicylato cobalt complexes formed from russet ammine salicylato cobalt(III) complexes.[6,7] Inasmuch as these deep green compounds have oxidizing power and are paramagnetic, the earlier papers formally denoted them as cobalt(IV) compounds. However, examination of electric resistivity,[3] ESR,[3] IR,[4] and NMR[4] spectra suggested that the electron deficiency is not centered at cobalt, but is delocalized over the system composed of the cobalt atom and the organic ligand. In this sense we have changed the series title to the present one.[5]

The situation is in a sense similar to the case of some paramagnetic μ-O_2 dicobalt complexes which were formerly described as Co(III)–Co(IV) complexes,[8] but which are now usually formulated as μ-hyperoxo-dicobalt(III) complexes on the basis of structural,[9] ESR,[10] vibrational,[11] and other studies.[12]

The present study has been intended to elucidate the valency and related problems in paramagnetic ammine 5-nitrosalicylato cobalt complexes and μ-O_2 dicobalt complexes by means of X-ray photoelectron spectroscopy (XPS), which is becoming to give useful information as to the state of the constituent atoms.

Experimental

Materials. Tetraammine-5-nitrosalicylatocobalt complexes were prepared after Yamamoto *et al.*,[1–5] whereas μ-O_2 dicobalt complexes were prepared according to the description by Mori *et al.*[13,14]

XPS Measurements. The spectra were obtained by irradiating the compounds with Mg $K\alpha$ X-rays (120 W) in a vacuum at a pressure of less than 3×10^{-7} Pa and at room temperature or around 220 K. The powdered compounds were uniformly mounted on Ni holders by using adhesive tape. The instrument used was a VG ESCA 3 electron spectrometer, and was calibrated with gold and copper, relative to the photoelectron peaks Au $4f_{7/2}$(84.0 eV), Cu $3s_{1/2}$(122.6 eV), and Cu $2p_{3/2}$(932.7 eV); FWHM (full width at half maximum) of the Au $4f_{7/2}$ peak was 1.18 eV, and C 1s peak due to the carbonaceous contamination formed on Au and Cu specimens in the instrument appeared at 284.8 eV. The peak shift caused by charge-up effect was corrected with the contamination C 1s peak.[15]

The spectra comprised of several components were deconvoluted with skewed Gaussian shape, where the same FWHM was assigned for components of the same element. The error of binding energy determination was estimated to be ±0.2 eV when the peaks were well-separated, whereas it was estimated to be ±0.4 eV when deconvolution was applied. The error of intensity estimation was around 5% in the former case while it was around 10% in the latter case.

Results and Discussion

XPS of Ammine 5-Nitrosalicylato Cobalt Complexes. The binding energies of C 1s, N 1s, O 1s, and Co 2p electrons of the cobalt complexes studied in this research are given in Table 1. The binding energies of Co 2p electrons as well as their spin-orbit separation ($\approx$15 eV) in the green paramagnetic complex $[Co(5\text{-}NO_2sal)(NH_3)_4]ClNO_3\cdot H_2O$ fell well within the range of those of cobalt(III) complexes[16] as of course did those of orange diamagnetic complexes $[Co(5\text{-}NO_2sal)(NH_3)_4]NO_3\cdot H_2O$ and $[Co(5\text{-}NO_2sal)(NH_3)_4]\text{-}Cl\cdot HCl\cdot H_2O$, the latter two being considered to be typical cobalt(III) complexes. This is consistent with the results of studies of electric conductivities, ESR,[3] IR, and NMR spectra[4] and suggests delocalization of the electron hole over the cobalt-ligand system in the former paramagnetic compound.

The following points, however, seem to be worth noting concerning the XPS of the paramagnetic $[Co(5\text{-}NO_2sal)(NH_3)_4]ClNO_3\cdot H_2O$: (1) Cobalt 2p peaks have satellites which show the presence of certain spin density at the cobalt atom (Fig. 1). Somewhat greater FWHM observed for the Co $2p_{3/2}$ peak (Table 1) may also be due to the presence of unpaired spin. (2) There are some carbon atoms (estimated to be 22.2% of the total carbon) that have high binding energies (Fig. 2). (1) is in apparent contradiction to the tervalence of cobalt as concluded from the binding energies and spin-orbit separation. These might be accommodated by assuming that although the unpaired spin is not centered at cobalt in the

TABLE 1. BINDING ENERGIES OBSERVED IN THE XPS OF AMMINE-5-NITROSALICYLATO COBALT COMPLEXES[a)]

Compound	Temp	C 1s	N 1s	O 1s	Co $2p_{3/2}$	$2p_{1/2}$
$[(NH_3)_4Co(O-C(=O)-C_6H_3(NO_2)-O)]^+ Cl\cdot NO_3\cdot H_2O$[a)]	room	285.1 ring+contam.[b)] 288.8 ring[c)]+CO shoulder	400.1 NH_3 405.4 NO_2 406.9 NO_3	532.2 max FWHM 3.0	782.1 FWHM 2.6 satellites medium	797.0
	220K	285.4 ring+contam. 288.6 ring[c)]+CO shoulder	400.2 NH_3 405.6 NO_2 407.2 NO_3	532.4 max FWHM 3.1	782.2 FWHM 2.4 satellites medium	797.0
$[(NH_3)_4Co(O-C(=O)-C_6H_3(NO_2)-O)]^+ NO_3\cdot H_2O$	room	285.2 ring+contam. 288.5 =CO shoulder	400.2 NH_3 405.3 NO_2 407.0 NO_3	532.5 max FWHM 2.9	782.3 FWHM 2.1 satellites very weak	797.1
$[(NH_3)_4Co(O-C(=O)-C_6H_3(NO_2)-O)]^+ Cl\cdot HCl\cdot 2H_2O$[a)]	220K	285.2 ring+contam. 288.3 =CO shoulder	400.2 NH_3 405.3 NO_2	532.3 max FWHM 3.2	782.1 FWHM 2.3 satellites very weak	796.9

a) In eV. The maximum of Cl $2p_{3/2}$ has been taken to be at 198.2 eV. b) The peak due to ring carbon admixed with that due to contaminating hydrocarbon from instrument.[15] c) Ring carbon of high binding energy.

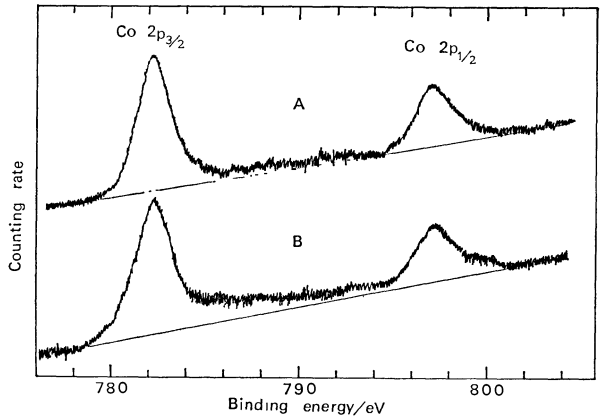

Fig. 1. XPS of $[(NH_3)_4Co(O-C(=O)-C_6H_3(NO_2)-O)]Cl\cdot HCl\cdot 2H_2O$ (A) and $[(NH_3)_4Co(O-C(=O)-C_6H_3(NO_2)-O)]Cl\cdot NO_3\cdot 2H_2O$ (B) in the Co 2p region at 220 K.

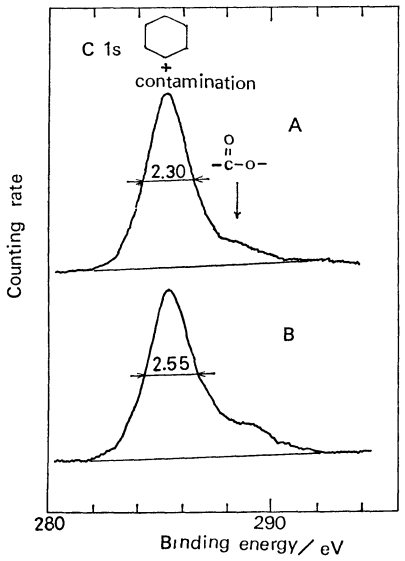

Fig. 2. XPS of $[(NH_3)_4Co(O-C(=O)-C_6H_3(NO_2)-O)]Cl\cdot HCl\cdot 2H_2O$ (A) and $[(NH_3)_4Co(O-C(=O)-C_6H_3(NO_2)-O)]Cl\cdot NO_3\cdot 2H_2O$ (B) in the C 1s region at 220 K.

sense that cobalt is quadrivalent, yet some fraction of the spin density remains on cobalt. However, a considerable part of the spin density or the electron deficiency seems to be also distributed over some carbon atoms of the 5-nitrosalicylato ligand as evidenced by (2), *i.e.* by the high binding energies observed for certain portion of the carbon atoms. In the case of orange diamagnetic $[Co(5\text{-}NO_2sal)(NH_3)_4](NO_3)\cdot H_2O$, a shoulder appeared at the high energy side of the main C 1s peak, and from its area (estimated to be 6.7% of the total carbon), it is considered to correspond to the carboxylato carbon.

In the green paramagnetic as well as the orange diamagnetic complexes the nitrogen 1s electrons appear as two peaks separated by 6.4—6.8 eV. The peak at *ca.* 400 eV was assigned to NH_3 nitrogen. The peak at higher energy could be deconvoluted to the one at 405—406 eV assignable to NO_2 nitrogen and to the one at *ca.* 407 eV assignable to NO_3 ni-

Table 2. Binding energies observed in the XPS of μ-O_2 dicobalt complexes

Compound	Temp	C 1s	N 1s	O 1s	Co $2p_{3/2}$	$2p_{1/2}$
$\left[(NH_3)_4Co\begin{smallmatrix}NH_2\\ \\ OO\end{smallmatrix}Co(NH_3)_4\right]$- $Br_4\cdot H_2O$[b]	room	284.8 contam.[a]	398.2 $-NH_2$-[e]	531.5 -OO-	781.6 FWHM 2.4	796.5
			400.0 NH_3	533.2 H_2O	satellites very weak	
$\left[(en)_2Co\begin{smallmatrix}NH_2\\ \\ OO\end{smallmatrix}Co(en)_2\right]Cl_4\cdot xH_2O$[b]	room	284.8 contam.	398.5 $-NH_2$-[e]	531.9 -OO-	781.9 FWHM 2.4	796.7
		286.1 en	400.3 en	533.4 H_2O	satellites very weak	
$\left[(en)_2Co\begin{smallmatrix}NH_2\\ \\ OO\end{smallmatrix}Co(en)_2\right]Br_4\cdot 4H_2O$[b]	room	284.8 contam.	398.4 $-NH_2$-[e]	531.9 -OO-	781.8 FWHM 2.1	796.7
		286.0 en	400.3 en	533.4 H_2O	no satellite	
$\left[(en)_2Co\begin{smallmatrix}NH_2\\ \\ OO\end{smallmatrix}Co(en)_2\right]$- $(NO_3)_4\cdot 2H_2O$[b]	room	284.8 contam.	398.2 $-NH_2$-[f]	531.6 -OO-	781.9 FWHM 2.3	796.6
		286.0 en	400.2 en	532.7 NO_3 $+H_2O$	satellites very weak	
			407.0 NO_3			
	220K	284.8 contam.	398.3 $-NH_2$-[e]	531.7 -OO-	781.8 FWHM 2.3	796.7
		286.0 en	400.3 en	532.7 NO_3 $+H_2O$	no satellite	
			406.9 NO_3			
$\left[(en)_2Co\begin{smallmatrix}NH_2\\ \\ OO\end{smallmatrix}Co(en)_2\right]$- $(NO_3)_3\cdot 2.5\,H_2O$[c]	room	284.8 contam.	398.3 $-NH_2$-[f]	530.8 -OO-	781.3 FWHM 2.6	795.9
		286.0 en	400.2 en	532.3 NO_3 $+H_2O$	satellite weak	
			406.8 NO_3			
	220K	284.8 contam.	398.2 $-NH_2$-[e]	530.6 -OO-	781.1 FWHM 2.6	795.9
		286.0 en	400.1 en	532.5 NO_3 $+H_2O$	no satellite	
			406.7 NO_3			
$\left[(en)_2Co\begin{smallmatrix}NH_2\\ \\ O\\ \\ OH\end{smallmatrix}Co(en)_2\right]$- $Br_4\cdot H_2O$[d]	room	284.8 contam.	398.4 $-NH_2$-[e]	531.4 OH	781.7 FWHM 2.0	796.2
		285.8 en	400.2 en	532.2 -O=	no satellite	
				533.5 H_2O		

a) The C 1s peak due to hydrocarbon contamination from the instrument has been taken to be at 284.8 eV.[15] b) Green paramagnetic hyperoxo complex. c) Brown diamagnetic peroxo complex. d) Red diamagnetic hydroperoxo complex. e) I_{NH_2}/I_{NH_3}(or en) $\fallingdotseq$ 1/8. f) The above ratio is not equal to 1/8. The reason is not clear.

trogen. It has not so far been possible to deconvolute the peak of O 1s (half width=3.3 eV) into those of different types of atoms in the compound.

XPS of μ-NH_2-μ-O_2 Dicobalt Complexes. Okamoto *et al.* who studied the XPS of various cobalt compounds in connection with the catalytic activities reported that the Co 2p binding energies and their spin orbit separation of $[(NH_3)_5CoO_2Co(NH_3)_5](NO_3)_4$ (diamagnetic) and $[(NH_3)_5CoO_2Co(NH_3)_5]Cl_5$ (paramagnetic) were in the same range as those of usual cobalt(III) complexes.[17] Burness *et al.* studied the XPS of Shiff-base complexes and their O_2 adducts, found similar results,[18] and concluded that the oxygenated compounds contain tervalent cobalt, so that O_2 is a peroxo (diamagnetic) or a hyperoxo (paramagnetic) ligand. The peroxo compounds they studied included both mononuclear and dinuclear (*i.e.* μ-O_2) complexes, whereas the hyperoxo compounds they studied were all mononuclear. They also found that the O 1s binding energies of the hyperoxo complexes are *ca.* 1 eV higher than those of the peroxo complexes in conformity with the reduction of the charge on the O_2 moiety. The result of the present XPS study (Table 2) on the μ-NH_2-μ-O_2 dicobalt complexes also showed a similar trend. A slightly lower binding energies of Co 2p electrons in the peroxo as compared with those in the hyperoxo complex might be accounted for in terms of the donation of the extra antibonding π-electron of O_2 to cobalt in the former. Satellites were either inperceptible or very weak indicating low spin density on the cobalt atom (Fig. 3), again rationalizing the formulation of the paramagnetic compound as μ-hyperoxo-dicobalt(III) complex.

In $[(en)_2Co(NH_2)(OOH)Co(en)_2]Br_4\cdot H_2O$ spectrum, the O 1s band could be deconvoluted into three peaks at 531.4, 532.2, and 533.5 eV assigned to -OH, >O-, and H_2O oxygens, respectively, supporting the μ-OOH structure reported for the corresponding nitrate.[19] The higher binding energy of >O- in >O-OH as compared with that of usual peroxo oxygen might be due to the lower electron density caused by coordination of one peroxo oxygen to two cobalt ions in the former case. It has also been possible to dif-

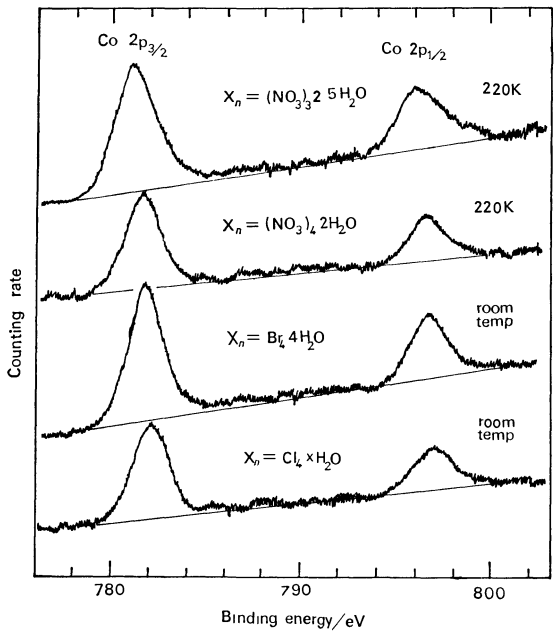

Fig. 3. XPS of $\left[(en)_2Co\begin{matrix}\diagup NH_2\diagdown \\ \diagdown OO\diagup\end{matrix}Co(en)_2\right]X_n$ in the Co 2p region.

ferentiate the nitrogen atom present as NH_2 from those present as NH_3 or en with the intensity ratio of 1:8 in most μ-NH_2-μ-O_2 complexes studied (*cf.* Table 2).

Comparison between the Two Series of Paramagnetic Cobalt Complexes. As discussed above, the deep green ammine-5-nitrosalicylatocobalt complex and the green μ-hyperoxo-dicobalt complex are in a sense similar in that one unpaired spin (an electron hole) has the probability of existence partly on the cobalt atom and partly on some of the ligand molecules. In the case of the paramagnetic μ-O_2 complex, the large hyperfine coupling constant due to ^{17}O nucleus in the ESR spectrum established that the spin density is much higher on the O_2 bridge,[10] rationalizing the μ-hyperoxo nomenclature. This seems to be in line with inperceptible or very weak satellites of Co 2p lines in the XPS of the μ-amido-μ-hyperoxo complex. On the other hand the appearance of satellites in the Co 2p lines in the XPS of the deep green tetraammine-5-nitrosalicylatocobalt complex seems to suggest a higher spin density on cobalt as compared with the μ-hyperoxo-dicobalt case. Yamamoto[3] observed eight hyperfine lines in the aqueous esr spectrum of deep green bis(ethylenediamine)-5-nitrosalicylatocobalt chloride nitrate in the narrow concentration range of ca. 10^{-2}—10^{-3} M, which may possibly be due to ^{59}Co nucleus, but simultaneous appearance of one sharp line leaves some ambiguity as to the state of the complex in aqueous solution. Thus, quantitative estimation of the spin density by use of more stable complex of this series containing isotopically labeled ligand seems to be very desirable.

References

1) Y. Yamamoto, K. Ito, H. Yoneda, and M. Mori, *Bull. Chem. Soc. Jpn.*, **40**, 2580 (1967).
2) Y. Yamamoto, M. Mori, H. Yoneda, S. Misumi, and K. Ito, *Bull. Chem. Soc. Jpn.*, **42**, 984 (1969).
3) Y. Yamamoto, *Bull. Chem. Soc. Jpn.*, **42**, 999 (1969).
4) Y. Yamamoto, *Bull. Chem. Soc. Jpn.*, **51**, 2894 (1978).
5) Y. Yamamoto, E. Toyota, and N. Mitsudera, *Bull. Chem. Soc Jpn.*, **53**, 3517 (1980).
6) G. T. Morgan and J. D. M. Smith, *J. Chem. Soc.*, **1922**, 1956; **1924**, 1924.
7) Y. Yamamoto and E. Toyota, *Chem. Pharm. Bull.*, **26**, 2275 (1978); *Bull. Chem. Soc. Jpn.*, **52**, 2540 (1979).
8) A. Werner, *Ann.* **375**, 1 (1910).
9) G. G. Christoph, R. E. Marsh, and W. P. Schaefer, *Inorg. Chem.*, **8**, 291 (1969).
10) E. A. V. Ebsworth and J. A. Weil, *J. Phys. Chem.*, **63**, 1890 (1959); J. A. Weil and J. K. Kinnaird, *J. Phys. Chem.*, **71**, 3341 (1967).
11) T. Shibahara, *J. Chem. Soc., Chem. Commun.*, **1973**, 864; T. Shibahara and M. Mori, *Bull. Chem. Soc. Jpn.*, **51**, 1374 (1978).
12) A. G. Sykes and J. A. Weil, "Progress in Inorganic Chemistry," Interscience Publishers, New York (1970), Vol. 13, p. 33.
13) M. Mori and J. A. Weil, *J. Am. Chem. Soc.*, **89**, 3732 (1967).
14) M. Mori, J. A. Weil, and M. Ishiguro, *J. Am. Chem. Soc.*, **90**, 615 (1968).
15) C. J. Powell, N. E. Erickson, and T. E. Madey, *J. Electron Spectrosc. Relat. Phenom.*, **17**, 361 (1980).
16) D. C. Frost, C. A. McDowell, and I. S. Woolsey, *Mol. Phys.*, **27**, 1473 (1974).
17) Y. Okamoto, H. Nakano, T. Imanaka, and S. Teranishi, *Bull. Chem. Soc. Jpn.*, **48**, 1163 (1975).
18) J. H. Burness, J. G. Dillard, and L. T. Tayler, *J. Am. Chem. Soc.*, **97**, 6080 (1975).
19) U. Thewalt and R. E. Marsh, *J. Am. Chem. Soc.*, **89**, 6364 (1967).

  Bull. Chem. Soc. Jpn., 54, 1999—2004 (1981)

Negative Ions Formed by Vacuum Spark Discharge. III.[1] Polyatomic Negative Ions of the Elements in A-Subgroups on the Periodic Table

Hiroshi KISHI†

Department of Chemistry, Faculty of Science, Kyoto University, Sakyo-ku, Kyoto 606

(Received December 15, 1980)

Polyatomic negative ions for almost all of the elements in A-subgroups on the periodic table were tested by the spark discharge type ion source mass spectroscopy. A large number of polyatomic negative ions such as "polymer" negative ions, hydride negative ions, oxide negative ions, and carbide negative ions, could be detected. The results are discussed with reference to the reported values of electron affinities of the molecules and to the reported results by other methods of formation.

A study on negative ion spark source mass spectroscopy using a Mattauch-Herzog type double focusing mass spectrograph has been carried out. Formation of atomic negative ions of 48 elements has previously been reported,[2] and the relative sensitivity coefficients for negative ions has also been reported.[1]

The significant features of the Mattauch-Herzog type double focusing mass spectroscopy[3] are (1) all ions of a given mass (m/z) range can be detected at the same time on a photographic emulsion plate, and (2) by the cumulative nature of the ion detection on the photographic emulsion plate, it is possible to detect ions of weak intensity: the exposure time is long and all ions formed during the exposure time are collected. In the experiment of atomic negative ions with the use of a spark discharge type ion source,[2] a large number of polyatomic negative ions were detected in addition to the atomic negative ions.

On the polyatomic negative ions detected by spark source mass spectroscopy, there are only a few reports in the literature.[4,5] This might reflect the difficulty of the formation of negative ions by spark discharge type ion sources, compared with the case of formation of positive ions. The probability of formation of negative ions versus the positive ions is 10^{-3} to 1, in an electron-impact type ion source.[6] In the spark discharge type ion source, the probability appears to be close to this value.

In the present experiment, the following testing materials were used: (1) elementary materials in the form of solid metals or powdered metals, (2) gases, (3) oxide compounds, (4) inter-elementary compounds such as GaAs or LiF, (5) other types of compounds, including almost all of the elements in A-subgroups (typical elements) on the periodic table, except for Po, At, Fr, and Ra.

In this report, the ionic species of polyatomic negative ions detected in the experiment are described, along with some polyatomic positive ions. The negative ions are classified into the following five types: (1) "polymer" negative ions, (2) hydride negative ions, (3) oxide negative ions, (4) carbide negative ions, and (5) other types of negative ions.

Electron affinity of molecules is important to the understanding of molecular phenomena. Reported values of electron affinities are available for some molecules in the literature;[7,57] however, the experimental determination and theoretical calculation both present great difficulties. The results given here present experimental evidence that molecular ions detected here have positive electron affinity values. The results are discussed with reference to the reported values of electron affinities.[32-56]

The results are also compared with those obtained from negative ion formation by means of the spark discharge, electron impact, surface ionization, and other methods.

Experimental

Apparatus. The instrument used was a Mattauch-Herzog type double focusing mass spectrograph, equipped with an r f spark discharge type ion source (Mitsubishi Denki Electric Co. Ltd.). Since details of the instrumentation were reported elsewhere,[8-10] only the operationing conditions are given here: spark voltage 20 kV, pulse width 200 μs, repetition rate 100 s^{-1}, ion accelerating voltage 15 kV for positive and negative ions.

Materials. Sample materials studied are (1) elementary materials in the form of solid metals or powdered metals, (2) gases, (3) oxide compounds, (4) binary compounds such as GaAs or LiF, (5) other types of compounds. They are listed in Table 1.

When the samples are solid materials, the discharge electrodes of the ion source, about 1 $mm^2 \times 5$ mm, are made from them. In this case, it is convenient to maintain a discharge between the electrodes, and to have a long exposure time. When the samples are fine powders, they are packed inside a small ($\approx$1 mm diameter) metal tube, made of gold or nickel, and a platinum counterelectrode is applied. When they are electrical insulators, some oxides for instance, powdered materials are mixed well with pure aluminium powder of equal weight, and pressed[11] to form rigid electrodes. Some insulators, lithium fluoride crystal for instance, can be ionized with a platinum counterelectrode.

When the samples are gaseous materials, they are introduced into the region of the spark discharge of Pt/Pt electrodes through a capillary leak. In "A/B spark discharge," A and B mean the electrode materials in the spark discharge ion source. This notation will be used throughout this report.

Vacuum discharge ionization is difficult to maintain when the melting point of the electrode is low. Gallium, for instance, is ionized using a gallium arsenide crystal.

† Present address: Oyama Technical College, Nakakuki, Oyama, Tochigi 323.

TABLE 1. SAMPLE MATERIALS FOR THE POLYATOMIC NEGATIVE IONS

Group	Element	Sample materials	Group	Element	Sample materials
IA	H	Hydrogen gas		Ge	Germanium, Crystal
	Li	Lithium fluoride, Crystal			Germanium dioxide, Powder
		Lithium carbonate, Powder		Sn	Tin metal
	Na	Sodium chloride, Crystal			Tin(IV) oxide
		Sodium carbonate, Powder		Pb	Lead metal
	K	Potassium bromide, Crystal	VA	N, P	Ammonium hydrogenphosphate, Powder
		Potassium chloride, Crystal			
		Potassium carbonate, Powder		N	^{15}N-Ammonium sulfate, Powder
	Rb	Rubidium chloride, Crystal		As	Gallium arsenide, Crystal
		Rubidium chloride, Powder			Diarsenic trioxide, Power
	Cs	Caesium bromide, Crystal		Sb	Indium antimonide, Crystal
		Caesium nitrite, Powder			Diantimony trioxide, Powder
IIA	Be	Beryllium, Flake		Bi	Dibismuth trioxide, Powder
		Beryllium oxide, Powder	VIA	O	Metal oxides, Powder
	Mg	Magnesium			Air, Gas
		Magnesium oxide, Powder		S	Cadmium sulfide, Crystal
	Ca	Calcium, Metal			Barium sulfide
		Calcium fluoride, Powder		Se	Zinc selenide, Crystal
	Sr	Strontium carbonate, Powder			Selenium dioxide, Powder
	Ba	Barium sulfide		Te	Tellurium
		Barium carbonate, Powder			Cadmium telluride, Crystal
IIIA	B	Boron, Powder	VIIA	F	Lithium fluoride, Crystal
		Diboron trioxide			Calcium fluoride, Powder
	Al	Aluminium, Wire		Cl	Sodium chloride, Crystal
		Aluminium, Powder			Potassium chloride, Crystal
	Ga	Gallium arsenide, Crystal			Rubidium chloride, Crystal
	In	Indium antimonide, Crystal			Ammonium chloride, Powder
	Tl	Dithallium trioxide, Powder		Br	Potassium bromide, Crystal
IVA	C	Graphite			Caesium bromide, Crystal
	Si	Silicon, Crystal			Silver bromide, Powder
		Silicon, Powder		I	Ammonium iodide, Powder

Results and Discussion

Method and procedure for the assignment of the mass spectral peaks obtained by the spark ion source mass spectroscopy are essentially the same as the experiment of the atomic negative ions.[2]

Experimental results for the polyatomic negative ions are tabulated in Table 2, along with the experimental results for atomic negative ions[2] and for polyatomic positive ions which were detected in the positive ion spark source mass spectra using the same samples.

Reported values of electron affinities of the molecules available in the literature[7] are tabulated in Table 3. In this table, the experimental or theoretical method used to determine the values of electron affinities are given in parentheses by an abbreviation.

Group IA Elements. By spark discharge of Pt/Pt electrodes in an atmosphere of H_2 gas, H^-, H_2^+, H_3^+ ions are detected, but H_2^- ion can not be detected. For the molecular ion of hydrogen, there are many reports in the literature. H_3^+ ion was detected by the parabola-type mass spectrograph, but H_2^- ion could not be detected.[12] The reported value of the electron affinity of H_2^- ion by the calculation is negative,[50,51] although H_2^- ion was detected by charge exchange of H_2^+ ion with H_2 gas,[13] and in a duoplasmatron ion source.[14] H_3^+, H_5^+, and H_5O^+ ions were detected by glow discharge.[15]

For the experiment of alkali-metal elements, alkali halide crystals are used as spark discharge electrodes. The polyatomic negative ions of $RbCl^-$, and the polyatomic positive ions of Li_2^+ and LiF^+ are detected in the spark discharge of LiF(crystal)/Pt electrodes.

For the polyatomic ions of alkali-metal elements, there are reports in the literature: MX^-, and MX_2^- ions (M=Li, Na, K, Rb, Cs; X=F, Cl, Br, I) are formed by surface ionization,[16] LiH_2^- ion by Penning discharge,[17] $LiCl^+$, $NaCl^+$, Na_2Cl^+, $Na_2Cl_2^+$, KCl^+, and $LiBH_2^+$ by spark discharge.[18]

Group IIA Elements. In the present experiment, only the Be^- ion is detected for negative ions. No polyatomic negative and positive ions are detected. The positives ions Be^+—Be_{25}^+, $Be_p(BeO)_q^+$,[19] and Mg^+—Mg_5^+ [4] are reported to form by spark discharge.

Group IIIA Elements. In this group, many polyatomic negative ions are detected. For the element Al, "polymer" negative ions of Al_2^-—Al_{13}^- are detected by Al/Al spark discharge. The results of detection of Al_2^-—Al_7^- and their relative intensities were already reported.[20] In addition to these ions, oxide negative ions AlO^-, and AlO_2^- are also detected.

TABLE 2. POLYATOMIC NEGATIVE IONS AND POSITIVE IONS

Group	Element	Atomic	Polyatomic negative ions	Polyatomic positive ions	Group	Element	Atomic	Polyatomic negative ions	Polyatomic positive ions
IA	H	D[a]		H_2^+, H_3^+				SiC_2^-	
	Li	D		Li_2^+, LiF^+		Ge	D	Ge_2^-—Ge_4^-;	Ge_2^+—Ge_4^+
	Na	D						GeC^-, GeC_2^-	
	K	D				Sn	D	SnC^-, SnC_2^-	
	Rb	D	$RbCl^-$			Pb	D	PbC^-	
	Cs	D			VA	N	ND		
IIA	Be	D				P	D	PO^-—PO_4^-	
	Mg	(ND)				As	D	As_2^-; AsO^-;	As_2^+, AsH^+
	Ca	ND[b]						AsH^-, As_2H^-;	
	Sr	ND						AsC^-—AsC_3^-	
	Ba	ND				Sb	D	Sb_2^-	
IIIA	B	D				Bi	D		
	Al	D	Al_2^-—Al_{13}^-; AlO^-, AlO_2^-	Al_2^+	VIA	O	D	O_2^-; OH^-, O_2H^-	O_2^+
	Ga	D	Ga_2^-; GaO^-, GaO_2^-; $GaAs^-$, $GaAsH^-$	Ga_2^+		S	D	S_2^-, S_3^-	S_2^+
						Se	D	Se_2^-—Se_4^-	Se_2^+
						Te	D	Te_2^-	
	In	D			VIIA	F	D		F_2^+; FH^+; LiF^+
	Tl	D	TlO^-; TlC^-			Cl	D	Cl_2^-; $RbCl^-$	
IVA	C	D	C_2^-—C_{15}^-; CH^-—$C_{13}H^-$	C_2^+—C_{15}^+		Br	D	Br_2^-, Br_3^-; BrH^-; Br_2O^-	Br_2^+; BrH^+; Br_2O^+, $Br_2O_2^+$
	Si	D	Si_2^-; SiC^-,	Si_2^+—Si_4^+		I	D		

a) Detected. b) Not detected.

TABLE 3. REPORTED VALUES OF THE ELECTRON AFFINITIES OF THE MOLECULES
(—: No data are available in the literature)

Element	Present study	Electron affinity values/eV	Element	Present study	Electron affinity values/eV
Rb	$RbCl^-$	—	P	PO^-	$\leqslant$1.13(HF, 37)
Al	Al_2^-—Al_{13}^-	—		PO_2^-—PO_4^-	—
	AlO^-	3.68±0.13(SI, 32), 2.60(AA, 33)	As	As_2^-	—
	AlO_2^-	4.11±0.13(SI, 32)		AsO^-	—
Ga	Ga_2^-	—		AsH^-	—
	GaO^-	—		As_2H^-	—
	GaO_2^-	—		AsC^-—AsC_3^-	—
Tl	TlO^-	—	Sb	Sb_2^-	>0(OBS, 38)
	TlC^-	—	O	O_2^-	0.440±0.008(PE, 39),
C	C_2^-	$\leqslant$3.54±0.05(P, 34), 4.0(SI, 35), >2.9±0.5(DEC, 36)			0.5±0.1(CE, 40), $\geqslant$0.48(CE, 41), 0.42(DE, 42), 0.15±0.05(P, 43)
	C_3^-	2.5(SI, 35)		OH^-	1.91±0.10(HF, 44)
	CH^-	0.74±0.05(P, 34), $\geqslant$4.1±0.4(DEC, 36)		O_2H^-	4.6(BH, 45)
S	S_2^-	>2.0(ATT, 46)		C_2H^-	$\leqslant$3.73±0.05(P, 34), >2.3±0.7(DEC, 36)
	S_3^-	—		C_4^-—C_{15}^-	—
Se	Se_2^-—Se_4^-	>0(OBS, 38)		C_3H^-—$C_{13}H^-$	—
Te	Te_2^-	>0(OBS, 38)	Si	Si_2^-	—
Cl	Cl_2^-	2.45±0.15(CE, 40), 2.46±0.14(CE, 47), <1.7(ATT, 48)		SiC^-	—
	$RbCl^-$	—		SiC_2^-	—
Br	Br_2^-	2.55±0.10(CE, 40), >0(OBS, 49), 2.51±0.10(CE, 58)	Ge	Ge_2^-—Ge_4^-	—
	Br_3^-	—	Sn	SnC^-	—
	BrH^-	—		SnC_2^-	—
	Br_2O^-	—	Pb	PbC^-	—

SI: Surface ionization. AA: Constituent atom electron affinity(dissociation energy). P: Incoherent photon detachment. DEC: Electron impact with analytic deconvolution. HF: Hartree-Fock calculation. OBS: Observation in mass spectrum. PE: Photoelectron spectroscopy with fixed frequency. CE: Charge exchange. DE: Dissociation energy. BH: Born-Haber cycle calculation. ATT: Dissociative electron attachment.
(Numbers in the parentheses are reference numbers.)

TABLE 4. "POLYMER" NEGATIVE IONS

Group	IA	IIA	IIIA		IVA			VA		VIA				VIIA	
Element	Li	Be	Al	Ga	C	Si	Ge	As	Sb	O	S	Se	Te	Cl	Br
M^-	D	D	D	D	D	D	D	D	D	D	D	D	D	D	D
M_2^-		D	D	D	D	D	D	D	D	D	D	D	D	D	D
M_3^-			D		D		D				D	D			D
M_4^-			D		D		D					D			
⋮			⋮		⋮										
M_{13}^-			D		⋮										
⋮					⋮										
M_{15}^-					D										

For the element Ga, the diatomic negative ion Ga_2^- and the oxide negative ions GaO^- and GaO_2^- are detected by spark discharge of GaAs/GaAs. In this experiment, $GaAs^-$ and $GaAsH^-$ ions are also detected. For the element Tl, TlO^-, and TlC^- ions are detected.

For polyatomic positive ions of these elements, Al_2^+ and Ga_2^+ ions are detected; these results were already reported.[20]

Al_2^+—Al_{14}^+ ions were reported to form by spark discharge,[19] and BO^- and BO_2^- ions are reported to form by surface ionization.[21] Electron affinity values are available for AlO^- (2.60, 3.68 eV) and AlO_2^- (4.11 eV) (Table 3).

Group IVA Elements. In this group, many polyatomic negative ions are detected. For the element C, "polymer" negative ions C_2^-—C_{15}^-, and hydride negative ions CH^-—$C_{13}H^-$ are detected. For Si: Si_2^- and SiC^- and SiC_2^- ions are detected; for Ge: Ge_2^-, Ge_3^- and Ge_4^-; GeC^- and GeC_2^- ions; for Sn: SnC^- and SnC_2^- ions; and for Pb: PbC^- ions. The following positive ions are detected in these elements: C_2^+—C_{15}^+; Si_2^+—Si_4^+. Ge_2^+—Ge_4^+ "polymer" positive ions are also detected.

In the literature,[22,23] CS^-, CS_2^-, OCN^-, SCN^- ions are reported to form by ion-molecule reactions. SiO_2^- ions are reported by surface ionization.[24] Several positive "polymer" ions of C, C_2^+—C_{31}^+, are reported to form by spark discharge.[18,25,26,27]

The electron affinity values are available for the molecules C_2^-(2.9—4.0 eV), CH^-(0.74—4.1 eV), C_2H^-(2.3—3.73 eV) (Table 3).

Group VA Elements. In this group, for the element N, no atomic negative ion was detected,[2] and no polyatomic negative ion was detected. For the element P: PO^-, PO_2^-, PO_3^-, and PO_4^- are detected. For the element As: As_2^-; AsH^-, and As_2H^-; AsO^-; AsC^-, AsC_2^-, and AsC_3^- ions are detected. For the element Sb: Sb_2^- ion is detected. For the polyatomic positive ions of this group, As_2^+ and AsH^+ ions are detected.

The literature reports PH^- and PH_2^-, AsH^- and AsH_2^- ions by electron impact,[28] and N_3^-, CN^-, $C_2N_3^-$, C_3NO^-, $C_2N_4^-$, $C_2N_6^-$, $C_3N_2O^-$, $C_2N_5^-$, *etc.* ions by glow discharge.[29]

The electron affinity values are available for the molecules PO^- (<1.13 eV), and Sb_2^- (>0 eV) (Table 3).

Group VIA Elements. For the element O: O_2^-, O_2H^- and OH^- negative ions are detected. For the element S: S_2^- and S_3^-; for Se: Se_2^-, Se_3^-, and Se_4^-; and for Te, Te_2^-. These "polymer" negative ions are detected by the spark discharges of CdS(crystal)/Pt, CdSe(crystal)/Pt, and CdTe(crystal)/Pt, respectively. Positive ions of O_2^+, S_2^+, and Se_2^+ are also detected.

The literature reports O_3^-, OH^-, NO_2^-, SO_2^-, CS^-, CS_2^-, S_n^- (n=2—6) ions,[22] SF_6^-,[30] SCN^-, OCN^-, HS^-, NH_2S^- ions,[23] and S_{12}^+ ion.[31]

Electron affinity values are available for the molecules O_2^- (0.15—0.5 eV), OH^- (1.825—1.91 eV), O_2H^- (4.6 eV), S_2^- (2.0 eV), Se_n^- (n=2—4: >0 eV), and Te_2^- (>0 eV) (Table 3).

Group VIIA Elements. For Cl, Cl_2^-, and $RbCl^-$ ions are detected by spark discharge of RbCl/Pt. For Br, Br_2^-, Br_3^-, BrH^-, and Br_2O^- ions are detected

TABLE 5. HYDRIDE NEGATIVE IONS

Group	IVA	VA	VIA	VIIA	
Element	C	As	O	Cl	Br
M^-	D	D	D	D	D
MH^-	D	D	D		D
MH_2^-	D	D	—		
M_2H^-	D	D	D		

TABLE 6. OXIDE NEGATIVE IONS

Group	IA	IIIA			VA		VIIA
Element	H	Al	Ga	Tl	P	As	Br
M^-	D	D	D	D	D	D	D
MO^-	D	D	D	D	D	D	—
MO_2^-	D	D	D		D		—
MO_3^-					D		—
MO_4^-					D		—
M_2O^-							D

TABLE 7. CARBIDE NEGATIVE IONS

Group	IVA				VA	
Element	Si	Ge	Sn	Pb	As	Sb
M^-	D	D	D	D	D	D
MC^-	D	D	D	D	D	D
MC_2^-	D	D	D		D	D
MC_3^-					D	

Table 8. "Polymer" positive ions

Group	IA		IIIA		IVA			VA	VIA			VIIA	
Element	H	Li	Al	Ga	C	Si	Ge	As	O	S	Se	F	Br
M_2^+	D	D	D	D	D	D	D	D	D	D	D	D	D
M_3^+	D				D	D	D			D			
M_4^+					D	D	D						
⋮					⋮								
M_{15}^+					D								

Table 9. Hydride positive ions

Group	VA	VIIA	
Element	As	F	Br
MH^+	D	D	D
M_2H		D	

Table 10. Oxide positive ions

Group Element	VIIA Br
M_2O^+	D
$M_2O_2^+$	D

Table 11. Other types of positive ions

LiF^+	Li_2F^+

by AgBr/Pt spark discharge. Some polyatomic positive ions of the elements in this group are found: F_2^+, F_2H^+, and LiF^+ ions for the element F, and Br_2^+, Br_2O^+, $Br_2O_2^+$, and BrH^+ ions for the element Br. These are detected by the spark discharge of LiF/Pt and AgBr/Pt, respectively.

Electron affinity values are available for the molecules Cl_2^- (1.7—2.46 eV) and Br_2^- (>0—2.55 eV) (Table 3).

In summary, we have described the ionic species of polyatomic negative ions formed by the spark discharge type ion source for the elements in A-subgroups on the periodic table, along with the polyatomic positive ions. For the molecules that are detected as negative ions in this experiment, the reported values of the electron affinities are all positive. For the molecules having negative electron affinity values, available in the literature: (H_2^-: <0 eV,[50] −2.85 eV;[51] CO^-: −1.8 eV;[52] CO_2^-: >−0.9 eV;[53] N_2^-: −1.6 eV,[54] −11.345 eV;[55] HF^-: <0 eV[56]); no polyatomic negative ions can be detected in this experiment. Therefore, it seems that the electron affinity values are positive for the molecules which are detected as negative ions in this experiment, although there are many examples that the molecules can not be detected as negative ions in spite of the positive electron affinity values of them. This conclusion is in line with the case of atomic negative ions.[2] If this assumption is correct, the experimental results described in this report give experimental evidence that the ionic species that are detected as negative ions have the positive electron affinity values.

The polyatomic negative ions described in this report are classified into the following four types: (1) "polymer" negative ions, (2) hydride negative ions, (3) oxide negative ions, and (4) carbide negative ions. They are tabulated in Tables 4—7. Polyatomic positive ions detected can also be classified into the following four types: (1) "polymer" positive ions, (2) hydride positive ions, (3) oxide positive ions, and (4) other types of positive ions. They are tabulated in Tables 8—11. These tables indicate the following features for the formation of the polyatomic negative and positive ions by the spark discharge type ion source in the elements of A-subgroups on the periodic table.

(1) In the elements for which atomic negative ions can not be detected, no polyatomic negative ions can be detected.

(2) The elements, whose negative and positive "polymer" ions can easily be detected are identical, except for the elements H, Be, Sb, F, and Cl. They belong mostly to the IIIA, IVA, VA, VIA groups in the periodic table.

(3) Few hydride positive ions are detected, compared to the number of hydride negative ions; these are observed for the elements C, As, O, Cl, Br.

(4) Oxide negative ions are observed for the elements H, Al, Ga, Tl, P, As, and Br, whereas oxide positive ions are observed only for the element Br.

(5) Carbide negative ions are observed for the elements Si, Ge, Sn, Pb, As, and Sb. No carbide positive ions can be detected in this experiment.

The author would like to express his hearty thanks to Dr. K. Kodera and Dr. T. Makita, Kyoto University, for their encouragement and helpful suggestions throughout this work.

References

1) Part II: H. Kishi, *Bull. Chem. Soc. Jpn.*, **54**, 703 (1981).
2) T. Makita, H. Kishi, and K. Kodera, *Mass Spectroscopy (Japan)*, **21**, 293 (1973).
3) J. Mattauch and R. Herzog, *Z. Phys.*, **89**, 786 (1934).
4) H. Hintenberger, J. Franzen, and K. D. Schuy, *Z. Naturforsch., Teil A*, **18**, 1236 (1963).
5) K. D. Schuy, J. Franzen, and H. Hintenberger, *Z. Naturforsch., Teil A*, **19**, 153 (1964).
6) C. E. Melton, "Mass Spectrometry of Organic Ions," ed by F. W. McLafferty, Academic Press (1963), p. 163.
7) H. R. Rosenstock, K. Draxl, B. W. Steiner, and J. T. Herron, "Energetics of Gaseous Ions," National Bureau of Standards, Washington, D. C., 20234 (1977).
8) N. Sasaki and J. Kai, *Mass Spectroscopy (Japan)*, **7**, 64 (1959).

9) M. Gotoh and J. Kai, *Mitsubishi Denki Lab. Report*, **1**, 51 (1960).
10) T. Makita and K. Kodera, *Mass Spectroscopy (Japan)*, **12**, 1 (1964).
11) F. Konishi, *Mass Spectroscopy (Japan)*, **16**, 251 (1968).
12) J. W. Hiby, *Ann. Phys.*, **34**, 473 (1939).
13) V. I. Khvostenko and V. M. Dukelsky, *Soviet Phys. -JETP*, **7**, 709 (1958).
14) E. B. Carter and R. H. Davis, *Rev. Sci. Instrum.*, **34**, 93 (1963).
15) P. H. Dawson and A. W. Tickner, *J. Chem. Phys.*, **37**, 672 (1962).
16) H. Ebinghaus, *Z. Naturforsch., Teil A*, **19**, 727 (1964).
17) H. Baumann, K. Bethge, and E. Heinicke, *Nucl. Instrum. Methods*, **46**, 43 (1967).
18) K. Goshgarian and J. Jensen, ASTM-E14, 12th Annual Meeting, preprint, p. 350, (1964).
19) J. Franzen and H. Hintenberger, *Z. Naturforsch., Teil A*, **16**, 535 (1961).
20) K. Kodera and T. Makita, Twelfth Annual Conference on Mass Spectrometry and Allied Topics, p. 486 (1964).
21) S. Taniguchi, *Mass Spectroscopy (Japan)*, **14**, 139 (1966).
22) J. G. Dillard and J. L. Franklin, *J. Chem. Phys.*, **48**, 2349 (1968).
23) J. G. Dillard and J. L. Franklin, *J. Chem. Phys.*, **48**, 2353 (1968).
24) D. C. Newton, J. Sanders, and A. C. Tyrrell, *Nature*, **187**, 683 (1960).
25) W. L. Baun, F. N. Hodgson, and M. Desgardino, *J. Chem. Phys.*, **38**, 2787 (1963).
26) M. S. Chupakhin, G. G. Glavin, and L. T. Duev, *Zh. Tekh. Fiz.*, **33**, 1281 (1963).
27) K. Dornenberg, H. Hintenberger, and J. Franzen, *Z. Naturforsch., Teil A*, **19**, 532 (1961).
28) H. Ebinghaus, K. Kraus, W. Müller-Duysing, and H. Neuert, *Z. Naturforsch., Teil A*, **19**, 732 (1964).
29) A. N. Hayhurst and P. J. Padley, *Trans. Faraday Soc.*, **63**, 1620 (1967).
30) A. J. Ahearn and N. B. Hannay, *J. Chem. Phys.*, **21**, 119 (1953).
31) J. Buckler, *Angew. Chem., Int. Ed. Engl.*, **5**, 965 (1966).
32) R. D. Srivastava, O. M. Uy, and M. Farber, *J. Chem. Soc., Faraday Trans. 2*, **68**, 1388 (1972).
33) A. F. Gaines and F. M. Page, *Trans. Faraday Soc.*, **62**, 3086 (1966).
34) D. Feldmann, *Z. Naturforsch., Teil A*, **25**, 621 (1970).
35) R. E. Honig, *J. Chem. Phys.*, **22**, 126 (1954).
36) J. C. J. Thyne and K. A. G. MacNeil, *J. Phys. Chem.*, **75**, 2584 (1971).
37) D. B. Boyd and W. N. Lipscomb, *J. Chem. Phys.*, **46**, 910 (1967).
38) V. M. Dukelskii and N. I. Ionov, *Dokl. Akad. Nauk SSSR*, **81**, 767 (1951).
39) R. J. Cellotta, R. A. Bennett, J. L. Hall, M. W. Siegel, and J. Levine, *Phys. Rev. A*, **6**, 631 (1972).
40) A. P. M. Baede, *Physica*, **59**, 541 (1972).
41) J. Berkowitz, W. A. Chupka, and D. Gutman, *J. Chem. Phys.*, **55**, 2733 (1971).
42) W. T. Zemke, G. Das, and A. C. Wahl, *Chem. Phys. Lett.*, **14**, 310 (1972).
43) S. Burch, S. J. Smith, and L. M. Branscomb, *Phys. Rev.*, **112**, 171 (1958).
44) P. E. Cade, *J. Chem. Phys.*, **47**, 2390 (1967).
45) J. Weiss, *Trans. Faraday Soc.*, **31**, 966 (1935).
46) K. Jäger and A. Henglein, *Z. Naturforsch., Teil A*, **21**, 1251 (1966).
47) D. B. Dunkin, F. C. Fehsenfeld, and E. E. Ferguson, *Chem. Phys. Lett.*, **15**, 257 (1972).
48) R. F. Baker and J. T. Tate, *Phys. Rev.*, **53**, 683 (1938).
49) J. P. Blewett, *Phys. Rev.*, **49**, 900 (1936).
50) T. E. Sharp, Lockheed Report LMSC 5-10-69-9 (1969).
51) H. Eyring, J. O. Hirschfelder, and H. S. Taylor, *J. Chem. Phys.*, **4**, 479 (1936).
52) R. D. Rempt, *Phys. Rev. Lett.*, **22**, 1034 (1969).
53) J. N. Bardsley, *J. Chem. Phys.*, **51**. 3384 (1969).
54) F. R. Gilmore, *J. Quant. Spectrosc. Radiat. Transfer*, **5**, 369 (1965).
55) J. Comer and F. H. Read, *J. Phys. B*, **4**, 1055 (1971).
56) V. Bondybey, P. K. Pearson, and H. F. Schaefer, *J. Chem. Phys.*, **57**, 1123 (1972).
57) Sir Harrie Massey, "Negative Ions, Third Edition," Cambridge University Press (1976).
58) W. A. Chupka, J. Berkowitz, and D. Gutman, *J. Chem. Phys.*, **55**, 2724 (1971).

  Bull. Chem. Soc. Jpn., 54, 2005—2009 (1981)

Negative Ions Formed by Vacuum Spark Discharge. IV.[1] Polyatomic Negative Ions of the Elements in B-Subgroups on the Periodic Table

Hiroshi KISHI†

Department of Chemistry, Faculty of Science, Kyoto University, Sakyo-ku, Kyoto 606

(Received December 15, 1980)

Polyatomic negative ions for almost all of the elements in B-subgroups on the periodic table were tested by the spark discharge type ion source mass spectroscopy. Polyatomic negative ions such as hydride negative ions, oxide negative ions, and carbide negative ions could be detected. The results are discussed with reference to the reported results by other methods of formation.

A study on negative ion spark source mass spectroscopy has been carried out using a Mattauch-Herzog type double focusing mass spectrograph. Formation of atomic negative ions of 48 elements,[2] relative sensitivity coefficients for negative ions,[3] and polyatomic negative ions of the elements in A-subgroups on the periodic table[1] have already been reported.

In the previous report,[1] polyatomic negative ions of the elements in A-subgroups on the periodic table were described; these were formed by the spark discharge type ion source and were detected with use of the Mattauch-Herzog type double focusing mass spectrograph. They were classified into five types: (1) "polymer" negative ions, (2) hydride negative ions, (3) oxide negative ions, (4) carbide negative ions and (5) other types of negative ions. The results were discussed with reference to the reported values of electron affinities and to the other methods of formation.

In the present report, polyatomic negative ions of the elements in B-subgroups on the periodic table which can be detected experimentally by a spark discharge type ion source are described, along with the polyatomic positive ions. Sample materials used were: (1) elementary materials in the form of solid metals or powdered metals, (2) oxide compounds, (3) binary compounds such as ZnSe or CdS, (4) various metal alloys, and (5) other types of compounds, including almost all of the elements in B-subgroups (transition metal elements) on the periodic table, except for the element Tc.

The detected polyatomic negative ions are classified into three types: (1) hydride negative ions, (2) oxide negative ions, and (3) carbide negative ions. No "polymer" negative ions can be detected for these elements in this experiment, in contrast to the case of the elements in A-subgroups (typical elements), in which many "polymer" negative ions were detected.[1]

Although there are fewer examples in the literature that describe the formation of polyatomic negative ions of the elements of B-subgroups by various methods of formation, as compared with the case of A-subgroups, the results obtained here are compared with such reports as do exist.

Few electron affinity values for the molecules containing transition metal elements are also available in the literature,[4,5] except for those of the molecular ions WO_3^-,[6] HWO_4^-,[6] and PtN^-.[7] This is just the opposite situation to the case of the molecular ions of the A-subgroups (typical elements), in which many examples of determination of the values of the electron affinities are reported. For example, experimental techniques for determining the electron affinity values include the following: photodetachment,[8,9] spectroscopy,[10] photoelectron spectroscopy,[11] photoionization,[12,13] charge exchange,[14] dissociative electron attachment,[15,16] thermochemistry,[17] surface ionization,[18,19] and electron impact.[20,21] Empirical techniques applied to the electron affinity values of molecular ions is the method of isoelectronic model (NO^- [22]).

Few theoretical calculations of the electron affinity values for the molecules containing transition metal elements are in the literature, though some for molecular ions containing the typical elements are reported.[4,5] Methods include variational calculation,[23] Hartree-Fock calculation,[24] configuration interactions,[25] and Rydberg-Klein-Rees calculations.[26]

The experimental results given here are thus considered to be very valuable from the standpoint of the study of electron affinity values for the molecular ions of the transition metal elements. They give experimental evidence that the molecular ions detected here have the positive electron affinity values. The results are also very valuable in the interpretation of negative ion mass spectra formed by the spark discharge type ion source.

Experimental

Apparatus. The instrument used was a Mattauch-Herzog type double focusing mass spectrograph equipped with an r. f. spark discharge type ion source (Mitsubishi Denki Electric Co., Ltd.). Since details of the instrumentation were reported elsewhere,[27-29] only the operationing conditions are given here: spark voltage 20 kV, pulse width 200 μs, repetition rate 100 s^{-1}, ion accelerating voltage 15 kV for both positive and negative ions.

Materials. Sample materials studied are (1) elementary materials in the form of solid metals or powdered metals, (2) oxide compounds, (3) binary compounds such as ZnSe or CdS, (4) various metal alloys, (5) other types of compounds. They are listed in Table 1.

Experimental procedures for measuring mass spectra o negative ions for these sample materials, and the method and procedure for the assignment of the mass spectral peaks obtained, are essentially the same as described in the previous report.[1,2]

† Present address: Oyama Technical College, Nakakuki, Oyama, Tochigi 323.

TABLE 1. SAMPLE MATERIALS FOR THE POLYATOMIC NEGATIVE IONS

Group	Element	Sample materials
IB	Cu	Copper metal
		Copper alloy
	Ag	Silver metal
		Silver alloy
		Silver(I) oxide, Powder
		Silver bromide, Powder
	Au	Gold metal
		Gold, powder
		Gold alloy
IIB	Zn	Zinc(II) selenide
		Zinc(II) oxide, Powder
	Cd	Cadmium(II) telluride, Crystal
		Cadmium(II) sulfide, Crystal
		Cadmium(II) oxide, Powder
	Hg	Mercury(I) chloride, Powder
		Mercury(II) oxide, Powder
IIIB	Sc	Scandium metal
		Scandium(III) oxide, Powder
	Y	Yttrium metal
		Yttrium(III) oxide, Powder
	La	Lanthanum metal
		Lanthanum(III) oxide, Powder
		Monazite
IVB	Ti	Titanium metal
		Titanium(IV) oxide, Powder
	Zr	Zirconium metal
		Zirconium (IV) oxide, Powder
		Monazite
	Hf	Hafnium metal
VB	V	Vanadium metal
		Vanadium(V) oxide, Powder
	Nb	Niobium metal
		Niobium(V) oxide, Powder
	Ta	Tantalum metal
		Tatalum(V) oxide, Powder
VIB	Cr	Chromium metal
		Chromium(III) oxide, Powder
	Mo	Molybdenum metal
		Ammonium molybdate, Powder
	W	Tungsten metal
		Tungsten(VI) oxide, Powder
VIB	Mn	Manganese metal
		Manganese(II) carbonate
	Re	Rhenium, Filament
		Rhenium, Powder
VIII	Fe	Iron metal
		Iron alloy
		Iron(III) oxide, Powder
		Meteorite
	Co	Cobalt alloy
		Meteorite
	Ni	Nickel metal
		Nickel alloy
		Meteorite
	Ru	Ruthenium, Powder
	Rh	Rhodium, Powder
		Rhodium-platinum alloy
	Pd	Palladium metal
		Palladium alloy
	Os	Osmium, Powder
	Ir	Iridium, Powder
	Pt	Platinum metal
		Platinum alloy

Results and Discussion

Experimental results for the polyatomic negative ions are tabulated in Table 2, along with the experimental results for atomic negative ions[2] and for polyatomic positive ions which were detected in the positive ion spark source mass spectra using the same samples.

Group IB Elements. In this group, for the elements Cu, the oxide ion CuO^- and the carbide ions CuC^- and CuC_2^- are detected. For the element Ag, the carbide negative ion AgC^-; for the element Au, oxide negative ions AuO^- and AuO_2^-, and carbide negative ions AuC^-, AuC_2^-, AuC_3^-, and AuC_4^- are detected. The positive ion Ag_2^+ is detected.

In the literature,[30] Cu^+—Cu_5^+ ions were detected by spark source mass spectroscopy. NO electron affinity values for the molecules that are detected in this experiment are available in the literature.

Group IIB Elements. For all of the elements in this group, no polyatomic negative or positive ions are detected by the experiment. Spark electrodes in this experiment were ZnSe(crystal)/Pt, or ZnO(powder)/Pt, Zn-alloy/Pt; CdS(crystal)/Pt, CdTe(crystal)/Pt, CdO(powder)/Pt; Hg_2Cl_2(powder)/Pt, HgO(powder)/Pt.

In the literature,[31] CdO^-, CdO_3^-, CdO_6^-, and CdO_7^- ions are reported to form by surface ionization. No electron affinity values are available for the molecules in this group.

Group IIIB Elements. In this group, negative ions of YO^-, LaO^-, LaO_2^-, LaO_3^-, $LaOH_2^-$, and $LaO_2H_2^-$ are detected. Positive ions of YO^+, YOH_3^+, and LaO^+ are also detected. When the pure metals of Y/Y and La/La electrodes are used as sample materials, these ions are detected. The oxygen and hydrogen atoms in these detected ions may derive from the contamination on the electrodes or from the background gas molecules. Carbide negative ions for these elements can not be detected. There are no reports on polyatomic negative ions or electron affinity values

Table 2. Polyatomic negative ions and positive ions

Group	Element	Atomic	Polyatomic negative ions	Polyatomic positive ions
IB	Cu	D[a]	CuO^-; CuC^-, CuC_2^-	
	Ag	D	AgC^-	Ag_2^+
	Au	D	AuO^-, AuO_2^-; AuC^-—AuC_4^-	
IIB	Zn	ND[b]		
	Cd	ND		
	Hg	ND		
IIIB	Sc	ND		
	Y	D	YO^-	YO^+, YOH_3^+
	La	D	LaO^-—LaO_3^-; $LaOH_2^-$, $LaO_2H_2^-$	LaO^+
IVB	Ti	ND		
	Zr	D	ZrO^-	ZrO^+
	Hf	ND		
VB	V	(ND)		
	Nb	D	NbO^-—NbO_3^-; NbO_2H^-, NbO_3H^-; NbC^-, NbC_2^-	
	Ta	ND		TaO^+—TaO_3^+
VIB	Cr	D	CrO^-—CrO_3^-	
	Mo	D	MoO^-—MoO_4^-; MoC^-—MoC_4^-; $MoOH^-$—MoO_3H^-; MoH^-	
	W	D	WO^-—WO_4^-; WC^-—WC_3^-	
VIIB	Mn	ND		
	Tc			
	Re	ND		
VIII	Fe	D		
	Ru	D		
	Os	D		
	Co	D		
	Rh	D	RhH^-; RhO^-; RhC^-, RhC_2^-	
	Ir	D		
	Ni	D		
	Pd	D	PdH^-	
	Pt	D	PtO^-, PtO_2^-; PtC^-—PtC_4^-; PtH^-; $PtCH^-$—PtC_3H^-	

a) Detected. b) Not detected.

of these elements.

Group IVB Elements. In this group, ZrO^- and ZrO^+ are detected by this experiment, For the elements Ti and Hf, no polyatomic negative and positive ions are detected.

In the literature,[30] Ti^+—Ti_5^+ ions were reported to form by the spark discharge ion source. No electron affinity values are available in the literature.

Group VB Elements. For the element Nb, we detected in the Nb/Pt spark discharge oxide negative ions, NbO^-, NbO_2^-, and NbO_3^-; hydride oxide negative ions NbO_2H^- and NbO_3H^-; and carbide ions NbC^-, and NbC_2^-. For the elements V and Ta, no atomic or polyatomic negative ions are detected. The positive ions TaO^+, TaO_2^+, and TaO_3^+ ions are detected.

There are no reports on the polyatomic negative ions for these elements and their electron affinity values.

Group VIB Elements. For the element Cr, oxide negative ions CrO^-, CrO_2^-, and CrO_3^- are detected by Cr/Cr spark discharge, for Mo, we detected oxide negative ions MoO^-, MoO_2^-, MoO_3^-, and MoO_4^-; hydride oxide negative ions $MoOH^-$, MoO_2H^-, and MoO_3H^-; carbide negative ions MoC^-, MoC_2^-, MoC_3^-, and MoC_4^-; and hydride negative ions MoH^- by Mo/Mo spark discharge. For the element W, oxide negative ions WO^-, WO_2^-, WO_3^-, and WO_4^- and carbide negative ions WC^-, WC_2^-, WC_3^- are detected by W/W spark discharge. No polyatomic positive ions for these elements are detected.

Table 3. Hydride negative ions

Group	VIB	VIII		
Element	Mo	Rh	Pd	Pt
M^-	D	D	D	D
MH^-	D	D	D	D

The literature reports detection of WO_6^- and WO_8^- ions by surface ionization,[31] and WO^+, WO_2^+, and WO_3^+ ions by the reaction of incandescent W-filament with oxygen gas followed by the electron-impact.[32] Electron affinity values for the molecular ions WO_3^- and HWO_4^- are reported to be 3.6 eV and 4.4 eV respectively from a thermochemical measurement,[6] but HWO_4^- ion could not be detected in this experiment.

Group VIIB Elements. For this group, no atomic or polyatomic negative ions are detected, nor are any

TABLE 4. OXIDE NEGATIVE IONS

Group	IB		IIIB		IVB	VB	VIB			VIII	
Element	Cu	Au	Y	La	Zr	Nb	Cr	Mo	W	Pt	Rh
M^-	D	D	D	D	D	D	D	D	D	D	D
MO^-	D	D	D	D	D	D	D	D	D	D	D
MO_2^-		D		D		D	D	D	D	D	
MO_3^-				D		D	D	D	D		
MO_4^-				—		—		D	D		
MOH_2^-				D		—					
MO_2H^-				—		D					
$MO_2H_2^-$				D		—					
MO_3H^-						D					

TABLE 5. CARBIDE NEGATIVE IONS

Group	IB			VIB		VIII	
Element	Cu	Ag	Au	Mo	W	Rh	Pt
M^-	D	D	D	D	D	D	D
MC^-	D	D	D	D	D	D	D
MC_2^-	D		D	D	D	D	D
MC_3^-			D	D	D		D
MC_4^-			D	D			D
MCH^-							D
MC_2H^-							D
MC_3H^-							D

TABLE 6. "POLYMER" POSITIVE IONS

Group	IB
Element	Ag
M_2^+	D

TABLE 7. OXIDE POSITIVE IONS

Group	IIIB		IVB	VB
Element	Y	La	Zr	Ta
MO^+	D	D	D	D
MO_2^+	—			D
MO_3^+	—			D
MOH_3^+	D			

positive polyatomic ions.

In the literature,[31] ReO_2^- and ReO_4^- ions were reported to form by surface ionization. No electron affinity values are available here.

Group VIII Elements. For the element Rh, hydride RhH^-, oxide RhO^-, and carbide negative ions RhC^- and RhC_2^- are detected by Pt–Rh/Pt–Rh spark discharge. For Pd, the hydride negative ion PdH^- is detected by Pd/Pd spark discharge. For the element Pt, we detected hydride negative ion PtH^-, oxide negative ions PtO^- and PtO_2^-, carbide negative ions PtC^-, PtC_2^-, PtC_3^-, and PtC_4^-; and carbide hydride negative ions $PtCH^-$, PtC_2H^-, and PtC_3H^-, by Pt/Pt spark discharge. For the other elements in this group, no polyatomic negative or positive ions are detected.

Fe_2^+—Fe_6^+ ions were detected by spark discharge.[30] The electron affinity value for PtN^- ion was reported to be >0 eV.[7]

In summary, we described the ionic species of polyatomic negative ions for the elements in B-subgroups on the periodic table, in addition to the polyatomic positive ions which are detected in this experiment. The polyatomic negative ions described here are classified into the following three types: (1) hydride negative ions, (2) oxide negative ions, and (3) carbide negative ions. They are tabulated in Tables 3, 4, and 5. Polyatomic positive ions are classified into (1) "polymer" positive ions, and (2) hydride positive ions. They are shown in Tables 6 and 7. From these tables, the following features are observed concerning the formation of polyatomic negative and positive ions by the spark discharge type ion source in the elements of B-subgroups on the periodic table.

(1) No polyatomic negative ions can be detected for the elements in which atomic negative ions can not be detected. (Zn, Cd, Hg, Sc, Ti, V, Ta, Re).

(2) No "polymer" negative ions can be detected for the elements of the B-subgroups, in contrast to the case of the elements of A-subgroups, in which many "polymer" negative and positive ions are detected. The only "polymer" positive ion detected in an element of B-subgroup is Ag_2^+.

(3) Hydride negative ions can be detected for the elements Mo, Rh, Pd, and Pt. No hydride positive ion can be detected.

(4) Oxide negative ions are detected in a large number of the ionic species, than in the case of the elements of A-subgroups.[1] Oxide positive ions are detected for the elements Y, La, Zr, and Ta.

(5) Carbide negative ions are also detected in a large number of ionic species than in the elements of A-subgroups.[1] No carbide positive ions can be detected in the elements of B-subgroups.

The electron affinity values for the molecular ions detected here are not available in the literature, except for the molecular ion of WO_3^- (3.6 eV[6]). Therefore, the comparison between the experimental results given here and the reported values of electron affinities is impossible. However, in the case of atomic negative ions,[2] and in the polyatomic negative ions of the elements of A-subgroups,[1] there were no exceptions to the assumption that the ionic species detected in these experiments had positive electron affinity

values in the literature. If this assumption is correct also in the case of the polyatomic negative ions of the elements of B-subgroups on the periodic table, the results presented here give experimental evidence that the ionic species described in this report have positive electron affinity values.

The author would like to express his hearty thanks to Dr. K. Kodera and Dr. T. Makita, of Kyoto University, for their encouragement and helpful suggestions throughout this work.

References

1) Part III: H. Kishi, *Bull. Chem. Soc. Jpn.*, **54**, 1999 (1981).
2) T. Makita, H. Kishi, and K. Kodera, *Mass Spectroscopy (Japan)*, **21**, 293 (1973).
3) H. Kishi, *Bull. Chem. Soc. Jpn.*, **54**, 703 (1981).
4) H. R. Rosenstock, K. Draxl, B. W. Steiner, and J. T. Herron, "Energetics of Gaseous Ions," National Bureau of Standards, Washington, D. C., 20234 (1977).
5) Sir Harrie Massey, "Negative Ions, Third Edition," Cambridge University Press (1976).
6) D. E. Jensen and W. J. Miller, *J. Chem. Phys.*, **53**, 3287 (1970).
7) H. Hotop and W. C. Lineberger, *J. Chem. Phys.*, **58**, 2379 (1973).
8) D. Feldmann, *Z. Naturforsch., Teil A*, **25**, 621 (1970).
9) K. C. Smyth and J. I. Brauman, *J. Chem. Phys.*, **56**, 4620 (1972).
10) K. Hermann and P. A. Giguere, *Can. J. Chem.*, **43**, 1746 (1965).
11) W. C. Lineberger, "Laser Negative Ion Spectroscopy," in "Laser Spectroscopy," ed by R. G. Brewer and A. Mooradian, Plenum Press, New York (1974).
12) J. A. R. Samson and R. B. Cairns, *J. Opt. Soc. Am.*, **56**, 769 (1966).
13) J. Berkowitz, W. A. Chupka, and T. A. Walter, *J. Chem. Phys.*, **50**, 1497 (1969).
14) J. Berkowitz, W. A. Chupka, and D. Gutman, *J. Chem. Phys.*, **55**, 2733 (1971).
15) W. E. Wentworth, E. Chen, and R. Freeman, *J. Chem. Phys.*, **55**, 2075 (1971).
16) F. H. Dorman, *J. Chem. Phys.*, **44**, 3856 (1966).
17) P. Gray and T. C. Waddington, *Proc. R. Soc. London, Ser. A*, **235**, 481 (1956).
18) A. L. Farragher, F. M. Page, and R. C. Wheeler, *Discuss. Faraday Soc.*, **37**, 203 (1964).
19) R. Napper and F. M. Page, *Trans. Faraday Soc.*, **59**, 1086 (1963).
20) R. Locht and J. Momigny, *Chem. Phys. Lett.*, **6**, 273 (1970).
21) J. M. Williams and W. H. Hamill, *J. Chem. Phys.*, **49**, 4467 (1968).
22) F. R. Gilmore, *J. Quant. Spectrosc. Radiat. Transfer*, **5**, 369 (1965).
23) H. Eyring, J. O. Hirschfelder, and H. S. Taylor, *J. Chem. Phys.*, **4**, 479 (1936).
24) P. A. G. O'Hare and A. C. Wahl, *J. Chem. Phys.*, **56**, 4516 (1972).
25) H. S. Taylor, *Proc. Phys. Soc. (London)*, **90**, 877 (1967).
26) T. E. Sharp, Lockheed Report LMSC 5-10-69-9 (1969).
27) N. Sasaki and J. Kai, *Mass Spectroscopy (Japan)*, **7**, 64 (1959).
28) M. Gotoh and J. Kai, *Mitsubishi Denki Lab. Report*, **1**, 51 (1960).
29) T. Makita and K. Kodera, *Mass Spectroscopy (Japan)*, **12**, 1 (1964).
30) J. Franzen, H. Hintenberger, and K. D. Schuy, *Z. Naturforsch., Teil A*, **18**, 1236 (1963).
31) S. Taniguchi, *Mass Spectroscopy (Japan)*, **14**, 139 (1966).
32) K. Kodera, I. Kusunoki, Y. Kita, H. Kishi, and A. Sakiyama, *Bull. Chem. Soc. Jpn.*, **42**, 3124 (1969).

Preparation and Properties of Monoalkylnickel(II) Complexes Having a Phenoxo, Benzenethiolato, Oximato, β-Diketonato, or Halo Ligand

Takakazu YAMAMOTO,* Teiji KOHARA, and Akio YAMAMOTO
Research Laboratory of Resources Utilization, Tokyo Institute of Technology, 4259 Nagatsuta, Midori-ku, Yokohama 227

(Received January 22, 1981)

Thirteen complexes of a type $NiR(Y)L_n$ (R=CH_3 (Me), C_2H_5 (Et); Y=OC_6H_5, *p*-cyanophenoxo, *p*-phenylphenoxo, 8-quinolinolato, OCOEt, OCOPh, acetophenone oximato, acetylacetonato, benzoylacetonato, Cl; L=triethylphosphine (PEt_3), 2,2′-bipyridine (bpy)) have been prepared by reactions of dialkylnickel(II) complexes NiR_2L_2 (**1**) with the corresponding active hydrogen compounds HY. Reactions of **1** with R′COY (Y=OC_6H_5, $OCOC_6H_5$, Cl) also afford the $NiR(Y)L_n$ type complexes with formation of unsymmetrical ketones RCOR′. Reactions of **1** with alcohols lead to dehydrogenation of alcohols to afford aldehydes or ketones. The $NiR(Y)L_n$ type complexes have been characterized by elemental analysis and spectroscopies (IR, NMR, visible). NMR spectra of *trans*-NiMe(OCOPh)(PEt_3)$_2$, NiMe(acetophenone oximato)(PEt_3) (**11**), NiMe(benzoylacetonato)(PEt_3) show temperature dependence, indicating occurrence of rapid dynamic reactions on NMR time scale in these complexes. The acetophenone oximato ligand in **11** is proposed to serve as an oxa-, aza-π-allylic ligand on the bases of IR and NMR spectroscopies. NiEt($OCOC_2H_5$)(bpy) (**8**), NiEt($OCOC_6H_5$)(bpy), and NiEt(Cl)(bpy) (**14**) undergo disproportionation reaction to give $NiEt_2$(bpy) and NiY_2(bpy) type complexes. Diethyl ketone is also produced during the disproportionation of **8**. Reactions of **14** with olefins having electron-withdrawing substituents afford $NiCl_2$(bpy) and Ni(olefin)$_2$(bpy).

Nickel complexes of a type $NiR(Y)L_n$, where R is an alkyl, alkenyl, or aryl group and Y is an anionic ligand such as Cl, OPh, or NR^1R^2, are often assumed as key intermediates in various Ni-catalyzed reactions such as isomerization of olefin and polymerization or oligomerization of olefins and dienes.[1-4] However, only a few papers[5-7] have reported on the isolation and chemical properties of the $NiR(Y)L_n$ type complexes except for monoaryl(halo)nickel(II) complexes such as Ni(aryl)X(PR_3)$_2$[8,9] and Ni(aryl)X(bpy).[10]

In our preceding paper[11] we reported preparation of monoalkyl(amido)nickel(II) complexes, $NiR(NR^1R^2)L_2$, by reactions of dialkylnickel(II) complexes, NiR_2L_2, with corresponding N–H compounds. As an extention of the work we have carried out reactions of NiR_2L_2 with phenols, alcohols, benzenethiol, carboxylic acids, oximes, β-diketones, and hydrogen halides and isolated several new $NiR(Y)L_n$ type complexes from the reaction mixtures. This paper deals with the preparation and chemical properties of the complexes. In some cases the $NiR(Y)L_n$ type complexes can be prepared also by reactions of NiR_2L_2 with carbonyl compounds such as CH_3COCl, $CH_3COOC_6H_5$, and $(C_6H_5CO)_2O$, and the results are included in this paper.

Results and Discussion

Preparation of NiR(Y)L$_n$. Reactions of NiR$_2$L$_2$ with Active Hydrogen Compounds HY: Dialkylnickel(II) complexes, NiR_2L_2, react with equimolar amounts of active hydrogen compounds to give monoalkylnickel(II) complexes of the type $NiR(Y)L_n$:

$$NiR_2L_2 + HY \longrightarrow NiR(Y)L_n + RH \quad (1)$$

(1 : 1; **2**—**14**)

1a: $NiMe_2$(bpy)
1b: $NiEt_2$(bpy)
1c: $NiMe_2(PEt_3)_2$

NiMe(OC_6H_5)(bpy)
2

NiMe(OC_6H_4-*p*-CN)(bpy)
3

NiEt(OC_6H_4-*p*-CN)(bpy)
4

trans-NiMe(OC_6H_4-*p*-C_6H_5)(PEt_3)$_2$
5

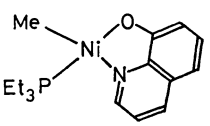

6

trans-NiMe(SC_6H_5)(PEt_3)$_2$
7

NiEt(OCOEt)(bpy)
8

NiEt(OCOPh)(bpy)
9

trans-NiMe(OCOPh)(PEt_3)$_2$
10

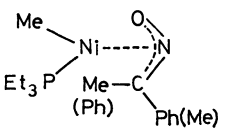

11

NiMe(acac)(PEt_3)
12

NiMe(benzoylacetonato)(PEt_3)
13

NiEt(Cl)(bpy)
14

Me=CH_3. Et=C_2H_5. Ph=C_6H_5. acac=2,4-pentanedionato (acetylacetonato). PEt_3=triethylphosphine. bpy=2,2′-bipyridine. benzoylacetonato=1-phenyl-1,3-butanedionato (bzac).

Table 1. Preparative conditions, yields, and analytical data of complexes **2**—**14**

Complex[a]	Preparative conditions				Yield	Color[b]	Mp[c]	Found (Calcd) (%)				
	NiR_2L_2 mmol	Temp °C	Solv. (cm^3)	Time h	%		°C	C	H	N	Ni	Cl
NiMe(OPh)(bpy)	0.56	r.t.	THF	24	87	p.	145	63.0	5.1	8.2		
2			(0.5)				(dec)	(63.2)	(5.0)	(8.7)		
NiMe(OC_6H_4CN)(bpy)	1.4	r.t.	THF	0.2	71	brown	137	62.9	4.5	12.0		
3			(7)				(dec)	(62.1)	(4.3)	(12.1)		
NiEt(OC_6H_4CN)(bpy)	2.7	r.t.	THF	0.2	62	p.	116	63.4	4.5	11.2		
4			(15)				(dec)	(63.0)	(4.7)	(11.6)		
trans-NiMe(OC_6H_4Ph)(PEt_3)$_2$	2.4	r.t.	Ether	0.2	78	yellow	109	62.3	9.0			
5			(14)					(62.6)	(8.8)			
NiMe(8-quinolinolato)(PEt_3)	3.0	r.t.	Ether	0.5	76	red	74—75	56.8	7.4	4.0		
6			(5)					(57.2)	(7.2)	(4.2)		
trans-NiMe(SPh)(PEt_3)$_2$	2.7	−20	Ether	0.2	53	red	<r.t.		d)		14.1	
7			(10)								(14.0)	
NiEt(OCOEt)(bpy)	0.84	r.t.	THF	0.2	62	red	110	57.2	5.0	8.9		
8			(10)				(dec)	(56.8)	(5.7)	(8.8)		
NiEt(OCOPh)(bpy)	1.5	r.t.	Toluene	0.2	80	p.	130	61.5	4.8	7.5		
9			(25)				(dec)	(62.5)	(5.0)	(7.7)		
trans-NiMe(OCOPh)(PEt_3)$_2$	0.59	r.t.	Ether	0.1	85	yellow	76—77	55.2	8.1			
10			(5)					(55.7)	(8.9)			
NiMe(acetophenone oximato)(PEt_3)	1.9	0—15	Ether	0.2	75	yellow	145	55.0	8.4	3.6	Mw: 310[e]	
11			(5)				(dec)	(55.3)	(8.0)	(4.3)	(326)	
NiMe(acac)(PEt_3)	0.41	r.t.	Ether	24	45	y.b.	<r.t.		d)		19.9	
12			(1.5)								(20.2)	
NiMe(bzac)(PEt_3)	3.2	r.t.	Ether	0.5	62	y.b.	63—64	57.7	7.9			
13			(15)					(57.8)	(7.7)			
NiEt(Cl)(bpy)	3.4	r.t.	THF-Ether	0.1	36	p.	110	51.2	4.5	9.9		12.2
14			(39)				(dec)	(51.6)	(4.7)	(10.0)		(12.7)

a) bzac: benzoylacetonato. b) p.=purple. y.b.=yellowish brown. c) dec=decomposed. d) Microanalysis was not feasible due to the low melting point and high sensitivity to air. e) Cryoscopic in benzene.

TABLE 2. FORMATION OF KETONE OR ALDEHYDE BY REACTIONS OF DIALKYLNICKEL(II) COMPLEXES WITH ALCOHOLS[a)]

No.	NiR_2L_2	Alcohol	Product (mol/NiR_2L_2)
1	$NiMe_2$ (dpe)	$PhCH_2OH$	PhCHO (0.65), CH_4 (1.1)
2	$NiMe_2$ (dpe)	*i*-PrOH	Me_2CO (0.10), CH_4 (0.31)
3	$NiMe_2(PEt_3)_2$	$PhCH_2OH$	PhCHO (0.79), CH_4 (1.2)
4	$NiMe_2(PEt_3)_2$	*i*-PrOH	Me_2CO (1.0), CH_4 (2.0)
5	$NiMe_2(PEt_3)_2$	$PhCH{=}CHCH_2OH$	$PhCH{=}CHCHO$ (0.48), CH_4 (1.4), C_2H_6 (0.06)

a) Alcohol/dialkylnickel(II) complex=2. At room temperature.

TABLE 3. PRODUCTS OF REACTIONS BETWEEN NiR_2L_2 AND R'COY[a)]

Run	NiR_2L_2	R'COY (R'COY/Ni)	Solvent	Product (mol%/NiR_2L_2)		
				$NiR(Y)L_n$	RCOR'	Others
1	**1b**	CH_3COCl (1)	Toluene	**14** (47)	$CH_3COC_2H_5$ (96)	
2	**1b**	C_2H_5COCl (1)	THF	**14** (68)	$(C_2H_5)_2CO$ (80)	
3	**1b**	CH_3COBr (1)	Toluene	**16** (35)	$CH_3COC_2H_5$ (76)	
4	**1c**	$CH_3COOC_6H_5$ (2)	Ether	**15** (60)	CH_3COCH_3 (56),	CH_4 (15), C_2H_6 (17)
5	**1c**	$(C_6H_5CO)_2O$ (1)	Ether	**10** (66)	$CH_3COC_6H_5$ (70)	

a) At room temperature. Reaction time: *ca.* 10 min for Runs 1—3, 1 d for Runs 4 and 5.

Preparation of $NiEt(OC_6H_5)(bpy)$ and $NiMe(OC_6H_5)$-(dpe) (dpe=1,2-bis(diphenylphosphino)ethane) by a similar method has been reported.[5,6)]

The reactions proceed more rapidly than the reactions of NiR_2L_2 with N–H compounds[11)] due to the higher acidity of the HY compounds than the N–H compounds. Addition of an excess HY afforded the same product as in the 1:1 reactions when the acidity of the HY was not so high (*e.g.*, phenols and benzenethiol), whereas addition of an excess of a highly acidic HY (carboxylic acids and HCl) led to a further reaction to give NiY_2L_2.

Table 1 shows preparative conditions, yield, melting points and analytical data of the complexes **2**—**14**. Coordination of two PEt_3 to Ni in the phenoxo complex **5** indicates that the phenoxo group bonds to Ni through oxygen serving as a monodentate ligand, although it sometimes coordinates to transition metal through the aromatic ring.[12)] The SC_6H_5 group in **7** also seems to coordinate to Ni through sulfur. The coordination of only one PEt_3 ligand to Ni in **6** and **11** suggests that the 8-quinolinolato and acetophenone oximato ligands serve as 3-electron ligands. As for the 8-quinolinolato ligand it is reasonable to assume intramolecular coordination of nitrogen to nickel to form a stable 5-membered chelate ring as observed in many such known complexes. As for the acetophenone oximato ligand we propose that it serves as an oxa-, aza-π-allylic ligand in the mononuclear (for Mw, see Table 1) complex **11**, whose IR and NMR data are consistent with the π-allylic coordinating mode of the acetophenone oximato ligand (*vide infra*). A THF solution of **14** shows only a minor electric conductivity indicating that the complex does not have an ionic structure. $NiMe(OC_6H_5)(PEt_3)_2$ **15** and NiEt-(Br)(bpy) **16** were also obtained by similar reactions as expressed by Eq. 1. However, isolation of analytically pure samples was not feasible due to instability in solutions (for **15**) or lack of a suitable solvent for recrystallization (for **16**).

In contrast to the reactions of phenols, reactions of alcohols with NiR_2L_2 do not give monoalkylnickel-(II) complexes but they lead to dehydrogenation of alcohols to yield aldehydes or ketones as shown in Table 2. The reaction most probably proceeds through abstraction of β-hydrogen by R group in an intermediate species formulated as $NiR(alkoxo)L_2$:

$$NiR_2L_2 + R^1R^2CHOH \xrightarrow{-RH} \left[L_2Ni\begin{matrix}OCHR^1R^2\\ \diagdown\\ R\end{matrix}\right] \quad \textbf{17}$$

$$\longrightarrow \begin{matrix}R^1\\ \diagdown\\ R^2\end{matrix}\!\!>C{=}O + RH. \qquad (2)$$

Among the reactions examined, treatment of **1c** with *i*-C_3H_7OH (No. 4 in Table 2) gave quantitative yields of methane and acetone. The other reactions may follow the similar course but they were not pursued further.

Reactions of NiR_2L_2 with Organic Acyl Compounds R'COY: The monoalkylnickel(II) complexes, NiR-(Y)L_2, can be prepared also by reactions of NiR_2L_2 with organic acyl compounds with simultaneous formation of unsymmetrical ketone.

$$NiR_2L_2 + R'COY \longrightarrow NiR(Y)L_n + RCOR' \qquad (3)$$

R'COY: phenyl carboxylate (Y=OC_6H_5)
carboxylic anhydride (Y=OCOR')
acyl chloride (Y=Cl)

The results suggest a four-centered mechanism,

$$NiR_2L_2 + R'COY \longrightarrow \begin{matrix}O\\ \|\\ \overset{\delta-}{Y}-\overset{\delta+}{C}-R'\\ \vdots\quad\vdots\\ L_2\overset{\delta+}{Ni}-\overset{\delta-}{R}\\ |\\ R\end{matrix} \longrightarrow NiR(Y)L_2 + RCOR'. \qquad (4)$$

Table 4. Spectral data of complexes **2**—**14**

Complex	IR[a] $\tilde{\nu}$/cm^{-1}	Conditions	^{1}H-NMR δ/ppm[b] Ni-R	Ni-Y	L	^{31}P{^{1}H}-NMR/ppm[c]	Visible λ/nm
2	1585 1480 1295	d)	0.10(3H, s)	6.48(1H, t, 6 Hz, *p*-Ph) 6.9—7.6(6H, m, *o*, *m*-Ph +bpy)	7.7(4H, m) 8.5(2H, m)		508(THF)
3	2190 1500 1330	d)	0.06(3H, s)	7.2—7.6(6H, m) 7.8—8.0(4H, m) 8.2(2H, m) +bpy	OC_6H_4CN		490(THF)
4	1585 1500 1335	d)	0.58(3H, t, 7 Hz, CH_3) 1.00(2H, q, 7 Hz, CH_2)	7.1—7.6(6H, m) 7.7—8.1(4H, m) 8.3(1H, m) 8.5(1H, m) +bpy	OC_6H_4CN		503(THF)
5	1580 1480 1325	e)	−1.04(3H, t, 10 Hz)	7.0—7.8(9H, m)	1.04(qui, 7 Hz) 1.2(m) 30H[i]	32.3 s	
6	1495 1460 1320	e)	−0.46(3H, s)	6.63(1H, dd, 8 Hz and 5 Hz) 6.72(1H, d, 7 Hz) 7.15(1H, d, 7 Hz) 7.39(1H, t, 7 Hz) 7.60(1H, d, 8 Hz) 8.10(1H, d, 5 Hz)	0.9—1.7(15 H, m)	45.5 s	
		f)	−0.68(3H, s)	6.68(1H, d, 8 Hz) 6.96(1H, d, 8 Hz) 7.40(1H, t, 8 Hz) 7.60(1H, dd, 8 Hz and 5 Hz) 8.4(2H, m)	1.3(9H, m) 1.7(6H, m)		
7	2960 2930 1465	e)	−0.42(3H, t, 9 Hz)	7.1(3H, m, *m*, *p*-Ph) 8.18(2H, d, *o*-Ph)	1.00(18H, qui, 7 Hz) 1.50(12H, m)	44.4 s	
8	1560* 1435 1395			j)			
9	1610* 1360 760	d)	0.60(3H, t, 7 Hz, CH_3) 1.10(2H, q, 7 Hz, CH_2)	7.4—8.4(13H, Ph +bpy)			522(THF) 535 (Toluene)
10	1605* 1350 720	e) f)	−0.92(3H, s) −1.16(3H, t, 10 Hz)	7.2(3H, m, *m*, *p*-Ph) 8.45(2H, m, *o*-Ph) 7.42(3H, m, *m*, *p*-Ph) 7.90(2H, m, *o*-Ph)	1.10(t, 6 Hz) 1.38(q, 6 Hz) 30H[i] 1.22(qui, 7 Hz) 1.5(m) 30H[i]	32.5 s	
11	1030 965 750	g)	−1.04(1.2H, d, 6 Hz) 0.00(1.8H, d, 6 Hz)	2.2(1.2H, s, CH_3) 2.3(1.8H, s, CH_3)	0.8—2.0(15H, m)		
		h)	−0.6(3H, br)	2.26(3H, s, CH_3)	1.0—2.0(15H, m)		
12	k)	e)	−0.20(3H, d, 6 Hz)	1.68(3H, s, CH_3) 1.88(3H, s, CH_3) 5.37(1H, s, CH)	0.9—1.5(15H, m)		
13	1565* 1510 1390	e)	−0.10(3H, s)	1.89(3H, s, CH_3) 6.10(1H, s, CH) 7.2—7.9(5H, m, Ph)	1.1—1.3(15H, m)	46.3 s	
		f)	−0.69(1.5H, d, 6 Hz) −0.65(1.5H, d, 6 Hz)	1.88(1.5H, s, CH_3) 1.99(1.5H, s, CH_3) 6.24(0.5H, s, CH) 6.28(0.5H, s, CH) 7.5—8.0(5H, m, Ph)	1.0—1.8(15H, m)		
14	2840 1450 760	d)	0.60(3H, t, 7 Hz, CH_3) 1.10(2H, q, 7 Hz, CH_2)		7.48(2H, br) 7.90(4H, br) 8.48(1H, br) 9.10(1H, br)		533(THF) 555 (Toluene)

a) Strongest three peakes are given. The peak with * mark is assigned to ν(C=O). b) s=singlet, d=doublet, t=triplet, q=quartet, qui=quintet, m=multiplet, br=broad. c) From external H_3PO_4 (downfield positive). Measured at r.t. in C_6D_6. d) In CD_2Cl_2 at r.t. e) In C_6D_6 at r.t. f) In acetone-d_6 at −60 °C. g) In pyridine-d_5 at r.t. ^{1}H-NMR spectrum of **11** in acetone-d_6 at r.t. shows almost the same pattern as that in pyridine-d_5. h) In pyridine-d_5 at 86 °C. i) Two signals are overlapped with each other. j) Good spectrum was not obtained due to instability of the complex in solutions (see text). k) IR spectrum was not taken due to the low melting point and high sensitivity of **12** to air.

Preparation of the $NiR(Y)L_n$ type complex by the method expressed by Eq. 3 has no precedent.

Characterization of the Complexes by Means of Spectroscopy. IR, NMR, and visible spectroscopic data are summarized in Table 4.

IR Spectra: All of the IR spectra of the complexes are consistent with the formulation of the complexes given in Table 1, showing bands due to R, Y, and L ligands. IR spectra of the bpy-coordinated compounds show δ(C–H) bands of bpy at 750—780 cm^{-1}, and those of the PEt_3-coordinated complexes do strong ν(C–H) bands of the PEt_3 ligand in a region of 2850—3000 cm^{-1}. IR spectra of the phenoxo type complexes **2**—**6** shows strong ν(C–O) at about 1300 cm^{-1} characteristic of transition metal phenoxides. ν(C≡N) bands of **3** and **4** are observed at about 2200 cm^{-1}.

The benzoato complexes **9** and **10** give rise to ν(C=O) bands in a region where the ν(C=O)| bands of unidentate carboxylato complexes appear.[13] The ν(C=O) band of the propionato complex **8** appears at a somewhat lower frequency, suggesting the presence of some interaction between Ni and the carbonyl oxygen of the propionato ligand. The benzoylacetonato complex **13** shows ν(C=O) band at 1565 cm^{-1}, indicating the formation of an *O,O'*-bonded six-membered chelate ring.[13] The IR spectrum of the oximato complex shows no ν(O–H) band, excluding the possibility that the oxime bonds to nickel as a neutral base through nitrogen[14] or as a chelating ligand through *ortho*-metalated carbon of the aromatic ring and nitrogen.[15]

NMR Spectra: In ^{1}H-NMR spectra of the methylnickel complexes **2**, **3**, **5**—**7**, and **10**—**13** the CH_3 signals are observed at normal regions where CH_3 signals of methylnickel(II) complexes are expected.[1,11] Similarly to ^{1}H-NMR spectra of the monoethyl(amido)nickel complexes the ^{1}H-NMR spectra of **4**, **9**, and **14** show CH_2 signals of the ethyl ligand at lower field than CH_3 signals, indicating the electronegativity of nickel is increased through replacement of one of the Et ligands of **1b** by the electron-withdrawing Y ligand.[11]

Coupling patterns of the Ni–CH_3 signals of $NiMe(Y)(PEt_3)_n$ also reflect the increase in the electronegativity of nickel through the replacement of one of the two Me ligands of **1c**, whose ^{1}H-NMR shows no coupling between ^{31}P of PEt_3 and ^{1}H of CH_3 even at −60 °C due to a rapid exchange reaction between the coordinated PEt_3 and free PEt_3 in solution partly liberated from **1c**. Similarly to the ^{1}H-NMR spectra of the complexes of the type $NiMe(amido)(PEt_3)_2$,[11] the ^{1}H-NMR spectra of **5**, **7**, **11**, and **12** at room temperature clearly show the coupling between ^{1}H of the CH_3 ligand and ^{31}P of the PEt_3 ligand, indicating that the Ni–PEt_3 bonding becomes stronger due to the increase in the electronegativity of Ni through the replacement of the Et ligand by the Y ligand. In contrast to the ^{1}H-NMR spectra of **5**, **7**, **11**, and **12**, the ^{1}H-NMR spectra of **6**, **10**, and **13** do not show the ^{1}H–^{31}P coupling at room temperature. In the case of **6** the weak bonding between Ni and PEt_3 is attributable to an increase in the basicity of Ni through the intramolecular coordination of N of the 8-quinolinolato ligand. The CPK molecular model shows steric repulsion between the OCOPh ligand and PEt_3 ligands in **10**, accounting for the rapid dissociation of PEt_3 from **10** on NMR time scale. In the case of the benzoylacetonato complex **13**, however, the molecular model shows no special steric repulsion between the Ph group of the bzac ligand and PEt_3, and therefore the difference in the dynamic behavior of the PEt_3 ligand between **12** and **13** at room temperature seems to be attributable to a difference in an electronic effect between the acac and bzac ligands. In cases of **10** and **13** the rapid exchange of the PEt_3 ligand is frozen on lowering the temperature to −60 °C where the NMR spectra show the ^{31}P–^{1}H coupling. The NMR spectrum of **13** at −60 °C reveals that **13** is composed of a 1:1 mixture of the following isomers

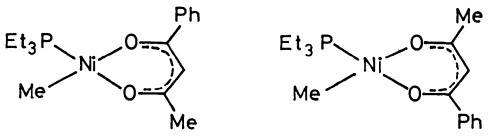

13a **13b**

at the temperature. The exchange of the PEt_3 ligand in **6** is not frozen even at −60 °C.

The ^{1}H-NMR spectrum of **11** at room temperature shows two sets of signals with a peak area ratio of 1.2:1.8, suggesting that there exist the following two stereoisomers in the solution,[16] The fairly large difference in chemical shifts of the Ni–CH_3 signal between the two steroisomers may be due to a large difference in the anisotropic magnetic effect of the phenyl ring of the oxa, aza-π-allyl ligand. On raising temperature to 86 °C, the ^{1}H-NMR spectrum shows averaged somewhat broad signals, demonstrating occurrence of a rapid exchange reaction between the two stereoisomers. Such a dynamic exchange reaction is often observed for nickel π-allyl complexes[1,17] and the following exchange process involving formation of an 1-nitrosoalkylnickel intermediate is suggested for the present complex,

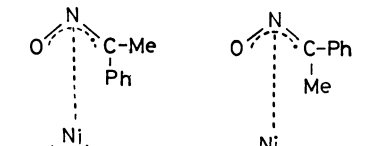

Z-form *E*-form

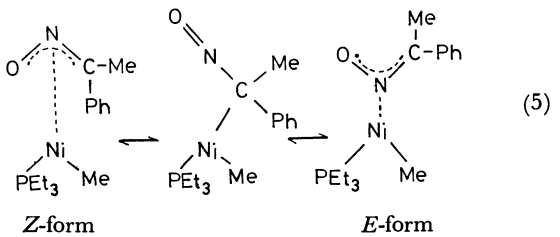

(5)

Z-form *E*-form

Visible Spectra: Similarly to visible spectra of NiR(imido)(bpy) type complexes,[11] those of **2**, **3**, **4**, **9**, and **14** show Ni→bpy CT bands at about 500 nm ($\varepsilon = 3 \times 10^3$), which are shifted to shorter wavelength by about 150 nm from the position of Ni→bpy CT

bands of $NiR_2(bpy)$,[18] demonstrating that the highest occupied level of Ni is lowered by the replacement of the R ligand by the Y ligand.

Chemical Properties. Thermolysis, Acidolysis, and Degradation in Air: Although complexes **2**—**14** have higher thermal stabilities than the original dialkylnickel complexes, their thermal stabilities are not so high as the $NiR(NR^1R^2)L_n$ type complexes[11] presumably due to lower stability of the Ni–Y bond than the Ni–NR^1R^2 bond against the thermolysis. The ethyl complex evolves a *ca.* 1:1 mixture of C_2H_4 and C_2H_6 on the thermolysis, and the methyl complex does a mixture of CH_4 and C_2H_6, the CH_4/C_2H_6 ratio varying from *ca.* 2.0 to 0.5 depending on the complex. Acidolysis of $NiR(Y)L_n$ by HCl gives RH and HY (Y=OC_6H_5, OCOR) with formation of $NiCl_2L_n$. The complexes with bpy have moderate stabilities to air in solid, whereas those with PEt_3 are very sensitive to air even in the solid state. All of the complexes are very sensitive to air in solutions. On exposure of an ethereal solution of **14** to air C_2H_4 (0.2 mol/Ni) was evolved exclusively as a gaseous product, suggesting β-hydrogen elimination promoted by oxygen.

Disproportionation: On standing a THF solution of **14** at room temperature the color gradually changes from purple to deep green with eventual formation of a light green precipitate of $NiCl_2(bpy)$, indicating that a disproportionation reaction proceeds in the solution,

$$\underset{\text{purple}}{2\,NiEt(Cl)(bpy)} \longrightarrow \underset{\text{deep green}}{NiCl_2(bpy)} + \mathbf{1b}. \qquad (6)$$

The disproportionation reaction is greatly accelerated by adding π-acids such as acrylonitrile and maleic anhydride, although in these cases the products are $NiCl_2(bpy)$, butane, ethane, ethylene, and $Ni(\pi\text{-acid})_n(bpy)$ (n=1 or 2), since **1b** once formed reacts with the π-acid to afford $Ni(\pi\text{-acid})_n(bpy)$ with evolution of a gas mainly composed of butane.[18] The carboxylato complexes **8** and **9** also undergo similar disproportionation reactions to give Ni(carboxylato)$_2$(bpy) and **1b**. In the case of **8** formation of diethyl ketone (*ca.* 50%/Ni) takes place besides the disproportionation reaction, the result suggesting occurrence of a coupling reaction between the COR group in the OCOR ligand and the Et ligand.[19]

Reactions with Other Reagents: Complex **10** reacts with excess EtBr to afford PhCOOEt (0.73 mol/Ni). Acetylene is trimerized to benzene by **13** and aldehydes (CH_3CHO, C_2H_5CHO) are dimerized by **2** or **3**. A reaction between **14** and i-C_3H_7ONa affords acetone (0.72 mol/Ni) with evolution of C_2H_6. Acetone seems to be formed through a metathesis reaction between the two reactants to produce an intermediate ethyl(propoxo)nickel species **18** and β-hydrogen elimination from **18**.

$$\mathbf{14} + i\text{-}C_3H_7ONa \xrightarrow{-NaCl} \underset{\mathbf{18}}{\left[(bpy)Ni\begin{matrix}C_2H_5\\OC_3H_7\end{matrix}\right]} \longrightarrow \text{acetone} + C_2H_6 \qquad (7)$$

Experimental

General, Materials, Analysis, and Spectroscopic Measurements. Reactions, analysis, and spectroscopic measurements were carried out as reported in the preceding paper.[11] Complexes **1a**—**1c** were prepared according to literature.[18,20]

Preparation of Complexes. Phenoxo and Benzenethiolato Complexes 2—7 and 15 (cf. *Table 1*): THF (0.5 cm^3) containing 53 mg (0.57 mmol) of phenol was added to 140 mg (0.57 mmol) of **1a** and the mixture was stirred for 24 h at room temperature to obtain a purple solution. Hexane (10 cm^3) was added to the solution to obtain a purple solid, which was recrystallized from acetone to yield 160 mg (89%) of **2**. The other phenoxo and benzenethiolato complexes were prepared in similar ways under conditions shown in Table 1 (phenol:**1**=1:1). Solvents for recrystallization were actone for **3** and **4** and diethyl ether for **5**—**7**. A reaction between **1c** (150 mg, 0.47 mmol) and phenol (45 mg, 0.47 mmol) at room temperature in 1.4 cm^3 of benzene afforded **15**, whose NMR shows a Ni–CH_3 signal at δ −1.08 (3H, t, 8.5 Hz) and PEt_3 signals around δ 1 ppm (30H, m). However, isolation of the complex failed.

Carboxylato Complexes 8—10: Propionic acid (0.062 cm^3, 0.84 mmol) was added to a THF (10 cm^3) solution of **1b** (230 mg, 0.84 mmol) at −78 °C. The mixture was warmed to room temperature and stirring the solution at the temperature for 20 min gave 0.75 mmol of C_2H_6 and a deep red solution, which was condensed to 2 cm^3 to obtain a dark red solid of **8** (170 mg, 62%). Longer reaction time led to the disproportionation reaction (see text) and the complex obtained was not recrystallized due to the instabilities of **8** in solutions.

Toluene (5 cm^3) containing 180 mg (1.5 mmol) of benzoic acid was added to a toluene (20 cm^3) solution of **1b** (400 mg, 1.5 mmol) and the mixture was stirred at room temperature. The color of the solution instantly changed from deep green to purple. Hexane (10 cm^3) was added to the solution immediately after changing of the color to obtain a purple solid (430 mg, 80%). The disproportionation of **9** is not so fast as that of **8** and a sample for analysis could be obtained by recrystallization from acetone. Complex **10** was prepared analogously and crystallized from ether.

Acetophenone Oximato Complex 11: Diethyl ether (5 cm^3) was added to a mixture of **1c** (600 mg, 1.9 mmol) and acetophenone oxime (250 mg, 1.9 mmol) at −10 °C. Stirring the mixture for 10 min at room temperature led to formation of a yellow precipitate, which was recrystallized from THF to yield 450 mg (75%) of **11**.

β-Diketonato Complexes 12 and 13: Acetylacetone (0.042 cm^3, 0.41 mmol) was added to an ethereal solution of **1c** (130 mg, 0.41 mmol) and the mixture was stirred at room temperature for 24 h to obtain a brown solution. Cooling the solution to −78 °C gave yellowish brown crystals of **12** (74 mg, 45%). Complex **13** was prepared analogously.

Chloro Complex 14: Diethyl ether (19 cm^3) containing 3.4 mmol of dry HCl was added to a THF (20 cm^3) solution of **1b** (940 mg, 3.4 mmol). Color of the solution changed instantly from deep green to dark purple and then excess hexane was added to the solution to yield a dark purple precipitate, which was recrystallized from THF–hexane to yield 350 mg (36%) of **14**.

Reactions of Dialkylnickel(II) Complexes with R'COY (cf. *Table 3*). Propionyl chloride (0.46 cm^3, 5.3 mmol) was added to a THF (60 cm^3) solution of **1b** (1.4 g, 5.2 mmol). The color of the solution instantly changed from deep green to dark purple. Addition of hexane (50 cm^3) gave a yellow

precipitate (1.0 g, 68%) whose IR spectrum was identical to that of **14**. GLC analysis of the solution revealed formation of 4.2 mmol (80%) of diethyl ketone. A similar reaction between **1b** (200 mg, 0.74 mmol) and acetyl bromide (0.059 cm^3, 0.74 mmol) in toluene (10 cm^3) gave a purple powder of **16** (220 mg, 90%) with formation of ethyl methyl ketone (76%). IR spectrum of the purple powder showed almost a similar absorption pattern to that of **14** and the analytical data (Found: C, 42.1; H, 3.0; N, 8.2; Br, 24.6%. Calcd for: C, 44.5; H, 4.0; N, 8.7; Br, 24.7%) roughly agreed with the composition of NiEt(Br)(bpy). The reaction of dialkylnickel(II) complexes with $CH_3COOC_6H_5$ and $(C_6H_5CO)_2O$ were carried out analogously.

Reactions of Dialkylnickel(II) Complexes with Alcohol (cf. Table 2). Benzyl alcohol (0.073 cm^3, 0.71 mmol) was added to an ethereal (1 cm^3) solution of **1c** (110 mg, 0.35 mmol). Although no apparent change was observed after stirring the mixture for 12 h, GLC analysis and measurement of the amount of gas evolved with a Toepler pump showed formation of 0.40 mmol of CH_4 and 0.28 mmol of benzaldehyde. The other reactions listed in Table 2 were carried out analogously.

Disproportionation Reaction. A mixture of acrylonitrile (1.0 cm^3) and THF (1.5 cm^3) was added to **14** (140 mg, 0.51 mmol) to obtain a deep reddish purple homogeneous solution. A light green solid started to precipitate after stirring the mixture for 40 min at room temperature. After 1.5 h GLC analysis of the gas phase indicated evolution of 0.11 mmol of C_2H_4 and 0.03 mmol of n-C_4H_{10}.[21] On adding 20 ml of THF to the reaction mixture, the solid precipitated (54 mg, 37%) was separated by filtration and characterized as $NiCl_2$(bpy) by its IR spectrum.[18] The filtrate was condensed to 2 ml and then 20 ml of hexane was added to obtain 26 mg (19%) of a precipitate whose IR spectrum coincides with that of Ni(acrylonitrile)(bpy).[18]

Benzene (4 cm^3) was added to 140 mg (0.44 mmol) of **8** and the mixture was stirred for 20 h at 70 °C. GLC analysis of the solution showed formation of 0.20 mmol of diethyl ketone. A light yellow solid precipitated was $Ni(OCOC_2H_5)_2$(bpy) as proved by its IR spectrum.

References

1) P. W. Jolly and G. Wilke, "The Organic Chemistry of Nickel," Vol. 1 (1974) and Vol. 2 (1975), Academic Press, New York.

2) R. F. Heck, "Organotransition Metal Chemistry," Academic Press, New York (1974).

3) J. Tsuji, "Organic Synthesis by Means of Transition Metal Complexes," Springer, Berlin (1975).

4) C. W. Bird, "Transition Metal Intermediates in Organic Synthesis," Academic Press, New York (1967).

5) G. Wilke and G. Herrman, *Angew. Chem.*, **78**, 591 (1966).

6) M. L. H. Green and M. J. Smith, *J. Chem. Soc., A*, **1971**, 639.

7) H. F. Klein and H. H. Karsch, *Chem. Ber.*, **105**, 1433 (1973).

8) M. Hidai, T. Kashiwagi, T. Ikeuchi, and Y. Uchida, *J. Organomet. Chem.*, **30**, 279 (1971).

9) D. G. Morrell and J. K. Kochi, *J. Am. Chem. Soc.*, **97**, 7262 (1975).

10) M. Uchino, A. Yamamoto, and S. Ikeda, *J. Organomet. Chem.*, **24**, C63 (1970); M. Uchino, K. Asagi, A. Yamamoto, and S. Ikeda, *ibid.*, **84**, 93 (1975).

11) T. Yamamoto, T. Kohara, and A. Yamamoto, *Bull. Chem. Soc. Jpn.*, **54**, 1720 (1981).

12) D. J. Cole-Hamilton, R. J. Young, and G. Wilkinson, *J. Chem. Soc., Dalton Trans.*, **1976**, 1995.

13) K. Nakamoto, "Infrared and Raman Spectra of Inorganic and Coordination Compounds," John Wiley, New York (1978).

14) S. Imamura, T. Kajimoto, Y. Kitano, and J. Tsuji, *Bull. Chem. Soc. Jpn.*, **42**, 805 (1969).

15) H. Onoue and I. Moritani, *J. Organomet. Chem.*, **44**, 189 (1972).

16) It is also conceivable that the observation of the two sets of peaks is due to the presence of two stereoisomers according to the difference in a relative position of the oxa, aza-π-allylic ligand to the PEt_3 and Me ligands. However, the rotation of π-allylic ligands around metal–π-allyl bonds is generally a more rapid process compared with the *Z*-form-*E*-form isomerization,[1,17] and therefore in the text we ignore the isomerism according to the difference in a relative position of the π-allylic ligand.

17) K. Vrieze, "Dynamic Nuclear Magnetic Resonance Spectroscopy," ed by L. M. Jackman and F. A. Cotton, Academic Press, New York (1975).

18) T. Yamamoto, A. Yamamoto, and S. Ikeda, *J. Am. Chem. Soc.*, **93**, 3350 (1971); T. Saito, Y. Uchida, A. Misono, A. Yamamoto, K. Morifuji, and S. Ikeda, *ibid.*, **88**, 5198 (1966).

19) T. Yamamoto and A. Yamamoto, *Chem. Lett.*, **1978**, 615.

20) A. Yamamoto, T. Yamamoto, M. Takamatsu, T. Saruyama, and Y. Nakamura, "Organotransition Metal Chemistry," ed by Y. Ishii and M. Tsutsui, Plenum, New York (1975).

21) A more amount of n-C_4H_{10} seems to be formed, since n-C_4H_{10} has a high solubility in THF and it is difficult to catch all of n-C_4H_{10}.

  Bull. Chem. Soc. Jpn., 54, 2017—2022 (1981)

Digitally Controlled Automatic Coulometric Karl Fischer Titrator

Kisaburo UMEMOTO

Department of Pure and Applied Sciences, College of General Education, The University of Tokyo, Komaba, Meguro-ku, Tokyo 153

(Received October 22, 1980)

An automatic coulometric Karl Fischer titrator capable of direct readout of the water titrated and the background of titration was constructed. Control of the generation of reagent was carried out by a digital counting method. The over- and under-titration was minimized by holding the level of reagent at the start and the end of titration as close as possible. Details of the circuit configuration were presented. The precision of determination was *ca.* ±2 μg and ±1—±2 μg for the automatic titration of 1 mg and 10—500 μg of water, respectively. Water of less than 20 μg was titrated within a precision of 1 μg by watching the drift and subsequent recovery of the blank level.

Karl Fischer determination of water is based on a reaction in which 1 mol of iodine is consumed in the titration of 1 mol of water in a methanolic solution of pyridine, sulfur dioxide and iodine. In the coulometric determination of water, iodine is generated by electrolysis and the amount of water is determined by measuring the quantity of the current consumed during titration, since 10.71 mC is required for each microgram of water.[1] At the end point of titration excess iodine is generated, which is detected by the depolarization of platinum indicator electrodes. The coulometric Karl Fischer titration was found to be suitable for the determination of a trace of water.[1–12] For the purpose to automate the titration, Kelly *et al.* designed an automatic cutoff attachment to a pH meter[2] but the current for compensating the background of titration was set manually. Hoyt constructed an automatic end point indicator[7] but no care was taken for compensation of the background of titration. Miyake and Sudo constructed an instrument capable of automatic control of the generation of iodine and also capable of automatic elimination of the blank,[12] but compensation of the background of titration was not performed. Recently, automatic coulometric Karl Fischer titrators capable of automatic compensation of the background of titration have appeared.[17,18] The electrolysis current of Mitsubishi Kasei Model CA-02 titrator is controlled to be proportional to the drift of the potential of the indicator electrodes, the titration being terminated when the electrolysis current substantially returns to the blank level. However, insufficient period of time for anticipation of the end point restricts the accuracy of determination of a micro amount of water, since the Karl Fischer reaction is not fast enough to assure the instant completion of reaction.[14–16] Hiranuma Sangyo Model AQ-3B titrator was constructed on the basis of constant current coulometry; near the end of titration the current is periodically interrupted with subsequent anticipation of the end point. In the method of anticipation of the end point, some overshoot at the end point is present since the end point is determined when the potential of the indicator electrodes lasts above the cutoff potential over a given anticipated period of time. No care has been taken for minimizing this type of over-titration except for restricting the generation of iodine near the end point. Moreover, in constant current coulometry, inaccuracy in the count of current was caused by the switching time delay in each on-off operation of the electrolysis current.[12]

The automatic coulometric Karl Fischer titrator presented in this paper was designed with the following improvements. (i) The electrolysis current is so adjusted that 100% current efficiency is guaranteed for any size of working electrode and concentration of the reagent. The current was measured by current-to-frequency conversion with subsequent counting for integration. (ii) The method of anticipation of end point is preferred in order to avoid the risk of under-titration since the Karl Fischer reaction is not instantaneous in spite of much improvement in the reagents.[13–16] Care was taken to minimize the overshoot at the end point not only by restricting the rate of generation of iodine near the end point but also by holding the potential of the indicator electrodes at the start and the end of titration as close as possible. (iii) With the use of digitally controlled counting method of the blank, the waving drift in the level of iodine during the standby state[12] is minimized by controlling the generation of iodine to one count for each detection of the blank. (iv) The background of titration is directly read out by integrating the level of the blank instead of compensating it. This method is more simple than the method of compensation since no extra precise control of the constant current power supply is required. (v) The blank level is directly read out so that micro amount of water can be accurately determined by watching the drift and the subsequent recovery of the blank level.

Apparatus

A block diagram of the instrument is shown in Fig. 1. The blank level is held prior to introduction of the sample in order to integrate it for counting the background of titration. After introduction of the sample, electrolysis is started by opening the gate of the transistor switching circuit. The electrolysis current is fed into the current measuring circuit and converted into the frequency of one count equivalent to one microgram of water, the count being read out on the display unit. The background counting circuit integrates the blank level until the end of titration is reached, the count being read out on another display unit. The monitoring circuit detects any excess or

deficiency of iodine, giving out "on" and "off" signals for controlling the electrolysis. The end point determining circuit detects the approach of end of titration; near the end point the amount of generating iodine is restricted by the controlling circuit. At the end point of titration, the controlling circuit starts to control the counting of the blank and holding of the blank level. During this standby state for subsequent titration, the blank level can be read out on the diplay unit with the operation of the selection switch. Details of the circuit configurations are given below, where all the TTL logic gates are composed of SN74LS series and the power supplies are regulated by the standard method.

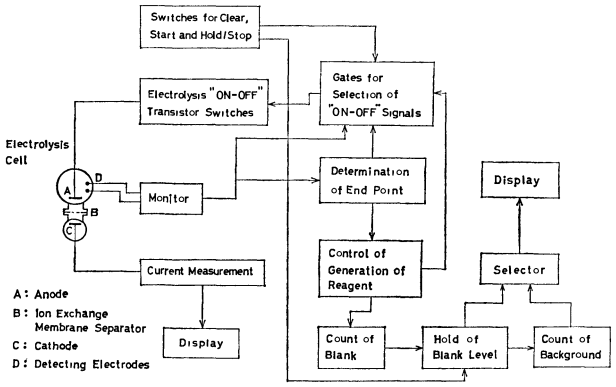

Fig. 1. Block diagram of the functional construction of the instrument.

Operation for Start, Hold/Stop, and Clear. The circuit is shown in Fig. 2. The whole circuit is reset by signal *a* from gate G_1; automatically by a delay circuit when power is switched on or manually by pushing spring switch S_1. When spring switch S_2 is pushed to "Hold/Stop" position, latch L_1 is reset to stop the electrolysis. This operation is performed prior to introduction of the sample. In order to start titration, switch S_2 is pushed to "Start" position, triggering timer T_1 to give a pulse *c* which resets the results of the previous titration. At the end of pulse *c*, latch L_1 is set to activate gate G_3 to start electrolysis. The electrolysis current power supply is adjustable in the range 5—25 V.

Monitoring Circuit. A potential difference of a few millivolts is given between the detecting electrodes (Fig. 2). When excess water is present in the cell, the cathode of the detecting electrodes is polarized, no current flowing. However, when iodine is in excess the cathode is depolarized and a small current flows, resulting in a voltage drop across a resistor of 1 kΩ. The voltage drop is fed into operational amplifier A_1. The noise involved in the voltage due to the turbulent mixing of the solution is substantially filtered off by placing a capacitor in the feedback loop of A_1. A_1 is balanced *ab initio* so that its output is nega-

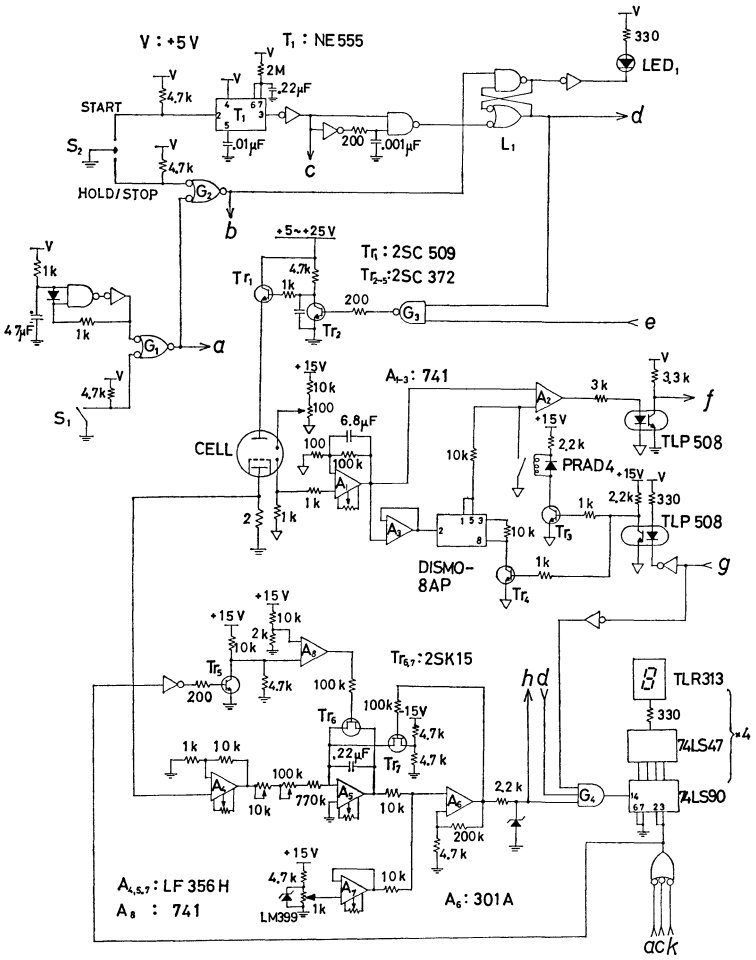

Fig. 2. Operational, monitoring, and current measuring circuits.

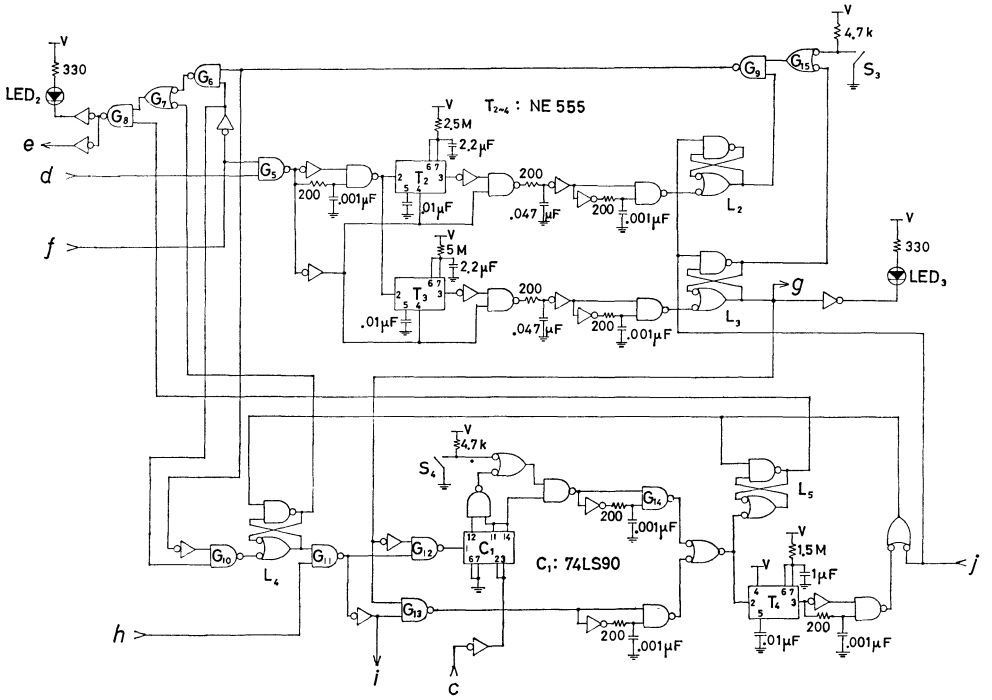

Fig. 3. End point determining and controlling circuits.

tive when excess water is present in the cell. The output of A_1 increases as the titration approaches the end point, turning to positive when excess iodine is detected. The output of A_1 is fed into comparator A_2 which is used as a zero cross detector during the course of titration. The output of A_2 is fed into a photocoupler whose output signal *f* controls the "on" or "off" of the electrolysis depending on whether iodine is deficient or excess in the cell. Isolation of the monitoring circuit is necessary for the electrolysis cell current not to flow into it. The monitoring circuit is operated with an isolated power supply.

The sample-hold circuit DISMO 8AP(Xebec) was used to minimize the overshoot at the end point. At the end point of each titration, the potential of the detecting electrodes was found to concentrate around a potential which is a little higher than zero, indicating that the amount of excess iodine present at the end point of titration is about the same for each titration. The overshoot at the end point is minimized by starting subsequent titration from this level of excess iodine to make the level of iodine at the start and the end of titration as close as possible. In order to maintain this level of excess iodine constant during the standby state, the cutoff potential of the monitoring circuit is switched from zero to a potential which is held by the sample-hold circuit DISMO 8AP at the end point of titration.

Current Measuring Circuit. The current through the cell is measured with a voltage drop across a high quality precision resistor of 2 Ω and converted into frequency with a V-F converting circuit (Fig. 2). High quality metal film resistors and a polycarbonate capacitor were used to ensure the accuracy and stability of this circuit. The time required for resetting the integrator was *ca.* 15 μs. The integrator was so adjusted that the V-F converter advances one count within an accuracy of 0.1% on flowing a current of 10.71 mC through the current measuring resistor and the amount of water titrated is directly read out in microgram unit. The output of the V-F converter is fed into the counter of the display unit *via* gate G_4 which is opened by the start signal *d* and closed by the end point signal *g* to register the result of the titration.

End Point Determining and Controlling Circuit. The end point determining circuit and the controlling circuit are shown in Fig. 3. At an early stage of titration, the signal *f* passes through gates G_6, G_7, and G_8, and controls the "on-off" of the electrolysis. On approaching the end point, the rate of generation of iodine exceeds that of consumption and the electrolysis stops temporarily. The excess iodine is soon consumed by the residual water, electrolysis starting again. This procedure is repeated, the interval of "on" being elongated with approach to the end point. Titration has been completed to 98—99% and to 100% when the electrolysis "off" continues for 8 and 20 s, respectively. Timers T_2 and T_3 are used to detect the approach or reach of the end point, each delay time being determined as 8 and 20 s, respectively. Both timers are triggered at the instant the signal *f* turns to "off" and reset when *f* turns to "on" before each delay time is over. When the electrolysis "off" begins to last over 8 s, latch L_2 is set and signal *f* is introduced into the controlling circuit *via* gate G_{10} so that the subsequent electrolysis is controlled at gates G_7 and G_8 by latches L_4 and L_5. When signal *f* turns to "on," L_4 is set to make the electrolysis "on," and the current counting pulse *h* is fed into the counter C_1 *via* gates G_{11} and G_{12}. The outputs of C_1 are wired into a scaler so that L_5 is set to stop the electrolysis at 5 or 10 counts advance depending on whether preset switch S_4 is open or closed. Timer T_4 is used

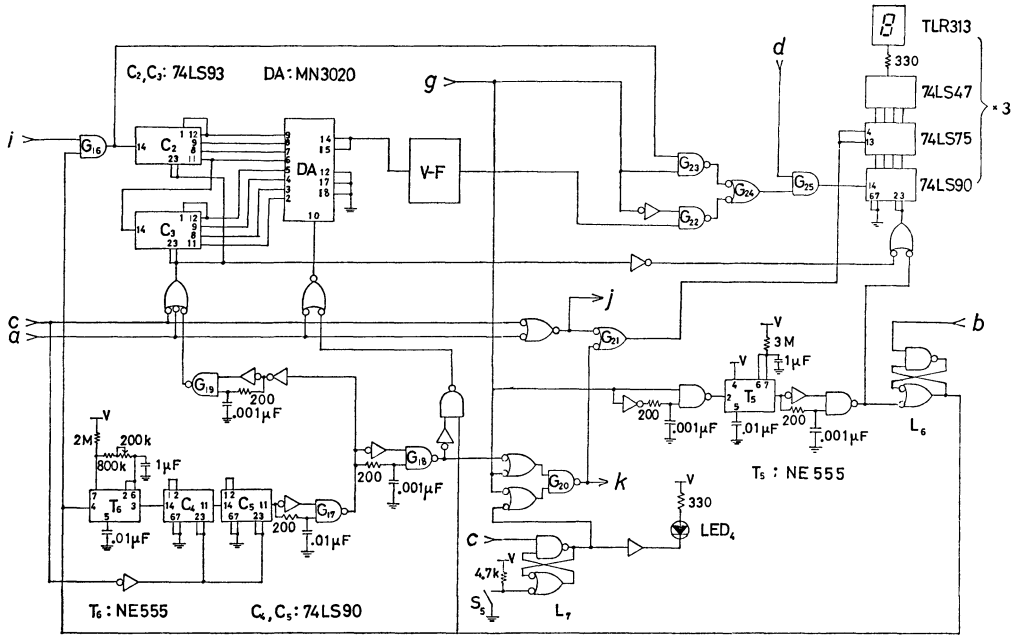

Fig. 4. Circuits for counting the blank, holding the blank level, and counting the background of the titration.

to provide a time delay of about 1.2 s before the reset of L_4 and L_5 to ensure the generated iodine to reach the detecting electrodes. Generation of a preset amount of iodine and subsequent waiting is repeated whenever the signal *f* turns to "on" until the end point of titration is reached. When the electrolysis "off" lasts over 20 s, latch L_3 is set to stop titration. With the signal *g*, gates for counting the electrolysis current and the background of titration are closed, DISMO being switched to "hold" mode and counting of the blank is started.

Circuits for Counting the Blank and Holding the Blank Level. The circuit for compensating the blank is shown in Fig. 3. The signal *g* closes gate G_{12} and opens gate G_{13} at the end of titration, the rate of generating iodine being restricted to one count whenever the blank is detected. The waving drift in the level of iodine[12] is minimized at most to one count during the standby state.

The blank level is defined as the number of blank for 30 s and determined by counting the blank current counting pulse *i* by a controlling method as shown in Fig. 4. The pulse *i* is fed into gate G_{16} which is activated at 5 s after the end of titration with latch L_6 and timer T_5. The delay is required for waiting for the cutoff operation of the monitoring circuit to settle at a voltage held by DISMO 8AP. When L_6 is set, G_{16} is opened for introducing *i* into counters C_2 and C_3, oscillator T_6 being activated simultaneously. T_6 is *ab initio* adjusted so that pulses with 30 s interval are obtained from G_{17}. From the leading and trailing edge of this pulse, non-overlapping pulses are obtained from gates G_{18} and G_{19}. The pulse from G_{18} registers the count of C_2 and C_3 into the D/A converter, and the pulse from G_{19} clears the counters. In this manner, the counters count the numbers of the blank and transfer it to the D/A converter before being cleared at every 30 s to hold the latest blank level.

In parallel with these operation, the blank is also counted with the BCD counters of the display unit. When the blank level is required to be displayed, spring switch S_5 is pushed to set latch L_7, which opens gate G_{20} so that the pulse from G_{18} is given to the shift registers as a strobe to show the blank level.

Circuit for Counting the Background of Titration. The background of titration is counted by integrating the blank level held just before the start of titration. The circuit for counting the background of titration is shown in Fig. 4. By pushing switch S_2 to "Hold/Stop" position (Fig. 2), latch L_6 is reset by signal *b* to make gate G_{16} and oscillator T_6 inactive so that the D/A converter continues to hold the last blank level until the end of titration is reached. The output of the D/A converter is fed into a V-F converter consisting of the same circuit configuration as that used in the electrolysis current measuring circuit. The time constant of the V-F converter is *ab initio* adjusted so that the counting rate coincides with the blank level. The output of the V-F converter is fed into BCD counters through gates G_{22}, G_{24}, and G_{25}. The shift registers of the display unit are kept active while titration proceeds, but made inactive by signal *g* to keep the counted background of titration on the display unit after the end of titration. The count of the background of titration is subtracted from the reading of the electrolysis current to obtain the net amount of water titrated.

Experimental

Aqualyte G (generator electrolyte) and aqualyte C (counter electrolyte) from Hiranuma Sangyo were used as Karl Fischer reagent. The water–methanol solution was prepared by diluting 247.0 mg of water with dehydrated methanol in a measuring flask of 25.00 ml calibrated by weighing pure

water. The density of pure water was taken into consideration for calibration. The water content in the methanol taken in the measuring flask was determined to be 0.440 mg/ml. The water content in the water–methanol solution was calculated to be 10.32 mg/ml. The solution was transferred into a sample bottle in a dry bag and sealed with a serum-type rubber stopper. The water–methanol solution was taken with a 100 μl(# 710) or 10 μl(# 701) Hamilton micro syringe which has an accuracy of 1% full scale. The titration vessel was a separable H-type cell with an assembly similar to that reported.[1,13]

Results and Discussion

In order to examine the effect of the rate of iodine generation, the voltage applied to electrolysis was changed in the range 5—25 V. The corresponding rate of iodine generation was 3—18 counts/s, for which the titration of a given amount of water gave an identical result. This indicates that the condition of 100% current efficiency is preserved in this range of applied voltage. The voltage for the routine use was adjusted to approximately 15 V in order to limit the rate of iodine generation to *ca.* 10 counts/s, sufficiently lower than the safety limit. Incomplete titration was avoided by confirming that the blank level returned to the original level at the end of titration.

Accuracy and precision of titration is affected by the stability of the blank level. If the blank level is not settled, error is caused in the counting of the background of titration. When a fine porosity glass filter was used as a separator of the two compartments of the titration vessel, the blank level was high and unstable. The blank level increases after each titration unless the level of the counter electrolyte is kept lower than that of the generating electrolyte. This indicates that use of this type of separator is restricted by the leakage of counter electrolyte. When an ion-exchange membrane[12] was used as separator, the blank level was kept low and stable. The following determinations were carried out with an ion-exchange membrane as separator.

The results of titration of the standard water-methanol solution are given in Table 1. The precision was *ca.* ±2 μg and ±1—±2 μg for automatic titration of 1 mg and 10—500 μg of water, respectively. The time needed for the titration of 1 mg of water was *ca.* 150 s. The precision is better than that reported for the automatic coulometric Karl Fischer titrator.

The over- and under-titration was minimized by holding the level of iodine at the start and the end of titration as close as possible by using a sample-hold circuit (Fig. 2). The waving drift in the level of iodine during the standby state was minimized by restricting the rate of iodine generation to one count for each detection of the blank level by digitally controlled counting method (Fig. 3). The effect of these circuit devices was examined as follows.

When a small amount of water is introduced into the cell, the reading of the blank level increases but it soon returns to the original level. The amount of water is determined by taking the summation of the differences obtained by subtracting the original blank level from those read out at 30 s intervals. Over- or under-titration is thus completely avoided. The results are given in Table 2. The amount of water less than 50 μg was determined with a precision of ±1 μg. By comparing the results shown in Tables 1b) and 2, the average values were found to agree within an accuracy of 1 μg, indicating that the error due to over- or under-titration does not exceed 1 μg.

An example showing absolute accuracy of the method of determination of water by watching the drift and subsequent recovery of the blank level was given for the determination of atmospheric humidity. Air was taken with a 1 ml tuberculin syringe. The results are given in Table 3. The experimentally obtained values agree with the values calculated from the relative humidity within an accuracy of 1 μg with a preci-

Table 1. Repeadability of titration of water–methal solution (10.32 mg H_2O/ml)

Amount of sample / μl	No. of runs	Found / μg
a) Sample taken with 100 μl micro syringe.		
100	7	1035.6±1.9
50	7	520.4±1.7
10	5	109.6±1.0
b) Sample taken with 10 μl micro syringe.		
10	5	104.2±1.9
5	6	52.0±1.7
2	5	22.2±1.5
1	5	11.2±1.5

Table 2. Repeadability of titration of water–methanol solution (10.32 mg H_2O/ml)[a]

Amount of sample / μl	No. of runs	Found / μg
5	6	52.1±1.0
2	6	22.2±1.0
1	6	11.4±0.8

a) The end point of titration was determined by watching the drift and subsequent recovery of the blank level. Sample was taken with 10 μl micro syringe.

Table 3. Determination of water content in 1.0 ml of atmospheric air

Temperature / °C	Relative humidity / %	No. of runs	Found / μg	Calculated / μg
23.8	53	12	11.1±0.4	11.7
24.0	70	10	15.7±0.8	15.3
23.0	23	8	5.9±0.7	5.4

sion of less than ± 1 μg. The discrepancy observed in the titration of 10 μl of the standard water–methanol solution taken with different micro syringes (Table 1) is due to the inaccuracy in the scale of the micro syringe.

In conclusion, the circuit devices presented in this work are useful for improving the accuracy and precision of the automatic coulometric Karl Fischer titration of water.

The author wishes to thank Dr. Tadashi Aoki for his advice in the construction of the V-F converter.

References

1) A. S. Mayer, Jr., and C. M. Boyd, *Anal. Chem.*, **31**, 215 (1959).
2) M. T. Kelly, R. W. Stelzer, W. R. Laig, and D. J. Fisher, *Anal. Chem.*, **31**, 220 (1959).
3) R. F. Swensen and D. A. Keyworth, *Anal. Chem.*, **35**, 863 (1963).
4) G. A. Rechnitz and K. Srinivasan, *Z. Anal. Chem.*, **210**, 9 (1965).
5) M. R. Lindbeck and H. Freund, *Anal. Chem.*, **37**, 1641 (1965).
6) J. Bizot, *Bull. Soc. Chim. Fr.*, **1967**, 151.
7) J. L. Hoyt, *Anal. Chim. Acta*, **44**, 369 (1969).
8) R. Karlsson and K. J. Karrman, *Talanta*, **18**, 459 (1971).
9) R. Karlsson, *Talanta*, **19**, 1639 (1972).
10) T. H. Beasely, H. W. Ziegler, R. L. Charles, and P. King, *Anal. Chem.*, **44**, 1833 (1972).
11) A. Cedergren, *Talanta*, **21**, 367 (1974).
12) S. Miyake and T. Sudo, *Jpn. Analyst*, **23**, 482 (1974).
13) S. Miyake and T. Sudo, *Jpn. Analyst*, **23**, 476 (1974).
14) K. Muroi and M. Ono, *Jpn. Analyst*, **20**, 975 (1971).
15) A. Cedergren, *Talanta*, **21**, 265 (1974); **25**, 229 (1978).
16) J. C. Verhoef and E. J. Baredrecht, *J. Electroanal. Chem. Interfacial Electrochem.*, **71**, 305 (1976); **75**, 705 (1977); *Anal. Chim. Acta*, **94**, 395 (1977).
17) Mitsubishi Kasei Kogyo Co. Ltd. Private communication and catalog of Model CA-02 Titrator.
18) Hiranuma Sangyo Co. Ltd. Private communication and catalog of Model AQ-3B Titrator.

The Study of Transition-metal Complexes with Ethylenediamine and Cyano Ligands by Means of the X-Ray Photoelectron Spectra

Mitsuru SANO and Hideo YAMATERA*

Department of Chemistry, Faculty of Science, Nagoya University, Chikusa-ku, Nagoya 464

(Received November 12, 1980)

The X-ray photoelectron spectra (XPS) were measured in order to obtain the N1s and C1s core-orbital energies of ten ethylenediamine and 21 cyano complexes of transition metals. The difference between the N1s and C1s energies, ΔE, which was found to be hardly affected by the counter ion or by charging, was accurately determined for each complex. The trends observed in the ΔE values for these series of complexes are correlated with the electronic structures of the complexes by the use of Siegbahn's equation. For the ethylenediamine complexes, the ΔE values are shown to be related to the σ donation. For the cyano complexes, the ΔE values are mainly controlled by the nitrogen charge, which is itself closely connected with the π back-donation. Demonstrative of the importance of the π back-donation are the cases of $[Fe(CN)_6]^{4-}$ and $[Fe(CN)_6]^{3-}$, where the decrease in the negative charge from the former to the latter is found to occur dominantly (76%) in the nitrogen atoms. Molecular orbital (MO) calculations in the discrete variational Xα (DV-Xα) scheme were performed for a few series of the cyano complexes, giving results consistent with the XPS results.

The X-ray photoelectron spectrum (XPS) gives information about the charge distribution in a molecule and, accordingly, can be expected to provide a clue to clarifying the electronic structure. However, the chemical shifts of the inner-shell electrons of the metal and ligand atoms of transition-metal complexes have not been well related to the electronic structures because of several difficulties. One is the phenomenon of sample charging, which is serious for insulators. This phenomenon hinders one from making accurate measurements of electron binding energies. In order to overcome this difficulty, the 4f peaks of sputtered gold are usually used as a reference. This is not satisfactory, however, for measuring small chemical-shift differences, since the Au4f levels are influenced by the quantity of the gold and sometimes also by the chemical reaction of the gold with the sample, as is the case with cyanides. Another problem is that the electron binding energies of a complex ion to be measured may be influenced by the counter ion. These difficulties can be removed by the use of an internal reference or by the observation of the difference between the binding energies of different electrons in the same complex.

We investigated how the difference between two core binding energies of ligand atoms is related to the electronic structure of the complex. Transition-metal complexes coordinated with ethylenediamine and cyano ligands were selected for the investigation for the following reasons. Firstly, they are stable enough under a high vacuum and against X-ray irradiation to show reproducible results at −50 °C or below. Secondly, they contain carbon and nitrogen atoms in the ligand, and their coordination bonds show a striking contrast between the mainly σ character in the ethylenediamine complexes and both σ and π characters in the cyano complexes.

The XPS studies of some cyano complexes have been reported on the valence-region spectra by Calabrase and Hayes[1] and on the chemical shifts of the ligand core orbital by Vannerberg.[2]

In this paper, the XPS experimental results are presented for the N1s and C1s binding energies in ethylenediamine and cyano complexes of various transition-metal ions, and trends observed for the differences between the N1s and C1s energies are discussed in relation to the electronic structures of the complexes.

Experimental

The spectra were recorded on a JEOL Model JESCA-3A spectrometer. Aluminium $K\alpha_{1,2}$ radiation (1486.6 eV) was used as the X-ray excitation source, and the measurements were carried out at 5×10^{-8} Torr (1 Torr = 133.3 Pa) or below. For the calibration of the electron binding energies, we used both $Au4f_{7/2}$ (83.8 eV) and $Ag3d_{5/2}$ (368.2 eV) peaks[3] from a thin layer of gold and/or silver deposited onto an aluminium plate. Commercially available potassium salts of cyanide complexes, $K_3[Mn(CN)_6]$, $K_3[Fe(CN)_6]$, $K_3[Co(CN)_6]$, $K[Cu(CN)_2]$, $K[Ag(CN)_2]$, and $K[Au(CN)_2]$, were used without further purification. Other compounds were prepared according to standard methods. A small amount of each sample was ground in ethanol, and a droplet of this ethanolic suspension was placed on a gold plate and dried, or the crystals were ground without solvent and were deposited on an adhesive tape. Care was taken to make sure that the spectra did not contain any features due to contaminants. Carbon contaiminations were examined by comparing the integrated intensities of the carbon 1s and nitrogen 1s peaks. All the spectra reported here were proved to be free from any appreciable contamination. In order to avoid any significant decomposition of the sample by high-vacuum and X-ray irradiation, the sample was cooled at about −50 °C or below. We obtained the difference between the C1s and N1s binding energies by measuring them at the same time. This procedure was repeated several times for each sample, yielding consistent results. The average binding-energy difference was determined with an accuracy of about ±0.1 eV in several runs on a given compound.

We tried to obtain the absolute binding energies by calibrating the nitrogen 1s and carbon 1s peaks against the $4f_{7/2}$ peak of the gold sputtered onto the sample. This method was not, however, satisfactory for giving the absolute values of the binding energies, because the measured chemical shifts of the N1s and C1s binding energies were dependent upon the quantity of the sputtered gold[4] and it is not certain that the Fermi level in the gold should coincide with that in the sample. However, the uncertainty associated with the binding energies can, for the most part, be eliminated

TABLE 1. THE ELECTRON BINDING ENERGIES OF N1s AND Cl s AND THEIR DIFFERENCES FOR VARIOUS TRIS(ETHYLENEDIAMINE)COBALT(III) SALTS ($Au4f_{7/2}$=83.8 eV)

Compound $[Co(en)_3]X_3$	Binding energy/eV		
	N1s	Cl s	ΔE(N1s−Cl s)
X=Cl	399.4	285.3	114.1
Br	399.5	285.4	114.1
NO_3	399.6	285.5	114.1
ClO_4	399.7	285.5	114.2

TABLE 2. THE ELECTRON BINDING ENERGIES OF N1s AND Cl s AND THEIR DIFFERENCES FOR VARIOUS ETHYLENEDIAMINE COMPLEXES ($Au4f_{7/2}$=83.8 eV)

Compound	Binding energy/eV		
	N1s	Cl s	ΔE(N1s−Cl s)
$[Cr(en)_3]Cl_3$	400.4	286.5	113.9
$[Co(en)_3]Cl_3$	399.4	285.3	114.1
$[Ni(en)_3]Cl_2$	399.4	285.7	113.7
$[Cu(en)_3]SO_4$	399.4	285.4	114.0
$[Zn(en)_3]Cl_2$	400.0	285.9	114.1
$[Pd(en)_2]Cl_2$	399.7	285.7	114.0
$[Pt(en)_2]Cl_2$	400.2	285.9	114.4

by making use of their difference. For the convenience of comparison, the binding energies in ethylenediamine complexes were standardized against the sputtered-gold $4f_{7/2}$ peak (83.8 eV), and those in cyanide complexes, against the internal-potassium $2p_{3/2}$ peak (293.5 eV).[2)]

Results

In order for us to correlate the chemical shift of the electron binding energy from XPS with the electronic structure of the complex, an accurate determination of the chemical shift is needed. The chemical shift is, however, influenced considerably by the charging effect and also by the counter-ion effect. We first investigated these two effects on the chemical shift using Λ-$[Co(en)_3]X_3$ (X=Cl^-, Br^-, NO_3^-, and ClO_4^-) as the samples. The Cl s and N1s electron binding energies, as measured for the complex salts, are shown in Table 1, along with the energy difference (ΔE) between N1s and Cl s. Both the N1s and Cl s energies increase in the order of Cl^-, Br^-, NO_3^-, and ClO_4^- salts, but the ΔE value remains almost unchanged (114.1—114.2 eV), suggesting that ΔE is hardly affected by the counter ion. In addition, the ΔE value is not influenced by sample charging. Thus, the ΔE values can be used with advantage for the discussion of the electronic structures of the metal complexes. The Cl s and N1s energies were measured on various ethylenediamine complexes; the meaningful and reproducible data are listed in Table 2 in the order of the increasing atomic number of the metal. The N1s and Cl s binding energies listed in Columns 2 and 3 of this table show scattered values, without any apparent trend, but their differences, ΔE, given in Column 4, clearly show the following trends:

TABLE 3. THE ELECTRON BINDING ENERGIES OF N1s AND Cl s AND THEIR DIFFERENCES FOR VARIOUS CYANO COMPLEXES ($K2p_{3/2}$=293.5 eV)

Compound	Binding energy/eV		
	N1s	Cl s	ΔE(N1s−Cl s)
$K_3[Cr(CN)_6]$	399.1	285.5	113.6
$K_3[Mn(CN)_6]$	399.1	285.7	113.4
$K_3[Fe(CN)_6]$	399.0	285.7	113.3
$K_3[Co(CN)_6]$	398.9	285.7	113.2
$K_3[Rh(CN)_6]$	399.0	285.8	113.2
$K_4[Mn(CN)_6]$	398.4	285.2	113.2
$K_4[Fe(CN)_6]$	398.4	285.3	113.1
$K_4[Os(CN)_6]$	398.1	285.4	112.7
$K_2[Ni(CN)_4]$	399.0	285.6	113.4
$Ni(CN)_2$	405.1[a)]	291.6[a)]	113.5
$K_2[Pd(CN)_4]$	399.0	285.7	113.3
$K_2[Pt(CN)_4]$	398.9	285.7	113.2
$K[Cu(CN)_2]$	398.8	285.3	113.5
AgCN	405.5[a)]	291.8[a)]	113.7
$K[Ag(CN)_2]$	399.1	285.7	113.4
$K_3[Ag(CN)_4]$	398.9	285.6	113.3
$K[Au(CN)_2]$	399.2	286.0	113.2
$K_2[Zn(CN)_4]$	399.4	285.7	113.7
$K_2[Cd(CN)_4]$	399.3	285.7	113.6
$K_2[Hg(CN)_4]$	399.1	285.6	113.5
$Hg(CN)_2$	406.7[a)]	293.2[a)]	113.5
KCN	399.0	285.4	113.6

a) Uncalibrated value.

(1) The ΔE value increases in going from left to right, or from top to bottom, of the periodic table in each series of bi- and tervalent metal complexes: 113.9→114.1 eV for Cr^{3+}→Co^{3+}, 113.7→114.1 eV for Ni^{2+}→Zn^{2+}, and 113.7→114.4 eV for Ni^{2+}→Pt^{2+}.

(2) The ΔE value is larger for tervalent metal complexes than for bivalent ones if a comparison is made between complexes of the metals near to each other in the periodic table: $Ni^{2+}<Cr^{3+}<Cu^{2+}<Co^{3+}$, Zn^{2+}.

Measurements were also made of various cyanide complexes, for which the N1s and Cl s binding energies and the ΔE values are given in Table 3. The following trends are observed:

(3) The ΔE values for $[M(CN)_6]^{3-}$ and $[M(CN)_6]^{4-}$ decrease with an increase in the atomic number of the metal of the first transition series: 113.6→113.2 eV for Cr^{3+}→Co^{3+} and 113.2→113.1 eV for Mn^{2+}→Fe^{2+}.

(4) The ΔE value is greater for a tervalent-metal complex than for the complex of the same metal of a bivalent state: Fe^{3+} (113.3)>Fe^{2+} (113.1), and Mn^{3+} (113.4)>Mn^{2+}(113.2).

(5) The ΔE value is also greater for the higher oxidation number of the metal if a comparison is made between complexes of different metals with the same structure and the same electronic configuration: Hg^{2+}(113.5)>Au^{+}(113.2) for $[M(CN)_2]^{(2-n)-}$, and Co^{3+}(113.2)>Fe^{2+}(113.1) and Fe^{3+}(113.3)>Mn^{2+} (113.2) for $[M(CN)_6]^{(6-n)-}$.

(6) The ΔE value decreases with an increase in the atomic number of the metal in the same family: $Fe^{2+}(113.1)>Os^{2+}(112.7)$, $Ni^{2+}(113.4)>Pd^{2+}(113.3)>Pt^{2+}(113.2)$, $Ag^{+}(113.4)>Au^{+}(113.2)$, and $Zn^{2+}(113.7)>Cd^{2+}(113.6)>Hg^{2+}(113.5)$.

(7) In contradistinction to the trend described under (3), ΔE shows an increase with an increase in the atomic number in the series: $[Fe(CN)_6]^{4-}(113.1)<[Ni(CN)_4]^{2-}(113.4)<[Zn(CN)_4]^{2-}(113.7)$, $[Pd(CN)_4]^{2-}(113.3)<[Cd(CN)_4]^{2-}(113.6)$, and $[Os(CN)_6]^{4-}(112.7)<[Pt(CN)_4]^{2-}(113.2)<[Hg(CN)_4]^{2-}(113.5)$. This may be due to different symmetries of the complexes. The order of increasing ΔE is $O_h<D_{4h}<T_d$.

(8) The ΔE values for cyanide complexes are smaller than that for KCN; AgCN and $K_2[Zn(CN)_4]$ are exceptions, however.

These trends (1)—(8) will be discussed in more detail in the following section.

Discussion

The trends observed for ethylenediamine and cyanide complexes will be discussed in order to correlate them with the electronic structure. The charge-potential model developed by Siegbahn and his co-workers[5] is used to relate the shift in the core-electron binding energy to the charge distribution in a molecule. According to the model, the binding energy of the relevant electron of the i atom can be given by:

$$E_i = E_i^\circ + k_i q_i + \sum_{j\neq i} q_j/r_{ij}. \quad (1)$$

In this equation, E_i° is the energy of a reference level; q_i and q_j, the charges on the i and j atoms respectively, and r_{ij}, the internuclear distance between the i and j atoms. The last term of Eq. 1 represents an intramolecular Madelung-type potential. The value of the k parameter depends on the atomic species and can be obtained experimentally from the chemical-shift data in small molecules. Using Eq. 1, the difference between N1s and C1s can be expressed as follows:

$$\Delta E = k_N q_{N^*} - k_C q_{C^*} + \left(\sum_{i\neq N^*} q_i/r_{iN^*} - \sum_{j\neq C^*} q_j/r_{jC^*}\right) + E_{N^*}^\circ - E_{C^*}^\circ, \quad (2)$$

where the subscripts, N* and C*, denote, respectively, the particular nitrogen and carbon atoms under consideration and where r_{iN^*} and r_{jC^*} are the distances of the i and j atoms from the particular nitrogen and carbon atoms. The k_N and k_C values are taken as 21.5 and 21.9 for N1s and C1s respectively. (The units of the charge and the potential are e and V respectively.)[5]

The Trends (1) and (2) Observed for Ethylenediamine Complexes. The trends will be discussed by using Eq. 2. For the sake of simplicity, all the bond lengths and the charges on the carbon and hydrogen atoms are assumed to remain unchanged when the central metal is changed. Then, the difference in ΔE between two complexes can be obtained as follows:

$$\Delta(\Delta E) = \Delta E' - \Delta E = k_N(q_{N^*}' - q_{N^*}) + (q_M' - q_M)/r_{MN^*} + (q_N' - q_N)(1+4\sqrt{2})/2r_{MN^*}, \quad (3)$$

where M refers to metal atoms, and N to nitrogen atoms different from N*, although $q_N=q_{N^*}$, $q_N'=q_{N^*}'$, and $r_{MN}=r_{MN^*}$. In this and the following equations, the primed symbols refer to the complex containing the metal of higher atomic number. From the conservation of the charge, one obtains:

$$q_M' - q_M = -6(q_N' - q_N). \quad (4)$$

By substituting Eq. 4 in Eq. 3, one obtains:

$$\Delta(\Delta E) = (q_N' - q_N)(k_N - 6/r_{MN} + (1+4\sqrt{2})/2r_{MN}). \quad (5)$$

If the bond length, r_{MN}, is taken to be 2.0 Å, then the term, $(k_N - 6/r_{MN} + (1+4\sqrt{2})/2r_{MN})$, has a positive value of 2.3 V.

The trend (1) shows that the $\Delta(\Delta E)$ values are positive for the sequence of Cr^{3+} and Co^{3+} ($\Delta E_{Co} - \Delta E_{Cr} = 0.2$ eV) and for Ni^{2+} and Zn^{2+} ($\Delta E_{Zn} - \Delta E_{Ni} = 0.4$ eV). Therefore, the term of $(q_N' - q_N)$ is positive and the negative nitrogen charge decreases in going from Cr^{3+} to Co^{3+} and from Ni^{2+} to Zn^{2+}. This change in the nitrogen charge results from an increase in the nitrogen-to-metal σ donation with an increase in the atomic number, that is, with an increase in the effective nuclear charge.

For square-planar bis ethylenediamine complexes of Pd^{2+} and Pt^{2+}, Eq. 2 leads to the following equation instead of Eq. 5:

$$\Delta(\Delta E) = (q_N' - q_N)(k_N - 4/r_{MN} + (1+2\sqrt{2})/2r_{MN}). \quad (5')$$

The substitution of parameter values in Eq. 5′ gives:

$$\Delta E_{Pt} - \Delta E_{Pd} = 6.5(q_N' - q_N).$$

The corresponding experimental $\Delta(\Delta E)$ value is 0.4 eV; thus, $(q_N' - q_N)$ is positive. This means a greater σ donation in the Pt^{2+} complex, which is consistent with the general tendency for the electronegativity to increase in going down the periodic table in its middle part, where the noble metals appear.

The same argument applies to the trend described under (2) for a tervalent-metal complex to show a larger ΔE value when compared with the complex of a bivalent metal of a similar atomic number. A metal ion of a higher oxidation state is usually more electronegative and usually accepts a larger amount of negative charge from the coordinated nitrogen atoms. Thus, the trends observed in the ΔE values of ethylenediamine complexes can be well explained on the basis of Eq. 3 and correlated with the extent of the σ donation.

The Trends (3) Observed for the Octahedral Cyanide Complexes. Now, we shall turn to the cyanide complexes, $[M(CN)_6]^{3-}$ (M=Cr, Mn, Fe, and Co) and $[M(CN)_6]^{4-}$ (M=Mn and Fe). For these complexes, Eq. 2 leads to:

$$\Delta E = k_N q_N + q_C/r_{CN} + q_M/r_{MN} + 4q_C/\sqrt{r_{MC}^2 + r_{MN}^2} + 4q_N/\sqrt{2}\,r_{MN} + q_C/(r_{MN}+r_{MC}) + q_N/2r_{MN} - (k_C q_C + q_N/r_{NC} + q_M/r_{MC} + 4q_C/\sqrt{2}\,r_{MC} + 4q_N/\sqrt{r_{MC}^2 + r_{MN}^2} + q_C/2r_{MC} + q_N/(r_{MN}+r_{MC})),$$

which gives the following equation for $\Delta(\Delta E)$ with the metal–carbon and carbon–nitrogen bond lengths of 2.0 and 1.15 Å respectively:

$$\Delta(\Delta E) = \Delta E' - \Delta E = 6.0(q_N' - q_N) - 15.1(q_C' - q_C) - 2.6(q_M' - q_M). \quad (6)$$

Table 4. The Mulliken charges (in e) and core-orbital energy differences (in eV) for $[M(CN)_6]^{3-}$ (M=Cr, Mn, Fe, and Co) and $[Fe(CN)_6]^{4-}$, as estimated by DV-Xα MO calculations

	Cr^{3+}	Mn^{3+}	Fe^{3+}	Fe^{2+}	Co^{3+}
Metal	+1.21	+1.13	+0.98	+0.83	+0.84
Carbon	−0.17	−0.14	−0.05	−0.06	−0.04
Nitrogen	−0.53	−0.55	−0.61	−0.74	−0.60
ΔE(N1s−C1s)	110.0	109.9	109.9	109.8	109.6

With the relation between the charges given by:

$$6(q_N'-q_N) + 6(q_C'-q_C) = -(q_M'-q_M), \quad (7)$$

Eq. 6 can be written as:

$$\Delta(\Delta E) = 21.6(q_N'-q_N) + 0.5(q_C'-q_C). \quad (8)$$

On the basis of this equation, the relation between the atomic charges and $\Delta(\Delta E)$ will be discussed in this and the following sections.

Since the coefficient of $(q_C'-q_C)$ is much smaller than that of $(q_N'-q_N)$ in Eq. 8, we shall, for the present, ignore the $(q_C'-q_C)$ term. With the XPS result, $\Delta(\Delta E)=-0.4$ eV, for Cr^{3+} and Co^{3+}, Eq. 8 gives $q_N'-q_N=-0.02$. The negative value is to be expected from the qualitative consideration that the cobalt complex with a larger number of $d\pi$ electrons will show a greater π back-donation, which increases the electron density at the nitrogen atom; this tendency is, however, partially compensated for by the greater effective nuclear charge of Co^{3+}. This may explain why the charge on nitrogen is slightly more negative in the cobalt complex than in the chromium complex. Consistent results are obtained from the infrared spectroscopy, which shows that the force constant of the M–C vibration is greater for Co^{3+} than for Cr^{3+}, while that of C–N remains nearly constant.[6] Table 4 shows the results of our DV-Xα MO calculation,[7] which are in qualitative agreement with the above findings, although the $(q_N'-q_N)$ value (−0.07) and the $\Delta(\Delta E)$ value (1.5 eV) derived from the calculated atomic charges are greater (in absolute values) than those obtained from the experimental results. The $(q_C'-q_C)$ value is positive and greater than $-(q_N'-q_N)$, showing that the σ donation increases in going from the Cr^{3+} to the Co^{3+} complex by a larger amount than the increase in the π back-donation. The $\Delta(\Delta E)$ value (0.4 eV) obtained as the difference of calculated N1s and C1s energies showed a good agreement with the XPS result (0.4 eV).

The Trend (4) Observed between $[M(CN)_6]^{4-}$ and $[M(CN)_6]^{3-}$ (M=Mn and Fe). The relation of the charges between bivalent and tervalent complexes is:

$$q_M' + 6q_C' + 6q_N' = q_M + 6q_C + 6q_N + 1.0, \quad (9)$$

where the prime refers to the tervalent complexes. If the geometry of complexes is the same as has been described above, the equation for $\Delta(\Delta E)$ can be obtained as follows:

$$\Delta(\Delta E) = \Delta E(M^{3+}) - \Delta E(M^{2+}) = 21.6(q_N'-q_N) + 0.5(q_C'-q_C) - 2.6. \quad (10)$$

Experimentally, the $\Delta(\Delta E)$ value was found to be about 0.2 eV, so that we may write;

$$0.2 + 2.6 = 21.6(q_N'-q_N) + 0.5(q_C'-q_C). \quad (11)$$

Disregarding $0.5(q_C'-q_C)$, we obtain $q_N'-q_N=0.13$. According to the orbital mixing rule,[8,9] a π back-donation from metal to ligand will result in an increased population at the nitrogen atom, but in an almost unchanged or even decreased population at the carbon atom. Thus, the XPS result can be taken as showing the effect of π back-donation; the extent of π back-donation is greater in the Fe^{2+} than in the Fe^{3+} complex. This is also shown by the force constants reported for the M–C and C–N vibrations. Thus, the M–C force constant is greater for Fe^{2+} than for Fe^{3+}, while the C–N force constant is smaller for the Fe^{2+} complex.[10] The results of our MO calculations (given in Table 4) are also in good agreement with the XPS results. Thus, the charges at the nitrogen atom of the complexes are −0.74 (Fe^{2+}) and −0.61 (Fe^{3+}), which give $q_N'-q_N=0.13$. This agrees excellently with the result (0.13) derived from the XPS data by disregarding the $q_C'-q_C$ term. Therefore, $q_C'-q_C$ can be expected to be small, and a consistent result of $q_C'-q_C=0.01$ is shown by the MO calculation. Thus, the positive $\Delta(\Delta E)$ shows that the major part (more than 72%) of the decreased negative charge of the complex has been lost from the nitrogen atoms; for $\Delta(\Delta E)=0.2$ in the case under consideration, the loss from the nitrogen atoms amounts to 76%. This means that the π back-donation greatly decreases in going from the Fe^{2+} to the Fe^{3+} complex.

The Trend (5) Observed for the Isoelectronic Cyanide Complexes. The trend (5) will be discussed in the case of the octahedral complexes, *e.g.*, $[Fe(CN)_6]^{4-}$ and $[Co(CN)_6]^{3-}$. If $0.5(q_C'-q_C)$ is ignored in comparison with $21.6(q_N'-q_N)$ in Eq. 8, we obtain:

$$0.1 + 2.6 = 21.6(q_N'-q_N), \quad (12)$$

where the prime refers to tervalent complexes. Equation 12 gives 0.13 for the value of $(q_N'-q_N)$, which is in good agreement with the value of 0.14 obtained from the DV-Xα MO calculation for the Fe^{2+} and Co^{3+} complexes.[10] The above argument on the basis of XPS results is also supported by the small value of $(q_C'-q_C)$ (=0.02) from DV-Xα.

In the cases of $[Au(CN)_2]^-$ and $[Hg(CN)_2]$ with $D_{\infty h}$ symmetry (N–C–M–C–N), the metal–carbon and carbon–nitrogen bond lengths are taken to be 2.0 and 1.15 Å respectively, and the relation between the charges is given by:

$$2q_N' + 2q_C' + q_M' = 2q_N + 2q_C + q_M + 1.0, \quad (13)$$

where the prime refers to $[Hg(CN)_2]$. Then, the following equation can be obtained:

$$\Delta(\Delta E) = 13.7(q_N'-q_N) - 4.9(q_C'-q_C) - 2.6. \quad (14)$$

As a first approximation, $(q_C'-q_C)$ is disregarded, as

Table 5. The Mulliken charges (in e) and core-orbital energy differences (in eV) for $D_{\infty h}$ symmetry complexes, as estimated by DV-Xα MO calculation

	$[Ag(CN)_2]^-$	$[Au(CN)_2]^-$	$[Hg(CN)_2]$
Metal	+0.42	+0.33	+1.11
Carbon	−0.22	−0.17	−0.26
Nitrogen	−0.50	−0.49	−0.30
ΔE(N1s−C1s)	110.2	109.7	110.5

in the above cases. Then, with the observed $\Delta(\Delta E)$ value of 0.3 eV, we obtain $q_N'-q_N=0.21$, which means a smaller π back-donation in $[Hg(CN)_2]$ than in $[Au(CN)_2]^-$. This can be expected from the higher nuclear charge of the central ion for the former. The MO calculation gave a consistent result, $q_N'-q_N=0.19$.[11] However, the MO calculation showed that $(q_C'-q_C)$ $(=-0.09)$ is not so small (in absolute value) as to be neglected.[12] The negative value means that the carbon atom has a more negative charge when it is coordinated to Hg^{2+} than when linked to Au^+. This might seem to contradict the higher electronegativity of Hg^{2+}; however, it can be understood electrostatically by considering the higher polarizing power of Hg^{2+}. It is also consistent with the molecular orbital consideration that the greater π back-donation in the Au^+ complex will cause a more extensive mixing of the antibonding CN^- π orbital into the bonding CN^- π, in-phase at N and out-of-phase at C. The importance of the change in π back-donation has also been demonstrated in this case. Calculating $\Delta(\Delta E)$ with the atomic charges from the MO calculation, we obtain 0.4 eV for $\Delta(\Delta E)$, which is nearly equal to the XPS result (0.3 eV). (The ΔE(N1s−C1s) values directly obtained from the MO calculation (Table 5) also show a consistent trend, although the $\Delta(\Delta E)$ value is twice as large.)

The Trend (6) Observed for Complexes of the Metals of the Same Family. The ΔE value slightly decreased in going down the periodic table in each family. A discussion of $\Delta(\Delta E)$ similar to those made above cannot be made here, because the differences in the M–C distance are appreciable in the present case. With the calculated atomic charges for the Ag^+ and Au^+ complexes (Table 5), however, Siegbahn's equation gave a $\Delta(\Delta E)$ value (−0.1 eV) consistent with the XPS result (−0.2 eV).

The Trend (7) Observed between Complexes of Different Symmetries. The coordination of cyanide ions to a metal ion results in a shift of the negative charge from the ligands to the metal ion. When the oxidation number of the metal ion remains the same, the total charge received by the metal ion will not remarkably change from one metal ion to another. Thus, the donation per ligand will be less in $[Fe(CN)_6]^{4-}$ than in $[Ni(CN)_4]^{2-}$, for example. The smaller net donation can be attributed to a smaller σ donation or to a larger π back-donation; the former leaves more negative charge on C, and the latter increases the electronic density on N. The observed tendency for the ΔE value to be smaller for a hexacyano than for a tetracyano complex implies the importance of the effect of the π back-donation. Among the tetracyano complexes, the observed ΔE value is smaller for a planar than for a tetrahedral coordination. This may also indicate a greater π back-donation in the planar complexes.

The Trend (8) Observed for Most of the Cyano Complexes. As has been described above, the electronic density of the cyanide ion is decreased on C, and increased on N, by the ligation of the cyanide ion to a metal ion. Thus, compared with the free cyanide ion, the ΔE value can be expected to be smaller in a complex. This is demonstrated by the XPS results (Table 3). The exceptionally high ΔE value for $[Zn(CN)_4]^{2-}$ may be attributed to the poor π back-donation and/or the polarization of the CN^- ligand. Though less pronounced, a similar situation is also found in other tetrahedral complexes. The Cr^{3+} ion is the hardest of the metal ions listed in Table 3 and has only three $d\pi$ electrons. Thus, a large ΔE value can be expected for $[Cr(CN)_6]^{3-}$, in agreement with the XPS results.

Conclusion

The ΔE value, the difference between the N1s and C1s orbital energies, was measured for various ethylenediamine complexes and cyano complexes. The following trends were observed.

1) The ΔE value was not influenced by the counter ion or by the charging-up of the sample, and the observed trends could be related to the trends in the charge distribution of the complex and the character of the coordinate bond by making use of Siegbahn's equation and also by means of the DV-Xα MO calculation.

2) For ethylenediamine complexes, the ΔE value increased in the following orders: $Cr^{3+}<Co^{3+}$, $Ni^{2+}<Cu^{2+}<Zn^{2+}$, and $Ni^{2+}<Pd^{2+}<Pt^{2+}$. These indicate the sequences of the decreasing negative charge of the nitrogen atom or the increasing donation of electrons from ligand to metal.

3) For cyanide complexes, the following trends are found and explained. The ΔE value increased in the following orders: $Cr^{3+}<Mn^{3+}<Fe^{3+}<Co^{3+}$, $Mn^{2+}<Fe^{2+}$, $Mn^{2+}<Mn^{3+}$, $Fe^{2+}<Fe^{3+}$, $Mn^{2+}<Fe^{3+}$, $Fe^{2+}<Co^{3+}$, $Au^+<Hg^{2+}$, $Os^{2+}<Fe^{2+}$, $Pt^{2+}<Pd^{2+}<Ni^{2+}$, $Au^+<Ag^+$, $Hg^{2+}<Cd^{2+}<Zn^{2+}$ (for complexes of the same symmetries), and $O_h<D_{4h}<T_d$ (for those of different symmetries). In the $[M(CN)_6]^{3-}$ (M: Cr→Co) and $[M(CN)_6]^{4-}$ (M: Mn→Fe) series, Siegbahn's equation shows that the tendency observed in ΔE reflects mainly the change in the nitrogen charge. The greater change in the carbon charge, as shown by the DV-Xα calculation, has a minor effect on the ΔE value. In $[M(CN)_6]^{n-}$ (M=Mn and Fe), the nitrogen charge becomes less negative by about 0.1 in going from the M^{2+} to the M^{3+} complex with a decreasing π back-donation, whereas the carbon charge remains almost unchanged. For complexes of different metal ions with the same electronic configuration, the ΔE value is controlled by the nitrogen charge, whose difference is about 0.2 between Hg^{2+} and Au^+ and 0.13 between Mn^{2+} and Fe^{3+} and between Fe^{2+}

and Co^{3+}. The π back-donation is shown to be also important in accounting for the trend observed in the ΔE values of complexes of different geometries and of free CN^-.

4) The DV-Xα MO calculation gave results consistent with the XPS results, thus showing its usefulness for the interpretation of the XPS results.

This work was supported in part by a Grant-in-Aid for Scientific Research No. 510806 from the Ministry of Education, Science and Culture.

References

1) A. Calabrase and R. G. Hayes, *J. Am. Chem. Soc.*, **96**, 5054 (1974).
2) N. G. Vannerberg, *Chemi. Scripta*, **9**, 122 (1976).
3) G. Johansson, J. Hedman, A. Berndtsson, M. Klasson, and R. Nilsson, *J. Electron Spectrosc. Relat. Phenom.*, **2**, 295 (1973).
4) M. Sano and H. Yamatera, unpublished results.
5) K. Siegbahn *et al.*, "ESCA Applied to Free Molecules," North-Holland Pub., Amsterdam (1969).
6) L. H. Jones, *Inorg. Chem.*, **2**, 777 (1963).
7) M. Sano, H. Adachi, and H. Yamatera, *Bull. Chem. Soc. Jpn.*, in press.
8) S. Inagaki and K. Fukui, *Chem. Lett.*, **1974**, 509.
9) M. Sano, Y. Hatano, H. Kashiwagi, and H. Yamatera, *Bull. Chem. Soc. Jpn.*, **54**, 1523 (1981).
10) K. Nakamoto, "Infrared and Raman Spectra of Inorganic and Coordination Compounds," 3rd ed, John Wiley & Sons, New York (1978).
11) M. Sano, H. Adachi, and H. Yamatera, 42th National Meeting of the Chemical Society of Japan, Tokyo, April 1981, Abstr. I, p. 18.
12) A calculation of $q_N'-q_N$ with Eq. 14, allowing for $q_C'-q_C=-0.09$, gives $q_N'-q_N=0.18$, which is in closer agreement with the DV-Xα MO value (0.19).

The Stereochemistry and Reactivity of Metal-Schiff Base Complexes. IV. The Stereoselectivity of *N,N'*-Ethylenebis(α-methylsalicylideneaminato)-cobalt(III) Complexes with *N*-Benzyl-L-alanine, *N*-Methyl-L-alanine, and *N*-Benzyl-*N*-Methyl-L-alanine, and the Stereospecificity of (1*S*, 2*S*)-*N,N'*-1,2-Cyclohexylenebis(salicylideneaminato)-cobalt(III) Complexes toward *N*-Benzyl-L-alanine

Yuki Fujii,* Makoto Matsufuru, Akira Saito, and Sakiko Tsuchiya

Department of Chemistry, Faculty of Science, Ibaraki University Bunkyo-cho, Mito, Ibaraki 310

(Received November 14, 1980)

Cobalt(III) complexes containing *N*-alkyl-L-alanine and a Schiff base ligand, β_2-[Co(α-Me-sal$_2$en)(*N*-R-L-ala)] (where α-Me-sal$_2$en represents the dianion of *N,N'*-ethylenebis(α-methylsalicylideneamine) and *N*-R-L-ala denotes the anion of titled amino acids), have been prepared. They were characterized by the use of the absorption, circular dichroism, and ^{1}H NMR spectra of the complexes. They showed quite high stereoselectivity for Λ_{RS}-β_2-configuration: 93% for *N*-methyl-L-alanine, and almost 100% for *N*-benzyl-L-alanine and *N*-benzyl-*N*-methyl-L-alanine. The similar β_2-Co(sal$_2$-(*S,S*)-chxn) complexes with *N*-benzyl-L- and *N*-benzyl-D-alanines, where sal$_2$-(*S,S*)-chxn represents the dianion of (1*S*,2*S*)-*N,N'*-1,2-cyclohexylenebis(salicylideneamine), have been synthesized to investigate the stereospecificity of the complex toward *N*-benzyl-L-alanine. It was found that Co(sal$_2$-(*S,S*)-chxn) complex reacts with *N*-benzyl-L-alanine in a high stereospecificity (93—94% at the 1:2 reaction molar ratio between the complex and racemic *N*-benzylalanine, and almost 100% at the 1:100 molar ratio). The above phenomena were explained in terms of the thermodynamic selectivity of the complexes.

The steric control of the diastereoisomers of metal complexes is one of the interesting subjects in the stereochemistry of coordination compounds. Many studies have been directed toward the stereoselectivity or stereospecificity of Co(N$_4$) complexes with a chiral amino acid,[1] where (N$_4$) denotes a tetramine ligand such as (en)$_2$ or trien. However, the stereoselectivity of the [Co(N$_4$)(aa)]$^{2+}$ complexes is not so high. For examples, the isomeric ratio of the diastereoisomers, Λ/Δ, at the equilibrium conditions is about 50/50 in [Co(en)$_2$(L-ala)]$^{2+}$,[2] 37/63 in [Co(en)$_2$(L-val)]$^{2+}$,[2] 33/67 in β_2-[Co(trien)(L-pro)]$^{2+}$,[3] and 18/82 in β_2-[Co(pyht)(L-ala)]$^{2+}$.[4] In the case of Co(N$_4$) complexes with *N*-alkyl-L-amino acid, the stereoselectivity is higher than the corresponding L-amino acidato complex; but the Λ/Δ ratio is 80/20, 60/40, or 90/10 in [Co(en)$_2$(*N*-Me-L-ala)]$^{2+}$,[5] β_2-[Co(trien)(*N*-Me-L-ala)]$^{2+}$,[6] or β_2-[Co(2(*S*)10(*S*)-Me$_2$-2,3,2-tet)(*N*-Me-L-ala)]$^{2+}$ [7] respectively.[8]

We have recently found that the stereoselectivity of cobalt(III)–Schiff base complexes with a chiral amino acid, β_2-[Co(Schiff base)(L-aa)], is much higher than that of the corresponding Co(N$_4$) complexes: Λ/Δ is 67/33 in the L-ala complex, 90/10 in the L-phe complex, and about 0/100 in the L-pro complex.[9,10] It is most interesting that the stereoselectivity of the L-pro complex reaches almost 100%. This quite high stereoselectivity of the L-pro complex comes from the strong intramolecular steric repulsion between the Schiff base ligand and the pyrrolidine ring, a kind of *N*-alkyl group, of L-proline. Therefore, in the Co(III)–Schiff base system, it can be expected that the *N*-alkyl amino acidato complex may show quite high stereoselectivity.

In this paper, the preparation and the stereoselectivity of Co(α-Me-sal$_2$en) complexes with *N*-methyl-L-alanine, *N*-benzyl-L-alanine, and *N*-benzyl-*N*-methyl-L-alanine will be studied to establish a quite high steric control of the diastereoisomers of amino acidato cobalt(III) complexes. The optical resolution of amino acids[11] will be used to study the stereospecificity of Co(sal$_2$-(*S,S*)-chxn) complex toward *N*-benzyl-L-alanine.

Experimental

Preparation of the Complexes. [Co(α-Me-sal$_2$en)] was prepared by the method of Bigotto *et al.*[12] [Co(sal$_2$-(*S,S*)-chxn)] was prepared by the method described in Ref. 13. (1*S*,2*S*)-1,2-Cyclohexanediamine was resolved by the method reported in Ref. 13. *N*-Alkyl amino acids were prepared by the method of Quitt *et al.*[14]

[Co(α-Me-sal$_2$en)(N-Bz-L-ala)]. 1:1 Mixture of Λ_{RS}- and Δ_{SS}-β_2-Isomers (Complex I): *N*-Benzyl-L-alanine (2.1 g, 1.2×10^{-2} mol) in a mixed solvent of water (20 cm^3) and methanol (130 cm^3) was added to a slurry of [Co(α-Me-sal$_2$en)] (3.8 g, 1.1×10^{-2} mol) in chloroform (250 cm^3). The mixture was stirred vigorously in the open air for about 7 min until the color of the solution became green. After a trace amount of unreacted [Co(α-Me-sal$_2$en)] had then been filtered off, water (about 500 cm^3) was added to the filtrate; then the water-soluble component was extracted into water (twice). The chloroform layer was filtered, and petroleum ether (about 2 dm^3) was added to the filtrate to give a green powder. Since the reaction product is labile in isomerization in solution, the above procedure should be carried out as quickly as possible. When the procedure took about 15 min, the green precipitate thus obtained showed the molar rotation at 435 nm of -1.95×10^4° ($c=1.0\times10^{-3}$ mol dm^{-3}; chloroform, soon after dissolution), which corresponds to a 1:2 mixture of Δ_{SS}- and Λ_{RS}-β_2-isomers of [Co(α-Me-sal$_2$en)(*N*-Bz-L-ala)]. Yield, about 4.0 g. Found: C, 62.27; H, 5.61; N, 7.77%. Calcd for $CoC_{28}H_{30}N_3O_4\cdot0.5H_2O$: C, 62.22; H, 5.78; N, 7.77%. The 1:1 mixture was obtained by treating the 1:2 mixture as follows. The 1:2 mixture (0.4 g) was dissolved in chloroform (20 cm^3), and acetone (30 cm^3) was added to it. The solution was concentrated to a small volume with a rotary vacuum evaporator at about 40 °C. The green powder thus obtained was washed with acetone and dried under vacuum. Yield, about 0.2 g. Found: C, 59.30; H,

5.36; N, 7.36%. Calcd for $CoC_{28}H_{30}N_3O_4 \cdot 0.5H_2O \cdot 0.5 CHCl_3$: C, 59.49; H, 5.52; N, 7.37%. $[M]_{435} = -2.50 \times 10^3°$ ($c = 1.0 \times 10^{-3}$ mol dm^{-3}; chloroform, soon after dissolution).

Λ_{RS}-β_2-Isomer (Complex II): Method A. One gram of the green powder ($[M]_{435} = -1.95 \times 10^4°$) obtained above was dissolved in the mixed solvent of chloroform (30 cm^3) and methanol (30 cm^3). The solution was slowly concentrated to a small volume at room temperature to give green crystals in about an 85% yield. Found: C, 51.48; H, 5.13; N, 6.26%. Calcd for $CoC_{28}H_{30}N_3O_4 \cdot 1.5H_2O \cdot CHCl_3$: C, 51.38; H, 5.05; N, 6.20%. $[M]_{435} = -4.38 \times 10^4°$ ($c = 1.0 \times 10^{-3}$ mol dm^{-3}; chloroform soon after dissolution).

Method B. *N*-Benzyl-L-alanine (2.1 g, 1.2×10^{-2} mol) in a mixed solvent of water (20 cm^3) and methanol (130 cm^3) was added to the slurry of [Co(α-Me-sal$_2$en)] (3.8 g, 1.1×10^{-2} mol) in chloroform (175 cm^3). The mixture was stirred vigorously in the open air for 2 h. After a trace amount of brownish by-product had been filtered off, the filtrate was slowly concentrated to a small volume. The green crystals thus obtained were recrystallized from a mixed solvent of chloroform and methanol (1:1 in volume). Yield, about 4.2 g. Found: C, 51.67; H, 5.06; N, 6.32%. Calcd for $CoC_{28}H_{30}N_3O_4 \cdot 1.5H_2O \cdot CHCl_3$: C, 51.38; H, 5.06; N, 6.20%. $[M]_{435} = -4.38 \times 10^4°$ ($c = 1.0 \times 10^{-3}$ mol dm^{-3}; chloroform, soon after dissolution). When the complex was recrystallized from methanol and water, green crystals without any crystalline chloroform were obtained. Found: C, 58.36; H, 6.10; N, 7.29%. Calcd for $CoC_{28}H_{30}N_3O_4 \cdot 2.5H_2O$: C, 58.33; H, 6.12; N, 7.29%. $[M]_{435} = -4.38 \times 10^4°$ ($c = 1.0 \times 10^{-3}$ mol dm^{-3}; chloroform, soon after dissolution).

[Co(α-Me-sal$_2$en)(N-Me-L-ala)]. 1:1 Mixture of Λ_{RS}-β_2-Isomer and Δ-β_2-Isomers (Complex III): *N*-Methyl-L-alanine (1.3 g, 1.2×10^{-2} mol) in a mixed solvent of water (10 cm^3) and methanol (100 cm^3) was added to the slurry of [Co(α-Me-sal$_2$en)] (3.7 g, 1.1×10^{-2} mol) in chloroform (250 cm^3). The mixture was stirred vigorously in the open air for about 10 min, until the solution became green. After a trace amount of unreacted [Co(α-Me-sal$_2$en)] had been filtered off, water (500 cm^3) was added to the filtrate to extract the water-soluble component into water (twice). The chloroform layer thus obtained was filtered, and petroleum ether (about 2 dm^3) was added to the filtrate to give green powder in about a 3.5 g yield. It was dried under vacuum. When this procedure took about 20 min, the green product thus obtained showed $[M]_{435}$ of $-1.44 \times 10^4°$ ($c = 1.0 \times 10^{-3}$ mol dm^{-3}; chloroform, soon after dissolution), which corresponds to the 1:2 mixture of Δ- and Λ_{RS}-β_2-isomers. The 1:1 mixture was obtained by the following procedure. The green powder (0.8 g) obtained above was dissolved in chloroform (20 cm^3), and acetone (20 cm^3) was added to it. When the solution was concentrated to a small volume with a rotary vacuum evaporator at about 40 °C, the 1:1 mixture was precipitated as a green powder in about a 40% yield. Found: C, 56.47; H, 5.82; N, 8.95%. Calcd for $CoC_{22}H_{26}N_3O_4 \cdot 0.5H_2O$: C, 56.90; H, 5.86; N, 9.05%. $[M]_{435} = -6.1 \times 10^3°$ ($c = 1.0 \times 10^{-3}$ mol dm^{-3}; chloroform, soon after dissolution).

Λ_{RS}-β_2-Isomer (Complex IV): One gram of the green powder obtained above (the 1:2 mixture of Δ- and Λ_{RS}-β_2-isomers) was dissolved in a mixed solvent of chloroform (10 cm^3) and methanol (30 cm^3), and the solution was warmed at about 50 °C for 7 h. When petroleum ether (about 300 cm^3) was added to the solution, the Λ_{RS}-β_2-isomer was precipitated as a green powder in about an 80% yield. It was dried under vacuum. Found: C, 56.64; H, 5.91; N, 8.82%. Calcd for $CoC_{22}H_{26}N_3O_4 \cdot 0.5H_2O$: C, 56.90; H, 5.86; N, 9.05%. $[M]_{435} = -4.15 \times 10^4°$ ($c = 1.0 \times 10^{-3}$ mol dm^{-3}; chloroform, soon after dissolution).

When the 1:2 mixture obtained above was recrystallized from a mixed solvent of methanol and water, green crystals with $[M]_{435}$ of $-2.40 \times 10^4°$ ($c = 1.0 \times 10^{-3}$ mol dm^{-3}; chloroform, soon after dissolution) were isolated in an 85% yield. The product corresponds to the 1:4 mixture of Δ- and Λ_{RS}-β_2-isomers. Found: C, 56.72; H, 5.99; N, 8.93%. Calcd for $CoC_{22}H_{26}N_3O_4 \cdot 0.5H_2O$: C, 56.90; H, 5.86; N, 9.05%.

Λ_{RS}-β_2-[Co(α-Me-sal$_2$en)(N-Bz,Me-L-ala)] (Complex V). This complex was prepared by a method similar to that employed for the preparation of Λ_{RS}-β_2-[Co(α-Me-sal$_2$en)-(*N*-Bz-L-ala)] (Complex II), as mentioned above (Method B). When the complex was recrystallized from methanol and water, it was obtained as a green powder in about a 70% yield. Found: C, 60.61; H, 6.22; N, 7.15%. Calcd for $CoC_{29}H_{32}N_3O_4 \cdot 1.5H_2O$: C, 60.84; H, 6.16; N, 7.34%. $[M]_{435} = -4.12 \times 10^4°$ ($c = 1.0 \times 10^{-3}$ mol dm^{-3}; chloroform).

Λ_{RS}-β_2-[Co(sal$_2$-(S,S)-chxn)(N-Bz-L-ala)] (Complex VI). *N*-Benzyl-L-alanine (0.27 g, 1.5×10^{-3} mol) in a mixed solvent of water (10 cm^3) and methanol (20 cm^3) was added to a slurry of [Co(sal$_2$-(*S,S*)-chxn)] (0.5 g, 1.3×10^{-3} mol) in methanol (40 cm^3). The mixture was stirred vigorously in the open air for about 1 h to give a green solution. When the green solution was concentrated to a small volume, green crystals were obtained in about an 0.6 g yield. They were recrystallized from methanol. Found: C, 60.70; H, 6.21; N, 7.18%. Calcd for $CoC_{30}H_{32}N_3O_4 \cdot 2H_2O$: C, 60.71; H, 6.11; N, 7.08%. $[M]_{435} = -3.94 \times 10^4°$ ($c = 1.0 \times 10^{-3}$ mol dm^{-3}; methanol).

1:1.5 Mixture of Δ-$_{RS}$ and Λ_{RR}-β_2-[Co(sal$_2$-(S,S)-chxn)(N-Bz-D-ala)] (Complex VII). This complex was prepared by a method similar to that employed for the preparation of Complex VI. It was obtained as a green powder in about a 70% yield. Found: C, 60.56; H, 6.18; N, 7.27%. Calcd for $CoC_{30}H_{32}N_3O_4 \cdot 2H_2O$: C, 60.71; H, 6.18; N, 7.08%. $[M]_{435} = -8.6 \times 10^3°$ ($c = 1.0 \times 10^{-3}$ mol dm^{-3}; methanol).

The Optical Resolution of N-Benzylalanine with [Co(sal$_2$-(S,S)-chxn)]. Racemic *N*-benzylalanine (0.47 g, 2.64×10^{-3} mol) in water (20 cm^3) was added to the slurry of [Co(sal$_2$-(*S,S*)-chxn)] (0.5 g, 1.32×10^{-3} mol) in methanol (100 cm^3). The mixture was stirred in the open air for about 1 h. To the resulting green solution, chloroform (250 cm^3) and water (250 cm^3) were added, and the mixture was shaken for about 5 min. The chloroform layer (A) and the water layer (B) were separated with a separatory funnel. Water (150 cm^3) was added to the chloroform layer (A), and a residual trace amount of *N*-benzylalanine was extracted into the water layer (C). Then, chloroform (150 cm^3) was added to the water layer (B), and a residual trace amount of green complex was extracted into chloroform layer (D). The water solutions (B) and (C) were mixed together, and the resulting mixture was evaporated to dryness. A white precipitate was obtained in about an 0.23 g (98%) yield. The precipitate was confirmed to be *N*-benzylalanine from its ^{1}H NMR spectrum and the elemental analysis. The optical purity of the *N*-benzylalanine was determined to be 93% (D-form) by the method of Ref. 15.

The chloroform solutions (A) and (D) were combined and the mixture was evaporated to dryness. The green powder thus obtained was washed with water. This green powder was then partially dissolved in a mixed solvent of methanol (50 cm^3) and water (100 cm^3), $NaBH_4$ (0.05 g, 1.32×10^{-3} mol) was added to the mixture. The mixture

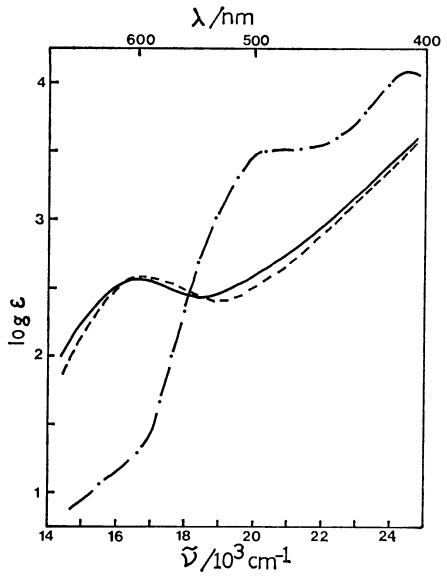

Fig. 1. The absorption spectrum of [Co(α-Me-sal$_2$en)] in $CHCl_3$ under nitrogen (—·—·), and those for the reaction solution of [Co(α-Me-sal$_2$en)] (1.0×10^{-3} mol dm^{-3}) and *N*-benzyl-L-alanine (1.1×10^{-3} mol dm^{-3}) in a mixed solvent of $CHCl_3$ and CH_3OH (4:1) under the air-oxidation conditions. (——): Soon after reaction, (----): at the equilibrium conditions.

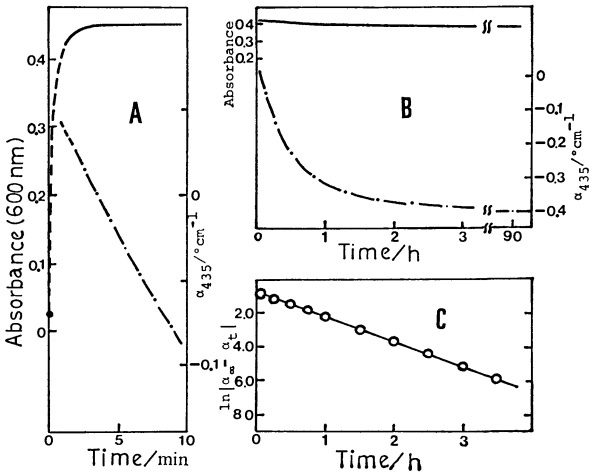

Fig. 2. The time dependences of the absorbance at 600 nm (——) and the rotation at 435 nm (—·—·) for the reaction solution of [Co(α-Me-sal$_2$en)] (1.0×10^{-3} mol dm^{-3}) and *N*-benzyl-L-alanine (1.1×10^{-3} mol dm^{-3}) in a mixed solvent of $CHCl_3$ and CH_3OH (4:1) under the air-oxidation conditions at 35 °C. Cell length = 1.0 cm.
A: Those for the initial reaction, B: those for the full reaction, C plot of $\ln|\alpha_\infty-\alpha_t|$ *vs.* the time.

was stirred vigorously for about 15 min until an orange precipitate of [Co(sal$_2$-(*S*,*S*)-chxn)] appeared. The precipitate was filtered, and water (250 cm^3) and chloroform (250 cm^3) were then added to the filtrate to extract a trace amount of orange complex into the chloroform. The pH of the water solution was adjusted to about 7 with dil HCl, and then the solution was evaporated to dryness to give a white powder. Methanol (150 cm^3) was added to the white precipitate to extract *N*-benzylalanine into methanol. When the methanol solution was concentrated to a small volume, a white precipitate was obtained in about an 0.24 g yield. The precipitate was confirmed to be *N*-benzylalanine, contaminated by a small amount of H_3BO_3 from the ^{1}H NMR spectrum and the elemental analysis. No further purification was attempted. The optical purity of the *N*-benzylalanine was 94% (L-form).[15]

Measurements. The electronic absorption spectra were recorded with a Hitachi EPS-3 Spectrophotometer at 23 °C. The CD spectra were measured with a JASCO J-20 Automatic Recording Spectropolarimeter at room temperature. The optical rotation at 435 nm was measured with a JASCO DIP-140 Digital Polarimeter. The ^{1}H NMR spectra were recorded with a Hitachi R-20 Spectrometer (60 MHz) using TMS as the internal reference at 35 °C.

Results and Discussion

The Reaction of [Co(α-Me-sal$_2$en)] with N-*Alkyl*-L-*alanine, and the Preparation and Properties of β$_2$-[Co(α-Me-sal$_2$en)(*N*-*R*-L-ala)] Complexes.* *1) β$_2$-[Co(α-Me-sal$_2$en)(*N*-Bz-L-ala)]*: Figure 1 shows the absorption spectrum of [Co(α-Me-sal$_2$en)] and that of the reaction solution of [Co(α-Me-sal$_2$en)] and *N*-benzyl-L-alanine under air-oxidation conditions. Figure 2 shows the time dependences of the absorbance at 600 nm and the rotation at 435 nm for the reaction solution. The absorbance at 600 nm becomes almost constant within a few minutes after the initiation of the reaction, and the absorption spectrum soon after reaction closely resembles that at the equilibrium conditions. Further, the absorption spectra are very similar to those of the β$_2$-[Co(α-Me-sal$_2$en)(L-aa)].[8,9,16] Accordingly, it seems that the complexation between [Co(α-Me-sal$_2$en)] and *N*-benzyl-L-alanine proceeds quite rapidly to form β$_2$-[Co(α-Me-sal$_2$en)(*N*-Bz-L-ala)]. On the other hand, the rotation at 435 nm of the reaction solution shows a small plus value soon after reaction, but it changes gradually to show a large minus value at the equilibrium conditions. The plot of $\ln|\alpha_\infty-\alpha_t|$ *vs.* the time for the mutarotation gives a straight line, as is shown in Fig. 2. These facts indicate that the reaction produces a mixture of two species: $(+)_{435}$- and $(-)_{435}$-isomers of β$_2$-[Co(α-Me-sal$_2$en)(*N*-Bz-L-ala)] complex, and then the $(+)_{435}$-isomer thus formed isomerizes slowly to the $(-)_{435}$-isomer. In fact, as has been mentioned in the Experimental section, from the initial reaction solution, a green powder with a small minus rotation at 435 nm (represented as Complex I) was isolated. From the equilibrium solution, green crystals with a large minus rotation at 435 nm (Complex II) were isolated. Both complexes had the same composition that corresponding to [Co(α-Me-sal$_2$en)(*N*-Bz-L-ala)], and their absorption spectra resemble not only each other but also those of the reaction solution mentioned above. Further, the mutarotation curve for Complex I was very similar to that for the reaction solution: the slopes of the plots of $\ln|\alpha_\infty-\alpha_t|$ *vs.* the time for both mutarotations were the same. Therefore, it can be concluded that [Co(α-Me-sal$_2$en)] reacts with *N*-benzyl-L-alanine quite rapidly to form a mixture of the $(+)_{435}$- and $(-)_{435}$-isomers of β$_2$-[Co(α-Me-sal$_2$en)-

Table 1. The ^{1}H NMR spectral data of the complexes (δ)[a),d)]

Complex	C-CH_3[c)]	N-CH_3	CH_3-C=N	Others
I[b)]	0.70, 0.82 [1.5]; 1.29, 1.41 [1.5]		2.73 [3]; 2.82 [3]	4.0(HDO), 4.1(multiplet of N-C$\underline{H}_2$-ϕ), 3.8—4.6 (broad multiplet of N-CH_2-CH_2-N), 6.4—7.8 (multiplet of phenyl protons)
II[b)]	0.70, 0.82 [3]		2.73 [3]; 2.82 [3]	4.0(HDO), 4.1(multiplet of N-C$\underline{H}_2$-ϕ), 3.8—4.6 (broad multiplet of N-CH_2-CH_2-N), 6.4—7.8 (multiplet of phenyl protons)
III[b)]	1.32, 1.44 [1.5]; 1.39, 1.51 [1.5]	2.15, 2.24 [3][c)]	2.68 [3]; 2.77 [3]	4.1(HDO), 3.6—4.7(broad multiplet of N-CH_2-CH_2-N), 6.5—7.7(multiplet of phenyl protons)
IV[b)]	1.32, 1.44 [3]	2.15, 2.24 [3][c)]	2.68 [3]; 2.77 [3]	4.1(HDO), 3.6—4.7(broad multiplet of N-CH_2-CH_2-N), 6.5—7.7(multiplet of phenyl protons)
V	0.40, 0.51 [3]	2.15 [3]	2.66 [3]; 2.79 [3]	4.1(HDO), 3.5—4.7(broad multiplet of N-CH_2-CH_2-N), 6.5—7.7(multiplet of phenyl protons)
VI	0.83, 0.92 [3]		7.85 [1]; 8.05 [1] (H-C=N)	1.5—2.3(multiplet of C_6H_{10}), 4.1(HDO), 3.4—3.7 (C$\underline{H}_2$-ϕ), 6.5—7.7(multiplet of phenyl protons)
VII	1.12, 1.24 [1.8]; 1.35, 1.48 [1.2]		7.79 [2] (H-C=N)	1.5—2.3(multiplet of C_6H_{10}), 4.1(HDO), 3.37 (C$\underline{H}_2$-ϕ), 6.5—7.7(multiplet of phenyl protons)

a) Solvent = $CD_3OD + CDCl_3$(1 : 4). b) Soon after dissolution. c) Doublet. d) [ ] represents relative peak area.

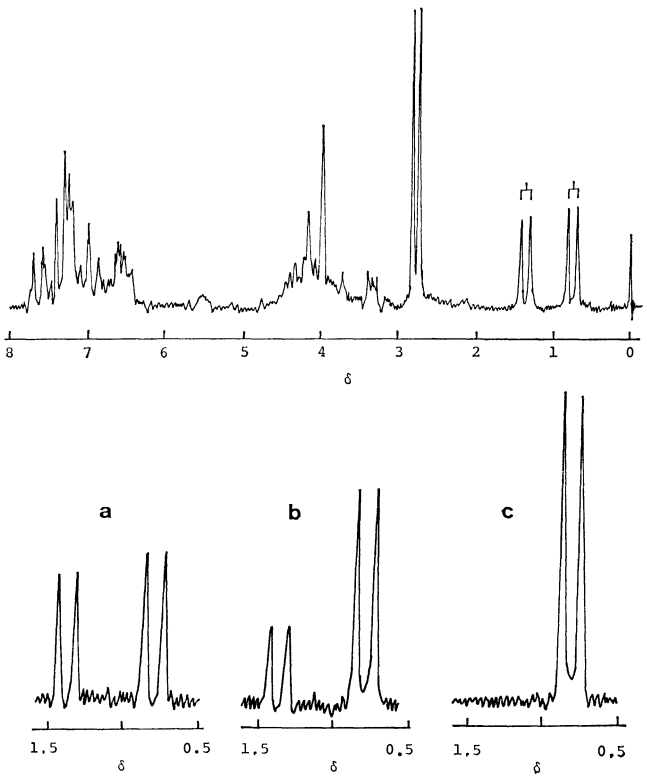

Fig. 3. The ^{1}H NMR spectrum of Complex I (1:1 mixture of Δ_{SS}- and Λ_{RS}-β_2-[Co(α-Me-sal$_2$en)(*N*-Bz-L-ala)]) in a mixed solvent of $CDCl_3$ and CD_3OD (4:1) soon after dissolution.
a, b, and c are the time dependences of C-CH_3 signal of the coordinated *N*-benzyl-L-alaninate.
a: About 3 min after dissolution, b: about 10 min after, c: at the equilibrium conditions.

(*N*-Bz-L-ala)] complex, and the $(+)_{435}$-isomer thus formed isomerizes slowly to the $(-)_{435}$-isomer. It has already been shown that β_2-Co(α-Me-sal$_2$en) complexes with L-amino acids are labile in isomerization between Δ- and Λ-configurations.[8,9] On the other hand, no mutarotation was observed for Complex II.

Figure 3 shows the ^{1}H NMR spectra of the *N*-Bz-L-ala complexes. The numerical data are listed in Table 1. The ^{1}H NMR spectrum of Complex I exhibited a time dependence in its methyl signal of the coordinated *N*-benzyl-L-alaninato ligand, and that of the complex at the equilibrium conditions coincided with that of Complex II. The methyl signal of Complex I soon after dissolution consists of two doublets at 0.77 and 1.35 ppm (center of the doublet) with the relative intensity ratio of about 1:1. Complex II shows only one doublet at 0.77 ppm. No other peaks or shoulders were observed for the methyl signal. These facts strongly support the assertion that only two species, the $(+)_{435}$- and $(-)_{435}$-isomers, are involved in the mutarotation of Complex I. From the ^{1}H NMR spectra, it can be concluded that 1) Complex I is the 1:1 mixture of the $(+)_{435}$- and $(-)_{435}$-isomers of β_2-[Co(α-Me-sal$_2$en)(*N*-Bz-L-ala)], 2) Complex II is the pure $(-)_{435}$-isomer of the *N*-Bz-L-ala complex, and 3) the stereoselectivity at the equilibrium conditions of the *N*-Bz-L-ala complex is almost 100%. As will be mentioned later, the Λ_{RS}-β_2-structure is assigned to the $(-)_{435}$-isomer, and the Δ_{SS}-β_2-structure to the $(+)_{435}$-isomer. Here, it should be noted that 1) the formation of both $(+)_{435}$- and $(-)_{435}$-isomers in the initial reaction between [Co(α-Me-sal$_2$en)] and *N*-benzyl-L-alanine can be regarded as kinetic in origin,[9] 2) the isolation of the 1:1 mixture of $(+)_{435}$- and $(-)_{435}$-isomers from the solution of the 1:2 mixture may be due to the lower solubility

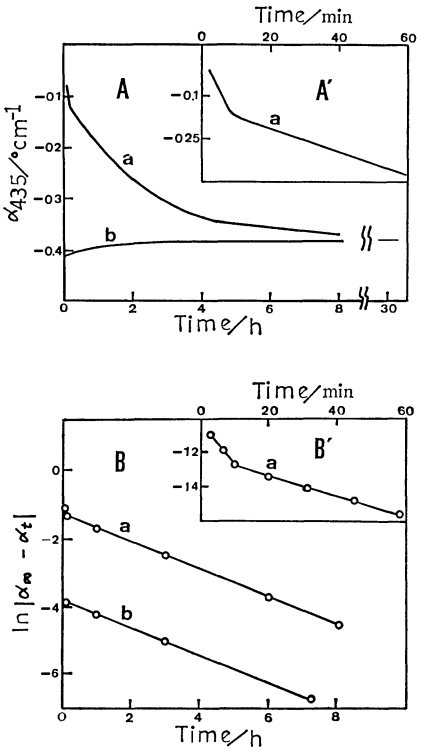

Fig. 4. The mutarotation (A) and the plot of ln$|\alpha_\infty - \alpha_t|$ *vs.* the time (B).
A′ and B′ show those of the initial reaction solution.
a: The reaction solution of [Co(α-Me-sal$_2$en)] (1.0×10^{-3} mol dm^{-3}) with *N*-methyl-L-alanine (1.1×10^{-3} mol dm^{-3}) in a mixed solvent of $CHCl_3$ and CH_3OH (4:1) under the air-oxidation conditions at 35 °C,
b: Complex IV (Δ_{RS}-β_2-[Co(α-Me-sal$_2$en)(*N*-Me-L-ala)]) (1.0×10^{-3} mol dm^{-3}) in the same conditions as a.

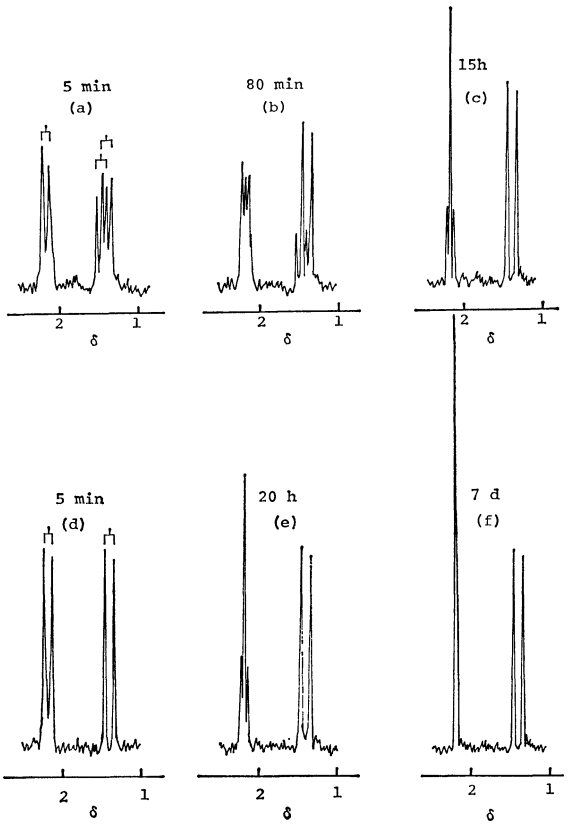

Fig. 5. The ^{1}H NMR spectra of β_2-[Co(α-Me-sal$_2$en)-(*N*-Me-L-ala)] complexes in a mixed solvent of $CDCl_3$ and CD_3OD (4:1).
(a), (b), (c), and (f) are the time dependences of N–CH_3 and C–CH_3 signals of the coordinated *N*-methyl-L-alaninate for Complex III. (d), (e), and (f) are those for Complex IV.

of the 1:1 mixture as compared with the solubility of the 1:2 mixture, and 3) the preference of the $(-)_{435}$-isomer at the equilibrium conditions should come from a thermodynamic origin. The thermodynamic stereoselectivity of the *N*-Bz-L-ala complex will be mentioned later in detail.

*2) β_2-[Co(α-Me-sal$_2$en)(*N*-Me-L-ala)]*: In the reaction for [Co(α-Me-sal$_2$en)] and *N*-methyl-L-alanine, the absorption spectra of the reaction solution soon after reaction and at the equilibrium conditions resembled each other quite closely, and they were very similar to those for β_2-[Co(α-Me-sal$_2$en)(L-aa)]. The absorbance at 600 nm of the reaction solution became almost a constant within a few minutes after initiation of the reaction: the complexation is very fast. The rotation at 435 nm of the reaction solution changed gradually to show a large minus rotation at the equilibrium conditions. These spectral and rotational properties of the *N*-Me-L-ala complex are very similar to those of the *N*-Bz-L-ala complex. However, as is shown in Fig. 4, the plot of ln$|\alpha_\infty - \alpha_t|$ *vs.* the time for the mutarotation gives two straight lines crossing at about $t=10$ min. A quite similar mutarotation was observed for Complex III, which was isolated from the initial reaction solution between [Co(α-Me-sal$_2$en)] and *N*-methyl-L-alanine. These facts indicate that three species at least, two $(+)_{435}$-isomers and one $(-)_{435}$-isomer of β_2-[Co(α-Me-sal$_2$en)(*N*-Me-L-ala)] complex, are involved in the mutarotation, and one of the two $(+)_{435}$-isomers isomerizes much faster to the $(-)_{435}$-isomer than the other $(+)_{435}$-isomer does. As mentioned later, four diastereoisomers are thought to be available for the β_2-[Co(α-Me-sal$_2$en)(*N*-Me-L-ala)] complex; their relative stability is as follows: Δ_{RS}->Δ_{SS}->Δ_{RS}->Δ_{SS}-isomers. Therefore, the $(+)_{435}$-isomer, which isomerizes first, may correspond to the less stable Δ_{RS}-isomer, and the other $(+)_{435}$-isomer may correspond to the Δ_{SS}-isomer.

As is shown in Fig. 4, Complex IV also exhibits a mutarotation; it has a smaller minus rotation at the equilibrium conditions than that soon after dissolution, although the degree of the mutarotation is very small. This fact indicates that the stereoselectivity of the *N*-Me-L-ala complex is less than 100%.

Figure 5 shows the ^{1}H NMR spectra of Complexes III and IV. The ^{1}H NMR spectrum of Complex III exhibited a time dependence in the *C*-methyl signal of the coordinated *N*-methyl-L-alaninato ligand. The methyl signal of Complex III soon after dissolution consists of two doublets at 1.34 and 1.55 ppm (center of the doublet) with the relative intensity of about 1:1. At the equilibrium conditions, only one doublet at 1.34 ppm is observed, and the ^{1}H NMR

Table 2. The isomeric ratio of β_2-[Co(α-Me-sal$_2$en)(*N*-R-L-ala)] at the equilibrium conditions[a)]

N-R-L-ala	Λ_{RS}-Isomer/Λ_{SS}-Isomer	Stereoselectivity
N-Bz-L-ala	≈100/≈0	≈100%
N-Me-L-ala	96.5/3.5	93%
N-Bz,Me-L-ala	≈100/0	≈100%

a) Solvent=$CH_3OH+CHCl_3$(1 : 4 in volume), Temp=35 °C.

spectrum is identical with that for Complex IV. Complex IV showed no observable time dependence in its ^{1}H NMR spectrum, except that the *N*-methyl signal became a singlet due to the H-D exchange of N–H proton on the *N*-methyl-L-alaninato ligand with deuterium of the solvent. Such ^{1}H NMR spectral behavior suggests that 1) Complex III is the 1:1 mixture of two species of isomer of [Co(α-Me-sal$_2$en)(*N*-Me-L-ala)] complex, 2) Complex IV is the pure $(-)_{435}$-isomer of the *N*-Me-L-ala complex, and 3) the stereoselectivity at the equilibrium conditions of the *N*-Me-L-ala complex is almost 100%. However, the above suggestions 1) and 3) somewhat disagree with the results obtained from the rotational measurements for the *N*-Me-L-ala complexes mentioned above. The disagreement in suggestion 1) may come from the overlap of peaks in the ^{1}H NMR spectrum, low sensitivity of the ^{1}H NMR spectrum as compared with the rotational measurement, or the rapid isomerization of one of the two $(+)_{435}$-isomers to the $(-)_{435}$-isomer in the course of the ^{1}H NMR spectral measurement for Complex III. The discrepancy in suggestion 3) should come from the low sensitivity of the ^{1}H NMR spectrum as compared with that of the rotational measurement. Here, the stereoselectivity at the equilibrium conditions of the *N*-Me-L-ala complex was estimated by the use of the following equation:

$$\text{Stereoselectivity (\%)} = [M]^B_{435}/[M]^A_{435} \times 100,$$

where $[M]^A_{435}$ and $[M]^B_{435}$ denote the molar rotations at 435 nm of Complex IV soon after dissolution (A) and at the equilibrium conditions (B) respectively. The estimated stereoselectivity is listed in Table 2.

3) β_2-[Co(α-Me-sal$_2$en)(N-Bz,Me-L-ala)]: The absorbance at 600 nm of the reaction solution between [Co(α-Me-sal$_2$en)] and *N*-benzyl-*N*-methyl-L-alanine became a constant value within a few minutes after the start of the reaction: the complexation of *N*-benzyl-*N*-methyl-L-alanine is quite fast, as are those of *N*-benzyl-L-alanine and *N*-methyl-L-alanine. Unlike the above two amino acids, however, the reaction solution of *N*-benzyl-*N*-methyl-L-alanine showed a large minus rotation at 435 nm from the beginning of the reaction, and no mutarotation was observed. The rotation of free *N*-benzyl-*N*-methyl-L-alanine itself is negligibly small at 435 nm under the experimental conditions employed ($c=1.0\times10^{-3}$ mol dm^{-3}). These facts indicate that only the $(-)_{435}$-isomer of β_2-[Co(α-Me-sal$_2$en)(*N*-Bz,Me-L-ala)] complex is produced by the formation reaction, and that the other isomers are not produced. As mentioned later, the other isomers may be too unstable to be produced. In fact, only the $(-)_{435}$-isomer (Complex V) was isolated from the reaction solution. Complex V itself is not so stable; thus, it decomposes at a higher temperature in methanol.

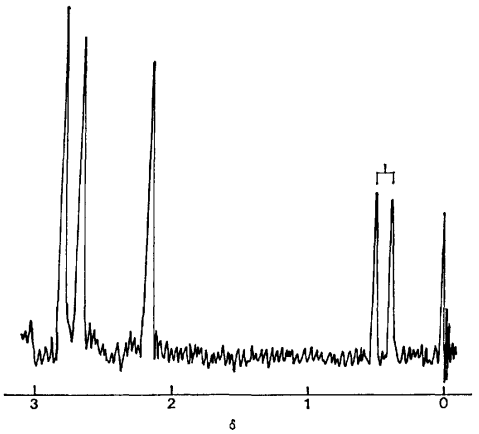

Fig. 6. The ^{1}H NMR spectrum of Λ_{RS}-β_2-[Co(α-Me-sal$_2$en)(*N*-Bz,Me-L-ala)] in $CDCl_3+CD_3OD$ (4:1).

Figure 6 shows the ^{1}H NMR spectrum of Complex V. The ^{1}H NMR spectrum corresponds to that of the only species of isomer, and no time dependence is observed. Since Complex V exhibits no mutarotation at 435 nm and no time dependence in its ^{1}H NMR spectrum, the stereoselectivity under the equilibrium conditions is estimated to be almost 100%.

The Structure and the Stereoselectivity of β_2-[Co(α-Me-sal$_2$en)(N-R-L-ala)] Complexes. 1) The Structure of the Complexes: The electronic absorption (AB) and the circular dichroism (CD) spectra of the isolated Complexes I—V are shown in Fig. 7. The CD spectra of Complexes I, III, and IV exhibited mutarotations The CD spectrum of Complex I gradually increased in its intensity, and that of Complex I at the equilibrium conditions corresponded to that of Complex II. The CD spectrum of Complex III gradually increased in its intensity, whereas that of Complex IV slowly decreased in its intensity, and the CD spectra of both Complexes at the equilibrium conditions coincided with each other. Further, the AB spectrum of Complex I soon after dissolution was very similar to that at the equilibrium conditions, and the AB spectrum at the equilibrium conditions coincided with that of Complex II. For Complexes III and IV, each AB spectrum soon after dissolution was very similar to that at the equilibrium conditions; AB spectra of both Complexes at the equilibrium conditions were the same.

Since the AB spectra of all the complexes isolated here resemble each other quite closely, it can be assumed that the geometrical structure with respect to the coordinated atoms is the same for all the complexes. The CD spectra of Complexes II, IV, and V, which correspond to the pure $(-)_{435}$-isomer of each *N*-R-L-ala complex, are very similar to that of $(-)_{435}$-Λ-β_2-[Co(α-Me-sal$_2$en)(L-ileu)].[8,16] Therefore, the Λ-β_2-structure can be assigned to the $(-)_{435}$-isomers. Figure 8 shows the vicinal effect of the coordinated *N*-R-L-ala in Complexes II, IV, and V. The vicinal effect was calculated by the use of the

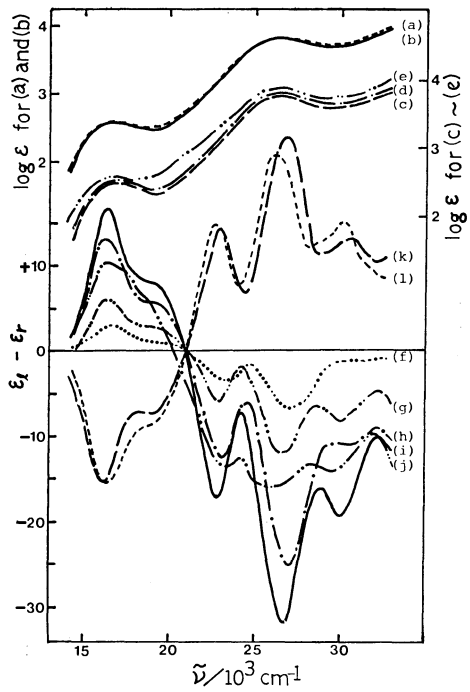

Fig. 7. AB and CD spectra of the complexes in a mixed solvent of $CHCl_3$ and CH_3OH (4:1).
(a): Complex I soon after dissolution, (b): Complex II, (c): Complex III soon after dissolution, (d): Complex IV soon after dissolution, (e) Complex V, (f): CD spectrum of Complex III at the isomeric ratio of 1:2 (Δ_{SS}-:Δ_{RS}-isomers), (g): Complex I at the isomeric ratio of 1:2 (Δ_{SS}-:Δ_{RS}-isomers), (h): Complex IV soon after dissolution, (i): Complex II, (j): Complex V, (k): the estimated CD spectrum of Δ_{SS}-β_2-[Co(α-Me-sal$_2$en)(*N*-Bz-L-ala)], and (l): the estimated CD spectrum of Δ_{SS}-β_2-[Co(α-Me-sal$_2$en)(*N*-Me-L-ala)].

following equation:[17]

$$\text{CD(vicinal) in } (-)_{435}\text{-isomer} = \text{CD}^{\text{A}} - 3(\text{CD}^{\text{B}} - \text{CD}^{\text{C}}), \quad (1)$$

where CD^A represents the CD for the pure $(-)_{435}$-isomer of β_2-[Co(α-Me-sal$_2$en)(*N*-R-L-ala)], and CD^B and CD^C represent the CD's of the 1:2 (B) and 1:1 (C) mixtures of Δ- and Δ-β_2-[Co(α-Me-sal$_2$en)(L-ala)][8,16] respectively. The vicinal effects of all the *N*-R-L-ala closely resemble each other; they are very similar to that of the L-pro complex,[9] except for the reversed CD sign. It is well known that L-proline can chelate to metal ion with *N(S)C(S)*-configuration, and that the vicinal effect of the asymmetric coordinated atom is much larger than that of the asymmetric atom far from the metal ion. Thus, *N(R)C(S)*-configuration can safely be assigned to the coordinated *N*-R-L-ala in Complexes II, IV, and V. The X-ray study for Complex II is now going on, and we have recently confirmed that Complex II takes the Δ_{RS}-β_2-structure.[18]

The estimated CD curves for the $(+)_{435}$-isomers of the *N*-Me-L-ala and *N*-Bz-L-ala complexes, which exist in the course of the isomerization of Complexes I and III, are shown in Fig. 7. These CD curves were calculated by the use of the following equation:

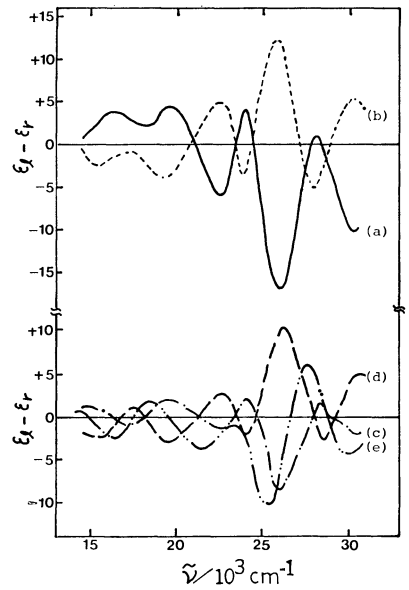

Fig. 8. The vicinal CD of the complexes.
(a) and (b) are those for Δ_{RS}- and Δ_{SS}-β_2-isomers of *N*-Bz-L-ala-complex respectively, (c) and (d) are those for Δ_{RS}- and Δ_{SS}-β_2-isomers of *N*-Me-L-ala-complex respectively, and (e) is the vicinal CD for Δ_{RS}-β_2-isomer of *N*-Bz,Me-L-ala-complex.

$$\text{CD}((+)_{435}\text{-isomer}) = 3\text{CD}^{\text{D}} - 2\text{CD}^{\text{A}}, \quad (2)$$

where CD^D represents the CD of the 1:2 mixture of the $(+)_{435}$- and $(-)_{435}$-isomers of the *N*-R-L-ala complex. The CD spectra could be measured in the course of the isomerization of the 1:1 mixture (Complexes I and III).[19] CD^A denotes the CD of the pure $(-)_{435}$-isomer of the *N*-R-L-ala complex. It is observed that the estimated CD curves for the $(+)_{435}$-isomers are almost mirror images of the CD spectra of the $(-)_{435}$-isomers. Thus, the Δ-β_2-structure can be assigned to the $(+)_{435}$-isomers. The vicinal effect of the *N*-R-L-ala in the $(+)_{435}$-isomers is shown in Fig. 8. The vicinal CD was calculated by the use of the following equation:

$$\text{CD(vicinal) in } (+)_{435}\text{-isomer} = \text{CD}^{\text{E}} - 3(\text{CD}^{\text{B}} - \text{CD}^{\text{C}}), \quad (3)$$

where CD^B and CD^C have been described above, and CD^E denotes the CD of the pure $(+)_{435}$-isomer. Since the vicinal effect is almost a mirror image of that of the corresponding *N*-R-L-ala in the $(-)_{435}$-isomers, the *N(S)C(S)*-configuration can be assigned to the *N*-R-L-ala in the $(+)_{435}$-isomers.

From these results and discussion, it can be concluded that the $(-)_{435}$-isomers of *N*-R-L-ala complex (Complexes II, IV, and V) take the Δ_{RS}-β_2-structure, whereas the $(+)_{435}$-isomer of the *N*-Bz-L-ala complex and one of the two $(+)_{435}$-isomers of the *N*-Me-L-ala complex, which isomerizes more slowly, take the Δ_{SS}-β_2-structure.

2) The Stereoselectivity: The stereoselectivity at the equilibrium conditions of *N*-R-L-ala complex is listed in Table 2. A quite high stereoselectivity can be established in the Co(Schiff base) complexes of *N*-R-L-ala, and the stereoselectivity is much higher than

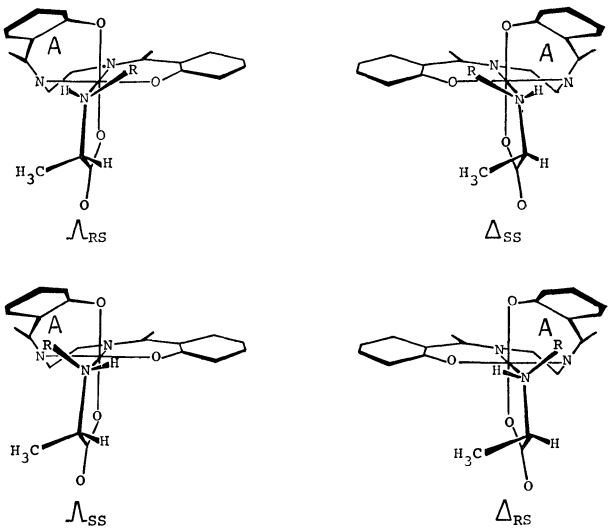

Fig. 9. Structure of four diastereoisomers of β_2-[Co(α-Me-sal$_2$en)(*N*-R-L-ala)].

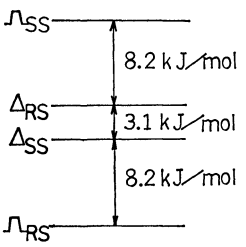

Fig.10. The relative energy difference among four diastereoisomers of *N*-Me-L-ala-complex.

that of Co(trien) complexes. Since the stereoselectivity under the equilibrium conditions can be regarded as thermodynamic in origin, the sterochemical reason why there is a large difference in the thermodynamic stability among the diastereoisomers of Co(Schiff base) complexes is developed as follows.

(a) N-*Me*-L-*ala Complex*: The possible four β_2-isomers are shown in Fig. 9. It is characteristic of a tetradentate Schiff base ligand with β-configuration that the chelate ring (A) in Fig. 9 inclines toward the side of the coordinated amino acid about 30° from the N–Co–O plane of (A). In the cases of Λ_{RS}- and Λ_{SS}-β_2-isomers, the molecular models indicate that the inclination of the chelate ring (A) brings about an extreme steric closeness (1.2—1.4 Å) between the distored chelate ring (A) and the *N*-methyl group of the coordinated amino acid. However, in the cases of Λ_{RS}- and Δ_{SS}-β_2-isomers, there is no abnormal steric closeness between them. In the cases of Λ_{RS}- and Δ_{SS}-β_2-isomers, the *N*-methyl group somewhat approaches to the two phenolic oxygen atoms of α-Me-sal$_2$en ligand (about 2.3 Å), but the steric repulsion seems to be much weaker than that between the chelate ring (A) and the *N*-methyl group in the Δ_{RS}- and Λ_{SS}-β_2-isomers. Thus, it can be assumed that Λ_{RS}- and Δ_{SS}-β_2-isomers are much more stable than Δ_{RS}- and Λ_{SS}-β_2-isomers. In the case of L-pro complex, it has been reported that the Δ_{SS}-β_2-isomer is more stable than the Λ_{SS}-β_2-isomer at about 11.3 kJ mol^{-1} or more.[9]

On the other hand, the conformational relationship between the *N*-methyl and *C*-methyl groups of the *N*-methyl-L-alaninato ligand is staggered (*trans*) in the Λ_{RS}- and Λ_{RS}-β_2-isomers, but it is nearly eclipsed (*cis*) in the Λ_{SS}- and Δ_{SS}-β_2-isomers. And, staggered is more stable than eclipsed. In the case of Co(α-Me-sal$_2$en) complex with *N*-methyl-L-alanine, the energy difference is estimated to be about 8.2 kJ mol^{-1} from the isomeric ratio, Λ_{RS}-isomer/Λ_{SS}-isomer, at the equilibrium conditions, and it is clearly smaller than the steric repulsion energy difference, 11.3 kJ mol^{-1}, between the Schiff base ligand and the *N*-methyl group mentioned above.

Consideration of the above two factors, which are though to contribute greatly to the stability of the diastereoisomers, allows the relative stability among the four isomers to be estimated to be Λ_{RS}->Δ_{SS}->Λ_{RS}->Λ_{SS}-β_2-isomers. The estimated energy differences among the four isomers are shown in Fig. 10.

In the cases of Co(trien) and Co((3*S*,8*S*)-dimetrien) complexes with *N*-methyl-L-alanine,[1,6] the isomeric ratio at the equilibrium conditions is Λ_{RS}-:Δ_{SS}-:Λ_{RS}-isomers=about 60:20:20 and about 85:11:4 respectively. On the other hand, in the case of the Co(α-Me-sal$_2$en) complex, the isomeric ratio at the equilibrium conditions is Λ_{RS}-:Λ_{SS}-isomers=96.5:3.5. The difference in the stereoselectivity between the Co(N$_4$) and Co(Schiff base) complexes seems to come from the following steric reasons: 1) the steric interaction between *N*-methyl group and the tetradentate ligand is much stronger in a Co(Schiff base) complex than a Co(N$_4$) complex, so that Λ_{RS}- and Λ_{SS}-isomers are too unstable to exist at the equilibrium conditions in the case of the Co(Schiff base)-system. 2) In order to decrease the steric closeness between *N*-methyl and *C*-methyl groups in the *N(S)C(S)*-configuration, the chelate ring of *N*-methyl-L-alanine in Co(trien) complex takes a nearly puckered conformation.[20] However, in the case of Co(Schiff base) complex, when the chelate ring takes this nearly puckered conformation, the *N*-methyl group comes close to one of the phenolic oxygen atoms of the Schiff base ligand. Thus, the energy difference between Λ_{RS}- and Λ_{SS}-isomers is much larger in the Co(Schiff base)-system than in the Co(N$_4$)-system.

(b) N-*Bz*-L-*ala Complex*: The steric crowding brough about by a *N*-benzyl group is much larger than that by a *N*-methyl group. Accordingly, the steric interaction between the *N*-alkyl group and the chelate ring (A) in Fig. 9 is much stronger in the *N*-Bz-L-ala complex than in the *N*-Me-L-ala complex, when they take Δ_{RS}- and Λ_{SS}-β_2-configurations. The Δ_{RS}- and Λ_{SS}-isomers of the *N*-Bz-L-ala complex are thus thought to be more unstable than those of the *N*-Me-L-ala complex. Further, the *cis* interaction between the *N*-alkyl group and the *C*-methyl group of the chelated amino acid in the *N(S)C(S)*-configuration is also much stronger in the *N*-Bz-L-ala complex than in the *N*-Me-L-ala complex. Thus, in the case of *N*-Bz-L-ala complex, only the Λ_{RS}-β_2-isomer is favored stereoselectively under the equilibrium conditions.

(c) N-*Bz,Me*-L-*ala Complex*: From the strong steric

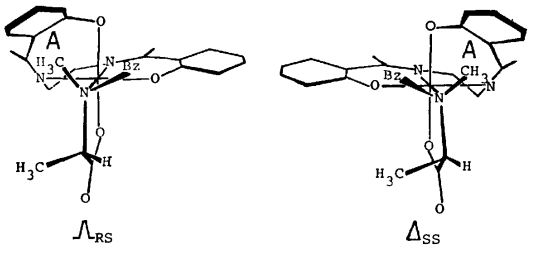

Fig. 11. The steric structure of Λ_{RS}- and Λ_{SS}-β_2-isomers of *N*-Bz,Me-L-ala-complex.

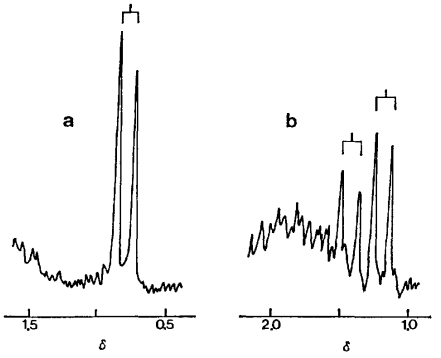

Fig. 12. The ^{1}H NMR spectra of Co(sal$_2$-(*S*,*S*)-chxn)-complexes in a mixed solvent of $CDCl_3$ and CD_3OD (4:1).
a: Λ_{RS}-β_2-[Co(sal$_2$-(*S*,*S*)-chxn)(*N*-Bz-L-ala)], b: a mixture of Λ_{RR}- and Δ_{SR}-β_2-isomers of [Co(sal$_2$-(*S*,*S*)-chxn)(*N*-Bz-D-ala)].

intereaction between the *N*-benzyl group and the distored chelate ring (A), the Λ_{RS}- and Λ_{SS}-β_2-isomers of the *N*-Bz,Me-L-ala complex are though to be relatively unstable as compared with the Λ_{RS}- and Δ_{SS}-isomers of the complex. Further, as shown in Fig. 11, even when the complex takes Λ_{RS}- and Δ_{SS}-configurations, the strong steric repulsion between the *N*-methyl group and the chelate ring (A) is inevitable: the *N*-Bz,Me-L-ala complex is thought to be more unstable than the *N*-Me-L-ala and *N*-Bz-L-ala complexes. In fact, Complex V decomposes at a higher temperature. The *cis* interaction between *N*-alkyl group and *C*-methyl group is also inevitable in the case of the *N*-Bz,Me-L-ala complex. However, the *cis* interaction between *N*-methyl group and *C*-methyl group in the Λ_{RS}-configuration is weaker than that between *N*-benzyl group and *C*-methyl group in the Δ_{SS}-configuration. Thus, the *N*-Bz,Me-L-ala complex takes the Λ_{RS}-β_2-structure stereoselectively.

Stereospecificity of Co(sal$_2$-(S,S)-chxn) Complex. It has been reported that a Co(sal$_2$-(*S*,*S*)-chxn) complex assumes the Λ-β_2-structure excusively when it reacts with amino acids such as L- and D-alanines and L- and D-valines.[11] Accordingly, it can be expected that the Co(sal$_2$-(*S*,*S*)-chxn) complex produces a complex containing *N*-benxyl-L-alanine stereospecifically, when it is allowed to react with racemic *N*-benzylalanine, because the Co(α-Me-sal$_2$en) complex with *N*-benzyl-L-alanine, which is similar, shows almost 100% stereoselectivity for the Λ_{RS}-β_2-configuration, as has been mentioned above.

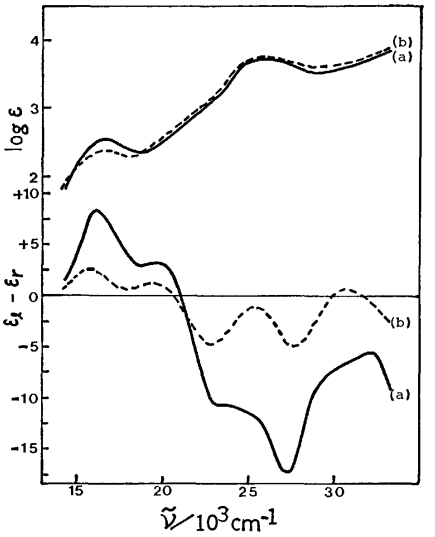

Fig. 13. AB and CD spectra of Co(sal$_2$-(*S*,*S*)-chxn)-complexes in the same solvent as that in Fig. 7.
a: *N*-Bz-L-ala, b: *N*-Bz-D-ala.

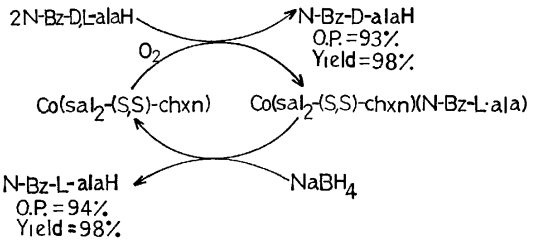

Fig. 14. The scheme for the optical resolution of *N*-benzylalanine with Co(sal$_2$-(*S*,*S*)-chxn)-complex.
The optical purity shown in this figure is the value when the reaction molar ratio between [Co(sal$_2$-(*S*,*S*)-chxn)] and racemic *N*-benzylalanine is 1:2.

Figure 12 shows the ^{1}H NMR spectra of the Co(sal$_2$-(*S*,*S*)-chxn) complexes with *N*-Bz-L-ala and *N*-Bz-D-ala. From the *C*-methyl signals of the coordinated *N*-benzyl amino acids, it is clear that the *N*-Bz-L-ala complex (Complex VI) exists as only one species of isomer but the *N*-Bz-D-ala complex (Complex VII) exists as a mixture of two species of isomer at about 1:1.5 isomeric ratio.

Figure 13 shows the AB and CD spectra of the complexes. Since the AB and CD spectra of the *N*-Bz-L-ala complex are very similar to those of $(-)_{435}$-Λ-β_2-[Co(α-Me-sal$_2$en)(L-ileu)],[8,16] the Λ_{RS}-β_2-structure can be assigned to it. In the case of the *N*-Bz-D-ala complex, the AB and CD spectra are also similar to those of $(-)_{435}$-Λ-β_2-[Co(α-Me-sal$_2$en)(L-ileu)]; however, the CD intensity is much smaller than that of the *N*-Bz-L-ala complex. The molecular model of Co(sal$_2$-(*S*,*S*)-chxn) complexes suggests that the sal$_2$-(*S*,*S*)-chxn moiety can take Λ-β-configuration as well as Λ-β-form, although the strain energy is much larger in Λ-β-configuration. Therefore, the *N*-Bz-D-ala complex may be a mixture of Λ_{RR}-β_2- and Δ_{SR}-β_2-isomers with the isomeric ratio of about 1.5:1.

The formation of the Δ_{SR}-β_2-isomer was not expected. It is expected that the Δ_{SR}-β_2-isomer will be more unstable than the Λ_{RR}-β_2-isomer and the Λ_{RR}-

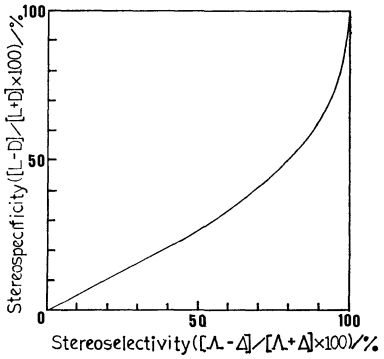

Fig.15. The estimated relationship between stereoselectivity of Co(α-Me-sal$_2$en)-complex and stereospecificity in the reaction of [Co(sal$_2$-(*S*,*S*)-chxn)] with racemic amino acid (the molar ratio=1:2).

β_2-isomer will be much more unstable than the Λ_{RS}-β_2-isomer of *N*-Bz-L-ala complex. Thus, our initial expectations may still be satisfied.

In order to estimate the stereospecificity of the Co(sal$_2$-(*S*,*S*)-chxn) complex toward *N*-benzyl-L-alanine, we examined the reaction of [Co(sal$_2$-(*S*,*S*)-chxn)] and racemic *N*-benzylalanine at 1:2 reaction molar ratio under the air-oxidation conditions. The reaction scheme is shown in Fig. 14. The detailed experimental procedure is described in the Experimental section. Two points should be noted; 1) no racemization of *N*-benzylalanine is observed in the employed experimental conditions, and 2) the recovered [Co(sal$_2$-(*S*,*S*)-chxn)] can be used repeatedly.

From the optical purity of the isolated *N*-benzylalanine, it can be concluded that *N*-benzyl-L-alanine coordinates to the Co(sal$_2$-(*S*,*S*)-chxn) complex in a high stereospecificity (93—94%). However, the stereospecificity did not reach 100%. Figure 15 shows the relationship between the stereoselectivity for Δ- and Λ-isomers in the Co(α-Me-sal$_2$en) complex and the stereospecificity in the reaction of similar Co(sal$_2$-(*S*,*S*)-chxn) complex with a racemic amino acid at 1:2 reaction molar ratio. The relationship was calculated by the use of Equations (3) and (4) in Ref. 11. This figure indicates that the higher the stereoselectivity, the higher the stereospecificity, but their values are not the same. For example, when the stereoselectivity is 98%, the stereosepecificity is 82%. and when it is 99.7%, the stereospecificity is 93%. From these calculations, it is estimated that the stereoselectivity of β_2-[Co(α-Me-sal$_2$en)(*N*-Bz-L-ala)] is not complete but it may reach about 99.7%.

It should be noted that when the reaction molar ratio between [Co(sal$_2$-(*S*,*S*)-chxn)] and racemic *N*-benzylalanine was 1:100, the optical purity of the *N*-benzylalanine recovered from the produced complex was almost 100% (L-form).

The authors whish to express their deep thanks to Professor J. Hidaka of Tsukuba University and to Professor K. Sone and Dr. Y. Fukuda of Ochanomizu University for their kind assistance with the CD spectral measurements. This work was partly supported by a Grant-in-Aid for Scientific Research No. 547038 from the Ministry of Education, Science and Culture.

References

1) M. Saburi and S. Yoshikawa, "Chemistry of Octahedral Complexes," Kagaku Sosetsu, Gakkai Shuppan Center, Tokyo (1976), Vol. 13, p. 109.
2) D. A. Buckingham, L. G. Marzilli, and A. M. Sargeson, *J. Am. Chem. Soc.*, **89**, 5133 (1967).
3) M. H. Ghandehari, T. N. Anderson, D. R. Boone, and H. Eyring, *J. Am. Chem. Soc.*, **92**, 6466 (1970).
4) The data cited here is the isomeric ratio between Λ_L- and Λ_D-isomers: M. Yamaguchi, S. Yamamatsu, T. Furusawa, S. Yano, M. Saburi, and S. Yoshikawa, *Inorg. Chem.*, **19**, 2010 (1980).
5) D. A. Buckingham, J. Dekkers, A. M. Sargeson, and M. Wein, *Inorg. Chem.*, **12**, 2019 (1973).
6) D. A. Buckingham, I. E. Maxwell, and A. M. Sargeson, *Inorg. Chem.*, **9**, 2663 (1970).
7) M. Yamaguchi, S. Yano, M. Saburi, and S. Yoshikawa, *Bull. Chem. Soc. Jpn.*, **53**, 691 (1980).
8) Y. Fujii, T. Isago, M. Sano, N. Yanagibashi, S. Hirasawa, and S. Takahashi, *Bull. Chem. Soc. Jpn.*, **49**, 3509 (1976).
9) Y. Fujii, K. Shiono, K. Ezuka, and T. Isago, *Bull. Chem. Soc. Jpn.*, **53**, 3537 (1980).
10) The following abbreviations are used: *N*-Bz-L-ala=anion of *N*-benzyl-L-alanine, *N*-Me-L-ala=anion of *N*-methyl-L-alanine, *N*-Bz,Me-L-ala=anion of *N*-benzyl-*N*-methyl-L-alanine, *L*-ala=anion of L-alanine, L-val=anion of L-valine, L-ileu=anion of L-isoleucine, L-phe=anion of L-phenylalanine, L-pro=anion of L-proline. In the notations used in this paper: Λ_{RS}, Δ_{SS}, Δ_{RS}, and Λ_{SS}, the first suffix (R or S) represents the configuration of the asymmetric nitrogen atom of the coordinated *N*-alkyl amino acid, and the second suffix (S) denotes that of the asymmetric carbon atom of the amino acid.
11) Y. Fujii, M. Sano, and Y. Nakano, *Bull. Chem. Soc. Jpn.*, **50**, 2609 (1977).
12) A Biggoto, G. Costa, G. Mestroni, G. Pellizer, A. Puxeddu, E. Reisenhofer, L. Stefani, and T. Tauzer, *Inorg. Chem. Acta, Reviews*, **4**, 41 (1970).
13) H. Aoi, M. Ishimori, S. Yoshikawa, and T. Tsuruta, *J. Organomet. Chem.*, **85**, 241 (1975).
14) P. Quitt, J. Hellerbach, and K. Vogler, *Helv. Chim. Acta*, **46**, 327 (1963).
15) Y. Fujii, S. Hirasawa, and S. Takahashi, *Chem. Lett.*, **1976**, 817.
16) In previous paper,[8,11] the β_1-structure was assigned tentatively to the [Co(Schiff base)(amino acid)] complexes; however, it has been found recently, in our X-ray study for $(-)_{435}$-[Co(α-Me-sal$_2$en)(L-ileu)]·1.5H$_2$O, that the complex has the β_2-structure: K. Kushi, R. Tamura, M. Kuramoto, T. Yoshizawa, H. Yoneda, and Y. Fujii, *J. Chem. Soc., Chem. Commun.*, **1978**, 266.
17) $3(CD^B - CD^C)$ corresponds to the configurational effect in the β_2-[Co(α-Me-sal$_2$en)(L-ala)] complex.
18) Will be published elsewhere.
19) In the case of the *N*-Me-L-ala complex, Complex I contains three isomers: two $(+)_{435}$-isomers and one $(-)_{435}$-isomer. However, one of the two $(+)_{435}$-isomers isomerizes quite rapidly. Thus, the contribution of one of the two $(+)_{435}$-isomers to the CD intensity at the isomeric ratio of 1:2 between $(+)_{435}$- and $(-)_{435}$-isomers can be neglected.
20) B. F. Anderson, D. A. Buckingham, G. J. Gainsford, G. B. Robertson, and A. M. Sargeson, *Inorg. Chem.*, **14**, 1658 (1975).

  Bull. Chem. Soc. Jpn., 54, 2039—2044 (1981)

Substituent and Solvent Effects in the Reactions of Diaryldiazomethanes with 2,3-Dichloro-5,6-dicyanobenzoquinone

Takumi Oshima and Toshikazu Nagai*

Institute of Chemistry, College of General Education, Osaka University, Toyonaka, Osaka 560

(Received August 18, 1980)

Kinetic studies have been made of the reactions of fifteen *meta*- and *para*-substituted diphenyldiazomethanes(DDMs) with 2,3-dichloro-5,6-dicyanobenzoquinone(DDQ) in benzene. The second-order rate constants, k, increased with the electron-donability of the substituents, and the value could be correlated with the Yukawa-Tsuno equation: $\log k/k_0 = -2.33(\sigma^0 + 0.47\Delta\bar{\sigma}_R^+) + 0.017$, ($r$=0.996,30 °C). The ρ value, −2.33, indicates the development of a positive charge at the diazo carbon in the transition state, while the R value, 0.47, confirms the moderate stabilization of the positive charge by the π-electronic contribution of the para substituents. The rate constants have also been determined for the reaction of diphenyldiazomethane(DDM) with DDQ in 28 aprotic solvents. The effects of solvents can be interpreted in terms of the basicity and the steric nature of the solvents. The products of these reactions were poly(2,3-dichloro-5,6-dicyanohydroquinone benzhydryl ether)s, which were easily convertible into benzophenones and α,α-dimethoxydiphenylmethane, together with 2,3-dichloro-5,6-dicyanohydroquinone, under the influence of water and methanol. These solvolysis products were also obtained in excellent yields in the initial presence of these additives.

In view of the general interest in reactions of diazoalkanes with quinones, most of the synthetic and mechanistic works have been carried out by use of the simplest diazoalkane, *e.g.*, diazomethane.[1] However, little is known of the reactions of aryl- and diaryldiazomethanes[2] with quinones or of kinetic studies of these systems.

We previously reported that chloranil decomposed a variety of substituted diphenyldiazomethanes(DDMs) to produce poly(2,3,5,6-tetrachlorohydroquinone benzhydryl ether)s and that the second-order rate constants were very dependent on the substituents and the solvents.[3] In this paper, we extend our studies of substituent and solvent effects to the kinetics of the reactions of DDMs with 2,3-dichloro-5,6-dicyanobenzoquinone(DDQ).

Results and Discussion

Product Studies. As well as in the case of chloranil,[3] the reactions of fifteen *meta*- and *para*-substituted DDMs with an equimolar amount of DDQ in benzene at 30 °C were much more accelerated with the increase in the electron-donating abilities of the substituents. All these reactions, more or less accompanied by an evolution of N_2, gave resinous products which were highly sensitive to hydroxylic solvents. When these products were hydrolyzed, corresponding benzophenones (**3**) and 2,3-dichloro-5,6-dicyanohydroquinone($DDQH_2$) were isolated in most cases greater than 95%. Moreover, the methanolysis of the product in the case of diphenyldiazomethane(DDM) afforded α,α-dimethoxydiphenylmethane (**5**) in an 81% yield, together with **3** (15%) and $DDQH_2$ (96%). These chemical findings strongly suggest the structure of the 1:1 reaction products to be a hydroquinone polyether linkage similar to that previously considered for the chloranil–DDMs systems.[3] This suggestion is also supported by the representative IR spectrum of the DDM–DDQ system, which exhibited a complete loss of the characteristic carbonyl absorption of DDQ.

The ether linkage may be made up by the successive combination of intermediary diazonium betaines(I) or carbonium betaines(II), as is predicted in Scheme 1. The propagation may be terminated by the action of the residual water present in the solvent. Further action of water and methanol can cause the hydrolytic and methanolytic cleavage of the ether bonds to give *gem*-diols (**2**) and **5**, together with $DDQH_2$; the *gem*-diols are transformed into **3**. In the case of methanolysis, the formation of **3** as a by-product is attributable to the terminal benzhydrol moiety, which primarily degrades into α-methoxy-α-phenylbenzyl alcohol (**4**), which is itself easily convertible into **3**. Therefore, it is possible to estimate the average polymerization degree (n) from the ratio of **5** (81%) to **3** (15%); the value over 5 corresponds to n=6—7.

On the other hand, the initial presence of water and methanol as additives induced solvolysis reactions giving, respectively, **3** and **5**, along with $DDQH_2$. These products are thought to be yielded by the successive nucleophilic attack of these additives on the betaine intermediate, as is also depicted in Scheme 1. These reactions were accompanied by trace amounts of benzhydrol (**8**) and 2,3-dichloro-5,6-dicyanohydroquinone dibenzhydryl ether (**7**) arising from the acid-induced decomposition of DDM by the resulting $DDQH_2$; **8** seems to be afforded by the hydrolysis of 2,3-dichloro-5,6-dicyanohydroquinone benzhydryl ether (**6**).

Apparently, the susceptibility of rates to the substituents, the stoichiometry of the reactions, and the solvolysis evidence all confirm that the present diaryldiazomethanes(DDMs)–DDQ systems proceed through a reaction course similar to that of chloranil systems.[3]

Kinetic Studies. Substituent Effects: The reactions of DDMs with DDQ in benzene can be followed spectrophotometrically by monitoring the disappearance of the absorption of DDQ at 408 nm or that of the combined absorptions of both components at 500 nm in the case of nitro-substituted DDMs. These reactions have been found to obey a second-order kinetic law. The rate constants, k, determined for the fifteen *meta*- and *para*-substituted DDMs at various temperatures are listed in Table 1, together

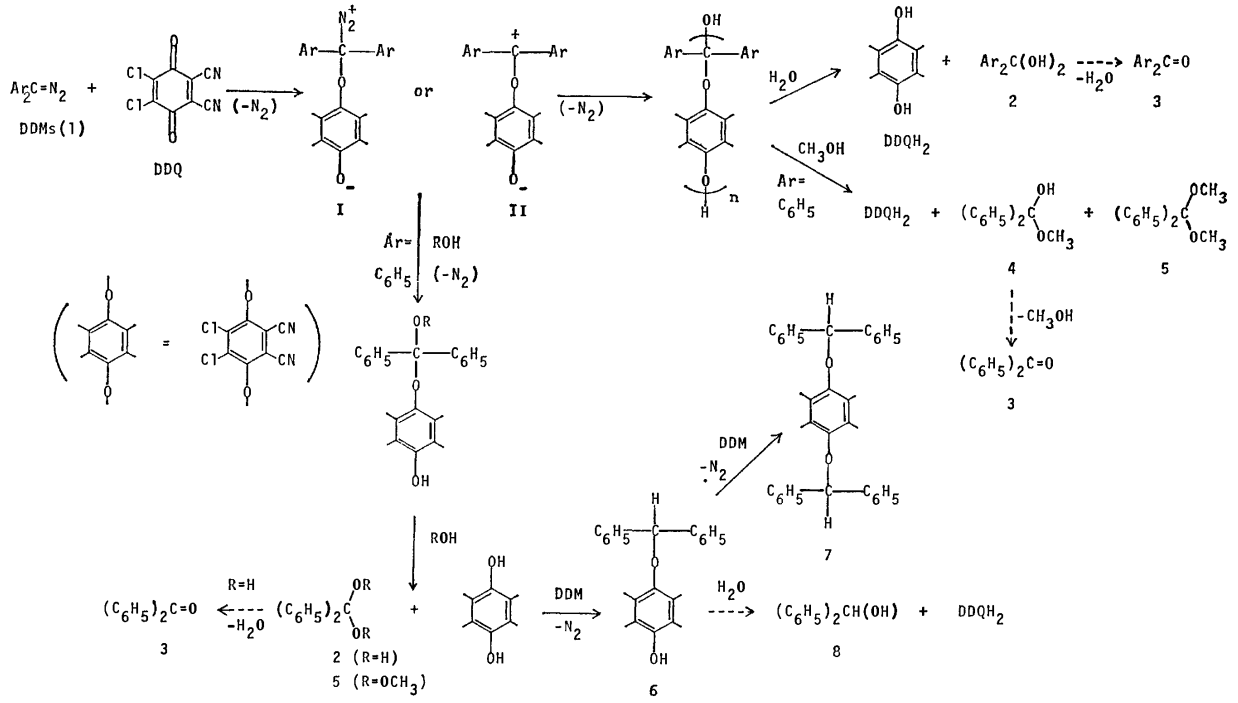

Scheme 1.

Table 1. Second-order rate constants, and activation parametes for the reactions of the substituted DDMs(**1a—o**) with DDQ in benzene

DDMs	Substituents	$k^{a)}$/l mol^{-1} g^{-1}			$\Delta H^{\neq}$	$\Delta S^{\neq}$
		30 °C	40 °C	50 °C	kJ mol^{-1}	J mol^{-1} K^{-1}
1a	*p,p'*-OCH_3	256 (1.11×10^{-1})	—	—	—	—
1b	*p*-OCH_3, *p'*-CH_3	88.4 (4.06×10^{-2})	—	—	—	—
1c	*p*-OCH_3	29.1 (1.95×10^{-2})	—	—	—	—
1d	*p,p'*-CH_3	25.4 (1.42×10^{-2})	—	—	—	—
1e	*p*-OPh	10.3 (6.85×10^{-3})	—	—	—	—
1f	*p*-CH_3	8.58 (6.67×10^{-3})	—	—	—	—
1g	*m*-CH_3	5.49 (3.41×10^{-3})	8.55	12.1	29.5	−133
1h	*p*-Ph	3.26 (3.15×10^{-3})	4.74	6.68	26.6	−147
1i	*p*-H	3.05 (2.66×10^{-3})	4.96	7.72	35.2	−119
1j	*p*-F	1.88 (2.87×10^{-3})	3.04	4.80	35.6	−126
1k	*p*-Cl	0.935 (2.07×10^{-3})	1.45	2.28	33.7	−134
1l	*m*-Cl	0.322 (1.05×10^{-3})	0.505	0.778	33.3	−144
1m	*p,p'*-Cl	0.283 (—)	0.510	0.831	41.2	−119
1n	*m*-NO_2	0.102 (5.17×10^{-4})	0.188	0.338	46.2	−112
1o	*p*-NO_2	0.0295 (1.15×10^{-4})	0.0594	0.113	52.1	−112

a) The values in parentheses are the second-order rate constants for the reactions of DDMs with chloranil in benzene.

with the activation parameters. This table also includes the comparable kinetic data of the reactions of DDMs with chloranil in benzene at 30 °C. It is noteworthy that the present reactions were much more accelerated with an increase in the electron-releasing abilities of the substituents; the *p,p'*-dimethoxy substituents caused a *ca.* 9000-fold increase in the rates compared with the *p*-nitro substituent, though the chloranil system showed only a 960-fold increase.

The dependency of log k/k_0 on the Hammett σ[4] and Brown σ^+[5] constants is shown in Fig. 1. As may be noticed, the additivity of the substituent constants holds for the disubstituted DDMs. Four *meta*-substituted DDMs gave a sufficient linear dependence ($\rho=-2.19$), $r=0.990$ (correlation coefficient) when the simple Hammett equation and normal σ values were used. When correlating all the DDMs and using the normal σ values, we obtained slighlty worse results ($\rho=-2.65$, $r=0.983$). The correlation line curved somewhat upward from the meta line. The replacement of σ by σ^+ displayed a significant curvature with a ρ value of −1.67 ($r=0.976$), wherein the meth-

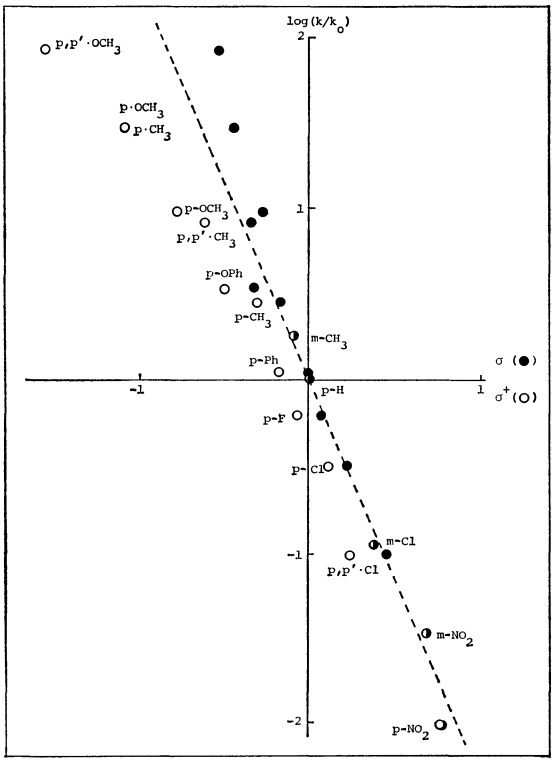

Fig. 1. Plot of $\log k/k_0$ against the Hammett σ(●) and Brown σ^+(○) constants.

oxy substituents induced the marked deviation from the meta line. Thus, the one-parameter equation did not well fit the correlation of *para*-substituted DDMs. We used, therefore, the two-parameter Yukawa-Tsuno equation,[6] $\log k/k_0 = \rho(\sigma^0 + R\Delta\bar{\sigma}_R^+)$, where σ^0, R, and $\Delta\bar{\sigma}_R^+$ are the normal substituent constant, the resonance reaction constant, and the resonance substituent constant respectively. The two-parameter treatment provided a better correlation (Eq. 1):

$$\log k/k_0 = -2.33(\sigma^0 + 0.47\Delta\bar{\sigma}_R^+) + 0.017(r=0.996,\ s=0.09,\ n=15). \quad (1)$$

The ρ value of -2.33 is consistent with the development of a positive charge at the diazo carbon in the transition state, while the R value of 0.47 indicates an almost equivalent stabilization of the positive charge by both the inductive and the resonance contributions of the *para* substituents.

When a similar regression analysis was applied to the chloranil–DDMs reactions in benzene (Table 1), a sufficient correlation (Eq. 2) was also obtained with a ρ value of -1.39 and an R value of 0.69:†

$$\log k/k_0 = -1.39(\sigma^0 + 0.69\Delta\bar{\sigma}_R^+) + 0.0314(r=0.989,\ s=0.12,\ n=14). \quad (2)$$

A comparison of the Hammett parameters in the two systems is of usefulness in obtaining some information about the transition state. As well as the chloranil–DDMs reactions[3] the present DDQ reactions are postulated to proceed through the polar transition state depicted below, though the polar transition state of 1,3-dipolar addition can not be ruled out. The negatively larger ρ value for DDQ reactions implies that DDQ induces a more positive charge in the diazo carbon, probably because its electron acceptability is stronger than that of chloranil.[7] How-

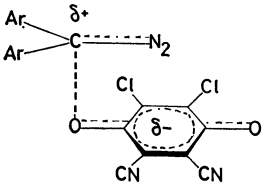

ever, the extent of the resonance stabilization of the positive charge is somewhat lower in DDQ reactions (0.47) than in chloranil reactions (0.69). This discrepancy can be explained by speculating that the higher electron-acceptor ability of DDQ tends to develop more the bond between the diazo carbon and the quinone oxygen. That is, the sp^2 hybridization of the diazo carbon is reduced, and the effect of resonance contribution is thereby lessened, compared to the case of chloranil.

Solvent Effects: In a previous paper, we discussed the kinetics of the reaction of DDM with chloranil in several aprotic solvents.[3] The kinetic solvent effects were tentatively interpreted in terms of the stabilization of the initial state relative to the transition state. We have now extended these studies of solvent effects to the kinetics of the present reaction. As is shown in Table 2, the rates were much more accelerated in the halogenated solvents, while they were decelerated in tetrahydrofuran or toluene; the k values for chloroform and carbon tetrachloride are *ca.* 110—160 times greater than for toluene. Nonpolar carbon tetrachloride is also noticiable for bringing about a 10—50-fold increase in the rate compared to the polar acetonitrile and acetone. These kinetic results imply that the reaction rate is primarily influenced by the solvation of the initial state rather than by that of the transition state for which the polar-activated complex was deduced from the kinetic substituent effects. This situation is represented in the free-energy profile, where the stronger solvation of initial reactants overcomes the accelerating solvation of the present polar-activated complex, consequently increasing the free activation energy (Fig. 2).

Since DDQ is a strong electron-acceptor, like chloranil and TCNE,[7] such specific solute-solvent interactions as the formation of a charge-transfer complex may be expected, especially in the solvents with a high basicity.[8] Therefore, we attempted to correlate $\log k$ with some of the solvent-basicity parameters, *e.g.*, $\Delta\nu_D$,[9] β,[10] and DN.[11] The symbols have the following meanings: $\Delta\nu_D$ is defined as the relative difference between the O–D absorption band of methanol-*d* observed in a given solvent and that in benzene; β, as the hydrogen-bonding acceptor basicity, and DN (donor number), as the negative ΔH values for 1:1 adduct formation between antimony pentachloride and electron-pair donor solvents in 1,2-dichloroethane.

† We have reported in our previous paper[3] that in the THF medium the chloranil systems also gave an excellent correlation with a somewhat large negative ρ value of -1.67 and a substantially equal R value of 0.66.

Table 2. Rate constants and activation parameters for the reaction between DDM and DDQ in aprotic solvents, with solvent basicity parameters

	Solvents	k/l mol^{-1} s^{-1} 30 °C	40 °C	50 °C	$\Delta H^{\ddagger}$ kJ mol^{-1}	$\Delta S^{\ddagger}$ J mol^{-1} K^{-1}	$\Delta\nu_D$	β	DN
1	Chloroform	169	—	—	—	—	−17	—	—
2	Dichloromethane	146	—	—	—	—	−12	—	—
3	Carbon tetrachloride	136	—	—	—	—	−21	—	0
4	1,2-Dichloroethane	134	—	—	—	—	2	—	0
5	Diisopropyl ether	56.8	—	—	—	—	75	0.466	—
6	Bromobenzene	39.2	—	—	—	—	−1	0.062	—
7	Chlorobenzene	30.8	—	—	—	—	−2	0.071	—
8	Nitrobenzene	30.3	—	—	—	—	21	—	4.4
9	Fluorobenzene	27.6	—	—	—	—	—	—	—
10	Methyl chloroacetate	25.1	—	—	—	—	27	—	—
11	Dibutyl ether	12.8	18.7	24.8	24.3	−144	—	0.453	—
12	Acetonitrile	11.2	14.3	18.2	17.2	−170	49	0.31	14.1
13	Diethyl ether	10.3	—	—	—	—	78	0.466	19.2
14	Propionitrile	7.85	10.6	12.9	17.6	−170	52	—	16.1
15	1,2-Dimethoxyethane	4.20	7.27	11.5	38.4	−107	71	0.405	24
16	Benzene	3.05	4.56	7.72	35.2	−119	0	0.1	0
17	Acetone	2.91	—	—	—	—	64	0.478	17
18	Ethyl methyl ketone	2.58	—	—	—	—	57	—	—
19	1,4-Dioxane	2.22	3.08	4.56	26.8	−150	77	0.369	14.8
20	Dimethoxymethane	2.10	—	—	—	—	—	—	—
21	Ethyl acetate	1.81	2.74	3.93	29.0	−145	39	0.446	17.1
22	Ethylbenzene	1.56	2.44	4.78	43.1	−99.5	4	—	—
23	Isopropyl acetate	1.38	2.02	3.00	29.0	−147	—	—	—
24	Methyl acetate	1.34	2.16	3.42	35.6	−125	36	0.454	16.5
25	Tetrahydrofuran	1.27	2.24	3.46	38.2	−117	90	0.550	20
26	Propyl acetate	1.13	1.92	3.05	37.8	−119	—	—	—
27	Tetrahydropyran	1.12	—	—	—	—	93	0.544	—
28	Toluene	1.03	1.85	3.20	43.6	−101	2	0.112	—

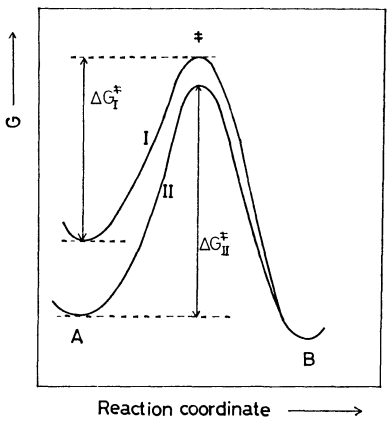

Fig. 2. Schematic free energy profiles for the reaction with non-solvated(I) and solvated(II) reactants (preferential solvation of the initial reactants).
$\Delta G^{\ddagger}_{I}$, $\Delta G^{\ddagger}_{II}$=Free activation energy in nonpolar(I) and polar solvents(II) respectively. A=Initial reactants; ‡=activated complex; B=products.

The values of $\Delta\nu_D$, β, and DN are available for 23, 15, and 13 of our solvents respecitvely, and inspection (Table 2) shows that the reaction tends to be fast in weakly basic solvents and slow in strongly basic solvents.

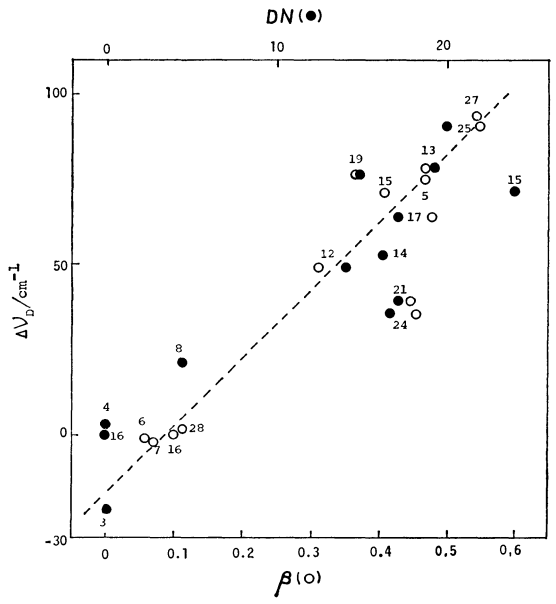

Fig. 3. Relationships between $\Delta\nu_D$ and β, and DN; for point numbers, see Table 2.

A comparison of these parameters substantially presented the linear relationship shown in Fig. 3. We adopted the widely available $\Delta\nu_D$ values as the solvent

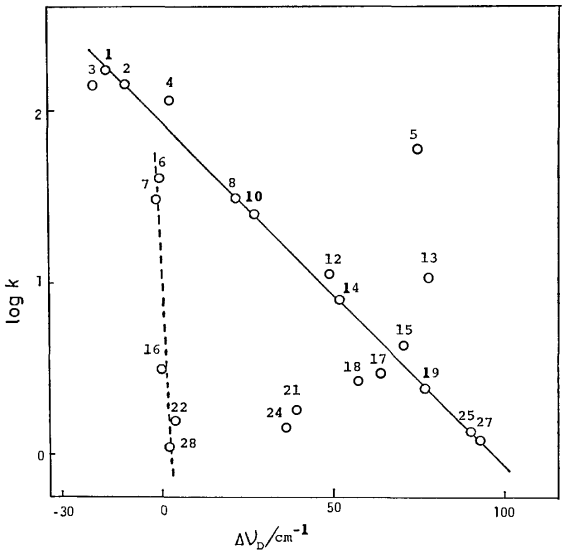

Fig. 4. Plot of log k against $\Delta\nu_D$; for point numbers, see Table 2.

basic parameter. As is shown in Fig. 4, a plot of log k against the $\Delta\nu_D$ values provided two correlation groups, excluding six solvents (Solv. Nos. 5, 13, 17, 18, 21, 24). The first solvent group, including aliphatic chlorinated solvents, nitriles, and cyclic ethers, moderately decreased the logarithmic rate with the increase in the solvent basicities. The regression analysis gave an excellent correlation (Eq. 3, solid line). The second group, consisting of five aromatic solvents, brought about a steeper decrease (slope −0.259, broken line). The correlation equation (r= 0.848), however, is not so good, probably because the $\Delta\nu_D$ values of these aromatic solvents are too narrow (ranging from −2 to 4 cm^{-1}) to avoid the uncertainty due to the error (±1 cm^{-1}) in the measured shift of O–D stretching.

$$\log k = -0.0196\Delta\nu_D + 1.92 \quad (r=0.991,\ s=0.005,\ n=12) \qquad (3)$$

These phenomena confirm that the present reaction is essentially governed by the extent of the interaction between solvents and DDQ in the initial state. Two solvent groups are given because of the difference in the solvent basic nature. Of the solvents, alkyl halides are σ-donors; ethers, nitriles, and ketones are n-donors, and aromatic hydrocarbons are π-donors.[12] According to the HSAB concept,[13] DDQ is a soft acid π-acceptor and prefers to bind soft bases, such as benzene and toluene. Therefore, the specific stability of the π-donor–π-acceptor complexes between the aromatic solvents and DDQ seems to give a separate correlation line from the first solvent group. These aromatic solvents are strong bases toward such π-acceptors as DDQ, while they are weak toward a typical hard acid methanol, as judged by the small $\Delta\nu_D$ values. However, nitrobenzene was an exceptional aromatic solvent, probably because the negatively charged nitro group acts overwhelmingly as an associating site.

It can also be seen in Fig. 4 that the log k values for the solvents containing carbonyl groups (Nos. 17, 18, 21, 24) and for diethyl ether (No. 13) and diisopropyl ether (No. 5) are smaller and larger respectively than called for by Eq. 3. We assume that these carbonyl solvents possess, to some extent, a softness toward DDQ, the property of which can not be evaluated by the interaction with hard acid methanol-*d*. Methyl chloroacetate, however, belongs to the first solvent group because the chlorine substituent weakens the basicity. The upper deviation of diethyl and diisopropyl ethers is attributable to the steric hindrance, which is of some importance in estimating the strength of the solvent-DDQ interaction. A bulky substituent adjacent to the oxygen atom undoubtedly causes an increase in the rate, probably because of the poor solvation of DDQ. This phenomenon can be understood in terms of the Taft steric constants,[14] E_S, which predict the present increase in k in the series of diisopropyl ether (E_S=−0.47)>dibutyl ether (−0.39)>diethyl ether (−0.07).

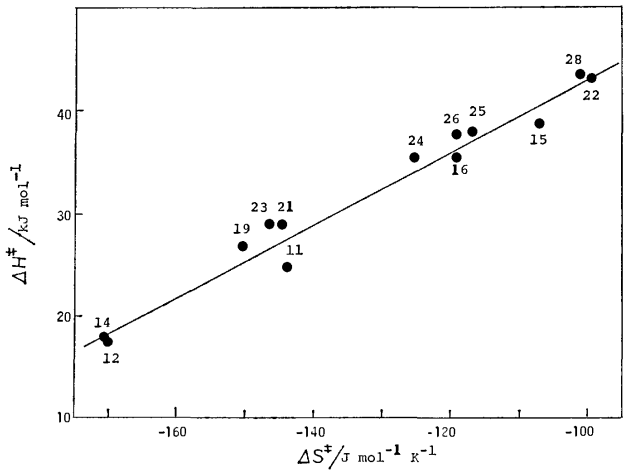

Fig. 5. Plot of ΔH^* *vs.* ΔS^*; for point numbers, see Table 2.

With regard to the enthalpies and entropies of activation, a plot of ΔH^* against ΔS^* displayed a linear correlation (r=0.98, Fig. 5). The ΔH^* values vary from 17.2 to 43.6 kJ mol^{-1} in going from acetonitrile to toluene, while the ΔS^* values vary from −99.5 to −170 J mol^{-1} K^{-1} in going from ethylbenzene to acetonitrile. The larger ΔH^* values for toluene and ethylbenzene are indicative of the high stabilization of the DDQ molecule, consistent with the favorable π-π donor acceptor interaction in the initial state, by which the negatively smaller ΔS^* values of these solvents can be explained.

Experimental

The IR and NMR spectra were recorded on Hitachi 215 and Varian EM-360 spectrometers respectively. The UV spectra were observed with Hitachi 323 and JASCO UVIDEC 505 instruments.

Materials. All the diaryldiazomethanes were made by the oxidation of the corresponding hydrazones with yellow mercury(II) oxide, as has previously been described.[15] The physical properties of these diazoalkanes were listed in previous papers.[3,16] The 2,3-dichloro-5,6-dicyanobenzoquinone(DDQ) was of commercial origin and was recrystal-

lized from dichloromethane; orange yellow needles, mp 213 °C. All the solvents were dried and purified according to the standard procedures.[17]

Kinetic Measurements. The kinetic data were obtained according to the standard spectrophotometric methods. Solutions for kinetic experiments were prepared separately just before use in a volumetric flask equipped with a stopper. The DDQ solution (10^{-5}—10^{-3} mol dm^{-3}) was introduced into a stoppered quartz optical cell (10 mm) and kept at the given temperature within ±0.1 °C in a thermostat-controlled cell-holder of a Hitachi 323 spectrophotometer. The reaction was initiated by the quick addition of the requisite volume of a DDM slution(10^{-5}—10^{-3} mol dm^{-3}), which had been preheated in a water bath to the same temperature as the above cell-holder. The change in the maximum absorption (408 nm, ε=2750) of DDQ in benzene was conveniently monitored over at least two half-lives in the cases of the DDMs (**1a**—**m**), for these diazoalkanes and the products are essentially transparent at this wavelength. In the cases of nitrosubstituted DDMs(**1n**—**o**), the additive absorption of these diazoalkanes(**1n**; ε=122, **1o**; ε=290) and DDQ(ε=361) at 500 nm in benzene was followed. The measurements in the other solvents were made by following the appropriate absorption of DDQ in the regions of 380—410 nm. The second-order rate constants, k, were determined graphically from the plots of $\ln\{b(a-x)/a(b-x)\}/(a-b)$ against the time, where a and b are the initial concentrations of the DDMs or DDQ respectively, x being the consumed DDMs or DDQ. The rate constants were reproducible within ±3%(usually two determinations).

Reactions of Diaryldiazomethanes(DDMs) with DDQ in Benzene. General Procedures: A benzene solution (10 ml) of diphenyldiazomethane(DDM) (0.50 g, 2.58 mmol) was added, all at once, to a solution of DDQ (0.59 g, 2.60 mmol) in benzene (20 ml). The purple color of DDM suddenly disappeared with the vigorous evolution of N_2. After stirring for 1 h (one overnight standing for the nitro-substituted DDMs), the solvent was evaporated *in vacuo* to give an essentially colorless, resinous product, the IR spectrum of which showed no absorption in the C=O region. The product was then treated with a ten-fold excess of water or methanol for 10 min, with occasional shaking and dried under reduced pressure. The pasty residue thus obtained was triturated with 50 ml of benzene. Filtration gave $DDQH_2$ (0.56—0.57 g, 94—96%). The filtrate was washed with aqueous sodium carbonate and dried over anhydrous sodium sulfate. The subsequent evaporation of benzene gave benzophenone (0.45 g, 96%) in the case of treatment with water or α,α-dimethoxydiphenylmethane(**5**) (0.48 g, 81%) and benzophenone (70 mg, 15%) in the case of treatment with methanol. The relative yields of **5** and benzophenone were determined by means of the NMR spectrum of the product mixture, while pure **5** was obtained by fractional crystallization from pentane. The benzophenones and **5** were identified by a comparison of the IR and NMR spectra with those of authentic samples.[3]

Reaction of Diphenyldiazomethane(DDM) with DDQ in H_2O–Benzene. A benzene solution (10 ml) of DDM (0.50 g, 2.58 mmol) and H_2O (0.23 g, 13 mmol) was added, all at once, to a solution of DDQ (0.59 g, 2.60 mmol) in benzene (20 ml). After stirring for 1 h, the removal of the solvent, followed by column chromatography(silica gel), gave 2,3-dichloro-5,6-dicyanohydroquinone dibenzhydryl ether(**7**) (35 mg, 5% based on the DDM used), and benzophenone (0.40 g, 85%) with a petroleum ether–benzene mixture, and then $DDQH_2$ (0.49 g, 83%) and benzhydrol(**8**) (30 mg, 6%) with a benzene–ether mixture. The product, **7**, had a mp of 190—191 °C (from benzene) (lit,[18] mp 189—190 °C), IR(KBr): 2235, 1412, 993, 928, and 695 cm^{-1}; NMR (δ, $CDCl_3$): 6.67(2H, s) and 7.33(20H, s); Found: C; 72.94, H; 4.15, N; 4.94%. Calcd for $C_{34}H_{22}Cl_2N_2O_2$: C; 72.72, H; 3.95, N; 4.99%. Compound **8** was identified by a comparison of its IR and NMR spectra with those of a commercial sample.

Reaction of DDM with DDQ in CH_3OH–Benzene. A benzene solution (10 ml) of DDM (0.50 g, 2.58 mmol) and CH_3OH (0.42 g, 13 mmol) was added, all at once, to a solution of DDQ (0.59 g, 2.60 mmol) in benzene (20 ml). After stirring for 1 h, the reaction mixture was evaporated *in vacuo* and the pasty residue was triturated with benzene (50 ml). Filtration gave pure crystalline $DDQH_2$ (0.54 g, 91%). The filtrate part was divided in equal parts and was examined by two different methods. One part was washed with aqueous sodium carbonate (5%), dried over sodium sulfate, and evaporated to dryness to give crystalline **5** (0.26 g, 87%). The other part was evaporated, followed by column chromatography(silica gel) to give **7** (30 mg, 4%) and benzophenone (0.20 g, 85%) with a petroleum ether–benzene mixture, and **8** (15 mg, 6%) with a benzene–ether mixture. Thus, acetal **5** was completely changed into benzophenone on silica-gel-column chromatography.

References

1) C. D. Gutsche, *Org. React.*, **8**, 364 (1954); K. T. Finley, "The Chemistry of the Quinonoid Compounds," ed by S. Patai, John Wiley & Sons (1974), Chap. 17.
2) T. Oshima and T. Nagai, *Bull. Chem. Soc. Jpn.*, **53**, 726 (1980); A. R. Bader and M. G. Ettlinger, *J. Am. Chem. Soc.*, **75**, 730 (1953); P. G. Jones, *J. Chem. Soc., Chem. Commun.*, **1966**, 894.
3) T. Oshima and T. Nagai, *Bull. Chem. Soc. Jpn.*, **53**, 3284 (1980).
4) D. H. McDaniel and H. C. Brown, *J. Org. Chem.*, **23**, 420 (1958).
5) H. C. Brown and Y. Okamoto, *J. Am. Chem. Soc.*, **80**, 4979 (1958).
6) Y. Yukawa, Y. Tsuno, and M. Sawada, *Bull. Chem. Soc. Jpn.*, **39**, 2274 (1966).
7) G. Briegleb, *Angew. Chem.*, **76**, 326 (1964).
8) D. F. Ilten and M. Calvin, *J. Chem. Phys.*, **42**, 3760 (1965); R. Vars, L. A. Tripp, and L. W. Pickett, *J. Phys. Chem.*, **66**, 1754 (1962); K. Kimura, Y. Achiba, and S. Katsumata, *J. Phys. Chem.*, **77**, 2520 (1973).
9) T. Kagiya, Y. Sumida, and T. Inoue, *Bull. Chem. Soc. Jpn.*, **41**, 767 (1968).
10) M. J. Kamlet and R. W. Taft, *J. Am. Chem. Soc.*, **98**, 377 (1976); M. J. Kamlet, A. Solomonovici, and R. W. Taft, *ibid.*, **101**, 3734 (1979).
11) V. Gutmann, "Coordination Chemistry in Non-Aqueous Solutions," Springer-Verlag (1968), Chap. 2.
12) C. Reichardt, "Solvent Effects in Organic Chemistry," Verlag Chemie (1979), Chap. 2.
13) T.-L. Ho, "Hard and Soft Acids and Bases Principle in Organic Chemistry," Academic Press (1977), Chap. 2; R. G. Pearson, *J. Chem. Educ.*, **45**, 581 (1968).
14) R. W. Taft, "Steric Effects in Organic Chemistry," ed by M. S. Newman, Wiley (1956), Chap. 13.
15) L. I. Smith and K. L. Howard, *Org. Synth.*, Coll. Vol. III, 351 (1955).
16) T. Oshima, A. Yoshioka, and T. Nagai, *J. Chem. Soc., Perkin Trans. 2*, **1978**, 1283.
17) J. A. Riddick and W. B. Bunger, "Techniques of Chemistry, Vol. II, Organic Solvents," 3rd ed, ed by A. Weissberger, Wiley (1970).
18) H.-D. Becker, *J. Org. Chem.*, **34**, 1203 (1969).

Acetylenic and Polyacetylenic Compounds Derived from Thiophene, Furan, and *p*-Dibromobenzene Using 1,1-Dichloro-2,2-difluoroethene

Kunio Okuhara

Government Industrial Research Institute, Nagoya, Hirate Machi, Kita-ku, Nagoya 462

(Received September 1, 1980)

Compounds of the type AZCF=CCl_2, prepared from AZA (thiophene, furan, and *p*-dibromobenzene; Z= 2,5-thiophenediyl, 2,5-furandiyl, and *p*-phenylene; A=H or Br), were converted into CCl_2=CFZC≡CH, CCl_2=CFZC≡CCF=CCl_2, and CCl_2=CFZC≡C$Si(CH_3)_3$ in a one-flask procedure *via* LiZC≡CLi. The products were further converted into acetylenic compounds such as $(CH_3)_3$SiC≡CZC≡C$Si(CH_3)_3$ and $(CH_3)_3$SiC≡CZC≡C–C≡C$Si(CH_3)_3$. 1-Ethynyl-4-(1,3-butadiynyl)benzene was isolated. 2,5-Diethynylthiophene and -furan were prepared in two steps from thiophene and furan, respectively, *via* CCl_2=CFZCF=CCl_2. By treatment with copper (II) acetate hydrate in pyridine, (CCl_2=CFZC≡C–)$_2$ were obtained not only from CCl_2=CFZC≡CH but also from CCl_2=CFZC≡C$Si(CH_3)_3$.

For introduction of the ethynyl group, the method using CF_2=CCl_2 (**1**)[1] is useful where R is aryl[2,3] and the organolithium and/or magnesium compounds are available. The method is particularly attractive when

$$RLi \longrightarrow RCF{=}CCl_2 \longrightarrow RC{\equiv}CLi$$

an appropriate lithium compound is easily obtained by lithiation[4] rather than by halogen-lithium exchange.[5] Lithium compounds easily obtained by lithiation are also expected to give rise to the desired substitution in high proportion (undesirable Cl-Li exchange in low proportion) in the reaction with **1**, since the partial negative charge is considerably delocalized in such compounds.[6] A typical example is the preparation of 2-ethynylthiophene from thiophene.[1] A good overall yield is also expected for the preparation of 2-ethynylfuran from furan *via* 2-(2,2-dichloro-1-fluoroethenyl)furan (**4b**).[7]

In the previous study,[1] however, only one position in each compound[8] was used for introduction of Li followed by reaction with **1** and subsequent transformations even where more than one position are available. In the present study two positions in each compound have been used in order to expand the synthetic possibility of the proposed method. 2,5-Diethynylthiophene (**23a**) and 2,5-diethynylfuran (**23b**) were prepared from thiophene and furan by this method. For the synthesis of these new diethynyl compounds, other methods used for the synthesis of 2-ethynylthiophene[9–13] and 2-ethynylfuran[14–16] do not seem to be feasible.[17] *p*-Dibromobenzene was also subjected to similar conversions, though preparation of *p*-diethynylbenzene was not attempted because of its known preparation from divinylbenzene (isomeric mixture),[18] diethylbenzene,[19] and *p*-diacetylbenzene.[20]

Results and Discussion

Treatment of 2-(2,2-dichloro-1-fluoroethenyl)thiophene (**4a**) and 2-(2,2-dichloro-1-fluoroethenyl)furan (**4b**) with two equivalents of butyllithium affords lithium acetylides **5**[1] (Scheme 1). Further addition of butyllithium lithiated the 5-position of the heterocycles to give dilithium compounds (**6a** and **6b**). A similar dilithium compound (**6c**) was formed, together with butyl bromide, from **4c** *via* Li-Br exchange between **5c** and butyllithium. When a portion of a mixture obtained in this way was left standing in the absence of **1**, 1-butyl-4-lithioethynylbenzene (**18**) was formed by the reaction of **6c** with butyl bromide.

$$p\text{-}BrC_6H_4CF{=}CCl_2 + 2\,n\text{-}C_4H_9Li \quad (\mathbf{4c})$$
$$\longrightarrow p\text{-}BrC_6H_4C{\equiv}CLi + 2\,n\text{-}C_4H_9Cl + LiF \quad (\mathbf{5c})$$

$$\mathbf{5c} + n\text{-}C_4H_9Li \longrightarrow p\text{-}LiC_6H_4C{\equiv}CLi + n\text{-}C_4H_9Br \quad (\mathbf{6c})$$
$$\longrightarrow p\text{-}(n\text{-}C_4H_9)C_6H_4C{\equiv}CLi + LiBr \quad (\mathbf{18})$$

Compounds **6** serve as key intermediate in the transformations shown in Scheme 1. Treatment with **1** under refluxing conditions afforded compounds (**10**) having two –CF=CCl_2 groups. As the nucleophilicity of the acetylide carbanion is much smaller than that of the ring carbanion, the reaction can be carried out in such a way that only the latter takes part in the reaction. Thus the reaction of **6** with **1** at about 15 °C for a short time or at 0 °C for 1—2 h led to the formation of lithium acetylides **9** as the predominant product. Hydrolytic work-up afforded terminal acetylenes **11**, and quenching with chlorotrimethylsilane gave **12**. Compound **11a** was relatively unstable,[21] no procedure for its isolation in satisfactory yield being found. Thus the isolated yield of **11a** from **4a** was only 29%, whereas **12a** (a silylated acetylene)[22] was obtained in 78% yield together with 7% crude yield of **10a**. (At present the best way to prepare **11a** is the hydrolysis of **12a** by alkali.) Compounds **11b** and **11c** were much more stable than **11a**.

The 2,2-dichloro-1-fluoroethenyl group in **12** can also be converted into the lithioethynyl group by treatment with butyllithium. The conversion *via* **12** thus illustrates a method for the preparation of compounds of the type $A_1C{\equiv}CZC{\equiv}CA_2$, though there are limitations regarding the types of A_1 and A_2 for the conversion to be applicable. The conversions of **4** into **10**, **11**, and **12**, *via* several steps each, were conveniently carried out by a one-flask procedure.

Terminal acetylenes were oxidatively coupled in order to obtain more stable crystalline "derivatives." Compounds **11a**, **11b**, and **11c** were satisfactorily converted into the symmetrically substituted butadiynes **13** by Eglinton coupling.[23,24] However, the use of

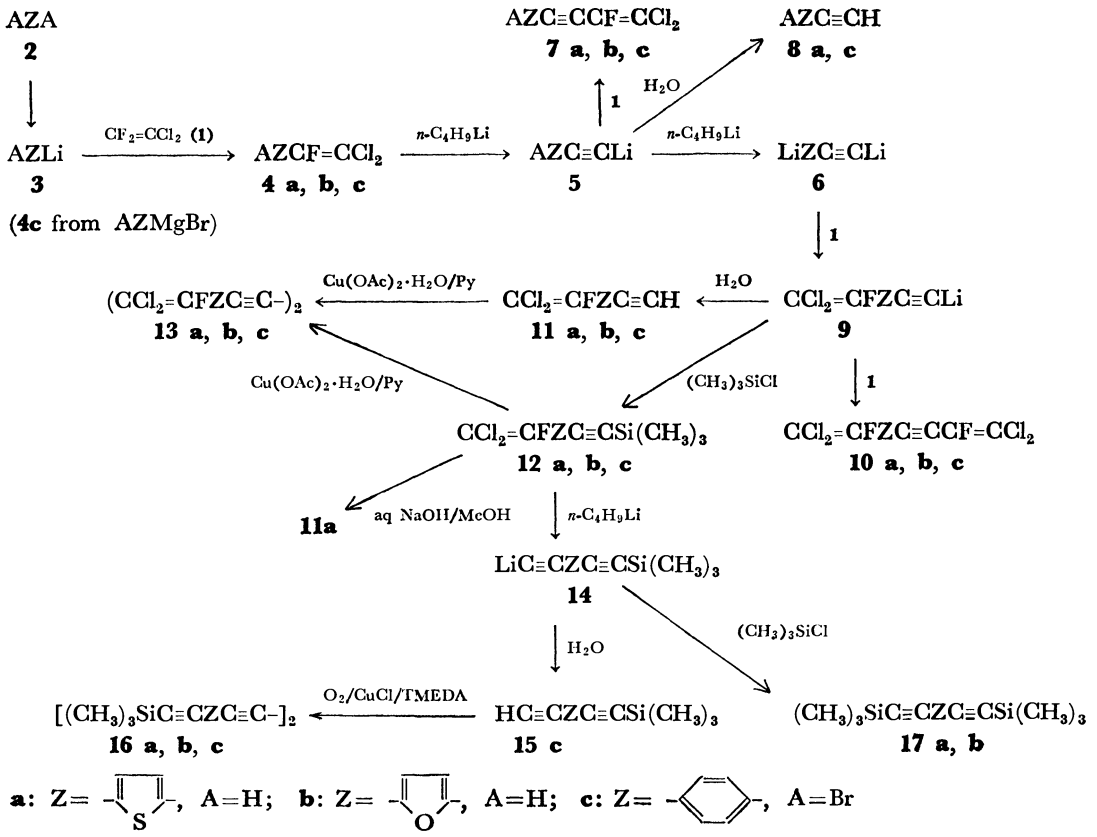

Scheme 1.

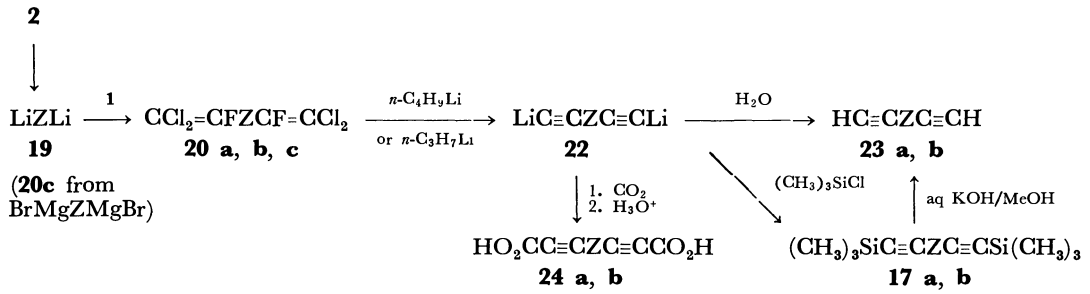

Scheme 2.

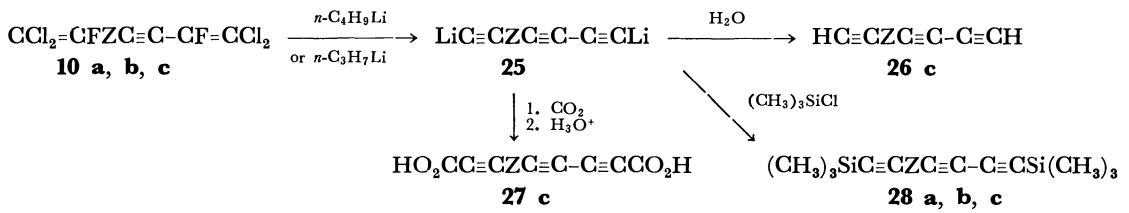

Scheme 3.

this method in the case of **15b** (curde product obtained from **12b**) resulted in the formation of a black, insoluble substance instead of **16b**, suggesting the cleavage of the Si–C (acetylenic) bond followed by a coupling reaction. Thus **12b** was subjected to the conditions for Eglinton coupling of **11b**, formation of **13b** being expected. Compound **13b** was indeed obtained in 77% isolated yield, higher than the yield (58%) of this compound obtained from **11b**. Likewise **13c** was obtained in an excellent yield from **12c** as well as from **11c**. On the other hand, the yield of **13a** obtained from **12a** was considerably lower than that obtained from **11a**. Under the reaction conditions compound **12a** (or a compound derived therefrom) probably undergoes a side reaction, such as ring cleavage, whereas compound **11a** is rapidly converted into the coupling product (**13a**). The coupling product formed from **11a** soon crystallizes, remaining mostly intact. The conversion of **15** into **16** was effected by use of Hay's procedure.[25]

Scheme 2 shows the conversion of thiophene and furan into 2,5-diethynylthiophene (**23a**) and 2,5-di-

TABLE 1. YIELDS, PHYSICAL PROPERTIES, AND ELEMENTAL ANALYSIS DATA OF ACETYLENES AND RELATED COMPOUNDS OBTAINED BY USING $CF_2=CCl_2$

Compd	Yield/%[a]		Bp/°C(mmHg)	n_D^{20} or [Mp/°C]	^{19}F NMR[b,c] δ/ppm	^1H NMR[b] δ/ppm I[d]	^1H NMR[b] δ/ppm II[e]	IR[f] $\tilde{\nu}$/cm^{-1}	C (%) (Calcd) Found	H (%) (Calcd) Found
10a	73	(**4a**)		[46—47]	22.7 (t 0.9) **24.8** (d 0.6)		7.36+7.44(4.0) (d 1.0) (t 0.7)	1612 1620 sh **2190**	(35.96) 35.70	(0.60) 0.59
11a	29	(**4a**)	96—98(6)	[42—43]	22.5 (t 0.9)	*3.48* (d 0.5)	7.25+7.39(4.0) (d 0.9) (d 1.0) (d 0.4)	1628 **2110** *3300*	(43.46) 43.35	(1.37) 1.21
	97[g]	(**12a**)								
12a	78	(**4a**)	126—128(2.5)	[76.5—78]	22.7 (t 0.9)	0.26	7.20+7.36 (4) (d 0.9) (d 0.9)	1620 **2145**	(45.05) 44.78	(3.78) 3.70
13a	77	(**11a**)		[197—198] dec	20.1[h]			1618	(43.66)	(0.92)
	38	(**12a**)						**2140**	43.41	0.97
16a	78	(**12a**)		[135.5—136.5]		0.25[i]	7.08+7.17[i] (3.9)	**2145**	(64.97) 64.76	(5.45) 5.29
17a	95	(**12a**)		[82.5—83.5]		0.24	7.06	**2145**	(60.80)	(7.29)
	95	(**20a**)							60.70	7.51
20a	64	(**2a**)	130—133(2)	[85—86]	22.2 (t 0.9)		7.47 (t 0.9)	1616	(30.99) 30.64	(0.65) 0.59
21a[j]		(**2a**)	*ca.* 80(2)	1.6114	24.0 (t 0.9)		6.90+7.25(4.2) (d 0.6) (d 0.8)	1628	(31.13) 31.30	(0.87) 0.90
23a	85	(**17a**)		1.636[k]		*3.35*[i]	7.11[i]	**2106**	(72.69)	(3.05)
	85	(**20a**)						*3290*	72.46	3.08
24a	72[g]	(**20a**)		1)		5.11[m,n]	7.49[m]	**2210**	(54.54) 54.17	(1.83) 1.54
28a	59	(**10a**)	*ca.* 182(2)	1.6231		0.23 0.24	7.09+7.12(3.8)	**2090**[o] **2135**[o] **2180**[o]	(63.93) 63.63	(6.71) 6.79
10b	51	(**4b**)	130—135(2)	[52—53]	35.3 (t 1.1) **26.1**		6.92 (d 1.0)	1624 **2205**	(37.77) 37.66	(0.63) 0.62
11b	44	(**4b**)	85(7)	1.5912	35.1 (d 1.3) (d 0.6)	*3.48* (d 0.4)	6.73+6.83(3.6) (d 1.4) (d 0.6) (d 0.5)	1630 **2119** *3295*	(46.87) 46.72	(1.48) 1.68
12b	49[p]	(**4b**)	118—122(2.5)	1.5673	35.0 (d 1.4) (d 0.6)	0.26	6.69+6.82(3.5) (d 1.5) (d 0.5)	1628 **2153**	(47.66) 47.58	(4.00) 4.08
13b	58	(**11b**)		[123—124] dec	35.6[i]		6.88[i]	1637	(47.10)	(0.99)
	77	(**12b**)			(t 1.0)		(d 1.0)	**2149**	46.97	0.98
16b	64	(**12b**)		[128—129]		0.26	6.60+6.76(3.6)	**2154** **2184** w	(70.54) 70.47	(5.92) 5.94
17b	88	(**12b**)		[72—72.5]		0.24	6.55	**2158**	(64.55)	(7.74)
	93	(**20b**)						**2192** w	64.41	7.58
20b	37	(**2b**)	116(4)	[65.5—66.5]	35.4 (t 1.0)		6.93 (t 1.0)	1625	(32.69) 32.68	(0.69) 0.55
21b[j]		(**2b**)	*ca.* 75(5)	1.5556	35.3 (d 1.4)		6.31+6.83(3.6) (d 1.4)	1635	(33.45) 33.29	(0.94) 0.96
23b	72	(**17b**)		1.5654[k]		*3.39*[i]	6.62[i]	**2107**	(82.75)	(3.47)
	86	(**20b**)						*3290*	82.90	3.40
24b	73[g]	(**20b**)		1)		5.30[m,n]	7.11[m]	**2225**	(58.83) 58.89	(1.98) 1.97
28b	50	(**10b**)	153—158(2)	[50—52]		0.22 0.24	6.58+6.62(3.6)	**2100**[o] **2152**[o] **2200**[o]	(67.54) 67.44	(7.09) 7.06
10c	72	(**4c**)		[74.5—75.5]	19.7 br **24.4** br		7.59+7.76(8.6)[q]	1624 1630 sh **2200**	(43.94) 43.66	(1.23) 1.14

Table 1. (continued)

Compd	Yield/%[a]	Bp/°C(mmHg)	n_D^{20} or [Mp/°C]	^{19}F NMR[b,c] δ/ppm	^1H NMR[b] δ/ppm I[d]	^1H NMR[b] δ/ppm II[e]	IR[f] $\tilde{\nu}$/cm^{-1}	C (%) (Calcd) Found	H (%) (Calcd) Found
11c	60 (**4c**)		[50—51]	19.2 br	*3.20*	7.57+7.71 (8.8)[q]	1634 r)	(55.85) 55.74	(2.34) 2.42
							3275		
							3300 w		
12c	55 (**4c**)	129—137 (3)	[56—57]	19.3 br	0.26	7.52+7.66 (8.4)[q]	1628[s]	(54.36)	(4.56)
							2154	54.33	4.50
13c	93 (**11c**)		[161—162]	19.7[l]		7.61+7.75[l] (9)[q]	1634 r)	(56.11) 55.64	(1.88) 1.77
	96[g] (**12c**)								
15c[t]	71 (**12c**)		[55—56]		0.25	7.45	**2152**		
					3.16		*3259*		
16c	78 (**12c**)		[231—232]		0.26[l]	7.44[l]	**2152**	(79.12) 78.98	(6.64) 6.45
20c[u]			[119—120.5]	19.6 br[l]		7.82[l]	1634	(39.51) 39.48	(1.33) 1.39
26c	79 (**10c**)		1)		*2.52*[l]	7.47[l]	**2205**	(95.97)	(4.03)
					3.20[l]		*3295* sh	95.18	3.99
							3270		
27c	85[g] (**10c**)		1)		4.90[m,n]	7.65[m]	**2165** w	(70.59)	(2.54)
							2209 sh	70.10	2.71
							2230		
28c	81 (**10c**)		[107.5—108.5]		0.22	7.43	**2103**[o]	(73.40)	(7.53)
					0.24		**2153**[o]	73.32	7.53
							2205[o]		

a) Isolated yield, calculation being based on the starting compound indicated in parentheses. b) 20% Solution in $CDCl_3$ unless otherwise stated. ^1H and ^{19}F chemical shifts measured downfield relative to internal tetramethylsilane and upfield relative to external CF_3CO_2H, respectively. Splitting pattern and (apparent) coupling constant (Hz) indicated in parentheses. c) ^{19}F chemical shift for $-C\equiv C-CF=CCl_2$ indicated by bold face; broad signals at expanded scale (half-height width of roughly 1 Hz) denoted by br. ^{19}F chemical shifts and splitting patterns (in parentheses) not given in the Table are as follows: **4a**, 20.7(d 2.8)(t 1.1); **7a**, 23.9(d 0.6); **4b**, 34.1(t 1.4)(t 0.5); **7b**, 25.2 br; **4** (Z=*p*-phenylene, A=H), 15.6 br; **7** (Z=*p*-phenylene, A=H), 23.6; **4c**, 18.8 br; **7c**, 24.2 br. d) $Si(CH_3)_3$ (0.22—0.26 ppm), CO_2H (4.90—5.30 ppm), and C≡CH (2.52—3.48 ppm, in italics). e) Aromatic ring proton. Data for (gross) AB pattern: chemical shift of A+chemical shift of B (coupling constant: J_{AB} in Hz). Further splittings indicated under the respective chemical shifts. f) νC=C of $-CF=CCl_2$, νC≡C (in bold face), and νC-H of -C≡CH (in italics) are given. Neat for liquid and in KBr pellet for crystals. w, weak; sh, shoulder; br, broad. g) Crude yield. h) Saturated solution in thiophene. This compound is sparingly soluble in organic solvents. i) Concentration smaller than 10%. j) Obtained in *ca.* 7% crude yield as by-product of **20a** or **20b**. k) Melting point *ca.* 15 °C. l) No melting point observed; turning dark with rise in temperature. m) CD_3OD used as solvent. n) Chemical shift probably concentration-dependent due to the equilibrium: $-COOH+CD_3OD \rightleftharpoons -COOD+CD_3OH$. o) The three bands of νC≡C of comparable strength. p) 2-(Trimethylsilylethynyl)furan obtained in 17% yield. q) Approximate value of J_{AB} of AA'BB' (or AA'BB'X) system. Since J_{AB} is the coupling constant between protons in mutually ortho positions and is expected to be much larger than other coupling constants, the spectrum has been treated as a (gross) AB pattern. r) νC≡C not observed: apparently IR-inactive. s) A stronger band, probably not due to the $-CF=CCl_2$ group, present at 1608 cm^{-1}. t) Previously reported (Ref. 23). u) Obtained in 9% yield together with 52% yield of **4c** when excess **1** was refluxed for a total of 19 h (in 3 days) in a Grignard reagent mixture prepared from *p*-dibromobenzene (0.5 mol) and magnesium (0.62 g-atom: Ventron chips).

ethynylfuran (**23b**), as well as their derivatives. The yields of 2,5-bis(2,2-dichloro-1-fluoroethenyl)thiophene (**20a**) and -furan (**20b**) obtained *via* lithiation of thiophene and furan followed by treatment with **1** were 64 and 37%, respectively. The low yields are apparently due to incomplete dilithiation of the heterocycles (and to possible decomposition of the dilithium compounds), particularly in the case of furan,[26] rather than to the yield of the reaction of the dilithium compounds with **1**. In the lithiation an increase in the proportion of butyllithium is expected to increase the extent of conversion of the heterocycles into dilithium compounds. However, the use of a large excess of butyllithium is undesirable since remaining butyllithium reacts with **20** as well as with **1**. In the present experiments a 50% excess of butyllithium (a total of three equivalents) was used for the dilithiation of thiophene and furan with a refluxing time of 9.5—11 h. In the reaction with **1**, the inverse addition method was not used since a significant portion of the butyllithium was considered to remain and to offset the advantage of use of this less convenient method.

The by-products of these reactions are 2-chloro-5-(2,2-dichloro-1-fluoroethenyl)thiophene (**21a**) and

-furan (**21b**) besides **4a** and **4b**, which were formed from the monolithiated compounds (**3a** and **3b**). Compounds **21a** and **21b** were isolated by preparative GC for identification. The formation of $ClZCF{=}CCl_2$ (**21**) from LiZLi seems to proceed *via* ClZLi rather than *via* $LiZCF{=}CCl_2$ since LiZLi is expected to give much higher proportion of the Li-Cl exchange to the substitution than $LiZCF{=}CCl_2$, in view of stabilization to a much smaller extent of the negative charge[6] in LiZLi than in $CCl_2{=}CFZLi$.

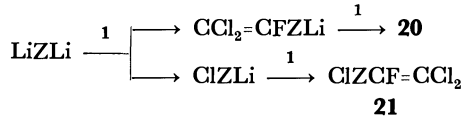

Treatment of **20a** and **20b** with excess butyllithium (or propyllithium) followed by work-up and rotary evaporation of the solvent and butyl chloride (or propyl chloride) afforded crude 2,5-diethynylthiophene (**23a**) and 2,5-diethynylfuran (**23b**), respectively. The yields were high, but the samples contained hydrocarbon impurities, apparently originating from lithium reagent solutions and not effectively removable by rotary evaporation. 2,5-Diethynylthiophene (**23a**) was not sufficiently stable to be purified by preparative GC; purification was successfully performed through conversion into the disilver diacetylide. 2,5-Diethynylfuran (**23b**) was more stable, pure samples being obtained by careful preparative GC as well as through conversion into its disilver diacetylide.

Alkali hydrolysis of the bis(trimethylsilyl) derivatives (**17**), obtained by treatment of the dilithium diacetylides (**22**) with chlorotrimethylsilane as well as by a one-flask procedure from **12** (Scheme 1), also afforded 2,5-diethynylthiophene (**23a**) and -furan (**23b**). However, the crude samples obtained from **17** contained $(CH_3)_3SiOSi(CH_3)_3$, and its removal required the use of the methods by which the samples obtained from **20** were purified.

The conversion of 1,4-bis(2,2-dichloro-1-fluoroethenyl)benzene (**20c**) into 1,4-diethynylbenzene (**23c**) was not undertaken. 1-Ethynyl-4-(1,3-butadiynyl)benzene (**26c**) was, however, prepared for the first time by treatment of **10c** with butyllithium (or propyllithium) as shown in Scheme 3. This is probably the easiest route for preparation of **26c**. The dicarboxylic acid (**27c**) and the bis(trimethylsilyl) derivative (**28c**) were also obtained. The corresponding bis(trimethylsilyl) derivatives (**28a** and **28b**) of thiophene and furan were similarly obtained. Compound **28a** remained as a viscous oil even after being purified by preparative GC.

Each of the compounds **28** obtained from **10** was accompanied by a by-product resulting from addition of butyllithium to **25** and subsequent replacement of three lithium atoms by trimethylsilyl groups. Propyllithium was not used for the preparation of **28**. On the basis of the infrared spectrum (ν C≡C 2122 and 2158 cm^{-1} for **30a** as compared with ν C≡C 2090, 2135, and 2180 cm^{-1} for **28a**) and from the fact that no addition of butyllithium to **22** takes place in the treatment of **20** with excess butyllithium, as confirmed by GC-mass spectroscopic examination of crude **17** obtained from the route given in Scheme 2, the by-product is considered as formed *via* 1,2-addition of butyllithium to one of the triple bonds in the lithiobutadiynyl group of **25**. Structure **29** is most likely for the adduct, structure **30** being tentatively assigned to the trisilylated compound. The addition of butyllithium to **25** was particularly conspicuous in the case of the thiophene derivative.

$LiC{\equiv}CZC(C_4H_9\text{-}n){=}C(Li)C{\equiv}CLi$ (**29**)

$(CH_3)_3SiC{\equiv}CZC(C_4H_9\text{-}n){=}C[Si(CH_3)_3]C{\equiv}CSi(CH_3)_3$ (**30**)

The following remarks are given on the NMR data summarized in Table 1: (1) The unusually high ^{19}F NMR chemical shifts of the $-CF{=}CCl_2$ group of furan derivatives are clearly associated with a similar trend of the ^1H NMR chemical shifts of the ring protons. Note that the ^{19}F NMR and ^1H NMR chemical shifts are measured in mutually opposite directions. (2) The coupling patterns in ^1H NMR spectra of thiophene and furan derivatives are much simpler than those of benzene derivatives. In many cases, the coupling constant between the fluorine of the $-CF{=}CCl_2$ group (attached to the 2-position of the ring) and the proton at the 3-position is comparable to the one between the fluorine and the proton at the 4-position. However, of the two coupling constants or of the two ^1H chemical shifts, it is not clear which one is for the proton at the 3-position.

Experimental

Caution should be taken in the handling of acetylenic compounds. Some terminal acetylenes are liable to exothermic decompostion upon heating (*cf.* descriptions for **11a** and **23a**).

Temperature readings are uncorrected. Pressure readings are given in terms of mmHg (1 mmHg=133.322 Pa). ^{19}F NMR and ^1H NMR spectra were recorded on a Hitachi R-20BK operated at 56.451 MHz and on a Hitachi R-22 operated at 90 MHz, respectively. IR spectra were recorded on a Hitachi EPI-G3, and mass spectra[27] on a Shimadzu GCMS-7000. All reactions of butyllithium and propyllithium were conducted under an atmosphere of nitrogen with use of sodium-dried ether. Butyllithium and propyllithium were prepared from butyl bromide and propyl bromide, respectively, by the reaction with cut pieces of lithium in ether and stored at −20 °C. The amounts of these reagents are calculated from nominal concentration.

*2-Ethynyl-5-(2,2-dichloro-1-fluoroethenyl)thiophene (**11a**).* Compound **4a**[1] (19.06 g, 96.7 mmol) was treated with butyllitium, **1** being added as described in the section for **12a**. The resulting mixture was allowed to warm to 0 °C, at which it was stirred for 1.3 h. The worked-up mixture was crystallized by cooling to −20 °C, crystals of **11a** (4.32 g) remaining unmelted at room temperature being filtered off. Vacuum distillation of the mother liquor afforded an additional amount of **11a** (1.95 g, bp 96—98 °C/6 mmHg), increasing the total isolated yield to 29%. A large amount (11.86 g) of distillation residue remained. The experiment was repeated, and the total worked-up mixture was subjected to vaccum distillation. A few minutes after air[28] had been admitted into the apparatus in order to replace the condenser, in which the first portion of **11a** had crystallized, the content of the still pot decomposed with ignition. The analytical sample (mp 42—43 °C) of **11a** was obtained by

recrystallization (from methanol) of a sample obtained by alkaline hydrolysis of **12a**. MS *m/e*, 220 (M).

2-(2,2-Dichloro-1-fluoroethenyl)-5-(trimethylsilylethynyl) thiophene (12a). Ethereal butyllithium (322 mmol, 192 ml) was added to a stirred solution of **4a** (19.70 g, 100 mmol) in ether (100 ml) cooled with Dry Ice–acetone below −50 °C. The resulting mixture was stirred for 1.5 h at *ca.* 20 °C and re-cooled with Dry Ice–acetone. After addition of **1** (36 g, 270 mmol) in one portion, the Dry Ice–acetone bath was replaced by an ice–water bath. The internal temperature rose rapidly to reach a maximum of 20 °C and then began to fall. The resulting mixture was stirred at 13—17 °C for 16 min after that moment, re-cooled with Dry Ice–acetone, and chlorotrimethylsilane (24.5 g, 225 mmol) was added. After the cooling bath had been removed, the whole mixture was stirred for 2 h and poured onto a mixture of crushed ice and concd hydrochloric acid. Distillation of 94% of the worked-up mixture afforded 21.47 g (78% yield) of **12a**, bp 126—128 °C/2.5 mmHg. The distillation residue (2.2 g, corresponding to 7% yield) was found to be mainly **10a** by IR and ^{19}F NMR spectroscopy. No crystallization of **12a** took place in the condenser during the course of distillation, though crystallization was easily induced by seeding. The analytical sample (mp 76.5—78 °C) was obtained by recrystallization from ethanol. MS *m/e* (rel intensity), 292 (M, 46), 277 (M−CH_3, 100).

Bis[5-(2,2-dichloro-1-fluoroethenyl)-2-thienyl]butadiyne (13a). Compound **11a** (2.00 g, 9.0 mmol) and copper(II) acetate hydrate (3.00 g) was stirred in pyridine (30 ml) in a bath at 50 °C. The solution turned into a bright brown slurry in a few minutes. After being stirred for 30 min, the resulting mixture was poured onto water (*ca.* 500 ml) with agitation. The precipitate was collected by filtration and dried (mp 195—199 °C; 1.93 g, corresponding to 97% yield of **13a**). The first crop of recrystallization of **13a** from dioxane was 1.54 g, (77%; mp 197—198 °C with decomposition as judged from formation of a black melt). MS *m/e* (rel intensity), 438 (M, 100), 368 (M−2Cl, 22).

When compound **12a** (2.00 g, 6.8 mmol) was subjected to essentially the same treatment as described above, the crude product obtained by pouring the reaction mixture onto water amounted to 1.44 g, corresponding to 96% yield of **13a**. However, only 38% yield (0.57 g) of **13a** was obtained from this. The rest of the material was more strongly adsorbed on alumina and is suggested to be a mixture by its elution behavior.

2,5-Bis(trimethylsilylethynyl) thiophene (17a). Ethereal butyllithium (31 mmol, 19 ml) was added to a cooled stirred suspension of **12a** (3.36 g, 11.5 mmol) in ether (60 ml) over a period of 12 min below −58 °C. After addition of chlorotrimethylsilane (6 g, 55 mmol) at −5 °C, the resulting mixture was stirred for 1.5 h without cooling. Hydrolysis, workup, and solvent evaporation afforded a crystalline residue, from which 2.65 g (mp 82.5—83.5 °C) of **17a** was obtained by digestion with ethanol followed by filtration. From the filtrate, less pure **17a** (mp 79—81 °C. 0.36 g; total 95%) was recovered. Recrystallization from ethanol afforded the analytical sample (mp 82.5—83.5 °C). MS *m/e* (rel intensity), 276 (M, 100), 261 (M−CH_3, 51).

The same compound was obtained in 95% yield from **20a** by the same procedure, its identity being confirmed by undepressed mixed melting point.

1,4-Bis[p-*(trimethylsilylethynyl)phenyl*]*-1,3-butadiyne (16c).* An acetone (10 ml) solution of crude **15c**[29] obtained from **12c** (2.00 g, 7.0 mmol) by treatment with butyllithium (19 mmol) was added to an oxygen-bubbled solution of *N,N,N′,N′*-tetramethylethylenediamine (0.12 g) and copper(I) chloride (0.10 g) in acetone (20 ml). The resulting mixture, which became a crystalline slurry in a few minutes, was stirred for 39 min with continued oxygen bubbling and treated with a mixture of ether (*ca.* 150 ml) and aqueous hydrochloric acid. Crystals of **16c** remaining insoluble even after addition of benzene (50 ml) followed by shaking of the total mixture were filtered off (dried 0.28 g, mp 231—232 °C). An additional amount (0.79 g) of crystals of **16c** was obtained from the organic layer after washing (with aqueous hydrochloric acid and then with water), drying, and concentration, with increase in the total isolated yield of **16c** to 78% (based on **12a**). A mixture (0.20 g, 15%) of **15c** and **16c** recovered from the mother liquor is excluded from the above yield. Recrystallization from benzene afforded the analytical sample (mp 231—232 °C). MS *m/e* (rel intensity), 394 (M, 100), 279 (M−CH_3, 94). The corresponding thiophene and furan derivatives (**16a** and **16b**) were much more soluble in organic solvents than **16c**; most of the acetone was removed by evaporation before similar work-up.

2,5-Bis(2,2-dichloro-1-fluoroethenyl)thiophene (20a). Ethereal butyllithium (300 mmol, 180 ml) was added (exothermic) to a stirred solution of thiophene (8.41 g, 100 mmol) in ether (100 ml) in a 500 ml four-necked flask equipped with a thermometer, a dropping funnel, and a Dimroth condenser. The solution was refluxed for 12 h to give a slurry. Compound **1** (51 g, 380 mmol) was added over a period of 43 min, during which time the internal temperature was kept below −50 °C by cooling with Dry Ice–acetone. Circulation of ice water through the Dimroth condenser was initiated, and the dropping funnel was replaced by an additional condenser, two condensers being necessary to control the excessive exothermicity. The cooling bath was replaced with a vacant bath vessel, which was filled with ice water to the necks of the flask as soon as the internal temperature reached 0 °C. The temperature rose slowly up to 20 °C but very rapidly to refluxing temperature (30—32 °C) from 20 °C. After vigorous boiling subsided, the cooling bath and the additional condenser were removed, the mixture was heated to reflux for 2 h, and poured onto a mixture of crushed ice and concd hydrochloric acid (30 ml). The ether layer was separated, washed (with water and with aq $NaHCO_3$), dried, and 95% of the solution was evaporated to leave a crystalline residue. Digestion with ethanol followed by filtration afforded **20a** (14.50 g). Fractional distillation of the filtrate with a short Vigreux column gave an additional amount (4.51 g) of **20a** (bp 130—132 °C/2 mmHg), increasing its total yield to 64%, besides an approximately 1:1 mixture (3.02 g, in three fractions) of **4a** (7% yield) and **21a** (7% yield). The analytical sample of **20a**, mp 85—86 °C, obtained from a distilled sample by recrystallization from ethanol, was colorless. MS *m/e* (rel intensity), 308 (M, 100), 273 (M−Cl, 6), 238 (M−2Cl, 32). A pure sample of **21a** was obtained by preparative GC. MS *m/e* (rel intensity), 230 (M, 100), 195 (M−Cl, 30), 160 (M−2Cl, 42). By a similar procedure with an externally heated refluxing time of 2 h for lithiation of thiophene using 2.4 equivalents of butyllithium, **4a** and **20a** were isolated 31 and 35% yields, respectively.

2,5-Diethynylthiophene (23a). Ethereal butyllithium (20 mmol, 12 ml) was added below −58 °C over a period of 10 min to a cooled stirred slurry of **20a** (1.00 g, 3.2 mmol) in ether (50 ml). The resulting mixture was allowed to warm to −10 °C and poured onto a mixture of concd hydrochloric acid (4 ml) and crushed ice. The whole mixture was shaken, the ether layer separated, washed (with water and with aq sodium hydrogencarbonate), and dried (Na_2-

SO_4). The oil (0.57 g; *caution*[30]) obtained after brief rotary evaporation was dissolved in ethanol (20 ml), and a solution of silver nitrate (2.00 g) in water (2 ml) was added giving a bright yellow precipitate, which was filtered off and washed with ethanol and with ether. The precipitate was stirred in ether (100 ml). An aqueous solution (15 ml) containing 3 ml of concd hydrochloric acid was added, the ether layer separated (after complete conversion of the precipitate), then washed (aq hydrochloric acid, water, and aq sodium hydrogencarbonate), dried and evaporated (up to 45 °C bath temp) to give **23a** as an oil (0.37 g, 87%). IR and ^{1}H NMR examination indicated the presence of ether (2%), the yield of **23a** being 85%. Pure **23a** was obtained by further evaporation.

Aqueous potassium hydroxide (a 0.08g pellet dissolved in 2 ml of water) was added to a solution of **17a** (1.00 g, 3.6 mmol) in methanol (50 ml) stirred in a bath kept at 20 °C. After 20 min, the resulting solution was shaken with a mixture of ether (100 ml) and water (100 ml). Crude **23a** was obtained from the ether layer and purified by conversion *via* the disilver diacetylide. Regenerated **23a** (0.42 g) contained 3% of ether (yield of **23a**: 85%). A 0.20 g portion of this sample was further evaporated to give 0.18 g of pure **23a** (79% from **17a**). MS *m/e* (rel intensity), 132 (M, 100), 82 (M−C_4H_2, 16), 69 (M−C_5H_3, 23), 63 (C_5H_3, 11); IR (neat),[31] 3290 [1], 3100 [2], 3090 sh [2], 2590 w, 2106 [3], 1784 [4], 1620 [5], 1518 [6], 1513 sh [6], 1442 [7], 1340 br [8], 1235 sh, 1219, 1152, 1138, 1034 [9], 813 [10], 705, 676 sh [11], 670 [11], 608 [12], 548, 495, 442 cm^{-1} [13].

*2,5-Diethynylfuran (**23b**).* MS *m/e* (rel intensity), 116 (M, 100), 88 (M−CO, 12), 63 (C_5H_3, 13), 62 (C_5H_2, 13), 53 (M−C_5H_3, 10); IR (neat),[31] 3290 [1], 3146 [2], 3110 w [2], 2692 w, 2107 [3], 1730 [4], 1600 [5], 1570 [6], 1565 sh [6], 1497 [7], 1380 br [8], 1347, 1310, 1214, 1200, 1022 [9], 965, 800 [10], 688 [11], 670 sh [11], 604 [12], 453 cm^{-1} [13].

*1-Ethynyl-4-(1,3-butadiynyl)benzene (**26c**).* Compound **10c** (1.00 g, 3.1 mmol each time) was treated with butyllithium or propyllithium (20 mmol) below −50 °C in order to find an appropriate isolation procedure for **26c**, an unstable compound. The ether solution obtained after work-up from each run was dried (Na_2SO_4) and subjected to rotary evaporation to leave a crystalline residue (0.5—0.6 g, corresponding to 109—130% yield of **26c**). All samples showed ^{1}H NMR signals at the alkyl hydrogen region, impurities not being completely removable by continued evaporation. Digestion with cold ethanol (or methanol) followed by filtration afforded pure **26c**, the yields being less than 50% even after combining the crystals obtained by cooling the filtrates to −20 °C. Conversion into the disilver diacetylide led to the highest isolated yield of pure **26c**. Thus the crude sample obtained from a butyllithium run was dissolved in ethanol (25 ml), and a solution of silver nitrate (2.00 g) in water (2 ml) was added to give a pale yellow precipitate, which was filtered off, washed, and treated with aqueous hydrochloric acid as in the case of **23a**. The sample of regenerated **26c** (0.36 g, 79%) showed no ^{1}H NMR signal other than three single peaks (2.52, 3.20, 7.47 ppm) in 1:1:4 relative intensities. The crystals of **26c** first appearing on the inside wall of the flask upon evaporation of every worked-up solution were nearly white, indicating that **26c** is stable in ether. However, the crystals turned rapidly to beige and to brown black. The compound showed no melting point and turned dark with rise in temperature. Cooling to or below −20 °C was neccessary for storage even for a short time (*e.g.* 2 h). The spectroscopic data of freshly prepared samples are as follows. MS *m/e* (rel intensity), 150 (M, 100), all other peaks (<7); IR (KBr), 3295 sh(w), 3275 sh, 3270, 2205, 1920, 1670, 1505 sh, 1497, 1403, 1378 w, 1269, 1258, 1109, 1020, 838, 711, 679, 668, 641, 636 sh, 548, 508, 451 cm^{-1}. The KBr discs of IR measurement turned black in one day upon standing in the dark at room temperature. The IR spectrum at this stage was nearly the same as the spectrum obtained after several months. Notable spectral changes were: (1) broadening and decrease in intensity of the 3270, 1403, 1109, 1020, 838, 668, 641, and 548 cm^{-1} bands, (2) disappearance of 2205, 1920, 1670, 1378, 1269, 1258, 711, 679, 508, and 451 cm^{-1} bands, and (3) replacement of the bands at 711—636 cm^{-1} by two broad bands (of decreased intensity) at 650 and 618 cm^{-1}.

*5-[p-(Carboxyethynyl)phenyl]-2,4-pentadiynoic Acid (**27c**).* Compound **10c** (1.00 g, 3.1 mmol) was treated with butyllithium as above, several pieces of Dry Ice (*ca.* 10 g) being added to the resulting active mixture. After stirring for 1.5 h water was added, the whole mixture shaken, filtered, the aqueous layer separated, washed with ether, and acidified with aqueous hydrochloric acid. The resulting faintly yellow crystalline precipitate was filtered off and dried (0.62 g, 85% yield of **27c**) over calcium chloride in a vacuum desiccator. Recrystallization of a portion of the sample from a small amount of methanol by cooling to −20 °C gave a colorless analytical sample showing no melting point and turning dark above *ca.* 190 °C. Recrystallization from water was inappropriate. Heating the compound in boiling water appeared to induce decarboxylation, the product (not purely isolated) suspected to be $HO_2CC{\equiv}CC_6H_4C{\equiv}C{-}C{\equiv}CH$. (The analytical samples of **24a** and **24b** were obtained by recrystallization from acetone and from water, respectively.)

*1-(Trimethylsilylethynyl)-4-(4-trimethylsilyl-1,3-butadiynyl)-benzene (**28c**).* Compound **10c** (2.00 g, 6.1 mmol) was treated with butyllithium (40 mmol), and the resulting active mixture with chlorotrimethylsilane. From the crystalline mixture obtained after work-up, **28c** (1.45 g, 81%; mp 107.5—108.5 °C) was obtained by digestion with methanol followed by filtration. The filtrate upon standing for one week, precipitated crystals (0.21 g, mp *ca.* 75—97 °C), which were found to be a mixture (*ca.* 3:2) of **28c** and a compound whose mass spectroscopic molecular weight is greater than that of **28c** by 130 [$(CH_3)_3SiC_4H_9$]. The latter seems to have the structure **30c**.

References

1) K. Okuhara, *J. Org. Chem.*, **41**, 1487 (1976).

2) The reaction observed between **1** and butyllithium is lithium-chlorine exchange (Ref. 1). See also D. Masure, R. Sauvetre, J. F. Normant, and J. Villieras, *Synthesis*, **1976**, 761.

3) The reaction of **1** with alkyl Grignard reagents is complicated and explained in terms of radical mechanism involving β-hydrogen atom abstraction from Grignard reagents: K. Okuhara, *J. Am. Chem. Soc.*, **102**, 244 (1980).

4) H. Gilman, *Org. React.*, **8**, 258—304 (1954); J. M. Mallan and R. L. Bebb, *Chem. Rev.*, **69**, 693—755 (1969); U. Schöllkopf, *Methoden Org. Chem.*, **13**, part 1, 97—127 (1970); B. J. Wakefield, "The Chemistry of Organolithium Compounds," Pergamon Press, New York (1974), pp. 26—50; H. W. Gschwend and H. R. Rodriguez, *Org. React.*, **26**, 1—360 (1979).

5) R. G. Jones and H. Gilman, *Org. React.*, **6**, 339—366 (1951); U. Schöllkopf, *Methoden Org. Chem.*, **13**, part 1, 134—160 (1970); B, J. Wakefield, "The Chemistry of Organolithium Compounds," Pergamon Press, New York (1974),

pp. 51—65.

6) In the reaction of **1** with organolithium compounds (RLi), the proportion of the Cl-Li exchange to the sum of the exchange and substitution varies widely depending on the nature of R. It is suggested that the smaller the extent of delocalization of the negative charge in the reagent, the higher the proportion of the exchange (Ref. 1). The word "delocalization" may be replaced by "stabilization."

7) The isolated yield of **4b** was improved to 76% from the yield (53%) reported in Ref. 1. The major difference in reaction conditions is that the refluxing time for lithiation of furan with butyllithium was extended from 1 h (used after standing overnight) to 4 h (used at once). Compound **4b**, though turning intensely colored and then darkend on exposure to air, remained colorless when stored at −20 °C in an ampule filled with nitrogen.

8) Ferrocene was an exception, where 1,1′-disubstituted as well as monosubstituted derivatives were obtained.

9) A. Vaitiekunas and F. F. Nord, *J. Org. Chem.*, **19**, 902 (1945).

10) L. Brandsma, "Preparative Acetylenic Chemistry," Elsevier, Amsterdam (1971), p. 117.

11) R. E. Atkinson, R. F. Curtis, D. M. Jones, and J. A. Taylor, *J. Chem. Soc., C*, **1969**, 2173.

12) T. B. Patrick, J. M. Disher, and W. J. Probst, *J. Org. Chem.*, **26**, 4467 (1972).

13) C. Wentrup and H. W. Winter, *Angew. Chem.*, **90**, 643 (1978).

14) I. Iwai and U. Yura, *Takamine Kenkyusho Nempo*, **10**, 30 (1958); *Chem. Abstr.*, **55**, 4400f (1961).

15) S. Holand, F. Mercier, N. Le Goff, and R. Epsztein, *Bull. Soc. Chim. Fr.*, **1972**, 4357.

16) M. Schlosser and V. Ladenberger, *Chem. Ber.*, **100**, 3901 (1967).

17) These diacetylenes seem to be obtainable from 2,5-thiophene- and 2,5-furandicarbaldehyde *via* the route of Ref. 16: RCHO→RCH=CHCl→RC≡CLi. However, the existence of the 2-chloroethenyl group in cis and trans forms might seriously complicate the isolation and purification of intermediates, particularly in cases where there are more than one 2-chloroethenyl group. The method given in the following paper, with use of $RCH{=}CBr_2$ as an intermediate, gives no such complication: E. J. Corey and P. L. Fuchs, *Tetrahedron Lett.*, **1972**, 3769.

18) A. S. Hay, *J. Org. Chem.*, **25**, 637 (1960).

19) Mixtures of *m*- and *p*-isomer were prepared: J. M. Watson, *Macromolecules*, **6**, 815 (1973).

20) J. M. Watson, *Macromolecules*, **5**, 331 (1972).

21) Compound **11a** in a sealed NMR tube as a 20% benzene solution decomposed almost completely in several years whereas compound **11c** under the same conditions showed no sign of decomposition. See Experimental for exothermic decomposition of **11a**.

22) Trialkylsilyl groups are often used for the protection of terminal acetylenes. For example: R. Eastmond, T. R. Johnson, and D. R. M. Walton, *Tetrahedron*, **28**, 4601 (1972).

23) G. Eglinton and A. R. Galbraith, *Chem. Ind. (London)*, **1956**, 737.

24) G. Eglinton and A. R. Galbraith, *J. Chem. Soc.*, **1959**, 889.

25) A. S. Hay, *J. Org. Chem.*, **27**, 3320 (1962).

26) Treatment of furan with a three-fold excess of butyllithium in refluxing ether for 4 h followed by quenching with D_2O gave furan-2,5-d_2: G. R. Ziegler and G. S. Hammond, *J. Am. Chem. Soc.*, **90**, 513 (1968). The material is reported to be 80% dideuterated. However, the absolute yield of furan-2,5-d_2 may be considerably lower than 80%.

27) None of the peaks due to ^{37}Cl-containing species is given. Such a peak is not taken as a base peak (intensity 100) even if it is the strongest (*e.g.*, *m/e* 310 in the case of **20a**).

28) Admission of nitrogen is instructed after termination of distillation of acetylenic compounds *in vacuo*: Ref. 10, p. 13.

29) This compound was previously reported: V. D. Ermakova, M. G. Chauser, J. S. Nesterova, and M. I. Cherkoshin, *Tesisy Dokl. Vses, Konf. Khim. Stsetilena*, 5th, 1975, 505; *Chem. Abstr.*, **88**, 153350r (1978).

30) In an earlier experiment of the same scale, such an oil (crude **23a**) was further evaporated, and GC examination of the resulting oil (0.30 g, not pure according to IR) was attempted. As soon as the needle of the microsyringe was inserted into the injection port (*ca.* 250 °C), the content (1 μl+needle volume) decomposed with ignition. Although crude samples of lower **23a** content (and solutions of **23a** in ether) were injectable, a considerable decomposition of **23a** was apparent in its low sensitivity.

31) The figures in square brackets indicate the correspondence of frequencies of **23a** and **23b** suggested from comparative inspection of the two spectra (aside from rigorous assignments of frequencies).

Specific Catalysis by α-Cyclodextrin on the Dichlorocarbene Attack at Phenolate

Makoto KOMIYAMA* and Hidefumi HIRAI

Department of Industrial Chemistry, Faculty of Engineering, The University of Tokyo, Hongo, Bunkyo-ku, Tokyo 113

(Received October 14, 1980)

A selective attack of dichlorocarbene at the para-position of phenolate has been achieved by using α-cyclodextrin and the reaction mechanism has been studied by the ^{13}C-NMR and ^{1}H-NMR spectroscopy. The attack of the carbene at the para-position of phenolate (82%) is dominant over the attack at the ortho-position (18%) in the presence of 0.15 mol dm^{-3} of α-cyclodextrin, which is in contrast with the predominance of the ortho-attack (59%) over the para-attack (41%) in the absence of α-cyclodextrin.

Specificity is one of the important characteristics of the cyclodextrin catalyses.[1] This specificity has been attributed to the complex formation of the substrate with cyclodextrin prior to the chemical transformation. However, detailed analysis on the origin of the specificity has been scant, mainly because of poor information on the structures of the inclusion complexes of cyclodextrin in solution.

In previous papers, the time-averaged conformations of the inclusion complexes were determined by use of the ^{1}H-NMR[2,3] and ^{13}C-NMR[4] spectroscopy. Furthermore, a much larger magnitude of the catalysis of α-cyclodextrin in the cleavage of *m*-nitrophenyl acetate than that in the cleavage of *p*-nitrophenyl acetate was satisfactorily interpreted in terms of the structures of the inclusion complexes of the substrates and α-cyclodextrin.[5]

In the present paper, the α-cyclodextrin-catalyzed para-selective attack of dichlorocarbene at phenolate is shown. Furthermore, the origin of the selectivity is clarified by using the time-averaged structure of the α-cyclodextrin-phenolate complex, determined by the ^{13}C-NMR and ^{1}H-NMR spectroscopy.

Experimental

Determination of the Para-Ortho Selectivity in the Dichlorocarbene Attack at Phonolate. Dichlorocarbene, prepared *in situ* from chloroform and sodium hydroxide, was allowed to react with phenolate as shown in Eqs. 1—3 (Reimer-Tiemann reaction).[6] The reactions were carried out in 0.2 mol dm^{-3} NaOH solution at 30 °C, and the initial concentrations of phenolate, chloroform, and α-cyclodextrin, respectively, were in the regions of 5×10^{-3}—2×10^{-2}, 1×10^{-2}—4×10^{-2}, and 0—1.5×10^{-1} mol dm^{-3}. The rate and the selectivity in the attack at phenolate were determined by the absorption spectroscopy on the hydrolysis products, hydroxybenzaldehydes, of the adducts of dichlorocarbene with phenolate.[7] The concentrations of *p*- and *o*-hydroxybenzaldehydes were determined by using the absorptions at 330 and 378 nm, respectively.

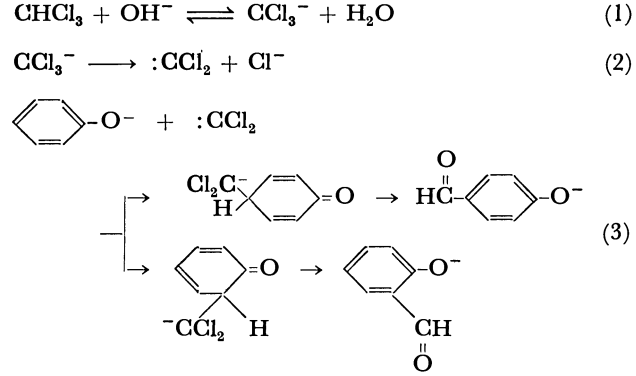

Table 1. The para : ortho selectivity in the dichlorocarbene attack at phenolate in the presence of α-cyclodextrin[a,b]

[α-Cyclodextrin]$_0$ / 10^{-1} mol dm^{-3}	Conversion of phenolate / %	Products: Para : Ortho molar ratio	Products: Para selectivity/%
0	12	0.71	41
0.071	9.7	0.77	44
0.15	8.1	0.85	46
0.25	6.0	0.99	50
0.35	4.3	1.11	53
0.60	2.3	1.71	63
1.0	1.5	3.55	78
1.5	0.95	4.65	82

a) In 0.2 mol dm^{-3} NaOH solution; [phenolate]$_0=10^{-2}$ and [chloroform]$_0=3\times10^{-2}$ mol dm^{-3}; the reaction time is two days. b) The subscript 0 refers to the initial concentration.

Determination of the Time-averaged Position of Phenolate in the Cavity of α-Cyclodextrin. The time-averaged position of phenolate was determined by use of the position of each of the carbon atoms of phenolate in the cavity of α-cyclodextrin, estimated by the ^{13}C-NMR spectrsocopy. The depths of the penetration of the carbon atoms of phenolate were estimated from the observed ^{13}C-NMR chemical shift changes by using the relationship between the depth of the penetration and the ^{13}C-NMR chemical shift changes reported in the previous paper.[5] As shown previously,[5] the change of the ^{13}C-NMR chemical shift of the aromatic carbon atom of the guest compound on the complex formation with α-cyclodextrin is governed by the depth of the penetration of the carbon atom in the cavity, irrespective of the substituents of the benzene moieties of the guest compounds.

The ^{13}C-NMR spectrometry was run in 0.2 mol dm^{-3} NaOD solution on a JEOL PFT-100 spectrometer operating at 25.03 MHz, connected with JEOL EC-100 computer. The ^{13}C-NMR chemical shifts were determined by use of sodium formate as the internal standard. The ^{1}H-NMR spectra were taken on a JEOL PS-100 spectrometer in 0.2 mol dm^{-3} NaOD solution. The signal of HOD was used as the internal reference.

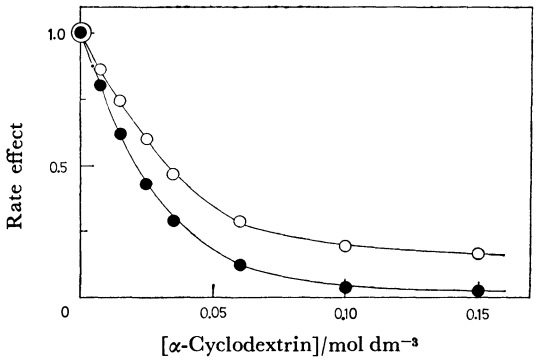

Fig. 1. Effects of α-cyclodextrin on the rates of the para-attack (○) and the ortho-attack (●) of dichlorocarbene at phenolate; the rates of the para-attack and the ortho-attack in the absence of α-cyclodextrin are taken as unity.

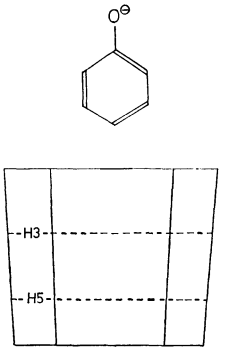

Fig. 2. Time-averaged conformation of the α-cyclodextrin–phenolate complex; ---H3--- and ---H5--- show the planes comprised of the corresponding six atoms of α-cyclodextrin.

Results

Effect of α-Cyclodextrin on the Orientation of the Dichlorocarbene Attack at Phenolate. Table 1 shows the dependence of the para-ortho ratio in the dichlorocarbene attack at phenolate on the concentration of α-cyclodextrin. In the absence of α-cyclodextrin, the attack at the ortho-carbon atom (59%) was dominant over the attack at the para-carbon atom (41%). However, α-cyclodextrin changed the specificity of this reaction from the ortho-selectivity to the para-selectivity. The ratio of the para-attack to the ortho-attack increased with the increase of the concentration of α-cyclodextrin. At the concentration of 0.15 mol dm^{-3}, the ratio was 4.65, which corresponded to 82% para-selectivity.

The variations of the initial concentrations of phenolate and chloroform in the regions of 5×10^{-3}—2×10^{-2} and 1×10^{-2}—4×10^{-2} mol dm^{-3}, respectively, showed little effect on the para-ortho ratio at a fixed initial concentration of α-cyclodextrin.

The para-selectivity in the presence of α-cyclodextrin came from the larger magnitude of the suppression of the ortho-attack by α-cyclodextrin than that of the para-attack as shown in Fig. 1. For example, 0.15 mol dm^{-3} of α-cyclodextrin decreased the rate of the ortho-attack and that of the para-attack, respectively, by 41 and 6.3 fold with respect to the rates in the absence of α-cyclodextrin, which resulted in the para-ortho ratio of 4.65. The ratio in the absence of α-cyclodextrin was 0.71.

No reaction product between α-cyclodextrin and dichlorocarbene was detected in the present reactions. Thus, the reaction mixture with the initial concentrations of phenolate, chloroform, and α-cyclodextrin, respectively, of 10^{-2}, 4×10^{-2}, and 5×10^{-2} mol dm^{-3} was acidified with hydrochloric acid after 2 d at 30 °C, and was then vigorously extracted with chloroform. The ^{1}H-NMR and IR spectroscopy on the white powder, obtained after the evaporation of the aqueous layer, showed that all α-cyclodextrin remained intact during the reaction.

Time-averaged Position of Phenolate in the Cavity of α-Cyclodextrin. Figure 2 depicts the time-averaged position of phenolate in the cavity of α-cyclodextrin determined by the ^{13}C-NMR spectroscopy. The depths of the penetration of the carbon atoms of phenolate in the cavity, determined from the changes of the ^{13}C-NMR chemical shifts on the complex formation (see Experimental Section) and listed in Table 2, were used here. The agreements between the observed changes of the ^{13}C-NMR chemical shifts and the calculated ones are fair as shown in Table 2.

In the time-averaged conformation of Fig. 2, phenolate penetrates in the cavity with the hydrogen atom on the para-carbon atom as a head from the secondary hydroxyl side of α-cyclodextrin.

The validity of this conformation of the complex was further supported by the ^{1}H-NMR spectroscopy. In this conformation, the anisotropic shielding effects of the aromatic ring of phenolate on the H-3 and H-5 atoms of α-cyclodextrin (see Fig. 2), estimated by using the table of Johnson and Bovey[8] as described previously,[2] are −0.07 and −0.07 ppm, respectively.

TABLE 2. OBSERVED AND CALCULATED VALUES OF THE ^{13}C-NMR CHEMICAL SHIFT CHANGES OF PHENOLATE ON THE COMPLEX FORMATION WITH α-CYCLODEXTRIN, AND THE DEPTHS OF THE PENETRATION OF THE CARBON ATOMS IN THE CAVITY

Carbon atoms[a]	^{13}C-NMR chemical shift change/ppm[b]		Depth of the penetration/Å[c]
	Obsd	Calcd	
1	+0.33	—[d]	−3.7
2	+0.54	+0.55	−2.3
3	+0.12	+0.07	−1.6

a) The numbering system is as follows;

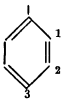

b) The positive sign shows the increase of the shielding. c) The depth from the plane comprised of the six H-3 atoms (see Fig. 2) of α-cyclodextrin. The negative sign refers to the region in the side of the secondary hydroxyl groups. d) The position of the carbon atom was so far away from the region examined previously (Ref. 4) that the calculation was not made.

Table 3. Effect of chloroform on the ^{13}C-NMR chemical shift changes due to the complex formation of α-cyclodextrin with phenolate

System[a]	Changes of ^{13}C-NMR chemical shifts of phenolate/ppm[b]		
	C-1	C-2	C-3
α-Cyclodextrin(10^{-1}) -phenolate(3×10^{-2})	+0.28	+0.43	+0.10
α-Cyclodextrin(10^{-1}) -phenolate(3×10^{-2}) -chloroform(3×10^{-2})	+0.02	+0.02	0.00

a) The numbers in parentheses are the concentrations in mol dm^{-3} unit in 0.2 mol dm^{-3} NaOD solution. b) The numbering system of the carbon atoms is shown in the footnote a) of Table 2. The positive sign shows the increase of the shielding.

Here the negative sign refers to the decrease of the shielding. These values show fair agreements with the corresponding observed changes of the ^{1}H-chemical shifts (−0.07 and −0.08 ppm, respectively, for the H-3 and H-5 atoms).

Effect of Chloroform on the Complex Formation between α-Cyclodextrin and Phenolate. The changes of the ^{13}C-NMR chemical shifts of phenolate on the complex formation with α-cyclodextrin were highly suppressed by the addition of chloroform (Table 3). The changes of the chemical shifts of all the carbon atoms of phenolate were virtually none in the presence of 3×10^{-2} mol dm^{-3} of chloroform. This result indicates that the complex formation between chloroform and α-cyclodextrin takes place competitively with that between phenolate and α-cyclodextrin. Almost all of phenolate are free from the complex formation with α-cyclodextrin in the reaction mixtures used in the present study.

Discussion

The reaction between dichlorocarbene and phenolate in the presence of α-cyclodextrin proceeds as the one between the carbene complexed with α-cyclodextrin and free phenolate. The complex formation of chloroform with α-cyclodextrin almost completely inhibits the complex formation of phenolate with α-cyclodextrin in the reaction mixture as shown in Table 3. Chloroform, complexed with α-cyclodextrin, is converted to dichlorocarbene according to Eqs. 1 and 2. Alternative pathway of the formation of the complex between α-cyclodextrin and the carbene, where the carbene is formed in solution followed by complexation with α-cyclodextrin, is unlikely, since the carbene in solution is so unstable that its life-time is short.

Figure 3 schematically depicts the mechanism of the para-selectivity of the catalysis by α-cyclodextrin in the dichlorocarbene attack at phenolate. Toward the carbene, formed inside the cavity of α-cyclodextrin, phenolate can approach in two ways such as A and B, which should predominantly result in the para-attack and the ortho-attack, respectively, because of a sterical reason. The para-selectivity observed in

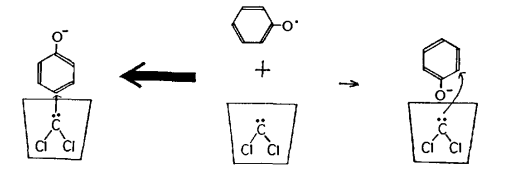

Fig. 3. Proposed mechanism of the α-cyclodextrin-catalyzed selective para attack of dichlorocarbene at phenolate.

the present study is attributable to the predominant occurrence of the approach of the phenolate in the type A, which is due to the fact that the penetration of the hydrogen atom on the para-carbon atom of the phenolate in the cavity as a head is more favorable than the penetration of the phenoxide oxygen atom as a head. The approach in the type A should be easier than that in the type B, since the penetration of the apolar aromatic moiety of phenolate in the apolar cavity of α-cyclodextrin is more stable than the penetration of the polar phenoxide oxygen atom in the apolar cavity.

The above argument is definitely supported by the time-averaged conformation of the α-cyclodextrin–phenolate inclusion complex shown in Fig. 2. Penetration of phenolate in the cavity with the side of the para-carbon as a head in the complex strongly indicates the predominant formation of the transition state involving the penetration of the para-carbon of phenolate in the cavity (type A).

The mechanism involving the dichlorocarbene formed inside the cavity is consistent with the suppression of the rates of the reactions between phenolate and dichlorocarbene by α-cyclodextrin (Fig. 1). Since the carbene is formed *via* anion of chloroform as shown in Eq. 1, the negative charges of the secondary hydroxyl groups electrostatically prevent the formation of the carbene. The secondary hydroxyl groups of α-cyclodextrin exist mostly in the anionic forms in the reaction mixture, since their pK_a is around 12.[1] Steric hindrance by α-cyclodextrin should also reduce the reactivity of the carbene. The suppression of the reaction by α-cyclodextrin also indicates that the formation of dichlorocarbene by the reaction of chloroform with the alkoxide ion of α-cyclodextrin (in place of hydroxide ion in Eq. 1) is less important.

The para-selectivity in the present reaction is consistent with those in the β-cyclodextrin-catalyzed Reimer-Tiemann reaction of phenolate[9] and the α-cyclodextrin-catalyzed chlorination of anisole.[10]

In conclusion, a selective attack of dichlorocarbene at the para-position of phenolate was achieved by using α-cyclodextrin. α-Cyclodextrin regulated the orientation of phenolate with respect to the carbene on the mutual access, resulting in the specific catalysis.

This work was partially supported by a Grant-in-Aid for Scientific Research from the Ministry of Education, Science and Culture. The support by the Kawakami Foundation is acknowledged.

References

1) M. L. Bender and M. Komiyama, "Cyclodextrin Chemistry," Springer-Verlag, Berlin (1978).
2) M. Komiyama and H. Hirai, *Polym. J.*, **13**, 171 (1981).
3) M. Komiyama and H. Hirai, *Chem. Lett.*, **1980**, 1467.
4) M. Komiyama and H. Hirai, *Bull. Chem. Soc. Jpn.*, **54**, 828 (1981).
5) M. Komiyama and H. Hirai, *Chem. Lett.*, **1980**, 1471.
6) H. Wynberg, *Chem. Rev.*, **60**, 169 (1960).
7) J. Hine and J. M. van der Veen, *J. Am. Chem. Soc.*, **81**, 6446 (1959).
8) C. E. Johnson and F. A. Bovey, *J. Chem. Phys.*, **29**, 1012 (1958).
9) M. Ohara and J. Fukuda, *Pharmazie*, **33**, 467 (1978).
10) R. Breslow and P. Campbell, *J. Am. Chem. Soc.*, **91**, 3085 (1969).

  Bull. Chem. Soc. Jpn., 54, 2057—2060 (1981)

Photo-promoted Hypochlorite Oxidation of α-Amino Acids. Kinetics and Irradiation Effect for the Strecker Degradation[1)]

Yoshiro OGATA,* Makoto KIMURA, and Yoshinori KONDO

Department of Applied Chemistry, Faculty of Engineering, Nagoya University, Furo-cho, Chikusa-ku, Nagoya 464

(Received July 9, 1980)

Hypochlorite oxidation of simple α-amino acids (the Strecker degradation) in aqueous solutions has been studied in the dark and under UV-irradiation. UV-spectra, iodometry, and amino acid determination (2,4-dinitrofluorobenzene method) suggest that the intermediate *N*-chloro amino acid is formed quickly at an initial stage, then its slow oxidative decomposition takes place to give aldehyde, carbon dioxide, and ammonia. The mechanism is also supported by the fact that the oxidation follows the first-order rate expression; $-d[RCH(NH_2)CO_2H]/dt = k_1[RCH(NHCl)CO_2H]$. UV-irradiation was found to promote remarkably the degradation of *N*-chloro amino acid. When equimolar amounts of amino acid and hypochlorite were used, the products such as unreacted amino acid, ammonia, and aldehyde were analogous to those of the dark reaction. The use of a large excess of hypochlorite under irradiation enables complete oxidative degradation of amino acid to carbon dioxide, water, and nitrogen. Its application to waste water treatment is discussed.

Simple α-amino acids often present in municipal waste water may be one of the major organic pollutants causing serious eutrophication in seas and lakes. Treatment of α-amino acids with sodium hypochlorite in the dark is known to cause the Strecker degradation leading to carbon dioxide, ammonia, and aldehydes possessing one less carbon atom.[2)] Langheld postulated a mechanism involving *N*-chloro amino acid (Eq. 1),[3)] but only limited information is available as to the kinetics and mechanism.[4,5)]

$$RCHCO_2H \xrightarrow[NH_2]{NaOCl} RCHCO_2Na \xrightarrow[NHCl]{-HCl} RCCO_2Na \xrightarrow[NH]{} \xrightarrow{-CO_2}$$

$$RCH{=}NH \xrightarrow{H_2O} RCHO + NH_3 \qquad (1)$$

Sodium hypochlorite exhibits under UV-irradiation a high oxidation power, decomposing effectively organic compounds and ammonia.[6)] It has been reported that irradiated hypochlorite effectively oxidizes some sulfonic acids,[7)] ethers,[8)] and aliphatic acids,[9)] which are fairly stable against hypochlorite in the dark. Hypochlorite oxidation of ammonia to nitrogen is greatly accelerated by irradiation.[10)] This photo-oxidation method might be important for waste water treatment, in which pollutants should be eliminated completely.

The present paper describes the kinetic behavior of the Strecker degradation in order to clarify the rate-determining step and also the effect of irradiation. We have found that on irradiation in the presence of large excess of NaOCl amino acids are decomposed rapidly into carbon dioxide and nitrogen.

Results and Discussion

Dark Reaction and Its Kinetics. The dark reactions of 5—10 mM (1 mM=10^{-3} mol dm^{-3}) glycine, alanine, and valine with NaOCl were examined in various buffer solutions at room temperature by monitoring the concentration of amino acid and oxidant. Analysis was based on (A) iodometry which gives concentration of hypochlorite and even *N*-chloro amino acids, and (B) determination of amino acids by 2,4-dinitrofluorobenzene method after converting *N*-chloro amino acids into amino acids. When hypochlorite was used in a 5—10-fold amount to amino acid at various pH, degradation of amino acid at pH 3—11 was too fast to determine the accurate rate of oxidation.

Table 1. First-order rate constants (k_1)[a)] for the dark reaction of α-amino acids with NaOCl at 20 °C

Amino acid	pH	$k_1 \times 10^5$/s^{-1}
Glycine	7.0	0.74
Alanine	6.0	7.5
	7.0	8.0 (9.8)
	9.0	8.5 (9.0)
Valine	7.0	10.3 (12.0)

a) Determined by iodometry (method A). Figures in parentheses are based on consumed amino acid (method B).

When equimolar (1:1 mol) amounts of hypochlorite and amino acid were used, oxidation became slow enough to be followed by spectrophotometry, iodometry, and amino acid determination. The UV spectroscopy of the equimolar solution indicated the instantaneous and quantitative formation of *N*-monochloro amino acid at pH 5—11. Each *N*-chloro amino acid was assigned by its absorption maximum at *ca.* 250 nm and its observed molar absorption coefficient (see Experimental). In acidic solutions at pH 2—4, *N*,*N*-dichloro amino acids were detected.

For the reaction of one mole of amino acid with one mole of hypochlorite, the change in amino acid concentration (c) was measured from time to time by methods (A) and (B). The observed values were found to fit the first-order rate expression ($\ln c_0/c = k_1 t$), though an apparent deviation from the first-order was observed at conversion higher than 70%. The first-order rate constants (k_1) analogous in methods (A) and (B) are given in Table 1.

The observed first-order rate suggests that the Strecker degradation with hypochlorite involves the decomposition of *N*-chloro amino acids at a rate-determining step. Thus the rate is first-order with respect to *N*-chloro amino acid:

$-d[RCH(NH_2)CO_2H]/dt = k_1[RCH(NHCl)CO_2H]$.

TABLE 2. PHOTOLYSIS AND DARK REACTION OF AMINO ACID WITH HYPOCHLORITE[a]

Light	Substrate	Amino acid		Ammonia		Aldehyde	
		Unreacted (mM)	Consumed (%)	Produced (mM)	Yield[b] (%)	Produced (mM)	Yield[b] (%)
>290 nm	Glycine	1.50	70	3.57	102	1.35	39
	Alanine	1.07	78	3.53	90	c)	
	Valine	0.85	83	4.28	97	c)	
None	Glycine	1.90	62	2.30	74	0.50	17
	Alanine	0.96	81	4.11	102	c)	
	Valine	0.75	85	4.61	108	c)	

a) Initial concentration; amino acid 5.0 mM; NaOCl 5.02 mM. Photolysis at 22 °C for 2.0 h, dark reaction at 25±2°C for 52 h. b) Yield based on consumed amino acid. c) Unsuccessful in quantitative determination, but positive to 2,4-dinitrophenylhydrazine reagent.

This is in accord with the UV spectroscopic measurements indicative of rapid and quantitative *N*-chlorination of amino acid. Though monochlorination of amino acid with chloramine T giving nitrile is slow,[5] the *N*-chlorination with hypochlorite leading to Strecker degradation is very rapid as is seen in ammonia and alkylamines.[11]

Chloramine NH_2Cl is in equilibrium with ammonia and hypochlorite.[12] Thus, the following mechanism is proposed:

$$\underset{\underset{NH_2}{|}}{RCHCO_2H} + HOCl \underset{\text{fast}}{\overset{\text{very fast}}{\rightleftharpoons}} \underset{\underset{NHCl}{|}}{RCHCO_2H} + H_2O \quad (2a)$$

$$\underset{\underset{NHCl}{|}}{RCHCO_2H} \xrightarrow{\text{slow}} RCHO + NH_3 + CO_2. \quad (2b)$$

Fast *N*-chlorination takes place with the equilibration of Eq. 2a (the equilibrium is extremely shifted to the right), followed by slow decomposition of *N*-chloro amino acid (Eq. 2b), indicating that the reverse process in pre-equilibrium (Eq. 2a) should be faster than decomposition (Eq. 2b). Otherwise, the second-order rate instead of first-order would have been observed.

The oxidation rate at pH 7 increases in the order glycine<alanine<valine (Table 1). The order might indicate that the electron-releasing group (CH_3) accelerates the reaction by stabilizing the developing positive charge during the course of oxidation. The effect of pH on the rate is not significant.

Photo-oxidation. Equimolar solutions (5—10 mM) of hypochlorite and amino acid were irradiated with light of wavelength>290 nm at pH 2—11. By means of iodometry and UV spectroscopy, *N*-chlorinated amino acids were found to decompose quite readily at any pH. To attain 95% consumption of *N*-chloro amino acid (oxidant), only 15 min was sufficient with an internal irradiation (see Experimental), whereas a period of over two days was necessary with the dark reaction. In spite of the presence of *N,N*-dichloro amino acid at pH 2—4, the decomposition rate was the same as that at pH 5—11; the effect of pH on decomposition rate of *N*-chlorinated amino acids was negligible. This may be due to the rapid interconversion between *N,N*-dichloro amino acid and *N*-chloro amino acid.

$$\underset{\underset{NCl_2}{|}}{RCHCO_2H} + \underset{\underset{NH_2}{|}}{RCHCO_2H} \longrightarrow 2\underset{\underset{NHCl}{|}}{RCHCO_2H} \quad (3)$$

Aldehydes, ammonia, carbon dioxide, and nitrogen were identified as products of the equimolar reaction together with unchanged amino acids. These products are the same as those of the corresponding dark reaction. A parallel experiment between irradiated and dark reactions was conducted with an equimolar solution at pH 7.0 in order to examine their product distribution. The results are summarized in Table 2.

The consumption extent of amino acid is in the order glycine<alanine<valine, irrespective of irradiated and dark reactions. In irradiated and dark reactions (Table 2), each case of amino acid shows similar amounts of unreacted amino acid and produced ammonia. UV irradiation might essentially affect the rate of decomposition of *N*-chlorinated amino acid, accelerating the Strecker degradation. This is energetically possible since light energy supplied as high as 400 kJ/mol surpassed the N–Cl bond energy (about 190 kJ/mol) in *N*-chloro amino acid. Formation of formaldehyde resulted in a lower yield than expected from the stoichiometry (Eq. 1), though high yield was observed for ammonia (Table 2). Reactions of amino acid with one mole of hypochlorite were carried out in the presence of five moles of aldehyde. Increase in the amount of recovered amino acid was observed. Aldehydes produced should reduce *N*-chloro amino acid to the original amino acid.

Another kind of irradiation was carried out in order to attain complete oxidation of amino acid in water. According to the theoretical equation (*e.g.* Eq. 4), 5, 8, and 15 equivalent amounts (only slight excess) of hypochlorite were irradiated (>290 nm) with glycine, alanine, and valine, respectively.

$$2H_2NCH_2CO_2H + 9NaOCl \longrightarrow 4CO_2 + 5H_2O + N_2 + 9NaCl \quad (4)$$

Iodometry showed rapid comsumption of oxidants such as OCl^- (alkaline solution) or HOCl (in acidic solution). After completion of the reaction, no significant amount of starting amino acids nor their primary products (ammonia and aldehydes) was detected. Estimation of carbon dioxide produced gave 60, 43, and 23% yields for glycine, alanine, and valine, respectively, based on the complete oxidation stoichiometry. Attempts to detect formic acid as a pos-

sible oxidation product of glycine were unsuccesful. However, acetic acid for alanine, and 2-methylpropanoic acid for valine could be detected by analysis of their crude reaction mixtures. Carboxylic acids can be completely oxidized with a large excess of hypochlorite under irradiation,[9] the oxidation of ammonia to nitrogen being considerably accelerated under irradiation.[10] Photochemical oxidation of sulfonic acids,[7] ethers,[8] and carboxylic acids[9] has been attributed to active oxygen species derived from hypochlorite ion. The oxygen atom might take part in the complete oxidation of aldehyde and carboxylic acid. It is evident that the initial stage for amino acid oxidation involves the formation and subsequent decomposition of *N*-chloro amino acid.

Experimental

General. Aqueous sodium hypochlorite (1 M) was prepared by introducing gaseous chlorine to aqueous NaOH (2.1 M) at 0 °C, the concentration of which was determined by iodometry. All amino acids (guaranteed grade) were DL-compounds. A buffer solution of pH 7 for the reactions was prepared with 0.2 M KH_2PO_4 added to NaOH. Commercial reagents (guaranteed grade) were used for analysis. Visible and UV absorption spectra were measured on a Hitachi 124 spectrophotometer in 1 cm cells. The internal irradiation was carried out in a vessel equipped with a Halos 100 W high-pressure mercury lamp, and external irradiation with a merry-go-round apparatus equipped with a Halos 300 W high-pressure mercury lamp.

Analysis. The 2,4-dinitrofluorobenzene (DNFB) method[13] was selected for the determination of amino acid. To a sample adjusted at pH 10 (1+1 ml) was added 1 w/v % 2,4-dinitrofluorobenzene in 2-propanol (1 ml). After being kept at 40 °C for 15 min, 1 M HCl solution (2 ml) of 2-propanol (1:1) was added. The resulting coloration was determined spectrophotometrically at 460 nm. The presence of equal mol of ammonia was found to increase the estimation of glycine, alanine, and valine by 29, 22, or 17±2%, respectively. Hence, we corrected the apparent values of amino acid by substracting the contribution due to eventual amount of ammonia.

The estimation of ammonia was based on the Nessler method[14] according to the procedure of JIS K 0101-1976. Chloramine, which is formed from ammonia and hypochlorite, disturbed the colorimetry at 450 nm. No interference was observed in the presence of amino acids. The presence of equimolar formaldehyde in an ammonia solution gave positive 28±3% error, acetaldehyde and 2-methylpropanal giving only *ca.* 5% error. No correction was made in the reactions of alanine and valine.

As regards aldehydes, 2,4-dinitrophenylhydrazine method was restricted only to qualitative analysis because of low sensitivity for quantitative analysis. Chromotropic acid reagent[15] was used for determination of formaldehyde, which was confirmed to be specific for formaldehyde. Colorimetry was carried out at 570 nm.

Dark Reaction. An equimolar amount of aqueous sodium hypochlorite was added to buffered solution of amino acid. Immediate iodometry showed a slight decrease in oxidant concentration, the concentration of amino acid based on DNFB method decreasing to 5—10% of the initial concentration. UV inspection of the solution showed a new absorption instead of HOCl (at 235 nm) and OCl^- (at 292 nm). After reduction with sodium thiosulfate solution, the DNFB method gave the expected value. This shows that since *N*-chloro amino acid is formed quickly, it is determined by iodometry but not by the DNFB method. The UV absorption data for *N*-chloro amino acid are as follows: absorption maximum (molar coefficient), *N*-chloroglycine 254 nm (342) (lit,[16] 256 nm (350)), *N*-chloroalanine 252 nm (349) (lit,[16] 253 nm (385)), and *N*-chlorovaline 254 nm (338). Each acidic (pH 2—4) solution of glycine, alanine, and valine containing an equimolar amount of hypochlorite showed an absorption at 302, 293, and 295 nm, respectively. These absorptions were assigned to the corresponding *N,N*-dichloro amino acid, based on lit.[16]

Kinetic runs were conducted with an equimolar solution of amino acid (7.0 mM) and sodium hypochlorite (7.0 mM) in buffer solutions at 20±1 °C. The change of concentration of *N*-chloro amino acid with time was followed by iodometry (method A). In order to know the true consumption of amino acid, determination by the DNFB method was applied after reduction of *N*-chlorinated amino acid with aqueous thiosulfate (method B). The results are given in Table 1.

Photo-oxidation. Internal irradiation was started immediately after addition of aqueous sodium hypochlorite to a buffer solution of glycine, alanine, and valine. Progress of each reaction was followed by iodometry together with UV spectroscopy. The irradiation was continued for 15—20 min. In order to detect aldehydes, the irradiated solution was treated with 2,4-dinitrophenylhydrazine dissolved in sulfuric acid and ethanol. 2,4-Dinitrophenylhydrazones of aldehydes (recrystallized from ethanol), obtained from glycine, alanine, and valine, respectively, showed following mps (mixed mps) and ^{1}H-NMR spectra: formaldehyde 168—169 °C (lit,[17] 166 °C), δ (d_6-DMSO) ppm 6.90 (d, J=12 Hz, N=$\underset{|}{\text{C}}$–H) 7.71 (d, J=12 Hz, N=$\underset{|}{\text{C}}$–H) 8.03 (d, J=10 Hz, arom. H^6) 8.44 (d, d, J=10 Hz, J'=2 Hz, H^5) 9.02 (d, J'=2 Hz, H^3) 11.7 (broad s, N–H); acetaldehyde 168—170 °C (lit,[18] 168 °C) δ ($CDCl_3$) 2.15 (d, J=6 Hz, CH_3) 7.63 (q, J=6 Hz, =$\underset{|}{\text{C}}$H); 2-methylpropanal 180—182 °C (lit,[19] 182 °C) δ ($CDCl_3$) 1.20 (d, J=6 Hz, CH_3) 2.68 (m, >CH). Carbon dioxide was trapped on acidification of the solution with $Ba(OH)_2$ solution as $BaCO_3$. Nitrogen was ascertained by GLC with a column packed with Molecular Sieve 5A.

A solution of amino acid and sodium hypochlorite (50 mM, 5-fold equivalent to glycine, 8-fold to alanine and 15-fold to valine) was irradiated internally at pH 4, 7, and 10 until over 99% hypochlorite was consumed (for 15—20 min), 100% amino acid was consumed with negligible formation of ammonia and aldehydes. By titration using $Ba(OH)_2$, the yield of carbon dioxide was 60, 43, and 23% (average values) for glycine, alanine, and valine, respectively. Several kinds of detection of formic acid (reduction with magnesium in acidic solution followed by coloration of resulting formaldehyde with chromotropic acid; IR spectroscopy of the dried-up material) were attempted, but were unsuccessful. Acetic acid and 2-methylpropanoic acid were detected successfully by GLC method (with a column packed Chromosorb WAW).

Comparison of Products between Photo Reaction and Dark Reactions. To a 10.0 mM amino acid solution prepared in a buffer solution of 7.0 was added in one portion 50 ml of a buffered 10.3 mM NaOCl (existing as HOCl). Two samples of the solution (each 25 ml) were subjected to external irradiation at 22 °C until iodometry showed zero titer (for 2.0 h). The other two quarters were kept in the dark at 25±2 °C for 52 h. In the case of glycine, the oxidant

remained 6% after 52 h. All determinations were performed within 1 d. The results are given in Table 2.

Decomposition of N-*Chloro Amino Acid in the Presence of Aldehydes.* Solutions containing 5.0 mM amino acid, 5.0 mM hypochlorite, and 12.5 mM aldehyde were kept standing in the dark for 2 d. Addition of aldehyde increased the recovery yield of starting amino acid from 19% to 36% in the case of alanine and from 15% to 34% in the case of valine.

References

1) Contribution No. 279.
2) A. Schönberg and R. Moubacher, *Chem. Revs.*, **50**, 261 (1952).
3) K. Langheld, *Ber. Dtsch. Chem. Ges.*, **42**, 2360 (1909).
4) H. L. Slates, D. Taub, C. H. Kuo, and N. L. Wendler, *J. Org. Chem.*, **24**, 1424 (1964); E. E. van Tamelen, V. B. Haarstad, and R. L. Orvis, *Tetrahedron*, **24**, 687 (1968); N. Konigsberg, G. Stevenson, and J. M. Luck, *J. Biol. Chem.*, **235**, 1341 (1960); Y. Matsushima, *Bull. Chem. Soc. Jpn.*, **24**, 17 (1951).
5) A. Kumar, A. K. Bose, and S. P. Mushran, *Monatsch. Chem.*, **106**, 13 (1975).
6) Reviews; Y. Ogata and M. Kimura, *Yuki Gosei Kagaku*, **37**, 581 (1979); S. K. Chakrabartty "Oxidation in Organic Chemistry," ed by W. S. Trahanovsky, Academic Press, New York (1978), Chap. V.
7) M. Nakamura and Y. Ogata, *Bull. Chem. Soc. Jpn.*, **50**, 2396 (1977).
8) Y. Ogata, K. Takagi, and T. Suzuki, *J. Chem. Soc. Perkin Trans. 2*, **1978**, 562.
9) Y. Ogata, T. Suzuki, and K. Takagi, *J. Chem. Soc. Perkin Trans. 2*, **1979**, 1715.
10) M. Kimura and Y. Ogata, *Bull. Chem. Soc. Jpn.*, **53**, 3198 (1980).
11) I. Weil and J. C. Morris, *J. Am. Chem. Soc.*, **71**, 1664 (1949); C. R. Edmond and F. G. Soper, *J. Chem. Soc.*, **1949**, 2942.
12) R. E. Corbett, W. S. Metcalf, and F. G. Soper, *J. Chem. Soc.*, **1953**, 1927.
13) D. T. Dubin, *J. Biol. Chem.*, **235**, 783 (1960); F. C. McIntire, L. M. Clements, and M. Sproull, *Anal. Chem.*, **25**, 1757 (1953).
14) W. Massmann, *Z. Anal. Chem.*, **193**, 332 (1963).
15) E. Eegriwe, *Z. Anal. Chem.*, **110**, 22 (1937); C. E. Bricker and W. A. Vail, *Anal. Chem.*, **22**, 720 (1950).
16) W. S. Metcalf, *J. Chem. Soc.*, **1942**, 148.
17) N. R. Campbell, *Analyst*, **61**, 391 (1936).
18) B. E. Gordon, F. Wopat, Jr., H. D. Burnham, and L. C. Jones, Jr., *Anal. Chem.*, **23**, 1754 (1951).
19) O. L. Brady and G. V. Elsmie, *Analyst*, **51**, 78 (1926).

Reactivity of Peroxomonophosphoric Acid in the Oxidation of Benzaldehydes and Dimethyl Sulfoxide in Aqueous Ethanol[1)]

Yoshiro OGATA,* Yasuhiko SAWAKI, and Yasuyuki TSUKAMOTO
Department of Applied Chemistry, Faculty of Engineering, Nagoya University, Chikusa-ku, Nagoya 464
(Received October 14, 1980)

Oxidation of benzaldehydes and dimethyl sulfoxide with peroxomonophosphoric acid (PMPA) has been studied in 40% aqueous EtOH in order to examine the reactivity of undissociated and dissociated PMPA in comparison with that of peroxycarboxylic acid. The reactivity for DMSO was in the order $RCO_3^- > H_3PO_5 > H_2PO_5^- > RCO_3H > HPO_5^{2-}$. As in the peroxycarboxylic acid oxidation, PMPA oxidation of substituted benzaldehydes afforded phenols by aryl migration and benzoic acids by hydride migration. The product ratio changed with substituents and pH; salicylaldehyde (*o*-HO) gave only catechol by aryl migration, while *p*-chloro- and unsubstituted benzaldehydes afforded benzoic acids predominantly. The oxidation of aldehydes bearing *p*-MeO and *p*-Me was a borderline case and the migratory ratio of Ar~/H~ was higher at lower pH, *i.e.*, the order being $H_3PO_5 > H_2PO_5^- > HPO_5^{2-}$. The substituent effect in the apparent k_{obsd} values was very small (*i.e.*, $\rho \approx 0$), but the effect for aryl migration ($k_{Ar\sim}$) estimated from product selectivity gave $\rho = -2.88$ (σ). The rate for hydride migration ($k_{H\sim}$) resulted in $\rho = 1.7$ and 2.0 (σ). Reactivity of PMPA in each dissociated form was compared with that of RCO_3H.

Peroxomonophosphoric acid (PMPA) has been known for a long time,[2)] but its reactivity has not been clarified. Its decomposition[3)] and reactions with bromide[4)] and iodide ions[5)] were studied kinetically. Reports have been given on PMPA oxidation of organic substances, including the hydroxylation of aromatic rings,[6)] the Baeyer-Villiger(B-V) reaction of acetophenones,[7)] the epoxidation of *trans*-stilbene,[8)] and the oxidation of tertiary amines.[9)]

PMPA is a tribasic acid having three dissociated forms.[10)] We were interested in the reactivity of each form of PMPA as well as in their possibility as an oxidant with bifunctional catalysis since phosphoric acid is known as such a catalyst.[11)] The reaction of PMPA is also of interest from a biochemical standpoint, since PMPA might be produced by perhydrolysis of pyrophosphoric acids[12)] with oxygen species such as H_2O_2 or $O_2^{\cdot-}$.[13)] When we had almost completed our experiment a kinetic study on the PMPA oxidation of benzaldehydes was reported,[14)] the conclusion of which differing from ours.

Results and Discussion

Peroxomonophosphoric acid (PMPA) dissociates into three forms, affording $pK_1 = 1.1$, $pK_2 = 5.2$, and $pK_3 = 12.7$ in water.[10)] Oxidation of dimethyl sulfoxide (DMSO) and benzaldehydes with PMPA was carried out in the presence of 0.4 mM EDTA in 40% aqueous ethanol at 25 °C. The decrease of PMPA was monitored by iodometric titration in 5% AcOH; its spontaneous decompositition was very slow in the absence of added substrates. Products were determined by GLC directly or after methylation with dimethyl sulfate for phenols or with diazomethane for carboxylic acids.

$$H_3PO_5 \overset{K_1}{\rightleftharpoons} H_2PO_5^- + H^+ \quad (1)$$

$$H_2PO_5^- \overset{K_2}{\rightleftharpoons} HPO_5^{2-} + H^+ \quad (2)$$

$$HPO_5^{2-} \overset{K_3}{\rightleftharpoons} PO_5^{3-} + H^+ \quad (3)$$

Oxidation of DMSO. Dimethyl sulfoxide was easily oxidized to sulfone in over 90% yield based on PMPA consumed. The oxidation follows the second-order rate equation (Eq. 4). The pH-rate profile

$$v = k_{obsd}[\text{PMPA}][\text{Substrate}] \quad (4)$$

is shown in Fig. 1. The resulting second-order rate constant are 210, 45, and 1.2 $M^{-1} s^{-1}$ for H_3PO_5, $H_2PO_5^-$, and HPO_5^{2-}, respectively. The kinetically determined pK_1 and pK_2 values for PMPA in 40% EtOH are 1.6 and 4.6, respectively, close to the reported pK_a values 1.1 and 5.2, respectively, in water.[10)] The difference of *ca.* 0.5 might be partly due to the solvent effect on pK_a of PMPA.

The Baeyer-Villiger Oxidation of Benzaldehydes. Products. Products from the B-V oxidation of benzaldehydes with PMPA vary with substituents and pH (Table 1). Salicylaldehyde with strong electron-releasing *o*-HO afforded only catechol by aryl migration. The relatively low yields (*i.e.*, 65—75%) of catechol can be ascribed to further oxidation by PMPA. The other aldehydes resulted in the simultaneous formation of phenols by aryl migration and benzoic acids by hydride migration.

$$\text{ArCHO} \xrightarrow{\text{PMPA}} \begin{cases} \xrightarrow{Ar\sim} \text{ArOCHO} \xrightarrow{H_2O} \text{ArOH} & (5a) \\ \xrightarrow{H\sim} \text{ArCO}_2\text{H} & (5b) \end{cases}$$

We see from Table 1 that the aryl migration is facilitated by an increase in electron-releasing power of ring substituents and by a decrease of pH. Higher pH and electron-attracting groups favor the hydride

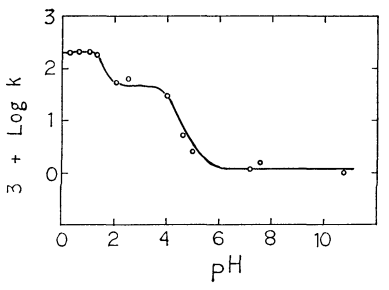

Fig. 1. The pH-rate profile for the [PMPA oxidation of DMSO in 40% aqueous EtOH at 25 °C.

Table 1. Products (%) from the B-V reaction of substituted benzaldehydes by PMPA[a]

Substituent	pH 1.3		pH 4.0		pH 7.3		pH 10	
	$ArCO_2H$	ArOH	$ArCO_2H$	ArOH	$ArCO_2H$	ArOH	$ArCO_2H$	ArOH
o-HO	0	65	0	72	0	75	0	73
p-MeO	0	74	2	78	7	45	23	21
p-Me	22	63	42	8	45	4	49	1
H	75	14	83	0	98	0	81	0
p-Cl	61	3	85	0	72	0.4	72	1

a) Reaction with 0.04 M each of H_3PO_5 and ArCHO in 40% EtOH at 25 °C. % Yields are based on the aldehyde consumed and determined by GLC after methylation with dimethyl sulfate for phenols or with diazomethane for carboxylic acids.

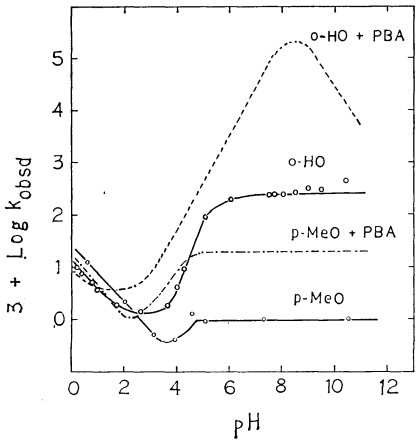

Fig. 2. pH-rate profiles for the PMPA oxidation of substituted benzaldehydes in 40% EtOH at 25.0 °C. The dotted lines are plots for perbenzoic acid (PBA) oxidation from Ref. 15. The solid line for *o*-HO is calculated according to the rate data in Table 3.

migration leading to carboxylic acids. The trend is similar to that of the B-V oxidation with perbenzoic acid (PBA).[15]

Mechanism. In case of the PBA oxidation of salicylaldehyde the rate-determining step is the addition of PBA to C=O.[15] Since the pK_a values of the aldehydes and PBA are 8.45 and 8.5, respectively, in 40% EtOH,[15] the pH-rate profile gives a bell-shaped curve (dotted line, Fig. 2). The oxidation with PMPA afforded a similar profile (Fig. 2); the observed slopes of *ca.* −0.5 at pH<2 suggest an acid-catalysis, while horizontal lines at pH 5—10 indicate no catalysis by H^+ or HO^-. If the addition of PMPA to C=O were rate-limiting, the rate should slow down at pH above 9 on the basis of the dissociation of salicylaldehyde, which was not the case. This is in contrast to the PBA case, suggesting that the addition to C=O is not rate-determining. The rate is determined by the migration step (Eq. 7). Here, YOOH

$$ArCHO + YOOH \overset{K_6}{\rightleftharpoons} \underset{\underset{OOY}{|}}{\overset{OH}{|}}{ArCH} \quad (6)$$

1

$$\mathbf{1} \xrightarrow{k_7} \text{Products} + YOH \quad (7)$$

is H_3PO_5, $H_2PO_5^-$, or HPO_5^{2-}. In the neutral region, the most prevalent species is $H_2PO_5^-$, so that the

Table 2. Substituent effect on the B-V reaction of benzaldehydes with PMPA in 40% EtOH at 25.0 °C[a]

Substituent	$10^3\,k/M^{-1}\,s^{-1}$			
	pH 1.3	pH 4	pH 7.3	pH 10
A) Observed second-order rate constant (k_{obsd})[b]				
p-MeO	13.9 (2.1)[c]	0.43 (9)[c]	1.08 (13)[c]	0.93 (13)[c]
p-Me	8.6	0.35	0.49	0.98
H	8.0	0.39	0.45	1.17
p-Cl	10.1 (4.4)[c]	0.98 (14)[c]	1.22 (18)[c]	0.97 (220)[c]
B) Rates for aryl migration ($k_{Ar\sim}$)[d]				
p-MeO	10.3	0.33	0.49	0.19
p-Me	5.4	0.028	0.020	0.014
H	1.2	0	≈0	≈0
p-Cl	0.27	0	0.004	0.01
ρ (*vs.* σ)	−2.88	e)	e)	e)
C) Rates for hydride migration ($k_{H\sim}$)[d]				
p-MeO	0	0.010	0.075	0.22
p-Me	1.9	0.15	0.22	0.48
H	5.9	0.33	0.44	0.95
p-Cl	6.2	0.83	0.87	0.70
ρ (*vs.* σ)	e)	1.74	*ca.* 2.0	e)

a) Reaction with 0.01—0.05 M each of benzaldehyde and PMPA. b) Observed rate constant determined iodometrically. c) For comparison, the k_{obsd} values for PBA (Ref. 17) are shown in parentheses. d) Rate constants for aryl or hydride migration obtained by dividing k_{obsd} values by product selectivities in Table 1. e) Numbers of data were too small, the correlation being poor.

departing group YOH from **1** is $H_2PO_4^-$ (pK_a= 7.2), which is significantly less potent as a departing group than benzoic acid (pK_a=4.2) in the PBA oxidation. The rate of rearrangement of **1** (*i.e.*, k_7) is then substantially lowered, leading to the establishment of preequilibrium 6 for the PMPA case.

The PMPA oxidation of *p*-anisaldehyde (*p*-MeO) is substantially slower than that of salicylaldehyde at pH>3, but slightly faster at pH<2 (Fig. 2). The rates for the other aldehydes are similar to that of anisaldehyde, the k_{obsd} values not varying with substituent, *i.e.*, $\rho \approx 0$ (Table 2-A). It can be assumed that the ρ value for K_6 is close to the ρ value of 1.6

Table 3. Comparison of the reactivities of PMPA and peroxycarboxylic acid toward various substrates

Oxidant YOOH	pK_a of YOH[b]	Second-order rate constant, $10^3\,k/M^{-1}\,s^{-1}$[a]					
		I^- [c]	Br^- [d]	Stilbene[e]	DMSO	o-HOC_6H_4CHO	PhCOMe[f]
Mechanism[g]		one	one	one	one	two	two
Solvent		H_2O	H_2O	dioxane	40% EtOH	40% EtOH	MeCN
H_3PO_5	2.1	2×10^6	8×10^3	0.11	210	≈1[h]	2.9
$H_2PO_5^-$	7.2	6×10^4	32		45	≈1	
HPO_5^{2-}	12.7	4×10^2			1.2	230	
$PhCO_3H$	4.2	3×10^6	3×10^2	0.20[i]	26	5	0.015[i]
$PhCO_3^-$					(330)[j]	1×10^6	

a) Rate constant at 25 °C. b) The pK_a of parent acid in water. c) Ref. 5. d) J. O. Edwards, "Peroxide Reaction Mechanism," Interscience, New York (1962), p. 73. e) Ref. 8. f) Ref. 7. g) One: one-step electrophilic oxidation. Two: two-step reaction involving an addition and a rearrangement step. h) Rate constant for the acid catalysis at pH<1 is $k_H=9\times10^{-3}\,M^{-2}\,s^{-1}$, obtained from a rate equation: $v=k_H[HClO_4][\text{aldehyde}]\times[\text{PMPA}]$. i) Peracetic acid. j) Nucleophilic oxidation of sulfoxide *via* two-step reaction.

(σ) for the H_2O_2 addition (Y=H, Eq. 6).[15] The apparent zero value of ρ for k_{obsd} might be due to the cancellation, since $k_{obsd}=k_7K_6$, between a positive ρ value for K_6 and a negative ρ value for k_7. Negative ρ values for aryl and hydride migration are well known.[15–17] Such a cancellation is often observed in reactions involving carbonyl addition.[18]

A mechanism was postulated for the PMPA oxidation of benzaldehydes, which involves a rate-determining attack of PMPA on benzaldehyde hydrates, $ArCH(OH)_2$.[14] However, the scheme is questionable. (i) No reaction is known in which the nucleophilic attack on tetrahedral carbons such as aldehyde hydrate is much faster than that on free aldehyde ArCHO. (ii) Benzaldehydes exist essentially as free aldehydes ArCHO under these conditions of aqueous EtOH; an exception is *p*-nitrobenzaldehyde, where 20% of the aldehyde exists as its hydrated form.[19] Likewise, the addition equilibrium of HO^- instead of H_2O shifts to the free ArCHO rather than to the adduct $ArCH(OH)O^-$ at pH<14.[20] Thus the C=O addition scheme is favorable, since both concentration and reactivity of the free aldehydes are much higher than those of the hydrates.

Polybasic acids such as phosphoric acid are sometimes effective as a bifunctional catalyst.[11] We intended to examine such a possibility in the addition to C=O, *e.g.*, an intermolecular acid-catalysis (**2a**) or an intramolecular base-catalysis (**2b**). However,

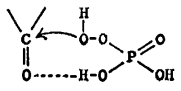

2a

or

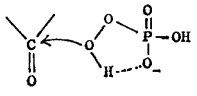

2b

the addition to C=O was not rate-determining even in the case of salicylaldehyde with the most facile migratory aptitude; no such catalysis could be examined.

Aryl and Hydride Migration. Although the k_{obsd} values in Table 2-A are little affected by substituents (*i.e.*, $\rho\approx0$), interesting results for the relative migratory aptitudes were obtained by multiplying the k_{obsd} values by products selectivities in Table 1. The aryl migration ($k_{Ar\sim}$) at pH 1.3 affords $\rho=-2.88$ (σ) (Table 2-B). Similar results ($\rho=-2.55$ *vs.* σ) are known for the PMPA oxidation of acetophenones.[7] These correlations are in contrast to the σ^+ correlation for the B-V reaction with PBA.[15,16] The difference might be due to the fact that in the rearrangement of **1** at pH<2 the departing phosphoric acid (pK_a=2.1) is a much stronger acid than benzoic acid (pK_a=4.2). The loosening of O–O bond in the PMPA oxidation is relatively weak, and hence the developing cationic charge (δ^+) in **3** is much lower than in the

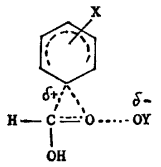

3

PBA case. The interpretation seems to be in line with the observed high rate ratios of *p*-MeO/*p*-Me for the reaction at pH 4 (*i.e.*, $H_2PO_5^-$) and pH 7 or 10 (*i.e.*, HPO_5^{2-}), suggesting a σ^+ correlation. Since $H_2PO_4^-$ (pK_a=7.2) and HPO_4^{2-} (pK_a=12.7) are much less potent departing groups as compared with H_3PO_4, the cationic charge in **3** increases leading to the σ^+ correlation at pH>4. High rate ratios of *p*-MeO/*p*-Me correspond to a σ^+ correlation, small ratios giving rise to σ correlation.

On the other hand, Hammett's equation for the hydride shift gives $\rho=1.74$ (pH 4) and 2.0 (pH 7.3) with σ correlation (Table 2-C). The same reaction with PMPA in the presence of 0.2 M NaOH gives a ρ value 1.27 (σ) in water.[14] These ρ values are close to 1.6 (σ) for the addition equilibrium of H_2O_2 (Eq. 6).[15] Since $k_{obsd}=k_7K_6$, the net ρ value for the hydride shift (*i.e.*, k_7) might be close to zero. Similar ρ values of 1.1—1.8 were obtained at pH 1—12 in the PBA oxidation of benzaldehydes affording hydride shift,[17] which is rather insensitive to acid and base catalysis.[15] The same might be the case for the PMPA oxidation.

Comparison with Peroxycarboxylic Acid. The reac-

tivity of PMPA was compared with that of peroxycarboxylic acids (Table 3). In one-step electrophilic oxidation, relative reactivities of PMPA and RCO_3H change with substrate. For example, the relative reactivity in the oxidation of bromide ion differs from the corresponding order for iodide ion. The rate order for olefin epoxidation is $RCO_3H \gtrsim H_3PO_5$,[8] that for the oxidation of DMSO, $H_3PO_5 > H_2PO_5^- > RCO_3H > HPO_5^{2-}$. The DMSO oxidation with RCO_3^- is of a different mechanism and excluded from the comparison; the alkaline reaction involves two steps, a nucleophilic addition to sulfoxide and its decomposition to sulfone and carboxylate ion,[21] just as the B-V reaction.

The relative reactivity for the B-V reaction also changes with substrates and pH (Fig. 2, Table 2-A, and Table 3). The rate order for the B-V reaction of benzaldehydes at pH 3—10 is $RCO_3H > PMPA$, but changes to the order $PMPA > RCO_3H$ at the lower pH. This is due to the higher sensitivity of PMPA to acid-catalysis as compared with that of RCO_3H.

Experimental

GLC analysis was performed with a Yanagimoto 550F gas chromatograph using a column of PEG 20 M on Chromosorb (1 m).

Materials. Peroxomonophosphoric acid (PMPA) was prepared from P_2O_5 and 90% H_2O_2.[9] Commercial benzaldehydes were used.

Typical Procedure. The reaction with 0.04 M each of PMPA and benzaldehyde was carried out in 40 vol % EtOH at 25.0 °C. EDTA (0.4 mM) was added to minimize a metallic ion-catalyzed decomposition of PMPA. The pH of solution was maintained with perchloric acid ($pH < 1$), 0.5 M acetate (pH 2.5—4.4), 0.5 M phosphate (pH 3.7—6.1), and 0.5 M carbonate buffers (pH 7.5—10). The pH values were determined with a glass electrode before and after the reaction. The decrease of PMPA was monitored by iodometric titration in 5% aqueous AcOH. The spontaneous decomposition of PMPA was very slow in the absence of substrate added. Reproducibility of the oxidation kinetics was ascertained to be adequate (*i.e.*, within ±5%).

Reaction products were determined by means of GLC directly or after methylation with diazomethane using biphenyl or propiophenone as an internal standard. Catechol was determined after methylation with dimethyl sulfate.

References

1) Contribution No. 283.
2) a) J. Schmidlin and P. Massini, *Chem. Ber.*, **43**, 1102 (1910); b) G. Toennies, *J. Am. Chem. Soc.*, **59**, 555 (1937).
3) E. Koubek, M. L. Hagget, C. J. Battaglia, K. M. Ibne-Rasa, H. Y. Pyrun, and J. O. Edwards, *J. Am. Chem. Soc.*, **85**, 2263 (1963).
4) D. H. Fortum, C. J. Buttaglia, S. R. Cohen, and J. O. Edwards, *J. Am. Chem. Soc.*, **82**, 778 (1960).
5) F. Secco and M. Venturini, *J. Chem. Soc., Dalton Trans.*, **1976**, 1410.
6) Y. Ogata, I. Urasaki, K. Nagura, and N. Satomi, *Tetrahedron*, **30**, 3021 (1974).
7) Y. Ogata, K. Tomizawa, and T. Ikeda, *J. Org. Chem.*, **43**, 2417 (1978).
8) Y. Ogata, K. Tomizawa, and T. Ikeda, *J. Org. Chem.*, **44**, 2362 (1979).
9) Y. Ogata, K. Tomizawa, and T. Morikawa, *J. Org. Chem.*, **44**, 352 (1979).
10) C. J. Battaglia and J. O. Edwards, *Inorg. Chem.*, **4**, 552 (1965).
11) Y. -N. Lee and G. L. Schmir, *J. Am. Chem. Soc.*, **101**, 6277 (1979), and references cited therein.
12) E. E. Conn and P. K. Stumpf, "Outlines of Biochemistry," 4th ed, John Wiley & Sons, Inc., New York, N. Y. (1976), Chaps. 6 and 14.
13) The perhydrolysis of acid anhydrides or chlorides with H_2O_2 is very facile to afford peroxycarboxylic acids; Y. Ogata and Y. Sawaki, *Tetrahedron*, **23**, 3327 (1967).
14) G. P. Panigrahi and R. Panda, *Bull. Chem. Soc. Jpn.*, **52**, 3084 (1979).
15) Y. Ogata and Y. Sawaki, *J. Am. Chem. Soc.*, **94**, 4189 (1972).
16) Y. Ogata and Y. Sawaki, *J. Org. Chem.*, **37**, 2953 (1972).
17) Y. Ogata and Y. Sawaki, *J. Org. Chem.*, **34**, 3985 (1969).
18) For example, Y. Ogata and A. Kawasaki, "The Chemistry of the Carbonyl Group," ed by J. Zabicky, Interscience Publishers, London (1970), Vol. 2, p. 42.
19) J. M. Sayer, *J. Org. Chem.*, **40**, 2545 (1975).
20) a) W. J. Bover and P. Zuman, *J. Chem. Soc., Perkin Trans. 2*, **1973**, 786; b) W. J. Bover and P. Zuman, *J. Am. Chem. Soc.*, **95**, 2531 (1973).
21) R. Curci and G. Modena, *Tetrahedron*, **22**, 1227, 1235 (1966).

  Bull. Chem. Soc. Jpn., 54, 2065—2067 (1981)

The Reactions of Phenylmagnesium Halides with Seleninyl Chloride, Diphenyl Selenoxide, and Dibromodiphenylselenium

Yasunori Iwama, Masashi Aragi, Motohide Sugiyama, Kasumi Matsui, Yasutaka Ishii, and Masaya Ogawa*

Department of Applied Chemistry, Faculty of Engineering, Kansai University, Senriyama, Suita, Osaka 564

(Received October 21, 1980)

Triphenylselenonium halides were readily prepared in good yields by the one-step reaction of seleninyl chloride with phenylmagnesium halides, followed by treatment with hydrogen halides. The yields of triphenylselenonium halides are markedly affected by the molar ratio of seleninyl chloride to the phenylmagnesium halides. In order to interpret the above results, some probable intermediates, such as diphenyl selenoxide, dibromodiphenylselenium, and diphenyl selenide, were investigated by allowing them to react with the phenylmagnesium halides. A pathway which consists of competitive and successive reactions is discussed.

Trimethylselenonium hydroxide ($(CH_3)_3Se^+OH^-$) is a very useful methylation reagent for carboxylic, thiol, and aromatic hydoroxyl groups.[1] Hampton[2] has reported on the use of diphenyliodonium chloride ($Ph_2I^+Cl^-$) for terminal phenylation. Triarylselenonium halides ($Ar_3Se^+X^-$), which may be expected as arylation reagents, could be prepared by a convenient one-step synthesis.[3] Strecker and Willing[4] have obtained only diphenyl selenide (Ph_2Se) and diphenyl (Ph_2) by the reaction of seleninyl chloride ($SeOCl_2$) with phenylmagnesium bromide (PhMgBr); they have not described the formation of selenonium salt. However, the addition of about three moles of arylmagnesium halides to one mole of $SeOCl_2$ afforded the corresponding triarylselenonium salts, together with Ph_2Se and Ph_2.[3] This method is useful for the preparation of selenonium salts, since the usual methods require several steps.[5,6]

In order to clarify the formation path of triphenylselenonium halides ($Ph_3Se^+X^-$), the reaction of phenylmagnesium halides (PhMgX) with such probable intermediates as diphenyl selenoxide (Ph_2SeO), dibromodiphenylselenium (Ph_2SeBr_2), and diphenyl selenide (Ph_2Se) were investigated.

Results and Discussion

Reaction of PhMgX with $SeOCl_2$. After the addition of 3.5-fold mole of various PhMgX's to $SeOCl_2$ in THF or ether, the solution was maintained at the reflux temperature for 2 h.[7] The hydrolysis of the reaction mixtures with aqueous hydrobromic acid (HBr *ca.* 1 mol dm^{-3}) gave $Ph_3Se^+X^-$, Ph_2Se, and Ph_2, as is shown in Table 1. It is of interest that $Ph_3Se^+Br^-$ appeared in the reaction of $SeOCl_2$ with the PhMgCl was afforded by the treatment of the resulting reaction mixtures with HBr. In the case of PhMgI, $Ph_3Se^+I^-$ was produced, even though the mixtures were similarly treated with HBr.[8]

The reaction with PhMgCl, followed by treatment with HBr, gave $Ph_3Se^+Br^-$ in a 56% yield, but the yield of selenonium salt in the same reaction in the presence of $MgBr_2$ fell to 39%, which is comparable to the yield of the reaction with PhMgBr,[9] as is shown in Table 1. These findings indicate the occurrence of halogen exchange in the reaction system during the period of reaction and the treatment with HBr. It is considered that the lower yield of selenonium salt in the reaction with PhMgBr results from the formation of more reactive, but less selective, $SeOBr_2$ by halogen exchange between $SeOCl_2$ and the resulting $MgBr_2$ during the reaction. The considerable lowering in the yield in the case of PhMgI is thought to be due to the decomposition of the unstable $SeOI_2$.[10]

These results indicate that the seleninyl halides ($SeOX_2$) generated by halogen exchange react with three moles of PhMgX to give triphenylselenonium halogenomagnesium oxide ($Ph_3Se^+OMgX^-$), which then affords $Ph_3Se^+X^-$ upon subsequent hydrolysis with HBr.

The product distributions of $Ph_3Se^+Br^-$, Ph_2Se, and Ph_2 varied with the ratio of PhMgX to $SeOCl_2$. Figure 1 shows a typical curve for the yield of each product obtained by the addition of PhMgBr to $SeOCl_2$ in ether. The production of Ph_2SeBr_2 was at its maximum at the molar ratio of 1.5; thereafter, it decreased rapidly to zero at the ratio of 2.5, in contrast to the increase in Ph_2Se and Ph_2. The amount of selenonium salt increased gradually with the increase in PhMgBr until the molar ratio of 3.5. At more than 3.5, a rapid decrease in the selenonium salt led to the formation of Ph_2Se and Ph_2. Thus, the present reaction is considered to be a complicated successive reaction.

Reaction of PhMgBr with Ph_2SeBr_2. A solution of PhMgBr in ether was added to equimolar amounts of Ph_2SeBr_2, and then the mixture was worked-up as above. The selenonium salt which was expected as the primary product was not obtained at all, but

Table 1. Addition of PhMgX to a solution of $SeOCl_2$[a] (Followed by HBr work-up)

X PhMgX	MgX_2	Yield[b]/mmol		
		$Ph_3Se^+Br^-$	Ph_2Se	Ph_2[c]
Cl	—	16.9(56.2)	11.7(39.0)	4.2(14.3)
Br	—	11.2(37.3)	14.9(49.5)	7.9(26.3)
I[d]	—	0.8(2.5)[e]	10.6(35.2)	9.9(33.1)
Cl	$MgCl_2$	16.4(54.5)	12.1(40.2)	5.4(18.1)
Cl	$MgBr_2$	11.7(39.0)	15.1(50.5)	9.6(32.0)

a) PhMgX (105 mmol) was added to a solution of $SeOCl_2$ (30 mmol) in THF (100 ml). b) Yields given in parentheses indicate the mol% based on $SeOCl_2$. c) Formation from Ph_4Se was assumed. d) Ether was used as the solvent. e) $Ph_3Se^+I^-$.

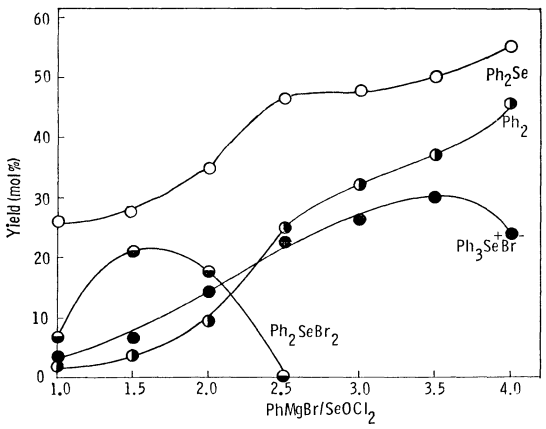

Fig. 1. Dependence of the yield of each product on the molar ratio of PhMgBr to $SeOCl_2$.

equimolar amounts of Ph_2Se and Ph_2 were.[11] This fact shows that Ph_2SeBr_2 reacts with PhMgBr to give, probably, an unstable tetraphenylselenium (Ph_4Se), which then immediately decomposed to Ph_2Se and Ph_2. It was found that Ph_2SeBr_2 is not connected with the production of selenonium salt.

On the other hand, no product was furnished by the reaction of Ph_2Se with PhMgBr.

Reaction of PhMgBr with Ph_2SeO. Ph_2SeO could not be isolated in the reaction of $SeOCl_2$ with PhMgBr, but it appeared to be one of the most probable intermediates. Wildi[12] has reported the production of triphenylsulfonium bromide ($Ph_3S^+Br^-$) by the reaction of diphenyl sulfoxide (Ph_2SO) with PhMgBr.

The reaction of Ph_2SeO with PhMgBr, followed by hydrolysis with HBr, gave $Ph_3Se^+Br^-$, Ph_2Se, and Ph_2 in yields of 25, 63, and 10% respectively. It seems that selenonium salt was produced through triphenylselenonium bromomagnesium oxide (Ph_3Se^+-$OMgBr^-$) according to the following equation.

$$Ph_2SeO + PhMgBr \longrightarrow Ph_3Se^+OMgBr^-$$

$$Ph_3Se^+OMgBr^- + HBr \longrightarrow Ph_3Se^+Br^- + MgBr(OH)$$

Some of the $Ph_3Se^+OMgBr^-$ reacts further with PhMgBr to afford Ph_2Se and Ph_2 *via* Ph_4Se:

$$Ph_3Se^+OMgBr^- + PhMgBr \longrightarrow Ph_4Se + (MgBr)_2O$$

$$Ph_4Se \longrightarrow Ph_2Se + Ph_2$$

However, the significant formation of Ph_2Se can not be interpreted by considering only the above reaction. It may be supposed that Ph_2Se is produced by the elimination of oxygen from Ph_2SeO, which is liable to be reduced, but the detailed process has not been ascertained.[13]

Consequently, the reaction proceeds first through halogen exchange between $SeOCl_2$ and PhMgX, as well as, the MgX_2 which is generated during the period of reaction, and the resulting $SeOX_2$ reacts with PhMgBr to give Ph_2SeO and Ph_2SeBr_2. Selenonium salts are chiefly derived from Ph_2SeO, and Ph_2Se and Ph_2, from Ph_2SeBr_2. From these results, it seems reasonable that the maximum yield of selenonium salts is at the molar ratio of PhMgX to $SeOCl_2$ of 3.5, and that the reaction proceeds through competitive and successive paths which are complicated by halogen exchange.

Experimental

The melting points, determined on a Yanagimoto micro-melting-point apparatus (MP-J3), are uncorrected. The IR spectra were obtained with a Shimadzu IR-27G spectrophotometer. The mass spectra were measured with a JEOL JMS-01SG apparatus. The general procedure for the reaction of PhMgX with $SeOCl_2$ was the same as in a previous paper.[3] The yields of $Ph_3Se^+X^-$ and Ph_2Se, based on the $SeOCl_2$ used, and of Ph_2 were estimated and considered to result from the decomposition of Ph_4Se to Ph_2Se and Ph_2.

Reaction of PhMgCl with $SeOCl_2$ in the Presence of $MgBr_2$. Anhydrous $MgBr_2$ (5.5 g, 30 mmol) was added to a solution of $SeOCl_2$ (5.0 g, 30 mmol) in THF (100 ml). The mixture gradually became brownish and was then allowed to react with PhMgCl (105 mmol) in THF under reflux for 2 h. After the THF had been evaporated *in vacuo*, the mixture was hydrolyzed with HBr (*ca.* 1 mol dm^{-3}) and extracted with benzene; the remaining aqueous solution was further extracted with chloroform. The benzene extract was dried over sodium sulfate, and the benzene was evaporated *in vacuo*. The residue was distilled under reduced pressure to give Ph_2 (1.5 g; 32%) and Ph_2Se (3.6 g; 50.5%).

Ph_2: mp 69—70 °C; IR 3055, 3025, 1473, 1423, 902, 725, 690 cm^{-1}. These values were identical with those of an authentic sample.

Ph_2Se: bp 106 °C/2 mmHg; IR 3060, 1575, 1475, 1440, 1000, 735 cm^{-1}; MS *m/e* 234 (M^+), 154 (M^+—Se). Found: C, 61.77; H, 4.42%. Calcd for $C_{12}H_{10}Se$; C, 61.81; H, 4.32%.

The chloroform extract afforded $Ph_3Se^+Br^-$ (4.6 g; 37%) upon recrystallization from chloroform–acetone(1:5): mp 236 °C decomposed; IR 3050, 1580, 1430, 990, 765, 745, 734 cm^{-1}; MS *m/e* 234 (M^+—PhBr), 157 (M^+—Ph_2). Found; C, 55.32; H, 3.79%. Calcd for $C_{16}H_{15}SeBr$: C, 55.42; H, 3.88%.

Reaction of PhMgBr with Ph_2SeBr_2. $SeOCl_2$ (5.0 g; 30 mmol) was added to PhMgBr (45 mmol) in ether (100 ml), and the mixture was stirred under reflux for 1 h. After the removal of the ether, the reaction mixtures were treated with HBr (*ca.* 1 mol dm^{-3}), and then crude Ph_2SeBr_2 was precipitated. The crystals were collected and recrystallized from ether to afford Ph_2SeBr_2 (2.4 g; 21.6%): mp 147.5 °C decomposed; IR 1600, 1460, 1150, 990, 738, 681 cm^{-1}. Found: C, 36.62; H, 2.61%. Calcd for $C_{12}H_{10}Br_2Se$: C, 36.67; H, 2.57%.

Ph_2SeBr_2 (12.3 g; 31 mmol) was added to a solution of PhMgBr (31 mmol) in ether (50 ml) at 34 °C, and the mixture was hydrolyzed with HBr (*ca.* 1 mol dm^{-3}) and extracted with benzene and then with chloroform. Ph_2Se (3.5 g; 47.9%), Ph_2 (1.9 g; 42.4%), and unreacted Ph_2SeBr_2 (4.9 g; 40%) were obtained from the benzene extracts. From the chloroform extract, though, no product was obtained.

Reaction of PhMgBr with Ph_2SeO. Ph_2SeO was prepared by the method of Rheinboldt.[14] PhMgBr (60 mmol) was added, drop by drop, over a period of 1 h at 34 °C to an equimolar amount of Ph_2SeO (60 mmol) in ether (50 ml). After the addition, the ether was removed and the residue was hydrolyzed with HBr (*ca.* 1 mol dm^{-3}), and then extracted with benzene and subsequently with chloroform, as has been described above. From the extracts, Ph_2Se (6.2 g; 63.5%), $Ph_3Se^+Br^-$ (5.9 g; 25.2%), and Ph_2 (0.86 g; 10.0%) were afforded.

References

1) K. Yamauchi, K. Nakamura, and M. Kinoshita, *Tetrahedron Lett.*, **1979**, 1787.
2) K. G. Hampton, T. M. Harris, and C. R. Hauser, *J. Org. Chem.*, **29**, 3511 (1964).
3) Y. Ishii, Y. Iwama, and M. Ogawa, *Synth. Commun.*, **8**, 93 (1978).
4) W. Strecker and A. Willing, *Ber.*, **48**, 204 (1915).
5) T. Hashimoto, M. Sugita, H. Kitano, and K. Fukui, *Nippon Kagaku Zasshi*, **88**, 991 (1967).
6) "Organic Selenium Compound: their Chemistry and Biology," ed by D. L. Klayman and W. H. Gunther, John Wiley & Sons, N. Y. (1973), p. 173.
7) In the opposite addition of $SeOCl_2$ to PhMgX, almost no $Ph_3Se^+X^-$ was formed, but Ph_2Se and Ph_2 were.
8) Anion exchange in selenonium salts is possible using either the solubility differences between these salts or by taking advantage of the insolubility of certain metal salts: "Selenium," ed by R. A. Zingaro and W. C. Cooper, Van Nostrand Reinhold, N. Y. (1974), p. 507.
9) The addition of $MgBr_2$ to $SeOCl_2$ in THF led to a rapid color change indicating the formation of $SeOBr_2$.
10) The deposition of metallic selenium and the liberation of iodine are observed; $SeOI_2$ may be decomposed according to the following equation:

$$2SeOI_2 \longrightarrow SeO_2 + Se + 2I_2.$$

11) About 40% of the starting material, Ph_2SeBr_2, was recovered.
12) B. S. Wildi, S. W. Taylor, and H. A. Potratz, *J. Am. Chem. Soc.*, **73**, 1965 (1951).
13) In the reaction of PhSeO with PhMgBr, benzene is detected by gas chromatography in the light fraction of the resulting mixture, and the resinous residue obtained after the distillation shows a typical ^{13}C-NMR spectrum of polyphenylene. Thus, the direct reduction of Ph_2SeO may take place through the following radical reaction:

$$Ph_2SeO + 2PhMgX \longrightarrow Ph_2Se + 2Ph\cdot + (MgX)_2O,$$

$$n Ph\cdot \longrightarrow \text{benzene} + \text{polyphenylene}.$$

14) H. Rheinboldt and E. Giesbrecht, *J. Am. Chem. Soc.*, **69**, 664 (1947).

Effects of Chelated and Non-chelated Transition Metal Ions on the Photoreactions of Pyridinecarboxylic Acids in Aqueous Solutions

Akira SUGIMORI,* Kōtarō TAKADA, Tsutomu KIMURA, and Junji KAMIMURA

Department of Chemistry, Faculty of Science and Technology, Sophia University, Kioi-cho 7-1, Chiyoda-ku, Tokyo 102

(Received October 23, 1980)

Iron(III) and copper(II) chelated by 2-pyridinecarboxylate bring about the photochemical decarboxylation of the ligand *via* the electron transfer from carboxylate to metal ions to give pyridine and 2,2′-bipyridine (for Fe(III)) or 2-pyridinol (for Cu(II)). In the presence of iron(III), ruthenium(III), and copper(II), 3-pyridinecarboxylic acid gives photochemically 2,2′-bipyridine-3,5′-dicarboxylic acid without decarboxylation. 4-Pyridinecarboxylic acid is photo-resistant both in the presence and in the absence of iron(III) and copper(II).

Metal ions, especially transition metal ions, have profound effects on the photoreactions of organic compounds.[1] Recently, long range electron transfer mechanism has been proposed for the metal ion-catalyzed photo-oxidation of olefins.[2] Effects of metal ions on the photoreactions of carboxylic acids have extensively been studied,[3] together with their photoreactions in the absence of metal ions.[4] A metal ion may have different effects on the photoreaction depending on whether it is coordinated by an organic ligand or not. Pyridinecarboxylic acids afford a good system to investigate the differences between the coordinated and the non-coordinated metal ions: 2-pyridinecarboxylic acid forms very stable chelate bonds with many metal ions, whereas 3- and 4-pyridinecarboxylic acid form no such stable chelate bonds.[5]

We have reported some results on the photoreactions of 2- and 3-pyridinecarboxylic acid in the absence of metal ions. The irradiation of 3-pyridinecarboxylic acid in an aqueous solution with 254 nm light gives 2-hydroxy-3-pyridinecarboxylic acid in the pH range of 0—2 and 2,3′-bipyridine-5-carboxylic acid in the pH range of 4—6.[6] 2-Pyridinecarboxylic acid gives photochemically 6-hydroxy-2-pyridinecarboxylic acid in an acidic aqueous solution.[7]

Results and Discussion

The photoreactions of pyridinecarboxylic acids in the presence of several metal ions are summarized in Tables 1 and 2. Among the metal ions, iron(III) and copper(II) have remarkable effects on the photochemical processes of the acids. The metal ion effects on 2-pyridinecarboxylic acid (**1**) are different from those on 3-pyridinecarboxylic acid (**2**). In the case of **1**, which forms stable chelate bonds with metal ions,[8] the products *via* decarboxylation are significant. The 254 nm light irradiation of 2-pyridinecarboxylatoiron(III) complex gives pyridine (**3**), 2,2′-bipyridine (**4**) and a trace of 2-pyridinol. The photoreaction

Table 1. Photoreactions of 2-pyridinecarboxylatometal complexes in aqueous solutions
2-PyCOO = 2-Pyridinecarboxylato, Irradiated with a low pressure mercury lamp.

Complex	10^4[Complex] / mol dm^{-3}	Additive and its concn	Irr. time / h	Yield of product/%[a]			Recovery of starting material/%
				3	**4**	**5**	
$[Fe_2(2\text{-PyCOO})_4(OH)_2]$	1.34		2.5	12	8		56[b]
	1.34		6	17	15	3	39[b]
	1.34	Hydroquinone 6.7×10^{-6} mol dm^{-3}	6	62	trace		23[b]
$[Cu(2\text{-PyCOO})_2]$	2.0		6	trace		15	24[b]
$[Cr(2\text{-PyCOO})_3]$	1.0		48			trace	
$[Zn(2\text{-PyCOO})_2]$	1.0		3			trace	
$[Mg(2\text{-PyCOO})_2]$	1.0		3			trace	67[c]

a) Yield = $\frac{\text{Amount of product with respect to pyridine nucleus}}{\text{Amount of 2-pyridinecarboxylate contained in the starting complex}}$. b) With respect to 2-pyridinecarboxylate. c) With respect to metal complex.

Table 2. Photoreactions of 3-pyridinecarboxylic acid–metal salt systems in aqueous solutions
[3-Pyridinecarboxylic acid] = 6×10^{-4} mol dm^{-3}, Irradiated with a low pressure mercury lamp.

Metal salt	10^4[Metal salt] / mol dm^{-3}	pH	Irr. time / h	Yield of product/%[a]		Recovery of **2** / %
				7	**8**	
$FeCl_3$	1.0	4.9—5.3	4	12	24	41
$RuCl_3$	1.0	4.4—4.8	4	6	17	31
$CuSO_4$	3.0	4.9—5.2	4	7	4	53

a) The yields of the bipyridine derivatives are expressed with respect to the pyridine nucleus.

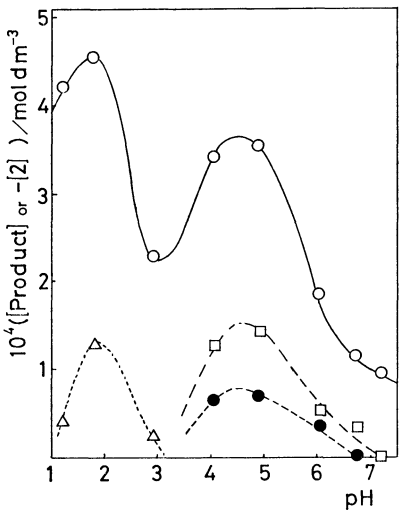

Fig. 1. Dependence of photoreactions of 3-pyridinecarboxylic acid–$FeCl_3$ systems on pH.
[3-Pyridinecarboxylic acid] = 6×10^{-4} mol dm^{-3}; [$FeCl_3$] = 1×10^{-4} mol dm^{-3}; Irradiation time, 4 h. The yields of the bipyridine derivatives are expressed with respect to the pyridine nucleus.
···△···: **6**, --●--: **7**, —·—□—·—: **8**, —○—: **2** reacted.

of 2-pyridinecarboxylatocopper(II) complex gives 2-pyridinol and a trace of pyridine.

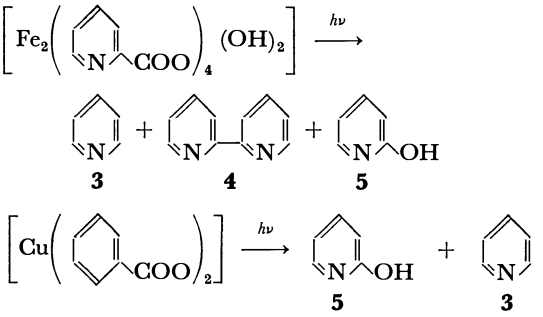

In the absence of metal ions, the UV-irradiation of 2-pyridinecarboxylic acid in the pH range of 4—6 gives 2,3′-bipyridine in 20% yield.

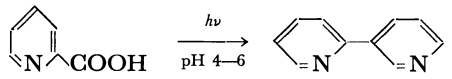

The addition of hydroquinone, a radical scavenger, to the iron(III) complex solution inhibits the formation of 2,2′-bipyridine and increases the yield of pyridine.

The coordinated cobalt(II) and magnesium(II), the lower oxidation states of which are unstable, stabilyze the coordinating 2-pyridinecarboxylate under illumination.

The photoreaction of 3-pyridinecarboxylic acid, which forms no stable chelate bond with metal ions, is affected by iron(III) ions differently from that of 2-pyridinecarboxylic acid. 3-Pyridinecarboxylic acid exists in three forms depending on the pH of the solutions. The effects of iron(III) on the photoreaction of 3-pyridinecarboxylic acid is pH dependent (Fig. 1). At pH 4—6, where the form of 3-pyridinecarboxylic

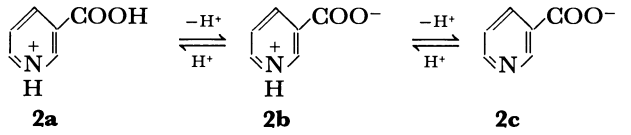

2a pK_a at 25 °C, 2.07[9] **2b** pK_a at 25 °C, 4.81[9] **2c**

acid is a mixture of **2b** and **2c**, the UV-irradiation in the presence of Fe(III) gives 2,2′-bipyridine-3,5′-dicarboxylic acid (**7**), which is obtained as an iron(II) complex, in addition to 2,3′-bipyridine-5-carboxylic acid (**8**), which is the main product in the absence of Fe(III).[6]

At pH 1—3, where the form of 3-pyridinecarboxylic acid is **2a**, the irradiation in the presence of Fe(III) gives 2-hydroxy-3-pyridinecarboxylic acid (**6**), the same product as in the photoreaction in the absence of Fe(III).[6]

In higher pH range, iron(III) is precipitated as hydroxide or oxide, and hence the effect of iron(III) can not be studied.

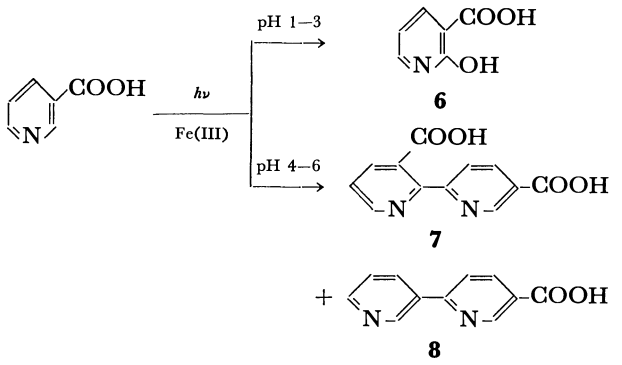

The effects of ruthenium(III) and copper(II) are practically the same as those of iron(III). The UV-irradiation of **2** in the presence of Ru(III) or Cu(II) in the pH range of 4—5 gives **7** and **8**.

Figure 2 shows the effects of iron(III) as a function of iron(III) concentration. Here the efficiency of Fe(III) effect (Q) on the photoreaction is expressed on the basis of the light absorbed by 3-pyridinecarboxylic acid according to the following equation.

$$Q = \frac{[\text{Product}] \text{ or } -[\mathbf{2}]}{\dfrac{\text{Light absorbed by } \mathbf{2}}{\text{Light absorbed by } \mathbf{2} \text{ and } FeCl_3}}$$

(The Q-value is a relative quantum yield calculated for the light absorbed by 3-pyridinecarboxylic acid.)

The saturation of the effect of Fe(III) at relatively low concentration and the constant Q-values over the wide range of Fe(III) concentration suggest that the photoreaction originates from the excited **2** not from the excited Fe(III), and the reaction between the excited **2** and Fe(III) should be rapid.

For the photoreaction of 4-pyridinecarboxylic acid, iron(III) and copper(II) have practically no effects. Four hours' irradiation of 5×10^{-4} mol dm^{-3} solutions of 4-pyridinecarboxylic acid at pH 4.7 gave slight UV-spectral changes both in the presence and in the absence of iron(III) and copper(II).

The photochemical decarboxylation of 2-pyridinecarboxylate attached to iron(III) and copper(II) under

Table 3. Composition of 2-pyridinecarboxylatometal complexes
2-PyCOO = 2-Pyridinecarboxylato

Complex	Found (%)			Calcd (%)		
	C	H	N	C	H	N
$[Fe_2(2\text{-PyCOO})_4(OH)_2]$	44.78	2.68	8.82	45.46	2.86	8.83
$[Cu(2\text{-PyCOO})_2]$	46.32	2.72	8.87	46.83	2.62	9.10
$[Zn(2\text{-PyCOO})_2]4H_2O$	37.52	3.99	7.33	37.96	4.25	7.38
$[Cr(2\text{-PyCOO})_3]H_2O$	49.69	2.96	9.73	49.55	3.23	9.63
$[Mg(2\text{-PyCOO})_2]2H_2O$	45.76	3.97	8.89	47.33	3.97	9.20

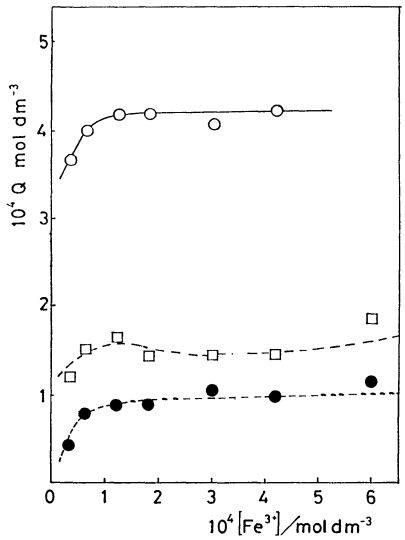

Fig. 2. Dependence of photoreactions of 3-pyridinecarboxylic acid on Fe(III) concentration ([2]=6×10^{-4} mol dm^{-3}, pH≈4.4).
The efficiency of the photoreaction is defined as,

$$Q = \frac{[\text{Product}] \text{ or } -[\mathbf{2}]}{\text{Light absorbed by } \mathbf{2}} \Big/ \frac{\text{Light absorbed by } \mathbf{2} \text{ and } FeCl_3}{\text{Light absorbed by } \mathbf{2}}$$

--●--: **7**, —·—□—·—: **8**, —○—: **2** reacted.

illumination can be explained by the effective electron transfer from the carboxylate to the coordinated metal ions to give carbonyloxy radicals which easily decarboxylate to form 2-pyridyl radicals.

2,2′-Bipyridine is considered to be a coupling product of 2-pyridyl radicals. The fact that the addition of hydroquinone, an effective hydrogen donor, inhibits the photochemical formation of 2,2′-bipyridine and promotes that of pyridine supports the suggested mechanism (Scheme 1).

The promotion of radical coupling in the presence of transition metal ions has been reported,[10] and a long lived free radical-metal complex has been proposed.[11]

The formation of 2-pyridinol in the photoreaction of 2-pyridinecarboxylatocopper(II) complex can be explained by the subsequent oxidation of 2-pyridyl radicals by copper(I). The formation of a copper mirror on the reaction vessel was observed during the irradiation (Scheme 2).

The process of the formation of 2,2′-bipyridine-3,5′-dicarboxylic acid in the photoreaction of the 3-pyridinecarboxylic acid–iron(III) system is different from that

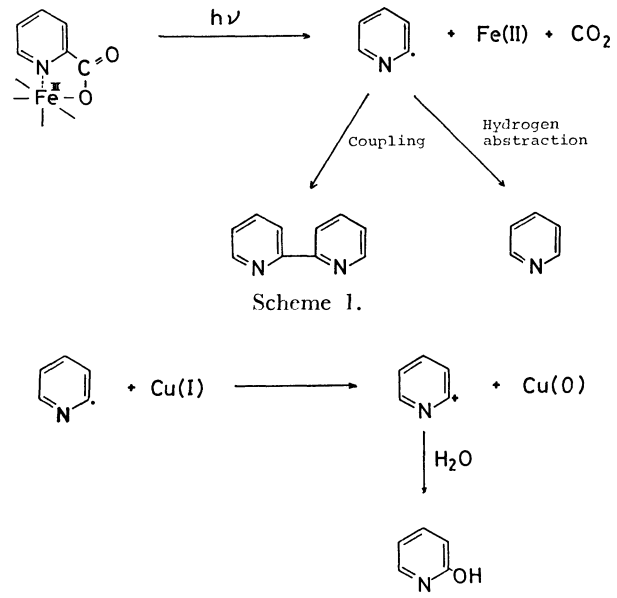

Scheme 1.

Scheme 2.

of the formation of 2,2′-bipyridine in the photoreaction of 2-pyridinecarboxylatoiron(III) complex.

The formation of a bipyridine derivative and iron(II) indicates the electron transfer from 3-pyridinecarboxylic acid to iron(III). At pH=5, no evidence for the complex formation between 3-pyridinecarboxylic acid and iron(III) in the ground state, because the UV-absorption spectrum of the mixture of 3-pyridinecarboxylic acid and iron(III) is almost the same as the sum of those of the components. As is shown earlier, only the light absorbed by 3-pyridinecarboxylic acid is effective for the formation of **7**. These facts suggest that the formation of **7** occurs *via* charge transfer interaction between an excited 3-pyridinecarboxylic acid and a ground state iron(III) ion.

Thermal oxidation of pyridine by iron(III) at high temperature is an example in which the oxidation of pyridine gives bipyridine.[12]

Experimental

Materials. Commercial 2-, 3-, and 4-pyridinecarboxylic acid (G.R. grade reagents of Tokyo Kasei Co. or Wako Junyaku Co.) were used without further purification. 2-Pyridinecarboxylatometal complexes were prepared in the crystalline form by refluxing the metal salt and sodium 2-pyridinecarboxylate in water. The composition of the metal complexes were determined by elemental analysis (Table 3).

UV-irradiation. The solutions of 2-pyridinecarboxylatometal complexes were prepared by dissolving the complexes in water. The sample solutions of 3- and 4-pyridinecarboxylic acid–transition metal salt systems were prepared by adding the metal salts to the solutions of sodium pyridinecarboxylates. The pH of the solution was adjusted with hydrochloric acid or sodium hydrogencarbonate.

For the identification of the photoproducts 2—3 dm^3 of the solution were irradiated with a low pressure mercury lamp under the bubbling of nitrogen. For the quantitative analysis 50—100 cm^3 of the solution deaerated by bubbling nitrogen or argon for at least 30 min were irradiated with a low pressure mercury lamp under magnetic stirring.

Separation, Identification, and Quantitative Analysis of the Photoproducts. Photoproducts from 2-Pyridinecarboxylatometal Complexes: Pyridine was extracted with dichloromethane from the irradiated solutions and identified by means of UV-spectra. Other products were separated by anion exchange chromatography (column, Dowex-1 formate; eluent, formic acid).

2,2′-Bipyridine was obtained as tris(2,2′-bipyridine)iron-(II). 2,2′-Bipyridine liberated by refluxing it in a sodium hydroxide solution was steam-distilled. By comparing its NMR spectra with those of the authentic 2,2′-bipyridine, 2,2′-bipyridine in the photoproducts was identified. The UV- and visible spectra of the iron(II) complex supports this conclusion.

2-Pyridinol and 2,3′-bipyridine were identified by the comparison of UV-, IR-, and NMR spectra with those of the authentic samples.

Quantitative analysis was done by means of the ion exchange chromatography and spectroscopy.

Photoproducts from the 3-Pyridinecarboxylic Acid–$FeCl_3$ System: After the irradiated solution was concentrated under reduced pressure, iron(II) and iron(III) were precipitated with hydrogen sulfide. The photoproducts were separated by means of the anion exchange chromatography (column, Dowex-1 formate; eluent, formic acid) and by means of gel-filtration with Sephadex G-10. Two photoproducts were identified.

Iron(II) Complex of 2,2′-Bipyridine-3,5′-dicarboxylic Acid. In order to liberate the ligand the complex was refluxed with aqueous sodium hydroxide. After the evaporation of the solvent the residue was extracted in a Soxhlet's extractor with dry 1,4-dioxane. The crystalline product thus obtained was converted to the methyl ester by diazomethane. The compound was identified as dimethyl 2,2′-bipyridine-3,5′-dicarboxylate from the following data; mp 115—116 °C; IR (KBr disk) 2900 (CH_3), 1735, 1730, 1720 (C=O), and 1295 cm^{-1} (ester C–O); NMR ($CDCl_3$) δ=9.25 (1H, dd, J=2.1 and 0.9 Hz, H at the 6′-position), 8.82 (1H, dd, J=4.9 and 1.6 Hz, H at the 6-position), 8.49 (1H, dd, J=8.0 and 2.1 Hz, H at the 4′-position), 8.27 (1H, dd, J=8.0 and 0.9 Hz, H at the 3′-position), 8.10 (1H, dd, J=7.8 and 1.6 Hz, H at the 4-position), 7.44 (1H, dd, J=7.8 and 4.9 Hz, H at the 5-position), 4.00 (3H, s, CH_3), and 3.82 (3H, s, CH_3); The above assignment is based on the decoupling experiment; MS (70 V) *m/e*(relative intensity), 272(20), 257(54), 242(19), 241(100), 214(10), 213(8), 198 (7), 183(11), 105(12), 91(12), 78(10), 77(10). Found: C, 61.62; H, 4.41; N, 10.43%; M^+, 272. Calcd for $C_{14}H_{12}N_2O_4$: C, 61.76; H, 4.44; N, 10.29%; M, 272.

UV spectra of the iron(II) complex, λ_{max}=515 (shoulder) and 550 nm.

2,3′-Bipyridine-5-carboxylic Acid. The product eluted by 0.5 mol dm^{-3} formic acid was identified as 2,3′-bipyridine-5-carboxylic acid by comparing its spectra with those reported previously.[6]

Determination of the Yields of Products. The quantitative analyses of the photoproducts from 3-pyridinecarboxylic acid–metal salt systems were carried out spectrophotometrically after the separation with anion exchange chromatography.

The authors are grateful to Mr. Susumu Kumon of Shinnihon Jitsugyo Co. for MS measurement. The present work was partially supported by the fund of the Asahi Glass Foundation for Industrial Technology and by a Grant-in-Aid for Scientific Research No. 547045 from the Ministry of Education, Science and Culture.

References

1) Reviews, T. Sato, *Yuki Gosei Kagaku Kyokai Shi*, **32**, 989 (1974); A. Sugimori and T. Akiyama, *Kagaku No Ryoiki*, **31**, 1114 (1977); Y. Matsushima and M. Maeda, "Kireto Kagaku (Chelate Chemistry)," ed by K. Ueno, Nankodo, Tokyo (1977), Vol. 3, Chap. 4.

2) E. Maruyama, A. Kohda, and T. Sato, *J. Chem. Soc., Perkin Trans. 1*, **1980**, 947.

3) J. K. Kochi, "Organometallic Mechanisms and Catalysis," Academic Press, New York (1978), pp. 99—106.

4) R. S. Givens and N. Levi, "The Chemistry of Functional Groups," Suppliment B, "The Chemistry of Acid Derivatives," ed by S. Patai, John Wiley & Sons (1979), Part 1, Chap. 11.

5) A preliminary report on the photoreactions of the metal complexes of 2-pyridinecarboxylic acid; T. Kimura, J. Kamimura, K. Takada, and A. Sugimori, *Chem. Lett.*, **1976**, 237.

6) F. Takeuchi, T. Sugiyama, T. Fujimori, K. Seki, Y. Harada, and A. Sugimori, *Bull. Chem. Soc. Jpn.*, **47**, 1245 (1974).

7) H. Kurokawa, T. Furihata, F. Takeuchi, and A. Sugimori, *Tetrahedron Lett.*, **1973**, 2623.

8) Considering the following equilibria,
$Fe(III)+2L+OH^- \rightleftarrows [Fe(III)L_2(OH)]$ $K_1=10^{23.84}$ mol^{-3} dm^9
$2[Fe(III)L_2(OH)] \rightleftarrows [Fe(III)_2L_4(OH)_2]$ $K_2=10^{3.06}$ mol^{-1} dm^3
$[Fe(III)L_2(OH)]+H^+ \rightleftarrows [Fe(III)L_2]+H_2O$ $K_3=10^{2.96}$
where L represents 2-pyridinecarboxylate, it was found that 30% of iron(III) is in the form of $[Fe(III)_2L_4(OH)_2]$ and 70% of iron(III) is in the form of $[Fe(III)L_2(OH)]$ in 1.3×10^{-4} mol dm^{-3} solution of $[Fe(III)_2L_4(OH)_2]$ at pH=6. Almost all the iron(III) ions are coordinated by 2-pyridinecarboxylate (G. Anderegg, *Helv. Chim. Acta*, **43**, 1530 (1960)).

A similar calculation on the following equilibria:
$Cu(II)+L \rightleftarrows [Cu(II)L]$ $K_1=10^{7.95}$ mol^{-1} dm^3
$[Cu(II)L]+L \rightleftarrows [Cu(II)L_2]$ $K_2=10^{7.00}$ mol^{-1} dm^3
showed that 98% of copper(II) is in the form of $[Cu(II)L_2]$ in 2.0×10^{-4} mol dm^{-3} solution of $[Cu(II)L_2]$ at pH=6 (G. Anderegg, *Helv. Chim. Acta*, **43**, 414 (1960)).

9) Nippon Kagaku Kai, "Kagaku Benran, Kiso Hen," 2nd ed, Maruzen, Tokyo (1975), p. 997.

10) J. K. Kochi and F. F. Rust, *J. Am. Chem. Soc.*, **83**, 2017 (1961).

11) S. Richter, C. Daul, and A. von Zelewsky, *Inorg. Chem.*, **15**, 943 (1976).

12) F. H. Case, *J. Am. Chem. Soc.*, **68**, 2574 (1946).

Nucleophilic Cleavage of Phosphate Triesters in Dialkylammonium Bilayer Membranes[1)]

Yoshio Okahata, Hirotaka Ihara, and Toyoki Kunitake*

Department of Organic Synthesis, Faculty of Engineering, Kyushu University, Higashi-ku, Fukuoka 812

(Received October 27, 1980)

A study was carried out on the reaction of *p*-nitrophenyl phosphates with hydroxamate nucleophiles in water in the presence of dialkylammonium bilayer membranes. With ethyl bis(*p*-nitrophenyl) phosphate, clean second-order kinetics was observed for all the hydroxamate nucleophiles, two equivalents of *p*-nitrophenol being released in most cases. In contrast, a complex kinetics was observed for octadecylbis(*p*-nitrophenyl)phosphate. The second cleavage process of this long-chain substrate by a long-chain hydroxamate was affected by the fluidity of the matrix membrane, an inflection region being present in the Arrhenius plots near the phase transition temperature(T_c) of the $2C_{16}N^+2C_1$ membrane. The activation energy was 14 and 21 kcal/mol at temperatures above and below T_c, respectively. Similar changes in the activation energy had been observed for decarboxylation and proton abstraction.

Since it was first found that bilayer membranes are formed from dialkylammonium salts,[2,3)] physicochemical characterization of the dialkylammonium bilayer has been extensively carried out. One important characteristic is the occurrence of the crystal-to-liquid crystal phase transition similar to that of biolipid bilayers, as confirmed by differential scanning calorimetry,[4,5)] NMR spectroscopy,[6)] fluorescence depolarization,[6,7)] and positron annihilation.[7)]

The unique organization of the dialkylammonium bilayer was subsequently used as site for several kinds of organic reaction. A large rate difference was observed between the intra-vesicle and inter-vesicle reactions of nucleophiles and a phenyl ester.[8)] A cholesteryl nucleophile was specifically activated in the ammonium membrane,[9)] and the reaction rate was influenced by the phase transition in acyl transfer,[10)] proton abstraction,[11)] and decarboxylation.[12)]

In this article we report on the hydrolysis of activated phosphoric triesters by hydrophobic hydroxamate nucleophiles in the presence of hexadecyltrimethylammonium bromide (CTAB) micelle and dialkylammonium ($2C_nN^+2C_1$) bilayer membranes.[13)] The hydrolysis of phosphoric triesters proceeds *via* general-base or nucleophilic pathways. The relative ease of these pathways is determined by structural combinations of substrates and bases, the relative basicity of leaving group and nucleophile and steric crowding in the transition state being concluded to be the two most important factors.[14—16)]

The micellar effect on the cleavage of phosphoric triesters was studied by Bunton and Ihara[17)] and Epstein *et al.*[18)] for oximate nucleophiles and by Tagaki *et al.*[19)] for imidazole nucleophiles. It was found that cationic micelles accelerate the reaction and change the mechanism. It is of particular interest to see how the peculiar molecular organization of the bilayer membrane affects the cleavage of phosphoric esters.

The structures of nucleophiles, substrates and membrane-forming ammonium salts used in this study are given below together with their abbreviations.

Ammonium salt

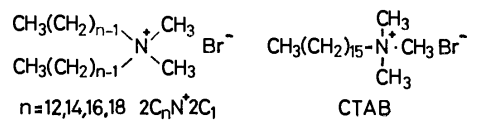

Nucleophile

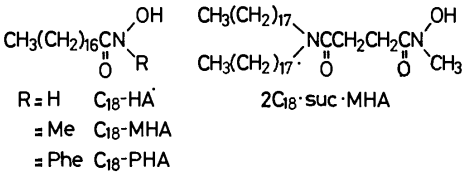

Substrate

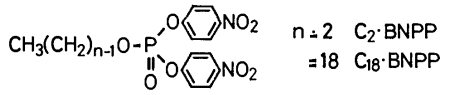

Experimental

Nucleophiles. Octadecanehydroxamic acid (C_{18}-HA), *N*-methyloctadecanehydroxamic acid (C_{18}-MHA), and *N*-phenyloctadecanehydroxamic acid (C_{18}-PHA) were prepared from octadecanoyl chloride and the corresponding hydroxylamines, and identified by NMR and IR spectroscopy and elemental analysis. C_{18}-HA: mp 102—104 °C. Found: C, 71.86; H, 12.46; N, 4.65%. Calcd for $C_{18}H_{37}NO_2$: C, 72.19; H, 12.45; N, 4.68%. C_{18}-MHA: mp 60—62 °C. Found: C, 72.59; H, 12.39; N, 4.40%. Calcd for $C_{19}H_{37}NO_2$: C, 72.79; H, 12.54; N, 4.47%. C_{18}-PHA: mp 88—89 °C. Found: C, 76.33; H, 10.97; N, 3.70%. Calcd for $C_{24}H_{41}NO_2$: C, 76.74; H, 11.00; N, 3.73%.

Mono-*N*,*N*-dioctadecylamide of succinic acid (9.3 g, 15 mmol) as prepared from dioctadecylamine and succinic anhydride, and 2 g (18 mmol) of *N*-hydroxysuccinimide were dissolved in 70 ml of tetrahydrofuran (THF), 3.7 g (18 mmol) of dicyclohexylcarbodiimide being added with stirring at ice-bath temperature. The reaction mixture was warmed to room temperature after 1 h and stirred for 24 h. *N*,*N*'-Dicyclohexylurea was filtered. After the solvent had been removed, the residue was recrystallized from 1:10 ether–methanol to give colorless powder: yield 9.3 g (86%), mp 64—67 °C. The succinimide ester obtained (5 g, 8 mmol) was dissolved in 30 ml of $CHCl_3$, and 2.5 g (30 mmol) of *N*-methylhydroxylamine and 3 g (30 mmol) of triethylamine in 60 ml of $CHCl_3$ were slowly added with stirring. After the mixture had been stirred for 6 h at room temperature, the solvents were evaporated and the residue was dissolved in ether, washed with dilute hydrochloric acid and water, and dried over Na_2SO_4. The solution was concentrated and 3 g of solids was recovered by addition of methanol. Colorless powder was obtained by repeated recrystalliza-

tion from 1:1 acetone–ether: yield 1.4 g (30%), mp 50—52 °C. The product, *N*-methyl-3-(dioctadecylcarbamoyl)propanehydroxamic acid, ($2C_{18}$-suc-MHA) was confirmed by IR and NMR spectroscopy and by elemental analysis. Found: C, 75.62; H, 12.80; N, 4.20%. Calcd for $C_{41}H_{82}N_2O_3$: C, 75.63; H, 12.69; N, 4.30%.

Preparation and purification of *N*-dodecylbenzohydroxamic acid (C_{12}-BHA),[20] and *N*-benzylbenzohydroxamic acid (BBHA)[21] were reported. $C_{12}N^+C_2$-MHA was supplied by T. Sakamoto.[22]

Substrates. Tris(*p*-nitrophenyl) phosphate (1 g, 2.2 mmol) was refluxed for 1 d in 10 ml of dry ethanol, coloreless needles of C_2-BNPP being obtained on cooling: yield 0.7 g (90%), mp 134—135 °C (lit,[23] mp 133 °C). The purity was confirmed by NMR spectroscopy and elemental analysis. Found: C, 45.50; H, 3.57; N, 7.68%. Calcd for $C_{14}H_{13}N_2O_8P$: C, 45.67; H, 3.56; N, 7.61%.

Triethylamine (3.7 g, 37 mmol) and 10.0 g (37 mmol) of octadecyl alcohol were dissolved in 100 ml of dry ether, 21 g (137 mmol) of $POCl_3$ being added with stirring at ice-bath temperature. The mixture was then stirred for 3 h at room temperature and precipitates were removed. The solvent was evaporated and the residual white solid was recrystallized from acetonitrile: yield 15 g, mp<30 °C. The acid chloride obtained and 21.5 g (155 mmol) of *p*-nitrophenol were dissolved in 100 ml of dry ether, 15.5 g (155 mmol) of triethylamine being added dropwise with stirring at ice-bath temperature. After stirring for one day at room temperature, precipitates were removed and the solution was concentrated to give a waxy product. Recrystallization twice from acetone and methanol gave colorless needles of C_{18}-BNPP: yield 3 g (13%), mp 59—60 °C. The NMR spectrum was consistent with the expected structure. Found: C, 60.80; H, 7.68; N, 4.89%. Calcd for $C_{10}H_{45}N_2O_8P$: C, 60.79; H, 7.65; N, 4.83%.

Other Materials. Commercial CTAB was recrystallized twice from ethanol. Dialkyldimethylammonium bromides ($2C_nN^+2C_1$) were prepared by stepwise alkylation.[3,9]

Kinetics. Hydrolysis was initiated by injecting substrate solutions (in ethanol or acetonitrile) into aqueous solutions of surfactants containing given amounts of catalyst. The progress of the reaction was followed by the appearance of *p*-nitrophenolate anion (λ_{max}=400 nm in CTAB micelles and 390 nm in ammonium membranes, ε=18100) with a Hitachi 124 spectrophotometer. The surfactant concentration was 1×10^{-3} M (1 M=1 mol dm^{-3}), which is larger than the cmc of CTAB and $2C_nN^+2C_1$. The reaction conditions were 3 v/v% organic solvent–H_2O, μ=0.01 (KCl), 0.01—0.02 M borate buffer (pH 7—10), unless stated otherwise. The pH measurement was carried out with a Toa Digital pH meter (Type HM-10A), the pH variation of the reaction medium being smaller than 0.05.

Results

Course of Phosphoric Ester Cleavage. Ethyl bis(*p*-nitrophenyl) phosphate (C_2·BNPP) undergoes slow hydrolysis in alkaline CTAB solutions (pH 8—10). The UV absorption of C_2·BNPP (λ_{max}=270 nm) diminishes with time, new absorptions appearing at 400 and 290 nm (Fig. 1). The 400-nm band is attributable to *p*-nitrophenolate anion, one equivalent of which is formed eventually. The 290-nm band is ascribable to ethyl *p*-nitrophenyl phosphate anion (ε=9500)(C_2·MNPP$^-$) which is stable under these conditions. Tagaki *et al.*[19] confirmed that phenyl *p*-nitrophenyl phosphate anion is hydrolyzed very slowly even at 55 °C, pH 12.5. Brass and Bender[16] similarly observed the formation of *p*-nitrophenyl methylphosphonate anion at 288 nm (ε=9560) in the alkaline hydrolysis of bis(*p*-nitrophenyl) methylphosphonate.

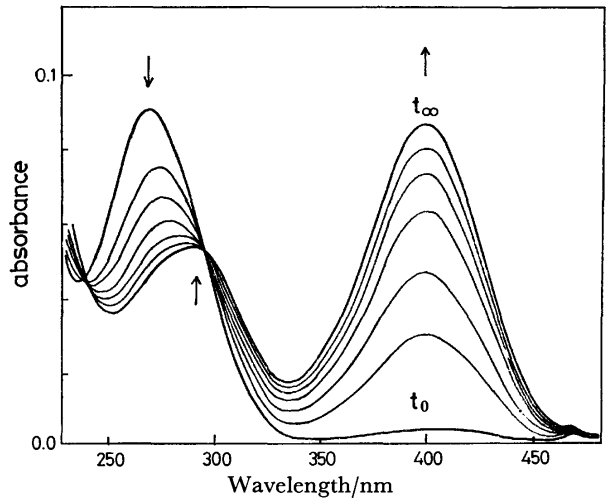

Fig. 1. Spontaneous hydrolysis of C_2-BNPP in the CTAB micelle.
pH 9.6, 30 °C, 0.01 M borate buffer, μ=0.01(KCl), 3 v/v%EtOH–H_2O. [CTAB]=1.00×10^{-3} M, [C_2-BNPP]=5.00×10^{-6} M.

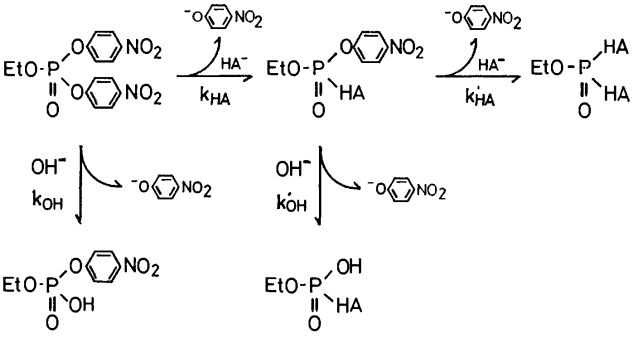

Fig. 2. The course of the ester cleavage of C_2-BNPP.

In the presence of excess hydroxamate nucleophiles, the predominant course of reaction is the release of two equivalents of *p*-nitrophenol without formation of ethyl *p*-nitrophenyl phosphate anion.

The courses of the phosphoric ester cleavage are summarized in Fig. 2. The alkaline hydrolysis (k_{OH} process) is negligible in the presence of excess of most hydroxamates, since the UV peak (λ_{max} 290 nm) characteristic of diester product C_2-MNPP$^-$ (Fig. 1) cannot be detected in the reaction mixture.

On the other hand, if equimolar amounts of substrate and nucleophile (C_{18}·MHA) are present, we observe, upon correction for the alkaline hydrolysis, rapid formation of one equivalent of *p*-nitrophenol followed by much slower *p*-nitrophenol release. These steps correspond to the k_{HA} and k'_{OH} processes (Fig. 2). Introduction of additional C_{18}·MHA during the second stage induces rapid *p*-nitrophenol release of the k'_{HA} process.

Behavior of Different Hydroxamate Nucleophiles toward C_2·BNPP. Figure 3 shows the time course of

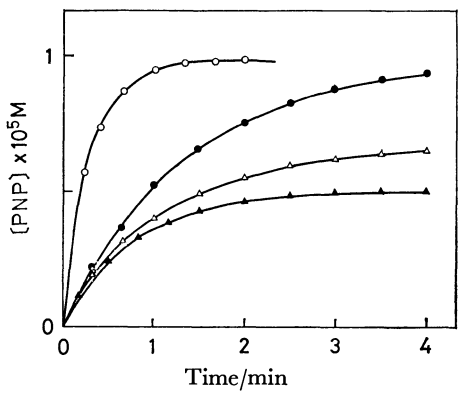

Fig. 3. The time course of the *p*-nitrophenol (PNP) release from C_2-BNPP by several hydroxamates in the presence of the CTAB micelle.
30 °C, pH 8.8, 0.02 M borate buffer, $\mu=0.01$ (KCl), [CTAB] $=1.00\times10^{-3}$ M, [hydroxamate] $=5.00\times10^{-5}$ M, [C_2-BNPP] $=5.00\times10^{-6}$ M. *p*-Nitrophenolate anion: λ_{max} 400 nm, $\varepsilon=1.81\times10^4$. C_{18}-MHA: —○—, C_{18}-HA: —●—, C_{18}-PHA: —△—, $C_{12}N^+C_2$-MHA: —▲—.

p-nitrophenol release from C_2-BNPP by a series of long-chain hydroxamate nucleophiles in the CTAB micelle.

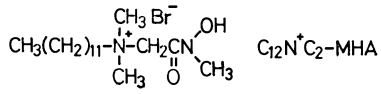

$C_{12}N^+C_2$-MHA

The ultimate *p*-nitrophenol release varies considerably with nucleophile. Excess of C_{18}-HA, C_{18}-MHA, and $2C_{18}$-MHA (not shown in Fig. 3) releases two equivalents of *p*-nitrophenol due to k_{HA} and k'_{HA} processes of Fig. 2. However, C_{18}-PHA produces 1.4—1.6 equivalents, the release by $C_{12}N^+C_2$-MHA being one equivalent. In the reaction with C_{18}-PHA, the difference spectrum indicates increases in absorbance at 245 and 300 nm (shoulder). The 245-nm absorption can be attributed to the monosubstitution product, the shoulder at 300 nm suggesting the formation of C_2-MNPP$^-$ (λ_{max} 290 nm, see above). The simple alkaline hydrolysis is too slow to explain the results. General base catalysis (Eq. 1) might become com-

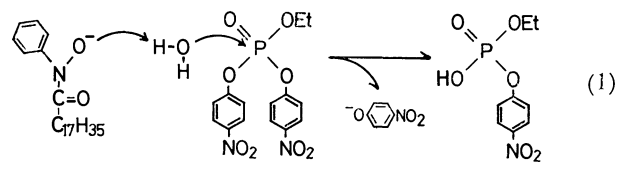

(1)

petitive with the nucleophilic process, since the latter process is rendered less efficient due to steric hindrance of the phenyl substituent near the nucleophilic center. Similarly, less than two equivalents of *p*-nitrophenol were released with related nucleophiles, BBHA and C_{12}-BHA. The release of one equivalent of *p*-ni-

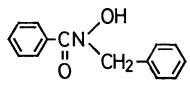

BBHA

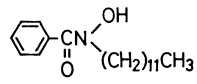

C_{12}-BHA

Table 1. Values of k_1 for *p*-nitrophenol release from C_2-BNPP with hydroxamate nucleophiles

Nucleophile	$10^3 k_1/s^{-1}$		
	CTAB	$2C_{12}N^+2C_1$	$2C_{16}N^+2C_1$
None(OH^-)	1.0	1.8	1.4
C_{18}-HA	9.1	35	28
C_{18}-MHA	88	100	74
C_{18}-PHA	8.3	45	50
$2C_{18}$-MHA	45	40	28

30 °C, pH 8.8, 0.02 M borate buffer, $\mu=0.01$(KCl), [Ammonium] $=1.00\times10^{-3}$ M, [hydroxamate] $=5.00\times10^{-5}$ M, [C_2-BNPP] $=5.00\times10^{-6}$ M.

trophenol by $C_{12}N^+C_2$-MHA is ascribed to the very low reactivity of the first substitution product **1** in the subsequent nucleophilic attack. There is no indication of the general base catalysis (formation of C_2-MNPP$^-$) in this case.

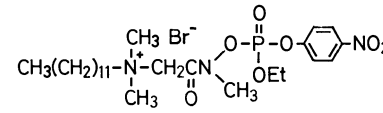

1

The presence of the $C_{12}N^+C_2$-MHA moiety in the intermediate and/or nucleophile appears to interfere with the second nucleophilic attack. This presumption is supported by the following experiments: (a) no *p*-nitrophenol release was observed when C_{18}-MHA was added to an equimolar reaction mixture (1:1 adduct formed) of C_2-BNPP and $C_{12}N^+C_2$-MHA, (b) addition of $C_{12}N^+C_2$-MHA did not promote *p*-nitrophenol release from an equimolar reaction mixture (1:1 adduct formed) of C_{18}-MHA and C_2-BNPP.

In spite of the varying extent of *p*-nitrophenol release, all the time courses of Fig. 3 obeyed the pseudo first-order kinetics (Eq. 2) for up to 80% conversion.

$$k\cdot t = -\ln\frac{A_\infty - A_t}{A_\infty}, \qquad (2)$$

where A_∞ and A_t are absorbances at the infinite time and at time t, respectively. The results indicate that the second nucleophilic attack is not slower than the first one ($k_{HA}\leqq k'_{HA}$) in the two-step nucleophilic attack toward C_2-BNPP, except in the case of $C_{12}N^+$-C_2-MHA.

The kinetic pattern of the C_2-BNPP cleavage was the same in the CTAB micelle as well as in the dialkylammonium membrane for given nucleophilics. The pseudo first-order rate constants with various hydroxamates in micellar and membrane systems are summarized in Table 1. The effective nucleophile is the hydroxamate anion. The true nucleophilic reactivity of the anion cannot be compared, since the pK_a value and consequently the fraction of the dissociated species was not determined.

Cleavage of C_{18}-BNPP. The reaction scheme for the cleavage of long-chain substrate C_{18}-BNPP is fundamentally the same as that for C_2-BNPP (Fig. 2). However, the kinetic patterns are quite different. In the reaction with excess C_{18}-HA, the first-order

kinetics holds only approximately, two equivalents of *p*-nitrophenol being released. The reaction with C_{18}-PHA was very slow ($k_{HA} \ll k_{OH}$), no further kinetic examination being performed.

In the reaction with excess C_{18}-MHA, the first-order plots in the CTAB micelle consist of two lines (Fig. 4). Since the ultimate *p*-nitrophenol release is two equivalents per mole of C_{18}-BNPP, the result

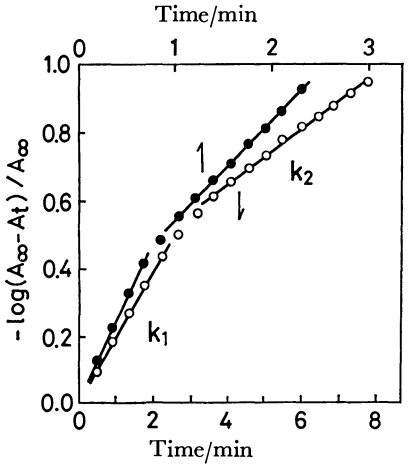

Fig. 4. Pseudo first order plots of the reaction of C_{18}-BNPP with C_{18}-MHA in the presence of the CTAB micelle.
pH 8.7, 0.02 M borate buffer, μ=0.01 (KCl), [CTAB] = 1.00×10^{-3} M, [C_{18}-MHA] = 1.00×10^{-4} M, [C_{18}-BNPP] = 1.00×10^{-5} M. 30 °C: —○—, 43 °C: —●—.

indicates that the second stage of the nucleophilic displacement (k'_{HA} process) is appreciably slower than the first stage (k_{HA} process). Similar kinetic results were obtained in the membrane system. Figure 5a shows the first order plots obtained at 30 °C. The slopes for the initial release do not vary much with the membrane. On the other hand, the slope for the second stage is suppressed increasingly with increasing lengths of the alkyl chain of the membrane. At a higher reaction temperature of 43 °C, the changes in slope are smaller except for the $2C_{18}N^+2C_1$ membrane (Fig. 5b). The apparent rate constants of the first and second steps of the reaction, k_1 and k_2, respectively, are given in Table 2. The k_1 value was determined from the initial linear portion of the first-order plots, k_2 being obtained from the second linear portions corresponding to 60—90% conversion. These two steps approximately correspond to the k_{HA} and k'_{HA} processes. The k_1 value is $(7.8\pm1.0)\times10^{-3}$

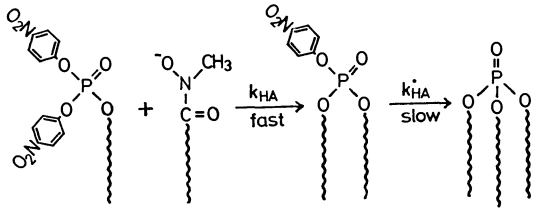

(3)

s^{-1} at 30 °C and $(18\pm3)\times10^{-3}$ s^{-1} at 43 °C, indicating that the magnitude of k_1 is not influenced by the membrane (or micelle) used.[24] In contrast, k_2 is dependent

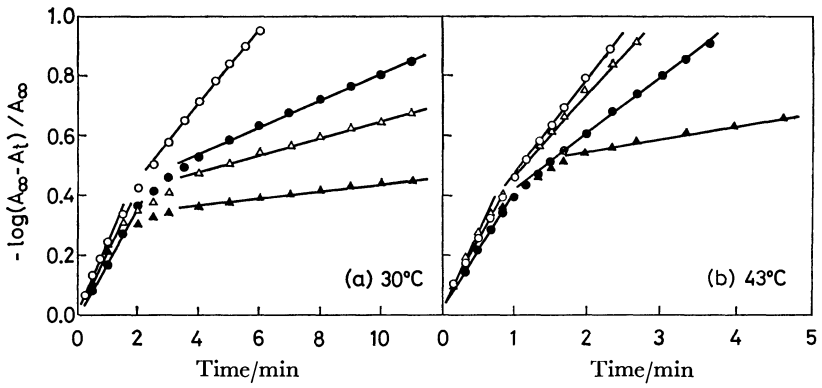

Fig. 5. Pseudo first-order plots of the reaction of C_{18}-BNPP with C_{18}-MHA in the presence of dialkylammonium membranes.
pH 8.7, 0.02 M borate buffer, μ=0.01(KCl), [C_{18}-BNPP] = 1.00×10^{-5} M, [C_{18}-MHA] = 1.00×10^{-4} M, [$2C_nN^+2C_1$] = 1.00×10^{-3} M. $2C_{12}N^+2C_1$: —○—, $2C_{14}N^+2C_1$: —●—, $2C_{16}N^+2C_1$: —△—, $2C_{18}N^+2C_1$: —▲—.

TABLE 2. VALUES OF k_1, k_2, AND k_2/k_1 IN THE REACTION OF C_{18}-BNPP WITH C_{18}-MHA

Micelle and membrane	At 30 °C			At 43 °C		
	$10^3 k_1/s^{-1}$	$10^3 k_2/s^{-1}$	k_2/k_1	$10^3 k_1/s^{-1}$	$10^3 k_2/s^{-1}$	k_2/k_1
CTAB	7.8	2.3	1/3.4	16	5.1	1/3.0
$2C_{12}N^+2C_1$	8.8	4.5	1/2.0	17	9.9	1/1.7
$2C_{14}N^+2C_1$	6.9	1.7	1/4.1	15	6.8	1/2.2
$2C_{16}N^+2C_1$	8.6	1.0	1/8.6	21	9.8	1/2.2
$2C_{18}N^+2C_1$	8.3	0.52	1/15.8	20	1.4	1/13.8

pH 8.7 (30 °C), pH 8.8 (43 °C), 0.02 M borate buffer (μ=0.01), [Ammonium] = 1.00×10^{-3} M, [C_{18}-MHA] = 1.00×10^{-4} M, [C_{18}-BNPP] = 1.00×10^{-5} M.

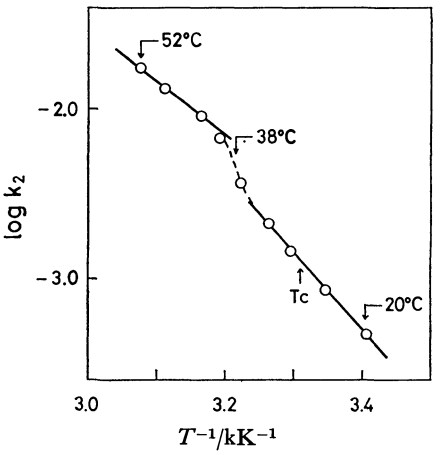

Fig. 6. Arrhenius plots for $k_{2,obsd}$ for the reaction of C_{18}-BNPP with C_{18}-MHA in the $2C_{16}N^+2C_1$ membrane.
pH 9.4, 0.02 M borate buffer, $\mu=0.01$(KCl), $[2C_{16}N^+2C_1]=1.00\times10^{-3}$ M, $[C_{18}$-MHA$]=1.00\times10^{-4}$ M, $[C_{18}$-BNPP$]=1.00\times10^{-5}$ M.

of the ammonium membrane used, decreasing with increasing alkyl chain lengths of the dialkylammonium membrane at 30 °C but not necessarily at 43 °C. A smaller k_2 value was obtained only for the $2C_{18}N^+2C_1$ membrane at higher temperature. The rate depressing effect for k_2 can be seen more clearly by comparing the ratio of the rate constants k_2/k_1. The ratio is *ca.* 1/3 for the CTAB system at both temperatures, the temperature effect being similarly small for the $2C_{12}N^+2C_1$ system. It is smaller at 30 °C than at 43 °C for the $2C_{14}N^+2C_1$ and $2C_{16}N^+2C_1$ systems, but small and constant at the two temperatures for the $2C_{18}N^+2C_1$ membrane. Since the change in k_2/k_1 due to temperature is the largest for the $2C_{16}N^+2C_1$ system, the temperature effect was studied carefully in this system. Figure 6 shows the Arrhenius plots for k_2. The plots are represented by two lines with inflection at 35 to 40 °C.

Discussion

The kinetic behavior of the nucleophilic attack of a series of long-chain hydroxamates toward phosphoric esters is summarized in Table 3. Clean second-order kinetics was observed for all the hydroxamates in the case of C_2-BNPP. This indicates that the first substitution is not faster than the second: $k_{HA}\leqq k'_{HA}$ in Fig. 1. A C_{18} alkyl chain is introduced in the first substitution. The resulting monosubstitution product is hydrophobic and the second substitution would be accelerated more efficiently in the micelles and membranes. Micellar acceleration is greater with hydrophobic substrates.

In sharp contrast with C_2-BNPP, no clean second-order kinetics could be found for C_{18}-BNPP. It appears that the steric constraint considerably retards the reaction with C_{18}-PHA and $2C_{18}$-MHA. The monosubstitution products of C_{18}-BNPP possess structures **2** and **3**. The CPK molecular model shows that the steric interference due to *N*-substituents (R)

Table 3. Kinetic behavior of various combinations of nucleophile and substrate

Nucleophile	Substrate: C_2-BNPP	Substrate: C_{18}-BNPP
C_{18}-HA	Clean second order: $k_{HA}\ll k'_{HA}$. 2 equiv. PNP released.	Approximate pseudo first order: $k_1\leqq k_2$. 2 equiv. PNP released.
C_{18}-MHA	Clean second order: $k_{HA}\ll k'_{HA}$. 2 equiv. PNP released.	Two steps in the first order plots: $k_1>k_2$. Membrane fluidity influential. 2 equiv. PNP released.
C_{18}-PHA	Clean second order: 1.4—1.6 equiv. PNP released.	PNP release very slow.
$2C_{18}$-MHA	Clean second order: $k_{HA}\ll k'_{HA}$. 2 equiv. PNP released.	Two steps in the first order plots: $k_1\gg k_2$. k_2 very small. More than equiv. PNP released.

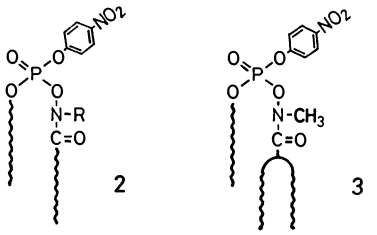

is appreciable in **2**. Thus, when R=H, mono- and disubstitutions proceed smoothly, but when R=phenyl, even the monosubstitution virtually does not proceed. When R=methyl, the monosubstitution is smooth but the disubstitution is slower. When the attacking nucleophile is a double-chain compound, even the monosubstitution is extremely slow with a *N*-methylhydroxamate ($2C_{18}$-MHA). Disubstitution proceeds faster than monosubstitution for the combination of C_2-BNPP and $2C_{18}$-MHA (Eq. 4). The double alkyl chain in $2C_{18}$-MHA may be not very demanding sterically since the double chain is removed from the phosphorus center.

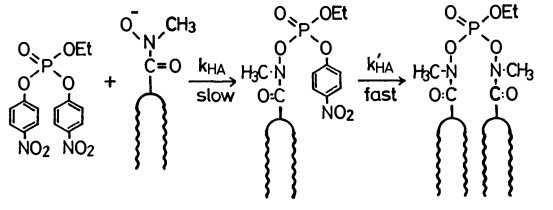

(4)

The rate constant for the pair of C_{18}-BNPP and C_{18}-MHA shows a characteristic variation with the membrane matrix. k_2 (*i.e.*, k'_{HA}) appears to be sensitive to membrane fluidity (Table 2).

The phase transition temperature (T_c) of the dialkylammonium bilayer membrane has been determined by various physicochemical means. The results determined by differential scanning calorimetry

Table 4. Phase transition temperature of dialkylammonium ($2C_nN^+2C_1Br^-$) membranes

n	12	14	16	18
T_c °C	0—5	18	28	45

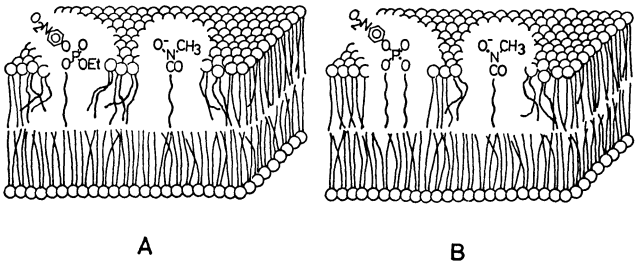

Fig. 7. Schematic illustration of nucleophiles and substrates in the membrane matrix.
Note that the double-chain substrate in B perturbs the neighboring membrane less than the single-chain substrate in A.

seems to be most reliable. The T_c data are given in Table 4. At reaction temperature 30 °C, the $2C_{16}N^+2C_1$ and $2C_{18}N^+2C_1$ membranes are in the crystalline phase, their k_2 values being smaller than those in the other membranes. At reaction temperature 43 °C, only the $2C_{18}N^+2C_1$ membrane is in the crystalline state, giving a small k_2 value. The influence of the membrane fluidity is more apparent when k_2/k_1 values are compared. The membranes in the liquid crystalline state (above T_c) give k_2/k_1 ratios of 1/2—1/4, but the rigid membranes at temperatures below T_c give smaller ratios.

It may be asked why the k'_{HA} process and not the k_{HA} process is affected by membrane fluidity. The k_{HA} process is a reaction between a single-chain nucleophile and a single-chain substrate. The same type of reaction between a single-chain imidazole and a single-chain phenyl ester is influenced by phase transition.[10] The presence or absence of the influence of the membrane fluidity might depend on particular combinations of the single-chain reagents.

The k'_{HA} process is a reaction between a single-chain nucleophile and a double-chain monosubstitution product. Since the reactivity of the nucleophile (C_{18}-MHA) is not affected by membrane fluidity (k_{HA} invariant), the dependence of k'_{HA} on the membrane fluidity should arise from the varying reactivity of the double-chain intermediate. If we assume that the double-chain compound does not destroy the neighboring dialkylammonium membrane matrix, its reactivity would be affected by membrane fluidity more than the reactivity of the single-chain substrate. That is, the dialkyl species can be a part of the membrane matrix but the single-chain species should act as an impurity for the membrane. The situation is illustrated in Fig. 7.

The inflection of the Arrhenius plots (Fig. 5) is similarly associated with the phase transition, although the inflecting temperature region centered at 38 °C is 10 °C higher than T_c of the $2C_{16}N^+2C_1$ membrane (28 °C).

Table 5. Activation energy in $2C_{16}N^+2C_1$ membrane

Reaction	E_a/kcal mol^{-1} Below T_c	E_a/kcal mol^{-1} Above T_c	Remark
Nucleophilic displacement (k_{HA}' process)	21	14	This study
Decarboxylation (Eq. 5)	25	19	Ref. 12
Proton abstraction (Eq. 6)	46	20	Ref. 11

The presence of two sets of the activation energy in the membrane system has been detected in the cleavage of a phenyl ester,[10] in decarboxylation (Eq. 5),[12] and in the proton abstraction (Eq. 6).[11]

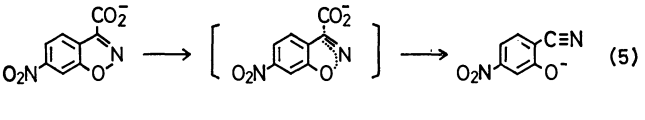

(5)

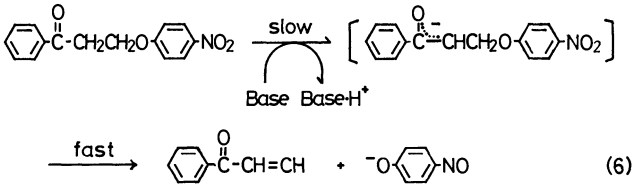

fast

(6)

The E_a value determined from Fig. 6 is 14 kcal/mol at temperatures above T_c and 21 kcal/mol at temperatures below T_c. E_a values obtained in the temperature ranges above and below T_c for different types of reaction are compared in Table 5. In all cases, E_a below T_c is appreciably larger than E_a above T_c. It becomes more difficult for these reactions to proceed at low temperatures due to increased rigidity of the $2C_{16}N^+2C_1$ membrane matrix.

Conclusion

Phase transition is associated with the regulation of physiological functions of the biomembrane. For example, the activity of succinic acid oxidase of sheep liver mitochondria membrane changes with phase transition, the activation energy being 2 and 12 kcal/mol at temperatures above and below T_c, respectively.[25] These biochemical results are very similar to those observed for some common organic reactions: nucleophilic displacement, base-catalyzed proton abstraction, and unimolecular decarboxylation (Table 5). It is presumed that the regulation of the reaction rate by phase transition becomes possible for a large variety of organic reactions.

This study was supported in part by Grant-in-Aid for Scientific Research No. 447079 from Ministry of Education, Science and Culture.

References

1) Contribution No. 610 from the Department of Organic Synthesis.
2) T. Kunitake and Y. Okahata, *J. Am. Chem. Soc.*, **99**,

3860 (1977).
3) T. Kunitake, Y. Okahata, K. Tamaki, F. Kumamaru, and M. Takayanagi, *Chem. Lett.*, **1977**, 387.
4) T. Kajiyama, A. Kumano, M. Takayanagi, Y. Okahata, and T. Kunitake, *Chem. Lett.*, **1979**, 645.
5) Y. Okahata, R. Ando, and T. Kunitake, *Ber. Bunsenges Phys. Chem.*, in press.
6) T. Nagamura, S. Mihara, Y. Okahata, T. Kunitake, and T. Matsuo, *Ber. Bunsenges. Phys. Chem.*, **82**, 1093 (1978).
7) K. Kano, A. Romero, B. Djermouni, H. J. Ache, and J. H. Fendler, *J. Am. Chem. Soc.*, **101**, 4030 (1979).
8) T. Kunitake and T. Sakamoto, *J. Am. Chem. Soc.*, **100**, 4615 (1978).
9) Y. Okahata, R. Ando, and T. Kunitake, *Bull. Chem. Soc. Jpn.*, **52**, 3647 (1979).
10) T. Kunitake and T. Sakamoto, *Chem. Lett.*, **1979**, 1059.
11) Y. Okahata, S. Tanamachi, and T. Kunitake, *Nippon Kagaku Kaishi*, **1980**, 442.
12) T. Kunitake, Y. Okahata, R. Ando, S. Shinkai, and S. Hirakawa, *J. Am. Chem. Soc.*, **102**, 7877 (1980).
13) Earlier examples of the use of micellar hydroxamate nucleophiles toward carboxylic acid esters include I. Tabushi, Y. Kuroda, and S. Kita, *Tetrahedron Lett.*, **1974**, 643; I. Tabushi, and Y. Kuroda, *ibid.*, **1974**, 3613; T. Kunitake, Y. Okahata, and T. Sakamoto, *Chem. Lett.*, **1975**, 459.
14) S. A. Khan and A. J. Kirby, *J. Chem. Soc., B*, **1970**, 1172.
15) A. Williams and R. A. Naylon, *J. Chem. Soc., B*, **1971**, 1967.
16) H. J. Brass and M. L. Bender, *J. Am. Chem. Soc.*, **94**, 7421 (1972).
17) C. A. Bunton and Y. Ihara, *J. Org. Chem.*, **42**, 2865 (1977).
18) J. Epstein, J. J. Kaminski, N. Bodor, R. Enever, J. Sowa, and T. Higuchi, *J. Org. Chem.*, **43**, 2816 (1978).
19) W. Tagaki, T. Eiki, and H. Kaneko, The 28th Symposium on Organic Reaction Mechanisms, November 1977, Yokohama, Preprint, p. 207.
20) T. Kunitake, Y. Okahata, and T. Sakamoto, *J. Am. Chem. Soc.*, **98**, 7799 (1976).
21) T. Kunitake, Y. Okahata, and T. Tahara, *Bioorg. Chem.*, **5**, 155 (1976).
22) T. Sakamoto, unpublished synthesis in these laboratories.
23) M. Rapp, *Liebigs. Ann. Chem.*, **224**, 161 (1884).
24) The k_1 and k_2 values in the $2C_{14}N^+2C_1$ membrane are slightly smaller than expected. Small deviations from the first-order plot were observed in the initial stage of the *p*-nitrophenol release, the reaction mixture becoming turbid in some cases. These observations suggest that the reacting species are not entirely miscible with the $2C_{14}N^+2C_1$ membrane, and explain the small, negative deviations of k_1 and k_2.
25) E. J. McMurchie and J. K. Raison, *Biochim. Biophys. Acta*, **554**, 364 (1979).

Synthesis of [3.3](1,1′)- and [5.5](1,1′)Ruthenocenophanes and Their Ferrocenoruthenocenophane Homologs

Shin-ichi KAMIYAMA,* Akira KASAHARA,** Taeko IZUMI,**
Iwao SHIMIZU,** and Hiroyuki WATABE**

Government Industrial Research Institute, Tohoku, Nigatake, Haranomachi, Sendai 983
***Department of Applied Chemistry, Faculty of Engineering, Yamagata University, Yonezawa 992*

(Received October 27, 1980)

[3.3](1,1′)Ruthenocenophane-2,14-diene-1,16-dione, [5.5](1,1′)ruthenocenophane-2,14,17,29-tetraene-1,16-dione and their ferrocenoruthenocenophane homologs were synthesized by using an intermolecular base-catalyzed condensation.

A variety of layered compounds have been synthesized and their physical and chemical properties have been studied.[1-4] Cyclophanes in which aromatic rings are mutually stratified have been well investigated from a viewpoint of transannular π-electronic interactions. In contrast to the active interest in cyclophanes, little attention has been focused on [2.2](1,1′)ferrocenophane-1,13-diyne,[5] [2.2](1,1′)ferrocenophane-1,13-diene,[6] [2]paracyclo[2]paracyclo[2](1,1′)-ferrocenophane derivatives,[7] [3.3](1,1′)ferrocenophane-1,15-diene-3,14-dione,[8] [5.5](1,1′)ferrocenophane1,4,-16,19-tetraene-3,18-dione,[8] and [0]metacyclo[2]-metacyclo[0](1,1′)ferrocenophan-7-ene.[9] In addition, there are only a few synthetic investigations of [5]-ruthenocenophane derivatives[10] and [3]- and [4]-ruthenocenophane derivatives.[11] This paper is concerned with the synthesis of [3.3](1,1′)- and [5.5]-(1,1′)ruthenocenophanes and their ferrocenoruthenocenophane homologs, including olefinic and carbonyl groups between metallocene systems, in order to examine the transannular π-electronic interactions of the chromophores.

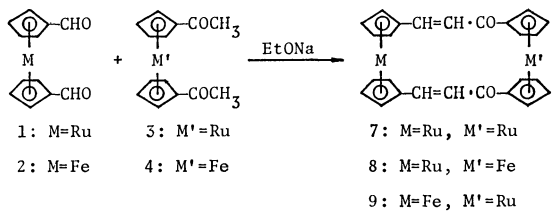

Scheme 1.

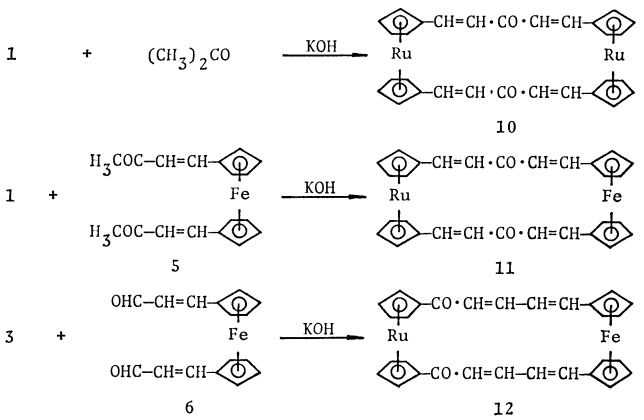

Scheme 2.

Results and Discussion

Synthesis of [3.3](1,1′)Ruthenocenophane. In the presence of sodium ethoxide, the reaction of 1,1′-ruthenocenedicarbaldehyde (**1**) with 1,1′-diacetylruthenocene (**3**)[12] in ethanol gave a good yield of [3.3]-(1,1′)ruthenocenophane-2,14-diene-1,16-dione (**7**).[13] Under the same conditions, the internal base-catalyzed condensations of **1** with 1,1′-diacetylferrocene (**4**)[17] and 1,1′-ferrocenedicarbaldehyde (**2**)[16] with **3** gave rise to the formation of [3.3](1,1′)ferrocenoruthenocenophane-13,25-diene-1,12-dione (**8**)[13] and [3.3](1,1′)-ferrocenoruthenocenophane-2,14-diene-1,16-dione (**9**),[13] respectively (Scheme 1).

Synthesis of [5.5](1,1′)Ruthenocenophane. In the presence of KOH, the base-catalyzed condensation of **1** with acetone led to the formation of [5.5]-(1,1′)ruthenocenophane-2,14,17,29-tetraene-1,16-dione (**10**).[13] In the same manner, the reactions of **1** with 1,1′-bis(2-acetylvinyl)ferrocene (**5**)[18] and of **3** with 1,1′-bis(2-formylvinyl)ferrocene (**6**)[18] also gave [5.5](1,1′)-ferrocenoruthenocenophane-2,14,17,29-tetraene-1,16-dione (**11**)[13] and [5.5](1,1′)ferrocenoruthenocenophane-2,4,16,18-tetraene-1,20-dione (**12**),[13] respectively (Sceheme 2).

Characterization and Spectral Data. The structures of the phane compounds **7**—**12** and the other compounds were determined on the basis of IR, ^{1}H NMR, and mass spectra and elemental analyses. The ^{1}H NMR spectral data of the phane compounds **7**—**12** are summarized in Table 1. The coupling constants of doublets for olefinic protons in **7**—**12** are 15 or 16 Hz, except for the case of **12**. On the other hand, the IR spectral data of olefinic linkages in **7**—**12** exhibit two bands at *ca.* 1600 and 960 cm^{-1} (Table 2). The J values in the ^{1}H NMR spectra and the IR spectral data support the conclusion that the olefinic protons occupy a *trans* position relative to each other. The ^{1}H NMR signal of the olefinic protons in **7** (δ, 6.34 and 6.91 ppm) is shifted upfield by about 0.37 ppm, as compared with that of the reference compound, 1,3-diruthenocenyl-2-propen-1-one (**13**) (δ, 6.71 and 7.29 ppm) (Fig. 1). The upfield shift of the olefinic protons in **7** should be due to the magnetic anisotropy of the other olefinic bond. Similarly, the protons of the olefinic bonds in **8**, **9**, **10**, **11**, and **12** are shifted somewhat upfield, as compared with the positions of the reference compounds, 1-ferrocenyl-3-ruthenocenyl-2-propen-1-one (**14**), 3-ferrocenyl-1-ruthenocenyl-2-propen-1-one (**15**), 1,5-diruthenocenyl-1,4-pentadien-3-one (**16**), 1-ferrocenyl-5-ruthenocenyl-1,4-

Table 1. ^{1}H NMR spectral data of phane compounds (**7**—**12**) and the reference compounds (**13**—**18**) (δ)[a]

Compound	Olefinic proton	Cp ring proton	Compound	Olefinic proton	Cp ring proton
7	6.34 (d,[c] J=16 Hz)	4.76 (t)[d]	**14**	6.91 (d, J=15 Hz)	4.17 (s)
	6.91 (d, J=16 Hz)	4.84 (t)		7.39 (d, J=15 Hz)	4.56 (s)
		5.12 (t)			4.61 (t)
		5.37 (t)			4.79 (t)
8	6.29 (d, J=16 Hz)	4.55 (t)			4.92 (t)
	6.80 (d, J=16 Hz)	4.80 (t)			5.21 (s)
		5.03 (t)	**15**	6.77 (d, J=16 Hz)	4.16 (s)
		5.10 (t)		7.44 (d, J=16 Hz(	4.51 (t)
9	6.48 (d, J=15 Hz)	4.48 (t)			4.60 (s)
	7.06 (d, J=15 Hz)	4.76 (t)			4.76 (t)
		4.80 (t)			4.89 (t)
		4.91 (t)			5.28 (t)
10	6.14 (d, J=16 Hz)	4.80 (t)	**16**	6.63 (d, J=16 Hz)	4.57 (s)
	6.73 (d, J=16 Hz)	5.04 (t)		7.39 (d, J=16 Hz)	4.77 (t)
11[f]	6.05 (d, J=16 Hz)	4.45 (t)			5.07 (t)
	6.17 (d, J=16 Hz)	4.54 (t)	**17**[f]	6.54 (d, J=16 Hz)	4.17 (s)
	7.05 (d, J=16 Hz)	4.77 (t)		6.55 (d, J=16 Hz)	4.47 (t)
	7.21 (d, J=16 Hz)	4.89 (t)		7.49 (d, J=16 Hz)	4.56 (s)
12	6.3—7.1 (m)[e]	4.44 (t)		7.59 (d, J=16 Hz)	4.73 (t)
	7.19 (d, J=15 Hz)	4.47 (t)			4.93 (t)
		4.92 (t)	**18**	6.8—7.2 (m)	4.16 (s)
		5.28 (t)		7.30 (d, J=15 Hz)	4.42 (t)
13	6.71 (d, J=16 Hz)	4.55 (s)[b]			4.58 (t)
	7.29 (d, J=16 Hz)	4.57 (s)			4.61 (s)
		4.77 (t)			4.87 (t)
		4.87 (t)			5.18 (t)
		5.13 (t)			
		5.20 (t)			

a) In DMSO-d_6 except where indicated otherwise. b) Singlet. c) Doublet. d) Triplet. e) Multiplet. f) In $CDCl_3$.

Table 2. IR spectral data of phane compounds (**7**—**12**) and the reference compounds (**13**—**18**)

Compound	$\tilde{\nu}$(-HC=CH-)/cm^{-1}	$\tilde{\nu}$(>C=O)/cm^{-1}
7	1591, 961	1651
8	1591, 959	1655
9	1592, 972	1659
10	1587, 968	1610
11	1560, 982	1655
12	1580, 960	1645
13	1586, 965	1652
14	1574, 975	1642
15	1585, 966	1649
16	1562, 978	1610
17	1575, 986	1626
18	1585, 1002	1650

pentadien-3-one (**17**), and 5-ferrocenyl-1-ruthenocenyl-2,4-pentadien-1-one (**18**), respectively (see Table 1). These upfield shifts may also be caused by the magnetic anisotropy of the other olefinic group.

The electronic spectra of phane compounds **7**, **10**, and **12** and the reference compounds **13**, **16**, and **18** in chloroform are shown in Figs. 2—4. The electronic

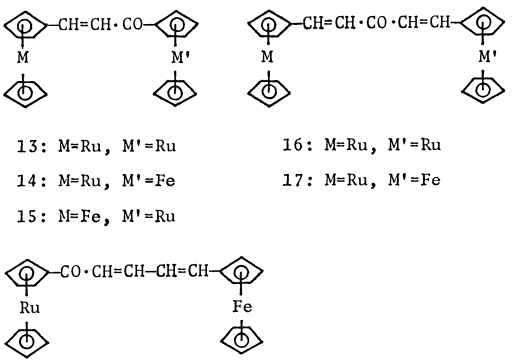

18

Fig. 1.

spectra of d^6 metallocenes have been thoroughly studied.[14] It is well known that the bathochromic and hyperchromic shifts of absorption bands of metallocenes are caused by the conjugations of the olefinic and carbonyl groups with cyclopentadienyl rings.[15] Thus, the absorption bands of **13**, **16**, and **18** in the 400 and 500 nm regions correspond to the spin-allowed d-d transitions of ruthenocene and ferrocene, respectively. The intense bands of **13**, **16**, and **18** at *ca.* 300 nm are associated with the charge transfer

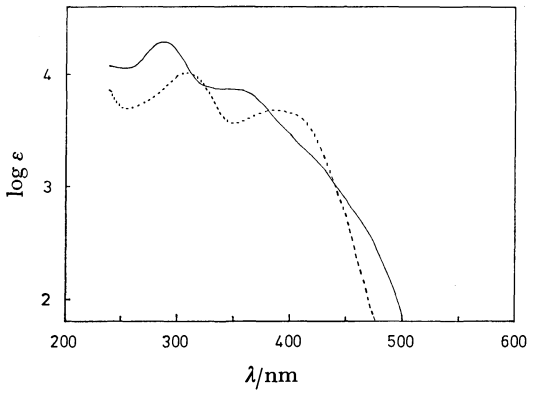

Fig. 2. The electronic spectra of phane compound **7** (——) and the reference compound **13** (----) in chloroform.

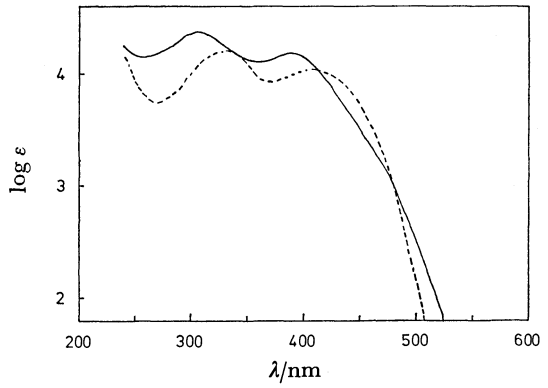

Fig. 3. The electronic spectra of phane compound **10** (——) and the reference compound **16** (----) in chloroform.

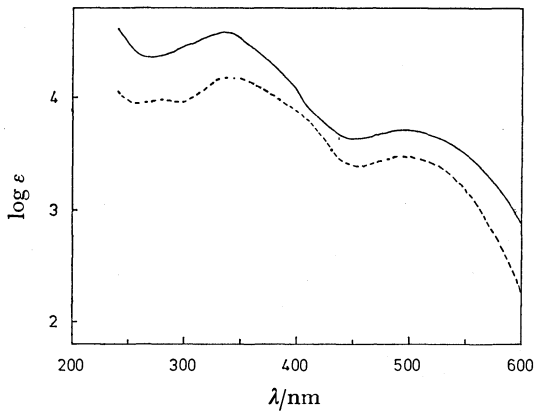

Fig. 4. The electronic spectra of phane compound **12** (——) and the reference compound **18** (----) in chloroform.

transitions between metal and ligand. The electronic spectra of **7** and **10** show new shoulder bands at longer wavelengths and the broadening of absorption curves, and the absorption bands of charge transfer and d-d transitions are located at shorter wavelengths and the intensity increases, as compared with the spectra of **13** and **16**. On the other hand, three bands of **12** are located at similar positions to the bands of **18**, and the intensity of **12** is much higher than those of **18**.

Experimental

Measurements. The ^{1}H NMR spectra were obtained with a JEOL JNM-FX 100 spectrometer (100 MHz) at 26 °C. All the chemical shifts are expressed in δ (ppm: downfield from internal Me_4Si). The IR spectra were measured in KBr pellets with a Hitachi Model 285 infrared spectrometer. The electronic spectra were recorded with a Shimadzu Double 40-R spectrophotometer at room temperature.

Materials. All the melting points are uncorrected. The following compounds were synthesized by the methods described in the literature: 1,1′-ruthenocenedicarboxylic acid,[12] 1,1′-ferrocenedicarbaldehyde (**2**),[16] 1,1′-diacetylruthenocene (**3**),[12] 1,1′-diacetylferrocene (**4**),[17] 1,1′-bis(2-acetylvinyl)ferrocene (**5**),[18] and 1,1′-bis(2-formylvinyl)ferrocene (**6**).[18]

Dimethyl 1,1′-Ruthenocenedicarboxylate. A methanol solution (120 ml) containing 1,1′-ruthenocenedicarboxylic acid (3.8 g, 11.9 mmol) and concentrated sulfuric acid (0.30 ml) was refluxed for 20 h under a nitrogen atmosphere. After the mixture was poured into water, the solution was extracted by chloroform. The chloroform extract was washed by saturated sodium hydrogencarbonate, water and brine, and then dried over anhydrous sodium sulfate. After purification by column-chromatography (silica gel–chloroform), 4.0 g (98%) of this compound was obtained; mp 165—167 °C (chloroform). ^{1}H NMR ($CDCl_3$): δ 3.74 (6H, s, $-COOCH_3$), 4.73 (4H, t, J=1.8 Hz, Rc ring protons), 5.17 ppm (4H, t, J=1.8 Hz, Rc ring protons). IR (KBr): 1709 cm^{-1} ($-COOCH_3$). MS: *m/e* 347 (M^+) and 101 (Ru^+). Found: C, 48.59; H, 4.32%. Calcd for $C_{14}H_{14}O_4Ru$: C, 48.41; H, 4.06%.

1,1′-Bis(hydroxymethyl)ruthenocene. A solution of dimethyl 1,1′-ruthenocenedicarboxylate (2.7 g, 7.78 mmol) in benzene (150 ml) was added dropwise to a mixture of lithium aluminum hydride (0.65 g) in ether (150 ml). After the solution was refluxed for 4 h under a nitrogen atmosphere, the excess lithium aluminum hydride was decomposed with a small amount of cold water. The resulting mixture was extracted with chloroform. The chloroform extract was dried over anhydrous sodium sulfate. The removal of chloroform yielded 2.2 g (98%) of this compound; mp 125—127 °C (chloroform). ^{1}H NMR ($CDCl_3$): δ 1.80 (4H, br-s, $-CH_2-$), 4.16 (2H, br-s, –OH), 4.58 (4H, t, J=1.8 Hz, Rc ring protons), and 4.71 ppm (4H, t, J=1.8 Hz, Rc ring protons). IR (KBr): 3176 cm^{-1} (–OH). MS: *m/e* 291 (M^+) and 101 (Ru^+). Found: C, 49.99; H, 4.42%. Calcd for $C_{12}H_{14}O_2Ru$: C, 49.48; H, 4.84%.

*1,1′-Ruthenocenedicarbaldehyde (**1**).* A solution of 1,1′-bis(hydroxymethyl)ruthenocene (1.5 g, 5.15 mmol) and active manganese dioxide (12 g) in chloroform (100 ml) was shaken for 24 h at room temperature. After filtration of active manganese dioxide, the removal of chloroform left 1.0 g (70%) of **1**; mp 235 °C (dec) (hexane–dichloromethane). ^{1}H NMR ($CDCl_3$): δ 4.94 (4H, t, J=1.8 Hz, Rc ring protons), 5.18 (4H, t, J=1.8 Hz, Rc ring protons), and 9.71 ppm (2H, s, –CHO). IR (KBr): 1655 cm^{-1} (–CHO). MS: *m/e* 287 (M^+) and 101 (Ru^+). Found: C, 50.44; H, 3.28%. Calcd for $C_{12}H_{10}O_2Ru$: C, 50.17; H, 3.51%.

General Procedure for an Intermolecular Base-catalyzed Condensation.

*[3.3](1,1′)Ruthenocenophane-2,14-diene-1,16-dione (**7**).* A mixture of **1** (1.0 g, 3.48 mmol), **3** (1.1 g, 3.48 mmol), and sodium (0.5 g) in ethanol (100 ml) was stirred at 60 °C for 6 h under a nitrogen atmosphere. After the crude product was filtered off, washed with water, ethanol, and

TABLE 3. ANALYSIS AND PROPERTY OF PHANE COMPOUNDS (**7**—**12**) AND THE REFERENCE COMPOUNDS (**13**—**18**)

Compound	
7	mp>300 °C (chloroform). Found: C, 55.46; H, 3.77%. Calcd for $C_{26}H_{20}O_2Ru_2$: C, 55.12; H, 3.56%. MS: *m/e* 566 (M^+) and 101 (Ru^+).
8	mp 270 °C (dec) (chloroform). Found: C, 60.14; H, 3.52%. Calcd for $C_{26}H_{20}O_2RuFe$: C, 59.90; H, 3.87%. MS: *m/e* 521 (M^+), 101 (Ru^+), and 56 (Fe^+).
9	mp 280 °C (dec) (chloroform). Found: C, 59.34; H, 3.56%. Calcd for $C_{26}H_{20}O_2RuFe$: C, 59.90; H, 3.87%. MS: *m/e* 521 (M^+), 101 (Ru^+), and 56 (Fe^+).
10	mp 287 °C (dec) (chloroform). Found: C, 58.52; H, 3.56%. Calcd for $C_{30}H_{24}O_2Ru_2$: C, 58.24; H, 3.91%. MS: *m/e* 619 (M^+) and 101 (Ru^+).
11	mp 118—120 °C (chloroform). Found: C, 62.44; H, 3.97%. Calcd for $C_{30}H_{24}O_2RuFe$: C, 62.84; H, 4.22%. MS: *m/e* 573 (M^+), 101 (Ru^+), and 56 (Fe^+).
12	mp 270 °C (dec) (chloroform). Found: C, 62.27; H, 4.86%. Calcd for $C_{30}H_{24}O_2RuFe$: C, 62.84; H, 4.22%. MS: *m/e* 577 (M^+), 101 (Ru^+), and 56 (Fe^+).
13	mp 255—258 °C (hexane-chloroform). Found: C, 53.64; H, 3.79%. Calcd for $C_{23}H_{20}ORu_2$: C, 53.69; H, 3.92%. MS: *m/e* 514 (M^+) and 101 (Ru^+).
14	mp 257—259 °C (hexane-chloroform). Found: C, 58.42; H, 4.11%. Calcd for $C_{23}H_{20}ORuFe$: C, 58.86; H, 4.30%. MS: *m/e* 469 (M^+), 101 (Ru^+), and 56 (Fe^+).
15	mp 218—220 °C (hexane-chloroform). Found: C, 58.74; H, 4.45%. Calcd for $C_{23}H_{20}ORuFe$: C, 58.86; H, 4.30%. MS: *m/e* 469 (M^+), 101 (Ru^+), and 56 (Fe^+).
16	mp 131—134 °C (chloroform-ether). Found: C, 55.84; H, 3.82%. Calcd for $C_{25}H_{22}ORu_2$: C, 55.55; H, 4.10%. MS: *m/e* 540 (M^+) and 101 (Ru^+).
17	mp 214—217 °C (chloroform). Found: C, 59.18; H, 4.13%. Calcd for $C_{25}H_{22}ORuFe$: C, 60.62; H, 4.48%. MS: *m/e* 495 (M^+), 101 (Ru^+), and 56 (Fe^+).
18	mp 195—196 °C (hexane-dichloromethane). Found: C, 60.26; H, 4.87%. Calcd for $C_{25}H_{22}ORuFe$: C, 60.62; H, 4.48%. MS: *m/e* 495 (M^+), 101 (Ru^+), and 56 (Fe^+).

ether, and then dried, 1.6 g (80%) of **7** was obtained.

*[5.5](1,1')Ruthenocenophane-2,14,17,29-tetraene-1,16-dione (**10**).* A mixture of **1** (2.0 g, 6.96 mmol), acetone (0.2 g, 3.48 mmol), and potassium hydroxide (3.5 g) in ethanol (100 ml) was heated at 60 °C for 6 h under a nitrogen atmosphere. After the crude product was filtered off, washed with water, ethanol, and ether, and then dried, 1.6 g (75%) of **10** was yielded.

The yields of phane compounds **8**, **9**, **11**, and **12** were 78, 80, 75, and 79%, respectively.

*1,3-Diruthenocenyl-2-propen-1-one (**13**).* A solution of formylruthenocene[11] (1.0 g, 3.86 mmol), acetylruthenocene[16] (1.05 g, 3.86 mmol), and sodium (0.5 g) in ethanol (50 ml) was stirred at 60 °C for 6 h under a nitrogen atmosphere. After the crude product was filtered off, washed with water, ethanol, and ether, and then dried, 1.6 g (81%) of **13** was obtained.

*1,5-Diruthenocenyl-1,4-pentadien-3-one (**16**).* A mixture of formylruthenocene[11] (1.0 g, 3.86 mmol), acetone (0.11 g, 1.93 mmol), and potassium hydroxide (1.9 g) in ethanol (50 ml) was heated at 60 °C for 6 h under a nitrogen atmosphere. After the crude product was filtered off, washed with water, ethanol, and ether, and then dried, 1.4 g (66%) of **16** was yielded.

1-Ferrocenyl-3-ruthenocenyl-2-propen-1-one (**14**) and 3-ferrocenyl-1-ruthenocenyl-2-propen-1-one (**15**) were prepared in 69 and 70% yields from formylruthenocene[11] and acetylferrocene[19] and from formylferrocene[20] and acetylruthenocene[16] under the same conditions as **13**, respectively. 1-Ferrocenyl-5-ruthenocenyl-1,4-pentadien-3-one (**17**) and 5-ferrocenyl-1-ruthenocenyl-2,4-pentadien-1-one (**18**) were prepared in 62 and 60% yields from formylruthenocene[11] and (2-acetylvinyl)ferrocene[18] and from acetylruthenocene[16] and (2-formylvinyl)ferrocene[18] under the same conditions as **16**, respectively.

References

1) R. W. Griffin, Jr., *Chem. Rev.*, **63**, 45 (1963).
2) S. Misumi, *Kagaku No Ryoiki*, **28**, 927 (1974); **32**, 651 (1978).
3) Y. Sakata, *Kagaku No Ryoiki*, **28**, 947 (1974).
4) S. Misumi and T. Otsubo, *Acc. Chem. Res.*, **11**, 251 (1978).
5) M. Rosenblum, N. M. Brawn, D. Clappenelli, and J. Tancrede, *J. Organomet. Chem.*, **24**, 469 (1970).
6) A. Kasahara and T. Izumi, *Chem. Lett.*, **1978**, 21.
7) A. Kasahara, T. Izumi, and I. Shimizu, *Chem. Lett.*, **1979**, 1119.
8) A. Kasahara, T. Izumi, and I. Shimizu, *Chem. Lett.*, **1979**, 1317.
9) A. Kasahara, T. Izumi, and H. Umezawa, *Chem. Lett.*, **1980**, 1039.
10) A. N. Nesmeyanov, G. B. Shul'pin, D. V. Zagorevskii, and M. I. Rybinskaya, *Dokl. Akad. Nauk SSSR*, **229**, 881 (1976).
11) S. Kamiyama, T. M. Suzuki, T. Kimura, and A. Kasahara, *Bull. Chem. Soc. Jpn.*, **51**, 909 (1978).
12) M. D. Rausch, E. O. Fischer, and H. Grubert, *J. Am. Chem. Soc.*, **82**, 76 (1960).
13) The nomenclature is that proposed by B. H. Smith ("Bridged Aromatic Compounds," Academic Press Inc., New York, N. Y. (1964)).
14) Y. S. Sohn, D. N. Hendrickson, and H. B. Gray, *J. Am. Chem. Soc.*, **93**, 3603 (1971).
15) M. Rosenblum, "Chemistry of the Iron Group Metallocene," Interscience Publishers, New York (1965), p. 39.
16) J. M. Osgerby and P. L. Pauson, *J. Chem. Soc.*, **1961**, 4604.
17) K. Yamakawa, H. Ochi, and K. Arakawa, *Chem. Pharm. Bull.*, **11**, 905 (1963).
18) A. Kasahara, T. Izumi, G. Saito, M. Yodono, R. Saito, and Y. Goto, *Bull. Chem. Soc. Jpn.*, **45**, 895 (1972).
19) G. D. Broadhead, J. M. Osgerby, and P. L. Pauson, *J. Chem. Soc.*, **1958**, 650.
20) M. Rosenblum, A. K. Banerjee, N. Danieli, R. W. Fish, and V. Schlatter, *J. Am. Chem. Soc.*, **85**, 316 (1963).

  Bull. Chem. Soc. Jpn., 54, 2083—2088 (1981)

Prerequisites for the Enhancement of Formose Formation in the Presence of Hydroxy Oxo Compounds

Tomoya Sakai,* Masahiko Ishizaki, Katsuaki Kobayashi, and Masafumi Goto

Department of Chemical Reaction Engineering, Faculty of Pharmaceutical Sciences, Nagoya City University, Mizuho-ku, Nagoya 467

(Received October 28, 1980)

The enhancement of formose formation in the presence of several hydroxy oxo compounds was examined in an aqueous $Ca(OH)_2$ solution. Four terminal hydroxy oxo compounds, 2-hydroxyacetophenone, 1,3-dihydroxyacetone, DL-glyceraldehyde, and D-glucose, were confirmed to accelerate the reaction, but two internal hydroxy oxo compounds, 2-hydroxypropiophenone and acetoin, were found not to be effective. The acceleration efficiency was larger for a system in which hydroxy oxo compounds were introduced to an aqueous mixture of $Ca(OH)_2$ and formaldehyde than for a system in which formaldehyde was introduced to an aqueous mixture of $Ca(OH)_2$ and the hydroxy oxo compounds. The difference in the acceleration efficiencies between the two procedures of reagent introduction was large for 2-hydroxyacetophenone and 1,3-dihydroxyacetone. This is accounted for by the rapid conversions of the added hydroxy oxo compounds in an aqueous $Ca(OH)_2$ solution.

The typical formose formation in the absence of accelerators takes place in an aqueous mixture of $Ca(OH)_2$ and formaldehyde(C_{1A}) at about 50 °C. The initial heterogenous suspension of $Ca(OH)_2$ turns into a homogeneous solution as the reaction proceeds. The consumption rate of C_{1A} for the formose formation shows a characteristic feature of an auto-catalysis, accompanied by a long induction period. After the maximum rate of C_{1A} consumption, the reaction mixture is tinged with pale yellow. At this "yellowing point," the yield of formose sugars reaches its maximum; after that the dehydration of sugars proceeds gradually. The main products at the "yellowing point" have been reported to be C_2—C_8 sugars centering around C_6, including reducing sugars and sugar alcohols.[1] The reaction scheme proposed by Mizuno and Weiss[1] is summarized in a series of reactions: (1) the slow dimerization of C_{1A} to glyceraldehyde (C_{2A}), (2) the rapid aldol addition of C_{1A} to C_{2A} and higher carbohydrates, (3) Lobry de Bruyn-Alberda van Ekenstein(L·V) transformation, and (4) Cannizzaro and cross-Cannizzaro reactions among the products and C_{1A}.

The presence of such hydroxy oxo compounds as C_{2A} and D-glucose (Glu) in the reaction system has been known to shorten or to eliminate the induction period and to cause the reaction to proceed rapidly through C–C chain growth. Most of the hydroxy oxo compounds so far examined have the terminal 1-hydroxy-2-oxo structure: the order of the acceleration efficiency has been reported by Kusin[2] as D-fructose (Fru) > Glu > maltose; by Langenbeck,[3] as 1,3-dihydroxyacetone (C_{3K}) > C_{2A} > Fru, and by Langenbeck[4] and Monozov and Lavanevskii,[5] as will be described in a later section.

This study deals with the efficiencies of seven hydroxy oxo compounds, 2-hydroxyacetophenone (HAP), C_{3K}, DL-glyceraldehyde (C_{3A}), Glu, 2-hydroxypropiophenone (HPP), and acetoin, as accelerators of the formose formation. Among them, C_{3A} and C_{3K} represent the initial products of the typical formose formation. Glu was used because the major products at the "yellowing point" are hexoses. One of the most efficient accelerators, HAP, is unique because it is not involved in the typical formose formation. HPP and acetoin have the internal hydroxy oxo structure and are employed to examine whether or not these compounds show the acceleration effect.

The accelerators with terminal 1-hydroxy-2-oxo structure all shared large acceleration efficiencies with regard to the formose formation. It was also noted that the procedure of reagent introduction, *i.e.*, either the reaction was started with the introduction of accelerators into an aqueous mixture of $Ca(OH)_2$ and C_{1A} or it was started with the introduction of C_{1A} into an aqueous mixture of $Ca(OH)_2$ and hydrox oxo compounds, affected the efficiency of each accelerator. The phenomenon was attributed to the rapid transformation of the hydroxy oxo compounds in an aqueous $Ca(OH)_2$ solution in the absence of C_{1A}.

Experimental

Materials. A commercially available 37% C_{1A} solution (Wako) was used for the C_{1A} stock solution without further purification. This contained 3 to 4% methanol as a stabilizer. Commercially available guaranteed-reagent-grade calcium hydroxide (Katayama), C_{3K} (Wako), and C_{3A} (Tokyo Kasei) were used without further treatment. The C_{3K} and C_{3A} are dimers, but these have been known to dissociate to the respective monomers immediately in an aqueous $Ca(OH)_2$ solution.[6]

HAP was prepared according to the method of Cebrian:[7] mp 76—78 °C (lit, 75—76 °C). HPP was prepared according to the method of Temnikowa;[8] the material thus obtained was found by GLC measurements to contain an isomer, 1-hydroxy-1-phenyl-acetone, in a 27% amount, but it was used without further purification: bp 115—120 °C/12 Torr (lit,[8] for HPP 123—124 °C/13 Torr) (1 Torr= 133.322 Pa).

Product Analysis. The products of formose formation have been reported to consist of formose sugars, including reducing sugars, sugar alcohols, and formic acid, produced by the side Cannizzaro reaction.[1] The amounts of remaining C_{1A} and formic acid were measured on a Kyowa K-880 high-performance liquid (HPL) chromatograph, using a column of Shodex Ionpak C-811 and an aqueous eluent of 0.1% phosphoric acid under a pressure of 50 bar at room temperature, and with an UV monitor (Kyowa KUV-254)

at 254 nm and a refractive index monitor (Shodex RISE-11) connected in series. The accuracy of the quantitative measurement of C_{1A} was confirmed to be in agreement with the photometric method with chromotropic acid[9] within a 2—3% error. Higher formose sugars, such as C_5 and C_6, were not fully separated in this HPL chromatogram, though.

The spectral change between 210—300 nm of an aqueous HAP and $Ca(OH)_2$ solution was recorded at 5-min interval with a Shimadzu UV-210A spectrophotometer with a Shimadzu WP-1 wavelength programmer and an X-Y recorder (Rika Denki) attached. The amounts of HPP and its isomer were measured with a postulation of equal molar sensitivities for the two isomers on an Ohkura Model 802 gas-liquid chromatograph, with FID by means of a silicone grease (SE-30) column at 150 °C.

Formose-formation Procedures. In a three-necked, round-bottomed flask, either an aqueous or a 40% methanol aqueous solution of $Ca(OH)_2$ was placed and thermostated at 35—50 °C. The reaction was initiated with two different procedures. In the normal procedure, first a thermostated C_{1A} solution was mixed with the $Ca(OH)_2$ solution; then after 1 or 3 min, a reaction was initiated by the introduction of a thermostated aqueous accelerator solution. In the reverse procedure, first, a thermostated aqueous accelerator solution was mixed with the $Ca(OH)_2$ solution; then, after 1 or 3 min, a reaction was initiated with the introduction of a thermostated C_{1A} solution. The reaction mixture was stirred magnetically and thermostated in a water bath. Aliquots of the reaction mixture were pipetted out at appropriate time intervals and were then dissolved in a dilute hydrochloric acid to quench the reaction (litmus). The amounts of remaining C_{1A} and formic acid were determined with the HPL chromatograph. The conversion of C_{1A} to formose was calculated by Eq. 1, where the formation of formic acid was assumed to be caused through the cross-Cannizzaro reaction between C_{1A} and aldoses.

$$C_{1A} \text{ conversion to formose} = 1 - \frac{[C_{1A}]_{remained} - [HCOOH]}{[C_{1A}]_{initial}} \quad (1)$$

Deactivation of Accelerators. An aqueous solution of an accelerator was added to a $Ca(OH)_2$ solution in the absence of C_{1A}. At appropriate time intervals, aliquots of the reaction mixture were pipetted out and examined by means of an HPL chromatograph after acid treatment.

Results and Discussion

Essential Structure for Acceleration. C_{1A} consumption in a typical formose formation in the absence of accelerators is shown in Fig. 1. This shows the autocatalytic nature of the formose formation. The change in the HPL chromatogram with reaction periods is illustrated in Fig. 2. The arrow indicates the retention time of each authentic sample, measured separately under the same conditions of HPL chromatography. C_{4A} and C_{5A} denote D-erythrose and D-arabinose respectively. The final chart at 60 min shows product peaks distributing between C_{5A} and Glu, suggesting that they are mostly aldo- and ketohexoses including sugar alcohols, in accordance with the literature.[1] Figure 3 shows a change in the HPL chromatogram in the presence of an accelerator, C_{3A} (0.01 mmol cm^{-3}), with the normal procedure. The products of formose formation gave similar HPL chromatograms irrespective of the introduction of a small amount of C_{3A} (compare Figs. 2 and 3), although the consumption of C_{1A} was rapid for the reaction with added C_{3A}. The reaction shown in Fig. 3 was carried out in an aqueous solution.

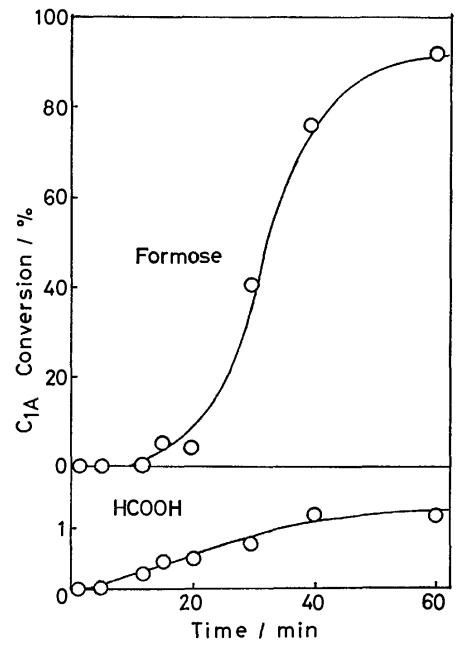

Fig. 1. Autocatalytic nature of formose formation in the absence of accelerators.
50 °C, 20 vol% methanol–H_2O, $Ca(OH)_2$: 0.10 mmol cm^{-3}, C_{1A}: 2.45 mmol cm^{-3}.

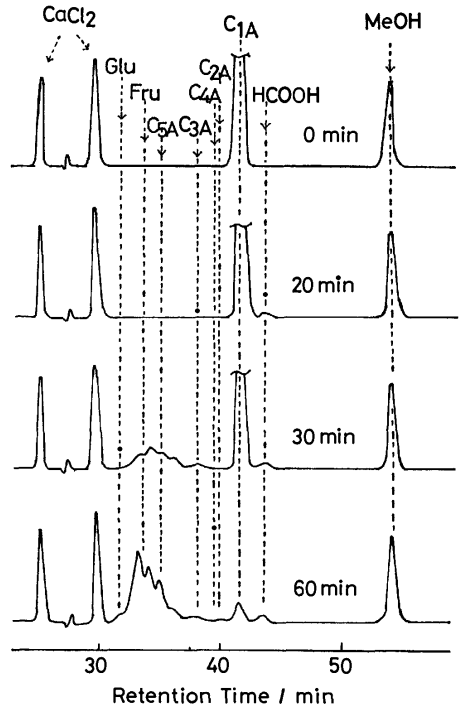

Fig. 2. Change in HPL chromatogram with reaction period in the absence of accelerators.
50 °C, 20 vol% methanol–H_2O, $Ca(OH)_2$: 0.10 mmol cm^{-3}, C_{1A}: 2.45 mmol cm^{-3}.

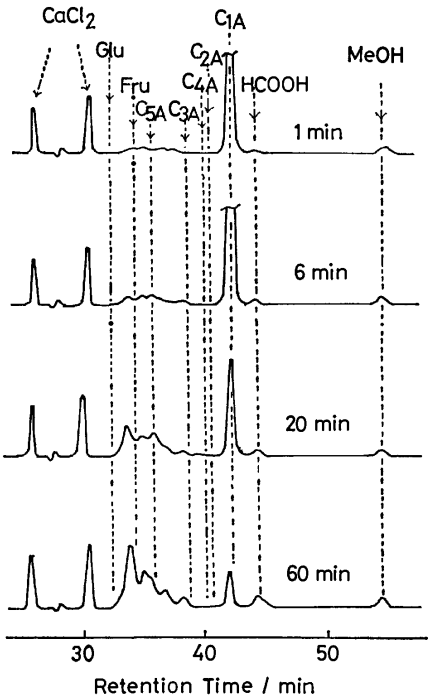

Fig. 3. Change in HPL chromatorgam with reaction period in the presence of C_{3A}.
50 °C, H_2O, $Ca(OH)_2$: 0.10 mmol cm^{-3}, C_{1A}: 2.45 mmol cm^{-3}, C_{3A}: 0.01 mmol cm^{-3}.

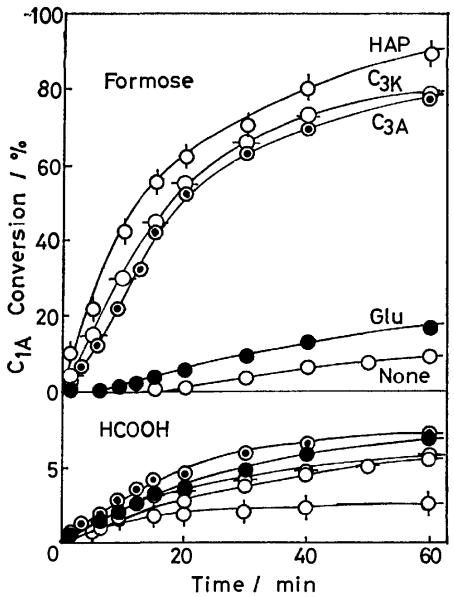

Fig. 4. Acceleration efficiencies of HAP, C_{3K}, C_{3A}, and Glu.
50 °C, H_2O, $Ca(OH)_2$: 0.10 mmol cm^{-3}, C_{1A}: 2.45 mmol cm^{-3}, accelerator: 0.01 mmol cm^{-3}.

The efficiencies of the acceleration of various hydroxy oxo compounds, HAP, C_{3K}, C_{3A}, or Glu, are compared in Fig. 4 with the normal procedure. The concentration of each accelerator is 0.01 mmol cm^{-3}, while that of C_{1A} is 2.45 mmol cm^{-3}. The conversion of C_{1A} amounted to 80% at 60 min for HAP, C_{3K}, and C_{3A}, so that the molar amounts of the converted C_{1A} are more than 200 times those of the introduced accelerators. A comparison of the results shown in Fig. 4 with those in Fig. 1 suggests that the steep rising of the conversion of C_{1A} in the middle and the leveling off in the later stage of the reaction periods in Fig. 1 correspond to the rapid C_{1A} additions to lower carbohydrates, such as C_{3A} and C_{3K}, and to the slow C_{1A} additions to higher carbohydrates, such as Glu, respectively, based on the different acceleration efficiencies of the compounds shown in Fig. 4.

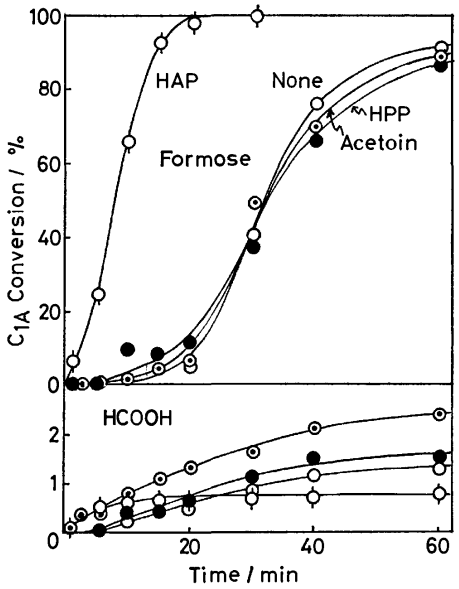

Fig. 5. Non-effectiveness of internal hydroxy oxo compounds, HPP and acetoin, as accelerator.
50 °C, 20 vol% methanol–H_2O, $Ca(OH)_2$: 0.10 mmol cm^{-3}, C_{1A}: 2.45 mmol cm^{-3}, accelerator: 0.01 mmol cm^{-3}.

HAP is a unique compound in that it belongs to the most effective class of accelerators for the formose formation and in that it is not formed in a typical formose reaction. Langenbeck[4] has reported that the efficiency of the acceleration of hydroxy oxo compounds decreases in the following order; HAP > 2-hydroxyacetonaphthone > 1-hydroxy-2-propanone > C_{3K} > C_{2A} > 5-(2-hydroxyacetyl)acenaphthene > Fru > Glu. Further, Monozov and Levanevskii[5] have reported that the efficiencies of HAP derivatives follow a Hammett-type LFER; *i.e.*, 2′,5′-dichloro-HAP>4′-chloro-HAP=3′-chloro-HAP>HAP>4′-methyl-HAP>4′-methoxy-HAP. These compounds have, without exception, terminal 1-hydroxy-2-oxo structure. The accelerations by internal hydroxy oxo compounds deserve to be examined. Langenbeck[3] reported the acceleration efficiencies of benzoin, anisoin, and acetoin to be smaller than that of Glu. The present results with HPP and acetoin as internal hydroxy oxo compounds are shown in Fig. 5. A mixture of methanol and water (2:8 in volume) was employed in this case because of the poor solubility of these substances in water. It is concluded that internal hydroxy oxo compounds have no acceleration efficiency.

Influence of the Procedures of Reagent Introduction. The procedures of the reagent introduction for starting

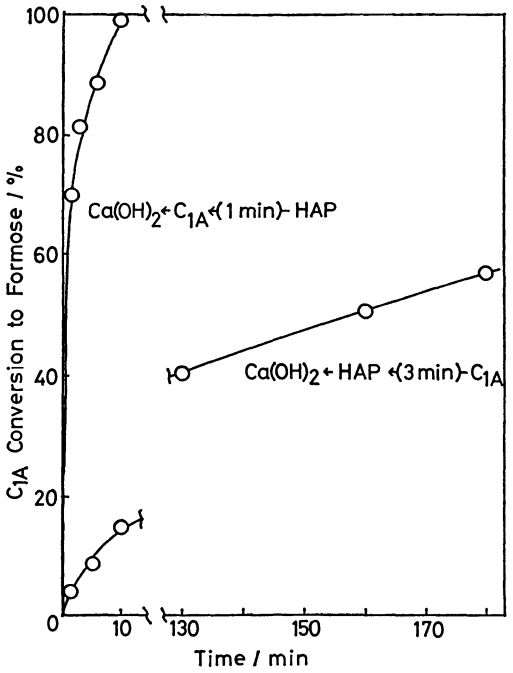

Fig. 6. Difference in acceleration efficiency of HAP with normal or reverse procedure.
35 °C, 40 vol% methanol–H_2O, $Ca(OH)_2$: 0.10 mmol cm^{-3}, C_{1A}: 1.0 mmol cm^{-3}, HAP: 0.20 mmol cm^{-3}.

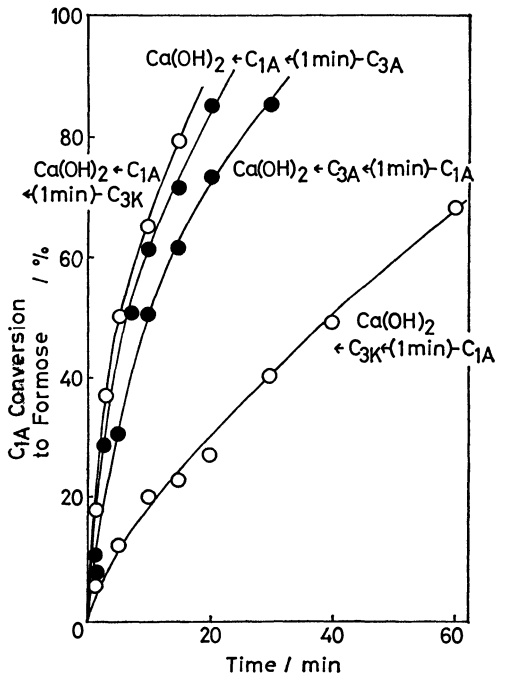

Fig. 7. Differences in acceleration efficiencies of C_{3K} and C_{3A} with normal or reverse procedure.
35 °C, H_2O, $Ca(OH)_2$: 0.10 mmol cm^{-3}, C_{1A}: 0.98 mmol cm^{-3}, C_{3A}: 0.20 mmol cm^{-3}, C_{3K}: 0.20 mmol cm^{-3}.

formose formation greatly influenced the efficiency of acceleration, whether by the normal procedure, $Ca(OH)_2$←C_{1A}←accelerator, or by the reverse procedure, $Ca(OH)_2$←accelerator←C_{1A}. A large difference in the acceleration efficiencies was observed for

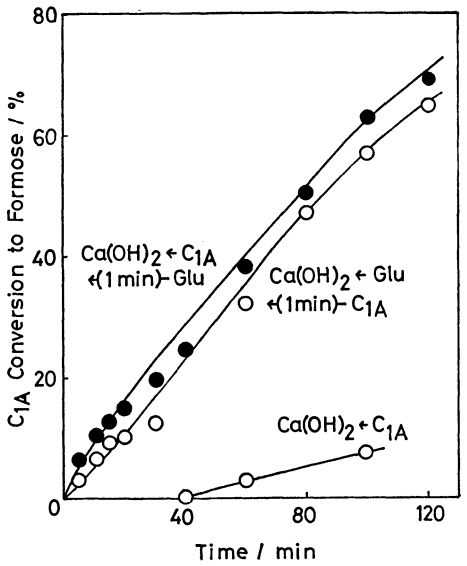

Fig. 8. Difference in acceleration efficiency of Glu with normal or reverse procedure.
35 °C, 40 vol% methanol–H_2O, $Ca(OH)_2$: 0.10 mmol cm^{-3}, C_{1A}: 1.0 mmol cm^{-3}, Glu: 0.20 mmol cm^{-3}.

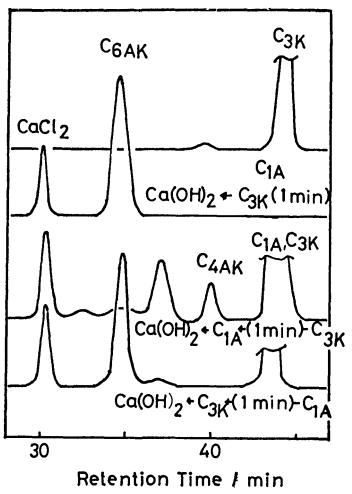

Fig. 9. HPL chromatographic change of C_{3K} by mixing with $Ca(OH)_2$ and C_{1A} in different procedures.
35 °C, H_2O, $Ca(OH)_2$: 0.10 mmol cm^{-3}, C_{3A}: 0.20 mmol cm^{-3}, C_{1A}: 1.0 mmol cm^{-3}.

HAP, as is shown in Fig. 6. The results for C_{3A} and C_{3K} are shown in Fig. 7. The difference is larger for C_{3K} than for C_{3A}. The difference for Glu was small, as shown in Fig. 8.

To investigate the difference in the acceleration efficiencies between the two procedures, the HPL chromatographic change of the accelerator with a duration time of 1 min was examined for the case of C_{3K} in Fig. 9. The chromatogram of the mixture of C_{3K} and $Ca(OH)_2$ solution, 1 min after the mixing, showed a complete consumption of C_{3K} and the formation of C_6 sugars (C_{6AK}) containing DL-dendroketose, Fru, and D-sorbose.[10] A chromatogram obtained with the normal procedure (a C_{3K} solution was mixed 1 min

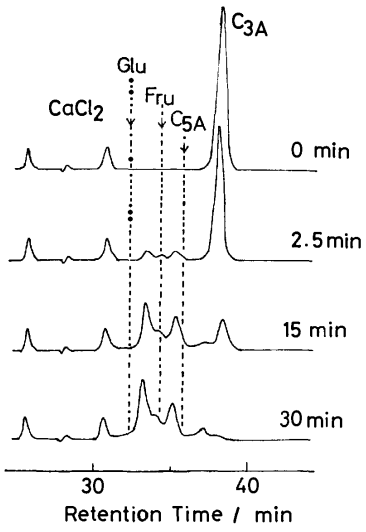

Fig.10. HPL chromatographic change of C_{3A} in an aqueous $Ca(OH)_2$ solution.
20 °C, H_2O, $Ca(OH)_2$: 0.05 mmol cm^{-3}, C_{3A}: 0.20 mmol cm^{-3}.

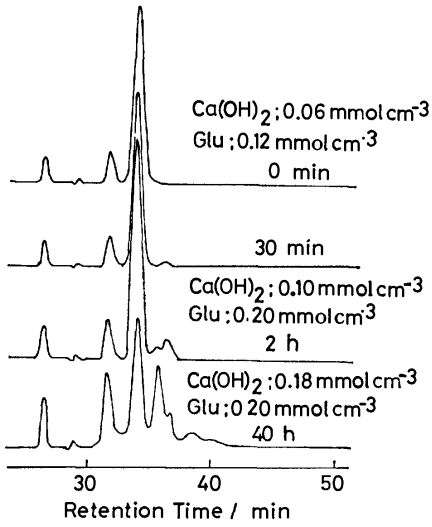

Fig.11. HPL chromatographic change of Glu in an aqueous $Ca(OH)_2$ solution.
18—20 °C, H_2O.

after the preparation of an aqueous mixture of C_{1A} and $Ca(OH)_2$) exhibited few dimerization products, but a peak corresponding to C_{4A} (D-erythrose), presumably a mixture of tetroses (C_{4AK}), appeared. On the other hand, the chromatogram of the reaction mixture with the reverse procedure (a C_{1A} solution was mixed 1 min after the preparation of an aqueous mixture of C_{3K} and $Ca(OH)_2$) showed that C_{3K} had already been converted to dimerization products and that no tetrose peak had appeared. Thus, the high efficiency of C_{3K} with a normal procedure, as is shown in Fig. 7, corresponds to the process which involves C_{1A} addition to C_{3K}, where the dimerization of C_{3K} is excluded. With the reverse procedure, however, the dimerization takes place prior to the addition of C_{1A} to C_{3K} and the weak acceleration efficiencies of such dimerization products, like that of Glu, govern

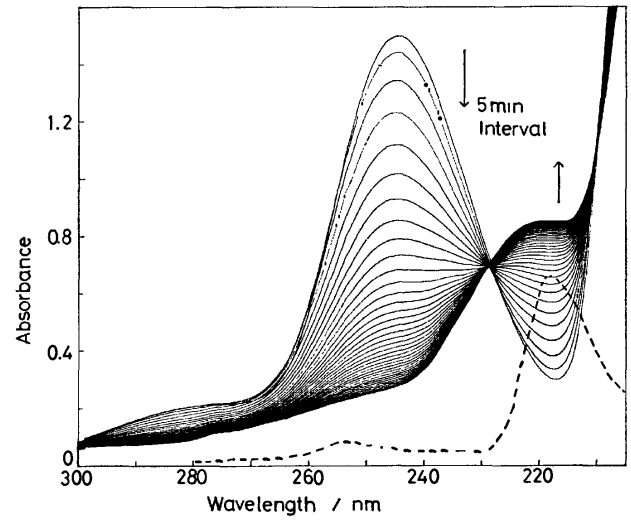

Fig. 12. UV spectral change of HAP in an aqueous $Ca(OH)_2$ solution.
25 °C, H_2O, $Ca(OH)_2$: 2.0×10^{-3} mmol cm^{-3}, HAP: 1.3×10^{-4} mmol cm^{-3}.

the formose formation. For C_{3A}, the dimerization in the presence of $Ca(OH)_2$ is slower than for C_{3K}, as is shown in Fig. 10. The difference with different procedures for reagent introduction is not significant for this accelerator, as is shown in Fig. 7. The dimerization of either C_{3A} or C_{3K} has been reported by Gutche *et al.*[10] and Berl and Feazel.[11] Glu changed little in a $Ca(OH)_2$ solution, as is shown in Fig. 11; consequently, no apparent difference between the two procedures was observed.

The significant difference observed for HAP with the procedure of reagent introduction *cf.* Fig. 6 is not fully understood. A spectral change in the ultraviolet spectrum of HAP in an aqueous $Ca(OH)_2$ solution (shown in Fig. 12) exhibits a decrease in absorbance at the absorption maximum, 246 nm, and an increase in the region of wavelength shorter than the isosbestic point at 227 nm. This suggests a loss of absorption due to the carbonyl group conjugated with the phenyl group of HAP by the reaction below. However, the HPL chromatographic separation of these compounds was not attained.

This postulation is in agreement with the facts that no significant absorption appears around 246 nm for phenylethylene glycol, as is shown by the broken curve in Fig. 12, and that 2-hydroxybutyrophenone forms an equilibrium mixture with 1-hydroxy-1-phenyl-2-butanone in the presence of OH^-.[12] The addition of one molecule of C_{1A} to the isomerized product of HAP, *i.e.*, 2-hydroxy-2-phenylacetaldehyde (HPA), would yield 2-phenylglyceraldehyde, which has saturated α-carbon next to carbonyl group, and thus is not susceptible to the addition of further C_{1A}. Although HPA has not yet been isolated from the reaction mixture with HAP, the isomerization of HAP in a $Ca(OH)_2$ solution is a plausible reason why the

large difference was observed between the different procedures of HAP introduction.

On the Mechanism of Formose Reaction. The finding of the present study, that the acceleration does not originate from the internal hydroxy oxo structure, but from the terminal hydroxy oxo structure of the accelerator, indicates that the C–C chain growth in formose formation is attained by successive additions of C_{1A} to the α-carbon to the carbonyl group, accompanied by the successive L-V transformation of the carbonyl group to the terminal position. The internal hydroxy oxo compound exhausts the hydrogen attached to α-carbon by the addition of one molecule of C_{1A} and then terminates, provided that there is no cleavage of the C–C bond of the accelerator during the reaction. Another finding, that the procedures of reagent introduction considerably influence the efficiencies of the accelerators, also suggests the aldol addition mechanism for the C–C chain growth of formose formation, because the acceleration by the hydroxy oxo compound occurs through the reaction between the hydroxy oxo compound and C_{1A}, as is shown in Fig. 9 for C_{3K}.

Moreover, the findings, that the acceleration efficiencies of Glu and Fru are small compared with those of C_{3A} and C_{3K}[4] and that the molar amounts of the consumption of C_{1A} are more than 200 times those of the introduced accelerators, as is shown in Fig. 4, suggest a degradation by a retro aldol reaction in order to account for the high activity being retained throughout the reaction until most of the C_{1A} is consumed.

References

1) T. Mizuno and A. H. Weiss, *Adv. Carbohydr. Chem. Biochem.*, **29**, 173 (1974).
2) A. Kusin, *Chem. Ber.*, **68**, 619, 1494 (1935).
3) W. Langenbeck, *Naturwissenschaften*, **30**, 30 (1942); *Chem. Abstr.*, **37**, 3733 (1943).
4) W. Langenbeck, *Angew. Chem.*, **61**, 186 (1949).
5) A. A. Monozov and O. E. Levanevskii, *Kinet. Katal.*, **19** (3), 580 (1978).
6) R. P. Bell and E. C. Baughan, *J. Chem. Soc.*, **III**, 1947 (1937).
7) G. R. Cebrián, *Anales Real Soc. Espan. Fis. y Quim., Ser. B.*, **44**, 587 (1948); *Chem. Abstr.*, **42**, 8176 (1948).
8) T. I. Temnikova, *J. Gen. Chem. USSR*, **10**, 468 (1940); *Chem. Abstr.*, **34**, 7876 (1940).
9) AD S. Olansky and S. N. Deming, *Anal. Chim. Acta*, **83**, 241 (1976).
10) C. D. Gutche, D. Redmore, R. S. Buriks, K. Nowothy, H. Grassner, and C. D. Armbruster, *J. Am. Chem. Soc.*, **89**, 1235 (1967).
11) W. G. Berl and C. E. Feazel, *J. Am. Chem. Soc.*, **73**, 2054 (1951).
12) T. I. Temnikova and E. F. Afanas'eva, *J. Gen. Chem. USSR*, **11**, 70 (1941); *Chem. Abstr.*, **35**, 6580 (1941).

  Bull. Chem. Soc. Jpn., 54, 2089—2092 (1981)

Applications of Homogeneous Water-gas Shift Reaction. III. A Further Study of the Hydrocarbonylation. A Highly Selective Formation of Diethyl Ketone from Ethene, CO, and H_2O

Kazuhisa MURATA* and Akio MATSUDA

National Chemical Laboratory for Industry, Tsukuba Research Center, Yatabe, Tsukuba, Ibaraki 305

(Received November 12, 1980)

The hydrocarbonylation of ethene with CO and H_2O produces diethyl ketone with a high selectivity of 99±1%(propanal 1±1%); a $Co_2(CO)_8$–phosphine system is used as an efficient catalyst, which is also active for the homogeneous water-gas shift reaction. The effects of the reaction parameters(CO pressure, temperature, and ethene and H_2O concentrations) on the selectivity and activity are examined for the $Co_2(CO)_8$–1,2-bis(diphenylphosphino)ethane (diphos) system; the selectivity to yield the ketone is fairly high under the variety of conditions studied here. Evidence suggests that the active species which catalyze the water-gas shift reaction participate in the hydrocarbonylation of ethene.

Diethyl ketone(3-pentanone) is produced under normal oxo conditions using a transition-metal catalyst;[1] it was previously reported that a maximum molar ratio of the ketone to propanal up to *ca.* 3 was achieved using $Co_2(CO)_8$ as the catalyst.[2,3]

In preceding papers[4,5] we described the hydrocarbonylation of propene with CO and H_2O, using a $Co_2(CO)_8$-phosphine catalyst system, to yield a mixture of dipropyl ketones(4-heptanone+2-methyl-3-hexanone+2,4-dimethyl-3-pentanone) as primary products.[6] Therefore, the hydrocarbonylation of ethene has become of great interest to us, because a selective and efficient industrial route to obtain diethyl ketone may be realized.

In the present study, optimum conditions are explored for the ketone formation and the catalytic behavior of hydrocarbonylation is discussed further.

Experimental

Materials. The ethene (Research Grade), phosphine, dioxane, and acetone were obtained commercially and used without further purification.

Reaction Procedure. The hydrocarbonylation reactions were carried out in a 100-ml stainless-steel autoclave in which $Co_2(CO)_8$, phosphine, H_2O, and solvent had been placed. The vessel was sealed and degassed by three 10 kg/cm² pressurization/depressurization cycles with CO. Into the vessel both ethene and CO were introduced. The vessel was heated with stirring to a definite reaction temperature for a certain reaction period and then cooled down to room temperature.

Analytical Methods. The liquid products were analyzed at 100 °C by means of a gas chromatograph equipped with FID using a 6-m column packed with polyethylene glycol adipate. The infrared and ^{1}H-NMR spectra of the catalyst solutions were recorded on a Hitachi type 215 spectrometer and a Hitachi type R-40 spectrometer respectively.

Results and Discussion

Time Course of Diethyl Ketone Formation. A typical example of the reaction is shown in Fig. 1, where the molar ratio ethene/$Co_2(CO)_8$ of 150/2 was used. At 165 °C, the selectivity of the ketone was as high as 97±1% (propanal 3±1%, 32:1 ratio). An induction period of about 1 h preceded the onset of catalysis; this is roughly the same as that observed in the formation of dipropyl ketones.[4]

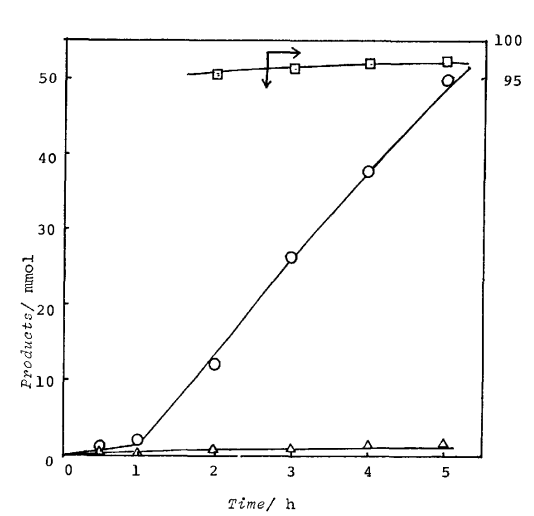

Fig. 1. Cobalt-catalyzed hydrocarbonylation as a function of time.
$Co_2(CO)_8$ 2 mmol, diphos 2 mmol, dioxane 50 ml, H_2O 60 mmol, CO 70 kg/cm²(const.), temp. 165 °C, ethene 150 mmol.
—○— Diethyl ketone, —△— propanal, —□— selectivity; [diethyl ketone]$_t$/([diethyl ketone]$_t$+[propanal]$_t$), t: time.

No trace of propanoic acid was detected under the conditions described here. Moreover, neither the hydrogenation of propanal to 1-propanol[7] nor aldol condensation occurred, partly because the amount of propanal formed was too small.

The extremely high selectivity suggests that the cobalt-catalyzed hydrocarbonylation of ethene may have some industrial importance. Thus, the optimum conditions were explored in detail in the hope of developing a feasible industrial process.

Effect of Reaction Parameters. Table 1 shows the effect of the phosphorus ligand on the selectivity(S) and activity(r^{max}). The S value was slightly affected by both the phosphine structure(Runs 1—6) and the ratio of diphos to $Co_2(CO)_8$(Runs 7—10), although excess amounts of diphos decreased the S value (Run 7). The use of an equimolar amount of H_2 (60 mmol) instead of H_2O drastically decreased the S value (Run 12). The use of MeOH (60 mmol) resulted in a

decrease in the activity r^{max} (Run 13).

The selectivity and activity were examined as a function of the ethene([C_2']) and H_2O([H_2O]) concentration as well as of the CO pressure (Table 2). The S value slightly increased with the increase in ethene from 75 to 190 mmol. The r^{max} value increased with the initial increase in [C_2'], but reached a maximum at *ca.* 150 mmol and decreased thereafter (Runs 1—4). The S value slightly increased with the increase in CO pressure(P_{CO}), while r^{max} reached a maximum at *ca.* 100 kg/cm² of P_{CO}. Excess water reduced the S value (Run 9). The S value decreased with the increase in reaction temperature, but it was still high at 180 °C (Fig. 2). The use of acetone as a solvent resulted in a decrease in the activity, especially at 135 °C.

Thus, the selectivity to diethyl ketone is fairly high under the variety of conditions studied here. However, the mode of the influence of these parameters on the activity r^{max} is similar to that observed in the case of propene.[4]

Table 1. Hydrocarbonylation of ethene using CO-H_2O catalyzed by $Co_2(CO)_8$-phosphine system
$Co_2(CO)_8$: 2 mmol, phosphine: 1.5 mmol, dioxane: 50 ml, ethene: 150 mmol, H_2O: 60 mmol, CO: 70 kg/cm² (initial), temp: 180 °C (Runs 1—6), 165 °C (Runs 7—13).

Run No.	Added phosphine	Rate[a] r_k^{max} / mmol h⁻¹	Rate[a] r_a^{max} / mmol h⁻¹	S[b] (—)
1	$Ph_2PCH_2PPh_2$	14.9	0.29	98.1
2	$Ph_2P(CH_2)_2PPh_2$	22.9	0.55	97.6
3	$Ph_2PC{\equiv}CPPh_2$	13.0	0.61	95.5
4	$Ph_2P(CH_2)_3PPh_2$	21.6	0.3	98.6
5	$Ph_2As(CH_2)_2PPh_2$	4.6	0.26	94.6
6	PPh_3	16.4	0.17	99.0
7	$Ph_2P(CH_2)_2PPh_2$ (2.5 mmol)	6.0	1.4	81.1
8	$Ph_2P(CH_2)_2PPh_2$ (2.0 mmol)	12.4	0.44	96.6
9	$Ph_2P(CH_2)_2PPh_2$ (1.5 mmol)	13.2	0.13	99.0
10	$Ph_2P(CH_2)_2PPh_2$ (1.0 mmol)	7.5	0.21	97.3
11	None	2.2	1.2	64.7[c]
12[d]	$Ph_2P(CH_2)_2PPh_2$ (2.0 mmol)	12.8	15.5	45.2
13[e]	$Ph_2P(CH_2)_2PPh_2$ (2.0 mmol)	1.2	—	—

a) r^{max}: the slope of the linear portion of the maximum rate region (see Fig. 1). The suffix 'k': diethyl ketone, 'a': propanal. b) $S=\frac{r_k}{r_k^{max}+r_a^{max}}$. c) The decomposition of $Co_2(CO)_8$ occurs.[4] d) H_2: 60 mmol, CO: 90 kg/cm² (initial). e) CH_3OH: 60 mmol, CO: 50 kg/cm² (initial), ethene: 185 mmol.

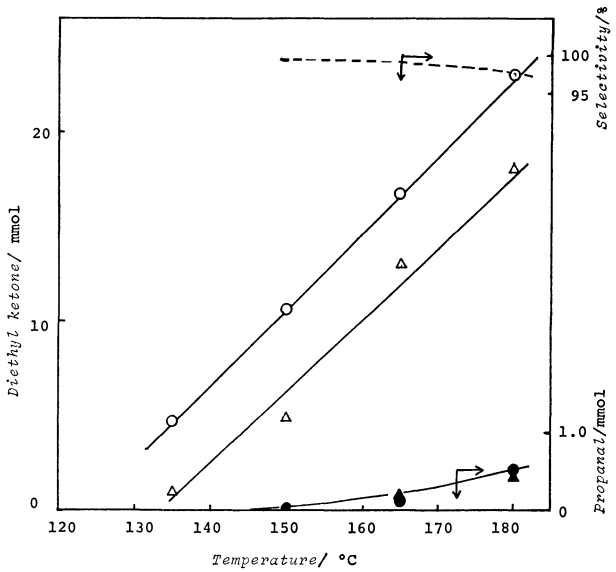

Fig. 2. Effect of temperature.
$Co_2(CO)_8$ 2 mmol, diphos 1.5 mmol, H_2O 60 mmol, dioxane 50 ml, CO 80 kg/cm² (initial), ethene 150 mmol.
Dioxane solution; —○— [r_k^{max}], —●— [r_a^{max}].
Acetone solution; —△— [r_k^{max}], —▲— [r_a^{max}].
---- Selectivity [S].
Notations: See footnote of Table 1.

Table 2. Effect of reaction parameters
$Co_2(CO)_8$: 2 mmol, diphos: 2 mmol, dioxane: 50 ml, temp: 165 °C.

Run No.	[Ethene] / mmol	P_{CO}[a] / kg cm⁻²	[H_2O] / mmol	Rate[b] r_k^{max} / mmol h⁻¹	Rate[b] r_a^{max} / mmol h⁻¹	S (—)
1	74	70	60	12.0	0.5	96.0
2	111	70	60	12.5	0.17	98.6
3	150	70	60	13.2	0.13	99.0
4	185	70	60	12.5	0.06	99.5
5	150	50	60	7.6	0.07	99.1
6	150	90	60	19.6	0.13	99.3
7	150	120	60	17.3	0.09	99.5
8	150	70	120	11.4	0.1	99.0
9	150	70	180	13.6	0.28	97.9

a) Initial pressure. b) See footnote of Table 1.

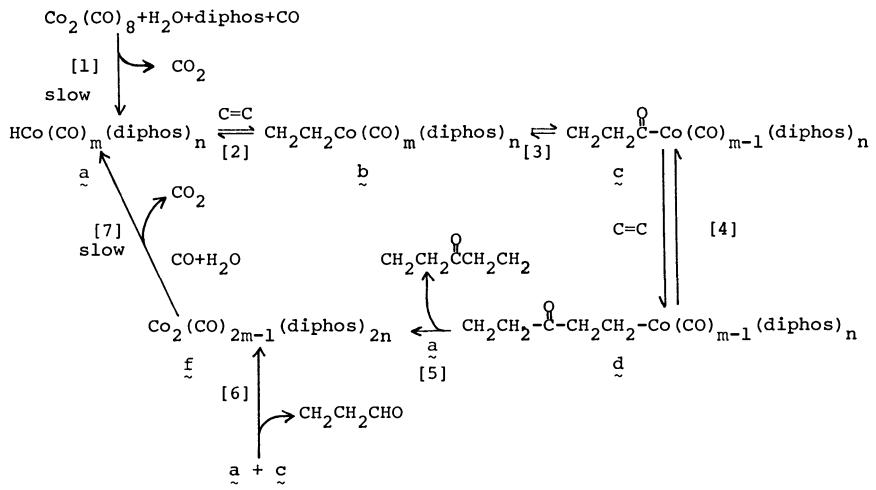

Scheme 1. A possible reaction scheme of the hydrocarbonylation of ethene with CO and H_2O.

The Nature of Catalytically Active Species. The active species responsible for the hydrocarbonylation of ethene may be assumed to be $HCo(CO)_m(diphos)_n$, as in the case of propene.[4,8] In fact, an induction period of *ca.* 1 h was also observed for the diethyl ketone formation (Fig. 1) and the catalytic behavior was generally similar (Tables 1 and 2 and Fig. 2).

A catalyst solution[8] consisting of $Co_2(CO)_8$, diphos, H_2O, and dioxane, which is active in the water-gas shift reaction, has a characteristic ^{1}H-NMR resonance at δ −17.2.[9,10] Some experiments were performed in order to elucidate the NMR behavior in connection with the catalytic properties. The results may be summarized as follows.

(1) In the absence of CO, a stoichiometric reaction of the water-gas shift catalyst solution with ethene occurred, even at room temperature, to give diethyl ketone[11] selectively. The intensity of the ^{1}H-NMR resonance of the solution decreased significantly after the 3 h-reaction.[12]

(2) The NMR spectrum exhibited no resonance on a short-time (5 min) treatment of a solution ($Co_2(CO)_8$ (4 mmol), diphos (4 mmol), and dioxane (5 ml) with both CO (70 kg/cm^2) and H_2O (60 mmol) at 165 °C; this is in contrast to the reaction of a matured solution[8] (see Fig. 1).

(3) No NMR resonance could be observed during the catalytic hydrocarbonylation of ethene at 165 °C under a CO pressure of 80 kg/cm^2, indicating a rapid consumption of the active species.

(4) The NMR spectrum of a solution in the absence of diphos or H_2O showed no resonance in either case.

(5) When an acetone solution consisting $Co_2(CO)_8$, diphos, and H_2O was treated at 135 °C for 3 h under CO(70 kg/cm^2), its ^{1}H-NMR spectrum exhibited a resonance at δ −17.2, although it was weak in comparison with that of the dioxane solution prepared under the same conditions[13] (see Fig. 2).

Thus, the active species which catalyze the water-gas shift reaction can be expected to participate in the hydrocarbonylation of ethene and to exhibit the ^{1}H-NMR resonance at δ −17.2.

A possible reaction scheme is illustrated in Scheme 1:[14,15] The species, **a**, formed during the course of the water-gas shift reaction[1] is trapped by ethene to form a alkyl cobalt complex, **b**, [2]; CO insertion [3] and succeeding ethene addition to **c**[4] give a 2-propyonylethyl cobalt complex, **d**, and the reaction of **a** with **d** produces diethyl ketone[5].[16] Step [6] accounts for the aldehyde formation, though it may be disregarded because of the high selectivities of the ketone formation. (Figs. 1 and 2 and Tables 1 and 2). The resulting complex, **f**, is converted into **a** by the WGSR pathway[7] again, and thus the catalytic cycle is completed.

Reactions 2—6 proceed rapidly, even under mild conditions, as has been mentioned above((1) and (2)). Reactions 1 and 7, on the other hand, proceed only at a relatively high temperature (120 °C or above (2), Figs. 1 and 2).

Although there is no direct evidence that the ^{1}H-NMR peak is due to $HCo(CO)_m(diphos)_n$, the present reaction scheme of the cobalt-catalyzed hydrocarbonylation using CO and H_2O seems to be probable.

References

1) I. Wender and P. Pino, "Organic Synthesis *via* Metal Carbonyls," Wiley, New York (1977), Vol. 2.

2) M. Dokiya and K. Bando, *Kogyo Kagaku Zasshi*, **71**, 1866 (1968).

3) Better yields can be obtained by using a heterogeneous catalyst, according to the patent literature.[1]

4) K. Murata and A. Matsuda, *Bull. Chem. Soc. Jpn.*, **54**, 249 (1981).

5) K. Murata and A. Matsuda, *Chem. Lett.*, **1980**, 11.

6) K. Murata, A. Matsuda, K. Bando, and Y. Sugi, *J. Chem. Soc., Chem. Commun.*, **1979**, 785.

7) Under the conditions given in Fig. 1, propanal (10 mmol) introduced independently can be hydrogenated to yield 1-propanol (2 mmol) in a 4 h-reaction.

8) A standard sample of the catalyst solution which is subjected to the ^{1}H-NMR analysis was prepared as follows: in a stainless-steel autoclave (50 ml volume) were mixed 4 mmol of $Co_2(CO)_8$, 4 mmol of diphos, 30 mmol of H_2O, and 5 ml of dioxane. The vessel was then sealed, and CO (70 kg/cm^2, room temp) was introduced. After the vessel had been heated to 165 °C with stirring for 3 h, an aliquot sample was quickly withdrawn from the vessel at 0 °C.

9) K. Murata and A. Matsuda, *Bull. Chem. Soc. Jpn.*, **54**, 245 (1981).
10) C. Ungermann, V. Landis, S. A. Moya, H. Cohen, H. Walker, R. G. Pearson, R. G. Rinker, and P. C. Ford, *J. Am. Chem. Soc.*, **101**, 5922 (1979).
11) The product was identified by gas chromatography.
12) When the solution was allowed to react with ethene at 50 °C for 4 h, no ^{1}H-NMR peak was observed at δ −17.2.
13) In these cases, the pH values of the acetone and dioxane solutions were 2.5 and 1.5 respectively. Further investigations concerning the pH effects on the activity are in progress.
14) The participation of the acyl cobalt complex, **c**, has already been described in a previous paper on the hydrocarbonylation of propene.[4]
15) R. F. Heck and D. S. Breslow, *J. Am. Chem. Soc.*, **83**, 4023 (1961); J. A. Bertrand, C. L. Aldrige, S. Husebye, and H. B. Jonassen, *J. Org. Chem.*, **29**, 790 (1964).
16) There is an alternative route: the acyl complex, **c**, reacts with alkyl complex, **b**, to yield the ketone and dimeric cobalt complex, **f**.

Intramolecular Hydrogen Bonding and Conformations of α,α-Dialkyl- and α-Alkyl-o-methoxybenzyl Alcohols. II. Enthalpies of Hydrogen Bond Formation and Molecular Force Field Calculations on α-Alkyl-substituted Benzyl Alcohols

Masayuki Ito and Minoru Hirota*

Department of Applied Chemistry, Faculty of Engineering, Yokohama National University, Hodogaya-ku, Yokohama 240

(Received November 17, 1980)

Enthalpies of intramolecular hydrogen bond formation (ΔH) were determined for a series of α-mono- and α,α-dialkyl-o-methoxybenzyl alcohols and related compounds. The $-\Delta H$ values of the unsubstituted and α,α-dialkyl-o-methoxybenzyl alcohols are more than 2.5 kJ mol^{-1}, while those for the corresponding α-monoalkyl derivatives are at most 1 kJ mol^{-1}. This tendency is in accordance with the results on their $\Delta\nu_{OH}$ and $\varepsilon_b/\varepsilon_f$ values, showing the hydrogen bonded conformations of the α-monoalkyl derivatives are less favorable than those of the other alcohols in discussion. Molecular force field calculations on α-alkyl- and α,α-dialkylbenzyl alcohols were also carried out. The results shows that the hydroxyl/aryl coplanar conformation ($\omega=0°$) is the most stable for the unsubstituted and α,α-dialkylbenzyl alcohols and the hydroxyl/aryl non-coplanar conformation ($\omega=30°$) for α-alkylbenzyl alcohols. Since the OH···O distance might be farther and, hence, the overlap between the unshared electron pairs on the methoxyl oxygen and the anti-bonding OH orbital might be less in the non-coplanar conformation, α-monoalkyl-o-methoxybenzyl alcohols are less favorable than the corresponding α,α-dialkyl derivatives in the intramolecular hydrogen bond formation.

The conformations of several benzyl alcohols have been discussed by the measurement of infrared and NMR spectra. Thus Ōki and Iwamura have concluded the existence of weak attractive interaction similar to hydrogen bonding between hydroxyl group and aromatic π-electron system.[1] The OH···π interaction might be favored when the hydroxyl group approached from upright the plane of aromatic nucleus, taking conformation II. On the other hand, α,α-di-

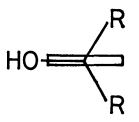

I

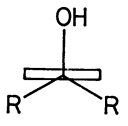

II

t-butylbenzyl alcohol is a highly crowded molecule, the rotation around the C(benzyl)–C(aromatic) bond being so slow as to make it possible to observe the signals of 2- and 6-protons separately by ^{1}H-NMR measurement.[2,3] This fact strongly suggests that conformer I or a similar one predominates over conformer II. We have also measured the infrared OH stretching absorptions and ^{1}H-NMR of α-alkyl-o-methoxybenzyl alcohols and discussed on their conformations.[4] A remarkable difference in the preference of hydrogen-bonded conformer has been observed between the α-monoalkyl and α,α-dialkyl-substituted derivatives.

In order to study further on this point, the enthalpies of the intramolecular hydrogen bond formation are determined with these alcohols. The most favorable conformers are also estimated theoretically by the molecular force field approaches.

Experimental

Preparation of Materials. Unsubstituted and α,α-dialkylbenzyl alcohols were prepared by the known procedures.[5,6] α-Monoalkylbenzyl alcohols were obtained by the Grignard reactions of o-methoxybenzaldehyde with the corresponding alkylmagnesium bromides. 2-Methoxy-α,α,3,5-tetramethylbenzyl alcohol was prepared similarly by the addition reaction to acetone of 2-methoxy-3,5-dimethylphenylmagnesium bromide, which was derived from 2,4-xylenol. Bp 89.0—90.0 °C/2 mmHg; MS (70 eV) *m/e*, 194.

Measurement of Infrared Spectra. Infrared OH stretching absorptions were recorded with a Hitachi Model 225 grating infrared spectrophotometer. The temperature dependence measurements were carried out on the dilute carbon tetrachloride solutions at the temperature ranging from 290 to 312 K. Throughout each measurement, temperature of the solution was kept sufficiently constant (The temperature variation was kept within 0.5 K). The results are given in Table 1. The enthalpies of the hydrogen bond formation was obtained as the gradients of the $\log_{10}(\varepsilon_b/\varepsilon_f)$ *vs.* $1/T$ plot by the least squares calculations.

The measurements were carried out within a relatively narrow range of temperature. Since the influence of temperature dependent broadening were shown to be negligible with some typicals of the absorption bands in this range of temperature, the peak heights (absorbance) of the bands were used to evaluate the relative equilibrium constants instead of integrated intensities. Fortunately the free and the hydrogen-bonded bands were rather well resolved, which made possible to use the peak intensities without any correction for the effect of the overlapping bands in most instances.

Molecular Force Field Calculations. We have employed the empirical force field proposed by Allinger and coworkers[7] to calculate steric energies and geometries of the benzyl alcohols. The geometries corresponding to the potential minima were obtained by the full optimization calculations, while the other labile conformations were calculated by restricting the torsional angle around C(aryl)–C(benzyl) bond.

Results and Discussion

The infrared OH absorptions of some newly prepared α,α-dialkylbenzyl alcohols, 1-(o-methoxyphenyl)cycloalkanols and 2-(8-chromanyl)-2-propanol are given in Table 2. The strength of hydrogen bond can be evaluated by the hydrogen bond shift ($\Delta\nu_{OH}$) of the

Table 1. The temperature dependence data

T/K	ε_f/l mol^{-1} cm^{-1}	ε_b/l mol^{-1} cm^{-1}
a) *o*-Methoxybenzyl alcohol (**3**), $c=4.95\times10^{-3}$ mol/l.		
295.7	27.6	54.3
303.1	29.0	54.2
309.2	28.4	52.1
315.3	29.1	50.5
321.2	29.4	50.0
b) α-Methyl-*o*-methoxybenzyl alcohol (**4**), $c=4.84\times10^{-3}$ mol/l.		
292.8	51.4	27.2
297.8	51.7	27.0
302.8	51.8	26.9
309.8	50.7	25.8
317.8	49.0	24.8
c) α-Ethyl-*o*-methoxybenzyl alcohol (**5**), $c=3.94\times10^{-3}$ mol/l.		
293.0	51.9	28.6
300.4	51.1	28.0
307.2	50.5	27.4
314.2	50.5	28.1
321.3	50.2	26.9
d) α-Isopropyl-*o*-methoxybenzyl alcohol (**6**), $c=5.00\times10^{-3}$ mol/l.		
292.6	59.5	30.1
299.3	58.8	29.3
307.2	57.2	28.6
313.8	55.6	27.0
320.1	56.5	27.6
e) α-*t*-Butyl-*o*-methoxybenzyl alcohol (**7**), $c=4.28\times10^{-3}$ mol/l.		
293.5	49.1	24.3
299.6	47.8	23.8
307.3	46.1	22.7
313.6	45.9	22.6
319.7	45.7	22.4
f) α,α-Dimethyl-*o*-methoxybenzyl alcohol (**8**), $c=4.98\times10^{-3}$ mol/l.		
293.2	22.8	97.9
300.0	22.9	92.7
308.1	22.9	87.3
314.8	23.7	86.0
321.3	24.9	85.1
g) α,α-Diethyl-*o*-methoxybenzyl alcohol (**9**), $c=5.07\times10^{-3}$ mol/l.		
293.3	40.6	68.1
299.9	40.7	65.8
308.8	39.6	62.6
316.2	38.5	60.6
322.8	38.2	58.2
h) α,α-Dipropyl-*o*-methoxybenzyl alcohol (**10**), $c=4.70\times10^{-3}$ mol/l.		
292.4	38.4	60.7
297.9	37.1	58.0
305.8	37.5	56.6
312.9	38.0	55.5
318.6	38.1	54.9
i) α,α-Diisopropyl-*o*-methoxybenzyl alcohol (**11**), $c=3.10\times10^{-3}$ mol/l.		
292.6	24.2	132.9
297.3	24.4	130.6
302.2	24.5	128.4
310.2	25.0	124.5
318.6	25.5	120.1
j) α,α-Dibutyl-*o*-methoxybenzyl alcohol (**12**), $c=4.54\times10^{-3}$ mol/l.		
292.6	40.7	67.1
297.2	40.7	65.6
304.3	40.1	63.0
310.0	39.4	62.3
315.6	38.4	60.0
k) α,α-Di-*t*-butyl-*o*-methoxybenzyl alcohol (**13**), $c=3.22\times10^{-3}$ mol/l.		
295.6	20.0	118.0
301.6	20.1	114.5
307.7	20.3	110.2
314.7	21.0	108.5
319.2	21.3	108.2
l) α,α-Dipentyl-*o*-methoxybenzyl alcohol (**14**), $c=4.45\times10^{-3}$ mol/l.		
293.1	40.8	66.5
299.1	41.6	64.8
307.4	41.2	63.0
314.2	41.2	60.9
319.3	40.5	60.1
m) 1-(*o*-Methoxyphenyl)cyclopentanol (**15**), $c=4.06\times10^{-3}$ mol/l.		
294.2	22.0	62.6
301.2	22.1	60.8
309.5	22.1	59.5
316.9	22.2	58.5
322.0	22.2	57.1
n) 1-(*o*-Methoxyphenyl)cyclohexanol (**16**), $c=3.89\times10^{-3}$ mol/l.		
293.2	15.3	90.7
299.9	16.3	88.7
307.4	17.6	88.2
313.3	18.0	86.6
319.2	18.7	84.3
o) 1-(*o*-Methoxyphenyl)cycloheptanol (**17**), $c=4.37\times10^{-3}$ mol/l.		
291.4	14.2	82.5
298.0	14.0	79.5
303.8	14.2	77.8
308.5	15.0	76.8
315.0	14.5	73.9

Table 1. (Continued)

T/K	ε_f/l mol^{-1} cm^{-1}	ε_b/l mol^{-1} cm^{-1}	T/K	ε_f/l mol^{-1} cm^{-1}	ε_b/l mol^{-1} cm^{-1}
p) 2-(8-Chromanyl)-2-propanol (**18**), $c=4.05\times10^{-3}$ mol/l.			q) 2-Methoxy-α,α,3,5-tetramethylbenzyl alcohol (**19**), $c=3.98\times10^{-3}$ mol/l.		
293.6	9.1	62.3	294.0	19.7	51.9
301.4	9.1	59.3	301.5	19.8	49.6
308.7	9.1	56.3	309.4	20.2	48.6
315.0	9.8	56.6	315.8	20.2	47.2
321.9	10.0	55.2	322.2	20.3	46.1

Table 2. OH stretching absorptions of some *o*-methoxybenzyl alcohols and related compounds

Compd No.	Substituent R_1	Substituent R_2	ν_f (ε_f)[a]	ν_b (ε_b)[a]
3	H	H	3637 (27.6)	3607[c] (54.3)
10	*n*-C_3H_7	*n*-C_3H_7	3619 (38.4)	3557 (60.7)
11	*i*-C_3H_7	*i*-C_3H_7[b]	3616 (24.3)	3542 (132.9)
12	*n*-C_4H_9	*n*-C_4H_9	3619 (40.7)	3557 (67.1)
13	*t*-C_4H_9	*t*-C_4H_9[b]	3616 (20.1)	3508 (114.5)
14	*n*-C_5H_{11}	*n*-C_5H_{11}	3618 (40.1)	3556 (66.5)
15	-$(CH_2)_4$-		3603 (21.1)	3576 (63.4)
16	-$(CH_2)_5$-		3604 (18.8)	3567 (112.9)
17	-$(CH_2)_6$-		3600 (12.9)	3580 (78.1)
18	2-(8-Chromanyl)-2-propanol		3609 (9.1)	3560 (62.3)
19	2-Methoxy-α,α,3,5-tetramethylbenzyl alcohol		3607 (19.7)	3525 (51.9)

a) Frequencies in cm^{-1} and molar absorptivity in l·mol^{-1} cm^{-1}. Sufixes f and b refer to the free and the intramolecularly hydrogen-bonded species, respectively. b) Diisopropyl and di-*t*-butyl derivatives were re-examined and their spectral data were corrected. c) The ν_{OH} band of the OH···π interacted form of variously substituted benzyl alcohols ($XC_6H_4CH_2OH$) were shown to appear within a narrow frequency range between 3617.4 and 3616.0 cm^{-1}. (See Ref. 1) Since the frequency of this band is considerably lower, it was assigned to the OH···O interacted form of **3**.

Table 3. Enthalpies of hydrogen bond formation and ν_{OH} hydrogen bond shifts of *o*-methoxybenzyl alcohols and related compounds

Compd No.	Substituent R_1	Substituent R_2	ΔH/kJ mol^{-1}	$\Delta\nu$/cm^{-1}	$\varepsilon_b/\varepsilon_f$
3	H	H	4.72	30	1.97
4	H	CH_3	1.25	36	0.72
5	H	C_2H_5	0.79	48	0.57
6	H	*i*-C_3H_7	1.00	42	0.54
7	H	*t*-C_4H_9	0.42	60	0.42
8	CH_3	CH_3	6.40	58	3.70
9	C_2H_5	C_2H_5	2.59	64	1.64
10	*n*-C_3H_7	*n*-C_3H_7	2.88	62	1.58
11	*i*-C_3H_7	*i*-C_3H_7	5.48	74	5.47
12	*n*-C_4H_9	*n*-C_4H_9	2.51	62	1.65
13	*t*-C_4H_9	*t*-C_4H_9	5.85	108	5.70
14	*n*-C_5H_{11}	*n*-C_5H_{11}	2.80	62	1.63
15	-$(CH_2)_4$-		2.80	27	3.00
16	-$(CH_2)_5$-		7.94	37	6.01
17	-$(CH_2)_6$-		4.81	20	6.05
18	2-(8-Chromanyl)-2-propanol		6.06	49	6.85
19	2-Methoxy-α,α,3,5-tetramethylbenzyl alcohol		4.18	82	2.64

OH stretching band, which is defined as the difference in the OH frequencies of the free and the hydrogen bonded species. The $\Delta\nu_{OH}$ is often related with the OH···O distance of hydrogen bond system.[8] Thus it can be a measure for the strength of the hydrogen bond. The enthalpy of hydrogen bond formation serves as another scale for the strength of the hydrogen bond, being determined from the temperature dependence measurement of the OH absorption intensities of free and hydrogen bonded species.[9] Results are given in Table 3 together with the $\Delta\nu_{OH}$ and $\varepsilon_b/\varepsilon_f$ values.

Enthalpies of Hydrogen Bond Formation and the Hydrogen Bond Shifts of OH Stretching Bands. Enthalpies of intramolecular hydrogen bond formation is generally smaller than those of intermolecular hydrogen bond formation when hydrogen donating and accepting groups are similar. The hydrogen bond enthalpies for the benzyl alcohols are rather small even when compared with those of similar six-membered hydrogen-bonded chelates. The enthalpies of intramolecular hydrogen bond formation (ΔH) for *o*-methoxybenzoic acid (**1**)[10] and 3-methoxy-1-propanol (**2**)[11] have been determined to be −13.8 and −8.8 kJ/mol, respectively.

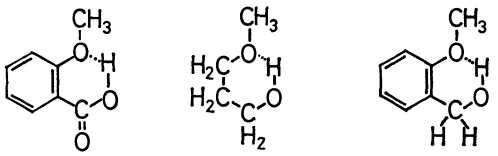

1 **2** **3**

On the other hands, the $-\Delta H$ values for the *o*-methoxybenzyl alcohols in Table 3 are at most 8 kJ/mol, most of them being less than 6 kJ/mol. This is due to the fact that the alcoholic hydroxyl group is a weak hydrogen donor and the oxygen atom of aromatic ether is a weak hydrogen acceptor in forming hydrogen bonds. In compound **1**, the carboxylic OH group is a very strong donor, while the aliphatic ether group in **2** is a stronger hydrogen acceptor than the aromatic ether group in **3**.

When compared among the benzyl alcohols, α-monoalkyl alcohols **4**—**7** have shown to have smaller $\Delta\nu_{OH}$ and $\varepsilon_b/\varepsilon_f$ values than the alcohols in other series, having been supposed to be less favorable in forming hydrogen bonds.[4] This tendency is again obvious with the $-\Delta H$ values in Table 3. The intramolecularly hydrogen bonded conformers of the α-monoalkyl alcohols are at most only 1 kJ/mol more stable than the free conformers, in contrast to the unsubstituted and α,α-dialkyl benzyl alcohols of which hydrogen-bonded conformers are more than 2.5 kJ/mol more stable than the free conformers.

In the series of α,α-dialkylbenzyl alcohols, α,α-diethyl and higher homologous α,α-di(*n*-alkyl) derivatives have considerably low $-\Delta H$ values around 2.5 kJ/mol. The anomalous behavior was first suspected when the $\varepsilon_b/\varepsilon_f$ and $-\Delta H$ values were compared among a series of dialkyl derivatives carrying $CH_{3-n}(CH_3)_n$ groups, where *n* is 0, 1, 2, and 3. To investigate further on this point, infrared OH stretching absorptions of homologous di(*n*-alkyl) derivatives with propyl, butyl, and pentyl groups were measured, giving very similar ν_f, ν_b, $\Delta\nu_{OH}$, $\varepsilon_b/\varepsilon_f$, and $-\Delta H$ values as shown in Tables 2 and 3. The Hydrogen bond shifts ($\Delta\nu_{OH}$) of dialkyl derivatives increase in the order of the bulkiness of alkyl substituent [$CH_3<C_2H_5<CH(CH_3)_2<C(CH_3)_3$], revealing no indication of anomaly. The $\Delta\nu_{OH}$ value has been correlated to be nearly inversely proportional to the OH···O distance, giving a measure to the strength of intramolecular hydrogen bond. Thus, the order is rationalized by taking the buttressing effect of the alkyl groups in the intramolecularly hydrogen-bonded conformation (III) into consideration. A

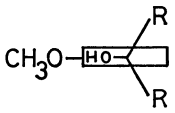

III

strong hydrogen bond is not necessary to be favorable in the equilibrium of its formation reaction, however. The hydrogen bonded conformation can be unfavorable when the steric hindrance and other unfavorable entropy effects in other parts of molecule is serious. Thus the lower $-\Delta H$, as well as the lower $\varepsilon_b/\varepsilon_f$, for **9** and its homologs should be related either to the unfavorable steric effect in other part of the intramolecularly hydrogen bonded conformation or to the favorable steric circumstances in the free conformation. The possible free conformation with extended chain (IV) of α,α-di-*n*-alkylbenzyl alcohols are presumably more stable than those for α,α-diisopropyl- and α,α-di-*t*-butylbenzyl alcohols, because the alkyl-methoxyl repulsion is less in the former. An evidence in support of this explanation was obtained from the measurements on 1-(2-methoxyphenyl)cycloalkanols. Anomalously low ΔH and $\varepsilon_b/\varepsilon_f$ values were not observed with these cyclic alcohols the end of whose alkyl chain are connected to each other. These compounds cannot take the extended chain conformation IV. 1-(2-Methoxyphenyl)cycloalkanols **15**—**17** have the ν_f bands considerably lower than those of other open chain alcohols investigated. They are located between 3604 and 3600 cm^{-1}, assignable to OH···π interacted hydroxyl groups according to the extensive works by Ōki and Iwamura[1b] who attributed the bands at 3620.5 and 3605.2 cm^{-1} of 1-phenylcyclohexanol to the free and the OH···π interacted forms, respectively. The higher ν_{OH} bands of the open chain alcohols **3**—**14**, on the contrary, lies in the frequency region higher than 3616 cm^{-1}. They were assigned to the free OH absorptions according to the fact that the free ν_{OH} bands of 2-phenyl-2-propanol and 3-phenyl-3-pentanol were shown to appear at 3620.6 and 3618.2 cm^{-1}, respectively.[1a]

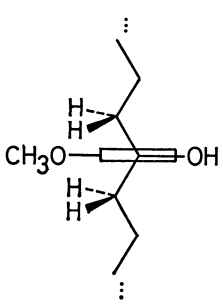

IV

From the results in molecular force field calculations, the free conformers of the dialkyl alcohols without ring structures are estimated to take the OH periplanar conformation V which is unfavorable to have the OH···π interaction. The methoxycycloalkanols **15**—**17**, on the contrary, takes preferably the free conformation (VI) in which the hydroxyl group is clinal to the plane of aromatic ring because of steric hindrance between the alicyclic ring and the *ortho*-methoxyl group expected in conformation V. The conformer VI is supposed to be sterically more crowded than the conformer V of the open chain series. This should be a reason for the larger $-\Delta H$ of the alcohols **15**—**17**. The clinal conformation VI is very favorable to have the OH···π interaction to which the low frequency shifts of the ν_f bands of **15**—**17** is due.

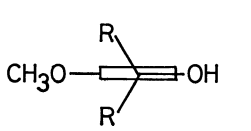

V

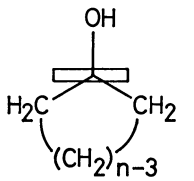

$n=5$, 6, and 7

VI

In order to investigate the effect of the conformation of hydrogen-accepting alkoxyl group upon the hydrogen bonding, 2-(8-chromanyl)-2-propanol (**18**) and 2-methoxy-α,α,3,5-tetramethylbenzyl alcohol (**19**) were prepared and their behavior in intramolecular hydrogen bond formation was examined. The intramolecularly hydrogen bonded conformer of **18** is supposed to take conformation VII, which is very similar to

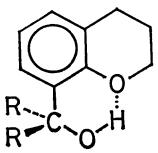

VII

Table 4. Steric energies(E)[a] and some geometrical parameters[b] of the benzyl alcohols $C_6H_5CR^1R^2OH$ calculated by use of MMI program

R^1	R^2	E/kJ mol^{-1}				$\angle OC_\alpha C_{ipso}$	$\angle C_\alpha C_{ipso} C_2$	$l(C_{ipso}-C_\alpha)$
		$\omega=0°$	$\omega=30°$	$\omega=60°$	$\omega=90°$			
H	H	47.40 (0.00)	47.90 (0.50)	48.66 (1.26)	50.70 (3.30)	112.34°	120.85°	1.510 Å
H	CH_3	48.23 (2.25)	45.98 (0.00)	49.78 (3.80)	—	109.53	120.45	1.515 Å
H	C_2H_5	54.59 (2.67)	51.92 (0.00)	54.67 (2.75)	—	109.18	120.36	1.515 Å
H	*i*-C_3H_7	59.36 (3.60)	55.76 (0.00)	58.31 (2.55)	—	108.90	120.51	1.515 Å
H	*t*-C_4H_9	76.20 (17.60)	58.60 (0.00)	71.85 (13.25)	—	108.22	120.37	1.524 Å
CH_3	CH_3	44.68 (0.00)	47.44 (2.76)	—	62.24 (17.56)	108.93	120.71	1.525 Å
C_2H_5	C_2H_5	57.89 (0.00)	64.08 (6.19)	—	87.15 (29.26)	109.00	120.64	1.523 Å
i-C_3H_7	*i*-C_3H_7	84.02 (0.00)	84.77 (0.75)	—	147.89 (63.87)	107.00	120.23	1.531 Å
t-C_4H_9	*t*-C_4H_9	141.45 (0.00)	146.30 (4.85)	—	251.47 (110.02)	103.75	119.73	1.541 Å

a) The relative values with reference to the most stable conformers are given in parentheses. b) The bond angles and the bond lengths for the most stable conformers are given.

that of **8**. In line with this consequence, the $\Delta\nu_{OH}$ and the $-\Delta H$ values of **18** are very close to those of **8**. The $\varepsilon_b/\varepsilon_f$ value of **18** is significantly larger than the corresponding ratio of **8**, however. The alkoxyl group in **18** is fixed antiperiplanar to the 2-hydroxy-2-propyl moiety by the condensed dihydropyran ring and is favorable entropically to the intramolecular hydrogen bond formation, causing the larger $\varepsilon_b/\varepsilon_f$. Introduction of the 3-methyl group onto the hydrogen bonded molecule as in **19** prevents the antiperiplanar conformation favorable for the hydrogen bonding. Thus, the $-\Delta H$ and $\varepsilon_b/\varepsilon_f$ values of **19** are considerably lower than the corresponding quantities of **8** due to the increase in steric energy and the restriction of the conformation in the hydrogen bonded conformer. In contrast, the $\Delta\nu_{OH}$ increases remarkably because the OH···O distance becomes closer due to the buttresing effect caused by the 3-methyl group. Thus, it is probable that the intramolecular hydrogen bonds can be persistent even in cases when the alkoxyl group is not coplanar to the chelate ring formed by the hydrogen bonding. Similar tendency has been observed with the hydrogen bond chelates containing carboxyl groups as hydrogen donors.[12] The ethereal oxygen atom can interact with hydroxyl and other hydrogen donating groups in various conformations because it has two pairs of unshared electrons. The alcohol **19** has a low frequency ν_f band locating at 3607 cm^{-1}. Since the 3-methyl group in **19** enforces the methoxyl group to take nonplanar conformation and to approach nearer to the 2-hydroxy-2-propyl moiety, the most favorable conformation of the free species tends to have a nonplanar hydroxyl group favorable to interact with the aromatic π-electrons (just illustrated schematically by VIII).

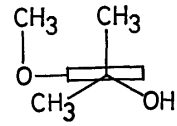

VIII

Estimation of the Most Stable Conformations by Molecular Force Field Approach. The probable conformations of these alcohols were then discussed on the basis of the molecular force field calculations carried out by use of the MMI version of the computer program developed by Allinger and co-workers.[7] As the force field involving hydrogen bond system has not yet been available, the calculations were carried out on benzyl alcohol and its α-substituted derivatives void of methoxyl group. The results are given in Table 4. Here, in this Table, the torsional angle ω refers to the dihedral angle between the aromatic ring and the hydroxyl group (as illustrated in IX—XII). The

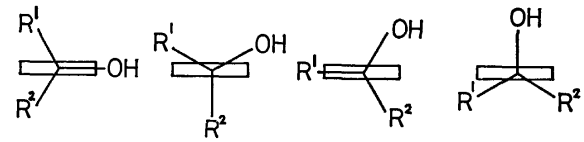

ω = 0° 30° 60° 90°

IX X XI XII

results show that the most stable conformation of α-monoalkylbenzyl alcohols are X in which ω is around 30° and that those of α,α-dialkylbenzyl alcohols are IX with $\omega=0°$.[13] The optimized torsional angles were calculated to be 31.3°, 32.2°, 33.1°, and 34.4° for the most stable conformers of α-methyl, α-ethyl, α-isopropyl, and α-*t*-butylbenzyl alcohols, respectively.

As expected from the repulsive force operating between the alkyl and the hydroxyl groups, the torsional angles increase in the same order. Since the methoxyl group on the aromatic ring is ignored in calculations, the results should be applied on the methoxy alcohols **3**—**14** with care. Nevertheless the hydrogen bonded conformations might be rather properly estimated since the methoxyl group lies far from the alkyl group(s).

The results which conclude the conformation X of **4**—**7** with non-coplanar hydroxyl group to be the most stable coincide with the fact that the hydrogen bonded conformers of these alcohols are less favorable than those of the α,α-dialkylbenzyl alcohols as revealed by both the $\varepsilon_b/\varepsilon_f$ and the ΔH values in Table 3. The OH···O distance might become farther and, moreover, the overlap between the unshared electron pairs and the anti-bonding OH orbital might be less in conformation X than in conformation IX. The OH proton signals of **4**—**7** have shown to appear at higher fields than those of the corresponding dialkylbenzyl alcohols. This can be ascribed to the magnetic anisotropy effect on the hydroxyl protons lying above the aromatic rings to induce the high field shifts.

The introduction of α-alkyl groups causes considerable C_α–C_{ipso} bond stretching and O–C_α–C_{ipso} bond angle decrease but little C_α–C_{ipso}–C_2 bond angle alteration. As a result, the estimated distance between the hydroxyl and the methoxyl oxygen atoms decreases from 2.34 to 2.14 Å when the two benzylic hydrogen atoms are replaced with *t*-butyl groups.[14] This explains the $\Delta\nu_{OH}$ increase caused by the introduction of α,α-dialkyl groups. The consequences from the calculations on α,α-di-*t*-butylbenzyl alcohol (**20**) agrees with the fact that the protons at 2- and 6-positions of **20** are not isochronous because of the very high rotational barrier around C_{ipso}–C_{benzyl} bond.[2,3] The conformation IX which is estimated to be the most stable explains the unisochronous ^{1}H-NMR spectrum of **20** together with the rotational barrier supposed to be a little higher than 110 kJ/mol. The extended conformation IV of **9** was also confirmed by the calculation giving the torsional angle near 180° (177.1 and 177.9° exactly) for both of the C_α–$CH_2(CH_3)$ bonds.

We wish to thank Prof. Eiji Osawa, Hokkaido University, for his valuable advice and kind permission to use their MMI program. We are also grateful to Prof. Hiizu Iwamura, the Institute of Molecular Sciences, for his valuable advice and facilitation in using the HITAC M-200H computer. The molecular force field calculations were carried out by using a HITAC 8800/8700 computer of the University of Tokyo and a HITAC M-200H computer of the Institute of Molecular Sciences.

References

1) M. Ōki and H. Iwamura, *Bull. Chem. Soc. Jpn.*, **32**, 950 (1959); **35**, 1552 (1962); **36**, 1 (1963).

2) G. P. Newsereff and S. Sternhell, *Tetrahedron Lett.*, **1967**, 2539.

3) P. D. Bartlett, T. R. Steadman, T. T. Tidwell, and P. Weber, *Tetrahedron Lett.*, **1970**, 2915.

4) A. Yamashita, K. Hara, S. Aizawa, and M. Hirota, *Bull. Chem. Soc. Jpn.*, **47**, 2508 (1974).

5) M. Ōki, M. Hirota, H. Satonaka, and T. Hagiwara, *Tetrahedron Lett.*, **1967**, 1785.

6) S. Natelson and S. P. Gottfried, *J. Am. Chem. Soc.*, **61**, 1001 (1939); P. D. Bartlett and A. Schneider, *ibid.*, **67**, 140 (1945).

7) N. L. Allinger and Y. H. Yuh, MMI/MMPI program (1973), QCPE, #318.

8) L. P. Kuhn, *J. Am. Chem. Soc.*, **74**, 2492 (1952); **76**, 4323 (1954); **80**, 5950 (1958).

9) Details of our experiments were reported previously. See, for example: M. Hirota, K. Shinozuka, and Y. Hamada, *Bull. Chem. Soc. Jpn.*, **47**, 2696 (1974).

10) M. Davies and D. M. F. Griffiths, *J. Chem. Soc.*, **1955**, 132. See also M. Ōki, M. Hirota, and S. Hirofuji, *Spectrochim. Acta*, **22**, 1537 (1966).

11) L. P. Kuhn and R. A. Wires, *J. Am. Chem. Soc.*, **86**, 2161 (1964).

12) M. Ōki and M. Hirota, *Bull. Chem. Soc. Jpn.*, **36**, 290 (1963).

13) It cannot be deduced straightforwardly from this conclusion that the OH···π interacted conformer is unfavorable in α,α-dialkylbenzyl alcohols. The OH..π interacted conformation is known to be rather flexible, the torsional angle varying in a considerably wide range. As the torsional barriers of benzyl alcohol and its α-methyl-substituted derivatives are rather low, the interacted conformer may become the most stable owing to the additional stabilization due to attractive OH···π interaction.

14) The OH···O(CH_3) distance was calculated by assuming that the coordinates of *ortho*-methoxyl group is exactly the same as those of anisole. Similar calculations on α,α-dimethyl, α,α-diethyl, and α,α-diisopropyl derivatives gave 2.28, 2.28, and 2.23 Å (=10^{-1} nm), respectively, as O···O distances.

Structure and Synthesis of (+)-Shonanol

Takashi MATSUMOTO,* Sachihiko IMAI, Hiroyuki KAWASHIMA, and Masanori MITSUKI

Department of Chemistry, Faculty of Science, Hiroshima University, Higashisenda-machi, Naka-ku, Hiroshima 730

(Received November 17, 1980)

The structure of shonanol was restudied and found to be 12-hydroxyabieta-2,8,11,13-tetraen-1-one (**1**) by the following synthesis. A Grignard reaction of methyl (+)-12-methoxyabieta-8,11,13-trien-18-oate with phenylmagnesium bromide, followed by treatment with lead tetraacetate and calcium carbonate afforded a mixture of Δ^3-, Δ^4-, and $\Delta^{4(18)}$-19-nor compounds. This was oxidized with selenium dioxide to give (+)-12-methoxy-19-norabieta-4(18),8,11,13-tetraen-3α-ol. This alcohol was converted to (+)-12-methoxyabieta-5,8,11,13-tetraen-3-one (**6**) by the known procedure. Reduction of **6** with lithium aluminium hydride, followed by catalytic hydrogenation, yielded (+)-12-methoxyabieta-8,11,13-trien-3β-ol (**8**) and a small amount of its *cis* isomer. The compound (**8**) was then converted to (+)-12-methoxyabieta-1,8,11,13-tetraen-3-one (**12**) by a series of reactions: oxidation with pyridinium chlorochromate, bromination with pyridinium tribromide, and dehydrobromination with lithium carbonate and lithium bromide. Demethylation of **12** with boron tribromide gave (+)-12-hydroxyabieta-1,8,11,13-tetraen-3-one. Oxidation of **12** with alkaline hydrogen peroxide, followed by treatment with hydrazine hydrate, gave (+)-12-methoxyabieta-2,8,11,13-tetraen-1α-ol; this was oxidized with Jones reagent to give the corresponding 1-oxo compound. The 1-oxo compound was finally demethylated with boron tribromide to yield (+)-**1**, whose spectra were identical with those of natural shonanol.

The structure of shonanol, a tricyclic diterpene phenol isolated from the sawdust of *Libocedrus formosana* by Lin and Liu[1] in 1965, has been tentatively assigned as 12-hydroxytotara-1,8,11,13-tetraen-3-one (I) on the basis of spectroscopic studies. To confirm this structure we synthesized (±)-I in our laboratory.[2] However, this synthetic (±)-I was shown to be different from natural shonanol by spectral comparison. Further synthetic studies on the structural isomers[3,4] possessing a hydroxyl group at the position meta to an isopropyl group in the C ring: (±)-12-hydroxytotara-2,8,11,13-tetraen-1-one (II), (±)-14-hydroxy-12-isopropylpodocarpa-1,8,11,13-tetraen-3-one (III), (±)-14-hydroxy-12-isopropylpodocarpa-2,8,11,13-tetraen-1-one (IV), (+)-11-hydroxyabieta-1,8,11,13-tetraen-3-one (V), and (+)-11-hydroxyabieta-2,8,11,13-tetraen-1-one (VI), led to the same result, whereas the spectral analyses of these synthetic materials I—VI and natural shonanol suggested that the structure of shonanol is 12-hydroxyabieta-2,8,11,13-tetraen-1-one (**1**).[4] To confirm the validity of our proposed structure, we now attempted the synthesis of **1**. This paper will describe the structural confirmation of natural shonanol by the synthesis of (+)-**1** starting from methyl (+)-12-methoxyabieta-8,11,13-trien-18-oate (**2**).[5,6]

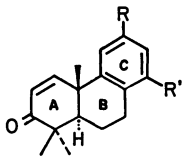

I R=OH, R'=i-Pr

III R=i-Pr, R'=OH

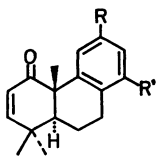

II R=OH, R'=i-Pr

IV R=i-Pr, R'=OH

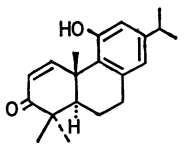

V

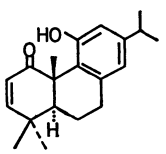

VI

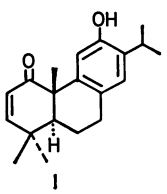

I

The Grignard reaction of **2** with phenylmagnesium bromide at 95—100 °C afforded a diphenylmethanol derivative (**3**: 80%). This was treated with lead tetraacetate and calcium carbonate in refluxing benzene to give a mixture (**4**: 78%) of Δ^3-, Δ^4-, and $\Delta^{4(18)}$-19-nor compounds in a ratio of *ca.* 1:2:7. The mixture was then oxidized with selenium dioxide in refluxing aqueous ethanol to yield (+)-12-methoxy-19-norabieta-4(18), 8,11,13-tetraen-3α-ol (**5**: 51%).[7,8] This alcohol (**5**) was subsequently converted to (+)-12-methoxyabieta-5,8,11,13-tetraen-3-one (**6**) by a series of known procedures:[7] isomerization with lithium in ethylenediamine to 12-methoxy-19-norabieta-4,8,11,13-tetraen-3α-ol, Jones oxidation, and methylation with methyl iodide in the presence of potassium *t*-butoxide. Reduction of **6** with lithium aluminium hydride in ether afforded (−)-12-methoxyabieta-5,8,11,13-tetraen-3β-ol (**7**: 90%), which was submitted to catalytic hydrogenation over 5% Pd–C in methanol to yield (+)-12-methoxyabieta-8,11,13-trien-3β-ol (**8**: 68%)[9,10] as a major product and its *cis* isomer (**9**: 11%) as a minor one. The stereochemistry of the hydroxyl group at the C-3 position in **7**, which was expected to be β-configuration from many literature precedents,[2,3,10,11] was confirmed by the conversion to the known compound (**8**).[9,10] The *cis*-configuration of the A/B ring junction in **9** was supported by the appearance of a signal due to one of the *gem*-dimethyl groups at the C-4 position in very high field (δ 0.42 ppm) owing to the shielding effect of the aromatic C ring. The β-configuration of the hydroxyl group at the C-3 position was also supported by a signal at δ 3.22 ppm with half-height width of 9 Hz, suggesting the presence

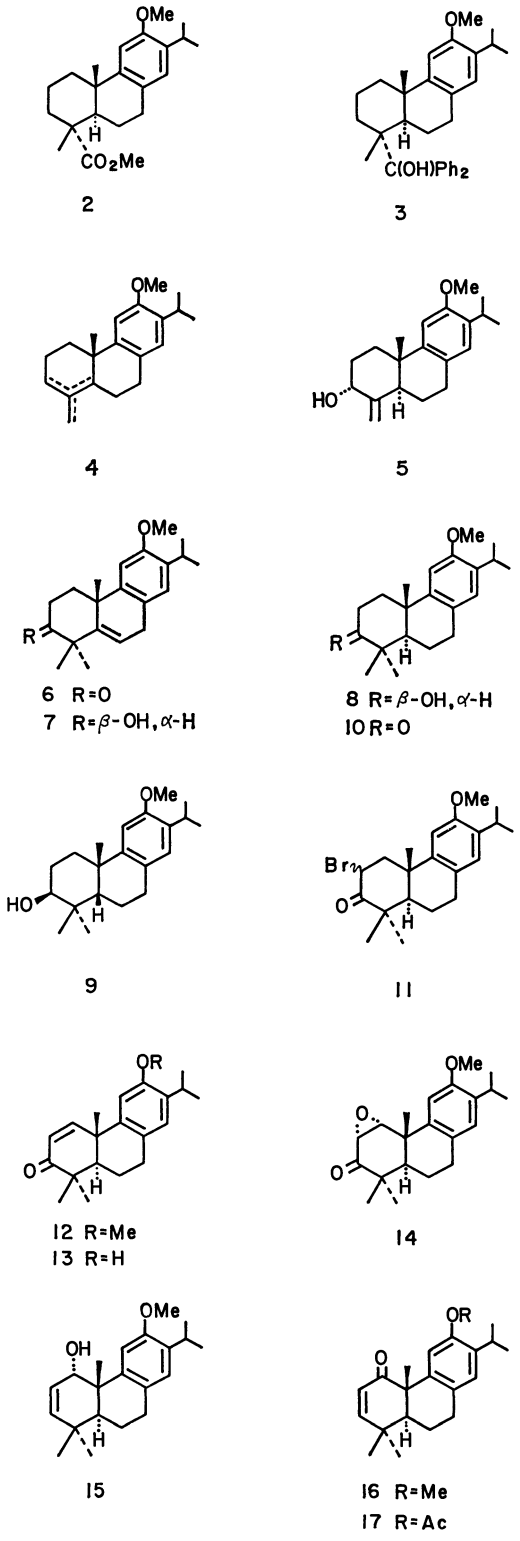

of an equatorial α hydrogen. Oxidation of the *trans*-compound (**8**) with pyridinium chlorochromate in dichloromethane afforded (+)-12-methoxyabieta-8,11,13-trien-3-one (**10**: 73%).[7,9,10] On bromination with pyridinium tribromide in ethanol and chloroform, this was converted to a mixture of the epimeric 2-bromo derivatives (**11**: 69%). The mixture (**11**), without purification, was immediately treated with lithium carbonate and lithium bromide in *N*,*N*-dimethylformamide at 120—125 °C to produce (+)-12-methoxyabieta-1,8,11,13-tetraen-3-one (**12**: 63%), which was demethylated with boron tribromide in dichloromethane to give (+)-12-hydroxyabieta-1,8,11,13-tetraen-3-one (**13**: 82%).[12] The physical and spectral data of **13** were different from those of natural shonanol.

Subsequently, 1,3-carbonyl transposition[3,4,13] of the α,β-unsaturated carbonyl group in **12** was carried out as follows. Oxidation of **12** with alkaline hydrogen peroxide in methanol and dichloromethane at −10—−5 °C, followed by treatment of the resulting epoxy ketone (**14**)[14] with hydrazine hydrate in refluxing methanol containing a small amount of acetic acid, yielded (+)-12-methoxyabieta-2,8,11,13-tetraen-1α-ol (**15**: 49% from **12**). This alcohol (**15**) was then oxidized with Jones reagent. The resulting (+)-12-methoxyabieta-2,8,11,13-tetraen-1-one (**16**: 78%) was demethylated with boron tribromide to give (+)-12-hydroxyabieta-2,8,11,13-tetraen-1-one (**1**: 74%), whose melting point and spectra (IR and ^{1}H NMR) were identical with those of natural shonanol. The synthetic **1** was further characterized as its acetate (**17**).

From the present study, the structure of shonanol was conclusively assigned as **1**.

Experimental

All melting points are uncorrected. The IR spectra and optical rotations were measured in chloroform, and the NMR spectra in carbon tetrachloride at 60 MHz, with tetramethylsilane as an internal standard, unless otherwise stated. The chemical shifts are presented in terms of δ values; s: singlet, bs: broad singlet, d: doublet, t: triplet, m: multiplet. Column chromatography was performed using Merck silica gel (0.063 mm).

Grignard Reaction of Methyl 12-Methoxyabieta-8,11,13-trien-18-oate (2) with Phenylmagnesium Bromide. A solution of **2**[5,6] (43.985 g) in dry ether (90 ml) was added to a refluxing ethereal solution of phenylmagnesium bromide prepared from magnesium turnings (12.4 g) and bromobenzene (80.2 g) in dry ether (180 ml). The mixture was refluxed for 1 h, the ether was removed, and the viscous residue was heated at 95—100 °C for 8 h. After standing overnight at room temperature, the mass was carefully hydrolyzed with a mixture of dilute hydrochloric acid and ice, and then extracted with ether. The ether extract was washed successively with aqueous sodium thiosulfate and brine, dried over sodium sulfate, and evaporated. The residue was recrystallized from acetone–hexane to give a diphenylmethanol derivative (**3**) (34.796 g), mp 205—207.5 °C, $[\alpha]_D$ +97.4° (*c* 2.73), IR: 3591 cm^{-1}; NMR: 1.10 (6H, d, J=7 Hz, $-CH(C\underline{H}_3)_2$), 1.22 and 1.34 (each 3H and s, C_4–CH_3 and C_{10}–CH_3), 2.33 (1H, s, –OH, disappeared on deuteration), 3.14 (1H, m, $-C\underline{H}(CH_3)_2$), 3.69 (3H, s, $-OCH_3$), 6.53 (2H, s, C_{11}–H and C_{14}–H), 7.0—7.9 (10H, m, 2-C_6H_5). Found: C, 84.79; H, 8.86%. Calcd for $C_{33}H_{40}O_2$: C, 84.57; H, 8.60%.

The mother liquor of recrystallization was evaporated *in vacuo* and the residue was purified by column chromatography on silica gel (300 g), using hexane–benzene (6:4 and then 4:6) as the eluent, to give an additional alcohol (**3**: 10.047 g).

Fragmentation of 3 with Lead Tetraacetate. A solution of **3** (18.383 g) in dry benzene (100 ml) was added to a stirred suspension of 87% lead tetraacetate (24.0 g) and

calcium carbonate (23.5 g) in dry benzene (150 ml). The mixture was refluxed for 8 h, cooled, and then filtered. The filtrate was diluted with ether and the solution was washed successively with 10% aqueous potassium iodide, aqueous sodium thiosulfate, aqueous sodium hydrogencarbonate, and brine. The dried solution was evaporated *in vacuo* and the residue was purified by column chromatography on silica gel (200 g), using hexane as the eluent, to give a mixture of Δ^3-, Δ^4-, and $\Delta^{4(18)}$-19-nor compounds (**4**) (8.654 g: 77.6%). The NMR spectrum of the mixture indicated that it was composed of approximately 7% of Δ^3- (δ 1.02 ppm, C_{10}–CH_3; 5.38 ppm, C_3–H), 21% of Δ^4- (δ 1.36 ppm, C_{10}–CH_3), and 72% of $\Delta^{4(18)}$-19-nor compound (δ 0.99 ppm, C_{10}–CH_3; 4.57 and 4.81 ppm, CH_2=C–).

*12-Methoxy-19-norabieta-4(18),8,11,13-tetraen-3α-ol (**5**).* A solution of selenium dioxide (1.494 g) in ethanol (48 ml) and water (2.0 ml) was added dropwise to a stirred suspension of **4** (7.661 g) in ethanol (50 ml). The mixture was refluxed for 4 h, cooled, and then filtered. The filtrate was diluted with chloroform, evaporated *in vacuo*, and the residue was chromatographed on aluminium oxide (Merck activ. II—III: 150 g), using ether–benzene (1:9 and then 4:6) as the eluent, to give **5**[7,8] (4.097 g: 50.6%) which was recrystallized from hexane, mp 59—61 °C, $[\alpha]_D$ +159° (*c* 5.80); IR: 3610, 3415 cm^{-1}; NMR: 0.91 (3H, s, C_{10}–CH_3), 1.17 (6H, d, J=7 Hz, $-CH(C\underline{H}_3)_2$), 2.58 (1H, s, –OH, disappeared on deuteration), 3.22 (1H, m, $-C\underline{H}(CH_3)_2$), 3.73 (3H, s, $-OCH_3$), 4.17 (1H, bs, $W_{1/2}$=5 Hz, C_3–H), 4.60 and 4.92 (each 1H and bs, CH_2=C–), 6.63 and 6.77 (each 1H and s, C_{11}–H and C_{14}–H). Found: C, 79.86; H, 9.55%. Calcd for $C_{20}H_{28}O_2$: C, 79.95; H, 9.39%.

*12-Methoxyabieta-5,8,11,13-tetraen-3-one (**6**).* The 3α-ol (**5**) was converted to **6** by the known procedure.[7] The crude product was purified by column chromatography on silica gel, using ether–benzene (1.5:98.5) as the eluent, to give **6** which was recrystallized from hexane, mp 92.5—93.5 °C, $[\alpha]_D$ +41.3° (*c* 3.25), IR: 1705 cm^{-1}; NMR: 1.18 (6H, d, J=7 Hz, $-CH(C\underline{H}_3)_2$), 1.18, 1.24, and 1.32 (each 3H and s, $-C(CH_3)_2$ and C_{10}–CH_3), 3.32 (2H, d, J=4 Hz, $=CHC\underline{H}_2$–), 3.78 (3H, s, $-OCH_3$), 5.90 (1H, t, J=4 Hz, C_6–H), 6.72 and 6.85 (each 1H and s, C_{11}–H and C_{14}–H). Found: C, 80.77; H, 9.14%. Calcd for $C_{21}H_{28}O_2$: C, 80.73; H, 9.03%.

*12-Methoxyabieta-5,8,11,13-tetraen-3β-ol (**7**).* A mixture of **6** (502 mg) and lithium aluminium hydride (61 mg) in dry ether (15 ml) was stirred at room temperature for 80 min, poured into a mixture of ice and dilute hydrochloric acid, and extracted with ether. The ether extract was washed with brine, dried over sodium sulfate, and evaporated. The residue was purified by column chromatography on silica gel (15 g), using ether–benzene (2:98) as the eluent, to give **7** (457 mg: 90.5%), which was recrystallized from hexane, mp 69—71 °C, $[\alpha]_D$ −53.5° (*c* 3.10); IR: 3616, 3454 cm^{-1}, NMR: 1.13, 1.21, and 1.28 (each 3H and s, $-C(CH_3)_2$ and C_{10}–CH_3), 1.17 (6H, d, J=7 Hz, $-CH(C\underline{H}_3)_2$), 2.17 (1H, s, –OH, disappeared on deuteration), 3.26 (2H, d, J=4 Hz, $=CHC\underline{H}_2$–), 3.75 (3H, s, $-OCH_3$), 5.97 (1H, t, J=4 Hz, C_6–H), 6.68 and 6.80 (each 1H and s, C_{11}–H and C_{14}–H). Found: C, 79.92; H, 9.91%. Calcd for $C_{21}H_{30}O_2$: C, 80.21; H, 9.62%.

*Catalytic Hydrogenation of **7**.* A mixture of **7** (456 mg) and 5% Pd–C (450 mg) in methanol (10 ml) was subjected to catalytic hydrogenation at room temperature for *ca.* 24 h. After the usual work-up, the crude product was purified by column chromatography on silica gel (40 g), using ether–benzene (1:99) as the eluent, to give 12-methoxy-5β*H*-abieta-8,11,13-trien-3β-ol (**9**) (51 mg: 11.1%) $[\alpha]_D$ +41.2° (*c* 1.68); IR: 3630, 3455 cm^{-1}; NMR: 0.42, 0.99, and 1.18 (each 3H and s, $-C(CH_3)_2$ and C_{10}–CH_3), 1.15 (6H, d, J=7 Hz, $-CH(C\underline{H}_3)_2$), 1.60 (1H, s, –OH, disappeared on deuteration), 3.22 (1H, m, $W_{1/2}$=9 Hz, C_3–H), 3.75 (3H, s, $-OCH_3$), 6.67 and 6.70 (each 1H and s, C_{11}–H and C_{14}–H). Found: C, 79.42; H, 10.33%. Calcd for $C_{21}H_{32}O_2$: C, 79.70; H, 10.19%.

Further elution with ether–benzene (5:95) afforded 12-methoxyabieta-8,11,13-trien-3β-ol (**8**)[9,10] (314 mg: 68.4%) which was recrystallized from hexane, mp 104—105 °C (softened at *ca.* 95 °C), $[\alpha]_D$ +60.7° (*c* 2.39); IR: 3625, 3455 cm^{-1}; NMR: 0.85, 1.04, and 1.19 (each 3H and s, $-C(CH_3)_2$ and C_{10}–CH_3), 1.16 (6H, d, J=7 Hz, $-CH(C\underline{H}_3)_2$), 1.95 (1H, s, –OH, disappeared on deuteration), 3.20 (1H, m, $W_{1/2}$=15 Hz, C_3–H), 3.74 (3H, s, $-OCH_3$), 6.58 and 6.72 (each 1H and s, C_{11}–H and C_{14}–H). Found: C, 79.94; H, 10.30%. Calcd for $C_{21}H_{32}O_2$: C, 79.70; H, 10.19%.

*12-Methoxyabieta-8,11,13-trien-3-one (**10**).* Pyridinium chlorochromate (2.74 g) was added at 0—5 °C to a stirred solution of **8** (2.649 g) in dry dichloromethane (30 ml) over a 5 min period. The mixture was stirred at room temperature for 2 more hours and then diluted with ether. After the addition of water, the mixture was extracted with ether. The ether extract was washed with brine, dried over sodium sulfate, and evaporated *in vacuo*. The residue was chromatographed on silica gel (80 g), using ether–benzene (1:99) as the eluent, to give **10** (1.911 g: 72.6%), whose IR and NMR spectra were identical with those of authentic hinokione methyl ether.[10]

*12-Methoxyabieta-1,8,11,13-tetraen-3-one (**12**).* A mixture of **10** (1.295 g) and 80% pyridinium tribromide (1.482 g) in ethanol (13.3 ml) and chloroform (26.6 ml) was stirred at room temperature for 30 min. After the addition of aqueous sodium thiosulfate, the mixture was extracted with ether. The ether extract was washed with dilute hydrochloric acid and brine, dried over sodium sulfate, and then evaporated *in vacuo*. The residue was chromatographed on silica gel (100 g), using hexane–benzene (1:1) as the eluent, to give a mixture of epimeric 2-bromo derivatives (**11**) (1.115 g: 68.9%), which was immediately submitted to dehydrobromination.

A mixture of **11** (1.009 g), lithium carbonate (570 mg), and lithium bromide (446 mg) in *N*,*N*-dimethylformamide (16 ml) was stirred at 120—125 °C for 3 h in a stream of nitrogen. The reaction mixture was cooled, poured into dilute sulfuric acid, and extracted with ether. The ether extract was washed with aqueous sodium thiosulfate and brine, dried over sodium sulfate, and then evaporated *in vacuo*. The residue was purified by column chromatography on silica gel (30 g), using benzene as the eluent, to give **12** (505 mg: 62.9%), which was recrystallized from hexane, mp 145.5—146.5 °C, $[\alpha]_D$ +158° (*c* 0.505), IR: 1665 cm^{-1}; NMR: 1.14, 1.17, and 1.39 (each 3H and s, $-C(CH_3)_2$ and C_{10}–CH_3), 1.15 (6H, d, J=7 Hz, $-CH(C\underline{H}_3)_2$), 3.19 (1H, m, $-C\underline{H}(CH_3)_2$), 3.73 (3H, s, $-OCH_3$), 5.89 (1H, d, J=10 Hz, C_2–H), 6.72 and 6.77 (each 1H and s, C_{11}–H and C_{14}–H), 7.46 (1H, d, J=10 Hz, C_1–H). Found: C, 80.70; H, 9.16%. Calcd for $C_{21}H_{28}O_2$: C, 80.73; H, 9.03%.

*12-Hydroxyabieta-1,8,11,13-tetraen-3-one (**13**).* A solution of **12** (58.4 mg) and boron tribromide (0.05 ml) in dichloromethane (1.5 ml) was allowed to stand at 0—5 °C for 30 min, poured into a mixture of ice and water, and extracted with ether. The ether extract was washed successively with aqueous sodium thiosulfate and water, dried over sodium sulfate, and then evaporated *in vacuo*. The

crude product was chromatographed on silica gel (3.0 g), using ether–benzene (3:97) as the eluent, to give **13** (45.9 mg: 82.3%), which was recrystallized from acetone–hexane, mp 175.5—176.5 °C, $[\alpha]_D$ +162° (*c* 0.500, EtOH) (lit,[12] mp 175—178 °C, $[\alpha]_D$ +163° (EtOH)); IR: 3607, 3357, 1665 cm^{-1}; NMR (90 MHz): 1.16, 1.18, and 1.36 (each 3H and s, $-\dot{C}(CH_3)_2$ and C_{10}–CH_3), 1.22 (6H, d, J=7 Hz, $-CH(C\underline{H}_3)_2$), 3.15 (1H, m, $-C\underline{H}(CH_3)_2$), 5.73 (1H, s, –OH), 5.94 (1H, d, J=10 Hz, C_2–H), 6.69 and 6.78 (each 1H and s, C_{11}–H and C_{14}–H), 7.43 (1H, d, J=10 Hz, C_1–H). Found: C, 80.21; H, 8.92%. Calcd for $C_{20}H_{26}O_2$: C, 80.49; H, 8.78%.

*12-Methoxyabieta-2,8,11,13-tetraen-1α-ol (**15**).* A solution of **12** (500 mg) in methanol (75 ml) and dichloromethane (25 ml) was cooled to −15 °C and over *ca.* 6 min was added dropwise 30% hydrogen peroxide (0.92 ml), followed by 10% aqueous sodium hydroxide (3.24 ml), in a stream of nitrogen. The solution was stirred at −10——5 °C for 2 h, poured into water (50 ml), and extracted with ether. The ether extract was washed with brine, dried over sodium sulfate, and then evaporated to give the corresponding epoxy ketone (**14**) (525 mg).

A solution of the crude epoxy ketone (**14**: 140 mg) in methanol (10 ml) was cooled to 0 °C in a stream of nitrogen and a mixture of hydrazine hydrate (0.65 ml) and acetic acid (0.13 ml) was added dropwise over a 3 min period. The reaction mixture was stirred at 0—5 °C for an additional 15 min, at room temperature for 15 min, and then refluxed for 13.5 h. After the methanol had been evaporated *in vacuo*, the residue was extracted with ether. The ether extract was washed successively with aqueous sodium hydrogencarbonate and brine, dried over sodium sulfate, and then evaporated *in vacuo*. The crude product was chromatographed on silica gel (10 g), using ether–benzene (1:99) as the eluent, to give **15** (65.6 mg: 48.9% from **12**) as an oil, $[\alpha]_D$ +251° (*c* 3.49), IR: 3550 cm^{-1}; NMR: 0.98, 1.08, and 1.17 (each 3H and s, $-\dot{C}(CH_3)_2$ and C_{10}–CH_3), 1.19) (6H, d, J=7 Hz, $-CH(C\underline{H}_3)_2$), 1.41 (1H, s, –OH, disappeared on deuteration), 3.21 (1H, m, $-C\underline{H}(CH_3)_2$), 3.78 (3H, s, $-OCH_3$), 4.23 (1H, d, J=5 Hz, C_1–H), 5.64 (2H, m, C_2–H and C_3–H), 6.59 and 6.77 (each 1H and s, C_{11}–H and C_{14}–H). Found: C, 80.16; H, 9.90%. Calcd for $C_{21}H_{30}O_2$: C, 80.21; H, 9.62%.

*12-Methoxyabieta-2,8,11,13-tetraen-1-one (**16**).* A solution of **15** (170 mg) in acetone (3.0 ml) was oxidized at −12——6 °C for 5 min with Jones reagent (2.5 M: 0.2 ml) and then diluted with ether. The ether solution was washed with brine, dried over sodium sulfate, and evaporated *in vacuo*. The crude product was purified by column chromatography on silica gel (10 g), using benzene as the eluent, to give **16** (133 mg: 78.2%), which was recrystallized from hexane, mp 106.5—107 °C, $[\alpha]_D$ +333° (*c* 4.60), IR: 1677 cm^{-1}; NMR: 1.17 (6H, d, J=7 Hz, $-CH(C\underline{H}_3)_2$), 1.19 (6H, s, $-\dot{C}(CH_3)_2$), 1.47 (3H, s, C_{10}–CH_3), 3.21 (1H, m, $-C\underline{H}(CH_3)_2$), 3.74 (3H, s, $-OCH_3$), 5.78 (1H, d, J=10 Hz, C_3–H), 6.38 (1H, d, J=10 Hz, C_2–H), 6.66 and 7.22 (each 1H and s, C_{11}–H and C_{14}–H). Found: C, 80.77; H, 9.13%. Calcd for $C_{21}H_{28}O_2$: C, 80.73; H, 9.03%.

*12-Hydroxyabieta-2,8,11,13-tetraen-1-one (Shonanol) (**1**).* A solution of **16** (108.2 mg) and boron tribromide (0.10 ml) in dichloromethane (3.0 ml) was allowed to stand at 0—5 °C for 1 h. After the same work-up as described for the preparation of **13**, the crude product was chromatographed on silica gel (10 g), using ether–benzene (1:99 and then 3:97) as the eluent, to give **1** (76.9 mg: 74.4%) which was recrystallized from ether–hexane, mp 188—189 °C, $[\alpha]_D$ +326° (*c* 0.500, EtOH) (natural shonanol,[1] mp 187—188 °C, $[\alpha]_D$ +3.01 (EtOH)[15]); IR (KBr): 3375, 2960, 1670, 1618, 1515, 1470, 1425, 1376, 1362, 1265, 1205, 1177, 1053, 1020, 947, 883, 825, 816, 750, 715 cm^{-1}; NMR (90 MHz): 1.16 and 1.18 (each 3H, d, and J=7 Hz, $-CH(C\underline{H}_3)_2$), 1.19 (6H, s, $-\dot{C}(CH_3)_2$), 1.49 (3H, s, C_{10}–CH_3), 3.18 (1H, m, $-C\underline{H}(CH_3)_2$), 5.95 (1H, d, J=10 Hz, C_3–H), 6.50 (1H, d, J=10 Hz, C_2–H), 6.67 (1H, s, C_{14}–H), 6.74 (1H, s, C_{12}–OH, disappeared on deuteration), 7.33 (1H, s, C_{11}–H). Found: C, 80.42; H, 8.91%. Calcd for $C_{20}H_{26}O_2$: C, 80.49; H, 8.78%. The IR and NMR spectra of the synthetic **1** were identical with those of natural shonanol.

*12-Acetoxyabieta-2,8,11,13-tetraen-1-one (**17**).* A solution of **1** (39.4 mg) and acetic anhydride (0.3 ml) in pyridine (1.0 ml) was heated at 80—85 °C for 1.5 h. After the usual work-up, the crude product was chromatographed on silica gel (5.0 g), using ether–benzene (1:99) as the eluent, to give **17** (37.0 mg: 82.3%) as an oil, $[\alpha]_D$ +295° (*c* 0.285); IR: 1752, 1678 cm^{-1}; NMR (90 MHz): 1.17 (6H, s, $-\dot{C}(CH_3)_2$), 1.18 (6H, d, J=7 Hz, $-CH(C\underline{H}_3)_2$), 1.47 (3H, s, C_{10}–CH_3), 2.25 (3H, s, $-OCOCH_3$), 5.80 (1H, d, J=10 Hz, C_3–H), 6.40 (1H, d, J=10 Hz, C_2–H), 6.82 (1H, s, C_{14}–H), 7.31 (1H, s, C_{11}–H). Found: C, 77.71; H, 8.48%. Calcd for $C_{22}H_{28}O_3$: C, 77.61; H, 8.29%.

The authors are grateful to Arakawa Chemical Co. Ltd. for a generous gift of rosin. Thanks are also due to Professor Y. T. Lin for kindly supplying the spectral data of natural shonanol.

References

1) Y. T. Lin and K. T. Liu, *J. Chinese Chem. Soc. Taiwan*, **12**, 51 (1965); *Chem. Abstr.*, **63**, 16772 (1965).
2) T. Matsumoto, I. Tanaka, T. Ohno, and K. Fukui, *Chem. Lett.*, **1973**, 321.
3) T. Matsumoto, T. Ohno, H. Fujita, and K. Fukui, *Chem. Lett.*, **1973**, 1117.
4) T. Matsumoto, S. Imai, and S. Yuki, *Bull. Chem. Soc. Jpn.*, **54**, 1448 (1981).
5) W. P. Campbell and D. Todd, *J. Am. Chem. Soc.*, **62**, 1287 (1940).
6) R. C. Cambie and R. A. Franich, *Aust. J. Chem.*, **24**, 117 (1971).
7) R. C. Cambie and T. J. Fullerton, *Aust. J. Chem.*, **24**, 2611 (1971).
8) E. E. van Tamelen and E. G. Taylor, *J. Am. Chem. Soc.*, **102**, 1202 (1980).
9) Y. Yoshiki and T. Ishiguro, *Yakugaku Zasshi*, **53**, 73 (1933).
10) T. Matsumoto, S. Usui, H. Kawashima, and M. Mitsuki, *Bull. Chem. Soc. Jpn.*, **54**, 581 (1981).
11) M. Fetizon and G. Moreau, *Bull. Soc. Chim. Fr.*, **1965**, 3479.
12) Y. L. Chow and H. Erdtman, *Acta Chem. Scand.*, **16**, 1296 (1962).
13) H. W. Whitlock, Jr., P. B. Reichardt, and F. M. Silver, *J. Am. Chem. Soc.*, **93**, 485 (1971).
14) It is well known that epoxidation occurs preferentially from the less hindered α face of the molecule.[3,4,13]
15) It seems that the low specific rotation value for natural shonanol was obtained by a miscalculation.

  Bull. Chem. Soc. Jpn., 54, 2103—2106 (1981)

Improvement of Furan Yield in Oxidation of Crotonaldehyde by Modifying 12-Molybdophosphoric Acid Catalysts

Tian-hsi Tsai, Mamoru Ai,* and Atsumu Ozaki

Research Laboratory of Resources Utilization, Tokyo Institute of Technology, 4259 Nagatsuta, Midori-ku, Yokohama 227

(Received December 1, 1980)

12-Molybdophosphoric acid effective for oxidation of crotonaldehyde to furan was modified in two ways; by adding various cations and by replacing Mo with V or W. Among cations caesium was proved to be most effective in improving the furan yield, by decreasing reactivity of product furan relative to crotonaldehyde, thus minimizing the secondary oxidation of furan to maleic anhydride. The highest efficiency of caesium is associated with its high basicity, while the active catalyst species responsible for the furan formation is acidic in nature. The replacement of Mo by V or W gave rise to decreased activity, in contrast to other oxidations on the same catalyst. The unique character of crotonaldehyde oxidation is discussed.

It is known that acrylaldehyde and methacrylaldehyde are oxidized to acrylic acid and methacrylic acid, respectively, over V_2O_5- or MoO_3-based catalysts, while crotonaldehyde is oxidized to furan, instead of crotonic acid on the same catalyst.[1] Recently, it was found that heteropoly compounds such as 12-molybdophosphoric acid are effective as catalyst for the furan formation from crotonaldehyde and that an acidic caesium salt of 12-molybdophosphoric acid gives a higher yield than the 12-molybdophosphoric acid.[2]

It would be of interest to see how the yield of furan is affected by modification of the 12-molybdophosphoric acid catalyst. The present paper deals with the effect of partial relpacement of the catalyst protons by various cations and that of the catalyst molybdenum by vanadium or tungsten on the catalytic performance.

Experimental

Catalysts. Two series of supported heteropoly compounds were used: (i) The first series of catalysts are represented by a general equation of $M_{x/n}H_{3-x}PMo_{12}O_{40}$ where M represent an n valent cation and $O \leqslant x \leqslant 3$ is the extent of proton replacement. The cation M was introduced by adding carbonate (alkali, Ag, and Ba), acetate (Mn, Co, Cu, and Ni), or nitrate (Fe and Bi) to aqueous solution of $H_3PMo_{12}O_{40}$ followed by deposition on pumice by evaporation to dryness. Other procedures were the same as previously reported.[2] (ii) The second series of catalysts are $H_3PMo_6W_6O_{40}$, $H_4PMo_{11}VO_{40}$, and $H_5PMo_{10}V_2O_{40}$. The $H_3PMo_6W_6O_{40}$ catalyst was prepared by mixing aqueous solutions of $H_3PMo_{12}O_{40}$ and $H_3PW_{12}O_{40}$ (Kanto Chemical Co. Inc.). $H_5PMo_{10}V_2O_{40}$ was synthesized following a procedure reported by Tsigdinos.[3] The $H_4PMo_{11}VO_{40}$ catalyst was prepared by mixing aqueous solutions of $H_5PMo_{10}V_2O_{40}$ and $H_3PMo_{12}O_{40}$. Other procedures were the same as those for the series (i).

Reaction Procedures. The vapor-phase oxidation of crotonaldehyde was carried out in an ordinary continuous-flow system. The reactor and the experimental procedures were the same as those employed in the preceding work.[2]

Results

Effect of Cs^+. The oxidation of crotonaldehyde was carried out over a series of $Cs_xH_{3-x}PMo_{12}O_{40}$ catalysts with $x=0$, 0.5, 1.0, 1.5, and 2.0 (amount of catalyst used=20 g), using a fixed concentration of reaction mixture: $C_4H_6O/O_2/H_2O/N_2=1.66/6.6/7.6/84.1$ mol% and a total flow rate of 1.0 l/min. Variation of furan yield with reaction temperature are shown for the Cs-exchanged catalysts in Fig. 1. The catalytic activity to give furan clearly decreases with increase in the caesium content at a fixed temperature, while the maximum yield of furan attained at a different temperatures increases with increase in caesium content up to $x=1.0$, and remains constant at about 40 mol% in the range of $x=1$ to 2.

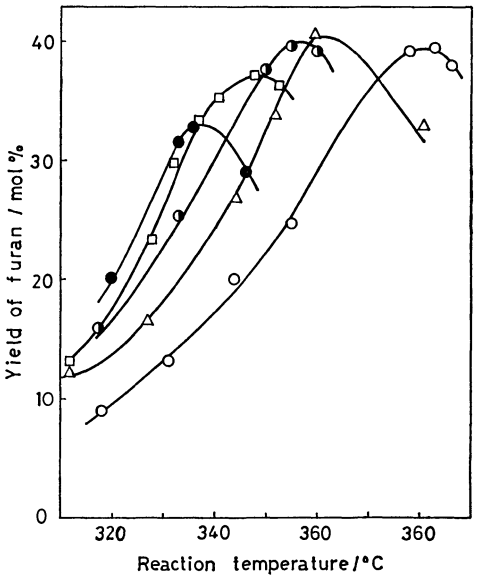

Fig. 1. Variation of furan yield with reaction temperature.
Catalysts=$Cs_xH_{3-x}PMo_{12}O_{40}$. Caesium content($x$): (●)=0, (□)=0.5, (◑)=1.0, (△)=1.5, (○)=2.0.

The yield of furan is plotted as a function of the overall conversion of crotonaldehyde in Fig. 2. The furan yield increases with increase in the conversion and passes a maximum. The conversion of crotonaldehyde to give the maximum yield of furan increases from 83 to 92% with the addition of caesium up to $x=1.0$ and remains almost constant at 92 to 95% in the range of $X=1.0$ to 2.0. As demonstrated in the preceding papers the product furan is consecutively oxidized to maleic anhydride on the heteropoly-acid catalyst so that the maximum yield of furan is determined by reactivity of furan relative to crotonaldehyde

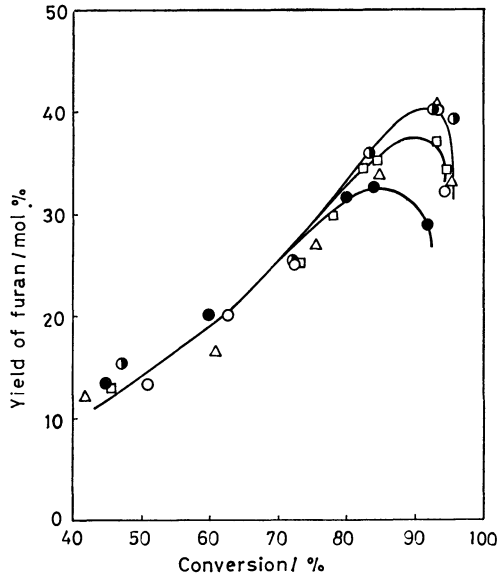

Fig. 2. Yield of furan as a function of the overall conversion of crotonaldehyde.
Catalysts=$Cs_xH_{3-x}PMo_{12}O_{40}$. Casesium content($x$): (●)=0, (□)=0.5, (◑)=1.0, (△)=1.5, (○)=2.0.

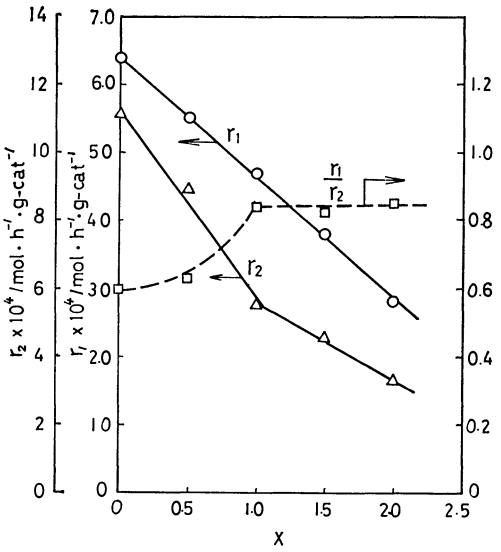

Fig. 3. Effect of the caesium content on the rate of furan formation and that of furan consumption. r_1=Rate of furan formation from crotonaldehyde, r_2=rate of furan consumption, catalysts=$Cs_xH_{3-x}PMo_{12}O_{40}$.

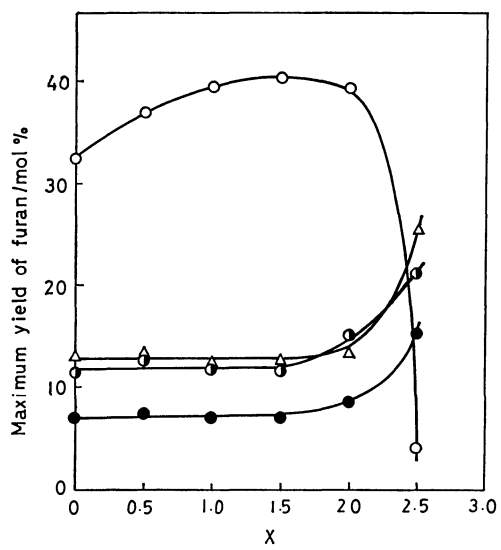

Fig. 4. Effect of caesium content on the yields of furan, maleic anhydride, CO, and CO_2 at a conversion of 85 to 90%.
(○)=Furan, (△)=maleic anhydride, (●)=1/4 CO, (◑)=1/4 CO_2, catalysts=$Cs_xH_{3-x}PMo_{12}O_{40}$.

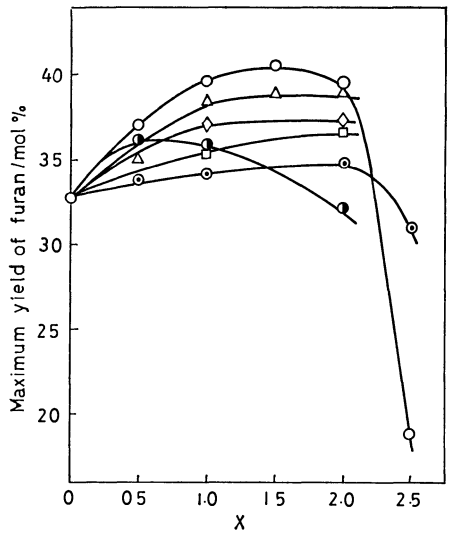

Fig. 5. Effect of the content of univalent cations on the maximum yield of furan.
Catalysts=$M_xH_{3-x}PMo_{12}O_{40}$, (○)=Cs^+, (◇)=Rb^+, (□)=K^+, (⊙)=Na^+, (◑)=Li^+, (△)=NH_4^+.

on the catalyst. The observed increase in the maximum yield of furan suggests that the reactivity ratio of furan to crotonaldehyde decreases with the caesium addition up to $x=1.0$.

In order to examine the relative reactivity of furan, initial rate of furan formation from crotonaldehyde (concentration=1.66 mol%), r_1, and that of furan consumption (concentration=0.96 mol%), r_2, were determined at 330 °C over the Cs-exchanged catalysts. The results are shown in Fig. 3. The ratio r_1/r_2 really increases with x up to $x=1.0$ and remains constant in the range of $x=1.0$ to 2.0 in agreement with the above suggestion.

The yield of furan, maleic anhydride, CO, and CO_2 obtained at a conversion of 85 to 90% are shown in Fig. 4 as a function of x. It is seen that the product distribution is much less affected by the caesium content up to $x=2.0$ than in the range $x>2$. It is clear that the x value should be kept below 2 to give higher yield of furan.

Effect of Univalent Cations. Analogous effect of other univalent cations was examined with Li^+, Na^+, K^+, Rb^+, and NH_4^+. Figure 5 shows variation of the maximum yield of furan as a function of x. The maximum yield was mostly attained at the aldehyde conversion of about 90 to 95%. It is seen that the maximum yield of furan generally increases with x

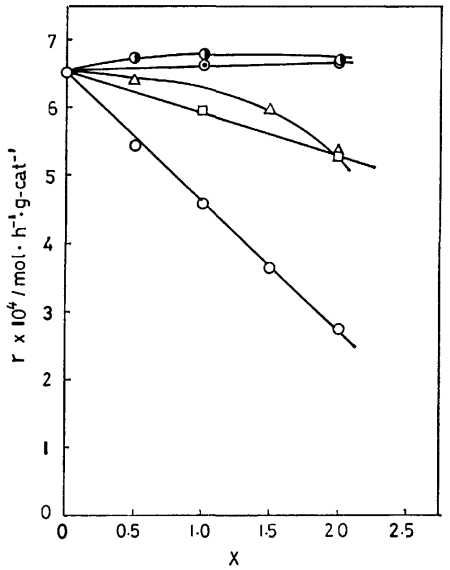

Fig. 6. Effect of the content of univalent cations on the rate of furan formation.
Temperature=330 °C. Catalysts=$M_xH_{3-x}PMo_{12}O_{40}$, (○)=Cs^+, (□)=K^+, (⊙)=Na^+, (◑)=Li^+, (△)=NH_4^+.

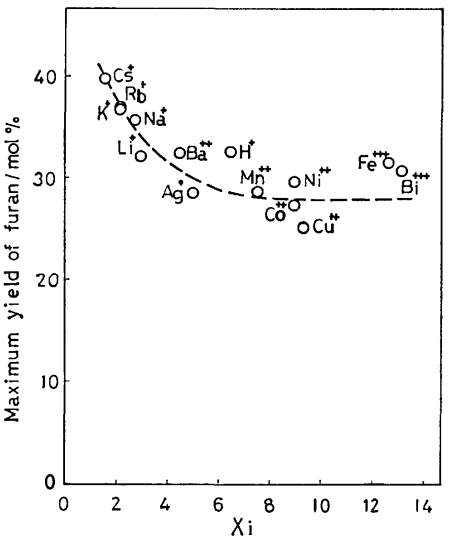

Fig. 7. Maximum yield of furan obtained with the $M_{2/n}HPMo_{12}O_{40}$ catalysts as a function of the electronegativity of metal cation, X_i.

value up to respective maximum, while the yield of furan at the maximum decreases in the order of $Cs^+ > NH_4^+ > Rb^+ > K^+ > Na^+$. It is clear that caesium is the most effective in improving the furan yield.

Thus, the effect of alkali substitution on the initial rate of furan formation was examined at 330 °C. As shown in Fig. 6 as a function of x value, the inhibitive effect of cation is largest with Cs^+, less marked with K^+ and NH_4^+, and nondetectable with Li^+ and Na^+. The large inhibitive effect of Cs^+ seems to be associated with the favorable results on Cs-catalyst.

Effect of Other Cations. Analogous effect of other cations was studied with Fe^{3+}, Bi^{3+}, Cu^{2+}, Ni^{2+}, Co^{2+}, Mn^{2+}, Ba^{2+}, and Ag^+. No clear improvement in the oxidation activity was observed by the addition of

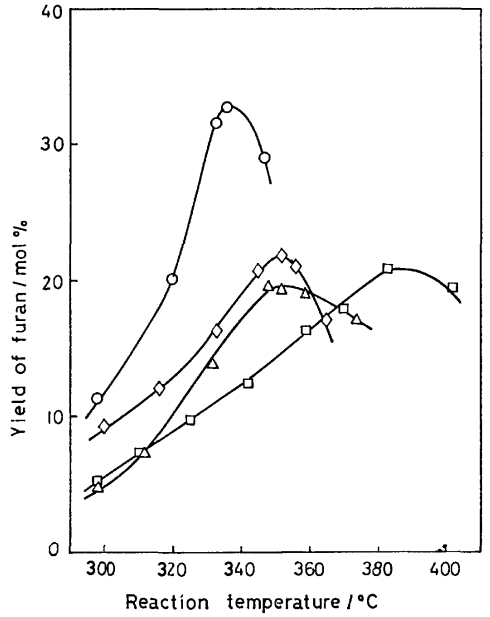

Fig. 8. Yield of furan obtained on $H_3PMo_{12}O_{40}$, $H_3PMo_6W_6O_{40}$, $H_4PMo_{11}VO_{40}$, and $H_5PMo_{10}V_2O_{40}$ catalysts.
(○)=$H_3PMo_{12}O_{40}$, (△)=$H_3PMo_6W_6O_{40}$, (◇)=$H_4PMo_{11}VO_{40}$, (□)=$H_5PMo_{10}V_2O_{40}$.

these cations up to $x=2$. Summarizing the effect of metal cations examined above, imporvement in furan yield is generally made by more basic elements. Thus, the maximum yield of furan obtained on the series (i) catalysts with $x=2$ are plotted against the electronegativity of metal cation, X_i, which can be regarded a parameter of acidity of cation. Although the reaction temperature to give the maximum yields were different from each other, it is apparent from Fig. 7 that the maximum furan yield decreases with increase in the acidity of metal cation added, in agreement with the above generalization.

Replacement of Mo Atom in $H_3PMo_{12}O_{40}$ by W or V. The oxidation of crotonaldehyde was carried out on the series (ii) catalysts under the same reaction conditions as adopted for the series (i) catalysts. The results obtained on $H_3PMo_6W_6O_{40}$, $H_4PMo_{11}VO_{40}$, and $H_5PMo_{10}V_2O_{40}$ catalysts are compared with those of $H_3PMo_{12}O_{40}$ catalyst in Fig. 8. It is clear that the replacement of Mo atom of $H_3PMo_{12}O_{40}$ by W or V results in decreases in the oxidation activity as well as in the maximum yield of furan.

Discussion

As demonstrated by the above results, the attainable furan yield in the oxidation of crotonaldehyde on the heteropoly acid catalysts is improved by adding basic element to the catalyst. Since complete replacement of the acidic proton results in loss of the catalytic activity, the improvement is likely caused by a partial neutralization of the acid. The result shown in Fig. 3 clearly demonstrated that the high furan yield is realized by increase in stability or decrease in reactivity of furan relative to crotonaldehyde on the catalyst surface. The reactivity decrease by the incorpora-

tion of caesium ion is associated with a decrease in acidity,[4] in conformity with the partial neutralization suggested above. The results shown in Fig. 7 suggest that the highest yield obtained with the Cs–HPA catalyst is ascribed to the highest basicity of caesium. Indeed other elements of less basicity are less efficient in reducing reactivity of crotonaldehyde as shown in Fig. 6.

On the other hand, the reactivity decrease caused by the incorporation of basic element indicates an active site acidic in nature. It is reported in the preceding paper that the rate of furan formation increases with partial pressure of water vapor.[2] In connection with this, it is known that enolization of crotonaldehyde requires water, *i.e.*[5]

$$CH_3\text{-}CH{=}CHCHO \overset{H^+,\ H_2O}{\rightleftharpoons} CH_3\text{-}\underset{OH}{CH}\text{-}CH{=}CHOH.$$

Since the trans-form predominates in crotonaldehyde, it is required to take a cis-form before cyclization to furan. The water-enhanced enolization would provide a chance for cyclization. Thus the water-promoted furan formation can be understood in terms of acid catalysis as suggested by the inhibitive effect of caesium. The enhancement of enolization would be another role of water in addition to the enhancement of furan desorption as suggested in the previous paper.[2]

The effect of caesium addition to heteropoly acid catalyst is also known with oxidation of methacrylaldehyde,[4] isobutyraldehyde,[6] butadiene,[7] and ethyl methyl ketone.[4] It is commonly observed that the catalytic activity increases with the caesium addition up to $x=2$, in a striking contrast to the present result. It is accordingly suggested that the nature of present oxidation of crotonaldehyde is quite different from others. Indeed, the oxidation of crotonaldehyde is unique in the kinetic behavior. The rate of furan formation is nearly zero order with respect to oxygen pressure,[2] whereas the rates of other oxidations are 0.5 to 1.0 order in oxygen.[4] This would be reasonable in view of the difference in the oxidation reaction to be undertaken. Methacryladehyde is oxidized to methacrylic acid, while crotonaldehyde is oxidized to furan, on the same catalyst. Since no furan formation was found in the oxidation of crotonic acid on the heteropoly-acid catalyst, crotonic acid cannot be the intermediate from crotonaldehyde to furan. Thus it is clear that the oxidation of crotonaldehyde is completely different from that of methacrylaldehyde although they are structural isomers. This difference in the nature of oxidation reaction should give rise to difference in the type of activation of reactant molecule.[4]

The last results shown in Fig. 8 may be understood on the ground of above concept. Partial replacement of Mo in $H_3PMo_{12}O_{40}$ with V is reported to enhance the oxidation of methacrylaldehyde[8] or isobutyraldehyde,[9] while it results in decrease in the activity to form furan from crotonaldehyde. It is likely that the replacement with V increases oxidizing activity which is essential for those oxidations, while modifies the acidic nature which is essential for the furan formation.

References

1) M. Ai and M. Ishihara, *Kogyo Kagaku Zasshi*, **73**, 2152 (1970).
2) M. Ai, T. Tsai, and A. Ozaki, *Bull. Chem. Soc. Jpn.*, **53**, 2647 (1980).
3) G. A. Tsigdinos, *Ind. Eng. Chem., Prod. Res. Dev.*, **13**, 267 (1974).
4) M. Ai, Preprint, 46th Disc. Meeting, Cat. Soc. Jpn., 1980, A3P14; *J. Catal.*, in press.
5) W. A. Waters and J. S. Littler, "Oxidation in Organic Chemistry," ed by K. Wiberg, Academic Press (1965).
6) M. Akimoto, Y. Tsuchida, and E. Echigoya, Preprint, 46th Disc. Meeting, Cat. Soc. Jpn., 1980, B-1C04; *Shokubai*, **22**, 214.
7) M. Ai, *J. Catal.* **67**, 110 (1981).
8) S. Nakamura and H. Ichihashi, Preprint, 7th Int. Congr. Catal. Tokyo, 1980, B1.
9) M. Otake and T. Onoda, *Shokubai*, **18**, 169 (1976).

Stereospecific and Stereoselective Reactions. V.[1] Alkylation of Active Methylene Compounds by the Use of Alcohols, Diethyl Azodicarboxylate, and Triphenylphosphine[2]

Toshio KURIHARA, Masaru SUGIZAKI, Itaru KIME, Makoto WADA, and Oyo MITSUNOBU*

Department of Chemistry, College of Science and Engineering, Aoyama Gakuin University, Chitosedai, Setagaya-ku, Tokyo 157

(Received December 4, 1980)

The reagent formed by the reaction of diethyl azodicarboxylate (**1**) and triphenylphosphine (**2**) reacted with alcohols and ethyl cyanoacetate (**6**) to give alkylated products in 30—80% yields. When ethyl acetoacetate, 1,3-cyclopentanedione, or 1,3-cyclohexanedione was used in place of **6**, the corresponding *O*-alkylated products were obtained. The reaction of either (*S*)-(−)-ethyl lactate or (*S*)-(−)-ethyl 2-hydroxy-3-phenylpropionate with **1**, **2**, and **6**, followed by hydrolysis resulted in the formation of (*S*)-(−)-methylsuccinic acid or (*S*)-(−)-benzylsuccinic acid. The results indicate that nearly complete inversion of the configuration takes place in the alkylation step.

Alkylation of anions derived from active methylene compounds furnishes a synthetically useful reaction producing carbon to carbon bonds. A number of bases are effective for removing a proton from the carbon atom alpha to an electron-withdrawing group, but only a few alkylating reagents are utilized in the alkylation of the carbanions.[3]

It was reported that the reaction of diethyl azodicarboxylate (**1**) and triphenylphosphine (**2**) in the presence of an alcohol and an acidic component gives an alkoxyphosphonium salt intermediate (**5**) which functions as a versatile alkylating reagent.[4] The reaction seems to proceed through (a) addition of **2** to **1** giving a quaternary phosphonium salt (**3**),[5] (b) protonation of **3**, (c) formation of an alkoxyphosphonium salt (**5**), and (d) S_N2 type displacement of the resulting species **5** as shown in Scheme 1.

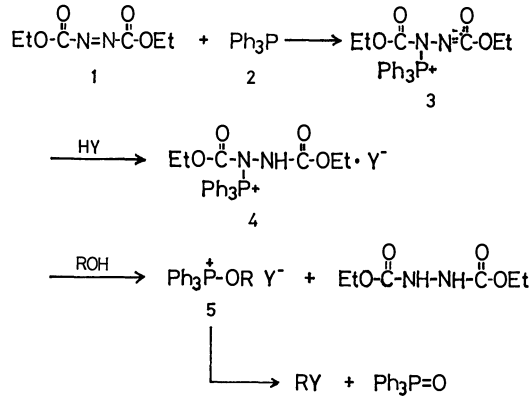

Scheme 1.

Acidic components (Scheme 1; YH) alkylated by this method include phosphoric mono- and diesters, carboxylic acids, imides, phenols, and oximes. Not only simple alcohols but also complex hydroxy compounds such as nucleosides, carbohydrates, and steroids can be used.[4] This paper deals with the alkylation of acyclic and cyclic active methylene compounds by the above reaction.

Alkylation of Ethyl Cyanoacetate. The alkylation of ethyl cyanoacetate (**6**) was carried out under the same conditions as for the preparation of carboxylic esters.[6] Thus, **1** was added to a solution of 1-propanol, **2**, and **6** in tetrahydrofuran (THF) at room temperature (Procedure A). No alkylation of **6** took place, 45% of **6** being recovered. Similarly, no alkylated product was obtained when the reaction was carried out at −10——15 °C. On the other hand, when **1** was added to **2** in THF at −10——15 °C, followed by the addition of **6** and 1-propanol (Procedure B) and the reaction was continued for 1 h, ethyl 2-cyanopentanoate (**7**; R=C_3H_7) was isolated in 29% yield along with dialkylated product, ethyl 2-cyano-2-propylpentanoate (**8**; R=C_3H_7; 3—4%). A small amount of diethyl *N*-propylhydrazine-*N*,*N*′-dicarboxylate (**9**; R=C_3H_7) was also obtained (Scheme 2).

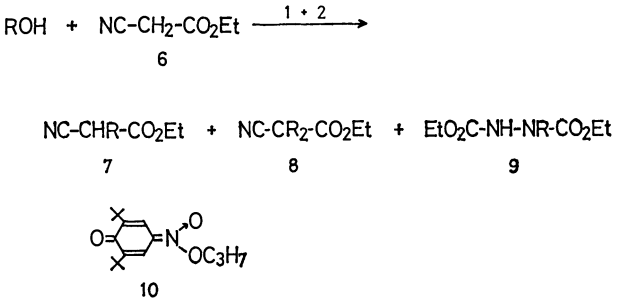

Scheme 2.

In Procedure B, a white fine precipitate is sometimes observed in the initial 5—10 min (1—2 mmol each of **1** and **2**/2—3 ml of THF). Complete disolution takes place on addition of alcohol and **6**, **7** (R=C_3H_7) being obtained in a comparable yield as above. No identification has yet been made but the precipitate seems to be an intermediate in the reaction. Since stirring of the slurry of the adduct is difficult, the alcoholic and acidic components are added preferably before the precipitation of adduct.

It was found that various alcohols can also enter into the reaction under similar conditions. The results are summarized in Table 1.

The formation of **9** suggests that both ethyl cyanoacetate anion and diethyl hydrazinedicarboxylate anion exist in the reaction mixture at equiliblium, the product ratio (**7**/**9**) depending on relative acidity of **6** and diethyl hydrazinedicarboxylate as well as the nucleophilicity of their anions (Scheme 3).[7]

TABLE 1. ALKYLATION OF ETHYL CYANOACETATE (**6**) BY PROCEDURE B

Reactant (mmol) ROH R	1 and 2	6	OH	Reaction time/h (°C; rt, room temperature)	$NC-CHR-CO_2C_2H_5$ Yield %	NMR (CCl_4) δ/ppm
C_3H_7	2 3	2	0	1(−20), 7(−20—0), 10(rt)	51[a]	0.8—1.2(m, $CH_3CH_2CH_2$-), 1.35(t, CH_3CH_2O-), 1.1—2.2(m, $CH_3CH_2CH_2$-), 3.35 (t, NCCH-), 4.3(q, CH_3CH_2O-)
	4 3	2	0	1(−20)[b]	29[c]	
	4 3	2	0	48(−20)[b]	30[d]	
$CH_2=CHCH_2$	4 2	2	0	2(rt)	43[e]	1.3(t, CH_3), 2.5—2.75(3 lines, $=CHCH_2$-), 3.4—3.65(3 lines, NCCH-), 4.22(q, CH_2O-), 4.9—6.2(m, vinyl H)
	1.3 1.5	1	1	10(rt)	24[f]	
EtO_2C CH_3 CH (*dl*)	3 4.5	3	0	24(rt)	45[g]	1.3 and 1.32(two t, CH_3CH_2-), 1.4(d, CH_3CH<), 2.7—3.35(m, CH_3CH<), 3.45—3.9(4 lines, NCCH-), 4.15 and 4.25 (two q, CH_3CH_2O-)
	3 4.5	3	3	24(rt)	62[g]	
EtO_2C C_5H_{11} CH (*dl*)	54 70	54	0	5(−30——20), 12(−10), 10(0), 120 (rt)	83	0.9(m, $CH_3(CH_2)_4$-), 1.3 and 1.35(two t, CH_3CH_2O-), 1—2.2(m, $CH_3(CH_2)_4$-, 2.7—3.2(m, $C_5H_{11}CH$-), 3.65—3.95(4 lines, NCCH-), 4.18 and 4.25(two q, CH_3CH_2-)
	30 40	30	40	12(0), 120(rt)	74	
MeO_2C CH_3CH (*dl*)	2 1.5	1	0	24(rt)	67	1.15 and 1.2(two t, CH_3CH_2-), 1.5(d, CH_3CH-), 3.25—3.8(m, NC-CHCH-), 4.1 and 4.15(two q, CH_3CH_2-), 7.35 and 7.95 (AA'BB', aromatic H)
	2 1.5	1	1.5	24(rt)	79	

a) 12 and 17% yields of **8**($R=C_3H_7$) and **9**($R=C_3H_7$), respectively, 23% of **6** recovered. b) Procedure C. c) 3—4% yield of **8**($R=C_3H_7$). d) 7% yield of **8**($R=C_3H_7$). e) 10% yield of **8**($R=CH_2=CHCH_2$-). f) 21% yield of **8**($R=CH_2=CHCH_2$-), 29% of **6** recovered. g) 10% yield of **9**($R=EtO_2C(CH_3)CH$).

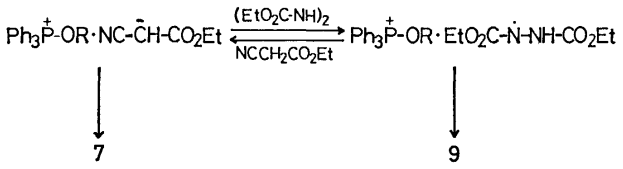

Scheme 3.

The yields of the alkylated products are not so high as compared with those obtained in the alkylation of relatively strong acid such as phosphoric diesters,[8] carboxylic acids,[6] or imides.[9] A possible explanation of the difference is obtained if a protonated phosphonium salt (**4**) is assumed to be an active intermediate for the formation of an alkoxyphosphonium salt (**5**). In the reaction of **6**, equilibrium is not favorable to protonated form (**4**; $Y=CH(CN)CO_2Et$) because of its low acidity. In order to increase the concentration of the protonated form in equilibrium, alkylation of **6** by various alcohols was examined in the presence of 2,6-di-*t*-butylphenol as a proton source. The yields of alkylated products increased to some extent, but no marked effect of the proton source was observed (Table 1). When 2,6-di-*t*-butyl-4-nitrophenol was used in place of 2,6-di-*t*-butylphenol, an *aci*-nitro ester (**10**)[10] was obtained in 70% yield with a 67% recovery of **6**.

Alkylation of Ethyl Acetoacetate. The reaction of ethyl acetoacetate (**11**) with **1**, **2**, and 2-propanol was carried out by Procedure B giving ethyl 3-isopropoxy-2-butenoate (**12a**), 3-[1,2-bis(ethoxycarbonyl)hydrazino]-2-butenoate (**14**), and 3-[2-isopropyl-1,2-bis(ethoxycarbonyl)hydrazino]-2-butenoate (**15a**) in 17, 16, and 12% yields, respectively. Contrary to the case of alkylation of **6**, that of **11** took place even at room temperature by Procedure A giving **12a**, **14**, and **15a** in 6, 40, and 8% yields, respectively (Scheme 4). No *C*-alkylated product (**13a**) could be isolated in these reactions.

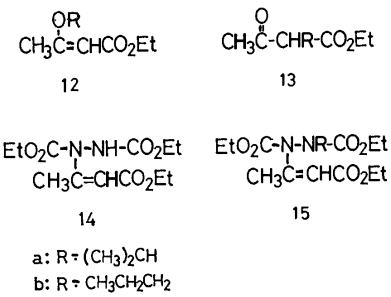

Scheme 4.

The side product **14** would be formed *via* a vinyloxyphosphonium salt (**16**) which arises from the reaction of **3** with **11** (enol form). Collapse of **16** by an addition-elimination process gave rise to **14** and triphenylphosphine oxide (Scheme 5). The assumption is supported by the reaction of **11** with **1** and **2** in

Table 2. Alkylation of ethyl acetoacetate (**11**)

R	ROH	Reactant(mmol) 1 and 2	Reactant(mmol) 11	Procedure	Reaction time/h (°C; rt, room temperature)	Products yield/% 12	Products yield/% 13
$(CH_3)_2CH$	4	3	2	A	48 (rt)	6[a]	0
	4	3	2	B	48 (−20)	17[b]	0
	4	3	2	C	48 (−20)	35	0
C_3H_7	4	3	2	A	24 (rt)	18[c]	0
	8	5	4	B	24 (−20)	18	0
	8	5	4	C	48 (−20)	37	0
	40	5	4	A	72 (rt)	29	6
	40	5	4	C	72 (−20)	30	6

a) 40 and 8% yields of **14** and **15a**, respectively. b) 16 and 12% yields of **14** and **15a**, respectively. c) 8 and 6% yields of **14** and **15b**, respectively.

Table 3. Alkylation of 1,3-cyclohexanedione

ROH	Reactant(mmol)[a] 1 and 2	Procedure	Reaction time/min (°C; rt, room temperature)	Products yield/% 18	Products yield/% 19
$(CH_3)_2CH$	2	A	35 (rt)	81	
	2	B	50 (−20)	74	
C_2H_5>CH $CH_2=CH$	3	A	60 (rt)	36	8
	3	B	60 (−20)	40	13

a) 1,3-Cyclohexanedione; 1.5 mmol.

the absence of an alcoholic component where **14** was obtained in 68% yield. Compound **15** would be produced through a similar intermediate **17**.

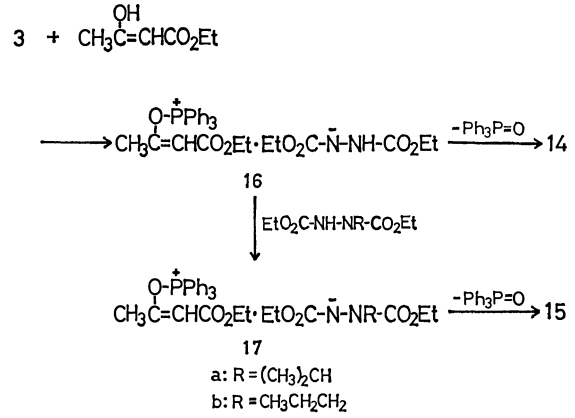

Scheme 5.

In order to suppress the formation of undesirable **14** and **15a**, 2-propanol (2 equivalents) and **11** were successively added to the reaction mixture of **1** with **2** at −10——20 °C (Procedure C). By this procedure, the yield of **12a** increased to 35%.

Similarly, the reaction of 1-propanol with **11** by Procedure A or B resulted in the formation of *O*-alkylated product (**12b**) in 18% yield, the yield increasing to 37% by Procedure C. When 1-propanol was used in large excess (10 equivalents), the *C*-alkylated product (**13b**) was formed in 6—10% yield along with **12b** (30%). The results are summarized in Table 2.

Alkylation of Cyclic 1,3-Diketone. In contrast to the case of acyclic active methylene compounds, the alkylation of cyclic 1,3-diketones proceeded smoothly in a perior of 0.5—1 h, giving *O*-alkylated products in good yields. Thus, when 1,3-cyclohexanedione was allowed to react with 2-propanol, **1**, and **2**, 3-isopropoxy-2-cyclohexenone (**18a**) was isolated by Procedures A and B in 74% and 81% yields, respectively. When 1-penten-3-ol was used in this reaction (Procedure B), 3-(1-ethyl-2-propenyloxy)-2-cyclohexenone (**18b**) and 3-(1-ethyl-2-propenyloxy)-2-(1-ethyl-2-propenyl)-2-cyclohexenone (**19**) were obtained in 40 and 13% yields, respectively (Scheme 6; Table 3). The reaction of 1,3-cyclopentanedione with 1-penten-3-ol by Procedure A resulted in the formation of 3-(1-ethyl-2-propenyloxy)-2-cyclopentenone (**20**) in nearly quantitative yield.

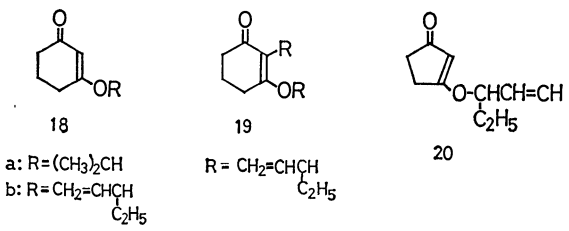

Scheme 6.

Stereochemistry. Intermolecular dehydration between an optically active alcohol and active hydrogen compounds by the use of **1** and **2** proceeds through the inversion of the configuration at the carbon atom bonded to hydroxyl group.[4]

The inversion of configuration was observed in the alkylation of **6**. Thus, (*S*)-(−)-ethyl lactate (**21a**) reacted with **6** in the presence of **1** and **2** to give diethyl 2-cyano-3-methylsuccinate in 61% yield. On hydrolysis, methylsuccinic acid (**22a**) with $[\alpha]_D$ −15.1° was obtained. This indicates that complete or nearly complete inversion of the configuration at the reaction site takes place in the alkylation step. Similarly, (*S*)-

(−)-ethyl 2-hydroxy-3-phenylpropionate (**21b**) was converted into opticcally pure (*S*)-(−)-benzylsuccinic acid (**22b**) (Scheme 7).

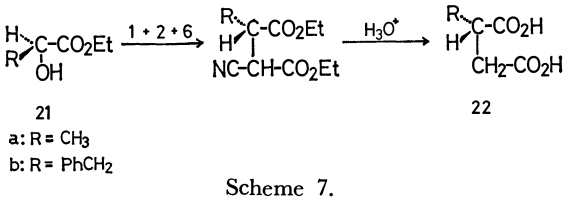

Scheme 7.

Concluding Remarks. The reagent formed by the reaction of **1** and **2** could be utilized in direct condensation between alcohols and active methylene compounds. The reaction proceeds under mild neutral conditions with inversion of configuration at the reaction site. In spite of some reduced yields, a high degree of stereospecificity is observed. The reaction might provide an effective procedure for the synthesis and transformation of natural products.

The fact that the alkylation of 1,3-dicarbonyl compounds mainly gives *O*-alkylated products suggests that the alkoxyphosphonium salt intermediate is a harder alkylating reagent than alkyl halides and alkyl sulfonates.[11] Steric interaction between alkoxyphosphonium salt having three bulky phenyl groups and ambident anion derived from the dicarbonyl compound would also favor *O*-alkylation.

Diethyl malonate can not enter into the alkylation reaction,[2b] suggesting that an active methylene compound to be alkylated should be more acidic than diethyl hydrazinedicarboxylate for achievement of the reaction.

Experimental

The reaction was carried out under anhydrous conditions. Anhydrous tetrahydrofuran (THF) was obtained by distillation from sodium benzophenone ketyl. Unless otherwise stated, the products were isolated by preparative layer chromatography (PLC) carried out on Kieselgel 60 PF_{254} (Merck) or Wakogel-B5 plates (20 cm × 20 cm or 20 cm × 30 cm), visualization being made by UV light or iodine vapor. Nuclear magnetic resonance spectra were measured on a Hitachi R-20 spectrometer (60 MHz) using tetramethylsilane as an internal standard.

Alkylation of Ethyl Cyanoacetate. Procedure A: A solution of **1** (522 mg, 3 mmol) in THF (2 ml) was added dropwise to a solution of **2** (787 mg, 3 mmol), **6** (226 mg, 2 mmol), and 1-propanol (240 mg, 4 mmol) in THF (6 ml) at room temperature. The solution was stirred at room temperature for 2 d. No alkylated product could be obtained, 45% of **6** being recovered.

Procedure B: A solution of **1** (1.3—1.5 mmol) in THF (0.5 ml) was added dropwise to a solution of an equimolar amount of **2** in THF (3 ml) stirred in an ice–salt bath. The intermediate formed in solution by this procedure will be referred to as "adduct." A few min after mixing the components, a solution of **6** (1 mmol) and an alcohol (1—2 mmol) in THF (3 ml) was added at this temperature. Stirring was continued under the conditions shown in Table 1.

Reaction in the Presence of 2,6-Di-t-butylphenol. To the adduct was added a solution of 1 mmol each of **6**, 2,6-di-*t*-butylphenol, and an alcohol in THF (3 ml) at −20 °C. The solution was stirred for appropriate periods of time (Table 1).

Reaction in the Presence of 2,6-Di-t-butyl-4-nitrophenol. To the adduct prepared from 3 mmol each of **1** and **2** in THF (4.5 ml) was added all at once a solution of 1-propanol (4 mmol) and 2,6-di-*t*-butyl-4-nitrophenol (754 mg, 3 mmol) in THF (3 ml). A solution of **6** (2 mmol) in THF (2.5 ml) was then immediately added over a period of 20 min and the resulting solution was kept standing at −20 °C for 10 h. The products were separated by PLC (benzene) giving **10** in 70% (617 mg) yield and recovered **6** (67%). Compound **10** was again applied to silica-gel plates and developed with ether–petroleum ether (1:5) to give semicrystalline sirup which crystallized on trituration with petroleum ether, subliming at 138—141 °C. NMR (CCl_4) δ 1.8—2 (m, $C\underline{H}_3C\underline{H}_2$), 1.13 (s, *t*-$C_4H_9$), 4.25 (t, CH_2O), 7.28 and 7.5 (AB q, J=3 Hz, 2H, vinyl H).

Preparative Scale Experiment. Reaction with Ethyl 2-Hydroxyheptanoate. A solution of **6** (54 mmol) and ethyl 2-hydroxyheptanoate (9.387 g, 54 mmol) in THF (25 ml) was added dropwise at −20——30 °C to a solution of the adduct prepared from 70 mmol each of **1** and **2** in THF (20 ml). After the solution had been stirred at −30——20 °C for 5 h, −10 °C for 12 h, at 0 °C for 10 h, and then at room temperature for 5 d, the solvent was removed under reduced pressure. Ether (30 ml) was added to the residue and precipitate was filtered off. The filtrate was evaporated and the residue was applied to a silica-gel column (Wakogel C-200, 4 cm × 30 cm) and eluted with benzene. Diethyl 2-cyano-3-pentylsuccinate was obtained in 83% yield and purified by distillation; 64%, bp 119—122 °C/0.25 Torr (1 Torr = 133.322 Pa).

The ester was treated with concd HCl under reflux for 15 h. The mixture was extracted with ether and organic layer was evaporated giving pentylsuccinic acid which was recrystallized from hexane; 84% yield, mp 82—83 °C (lit,[12] mp 82.5—83.5 °C) (*R*-(+)-form). NMR (acetone-d_6) δ 1.6—2.0 (m, 11H, C_5H_{11}), 2.3—3.2 (m, 3H, $CHCH_2$), 9.51 (s, 2H, COOH).

Alkylation of Ethyl Acetoacetate. Procedure A: A solution of **1** (3 mmol) in THF (3 ml) was added dropwise to a solution of **2** (3 mmol), **11** (260 mg, 2 mmol), and 2-propanol (4 mmol) in THF (7 ml) at room temperature, and the solution was stirred at room temperature for 2 d. After removal of the solvent *in vacuo*, the residue was applied to silica-gel plates, developed with benzene giving **12a** in 6% (20 mg) yield. The zone containing **14** and **15a** was rechromatographed (AcOEt–CCl_4 = 1:3) affording chromatographically homogeneous **14** and **15a** in 40% (231 mg) and 8% (55 mg) yields, respectively. NMR, **12a** (CCl_4) δ 1.20 (t, $C\underline{H}_3C\underline{H}_2$) and 1.25 (d, $(CH_3)_2CH$); total 9H, 2.15 (s, $C\underline{H}_3$–$\underline{C}$=C<), 3.9 (q, $CH_3C\underline{H}_2$) and 4.3 (septet, $(CH_3)_2C\underline{H}$); total 3H, 4.7 (s, >C=C$\underline{H}$). **14** ($CDCl_3$) δ 1.25 (superimposed t, 9H, three $C\underline{H}_3CH_2$), 2.45 (s, $C\underline{H}_3$–$\underline{C}$=C<), 3.84—4.4 (superimposed q, 6H, $CH_3C\underline{H}_2$), 5.85 (s, >C=C$\underline{H}$–), 7.2—7.5 (br s, NH). **15a** (CCl_4) δ 1.1 (d, $(C\underline{H}_3)_2CH$) and 1.25 (superimposed t, three $C\underline{H}_3CH_2$); total 15H, 2.35 (s, $C\underline{H}_3$–C=C<), 3.7—4.35 (septet and superimposed q, total 7H, three $CH_3C\underline{H}_2$ and $(CH_3)_2C\underline{H}$), 5.5 (s, >C=CH–).

Procedure B: A solution of **1** (3 mmol) in THF (3 ml) was added dropwise to a solution of **2** (3 mmol) in THF (3 ml) stirred in an ice–salt bath. A few min after the components had been mixed, a solution of **11** (2 mmol) and 2-propanol (4 mmol) in THF (4 ml) was added and stirring was continued for 5 h. After the solution had been kept standing for 2 d at *ca.* −20 °C, **12a** **14**, and **15a** were obtained in 17, 16, and 12% yields, respectively.

Procedure C: A solution of 2-propanol (4 mmol) in THF (2 ml) was added all at once at −20 °C to a solution of the adduct prepared from 3 mmol each of **1** and **2** in THF (4 ml). Immediately after the addition of 2-propanol, a solution of **11** (2 mmol) in THF (2 ml) was added dropwise over a period of 15 min at −20 °C. The reaction mixture was stirred for 1.5 h and then kept standing at −20 °C for 2 d. The products were separated by PLC giving **12a** in 35% yield. Small amounts of **14** and **15a** were also formed as indicated by thin layer chromatography of the crude reaction mixture, no attempt being made to isolate them.

When 1-propanol was used in large excess (10 equivalents), a mixture of *C*-alkylated and *O*-alkylated products were obtained. The ratio was estimated from integration of the signal of NMR spectrum.

*Preparation of **14***. Compound **1** (3 mmol) in THF (2 ml) and **11** (2 mmol) in THF (2 ml) were successively added to a solution of **2** (3 mmol) in THF (3.5 ml) at −20 °C, and the mixture was kept standing at −20 °C for 2 d. Compound **14** was isolated by PLC (AcOEt–CCl_4=1:3) in 68% (390 mg) yield.

Alkylation of 1,3-Cyclohexanedione. Procedure A: A solution of **1** (2 mmol) in THF (3 ml) was added dropwise over a period of 10 min to a solution of **2** (2 mmol), 2-propanol (2 mmol), and 1,3-cyclohexanedione (1.5 mmol) in THF (6 ml) at room temperature. After the solution had been stirred at room temperature for 35 min, water (4 ml) was added, and extracted with $CHCl_3$. The organic layer was evaporated and the residue was separated by PLC (AcOEt–petroleum ether=1:1) giving **18a** which was contaminated with a small amount of diethyl hydrazinedicarboxylate. The crude product was suspended in CCl_4, stirred, and filtered in order to remove undissolved diethyl hydrazinedicarboxylate to give practically pure **18a**, 188 mg (81%). A pure sample was obtained by distillation, bp (oven temperature) 58—68 °C/35 Torr. NMR (CCl_4) δ 1.25 (d, $(C\underline{H}_3)_2CH$), 1.6—2.5 (m, $-(CH_2)_3-$), 4.4 (septet, $(CH_3)_2C\underline{H}$), 5.13 (s, $>C{=}C\underline{H}-$).

Procedure B: A solution of 1-penten-3-ol (258 mg, 3 mmol) and 1,3-cyclohexanedione (168 mg, 1.5 mmol) in THF (3 ml) was added over a period of 15 min to a solution of the adduct prepared from 3 mmol each of **1** and **2** in THF (7 ml) cooled in an ice–salt bath. Thin layer chromatography of the reaction mixture revealed that the cyclohexanedione disappeared in 10 min after the addition. The reaction mixture was stirred for 1 h and water was added. The mixture was extracted with $CHCl_3$ and the organic layer was evaporated. The residue was applied to silica-gel plates and developed with ether–petroleum ether=3:1 giving **18b** (108 mg, 40%) and **19** (48 mg, 13%). NMR; **18b** (CCl_4) δ 0.9 (t, CH_3), 1.25—2.55 (m, CH_3CH_2 and $-(CH_2)_3-$), 4.37 (q, CH–O), 4.85—5.95 (m, 4H, vinyl H). **19** (CCl_4) δ 0.75 (t, CH_3), 0.95 (t, CH_3), 0.9—2.6 (m, two $CH_3C\underline{H}_2$ and $-(CH_2)_3-$), 3.35 (q, $\equiv C-C\underline{H}(C_2H_5)CH{=}CH_2$), 4.4 (q, CH–O), 4.5—6.2 (m, 6H, vinyl H).

Alkylation of 1,3-Cyclopentanedione. A solution of 1,3-cyclopentanedione (147 mg, 1.5 mmol) and 1-penten-3-ol (172 mg, 2 mmol) in *N,N*-dimethylformamide (1 ml) was added at −17 °C to the adduct prepared by the reaction of 2 mmol each of **1** and **2** in THF (2 ml). The solution was stirred at −17——12 °C for 1.5 h and then at room temperature overnight. The products were separated by PLC (ether) to give **20** in 93% yield. NMR (CCl_4) δ 1.0 (t, CH_3), 1.7 (m, $CH_3C\underline{H}_2$), 2.1—2.8 (A_2B_2, $-CH_2CH_2-$), 4.5 (q, CH–O), 5—6.15 (m, 5H, vinyl H).

Preparation of (S)-(−)-*Methylsuccinic Acid*. A solution of (*S*)-(−)-ethyl lactate [1.53 g, 13 mmol, $[\alpha]_D^{19}$ −10.9° (neat)], **6** (1.13 g, 10 mmol), and 2,6-di-*t*-butylphenol (2.06 g, 10 mmol) in THF (17 ml) was added dropwise to a solution of the adduct prepared from 15 mmol each of **1** and **2** in THF (5 ml) at −20 °C. After the solution had been stirred at −20 °C for 3 h and then at room temperature for 1 d the solvent was removed *in vacuo*. Ether was added and the precipitate was filtered off. The filtrate was concentrated and the products were separated by PLC ($CHCl_3$) giving diethyl 2-cyano-3-methylsuccinate in 61% (1.29 g) yield, $[\alpha]_D^{20}$ −2.76° (*c* 6.03, CCl_4). The product was contaminated by small amounts of two side products as indicated by gas chromatography (OV-1, 1 m, column temperature was 140 °C in initial 6 min and then raised at a rate of 5 °C/min, retention time; the succinate, 2.3 min, unknown side products, 4 and 12.5 min, respectively).

The succinate (1.13 g, 5.3 mmol) was treated with acetic acid (1 ml) and concd HCl (4 ml) under reflux for 6 h and then 4 ml of concd HCl was added. After the mixture had been refluxed for 10 h, ether was added. Organic layer was concentrated to dryness giving crude methylsuccinic acid (502 mg, mp 80—85 °C). Recrystallization from hexane–CH_2Cl_2 (1:1) caused a rise in the melting point to 100—103 °C, $[\alpha]_D^{20}$ −12.5° (*c* 1.82, EtOH). Recrystallization for the second time from the same solvent system gave a pure sample, mp 109—109.5 °C, $[\alpha]_D^{19}$ −15.1° (*c* 0.818, EtOH) [lit,[13] mp 111—113 °C, $[\alpha]_D^{24.2}$ −15.0 (*c* 1.89, EtOH)].

Preparation of (S)-(−)-Benzylsuccinic Acid. (*S*)-(−)-Ethyl 2-hydroxy-3-phenylpropionate [1.94 g, 10 mmol, $[\alpha]_D$ −22.7° (*c* 0.852, benzene), lit [14] $[\alpha]_D$ −22.6° (*c* 4.33, benzene)] was allowed to react with 10 mmol each of **1**, **2**, and **6** by Procedure B. After the addition of the hydroxy ester and **6**, the solution was stirred at room temperature for 2 h. Diethyl 2-benzyl-3-cyanosuccinate was isolated by distillation (250 mg, 8.7%, bp 130 °C/0.25 Torr). The succinate was treated with a mixture of acetic acid (2.5 ml) and concd HCl (11.3 ml) under reflux for 10 h giving (*S*)-(−)-benzylsuccinic acid (159 mg, 88%) which was recrystallized from water, mp 153—154 °C, $[\alpha]_D^{21}$ −28.9° (*c* 0.665, AcOEt) [lit,[14] mp 159—161 °C, $[\alpha]_D^{26}$ −26° (*c* 1.5, AcOEt)].

References

1) Part IV: O. Mitsunobu, T. Kudo, M. Nishida, and N. Tsuda, *Chem. Lett.*, **1980**, 1613.

2) a) Taken in part from M. Sc. Tesis of Toshio Kurihara, Aoyama Gakuin University, Tokyo, 1976; b) Preliminary communication; M. Wada and O. Mitsunobu, *Tetrahedron Lett.*, **1972**, 1279.

3) H. O. House, "Modern Synthetic Reactions," 2nd ed, W. A. Benjamin, Inc., Menlo Park, California (1972), pp. 492—628.

4) For reviews, see O. Mitsunobu, *Synthesis*, **1981**, 1; A. G. Rowley in "Organophosphorus Reagents in Organic Synthesis," ed by J. I. G. Cadogan, Academic Press, London (1979), pp. 327—335.

5) E. Brunn and R. Huisgen, *Angew. Chem., Int. Ed. Engl.*, **8**, 513 (1969).

6) O. Mitsunobu and M. Yamada, *Bull. Chem. Soc. Jpn.*, **40**, 2380 (1967); O. Mitsunobu, J. Kimura, K. Iiizumi, and N. Yanagida, *ibid.*, **49**, 510 (1976).

7) See for example, G. Grynkiewicz, J. Jurczak, and A. Zamojski, *Bull. Acad. Pol. Sci.*, **XXIV**, 83 (1976); G. Grynkiewicz and J. Jurczak, *Carbohydr. Res.*, **43**, 188 (1975).

8) O. Mitsunobu and M. Eguchi, *Bull. Chem. Soc. Jpn.*,

44, 3427 (1971).

9) O. Mitsunobu, M. Wada, and T. Sano, *J. Am. Chem. Soc.*, **94**, 679 (1972); M. Wada, T. Sano, and O. Mitsunobu, *Bull. Chem. Soc. Jpn.*, **46**, 2833 (1973).

10) J. Kimura, A. Kawashima, M. Sugizaki, N. Nemoto, and O. Mitsunobu, *J. Chem. Soc., Chem. Commun.*, **1979**, 303.

11) T. -L. Ho, "Hard and Soft Acids and Bases Principle in Organic Chemistry," Academic Press, New York, N. Y. (1977). For the alkylation of ambident nucleophiles by the use of **1**, **2**, and an alcohol, see also H. Loibner and E. Zbiral, *Helv. Chim. Acta*, **59**, 2100 (1976); H. Nagasawa and O. Mitsunobu, *Bull. Chem. Soc. Jpn.*, **54**, 2223 (1981).

12) J. J. Gordon J. P. Devlin, A. J. East, W. D. Ollis, I. O. Sutherland, D. E. Wright, and L. Ninet, *J. Chem. Soc., Perkin Trans. 1*, **1975**, 819.

13 E. J. Eisenbraum and S. M. McElvain, *J. Am. Chem. Soc.*, **77**, 3383 (1955).

14) S. G. Cohen and S. Y. Weinstein, *J. Am. Chem. Soc.*, **86**, 5326 (1964).

15) S. G. Cohen and A. Milovanovic, *J. Am. Chem. Soc.*, **90**, 3495 (1968).

  Bull. Chem. Soc. Jpn., 54, 2113—2119 (1981)

An Occurrence of Attractive Alkyl-Phenyl Interaction. The Conformations of Several 1-Phenyl-2-alkanols

Shoji Zushi, Yoshio Kodama, Yoshimasa Fukuda, Ken Nishihata, Motohiro Nishio,* Minoru Hirota†, and Jun Uzawa††

Central Research Laboratories, Meiji Seika Kaisha, Ltd., Morooka, Kohoku-ku, Yokohama 222

† *Department of Applied Chemistry, Faculty of Engineering, Yokohama National University, Tokiwadai, Hodogaya-ku, Yokohama 240*

†† *The Institute of Physical and Chemical Research, Wako 351*

(Received December 5, 1980)

The conformations have been studied, by means of NMR spectroscopy, for a series of 1-alkyl-substituted 2-phenylethyl alcohols with the structure $C_6H_5CH_2CH(OH)$-R, where R=CH_3 (**1**), C_2H_5 (**2**), i-C_3H_7 (**3**), and t-C_4H_9 (**4**). It has been suggested that a rotamer in which the phenyl group is oriented *gauche* to the alkyl (R) and *anti* to the hydroxyl group is most populated in the conformational equilibria of **1**—**3**. Another rotamer (in which Ph is *anti* to R) has, on the other hand, been suggested to be preferred in the conformational equilibrium of **4**. The results have been discussed in the light of the presence of an attractive alkyl-phenyl interaction (CH-π interaction).

In connection with the general interest in the conformational problems of acyclic compounds, we have now studied the conformations of a series of benzylic alcohols with the following structures:

$C_6H_5CH_2CH(OH)$-R

R=CH_3 (**1**), C_2H_5 (**2**), i-C_3H_7 (**3**), and t-C_4H_9 (**4**).

Results

Tables 1 and 2 list the proton and carbon NMR parameters, respectively, for a series of 1-alkyl-substituted 2-phenylethyl alcohols: 1-phenyl-2-propanol (**1**), 1-phenyl-2-butanol (**2**), 3-methyl-1-phenyl-2-butanol (**3**), 3,3-dimethyl-1-phenyl-2-butanol (**4**). Parts of the ^{1}H NMR spectra are reproduced in Fig. 1.

An inspection of the tables and figures reveals several interesting facts. First, the signal attributed to the OH proton moves progressively to a higher magnetic field as the alkyl group, R, goes from the methyl group through the ethyl and isopropyl groups and then to the t-butyl group. The shape of the OH peak is a sharp singlet for **1**, **2**, and **3**; this suggests that the OH group is largely free from the OH-π complexation in these alcohols.[1] For the t-butyl homologues (**4**), the signals ascribed to the OH and the proton adjacent to this (labeled H_x) are a little bit broader than those in the lower alkyl compounds. Second, the benzylic protons are magnetically nonequivalent, except for **1**, giving rise to a pair of quartets. The spin-coupling constants[2] with the vicinal proton (H_x) are larger for the higher part (H_a) of the double quartets than for the lower one (H_b). The coupling constant,

Table 1. Proton chemical shifts[a] and vicinal coupling constants[b] for alcohols, $C_6H_5CH_2CH(OH)$-R

R	Ar	H_a	H_b	H_x	H_y	H_z	OH[c]	J_{HaHx}	J_{HbHx}	J_{HyHx}
Me (**1**)	7.17	2.62	2.62	3.87	1.11	—	2.20	6.5	6.5	—
Et (**2**)	7.17	2.57	2.70	3.56	1.41[d]	0.93	1.78	7.5	4.5	6.5, 2.0
Pr^i (**3**)	7.17	2.50	2.76	3.45	1.61	0.94[e]	1.44	9.0	4.0	6.0
Bu^t (**4**)	7·12	2.37	2.77	3.25[f]	—	0.95	1.26[f]	10.5	2.5	—

a) Ppm downfield from internal TMS in CCl_4. b) The $^3J_{HH}$'s are the approximate values (in Hz) obtained by the first-order analysis. c) Sensitive to the experimental conditions. d) Almost equivalent for the diastereotopic protons. e) Equivalent for the diastereotopic methyls. f) Broad relative to the respective peak(s) in the lower homologues (see text).

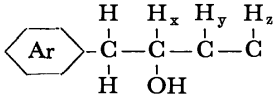

Table 2. Carbon chemical shifts[a] for the alcohols, $C_6H_5CH_2CH(OH)$-R

R	1	2, 6	3, 5	4	7	8	9	10
R	138.6	129.4	128.4	126.4	45.7	68.7	22.7	—
Et	138.7	129.4	128.4	126.3	43.6	74.0	29.5	10.0
Pr^i	139.1	129.3	128.4	126.3	40.7	77.4	33.1	17.4, 18.0
Bu^t	139.9	129.3	128.4	126.1	38.3	80.5	34.7	25.8

a) Ppm downfield from internal TMS in $CDCl_3$.

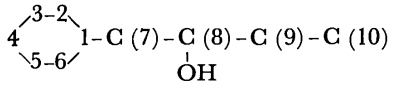

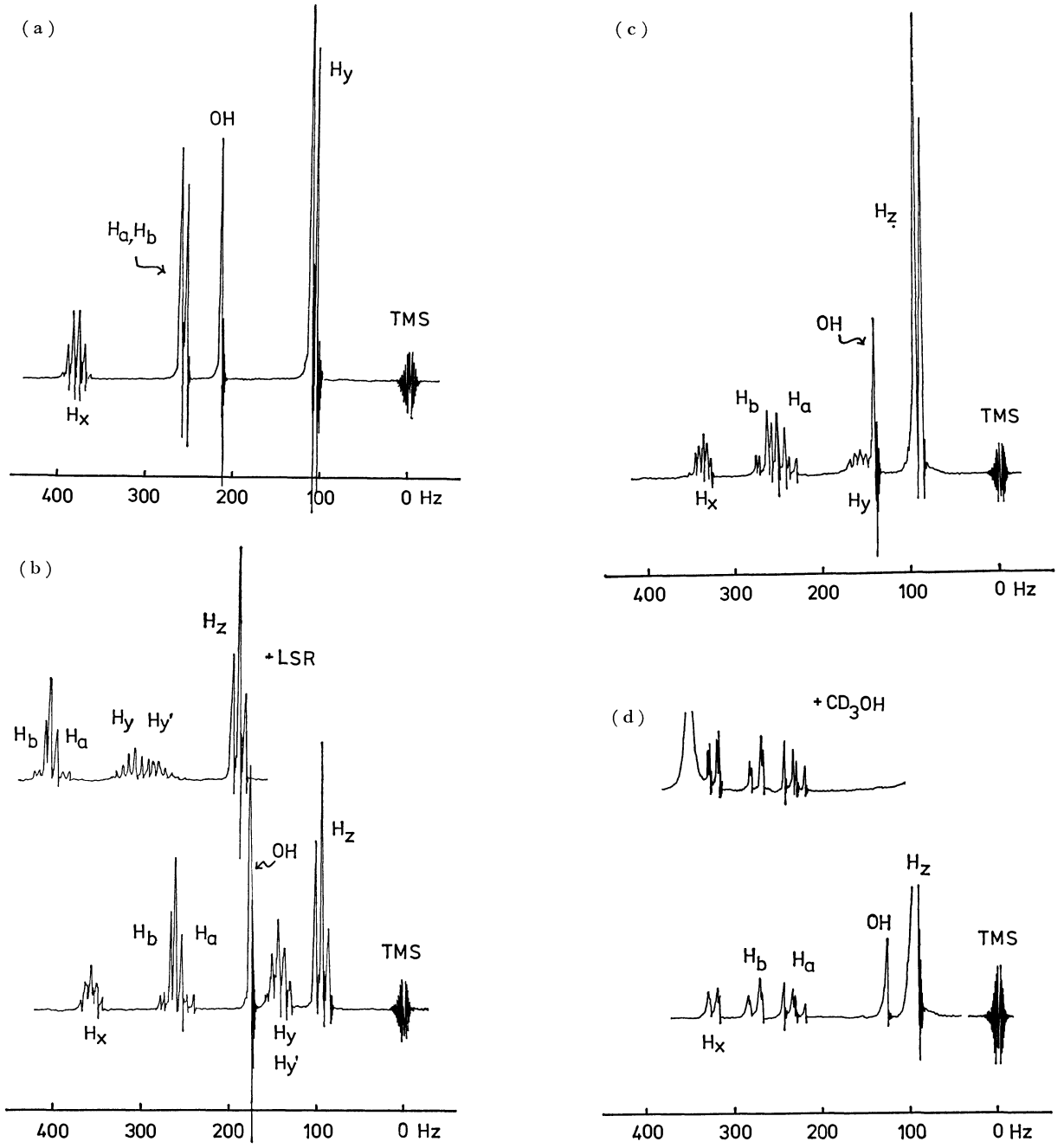

Fig. 1. Proton NMR spectra of (a) 1-phenyl-2-propanol (**1**); (b) 1-phenyl-2-butanol (**2**), insert shows the effect of LSR; (c) 3-methyl-1-phenyl-2-butanol (**3**); and (d) 3,3-dimethyl-1-phenyl-2-butanol (**4**), insert shows the effect of added CD_3OH.

$^3J_{HaHx}$, becomes progressively larger as the methyl group in **1** is replaced by the ethyl, isopropyl, and then *t*-butyl groups; the reverse is true for $^3J_{HbHx}$. Third, the lanthanoid shift-reagent[3] (LSR) induced shift[4] (LIS, Table 3) is greater for H_a than for H_b, the difference in the LIS is most remarkable for **4** (R=Bu^t). The LIS values for the benzylic protons are virtually the same in the cases of **1** and **2**. A signal assignment is possible for the diastereotopic protons if the LIS data are combined with information obtained by the coupling constants. These points will be discussed later.

The conformations of **1**—**4** were then studied by means of a computer simulation[5] of the LIS. Ac-

Table 3. Lanthanoid shift-reagent-induced shifts[a]
$C_6H_5CH_2CH(OH)$-R

R		H_o	H_m	H_a	H_b	H_x	H_y	H_z
Me	(**1**)	31.7	14.5	61.4	61.4	100	62.1	—
Et	(**2**)	36.7	16.1	64.6	64.6	100	72.7[b] 61.4	43.6
Pr^i	(**3**)	31.7	11.1	60.0	54.8	100	59.5	38.0[b] 43.0
Bu^t	(**4**)	29.9	3.7	67.7	40.0	100	—	38.1

a) Relative chemical shifts induced by the addition of $Eu(fod)_3$ to CCl_4 solutions. The data are normalized to the value for H_x ($LIS_{rel}=100$). b) Average values were used in the computations.

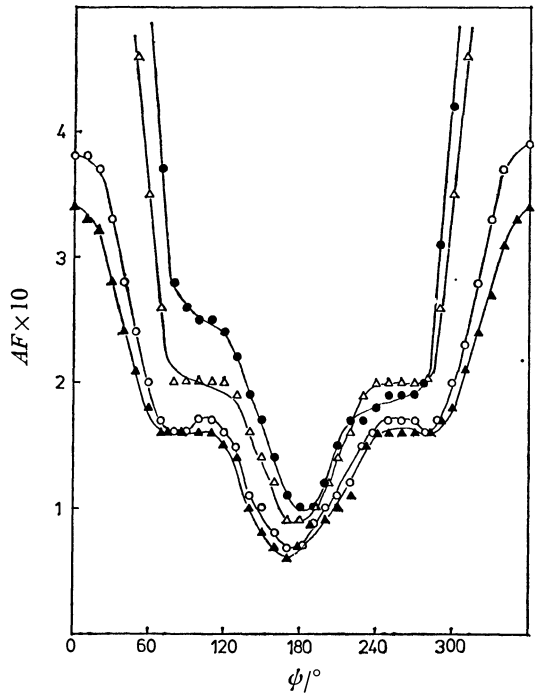

Fig. 2. Plots of AF *vs.* ϕ for **1**. R is kept constant at 0.32 nm.
●: A=0.0, △: 0.4, ○: 0.8, ▲: 1.2.

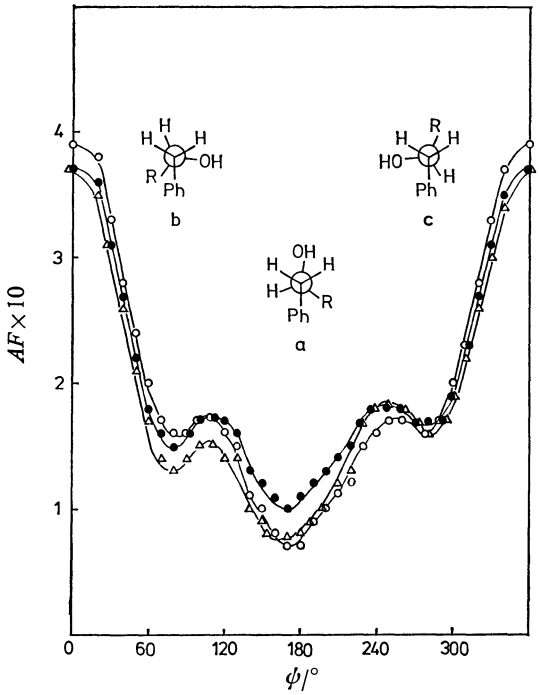

Fig. 3. Plots of AF *vs.* ϕ for **1**, **2**, and **3**. A and R are kept constant at 0.8 and 0.32 nm respectively.
○: R=Me (**1**), ●: R=Et (**2**), △: R=Pr^i (**3**).

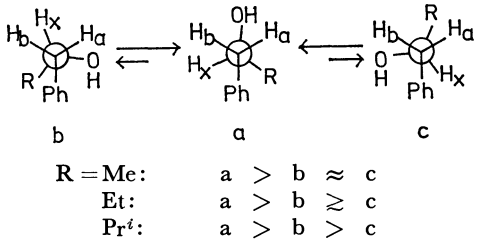

Fig. 4. Relative stabilities of the rotamers **a**, **b**, and **c**, suggested for the conformational equilibria of **1**, **2**, and **3**.

cording to the procedure described in an earlier paper,[1b] the positions of the LSR and the geometry of the substrate were varied, step by step, in the search for a reasonable agreement of the computed LIS's with the observed values.[6]

Figure 2 plots the Hamilton reliability factors (AF)[7] against the O–C(8)–C(7)–Ph dihedral angle, ϕ, for a representative case of Compound **1**. Here, the Ln–O distance, R, is fixed at 0.32 nm,[8] while the LSR-distribution index A,[6] is varied from 0.0 to 1.2. A good fit is obtained at ϕ *ca.* 180° in every case. The agreement is worst at ϕ around 0°, but it becomes better with a larger value of A; this is reasonable, since the rotation of the LSR will be hindered if OH (the LSR-complexation site) comes close to the phenyl group. The values of ϕ at the AF-minima do not vary significantly with the change in A; however, the presence of the second (or third) minimum becomes more apparent with a higher value of A.

Figure 3 summarizes the results obtained for **1**, **2**, and **3**. (A and R are fixed at 0.8 and 0.32 nm respectively). A notable feature of these profiles is the presence of three minima in every case. The AF at these ϕ-values are not necessarily good enough to be acceptable, except for the best-fit position. It should be kept in mind that the value of AF represents the plausibility for a single, hypothetical conformation and by no means corresponds to the potential energy or the population of the respective rotamer. However, for reasons previously cited,[1,9] we believe it likely that the appearance of the second and third minima reflects the contribution from other, less populated rotamers. The values of ϕ and AF might thus reflect, though in an indirect manner, the geometry and the relative stability of the respective rotamers.

An inspection of Fig. 3 suggests that the rotamer with the hydroxyl group *anti* to the phenyl group (ϕ *ca.* 170°, rotamer **a**) is the most populated one in the rotameric mixture of these alcohols. The **b** (ϕ *ca.* 80°) and **c** (ϕ *ca.* 280°) rotamers seem to be of about the same importance for **1** and **2**; the **b** rotamer appears to be more stable than the **c** rotamer in the case of the isopropyl-substituted alcohol (**3**).

A configuration assignment is given in Fig. 4 for the benzylic hydrogens in alcohol **3** (R=Pr^i). With this assignment, the coupling data ($J_{HaHx} > J_{HbHx}$) and the LIS data (larger for H_a) are consistent with the suggested geometries and the equilibrium; a conflict occurs, however, with the alternative assignment. The same conclusion can be reached for **2** and **1**; in the latter case, the chemical shifts of the diastereotopic protons are virtually equivalent.

For the *t*-butyl homologue (**4**), however, a paradoxical result is obtained. With the same signal assignment, the simulation indicates the coexistence of rotamers with ϕ *ca.* 90° and 140° (Figs. 5 and 6a). This conclusion is unacceptable in view of the coupling data (Table 1: 10.5 Hz for H_a and 2.5 Hz for H_b).

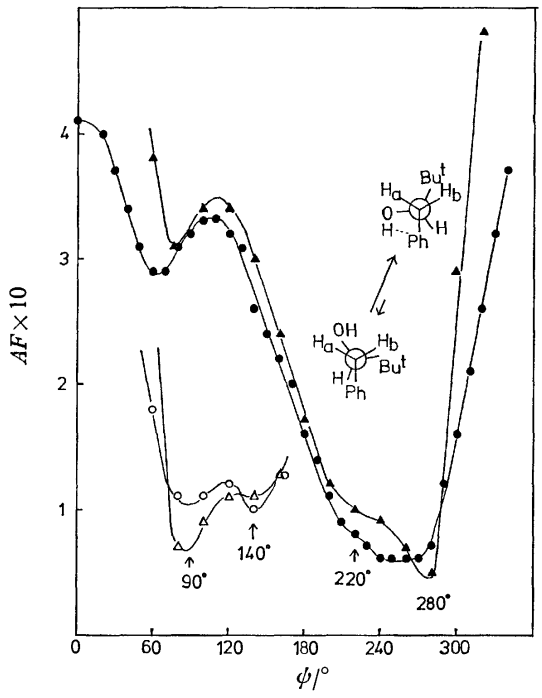

Fig. 5. Plots of AF *vs.* ϕ for **4**. Assignment for the benzylic protons is made as indicated. ▲: A=0.4, ●: A=0.8. Insert shows the profiles obtained with the reversed assignment; this equals to the assignment given for the lower alkyl homologues. △: A=0.4, ○: A=0.8. R is kept constant at 0.32 nm.

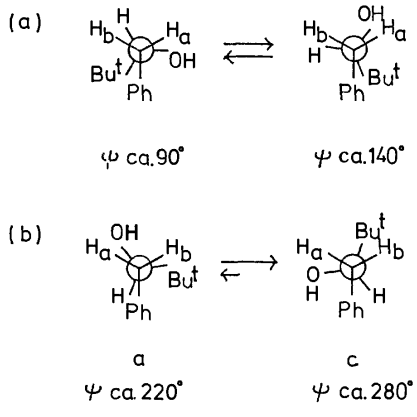

Fig. 6.

A more reasonable conclusion is reached with the alternative assignment. Thus, with an inversed signal assignment, the concomitant presence of rotamers corresponding to the **c** rotamer (ϕ *ca.* 280°) and the **a** rotamer (ϕ *ca.* 220°) is suggested, the former being likely to be predominant (Figs. 5 and 6b). In this case, the conclusion is compatible with the coupling data.

Support for the above suggestions regarding the rotameric equilibria of **1**—**4** is provided by an inspection of the NMR data. In the **c** rotamer (and **b**), the hydroxyl group is *gauche* to Ph and is expected to participate in the OH–π complexation.[10] The hydroxyl group in the **a** rotamer, in contrast, lies *anti* to the phenyl group. The OH proton in the **c** rotamer can, therefore, be expected to be magnetically more

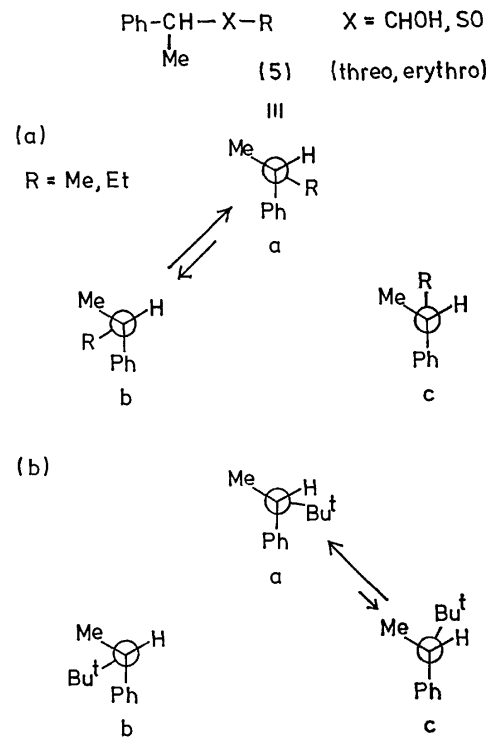

Fig. 7. Rotameric equilibria suggested for the diastereoisomeric pairs of sulfoxides (**5**, X=SO) and alcohols (X=CHOH).

shielded and free from proton exchange, than that in the **a** rotamer.[1] In fact, the hydroxyl proton of **4** gives rise to the highest peak in the series, and it is broader (due to the slow exchange) than that in the lower alkyl homologues. This can be understood by considering the important contribution of the **c** rotamer to **4** and the relative non-importance of this rotamer (and the **b** rotamer) for the other alcohols.

In the **a** rotamer, whereby the OH group is flanked by the two benzylic hydrogens, H_a and H_b, the LIS is anticipated to be about the same for these nuclei. The LIS for H_a and H_b should be very different in the **b** and **c** rotamers, but the effect will be cancelled if these rotamers are populated at an approximately equal concentration. This is what we observed in the proton NMR spectra of **1** and **2**; the trend is reflected in the simulated results. The tendencies observed for the coupling constants as well as the shift data are compatible with the computed results, judging from the assignments given in Figs. 4 and 6b.

Discussion

A remarkable feature of the present result is the finding that the **a** rotamer (Fig. 4) is most populated in the rotameric mixtures of **1**, **2**, and **3**. In the **a** rotamer, the alkyl group lies close to the phenyl group. Note that the benzylic methyl group, which is present in compounds previously studied (Fig. 7), is absent in these molecules. We believe that the above finding can be accommodated only in terms of an attractive force operating between an alkyl and a phenyl group (the CH/π interaction).[1,11]

With regard to the *t*-butyl homologue (**4**), the most populated rotamer has been suggested to be the **c** rotamer (Fig. 6b). In this conformation, the *t*-butyl group is oriented *anti* (Bu^t–Ph torsional angle *ca.* 160°) to the phenyl group. The geometry corresponding to the **a** rotamer (Bu^t–Ph torsional angle *ca.* 100°) is found to be the second most stable one in this case. A comment is required on the apparent discrepancy that the **a** rotamer is most stable for **1**, **2**, and **3**, while the **c** rotamer is more important than **a** in the case of **4**. This result is in contrast to the earlier finding that in compounds such as **5** (Fig. 7) the most stable rotamer always has its alkyl group *gauche* to Ph, irrespective of the nature of Groups R and X. The conformational equilibria suggested for sulfoxides (**5**, X=SO)[9a] and alcohols (**5**, X=CHOH)[1b] are illustrated in Fig. 7. In both of these cases, the rotameric mixtures have been shown to consist, principally, of the **a** and **b** rotamers for the lower alkyl homologues and of the **a** and **c** rotamers for the *t*-butyl derivatives, the more stable one being the **a** rotamer in every case.[12] The position of the alkyl group in the most stable geometries has been found to be shifted (slightly, but distinctly) to give a larger R–Ph torsional angle for the *t*-butyl compounds (compare the **a** rotamers in Figs. 7a and 7b) as compared with the lower alkyl homologues.

The conformation of a molecule is, indeed, a consequence of a compromise of a number of interactions. In compounds such as **5**, where a methyl group is present in the benzylic position, the geometry of a molecule is controlled, primarily, by the balance of two interactions: R *vs.* CH_3, and R *vs.* Ph. These interactions may be attractive at an appropriate distance (the dispersion force[13] and/or the CH–π interaction[11]) or repulsive if the relevant groups come too close.

The suggestion that the **c** rotamer (ψ *ca.* 280°) represents the most stable conformation for **4** is understood in view of the absence of the benzylic methyl; the **a** rotamer might have become energetically less favorable than **c** in the present molecular environment. The **a** rotamer may be destabilized by the unfavorable (repulsive van der Waals) interaction between Bu^t and a benzylic hydrogen (H_b). This situation might occur when a methyl group in Bu^t takes a suitable position for the CH–π bonding.

Other possible factors which may contribute to controlling the rotameric equilibria of these compounds are the OH–π hydrogen bonding and the O–Ph dipole-quadrupole and *gauche*-vicinal H–H interactions. Some speculations will be made, on the basis of the suggested geometries of the preferred conformations, as to the factors influencing the molecular geometries of these alcohols.

The operation of the attractive CH–π interaction is possible in both the **a** and **b** rotamers (Fig. 4). However, the **a** rotamer has been found to be more stable than **b** in all cases. To accommodate this, it may be pointed out that there are two vicinal H–H interactions in the **b** rotamer. According to Wertz and Allinger, this interaction is very destabilizing.[14] The O–Ph dipole-quadrupole interaction[15] may also destabilize the **b** rotamer (and **c**).[16] The OH–π interaction[10,17] is undoubtedly attractive, but the other unfavorable interactions might override its effect. In this respect, it should be noted that OH–π bonding has not been observed in such compounds as **6** and **7**[18] even though these molecules appear to be ideally

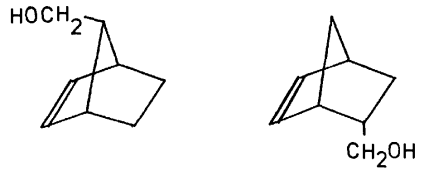

6 7

constituted for such interactions to take place. The observance of the OH–π hydrogen bonding might, therefore, be merely a consequence of a given (somewhat compelled) geometry of a molecule.

To conclude, we suggest that the attractive CH–π interaction is very important in the consideration of the conformational problems of flexible molecules. It may be more important than the OH–π hydrogen bonding. The stabilization energy is probably very small for a single CH–π interaction. In some molecular dispositions, however, the sum total of the stabilization energy may become sufficiently large to ensure a low-entropy structure of a complex molecule.

The recognition of the above facts would be of help in elucidating certain well-known, but poorly understood phenomena. Possible examples have been given in earlier papers,[9b,19] so here we will confine ourselves to illustrating a probable case from terpene chemistry. It has been established that levopimaric acid (**8**) exists in a folded conformation.[20,21] It is also well known that a considerable fraction of the folded conformer (with an axially oriented isopropyl group) contributes to conformational equilibrium of α-phellandrene (**9**).[20,22] These results were once at-

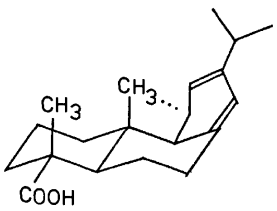

8

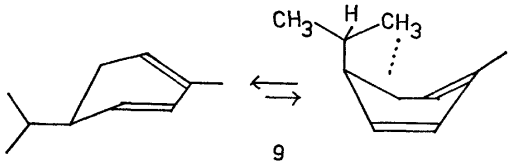

9

tributed, by Burgstahler *et al.*[20] to the presence of some type of attractive interaction which stabilizes an otherwise unfavorable conformation. The above interpretation was later replaced by alternative ones based principally on repulsive steric effects.[21,23]

The well-known diene chirality rule, in its original form,[24] states that the long wavelength π→π*-transition Cotton effect is mainly controlled by the helicity and the amount of twist of a conjugated diene. Re-

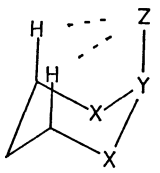

Fig. 8. A possible explanation (in terms of the CH–π or CH–n[9b]) interactions) for the axial preference of the Group Z.
Z: unsaturated groups or hetero atoms. X: O, S, CH_2 *etc.* Y: CH, S, or P.

cently, Burgstahler and his associates presented evidence[25] that the Cotton effects of 1,3-cyclohexadienes are primarily determined by the chirality contributions of allylic axial substituents according to the size or polarizability of the group. The suggestion has gained rapid acceptance and has been followed by quantum mechanical studies[26] and the proposal of an empirical quadrant rule.[27] In particular, Rosenfield and Charney presented evidence,[26a] obtained by MO calculations, that an axially oriented allylic hydrogen and methyl group contribute significantly to the rotatory strength of cisoid diene, a methyl group being *ca.* twice as effective as a hydrogen atom.

We suggest that these results are better accommodated in terms of the CH–π interaction. In our view, the folded conformations of **8** and **9** are consequences of an attractive interaction.[28] Also, it seems reasonable to suggest that the axial allylic (or homoallylic[29]) effect[25] operates mainly through the dissymmetric perturbation of the π^* orbital of the chromophore by virtue of the C–H groups,[30] which are oriented suitably for this interaction to take place. Inspections of Dreiding models suggest, in fact, that such an interaction is possible between CH groups and conjugated π-systems whenever a significant contribution of axial allylic or homoallylic (or even remoter) groups is present.[25,27,29] The same kind of argument will perhaps apply to the theoretical background, at least in part, of the Octant rules of ketones[31] and olefins,[32] and to the genesis of the 2-axial ketone effect.[33] Also noteworthy in this regard is the tendency for a group which bears π- or unshared-electrons to adopt the axial conformation (configuration) in saturated six-membered heterocycles (Fig. 8).[34] It is tempting to speculate about the possibility that the above effect (the generalized anomeric effect) is ascribable, at least in part, to the CH–π (and CH–n[9b]) interaction.[35]

Experimental

Materials. The alcohols (**1**—**4**) were prepared by treating phenylacetaldehyde with an appropriate Grignard reagent, RMgCl. The samples were purified as usual and shown gas-chromatographically to be pure.

NMR Spectra. ^{1}H NMR spectra were recorded at 30 °C on a JEOL MH-100 spectrometer (100 MHz) for *ca.* 0.2 M solutions in CCl_4 (locked to internal TMS; sweep-rate, 4 Hz s^{-1}). The calibrations of the chemical shifts (reported in ppm relative to internal TMS) were made by referring to the signals of standard samples. The coupling constants were determined by an inspection of the spectra and are accurate to $\pm$0.5 Hz. The ^{13}C NMR spectra were obtained at 27 °C on a JEOL FX-100 instrument (25.05 MHz) for $CDCl_3$ solutions in 10 mm ϕ-sample tubes (FT-conditions: data points, 8 K; spectral width, 4 kHz; flip angle, 45°; repetition time, 1.2 s). The signal assignments were made by the use of selective and gated decoupling techniques. The chemical shifts are reported in ppm downfield from internal TMS (δ=0) and are accurate to $\pm$0.04 ppm.

LIS Measurements. Weighted LSR [Eu(fod)$_3$] was added, step by step, to a solution containing a known amount of a substrate, and the signals were followed in the spectra. A least-squares fit of the experimental points was used to obtain the observed LIS's used in the computations. In all cases straight lines were obtained with correlation coefficients of $r>0.998$.

We wish to thank Professor Naoya Nakagawa (The University of Electro-communications) for his useful discussions, and Drs. Teiichiro Ito and Koshiro Umemura (Meiji Seika Kaisha) for their encouragement.

References

1) a) Y. Kodama, K. Nishihata, S. Zushi, M. Nishio, J. Uzawa, K. Sakamoto, and H. Iwamura, *Bull. Chem. Soc. Jpn.*, **52**, 2661 (1979); b) J. Uzawa, S. Zushi, Y. Kodama, Y. Fukuda, K. Nishihata, K. Umemura, M. Nishio, and M. Hirota, *ibid.*, **53**, 3623 (1980).

2) It was shown that the coupling constants were not appreciably affected by the addition of the LSR; perturbation to the conformational equilibria by the complexation is unimportant in the present case.

3) C. C. Hinckley, *J. Am. Chem. Soc.*, **91**, 5160 (1969).

4) "NMR Shift Reagents," ed by R. E. Sievers, Academic Press, New York (1973).

5) For the leading references of this subject, see O. Hofer, *Top. Stereochem.*, **9**, 111 (1976).

6) The lanthanoid (Ln)–O–C angle was fixed at 130°, but the Ln–O distance was varied incrementally. A Gaussian weight factor $w(\theta)=A/\sqrt{\pi}\exp[-A^2(\theta-\theta_0)^2]$ was used for describing a localized distribution of the LSR. The free rotation of LSR corresponds to $A=0$, whereas a higher value of A denotes a localized distribution of the LSR.

7) $AF=[\sum_i(\mathrm{LIS}_i^{\mathrm{obsd}}-\mathrm{LIS}_i^{\mathrm{calcd}})^2/\sum_i(\mathrm{LIS}_i^{\mathrm{obsd}})^2]^{1/2}$. The calculated shifts were normalized to the average experimental LIS in the computational process.

8) The reasonable fit has invariably been found at about this value.

9) a) Y. Kodama, S. Zushi, K. Nishihata, M. Nishio, and J. Uzawa, *J. Chem. Soc., Perkin Trans. 2*, **1980**, 1306; b) S. Zushi, Y. Kodama, K. Nishihata, K. Umemura, M. Nishio, J. Uzawa, and M. Hirota, *Bull. Chem. Soc. Jpn.*, **53**, 3631 (1980).

10) M. Ōki, H. Iwamura, T. Onoda, and M. Iwamura, *Tetrahedron*, **24**, 1905 (1968); M. Ōki and H. Iwamura, *Bull. Chem. Soc. Jpn.*, **33**, 1600 (1960), and the references cited therein.

11) Y. Kodama, K. Nishihata, M. Nishio, and N. Nakagawa, *Tetrahedron Lett.*, **1977**, 2105; M. Nishio, *Kagaku No Ryoiki*, **31**, 834, 998 (1977).

12) The only exception is the case of 3-phenyl-2-butanol with the *threo* configuration, where the **b** rotamer is the most stable one.[1b]

13) R. E. Carter and P. Stilbs, *J. Am. Chem. Soc.*, **98**, 7515 (1976).
14) D. H. Wertz and N. L. Allinger, *Tetrahedron*, **30**, 1579 (1974). See E. Osawa, J. B. Collins, and P. v. R. Schleyer, *ibid.*, **33**, 2667 (1977), for criticism.
15) N. Nakagawa, K. Nikki, Y. Takeuchi, and I. Kumagai, *Chem. Lett.*, **1972**, 1239.
16) It is noteworthy, in this respect, that the rotamer with the eclipsed OH (or CO)/Ph conformation has been suggested to be the least stable for the alcohols[1b] and ketones[9b] examined thus far.
17) G. C. Pimentel and A. L. McClellan, "The Hydrogen Bond," W. H. Freeman, New York (1960), Chap. 6.
18) L. P. Kuhn, P. von R. Schleyer, W. F. Baitinger, Jr., and L. Eberson, *J. Am. Chem. Soc.*, **86**, 650 (1964).
19) M. Nishio, *Kagaku No Ryoiki*, **33**, 422 (1979).
20) A. W. Burgstahler, H. Ziffer, and U. Weiss, *J. Am. Chem. Soc.*, **83**, 4660 (1961).
21) A. W. Burgstahler, J. Gawronski, T. F. Niemann, and B. A. Feinberg, *Chem. Commun.*, **1971**, 121; U. Weiss, W. B. Whalley, and I. L. Karle, *ibid.*, **1972**, 160; I. L. Karle, *Acta Crystallogr., Sect B*, **28**, 2000 (1972).
22) H. Ziffer, E. Charney, and U. Weiss, *J. Am. Chem. Soc.*, **84**, 2961 (1962); G. Horsman and C. A. Emeis, *Tetrahedron*, **22**, 167 (1966); G. Snatzke, E. Sz. Kovats, and G. Ohloff, *Tetrahedron Lett.*, **1966**, 4551.
23) G. A. Lane and N. L. Allinger, *J. Am. Chem. Soc.*, **96**, 5825 (1974).
24) A. Moscowitz, E. Charney, U. Weiss, and H. Ziffer, *J. Am. Chem. Soc.*, **83**, 4663 (1961); U. Weiss, H. Ziffer, and E. Charney, *Tetrahedron*, **21**, 3105 (1965); E. Charney, *ibid.*, **21**, 3127 (1965).
25) A. W. Burgstahler and R. C. Barkhurst, *J. Am. Chem. Soc.*, **92**, 7601 (1970); A. W. Burgstahler, L. O. Weigel, and J. K. Gawronski, *ibid.*, **98**, 3015 (1976); A. W. Burgstahler, D. L. Boger, and N. C. Naik, *Tetrahedron*, **32**, 309 (1976). See also A. Yogev, D. Amar, and Y. Mazur, *Chem. Commun.*, **1967**, 339; N. H. Andersen, C. R. Costin, D. D. Syrdal, and D. P. Svedberg, *J. Am. Chem. Soc.*, **95**, 2049 (1973).
26) a) J. S. Rosenfield and E. Charney, *J. Am. Chem. Soc.*, **99**, 3209 (1977); b) E. Charney, C. H. Lee, and J. S. Rosenfield, *ibid.*, **101**, 6802 (1979); O. E. Weigang, Jr., *ibid.*, **101**, 1965 (1979).
27) R. M. Moriarty, H. E. Paaren, U. Weiss, and W. B. Whalley, *J. Am. Chem. Soc.*, **101**, 6804 (1979).
28) This possibility was first suggested to us by Professor E. Wenkert (Rice University). We wish to thank Professor Wenkert for calling our attention to the conformational problems of 1,3-cyclohexadienes.
29) J. K. Gawronski and M. A. Kielczewski, *Tetrahedron Lett.*, **1971**, 2493.
30) We noticed recently that Kuriyama had commented upon the possibility of σ/π interaction in order to explain the CD data of α-phellandrene. K. Kuriyama, "Optical Rotation," ed by K. Imahori, Tokyo Kagaku Dojin, Tokyo (1967), Chap. 4.
31) W. Moffitt, R. B. Woodward, A. Moscowitz, W. Klyne, and C. Djerassi, *J. Am. Chem. Soc.*, **83**, 4013 (1961); C. Djerassi, "Optical Rotatory Dispersion," McGraw-Hill, New York (1960).
32) A. I. Scott and A. W. Wrixon, *Tetrahedron*, **26**, 3695 (1970); J. Hudec and D. N. Kirk, *ibid.*, **32**, 2475 (1976).
33) W. Klyne, *Experientia*, **12**, 119 (1956); N. L. Allinger and H. B. Blatter, *J. Am. Chem. Soc.*, **83**, 994 (1961); B. Rickborn, *ibid.*, **84**, 2414 (1962); W. D. Cotterill and M. J. T. Robinson, *Tetrahedron*, **20**, 765 (1964).
34) For leading references of this subject, see C. Romers, C. Altona, H. R. Buys, and E. Havinga, *Top. Stereochem.*, **4**, 39 (1967); W. F. Bailey and E. L. Eliel, *J. Am. Chem. Soc.*, **96**, 1798 (1974); E. L. Eliel, W. F. Bailey, K. B. Wiberg, H. Connon, and F. W. Nader, *Ann.*, **1976**, 2240. See also G. M. Kellie, P. Murray-Rust, and F. G. Riddell, *J. Chem. Soc., Perkin Trans. 2*, **1972**, 2384; W. G. Bentrude and K. C. Lee, *Tetrahedron Lett.*, **1970**, 3999; A. T. McPhail, J. J. Breen, J. H. Somers, J. C. H. Steele, Jr., and L. D. Quin, *Chem. Commun.*, **1971**, 1020; A. T. McPhail, J. J. Breen, and L. D. Quin., *J. Am. Chem. Soc.*, **93**, 2574 (1971); R. O. Hutchins and B. E. Maryanoff, *ibid.*, **94**, 3266 (1972); R. C. G. Killean, J. L. Lawrence, and I. M. Magennis, *Acta Crystallogr., Sect B*, **27**, 189 (1971); W. H. De Camp and F. R. Ahmed, *ibid.*, **28**, 1796 (1972). See also K. D. Kopple and D. H. Marr, *J. Am. Chem. Soc.*, **89**, 6193 (1967); K. D. Kopple and M. Ohnishi, *ibid.*, **91**, 962 (1969) and L. E. Webb and C-F. Lin, *ibid.*, **93**, 3818 (1971), for folded conformations in cyclic dipeptides (diketopiperazines).
35) This suggestion of the attractive 1,3-diaxial interaction is not without precedent. See R. J. Abraham and Z. L. Rossetti, *J. Chem. Soc., Perkin Trans. 2*, **1973**, 582; N. Nogami, Thesis, Univ. of Tokyo (1977).[19]

The Formylation of an Aromatic Nucleus by the Use of 2-Ethoxy-1,3-dithiolane

Shigeo Jo, Shigeo Tanimoto,* Toyonari Sugimoto, and Masaya Okano
Institute for Chemical Research, Kyoto University, Uji, Kyoto 611

(Received December 8, 1980)

The reaction of various phenols with 2-ethoxy-1,3-dithiolane proceeded smoothly in the presence of $BF_3 \cdot Et_2O$ to afford 1,3-dithiolan-2-ylated phenols, which were readily hydrolyzed to the corresponding aldehydes. This process was also extended to *N,N*-dimethylaniline and indole.

Considerable efforts have been devoted towards the discovery of methods for the introduction of a formyl moiety onto an aromatic nucleus. The Gattermann-Koch reaction,[1] the Reimer-Tiemann reaction,[2] the Vilsmeier reaction,[3] the Duff reaction,[4] the Friedel-Crafts reaction with dichloromethyl alkyl ether or with trialkyl orthoformate,[5] *etc.* are well known and widely used. Recently, Gassman and Amick have reported a process which involves the reaction of phenols with a salt formed through the mixing of *N*-chlorosuccinimide and dithiane.[6] However, all these reactions give relatively poor yields or can be used only with electron-rich aromatic compounds. It is proper to say that no reaction for formylating aromatic compounds which would not be subjected to either one of the above limitations has been found.

We have now found that 2-ethoxy-1,3-dithiolane in dichloromethane with a Lewis acid catalyst is an efficient reagent for the introduction of the 1,3-dithiolan-2-yl group to some phenols and that the resulting cyclic thioacetal derivatives (protected formylated phenols) are easily hydrolyzed to the corresponding aldehydes. This process for the formylation of phenols could also be extended to *N,N*-dimethylaniline and indole. Although this formylation process is also subject to limitations similar to those of the earlier methods, that is, it is applicable only to electron-rich aromatic compounds, such as phenols, *N,N*-dimethylaniline, and indole, and the yields of the obtained aldehydes are roughly the same as those in the previously reported reactions, it has such advantages that the starting 2-ethoxy-1,3-dithiolane is readily available, and can be stored for a long time, and the reaction smoothly proceeds under relatively mild conditions.

Results and Discussion

The first attempt was directed toward establishing the most effective Lewis acid catalyst for the reaction of *p*-cresol (**1d**) with 2-ethoxy-1,3-dithiolane in dichloromethane. The yields of 2-(1,3-dithiolan-2-yl)-*p*-cresol (**2d**) formed in the reaction with various Lewis acid catalysts are shown in Table 1.

As is evident from Table 1, the best yield (55%) was achieved in a run involving a 1.5 molar ratio of 2-ethoxy-1,3-dithiolane and a 0.75 molar ratio of $BF_3 \cdot Et_2O$ for **1d**. The $BF_3 \cdot Et_2O$ catalyst, therefore, would be a very effective catalyst for the 1,3-dithiolan-2-ylation of phenols other than **1d**. Thus, we have studied the $BF_3 \cdot Et_2O$-catalyzed reaction of 2-ethoxy-1,3-dithiolane with several phenols in dichloromethane at room temperature. The results are summarized in Table 2.

It seems plausible that the reaction path involves the coordination of $BF_3 \cdot Et_2O$ with 2-ethoxy-1,3-dithiolane to give the 1,3-dithiolan-2-ium ion and the subsequent attack on the aromatic nucleus. As can be seen from Table 2, the exclusive attack occurs in the 2- and 3-positions of **1d** and *p*-hydroxyanisole (**1f**) respectively and also in the 4-positions of *o*-cresol (**1b**) and guaiacol (**1e**). Phenol (**1a**) was 1,3-dithiolan-

Table 1. Reaction of *p*-cresol (**1d**) with 2-ethoxy-1,3-dithiolane in the presence of various Lewis-acid catalysts

Mole ratio, 2-ethoxy-1,3-dithiolane/**1d**	Lewis acid (Mole ratio, Lewis acid/2-ethoxy-1,3-dithiolane)	Reaction[a,b]		Yield/% of **2d**[c]
		Temp/°C	Time/h	
1.0	$ZnCl_2$ (0.2)	rt	24	31 (61)
1.5	$ZnCl_2$ (0.2)	77[d]	8	37 (87)
1.5	$ZnCl_2$ (0.2)	rt	22	37 (90)
1.0	$ZnCl_2$ (1.0)	rt	1	27 (98)
1.5	$ZnCl_2$ (0.5)	rt	14	45 (84)
2.0	$ZnCl_2$ (0.5)	rt	14	34 (64)
1.5	$FeCl_3$ (0.5)	rt	6	41 (59)
1.5	$HgCl_2$ (0.5)	rt	6	22 (43)
1.5	$BF_3 \cdot Et_2O$ (0.5)	rt	14	55 (94)
1.5	$TiCl_4$ (0.5)	rt	14	40 (66)

a) Dichloromethane was used as the solvent unless otherwise noted. b) In almost all runs, the formation of a small amount of 2,2′-[1,2-ethanediylbis(thio)]bis-1,3-dithiolane[7] as a by-product was observed. c) The values in parentheses are the percentages of conversion, corrected for the recovered **1d**. d) The solvent here is carbon tetrachloride.

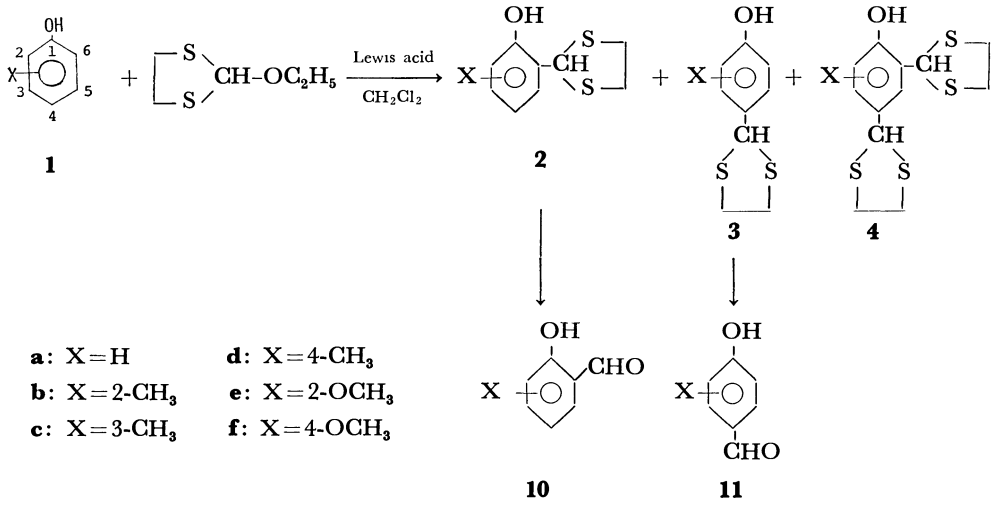

Table 2. Reaction of phenols (**1**) with 2-ethoxy-1,3-dithiolane in the presence of $BF_3 \cdot Et_2O$

1, 20 mmol; 2-ethoxy-1,3-dithiolane, 30 mmol; $BF_3 \cdot Et_2O$, 15 mmol; dichloromethane, 40 ml. Reaction conditions: room temperature, 14 h.

Starting phenol	Total yield/% of products[a)]	Composition of product (%)		
1a	69 (100)	**2a**[b)] (22)	**3a**[b)] (65)	**4a**[b)] (13)
1b	89 (96)	**2b** (0)	**3b**[c)] (94)	**4b**[d)] (6)
1c	49 (58)	**2c**[b)] (33)	**3c**[b)] (49)	**4c**[b)] (18)
1d	55 (94)	**2d**[c)] (100)	**3d** (0)	**4d** (0)
1e	38 (81)	**2e** (0)	**3e**[c)] (100)	**4e** (0)
1f	40 (74)	**2f**[c)] (100)	**3f** (0)	**4f** (0)

a) The values in parentheses are the percentages of conversion, corrected for the recovered starting phenols. b) Isolated by column chromatography on silica gel, using dichloromethane as the eluent. c) Isolated by distillation. d) After the evaporation of **3b** from the crude reaction product, the residue was column-chromatographed on silica gel, using dichloromethane as the eluent, to afford **4b**.

2-ylated in both the 2- and 4-positions in an approximate ratio of 1:3; *m*-cresol (**1c**) was attacked similarly in both the 6- and 4-positions in an approximate ratio of 2:3. These results are in accordance with the above suggestion that the reaction proceeds by means of a nucleophilic aromatic substitution.

The reaction of *N*,*N*-dimethylaniline (**5**) with 2-ethoxy-1,3-dithiolane proceeded smoothly in the presence of a large amount of acetic acid to afford *p*-(1,3-dithiolan-2-yl)-*N*,*N*-dimethylaniline (**6**), whereas the same reaction using $ZnCl_2$ as a catalyst gave only a trace of **6**.

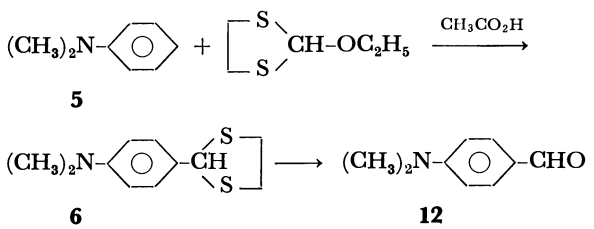

Table 3. Reaction of *N*,*N*-dimethylaniline (**5**) or of indole (**7**) with 2-ethoxy-1,3-dithiolane

5 (or **7**), 13 mmol; 2-ethoxy-1,3-dithiolane, 20 mmol.

Starting aromatics	Catalyst	Reaction conditions	Products (yields %[a)])
5	$ZnCl_2$	rt, 24 h, in dichloromethane	**6** (trace)
5	Acetic acid	110 °C, 5 h, in acetic acid	**6** (77)
7	$BF_3 \cdot Et_2O$[b)]	rt, 24 h, in dichloromethane	**8** (33) **9** (26)
7	Acetic acid	110 °C, 5 h, in acetic acid	**8** (64) **9** (8)
7	Acetic acid	rt, 14 h, in acetic acid	**8** (81)

a) Yield is based upon **5** or **7**. b) 0.75 molar ratio of $BF_3 \cdot Et_2O$ for **7**.

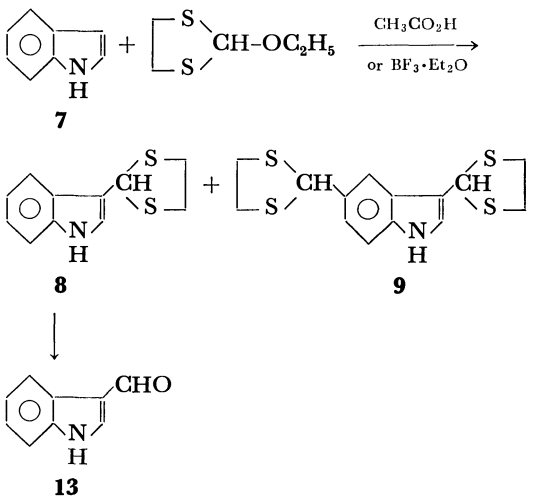

The 1,3-dithiolan-2-ylation of indole (**7**) was also promoted by using acetic acid as both catalyst and solvent. When the reaction was carried out at 110 °C, the products were 3-(1,3-dithiolan-2-yl)indole (**8**) (64%) and 3,5-bis(1,3-dithiolan-2-yl)indole (**9**) (8%), a hitherto unknown compound; only the former was produced in a good yield (81%) in the reaction conducted at room temperature.

Most of the 1,3-dithiolan-2-ylated aromatics obtained in this work were hydrolyzed to the correspond-

Table 4. Physical properties of 1,3-dithiolan-2-ylated aromatics

Compound[a]	Mp/°C or Bp/°C [Pressure/Torr]	^{1}H-NMR(δ/ppm, $CDCl_3$) ArH	OH	Methine H	SCH_2CH_2S	CH_3 or OCH_3	Other
2a	—[b]	7.4—6.7 (m, 4H)	6.76 (bs, 1H)	5.80 (s, 1H)	3.7—3.1 (m, 4H)		
3a	115—116.5 (chloroform) (lit,[8] 119—120 °C)	7.6—7.4 (m, 2H) 6.9—6.7 (m, 2H)	5.62 (bs, 1H)	5.70 (s, 1H)	3.7—3.1 (m, 4H)		
4a	—[b]	7.4—6.7 (m, 3H)	6.73 (bs, 1H)	5.74 (s, 1H) 5.52 (s, 1H)	3.7—3.1 (m, 8H)		
3b	168—170[1.0]	7.2—7.0 (m, 2H) 6.6—6.4 (m, 1H)	5.30 (bs, 1H)	5.48 (s, 1H)	3.6—3.0 (m, 4H)	2.14 (s, 3H)	
4b	—[b]	7.21 (bs, 2H)	6.86 (bs, 1H)	5.70 (s, 1H) 5.52 (s, 1H)	3.7—3.0 (m, 8H)	2.20 (s, 3H)	
2c	—[b]	7.2—7.0 (m, 1H) 6.7—6.4 (m, 2H)	6.7—6.4[c] (bs, 1H)	5.72 (s, 1H)	3.6—3.0 (m, 4H)	2.18 (s, 3H)	
3c	173—174[1.0]	7.6—7.4 (m, 1H) 6.6—6.4 (m, 2H)	6.28 (bs, 1H)	5.71 (s, 1H)	3.5—2.9 (m, 4H)	2.23 (s, 3H)	
4c	—[b]	7.73 (bs, 1H) 6.57 (bs, 1H)	6.73 (bs, 1H)	5.73 (s, 2H)	3.7—3.0 (m, 8H)	2.30 (s, 3H)	
2d	173—173.5[1.5]	7.1—6.7 (m, 3H)	6.50 (bs, 1H)	5.78 (s, 1H)	3.7—3.1 (m, 4H)	2.23 (s, 3H)	
3e	163—165[1.5]	7.15 (bs, 1H) 7.0—6.9 (m, 2H)	5.94 (bs, 1H)	5.66 (s, 1H)	3.6—3.2 (m, 4H)	3.85 (s, 3H)	
2f	176—177[0.5]	7.1—6.9 (m, 1H) 6.8—6.7 (m, 2H)	6.58 (bs, 1H)	5.81 (s, 1H)	3.4—3.1 (m, 4H)	3.69 (s, 3H)	
6	100—101 (ethanol) (lit,[9] 105 °C)	7.5—7.3 (m, 2H) 6.7—6.5 (m, 2H)		5.62 (s, 1H)	3.5—3.1 (m, 4H)	2.90 (s, 6H)	
9	154—155.5 (50% diisopropyl ether-dichloromethane)	7.2—7.0 (m, 3H)		6.41 (s, 1H) 6.29 (s, 1H)	3.8—3.0 (m, 8H)		8.57 (bs, 1H, NH) 8.0—7.7 (m, 1H, NCH)

a) The data of **8** can be seen in the literature.[10] b) The mp or bp could not be exactly determined because of the limited amounts. c) The line assigned to the OH is involved in that of the ArH.

ing aldehydes. The procedure used to accomplished the hydrolysis involved the treatment of the aromatic thioacetals with HgO and $BF_3 \cdot Et_2O$, followed by neutralization with aqueous Na_2CO_3.[11] As can be seen from Table 6, the overall yields of the aldehydes from the starting aromatics (**1**, **5**, and **7**) ranged from 15 to 77%.

Experimental

Reaction of Phenols (1) with 2-Ethoxy-1,3-dithiolane. General Procedure: To a mixture of **1** (20 mmol) and 2-ethoxy-1,3-dithiolane (4.5 g, 30 mmol) in dichloromethane (40 ml), we added, drop by drop, $BF_3 \cdot Et_2O$ (2.1 g, 15 mmol) at 0 °C. The mixture was brought to room temperature, stirred for 14 h, and then poured into about 200 ml of water. The organic layer was separated, and the aqueous phase was thoroughly extracted with dichloromethane. The combined dichloromethane solution was washed successively with water, 5% aqueous $NaHCO_3$, and again with water, dried over anhydrous $MgSO_4$, filtered, and concentrated *in vacuo* to give the crude product. The crude 1,3-dithiolan-2-ylated phenols thus obtained were purified by distillation under reduced pressure or by column chromatography on silica gel (see footnote to Table 2).

Reaction of N,N-*Dimethylaniline (**5**) with 2-Ethoxy-1,3-dithiolane in Acetic Acid.* To a solution of **5** (1.6 g, 13 mmol) in acetic acid (30 ml) we added, drop by drop, 2-ethoxy-1,3-dithiolane (3.0 g, 20 mmol) at 110 °C. The mixture was stirred for 5 h at the same temperature, cooled, and then poured into about 150 ml of saturated brine. The resulting acidic solution was thoroughly extracted with ether and backwashed repeatedly with saturated brine containing Na_2CO_3, saturated brine, and a small amount of water, dried over anhydrous $MgSO_4$, filtered, and concentrated *in vacuo* to give a residue. It was chromatographed on silica gel, using 15% ether–hexane as eluent, to provide 2.3 g (77%) of **6**.

*Reaction of Indole (**7**) with 2-Ethoxy-1,3-dithiolane in Acetic Acid.* To a solution of **7** (1.5 g, 13 mmol) in acetic acid (30 ml) we added, drop by drop, 2-ethoxy-1,3-dithiolane (3.0 g, 20 mmol) at 110 °C. The mixture was stirred for 5 h at the same temperature and then worked up as described in the above experiment using **5**. Subsequent column chromatography on silica gel, using 50% chloroform–hexane as the eluent, gave two products, **8** (1.8 g, 64%) and **9** (0.34 g, 8%). When the reaction temperature was varied from 110 °C to room temperature, only the former, **8**, was obtained in an 81% yield.

Preparation of Aldehydes from 1,3-Dithiolan-2-ylated Aromatics. To a suspension of red HgO (3.9 g, 18 mmol) in 20 ml of 15% aqueous tetrahydrofuran, maintained under N_2 at 0 °C, we added, drop by drop, $BF_3 \cdot Et_2O$ (2.6 g, 18 mmol). The mixture was then allowed to warm to room temperature. A 1,3-dithiolan-2-ylated aromatic (9 mmol) was added over a period of 20 min, after which the mixture was stirred for 1 h. The resulting insoluble precipitate was filtered and washed thoroughly with a large amount of ether. The foregoing filtrate was extracted repeatedly with the washings and once with ether. The combined ethereal extracts were washed successively with saturated brine containing Na_2CO_3 (pH 10), saturated brine, and a small amount of water, dried over anhydrous $MgSO_4$, filtered, and concentrated *in vacuo* to give the crude aldehyde, which was then purified.

Table 5. Analytical data of 1,3-dithiolan-2-ylated aromatics

Compound	Found(%)			Calcd(%)		
	C	H	N	C	H	N
2a	54.09	5.32		54.51	5.08	
3a	54.41	5.30		54.51	5.08	
4a	47.60	4.90		47.65	4.66	
3b	56.47	5.61		56.57	5.70	
4b	49.14	5.26		49.33	5.10	
2c	56.37	5.57		56.57	5.70	
3c	56.57	5.90		56.57	5.70	
4c	49.67	5.02		49.33	5.10	
2d	56.53	5.72		56.57	5.70	
3e	52.44	5.32		52.60	5.30	
2f	52.53	5.43		52.60	5.30	
6	58.87	6.79	5.99	58.62	6.71	6.22
9	51.61	4.67	4.17	51.65	4.64	4.30

References

1) L. Gattermann and J. A. Koch, *Ber.*, **30**, 1622 (1897); N. N. Crounse, *Org. React.*, **5**, 290 (1957).
2) K. Reimer and F. Tiemann, *Ber.*, **9**, 824, 1268 (1876); H. Wynberg, *Chem. Rev.*, **60**, 169 (1960).
3) A. Vilsmeier and A. Haack, *Ber.*, **60**, 119 (1927); L. N. Ferguson, *Chem. Rev.*, **38**, 227 (1946).
4) J. C. Duff and E. J. Bills, *J. Chem. Soc.*, **1932**, 1987; J. C. Duff, *J. Chem. Soc.*, **1941**, 547; W. E. Smith, *J. Org. Chem.*, **37**, 3972 (1972).
5) H. Goss, A. Rieche, and G. Matthey, *Chem. Ber.*, **96**, 308 (1963); T. M. Cresp, M. V. Sargent, and J. A. Elix, *J. Chem. Soc., Chem. Commun.*, **1972**, 214.
6) P. G. Gassman and D. R. Amick, *Tetrahedron Lett.*, **1974**, 3463.
7) S. Tanimoto, T. Miyake, and M. Okano, *Bull. Inst. Chem. Res., Kyoto Univ.*, **55**, 276 (1977).
8) R. H. Jones, G. E. Lukes, and J. T. Bashour, U. S. Patent 2701253; *Chem. Abstr.*, **50**, 1086 (1956).
9) R. Wizinger and D. Dürr, *Helv. Chim. Acta*, **46**, 2167 (1963).
10) P. Stütz and P. A. Stadler, *Helv. Chim. Acta*, **55**, 75 (1972).
11) E. Vedejs and P. L. Fuchs, *J. Org. Chem.*, **36**, 366 (1971).

Table 6. Preparation of aldehydes from 1,3-dithiolan-2-ylated aromatics

1,3-Dithiolan-2-ylated aromatics	Aldehyde[a]	Yield/% of aldehyde from 1,3-dithiolan-2-ylated aromatics[b]	Overall yield/% of aldehyde from the starting aromatics	Chemical shift of aldehyde H (δ/ppm, $CDCl_3$)
3a	**11a**	77	35	9.92
3b	**11b**	92	77	9.87
3c	**11c**	91	22	10.13
2d	**10d**	84	46	9.82
3e	**11e**	39	15	9.96
2f	**10f**	47	19	9.50
6	**12**	90	69	9.83
8	**13**	84	68	10.07[c]

a) All the aldehydes here are known compounds. Their ^{1}H-NMR spectra and analytical data satisfied all the given structures. b) Represents isolated yield. c) The solvent here was a mixture of $CDCl_3$ and DMSO-d_6.

Asymmetric Reactions. X. Asymmetric Hydrogenation Catalyzed by Bis(dimethylglyoximato)cobalt(II)–Chiral Cocatalyst (Amino Alcohol) System

Yoshiaki Ohgo,* Seiji Takeuchi, Yukikazu Natori, and Juji Yoshimura†

Niigata College of Pharmacy, 5829 Kamishin'ei-cho, Niigata 950-21

† *Laboratory of Chemistry for Natural Products, Tokyo Institute of Technology, Nagatsuta, Midori-ku, Yokohama 227*

(Received December 16, 1980)

The catalytic asymmetric hydrogenations of α-diketones, α-keto carboxylates, α-(acylamino)acrylates, α-phenylacrylophenone, and α-phenylacrylate were examined with bis(dimethylglyoximato)cobalt(II)–chiral cocatalyst (amino alcohol) and with simple achiral base coordinated bis(dimethylglyoximato)cobalt(II)–chiral cocatalyst (amino alcohol) systems. These gave corresponding optically active reduction products, and in some cases, optically active reductive dimerization products. High degrees of enantioselectivities (≈78%) are achieved in the hydrogenation of α-diketones. Evidence for non-binding of chiral base to cobalt complexes was presented in the case of latter system, *i.e.*, it was shown that the catalytic site and the enantioselectivity-determining site are separated in this system, as in enzymes. The importance of protonated chiral bases for enantioselection was also shown. Based on these results and the stereochemical correlations between structures of the chiral bases and those of the products, a mechanism for this asymmetric hydrogenation was proposed.

Considerable attention has recently been paid to metal complex-catalyzed asymmetric hydrogenation.[1,2] Most of the researches in this area concentrate on the chiral phosphine rhodium complexes which have given successful results in the asymmetric hydrogenation of olefinic compounds.[1,2] In spite of the obvious advantages of being easily accessible and versatile, catalytic asymmetric hydrogenation using cobalt complexes and/or chiral cocatalysts has scarcely been studied.[3–6]

From the viewpoint of chemical evolution, the authors began to study asymmetric hydrogenation with one of the simplest catalysts, cyanocobalt–chiral amine systems.[3,4] The limitations of these systems suggested that we should use a complex whose framework is stable during the reaction. On the other hand, bis(dimethylglyoximato)cobalt(II) complex (Fig. 1)[7]

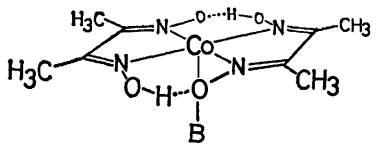

Fig. 1. Bis(dimethylglyoximato)cobalt(II).

was shown to be an effective catalyst for hydrogenation of activated olefinic compounds, α-diketones, α-keto carboxylates, and unsaturated nitrogen compounds.[8,9] We expected that a polyfunctional asymmetric substance bound weakly to cobalt or dimethylglyoxime ligand could draw a substrate into the reaction center with an attractive interaction and should bring about asymmetric induction. Thus, we have found two unique and excellent catalyst systems, bis(dimethylglyoximato)cobalt(II)–chiral amino alcohol and achiral base coordinated bis(dimethylglyoximato)-cobalt(II)–chiral amino alcohol, which catalyze asymmetric hydrogenation of α-diketones, α-keto carboxylates, and olefinic compounds. These have, in part, been communicated previously.[5]

The purpose of this paper is to describe more detailed results and the mechanism of this asymmetric hydrogenation which revealed the unique characteristic of these systems: the catalytic site and the enantioselectivity-determining site are separated, as in enzymes.

Results and Discussion

Catalytic Asymmetric Hydrogenation of α-Keto Carbonyl Compounds and Olefinic Compounds with Bis(dimethylglyoximato)cobalt(II)–Chiral Base System. (a) Substrate Study: Catalytic hydrogenations of various keto carbonyl compounds were examined using bis(dimethylglyoximato)cobalt(II)–quinine under an atmospheric pressure of hydrogen in benzene solution. α-Diketones and α-keto carboxylates were catalytically hydrogenated with this catalyst system to give the corresponding optically active reduction products as shown in Table 1. However, β-keto carboxylates, α-keto carboxamides, and 1,4-dibenzoylbenzene resisted reduction under the given conditions.

Asymmetric hydrogenation of benzil gave *S*(+)-benzoin almost quantitatively with 71% optical yield at 10 °C. The carbonyl group adjacent to the phenyl group of methyl phenyl diketone was preferentially reduced to give *S*(+)-α-hydroxy-α-phenylacetone in 56% optical yield. This compound was shown to racemize under the reaction conditions, and the true enantioselectivity (about 67%) was obtained by extrapolation of the linear log $[\alpha]_D$ *vs.* reaction time to $t=0$. The hydrogenation of biacetyl gave not only the simple reduction product, but also reductive dimerization products. The simple reduction product, acetoin, and reductive dimerization products, 3,4-dihydroxy-3,4-dimethyl-2,5-hexanedione, were separated by silica gel column chromatography. The ratio of *erythro* isomer (78%) and *threo* isomer (22%) in the dimerization products was determined from the intensities of NMR signals of C–CH_3 [δ 1.25 (*erythro*) and δ 1.30 (*threo*)] and CH_3CO [δ 2.36 (*erythro*) and δ 2.23 (*threo*)].[10] Reduction of 1,2-cyclohexanedione gave 2-hydroxycyclohexanone with $[\alpha]_D$ −2.44° in 54% chemical yield. The optical yield can not be

Table 1. Asymmetric hydrogenation of α-ketocarbonyl compounds catalyzed by $Co(dmg)_2$-quinine[a]

Substrate	S/Co[g]	Reaction temp °C	Products: Structure	Yield/%	$[\alpha]_D$/°	Optical yield/%	Conf.
PhCOCOPh (**1**)	10	30	PhCHCOPh (**7**) OH	99	+73[h]	61.6	*S*
PhCOCOCH$_3$ (**2**)	10	R.T.	PhCHCOCH$_3$ (**8**) OH	87—88	+88.8[b]	56.1	*S*
			PhCOCHCH$_3$ (**9**) OH	7— 8			
			CH$_3$CHCOCH$_3$ (**10**) OH		−2.0[c]	2.5	*R*
CH$_3$COCOCH$_3$ (**3**)	10	30	[CH$_3$ -COH COCH$_3$]$_2$ *erythro* (**11**-E)	42.9			
			threo (**11**-T)	12.1	−33[d]		
(**4**)	10	R.T.	(**12**)	54	−2.44		
			PhCHCOOC$_2$H$_5$ (**13**) OH	32	+28.2[e]	13.7	*S*
PhCOCOOC$_2$H$_5$ (**5**)	20	30	[Ph -COH COOC$_2$H$_5$]$_2$ (**14**)	54			
5	10	15	**13**	71—73	+40	19.5	*S*
			14	20—23			
			PhCHCOOCH(CH$_3$)$_2$ (**15**) OH	62	+18[f]	11.4	*S*
PhCOCOOCH(CH$_3$)$_2$ (**6**)	10	15	[Ph -COH COOCH(CH$_3$)$_2$]$_2$ (**16**)	24			

a) Catalytic hydrogenation was carried out in benzene under the atmospheric pressure of hydrogen. In every experiment, equimolar amounts of quinine (Q*) and its HCl salt (Q*HCl) were used (Q*/Co=Q*HCl/Co=1). b) Specific rotation of pure *R*(−)-α-hydroxy-α-phenylacetone, $[\alpha]_D^{20}$ −158.3° (*c* 2.5, ethanol).[11] c) Specific rotation of pure (*R*(−)-acetoin, $[\alpha]_D$ −82° (*c* 0.844, water)[12] d) This value was based upon the concentration of *threo* derivative calculated from the ratio of *threo* to *erythro*. e) Specific rotation of pure ethyl *S*(+)-mandelate, $[\alpha]_D^{20}$ +205.1° (*c* 0.7, carbon disulfide).[13] f) Specific rotation of mandelic acid derived by hydrolysis of the product (isopropyl mandelate); Specific rotation of pure *S*(+)-mandelic acid, $[\alpha]_D^{20}$ +157.5 (*c* 2.1875, water)[14] g) S/Co: molar ratio of substrate to cobalt. h) Specific rotation of pure benzoin, $[\alpha]_D$ ±118.5 (*c* 1, acetone).[15]

determined because the optically pure enantiomer is unknown. Hydrogenation of ethyl phenylglyoxylate and isopropyl phenylglyoxylate gave ethyl *S*(+)-mandelate and isopropyl *S*(+)-mandelate in optical yields of 19.5 and 11.4%, respectively. In these cases, reductive dimerization products which had positive rotation were also obtained. The yields of reductive dimerization products increase with increasing molar ratio of substrate to cobalt. The details of these reductive dimerizations will be published separately.

Catalytic asymmetric hydrogenations of olefinic compounds were also carried out in benzene solution. The reaction products were purified by distillation, except for the case of methyl (*S*)-*N*-(phenylacetyl)-alaninate (**23**). All these samples were checked by ^{1}H NMR. Optical yields were calculated from the specific rotations of the products by reference to the maximum optical rotation reported in the literature, except for **23** which was obtained by methylation of (*S*)-*N*-(phenylacetyl)alanine ($[\alpha]_D$ −30°)[19] with diazomethane, $[\alpha]_D$ −56.9° (*c* 2, methanol) (see experimental part). The results are shown in Table 2. Olefinic double bonds of both the olefinic ketone and olefinic carboxylates are chemospecifically hydrogenated with this catalyst system to give the corresponding saturated optically active ketone and carboxylates.

In general, the optical yields with the substrates carrying acyl groups were much higher than those with the substrates carrying alkoxycarbonyl groups (Tables 1 and 2).

(b) Effect of Solvent: Catalytic hydrogenation of benzil was examined in several solvent systems (Table

Table 2. Asymmetric hydrogenation of olefinic compounds catalyzed by Co(dmg)$_2$-quinine

Substrate	S/Co[a]	Reaction temp °C	Products: Structure	Yield/%	$[\alpha]_D$/°	Conf.	Optical yield/%
$H_2C{=}C(Ph)(COOCH_3)$ (**17**)	9	R.T.[b]	$H_3C{-}CH(Ph)(COOCH_3)$ (**21**)	80	+7.7[c]	*S*	7.1
$H_2C{=}C(Ph)(COOCH_3)$	17	9	$H_3C{-}CH(Ph)(COOCH_3)$	92	+11.3	*S*	10.4
$H_2C{=}C(NHCOCH_3)(COOCH_3)$ (**18**)	8.4	R.T.	$H_3C{-}CH(NHCOCH_3)(COOCH_3)$ (**22**)	62	−17.0[d]	*S*	18.5
$H_2C{=}C(NHCOCH_2Ph)(COOCH_3)$ (**19**)	8	R.T.	$H_3C{-}CH(NHCOCH_2Ph)(COOCH_3)$ (**23**)	60	−4.0	*S*	7.0
$H_2C{=}C(Ph)(COPh)$ (**20**)	10	R.T.	$H_3C{-}CH(Ph)(COPh)$ (**24**)	95	+99.4[e]	*S*	49.2

a) Molar ratio of substrate to cobalt complex. b) Room temperature. c) Optical rotation of pure (*S*)-isomer; $[\alpha]_D$ +109.2° (*c* 6.2, toluene).[16] d) Optical rotation of pure (*S*)-isomer; $[\alpha]_D$ −91.7° (*c* 2, water).[17] e) Optical rotation of pure (*S*)-isomer; $[\alpha]_D$ +202° (*c* 3.5, chloroform).[18]

Table 3. Effect of solvent on the asymmetric hydrogenation of benzil catalyzed by Co(dmg)$_2$-quinine[a]

Run	S/Co[b]	B/Co[c]	Solvent (ratio)[d]	Yield %	$[\alpha]_D^{21}$/°	Optical yield/%
1	5	3	M	98.5	+10.3	8.7
2	20	3	M/B (1.4)	99.0	+27.8	23.5
3	50	3	M/B (1.07)	85.0	+33.5	28.3
4	20	1	M/B (1.4)	96.5	+29.7	25.1
5	20	2	M/B (1.4)	99.0	+30.2	25.5
6	20	2	M/B (0.43)	96.5	+50.1	42.3
7	20	2	A	96.0	+12.0	10.1
8	20	2	THF	95.5	+42.6	36.0
9	20	2	THF/B (0.6)	97.0	+59.0	49.8
10	10	2	B	98.0	+72.7	61.4

a) Hydrogenation was carried out under the atmospheric pressure of hydrogen at room temperature. In this series of experiments eqimolar amounts of quinine(Q*) and its HCl salt (Q*HCl) were used. b) Molar ratio of substrate to cobalt. c) Molar ratio of quinine to cobalt. d) Ratio of solvents in volume; M=methanol, B=benzene, A=acetone, THF=tetrahydrofuran. e) Specific rotations were measured in acetone (*c*=2—5). The specific rotation of optically pure benzoin, $[\alpha]_D$ ±118.5° (*c* 1, acetone).[15]

3). As is seen from Table 3, the optical yield increases with decreasing polarity of the solvent used. The reaction in benzene gave maximum optical yield under the given conditions. The carbonyl and hydroxyl groups in the solvent molecules decrease the enantioselectivity considerably, suggesting that these groups are concerned with the enantioselection mechanism.

(c) Effect of Temperature and Activation Parameters: The enantioselectivities and pseudo-first-order rate constants were determined at 10°, 20°, and 30 °C in the Co(dmg)$_2$–quinine catalyzed hydrogenation of benzil. The results are summarized in Table 4. From the Arrhenius plot of the rate constants, the apparent activation energy (ΔE_a^*) and the activation entropy (ΔS^*) were estimated to be 8.3 kcal/mol and −50 eu, respectively. Plotting logarithms of the enantiomeric ratio (*S*-isomer/*R*-isomer) *vs.* $1/T$ gave fairly good linearity. From the slope and the intercept at $1/T=0$, the difference between the activation enthalpies for the formation of *R*-isomer and that of

Table 4. Enantioselectivities and pseudo-first-order rate constants in variation of temperatures in the hydrogenation of benzil[a]

Reaction temp °C	Chemical yield	Rate constant, k/min^{-1}	$[\alpha]_D^{21}$/°	Optical yield/%
10	95	5.2×10^{-3}	+94	70.9
20	95	9.1×10^{-3}	+79	66.7
30	99	1.4×10^{-2}	+73	61.6

a) Hydrogenation was carried out in benzene under the atmospheric pressure of hydrogen. Reaction conditions: Co(DMG)$_2$, 2.1×10^{-2} mol dm^{-3}; quinine, 2.1×10^{-2} mol dm^{-3}; quinine hydrochloride, 2.1×10^{-2} mol dm^{-3}; benzil, 2.1×10^{-1} mol dm^{-3} in benzene.

Table 5. Effect of structural variation of chiral amine on the asymmetric hydrogenation of benzil[a)]

Run	Amine	Solvent (ratio)	Yield %	$[\alpha]_D^{21}$/°	Optical yield/%	Conf.[b)]
1	Quinine	T/B (0.6)[c)]		+40.0	33.8	*S* (+)
2	Quinidine	T/B (0.64)	92	−39.4	33.2	*R* (−)
3	Cinchonidine	T/B (0.64)	98	+39.9	33.7	*S* (+)
4	Quinidine	B	95	−56.0	47.3	*R* (−)
5	Ephedrine	M/B (0.36)	99.5	+12.6	10.6	*S* (+)
6	Ephedrine	B	94	+19.8	16.7	*S* (+)
7	*Ψ*-Ephedrine	B	96	−9.2	7.8	*R* (−)
8	*N*-Methylephedrine	B	95	+33.2	28.0	*S* (+)
9	(1*R*,2*S*)-ADPE[e)]	B (5—7 °C)	89	+8.3	7.0	*S* (+)
10	(1*S*,2*S*)-ADPE[g)]	B[d)]	90	−2.0	1.7	*R* (−)
11	(1*R*,2*S*)-MADPE[f)]	B[d)]	98	+15.4	13.0	*S* (+)
12	Brucine	T/B (0.64)	96	−1.55	1.3	*R* (−)
13	*O*-Acetylquinine	T/B (0.6)	99	−5.35	4.5	*R* (−)
14	*S*(−)-α-Methylbenzylamine	T/B (0.6)	95	0.00	0	

a) In this series of experiments free bases were used (Base/Cobalt=2; Substrate/Cobalt=20). Hydrogenation was carried out under atmospheric pressure of hydrogen at room temperature. b) Configuration of predominant isomer. c) T=tetrahydrofuran; B=benzene; M=methanol. d) Benzene solution containing a small amount of methanol. e) (1*R*,2*S*)-2-Amino-1,2-diphenylethanol. f) (1*R*,2*S*)-2-Dimethylamino-1,2-diphenylethanol.[27] g) (1*S*,2*S*)-2-Amino-1,2-diphenylethanol.

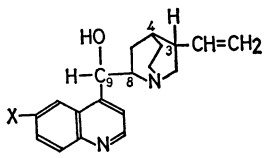

Quinine (X=OCH_3)
Quinidine (X=OCH_3)
Cinchonidine (X=H)

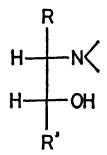

Quinine
Cinchonidine
Ephedrine
(R=CH_3, R′=Ph)
(1*R*,2*S*)-ADPE
(R=R′=Ph)

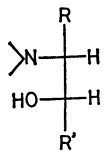

Quinidine

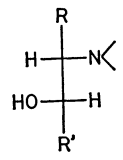

ψ-Ephedrine
(R=CH_3, R′=Ph)
(1*S*,2*S*)-ADPE
(R=R′=Ph)

Fig. 2. Structures and Fischer projections of chiral amino alcohols.

S-isomer ($\Delta\Delta H^{*}_{R\text{-}S}$), and the corresponding entropy difference of activation ($\Delta\Delta S^{*}_{R\text{-}S}$) were estimated to be 2.9 kcal/mol and 6.5 eu, respectively. It should be mentioned that in spite of the rather large difference in activation enthalpies, activation free energy difference became rather small ($\Delta\Delta G^{*}_{R\text{-}S}$=1.1 kcal/mol at 10 °C) since the contribution of the activation entropy term of the same sign is also large ($T\cdot\Delta\Delta S^{*}_{R\text{-}S}$=1.8 kcal/mol).

(d) Effect of Structure of Chiral Amines: In order to obtain some information on the structural parts which have effective interactions in enantioselection, several amines were tested for this catalytic asymmetric hydrogenation of benzil. Only free bases were used in this series of experiments. The results are shown in Table 5; the structures of chiral amines needed for this explanation are shown in Fig. 2. Quinine, quinidine, and cinchonidine have the same configuration at C_3 and C_4 (3*R*,4*S*).[20] The configuration at C_8 and C_9 of quinine and cinchonidine is (8*S*,9*R*), while that of quinidine is (8*R*,9*S*).[20] (−)-Ephedrine,[21] (−)-*N*-methylephedrine,[22] (1*R*,2*S*)-2-amino-1,2-diphenylethanol[23] have the same configurations as quinine at carbon atoms which are attached to amino and hydroxyl groups, *i.e.*, (C_N–*S*,C_{OH}–*R*). *Ψ*-Ephedrine,[24] and (1*S*,2*S*)-2-amino-1,2-diphenylethanol[23] have the (C_N–*S*,C_{OH}–*S*) configuration.

The results indicate that the chiral structure at C_3 and C_4 of quinine, quinidine, and cinchonidine does not affect enantioselectivity (runs 1—4), and that the configuration of predominant isomer is unequivocally determined by those of the vicinal carbons which are attached to amino and hydroxyl groups, *i.e.*, (C_N–*S*,C_{OH}–*R*) and (C_N–*R*,C_{OH}–*S*) give *S*(+)- and *R*(−)-benzoin, respectively. Brucine and *O*-acetylquinine gave extremely low enantioselectivity and moreover, *S*(−)-α-methylbenzylamine could not bring about asymmetric hydrogenation. These facts show again that the hydroxyl group of chiral amines plays an extremely important role in the enantioselection, as already pointed out in a previous section (b). The enantioselectivity of chiral amino alcohol seems to increase in the order of primary, secondary, and tertiary amines.

Asymmetric Hydrogenation Catalyzed by a Conjugated System Composed of Achiral Base Coordinated Bis(dimethylglyoximato)cobalt(II) and Chiral Amino Alcohols (Cocata-

Table 6. Asymmetric hydrogenation of benzil catalyzed by $Co(dmg)_2$·B-Q* [a]

Run	Base	Reaction temp °C	B/Co[c]	Q*/Co[d]	Q*HCl/Co[e]	Benzoin $[\alpha]_D^{22}$/°	Benzoin O.Y.[f] %	Benzoin Conf.	V[g] 10^{-3} s^{-1}
1	Quinidine	R.T.	0	2	0	−56	47.3	*R*	
2	BA[b] Quinidine	26—27	1	1	0	−57	48.1	*R*	6.0
3	BA Quinidine	30	1	3	0	−60	50.6	*R*	12.0
4	Quinine	30	0	1	1	+73	61.6	*S*	1.5
5	BA Quinine	30	1	1	0	+54	45.6	*S*	
6	BA Quinine	30	1	1	1	+72.3	61.0	*S*	13.6
7	Ph_3P Quinine	R.T.	1	1	1	+72.8	61.4	*S*	0.3
8	Pyridine Quinine	30	1.5	1	1	+67.1	56.6	*S*	2.5
9	BA Quinine	−10	1	1	1	+92	77.6	*S*	

a) Every experiment was carried out in benzene solution except for run 9 (in mesitylene); Substrate/Cobalt=10. b) BA: benzylamine. c) B: achiral base. d) Q*: chiral amino alcohol. e) Q*HCl: hydrochloride of Q*. f) O.Y.: optical yield. g) V: initial velocity (H_2 moles consumed/s/mol of catalyst). h) In every case, chemical yield was almost quantitative.

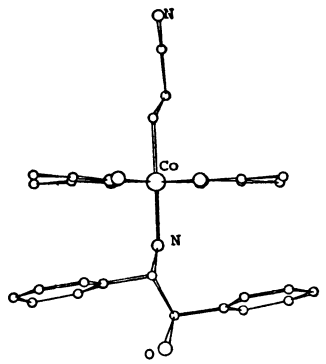

Fig. 3. Perspective view of **25** looking along equatorial plane.[26]

lysts). (a) Evidence for Non-binding of Chiral Base to Cobalt Complexes: Our primary concern is to disclose the mechanism by which chiral amine brings about asymmetric induction. Two dimethylglyoxime monoanions are in planar coordination to cobalt. If chiral amine would coordinate to cobalt, the catalytically active site must be at the site trans to the chiral amine which can not interact with the substrate directly. All attempts to isolate a quinine or quinidine coordinated complex were unsuccessful. However, (1*R*, 2*S*)-2-amino-1,2-diphenylethanol coordinated (2-cyanoethyl)bis(dimethylglyoximato)cobalt(III) (**25**) was isolated. From NMR and circular dichroism spectra of the complex and from the importance of the hydroxyl group of chiral amine, asymmetric induction had, first, been assumed to be brought about by an asymmetric field induced at the site trans to chiral axial base through hydrogen bonding between the oxygen of the dimethylglyoxime ligand and the hydroxyl group of chiral amino alcohol. However, X-ray analysis of the complex (**25**) revealed that the amino nitrogen and the hydroxyl group of amino alcohol are fully transoid; there exists no hydrogen bonding between the oxygen of the inplane ligand and the hydroxyl group of amino alcohol and also no significant asymmetric distortion of the inplane ligand (Fig. 3).[25] The optical yields increase in the order of primary, secondary, and tertiary amines. This order is consistent with that of the difficulty in coordination of the amine. Such results suggested the possibility that asymmetric induction was brought about by an amino alcohol molecule other than that coordinated to the cobalt atom. Thus, asymmetric hydrogenation was examined in the presence of both chiral amino alcohol and an achiral simple base such as benzylamine, pyridine, and triphenylphosphine. The results are summarized in Table 6. A comparison of runs 4 and 6 (or 1 and 2) shows the optical yields did not decrease, while the reaction rates were extremely enhanced on addition of benzylamine to bis(dimethylglyoximato)cobalt(II)–quinine or –quinidine system. The reaction rates increase in the order of increasing electron donor ability of the achiral simple base added. This seems to suggest that the achiral simple base is coordinated to a cobalt atom. The rate acceleration made it easy to react at a lower temperature. At −10 °C in mesitylene the optical yield reached 78%.

In order to obtain more precise information on the coordinated base, the circular dichroism was examined. If an optically active amine is coordinated to a cobalt atom, the CD band due to vicinal effect[26] of the amine should be observed in the d-d transition region of cobalt. The CD spectra of mixtures of methylbis(dimethylglyoximato)cobalt(III) and quinidine were measured for various molar ratios (Fig. 4). The CD Cotton effect in the d-d transition region of cobalt increased with the increasing molar ratio of quinidine to cobalt complex, showing an equilibrium between the states of quinidine coordinated and non-coordi-

Table 7. Effect of HCl salt on the asymmetric hydrogenation of benzil[a)]

Run	Solvent (ratio)	BA[b)]	Q*[c)]	Q*HCl	BHCl (BHCl/Co)	$[\alpha]_D^{22}$/°	O.Y./%	$\frac{V}{10^{-3}\ s^{-1}}$
1	Benzene	1	1	0	0	+54	45.6	9
2	Benzene	1	0	1	0	+70	59.0	6.5
3	Benzene	1	1	1	0	+72.3	61.0	13.6
4	B/M(4/1)[d)]	1	0	1	0	+33.6	28.4	6.5
5	B/M(4/1)	1	0	1	Quinuclidine HCl (1)	+8.6	7.3	7.6

a) The reaction was carried out under the atmospheric pressure of hydrogen at about 30 °C. b) BA: benzylamine. c) Q*: quinine. d) B/M: a mixture of benzene and methanol.

Table 8. Effect of HCl salt on the asymmetric hydrogenation of α-phenylacrylophenone[a)]

Run	Reaction temp °C	BA	Q*	Q*HCl	$[\alpha]_D$/°	O.Y./%	$\frac{V}{10^{-3}\ s^{-1}}$
1	R.T.	0	1	1	+99.4	49	—
2	30	1	1	0	+20.2	10	13
3	30	1	0	1	+91.4	45	11

a) The reaction was carried out in benzene. See also the footnotes of Tables 6 and 7.

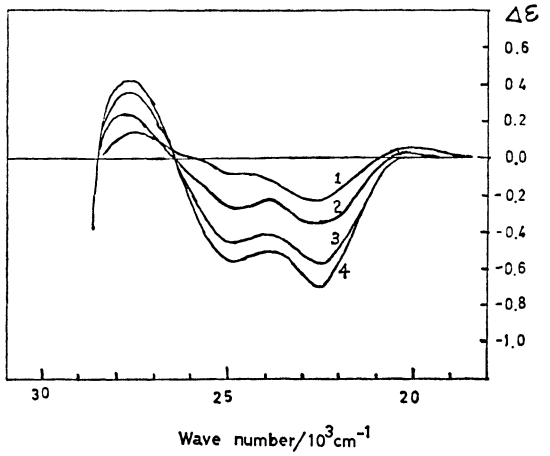

Fig. 4. CD Spectra of dichloromethane solutions of $CH_3Co(dmg)_2$ (A) and quinidine (B) in variation of molar ratio of (B) to (A).
Spectrum 1: $[A]=[B]=10^{-3}$ mol/l,
Spectrum 2: $[A]=10^{-3}$ mol/l; $[B]=1.5\times10^{-3}$ mol/l,
Spectrum 3: $[A]=10^{-3}$ mol/l; $[B]=4\times10^{-3}$ mol/l,
Spectrum 4: $[A]=10^{-3}$ mol/l; $[B]=8\times10^{-3}$ mol/l.

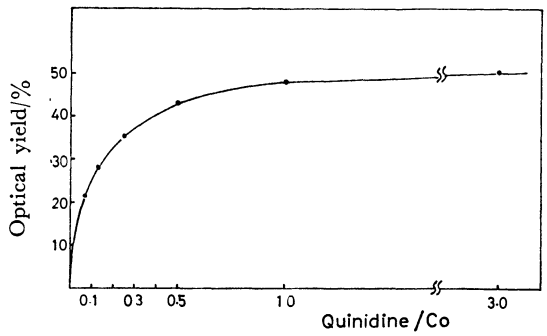

Fig. 5. Non-linear correlation between optical yields and molar ratio of quinidine to $Co(dmg)_2$ in the hydrogenation of benzil catalyzed by $Co(dmg)_2$·benzylamine-quinidine.

nated to the cobalt complex. Addition of an equimolar amount of benzylamine to the above system erased the Cotton effect. This clearly indicates that benzylamine coordinates selectively to cobalt in the system:

$$[CH_3Co(dmg)_2\cdot Q^* \rightleftarrows CH_3Co(dmg)_2 + Q^*] \xrightarrow{PhCH_2NH_2} CH_3Co(dmg)_2\cdot NH_2CH_2Ph + Q^*$$

However, the results still do not rule out the possibility that the amino alcohol have some interaction with some part of the ligands. In order to check this possibility, we studied the change in optical yield with variation of molar ratio of quinidine to cobalt complex in the hydrogenation of benzil by this system. If chiral amine and cobalt complex have a 1:1 interaction or binding, then the optical yields will increase linearly up to the ratio of Q*/Co=1. However, the results do not show a linear correlation (Fig. 5). These results clearly indicate that this enantioselection is brought about by chiral amino alcohol which does not bind firmly to any part of the complex. This fact is quite surprising in view of how asymmetric induction is brought about.

(b) Importance of Protonated Chiral Base for Enantioselection, and Mechanism of Asymmetric Hydrogenation: As is seen from Table 7, when free quinine only is used as the chiral substance in the hydrogenation of benzil, the optical yield is only 46%. However, when the hydrochloride of quinine is used, the optical yield becomes much higher. The optical yield increases a little more when both free quinine and its hydrochloride salt are used. Moreover, the addition of hydrochloride of achiral quinuclidine caused a remarkable decrease in enantioselectivity. A similar effect of hydrochloride salt was also observed in the hydrogenation of α-phenylacrylophenone (Table 8). These facts suggest that protonated chiral amino alcohol plays a decisive role in this enantioselection and also that the proton pulled out of the hydridobis(dimethylglyoxi-

Table 9. Effect of tertiary amines on the asymmetric hydrogenation of benzil with $Co(dmg)_2 \cdot BA\text{-}Q^*$

Run	Reaction temp/°C	BA[a]	Q_1^*	Q_1^*HCl[b]	Q_2^*[c]	Tertiary base(B/Co)	Optical yield/%	Conf.	V[d] / 10^{-3} s^{-1}
1	30	1	1	1	0	0	61.0	*S*	13.6
2	30	1	1	1	0	Pyridine (2)	61.0	*S*	10.0
3	30	1	1	1	0	$(n\text{-}C_6H_{13})_3N$ (2)	58.0	*S*	11.1
4	R.T.	1	1	1	0	$(C_2H_5)_3N$ (2)	51.8	*S*	14.9
5	30	1	1	1	0	Quinuclidine (2)	8.5	*S*	
6	30	1	1	0	0	0	45.6	*S*	9.0
7	27	1	0	0	1	0	48.1	*R*	6.0
8	30	1	0	0	3	0	51.0	*R*	12.0
9	30	1	0	0	1	$(n\text{-}C_6H_{13})_3N$ (1)	37.0	*R*	8.2
10	30	1	0	0	1	$(C_2H_5)_3N$ (1)	32.0	*R*	9.9
11	30	1	0	0	1	Quinuclidine (1)	12.0	*R*	10.6

a) BA: benzylamine. b) Q_1^*: quinine, Q_1^*HCl: hydrochloride of quinine. Q_2^*: quinidine. d) V: initial velocity (H_2 moles consumed/s/mol of catalyst). For reaction conditions see the footnote of Table 6.

Table 10. Asymmetric hydrogenation of benzil catalyzed by $Co(dmg)_2 \cdot B$-bulky chiral base

Run	Base	Reaction temp/°C	B/Co[a]	B*/Co[b]	$[\alpha]_D$/°	Optical yield/%	Conf.	V[c] / 10^{-3} s^{-1}
1	*N*-Methylephedrine	R.T.	0	1	+33.2	28.0	*S*	
2	[Benzylamine *N*-Methylephedrine	30	1	1	+9.1	7.7	*S*	5.0
3	[Pyridine *N*-Methylephedrine	30	1	1	+18.2	15.4	*S*	0.7
4	[Triphenylphosphine *N*-Methylephedrine	30	1	1	+51.0	43.0	*S*	0.2
5	(1*R*,2*S*)-MADPE	R.T.	0	1	+15.4	13.0	*S*	
6	[Benzylamine (1*R*,2*S*)-MADPE	30	1	1	+1.3	1.1	*S*	7.1

a) Molar ratio of B(non-chiral base) to cobalt. b) Molar ratio of bulky chiral base(B*) to cobalt. c) V: initial velocity, see the footnot of Table 6. d) (1*R*,2*S*)-2-Dimethyl-amino-1,2-diphenylethanol.[27]

mato)cobalt complex by the amine reacts with substrate or substrate-bound complexes in a bound state. Addition of an achiral base stronger than the chiral base gives a protonated achiral base (t-BH^+), in competition with the formation of a protonated chiral base (B^*H^+). This is expected to cause a decrease in enantioselectivity. As expected, addition of a

$$[B^* + t\text{-}B + HCo(dmg)_2 \cdot B \rightleftharpoons Co(dmg)_2 \cdot B^- + B^*H^+ + t\text{-}B \rightleftharpoons Co(dmg)_2 \cdot B^- + B^* + t\text{-}BH^+]$$

stronger base to the system caused a remarkable decrease in enantioselectivity (Table 9). Even though these tertiary amines have almost the same basicity, their effects on the enantioselectivities are considerably different. The differences can be understood in terms of steric hinderances which prevent these protonated bases from approaching the reaction center. The same kind of steric effect is observed in cases of sterically hindered chiral amine (Table 10). On using quinine or quinidine, whose effective bulk around nitrogen atom is relatively small owing to the cage structure, optical yields did not vary with achiral weak bases such as benzylamine, pyridine, and triphenylphosphine. However, when *N*-methylephedrine was used as the chiral base, optical yields varied remarkably with variation of the above achiral bases. In this case, even a small amount of a protonated simple base (for example, dissociated benzylamine) or hydride complex seems to compete seriously. Thus, a fairly good result is obtained using triphenylphosphine as the axial base which has very low basicity toward protons.

Thus, protonated chiral amino alcohol must recognize enantiotopic face on giving its proton to the substrate or substrate-bound complexes. This, in turn, requires an electron donor at some stages. The species must be a Co(I) anion which is released by abstraction of H^+ from a hydride complex. The rate accelerations with increasing basicity and with addition of proton sources are in accord with the mechanism comprised of an electron donor [Co(I) anion] and a proton donor. In addition, the catalytic hydrogenation by this system has been shown to proceed through an α-alkyl complex, followed by the reductive cleavage of Co–C bond with a Co(I) anion.[9,28] The mechanism of this hydrogenation is schematically delineated in Scheme 1.

A hydridobis(dimethylglyoximato)cobalt complex is produced by the reaction of bis(dimethylglyoximato)-cobalt(II)–base and molecular hydrogen. The hydride complex dissociates into proton and Co(I) anion with an aid of a basic solute in equilibrium. The proton is captured by bases in this system. The substrate

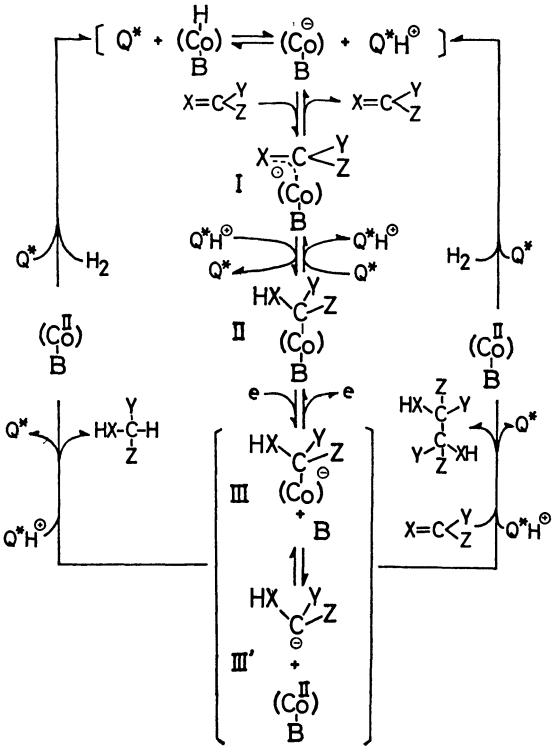

Scheme 1. Catalytic cycle in the hydrogenation with $Co(dmg)_2$·B-Q*.
Electron (e) is supplied from hydrogen probably *via* $(Co^{I})\cdot B^{-}$. (Co), B, and Q* represent bis(dimethylglyoximato)cobalt, axial base and chiral cocatalyst (chiral amino alcohol), respectively.

gains an electron from the Co(I) anion to give an intermediate (anionic alkyl complex or radical anion) which undergoes the attack of the protonated base to give an alkyl complex (II). The reaction of the alkyl complex (II) with the electron donor, Co(I) anion, will form the reduced state of the alkyl complex, III, and/or carbanion, III'. The subsequent attack of the protonated base, Q^*H^+, and/or the protonated basic solute including the hydridobis(dimethylglyoximato)cobalt complex will give the simple reduction product. But if the reduced state of the alkyl complex or carbanion (III or III') undergoes the attack of another substrate followed by protonation, the reductive dimerization product may be formed. Enantioselection will take place in two stages when Q^*H^+ gives its proton to the intermediates I and III and/or III'. The latter stage of enantioselection will be more important for the following reasons. The former stage was shown to be in an equilibrium;[9] also, deuterium cleavage of optically pure [(*R*)-1-(methoxycarbonyl)ethyl](pyridine)bis(dimethylglyoximato)cobalt(III), which was easily derived by displacement of the axial base of [(*R*)-1-(methoxycarbonyl)ethyl] [*R*(+)-methylbenzylamine]bis(dimethylglyoximato)cobalt(III)[29] with pyridine, gave the inversion product predominantly, but the stereoselectivity was extremely low (lower than 1%).[30] This result implies that the reduced state of alkyl complex III is also in an equilibrium with carbanion III'.

Before presenting the mechanism of chiral recognition it is necessary to discuss the conformations of alkyl complexes or carbanions ejected from the reduced state of alkyl complexes. They will be able to exist in two forms of rotamers with respect to the rotating axis of C_α–COR' bond:

Transoid (*T*) Cisoid (*C*)

One is the rotamer in which substituents, R and R' are transoid, and the other is one in which they are cisoid. The stability of each form will be determined by the balance of the attractive interaction between O and HX, and the repulsive interaction between R and R'. Considering that Q^*H^+ selects the favored chirality of two enantiomers (or the favored prochiral face of carbanion) in the more stable rotamer (*T* or *C*) to furnish its proton, we can predict the configuration of the predominant enantiomer in all the cases examined.

In cases of substrates having large substituents such as benzil and α-phenylacrylophenone, two substituents have to situate in trans form, because of the large steric repulsion between these groups. Protonated quinine will approach the reduced alkyl complex (III) or carbanion (III') with an attractive interaction between the OH group of quinine and carbonyl group of substrate and also between the positive charge of protonated quinine and the negative charge of reduced alkyl complexes or carbanion (Fig. 6). The assumption of the attractive interaction between the hydroxyl group of amino alcohol and the carbonyl group of the substrate may be substantiated by solvent

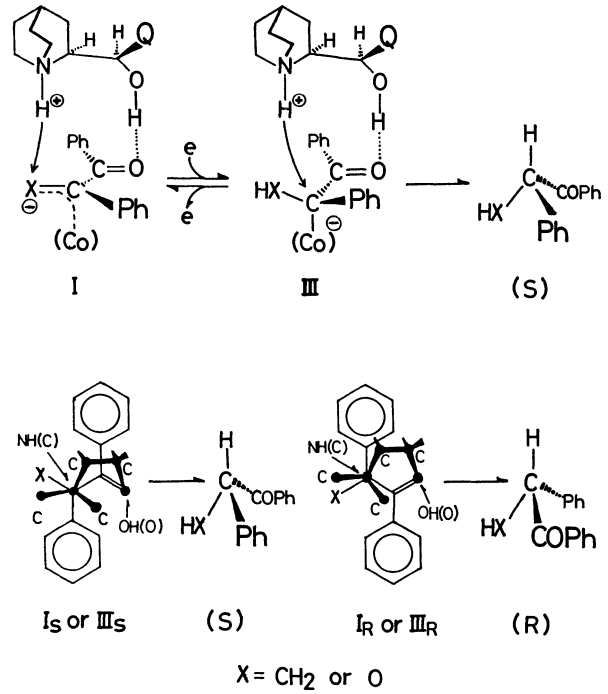

Fig. 6. A proposed mechanism for enantioselection in the hydrogenation of benzil, α-phenylacrylophenone, and methyl phenyl diketone.

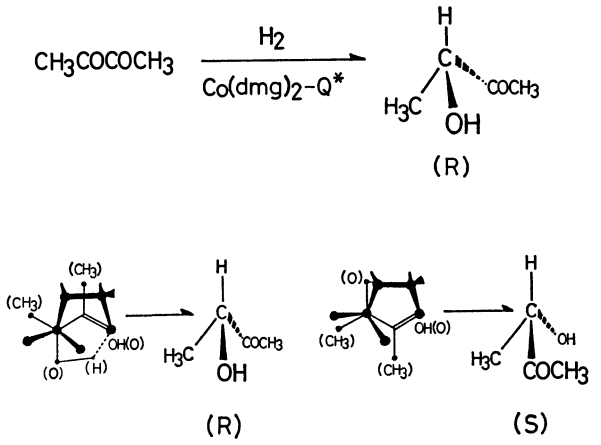

Fig. 7. A proposed mechanism for enantioselection in the hydrogenation of biacetyl.

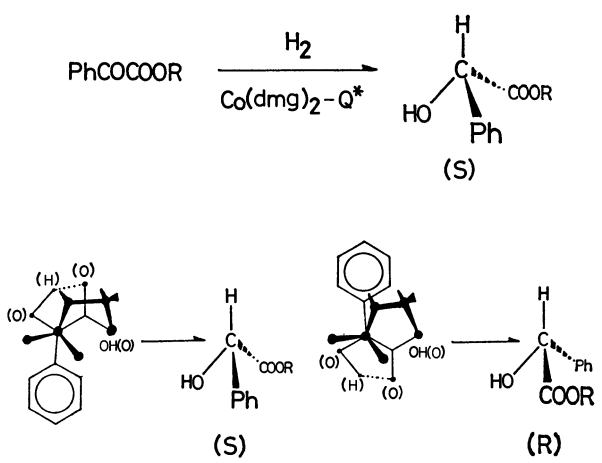

Fig. 8. A proposed mechanism for enantioselection in the hydrogenation of phenylglyoxylates.

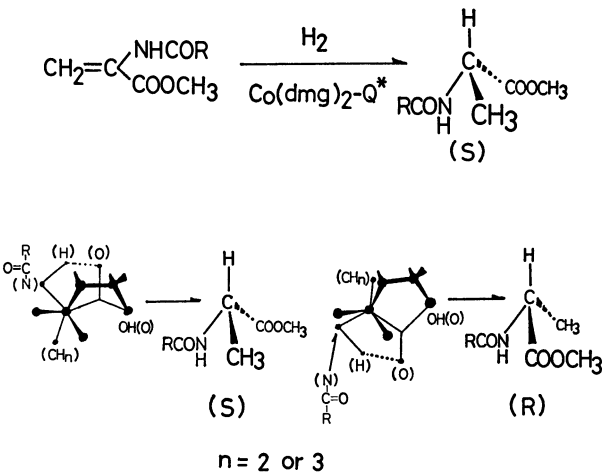

Fig. 9. A proposed mechanism for enantioselection in the hydrogenation of dehydroalanine derivatives.

effect: that solvents having hydroxyl and carbonyl groups decrease enantioselectivity, and also by the importance of hydroxyl group of chiral amine for the enantioselection. Is (or IIIs) and Ir (or IIIr) are the projections which are obtained by viewing I (or III) from above. As is seen, an approach like Is (or IIIs) which gives the predominant enantiomer (*S*) is well fitting and has no substantial repulsion, while the other (*R*) will result in a serious repulsion because the substituents around the reaction site are nearly eclipsed. In cases of the substrates having small substituents or substituents compelled to be in cisoid form, such as biacetyl and 1,2-cyclohexanedione, hydrogen bonded cis form will be favored. Thus, the attack of protonated quinine to the cis form (***C***) will reasonably be assumed in cases of substrates having small substituents or substituents compelled to be in cis form. The transition state which gives *R* isomer is more stable than that giving *S* isomer (Fig. 7). The same explanation will be made in the cases of α-keto carboxylates and α-(acylamino)acrylates (Figs. 8 and 9). Although only quinine was used for the explanation of the enantioselection mechanism, the enantioselectivity of other chiral amino alcohols can also be explained in the same way.

Features and Limitations of This Catalyst System. Thus, the attempt to overcome the shortcomings of the previously studied catalyst system, the cyanocobalt–chiral amine system, have led us to explore a unique catalyst system, bis(dimethylglyoximato)cobalt(II)·B–chiral amino alcohol system, which resembles enzymes. The catalytic site and the enantioselectivity-determining site of this catalytic system are separated: bis(dimethylglyoximato)cobalt complex and chiral amino alcohol are considered to correspond to NAD (or NADP) and apoenzyme, respectively. This makes it possible to improve these two catalytic features almost independently. In fact, catalytic activity was enhanced by increasing electron density on cobalt atom without decreasing enantioselectivity, when the chiral base used was the same.

On the other hand, enantioselection of this catalytic system is performed when the chiral proton carrier gives the proton. In consequence, the existence of achiral proton carrier makes enantioselectivity lower. This is an inherent shortcoming of this catalytic system. However, this is not one which is impossible to overcome: Directed proton transfer with complete enantioselectivity seems to be involved in biological redox systems.

Another aspect is concerned with kinetic parameters. As described in a previous section, in spite of the rather large difference of activation enthalpies ($\Delta\Delta H^{*}_{R\text{-}S}=2.9$ kcal/mol), the activation free energy difference becomes rather small ($\Delta\Delta G^{*}_{R\text{-}S}=1.1$ kcal/mol at 10 °C) because of large difference in activation entropy term which has the same sign. If it would be possible to make the entropy term zero, almost complete enantioselectivity (99%) should be achieved. Thus, controlling the entropy term is an essential problem to be solved.

Experimental

Melting points were measured by a Yanagimoto micro-melting point apparatus and are uncorrected. Nuclear magnetic resonance spectra were recorded on a JEOL JNM-4H-100 spectrometer, using TMS as the internal standard.

Gas liquid chromatography was performed on a Shimadzu GC-4CM using 10% PEG 4000-Celite column. Optical rotations were measured on a Carl Zeiss photoelectric precision polarimeter. Circular dichroism spectra were measured by JASCO ORD/UV-5 spectrometer. Infrared spectra were taken on a Hitachi EPI-G2 spectrophotometer.

General Procedure for Asymmetric Hydrogenation Catalyzed by Bis(dimethylglyoximato)cobalt(II)-Puinine. A 200 ml flask which have a side neck with a rubber cap was used as the reaction vessel. To a methanol (10 ml) solution of $CoCl_2 \cdot 6H_2O$ (0.25 g) was added a hot solution of dimethylglyoxime (0.244 g) in methanol (14 ml) under nitrogen atmosphere with stirring. The solution was stirred for 5—10 min and then 1 ml of 2.35 mol dm^{-3} sodium methoxide solution was added to this solution. After 1—2 min, a degassed methanol solution of an equimolar mixture of quinine and quinine hydrochloride (which is prepared by adding 0.46 ml of 2.35 mol dm^{-3}-sodium methoxide solution to a solution of quinine $HCl \cdot 2H_2O$ (0.84 g) in methanol (5 ml)) was added to the above reaction vessel. The reaction vessel was connected to a gas burret and a vacuum system through a three-way tap. Methanol in the resulting catalyst solution was evaporated under a reduced pressure with warming and stirring to a wet paste (in this case, caution should be taken not to dry the catalyst). To this paste 10 ml of degassed benzene was added by a syringe under atmospheric pressure of hydrogen, and the mixture was then evaporated again to a wet paste under a reduced pressure in order to eliminate the residual methanol (the above caution should be repeated). To the resulting catalyst was added a degassed benzene solution of substrate with a syringe under atmospheric pressure of hydrogen; hydrogenation was then initiated with vigorous stirring. After the theoretical amount of hydrogen was absorbed, about 300 ml of benzene or ether was added to the reaction mixture, and then successively washed with water (several times), 6 mol dm^{-3} or dilute hydrochloric acid (several times), and water. The organic layer was dried over anhydrous sodium sulfate, and concentrated under a reduced pressure to give the corresponding reduction products.

Asymmetric Hydrogenation of Benzil. In this case, the crude product obtained according to the general procedure was shown to contain substantially no impurity by TLC and GLPC; optical rotation was therefore measured without further purification. The IR and NMR spectra were identical with those of the authentic sample (benzoin). Yields were almost quantitative (Tables 1 and 3).

Asymmetric Hydrogenation of Methyl Phenyl Diketone. After carrying out the usual workup (general procedure) described above, 1.4 g of a syrupy product was obtained from 1.48 g of methyl phenyl diketone. The reaction products were adsorbed on a silica-gel column (Kiesel gel H, Merck) and successively eluted by hexane, benzene, and ethyl acetate. α-Hydroxy-α-phenylacetone (**8**) and α-hydroxypropiophenone (**9**) were thus isolated and characterized by NMR as follows. **8**: NMR ($CDCl_3$) δ 7.20 [s, 5H, phenyl], 5.05 [s, 1H, α-CH–], 3.70 [s, 1H, OH], 2.05 [s, 3H, $COCH_3$]. $[\alpha]_D^{22}$ +88.8° (*c* 2.3, ethanol). TLC R_f 0.27 (benzene/hexane/ethyl acetate=4.5/4.5/1). **9**: NMR ($CDCl_3$) δ7.85 [2H, ortho H of phenyl], 7.20 [mc, 3H, metha and para H of phenyl], 5.00 [q, 1H α-CH–], 1.45 [d, 3H, methyl). TLC R_f 0.41 (benzene/hexane/ethyl acetate=4.5/4.5/1). The ratio of **8** and **9** was determined by NMR of the crude products.

Asymmetric Hydrogenation of Biacetyl. The catalyst was prepared according to the general procedure, except for using twice the amounts of the reagents. To the catalyst was added a solution of 1.81 g of biacetyl in 50 ml of benzene. The mixture was stirred under the atmospheric pressure of hydrogen. The reaction was stopped when 97 ml of hydrogen was absorbed (this took 2 h). The reaction mixture was adsorbed on a silica-gel column (40 g of Wako gel C-200) and eluted by ether/petroleum ether (2/1). The eluate was checked by thin layer chromatography. The first fraction contained biacetyl; the next ones contained *erythro*- and *threo*-3,4-dihydroxy-3,4-dimethyl-2,5-hexanedione (**11**-E and **11**-T). The fractions containing reductive dimerization products were combined and concentrated under a reduced pressure to give 1.0 g of a syrup. The syrup was dissolved in benzene and the optical rotation was measured. The ratio of *threo* and *erythro* products was determined from the intensities of NMR signals of C–CH_3 and CH_3CO to be 22/78. From the ratio and the optical rotation of the mixture (**11**-E and **11**-T), the specific rotation of **11**-T produced was determined: $[\alpha]_D$ −33° (*c* 2.02, benzene). The fractions containing only acetoin were combined. The solvent was evaporated by bubbling N_2 gas into the eluate. The residue was distilled at 25—25.5 °C/29 mmHg (1 mmHg=133.322 Pa.) $[\alpha]_D$ −2° (*c* 0.8, water). From the optical rotation, the optical yield was calculated by reference to that of the optically pure acetoin.[12] Optical yield, 2.5%.

Asymmetric Hydrogenation of 1,2-Cyclohexanedione. The reaction was performed according to the general procedure, except for using benzene/methanol (4/1) as a solvent. After a theoretical amount of hydrogen was absorbed, the reaction mixture was extracted with chloroform and the chloroform layer was washed with NaCl-saturated water, dil HCl and water, successively. The chloroform layer was dried over anhydrous sodium sulfate, and concentrated under a reduced pressure to give a syrup which crystallized gradually. $[\alpha]_D$ −2.44° (*c* 0.35, chloroform).

Asymmetric Hydrogenation of Ethyl Phenylglyoxylate. After carrying out the general procedure, 1.6 g of a syrupy product was obtained from 1.78 g of ethyl phenylglyoxylate. The yields of ethyl mandelate and reductive dimerization products were calculated by ^1H NMR spectra and yield of the crude product. The crude product crystallized partially (about 0.31 g), mp 118—121 °C; it was recrystallized by hexane to give cubic crystals, mp 124 °C. Found: C, 67.02; H, 6.10; MS *m/e* 359[$(M+1)^+$]. Calcd for $C_{20}H_{22}O_6$: C, 67.02; H, 6.15. ^1H NMR ($CDCl_3$) δ 7.15 [10H, phenyl], 5.07 [s, 2H, OH], 4.30 [q, 4H, $-CH_2-$], 1.27 [t, 6H, methyl]. The syrup obtained after removal of crystals (by filtration) was chromatographed on a silica-gel column using hexane–benzene (with increasing polarity of the solvent) as the solvent, giving ethyl phenylglyoxylate (0.3 g), dimerization products (0.06 g), and ethyl mandelate (0.42 g). The specific rotations of ethyl mandelate are given in Table 1.

Asymmetric Hydrogenation of Isopropyl Phenylglyoxylate. After carrying out the general procedure, the crude products were adsorbed on a silica-gel column (Kiesel gel H, Merck) and eluted by hexane/benzene; the polarity of the solvent was gradually increased. Diisopropyl α,α′-diphenyltartrate and isopropyl mandelate were thus isolated and characterized by ^1H NMR spectra. ^1H NMR of diisopropyl α,α′-diphenyltartrate ($CDCl_3$) δ 7.02 [m, 10H, phenyl], 5.1 [q, 2H, methine H of isopropyl], 4.9 [s, 2H, OH], 1.14 [t, 12H, methyl]. ^1H NMR of isopropyl mandelate ($CDCl_3$) δ 7.35 [m, 5H, phenyl], 5.09 [s, 1H, methine H of α-carbon], 5.02 [m, 1H, methine H of isopropyl], 3.4 [broad s, 1H, OH], 1.28 [d, 3H, methyl], 1.11 [d, 3H, methyl].

Isopropyl mandelate thus isolated was hydrolyzed by refluxing with 4 mol dm^{-3}-sulfuric acid for 24 h. The reaction mixture was made alkaline and washed with benzene.

The aqueous layer was acidified and extracted with benzene. The organic layer was washed with water, and concentrated *in vacuo* to give 0.1 g of mandelic acid, $[\alpha]_D$ +18° (*c* 2.0, water).

Asymmetric Hydrogenation of Methyl α-(Acetylamino)acrylate. After carrying out the usual workup (general procedure), an oily product was obtained which was chromatographed on a silica-gel column using ether as a solvent. 0.8 g of an oily substance (*N*-acetylalanine methyl ester) was obtained starting from 1.2 g of the substrate; this was further purified by distillation at 70—82 °C/1—2 mmHg, 0.4 g, $[\alpha]_D$ −17.2° (*c* 1.2, water).

Asymmetric Hydrogenation of Methyl α-(Phenylacetylamino)acrylate. 187 ml of hydrogen was absorbed for 2.2 h. The reaction mixture was treated as usual (general procedure) to give 1 g of *N*-(phenylacetyl)alanine methyl ester (starting from 1.67 g of substrate), $[\alpha]_D$ −4° (*c* 2, methanol). The IR and ^{1}H NMR spectra of the product were identical with those of the authentic sample prepared by the reaction of (*S*)-*N*-(phenylacetyl)alanine with diazomethane.

(S)-N-(Phenylacetyl)alanine Methyl Ester. (*S*)-*N*-(Phenylacetyl)alanine was esterified with diazomethane. The crude product was purified by recrystallization from ether–petroleum ether, mp 68.5—70.5 °C, $[\alpha]_D$ −56.9° (*c* 2, methanol). ^{1}H NMR ($CDCl_3$) δ 7.30 [s, 5H, phenyl], 6.32 [broad d, 1H, NH], 4.57 [qt, 1H, CH], 3.68 [s, 3H, OCH_3], 3.57 [s, 2H, CH_2], 1.34 [d, 3H, C–CH_3]. IR (KBr), 3340 cm^{-1} (NH), 1745 cm^{-1} (ester), 1640 cm^{-1} (amide).

Asymmetric Hydrogenation of Methyl 2-Phenyl-2-propenoate. After carrying out the usual workup (general procedure), 2.5 g of a syrup was obtained from 2.7 g of substrate, $[\alpha]_D$ +7.7° (*c* 6.2, toluene). This was distilled at 67—68 °C/2 mmHg and 0.9 g of purified product (methyl 2-phenylpropanoate) was obtained, $[\alpha]_D$ +11.5° (*c* 6.2, toluene).

Asymmetric Hydrogenation of α-Phenylacrylophenone. After carrying out the usual workup (general procedure) 1.9 g of a syrup (crude α-phenylpropiophenone) was obtained from 2 g of substrate, $[\alpha]_D$ +88.6° (*c* 3.5, chloroform). The syrup was distilled at 115—116 °C/1 mmHg, 1.0 g $[\alpha]_D$ +99.4° (*c* 3.57, chloroform).

Reaction Rate. A 200 ml Erlenmeyer flask which has a side neck with a rubber cap was used as the reaction vessel. The catalyst was prepared according to the general procedure using $CoCl_2 \cdot 6H_2O$ (0.25 g), dimethylglyoxime (0.244 g), and quinine $HCl \cdot 2H_2O$ (0.84 g) (a half of which was neutralized with sodium methoxide). To the reaction vessel containing the catalyst was added a degassed benzene solution (50 ml) of benzil (2.24 g) by a syringe. The reaction was initiated with vigorous stirring. The reaction temperature was maintained constant within ±0.2 °C. The quantity of hydrogen absorbed was measured by a gas burret. The pseudo-first-order rate constants are listed in Table 4.

General Procedure for Asymmetric Hydrogenation Catalyzed by a Conjugated System Composed of Achiral Base Coordinated Bis-(dimethylglyoximato)cobalt(II) and Chiral Amino Alcohols. To a methanol solution (10 ml) of $CoCl_2 \cdot 6H_2O$ (0.25 g) was added a hot solution of dimethylglyoxime (0.244 g) in methanol (14 ml) under nitrogen atmosphere with stirring. The solution was stirred for 5—10 min and then 1 ml of 2.35 mol dm^{-3}-sodium methoxide solution was added to this solution. After 1—2 min, achiral base, additives, and a degassed methanol solution of equimolar mixture of quinine and quinine hydrochloride (which is prepared by adding 0.46 ml of 2.35 mol dm^{-3}-sodium methoxide solution to a solution of quinine $HCl \cdot 2H_2O$ (0.84 g) in methanol (5 ml)) were added to the above reaction vessel, one by one. The procedure hereafter was the same as in the "General Procedure for Asymmetric Hydrogenation Catalyzed by Bis-(dimethylglyoximato)cobalt(II)–Quinine."

Circular Dichroism Study. To each methanol solution of 9.15 g of methyl(dimethyl sulfide)bis(dimethylglyoximato)-cobalt(III)[31] 8.1 mg (1 molar equivalent), 12.1 mg (1.5 molar equivalent), 32.4 mg (4 molar equivalent), or 64.8 mg (8 molar equivalent) of quinidine was added. The resulting solution was evaporated *in vacuo* to dryness. The residue was dissolved in methanol and the resulting solution was again evaporated *in vacuo* to dryness. The procedure was repeated several times, during which dimethyl sulfide was completely expelled. Circular dichroism spectrum of 25 ml dichloromethane solution of each sample thus prepared was measured by JASCO ORD/UV-5 Spectrometer. The results are shown in Fig. 4.

The authors are grateful to Dr. Yuji Ohashi and Professor Yoshio Sasada, Tokyo Institute of Technology, for their valuable discussions. This work was supported by a Grant-in-Aid for Scientific Research from the Ministry of Education, Science and Culture (Japan) and by the Kawakami Foundation. The authors are also indebted to Professor Hiroshi Kobayashi, Tokyo Institute of Technology, for CD measurements, and Mr. Hitoshi Matsumoto for NMR measurements.

References

1) B. Bogdanović, *Angew. Chem.*, **85**, 1013 (1973); R. E. Harmon, S. K. Gupta, and D. J. Brown, *Chem. Rev.*, **73**, 21 (1973); J. W. Scott and D. Valentine, *Science*, **184**, 943 (1974); J. D. Morrison, W. F. Masler, and M. K. Neuberg, *Adv. Catal.*, **25**, 81 (1976); J. D. Morrison, W. F. Masler, and S. Hathaway, "Catalysis in Organic Synthesis," ed by P. N. Rylander and H. Garfield, Acadmic Press, New York (1976), p. 203; H. B. Kagan and J. C. Fiaud, "Topics in Stereochemistry," ed by N. L. Allinger and E. L. Eliel, Wiley-Interscience, New York (1978), Vol. 10, p. 175; B. R. James "Advances in Organometallic Chemistry," ed by F. G. A. Stone and R. West, Academic Press, New York (1979), Vol. 17, p. 319.

2) W. S. Knowles, M. J. Sabacky, B. D. Vineyard, and D. J. Weinkauf, *J. Am. Chem. Soc.*, **97**, 2567 (1975); B. D. Vineyard, W. S. Knowles, M. J. Sabacky, G. L. Backman, and D. J. Weinkauf, *ibid.*, **99**, 5946 (1977); H. B. Kagan and T. P. Dang, *ibid.*, **94**, 6429 (1972); H. B. Kagan, N. Langlois, and T. P. Dang, *J. Organomet. Chem.*, **90**, 353 (1975); M. Tanaka and I. Ogata, *J. Chem. Soc., Chem. Commun.*, **1975**, 735; T. Hayashi, T. Mise, S. Mitachi, K. Yamamoto, and M. Kumada, *Tetrahedron Lett.*, **1976**, 1133; K. Achiwa, *J. Am. Chem. Soc.*, **98**, 8265 (1976); M. D. Fryzuk and B. Bosnich, *ibid.*, **99**, 6262 (1977); **100**, 5491 (1978).

3) Y. Ohgo, S. Takeuchi, and J. Yoshimura, *Bull. Chem. Soc. Jpn.*, **43**, 505 (1970).

4) Y. Ohgo, K. Kobayashi, S. Takeuchi, and J. Yoshimura, *Bull. Chem. Soc. Jpn.*, **45**, 933 (1972).

5) Y. Ohgo, S. Takeuchi, and J. Yoshimura, *Bull. Chem. Soc. Jpn.*, **44**, 583 (1971); S. Takeuchi, Y. Ohgo, and J. Yoshimura, *Chem. Lett.*, **1973**, 265; Y. Ohgo, Y. Natori, S. Takeuchi, and J. Yoshimura, *ibid.*, **1974**, 709; Y. Ohgo, S. Takeuchi, Y. Natori, and J. Yoshimura, *ibid.*, **1974**, 33; Y. Ohgo, Y. Natori, S. Takeuchi, and J. Yoshimura, *ibid.*, **1974**, 1327.

6) R. W. Wadron and J. H. Weber, *Inorg. Chim. Acta*, **18**, L3 (1976).

7) G. N. Schrauzer and R. J. Windgassen, *J. Am. Chem.*

Soc., **89**, 1999 (1967).
8) Y. Ohgo, S. Takeuchi, and J. Yoshimura, *Bull. Chem. Soc. Jpn.*, **44**, 283 (1971).
9) S. Takeuchi, Y. Ohgo, and J. Yoshimura, *Bull. Chem. Soc. Jpn.*, **47**, 463 (1974).
10) F. Ramirez, R. Ramanthan, and N. B. Desai, *J. Am. Chem. Soc.*, **85**, 3465 (1963).
11) R. Roger, *Biochem. Z.*, **230**, 320 (1930); J. H. Brewster, *J. Am. Chem. Soc.*, **78**, 4061 (1956).
12) S. Berl and E. Bueding, *J. Biol. Chem.*, **191**, 401 (1951).
13) R. Willstätter, R. Kuhn, and E. Bamann, *Chem. Ber.*, **61**, 866 (1928).
14) R. Roger, *J. Chem. Soc.*, **1932**, 2168.
15) I. V. Hopper and F. J. Wilson, *J. Chem. Soc.*, **1928**, 2483.
16) H. Pracejus, *Ann. Chem.*, **634**, 9 (1960).
17) J. P. Wolf, III, and C. Nieman, *Biochim.*, **2**, 493 (1963).
18) F. A. A. ELhafez and D. J. Cram, *J. Am. Chem. Soc.*, **74**, 5846 (1952).
19) T. Suyama, T. Toyoda, and S. Kanao, *J. Pharm. Soc. Jpn.*, **85**, 279 (1965).
20) W. Klyne and J. Buckingham, "Atlas of Stereochemistry," Chapman and Hall, London (1974), p. 146 and references cited therein; V. Prelog and E. Zalán, *Helv. Chim. Acta*, **27**, 535 (1944); G. G. Lyle and L. K. Keefer, *Tetrahedron*, **23**, 3253 (1967); O. L. Carter, A. T. McPail, and G. A. Sim, *J. Chem. Soc., A*, **1967**, 365.
21) W. Klyne and J. Buckingham, "Atlas of Stereochemistry," Chapman and Hall, London (1974), p. 25; W. Leithe, *Chem. Ber.*, **65**, 660 (1932); G. N. Ramachandran and S. Raman, *Curr. Sci. (India)*, **25**, 348 (1956).
22) N. Nagai, *Ann. Chem.*, **470**, 178 (1929).
23) J. Weijilard, K. Phister, E. F. Swanezy, C. A. Robinson, and M. Tishler, *J. Am. Chem. Soc.*, **73**, 1216 (1951); W. Klyne and J. Buckingham, "Atlas of Stereochemistry," Chapman and Hall, London (1974), p. 24.
24) H. Takamatsu, *J. Pharm. Soc. Jpn.*, **76**, 1227 (1956); W. Klyne and J. Buckingham, "Atlas of Stereochemistry," Chapman and Hall, London (1974), p. 25.
25) Y. Ohashi, Y. Sasada, Y. Tashiro, Y. Ohgo, S. Takeuchi, and J. Yoshimura, *Bull. Chem. Soc. Jpn.*, **46**, 2589 (1973).
26) C. J. Hawkins, "Absolute Configuration of Metal Complexes," Wiley-Interscience, New York (1971), p. 176.
27) Y. Yamakawa, *J. Pharm. Soc. Jpn.*, **80**, 295 (1960).
28) G. N. Schrauzer, *Acc. Chem. Res.*, **1**, 97 (1968).
29) The absolute configuration of this compound was determined by X-ray analysis: Y. Ohashi and Y. Sasada, *Bull. Chem. Soc. Jpn.*, **50**, 1710 (1977).
30) The Co–C bond of a bulkier alkyl complex is expected to cleave more easily and then lose its chirality to a greater extent. Preparation of chiral alkyl cobaloximes and their reactions, including deuterium cleavage, will be reported separately.
31) G. N. Schrauzer, *Inorg. Synth.*, **11**, 66 (1968).

Asymmetric Hydrogenation Catalyzed by the (Achiral Base)bis(dimethylglyoximato)cobalt(II)-Chiral Cocatalyst System. The Preparation of a New Type of Chiral Cocatalyst and Its Application to the Asymmetric Hydrogenation of Methyl *N*-(Acetylamino)acrylate and Benzil[1)]

Seiji Takeuchi* and Yoshiaki Ohgo

Niigata College of Pharmacy, 5829 Kamishinei-cho, Niigata 950-21

(Received December 16, 1980)

As a new type of chiral cocatalyst in the achiral base-coordinated bis(dimethylglyoximato)cobalt(II)–chiral cocatalyst system, tertiary amines with an amide group at α- or β-carbon were prepared, and asymmetric hydrogenation was examined by using them. The optical yield reached 34.5% enantiomeric excess(ee) by using *N*-[(2*S*,3*S*)-2-acetoxy-3-dimethylamino-3-phenylpropionyl]-(*R*)-α-methylbenzylamine; this is the highest value attained so far in the asymmetric hydrogenation of methyl *N*-(acetylamino)acrylate with this system. The enantioselectivity in the hydrogenation of methyl *N*-(acetylamino)acrylate was reversed with a configurational alteration of the α-methylbenzylamine moiety of *N*-[*N*,*N*-dimethyl-(*S*)-phenylalanyl]-α-methylbenzylamine, while it was not reversed in the hydrogenation of benzil by the configurational alteration. From these facts, it is deduced that the hydrogen bond between amide groups of the chiral amino carboxamides and methyl *N*-(acetylamino)acrylate may act as an attractive force to enhance the enantioselectivity of the asymmetric hydrogenation.

The authors have previously reported the asymmetric hydrogenation of α-diketones, α-keto carboxylates, and olefinic compounds catalyzed by an achiral base-coordinated bis(dimethylglyoximato)cobalt(II)–chiral base system (hereafter abbreviated as $Co(dmg)_2$·B–B*: B and B* are achiral and chiral bases respectively). This system resulted in high optical yields (up to 78%ee) and high reactivities for such α-diketone as benzil, but in low optical yields (up to 19%ee) and low reactivities for dehydro amino acid derivatives.[2)]

The catalytic system comprises two independent elementary processes, *i.e.*, electron-donation to a substrate by $[Co(dmg)_2 \cdot B]^-$ and proton-donation to a reduced state of the substrate by a protonated chiral base, of which only the proton-donation by the protonated chiral base is responsible for the asymmetric induction. Another important characteristic of this catalytic system is that the hydrogen bond between the hydroxyl group of the chiral base (chiral amino alcohol) and the carbonyl group of the substrate extremely enhances the enantioselectivity of the proton-donation reaction (Scheme 1).[1,2)]

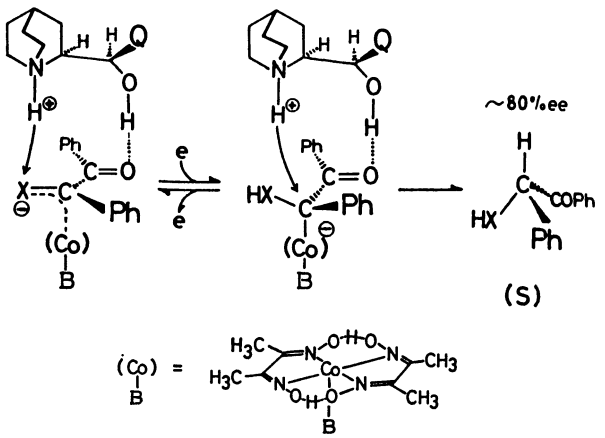

Scheme 1.

Therefore, the chiral base can be modified arbitrarily so long as the characteristics are retained. If the hydrogen bond between amide groups of a chiral amine having a secondary amide group and a dehydro amino acid derivative will act as an effective attractive force in the enantioselective proton-donation steps, the chiral amine can be expected to afford better results for the enantioselective hydrogenation of dehydro amino acid derivatives (Scheme 2).

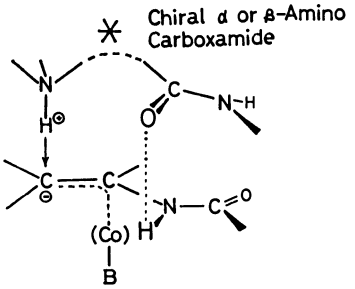

Scheme 2.

Here, we would like to describe the preparation of chiral tertiary amines bearing an alkylcarbamoyl group at the α- or β-carbon and the enantioselective hydrogenation of benzil and methyl *N*-(acetylamino)acrylate by their use of as cocatalysts.

Results and Discussion

Tertiary amines with an alkylcarbamoyl group at the α-carbon were prepared by the condensation of *N*-benzyloxycarbonyl derivatives of α-amino acids (L-phenylalanine, D-phenylglycine, L-isoleucine, and L-proline) with the corresponding amines (benzylamine, (*R*)- and (*S*)-α-methylbenzylamine), followed by reductive methylation. *N*-[(2*S*,3*S*)-3-dimethylamino-2-hydroxy-3-phenylpropionyl]-(*R*)-α-methylbenzylamine and its antipode were prepared by the condensation of (2*S*,3*R*)-2,3-epoxy-3-phenylpropionic acid and the (2*R*,3*S*)-isomer with (*R*)- and (*S*)-α-methylbenzylamine

Table 1. Structures and abbreviations of the chiral α- and β-amino carboxamides

(a) α-Amino carboxamides: $R^1-CH(N(CH_3)_2)-CONH-CH(R^2)-Ph$

R^1	Config.[a] of $R^1-CH<N/CO$	R^2	Config. of $Ph-CH<R^2/NH$	Abbreviation
$Ph-CH_2$	(*S*)	H		Pha-*S*,0
	(*S*)	CH_3	(*S*)	Pha-*S*,*S*
	(*S*)	CH_3	(*R*)	Pha-*S*,*R*
Ph	(*R*)	CH_3	(*S*)	Phg-*R*,*S*
CH_3, C_2H_5 CH	(*S*)	CH_3	(*S*)	Il-*S*,*S*
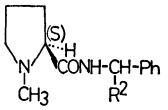		CH_3	(*S*)	Pr-*S*,*S*
		CH_3	(*R*)	Pr-*S*,*R*

(b) β-Amino carboxamides: $Ph-CH(OR)-CH(N(CH_3)_2)-CONH-CH(CH_3)-Ph$

Config. of CH-OR	Config. of CH-$N(CH_3)_2$	Config. of CH-CH_3	R	Abbreviation
(*R*)	(*R*)	(*S*)	H	DHP-(*R*,*R*)*S*
(*S*)	(*S*)	(*R*)	H	DHP-(*S*,*S*)*R*
(*S*)	(*S*)	(*R*)	CH_3-CO	DHP-*OAc*-(*S*,*S*)*R*

a) Configuration.

respectively (using the DCC method), followed by opening the epoxide ring by the use of dimethylamine (see Experimental section).

The structures and abbreviations of these amino carboxamides are listed in Table 1.

The asymmetric hydrogenation of benzil and methyl *N*-(acetylamino)acrylate with $Co(dmg)_2$·B–B* was carried out in benzene under an atmospheric pressure of hydrogen at room temperature by using these amino carboxamides as chiral cocatalysts (B*). The hydrogenation rate with $Co(dmg)_2$·BA is much faster than that with $Co(dmg)_2$·PPh_3 (BA and PPh_3 are abbreviations of benzylamine and triphenylphosphine respectively). However, triphenylphosphine was used as B when B* was the chiral α-amino carboxamides, since the optical yield of benzoin with benzylamine (5.7%ee) was considerably lower than that with triphenylphosphine (15.7%ee). The amine released in some stage of the catalytic cycle competes with chiral α-amino carboxamides in catching and in transferring the proton to a reduced state of the substrate. Because of the lower basicity of α-amino carboxamides, the competition is rather more serious when benzylamine is used as B than when triphenylphosphine[1,2] (which has a very low basicity toward proton) is so used. Both benzylamine and triphenylphosphine were employed when B* was the chiral β-amino carboxamides.

The results are summarized in Tables 2 and 3.

As the chemical yield of methyl *N*-acetylalaninate was lowered during isolation, and as the amount of the enantiomeric excess did not exceed that of the loss in chemical yield, the possibility of enantiomer enrichment during the isolation procedure was checked. The methyl *N*-acetylalaninate had no optical rotation such as was isolated after the treatment of the racemic one under the same conditions as in the catalytic hydrogenation. Therefore, it is evident that the optical activities of methyl *N*-acetylalaninate shown in Tables 2 and 3 are those brought about only by the asymmetric hydrogenation.

As may be seen in Table 2, the optical yields of methyl *N*-acetylalaninate were up to 17.2%ee and did not exceed that attained with the $Co(dmg)_2$–quinine system, but an interesting difference in the direction of stereoselectivities for benzil and methyl *N*-(acetylamino)acrylate was observed. The reaction using *S*-amino acid derivatives as the chiral cocatalysts gave *S*-benzoin predominantly, irrespective of the configuration of the α-methylbenzylamine moiety (Runs 1,2, 3,6, and 7), but the enantioselectivity of methyl *N*-acetylalaninate was reversed with a configurational change in the α-methylbenzylamine moiety (Runs 2 and 3). Furthermore, methyl *N*-acetylalaninate with the same configuration as that of the α-carbon of the α-amino carboxamides used as chiral cocatalysts was produced predominantly, except for Run 3.

The reversal of enantioselectivity by changing the configuration of α-methylbenzylamine (Runs 2 and 3 of methyl *N*-acetylalaninate) makes us imagine that the hydrogen bond between the amide groups of Pha-*S*,*R* and methyl *N*-(acetylamino)acrylate may be formed in the proton-donation steps; such a phenomenon may be brought about only when chiral α-amino carboxamides are able to be in a conformation suitable

TABLE 2. THE ASYMMETRIC HYDROGENATION OF BENZIL AND METHYL *N*-(ACETYLAMINO)ACRYLATE WITH $Co(dmg)_2 \cdot PPh_3$-CHIRAL α-AMINO CARBOXAMIDES[a]

Run	Chiral carboxamides	Benzoin				Methyl *N*-acetylalaninate			
		Yield	$[\alpha]_D$/°	Config.	Optical yield/%ee	Yield/%	$[\alpha]_D$/°	Config.	Optical yield/%ee
1	Pha-*S*,0	q [b]	+12.8[c]	(*S*)	10.8	54.0	−7.7[d]	(*S*)	8.3
2	Pha-*S*,*S*	q	+12.7	(*S*)	10.8	75.3	−13.1	(*S*)	14.3
3	Pha-*S*,*R*	q	+19.5	(*S*)	16.4	50.6	+15.8	(*R*)	17.2
4	Phg-*R*,*S*	q	−3.5	(*R*)	3.0	53.3	+3.5	(*R*)	3.9
5	Il-*S*,*S*	q	+2.2	(*S*)	1.9	68.0	−1.6	(*S*)	1.8
6	Pr-*S*,*S*	q	+11.0	(*S*)	9.3	45.0	−5.6	(*S*)	6.1
7	Pr-*S*,*R*	q	+17.8	(*S*)	15.0	45.0	−6.4	(*S*)	7.0

a) The molar ratio of the substrate to cobalt was 10 : 1, while those of triphenylphosphine, the chiral α-amino carboxamide, and its hydrochloride to cobalt were all 1 : 1. b) Quantitative yield. c) Optically pure *S* isomer: $[\alpha]_D$ +118.5° (*c* 1, acetone). d) Optically pure *S* isomer: $[\alpha]_D$ −91.7° (*c* 2, water).

TABLE 3. THE ASYMMETRIC HYDROGENATION OF BENZIL AND METHYL *N*-(ACETHYLAMINO)ACRYLATE WITH $Co(dmg)_2 \cdot$B-CHIRAL β-AMINO CARBOXAMIDES[a]

Run	[Achiral base Chiral base	Benzoin				Methyl *N*-acetylalaninate			
		Yield	$[\alpha]_D$/°	Config.	Optical yield/%ee	Yield/%	$[\alpha]_D$/°	Config.	Optical yield/%ee
1	[BA DHP-(*R*,*R*)*S*	q	+26.4	(*S*)	22.2	55.3	−1.8	(*S*)	2.0
2	[BA DHP-(*R*,*R*)*S*·HCl[b]	q	+0.8	(*S*)	0.7				
3	[BA DHP-(*R*,*R*)*S* DHP-(*R*,*R*)*S*·HCl	q	−3.7	(*R*)	3.1				
4	[PPh_3 DHP-(*S*,*S*)*R*	q	−3.8	(*R*)	3.2	45.3	+5.5	(*R*)	6.0
5	[BA DHP-*OAc*-(*S*,*S*)*R* DHP-*OAc*-(*S*,*S*)*R*·HCl[b]	q	−1.4	(*R*)	1.2	47.0	+17.7	(*R*)	19.3
6	[PPh_3 DHP-*OAc*-(*S*,*S*)*R* DHP-*OAc*-(*S*,*S*)*R*·HCl					45.5	+31.6	(*R*)	34.5

a) The molar ratio of the substrate to cobalt was 10 : 1, while those of achiral base, the chiral β-amino carboxamide, and its hydrochloride to cobalt were all 1 : 1. b) Hydrochloride of the corresponding chiral β-amino carboxamide.

for hydrogen bonding between the amide groups of the chiral α-amino carboxamides and the substrates.

If the above consideration is reasonable, it is possible to explain the enantioselectivities (the configurations and optical yields of products) in terms of the following factors: I) the bulkiness and arrangement of substituents around the α-carbon atom of the α-amino acid moiety, II) the conformation of the chiral α-amino carboxamides, and III) the hydrogen bonding between the amide groups of the chiral α-amino carboxamides and the substrates. The configurations and optical yields of the products are determined by the I) and II) factors, while the reversal enantioselectivity and/or the relatively high optical yields are obtained when the III) factor brought about by the II) factor becomes predominant.

It is impossible here to infer what conformation of the chiral α-amino carboxamide, Pha-*S*,*R*, is most effective and suitable for hydrogen bonding between the amide groups of Pha-*S*,*R* and methyl *N*-(acetylamino)acrylate in the proton-donation steps.

As may be seen in Table 3, the optical yield of methyl *N*-acetylalaninate rose to 34.5%ee, which is the highest value attained so far in the asymmetric hydrogenation of methyl *N*-(acetylamino)acrylate with the $Co(dmg)_2$·B–B* system, and a marked difference in the enantioselectivities for benzil and for methyl *N*-(acetylamino)acrylate was observed. The optical yield of benzoin was 22.2%ee (Run 1), but that of methyl *N*-acetylalaninate was 6.2%ee at most (Runs 1 and 4) when chiral β-amino carboxamides used had a hydroxyl group. On the other hand, the optical yield of methyl *N*-acetylalaninate rose to 34.5%ee (Run 6), while that of benzoin was lowered to 1.1%ee (Run 5), when the chiral β-amino carboxamide used had no free hydroxyl group, but an acetoxyl group.

From these results it may be deduced that the hydroxyl group of DHP-(*R*,*R*)*S* and DHP-(*S*,*S*)*R* in Runs 1 and 4, and the amide group of DHP-*OAc*-(*S*,*S*)*R* in Runs 5 and 6, are operative in forming the hydrogen bond to the carbonyl group of benzil and to the amide group of methyl *N*-(acetylamino)acrylate respectively,

in their enantioselectivity-determining step.

The findings that the optical yield of benzoin was considerably lowered (Run 4) when triphenylphosphine was used as the achiral base, as compared with that using benzylamine (Run 1), and that the enantioselectivity was reversed by change from the presence of the hydrochloride of DHP-(*R,R*)*S* to its absence (Runs 1 and 3), differ from those observed when a simple chiral amino alcohol such as *N*-methylephedrine was employed as the chiral base of the $Co(dmg)_2$·B–B* system, although it is not evident why these differences are brought about.

In conclusion, new type of chiral cocatalysts, α- and β-amino carboxamides, were explored; of them, DHP-*OAc*-(*S,S*)*R* is one of the most promising chiral bases of the $Co(dmg)_2$·B–B*-catalyzed asymmetric hydrogenation of methyl *N*-(acetylamino)acryrate. It can also be mentioned that the hydrogen bond between the amide groups of DHP-*OAc*-(*S,S*)*R* and methyl *N*-(acetylamino)acrylate may play an important role in the asymmetric hydrogenation.

Experimental

The melting points were determined by a Yanagimoto micro-melting-point apparatus and were uncorrected. The IR spectra were recorded on a JASCO A-3 spectrometer. The NMR spectra were obtained on JEOL JNM-PMX60 and JNM-PS-100 spectrometers. The optical rotations were measured with a Perkin Elmer 241 polarimeter.

Preparation of Chiral α-Amino Carboxamides. The chiral α-amino carboxamides (Pha-*S,0*, Pha-*S,S* Pha-*S,R*; Phg-*R,S*; Il-*S,S* and Pr-*S,S* Pr-*S,R*) were prepared by essentially the same procedure. Benzylamide and (*R*)- or (*S*)-α-methylbenzylamides of *N*-benzyloxycarbonylated α-amino acids (purchased from the Peptide Institute, Osaka) were prepared from the corresponding amines and α-amino acid derivatives by a modified DCC method,[3] and then the reductive *N,N*-dimethylation or *N*-methylation of them with formalin[4] was carried out.

The preparation of Pha-*S,R* as a typical procedure and that of Phg-*R,S* as an exceptional one are shown below.

N-[N-*Benzyloxycarbonyl-(S)-phenylalanyl*]-(R)-*α-methylbenzylamine.* To a solution of *N*-benzyloxycarbonyl-(*S*)-phenylalanine (15.0 g, 50 mmol) and (*R*)-α-methylbenzylamine (purchased from Aldrich: $[\alpha]_D^{23}$ +38° (neat); 6.47 ml, 50 mmol) in DMF (100 ml) was added a solution of DCC (10.73 g, 52 mmol) and 1-hydroxybenzotriazole (7.43 g, 55 mmol) in DMF (100 ml) during 1 h on ice-cooling with stirring. The reaction mixture was then allowed to stand overnight at room temperature. The dicyclohexylurea separated out was filtered off, and the filtrate was concentrated *in vacuo* at 30—40 °C. The residue was dissolved in ethyl acetate (*ca.* 500 ml), and the solution was washed successively with a 1 mol dm^{-3}-hydrochloric acid (100 ml), a 1 mol dm^{-3}-sodium hydrogencarbonate solution (100 ml), and a sodium chloride solution (100 ml) and then dried over anhydrous sodium sulfate. The solution was concentrated to a half, and the crystals separated out were thoroughly dissolved on heating. To the solution was added petroleum ether carefully. 13.1 g of a first crop (needles) and from the filtrate after similar recrystallization, 3.15 g of a second crop (needles) were obtained: first crop, mp 135.0—146.0 °C, $[\alpha]_D^{22.0}$ +24.9° (*c* 1.018, $CHCl_3$) and second crop, mp 134.0—135.0 °C, $[\alpha]_D^{22.0}$ +24.1° (*c* 1.045, $CHCl_3$); IR (KBr) 3340 (NH), 1690 (carbamate C=O) and 1650 cm^{-1} (amide C=O); NMR ($CDCl_3$) δ=1.26 (3H, d, *J*=7 Hz, $C\underline{H}_3$–CH), 3.10 (2H, dd, Ph–$C\underline{H}_2$–CH), 4.40 (1H, q, Ph–CH_2–$C\underline{H}$), 5.00 (1H, quintet, *J*=7 Hz, CH_3–$C\underline{H}$), 5.08 (2H, s, Ph–$C\underline{H}_2$–O), 5.46 (1H, d, N$\underline{H}$), 5.90 (1H, d, N$\underline{H}$), 7.30 (15H, d, Ph).

N-[N,N-*Dimethyl-(S)-phenylalanyl*]-(R)-*α-methylbenzylamine, (Pha-S,R).* *N*-[*N*-Benzyloxycarbonyl-(*S*)-phenylalanyl]-(*R*)-α-methylbenzylamine (6.0 g, 15 mmol: the first crop obtained above) was dissolved in methanol (*ca.* 200 ml) on heating, and to the solution glacial acetic acid (0.85 ml, 15 mmol) was then added. Under a weak nitrogen-gas flow, the solution was poured into an Erlenmeyer flask (with a special neck stoppered with a silicone gum cap) in which a 10% palladium charcoal catalyst (1.0 g) has been placed. Setting up the equipment for hydrogenation, the flask was degassed and charged with hydrogen gas, and then hydrogenation was carried out under atmospheric pressure at room temperature with stirring. About a theoretical amount of hydrogen was absorbed during 1 h; then, after degassing and the introduction of hydrogen, 37% formalin (2.4 ml, 32 mmol) was injected through the silicone gum cap and the hydrogenation was continued overnight. About two equivalents of hydrogen were absorbed. The reaction mixture was then filtered through celite, and the filtrate was concentrated *in vacuo*. The residue was dissolved in ether (*ca.* 200 ml) and washed twice with sodium hydrogencarbonate solution, and then the ether layer was dried over anhydrous sodium sulfate. The solution was concentrated *in vacuo* to afford 4.26 g of crystalline materials. This was recrystallized from ether–petroleum ether to yield 2.90 g of a first crop (needles) and 0.98 g of a second crop (needles): first crop, mp 79.5—80.5 °C, $[\alpha]_D^{12.5}$ +72.0° (*c* 1.005, $CHCl_3$) and second crop, mp 78.0—79.0 °C, $[\alpha]_D^{22.0}$ +70.8° (*c* 1.016, $CHCl_3$); IR (KBr) 3300 (NH) and 1630 cm^{-1} (amide C=O); NMR ($CDCl_3$) δ=1.38 (3H, d, *J*=7 Hz, $C\underline{H}_3$–CH), 2.28 (6H, s, $N(C\underline{H}_3)_2$), 3.13 (3H, m, Ph–$C\underline{H}_2$–CH), 5.10 (1H, quintet, *J*=7 Hz, CH_3–$C\underline{H}$), 7.03 (1H, d, N$\underline{H}$), 7.28 (10H, d, Ph).

N-[N,N-*Dimethyl-(R)-phenylglycyl*]-(S)-*α-methylbenzylamine, (Phg-R,S).* The reductive *N,N*-dimethylation of *N*-[*N*-benzyloxycarbonyl-(*R*)-phenylglycyl]-(*S*)-α-methylbenzylamine gave *N,N*-dimethylated, *N*-monomethylated and deaminated products; the yield of the *N,N*-dimethylated product, Phg-*R,S*, among them was very low. Therefore, *N*-[*N*-methyl-(*R*)-phenylglycyl]-(*S*)-α-methylbenzylamine was prepared in a 75% yield by using an equimolar amount of formardehyde and stopping the reductive methylation when equimolar amount of hydrogen had been absorbed. The isolated *N*-methylated product was further *N*-methylated by the following procedure.

A solution of *N*-[*N*-methyl-(*R*)-phenylglycyl]-(*S*)-α-methylbenzylamine (6.5 g, 24 mmol), 37% formalin (2.17 ml, 29 mmol) and 88% formic acid (3.7 g, 71 mmol) was refluxed for 3.5 h. After cooling, the solution was acidified with conc hydrochloric acid and extracted with ether (*ca.* 50 ml). By making the water layer basic with sodium hydroxide, an oily material was separated out and then crystallized. The crystalline products were extracted with ether (100 ml), and the solution was dried over sodium sulfate. The solution was concentrated *in vacuo* to afford 5.82 g of crystalline products. This was recrystallized from ether-petroleum ether to yield 4.27 g of white needles: mp 92.5—93.5 °C, $[\alpha]_D^{12.5}$ −146.6° (*c* 1.006, $CHCl_3$); IR (KBr) 3300 (NH) and 1660 cm^{-1} (amide C=O); NMR ($CDCl_3$) δ=1.56 (3H, d, *J*=7 Hz, $C\underline{H}_3$–CH), 2.20 (6H, s, $N(C\underline{H}_3)_2$), 3.72 (1H, s, Ph–$C\underline{H}$–CONH), 5.15 (1H, quintet, *J*=7 Hz, CH_3–$C\underline{H}$), 7.24 (11H, m, N$\underline{H}$ and Ph).

The hydrochlorides of the α-amino carboxamides were

Table 4. Physical constants and elemental analyses of chiral α-amino carboxamides

Chiral α-amino carboxamides	Mp/°C	$[\alpha]_D$/°	Elemental analyses (%) C H N	(Calcd) (Found)
Pha-*S*,0	61.0—62.0	+3.6 (*c* 1.026, $CHCl_3$)	76.56 7.85 9.92 75.76 7.68 9.69	($C_{18}H_{22}N_2O$)
Pha-*S*,0·HCl	147.0—148.0	+35.7 (*c* 1.026, CH_3OH)		
Pha-*S*,*S*	77.0—78.0	−46.1 (*c* 1.005, $CHCl_3$)	76.99 8.16 9.45 77.63 8.24 9.59	($C_{19}H_{24}N_2O$)
Pha-*S*,*S*·HCl	170.0—171.0	−14.3 (*c* 1.041, CH_3OH)		
Pha-*S*,*R*	79.5—80.5	+72.0 (*c* 1.005, $CHCl_3$)	77.01 8.38 9.52	(Found)
Pha-*S*,*R*·HCl	206.0—207.0	+128.0 (*c* 1.028, CH_3OH)		
Phg-*R*,*S*	92.5—93.5	−146.6 (*c* 1.006, $CHCl_3$)	76.56 7.85 9.92 77.08 8.22 10.00	($C_{18}H_{22}N_2O$)
Phg-*R*,*S*·HCl	214.0—216.0 (dec)	−117.4 (*c* 1.007, CH_3OH)		
Il-*S*,*S*	95.5—98.5	−70.6 (*c* 1.034, $CHCl_3$)	73.80 9.29 10.76 72.65 10.24 10.60	($C_{16}H_{26}N_2O$)
Il-*S*,*S*·HCl[a]	200.0—201.0	−59.1 (*c* 1.280, CH_3OH)		
Pr-*S*,*S*[b]	58.0—60.0	−170.0 (*c* 0.165, CH_3OH)	72.38 8.68 12.07 73.13 8.90 11.39	($C_{14}H_{26}N_2O$)
Pr-*S*,*R*	85.5—87.0	−2.17 (*c* 0.277, CH_3OH)	72.15 8.91 12.01	(Found)

a) Very hygroscopic. b) Hydrochloride did not crystallize.

prepared by bubling dry hydrogen chloride gas into an ether solution of α-amino carboxamides and recrystallized from methanol–ethyl acetate or methanol–ether–ethyl acetate.

The physical constants and data of the elemental analyses of the chiral α-amino carboxamides and their hydrochlorides are summarized in Table 4.

Preparation of Chiral β-Amino Carboxamides.

N-[(2S,3R)-2,3-Epoxy-3-phenylpropionyl]-(R)-α-methylbenzylamine and Its Antipode. (*R*)-α-methylbenzylammonium (2*S*,3*R*)-2,3-epoxy-3-phenylpropionate and its antipode were prepared by Harada's method.[5]

To a suspension of (*R*)-α-methylbenzylammonium (2*S*, 3*R*)-2,3-epoxy-3-phenylpropionate ($[\alpha]_D^{24.0}$ +126.3° (*c* 1.001, 99% ethanol), lit,[5] $[\alpha]_D$ +125.5° (*c* 0.96, abs ethanol); 15.3 g, 54 mmol) in DMF (300 ml) was added a solution of DCC (11.2 g, 54 mmol) and 1-hydroxybenzotriazole (7.3 g, 54 mmol) in DMF (100 ml) during 1.5 h on ice-cooling with stirring. The reaction mixture gradually became homogeneous and then heterogeneous again. Stirring was continued overnight at room temperature. After the filtration of the precipitates, the filtrate was concentrated *in vacuo* at 30—40 °C. The residue was dissolved in ethyl acetate (*ca.* 800 ml), after which the solution was washed successively with a 10% citric acid solution (200 ml), a 4% sodium hydrogencarbonate solution (200 ml), and a sodium chloride solution (200 ml) and then dried over anhydrous sodium sulfate. The solution was subsequently concentrated to 500—600 ml, and the crystals separated out were dissolved thoroughly on heating. To the solution was added petroleum ether carefully. 10.2 g of a first crop (needles) and, from the filtrate, 3.3 g of a second crop (needles) were obtained: first crop, mp 168.0—169.0 °C, $[\alpha]_D^{23.0}$ +143.1° (*c* 0.997, $CHCl_3$) and second crop, mp 167.0—168.0 °C, $[\alpha]_D^{23.0}$ +143.2° (*c* 0.997, $CHCl_3$): IR (KBr) 3300 (NH) and 1660 cm^{-1} (amide C=O); NMR ($CDCl_3$) δ=1.50 (3H, d, *J*=6.5 Hz, $C\underline{H}_3$–CH), 3.50 (1H, d, *J*=2 Hz, Ph–C<u>H</u>–O), 3.68 (1H, d, *J*=2 Hz, C<u>H</u>–CONH), 5.07 (1H, quintet, *J*=6.5 Hz, CH_3–C<u>H</u>), 6.43 (1H, d, N<u>H</u>), 7.17 (10H, Ph).

Its antipode was likewise prepared from (*S*)-α-methylbenzylammonium (2*R*,3*S*)-2,3-epoxy-3-phenylpropionate (18.0 g, 63 mmol) to afford 14.4 g of a first crop (needles) and 2.3 g of a second crop (needles): first crop, mp 169.0—170.0 °C, $[\alpha]_D^{22.0}$ −144.5° (*c* 0.996, $CHCl_3$) and second crop, mp 167.0—168.0 °C, $[\alpha]_D^{22.0}$ −138.7° (*c* 0.990, $CHCl_3$).

N-[(2S,3S)-3-Dimethylamino-2-hydroxy-3-phenylpropionyl]-(R)-α-methylbenzylamine, (DHP-(S,S)R) and Its Antipode (DHP-(R,R)S). A suspension of the first and second crops of *N*-[(2*S*,3*R*)-2,3-epoxy-3-phenylpropionyl]-(*R*)-α-methylbenzylamine (13.1 g, 49 mmol) prepared above in a 50% dimethylamine aqueous solution (250 ml) was stirred for 4 h at room temperature. The undissolved crystals were then filtered off, and the filtrate was evaporated *in vacuo*. A crystalline mass was separated out when the water began to evaporate and was then filtered off. After drying, the crystals were recrystallized from benzene to yield 7.4 g of a first crop (needles): mp 157.0—157.5° C, $[\alpha]_D^{26.5}$ +52.7° (*c* 1.028, $CHCl_3$); IR (KBr) 3400 (NH), 3200 (OH) and 1660 cm^{-1} (amide C=O); NMR ($CDCl_3$) δ=1.40 (3H, d, *J*=7 Hz, $C\underline{H}_3$–CH), 2.26 (6H, s, $N(C\underline{H}_3)_2$), 3.59 (1H, d, *J*=5 Hz, N–C<u>H</u>–CH–CONH), 4.20 (1H, s, OH), 4.60 (1H, d, *J*=5 Hz, C<u>H</u>–CONH), 4.90 (1H, quintet, *J*=7 Hz, CH_3–C<u>H</u>), 6.75 and 7.20 (11H, m, N<u>H</u> and Ph); Found: C, 73.23; H, 7.76; N, 9.03%; Calcd for $C_{19}H_{24}N_2O_2$: C, 73.04; H, 7.74; N, 8.97% and 1.43 g of a second crop (needles): mp 157.0—157.5 °C, $[\alpha]_D^{26.0}$ +53.1° (*c* 1.018, $CHCl_3$). The crystals obtained above by the filtration of the reaction mixture were also recrystallized from benzene to yield 2.7 g of a third crop (needles): mp 156.5—157.5 °C, $[\alpha]_D^{26.0}$ +51.3° (*c* 1.082, $CHCl_3$).

Its antipode, DHP-(*R*,*R*)*S*, was likewise prepared from *N*-[(2*R*,3*S*)-2,3-epoxy-3-phenylpropionyl]-(*S*)-α-methylbenzylamine (14.0 g, 52 mmol) to afford 7.82 g of a first crop: mp 156.5—157.5 °C, $[\alpha]^{26.5}$ −52.7° (*c* 1.007, $CHCl_3$); Found: C, 72.32; H, 7.74; N, 8.88%, a second crop (1.37 g): mp 156.5—157.5 °C, $[\alpha]_D^{26.5}$ −52.9° (*c* 1.007, $CHCl_3$) and a third crop (3.18 g): mp 156.0—157.0 °C, $[\alpha]_D^{26.5}$ −51.1° (*c* 1.101, $CHCl_3$).

The hydrochloride of DHP-(*R*,*R*)*S* was prepared by the procedure described above from the first crop of DHP-(*R*, *R*)*S*: mp 211.5—212.5 °C, $[\alpha]_D^{20.0}$ −38.7° (*c* 1.004, CH_3OH).

N-[*(2S,3S)-2-Acetoxy-3-dimethylamino-3-phenylpropionyl*]-*(R)*-*α-methylbenzylamine, (DHP*-OAc-*(S,S)R)*. To a solution of the first crop of DHP-*(S,S)R* prepared above (2.0 g, 64 mmol) in dry ethyl acetate (150 ml) was added acetyl chloride (0.54 g, 64 mmol). The solution was allowed to stand for 2 d at room temperature and then concentrated *in vacuo*. The residue was solidified by scratching the flask with ether. The solids were filtered off and dissolved in water. The solution was washed with ether, and the aqueous layer was made basic with a sodium hydrogencarbonate solution. The solution was extracted with ether, and the ether layer was dried over anhydrous sodium sulfate. The solution was concentrated *in vacuo* to afford 1.8 g of a crystalline material. This was recrystallized from ether–petroleum ether to yield 1.35 g of needles: mp 83.0—84.0 °C, $[\alpha]_D^{23.0}$ +21.6° (*c* 1.008, $CHCl_3$); IR (KBr) 3400 (NH), 1725 (ester C=O) and 1675 cm^{-1} (amide C=O); NMR ($CDCl_3$) δ=1.46 (3H, d, *J*=7 Hz, $C\underline{H}_3$-CH), 2.03 (3H, s, $C\underline{H}_3COO$), 2.23 (6H, s, N-($C\underline{H}_3$)$_2$), 3.89 (1H, d, *J*=7 Hz, N-C$\underline{H}$-CH-CONH), 5.03 (1H, quintet, *J*=7 Hz, CH_3-C$\underline{H}$), 5.78 (1H, d, *J*=7 Hz, C$\underline{H}$-CONH), 7.00 and 7.22 (10H, m, Ph), 7.62 (1H, d, N$\underline{H}$); Found: C, 70.28; H, 7.61; N, 7.78%; Cacld for $C_{21}H_{26}N_2O_3$: C, 71.16; H, 7.39; N, 7.90%.

Its hydrochloride was prepared by the procedure described above: mp 212.0—213.0 °C (dec), $[\alpha]_D^{20.0}$ +48.6° (*c* 0.693, CH_3OH).

Hydrogenation of Benzil and Methyl N-*(Acetylamino)acrylate with the Co(dmg)*$_2$·*B-Chiral Amino Carboxamide System.* The preparation of the catalyst system and the hydrogenation of the two substrates with it were identical to those described in the previous paper[1] except for using the chiral amino carboxamide as the chiral base; hence, only the typical procedure of the isolation of methyl *N*-acetylalaninate in Run 2 of Table 2 is given below.

After theoretical amounts of hydrogen (1.5 g, 10.5 mmol of methyl *N*-(acetylamino)acrylate was used) had been absorbed, the benzene solution was filtered through a short (*ca.* 10 cm×1.5ϕ) silica-gel column (Wako gel C-300), and then the column was washed with ethyl acetate (*ca.* 300 ml). The filtrate was concentrated *in vacuo*, and the residue was dissolved in ether (*ca.* 100 ml). Into the ether solution dry hydrogen chloride gas was bubbled until the solution became acidic. The amorphous solid which separated out was filtered off, and the filtrate was concentrated *in vacuo* to 5—10 ml. The residual ether solution was again filtered through a short silica-gel column (similar to the one above), and the column was washed with ethyl acetate (*ca.* 300 ml). The filtrate was neutralized and dried over anhydrous sodium carbonate and sodium sulfate. The solution was concentrated *in vacuo*, and to the residue was added water (100 ml). The crystalline materials which separated out were filtered off through celite and washed with water (150 ml). The filtrate was concentrated *in vacuo*, the residue was dissolved in ether (100 ml), and the ether solution was dried over anhydrous sodium sulfate. After the concentration of the solution, 1.13 g (75.3% yield) of an oily product, $[\alpha]_D^{25.0}$ −12.0° (*c* 2.121, water) was obtained. This was distilled at 98—99 °C/3 mmHg to give 0.49 g of a colorless liquid: $[\alpha]_D^{25.0}$ −13.1° (*c* 2.091, water).

No contamination of the chiral α-amino carboxamide, Pha-*S,S*, in the distilled product was observed in the NMR spectra.

Examination of Enantiomer Enrichment during Isolation. 2.0 g of racemic methyl *N*-acethylalaninate were treated under the same conditions as were used for the hydrogenation in Run 2 of Table 2 and were then isolated by the procedure described above. 1.1 g of an oily material was thus obtained: $[\alpha]_D^{13.0}$ −0.1° (*c* 2.108, water). This was subsequently distilled at 99—101 °C/3 mmHg to give 0.4 g of a colorless liquid: $[\alpha]_D^{15.6}$ 0.0° (*c* 2.010, water).

The NMR spectra of the colorless liquid was identical to that observed above.

The authors wish to express their thanks to Professor Juji Yoshimura, Dr. Ken'ichi Sato, and Mr. Yuzuru Ishida of the Laboratory of Chemistry for Natural Products, Tokyo Institute of Technology, for their NMR measurements and elemental analyses. The present work was partially supported by two Grants-in-Aid for Scientific Research (No. 264149 and No. 454159) from the Ministry of Education, Science and Culture.

References

1) Part XI on Asymmetric Reactions. Part X: Y. Ohgo, S. Takeuchi, Y. Natori, and J. Yoshimura, *Bull. Chem. Soc. Jpn.*, **54**, 2124 (1981).

2) Y. Ohgo, S. Takeuchi, and J. Yoshimura, *Bull. Chem. Soc. Jpn.*, **44**, 283, 583 (1971); S. Takeuchi, Y. Ohgo, and J. Yoshimura, *Chem. Lett.*, **1973**, 265; Y. Ohgo, S. Takeuchi, Y. Natori, and J. Yoshimura, *ibid.*, **1974**, 33; Y. Ohgo, Y. Natori, S. Takeuchi, and J. Yoshimura, *ibid.*, **1974**, 709, 1327.

3) W. König and R. Geiger, *Chem. Ber.*, **103**, 788 (1970).

4) R. E. Bowmann and H. H. Stroud, *J. Chem. Soc.*, **1950**, 1342.

5) K. Harada, *J. Org. Chem.*, **31**, 1407 (1966).

The Acid-catalyzed Decomposition of α-Diazo β-Hydroxy Ketones

Kazuo Miyauchi, Kimiaki Hori, Tsuguji Hirai, Matsuji Takebayashi,* and Toshikazu Ibata†

Department of Chemistry, Faculty of Science and Technology, Kinki University, Higashi-osaka, Osaka 577

† *Institute of Chemistry, College of General Education, Osaka University, Toyonaka, Osaka 560*

(Received December 12, 1980)

The proton acid-catalyzed decomposition of 3-aryl-2-diazo-3-hydroxy-1-phenylpropanone (**1**) gave aryl and hydrogen migration products. The former was the enol-form (**2**) of 2-aryl-3-phenyl-1,3-propanedione and the latter was the enol- (**3**) and keto-form (**4**) of 1-aryl-3-phenyl-1,3-propanedione. The product ratios, **2**/(**3**+**4**), were affected by the catalysts and solvents used. More polar solvents favored the formation of aryl migration products (**2**). On the other hand, the BF_3-catalyzed decomposition of **1** gave acetylenic ketones as main products along with **2**, **3**, and **4**. The TsOH-catalyzed decomposition of 2-diazo-3-hydroxy-3-phenyl-1-indanone, (cyclic α-diazo β-hydroxy ketone), gave 2-phenyl-1,3-indandione quantitatively through phenyl migration.

The acid-catalyzed decomposition of diazo compounds has been studied extensively from the synthetic and mechanistic view points.[1] However, only a few papers have been published on the acid-catalyzed decomposition of diazo carbonyl compounds bearing a hydroxyl group on the carbon atom adjacent to the diazomethyl-carbon. Wenkert and McPherson have reported the BF_3-catalyzed decomposition of α-diazo β-hydroxy esters and ketones to give the corresponding acetylenic esters and ketones.[2] Schöllkopf and his co-workers obtained ethyl 2-methyl-3-oxobutanoate as a methyl migration product in the HCl-catalyzed reaction of ethyl 2-diazo-3-hydroxy-3-methylbutanoate.[3] Similar observations were also reported by Disteldorf and Regitz in the BF_3- or HCl-catalyzed decomposition of 1-diazo-2-hydroxyethyldiphenylphosphine oxide.[4]

As an extension on the acid-catalyzed reaction of diazo carbonyl compounds,[5] we describe here the protonic or Lewis acids-catalyzed decomposition of 3-aryl-2-diazo-3-hydroxy-1-phenyl-1-propanones (**1**) to give aryl and hydrogen migration products and acetylenic ketones depending on the catalysts used.

Results and Discussion

An acetonitrile solution of 3-(*p*-chlorophenyl)-2-diazo-3-hydroxy-1-phenyl-1-propanone (**1a**) was treated with a catalytic amount of acid at 30 °C. In the proton acid-catalyzed reaction, the major product was the enol-form (**2a**) of 2-(*p*-chlorophenyl)-1,3-propanedione accompanying the enol- (**3a**) and keto-form (**4a**) of 1-(*p*-chlorophenyl)-3-phenyl-1,3-propanedione. In the BF_3-catalyzed reaction, however, 3-(*p*-chlorophenyl)-1-phenyl-2-propyn-1-one (**6a**) was obtained as a major product along with **2a**, **3a**, and **4a**. 3-(*p*-Nitrophenyl)-2-diazo-3-hydroxy-1-phenyl-1-propanone (**1b**) also gave similar products, with a few differences in the product ratios. The main difference is that **2b** is still the main product in the BF_3-catalyzed reaction of **1b** contrary to the case of **1a**. The other point is that the yield of the chlorinated product (**5b**) is much higher than that of **5a** in the HCl- and $AlCl_3$-catalyzed reactions of **1b**. The results are summarized in Table 1.

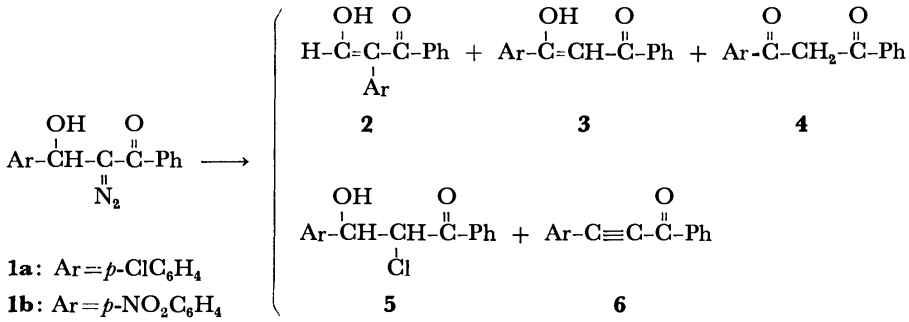

Scheme 1.

Table 1. Yields of products in the acid-catalyzed decomposition of **1** in acetonitrile at 30 °C

	Acid	**2**	**3**	**4**	**5**	**6**	**2**/(**3**+**4**)
1a	TsOH	84.3	3.0	8.0	—	—	7.7
	aq.HCl	76.1	5.5	2.6	14.5	—	9.4
	$AlCl_3$	68.8	8.0	3.1	18.8	—	6.2
	$BF_3(OEt_2)$	11.9	1.2	—	—	75.2	9.9
1b	TsOH	64.1	23.3	10.9	—	—	1.9
	aq.HCl	38.0	16.7	5.7	34.6	—	1.7
	$AlCl_3$	24.6	22.2	trace	47.1	—	1.1
	$BF_3(OEt)_2$	50.8	4.1	4.8	—	29.8	5.7

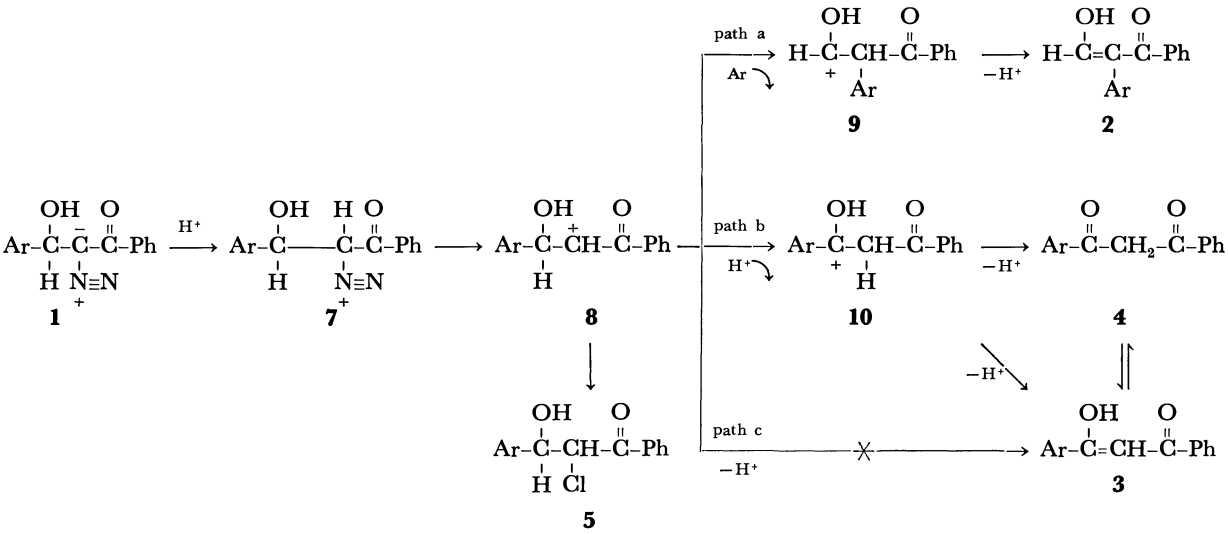

Scheme 2.

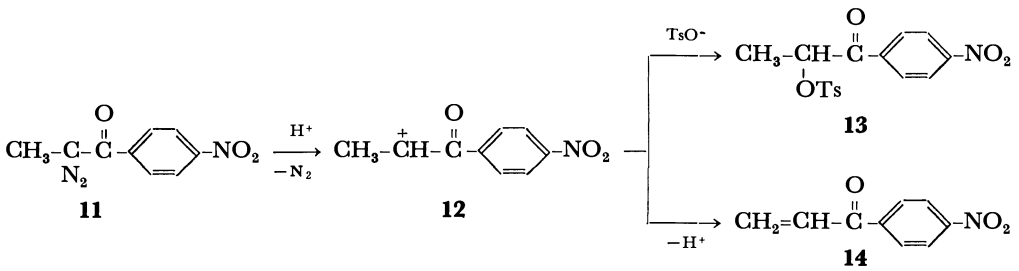

Scheme 3.

The difference between the behavior of proton acid and that of BF_3 may be attributed to the difference of the catalytic actions on the starting diazo ketones (**1**) as is described below.

In the proton acid-catalyzed reaction, the reaction may be initiated by protonation on the diazomethyl-carbon of **1** to give diazonium ion (**7**).[3,4] Successive elimination of nitrogen, aryl migration, and deprotonation lead to the enol ketone (**2**) through carbonium ion intermediate (**8** and **9**) (path a in Scheme 2). The hydrogen migration of **8** will afford diaroylmethane (**4**) and its enol-isomer (**3**) *via* deprotonation of intermediate (**10**) (path b in Scheme 2). Although direct deprotonation from the carbon attached by the hydroxyl group of **8** seems to give the enol-isomer (**3**) directly (path c in Scheme 2), this process can be excluded based on the results of the pinacol rearrangement of 1,1,2-triphenylethane-2-*d*-1,2-diol.[6]

The HCl-catalyzed reaction of **1** gave 3-aryl-2-chloro-3-hydroxypropiophenone (**5**) along with **2**, **3**, and **4**. This chlorinated compound may be produced by the attack of chloride ion with its high nucleophilicity on the carbonium ion intermediate (**8**) in competition with the aryl and hydrogen migrations. The higher yield of chlorinated product (**5b**) in the reaction of **1b** than that of **5a** may be explained by the high positive charge density on carbonium carbon in **8b** caused by the electron attracting nitro group on the phenyl ring. The behavior of $AlCl_3$ was quite similar to that of hydrochloric acid. This may be due to hydrogen chloride produced by the reaction with moisture in the reaction system. However, no tosylate[7] corresponding to **5** was obtained in the reaction when *p*-toluenesulfonic acid was used as a catalyst. And neither oxazoles[5a] nor oxazolium salts,[8] which might be produced by the reaction of **8** with acetonitrile used as a solvent, were recognized in the reaction products.

When α-diazo-*p*-nitropropiophenone (**11**), instead of **1**, was treated with an equivalent amount of TsOH in acetonitrile at 0—5 °C, the reaction gave 1-(*p*-nitrobenzoyl)ethyl tosylate (**13**) as a main product in 69% yield accompanying a small amount (13%) of *p*-nitrophenyl vinyl ketone (**14**) without formation of the corresponding oxazoles (Scheme 3). Therefore, the preference of the migration of aryl group or hydrogen atom to the intermolecular nucleophilic attack of tosylate ions or the nitrogen atom of acetonitrile to the carbonium ion intermediate (**8**), as has been observed in the decomposition of **1**, seems to be attributable to the effect of hydroxyl group attached to the carbon atom adjacent to the diazo carbon.

As listed in Table 1, the yields of aryl migration products (**2**) were larger than those of hydrogen migration products (**3**+**4**). The results may be due to the difference of resonance stabilities in the transition states of aryl- and hydrogen-migrations. Moreover the product ratios, **2**/(**3**+**4**), in the reaction of **1b** (Ar=*p*-$NO_2C_6H_4$) were observed to be smaller than those in the reaction of **1a** (Ar=*p*-ClC_6H_4), suggesting that the migratory aptitude of *p*-nitrophenyl group is smaller than that of *p*-chlorophenyl group. The

Table 2. Solvent effect on the yields of products in the TsOH-catalyzed decomposition of **1a** at 30 °C

Solvent	μ(D)	ε	Products yield/% 2	3	4	2/(2+4)
Cyclohexane	0.00	2.02	46	38	14	0.9
CCl_4	0.00	2.24	44	22	16	1.2
Benzene	0.00	2.28	54	24	17	1.3
Dioxane	0.45	2.21	66	25	8	2.0
$C_2H_5OC_2H_5$	1.15	4.81	68	9	11	3.3
$CHCl_3$	1.15	4.81	68	9	11	3.4
$CH_3OCH_2CH_2OCH_3$	1.71	7.20	67	9	9	3.7
THF	1.75	7.58	66	7	11	3.7
CH_2Cl_2	1.14	8.93	71	7	8	4.7
CH_3CN	3.44	33.0	84	3	8	7.7

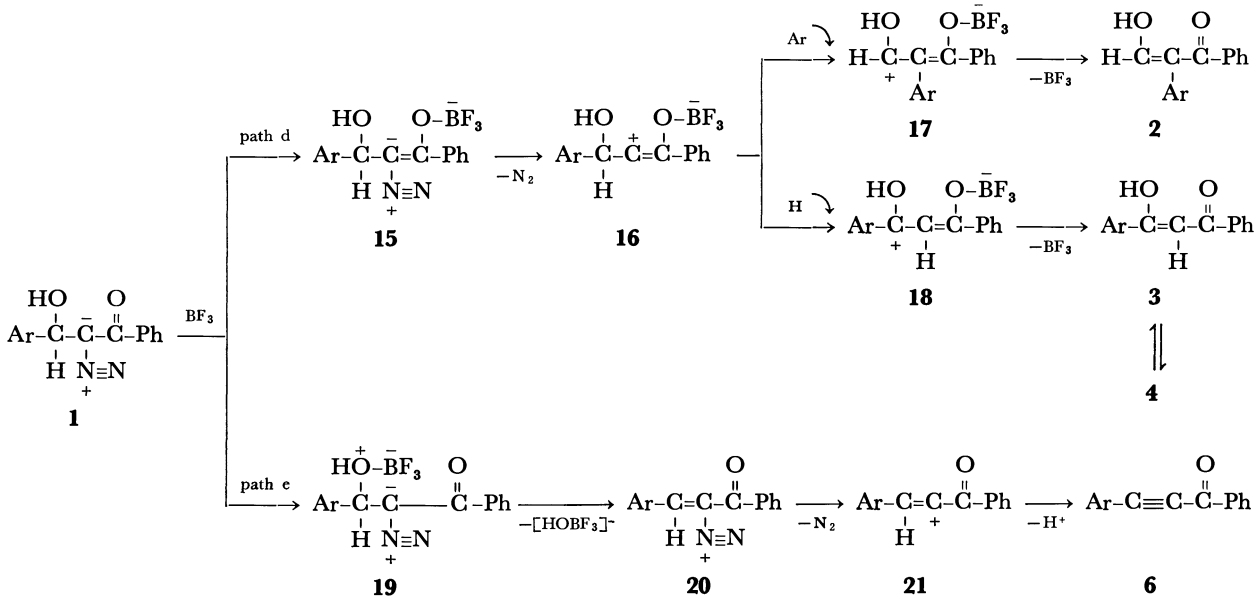

Scheme 4.

results further seem to accord with the view that the electron-withdrawing substituents reduce the migratory aptitude of aryl groups in the pinacol rearrangement.[9]

When the TsOH-catalyzed decomposition of **1a** was carried out in various solvents at 30 °C, it was recognized that the more polar solvents favored the migration of *p*-chlorophenyl group. In this case, the tendency of the migration of *p*-chlorophenyl in comparison to that of hydrogen, **2**/(**3**+**4**), seems to fit better to dielectric constant (ε) than to dipole moment (μ) (Table 2). The large migratory aptitude of aryl groups in polar solvent may be explained by the "principle of reactivity and selectivity relationship."[10] In other words, solvation stabilization of the carbonium ion intermediate (**8**) in polar solvents increases the amount of aryl migration products (**2**), owing to the large selectivity of **8** to the reaction paths (a and b).

In the BF_3-catalyzed reaction, two kinds of initial attack of BF_3 are expected. When the initial attack of BF_3 occured on the carbonyl-oxygen atom of **1**, the reaction will proceed to give diazonium ion intermediate (**15**),[5,11] from which two kinds of enol ketones (**2** and **3**) and β-diketone (**4**) may be derived *via* carbonium ion intermediates (**16**, **17**, and **18**) in a similar manner as described above (path d in Scheme 4). If the initial attack of BF_3 took place on hydroxyl-oxygen atom of **1** to afford oxonium ion intermediate (**19**), diarylpropynones (**6**)[2,12] will be given via intermediates (**20** and **21**) (path e in Scheme 4). Although the path e is the main path of the reaction of **1a**, the electron attracting nitro group retards the path e in the reaction of **1b** to give the small amount of **6b**.

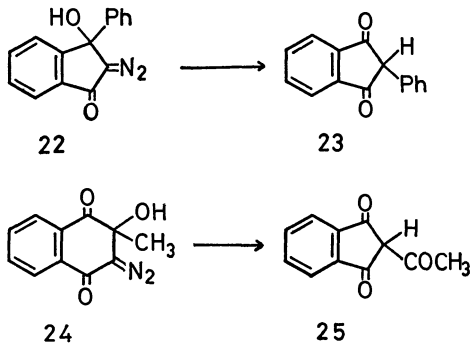

Scheme 5.

In another experiment, the TsOH-catalyzed decomposition of 2-diazo-3-hydroxy-3-phenyl-1-indanone (**22**) was carried out in order to compare with that of acyclic α-diazo β-hydroxy ketones. The reaction led to 2-phenyl-1,3-indandione (**23**) quantitatively without formation of the corresponding tosylate. In this reaction, the phenyl migration was observed also. However, Moore and his co-workers showed that the acid-catalyzed decomposition of 2-diazo-3-hydroxy-3-methyl-1,4-(2*H*,3*H*)-naphthalenedione (**24**) gave 2-acetyl-1,3-indandione (**25**) caused by ring contraction in a quantitative yield without methyl migration products.[13] The ring size seems to exert an influence on the course of the acid-catalyzed decomposition of cyclic α-diazo β-hydroxy ketones.

Experimental

All melting points were measured with a Yanagimoto Melting Point Apparatus and are not corrected. The IR spectra were measured on a JASCO IR Spectrometer model IR-G. NMR spectra were recorded in $CDCl_3$ solution at 60 MHz on a Varian Spectrometer model EM-360 using TMS as an internal standard.

Materials. *3-Aryl-2-diazo-3-hydroxy-1-phenyl-1-propanones (**1**)* were prepared by the reaction of α-diazoacetophenone and corresponding benzaldehydes according to the method described by Wenkert.[14] The obtained α-diazo β-hydroxy ketones were purified by recrystallization from benzene-heptane.

1a (Ar=*p*-ClC_6H_4): mp 126—127 °C; IR (KBr) 3350 (OH), 2070 (diazo), 1600 cm^{-1} (diazo C=O); ^{1}H-NMR ($CDCl_3$) δ 3.97 (d, 1H, OH, J=3.6 Hz), 6.14 (d, 1H, CH, J=3.6 Hz), 7.23—7.73 (m, 9H, arom). Found: C, 63.01; H, 3.82; N, 9.77%. Calcd for $C_{15}H_{11}O_2N_2Cl$: C, 62.84; H, 3.87; N, 9.77%.

1b (Ar=*p*-$NO_2C_6H_4$): mp 120—121 °C; IR (KBr) 3360 (OH), 2060 (diazo), 1600 (diazo C=O), 1515, 1340 cm^{-1} (NO_2); ^{1}H-NMR ($CDCl_3$) δ 4.15 (d, 1H, OH, J=3.8 Hz), 6.30 (d, 1H, CH, J=3.8 Hz), 7.38—7.95 (m, 9H, arom). Found: C, 60.63; H, 3.83; N, 13.91%. Calcd for $C_{15}H_{11}O_4N_3$: C, 60.60; H, 3.73; N, 14.14%.

*α-Diazo-*p*-nitropropiophenone (**11**)* was synthesized by the reaction of *p*-nitrobenzoyl chloride with an excess of diazoethane in the presence of an equimolar amount of triethylamine at 0 °C under vigorous stirring.[15] Mp 106—107 °C; IR (KBr) 2070 (diazo), 1610 (diazo C=O), 1510, 1340 cm^{-1} (NO_2). Found: C, 52.47; H, 3.47; N, 20.75%. Calcd for $C_9H_7O_3N$: C, 52.68; H, 3.44; N, 20.48%.

*2-Diazo-3-hydroxy-3-phenylindanone (**22**)* was synthesized by the triethylamine-catalyzed isomerization of 2-benzoyl-α-diazoacetophenone, which was prepared by the reaction of DCC-complex of 2-benzoylbenzoic acid with an excess of diazomethane,[16] according to the method of Burkoth.[17] Mp 179—180 °C; IR (KBr) 3280 (OH), 2090 (diazo), and 1662 cm^{-1} (diazo C=O). Found: C, 71.71; H, 3.60; N, 11.26%. Calcd for $C_{15}H_{10}O_2N_2$: C, 71.99; H, 4.03; N, 11.20%.

Acid Catalysts. Reagent grade chemicals were used as catalyst without further purification.

All solvents were purified by distillation over appropriate drying reagents just before use.

General Procedure of the Acid-catalyzed Decomposition of α-Diazo β-Hydroxy Ketones. To a solution of diazo ketone (**1**; 2 mmol) in an appropriate solvent (30 ml) were added an acid catalyst (0.2—0.4 mmol) under vigorous magnetic stirring at 30 °C. After evolution of N_2 ceased the reaction mixture was poured into 50 ml of water and the products were extracted with ether (20 ml) three times. The ether extract was column-chromatographed on silica gel after usual work-up.

2a (Ar=*p*-ClC_6H_4): mp 132—133 °C; $FeCl_3$ test, positive; IR (KBr) 3054 (OH), 1584 cm^{-1} (C=O); ^{1}H-NMR ($CDCl_3$) δ 7.12 (ABq, 4H, arom), 7.32 (s, 5H, Ph), 8.59 (d, 1H, =CH, J=4.8 Hz), and 16.93 (d, 1H, enol-OH); Found: C, 69.59; H, 4.24%. Calcd for $C_{15}H_{11}O_2Cl$: C, 69.64; H, 4.29%.

2b (Ar=*p*-$NO_2C_6H_4$): mp 144—146 °C; $FeCl_3$ test, positive; IR (KBr) 3000 (OH), 1595 (C=O), 1525, 1340 cm^{-1} (NO_2); ^{1}H-NMR ($CDCl_3$) δ 7.16—8.22 (m, 9H, arom), 8.66 (s, 1H, =CH), 13.00 (broad s, 1H, enol-OH). Found: C, 66.74; H, 4.08; N, 5.27%. Calcd for $C_{15}H_{11}O_4N$: C, 66.91; H, 4.12; N, 5.20%.

3a (Ar=*p*-ClC_6H_4): mp 90—92 °C; $FeCl_3$ test, positive; IR (KBr) 3050 (OH), 1490 cm^{-1} (C=O); ^{1}H-NMR ($CDCl_3$) δ 6.76 (s, 1H, =CH), 7.13—8.05 (m, 5H, Ph), 7.68 (ABq, 4H, arom), 17.80 (broad s, 1H, enol-OH). Found: C, 69.55; H, 4.53%. Calcd for $C_{15}H_{11}O_2Cl$: C, 69.64; H, 4.29%.

3b (Ar=*p*-$NO_2C_6H_4$): mp 166—167 °C; $FeCl_3$ test, positive; IR (KBr) 3100 (OH), 1585 (C=O), 1510, 1340 cm^{-1} (NO_2); ^{1}H-NMR ($CDCl_3$) δ 6.90 (s, 1H, =CH), 7.38—8.08 (m, 9H, arom), 17.10 (broad s, 1H, enol-OH). Found: C, 66.47; H, 4.12; N, 5.26%. Calcd for $C_{15}H_{11}O_4N$: C, 66.91; H, 4.12; N, 5.20%.

4a (Ar=*p*-ClC_6H_4): mp 108—110 °C; IR (KBr) 1685 cm^{-1} (C=O); ^{1}H-NMR ($CDCl_3$) δ 4.66 (s, 2H, CH_2), 7.16—8.11 (m, 9H, arom). Found: C, 69.58; H, 4.30%. Calcd for $C_{15}H_{11}O_2Cl$: C, 69.64; H, 4.29%.

4b (Ar=*p*-$NO_2C_6H_4$): mp 121—122 °C; IR (KBr) 1680 (C=O), 1518, 1348 cm^{-1} (NO_2); ^{1}H-NMR ($CDCl_3$) δ 4.60 (s, 2H, CH_2), 7.26—8.16 (m, 9H, arom). Found: C, 67.00; H, 4.15; N, 5.28%. Calcd for $C_{15}H_{11}O_4N$: C, 66.91; H, 4.12; N, 5.20%.

5a (Ar=*p*-ClC_6H_4): mp 125—126 °C; IR (KBr) 3350 (OH), 1650 cm^{-1} (C=O); ^{1}H-NMR ($CDCl_3$) δ 5.08 (d, 1H Cl-CH), 5.16 (q, 1H, O-CH), 16.63 (d, 1H, enol-H). Found: C, 61.23; H, 3.90%. Calcd for $C_{15}H_{12}O_2Cl_2$: C, 61.04; H, 4.10%.

5b (Ar=*p*-$NO_2C_6H_4$): mp 139—140 °C; IR (KBr) 3350 (OH), 1650 (C=O), 1510, 1350 cm^{-1} (NO_2); ^{1}H-NMR ($CDCl_3$) δ 5.03 (d, 1H, Cl-CH), 5.30 (q, 1H, O-CH), 16.46 (d, 1H, enol-OH). Found: C, 59.10; H, 3.66; N, 4.61%. Calcd for $C_{15}H_{12}O_4NCl$: C, 58.93; H, 3.96; N, 4.58%.

6a (Ar=*p*-ClC_6H_4): mp 107—109 °C; IR (KBr) 2200 (C≡C), 1630 cm^{-1} (C=O); ^{1}H-NMR ($CDCl_3$) δ 7.23—8.28 (m, 9H, arom). Found: C, 74.36; H, 3.80%. Calcd for $C_{15}H_9OCl$: C, 74.85; H, 3.77%.

6b (Ar=*p*-$NO_2C_6H_4$): mp 154—156 °C; IR (KBr) 2210 (C≡C), 1630 (C=O), 1528, 1352 cm^{-1} (NO_2); ^{1}H-NMR ($CDCl_3$) δ 7.50—8.54 (m, arom). Found: C, 71.61; H, 3.67; N, 5.58%. Calcd for $C_{15}H_9O_3N$: C, 71.71; H, 3.61: N, 5.57%.

*p-Toluenesulfonic Acid-catalyzed Decomposition of α-Diazo-*p*-nitropropiophenone (**11**).* To a solution of **11** (0.41 g, 2 mmol) in an acetonitrile (10 ml) was added an equimolar amount of TsOH·H_2O (0.38 g, 2 mmol) in small portions at 0—5 °C under vigorous stirring. After evolution of N_2 ceased the reaction mixture was poured into 50 ml of cold water and the organic layer was extracted with each 30 ml of ether three times. Combined ether solution was dried over $MgSO_4$ and separated with silica gel column chromatography. Major product was characterized to 1-(*p*-nitrobenzoyl)ethyl tosylate (**13**); white crystals; 0.48 g, 69%;

mp 146—147.5 °C; IR (KBr) 1685 (C=O), 1520, 1345 (NO_2), 1365, 1195 cm^{-1} (SO_2); ^{1}H-NMR ($CDCl_3$) δ 1.60 (d, 3H, CH_3 J=6.6 Hz) 2.43 (s, 3H, CH_3), 5.68 (q, 1H, CH, J=6.6 Hz), and 7.2—8.4 (two pairs of ABq, 8H, arom). Found: C, 54.95; H, 4.27; N, 4.12%. Calcd for $C_{16}H_{15}O_6NS$: C, 55.01; H, 4.33; N, 4.01%. The minor product was determined to *p*-nitrophenylvinylketone (**14**): 0.046 g, 13%; mp 87—87.5 °C; IR (KBr) 1645 (enone), 1490, 1320 cm^{-1} (NO_2); ^{1}H-NMR ($CDCl_3$) δ 6.03 (dd, 1H, Hx), 6.42 (dd, 1H, Hb (*cis* to Hx), 9.13 (dd, 1H Ha (*trans* to Hx)) and 8.0—8.4 (ABq, 4H, arom), (Jab=16.0, Jax=10.0, and Jbx=2.0 Hz). Found: C, 60.95; H, 4.07; N, 7.59%. Calcd for $C_9H_7O_3$: C, 61.01; H, 3.98; N, 7.91%.

p-*Toluenesulfonic Acid-catalyzed Decomposition of 2-Diazo-3-hydroxy-3-phenyl-1-indandione (**22**).* To an acetonitrile solution (10 ml) of **22** (0.500 g, 2 mmol) was added a catalytic amount of $TsOH \cdot H_2O$ at room temperature. Pouring the reaction mixture into 50 ml of water gave a white crystalline product (**23**) in quantitative yields. The structure was determined by the comparison of its IR spectra with that of authentic sample prepared by the alkali-catalyzed reaction of 3-benzylidenephthalide.[18]

References

1) H. Zollinger, "Azo and Diazo Chemistry," Interscience Publishers Inc., New York (1961), pp. 69, 103; S. Patai, "The Chemistry of Diazonium and Diazo Groups," John Wiley and Sons, New York (1978), p. 179.

2) E. Wenkert and C. A. McPherson, *Synth. Commun.*, **2**, 331 (1972).

3) U. Schöllkopf, B. Banhidai, H. Fransnelli, R. Meyer, and H. Beckhaus, *Ann.*, **1974**, 1767.

4) W. Disteldorf and M. Regitz, *Chem. Ber.*, **109**, 546 (1976).

5) a) T. Ibata and R. Sato, *Chem. Lett.*, **1978**, 1129; *Bull. Chem. Soc. Jpn.*, **52**, 3597 (1979); b) T. Ibata. K. Miyauchi, and S. Nakata, *Bull. Chem. Soc. Jpn.*, **52**, 3467 (1979).

6) K. Mislow and M. Siegel, *J. Am. Chem. Soc.*, **74**, 1060 (1952).

7) A. L. Crowther and G. Holt, *J. Chem. Soc.*, **1963**, 2818.

8) R. M. Acheson and M. W. Cooper, *J. Chem. Soc., Perkin Trans.* 1, **1980**, 1185.

9) There has been reported no migratory aptitude value of *p*-nitrophenyl group in the pinacol rearrangement; W. E. Bachmann and J. W. Ferguson, *J. Am. Chem. Soc.*, **56**, 2081 (1934); C. J. Collins, *Quatarl Rew.*, **14**, 357 (1960).

10) M. Auriel, E. de Hoffmann, *J. Am. Chem. Soc.*, **97**, 7433 (1975); b) B. Giese, *Angew. Chem. Int. Ed. Engl.*, **16**, 125 (1977).

11) H. E. Sheffer and J. A. Moore, *J. Org. Chem.*, **28**, 129 (1963).

12) R. Pellicciari, E. Castagnino R. Fringuelli and S. Corsano, *Tetrahedron Lett.*, **1979**, 481.

13) G. J. B. Cajipe, G. Landen, B. Semler, and H. W. Moore, *J. Org. Chem.*, **40**, 3874 (1975).

14) E. Wenkert and C. A. McPherson, *J. Am. Chem. Soc.*, **94**, 8084 (1972).

15) M. S. Newman and P. B. Beal, III, *J. Am. Chem. Soc.*, **71**, 1506 (1949).

16) L. Horner and H. Schwarz, *Ann.*, **747**, 21 (1971).

17) T. L. Burkoth, *Tetrahedron Lett.*, **1969**, 5049.

18) F. Nathanson, *Ber.*, **26**, 2576 (1893).

Structure of Octa-*O*-acetyl-tris(*N*-ethoxycarbonyl)destomycin A

Shigeomi Horito, Yuji Ohashi, Nobert Gassner, Juji Yoshimura,* and Yoshio Sasada

Laboratory of Chemistry for Natural Products, Faculty of Science, Tokyo Institute of Technology, Nagatsuta, Midori-ku, Yokohama 227

(Received January 16, 1981)

The molecular and crystal structure of octa-*O*-acetyl-tris(*N*-ethoxycarbonyl)destomycin A tetrahydrate, $C_{45}H_{65}N_3O_{27}\cdot 4H_2O$, has been determined by X-ray analysis. The space group is $P2_1$ with $a=14.738(4)$, $b=17.391(4)$, $c=12.171(4)$ Å, $\beta=105.58(4)°$, and $Z=2$. The structure was solved by the direct method, and the least-squares refinement using 4008 reflections led to the final R value of 0.12. The configuration of the ortho ester carbon atom is (*R*). The D-talose moiety has the boat conformation whereas the other rings are in the chair form.

A group of antibiotics such as everninomicins, flambamycin, curamycin, avilamycins, destomycins, hygromycin B, the antibiotics A-396-I and SS-56C was recently named as the orthosomycin family,[1] because they commonly include a very unique ortho ester linkage of a glyconic acid lactone to an α-diol function of an aldose in their molecules. This interlinkage provides two possible stereoisomers depending on the (*R*) or (*S*) configuration at the ortho ester carbon atom; however, no absolute configuration has been determined except for one of the two orthoester linkages in everninomicin D.[2] The difficulties in the elucidation of the configuration is attributed to that only X-ray analysis is applicable for this purpose at the present stage and that these sugar derivatives are not easily crystallizable.

In this paper, we intended to confirm the proposed structure and to determine the absolute configuration of the ortho ester linkage of destomycin A (Fig. 1),[3] which is the main aminoglycoside antibiotic produced by a strain of *Streptomyces rimofaciens*. By the examination of several derivatives, octa-*O*-acetyl-tris(*N*-ethoxycarbonyl)destomycin A (**1**) was obtained as crystals, and its X-ray analysis disclosed the structure to be 4,6-di-*O*-acetyl-3-ethoxycarbonylamino-1-[*N*-(ethoxycarbonyl)methylamino]-5-*O*-[4,6-di-*O*-acetyl-2,3-*O*-(2,3,7-tri-*O*-acetyl-6-deoxy-6-ethoxycarbonylamino-L-*glycero*-D-*galacto*-(*R*)-heptopyranosylidene)-β-D-talopyranosyl]-1D-1,2,3-trideoxy-*myo*-inositol.

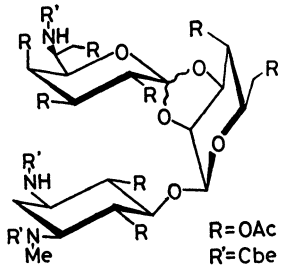

Fig. 1. The chemical structure.

Experimental and Structural Determination

Preparation of Octa-O-acetyl-tris(N-ethoxycarbonyl)destomycin A (1). To an ice-chilled aqueous solution of destomycin A (0.53 g, 1.0 mmol) and sodium carbonate (0.42 g, 4.0 mmol) was added ethoxycarbonyl chloride (0.35 g, 3.2 mmol) with stirring, and the resulting mixture was stirred overnight at room temperature, neutralized with dilute hydrochloric acid, and evaporated. The residue was fractionated on a silica gel column (1-butanol–methanol–water 3:2:1), and evaporation of the fractions showing one spot on TLC gave pure tri-*N*-ethoxycarbonyl derivative as a light yellow, hygroscopic hard syrup. Yield, 0.53 g (70.9%); $[\alpha]_D$ −17.0° (*c* 0.4, ethanol).

A solution of the above tri-*N*-ethoxycarbonyl derivative (0.74 g, 1 mmol) and acetic anhydride (1 ml, 10.6 mmol) in chloroform (10 ml) and pyridine (1 ml) was allowed to stand overnight at room temperature, diluted with water, and the organic layer was washed with aqueous sodium hydrogencarbonate and three time with water. The organic layer was evaporated, and the residual sirup was purified on a silica gel column with ethyl acetate as an eluent to give crystalline (**1**) which was recrystallized twice from ethanol–water (1:1). Single crystals suitable for X-ray studies were obtained as well-formed parallelepipeds. Yield, 0.75 g (69.8%), mp 143—145 °C, $[\alpha]_D$ +20.4°, (*c* 1.07, pyridine); NMR (δ): *ca.* 1.22 (3×C–CH_3, t), 1.98, 2.30, 2.08, 2.10, 2.12, 2.14 (8×Ac, each s), 2.74 (N–CH_3, s). Found: C, 50.01; H, 6.14; N, 4.01%. Calcd for $C_{45}H_{65}N_3O_{27}$: C, 50.04; H, 6.07; N, 3.89%.

X-Ray Analysis. Preliminary unit-cell dimensions and space group were obtained from photographs. The space group was determined as $P2_1$ from the systematic absences of reflections for $0k0$ with odd k. A crystal with dimensions of $0.5\times0.4\times0.2$ mm³ was used for data collection on a Rigaku automated four-circle diffractometer with Ni-filtered Cu $K\alpha$ radiation ($\lambda=1.54184$ Å). Accurate cell dimensions were determined by least-squares calculation with 2θ values of 16 high-angle reflections measured on the diffractometer. Crystal data are summarized in Table 1. Intensity data

Table 1. Crystal data

$C_{45}H_{65}N_3O_{27}\cdot 4H_2O$	
$M.W.=1152.1$	
Monoclinic	
$P2_1$	
$a=14.738(4)$ Å	$a=14.65(1)$ Å[a]
$b=17.391(4)$ Å	$b=17.41(1)$ Å
$c=12.171(4)$ Å	$c=12.16(1)$ Å
$\beta=105.58(4)°$	$\beta=105.5(1)°$
$V=3005(2)$ Å³	$V=2989(4)$ Å³
$Z=2$	
$D_x=1.273$ g cm⁻³	
$D_m=1.275$ g cm⁻³	
μ(Cu $K\alpha$) = 10.6 cm⁻¹	

a) The values after the data collection.

TABLE 2. FINAL ATOMIC COORDINATES WITH THEIR ESTIMATED STANDARD DEVIATIONS, MULTIPLIED BY 10^4 FOR NON-HYDROGEN AND 10^3 FOR HYDROGEN ATOMS

Atom	x	y	z	B_{eq}[a)] or B/Å^2	Atom	x	y	z	B_{eq}[a)] or B/Å^2
C(1)	3430(8)	6308(7)	9888(9)	65(4)	C(2″1)	1258(8)	4806(8)	2891(20)	151(9)
C(2)	2428(9)	6333(7)	10034(10)	76(5)	O(2″2)	1425(9)	4835(8)	1860(13)	197(7)
C(3)	1773(7)	6836(7)	9123(10)	65(4)	C(2″3)	423(14)	4866(14)	3385(39)	317(25)
C(4)	1833(8)	6584(6)	7914(9)	67(4)	O(3″)	2747(5)	3219(4)	3672(6)	62(2)
C(5)	2803(7)	6477(5)	7798(8)	55(3)	C(3″1)	2632(10)	2624(9)	4312(13)	115(6)
C(6)	3475(9)	6005(6)	8702(9)	72(4)	O(3″2)	2953(14)	2586(10)	5194(12)	157(8)
O(1′)	2713(6)	6148(4)	6699(6)	69(3)	C(3″3)	2103(10)	1994(7)	3461(15)	119(7)
O(0′)	2027(5)	6599(4)	4930(5)	63(2)	O(4″)	4336(5)	3640(4)	3017(6)	59(2)
C(1′)	2866(8)	6563(6)	5832(8)	64(4)	C(4″1)	4614(10)	3001(7)	2738(11)	86(5)
C(2′)	3643(7)	6246(5)	5378(8)	48(3)	O(4″2)	4886(10)	2455(6)	3421(9)	151(6)
C(3′)	3617(7)	6549(5)	4206(7)	46(3)	C(4″3)	4656(12)	2999(9)	1504(12)	118(7)
C(4′)	3044(8)	7267(5)	3934(8)	56(4)	O(7″)	7370(5)	5137(4)	5389(7)	82(3)
C(5′)	2024(8)	7167(6)	4120(9)	69(4)	C(7″1)	8028(11)	4668(8)	6116(14)	110(6)
C(6′)	1363(7)	6894(8)	2997(11)	81(5)	O(7″2)	7696(7)	4302(9)	6835(8)	145(5)
O(2′)	3478(5)	5427(4)	5216(5)	59(2)	C(7″3)	8967(9)	4761(10)	5929(18)	137(8)
O(3′)	3195(4)	5923(4)	3465(5)	52(2)	N(6″)	6014(6)	4496(5)	3554(7)	62(3)
O(0″)	4442(5)	5130(4)	4064(5)	53(2)	C(6″1)	6679(10)	4102(7)	3188(12)	93(5)
C(1″)	3511(7)	5276(6)	4112(7)	52(3)	O(6″2)	7138(8)	3576(5)	3779(8)	115(4)
C(2″)	2910(8)	4585(6)	3692(11)	71(4)	O(6″3)	6718(7)	4302(7)	2194(6)	110(4)
C(3″)	3285(7)	3866(6)	4277(8)	54(3)	C(6″4)	7493(15)	3993(11)	1748(13)	149(9)
C(4″)	4331(8)	3769(6)	4247(8)	63(4)	C(6″5)	7864(21)	4559(18)	1130(24)	242(17)
C(5″)	4887(7)	4455(6)	4696(8)	55(3)	O(W1)	325(15)	5251(11)	9506(22)	200(12)
C(6″)	5907(7)	4485(6)	4677(8)	55(3)	O(W2)	1251(18)	4257(21)	8044(23)	335(16)
C(7″)	6429(7)	5109(8)	5441(10)	76(4)	O(W3)	9037(22)	4279(24)	8812(26)	130(14)
N(1)	4093(7)	5894(6)	10822(7)	80(4)	O(W4)	2167(27)	4428(21)	6510(22)	94(14)
C(11)	3920(12)	5084(8)	10966(11)	112(7)	H(1)	350(7)	708(6)	1018(8)	90(28)
C(12)	4875(12)	6222(9)	11432(12)	112(7)	H(151)	683(5)	705(5)	1201(6)	59(21)
O(13)	5438(7)	5897(7)	12258(9)	133(5)	H(152)	580(4)	727(4)	1248(5)	32(15)
O(14)	4993(7)	6970(6)	11291(7)	104(4)	H(21)	238(6)	652(5)	1103(7)	67(22)
C(15)	5883(14)	7447(21)	11946(14)	215(14)	H(22)	202(6)	606(6)	982(7)	75(24)
C(16)	6026(30)	8178(26)	11560(30)	362(29)	H(3)	209(5)	734(5)	933(6)	54(20)
N(3)	832(8)	6889(7)	9241(10)	97(5)	H(N3)	58(7)	679(7)	899(9)	114(33)
C(31)	368(10)	7514(7)	9459(11)	87(5)	H(341)	−111(6)	820(5)	896(7)	68(23)
O(32)	814(7)	8122(6)	9554(11)	125(5)	H(342)	−66(4)	821(4)	1008(5)	30(15)
O(33)	−502(6)	7410(7)	9379(10)	124(5)	H(4)	144(4)	618(4)	788(5)	32(16)
C(34)	−971(15)	8007(20)	9678(20)	227(16)	H(5)	328(4)	702(4)	792(5)	35(16)
C(35)	−1941(11)	7773(21)	9616(18)	223(15)	H(6)	322(5)	552(5)	843(6)	57(20)
O(4)	1334(5)	7176(4)	7139(6)	72(3)	H(1′)	320(5)	703(4)	604(6)	45(18)
C(41)	472(8)	7088(8)	6447(11)	88(5)	H(2′)	418(5)	634(4)	600(6)	47(19)
O(42)	112(6)	6479(6)	6301(8)	105(4)	H(3′)	422(4)	674(4)	421(5)	22(14)
C(43)	111(11)	7794(9)	5758(14)	113(7)	H(4′)	347(4)	787(4)	435(5)	28(15)
O(6)	4377(6)	6086(4)	8578(6)	78(3)	H(5′)	168(6)	774(6)	448(7)	75(24)
C(61)	4906(13)	5512(8)	8559(12)	114(7)	H(6′1)	212(5)	659(4)	292(6)	48(19)
O(62)	4550(9)	4860(6)	8460(11)	154(6)	H(6′2)	125(7)	732(7)	212(9)	108(32)
C(63)	5914(10)	5724(9)	8424(14)	110(7)	H(2″)	280(5)	448(5)	318(6)	51(19)
O(4′)	2905(5)	7520(4)	2784(5)	62(2)	H(3″)	350(5)	396(4)	517(6)	48(19)
O(4′1)	3579(5)	8044(6)	2624(9)	73(4)	H(4″)	469(4)	343(4)	463(5)	37(17)
O(4′2)	4239(5)	8264(5)	3376(6)	75(3)	H(5″)	488(5)	432(5)	567(6)	53(20)
C(4′3)	3316(9)	8334(7)	1375(8)	76(4)	H(6″)	638(5)	410(4)	508(5)	38(17)
O(6′)	438(6)	6775(8)	3261(8)	132(5)	H(N6″)	551(8)	496(8)	325(10)	134(39)
C(6′1)	315(14)	2028(12)	7210(17)	148(9)	H(641)	694(5)	358(5)	75(7)	64(22)
O(6′2)	21(9)	2832(8)	7200(11)	157(6)	H(642)	761(6)	380(6)	219(8)	84(26)
C(6′3)	1134(10)	1751(11)	6914(14)	120(7)	H(7″1)	612(5)	507(4)	593(5)	42(17)
O(2″)	1995(5)	4683(4)	3792(10)	107(4)	H(7″2)	625(5)	545(4)	496(6)	48(19)

a) $B_{eq}=\frac{4}{3}\sum_i\sum_j \beta_{ij}\boldsymbol{a}_i\cdot\boldsymbol{a}_j$, where $\boldsymbol{a}_i$ and $\boldsymbol{a}_j$ are the base vectors in real space, and β_{ij}'s are anisotropic thermal parameters.

within the range of $3° \leq 2\theta \leq 125°$ were collected in the ω-2θ scan mode at a scanning rate of 8° (2θ) min^{-1}. Stationary background counts were accumulated for 5 s before and after each scan. The periodic check of the intensity values of three standard reflections revealed a slight change. The intensities decreased by 5—6% during the data collection. The cell dimensions also changed appreciably; the values after the data collection are also listed in Table 1. This is probably due to the dehydration of the crystal. As this change did not seem to be serious, it was ignored in the structure determination. A total of 4957 independent reflections was obtained, of which 4008 $[|F_o| \geq 3\sigma(|F_o|)]$ were used for the structure determination. Any correction for absorption or extinction was not applied.

Structure Determination. The structure was solved by direct methods with the MULTAN 78 program.[4] At the first stage, only 40 chemically significant peaks were found on the *E*-map. The other non-hydrogen atoms were obtained by the subsequent Karle recycling procedure. The structure was refined by the block-diagonal least-squares method with the modified HBLS program. The difference synthesis revealed that several substituents were disordered. This is probably due to the rearrangement of the substituents after the dehydration. Since the volume of the disordered portion, however, was probably less than 20%, the disordered model was not taken into account. All the hydrogen atoms except for those of the methyl groups and water molecules were located geometrically. Refinement using the anisotropic and isotropic temperature factors for the non-hydrogen and hydrogen atoms, respectively, gave the final *R* value of 0.12 for 4008 reflections. The weighting scheme used in the final stage was $w=[(|F_o|)^2+(0.015|F_o|)^2]^{-1}$. Atomic scattering factors were taken from "International Table for X-Ray Crystallography."[5] The final positional and thermal parameters are given in Table 2.†

The stereoscopic drawing of the molecular structure is shown in Fig. 2. The numbering of the atoms and the bond distances and angles are illustrated in Fig. 3.

Results and Discussion

The structure of destomycin A was previously elucidated as 5-*O*-[2,3-(6-amino-6-deoxy-L-*glycero*-D-*galacto*-heptopyranosylidene)-β-D-talopyranosyl]-1D-3-amino-1-methylamino-1,2,3-trideoxy-*myo*-inositol by chemical and spectroscopic studies[6] as shown in Fig. 1. The structure of aminocyclitol[7] and 6-aminoheptonic acid[8] (destomic acid) moieties were also proved by syntheses. The analyzed structure confirmed the above-mentioned spectroscopic and chemical elucidations. From the spatial interrelation of the destomic acid and D-talose moieties, the absolute configuration of the orthoester carbon atom was determined to be (*R*). The torsional angles around several bonds are listed in Table 3.

Surprisingly, the D-talopyranose moiety has $B_{1,4}$ conformation. In the case of everninomicin D in which a pentono-1,5-lactone makes a spiro cyclic ortho ester with the *trans*-diequatorial 3,4-diol function of L-lyxopyranose moiety,[2] the pyranose ring exists in $^1C_4$ conformation, because $B_{1,4}$ conformation causes an additional distortion to the five-membered ortho ester

† The table of the observed and calculated structure factors and the list of the anisotropic temperature factors are kept as Document No. 8140 at the office of the Chemical Society of Japan.

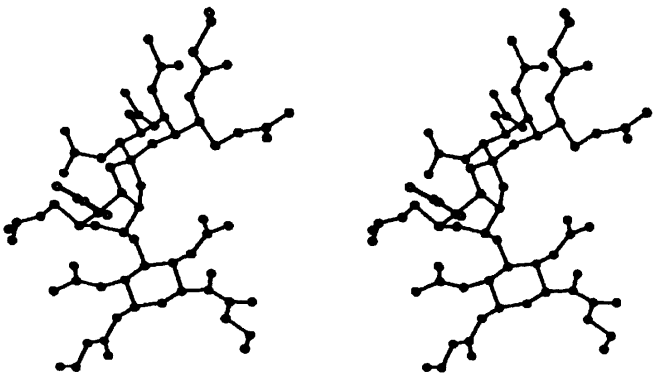

Fig. 2. A stereoscopic drawing of the molecule. This was drawn by TSD:XTAL, which is a computer-graphics interactive modeling program for NOVA 3 computer.[12]

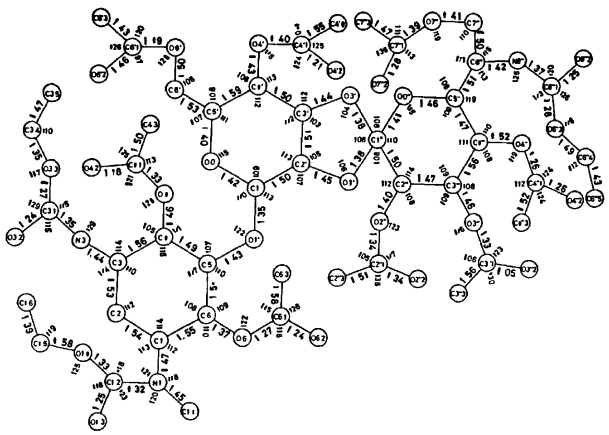

Fig. 3. Bond distances (l/Å) and angles (ϕ/°). Their standard deviations are 0.02—0.04 Å and 1—2°, respectively. Bond angles of O(2′)-C(1″)-O(0″) and O(3′)-C(1″)-C(2″) are 111° and 112°, respectively.

TABLE 3. TORSIONAL ANGLES (ϕ/°)

C(4)-C(5)-O(1′)-C(1′)	128
C(6)-C(5)-O(1′)-C(1′)	−106
C(5)-O(1′)-C(1′)-O(0′)	−118
C(5)-O(1′)-C(1′)-C(2′)	120
O(1′)-C(1′)-C(2′)-O(2′)	47
O(0′)-C(1′)-C(2′)-O(2′)	−75
O(1′)-C(1′)-C(2′)-C(3′)	40
O(0′)-C(1′)-C(2′)-C(3′)	162
O(2′)-C(2′)-C(3′)-O(3′)	15
C(1′)-C(2′)-C(3′)-C(4′)	19
O(3′)-C(3′)-C(4′)-O(4′)	−58
C(2′)-C(3′)-C(4′)-C(5′)	−52
C(2′)-C(3′)-O(3′)-C(1″)	−33
C(4′)-C(3′)-O(3′)-C(1″)	−153
C(1′)-C(2′)-O(2′)-C(1″)	129
C(3′)-C(2′)-O(2′)-C(1″)	9
C(2′)-O(2′)-C(1″)-O(3′)	−31
C(2′)-O(2′)-C(1″)-O(0″)	87
C(2′)-O(2′)-C(1″)-C(2″)	−153
C(3′)-O(3′)-C(1″)-O(2′)	41
C(3′)-O(3′)-C(1″)-O(0″)	−79
C(3′)-O(3′)-C(1″)-C(2″)	160
O(2″)-C(2″)-C(1″)-O(2″)	55
O(2″)-C(2″)-C(1″)-O(3′)	−64
O(2″)-C(2″)-C(1″)-O(0″)	174

Table 4. Least-squares planes and deviations (l/Å) for four atoms of the five-membered ortho ester ring

X,Y, and Z in Å referred to **a**, **b**, and **c***) respectively.
$-0.9615X+0.0951Y-0.2580Z+4.0005=0$

C 2′	−0.05[a]
C 3′	0.03[a]
O 2′	0.05[a]
C 1″	−0.03[a]
O 3′	0.51

a) Atoms included in the least-squares calculation.

ring.[9] Besides, in the case of (**1**) in which the 6-aminoheptono-1,5-lactone links to the *cis*-2,3-diol function of D-talopyranose moiety, $B_{1,4}$ conformation assists the formation of five-membered ortho ester ring, and erases the non-bonded interactions caused by C4′-hydroxyl group previously in axial orientation. In fact, the dihedral angle of C(2′)–O(2′) and C(3′)–O(3′) is 15°. These facts must also be true in the natural destomycin A itself.

From the synthetic studies,[10] it was suggested that the five-membered ring has a twist or envelope conformation to avoid the non-bonded interactions. The determined structure proved that the ring takes an envelope conformation in which the O(3′) atom of D-talopyranose moiety deviated significantly from the average plane of other four atoms. The equation of the plane and the deviation of each atom from the plane in the five-membered ring are shown in Table 4.

It is characteristic that the both C–O bonds in the five-membered ring concerned with ortho ester carbon is slightly short as was observed in the anomeric C–O bond in the usual aldopyranosides.[11] Other bond distances and angles show the values common in carbohydrate derivatives.

The crystal structure viewed along the b axis is shown in Fig. 4. The hydrogen bonds, listed in Table 5, make a three-dimensional network through the water molecules.

One of the authors (J.Y.) is grateful to Meiji Seika Co. Ltd. for the gift of destomycin A.

Table 5. Hydrogen bond lengths (l/Å)

O(13)···N(6″)[III]	2.90 (2)
O(W1)···N(3)[I]	2.99 (3)
O(W1)···O(W2)[I]	3.05 (5)
O(W1)···O(2″2)[III]	2.98 (3)
O(W1)···O(W3)[II]	2.51 (5)
O(W2)···O(W4)[I]	2.60 (6)
O(W2)···O(6′2)[I]	3.08 (4)
O(W2)···O(7″2)[I]	2.67 (5)

I. (0.0+x, 0.0+y, 0.0+z)
II. (−1.0+x, 0.0+y, 0.0+z)
III. (1.0+x, 0.0+y, 1.0+z)

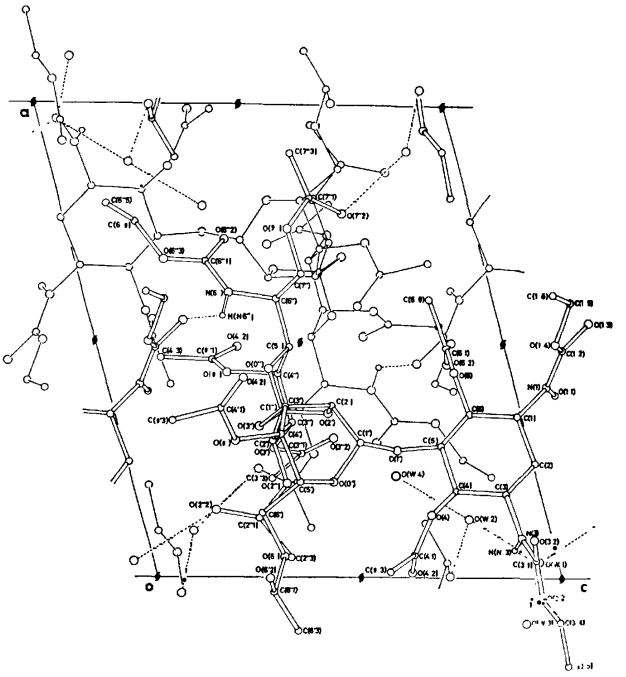

Fig. 4. Projection of the crystal structure along the b axis. The dotted lines indicate the hydrogen bonds.

References

1) W. D. Ollis, C. Smith, and D. E. Wright, *Tetrahedron*, **35**, 105 (1979).
2) A. K. Ganguly, O. Z. Sarre, A. T. McPhall, and R. W. Miller, *J. Chem. Soc., Chem. Commun.*, **1979**, 22.
3) S. Kondo, M. Sezaki, M. Koike, M. Shimura, E. Akita, K. Satoh, and T. Hara, *J. Antibiotics*, **18**, 38 (1965).
4) "International Tables for X-Ray Crystallography," The Kynoch Press, Birmingham (1974), Vol. IV, p. 72.
5) P. Main, S. E. Hull, L. Lessinger, G. Germain, J. P. Declercq, and M. M. Woolfson, "MULTAN 78, A System of Computer programmes for the Automatic Solution of Crystal Structures from X-Ray Diffraction Data," University of York, England (1978).
6) S. Kondo, K. Iinuma, H. Naganawa, M. Shimura, and Y. Sekizawa, *J. Antibiotics*, **28**, 79 (1975); S. Kondo, E. Akita, and M. Koike, *ibid.*, **19**, 139 (1966); S. Kondo, E. Akita, and M. Sezaki, *ibid.*, **19**, 137 (1966); S. Kondo, M. Sezaki, M. Koike, and E. Akita, *ibid.*, **18**, 192 (1965).
7) S. Kondo, K. Iimura, H. Yamamoto, K. Maeda, and H. Umezawa, *J. Antibiotics*, **26**, 412 (1973); N. Kurihara, K. Hayashi, and M. Nakajima, *Agric. Biol. Chem.*, **33**, 256 (1969); T. Suami, S. Ogawa, N. Tanno, M. Suguro, and K. L. Rinehart, Jr., *J. Am. Chem. Soc.*, **95**, 8734 (1973).
8) H. Hashimoto, K. Asano, F. Fujii, and J. Yoshimura, *Chem. Lett.*, **1980**, 1439.
9) According to information from Prof. W. Keller-Schierline of the Eidgenössische Technische Hochschule, Zurich, the structure of one of two ortho ester linkages of avilamycin C, in which a hexono-1,5-lactone attaches to *trans*-diequatorial 3,4-diol function of L-lyxopyranose moiety, was almost the same as that of everninomicin D.
10) J. Yoshimura and M. Tamaru, *Carbohydr. Res.*, **72**, C9 (1979); M. Tamaru, S. Horito, and J. Yoshimura, *Bull. Chem. Soc. Jpn.*, **53**, 3686 (1980).
11) H. M. Berman, S. S. C. Chu, and G. A. Jeffrey, *Science*, **157**, 1576 (1967).
12) A. Takenaka and Y. Sasada, *J. Crystallogr. Soc. Jpn.*, **22**, 214 (1980).

Reaction of Organoaluminium Reagents with Cyclopropylmethyl Acetates and 2-Vinylcyclopropane-1,1-dicarboxylate Esters

Tamejiro HIYAMA,* Yoshitomi MORIZAWA, Hajime YAMAMOTO, and Hitosi NOZAKI

Department of Industrial Chemistry, Kyoto University, Yoshida, Sakyo-ku, Kyoto 606

(Received January 20, 1981)

Ring-opening alkylation of cyclopropylmethyl acetates was studied. The acetoxyl group of 7-(1-acetoxyheptyl)norcarane is substituted by the alkyl group upon treatment with trialkylaluminium, but alkylation of *trans*-1-(1-acetoxyethyl)-2-phenylcyclopropane with trialkylaluminium gives rise to *trans*-5-phenyl-2-alkenes. The reaction of (1*S*,2*S*)-2-phenylcyclopropylmethyl acetate with trimethylaluminium resulted in the complete loss of optical activity to give racemic 4-phenyl-1-pentene. Alkylation of *trans*-1-(1-acetoxy-3-phenylpropyl)-2-vinylcyclopropane with trialkylaluminium proceeds under regioselective ring-opening to give 3-alkylated *trans*-8-phenyl-1,5-octadiene (selectivity 73—83%). The regio- and stereochemistry of homoconjugate addition to activated vinylcyclopropanes having a doubly carbonyl substituted ring carbon was studied. Trialkylaluminium on addition to diethyl 2-vinylcyclopropane-1,1-dicarboxylate in a 1,5-manner afford diethyl (2-alkyl-3-butenyl)-propanedioate (over 96% selectivity). In contrast, the reaction of this cyclopropane with tetraalkylaluminiumlithium takes place in a 1,7-manner to give diethyl (*trans*-4-alkyl-2-butenyl)propanedioate with 88—92% selectivity. Clean regiocontrol of the reaction is observed in the methylation of ethyl *exo*-6-(*trans*-1-propenyl)-2-oxobicyclo[3.1.0]hexane-1-carboxylate with trimethylaluminium or tetramethylaluminiumlithium. Alkylation with trimethylaluminium proceeds with 86% inversion of the configuration at C(6) of the substrate, affording (2*R**,3*R**)-2-ethoxycarbonyl-3-[(*S**)-*trans*-1-methyl-2-butenyl]cyclopentanone which is transformed into neonepetalactone.

Reagents of main group elements have furnished manifold synthetic methodologies.[1] The reaction of organolithium and -magnesium compounds provides a basic C–C bond forming process. The organometallics of electron-deficient elements such as boron and aluminium have intrinsic Lewis acidity and thus show to some extent Lewis acid catalysis. Examples are found in oxirane-allyl alcohol rearrangement, cyclization of neryl phosphate and alkylation of geranyl phosphate with the aid of organoaluminium reagents.[2] We have studied the reaction of organoaluminium reagents with cyclopropanes and found that (a) cyclopropylmethyl acetates undergo alkylation with or without ring-opening depending on the substituent on the cyclopropane ring and (b) regiochemistry in the homoconjugate addition of an alkyl group to 2-vinylcyclopropane-1,1-dicarboxylate esters is controlled by means of appropriate organoaluminium reagents.

Alkylation of Cyclopropylmethyl Acetates. The transformation of cyclopropylmethyl alcohols into (*E*)-homoallyl bromides is important for the stereoselective synthesis of olefins.[3,6] Strong Lewis acid such as hydrobromic acid or zinc bromide (plus phosphorus tribromide) is essential for the generation of homoallyl cations which react with bromide anion. The resulting homoallyl bromides should be treated with organometallics for the sake of carbon skeleton extention. We have found trialkylaluminium reagents can produce homoallylic cations in the presence of carbanionic species, attaining the C–C bond formation in a single step.

The cyclopropylmethyl esters **1a**, **1b**, and **3** were prepared starting with 7,7-dibromonorcarane (Scheme 1).[7] 7,7-Dibromonorcarane was treated with butyllithium at −95 °C, the lithium carbenoid generated being allowed to react with heptanal. The adduct was then treated with potassium *t*-butoxide to give *exo*-7-heptanoylnorcarane which was subsequently reduced with sodium borohydride to an alcohol, the acetylation and benzoylation of which gave **1a** and

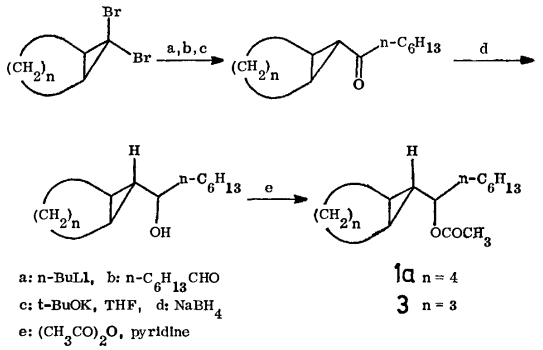

Scheme 1.

1b, respectively. **3** was prepared from 6,6-dibromobicyclo[3.1.0]hexane in a similar way.

When the acetate **1a** was treated with 2.8 mol of triethylaluminium at room temperature, the acetoxyl group was substituted by ethyl group without ring-opening, giving **2a** in 91% yield.[8] The reaction took place likewise in benzene (98% yield) or hexane (93%) and even in dichloromethane at −78 °C (93%).

The benzoate **1b** was also converted into **2a** in 68% yield. Alkylation of **3** was somewhat less effective to give **4** in 57% yield. A mixed aluminium reagent $Et_2AlC{\equiv}CC_4H_9$, prepared by treatment of diethylaluminium chloride with an equimolar amount of 1-lithio-1-hexyne, afforded **2b** only upon reaction with **1a** (56% yield). Thus, ethynyl group is more reactive than the ethyl group.[9]

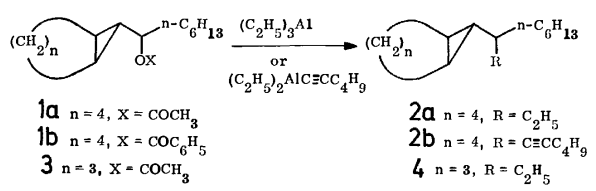

The reaction can be explained in terms of cyclopropylmethyl cation intermediates, since both *exo*- and

endo-2-acetoxynorcarane (**5a** and **5b** respectively) give *endo*-2-methylnorcarane **6** almost exclusively.[10]

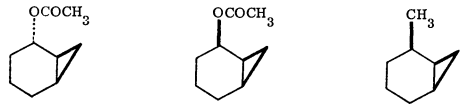

5a **5b** **6**

In contrast to the alkylation of **1a**, **1b**, **3**, or **5a,b**, the phenyl substituted cyclopropylmethyl acetates underwent alkylation under ring-opening. The cyclopropylmethyl acetate **7** was prepared by the reaction of *trans*-2-phenylcyclopropanecarbaldehyde with methylmagnesium iodide followed by acetylation. When **7** (45:55 diastereomeric mixture) was treated with 3 mol of trimethylaluminium, *trans*-5-phenyl-2-hexene (**8a**) was produced in 86% yield. The newly produced C=C bond was found to be *trans* (over 97% purity). By a similar reaction **8a** (>94% *trans*) and **8c** (>96% *trans*) were produced as the sole products from **7** upon treatment with triethylaluminium and triisobutylaluminium, respectively. For the sake of stereochemical confirmation, both diastereomers of **7** were isolated and subjected to the alkylation with triethylaluminium. The sole product was found to be **8b** resulting from each diastereomer (75, 63% yield respectively). Similarly both the diastereomers of the *cis* isomer of **7** gave **8b** (53% and 67% yields from each diastereomer). The reaction was entirely independent of the stereochemistry of the starting material. The primary acetate **9a** was less reactive than the secondary one, **7**, giving **10a** in 59% yield.

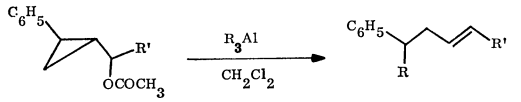

7 R' = CH_3
9a R' = H
9b R' = H (1S, 2S)

8a R' = CH_3, R = CH_3
8b R' = CH_3, R = C_2H_5
8c R' = CH_3, R = n-C_4H_9
10a R' = H, R = C_2H_5
10b R' = H, R = CH_3

In order to study the stereochemical aspect of alkylation, we prepared (1*S*,2*S*)-2-phenylcyclopropylmethyl acetate **9b** (optical purity >98%) by lithium aluminium hydride reduction of (1*S*,2*S*)-2-phenylcyclopropanecarboxylic acid followed by acetylation with acetic anhydride and pyridine. When **9b** was treated with trimethylaluminium, 4-phenyl-1-pentene (**10b**) having no optical activity was obtained. Since the carboxylic acid derived from **10b** by potassium permanganate-sodium periodate oxidation also showed no optical rotation, we can conclude that alkylation proceeds through a planar cationic intermediate.

Alkylation of 7-acetoxymethyl-1-phenylnorcarane **11a,b** showed a similar stereochemical feature. The starting materials were prepared by bromine-lithium exchange of 7,7-dibromonorcarane with butyllithium, carbonation with carbon dioxide gas, lithium aluminium hydride reduction, and the final acetylation (Scheme 2). First, a 1:3 mixture of **11a** and **11b** thus prepared was treated with trimethylaluminium in dichloromethane to produce an inseparable mixture (35:65) of **12** and **13**. The stereochemical assignment is based on the observation that isomer **13** should give a methyl singlet signal at higher field due to the shielding effect of C=C bond.[11] When the stereoisomer of the starting acetate was separated and subjected to the alkylation reaction with trimethylaluminium, the same mixture was obtained. Thus, the aluminium-mediated alkylation proceeds through a common intermediate irrespective of the stereochemistry of the starting material.

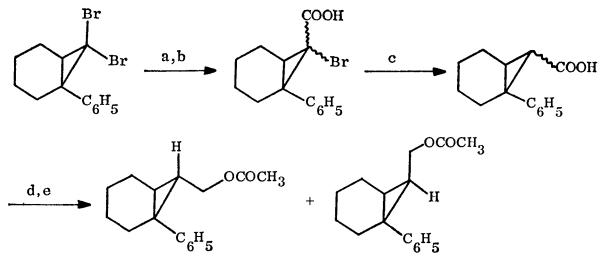

11a **11b**

a: n-BuLi, b: CO_2, c: 2 n-BuLi, -78°C, d: $LiAlH_4$, e: $(CH_3CO)_2O$, pyridine

Scheme 2.

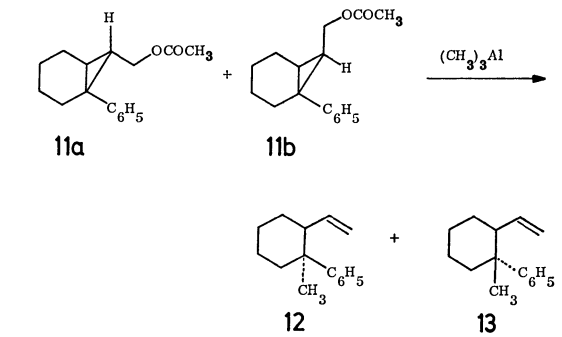

11a **11b**

12 **13**

Since a vinyl group also stabilizes a carbocation, we prepared the model compound **14** (Scheme 3).

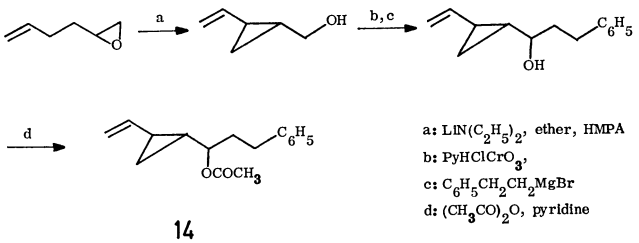

14

a: $LiN(C_2H_5)_2$, ether, HMPA
b: $PyHClCrO_3$,
c: $C_6H_5CH_2CH_2MgBr$
d: $(CH_3CO)_2O$, pyridine

Scheme 3.

2-Vinylcyclopropylmethanol was obtained by the reaction of 1,5-hexadiene monoepoxide with lithium diethylamide in ether-hexamethylphosphoric triamide.[12] Subsequent oxidation with pyridinium chlorochromate and Grignard reaction with 2-phenylethylmagnesium bromide gave an alcohol the acetylation of which gave **14** as a 55:45 diastereomeric mixture (two epimers at the acetoxyl group-bearing carbon). Both diastereomers were isolated and subjected to alkylation with trimethylaluminium at 0 °C. Isomers as well as their mixture gave almost the same mixture of **15a** and **16a** (Table 1, run 11). Methylation takes place predominantly at the cyclopropane carbon rather than the terminal methylene carbon, the newly pro-

Table 1. Reaction of cyclopropane derivatives with organoaluminum reagents

Run	Substrate (mg, mmol)	Aluminium reagent (mmol)	Solvent[a] (ml)	Temp °C	Time h	Products (mg, %yield, ratio)
1	**1a** (250, 1.0)	Et_3Al[b] (2.8)	D (3)	r.t.	2	**2a** (200, 91)
2	**1b** (310, 1.0)	Et_3Al[b] (2.8)	D (5)	r.t.	2	**2a** (151, 68)
3	**1a** (250, 1.0)	$Et_2AlC{\equiv}CC_4H_9$[c] (5.0)	C (5)	0	2	**2b** (151, 56)
4	**3** (25, 0.10)	Et_3Al[b] (0.74)	D (3)	r.t.	2.5	**4** (12, 57)
5	**9a** (190, 1.0)	Et_3Al[d] (3.0)	D (2)	r.t.	2	**10a**[e] (94, 59)
6	**9b** (480, 2.5)	Me_3Al[d] (10)	D (7)	r.t.	12	**10b**[f] (148, 40)
7	**7**[g] (38, 0.19)	Et_3Al[d] (0.47)	D (5)	r.t.	1	**8b**[h] (24, 75)
8	**7**[i] (101, 0.51)	Me_3Al[d] (1.25)	D (5)	0	2	**8a** (71, 86)
9	**7**[i] (103, 0.50)	i-Bu_3Al[j] (1.52)	D (2)	r.t.	3	**8c**[k] (76, 75)
10	**11a,b**[l] (39, 0.16)	Me_3Al[d] (0.40)	D (5)	0	1.5	**12**+**13** (29, 91, 35:65)[m]
11	**14**[n] (115, 0.47)	Me_3Al[d] (1.18)	D (8)	0 r.t.	0.5 0.6	**15a**+**16a** (78, 81, 83:17)[o]
12	**14** (133, 0.54)	Et_3Al[d] (1.35)	D (8)	0	1.5	**15b**+**16b** (94, 80, 83:17)
13	**14** (116, 0.48)	i-Bu_3Al[j] (1.22)	D (8)	0	4.5	**15c**+**16c** (64, 56, 73:27)
14	**17** (40, 0.19)	Me_3Al[d,p] (0.56)	B (8)	0	0.1	**18a**+**19a** (38, 88 (94)[q], 96:4)[r]
15	**17** (50, 0.24)	Me_4AlLi (0.71)	E (7)	0	0.5	**18a**+**19a** (42, 78 (90)[q], 8:92)
16	**17** (50, 0.24)	Et_3Al[p] (0.62)	B (7)	0	0.5	**18b**+**19b** (44, 76, 98:2)
17	**17** (51, 0.24)	Et_4AlLi (0.71)	E (2)	0	0.5	**18b**+**19b** (39, 68, 12:88)
18	**17** (50, 0.24)	$Et_2AlC{\equiv}CC_6H_5$[s] (0.71)	D (6)	0	0.8	**18c** (52, 70)
19	**20** (730, 3.5)	Me_3Al (10.6)	D (12)	−20	0.5	**21**+**22** (680, 87, 86:14)[t]
20	**20** (47, 0.23)	Me_4AlLi (0.68)	E (3.5)	0	1	**23** (36, 71)
21	**29** (48, 0.23)	Me_3Al (0.69)	D (1.8)	0	0.2	**30** (42, 81)[u]
22	**29** (35, 0.17)	Me_4AlLi (0.50)	E (6)	0	0.3	**31** (30, 80)

a) D: dichloromethane, C: dichloroethane, B: benzene, E: ether. b) A hexane solution (1.84 M) used. c) Prepared from 1-hexyne (0.45 g, 5.5 mmol), butyllithium (5.0 mmol), and diethylaluminium chloride (5.0 mmol) in hexane. d) A hexane solution (1.0 M) used. e) A by-product, *trans*-2-phenylcyclopropylmethanol (43 mg, 25%), also formed. f) α_D^{18} −0.002 to −0.005° in 5 ml of $CHCl_3$, 5 cm cell. g) One diastereomer used. The same product was invariably produced from the other diastereomer of **7** and the two diastereomers derived from the *cis*-**7**. In another experiment with the diastereomeric mixture of **7**, **8b** was produced in 89% yield. h) GLC analysis (Apiezon L, 5%, on Chromosorb WAW DMCS, KOH 1%, 2 m, 110 °C) revealed over 94% purity. i) Diastereomeric mixture of **7** used. j) A hexane solution of reagent (0.76 M) used. k) GLC analysis of the crude product showed the presence of a trace amount of 5-phenyl-2-pentene. l) A 24:76 mixture of **11a** and **11b** used. With the stereochemically pure starting material of **11a** and **11b**, the following results were obtained: yield of **12** and **13**, **12** to **13** ratio; 75%, 38:62; 86%, 36:64 respectively. m) GLC assay (PEG 20 M, 20%, on Celite 545, 2 m, 142 °C) showed the R_t of **12**, 15.8 min and the R_t of **13**, 16.8 min. n) A diastereomeric mixture (55:45) used. Both diastereomers of **14** gave nearly identical results, or the total yield of 59% or 63%, and the ratio of **15a** to **16a**, 83:17, or 83:16. When $NiCl_2(PPh_3)_2$ (10 mol% or 100 mol% was added, the total yield and the ratio of **15a** to **16a** changed to 79%, 69:31 for one isomer and 63%, 52:48 for the other. o) GLC analysis (PEG 20 M, 5% on Cellite 545, 1.5 m, 160 °C). p) The substrate **17** added to the trialkylaluminium reagent solution. q) GLC yield. r) The following results were obtained under different conditions: solvent, temperature, total yield of **18a** and **19a** (ratio); benzene, r.t., 74% (92:8); dichloromethane, 0 °C, 62% (86:14). In dichloromethane a dimeric by-product (24%) was also produced. In ether or THF at 0 °C or r.t. no trace of the product was formed, **17** being recovered unchanged. s) Reagent prepared from butyllithium (0.71 mmol), phenylacetylane (0.71 mmol) and diethylaluminium chloride (0.71 mmol) in hexane at 0 °C. t) Under other conditions, the following results were obtained: solvent, temperature, total yield of **21** and **22** (ratio); dichloromethane, 0 °C, 55% (79:21); hexane, 0 °C, 66% (86:14), toluene, 0 °C, 63% (85:15). In ether or THF no trace of the product was produced. u) GLC (PEG 20 M, 5%, on Celite 545, 1.5 m, 143 °C) showed 87% purity, the major product assumed to be **30**, the minor one being its epimer.

duced C=C bond being deduced to be *trans* (see Experimental). The regioselective alkylation takes place also with triethyl- and triisobutylaluminum. An attempt to change the regioselectivity by adding transition metal complexes failed except $NiCl_2(PPh_3)_2$ which accelerated the formation of **16a**.

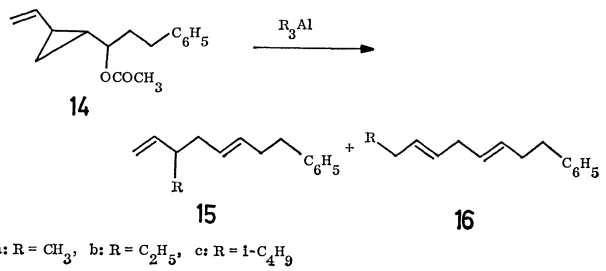

a: R = CH_3, b: R = C_2H_5, c: R = 1-C_4H_9

Regio- and Stereochemistry of Homoconjugate Addition to Activated Vinylcyclopropanes. Introduction of an alkyl group into 2-vinylcyclopropane-1,1-dicarboxylate esters or related compounds would control the regioselectivity, *i.e.* 1,5- or 1,7-homoconjugate addition.[13] Dialkylcopperlithium[14] would be a suitable reagent for 1,7-alkyl addition. However, none is known for 1,5-alkyl introduction. We have found that trialkylaluminium performs 1,5-homoconjugate addition and tetraalkylaluminiumlithium prepared from equimolar amounts of trialkylaluminium and alkyllithium effects 1,7-homoconjugate addition.

The vinylcyclopropane **17** was allowed to react with 3 mol of trimethylaluminium. The reaction took place immediately and ended usually in 10 min at 0 °C. Quenching with aq satd. sodium citrate solution, followed by work-up and isolation, gave a 96:4 mixture of **18a** and **19a**[14a] (Table 1, run 14). Among the solvents tested benzene gave best results as regards yield and selectivity. In dichloromethane a dimeric by-product was obtained. In a coordinating solvent such as ether the starting material was recovered unchanged. In order to accelerate the conversion of **17** into the products, use of 2.5 to 3 mol of trialkylaluminium is preferable, with less than 2 mol the reaction being extremely slow. Regioselectivity with triethylaluminium was almost perfect to give **18b** exclusively. Using the reagent of $Et_2AlC{\equiv}CPh$, **18c** only was produced. Thus, ethynyl carbon reacts in preference to ethyl group.[9]

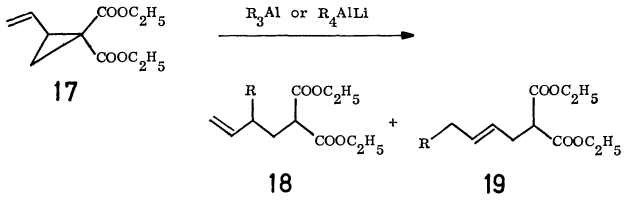

a: R = CH_3, b: R = C_2H_5, c: R = $C{\equiv}CC_6H_5$

The regioselectivity was reversed when tetramethylaluminiumlithium was used, the **18a**/**19a** ratio being 8:92 comparable to the cuprate reaction.[14] In a similar way tetraethylaluminiumlithium gave mainly **19b**. In these alanate reactions ether solvent was found to give the highest regioselectivity. Dilution with hexane gives rise to a decrease in the formation of 1,7-adduct **19**.

The regio-control of the homoconjugate addition was also attained in the reaction of a bicyclic β-keto ester **20** prepared according to the procedure shown in Scheme 4. With trimethylaluminium, **20** gave 1,5-homoconjugate adducts **21** and **22** as the sole products (Table 1, run 19). The reaction carried out in dichloromethane at −20 °C gave the adduct with the best yield. The product ratio **21**:**22** was almost independent of solvent except ether or tetrahydrofuran (THF) in which no reaction took place. The amount of trimethylaluminium necessary for alkylation was found to be more than 2 mol, 2.5 mol being usually employed.

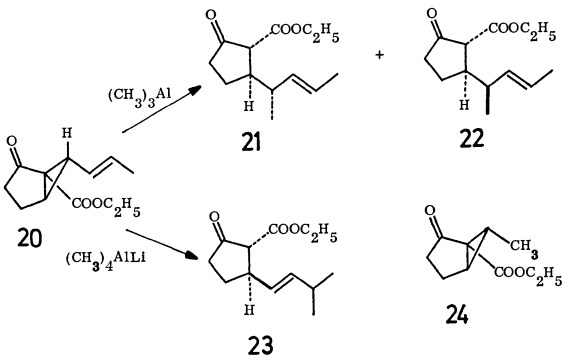

The stereochemistry of the products was determined by hydrogenating **21** and **22** and by comparing the spectral properties of the dihydro derivatives **26** and **28**, respectively. Each authentic sample was obtained by the reaction of **25** or **27** with dimethylcopperlithium.[15] We conclude that the 1,5-homoconjugate addition proceeds with *ca.* 86% inversion of the configuration at the cyclopropane carbon. This is in sharp contrast to the alkylation of **9** or **11a,b** in which complete loss of stereochemical integrity took place.

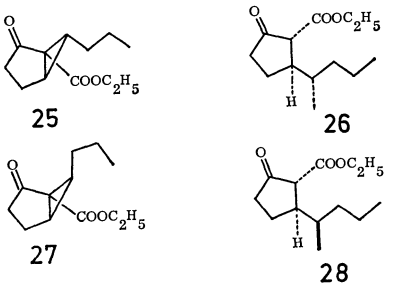

For successful homoconjugate addition, two necessary factors are (a) two activating carbonyl groups since ethyl chrysanthemate does not undergo conjugate addition, and (b) a vinyl group on the cyclopropane ring since compound **24** was recovered unchanged. Prolonged reaction of **24** with trimethylaluminium gave rise only to 1,2-methyl addition to the ketonic carbonyl.[16]

A similar regio- and stereochemical control was realized with **29** prepared according to Scheme 5. Using trimethylaluminium we obtained a 1,5-adduct of over 87% purity in 81% yield. We may assume

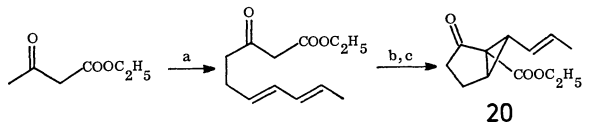

a: NaH, n-BuLi, $ClCH_2CH{=}CHCH{=}CHCH_3$, b: p-$CH_3C_6H_4SO_2N_3$, $(C_2H_5)_3N$
c: $Cu(acac)_2$, $C_6H_5CH_3$ reflux

Scheme 4.

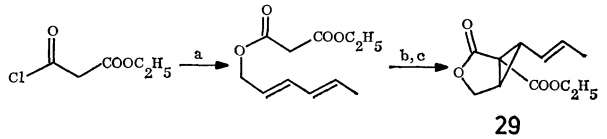

a: $HOCH_2CH{=}CHCH{=}CHCH_3$, pyridine, b: p-$CH_3C_6H_4SO_2N_3$, $(C_2H_5)_3N$
c: $Cu(acac)_2$, $C_6H_5CH_3$ reflux

Scheme 5.

the reaction proceeded mainly with inversion in analogy to the case of **20**. The present major product would have the structure shown in the formula **30**. In contrast, the reaction of **29** with tetramethylaluminiumlithium gave **31** only in 80% yield.

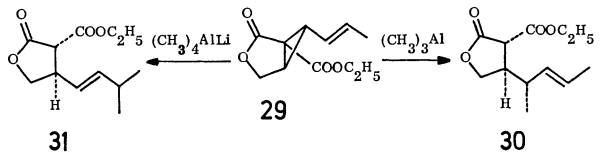

Thus we control the stereochemistry of the α-carbon of a side chain (*e.g. cf.* structure **21**). This is particularly useful for the synthesis of neonepetalactone,[17] and should be extended to the preparation of such terpenes having the same structural unit as chrysomelidial[18] and juvabione.[19]

The synthesis of neonepetalactone **34** (Scheme 6) was carried out as follows. The β-keto ester **21** was freed from its epimer **22** by preparative TLC and converted into an enol phosphate which was then allowed to react with dimethylcopperlithium to give **32**. The two C=C bonds in **32** may be differentially cleaved. Ozonolysis of **32** at −78 °C followed by reductive work-up gave a hydroxy ester **33** whose lactonization gave neonepetalactone **32** exhibiting consistent spectral properties.[17]

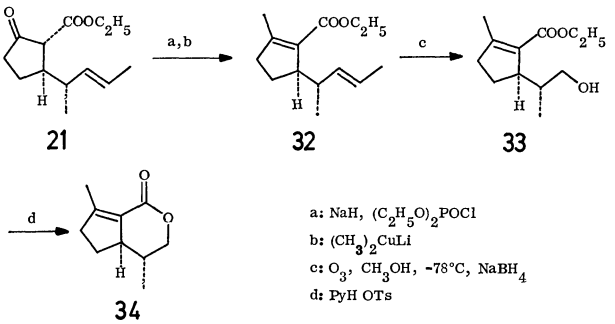

Scheme 6.

Experimental

Temperatures are uncorrected. Distillation of small amount of samples (less than 1 g) was carried out with Kugelrohr. ^{1}H-NMR spectra (tetramethylsilane as an internal standard) were taken on a Varian EM 390 spectrometer or JEOL PMX-60 spectrometer, chemical shifts being given in ppm unit. IR spectra were obtained on a Shimadzu IR-27G spectrometer, MS on a Hitachi RMU-6L spectrometer. Trialkylaluminium (Nippon Alkyl Aluminium Co., Ethyl Corp., or Alfa Division of Ventron Corp., a neat liquid) was diluted with specified solvents. All the reactions with organometallics were carried out under an argon atmosphere. Preparative TLC plates (20 cm×20 cm) were prepared by use of Merck Kiesel-gel PF_{254}. Column chromatography was carried out with silica gel at atmosphereic pressure (Wacogel C-100) or under pressure of 4—6×10^5 N/m^2 (Wacogel C-300).

Synthesis of exo-*7-(1-Acetoxyheptyl)norcarane (**1a**) and* exo-*7-(1-Benzoyloxyheptyl)norcarane (**1b**).* Butyllithium (1.80 M hexane solution, 19.0 ml, 34 mmol) was added to a THF (50 ml) solution of 7,7-dibromonorcarane (7.2 g, 28 mmol) at −95 °C over a period of 7 min. After stirring for 10 min heptanal (4.6 ml, 34 mmol) was added at −95 °C and the reaction mixture was stirred at −95 °C for 30 min, at −78 °C for 1 h, then at room temperature for 15 min. Work-up gave a crude β-bromo alcohol which was dissolved in THF (20 ml) and the mixture was stirred overnight with potassium *t*-butoxide (4.0 g, 35 mmol). Work-up followed by column chromatography (hexane–ether 10:1) gave *exo*-7-heptanoylnorcarane (4.7 g, 73% yield), which was dissovled in ethanol (10 ml) and treated under a nitrogen atmosphere at 0 °C with sodium borohydride (0.43 g, 11.2 mmol). Work-up and column chromatography (hexane–ether 10:1) gave *exo*-7-(1-hydroxyheptyl)norcarane (3.7 g, 57% yield from 7,7-dibromonorcarane), bp 83—85 °C (bath temp)/1 Torr; IR (neat): 3350, 1065, 1024 cm^{-1}; MS: *m/e* 192 (M^+-18). Found: C, 80.10; H, 12.58%. Calcd for $C_{14}H_{24}O$: C, 79.93; H, 12.46%.

The alcohol (0.22 g, 1.10 mmol) was mixed with pyridine (1 ml), and acetic anhydride (0.8 ml), and allowed to react at room temperature overnight. All the volatile material was then evaporated under reduced pressure and the residue was purified with short silica-gel column to give **1a** (0.26 g, 96% yield), bp 98—100 °C (bath temp)/1 Torr. ^{1}H-NMR (CCl_4): δ 1.4—2.1 (m+s (δ 1.92), 27H), 4.12 (dt, J=8, 5 Hz, 1H); IR (neat): 2940, 2870, 1730, 1450, 1365, 1235, 1020 cm^{-1}; MS: *m/e* (rel intensity) 210 (M^+-CH_2CO, 7), 192 (15), 135 (18), 125 (32), 121 (34), 79 (43), 67 (44), 43 (100). Found: C, 76.36; H, 11.38%. Calcd for $C_{16}H_{28}O_2$: C, 76.14; H, 11.18%.

The benzoate (**1b**) (1.22 g, 96% yield) was obtained by treating the alcohol (0.85 g, 4.0 mmol) with benzoyl chloride (0.49 ml, 4.2 mmol) and pyridine (2 ml) in dichloromethane (3 ml) at 0 °C for 1 h. Work-up and column chromatography (hexane–ether 10:1) gave **1b** as a colorless viscous oil, bp 165—170 °C (bath temp)/1 Torr. ^{1}H-NMR (CCl_4): δ 0.5—2.1 (m, 24H), 4.2—4.7 (m, 1H, CHOBz), 7.1—7.5 (m, 3H), 7.7—8.1 (m, 2H); IR (neat): 1715, 1605, 1587, 1110, 1025, 718 cm^{-1}; MS: *m/e* (rel intensity) 192 ($M^+-C_6H_5COOH$, 25), 135 (20), 122 (22), 105 (100), 94 (33), 79 (47), 77 (45), 41 (32). Found: C, 80.46; H, 9.74%. Calcd for $C_{21}H_{30}O_2$: C, 80.21; H, 9.62%.

Preparation of exo-*7-(1-Ethylheptyl)norcarane (**2a**). A Typical Procedure for the Reaction with Trialkylaluminium.* A hexane solution of triethylaluminium (1.84 M, 1.5 ml, 2.8 mmol) was added to a dichloromethane (3 ml) solution of **1a** (0.25 g, 1.0 mmol) at room temperature. The reaction mixture was stirred for 2 h and then quenched with satd. aq sodium sulfate solution (few drops). This was stirred vigorously, diluted with dichloromethane and filtered through a short column of anhydrous sodium sulfate. Concentration followed by column chromatography gave **2a** (0.20 g, 91% yield), bp 160—168 °C/16 Torr; ^{1}H-NMR (CCl_4): δ 0.0—2.1 (m); IR (neat): 3020, 1370, 1070, 968 cm^{-1}; MS: *m/e* (rel intensity) 222 (M^+, 10), 193 (12), 137 (24), 110 (53), 95 (82), 81 (91), 70 (98), 68 (100), 55 (85), 40 (86). Found: C, 86.37; H, 13.62%. Calcd for $C_{16}H_{30}$: C, 86.40; H, 13.60%.

Reaction with Diethyl(1-Alkynyl)aluminium. Butyllithium (1 mol) hexane solution was added to 1-alkyne (slightly more than 1 mol) at 0 °C. After 10 min diethylaluminium chloride (1 mol) hexane solution was added, stirring being carried out for 15 min at 0 °C. The reaction mixture was concentrated *in vacuo* below room temperature. The residue was dissolved in a specified solvent, and a substrate was added.

Tetraalkylaluminiumlithium. This reagent was prepared by mixing equimolar amounts of trialkylaluminium (hexane solution) and alkyllithium (ether solution) at 0 °C for 20 min. Substrate dissolved in ether was added to the solution.

exo-*7-(1-Hexyl-2-heptynyl)norcarane* (**2b**): Bp 135—139 °C (bath temp)/2 Torr; ^{1}H-NMR (CCl_4): δ 0.2—2.3 (m); IR (neat): 2950, 2880, 1450 cm^{-1}; MS: *m/e* (rel intensity) 274 (M^+, 1.4), 217 (23), 189 (32), 147 (32), 133 (46), 107 (54), 91 (79), 79 (79), 43 (60), 41 (100). Found: C, 87.54; H, 12.76%. Calcd for $C_{20}H_{34}$: C, 87.51; H, 12.49%.

Synthesis of exo-*6-(1-Acetoxyheptyl)bicyclo[3.1.0]hexane* (**3**). The procedure for the synthesis of **1a** was applied to the one of *exo*-6-heptanoylbicyclo[3.1.0]hexane, bp 80—83 °C (bath temp)/0.04 Torr. Found: C, 80.51; H, 11.73%. Calcd for $C_{13}H_{22}O$: C, 80.35; H, 11.41%.

Sodium borohydride reduction of this ketone followed by acetylation gave **3** quantitatively. Bp 87—91 °C (bath temp)/0.04 Torr; ^{1}H-NMR (CCl_4): δ 0.5—2.5 (m+S (δ 1.92), 25H), 3.9—4.3 (m, 1H); IR (neat): 3030, 1728, 1235, 1018 cm^{-1}; MS: *m/e* (rel intensity) 196 (M^+-CH_2CO, 4), 178 (9), 135 (9), 121 (20), 111 (22), 93 (33), 79 (42), 67 (38), 55 (24), 43 (100). Found: C, 75.63; H, 11.29%. Calcd for $C_{15}H_{26}O_2$: C, 75.58; H, 11.00%.

exo-*6-(1-Ethylheptyl)bicyclo[3.1.0]hexane* (**4**): ^{1}H-NMR (CCl_4): δ 0.1—1.9 (m); MS: *m/e* (rel intensity) 208 (M^+, 3), 189 (4), 140 (10), 123 (14), 111 (22), 95 (33), 81 (54), 70 (100), 55 (65), 41 (81). Due to the lack of sample confirmation of the structure was not carried out.

Preparation of (1S,2S)-2-Phenylcyclopropylmethyl Acetate (**9b**). Optical resolution of *trans*-2-phenylcyclopropanecarboxylic acid with quinine[20] gave a sample of $[\alpha]_D^{16}$ +375° (*c* 2.3, $CHCl_3$), estimated to be 98% optically pure based on the reported value $[\alpha]_D^{14}$ +381° ($CHCl_3$),[20] $[\alpha]_D^{20}$ +376° ($CHCl_3$).[21] The carboxylic acid was reduced with lithium aluminium hydride and acetylated with acetic anhydride to give **9b**, $[\alpha]_D^{19}$ +87.6° (*c* 2.0, $CHCl_3$) quantitatively. Bp 75—79 °C (bath temp)/0.03 Torr; ^{1}H-NMR (CCl_4): δ 1.0—2.0 (m, 4H), 2.04 (s, 3H), 4.04 (d, J=6.4 Hz, 2H), 7.0—7.4 (m, 5H); IR (neat): 3035, 1743, 1608, 1500, 1237, 1030, 757, 698 cm^{-1}; MS: *m/e* (rel intensity) 190 (M^+, 10), 149 (15), 130 (100), 115 (48). Found: C, 75.87; H, 7.42%. Calcd for $C_{12}H_{14}O_2$: C, 75.76; H, 7.42%.

trans-*7-(1-Acetoxyethyl)-2-phenylcyclopropane* (**7**). Methylmagnesium iodide (0.88 M ethereal solution, 0.99 ml, 0.87 mmol) was added to *trans*-2-phenylcyclopropanecarbaldehyde[22] (84 mg, 0.58 mmol) dissolved in ether (5 ml) at 0 °C, and the reaction mixture was stirred for 3 h, quenched with aq satd. ammonium chloride solution (10 ml) and extracted with dichloromethane. The combined dried organic phase was concentrated and the residue chromatographed with preparative TLC (dichloromethane) to give two diastereomers of *trans*-1-(1-hydroxyethyl)-2-phenylcyclopropane (R_f 0.4, 30 mg; R_f 0.3, 36 mg, 75% total yield). The more polar diastereomer gave ^{1}H-NMR (CCl_4): δ 0.7—1.4 (m, 3H), 1.26 (d, J=6.2 Hz, 3H), 1.5—2.0 (m, 1H), 2.08 (s, 1H), 3.1—3.7 (m, 1H), 6.7—7.4 (m, 5H). The less polar alcohol was acetylated with acetic anhydride (0.2 ml) and pyridine (0.2 ml) (r.t., 5 h) to give one diastereomer of **7** (38 mg, 95% yield). ^{1}H-NMR (CCl_4): δ 0.7—1.5 (m+d (δ 1.31, J=6.4 Hz, 6H), 1.8—2.2 (m+s (δ 1.97), 4H), 4.50 (quintet, J=6.4 Hz, 1H), 6.8—7.3 (m, 5H); IR (neat): 1735, 1605, 1503, 1372, 1242 cm^{-1}. The more polar alcohol was acetylated to give the other diastereomer of **7** (38 mg, 79% yield), bp 84—87 °C (bath temp)/0.05 Torr. ^{1}H-NMR (CCl_4): δ 0.8—1.6 (m+d(δ 1.33, J=6.4 Hz), 6H), 1.6—2.1 (m+s(δ 1.99), 4H), 4.99 (quintet, J=6.4 Hz, 1H), 6.8—7.3 (m, 5H); IR (neat): 1737, 1610, 1507, 1377, 1245 cm^{-1}; MS: *m/e* 204 (M^+). Found: C, 76.41; H, 8.01%. Calcd for $C_{13}H_{16}O_2$: C, 76.44; H, 7.90%.

Physical properties of the *cis* isomers of **7** (prepared from *cis*-2-phenylcyclopropanecarboxylic acid): bp 102—104 °C (bath temp)/0.09 Torr. Found: C, 76.71; H, 8.00%. Calcd for $C_{13}H_{16}O_2$: C, 76.44; H, 7.90%.

Each diastereomer was separated at the stage of alcohol (dichloromethane, R_f 0.6 and 0.4). The acetate of the less polar alcohol showed following spectra. ^{1}H-NMR (CCl_4): δ 0.7—1.6 (m+d (δ 1.23, J=6.2 Hz), 6H), 1.67 (s, 3H), 1.9—2.5 (m, 1H), 3.6—4.2 (m, 1H), 7.16 (s, 5H). IR (neat): 1733, 1605, 1503, 1370, 1245 cm^{-1}. The acetate of the more polar alcohol exhibited ^{1}H-NMR (CCl_4): δ 0.8—1.1 (m+d (δ 0.98, J=6.2 Hz), 6H), 1.9—2.4 (m+s (δ 1.92), 4H), 4.1—4.5 (m, 1H), 7.15 (s, 5H); IR (neat): 1730, 1605, 1503, 1370, 1245 cm^{-1}; MS: *m/e* (rel intensity) 204 (M^+, 4), 149 (34), 129 (100), 107 (70).

trans-*5-Phenyl-2-hexane* (**8a**): Bp 68—75 °C (bath temp)/1 Torr; ^{1}H-NMR (CCl_4): δ 1.22 (d, J=6.9 Hz, 1H), 1.60 (d, J=3.9 Hz, 3H), 2.1—2.4 (m, 2H), 2.67 (sextet, J=6.9 Hz, 1H), 5.2—5.4 (m, 2H), 7.0—7.3 (m, 5H); IR (neat): 3045, 1610, 1502, 968, 760, 704 cm^{-1}; MS: *m/e* (rel intensity) 160 (M^+, 6), 144 (2), 105 (100), 91 (5), 79 (5), 77 (5). Found: C, 90.17; H, 10.30%. Calcd for $C_{12}H_{16}$: C, 89.94; H, 10.06%.

trans-*5-Phenyl-2-heptene* (**8b**): Bp 81—88 °C (bath temp)/1 Torr; ^{1}H-NMR (CCl_4): δ 0.77 (t, J=7.5 Hz, 3H), 1.3—2.1 (m+d (δ 1.56, J=4 Hz), 5H), 2.1—2.7 (m, 3H), 5.2—5.5 (m, 2H), 6.9—7.3 (m, 5H); IR (neat): 3030, 1604, 1497, 966, 756, 698 cm^{-1}; MS: *m/e* (rel intensity) 174 (M^+, 3), 145 (1), 119 (56), 91 (100), 77 (5). Found: C, 89.58; H, 10.53%. Calcd for $C_{13}H_{18}$: C, 89.59; H, 10.41%.

trans-*7-Methyl-5-phenyl-2-octene* (**8c**): Bp 89—96 °C (bath temp)/1 Torr; ^{1}H-NMR (CCl_4): δ 0.7—1.0 (m, 6H), 1.1—1.7 (m+d (δ 1.52, J=4 Hz), 5H), 2.1—2.4 (m, 2H), 2.5—2.8 (m, 1H), 5.2—5.5 (m, 2H), 6.9—7.3 (m, 5H); IR (neat): 3040, 1606, 1500, 1468, 1456, 968, 760, 701 cm^{-1}; MS: *m/e* (rel intensity) 202 (M^+, 1), 147 (27), 105 (28), 91 (100), 77 (4). Found: C, 89.28; H, 10.81%. Calcd for $C_{15}H_{22}$: C, 89.04; H, 10.96%.

Preparation of endo- *and* exo-*7-Acetoxymethyl-1-phenylnorcarane* (**11a** *and* **11b**). Bromoform (0.36 ml, 4.1 mmol) was added to a mixture of 1-phenylcyclohexane (0.55 g, 3.5 mmol), potassium *t*-butoxide (4.3 mmol), and hexane (5 ml) at ice–salt temperature over a period of 30 min. After the addition was completed, the reaction mixture was warmed to room temperature, stirred for 1.5 h, then poured into water (20 ml). Extraction with dichloromethane (10 ml× 3 times) followed by the usual work-up and column chromatography gave 7,7-dibromo-1-phenylnorcarane (0.67 g, 58% yield; 79% yield based on the consumed olefin) as a viscous oil, bp 98—100 °C (bath temp)/0.03 Torr. ^{1}H-NMR (CCl_4): δ 1.2—1.7 (m, 5H), 1.9—2.5 (m, 4H), 7.24 (s, 5H); IR (neat): 3035, 1603, 1496, 1449, 753, 747, 697 cm^{-1}; MS: *m/e* (rel intensity) 264 (1.2), 262 (2.2), 260 (1.2), 251 (24), 249 (24), 169 (100), 141 (80), 126 (52), 115 (53), 91 (68). Found: C, 47.46; H, 4.20%. Calcd for $C_{13}H_{14}Br_2$: C, 47.31; H, 4.28%.

To a THF (10 ml) solution of the dibromonorcarane (0.33 g, 1.0 mmol) was added butyllithium (1.60 M hexane solution, 0.69 ml, 1.1 mmol) at −95 °C over a period of 5 min and the reaction mixture stirred for 20 min. Dry carbon dioxide gas was bubbled at −95 °C for 25 min into the reaction mixture which was then warmed to room temperature and acidified with dil hydrochloric acid. Work-up gave a crude bromo carboxylic acid (0.30 g, quantitative yield). ^{1}H-NMR ($CDCl_3$): δ 1.1—2.5 (m, 9H), 7.3—7.7 (m, 5H), 9.3—10.1 (br s, 1H); IR (neat): 3400, 2500, 1737, 1704, 1603, 1496, 1266, 760, 698 cm^{-1}; MS: *m/e* (rel intensity) 256 (1), 214 (77), 187 (28), 169 (79), 142 (83), 141

(77), 129 (60), 115 (70), 91 (100).

The bromocarboxylic acid (0.83 g, 2.8 mmol) was dissolved in THF (10 ml) and to this solution was added butyllithium (1.53 M hexane solution, 3.8 ml, 5.9 mmol) at −78 °C over a period of 8 min. The reaction mixture was stirred for 25 min, then treated with ethanol (1 ml) and warmed to room temperature. Acidification with dil hydrochloric acid followed by the work-up gave a crude carboxylic acid (0.50 g). Preparative TLC (hexane–ethyl acetate 2:1 double development) of the crude product (0.10 g) gave *endo*-carboxylic acid (R_f 0.6—0.7, 72 mg) and its *exo* isomer (R_f 0.5—0.6, 25 mg) in 80% total yield.

The *endo* isomer, 1-phenylnorcarane-*endo*-7-carboxylic acid (colorless prisms, mp 75—76 °C (hexane)), gave ^{1}H-NMR ($CDCl_3$): δ 1.1—2.4 (m, 10H), 7.41 (br s, 5H), 8.6—9.5 (m, 1H); IR (neat): 3400—2500, 3040, 1698, 1604, 760, 700 cm^{-1}; MS: *m/e* (rel intensity) 217 (4), 216 (M^+, 36), 198 (14), 171 (80), 129 (83), 115 (57), 91 (100). Found: C, 77.78; H, 7.44%. Calcd for $C_{14}H_{16}O_2$: C, 77.75; H, 7.46%.

The *exo* isomer, 1-phenylnorcarane-*exo*-7-carboxylic acid (colorless prisms, mp 139—140 °C (benzene)); ^{1}H-NMR ($CDCl_3$): δ 1.1—2.4 (m, 10H), 7.35 (br s, 5H), 8.0—9.0 (m, 1H); IR ($CHCl_3$): 3450—2500, 3060, 1693, 1604, 694 cm^{-1}; MS: *m/e* (rel intensity) 217 (M^+ +1, 7), 216 (M^+, 36), 198 (14), 171 (80), 129 (83), 115 (57), 91 (100). Found: C, 78.00; H, 7.37%. Calcd for $C_{14}H_{16}O_2$: C, 77.75; H, 7.46%.

The *exo* carboxylic acid (23 mg, 0.11 mmol) was reduced with lithium aluminium hydride (8.0 mg, 0.22 mmol) in ether (1 ml) to give *exo*-7-hydroxymethyl-1-phenylnorcarane, bp 93—98 °C (bath temp)/0.03 Torr; ^{1}H-NMR (CCl_4): δ 1.0—2.3 (m, 11H), 3.12 (dd, J=6.6, 3.0 Hz, 2H), 7.2 (br s, 5H); IR (neat): 3320, 2930, 1603, 1497, 1447, 1018, 759, 700 cm^{-1}; MS: *m/e* (rel intensity) 202 (M^+, 4), 184 (40), 171 (69), 141 (57), 129 (82), 115 (65), 91 (100). Found: C, 83.25; H, 9.20%. Calcd for $C_{14}H_{18}O$: C, 83.12; H, 8.97%.

The alcohol was acetylated with acetic anhydride (0.2 ml) and pyridine (0.2 ml) (r.t., 13 h) to give **11a** (27 mg, 97% yield for 2 steps). bp 108—110 °C (bath temp)/0.04 Torr; ^{1}H-NMR (CCl_4): δ 1.0—2.3 (m+s (δ 1.94), 13H), 3.56 (d, J=6.6 Hz, 2H), 7.17 (s, 5H); IR (neat): 3035, 1738, 1603, 1252, 1028, 960, 701 cm^{-1}; MS: *m/e* (rel intensity) 244 (M^+, 2), 184 (85), 141 (100), 129 (49), 115 (41), 91 (78). Found: C, 78.72; H, 8.24%. Calcd for $C_{16}H_{20}O_2$: C, 78.65; H, 8.25%.

The *endo* acetate **11b** was prepared similarly. *endo*-7-Hydroxymethyl-1-phenylnorcarane: bp 114—116 °C (bath temp)/0.06 Torr; ^{1}H-NMR (CCl_4): δ 1.1—2.3 (m, 11H), 3.8 (d, J=6.9 Hz, 2H), 6.9—7.3 (m, 5H); IR (neat): 3350, 3030, 1603, 1494, 1449, 1018, 749, 700 cm^{-1}; MS: *m/e* (rel intensity) 203 (0.8), 202 (M^+, 4), 184 (37), 171 (77), 141 (51), 129 (83), 91 (100). Found: C, 82.91; H, 8.93%. Calcd for $C_{14}H_{18}O$: C, 83.12; H, 8.97%.

Acetylation of the alcohol gave **11b**, bp 90—93 °C (bath temp)/0.04 Torr; ^{1}H-NMR (CCl_4): δ 1.2—2.1 (m+s (δ 2.06), 13H), 4.27 (d, J=5.4 Hz, 2H), 7.16 (br s, 5H); IR (neat): 3035, 1739, 1604, 1494, 1242, 1028, 759, 700 cm^{-1}; MS: *m/e* (rel intensity) 244 (M^+, 1), 184 (82), 141 (100), 91 (82). Found: C, 78.89; H, 8.47%. Calcd for $C_{16}H_{20}O_2$: C, 78.65; H, 8.25%.

1-Methyl-1-phenyl-2-vinylcyclohexane. This was obtained as a *ca.* 2:3 mixture of **12** and **13**: bp 117—123 °C (bath temp)/5 Torr; ^{1}H-NMR (CCl_4): δ 1.21 (s, 1.05 H, CH_3 for **12**), 1.32 (s, 1.95 H, CH_3 for **13**), 1.7—2.3 (m, 8H), 2.3—2.7 (m, 1H), 4.6—5.0 (m, 2H), 5.2—6.0 (m, 1H), 7.0—7.5 (m, 5H); IR (neat): 3070, 3040, 1638, 1602, 1497, 990, 908, 762, 697 cm^{-1}; MS: *m/e* (rel intensity) 200 (M^+, 29), 184 (45), 131 (56), 118 (100), 105 (64), 91 (45). Found: C, 89.67; H, 10.08%. Calcd for $C_{15}H_{20}$: C, 89.94; H, 10.06%.

Synthesis of trans-*1-(1-Acetoxy-3-phenylpropyl)-2-vinylcyclopropane (**14**).* The major isomer of 2-vinylcyclopropylmethanol[12] (93:7 isomeric mixture based on GLC (PEG 20 M, 5%, on Celite 545, 1.5 m, 72 °C)) was assigned to be *trans* on the basis of ^{13}C-NMR (CCl_4): chemical shift (δ from TMS) (intensity), 112.25 (100) and 115.36 (8), 140.76 (64) and 136.72 (5), 66.00 (100) and 62.88 (7). Pyridinium chlorochromate (0.63 g) oxidation (0 °C, 16 h) of this alcohol (0.100 g, 2.0 mmol) followed by the reaction (0 °C, 2.5 h) with 2-phenylethylmagnesium bromide (2.4 mmol) and preparative TLC (hexane–ether 5:1) gave two diastereomers of (1*R**,2*S**)-1-(1-hydroxy-3-phenylpropyl)-2-vinylcyclopropane (R_f 0.3, 136 mg; R_f 0.2, 131 mg) totally in 65% yield. The less polar alcohol showed ^{1}H-NMR (CCl_4): δ 0.5—0.7 (m, 2H), 0.8—1.1 (m, 1H), 1.2—1.5 (m, 1H), 1.7—2.1 (m, 3H), 2.72 (dt, J=8.7, 3.0 Hz, 2H), 3.00 (q, J=6.6 Hz, 1H), 4.7—5.6 (m, 3H), 7.13 (s, 5H). The more polar alcohol gave ^{1}H-NMR (CCl_4) spectrum: δ 0.4—1.0 (m, 3H), 1.1—1.4 (m, 1H), 1.7—2.0 (m, 3H), 2.70 (dt, J=8.1. 2.6 Hz, 2H), 2.98 (q, J=6.6 Hz, 1H), 4.7—5.6 (m, 3H), 7.14 (s, 5H).

Acetylation of the less polar alcohol gave one diastereomer of **14**, ^{1}H-NMR (CCl_4): δ 0.5—1.7 (m, 3H), 1.8—2.1 (m+s (δ 1.95), 5H), 2.4—2.7 (m, 2H), 4.2—4.5 (m, 1H), 4.7—5.6 (m, 3H), 7.0—7.3 (m, 5H). The more polar alcohol afforded the other diastereomer of **14**, ^{1}H-NMR (CCl_4): δ 0.4—1.4 (m, 3H), 1.8—2.1 (m+s (δ 1.95), 5H), 2.5—2.7 (m, 2H), 4.2—4.5 (m, 1H), 4.8—5.6 (m, 3H), 7.0—7.3 (m, 5H). Physical properties of the diastereomeric mixture of **17** were as follows: bp 124—127 °C (bath tem)/0.1 Torr; IR (neat): 3080, 3040, 1730, 1638, 1605, 1497, 1240, 1020, 700 cm^{-1}; MS: *m/e* (rel intensity) 224 (M^+, 4), 184 (11), 160 (8), 130 (52), 117 (34), 104 (35), 91 (100), 77 (25), 65 (20). Found: C, 78.44; H, 8.41%. Calcd for $C_{16}H_{20}O_2$: C, 78.65; H, 8.25%.

*(E)-3-Methyl-8-phenyl-1,5-octadiene (**15a**) and (E,E)-1-Phenyl-3,6-nonadiene (**16a**).* The reaction product formed an 83:17 mixture of **15a** and **16a**, bp 83—93 °C (bath temp)/1 Torr; ^{1}H-NMR (CCl_4): δ 0.93 (d, J=6.6 Hz, 3H), 1.8—2.4 (m, 5H), 2.5—2.8 (m, 2H), 4.7—5.1 (m, 2H), 5.3—5.9 (m, 3H), 7.0—7.3 (m, 5H). Preparative GLC separation (PEG 20 M, 30%, on celite 545, 3 m, 180 °C) gave pure components. The product **15a** showed practically the same ^{1}H-NMR spectrum and IR (994, 969, 910 cm^{-1}) as those of the mixture. MS: *m/e* 200 (M^+). Found: C, 89.86; H, 10.30%. Calcd for $C_{15}H_{20}$: C, 89.94; H, 10.06%. The geometry of the newly produced carbon-carbon double bond was inferred to be *trans* based on the IR absorptions at 969 cm^{-1}. The other product **16a** was characterized spectrometrically. MS: *m/e* 200 (M^+); IR (neat): 969 cm^{-1}; ^{1}H-NMR: (CCl_4): δ 0.97 (t, 3H), 1.7—2.5 (m, 6H), 2.5—2.8 (m, 2H), 5.2—5.6 (m, 4H), 7.10 (s, 5H). The IR absorption at 969 cm^{-1} was almost twice as intense as that of **16a** (based on the intensity of the phenyl absorptions), no absorptions near 800—750 cm^{-1} being detected. Consequently both of the C=C bonds in **16a** were assigned to be *trans*.

*(E)-3-Ethyl-8-phenyl-1,5-octadiene (**15b**) and (E,E)-1-Phenyl-3,6-decadiene (**16b**).* The reaction product formed an 83:17 mixture of **15b** and **16b**, bp 105—110 °C (bath temp)/1 Torr. Found: C, 89.49; H, 10.40%. Calcd for $C_{16}H_{22}$: C, 89.65; H, 10.35%. Each product was separated by

preparative GLC. The product **15b** showed IR (neat): 995, 970, 910, 745, 700 cm^{-1}; ^1H-NMR (CCl_4): δ 0.80 (t, J=7 Hz, 3H), 1.0—1.5 (m, 2H), 1.5—2.1 (m, 3H), 2.1—2.4 (m, 2H), 2.5—2.7 (distorted t, 2H), 4.7—5.0 (m, 2H), 5.2—5.7 (m, 3H), 7.0—7.3 (m, 5H); MS: *m/e* 214 (M^+). The isomer **16b** exhibited ^1H-NMR (CCl_4): δ 0.90 (t, J=6 Hz, 3H), 1.1—1.7 (m, 2H), 1.7—2.1 (m, 2H), 2.1—2.5 (m, 2H), 2.5—2.8 (m, 4H), 5.2—5.6 (m, 4H), 7.0—7.3 (m, 5H).

*(E)-3-Isobutyl-8-phenyl-1,5-octadiene (**15c**) and (E,E)-10-Methyl-1-phenyl-3,6-undecadiene (**16c**)*: Bp 89—93 °C (bath temp)/0.05 Torr; IR (neat): 3030, 1641, 1607, 1497, 994, 966, 909, 745, 700 cm^{-1}. Found: C, 89.16; H, 11.03%. Calcd for $C_{18}H_{26}$: C, 89.19; H, 10.81%. Preparative GLC separation gave pure **15c**: ^1H-NMR (CCl_4): δ 0.80 (d, J=6 Hz, 3H), 0.83 (d, J=6 Hz, 3H), 1.0—1.4 (m, 2H), 1.4—1.7 (m, 1H), 1.7—2.4 (m, 5H), 2.5—2.8 (m, 2H), 4.7—5.0 (m, 2H), 5.2—5.6 (m, 3H), 7.0—7.3 (m, 5H).

*Diethyl (2-Methyl-3-butenyl)propanedioate (**18a**)*: Bp 75—77 °C (bath temp)/0.05 Torr; ^1H-NMR (CCl_4): δ 1.04 (d, J=6.6 Hz, 3H), 1.29 (t, J=6.9 Hz, 6H), 1.7—1.9 (m, 2H), 1.9—2.2 (m, 1H), 3.21 (dd, J=8.4, 2.4 Hz, 1H), 4.10 and 4.12 (2q, J=6.9 Hz each, 4H), 4.8—5.1 (m, 2H), 5.4—5.8 (m, 1H); IR (neat): 3090, 1756, 1737, 1645, 1373, 1270, 1240, 1180, 1150, 1031, 998, 917 cm^{-1}; MS: *m/e* (rel intensity) 228 (M^+, 2), 183 (11), 160 (100), 137 (55), 109 (59), 81 (58), 68 (55). Found: C, 63.29; H, 8.95%. Calcd for $C_{12}H_{20}O_4$: C, 63.13; H, 8.83%.

Spectral data of **19a**[14a] are as follows. ^1H-NMR (CCl_4): δ 0.95 (t, J=7.8 Hz, 3H), 1.27 (t, J=6.9 Hz, 6H), 1.8—2.2 (m, 2H), 2.43 (dd, J=7.5, 6.3 Hz, 2H), 3.19 (t, J=7.5 Hz, 1H), 4.12 (q, J=6.9 Hz, 4H), 5.1—5.6 (m, 2H); IR (neat): 1755, 1739, 1372, 1152, 1024, 969 cm^{-1}; MS: *m/e* 228 (M^+).

*Diethyl(2-Ethyl-3-butenyl)propanedioate (**18b**)*: Bp 123—126 °C (bath temp)/0.2 Torr. ^1H-NMR (CCl_4): δ 0.87 (t, J=7.8 Hz, 3H), 1.29 (t, J=6.9 Hz, 6H), 1.2—2.2 (m, 5H), 3.1—3.4 (m, 1H), 4.11 and 4.13 (2q, J=6.9 Hz each, 4H), 4.9—5.1 (m, 2H), 5.2—5.7 (m, 1H); IR (neat): 3080, 1752, 1736, 1645, 1252, 1225, 1178, 1145, 1031, 998, 917 cm^{-1}; MS: *m/e* (rel intensity) 242 (M^+, 1), 213 (2), 197 (15), 160 (100), 151 (38), 132 (48), 123 (48), 95 (55), 67 (57). Found: C, 64.26; H, 9.30%. Calcd for $C_{13}H_{22}O_4$: C, 64.44; H, 9.15%.

Alternative Synthesis of Diethyl trans-*2-Hexenylpropanedioate (**19b**)*. Diethylcopperlithium (0.71 mmol) was allowed to react with **17** (50 mg, 0.24 mmol) in ether (2 ml) at −23 °C. Work-up and preparative TLC (hexane–ethyl acetate 5:1, R_f 0.4—0.5) gave a mixture (5:95 by GLC) of **18b** and **19b** (40 mg, 70% yield), bp 114—116 °C (bath temp)/0.1 Torr; ^1H-NMR (CCl_4): δ 0.87 (t, J=7.8 Hz, 3H), 1.2—1.5 (m+t (δ 1.29, J=6.9 Hz), 8H), 1.8—2.1 (m, 2H), 2.4—2.6 (distorted t, 2H), 3.21 (t, J=7.8 Hz, 1H), 4.13 (q, J=6.9 Hz, 4H), 5.3—5.5 (m, 2H); IR (neat); 1753, 1738, 1230, 1174, 1150, 1034, 969 cm^{-1}; MS: *m/e* (rel intensity) 242 (M^+, 7), 197 (11), 160 (75), 125 (100), 95 (69), 67 (55). Found: C, 64.37; H. 9.30%. Calcd for $C_{13}H_{22}O_4$: C, 64.44; H, 9.15%.

*Diethyl [2-(Phenylethynyl)-3-butenyl]propanedioate (**18c**)*. Bp 163—167 °C (bath temp)/0.15 Torr; ^1H-NMR (CCl_4): δ 1.28 (t, J=6.9 Hz, 6H), 1.9—2.3 (m, 2H), 4.2—4.5 (m, 1H), 4.51 (dd, J=8.4, 2.1 Hz, 1H), 4.13 and 4.16 (2q, J=6.9 Hz each, 4H), 5.1—5.5 (m, 2H), 5.6—6.0 (m, 1H), 7.2—7.5 (m, 5H); IR (neat): 2220, 1734, 1643, 1602, 1494, 1260, 1230, 1178, 1156, 1030, 990, 925, 759, 693 cm^{-1}; MS: *m/e* (rel intensity) 314 (M^+, 6), 285 (1), 241 (10), 240 (11), 213 (11), 211 (11), 195 (34), 167 (39), 154 (100), 141 (32), 115 (69). Found: C, 72.35; H, 7.10%. Calcd for $C_{19}H_{22}O_4$: C, 72.59; H, 7.05%.

*Synthesis of Ethyl 2-Oxo-*exo*-6-(*trans*-1-propenyl)bicyclo[3.1.0]hexane-1-carboxylate (**20**)*. Ethyl (*E,E*)-3-oxo-6,8-decadienoate (1.32 g, 6.3 mmol)[23] was treated with *p*-toluenesulfonyl azide (TsN_3) (1.26 g, 6.4 mmol) and triethylamine (0.88 ml, 6.4 mmol) in acetonitrile (25 ml) (r.t., 7 h). Work-up gave the α-diazo β-keto ester (IR: 2140, 1723, 1662 cm^{-1}). The diazo compound was dissolved in benzene (27 ml) and heated to reflux in the presence of copper(II) acetylacetonate (0.18 g) for 7 h. Work-up followed by column chromatography (hexane–ethyl acetate 10:1 to 5:1) gave **20** (1.13 g, 86% yield); bp 132—134 °C (bath temp)/0.09 Torr; ^1H-NMR (CCl_4): δ 1.29 (t, J=6.9 Hz, 3H, $COOCH_2C\underline{H}_3$), 1.70 (dd, J=6.3, 1.8 Hz, 3H, $=CH-C\underline{H}_3$), 1.9—2.3 (m, 5H), 2.4—2.5 (m, 1H), 4.14 (q, J=6.9 Hz, 2H, $COOC\underline{H}_2CH_3$); IR (neat): 3000, 1750, 1730, 1374, 1296, 1184, 1033, 967 cm^{-1}; MS: *m/e* (rel intensity) 208 (M^+, 22), 179 (27), 162 (68), 151 (40), 91 (73), 79 (100). Found: C, 69.32; H, 7.80%. Calcd for $C_{12}H_{16}O_3$: C, 69.21; H, 7.74%.

(2R,3R*)-2-Ethoxycarbonyl-3-[(S*)-*trans*-1-methyl-2-butenyl]-cyclopentanone (**21**) and Its Epimer (**22**)*: Bp 70—78 °C (bath temp)/0.15 Torr; ^1H-NMR (CCl_4): δ 1.03 and 0.98 (d, J=7.2 Hz, totally 3H, $CH-C\underline{H}_3$), 1.29 (t, J=6.9 Hz, 3H, $COOCH_2C\underline{H}_3$), 1.60 (d, J=5.4 Hz, 3H, $=CHC\underline{H}_3$), 1.8—2.6 (m, 6H), 2.71 and 2.76 (d, J=10.8 Hz, totally 1H), 4.08 and 4.10 (2q, J=6.9 Hz, totally 2H, $OC\underline{H}_2CH_3$), 5.0—5.4 (m, 2H); IR (neat): 3060, 1760, 1726, 1460, 1370, 1276, 1180, 970 cm^{-1}; MS: *m/e* (rel intensity) 224 (M^+, 2), 206 (9), 178 (18), 155 (42), 109 (55), 95 (36), 83 (40), 69 (100). Found: C, 69.34; H, 9.10%. Calcd for $C_{13}H_{20}O_3$: C, 69.61; H, 8.99%.

(2R,3R*)-2-Ethoxycarbonyl-3-(*trans*-3-methyl-1-butenyl)cyclopentanone (**23**)*: Bp 109—112 °C (bath temp)/0.03 Torr; ^1H-NMR (CCl_4): δ 0.99 (d, J=7.2 Hz, 6H, $CH(C\underline{H}_3)_2$), 1.27 (t, J=6.9 Hz, 3H, $OCH_2C\underline{H}_3$), 1.5—1.8 (m, 1H), 1.9—2.5 (m, 5H), 2.75 (d, J=11.1 Hz, 1H), 4.14 (q, J=6.9 Hz, 2H, $OC\underline{H}_2CH_3$), 5.1—5.5 (m, 2H); IR (neat): 1753, 1726, 1630, 1370, 967 cm^{-1}; MS: *m/e* (rel intensity) 224 (M^+, 1), 223 (1), 205 (1), 152 (30), 109 (24), 96 (56), 81 (71), 69 (100), 55 (55). Found: C, 69.67; H, 9.17%. Calcd for $C_{13}H_{20}O_3$: C, 69.61; H, 8.99%.

Synthesis of Ethyl exo-*6-Propyl-2-oxobicyclo[3.1.0]hexane-*1*-carboxylate (**25**)*. Ethyl acetoacetate (0.39 g, 3.0 mmol) dissolved in THF (5 ml) was added to sodium hydride (50% in oil, 0.16 g, 3.3 mmol) suspended in THF (10 ml) at 0 °C. After 15 min butyllithium hexane solution (1.70 M, 1.88 ml, 3.2 mmol) was added and the reaction mixture was stirred for 15 min at 0 °C. *Trans*-1-bromo-2-hexene (0.60 g, 3.7 mmol) dissolved in THF (4 ml) was then added and the reaction mixture was stirred for 50 min. Column chromatography (ethyl acetate–hexane 1:10) gave ethyl 3-oxo-trans-6-decenoate (0.34 g, 53% yield). IR (neat): 1750, 1723, 970 cm^{-1}; ^1H-NMR (CCl_4): δ 0.88 (t, J=6.9 Hz, 3H), 1.2—1.7 (m+t (δ 1.28 J=6.9 Hz, 5H), 1.8—2.6 (m, 6H), 3.28 (s, 2H), 4.16 (q, J=6.9 Hz, 2H), 5.3—5.5 (m, 2H).

The compound (0.34 g, 1.6 mmol) was converted into the diazo compound with TsN_3 (0.31 g, 1.6 mmol) and triethylamine (0.24 ml, 1.75 mmol) in acetonitrile (10 ml) (r.t., 15 h). The diazo compound was then heated in benzene (10 ml) with $Cu(acac)_2$ (49 mg) at reflux for 2.5 h. Concentration and column chromatography gave **25** (0.25 g, 74% yield), bp 124—127 °C (bath temp)/0.07 Torr; ^1H-NMR (CCl_4): δ 0.94 (t, J=6.3 Hz, 3H), 1.1—2.5 (m+t (δ 1.31, J=6.9 Hz), 13H), 4.16 (q, J=6.9 Hz, 2H); IR (neat): 3060, 1738, 1183, 1037 cm^{-1}. Found: C, 68.36; H, 8.69%. Calcd for $C_{12}H_{18}O_3$: C, 68.54; H, 8.63%.

*Reaction of **25** with Dimethylcopperlithium.* Compound **25** (27 mg, 0.13 mmol) was allowed to react at 0 °C for 30 min with dimethylcopperlithium generated from CuI (122 mg, 0.64 mmol), methyllithium (1.41 M ethereal solution, 0.64 ml, 1.28 mmol) and ether (3 ml). Preparative TLC (hexane–ethyl acetate 5:1, R_f 0.4—0.5) gave (2*R**,3*R**)-2-ethoxycarbonyl-3-[(*S**)-1-methylbutyl]cyclopentanone (**26**) (23 mg, 83% yield), bp 98—103 °C (bath temp)/1 Torr; ^{1}H-NMR (CCl_4): δ 0.75—1.8 (m+d (δ 0.91, J=7.2 Hz) +t (δ 1.28, J=6.9 Hz), totally 14H), 1.8—2.6 (m, 5H), 2.75 (d, J=11.1 Hz, 1H), 4.13 (q, J=6.9 Hz, 2H); IR (neat): 1757, 1726, 1184, 1116, 1024 cm^{-1}; MS: *m/e* (rel intensity) 226 (M^+, 3), 208 (3), 181 (6), 180 (6), 155 (19), 109 (44), 83 (100), 55 (96). Found: C, 69.14; H, 9.88%. Calcd for $C_{13}H_{22}O_3$: C, 68.99; H, 9.80%.

(2R,3R*)-2-Ethoxycarbonyl-3-[(R*)-1-methylbutyl]cyclopentanone (**28**).* This compound was prepared similarly starting with *cis*-1-bromo-2-hexene and characterized spectrometrically. ^{1}H-NMR (CCl_4): δ 0.8—2.5 (m+d (δ 0.89, J=6.3 Hz) +t (δ 1.30, J=6.9 Hz), totally 19H), 2.75 (d, J=11.1 Hz, 1H), 4.15 (q, J=6.9 Hz, 2H); IR (neat): 1757, 1727, 1249, 1180, 1113 cm^{-1}; MS: *m/e* (rel intensity) 226 (M^+, 5), 208 (3), 181 (14), 155 (41), 137 (40), 109 (100), 83 (45), 55 (70).

*Hydrogenation of a Mixture of **21** and **22**.* A mixture of **21** and **22** (56 mg, 0.25 mmol) dissolved in ethanol (5 ml) was stirred in the presence of 10% palladium on charcoal (*ca.* 10 mg) under a hydrogen atmosphere for 2 h. Removal of the catalyst by filtration, concentration, and preparative TLC (hexane–ethyl acetate 5:1, R_f 0.5) gave a mixture of dihydro derivatives of **26** and **28** (49 mg, 87% yield). The ^{1}H-NMR (CCl_4) was practically the same as that of the authentic specimen of **26** except for two doublets at δ 0.89 (attributable to that of **28**) and δ 0.91 (identical with the doublet of **26**). MS: *m/e* 226 (M^+).

Synthesis of Ethyl exo-*6-Methyl-2-oxobicyclo[3.1.0]hexane-1-carboxylate (**24**).* This compound was prepared from ethyl *trans*-3-oxo-6-octenoate[24] (0.62 g, 3.4 mmol) *via* diazotization (TsN_3 0.66 g, 3.4 mmol), Et_3N (0.47 ml, 3.4 mmol, CH_3CN (18 ml), r.t., 3 h) and decomposition (Cu(acac)$_2$ (34 mg), toluene (7 ml), reflux, 3 h) in 84% yield. Bp 99—103 °C/0.06 Torr; ^{1}H-NMR (CCl_4): δ 1.22 (d, J=6.3 Hz, 3H), 1.31 (t, J=6.9 Hz, 3H), 1.62 (dq, J=4.0, 6.3 Hz, 1H), 1.8—2.5 (m, 5H), 4.15 (q, J=6.9 Hz, 2H); IR (neat): 1732, 1193, 1034 cm^{-1}; MS: *m/e* (rel intensity) 182 (M^+, 28), 155 (42), 137 (92), 112 (89), 67 (100). Found: C, 65.72; H, 7.87%. Calcd for $C_{10}H_{14}O_3$: C, 65.91; H, 7.74%.

*Reaction of **24** with Trimethylaluminium.* A hexane solution of trimethylaluminium (1.0 M, 0.32 ml, 0.32 mmol) was added to a hexane (4 ml) solution of **24** (23 mg, 0.13 mmol) at 0 °C and the mixture was stirred for 1.5 h. Preparative TLC (hexane–ethyl acetate 2:1, double development, R_f 0.5—0.6) gave ethyl 2-hydroxy-2-*exo*-6-dimethylbicyclo[3.1.0]-hexane-1-carboxylate (18 mg, 72% yield), bp 88—90 °C (bath temp)/1 Torr; ^{1}H-NMR (CCl_4): δ 1.03 (d, J=5.9 Hz, 3H), 1.1—1.9 (m+t (δ 1.28, J=6.9 Hz) +s (δ 1.30), 12H), 2.2 (br s, 1H), 4.15 (q, J=6.9 Hz, 2H); IR (neat): 3500, 1714, 1117, 1050, 1010, 948 cm^{-1}; MS: *m/e* (rel intensity) 198 (M^+, 19), 183 (33), 137 (100), 124 (58). Found: C, 66.41; H, 9.14%. Calcd for $C_{11}H_{18}O_3$: C, 66.64; H, 9.15%.

Synthesis of Ethyl exo-*6-(*trans-*1-Propenyl)-3-oxa-2-oxo-bicyclo-[3.1.0]hexane-1-carboxylate (**29**).* Ethoxycarbonylacetyl chloride (1.82 g, 12.1 mmol) dissolved in ether (15 ml) was added at 0 °C to a mixture of (2*E*,4*E*)-2,4-hexadien-1-ol (0.99 g, 10.1 mmol) and pyridine (0.98 ml, 12.1 mmol) and the reaction mixture was stirred for 1.5 h. Work-up followed by column chromatography (hexane–ethyl acetate 10:1) gave ethyl (2*E*,4*E*)-2,4-hexadienyl propanedioate (1.96 g, 92% yield).

The mixed malonate (1.96 g, 9.3 mmol) was converted (Et_3N (1.42 ml), TsN_3 (1.82 g), CH_3CN (15 ml), r.t., 22 h) into the corresponding diazo compound which decomposed (Cu(acac)$_2$ (0.13 g), toluene (20 ml), reflux, 7 h). Work-up and column chromatography gave **29** (0.57 g, 63% yield), bp 154—157 °C (bath temp)/0.1 Torr; ^{1}H-NMR (CCl_4): δ 1.35 (t, J=6.9 Hz, 3H), 1.77 (dd, J=6.6, 2.1 Hz 3H) 2.21 (dd, J=8.7, 5.1 Hz, 1H), 2.61 (t, J=4.6 Hz, 1H), 4.1—4.4 (m+q (δ 4.23, J=6.9 Hz), 4H), 5.31 (dd, J=9.0, 15.6 Hz, 1H), 5.80 (dq, J=6.6, 15.6 Hz, 1H); IR (neat): 1785, 1723, 1184, 1051, 962 cm^{-1}; MS: *m/e* (rel intensity) 210 (M^+, 5), 164 (34), 137 (86), 93 (100), 79 (95). Found: C, 62.83; H. 6.67%. Calcd for $C_{11}H_{14}O_4$: C, 62.84; H, 6.71%.

(3R,4R*)-3-(Ethoxycarbonyl-4-[(S*)-*trans*-1-methyl-2-butenyl]oxolan-2-one (**30**)*: Bp 150—152 °C (bath temp)/0.09 Torr; ^{1}H-NMR (CCl_4): δ 1.00 (d, J=6.3 Hz, 3H), 1.30 (t, J=6.6 Hz, 3H), 1.63 (d, J=6.0 Hz, 3H), 1.9—2.4 (m, 1H), 2.6—3.1 (m, 1H), 3.13 (d, J=9.3 Hz, 1H), 3.87 (t, J=8.4 Hz, 1H), 4.1—4.6 (m+q (δ 4.18, J=6.6 Hz), 3H), 5.0—5.8 (m, 2H); IR (neat): 1782, 1736, 1146, 1017, 973 cm^{-1}; MS: *m/e* (rel intensity) 226 (M^+, 2), 181 (8), 180 (8), 157 (17), 107 (21), 69 (100). Found: C, 63.41; H, 8.13%. Calcd for $C_{12}H_{18}O_4$: C, 63.70; H, 8.02%.

*3-Ethoxycarbonyl-4-(*trans*-3-methyl-1-butenyl)oxolan-2-one (**31**)*: Bp 134—136 °C (bath temp)/0.1 Torr; ^{1}H-NMR (CCl_4): δ 1.01 (d, J=6.6 Hz, 3H), 1.31 (t, J=6.5 Hz, 3H), 2.24 (heptet, J=6.4 Hz, 1H), 3.20 (d, J=9.6 Hz, 1H), 3.2—3.7 (m, 1H), 3.89 (t, J=8.4 Hz, 1H), 4.1—4.5 (m, 1H), 4.23 (q, J=6.5 Hz, 2H), 5.28 (dd, J=15.8, 7.1 Hz, 1H), 5.65 (dd, J=15.8, 6.4 Hz, 1H); IR (neat): 1787, 1738, 1150, 1020, 973 cm^{-1}; MS: *m/e* (rel intensity) 226 (M^+, 5), 182 (22), 139 (56), 107 (89), 95 (100), 81 (77), 79 (79). Found: C, 63.45; H, 7.86%. Calcd for $C_{12}H_{18}O_4$: C, 63.70; H, 8.02%.

*Transformation of **21** into **32**.* The β-keto ester **21** (142 mg, 0.63 mmol) dissolved in THF (5 ml) was added at 0 °C to sodium hydride (50% in oil, 33 mg, 0.70 mmol) suspended in THF (2 ml) and the reaction mixture was stirred for 15 min. Diethyl phosphorochloridate (101 μl, 0.70 mmol) was added and the mixture was stirred for 30 min. Work-up and preparative TLC (hexane–ethyl acetate 10:1, R_f 0.6—0.7) gave ethyl (5*R**)-2-methyl-5-[(*S**)-*trans*-1-methyl-2-butenyl]cyclopentene-1-carboxylate (**32**) (96 mg, 69% yield), bp 107—110 °C (bath temp)/0.08 Torr; ^{1}H-NMR (CCl_4): δ 0.81 (d, J=7.8 Hz, 3H), 1.30 (t, J=6.9 Hz, 3H), 1.6—2.0 (m+d (δ 1.65, J=3.9 Hz), 5H), 2.04 (br s, 3H), 2.2—2.8 (m, 3H), 2.8—3.2 (m, 1H), 4.12 (q, J=6.9 Hz, 2H), 5.2—5.4 (m, 2H); IR (neat): 1714, 1648, 1632, 1098, 970 cm^{-1}; MS: *m/e* (rel intensity) 222 (M^+, 6), 179 (14), 177 (15), 153 (70), 107 (74), 69 (100). Found: C, 75.42; H, 10.04%. Calcd for $C_{14}H_{22}O_2$: C, 75.63; H, 9.97%.

*Transformation of **32** into Neonepetalactone (**34**).* Ozone was bubbled into a methanol (1 ml) solution of **32** (40 mg, 0.18 mmol) at −78 °C under monitoring by TLC. When all the starting material was consumed, sodium borohydride (*ca.* 20 mg) was added to the reaction mixture, which was then allowed to react at room temperature. After most of the methanol was removed *in vacuo*, the residue was treated with brine and extracted with dichloromethane. Concentration of the extract followed by preparative TLC (hexane–ethyl acetate 2:1, R_f 0.3) gave an alcohol **33** (8 mg, 21%

yield). ^{1}H-NMR (CCl_4): δ 0.80 (d, J=6.3 Hz, 3H), 1.33 (t, J=6.9 Hz, 3H), 1.5—2.2 (m+br s (δ 2.09), 7H), 2.2—2.6 (m, 2H), 2.9—3.3 (m, 1H), 3.36 (d, J=6.0 Hz, 2H), 4.17 (q, J=6.9 Hz, 2H); IR (neat): 3450, 1705, 1108, 1054 cm^{-1}; MS: *m/e* (rel intensity) 212 (M^+, 2), 194 (4), 166 (30), 107 (44), 79 (100).

The alcohol (8 mg) was mixed with pyridinium *p*-toluenesulfonate (3 mg) in dichloromethane (1 ml) and the mixture heated to reflux for 7 h. Concentration and preparative TLC (hexane–ethyl acetate 2:1, R_f 0.7) gave neonepetalactone (**34**) (2 mg, 35% yield) having spectra consistent with the recorded ones. ^{1}H-NMR (CCl_4): δ 0.96 (d, J=6.9 Hz, 3H), 1.2—1.8 (m, 4H), 2.9 (br s, 3H), 2.3—2.7 (m, 2H), 3.78 (dd, J=12.4, 10.7 Hz, 1H), 4.17 (dd, J=4.7, 10.7 Hz, 1H); IR (CCl_4): 1722, 1645, 1244, 1197, 1105, 1056 cm^{-1}; MS: *m/e* (rel intensity) 166 (M^+, 46), 151 (16), 124 (61), 79 (100).

References

1) E. Negishi, "Organometallics in Organic Synthesis," John Wiley and Sons, New York (1980), Vol. 1.

2) H. Yamamoto and H. Nozaki, *Angew. Chem. Int. Ed.*, **17**, 169 (1978).

3) D. Tsunemoto and K. Kondo, *J. Synth. Org. Chem. (Japan)*, **35**, 1070 (1977).

4) M. Julia, S. Julia, and R. Guegan, *Bull. Soc. Chim. Fr.*, **1960**, 1072; M. Julia, S. Julia, and S. Y. Tchen, *ibid.*, **1961**, 1849.

5) W. S. Johnson, T. T. Li, D. J. Faulkner, and S. F. Campbell, *J. Am. Chem. Soc.*, **90**, 6225 (1968); W. S. Johnson, M. F. Semmelhack, M. U. S. Sultanbawa, and L. A. Dolak, *ibid.*, **90**, 2994 (1968).

6) H. Nakamura, H. Yamamoto, and H. Nozaki, *Tetrahedron Lett.*, **1973**, 111.

7) T. Hiyama, S. Takehara, K. Kitatani, and H. Nozaki, *Tetrahedron Lett.*, **1974**, 3295; M. Braun, R. Dammann, and D. Seebach, *Chem. Ber.*, **108**, 2368 (1975).

8) Part of this article was published in a preliminary form: A Itoh, K. Oshima, S. Sasaki, H. Yamamoto, T. Hiyama, and H. Nozaki, *Tetrahedron Lett.*, **1979**, 4751.

9) Similar reactivity preference has been observed: G. "The Use of Aluminium Alkyls in Organic Synthesis," ed by G. Bruno, Ethyl Corp., Baton Rouge, La., U.S.A. (1973), Supplement (1969—1972), p. 90; K. Takai, K. Oshima, and H. Nozaki, *Tetrahedron Lett.*, **21**, 2531 (1980).

10) A. Itoh, S. Ozawa, K. Oshima, S. Sasaki, H. Yamamoto, T. Hiyama, and H. Nozaki, *Bull. Chem. Soc. Jpn.*, **53**, 2357 (1980).

11) L. M. Jackman and S. Sternhell, "Applications of Nuclear Magnetic Resonance Spectroscopy in Organic Chemistry," Pergamon Press, Oxford (1969), p. 83.

12) M. Apparu and M. Barrelle, *Tetrahedron*, **34**, 1691 (1978).

13) S. Danishefsky, *Acc. Chem. Res.*, **12**, 66 (1979).

14) a) P. A. Grieco and R. Finkelhor, *J. Org. Chem.*, **38**, 2100 (1973); b) G. Daviaud and Ph. Miginiac, *Tetrahedron Lett.*, **1972**, 997; c) N. Miyaura, M. Itoh, N. Sasaki, and A. Suzuki, *Synthesis*, **1975**, 317; N. Miyaura, M. Itoh, and A. Suzuki, *Tetrahedron Lett.*, **1976**, 255.

15) B. M. Trost, D. F. Taber, and J. B. Alper, *Tetrahedron Lett.*, **1976**, 3857.

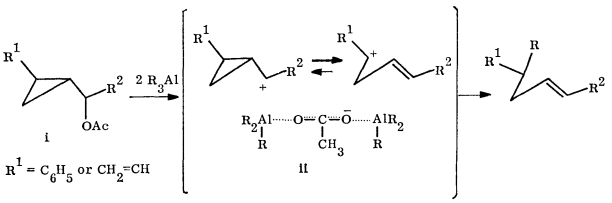

16) The reaction of **7**, **9**, **11a,b**, and **14** with trialkylaluminium can be understood in terms of the tight ion pairs shown in the bracket below. Trialkylaluminum dimer interacts with the leaving acetoxyl group of i to form fairly less nucleophilic complex ii whose R group on aluminium atom is in turn activated to some extent to attack an electron-deficient center. The cyclopropylmethyl cation generated undergoes rearrangement to the homoallyl cation stabilized by a phenyl or vinyl group. Thus, the overall reaction is reminiscent of an S_N1 type reaction[10] which proceeds in the absence of a polarizing solvent.

In contrast, the homoconjugate 1,5-addition to activated vinylcyclopropanes is explained by an S_N2-like mechanism illustrated in iii. Use of more than two mol of trialkylaluminium reagent as well as the presence of two activating carbonyls and a vinyl group in the substrate is essential for the reaction. Trialkylaluminium acid should possibly coordinate both of the carbonyls. The cyclopropane C–C bond is thus loosened and cleaved by the attack of an alkyl anion liberated from the third molecule of trialkylaluminium possibly coordinated on another substrate molecule.

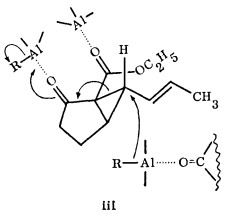

The 1,7-homoconjugate addition may be explained by an electron-transfer mechanism as discussed in the conjugate addition of lithium organocuprate.[25]

17) T. Sakan, S. Isoe, S. B. Hyeon, R. Katsumura, T. Maeda, J. Wolinsky, D. Dickerson, M. Slabaugh, and D. Nelson, *Tetrahedron Lett.*, **1965**, 4097.

18) K. Kon and S. Isoe, *Tetrahedron Lett.*, **21**, 3399 (1980); J. Meinwald and T. H. Jones, *J. Am. Chem. Soc.*, **100**, 1883 (1978); J. Meinwald, T. H. Jones, T. Eisner, and K. Hicks, *Proc. Nat. Acad. Sci. U.S.A.*, **74**, 2189 (1977); T. H. Jones, M. S. Blum, and H. M. Fales, *Tetrahedron Lett.*, **21**, 1701 (1980).

19) D. A. Evans and J. V. Nelson, *J. Am. Chem. Soc.*, **102**, 774 (1980) and references cited therein.

20) Y. Inoue, T. Sugita, and H. Walborsky, *Tetrahedron*, **20**, 1695 (1964).

21) T. Aratani, Y. Nakanishi, and H. Nozaki, *Tetrahedron*, **26**, 1675 (1970).

22) S. Pierre and W. Joseph, *Bull. Soc. Chim. Fr.*, **1971**, 2268.

23) G. Beck and F. Henseleit, *Chem. Ber.*, **104**, 21 (1971).

24) L. Crombie, A. J. B. Edgar, S. H. Harper, M. W. Lowe, and D. Thompson, *J. Chem. Soc.*, **1950**, 3552.

25) H. O. House, *Acc. Chem. Res.*, **9**, 59 (1976).

Insertion of Carbon Monoxide into Nickel-Alkyl Bonds of Monoalkyl- and Dialkylnickel(II) Complexes, $NiR(Y)L_2$ and NiR_2L_2. Preparation of $Ni(COR)(Y)L_2$ from $NiR(Y)L_2$ and Selective Formation of Ketone, Diketone, and Aldehyde from NiR_2L_2

Takakazu YAMAMOTO,* Teiji KOHARA, and Akio YAMAMOTO
Research Laboratory of Resources Utilization, Tokyo Institute of Technology,
4259 *Nagatsuta, Midori-ku, Yokohama* 227

(Received January 22, 1981)

Reactions of monoalkylnickel(II) complexes, $NiR(Y)L_2$ (R=CH_3, C_2H_5; Y=Cl, suc(succinimido), pht-(phthalimido), OC_6H_4-*p*-CN; L=1/2 bpy (2,2′-bipyridine), PEt_3 (triethylphosphine)), with CO afford monoacylnickel(II) complexes, $Ni(COR)(Y)L_2$, which are characterized by elemental analysis and spectroscopies (IR and NMR). Reactions of the acylnickel(II) complexes with alcohols and aniline give the corresponding esters and amides, respectively. Exposure of $Ni(COR)(Y)L_2$ to dry air leads to oxidation of RCO to a RCOO ligand giving a complex formulated as $Ni(OCOR)(Y)L_2$. Reactions of dimethylnickel(II) complexes, $Ni(CH_3)_2L_2$ (L=1/2 bpy, PEt_3, 1/2 dpe (1,2-bis(diphenylphosphino)ethane, 1/2 dpp (1,3-bis(diphenylphosphino)propane), with carbon monoxide afford acetone and/or 2,3-butanedione in medium to high yields, the acetone/2,3-butanedione ratio varying with the ligand L, reaction temperature, and additives such as maleic anhydride and triphenylphosphine. Generally the acetone/2,3-butanedione ratio decreases with increase in thermal stabilities of $Ni(CH_3)_2L_2$. $Ni(C_2H_5)_2$(bpy) and $Ni(n\text{-}C_3H_7)_2$(bpy) give 3-pentanone and 4-heptanone, respectively, on treating them with CO, whereas $Ni(C_2H_5)_2$(dpe) produces C_2H_5CHO and C_2H_4.

Insertion of carbon monoxide into transition metal-carbon bond constitutes a crucial step in industrially important processes.[1] It is known that transition metal (Ni, Pd, *etc.*) compounds catalyze carbonylation of unsaturated compounds and organic halides in the presence of alcohols and amines to afford esters and amides, respectively,[1,2] and a mechanism involving nucleophilic attack of alcohol or amine to an acyltransition metal intermediate is sometimes proposed for the reactions. However, in contrast to the well explored catalytic reactions, fundamental studies of the carbonylation process dealing with well characterized transition metal alkyl compounds are still limited[3] and chemical reactivities of acyltransition metal complexes prepared by the CO insertion reaction have not been well explored.

We have carried out reactions of isolated monoalkyl- and dialkylnickel(II) complexes, $NiR(Y)L_2$ and NiR_2L_2, with CO to find out that several isolable acylnickel(II) complexes are obtained in the reactions of the monoalkylnickel complexes with CO, whereas the reaction of NiR_2L_2 with CO gives ketone, diketone, and/or aldehyde. The paper deals with the results of the reactions of $NiR(Y)L_2$ and NiR_2L_2 with CO and chemical behavior of $Ni(COR)(Y)L_2$ with compounds such as alcohols and amines. A part of the results given in this paper has been reported in a communication form.[4]

Results and Discussion

I. Preparation of Acylnickel(II) Complexes. The following five acylnickel complexes can be prepared by reactions of the $NiR(Y)L_2$ type complexes[5] with CO. Although several acetylnickel(II) complexes have been prepared by several groups of researchers,[6,7] the propionylnickel complex has only one precedent.[7a] The acylnickel(II) complexes having the Cl, suc, or pht ligand can be prepared under a wide range of reaction conditions, whereas the complexes with the OC_6H_4-*p*-CN ligand can be prepared only by 1:1 reactions of $NiR(OC_6H_4\text{-}p\text{-}CN)$(bpy) with CO at low temperature (−78 °C). Carrying out the reaction of $NiR(OC_6H_4\text{-}p\text{-}CN)$(bpy) at −78 °C or above in the presence of excess CO leads to the formation of $RCOOC_6H_4$-*p*-CN and $Ni(CO)_2$(bpy), suggesting that coordination of CO to **3** and **4** enhances reductive coupling of the RCO and OC_6H_4-*p*-CN groups. In fact, **3** and **4** once isolated have considerably high stabilities in organic solvents even at room temperature, whereas addition of CO to the solution of **3** or **4** leads to rapid formation of $RCOOC_6H_4$-*p*-CN and $Ni(CO)_2$(bpy) almost quantitatively even at −78 °C,

$$NiR(Y)L_2 + CO \longrightarrow Ni(COR)(Y)L_2 \quad (1)$$

	R	Y	L
1	Et	Cl	1/2 bpy
2	Et	suc	1/2 bpy
3	Et	OC_6H_4-*p*-CN	1/2 bpy
4	Me	OC_6H_4-*p*-CN	1/2 bpy
5	Me	pht	PEt_3

Me=CH_3, Et=C_2H_5, suc=succinimido, pht=phthalimido, bpy=2,2′-bipyridine

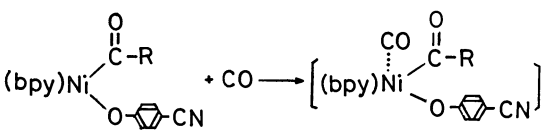

$$\xrightarrow{+CO} RCOOC_6H_4\text{-}p\text{-}CN + Ni(CO)_2(bpy). \quad (2)$$

Complexes **1**, **2**, and **5** are stable in solutions and do not undergo the reductive coupling to produce RCOY even in the presence of excess CO, presumably due to high stabilities of the Ni–Cl, Ni–suc, and Ni–pht bonds.

The reductive coupling is considered to proceed through a concerted mecahnism involving simultaneous loosening of the Ni–COR and Ni–Y bonds and overlapping of bonding orbitals of the COR and Y groups. When there is a difference in bond energies

TABLE 1. IR, NMR, AND VISIBLE SPECTROSCOPIC DATA OF Ni(COR)(Y)L_2

Complex	IR[a] $\tilde{\nu}$/cm^{-1}	^{1}H-NMR δ/ppm[b] COR[d]	Y	L	^{31}P-NMR[b] δ/ppm	^{13}C{^{1}H}-NMR[b] δ/ppm	λ_{max}[c] nm
Ni(COEt)(Cl)(bpy) **1**	2950, 1655*, 1595, 1440, 880, 765	1.14(CH_3), 3.19(CH_2)		7.3(2H, m), 7.9(5H, m), 8.7(1H, d, 5 Hz)			503
Ni(COEt)(suc)(bpy) **2**	1620*, 1445, 1345, 1220, 770	0.98(CH_3), 3.11(CH_2)	2.60(s, CH_2)	7.1—8.2			480
Ni(COEt)(OC_6H_4-*p*-CN)(bpy) **3**	2200, 1650*, 1580, 1320, 1145, 770	0.99(CH_3), 3.04(CH_2)		7.2—8.6 (Y + L)			482
Ni(COMe)(OC_6H_4-*p*-CN)(bpy) **4**	2190, 1645*, 1580, 1330, 1155, 765	2.42(CH_3)		7.2—8.6 (Y + L)			488
Ni(COMe)(pht)-(PEt_3)$_2$ **5**	2960, 1650*, 1600, 1300, 1120, 760, 535	2.65(CH_3)	7.03(2H, dd, 5 Hz and 7 Hz), 7.72(2H, dd, 5 Hz and 7 Hz)	0.98(18H, qui, 7 Hz, CH_3), 1.3(12H, m, CH_2)	32.5(s) (in C_6D_6)	7.84(s, PCH_2-CH_3), 13.46(s, P-CH_2), 32.47(t, 8 Hz, $COCH_3$), 121.16, 132.22, 138.10 (aromatic ring of pht), 180.51(d, 16 Hz, -N(CO)$_2$), 258.31(t, 22 Hz, COMe)	

a) In KBr. The band with an asterisk is assigned to ν(C=O) of the RCO ligand. b) s=singlet, d=doublet, dd=double doublet, qui=quintet, m=multiplet. Chemical shifts of ^{31}P- and ^{13}C{^{1}H}-NMR spectra are referred to external PEt_3 and internal TMS, respectively (downfield positive). Solvents for ^{1}H-NMR: CD_2Cl_2 for **1** and **2**, acetone-d_6 for **3** and **4**, and C_6D_6 for **5**. The solvent for ^{13}C{^{1}H}-NMR: THF-d_8. c) Measured in THF. d) The CH_3 and CH_2 groups of COEt give rise to a triplet and a quartet, respectively, with the J value of 7—8 Hz.

between the Ni–COR and Ni–Y bonds, however, the ease of reductive elimination may be critically dependent on the ease of activation of the stronger bond, Ni–Y in this case. If the Ni–Y bond is too stable, the complex may be decomposed by other route than reductive elimination.

Reactions of NiMe(OC_6H_5)(bpy),[5] NiEt(OC_6H_5)(bpy),[8] and NiMe(OC_6H_4-*p*-C_6H_5)(PEt_3)$_2$[5] with an equimolar amount of CO at −78 °C gave nickel carbonyl complexes, Ni(CO)$_2L_2$, and the corresponding esters, $CH_3COOC_6H_5$, $C_2H_5COOC_6H_5$, and $CH_3COOC_6H_4$-*p*-C_6H_5, respectively, but the acylnickel(II) complexes were not obtained in these reactions. The Ni–OC_6H_5 and Ni–OC_6H_4-*p*-C_6H_5 bonds in these complexes are expected to have lower stabilities than the Ni–OC_6H_4-*p*-CN bonds in NiR(OC_6H_4-*p*-CN)(bpy) since an OR group generally binds to metals more strongly when the electron-withdrawing ability of the OR group increases. This effect may account for the successful isolation of the *p*-cyanophenoxo(acyl)-nickel complexes **3** and **4** and failure of isolation of the supposed intermediates Ni(acyl)(OC_6H_5)L_2 and Ni(acyl)(OC_6H_4-*p*-C_6H_5)L_2 which may reductively eliminate esters even in the absence of excess CO and at −78 °C.

The isolated acylnickel(II) complexes **1**—**5** have relatively high thermal stabilities but are sensitive to air to give carboxylatonickel(II) complexes (*vide infra*).

IR, NMR, and Visible Spectroscopic Data. Table 1 summarizes spectroscopic data of the complexes. IR spectra of the acylnickel(II) complexes show ν(C=O) bands at about 1650 cm^{-1} which may be compared with the ν(C=O) bands of reported acylnickel(II) complexes observed in the region of 1680 to 1625 cm^{-1}.[6,7]

In the ^{1}H-NMR spectrum, the CH_3 signal of the Et ligands in the ethyl complexes NiEt(Y)L_2[5] is only slightly shifted by the CO insertion into the Ni–Et bond, whereas the CH_2 signals of the Et ligand is considerably shifted to lower field. The acetyl complexes, **4** and **5**, give rise to signals of $COCH_3$ in a region where the signal of $COCH_3$ of acetyltransition metal complexes is usually observed.[1,3,6,7] The complexes are stable in solutions and signals of decarbonylated complexes (NiR(Y)L_2) are not observed at room temperature.

^{13}C{^{1}H}-NMR spectrum of **5** shows a triplet (J=

Table 2. Reactivities of acylnickel complexes

No.	Complex	Reactant[a] mol/complex	Solvent	Temp °C	Time h	Products (mol%/complex)
I.	Thermolysis					
1	**1**		none	200	5	CO(27), C_2H_4(17), C_2H_6(7), EtCOEt(6)
2	**1**		toluene	80	3	CO(27), C_2H_4(13), C_2H_6(4), EtCOEt(13)
3	**2**		none	200	5	CO(31), C_2H_4(34), C_2H_6(19), EtCOEt(2)
4	**3**		toluene	80—90	1	CO(17), C_2H_4(12), C_2H_6(4), $EtCOOC_6H_4$-*p*-CN(12)
5	**4**		toluene	80—85	1	CO(43), CH_4(4),$MeCOOC_6H_4$-*p*-CN(3)
6	**5**		*p*-xylene	90	2	CO(10), MeCOMe(12)
II.	Reactions with alcohols or aniline					
7	**1**	MeOH(ex)	none	50—60	2	EtCOOMe(14)
8[b]	**1**	MeOH(ex)	none	r.t.	8	EtCOOMe(92)
9[b]	**1**	*i*-PrOH(ex)	none	r.t.	24	EtCOO-*i*-Pr(72)
10[b]	**2**	MeOH(ex)	none	r.t.	9	EtCOOMe(82)
11[b]	**2**	EtOH(ex)	none	r.t.	1	EtCOOEt(73)
12[b]	**2**	*n*-PrOH(ex)	none	r.t.	1	EtCOO-*n*-Pr(76)
13[b]	**2**	*i*-PrOH(ex)	none	r.t.	1	EtCOO-*i*-Pr(78)
14	**3**	MeOH(ex)	none	r.t.	24	EtCOOMe(30)
15	**1**	$PhNH_2$(ex)	none	r.t.	48	EtCOONHPh(41)
16[b]	**1**	$PhNH_2$(ex)	none	r.t.	24	EtCOONHPh(40)
17	**2**	$PhNH_2$(ex)	none	r.t.	24	EtCOONHPh(53), succinimide(56)
18	**4**	$PhNH_2$(ex)	none	r.t.	1	MeCOONHPh(45)
III.	Reactions with O_2[c]					
19	**1**	O_2(1)	none	r.t.	48	EtCOOH(63), $NiCl_2$(bpy)(100)
20	**1**	O_2(1.2)	benzene	r.t.	48	EtCOOH(82)
21	**2**	O_2(ex)	none	r.t.	15	EtCOOH(56), succinimide(45)
22	**2**	O_2(1.1)	benzene	r.t.	24	EtCOOH(75), succinimide(56)
23	**4**	O_2(1.3)	benzene	r.t.	24	MeCOOH(100)
IV.	Reactions with π-acids					
24	**3**	MAH(3.8)	THF	r.t.	24	$EtCOOC_6H_4$-*p*-CN(62), Ni(MAH)$_2$(bpy)(90)
25	**3**	EMA(ex)	none	r.t.	6	$EtCOOC_6H_4$-*p*-CN(31)
26	**5**	MAH(ex)	THF	r.t.	4	$MeCOOC_6H_4$-*p*-CN(70), Ni(MAH)$_2$(bpy)(77)
27	**3**	CO(ex)	THF	r.t.	1	$EtCOOC_6H_4$-*p*-CN(79), Ni(CO)$_2$(bpy)(42)
V.	Reactions with NiR_2(bpy)					
28[d]	**5**	$NiMe_2$(bpy) (1.0)	C_6D_6	40	72	MeCOMe(33), NiMe(pht)$(PEt_3)_2$(100), Ni(CO)$_2$(bpy)[e]
29	**5**	$NiEt_2$(bpy) (1.0)	C_6D_6	40	24	EtCOEt(12), MeCOEt(2), NiMe(pht)$(PEt_3)_2$[e] Ni(CO)$_2$(bpy)[e]

a) ex=excess, Me=CH_3, Et=C_2H_5, Ph=C_6H_5, Pr=C_3H_7, MAH=maleic anhydride, EMA=ethyl methacrylate. b) The reaction was carried out under an atmosphere of CO. c) Dry air (not pure O_2) was added. The last column shows compounds recovered after treating the produced complex with dry HCl. d) Followed by NMR. e) Formation of the complex was confirmed by IR but the amount not measured.

22 Hz) at 258.31 ppm assignable to the CO carbon of the $COCH_3$ ligand, the triplet pattern indicating that **5** has a *trans* configuration. The *trans* configuration is consistent with an observation of an only one sharp singlet in ^{31}P-NMR spectrum of **5**.

Visible spectra of the bpy-coordinated complexes, **1**—**4**, in THF show Ni→bpy CT-band ($\varepsilon \fallingdotseq 3\times10^3$) at 480—503 nm, the λ_{max} values being shifted to shorter wave length by 20—30 nm from the starting NiR(Y)-(bpy) type complexes.[5] The shift suggests that the electronegativity of Ni is increased by replacing the R ligand with the COR ligand.[9]

Chemical Reactivities of Ni(COR)(Y)L_2. Products of thermolysis and reactions of NiR(Y)L_2 with various compounds are summarized in Table 2.

Thermolysis: Although the acylnickel(II) complexes have fairly high thermal stabilities, they undergo decarbonylation reaction at 100—150 °C in solid to liberate CO and a mixture of C_2H_4 and C_2H_6 from the propionyl complexes or CH_4 from the acetyl complex (Nos. 1—6 in Table 2). Formation of ester in the thermolysis of **3** and **4** indicates occurrence of the reductive coupling of the RCO and OC_6H_4-*p*-CN groups at the elevated temperature. Thermolyses of **1**, **2**, and **5** which have stronger Ni–Y bonds, on the other hand, do not give the reductive coupling product RCOY even at the elevated temperature, but they afford ketone RCOR presumably through a coupling reaction between Ni(COR)(Y)L_2 and NiR(Y)L_n formed in the thermolysis. The thermolysis of Ni(COR)-

TABLE 3. REACTIONS OF NiR_2L_2 WITH CO[a]

No.	Complex	Dp[b] °C	Additive (mol/Ni)	Solvent	Temp °C	Time h	Products (% yield/Ni) RCOCOR	RCOR	RCHO	R(-H)
I.	Reactions at −78 °C (effects of R and L).									
1	**6** (R=Me, L_2=bpy)	160	none	Et_2O	−78	24	89	0	0	0
2	**6**		none	THF	−78	24	76	0	0	0
3	**7** (R=Me, L_2=dpe)	140	none	Et_2O	−78	12	76	4	0	0
4	**7**		none	toluene	−78	6.5	48	25	0	0
5	**8** (R=Me, L_2=dpp)	95	none	THF	−78	24	21	75	0	0
6	**8**		none	Et_2O	−78	24	44	47	0	0
7	**9** (R=Me, L_2=$2PEt_3$)	40	none	Et_2O	−78	0.2	0	98	0	0
8	**10** (R=Et, L_2=bpy)	105	none	THF	−78	0.1	0	100	0	0
9	**11** (R=*n*-C_3H_7, L_2=bpy)	50	none	THF	−78	0.1	0	100	0	0
10	**12** (R=Et, L_2=dpe)	50	none	THF	−78	6.5	0	0	38	c)
11	**12**		none	Et_2O	−78	24	0	0	15	c)
II.	Reactions at temperatures higher than −78 °C (effect of temperature).									
12	**6**		none	Et_2O	−45	5	89	0	0	0
13	**6**		none	Et_2O	−17	24	68	8	0	0
14	**6**		none	Et_2O	1	7	42	39	0	0
15	**6**		none	Et_2O	13	3	0	90	0	0
16	**7**		none	Et_2O	r.t.	48	0	73	0	0
17	**7**		none	toluene	r.t.	8	3	83	0	0
18	**8**		none	THF	r.t.	2	0	80	0	0
19	**9**		none	Et_2O	r.t.	1.5	0	93	0	0
20	**10**		none	THF	r.t.	0.1	0	90	0	0
21	**11**		none	acetone	r.t.	0.1	0	79	0	0
22	**12**		none	THF	−40	3.5	0	0	58	c)
23	**12**		none	THF	r.t.	24	0	2	24	59
24	**12**		none	toluene	r.t.	3	0	0	29	41
III.	Reactions in the presence of additives.									
									(Remarks)	
25	**6**		bpy(5.3)	THF	r.t.	0.1	0	100	no effect	
26	**6**		dpe(excess)	THF	−78	1.5	50	5	ligand exchange	
27	**6**		MAH(3.2)	THF	−78	24	2	37	RCOR increases	
28	**7**		MAH(3.3)	THF	−78	1	27	73	RCOR increases	
29	**9**		PEt_3(3.2)	Et_2O	r.t.	1.5	0	98	no effect	

a) Reactions are carried out in the presence of excess (more than 3 mol/Ni) CO. b) Decomposition temperature of the complex (see Refs. 9, 12, and 13). c) Evolution of C_2H_4 was confirmed by GLC, but measurement of its amount was not feasible due to high solubility of C_2H_4 in the solvent at the temperature.

$$Ni(COR)(Y)L_2 \rightleftarrows NiR(Y)L_2 + CO \quad (3)$$
$$\downarrow +Ni(COR)(Y)L_2$$
$$RCOR$$

$(Y)L_2$ proceeds at lower temperature in solutions.

Reactions with Alcohols and Aniline: $Ni(COR)(Y)L_2$ reacts with alcohols and aniline to afford esters and amides, respectively,

$$Ni(COR)(Y)L_2 + R'OH \longrightarrow RCOOR', \quad (4)$$
$$Ni(COR)(Y)L_2 + C_6H_5NH_2 \longrightarrow RCOONHC_6H_5. \quad (5)$$

Carrying out the reaction with R'OH in the absence of excess CO gives RCOOR' only in a low yield presumably due to a partial decarbonylation of $Ni(COR)(Y)L_2$ in the presence of R'OH, and the yield increases considerably when the reaction is carried out in the presence of excess CO. In the reaction with aniline,

$$Ni(COR)(Y)L_2 \rightleftarrows NiR(Y)L_2 + CO \quad (6)$$
$$\downarrow +R'OH$$
$$RCOOR'$$

on the contrary, the yield of amide is virtually independent of the presence or absence of excess CO. These reactions which may be regarded as nucleophilic attack of alcohol or amine on the acyl ligand are relevant to the transition metal-catalyzed synthesis of esters or amides from organic halide, CO, and alcohols

or amines.[1,2]

Oxidation of the RCO Ligand: $Ni(COR)(Y)L_2$ absorbs O_2 (about 0.5 mol/Ni) in dry air. Acidolysis of the paramagnetic product by dry HCl gives RCOOH in 56—100% yield, indicating that oxidation of the acyl to a carboxylato ligand takes place on exposure of $Ni(COR)(Y)L_2$ to dry air,

$$Ni(COR)(Y)L_2 + O_2 \longrightarrow [Ni(OCOR)(Y)L_n] \xrightarrow{+HCl} RCOOH \quad (7)$$

Isolation of $Ni(OCOR)(Y)L_n$ was not feasible due to the lack of suitable solvents for recrystallization, but IR spectrum of a complex formed by the reaction of **2** with dry air is identical to that of a product formed by an 1:1 reaction of NiEt(suc)(bpy) with C_2H_5-COOH, supporting the occurrence of the reaction expressed by Eq. 7.

π-Acid Induced Reductive Elimination of Ester from 3 and 4: As described above, reductive elimination of $RCOOC_6H_4$-*p*-CN from $Ni(COR)(OC_6H_4$-*p*-CN)-(bpy) is enhanced by addition of CO, which is regarded as a typical π-acid. Addition of other π-acids such as maleic anhydride (MAH) and ethyl methacrylate (EMA) also enhances the reductive elimination (No. 24—26). The Ni–COR and/or Ni–OC_6H_4-*p*-CN bond seems to be activated by coordination of the π-acid to cause the reductive elimination,

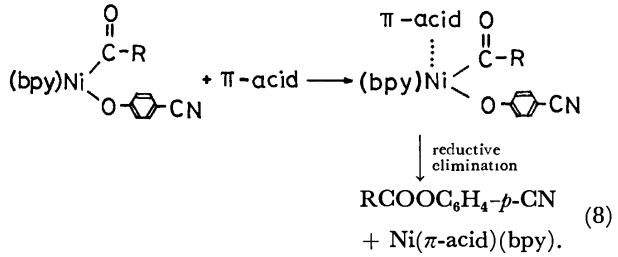

$$RCOOC_6H_4\text{-}p\text{-}CN + Ni(\pi\text{-acid})(bpy). \quad (8)$$

Similar enhancement of reductive elimination of R–R from $NiR_2(bpy)$ by coordination of π-acid to Ni has been reported.[9] A stronger π-acid, MAH, affords the ester in a higher yield than a weaker π-acid, EMA. The reaction (8) can be regarded as a reverse process of oxidative addition of ester to a Ni(0) complex.[10] Addition of MAH does not induce such a reductive elimination of RCOY from complexes **1**, **2**, and **5** having stronger Ni–Y bonds.

Reactions with Ni(0)- and Dialkylnickel(II) Complexes: Addition of $Ni(PPh_3)_4$ (PPh_3=triphenylphosphine) to a solution of **4** leads to formation of a mixture of NiMe-$(OC_6H_4$-*p*-CN)(bpy) and $Ni(CO)(PPh_3)_3$. The reaction is considered to proceed through partial decarbonylation of **4** and trapping of CO by $Ni(PPh_3)_4$. A similar decarbonylation of an acetylnickel(II) complex enhanced by Ni(0) complexes has been observed.[6a] The acylnickel(II) complexes are also decarbonylated on treatment with dialkylnickel(II) complexes. For example, a reaction of **5** with $NiMe_2(bpy)$ **6** (1:1) at 40 °C (No. 28) gives acetone (33%, determined by ^{1}H-NMR), the decarbonylated product NiMe(pht)-$(PEt_3)_2$ (100%), $Ni(CO)_2(bpy)$,[11] and intact **6** (67%), suggesting CO partly liberated from **5** is trapped by **6** to release acetone and $Ni(CO)_2(bpy)$ according to the following stoichiometry,

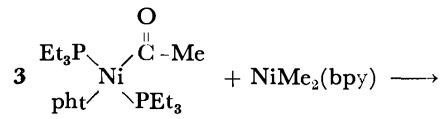

$$MeCOMe + 3NiMe(pht)(PEt_3)_2 + Ni(CO)_2(bpy). \quad (9)$$

When $NiEt_2(bpy)$ is added to a solution of **5**, a cross coupling reaction to give MeCOEt takes place (No. 29) besides the simple CO trapping reaction by $NiEt_2$-(bpy) to give EtCOEt. The results suggest the occurrence of intermolecular alkyl or acyl transfer reactions.

II. Reactions of NiR_2L_2 with CO. In contrast to the reactions of monoalkylnickel(II) complexes with CO, reactions of dialkylnickel(II) NiR_2L_2 with CO did not afford any isolable acylnickel complexes, but they produced carbonylated compounds of the alkyl ligands, ketone, diketone, and/or aldehyde:

$$NiR_2L_2 + CO \longrightarrow RCOR, RCOCOR, \text{and/or } RCHO. \quad (10)$$

6 $NiMe_2(bpy)$
7 $NiMe_2(dpe)$
8 $NiMe_2(dpp)$ dpe=1,2-bis(diphenylphosphino)-ethane
9 $NiMe_2(PEt_3)_2$
10 $NiEt_2(bpy)$ dpp=1,3-bis(diphenylphosphino)-propane
11 $Ni(n\text{-}C_3H_7)_2(bpy)$
12 $NiEt_2(dpe)$

Table 3 summarizes results of the reactions. It is seen in Table 3 that the product of the reaction (10) varies with changes in the R and L ligands and reaction conditions. Following is details of effects of the ligands and reaction conditions on the product.

Effects of R and L: Reactions of dimethylnickel complexes **6**—**9** with CO give 2,3-butanedione and acetone and the ratio of the two products varies with the nature of L and the reaction temperature. At −78 °C the fraction of the diketone increases in an increasing order of a thermal stability of $NiMe_2L_2$, **9**<**8**<**7**<**6**.[9,12,13]

Among the complexes of a type $NiR_2(bpy)$ examined, only the methyl complex which has the higher thermal stability than the ethyl and propyl homologs gives diketone at −78 °C, and less stable complexes **10** and **11** afford ketones exclusively at −78 °C. These results suggest that the ketone/diketone ratio at −78 °C may be related to the thermal stability of NiR_2L_2 (or the strength of the Ni–R bond). The reaction of **12** with CO gives a different type of product, propanal, with evolution of ethylene.

Effect of Temperature: On raising the reaction temperature, the fraction of acetone formed in the reaction of **6** with CO increases and at 13 °C or above acetone becomes a sole liquid product. Similar increases in the proportion of acetone on raising the reaction temperature to room temperature are observed in the reactions of diphosphine-containing complexes **7** and **8** with CO. Complexes **9**, **10**, and **11** which give ketones as the sole liquid products at −78

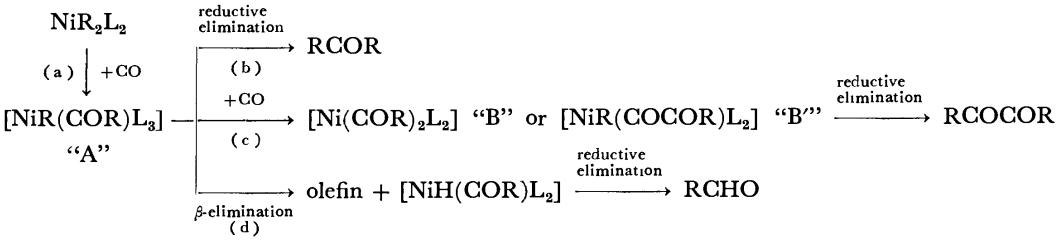

Scheme 1.

°C afford the same products at room temperature.

Effect of Additive: Addition of maleic anhydride increases the fraction of acetone formed in the reactions of **6** and **7** with CO at −78 °C presumably due to the activating effect of the alkyl and/or acyl ligands by coordination of the π-acid. Addition of bpy and PEt_3 in the reactions of the dimethyl complexes **6** and **9** with CO, respectively, seems to affect neither the product nor the rate of the reaction.

Other Factors: Table 3 shows results of the reactions carried out in the presence of excess CO (more than 3 mol/Ni) which left no intact NiR_2L_2. When the reaction is carried out in the presence of a less amount of CO, however, the yield of the product decreases. For example, reactions of **9** in the presence of 1.0 and 2.0 mol of CO per **9** at −78 °C afford acetone in 21 and 68% yields, respectively. Since $Ni(CO)_2(PEt_3)_2$ is isolated from the reaction mixture, the stoichiometry of the reaction of **9** with CO can be written as follows,

$$NiMe_2(PEt_3)_2 + 3CO \longrightarrow MeCOMe + Ni(CO)_2(PEt_3)_2 \quad (11)$$

and the yields obtained in the presence of 1.0 and 2.0 mol of CO per **9** roughly agree with the stoichiometry. $Ni(CO)_2(dpe)$[14] (isolated yield=76%), $Ni(CO)_2(dpp)$[14] (81%), and $Ni(CO)_2(bpy)$[11] (50%) are obtained in the reaction Nos. 3, 5, and 20 (see Table 3), respectively.

Although detailed examination has not been made concerning rates of the reactions, among the phosphine-coordinated complexes the monodentate PEt_3-coordinated complex **9** seems to react with CO at a faster reaction rate than the bidentate phosphine coordinated complexes **7** and **8**.

Among the complexes of the type $NiR_2(bpy)$, the dimethyl complex **6** reacts with CO most slowly. At −78 °C the reaction of **6** with CO requires more than 10 h to be completed, whereas the reactions of **10** and **11** with CO are completed in few minutes even at the temperature. A competitive reaction between the dimethyl and diethyl complexes, **6** and **10**, (1:1) in the presence of 1 mol of CO per Ni (**6**+**10**) at room temperature produces 3-pentanone (30%/**10**) exclusively and all of **6** remains intact, indicating **10** reacts with CO much faster than **6**. The difference in the rate may be related to the difference in relative strength of the Ni–C bond of the complex and/or to the difference in relative affinity of the complex to CO. It is known that the Ni–CH_3 bond in **6** is stronger than the Ni–C_2H_5 and Ni–C_3H_7 bonds in **10** and **11** and that **6** has a weaker affinity toward π-acids than **10** and **11** due to its weaker Lewis basicity.[9]

Reaction Scheme and Factors Controlling the Distribution of Products. These results of the reactions of NiR_2L_2 with CO can be reasonably explained by a scheme involving formation of a monoalkyl(acyl)nickel(II) complex "A" as the key reaction intermediate (Scheme 1). In the reaction scheme CO inserts into one of the Ni–R bonds of NiR_2L_2 (step (a)) to form an intermediate monoalkyl(acyl)nickel(II) complex "A". The intermediate "A" undergoes reductive elimination to give ketone (step (b)). Further CO-insertion reaction may give a diacylnickel(II) complex "B" or alkyl(pyruvoyl)nickel(II) complex "B'" from which diketone is produced (step (c)). When the ethyl group is employed, β-elimination reaction from "A" may produce olefin (R(−H)) and aldehyde. Formation of acetone from isolated platinum (IV) complexes having both methyl and acetyl groups have been reported.[15] In the case of the reaction of **6** with CO, the intermediacy of "A" is supported by production of 2-butanone on carrying out the reaction in the presence of C_2H_5Br. Attempts to isolate NiMe(COMe)(bpy), however, have not been successful presumably due to instability of the complex.

As described above, $CH_3COC_2H_5$ is produced in the reaction of **6** with CO at −78 °C in the presence of C_2H_5Br, whereas no $CH_3COCOC_2H_5$ was detected in the product. This suggests that 2,3-butanedione is produced through the intermediate diacyl species "B" rather than "B'". However, at present it is not possible to exclude the possibility for the intermediacy of the doubly CO-inserted species, since a transition metal complex having a CH_3COCO ligand is known[16] and evidence for the double CO-insertion has been obtained for carbonylation of a dimethylpalladium complex.[17]

According to Scheme 1, the distribution of the products is determined by relative rates of the elemental reactions (b)—(d), and the results described above indicate that the relative rates depend on the R and L ligands, reaction temperature, and additives in following ways.

(i) Effect of R and L: The relative rate of the reaction (b) at −78 °C to that of the reaction (c) increases when the thermal stability of the starting dialkylnickel(II) complex NiR_2L_2 decreases. If the strength of either or both of the Ni–R and Ni–COR bonds in "A" is controlled by the nature of the R and L ligands in a similar way to that of the Ni–R bonds in NiR_2L_2, these results indicate that the reductive elimination of RCOR from "A" takes place prior

to the further attack of CO at "A" (step (c) in Scheme 1) when the Ni–R and/or Ni–COR bond is weak. On the contrary, when the bonds are stronger, the intermediate "A" can wait for the further attack of CO to form "B" or "B‴" and diketone is formed in this case.

(ii) Effect of Temperature: When the reaction temperature is raised, the Ni–R and Ni–COR bonds in "A" will be activated to cause the reductive elimination and the proportion of ketone will thus increase.

(iii) Effect of Additive: The effect of MAH to increase the proportion of ketone may be related to the MAH-induced reductive elimination of $RCOOC_6H_4$-*p*-CN from **3** and **4**. Namely, coordination of MAH to "A" may lead to activation of the Ni–R and Ni–COR bonds as in the case of **3** and **4**, and therefore the fraction of ketone will increase on the addition of MAH. An alternative explanation of the effect of MAH is that MAH coordinates to "A" to block the coordination site to prevent the further attack of CO at "A". We consider that the former explanation is more reasonable since the effect of MAH on the reductive elimination of esters and R–R from the acyl(phenoxo)-type complexes and $NiR_2(bpy)$ (R=Me, Et),[9] respectively, is so pronounced.

*(iv) Difference between **10** and **12***: The difference in the products of the reaction of **10** with CO and that of **12** with CO may be related to the difference of thermolysis between **10** and **12**; the former gives mainly the coupling product C_4H_{10} on the thermolysis,[9] whereas the latter exclusively affords the disproportionation products, C_2H_6 and C_2H_4,[12] indicating that the β-elimination in **12** proceeds more easily than that in **10**. If coordination of dpe to Ni having ethyl ligand(s) makes the abstraction of the β-hydrogen in the Et ligand by Ni easier, the formation of C_2H_5CHO and C_2H_4 through the path (d) in Scheme 1 can be reasonably explained. Lower yield of C_2H_5CHO than that of C_2H_4 seems to be due to partial polymerization of C_2H_5CHO catalyzed by Ni complexes.[18]

Conclusion and Scope

Carbon monoxide inserts into Ni–R bonds of monoalkyl- and dialkylnickel(II) complexes, $NiR(Y)L_2$ and NiR_2L_2, to give complexes of a type $Ni(COR)(X)L_n$ (X=R, Cl, phenoxo, imido). When the X ligand has a moderate or strong bonding ability to Ni as in Cl, OC_6H_4-*p*-CN, and imido ligands, the acylnickel(II) complex can be isolated. On the contrary, when X has only a weak bonding ability as R, OC_6H_5, and OC_6H_4-*p*-C_6H_5, the reductive elimination of RCOX takes place under the reaction conditions and the acylnickel(II) complex could not be isolated. In the case of $NiR(COR)L_n$, other types of reactions, namely, further insertion of CO to form "B" (or "B‴") and β-elimination of C_2H_5CHO and C_2H_4, can also take place depending on nature of the R and L ligands and the reaction conditions. The acylnickel(II) complexes having a moderately strong bonding ligand, OC_6H_4-*p*-CN, are activated by coordination of π-acids (CO, MAH, EMA) to cause the reductive elimination of $RCOOC_6H_4$-*p*-CN. Such a reductive elimination, however, is not induced on adding the π-acids to complexes having stronger Ni–X bonds such as Ni–Cl and Ni–imido. The isolated acylnickel(II) complexes afford esters, amides, and carboxylato complexes in the reactions with alcohols, aniline, and O_2, respectively.

These results obtained in this work may be useful in planning carbonylation of organic compounds by CO. The formation of ketone from NiR_2L_2 has been actually applied to nickel-catalyzed synthesis of ketone from RMgX, RX, and CO.[4a]

Experimental

General. Manipulation of nickel complexes was carried out under deoxygenated nitrogen or argon or in a vacuum. IR spectra were taken on a Hitachi Model 295 spectrometer using KBr discs under nitrogen. NMR spectra were taken by using a Japan Electron Optics Lab. JNM-PS-100 spectrometer. Microanalysis of C, H, and N was performed by T. Saito in our laboratory with a Yanagimoto CHN Autocorder Type MT-2. High sensitivities of the nickel complexes to air should be taken into account concerning the microanalysis. Nickel contents of the complexes were measured by volumetric titration after acidolysis of the complexes. Gases evolved were analyzed with a Hitachi RMU 5B mass-spectrometer and a Shimadzu GC-5B gas chromatograph, their volumes being measured with a Toepler pump. Liquid products were analyzed with a Shimadzu GC-5B gas chromatograph.

Material. The monoalkyl-[5] and dialkylnickel(II)[9,12,13] complexes were prepared as described in literature. Solvents were dried over Na wires or CaH_2, distilled under N_2, and stored under N_2. CO gas was dried by bubbling through concd H_2SO_4.

*Preparation of the Acylnickel Complexes. Propionyl(chloro)(2,2′-bipyridine)nickel(II) **1***: A reaction vessel (60 cm³) containing a THF (10 cm³) solution of NiEt(Cl)(bpy) (420 mg, 1.5 mmol) was evacuated and then CO (50 cm³, 1 atm) was introduced into the vessel. Stirring the solution for 10 min at room temperature gave a reddish brown solution, into which 40 cm³ of hexane was added to obtain 440 mg of a reddish brown solid. The reddish brown solid was recrystallized from THF–hexane to yield brown crystals of **1** (220 mg, 48%); mp 130 °C (dec). Found: C, 51.2; H, 4.2; N, 9.1; Cl, 11.2%. Calcd for $C_{13}H_{13}ClN_2NiO$: C, 50.8; N, 4.3; N, 9.1; Cl, 11.5%.

*Propionyl(succinimido)(2,2′-bipyridine)nickel(II) **2***: A reaction vessel (60 cm³) containing a CH_2Cl_2 (10 cm³) solution of NiEt(suc)(bpy) (630 mg, 1.8 mmol) was evacuated and CO (50 cm³, 1 atm) was introduced into the vessel. Stirring the solution for 30 min at room temperature gave a red solution and a small amount of a precipitate. The solution was separated by filtration and hexane was added to the filtrate to obtain a dark brown precipitate, which was recrystallized from THF–hexane to yield a reddish brown microcrystals of **2** (450 mg, 73%); mp 150 °C (dec). Found: C, 54.1; H, 4.9; N, 10.0%. Calcd for $C_{17}H_{17}N_3NiO_3$: C, 55.2; H, 4.6; N, 11.2%.

*Propionyl(p-cyanophenoxo)(2,2′-bipyridine)nickel(II) **3***: A reaction vessel containing a THF (7 cm³) solution of NiEt(OC_6H_4-*p*-CN)(bpy) (420 mg, 1.2 mmol) was connected to a vacuum line and the vessel was evacuated. After cooling the solution to −78 °C, CO gas (1.2 mmol) whose amount was measured by a manometer was introduced and the solu-

tion was stirred for 3 h at −78 °C to obtain a reddish purple homogeneous solution. An excess amount of hexane was added to the solution to yield 430 mg (94%) of reddish purple crystals of **3**. A sample for the microanalysis was obtained by recrystallization from acetone–hexane; mp 120 °C (dec). Found: C, 60.8; H, 3.9; N, 11.1; Ni, 14.7%. Calcd for $C_{20}H_{17}N_3NiO_2$: C, 61.6; H, 4.4; N, 10.8; Ni, 15.1.

Acetyl(p-cyanophenoxo)(2,2'-bipyridine)nickel(II) **4**: A vessel containing a THF (20 cm³) solution of NiMe(OC_6H_4-*p*-CN)(bpy) (1.0 g, 2.8 mmol) was connected to a vacuum line and the vessel was evacuated. After cooling the solution to −78 °C, a measured amount of CO (2.8 mmol) was introduced into the vessel and the solution was stirred at −78 °C for 5 h. Hexane (excess) was added to the solution to obtain a brown powder, which was recrystallized from acetone to yield reddish brown crystals of **4** (380 mg, 36%); mp 140 °C (dec). Found: C, 59.5; H, 4.1; N, 10.5; Ni, 15.6. Calcd for $C_{19}H_{15}N_3NiO_3$: C, 60.7; H, 4.0; N, 11.2; Ni, 15.6%.

Acetyl(phthalimido)bis(triethylphosphine)nickel(II) **5**: A vessel containing an ethereal solution (20 cm³) of NiMe(pht)(PEt_3)$_2$ was evacuated and then CO (100 cm³, 1 atm) was introduced into the vessel. Stirring the solution for 10 min at room temperature gave a yellow solution and a small amount of a precipitate. The yellow solution was separated by filtration and cooling the solution to −78 °C gave yellow crystals of **5** (470 mg, 83%); mp 100 °C (dec). Found: C, 54.0; H, 7.8; N, 2.9; Ni, 12.4%. Calcd for $C_{22}H_{37}NNiO_3P_2$: C, 54.6; H, 7.7; N, 2.9; Ni, 12.1%.

Reactions of NiR_2L_2 with CO (cf. Table 3). *No. 1*: Carbon monoxide (3.2 mmol) was introduced at −78 °C into an evacuated vessel containing 130 mg (0.53 mmol) of **6** in 6.5 ml of diethyl ether. The dimethylnickel(II) complex was partly soluble in diethyl ether at −78 °C and the solution was colored deep green (color of **6**) at the initial stage of the reaction. On stirring the mixture at −78 °C, the color of the solution gradually turned to red. After 1 d, a homogeneous red solution was obtained and GLC analysis of the solution indicated formation of 0.48 mmol of 2,3-butanedione. Drying up the solution in vacuum at −78 °C gave almost pure bpy, whereas drying up the solution after warming the solution to room temperature gave a mixture of bpy and Ni(CO)$_2$(bpy),[11] indicating that there exists an equilibrium, Ni(CO)$_4$+bpy$\rightleftharpoons$Ni(CO)$_2$(bpy)+2CO, and the equilibrium lies to the left at −78 °C.

Other Reactions of NiR_2L_2 with CO: Other reactions listed in Table 3, except for reactions in the presence of MAH, were carried out in similar ways to the reaction of **6** at −78 °C. Reactions of NiR_2(bpy) with CO at room temperature gave Ni(CO)$_2$(bpy) in high yields. Nickel carbonyl complexes, Ni(CO)$_2$(bpy),[11] Ni(CO)$_2$(PEt_3)$_2$,[14] Ni(CO)$_2$(dpe),[14] and Ni(CO)$_2$(dpp)[14] were identified by their IR spectra. Reactions in the presence of MAH require the following special attention to prevent NiR_2L_2 to decompose before the reaction with CO since MAH strongly activates the Ni–R bond of NiR_2L_2. A solution of NiR_2L_2 in THF was solidified by cooling to −196 °C and then MAH was added to the reaction system. CO was added immediately after the solution melted on raising temperature.

References

1) J. Falbe, "Carbon Monoxide in Organic Synthesis," Springer, Berlin (1970); R. F. Heck, "Organotransition Metal Chemistry," Academic Press, New York (1974); J. Tsuji, "Organic Synthesis by Means of Transition Metal Complexes," Springer, Berlin (1975); I. Wender and P. Pino, "Organic Syntheses *via* Metal Carbonyls," John Wiley & Sons, New York (1977); M. M. Taqui Khan and A. E. Martell, "Homogeneous Catalysis by Metal Complexes," Academic Press, New York (1974), Vol. I.

2) A. Schoenberg and R. F. Heck, *J. Org. Chem.*, **39**, 3318, 3327 (1974); D. E. James and J. K. Stille, *J. Am. Chem. Soc.*, **98**, 1810 (1976); D. E. James, L. F. Hines, and J. K. Stille, *ibid.*, **98**, 1806 (1976); Y. Becker and J. K. Stille, *ibid.*, **100**, 838 (1978), M. Hidai, M. Kokura, and Y. Uchida, *J. Organometal. Chem.*, **52**, 431 (1973); M. Hidai, T. Hikita, Y. Wada, Y. Fujikura, and Y. Uchida, *Bull. Chem. Soc. Jpn.*, **48**, 2075 (1975).

3) F. Calderazzo, *Angew. Chem.*, **89**, 305 (1977) and references therein.

4) a) T. Yamamoto, T. Kohara, and A. Yamamoto, *Chem. Lett.* **1976**, 1217; b) T. Kohara, S. Komiya, T. Yamamoto, and A. Yamamoto, *ibid.*, **1979**, 1513.

5) T. Yamamoto, T. Kohara, and A. Yamamoto, *Bull. Chem. Soc. Jpn.*, **54**, 1720, (1981); **54**, 2010 (1981).

6) a) H.-F. Klein and H. H. Karsch, *Chem. Ber.*, **109**, 2524 (1976); b) D. R. Fahey and J. E. Mahan, *J. Am. Chem. Soc.*, **99**, 2501 (1977); c) P. E. Garrou and R. F. Heck, *ibid.*, **98**, 4115 (1976).

7) a) T. Saruyama, T. Yamamoto, and A. Yamamoto, *Bull. Chem. Soc. Jpn.*, **49**, 546 (1976); b) K. Maruyama, T. Ito, and A. Yamamoto, *J. Organometal. Chem.*, **157**, 463 (1978).

8) G. Wilke and G. Herrmann, *Angew. Chem.*, **78**, 591 (1966).

9) T. Yamamoto, A. Yamamoto, and S. Ikeda, *J. Am. Chem. Soc.*, **93**, 3350, 3360 (1971).

10) T. Yamamoto, J. Ishizu, T. Kohara, S. Komiya, and A. Yamamoto, *ibid.*, **102**, 3758 (1980).

11) R. S. Nyholm and L. N. Short, *J. Chem. Soc.*, **1953**, 2670.

12) A. Yamamoto, T. Yamamoto, M. Takamatsu, T. Saruyama, and Y. Nakamura, "Organotransition-Metal Chemistry," ed by Y. Ishii and M. Tsutsui, Plenum, New York (1975); M. Takamatsu, Thesis for M. Eng. Tokyo Institute of Technology (1974).

13) T. Kohara, T. Yamamoto, and A. Yamamoto, *J. Organometal. Chem.*, **192**, 265 (1980).

14) P. W. Jolly and G. Wilke, "The Organic Chemistry of Nickel," Academic Press, New York (1975) Vol. 1; J. Chatt, and F. A. Hart, *J. Chem. Soc.*, **1960**, 1378.

15) J. D. Ruddick and B. L. Shaw, *J. Chem. Soc., A*, **1969**, 2969; M. P. Brown, R. J. Puddephatt, C. E. E. Upton, and S. W. Lavington, *J. Chem. Soc., Dalton Trans.*, **1974**, 1613.

16) C. P. Casey, C. A. Bunnell, and J. C. Calabrese, *J. Am. Chem. Soc.*, **98**, 1166 (1976).

17) F. Ozawa and A. Yamamoto, *Chem. Lett.*, **1981**, 289.

18) T. Yamamoto, S. Konagaya, and A. Yamamoto, *J. Polym. Sci., B*, **16**, 7 (1978).

Branched-chain Sugars. XXII. Synthesis of Benzyl 2,3-Di-*O*-benzyl- and 2,3-*O*-Methylene-β-L-*threo*-pentopyranosid-4-uloses, and the Corresponding 6-Deoxy-α-D-*xylo*-hexopyranosid-4-uloses[1]

Masafumi MATSUZAWA, Kazusuke KUBO, Hisashi KODAMA, Masuo FUNABASHI,† and Juji YOSHIMURA*

Laboratory of Chemistry for Natural Products, Faculty of Science, Tokyo Institute of Technology, Nagatsuta, Midori-ku, Yokohama 227

(Received February 2, 1981)

The title compounds were synthesized from L-arabinose and D-glucose as intermediates to a few naturally occuring branched-chain sugars. Oxidation conditions of precursors to the corresponding 4-uloses were examined.

In previous papers of this series, stereoselectivities in nucleophilic reactions of hexopyranosid-2-uloses[2] and 3-uloses[3] have been extensively examined, from the views of non-bonded interactions, electrostatic interaction in the transition state,[4] and kinetic or thermodynamic control in reversible reactions.[5] In order to examine the stereoselectivities in similar reactions of 4-uloses and to utilize the results for the stereoselective synthesis of 2,3-*O*-methylene-4-*C*-substituted aldono-1,5-lactones found in everninomicins,[6] flambamycin,[7] and avilamycins,[8] benzyl 2,3-*O*-benzyl-(**1**) and 2,3-*O*-methylene-β-L-*threo*-pentopyranosid-4-uloses (**2**), benzyl 2,3-*O*-benzyl-6-deoxy-(**3**) and 6-deoxy-2,3-*O*-methylene-α-D-*xylo*-hexopyranosid-4-uloses (**4**), together with benzyl 2,3-di-*O*-benzyl-6-*O*-trityl-α-D-*xylo*-hexopyranosid-4-ulose (**5**) and methyl 6-deoxy-2,3-*O*-methylene-α-D-*ribo*-hexopyranosid-4-ulose (**6**), were synthesized in this paper.

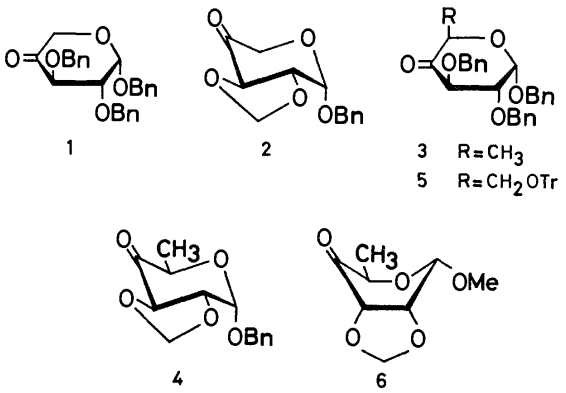

Fig. 1.

Results and Discussion

Treatment of benzyl 2,3-di-*O*-benzoyl-α-L-arabinopyranoside[9] in acetic acid with dimethyl sulfoxide and acetic anhydride[10] at room temperature for 2 days gave the corresponding 4-*O*-methylthiomethyl derivative (**7**) in 88% yield, which was converted into de-*O*-benzoylated derivative (**8**) by treatment with sodium methoxide in 57% yield. Treatment of **8** in *N*,*N*-dimethylformamide with sodium hydride and benzyl chloride or dichloromethane[11] gave the corresponding 2,3-di-*O*-benzyl (**9**) and 2,3-*O*-methylene derivatives (**10**) in 81% and 46% yields, respectively. In the case of **10**, a small amount of dimers were formed, however, they could not be characterized. Treatment of **9** and **10** in aqueous acetonitrile with mercury(II) chloride and calcium carbonate gave the corresponding de-*O*-methylthiomethyl derivatives (**11** and **12**) in quantitative and 62% yields, respectively.

On the other hand, treatment of benzyl 4,6-*O*-benzylidene-α-D-glucopyranoside[12] in *N*,*N*-dimethylformamide with sodium hydride and dichloromethane gave the corresponding 2,3-*O*-methylene derivative (**13**)[11] and two dimers (**14** and **15**) in 43%, 6.2%, 7.2% yields, respectively. The dimers showed no absorption of a hydroxyl group in IR spectra, and the parent ion peak of *m/e* 741 in MS spectra. Configurations of 2,3′:2′,3-bis-*O*-methylenedi(benzyl 4,6-*O*-benzylidene-α-D-glucopyranoside) (**14**) and the corresponding 2,2′:3,3′-bis-*O*-methylene isomer (**15**) were assigned from the *O*-methylene proton signals in NMR spectra. Compound **14** showed AB quartet indicating two magnetically nonequivalent protons in equivalent two methylene groups, whereas **15** two singlets indicating each two equivalent protons in non-equivalent two methylene groups. Analogous two dimers were also obtained by the reaction of the corresponding methyl glucoside with dibromomethane in each 22% yield, together with 2,3-*O*-methylene derivative (**16**),[11,13] but their structures were not assigned. While, similar reaction of methyl 4,6-*O*-benzylidene-α-D-allopyranoside[14] gave the corresponding 2,3-*O*-methylene derivative (**17**) in 65% yield.

For the deoxygenation of *C*-6 position, **13** was treated with 80% acetic acid at room temperature for one day to give de-*O*-benzylidenated product (**18**) in 64% yield. Selective tosylation of **18** in pyridine at 0 °C with 1.4 equivalent *p*-toluenesulfonyl chloride gave 6-*O*-tosyl (**19**) and 4,6-di-*O*-tosyl (**20**) derivatives in 80% and 8% yields, respectively. Reduction of **19** in *N*,*N*-dimethylformamide with lithium aluminium hydride gave the corresponding 6-deoxy derivative (**21**) in 81% yield. For the preparation of **21**, oxidative ring-opening of the 4,6-*O*-benzylidene group of **13** with *N*-bromosuccinimide was unsuccessful, probably due to the reaction of the strained 2,3-*O*-methylene group. By the same route, **16** and **17** were also converted into methyl 6-deoxy-2,3-*O*-methylene-α-D-glucopyranoside (**22**) and -allopyranoside (**23**), respectively. While, monotosylation of benzyl 2,3-di-*O*-ben-

† Present address: College of Arts and Science, Chiba University, Yayoicho, Chiba 260.

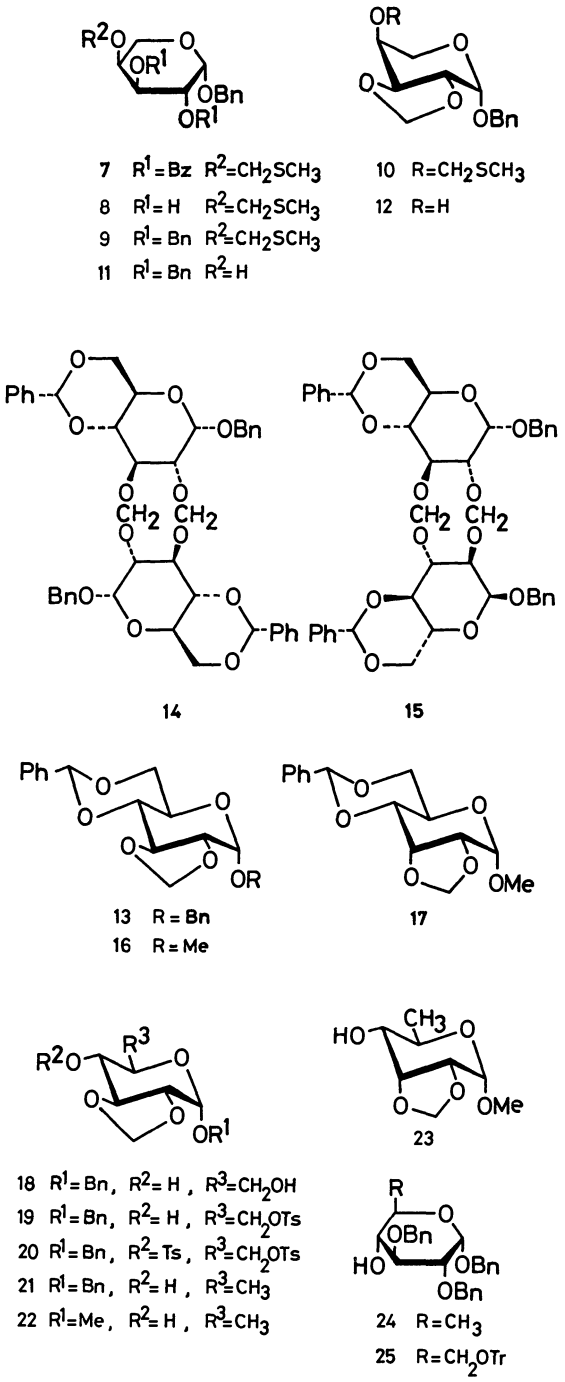

Fig. 2.

zyl-α-D-glucopyranoside[10] and successive reduction of the product with lithium aluminium hydride gave benzyl 2,3-di-*O*-benzyl-6-deoxy-α-D-glucopyranoside (**24**) in 38% overall yield.

Oxidation of **11**, **12**, **21**—**24**, and benzyl 2,3-di-*O*-benzyl-6-*O*-trityl-α-D-glucopyranoside (**25**)[12] into the corresponding 4-uloses was examined by a few methods, and the results were summarized in Table 1. The chromium trioxide-pyridine oxidation of 2,3-di-*O*-benzyl derivatives, (**11**, **24**, and **25**) was unsuccessful, probably due to the oxidation of the benzyl groups as was reported by Stevens and Czernecki[15] in the case of oxidation of methyl 6-deoxy-2,3-di-*O*-benzyl-α-D-galactopyranoside with ruthenium tetraoxide. A similar oxidation of **22** was accompanied by the epimerisation at *C*-3 position to give **6** in 45% yield. The epimerization of equatorial C–O bond to axial configuration implies that the 2,3-*O*-methylene ring from *trans*-diequatorial hydroxyl groups contains a fairly large steric strain. Configuration of 6 obtained above was confirmed by the comparison with that obtained by the oxidation of **23** with chromium trioxide in 63% yield. Oxidation of **11** with dimethyl sulfoxide (DMSO)–acetic anhydride gave the corresponding 4-ulose in 60% yield, together with a small amount of 4-*O*-methylthiomethyl derivative (**9**), however, similar oxidation of 2,3-*O*-methylene derivatives (**12** and **22**) gave only a small amount of 4-*O*-methylthiomethyl derivative. Although DMSO–acetic anhydride oxidation of the corresponding methyl glucoside of **24** was reported to be unsuccessful,[15] DMSO–trifluoroacetic anhydride oxidation[16] gave commonly good results. Thus 4-uloses, **1**—**6**, could be obtained from **11**, **12**, **24**, **21**, **25**, and **23**, respectively.

Table 1. Preparation of 4-uloses

Substrates	Oxidation methods[a]	Products (%)	
		4-Uloses	4-*O*-Methylthiomethyl derivatives
11	B	**1** (60)	**9** (7.8)
	C	**1** (82)	
24	C	**3** (72)	
25	C	**5** (98)	
12	B		**10** (10)
	C	**2** (quant)	
21	C	**4** (quant)	
22	B		(10)
	A	**6** (45)	
23	A	**6** (63)	

a) Method A, B, and C indicate the oxidation with CrO_3–pyridine, DMSO–Ac_2O, and DMSO–$(CF_3CO)_2O$, respectively.

^{1}H NMR parameters of 4-uloses thus obtained were shown in Table 2. The results indicate that **1**—**5** exist in *C*1 conformation, and **6** in ^{1,4}B. Because **23** takes *C*1 conformation (see Experimental), the conformational difference between **6** and **23** will be attributed to the larger bond angle of sp^2-carbon than that of sp^3-carbon at *C*-4, and the trend of coplanarity of 2,3-*O*-methylene ring.

Experimental

General Methods. Melting points were determined with a Mel-Temp melting point apparatus and not corrected. Optical rotations were measured with Carl Zeiss LEP-Al or JASCO DIP-4 polarimeter, using a 0.5 dm tube. IR spectra were recorded with a Hitachi EPI-G2 grating spectrometer. NMR spectra were recorded with a JEOL JNM PS-100 spectrometer in chloroform-*d* containing tetramethylsilane as the internal reference. Chemical shifts and coupling constants were recorded in δ(ppm) and Hz units, and IR frequencies in cm^{-1}. Evaporations were conducted under diminished pressure.

Benzyl 2,3-Di-O-benzoyl-4-O-methylthiomethyl-β-L-arabinopyranoside (7). A solution of benzyl 2,3-di-*O*-benzoyl-β-L-

Table 2. ^{1}H NMR parameters of 4-uloses

4-Uloses	Chemical shifts (δ) and coupling constants (Hz)							Other protons
	H-1 ($J_{1,2}$)	H-2 ($J_{2,3}$)	H-3 ($J_{3,5e}$)	H-5e ($J_{5e,5a}$)	H-5a ($J_{5,6}$)	H-6 ($J_{5,6'}$)	H-6′ ($J_{6,6'}$)	
1	4.96 d (3.0)	3.74 dd (10.0)	4.46 d	4.14 d (15.0)	3.86 d			5.04—4.44 (3×CH_2Ph; m)
2	5.50 d (3.0)	3.67 dd (10.8)	4.72 dd (1.0)	4.02 dd (15.0)	3.92 d			7.52—7.21 (Ph; m), 5.20 and 5.10 (OCH_2O; ABq, J=0.8), 4.86 and 4.76 (CH_2Ph; ABq, J=11.6)
3	4.92 d (4.0)	3.73 dd (10.5)	4.49 d		4.21 q (7.0)	1.22 d		7.14—7.50 (Ph; m), 4.48—5.00 (3×CH_2Ph; m)
4	5.47 d (3.0)	3.67 dd (10.5)	4.70 dd (1.0)		4.12 q (3.5)	1.35 d		ca. 7.38 (Ph; m), 5.19 and 5.10 (OCH_2O; ABq, J=0.8), 4.82 (CH_2Ph; s)
5	5.03 d (3.8)	3.78 dd (10.0)	4.44 d		4.34 dd (3.3)	3.56 dd (7.5)	3.40 dd (10.5)	7.60—7.10 (Ph; m), 4.98—4.55 (3×CH_2Ph; m)
6[a]	5.02 d (4.2)	4.8—4.6m (8.8)			4.13 q (7.0)	1.38 d		3.46 (OMe), 4.95 and 5.04 (OCH_2O, each s)

a) $J_{1,2}$ and $J_{2,3}$ were observed by the use of a shift reagent, Pr(FOD)$_3$.

arabinopyranoside[9] (50 g, 0.109 mol) in dimethyl sulfoxide (DMSO, 400 ml), acetic anhydride (240 ml) and acetic acid (80 ml) was kept at room temperature for 2 d, then poured into saturated sodium hydrogencarbonate, and the resulting solution was extracted with ether. The extract was evaporated and the residue was purified on a silica gel column to give **7** (50 g, 88%) as a syrup. $[\alpha]_D$ +176.8° (c 1.24, $CHCl_3$), NMR: 8.2—7.94 and 7.60—7.10 (Ph; m), 5.82 (H-3; q, $J_{2,3}$=10.8, $J_{3,4}$=2.0), 5.71 H-2; q, $J_{1,2}$=3.0), 5.31 (H-1; d), 4.74 (SCH_2O; s), 4.68 ($PhCH_2$; ABq, J=13.0), 4.46 (H-4; m, $J_{4,5e}$=1.8, $J_{4,5a}$=2.0), 4.00 (H-5e; q, $J_{5e,5a}$=13.2), 3.84 (H-5e; q), 1.98 (CH_3S, s). Found: C, 65.59; H, 5.66; S, 6.98%. Calcd for $C_{28}H_{28}O_7S$: C, 66.12; H, 5.55; S, 6.31%.

Benzyl 4-O-Methylthiomethyl-β-L-arabinopyranoside (8). A solution of **7** (600 mg, 1.18 mmol) in methanol (8 ml) containing sodium (60 mg, 2.6 mmol) was kept at room temperature for 6 h, evaporated, and the residue was purified on a silica gel column (benzene–ethyl acetate–ethanol 6:1:1) to give pure crystals in 57% (200 mg) yield. Mp 72—73 °C ($CHCl_3$–hexane), $[\alpha]_D$ +193.9° (c 0.72, $CHCl_3$), NMR: 7.34 (Ph; s), 5.00 (H-1; d, $J_{1,2}$=3.0), 4.73 and 4.85 (SCH_2O, ABq, J=11.3), 4.52 and 4.75 ($PhCH_2$; ABq, J=12.0), 4.02 (H-4; m, $J_{3,4}$=2.0), 3.84—3.70 (H-2, H-3, H-5e, and H-5a; m), 2.18 (CH_3S, s). Found: C, 55.53; H, 6.69; S, 10.73%. Calcd for $C_{14}H_{20}O_5S$: C, 55.98; H, 6.71; S, 10.68%.

Benzyl 2,3-Di-O-benzyl-4-O-methylthiomethyl-β-L-arabinopyranoside (9). To a solution of **8** (1 g, 3.3 mmol) in *N*,*N*-dimethylformamide (DMF, 10 ml) was added with stirring sodium hydride (0.35 g, 14.5 mmol) washed with hexane and then benzyl chloride (1.01 g, 7.9 mmol). After stirring one day at room temperature, the reaction mixture was poured into water, and the resulting solution was extracted with chloroform. The extract was evaporated, and the residue was purified on a silica gel column (hexane–ethyl acetate 10:1) to give a syrup (1.3 g) in 81.3% yield. $[\alpha]_D$ +91.4° (c 1.1, $CHCl_3$), NMR: 7.6—7.2 (Ph; m), 4.96—4.47 (4×$PhCH_2$, m), 4.91 (H-1; d, $J_{1,2}$=3.0), 4.18 (H-4; m, $J_{4,5e}$=1.6, $J_{4,5a}$=2.8), 4.01 (H-3; dd, $J_{2,3}$=10.3, $J_{3,4}$=2.5), 3.90 (H-2; dd), 3.80 (H-5e; dd, $J_{5e,5a}$=13.0), 3.66 (H-5a; dd), 2.13 (CH_3S; s). Found: C, 69.65; H, 6.81; S, 6.34%. Calcd for $C_{28}H_{32}O_5S$: C, 69.97; H, 6.71; S, 6.67%.

Benzyl 2,3-O-Methylene-4-O-methylthiomethyl-β-L-arabinopyranoside (10). To a solution of **8** (0.5 g, 1.66 mmol) in DMSO (30 ml) was added with stirring sodium hydride (170 mg, 7.1 mmol) washed with hexane, and then excess dichloromethane (1 ml). The usual work-up of the reaction mixture as **13** gave a syrup (0.4 g) which was purified on a silica gel column (benzene–acetone 4:1) to give pure **10** (240 mg, 46%). $[\alpha]_D$ +110.1° (c 1.0, $CHCl_3$), NMR: 7.33 (Ph, s), 5.36 (H-1; d, $J_{1,2}$=2.8), 5.06 and 5.09 (OCH_2O; ABq, J=1.0), 4.82 (SCH_2O; s), 4.66 and 4.73 ($PhCH_2$; ABq, J=13.0), 4.48 (H-4; m), 3.95 (H-3; dd, $J_{3,4}$=2.0), 3.87 (H-2; dd, $J_{2,3}$=10.0), 3.78 (H-5e; dd, $J_{4,5e}$=1.5, $J_{5e,5a}$=13.0), 3.65 (H-5a; dd, $J_{4,5a}$=1.0), 2.16 (CH_3S). Found: C, 57.47; H, 6.62; S, 9.97%. Calcd for $C_{15}H_{20}O_5S$: C, 57.67; H, 6.45; S, 10.27%.

Benzyl 2,3-Di-O-benzyl-β-L-arabinopyranoside (11). A supension of **9** (1.2 g, 2.5 mmol), mercury(II) chloride (1.36 g, 5.0 mmol), and calcium carbonate (0.75 g, 7.5 mmol) in aqueous acetonitrile (75%, 30 ml) was refluxed for 7 h, filtered, and the filtrate was evaporated. A dichloromethane solution of the residue was washed twice with aqueous sodium iodide (10%), and then evaporated to give a syrup (1.0 g) quantitatively. $[\alpha]_D$ +105.9° (c 3.2, $CHCl_3$). Found: C, 74.28; H, 6.37%. Calcd for $C_{26}H_{28}O_5$: C, 74.26; H, 6.71%.

Benzyl 2,3-O-Methylene-β-L-arabinopyranoside (12). A similar work up of **10** (240 mg, 0.77 mmol) as above and purification of syrupy product on a silica gel column (benzene–acetone 4:1) gave pure **12** (120 mg, 62%). $[\alpha]_D$ +212.2° (c 1.6, $CHCl_3$); NMR: 7.28—7.40 (Ph; m), 5.36 (H-1; d, $J_{1,2}$=1.0), 5.04 and 5.11 (OCH_2O, ABq, J=1.0), 4.64 and 4.75 (CH_2Ph; ABq, J=12.5), 4.30 (H-4; m), 3.89 (H-3; dd, $J_{3,4}$=1.0), 3.79 (H-2; dd, $J_{2,3}$=10.0), 3.73 (H-5e; dd, $J_{4,5e}$=2.0), 3.58 (H-5a; dd, $J_{4,5a}$=1.8, $J_{5e,5a}$=13.2). Found: C, 61.83; H, 6.39%. Calcd for $C_{13}H_{16}O_5$: C, 61.89; H, 6.39%.

Benzyl 4,6-O-Benzylidene-2,3-O-methylene-α-D-glucopyranoside (13). To a solution of benzyl 4,6-*O*-benzylidene-α-D-glucopyranoside[11] (50 g, 150 mmol) in DMF (500 ml) was added with stirring sodium hydride (21.6 g, 450 mmol) and then dichloromethane (28.6 ml, 450 mmol) dropwise, and the resulting suspension was stirred overnight at room temperature. A mixture of ethyl acetate and water was added to the reaction mixture, and the resulting solution was extracted with chloroform. The extract was washed

with water, dried, and evaporated. The residue was separated on a silica gel column (hexane–ethyl acetate 8:1) to give **13** (22.4 g, 43.3%) and a mixture of two dimers (7.2 g, 13.9%). The dimers were separated on a preparative TLC (developed three times with hexane–ethyl acetate 3:1) to give 2,3′:2′,3-bis-*O*-methylenedi(benzyl 4,6-*O*-benzylidene-α-D-glucopyranoside) (**14**) and the corresponding 2,2′:3,3′-bis-*O*-methylene isomer (**15**) in 6.2% and 7.2% yields, respectively.

13: Mp 107—108 °C, $[\alpha]_D$ +123° (*c* 1.0, $CHCl_3$); NMR: 7.6—7.2 (Ph; m), 5.58 (PhCH; s), 5.35 (H-1; d, $J_{1,2}=3.5$), 5.17 (OCH_2O, s), 4.64 and 4.67 (CH_2Ph, ABq, $J=12.8$), 3.45 (H-2; dd, $J_{2,3}=9.0$), 3.68—4.30 (H-3, H-4, H-5, H-6, and H-6′, m). Found: C, 67.99; H, 5.86%. Calcd for $C_{21}H_{22}O_6$: C, 68.09; H, 5.99%.

14: Mp 111—113 °C, $[\alpha]_D$ +171° (*c* 0.98, $CHCl_3$); NMR: 7.14—7.53 (Ph; m), 4.75 and 4.96 (OCH_2O, ABq, $J=7.0$), 4.90 (H-1; d, $J_{1,2}=4.0$), 4.63 and 4.74 ($PhCH_2$; ABq, $J=12.0$), 4.18 (H-6e; dd, $J_{6e,6a}=9.5$, $J_{5,6a}=4.0$), 4.12 (H-3; t, $J_{2,3}=J_{3,4}=9.0$), 3.87 (H-5; dd, $J_{4,5}=9.0$), 3.71 (H-6e; d), 3.49 (H-4; t), 2.57 (H-2; dd); MS (70 eV): *m/e* 741. Found: C, 68.00; H, 5.87%. Calcd for $C_{42}H_{44}O_{12}$: C, 68.09; H, 5.99%.

15: Mp 114—116 °C, $[\alpha]_D$ +196° (*c* 0.8, $CHCl_3$); NMR: 7.10—7.60 (Ph; m), 4.92 (H-1; d, $J_{1,2}=3.5$), 3.71 and 4.90 (OCH_2O; each s), 5.49 (PhCH, s), 4.58 and 4.76 ($PhCH_2$; ABq, $J=12.0$), 4.17 (H-6e; dd, $J_{5,6e}=4.0$, $J_{6e,6a}=9.5$), 4.00 (H-3; t, $J_{2,3}=J_{3,4}=9.5$), 3.80 (H-5; dt, $J_{4,5}=J_{5,6a}=9.5$), 3.68 (H-6a; t), 3.66 (H-2; dd), 3.49 (H-4; t); MS (70 eV): *m/e* 740. Found: C, 68.47; H, 6.21%. Calcd for $C_{42}H_{44}O_{12}$: C, 68.09; H, 5.99%.

*Methyl 4,6-O-Benzylidene-2,3-O-methylene-α-D-glucopyranoside (**16**) and -α-D-allopyranoside (**17**).* *(A)*: Reaction of 4,6-*O*-benzylidene-α-D-glucopyranoside (1 g, 3.5 mmol) in DMF (50 ml) with sodium hydride (0.27 g, 10.6 mmol) and dibromomethane (1.85 g, 10.6 mmol) as above, and the usual work up of the reaction mixture gave **16** [mp 103—104 °C, $[\alpha]_D$ +124.1° (*c* 1.0, $CHCl_3$); MS: *m/e* 294; lit,[11] mp 104—105 °C, $[\alpha]_D$ +122.9° (*c* 0.21, $CHCl_3$); Found: C, 61.03; H, 6.07%. Calcd for $C_{15}H_{18}O_6$: C, 61.21; H, 6.17%], and two dimers [mp 209—212 °C and 225—229 °C; each MS: *m/e* 588. Found: C, 61.69; H, 6.20%. Calcd for $C_{30}H_{36}O_{12}$: C, 61.21; H, 6.17%] in 28% (290 mg), 22% (230 mg), and 13% (140 mg) yields, respectively.

(B): A similar reaction of methyl 4,6-*O*-benzylidene-α-D-allopyranoside[14] (3.7 g, 13.1 mmol) gave the corresponding 2,3-*O*-methylene derivative (**17**) in 50% (1.93 g) yield. Mp 162—164 °C, $[\alpha]_D$ +102.8° (*c* 1.0, $CHCl_3$); NMR: 7.5—7.2 (Ph; m), 5.54 (PhCH; s), 5.32 and 5.06 (OCH_2O; ABq, $J=1.8$), 4.74 (H-1; dd, $J_{1,2}=4.0$, $J_{1,3}=1.6$), 4.44—4.20 (H-2, H-5, H-6e; m, $J_{5,6e}=5.2$, $J_{6e,6a}=10.5$), 4.12 (H-4; dd, $J_{4,5}=10.0$, $J_{3,4}=5.0$), 3.80 (H-3; m, $J_{2,3}=8.4$), 3.68 (H-6a; t, $J_{5,6a}=10.0$), 3.40 (OMe).

*Benzyl 2,3-O-Methylene-α-D-glucopyranoside (**18**).* A solution of **13** (22.4 g, 60.5 mmol) in 80% acetic acid (400 ml) was stirred 1 d at room temperature. The solution was extracted with petroleum ether to remove benzaldehyde, and the water layer was evaporated to give crystals which were recrystallized from ethanol–hexane. From the mother liquor, the second crop was obtained by separation on a silica gel column (hexane–ethyl acetate 3:1). The combined yield was 63.7% (10.8 g). Mp 108—110 °C, $[\alpha]_D$ +176° (*c* 1.0, $CHCl_3$). Found: C, 59.17; H, 6.38%. Calcd for $C_{14}H_{18}O_6$: C, 59.56; H, 6.43%.

*Benzyl 2,3-O-Methylene-6-O-(p-tolylsulfonyl)-α-D-glucopyranoside (**19**).* To an ice-cooled solutions of **18** (10 g, 35.4 mmol) in pyridine (150 ml) was added portionwise with stirring *p*-toluenesulfonyl chloride (9.9 g, 50 mmol). After keeping at room temperature overnight, the reaction mixture was poured into ice–water and extracted with chloroform. Evaporation of the chloroform solution gave a syrup which was separated on a silica gel column (hexane–ethyl acetate 8:1) to give **19** (12.3 g, 80%) and the corresponding di-*O*-tosylate (**20**: 1.7 g, 8%).

19: Mp 80—82 °C, $[\alpha]_D$ +78.9° (*c* 1.2, $CHCl_3$), NMR: 7.84—6.70 (Ph; m), 5.02 (H-1; d, $J_{1,2}=3.0$), 4.90 and 4.88 (OCH_2O; ABq, $J=0.8$), 4.81 (H-4; t, $J_{4,5}=9.0$), 4.50 and 4.48 (CH_2Ph; ABq, $J=12.0$), *ca.* 4.32 (H-6a and H-6e; m), 4.00 (H-3; t, $J_{3,4}=9.0$), 3.62 (H-5; m), 3.10 (H-2; dd, $J_{2,3}=9.0$), 2.94 (OH; s), 2.44 (CH_3Ph; s). Found: C, 58.14; H, 5.60; S, 7.59%. Calcd for $C_{21}H_{24}O_8S$; C, 57.79; H, 5.54; S, 7.35%.

20: Mp 144—145 °C, $[\alpha]_D$ +87.6° (*c* 1.1, $CHCl_3$), NMR: 7.15—7.85 (Ph; m), 5.21 (H-1; d, $J_{1,2}=3.0$), 5.04 (OCH_2O; s), 4.72 (H-4; t, $J_{3,4}=J_{4,5}=10.0$), 4.57 and 4.70 (CH_2Ph; ABq, $J=11.0$), 4.25 (H-6e; dd, $J_{5,6e}=2.5$, $J_{6e,6a}=11.0$), 4.03 (H-6a; dd, $J_{5,6a}=5.5$), 3.95 (H-3; t, $J_{2,3}=10.0$), 3.70 (H-5; sex), 3.30 (H-2; dd), 2.45 ($2\times CH_3Ph$). Found: C, 57.54; H, 5.16; S, 10.7%. Calcd for $C_{28}H_{30}O_{10}S_2$: C, 56.93; H, 5.12; S, 10.7%.

*Benzyl 6-Deoxy-2,3-O-methylene-α-D-glucopyranoside (**21**).* A mixed solution of **19** (8 g, 18.4 mmol) and sodium borohydride (1.7 g, 45.7 mmol) in DMSO (100 ml) was heated at 80 °C for 3 h, and then poured into ice–water. The resulting solution was extracted with ether, and the extract was evaporated. The residual syrup was purified on a silica gel column (hexane–ethyl acetate 8:1) to give **21** (6.1 g, 81%) as a syrup. $[\alpha]_D$ +154° (*c* 0.85, $CHCl_3$), NMR: 7.50—7.20 (Ph; m), 5.24 (H-1; d, $J_{1,2}=3.0$), 5.13 (OCH_2O; s), 4.63 and 4.80 (CH_2Ph; ABq, $J=10.5$), 3.87 (H-3; t, $J_{2,3}=J_{3,4}=9.5$), 3.56 (H-5; dq, $J_{4,5}=9.5$, $J_{5,6}=6.5$), 3.45 (H-4; t), 3.35 (H-2; dd), 1.30 (H-6; d). Found: C, 62.64; H, 6.95%. Calcd for $C_{14}H_{18}O_5$: C, 63.14; H, 6.81%.

*Methyl 6-Deoxy-2,3-O-methylene-α-D-glucopyranoside (**22**).* Compound **16** was converted into **22** in a similar manner to that of **13** into **21**. Partial hydroxysis of **16** (24 gr, 8.16 mmol) in aqueous acetic acid (80%, 500 ml) at 35 °C for 1 d gave methyl 2,3-*O*-methylene-α-D-glucopyranoside (12 g, 68.5%) as a syrup. Monotosylation of the syrup (9.4 gr, 45.6 mmol) in pyridine (200 ml) with *p*-toluenesulfonyl chloride (9.9 g, 52 mmol) and purification of the products on a silica gel column (benzene–acetone 50:1) gave the 6-*O*-tosylate (12.6 g, 77%) as a syrup. NMR: 7.80 and 7.34 (Ph; each d, $J=8.0$), 5.13 (OCH_2O; s), 5.05 (H-1; d, $J_{1,2}=3.2$), 4.36 (H-6; dd, $J_{5,6}=4.0$, $J_{6,6'}=11.0$), 4.30 (H-6′; dd, $J_{5,6'}=2.4$), 3.9—3.4 (H-3, H-4, and H-5; m), 3.44 (OMe; s), 3.28 (H-2; dd, $J_{2,3}=9.5$), 2.44 (CMe; s). Found: C, 50.00; H, 5.60; S, 8.88%. Calcd for $C_{15}H_{20}O_8S$: C, 49.99; H, 5.59; S, 8.90%.

Reduction of 6-*O*-tosylate (9.18 g, 25.5 mmol) in THF (400 ml) with lithium aluminium hydride (LAH) (1.94 g, 50 mmol) and the purification of the product on a silica gel column gave pure **24** (2.0 g, 41.3%) as a syrup. $[\alpha]_D$ +202.3° (*c* 1.0, $CHCl_3$). Found: C, 50.21; H, 7.71%. Calcd for $C_8H_{14}O_5$: C, 50.52; H, 7.42%.

*Methyl 6-Deoxy-2,3-O-methylene-α-D-allopyranoside (**23**).* Compound **17** was converted into **23** as above. Partial hydrolysis of **17** and successive monotosylation of the product gave methyl 2,3-*O*-methylene-6-*O*-tosylsulfonyl-α-D-allopyranoside as a syrup in 62% yield. $[\alpha]_D$ +65.3° (*c* 1.0, $CHCl_3$). NMR: 7.79 and 7.36 (Ph; each d, $J=8.0$), 5.02 and 4.80 (OCH_2O; ABq, $J=2.0$), 4.58 (H-1; d, $J_{1,2}=5.0$), 4.4—4.1 (H-6 and H-6′; $J_{5,6}=2.4$, $J_{5,6'}=5.0$, $J_{6,6'}=10.8$), 4.06 (H-2; t, $J_{2,3}=5.0$), 3.95—3.65 (H-3 and H-5;

m, $J_{3,4}=3.0$, $J_{4,5}=10.0$), 3.50 (H-4; m), 3.34 (OMe; s), 3.24 (OH; s), 2.47 (CMe; s). Found: C, 49.76; H, 5.65; S, 8.75%. Calcd for $C_{15}H_{20}O_8S$: C, 49.99; H, 5.59; S, 8.90%.

Reduction of the above 6-*O*-tosylate with LAH gave **23** as a syrup in 83% yield. $[\alpha]_D$ +88.4° (*c* 2.75, $CHCl_3$); NMR: 5.27 and 5.03 (OCH_2O; ABq, $J=2.0$), 4.69 (H-1; d, $J_{1,2}=5.0$), 4.35—4.10 (H-3 and H-4; m), 3.64 (H-5; dq, $J_{5,6}=6.3$, $J_{4,5}=10.0$), 3.25 (H-4; dd, $J_{3,4}=3.5$), 3.40 (OMe; s), 2.56 (OH; s), 1.29 (H-6; d). Found: C, 50.41; H, 7.56%. Calcd for $C_8H_{14}O_5$: C, 50.52; H, 7.42%.

The coupling constants mentioned above indicate that **23** and the precursor exist in a flattened *C*1 conformation.

*Benzyl 2,3-Di-*O*-benzyl-6-deoxy-α-*D*-glucopyranoside (**24**).* To an ice-cooled solution of benzyl 2,3-di-*O*-benzyl-α-D-glucopyranoside[10] (28 g, 62 mmol) in pyridine (400 ml) was added *p*-toluenesulfonyl chloride (15.7 g, 82 mmol) portionwise for 4 h with stirring. After keeping overnight at room temperature, the reaction mixture was poured into ice-water and extracted with chloroform. The chloroform solution was evaporated, and the residual syrup was dried and dissolved in THF, and LAH (2.8 g, 74 mmol) was added to THF solution with stirring. After stirring for 3 h at room temperature, a mixture of ethyl acetate and water was added to the reaction mixture and the precipitates deposited were filtered off. The filtrate was extracted with chloroform, and evaporation of the extract gave a syrup (13.2 g) which was purified on a silica gel column (hexane–ethyl acetate 10:1) to give **24** as a syrup (10.2 g, 38%). $[\alpha]_D$ +51.5° (*c* 0.84, $CHCl_3$), NMR: 7.44—7.22 (Ph; m), 4.79 (H-1; d, $J_{1,2}=3.0$), 4.42—5.09 (CH_2Ph; m), 3.81 (H-4; t, $J_{3,4}=J_{4,5}=9.5$), 3.75 (H-5; dq, $J_{5,6}=5.5$), 3.50 (H-2; dd, $J_{2,3}=9.5$), 3.17 (H-3; t), 1.23 (H-6; d). Found: C, 71.60; H, 6.98%. Calcd for $C_{27}H_{30}O_6$: C, 71.98; H, 6.71%.

Preparation of 4-Uloses. Method A: Oxidation with chromium oxide-pyridine is illustrated by the preparation of methyl 6-deoxy-2,3-*O*-methylene-α-D-*ribo*-hexopyranosid-4-ulose (**6**). To a mixture of pyridine (1.79 g, 22.6 mmol) and dichloromethane (40 ml) was added chromium trioxide (1.81 g, 18.1 mmol) in two portions, and the mixture was stirred for 20 min. To the mixture was added a solution of **22** (860 mg, 45 mmol) in dichloromethane (10 ml) and it was stirred for 20 min until **22** had disappeared on TLC. The mixture was poured into saturated sodium hydrogencarbonate, and the organic layer was processed conventionally to give a syrup which was purified on a silica gel column (benzene–acetone 5:1) to give **6** (382 mg, 45%). This fact implies the epimerrization at *C*-3 during the oxidation. IR: 1745 (C=O). Found: C, 50.82; H, 6.21%. Calcd for $C_8H_{12}O_5$: C, 51.06; H, 6.43%.

Method B: The DMSO–acetic anhydride oxidation is typically shown by the preparation of benzyl 2,3-di-*O*-benzyl-β-L-*threo*-pentopyranosid-4-ulose (**1**). A solution of **11** (0.5 g, 1.19 mmol) in DMSO (8 ml) and acetic anhydride (4 ml) was kept overnight at room temperature, poured into ice–water, and extracted with ether. The usual work up of the extract gave **1** as a syrup in 60% (0.3 g) yield. $[\alpha]_D$ +98.3° (*c* 1.25, $CHCl_3$), IR: 1740 (C=O). Found: C, 74.08; H, 6.51%. Calcd for $C_{26}H_{26}O_5$: C, 74.62; H, 6.26%.

Method C: The DMSO–trifluoroacetic anhydride oxidation is illustrated by the preparation of benzyl 2,3-di-*O*-benzyl-6-*O*-trityl-α-D-*xylo*-hexopyranosid-4-ulose (**5**). To a chilled solution of DMSO (143 mg, 2.01 mmol) and dichloromethane (2 ml) at −78 °C was added trifluoroacetic anhydride (318 mg, 1.51 mmol) in dichloromethane (2 ml) with stirring, and after 10 min, subsequently a solution of benzyl 2,3-di-*O*-benzyl-6-*O*-trityl-α-D-glucopyranosid (**25**)[12] (349 mg, 0.58 mmol) in dichloromethane (4 ml) dropwise. After stirring for 1 h, the reaction mixture was carefully neutralized at −78 °C with triethylamine, and then poured into ice-water. The resulting solution was extracted with chloroform, and the usual work up of the extract and purification of the product on a silica gel column gave pure **5** in 98% (341 mg) yield, which was crystallized from ethanol. Mp 131—136 °C; $[\alpha]_D$ +41.5° (*c* 1.42, $CHCl_3$). Found: C, 79.50; H, 6.01%. Calcd for $C_{46}H_{42}O_6$: C, 79.98; H, 6.13%.

In a similar manner, benzyl 2,3-*O*-methylene-β-L-*threo*-pentopyranosid-4-ulose (**2**), benzyl 2,3-*O*-benzyl-6-deoxy-α-D-*xylo*-hexopyranosid-4-ulose (**3**), benzyl 2,3-*O*-methylene-6-deoxy-α-D-*xylo*-hexopyranosid-4-ulose (**4**) were also obtained as syrups from **12**, **24**, and **21**, respectively. These compounds showed the correct analytical values, and the structures were confirmed by the NMR and IR spectra. However, the rotational values were not measured, because a small amount of impurities could not be removed, and they were directly used to the next reaction.

The present work was partially supported by a Grand-in-Aid for Scientific Research No. 347023 from Ministry of Education, Science and Culture.

References

1) Part XXI: M. Iwakawa, J. Yoshimura, and M. Funabashi, *Bull. Chem. Soc. Jpn.*, **54**, 496 (1981).
2) J. Yoshimura, K. Mikami, K. Sato, and C. Shin, *Bull. Chem. Soc. Jpn.*, **49**, 1686 (1976).
3) J. Yoshimura, K. Sato, K. Kobayashi, and C. Shin, *Bull. Chem. Soc. Jpn.*, **46**, 1515 (1973).
4) K. Sato and J. Yoshimura, *Bull. Chem. Soc. Jpn.*, **51**, 2116 (1978); *Carbohydr. Res.*, **73**, 75 (1979).
5) K. Sato, J. Yoshimura, and C. Shin, *Bull. Chem. Soc. Jpn.*, **50**, 1191 (1977); K. Sato, K. Koga, H. Hashimoto, and J. Yoshimura, *ibid.*, **53**, 2639 (1980).
6) A. K. Ganguly, "Oligosaccharide Antibiotics," in "Topics in Antibiotic Chemistry," ed by P. G. Sammes, Billis Horwood Ltd, Chichester, John Wiley and Sons, Chichester, New York, Brisbane, Toronto (1978), Vol. 2, p. 61.
7) W. D. Ollis, C. Smith, and D. E. Wright, *Tetrahedron*, **35**, 105 (1979); W. D. Ollis, I. O. Sutherland, and B. F. Taylor, *ibid.*, **35**, 993 (1979); W. D. Ollis, S. Jonest, and C. Smith, *ibid.*, **35**, 1003 (1979).
8) W. Heilman, E. Kupfer, W. Keller-Schierlein, H. Zähner, H. Wolf, and H. H. Peter, *Helv. Chim. Acta*, **61**, 1 (1978); F. Buzzetti, F. Eisenberg, H. N. Grant, W. Keller-Schierlein, W. Voser, and H. Zähner, *Experientia*, **24**, 320 (1968).
9) T. Sivakumaran and J. K. N. Jones, *Can. J. Chem.*, 45, 2493 (1967).
10) P. M. Pojer and S. J. Angyal, *Tetrahedron Lett.*, **1967**, 3067.
11) J. S. Brimacombe, A. B. Foster, B. D. Jones, and J. J. Willard, *J. Chem. Soc., C*, **1967**, 2407.
12) A. Lubinean, A. Thieffry, and A. Veyrieres, *Carbohydr. Res.*, **46**, 143 (1976).
13) K. S. Kim and W. A. Szarek, *Synthesis*, **1978**, 48.
14) Y. Kondo, *Carbohydr. Res.*, **30**, 386 (1973).
15) C. L. Stevens and S. H. Czernecki, *Carbohydr. Res.*, **63**, 307 (1978).
16) J. Yoshimura, K. Sato, and H. Hashimoto, *Chem. Lett.*, **1977**, 1327.

Determination of the Non-stoichiometry of Zeolite A

Tatsuo OHGUSHI

School of Materials Science, Toyohashi University of Technology, Tempaku-cho, Toyohashi 440

(Received September 29, 1980)

Zeolite A was synthesized in the sodium form with the composition $Na_{12}(AlO_2 \cdot SiO_2)_{12}(NaAlO_2)_\delta \cdot nH_2O$, $0 \leqq \delta \leqq 1$. A new method was developed for the determination of the δ-value of the non-stoichiometric part in the product. It consists of repeated ion exchanges of zeolite with $TlNO_3$ (or $BaCl_2$), and determination of the residual amount of Na^+ in the zeolite as a function of the number of treatments. The K_δ/δ value was determined from a linear plot, where K_δ is a selectivity coefficient of the ion exchange reaction between Tl^+ (or Ba^{2+}) and Na^+ in the non-stoichiometric part. The K_δ value was taken from the observed K_δ/δ value, the δ-value being obtained by chemical analysis. The δ-value of a sample can be determined by introducing the K_δ-value into K_δ/δ. An approximate δ-value can be estimated from a break point of the curve, log(residual amount of Na^+) *vs.* the number of times of treatment.

Zeolite A was synthesized in the sodium form, having the composition $Na_{12}(AlO_2 \cdot SiO_2)_{12}(NaAlO_2)_\delta \cdot nH_2O$, with $0 \leqq \delta \leqq 1$.[1,2] The $(AlO_2 \cdot SiO_2)_{12}$ constitutes the framework of the crystal, twelve Na^+ undergoing ion exchange with other cations.[1-4] The non-stoichiometric part, $NaAlO_2$, abbreviated as the δ-part, is occluded in the β-cage of sodalite unit.[2,5] This model for the δ-part, however, has not been confirmed as yet by X-ray analysis, since the structural studies have usually been carried out with single crystals synthesized by Charnell's method,[6] which are said to contain no non-stoichiometric part.[7,8] On the other hand, most studies on ion exchange, thermal measurement, gas sorption, and catalysis are carried out with commercial zeolite (hydrothermally synthesized), and their non-stoichiometry cannot be ignored. The physical and chemical properties of zeolite A, which might be influenced by the δ-value are as follows. In entirely Ca-exchanged zeolite A, $(1+\delta)Ca^{2+}$ ions are located on the 8-membered oxygen ring,[9] Ca^{2+} acting as a highly active center for the isomerization reaction of 1-butene.[10] In (K,Zn)–A systems, discrepancy was found between the conclusions obtained by X-ray analysis[11] and ion exchange isotherm.[12] This was explained by a difference in δ-values of samples.[9] Recently Rees analyzed ion exchange isotherms on (Na,Ca)–A systems and found that there is considerable divergence in data obtained by different authors.[13] He suggested that such divergence is partly attributable to the difference in δ-values.[14]

It is desirable to work out a reliable method to determine the δ-value. The one proposed by Barrer and Meier is too laborious.[15] In the present paper new methods are proposed.

Experimental

Pretreatment. Commercial molecular sieves 4A powder (Shōwa-Unox Co., Lot No. 410713) was used as the starting material. The powder, which was passed through a 200-mesh sieve, contained some sodium hydroxide and iron oxide. In order to remove these impurities, the powder was shaken with a vibrator washer fifteen times in 0.2—0.02 mol dm^{-3} sodium acetate and then washed with distilled water three times. The residual iron impurity was less than 50 ppm as checked by spectrophotometry.

Chemical Analysis. The pretreated zeolite (*ca.* 0.6 g) was dehydrated at 400 °C in a vacuum of 10^{-3} Pa for 4 h and weighed *in situ* with a quartz spring balance. The sensitivity and sensibility of the balance were 0.5 mm/mg and 0.2 mg, respectively. The sample was dissolved in 2 mol dm^{-3} HCl with sodium impurity less than 0.65 ppm in 37% concentration. The amount of silicon, aluminum, and sodium in the dissolved solution was analyzed by gravimetry. Silicon was precipitated as silica, and the filtrate, free from silica, was analyzed. Aluminum and sodium were precipitated as complexes with oxine and zinc uranyl acetate, respectively, and weighed after filtration.[16]

Activation Analysis. Residual amounts of sodium, in ion exchanged Tl–A, Ba–A, and Sr–A zeolite, were determined by neutron activation analysis. Dehydrated samples weighed were irradiated in a TRIGA MARK II REACTOR of Rikkyo (St. Paul's) University for 1—5 h. After a cooling time of 20 h, 1368.4 and 2753.6 keV γ-rays from ^{24}Na in the sample were measured with a γ-ray spectrometer (CANBERRA Ge(Li)-4K-PHA). The absolute amount of ^{24}Na in the sample was determined by comparison with a standard sample. Dehydrated Na_{12}–A zeolite was used as a standard since neutrons are absorbed and reflected by it in a way similar to that of the sample concerned. The sodium content of the standard was determined by chemical analysis.[16]

Results

Chemical Analysis. Results of the chemical analysis of Na–A are given in Table 1. The δ-value was determined from the ratio [Si]/[Al] but not from [Si]/[Na]. When zeolite A is washed a certain amount of Na^+'s is replaced by proton,[17-19] and hence the ratio [Si]/[Na] cannot be used as a means to determine the δ-value. The unfavorable proton exchange is estimated to be 0.5 protons per unit cell from the ratio [Na]/[Al] (Table 1), since [Na]/[Al] would have been unity if no hydrolysis took place.† The observed value for the ratio [Si]/[Al] is 0.988 ± 0.05, giving $\delta = 0.15 \pm 0.05$.

Ion Exchange. (a) Na_{12}–A zeolite (2 g) was subjected to ion exchange in 30 ml of a 0.2 mol dm^{-3} $TlNO_3$ or $BaCl_2$ solution at 82 ± 2 °C. (b) The same amount of zeolite was treated in 50 ml of a 0.05 mol dm^{-3} $BaCl_2$, $SrCl_2$, or $TlNO_3$ solution at 82 ± 2 °C.

† The decrease in the total sum of the components resulted from both partial hydrolysis and incomplete dehydration. No analysis of protons and water was carried out. The residual amount of H_2O molecules is estimated to be *ca.* 2 molecules per unit cell.

Table 1. Results of the chemical analysis of Na-A

No.	Dehydrated zeolite wt / mg	SiO_2 wt%	Al_2O_3 [a] wt%	Na_2O [b] wt%	Total wt%	[Si]/[Al] $=\delta/(12+\delta)$	δ
1	644.7	41.82	—	—	—	—	—
2	561.4	41.86	36.02	—	—	0.986	0.17
3	642.5	41.66	35.78	—	—	0.988	0.15
4	660.5	—	35.82	21.0	—	—	—
5	693.6	41.74	35.86	20.8	98.4	0.988	0.15
Ave.		41.77±0.11	35.87±0.14	20.9±0.3	98.5±0.4	0.988±0.005	0.15±0.05

a) The weight of Al_2O_3 was calculated from that of $Al(C_9H_6ON)_3$. The conversion factor is 0.1109. b) The weight of Na_2O was calculated by multipling the weight of $NaZn(UO_2)_3(CH_3COO)_9\cdot 6H_2O$ by 0.01495.

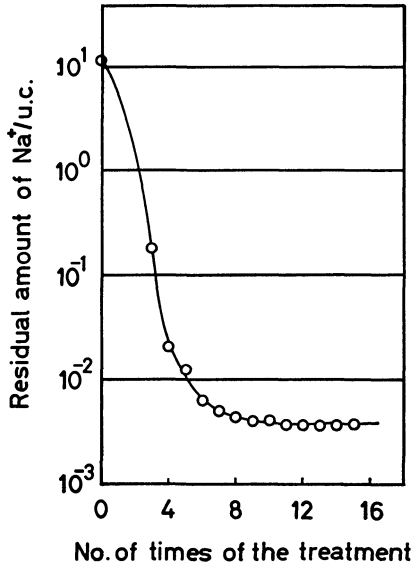

Fig. 1. Residual amount of Na^+ per unit cell in Tl-exchanged zeolites *vs.* the number of times of the treatment.

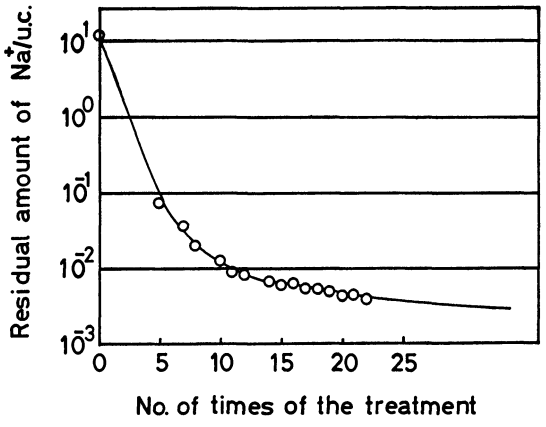

Fig. 2. Residual amount of Na^+ per unit cell in Ba-exchanged zeolites *vs.* the number of times of the treatment.

After equilibration the zeolite and the solution were separated, the zeolite being subjected to the same treatment. The process was repeated. We prepared samples subjected to the treatment 1, 2,……ν-times. The residual amount of sodium in the sample treated n-times, $[Na]_n$, was determined by activation analysis.

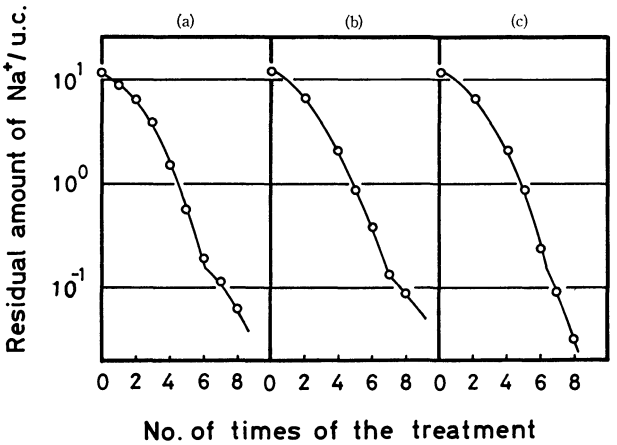

Fig. 3. Residual amount of Na^+ per unit cell in zeolites ion exchanged with dilute solutions.
a): Ba-exchanged zeolite, b): Sr-exchanged zeolite, c): Tl-exchanged zeolite.

The value for $\log [Na]_n$, thus determined, is plotted against n, the number of times of treatment (Figs. 1—3).

Analysis and Discussion

Determination of the Selectivity Coefficient. After repetition of ion exchange, all Na^+ ions on easily exchangeable sites (normal site) are replaced by the ion exchanging cations. Further exchange deals with the Na^+ ions on the δ-site. However, the amount of sodium includes the contribution from a nuclear side-reaction $^{27}Al(n,\alpha)^{24}Na$. This is negligibly small in the initial part of the curves (Figs. 1 and 2) but significant in the final part. The contribution corresponds to a spurious 1.83×10^{-3} Na per unit cell.[20] Subtracting this we obtain the curves for the residual amount (Figs. 4 and 5).

Let us analyze the curve (Fig. 4) by means of the equation

$$[Na]_n = \frac{[Na]_{n-1}}{1+m'(Tl)_s K_\delta(Na,Tl)/\delta} + \frac{m'(Tl)_s K_\delta(Na,Tl)[Na]_\infty/\delta}{1+m'(Tl)_s K_\delta(Na,Tl)/\delta}, \quad (1)$$

where $[Na]_n$ and $[Na]_\infty$ denote the residual amount of sodium after repetition of treatment n-times and infinite number of times, respectively, $K_\delta(Na,Tl)$ the

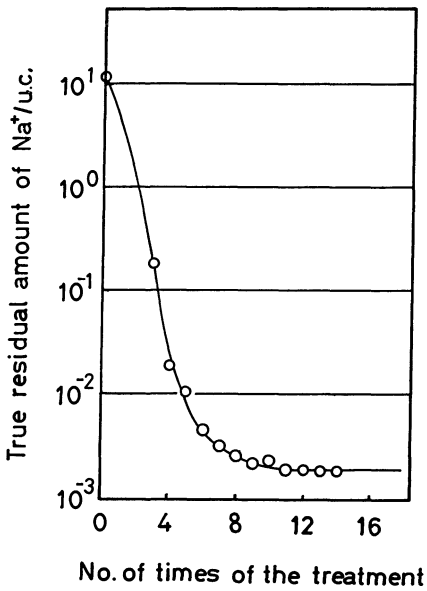

Fig. 4. True residual amount of Na^+ per unit cell in Tl-exchanged zeolites *vs.* the number of times of the treatment.

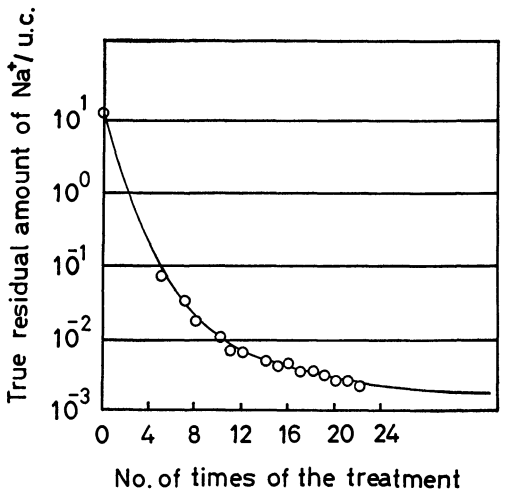

Fig. 5. True residual amount of Na^+ per unit cell in Ba-exchanged zeolites *vs.* the number of the times of the treatment.

selectivity coefficient of the ion exchange reaction between Tl^+ and Na^+ on δ-site, $m'(Tl)_s$ the amount of Tl^+, in mole, contained in the exchanging solution initially loaded. The derivation of Eq. 1 is given in the Appendix. Figure 4 gives the value of $[Na]_\infty$:

$$[Na]_\infty = 1.90\times10^{-3}\,Na^+/u.c.$$

When $[Na]_n$ is plotted against $[Na]_{n-1}$, we have a straight line (Fig. 6). The line crosses a line having a slope of unity at $[Na]_\infty(=1.90\times10^{-3})$. The straight line is represented by

$$[Na]_n = 0.53[Na]_{n-1} + 9.0\times10^{-4}. \quad (2)$$

Comparing Eqs. 1 and 2, we get

$$K_\delta(Na,Tl) = 0.89\ \delta/m'(Tl)_s.$$

Introducing the experimental value $m'(Tl)_s=6.67$, we have

$$K_\delta(Na,Tl) = 0.13\delta.$$

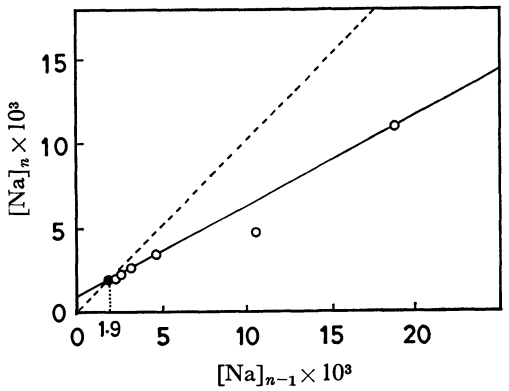

Fig. 6. Plots of $[Na]_n$ *vs.* $[Na]_{n-1}$ for (Na,Tl)–A system. The solid line is a most probable line to the plotts and the broken line is that of unity slope.

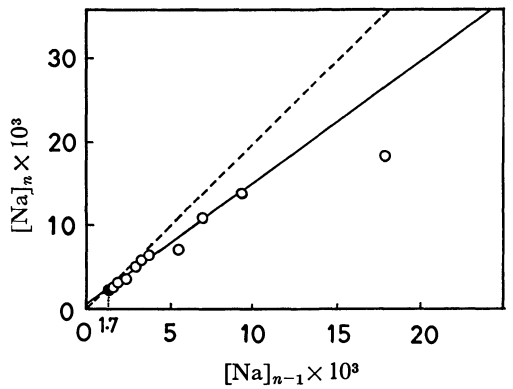

Fig. 7. Plots of $[Na]_n$ *vs.* $[Na]_{n-1}$ for (Na,Ba)–A system. Broken line is that of unity slope.

If we use the δ-value obtained by chemical analysis, the value for $K_\delta(Na,Tl)$ is determined as

$$K_\delta(Na,Tl) = (2.0\pm0.4)\times10^{-2}. \quad (3)$$

Similar analysis can be carried out for a (Na,Ba)–A system by use of the equation

$$[Na]_n = \frac{[Na]_{n-1}}{1+\frac{m'(Ba)_s}{\delta}\sqrt{\frac{2K_\delta(Na,Ba)}{T_n}}} + \frac{[Na]_\infty\frac{m'(Ba)_s}{\delta}\sqrt{\frac{2K_\delta(Na,Ba)}{T_n}}}{1+\frac{m'(Ba)_s}{\delta}\sqrt{\frac{2K_\delta(Na,Ba)}{T_n}}} \quad (1')$$

where $K_\delta(Na,Ba)$ is the selectivity coefficient of the ion exchange reaction between Ba^{2+} and Na^+ on the δ-site and T_n the total normality of the solution. From Fig. 5, $[Na]_\infty$ was chosen for the (Na,Ba)–A as

$$[Na]_\infty = 1.7\times10^{-3}\ Na^+/u.c.$$

Plots of $[Na]_n$ *vs.* $[Na]_{n-1}$ for the system are shown in Fig. 7. A straight line for the plots, passing through the point $[Na]_\infty$, is represented by

$$[Na]_n = 0.77[Na]_{n-1}+3.9\times10^{-4}. \quad (2')$$

From Eqs. 1′ and 2′, we obtain

$$K_\delta(Na,Ba) = 4.5\times10^{-2}\,\delta^2T_n/m'(Ba)_s.$$

Since $m'(Ba)_s=3.33$ and $T_n=0.20$, we have

$$K_\delta(Na,Ba) = 8.0\times10^{-4}\,\delta^2.$$

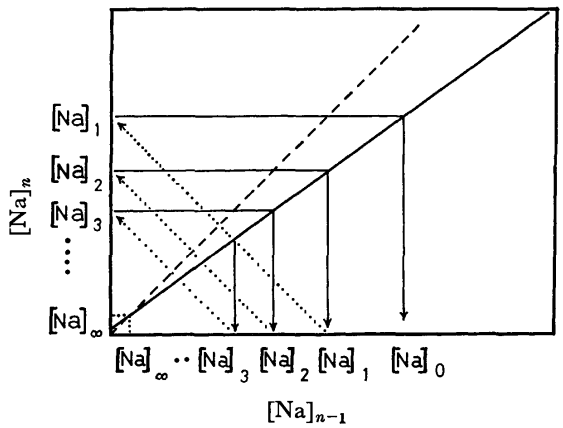

Fig. 8. Schematic diagram which shows a procedure to obtain $[Na]_0$ by using $[Na]_n$-$[Na]_{n-1}$ plotts.

By use of the δ-value determined by chemical analysis, K_δ(Na,Ba) is calculated as

$$K_\delta(\mathrm{Na,Ba}) = (1.8\pm0.4)\times10^{-5}.$$

Determination of the δ-Value. Use of Eq. 1: For the sake of brevity, let us discuss the case of Tl-exchanges.

Introducing Eq. 3 into Eq. 1, we get

$$[\mathrm{Na}]_n = \frac{[\mathrm{Na}]_{n-1}}{1+2.0\times10^{-2}\,m'(\mathrm{Tl})_s/\delta} + \frac{2.0\times10^{-2}m'(\mathrm{Tl})_s[\mathrm{Na}]_\infty/\delta}{1+2.0\times10^{-2}\,m'(\mathrm{Tl})_s/\delta}. \quad (4)$$

When the same experiments are carried out with an unknown sample, values for $[Na]_n$, $[Na]_{n+1}$ *etc.* being measured, its δ-value is determined by means of Eq. 4.

Approximate Methods: The principle of the method is schematically given in Fig. 8. The value for $[Na]_{\nu-1}$ is given from $[Na]_\nu$. The final value for $[Na]_0$ is obtained by repeating the procedure. According to Eq. 1, the $[Na]_0$ value corresponds to the initial amount of sodium in the δ-part. In the present case, we have

$$\delta = 0.12\pm0.05,$$

in agreement with the result of the chemical analysis.

Empirical Methods: When Na–A zeolite is treated with a dilute solution, we obtain curves as shown in Fig. 3. Break points in the curves roughly correspond to the point where easy exchange stops and hard exchange starts. The δ-value is determined from the break as follows.

$\delta = 0.16\pm0.02$ in $BaCl_2$ solution

$\delta = 0.14\pm0.02$ in $SrCl_2$ solution

and

$\delta = 0.15\pm0.04$ in $TlNO_3$ solution.

These values agree with those given by chemical analysis, in spite of the crude procedure.

Conclusion

As compared with the method of Barrer and Meier, the present method is efficient.

Systems (Na,Tl)–A and (Na,Ba)–A were used for determination of the δ-value; the former seems superior.

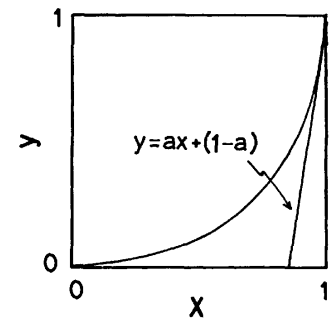

Fig. 9. Ion exchange isotherm for the δ-site. x and y are equivalent cation fractions in a solution and on the δ-site, respectively. Solid line is an asymptote.

Determination of the $[Na]_\infty$ value is easier in (Na, Tl)–A. In the empirical method, systems (Na,Ba)–A and (Na,Sr)–A are superior to system (Na,Tl)–A since Na^+ on the δ-site is not easily replaced by Ba^{2+} or Sr^{2+}, a sharp break appearing in the curve of $\log [Na]_n$ *vs.* n.

Tl^+ and Ba^{2+} do not seem to enter into the δ-part.[15,21] However, the present results show that this is not the case. As for Sr^{2+}, Sherry and Walton concluded that it enters into the δ-part,[21] in line with the present results.

Appendix

An ion exchange isotherm for the δ-site has a form shown in Fig. 9, where x and y are equivalent cation fractions in a solution and on the δ-site, respectively.[15] In the case of (Na,Tl)–A system, they are defined by

$$x = \frac{m(\mathrm{Tl})_s}{m(\mathrm{Tl})_s+m(\mathrm{Na})_s} \quad (5)$$

and

$$y = \frac{m(\mathrm{Tl})_\delta}{m(\mathrm{Tl})_\delta+m(\mathrm{Na})_\delta}, \quad (6)$$

where $m(Tl)_s$ and $m(Tl)_\delta$ denote the amount of Tl^+ in mole unit in the solution and on the δ-site, respectively. In the final range of the exchange, the most part of the δ-site has been occupied by Tl^+ and the final part of the exchange isotherm might converge to an asymptote

$$y = ax + (1-a). \quad (7)$$

Consider the case in which one mole of zeolite is repeatedly treated with a solution having a certain composition. The solution initially contains $m'(Tl)_s$ mole of Tl^+ ion and $r\cdot m'(Tl)_s$ of trace impurity Na^+ ion, where r denotes the proportion of the amount of Na^+ to that of Tl^+. From Eqs. 5, 6 and the material balance, we have

$$(1+r)m'(\mathrm{Tl})_s x = m(\mathrm{Tl})_s,$$
$$\delta y = m(\mathrm{Tl})_\delta,$$

and

$$(1+r)m'(\mathrm{Tl})_s x + \delta y = m(\mathrm{Tl})_t, \quad (8)$$

where $m(Tl)_t$ is the total amount of Tl^+ in the system. From Eqs. 7 and 8, we obtain

$$1-y = \frac{\delta+(1+r)m'(\mathrm{Tl})_s-m(\mathrm{Tl})_t}{\delta+(1+r)m'(\mathrm{Tl})_s/a}.$$

After ion exchange n-times, we get

$$1-y_n=\frac{\delta+(1+r)m'(\mathrm{Tl})_s-m(\mathrm{Tl})_{t,n}}{\delta+(1+r)m'(\mathrm{Tl})_s/a}. \quad (9)$$

From the material balance we have

$$m(\mathrm{Tl})_{t,n}=\delta y_{n-1}+m'(\mathrm{Tl})_s.$$

Introducing this into Eq. 9, we get

$$1-y_n=\frac{\delta(1-y_{n-1})}{\delta+(1+r)m'(\mathrm{Tl})_s/a}+\frac{r\cdot m'(\mathrm{Tl})_s}{\delta+(1+r)m'(\mathrm{Tl})_s/a}$$
$$\approx\frac{\delta(1-y_{n-1})}{\delta+m'(\mathrm{Tl})_s/a}+\frac{r\cdot m'(\mathrm{Tl})_s}{\delta+m'(\mathrm{Tl})_s/a}, \quad (10)$$

where the equation was simplified by the condition $r\ll 1$. In the present experiments, the residual amount of sodium per unit cell, $[\mathrm{Na}]_n$, is measured as a function of n, and is given by

$$[\mathrm{Na}]_n=\delta(1-y_n).$$

Thus Eq. 10 becomes

$$[\mathrm{Na}]_n=\frac{[\mathrm{Na}]_{n-1}}{1+m'(\mathrm{Tl})_s/a\delta}+\frac{r\cdot m'(\mathrm{Tl})_s}{1+m'(\mathrm{Tl})_s/a\delta}. \quad (11)$$

By repetition of ion exchange, $[\mathrm{Na}]_n$ decreases, converging to a definite value:

$$\lim_{n\to\infty}\frac{[\mathrm{Na}]_n}{[\mathrm{Na}]_{n-1}}=1.$$

Combining the above two equation, we get

$$[\mathrm{Na}]_\infty=a\delta r,$$

where $[\mathrm{Na}]_\infty$ is the converged value and determined from the flat part of the curve in Fig. 5. Thus, the unknown parameter r is eliminated from Eq. 11, and we have

$$[\mathrm{Na}]_n=\frac{[\mathrm{Na}]_{n-1}}{1+m'(\mathrm{Tl})_s/a\delta}+\frac{m'(\mathrm{Tl})_s[\mathrm{Na}]_\infty/a\delta}{1+m'(\mathrm{Tl})_s/a\delta}. \quad (12)$$

This shows that when $[\mathrm{Na}]_n$ is plotted against $[\mathrm{Na}]_{n-1}$, we get a straight line which crosses at $[\mathrm{Na}]_\infty$ with a line having a slope of unity.

The slope of straight line in Eq. 7, a, is related to a selectivity coefficient of the exchange reaction on the δ-site. The selectivity coefficient for the (Na,Tl)–A system, $K_\delta(\mathrm{Na,Tl})$, is given by

$$K_\delta(\mathrm{Na,Tl})=\frac{Na_s\cdot Tl_\delta}{Tl_s\cdot Na_\delta},$$

where Tl_s and Tl_δ denote the equivalent cation fractions of Tl^+ in the solution and on the δ-site, respectively. Such an equation was found to hold for the exchange reaction on the δ-site.[13,15] Introducing Eqs. 5 and 6 into the above equation, we have

$$K_\delta(\mathrm{Na,Tl})=\frac{(1-x)y}{x(1-y)}.$$

Since $a=(\mathrm{d}y/\mathrm{d}x)_{x=1}$, we get

$$a=\frac{1}{K_\delta(\mathrm{Na,Tl})}.$$

Eliminating the parameter a from this equation and Eq. 12, we obtain

$$[\mathrm{Na}]_n=\frac{[\mathrm{Na}]_{n-1}}{1+m'(\mathrm{Tl})_sK_\delta(\mathrm{Na,Tl})/\delta}+\frac{m'(\mathrm{Tl})_sK_\delta(\mathrm{Na,Tl})[\mathrm{Na}]_\infty/\delta}{1+m'(\mathrm{Tl})_sK_\delta(\mathrm{Na,Tl})/\delta}. \quad (13)$$

This is the fundamental equation in the present analysis and is reduced to Eq. 1 when numerical values determined experimentally are introduced.

As for the (Na,Ba)–A system, minor changes should be introduced as

$$[\mathrm{Na}]_n=\frac{[\mathrm{Na}]_{n-1}}{1+2m'(\mathrm{Ba})_s/a\delta}+\frac{2m'(\mathrm{Ba})_s[\mathrm{Na}]_\infty/a\delta}{1+2m'(\mathrm{Ba})_s/a\delta} \quad (12')$$

and

$$K_\delta(\mathrm{Na,Ba})=\frac{2Ba_\delta\cdot(Na_s)^2}{(Na_\delta)^2\cdot Ba_s}\cdot T_n,$$

where Ba_δ means the equivalent cation fraction of Ba^{2+} on the δ-site, Ba_s that in the solution and T_n a total normality of the solution. Thus, we have

$$a=\sqrt{\frac{2T_n}{K_\delta(\mathrm{Na,Ba})}}$$

and

$$[\mathrm{Na}]_n=\frac{[\mathrm{Na}]_{n-1}}{1+\frac{m'(\mathrm{Ba})_s}{\delta}\sqrt{\frac{2K_\delta(\mathrm{Na,Ba})}{T_n}}}+\frac{[\mathrm{Na}]_\infty\cdot\frac{m'(\mathrm{Ba})_s}{\delta}\sqrt{\frac{2K_\delta(\mathrm{Na,Ba})}{T_n}}}{1+\frac{m'(\mathrm{Ba})_s}{\delta}\sqrt{\frac{2K_\delta(\mathrm{Na,Ba})}{T_n}}}. \quad (13')$$

The author is grateful to Prof. T. Takaishi, Toyohashi University of Technology, for his support and valuable discussions. He also wishes to thank Prof. Y. Sensui, Rikkyo (St. Paul's) University, for his encouragement and γ-ray spectra measurements. The present work was supported in part by a Grant-in-Aid for Research from the Ministry of Education, Contract No. 443001.

References

1) D. W. Breck, E. C. Eversole, R. M. Milton, T. B. Reed, and T. L. Thomas, *J. Am. Chem. Soc.*, **78**, 5963 (1956).
2) R. M. Barrer and W. M. Meier, *Trans. Faraday Soc.*, **54**, 1078 (1958).
3) T. B. Reed and D. W. Breck, *J. Am. Chem. Soc.*, **78**, 5972 (1957).
4) A. A. Amaro, C. L. Kovaciny, K. B. Kunz, P. E. Riley, T. B. Vance Jr., R. Y. Yanagida, and K. Seff, "Proceeding of the 3rd International Conference on Molecular Sieves," Leuven University Press, Belgium (1973), p. 113.
5) "Properties and Applications of Zeolites," R. P. Townsend, The Chemical Society, London (1979), p. 293.
6) J. F. Charnell, *J. Cryst. Growth*, **8**, 291 (1971).
7) P. E. Riley and K. Seff, *J. Chem. Soc., Chem. Commun.*, 1972, 1287.
8) R. L. Firror and K. Seff, *J. Am. Chem. Soc.*, **100**, 3091 (1978).
9) T. Ohgushi, A. Yusa, and T. Takaishi, *J. Chem. Soc., Faraday Trans. 1*, **74**, 613 (1978).
10) T. Takaishi and H. Hattori, *J. Am. Chem. Soc.*, **99**, 7731 (1977).
11) N. V. Raghavan and K. Seff, *J. Phys. Chem.*, **80**, 2133 (1976).
12) T. Takaishi, Y. Yatsurugi, A. Yusa, and T. Kuratomi, *J. Chem. Soc., Faraday Trans. 1*, **71**, 97 (1975).
13) "Properties and Applications of Zeolites," ed by R. P. Townsend, The Chemical Society, London (1979), p. 218.
14) "Properties and Applications of Zeolites," ed by R. P. Townsend, The Chemical Society, London (1979), pp. 289, 290.

15) R. M. Barrer and W. M. Meier, *Trans. Faraday Soc.*, **55**, 130 (1959).
16) F. P. Treadwell and W. T. Hall, "Analytical Chemistry," 9th ed, Wiley, New York (1959), Vol. **II**, p. 278.
17) P. A. Howell, *Acta Crystallogr.*, **13**, 737 (1960).
18) P. C. W. Leung, K. B. Kunz, K. Seff, and I. L. Maxwell, *J. Phys. Chem.*, **79**, 2173 (1975).
19) T. Ohgushi, A. Yusa, K. Kinoshita, and Y. Yatsurugi, *Bull. Chem. Soc. Jpn.*, **51**, 419 (1978).
20) H. Higuchi, Ph. D. Thesis, The University of Tokyo (1973), p. 38.
21) H. S. Sherry and H. F. Walton, *J. Phys. Chem.*, **71**, 1457 (1967).

ESR Study of the Spin-labeled Poly(methyl methacrylate) Adsorbed on the Human Tooth and Hydroxyapatite

Harutoshi SAKAI,* Tetsuo ASAKURA,†,†† Kazuomi SUZUKI,† Kozo HORIE,†
Yukihiro MAESHIMA, and Yoshio IMAMURA

Department of Chemistry, Faculty of Science, Science University of Tokyo, Kagurazaka, Shinjuku-ku, Tokyo 162

† *Department of Dental Materials, Nihon University of Dentistry at Matsudo, Matsudo, Chiba 271*

(Received November 11, 1980)

The motion and the configurational behavior of the poly(methyl methacrylate) adsorbed on the surfaces of human tooth substances (dentin, enamel, and hydroxyapatite crystal) from a solution were clarified by using the electron-spin-resonance technique. The polymer molecules were more strictly bound by the surfaces of enamel and hydroxyapatite than the dentin. On both enamel and hydroxyapatite, the adsorbed molecules behaved in the same manner in their motion and configuration. However, the segments directly bound by each tooth substance had a much higher degree of motional freedom than those by the silica surface. These results were discussed in relation to the interaction between the polymer and the tooth, and in relation to the clinical adhesive aspects.

Electron spin resonance (ESR), coupled with a spin-labeling technique, has been successfully applied to the study of the adsorption behavior of several polymers.[1-4]

The bound segments in the adsorbed polymers (train) are easily distinguishable from the segments in loops or tails on the basis of the difference in the ESR line shape, which corresponds to the difference in mobility among these segments. Thus, the ESR study is very useful in clarifying the detailed aspects of the interaction between a polymer and a solid surface.

On the other hand, restorative materials which consist of polyfunctional methacrylates and glass filler have often been used to fill the missing tooth produced by dental caries.[5,6] However, the failure of the restorative materials to hold or secondary caries sometimes occur because of a lack of adhesiveness with tooth surface. In order to develop restorative materials which have a good adhesiveness with the tooth, it is necessary to obtain information on the adhesive mechanism between the materials and the tooth surface.

In our previous papers, the interaction between spin-labeled poly(methyl methacrylate) (PMMA) and a silica surface has been studied in detail by means of the ESR method.[3,4] In this paper, the ESR study was performed in order to obtain information on the interaction between PMMA and the surfaces of three tooth substances, *i.e.*, dentin, enamel, and hydroxyapatite.

Experimental

A human tooth, dried at 60 °C for two weeks, was cut into two parts, the enamel and the dentin. Each part was then crushed with a ball mill to obtain a powder which could be used for the adsorption experiments. A sample of finely powdered hydroxyapatite, $Ca_{10}(PO_4)_6(OH)_2$, was purchased from the Seikagaku Kogyo Co., Ltd. The electron micrographs of these samples were obtained with a HITAC S-500 Scanning Electron Microscope. The diameters of these particles had a wide distribution in each case, 1—10 μm.

† Present address: Faculty of Technology, Tokyo University of Agriculture and Technology, Koganei, Tokyo 184.

Spin-labeled PMMA was prepared by the method described in a previous paper.[3] The sample used had a number-average molecular weight of 1.2×10^5 and a narrow mol wt distribution. The stereoregularity of the sample was highly isotactic.

The solid powder, 0.2 g, was added to 5 cm^3 of a CCl_4 polymer solution, after which the mixture was stirred for 4 h at 25±2 °C. The adsorbents were centrifuged after the adsorption equilibrium had been attained and separated from the supernatant solutions. The solids were rinsed with pure CCl_4 and 0.1 g of each sample was placed in a quartz sample tube. The ESR signals from the adsorbed polymer were measured on a JEOL JES FE 3-X spectrometer, applying a temperature control. On the other hand, the amount of adsorption was determined by means of ESR measurements of the changes in the polymer concentrations of the supernatant solution before and after the adsorption. The polymer concentration was calculated from the signal intensities of the polymer solution of a constant volume, approximately 0.1 cm^3, relative to those of the standard solutions. The other experimental methods have been described in previous papers.[3,4]

Results and Discussion

The adsorption isotherms of PMMA on three kinds of tooth substances, *i.e.*, dentin, enamel, and hydroxyapatite, in CCl_4 at 25 °C are shown in Fig. 1. Each curve reaches a plateau at a low concentration of the polymer solution, with a slight increase at a higher concentration. This behavior is independent of the kinds of tooth substance. The saturated amount of adsorption, A_s, increased in the order of dentin (10 mg/g), enamel (30 mg/g), and hydroxyapatite (90 mg/g).

Let us now examine in detail the ESR spectra of the spin-labeled PMMA adsorbed on these tooth substances in the unsaturated stages. Figure 2 shows the ESR spectra of the PMMA adsorbed on hydroxyapatite crystals. These spectra can be assumed to be composed of three portions of the local chain, *i.e.*, train, short loop, and long loop.[4] It should be noted that there is a significant change in the ESR line shapes with the degree of adsorption; this corresponds to the change in the conformation of PMMA

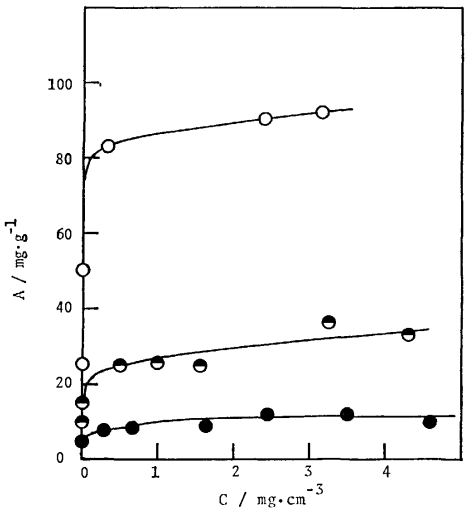

Fig. 1. The adsorption isotherms of PMMA on the tooth substances from CCl_4 dilute solution at 25 °C. ○: On hydroxyapatite, ◓: enamel, ●: dentin.

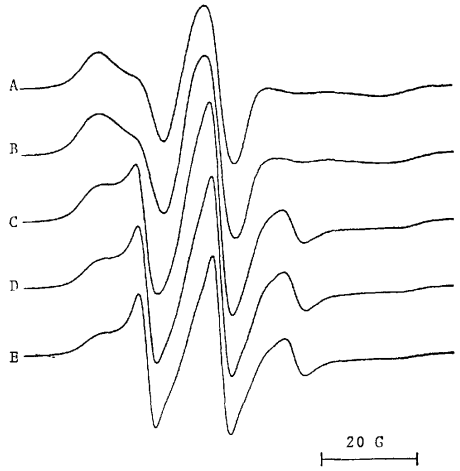

Fig. 2. The ESR spectra of the spin-labeled PMMA adsorbed on hydroxyapatite crystal at 25 °C. The relative amounts of adsorption (θ) are A: 0.3, B: 0.5, C: 0.8, D: 0.9, and E: 1.0, respectively. Here, 1 G is equal to 10^{-4} T.

adsorbed on the hydroxyapatite surface. The adsorbed molecules initially tend to adsorb in a relatively flat conformation (train) and to become more looped as the saturation adsorption is approached. The spectral behavior of PMMA in the unsaturated stage was also qualitatively the same as in the cases of enamel and dentin, as is shown in Fig. 3 and 4 respectively. Moreover, there was no difference between the ESR spectrum of PMMA adsorbed on hydroxyapatite and that adsorbed on enamel, even at the saturated stage ($\theta \approx 1$). Here, θ is the amount of adsorption relative to the maximum amount of adsorption. On the other hand, a looser adsorption behavior was observed in the case of dentin, as is shown in Fig. 4. In order to clarify this difference, the fraction and the correlation time of the segments in the train conformation were calculated when $\theta = 1$. As has been mentioned above, these ESR spectra of the adsorbed PMMA can be assumed to be com-

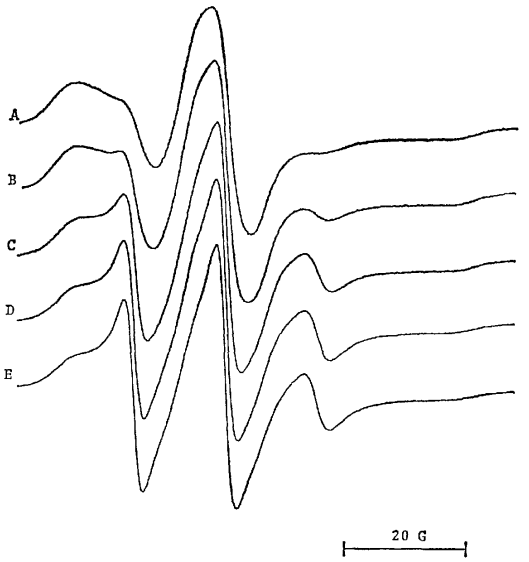

Fig. 3. The ESR spectra of the spin-labeled PMMA adsorbed on enamel at 25 °C. The relative amounts of adsorption (θ) are A: 0.3, B: 0.5, C: 0.8, D: 0.9, and E: 1.0, respectively.

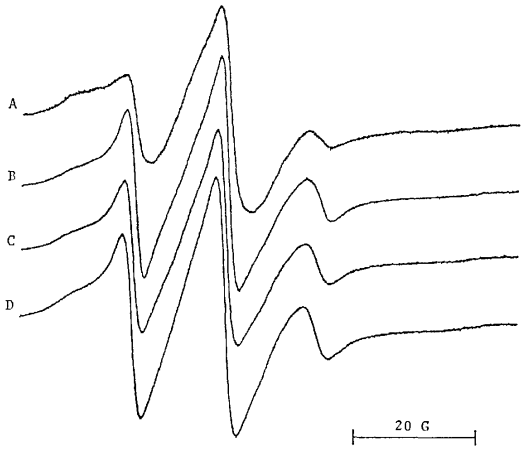

Fig. 4. The ESR spectra of the spin-labeled PMMA adsorbed on dentin at 25 °C. The relative amounts of adsorption (θ) are A: 0.2, B: 0.8, C: 0.9, and D: 1.0, respectively.

posed of three portions of the local chain. The fraction of each portion was evaluated by fitting the spectrum calculated from the superposition of appropriate three model spectra to the observed spectrum on a computer.[4] The correlation time, τ_c, of the bound segments is considered to be in the region of relatively slow motion from 10^{-7} to 10^{-9} s and can be calculated by the following equation, derived by Goldman *et al.*:[7]

$$\tau_c = a(1-S)^b,$$

where $S = A'_z/A_z$, A'_z is one-half the separation width of the hyperfine extrema (W) and where A_z corresponds to the rigid limit value (W_{max}). The parameters, a and b, are dependent on the rotational diffusion models and the intrinsic line-width in the spectrum. In this calculation, the values for the moderate jump diffusion model, $a = 1.10 \times 10^{-9}$ and $b = -1.01$,

Table 1. The correlation time, τ, and the fraction of bound segments of adsorbed PMMA

Sample	τ/s	Segment fraction
Hydroxyapatite	2.2×10^{-8}	0.55
Enamel	2.2×10^{-8}	0.54
Dentin	1.5×10^{-8}	0.44
Silica	$>10^{-6}$	0.48

were used. The results were summarized in the table, together with the data on silica reported previously.[4] The fraction of bound segments decreased considerably, and the mobility increased significantly, in dentin compared with the values for hydroxyapatite and enamel. These results correspond to the difference in composition between dentin and enamel. The composition of dentin on a wet-weight basis is generally considered to be approximately 70% inorganic material, 18% organic material, and 12% water.[8] The inorganic portion consists mainly of hydroxyapatite crystals, while the organic portion consists mainly of collagen. On the other hand, the composition of the enamel is 92—96% inorganic material, 1—2% organic material, and 3—4% water. Most of the inorganic material is hydroxyapatite here, also. Thus, the composition of the inorganic material (hydroxyapatite) decreases considerably in the dried dentin compared with that in the dried enamel used here. The carbonyl groups of PMMA are able to form a hydrogen bond with OH groups in the hydroxyapatite, and this interaction is considered to be a predominant force for the adsorption rather than other van der Waals interactions.[9] Thus, a decrease in the amount of hydroxyapatite in dentin would cause a decrease in the fraction of bound segments and an increase in the mobility of the bound segments compared with the cases of enamel and hydroxyapatite. These conclusions derived from the ESR study are in agreement with the clinical results where polyfunctional methacrylates are found to be more adhesive to enamel than dentin.[10—12]

It should be noted that the motion of PMMA adsorbed on silica is significantly slower than those of PMMA adsorbed on hydroxyapatite, enamel, and dentin; *i.e.*, the correlation time of the bound segments is longer than 10^{-6} s for silica, while it is approximately 10^{-8} s for the tooth substances. Such a difference was also observed in the temperature dependence of the extreme separation width. The spectral change of PMMA adsorbed on enamel is shown in Fig. 5 at various temperatures. The value of W decreased gradually with a rise in the temperature. In contrast, the value remained constant over the wide temperature range of −120 to 70 °C in the case of the bound segments on silica, as has been described previously.[4] These observations indicate that PMMA interacts with

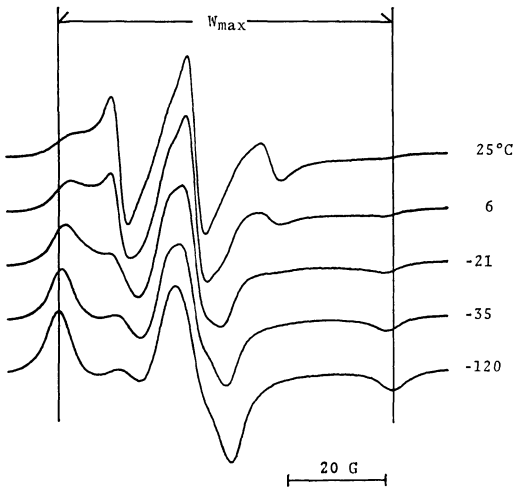

Fig. 5. The ESR spectral change of the spin-labeled PMMA adsorbed on enamel with temperature change. W_{max} is a rigid limit value in the extreme separation widths.

silica more strongly than with a tooth. This is interesting because composite resin, which is widely used as a restorative material for teeth, consists of polyfunctional methacrylates and silica powder.

Thus, the ESR method, coupled with the spin-labeling technique, is very useful in studying the interaction between synthetic polymer and the tooth surface.

References

1) K. K. Fox, I. D. Robb, and R. Smith, *J. Chem. Soc., Faraday Trans.* 1, **70**, 1186 (1974).
2) I. D. Robb and R. Smith, *Polymer*, **18**, 500 (1977).
3) H. Sakai and Y. Imamura, *Bull. Chem. Soc. Jpn.*, **53**, 1749 (1980).
4) H. Sakai, T. Fujimori, and Y. Imamura, *Bull. Chem. Soc. Jpn.*, **53**, 3457 (1980).
5) R. W. Phillips, "Science of Dental Materials," W. B. Saunders Co., Philadelphia (1973), p. 231.
6) R. L. Bowen, U. S. Patent 306-6112 (1962).
7) S. A. Goldman, G. V. Bruno, and J. H. Freed, *J. Phys. Chem.*, **76**, 1858 (1972).
8) I. A. Mjör and J. J. Pindborg, "Histology of the Human Tooth," Munksgaard Co., Copenhagen (1973), p. 46.
9) B. J. Fontana and J. R. Thomas, *J. Phys. Chem.*, **65**, 480 (1961).
10) E. H. Greener, J. K. Harcount, and E. P. Lautenschlager, "Materials Science in Dentistry," The Williams & Wilkins Co., Baltimore (1972), p. 346.
11) N. Kurosaki, M. Nakamura, T. Tobimatsu, H. Node, and M. Iwaku, *Jpn. J. Conserv. Dent.*, **21**, 112 (1978).
12) K. Suzuki, T. Munechika, S. Matsukawa, and K. Horie, *J. Jpn. Res. Soc. Dent. Mater. Appl.*, **37**, 114 (1980).

  Bull. Chem. Soc. Jpn., 54, 2183—2188 (1981)

The Fluidity and Electrolytic Conductivity of Alkali-metal Chloride/Poly(ethylene oxide)-H_2O Systems. The Effects of the Polymer Concentration and the Temperature

Toshiaki Isono,* Katsuo Takahashi, and Reita Tamamushi

The Institute of Physical and Chemical Research, 2-1 Hirosawa, Wako, Saitama 351

(Received December 17, 1980)

The fluidities of poly(ethylene oxide) (PEO)–H_2O mixtures and the electrolytic conductivities of alkali-metal chlorides in the PEO–H_2O mixtures were measured at different PEO compositions and temperatures (25—50 °C). The extended Walden's rule was found to be satisfied when the fluidity and conductivity were changed by the temperature variation at a constant composition, whereas a large deviation from Walden's rule was observed upon the isothermal variation of the PEO composition. The Arrhenius activation parameters were determined from the temperature dependence of the fluidities and conductivities, and some correlations between pairs of parameters were examined.

The mobility of ions and molecules in solution generally decreases with a decrease in the fluidity of the solution; the simplest relationship between the ionic mobility and fluidity is given by the well-known Stokes law (or Walden's rule);

$$\lambda^\infty/\phi = \text{const}, \quad (1)$$

where λ^∞ is the limiting ionic conductivity, and ϕ, the fluidity of the solution. In viscous solutions containing large polymer molecules, however, the mobility of small particles has been known to show significant deviations from Walden's rule;[1] but it can be approximately represented by the empirical equation;[2-4]

$$\lambda^\infty\phi^{-p} = \text{const}, \quad (2)$$

where $0<p<1$.

Different theoretical approaches, such as the concepts of "microscopic viscosity" and "obstruction effect," have attempted to interpret the influence of large neutral molecules on the mass-transport properties of small ions and molecules.[2,5] From the experimental point of view, it seems important to find empirical correlations between pairs of various physical quantities concerning the mass-transport process; although the physical meaning of some of these correlations may be difficult to understand, they may be expected to provide useful information for the theoretical study of the structure of solutions and the mechanism of mass-transport phenomena.

In the present work, we have measured the fluidities of aqueous solutions containing poly(ethylene oxide)s (PEO) with relative molecular masses of 200—20000 and the electrolytic conductivities of alkali-metal chlorides (MX) in PEO–H_2O mixtures at different polymer concentrations and temperatures. This PEO series was chosen for the following reasons: (i) pure samples of sufficiently low conductivities are available; (ii) aqueous solutions of a wide range of fluidity can be prepared, and (iii) PEO is a material of practical importance, being very much used for surfactants, detergents, drugs, and polymer solvents in chemical reactions. The Arrhenius activation parameters have been determined from the temperature dependence of the fluidity and conductivity, and some phenomenological correlations between pairs of these parameters will be discussed.

Experimental

Materials. The poly(ethylene oxide)s used were Polyethylene Glycols (PEG 200, PEG 4000, and PEG 20000) as supplied by Wako Pure Chemical Industries, Ltd. The average relative molecular masses of these polymers, as determined by the vapor-pressure method, were 200 for PEG 200, 3300 for PEG 4000, and 11700 for PEG 20000.

The samples of alkali-metal chlorides were special-reagent-grade chemicals and were used without further purification.

All solutions were prepared gravimetrically by using redistilled water. In this paper, the composition of the PEO–H_2O mixture is given in terms of the mass fraction of PEO, and the PEO–H_2O mixture is regarded as the solvent of the MX/PEO–H_2O system.

Fluidity and Conductivity Measurements. The PEO–H_2O mixtures used in this work were assumed to be Newtonian fluids, because a preliminary study using a rotational viscometer showed an approximate proportionality between the shearing stress and the velocity gradient.

Cannon-Fenske and Ubbelohde viscometers were used to measure the fluidity of the solutions of $\phi>5$ Pa^{-1} s^{-1} (aqueous solutions of PEG 200 and PEG 4000, and those of PEG 20000 at lower concentrations). Capillary diameters were chosen to give flow times of 60 seconds at least. The fluidities of highly viscous mixtures (aqueous solutions of PEG 20000 at higher concentrations) were measured by means of a falling-ball viscometer consisting of a glass cylindrical tube (inner diameter, 17 mm) and a stainless steel ball (diameter, 1 mm) used in ball bearings. Weld pycnometers were employed to determine the densities of the solutions.

The electrolytic conductivities of 0.1 mol kg^{-1} MX/PEO–H_2O systems were measured by the four-electrode a.c. method that has been described in a previous paper;[6] the electrodes were Pt-wires (diameter, 0.5 mm), and the frequency was 125 Hz, no frequency effect being observed in the range of 60 Hz—1 kHz. This method has definite advantages over the conventional two-electrode method when applied to highly viscous mixtures. The conductivities of the PEO–H_2O mixtures were always less than 1% of those due to the electrolytes and so could be neglected in the calculation of the molar conductivities of MX.

All measurements were made in a constant-temperature water bath which was capable of a controlled temperature of better than T ±0.05 K. The accuracy of the measurements was estimated to be better than ±1% for the molar conductivity, ±0.1% for $\phi>5$ Pa^{-1} s^{-1}, and ±1% for $\phi<1$ Pa^{-1} s^{-1}; no correction of ϕ was made for the kinetic energy term.

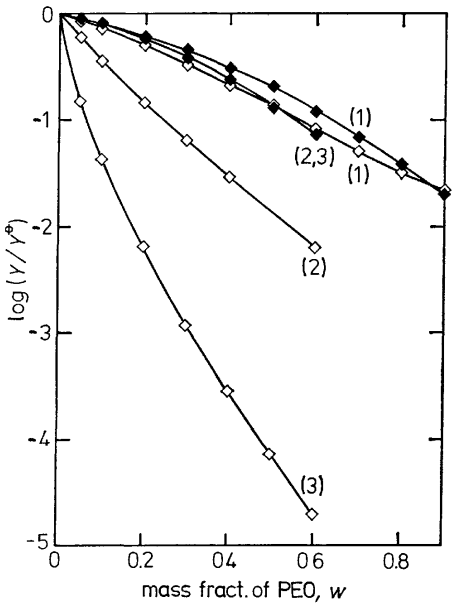

Fig. 1. Changes in the fluidity ($Y=\phi$, —◇—) and the molar conductivity of 0.1 mol kg^{-1} NaCl ($Y=\Lambda$, —◆—) in the PEO–H_2O mixtures at 25 °C as a function of the mass fraction of PEO: (1) PEG 200, (2) PEG 4000, and (3) PEG 20000. Y° represents the fluidity of pure water in the case of $Y=\phi$, and the molar conductivity of 0.1 mol kg^{-1} NaCl in H_2O in the case of $Y=\Lambda$, respectively.

Further details of the experimental procedures and the full experimental data obtained in this work have been reported in a separate paper.[7]

Results and Discussion

Effect of the Polymer Concentration on the Fluidity and Conductivity. The fluidity of a PEO–H_2O mixture and the molar conductivity of MX in the 0.1 mol kg^{-1} MX/PEO–H_2O system are functions of the polymer concentration and the temperature:

$$Y = Y(w,T) \quad ; \quad Y \equiv \phi \text{ and } \Lambda_{MX}, \tag{3}$$

where the symbol Y represents the fluidity (ϕ) and the molar conductivity of MX (Λ_{MX}), w is the mass fraction of PEO, and T is the absolute temperature. The fluidity and conductivity changes produced by the isothermal variation in the polymer concentration are different in nature from those produced by the temperature variation at a constant composition; this difference should be considered when the relationship between the fluidity and conductivity is to be analyzed.[2]

Figure 1 shows the fluidity and conductivity changes in 0.1 mol kg^{-1} NaCl/PEO–H_2O systems at 25 °C as a function of the mass fraction of PEO, w; both the fluidity and conductivity decrease with the increase in w. The change in ϕ with the mass fraction, w, was more pronounced with PEO's of larger relative molecular masses, while the change in Λ_{NaCl} was very much less than that of ϕ and was almost independent of the relative molecular mass of PEO. A similar tendency in the fluidity and conductivity changes with the solution composition has also been known in colloidal solutions (sols and/or gels) including large neutral molecules such as gelatin and agar-agar.[1,2]

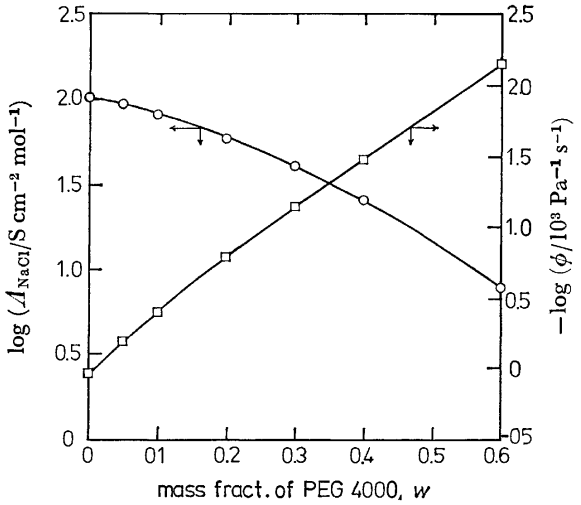

Fig. 2. Composition dependence of the fluidity of PEG 4000–H_2O mixtures and that of the molar conductivity of 0.1 mol kg^{-1} NaCl in PEG 4000–H_2O mixtures (temperature 25 °C): □ and ○ are experimental points; the best-fit equations (4) determined by the least-squares method are shown by solid lines.

Empirically, the isothermal variation in ϕ and Λ_{MX} of the MX/PEO–H_2O system with the mass fraction of PEO can be approximately represented by the equation:

$$\log Y = \sum_{i=0}^{n} a_{i,Y} w^i \quad ; \quad Y \equiv \phi \text{ and } \Lambda_{MX}. \tag{4}$$

In most cases, sufficient accuracy was obtained with $n=3$ for the fluidity of the systems containing PEG 200 and 4000, $n=4$ for the fluidity of the PEG 20000 systems, and $n=2$ for the conductivity. Examples of fitting experimental points by the use of Eq. 4 are given in Fig. 2, where the solid lines represent the empirical equations determined by the method of least-squares.

Temperature Dependence of the Fluidity and Conductivity. The temperature dependence of the fluidities and conductivities of aqueous electrolyte solutions may be represented by an empirical expression of the Arrhenius-type:[8,9]

$$Y = A_Y \exp(-E_Y/RT) \quad ; \quad Y \equiv \phi \text{ and } \Lambda_{MX}, \tag{5}$$

where E_Y and A_Y are the Arrhenius activation energy and the pre-exponential frequency factor respectively for the viscous flow ($Y\equiv\phi$) and the conductivity ($Y\equiv\Lambda_{MX}$). Over a wide range of temperatures, the Arrhenius plot (ln Y *vs.* T^{-1} plot) for the fluidity of aqueous solutions has been known to deviate from linearity,[10] which suggests that the activation parameters (E_Y and A_Y) are temperature-dependent or that the Arrhenius-type expression is inadequate. Within a limited range of temperatures, however, the Arrhenius plot generally gives a reasonably straight line and the activation parameters may be regarded as constant.

Some typical Arrhenius plots for the conductivity of the MX/PEO–H_2O systems are shown in Fig. 3, the plots being almost linear over the temperature

Table 1. Activation energies, E_ϕ, and pre-exponential factors, A_ϕ, for the viscous flow of the PEO-H_2O mixtures
(± represents the standard deviation)

System	Mass fraction of PEO	E_ϕ / kJ mol^{-1}	$R\ln(A_\phi/10^3\ \mathrm{Pa^{-1}\ s^{-1}})$ / J mol^{-1} K^{-1}
PEG 200-H_2O	0.05	16.5±0.2	55.0±0.6
	0.1	17.4±0.2	56.7±0.7
	0.2	19.3±0.2	59.8±0.6
	0.3	20.2±0.3	59.7±0.9
	0.4	22.8±0.3	64.6±0.9
	0.5	25.4±0.3	69.4±1.1
	0.6	28.2±0.4	75.0±1.2
	1.0	33.9±0.6	81.6±1.8
PEG 4000-H_2O	0.05	17.3±0.1	54.6±0.5
	0.1	18.9±0.1	56.0±0.4
	0.2	21.2±0.1	56.1±0.4
	0.3	22.6±0.3	53.9±0.8
	0.4	24.8±0.2	54.8±0.7
	0.6	32.6±0.5	68.3±1.5
PEG 20000-H_2O	0.05	21.4±0.2	56.8±0.5
	0.1	21.6±0.1	47.1±0.4
	0.2	20.5±0.1	27.9±0.3
	0.3	21.9±0.2	18.4±0.7
	0.4	23.9±0.2	13.3±0.7
	0.5	27.6±0.4	14.5±1.3
	0.6	33.1±0.5	21.8±1.7

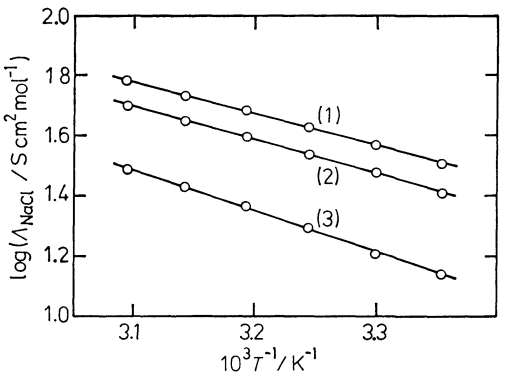

Fig. 3. Arrhenius plots for the molar conductivity of 0.1 mol kg^{-1} NaCl in PEO-H_2O mixtures: (1) PEG 200, w=0.4; (2) PEG 4000, w=0.4; and (3) PEG 20000, w=0.5.

range of 25—50 °C. Similar Arrhenius plots were also obtained for the fluidity of PEO-H_2O mixtures. Tables 1 and 2 present the activation parameters determined from the Arrhenius plots by using the method of least-squares.

Relationship between the Fluidity and Conductivity. The change in the fluidity and conductivity due to the variation of the polymer concentration and temperature can be obtained from Eq. 3 as:

$$dY = \left(\frac{\partial Y}{\partial w}\right)_T dw + \left(\frac{\partial Y}{\partial T}\right)_w dT \tag{6}$$

or:

$$d\ln Y = \left(\frac{\partial \ln Y}{\partial w}\right)_T dw - \frac{1}{T^2}\left(\frac{\partial \ln Y}{\partial T^{-1}}\right)_w dT. \tag{7}$$

Table 2. Activation energies, E_Λ, and pre-exponential factors, A_Λ, for the molar conductivities of 0.1 mol kg^{-1} MX in PEO-H_2O mixtures
(± represents the standard deviation)

System	Mass fraction of PEO	E_Λ / kJ mol^{-1}	$R\ln(A_\Lambda/\mathrm{S\ cm^2\ mol^{-1}})$ / J mol^{-1} K^{-1}
NaCl/PEG 200-H_2O	0.05	14.9±0.1	88±0.4
	0.1	15.5±0.1	89±0.3
	0.2	16.7±0.2	91±1
	0.3	18.4±0.3	94±1
	0.4	20.5±0.3	98±1
	0.5	23.0±0.4	102±1
	0.6	27.1±0.5	112±2
	1.0	30.3±0.9	101±3
KCl/PEG 200-H_2O	0.5	23.6±0.4	105±1
	0.6	27.5±0.5	113±2
NaCl/PEG 4000-H_2O	0.1	15.4±0.1	88±0.3
	0.2	16.7±0.3	90±1
	0.3	18.9±0.2	94±1
	0.4	21.5±0.4	99±1
	0.6	30.1±0.5	118±2
LiCl/PEG 20000-H_2O	0.3	19.0±0.3	93±1
	0.4	21.7±0.4	98±1
	0.5	25.3±0.5	106±2
	0.6	28.9±0.6	113±2
NaCl/PEG 20000-H_2O	0.05	14.7±0.2	87±1
	0.1	15.3±0.3	88±1
	0.2	16.8±0.2	90±1
	0.3	18.9±0.2	94±1
	0.4	21.8±0.4	100±1
	0.5	26.1±0.6	110±2
	0.6	29.8±0.5	117±2
KCl/PEG 20000-H_2O	0.3	19.3±0.2	96±1
	0.4	22.7±0.3	103±1
	0.5	26.9±0.6	112±2
	0.6	30.9±0.5	120±2
RbCl/PEG 20000-H_2O	0.3	19.1±0.3	96±1
	0.4	22.5±0.3	103±1
	0.5	26.9±0.5	112±2
	0.6	30.7±0.4	119±1
CsCl/PEG 20000-H_2O	0.3	18.9±0.2	95±1
	0.4	22.4±0.4	102±1
	0.5	26.9±0.5	112±2
	0.6	30.6±0.6	119±2

The first term on the right-hand side of Eq. 6 or 7 represents the effect of the polymer concentration on the viscous flow and conductivity at a constant temperature, whereas the second term represents the temperature effect at a constant composition.

Using the empirical equations 4 and 5, we can obtain the following expressions:

$$\left(\frac{\partial \ln Y}{\partial w}\right)_T = 2.303 \sum_{i=1}^{n} i a_{i,Y} w^{i-1} \tag{8}$$

and:

$$\left(\frac{\partial \ln Y}{\partial T^{-1}}\right)_w = -\frac{E_Y}{R}, \tag{9}$$

where n=3 or 4 for the fluidity and n=2 for the conductivity.

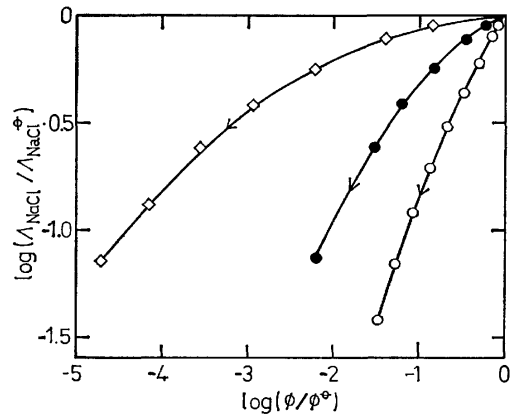

Fig. 4. Plots of $\log(\Lambda_{NaCl}/\Lambda^*_{NaCl})$ against $\log(\phi/\phi^*)$ by the composition variation at 25 °C, where Λ^*_{NaCl} and ϕ^* are the values at $w=0$: —○— PEG 200, —●— PEG 4000, and —◇— PEG 20000. Arrows indicate the direction of increasing PEO-concentration.

From Eqs. 7 and 8, the isothermal change in $\ln \Lambda_{MX}$ with respect to $\ln \phi$ can be given by:

$$\left(\frac{d \ln \Lambda_{MX}}{d \ln \phi}\right)_T = \left(\frac{\partial \ln \Lambda_{MX}}{\partial w}\right)_T \Big/ \left(\frac{\partial \ln \phi}{\partial w}\right)_T = \frac{a_{1,\Lambda} + 2a_{2,\Lambda} w}{a_{1,\phi} + 2a_{2,\phi} w + 3a_{3,\phi} w^2 + 4a_{4,\phi} w^3}. \quad (10)$$

This result suggests that, when the concentration of PEO is changed at a constant temperature, the plot of $\ln \Lambda_{MX}$ against $\ln \phi$ does not give a straight line; in other words, the relation between Λ_{MX} and ϕ deviates from the extended Walden's rule as represented by Eq. 2. Only at sufficiently low concentrations of PEO ($w \ll 1$), the right-hand side of Eq. 10 can be approximated by $a_{1,\Lambda}/a_{1,\phi}$, and the extended Walden's rule may be satisfied.

Similarly, from Eqs. 7 and 9, when the temperature is varied at a constant composition, the change in $\ln \Lambda_{MX}$ with respect to $\ln \phi$ is given by:

$$\left(\frac{d \ln \Lambda_{MX}}{d \ln \phi}\right)_w = \left(\frac{\partial \ln \Lambda_{MX}}{\partial T^{-1}}\right)_w \Big/ \left(\frac{\partial \ln \phi}{\partial T^{-1}}\right)_w = \frac{E_\Lambda}{E_\phi}. \quad (11)$$

Since the activation energies, E_Λ and E_ϕ, are nearly independent of the temperature, the $\ln \Lambda_{MX}$ *vs.* $\ln \phi$ plot by the temperature variation is expected to be linear in accordance with the extended Walden's rule. A comparison of Eqs. 2 and 11 gives the following expression for the p coefficient:

$$p = E_\Lambda / E_\phi. \quad (12)$$

The experimental data are consistent with the above-mentioned consideration. Some examples of the relation between $\log \Lambda_{NaCl}$ and $\log \phi$ upon the isothermal variation in the PEO composition are given in Fig. 4. Upon the variation in the temperature at a constant composition, however, $\log \Lambda_{NaCl}$ changes linearly with $\log \phi$, as is shown in Fig. 5.

Correlations between Pairs of Activation Parameters. The values of the p coefficient as determined from the $\log \Lambda_{MX}$ *vs.* $\log \phi$ plots were nearly independent of the composition of the MX/PEO–H_2O system, the average value being 0.89±0.07. Because of the relationship given by Eq. 12, this result is equivalent to the existence of a linear correlation between E_Λ and E_ϕ, as is shown in Fig. 6. In this figure, the broken line represents the relation, $E_\Lambda/E_\phi = 0.89$ while the solid line corresponds to the best-fit equation:

$$E_\Lambda = (0.97 \pm 0.04) E_\phi - (2.52 \pm 0.92)\text{kJ mol}^{-1}, \quad (13)$$

where ± represents the standard deviation. The relatively large standard deviations for these two lines suggest that the difference between them can not be regarded as very significant.

In contrast to the activation energy (enthalpy term), no significant correlation can be observed between the frequency factors (entropy term), A_Λ and A_ϕ, except in the case of PEG 200–H_2O systems (see Fig. 7).

A number of empirical entropy-enthalpy relationships have been known in the study of chemical reactions, both static and kinetic, in solution.[11,12] The

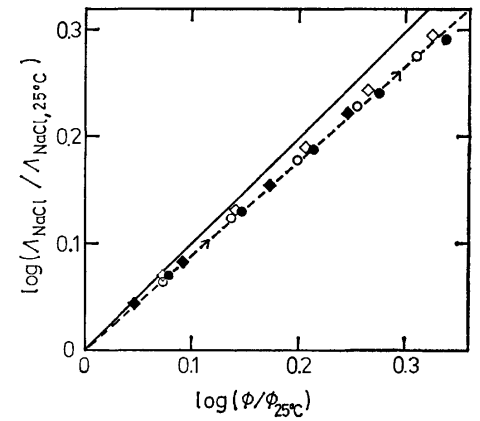

Fig. 5. Plots of $\log(\Lambda_{NaCl}/\Lambda_{NaCl,25°C})$ against $\log(\phi/\phi_{25°C})$ by the temperature variation at constant composition, where $\Lambda_{NaCl,25°C}$ and $\phi_{25°C}$ are the values at 25 °C: —◆— H_2O; —○— PEG 200, $w=0.4$; —●— PEG 4000, $w=0.4$; and —◇— PEG 20000, $w=0.4$. The straight line corresponds to the classical Walden's rule ($p=1$) and the broken line to the extended Walden's rule with $p=0.89$. Arrows indicate the direction of increasing temperature.

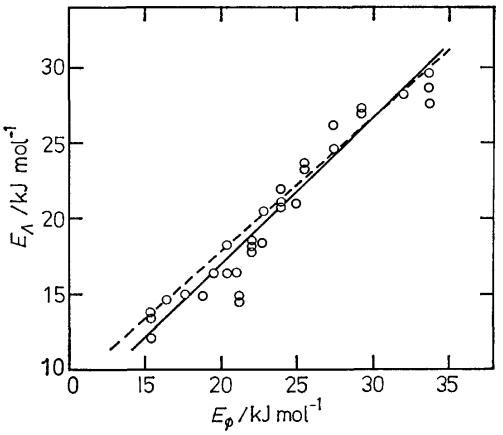

Fig. 6. Correlation between the activation energies for fluidities and molar conductivities of the 0.1 mol kg^{-1} MX/PEO-H_2O systems. The broken line represents Eq. 12 with $p=0.89$ and the solid line represents the best-fit equation (13).

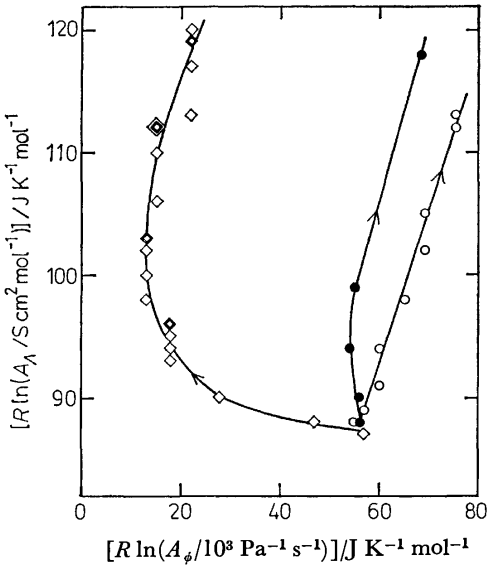

Fig. 7. Plots of $R\ln A_\Lambda$ against $R\ln A_\phi$ of the MX/PEO–H_2O systems: —○— PEG 200, —●— PEG 4000, and —◇— PEG 20000. Arrows indicate the direction of increasing PEO-concentration.

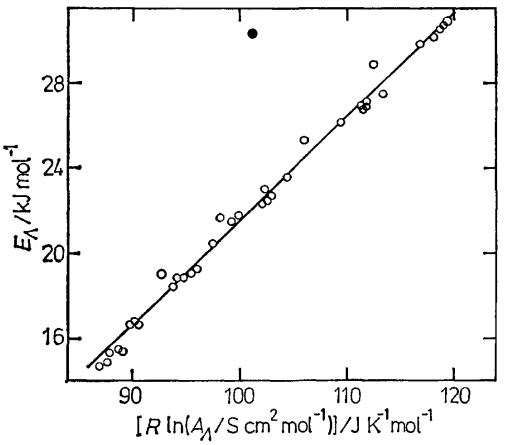

Fig. 8. Correlation between E_Λ and $R\ln A_\Lambda$ (isokinetic relationship) for the molar conductivities of MX in 0.1 mol kg^{-1} MX/PEO–H_2O systems. The solid circle corresponds to the NaCl/pure PEG 200 system, and the solid line represents the best-fit equation (14).

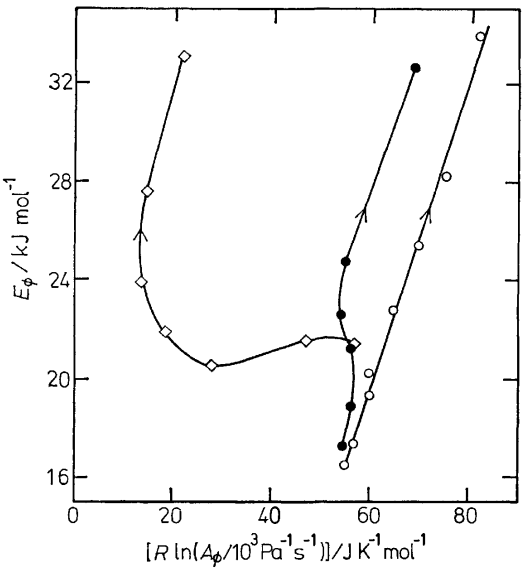

Fig. 9. Plots of E_ϕ against $R\ln A_\phi$ for the fluidity of PEO–H_2O mixtures: —○— PEG 200, —●— PEG 4000, and —◇— PEG 20000. Arrows indicate the direction of increasing PEO-concentration.

analysis of the activation parameters for the viscous flow and conductivity of the MX/PEO–H_2O systems has revealed a good correlation between E_Λ and $\ln A_\Lambda$, but no correlation between E_ϕ and $\ln A_\phi$, as is shown in Figs. 8 and 9. Except for the point corresponding to the NaCl/pure PEG 200 system, the analysis of 37 sets of data in Fig. 8 gives the following equation, representing the E_Λ *vs.* $R\ln A_\Lambda$ relationship:

$$E_\Lambda = T_c R \ln \frac{A_\Lambda}{\mathrm{S\,cm^2\,mol^{-1}}} - (27.5\pm0.74)\ \mathrm{kJ\,mol^{-1}} \quad (14)$$

with $T_c=489.6\pm7.3$ K and the correlation coefficient $r=0.9962$, and where T_c, the slope of the E_Λ *vs.* $R\ln A_\Lambda$ plot, is called the isokinetic or compensation temperature.[12] This relationship means that, in the case of the conductivity of the MX/PEO–H_2O system, the enthalpy of activation is partly compensated for by the entropic term (the enthalpy-entropy compensation effect) upon the variation in the composition of the system. Although the physical meaning of this correlation is not well known, the relation may be expected to originate in the solvent-solute interactions.[11,12] The significant deviation of the NaCl/pure PEG 200 system from the above-mentioned correlation suggests that the thermodynamic factors controlling the electric conduction will be different in pure PEO media from those in solutions containing water.

Conclusion. Our observations on the composition and temperature dependence of the fluidity and conductivity of the 0.1 mol kg^{-1} MX/PEO–H_2O systems can be summarized as follows: (1) The systems exhibited a linear relationship between $\ln \Lambda_{MX}$ and $\ln \phi$ (extended Walden's rule) upon the temperature variation at a constant composition, but not upon an isothermal variation in the PEO-concentration. (2) A good correlation was observed between the activation energies of the viscous flow and the conductivity, but not between the corresponding entropy terms (frequency factors). (3) The conductivity exhibited an enthalpy-entropy compensation effect (the isokinetic relationship) upon a variation in the composition of the system, while such a relationship could not be obtained in the case of the viscous flow.

When the PEO concentration increases at a constant temperature, the molar conductivity of 0.1 mol kg^{-1} MX in PEO–H_2O mixtures will decrease not only upon a lowering of the fluidity, but also by an increase in the ion association due to the decrease in the dielectric constant of the solution. The dielectric constants of PEO–H_2O mixtures have been reported to decrease almost linearly with an increase in the volume fraction of PEO, independent of the molar mass of PEO, in nearly the same way as in the case of dioxane–H_2O mixtures.[13] A rough estimation based on the knowl-

edge concerning the ion-association constants for some alkali halides in dioxane–H_2O mixtures[14] shows that the degree of dissociation of 0.1 mol kg^{-1} MX in the PEO–H_2O mixtures will begin to decrease from unity at the mass fraction of PEO $w \simeq 0.4$ and reach about 0.3 at $w \simeq 0.6$. If the conductivity of the MX/PEO–H_2O system is corrected for the ion-association effect, the deviation from Walden's rule for the ionic mobilities of the ions should become greater than that observed for the molar conductivities. The above-mentioned consideration suggests that the ion-association effect cannot be ignored in discussing the conductivity of the MX/PEO–H_2O system. In this paper, however, no further consideration will be made of the ion-association effect because the present study is intended to examine some phenomenological relationships and not to make detailed mechanistic discussions.

It is suggested that the mechanisms controlling the viscous flow and electric conduction of the MX/PEO–H_2O system may be similar from the enthalpic standpoint, but may be significantly different from the entropic point of view. In the aqueous solutions of PEO, the long-chain polymer molecules will typically exist as random coils and will occasionally from a loosely coupled network. The Arrhenius-type expression (Eq. 5) shows that very low values of the macroscopic fluidity of the solutions containing large PEO molecules can be attributed to the decrease in the pre-exponential factor (entropy term), which is itself due to the formation of the very loose network structure consisting of the polymer chains and which cannot be compensated for by the enthalpy term. For small ions, however, there remain in the solution sufficiently large spaces to move around in, filled with water molecules in the normal condition, and the movement of the ions would not be appreciably disturbed by the low macroscopic fluidity. The correlations between pairs of the activation parameters observed in this study are consistent with the above-mentioned consideration of the ion-transport mechanism in the PEO–H_2O mixtures.

We wish to thank Dr. Yoshihiko Sugiura for the viscosity measurements using a rotational viscometer, and Dr. Haruo Honma for the determination of the relative molecular masses of the PEO samples.

References

1) For example: D. J. Jloyd, "The Problem of Gel Structure," in "Colloid Chemistry," ed by J. Alexander, The Chemical Catalog Company, New York (1926), Vol. I, pp. 775-776; P. H. Hermans, "Gels," in "Colloid Science," ed by H. R. Kruyt, Elsevier, Amsterdam (1949), Vol. II, Chap. XII; R. L. Kay, "Ionic Transport in Water and Mixed Aqueous Solvents," in "Water, A Comprehensive Treatise," ed by F. Franks, Plenum Press, New York (1973), Vol. 3, Chap. 4.

2) R. A. Robinson and R. H. Stokes, "Electrolyte Solutions," Butterworths, London (1965), Revised Ed., pp. 302—313.

3) J. M. Stokes and R. H. Stokes, *J. Phys. Chem.*, **62**, 497 (1958).

4) C. Treiner and R. M. Fuoss, *J. Phys. Chem.*, **69**, 2576 (1965).

5) R. H. Stokes and R. Mills, "Viscosity of Electrolytes and Related Properties," Pergamon, Oxford (1965), Chap. 6.

6) R. Tamamushi and K. Takahashi, *J. Electroanal. Chem.*, **50**, 277 (1974).

7) T. Isono, *Rikagaku Kenkyusho Hokoku*, **56**, 55 (1980).

8) R. H. Stokes and R. Mills, "Viscosity of Electrolytes and Related Properties," Pergamon, Oxford (1965), Chap. 7.

9) S. Glasstone, K. J. Laidler, and H. Eyring, "The Theory of Rate Processes," McGraw-Hill, New York (1941), Chaps. IX and X.

10) J. Jarzynski and C. M. Davis, "The Viscosity of Water," in "Water and Aqueous Solutions," ed by R. A. Horne, Wiley-Interscience, New York (1972), Chap. 17.

11) E. A. Moelwyn-Hughes, "Chemical Statics and Kinetics of Solutions," Academic Press, London (1971), Chap. 15.

12) J. B. F. N. Engberts, "Mixed Aqueous Solvent Effects on Kinetics and Mechanisms of Organic Reactions," in "Water, A Comprehensive Treatise," ed by F. Franks, Plenum Press, New York (1979), Chap. 4.

13) U. Kaatze, *Prog. Colloid Polym. Sci.*, **65**, 214 (1978).

14) J. E. Lind, Jr. and R. M. Fuoss, *J. Phys. Chem.*, **65**, 999 (1961); C. F. Mattina and R. M. Fuoss, *ibid.*, **79**, 1604 (1975).

Electrochemical Oxidation-Reduction Properties of Covalently Bound FAD of Cholesterol Oxidase Adsorbed on Mercury Electrode Surface

Tokuji IKEDA,* Shinji ANDO, and Mitsugi SENDA

Department of Agricultural Chemistry, Faculty of Agriculture, Kyoto University, Sakyo-ku, Kyoto 606

(Received January 14, 1981)

Cholesterol oxidase from *Schizophyllum commune* was studied by cyclic d.c. and a.c. voltammetry with a hanging mercury drop electrode. The enzyme gave d.c. and a.c. waves due to covalently bound FAD of the enzyme adsorbed on an electrode surface. The waves were interpreted in terms of d.c. and a.c. voltammetry of a two-step surface redox reaction. The standard surface oxidation-reduction potential of the enzyme adsorbed on the electrode surface, E'_s, was -0.32_5 V *vs.* SCE, the semiquinone formation constant being 1.5 ± 1.0 at pH 7.4 (25 °C). The pH dependence of E'_s was -60 mV/pH (pH 2.0—6.4), -30 mV/pH (pH 6.4—8.5), and -60 mV/pH (pH 8.5—12.0). The apparent charge transfer rate constant of the surface redox reaction was $1.6\pm0.5\times10^3$ s^{-1} at pH 5.4.

Flavoprotein oxidase is a flavin-containing enzyme which catalyzes the oxidation of a substrate by dioxygen.[1] Knowledge of the oxidation-reduction properties of this class of enzymes is important in utilizing the enzymes in electrocatalysis and for understanding the enzymatic reaction. Electrochemical methods seem to be advantageous for the study.[2] Scheller *et al.*[3] studied glucose oxidase from *Penicillium notatum* by differential pulse polarography and observed a wave with a peak at -0.34 V *vs.* SCE (pH 7.0). We[4] have studied glucose oxidase from *Aspergillus nigar* using a.c. polarography and observed a wave with a peak at -0.38 V *vs.* SCE (pH 7.0). Kuznetsov *et al.*[5] studied D-amino acid oxidase from pig kidney and observed an a.c. wave with a peak at -0.36 V *vs.* SCE (pH 7.0). In these flavoproteins FAD is bound to the apoprotein by noncovalent bond.[6] On the other hand the proteins are strongly adsorbed on the electrode surface, and thus FAD might be dissociated from the enzyme on this surface. The polarographic waves of the flavoproteins could, under certain conditions, be the waves due to the redox reaction of FAD dissociated from the enzymes on the electrode surface.

In this study we have investigated cholesterol oxidase from *Schizophyllum commune*, a flavoprotein in which FAD is covalently bound to its apoprotein,[7] by means of cyclic d.c. and a.c. voltammetry with a hanging mercury drop electrode. The enzyme gave d.c. and a.c. waves assignable to the covalently bound FAD of the enzyme adsorbed on the electrode surface. By interpreting the waves by means of cyclic d.c. and a.c. voltammetry of the two-step surface redox reaction,[8] we were able to determine the thermodynamic and kinetic parameters of the electrochemical oxidation-reduction reaction of the enzyme adsorbed on the electrode surface. The results and discussion are presented in this paper.

Experimental

Cholesterol oxidase (from *Schizophyllum commune* (ChOD), Toyobo Co., grade II, lot No. 9316) was used. This was dialyzed against 0.05 mol dm^{-3} phosphate buffer of pH 6.0 before use. The concentration of ChOD was determined spectrophotometrically, the molar extinction coefficient being 1.13×10^4 mol^{-1} dm^3 cm^{-1} at 455 nm.[9]

Voltammetric measurements were performed in the dark in an H-type cell immersed in a thermostat controlled at 25 ± 0.5 °C. The working electrode was a hanging mercury drop electrode (hmde), Metrohm E410, with surface area 0.0187 ± 0.0003 cm^2. The following buffer solutions were used: 0.1 mol dm^{-3} nitric acid–sodium acetate for pH 2.0—4.0; 0.1 mol dm^{-3} acetic acid–sodium acetate for pH 4.0—6.0; 0.1 mol dm^{-3} sodium dihydrogenphosphate–disodium hydrogenphosphate for pH 6.0—8.0; 0.1 mol dm^{-3} nitric acid–tris(hydroxymethyl)methanamine for pH 8.0—9.2; 0.1 mol dm^{-3} borax–sodium hydroxide for pH 9.2—12.0. The ionic strength of the base solution was adjusted to 0.5 mol dm^{-3} with potassium nitrate. All chemicals used were of standard reagent grade.

D.c. and a.c. voltammograms were recorded after a fresh mercury drop from the hmde had been exposed to a test solution for a given period of time, exposure time t_{exp}, and at a constant potential, initial potential E_i. All potentials were measured against a saturated calomel electrode (SCE). Other details on apparatus and methods of electrochemical measurements were reported.[10]

Results and Discussion

Adsorption of ChOD on Electrode Surface. Figure 1 shows a cyclic d.c. voltammogram of 0.33 μmol dm^{-3} ChOD in a solution of pH 7.4. The voltammogram was recorded after $t_{exp}=3$ min at $E_i=-1.4$ V and with a potential sweep rate, v, 0.33 V s^{-1}. Two pairs of peak-shaped anodic and cathodic waves, (I_a and I_c, and II_a and II_c) and a cathodic wave (III_c) appear at -0.33 V, -0.64 V, and -1.2 V, respectively. The waves grow to a certain limit with increasing t_{exp} at a given concentration of ChOD, c_{ChOD}. The peak heights of the waves corrected for base current, i_p, increase linearly with $t_{exp}^{1/2}$ for small t_{exp} values, reaching a saturation value, i_p^{max}, for large t_{exp} values. Figure 2 shows i_p *vs.* $t_{exp}^{1/2}$ plots for wave I_c at three different ChOD concentrations. The slope of the linear part of i_p *vs.* $t_{exp}^{1/2}$ plots is proportional to c_{ChOD}. The results indicate that[10] ChOD is accumulated by adsorption on the hmde surface and the adsorption is controlled by diffusion of ChOD to the electrode surface, the current being assumed to be proportional to the amount of the adsorbed ChOD. The maximum amount of the adsorbed ChOD per unit surface area, Γ_{ChOD}^{max}, was determined to be $4\pm0.5\times10^{-12}$ mol cm^{-2} by means of a theoretical equation,[10] $\Gamma_{ChOD}^{max}=2(D_{ChOD}/\pi)^{1/2}c_{ChOD}i_p^{max}t_{exp}^{1/2}/i_p$, where the diffusion coefficient of

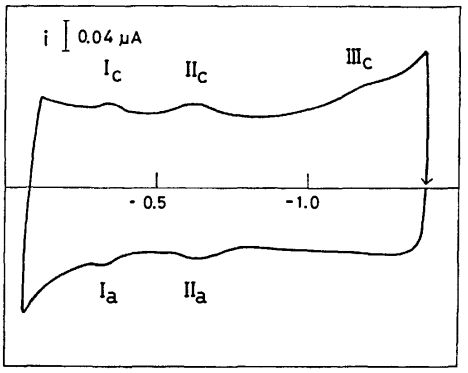

(*E vs.* SCE)/V

Fig. 1. Cyclic d.c. voltammogram of 0.33 μmol dm^{-3} ChOD at pH 7.4; t_{exp}=3 min at E_i=−1.4 V and v=0.33 V s^{-1}.

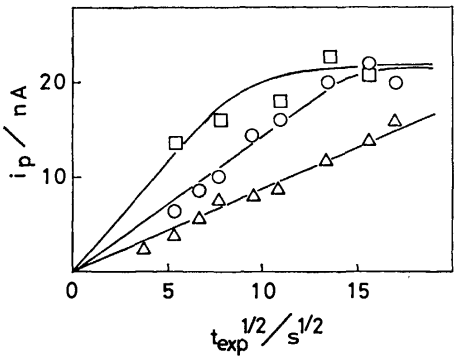

Fig. 2. Plots of i_p against $t_{exp}^{1/2}$ of waves I_c at pH 7.4. c_{ChOD}: (△) 0.24, (○) 0.38, and (□) 0.61 μmol dm^{-3}.

ChOD, D_{ChOD}, was estimated as 7.5×10^{-7} cm^2 s^{-1} on the basis of the diffusion coefficient of proteins[11] of about the same molecular weight as ChOD.

The following experiment gave another evidence that the voltammogram shown in Fig. 1 is due to the surface redox reaction of ChOD irreversibly adsorbed on the electrode surface. The hmde was dipped into 4×10^{-5} mol dm^{-3} ChOD solution allowing ChOD to be adsorbed on the electrode surface, washed gently with distilled water, then immersed in the same solution (Fig. 1) but containing no ChOD. The same cyclic voltammogram as in Fig. 1 was obtained.

Assigment of D.c. Waves of ChOD. The pair of waves II_a and II_c should be assigned to the half-cystine residues[9] of ChOD, since their peak potential coincides with that of the waves of apoferredoxin,[10] an SH-protein, adsorbed on the mercury electrode surface. The dependence of the peak heights, peak potentials, half-peak widths of the waves on the potential sweep rate, and that of the peak potentials on pH were explained by assigning the waves to a surface redox process,[10] $Hg+(RSH)_{ad}\rightleftharpoons(RSHg)_{ad}+H^++e^-$. The height of wave III_c increased with decrease in pH and with increase in the concentration of buffer salts of the test solutions. Riboflavin and its derivatives give catalytic hydrogen evolution current at *ca.* −1.3 V on mercury electrode in neutral and acidic solutions.[12] Thus we conclude that the wave III_c is due to catalytic hydrogen evolution by covalently bound FAD of the enzyme.

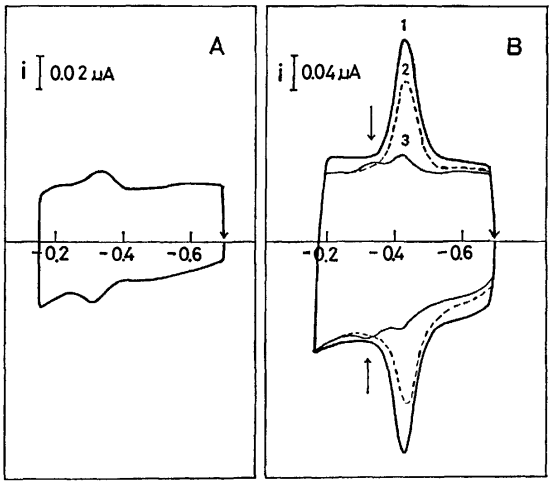

(*E vs.* SCE)/V

Fig. 3. (A): Cyclic d.c. voltammogram of 0.61 μmol dm^{-3} ChOD at pH 7.4, t_{exp}=3 min at E_i=−0.7 V and v=0.10 V s^{-1}.
(B): Cyclic d.c. voltammograms of 1.0 μmol dm^{-3} FAD and 0.14 μmol dm^{-3} ChOD at pH 7.4; t_{exp}= (1) 30 s, (2) 5 min, and (3) 20 min at E_i=−0.7 V and v=0.33 V s^{-1}.

The pair of waves I_a and I_c should be attributed to the redox reaction of covalently bound FAD of the enzyme. In order to confirm that the waves are due to FAD bound to the protein and not to the free FAD which might be present in trace amount in the stock solution of ChOD, we compared the voltammogram of ChOD with that of free FAD. FAD was adsorbed on the mercury electrode surface.[13] Figure 3(B) shows cyclic d.c. voltammograms of a solution containing both 1.0 μmol dm^{-3} FAD and 0.14 μmol dm^{-3} ChOD (pH 7.4) at t_{exp}=30 s, 5 min, or 20 min at E_i=−0.7 V. FAD gives a pair of d.c. waves with the peak potential −0.43 V, 100 mV more negative than the peak potential of waves I_a and I_c (Fig. 3(A)), indicating that the latter waves are due to FAD covalently bound to the protein. The peak heights of the waves due to free FAD in the presence of ChOD decrease with increasing t_{exp}, while the waves due to ChOD begin to appear (curves 1, 2, and 3, Fig. 3(B)). This indicates that at the begining of the exposure of hmde to the test dolution the electrode surface is covered dominantly by free FAD (both the diffusion coefficient and the bulk concentration of free FAD are much larger than ChOD), but with the elapse of time the adsorbed free FAD is replaced by ChOD, probably owing to the heigher affinity of ChOD to mercury electrode than FAD.

D.c. Waves of Covalently Bound FAD of ChOD. The anodic and cathodic peak currents, i_{ap} and i_{cp}, the peak potentials, E_{ap} and E_{cp}, and the half-peak widths, $\Delta E_{a,\,p/2}$ and $\Delta E_{c,\,p/2}$, of waves I_a and I_c as a function of the potential sweep rate, v, at pH 7.4 are summarized in Table 1. Q_a and Q_c are the charges required to electrooxidize or electroreduce the

Table 1. Peak current, peak potential, half-peak width, and Integrated current of d.c. waves I_a and I_c of ChOD at pH 7.4

v / V s^{-1}	i_{ap} / nA	i_{cp} / nA	$-E_{ap}$ *vs.* SCE / V	$-E_{cp}$ *vs.* SCE / V	$\Delta E_{ap/2}$ / mV	$\Delta E_{cp/2}$ / mV	Q_a / 10^{-9} C	Q_c / 10^{-9} C
0.05	4.0	4.0	0.32	0.33	60	75	6.2	6.6
0.10	7.6	8.0	0.32	0.33	55	60	5.5	6.9
0.20	14	14	0.32	0.33	60	80	5.3	7.3
0.33	17	18	0.32	0.33	60	70	4.4	5.2

adsorbed ChOD, respectively, and estimated from the area under the waves I_a and I_c corrected for the base current. Peak heights, i_{ap} and i_{cp}, are both proportional to v, the ratio i_{ap}/i_{cp} being unity. The peak potentials and the half-peak widths are both independent of v, and E_{ap} and $\Delta E_{a,p/2}$ coincide with E_{cp} and $\Delta E_{c,p/2}$, respectively. Q_a and Q_c also coincide with each other and are independent of v. The results are in line with theoretical predictions (1) to (4), for two-step surface redox reaction which can be expressed by

$$(\mathrm{Fp.FAD^{ox}H_p})_{ad} + e^- + (q-p)H^+ \rightleftharpoons (\mathrm{Fp.FAD^{sem}H_q})_{ad} \quad \text{I-a}$$

$$(\mathrm{Fp.FAD^{sem}H_q})_{ad} + e^- + (r-q)H^+ \rightleftharpoons (\mathrm{Fp.FAD^{red}H_r})_{ad} \quad \text{I-b}$$

for ChOD adsorbed on the electrode surface. $(\mathrm{Fp.FAD^{sem}H_p})_{ad}$, $(\mathrm{Fp.FAD^{sem}H_q})_{ad}$, and $(\mathrm{Ap.FAD^{red}H_r})_{ad}$ denote the oxidized, intermediate (semiquinone), and reduced forms of the adsorbed ChOD, respectively. Theoretical expressions[8] of the d.c. anodic and cathodic currents in cyclic voltammetry, i_a and i_c, of the two-step surface redox reaction are given in a simplified case[14] by

$$i = i_a = -i_c = FA(F/RT)\Gamma v\rho[\rho(K^{1/2}\rho+2) + (K^{1/2}+2\rho)]/(1+K^{1/2}\rho+\rho^2)^2 \quad (1)$$

where $\rho=\exp[(F/RT)(E-E_s')]$, $E_s'=(E_1'+E_2')/2$, and $K=\exp[(F/RT)(E_1'-E_2')]$, Γ is the amount of adsorbed ChOD per unit surface area, K the semiquinone formation constant defined by $K=[(\mathrm{Fp.FAD^{sem}H_q})_{ad}]^2/[(\mathrm{Fp.FAD^{ox}H_p})_{ad}][(\mathrm{Fp.FAD^{red}H_r})_{ad}]$, and E_s', E_1', and E_2' are the standard surface oxidation-reduction potentials of the redox couples $(\mathrm{Fp.FAD^{ox}H_p})_{ad}/(\mathrm{Fp.FAD^{red}H_r})_{ad}$, $(\mathrm{Fp.FAD^{ox}H_p})_{ad}/(\mathrm{Fp.FAD^{sem}H_q})_{ad}$, and $(\mathrm{Fp.FAD^{sem}H_q})_{ad}/(\mathrm{Fp.FAD^{red}H_r})_{ad}$, respectively. When $K\leqslant 16$, the peak currents are given by

$$i_p = i_{ap} = -i_{cp} = FA(F/RT)\Gamma v[2/(2+K^{1/2})] = (F/RT)Qv/(2+K^{1/2}) \quad (2)$$

where $Q(=Q_a=Q_c)$ is the charge required to electrooxidize or electroreduce the adsorbed ChOD. The peak potentials are equal to E_s':

$$E_p = E_{ap} = E_{cp} = E_s' \quad (3)$$

and the half-peak widths are given by

$$\Delta E_{p/2} = \Delta E_{a,p/2} = \Delta E_{c,p/2} = (2RT/F)\ln[f(K)] \quad (4)$$

where $f(K)$ is a function of K.[8]

The results satisfy the predictions, indicating that $E_p=E_s'=-0.32_5$ V *vs.* SCE at pH 7.4. Thus the K value at pH 7.4 was determined to be 1.8 ± 1.1 by Eq. 2 and 1.1 ± 0.8 by Eq. 4. The values agree,

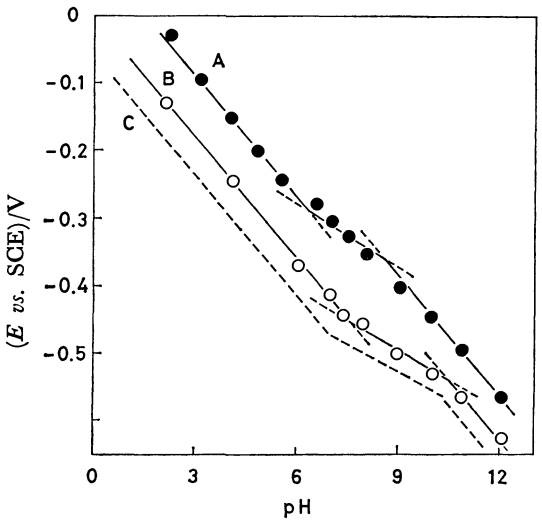

Fig. 4. Plots of $E_p(=E_s')$ against pH; (A): ChOD adsorbed on mercury electrode surface, (B): FAD adsorbed on mercury electrode surface. (C): Broken line represents E_m' *vs.* pH curve for FAD in the bulk of solution (taken from Ref. 13).

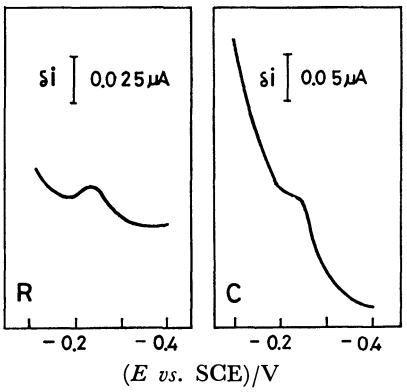

Fig. 5. A.c. voltammograms of 0.67 μmol dm^{-3} ChOD at pH 5.4 (R): Real component and (C): imaginary component at $f=100$ Hz; $t_{exp}=3$ min at $E_i=-0.4$ V and $v=0.02$ V s^{-1}.

giving the average value of $K=1.5\pm1.0$ at pH 7.4. The waves I_a and I_c obtained in the pH region 2—12 satisfy the predictions by Eqs. 1—4. Figure 4(A) shows plot of $E_p(=E_s')$ against pH; three linear relations of $E_p(=E_s')$ against pH, the slopes being −60 mV/pH (pH 2.0—6.4), −30 mV/pH (pH 6.4—8.5), and −60 mV/pH (pH 8.5—12.0). The first and second inflection points, 6.4 and 8.5, indicate the pK of acid dissociation constants[15] of reduced and oxidized forms of ChOD adsorbed on electrode surface, respectively. Plots of $E_p(=E_s')$ *vs.* pH of free FAD

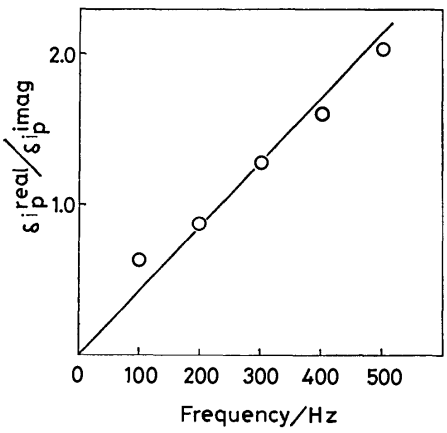

Fig. 6. Dependence of $\delta i_p^{real}/\delta i_p^{imag}$ on f for a.c. waves at pH 5.4.

adsorbed on mercury electrode surface and of the standard oxidation-reduction potential[13] of free FAD in the bulk of solution, $E'_{m,\,FAD}$, are given in Figs. 4(B) and (C), respectively.

No standard oxidation-reduction potential of ChOD in the bulk of solution, $E'_{m,\,ChOD}$, has been determined. We tried to determine $E'_{m,\,ChOD}$ by the potentiometric titration method with dithionate as a titrant using a Pt electrode in the presence of indigo carmine la (Chroma Chemical Co., the standard oxidation-reduction potential being determined as -0.305 ± 0.015 V *vs.* SCE at pH 7.0) as a mediator. We confirmed spectrophotometrically that ChOD can be reduced by dithionate without forming a complex[16] with sulfite, the oxidation product of dithionate. However, the system reached equilibrium only after very long time on each addition of sodium dithionate, preventing accurate determination of $E'_{m,\,ChOD}$. The $E'_{m,\,ChOD}$ value at pH 7.0 was tentatively determined to be $-0.26+0.03$ V *vs.* SCE, which is 210 mV more positive than $E'_{m,\,FAD}$ at pH 7.0. It has been suggested that covalent linkage of flavin to apoprotein shifts the oxidation-reduction potential of the flavin positively, which facilitate catalysis,[17] a model compound hystidyl-8α-flavin being reported to have the standard oxidation-reduction potential 30 mV more positive than that of the nonsubstituted flavin.

The standard oxidation-reduction potential of a redox couple adsorbed on the electrode surface, the standard surface oxidation-reduction potential, can be shifted from the standard oxidation-reduction potential of the redox couple in the bulk of solution. This might be attributed to a difference in adsorption free energy between the oxidized and reduced species, a positive shift being observed with FMN adsorbed on mercury electrode surface.[18] This is also the case with FAD (plots B and C, Fig. 4). In contrast, a negative shift was observed in the case of ChOD. This shift could be attributed not only to a difference in adsorption free energy but also to a change in conformation (surface denaturation) of the protein which could be associated with adsorption of the protein on electrode surface.

A.c. Waves of Covalently Bound FAD of ChOD. In a.c. voltammetry with hmde, ChOD gave a peak-shaped wave at the potential of waves I_a and I_c in the d.c. voltammetry of ChOD with hmde. Figure 5 shows the real and imaginary component of the a.c. voltammogram of anodic scan at pH 5.4. The a.c. voltammogram of cathodic scan coincided both in height and shape with that of anodic scan. The peak potentials of the two components, E_p^{real} and E_p^{imag}, coincide with each other and with the peak potential of the d.c. wave (waves I_a and I_c) at the same pH. $E_p^{real}(=E_p^{imag})$ was independent of a.c. frequency, f, in the range 100—500 Hz. The ratio of the peak current of the real component to that of the imaginary component, $\delta i_p^{real}/\delta i_p^{imag}$, is proportional to f (Fig. 6). The result is in line with the prediction by a simplified equation[8,19] of a.c. voltammograms for the two-step surface redox reaction (I-a and I-b):

$$\delta i_p^{real\prime}\delta i_p^{imag} = 2\pi f/(k_{sap}K^{1/4}), \qquad (5)$$

where k_{sap} is the apparent charge transfer rate constant of the surface redox reaction. From the plot we have $k_{sap}=1.6\pm0.5\times10^3\ s^{-1}$ at pH 5.4, where $K=1.2\pm1.0$. The half-peak widths of the two components at various frequencies at pH 5.4 and their values calculated by equations[8] using the above values of k_{sap} and K are given in Table 2. Agreement between observed and calculated values is fair.

Table 2. Half-peak widths of real and imaginary components of a.c. wave of ChOD adsorbed on HMDE surface at pH 5.4

Frequency / Hz	$\Delta E_{p/2}^{real}$/mV		$\Delta E_{p/2}^{imag}$/mV	
	Obsd	Calcd[a]	Obsd	Calcd[a]
100	60	55	70	72
200	60	60	75	82
300	65	66	—	95
400	70	72	—	110
500	70	76	—	124

a) Calculated by using $K=1.2$ and $k_{sap}=1.6\times10^3\ s^{-1}$.

Thermodynamic and kinetic information on the redox reaction of ChOD adsorbed on an electrode surface would be useful in designing an immobilized ChOD electrode where the electrode functions as an electron acceptor from (or electron donor to) the flavoprotein.

This work was supported by a Grant-in-Aid for Scientific Research No. 510804 from the Ministry of Education, Science and Culture.

References

1) H. J. Bright and D. J. T. Porter, "The Enzymes," ed by P. D. Boyer, Academic Press, New York (1975), Vol. XII B, p. 421.
2) M. Senda, T. Ikeda, T. Kakutani, H. Kinoshita, and K. Kano, *Bioelectrochem. Bioenerg.*, in press.
3) F. Scheller, G. Strnad, B. Neumann, K. Kühn, and W. Ostrowski, *Bioelectrochem. Bioenerg.*, **6**, 117 (1979).
4) Unpublished results.
5) B. A. Kuznetsov, N. M. Mestechkina, and G. P. Shumakovich, *Bioelectrochem. Bioenerg.*, **4**, 1 (1977).
6) D. E. Metzler, "Biochemistry. The Chemical, Reac-

tions in Living Cells," Academic Press, New York (1977), p. 476.

7) W. C. Kenney, T. P. Singer, M. Fukuyama, and Y. Miyake, *J. Biol. Chem.*, **254**, 4689 (1979).

8) T. Kakutani and M. Senda, *Bull. Chem. Soc. Jpn.*, **53**, 1942 (1980).

9) M. Fukuyama and Y. Miyake, *J. Biochem.*, **85**, 1183 (1979).

10) T. Ikeda, K. Toriyama, and M. Senda, *Bull. Chem. Soc. Jpn.*, **52**, 1937 (1979).

11) "CRC Handbook of Biochemistry," ed by H. A. Sober, Chemical Rubber Co., Cleveland Ohio (1968), p. C-10.

12) E. Knobloch, *Collect. Czech. Chem. Commun.*, **31**, 4503 (1966).

13) G. Dryhurst, "Electrochemistry of Biological Molecules," Academic Press, New York (1977), p. 315.

14) This is the case[8] when all the interaction parameters a_{ij} (i,j=ox, sem, or red) between the adsorbed reactants are of the same value. This seems a reasonable assumption since the interaction between the adsorbed protein molecules would not appreciably be affected by the change in the oxidation state of the FAD moiety of the protein because of the large size of the protein molecule. Assumption that m/n=1[8] is made.

15) W. M. Clark, "Oxidation-Reduction Potentials of Organic Systems," The Williams & Wilkins Co., Baltimore (1960), p. 118.

16) V. Massey, F. Müller, R. Feldberg, M. Schuman, P. A. Sullivan, L. G. Howell, S. G. Mayhew, R. G. Mathews, and G. P. Foust, *J. Biol. Chem.*, **244**, 3999 (1969).

17) D. E. Edmondson and T. P. Singer, *J. Biol. Chem.*, **248**, 8144 (1973).

18) T. Kakutani, K. Kano, S. Ando, and M. Senda, *Bull. Chem. Soc. Jpn.*, **54**, 884 (1981).

19) In addition to the assumption,[14] it is assumed[8] that $k_{sap}(1)=k_{sap}(2)=k_{sap}$ and $\alpha_n=\beta_n$, where $k_{sap}(1)$ and $k_{sap}(2)$ are respectively the rate constants of the first and second charge transfer steps and α_n and β_n ($n=1$ or 2) are the transfer coefficients for cathodic and anodic charge transfer of the n-th step, respectively.

Transfer Free Energies of Fluoride Ion in Aqueous Mixtures of Some Organic Solvents

Abhijit BHATTACHARYA, Kaushik DAS, Asim Kumar DAS, and Kiron Kumar KUNDU*

Physical Chemistry Laboratories, Jadavpur University, Calcutta-700032, India

(Received June 6, 1980)

Standard free energies of transfer, ΔG_t°, of potassium fluoride (KF) from water to aqueous mixtures of dimethyl sulfoxide (DMSO), *N,N*-dimethylformamide (DMF), acetonitrile (ACN), 1,2-dimethoxyethane (DME), and 2-methoxyethanol (ME) have been determined at 25 °C from emf measurements performed on the double cell: Pb(Hg)–PbF_2/KF(m), solvent/K(Hg)/KF(m), water/PbF_2–Pb(Hg). ΔG_t° values of F^- were obtained from these values using the corresponding values of K^+, as obtained earlier by use of tetraphenylarsonium tetraphenylborate reference electrolyte assumption. In each solvent system $\Delta G_t^\circ(F^-)$ values are found to be increasingly positive with cosolvent composition reflecting the pronounced destabilization of F^- and their relative order : DME > DMSO ≥ DMF ≫ ACN ≈ ME conforms to what is expected from the relative 'aproticity' of the dipolar aprotic cosolvents and that induced in the protic ME by the possible intramolecular H-bonding. The observed larger destabilization of F^- compared to OH^- in ME–water system has been attributed to the H-bonding effect of the protic cosolvent ME and the reverse behaviour in DME–water and DMSO–water systems to the absence of such effect of these cosolvents. Moreover, tests of Feakins-type extrapolation for assigning individual ion contribution using ΔG_t°(KF) values along with those of other potassium halides, provided some important reflections on the inadequacy of such plots made without the data points of F^-.

It is well known that the dipolar aprotic solvents exert pronounced effects on the acidity functions[1] or rates of reactions involving nucleophiles. But the elucidation of the thermodynamic basis of such effects is yet far from complete. Recent years have therefore witnessed increased interests on this topic as are evidenced from various studies[2–7] on the transfer energetics of different ions based on the widely accepted tetraphenylarsonium tetraphenylborate (TATB) assumption[2–8] in various pure and mixed solvents, including some typical dipolar aprotic solvents.

Strikingly enough, although F^- is often used[9] in organic synthesis for proton abstraction reactions in dipolar aprotic solvents because of its possible pronounced "desolvation" in the solvents, transfer free energies of F^- have been reported, so far as we know, only in protic solvent D_2O.[10] So, in continuation of our previous studies[7] on transfer free energies, ΔG_t°, of different ions based on TATB assumption, we are now reporting ΔG_t° of F^- in aqueous mixtures of some dipolar aprotic cosolvents like dimethyl sulfoxide (DMSO), *N,N*-dimethylformamide (DMF), acetonitrile (ACM), and 1,2-dimethoxyethane (DME) and of a protic solvent like 2-methoxyethanol (ME). While the compositions studied in the first three cases are 20, 40, and 60 wt% cosolvents and for DME are 10, 30, and 50 wt%, those for ME are 10, 30, 50, and 70 wt % cosolvent.

For the purpose in view, we have obtained the standard free energies of transfer of potassium fluoride (KF) from water to these mixed solvents by determining the standard emf's (ΔE°) of the double cell I

Pb(Hg)–PbF_2/KF(m), Solvent/K(Hg)/KF(m), Water/PbF_2–Pb(Hg) (I)

using a procedure similar to that used by Voice[10] in D_2O. These values helped evaluate $\Delta G_t^\circ(F^-)$ values as the values for K^+, based on TATB assumption, for each of the solvent systems are known from our previous studies.[7b–e] Moreover, it is well known that Feakins-type extrapolation[11] for assigning individual ion contributions to the ΔG_t° values being usually based on the adjacent data points of three larger sized halide ions, are susceptible to intrinsic limitations of long extrapolation. So, attempts have also been made to test if the inclusion of data point for F^- can improve the extrapolation procedure or not.

Experimental

The fluoride electrode consisting of a two-phase lead amalgam covered with insoluble lead(II) fluoride (PbF_2) was prepared in a manner essentially similar to that described by Voice.[10] The lead amalgam was prepared by electrolysing an aqueous solution (@ 10%) of $Pb(NO_3)_2$ (A.R., B.D.H.) using mercury (triply distilled) pool as cathode and Pt electrode as anode. The amalgam thus prepared was preserved in a sealed bottle under H_2 atmosphere. Before using it was repeatedly washed with a very dilute HNO_3 (AR., B.D.H.) to remove the ash or film, if any, and then by deionized CO_2-free water. The PbF_2 was prepared by mixing aqueous solution of $Pb(NO_3)_2$ and NaF (Merck, GR) with constant stirring. The white precipitate so obtained was filtered, washed repeatedly by magnetic stirring with CO_2- and O_2-free deionized water, and dried.

The base of the Pb(Hg)–PbF_2 electrode was a J-shaped glass tube with two limbs separated by a glass seal and connected electrically through a Pt-wire fused in the glass seal. The longer limb was fitted with a B-19 standard joint to hold the electrode in the cell vessel and the shorter limb at the other end serving as the electrode "cup" contained the electrode materials and was dipped in the cell solution. Before introducing the Pb-amalgam into cups, one each-side of the double cell, the Pb-amalgam was warmed in a closed vessel until it became mobile to attain its two phase character properly. The cooled two-phase amalgam was masked with a thick layer of PbF_2 crystals. It was observed that asymmetry potential was fairly high when a thin layer of PbF_2 was used. But it was considerably reduced if the layer of PbF_2 over Pb-amalgam become thick and was found to be practically within the range of experimental accuracy (± 0.3 mV). So, the measurement of bias potential before each set of experiment was not necessary.

Preparation and preservation of K-amalgam as well as the cell design have been described elsewhere.[12] The solvents used are of the following grades: DME (Reidel), DMSO

(L.R., B.D.H.), DMF (L.R., B.D.H.), ACN (L.R., B.D.H.), and ME (E. Merck). The method of purification of DME,[7f] DMSO,[13a] DMF,[13b] ACN,[13c] and ME[7e] were similar to those described earlier. Triply distilled and CO_2- and O_2-free water was used for the preparation of solvents as well as the cell solutions.

Anhydrous KF (Merck GR) was dried in a vacuum desiccator for about two weeks. Heating at high temperature was avoided due to the possibility of formation of insoluble material as reported earlier.[14] Because of highly hygroscopic nature of KF, F^- concentrations of the stock solutions were checked by standard gravimetric method. Solutions of different materials were made by weight dilution of the stock solutions. General experimental procedure, including the emf measurements with the help of a Leeds Northrup K_4-potentiometer and a moving coil galvanometer (Cambridge Instrument) as a null-point detector, has been described.[12]

The conditions for equilibrium were different for different solvents. Actually, in pure water as well as up to 50 wt% aqueous mixtures of ME the equilibrium was established within around 2 h and the constancy of emf readings to ± 0.2 mV for 1 h was considered to be the criterion of equilibrium and for 70% ME–water solution the equilibrium was attained after about 4 h. In aqueous dipolar aprotic solvents, however, overnight ageing of the electrode in the respective solution was essential to get stable emf readings. The final emf readings were often checked by introducing separate fluoride electrodes or by measuring emf of the cell I taking pair of solutions having exactly same molality.

Results

The observed emf values (ΔE) of the double cell I for different molalities (m) of KF in different cosolvent–water mixtures are listed in Table 1. These were used to construct the following function.[12b]:

$$\Delta E^{o\prime} = \Delta E - 2k[f_s(m) - f_w m)] = \Delta E^\circ_m - 2k\Delta b m, \quad (1)$$

where

$$f(m) = -A_0B_0m^{1/2}(1+a_0B_0m^{1/2})^{-1} - \ln(1+0.002Mm). \quad (2)$$

The subscripts s and w denote the mixed solvent and water respectively, $k=RT/F$, M is the appropriate molecular weight of the solvent, a_0 is the ion-size parameter, A_0B_0 and B_0 are the Debye-Hückel constants in S.I. units as given by[13c]

$$A_0B_0 = 1.824\times10^6 \ln 10 d^{1/2}(\varepsilon_0 T)^{-3/2} \text{ mol}^{-1/2}\text{ kg}^{1/2}, \quad (3)$$

$$B_0 = 50.29\times10^{10} d^{1/2}(\varepsilon_0 T)^{-1/2} \text{ m}^{-1/2}\text{ mol}^{-1}\text{ kg}^{1/2}, \quad (4)$$

where ε_0 is the dielectric constant, d the density of the solvent, T is the temperature in absolute scale. Since alteration of a_0 values caused no significant change in ΔE°_m values, the values of $a_0=0$ was used in all the cases. In Eq. 1 Δb is the difference of b values in the solvent and water, which are empirical constants depending on the nature of solvent, temperature and on the assumed a_0-values.

$\Delta E^{o\prime}$ values were calculated by Eq. 1 and the plots of $\Delta E^{o\prime}$ *vs.* m were found to be linear in all the cases and when extrapolated to $m=0$ yielded the values of ΔE°_m as intercepts. The values of ΔE°_m in the respective solvents are given in Table 2 and are correct within ± 0.3 mV.

Transfer free energies of *KF*, ΔG°_t(KF) from the standard state in water to the standard state in the respective solvents were obtained on mole fraction scale by Eq. 5

$$\Delta G^\circ_t(\text{KF}) = F\Delta E^\circ_m - 2RT \ln(M_s/M_w), \quad (5)$$

where M_w is the molecular weight of water. The ΔG°_t(KF) values are given in Table 2 and correct within ± 0.03 kJ mol^{-1}.

The transfer free energies of F^-, $\Delta G^\circ_t(F^-)$, in all the solvents were evaluated from the respective ΔG°_t(KF) values using the corresponding ionic contributions of K^+, *i.e.* $\Delta G^\circ_t(K^+)$, taken from our earlier work based on TATB method[7b–f] and are presented in Table 2. For the sake of comparison ΔG°_t (i) values of Cl^-, Br^-, and I^-[7b–f] and OH^- [7b,g,h] in some of the mixed solvents, are also presented in Table 2. Moreover, in order to draw important implications of the observed results, ΔG°_t-composition profiles of OH^- for DMSO–water,[7b] DME–water[7h] and ME–water[7g] systems have also been shown in Fig. 1, where those of F^- for all the solvent systems are illustrated.

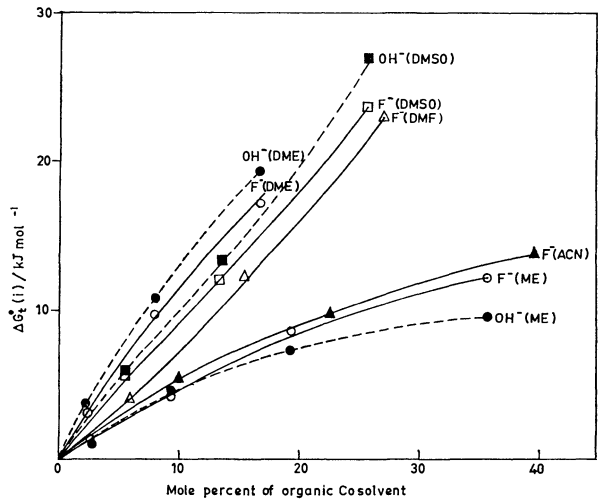

Fig. 1. Variation of $\Delta G^\circ_t(F^-)$ (solid line) and ΔG°_t (OH^-) (dotted line) in various aqueous-organic solvents.

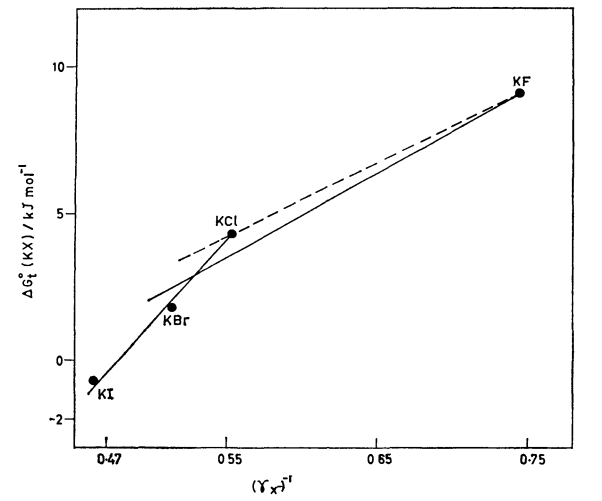

Fig. 2. Typical Feakin's type plots of ΔG°_t(KX) [X=F, Cl, Br, or I] *vs.* $(r_x)^{-1}$ in 40 wt% DMSO–water mixture at 298.16°A.

Table 1. EMF (ΔE) in volt of the double cell (I) in different aqueous-organic solvents at 25 °C

System	m/mol kg^{-1}	ΔE/V	m/mol kg^{-1}	ΔE/V	m/mol kg^{-1}	ΔE/V	m/mol kg^{-1}	ΔE/V
	20% DMSO		40% DMSO		60% DMSO			
DMSO-H_2O	0.0978	0.0434	0.0934	0.1053	0.0761	0.1970		
	0.0773	0.0447	0.0773	0.1062	0.0593	0.1974		
	0.0589	0.0456	0.0604	0.1086	0.0493	0.2013		
	0.0490	0.0473	0.0407	0.1106	0.0382	0.2024		
	0.0401	0.0478	0.0305	0.1124	0.0276	0.2032		
	0.0184	0.0495	0.0208	0.1134	0.0196	0.2019		
DMF-H_2O	0.0900	0.0459	0.0972	0.1084	0.0957	0.1956		
	0.0795	0.0464	0.0756	0.1090	0.0799	0.1958		
	0.0564	0.0468	0.0549	0.1100	0.0596	0.1977		
	0.0491	0.0474	0.0496	0.1104	0.0382	0.1991		
	0.0378	0.0476	0.0371	0.1110	0.0808	0.1990		
	0.0163	0.0478	0.0174	0.1115	0.0195	0.2002		
ACN-H_2O	0.1054	0.0390	0.0954	0.0758	0.0921	0.1231		
	0.0971	0.0404	0.0754	0.0791	0.0807	0.1245		
	0.0787	0.0410	0.0574	0.0810	0.0613	0.1275		
	0.0587	0.0414	0.0401	0.0824	0.0527	0.1291		
	0·0398	0.0424	0.0306	0.0830	0.0310	0.1325		
	0.0205	0.0430	0.0190	0.0842	0.0207	0.1358		
	10% DME		30% DME		50% DME			
DME-H_2O	0.1013	0.0253	0.1019	0.0824	0.1014	0.1403		
	0.0842	0.0256	0.0837	0.0830	0.0839	0.1418		
	0.0667	0.0266	0.0667	0.0834	0.0672	0.1452		
	0.0524	0.0270	0.0545	0.0840	0.0535	0.1472		
	0.0403	0.0276	0.0364	0.0846	0.0406	0.1480		
	0.0233	0.0285	0.0239	0.0851	0.0223	0.1474		
	10% ME		30% ME		50% ME		70% ME	
ME-H_2O	0.1218	0.0144	0.1231	0.5776	0.1259	0.1006	0.1100	0.1472
	0.1100	0.0151	0.1100	0.0583	0.1100	0.1019	0.0981	0.1484
	0.0953	0.0154	0.0982	0.0597	0.0977	0.1035	0.0870	0.1500
	0.0739	0.0180	0.0904	0.0600	0.0739	0.1038	0.0735	0.1504
	0.0546	0.0186	0.0754	0.0602	0.0594	0.1052	0.0552	0.1506
	0.0469	0.0215	0.0537	0.0606	0.0500	0.1059	0.0395	0.1510
	0.0301	0.0201	0.0350	0.0616	0.0381	0.1069	0.0303	0.1513
	0.0184	0.0213	0.0248	0.0618	0.0238	0.1071	0.0263	0.1515

Tests of Feakins-type extrapolation[11] by use of data points for all the potassium halides *i.e.* from the plots of $\Delta G_t^\circ(KX)$ [X=F, Cl, Br, and I] *vs.* $(r_{x^-})^{-1}$ showed that no straight line was obtainable through the data points for all the four anions simultaneously in any of the solvents. Consequently, in each of the solvent systems, three values of $\Delta G_t^\circ(K^+)$ were evaluated by extrapolating the mean deviation lines through the data points for X=Cl, Br, I, and for X=F, Cl, Br, and the 'ideal' line through the data points for X=F and Cl. These value of K^+ are compared with the corresponding values obtained by TATB in Table 3. Figure 2 illustrates the plots of $\Delta G_t^\circ(KX)$ against $(r_{x^-})^{-1}$ referred to above for 40 wt % DMSO–water system.

Discussion

As Table 2 shows, the transfer free energies of F^- from water to all the aqueous-organic solvents are increasingly positive indicating that the ion becomes increasingly destabilized as the proportion of the cosolvents increases. Thus, the observed destabilization of F^- from this thermodynamic consideration also corroborates the widely recognized phenomenon of increased "desolvation" of the anions caused by the addition of dipolar aprotic solvents. This in fact stems from the increasing loss of hydrogen-bonded stability of the anions[13c] and decreasing interactions with the mixed solvents resulting from the increased proportion of the cosolvents which either have little H-bond donating propensity or sterically shielded interacting positive charge centres. From Table 2 it is also evident that for any given solvent the extent of destabilization of halide ions (X^-) decreases with the increased size of the ions. Expectedly, this is the amalgamated effects of decreasing strength of H-bonded interactions with water on the one hand and increasing strength of "soft-soft"[14] and dispersion interactions[15] between the dipolar aprotic cosolvents and the increasing anion size on the other.

Table 2. Values of standard EMF's $\Delta E°$/V of the cell (I) and free energies of transfer $\Delta G_t°$ for KF and other single ions from water to aqueous mixtures of cosolvents

System	Wt%	At 25°C			$\Delta G_t°$(i)/kJ mol^{-1}					
		Mole %	$\Delta E°$/V	$\Delta G_t°$(KF)/kJ	K^+	F^- [f]	Cl^-	Br^-	I^-	OH^-
DMSO-H_2O[a]	20	5.46	0.0507	4.06	−1.6	5.7	3.3	2.1	0.8	5.9
	40	13.33	0.1144	9.22	−2.8	12.0	7.2	4.6	2.1	13.4
	60	25.70	0.2080	17.00	−6.6	23.6	14.3	10.5	5.0	27.0
DMF-H_2O[b]	20	5.81	0.0479	3.81	−0.2	4.0	2.1	1.2	−0.2	—
	40	14.11	0.1109	8.92	−3.4	12.3	7.7	5.6	2.6	—
	60	27.00	0.1984	16.17	−6.6	22.8	15.9	11.0	4.9	—
ACN-H_2O[c]	20	9.88	0.0429	3.55	−2.0	5.5	3.6	2.6	1.6	—
	40	22.63	0.0838	6.83	−2.6	9.4	6.4	4.7	2.0	—
	60	39.71	0.1453	11.99	−1.8	13.8	8.9	6.3	2.6	—
DME-H_2O[d]	10	2.17	0.0308	2.56	−0.7	3.3	2.3	1.3	0.7	3.7[g]
	30	7.89	0.0874	7.07	−2.6	9.7	6.9	4.8	2.8	10.9[g]
	50	16.66	0.1448	11.44	−5.7	17.1	12.7	10.0	5.8	19.4[g]
ME-H_2O[e]	10	2.56	0.0218	1.71	0.6	1.2	0.5	0.01	−0.2	1.0[h]
	30	9.21	0.0603	3.83	−0.3	4.2	3.1	2.0	0.6	4.6[h]
	50	19.14	0.1019	7.45	−1.3	8.7	6.1	4.4	1.2	7.2[h]
	70	35.59	0.01367	9.40	−2.8	12.2	9.6	7.2	2.5	9.6[h]

a) Ref. 7b. b) Ref. 7c. c) Ref. 7d. d) Ref. 7g. e) Ref. 7e. f) Present study. g) Ref. 7h. h) Ref. 7g.

Table 3. Values of $\Delta G_t°(K^+)$/kJ mol^{-1} based on extrapolation and R.E. methods

System	Wt%	Feakins-type extrapolation with data points of K-salts of			R.E.M.[a]
		(Cl^-, Br, I^-)	(F^-, Cl^-, Br^-)	(F^-, Cl^-)	
DMSO	20	−10.0	−6.1	−4.9	−1.6
	40	−27.2	−11.4	−8.8	−2.8
	60	−23.6	−20.0	−17.9	−6.6
DMF	20	−11.3	−4.1	−3.3	−0.2
	40	−26.6	−10.6	−8.4	−3.4
	60	−52.5	−17.0	−14.2	−6.6
ACN	20	−10.5	−4.4	−3.6	−2.0
	40	−22.1	−6.3	−4.5	−2.6
	60	−32.7	−8.6	−6.1	−1.8
DME	10	−8.1	−4.6	−3.3	−0.7
	30	−19.4	−6.3	−3.7	−2.6
	50	−29.1	−8.4	−5.4	−5.7
ME	10	−3.1	−1.4	−1.0	0.6
	30	−11.5	−1.7	−0.4	−0.3
	50	−21.2	−4.2	−2.5	−1.3
	70	−27.6	−4.0	−0.7	−2.8

a) R.E.M.: Reference electrolyte method on TATB assumption (Refs. 7b, c, d, e, f).

It is interesting to note, as $\Delta G_t°(F^-)$-composition profiles for the solvents (Fig. 1) show, that at any composition the destabilizing capacity of the cosolvents decreases in the order DME>DMSO≥DMF≫ACN≈ ME. Significantly enough, similar order has also been observed[1] in the enhancement of H_- function by these dipolar aprotic cosolvents, excepting DME, when added to 0.1 m disodium 1,2-ethanediolate solution in 1,2-ethanediol, which of course chiefly reflects the relative destabilization of the 1,2-ethanediolate anion.

As this order reflects the effects of relative "aproticity" of the cosolvents resulting chiefly from the combined effects of relative magnitudes and approachability of the positive charge centres of the cosolvents, these results appear to suggest that the "aproticity" of DMF is slightly less than that of DMSO. Although it is difficult at this stage to differentiate the relative percentages of the two possible forms of DMF: A and B[17] one may wonder if the slightly less destabilization of F^- and other X^- ions relative to those in DMSO–water arises from the weak H-bonding effect of H-atom attached to the positively charged C atom of the form A. Alternatively, the formal positive charge on S atom in

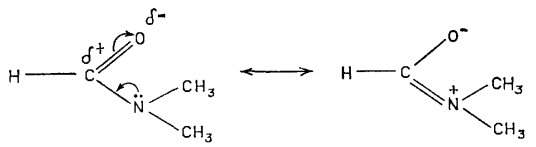

A B

DMSO molecule appears to be sterically more unapproachable than that in DMF molecule, affecting the ion-dipole interactions. Either of these effects will be of course more predominant in the cases of pure solvents than in the mixed solvents as has been observed.[2]

On the other hand, the relatively less destabilization of F^- and other X^- ions in ACN–water mixtures compared to those in DMSO or DMF–water mixtures is indicative of the fact that "aproticity" of ACN is smaller than that of the other two dipolar aprotic solvents as is expected from its relatively smaller size, less shielded positive charge centre and also weak H-bonding propensity.[18] Besides, this is also expected, if, as has been suggested by Kebarle *et al.*,[19] X^- approaches $\begin{matrix}H\\ H\text{-}C\text{-}C\equiv N\\ H\end{matrix}$ molecule along the C_3-axis of the latter and bonding occurs symmetrically through all 3H atoms. Since the overall strength of such H-bonds should increase as the X^- becomes larger and more accommodative,[20] $\Delta G_t^\circ(F^-) \gg \Delta G_t^\circ(Cl^-) > \Delta G_t^\circ(Br^-) > \Delta G_t^\circ(I^-)$, as has been observed.

But strikingly enough, in spite of the fact that ME is a protic solvent with a relatively strong H-bonding centre compared to ACN, the observed comparable destabilization of F^- in these two solvent systems suggests that the inductive effect of CH_3^- group in ME possibly imparts "aproticity" comparable to that of ACN through intramolecular H-bonding[21] or alternatively, makes the protic character of the hydroxylic H atom fairly less than that of pure water. On the other hand, the observed pronounced destabilization of F^- in DME–water system is indicative of the effect of pronounced "aproticity" of DME which results from the absence of any localized positive charge centres suitable for anion solvation. Also, the enhanced negative charge density on the O atoms of two methoxyl groups will also help destabilization of F^-. Apart from these, the DME–water complexes C in water-rich composition which are capable of anion solvation, are likely to be replaced by complexes of the type D in

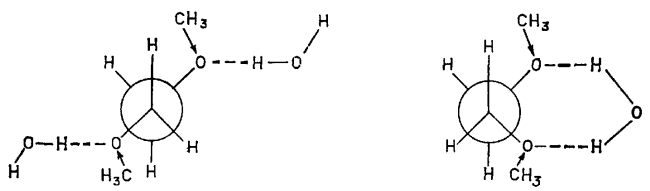

C D

water deficient composition thus imparting decreasing acidity to the mixed solvents. Moreover, the inductive effect of two CH_3^- groups relayed through co-operative hydrogen bonded structures, diminishes the proticity of the hydrogen-bonded water in the water–cosolvent complexes. All these together are likely to result in the decreasing acidity of the mixed solvents.

It is interesting to note that while in DMSO–water and DME–water mixtures the ΔG_t°-composition profiles for OH^- lie above the corresponding profiles for F^-, the reverse is true in ME–water system (Fig. 1). This larger destabilization of OH^- compared to F^- in DMSO–water and DME–water mixtures can be attributed to its pronounced stabilization in water because of its intrinsic protophilicity and natural propensity of fitting in water structures[13b] and the relatively poor H-bond denating capacity of the aqueous DMSO and DME solutions. But the observed reverse behaviour of OH^- compared to F^- in ME–water system indicates that ME being itself a protic solvent stabilizes the protophilic OH^- through H-bonding more than F^-. Thus, the present results suggest that while the stability of OH^- is governed more by H-bond donating capacity of water and the protic cosolvents, that of F^- is dictated partly by H-bond donating capacity and partly by "aproticity" of the cosolvents, which is chiefly guided by the magnitudes and the location of formal positive charges of the cosolvent dipoles.

Tests of Feakins-type extrapolation using $\Delta G_t^\circ(KF)$ values along with the corresponding values of other potassium halides (Fig. 2) reveral that the "ideal plots' of $\Delta G_t^\circ(KX)$ *vs.* $(r_x)^{-1}$ through the data points of KF and KCl yield single-ion contributions (Table 3) that are nearer to those obtained by TATB method.[7b-e] But those obtained from the mean deviation lines drawn through the data points of KF, KCL, and KBr or of KCl, KBr, and KI are increasingly far off from the respective values by TATB method, indicating that the superimposed soft-soft interactions[20] on Br^- and I^- make the latter plots more untenable.

The authors express their thanks to the Council of Scientific and Industrial Research, New Delhi, for financial assistance.

References

1) K. K. Kundu and L. Aiyar, *J. Chem. Soc., Perkin Trans. 2*, **1972**, 715.

2) B. G. Cox, B. R. Hedwig, A. J. Parker, and I. W. Watts, *Aust. J. Chem.*, **27**, 477 (1974).

3) a) O. Popovych, *Crit. Rev. Anal. Chem.*, **73**, 1 (1970); b) O. Popovych, A. Gibofsky, and D. H. Berne, *Anal. Chem.*, **44**, 811 (1972); c) O. Popovych, *ibid.*, **46**, 2009 (1974).

4) I. M. Kolthoff and M. K. Chantooni, *J. Phys. Chem.*, **76**, 2024 (1972).

5) a) M. H. Abraham, *J. Chem. Soc., Faraday Trans. 1*, **74**, 2101 (1972); b) M. H. Abraham and A. Nasehzadeh, *Can. J. Chem.*, **57**, 71 (1979).

6) C. Tissier and C. R. Hebd, *Seances, Acad. Sci. Ser. C.*, **286**, 35 (1978).

7) a) A. K. Das and K. K. Kundu, *Ind. J. Chem.*, **16A**, 467 (1978); b) A. K. Das and K. K. Kundu, *J. Solution Chem.*, **8**, 259 (1979); c) K. Das, A. K. Das, and K. K. Kundu, *Electrochim. Acta*, **26**, 471 (1981); d) K. Das, K. Bose, and K. K. Kundu, *ibid.*, **26**, 479 (1981); e) A.

Bhattacharya, A. K. Das, and K. K. Kundu, *Ind. J. Chem.*, **20A**, 347 (1981); f) A. Bhattacharya, A. K. Das, and K. K. Kundu, *ibid.*, **20A**, 353 (1981); g) A. Bhattacharya, A. K. Das, and K. K. Kundu, *Can. J. Chem.*, in press; h) A. Bhattacharya and K. K. Kundu, Unpublished results : detailed data can be had from the authors on request.

8) J. I. Kim, *J. Phys. Chem.*, **82**, 191 (1978).

9) a) L. A. Carpine and A. C. Sau, *J. Chem. Soc., Chem. Commun.*, **1979**, 470; also see various references therein. b) J. Hayami, N. Ono, and A. Kaji, *Tetrahedron Lett.*, **1968**, 1385.

10) P. J. Voice, *J. Chem. Soc., Faraday Trans. 1*, **70**, 498 (1974).

11) a) D. Feakins and P. Watts, *J. Chem. Soc., A*, **1967**, 4734; b) D. Feakins, cited in Physico-chemical process in mixed aqueous solvents, ed by F. Franks, Heinemann Educational Books, London (1967), p. 71.

12) a) K. K. Kundu, A. K. Rakshit, and M. N. Das, *Electrochim. Acta*, **17**, 1921 (1972); b) K. Bose and K. K. Kundu, *J. Solution Chem.*, **8**, 195 (1979); c) I. N. Basu Mullick and K. K. Kundu, *Can. J. Chem.*, **58**, 79 (1980).

13) a) A. K. Das and K. K. Kundu, *J. Chem. Soc., Faraday Trans. 1*, **69**, 730 (1973); b) *Electrochim. Acta*, **23**, 685 (1978); c) K. Bose and K. K. Kundu, *J. Chem. Soc., Faraday Trans. 1*, **73**, 284 (1977).

14) N. M. Burns, *Can. J. Chem.*, **51**, 3123 (1973).

15) a) R. G. Pearson, *J. Am. Chem. Soc.*, **85**, 3533 (1963); b) D. Feakins and P. J. Voice, *J. Chem. Soc., Faraday Trans. 1*, **68**, 1390 (1972); c) A. K. Das and K. K. Kundu, *J. Solution Chem.*, **5**, 43 (1976).

16) J. F. Coetzee and W. R. Sharpe, *J. Solution Chem.*, **4**, 72 (1972).

17) T. Yonezawa and I. Morishima, *Bull. Chem. Soc. Jpn.*, **39**, 2346 (1966); C. de Visser, C. Perron, J. E. Desnoyers, W. J. M. Heuverland, and G. Somsen, *J. Chem. Eng. Data*, **1971**, 22, 74.

18) I. M. Kolthoff, *Pure Appl. Chem.*, **25**, 305 (1971).

19) R. Yamdagni and P. Kebarle, *J. Am. Chem. Soc.*, **94**, 2940 (1972).

20) K. Bose and K. K. Kundu, *Can. J. Chem.*, **57**, 2476 (1979).

21) a) L. S. Prabhuminash and C. K. Jose, *J. Chem. Soc., Faraday Trans. 2*, **71**, 1545 (1975); b) R. Iwamoto, *Spectrochim. Acta, Part A*, **27**, 2385 (1971).

22) F. Franks and G. J. Ives, *Quart. Rev.*, **20**, 1 (1966).

23) A. Jeanes and R. Adams, *J. Am. Chem. Soc.*, **59**, 2608 (1937).

24) a) R. E. Robertson and S. E. Stugamari, *Can. J. Chem.*, **50**, 1353 (1972); b) K. W. Morcom and R. W. Smith, *J. Chem. Thermodyn.*, **1**, 503 (1969); c) C. Moreau and G. Douheret, *Tehermochim. Acta*, **385**, 13; *J. Chem. Thermodyn.*, **8**, 403 (1976). d) S. Schiavo and B. Scrosati, *Z. Phys. Chem.*, **9**, 102 (1976).

25) I. S. Perelygin and N. R. Sibinllina, *Teplo Dvizhnic Mol. Mezmol Vrimodeistvic Zhidk. Rastvorakh*, **1969**, 180.

26) A. Le Narvor, E. Gentric, and P. Sauragne, *Can. J. Chem.*, **49**, 1933 (1971).

27) E. L. Zukhova, *Opt. Spektrosk*, **4**, 750 (1958).

28) A. U. Saum, *J. Polym. Sci.*, **42**, 57 (1961).

Ultrasonic Investigation on the Structure of Aqueous Solutions of *N,N*-Dimethylformamide and Dimethyl Sulfoxide

Kopparapu Subbarangaiah, Neriyanuri Manohara Murthy, and Saraswatula Venkata Subrahmanyam*

Department of Physics, S.V.U.A.P.G. Centre, Anantapur-515 003, India

(Received June 23, 1980)

The effects of *N,N*-dimethylformamide and dimethyl sulfoxide on the temperature of adiabatic compressibility minimum (T_β) and sound velocity maximum (T_u) of water have been studied. The structural contributions to the shift in T_β and T_u, $[\Delta T_{\beta\ \mathrm{str.}}]_{\mathrm{exp.}}$ and $[\Delta T_{u\ \mathrm{str.}}]_{\mathrm{exp.}}$, have been found to be negative for both solutes. Both $[\Delta T_{\beta\ \mathrm{str.}}]_{\mathrm{exp.}}$ and $[\Delta T_{u\ \mathrm{str.}}]_{\mathrm{exp.}}$ are higher for dimethyl sulfoxide than *N,N*-dimethylformamide indicating that the sulfinyl group (>SO) is more efficient in structure disruption than the formylimino group (>F). The results have been explained in the light of hydrogen bonding equilibria by the solutes.

In recent years the effect of nonelectrolytes on the hydrogen-bonded structure of water has been studied extensively by observing the non-ideal thermodynamic behavior such as viscosity composition maxima,[1] negative partial molal volumes[2-4] and partial molal heat capacity at infinite dilution.[5-7] The structure of aqueous nonelectrolyte solution may also be investigated by determining the shift in the extrema in various physical properties of water caused by the addition of nonelectrolytes. Effects of nonelectrolytes on the density maximum temperature (DMT) of water have been studied extensively[8-15] and the results have been utilized successfully to classify the solutes as structure promoters and disrupters. Recent studies on the effect of nonelectrolytes on the adiabatic compressibility minimum temperature[16-20] (ACMT) and sound velocity maximum temperature[21,22] (SVMT) have been found to be useful in understanding their structural behavior.

Aqueous solutions of *N,N*-dimethylformamide (DMF) and dimethyl sulfoxide (DMSO) are known to be the best mixtures and reaction media. DMSO and DMF interact with water through hydrogen-bonding, but details of such interactions are not well characterised. The studies on density maximum by Macdonald *et al.*,[11] excess Gibbs free energy by Clever and Piggott[23] and the infrared spectroscopy by Brink and Falk[24] on aqueous DMSO characterise DMSO as a structure disrupter, while studies on standard free energy by Oakenfull and Fenwick,[28] X-ray diffraction and neutron inelastic scattering by Safford *et al.*,[26] partial molar enthalpies by Rallo *et al.*[25] apparent molar volume and heat capacity by de Visser *et al.*[27] on water+DMSO system classify DMSO as a structure promotor. DMF is also representative of a class of solutes[29] including dioxane, dimethylsulfoxide and possibly acetone which are only weakly hydrophobic and probably have little overall influence on the structure of water.

In view of the growing importance of sulfoxides and amides as solutes in biochemical and physicochemical investigations involving water as solvent and also of the fact that contraversial conclusions in particular have been drawn regarding the solute-solvent interactions and structural propensity of DMSO, we have taken up the studies on the effect of DMSO and DMF on SVMT and ACMT of water and the results are reported in this paper.

Experimental

Analar grade DMF and DMSO were used after necessary purification.[30] The purity of the samples were checked by determining their densities at 25 °C using a bicapillary type pycknometer with an accuracy of 2 parts in 10^5, the values being in good agreement with literature data.[4,27] Ultrasonic velocity (u) was determined using a single crystal variable path interferometer working at 3 MHz with an accuracy of $\pm 0.003\%$. The details of the measurement of ultrasonic velocity were reported in a previous paper.[16] Triple distilled degassed water was used to prepare solutions of DMF and DMSO of various concentrations. Ultrasonic velocities and densities were determined at an interval of $\simeq 2$ °C over a range of 5 °C on either side of SVMT and ACMT. The velocities were corrected for diffraction effects following the procedure reported.[31] The adiabatic compressibilities calculated using the formula $\beta = u^{-2}\rho^{-1}$ are accurate to $\pm 0.01\%$. At low concentrations of the organic solute, the temperature dependence of the adiabatic compressibility and ultrasonic velocity in solutions is similar to that of the curves for pure water. Transparent templates of the curves of pure water were used to determine SVMT (T_u) and ACMT (T_β) of solutions. The accuracy of the values of T_β and T_u are ± 0.4 and ± 0.2 °C, respectively.

Results and Discussion

Results of the measurement of adiabatic compressibility and ultrasonic velocity as a function of temperature at different concentrations of dilute aqueous solutions of DMF and DMSO are shown graphically in Figs. 1—4.

Expressions for T_u and T_β in aqueous solutions are obtained by considering the basic expressions for u and β in pure components as a function of temperature and the expression for the β of the solution in terms of the compressibilities of pure components. The details of the derivation were reported.[19] The final expressions are as follows.

$$T_{\beta\ \mathrm{sol.}} = \left[64 - \frac{\phi_2 \alpha_\beta}{\phi_1 0.0032 \times 10^{-11}}\right] \times \left[1 + \frac{\phi_2 \alpha^1_\beta}{\phi_1 0.0016 \times 10^{-11}}\right]^{-1} - \frac{d\beta^E}{dt}(\phi_1 0.0032 \times 10^{-11})^{-1} \times \left[1 + \frac{\phi_2 \alpha^1_\beta}{\phi_1 0.0016 \times 10^{-11}}\right]^{-1}, \quad (1)$$

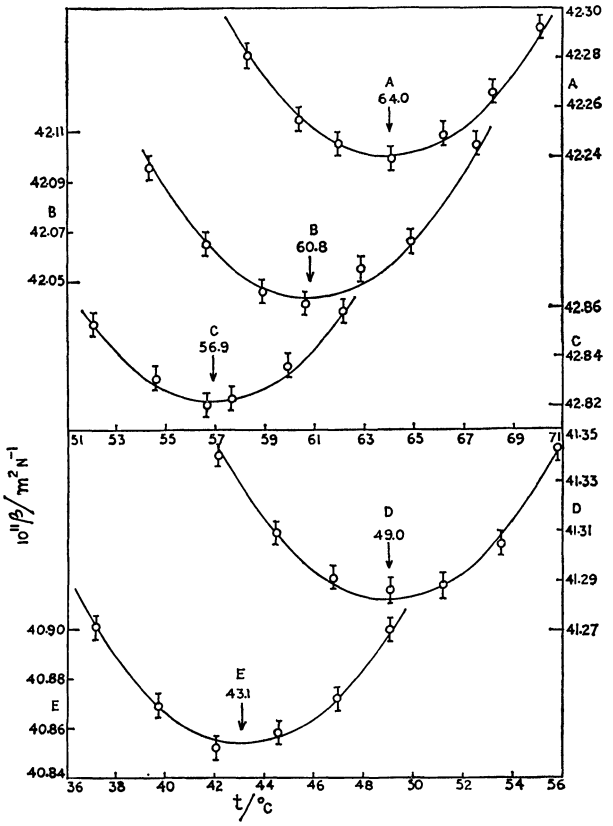

Fig. 1. Adiabatic compressibility, β, plotted against temperature of solutions of aqueous *N,N*-dimethylformamide.
A: $X_2=0.0000$, B: $X_2=0.0046$, C: $X_2=0.0095$, D: $X_2=0.0201$, E: $X_2=0.0279$.

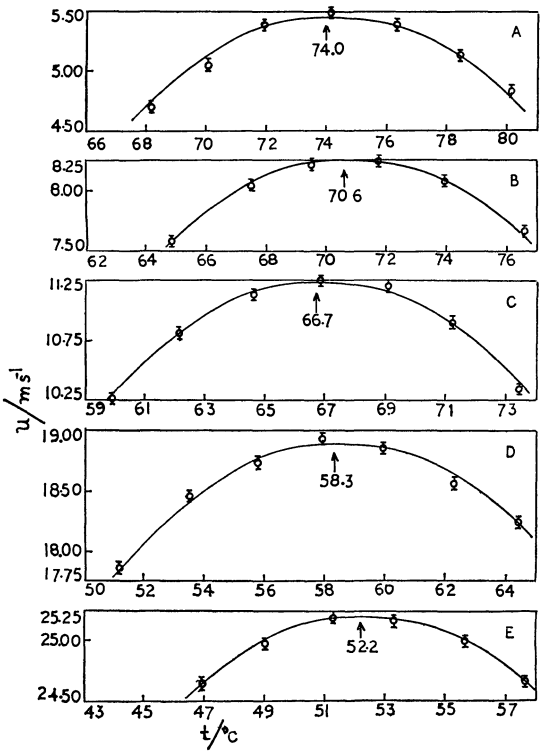

Fig. 2. Ultrasonic velocity, u, plotted against temperature, in solutions of aqueous *N,N*-dimethylformamide. The values given in the ordinate have to be added to 1550 ms^{-1}. A: $X_2=0.0000$, B: $X_2=0.0046$, C: $X_2=0.0095$, D: $X_2=0.0201$, E: $X_2=0.0279$.

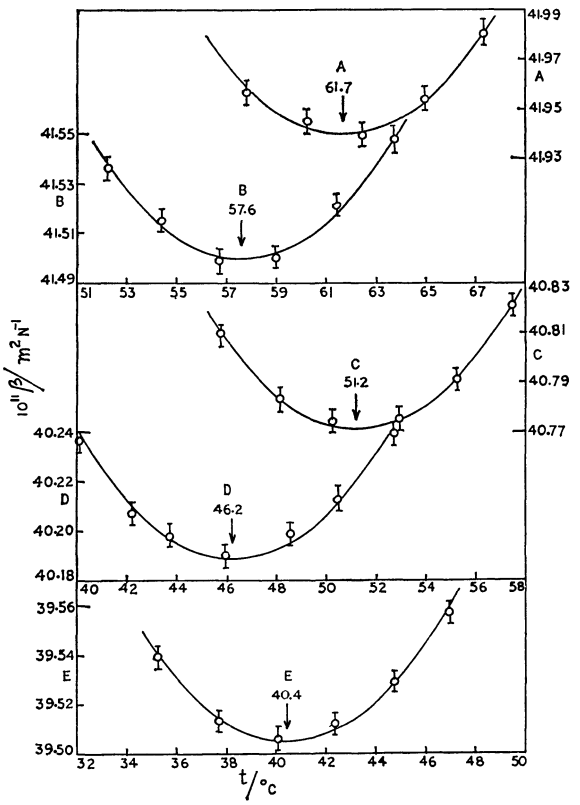

Fig. 3. Adiabatic compressibility, β, plotted against temperature of solutions of aqueous dimethyl sulfoxide.
A: $X_2=0.0044$, B: $X_2=0.0115$, C: $X_2=0.0225$, D: $X_2=0.0308$, E: $X_2=0.0402$.

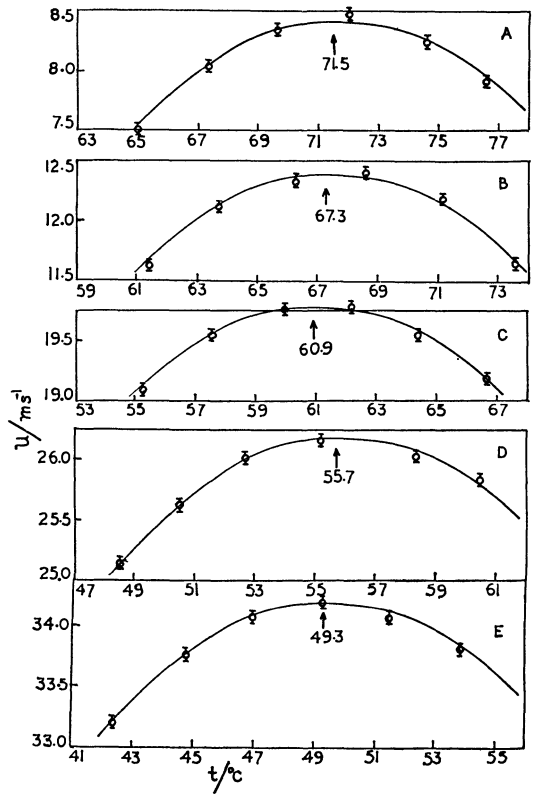

Fig. 4. Ultrasonic velocity, u, plotted against temperature, in solutions of aqueous dimethyl sulfoxide. The values given in the ordinate have to be added to 1550 ms^{-1}. A: $X_2=0.0044$, B: $X_2=0.0115$, C: $X_2=0.0225$, D: $X_2=0.0308$, E: $X_2=0.0402$.

TABLE 1. β_2^0, α_β, α_β^1, u_2^0, AND α_u FOR *N,N*-DIMETHYLFORMAMIDE AND DIMETHYL SULFOXIDE

Solute	$\beta_2^0 \times 10^{11}$ / $m^2\ N^{-1}$	$\alpha_\beta \times 10^{11}$ / $m^2\ N^{-1}\ °C^{-2}$	$\alpha_\beta^1 \times 10^{11}$ / $m^2\ N^{-1}\ °C^{-2}$	u_2^0 / ms^{-1}	α_u / $ms^{-1}\ °C^{-1}$
N,N-Dimethylformamide	43.046	0.21816	0.001740	1556.77	3.82470
Dimethyl sulfoxide	36.007	0.17048	0.000985	1576.98	3.34693

TABLE 2. $T_{\beta\ id.}$, $T_{\beta\ exp.}$, $(d\beta^E/dt)$, AND $\Delta T_{\beta\ str.}$ AT DIFFERENT MOLE FRACTION X_2 OF *N,N*-DIMETHYL FORMAMIDE AND DIMETHYL SULFOXIDE IN WATER

Solute	X_2	$T_{\beta\ id.}$ / °C	$T_{\beta\ exp.}$ / °C	$(d\beta^E/dt) \times 10^{14}$ / $m^2\ N^{-1}\ °C^{-1}$	$\Delta T_{\beta\ str.}$/°C Exptl	$\Delta T_{\beta\ str.}$/°C Calcd
N,N-Dimethylformamide	0.0046	61.3	60.8	0.7±0.3	−0.5±0.4	−0.2±0.1
	0.0095	58.5	56.9	2.1±1.1	−1.6±0.4	−0.7±0.3
	0.0201	52.8	49.0	9.2±4.1	−3.8±0.4	−2.9±1.3
	0.0279	48.9	43.1	17.0±8.5	−5.8±0.4	−5.3±2.6
Dimethyl sulfoxide	0.0044	62.4	61.7	1.0±0.6	−0.7±0.4	0.3±0.2
	0.0115	59.8	57.6	4.3±2.2	−2.2±0.4	−1.4±0.7
	0.0225	55.9	51.2	10.6±5.3	−4.7±0.4	−3.4±1.7
	0.0308	53.1	46.2	18.3±8.2	−6.9±0.4	−6.0±2.7
	0.0402	50.0	40.4	28.2±14.1	−9.6±0.4	−9.3±4.7

TABLE 3. $T_{u\ id.}$, $T_{u\ exp.}$, $(d\rho/dt)$, $(d\beta^E/dt)$, AND $\Delta T_{u\ str.}$ AT DIFFERENT MOLE FRACTIONS X_2 OF *N,N*-DIMETHYLFORMAMIDE AND DIMETHYLSULFOXIDE IN WATER

Solute	X_2	$T_{u\ id.}$ / °C	$T_{u\ exp.}$ / °C	$(d\rho/dt) \times 10^3$ / $kg\ m^{-3}\ °C^{-1}$	$(d\beta^E/dt) \times 10^{14}$ / $m^2\ N^{-1}\ °C^{-1}$	$\Delta T_{u\ str.}$/°C Exptl	$\Delta T_{u\ str.}$/°C Calcd
N,N-Dimethyl-formamide	0.0046	71.0	70.6	−59	−0.9±0.4	−0.4±0.2	0.2±0.2
	0.0095	67.9	66.7	−59	−0.5±0.2	−1.2±0.2	−0.1±0.1
	0.0201	61.7	58.3	−57	2.9±1.3	−3.4±0.2	−1.8±0.5
	0.0279	57.6	52.2	−57	8.7±3.9	−5.4±0.2	−4.5±1.6
Dimethyl sulfoxide	0.0044	72.2	71.5	−60	0.7±0.4	−0.7±0.2	−0.4±0.2
	0.0115	69.4	67.3	−60	2.2±1.1	−2.1±0.2	−1.1±0.4
	0.0225	65.2	60.9	−57	7.2±3.2	−4.3±0.2	−3.4±1.3
	0.0308	62.2	55.7	−58	11.2±5.6	−6.5±0.2	−5.4±2.4
	0.0402	59.0	49.3	−58	19.1±8.6	−9.7±0.2	−9.2±3.8

$$T_{u\ sol.} = \left[74 - \left(\frac{\phi_2}{\phi_1}\right)^2 \left(\frac{W_1}{W_2}\right) \left(\frac{\alpha_u}{0.049}\right) \frac{(u_1)^3}{(u_2)^3}\right] - \left(\frac{W_1}{\phi_1^2}\right) \left(\frac{u_1^3}{0.098}\right) \left[\rho \frac{d\beta^E}{dt} + \beta^E \frac{d\rho}{dt}\right]. \quad (2)$$

Where ϕ_1, ϕ_2 and W_1, W_2 represent the volume fractions and weight fractions of pure water and organic solute, respectively, in solution. α_β and α_β^1 are the coefficients involved in the relation for the adiabatic compressibility as a function of temperature (t) of organic solute given below:

$$\beta_2 = \beta_2^0 + \alpha_\beta t + \alpha_\beta^1 t^2. \quad (3)$$

Where α_u represents the coefficient involved in the expression for temperature dependence of velocity in the organic solute, namely

$$u_2 = u_2^0 - \alpha_u t. \quad (4)$$

Where u_1 and u_2 are velocities in pure water and organic solute, respectively. β^E represents the excess adiabatic compressibility. The values of β_2°, α_β, α_β^1, u_2°, and α_u for DMF and DMSO are evaluated using ultrasonic velocity determined experimentally and density data at different temperatures. The values are given in Table 1.

The shifts produced $\Delta T_\beta = (T_{\beta\ sol.} - T_{\beta\ water})$ and $\Delta T_u = (T_{u\ sol.} - T_{u\ water})$ may be divided into an ideal contribution ($\Delta T_{u\ id.}$ and $\Delta T_{\beta\ id.}$) and structural contribution ($\Delta T_{u\ str.}$ and $T_{\beta\ str.}$) according to Eqs. 1 and 2. The ideal contribution is always negative, but the structural contribution can either be positive or negative, indicating either structure promotion or structure disruption by the solute.

The second terms on the right hand side of Eqs. 1 and 2 represent $\Delta T_{\beta\ str.}$ and $\Delta T_{u\ str.}$, respectively. They can also be obtained experimentally using the following relations.

$$[\Delta T_{\beta\ str.}]_{exp.} = T_{\beta\ exp.} - T_{\beta\ id.}, \quad (5)$$

$$[\Delta T_{u\ str.}]_{exp.} = T_{u\ exp.} - T_{u\ id.}, \quad (6)$$

where $T_{\beta\ id.}$ and $T_{u\ id.}$ are given by the first terms of the right hand sides of Eqs. 1 and 2, respectively. These temperatures correspond to those at which adiabatic compressibility minimum of and sound velocity maximum in the solution would take place if ideal mixing occurs. Since the temperature dependence of ϕ_1 and ϕ is small, ϕ_1 and ϕ_2 used to determine $T_{\beta\ id.}$

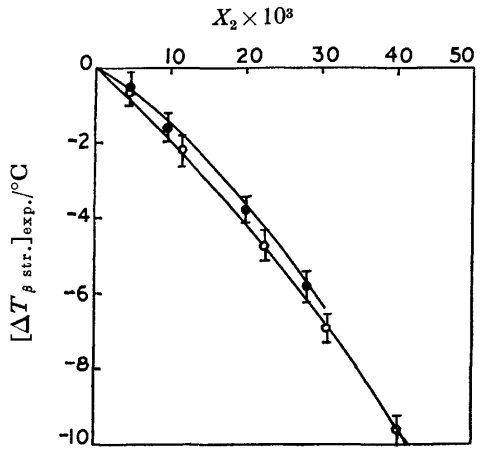

Fig. 5. Structural shifts, $[\Delta T_{\beta\,\mathrm{str.}}]_{\mathrm{exp.}}$, plotted against X_2 of *N,N*-dimethylformamide and dimethyl solfolxide. ●: *N,N*-Dimethyl formamide, ○: dimethyl solfoxide.

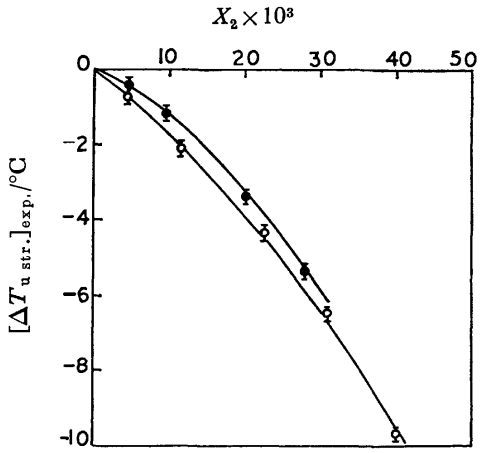

Fig. 6. Structural shifts, $[\Delta T_{\mathrm{u\,str.}}]_{\mathrm{exp.}}$, plotted against X_2 of *N,N*-dimethylformamide and dimethyl sulfoxide. ●: *N,N*-Dimethylformamide, ○: dimethyl sulfoxide.

and $T_{\mathrm{u\,id.}}$ were those calculated at T_β and T_u of the solution found experimentally. Successive approximation method was employed for evaluation of $T_{\mathrm{u\,id}}$. The values of $[\Delta T_{\beta\,\mathrm{str.}}]_{\mathrm{exp.}}$ and $[\Delta T_{\mathrm{u\,str.}}]_{\mathrm{exp.}}$ at different mole fractions (X_2) of DMF and DMSO are given in Tables 2 and 3 and shown graphically in Figs. 5 and 6, respectively. The negative shifts increase with increasing X_2, indicating that both DMF and DMSO promote disruption of the three dimensional structure of water.

The spectroscopic and thermodynamic studies of aqueous DMSO by Fox and Whittingham[32] indicate hydrophobic hydration of DMSO in water, only when DMSO is present in a small amount *i.e.* $X_2 \leq 0.005$. At higher concentration complex formation is predominant. The extrema that have been observed in the excess enthalpy,[32] isothermal compressibility,[33] viscosity[34] and activation volume for benzyl chloride solvolysis[35] around $X_2 \simeq 0.35$ indicate the formation of 2:1 (H_2O:DMSO) complexes, and do not correspond to hydrophobic hydration. As such, DMSO cannot be described as a structure promoter. The structural contribution to the shift in MDT of water for DMSO has been found to be negative,[11] indicating the structure disrupting character of DMSO which supports the present study. Studies on X-ray diffraction and neutron inelastic scattering by Safford *et al.*[26] indicate DMSO as structure promoter. The studies by Brink and Falk[24] show that addition of a few mol% of DMSO to water does not change the average value or the width of distribution of hydrogen-bond energies derived from infrared spectroscopy. The studies on the apparent molar volumes[4,27,36] and heat capacities[27,37] indicate both DMSO and DMF to be weakly hydrophobic. The minimum in the standard free energy of hydrophobic interaction ($\Delta G^\circ_{\mathrm{HI}}$) for both DMSO and DMF around $X_2 \simeq 0.25$ and 0.1 indicates that these solutes strengthen hydrophobic interaction.[28] DMF is weakly hydrophobic. However, the present study indicates that it does not enhance the long-range interaction in water. Ultrasonic velocity and adiabatic compressibility measurements carried out by Endo[38] on water+DMF system over the temperature range 20—50 °C indicate some complex formation, where the number of molecules of water per DMF molecule are 22.8, definitely not of clathrate hydrate type.[39] Thus DMF–water interactions are not of hydrophobic nature. Also ultrasonic absorption measurements made by Kawaizumi *et al.*[40] on this system indicate that added DMF molecules have the same effects as the temperature rise upon the ultrasonic absorption coefficient, and DMF has been characterized as a structure disrupter. The structural contribution to the shift in MDT is negative[12] which further confirms the structure disrupting nature of DMF. Since the structure promoting interactions are sensitive to temperature[20,41–44] different conclusions drawn only reflect the different experimental temperatures, *i.e.* 64 and 74 °C for ACMT and SVMT studies carried out in the present work, 4 °C for MDT studies, and 25 °C for the other studies. It is possible that various experimental techniques correspond to different phenomena.

One may regard the ability of the solute to perturb the structure of water as a sum of group effects as proposed by Wada and Umeda.[8] We see in Figs. 5 and 6 that the structure disrupting tendency of DMSO is greater than that of DMF. Since both solutes have a common dimethyl group, it is clear that the sulfinyl group (>SO) is more efficient in disrupting the structure of water than the formylimino group (>F).

The structural contribution to the shifts in T_β and T_u has also been calculated using the values of $\frac{d\beta^E}{dt}$ at each concentration. The excess adiabatic compressibility β^E was evaluated[11] at each temperature using experimental velocities of pure components and the mixtures. At all concentrations β^E was found to be a linear function of temperature within experimental error. The calculated structural shifts $[\Delta T_{\beta\,\mathrm{str.}}]_{\mathrm{cal.}}$ and $[\Delta T_{\mathrm{u\,str.}}]_{\mathrm{cal.}}$, are also given in Tables 2 and 3 and these values compare well with the experimental ones.

One of the authors (K. Subbarangaiah) is grateful to the authorities of S. V. U. Autonomous Post-

Graduate Centre for providing the necessary financial assistance from V Plan U. G. C. grants.

References

1) W. Hertz and E. Lorentz, *Z. Phys. Chem., A*, **140**, 406 (1929).
2) V. S. Griffiths, *J. Chem. Soc.*, **1952**, 860.
3) G. N. Malcolm and J. S. Rowlinson, *Trans. Faraday Soc.*, **53**, 921 (1957).
4) F. Kawaizumi, M. Ohno, and Y. Miyahara, *Bull. Chem. Soc., Jpn.*, **50**, 2229 (1977).
5) R. K. Mohanty, S. Sunder, and J. C. Ahluwalia, *J. Phys. Chem.*, **76**, 2577 (1972).
6) E. M. Arnett, W. B. Kover, and J. V. Carter, *J. Am. Chem. Soc.*, **91**, 4028 (1969).
7) G. C. Kresheck and I. Benjamin, *J. Phys. Chem.*, **68**, 2476 (1964).
8) G. Wada and S. Umeda, *Bull. Chem. Soc. Jpn.*, **35**, 646, 1797 (1962).
9) F. Franks and B. Watson, *Trans. Faraday Soc.*, **63**, 329 (1967).
10) M. Sakurai, T. Komatsu, and T. Nakagawa, *Bull. Chem. Soc. Jpn.*, **45**, 1038 (1972).
11) D. D. Macdonald, M. D. Smith, and J. B. Hyne, *Can. J. Chem.*, **49**, 2817 (1971).
12) D. D. Macdonald, M. E. Estep, M. D. Smith, and J. B. Hyne, *J. Solution Chem.*, **3**, 713 (1974).
13) G. Wada and M. Miura, *Bull. Chem. Soc. Jpn.*, **42**, 2498 (1969).
14) D. D. Macdonald, B. Dolan, and J. B. Hyne., *J. Solution Chem.*, **5**, 405 (1976).
15) D. D. Macdonald and J. B. Hyne, *Can. J. Chem.*, **54**, 3073 (1976).
16) S. V. Subrahmanyam and N. Manohara Murthy, *J. Solution Chem.*, **4**, 347 (1975).
17) N. Manohara Murthy and S. V. Subrahmanyam, *J. Acoust. Soc. India*, **5**, 88 (1977).
18) N. Manohara Murthy and S. V. Subrahamnyam, *Acustica.*, **40**, 263 (1978).
19) N. Manohara Murthy and S. V. Subrahmanyam, *Can. J. Chem.*, **56**, 2412 (1978).
20) N. Manohara Murthy and S. V. Subrahmanyam, *J. Chem. Soc., Faraday Trans. 1*, **75**, 2067 (1979).
21) S. V. Subrahmanyam and N. Manohara Murthy, *Z. Phys. Chem. (Neue Folge)*, **88**, 116 (1974).
22) N. Manohara Murthy and S. V. Subrahmanyam, *J. Acoust. Soc. India*, **7**, 79 (1979).
23) H. L. Clever and S. P. Piggott, *J. Chem. Thermodyn.*, **3**, 221 (1971).
24) G. Brink and M. Falk, *J. Mol. Struct.*, **5**, 27 (1970).
25) F. Rallo, F. Rodante, and P. Silvestroni, *Thermochim. Acta.*, **1**, 311 (1970).
26) G. J. Safford, P. C. Schaffer, P. S. Leung, G. F. Doebbler, G. W. Brady, and E. F. X. Lyden, *J. Chem. Phys.*, **50**, 2140 (1969).
27) C. de Visser, W. J. M. Heuvelsland, L. A. Dunn, and G. Somsen, *J. Chem. Soc., Faraday Trans. 1*, **74**, 1159 (1978).
28) D. Oakenfull and D. E. Fenwick, *J. Chem. Soc., Faraday Trans. 1*, **75**, 636 (1979).
29) J. E. Desnoyers, O. Kiyohara, G. Perron, and L. Avedikian, *Adv. Chem. Ser.*, **155**, 274 (1976).
30) D. D. Perrin, W. L. F. Armarego, and D. R. Perrin, "Purification of Laboratory Chemicals," Pergamon, Oxford (1966).
31) S. V. Subrahmanyam, V. Hyderkhan, and C. V. Raghavan, *J. Acoust. Soc. Am.*, **46**, 272, (1969).
32) M. F. Fox and K. P. Whittingham, *J. Chem. Soc., Faraday Trans. 1*, **71**, 1407 (1975).
33) K. H. Jung and J. B. Hyne, *Can. J. Chem.*, **48**, 2423 (1970).
34) S. A. Schichman and R. L. Amey, *J. Phys. Chem.*, **75**, 98 (1971).
35) D. D. Macdonald and J. B. Hyne, *Can. J. Chem.*, **48**, 2494 (1970).
36) A. R. Giaquinto, R. E. Lindstrom, J. Swarbrick, and A. LoSurdo, *J. Solution Chem.*, **6**, 687 (1977).
37) C. de Visser, G. Perron, J. E. Desnoyers, W. J. M. Heuvelsland, and G. Somsen, *J. Chem. Eng. Data.*, **22**, 74 (1977).
38) H. Endo, *Bull. Chem. Soc. Jpn.*, **46**, 1106 (1973).
39) A. D. Potts and D. W. Davidson, *J. Phys. Chem.*, **69**, 996 (1965).
40) F. Kawaizumi, H. Nomura, M. Ohno, and Y. Miyahara, *Bull. Chem. Soc. Jpn.*, **52**, 3135 (1979).
41) F. Franks and D. J. G. Ives, *Quart. Rev.*, **20**, 1 (1960).
42) F. Franks, "Hydrogen Bonded Solvent Systems" Taylor and Francis, London (1968).
43) R. K. Mohanty, T. S. Sarma, S. Subramanian, and J. C. Ahluwalia, *Trans. Faraday Soc.*, **67**, 305 (1971).
44) B. Kingston and M. C. R. Symons, *J. Chem. Soc. Faraday Trans. 2*, **69**, 978 (1973).

Mixed Monolayers of Long Normal-chain Fatty Acids with Long Normal Alkyl Esters. III. Pentadecanoic Acid-Esters System

Hirosi MATUO,* Kinsi MOTOMURA, and Ryohei MATUURA

Department of Chemistry, Faculty of Science, Kyushu University 33, Higashi-ku, Fukuoka 812

(Received June 28, 1980)

The surface pressures of mixed monolayers of pentadecyl acetate, hexadecyl acetate, heptadecyl acetate, and hexadecyl propionate with pentadecanoic acid were measured at various compositions and temperatures. The two-dimensional phase diagram and apparent molar entropy and energy changes were evaluated by means of a previously described thermodynamic treatment. They depend uniquely on the molecular structure of the film-forming substances and on the composition in the mixed monolayer. The phase diagrams of pentadecanoic acid–pentadecyl acetate and pentadecanoic acid–hexadecyl acetate systems are of a complicated type. There are positive and negative regions in the excess apparent molar energy changes. The pentadecanoic acid–heptadecyl acetate and pentadecanoic acid–hexadecyl propionate systems are of the positive azeotropic type. The excess apparent molar energy changes are positive over the whole range of mole fractions.

Previously we have reported unique behavior in the mixed monolayer of the pentadecanoic acid(C_{15})–hexadecyl acetate(HA) system.[1] It has maximum and minimum points in the phase diagram. To investigate this phenomenon in more detail, it is necessary to use esters which have a different chain length of the hydrophobic part from that of HA, such as pentadecyl acetate(PA), heptadecyl acetate(HpA), and hexadecyl propionate(HPr), which has the same chain length as HA, but with a different hydrophilic group. In the present study we have attempted to do experiments with these esters.

Experimental

Pentadecanoic acid(C_{15}) was purified by fractional distillation and recrystallization. Pentadecyl acetate(PA), hexadecyl acetate(HA), heptadecyl acetate(HpA), and hexadecyl propionate(HPr) were synthesized by the usual method[2] and were purified by reduced pressure distillations.

The surface pressure was measured by means of a Wilhelmy-type surface balance. The monolayer was compressed continuously with a constant velocity. The surface pressure-mean area (π-A) curves were reproducible within ± 0.2 mN m^{-1} in the same mean molecular area. Purified benzene was used as the spreading solvent. To prevent the ester from hydrolysis, a 0.1 mol dm^{-3} NaCl solution was used as the substrate; this was prepared from twice-distilled water and sodium chloride (Wako super special grade). The temperature was kept constant within ± 0.1 K during the experiment.

Results and Discussion

Representative π-A curves of the C_{15}–PA, C_{15}–HA,[1] C_{15}–HpA, and C_{15}–HPr systems at 298.2 K are shown in Figs. 1 to 4. These esters and fatty acid spread on the air–water interface formed an expanded monolayer at the experimental temperature. The transition from the liquid expanded to the liquid condensed state was observed for all systems over the whole range of composition. The transition pressure, π^{eq}, corresponds to the surface pressure at the break point of the π-A curve. The variations in π^{eq} with the mole fraction of esters, $x_2^{\pi,eq}$, are very different from each other, as is shown in Fig. 5. These curves depend significantly on the chain length and the structure of the hydrophilic group of esters. The

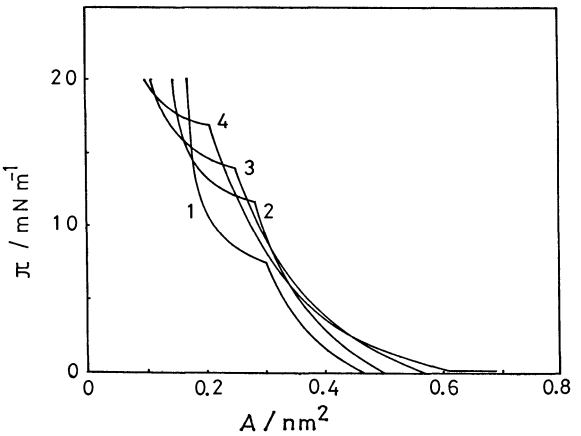

Fig. 1. Surface pressure *vs.* mean area curves of the pentadecanoic acid–pentadecyl acetate mixed monolayer at 298.2 K.
1: $x_2^{\pi}=0$ (pentadecanoic acid), 2: 0.3, 3: 0.7, 4: 1 (pentadecyl acetate).

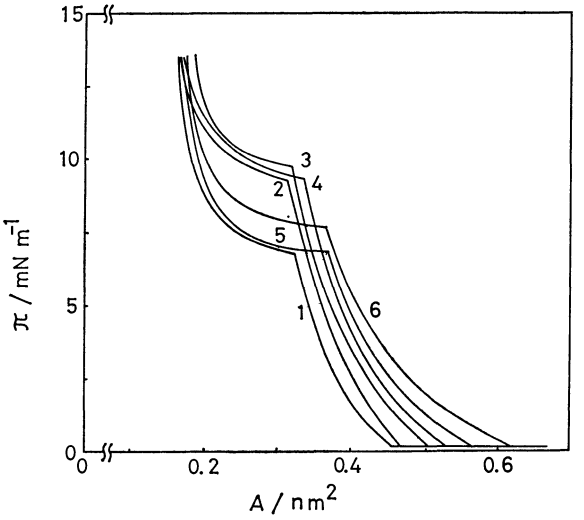

Fig. 2. Surface pressure *vs.* mean area curves of the pentadecanoic acid–hexadecyl acetate mixed monolayer at 298.2 K.
1: $x_2^{\pi}=0$ (pentadecanoic acid), 2: 0.2, 3: 0.3, 4: 0.4, 5: 0.8, 6: 1 (hexadecyl acetate).

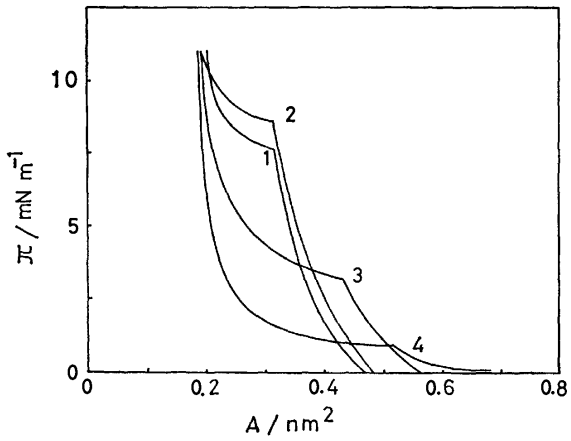

Fig. 3. Surface pressure *vs.* mean area curves of the pentadecanoic acid–heptadecyl acetate mixed monolayer at 298.2 K.
1: $x_2^{\pi}=0$ (pentadecanoic acid), 2: 0.2, 3: 0.7, 4: 1 (heptadecyl acetate).

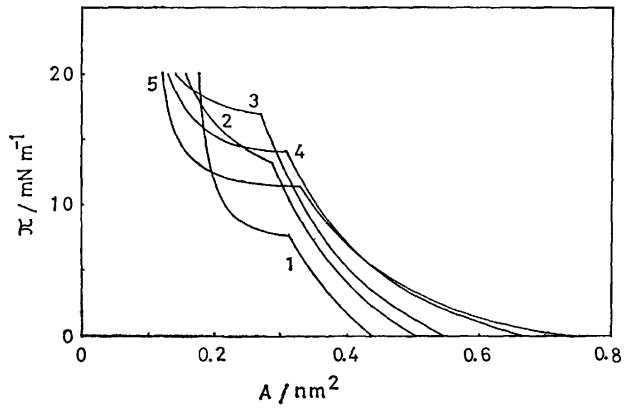

Fig. 4. Surface pressure *vs.* mean area curves of the pentadecanoic acid–hexadecyl propionate mixed monolayer at 298.2 K.
1: $x_2^{\pi}=0$ (pentadecanoic acid), 2: 0.2, 3: 0.6, 4: 0.8, 5: 1 (hexadecyl propionate).

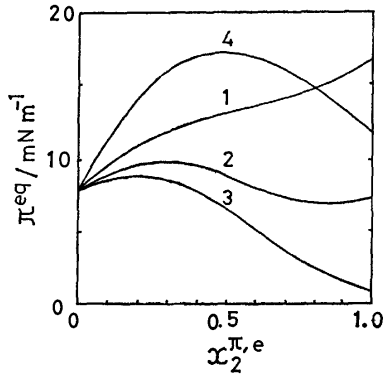

Fig. 5. π^{eq}-$x_2^{\pi,e}$ curves of several mixed monolayers at 298.2 K.
1: Pentadecanoic acid–pentadecyl acetate system, 2: pentadecanoic acid–hexadecyl acetate system, 3: pentadecanoic acid–heptadecyl acetate system, 4: pentadecanoic acid–hexadecyl propionate system.

hydrophilic group of PA, HA, and HpA is the same, that is, acetoxyl group (CH_3COO–), but the carbon number of the hydrophobic group is different in each. On the other hand, the hydrophilic group of HPr is different from that of HA, while the chain length is the same. In the C_{15}–PA system, π^{eq} increases gently with an increase in the mole fraction of the ester in the expanded state, $x_2^{\pi,e}$. There are maximum and minimum points in the C_{15}–HA system, as has previously been mentioned.[1] For the C_{15}–HpA system, a small maximum was observed, while the C_{15}–HPr system has a large maximum.

Recently thermodynamic equations of a multicomponent mixed monolayer in which the contribution of water is incorporated were derived by Motomura.[3-6] When two components are miscible in both the expanded and condensed states, the following equations (Eqs. 209, 201, and 205 in Ref. 6) have been reported:

$$x_2^{\pi,c} = x_2^{\pi,e} + (a^c-a^e)(\partial\pi^{eq}/\partial x_2^{\pi,e})_{T,p} / \{RT/x_1^{\pi,e}x_2^{\pi,e} + (\partial a^e/\partial x_2^{\pi,e})_{T,p,\pi}(\partial\pi^{eq}/\partial x_2^{\pi,e})_{T,p} + \int_0^{\pi}[\partial^2 a^e/(\partial x_2^{\pi,e})^2]_{T,p,\pi}d\pi\}, \quad (1)$$

$$\Delta s^r = [a^c-a^e-(x_2^{\pi,c}-x_2^{\pi,e})(\partial a^e/\partial x_2^{\pi,e})_{T,p,\pi}] \times [(\partial\pi^{eq}/\partial T)_{p,x_2^{\pi,e}}-(\partial\gamma^{\circ}/\partial T)_p], \quad (2)$$

and;

$$\Delta u^r = -(\pi^{eq}-\gamma^{\circ})[a^c-a^e-(x_2^{\pi,c}-x_2^{\pi,e})(\partial a^e/\partial x_2^{\pi,e})_{T,p,\pi}] + \Delta Ts^r, \quad (3)$$

where x_2^{π} is the mole fraction of the second component (ester) in the mixed monolayer; a is the mean area per mole of film-forming components; π^{eq} is the phase-equilibrium surface pressure, which corresponds to that of the break point of the π-A curve; the superscripts c and e represent the condensed and expanded states respectively; Δs^r and Δu^r are the apparent molar entropy and energy changes, and γ° is the surface tension of water.

Now we can obtain two curves; one is the experimental π^{eq}–$x_2^{\pi,e}$ curve, and the other is the π^{eq}–$x_2^{\pi,c}$ curve calculated using Eq. 1. A two-dimensional phase diagram is constructed by means of these two curves. The diagrams of the C_{15}–PA, C_{15}–HA, C_{15}–HpA, and C_{15}–HPr systems at 298.2 K are shown in Figs. 6 to 9. For all systems, two components are miscible in the expanded as well as the condensed states. At the maximum and minimum points, the mole fractions of the expanded($x_2^{\pi,e}$) and condensed ($x_2^{\pi,c}$) phases are equal. According to the previously presented classification of phase diagrams,[7,8] the C_{15}–PA and C_{15}–HA systems are of a complicated type, while the C_{15}–HpA and C_{15}–HPr systems are of a positive azeotropic type.

The apparent molar entropy change of these systems was evaluated by means of Eq. 2. They are shown in Fig. 10. In the C_{15}–PA system, Δs^r decreases gently with an increase in $x_2^{\pi,c}$. The Δs^r of the C_{15}–HA system has a small minimum. The value for the C_{15}–HpA system increases gradually with an increase in $x_2^{\pi,c}$. The C_{15}–HPr system has an obvious minimum. In this way, the apparent molar entropy changes of these systems depend also uniquely on the chain length and structure of the hydrophilic group of esters.

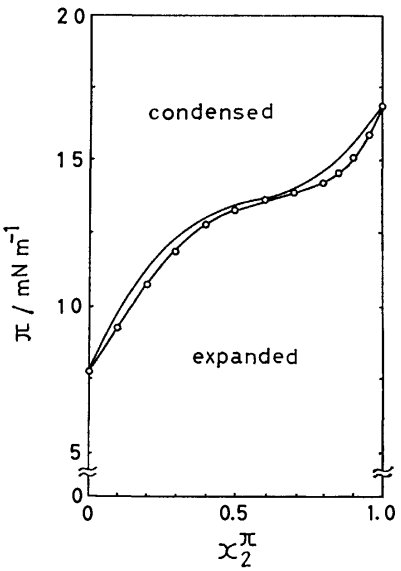

Fig. 6. Phase diagram of the pentadecanoic acid–pentadecyl acetate mixed monolayer at 298.2 K.

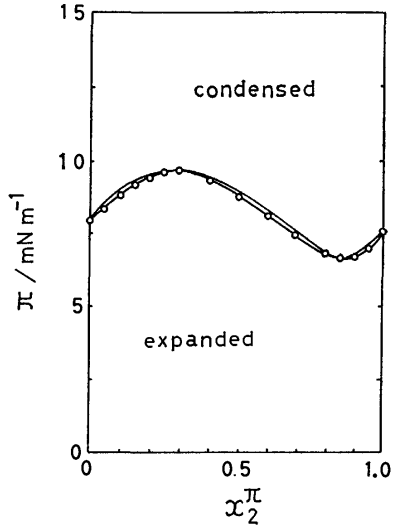

Fig. 7. Phase diagram of the pentadecanoic acid–hexadecyl acetate mixed monolayer at 298.2 K.

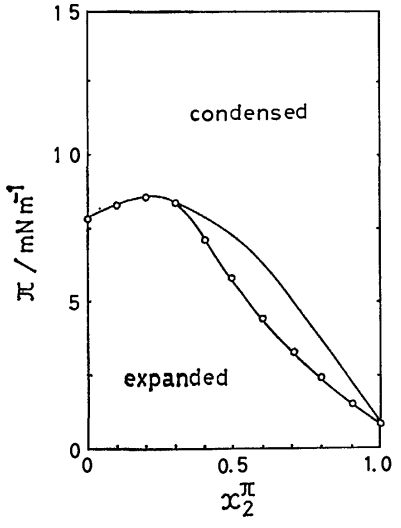

Fig. 8. Phase diagram of the pentadecanoic acid–heptadecyl acetate mixed monolayer at 298.2 K.

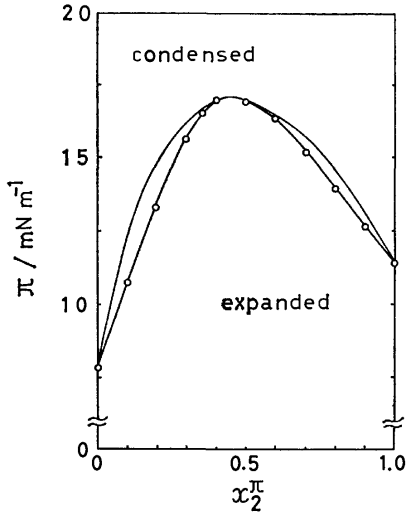

Fig. 9. Phase diagram of the pentadecanoic aicd–hexadecyl propionate mixed monolayer at 298.2 K.

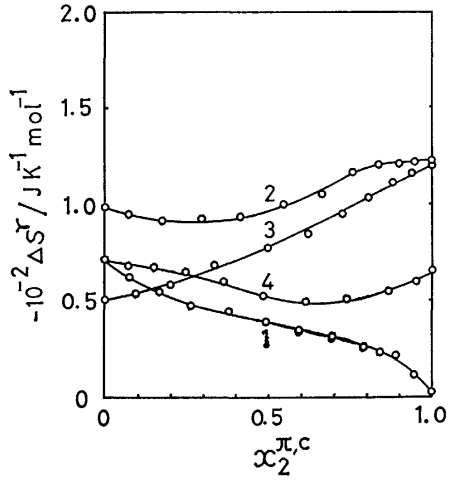

Fig.10. Δs^r *vs.* $x_2^{\pi,c}$ curves of several mixed monolayers.
1: Pentadecanoic acid–pentadecyl acetate system at 298.2 K, 2: pentadecanoic acid–hexadecyl acetate system at 295.7 K, 3: pentadecanoic acid–heptadecyl acetate system at 299.7 K, 4: pentadecanoic acid–hexadecyl propionate system at 298.2 K.

The excess apparent molar energy change is defined by $\Delta u^r - \overline{(\Delta u^r)}$, where $\overline{(\Delta u^r)}$ is the composition average of Δu^r. From Eq. 3 and the above definition, we can now calculate the excess apparent molar energy changes. They are given in Fig. 11. It is interesting that there are positive and negative regions in the energy change. This is why C_{15}–PA and C_{15}–HA systems show complicated phase diagrams. They indicate the following facts: (1) in the positive region, there are mutual interactions between the two components in the mixed monolayer which are weaker than the interactions between the pure component molecules themselves, and (2) in the negative region, there are mutual interactions between the two components in the mixed monolayer which are stronger than the interactions between the pure component molecules themselves. Upon comparing the C_{15}–PA,

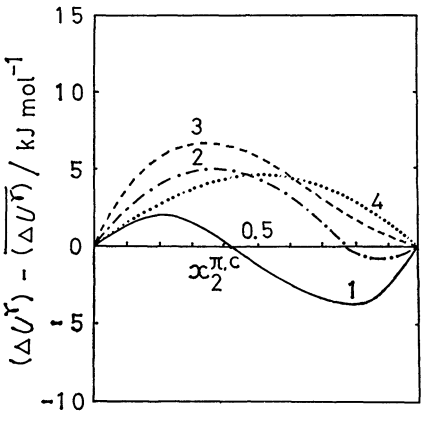

Fig.11. $(\Delta u^r) - \overline{(\Delta u^r)}$ *vs.* $x_2^{\pi,c}$ curves of several mixed monolayers.
1: Pentadecanoic acid–pentadecyl acetate system at 298.2 K, 2: pentadecanoic acid–hexadecyl acetate system at 295.7 K, 3: pentadecanoic acid–heptadecyl acetate system at 299.7 K, 4: pentadecanoic acid–hexadecyl propionate system at 298.2 K.

C_{15}–HA, and C_{15}–HpA systems, we find that the positive region increases with an increase in the chain length of the esters until, in the C_{15}–HpA system, the energy change is positive over the whole range of $x_2^{\pi,c}$. In these C_{15}–PA, C_{15}–HA, and C_{15}–HpA systems, the hydrophilic group of the esters is the same, but the chain length of the esters is different in each. Therefore, the above results show the following facts: (1) interactions between two components in the mixed monolayer decrease with an increase in the difference in chain length between the two components, and (2) in the low $x_2^{\pi,c}$ region, the contribution of the hydrophilic-hydrophilic steric hindrance becomes relatively large. The excess apparent molar energy change of the C_{15}–HPr system is positive over the whole range of $x_2^{\pi,c}$. This also indicate the weaker interactions. This is why C_{15}–HPr system shows a positive azeotropic transformation in mixed monolayers.[5,8,9] HPr has a propyl group(C_3H_8–) in its hydrophilic part, but PA, HA, and HpA have a methyl group(CH_3–) in their hydrophilic parts. The steric hindrance of the propyl group is much larger than that of the methyl group. Therefore, the steric hindrance of the propyl group may be supposed to play an important role in the positive azeotropic transformation.

References

1) H. Matuo, K. Motomura, and R. Matuura, *Bull. Chem. Soc. Jpn.*, **52**, 673 (1979).
2) J. C. Sauer, B. E. Hain, and P. W. Boutwell, *Org. Synth.*, Coll. Vol. 3, 605 (1955).
3) K. Motomura, *J. Colloid Interface Sci.*, **48**, 307 (1974).
4) K. Motomura, K. Sekita, and R. Matuura, *J. Colloid Interface Sci.*, **48**, 319 (1974).
5) K. Motomura, T. Yano, M. Ikematsu, H. Matuo, and R. Matuura, *J. Colloid Interface Sci.*, **69**, 209 (1979).
6) K. Motomura, *Adv. Colloid Interface Sci.*, **12**, 1 (1980).
7) H. Matuo, K. Motomura, and R. Matuura, *J. Colloid Interface Sci.*, **69**, 192 (1979).
8) H. Matuo, K. Motomura, and R. Matuura, *Chem. Phys. Lipids*, **28**, 385 (1981).
9) H. Matuo, N. Yosida, K. Motomura, and R. Matuura, *Bull. Chem. Soc. Jpn.*, **52**, 667 (1979).

NOTES

Bull. Chem. Soc. Jpn., 54, 2209—2210 (1981)

Effect of Hydrogen Bonding on the Phosphorescence of Benzo[c]cinnoline in Polyhydric Solvents

Hiroyasu Inoue,* Yukimi Hiroshima, and Kôichi Tomiyama
Department of Applied Chemistry, Faculty of Technology, Kanagawa University, Kanagawa-ku, Yokohama 221

(Received November 27, 1980)

Synopsis. Phosphorescence of benzo[*c*]cinnoline has been found to be enhanced in polyhydric solvents, such as ethylene glycol, glycerol, and aqueous ethanol. Enhancement of the phosphorescence emission can be attributed to the formation of the hydrogen bond in the triplet state of benzo[*c*]cinnoline with the solvent molecules.

Emission characteristics of ortho-diazines, such as pyridazine and benzo[*c*]cinnoline (9,10-diazaphenanthrene, abbreviated hereafter as BCC), have often been discussed.[1] BCC shows intense fluorescence, but its phosphorescence emission efficiency is very low.[2] Recently, Lin and Stikeleather[3] observed enhanced phosphorescence of BCC in the fluorinated alcohols. The alcohols act as a proton-donor in hydrogen bonding with BCC, thus inducing the phosphorescence of the substrate. They suggested that the lack of phosphorescence in hydrocarbon solvents was not due to a nonpopulated triplet state, but rather due to the $T_1 \rightarrow S_0$ radiationless rate being much faster than the radiative rate.

In general, the hydrogen bond between solute and solvent has some influence on the emission properties of the solute. As for cinnoline, for example, it is known that the formation of a hydrogen bond induces phosphorescence, although it is a poor phosphorescer in non proton-donating solvents.[4]

The formation of the hydrogen bond in the ground state BCC with proton-donating solvents was proved from a blue shift of the $n\pi^*$ absorption spectrum.[5] In the lowest excited singlet state of BCC, the hydrogen bond is formed at low temperature, but it is broken at room temperature.[6,7]

In this paper, we will report the enhanced phosphorescence emission of BCC in polyhydric alcohols and aqueous monohydric alcohols, and will discuss the hydrogen bonding in the lowest triplet state of BCC with those solvents.

Experimental

BCC was obtained from Aldrich Chem. Co. and was purified by recrystallization from ethanol. Emission spectra were recorded on a Shimadzu RF-500 spectrofluorimeter at 77 K. Excitation spectra were corrected for the intensity of incident light using a rhodamine B solution.

Results and Discussion

In monohydric alcohols, such as ethanol and 2-propanol, BCC shows no appreciable phosphorescence under our experimental conditions. However, it was found that in mixture of the monohydric alcohols and water (1:1 vol) the phosphorescence emission could be observed around 540 nm with a significant yield. In addition, ethylene glycol and glycerol were also found to be suitable solvents for the appearance of the phosphorescence of BCC. The observed phosphorescence spectra are presented in Fig. 1. None of the emission arises from the solvents used here. Moreover, the possible photochemical change of the sample was not detected.[8] The formation of a dimer of BCC at low temperature as reported by Hoytink *et al.*[9] can be ruled out as an origin of the observed phosphorescence, because polar solvents are used in this study. Hochstrasser and Marzzacco[10] reported the crystalline $T_1 \leftarrow S_0$ absorption spectrum and they assigned the lowest triplet at 5384.6 A (0—0 band) as the $\pi\pi^*$ type. The 0—0 band of $T_1 \leftarrow S_0$ absorption spectrum corresponds in position to that of the phosphorescence observed in this study.

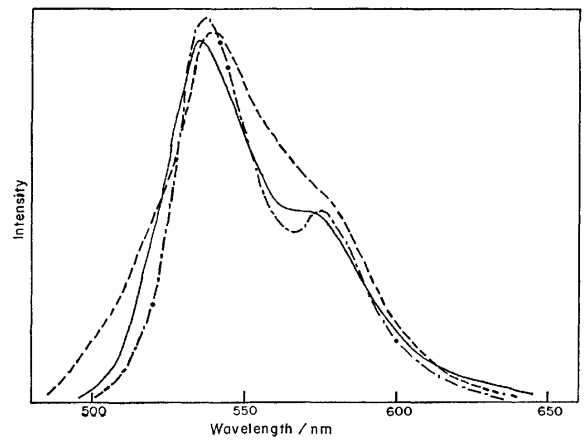

Fig. 1. Phosphorescence spectra of BCC.
—: In a mixture of ethanol and water (1:1), ——: in glycerol, ---: in ethylene glycol.

It should be noted that the phosphorescence of protonated BCC in 4 mol/dm^3 HCl aqueous 2-propanol, which was reported earlier,[11] was quite similar in shape to the spectra in Fig. 1, though the former has a maximum at somewhat longer wavelength.[12] In the present case, therefore, enhancement of the phosphorescence can reasonably be explained in terms of the hydrogen bonding between the solute and the solvents. In the aqueous alcohols, water seems to act as a proton-donor. It is worth noting that the solvent molecule which is suitable for the emission has at least two hydrogen atoms which can take part in the hydrogen bonding with the aza nitrogen atoms of BCC. Accordingly, the following hydrogen bonds are though to be formed. In fact, ethylene glycol

monoethyl ether, which could not form such hydrogen bonds, did not induce the phosphorescence. Therefore, there is a distinct difference in the hydrogen bonding with the triplet state BCC between the mono- and polyhydric alcohols.

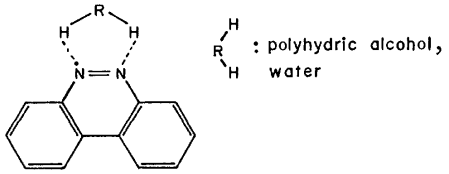

In order to see the difference in hydrogen bonding with the ground (S_0) and the lowest excited singlet (S_1) BCC between mono- and polyhydric alcohols, the absorption and fluorescence spectra were determined at room temperature. Owing to the hydrogen bonding, the $n\pi^*$ absorption band exhibits a large blue shift, thus appearing as a shoulder at the long wavelength of the first $\pi\pi^*$ band in both the mono- and polyhydric alcohols. The shape of the shoulder is the same in both solvents. The wavelengths of the fluorescence maxima in the polyhyric alcohols and the aqueous alcohols are almost the same as those in the monohydric alcohols, *e.g.*, 485 nm in ethylene glycol and 488 nm in ethanol. Therefore, we could not find any differences in hydrogen bonding properties of BCC in the S_0 and S_1 states between the mono- and polyhydric alcohols at room temperature.

Figure 2 shows the excitation spectra of the fluorescence at room temperature and of the phosphorescence at 77 K in glycerol. The phosphorescence excitation spectrum is shifted to somewhat longer wavelengths compared with the fluorescence excitation spectrum which corresponds to the absorption spectrum. This shift suggests that in polyhydric alcohols the hydrogen bonds are strengthened at low temperature, that is, the formation of the hydrogen bonds occurs as illustrated above.

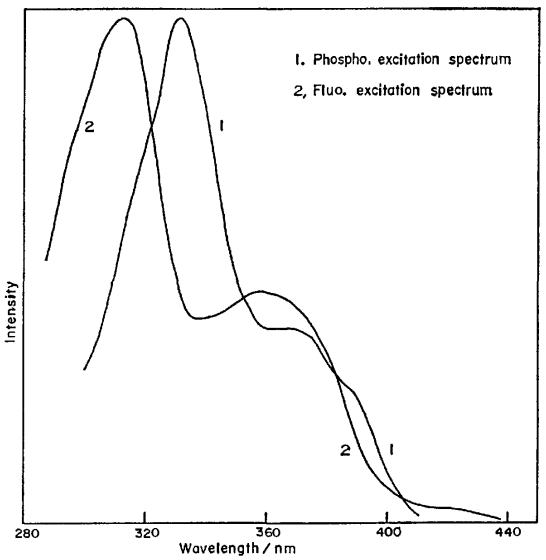

Fig. 2. Excitation spectra of phosphorescence at 77 K (1) and of fluorescence at room temperature (2) in glycerol (5×10^{-5} mol/dm^3).

References

1) S. P. McGlynn, T. Azumi, and M. Kinoshita, "Molecular Spectroscopy of the Triplet State," Prentice-Hall, Inc., New Jersey, p. 90 (1969).

2) E. Lippert, W. Lüder, F. Moll, W. Nägele, H. Boos, H. Prigge, and I. Seibold-Blankenstein, *Angew. Chem.*, **73**, 695 (1961).

3) C. T. Lin and J. A. Stikeleather, *Chem. Phys. Lett.*, **38**, 561 (1976).

4) J. A. Stikeleather, *Chem. Phys. Lett.*, **24**, 253 (1974).

5) C. Mugiya and H. Baba, *Bull. Chem. Soc. Jpn.*, **40**, 2201 (1967).

6) H. Baba and C. Mugiya, *Bull. Chem. Soc. Jpn.*, **43**, 13 (1970).

7) I. Yamazaki, H. Takeda, and H. Baba, *Bull. Chem. Soc. Jpn.*, **53**, 541 (1980).

8) BCC has been found to be photoreduced to give 5,6-dihydro BCC in ethylene glycol and glycerol to be published.

9) D. N. deVries Reilingh, R. P. H. Rettschnick, and G. J. Hoytink, *J. Chem. Phys.*, **54**, 2722 (1971).

10) R. M. Hochstrasser and C. Marzzacco, *J. Chem. Phys.*, **45**, 4681 (1966).

11) H. Inoue, Y. Hiroshima, and N. Makita, *Bull. Chem. Soc. Jpn.*, **52**, 351 (1979).

12) In glycerol and the acidic medium the phosphorescence band has two peaks. The separations of these peaks in both media are similar to each other (1200 cm^{-1}).

^{14}N Nuclear Quadrupole Resonance Spectra of $K_2SrCu(NO_2)_6$, $K_2BaCu(NO_2)_6$, and $Cs_2PbCu(NO_2)_6$

Tetsuo Asaji,* Jun Ishikawa, Ryuichi Ikeda, and Daiyu Nakamura
Department of Chemistry, Nagoya University, Chikusa-ku, Nagoya 464

(Received January 24, 1981)

Synopsis. The ^{14}N NQR frequencies of $K_2SrCu(NO_2)_6$, $K_2BaCu(NO_2)_6$, and $Cs_2PbCu(NO_2)_6$ were determined at various temperatures below about 155, 67, and 235 K, respectively. The results are discussed in referring to their crystal structure.

Recently, a number of structural studies[1-8] have been made on the compound $R_2MCu(NO_2)_6$ (R=K, Rb, Cs, NH_4, Tl and M=Pb, Ca, Sr, Ba) and it became obvious that this series of compounds can be classified into two distinct classes through the sort of the bivalent cation M. The compounds containing Pb form cubic crystals in their high-temperature phase and exhibit successive phase transitions with decreasing temperature. In their lowest-temperature commensurate phase, these crystals are thought to have a pseudotetragonal lattice with $c/a<1$.[1-6] On the other hand, the crystals containing the alkali earth metal atoms have a pseudotetragonal lattice with $c/a>1$ at room temperature[6-8] and the occurrence of phase transition has not been reported as yet.

In a preceding paper,[9] we reported the existence of at least two sets of ^{14}N nuclear quadrupole resonance (NQR) frequencies in the low-temperature phase of the former class compounds. However, there remains an unsolved problem on the assignment of the observed frequencies to nonequivalent nitrogen atoms in the crystals. Accordingly, we have undertaken the present investigation of the ^{14}N NQR of the latter compounds to clarify this point.

Experimental

The samples employed for the measurements of NQR and DTA (differential thermal analysis) were synthesized according to the method reported by Reinen *et al.*,[6] and identified by recording X-ray powder patterns. A modified Pound-Watkins type spectrometer operated in a frequency modulation mode[10] was used for the observation of ^{14}N NQR signals. The sample temperature was determined by employing the usual method already described elsewhere.[9] DTA curves were taken by means of a home-made apparatus previously described.[11]

Results and Discussion

Three NQR frequencies ν^{I}, ν^{II}, and ν^{III} defined below are usually observed for ^{14}N nuclei in compounds.

$$\left.\begin{aligned} &\nu^{I} = (3/4h)eQq(1+\eta/3),\ \nu^{II} = (3/4h)eQq(1-\eta/3) \\ &\nu^{III} = (1/2h)eQq\cdot\eta. \end{aligned}\right\} \quad (1)$$

Here, eQq and η denote the quadrupole coupling constant and the asymmetry parameter, respectively. The ν^{I} and ν^{II} frequencies and their signal-to-noise ratios (S/N) determined at various temperatures are given in Table 1.

A single pair of ν^{I} and ν^{II} frequencies was observed for both of $K_2SrCu(NO_2)_6$ and $K_2BaCu(NO_2)_6$. For the former compound ν^{I} and ν^{II} could be detected up to about 110 and 155 K, respectively, while for the latter up to about 45 and 67 K, respectively. Both frequencies of $K_2SrCu(NO_2)_6$ decreased smoothly with increasing temperature up to respective fade-out temperatures, indicating that no phase transition takes place below 155 K. To examine the thermal properties of $K_2SrCu(NO_2)_6$, we carried out the experiment of DTA and found no thermal anomaly in the temperature range of 143—323 K. Accordingly, it can be concluded that $K_2SrCu(NO_2)_6$ retains its crystal symmetry determined at room temperature unaltered down to liquid helium temperature. For $K_2BaCu(NO_2)_6$, the resonance frequencies decreased smoothly with increasing temperature, indicating the absence of phase transition between 2 and 67 K.

The caesium salt, $Cs_2PbCu(NO_2)_6$ yielded two sets of ν^{I} and ν^{II} lines at liquid helium temperature. With increasing temperature, these ν^{I} and ν^{II} lines decreased their frequency smoothly and disappeared in the noise level at about 124 and 235 K, respectively. The latter temperature is lower by 50 K than the lowest transition temperature of the caesium salt.[12]

According to Takagi *et al.*,[8] all the complex ions $[Cu(NO_2)_6]^{4-}$ having an orthorhombic symmetry are crystallographically equivalent in the crystals of $K_2SrCu(NO_2)_6$. Therefore, three kinds of crystallographically nonequivalent nitrogen atoms exist in the crystals: one kind of axially elongated nitrogen atoms (Cu–N: 2.31 Å) and two kinds of equatorial nitrogen atoms (Cu–N: 2.04 and 2.03 Å). The fact that the Sr compound shows only one set of ^{14}N NQR frequencies suggests that only the elongated nitrogen atoms afford detectable NQR signals. The NQR signals of the other nitrogen atoms may be undiscernibly broadened owing to the magnetic disturbance of the Cu(II) unpaired electron situated near to the nitrogen atoms.

The NQR parameters, eQq/h and η obtained at 4.2 K are given in Table 2 with those of $R_2PbCu(NO_2)_6$ for comparison. The $R_2PbCu(NO_2)_6$ type complexes except for $(NH_4)_2PbCu(NO_2)_6$ yield two sets of the parameters.[9] The ammonium salt shows an additional structural phase transition at 94.5 K, above which temperature the salt also yields two sets of the parameters. On the X-ray and neutron diffraction studies of $K_2PbCu(NO_2)_6$, Noda *et al.*[1] interpreted their experimental results in terms of a structural model proposed by Reinen *et al.*[6] In this model, local tetragonal elongation of a complex ion takes place and the axis of the elongation alternates between the a- and b-axis of the pseudotetragonal crystal. Taking into account of the configuration of oxygen atoms, this indicates that there exist two crystallographically different elongated complex ions. Accordingly, there are two nonequivalent nitrogen atoms

Table 1. ^{14}N NQR frequencies (± 0.1 kHz) and their signal-to-noise ratios (S/N) of $K_2SrCu(NO_2)_6$, $K_2BaCu(NO_2)_6$, and $Cs_2PbCu(NO_2)_6$ determined at various temperatures

Compound	Temp/K	ν^{I}/kHz	(S/N)	ν^{II}/kHz	(S/N)
$K_2SrCu(NO_2)_6$	2	4555.8	($\approx$200)	3527.9	($\approx$400)
	18	4555.8	(8)	3527.9	(35)
	77	4547.0	($\approx$4)	3525.3	($\approx$7)
	109	4536.7	(3)	3521.2	(5)
	155	—		3511.7	(5)
$K_2BaCu(NO_2)_6$	2	4572.8	(60)	3541.1	(170)
	20	4572.1	(4)	3540.9	(10)
	45	4566.5	(2)	3539.7	(5)
	67	—		3537.9	(3)
$Cs_2PbCu(NO_2)_6$	2	4496.2	(150)	3508.1	(200)
		4495.4	(150)	3512.1	(230)
	22	4496.0	(7)	3508.0	(6)
		4495.2	(7)	3512.0	(6)
	77	4490.5	($\approx$5)	3504.5	($\approx$4)
		4489.7	($\approx$5)	3508.5	($\approx$4)
	124	4478.2	(3)	3495.5	(3)
		4477.6	(3)	3499.7	(3)
	235	—		3458.4	(2)
		—		3463.2	(2)

Table 2. ^{14}N NQR parameters of $R_2MCu(NO_2)_6$ type complexes determined at 4.2 K

$R_2MCu(NO_2)_6$		Ref.	Quadrupole parameter	
R	M		(eQq/h)/kHz	η
K	Ba	this work	5409.3	0.3815
K	Sr	this work	5389.3	0.3815
K	Pb	9	5363.5	0.3752
			5360.5	0.3737
NH_4	Pb	9	5357.5	0.3744
Rb	Pb	9	5348.3	0.3743
			5345.5	0.3722
Cs	Pb	this work	5336.1	0.3703
			5338.3	0.3684
Tl	Pb	9	5296.1	0.3510
			5293.7	0.3498

having longer Cu–N distances and it is considered that these nitrogen atoms afford detectable NQR signals.[9,13]

References

1) Y. Noda, M. Mori, and Y. Yamada, *J. Phys. Soc. Jpn.*, **45**, 954 (1978).

2) B. V. Harrowfield and J. R. Pilbrow, *J. Phys. C*, **6**, 755 (1973).

3) S. Takagi, M. D. Joesten, and P. G. Lenhert, *Acta Crystallogr., Sect. B*, **32**, 1278 (1976).

4) D. Mullen, G. Heger, and D. Reinen, *Solid State Commun.*, **17**, 1249 (1975).

5) B. V. Harrowfield, A. J. Dempster, T. E. Freeman, and J. R. Pilbrow, *J. Phys. C*, **6**, 2058 (1973).

6) D. Reinen, C. Friebel, and K. P. Reetz, *J. Solid State Chem.*, **4**, 103 (1972).

7) S. Takagi, P. G. Lenhert, and M. D. Joesten, *J. Am. Chem. Soc.*, **96**, 6606 (1974).

8) S. Takagi, M. D. Joesten, and P. G. Lenhert, *Acta Crystallogr., Sect. B*, **32**, 2524 (1976); *ibid.*, **31**, 596 (1975).

9) T. Asaji, R. Ikeda, and D. Nakamura, *Z. Naturforsch., B*, **34**, 1722 (1979).

10) R. Ikeda, D. Nakamura, and M. Kubo, *J. Phys. Chem.*, **70**, 3626 (1966).

11) Y. Kume, R. Ikeda, and D. Nakamura, *J. Magn. Reson.*, **33**, 331 (1979).

12) M. Mori, Y. Noda, and Y. Yamada, *Solid State Commun.*, **27**, 735 (1978).

13) H. Chihara and N. Nakamura, "Advances in Nuclear Quadrupole Resonance," ed by J. A. S. Smith, Heyden, London (1980), Vol. 4, p. 62.

Kinetics of the Decarboxylation of Benzylmalonic Acid, Ethylmalonic Acid, and Dimethylmalonic Acid in Hydroxylic Solvents

Mihir K. Biswas and Dilip K. Majumdar*
Department of Chemistry, University of Kalyani, Kalyani 741235, W. Bengal, India
(Received May 6, 1980)

Synopsis. Kinetics of the decarboxylation of benzylmalonic acid, ethylmalonic acid, and dimethylmalonic acid have been shown to follow first order rate equation in several solvents, namely alkanediols and diethylene glycol (DEG), polyethylene glycol (PEG), and polypropylene glycol (PPG). The enthalpy and entropy of activation for the decarboxylation reactions were determined and the plot of ΔH^* *vs.* ΔS^* was found to be linear through all the solvents.

In the present Note, we report the results of our investigations into the kinetics of the decarboxylation of substituted malonic acids in hydroxylic solvents. The experimental set up is the same as was described previoulsy.[1,3,6] The decarboxylation was carried out in a thermostated bath controlled to within ±0.2 °C. The decarboxylation rates were measured by collecting the evolved carbon dioxide gas at atmospheric pressure at various time intervals. The solvents used are: ethylene glycol (Pfizer, India), 1,2-propanediol (B.D.H., L.R.), 1,3-butanediol (B.D.H., England), diethylene glycol (B.D.H., England), polyethylene glycol-400 (B.D.H., England), and polypropylene glycol-425 (Koch-Light, England). Benzylmalonic acid, ethylmalonic acid, and dimethylmalonic acid used were of Fluka, Switzerland. Ethylene glycol and 1,2-propanediol were distilled under reduced pressure before use. The solvents were previously saturated at the reaction temperature by passing a stream of pure and dry carbon dioxide gas. Stoichiometry was checked in all the solvents by collecting carbon dioxide gas when the reaction was complete. In each kinetic run, the amount of acid taken was about 0.17—0.18 g in 25 ml of the solvent.

Results and Discussion

The first order rate constants k given in Table 1 are mean values over at least four kinetic runs. We also observed that the decarboxylation of these acids obeys rate theory equation of Eyring. The thermodynamic parameters, enthalpy and entropy of activation, ΔH^* and ΔS^* have been evaluated and these are given in Table 2.

Figure 1 shows the enthalpy-entropy plot for the decarboxylation reaction of these acids in these solvents as well as in the molten state. Decarboxylation kinetics of benzylmalonic acid in the molten state have been reported by Clark.[7] We have also measured the decarboxylation rate in the molten state of these three acids at several temperatures.[8] It is seen that a straight line can be drawn through all the solvents including the melting point. The data for dimethylmalonic acid, however, is off as will be evident in Fig. 1. This is not unexpected because dimethylmalonic acid was seen to decarboxylate very fast in the molten state and there was some uncertainty in the values of the rate constant.[8] The linearity of $\Delta H^*-\Delta S^*$ plot implies one reaction series for each of these acids in these solvents. The slope of the enthalpy-entropy plot of Fig. 1 gives the isokinetic temperatures, which are very close to the respective melting points of the acids (Table 3). This is in harmony with the conclusions reached by Clark on the decarboxylation kinetics of alkyl-substituted malo-

Table 1. First order rate constants for the decarboxylation of substituted malonic acids in hydroxylic solvents

Temp °C	Rate constant, $k\times10^4/s^{-1}$					
	Ethylene glycol	1,2-Propanediol	1,3-Butanediol	Diethylene glycol	Polyethylene glycol	Polypropylene glycol
			Benzylmalonic acid			
120	7.85±0.38	11.40±0.36	7.75±0.85	6.64±0.36	5.42±0.32	6.16±0.06
130	10.90±0.14	14.10±0.02	16.80±0.15	14.32±0.46	8.89±0.25	9.59±0.05
140	22.50±0.23	19.67±0.23	26.20±0.90	18.06±0.14	15.99±0.19	18.30±0.08
			Ethylmalonic acid			
120	2.89±0.11	2.57±0.17	3.01±0.34	3.67±0.18	2.14±0.04	2.04±0.03
130	7.13±0.01	6.24±0.01	7.78±0.15	5.70±0.22	3.68±0.12	4.51±0.15
140	15.12±0.01	9.07±0.21	14.88±0.05	10.75±0.25	7.57±0.28	9.23±0.29
145	20.09±0.12	15.44±0.09	—	—	13.30±0.54	14.08±0.22
			Dimethylmalonic acid			
130	3.53±0.05	3.41±0.11	2.99±0.45	3.33±0.05	3.43±0.02	2.07±0.05
140	7.37±0.07	8.03±0.21	7.61±0.08	7.05±0.18	6.07±0.05	4.63±0.22
145	14.79±0.77	13.33±0.12	12.71±0.01	8.84±0.08	7.54±0.12	9.82±0.91

Table 2. Thermodynamic parameters of the decarboxylation reaction in solvents

Solvents	Benzylmalonic acid			Ethylmalonic acid			Dimethylmalonic acid		
	ΔH^* kcal mol^{-1}	ΔS^* e.u.	ΔF^* m.p. kcal mol^{-1}	ΔH^* kcal mol^{-1}	ΔS^* e.u.	ΔF^* m.p. kcal mol^{-1}	ΔH^* kcal mol^{-1}	ΔS^* e.u.	ΔF^* m.p. kcal mol^{-1}
Ethylene glycol	16.93	−30.39	28.90	27.09	−6.46	29.56	30.02	−0.52	30.26
1,3-Butanediol	20.40	−21.38	28.82	24.43	−12.90	29.37	30.07	−0.59	30.34
1,2-Propanediol	8.61	−50.72	28.59	23.12	−16.74	29.53	32.17	4.66	30.00
Diethylene glycol	15.52	−33.97	28.90	16.41	−33.11	29.09	21.08	−22.66	31.60
Polyethylene glycol	17.39	−29.87	29.19	22.19	−19.51	29.66	16.62	−33.73	32.27
Polypropylene glycol	18.26	−27.46	29.08	23.55	−16.00	29.68	31.79	2.85	30.46

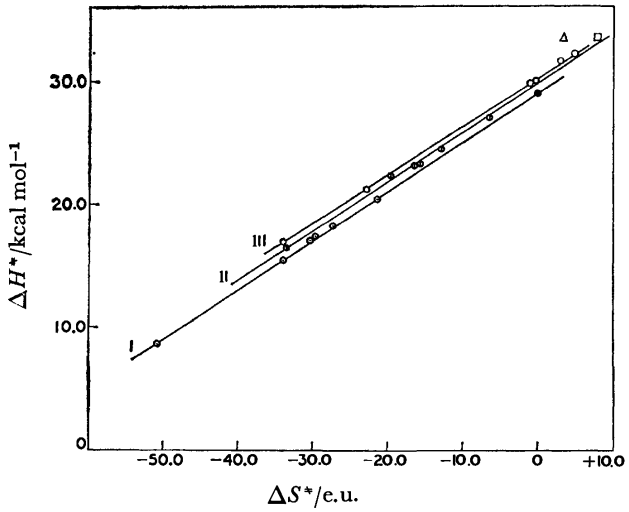

Fig. 1. Enthalpy-entropy plot for the decarboxylation of: benzylmalonic acid[line-I; solvents (⊙); molten state (●)], ethylmalonic acid[line-II; solvents (◫); molten state (□)], dimethylmalonic acid[line-III; solvents (○); molten state (△)].

Table 3. Analysis of the effect of errors in the $\Delta H^*-\Delta S^*$ relationship for the decarboxylation reaction in alkanediols, DEG, PEG, and PPG

Acids	2δ / kcal mol^{-1}	$d(\Delta H^*)$ / kcal mol^{-1}	$d(\Delta H^*/2\delta)$	Isokinetic temp
Benzylmalonic	3.25	11.79	3.6	120°C
Ethylmalonic	2.89	10.70	3.7	111°C
Dimethylmalonic	4.04	16.94	4.2	192°C

nic acids in alkanols and carboxylic acids. Peterson and coworkers,[5] however, suggested the criterion which must be satisfied for any valid conclusions from the linearity of ΔH^* *vs.* ΔS^* plot.

If the total maximum possible error in ΔH^* is 2δ and the range of ΔH^* values is designated as $d\Delta H^*$, then the ratio, $d\Delta H^*/2\delta \gg 1$. The maximum possible error in ΔH^*, may be calculated from the relation,[5,6]

$$\delta = 2R\frac{T'T}{T'-T}\alpha \quad \text{if } \alpha \ll 1.$$

Using this relation, we have given in Table 3 the maximum possible error 2δ in ΔH^*, the range of $d\Delta H^*$ values for a reaction series and the ratio, $d\Delta H^*/2\delta$.

It will be seen that the ratio $d\Delta H^*/2\delta$ is always greater than 1. So the observed linearity of ΔH^* *vs.* ΔS^* plot (Fig. 1) may be regarded as valid. Therefore at the isokinetic temperature, the rate constant is the same for a reaction series in all the solvents.

Diethylene glycol (DEG), polyethylene glycol (PEG), and polypropylene glycol (PPG) differ from the alkanediols in having oxygen in the middle of the chain in addition to having two hydroxyl groups at the ends. Therefore in the solvents, namely, DEG, PEG, and PPG, the activated complex may form either with the ether oxygen or the hydroxyl oxygen and the polarised carbonyl carbon of the acid. Accordingly the enthalpy-entropy plot for malonic acid and methylmalonic acid[4] shows two parallel straight lines-one passing through the alkanediols and the other through DEG, PEG, and PPG. The nature of the activated complex thus significantly differs in the two types of solvents. With benzylmalonic acid, ethylmalonic acid, and dimethylmalonic acid, the bulky substituents are likely to hinder coordination with the lone pair of electrons on ether oxygen of the solvents buried deep in the middle of the chain, so that effective participation of hydroxylic oxygen is only permitted. Thus in the decarboxylation of benzylmalonic acid, ethylmalonic acid, and dimethylmalonic acid the nature of the activated complex will be similar in alkanediols and DEG, PEG, and PPG. So it is natural to expect one straight line passing through all the solvents in respect of decarboxylation of a given acid in the series.

Now it is further noticed that the decarboxylation rate constant in these solvents decreases in the following order:

Benzylmalonic acid, ethylmalonic acid, dimethylmalonic acid. This is also the order in which the electron donating ability of alkyl group namely ethyl- and dimethyl-, decreases. If the Fraenkel[2] mechanism is accepted, then the C–C bond will be broken more easily, when the substituent is an electron attracting group. On the other hand, if the substituent is an electron donating group such as alkyl, the excess negative charge on the carbonyl carbon atom will hinder the process of C–C bond breaking and thus retard the rate of decarboxylation reaction. It is thus expected that the rate of decarboxylation should decrease as the electron donating ability of the substituent increases. The electron donating ability of two methyl-being greater than the ethyl, it is easy to understand the decreasing value of the rate constant as we go from ethylmalonic acid to dimethylmalonic acid. The benzyl group, on the other hand, may act either as an electron sink or as an electron donor; so it is difficult to locate its position in the inductivity scale. However, our kinetic studies suggest that the benzyl group has a low electron donating ability in the decarboxylation reactions-much less than the alkyl substituents. On these considerations we may place them in the following order of decreasing electron donating ability: benzylmalonic acid ethylmalonic acid and dimethylmalonic acid, and this is exactly the order in which the decarboxylation rate constant decreases.

Thanks of the authors are due to Kalyani University for award of a Research Scholarship to one of them (MKB). The authors also thank Dr. A. Mitra for helpful discussion.

References

1) L. W. Clark, "The chemistry of carboxylic acids and esters," ed by S. Patai, Interscience (1969), p. 589.
2) G. Fraenkel, R. L. Belford, and P. E. Yankwich, *J. Am. Chem. Soc.*, **76**, 15 (1954).
3) M. K. Biswas and D. K. Majumdar, *J. Ind. Chem. Soc.*, **56**, 280 (1979).
4) M. K. Biswas and D. K. Majumdar, *J. Ind. Chem. Soc.*, **56**, 874 (1979).
5) R. C. Peterson, J. H. Markgraf, and S. D. Ross, *J. Am. Chem. Soc.*, **83**, 3819 (1961).
6) L. W. Clark, *J. Phys. Chem.*, **67**, 1481 (1963).
7) L. W. Clark, *J. Phys. Chem.*, **67**, 138 (1963).
8) M. K. Biswas and D. K. Majumdar, *J. Ind. Chem. Soc.*, (communicated).

Magnetic Properties of Copper(II) Complexes of Phenylboronic Acid

Shuji EMORI, Hisayasu MASUO, and Yoneichiro MUTO*

Department of Chemistry, Faculty of Science and Engineering, Saga University, Saga 840

(Received August 29, 1980)

Synopsis. The magnetic susceptibilities of copper (II) phenylboronate obey the Bleaney-Bowers equation for dinuclear clusters. The exchange integral within the dinuclear copper(II) phenylboronate, J/k, is equal to -195 K. The structures for hydrolysis products of copper(II) phenylboronate are presumed to contain copper(II) phenylboronate dinuclear units connected together by diborate bridges.

Some copper(II) complexes of benzoic acid have copper(II) acetate-type dinuclear structures with strong antiferromagnetic coupling between the copper(II) ions of a pair.[1] It has been proposed that superexchange interaction predominates in the coupling of these compounds. The degree of superexchange depends to a great extent on the electronic structure of the bridging ligands. Although phenylboronic acid is a much weaker acid(pK_a=8.86)[2] than benzoic acid(pK_a=4.18),[3] both are isoelectronic. So copper(II) complexes of phenylboronic acid may also have a similar structure to that of copper(II) acetate monohydrate.[4]

The complex $Cu(PhBO_2H)_2(py)_2$ was obtained by concentrating a pyridine solution of phenylboronic acid and anhydrous copper(II) acetate. This pyridine adduct was warmed on a water bath to convert it into $Cu(PhBO_2H)_2$. When $Cu(PhBO_2H)_2$ is allowed to stand for a few days in air, it is partly hydrolysed into $Cu(PhBO_2H)_{3/2}(B_2O_5H_2)_{1/4}$. If the pyridine solution of this complex is concentrated gently on a water bath, the crystalline $Cu(PhBO_2H)_{4/3}(B_2O_5H_2)_{1/3}$ is obtained.

The magnetic susceptibilities of these complexes were measured at room temperature by the Gouy method. Their effective magnetic moments were calculated from expression 1:

$$\mu_{\text{eff}} = 2.83\sqrt{(\chi_A - N\alpha)\cdot T}, \quad (1)$$

where χ_A is the molar magnetic susceptibility corrected for the diamagnetism of all the atoms in the compounds by the use of Pascal's constants,[5] and $N\alpha$ is the temperature-independent paramagnetism per gram-ion of Cu(II). The $N\alpha$ was assumed to be 60×10^{-6} cgsu.† The results are given in Table 1. For $Cu(PhBO_2H)_2$, the magnetic measurement was made over the temperature range 80—300 K. The cryomagnetic data could be fitted well to the Bleaney-Bowers equation 2[6] for isotropic exchange in a copper-(II) dimer:

$$\chi_A = \frac{Ng^2\beta^2}{3kT}\left[1+\frac{1}{3}\exp\left(\frac{-2J}{kT}\right)\right]^{-1} + N\alpha, \quad (2)$$

where J is the exchange integral and g is the average g factor. The best fit yields $J/k=-195$ K and $g=2.15$ (Fig. 1). These results suggest the existence of dinuclear clusters in crystals. The values are almost the same as $J/k=-225$ K and $g=2.18$ for copper(II) benzoate.[7] This suggests that this compound has a copper(II) acetate-type of dinuclear structure, as shown in Fig. 2 A.

† The value of the molar magnetic susceptibility in $m^3\,mol^{-1}$(SI) can be obtained by multiplying the value in $cm^3\,mol^{-1}$(cgs) by $4\pi\times10^{-6}$.

TABLE 1. ANALYTICAL DATA AND EFFECTIVE MAGNETIC MOMENTS AT 17 °C

Compound	Cu (%) Found	Cu (%) Calcd	μ_{eff}[a] BM
$Cu(PhBO_2H)_2$	20.8	20.8	1.43
$Cu(PhBO_2H)_2(py)_2$	13.7	13.7	1.79
$Cu(PhBO_2H)_{3/2}(B_2O_5H_2)_{1/4}$	23.4	23.5	1.36
$Cu(PhBO_2H)_{4/3}(B_2O_5H_2)_{1/3}$	24.5	24.5	1.33

a) 1 BM=9.27×10^{-24} Am^2.

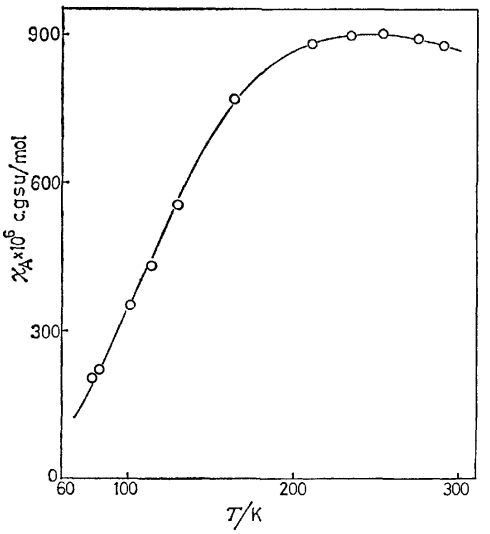

Fig. 1. Observed and calculated magnetic susceptibilities of $Cu(PhBO_2H)_2$: ○, experimental; solid curve, calculated by Eq. 2 with $J/k=-195$ K, $g=2.15$, and $N\alpha=60\times10^{-6}$ cgsu.

On the basis of the analytical data and the reactivity of phenylboronic acid, we assumed that the hydrolysis products, $Cu(PhBO_2H)_{3/2}(B_2O_5H_2)_{1/4}$ and $Cu(PhBO_2H)_{4/3}(B_2O_5H_2)_{1/3}$, have the B and C types of bridging structure shown in Fig. 2, respectively.

Since the magnitude of J should be proportional to the number of bridging ligands involved in the superexchange interaction,[8] the mean exchange integrals for these hydrolysis products can be predicted from Eq. 3 by assuming that no magnetic interaction operates through the >B–O–B< bridge between the dimers:

$$J = \frac{2n+2}{n}J_{PhBO_2H} + \frac{2n-2}{n}J_{B_2O_5H_2} \quad (n=2 \text{ and } 3), \quad (3)$$

where the J_{PhBO_2H} and $J_{B_2O_5H_2}$ are the exchange integrals per single phenylboronate and diborate bridge,

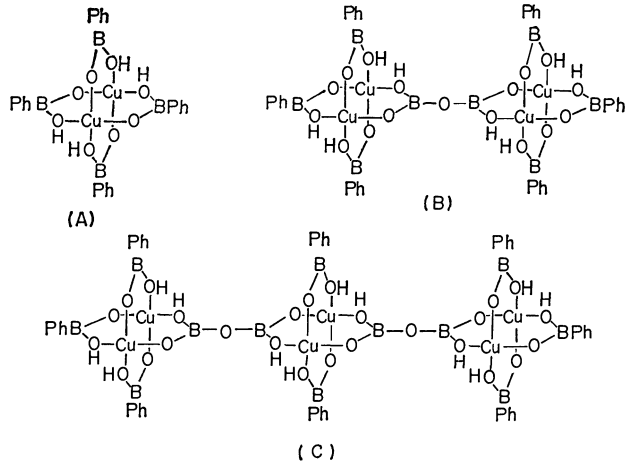

Fig. 2. Schematic representations of probable structure.
(A): $Cu(PhBO_2H)_2$, (B): $Cu(PhBO_2H)_{3/2}(B_2O_5H_2)_{1/4}$,
(C): $Cu(PhBO_2H)_{4/3}(B_2O_5H_2)_{1/3}$.

respectively. The observed magnetic moments of hydrolysis products are the same as the calculated ones (for $n=2$ and 3, 1.36 and 1.33 BM respectively) from the mean exchange integrals obtained with $J_{PhBO_2H}/k=-49$ K (a quarter of the J/k value evaluated by use of Eq. 2) and $J_{B_2O_5H_2}/k=-73$ K.[9,10] This close agreement supports the validity of the postulated structure of hydrolysis products.

The magnitude of superexchange interaction depends to a great extent on the electronic structure of the bridging ligand. Our result, where the J/k value of $Cu(PhBO_2H)_2$ is nearly equal to the value of $Cu(PhCO_2)_2$, can be explained by the isoelectronicity of the ligands. The other result, where the antiferromagnetic interaction operates more strongly in the hydrolysis products than in $Cu(PhBO_2H)_2$, can be explained by considering that diborate groups promote the migration of positive holes to a greater extent than phenylboronate groups.

References

1) M. Inoue, M. Kishita, and M. Kubo, *Inorg. Chem.*, **3**, 239 (1964).
2) B. Bettman, G. E. K. Branch, and D. L. Yabroff, *J. Am. Chem. Soc.*, **56**, 1865 (1934).
3) D. J. G. Ives, *J. Chem. Soc.*, **1933**, 731.
4) J. N. van Niekerk and F. R. L. Schoening, *Acta Crystallogr.*, **6**, 227 (1953).
5) G. Föex, "Constants Sélectionées, Diamagnétisme et Paramagnétisme," Masson, Paris (1957).
6) B. Bleaney and K. D. Bowers, *Proc. R. Soc. London, Ser. A*, **214**, 451 (1952).
7) J. Lewis, Y. C. Lin, L. K. Royston, and R. C. Thompson, *J. Chem. Soc.*, **1965**, 6464.
8) D. B. Brown, J. W. Hall, H. M. Helis, E. G. Walton, D. J. Hodgson, and W. E. Hatfield, *Inorg. Chem.*, **16**, 2675 (1977).
9) H. Rose, *Pogg. Ann.*, **87**, 587 (1852).
10) To be published.

Dimeric Copper(II) Nitrato and Chloro Complexes with *N*-(3-Dimethylaminopropyl)salicylideneaminato Ligand Protonated at the Terminal Nitrogen

Tadashi Tokii, Toshihiko Tenhiro, and Yoneichiro Muto*

Department of Chemistry, Faculty of Science and Engineering, Saga University, Saga 840

(Received November 10, 1980)

Synopsis. The title complexes have been prepared and characterized. The strong antiferromagnetic interaction observed for the complexes is interpreted in terms of a phenolic-oxygen-bridged dimeric structure with the metal ions in a square-pyramidal geometry.

Previously we reported that chloro[*N*-(3-dimethylaminopropyl)salicylideneaminato]copper(II), Cu(sal·pr·NMe_2)Cl, was obtained in two forms, one monomeric and the other dimeric;[1] the corresponding nitrato complex, Cu(sal·pr·NMe_2)NO_3, was obtained only in a monomeric form.[2] In order to study the effect of structural change upon the magnetic interaction in such complexes, we have prepared copper(II) nitrato and chloro complexes with the Schiff base ligand protonated at the terminal nitrogen, Cu(sal·pr·$\overset{+}{N}Me_2H$)X_2 (X=NO_3 or Cl), from the reaction of HX and Cu(sal·pr·NMe_2)X in ethanol. The analogous complex, Cu(sal·en·$\overset{+}{N}Et_2H$)Cl_2, has also been synthesized (*cf.* formula I).

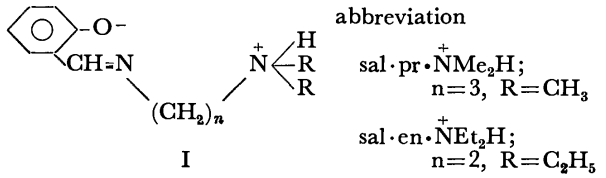

I

abbreviation

sal·pr·$\overset{+}{N}Me_2H$; n=3, R=CH_3

sal·en·$\overset{+}{N}Et_2H$; n=2, R=C_2H_5

The results of characterization studies on these complexes are presented in this paper.

Experimental

Synthesis. A typical synthetic method is as follows. A solution of one of the acids HX(5 mmol) in ethanol(5 ml) was added to a solution of one of the parent complexes(2 mmol), Cu(sal·pr·NMe_2)NO_3,[2] Cu(sal·pr·NMe_2)Cl (monomeric form)[1] and Cu(sal·en·NEt_2)Cl,[3] in ethanol (50 ml). After the resulting solution had been allowed to stand for several days at *ca.* 5 °C in a freezer, the separated crystals were filtered, washed with ethanol, and dried *in vacuo*. All crystals were orange. Anal. **1.** Cu(sal·pr·$\overset{+}{N}Me_2H$)-$(NO_3)_2$. Found: C, 36.33; H, 4.60; N, 14.01; Cu, 16.02%. Calcd for $C_{12}H_{18}N_4O_7Cu$: C, 36.60; H, 4.61; N, 14.23; Cu, 16.13%. **2.** Cu(sal·pr·$\overset{+}{N}Me_2H$)Cl_2. Found: C, 42.20; H, 5.32; N, 8.22; Cu, 18.65%. Calcd for $C_{12}H_{18}N_2OCl_2Cu$: C, 42.30; H, 5.35; N, 8.22; Cu, 18.65%. **3.** Cu(sal·en·$\overset{+}{N}Et_2H$)Cl_2. Found: C, 43.79; H, 5.69; N, 7.94; Cu, 17.76%. Calcd for $C_{13}H_{20}N_2OCl_2Cu$: C, 44.01; H, 5.68; N, 7.90; Cu, 17.91%.

Physical Measurements. The magnetic susceptibilities in the temperature range 80—300 K were determined by the Gouy method. The IR spectral measurements were made with a Hitachi EPI-G2 IR Spectrophotometer in the 400—4000 cm^{-1} region on Nujol mulls. The reflectance spectra were recorded with a Hitachi Recording Spectrophotometer 323.

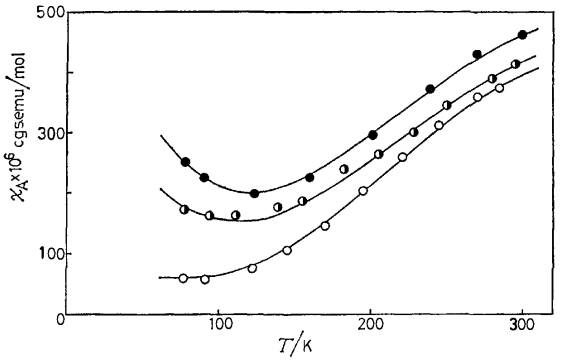

Fig. 1. Variation of magnetic susceptibilities with temperature.
(○): Complex **1**, (◑): Complex **2**, (●): Complex **3**.
The solid curves were obtained as described in text.

Results and Discussion

The variable-temperature magnetic susceptibility data observed for complex **1** have been analyzed by the Bleaney-Bowers equation for isotropic exchange in a copper(II) dimer:[4]

$$\chi_A = \frac{Ng^2\beta^2}{3kT}\left[1+\frac{1}{3}\exp\left(\frac{-2J}{kT}\right)\right]^{-1} + N\alpha, \qquad (1)$$

where each symbol has the usual meaning. The data fit the above expression very well: $-2J=554\ cm^{-1}$, $g=2.16$, and $N\alpha=60\times10^{-6}$ cgs emu† (Fig. 1). For complexes **2** and **3**, the cryomagnetic data at low temperatures have been found to be somewhat higher than those predicted by Eq. 1. This type of behavior is most likely due to a small amount of a monomeric Cu(II) impurity.[5] Assuming the magnetic moment of 1.8 BM†† for the Cu(II) impurity, the magnetic data have been fitted to a modified equation:[5]

$$\chi_A = \frac{Ng^2\beta^2}{3kT}\left[1+\frac{1}{3}\exp\left(\frac{-2J}{kT}\right)\right]^{-1}(1-P) + \frac{0.405P}{T} + N\alpha, \qquad (2)$$

where P is the mole fraction of the Cu(II) impurity. The best fit yields $-2J=554\ cm^{-1}$, $g=2.16$, $N\alpha=60\times10^{-6}$ cgs emu and $P=0.022$ for complex **2** and $-2J=542\ cm^{-1}$, $g=2.20$, $N\alpha=60\times10^{-6}$ cgs emu and $P=0.036$ for complex **3** (Fig. 1).

The IR spectra of the present complexes all show an intence band in the range 1550—1560 cm^{-1} (**1.** 1559; **2.** 1549; **3.** 1550 cm^{-1}), while the corresponding bands in the spectra of the parent monomeric com-

† 1 cgs emu $mol^{-1}=4\pi\times10^{-6}\ m^3\ mol^{-1}$.
†† 1 BM$=9.274\times10^{-24}\ Am^2$.

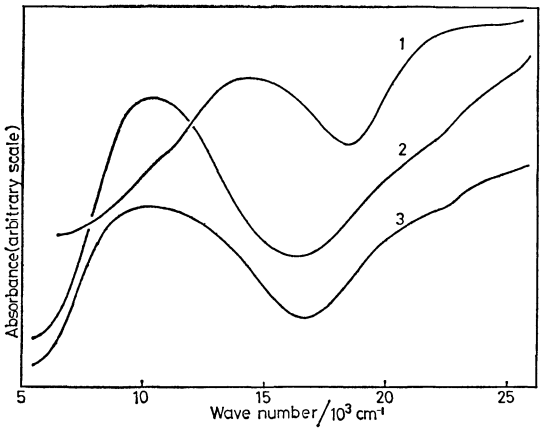

Fig. 2. Reflectance spectra of Complexes **1** (1), **2** (2), and **3** (3).

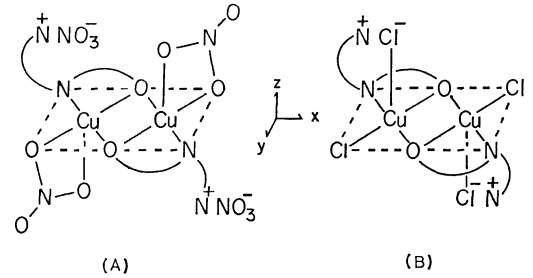

Fig. 3. Schematic representations of probable structure.
(A) Complex **1** and (B) Complexes **2** and **3**.

plexes, $Cu(sal\cdot pr\cdot NMe_2)NO_3$, $Cu(sal\cdot pr\cdot NMe_2)Cl$ and $Cu(sal\cdot en\cdot NEt_2)Cl$, appear at 1541, 1529, and 1530 cm^{-1}, respectively. Such band shift toward higher frequencies (15—20 cm^{-1}) is indicative of the presence of bridging phenolic oxygen atoms in the present complexes.[1,2] The band around 2500—2900 cm^{-1} (**1**. 2900; **2**. 2650; **3**. 2600 cm^{-1}) can be assigned to the $\nu(\overset{+}{N}\text{–H})$ mode, in agreement with the values of 2680 and 2540 cm^{-1} observed for this stretching frequency in *N*-methylpiperidine and triethylamine hydrochlorides.[6] This assignment is further supported by the fact that no band is observed in the same region for the parent monomeric complexes.

The reflectance spectral feature of complex **1** is nearly the same as that of the phenolic oxygen-bridged dimeric copper(II) complex with *N*-ethylsalicylideneaminato ligand, $[Cu(sal\cdot Et)NO_3]_2$, in which the metal ions are five-coordinated with four strong bonds and a weak fifth bond with a nitrato oxygen to complete a rough square-pyramid.[7] Complexes **2** and **3** show a broad band at *ca.* 10000 cm^{-1}: a spectral feature indicative of a five-coordination around the metal ion (Fig. 2).

All these results indicate that the complexes in the present study have a phenolic oxygen-bridged dimeric structure with a five-coordinated Cu(II) geometry. The most probable structures are shown in Fig. 3.

The $-2J$ values determined for the present complexes are more than twice those of $[Cu(sal\cdot pr\cdot NMe_2)X]_2$ ($-2J_{X=Cl}=248$ and $-2J_{X=Br}=260$ cm^{-1}),[1] to which a phenolic oxygen-bridged dimeric structure with the metal ions in a five-coordinated, essentially trigonal bipyramidal, geometry was previously assigned.[1] This result may be taken as evidence in favor of the previous conclusion that the strength of antiferromagnetic interaction in five-coordinated copper(II) dimers containing a $Cu\begin{smallmatrix}O\\O\end{smallmatrix}Cu$ bridging system decreases as the distortion of Cu(II) geometry from square-pyramid toward trigonal-bipyramid increases.[1] On the basis of the difference between the assumed structures, the pronounced difference in magnetic interaction can be explained as follows. In the square pyramidal coordination around the Cu(II) ions in the dimeric species shown in Fig. 3, the overlap of singly occupied $3d_{xy}$ orbitals of the two Cu(II) centers with the oxygen $2p_x$ orbital may yield an efficient pathway for superexchange (*cf.* the coordinate system given in Fig. 3).[8,9] However, a distortion of the Cu(II) geometry from square-pyramid toward trigonal-bipyramid will give rise to a decrease in successive orbital overlap of $Cu(d_{xy})$–$O(p_x)$–$Cu(d_{xy})$, leading to a weakening of spin-coupling, *i.e.*, a decrease in $|-2J|$ value.

References

1) Y. Muto and T. Tokii, *Bull. Chem. Soc. Jpn.*, **51**, 139 (1978).
2) T. Tokii, S. Emori, and Y. Muto, *Bull. Chem. Soc. Jpn.*, **52**, 2114 (1979).
3) L. Sacconi and I. Bertini, *Inorg. Chem.*, **5**, 1520 (1966).
4) B. Bleaney and K. D. Bowers, *Proc. R. Soc. London, Ser. A*, **214**, 451 (1952).
5) K. E. Hyde, G. Gordon, and G. F. Kokoszka, *J. Inorg. Nucl. Chem.*, **30**, 2155 (1968).
6) P. J. Stone, J. C. Craig, and H. W. Thomson, *J. Chem. Soc.*, **1958**, 52.
7) E. Sinn, *Inorg. Chem.*, **15**, 366 (1976).
8) M. Kato, K. Imai, Y. Muto, T. Tokii, and H. B. Jonassen, *J. Inorg. Nucl. Chem.*, **35**, 109 (1973).
9) H. E. LeMay, D. J. Hodgson, P. Pruettiangkura, and L. J. Theriot, *J. Chem. Soc., Dalton Trans.*, **1979**, 781.

The Synthesis of Anthglutin and Its Analogues

Takeshi KINOSHITA,* Hiroko WATANABE, and Sadamasa MINATO†

Central Research Laboratories, Sankyo Co., Ltd., Hiromachi, Shinagawa-ku, Tokyo 140

† *Fermentation Research Laboratories, Sankyo Co., Ltd., Hiromachi, Shinagawa-ku, Tokyo 140*

(Received August 6, 1980)

Synopsis. Anthglutin (1-γ-L-glutamyl-2-(2-carboxyphenyl)hydrazine) and its analogues were synthesized. Their inhibitory activity on γ-glutamyl transpeptidase was measured. 2-Carboxyphenyl derivatives, including anthglutin, showed inhibitory activity, while the other derivatives did not. The 2-carboxyl group seems to be essential for the inhibitory activity.

In previous papers,[1,2] we reported that anthglutin, an inhibitor of γ-glutamyl transpeptidase, was isolated from a cultured medium of Penicillium oxalicum, and Structure (**1**), 1-γ-L-glutamyl-2-(2-carboxyphenyl)hydrazine, was proposed. We have confirmed the structure of anthglutin by the synthesis of 1-γ-glutamyl-2-(2-carboxyphenyl)hydrazine (**1**).

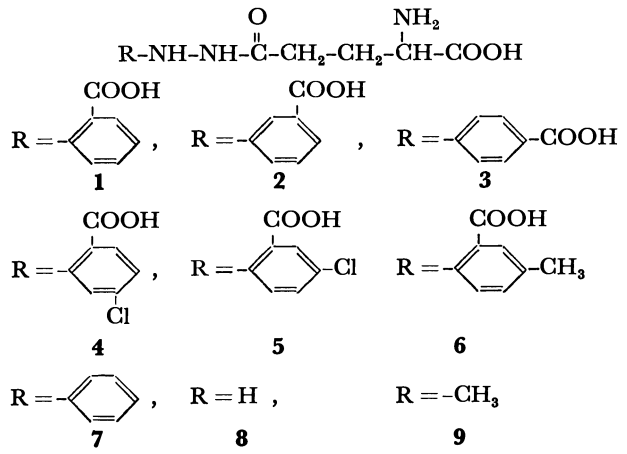

Several compounds related to anthglutin were synthesized and measured for their inhibitory activity on γ-glutamyl transpeptidase (Tables 1 and 2). 2-Carboxyphenyl hydrazine derivatives (**4**—**6**) inhibited an enzyme activity, showing that the 2-carboxyl group of anthglutin is a functional group for the inhibitory activity. As has been shown in a previous paper,[1] the α-carboxyl and α-amino groups of the glutamyl moiety of anthglutin also seem to be essential for forming a complex between the inhibitor and the enzyme.

Experimental

Materials. Commercially available aminobenzoic acid derivatives were used. The *N-t*-BOC-L-glutamic acid α-benzyl ester was obtained from the Sigma Chemical Company. γ-Glutamyl transpeptidase was partially purified by the method of Orlowski and Meister;[3] it was thereby purified about 140-fold from the whole homogenate of the hog kidney.

Synthesis. Carboxyphenylhydrazine compounds were synthesized, according to the method described by Stephenson,[4] from the appropriate aminobenzoic acid compounds. 1-γ-L-Glutamyl-carboxyphenylhydrazine compounds were prepared by condensation between the N-*t*-BOC-L-glutamic acid benzyl ester and the appropriate free base form of the hydrazine, according to the method described by F. Hoffmann-La Roche & Co.[5]

1-γ-L-Glutamyl-2-(2-carboxyphenyl) hydrazine (1). 2-Carboxyphenylhydrazine (0.96 g, 6.31 mmol), the *N-t*-BOC-L-glutamic acid α-benzyl ester (1.05 g, 3.11 mmol), and triethylamine (0.6 ml) were dissolved in dichloromethane (10 ml). To the solution we then added dicyclohexylcarbodiimide (0.88 g, 4.53 mmol) dissolved in dichloromethane (1.0 ml), and the mixture was stirred for 3 h at room temperature. After removing the precipitate thus obtained by filtration, the filtrate was subjected to column chromatography on silica gel, eluting with chloroform–methanol–acetic acid (400:10:1). After the solvent had been removed *in vacuo* at 30 °C, the residue was dissolved in ethanol (20 ml) containing cyclohexene (1.0 ml). To the solution we added palladium–charcoal (5%, 400 mg), after which the mixture was refluxed for 1 h with stirring. The catalyst was removed

Table 1. Yields, melting points, and analytical data

Compound	Yield/%	Mp/°C	Molecular formula	Found (Calcd)(%) C	H	N
2	18.3	187	$C_{12}H_{15}N_3O_5$	51.27 (51.24	5.31 5.38	14.84 14.94)
3	14.1	175	$C_{12}H_{15}N_3O_5$	51.44 (51.24	5.41 5.38	14.70 14.94)
4	24.4	165	$C_{12}H_{14}N_3O_5Cl$	45.75 (45.65	4.31 4.47	13.18 13.31)
5	16.8	172	$C_{12}H_{14}N_3O_5Cl$	45.90 (45.65	4.51 4.47	13.11 13.31)
6	25.4	165	$C_{13}H_{17}N_3O_5$	52.61 (52.88	5.97 5.80	14.08 14.23)
7	26.3	202	$C_{11}H_{15}N_3O_3$	55.57 (55.68	6.48 6.47	17.68 17.71)
8	24.6	164	$C_5H_{11}N_3O_3$	37.26 (37.26	6.87 6.88	26.10 26.08)
9	22.7	152	$C_6H_{13}N_3O_3$	41.26 (41.14	7.41 7.43	24.03 24.00)

Table 2. Inhibition of γ-glutamyl transpeptidase anthglutin analogues

Compounds (R–)	$K_i/\mu M$
Anthglutin (P. oxalicum)	5.7
2-Carboxyphenyl-(**1**)	5.9
3-Carboxyphenyl-(**2**)	200.0
4-Carboxyphenyl-(**3**)	>1000.0
2-Carboxy-5-chlorophenyl-(**4**)	7.5
2-Carboxy-4-chlorophenyl-(**5**)	11.6
2-Carboxy-4-methylphenyl-(**6**)	8.7
Phenyl-(**7**)	>1000.0
N-Unsubstituted (**8**)	Not inhibit
Methyl-(**9**)	Not inhibit

In the presence of the analogues (6.5 μM), inhibition was determined according to a method described previously.[1] Substrate (γ-glutamyl-*p*-nitroanilide), 0.42—4.21 mM; acceptor(glycylglycine), 47.9 mM; enzyme, hog kidney γ-glutamyl transpeptidase; incubation, pH 8.5, 37 °C, 15 min.

by filtration, and the filtrate was evaporated *in vacuo* at 30 °C to dryness to give a white powder. The powder thus obtained was treated with trifluoroacetic acid (1.0 ml) and anisole (0.25 ml) for 1 h in an ice bath.[6] The reaction product was thus precipitated by the addition of ether (25 ml). The precipitate thus obtained was purified on a column of Dowex 2×8 (formate form) according to the method described previously.[1] The product thus obtained (210 mg) was identical with a sample of natural anthglutin (yield, 24%; mp 170—171.5 °C; UV (water): 243 and 322 nm (pH 2.0), and 240 and 307 nm (pH 7.0); $[\alpha]_D^{30}$: +22.6° (*c*, 0.9, 0.05 mol dm^{-3} HCl)), as established by paper chrcmatography and the inhibitory activity (Table 2). Found: C, 51.21; H, 5.32; N, 14.88%. Calcd for $C_{12}H_{15}N_3O_5$: C, 51.24, H, 5.38; N, 14.94%.

Analogues Anthglutin. Analogues of anthglutin (**2**—**6**) were synthesized by the procedure described above using the appropriate hydrazine compound.

The 1-γ-L-glutamyl hydrazine compounds (**7**—**9**) were prepared by condensation between L-pyroglutamic acid and the appropriate free-base form of the hydrazine compound, under reflux overnight in 85% ethanol, according to the method described by Yale *et al.*[7] The results thus obtained are shown in Table 1.

References

1) S. Minato, *Arch. Biochem. Biophys.*, **192**, 235 (1979).
2) T. Kinoshita and S. Minato, *Bull. Chem. Soc. Jpn.*, **51**, 3282 (1978).
3) M. Orlowski and A. Meister, *J. Biol. Chem.*, **240**, 338 (1965).
4) E. F. M. Stephenson, *Org. Synth.*, Coll. Vol. **III**, 475 (1955).
5) F. Hoffmann-La Roche & Co., British Patent, 843372, Avg. 4, 1960.
6) F. C. McKay and W. F. Albertson, *J. Am. Chem. Soc.*, **79**, 4684 (1957).
7) H. L. Yale, K. Losee, S. J. Martin, M. Holsing, F. M. Perry, and J. Bernstein, *J. Am. Chem. Soc.*, **75**, 1933 (1953).

4-Dimethylaminopyridine *N*-Oxide as an Efficient Oxidizing Agent for Alkyl Halides

Shigemi MUKAIYAMA, Junji INANAGA, and Masaru YAMAGUCHI*

Department of Chemistry, Faculty of Science, Kyushu University 33, Hakozaki, Higashi-ku, Fukuoka 812

(Received October 21, 1980)

Synopsis. Various types of alkyl halides were converted into aldehydes or ketones in high yields with 4-dimethylaminopyridine *N*-oxide in the presence or absence of DBU.

Oxidation of alkyl halides with pyridine *N*-oxide[1] or trimethylamine *N*-oxide[2] has been known as a unique method to obtain carbonyl compounds. However, the former is only applicable to the relatively active substrates such as benzyl bromide[1a] because of the low nucleophilicity of pyridine *N*-oxide. While trimethylamine *N*-oxide can oxidize alkyl bromides and iodides, the yields are not satisfactory. In this paper is described the use of 4-dimethylaminopyridine *N*-oxide (DMAP *N*-oxide)[3] as an efficient oxidizing agent to afford aldehydes or ketones from primary or secondary alkyl halides, and α-keto esters from α-bromo esters, respectively.

The reaction was carried out in two steps, salt formation (1) and deprotonation (2).

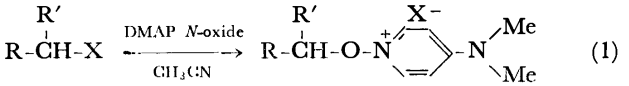

(1)

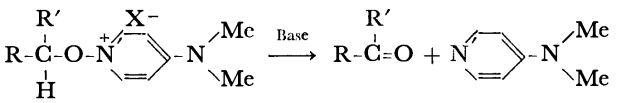

(2)

X=Br or Cl

Acetonitrile was used as the solvent in which DMAP *N*-oxide was moderately soluble and 1,8-diazabicyclo-[5.4.0]undec-7-ene (DBU) proved to be the best base for the deprotonation step (2). Alkyl halides were refluxed with the *N*-oxide in acetonitrile until the substrates were consumed, and then DBU was added. The reaction was followed by GLC by using appropriate internal standards. The results are summarized in Table 1.

Benzylic halides were easily oxidized to give the corresponding carbonyl compounds in quantitative yields. Primary alkyl halides (bromide and chloride) were converted into aldehydes. Secondary alkyl bromide also reacted to afford a ketone quantitatively. Cyclohexyl bromide, however, gave cyclohexanone in very low yield, and the formation of a large amount of cyclohexene was observed in the first step (1), though DMAP *N*-oxide is known to have a small pK_a value (3.88)[4] (entry 9).[5]

2-Formylpyridine was obtained in 82% yield by only heating 2-chloromethylpyridine hydrochloride[6] with three molar equivalents of the *N*-oxide in acetonitrile (entry 5).

Sliwa *et al.*[1b] reported the oxidation of α-bromo esters with pyridine *N*-oxide, but this method required the addition of silver nitrate to attain the effective formation of pyridinium salt. With 2.5 equivalents of DMAP *N*-oxide, however, α-bromo esters were rapidly oxidized to α-keto esters.

As is shown in Table 2, not only phenylglyoxylic acid ester but also aliphatic α-keto esters were produced in high yields.

Dimethyl sulfoxide is known to oxidize alkyl halides in a similar fashion.[7] However, it usually requires high reaction temperature (100—150 °C) and is only applicable to primary alkyl iodides, tosylates, or reactive substrates such as benzyl halides.[8] For the

Table 1. Oxidation of alkyl halides[a]

	Substrate	Salt formation		Deprotonation		Product	Yield/%[b]
		Temp	Time	Temp	Time		
1	$C_6H_5CH_2Br$	RT	1.5 h[c]	Refl	20 min	C_6H_5CHO	>98[d]
2	$C_6H_5CH_2Cl$	RT	2 h	Refl	20 min	C_6H_5CHO	>98
3	$C_6H_5CH(Br)CH_3$	Refl	8 min	Refl	5 h	$C_6H_5COCH_3$	>98
4	$C_6H_5CH(Br)C_6H_5$	Refl	10 min	Refl	3.3 h	$C_6H_5COC_6H_5$	>98
5	$C_5H_4NCH_2Cl\cdot HCl$[e]			Refl	3 h[f]	$C_5H_4N\cdot CHO$[g]	82
6	$C_8H_{17}Br$	Refl	15 h	Refl	40 min	$C_7H_{15}CHO$	83
7	$C_8H_{17}Cl$	Refl	10 h	Refl	1 h	$C_7H_{15}CHO$	88
8	$C_3H_7CH(Br)CH_3$	Refl	40 min	Refl	16 h	$C_3H_7COCH_3$	>98
9	$C_6H_{11}Br$[h]	Refl	6.5 h	Refl	2 h	$C_6H_{10}O$[i]	13[j]

a) Substrate (0.3 mmol), DMAP *N*-oxide (0.36 mmol), DBU (0.36 mmol), and CH_3CN (0.5 ml) were used except for entry 5. b) GLC yield. c) In a separate experiment, the salt, 1-benzyloxy-4-dimethylaminopyridinium bromide, was isolated. Mp 115 °C (sinter), 141 °C (decomp). Found: C, 54.50; H, 5.51; N, 9.16%. Calcd for $C_{14}H_{17}BrN_2O$: C, 54.38; H, 5.54; N, 9.06%. d) An 87% or 30% yield of benzaldehyde has been reported in the oxidation of benzyl bromide with pyridine *N*-oxide[1a] or with trimethylamine *N*-oxide,[2] respectively. e) 2-Chloromethylpyridine hydrochloride. f) Three molar equivalents of DMAP *N*-oxide was used *vs.* substrate without DBU. g) 2-Formylpyridine. h) Cyclohexyl bromide. i) Cyclohexanone. j) Cyclohexene (60—70%) was also produced.

Table 2. Oxidation of α-bromo esters[a)]

Substrate	Temp	Time/min	Product	Yield/%[b)]
$CH_3CH(Br)CO_2CH_3$	Refl	20	$CH_3COCO_2CH_3$	>90
$C_6H_{13}CH(Br)CO_2CH_3$	Refl	35	$C_6H_{13}COCO_2CH_3$	85[c)]
$C_6H_5CH(Br)CO_2C_2H_5$	Refl	26	$C_6H_5COCO_2C_2H_5$	92

a) Substrate (0.3 mmol), DMAP *N*-oxide (0.75 mmol), and CH_3CN (0.5 ml) were used. b) GLC yield. c) Isolated yield.

oxidation of α-bromo ester by dimethyl sulfoxide, one example is reported.[9)]

The high yields, mildness of the reaction conditions, and applicability to wide variety of alkyl halides are considered to make the present method synthetically useful one.

Experimental

All starting alkyl halides are commercially available except for 2-chloromethylpyridine hydrochloride[6)] and α-bromo esters which were obtained by esterification of the corresponding α-bromo acids. Products were identified with authentic samples by the comparison of their NMR and/or GLC data.

Two typical examples of oxidation are described below.

Oxidation of 2-Bromopentane. A mixture of 2-bromopentane (38 μl), DMAP *N*-oxide (41 mg), and absolute acetonitrile (0.5 ml) was refluxed for 40 min. Then, DBU (57.3 μl) was added and the reflux was continued. After 16 h quantitative formation of 2-pentanone was observed on GLC by the addition of toluene as an internal standard.

Oxidation of Methyl 2-Bromooctanoate. A mixture of the bromo ester (167 mg), DMAP *N*-oxide (201 mg), and acetonitrile (2 ml) was refluxed for 35 min. After cooling 1.1 equivalents of hydrochloric acid in acetonitrile (1 ml) was added. The resulting mixture was passed through a short silica gel column, concentrated, and chromatographed on preparative TLC (SiO_2, Merck) with benzene giving methyl 2-oxopentanoate[10)] (103 mg, 85%). NMR ($CDCl_3$) δ 0.89 (t, J=5.0 Hz, 3H), 1.0—2.0 (m, 8H), 2.84 (t, J=7.0 Hz, 2H), and 3.88 (s, 3H).

This work was partially supported by a Grant-in-Aid for Scientific Research No. 443008 from the Ministry of Education, Science and Culture.

References

1) a) W. Feely, W. L. Lehn, and V. Boekelheide, *J. Org. Chem.*, **22**, 1135 (1957) and references cited therein; b) H. Sliwa and A. Tartar, *J. Org. Chem.*, **41**, 160 (1976).

2) V. Franzen and S. Otto, *Chem. Ber.*, **94**, 1360 (1961); V. Franzen, *Org. Synth.*, Coll. Vol., 5, 872 (1973).

3) a) L. Pentimalli, *Gazz. Chim. Ital.*, **94**, 902 (1964). DMAP was oxidized according to the literature cited above, but the workup procedure was slightly modified as follows: The reaction mixture was passed through a column of anion-exchange resin (Dowex 1-X2) to remove benzoic acid and eluted with methanol giving the crude product. After the removal of a small amount of DMAP by washing with ethyl acetate, the product was recrystallized from acetone, and then sublimed at 150 °C (bath)/133 Pa. A hygroscopic white powder. Mp 214—215 °C (lit, 214—215 °C). NMR ($CDCl_3$) δ 3.08 (s, 6H), 6.48 (dd, J=5.8 Hz, J=1.5 Hz, 2H), and 7.98 (dd, J=5.8 Hz, J=1.5 Hz, 2H); b) R. Frampton, C. D. Johnson, and A. R. Katritzky, *Justus Liebigs Ann. Chem.*, **749**, 12 (1971).

4) J. N. Gardner and A. R. Katritzky, *J. Chem. Soc.*, **1957**, 4375; P. Forsythe, R. Frampton, C. D. Johnson, and A. R. Katritzky, *J. Chem. Soc., Perkin Trans.* 2, **1972**, 671.

5) Cyclohexyl iodide produced cyclohexene quantitatively in the salt formation step.

6) H. S. Mosher and J. E. Tessieri, *J. Am. Chem. Soc.*, **73**, 4925 (1951).

7) N. Kornblum, W. J. Jones, and G. J. Anderson, *J. Am. Chem. Soc.*, **81**, 4113 (1959); H. R. Nace and J. J. Monagle, *J. Org. Chem.*, **24**, 1792 (1959); A. P. Johnson and A. Pelter, *J. Chem. Soc.*, **1964**, 520.

8) Oxidation of secondary alkyl halides under the presence of $AgBF_4$ has been reported [B. Ganem and R. K. Boeckman Jr., *Tetrahedron Lett.*, **1974**, 917]. However, this method is not applicable to alkyl chlorides.

9) I. M. Hunsberger and J. M. Tien, *Chem. Ind. (London)*, **1959**, 88.

10) S. Cacchi, L. Caglioti, and P. Zappelli, *J. Org. Chem.*, **38**, 3653 (1973).

Alkylation of Thioureas and Related Compounds by Use of Alcohols, Diethyl Azodicarboxylate, and Triphenylphosphine

Hiroshi NAGASAWA and Oyo MITSUNOBU*

Department of Chemistry, College of Science and Engineering, Aoyama Gakuin University, Chitosedai, Setagaya-ku, Tokyo 157

(Received November 10, 1980)

Synopsis. The alkylation of ambident nucleophiles having a thiocarbonyl group by use of alcohols, diethyl azodicarboxylate, and triphenylphosphine was studied. Selective *S*-alkylation took place in the cases of *N*-benzoyl-*N'*-mono- and -disubstituted thioureas, while selective *N*-alkylation occurred in the reaction of *N*-phenyl-*N',N'*-diethylthiourea. 1-Methoxymethyl-2-thiouracil afforded both *N*-alkylated and *S*-alkylated products.

The reaction of either *N*-benzyloxycarbonylbenzamide[1] or ethyl acetoacetate[2] with an alcohol, diethyl azodicarboxylate (**1**), and triphenylphosphine (**2**) mainly gives *O*-alkylated products. The results indicate that the triphenylalkoxyphosphonium salt formed as a key intermediate of the present reaction[3] is a harder alkylating reagent than alkyl halides or alkyl tosylates.[4]

In order to examine the present alkylating system, we studied the alkylation of other ambident nucleophiles, *N*-acylthioureas and 1-methoxymethyl-2-thiouracile, ambident at N, S, and O, being chosen as reagents.

A series of *N*-benzoylthioureas, PhCO–NH–CS–NR^1R^2 with R^1=H, R^2=*t*-butyl (**3**), R^1=H, R^2=cyclohexyl (**4**), and $R^1=R^2$=ethyl (**5**) was prepared by the reaction of benzoyl isothiocyanate with amines. The reaction of 2-phenylethanol with **3**, **4**, and **5** in the presence of 1.5 molar equivalents each of **1** and **2** proceeded smoothly at room temperature giving the corresponding *S*-alkylated products (**6a**, **7a**, and **8a**) in good to excellent yields (Table 1).[5] The structure was confirmed by the reaction of the products with ammonia at room temperature, the corresponding *N*-benzoylguanidines and bis(2-phenylethyl) disulfide being isolated (Table 2). The reaction of **5** with **1**, **2**, and 2-phenoxyethanol also gave *S*-alkylated product (**8b**) almost quantitatively.

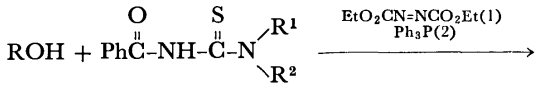

3: R^1=H, R^2=*t*-Bu
4: R^1=H, R^2=cyclo-C_6H_{11}
5: $R^1=R^2$=Et

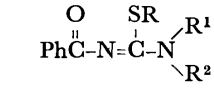

6: R^1=H, R^2=*t*-Bu
7: R^1=H, R^2=cyclo-C_6H_{11}
8: $R^1=R^2$=Et
a: R=$PhCH_2CH_2$–
b: R=$PhOCH_2CH_2$–
c: R=$CH_3CH(OH)CH_2CH_2$–
d: R=$PhCH(OH)CH_2CH_2$–
e: R=$CH_3CH(OH)CH_2CH_2CHCH_3$

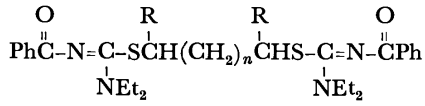

9

Selective *S*-alkylation also took place when sodium salt of **5** was treated with 2-phenylethyl bromide in tetrahydrofuran. Compound **8a** was obtained in 38% yield and 59% of **5** was recovered.

When primary, secondary-diol was allowed to react with **1**, **2**, and **5**, the primary hydroxyl group predominantly reacted to give 2-(hydroxylakyl)isothiourea (**8c**, **8d**). 2,5-Hexanediol also gave 2-(1-methyl-4-hydroxypentyl)isothiourea (**8e**). No detectable amount of bis(amidinothio) derivatives (**9**) could be obtained by preparative layer chromatography.

Contrary to the case of *N*-benzoylthioureas, the reaction of *N*-phenyl-*N',N'*-diethylthiourea with 2-phenylethanol, **1**, and **2** resulted in the formation of *N*-alkylated product in 48% yield rather than *S*-alkylated product. Diethyl 1-phenethyl-1,2-hydrazinedicarboxylate was isolated in 26% yield.

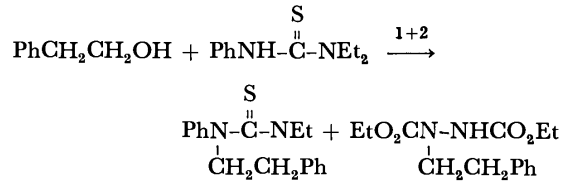

The alkylation of 1-methoxymethyl-2-thiouracil (**10**),[6] a cyclic analogue of **5**, with 2-phenylethanol in the presence of **1** and **2** resulted in the formation of *N*-alkylated (**11**) and *S*-alkylated (**12**) products in 64% and 18% yields, respectively.[7] The change in solvent scarcely affected the product ratio.

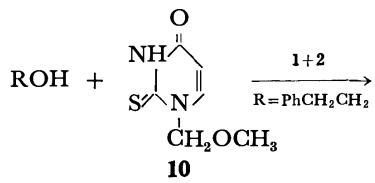

10

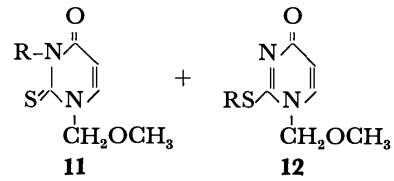

11 **12**

THF	64%	18%
DMF	64%	19%
THF-DMF(4:1)	60%	17%
Benzene-DMF(4:1)	66%	18%

Table 1. Alkylation of *N*-benzoylthioureas

	BzN=C(SR)-NR¹R² R	R¹	R²	Yield %	TLC[a]	NMR ($CDCl_3$), 60 MHz, δ/ppm from TMS[b]
6a	$PhCH_2CH_2$	H	*t*-Bu	82	C-EA 20:1	1.45 (s, *t*-Bu), 2.75—3.65 (A_2B_2, $PhCH_2CH_2S$), 7.15 (s, Ph), 7.2—8.3 (m, Bz)
7a	$PhCH_2CH_2$	H	cyclo-C_6H_{11}	90	C-EA 20:1	0.8—2.2 (m, C_6H_{11}), 2.7—3.6 (A_2B_2, $PhCH_2CH_2S$), 7.1 (s, Ph), 7.1—8.3 (m, Bz)
8a	$PhCH_2CH_2$	Et	Et	94	E	1.15 (t, CH_3), 2.5—3.25 (A_2B_2, $PhCH_2CH_2S$), 3.45 (q, CH_3CH_2), 6.65—7.1 (m, Ph), 7.1—8.2 (m, Bz)
8b	$PhOCH_2CH_2$	Et	Et	97	B-EA 1:1	1.19 (t,CH_3), 3.15 (t, CH_2S), 3.48 (q, CH_3CH_2), 4.0 (t, CH_2O), 6.55—7.15 (m, Ph), 7.1—8.3 (m, Bz)
8c	$CH_3CHCH_2CH_2$ (OH)	Et	Et	78	B-EA 1:1	1.0 (d, $CH_3CH(OH)$), 1.2 (t, CH_3CH_2), 1.6 (br. q, $CH_3CH_2CH(OH)$), 2.85 (t, SCH_2), 3.5 (q, CH_3CH_2), 3—4.1 (m, $CH(OH)$), 7.05—8.25 (m, Bz))
8d	$PhCHCH_2CH_2$ (OH)	Et	Et	36	B-EA 1:1 then E	1.2 (t, CH_3CH_2), 1.95 (br. $CH_2CH_2CH(OH)$), 2.85 (br. t, SCH_2), 3.5 (q, CH_3CH_2), 4.5 (t, $CH_2CH(OH)$), 7.25 (s, Ph), 7—8.1 (m, Bz)
8e	$CH_3CHCH_2CH_2CH$ (OH, CH_3)	Et	Et	31	B-EA 1:5	1—1.19 (m, CH_3CH_2, $CH_3CH(OH)CH_2CH_2CH(CH_3)S$), 2.8—4 (m, $CH(OH)$, $CH(CH_3)S$), 3.5 (q, CH_3CH_2), 7.05—8.1 (m, Bz)

a) Solvent systems used for isolation of products; C=CCl_4, EA=AcOEt, E=ether, B=benzene. b) NMR spectra of **6a** and **7a** were measured in CCl_4.

Table 2. Ammonolysis of **6a**, **7a**, and **8a**

Isothiourea	Reaction time / h	Products/% BzN=C(NH_2)-NR^1R^2 R^1	R^2		$(PhCH_2CH_2S)_2$	Recovered isothiourea / %
6a	20	H	*t*-Bu	29	38	47
7a	90	H	cyclo-C_6H_{11}	77	78	6
8a	72	Et	Et	51	81	17

Experimental

Alkylation of Thiocarbonyl Compounds. A solution of **1** (259 mg, 1.5 mmol) in tetrahydrofuran (THF, 2 ml) was added dropwise over a period of 15 min to a solution of a thiocarbonyl compound (1 mmol), an alcohol (1 mmol) and **2** (392 mg, 1.5 mmol) in THF (5 ml) at room temperature. After the solution had been stirred for 18 h, the solvent was removed and products were isolated by preparative layer chromatography (Merck PF_{254} 20 cm × 30 cm). The results are summarized in Table 1.

*Ammonolysis of **8a**.* Compound **8a** (215 mg, 0.6 mmol) was treated with ammonia saturated in methanol (10 ml) at room temperature for 72 h. After evaporation, *N*-benzoyl-*N'*,*N'*-diethylguanidine and diphenethyl disulfide were isolated by preparative layer chromatography in 51% and 81% yields, respectively.

*Alkylation of **10**.* A solution of **1** (519 mg, 3 mmol) in THF was added dropwise over a period of 30 min to a solution of **10** (345 mg, 2 mmol), 2-phenylethanol (243 mg, 2 mmol) and **2** (785 mg, 3 mmol) in a mixture of THF (6 ml) and DMF (2 ml) at room temperature. After the solution had been stirred at room temperature for 16 h, **11** and **12** were obtained by preparative layer chromatography (benzene–AcOEt=1:1) in 60% and 17% yield, respectively.

Compound **11** was recrystallized from petroleum ether (bp 30—60 °C); mp 73—75 °C. UV_{max} (MeOH) 282 nm. NMR ($CDCl_3$, 60 MHz) δ 2.75—3.2 (m, $PhCH_2$), 3.35 (s, CH_3), 4.4—4.85 (m, CH_2CH_2N), 5.5 (s, OCH_2), 5.95 (d, N–CH=), 7.1—7.5 ppm (d, O=C–CH= and m, Ph).

Compound **12** was recrystallized from CCl_4; mp 110—113 °C. UV_{max} (MeOH) 238 nm. NMR ($CDCl_3$) δ 2.75—3.2 (m, $PhCH_2$), 3.2—3.7 (s, CH_3, superimposed on m, SCH_2), 5.97 (d, N–CH=), 7.25 (s, Ph), 7.35 ppm (d, O=C–CH=).

References

1) H. Morimoto, T. Furukawa, K. Miyazima, and O. Mitsunobu, *Chem. Lett.*, **1973**, 821. For the alkylation of ambident anion such as NO_2^- or S=C=N$^-$ by the use of **1** and **2**, see H. Loibner and E. Zbiral, *Helv. Chim. Acta*, **59**, 2100 (1976).

2) T. Kurihara, M. Sugizaki, I. Kime, M. Wada, and O. Mitsunobu, *Bull. Chem. Soc. Jpn.*, **54**, 2107 (1981).

3) O. Mitsunobu and M. Eguchi, *Bull. Chem. Soc. Jpn.*, **44**, 3427 (1971).

4) For reviews of alkylation of ambident nucleophiles, see a) H. O. House, "Modern Synthetic Reactions," 2nd ed, W. A. Benjamin Inc., Menlo Park ,California (1972), pp. 492—628; b) R. Gompper and H. -U. Wagner, *Angew. Chem. Int. Ed. Engl.*, **15**, 321 (1976); c) T. -L. Ho, "Hard and Soft Acids and Bases Principle in Organic Chemistry," Academic Press, New York, N. Y. (1977), pp. 26—54; d) M. Ono, *Yuki Gosei Kagaku Kyokai Shi*, **38**, 836 (1980).

5) Two routes are possible for the formation of **6**—**8**, direct *S*-alkylation and one involving alkyl group rearrangement of initially formed *O*-alkylated product *via* six membered transition state. The latter process seems unlikely since alkylation proceeds under mild neutral conditions.

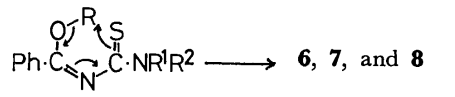

6, **7**, and **8**

6) H. Vorbrüggen and P. Strehlke, *Chem. Ber.*, **106**, 3039 (1973).

7) 1-Methyl-2-methylthio-4(1*H*)-pyrimidinone exhibits UV_{max}(MeOH) 231 nm.[6] Thus the alkylated product which absorbs light at 238 nm was assigned to be **12**.

The Direct Alkylamination of α-Substituted Anthraquinones Promoted by Metal Ions

Masaru MATSUOKA,* Toshio TAKEI, Isao NAKAMURA,
Katsuhira YOSHIDA,† and Teijiro KITAO

Department of Applied Chemistry, College of Engineering, University of Osaka Prefecture, Sakai, Osaka 591
† *Department of Chemistry, Faculty of Science, Kochi University, Akebono-cho, Kochi 780*

(Received December 4, 1980)

Synopsis. The reaction of 1-amino-4-acylaminoanthraquinones with piperidine in the presence of $CoCl_2$ and atmospheric oxygen gave the 2-aminated products in 75—80%, and similar reaction of 1-hydroxyanthraquinone or 1-aminoanthraquinone-2-sulfonic acid with butylamine gave the corresponding 4-aminated products, respectively. The effects of the α-substituents and the role of metal salts were discussed.

In our previous papers,[1-3] the new metal-promoted direct aminations of anthraquinone nucleus were reported. These are useful methods to prepare some aminoanthraquinone (aminoAQ) derivatives as dyes and dye intermediates.

In this paper, these metal-promoted direct aminations were applied to each of 1,4-diaminoAQs, 1-aminoAQ-2-sulfonic acid, and 1-hydroxyAQ which are the important intermediates for the preparation of some anthraquinonoid dyes.

The results of the reaction of 1,4-diaminoAQs with piperidine are shown in Scheme 1 and Table 1. The reaction of **1a** with piperidine resulted only in recovery of **1a** (Run 1). While, 1-amino-4-acylaminoAQs (**1b** and **1c**) gave the corresponding 2-aminated product (Runs 2 and 3). In the case of **1b**, hydrolysis of the 4-acetylamino group of **2b** was observed during the reaction, forming **2a** in 49.5%. The amination site of **1b** and **1c** were determined by ^{1}H-NMR spectra; the proton at 3(or 2)-position of **2a** was found at 6.40 ppm, while those of **2b** and **2c** were shifted downfield to 8.60, 8.66 ppm respectively, because of the deshielding effect of the neighboring 4-acylamino group. 1,4-Bis(benzoylamino)AQ (**1d**) did not react with piperidine, and **1d** was recovered in 93.6% (Run 4). These results imply that the mechanism of the 2-amination of **1** is the same as our previous case of 1-aminoAQ;[1] activation of 2-position by the formation of cobalt complex and reduction by 4-acylation in deactivating ability of 4-amino group play a cooperative roll for formation of 2-aminated products. Diacylation (**1d**) results in losing the ability of the complex formation and the amination does not take place.

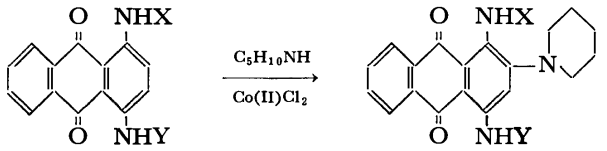

1 **a**: X=Y=H **b**: X=H, Y=$COCH_3$ **c**: X=H, Y=COC_6H_5 **d**: X=Y=COC_6H_5 **2**

Scheme 1.

TABLE 1. THE REACTION OF **1** WITH PIPERIDINE[a]

Run	Reactant	Time/h	**1**(Recovered)	Products (yield/%)
1	**1a**	50	94.0	None
2	**1b**	24	Trace	**2a** (49.5), **2b** (31.5)
3	**1c**	15	5.5	**2c** (74.5)
4	**1d**	50	93.6	None

a) Reactant (**1**, 2.92 mmol) was stirred with piperidine (50 ml) in the presence of $CoCl_2$ (2.92 mmol for **1b**—**1c**, 5.84 mmol for **1a**) at 30 °C.

The reaction of 1-aminoAQ-2-sulfonic acid (**3**) with butylamine gave the 4-aminated product (**4**), which is a very important compound as dye intermediate. In industry, **4** is produced by two-step method;[4] the bromination of **3** followed by the Ullmann amination of **6** (Path B in Scheme 2). Thus, the direct 4-amination of **3** affords a useful method for preparation of **4** (Scheme 2). The results are summarized in Table 2. Without $CoCl_2$, the amination did not take place at all (Runs 5 and 9). In the presence of $CoCl_2$, **3** gave rise to **4** in 23% yield together with 43% recovery of **3** (Run 6). The increase in molar ratio of $CoCl_2$ rather depressed the yield of **4** and a trace amount of **5** was formed along with **4** (Run 8). The yield of **4** could not be improved at higher temperature (Run 7).

The reaction of **7** with butylamine mainly afforded three products as shown in Scheme 3. The results are summarized in Table 3. The reaction hardly proceeded at room temperature (Run 15) and was carried out at 80 °C. Without metal salts, the reaction scarcely proceeded (Run 11), but an addition of $CoCl_2$ gave **9** in 23% and **10** in 2.4% yield together with 4-butylated product (**8**) in 48% yield (Run 12). A novel butylation of **7** at 4-position forming **8** was observed, but the mechanism was not obvious. The reaction did not proceed smoothly without solvent (Run 13). In the presence of $CuCl_2$, the reduction of copper ion to metal copper occured quantitatively, and a small amount of **8** (11%) and **10** (3%) were yielded (Run 14). From these results, it was concluded that the 4-amination of **7** hardly proceeds because of the

TABLE 2. THE REACTION OF **3** WITH BUTYLAMINE[a]

Run	$CoCl_2$/**3**	Solvent	**3**(Recovered)	Yield/% **4**
5	0	Pyridine	100	0
6	1	Pyridine	43	23
7[b]	1	Pyridine	7	27
8	2	Pyridine	33	11
9	0	1-Butanol	100	0
10	1	1-Butanol	Trace	41

a Reactant **3**(5.0 mmol) and butylamine(20 ml) were stirred with or without $CoCl_2$ at 30 °C for 24 h. b) Reaction was carried out at 80 °C for 24 h. A number of the unidentified by-products were obtained in a low yields.

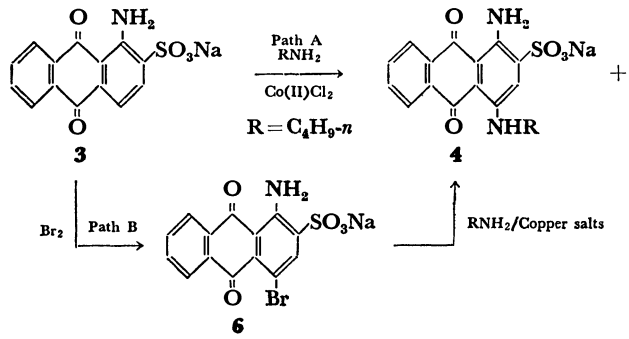

Scheme 2.

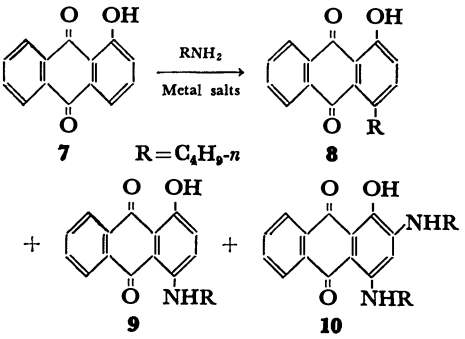

Scheme 3.

Table 3. The reaction of **7** with butylamine[a)]

Run	Metal salts	7(Recovered)	Yield/%			
			8	9	10	Cu°
11[b)]	None	Trace	3.8	0	0	—
12	$CoCl_2$	0	48.0	23.1	2.4	—
13[c)]	$CoCl_2$	53.0	32.0	8.5	0	—
14[b)]	$CuCl_2$	0	11.0	0	2.9	91
15[d)]	$CuCl_2$	58.9	Trace	2.9	0	—

a) Reactant (**7**, 5.0 mmol) was stirred with butylamine (22.5 ml) in 1-butanol(7.5 ml) in the presence of metal salts(5.0 mmol) at 80 °C for 5 h. b) A number of unidentified by-products were mainly obtained. c) Reaction was carried out without 1-butanol. d) Reaction was carried at 30 °C for 24 h.

formation of undesired product (**8**).

Experimental

Melting points are uncorrected. The spectra were measured on the instrumentals reported previously.[1-3)] Column chromatography were carried out on the activated alumina (Sumitomo KCG-30) or silica gel (Wacogel C-300).

*Reaction of **1** with Piperidine. General Procedures*: A mixture of **1c** (1.0 g, 2.92 mmol), $CoCl_2$ (1.37 g, 2.92 mmol), piperidine (50 ml) was stirred in a open flask at 30 °C. After the reaction, the solution was poured into water, and then H_2S gas was passed into the mixture. The precipitate was filtered, washed with water, dried, and extracted with chloroform. The extract was concentrated and chromatographed on alumina using benzene as an eluent.

*1,4-Diamino-2-piperidinoanthraquinone (**2a**)*: Mp 183.5—184 °C (xylene); lit,[5)] 185.5—186 °C. λ_{max} (benzene) (ε): 574 (8260), 538 (10100). Found: C, 71.16; H, 5.90; N, 12.84%. Calcd for $C_{19}H_{19}N_3O_2$: C, 71.01; H, 5.96; N, 13.07%. ^{1}H-NMR ($CDCl_3$) δ 1.70 (6H, m), 2.87 (4H, m), 6.40 (1H, s), 7.14 (2H, broad), 7.58 (2H, m), 7.60 (2H, broad), 8.25 (2H, m).

*1-Amino-2-piperidino-4-acetylaminoanthraquinone (**2b**)*: Mp 186—186.5 °C (xylene). λ_{max} (benzene) 568 (10600), 534 (13100). Found: C, 70.03; H, 5.75; N, 11.10%. Calcd for $C_{21}H_{21}N_3O_3$: C, 69.41; H, 5.82; N, 11.56%. ^{1}H-NMR ($CDCl_3$) δ 1.68 (6H, m), 1.80 (3H, s), 2.95 (4H, m), 7.64 (4H, m), 8.13 (2H, m), 8.60 (1H, s), 12.68 (1H, broad).

*1-Amino-2-piperidino-4-benzoylaminoanthraquinone (**2c**)*: Mp 195—195.5 °C (benzene). λ_{max} (benzene) 574 (10900), 538 (13200). Found: C, 73.00; H, 5.39; N, 9.51%. Calcd for $C_{26}H_{23}N_3O_3$: C, 73.40; H, 5.45; N, 9.88%. ^{1}H-NMR ($CDCl_3$) δ 1.70 (6H, m), 3.00 (4H, m), 7.55 (7H, m), 8.12 (4H, m), 8.66 (1H, s), 13.72 (1H, broad).

*Reaction of **3** with Butylamine. General Procedures*: A mixture of **3** (1.72 g, 5.0 mmol), $CoCl_2$ (0.65 g, 5.0 mmol), butylamine (20 ml) and pyridine (15 ml) or 1-butanol (15 ml) was stirred in a open flask at room temperature for 24 h. After the reaction, the mixture was poured into aqueous 30% HCl solution. The precipitate was filtered, washed with small amount of water, dried, and chromatographed on silica gel using benzene–acetone (5:5) as an eluent to give **4**. Small amount of **4** was also obtained from the filtrate by salting-out with NaCl. The recovery of **3** was determined by means of spectroscopy. The structure of **4** and **5** were determined by comparison with authentic samples.

*Reaction of **7** with Butylamine.* A mixture of **7** (5.0 mmol), metal salts (5.0 mmol), butylamine (22.5 ml) and 1-butanol (7.5 ml) was stirred under reflux for 5 h in a flask equipped with a reflux condenser. After the reaction, the mixture was poured into aqueous 10% HCl solution. The precipitate was filtered, washed with water, dried and chromatographed on silica gel using benzene as an eluent to give the products in the order of **8**, **9** and **10**, respectively.

*1-Hydroxy-4-butylanthraquinone (**8**)*: Mp 119.5—120 °C (benzene). λ_{max} (benzene) 435[s] (5120), 415 (6410), 395[s] (5480). Found: C, 77.16; H, 5.79%. Calcd for $C_{18}H_{16}O_3$: C, 77.12; H, 5.75%. ^{1}H-NMR ($CDCl_3$) δ 0.95—1.60 (7H, m), 2.73 (2H, t), 7.73 (4H, m), 8.25 (2H, m), 12.92 (1H, s). MS, *m/e* (rel intensity) 280 (M^+, 100), 251 (27), 238 (64), 237 (64).

*1-Hydroxy-4-butylaminoanthraquinone (**9**)*: Mp 122—123 °C (benzene). λ_{max} (benzene) 602 (10000), 561 (10600), 522[s] (6250). Found: C, 73.22; H, 5.82; N, 4.49%. Calcd for $C_{18}H_{17}NO_3$: C, 73.20; H, 5.80; N, 4.74%. ^{1}H-NMR ($CDCl_3$) δ 1.00 (3H, m), 1.62 (4H, m), 3.35 (2H, q), 7.15 (2H, s), 7.70 (2H, m), 8.30 (2H, m), 10.18 (1H, broad), 13.65 (1H, s). MS, *m/e* (rel intensity) 295 (M^+, 9), 294 (29), 251 (100), 223 (27).

*1-Hydroxy-2,4-bis(butylamino)anthraquinone (**10**)*: Mp 129—129.5 °C (hexane). λ_{max} (benzene) 598 (10100), 558 (10300), 518[s] (5900). Found: C, 71.45; H, 6.91; N, 7.34%. Calcd for $C_{22}H_{26}N_2O_3$: C, 72.11; H, 7.15; N, 7.64%. ^{1}H-NMR ($CDCl_3$) δ 0.69—2.20 (14H, m), 3.20 (4H, m), 5.30 (1H, broad), 5.77 (1H, s), 7.55 (2H, m), 8.14 (2H, m), 10.75 (1H, broad), 15.00 (1H, s). MS, *m/e* (rel intensity) 366 (M^+, 74), 323 (100), 262 (89).

References

1) K. Yoshida, M. Matsuoka, Y. Yamashita, and T. Kitao, *Chem. Lett.*, **1978**, 1317; *Bull. Chem. Soc. Jpn.*, **53**, 2552 (1980).

2) K. Yoshida, M. Matsuoka, Y. Yamashita, S. Nagamori, and T. Kitao, *Bull. Chem. Soc. Jpn.*, **53**, 3725 (1980).

3) M. Matsuoka, Y. Makino, K. Yoshida, and T. Kitao, *Chem. Lett.*, **1979**, 219; *Dyes and Pigments*, **1**, 27 (1980).

4) K. Venkataraman, "The Chemistry of Synthetic Dyes," Academic Press Inc., New York (1952), p. 840.

5) S. A. Russkikh. V. V. Loskutov, and V. V. Russkikh, *J. Gen. Chem. USSR.*, **44**, 162 (1974).

A Novel Synthesis of Phenyl Carboxylates

Shizunobu HASHIMOTO and Isao FURUKAWA*

Department of Applied Chemistry, Doshisha University, Karasuma-imadegawa, Kamigyo-ku, Kyoto 602

(Received December 12, 1980)

Synopsis. The direct synthesis of phenyl carboxylates from phenols and carboxylic acids is reported. The reactions proceeded easily when triphenylphosphine and carbon tetrachloride were used as dehydrating agents in the presence of a tertiary amine at room temperature, thus giving esters in high yields.

It has been known that the direct synthesis of phenyl carboxylates from carboxylic acids and phenols usually fails in the presence of common mineral acids. Therefore, the reaction has been carried out by using a special catalyst such as polyphosphoric acid,[1] a combination of boric acid and sulfuric acid,[2] and polymer-protected aluminium chloride[3] under heating. However, these methods can not be applied to the esters, which are unstable to heat and acid.

We have now investigated the direct acylation of phenols with acids under mild conditions, and have found that the reaction proceeds easily to form phenyl carboxylates when a combination of triphenylphosphine and carbon tetrachloride is used as the dehydrating agent in the presence of triethylamine. The results are shown in Table 1.

Although the reaction proceeded easily at room temperature to give esters in high yields, phenol and acid having a nitro group afforded the esters in a poorer yield because of the simultaneous formation of a colored matter from the phosphine and nitro compound.

Ester formation by the use of triphenylphosphine and carbon tetrachloride was investigated by Appel[4] for the esterification of an alcohol with a carboxylic acid. In this case, a high yield is obtained only when alcohol is added as the last component after reacting phosphine, carboxylic acid, and carbon tetrachloride in the presence of tertiary amine, when the alcohol and acid are added simultaneously into a mixture of phosphine, carbon tetrachloride and tertiary amine, the yield of the ester decreases because of the simultaneous formation of both alkyl halide and ester. On the other hand, the acylations of phenols with carboxylic acids in our work gave only esters in high yields, even when all reactants were reacted simultaneously. This difference may be attributed to the fact that phenol attacks selectively only the carbonyl carbon in the acyloxyphosphonium salt [II] assumed as an intermediate, while alcohol attacks both the phosphorus and the carbonyl carbon.[4]

From these results, we concluded that the esterification of phenols with carboxylic acids in the presence of a tertiary amine, when triphenylphosphine and carbon tetrachloride are used as dehydrating agents, proceeds through the process shown in the following scheme:

$$Ph_3P + CCl_4 \longrightarrow Ph_3\overset{+}{P}CCl_3 \cdot Cl^- \quad [I]$$

TABLE 1. PHENYL CARBOXYLATES

$RCOOC_6H_4X$ R:	X:	Yield %	Mp/°C (Torr)	Analysis IR $\tilde{\nu}$(C=O) cm^{-1}	IR $\tilde{\nu}$(C-O) cm^{-1}	MS(*m/e*) M+
CH_3	H	97	82—83(10)	1770	1230	136
$CH_3CH_2CH_2$	H	90	107(8)	1770	1205	164
C_6H_5	H	91	70—71	1725	1265	198
p-ClC_6H_4	H	85	100.5—101.5	1735	1280	232
p-$CH_3C_6H_4$	H	92	70.5—72.5	1735	1275	212
p-$CH_3OC_6H_4$	H	87	67.5—69	1730	1275	228
p-$NO_2C_6H_4$	H	34	107.5—111	1755	1280	243
$C_6H_5CH{=}CH$	H	86	74—75.5	1730	1205	224
C_6H_5	*p*-Cl	89	84—86	1745	1285	232
C_6H_5	*m*-Cl	92	69.5—70.5	1740	1260	232
C_6H_5	*p*-Br	72	104—106	1740	1260	276
C_6H_5	*p*-CH_3	78	70—71	1725	1275	212
C_6H_5	*m*-CH_3	89	51.5—53.5	1740	1270	212
C_6H_5	*p*-CH_3O	85	84—86	1735	1275	228
C_6H_5	*p*-NO_2	13	140—142	1750	1230	243
CH_3	*p*-Br	87	122—125(11)	1770	1230	214
$CH_3CH_2CH_2$	*p*-Br	66	144—149(11)	1770	1205	242
p-ClC_6H_4	*p*-Br	70	100—104	1750	1270	310
o-ClC_6H_4	*p*-Br	85	72—75.5	1760	1245	310
p-$CH_3C_6H_4$	*p*-Br	81	94—98	1740	1270	290
p-$CH_3OC_6H_4$	*p*-Br	62	103—104.5	1730	1270	306
$C_6H_5CH{=}CH$	*p*-Br	79	113—115	1750	1215	302

$$[I] + RCOOH \longrightarrow Ph_3\overset{+}{P}\text{-}O\text{-}COR\cdot Cl^- + CHCl_3$$
$$[II]$$

$$Ph_3\overset{+}{P}\text{-}O\text{-}COR\cdot Cl^- \xrightarrow[+R_3'N]{} Ph_3P{=}O + RCOOAr + R_3'N\cdot HCl$$
$$\uparrow$$
$$ArO\ddot{H}$$

Experimental

All the melting and boiling points are uncorrected. All the chemicals used were of an analytical reagent grade. Thin-layer chromatography (TLC) was performed on Merck's silica gel 60 (70—230 mesh). The IR spectra were recorded in KBr on a Shimazu IR-27C spectrometer, and the MS, on a Hitachi RM-50GC spectrometer with 60 eV.

Procedure. A mixture of benzoic acid (24 mmol), phenol (20 mmol), carbon tetrachloride (24 mmol), triethylamine (24 mmol), and triphenylphosphine (24 mmol) in 30 ml of acetonitrile was stirred at room temperature for 4 h. After the acetonitrile has been evaporated, hexane was added to the residue. The hexane solution was filtered off to remove the triphenylphosphine oxide and triethylamine hydrochloride precipitated, washed with an aqueous sodium hydroxide solution, and dried over anhydrous sodium sulfate, and then the hexane was removed. Subsequent distillation or recrystallization of the residual solid gave 3.6 g of phenyl benzoate (91% yield) as white crystals: mp 70—71 °C. A similar procedure has been applied successfully to a variety of substituted phenols, aliphatic, and aromatic carboxylic acids. The resulting products were identified by means of infrared and mass spectral analysis.

References

1) A. R. Bader and A. D. Kontowicz, *J. Am. Chem. Soc.*, **75**, 5416 (1953).
2) W. W. Lowrance, Jr., *Tetrahedron Lett.*, **1972**, 3453.
3) E. C. Blossey, L. M. Turner, and D. C. Neckers, *Tetrahedron Lett.*, **1973**, 1823.
4) R. Appel, *Angew. Chem.*, **87**, 863 (1975).

A Novel Preparation of Bicyclo[3.2.2]nonanes and Bicyclo[4.2.2]decanes Substituted at the Bridgeheads

Yasuo SAKAI,* Kaoru TERASHIMA, Yoshito TOBE, and Yoshinobu ODAIRA

Department of Petroleum Chemistry, Faculty of Engineering, Osaka University, Suita, Osaka 565

(Received December 23, 1980)

Synopsis. A novel preparation of 1,5-disubstituted bicyclo[3.2.2]nonanes and 1,6-disubstituted bicyclo[4.2.2]-decanes based on the one-pot reaction of [3.2.2]- and [4.2.2]-propellanecarboxylic acids with 2 equiv. of lead tetraacetate, followed by catalytic hydrogenation, is described.

The bicyclo[n.2.2]alkanes, having substituents on each bridgehead carbon atom, are of importance as models for examining through–bond and/or through–space orbital interactions and as a key intermediate for the synthesis of paddlanes.[1] Syntheses of the 1,4-disubstituted bicyclo[2.2.2]octanes (**1**) have been described.[2] However, only a few methods have been worked out for the higher homologues, bicyclo[3.2.2]-nonanes and bicyclo[4.2.2]decanes substituted at the bridgeheads.[2a,3] We have found that the oxidative decarboxylation of [4.2.2]propellanecarboxylic acid (**5**) with lead tetraacetate (Pb(IV)) gives rise to the formation of the cyclopropylcarbinyl type tricyclic acetate (**7**) in high efficiency.[4] Since the oxidation of highly strained bicyclo[*n*.1.0]alkanes with Pb(IV) proceeds with exclusive internal bond cleavage of cyclopropane ring,[5] it may be reasonable to expect the formation of 1,6-disubstituted bicyclo[4.2.2]decane derivatives such as **9** by the reaction of **7** with Pb(IV). In this connection, we wish to report a novel preparation of 1,5-disubstituted bicyclo[3.2.2]nonanes (**2a**, **b**) and 1,6-disubstituted bicyclo[4.2.2]decanes (**3a**, **b**) based on

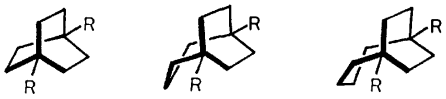

1 **2a** R=OAc, **2b** R=OH **3a** R=OAc, **3b** R=OH

the one-pot reaction of [3.2.2]- and [4.2.2]propellanecarboxylic acids (**4**) and (**5**) with Pb(IV), comprising two successive oxidations by Pb(IV), *i.e.*, oxidative decarboxylation of **4** and **5**, affording the strained tricyclic acetates (**6**) and (**7**), and subsequent oxidative cleavage of internal cyclopropane bond of **6** and **7** leading to the unsaturated diacetates (**8**) and (**9**), followed by catalytic hydrogenation (Scheme 1).

The reaction of **7** with Pb(IV) was examined. When **7** was treated with 1.2 equiv. of Pb(IV) in benzene at 80 °C for 14 h, the bridgehead diacetate (**9**) was obtained as a major product in 76% yield along with 6-acetoxybicyclo[4.2.2]dec-1(8)-ene (**10**)[6] (17%).[7] The structure of **9** was elucidated by the presence of a two-proton singlet at δ 5.83 ppm in the ^{1}H NMR spectrum and the ^{13}C NMR spectrum which showed only seven signals involving a two-carbon doublet at δ 131.56 ppm in the off-resonance decoupled spectrum. No detectable amounts of the triacetates from internal bond cleavage and/or the external bond cleavage products were formed.

The direct preparation of **9** from [4.2.2]propellanecarboxylic acid (**5**) by an one-pot procedure involving two successive Pb(IV) oxidations was attempted. When the reaction of **5** with 2.5 equiv. of Pb(IV) in benzene was carried out at 80 °C for 20 h, the expected product (**9**) was obtained in 58% yield together with **10** in 13% yield.

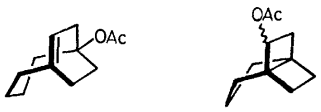

10 **11**

In order to prepare 1,5-disubstituted bicyclo[3.2.2]-nonanes, the reaction of [3.2.2]propellanecarboxylic acid (**4**) with 1.2 equiv. of Pb(IV) was examined. After 1 h, the bridgehead diacetate (**8**) was obtained as a major product in 47% yield along with the unrearranged 6-acetoxy[3.2.2]propellane (**11**) in 11% yield, while the tricyclic acetate (**6**) could not be detected even in a shorter reaction time. Similarly, the structure of **8** was determined by the ^{1}H NMR (a two-proton singlet at δ 6.04 ppm) and ^{13}C NMR spectra (seven signals involving a two-carbon doublet at δ 132.54 ppm in the off-resonance spectrum). In view of the fact that a considerable amount (30%) of the unreacted acid (**4**) was recovered, it can be assumed that **8** was formed by rapid oxidation of unstable intermediate (**6**) by Pb(IV) as in the case of **7**.

The catalytic hydrogenation of **8** and **9** over Pd/C gave **2a**, mp 72—73 °C, and **3a**,[6] mp 100—102 °C, respectively, in quantitative yields. The reductive cleavage of the diacetates (**2a**) and (**3a**) by lithium

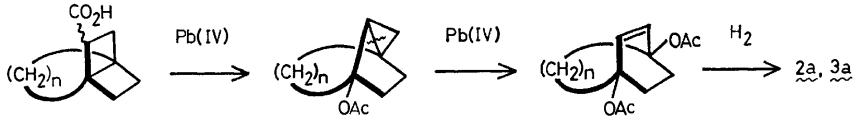

n=3 **4** **6** **8**
n=4 **5** **7** **9**

Scheme 1.

aluminum hydride afforded the corresponding diols (**2b**), mp 139—140 °C, and (**3b**), mp 158—160 °C, in moderate yields.

Experimental

Reaction of the Acetate (7) with Pb(IV). A mixture of 91 mg (0.47 mmol) of **7**,[4] 25 mg (0.32 mmol) of pyridine, and 250 mg (0.56 mmol) of lead tetraacetate in 5 ml of benzene was heated at 80 °C with stirring under nitrogen for 14 h. After filtration, the filtrate was washed with 1 mol dm^{-3} hydrochloric acid, sodium hydrogencarbonate solution, and water, and then dried over anhydrous sodium sulfate (Na_2SO_4). Evaporation of the solvent gave 109 mg of light brown oil. The products were analyzed by GLC (10% FFAP and 5% SE-30 columns) and separated by silica-gel column chromatography.

9 (76%); IR 3030, 1715, 1225, 1040, 1000 cm^{-1}; MS *m/e* 252 (M^+); ^1H NMR (CCl_4) δ 1.10—2.60 (m, 18H, s at 1.92), 5.83 (s, 2H); ^{13}C NMR ($CDCl_3$) δ 22.31 (q), 23.24 (t), 29.84 (t), 40.41 (t), 81.36 (s), 131.56 (d), 170.16 (s). Found: C, 66.54; H, 7.99%. Calcd for $C_{14}H_{20}O_4$: C, 66.64; H, 7.99%.

Reaction of [4.2.2]Propellanecarboxylic Acid (5) with Pb(IV). A mixture of 504 mg (2.6 mmol) of **5**,[4] 119 mg (1.5 mmol) of pyridine, and 2.88 g (6.5 mmol) of Pb(IV) in 40 ml of benzene was heated at 80 °C for 20 h. 606 mg of light brown oil was obtained by a similar work-up to that described above. The products were analyzed and separated as above.

Reaction of [3.2.2]Propellanecarboxylic Acid (4) with Pb(IV). A mixture of 2.40 g (14 mmol) of **4**,[3] 670 mg (8.5 mmol) of pyridine, and 8.36 g (17 mmol) of Pb(IV) in 120 ml of benzene was heated at 80 °C for 1 h. The same work-up as above gave 1.89 g of a product mixture, 860 mg (30%) of unreacted **4** being recovered by acidification of the sodium hydrogencarbonate washings followed by ether extraction. The products were analyzed and separated as above.

8 (47%); IR 3030, 1715, 1230, 1190, 1010 cm^{-1}; MS *m/e* 238 (M^+); ^1H NMR (CCl_4) δ 1.60—2.35 (m, 16H, s at 1.91), 6.04 (s, 2H); ^{13}C NMR ($CDCl_3$) δ 20.80 (t), 22.08 (q), 28.87 (t), 34.25 (t), 80.82 (s), 132.54 (d), 169.95 (s). Found: C, 65.50; H, 7.63%. Calcd for $C_{13}H_{18}O_4$: C, 65.53; H, 7.61%.

11 (11%; a mixture of epimers); IR 1725, 1220, 1020 cm^{-1}; MS *m/e* 180 (M^+); ^1H NMR (C_6D_6) δ 1.28—2.64 (m, 15H), 4.80 (t, 0.5H), 5.20 (t, 0.5H). Found: C, 73.03; H, 9.09%. Calcd for $C_{11}H_{16}O_2$; C, 73.30; H, 8.95%.

Catalytic Hydrogenation of 8 and 9. **8** and **9** were hydrogenated under atmospheric pressure of hydrogen over 5% Pd/C catalyst in methanol solvent to give **2a** and **3a**,[6] respectively, in quantitative yields. Pure samples of **2a** and **3a** were obtained by recrystallization from hexane–ether.

2a; mp 72—73 °C; IR 1715, 1235, 1200, 1000, 970 cm^{-1}; MS *m/e* 180 (M^+—AcOH); ^1H NMR (CCl_4) δ 1.60—2.40 (m, s at 1.92); ^{13}C NMR ($CDCl_3$) δ 20.02 (t), 22.35 (q), 30.65 (t), 38.54 (t), 82.51 (s), 170.04 (s). Found: C, 64.88; H, 8.52%. Calcd for $C_{13}H_{20}O_4$: C, 64.98; H, 8.39%.

3a; mp 100—102 °C; IR 1715, 1230 cm^{-1}; MS *m/e* 252 (M^+—2), 134 (M^+—2AcOH); ^1H NMR (CCl_4) δ 1.20—2.60 (m, s at 1.88); ^{13}C NMR ($CDCl_3$) δ 22.02 (q), 22.90 (t), 30.97 (t), 38.70 (t), 83.56 (s), 169.33 (s). Found: C, 65.76; H, 8.71%. Calcd for $C_{14}H_{22}O_4$: C, 66.11; H, 8.72%.

Lithium Aluminum Hydride Reduction of 2a and 3a. To a suspension of 1.5 equiv. of lithium aluminum hydride in ether was added dropwise a solution of **2a** or **3a** in the same solvent, the mixture being stirred at room temperature for 2 h. Water and then 1 mol dm^{-3} hydrochloric acid were added carefully. The organic layer was separated and washed with saturated sodium chloride solution and dried over Na_2SO_4. The aqueous layer was extracted with chloroform, the chloroform extracts being washed with saturated sodium chloride solution and dried (Na_2SO_4). Evaporation of both solvents gave **2b** and **3b** as white solids in 60—65% yields which were recrystallized from ether.

2b; mp 139—140 °C; IR 3250, 1030 cm^{-1}; MS *m/e* 156 (M^+); ^1H NMR ($CDCl_3$) δ 1.50—2.20 (m). Found: C, 69.11; H, 10.36%. Calcd for $C_9H_{16}O_2$: C, 69.19; H, 10.32%.

3b; mp 158—160 °C; IR 3250, 1060, 980 cm^{-1}; MS *m/e* 170 (M^+); ^1H NMR ($CDCl_3$) δ 1.40—2.20 (m). Found: C, 70.34; H, 10.71%. Calcd for $C_{10}H_{18}O_2$: C, 70.54; H, 10.66%.

References

1) P. v. R. Schleyer and C. W. Woodworth, *J. Am. Chem. Soc.*, **90**, 6528 (1968); C. A. Grob and R. Rich, *Tetrahedron Lett.*, **1978**, 663; G. A. Olah, G. Liang, P. v. R. Schleyer, E. M. Engler, M. J. S. Dewar, and R. C. Bingham, *J. Am. Chem. Soc.*, **95**, 6829 (1973); H. E. Zimmerman and R. D. McKelvey, *ibid.*, **93**, 3638 (1971); H. E. Zimmerman, T. D. Goldman, T. K. Hirzel, and S. P. Schmidt, *J. Org. Chem.*, **45**, 3933 (1980); E. H. Hahn, H. Bohm, and D. Ginsburg, *Tetrahedron Lett.*, **1973**, 507.

2) a) P. C. Guha, *Ber.*, **72**, 1359 (1939); b) J. D. Roberts, W. T. Moreland, Jr., and W. Frazer, *J. Am. Chem. Soc.*, **75**, 637 (1953); c) J. C. Kauer, French Patent 1345138 (1963); *Chem. Abstr.*, **62**, 14529e (1965); d) H. D. Holtz and L. M. Stock, *J. Am. Chem. Soc.*, **86**, 5183 (1964); e) J. C. Kauer, R. E. Benson, and G. W. Parshall, *J. Org. Chem.*, **30**, 1431 (1965).

3) P. E. Eaton and K. Nyi, *J. Am. Chem. Soc.*, **93**, 2786 (1971).

4) Y. Sakai, S. Toyotani, Y. Tobe, and Y. Odaira, *Tetrahedron Lett.*, **1979**, 3855; Y. Sakai, S. Toyotani, M. Ohtani, M. Matsumoto, Y. Tobe, and Y. Odaira, *Bull. Chem. Soc. Jpn.*, **54**, 1474 (1981).

5) R. Criegee and A. Rimmelin, *Chem. Ber.*, **90**, 414 (1957); R. J. Quellette, A. South, Jr., and D. L. Shaw, *J. Am. Chem. Soc.*, **87**, 2602 (1965); T. Katsushima, R. Yamaguchi, S. Iemura, and M. Kawanishi, *Bull. Chem. Soc. Jpn.*, **53**, 3318 (1980).

6) Y. Sakai, Y. Tobe, and Y. Odaira, *Chem. Lett.*, **1980**, 691.

7) The by-product **10** may be formed by the action of acetic acid generated during the course of reaction.[6]

Studies on Biologically Active Pteridines. VI.[1] Biopterin Conjugated to β-D-Galactosidase and Bovine Serum Albumine

Sadao MATSUURA,* Takashi SUGIMOTO, and Toshiharu NAGATSU†

Department of Chemistry, College of General Education, Nagoya University, Chikusa-ku, Nagoya 464

† *Laboratory of Cell Physiology, Department of Life Chemistry, Graduate School at Nagatsuta, Tokyo Institute of Technology, Midori-ku, Yokohama 227*

(Received January 16, 1981)

Synopsis. 4-Hydroxy-6-(L-*erythro*-1,2-dihydroxypropyl)-2-(methylthio)pteridine was converted by ethylenediamine to 2-(2-aminoethylamino)analogue of biopterin, which condensed with *N*-hydroxysuccimidyloxy *m*-maleimidobenzoate to give the maleimidobenzamide. The latter compound and β-D-galactosidase afforded a biopterin-galactosidase conjugate which showed the enzyme activity about 40% as compared to the unmodified enzyme.

The biosynthesis of neurotransmitting dopamine and serotonine from phenylalanine and tryptophan requires tetrahydrobiopterin cofactor at the oxygenation step of these amino acids. Therefore, a decrease of biopterin concentration in those tissues generating the neurotransmitting amines may cause neurological disorders. Several examples to support such assumption have been found recently: atypical hyperphenylalaninemia due to deficiency of biopterin[2] and anormalous low biopterin concentrations in human brain from parkinonian patients.[3] Consequently, assay of biopterin in tissue or serum becomes essential for basic and clinical studies of such diseases.

We have recently developed a radioimmunoassay for biopterin, which makes a merit of high specificity, sensitivity, and reproducibility.[4] The method, however, suffers from a disadvantage of using a radioactive antigen. In order to avoid this inherent drawback of radioimmunoassay, we aimed to develop an enzymeimmunoassay for biopterin by using a conjugate of biopterin to β-D-galactosidase as a labelled antigen. This paper describes a synthesis of biopterin conjugated to the galactosidase and to bovine serum albumine (BSA), of which the latter is to be used as an immunogenic antigen.

Previously we synthesized a biopterin-BSA conjugate by a mixed anhydride method, in which 6-(biopterinylamino)caproic acid was condensed to the free amino group of the protein *via* an anhydride and the condensation product was treated with 2 M sodium hydroxide at the final step of preparation.[4] This anhydride method is inapplicable to the present required biopterin-galactosidase conjugate, because alkaline treatment may inactivate the enzyme. Accordingly we sought for a different conjugation method and applied *N*-hydroxysuccimidyloxy *m*-maleimidobenzoate (MBS)[5] to conjugating biopterin to the mercapto groups of galactosidase and BSA. The enzyme contains a number of mercapto groups unconcerned with the enzyme activity and hence the conjugation of biopterin at such sites will not reduce the enzyme activity.

4-Hydroxy-6-(L-erythro-1,2-dihydroxypropyl)-2-(methylthio)pteridine (**1**)[6] underwent aminolysis on heating with ethylenediamine to give the 2-(2-aminoethylamino) analogue (**2**), which was then converted to the *m*-maleimidobenzoyl derivative (**3**) by MBS. Conjugation of **3** with BSA was achieved by incubating BSA with a large excess **3** in a pH 7 phosphate buffer at 25 °C for 1.5 h, and the product was purified by chromatography on Sepharose 6B (Fig. 1). The number of moles of biopterin per mole of BSA was estimated 0.66 from the UV and fluorescence spectra. Conjugation of **3** to β-galactosidase was carried out

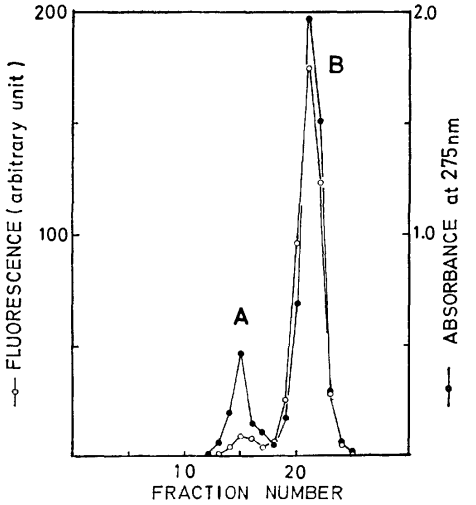

Fig. 1. Purification of biopterin-BSA conjugate on a Sepharose 6B column (1.8×30 cm) eluted by 0.05 M phosphate buffer, pH 7.0. The volume of each fraction was 5 ml. The intensity of fluorescence at 440 nm was measured by exciting at 360 nm. A: Conjugate, B: excess **3**.

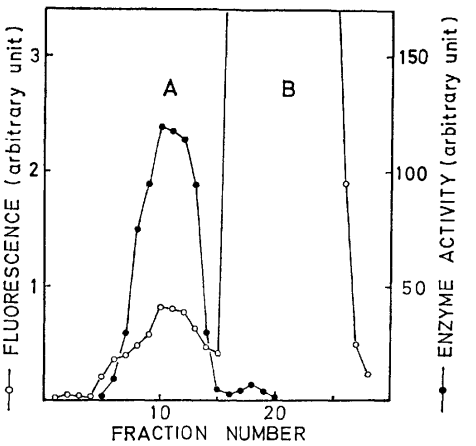

Fig. 2. Purification of biopterin-galactosidase conjugate on Sepharose 6B carried out in the same way as in Fig. 1. The enzyme activity was assayed as described in text.

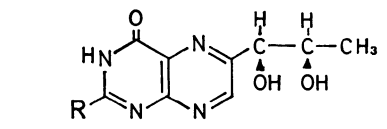

R

1 -S CH3

2 -NH CH2CH2NH2

3 -NH CH2CH2NH CO

4 -NH CH2CH2NH CO S-BSA

5 -NH CH2CH2NH CO S-βGAL

in the same way as above. The chromatography on Sepharose 6B was monitored by fluorescence spectra and by enzyme activity using 4-methylumbelliferyl β-D-galactoside as substrate.[7] As shown in Fig. 2, the enzymically active fractions show fluorescence due to the biopterin moiety, indicating a sucessful conjugation of **3** to galactosidase. The conjugate retained the enzyme activity about 40% as compared to the unmodified enzyme.

An enzymeimmunoassay for biopterin by employing the present synthesized conjugates is under progress and the detail will be reported elsewhere.

Experimental

*2-(2-Aminoethylamino)-4-hydroxy-6-(*L-erythro-*1,2-dihydroxypropyl)pteridine (2).* A solution of **1**[6] (500 mg) in ethylenediamine (5 ml) was heated at 110 °C under nitrogen for 4 h. The solution was fractionated on a Florisil column (2.5×30 cm), eluted gradiently with 0—3% ammonia (1.0 l), and then on a Dowex 50 W×8 column (2.5×20 cm), eluted with 0—3% ammonia. The eluate was evaporated to give a jellied residue, which on standing in a refrigerator for several days crystallized into a pale yellow needles (220 mg) of **2**. The compound darkened at 245 °C; pK_a at −1.0, 0.75, and 8.0 (measured by a spectroscopical method); λ_{max} (log ε) at H_o −3.0: 260 (4.08), 280 (sh., 3.99), 323 (3.65), and 392 (3.74); at H_o −0.25: 255 (4.11), 280 (3.96), 321 (3.75), and 392 (3.68); at pH 5.0: 261 (4.40), 350 (3.82); at pH 10.0: 240 (4.09), 277 (4.27), and 365 (3.88).

N-[*2-[4-Hydroxy-6-(*L-erythro-*1,2-dihydroxypropyl)-2-pteridinyl]-aminoethyl*]-m-*maleimidobenzamide (3).* To a solution of **2** (100 mg) in *N,N*-dimethylformamide (10 ml), MBS[5] (120 mg) was added and the solution was stirred at 25 °C for 2.5 h. The solution was then participated with water (40 ml) and dichloromethane (3×40 ml). The aqueous solution was evaporated *in vacuo* to almost dryness. Addition of tetrahydrofuran (1 ml) and chilling gave a solid (80 mg) of **3** which was used for the next reaction without further purification.

Preparation of Biopterin-BSA Conjugate (4). A solution of **3** (1 mg) in 0.5 ml of 0.1 M phsphate buffer, pH 7.0, was added to a solution of BSA (10 mg) in the same buffer (1 ml). The mixture was stirred at 25 °C for 1.5 h and then fractionated on a Sepharose 6B column (1.8×30 cm), eluted by a 0.05 M phosphate buffer, pH 7.0. The eluate was monitored by the fluorescence spectra and UV absorbance at 275 nm.

Preparation of Biopterin-galactosidase Conjugate (5). A solution of **3** (1 mg) in a 0.1 M phosphate buffer (pH 7.0, 0.5 ml) was added to a solution of β-D-galactosidase from E. Coli [EC 3.2.1.23] (1 mg) in the same buffer (1 ml), and the mixture was stirred at 25 °C for 2 h. Fractionation of the reaction products on a Sepharose 6B column (1.8×30 cm) using a 0.05 M phosphate buffer (pH 7.0) as solvent gave a chromatogram shown in Fig. 2. The enzyme activity was assayed as below.

Assay of β-D-Galactosidase Activity. A mixture of 4-methylumbelliferyl β-D-galactoside (1 mg/30 ml of 0.01 M phosphate buffer, pH 7.0; 50 μl) and 100 μl of each fraction diluted 50-fold by a 0.01 M phosphate buffer (pH 7.0) containing 0.1% BSA was incubated at 37 °C for 10 m. A 0.1 M glycine buffer (pH 10.3; 3 ml) was added to the mixture and the intensity of the fluorescence at 440 nm (excited at 360 nm) was measured on a Hitachi MPF-2A fluorescence spectrometer.

We thank Mrs. N. Nishioka for measuring the fluorescence spectra.

References

1) Part V. T. Sugimoto and S. Matsuura, *Bull. Chem. Soc. Jpn.*, **53**, 3385 (1980).

2) S. Kaufman, S. Berlow, G. K. Summer, S. Milstien, J. D. Schulman, S. Orloff, S. Spielberg, and S. Pueschel, *New Engl. J. Med.*, **299**, 673 (1978).

3) T. Nagatsu, T. Yamaguchi, T. Kato, T. Sugimoto, S. Matsuura, M. Akino, I. Nagatsu, R. Iizuka, and H. Narabayashi, *Clin. Chim. Acta*, **109**, 305 (1981).

4) T. Nagatsu, T. Yamaguchi, T. Kato, T. Sugimoto, S. Matsuura, M. Akino, S. Tsushima, N. Nakagawa, and H. Ogawa, *Proc. Jpn. Acad.*, **55**, **Ser. B**, 317 (1979).

5) T. Kitagawa and T. Aikawa, *J. Biochem. (Tokyo)*, **79**, 233 (1976).

6) T. Sugimoto, S. Matsuura, and T. Nagatsu, *Bull. Chem. Soc. Jpn.*, **53**, 2344 (1980).

7) K. Kato, Y. Yamaguchi, H. Fukui, and E. Ishikawa, *J. Biochem. (Tokyo)*, **78**, 235 (1975).

A Cationic [3,4] Sigmatropic Rearrangement[1)]

Mugio NISHIZAWA† and Ryoji NOYORI*
Department of Chemistry, Nagoya University, Chikusa-ku, Nagoya 464
(Received February 3, 1981)

Synopsis. The first example of the cationic [3,4] sigmatropic reaction has been achieved by the reaction of 1,3-dibromo-3-methyl-6-hepten-2-one and diiron nonacarbonyl.

There is currently much interest in electrocyclic reactions which involve carbocations.[2)] In 1971, Dewar has predicted that the [3,4]sigmatropic rearrangement, **1a**⇄**1b**, may take place *via* cyclic six-electron transition state.[3)] However, realization of such symmetry-allowed transformation has not yet been reported to date, at least to our knowledge. Here we report the first example of this type of cationic rearrangement.

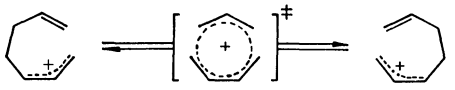

1a 1b

When the dibromo ketone **2** was treated with diiron nonacarbonyl in refluxing benzene, the dienone **3** was obtained as the sole isolable product, identical with authentic sample prepared independently. The reductive skeletal change is interpreted in terms of the title pericyclic process *via* the oxyallyl-Fe(II) intermediate **4** (R=H).[4)] The high stability of the resulting carboxonium ion **5** would facilitate the forward reaction. It should be noted that reaction course of the oxyallyl **4** is highly dependent on the substitution pattern of the internal olefinic bond. When the double bond is substituted by carbocation-stabilizing methyl groups, the cationic species **4** (R=CH_3) undergoes the stepwise, double cyclization to give (±)-camphor, **4**→**6**→**7**.[5,6)]

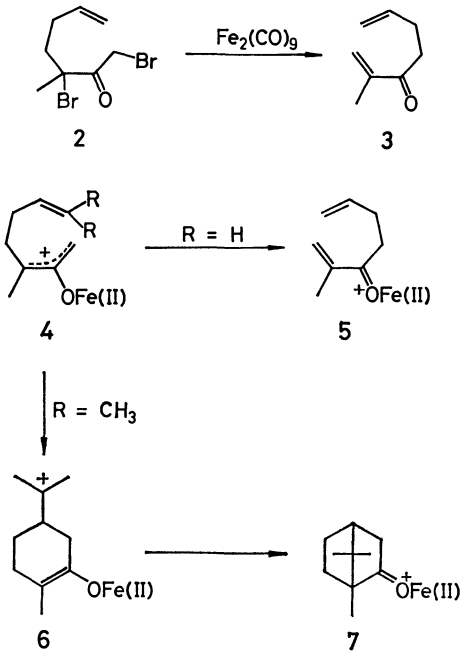

2 3 4 5 6 7

Experimental

2-Methyl-1,6-heptadien-3-one (3). A mixture of the dibromo ketone **2**[7)] (905 mg, 3.18 mmol) and diiron nonacarbonyl (2.13 g, 6.36 mmol) in dry benzene (12 ml) was heated at reflux for 2 h under argon atmosphere. The cooled mixture was filtered through a cotton-celite pad and the filtrate was concentrated under reduced pressure to give crude product (370 mg). The NMR and GLC analysis elucidated that this material contained **3** (80% GLC yield) and some unidentified minor products. An analytical sample (148 mg, 32%) was obtained by the preparative GLC (3% OV-1, 0.64×100 cm column, 100 °C). IR (neat) 3060 (=CH), 1680 (C=C), 1640 (C=C, enone), 1630 (C=C), 910 cm^{-1} (=CH). ^1H NMR (CCl_4) δ 1.85 (d, J=1.5 Hz, CH_3), 2.36 (t, J=7 Hz, =CHC$\underline{H}_2$), 2.70 (t, J=7 Hz, CH_2C=O), 4.94 (d, J=10 Hz, C$\underline{H}_2$=CHCH_2, a proton trans to CH_2), 4.98 (d, J=20 Hz, C$\underline{H}_2$=CHCH_2, a proton cis to CH_2), 5.70 (br s, C$\underline{H}_2$=CCH_3, a proton cis to CH_3), 5.80 (m, C$\underline{H}$=CH_2), 5.90 (s, C$\underline{H}_2$=CCH_3, a proton trans to CH_3). Found: *m/e* 124.08892. Calcd for $C_8H_{12}O$: (M^+), 124.08881.

2-Methyl-1,6-heptadien-3-ol (8). To a solution of 3-butenylmagnesium bromide prepared from 1-bromo-3-butene (1.5 g, 11.1 mmol) and magnesium (365 mg, 15 g-atom) in anhydrous ether (20 ml) was dropwise added a solution of methacrylaldehyde (770 mg, 11.1 mmol) in anhydrous ether (4 ml) over a period of 10 min at 0 °C. After stirring for 1 h at this temperature, aqueous saturated ammonium chloride (10 ml) was added, and the aqueous phase was extracted with ether. The combined organic materials was dried and concentrated. The resulting oil was subjected to column chromatography on silica gel using pentane–ether (8:1) as an eluent. The pure product was obtained as a colorless oil (1.21 g, 87%) after bulb-to-bulb distillation (110—118 °C, 15 mmHg). IR (neat) 3400 (OH), 3080 (=CH), 1640 (C=C), 910 cm^{-1} (=CH). NMR (CCl_4) δ 1.23 (s, OH), 1.76 (s, CH_3), 4.02 (t, H$\underline{C}$OH), 4.7—5.1 (m, 4H, =CH_2), 5.75 (m, C$\underline{H}$=CH_2). Found: C, 76.46; H, 11.27%. Calcd for $C_8H_{14}O$: C, 76.14; H, 11.18%.

Oxidation of 8. A suspension of the hydroxy compound **8** (150 mg, 1.19 mmol) and activated manganese dioxide (400 mg, 4.6 mmol) in pentane (3 ml) was stirred for 72 h at room temperature, and the resulting mixture was filtered through glass paper. The concentrated filtrate was subjected to column chromatography on silica gel using pentane–ether (50:1 and then 5:1) as an eluent to give 18 mg (12%, conversion yield 36%) of **3** and 101 mg (68%) of starting material **8**. The IR and NMR were identical with those of the product obtained from **2** and $Fe_2(CO)_9$.

References

1) Carbon-Carbon Bond Formation Promoted by Transition Metal Carbonyls. 30. Part 29: Ref. 5; Part 28: Ref. 6.
2) Review: T. S. Sorensen and A. Rank, "Pericyclic Reactions," ed by A. P. Marchand and R. E. Lehr, Academic Press, New York (1977), Vol. II, Chap 1.
3) M. J. S. Dewar, *Angew. Chem., Int. Ed. Engl.*, **10**, 761 (1971).

† Present address: Department of Chemistry, Osaka City University, Sumiyoshi-ku, Osaka 558.

4) R. Noyori, *Acc. Chem. Res.*, **12**, 61 (1979).
5) R. Noyori, M. Nishizawa, F. Shimizu, Y. Hayakawa, K. Maruoka, S. Hashimoto, H. Yamamoto, and H. Nozaki, *J. Am. Chem. Soc.*, **101**, 220 (1979).
6) Attempted reaction of the dibromo ketones i—iii with $Fe_2(CO)_9$ gave neither cyclization nor rearrangement products.

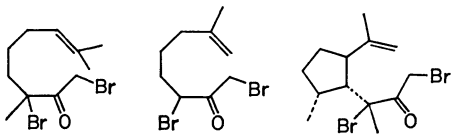

i ii iii

7) The dibromo ketone **2** was prepared from 4-methyl-6-acetoxy-4-hexenal.[5,8]
8) G. Stork, M. Gregson, and P. A. Grieco, *Tetrahedron Lett.*, **1969**, 1391.

Synthesis of Hypacrone

Fujio SAKAN,* Yukio MINAMI, Haruhisa SHIRAHAMA,† and Takeshi MATSUMOTO†

Department of Education, Fukui University, Fukui 910

† *Department of Chemistry, Faculty of Science, Hokkaido University, Sapporo 060*

(Received October 3, 1980)

Synopsis. Hypacrone, an illudoid sesquiterpene, was synthesized from 2,2-dimethyl-4-(3,3-ethano-4,4-ethylenedioxy-1-methylsulfinyl-2-oxopentyl)-1-cyclopentanone which is a key intermediate also in the synthesis of illudins.

Reports were given on the total synthesis of illudins (**1**)[1] employing a sulfoxide **2**[2] as the key intermediate. In this report, we wish to describe the synthesis of another illudoid[3] sesquiterpene, hypacrone (**3**),[4] with use of **2**.

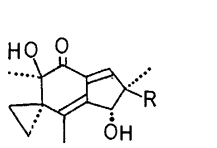

(1) illudin M R=CH_3
illudin S R=CH_2OH

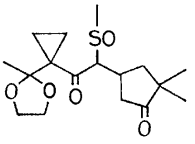

(2)

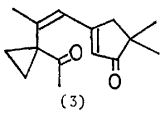

(3)

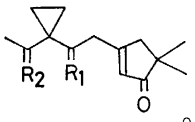

(4) R_1= O, R_2= 

(5) R_1=  , R_2=

(6) R_1=  , R_2= O

Elimination of sulfenic acid was carried out by boiling sulfoxide **2** in toluene for 5 h, diketone **4** being obtained in quantitative yield. Methylation of easily enolizable diketone **4**[5] by means of methyllithium gave **5** which upon deacetalization with a catalytic amount of *p*-toluenesulfonic acid in acetone gave diketone **6**. The spectral data of **6** (IR and NMR) are identical with those of an authentic sample.[4b] The total synthesis of hypacrone (**3**) through **6** was already reported by Nishizawa *et al.*[4b]

Experimental

IR spectra were recorded with a Hitachi EPI-G3 spectrometer. NMR spectra were obtained at 100 MHz on a JEOL JNM-4H-100 instrument using TMS as an internal standard, mass spectra on a JEOL JMS-01SG-2 mass spectrometer.

Diketone ***4***. Sulfoxide **2**(200 mg) was boiled in toluene for 5 h. The resulting reaction mixture was washed with $NaHCO_3$ and then with a NaCl solution, and dried over Na_2SO_4. Removal of the solvent gave a practically pure product **4**(160 mg) which on chromatography on silica gel gave pure **4**(140 mg, 86%) as a slightly yellow oil: IR (neat) 3070, 1700, 1615 and 1045 cm^{-1}; NMR $\delta(CDCl_3)$ 1.10 (6H s and 4H, m), 1.15 (3H, s), 2.50 (2H, bs), 3.73 (2H, bs), 3.95 (4H, m), and 5.95 (1H, bs); MS (*m/e*) 278 (M^+); Anal. Found: C, 69.35; H, 7.82, Calcd for $C_{16}H_{22}O_4$: C, 69.04; H, 7.94%.

Enone ***5***. To a solution of **4**(180 mg) in dry ether (10 ml) was added a 0.8 M ether solution of MeLi (1.2 ml)[6] at −40 to −30 °C under nitrogen atmosphere. After stirring for 2 h the reaction was quenched with a NH_4Cl solution, extraction being carried out with $CHCl_3$. The extracts were washed with a NaCl solution, dried, and evaporated. The crude material was purified by chromatography on silica gel (AcOEt–benzene) affording unchanged **4** (120 mg, 70%) and methylated product **5** (20 mg, 10%) as a colorless oil: IR(neat) 3450, 1695, 1610, and 1045 cm^{-1}; NMR $\delta(CDCl_3)$ 1.07 (4H, m), 1.10 (6H, s), 1.25 (3H, s), 1.47 (3H, s), 2.52 (2H, bs), 2.75 (2H, bs), 3.95 (4H, bs), and 5.96 (1H, bs); MS(*m/e*) 276 (M^+-H_2O); Anal. Found: C, 69.25; H, 8.72, Calcd for $C_{17}H_{26}O_4$: C, 69.36; H, 8.90%.

Diketone ***6***. A solution of acetal **5** (15 mg) and *p*-TsOH (1 mg) in acetone (2 ml) was refluxed for 2 h and quenched with solid $NaHCO_3$. After filtration, the solution was evaporated. Purification of the crude material was carried out by preparative TLC (silica gel, $CHCl_3$–ether) to give the known diketone **6** as a colorless oil: MS(*m/e*) 250 (M^+).[4b]

Thanks are due to Prof. Yuji Hayashi, Osaka City University, for supplying the authentic sample of **6**.

References

1) T. Matsumoto, H. Shirahama, A. Ichihara, H. Shin, S. Kagawa, F. Sakan, S. Matsumoto, and S. Nishida, *J. Am. Chem. Soc.*, **90**, 3280 (1968); T. Matsumoto, H. Shirahama, A. Ichihara, H. Shin, S. Kagawa, F. Sakan, and K. Miyano, *Tetrahedron Lett.*, **1971**, 2049 and references cited therein.

2) T. Matsumoto, H. Shirahama, A. Ichihara, H. Shin, S. Kagawa, T. Hisamitsu, T. Kamada, and F. Sakan, *Bull. Chem. Soc. Jpn.*, **45**, 1140 (1972).

3) Y. Ohfune, H. Shirahama, and T. Matsumoto, *Tetrahedron Lett.*, **1975**, 4377.

4) a) Y. Hayashi, M. Nishizawa, and T. Sakan, *Chem. Lett.*, **1973**, 63; *Tetrahedron*, **33**, 2509 (1977); b) M. Nishizawa, Y. Hayashi, and T. Sakan, *Chem. Lett.*, **1975**, 387; *Tetrahedron*, **33**, 2513 (1977).

5) This vinylogous 1,3-diketone was soluble in aqueous alkaline solution, giving methane on treatment with MeMgI.

6) Using a larger amount of MeLi did not improve the yield.

  Bull. Chem. Soc. Jpn., 54, 2237—2242 (1981)

Studies on the Complex Formation between *o*-Quinones and Metal Chlorides in Nitromethane Solution

Kazuaki KATAOKA,* Sumihisa KIMURA, Fumiko SHIRAKAWA, and Yoshio SASAKI

Faculty of Pharmaceutical Sciences, Osaka University, Yamadakami 133-1, Suita, Osaka 565

(Received June 21, 1980)

Complex formation between several kinds of metal chlorides and 4,5-dimethoxy-1,2-benzoquinone (**1**) or 4-methoxy-1,2-naphthoquinone (**2**) has been studied by means of NMR and spectrophotometry in CH_3NO_2. Stability constants of the 1 : 1 complex were found to decrease in the order of $SnCl_4 > InCl_3 > ZnCl_2 > BiCl_3 > SbCl_3 > HgCl_2$. $\Delta\delta_{ML}$ and $\Delta\nu_{max}$, which indicate the change in the chemical shift and the wavenumber on the formation of the 1 : 1 complex, were also arranged in the above order. The same order was reproduced from an electrostatic potential. Both $\Delta\delta_{ML}$ and $\Delta\nu_{max}$ were proved to be a convenient scale for the relative acceptor strength of metal chlorides. For the basicity of *o*-quinones, the order of **1**>**2** was obtained from the thermodynamic data and from the negative charge on the carbonyl oxygens. The solute-solvent interaction model was also found appliciable in this system.

o-Quinones have been reported to form intensively colored complexes with various kinds of metal chlorides.[1,2] An extensive study of these complexes was first carried out by Crowley and Haendler.[2] However, few reports have been published on the study of these complexes in solution, since they are liable to decompose in aqueous and/or polar solvents. Some *o*-quinones having ether type oxygen, such as cryptotanshinone (**3**), were observed to form complexes with $FeCl_3$ in nonaqueous media, and they are more stable than the similar complexes of 1,2-naphthoquinone or 9,10-phenanthraquinone.[3] In the previous work,[4] the complex formation between **3** and some metal chlorides in CH_3CN was examined by spectrophotometry, and the shift of wavenumber $\Delta\nu_{max}$ of the ligand absorption band due to complex formation was correlated to the stability constant K_c. In that work, however, a partial disagreement was observed between the order of $\Delta\nu_{max}$ and that of K_c; this was interpreted by the solvation effect of CH_3CN. In this work, CH_3NO_2 is chosen as a solvent, because it has a modest solubility for the metal chloride and a smaller donor strength than CH_3CN (*e.g.*, the donor numbers of CH_3CN and CH_3NO_2 are 14.1 and 2.7, respectively[5]). 4,5-Dimethoxy-1,2-benzoquinone (**1**) and 4-methoxy-1,2-naphthoquinone (**2**) are used as ligands. ^1H NMR signals of 3,6-H in **1** and 3-H in **2** and absorption bands between 400 and 600 nm are examined in detail.

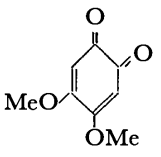

1

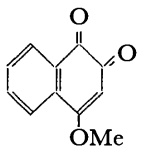

2

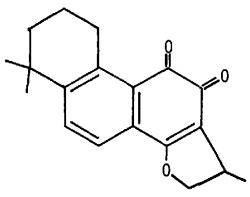

3

Experimental

Materials. **1** and **2** were prepared by the methods of Wanzlik[6] and Fieser,[7] respectively. 1,2,6,7,8,9-Hexahydro-1,6,6-trimethylphenanthro[1,2*b*]furan-10,11-dione (**3**) was isolated from the Chinese drug "Tan-shen" by Takiura.[8] Commercially available metal chlorides ($SnCl_4$, $InCl_3$, $SbCl_3$, $BiCl_3$, $ZnCl_2$, and $HgCl_2$) were purified by sublimation or distillation under reduced pressure. Commercially available CH_3NO_2 was purified by distillation after drying over $CaCl_2$, and the remaining water was removed by azeotropic distillation. Residual water in the rectified solvent was checked by the measurement of the degree of dissociation of **3**-$FeCl_3$ complex, which is liable to be decomposed by water,[3] and the data were found to be reproducible.

Preparation of Samples. In order to determine the stoichiometry by the continuous variation method, both solutions of ligand and metal chloride were prepared at the same concentration, and mixed in various ratios. For the determination of K_c, the solutions containing a fixed overall concentration of the ligand and a varying amount of the metal chloride were prepared: In the case of NMR, the concentrations of **1** and **2** were held constant at *ca.* 0.01 and 0.02 M (1 M=1 mol dm^{-3}), respectively, and the maximum concentration of the metal chloride was kept in the range of *ca.* 0.02 ($InCl_3$) to 0.13 M ($HgCl_2$). In the spectrophotometry, the concentrations of **1** and **2** were held constant at *ca.* 2.5×10^{-3} and 0.7×10^{-3} M, respectively, and the maximum concentration of the metal chloride was kept in the range of *ca.* 0.001 ($SnCl_4$) to 0.13 M ($HgCl_2$). The sample solutions were prepared by weight, and their final concentrations were calculated by taking the density of the solutions as equal to that of the pure solvent. These solutions were sealed in the NMR sample tubes or in the stoppered cells. All procedures described above were carried out in a dry box under N_2 atmosphere.

Measurements. Visible absorption spectra were measured on a Shimadzu UV-200 spectrophotometer at 34 °C. The change of absorbance due to complex formation was significant between 460 and 500 nm, and measurements were made at several wavelengths in this range. Proton NMR spectra were measured on a Hitachi R-22 spectrometer (90 MHz) at 34 °C. Chemical shifts of 3,6-H of **1** and 3-H of **2** were determined by a frequency counter within an error of ±0.1 Hz, relative to an internal reference TMS. Signals due to methoxyl groups were masked by the solvent peak. Variable temperature experiments of spectrophotometry were carried

out by using a Tajiri Kikai ECW-108 electronic cooling circulator in the range of 10 to 55 °C. Molar conductances of millimolar solutions of the metal chlorides in CH_3NO_2 were measured at room temperature on a Kyoto Denshi CM-07 conductivity meter. Λ/Ω^{-1} mol^{-1} cm^2: $HgCl_2$; 0, $ZnCl_2$; 1.7, $SbCl_3$; 2.6, $BiCl_3$; 2.4, $InCl_3$; 33.7, and $SnCl_4$; 21.8. The values of molar conductance of their complexes, which were prepared by adding an excess amount of the ligand to the solutions of the metal chlorides, were essentially unchanged from the above values.

Results and Discussion

Complex Formation between o-Quinones and Metal Chlorides in CH_3NO_2. Change of Spectra: **1** and **2** changed color from yellow to vermilion or red violet on addition of metal chloride in CH_3NO_2, suggesting formation of a complex. In the visible region, the absorption maxima of **1** and **2** due to the quinonoid π-π^* transition were observed at 407 and 400 nm, respectively. A typical example of the spectral change of **1** and **2** with metal chloride is shown in Fig. 1. The presence of isosbestic points in all systems except **2**+$InCl_3$ and **2**+$SnCl_4$ suggests the presence of only one kind of complex. It was found that the spectral change of **2** differed from

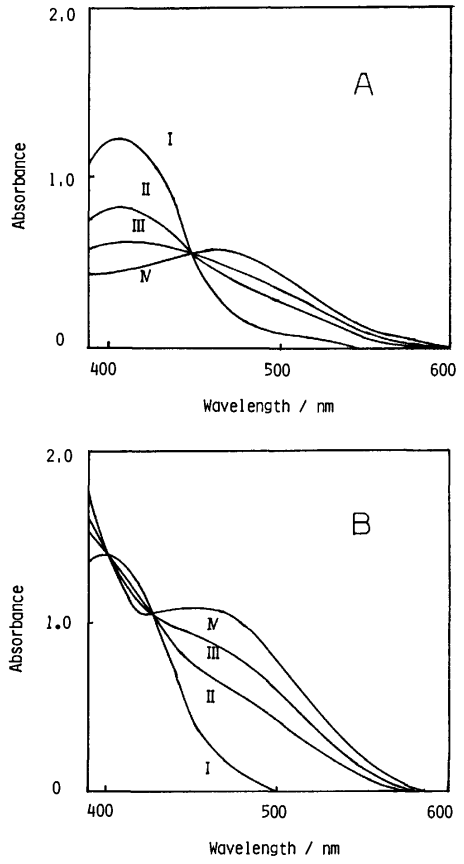

Fig. 1a. Spectral change of *o*-quinones with $ZnCl_2$ in CH_3NO_2. A: Concn of 4,5-dimethoxy-1,2-benzoquinone is maintained at 2.0×10^{-3} M, and concn of $ZnCl_2$ is varied as follows, I; 0, II; 2.0×10^{-3}, III; 3.8×10^{-3}, and IV; 1.0×10^{-2} M. B: Concn of 4-methoxy-1,2-naphthoquinone is maintained at 7.2×10^{-4} M, and concn of $ZnCl_2$ is varied as follows, I; 0, II; 3.6×10^{-3}, III; 5.9×10^{-3}, and IV; 1.0×10^{-2} M.

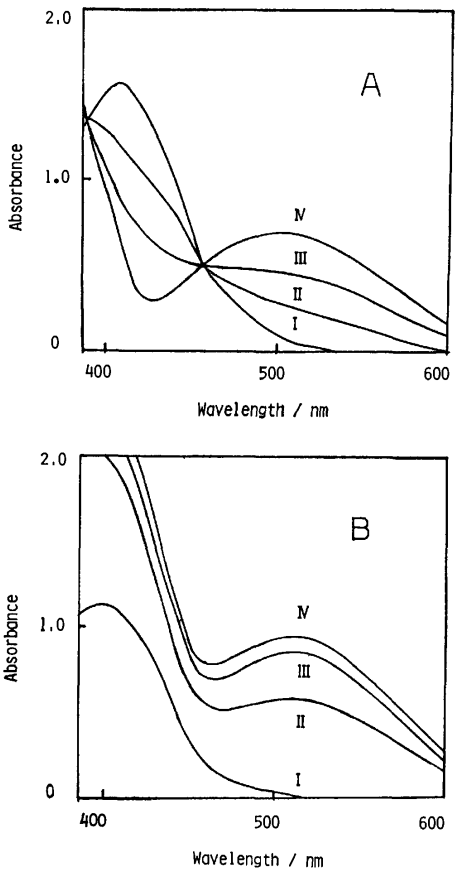

Fig. 1b. Spectral change of *o*-quinones with $SnCl_4$ in CH_3NO_2. A: Concn of 4,5-dimethoxy-1,2-benzoquinone is maintained at 2.6×10^{-3} M, and concn of $SnCl_4$ is varied as follows, I; 0, II; 6.4×10^{-4}, III; 1.8×10^{-3}, and IV=3.0×10^{-3} M. B: Concn of 4-methoxy-1,2-naphthoquinone is maintained at 5.7×10^{-4} M, and concn of $SnCl_4$ is varied as follows, I=0, II; 3.7×10^{-4}, III; 7.2×10^{-4}, and IV; 1.0×10^{-3} M.

that of **1** (*cf.* Fig. 1b). Existence of the absorption band in the neighborhood of 400 nm for the complex of **2** with $SnCl_4$ may be due to the red shift of the benzenoid π-π^* transition of **2**, since the latter transition is absent in **1**.[9]

In the ^{1}H NMR spectra, chemical shifts of 3,6-H of **1** and 3-H of **2** were observed at 5.76 and 5.99 ppm, respectively. When metal chloride was added to the solution of the *o*-quinone, the signal of the *o*-quinones was displaced to the downfield site, since the signals of free and complexed species were averaged; the downfield shift means an electron withdrawal by the metal chloride.

The metal chlorides in nonaqueous media are usually treated as nonelectrolytes, arguing from the conductance data.[10] In the present work also, the molar conductance of the metal chloride measured in CH_3NO_2 suggests the lack of dissociation. The relatively large values of the molar conductance found in the cases of $InCl_3$ and $SbCl_4$ are attributed to the hydrolysis of the metal chloride by the residual water in CH_3NO_2. When the ligand was added to the solution of metal chloride, the value of molar conductance remains essentially constant. In this experiment, a large excess amount of the

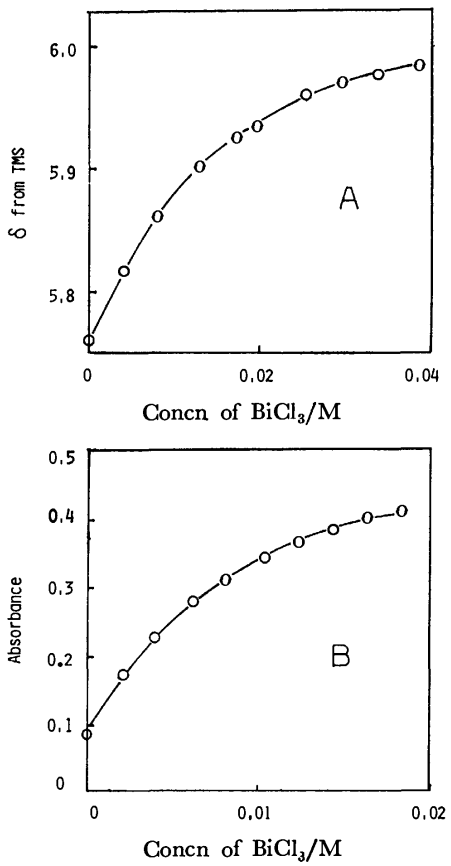

Fig. 2. Concentration dependence of the observed chemical shifts and absorbances. A: NMR method; ○: experimental point, —— : calculated curve with K_c=98.1 M^{-1}, δ_{ML}=6.057 ppm, δ_L=5.760 ppm, and concn of ligand=8.30×10^{-3} M. B: Spectrophotometric method; ○: experimental point, ——: calculated curve with K_c=115 M^{-1}, ε_{ML}=369, ε_L=77 and concn of ligand=1.56×10^{-3} M.

ligand was added, in the case of the metal chloride, giving a small value of K_c. From these results, the metal chloride and its complexes are treated as nonelectrolytes in this work.

Stability Constant and Complex Shift: The continuous variation method supported the formation of a 1 : 1 complex in all cases. To determine K_c, both absorbances and chemical shifts of solutions containing fixed amounts of ligand and varying amounts of metal chloride were measured. The results of the **1**+$BiCl_3$ system are shown in Fig. 2 as an example. The K_c values are calculated as follows. For an equilibrium of the formation of 1 : 1 complex, K_c is expressed as follows:

$$MX_n + L \overset{K_c}{\rightleftharpoons} MX_nL$$

$$K_c = [MX_nL]/[MX_n][L] = C_{ML}/(C_M^\circ - C_{ML})(C_L^\circ - C_{ML}), \quad (1)$$

where MX_n, L, and MX_nL mean metal chloride, ligand, and complex, C_{ML}, C_M° and C_L° are the equilibrium concentration of MX_nL, and the initial concentrations of MX_n and L, respectively. In an equilibrium state, Eqs. 2 and 2′ are appliciable:

$$A_{cal} = \varepsilon_{ML}C_{ML} + \varepsilon_L(C_L^\circ - C_{ML}), \quad (2)$$

$$\delta_{cal} = \delta_{ML}C_{ML}/C_L^\circ + \delta_L(C_L^\circ - C_{ML})/C_L^\circ, \quad (2')$$

where A_{cal}, ε_{ML}, and ε_L are the calculated absorbance and the molar absorption coefficients of MX_nL and L, and δ_{cal}, δ_{ML}, and δ_L are the calculated chemical shift and the chemical shifts of MX_nL and L, respectively. Equations 3 and 3′ are derived from Eqs. 1 and 2 or 2′.

$$A_{cal} = \varepsilon_L C_L^\circ + (\varepsilon_{ML}-\varepsilon_L)\{1+K_cC_M^\circ+K_cC_L^\circ - \sqrt{(1+K_cC_M^\circ+K_cC_L^\circ)^2-4K_c^2C_M^\circ C_L^\circ}\}/2K_c, \quad (3)$$

$$\delta_{cal} = \delta_L + (\delta_{ML}-\delta_L)\{1+K_cC_M^\circ+K_cC_L^\circ - \sqrt{(1+K_cC_M^\circ+K_cC_L^\circ)^2-4K_c^2C_M^\circ C_L^\circ}\}/2K_cC_L^\circ. \quad (3')$$

The root mean square deviations of the calculated and observed shifts were minimized by the curve fitting method. The results are listed in Table 1; the root mean square deviations of NMR and spectrophotometry were always<0.3 Hz and 0.003, respectively. In the case

Table 1. Stability constants and spectral data of complex formation between *o*-quinones and metal chlorides in CH_3NO_2 at 34 °C by NMR and spectrophotometry

L	MX_n	NMR		Spectrophotometry		
		log (K_c/M^{-1})	δ	log (K_c/M^{-1})	λ_{max}/nm	log ε_{max}
(1)	Free		5.76		407	2.78
	$SnCl_4$	Large	6.57	Large	503	2.45
	$InCl_3$	Large	6.39	Large	480	2.40
	$ZnCl_2$	2.62±0.06	6.35	2.61±0.06	471	2.49
	$BiCl_3$	1.99±0.01	6.06	2.06±0.01	455	2.67
	$SbCl_3$	0.68±0.05	6.04	0.96±0.09	460	2.75
	$HgCl_2$	0.63±0.03	6.00	0.64±0.02	440	2.63
(2)	Free		5.99		400	3.30
	$SnCl_4$	Large	6.76	4.75±0.03	509	3.23
	$InCl_3$	Large	6.71	4.28±0.10	485	3.26
	$ZnCl_2$	—	—	2.07±0.06	470	3.35
	$BiCl_3$	1.69±0.05	6.31	1.75±0.03	439	3.40
	$SbCl_3$	0.60±0.12	6.31	0.63±0.10	435	3.40
	$HgCl_2$	0.46±0.04	6.22	0.49±0.03	435	3.37

(1): 4,5-Dimethoxy-1,2-benzoquinone; (2): 4-methoxy-1,2-naphthoquinone.

of **2**+$ZnCl_2$, measurement of NMR spectra was unsuccessful, since the complex precipitated. The term "large" written in Table 1 means that the K_c value is too large to determine from the concentration dependence of the observed shift. However, approximate values of δ_{ML}, λ_{max}, and ε_{max} were obtained directly from the observed data, because the spectra were measured under the conditions where almost all ligands were transformed into the complex due to large K_c. In the case of smaller K_c, the visible absorption spectra were constructed as the sum of absorption bands of free and complexed species; accordingly, the ε_{ML} value at each wavelength of the spectra was calculated from Eq. 3, when C_M° and C_L° were known and the value of K_c was estimated. λ_{max} and ε_{max} of the complex were determined from the calculated spectra given by the calculated ε_{ML}.

The values of K_c determined by NMR and spectrophotometry were comparable with each other, as follows:

$$\log K_c(\text{NMR}) = 1.02 \log K_c(\text{spectrophotometry}) - 0.09 \quad (r=0.993). \quad (4)$$

The linear relation between $\Delta\delta_{ML}$ and $\Delta\nu_{max}$ is obvious as shown in Fig. 3. Furthermore, the other of the above parameters agree with those of K_c.

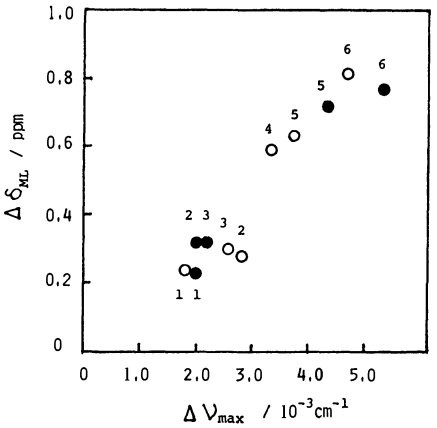

Fig. 3. Relationship between $\Delta\delta_{ML}$ and $\Delta\nu_{max}$.
○: 4,5-Dimethoxy-1,2-benzoquinone, ●: 4-methoxy-1,2-naphthoquinone, 1: $HgCl_2$, 2: $SbCl_3$, 3: $BiCl_3$, 4: $ZnCl_2$, 5: $InCl_3$, and 6: $SnCl_4$.

Electrostatic Model: The relative acceptor strengths of metal chloride toward *o*-quinones decrease in the order of $SnCl_4$>$InCl_3$>$ZnCl_2$>$BiCl_3$>$SbCl_3$>$HgCl_2$. Parameters of the metal ions are unable to explain the above order; this should be ascribed to the molecular (*i.e.*, non-ionic) property of the metal chloride. When the partial charge q on the metal atom of metal chloride was calculated by the method of Sanderson,[11] the electrostatic potential q/r (r means the distance between metal and chlorine) could be estimated. As shown in Fig. 4, the plots of log K_c against q/r are linear. This result suggests that the complex formation of this type is electrostatic in nature, and also supports the assumption that the metal chloride in CH_3NO_2 behaves as a nonelectrolyte.

Basicity of o-*Quinones*: In respect of the electronic

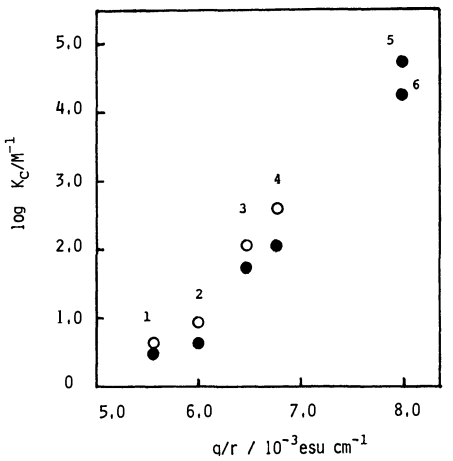

Fig. 4. Plots of log K_c against electrostatic potential (q/r) for metal chloride.
1: $HgCl_2$, 2: $SbCl_3$, 3:$BiCl_3$, 4: $ZnCl_2$, 5: $SnCl_4$, and 6: $InCl_3$.

structure of *o*-quinones, the negative charge on the carbonyl oxygen was reported to increase slightly in the order of 1,2-benzoquinone<1,2-naphthoquinone.[12] However, the values of K_c obtained in this work increased in the order of **2**<**1**. This disagreement is probably ascribable either to an inversion of the negative charge on the carbonyl oxygen or to an entropy effect due to the steric effect of aromatic moiety of **2**.

TABLE 2. π-ELECTRON CHARGE DENSITIES OF THE TWO CARBONYL OXYGEN ATOMS OF *o*-QUINONES CALCULATED BY HMO METHOD

o-Quinones	π-Electron density of oxygen atoms	
1,2-BQ	1.463	1.463
1,2-NQ	1.496	1.549
4-MeO-1,2-NQ	1.503	1.607
4,5-$(MeO)_2$-1,2-BQ	1.530	1.530
Cryptotanshinone	1.531	1.647

BQ: Benzoquinone; NQ: naphthoquinone.

In the first place, π-electron density of the carbonyl oxygen was calculated by the HMO method. As shown in Table 2, the contribution of the electron release from the methoxyl group is obvious, but an adequate elucidation of this disagreement is not given by this result alone.

TABLE 3. THERMODYNAMIC DATA OF COMPLEX FORMATION OF *o*-QUINONES WITH $BiCl_3$ AND $HgCl_2$ IN CH_3NO_2 (1 cal=4.184 J)

MX_n	Ligand	$-\Delta H^{a)}$ kcal/mol	$-\Delta S^{b)}$ e.u.
$HgCl_2$	4-MeO-1,2-NQ	1.8	3.4
	4,5-$(MeO)_2$-1,2-BQ	2.1	3.6
	Cryptotanshinone	2.8	4.9
$BiCl_3$	4-MeO-1,2-NQ	3.4	3.3
	4,5-$(MeO)_2$-1,2-BQ	4.2	4.1
	Cryptotanshinone	5.3	5.6

BQ: Benzoquinone; NQ: naphthoquinone. a) Error; ±10%. b) Error; ±20%.

Subsequently, thermodynamic data were determined from the temperature dependence of the K_c. These results are summarized in Table 3, where additional data for **3** are listed in order to test the steric contribution on the complex formation. The values of $-\Delta H$ in the complex formation of *o*-quinones with $BiCl_3$ or $HgCl_2$ increase in the same order as K_c. The values of ΔS are proportional to those of ΔH; this finding suggests that the steric contribution is not evident. Therefore, it is concluded that the contribution of the steric effect of aromatic moiety is negligible, and the number of the methoxyl groups influences the order of K_c.

Solute-Solvent Interaction Model. Formerly, the solute-solvent interaction model was established for the study of the weak association by NMR;[13] the solvent molecules play a much larger role in solution than the two solutes. A modified Benesi-Hildebrand type equation (*cf.* Eq. 5) derived from this model was introduced for the estimation of 1 : 1 bound chemical shift $\Delta\delta_{AD}$ and the free energy of the complex formation ΔG_{AD}.[13]

$$1/\Delta\delta_{obsd} = C_S/k\Delta\delta_{AD}\cdot 1/C_A^\circ x + 1/\Delta\delta_{AD}, \quad (5)$$

where C_S and C_A° are the molarity of solvent and the initial concentration of acceptor, respectively, k is the Boltzmann factor ($=\exp(-\Delta G_{AD}/RT)$), and x is C_A°/C_D° when $C_A^\circ<C_D^\circ$, which is approximated to 1.0 when $C_A^\circ>C_D^\circ$. Equation 5 was modified to Eq. 6 in order to use spectrophotometry:

$$1/\Delta\varepsilon_{obsd} = C_S/k\Delta\varepsilon_{AD}\cdot 1/C_A^\circ x + 1/\Delta\varepsilon_{AD}. \quad (6)$$

As both NMR and spectrophotometry are employed in this work, so proof of this model must be evaluated by the comparison of the results obtained from this model with those of the previous section. ΔG_{AD} and $\Delta\delta_{AD}$ or $\Delta\varepsilon_{AD}$ were estimated from the linear relations between $1/C_A^\circ x$ and $1/\Delta\delta_{obsd}$ or $1/\Delta\varepsilon_{obsd}$. For $\Delta\delta$ and $\Delta\varepsilon$, the linear relations illustrated in Figs. 5 and 6 were formulated by Eqs. 7 and 8:

$$\Delta\delta_{AD} = 0.95\cdot\Delta\delta_{ML} + 0.025 \quad (r=0.974), \quad (7)$$

$$\Delta\varepsilon_{AD} = 1.10\cdot\Delta\varepsilon_{ML} + 2.03 \quad (r=0.996). \quad (8)$$

The results of NMR and spectrophotometry for ΔG are expressed in Eqs. 9 and 10, respectively. These results

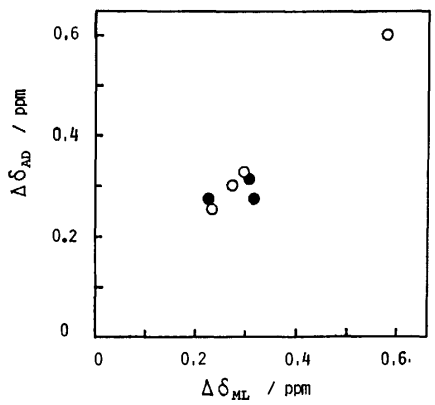

Fig. 5. Correlation between $\Delta\delta_{AD}$ and $\Delta\delta_{ML}$ in CH_3NO_2.
○: 4,5-Dimethoxy-1,2-benzoquinone+MX_c system,
●: 4-methoxy-1,2-naphthoquinone+MX_c system.

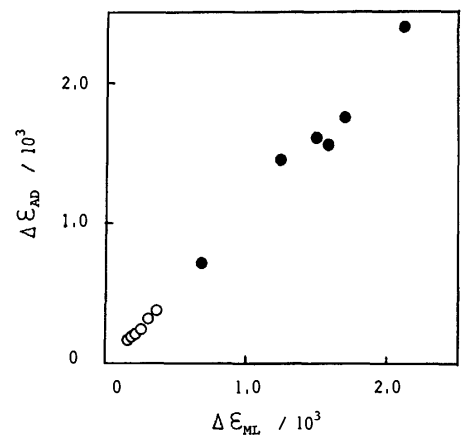

Fig. 6. Correlation between $\Delta\varepsilon_{AD}$ and $\Delta\varepsilon_{ML}$ at 490 nm in CH_3NO_2.
○: 4,5-Dimethoxy-1,2-benzoquinone+MX_n system,
●: 4-methoxy-1,2-naphthoquinone+MX_n system.

$$\Delta G_{AD} = 0.91\cdot\Delta G_{ML} + 1.77 \quad (r=0.996). \quad (9)$$

$$\Delta G_{AD} = 0.82\cdot\Delta G_{ML} + 2.05 \quad (r=0.994). \quad (10)$$

support the assertion that this model is reliable for the estimation of the thermodynamic parameter.

Lewis Acidity. Generally, Lewis acidity is evaluated by the change of the free energy or enthalpy of the complex formation. However, in the case of the complex formation between metal halide and Lewis base, the determination of the thermodynamic parameters is difficult for the wide range of metal halides. Therefore, several empirical scales have been presented to determine the relative acceptor strength of metal halides toward Lewis bases.[14] If these scales really represent a relative acceptor strength of metal halides, a correlation between them must occur. However, they are only qualitative.

In this work, the correlation between the values of K_c, $\Delta\nu_{max}$, and $\Delta\delta_{ML}$ is acknowledged. This result supports that $\Delta\nu_{max}$ and $\Delta\delta_{ML}$ are valid as a relative acidity scale. Formerly, in the study of the complex formation between benzamide and metal chloride in ether, Satchell *et al.*[15] concluded that the chemical shift was unlikely to represent the relative acidity. Unfortunately, they failed to account for the contribution of the solvation to K_c, since the donor strength of ether is evident. The effect of solvation on the order of K_c is ascertained in CH_3CN and CH_3NO_2; *i.e.*, the order of $ZnCl_2>BiCl_3$ was obtained in the latter, whereas the reverse order was obtained in the former;[4] the contribution of the solvation is considered to be much less for CH_3NO_2. The determination of $\Delta\nu_{max}$ and $\Delta\delta_{ML}$ is usually not so difficult as that of K_c, because the rigorous and quantitative experimental conditions are sometimes unnecessary for the former measurements. Therefore, these two parameters appear to offer a convenient scale for the Lewis acidity of metal halides.

References

1) K. H. Meyer, *Ber.*, **41**, 2568 (1908); J. Knox and H. R. Innes, *J. Chem. Soc.*, **105**, 1451 (1914).
2) P. J. Crowley and H. M. Haendler, *Inorg. Chem.*, **1**,

904 (1962).
3) K. Takiura, K. Kataoka, and Y. Sasaki, *Chem. Pharm. Bull. (Tokyo)*, **25**, 2477 (1977).
4) K. Kataoka, S. Kimura, and Y. Sasaki, unpublished data.
5) V. Gutmann, *Coord. Chem. Rev.*, **18**, 225 (1976).
6) H. W. Wanzlich and V. Jahnke, *Chem. Ber.*, **101**, 3744 (1968).
7) L. F. Fieser, *J. Am. Chem. Soc.*, **48**, 2922 (1926).
8) K. Takiura, *Yakugaku Zasshi*, **61**, 475 (1941).
9) S. Patai, "The Chemistry of the Quinonoid Compounds," John Wiley and Sons, Inc., New York (1974), p. 203.
10) For example, D. P. N. Satchell, and T. J. Weil, *J. Chem. Soc., Perkin Trans. 2*, **1977**, 592.
11) R. T. Sanderson, "Inorganic Chemistry," Reinhold Publishing Corp., New York (1967), p. 69.
12) A. Kuboyama, *Bull. Chem. Soc. Jpn.*, **32**, 1226 (1959).
13) J. Homer and A. R. Pudley, *J. Chem. Soc., Faraday Trans. 1*, **69**, 1996 (1973); Y. Sasaki, H. Fujiwara, H. Kawaki, and Y. Okazaki, *Chem. Pharm. Bull. (Tokyo)*, **26**, 1066 (1978).
14) R. S. Satchell, K. Bukka, and C. G. Payne, *J. Chem. Soc., Perkin Trans. 2*, **1975**, 541.
15) G. A. Olah, "Friedel-Crafts Chemistry," John Wiley and Sons, Inc., New York (1973), p. 393, and references cited therein.

  Bull. Chem. Soc. Jpn., 54, 2243—2247 (1981)

Interaction between Pyrazine and Halomethanes. I. Complex Formation between Pyrazine and Halomethanes at Room Temperature

Tatsuaki KUROI,* Yasuhiko GONDO,** Masamichi KUWABARA,**
Ryoichi SHIMADA,** and Yoshiya KANDA**

Chemical Institute, Faculty of Education, Oita University, Dannoharu, Oita 870-11
***Department of Chemistry, Faculty of Science, Kyushu University, Hakozaki, Higashi-ku, Fukuoka 812*

(Received October 27, 1980)

The absorption spectrum of pyrazine has been studied at room temperature in various mixed solvents of cyclohexane and halomethanes such as carbon tetrachloride, chloroform and dichloromethane. With increasing concentration of halomethane, the singlet-singlet (S-S) and singlet-triplet (S-T) $n\rightarrow\pi^*$ absorptions decrease in intensity and become structureless, whereas the S-S $\pi\rightarrow\pi^*$ absorption remains essentially unchanged. The observations are attributed to the complex formation between pyrazine and halomethanes involving the non-bonding electrons in pyrazine. From the concentration and temperature dependences of the $n\rightarrow\pi^*$ absorption spectra, the equilibrium constants, enthalpy and entropy changes have been obtained for the complex formation in all the systems studied. The equilibrium constants obtained from the S-S and S-T $n\rightarrow\pi^*$ absorptions are in good agreement with each other.

As is well known, the electronic spectra of organic compounds exhibit solvent effects. Burawoy,[1] Kasha,[2] and McConnell[3] proved that the solvent effect is useful for characterization of the $\pi\rightarrow\pi^*$ and $n\rightarrow\pi^*$ transitions, showing that the latter transition generally undergoes a blue shift in polar solvents. Brealey and Kasha[4] studied the blue shift of the $n\rightarrow\pi^*$ absorption spectra of benzophenone and pyridazine in hydroxylic mixed solvents, and attributed it to the hydrogen bonding between the solutes and the hydroxylic components of the solvents. But Pimentel[5] suggested that the Franck-Condon principle is significant in the blue shift. Krishna and Goodman[6] reported, on the solvent effects in the $n\rightarrow\pi^*$ absorption and $n\leftarrow\pi^*$ phosphorescence spectra of pyrazine and 2,5-dimethylpyrazine in EPA glass, that the weak hydrogen bonding and Franck-Condon strain resulting therefrom are operative. Baba *et al.*[7] examined the solvent effects on the absorption and fluorescence spectra of diazines, and discussed the dipole moments in the (n,π^*) excited states. Recently, Zalewski *et al.*[8] observed the absorption, fluorescence, and phosphorescence spectra of pyrazine in such matrices as durene, benzene, and cyclohexane, focusing on the nature of the first (n,π^*) excited state.

The present paper deals with the S-S and S-T $n\rightarrow\pi^*$ absorption spectra of pyrazine, which show a blue shift and a blurred structure in the presence of the halomethanes, carbon tetrachloride, chloroform, and dichloromethane. In view of the molecular symmetry of pyrazine and the nonpolar nature of carbon tetrachloride, the blue shift in carbon tetrachloride can not be interpreted in terms of the ground and excited state dipole moments. We here report evidence for the 1 : 1 complex formation between pyrazine and the halomethanes, and the related thermodynamic data obtained.

Carbon tetrachloride as solvent often gives rise to specific interaction with organic compounds such as benzene and pyrazine particularly at low temperatures, that is, to anomalous changes in the absorption and emission spectra.[9-13] In addition, carbon tetrachloride is known to form complexes as an electron acceptor not only with aromatic hydrocarbons[14-16] such as benzene, mesitylene, and hexamethylbenzene, but also with amines[17-19] such as triethylamine, butylamine, and triphenylamine.

Experimental

Pyrazine and all the solvents used were obtained from Wako Pure Chem. Ind., Ltd. Pyrazine was purified by repeated sublimation under vacuum. Cyclohexane (super special grade) was treated several times with a 200-mesh activated silica-gel column, and the benzene contained as an impurity was eliminated. Chloroform (absorption spectro grade) was passed several times just prior to use through a column packed with aluminium oxide Woelm basic (ICN Pharmaceutical Co.) in order to remove the ethanol contained as stabilizer. Carbon tetrachloride and dichloromethane (Dotite spectrosol) were used as received.

The absorption spectra were measured with a Shimadzu UV-200 spectrophotometer, equipped with a temperature-regulated cell holder adapted for the 1-cm cells. Circulating water of a constant temperature maintained the holder temperature constant to an accuracy of $\pm 0.5°$. The temperature was monitored with a thermocouple attached to the reference cell and displayed on a recorder throughout each measurement run. A pair of matched 1-cm fused silica cells were used for the S-S $n\rightarrow\pi^*$ absorption, and a pair of matched 5-cm cells for the S-T $n\rightarrow\pi^*$ absorption.

Results and Discussion

Pyrazine has three different absorptions in the ultraviolet region. One is the S-S $\pi\rightarrow\pi^*$ absorption in the region of 250—270 nm, and the others are the S-S and S-T $n\rightarrow\pi^*$ absorptions in the regions of 310—330 nm and 360—380 nm, respectively. Figures 1 and 2 show the latter two absorption spectra in cyclohexane and in three different halomethanes: carbon tetrachloride, chloroform, and dichloromethane. The spectra in the halomethanes, as in ethanol, are considerably blue-shifted and the vibrational structures are quite blurred compared to those in cyclohexane. The phenomenon is particularly prominent in chloroform and dichloromethane. On the contrary, the $\pi\rightarrow\pi^*$ absorption spectra in the halomethanes show only a slight red shift and the vibrational structure remains

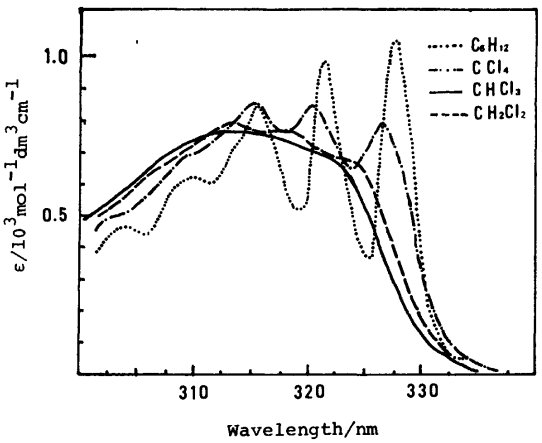

Fig. 1. S-S n→π* absorption spectra of pyrazine in cyclohexane (·····), carbon tetrachloride (·-·-), chloroform (——), and dichloromethane (------).

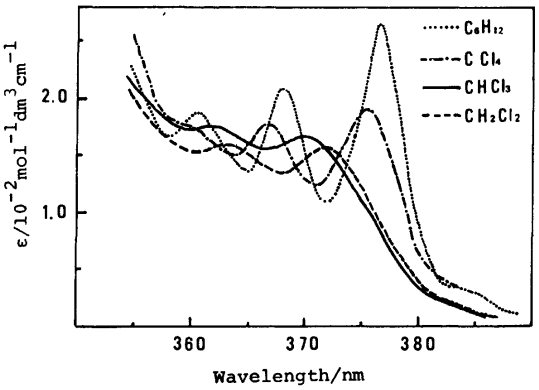

Fig. 2. S-T n→π* absorption spectra of pyrazine in cyclohexane (·····), carbon tetrachloride (·-·-), chloroform (——), and dichloromethane (----).

essentially the same as that in cyclohexane. These findings indicate that pyrazine undergoes a specific interaction with the halomethanes through its non-bonding electrons.

In order to study the interaction quantitatively, the S-S and S-T n→π* absorptions were investigated in detail in ternary systems consisting of pyrazine, the halomethanes, and cyclohexane, where the concentration of pyrazine was kept constant and those of the halomethanes were varied. For the convenience of discussion, the ternary system containing carbon tetrachloride, for example, will be referred to as the carbon tetrachloride system. The S-S and S-T n→π* absorption spectra thus obtained for the carbon tetrachloride system are shown in Figs. 3 and 4, respectively. Similar results have been observed for the chloroform and dichloromethane systems. With any one of the halomethanes, when the concentration of halomethane is relatively low, there always appear isosbestic points in a family of absorption curves, as can be seen in Figs. 3 and 4, suggesting formation of a 1 : 1 complex between pyrazine and the halomethane.

The equilibrium constant K of the complex formation can be determined from the S-S absorption data through the following relation, subject to the condition $[D]_0 \ll [A]_0$:

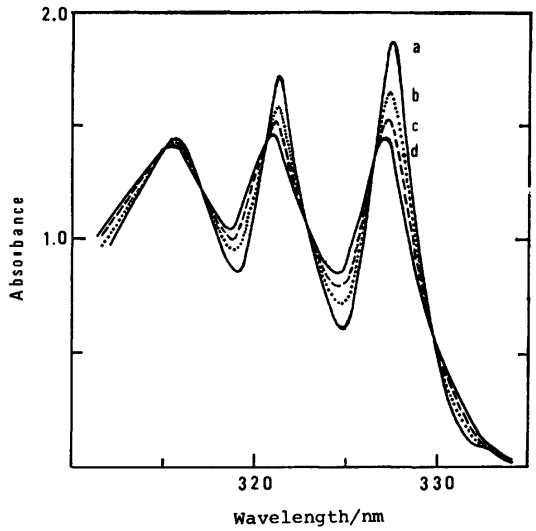

Fig. 3. S-S n→π* absorption spectra of pyrazine in the carbon tetrachloride–cyclohexane mixed solvents at 20 °C. Concentration of pyrazine: 1.654×10^{-3} mol dm^{-3}. Concentration of carbon tetrachloride: (a) 0, (b) 1.200, (c) 2.401, (d) 3.601 mol dm^{-3}.

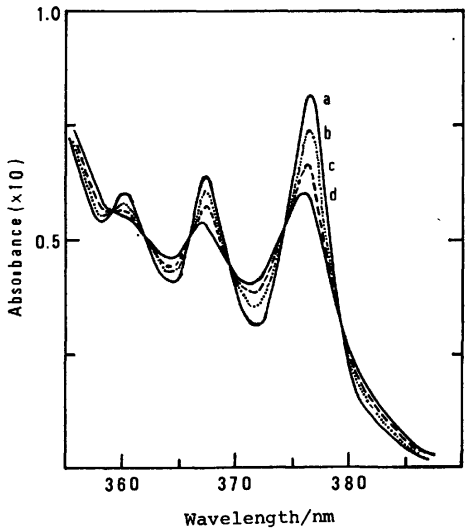

Fig. 4. S-T n→π* absorption specrta of pyrazine in the carbon tetrachloride–cyclohexane mixed solvents. Concentration of pyrazine: 0.622 mol dm^{-3}. Concentration of carbon tetrachloride: (a) 0, (b) 0.999, (c) 3.075, (d) 6.225 mol dm^{-3}.

$$d = (1/K)(\varepsilon_D[D]_0 - d)/[A]_0 + \varepsilon_C[D]_0, \qquad (1)$$

where $[D]_0$ and $[A]_0$ are the initial molar concentrations of the donor, pyrazine, and the acceptor, halomethane, d is the absorbance measured with 1-cm optical path, and ε_D and ε_C are the molar extinction coefficients of the free and complexed donor, respectively; the ε_D values were actually determined in cyclohexane. The apparent ε_D value decreases with increasing temperature, owing to the appearance of the hot band around 333 nm in the S-S n→π* absorption region. Therefore, in order to accurately evaluate the temperature dependence of the equilibrium constant K, we adopted the ε_D values measured at the corresponding temperatures. The concentrations of pyrazine used were 1.654×10^{-3}

mol dm^{-3} for the carbon tetrachloride system, and 1.608×10^{-3} mol dm^{-3} for the chloroform and dichloromethane systems, while the concentrations of halomethane covered the ranges of 0.600—3.601, 0.208—1.456, and 0.461—1.384 mol dm^{-3} for the carbon tetrachloride, chloroform, and dichloromethane systems, respectively. In order to estimate the heat of formation ΔH (the enthalpy change) and the entropy change ΔS, measurements were made at the following temperatures: 20, 25, 30, 35, and 40 °C for the carbon tetrachloride system; 20, 30, 40, and 50 °C for the chloroform system; 20, 30, 40, and 48 °C for the dichloromethane system. We monitored the absorption intensities at 327.5 nm and, if possible, those at 321.5 nm, corresponding to the first and second bands, respectively. Figure 5 shows the data thus obtained at 327.5 nm; the corresponding data at 321.5 nm are quite similar. From the K values estimated at the above-mentioned different temperatures, the ΔH values could be evaluated by means of

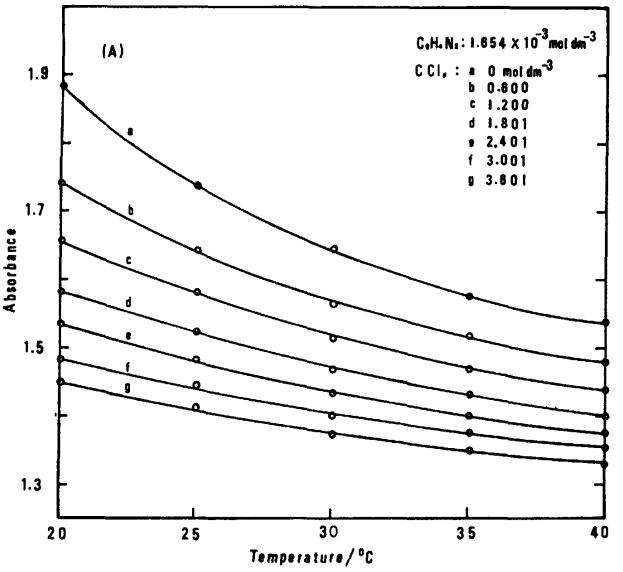

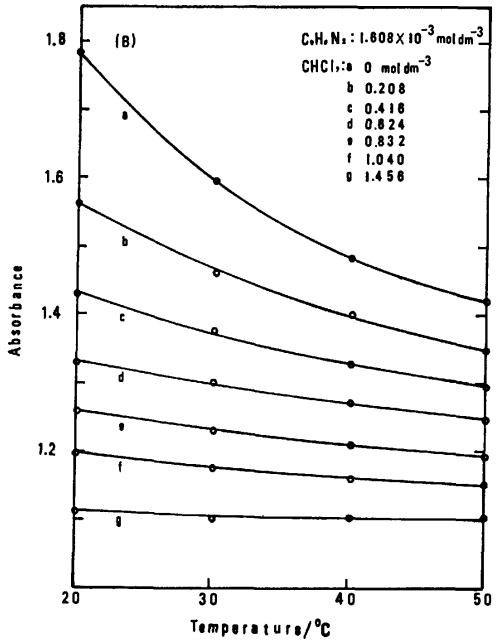

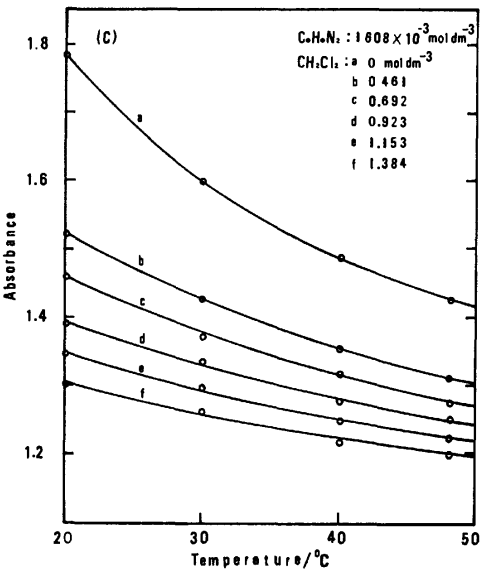

Fig. 5. Temperature dependence of the S-S n→π^* absorption monitored at 327.5 nm in the (A) carbon tetrachloride, (B) chloroform, and (C) dichloromethane systems.

the van't Hoff equation. The plots of d *vs.* $(\varepsilon_D[D]_0-d)/[A]_0$ and $-\ln K$ *vs.* $1/T$ gave fairly good straight-line relationships for any of the ternary systems studied, as exemplified in Figs. 6 and 7. The numerical results thus obtained in the S-S n→π^* absorption region are listed in Table 1, together with those in the S-T region to be described in the following paragraph. The thermodynamic data in Table 1 are found to fall in the ranges of magnitude expected for the molecular complexes.[20]

For the S-T n→π^* absorption, the concentrations of pyrazine used were fairly high because of its very low molar extinction coefficient: they were 0.622, 0.620, and 0.619 mol dm^{-3} for the carbon tetrachloride, chloroform, and dichloromethane systems, respectively. The halomethane concentrations covered the ranges of

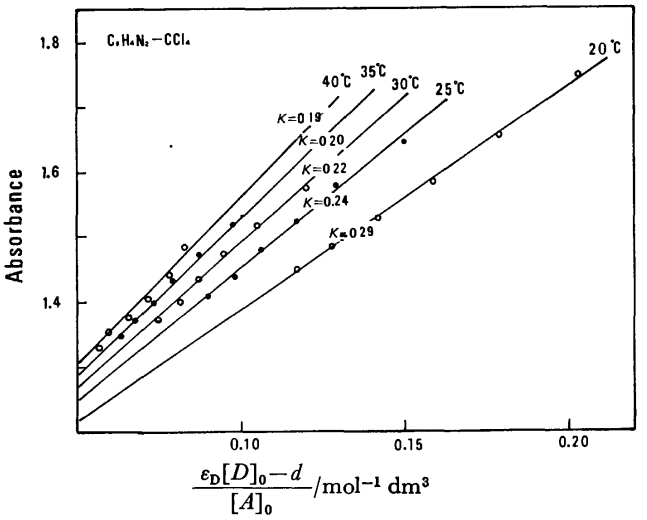

Fig. 6. Temperature dependence of the equilibrium constant K in the carbon tetrachloride system on the basis of the results in Fig. 5(A).

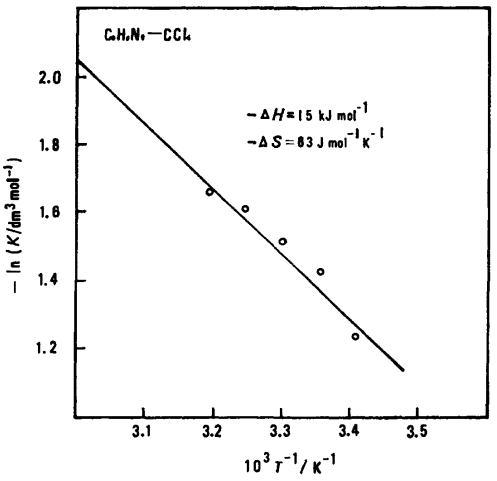

Fig. 7. Evaluation of the enthalpy and entropy changes in the carbon tetrachloride system.

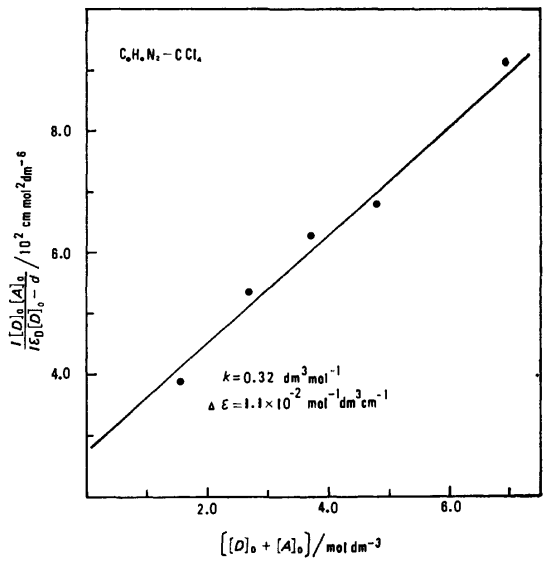

Fig. 8. Evaluation of the equilibrium constant by means of the modified Drago-Rose equation, Eq. 2, from the S-T n→π* absorption data obtained at 376 nm in the carbon tetrachloride system.

0.999—6.225, 0.244—2.493, and 0.326—1.244 mol dm^{-3} for the carbon tetrachloride, chloroform, and dichloromethane systems, respectively. Consequently, the relative concentrations of pyrazine and halomethanes no longer satisfy the condition $[D]_0 \ll [A]_0$. Therefore, the following modified Drago-Rose equation[21] was employed instead of Eq. 1:

$$\frac{l[D]_0[A]_0}{l\varepsilon_D[D]_0-d} = \frac{[D]_0+[A]_0}{\varepsilon_D-\varepsilon_C} + \frac{1}{K(\varepsilon_D-\varepsilon_C)}, \qquad (2)$$

where l is the optical path-length in cm. Equation 2 is applicable to the equilibrium system of relatively small K. The S-T n→π* absorption was studied only at room temperature (20—23 °C), since the 5-cm cells used did not fit the temperature-regulated cell holder. Figure 8 shows the plot of $(l[D]_0[A]_0)/(l\varepsilon_D[D]_0-d)$ *vs.* $[D]_0+[A]_0$, which gives a good straight-line fit. Here, the value of ε_D is 2.64×10^{-2} mol^{-1} dm^3 cm^{-1}, the molar extinction coefficient obtained at 376 nm in cyclohexane. The K's thus derived are listed in Table 1. Regarding Table 1, it should be emphasized that nearly the same values of K were obtained from the two different absorption regions, that is, the S-S and S-T n→π* absorption regions, and that the ε_C values listed as footnotes are in fairly good agreement with those in the

Table 1. Thermodynamic quantities for a 1 : 1 complex formation of pyrazine with halomethanes

	K[a] / mol^{-1} dm^3	$-\Delta H$ / kJ mol^{-1}	$-\Delta S$ / J mol^{-1} K^{-1}
CCl_4-system			
S-S absorption			
327.5 nm[b]	0.29[a] 0.24[b] 0.22[c] 0.19[d]	15	63
S-T absorption			
376 nm[b]	0.32[e]		
$CHCl_3$-system			
S-S absorption			
327.5 nm[b]	1.04[a] 0.73[c] 0.56[d] 0.47[f]	23	78
321.5 nm[b]	1.06[a] 0.76[c] 0.58[d] 0.43[f]		
S-T absorption			
376 nm[b]	0.90[e]		
CH_2Cl_2-system			
S-S absorption			
327.5 nm[b]	0.84[a] 0.68[c] 0.59[d] 0.54[g]	13	44
321.5 nm[b]	0.72[a] 0.65[c] 0.58[d] 0.52[g]		
S-T absorption			
376 nm[b]	0.69[e]		

a) The K values cited above were obtained at the following temperatures: *a*: 20 °C, *b*: 25 °C, *c*: 30 °C, *d*: 40 °C, *e*: 20—23 °C, *f*: 50 °C, *g*: 48 °C. b) The ε_c values obtained at 327.5 nm are 635, 400, and 560 mol^{-1} dm^3 cm^{-1} for the carbon tetrachloride, chloroform, and dichloromethane systems, while those at 321.5 nm are 613 and 676 mol^{-1} dm^3 cm^{-1} for the latter two systems. Those at 376 nm are *ca.* 1.5×10^{-2} mol^{-1} dm^3 cm^{-1} for the first system, and *ca.* 1.1×10^{-2} mol^{-1} dm^3 cm^{-1} for both the latter two systems.

pure halomethanes.

The results of the absorption measurements can be summarized as follows: (1) When the solvent is changed from hydrocarbon to halomethane, the pyrazine absorption due to the S-S $\pi \rightarrow \pi^*$ transition does not undergo any substantial change, showing only a slight red shift and a little increase in intensity. (2) On the other hand, the S-S and S-T $n \rightarrow \pi^*$ absorptions exhibit remarkable changes, indicating specific interaction of the non-bonding electrons of pyrazine with the halomethanes. (3) By use of the cyclohexane–halomethane mixed solvents, reasonable values could be obtained for the equilibrium constant in the 1 : 1 complex formation between pyrazine and the halomethanes.

In the case of the carbon tetrachloride system, the complex is most probably of the charge-transfer type, whereas in the chloroform and dichloromethane systems, the complexes may be due to charge transfer, hydrogen bonding, or to a combination of both of them. In this connection, we have undertaken a study of the phosphorescence spectra in the ternary systems investigated in this work, and obtained some significant results concerning the charge transfer nature of the complexes. These will be discussed in a separate, subsequent paper.[22]

References

1) A. Burawoy, *J. Chem. Soc.*, **1939**, 1177.
2) M. Kasha, *Discuss. Faraday Soc.*, **9**, 14 (1950).
3) H. McConnell, *J. Chem. Phys.*, **20**, 700 (1952).
4) G. Brealey and M. Kasha, *J. Am. Chem. Soc.*, **77**, 4462 (1955).
5) G. C. Pimentel, *J. Am. Chem. Soc.*, **79**, 3323 (1957).
6) V. G. Krishna and L. Goodman, *J. Chem. Phys.*, **33**, 381 (1960).
7) H. Baba, L. Goodman, and P. C. Valenti, *J. Am. Chem. Soc.*, **88**, 5410 (1966).
8) E. F. Zalewski, D. S. McClure, and D. L. Narva, *J. Chem. Phys.*, **61**, 2964 (1974).
9) H. Tsubomura and R. P. Lang, *J. Chem. Phys.*, **36**, 2155 (1962).
10) Y. Kanda, Y. Gondo, and R. Shimada, *Spectrochim. Acta*, **17**, 424 (1961).
11) Y. Kanda and R. Shimada, *Spectrochim. Acta*, **17**, 7 (1961).
12) R. Shimada, *Spectrochim. Acta*, **17**, 14 (1961).
13) R. J. McDonald, L. M. Logan, I. G. Ross, and B. K. Selinger, *J. Mol. Spectrosc.*, **40**, 137 (1971).
14) J. R. Coates, R. J. Sullivan, and J. B. Ott, *J. Phys. Chem.*, **63**, 589 (1959).
15) R. Anderson and J. M. Prausnitz, *J. Chem. Phys.*, **39**, 1225 (1963).
16) R. F. Weimer and J. M. Prausnitz, *J. Chem. Phys.*, **42**, 3643 (1965).
17) D. P. Stevenson and G. M. Coppinger, *J. Am. Chem. Soc.*, **84**, 149 (1962).
18) W. J. Lautenberger, E. N. Jones, and J. G. Miller, *J. Am. Chem. Soc.*, **90**, 1110 (1968).
19) T. Kuroi, N. Soeda, T. Tanaka, and R. Takashita, *Research Bull. Fac. Edu., Oita Univ. (Nat. Sci.)*, **4**(5), 7(1975).
20) G. Briegleb, "Elektronen-Donator-Acceptor-Komplexe," Springer-Verlag, Berlin (1961), p. 124.
21) R. S. Drago and N. J. Rose, *J. Am. Chem. Soc.*, **81**, 6138 (1959).
22) T. Kuroi, Y. Gondo, M. Kuwabara, R. Shimada, and Y. Kanda, *Bull. Chem. Soc. Jpn.*, **54**, 2248 (1981).

Interaction between Pyrazine and Halomethanes. II. Effects of Halomethanes on the Phosphorescence of Pyrazine at 77 K

Tatsuaki KUROI,* Yasuhiko GONDO,** Masamichi KUWABARA,**
Ryoichi SHIMADA,** and Yoshiya KANDA**

Chemical Institute, Faculty of Education, Oita University, Dannoharu, Oita 870-11
***Department of Chemistry, Faculty of Science, Kyushu University, Hakozaki, Higashi-ku, Fukuoka 812*

(Received October 27, 1980)

The phosphorescence and phosphorescence excitation spectra of pyrazine have been studied at 77 K in various mixed solvents of cyclohexane and halomethanes such as carbon tetrachloride, chloroform, and dichloromethane. When the halomethane concentration was low (below 10^{-2} mol dm^{-3}), only the cyclohexane-phase phosphorescence was observed at 77 K; the lower energy components of the well-known doublet band series in the cyclohexane-phase phosphorescence were found to decrease in intensity relative to the higher energy components, with increasing concentration of halomethane. When the halomethane concentration was raised to a range higher than 10^{-1} mol dm^{-3}, where the complex formation between pyrazine and the halomethanes was confirmed through absorption spectroscopy,[1] new phosphorescence bands appeared in the 373—375 nm region for all the systems studied. With further increase of the halomethane concentration, the new bands decreased in intensity or disappeared, and the phosphorescence approached to those in the pure halomethanes. Comparison of the absorption and phosphorescence excitation spectra shows that the new phosphorescence bands result from the 1 : 1 pyrazine–halomethane complexes. The possibility of hydrogen-bonding species formation with chloroform and dichloromethane has been discussed in the light of the phosphorescence spectra studied in the ethanol–cyclohexane mixed solvents.

The phosphorescence spectrum of pyrazine has been extensively studied in various crystalline matrices, rigid glasses, neat crystals, and in the vapor phase.[2-11] One of the unresolved problems is the anomalous phosphorescence of pyrazine observed by Shimada[2] in carbon tetrachloride matrix at 90 K. The phosphorescence shows doublet band-series structure, suggesting the existence of two different kinds of emitters with a separation of 290 cm^{-1}.[3,11] To explore the nature of the doublet structure, McDonald *et al.*[8] investigated the phosphorescence and absorption of pyrazine in carbon tetrachloride and in neat crystals at 77 K. From comparison of the phosphorescence and absorption spectra, they attributed the higher-energy components with origin at 377.4 nm to molecular pyrazine and the lower-energy components with origin at 381.4 nm to microcrystals of pyrazine. It should be noted that their measurements were restricted to concentrations higher than 10^{-4} mol dm^{-3}. In carbon tetrachloride at 77 K, the doublet band-series structure has been found to persist even at a concentration as low as 10^{-7} mol dm^{-3}, where the molecular aggregates or microcrystals are quite unlikely to occur. The anomalous phosphorescence should thus be attributed to a specific interaction between pyrazine and carbon tetrachloride. Such a specific interaction between pyrazine and the halomethanes, carbon tetrachloride, chloroform, and dichloromethane, is the main subject of this work. In order to examine the possibility of hydrogen-bond formation of pyrazine with chloroform and dichloromethane, we have also studied in detail the effect of ethanol on the phosphorescence of pyrazine.

Experimental

Pyrazine and all the solvents used were obtained from Wako Pure Chem. Ind., Ltd. The purification of the chemicals was described in the preceding paper.[1]

Measurements of the phosphorescence and phosphorescence excitation spectra were carried out with a Shimadzu RF-502 spectrophotofluorometer equipped with a cylindrical sector. The slit widths of 0.4 and 1.0 nm were adopted for the excitation and analyzing monochromators, respectively. It is often pointed out that the structures of the low-temperature spectra depend on the method of sample cooling. In this study, rapid cooling was adopted in order to diminish the possibility of formation of molecular aggregates in the course of cooling, since we intended to compare the results in this study with those of the preceding room-temperature study on the complex formation.[1]

Results and Discussion

General Remarks. In order to study the effect of the halomethanes on the phosphorescence spectrum of pyrazine, we have studied the ternary systems consisting of pyrazine, halomethane, and cyclohexane, where the halomethane is carbon tetrachloride, chloroform, or dichloromethane. For the convenience of discussion, the ternary system containing carbon tetrachloride, for example, will be referred to as the carbon tetrachloride system, following the preceding paper.[1] For comparison, we have also studied the ternary system containing ethanol in place of halomethane; this will be referred to as the ethanol system.

Phosphorescence of Pyrazine in Cyclohexane Matrix at 77 K. The phosphorescence spectrum of pyrazine in cyclohexane matrix at 77 K was observed and reexamined as a reference spectrum in some detail to determine the excitation-wavelength and solute-concentration dependences. Figure 1 shows the variation of the phosphorescence spectra with increasing wavelength of the excitation in the S-S n→π* absorption region. The general spectral appearance is quite similar to that reported previously.[3] As is seen in Fig. 1, the pyrazine phosphorescence consists of a doublet band-series structure, in which the origins are located at 377 and 378 nm for the higher and lower energy components, respectively. In addition, we could observe separately the excitation spectra for the higher and lower energy

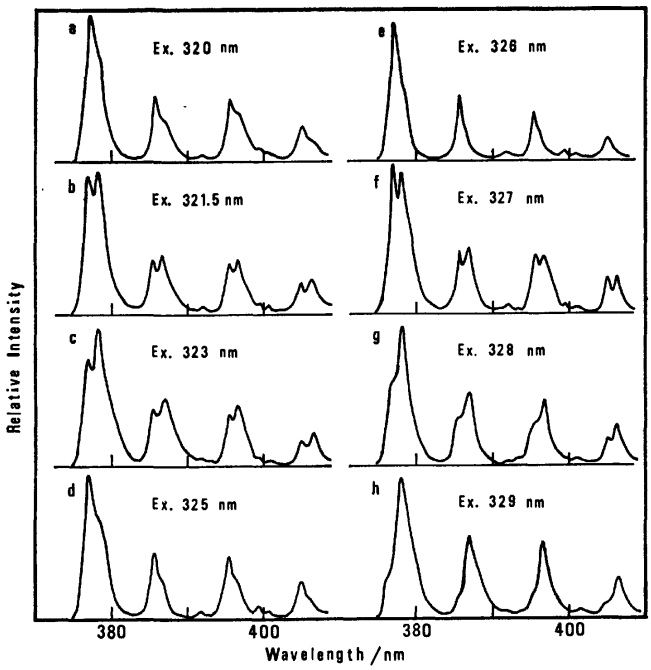

Fig. 1. Excitation-wavelength dependence of the phosphorescence spectrum of pyrazine in cyclohexane matrix at 77 K. Concentration of pyrazine: 1.647×10^{-4} mol dm^{-3}.

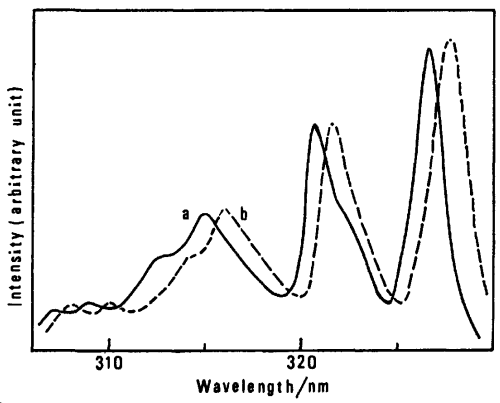

Fig. 2. Excitation spectra of the higher (a) and lower (b) energy components in the phosphorescence of pyrazine in cyclohexane matrix at 77 K. The spectra a and b were monitored at 376.0 and 378.5 nm, respectively. Concentration of pyrazine: 1.647×10^{-4} mol dm^{-3}.

components, as shown in Fig. 2. These observations clearly indicate that there exist at least two, different principal emitters in the cyclohexane matrix at 77 K. For the concentrations of pyrazine in the range of 10^{-7}—10^{-4} mol dm^{-3}, the phosphorescence spectrum remained essentially unchanged. Accordingly, we conclude that, in a cyclohexane solution of the order of 10^{-4} mol dm^{-3}, microcrystals or molecular aggregates are not formed at 77 K, contrary to the statement of McDonald *et al.*[8]

Phosphorescence of Pyrazine in the Ternary System Consisting of Pyrazine, Carbon Tetrachloride, and Cyclohexane at 77 K. Figure 3 shows the effect of carbon tetrachloride on the phosphorescence spectra of pyrazine excited at 324 nm; the relative intensities of the lower and higher energy

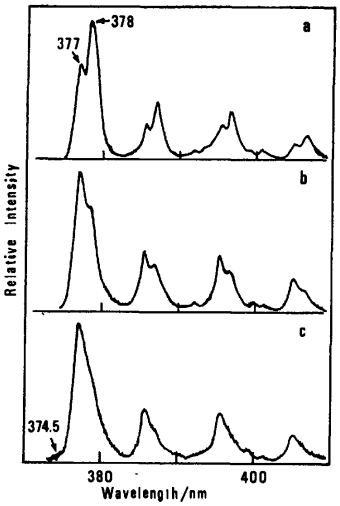

Fig. 3. Spectral changes of the pyrazine phosphorescence excited at 324 nm with the concentration variation of carbon tetrachloride from 10^{-3} to 10^{-1} mol dm^{-3} in the carbon tetrachloride–cyclohexane mixed solvents at 77 K. Concentration of pyrazine: 1.647×10^{-4} mol dm^{-3}. Concentration of carbon tetrachloride: (a) 1.494×10^{-3}, (b) 1.494×10^{-2}, (c) 1.494×10^{-1} mol dm^{-3}.

components, both inherent to the cyclohexane-phase phosphorescence as given in Fig. 1, show a systematic change for the carbon tetrachloride concentrations ranging from the order of 10^{-3} to 10^{-1} mol dm^{-3}; namely, with increasing carbon tetrachloride concentration, the lower energy components of the cyclohexane-phase phosphorescence decrease in relative intensity compared to the higher energy ones. As the concentration of carbon tetrachloride was increased to 10^{-1} mol dm^{-3}, a new phosphorescence band appeared around the 374—375 nm region as a very weak shoulder, and the spectral structure became rather obscure. Quite similar spectral changes were also observed for various excitation wavelengths other than 324 nm in the S-S $n \rightarrow \pi^*$ and $\pi \rightarrow \pi^*$ absorption regions. Therefore, it may be concluded that the doublet band series in the cyclohexane-phase phosphorescence depends not only on the excitation wavelength (Fig. 1), but also on the concentration of carbon tetrachloride (Fig. 3).

On the other hand, when the carbon tetrachloride concentration was increased up to just the same concentrations (in the range 0.562—9.233 mol dm^{-3}) as those used in the preceding paper on the complex formation,[1] the phosphorescence exhibited some complicated and interesting spectral features, as shown in Fig. 4; the pyrazine concentration was kept constant at 1.647×10^{-4} mol dm^{-3}. Such phosphorescence results strongly depend on the excitation wavelengths as well as the carbon tetrachloride concentrations. The excitations at 310, 323, and 324 nm show that the shoulder band in the 374—375 nm region grows with increasing concentration of carbon tetrachloride in the range of 0.5 to 2.0 mol dm^{-3}. In the preceding paper,[1] this concentration range was found to be the most suitable for the observation of the complex formation between pyrazine and carbon tetrachloride. Thus, the shoulder band in the 374—375 nm region seems to have a close connec-

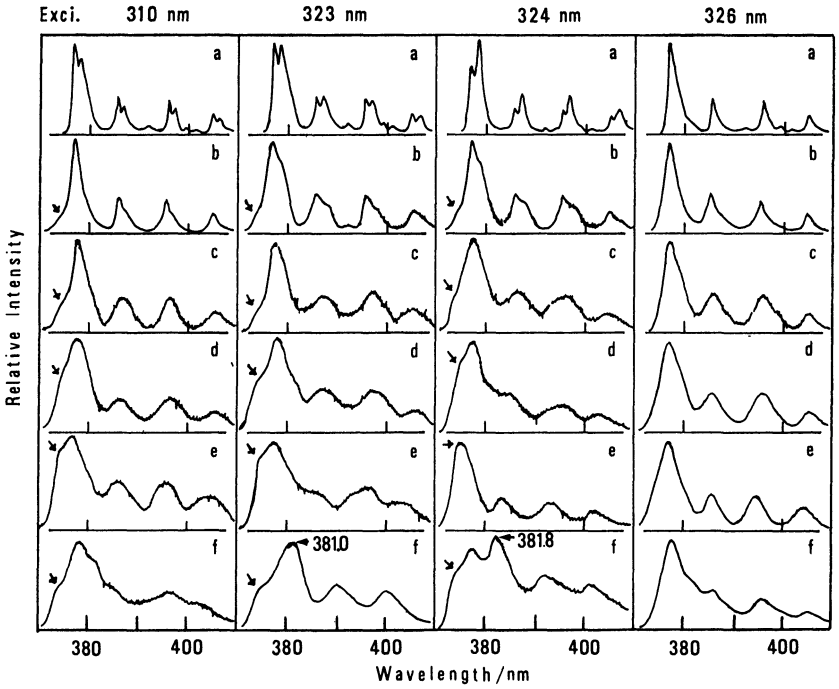

Fig. 4. Spectral changes of the pyrazine phosphorescence in the carbon tetrachloride–cyclohexane mixed solvents at 77 K excited at various wavelengths with the concentration variation of carbon tetrachloride over the range closely related to the complex formation. Concentration of pyrazine: 1.647×10^{-4} mol dm^{-3}. Concentration of carbon tetrachloride: (a) 0, (b) 0.517,(c) 1.022, (d) 1.530, (e) 2.048, (f) 9.223 mol dm^{-3}.

tion with the 1 : 1 charge-transfer complex. At the much higher concentrations, as is seen particularly in the phosphorescence spectra excited at 323 and 324 nm in Fig. 4, the 375-nm band is weaker and then there appears the doublet band-series structure with the origins at 378 and 382 nm, characteristic of the phosphorescence spectrum of pyrazine in carbon tetrachloride matrix at 77 K.

The phosphorescence excitation spectra monitored at the 375-, 378-, and 382-nm bands exhibit the first bands at 324.6, 327, and 330 nm, respectively, as shown in Fig. 5. Thus, the excitation spectra disclose that there are three principal kinds of phosphorescent species in the cyclohexane–carbon tetrachloride mixed solvents at 77 K, when the carbon tetrachloride concentrations are higher than *ca.* 0.5 mol dm^{-3}. Since the excitation spectrum responsible for 375-nm phosphorescence band is in good accord with the blue-shifted absorption spectrum of pyrazine observed in carbon tetrachloride at room temperature,[1] we suggest that the species giving rise to the 375-nm band is the 1 : 1 charge-transfer complex; the phosphorescence of the 375-nm species is much lower in intensity compared with those of the other species.

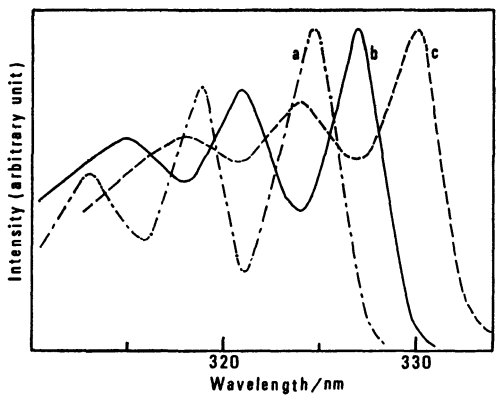

Fig. 5. Excitation spectra monitored at the (a) 375, (b) 378, and (c) 382 nm bands of the phosphorescence of pyrazine in the carbon tetrachloride–cyclohexane mixed solvents at 77 K. Concentration of pyrazine: (a) 1.647×10^{-4}, (b) and (c) 1.444×10^{-4} mol dm^{-3}. Concentration of carbon tetrachloride: (a) 1.530 mol dm^{-3}, (b) and (c) 90 vol%.

Phosphorescence of Pyrazine in the Ternary System Consisting of Pyrazine, Chloroform, and Cyclohexane at 77 K. Excitation-wavelength and chloroform-concentration dependences were also studied for the chloroform system in which the chloroform concentration was varied over the range 10^{-3}—1 mol dm^{-3}. Figure 6 shows the phosphorescence spectra excited at 323 nm; with increasing chloroform concentration, the lower energy components of the cyclohexane-phase phosphorescence decrease in relative intensity compared to the higher energy ones; this result is similar to the case of the carbon tetrachloride system. In this system, one can already see new phosphorescence bands, with the origin at 374.5 nm, at the chloroform concentrations of the order of 10^{-2} mol dm^{-3}. This is consistent with the results of the preceding study on the complex formation; the equilibrium constant for the chloroform

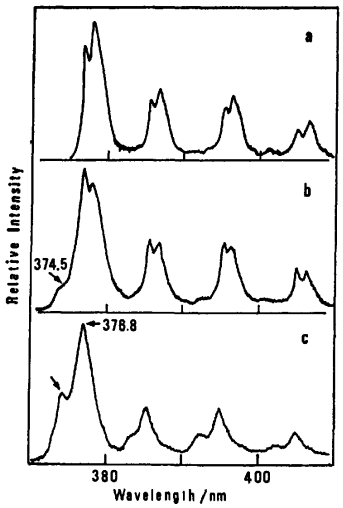

Fig. 6. Spectral changes of the pyrazine phosphorescence excited at 323 nm with the concentration variation of chloroform from 10^{-3} to 10^{-1} mol dm^{-3} in the chloroform–cyclohexane mixed solvents at 77 K. Concentration of pyrazine: 1.647×10^{-4} mol dm^{-3}. Concentration of chloroform: (a) 1.458×10^{-3}, (b) 1.458×10^{-2}, (c) 1.458×10^{-1} mol dm^{-3}.

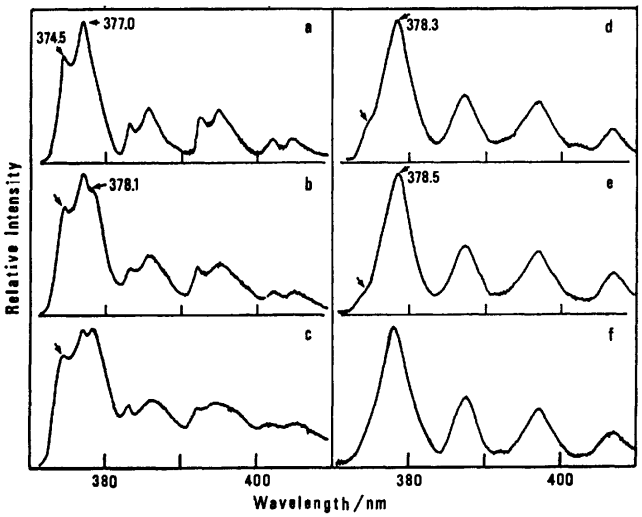

Fig. 7. Spectral changes of the pyrazine phosphorescence in the chloroform–cyclohexane mixed solvents at 77 K excited at 324 nm with the concentration variation of chloroform over the range closely related to the complex formation. Concentration of pyrazine: 1.647×10^{-4} mol dm^{-3}. Concentration of chloroform: (a) 0.219, (b) 0.292, (c) 0.365, (d) 0.693, (e) 0.924, (f) 1.155 mol dm^{-3}.

system is greater than that for the carbon tetrachloride system.[13]

In just the same range of chloroform concentration, 0.2—1.0 mol dm^{-3}, as that studied for the observation of the complex formation,[1] the phosphorescence showed remarkable spectral variations with excitation wavelength and chloroform concentration. The spectra excited at 324 nm are the most typical, and are shown in Fig. 7. In the chloroform concentration of 0.219 mol dm^{-3}, as is seen in Fig. 7, a new phosphorescence band-series with the origin at 374.5 nm clearly appears, while the lower energy components of the cyclohexane-phase phosphorescence completely disappear. With the chloroform concentration of 0.292 mol dm^{-3}, another new phosphorescence band-series, which is quite different both from the 374.5-nm band-series and from the lower energy components of the cyclohexane-phase phosphorescence, begins to appear around 378 nm, while the higher energy components of the cyclohexane-phase phosphorescence eventually disappear with increasing chloroform concentration. When the chloroform concentration is raised to 0.462 mol dm^{-3}, either the 323- or the 324-nm excitation gives exclusively the two new band-series with the origins at 374.5 and 378 nm. With further increase of the chloroform concentration, the intensity of the 374.5-nm band-series decreases; at the concentration of 1.155 mol dm^{-3}, the spectrum is close to that characteristic of the chloroform matrix at 77 K. The new band-series with the origin at 378 nm can thus be attributed to the chloroform-phase phosphorescence in the mixed solvent at 77 K.

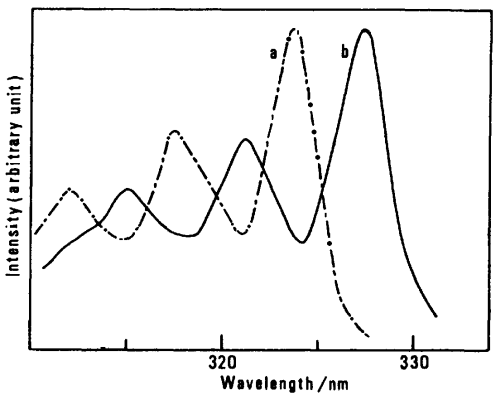

Fig. 8. Excitation spectra of the pyrazine phosphorescence monitored at (a) 373 and (b) 378 nm for the chloroform–cyclohexane mixed solvents at 77 K. Concentration of pyrazine: 8.564×10^{-4} mol dm^{-3}. Concentration of chloroform: 0.462 mol dm^{-3}.

Figure 8 shows the phosphorescence excitation spectra monitored at 373 and 378 nm for the chloroform concentration of 0.462 mol dm^{-3}; the two phosphorescence band-series with the origins at 374.5 and 378 nm are evidently attributable to different emitters. The excitation spectrum responsible for the 374.5-nm phosphorescence band is also blue-shifted in accord with the blue-shifted absorption spectrum in chloroform at room temperature, quite similarly to the case of the carbon tetrachloride system. It should also be noted that the 374.5-nm phosphorescence band-series appears with the strongest intensity in just the same range of chloroform concentration as that suitable for the observation of the 1 : 1 complex formation.[1]

Phosphorescence of Pyrazine in the Ternary System Consisting of Pyrazine, Dichloromethane, and Cyclohexane at 77 K.

Figure 9 shows the changes of the phosphorescence spectrum of pyrazine with the increase of the dichloromethane concentration from 10^{-3} to 10^{-1} mol dm^{-3}. In quite a similar manner to the cases of the carbon

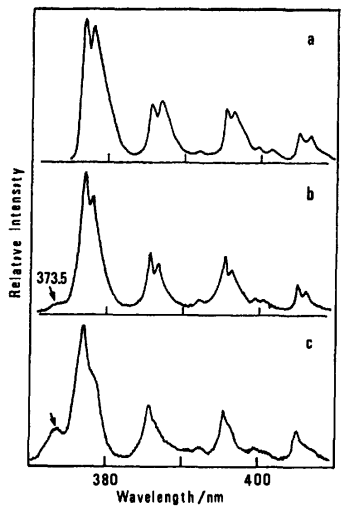

Fig. 9. Spectral changes of the pyrazine phosphorescence excited at 323 nm with the concentration variation of dichloromethane from 10^{-3} to 10^{-1} mol dm^{-3} in the dichloromethane–cyclohexane mixed solvents at 77 K. Concentration of pyrazine: 1.647×10^{-4} mol dm^{-3}. Concentration of dichloromethane: (a) 2.046×10^{-3}, (b) 2.046×10^{-2}, (c) 2.046×10^{-1} mol dm^{-3}.

tetrachloride and chloroform systems, the lower energy components of the cyclohexane-phase phosphorescence decrease with increasing concentration of dichloromethane. At the dichloromethane concentration of 2.0×10^{-2} mol dm^{-3}, a new phosphorescence band appears around 373.5 nm, as in the case of the chloroform system; this reflects the fact that nearly the same equilibrium constants for the complex formation are obtained in both systems at room temperature.[13]

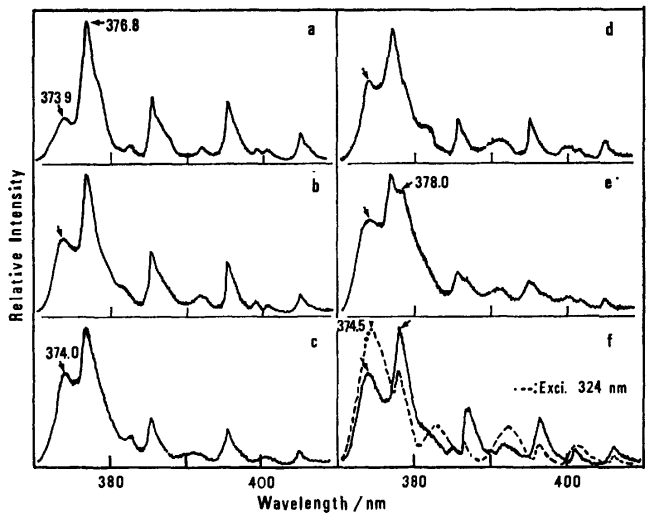

Fig. 10. Spectral changes of the pyrazine phosphorescence in the dichloromethane–cyclohexane mixed solvents at 77 K excited at 323 and/or 324 nm with the concentration variation of dichloromethane over the range closely related to the complex formation. Concentration of pyrazine: 1.444×10^{-4} mol dm^{-3}. Concentration of dichloromethane: (a) 0.255, (b) 0.511, (c) 0.766, (d) 1.021, (e) 1.277, (f) *ca.* 14 mol dm^{-3}.

Figure 10 shows the spectral changes of the phosphorescence excited at 323 and/or 324 nm with the increase of the dichloromethane concentration over just the same range as that studied on the complex formation.[1] At the concentration of 1.277 mol dm^{-3}, another new phosphorescence band appears as a shoulder at 378 nm. As in the cases of the carbon tetrachloride and chloroform systems, the new band is attributed to the dichloromethane-phase phosphorescence in the mixed solvent. In the dichloromethane concentration of about 14 mol dm^{-3}, either the 323-nm or the 324-nm excitation, even with very narrow slit width, no longer gives the higher energy components of the cyclohexane-phase phosphorescence, but gives exclusively the two new phosphorescence band-series mentioned above. The 374-nm band is somewhat dependent on the excitation wavelengths, as is seen in Fig. 10 (f); the 323- and 324-nm excitations give the bands at 373.8 and 374.5 nm, respectively. The excitation spectra monitored at 374 and 378 nm are quite similar to those of the carbon tetrachloride and chloroform systems; the excitation spectrum responsible for the 374-nm phosphorescence band is in accord with the blue-shifted absorption spectrum of pyrazine in dichloromethane at room temperature. Consequently, the 374-nm phosphorescence band can also be closely related to the 1 : 1 complex formation observed in the preceding study.[1]

Phosphorescence of Pyrazine in the Ternary System Consisting of Pyrazine, Ethanol, and Cyclohexane at 77 K. It is generally accepted that pyrazine in the ground state forms a hydrogen bond with ethanol. The ethanol system has been studied in order to examine whether the complexes in the chloroform and dichloromethane systems are of the charge-transfer type or the hydrogen-bonding one. Figure 11 shows the spectral changes of the phosphorescence excited at 323 nm with the increase of the ethanol concentration from 10^{-3} to 10^{-1} mol dm^{-3};

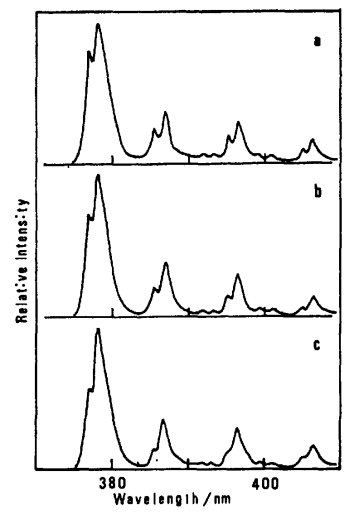

Fig. 11. Spectral changes of the pyrazine phosphorescence excited at 323 nm with the concentration variation of ethanol from 10^{-3} to 10^{-1} mol dm^{-3} in the ethanol–cyclohexane mixed solvents at 77 K. Concentration of pyrazine: 1.647×10^{-4} mol dm^{-3}. Concentration of ethanol: (a) 2.018×10^{-3}, (b) 2.018×10^{-2}, (c) 2.018×10^{-1} mol dm^{-3}.

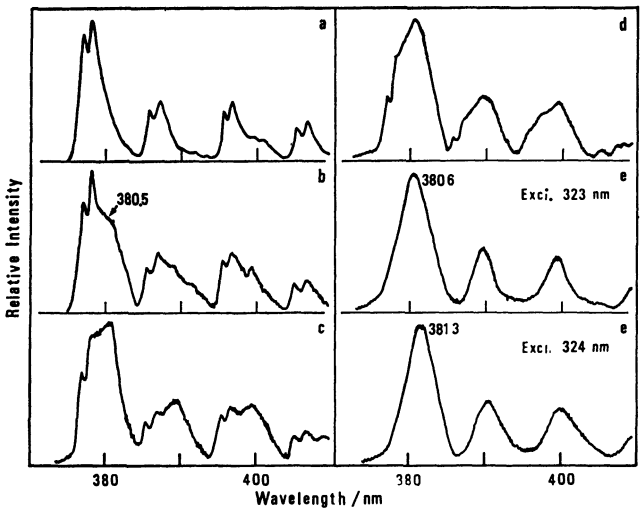

Fig. 12. Phosphorescence spectra of pyrazine excited at 323 and/or 324 nm in the ethanol-cyclohexane mixed solvents at 77 K. Concentration of pyrazine: 1.647×10^{-4} mol dm^{-3}. Concentration of ethanol: (a) 0.404, (b) 0.605, (c) 1.009, (d) 1.715 mol dm^{-3}, and (e) 90 vol%.

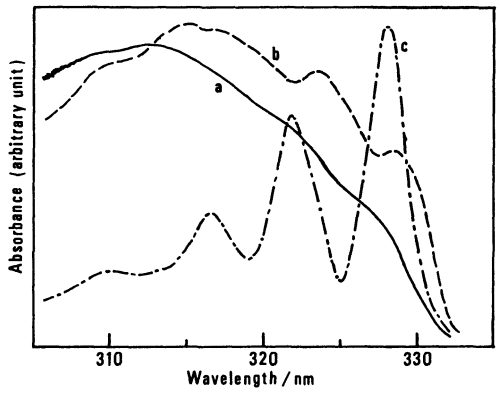

Fig. 13. Absorption and phosphorescence excitation spectra of pyrazine in the ethanol-containing mixed solvents. The absorption spectra a and b were obtained at room temperature and 77 K, respectively, in the mixed solvent of 93 vol% ethanol and 7 vol% methylcyclohexane. The excitation spectrum c monitored at 378 nm was obtained in the mixed solvent of 90 vol% ethanol and 10 vol% cyclohexane. Concentration of pyrazine: (a) and (b) 1.156×10^{-3}, (c) 1.647×10^{-4} mol dm^{-3}.

quite contrary to the cases of the halomethane systems, the lower energy components of the cyclohexane-phase phosphorescence increase in intensity relative to the higher energy ones with increasing ethanol concentration. Figure 12 shows the phosphorescence spectra at the ethanol concentrations ranging from 0.404 to 1.715 mol dm^{-3}. In contrast to the halomethane systems, the ethanol system shows no bands at wavelengths shorter than the higher energy components of the cyclohexane-phase phosphorescence. At ethanol concentrations higher than 0.605 mol dm^{-3}, new bands appear with their origin in the region 380—381 nm. Since the new phosphorescence bands are characteristic of the phosphorescence of pyrazine in ethanol glass at 77 K, they are attributed to the ethanol-phase phosphorescence in the mixed solvent. At a much higher ethanol concentration, 90% by volume, only the ethanol-phase phosphorescence has been observed, as shown in Fig. 12.

In order to examine the phosphorescence efficiences in the hydrogen bonding species, the phosphorescence excitation spectrum, curve c in Fig. 13, has been observed and compared with the absorption spectrum. The absorption spectrum of pyrazine in ethanol at room temperature loses some vibrational structure with blue shift of the spectrum due to hydrogen bonding; this is shown in Fig. 13 as curve a. The absorption spectrum at 77 K, curve b in Fig. 13, exhibits vibrational structure as shoulders at wavelengths longer than the vibrational bands observed in hydrocarbon solvents at room temperature. The absorption spectrum at 77 K is very similar to that observed at the same temperature by Krishna *et al.*[14] The phosphorescence excitation spectrum is apparently different from the absorption spectrum at 77 K. A comparison of the excitation and absorption spectra at 77 K indicates that the phosphorescence in ethanol at least mainly comes from the species which have vibrational structure in the absorption spectrum at 77 K. Therefore, it may be concluded that most of the hydrogen bonding species have very low phosphorescence efficiencies.

Krishna *et al.* proposed that the hydrogen bond was broken in the excited state, and hence the observed phosphorescence spectrum was consistent with the absence of hydrogen bonding in the triplet state; they did not perform any excitation spectrum measurement, however. Combining the results of Krishna *et al.* with our observations, the phosphorescence of pyrazine in ethanol at 77 K is thought to be emitted chiefly from the non-hydrogen bonding species, while the pyrazine molecules are modified by specific interactions such as cohesive forces between the solvent molecules or between the solute and solvent molecules. Thus, the phosphorescence bands observed around the region 373—374 nm in the chloroform and dichloromethane systems would not be attributed to hydrogen bonding species, but to the 1 : 1 charge-transfer complex species.

Origin of the New Phosphorescence Bands in the 373—375 nm Region. With the same halomethane concentrations as those suitable for the observation of the complex formation,[1] every halomethane system exhibits new phosphorescence bands with the origin in the 373—375 nm region; these are obviously different from the normal phosphorescence bands in the pure halomethane at 77 K. The 373—375 nm phosphorescence bands appear most clearly at the following halomethane concentrations: 2.048 mol dm^{-3} for the carbon tetrachloride system (Fig. 4, curve e; excited at 324 nm), 0.365 mol dm^{-3} for the chloroform system (Fig. 7, curve c; excited at 324 nm), and 0.766—1.021 mol dm^{-3} for the dichloromethane system (Fig. 10, curves c and d; excited at 323 nm). It has been previously established that the equilibrium constants for the complex formation

increase in the order of carbon tetrachloride, dichloromethane, and chloroform systems.[13] Accordingly, the chloroform and dichloromethane systems start to exhibit the new 373—375 nm bands at relatively low halomethane concentrations ($\approx 10^{-2}$ mol dm^{-3}) compared to the carbon tetrachloride system, as is seen in curve b of Fig. 6 and curve b of Fig. 9, respectively.

In addition, the excitation spectra of the 373—375 nm bands are blue-shifted in accord with the blue-shifted absorption spectra in the halomethane systems at room temperature. It should be emphasized that the results of the chloroform and dichloromethane systems are quite similar to those of the carbon tetrachloride system where no hydrogen-bonding species occurs. In contrast to the halomethane systems, the ethanol system exhibits no new phosphorescence bands in the 373—375 nm region. As for the relative intensities of the two well-known band series in the cyclohexane-phase phosphorescence of pyrazine, the halomethane systems show changes opposite to those in the ethanol system, with the increase of the halomethane and ethanol concentrations from 10^{-3} to 10^{-1} mol dm^{-3}, as is seen in Figs. 3, 6, 9, and 11. Thus, the halomethane effects on the phosphorescence of pyrazine differ from those of ethanol, and in particular the hydrogen-bonding species are independent of the appearance of the new 373—375 nm bands. In view of these observations, it is concluded that the new phosphorescence bands observed in the 373—375 nm region in the halomethane systems result from the 1 : 1 charge-transfer complexes.

References

1) Preceding paper in this series: Part 1, T. Kuroi, Y. Gondo, M. Kuwabara, R. Shimada, and Y. Kanda, *Bull. Chem. Soc. Jpn.*, **54**, 2243 (1981).

2) L. Goodman and M. Kasha, *J. Mol. Spectrosc.*, **2**, 58 (1958).

3) R. Shimada, *Spectrochim. Acta*, **17**, 14 (1961).

4) M. A. El-Sayed and G. W. Robinson, *Mol. Phys.*, **4**, 273 (1961).

5) L. M. Logan and I. G. Ross, *J. Chem. Phys.*, **43**, 2903 (1965).

6) W. R. Moomaw and M. A. El-Sayed, *J. Chem. Phys.*, **45**, 3890 (1966).

7) W. R. Moomaw and M. A. El-Sayed, *J. Chem. Phys.*, **48**, 2502 (1968).

8) R. J. McDonald, L. M. Logan, I. G. Ross, and B. K. Selinger, *J. Mol. Spectrosc.*, **40**, 137 (1971).

9) I. Suzuka and M. Ito, *Bull. Chem. Soc. Jpn.*, **45**, 2323 (1972).

10) C. J. Marzzacco and E. F. Zalewski, *J. Mol. Spectrosc.*, **43**, 239 (1972).

11) E. F. Zalewski, D. S. McClure, and D. L. Narva, *J. Chem. Phys.*, **61**, 2964 (1974).

12) M. Kuwabara, Master of Science Thesis, Kyushu University, March 1973.

13) For example, the equilibrium constants for complex formation at 20 °C are 0.29, 1.04, and 0.84 dm^3 mol^{-1} for the carbon tetrachloride, chloroform, and dichloromethane systems, respectively; see Ref. 1.

14) V. G. Krishna and L. Goodman, *J. Chem. Phys.*, **33**, 381 (1960).

  Bull. Chem. Soc. Jpn., 54, 2255—2259 (1981)

Molecular Structure of Trimethylphosphine-Boron Tribromide as Determined by Gas Electron Diffraction

Kinya IIJIMA, Eiichi KOSHIMIZU, and Shuzo SHIBATA*

Department of Chemistry, Faculty of Science, Shizuoka University, Oya, Shizuoka 422

(Received November 4, 1980)

The molecular structure of trimethylphosphine–boron tribromide $(CH_3)_3P\cdot BBr_3$ has been determined from gas electron-diffraction and vibrational-spectroscopic data. The molecular parameters and their uncertainties were r_g(B–Br)$=2.010\pm0.009$ Å, r_g(P–B)$=1.946\pm0.029$ Å, r_g(C–P)$=1.804\pm0.004$ Å, r_g(C–H)$=1.098\pm0.010$ Å, $\angle$BrBBr$=111.7\pm0.7°$, and $\angle$CPC$=108.0\pm0.7°$. The potential barrier around the P–B bond was also estimated to be about 10 kcal mol^{-1} (1 cal$=4.184$ J).

The molecular structures of trimethylamine–boron trihalides $(CH_3)_3N\cdot BX_3$ have been determined recently in both the gas and solid phases,[1-4] and the following conclusions have been drawn.[2] 1) On the formation of the complex the structural change of the acceptor molecule is greater than that of the donor molecule. 2) There is a correlation between the magnitude of the structural changes of the donor and acceptor molecules and the reorganization energy of the acceptor molecule.[5] 3) The donor-acceptor complex is stabilized and thus the N–B distance is shortened and the B–X distance is lengthened in the solid phase rather than in the gas phase.

On the other hand, the molecular structure of gaseous trimethylphosphine–boron trichloride $(CH_3)_3P\cdot BCl_3$[6] is essentially the same as that in the solid phase[7] and furthermore on the formation of the complex, the CPC angle in the donor molecule increases considerably and the C–P distance decreases, while in the case of the trimethylamine complexes the changes of the corresponding bond angle and distance are opposite. Thus it seems that trimethylphosphine and trimethylamine behave differently as a donor molecule.

In order to understand such interesting properties of trimethylphosphine donor, the structure of gaseous trimethylphosphine–boron tribromide $(CH_3)_3P\cdot BBr_3$ has been determined by an electron-diffraction method. The potential-barrier height of torsional vibration around the P–B bond has also been estimated from the combined analysis of electron-diffraction and vibrational-spectroscopic data.

Experimental

Trimethylphosphine–silver iodide complex was prepared by the procedure described in Ref. 8. The complex was decomposed under vacuum in an oil bath at 200 °C, and trimethylphosphine was collected in a trap cooled by liquid nitrogen after boron tribromide was condensed in advance. The mixture in the trap was warmed up to room temperature and was allowed to react. The crude complex obtained was recrystallized from acetone and water and was purified by repeated sublimations under vacuum.

In the electron-diffraction experiment the sample was vaporized at 200 °C by means of a high temperature nozzle. The photographs were taken using an r^3-sector on Kodak Electron-Image plates at camera distances 293.4 mm and 143.6 mm. The exposure time for the long camera distance was 17 s using an electron-beam current of 0.9 μA. For the short camera distance the exposure time was 65 s using a beam current of 0.8 μA. The pressure of the diffraction chamber was below 1×10^{-5} Torr (1 Torr$=133.3$ Pa) during the experiment. The electron wavelength was determined from the diffraction patterns of thallium chloride;[9] 0.06040 ± 0.00002 Å for the long camera distance and 0.06015 ± 0.00003 Å for the short camera distance. The optical densities of three plates taken at the long camera distance and three plates at the short camera distance were measured at 0.4 mm intervals by means of a digital microphotometer. The electron-diffraction unit and the digital microphotometer used in the present study were described in Ref. 10.

Analysis and Results

Molecular Intensity and Radial Distribution. The scattering intensites in the range of $s=2.5$—14.8 and 7.5—34.6 Å^{-1} were obtained from long and short camera distance plates, respectively. They were leveled by theoretical backgrounds, and then the intensities for each camera distance were averaged. The elastic and inelastic scattering factors were taken from the tables prepared by Schäfer *et al.*[11] and by Cromer and Mann,[12] respectively. The inelastic scattering factor for hydrogen atom was taken from the table by Tavard *et al.*[13]

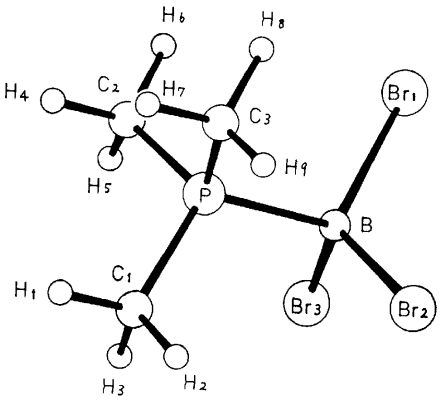

Fig. 1. Numbering of atoms in trimethylphosphine–boron tribromide (symmetry C_{3v}).

The background curves were drawn smoothly, and the molecular intensities shown in Fig. 2 were obtained.[14] Because of the large difference between the atomic numbers of bromine and other atoms in a trimethylphosphine–boron tribromide molecule, N_{ij} functions which fit μ_{ij} over the scattering-angle range for the experiment were calculated[15] and are given in Table 1. The radial distribution corrected by the N_{ij} functions is shown in Fig. 3.

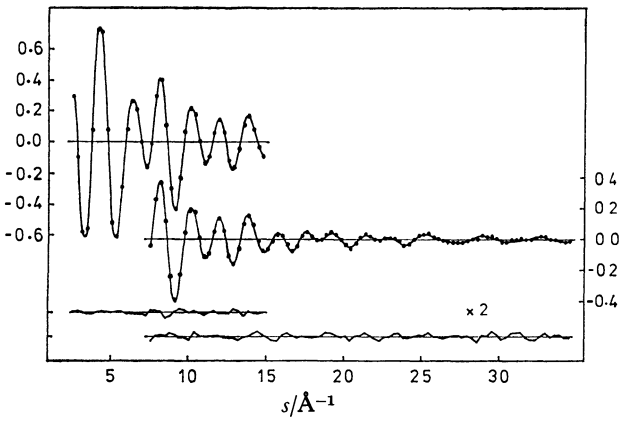

Fig. 2. Molecular intensities for trimethylphosphine–boron tribromide. The two upper curves are long and short camera-distance data. Dots represent observed ones, solid curves calculated ones, and their residuals are shown below.

TABLE 1. COEFFICIENTS OF N_{ij} FUNCTIONS

Atomic pair	a	b	c
B–Br	1.155	0.583	0.0213
B–P	1.317	1.438	0.0268
B–C	1.373	2.421	0.0222
B–H	1.485	3.227	0.0168
Br–Br	0.955	0.0	0.0
Br–P	1.080	0.0	0.0
Br–C	1.129	0.469	0.0128
Br–H	1.186	0.849	0.0070
P–C	1.282	1.133	0.0170
P–H	1.356	1.618	0.0101
C–C	1.339	2.114	0.0174
C–H	1.437	2.915	0.0136
H–H	1.529	4.014	0.0115

N_{ij} function fits μ_{ij} where $N_{ij}=a_{ij}+b_{ij}\exp(-c_{ij}s^2)$, $\mu_{ij}=|F_i|\cdot|F_j|/C_{ij}\sum(|F_k|^2+S_k)$, $C_{ij}=Z_iZ_j/\sum(Z_k^2+Z_k)$, and other notations follow Ref. 15.

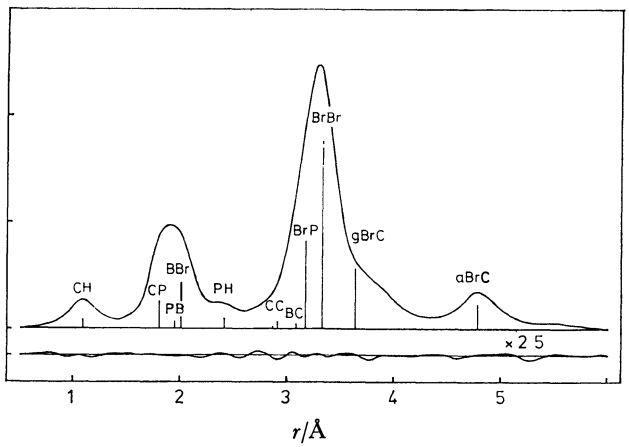

Fig. 3. Radial distribution curve for trimethylphosphine–boron tribromide. Solid curve, experimental; lower curve, 2.5 times the residuals.

Force Constant, Mean Amplitude of Vibration, and Shrinkage Effect. Drake *et al.* have studied the IR and Raman spectra of $(CH_3)_3P\cdot BBr_3$ in the solid phase and in solutions by the normal-vibration treatment.[16] We calculated the mean amplitudes of vibration, which are given in Table 5, on the basis of their force field. The calculated values for l(*gauche* Br···C), l(Br···Br), and l(B–Br), however, disagreed with the observed ones obtained from the analysis of electron-diffraction data.

The force field by Drake *et al.* was in disregard of the torsional vibrations around the P–B and C–P bonds. The torsional vibration around the P–B bond contributes significantly to l(*gauche* Br···C), and therefore the force constant of Y(P—B) was estimated so that the calculated l(*gauche* Br···C) is equal to the observed one.[1] The value obtained was 0.31×10^{-18} N m, which corresponds to the potential barrier of 9.9 kcal mol^{-1}.** The upper and lower limits of the barrier were estimated to be 18.2 and 6.7 kcal mol^{-1}, respectively. The force constant for the torsional vibration around the C–P bond was assumed to be 0.08×10^{-18} N m, which was estimated from the potential barrier for trimethylphosphine, 2.6 kcal mol^{-1}.[17] The force constants of K(B–Br) and F(Br···Br) are related mainly to l(B–Br) and l(Br···Br), respectively. These constants were also estimated as K(B–Br)$=2.0\times10^2$ N m^{-1} and F(Br···Br)$=0.30\times10^2$ N m^{-1} by the same method as used for Y(P–B).

TABLE 2. FORCE FIELD FOR $(CH_3)_3P\cdot BBr_3$

f(CH)	4.782	H(BrBBr)	0.44
f(HCH)	0.433	F(BrBr)	0.30†
f(HCP)	0.642	F(PBr)	0.25
f(CPC)	0.81	f(CH/CH′)	0.045
f(CPB)	0.84	f(HCP/HCP′)	−0.109
f(CP)	3.13	f(CP/CP′)	0.34
K(PB)	1.917	f(CPB/CPB′)	−0.06
K(BBr)	2.00†	Y(CP)	0.081†
H(PBBr)	0.42	Y(PB)	0.31†

In the present normal-coordinate calculation, general valence force constants f and Urey-Bradley force constants K, H, F, and Y were used with stretching and repulsion constants in 10^2 N m^{-1}, bending constants in 10^{-18} J rad^{-2}, and torsional constants in 10^{-18} N m. Linear constant F' was assumed as $-0.1F$. The values of the force constants were taken from Ref. 16, but those indicated by dagger were estimated in the present study.

The force constants of $(CH_3)_3P\cdot BBr_3$ modified in the present study are given in Table 2, and the mean amplitudes of vibration and the shrinkage effects,[18] r_a-r_α, calculated on the basis of these force constants are listed in Table 3. The force constants of K(B–Br) and F(Br···Br) obtained by Drake *et al.* (0.96 and 0.44×10^2 N m^{-1}, respectively)[16] are in disagreement with those from the present study. This may be due to the fact that the electron-diffraction experiment was carried out in the gas phase while the spectroscopic experiment was done in the solid phase and in solutions.

** The systematic error of the mean amplitude was taken into consideration because R_2 was slightly small as seen in Table 6, but it was quite small and thus the height of the potential barrier was not varied.

Table 3. Root-mean-square amplitudes and shrinkage effects for $(CH_3)_3P \cdot BBr_3$ (in 10^{-4} Å)

Atomic pair	l	$r_a - r_\alpha$	Atomic pair	l	$r_a - r_\alpha$
B–Br_1	596	39	P–C_1	548	194
P–B	621	18	P···H_1	1166	377
B···C_1	1059	107	C_1···C_2	1103	276
B···H_1	1268	251	C_1–H_1	783	524
B···H_2	2164	205	C_1···H_4	2236	288
Br_1···Br_2	1015	10	C_1···H_5	2283	308
Br_1···P	1061	−8	C_1···H_6	1277	506
Br_1···C_1	1079	42	H_1···H_2	1320	870
Br_1···C_2	2088	−17	H_1···H_4	3156	251
Br_1···H_1	1512	135	H_1···H_5	3577	147
Br_1···H_2	1941	128	H_1···H_6	2286	511
Br_1···H_4	2389	93	H_2···H_5	2269	551
Br_1···H_5	3433	−81	H_2···H_6	1527	670
Br_1···H_6	3152	24	H_2···H_9	3290	232

The numbering of the atoms is shown in Fig. 1. The calculated values were obtained for the same temperature (473 K) as the experiment was carried out.

Analysis of Electron Diffraction Intensities. The molecular parameters of $(CH_3)_3P \cdot BBr_3$ were determined by the least-squares analysis of molecular intensities. It was assumed that the molecule has a staggered form of C_{3v} symmetry with the methyl groups which also have C_{3v} symmetry in a staggered form with respect to the C–P bonds. The geometrical parameters determined by the least-squares analysis were as follows: r(B–Br), r(P–B), r(C–P), r(C–H), r(Br···Br), r(C···C), and ∠PCH. The mean amplitudes not listed in Table 5 and the shrinkage corrections for all the atomic pairs were fixed to the values listed in Table 3. The asymmetry parameter, κ, for the C–H bond was assumed to be 1.2×10^{-5} Å^3 by a diatomic approximation.[19] The asymmetry parameters for the other atomic pairs were ignored.

The r_α parameters determined by the least-squares calculation are listed in Table 4, where the r_g parameters and the limits of error are also listed. The random errors were given by 2.6 times the errors in least-squares calculations. The systematic errors were estimated from the errors in both the measurements of camera distance (0.04%) and wavelength (0.06%). The mean

Table 4. Molecular parameters obtained from least-squares analysis for $(CH_3)_3P \cdot BBr_3$

	r_α	r_g	σ[a]
B–Br	2.004	2.010	0.009
P–B	1.943	1.946	0.029
C–P	1.784	1.804	0.004
C–H	1.040	1.098	0.010
Br···Br	3.322	3.327	0.005
C···C	2.887	2.919	0.017
∠PCH	111.8		1.8
∠BrBBr[b]	112.0	111.7	0.7
∠CPC[b]	108.0	108.0	0.7

Bond distance: Å unit; bond angle: degree unit. a) Limits of error. b) Calculated from independent parameters.

Table 5. Root-mean-square amplitudes for $(CH_3)_3P \cdot BBr_3$ (in Å unit)

	Obsd[a]	Calcd[b]	Calcd[c]
B–Br	0.061(14)	0.060	0.073
P–B	0.035(28)	0.062	0.062
C–P	0.047(8)	0.055	0.055
C–H	0.081(12)	0.078	0.078
Br···Br	0.107(4)	0.102	0.087
Br···P	0.105(9)	0.106	0.109
anti Br···C	0.102(12)	0.108	0.113
gauche Br···C	0.207(11)	0.209	0.179
P···H	0.129(20)	0.117	0.119

a) Results obtained from the least-squares analysis of electron-diffraction data. Limits of error are shown in parentheses. b) Values calculated from the force constants in Table 2. c) Values calculated from the force constants in Ref. 16.

Table 6. Correlation matrix of $(CH_3)_3P \cdot BBr_3$

	r(BBr)	r(PB)	r(CP)	r(CH)	r(BrBr)	r(CC)	∠PCH	l(BBr)	l(BrBr)	l(BrP)	l(*a*BrC)	l(*g*BrC)	l(CP)	l(PH)	l(CH)	l(PB)	R_1[a]	R_2[a]
r(BBr)	1.0																	
r(PB)	−0.97	1.0																
r(CP)	−0.49	0.55	1.0															
r(CH)	−0.04	0.05	0.00	1.0														
r(BrBr)	0.18	−0.17	−0.06	0.04	1.0													
r(CC)	−0.11	0.22	0.60	−0.01	−0.27	1.0												
∠PCH	0.07	−0.12	−0.12	−0.31	−0.27	−0.12	1.0											
l(BBr)	−0.85	0.86	0.51	0.08	−0.19	0.15	−0.01	1.0										
l(BrBr)	0.00	0.10	−0.03	0.00	−0.69	0.11	0.14	0.16	1.0									
l(BrP)	−0.29	0.30	0.08	−0.02	−0.87	0.09	0.22	0.35	0.83	1.0								
l(*a*BrC)	0.00	0.00	−0.07	0.05	0.02	−0.10	−0.09	0.03	0.09	0.06	1.0							
l(*g*BrC)	0.01	0.04	0.00	−0.10	−0.11	0.01	0.11	0.03	0.35	0.24	0.02	1.0						
l(CP)	−0.67	0.65	0.35	0.08	−0.16	−0.02	−0.03	0.74	0.16	0.32	0.08	−0.03	1.0					
l(PH)	−0.31	0.28	0.21	−0.08	−0.14	0.15	0.04	0.27	−0.01	0.13	−0.03	−0.01	0.13	1.0				
l(CH)	0.00	−0.01	−0.08	−0.08	−0.03	−0.11	0.06	0.02	0.09	0.09	0.06	0.00	0.09	−0.04	1.0			
l(PB)	−0.61	0.58	0.35	0.05	−0.14	−0.01	−0.02	0.53	0.07	0.25	0.05	−0.04	0.77	0.09	0.06	1.0		
R_1	0.07	−0.12	−0.35	0.04	−0.11	−0.64	0.12	0.03	0.39	0.36	0.19	0.00	0.21	−0.12	0.17	0.14	1.0	
R_2	0.03	−0.05	−0.20	0.00	−0.06	−0.28	−0.14	0.07	0.38	0.27	0.23	−0.08	0.27	−0.02	0.19	0.16	0.52	1.0

a) R_1 and R_2 are the indices of resolution for the long and short camera-distance data respectively. The indices of resolution and their uncertainties are $R_1 = 0.88 \pm 0.02$ and $R_2 = 0.80 \pm 0.03$.

Table 7. Comparison of molecular parameters

	$(CH_3)_3P\cdot BCl_3$		$(CH_3)_3P\cdot BBr_3$		BCl_3,[d] $(CH_3)_3P$[e]	BBr_3[f]
	Gas[a]	Solid[b]	Gas[c]	Solid[b]		
r(P–B)/Å	1.941(16)	1.957(5)	1.946(29)	1.924(12)		
r(B–X)/Å	1.851(7)	1.855(5)	2.010(9)	2.022(7)	1.742(4)	1.893(5)
r(C–P)/Å	1.800(4)	1.81(1)	1.804(4)	1.81(1)	1.846(3)	
∠XBX/°	109.4(4)	111.2(2)	111.7(7)	110.4(5)	120	120
∠CPC/°	109.3(3)	107.9(3)	108.0(7)	107.2(5)	98.6(3)	

Bond distance: Å unit; bond angle: degree unit. The values in the gas phase represent r_g parameters. a) Ref. 6. b) Ref. 7. c) Present study. d) Ref. 22. e) Ref. 20. f) Ref. 21.

amplitudes and their limits of error obtained from the least-squares analysis and the calculated mean amplitudes are listed in Table 5. The large errors in the distances and the mean amplitudes for the B–Br and P–B bonds are probably attributable to the large correlation between their parameters.

The correlation matrix is listed in Table 6, and the best-fit theoretical molecular intensities are shown in Fig. 2. The calculations of the mean amplitudes and the shrinkage effects and the least-squares analysis were carried out on a HITAC 8800/8700 computer in the Computer Center of the University of Tokyo.

Discussion

On the formation of the $(CH_3)_3P\cdot BBr_3$ complex, the B–Br distance increases by 6.2% and the BrBBr angle decreases by 6.9% (Table 7), while the C–P distance decreases by 2.3% and the CPC angle increases by 9.5%. The ratios of the changes in the B–Br and C–P distances are in good agreement with the corresponding ones in $(CH_3)_3P\cdot BCl_3$.[6] The P–B distances in both complexes are also equal to each other in the gas phases. These structural changes represent that the valence orbital of the phosphorus atom in the donor molecule changes from p^3 to sp^3 and the valence orbital of the boron atom in the acceptor molecule from sp^2 to sp^3 on the formation of a complex.

On the other hand, in the solid phase the P–B distance in $(CH_3)_3P\cdot BBr_3$ is smaller than in the gas phase with the increment of the B–Br distance and the decrement of the BrBBr angle though these changes are not large as compared with their experimental errors. This is consistent with the foregoing remarks that the force constant of K(B–Br) is larger and the F(Br···Br) is smaller in the gas phase than in the solid phase. Thus it appears that the P–B dative bond in $(CH_3)_3P\cdot BBr_3$ is enhanced in the solid phase as well as the N–B bond in $(CH_3)_3N\cdot BX_3$.

Comparing the molecular structures of trimethylphosphine-boron trihalide complexes with those of trimethylamine-boron trihalide complexes, the boron-halogen bond distances in the trimethylphosphine complexes are a little larger than those in the trimethylamine complexes (r_g(B–Cl) = 1.836 ± 0.002 Å for $(CH_3)_3N\cdot BCl_3$ and r_g(B–Br) = 2.001 ± 0.003 Å for $(CH_3)_3N\cdot BBr_3$).[2] A stronger donor gives a larger change in an acceptor molecule on the formation of a complex, and thus it seems that trimethylphosphine is a stronger donor for boron trichloride and boron tribromide than trimethylamine.

The rotational barrier around the P–B bond of $(CH_3)_3P\cdot BBr_3$ is apparently higher than that of $(CH_3)_3P\cdot BCl_3$, 3.8 ± 0.7 kcal mol^{-1}.[6] It is interesting to note that this order is inverse to the order obtained for the trimethylamine complexes, $(CH_3)_3N\cdot BCl_3$ and $(CH_3)_3N\cdot BBr_3$.[2] The height of the rotational barriers for these complexes may be dominated by the repulsion due to the nonbonded atomic pairs, such as $Br_1\cdots H_6$ in the case of $(CH_3)_3N\cdot BBr_3$, which have the shortest distances among the atomic pairs between the methyl groups and halogen atoms. The above order for the trimethylamine complexes will be understandable because the $Br_1\cdots H_6$ distance (2.79 Å) in $(CH_3)_3N\cdot BBr_3$ is greater than the $Cl_1\cdots H_6$ distance (2.69 Å) in $(CH_3)_3N\cdot BCl_3$. However, the order for the trimethylphosphine complexes cannot be likewise understood because the $Br_1\cdots H_6$ distance (3.25 Å) in $(CH_3)_3P\cdot BBr_3$ is nearly equal to the $Cl_1\cdots H_6$ distance (3.27 Å) in $(CH_3)_3P\cdot BCl_3$.

References

1) K. Iijima and S. Shibata, *Bull. Chem. Soc. Jpn.*, **52**, 711 (1979).
2) K. Iijima and S. Shibata, *Bull. Chem. Soc. Jpn.*, **53**, 1908 (1980).
3) S. Geller and J. L. Hoard, *Acta Crystallogr.*, **4**, 399 (1951).
4) P. H. Clippard, J. C. Hanson, and R. C. Taylor, *J. Cryst. Mol. Struct.*, **1**, 363 (1971).
5) F. A. Cotton and J. R. Leto, *J. Chem. Phys.*, **30**, 993 (1959).
6) K. Iijima and S. Shibata, *Bull. Chem. Soc. Jpn.*, **52**, 3204 (1979).
7) D. L. Black and R. C. Taylor, *Acta Crystallogr., Sect. B*, **31**, 1116 (1975).
8) R. T. Markham, E. A. Dietz, Jr., and D. R. Martin, *J. Inorg. Nucl. Chem.*, **35**, 2659 (1973).
9) W. Witt, *Z. Naturforsch., Teil A*, **19**, 1363 (1964).
10) S. Shibata, K. Iijima, R. Tani, and I. Nakamura, *Rep. Fac. Sci. Shizuoka Univ.*, **9**, 33 (1974).
11) L. Schäfer, A. C. Yates, and R. A. Bonham, *J. Chem. Phys.*, **55**, 3055 (1971).
12) D. T. Cromer and J. B. Mann, *J. Chem. Phys.*, **47**, 1892 (1967); D. T. Cromer, *ibid.*, **50**, 4857 (1969).
13) C. Tavard, D. Nicolas, and M. Rouault, *J. Chim. Phys.*, **64**, 540 (1967).
14) Numerical experimental data of the leveled total intensity and the background have been deposited with the Chemical Society of Japan (Document No. 8141).

15) K. Iijima and S. Shibata, *Bull. Chem. Soc. Jpn.*, **47**, 1393 (1974).
16) J. E. Drake, J. L. Hencher, and B. Rapp, *Inorg. Chem.*, **16**, 2289 (1977).
17) "Kagaku Binran," 2nd ed, ed by the Chemical Society of Japan, Maruzen, Tokyo (1975), p. 1330.
18) K. Kuchitsu and S. J. Cyvin, "Molecular Structures and Vibrations," ed by S. J. Cyvin, Elsevier, Amsterdam (1972), Chap. 12.
19) K. Kuchitsu, *Bull. Chem. Soc. Jpn.*, **40**, 505 (1967).
20) L. S. Bartell and L. O. Brockway, *J. Chem. Phys.*, **32**, 512 (1960).
21) S. Konaka, T. Ito, and Y. Morino, *Bull. Chem. Soc. Jpn.*, **39**, 1146 (1966).
22) S. Konaka, Y. Murata, K. Kuchitsu, and Y. Morino, *Bull. Chem. Soc. Jpn.*, **39**, 1134 (1966).

Computer Counting of the Number of Water Molecules in the First Layer of Crystalline Water Clathrate

Iwao TABUSHI,* Yo-ichi KIYOSUKE, and Kazuo YAMAMURA
Department of Synthetic Chemistry, Kyoto University, Yoshida, Sakyo-ku, Kyoto 606
(Received November 4, 1980)

Semiempirical calculation of the number of water molecules in the first layer of water clathrates in crystalline state was developed by computer aided construction of hydrogen-bonded network of water molecules. In the generalized thermodynamic considerations on four possible types of "unit clathrate," van der Waals stabilization energy, "strain" energy of the unit clathrate, and entropy term due to the motional freedom of the guest were taken into account for the calculation of free energy change for the formation of the water clathrate. The results of calculations on 37 hydrophobic organic molecules well represented the trend of the reported experimental data of X-ray studies. The present calculation also disclosed such a large unfavorable strain energy (8.72 kcal·mol^{-1})† of pentakaidecahedron that it counteracts the van der Waals stabilization. The result is in a good agreement with the fact that pentakaidecahedral cavity is rarely seen in the gas hydrates. Most importantly, these semiempirical calculations of the energetics of water clathrates afforded valuable new insights into water assembly and may be extended to give better understandings of structured water in biological system and of water clusters that develop around apolar solutions in water.

Hydrophobic interaction is assumed to be one of the most significant factors that determine protein conformation and has provided a physicochemical basis for the concept of highly specific molecular recognition that many biological macromolecules exhibit.[1] Studies on properties of an apolar solute in water are particularly relevant to water structure study for elucidation and semiempirical determination of the hydrophobic interaction.[1,2a] However, the progress of an "iceberg" theory has been retarded by contradictory results from thermodynamic and spectroscopic studies.[2b-e] Moreover, no definitive evidence for the presence of strengthened water clusters around or in proximity to the hydrophobic surface of a solute molecule was obtained from spectroscopic experiments such as NMR.[2c,f]

Assumption of a generalized hypothetical process proposed for the molecular recognition between relatively simple host and guest and application of semiempirical force field potentials were found to claim a great advantage of the first layer model of water clusters in thermodynamic considerations.[3] Thus, in our most recent theoretical treatise on chemical model of biological molecular recognition, the observed free energy change for inclusion complexing of a hydrophobic guest by α-cyclodextrin in water could be successfully reproduced by applying the above concept of water clusters. Némethy and Scheraga had shown that the work requisite to break icelike structured water (water clusters) is proportional to the number of water molecules in the first layer of the water clusters developed around an apolar solute.[4a] Their treatment of cluster model has been continuously generalized and improved by use of modified partition function, incorporating the effects of cooperative hydrogen bonding on the continuous distribution of all possible cluster size.[4a-c]

Most importantly, the breaking of the water clusters around the guest is one of the most important and crucial factors associated with the process of biological molecular recognition and, in this context, greater sophistication is necessary in non- or semi-empirical evaluation of the number of water molecules in the first layer of water clusters around a guest molecule in order to derive the thermodynamic parameters rigorously. Fortunately a lot of insight have been accumulated into crystalline water clathrates from experiments,[5] although there is no direct physicochemical evidence from experiments for the presence of water clusters in a liquid state.[2]

A variety of hydrogen-bonded networks of water molecules in the crystalline state are thus far known, whose cavity includes various types of organic molecules. The unit structure of the water clathrate varies from dodecahedron composing of 20 water molecules to hexakaidecahedron composing of 28 water molecules, yet the actual hydrates involving so-called structure I or II have composite ratios of polyhedral cavities to form the complicated structures of the hydrate lattice.[5]

A semiempirical calculation of the number of water molecules in the first layer of water clathrate, the *unit clathrate*, was studied, by constructing and characterizing the hydrogen-bonded networks by computer method. Such the approach made a further progress in theoretical considerations of crystalline water clathrates, structured water in proteins[4d] and other molecules of biological interest, cyclodextrin[4e,f] being one of the simplest examples. In this article the authors wish to report the computer counting of the number of water molecules in the first layer for 37 hydrophobic molecules, where the predicted numbers are in good agreement with reported experimental data. In the extented procedure of the computer evaluation of the number of water molecules, we employed a fit criterion based on the thermodynamic consideration which takes van der Waals stabilization energy, "strain" energy of a polyhedron, and motional freedom of the guest into account. The present theoretical analyses have led us to the conclusions that (1) the rotational freedom of the guest is more critical than the van der Waals interaction for the stabilization of unit clathrates (2) pentakaidecahedron has too large "strain" energy to form a stable unit clathrate (3) a pentagon of hydrogen-bonded five water molecules is most appropriately used as the

† 1 cal=4.18 J.

metastable unit for the semiempirical constructions of the first layer of unit water clathrates. The energetics of water networks based on the semiempirical model was for the first time successfully developed to a simple expedient for the calculation of the number of water molecules. We are now in an advanced stage of the investigation of the water structure around apolar organic molecules in liquid water.

Method of Calculation

General Consideration of Network Construction and Computer Counting of Water Molecules. In Fig. 1a are shown fundamental parameters necessary to construct the hydrogen-bonded network of water molecules for the first layer model where r is the distance between two hydrogen-bonded oxygen atoms, and ϕ and ψ are bond angles defined by $O_2O_1O_3$ and $O_2O_1O_4$ in Fig. 1a, respectively. The fourth coordination of O_1 is neglected (first layer approximation), *viz.*, the hydrogen bond of O_1 to the water molecule in the second layer is regarded substantially the same as that in the bulk water.[6]

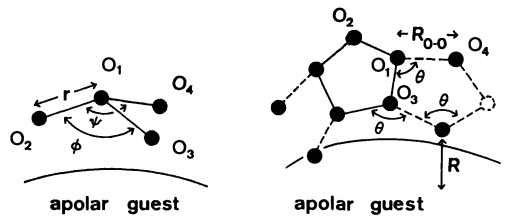

$R_{o-o}=2.8\pm0.1$ Å $\theta=108\pm5.8°$ $R_{vdw}\leq R\leq R_{vdw}+1.7$

Fig. 1. (a) Illustration of the distance r and the angles ψ, ϕ defined by hydrogen bond axis in the local structure of hydrogen-bonded networks of water molecules in the first layer of water clathrates. (b) Illustration of the distance R_{o-o} and the angle θ defined for the computer counting based on the method of "pentagon paving."

As preliminary trial of the network construction, we take three hydrogen bonds and van der Waals interaction between the guest and the surrounding network into consideration. Then, Cartesian coordinates (χ_j) of O_1 and O_2 are correlated by simple equations (1)—(3) to those of O_3 and O_4, of neighbored water molecules, where subscripts i and g refer to oxygen and guest,

$$\sum_{j=x,y,z}(\chi_{ji}-\chi_{j1})^2 = r^2 \quad (i=2,\ 3,\ \text{or}\ 4) \tag{1}$$

$$\sum_{j}(\chi_{j1}-\chi_{j2})(\chi_{j1}-\chi_{j2}) = r^2\cos\phi \ \text{ or } \ r^2\cos\psi \tag{2}$$

$$\sum_{j}(\chi_{ji}-\chi_{jg})^2 = R_{vdw}^2 \quad (i=1,\ 2,\ 3,\ \text{or}\ 4) \tag{3}$$

respectively, and R_{vdw} is the distance between the oxygen and the guest molecule.[7] Parameters were taken from structure I: $r=2.8$ Å, $\phi=\psi=108°$, and $R_{vdw}=3.32$ Å.[5] According to the requirements (1)—(3), consecutive determinations of coordinates of oxygen atoms were carried out for the case of argon, but the number of 12 obtained as the result of the iterative computer counting was much smaller than the X-ray results of 20 water molecules constructing a dodecahedron.[5]

Method of Pentagon Paving. Attempts to improve the disadvantage of the above somewhat complicated but still unsatisfactory treatment introduced to maximize both the vdw attractive interaction and the hydrogen bond energy, were made by introducing a pentagon which is composed of hydrogen-bonded five water molecules (Fig. 1b), since it is known that the pentagon is the important unit structure of the most stable forms of crystalline water[5] (structure I). The computer counting was executed iteratively, constructing pentagons in turn so as to satisfy geometrical relationships (4)—(6), where R_{o-o} is the distance between two

$$\sum_{j=x,y,z}(\chi_{ji}-\chi_{j1})^2 = R_{o\text{-}o}^2 \quad (i=2,\ 3,\ \text{or}\ 4) \tag{4}$$

$$\sum_{j}(\chi_{ji}-\chi_{j1})(\chi_{j2}-\chi_{j1}) = R_{o\text{-}o}^2\cos\theta \quad (i=3\ \text{or}\ 4) \tag{5}$$

$$\sum_{j}(\chi_{ji}-\chi_{j1})(\chi_{j3}-\chi_{j1}) = R_{o\text{-}o}^2\cos\theta \quad (i=2\ \text{or}\ 4) \tag{6}$$

hydrogen-bonded oxygen atoms, θ is the angle defined by three oxygen atoms (O–O\O), and χ are Cartesian coordinates of oxygen atom.[8]

Additional assumptions made for the present model are the followings: (1) The maximal allowancy of deformations of R_{o-o} and θ are 2.8 ± 0.1 Å and $108\pm5.8°$, respectively. Crystallographic data of water clathrate revealed that experimental values of R_{o-o} fall in the range of 2.8 ± 0.1 Å,[5p,g] and the allowancy of angle deformation ($\pm5.8°$) was, therefore, estimated on a basis of energetic equivalence to the bond deformation of 0.1 Å (0.112 kcal·mol^{-1}).

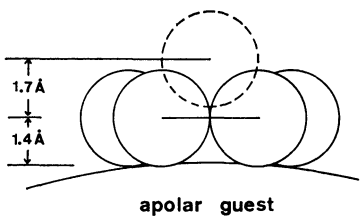

Fig. 2. A water molecule in contact with the pentagon illustrates the geometrical limit of the first layer water molecule ($R_{vdw}+1.7$ Å).

(2) A second water molecule comes into contact with the pentagon at a distance of 1.7 Å from the oxygen (Fig. 2). We, thus, assigned the distance of $R_{vdw}+1.7$ Å to the geometrical limit allowed for the first layer molecule, although the definition is a conceptual clue to the present semiempirical approach.

Fit Criterion Based on Thermodynamic Considerations. In view of the facts that hexagon appears in structure I and II which include relatively large guest molecules, four most probable polyhedra were employed as a *unit clathrate*; dodecahedron, tetrakaidecahedron, pentakaidecahedron, and hexakaidecahedron. At first the free energy change for the formation of the unit clathrate should be taken into the thermodynamic considerations.[8b] For the present purpose, all of possible free energies were introduced: van der Waals stabilization between the guest and the unit clathrate (ΔE_{vdw}),[9a] the "strain" energy of the hydrogen-bonded network of water molecules (ΔE_{strain}),[9b] and motional freedom

of the guest in the cavity (ΔS^g). The free energy change, ΔG, relevant to the formation of unit cell[9c] of crystalline water clathrate now can be calculated using Eq. 7. The number of water molecules in the first layer was calculated as shown in Scheme I, by combining the free energy calculation with the computer aided preconstruction of the network of water molecules for each postulated unit clathrate.

$$\Delta G = \Delta E_{vdw} + \Delta E_{strain} - T\Delta S^g$$
$$\Delta S^g = \Delta S^g_{rot} + \Delta S^g_{trans} + \Delta S^g_{vib} \quad (7)$$

	dodecahedron	tetrakaidecahedron	pentakaidecahedron	hexakaidecahedron
Guest	fit?	fit?	fit?	fit?
	yes	yes	yes	yes
Number of water molecule	20	24	26	28

Scheme 1.

Through the optimization of the atomic coordinates of the included guest molecule, the energy of van der Waals interaction (E_{vdw}) was maximized using Hill's potential[9d] (Eq. 8),

$$E_{vdw} = -2.25\varepsilon(r^*/r)^6 + 8.28 \times 10^5\varepsilon \exp(-r/0.0736r^*), \quad (8)$$

where r refers to the interatomic distance, r^* is the sum of the van der Waals radii of the two interacting atoms, and ε is a parameter which is defined individually for each pair of the two interacting atoms.[10]

The strain energy of the unit clathrate was calculated by use of semi-empirical force field potentials. The bond-stretching energy associated with the longitudinal deformation of the hydrogen bond is calculated by Eq. 9, where ΔR is the deviation from the equilibrium length of O···O distance (2.76 Å).[11] ΔE_θ and ΔE_α (Eqs. 10, 11) are angle strains relevant to deformations

$$\Delta E_R = \frac{1}{2}k_R(\Delta\bar{R})^2 \quad (9)$$

$$\Delta E_\theta = \frac{1}{2}k_\theta(\bar{R}-\bar{r})\bar{r}(\Delta\theta)^2 \quad (10)$$

$$\Delta E_\alpha = \frac{1}{2}k_\alpha r^{-2}(\Delta\alpha)^2 \quad (11)$$

$$\Delta E_{strain} = \Delta E_R + \Delta E_\theta + \Delta E_\alpha$$

of O–H···O angle and H–O–H angle, respectively, where R and r are the O···O and O–H bond lengths, respectively, and $\Delta\theta$ and $\Delta\alpha$ are the deformations from the equilibrium angles of O–H···O (180°) and H–O–H (109°28′), respectively. Reported parameters k_R= 22.7 kcal·mol^{-1}·Å^{-1}, k=12.7 kcal·mol^{-1}·Å^{-2}·rad^{-2}, and k_α=78.4 kcal·mol^{-1}·Å^{-2}·rad^{-2} were used.[11]

As to the motional freedom of the apolar guest,[9e] we calculated rotational freedom that makes largest contribution to the entropy term (ΔS^g). The vibrational entropy of a guest is assumed to be unchanged when the guest is sorbed within a unit clathrate of any cavity size. This assumption is supported by the following evaluation, *i.e.*, even a significant frequency change of 5 cm^{-1} for one vibration (1000 cm^{-1}) should accompany a very small entropy change of only 0.03 cal·deg^{-1}·mol^{-1}. One-dimensional, two-dimensional, and three-dimensional rotational entropies are given by Eqs. 12, 13, and 14, respectively, where N_A is Avogadro's number, κ is the Boltzman constant, h is the Planck constant, I is the moment of inertia, σ is the symmetry number, and T is the absolute temperature.

$$S^g_{rot(1\text{-}D)} = N_A\kappa\left\{\frac{1}{2}+\frac{1}{2}\ln\frac{8\pi^2 I\kappa T}{h^2}-\ln\sigma_1\right\} \quad (12)$$

$$S^g_{rot(2\text{-}D)} = N_A\kappa\left\{1+\ln\frac{8\pi^2 I\kappa T}{h^2\sigma_2}\right\} \quad (13)$$

$$S^g_{rot(3\text{-}D)} = N_A\kappa\left\{\frac{3}{2}+\frac{1}{2}\ln\frac{(8\pi^2\kappa T)^3 I_1 I_2 I_3}{h^6}-\ln\sigma_3\right\} \quad (14)$$

Calculations were aided by a digital computer FACOM M-190 OSIV/F4 at the Data Processing Center of Kyoto University.

Results and Discussion

The pentagon method was applied to eleven hydrophobic molecules and the counted number of water molecules in the first layer is listed in Table 1. The calculated results well reproduce experimental data. It is shown that rare gases and even methane or acetylene

Table 1. Results of counting of the number of water molecules in the first layer of unit clathrate based on the method of pentagon paving

Guest	Number of water molecules: Calcd	Number of water molecules: Exptl[5]
He	20 (dodecahedron)	
Ne	20 (dodecahedron)	
Ar	20 (dodecahedron)	20, 24
Kr	20 (dodecahedron)	20, 24
CH_4	20 (dodecahedron)	20, 24
HC≡CH	20 (dodecahedron)	20, 24
C_2H_6	unclosed 20	20, 24
Benzene	unclosed 20	28
Cl_2	20 (distorted dodecahedron)	20, 24
Br_2	unclosed 20	26
I_2	unclosed 20	

Table 2. The strain energy of unit clathrates (kcal·mol^{-1})

Unit Clathrate	ΔE_R[a]	ΔE_θ[b]	ΔE_α[c]	ΔE_{strain}
Dodecahedron	0.54	0.0	0.52	1.06
Tetrakaidecahedron	0.65	0.0	1.86	2.51
Pentakaidecahedron	3.84	0.0	4.88	8.72
Hexakaidecahedron	3.72	0.0	1.74	5.46

a) Longitudinal deformation of O···O from 2.76 Å, K_R= 22.7 kcal·mol^{-1}·Å^{-1}, Ref. 11. b) Angle deformation of O–H···O from 180°, K_θ=12.7 kcal·mol^{-1}·Å^{-2}·rad^{-2}, Ref. 11. c) Angle deformation of H–O–H from 109°28′, K_α=78.4 kcal·mol^{-1}·Å^{-2}·rad^{-2}, Ref. 11. d) Pentakaidecahedral cavity is very rare in the actual water clathrates. The extremely large strain energy (8.72 kcal·mol^{-1}) of unit pentakaidecahedron as well as the strain of ice lattice adjacent to pentakaidecahedron are reasonably attributed to the absence of pentakaidecahedral unit structure in clathrates.

TABLE 3. NUMBER OF WATER MOLECULES IN THE FIRST LAYER OF UNIT CLATHRATE AND CALCULATED VAN DER WAALS ENERGY AND STRAIN ENERGY

Guest		Calculated energies[a]				Number of water molecules	
		20	24	26	28	Calcd	Obsd[b]
He	A[b]	−0.76	−0.69	−0.76	−0.56		
	B[c]	0.30	1.82	7.96	4.90	n.s.[d]	
Ne	A	−1.66	−1.49	−1.67	−1.22		
	B	−0.60	1.02	7.04	4.24	20	
Ar	A	−4.82	−4.08	−4.40	−3.30		
	B	−3.67	−1.57	4.32	2.16	20	20, 24
Kr	A	−6.93	−5.58	−5.91	−4.46		
	B	−5.87	−3.07	2.80	1.00	20	20, 24
H_2	A	−1.67	−1.30	−1.30	−0.80		
	B	−0.61	1.21	7.42	4.66	20	
N_2	A	−3.58	−2.72	−2.68	−1.74		
	B	−2.52	−0.22	6.04	3.71	20	
O_2	A	−3.49	−2.65	−2.62	−1.69		
	B	−2.43	−0.14	6.10	3.78	20	
CO	A	−3.40	−2.90	−2.92	−2.10		
	B	−2.33	−0.40	5.80	3.36	20	
Cl_2	A	−9.20	−7.65	−7.31	−4.93		
	B	−8.14	−5.14	1.41	0.53	20	
Br_2	A	−9.05	−11.41	−11.30	−7.90		
	B	−8.00	−8.91	−2.56	−2.44	24	26
I_2	A	lp[e]	−15.01	−17.52	−13.11		
		lp	−12.50	−8.80	−7.66	24	
CH_4	A	−5.52	−4.21	−4.08	−2.62		
	B	−4.46	−1.71	4.64	2.84	20	20, 24
C_2H_6	A	−9.94	−7.17	−6.91	−4.38		
	B	−8.88	−4.66	1.88	1.08	20	20, 24
C_3H_8	A	lp	−11.48	−11.51	−9.41		
	B	lp	−8.99	−2.79	−3.96	24	28
$HC(CH_3)_3$	A	lp	−15.92	−14.75	−12.14		
	B	lp	−13.42	−6.03	−6.88	24	28
$C(CH_3)_4$	A	lp	lp	−16.52	−14.13		
	B	lp	lp	−7.81	−8.67	28	
$CH_2{=}CH_2$	A	−6.34	−5.27	−5.27	−4.29		
	B	−5.29	−2.77	3.45	1.17	20	20, 24
$HC{\equiv}CH$	A	−4.95	−4.03	−3.87	−2.66		
	B	−3.90	−1.53	4.85	2.80	20	20, 24
$CH_3CH{=}CH_2$	A	lp	−8.65	−8.99	−6.74		
	B	lp	−6.15	−0.28	−1.29	24	
$CH_3C{\equiv}CH$	A	lp	−7.64	−7.87	−5.69		
	B	lp	−5.13	0.85	−0.23	24	
$(CH_3)_2C{=}CH_2$	A	lp	−12.22	−11.52	−9.76		
	B	lp	−9.71	−2.80	−4.30	24	
$C_2H_5C{\equiv}CH$	A	lp	lp	lp	−7.38		
	B	lp	lp	lp	−1.92	28	
$CH_2{=}CH{\cdot}C{\equiv}CH$	A	lp	lp	lp	−5.80		
	B	lp	lp	lp	−0.35	28	
CH_3F	A	−6.23	−5.03	−4.93	−3.34		
	B	−5.18	−2.52	3.79	2.12	20	20, 24
CH_3Cl	A	−9.70	−7.69	−7.82	−5.63		
	B	−8.64	−5.18	0.90	−0.18	20	20, 24
CH_3Br	A	−10.98	−9.53	−9.29	−6.87		
	B	−9.92	−7.03	−0.57	−1.41	20	24
CCl_4	A	lp	lp	lp	−13.52		
	B	lp	lp	lp	−8.06	28	28
C_2H_3Cl	A	lp	−8.64	−8.96	−6.60		
	B	lp	−6.13	−0.24	−1.14	24	

Guest		Calculated energies[a]				Number of water molecules	
		20	24	26	28	Calcd	Obsd[5]
C_2F_4	A	−4.19	−8.22	−8.48	−6.85		
	B	−3.13	−5.72	0.24	−1.39	24	
C_3F_6	A	lp	lp	−10.52	−10.15		
	B	lp	lp	−1.79	−4.69	28	
Benzene	A	lp	−9.94	−6.76	−9.64		
	B	lp	−7.43	1.96	−4.19	24	28
Cyclopropane	A	−11.78	−9.67	−9.66	−6.93		
	B	−10.73	−7.17	−0.94	−1.47	20	
Ethylene oxide	A	−9.28	−7.17	−6.93	−4.49		
	B	−8.24	−4.66	1.79	0.97	20	24
CS_2	A	lp	−9.68	−10.34	−7.28		
	B	lp	−7.17	−1.62	−1.83	24	28

a) kcal·mol^{-1}. b) E_{vdw}. c) $E_{vdw}+E_{strain}$. d) Not stabilized. e) Largely positive.

can form a dodecahedron unit clathrate. In the case of chlorine molecule, the computer constructed network of twenty water molecules was found to have a structure of distorted dodecahedron, and each pentagons is to some extent constrained to take a puckered form. Further analyses of the results have disclosed that, incomplete constructions of water networks were seen for much larger molecules such as ethane, benzene, bromine, and iodine, and some portion of hydrophobic surfaces of those molecules are left uncovered by water molecules, four to eight more positions being open for water molecules to occupy in the region of the first layer (<1.7 Å). An advantageous clue to a priori prediction of the number of water molecules in the first layer is (a) thermodynamic consideration (*vide infra*) or (b) general modification of the paving method by incorporating the distribution of other possible diagrams than pentagon as well as with an improved concept of the first layer.

Table 3 shows the van der Waals energy and the quantitative effect of the strain energy of the polyhedron (Table 2) on the stabilization of the unit clathrate. It is apparent that the van der Waals stabilization energy decreases moderately and monotonously with the increase of the cavity size. However, since pentakaidecahedron and hexakaidecahedron have much larger strain energies (8.72 and 5.46 kcal·mol^{-1}, respectively) than the two smaller polyhedra (Table 2), the energy of the unit clathrate formation ($E_{vdw}+E_{strain}$) no longer correlates with the cavity size. For example, ethylene is most stabilized on forming the dodecahedron unit clathrate ($E=-5.29$ kcal·mol^{-1}), while the destabilization was greatest ($E=+3.45$ kcal·mol^{-1}) when it forms the pentakaidecahedron unit clathrate. Thus, the different extent of the contribution of E_{vdw} which counteracts E_{strain} resulted in a marked difference of formation energy ($E_{vdw}+E_{strain}$) of four unit clathrates (Table 3).

Remarkable van der Waals stabilizations obtained for cyclopropane ($E_{vdw}=-11.78$ kcal·mol^{-1}) and methyl bromide ($E_{vdw}=-10.98$ kcal·mol^{-1}) in dodecahedron, or isobutane ($E_{vdw}=-15.92$ kcal·mol^{-1}) and I_2 ($E_{vdw}=-15.01$ kcal·mol^{-1}) in tetrakaidecahedron, are most easily rationalized as a result of ideal fit of these molecules with the corresponding cavity size. Experimental values of ΔH for gases sorbed within preconstructed dodecahedral cavity are reported for only a few inert gases: Ar, $\Delta H=-6.1$ kcal·mol^{-1}; Kr, $\Delta H=-6.7$ kcal·mol^{-1}.[12] Therefore, the calculated values of E_{vdw}(−4.82 and −6.93 kcal·mol^{-1} for Ar and Kr, respectively) account for the most portion of the reported enthalpy changes. It is apparent from the results of Table 3 that the large portion of the net stabilization of the water clathrates originates in the large van der Waals stabilization, and the numbers of water molecules observed have been well reproduced by the present semi-empirical calculation. It has been approved, therefore, that many hydrates are stabler than ice I, those melting points being even higher than 0 °C.[1] In cases of small gas molecules (He, Ne, and H_2), however, the van der Waals attractive energy was too small to compensate the large strain energy of the unit clathrate (1.1 to 8.7 kcal·mol^{-1}). Thus the crucial magnitude of the strain energy resulted in no (or little) net stabilization of unit water clathrates of these molecules (Table 3). This result may explain why no X-ray study is thus far reported on these molecules.

In eight water clathrates (Ar, Kr, CH_4, C_2H_6, CH_2=CH_2, CH≡CH, CH_3F, and CH_3Cl), the present calculation gave the number of 20, *i.e.*, the dodecahedral unit brings more stabilization with these molecules than the tetrakaidecahedron does. Despite the above, two experimental numbers, 20 and 24, are known for those water clathrates[5] (structure I). It is most likely that the ensemble of the unit clathrate of dodecahedron alone hardly stabilizes the gross ice lattice. The enthalpy changes for the formation of structure I and structure II are reported by Child as 180 and 200 cal·mol^{-1}, respectively.[13a] This fact strongly indicates that even these actual clathrates have additional lattice energy, since the calculated energy (Table 2) predicts *ca.* one half of the observed value, *viz.*, 91 cal·mol^{-1} for 1 : 3 hybrid of dodecahedron and tetrakaidecahedron (structure I) and 110 cal·mol^{-1} for 12 : 8 hybrid of dodecahedron and hexakaidecahedron (structure II). This strongly indicates that, for the theoretical treat-

Table 4. Rotational entropy of guest molecules included by the cavity of each unit clathrate[a,b]

Guest	Dodecahedron	Tetrakaidecahedron	Pentakaidecahedron	Hexakaidecahedron
Br_2	0.0 (0)	0.0 (0)	16.03 (2)	16.03 (2)
I_2		0.0 (0)	0.0 (0)	17.57 (2)
C_3H_8		7.41 (1)	7.41 (1)	21.05 (3)
$HC(CH_3)_3$		0.0 (0)	8.68 (1)	22.12 (3)
$C(CH_3)_4$			0.0 (0)	20.52 (3)
$HC\equiv CH$	0.0 (0)	10.69 (2)	10.69 (2)	10.69 (2)
$CH_3C\equiv CH$		3.53 (1)	3.53 (1)	18.43 (3)
$(CH_3)_2C=CH_2$		0.0 (0)	0.0 (0)	22.68 (3)
CH_3Cl	3.52 (1)	3.52 (1)	17.56 (3)	17.56 (3)
CH_3Br	3.52 (1)	3.52 (1)	3.52 (1)	18.21 (3)
Benzene		0.0 (0)	0.0 (0)	20.47 (3)
CS_2		0.0 (0)	0.0 (0)	15.44 (2)

a) cal·mol^{-1}·deg^{-1}, 0°. b) Allowed mode of rotational freedom is given in the parenthesis.

ment of the lattice formation from unit clathrates, a semiempirical approach should be introduced to the mechanism of the strain relief over the gross crystalline lattice.

In addition, an exclusively new insight was given by the present calculations into the motional freedom of apolar molecules sorbed in water clathrates. In cases of relatively large molecules such as benzene, CS_2, and isobutane, a general trend is to be noted that the calculated number, 24, for those molecules (Table 3) is always smaller than the experimental value of 28. It is easily rationalized that in larger unit clathrates those molecules are endowed with much freedoms of restricted motions.[14] In Table 4 are listed the calculated entropies together with the rotational freedoms allowed for selected molecules. In Table 5 are given the numbers of water molecules predicted in the first layer of the water clathrate. As typically shown for propane, benzene, or CS_2, the rotational entropy drastically increases by the change of unit clathrate from pentakaidecahedron to hexakaidecahedron. As the result, the formation of hexakaidecahedral unit clathrate becomes more favorable, since the calculated ΔG value is large in the negative sign compared with those of other polyhedra (Table 5). In the case of benzene, the correct number of 28 was obtained. The results of Table 5 clearly indicate that the present calculation gives satisfactory number of water molecules in the first layer of unit clathrate, after the correction from rotational entropy term (see Table 5) is made. It is concluded, therefore, that the free energy minimization of unit clathrate can be used as the criterion for the formation of crystalline water clathrate.

The extraordinarily large strain energy of pentakaidecahedron (Table 2) rationalizes a fact that this unit structure is rare in the gas hydrates,[15] despite its appropriate cavity size for the accommodation of a relatively large guest molecule, or those large values of E_{vdw} in negative sign (Table 2) that is the intrinsically favorable factor for the formations of water clathrates.

In conclusion, it has been shown that the van der Waals interaction, the strain energy of the hydrogen-

Table 5. The free energy change (ΔG) for the formation of unit water clathrate and the calculated number of water molecules in the first layer of crystalline water clathrate

Guest	ΔG[a]				Number of water molecules	
	20	24	26	28	Calcd[b]	Found[5]
Ar	−3.76	−1.57	+4.32	+2.16	20 (24)	20, 24
Kr	−5.87	−3.07	+2.80	+1.00	20 (24)	20, 24
Cl_2	−11.93	−8.93	−2.38	−3.26	20 (24)	20, 24
CH_4	−7.16	−4.40	+1.94	+0.14	20 (24)	20, 24
C_2H_6	−13.26	−9.04	−2.50	−3.30	20 (24)	20, 24
$CH_2=CH_2$	−9.55	−7.03	−0.82	−3.10	20 (24)	20, 24
CH_3F	−9.62	−6.97	−0.66	−2.33	20 (24)	20, 24
CCl_4	lp	lp	lp	−14.44	28	28
	−13.60	−10.01	−3.56	−4.38	20	24
Br_2	−8.00	−8.91	−6.96	−6.82	24 (20)	26
I_2		−12.50	−8.80	−12.46	24, 28	
C_3H_8		−11.10	−4.82	−9.75	24 (28)	28
$HC(CH_3)_3$		−13.42	−8.40	−12.72	24 (28)	28
$C(CH_3)_4$			−7.81	−14.27	28	
$HC\equiv CH$	−3.90	−4.45	+1.93	−0.12	24 (20)	20, 24
$CH_3C\equiv CH$		−6.10	−0.12	−5.27	24 (28)	
$(CH_3)_2C=CH_2$		−9.71	−2.80	−10.57	28 (24)	
CH_3Cl	−9.60	−6.14	−3.90	−4.97	20	20, 24
CH_3Br	−10.89	−7.99	−1.53	−6.39	20	24
Benzene		−7.43	+1.96	−9.78	28	28
CS_2		−7.12	−1.62	−6.03	24 (28)	28

a) kcal·mol^{-1}. b) In parentheses are shown the number of water molecules of the penultimate unit clathrate which is the second most stable and less stable only within 2 kcal·mol^{-1} than the most stable unit clathrate.

bonded networks of water molecules, and the rotational freedom of the bound guest are the most important term which govern the formation of the water clathrates with hydrophobic molecules. The present study successfully provides the semiempirical basis for *a priori* computation of the number of water molecules in the first layer of the crystalline water clathrate and the present method may be fruitful enough to be extended to the significant problems of water clusters in solutions.

References

1) For example, M. H. Klapper, "Apolar Bond. A Re-evaluation," in "Progress in Bioorganic Chemistry," ed by E. T. Kaiser and F. J. Kezdy, John Wiley & Sons, New York (1973), Vol. 2, p. 55.

2) a) For example, R. A. Horne, "Water and Aqueous Solutions," John Wiley & Sons, New York (1972); b) H. S. Frank and M. W. Evans, *J. Chem. Phys.*, **13**, 507 (1945); c) W-Y. Wen and J. H. Hung, *J. Phys. Chem.*, **74**, 170 (1970), and references cited therein; d) A. H. Nartan and S. L. Lindenbaum, *J. Chem. Phys.*, **51**, 1108 (1969); e) K. Arakawa, "Ion and Solvents, (Kagaku Sosetsu)," ed by Chemical Society of Japan, Tokyo Univ. Press, Tokyo (1976), No. 11, Chaps. 2 and 3; f) A remarkable number of experimental approaches have been carried out in order to determine "total recognition" based on studies of "recognition element." Capped cyclodextrin: I. Tabushi, K. Shimokawa, N. Shimidzu, H. Shirakata, and K. Fujita, *J. Am. Chem. Soc.*, **98**, 7855 (1976); I. Tabushi, K. Fujita, and L. C. Yuan, *Tetrahedron Lett.*, **1977**, 2503. Metal capped cyclodextrin: I. Tabushi, N. Shimidzu, T. Sugimoto, M. Shiodzuka, and K. Yamamura, *J. Am. Chem. Soc.*, **99**, 7100 (1977). Water soluble heterocyclophane which binds $H_2PO_4^-$ I. Tabushi, Y. Kimura, and K. Yamamura, *ibid.*, **100**, 1304 (1978). Duplex cyclodextrin: I. Tabushi, K. Shimokawa, and Y. Kuroda, *ibid.*, **101**, 1614 (1979). Nucleosides binding lipophilic diammonium compound: I. Tabushi, J. Imuta, N. Seko, and Y. Kobuke, *ibid.*, **100**, 6287 (1978); R. Breslow and L. E. Overman, *ibid.*, **92**, 1075 (1970); R. Breslow and J. Emert, *ibid.*, **97**, 670 (1975); J. M. Lehn, E. Sonveaux, and A. K. Willard, *ibid.*, **100**, 4914 (1978).

3) a) I. Tabushi, Y. Kiyosuke, T. Sugimoto, and K. Yamamura, *J. Am. Chem. Soc.*, **100**, 916 (1978); b) That, by using pair potential, many Monte Carlo and molecular dynamics treatments well reproduce radical distribution, coordination number, or other properties of liquid water, strongly supports validity of the approximation of the first layer model of water clusters. MC: J. A. Barker and R. O. Watts, *Chem. Phys. Lett.*, **3**, 144 (1969); F. Abraham, *J. Chem. Phys.*, **61**, 1221 (1974); V. Sarkisov, V. G. Dashevsky, and G. G. Malenkov, *Mol. Phys.*, **27**, 1249 (1974); V. G. Dashevsky and G. N. Sarkisov, *ibid.*, **27**, 1271 (1974); (MC treatment of hydrophobic interaction); G. C. Lie, E. Clementi, and M. Yoshimine, *J. Chem. Phys.*, **64**, 2314 (1976), and references cited therein; A. J. C. Ladd, *Mol. Phys.*, **33**, 1039 (1977); M. R. Mruzik, *Chem. Phys. Lett.*, **48**, 171 (1977). MR: A. Rahman and F. H. Stillinger, *J. Chem. Phys.*, **55**, 3336 (1971); F. H. Stillinger and A. Rahman, *ibid.*, **57**, 1281 (1972); **60**, 1545, **61**, 4973 (1974).

4) a) G. Némethy and H. A. Scheraga, *J. Chem. Phys.*, **36**, 3401 (1962); *J. Phys. Chem.*, **66**, 1773, **67**, 2888 (1962); b) A. R. Hagler, H. A. Scheraga, and G. Némethy, *J. Phys. Chem.*, **76**, 3229 (1972); c) R. Lentz, A. T. Hagler, and H. A. Scheraga, *ibid.*, **78**, 1531 (1974); d) W. B. Dandliker and V. A. de Saussure, "Stabilization of Macromolecules by Hydrophobic Bonding," in "The Chemistry of Biosurfaces," ed by M. L. Hair, Marcel Dekker Inc., New York (1971), Chap. 1; e) Ref. 3 and references cited as Ref. 1; f) K. Lindner and W. Saenger, *Angew. Chem. Int. Ed. Engl.*, **17**, 694 (1978).

5) a) M. v. Stackelberg, *Die Naturwissenschaften*, **36**, 327 (1949); b) M. v. Stackelberg, *ibid.*, **36**, 359 (1949); c) M. v. Stackelberg and H. R. Muller, *Electrochem.*, **58**, 25 (1954); d) M. v. Stackelberg and W. Meinhold, *ibid.*, **58**, 40 (1954); e) M. v. Stackelberg and H. Fruhbuss, *ibid.*, **58**, 99 (1954); f) M. v. Stackelberg, *ibid.*, **58**, 104 (1954); g) M. v. Stackelberg and W. Jahns, *ibid.*, **58**, 162 (1954); h) M. v. Stackelberg and B. Meuthen, *ibid.*, **62**, 130 (1958); i) R. McMullan and G. A. Jeffrey, *J. Chem. Phys.*, **31**, 1231 (1959); j) D. Feil and G. A. Jeffrey, *ibid.*, **35**, 1963 (1961); k) M. Bonamica, G. A. Jeffrey, and R. K. McMullan, *ibid.*, **37**, 2219 (1962); l) G. A. Jeffrey and R. K. McMullan, *ibid.*, **37**, 2231 (1962); m) K. W. Allen and G. A. Jeffrey, *ibid.*, **38**, 2304 (1963); n) R. K. McMullan, M. Bonamica, and G. A. Jeffrey, *ibid.*, **39**, 3295 (1963); o) G. Beurskens, G. A. Jeffrey, and R. K. McMullan, *ibid.*, **39**, 3311 (1963); p) P. T. Beurskenss and G. A. Jeffrey, *ibid.*, **40**, 2800 (1964); q) R. K. McMullan and G. A. Jeffrey, *ibid.*, **42**, 2725 (1965); r) T. C. W. Mak and R. K. McMullan, *ibid.*, **42**, 2732 (1965).

6) A water molecule adjacent to the pentagon (first layer molecules) can independently form stable hydrogen bond, irrespective of the presence of an apolar solute, *i.e.*, as a safe approximation the local structure of water molecules in the second layer and at farther position was assumed to closely resemble that of bulk water.

7) We have encountered a difficulty that the number of sites possibly occupied by oxygens rapidly increases as the execution proceeds. A simple way of the counting to save the computing time was; two independently assigned positions of new oxygen atoms were compared after every loop of computer mapping, and if a site is judged to be doubly occupied within an error of 0.1 Å, then the computer program excludes one and reassigns a new serial number for all oxygens.

8) a) The pentagon method (Eqs. 4—6) employs preferential release of the strain energy (bond length and bond angle strain varying from 1.1 to 8.7 kcal·mol^{-1}) of an unit clathrate since van der Waals stabilization decreases only gradually with the increase of the distance of water molecule from the apolar guest. It, therefore, lightens restriction on the number of water molecules, leading to incorporation of sufficiently remote water molecules. The maximum limit allowed for the remote molecules is given by the elimination of the second layer water molecules from the present counting (Fig. 2). b) We deal with many different guest molecules which are in the gaseous state or in the liquid state at 0 °C, 1 atm. Therefore, it was necessary to constitute crystalline water clathrate from appropriate number of water molecules and a guest molecule, both in the same appropriate standard state, to allow comparison of the different ways that water molecules from the networks around apolar guest molecules of different shape and different size. Thus, for the present thermodynamic calculation, the clathrate was constituted from ice I and a guest molecule whose motional freedoms are freezed in a hypothetical isolated state.

9) a) At $r=\infty$, where r is the interatomic distance between the water molecule and the guest molecule, E_{vdw} equals zero. Therefore, the E_{vdw} value which was calculated by using Eq. 8 equals the van der Waals stabilization, ΔE_{vdw}. b) The "strain" energy of the unit clathrate, ΔE_{strain}, is given by $\Delta E_R+\Delta E_\theta+\Delta E_\alpha$ and designates the energy to form the unit clathrate from ice I whose "strain" energy is zero. c) Configuration change of a unit cell should be reflected in that of neighbors but as the first order approximation these trans-

mitting configuration effect is neglected in the present calculation. d) T. L. Hill, *J. Chem. Phys.*, **16**, 399 (1948), R. E. Hawkins, D. W. Davidson, *J. Phys. Chem.*, **70**, 1889 (1966). e) Based on the definition mentioned in Ref. 8b, motional freedom of the guest molecule allowed in the cavity is taken into the account. The rotational freedom of the guest molecule in the cavity made the largest contribution to ΔS^g, while the translational freedom should be negligible and the vibrational freedom is unchanged as discussed in the text.

10) a) Parameter ε is a geometrical mean of values for each of the two interacting atoms.

	H	C_{sp^3}	C_{sp^2}	C_{sp}	N
kcal·mol^{-1}	0.042	0.107	0.020	0.020	0.095
Ref	9d	10e	10b	10b	10b
	O	F	Cl	Br	I
kcal·mol^{-1}	0.116	0.109	0.314	0.434	0.623
Ref	10c	10b	10b	10b	10b
	S	He	Ne	Ar	Kr
kcal·mol^{-1}	0.314	0.017	0.07	0.235	0.326
Ref	10b	9d	9d	9d	9d

b) E. L. Eliel, N. L. Allinger, S. J. Angyal, and G. A. Morrison, "Conformational Analysis," John Wiley & Sons, New York (1965); c) N. L. Allinger, M. A. DaRooge, and R. B. Harmann, *J. Org. Chem.*, **26**, 3626 (1961); d) N. L. Allinger, J. A. Hirsch, M. A. Miller, and I. J. Tyminsky, *J. Am. Chem. Soc.*, **91**, 337 (1969); e) N. L. Allinger and W. Szkrybalo, *J. Org. Chem.*, **27**. 4601 (1962).

11) a) R. Zimmermann and G. C. Pimentel, "Advances in Molecular Spectroscopy," ed by A. Mangini, MacMillan, New York (1962); b) D. Eisenberg and W. Kauzmann, "The Structure and Properties of Water," Oxford at the Clarendon Press, London (1969); c) Potential functions used by us to calculate the "strain" energy of the unit clathrate were taken from a report by Zimmermann and Pimentel (Refs. 11a, b). They studied far-infrared spectrum of ice I at five temperatures and analyzed it as a five-atom system O···H-O-H···O. The k_R parameter reported was in a good agreement with force constants reported by others: Y. Kyogoku, *Nippon Kagaku Zasshi*, **81**, 1648 (1960); M. Tsuboi, *J. Chem. Phys.*, **40**, 1326 (1964); J. E. Bertie and E. Whalley, *ibid.*, **46**, 1271 (1967); d) Experiments of dielectric relaxation suggest that reorientation of the hydrogen bond of water molecule in gas hydrate is faster than that in ice I lattice and hydrogen atoms are randomly arranged in both gas hydrates and ice I (Refs. 11e—j). Therefore, in the framework of our thermodynamic treatment of isolated unit clathrate, it is a reasonable assumption that hydrogen atom is on the line of two oxygen atoms (O···H-O) in the unit clathrate; e) D. W. Davidson, M. M. Davies, and K. Williams, *J. Chem. Phys.*, **40**, 3449 (1964), and reference cited therein. f) R. P. Auty and R. H. Cole, *J. Chem. Phys.*, **20**, 1309 (1952); g) R. K. Chan, D. W. Davidson, and E. Whalley, *ibid.*, **43**, 2376 (1965); h) L. Pauling, *J. Am. Chem. Soc.*, **57**, 2680 (1935); i) S. W. Peterson and H. A. Levy, *Acta Crystallogr.*, **10**, 70 (1957); j) P. G. Owston, *Adv. Phys.*, **7**, 171 (1958).

12) R. M. Barrer and A. B. Edge, *Proc. R. Soc. London, Ser. A*, **300**, 1 (1967).

13) a) W. C. Child, Jr., *J. Phys. Chem.*, **68**, 1834 (1964); b) J. C. Platteeuw and J. H. van der Waals, *Mol. Phys.*, **1**, 91 (1958); c) J. H. van der Waals and J. C. Platteuw, *Adv. Chem. Phys.*, **2**, 1)1959); d) R. M. Barrer and D. J. Ruzicka, *Trans. Frady. Soc.*, **58**, 2239 (1962).

14) a) The entropy changes for dissociations of gases from gas hydrates were reported by Child (Ref. 13a): *e.g.*, CH_4, 20.5 ± 0.7 eu·mol^{-1}; CH_3Br, 23.6 ± 3.7 eu·mol^{-1}; C_3H_8, 26.2 ± 0.7 eu/mol at 273 K. The calculated entropy of translation of methane is 34.3 eu/mol at 273 K. This means that a portion of translational entropy and most of rotational entropy of methane are still preserved in the methane hydrate (structure, I, A 6.0 H_2O); b) That the rotational motion is partially allowed in water hydrates of ethers is supported by dielectric relaxation experiments: R. E. Hawkins and D. W. Davidson, *J. Phys. Chem.*, **70**, 1889 (1966).

15) a) Among the crystalline water clathrates investigated here, only Br_2 is known to be sorbed in a pentakaidecahedral cavity (Refs. 5k, m, 15b); b) S. Brownstein and D. W. Davidson, *J. Chem. Phys.*, **46**, 1454 (1967).

Resonance Energies of the Arenium Ions and Their Relevance to the Electrophilic Substitution Reactions

Jun-ichi AIHARA†

Department of Chemistry, Faculty of Science, Hokkaido University, Sapporo 060

(Received February 12, 1981)

Hyperconjugative interaction through the methylene group was incorporated in the framework of the Hückel molecular orbital model. Resonance energies of the arenium ions, derived from typical benzenoid hydrocarbons, were calculated using the graph theory of aromaticity. It was found that even a benzenium ion has a considerable degree of aromaticity. In general, the arenium ion with large localization energy has both large resonance energy due to hyperconjugation and large positive charge density at the methylene group. These two quantities are possibly responsible for the competition between substitution and addition reactions on the benzenoid hydrocarbons. An aromatic transition state tends to choose a reaction path to substitution products, at least, for these compounds.

It is widely known from the chemistry of aromatic hydrocarbons that solutions of these compounds in strong acidic media, such as concentrated sulfuric acid, show an intense color even if the pure compound is colorless.[1,2] The formation of an arenium ion, *i.e.*, a proton addition complex, is responsible for this phenomenon. An aromatic hydrocarbon is, therefore, characterized as a base, and the corresponding arenium ion as the conjugate acid. The cyclic π-electron system of an aromatic hydrocarbon is the electron source often sought not only by a proton but also by the reagent electrophile.[3,4] The arenium ions have been firmly established as intermediates in electrophilic substitution reactions, as well as numerous acid-catalyzed transformations of aromatics.[5,6] Thus, it is quite understandable that a considerable effort has been expended over the past years to elucidate the electronic structures of the arenium ions through their characterization by various theoretical as well as experimental methods.[1,2]

Above all, it has been argued that aromatic character of an aromatic hydrocarbon would be retained partly in the arenium ion.[7] This viewpoint is closely associated with possible hyperconjugation which should occur between the CH_2 group and the remaining π-electrons of the ring.[7,8] It has also been argued that the residual aromaticity in the arenium-type intermediate might be responsible for the occurrence of electrophilic substitution reactions.[4] The theoretical treatment of hyperconjugation shows that it should occur not only with the CH_2 group but also when one of the hydrogen atoms is replaced by any substituent group.[7,8] In this paper, I will first estimate the extent of hyperconjugation acting through the CH_2 group, and analyze in detail the electronic structure of arenium ions derived from typical benzenoid hydrocarbons. Our graph theory of aromaticity[9] will be applied to them to evaluate the resonance energies due to hyperconjugation. All the results will be examined in conjunction with the tendency of the benzenoid hydrocarbons to undergo electrophilic substitution reactions.

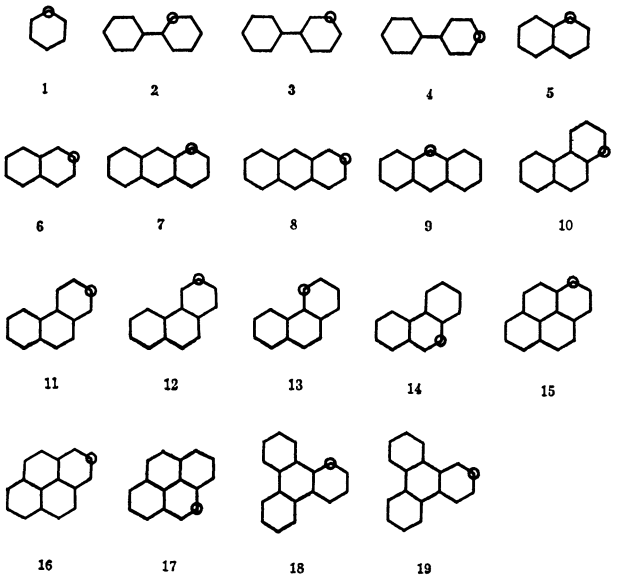

† Present address: Department of Chemistry, Faculty of Science, Shizuoka University, Oya, Shizuoka 422.

Hyperconjugation through the CH_2 Group

The graph theory of aromaticity has been described several times,[9,10] so it is not repeated here. The theory is based on the simple Hückel molecular orbital (HMO) model. The addition of a proton to the aromatic hydrocarbon destroys the sp^2-hybridized valence state of one of the carbon atoms, denoted by C*, and converts it into an sp^3-hybridized tetrahedral valence state.[7,8] In the arenium ion thus formed, one finds a CH_2 group adjacent to the remaining π-electron system. One hydrogen is believed to be above and the other below the plane,[11] the two hydrogens being denoted by H′ and H″.

In order to keep the algebra as simple as possible, we take one of the methylene orbital ϕ to be the composite bond orbital of π-symmetry,[12,13] namely,

$$\phi = \frac{1}{2}(\phi_1 - \phi_2), \qquad (1)$$

where ϕ_1 and ϕ_2 are the σ-bond orbitals localized along the C*–H′ and C*–H″ bonds, respectively. This constitutes a quasi-π orbital which functions like a π orbital in linear combinations with the $2p_z$ orbitals of the ring carbon atoms, in such a way as to yield a partial restoration of cyclic conjugation. This is nothing other than hyperconjugative interaction.

In order to incorporate the methylene orbital of π-symmetry in the HMO bonding model, two parameters,

h and k, must be determined for it. Here, h is related to the Coulomb integral for the quasi-π orbital, and k to the resonance integral for hyperconjugative interaction of this orbital with one of the adjacent $2p_z$ orbitals. By analogy with a hyperconjugative methyl orbital,[3] the value $h=2.0$ and $k=0.7$ may be applied to the methylene quasi-π orbital, too. Haddon recently reexamined hyperconjugation through the methylene group,[14] and suggested that a little smaller k value (≈ 0.5) might be more preferable for the methylene quasi-π orbital. At least, it gives a more reasonable diamagnetic anisotropy of cyclopentadiene.[14]

Heilbronner *et al.* adopted the simple bond orbital model to analyze the photoelectron spectra of cyclic alkanes,[13] and estimated the self-energy for the C–H bond orbital, A_{CH}, to be -15.67 eV and the cross term between two vicinal bond orbitals, $B_{CH,CH}$, to be -2.19 eV. In the simple HMO model, the self-energy corresponds to the Coulomb integral and the cross term to the resonance integral. From Eq. 1 the self-energy for the methylene quasi-π orbital can be set equal to $A_{CH}-B_{CH,CH}=-13.48$ eV. This represents a Coulomb integral for the methylene quasi-π orbital. For aromatic hydrocarbons, the resonance integral between two adjacent $2p_z$ orbitals has been estimated to be -2.7——-3.0 eV.[15] Then the Coulomb integral for each carbon $2p_z$ orbital lies in the -5.8——-6.5 eV range, depending upon the value adopted for the resonance integral. If we take all these numerical values into account, the $h=2.5$ value will become more suitable for the methylene quasi-π orbital.

Table 1. Energy separation between two occupied π orbitals for three dienes

Species	Experimental energy separation[a] eV[b]	HMO/β $h=2.0$ $k=0.5$	HMO/β $h=2.5$ $k=0.6$
1,4-Pentadiene	0.50	0.188	0.191
Cyclopentadiene	2.04	0.814	0.845
1,4-Cyclohexadiene	1.06	0.366	0.382

a) Ref. 16. b) 1 eV$=9.6525\times10^4$ J/mol.

Once this h value is adopted, the k value must next be determined in harmony with it. The simplest way of doing so is to make reference to the energy separations between the first and second π orbitals in such hydrocarbons as 1,4-pentadiene (0.50 eV), cyclopentadiene (2.04 eV), and 1,4-cyclohexadiene (1.06 eV).[16] The k value suitable for reproducing these energy separations were about 0.6. For this point, see Table 1. The set of HMO parameters suggested by Haddon, $h=2.0$ and $k=0.5$,[14] can likewise reproduce these energy separations. Conversely speaking, this kind of reproducibility supports the existence of hyperconjugative interaction through the CH_2 group. The above two sets of HMO parameters were employed to calculate resonance energies of arenium ions. For simplicity, all discussion will be made using the results based on our way of parametrization (*i.e.*, $h=2.5$ and $k=0.6$).

Resonance Energies of the Arenium Ions

Table 2 contains resonance energies of nineteen arenium ions derived from seven benzenoid hydrocarbons, together with their localization energies.[17] These resonance energies were calculated according to our graph theory of aromaticity.[9,10] An aromatic compound is characterized by the positive resonance energy, the magnitude of which indicates the degree of aromatic stabilization.[9,10,18] All energetic quantities are given in units of β or its absolute value β.

First, the simplest arenium ion, a benzenium ion, is predicted to have resonance energy of 0.094 β. If we adopt an effective β value reported for the resonance energies of benzenoid hydrocarbons ($\beta=3.562$ eV),[18] this resonance energy corresponds to 7.7 kcal/mol.†† Resonance energy of benzene is 0.273 β or 20.8 kcal/mol,[19,20] so the resonance energy of the benzenium ion amounts to about one-third that of benzene. Considering that benzene is one of highly aromatic compounds, the resonance energy of the benzenium ion is obviously far from negligible. Resonance energies of α-pyrone, γ-pyrone, furan, [10]annulene, and azulene are 0.044, 0.010, 0.010, 0.159, and 0.151, respectively, all in units of β.[9] Thus, the benzenium ion is much more aromatic than some weakly aromatic compounds, such as pyrones and furan, and is comparable in aromaticity to [10]annulene and azulene if the molecular sizes are taken into consideration.[21] As the benzenium ion is a monocyclic conjugated system, the whole resonance energy can be attributed to the hyperconjugative interaction through the CH_2 group; any resonance energy could not be anticipated without hyperconjugation.

In the case of polycyclic arenium ions, the situation is somewhat different. The contribution of the CH_2 group to aromaticity must be estimated relative to the resonance energy of some appropriate reference structure. A hypothetical compound with the same geometry but lacking conjugative interaction between the CH_2 group and the remaining π-electron system will serve for this purpose. The same structure has been used to calculate the localization energy.[17] The increment of resonance energy on introducing the hyperconjugative interaction in this reference structure can be interpreted as resonance energy due to hyperconjugation or hyperconjugative resonance energy (HRE). The HRE's are also listed in Table 2. It should be stressed that these HRE's are never negligible, either. Many of the polycyclic arenium ions indeed have HRE's comparable to that of the benzenium ion.

Hyperconjugative Resonance Energy and Electrophilic Substitution Reactions

The occurrence of electrophilic substitution reactions has been long regarded as an excellent indication of aromaticity.[3-16,22] However, we can easily show that

†† 1 $cal_{th}=4.184$ J.

TABLE 2. RESONANCE ENERGIES AND LOCALIZATION ENERGIES FOR TYPICAL ARENIUM IONS

Ion	LE[a]/β		RE[b]/β		HRE[c]/β	
	h=0.0 k=0.0	h=2.5 k=0.6	h=2.0 k=0.5	h=2.5 k=0.6	h=2.0 k=0.5	h=2.5 k=0.6
Benzenium (1)	2.536	2.953	0.085	0.094	0.085	0.094
2-Biphenylium (2)	2.400	2.774	0.289	0.297	0.082	0.091
3-Biphenylium (3)	2.544	2.963	0.337	0.345	0.082	0.090
4-Biphenylium (4)	2.447	2.830	0.294	0.303	0.085	0.092
1-Naphthalenium (5)	2.299	2.638	0.244	0.250	0.052	0.058
2-Naphthalenium (6)	2.480	2.873	0.209	0.217	0.080	0.089
1-Anthracenium (7)	2.231	2.544	0.344	0.348	0.041	0.045
2-Anthracenium (8)	2.423	2.789	0.308	0.315	0.067	0.074
9-Anthracenium (9)	2.013	2.279	0.403	0.406	0.020	0.023
1-Phenanthrenium (10)	2.318	2.663	0.378	0.385	0.063	0.070
2-Phenanthrenium (11)	2.498	2.898	0.352	0.362	0.091	0.101
3-Phenanthrenium (12)	2.454	2.836	0.356	0.365	0.081	0.090
4-Phenanthrenium (13)	2.366	2.726	0.373	0.380	0.070	0.078
9-Phenanthrenium (14)	2.299	2.637	0.411	0.417	0.054	0.060
1-Pyrenium (15)	2.190	2.494	0.447	0.452	0.044	0.049
2-Pyrenium (16)	2.549	2.969	0.414	0.424	0.101	0.112
4-Pyrenium (17)	2.274	2.601	0.470	0.475	0.047	0.052
1-Triphenylenium (18)	2.378	2.743	0.550	0.558	0.078	0.086
2-Triphenylenium (19)	2.477	2.869	0.541	0.550	0.090	0.099

a) Localization energy. b) Resonance energy. c) Hyperconjugative resonance energy.

TABLE 3. POSITIVE CHARGE DENSITY IN THE METHYLENE QUASI-π ORBITAL FOR TYPICAL ARENIUM IONS

Ion	PCD[a]	
	h=2.0 k=0.5	h=2.5 k=0.6
Benzenium (1)	0.146	0.139
2-Biphenylium (2)	0.129	0.124
3-Biphenylium (3)	0.147	0.140
4-Biphenylium (4)	0.133	0.128
1-Naphthalenium (5)	0.115	0.112
2-Naphthalenium (6)	0.137	0.132
1-Anthracenium (7)	0.106	0.104
2-Anthracenium (8)	0.128	0.124
9-Anthracenium (9)	0.083	0.084
1-Phenanthrenium (10)	0.118	0.114
2-Phenanthrenium (11)	0.140	0.154
3-Phenanthrenium (12)	0.133	0.128
4-Phenanthrenium (13)	0.124	0.119
9-Phenanthrenium (14)	0.115	0.112
1-Pyrenium (15)	0.101	0.099
2-Pyrenium (16)	0.147	0.140
4-Pyrenium (17)	0.111	0.108
1-Triphenylenium (18)	0.126	0.121
2-Triphenylenium (19)	0.137	0.131

a) Positive charge density in the methylene quasi-π orbital.

less aromatic compounds, in general, undergo electrophilic substitution reactions more rapidly. For example, furan undergoes substitution reactions much more rapidly than benzene when an appropriate electrophile attacks them.[23] In line with this, furan often reacts with electrophiles to form addition products.[23] Therefore, the tendency to undergo electrophilic substitution reactions is a vague criterion of aromaticity.[24]

In this connection, it seems quite likely that an electrophilic substitution reaction is not always an exothermic reaction. Let us consider the following pair of reactions: Suppose here that X and Y are hydrogen

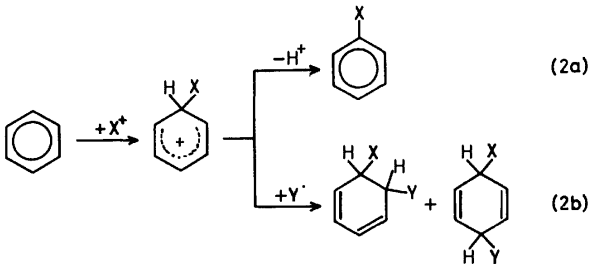

atoms. Heats of hydrogenation of benzene and 1,3-cyclohexadiene are 49.8 and 55.6 kcal/mol, respectively, in the gas phase.[25] 1,4-Cyclohexadiene also give a heat of hydrogenation comparable to that of 1,3-diene.[20] As stated before, benzene is highly aromatic with resonance energy of 20.8 kcal/mol.[19,20] If resonance energy of a given cyclic conjugated system were about 6 kcal/mol smaller than that of benzene, there would be no preference for substitution to addition reactions. Heats of reaction would become comparable for reactions of the types 2a and 2b. Many compounds are really considerably less aromatic than benzene.[9,10] Accordingly, such a situation might often be encountered even if X^+ and Y^- in Eq. 2 are replaced by an appropriate electrophile and nucleophile, respectively. In fact, it has been found that addition-accompanied substitution occurs in the chlorination of relatively simple benzenoid hydrocarbons, such as biphenyl and naphthalene.[26] As the situation is like this, the question may be raised why electrophilic substitution occurs preferentially.

By the way, localization energy (LE) has been successfully related to the rate of electrophilic substitution reaction.[3-6,17,27] The Wheland intermediate which appears during the reaction[17] is iso-π-electronic with a corresponding proton addition complex. According to the Hammond postulate,[28] the transition state must closely resemble the Wheland intermediate, because it is much higher in energy than the reactant and product. The effect of hyperconjugation has been neglected in the original LE theory,[3-6,17] but the present study shows that it must decrease the energy of the intermediate by 0.26—0.48 β (Table 2).

Now, let us return to the point. Stock suggested that the residual aromaticity in the transition state might be necessary for the occurrence of electrophilic substitution reactions.[4] The existence of this kind of resonance energy has already been clarified. The positive HRE is related exactly to the residual aromaticity. In this sence, Stock's suggestion appears to be worthy of serious consideration.

In order to obtain a clue to this problem, HRE was plotted against LE for the nineteen arenium ions (Fig. 1). Here and in Fig. 2, LE's defined for the systems with $h=0.0$ and $k=0.0$ are used. It was then found that HRE is closely related to LE, in such a manner that, when LE is large, HRE is large, too. This trend does not depend upon the type of the site to which a proton is attached. For example, the 9-anthracenium ion has both smaller LE and HRE than any other arenium ion investigated. The largest HRE is given by the 2-pyrenium ion, which necessarily has the largest LE. Since an electrophilic reaction takes place mostly *via* a Wheland intermediate with the smallest LE,[3-6] we might say that the reaction occurs mostly *via* the Wheland intermediate with the smallest HRE. This implies that most electrophilic reactions occur at the sites which are least favorable to the occurrence of substitution reactions.

This viewpoint is based on the fact that an aromatic species generally has not only thermodynamic but also

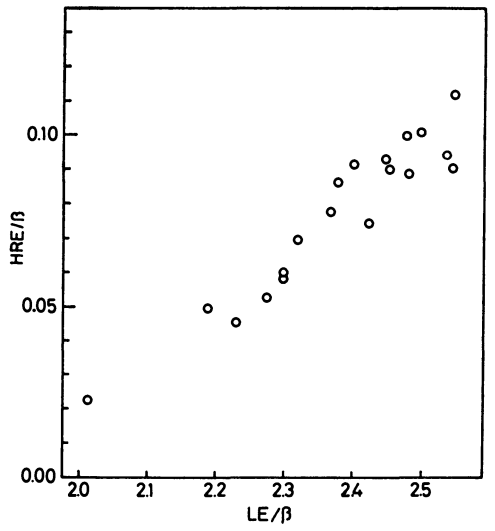

Fig. 1. Plot of hyperconjugative resonance energy (HRE) against localization energy (LE) for nineteen arenium ions.

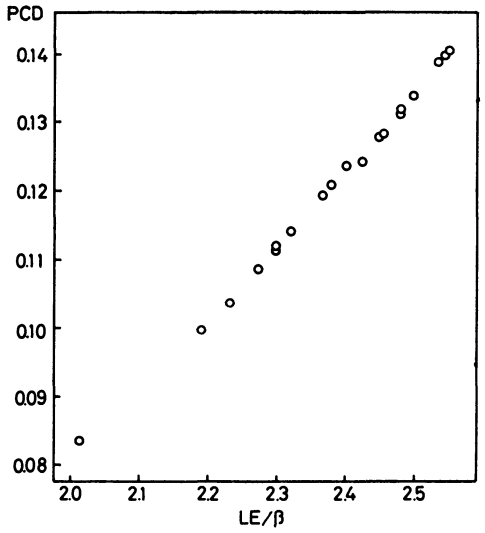

Fig. 2. Plot of positive charge density in the methylene quasi-π orbital (PCD) against localization energy (LE) for nineteen arenium ions.

kinetic stability.[29-31] In 1971, Hess and Schaad showed that the energy separation between the highest occupied molecular orbital and the lowest unoccupied molecular orbital is a linear function of the resonance energy per π-electron (REPE) for a variety of benzenoid hydrocarbons.[18,29] The REPE is a measure of aromatic stabilization, normalized with respect to the number of π electrons. Recently, Haddon and Fukunaga found an analogous relationship for the annulenes.[30] It then follows that an aromatic compound with larger resonance energy tends to retain its cyclic conjugated system, resisting addition-type reactions. Assigning such an attribute to the arenium ion and Wheland intermediates, we can reasonably infer that a highly aromatic intermediate would tend to refrain from taking paths to addition products. Addition products obviously break the cyclic conjugated system of the intermediate. On the other hand, a poorly aromatic intermediate would be willing to take paths to addition products.

The above inference is in fact supported by the work of de la Mare's group.[26] They studied the chlorination of benzenoid hydrocarbons with a molecular chlorine. The chlorine is a highly selective reagent.[32] It was found that significant proportions of by-products were formed by addition of chlorine or chlorine acetate derived from chlorine and acetic acid solvent.[26] There seems to be a general tendency for addition to become prominent as the reactivity of the hydrocarbon increases. Thus, the order of proportions of addition to substitution products was phenanthrene>naphthalene>triphenylene>biphenyl$\gg$benzene. This is exactly the same order as that of the overall reaction rates.[26] Anthracene probably comes first.[3] It is widely known that the 9 position of anthracene has a greater tendency toward electrophilic addition than the 9 position of phenanthrene.[4,33] It has been accepted that the overall reaction rate is determined by the smallest LE conceivable in the compound.[3,4] A greater overall reaction rate corresponds to the smaller LE, and a greater

proportion of the addition products to the smaller HRE. Competition between substitution and addition reactions can thus be related to the aromatic character of the Wheland intermediate.

Here, there is an exception to the order of experimental reaction rates; it is phenanthrene *vs.* naphthalene. LE of the 9-phenanthrenium ion is comparable to that of the 1-naphthalenium ion. However, the greater reactivity of phenanthrene than naphthalene is experimentally commonplace, and has been observed is several substitution reactions.[33] Unfortunately, this problem is beyond the scope of the HMO model, and should be treated by more sophisticated methods.[27]

Charge Density in the Methylene Quasi-π Orbital

When substitution occurs, the Wheland intermediate loses a proton to the nucleophile, and so reverts to an aromatic π-electron ring, now substituted with the electrophilic group.[3-6] It is noteworthy that salts of substituted benzenium ions can be isolated as crystalline materials or observed by spectroscopic techniques in non-nucleophilic solvents.[1,2,34] In this view, we may expect that, the greater the positive charge density (PCD) in the methylene orbital is, the easier should it be to remove hydrogen as a proton. If PCD is low in the methylene orbital, the chance that nucleophilic addition occurs to the remaining π-electron system would be great. In this connection, Dixon regarded the charge density on the protons of the CH_2 group as a measure of proton loss, leading to overall substitution.[12]

We can examine this effect by means of the present bonding model. Hyperconjugation permits a considerable migration of negative charge into the ring from the methylene quasi-π orbital. The PCD is induced as a result of partial equalization of the charge distribution. Table 2 and Fig. 2 indicate how the positive charge in the methylene quasi-π orbital correlates with LE for the benzenoid hydrocarbons studied. We see therefrom that PCD is almost linearly related to LE and, hence, to the overall reaction rate. This suggests that the leaving ability of hydrogen as a proton might be enhanced in the case of the arenium ions with large LE's. In other words, proton loss occurs more readily to restore the fully aromatic sextet when there is more extensive delocalization of the positive charge. This indicates that PCD reflects the magnitude of HRE straightforwardly. Accordingly, the tendency of a benzenoid hydrocarbon to undergo electrophilic substitution, predicted from the PCD, bears a close resemblance to the tendency predicted from the HRE. Both are naturally in good accord with experiment. The two effects seem to enhance cooperatively the preference for substitution reactions. In our chemical sence, it seems that HRE tends to avoid adding a nucleophile to the π-electron system, while PCD tends to eliminate a proton, both resulting in the same substitution reaction.

However, it should be stressed that HRE is not always a single determinant for the occurrence of substitution reactions. For example, pyrene is much more reactive than phenanthrene.[3,4,27,33] but the addition products have not been observed appreciably. Since HRE is at most 8 kcal/mol for any compound, the other factors, such as the size of an electrophile and a steric effect in the addition product, cannot be neglected in tracing a reaction path. By inspecting the molecular model, it was found that every ring in pyrene might be subject to some steric restriction when it undergoes an addition reaction. The restriction appears very severe in the case of addition reactions starting from the 1-pyrenium-type intermediate. In such a case, addition-elimination routes to substitution products become important.

Concluding Remarks

Three of the most characteristic properties of aromatic compounds are the thermodynamic stability, the diamagnetic susceptibility exaltation, and the tendency to undergo electrophilic substitution reactions. The first two properties can be analyzed consistently in terms of our graph theory of aromaticity.[9,10,35] For the first time, this theory succeeded in unifying the two concepts.[35] Along with these physical properties, the tendency to undergo electrophilic substitution reactions has been widely used as a purely chemical criterion of aromaticity.[22,36]

As stated before, this criterion is quite empirical. To make matters worse, it is not always related to aromaticity.[24,36] The tropylium ion, accepted as an example of a nonbenzenoid aromatic species, does not react with electrophiles.[36] On the contrary, a 2,3-dihydro-1,4-diazepinium ion undergoes many electrophilic substitution reactions, although it has no cyclic conjugated system.[36] In this sence, there is an obvious limitation in the present approach. It does not apply to the Wheland intermediates which are aromatically- or hetero-atom-stabilized species.[37] For example, the aromatically-stabilized intermediates are those derived from azulene and calicene. The azulenium and 2-calicenium ions are both Hückeloid aromatic cations with substituents. The hetero-atom-stabilized systems are exemplified by the Wheland intermediates derived from pyrrole and a 2,3-dihydro-1,4-diazepinium ion.

Electrophilic substitution is indeed a complicated chemical process.[5,6,38] To the best of my knowledge, there have been few logical approaches to the competition between substitution and addition reactions. Therefore, the present approach might be regarded as a first significant step forward, although its application is limited to benzenoid hydrocarbons. This approach not only unveiled some important features of aromatic substitution, but also enabled us to trace reaction routes to substitution products more closely than before. All the reasoning is relatively simple and understandable.

In summary, I have considered both the ability of the CH_2 group to function as a hyperconjugator and the ability to dissociate a proton. HRE represents the energy difference between a real hyperconjugative system and its hyperconjugative reference structure. Stock's suggestion that electrophilic substitution might

occur *via* an aromatic transition state[4] has been verified and generalized in terms of HRE. It was theoretically conciliated with Dixon's measure of proton loss defined using PCD.[12] If the Wheland intermediate were absolutely olefinic in nature, a significant proportion of addition products would be obtained, because there is no tendency for polyenic cations to undergo electrophilic substitution reactions. In general, if the parent compound is not aromatic, the corresponding proton addition complex has no HRE. This might be the main reason why electrophilic substitution is limited mostly to aromatic compounds.

The use of the facilities of the Hokkaido University Computing Center is gratefully acknowledged.

References

1) H.-H. Perkampus, *Adv. Phys. Org. Chem.*, **4**, 195 (1966).
2) D. M. Brouwer, E. L. Mackor, and C. MacLean, "Carbonium Ions," ed by G. A. Olah and P. v. R. Schleyer, Wiley, New York (1970), Vol. II, p. 837.
3) A. Streitwieser, Jr., "Molecular Orbital Theory for Organic Chemists," Wiley, New York (1961), Chap. 11.
4) L. M. Stock, "Aromatic Substitution Reactions," Prentice-Hall, Englewood Cliffs, N. J. (1968), Chap. 2.
5) T. H. Lowry and K. S. Richardson, "Mechanism and Theory in Organic Chemistry," Harper & Row, New York (1976), Chap. 7.
6) F. Badea, "Reaction Mechanisms in Organic Chemistry," Abacus Press, Tunbridge Wells, Kent (1977), Chap. 7.
7) N. Muller, L. W. Pickett, and R. S. Mulliken, *J. Am. Chem. Soc.*, **76**, 4770 (1954).
8) K. Fukui, T. Yonezawa, and C. Nagata, *Bull. Chem. Soc. Jpn.*, **27**, 423 (1954).
9) J. Aihara, *J. Am. Chem. Soc.*, **98**, 2750, 6840 (1976); I. Gutman, M. Milun, and N. Trinajstić, *ibid.*, **99**, 1692 (1977).
10) J. Aihara, *J. Am. Chem. Soc.*, **100**, 3339 (1978); *Bull. Chem. Soc. Jpn.*, **51**, 3540 (1978); *Chem. Phys. Lett.*, **73**, 104 (1980); A. Sabljić and N. Trinajstić, *J. Mol. Struct.*, **49**, 415 (1978); P. Ilić and N. Trinajstić, *J. Org. Chem.*, **45**, 1738 (1980); B. A. Hess, Jr., and L. J. Schaad, *ibid.*, **41**, 3058 (1976); B. A. Hess, Jr., L. J. Schaad, and I. Agranat, *J. Am. Chem. Soc.*, **100**, 5268 (1978); W. C. Herndon and C. Párkányi, *Tetrahedron*, **34**, 3419 (1978); W. C. Herndon, *Tetrahedron Lett.*, **1979**, 3283.
11) W. C. Ermler, R. S. Mulliken, and E. Clementi, *J. Am. Chem. Soc.*, **98**, 388 (1976).
12) W. T. Dixon, *J. Chem. Soc., B*, **1970**, 612.
13) G. Bieri, J. D. Dill, E. Heilbronner, and A. Schmelzer, *Helv. Chim. Acta*, **60**, 2234 (1977); E. Heilbronner, *ibid.*, **60**, 2248 (1977).
14) R. C. Haddon, *Aust. J. Chem.*, **30**, 1 (1977).
15) See, *e.g.*, J. H. D. Eland and C. J. Danby, *Z. Naturforsch. Teil. A*, **23**, 355 (1968); J. H. D. Eland, *Int. J. Mass Spectrom. Ion Phys.*, **9**, 214 (1972); R. Boschi, J. N. Murrell, and W. Schmidt, *Faraday Discuss. Chem. Soc.*, **54**, 116 (1972); W. Schmidt, *J. Chem. Phys.*, **66**, 828 (1977).
16) G. Bieri, F. Burger, E. Heilbronner, and J. P. Maier, *Helv. Chim. Acta*, **60**, 2213 (1977).
17) G. W. Wheland, *J. Am. Chem. Soc.*, **64**, 900 (1942).
18) J. Aihara, *J. Am. Chem. Soc.*, **99**, 2048 (1977).
19) M. J. S. Dewar and C. de Llano, *J. Am. Chem. Soc.*, **91**, 789 (1969).
20) R. B. Turner, B. J. Mallon, M. Ticky, W. v. E. Doering, W. R. Roth, and G. Schröder, *J. Am. Chem. Soc.*, **95**, 8605 (1973).
21) J. Aihara, *Bull. Chem. Soc. Jpn.*, **50**, 3057 (1977).
22) F. A. Carey and R. Sundberg, "Advanced Organic Chemistry," Plenum Press, New York (1977), Part A, Chap. 9.
23) L. A. Paquette, "Principles of Modern Heterocyclic Chemistry," W. A. Bemjamin, New York (1968), Chap. 4.
24) J. Aihara, *Bull. Chem. Soc. Jpn.*, **53**, 2689 (1980).
25) G. B. Kistiakovsky, J. R. Ruhoff, H. A. Smith, and W. E. Vaughan, *J. Am. Chem. Soc.*, **58**, 146 (1936).
26) P. B. D. de la Mare, *Acc. Chem. Res.*, **7**, 361 (1974); G. H. Beaven, P. B. D. de la Mare, M. Hassan, E. A. Johnson, and N. V. Klassen, *J. Chem. Soc.*, **1961**, 2749; G. H. Beaven, P. B. D. de la Mare, E. A. Johnson, and N. V. Klassen, *ibid.*, **1962**, 988; G. W. Burton, P. B. D. de la Mare, L. Main, and B. N. B. Hannan, *J. Chem. Soc., Perkin Trans. 2*, **1972**, 265.
27) A. Streitwieser, Jr., P. C. Mowery, R. G. Jesaitis, and A. Lewis, *J. Am. Chem. Soc.*, **92**, 6529 (1970).
28) G. S. Hammond, *J. Am. Chem. Soc.*, **77**, 334 (1955).
29) B. A. Hess, Jr., and L. J. Schaad, *J. Am. Chem. Soc.*, **93**, 305, 2413 (1971); *J. Org. Chem.*, **36**, 3418 (1971).
30) R. C. Haddon and T. Fukunaga, *Tetrahedron Lett.*, **1980**, 1191.
31) I. Gutman, *Z. Naturforsch., Teil. A*, **35**, 458 (1980).
32) S. F. Mason, *J. Chem. Soc.*, **1959**, 1233.
33) See, *e.g.*, L. Altschuler and E. Berliner, *J. Am. Chem. Soc.*, **88**, 5837 (1966).
34) G. A. Olah, J. S. Staral, G. Asencio, G. Liang, D. A. Forsyth, and G. D. Mateescu, *J. Am. Chem. Soc.*, **100**, 6299 (1978).
35) J. Aihara, *J. Am. Chem. Soc.*, **101**, 558, 5913 (1979).
36) D. Lloyd and D. R. Marshall, *Angew. Chem., Int. Ed. Engl.*, **11**, 404 (1972).
37) G. A. Olah, *Science*, **168**, 1298 (1970); *Angew. Chem., Int. Ed. Engl.*, **12**, 173 (1973).
38) See, *e.g.*, E. B. Pedersen, T. E. Petersen, K. Torssell, and S.-O. Lawesson, *Tetrahedron*, **29**, 579 (1973); C. L. Perrin, *J. Am. Chem. Soc.*, **99**, 5516 (1977).

Optical Properties of Undoped and AsF_5 Doped "Poly(4,4'-biphenylylene)" Films

Atsushi WATANABE, Hitoshi FUJIMOTO, Masashi TANAKA,* and Jiro TANAKA
Department of Chemistry, Faculty of Science, Nagoya University, Chikusa-ku, Nagoya 464
(Received September, 3, 1980)

Optical absorption and reflection measurements are carried out on undoped and AsF_5 doped films of "poly(4,4'-biphenylylene)" over a wide wavelength region (300—50000 cm^{-1}). In the doped polymer, the free carrier absorption band appears in the IR region and the dc conductivity is estimated from the observed spectrum. The obtained value (σ_0=376 S cm^{-1}) is two orders of magnitude larger than the value (σ_0=2 S cm^{-1}) observed by the conductivity measurement. The discrepancy may be due to the existence of many cracks on the films.

There is now a large and rapidly growing interest in conducting derivatives of organic polymers. Polymers such as doped polyacetylene,[1] doped poly(*p*-phenylene),[2] doped polypyrrole,[3-5] and doped poly(thio-*p*-phenylene)[6,7] were reported to exhibit high electrical conductivity. Polyacetylene is obtained as flexible and crystalline film, however, it is insoluble and infusible. Other polymers, such as electrochemically prepared polypyrrole, poly(thio-*p*-phenylene) are insoluble in common solvents.

We have recently reported the conducting polymer prepared by AsF_5 oxidation of benzene soluble polymer: "poly(4,4'-biphenylylene)."[8] In the present paper, we describe about the electrical and optical properties of pure and AsF_5 doped "poly(4,4'-biphenylylene)."

Experimental

"Poly(4,4'-biphenylylene)" was readily prepared by heating a suspension of the 4,4'-benzidinebis(diazonium) chloride–CuCl complex in pure water (80 °C, 1 h),[9,10] although poly(*p*-phenylene)[11,12] was synthesized by direct polymerization as is shown in Fig. 1. The dark-brown polymer was then separated into two fractions by extraction with benzene. The soluble portion was fractionally precipitated by adding petroleum ether and separated into two fractions by extraction with acetone.

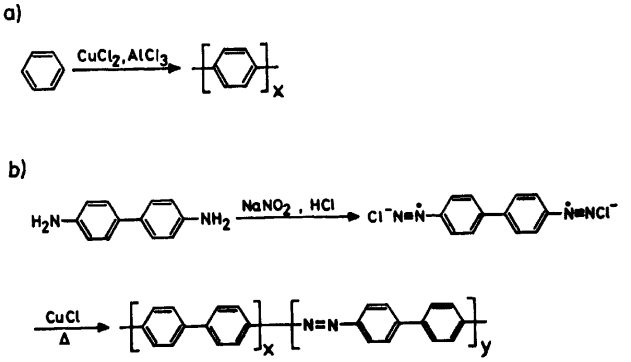

Fig. 1. Preparation of a) poly(*p*-phenylene), b) "poly(4,4'-biphenylylene)."

Reaction of AsF_5 gas with the benzene soluble and acetone insoluble polymer produced a blue-black material and the doped level were adjusted by doping time under 200 mmHg (1 mmHg=133.322 Pa) of AsF_5 gas. For the sample doped for 40 h, the uptake of AsF_5 measured by weight increases corresponds to *ca.* one AsF_5 molecule per phenyl group.

The film was made by dropping the dioxane solution of "poly(4,4'-biphenylylene)" on the four probe plate and then drying. The films were doped with AsF_5 and pumped for about one hour. After that, the doped films were connected to an apparatus for measuring the dc conductivity. The electrical conductivity was measured under nitrogen by the standard four probe method.

The absorption spectra of pure and AsF_5 doped films on a KBr or quartz plate were measured *in vacuo* with Hitachi IR 260-50 (300—4000 cm^{-1}) and Carl Zeiss M4Q (4000—50000 cm^{-1}) spectrophotometers. The reflection measurement of pure thick "poly(4,4'-biphenylylene)" film on a glass plate was made with Hitachi IR 260-50 and a microscopic spectrophotometer (4000—50000 cm^{-1}) made in our laboratory. It consists of an Olympus microscope, a Carl Zeiss Ultrafluar lens (×10), a Nikon crystal mount, a HTV 928 photomultiplier and a PbS tube, and an Intel 8080 microcomputer for data processing.

The Kramers-Kronig (K-K) transformation of the reflection spectra and the best fit of the absorption and reflection spectra by SALS program were made on a Facom M-200 computer of Nagoya University.

Results and Discussion

"Poly(4,4'-biphenylylene)" was identified to be a copolymer of 1,4-biphenyldiyl and azo-1,4-biphenyldiyl compounds (x : y=4 : 1).[9,10] Accordingly, the excited wave function (Ψ_e) of this polymer can be expressed by the superposition of the locally excited configurations of polyphenyl (Φ_{ph}) and azo (Φ_{azo}) groups and the charge transfer (Φ_{CT}) configurations between these two groups.[13]

$$\Psi_e = c_1\Phi_{ph} + c_2\Phi_{azo} + c_3\Phi_{CT} \quad (1)$$

and the transition moment between the ground (Ψ_0) and excited states can be given as follows,

$$(\Psi_e|M|\Psi_o) = c_1(\Phi_{ph}|M|\Psi_0) + c_2(\Phi_{azo}|M|\Psi_o). \quad (2)$$

However, the azo group has a weak absorption band at 350 nm whose intensity has been reported to be ε=5.[14] Therefore, the second term of the right side in Eq. 2 can be neglected and the visible absorption spectra of "poly(4,4'-biphenylylene)" may be considered to be similar to that of polyphenyl group. A benzene molecule has six π-electrons which are considered free to delocalize along the phenyl ring. These π-electrons form two single and two double degenerate π-orbitals (ϕ_i, i=1—6). In the polyphenyl system, π-bands $\psi_i(k)$ can be expressed by the linear combination of π-orbitals in each ring

$$\phi_i(k) = \frac{1}{\sqrt{N}}\sum_n e^{ikR_n}\phi_n^i \quad (i=1\text{—}6). \tag{3}$$

The energies $\varepsilon_i(k)$ of π-bands are calculated according to MO theory,

$$\begin{aligned}
\varepsilon_1(k) &= \alpha + 2\beta + \tfrac{1}{3}\beta' \cos(ka)\\
\varepsilon_2(k) &= \alpha + \beta - \tfrac{2}{3}\beta' \cos(ka)\\
\varepsilon_3(k) &= \alpha + \beta\\
\varepsilon_4(k) &= \alpha - \beta + \tfrac{2}{3}\beta' \cos(ka)\\
\varepsilon_5(k) &= \alpha - \beta\\
\varepsilon_6(k) &= \alpha - 2\beta - \tfrac{1}{3}\beta' \cos(ka),
\end{aligned} \tag{4}$$

where β is the resonance integral between successive carbon atoms in the same ring and β' in the different ring. All π-electrons are filled in the three bands of $\varepsilon_1(k)$, $\varepsilon_2(k)$, and $\varepsilon_3(k)$ as is shown in Fig. 2-a.

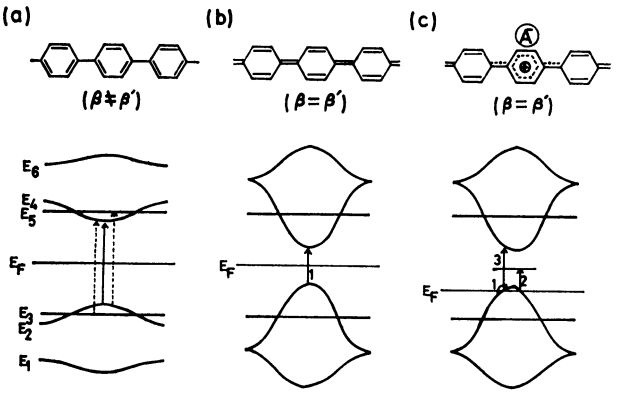

Fig. 2. Electronic structure of the polyphenyl system.

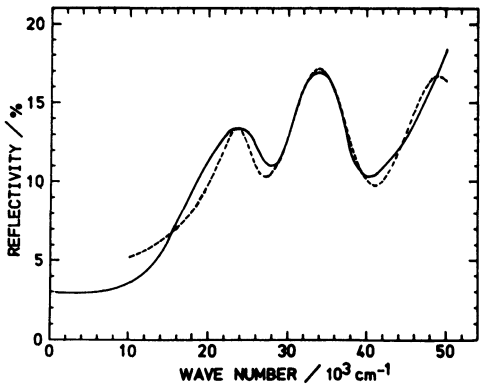

Fig. 3. Reflection spectra of "poly(4,4'-biphenylylene)." ——: Observed, ------: calculated (SALS).

Figure 3 shows the reflection spectrum of the pure polymer film of "poly(4,4'-biphenylylene)." The first band at 24000 cm^{-1} has the reflectivity of 13.4% and the second band at 34000 cm^{-1} has that of 17.1%. The third band is located in the region of higher wave number than 50000 cm^{-1}. Accordingly, the first band at 24000 cm^{-1} can be assigned to the transition from the $\varepsilon_2(k=0)$ band to the $\varepsilon_4(k=0)$ band. The second band consists of the overlap of two transitions of $\varepsilon_2(k=0)\rightarrow\varepsilon_5(k=0)$ and $\varepsilon_3(k=0)\rightarrow\varepsilon_4(k=0)$. The dielectric function of pure "poly(4,4'-biphenylylene)" can be expressed by the following equation.[15]

$$\varepsilon(\omega) = 1 + \sum_j \frac{\Omega_j^2}{\omega_j^2 - \omega^2 - i\omega\gamma_j}, \tag{5}$$

where

$$\Omega_j = \left(\frac{4\pi N_j e^2}{m} f_j\right)^{1/2}. \tag{6}$$

ω_j and γ_j are the transition energy and the band width of the j-th band. N_j is the number density of electron contributing to the j-th band, f_j is the oscillator strength of the j-th band and m is the electron mass.

The reflectivity R can be expressed by using the dielectric function of Eq. 5,[15-17]

$$R = \frac{1+|\varepsilon|-\sqrt{2(|\varepsilon|+\varepsilon_1)}}{1+|\varepsilon|+\sqrt{2(|\varepsilon|+\varepsilon_1)}} \tag{7}$$

and

$$|\varepsilon| = \sqrt{\varepsilon_1^2+\varepsilon_2^2}, \tag{8}$$

where ε_1 and ε_2 are the real and imaginary parts of the dielectric function. The parameters Ω_j, ω_j, and γ_j of undoped "poly(4,4'-biphenylylene)" can be determined by the best fit of the calculated reflection values to the observed spectra. The obtained parameters are shown in Table 1 and the best fit curve is plottted in Fig. 3 for comparison with the experimental curve.

The absorption coefficient $\alpha(\omega)$ based on these parameters can be obtained by the following equations,[15]

$$\alpha(\omega) = \frac{4\pi}{cn(\omega)}\omega\varepsilon_2(\omega) \tag{9}$$

and

$$n(\omega)^2 = \{\sqrt{\varepsilon_1^2+\varepsilon_2^2}+\varepsilon_1\}/2. \tag{10}$$

In Fig. 4, the obtained absorption spectrum is depicted together with the solution spectrum and the absorption spectrum calculated by the Kramers-Kronig transformation of the reflection spectrum.

Figure 5 shows the temperature dependence of the conductivity of the films doped with various concentrations of AsF_5. The room temperature conductivity was about $\sigma \simeq 2$ S cm^{-1} for the film doped for 40 h under

Table 1. Best fitted parameters of the dielectric function of pure and AsF_5 doped "poly(4,4'-biphenylylene)" film

Band j	Pure film			AsF_5 doped film[a]		
	Ω_j/cm^{-1}	ω_j/cm^{-1}	γ_j/cm^{-1}	Ω_j/cm^{-1}	ω_j/cm^{-1}	γ_j/cm^{-1}
1	16263.5	23742.5	5829.2	8678.9	0.0	3336.3
2	25736.2	32046.3	9400.9	26102.6	8933.6	10623.7
3	21906.9	44669.9	11791.3	25257.7	17488.5	7623.6
4				149223.0	51715.0	28382.0

a) Data of the "poly(4,4'-biphenylylene)" doped for 22 h under 200 mmHg of AsF_5 gas.

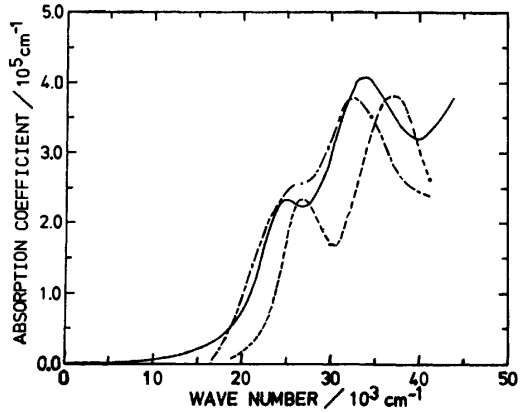

Fig. 4. Absorption spectra of pure "poly(4,4'-biphenylylene)."
------: Observed (dioxane solution), ——: calculated (SALS), —·—: calculated (Kramers-Kronig).

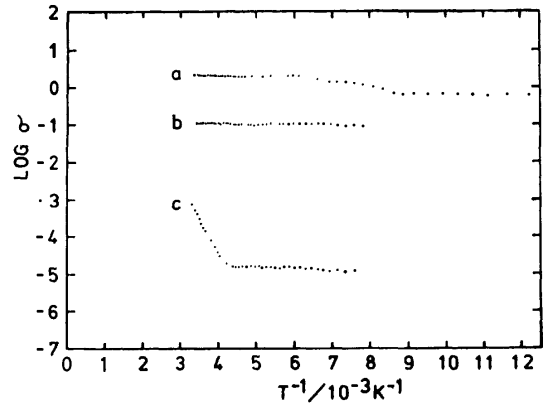

Fig. 5. Temperature dependence of the conductivity of the films doped with various concentrations of AsF_5.
a: 40 h, b: 20 h, c: 3 h.

200 mmHg of AsF_5 gas, although the conductivity for the undoped material is less than 10^{-4} S cm^{-1}. The plots of log σ *vs.* $1/T$ give straight lines near room temperature and the approximate thermal activation energy can be determined by the initial slope of $1/T$ plots. The resulting activation energy is about 0.36 eV for the sample doped for 4 h and reaches to almost zero for the films doped for more than 20 h.

Figures 6 and 7 are the visible and IR absorption spectra of thin "poly(4,4'-biphenylylene)" films doped with various concentrations of AsF_5. On doping the film with AsF_5, the absorption intensity of the 27000 cm^{-1} band decreases and the new band appears at about 18500 cm^{-1}. An isosbestic point at 23200 cm^{-1} may be explained by an equilibrium between the highly conjugated polymer ($\beta=\beta'$) and the twisting polymer ($\beta\neq\beta'$). That is, each phenyl ring seems to twist about the central bond in the pure polymer and $|\beta'|$ is smaller than $|\beta|$. For the lightly doped polymer, each phenyl group lies in the same plane and π-electrons become to be highly conjugated between phenyl rings ($|\beta'|=|\beta|$). As a consequence, the first band at 27000 cm^{-1} shifts to the shorter wave number region as is shown in Fig. 2-b. After that, doping produces the broad band in

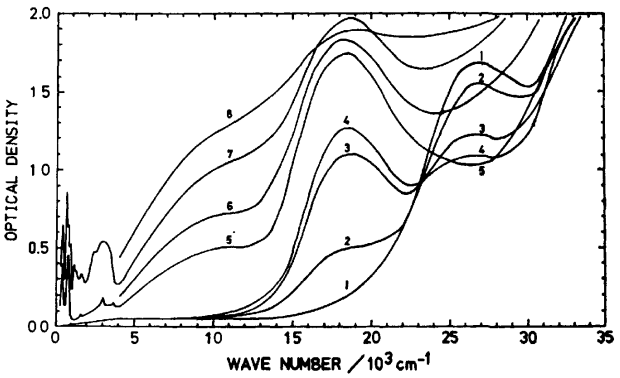

Fig. 6. Absorption spectra of AsF_5 doped "poly(4,4'-biphenylylene)."
1: 0 min, 2: 5 min, 3: 30 min, 4: 1 h, 5: 3 h, 6: 19 h, 7: 22 h, 8: 32 h.

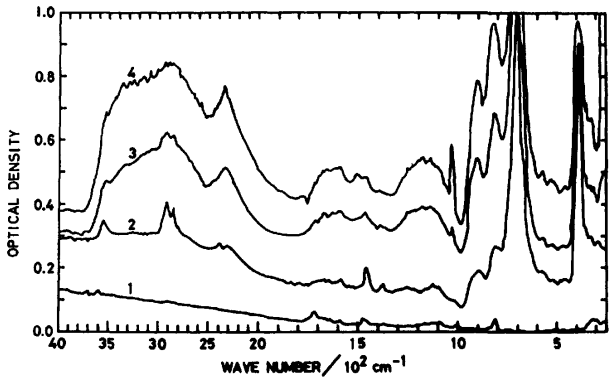

Fig. 7. IR absorption spectra of AsF_5 doped "poly(4,4'-biphenylylene)."
1: 0 min, 2: 2 h, 3: 4 h, 4: 22 h.

the region of 5000 cm^{-1} to 10000 cm^{-1} and a background absorption in the IR region in addition to the vibrational bands of $AsF_6^-H_3O^+$ at 400, 700, and 3000 cm^{-1}.[18] Figure 2-c shows that the Fermi level comes below the top of $\varepsilon_2(k)$ band by transfering a few π-electrons to AsF_5 molecules and the impurity level appears at the midpoint of the gap between the $\varepsilon_2(k)$ and $\varepsilon_4(k)$ bands. This broad band may be explained by the transition band from the $\varepsilon_2(k)$ band to the impurity level.

The maximum absorption coefficient of the 27000 cm^{-1} band of the pure film is determined to be 2.6×10^5 cm^{-1} in Fig. 4. Accordingly, the absorption coefficient of the AsF_5 doped film can be estimated as is shown in Fig. 8. Then, the parameters of the dielectric function of the doped film were decided by the optimum fit of Eq. 7 to the experimental data. The best fitted parameters are shown in Table 1. The calculated absorption spectrum based on these values is plotted for comparison with the experimental curve in Fig. 8.

The band 1 has the zero transition energy $\omega_j=0$ and is the back ground absorption in the IR region which can be assigned to the intraband transition. This means that doping makes the π-electrons in the polymer to be transferred to the AsF_5 molecule according to the following reaction,

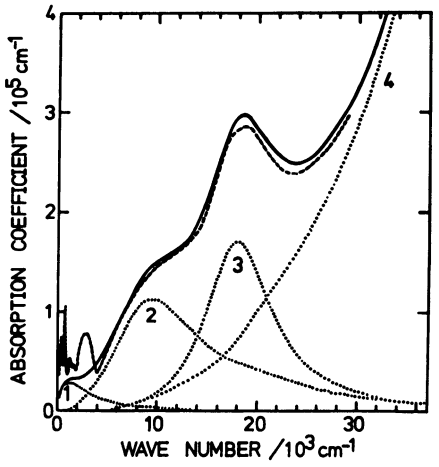

Fig. 8. Absorption spectra of "poly(4,4'-biphenylylene)" doped with AsF_5 (22 h).
——: Calcualted (SALS), ·····: calculated(SALS), ------: observed.

$$3AsF_5 + 2e \longrightarrow 2AsF_6^- + AsF_3 \quad (11)$$

and one of the π-bands becomes partially unfilled. The plasma frequency of the first band is given in Table 1.

$$\Omega_1 = \left(\frac{4\pi Ne^2}{m^*}\right)^{1/2} = 8678.9\,\mathrm{cm}^{-1} \quad (12)$$

Then, the number density (N) of the free carriers in the AsF_5 doped film can be estimated to be about $8\times10^{20}\,\mathrm{cm}^{-3}$ by substituting $m^*=m$ to the next equation,

$$N = \frac{\Omega_1^2 m^*}{4\pi e^2}. \quad (13)$$

This value corresponds to 1.4% of the total π-electrons ($6\times10^{22}\,\mathrm{cm}^{-3}$) in the polymer film, judging from the density of the film ($\rho=1.38\,\mathrm{g/cm}^3$). This means that a few holes in the unfilled π-band contribute to the transport phenomenon.

Furthermore, the dc conductivity, σ_0, is given by the following equation,[15]

$$\sigma_0 = \frac{\Omega_1^2}{4\pi\gamma_1} \quad (14)$$

and is calculated by using the observed plasma frequency, Ω_1, and the band width, γ_1. The obtained value ($\sigma_0\simeq376\,\mathrm{S\,cm}^{-1}$) is two orders of magnitude larger than the observed values ($\sigma_0\simeq2\,\mathrm{S\,cm}^{-1}$) of the dc conductivity of AsF_5 doped films. The discrepancy may be due to the existence of many cracks on the film.

References

1) H. Shirakawa, E. J. Louis, A. G. MacDiarmid, C. K. Chiang, and A. J. Heeger, *J. Chem. Soc., Chem. Commum.*, **1977**, 578.
2) D. M. Ivory, G. G. Miller, J. M. Sowa, L. W. Shacklette R. R. Chance, and R. H. Baughman, *J. Chem. Phys.*, **71**, 1506 (1979).
3) A. F. Diaz, K. K. Kanazawa, and G. P. Gardini, *J. Chem. Soc., Chem. Commun.*, **1979**, 635.
4) K. K. Kanazawa, A. F. Diaz, R. H. Geiss, W. D. Gill, J. F. Kwak, J. A. Logan, J. F. Rabolt, and G. B. Street, *J. Chem. Soc., Chem. Commun.*, **1979**, 854.
5) A. F. Diaz and J. I. Castillo, *J. Chem. Soc., Chem. Commun.*, **1980**, 397.
6) J. F. Rabolt, T. C. Clarke, K. K. Kanazawa, J. R. Reynolds, and G. B. Street, *J. Chem. Soc., Chem. Commun.*, **1980**, 347.
7) R. R. Chance, L. W. Shacklette, G. G. Miller, D. M. Ivory, J. M. Sowa, R. L. Elsenbaumer, and R. H. Baughman, *J. Chem. Soc., Chem. Commun.*, **1980**, 348.
8) M. Tanaka, A. Watanabe, H. Fujimoto, and J. Tanaka, *Chem. Lett.*, **1980**, 907.
9) A. A. Berlin, V. I. Liogon'kii, and V. P. Parini, *J. Polym. Sci.*, **55**, 675 (1961).
10) S. Hayama and S. Niino, *J. Polym. Sci., Polym. Chem. Ed.*, **12**, 357 (1974).
11) P. Kovacic and A. Kyriakis, *J. Am. Chem. Soc.*, **85**, 454 (1963).
12) P. Kovacic and J. Oziomek, *J. Org. Chem.*, **29**, 100 (1964).
13) H. C. Longuet-Higgins and J. N. Murrell, *Proc. R. Soc., London, Ser. A*, **68**, 601 (1955); J. N. Murrell, *ibid.*, **68**, 969 (1955); H. C. Longuet-Higgins, *ibid.*, **235**, 537 (1956).
14) J. N. Murrell, "The Theory of the Electronic Spectra of Organic Molecules," John Wiley & Sons, London (1963), p. 183.
15) F. Wooten, "Optical Properties of Solids," Academic Press, New York (1972).
16) M. Tanaka, A. Watanabe, and J. Tanaka, *Bull. Chem. Soc., Jpn.*, **53**, 3430 (1980).
17) A. A. Bright, A. F. Garito, and A. J. Heeger, *Phys. Rev. B*, **30**, 1328 (1974).
18) K. O. Christe, C. J. Schack, and R. D. Wilson, *Inorg. Chem.*, **14**, 2224 (1975).

Electrical and Optical Properties of a Stable Synthetic Metallic Polymer: Polypyrrole

Atsushi WATANABE, Masashi TANAKA,* and Jiro TANAKA
Department of Chemistry, Faculty of Science, Nagoya University, Chikusa-ku, Nagoya 464
(Received February 26, 1981)

Absorption and reflection spectra of the polypyrrole films prepared by electrochemical polymerization are shown over the wide wavelength region and the best fit of the calculated reflection spectra is presented to the observed spectra. Electrical conductivity of the film is measured as a function of temperature and a plot of log σ *vs.* $T^{-1/4}$ gives a straight line over the 4.2—300 K region. Furthermore, the thermoelectric-power, S, of the polypyrrole film is shown in the form of S *vs.* T on a linear scale. Based on these results, the conduction mechanism of polypyrrole film is discussed.

In recent years, many polymers such as polysulfur nitride, $(SN)_x$,[1] and AsF_5 doped polyacetylene, $(CH)_x$[2,3] have arrested attention because they exhibited metallic properties. These discoveries have encouraged the search for other polymeric systems with greater chemical stability and plasticity.

Diaz *et al.*[4-7] have synthesized a strongly adhered, durable film; polypyrrole, by electrochemical polymerization of pyrrole on platinum surface. The films have shiny blue-black color and show metallic properties like $(SN)_x$ and doped $(CH)_x$. The room temperature electrical conductivity of the present films is as high as 4.4 Ω^{-1} cm^{-1}. The films are stable in air.

In the present paper, we report the absorption spectra in the 250—4000 cm^{-1} region, the reflection spectra in the 250—33000 cm^{-1} region. The electrical conductivity and the thermoelectric-power of polypyrrole are measured over the wide temperature range and the conduction mechanism of polypyrrole is discussed based on these experimental results.

Experimental

The black films of polypyrrole (*ca.* 0.8 μm thick) were synthesized as described by Diaz *et al.*[4-7] Polypyrrloe was prepared on a platinum surface (1.0 × 3.0 cm^2) by passing 24 mC/cm^2 of charge in a cell containing 0.54 g (0.1 mol/dm^3) of Et_4NBF_4 and 0.10 g (0.06 mol/dm^3) of pyrrole in 25 cm^3 of 99% aqueous acetonitrile. The films adhere to the electrode surface strongly. The films were washed with distilled water and dried at room temperature in air. Tetraethylammonium tetrafluoroborate (Et_4NBF_4) was prepared by neutralizing 10% aqueous solution of tetraethylammonium hydroxide with 42% aqueous hydrofluoroboric acid.[8] Pyrrole and lithium perchlorate ($LiClO_4$) were products of Nakarai Chemicals Ltd. and they were used as received.

The absorption spectra of the thin polypyrrole film were measured with Hitachi IR 260-50 (250—4000 cm^{-1}), and the reflection spectra of polypyrrole film were measured with Hitachi IR 260-50 and a microscopic spectrophotometer (4000—33000 cm^{-1}) made in our laboratory. It consists of an Olympus microscope, a Carl Zeiss Ultrafluar lens (×10), a Nikon crystal mount, a HTV 928 photomultiplier and a PbS cell, and an Intel 8080 microcomputer for data processing.

The best fit of the calculated reflection spectra of polypyrrole film to the observed spectra were made on a Facom M-200 computer of Nagoya University by using SALS program.

For the thermoelectric-power measurements, a rectangular sample (4 × 15 mm^2) was mounted lengthwise between two copper blocks using pressure contacts. A temperature difference (ΔT) was established by heating one of the copper blocks, and the voltage generated by the thermal gradient across the sample was measured. The ΔT across the sample was measured with a copper-constantan differential thermocouple.

Results and Discussion

Figure 1 shows the IR absorption and reflection spectra of thin polypyrrole film prepared by using Et_4NBF_4 as supporting electrolyte. The color of the films prepared with Et_4NBF_4 is shiny black and the films prepared by using $LiClO_4$ is brown-black. IR absorption spectra show the bands characteristic of pyrrole confirming the presence of the pyrrole rings in the polymer.[9] For example, the skeletal stretching of the pyrrole ring is found at 1500 cm^{-1} region, the =C–H in-plane deformation is found at 1300 and 1180 cm^{-1}, the =C–H out-of-plane bending at 775 cm^{-1}, and the ring breathing at 920 cm^{-1}. The peak near 1035 cm^{-1} is assigned to the BF_4^- ion since this band is observed in the spectra of Et_4NBF_4 in KBr disk.

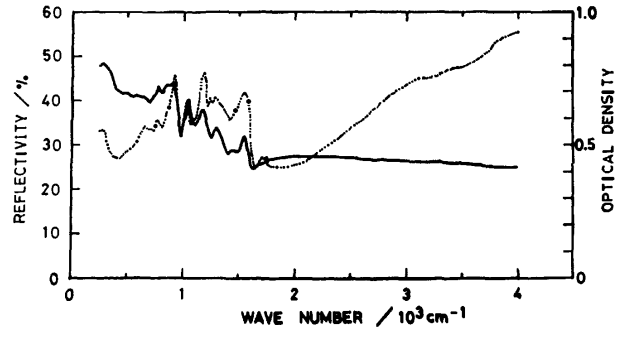

Fig. 1. Comparing between the absorption and the reflection spectra of polypyrrole film prepared by using Et_4NBF_4 in the IR region.
·····: Absorption spectrum, ——: reflection spectrum.

Figure 2 shows the reflection spectra of polypyrrole films prepared by different supporting electrolytes. The reflectivity in the lower energy region increases and a broad band around 3000—4000 cm^{-1} region is intensified with increasing conductivities. The lower energy

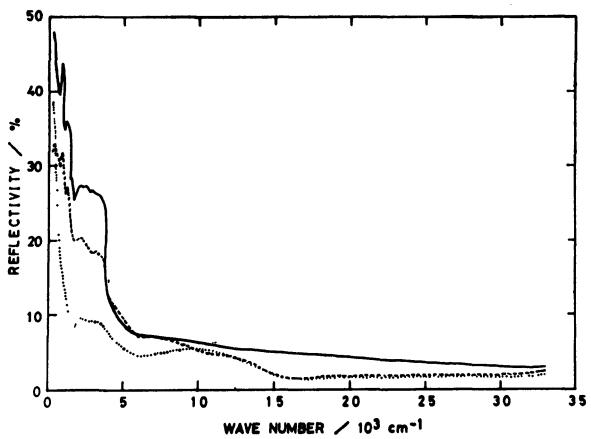

Fig. 2. Reflection spectra of polypyrrole film prepared by using different supporting electrolytes.
——: Et_4NBF_4 (σ_{295K}=4.4Ω^{-1} cm^{-1}), ------: Et_4NBF_4 (σ_{295K}=0.74 Ω^{-1} cm^{-1}), ……: $LiClO_4$ (σ_{295K}=0.016 Ω^{-1} cm^{-1}).

transition may be assigned to the zero-band gap transition. The origin of the peak around 3000 cm^{-1} region is not evident, but it may be correlated with the number of carriers because the intensity is enhanced with the conductivity.

Even if the same supporting electrolyte was used, the reflection spectra of the films were not the same from each other due to polymerization conditions. Comparing the reflection spectra of the films prepared with Et_4NBF_4, the film of lower dc conductivity (σ_{295K}=0.74 Ω^{-1} cm^{-1}) is shown to have a lower reflectivity throughout whole spectral region than the film of higher d.c. conductivity (σ_{295K}=4.4 Ω^{-1} cm^{-1}). The reflectivity at 300 cm^{-1} is 48% for the films of higher conductivity but 38% for the films which has lower d.c. conductivity.

It is noteworthy that the reflectivity is lower for the films prepared by using $LiClO_4$ which has the d.c. conductivity of σ_{295K}=0.016 Ω^{-1} cm^{-1}. However, the broad bands are clearly found at 3000 cm^{-1} and at 6000—16000 cm^{-1} region.

The dielectric function of a linear chain of zero-band gap may be expressed by the following equation,[10]

$$\varepsilon(\omega) = \varepsilon_{core} - \frac{\omega_p^2}{\omega^2 + i\omega\gamma}, \quad (1)$$

where

$$\omega_p = \left(\frac{4\pi Ne^2}{m^*}\right)^{1/2}. \quad (2)$$

γ is the band width, N is the number density of free carrier, and m^* is the effective electron mass.

The reflectivity R can be expressed by the following equation,[10-12]

$$R = \frac{1+|\varepsilon|-\sqrt{2(|\varepsilon|+\varepsilon_1)}}{1+|\varepsilon|+\sqrt{2(|\varepsilon|+\varepsilon_1)}}, \quad (3)$$

and

$$|\varepsilon| = \sqrt{\varepsilon_1^2+\varepsilon_2^2}, \quad (4)$$

where ε_1 and ε_2 are the real and imaginary parts of the dielectric function. Accordingly, the best fit of Eq. 3 to the observed reflection spectrum except the broad band around 3000—4000 cm^{-1} is obtained by using the following parameters with Eq. 1,

$$\omega_p = 17230\ \text{cm}^{-1},$$

$$\gamma = 39340\ \text{cm}^{-1},$$

and

$$\varepsilon_{core} = 2.4.$$

By using these values, the relaxation time is calculated as

$$1/\tau = 2\pi c\gamma = 7.41 \times 10^{15}\ \text{s}^{-1},$$

and we obtain

$$\tau = 0.135 \times 10^{-15}\ \text{s}.$$

This value is same magnitude with the value (σ_0= 0.277×10^{-15} s) obtained for the $ClSO_3H$ heavily doped polyacetylene.[11] The calculated reflection spectrum based on these values is in good agreement with the observed curve except the 3000—4000 cm^{-1} region as is shown in Fig. 3.

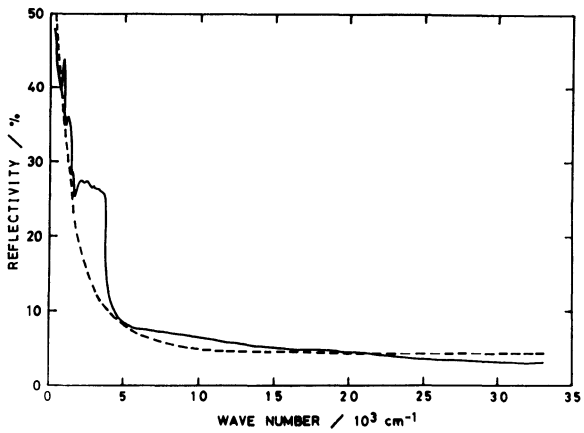

Fig. 3. Observed and calculated reflection spectra of polypyrrole film prepared by using Et_4NBF_4.
——: Observed spectrum, ------: calculated spectrum.

Then, the number density, N, of the free carrier in the polypyrrole film can be estimated as 3×10^{21} cm^{-3} by substituting $m^* = m_e$ to the next equation,[10-12]

$$N = \frac{\omega_p^2 m^*}{4\pi e^2}. \quad (5)$$

This value corresponds to *ca.* 5% of the total π-electrons (7×10^{22} cm^{-3}) which is estimated from the density of the film (ρ=1.48 g/cm^3).[5] This means that a few holes in the filled π-band contribute to the transport phenomenon.

Furthermore, the dc conductivity, σ_0, is given by the following equation,[10-12]

$$\sigma_0 = \frac{\omega_p^2}{4\pi\gamma}. \quad (6)$$

The value is calculated by using the observed plasma frequency, ω_p, and the band width, γ. The obtained value ($\sigma_0 \simeq 126$ Ω^{-1} cm^{-1}) is two order of magnitude larger than the observed value ($\sigma_0 \simeq 4.4$ Ω^{-1} cm^{-1}) of the d.c. conductivity of polypyrrole prepared by using Et_4NBF_4.

The difference between these two values may be

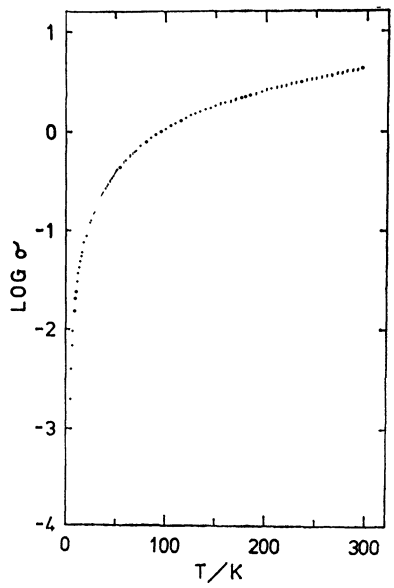

Fig. 4. Electrical conductivity of polypyrrole film prepared by using Et_4NBF_4 in the form of log σ *vs.* T.

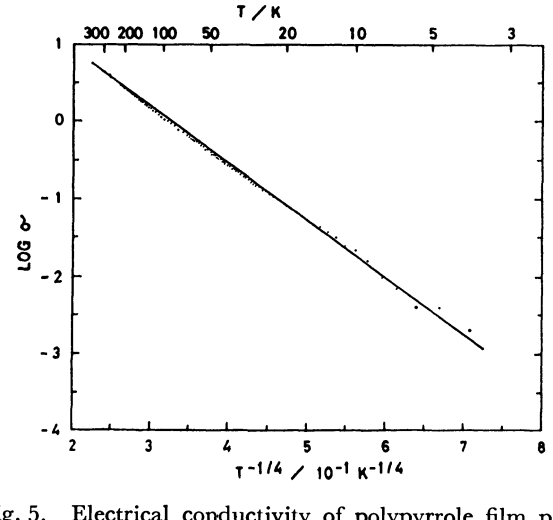

Fig. 5. Electrical conductivity of polypyrrole film prepared by using Et_4NBF_4 in the form of log σ *vs.* $T^{-1/4}$.

explained by the mechanism as shown below. Namely the temperature dependence of the electrical conductivity was measured on the polypyrrole films prepared by using Et_4NBF_4 as shown in Fig. 4 in the form of log σ *vs* T. A plot shows a smooth curve from $\sigma_{295K}=4.4\ \Omega^{-1}$ cm^{-1} to $\sigma_{4.2K}=6.72\times10^{-4}\ \Omega^{-1}\,cm^{-1}$. In fact, a plot of log . *vs.* $T^{-1/4}$ gives a straight line over the temperature region of 4.2—300 K as is shown in Fig. 5. The straight line is expressed by

$$\log\sigma = -7.35\ T^{-1/4} + 2.385. \tag{7}$$

Such behavior suggests a hopping model for the conduction mechanism. That is, the resistivity ($\rho=1/\sigma$) of the film is composed of the sum of the resistivity ($\rho_0=1/\sigma_0$) in the polypyrrole chain and the resistivity ($\rho_h=1/\sigma_h$) between the chains,

$$\rho = \rho_o + \rho_h. \tag{8}$$

The intrachain conductivity, σ_0, can be explained by

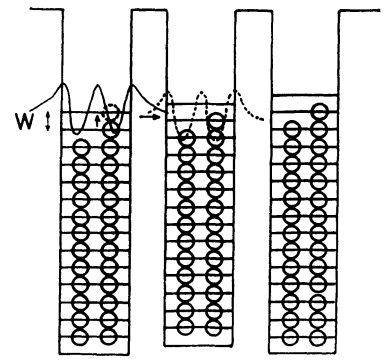

Fig. 6. A conduction mechanism of the hopping electron between the polypyrrole chain.

the conduction mechanism for the band model and corresponds to the optically determined value ($\sigma_0\simeq$ 126 $\Omega^{-1}\,cm^{-1}$), which is larger than the conductivity, σ_h, between the chains. Accordingly, the observed conductivity, σ, of the film may be correlated with the conductivity, σ_h, for the hopping electron between the chains. Mott[13] presented a conduction mechanism for a hopping process, which is depicted in Fig. 6. Every time an electron moves between the polymer chains, an electron just below the Fermi level jumps normally to a state just above it with energy W, and transfers from the one chain to the adjacent chain, of which the wave function overlaps that of the first chain. The hopping probability is then of the form,

$$\sigma \sim \nu_{ph}\exp(-2\alpha R - W/kT), \tag{9}$$

where α denotes the rate of a fall-off of the envelope of the wave function. The average spacing, W, between energy levels can be written by the density of state, $N(E)$, and the mean distance, a, between atoms as follows,

$$W = 1/(4\pi/3)a^3N(E). \tag{10}$$

If $a\simeq R$, the maximum conductivity can be found at $R\simeq(9/8\pi\alpha kTN(E))^{1/4}$ and can be expressed by the following equation,

$$\sigma \sim A\exp\{-(Q/kT)^{1/4}\}, \tag{11}$$

where

$$Q = 1.5/\alpha^3N(E). \tag{12}$$

A good consistency between the observed and the theoretical relation of log σ *vs.* $T^{-1/4}$ means that the mechanism of the conduction of polypyrrole films can be expressed by a hopping model.

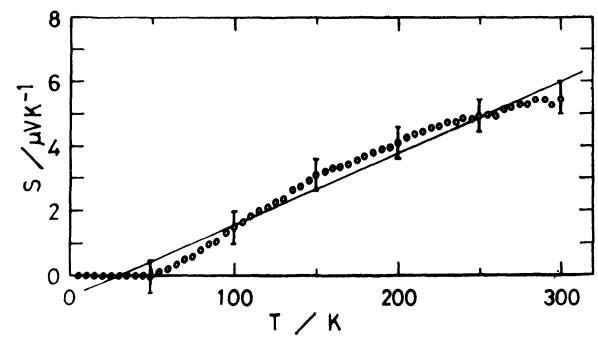

Fig. 7. Thermoelectric-power of polypyrrole film prepared by using Et_4NBF_4 in the form of S *vs.* T.

Thermoelectric-power, S, of the polypyrrole films is shown in Fig. 7, where S *vs.* T is plotted on a linear scale. The room temperature value of the thermoelectric-power is 6 μV/deg. The thermoelectric-power decreases with lowering temperature in a manner typical of a metal and the straight line in Fig. 7 is expressed by

$$S = 0.022\,T - 0.6 \quad (\mu\text{V/deg}). \tag{13}$$

The sign of S is positive in the range above 27.3 K indicating a p-type behavior. It means that the conduction occurs by the hole conduction.

For a nearly filled metallic band system (*i.e.* p-type), the thermoelectric-power can be written as follows,[13]

$$S = \frac{\pi^2}{3}\frac{k^2T}{e}\frac{\mathrm{d}\ln\sigma}{\mathrm{d}E}. \tag{14}$$

In the case that the interchain conduction occurs by hopping electrons, the thermoelectric-power can be expressed by using Eq. 9 as follows,[13]

$$S = \frac{\pi^2}{3}\frac{k}{e}\left(kT\frac{\mathrm{d}\ln\sigma_o}{\mathrm{d}E} - \frac{\mathrm{d}W}{\mathrm{d}E}\right). \tag{15}$$

$|S|$ is linearly increasing with T, and it falls down at certain temperature given by

$$T = \left(\frac{\mathrm{d}W}{\mathrm{d}E}\right)\Big/\left(k\frac{\mathrm{d}\ln\sigma_o}{\mathrm{d}E}\right) \tag{16}$$

and these theoretical predictions are in good agreement with the observed tendencies. The same result was obtained by Kanazawa *et al.*[14]

References

1) M. M. Labes, P. Love, and L. F. Nichols, *Chem. Rev.*, **7**, 79 (1979).
2) H. Shirakawa, E. J. Louis, A. G. MacDiarmid, C. K. Chiang, and A. J. Heeger, *J. Chem. Soc., Chem. Commun.*, **1977**, 578.
3) H. Shirakawa, E. J. Louis, A. G. MacDiarmid, C. K. Chiang, and A. J. Heeger, *J. Chem. Soc., Chem. Commun.*, **1977**, 578.
4) A. F. Diaz, K. K. Kanazawa, and G. P. Gardini, *J. Chem. Soc., Chem. Commun.*, **1979**, 635.
5) K. K. Kanazawa, A. F. Diaz, R. H. Geiss, W. D. Gill, J. F. Kwak, J. A. Logan, J. F. Rabolt, and G. B. Street, *J. Chem. Soc., Chem. Commun.*, **1979**, 854.
6) A. F. Diaz and J. I. Castillo. *J. Chem. Soc., Chem. Commun.*, **1980**, 397.
7) A. F. Diaz, W.-Y. Lee, and J. A. Logan, *J. Electroanal. Chem.*, **108**, 377 (1980).
8) N. S. Moe, *Acta Chem. Scand.*, **19**, 1023 (1965).
9) A. Kreutzberger and P. A. Kalter, *J. Phys. Chem.*, **65**, 624 (1961).
10) F. Wooten, "Optical Properties of Solids," Academic Press, New York (1972).
11) M. Tanaka, A. Watanabe, and J. Tanaka, *Bull. Chem. Soc., Jpn.*, **53**, 3430 (1980).
12) A. A. Bright, A. F. Garito, and A. J. Heeger, *Phys. Rev. B*, **30**, 1328 (1974).
13) S. N. Mott, "Metal-Insulator Transitions," Taylor & Francis London (1974).
14) K. K. Kanazawa *et al.*, *Synthetic Metals*, **1**, 329 (1980).

Determination of the Specific Heat Capacities of Aqueous Solutions of Pentose

Fumio KAWAIZUMI,* Shigemi KUSHIDA, and Yutaka MIYAHARA

Department of Chemical Engineering, Faculty of Engineering, Nagoya University, Chikusa-ku, Nagoya 464

(Received March 17, 1981)

A laboratory-constructed isoperibol twin calorimeter of dry shield type (*J. Chem. Thermodyn.*, **13**, 89 (1981)) was used for measurements of the specific heat capacities of aqueous solutions of D-xylose, D-ribose, D-, and L-arabinose at *ca.* 30 °C. The partial molar heat capacity at infinite dilution, $C^{\infty}_{p,2}$ was determined. Values of $C^{\infty}_{p,2}$ obtained are: D-xylose 281±2, D-ribose 271±2, D-arabinose 278±3, and L-arabinose 270±4 J K^{-1} mol^{-1}. Measurements of the heat capacity of these pentoses in the solid state, $C^{*}_{p,2}$ were carried out and the parameter $\Delta C^{\infty}_{p,2} \equiv C^{\infty}_{p,2} - C^{*}_{p,2}$ was evaluated. Values of $\Delta C^{\infty}_{p,2}$ are smaller than the corresponding values for hexose obtained previously. Similarly as had been the case for hexose, the additivity parameters of the group contribution on $C^{\infty}_{p,2}$ of solute estimated from the data on other nonelectrolytes were not acceptable for pentose. From this point the interactions working between solute of saccharide and the solvent water are considered to have characters largely different from those of other nonelectrolyte.

In the realm of the chemistry of aqueous solution of non-electrolyte, urea and saccharides, such as glucose and sucrose, have often been taken as the most basic solutes. This is because of the facts that these solutes are stable chemicals easily available at very high purity and that many physicochemical behaviors of their aqueous solutions are quasiideal, or at least vary linearly with the content of solute up to the moderate concentration. In addition to these facts, saccharide molecules have following two important features: First, they exist in cyclic structure. Secondly, they contain both many hydrophilic and hydrophobic groups and these groups having opposite nature are arranged in close proximity in each other.

Effect of hydrophobic molecule and group of a molecule on water structure, namely, hydrophobic interaction, has attracted attention of many investigators. Measurements of specific heat capacity of a solute are one of the most powerful methods to investigate the role played by hydrophobic group.[1] Furthermore, in spite of the rapid development of solution calorimetry stimulated by the commercial production of Picker's flow calorimeter,[2] data of the specific heat capacity of solutions of saccharide were rather scare. This situation pushed us to take the measurement of the specific heat capacity of aqueous solutions of saccharides, and results on hexose (D-fructose, D-galactose, D-glucose, and D-mannose), disaccharide (lactose and maltose), and trisaccharide raffinose have already been reported.[3]

In the present paper, results of the similar measurement on four kinds of pentose, D-xylose, D-ribose, D- and L-arabinose will be presented. To obtain the values of the partial molar heat capacity at infinite dilution, $C^{\infty}_{p,2}$, measurements of the specific heat capacity of the sample solutions were done at ten different concentrations of solute.

Experimental

Materials. D-Xylose and L-arabinose were supplied from Nakarai Chemical Co., Ltd. while D-arabinose and D-ribose were those of Pfanstiehl Laboratories Inc. The best quality obtainable was used. Samples were dried in an electric vacuum oven held in the temperature range 90—95 °C, (for D-ribose, in the temperature range 70—75 °C as its melting point is at 86 °C). These samples were used without further purification both for solution and solid state calorimetry. Water contents of the samples determined from the decrease of mass in drying process are as follows (expressed in wt%):

D-xylose	D-ribose	D-arabinose	L-arabinose
0.056	0.267	0.356	0.175

Solution Calorimetry. Specific heat capacities of aqueous solutions of pentose were determined using a laboratory-constructed isoperibol twin calorimeter of dry shield type. The heat reservoir of the calorimeter is an aluminium block which was kept at 30±0.1 °C. As details of this calorimeter and procedures of measurements have already been reported previously,[3,4] a brief mention may be sufficient here: i) Into one of the Dewar vessels, 100 grams of solution to be examined are introduced, while the other Dewar contains always 100 g of pure water as a reference liquid. ii) Two heaters with resistance of 45.45 and 45.42 Ω are connected in series and the e.m.f. applied to the terminals of the heaters was 20.0$_0$ V. This electric power was supplied from a stabilized source, Hewlett Packard Model 6266 B. iii) The temperature rise of the solution in Dewar vessel due to the supplied electric energy was 1—2 °C and the temperature differences between the two solutions in Dewar vessels in five minutes were detected by a pair of thermistors, amplified by laboratory-made bridge and then recorded on a strip-chart recorder. The time of five minutes was read off on the recorder chart from the instance of the sudden change of the voltage.

Calibration of the Solution Calorimeter. The calibration of this calorimeter was re-taken as an initial step of the present work. As before,[3,4] the calibration was carried out using aqueous solutions of NaCl and urea for which very accurate values of the specific heat capacity have been given.[2] Following relation was obtained between the specific heat capacity of the solution C_p and the potential difference in five minutes, ΔV.

$$C_p = A + B(\Delta V) + C(\Delta V)^2.$$

On expressing C_p and ΔV in J K^{-1} g^{-1} and V, respectively, the constants A, B, and C become:

$$A = 4.1299 \pm 0.006 \text{ J K}^{-1}\text{ g}^{-1}$$

$$B = -0.0673 \pm 0.0004 \text{ J K}^{-1}\text{ g}^{-1}\text{ V}^{-1}$$

$$C = 0.0014 \pm 0.00006 \text{ J K}^{-1}\text{ g}^{-1}\text{ V}^{-2}.$$

It may seem to be strange that the introduction of 100 g

of pure water in each of the Dewar vessels does not give rise to the result of $\Delta V=0$. The phenomenon of residual heat capacity difference of the present calorimeter may be ascribed to the inequality of the weight of the two Dewar vessels (207 and 191 g).

The concentration of sample solution was corrected for the water content of the sample.

Calorimetry of Pentose in Solid State. The determination of the specific heat capacity of the pentose in solid state was carried out in Governmental Industrial Research Institute, Osaka. An apparatus, Type SH-2000 manufactured by Tokyo Rikoh Co. Ltd. was used. Specific heat capacity data obtained are those of average values in the temperature range 28—41 °C.

Results

Solution Calorimetry. Specific heat capacities of the aqueous solutions of pentose determined in the present study are summarized in Table 1. The table contains the values of ϕ_{Cp}, apparent molar heat capacity of solute, and the values of $m\phi_{C_p}$ given by the equation

$$m\phi_{C_p} = (1000 + mM_2)C_p - 1000C_{p_1},$$

where C_{p1} is the specific heat capacity of the pure solvent, water (4.1785 J K^{-1} g^{-1}), M_2 is the molar mass, and m is the molality of the solute. Similarly as in our previous work,[3,5] values of ϕ_{C_p} at infinite dilution, $\phi^{\circ}_{C_p}=C^{\infty}_{p.2}$ were determined by the least-squares fitting of the relationship,

$$m\phi_{C_p} = bm + cm^2.$$

Evidently $C^{\infty}_{p.2}$ is equal to the coefficient b.

Specific Heat Capacities of Pentose in the Solid State. Results are given in Table 2. Values of $C^{*}_{p.2}$ of D-xylose, D-arabinose, and L-arabinose are equal while a little difference is observed between these values and that of D-ribose. If an estimation procedure of the specific heat capacity of saccharide in the solid state mentioned in a previous work[3] is adopted, the calculation leads to 184 J K^{-1} mol^{-1} for furanose form of pentose. In this calculation numbers of bond taken for the stretching and vibration are for C–C, C–O, C–H, and O–H bonds, 4, 6, 6, and 4, respectively, and the number of internal rotation is 5. The excellent agreement of this value with those in Table 2 supports the estimated value of $C^{*}_{p.2}$ of raffinose in the solid state reported in our previous work.[3]

Table 1. Heat capacities C_p and calculated values of $m\phi_{Cp}$ and apparent molar heat capacity ϕ_{Cp} of aqueous solutions of pentoses as functions of molality m

	m / mol kg^{-1}	C_p / J K^{-1} g^{-1}	$m\phi_{Cp}$ / J K^{-1}	ϕ_{Cp} / J K^{-1} mol^{-1}
D-Xylose	0.2045	4.109	56.66	277.1
	0.3025	4.075	81.57	269.7
	0.4027	4.048	114.2	283.6
	0.5026	4.018	142.7	283.9
	0.6021	3.987	168.9	280.5
	0.7026	3.959	198.1	282.0
	0.8015	3.929	223.3	278.6
	0.9007	3.903	252.3	280.1
	1.002	3.876	280.6	280.0
	1.105	3.849	309.0	279.6
D-Arabinose	0.1999	4.110	54.85	274.4
	0.2794	4.086	78.90	282.4
	0.4198	4.041	117.2	279.2
	0.5190	4.013	147.2	283.6
	0.6086	3.988	173.9	285.7
	0.7085	3.962	204.9	289.2
	0.7971	3.939	231.9	290.9
	0.8860	3.909	250.5	282.7
	0.9790	3.889	282.1	288.2
	1.079	3.867	314.9	291.8
D-Riboose	0.1901	4.116	54.97	289.2
	0.2791	4.086	78.71	282.0
	0.3713	4.056	103.6	279.0
	0.4587	4.029	128.0	279.0
	0.5480	4.008	159.3	290.7
	0.6384	3.981	184.1	288.4
	0.7384	3.957	217.2	294.1
	0.8237	3.935	243.1	295.1
	0.9263	3.911	276.4	298.4
	1.019	3.890	306.6	300.9
L-Arabinose	0.1822	4.118	52.15	286.2
	0.2693	4.089	75.82	281.5
	0.3820	4.055	109.1	285.6
	0.4811	4.024	136.2	283.1
	0.5725	3.996	161.0	281.2
	0.6682	3.966	185.4	277.5
	0.7626	3.939	211.5	277.3
	0.8591	3.918	244.8	284.9
	0.9515	3.895	272.9	286.8
	1.050	3.876	308.5	293.8

Discussion

In Table 2 are summarized the final results of the present work, where h is the hydration number. Hydration number was calculated from the data of the apparent molar compressibility[6] on the assumption that hydration waters are those bounded to solute which have the same compressibility as that of ice. For the sake of comparison, results on hexose obtained in our previous work[3] are also included in Table 2. Values of $C^{\infty}_{p.2}$ and $\Delta C^{\infty}_{p.2}$ are both positive, but smaller than the corresponding values of hexose. It has been demonstrated that the value of $C^{\infty}_{p.2}$ of a nonelectrolytic solute in aqueous solution can be assigned to the contribution of each component group of the solute.[7,8] In a word, the additivity rule holds for the quantity $C^{\infty}_{p.2}$. The application of the additivity parameters to saccharides, without taking account of the cyclic form of saccharide molecules, gives for pentose 161 J K^{-1} mol^{-1}, a value much smaller than those found in the present determination. This fact is not a new finding. Similar significant differences have already been found between estimated and experimental values of $C^{\infty}_{p.2}$ for monosaccharide hexose, disaccharide and trisaccharide.[3] Therefore it can be said that saccharide is not a "standard" solute as often is considered, but a solute showing very characteristic features from the point of thermochemical behavior of its aqueous solutions. The characteristic behavior of saccharide molecules in aqueous solutions

TABLE 2. VALUES OF $C^{\infty}_{p.2}$, $C^{*}_{p.2}$, $\Delta C^{\infty}_{p.2}$ (AT *ca.* 30 °C), AND HYDRATION NUMBER h (at 25 °C) OF PENTOSE AND HEXOSE IN AQUEOUS SOLUTION

	$C^{\infty}_{p.2}$ / J K^{-1} mol^{-1}	$C^{*}_{p.2}$ / J K^{-1} mol^{-1}	$\Delta C^{\infty}_{p.2}$ / J K^{-1} mol^{-1}	h / mol/mol
D-Xylose	281±2	184	97	2.6_7
D-Ribose	271±2	187	84	2.5_9
D-Arabinose	278±3	184	94	— 3.3[b]
L-Arabinose	270±4	184	86	4.0_0[c] 3.4[b]
D-Fructose	352±8	232±3	120	3.8[d]
D-Galactose	324±10	217±3	107	4.3_1
D-Glucose	331±7 322.6[a]	224±3	107	3.6_7
D-Mannose	337±5	216±3	121	3.3_1

a) Value obtained from the data found in Ref. 11. b) Value determined by the present authors. c) In Ref. 6, the distinction between D- and L-form is not mentioned. In our request, Dr. Høiland answered that they used L(+)-arabinose. d) Value found in Ref. 10.

may be interpreted as follows: The group contribution of $C^{\infty}_{p.2}$ have generally been derived for solutes which are monofunctional or α,ω-bifunctional molecules. For such solutes, effects of functional groups are isolated. However, as mentioned in the introductory part of this paper, in saccharide molecule, many functional groups are arranged in close proximity of each other on the cyclic skeleton of the molecule. As a result, effects of functional groups are overlapping and the values assigned to the contribution of each functional group on the partial molar heat capacity $C^{\infty}_{p.2}$ are not acceptable for solute of saccharide. Following values of $C^{\infty}_{p.2}$ have been observed:[3] for disaccharide lactose, 619±16 and maltose 614±20, and for trisaccharide raffinose, 931±7 J K^{-1} mol^{-1}. The $C^{\infty}_{p.2}$ varies from pentose to hexose, and from monosaccharide to di- and trisaccharide, in proportion to the molecular dimension of the saccharide molecule concerned. Therefore, the additivity rule of $C^{\infty}_{p.2}$ holds for saccharide, though the additivity parameters for saccharide should largely be different from the corresponding values obtained for other nonelectrolyte solutes. Experimental values of $C^{\infty}_{p.2}$ are much higher than those obtained by the application of the additivity rule. It follows that with regard to the contribution of group $-CH_2$, –OH, and –O– (ether), assigned respectively as 90, 9, and −57 J K^{-1} mol^{-1},[7] effects of $-CH_2$ and –OH groups seem to be strengthened, while those of –O– (ether) weakened.

Effects of solute upon the structure of solvent water are well reflected in the value of $\Delta C^{\infty}_{p.2}$, rather than that of $C^{\infty}_{p.2}$, as the intrinsic contribution of the solute in the pure state must be subtracted from the partial molar quantity, $C^{\infty}_{p.2}$. In Table 2, as the numerical values of $C^{*}_{p.2}$ are approximately constant for pentose, differences in $\Delta C^{\infty}_{p.2}$ result from differences in $C^{\infty}_{p.2}$. Values of $\Delta C^{\infty}_{p.2}$ increase with the molecular dimension of saccharide molecules, similarly as for the case of $C^{\infty}_{p.2}$. And the contribution of the structural unit of saccharide molecule to the quantity $\Delta C^{\infty}_{p.2}$ remains roughly constant in hexose, di- and trisaccharides. Here, the structural unit of saccharide is meant by

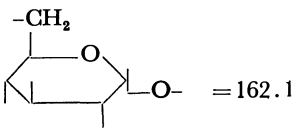

=162.1

Measurements on dextrans have shown[9] that the values of $\Delta C^{\infty}_{p.2}$ calculated for structural unit of dextran decrease with molecular weight and for dextran of M_w equal to 2.0×10^6, the value of $\Delta C^{\infty}_{p.2}$ amounts only to 3 J K^{-1} mol^{-1}.

In contrast to $C^{\infty}_{p.2}$ and $\Delta C^{\infty}_{p.2}$, hydration numbers vary randomly with solute species. Here, the term hydration corresponds to the existence of the compressed water molecules attached to solute. Hydration of saccharide is mainly ascribed to the effect of hydrophilic group –OH in the molecule. The fact that hydration number does not vary proportionally with the number of –OH group contained in saccharide molecule has been interpreted in terms of the intramolecular h dration bonding and the steric hindrance effect.[10]

The difference in the $\Delta C^{\infty}_{p.2}$ values of two stereoisomers of L- and D-arabinose is just the limit of experimental precision. This difference might be related to that the stable form of L-arabinose is pyranose form in solution, in contrast to furanose form of D-arabinose. In order to obtain further information on differences in the behavior of D- and L-arabinose, we have taken the determination of the hydration number of D- and L-arabinose at 25 °C. An ultrasonic interferometer which had long been used in our laboratory and a pycnometer were used. Results of this determination are included in Table 2, which indicate that the two stereoisomers of arabinose have the same amount of hydration. After considering these facts, it seems improper to place so much emphasis on the difference of values of $\Delta C^{\infty}_{p.2}$ of D- and L-arabinose.

The authors wish to express their thanks to Mr. Itsuki Uehara of Governmental Industrial Research Institute, Osaka, for the measurement of specific heat capacity of pentose in the solid state. The authors are also grateful to Associate Professor Hiroyasu Nomura of Nagoya University for his valuable suggestion and discussion.

References

1) P. White and G. C. Benson, *J. Phys. Chem.*, **64**, 599 (1960).

2) P. Picker, P.-A. Leduc, P. R. Philip, and J. E. Desoyers, *J. Chem. Thermodyn.*, **3**, 631 (1971).

3) F. Kawaizumi, N. Nishio, H. Nomura, and Y. Miyahara *J. Chem. Thermodyn.*, **13**, 89 (1981).
4) Y. Miyahara, H. Nomura, F. Kawaizumi, and N. Nishio, *Rep. Asahi Glass Found. Ind. Technol.*, **34**, 273 (1979).
5) F. Kawaizumi, T. Noguchi, and Y. Miyahara, *Bull. Chem. Soc. Jpn.*, **50**, 1687 (1977).
6) H. Hφiland and H. Holvik, *J. Solution Chem.*, **7**, 587 (1978).
7) N. Nichols, R. Sköld, C. Spink, J. Suurkuusk, and I Wadsö, *J. Chem. Thermodyn.*, **8**, 1081 (1976).
8) C. Jolicoeur and G. Lacroix, *Can. J. Chem.*, **54**, 624 (1976).
9) F. Kawaizumi, N. Nishio, H. Nomura, and Y. Miyahara, *Polym. J.*, **13**, 209 (1981).
10) H. Shiio, *J. Am. Chem. Soc.*, **80**, 70 (1958).
11) O. D. Bonner and P. L. Cerutti, *J. Chem. Thermodyn.*, **8**, 105 (1976).

Ion Association of Some 2 : 2 Electrolytes in Water at 25 °C. III. A New Interpretation of Experimental Results and the Determination of Formation Constants of Inner-sphere Ion-pairs

Haruhiko YOKOYAMA* and Hideo YAMATERA**

Department of Chemistry, Yokohama City University, 22-2 Seto, Kanazawa-ku, Yokohama 236
***Department of Chemistry, Faculty of Science, Nagoya University, Chikusa-ku, Nagoya 464*

(Received September 22, 1980)

The results of previous studies on ion association were re-examined. The formation constants of inner-sphere ion-pairs were obtained for several bivalent-metal sulfates by estimating the formation constants of outer-sphere ion-pairs with the help of the ion-association theory. The interactions between metal and sulfate ions were discussed by comparing these results.

Ion association usually refers to the formation of pairs of ions existing in the close vicinity of each other. In this concept, ion-pairs may be considered to be a chemical species, which is in equilibrium with the free ions in solution:

$$M^{n+} + A^{n-} \rightleftharpoons M^{n+}A^{n-}. \quad (1)$$

Sometimes they are classified into more than one chemical species, *e.g.* outer-sphere ion-pairs and inner-sphere ion-pairs, according to whether or not the ions of a pair are separated by at least one solvent molecule:

$$M^{n+} + A^{n-} \rightleftharpoons M^{n+}A^{n-}(os) \rightleftharpoons M^{n+}A^{n-}(is). \quad (2)$$

Another concept of ion-pairs has been shown in a previous paper.[1] There we have extended the Debye-Hückel theory[2] of strong electrolyte solutions, making approximation to the next higher order beyond that considered in the Debye-Hückel treatment. An expression was obtained for the chemical potential of an arbitrary central ion. This was compared with the corresponding Debye-Hückel expression. An extra term appearing in our equation arises from the excess interaction of the central ion with a counter-ion, since the probability of finding the latter in the vicinity of the central ion is greater than that assumed in the Debye-Hückel approximation. Although the counter-ion has probabilities of being found at various distances from the central ion and therefore of making different extents of contribution to the chemical potential of the latter, the total effect of the excess interactions can be regarded as equivalent to the effect of the conventional ion-pair formation. Accordingly, our concept of ion association complements the Debye-Hückel theory, which is not a good approximation for solutions of multivalent electrolytes and of solvents having a low dielectric constant.

The ion association expressed by Eq. 1 or 2 also complements the Debye-Hückel theory, since the free ions are regarded in these equations as hypothetical ions behaving in accordance with the Debye-Hückel theory. Therefore the above two concepts of ion association may be related to each other. From this point of view, we have derived the following expression for the ion-association constant at infinite dilution of a symmetrical electrolyte:

$$K = \frac{8\pi Na^3}{1000} \sum_{n=1}^{\infty} \frac{b^{2n+2}}{(2n+2)\,!\,(2n-1)}, \quad (3)\dagger$$

where N represents the Avogadro number, a the closest distance of approach between ions, and b the Bjerrum parameter given by $b = z^2e^2/\varepsilon kTa$.

It should be noted that Eq. 3 resulted from the consideration of the chemical potentials of the free and paired species, not from the counting of their numbers; however, the limiting expression ($b \to \infty$) of Eq. 3:

$$K(b \to \infty) = \frac{4\pi Na^3}{1000} \cdot \frac{\exp(b)}{b},$$

is the same as the corresponding limiting expression derived from the Bjerrum equation for ion-association constant,[1] which was obtained by counting the number of ions within the critical distance of a central ion.

Equation 3 has been utilized in the vapor-pressure osmometric, spectrophotometric, and conductivity investigations of several electrolytes for determining the *best* values of K and a.[3,4] Thus, when an appropriate value was chosen for a, the ion-association constant derived from the experimental results agreed with that predicted by the theoretical expression. Such a value of a was larger than the sum of the crystallographic radii of cation and anion ($r_M + r_A$) of each electrolyte, but smaller than the sum plus the diameter of a water molecule ($r_M + r_A + 2r_{H_2O}$, $r_{H_2O} = 1.4$ Å). From the viewpoint that the solvent is a continuous medium, the result can reasonably be taken as implying that the ions are hydrated to some extent. However, if a structual or microscopic view is taken of ions dissolved in water, the result can be interpreted as indicating that hydrated cations and anions may sometimes come so near to each other as to displace water molecules in the coordination spheres of ions to form inner-sphere ion-pairs. The latter view is preferred, since the water molecules in the first sphere of a bivalent-metal ion are strongly oriented or coordinated to the metal ion and consequently may have a different dielectric constant from that of the water in bulk. Then the solvent may not be regarded as a continuous medium of a certain dielectric constant, nor the ions as rigid spheres. Moreover, the interaction between ions may not be solely electrostatic in the first sphere of the ion. Thus, the conditions assumed in

† There are some misprints in our 1975 paper.[1] Equation 31 of the 1975 paper should be the same as Eq. 3 of the present paper ("when $b \to \infty$" should be deleted). For other misprints, refer to "Corrections" of the journal [*Bull. Chem. Soc. Jpn.*, **48**, 3002 (1975)].

deriving the Debye-Hückel theory[2] and our ion-association theory[1] may not be satisfied. Therefore, the value of a obtained in previous investigations[3,4] may not have a definite physical meaning, but may be only a measure of the closest distance of approach between ions. In this paper, another interpretation of the experimental results will be made by using the ion-association theory in a different way.

Basic Viewpoint

In this paper, we shall classify ion-pairs into inner-sphere ion-pairs and outer-sphere ion-pairs, and define an inner-sphere ion-pair as a pair of positive and negative ions with an inter-ionic distance less than the distance, $r_M+r_A+2r_{H_2O}$, which will be denoted by a_{os} in the following discussion. Then, for ions not forming an inner-sphere ion-pair, the so-called closest distance of approach can be taken to be equal to a_{os}. With this greater distance than usually assumed, the solvent may be reasonably approximated by a medium of a certain dielectric constant, and non-electrostatic interactions of the hydrated ions with further water molecules may be justifiably disregarded. Thus the theory is expected to give a satisfactory prediction for the formation of such outer-sphere ion-pairs.

The inner-sphere ion-pair can be regarded as a kind of neutral molecule, the presence of which has only a negligible effect on the theoretical treatment of very dilute solutions. Therefore, the theoretical ion-association constant can be derived in essentially the same way as that for Eq. 3[1] by employing the parameter a_{os} instead of a. The *theoretical* ion-association constant obtained here refers to the formation of all the ion-pair species†† except the inner-sphere ion-pair, namely to the formation of outer-sphere ion-pairs, for which the constant K_{os} becomes:

$$K_{os}=\frac{8\pi N a_{os}^3}{1000}\sum_{n=1}^{\infty}\frac{b^{2n+2}}{(2n+2)\,!\,(2n-1)} \qquad (4)$$

On the other hand, analysis of the *experimental* data by taking a_{os} as "the closest distance of approach of ions" gives us the overall constants for the ion-pair formation, K_Σ. When the value of K_Σ is larger than K_{os}, it is reasonable to assume the formation of inner-sphere ion-pairs in solutions. With such an assumption, we can estimate the formation constant of the inner-sphere ion-pair, K_{is}, from the difference of K_Σ and K_{os}.

Recently, Fuoss has proposed a new method of analysis of conductivity data for a purpose similar to ours but from a viewpoint different from ours.[5] He introduced the critical distance R as the closest distance of approach of unpaired ions (free ions), which is assumed to be equal to the sum of the radii of the Gurney cospheres of cation and anion. Ion-pairs are classified into solvent-separated pairs (diffusion pairs) and contact pairs (nearest-neighbor pairs). The solvent-separated pair is defined as a pair of a cation and an anion separated by at least one solvent molecule. His concept for the contact pair is similar to ours for the "inner-sphere ion-pair" as defined above, whereas that for the solvent-separated pair is very different from ours for the "outer-sphere ion-pair." That is, the solvent-separated pair is restricted to the pair of ions existing within the critical distance R of each other, and its formation constant is assumed to be given by the Fuoss 1958 equation[6] for the ion-pair formation, $K_R=4\pi NR^3\exp(b)/3000$.[5] His concept is specific in the respect that the solvent-separated pairs contribute to the transport current to the same extent as do the unpaired ions.

Fuoss's new method is of interest from the viewpoint that it precludes various problems at the vicinity of ions. However, some questions may be raised about his method: how his concept of ion-association can be thermodynamically connected with the Debye-Hückel theory; how the discontinuity at the distance of R can be justified; and what is the reasoning for the solvent-separated pair being equivalent to unpaired ions in the ionic conductance. On the other hand, our method of analysis of experimental data, which is simpler than Fuoss's method, has no adjustable parameter except for the distance a_{os} with a definite physical meaning, and is connected complementarily with the Debye-Hückel theory by Eq. 3.

Analysis of Experimental Data

The osmotic coefficient was measured on $MgSO_4$, $CaSO_4$, and $MnSO_4$ solutions with a vapor-pressure osmometer. The absorption at 250 nm was measured for copper sulfate solutions and mixed electrolyte solutions of copper sulfate and another bivalent-metal sulfate such as $MgSO_4$, $CaSO_4$, $MnSO_4$, and $ZnSO_4$. The experimental procedures and results have been described in previous papers.[3,4] In the present study, use was made of these experimental data as well as conductivity data given in the literature,[7-14] which are available for $CoSO_4$, $NiSO_4$, and $CdSO_4$ in addition to those mentioned above.

The analysis was made from the viewpoint described above: that is, with a a_{os} value characteristic of each electrolyte, the value of K_Σ was obtained from experimental data. In estimating a_{os}, r_M was assumed to be equal to Pauling's radius[15] and r_A to be 2.8_8 Å.[3] The former assumption seems to be reasonable, because the ionic radii of bivalent transition-metal ions from manganese(II) to zinc(II) obtained from X-ray scattering measurements in aqueous solutions[16] are in agreement with Pauling's radii within 0.1 Å.

The procedure used for deriving K_Σ values from experimental data of each kind is essentially the same as described in the previous papers,[3,4] except for the following modifications: (1) the parameter a_{os} was substituted for a; (2) the conventional expression for the concentration of the ion-pair, [MA], was (formally) replaced by the sum of the concentrations of outer-sphere ion-pairs and inner-sphere ion-pairs; (3) in the analysis of spectrophotometric data, in particular, the

†† A pair of cation and anion may not necessarily be divided strictly into two categories: a pair of the pure free ions and the pure ion-pair. There may be pairs which do not fully exhibit the characteristics of ion-pairs. These partial ion-pairs may be counted as fractions of an ion-pair.

conventional molar extinction coefficient, ε_{MA}, was (formally) replaced by $(\varepsilon_{MA(os)}K_{os}+\varepsilon_{MA(ls)}K_{ls})/K_{\Sigma}$, where $\varepsilon_{MA(os)}$ and $\varepsilon_{MA(ls)}$ are the extinction coefficients of the respective ion-pair species. The last two formal substitutions have arisen from the use of Eq. 2 instead of Eq. 1, and do not affect the K_{Σ} value to be obtained.

Results and Discussion

The experimental K_{Σ} values are given in Table 1, together with the values of K_{os} calculated by the use of Eq. 4. In each case, the value of K_{Σ} is larger than that of K_{os}, showing that the inner-sphere ion-pairs exist in the solution. Table 1 also lists the values of $K_{ls}(=K_{\Sigma}-K_{os})$ and K_{ls}/K_{Σ} for each electrolyte. We also calculated the values for K_{ls}/K_{Σ} based on a similar (but not exactly the same) definition, using the results of ultrasonic absorption studies;[17-19] the values are 0.10 for $MgSO_4$,[17] 0.48 for $MnSO_4$,[18] and 0.50 for $CuSO_4$,[19] which are close to those obtained in the present study. This implies that the above assumptions are reasonable.

The K_{ls} values for the first-row transition-metal ions (Table 1) appears to follow the order of the Irving-Williams series.[20] In order to discuss the formation of inner-sphere ion-pairs in more detail, we re-analyzed the conductivity data at various temperatures between 0 °C and 45 °C presented by Katayama.[8,11] The values of K_{Σ} and K_{ls} at each temperature were obtained in the same way as described above and their logarithmic values were plotted against T^{-1}. However, the plots showed curvatures like those found with the transition-metal dicarboxylates.[21,22] Therefore, according to the previously outlined procedure,[21,22] we evaluated the standard enthalpy and entropy of the ion-pair formation. The results are shown in Table 2. An approximately

Table 1. Ion-pair formation constants, K_{Σ}, K_{os}, and K_{ls},[a] for bivalent-metal sulfates in aqueous solutions obtained from various methods at 25 °C

Salt	From vapor-pressure osmometry[3]					From spectrophotometry[4]			From conductivity (re-calculated)			
	a_{os}/Å	K_{os}	K_{Σ}	K_{ls}	K_{ls}/K_{Σ}	K_{Σ}	K_{ls}	K_{ls}/K_{Σ}	K_{Σ}	K_{ls}	K_{ls}/K_{Σ}	Ref.
$MgSO_4$	6.3	86.7	127±6	40±6	0.31±0.04	107±7	20±7	0.19±0.06	124±3	37±3	0.30±0.02	7
									121±4	34±4	0.28±0.03	8
									118±2[b]	31±2	0.26±0.02	9
$CaSO_4$	6.7	79.0	155±24	76±24	0.49±0.10	131±14	52±14	0.40±0.08	131±12	52±12	0.40±0.06	10
									170±2	91±2	0.54±0.01	11
$MnSO_4$	6.5	82.7	185±4	102±4	0.55±0.01	130±11	47±11	0.36±0.06	152±6	69±6	0.45±0.03	12
									165±2	82±2	0.50±0.01	13
$CoSO_4$	6.4	84.7							163±4	78±4	0.48±0.02	11
$NiSO_4$	6.3	86.7							169±4	82±4	0.49±0.02	8
$CuSO_4$	6.4[c]	84.7				193±1	108±1	0.56±0.01	190±2	105±2	0.55±0.01	14
$ZnSO_4$	6.4	84.7				132±13	47±13	0.36±0.07	162±1	77±1	0.48±0.01	14
									175±3	91±3	0.52±0.01	11
$CdSO_4$	6.6	80.8							202±4	121±4	0.60±0.01	11

a) The values of the formation constants are expressed in $dm^3\ mol^{-1}$ except for the values obtained from vapor-pressure osmometry; in the latter case, the K_{Σ} and K_{ls} values are expressed in $kg\ mol^{-1}$. b) The K_{Σ} value has been re-calculated on the basis of a part of the reported conductivity data (at concentrations below 4.0×10^{-3} mol dm^{-3}). c) Since the hexa-aquacopper(II) ion is tetragonally distorted due to the Jahn-Teller effect, its average radius was used in the estimation of the a_{os} value for $CuSO_4$.

Table 2. Standard enthalpy and entropy of ion-pair formation of bivalent-metal sulfates in aqueous solutions at 25 °C obtained by the re-analysis of the conductivity data[8,11]

Salt	For overall ion-pair formation		For outer-sphere ion-pair for mation		For inner-sphere ion-pair formation	
	$\Delta H^{\circ}_{\Sigma}$[a] / kJ mol^{-1}	$\Delta S^{\circ}_{\Sigma}$[a] / J K^{-1} mol^{-1}	ΔH°_{os} / kJ mol^{-1}	ΔS°_{os} / J K^{-1} mol^{-1}	ΔH°_{ls} / kJ mol^{-1}	ΔS°_{ls} / J K^{-1} mol^{-1}
$MgSO_4$	6.78±0.08	62.7±0.3	4.01	50.5	12.96±0.26	73.1±0.9
$CaSO_4$	5.92±0.09	62.6±0.3	3.94	49.5	7.60±0.16	63.1±0.6
$CoSO_4$	5.33±0.11	60.2±0.4	3.99	50.3	6.74±0.22	58.9±0.8
$NiSO_4$	5.24±0.04	60.2±0.2	4.01	50.5	6.49±0.07	58.4±0.3
$ZnSO_4$	6.64±0.11	65.1±0.4	3.99	50.3	9.13±0.19	67.8±0.7
$CdSO_4$	8.07±0.06	71.2±0.2	3.95	49.8	10.75±0.10	75.9±0.4

a) Ten experimental data points between 0 °C and 45 °C were used for the evaluation of ΔH° and ΔS° values. The variation of log K with temperature was expressed by the equation $\log K=A+BT+CT^2$ (K represents K_{Σ} or K_{ls}) and the parameters A, B, and C were determined by the least-squares method. The values of the enthalpy and entropy changes were calculated from the equations $\Delta H^{\circ}=2.303\,RT^2(B+2CT)$ and $\Delta S^{\circ}=(\Delta H^{\circ}-\Delta G^{\circ})/T$. Uncertainties were estimated by using different combinations of experimental results at nine temperatures for the calculation of A, B, and C.

linear relationship exists between ΔH°_{is} and ΔS°_{is} and between ΔH°_{Σ} and ΔS°_{Σ} except for the case of magnesium sulfate. In each electrolyte, the values of ΔH°_{is} and ΔS°_{is}, are positive and larger than those of ΔH°_{os} and ΔS°_{os}, respectively; the difference is relatively small in the ΔS° values, however. The entropy changes favor the formation of both inner-sphere and outer-sphere ion-pairs, while the enthalpy changes oppose the reactions. Although the $T\Delta S^\circ$ terms predominate over the ΔH° terms, the differences between the ΔH° terms are significant for relative magnitudes of the formation constants given in Table 1.

The largest ΔH°_{is} value is shown by $MgSO_4$, reflecting the facts that the magnesium ion has the smallest ionic radius and accordingly the strongest hydration. The ΔH°_{is} value is considerably smaller for $NiSO_4$, in spite of the fact that the nickel ion has a radius close to that of the magnesium ion. This suggests that some interaction may exist between nickel and sulfate ions in addition to the electrostatic one. A similar argument seems to hold for the other transition-metal sulfates.

The enthalpy change is less unfavorable for cobalt and nickel sulfates than for zinc sulfate. On the contrary, the entropy change is more favorable for zinc sulfate. Such tendencies have also been observed with the malonates, succinates, and phthalates of these metals.[22,23] As regards the coordination of the acetate ion to the zinc ion, the comparatively large and positive enthalpy and entropy changes for the formation of ZnL_2 from ZnL^+ (where L=acetate ion) are considered to be consistent with the tendency of Zn(II) to form tetrahedral complexes.[23] If we take into account the above information and the ability of the dicarboxylate and sulfate ions to act as bidentate ligands, the formation of inner-sphere ion-pairs with the zinc ion would cause at least in part the change of the coordination number of the zinc ion from six to four. This will lead to increased positive ΔH° and ΔS° values, because a greater number of coordinated water molecules are released.

The speculation described above might seem to be opposed by the X-ray diffraction study[16] on aqueous zinc sulfate and zinc perchlorate solutions, which shows that the zinc ion is surrounded by six oxygen atoms in the solution. However, this does not seem to exclude the possibility that part of the zinc ions in inner-sphere ion-pairs are surrounded by four oxygen atoms; a majority of the zinc ions in the solutions exist as free ions and outer-sphere ion-pairs, and thus the decrease in the coordination number occurring in part on the formation of inner-sphere ion-pairs may have escaped detection.

The relatively large values of K_{is}, ΔH°_{is}, and ΔS°_{is} for $CdSO_4$ appear to show that more than one water molecule are released by the entrance of one sulfate ion into the inner-sphere of a cadmium ion; this may be supported by the fact that a cadmium ion in the $CdSO_4 \cdot 8/3\,H_2O$ is surrounded by sulfate ions (4 O of $2SO_4^{2-}$) and water molecules ($2H_2O$) in an entirely different way from that observed in the other metal sulfates.[24]

Conclusion

The theoretical formation constant for the outer-sphere ion-pairs was estimated by assuming a parameter a_{os} for the closest distance of approach for outer-sphere ion-pairs. Although some arbitrariness may be involved in the estimation of the a_{os} values, the present treatment has the merit of removing the theoretical difficulties encountered at the close vicinity of the ions in the application of the Debye-Hückel and ion-association theories.[1,2] Then from the re-analysis of various experimental data, the thermodynamic parameters were obtained for the formation of inner-sphere ion-pairs. The trends shown by the obtained parameters are consistent with other experimental findings and give useful information regarding the formation of inner-sphere ion-pairs.

References

1) H. Yokoyama and H. Yamatera, *Bull. Chem. Soc. Jpn.*, **48**, 1770, 3002 (1975).
2) P. Debye and E. Hückel, *Phys. Z.*, **24**, 185 (1923).
3) H. Yokoyama and H. Yamatera, *Bull, Chem. Soc. Jpn.*, **48**, 2708 (1975).
4) H. Yokoyama and H. Yamatera, *Bull. Chem. Soc. Jpn.*, **48**, 2719 (1975).
5) R. M. Fuoss, *Proc. Natl. Acad. Sci. U.S.A.*, **75**, 16 (1978); *J. Solution Chem.*, **7**, 771 (1978); *J. Phys. Chem.*, **82**, 2427 (1978).
6) R. M. Fuoss, *J. Am. Chem. Soc.*, **80**, 5059 (1958).
7) H. S. Dunsmore and J. C. James, *J. Chem. Soc.*, **1951**, 2925.
8) S. Katayama, *Bull. Chem. Soc. Jpn.*, **46**, 106 (1973).
9) A. D. Pethybridge and S. S. Taba, *Faraday Discuss. Chem. Soc.*, **64**, 274 (1977).
10) E. Inada, K. Shimizu, and J. Osugi, *Nippon Kagaku Zasshi*, **92**, 1096 (1971); *Rev. Phys. Chem. Jpn.*, **42**, 1 (1972).
11) S. Katayama, *J. Solution Chem.*, **5**, 241 (1976).
12) C. J. Hallada and G. Atkinson, *J. Am. Chem. Soc.*, **83**, 3759 (1961).
13) S. Petrucci, P. Hemmes, and M. Battistini, *J. Am. Chem. Soc.*, **89**, 5552 (1967).
14) B. B. Owen and R. W. Gurry, *J. Am. Chem. Soc.*, **60**, 3074 (1938).
15) L. Pauling, "The Nature of the Chemical Bond," 3rd ed, Cornell Univ. Press (1960), p. 514.
16) H. Ohtaki, T. Yamaguchi, and M. Maeda, *Bull. Chem. Soc. Jpn.*, **49**, 701 (1976).
17) G. Atkinson and S. Petrucci, *J. Phys. Chem.*, **70**, 3122 (1966).
18) G. Atkinson and S. K. Kor, *J. Phys. Chem.*, **71**, 673 (1967).
19) P. Hemmes and S. Petrucci, *J. Phys. Chem.*, **74**, 467 (1970).
20) H. Irving and R. J. P. Williams, *J. Chem. Soc.*, **1953**, 3192.
21) A. McAuley and G. H. Nancollas, *J. Chem. Soc.*, **1961**, 2215, 4458.
22) V. S. K. Nair, *J. Chem. Soc.*, **1965**, 1450.
23) G. H. Nancollas, "Interactions in Electrolyte Solutions," Elsevier Publishing Company (1966), p. 185; *Coodr. Chem. Rev.*, **5**, 379 (1970).
24) H. Lipson, *Proc. R. Soc., London, Ser. A*, **156**, 462 (1936).

Structure and Properties of Diaquabis(methylthioacetato)cobalt(II), $[Co(C_3H_5SO_2)_2(H_2O)_2]$, and Its Anhydride

Akira Ouchi,* Mamoru Shimoi, Toshio Takeuchi,† and Hideo Saito

Department of Chemistry, College of General Education, The University of Tokyo, Komaba 3-8-1, Meguro-ku, Tokyo 153

†*Department of General Sciences, Faculty of Science and Technology, Sophia University, Kioi-cho 7, Chiyoda-ku, Tokyo 107*

(Received October 1, 1980)

The crystal and molecular structure of the title complex has been determined by the X-ray diffraction method. The crystal was triclinic, space group $P\bar{1}$, $a=6.750(2)$, $b=9.214(4)$, $c=5.206(2)$ Å, $\alpha=102.57(6)$, $\beta=103.44(6)$, $\gamma=100.70(3)°$, $Z=1$, $D_x=1.702(3)$, $D_m=1.72(3)$ mg m^{-3}, μ(Mo $K\alpha$) = 1.89 mm^{-1}, and the final R value was 0.034 for 1175 reflections. The molecular arrangement has a center of symmetry and a distorted octahedron is formed around the central cobalt(II) atom; each methylthioacetato ligand forms a chelate ring by coordinating through a sulfur atom and a carbonyl oxygen atom, and two water molecules also coordinate to the central metal. Its amorphous anhydride as well as the other type anhydride, which resembles the bis(propylthioacetato)cobalt(II) hexamer in its infrared and visible spectra, is obtained by the dehydration process.

Alkylthioacetato complexes have interesting properties and they have been studied by many authors. We have already reported about their syntheses and spectroscopic properties.[1-5] Yamasaki also studied them,[6] and Pettit has shown the formation constants of their silver complexes.[7,8] More recently, many kinds of complexes containing the multi-dentates of this type of ligand were synthesized and actively investigated by Jones and others.[9-14]

One of the special properties of this type of complexes is the formation of a polymer-type structure, where the ligand bridges metal atoms. The hexamer of bis(propylthioacetato)cobalt(II) and bis(isopropylthioacetato)copper(II) dihydrate are the examples.[15,16] In the case of phenoxyacetato complexes of copper(II), the same type of the hexamer was already reported by Carruthers;[17] however, it was also shown that the ligand was able to form complexes with other structures.[18-21]

In the case of alkylthioacetato complexes, only a few structural reports have been published yet. We judge from the syntheses that the most stable form of the alkylthioacetates of cobalt(II), nickel(II), and copper(II) is the dihydrate, $ML_2 \cdot 2H_2O$ (some of which may be the diaqua complexes; here HL=alkylthioacetic acid), which are easily obtained from the aqueous solution. Therefore, we have started the structural research of this type of complexes. Although powder or fiber-like crystals of them were easily obtained, the formation of the single crystals suitable for the X-ray diffraction study was not easy. The single crystals of the title complex, obtained after many attempts, were used for its crystal and molecular structure determination.

The structural changes between the diaqua complex and the anhydride complex are also shown in the later part of this paper.

Experimental

Syntheses of Diaquabis(methylthioacetato)cobalt(II); $[Co(CH_3 \cdot S \cdot CH_2 \cdot CO_2)_2(H_2O)_2]$. The ligand was obtained by the slight modification of the method of Larsson:[22] a condensation reaction between dimethyl sulfate (in place of methyl iodide) and mercaptoacetic acid in the presence of sodium hydroxide in aqueous medium. The crude cobalt(II) complex was obtained by the reaction between cobalt(II) chloride and the sodium salt of the ligand in aqueous solution in the presence of a little sodium hydrogencarbonate. Then the concentrated aqueous solution of the complex was left standing for several weeks at 6 °C, and the crystals came out. Although many large crystals which looked like single crystals under microscopic observation were obtained, almost all of them consisted of many needle-like crystals in parallel, so they gave broad spots on Weissenberg photographs. From the 37 samples tried, only 2 crystals were obtained which could be used to obtain the diffraction data. Analyses of the complex. Found: Co, 19.38; C, 23.61; H, 4.61%, magnetic moment 4.8_2 BM** (per 1 mol of cobalt). Calcd for $CoC_6H_{14}S_2O_6$, Co, 19.31; C, 23.61; H, 4.62%.

Dehydration of Diaquabis(methylthioacetato)cobalt(II). When the title complex was heated to 140—150 °C for a few hours in air, the dark-red powder anhydride was obtained, this is amorphous, judging from the X-ray powder pattern. Analyses of the product. Found: Co, 21.90; C, 26.65; H, 3.84%, magnetic moment 4.9_0 BM** (per 1 mol of cobalt). Calcd for $CoC_6H_{10}S_2O_4$: Co, 21.89; C, 26.77; H, 3.74%. When the product was heated at 150 °C continuously, it decomposed slowly.

When the title complex was dehydrated by evaporating its benzene–ethanol mixed solvent solution two times, and then its benzene solution about five times (at 80 °C using rotary vacuum evaporator), another type of anhydride was obtained. (To complete the dehydration process, preferably, the anhydride obtained by the above mentioned process is to be kept in refluxed *p*-xylene for several hours.) The product was red-violet powder. Analyses Found: Co, 21.78; C, 27.15; H, 3.71%, magnetic moment 4.8_2 BM** (per 1 mol of cobalt). Calcd for $Co_6C_{36}H_{60}S_{12}O_{24}$: Co, 21.89; C, 26.77; H, 3.74%. As shown later, their infrared and visible spectroscopic properties of this anhydride resemble those of the bis(propylthioacetato)cobalt(II) hexamer *p*-xylene adduct,[15] and it is tentatively named as the hexamer-type anhydride.

X-Ray Measurement. The single crystals obtained were needle-like ones and were pale-red in color; they were stable in air. As they were too brittle, a crystal $0.4 \times 0.2 \times 0.2$ mm in size was used for X-ray measurement, without any additional reshaping process.

** 1 BM = $9.274078(36) \times 10^{-24}$ J T^{-1}.

The crystallographic data are as follows: $CoC_6H_{14}S_2O_6$, F.W.=305.24, triclinic, space group $P\bar{1}$, a=6.750(2), b=9.214(4), c=5.206(2) Å, α=102.57(6), β=103.44(6), γ=100.70(3)°, Z=1, D_x=1.702(3), D_m=1.72(3) mg m^{-3}, μ(Mo $K\alpha$)=1.89 mm^{-1}. The reflections within the range of $2\theta < 60°$ were collected on a Philips 1100 automated four-circle diffractometer, using Mo $K\alpha$ radiation (0.7107 Å) and applying the ω—2θ scan technique. The 1175 independent reflections with $|F_o| > 3\sigma(|F_o|)$ were used for the structure refinement. The intensities were corrected for Lorentz and polarization factors, but no correction was made for absorption and extinction.

All the calculations were carried out on a HITAC 8700/8800 computer at the Computer Center of The University of Tokyo, using the local version of UNICS program.[23] The atomic scattering factors were taken from the tables.[24]

Structure Determination. The structure was solved by the heavy-atom method. The positions of the cobalt and sulfur atoms were deduced from a three-dimensional Patterson map, and all the other non-hydrogen atoms were successively located by Fourier syntheses; their positions and their thermal parameters were refined by a repeated block-diagonal least squares method. Then the positions of all hydrogen atoms were obtained from a difference Fourier synthesis, and were also refined. In the last cycle of the refinement with anisotropic temperature factors for all non-hydrogen atoms, all the parameter shifts were less than one-third of the corresponding standard deviations. The final R value was 0.034.[25]

The Other Measurements. Magnetic moments of the solid powder samples were measured using a Gouy balance, at 25 °C.

The simultaneous thermogravimetric (TG) and differential thermal analysis (DTA) were carried out with Rigaku Denki M-8075 using a sample weighing 10 mg in each operation, with the heating rate of 10 °C min^{-1} in air, using α-alumina as the reference.

The infrared spectra of the samples were obtained by means of a JASCO infrared spectrophotometer, type 403G, using Nujol and hexachloro-1,3-butadiene mull.

The visible absorption spectra of the samples were obtained by a Hitachi 124 spectrophtometer, and their reflectance spectra by the same instrument using the appropriate attachment.

Results and Discussion

The final atomic parameters are listed in Table 1,[26] the atomic distances and the bond angles in Table 2. A perspective drawing of the complex and the numbering scheme of atoms are shown in Fig. 1, and a projection of the structure along b^* in Fig. 2. The crystal consists of discrete molecules of $[Co(CH_3 \cdot S \cdot CH_2 \cdot CO_2)_2(H_2O)_2]$, except for weak hydrogen bondings. The molecules has a center of symmetry, occupied by a cobalt atom. As shown in Fig. 1, the central metal in this complex is in a deformed octahedral environment, elongated in both the coordinated sulfur atom directions. Methylthioacetato ligand forms a five-membered chelate ring, coordinating through a sulfur atom and a carbonyl oxygen atom. Two water molecules also coordinate to the cobalt atom. The value of the magnetic moment of the complex shows no interaction between cobalt atoms.

The Co–S distance is 2.531(1) Å, which is almost the same as that in the bis(propylthioacetato)cobalt(II) hexamer,[15] and which is slightly longer than that of the four, five or six-membered ring chelate dithiolato complexes of cobalt(II).[27–29] As the sum of the covalent bond radii (Pauling) of Co(II) and S is 2.36 Å, the Co–S bond of this chelate is a little weaker than that of the common sulfur-coordinated cobalt(II) complexes. The distance C(1)–O(1) (where O(1) of the ligand coordinates to Co), is 1.278(3) Å; this is longer than C(1)–O(2): 1.228(4) Å. Therefore, the carboxyl group of the ligand is in rather a covalent character in the chelate, because the bond length C(1)–O(1) and C(1)–O(2) should be about equal when it has the ionic character.

The coordinated water molecule forms hydrogen bonds with the O(1) atom of the complex which is

Table 1. Final atomic coordinates ($\times 10^4$ for non-hydrogen atoms, and $\times 10^3$ for hydrogen atoms) and isotropic temperature factors (B/Å^2) with estimated standard deviations in parentheses

	x	y	z	B_{eq}/Å^2 [a]
Co	0	0	0	1.4
S	437 (1)	2744 (1)	−283 (1)	2.6
O(1)	−2045 (3)	595 (2)	2133 (4)	2.6
O(2)	−3945 (3)	2196 (2)	3395 (4)	3.2
O(W)	2397 (3)	596 (2)	3634 (4)	3.0
C(1)	−2751 (4)	1787 (3)	2091 (5)	2.3
C(2)	−2101 (4)	2774 (3)	262 (6)	2.9
C(3)	2115 (5)	3925 (3)	3034 (7)	3.8
	x	y	z	B_{iso}/Å^2
H(1)	−200 (5)	392 (3)	109 (6)	3.0 (7)
H(2)	−309 (5)	234 (4)	−157 (7)	3.5 (7)
H(3)	354 (6)	391 (4)	297 (8)	4.7 (8)
H(4)	204 (6)	503 (4)	332 (8)	4.9 (9)
H(5)	169 (6)	331 (4)	442 (8)	5.3 (9)
H(W1)	366 (5)	106 (4)	373 (7)	4.3 (8)
H(W2)	226 (5)	22 (4)	486 (7)	3.8 (8)

a) The equivalent isotropic temperature factors for non-hydrogen atoms were computed using the following expression: $B_{eq}=\frac{4}{3}(B_{11}a^2+B_{22}b^2+B_{33}c^2+B_{12}ab\cos\gamma+B_{13}ac\cos+\beta+B_{23}bc\cos\alpha)$. The B_{ij}'s are defined by: $\exp[-(h^2B_{11}+k^2B_{22}+l^2B_{33}+2klB_{23}+2hlB_{13}+2hkB_{12})]$.

Table 2. Interatomic distance (l/Å) and bond angles (ϕ/°) with estimated standard deviations in parentheses

Co–S	2.531 (1)	C(1)–C(2)	1.533 (4)
Co–O(1)	2.042 (2)	C(2)–S	1.805 (3)
Co–O(W)	2.066 (3)	C(3)–S	1.807 (4)
O(1)–C(1)	1.278 (3)	O(W)···O(2)^{I}	2.685 (3)
O(2)–C(1)	1.228 (4)	O(W)···O(1)^{II}	2.702 (3)
S–Co–O(1)	82.03 (6)	O(2)–C(1)–C(2)	117.0 (3)
S–Co–O(W)	93.29 (5)	C(1)–C(2)–S	115.0 (2)
O(1)–Co–O(W)	90.05 (8)	C(2)–S–C(3)	99.6 (1)
Co–O(1)–C(1)	123.0 (2)	Co–S–C(2)	91.2 (1)
O(1)–C(1)–C(2)	118.4 (3)	Co–S–C(3)	105.8 (1)
O(1)–C(1)–O(2)	124.6 (3)		

Key to symmetry operations: I. $1.0+x$, y, z; II. $-x$, $-y$, $1.0-z$.

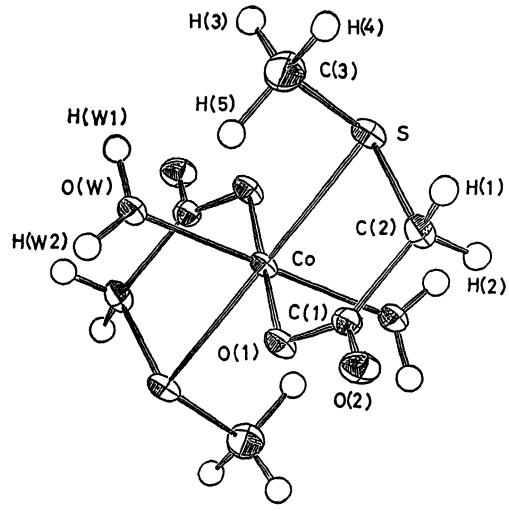

Fig. 1. A perspective drawing of the title compound with their numbering scheme of atoms.

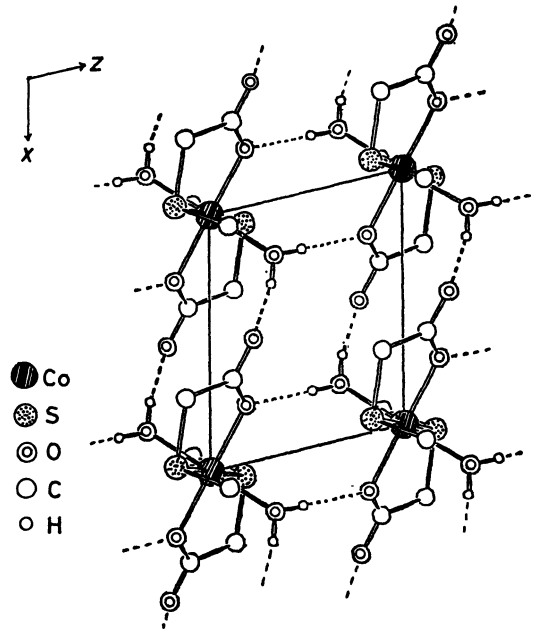

Fig. 2. Crystal packing diagram projected along b^*.

located next in the c-axis direction, as well as with the O(2) atom of the complex next in the a-axis direction. The crystal preferably grows in the c-axis direction, and a needle-like one is commonly obtained. The crystal cleaved along both of (100) and (010) planes, although the cleavage along the former plane must break hydrogen bondings between complexes.

The results of the simultaneous TG and DTA of [diaquabis(methylthioacetato)cobalt(II)] and of [diaquabis(propylthioacetato)cobalt(II)] are shown in Fig. 3. Their general features resemble each other, although the methylthioacetate is dehydrated in the higher temperature region. At the second step, a drastic mass loss occurs at about 230—300 °C in both cases. Their DTA curves show that several endo- and exo-thermal reactions occur in this region, and the complexes are completely decomposed into some tar-like

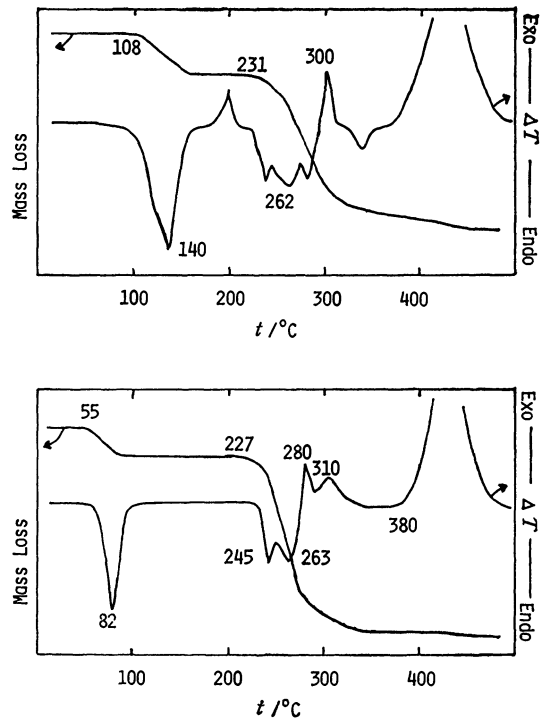

Fig. 3. Thermogravimetric and differential thermal analysis curves of a) diaquabis(methylthioacetato)-cobalt(II) (upper), and b) diaquabis(propylthioacetato)cobalt(II) (lower) (10 °C min^{-1}).

materials. The TG curve of the methylthioacetate shows a plateau between 140—230 °C. The anhydride corresponding with this region is an "amorphous anhydride" obtained by heating the diaqua complex at about 140—150 °C; this fact was determined from the X-ray powder pattern. From the propylthioacetate, the same type of anhydride was also obtained by the same process, but by heating at a lower temperature (100—110 °C).

When diaquabis(propylthioacetato)cobalt(II) was dehydrated by evaporation together with a benzene–ethanol mixture, and then with benzene, the obtained product was the amorphous anhydride; this has similar spectroscopic properties to those of the one obtained by heating the solid diaqua complex in air. However, when the amorphous anhydride was dissolved in some non-polar solvent, such as benzene, carbon tetrachloride, or xylene, and dried at room temperature, the anhydride hexamer or its organic solvent adducts were obtained. Its hexamer *p*-xylene adduct, used for the crystallographic analysis, was obtained by the gradual dissolution of petroleum ether into a xylene solution of the amorphous anhydride at room temperature.[15]

The infrared spectra of diaquabis(methylthioacetato)-cobalt(II), its amorphous anhydride, and its hexamer-type anhydride form, and those of diaquabis(propylthioacetato)cobalt(II) and its anhydride hexamer (*p*-xylene adduct), are all shown in Fig. 4. Although the wave number of each corresponding peak differs in some extent, the general features of the spectra of their diaqua complexes, and of the spectra of their hexamer or hexamer-type anhydride, are almost identical in the

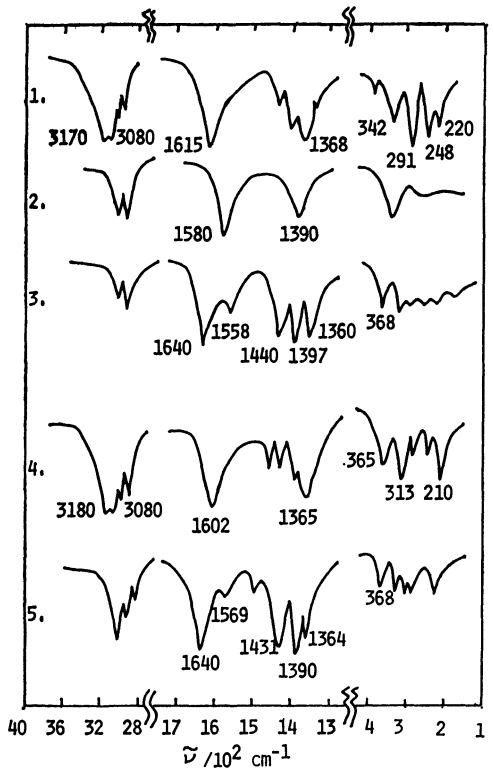

Fig. 4. Infrared spectra of the complexes. 1—3) Bis(methylthioacetato)cobalt(II); 1) diaqua complex, 2) amorphous anhydride, 3) hexamer-type anhydride. 4, 5) Bis(propylthioacetato)cobalt(II); 4) diaqua complex, 5) hexamer *p*-xylene adduct.

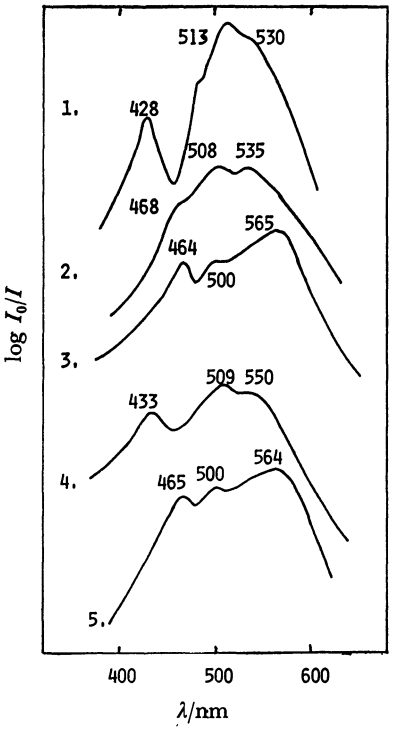

Fig. 5. Reflectance spectra of the complexes. 1—3) Bis(methylthioacetato)cobalt(II); 1) diaqua complex, 2) amorphous anhydride, 3) hexamer-type anhydride. 4, 5) bis(propylthioacetato)cobalt(II); 4) diaqua complex, 5) hexamer *p*-xylene adduct.

wave number region shown. The ν(O–H) peaks of both diaqua complexes appear at about 3100 cm^{-1} (split into 2 peaks), which is lower than those of common crystalline water in metal complexes. This fact is explained by the coordination of water to the central metal, as shown by the structure analysis of the title complex, diaquabis(methylthioacetato)cobalt(II). The wave numbers of ν_{as}(COO) and of ν_s(COO) are characteristic of each type of the complexes. In the case of both diaqua complexes, these peaks appeared at 1602 or 1615 and 1365 or 1368 cm^{-1}, those of the hexamer appeared as a strong ν_{as}(COO) peak at 1640 cm^{-1} (with a small one at 1569 or 1558 cm^{-1}), and the characteristic triplet ν_s(COO) peaks with the maxima at 1431 or 1440, 1390 or 1397, and 1364 or 1360 cm^{-1}. (The causes of the splitting and the shift of the peaks have not been analysed in detail, yet. At this stage, only the correspondence of those peaks in their general features was shown). As shown in Fig. 4, the amorphous anhydride of the methylthioacetate shows infrared spectral peaks different from those of either the diaqua complex or the hexamer-type one, in their maximum wave numbers as well as in their shapes. The far-infrared spectra of both types of complexes, diaqua and hexamer-type, also show characteristic patterns.

The reflectance spectra of these products are shown in Fig. 5. As in the case of infrared spectra, the spectra of the diaqua complexes of cobalt(II) methylthioacetate and of propylthioacetate are almost identical. Moreover, those of their hexamer-type anhydrides exhibit the same features.

From these infrared and reflectance spectral results, the diaqua complexes and the hexamer-type anhydrides of the methylthio- and propylthioacetate are likely to have the same types of structure. Their amorphous anhydrides have a structure different from the other two. It is likely to be in a polymer-type structure, but this is not yet clarified.

Although the hexamer of the propylthioacetate of cobalt(II) is soluble in many non-polar organic solvent, the methylthioacetate cannot be dissolved in benzene, xylene, toluene, or carbon tetrachloride at ambient temperature. The 1,1,2,2-tetrachloroethane solution of the methylthioacetate, stable at room temperature, can be obtained when its anhydride (hexamer-type one) is heated with the solvent and cooled.

The hexamer-type anhydride of methylthioacetate and propylthioacetate, dissolved in some non-polar organic solvent, show spectral patterns similar in their features. These patterns are similar to their reflectance spectra, too. Consequently, the hexamer structure shown by the crystallographic analysis of the propylthioacetate is kept in the solution, and the methylthioacetate complex is likely to have the same of a very similar structure in both its solid and its solution state. Beer's law is followed in the concentration region of 0.04—0.01 mol dm^{-3} (per monomer cobalt(II) complex). The high absorption coefficients of peaks, as well as the complicated splittings, correspond to the deformation from the octahedral configuration to an approximately

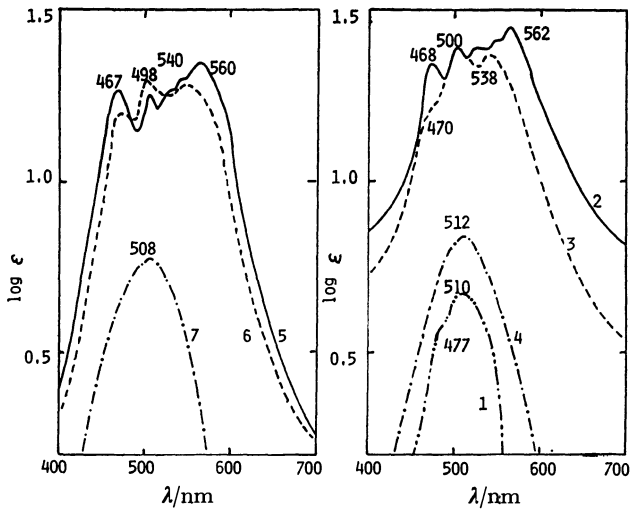

Fig. 6. Absorption spectra of the complexes in solution. 1) Cobalt(II) chloride hexahydrate in water, 2—4) bis(methylthioacetato)cobalt(II); 2) hexamer-type anhydride in 1,1,2,2-tetrachloroethane, 3) hexamer-type anhydride in the mixed solvent of 1,1,2,2-tetrachloroethane and ethanol (4 : 1, v/v), 4) diaqua complex in water (0.07 mol dm^{-3}), 5—7) bis(propylthioacetato)cobalt(II); 5) hexamer *p*-xylene adduct in benzene, 6) hexamer *p*-xylene adduct in the mixed solvent of benzene and ethanol (4 : 1, v/v), 7) diaqua complex in water (0.07 mol dm^{-3}).

squarepyramid one (Co–S is weak and elongated), around the cobalt(II) atoms.[15,30]

As shown in Fig. 6, when ethanol or some such slightly polar solvent was added to the solution of the hexamer-type anhydride mentioned above, the spectral pattern changed, and the destruction of the hexamer structure was suggested. The features of the spectra of their solutions in pure alcohols resemble those of their aqueous solution, although their absorption coefficients are higher.

When the diaqua complexes of both the alkylthioacetates were dissolved in water, the solutions showed neither the peak at 430 nm nor the shoulder about 530 nm, in their reflectance spectra. The spectra of their aqueous solution resemble those of the aqueous solution of cobalt(II) chloride. However, the intensities of the peak maxima of the former ones are higher than that of the latter one, when the former solutions are in higher concentrations (about 0.05—0.1 mol dm^{-3}). The absorption coefficients decrease as the concentration decreases, and the value tends to coincide with that of the hexaaquacobalt(II) ion. This fact shows that the methylthioacetate of cobalt(II) is decomposed in its aqueous solution, and that the ligand is almost completely dissociated in its dilute aqueous solution.

The authors wish to thank Professor Yoichi Iitaka of the Faculty of Pharmaceutical Sciences, The University of Tokyo, for the collection of the intensity data of X-ray diffraction.

References

1) A. Ouchi, Y. Ohashi, T. Takeuchi, and Y. Yoshino, *Bull. Chem. Soc. Jpn.*, **43**, 1088 (1970).
2) Y. Ohashi, T. Takeuchi, A. Ouchi, and Y. Yoshino, *Bull. Chem. Soc. Jpn.*, **43**, 2845 (1970).
3) A. Ouchi, T. Takeuchi, and Y. Ohashi, *Bull. Chem. Soc. Jpn.*, **44**, 731 (1971).
4) A. Ouchi. T. Takeuchi, and Y. Ohashi, *Bull. Chem. Soc. Jpn.*, **44**, 3461 (1971).
5) A. Ouchi, H. Honda, and S. Kitazima, *J. Inorg. Nucl. Chem.*, **37**, 2599 (1975).
6) K. Suzuki and K. Yamasaki, *J. Inorg. Nucl. Chem.*, **24**, 1093 (1962).
7) L. D. Pettit, A. Poyston, and R. J. Whewell, *J. Chem. Soc., A*, **1968**, 2009.
8) L. D. Pettit and C. Sherrington, *J. Chem. Soc., A*, **1968**, 3078.
9) M. M. Jones, T. Pratt, and C. H. Brown, *J. Inorg. Nucl. Chem.*, **36**, 1213 (1974).
10) M. M. Jones, A. J. Banks, and C. H. Brown, *J. Inorg. Nucl. Chem.*, **36**, 1833 (1974).
11) R. L. Coates and M. M. Jones, *J. Inorg. Nucl. Chem.*, **37**, 443 (1975).
12) M. M. Jones, A. J. Banks, and C. H. Brown, *J. Inorg. Nucl. Chem.*, **37**, 761 (1975).
13) T. H. Pratt and M. M. Jones, *J. Inorg. Nucl. Chem.*, **37**, 2403 (1975).
14) M. M. Jones, H. D. Coble, T. H. Pratt, and R. D. Harbison, *J. Inorg. Nucl. Chem.*, **37**, 2409 (1975).
15) M. Shimoi, F. Ebina, A. Ouchi, Y. Yoshino, and T. Takeuchi, *J. Chem. Soc., Chem. Commun.*, **1979**, 1132.
16) T. Ogawa, M. Shimoi, and A. Ouchi, *Acta Crystallogr., Sect. B*, **36**, 3114 (1980).
17) J. R. Carruthers, K. Prout, and F. J. C. Rossotti, *Acta Crystallogr., Sect. B*, **31**, 2044 (1975).
18) C. K. Prout, P. A. Armstrong, J. R. Carruthers, J. G. Forrest, P. Murray-Rust, and F. J. C. Rossotti, *J. Chem. Soc., A*, **1968**, 2791.
19) C. V. Goebel and R. J. Doedens, *Inorg. Chem.*, **10**, 2607 (1971).
20) C. K. Prout, J. R. Carruthers, and F. J. C. Rossotti, *J. Chem. Soc., A*, **1971**, 554: C. K. Prout, C. Walker, and F. J. C. Rossotti, *ibid.*, **1971**, 556.
21) J. G. Forrest, C. K. Prout, and F. J. C. Rossotti, *Chem. Commun.*, **1966**, 658.
22) E. Larsson, *Chem. Ber.*, **63**, 1347 (1930).
23) The Universal Crystallographic Computation Program System (UNICS), ed by T. Sakurai, Crystallographic Society of Japan, Tokyo (1967).
24) "International Tables for X-Ray Crystallography," Kynoch Press, Birmingham, U.K. (1974), Vol. IV.
25) $R=\sum||F_o|-|F_c||/\sum|F_o|$
26) The final coordinates, their thermal parameters, and the final F_o-F_c table, are kept at the Chemical Society of Japan as Document No. 8134.
27) R. Beckett and B. F. Hoskins, *J. Chem. Soc., Chem. Commun.*, **1967**, 909; *J. Chem. Soc., Dalton Trans.*, **1974**, 622.
28) J. D. Forrester, A. Salkin, and H. Templeton, *Inorg. Chem.*, **3**, 1500 (1964).
29) M. Shimoi, A. Ouchi, S. Sato, and Y. Saito, *Chem. Lett.*, **1979**, 319.
30) J. Catterick and P. Thornton, *J. Chem. Soc., Dalton Trans.*, **1976**, 1634.

Preparation of Graphite Intercalation Compounds of Thiazyl Salts

Tsuyoshi NAKAJIMA,* Masayuki KAWAGUCHI, and Nobuatsu WATANABE

Department of Industrial Chemistry, Faculty of Engineering, Kyoto University, Sakyo-ku, Kyoto 606

(Received October 22, 1980)

Thiazyl salts prepared from $S_3N_3Cl_3$ and MCl_3(M=Sb, Fe, Al) were intercalated into flaky or powdery natural graphite in CCl_4 or $SOCl_2$. Intercalation compounds prepared are $C_{24}S_4N_4\cdot 2SbCl_5$ [2nd stage, I_c(repeat distance) $=12.81\pm0.02$ Å], $C_{9.5}\cdot 0.2(S_3N_3Cl_3\cdot FeCl_2)\cdot 0.8(SOCl_2\cdot FeCl_2)$ [2nd stage, $I_c=12.77\pm0.03$ Å], $C_{11}S_3N_3Cl_3\cdot 2.4FeCl_2$ [a mixture of 1st and higher stage compounds, $I_c=9.17\pm0.05$ Å] and $C_{24}\cdot 0.4(S_3N_3Cl_3\cdot 2AlCl_2)\cdot 0.6(SOCl_2\cdot 2AlCl_2)$ [a mixture of 2nd and 3rd stage compounds, $I_c=12.89\pm0.03$ Å, 16.23 ± 0.03 Å]. Electrical conductivity of pyrolytic carbon–$S_4N_4\cdot 2SbCl_5$ [3rd stage] is higher than that of original pyrolytic carbon by one order.

In recent years, attention has been given to graphite intercalation compounds showing metallic behavior, *i. e.* high electrical conductivity. Alkali metal, acid or some halide compounds have such properties. Graphite compounds intercalated by strong Lewis acids such as SbF_5, AsF_5 are also of interest.[1] Most chlorides or fluorides of metals in higher oxidation states are hygroscopic and unstable. In many cases, their graphite intercalation compounds also have similar properties. However, such halides are stabilized to some extent forming ionic complexes with anion donor halides. Graphite intercalation compounds of the ternary system might be considered to be effective for preparing stable compounds with high electrical conductivity.

Ternary system compounds were prepared by the reaction of six-membered ring compound $S_3N_3Cl_3$ with metal chlorides ($SbCl_3$, $FeCl_3$, $AlCl_3$) in CCl_4 or $SOCl_2$ containing graphite. Electrical conductivity was measured for a relatively stable compound with pyrolytic carbon host, obtained in a form suitable for measurement.

Experimental

Flaky natural graphite from Madagascar consisting of two different grain sizes of over 500 μm(80%) and 297—500 μm (20%), and powdery natural graphite of less than 44 μm, were used. Purity was 99.4% after purification with a hydrogen fluoride solution. Trithiazyl trichloride $S_3N_3Cl_3$ (yellow crystals, mp 91 °C) was prepared by the usual method.[2] Commercial $SbCl_3$, $FeCl_3$, and $AlCl_3$ were used without further purification. All the reactions were carried out under nitrogen or dry atmosphere. Graphite intercalation compounds prepared were analysed by means of X-ray diffractometry and elemental analysis. The X-ray diffraction pattern for a moisture-sensitive compound was taken by wrapping the sample in thin, transparent poly(vinyl chloride) resin. Elemental analysis was performed at the Laboratory for Organic Elemental Microanalysis, Faculty of Pharmaceutical Science, Kyoto University for C, N, Cl, and at Kyoto Science Research Institute of Shimadzu Seisakusho Corporation for Sb, Fe, Al, and S. A-axis electrical conductivity was measured for pyrolytic carbon (PC), PC–$S_4N_4\cdot 2SbCl_5$, and PC–$SbCl_5$ by the 4-point DC-bridge method. The host material was a pyrolytic carbon plate (Nihon Carbon Comp. Ltd.) deposited at 2100 °C and further treated at 2400 °C.

The compounds were prepared as follows.

1) $C_{24}S_4N_4\cdot 2SbCl_5$. Flaky graphite (1.416 g), $SbCl_3$ (4.433 g, 19.4 mmol) and $S_3N_3Cl_3$ (1.589 g, 6.50 mmol) were added to 60 ml of dry CCl_4 in a 100 ml glass flask. The solution was then heated at 55 °C in an oil bath and stirred for 12 d. The reaction was completed in 1—2 h, a red-brown compound being precipitated from the solution. After 3 d, flaky graphite began to expand with insertion of the product. It took over a week for thiazyl salt to be intercalated completely. The product was filtered under nitrogen or dry atmosphere and dried in a vacuum.

2) $C_{9.5}\cdot 0.2(S_3N_3Cl_3\cdot FeCl_2)\cdot 0.8(SOCl_2\cdot FeCl_2)$ and $C_{11}S_3N_3Cl_3\cdot 2.4FeCl_2$. Flaky graphite (1.024 g), $FeCl_3$ (2.038 g, 12.60 mmol), $S_3N_3Cl_3$ (1.537 g, 6.28 mmol), and powdery graphite (0.693 g), $FeCl_3$ (1.397 g, 8.50 mmol), $S_3N_3Cl_3$ (1.040 g, 4.25 mmol) were added to 40 ml of $SOCl_2$. Each solution was then heated at 50 °C and stirred for 7 and 8 d, respectively. The compounds were isolated in the same way as for *1)*.

3) Reaction of Flaky Graphite with $S_3N_3Cl_3+2AlCl_3$. Flaky graphite (0.975 g), $AlCl_3$ (1.276 g, 9.57 mmol) and $S_3N_3Cl_3$ (1.170 g, 4.78 mmol) were added to 40 ml of $SOCl_2$. The solution was then heated. The compound was isolated in the same way as for *1)*.

4) PC–$S_4N_4\cdot 2SbCl_5$ *and PC–*$SbCl_5$. PC–$S_4N_4\cdot 2SbCl_5$ was prepared by the same method as for *1)*. PC(1 cm², *ca.* 0.1 cm in thickness) and $SbCl_5$ (70 g) were added to 15 ml of dry CCl_4 in a 100 ml flask. The solution was then heated at 100 °C in oil bath and stirred for 10 d.

Results and Discussion

Intercalation of $S_4N_4\cdot 2SbCl_5$. The reaction of $S_3N_3Cl_3$ with $SbCl_3$ gave two different compounds according to the mole ratio of the reactants: in the 1 : 1 reaction, ten-membered S, N ring compound $S_5N_5\cdot SbCl_6$ was crystallized from acetonitrille in orange color, in the 1 : 3 reaction, eight-membered ring compound $S_4N_4\cdot SbCl_5$ was isolated. The compounds were identified by IR spectra[3,4] and elemental analysis. IR (KBr): s (broad) 1166, s (broad) 1121, m 733, w 681, w 630 and vs 545 cm^{-1}. Elemental analysis: Found: S, 28.6; N, 12.6; Cl, 37.6; Sb, 21.1%. Calcd for $S_5N_5\cdot SbCl_6$: S, 28.4; N, 12.4; Cl, 37.7; Sb, 21.6%.

$$S_3N_3Cl_3 + SbCl_3 \xrightarrow[CH_3CN]{R.T.} S_5N_5\cdot SbCl_6 \quad (1)$$

IR (KBr): vs 1058, vs 976, s 808, vs 788, w 684, vs 512, m 413 cm^{-1}. Elemental analysis: Found: S, 24.7; N, 11.5; Cl, 36.9; Sb, 24.4%. Calcd for $S_4N_4\cdot SbCl_5$: S, 26.5; N, 11.6; Cl, 36.7; Sb, 25.2%.

$$S_3N_3Cl_3 + 3SbCl_3 \xrightarrow[CH_2Cl_2 \text{ or } CCl_4]{R.T.} S_4N_4\cdot SbCl_5 \quad (2)$$

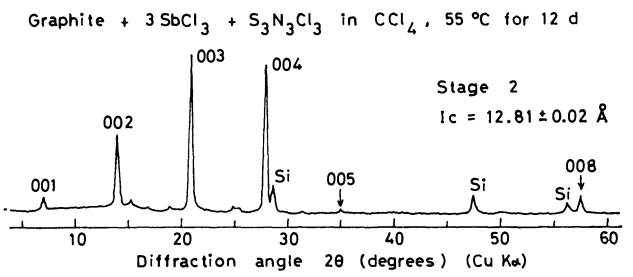

Fig. 1. X-Ray diffraction pattern for $C_{24}S_4N_4 \cdot 2SbCl_5$.

S_5N_5 ring is not as stable as S_4N_4 ring. Repeated recrystallization resulted in the change of the crystal structure from $S_5N_5 \cdot SbCl_6$ to $S_4N_4 \cdot SbCl_5$. When reaction (2) was carried out in the presence of graphite, a brown intercalation compound was obtained after 12

$$\text{Flaky graphite} + S_3N_3Cl_3 + 3SbCl_3 \xrightarrow[CCl_4]{55\,^\circ C} C_{24}S_4N_4 \cdot 2SbCl_5 \quad (3)$$

d. The X-ray diffraction pattern for this compound is shown in Fig. 1. The compound was so stable that the diffraction pattern could be taken without wrapping the sample. The repeat distance I_c is 12.81 ± 0.02 Å from the observed $(00l)$ diffraction lines. The result of elemental analysis for this compound coincides with $C_{24}S_4N_4 \cdot 2SbCl_5$. Found: C, 26.6; S, 10.8; N, 4.8; Cl, 32.4; Sb, 21.5%. Calcd for $C_{24}S_4N_4 \cdot 2SbCl_5$: C, 26.9; S, 12.0; N, 5.2; Cl, 33.1; Sb, 22.8%.

In general, the repeat distance of 1st stage compounds of metal chlorides is in the range of 9—10 Å.[5] 1st stage compound $C_{12}SbCl_5$ has 9.42 Å as the repeat distance,[5] indicating that the interlayer spacing of graphite is expanded by 6.07 Å with intercalation of $SbCl_5$. S_4N_4 reacts with metal chlorides ($SbCl_5$, $FeCl_3$, $AlCl_3$ *etc.*) to give mono- and diadducts.[4,8] The intercalant $S_4N_4 \cdot 2SbCl_5$ is regarded as a diadduct of S_4N_4. Considering that the dimension of monoadduct $S_4N_4 \cdot SbCl_5$ is *ca.* 6 Å,[7] it is possible that the intercalant $S_4N_4 \cdot 2SbCl_5$ is oriented between the interlayer spacing of 6.11 Å ($=12.81-3.35\times2$). Thus, $C_{24}S_4N_4 \cdot 2SbCl_5$ is assigned to a 2nd stage compound.

DTA and TG curves of $C_{24}S_4N_4 \cdot 2SbCl_5$ were obtained to determine the decomposition temperature. Decomposition of the intercalant began at *ca.* 150 °C and was completed at *ca.* 250 °C through $S_4N_3Cl \cdot SbCl_3$.

Reaction of Graphite with $S_3N_3Cl_3$+2FeCl$_3$. $S_3N_3Cl_3$ reacts with $FeCl_3$ to give 1 : 1 or 1 : 2 adduct.[9] In this case, $SOCl_2$ used as a solvent also forms an adduct with $FeCl_3$.[9] When the reaction was carried out in $SOCl_2$ containing flaky graphite, a black intercalation compound was isolated after 1 week. The repeat distance is calculated to be 12.77 ± 0.03 Å from the $(00l)$ diffraction lines shown in Fig. 2. The composition was derived from the elemental analysis as $C_{9.5} \cdot 0.2(S_3N_3Cl_3 \cdot FeCl_2) \cdot 0.8(SOCl_2 \cdot FeCl_2)$. The prepared compound contains much solvent.

$$\text{Flaky graphite} + S_3N_3Cl_3 + 2FeCl_3 \xrightarrow[SOCl_2]{50\,^\circ C} C_{9.5} \cdot 0.2(S_3N_3Cl_3 \cdot FeCl_2) \cdot 0.8(SOCl_2 \cdot FeCl_2) \quad (4)$$

Found: C, 29.2; S, 11.6; N, 2.2; Cl, 38.4; Fe, 14.4; (O), 3.5%. Calcd for $C_{9.5} \cdot 0.2(S_3N_3Cl_3 \cdot FeCl_2) \cdot 0.8(SOCl_2 \cdot FeCl_2)$: C, 29.6; S, 11.8; N, 2.2; Cl, 38.6; Fe, 14.5; (O), 3.3%.

$FeCl_2$ forms 1st stage intercalation compound with the composition $C_{4.7}FeCl_2$ and the repeat distance 9.56 Å.[5] The number of carbon is 9.5 per one intercalated molecule, in line with twice that for 1st stage compound. The repeat distance also indicates that the compound is a 2nd stage one.

The compound decomposed on exposure to the air, accompanied by decrease in weight and release of chlorine gas. After being left to stand for several hours, the diffraction lines for initial graphite appeared on the diffraction pattern.

When powdery graphite was used as host material instead of flaky graphite, another intercalation compound $C_{11}S_3N_3Cl_3 \cdot 2.4FeCl_2$ containing no solvent was formed.

$$\text{Powdery graphite} + S_3N_3Cl_3 + 2FeCl_3 \xrightarrow[SOCl_2]{50\,^\circ C} C_{11}S_3N_3Cl_3 \cdot 2.4FeCl_2 \quad (5)$$

Found: C, 19.9; S, 13.5; N, 6.3; Cl, 41.8; Fe, 18.9%. Calcd for $C_{11}S_3N_3Cl_3 \cdot 2.4FeCl_2$: C, 19.4; S, 14.1; N, 6.2; Cl, 40.6; Fe, 19.7%.

This is also black and a mixture of 1st and higher stage compounds. Powdery graphite has a much greater surface area than flaky graphite. However, no pure 1st stage compound could be obtained. The observed repeat distance for 1st stage compound is 9.17 ± 0.05 Å, and the strong peak at 27.2° corresponds to $(00l)$ line of higher stage compounds (Fig. 3). The characteristic of this compound is similar to that of $C_{9.5} \cdot 0.2(S_3N_3Cl_3 \cdot FeCl_2) \cdot 0.8(SOCl_2 \cdot FeCl_2)$.

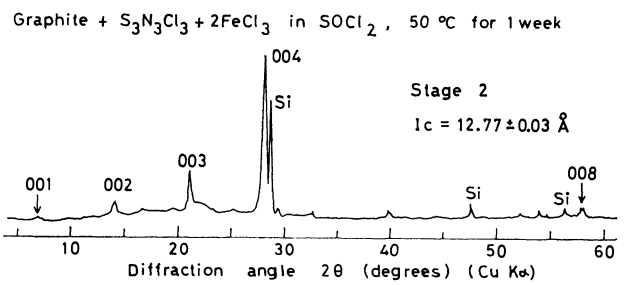

Fig. 2. X-Ray diffraction pattern for $C_{9.5}$ 0.2 ($S_3N_3Cl_3$-$FeCl_2$)0.8($SOCl_2FeCl_2$).

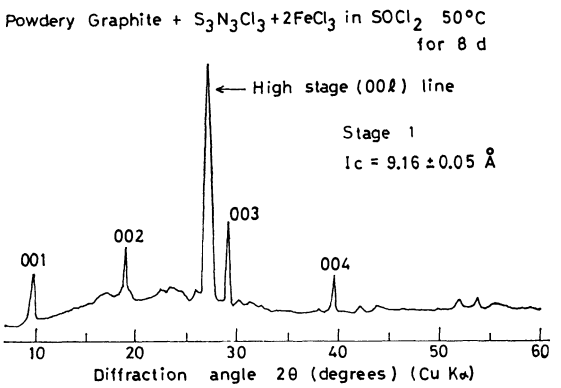

Fig. 3. X-Ray diffraction pattern for $C_{11}S_3N_3Cl_3 \cdot 2.4FeCl_2$.

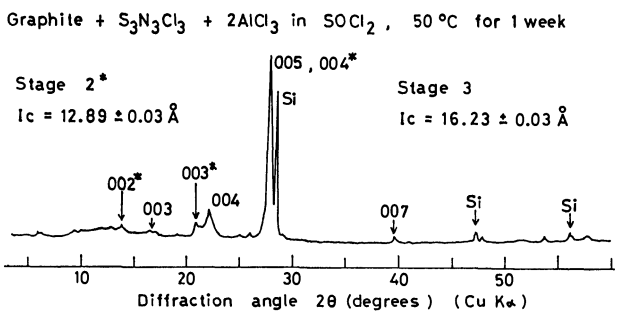

Fig. 4. X-Ray diffraction pattern for $C_{24}\cdot 0.4(S_3N_3Cl_3\text{-}2AlCl_2)\cdot 0.6(SOCl_2\cdot 2AlCl_2)$.

Reaction of Graphite with $S_3N_3Cl_3+2AlCl_3$. $S_3N_3Cl_3$ reacts also with $AlCl_3$ to give 1 : 1 or 1 : 2 adduct.[9] Reaction of flaky graphite with the adduct gave a green-black compound. X-Ray diffraction pattern (Fig. 4) indicates the coexistence of 2nd and 3rd stage compounds. No pure 2nd stage compound was obtained even by the reaction for *ca.* one month. The reaction rate from 3rd stage to 2nd stage might be low in this system. Their repeat distances are 12.89 ± 0.03 Å and 16.23 ± 0.03 Å, respectively. From the elemental analysis, the composition is approximated to $C_{24}\cdot 0.4(S_3N_3Cl_3\cdot 2AlCl_2)\cdot 0.6(SOCl_2\cdot 2AlCl_2)$.

$$\text{Flaky graphite} + S_3N_3Cl_3 + 2AlCl_3 \xrightarrow[SOCl_2]{50\,^\circ C} C_{24}\cdot 0\ 4(S_3N_3Cl_3\cdot 2AlCl_2)\cdot 0\ 6(SOCl_2\cdot 2AlCl_2) \quad (6)$$

Found: C, 44.1; S, 9.1; N, 2.2; Cl, 30.7; Al, 7.4; (O), 5.8%. Calcd for $C_{24}\cdot 0.4(S_3N_3Cl_3\cdot 2AlCl_2)\cdot 0.6(SOCl_2\cdot 2AlCl_2)$: C, 44.1; S, 8.8; N, 2.6; Cl, 34.7; Al, 8.3; (O), 1.5%.

A considerable discrepancy exists between analytical and calculated values for chlorine. The compound is very hygroscopic and unstable. As soon as it was taken out from a flask into the air, it decomposed liberating chlorine gas. The color turned from green-black to black. Analytical error occurred probably because of such property. Some unknown peaks appeared on the X-ray diffractogram for a decomposed compound, no peak corresponding to the original graphite being observed. The black substance may be a kind of residual compound.

Electrical Conductivity Measurement. The results of a-axis electrical conductivity for PC, PC–$SbCl_5$, and PC–$S_4N_4\cdot 2SbCl_5$ are given in Table 1. Both PC–$SbCl_5$ and PC–$S_4N_4\cdot 2SbCl_5$ were confirmed to be 3rd stage compounds by means of X-ray diffractometry. The electrical conductivity of PC–$SbCl_5$ and PC–$S_4N_4\cdot 2SbCl_5$ is obviously higher than that for original PC by one order. The chemical bond between S_4N_4 and $SbCl_5$ is the coordination of antimony atom of $SbCl_5$ as a Lewis acid to nitrogen atom of S_4N_4, the intercalant $S_4N_4\cdot 2SbCl_5$ having partially ionic character represented by $S_4N_4^{\delta+}\cdot 2SbCl_5^{\delta-}$.[7] It is likely that $S_4N_4\cdot 2SbCl_5$ is comparable with $SbCl_5$ in its ability as an electron acceptor which removes an electron from graphite and leaves behind a delocalized hole. Insertion of S_4N_4 increases the stability of the intercalation compound as compared with PC–$SbCl_5$.

Table 1. Electrical conductivities of PC, PC–$SbCl_5$, and PC–$S_4N_4$2$SbCl_5$ at 25 °C

Compound	σ_a/Ω^{-1} cm^{-1}
Pyrolytic carbon	3.9×10^3
PC–$SbCl_5$ (3rd stage)	4.1×10^4
PC–$S_4N_4\cdot 2SbCl_5$ (3rd stage)	4.4×10^4

The authors thank Dr. Rokuro Fujii, Government Industrial Research Institute, Osaka, for his assistance in the electrical conductivity measurement.

References

1) J. E. Fischer, "Physics and Chemistry of Materials with Layered Structures, Vol. 6, Intercalated Layered Materials," ed by F. A. Lévy, D. Reidel Pub. Comp. (1979), p. 481.
2) W. L. Jolly and K. D. Maguire, *Inorg. Synth.*, **9**, 107 (1967).
3) A. J. Banister and H. G. Clarke, *Inorg. Synth.*, **17**, 192 (1977).
4) K. J. Wynne and W. L. Jolly, *Inorg. Chem.*, **6**, 107 (1967).
5) K. Ohashi and I. Tsujikawa. *Tanso*, **1978**, 154.
6) H. Wölling, *Z. Anorg. Allg. Chem.*, **57**, 281 (1908).
7) D. Neubauer and J. Weiss, *Z. Anorg. Allg. Chem.*, **303**, 28 (1960).
8) A. J. Banister and P. J. Dainty, *J. Chem. Soc., Dalton Trans.*, **1972**, 2658.
9) A. Boeck and W. Rüdorff, *Z. Anorg. Allg. Chem.*, **397**, 179 (1973).

The *trans-cis* Isomerization of Potassium Diaquabis(oxalato)chromate(III) in Various Organic Solvent-Water Mixtures

Kengo UCHIDA* and Yoshinobu TAKINAMI

Department of Chemistry, Faculty of Science, Hirosaki University, Bunkyo-cho, Hirosaki 036

(Received October 31, 1980)

Kinetics of the *trans-cis* isomerization of $K[Cr(ox)_2(H_2O)_2]$ have been investigated in binary mixed solvents, including ethanol–, dioxane–, and acetone–water mixtures. The first-order rate constant decreases with an increase in the concentration of an organic solvent. A similar decrease by the addition of an organic solvent was observed in the presence of univalent and bivalent cations. These results are in contrast to those for the analogous malonato complex, and suggest that both dissociation and twist mechanisms are involved in the reaction.

Extensive investigations of the isomerization kinetics of *trans*-diaquabis(oxalato)chromate(III) ion have been reported.[1–12] A dissociation mechanism, where a bond rupture at Cr–oxalato is the rate determining step, has been reported and this has been supported by the catalytic effect of various cations,[1,3,11] while a twist mechanism has been suggested by Ashley and Lane.[13]

On the other hand, the studies on the influence of solvents are very few.[6] The authors have found that the rate of the isomerization of an analogous malonato complex increased with an increase of the concentration of organic solvents.[14] In this work, we have studied the effect of solvents on the rate of the isomerization. As the isomerization is catalyzed by some cations, the catalytic reaction is expected to be accelerated in organic solvents, because the reaction is ionic and depends on the relative permittivity of the solvent. Nevertheless, the reactions in the presence of univalent and bivalent cations are found to be retarded with increasing concentration of the organic solvent. We have also studied the reaction mechanism.

Experimental

Materials. Potassium *trans*-diaquabis(oxalato)chromate (III), *trans*-$K[Cr(ox)_2(H_2O)_2]\cdot 3H_2O$, was prepared by the standard method.[15] As considerable amount of by-products, $[Cr(ox)(H_2O)_4]^+$ and $[Cr(ox)_3]^{3-}$, were contained. The product was purified by using an ion exchange chromatography.[9] The absorption spectra (λ_{max}=400 nm (ε_{max}= 19.2), 532 nm (19.0)) agreed well with those reported in the literature.[4,9] The stock solutions containing the investigated cations were prepared by dissolving the chlorides of the cations in redistilled water. The chlorides of a guaranteed reagent grade were recrystallized from distilled water. Organic solvents of a guaranteed reagent grade were purified by the usual methods,[16] and ultraspecial grade solvents were used without further purification.

Procedures. Experimental methods were described previously.[14] The rates of the reactions were determined spectrophotometrically at the wavelength of 415 nm at 25.0 °C. The concentration of the complex was 8.0×10^{-3} mol dm^{-3} in all cases. The pH value of the solution was not adjusted but remained constant at about 4.5 throughout the reactions.

Results and Discussion

In the absence of excess cations, the isomerization rates were determined in aqueous mixtures of ethanol, dioxane, acetone and *N*-methylacetamide. The isomerization obeys good first-order kinetics even after 90% reaction, and the rate constant, k_{obsd}, decreased with increasing concentration (mole fraction) of the organic solvents, contrary to the case of the analogous malonato

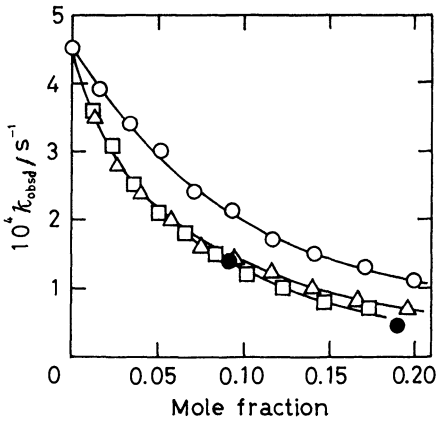

Fig. 1. Effects of the concentration of organic solvents on k_{obsd} in the absence of excess cation.
○: Ethanol, □: dioxane, △: acetone, ●: *N*-methylacetamide.

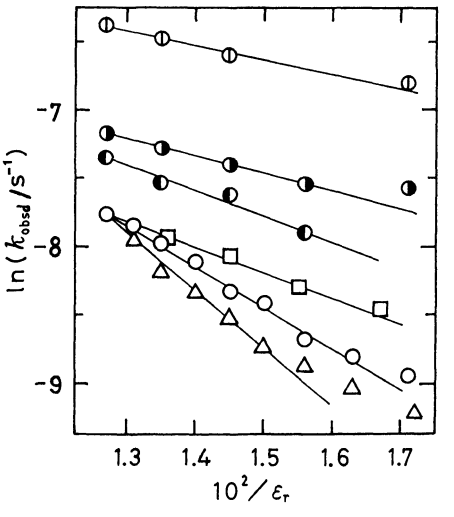

Fig. 2. Plots of $\ln(k_{obsd}/s^{-1})$ *vs.* the reciprocal of relative permittivity.
○: Ethanol, □: dioxane, △: acetone, ◐: $[Ca^{2+}]$= 0.0157 mol dm^{-3} (ethanol), ◑: $[Ca^{2+}]$=0.0314 mol dm^{-3} (ethanol), ⓘ: $[Sr^{2+}]$= 0.331 mol dm^{-3} (ethanol).

complex.[14] The results are shown in Fig. 1. As the relative permittivity, ε_r, of the solvents increased, k_{obsd} increased smoothly except in the solution of *N*-methylacetamide and formamide. Plots of $\ln k_{obsd}$ *vs.* $1/\varepsilon_r$ were found to be linear, though deviations could be seen in the high concentrations of the organic solvents. The ε_r values were properly interpolated from known values.[17] The plots are shown in Fig. 2. Even if the ε_r value was the same, different k_{obsd} values were obtained in other solvents. Therefore k_{obsd} did not depend on the ε_r value only.

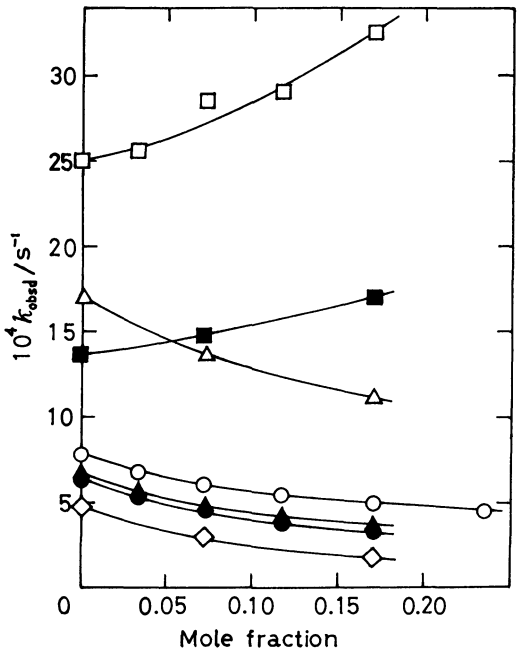

Fig. 3. Effects of the concentration of ethanol on k_{obsd} in the presence of some cations.
□: $[La^{3+}]=0.0040$ mol dm^{-3}, ■: $[La^{3+}]=0.0020$ mol dm^{-3}, △: $[Sr^{2+}]=0.331$ mol dm^{-3}, ▲: $[Sr^{2+}]=0.031$ mol dm^{-3}, ○: $[Ca^{2+}]=0.031$ mol dm^{-3}, ●: $[Ca^{2+}]=0.016$ mol dm^{-3}, ◇: $[K^+]=0.99$ mol dm^{-3}.

It has been shown that the rates in aqueous solutions are accelerated by the addition of cations, M^{n+}.[1,3,11] A similar acceleration was observed in a mixture of an organic solvent and water. The effects of the solvents on k_{obsd} in the presence of cations are shown in Fig. 3 and Table 1. The k_{obsd} values decreased with increasing concentration of the organic solvents, whereas they increased in the presence of La^{3+} in most of the solvents except *N*-methylacetamide, whose ε_r value is larger than that of water. The k_{obsd} value was also given by

$$k_{obsd} = k_o + k_M[M^{n+}], \quad (1)$$

when the ionic strength of the solution was kept constant by the addition of potassium chloride. The results are shown in Fig. 4, where the dashed curves mean the k_{obsd} values when the ionic strength was not adjusted. The acceleration effect of K^+ could be neglected, compared with those of the bivalent and the tervalent cations. Some k_M values are listed in Table 2.

Generally a rate constant, k, for an ionic reaction is given by

Table 1. The k_{obsd} values in various solvents in the presence of some cations

Cation	[Cation] / mol dm^{-3}	$10^4 \times k_{obsd}$ / s^{-1}				
Vol% of organic solvent		0.0	20.0	30.0	40.0	50.0
(a) Mol% of dioxane		0.0	5.04		12.4	
Na^+	0.99	6.5	3.6		2.0	
K^+	0.99	5.6	2.9		1.5	
Sr^{2+}	0.331	17.0	11.9		9.3	
(b) Mol% of acetone		0.0	5.80		14.17	
Sr^{2+}	0.331	17.0	11.4		8.7	
(c) Mol% of formamide		0.0	10.15		23.20	
K^+	0.99	5.6	3.5		2.6	
Sr^{2+}	0.331	17.0	12.9		9.4	
(d) Mol% of *N*-methylacetamide		0.0		9.14		19.01
Sr^{2+}	0.331	17.0		9.5		7.5
La^{3+}	0.0153	46		20.2		15.2

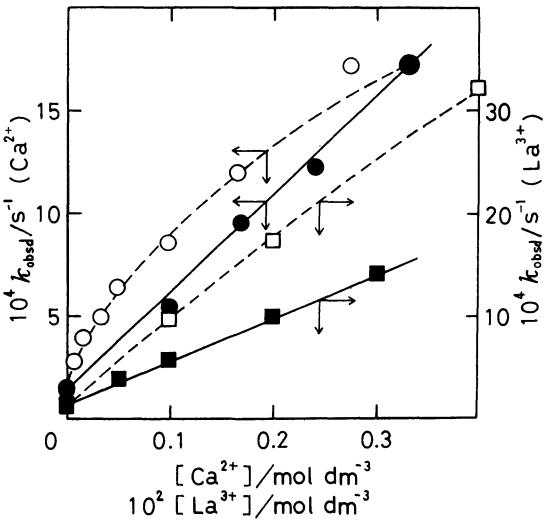

Fig. 4. Dependence of k_{obsd} upon the concentration of cations in 40 vol% ethanol–water.
○: Ca^{2+}, I is not adjusted, ●: Ca^{2+}, I is adjusted to 1.0 with KCl, □: La^{3+}, I is not adjusted, ■: La^{3+}, I is adjusted to 1.0 with KCl.

Table 2. The k_M values in various solvents (I=1.0)

Solvent	$10^4 \times k_M$/s^{-1}				
	Na^+	K^+	Ca^{2+}	Sr^{2+}	La^{3+}
40% Ethanol–H_2O		0.4	46	29	7900[b]
			121[a]	81[a]	7800[c]
40% Dioxane–H_2O	1.0	0.5	113[a]	26	
40% Acetone–H_2O				23	
40% Formamide–H_2O				21	
50% *N*-Methylacetamide–H_2O				22	970[a]
H_2O	2.0	1.1	105[a]	77[a]	4550[b]
					5130[c]

a) I=0.10. b) I=0.020. c) I=0.032.

$$\ln k = \ln k^\circ - \frac{z_A z_B e^2}{d_{AB} \kappa T} \cdot \frac{1}{\varepsilon_r}, \quad (2)$$

where z_A and z_B are charge numbers of ion A and B, respectively, e is the elementary charge, d_{AB} the radius of an activated complex, κ the Bolzmann constant, T temperature, and k° the k value when ε_r is extrapolated to infinity.[18] Plots of $\ln k_{obsd}$ *vs.* $1/\varepsilon_r$ gave a straight line, as shown in Fig. 2. The slope of the plot should be positive when a complex anion reacts with a catalytic cation. However, the observed results were completely contrary to that expected from Eq. 2.

According to the Brønsted-Bjerrum theory, the logarithm of the ionic reaction rate constant, k_M, is generally given for a dilute solution by

$$\ln k_M = \ln k_{M,o} + 2Qz_A z_B \varepsilon^{-3/2} I^{1/2}, \quad (3)$$

where $k_{M,o}$ is the k_M value when ionic strength, I, is zero, and Q is given by

$$Q = (2\pi L)^{1/2} e^3 / (1000)^{1/2} (\kappa T)^{3/2}, \quad (4)$$

where L is the Avogadro constant.[18] The $k_{M,o}$ value may be obtained from the plot of $\ln k_M$ *vs.* $I^{1/2}$. Strictly speaking, however, this method was not applicable when some cations were added to change the ionic strength of the solution, because the acceleration effect of these cations could not be neglected completely, especially in the study of the effect of a univalent cation. The k_M value decreased with increasing ionic strength. Therefore, the $k_{M,o}$ values were evaluated from Eq. 3 by subtracting the calculated second term of the right side of the equation from $\ln k_M$.

The plots of $\ln k_{M,o}$ *vs.* $1/\varepsilon_r$ were linear, as shown in Fig. 5, and the slope became positive when the bivalent and the tervalent cations were added. As the concentration of the organic solvent increased, k_0 in Eq. 1 decreased rapidly and k_M also decreased as the second term of the right side of Eq. 3 decreased, while $k_{M,o}$ increased. Consequently, in the presence of bivalent cations, k_{obsd} apparently decreased as ε_r decreased. On the other hand, the increase in $k_{M,o}$ in the presence of La^{3+}, was very large and k_{obsd} did not decrease with the concentration of the organic solvent. When the univalent cation was added, $k_{M,o}$ was small, and unfortunately the relationship between $\ln k_M$ and $1/\varepsilon_r$ was not clear. The radius of the activated complex, d_{AB}, may be obtained from the slopes of the plots in Fig. 5 and the values of 1.5 nm for Sr^{2+}: 1.4 nm for Ca^{2+} and 1.0 nm for La^{3+} were obtained tentatively. The values were slightly greater than those expected for the free ions. The ion of La^{3+} has a large charge and might come closer to the complex than the bivalent cations.

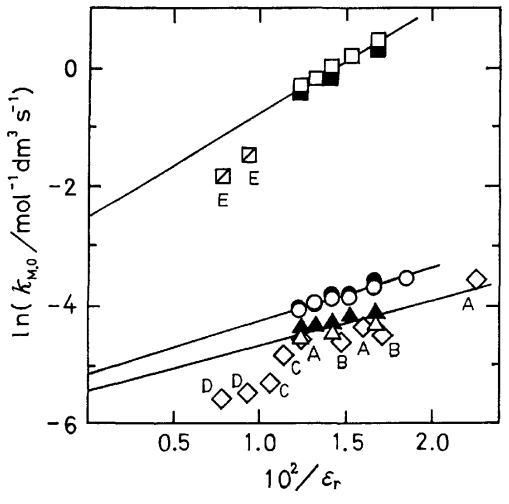

Fig. 5. Plots of $\ln(k_{M,o}/\mathrm{mol^{-1}\,dm^3\,s^{-1}})$ *vs.* the reciprocal of relative permittivity in ethanol–water system except A—E.
○: $[Ca^{2+}]=0.031$ mol dm^{-3}, ●: $[Ca^{2+}]=0.016$ mol dm^{-3}, △: $[Sr^{2+}]=0.33$ mol dm^{-3}, ▲: $[Sr^{2+}]=0.031$ mol dm^{-3}, ◇: $[Sr^{2+}]=0.33$ mol dm^{-3}; A: dioxane–H_2O, B: acetone–H_2O, C: formamide–H_2O, D: *N*-methylacetamide–H_2O, □: $[La^{3+}]=0.0040$ mol dm^{-3}, ■: $[La^{3+}]=0.0020$ mol dm^{-3}, ⊡: $[La^{3+}]=0.015$ mol dm^{-3} in *N*-methylacetamide–H_2O; E.

Although much work has supported a dissociation mechanism, a twist mechanism can not be excluded, since the activation parameters are more suitable for the twist mechanism,[13] and the ligand water is not liberated easily.[19] Then the reaction may involve two mechanisms. One is independent of ionic effects and would be the twist mechanism, the rate constant of which is k_0. Another is dependent on the cations and the dissociation mechanism would be predominant, the rate constant of which is k_M. When $\ln k_{obsd}$ was plotted *vs.* $1/\varepsilon_r$, without dividing k_{odsd} into k_0 and k_M, some linear plots of negative slope were obtained, as shown in Fig. 2, but the positive slopes, which are expected for reactions between ions of the opposite sign, were not obtained. With an increase in the concentration of the organic solvent, the k_0 value decreased, but on the other hand the $k_{M,o}$ value increased. These results suggest the existence of two different mechanisms. If the intermediate with a unidentate oxalato ligand formed by the dissociation is stabilized with an increase in the ε_r value of solvent, it is unreasonable that k_{obsd} becomes small in *N*-methylacetamide–water system. The ε_r value of *N*-methylacetamide is 182 and is much larger than that of water.[17] Kelm *et al.*[6] explained this decrease in terms of Grundwald-Winstein's Y-parameter. The rapid decrease of k_0 with an increase in the concentration of the organic solvent could be elucidated by such a solvent effect.

The authors wish to thank Professor Taro Isobe for useful suggestions during this work.

References

1) K. R. Ashley and R. E. Hamm, *Inorg. Chem.*, **4**, 1120 (1965).
2) H. Kelm, H. Stieger, and G. M. Harris, *Ber. Bunsenges. Phys. Chem.*, **73**, 939 (1969).
3) H. Kelm, H. Stieger, and G. M. Harris, *Z. Phys. Chem. (Frankfurt am Main)*, **67**, 98 (1969).
4) D. H. Huchital, *Inorg. Chem.*, **9**, 486 (1970).
5) M. W. Rophael and M. A. Malati, *J. Chem. Soc., A*, **1971**, 1903.

6) H. Kelm, H. Stieger, and G. M. Harris, *Chem. Ber.*, **104**, 2743 (1971).
7) M. Casula, G. Illuminati, and G. Ortaggi, *Inorg. Chem.*, **11**, 1062 (1972).
8) M. W. Rophael and M. A. Malati, *J. Inorg. Nucl. Chem.*, **36**, 1355 (1974).
9) M. B. Davies and J. W. Lethbridge, *J. Inorg. Nucl. Chem.*, **37**, 141 (1975).
10) Y. Harada and K. Uchida, *Sci. Rep. Hirosaki Univ.*, **23**, 68 (1976).
11) L. Goswami, S. Sarkar, and D. Banerjea, *Z. Anorg. Allg. Chem.*, **435**, 301 (1977).
12) P. L. Kendall, G. A. Lawrance, and D. R. Stranks, *Inorg. Chem.*, **17**, 1166 (1978).
13) K. R. Ashley and K. Lane, *Inorg. Chem.*, **9**, 1795 (1970).
14) K. Uchida and Y. Takinami, *Bull. Chem. Soc. Jpn.*, **53**, 3522 (1980).
15) M. Nakahara, "Mukikagōbutsu No Gōsei," in "Shin-Jikkenkagaku-kōza," ed by the Chemical Society of Japan, Maruzen, Tokyo (1977), Vol. 8, Part 3, p. 1102; A. Werner, *Ann.*, **406**, 286 (1914).
16) J. A. Riddic and W. B. Bunger, "Organic Solvents," in "Techniques of Chemistry," 3rd ed, ed by A. Weissberger, Wiley-Interscience, New York (1970), Vol. 2, p. 724.
17) G. Åkerlöf, *J. Am. Chem. Soc.*, **54**, 4125 (1932); "Landolt-Börnstein Zahlenwerte und Funktionen aus Physik, Chemie, Astronomie, Geophysik und Technik," 6 Aufl. Springer-Verlag, Berlin (1959), Vol. II-6-I, pp. 614—753.
18) K. J. Laidler, "Chemical Kinetics," McGraw-Hill, New York (1965), Chap. 5.
19) J. Aggett, I. Mawston, A. L. Odell, and B. E. Smith, *J. Chem. Soc., A*, **1968**, 1413.

Transition-metal Complexes of Pyrrole Pigments. XXI. One-electron Oxidation of Water Mediated by a Cobalt(III)-Tetradehydrocorrin Complex†

Yukito MURAKAMI,* Yasuhiro AOYAMA, and Toshito TADA

Department of Organic Synthesis, Faculty of Engineering, Kyushu University, Hakozaki, Higashi-ku, Fukuoka 812

(Received December 3, 1980)

The cobalt(III) complex of tetradehydrocorrin (TDHC), having pK_{a1} 6.15 and pK_{a2} 11.50 for successive acid-dissociation of axial aqua ligands, undergoes auto-reduction to the cobalt(II) complex in aqueous carbonate solutions. Kinetic analysis of the reaction indicates the following mechanism: a one-electron transfer from the axial hydroxo ligand to the metal site, subsequent homolytic cleavage of the Co-OH bond, and finally scavenging of the resulting hydroxyl radical with the carbonate ion. At relatively low concentrations of the carbonate ion, the scavenging step is rate-determining; while at $[CO_3^{2-}] \geqq 1.0 \times 10^{-2}$ mol dm^{-3} for [Co^{III}(TDHC)] of 7.62×10^{-5} —1.27×10^{-5} mol dm^{-3}, the initial bond homolysis becomes rate-determining. Analysis of the kinetic data in reference to relevant electrode potentials indicates that the powerful oxidation ability of Co^{III}(TDHC) is responsible for one-electron oxidation of the hydroxo ligand. Reduction of Co^{III}(TDHC) also takes place in the absence of the carbonate ion, the apparent rate increasing with rise of pH in the range 11—12; deprotonation of the hydroxyl radical, which may prevent the hydroxyl radical and the cobalt(II) species from backward recombination, takes place. The one-electron oxidation of the hydroxo ligand was also significantly accelerated by addition of acetonitrile or *t*-butyl alcohol.

The photosynthetic oxidation of water to dioxygen occurring in the photosystem-II has led to challenges to the discovery of chemical systems capable of oxidizing water. The manganese ion is believed to be an essential component of photosystem-II.[1] Thus, various types of manganese complexes,[2–5] mononuclear and binuclear, in homogeneous solutions or as coated on metal surfaces,[6,7] have been studied as models of biological water oxidation. Other homogeneous metal complex systems as regards water oxidation include the tris-(bipyridine) and tris(phenanthroline) complexes of iron(III),[8] osmium(III),[8,9] and ruthenium(III).[10] Another system of great importance employs heterogeneous noble-metal oxides such as RuO_2 which can mediate, when dispersed in aqueous media, oxidation of water to dioxygen by agents which have appropriate redox potentials such as $Ru(bpy)_3^{3+}$.[11,12]

Water can be oxidized most readily by a four-electron transfer process from a thermodynamic viewpoint; one-electron oxidation of water ($E^0 = +2.8$ V *vs.* SHE) or even hydroxide ion ($E^0 = +2.0$ V *vs.* SHE) is much less favorable than the four-electron process ($E^0 = +1.229$ V *vs.* SHE).[13] The four-electron transfer is not achieved by using ordinary mononuclear metal complexes in homogeneous phase even if the complexes have appropriate redox potentials, since such complexes can, in principle, oxidize water by a one-electron transfer process. However, clarification of the one-electron water-oxidation mechanism seems not only to provide a basis for understanding the mechanism of photosynthetic oxygen evolution reactions but also to offer relevant information for designing more elaborated multi-electron oxidation catalysis in homogeneous phase. No unambiguous demonstration has been presented for the direct one-electron oxidation of water or hydroxide ion, either free or metal-coordinated, with metal complexes, although the auto-reduction of manganese-(IV)–hematoporphyrin would involve such a process.[3]

† Contribution No. 615 from this Department.

The present study is based on the finding that a cobalt(II)-tetradehydrocorrin complex undergoes facile reduction to the corresponding cobalt(I) complex in an aprotic solvent with hydroxide ion.[14] In the course of our research on the mechanistic aspects of this and related reactions, we have investigated the reduction behavior of a cobalt(III) complex of tetradehydrocorrin in aqueous media, and demonstrated the one-electron oxidation of water as coordinated to the metal site in the form of the axial hydroxo ligand.

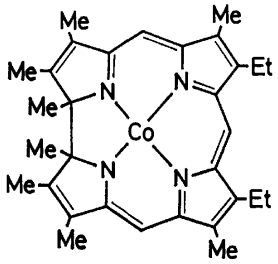

Co(TDHC)

Results

Formation of Co^{III}(TDHC). The cobalt(III) complex of 8,12-diethyl-1,2,3,7,13,17,18,19-octamethyltetradehydrocorrin (abbreviated as TDHC), Co^{III}-(TDHC), was obtained by oxidation of [Co^{II}(TDHC)]-ClO_4[14,15] in water–methanol (99 : 1 v/v); air-oxidation or chemical oxidation either with hypochlorite or chlorine, oxidation being carried out in acidic media. The apparent first-order rate constant for the air-oxidation at 20 °C was proportional to hydrogen ion concentration ($0.01 \leqq [H^+] \leqq 0.1$ mol dm^{-3}):[16] $k/s^{-1} = 0.29[H^+]$, as in the case of a related AD–didehydrocorrin complex.[17] The initial product, hydrogen peroxide, could not be detected since each peroxide readily oxidizes two more molecules of the cobalt(II) complex.[16] In fact, the oxidation rate was much larger in the presence of varying amounts of hydrogen peroxide than

in its absence and linearly dependent on $[H_2O_2]$: $k/s^{-1}=2.8\times10^{-3}+k'[H_2O_2]$ at $[H^+]=9.8\times10^{-3}$ mol dm^{-3} where $k'=196$ dm^3 mol^{-1} s^{-1}. The electronic spectrum of Co^{III}(TDHC) was dependent neither on the method of preparation described above nor on the nature of acid employed (hydrochloric, perchloric, or sulfuric acid). This indicates that a simple diaqua ligation takes place at the axial sites of Co^{III}(TDHC) in acidic media. The air-oxidation rate of Co^{II}(TDHC) was not affected to any detectable extent even in the presence of an equimolar amount of hydrogen cyanide, although the product was the aquacyano derivative, $[(CN)(H_2O)Co^{III}(TDHC)]^+$. This indicates that no cyanide ion is involved in the oxidation of Co^{II}(TDHC) and the oxidation product, $[(H_2O)_2Co^{III}(TDHC)]^{2+}$, is subsequently converted into $[(CN)(H_2O)Co^{III}$-(TDHC)$]^+$.

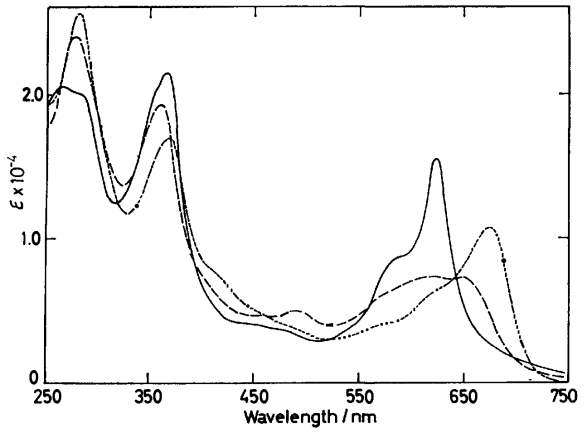

Fig. 1. Electronic absorption spectra of diaqua (——), aquahydroxo (— —), and dihydroxo (·····) species of Co^{III}(TDHC) in water–methanol (99.2 : 0.8 v/v) at 10 °C.

The spectral feature of Co^{III}(TDHC) varies as the axial ligands change from diaqua through cyanoaqua to dicyano in a similar manner as observed for the cobalt(III) complexes of AD–didehydrocorrin and cobinamide.[17] The successive acid dissociation of the two axial aqua ligands (Eq. 1) was confirmed by spectrophotometric titration of Co^{III}(TDHC) at 10 °C over a wide pH range: pK_{a1} 6.15 and pK_{a2} 11.50.[18] The choice of temperature (10 °C) is simply due to the fact that the reaction of the complex takes place at higher temperatures. Figure 1 shows the electronic spectra of the diaqua, aquahydroxo, and dihydroxo species.

$$\left[\begin{matrix}OH_2\\ |\\ Co^{III}\\ |\\ OH_2\end{matrix}\right]^{2+} \underset{}{\overset{pK_{a1}\ 6.15}{\rightleftharpoons}} \left[\begin{matrix}OH\\ |\\ Co^{III}\\ |\\ OH_2\end{matrix}\right]^{+} \overset{pK_{a2}\ 11.50}{\rightleftharpoons} \left[\begin{matrix}OH\\ |\\ Co^{III}\\ |\\ OH\end{matrix}\right] \quad (1)$$

Carbonate- and Hydroxide-induced Reduction of Co^{III}(TDHC). In aqueous carbonate solutions containing methanol (0.8% by volume) at 38.4 °C, Co^{III}(TDHC) underwent facile reduction to Co^{II}(TDHC) in quantitative yield. The product was identified by electronic spectroscopy and vapor pressure osmometric molecular weight determination. It was also converted into $(CN)_2Co^{III}$(TDHC),[15,19] which was identified by electronic and NMR spectroscopy. The results preclude any possible modification of the TDHC structure during the course of reduction. When the conversion Co(III)→Co(II) was followed spectrophotometrically, clear isosbestic points were observed at 264, 354, 443, and 579 nm. At carbonate concentrations greater than 1.0×10^{-2} mol dm^{-3} for $[Co^{III}(TDHC)]$ of 1.27×10^{-5} —7.62×10^{-5} mol dm^{-3}, the reduction of Co^{III}(TDHC) followed first-order kinetics with respect to Co^{III}-(TDHC) with the first-order rate constant independent of carbonate concentration; linear first-order plot almost to 100% conversion for any given run and no dependence of the rate constant on initial concentration of the complex. The first-order dependence of the reaction on Co^{III}(TDHC) rules out the participation of any equilibria involving a dimer such as the hydroxo-bridged one. The limiting (or leveled-off) rate constant (Fig. 2) depends neither on pH (Table 1) nor on concentration of chloride or perchlorate ion; for added chloride (0.07 mol dm^{-3}) or perchlorate (0.008 mol dm^{-3}) in addition to the carbonate ion, the rate constant remained the

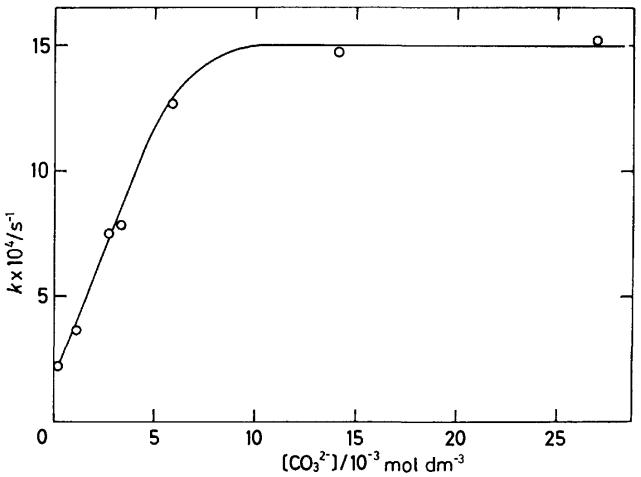

Fig. 2. Correlation of first-order rate constant with carbonate concentration for reduction of Co^{III}(TDHC) in water–methanol (99.2 : 0.8 v/v) at 38.4 °C and pH 9.5±0.2.

Table 1. Apparent first-order rate constants for carbonate- and hydroxide- induced reduction of Co^{III} (TDHC)[a]

Effective anion	pH	k/s^{-1}
Carbonate (0.11 mol dm^{-3})[b]	9.3	1.5×10^{-3}
(0.082 mol dm^{-3})[b]	9.7	1.5×10^{-3}
(0.082 mol dm^{-3})[b]	11.0	1.5×10^{-3}
Hydroxide[c]	10.7	2.6×10^{-4}
	11.4	6.1×10^{-4}
	11.7	8.1×10^{-4}
	12.2	1.1×10^{-3}
	13.1	*ca.* 1×10^{-4}

a) In water containing methanol (0.8% by volume) at 38.4 °C; initial concentration of Co^{III} (TDHC), 3.81×10^{-5} mol dm^{-3}. b) Total concentration of carbonate and hydrogencarbonate. c) Carbonate-free sodium hydroxide solution used.

Table 2. Activation parameters for homolysis of Co(III)–OH bond[a)]

Entry	Medium (composition)[b)]	$\Delta H^{\ddagger}$ / kcal mol^{-1}	$\Delta S^{\ddagger}$ / cal deg^{-1} mol^{-1}	$\Delta G^{\ddagger}$ / kcal mol^{-1}
1	H_2O–CH_3OH (99.2 : 0.8)	23.9	+4.7	22.4
2	H_2O–CH_3CN–CH_3OH (85.5 : 13.7 : 0.8)	21.6	+1.4	21.2
3	H_2O–CH_3CN–CH_3OH (77.3 : 21.9 : 0.8)	18.7	−6.6	20.8
4	H_2O–t-C_4H_9OH–CH_3OH (77.3 : 21.9 : 0.8)	18.5	−7.1	20.7

a) At 38.4 °C. Initial concentartion of Co^{III} (TDHC), 3.81×10^{-5} mol dm^{-3}. Other experimental conditions ([CO_3^{2-}], pH, temperature range): entry number 1, (1.5×10^{-2} mol dm^{-3}, 9.4, 20.0—47.7 °C); 2, (0.19 mol dm^{-3}, 11.4, 20.0—38.4 °C); 3, (0.19 mol dm^{-3}, 11.5, 24.5—38.4 °C); 4, (0.19 mol dm^{-3}, 11.9, 20.0—38.4 °C). b) Volume percent.

same. The rate constant showed linear dependence on [CO_3^{2-}] at lower concentrations of the carbonate ion (Fig. 2). Methanol (0.8% by volume) involved in the reaction medium as a cosolvent could be eliminated or replaced by acetonitrile or *N*,*N*-dimethylformamide at 0.8% by volume without affecting the limiting rate constant. Phosphate and borate ions in place of carbonate were less effective for promoting the reduction of Co^{III}(TDHC). The activation parameters were obtained at a carbonate concentration in the rate-saturation range (1.5×10^{-2} mol dm^{-3}, refer to Fig. 2) for the temperature range 20.0—47.7 °C (Table 2). Another important aspect of the carbonate-induced reduction is the photo-catalysis. Co^{III}(TDHC) (3.81×10^{-5} mol dm^{-3}) in 6.5×10^{-2} mol dm^{-3} carbonate was completely reduced to the Co(II) species at 0 °C in 90 min under irradiation with a 100-W high pressure mercury lamp from a distance of 11 cm, while the conversion was less than 10% in the dark in a period of 180 min under otherwise identical conditions.

In the absence of buffer salts, the reduction of Co^{III}-(TDHC) did occur with concomitant formation of hydrogen peroxide as detected by iodometry. The apparent first-order rate increased with rise of pH from 10.7 to 12.2 and approached the limiting rate constant

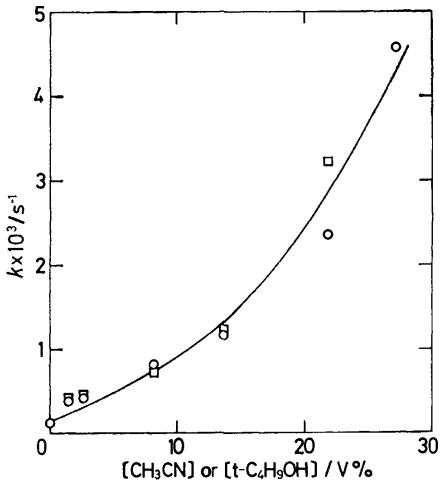

Fig. 3. Correlation of first-order rate constant with content of organic solvents for reduction of Co^{III}-(TDHC) in water–acetonitrile (○) and in water–*t*-butyl alcohol (□), both containing 0.19 mol dm^{-3} carbonate and 0.8% (v/v) methanol, at 20.0 °C.

for the carbonate-induced reaction (Table 1). The reaction was also photo-catalyzed in a similar way to that observed for the carbonate-induced reaction. The proton dissociation with pK_{a2} 11.50 resulted in an appreciable reduction in reactivity as seen from the rate constant at pH 13.1.

In the presence of the carbonate ion at rate-saturation level (0.19 mol dm^{-3}), the reduction of Co^{III}(TDHC) was facilitated by added organic cosolvents such as acetonitrile and *t*-butyl alcohol (Fig. 3). The activation parameters obtained are summarized in Table 2. The rate-acceleration upon addition of organic cosolvents is brought about by favorable activation enthalpy changes.

Discussion

Formation of Hydroxyl Radical and Its Scavenging. In order to establish the mechanism involved in the reduction of Co^{III}(TDHC) in aqueous carbonate solutions, we must identify the reductant (or species being oxidized), elucidate the electron transfer mechanism, and clarify the specific role of the carbonate ion. As regards the product, Co^{II}(TDHC), the TDHC ligand remains intact, no concomitant oxidation of the macrocyclic ligand taking place. This is in marked contrast to the base-induced reduction of Ni(III)[20] and Co(III)[21] complexes of N_4-macrocycles. An outer-sphere oxidation of water is highly unlikely because of the gross mismatch of the reduction potential (+0.59[17] or +0.54 V *vs.* SCE[22] in methanol) of L_2Co^{III}(TDHC) (L being a solvent molecule coordinated at the axial site) and the one-electron oxidation potential of water (E^0 = +2.8 V *vs.* SHE). A possibility that the free hydroxyl ion would act as a stoichiometric reductant can also be ruled out since the carbonate-induced reaction rate is independent of the pH in the range 9.3—11.0 (Table 1). Thus, the present oxido-reduction must be an intramolecular process involving the axial hydroxo ligand.[22] In view of one-electron transfer stoichiometry and the fact that the carbonate ion, which has no effect on the electronic spectrum of the present complex, is a powerful hydroxyl radical scavenger,[23-26] we can formulate the mechanism as follows: a reversible one-electron transfer from an axial hydroxo ligand to Co(III) and subsequent dissociation of the axial bond, followed by scavenging of the resulting

hydroxyl radical with the carbonate ion[27] (Eq. 2).

$$\text{Co(III)-OH} \underset{k_{-1}}{\overset{k_1}{\rightleftharpoons}} \text{Co(II)} + \cdot\text{OH}$$

$$\xrightarrow{k_2[CO_3^{2-}]} \text{Co(II)} + OH^- + CO_3^{\cdot-} \quad (2)$$

$$(CO_3^{\cdot-} \longrightarrow \text{further reaction})$$

The proposed mechanism involving homolytic cleavage of the Co(III)-OH bond is consistent with the photochemical acceleration as well as the observed dependency of the rate on carbonate concentration (Fig. 2). At relatively low concentrations of carbonate, the $k_2[CO_3^{2-}]$ process is rate-determining as reflected on the rate which is linearly dependent on the carbonate concentration. As the carbonate concentration is raised to the level where $k_2[CO_3^{2-}] \gg k_{-1}$, the k_1 process becomes the rate-determining step for which the rate is independent of carbonate concentration. The validity of Eq. 2 should be further examined by kinetic analysis of the data under steady state treatment. A steady state approximation is applied with respect to the hydroxyl radical, the steady state concentration, $[\cdot OH]_{ss}$, being given by

$$[\cdot OH]_{ss} = \frac{k_1[Co(III)]}{k_{-1}[Co(II)] + k_2[CO_3^{2-}]} \quad (3)$$

Eq. 3. The rate law for disappearance of Co^{III}(TDHC) is then represented by Eq. 4. A simple first-order

$$-\frac{d[Co(III)]}{dt} = k_1[Co(III)] - k_{-1}[Co(II)][\cdot OH]_{ss}$$

$$= k_2[CO_3^{2-}][\cdot OH]_{ss}$$

$$= \frac{k_1k_2[Co(III)][CO_3^{2-}]}{k_{-1}[Co(II)] + k_2[CO_3^{2-}]} \quad (4)$$

kinetics is derived under the conditions $k_2[CO_3^{2-}] \gg k_{-1}[Co(II)]$ with first-order rate constant k_1. Under the other extreme conditions as represented by $k_{-1}[Co(II)] \gg k_2[CO_3^{2-}]$, Eq. 4 is simplified to Eq. 5. The kinetic data for runs at carbonate concentrations of 2.3×10^{-4} and 1.7×10^{-3} mol dm^{-3} (the lowest two concentrations employed here) were satisfactorily analyzed by means of Eq. 5 or its integrated form, Eq. 6.[28]

$$-\frac{d[Co(III)]}{dt} = \frac{k_1k_2}{k_{-1}}[CO_3^{2-}]\frac{[Co(III)]}{[Co(II)]} \quad (5)$$

$$[[Co(III)] - [Co(III)]_0 \ln[Co(III)]]_0^t = \frac{k_1k_2}{k_{-1}}[CO_3^{2-}]t \quad (6)$$

Except for the early stage of reaction, a plot of $-d[Co(III)]/dt$ *vs.* $[Co(III)]/[Co(II)]$ yielded a straight line with the slope $k_1k_2[CO_3^{2-}]/k_{-1}$ (Fig. 4), where k_1 is the limiting rate constant in Fig. 2 (1.5×10^{-3} s^{-1}) (see Experimental). It is reasonable to assume that the highly exothermic k_{-1} process is diffusion-controlled, *i. e.*, $k_{-1} \cong 10^{10}$ dm^3 mol^{-1} s^{-1}. The k_2 values are calculated to be: 6×10^7 and 2×10^7 dm^3 mol^{-1} s^{-1} for runs at carbonate concentrations of 2.3×10^{-4} and 1.7×10^{-3} mol dm^{-3}, respectively. These values are comparable to the rate constant for bimolecular reaction of the hydroxyl radical with the carbonate ion obtained from a pulse-radiolysis study:[24] 4.2×10^8 dm^3 mol^{-1} s^{-1}.[29] The activation enthalpy as large as 23.9 kcal mol^{-1} and the positive activation entropy (+4.7 cal deg^{-1} mol^{-1}) (Table 2) for the k_1 process are consistent

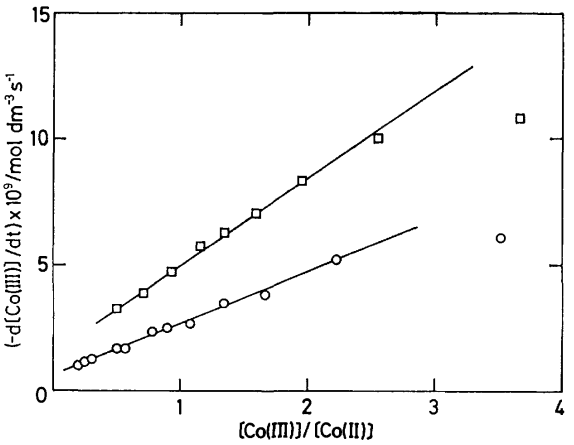

Fig. 4. Analysis of kinetic data (Eq. 5) for reduction of Co^{III}(TDHC) in water–methanol (99.2 : 0.8 v/v) in the presence of 2.3×10^{-4} mol dm^{-3} (○) and 1.7×10^{-3} mol dm^{-3} (□) carbonate at 38.4 °C.

with a highly endothermic unimolecular dissociation process.

Correlation with Electrode Potentials. Judging from the Co(II)/Co(III) redox potential for Co^{II}(TDHC) in methanol (+0.59[17] or 0.54 V *vs.* SCE[22]) and the one-electron oxidation potential of the hydroxide ion in water (+2.0 V *vs.* SHE),[13] the standard free energy change for an outer-sphere oxidation of the free hydroxide ion by L_2Co^{III}(TDHC) (L being a solvent molecule) would amount to *ca.* 27 kcal mol^{-1} and the process would proceed quite slowly at ordinary temperatures. The intramolecular oxidation of the hydroxo ligand can be regarded, from a thermodynamic viewpoint, as an oxidation of the coordination-free hydroxide ion by *naked* Co^{III}(TDHC) whose Co(II)/Co(III) potential may be assumed equivalent to that in a non-coordinating solvent; +0.97 V *vs.* SCE in CH_2Cl_2.[17] The accompanying free energy change would be reduced from 27 kcal mol^{-1} for an outer-sphere oxidation to *ca.* 18 kcal mol^{-1}. In the light of such evaluation, the free energy of activation for the bond dissociation (k_1 process), $\Delta G^{\ddagger} = \Delta H^{\ddagger} - T\Delta S^{\ddagger}$, 22.4 kcal mol^{-1} (Table 2) is reasonable in magnitude. In order to get further insight into the correlation with electrode potential, the kinetic data were analyzed on the basis of simplified reaction scheme; a reversible electron transfer between *naked* Co^{III}(TDHC) (*Co(III)*) and OH^- followed by scavenging of the hydroxyl radical with the carbonate ion as given by Eq. 7.

$$Co(III) + OH^- \underset{k_{-1}'}{\overset{k_1'}{\rightleftharpoons}} \text{Co(II)} + \cdot\text{OH}$$

$$\xrightarrow{k_2[CO_3^{2-}]} \text{Co(II)} + OH^- + CO_3^{\cdot-} \quad (7)$$

Under the conditions where scavenging is the rate-determining process, the apparent first-order rate constant is given by $(k_1'/k_{-1}')k_2[CO_3^{2-}]$; $(k_1'/k_{-1}')k_2$ corresponds to the slope (0.21 dm^3 mol^{-1} s^{-1}) of the linear portion of rate constant *vs.* $[CO_3^{2-}]$ profile in Fig. 2. If k_2 is taken for the range of 6×10^7 (calculated as above) through 1×10^9 dm^3 mol^{-1} s^{-1} (based on pulse radiolysis), the hypothetical equilibrium constant,

$K=k_1'/k_{-1}'$, would be in the range 3.5×10^{-9}—2.1×10^{-10}. A value of 1.23—1.16 V *vs.* SCE is obtained for $E_{Co(II)/Co(III)}$ at 38.4 °C ($E_{OH\cdot/OH^-}=+2.0$ V *vs.* SHE) by means of

$$-RT\ln K=\Delta G^0=F(E_{OH\cdot/OH^-}-E_{Co(II)/Co(III)}), \quad (8)$$

where F and E denote Faraday constant and electrode potential, respectively. The redox potential is consistent with the kinetic parameters based on Eq. 7 and close to the observed one in CH_2Cl_2 (+0.97 V *vs.* SCE). The argument may indicate that the one-electron oxidation of the hydroxide ion can be expected in the light of powerful oxidation capacity of Co^{III}(TDHC). In fact, the Co(II)/Co(III) redox potential of +0.97 V *vs.* SCE seems exceptional for the cobalt complexes of pyrrole pigments; +0.3 V for Co(etioporphyrin) in butyronitrile[30] and −0.26 V for Co(octaalkylcorrole) in CH_2Cl_2.[31]

Effects of Organic Cosolvents. Acetonitrile and *t*-butyl alcohol are known as potential hydroxyl radical scavengers. The scavenging efficiency of such solvents, however, does not seem to be the primary origin for the rate acceleration (Fig. 3) since the presence of sufficient amount of carbonate (0.19 mol dm^{-3}) assures that we are dealing with the rate-determining homolytic k_1 process which is free from the scavenging effect exercised by such organic solvents. Thus, the rate acceleration by organic cosolvents added must be solely due to their medium effects. The solvation status must change along the Co(III)–OH bond homolysis from highly solvated anionic hydroxo ligand at the initial state to the neutral hydroxyl radical which requires less solvation by water. As the content of an organic solvent increases, solvation of the hydroxo ligand becomes less effective with the consequence that the hydroxo ligand is less stabilized on the one hand and the surrounding water molecules get more translational freedom on the other at the ground state of reaction, resulting in the reduction of activation enthalpy with the compensating change in activation entropy. This is what was observed (Table 2). A major contributor to the potential energy to be overcome in the oxidation of both hydroxide ion and hydroxo ligand would be the stabilization of the ground state through solvation of such reactants. Desolvation of both hydroxide ion and hydroxo ligand, even to a small extent, would result in significant enhancement of their oxidation since the hydration energy of the hydroxide ion in water is greater than 100 kcal mol^{-1}.[32]

Reduction of Co^{III}(TDHC) without Radical Scavenger. Concerning the reduction of Co^{III}(TDHC) in the pH range 11—12 (Table 1) in the absence of the carbonate ion or other potential anions, the following remarks are given. (1) The reaction is photo-catalyzed in a manner similar to that in the carbonate system; (2) in reference to the mechanism for the carbonate system (Eq. 2), the hydroxide ion can never be regarded as a hydroxyl radical scavenger; and (3) the reaction rate increases with increasing [OH^-], approaching the limiting value for the carbonate-induced reaction. The pH-rate correlation seems to reflect the proton dissociation equilibrium (inactive form$\rightleftharpoons$active form$+H^+$) with pK_a around 11.5. This can not be referred to the conversion from the aquahydroxo into the dihydroxo form (Eq. 1) with pK_{a2} 11.50 in spite of numerical coincidence, since a sharp rate reduction is observed at pH 13.1 where the dihydroxo species predominates (Table 1). Thus, the reactive species should be the aquahydroxo species whose population becomes smaller while the overall rate constant increases with increasing pH. As an alternative and highly plausible equilibrium, we suggest the proton-dissociation of the hydroxyl radical whose pK_a is 11.8.[24] The hydroxyl radical is a super-oxidant and its most likely fate in the absence of its scavenger would be recombination with the Co(II) complex, *i. e.*, oxidation of the Co(II) species by the hydroxyl radical. This reverse process would not be effective for the anionic conjugate base ($O^{\cdot-}$) which is considered to be a far less effective oxidant. Under these circumstances, the dimerization of $O^{\cdot-}$ to peroxide, a well characterized reaction,[33] may compete with the backward recombination of the hydroxyl radical with the Co(II) species

$$\begin{aligned} &H_2O\text{-}Co(III)\text{-}OH \underset{k_{-1}}{\overset{k_1}{\rightleftharpoons}} H_2O\text{-}Co(II) + \cdot OH \\ &\underset{-OH^-;\ k_{-2}'}{\overset{OH^-;\ k_2'}{\rightleftharpoons}} H_2O\text{-}Co(II) + O^{\cdot-} + H_2O \\ &\qquad\qquad\qquad\qquad\qquad\qquad \hookrightarrow H_2O_2 \end{aligned} \quad (9)$$

(Eq. 9). This mechanism is consistent with the observed pH-dependence of reaction rate for the pH range 11—12. It involves the deprotonation of the hydroxyl radical and its subsequent reaction, and is thus important for water oxidation since the process requires no additional radical scavengers. It is unfortunate that the accidental coincidence of the pK_a values of the second aqua ligand of the complex and the hydroxyl radical makes a detailed analysis of the kinetic data difficult.

Conclusion

(1) One-electron oxidation of a hydroxo ligand coordinated to Co^{III}(TDHC) does take place in aqueous media. The Co(III)–OH bond undergoes homolytic cleavage to yield the hydroxyl radical first. This is an effective and conventional process for water oxidation. (2) For effective progress of the reaction, there must be some mechanism by which the back recombination of the hydroxyl radical and the Co(II) species can be prevented or depressed. (3) Oxidation of the hydroxide ion and possibly other anions, coordinated or not coordinated to metal complexes, may be accelerated by addition of organic cosolvents to aqueous media *via* a desolvation mechanism.

Experimental

Instruments and Materials. Electronic spectra were obtained with thermostated quartz cells (1-cm path length) set in either a Union Giken SM-401 high sensitive spectrophotometer or a Hitachi 124 spectrophotometer. ^1H NMR spectra were taken on a Hitachi R-24B spectrometer with tetramethylsilane as an internal reference. A Hitachi-Perkin Elmer 115 vapor pressure osmometer was used to determine molecular weights. pH-Measurements were carried out with a Beckman Expandomatic SS-2 pH meter equipped with a Metrohm EA-125 combined electrode, calibrated against standard aqueous buffers.

(8,12-Diethyl-1,2,3,7,13,17,18,19-octamethyltetradehydrocor-

rinato)cobalt(II) perchlorate, $[Co^{II}(TDHC)]ClO_4$, was prepared according to the procedure of Dolphin *et al.*[15] Found: C, 59.62; H, 5.92; N, 8.91%. Calcd for $C_{31}H_{37}ClCoN_4O_4$: C, 59.67; H, 5.98; N, 8.98%. Water was deionized and distilled with a Pyrex distilling apparatus. Acetonitrile and *t*-butyl alcohol were fractionally distilled just before use. All the other chemicals were of analytical grade.

Formation of Co^{III}(TDHC) and Acid Dissociation of Its Diaqua Complex. Oxidation of a reddish-purple solution of $[Co^{II}(TDHC)]ClO_4$ by three different oxidants (air, hypochlorite, and chlorine) under acidic conditions gave a greenish-blue solution of Co^{III}(TDHC) as confirmed by electronic spectroscopy. For air oxidation, the simplest procedure, a methanol solution of Co^{II}(TDHC) (1 part) was mixed with water (100 part) containing an appropriate amount of an acid and the mixture was exposed to the air at room temperature. Under anaerobic conditions neither oxidation nor spectral change was detected. For oxidation by hypochlorite or chlorine, a 100-μl sample of a methanol solution of Co^{II}(TDHC) (4.65×10^{-3} mol dm^{-3}) was injected into a deoxygenated 0.01-mol dm^{-3} HCl solution (3 ml) containing 2 μl of aqueous NaOCl solution (10% active chlorine) and 7 μl of saturated aqueous Cl_2 solution, respectively, at room temperature. Oxidation took place almost instantaneously.

A methanol solution of Co^{II}(TDHC) (4.65×10^{-3} mol dm^{-2}, 30 μl) was added to 3 ml of water containing an appropriate amount of hydrochloric acid, and hydrogen peroxide or hydrogen cyanide for specified experiments, at 20.0 ± 0.1 °C; the absorbance change at 490 nm then being measured at the same temperature. As regards the preparative scale experiment, 15 mg (2.4×10^{-5} mol) of Co^{II}(TDHC) was oxidized in water (50 ml) containing methanol (0.5 ml) and 1-mol dm^{-3} HCl (0.5 ml). The cobalt complex was extracted into dichloromethane, and the aqueous layer was found to be free of hydrogen peroxide by iodometric analysis. Co^{III}(TDHC) was relatively stable only when diluted in acidic aqueous media and quite readily reconverted into the original Co(II) complex during the course of isolation such as extraction with organic solvents (dichloromethane, benzene, and ether), precipitation from aqueous solution by adding an organic solvent, careful concentration (with partial regeneration of Co^{II}(TDHC)), and evaporation of aqueous solutions (with complete conversion into Co^{II}(TDHC)).

Spectra were recorded for a series of solutions of Co^{III}(TDHC) (2.79×10^{-5} mol dm^{-3}) in aqueous buffers at various pH (2.13—13.45) and at 10.0 °C. The absorbance at 620 nm ($2.13\leqq pH\leqq10.22$) or at 670 nm ($8.10\leqq pH\leqq13.45$) was plotted against pH, and the pK_a values for acid dissociation of the coordinated water molecules were determined graphically. The buffer systems used were as follows: pH 2.13—3.30, HCl; 3.75—5.58, acetate; 6.25—7.75, phosphate; 8.10, borate; 9.25—10.93, carbonate; 10.20—13.45, NaOH.

Kinetic Measurements. Acidic solutions of Co^{III}(TDHC) were prepared by mixing 30 μl of a methanol solution of Co^{II}(TDHC) (4.65×10^{-3} mol dm^{-3}) and water (appropriate amount) containing 30 μl of 1-mol dm^{-3} HCl and the resulting solutions were allowed to stand at room temperature for at least 30 min. Acetonitrile or *t*-butyl alcohol (appropriate amount) was added for specified experiments. No inorganic salts were added to the solutions unless otherwise stated because of their possible contribution to scavenging of the hydroxyl radical. The solutions were then placed in a specially designed quartz cell (1-cm path length) set in a spectrophotometer and preequilibrated at desired temperatures under nitrogen atmosphere. The reaction was initiated by injecting an appropriate amount of aqueous Na_2CO_3–$NaHCO_3$ (1.0 or 2.0 mol dm^{-3}) or aqueous NaOH (18.8 mol dm^{-3}). The final solutions were adjusted at a constant volume of 3.66 ml with 3.81×10^{-5} mol dm^{-3} of Co^{III}(TDHC). The course of reaction was followed by monitoring the absorbance change at 490 nm (an absorption maximum for Co^{II}(TDHC)). The concentrations of carbonate ion were calculated from the known amounts of ($[CO_3^{2-}]+[HCO_3^-]$) and pH of the solutions measured for every kinetic runs, in reference to the pK_a value of carbonate. The pK_a of carbonate in mixed solvents was independently determined by potentiometric titration: 10.7 in water–acetonitrile (86.3 : 13.7 v/v), and 10.6 in water–*t*-butyl alcohol (86.3 : 13.7 v/v). Analyses of kinetic data according to Eq. 5 were performed by evaluating [Co(II)] and [Co(III)] first at an appropriate time interval and then taking the average value for each time interval (Δt): $-d[Co(III)]/dt=([Co(III)]_t-[Co(III)]_{t+\Delta t})/\Delta t$; $[Co(III)]/[Co(II)]=([Co(III)]_t+[Co(III)]_{t+\Delta t})/([Co(II)]_{t+\Delta t}+[Co(II)]_t)$. Activation parameters were calculated as follows: $E_a=\Delta H^{\ddagger}+RT$ (E_a, activation energy from Arrhenius plot), $k_{38.4°C}=(kT/h)\exp(-\Delta G^{\ddagger}/RT)$, and $\Delta G^{\ddagger}=\Delta H^{\ddagger}-T\Delta S^{\ddagger}$.

Reduction of Co^{III}(TDHC) in Carbonate Solutions: Formation of Co^{II}(TDHC). A solution of Co^{III}(TDHC), prepared from $[Co^{II}(TDHC)]ClO_4$ (29 mg) in water (1 l) containing 1 mol dm^{-3} HCl (10 ml) and methanol (10 ml), was mixed with 110 ml of 1.0 mol dm^{-3} aqueous Na_2CO_3 solution. The mixture was allowed to stand at 40 °C for 30 min with occasional swirling, at room temperature for 4 h to complete the Co(III)→Co(II) conversion, and then extracted with dichloromethane (100 ml×2). The extract was washed with a saturated $NaClO_4$ solution (50 ml), dried (Na_2SO_4), and evaporated to give $[Co^{II}(TDHC)]ClO_4$ (25 mg, 86%). Its electronic spectrum and molecular weight (measured by vapor pressure osmometry for methanol solutions) were identical with those of the authentic sample. The Co(II) complex thus obtained was dissolved in methanol (10 ml), and potassium cyanide (30 mg) was added. The mixture was allowed to stand at room temperature for 10 h, the solvent was removed *in vacuo*, and the residue was extracted with chloroform. Evaporation of chloroform gave $(CN)_2Co^{III}$(TDHC)[15] (17 mg, 65% from the initial Co(II) complex): electronic and NMR spectra were identical with those of the authentic sample. ^1H NMR ($CDCl_3$): δ 6.91 (s, 2H, C(5)–H and C(15)–H), 6.87 (s, 1H, C(10)–H), 2.86 (q, 4H, $C\underline{H}_2CH_3$), 2.45 (s, 12H, CH_3's on C(3), C(7), C(13), and C(17)), 2.33 (s, 6H, CH_3's on C(2) and C(18)), 1.34 (t, 6H, $CH_2C\underline{H}_3$), and 0.76 (s, 6H, CH_3's on C(1) and C(9)).

Reduction of Co^{III}(TDHC) in the Absence of Carbonate: Detection of Hydrogen Peroxide. A solution of Co^{III}(TDHC), prepared in a manner similar to that described above by air oxidation of Co^{II}(TDHC) in acidic aqueous media with or without methanol (1%), was carefully concentrated at temperatures below 30 °C. A 10-ml portion of the resulting solution (*ca.* 1×10^{-3} mol dm^{-3} in Co^{III}(TDHC)) was mixed anaerobically with an appropriate amount of carbonate-free aqueous NaOH; pH of the solution, 12.3. The mixture was allowed to stand at room temperature for 40 min. The Co^{II}(TDHC) complex precipitated from the solution was removed by filtration, and the amount of hydrogen peroxide in the filtrate was determined by iodometric analysis. A solution to be examined was purged with argon for 5 min, and 10% aqueous KI solution (1 ml) and 4 mol dm^{-3} aqueous H_2SO_4 (2 ml) were added. After being bubbled with argon for 5 min, the mixture was titrated with 5.0×10^{-3} mol dm^{-3} aqueous $Na_2S_2O_3$; 30% yield at best on the basis of the Co(III) complex used. The low yield of hydrogen peroxide was at least due to its further reaction with Co^{II}(TDHC) to give unidentified product(s), as independently confirmed by spectrophotometric means.

References

1) G. M. Cheniae and I. F. Martin, *Biochim. Biophys. Acta*, **197**, 219 (1970).
2) M. Calvin, *Science*, **184**, 375 (1974); S. R. Cooper and M. Calvin, *ibid.*, **185**, 376 (1974); M. Calvin, *Acc. Chem. Res.*, **11**, 369 (1978).
3) I. Tabushi and S. Kojo, *Tetrahedron Lett.*, **1974**, 1577.
4) L. J. Boucher and C. G. Coe, *Inorg. Chem.*, **14**, 1289 (1975); **15**, 1334 (1976).
5) M. M. Morrison and D. T. Sawyer, *J. Am. Chem. Soc.*, **99**, 257 (1977); D. T. Sawyer, M. E. Bodini, L. A. Willis, T. L. Riechel, and K. D. Magers, in "Bioinorganic Chemistry-II," Advances in Chemistry Series 162, ed by K. N. Raymond, American Chemical Society, Washington, D. C. (1977), Chap. 19.
6) M. Aizawa, M. Hirano, and S. Suzuki, *Electrochim. Acta*, **24**, 89 (1979).
7) Y. Umezawa and T. Yamamura, *J. Electrochem. Soc.*, **126**, 705 (1979).
8) G. Nord and O. Wernberg, *J. Chem. Soc., Dalton Trans.*, **1972**, 866.
9) G. Nord and O. Wernberg, *J. Chem. Soc., Dalton Trans.*, **1975**, 845.
10) C. Creutz and N. Sutin, *Proc. Natl. Acad. Sci. U.S.A.*, **72**, 2858 (1975).
11) J. Kiwi and M. Grätzel, *Angew. Chem.*, **91**, 659 (1979); K. Kalyanasundaram and M. Grätzel, *ibid.*, **91**, 759 (1979).
12) J. M. Lehn, J. P. Sauvage, and R. Ziessel, *Nouv. J. Chim.*, **3**, 423 (1979).
13) D. Dovos, "Electrochemical Data," Elsevier, Amsterdam (1975), pp. 247—261.
14) Y. Murakami and Y. Aoyama, *Bull. Chem. Soc. Jpn.*, **49**, 683 (1976).
15) D. Dolphin, R. L. N. Harris, J. L. Huppatz, A. W. Johnson, and I. T. Kay, *J. Chem. Soc., C*, **1966**, 30.
16) Discussion on the mechanism of acid-catalyzed autoxidation of transition-metal complexes: J. J. Pignatello and F. R. Jensen, *J. Am. Chem. Soc.*, **101**, 5929 (1979). Autoxidation of vitamin B_{12r}: J. M. Pratt, "Inorganic Chemistry of Vitamin B_{12}," Academic Press, London (1972), pp. 202—204.
17) Y. Murakami, Y. Aoyama, and K. Tokunaga, *J. Am. Chem. Soc.*, **102**, 6736 (1980).
18) The pK_a values are reasonable for this type of Co(III) complexes: cobinamide, pK_{a1} 6.0 (G. C. Hayward, H. A. O. Hill, J. M. Pratt, N. J. Vanston, and R. J. P. Williams, *J. Chem. Soc.*, **1965**, 6485); AD-didehydrocorrin complex, pK_{a1} 6.2 and pK_{a2} 11.2 (Ref. 17); meso-tetrakis(1-methylpyridinium-4-yl)porphyrin complex, pK_{a1} 6.0 and pK_{a2} 10.0 (R. F. Pasternack and M. A. Cobb, *J. Inorg. Nucl. Chem.*, **35**, 4327 (1973)).
19) Y. Murakami, Y. Aoyama, and S. Nakanishi, *Chem. Lett.*, **1976**, 857; *Inorg. Nucl. Chem. Lett.*, **12**, 809 (1976).
20) E. K. Barefield and M. T. Mocella, *J. Am. Chem. Soc.*, **97**, 4238 (1975).
21) J. A. Switzer and J. F. Endicott, *J. Am. Chem., Soc.*, **102**, 1181 (1980).
22) An intramolecular reduction of a cobalt(III) complex of TDHC involving axial cyano ligands has been reported without mechanistic analysis: C. M. Elson, A. Hamilton, and A. W. Johnson, *J. Chem. Soc., Perkin Trans. 1*, **1973**, 775.
23) G. E. Adams, J. W. Boag, and B. D. Michael, *Trans. Faraday Soc.*, **61**, 1417 (1965); **61**, 1674 (1965).
24) J. L. Weeks and J. Rabani, *J. Phys. Chem.*, **70**, 2100 (1966).
25) D. Behar, G. Czapski, and I. Dochovny, *J. Phys. Chem.*, **74**, 2206 (1970).
26) J. P. Henry and A. M. Michelson, in "Superoxide and Superoxide Dismutases," ed by A. M. Michelson, J. M. McCord, and I. Fridovich, Academic Press, London (1977), pp. 283—290 and references therein.
27) For one-electron auto-reduction of iron(III)–porphyrin with concomitant oxidation of certain potential ligands to radicals: J. D. Gaudio and G. N. La Mar, *J. Am. Chem. Soc.*, **98**, 3014 (1976); G. N. La Mar and J. D. Gaudio, in "Bioinorganic Chemistry-II," Advances in Chemistry Series 162, ed by K. N. Raymond, American Chemical Society, Washington, D. C. (1977), Chap. 12.
28) The data shown in Fig. 2 have a non-zero intercept. This may be due to small rate contribution from scavenging of the hydroxyl radical with the hydrogencarbonate ion and from hydroxide-induced process (Table 1). The hydrogencarbonate-induced process is neglected in order to obtain a reasonable estimate of the scavenging rate constant for the hydroxyl radical with carbonate, the scavenging rate constant with hydrogencarbonate being 28 times smaller than that with carbonate.[24]
29) The linear correlations in Fig. 4 are for the range of $[Co(III)]/[Co(II)] \leqq 2.5$; *i.e.*, $[Co(II)] \geqq 1.0 \times 10^{-5}$ mol dm^{-3} ($[Co]_T = 3.81 \times 10^{-5}$ mol dm^{-3}); $k_{-1}[Co(II)] \geqq (10^{10})(1.0 \times 10^{-5}) = 10^5$. The product of calculated k_2 and [carbonate] is $(6 \times 10^7)(2.3 \times 10^{-4}) = 1.4 \times 10^4$ or $(2 \times 10^7)(1.7 \times 10^{-3}) = 3.4 \times 10^4$. Thus, the assumption, $k_{-1}[Co(II)] \gg k_2[carbonate]$, is satisfied for 2.3×10^{-4} mol dm^{-3} carbonate and to a lesser extent for 1.7×10^{-3} mol dm^{-3} carbonate. The calculated k_2 values are one- to two-order of magnitude (if corrected for temperature difference) smaller than that from the pulse radiolysis study. Since the experimental conditions are not identical, the difference may not be meaningful, but it could be due to an oversimplification of the k_{-1} process. The radical pair described as (Co(II)+·OH) in Eq. 2 would be more accurately represented as $\{Co(II) \cdot OH\} \rightleftharpoons Co(II) + \cdot OH$; an equilibrium between the intimate radical pair within a common solvent cage and the solvent separated radical pair. Recombination of the Co(II) species and ·OH in the cage would be much faster than in the bimolecular encounter process. If the limiting rate constant k_1 is to represent the true homolytic rate constant (*i.e.*, scavenging of the hydroxyl radical derived therefrom takes place with a 100% efficiency) and if the pulse-radiolysis rate for the scavenging step is the same under the present kinetic conditions, $k_{-1} \cong 10^{11}$—10^{12} dm^3 mol^{-1} s^{-1} (regarded as the effective recombination rate constant including the contribution from the in-cage process).
30) A. Stanienda and G. Biebl, *Z. Phys. Chem. (Frankfurt am Main)* [*N. F.*], **52**, 254 (1967).
31) M. Conlon, A. W. Johnson, W. R. Overand, D. Rajapaksa, and C. M. Elson, *J. Chem. Soc., Perkin Trans. 1*, **1973**, 2281.
32) F. A. Cotton and G. Wilkinson, "Advanced Inorganic Chemistry," 2nd ed, Interscience, New York (1966), p. 43.
33) J. Rabani and M. S. Matheson, *J. Phys. Chem.*, **70**, 761 (1966).

A Novel Cationic Optically Active Complex of Platinum(II) Containing 2-Methyl-2-butene and *o*-Benzenediamine. The Circular Dichroism Spectrum and Kinetics of Olefin Exchange

Shin'ya MIYA, Kazuo KASHIWABARA,† and Kazuo SAITO*

Department of Chemistry, Faculty of Science, Tohoku University, Sendai 980

†*Department of Chemistry, Faculty of Science, Nagoya University, Chikusa-ku, Nagoya 464*

(Received January 23, 1981)

An optically active cationic olefin complex, [PtCl(*o*-benzenediamine)((*S*)-2-methyl-2-butene)]$B(C_6H_5)_4$ was obtained for the first time as crystal stable in air at room temperature. It deteriorates slightly in solution, but is still stable enough to be characterized. Comparison of its CD spectrum with that of related complexes disclosed that the coordinating atoms at the *cis* sites to the olefin have a dominant influence upon the CD pattern in the region 20000—35000 cm^{-1}, as compared with those at the *trans* site. Substitution of *cis*-1,2-dichloroethylene for the coordinated (*S*)-2-methyl-2-butene (*S*-mbn) proceeds in accordance with the second order rate law; there is no contribution of the solvent path. The second order rate constant is smaller than that of *trans*-[$PtCl_2$(pyridine)-(*S*-mbn)]. The steric effect of the *o*-benzenediamine at the transition state seems responsible for the small rate rather than the basicity of the ligand at the *trans* site to mbn.

Asymmetric coordination of prochiral olefins to square planar complexes gives several circular dichroism (CD) peaks in the region 20000—45000 cm^{-1}. The pattern is largely dependent on the absolute configuration of the coordinated olefin,[1] but also on the ligands including asymmetric nitrogen donor atoms.[2,3] Studies were carried out on stereoselectivity accompanied by the olefin exchange of platinum(II) complexes of the types $[PtCl_3(olefin)]^-$ and [PtCl((*S*)-amino carboxylate)-(olefin)] both kinetically and thermodynamically in organic solvents.[4,5] However, all the known optically active platinum(II) olefin complexes are chargeless or negatively charged. Cationic platinum(II) complexes containing η^2-olefin are unstable.[6] Uguagliati *et al.* identified $[PtCl(C_2H_4)(bpy)]^+$ (bpy, bipyridine) as reaction intermediate. However, it liberates the ethylene almost instantaneously to give $[PtCl_2(bpy)]$.[7] Theophanides and Kong[8] suggested the formation of solid complex $[PtCl(C_2H_4)(en)]^+$ (en, ethylenediamine), which was not characterized because it decomposed quickly to give *cis*-$[PtCl_2(en)]$. Recently Tiripichio *et al.* obtained cationic complex $[PtCl(C_2H_4)\{(CH_3)_2NCH_2CH_2N(CH_3)_2\}]ClO_4$, the structure determined by the X-ray diffraction method,[10] and proposed the decomposition mechanism. They found that the cationic complex is stable enough to be characterized by recrystallization from water, and IR and ^1H NMR spectra.

We have synthesized a cationic optically active platinum(II) complex containing prochiral 2-methyl-2-butene (mbn) and *o*-benzenediamine (*o*-bzda) for the first time and compared the CD spectrum and the kinetics of olefin exchange reaction with those of related complexes.[1-5] The influence of various ligands *cis* and *trans* on the asymmetric olefin as well as of the overall charge of the complex is discussed.

Experimental

Preparation. The cationic optically active complex containing *o*-benzenediamine (*o*-bzda) and 2-methyl-2-butene (mbn), [PtCl(*o*-bzda)(*S*-mbn)]$B(C_6H_5)_4$, was prepared from optically active *trans*(*N*, mbn)-[PtCl(*S*-pro)(*S*-mbn)][3] (pro, prolinate) by the following method with retention of configuration. The original complex was converted into $P(C_6H_5)_4$-[$PtCl_3$(*S*-mbn)] by the method of Miya *et al.*[11] The complex (3.0×10^{-4} mol) was dissolved in methanol (25 cm^3) and treated with $NaB(C_6H_5)_4$ (3.0×10^{-4} mol) and *o*-bzda (3.0×10^{-4} mol). The white precipitate was removed to leave a yellow filtrate which was treated with $NaB(C_6H_5)_4$ (3.0×10^{-4} mol). Dripping of water first gave a small amount of yellowish precipitate, which was filtered off. Further dripping of water gave colorless crystals, which were washed with cold water, recrystallized from methanol and dried *in vacuo*. Found: C, 57.74; H, 5.26; N, 3.85%. Calcd for $C_{35}H_{38}N_2PtBCl$: C, 58.00; H, 5.40; N, 3.73%.

cis and *trans*(*N*, tbn)-[PtCl(*S*-pro)(*S*,*S*-btn)] (*S*-pro, (*S*)-prolinate; tbn, *trans*-2-butene),[3] *trans*-[$PtCl_2$(4-X-py)(*S*-mbn)][11] (4-X-py, 4-substituted pyridine; X=NH_2, H, and Cl), *trans*-[$PtCl_2$(4-X-ani)(*S*-mbn)][11] (4-X-ani, 4-substituted aniline; X=H, Cl, and CH_3) and *cis*-[$PtCl_2$((*S*)-α-methylbenzylamine)(*S*-mbn)][12] were synthesized by the methods reported. The solvents were purified by the usual methods.

Measurement. The visible and ultraviolet absorption and CD spectra were recorded with a Hitachi 323 spectrophotometer and a JASCO J-40 spectropolarimeter, respectively, at room temperature in acetone, acetonitrile, benzene, dichloromethane or ethanol. The rate of olefin exchange between $[PtCl(o\text{-bzda})(S\text{-mbn})]^+$ (3.0×10^{-3} mol dm^{-3}) and 1,2-dichloroethylene (dce) (0.1 to 5 mol dm^{-3}) was measured by recording the change in CD strength at 28170 cm^{-1} with time at 17.0 °C in acetone. Since the complex decomposes slightly with lapse of time, freshly prepared sample solutions were used. The results were analysed by a method previously reported.[11]

Results and Discussion

Synthesis. The formation of $[PtCl_3(S\text{-mbn})]^-$ from the (*S*)-prolinato complex proceeds with full retention of configuration in HCl.[11] The substitution of *o*-bzda for the two chloride ions proceeded quickly in methanol. The white precipitate first formed on the addition of $NaB(C_6H_5)_4$ was $(C_6H_5)_4P^+\cdot B(C_6H_5)_4^-$. The CD measurement suggests that the substitution causes no significant inversion of the coordinated olefin. (*vide infra*) The colorless product is stable in crystalline state. It is insoluble in benzene and dichloromethane, and

soluble in acetone and ethanol. The solutions turn slowly yellow, giving a black precipitate after a few days. However, the decomposition rate is amazingly smaller than that of the bpy[7] and en[8] complexes. It is remarkable that *o*-bzda gives a stable cationic platinum(II) complex containing η^2-olefin in spite of the fact that the diamine is believed to be a poor bidentate ligand to metal ions. The stability of this cationic complex might be comparable to that of $[PtCl(C_2H_4)\{(CH_3)_2NCH_2CH_2N(CH_3)_2\}]ClO_4$ prepared by Maresca *et al.*[9]

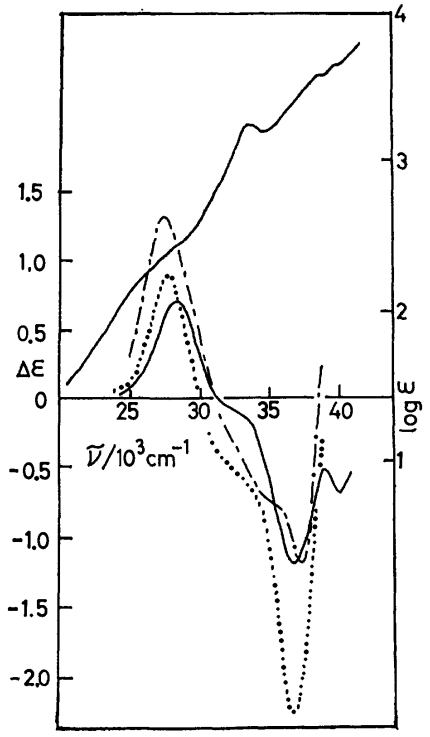

Fig. 1. Absorption and CD spectra in visible and UV region, 1) $[PtCl(o\text{-bzda})(S\text{-mbn})]B(C_6H_5)_4$ in ethanol (——), 2) The differential CD between *cis*(*N*, tbn)-[PtCl(L-pro)(*S*,*S*-tbn)] and *cis*(N, ethylene)-[PtCl(L-pro)(ethylene)] in acetonitrile (·····), 3) The differential CD between *cis*-$[PtCl_2((S)\text{-}\alpha\text{-methylbenzylamine})(S,S\text{-tbn})]$ and *cis*-$[PtCl_2((S)\text{-}\alpha\text{-methylbenzylamine})(ethylene)]$ in acetone (— · — · —).

Absorption and CD Spectra. The spectra are shown in Fig. 1 together with those of related complexes. The absorption spectrum of $[PtCl(o\text{-bzda})(S\text{-mbn})]^+$ changes slowly, the CD intensity decreasing in line with absorption change. However, the apparent rate constant is *ca.* 4×10^{-6} s^{-1} at 17.0 °C, affecting neither the spectroscopic measurement nor the kinetic study of olefin exchange with dce. (*vide infra*) The UV absorption gives a peak at 33000 cm^{-1} with log ε=3.22 and some peaks in the region 36000—39000 cm^{-1}. There is no absorption peak in the range 20000—30000 cm^{-1}, assigned to that of d-d transitions in platinum(II) olefin complexes,[3] but only a shoulder at *ca.* 28000 cm^{-1}. Such broad absorption spectra in the whole range would provide no useful means in investigation on the detailed spectroscopic properties.

On the other hand, the CD spectrum shows distinct strong peaks at 28300 and 37000 cm^{-1}. The former can be attributed to the d-d transition and the latter to the charge transfer between the metal and ligands, or intraligand transitions. The CD spectral data are summarized in Table 1 together with those of related complexes. CD spectra in the d-d transition region are generally affected by environmental changes around a metal ion. On the basis of the additivity rule held in platinum(II) olefin complexes,[4] we can estimate the contribution of asymmetric olefin in various types of complexes. Two cases are shown in Fig. 1, for L-prolinate and α-methylbenzylamine complexes, the differential CD spectra between the complexes containing (*S*,*S*)-*trans*-2-butene and ethylene being calculated. Although the solvents are not common because of the solubility of the complexes, the three CD patterns in Fig. 1 are very similar to each other, despite the big difference in overall charge and the donating atoms. The three complexes have Cl and N in common at the *cis* positions to the olefin, and N, O, and Cl at the *trans* site. The *trans* ligand appears to give only a minor contribution to the CD pattern and even to the peak energy, so far as the ligating atom at the *cis* site remains unchanged.

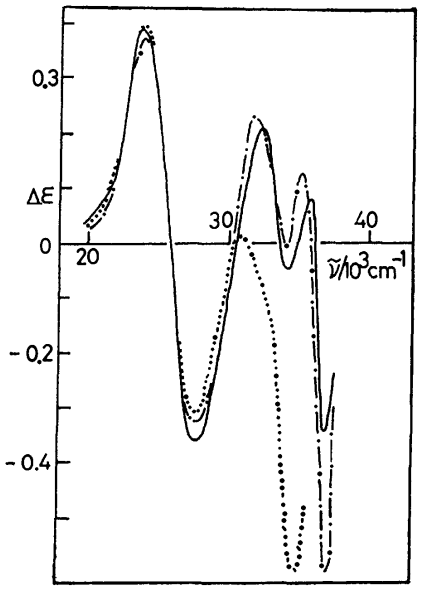

Fig. 2. CD spectra of *trans*-$[PtCl_2(4\text{-X-py})(S\text{-mbn})]$ in dichloromethane, X=NH_2 (·····), X=H (——), X=Cl (— · — · —).

This is also supported by the CD pattern of the complexes *trans*(*N*,mbn)-$[PtCl_2(4\text{-X-py})(S\text{-mbn})]$ and *trans*(*N*,mbn)-$[PtCl_2(4\text{-X-ani})(S\text{-mbn})]$. (Figs. 2 and 3) The changes of substituents X on both pyridine and aniline derivatives give no significant influence on the CD spectra, peak positions and strengths in the d-d transition region. In the higher frequency region, only the 4-aminopyridine complex shows a different spectrum from the other two. The strong peak of the 4-aminopyridine complex at 35000 cm^{-1} corresponds to the peaks of the aniline derivatives at the same position. The 4-aminopyridine ligand has two coordinate functions to a metal ion, the amino group and the pyridine

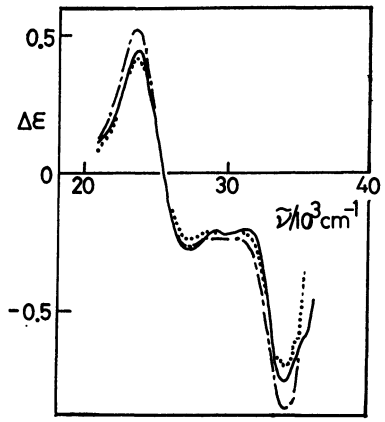

Fig. 3. CD spectra of *trans*-[$PtCl_2$(4-X-ani)(*S*-mbn)] in benzene, X=CH_3 (·····), X=H (——), X=Cl (—·—).

nitrogen atom. We have no definite evidence for the coordination mode, but the coordination through the pyridine nitrogen atom is highly probable from the fact that the CD spectrum of the 4-aminopyridine complex is in fair agreement with those of other pyridine derivative complexes in the d-d transition region (Table 1).

Comparison of the CD spectra between *cis*[2] and *trans*(*N*,C_2H_4)-[PtCl(*S*-pro)(C_2H_4)],[3] and between [$PtCl_3$(*S*,*S*-tbn)]$^-$ [4] and *cis*-[$PtCl_2$(α-methylbenzylamine)(*S*,*S*-tbn)][12] also indicates that the change in ligating atoms at the *cis* position to the olefin causes a big difference in the CD pattern, while that at the *trans* site gives only a slight difference. Since, the η^2-olefin gives a very remarkable *trans* influence, the variety of the ligating atom at the *trans* site should be cancelled, whereas change in atoms at the *cis* site causes a significant difference.

CD peaks at around 37000 cm^{-1} (Fig. 1) are also similar to each other despite the difference of the ligating atoms, so that the CD components might be due to the charge transfer between platinum(II) and olefins which are common in these three complexes.

Kinetics of Olefin Exchange. The rate of the following reaction was followed by recording the decrease in CD strength at 28170 cm^{-1} in the presence of a large excess of free *cis*-1,2-dichloroethylene(dce).

$$[PtCl(o\text{-bzda})(S\text{-mbn})]^+ + \text{dce} \longrightarrow [PtCl(o\text{-bzda})(\text{dce})]^+ + \text{mbn} \quad (1)$$

The observed rate constant is independent of the initial concentration of the complex ($\simeq 10^{-3}$ mol dm^{-3}) (Table 2), and proportional to that of free dce without intercept as shown in Fig. 4. Hence, the rate is expressed by,[11]

$$\text{Rate} = k_2[\text{complex}][\text{dce}]. \quad (2)$$

The concentration of free *o*-bzda added does not affect the rate in the concentration range 0—2.4×10^{-4} mol dm^{-3} (Table 2). We see that addition of $NaB(C_6H_5)_4$ does not affect the rate of olefin exchange. The complex seems to be in ion-paired in acetone, the observed rate

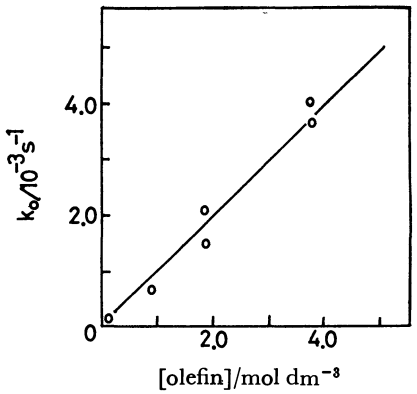

Fig. 4. Dependence of the observed first order rate constant for the substitution of *cis*-1,2-dichloroethylene for the (*S*)-2-methyl-2-butene in *trans*-[PtCl(*o*-bzda)-(*S*-mbn)]$B(C_6H_5)_4$ in acetone at 17 °C, [complex]= 0.0030 mol dm^{-3}.

Table 1. CD spectral data of platinum(II) complexes containing η^2-olefin

Complex	CD peaks, $\tilde{\nu}/10^3$ cm^{-1} ($\Delta\varepsilon$)				
[PtCl(*S*-mbn)(*o*-bzda]$B(C_6H_5)_4$[a]		28.3(+0.36)	32.8(−0.03)	37.0(−0.59)	40.3(−0.35)
cis-[$PtCl_2$(*S*,*S*-tbn)(mba)][b,c]		27.3(+1.32)	35.0(−0.72)	37.4(−1.19)	
cis(*N*,olefin)-[PtCl(pro)(*S*,*S*-tbn)][d,e]		27.6(+0.92)	33.2(−0.57)	37.0(−2.26)	
trans(*N*,olefin)-[PtCl(pro)(*S*,*S*-tbn)][e,f]		26.8(+1.08)	34.3(−1.90)		39.7(−0.54)
$P(C_6H_5)_4$[$PtCl_3$(*S*-mbn)][g]	22.9(+0.46)	26.5(−0.21)	29.4(+0.13)	34.3(−1.05)	
$P(C_6H_5)_4$[$PtCl_3$(*S*,*S*-tbn)][e]	24.0(+0.76)	28.0(−0.14)		35.1(−1.32)	39.5(+3.20)
trans-[$PtCl_2$(*S*-mbn)(4-Cl-ani)][h]	23.6(+0.51)	27.0(−0.28)		34.7(−0.86)	
trans-[$PtCl_2$(*S*-mbn)(4-CH_3-ani)][h]	23.6(+0.41)	27.1(−0.26)		34.5(−0.70)	
trans-[$PtCl_2$(*S*-mbn)(ani)][h]	23.6(+0.44)	27.2(−0.30)		34.3(−0.76)	
trans-[$PtCl_2$(*S*-mbn)(4-Cl-py)][g]	24.1(+0.35)	27.8(−0.34)	31.8(+0.26)	35.2(+0.17)	
			33.8(−0.01)	36.8(−0.60)	
trans-[$PtCl_2$(*S*-mbn)(py)][g]	24.0(+0.39)	27.8(−0.37)	32.4(+0.21)	35.7(+0.09)	
			34.4(−0.06)	37.1(−0.35)	
trans-[$PtCl_2$(*S*-mbn)(4-NH_2-py)][g]	24.0(+0.39)	27.8(−0.31)	30.8(+0.02)	35.0(−0.60)	
			32.4(−0.09)		

a) In ethanol. b) Differential CD between *cis*(*N*,olefin)-[$PtCl_2$(*S*,*S*-tbn)(*S*-mba)] and *cis*(*N*,olefin)-[$PtCl_2$(C_2H_4)(*S*-mba)], (mba, α-methylbenzyl amine). c) In acetone. d) Differential CD between *cis*(*N*,olefin)-[PtCl(*S*-pro)(*S*,*S*-tbn)] and *cis*(*N*, olefin)-[PtCl(*S*-pro)(C_2H_4)]. e) In acetonitrile. f) Differential CD between *trans*(*N*, olefin)-[PtCl(*S*-pro)(*S*,*S*-tbn)] and *trans*(*N*,olefin)-[PtCl(*S*-pro)(C_2H_4)]. g) In dichloromethane. h) In benzene.

Table 2. Dependence of the observed first order rate constant for the substitution of *cis*-1,2-dichloroethylene for the (*S*)-2-methyl-2-butene in [PtCl(*S*-mbn)(*o*-bzda)]$B(C_6H_5)_4$ in acetone at 17 °C on various factors, [dce]=1.89 mol dm^{-3}.

[complex] / 10^{-3} mol dm^{-3}	[*o*-bzda] / 10^{-4} mol dm^{-3}	$NaB(C_6H_5)_4$ / 10^{-2} mol dm^{-3}	k_0 / 10^{-3} s^{-1}
1.50	0	0	1.44
3.00	0	0	1.48
4.45	0	0	1.47
3.00	1.24	0	1.57
3.00	2.50	0	1.60
3.00	0	0.32	1.42
3.00	0	1.21	1.42
3.00	0	2.41	1.44

constants reflecting those of the ion-pairs rather than those of the free complex cation. The counter anions play an important role to stabilize the cationic complex. Bulky anions such as perchlorate or tetraphenylborate are good counter anions to stabilize the cationic complex, but not small ones such as chloride.[9] Strong ion-paired interactions between the complex cation and bulky anions might be a key effect to prevent nucleophilic attacks by reacting species such as solvent molecules or halides, stabilizing cationic olefin complexes.

The k_2 in Eq. 2 reflects the rate of direct olefin exchange, which should proceed by the S_N2 mechanism. The *o*-bzda ligand remains coordinated throughout the olefin exchange reaction, and the contribution of solvolysed species[11] being ignored. The result is compared with those of the related complexes in Table 3.

Table 3. Second order rate constants of the substituon of 1,2-dichloroethylene for some 2-methyl-2-butene complexes of platinum(II)

Complex	k_2/dm^3 mol^{-1} s^{-1}	pK_a
[PtCl(*o*-bzda)(*S*-mbn)]$^{+}$ [a]	1.09×10^{-3}	4.6
trans(*N*,olefin)-[PtCl(*S*-pro)(*S*-mbn)][a]	1.03×10^{-3}	10.6
trans-[$PtCl_2$(py)(*S*-mbn)][b]	4.66×10^{-2}	5.2

a) In acetone at 17.0 °C; k_2 for Eq. 2. b) From Ref. 11.

The basicity of the nitrogen base *trans* to the olefin in [$PtCl_2$(4-X-py)(*S*-mbn)] and [$PtCl_2$(4-X-ani)(*S*-mbn)] is the most important factor ruling the rate of olefin exchange.[11] The *o*-bzda complex has a much smaller k_2 than that of the pyridine complex, despite their similar pK_a values. Difference in the ligating atom at the *cis* site (Cl and N) could be responsible for the difference. However, the kinetic *cis* effect is understood to be in the percentage range of tens to hundreds and can not account for the big difference by 40 times. The difference may be ascribed to the presence of overall charge or of the chelate ring. The (*S*)-proline has pK_a 10.6 and the chargeless complex with one chelate gives $k_2=1.03\times10^{-3}$ dm^3 mol^{-1} s^{-1}. Its $\log k_2$ *vs.* pK_a plot falls almost on the common straight line for *trans*-[$PtCl_2$(4-X-py)(*S*-mbn)] and *trans*-[$PtCl_2$(4-X-ani)(*S*-mbn)] (figure in Ref. 11); *i. e.* the (*S*)-prolinato ligand does not seem to give significant effect on the rate expressed by Eq. 2.

The positive charge of the complex would decrease the effective electron density on platinum(II), and the nucleophilic attack of dce can be facilitated rather than retarded. Thus the overall plus charge cannot be the cause of slow substitution. Neither is its instability in organic solvents responsible for the slow exchange of olefin. Coordinated aniline derivatives in *trans*-[$PtCl_2$(ani)(*S*-mbn)] are replaced by donating solvent molecules to give *e. g.*, *trans*-[$PtCl_2$(S)(*S*-mbn)] (S, solvent molecule), which also participated in the olefin exchange.[11] If such a replacement had taken place prior to the attack of the nucleophilic olefin, the observed rate constant should have depended on the added free *o*-bzda concentration, as was the case for the complexes containing aniline derivatives.[11]

The *o*-bzda chelate may have a significant steric stress due to the rigid aromatic ring, particularly in the transition state; the trigonal bipyramidal intermediate may be formed with difficulty to decrease the second order rate constant. It is interesting that bulky ligands such as *N*,*N*,*N*′,*N*′-tetramethylethylenediamine stabilize the cationic platinum(II) olefin complex, probably preventing the nucleophilic attack by reacting species on a η-bonded olefin.[9] The *o*-bzda ligand might also have this effect.

The work was carried out with a Grant-in-Aid (No. 400016) from the Ministry of Education, Science and Culture.

References

1) I. Kinoshita, Y. Terai, K. Kashiwabara, H. Kido, and K. Saito, *J. Organomet. Chem.*, **127**, 237 (1977).
2) Y. Terai, H. Kido, and K. Saito, *Bull. Chem. Soc. Jpn.*, **50**, 3265 (1977).
3) K. Konya, J. Fujita, and K. Nakamoto, *Inorg. Chem.*, **10**, 1699 (1971).
4) Y. Terai and K. Saito, *Bull. Chem. Soc. Jpn.*, **51**, 503 (1978).
5) Y. Terai, H. Kido, K. Kashiwabara, and K. Saito, *Bull. Chem. Soc. Jpn.*, **51**, 3245 (1978).
6) M. Herberhold, "Metal π-Complexes," Elsevier, Amsterdam, (1972), Vol. 2, pp. 183—189.
7) P. Uguagliati, U. Belluco, U. Croatto, and R. Pietropaolo, *J. Am. Chem. Soc.*, **89**, 1336 (1967).
8) T. Theophanides and P. C. Kong, *Can. J. Chem.*, **48**, 1084 (1970).
9) L. Maresca, G. Natile, and G. Rizzardi, *Inorg. Chim. Acta*, **38**, 53 (1980).
10) A. Tiripichio, M. T. Camelini, L. Maresca, G. Natile, and G. Rizzard, *Cryst. Struct. Commun.*, **8**, 689 (1979).
11) S. Miya, K. Kashiwabara, and K. Saito, *Inorg. Chem.*, **19**, 98 (1980).
12) P. Corradini, G. Paiaro, and A. Panunzi, *J. Am. Chem. Soc.*, **88**, 2836 (1966).

Five-coordinate Copper(II) Complexes with a Thio Group as Type II Copper Models

Takeshi SAKURAI,* Shinnichiro SUZUKI, and Akitsugu NAKAHARA
Institute of Chemistry, College of General Education, Osaka University, Toyonaka, Osaka 560
(Received February 23, 1981)

Five-coordinate copper(II) complexes with a thio group were synthesized as non-blue copper(II) models by reactions of copper(II) perchlorate and condensation products of 2-pyridinecarbaldehyde or salicylaldehyde and bis(2-aminoethyl) sulfide or 2-aminoethyl 3-aminopropyl sulfide. In the complexes where thio group is coordinated to copper(II) at an equatorial position, the ESR spin Hamiltonian parameters $g_{//}$ and $A_{//}$ prominently decreased, and charge transfer bands due to sulfur to copper appeared at 300—350 nm and occasionally at 400—500 nm. On the other hand, complexes with a thio group at an axial position afforded slightly smaller $A_{//}$ values and charge transfer bands with lower intensity in the similar regions. The biological significance of a sulfur donation to non-blue copper(II) has been discussed.

Among the three types of copper ions found in copper-proteins the "non-blue" (type II) copper displays no remarkable properties as "blue"(type I) copper or "ESR-nondetectable"(type III) copper. The associated ESR parameters of the type II coppers are similar to those of common tetragonal copper(II) complexes: $-A_{//}$ values are in the range of 15—20($\times 10^{-4}$) cm^{-1} and $g_{//}$ values are of 2.2—2.3. The visible absorption spectra arising from type II copper have also been considered to be the same with those of low molecular weight copper(II) complexes,[1] although they are often obscured by the type I and III coppers in multi-copper oxidases such as laccase, ceruloplasmin, and ascorbate oxidases. Having no conspicuous properties, the type II copper has thus been unfamiliar compared with coppers of the other types.

However, non-blue coppers in galactose oxidase[2] and amine oxidase[3] have been convinced to be in the environment of square-pyramid based on their d-d absorption spectra. Although there are only limited data on the protein ligands around type II copper, coordination of 2 to 4 imidazolyl groups and some oxygens has been reasonably proposed. Of special interest is the suggestion that a thio group is possibly coordinated to type II copper in galactose oxidase[4,5] and amine oxidase.[3] Here we report spectral properties of five-coordinate copper complexes with a thio group in an equatorial or an axial position as non-blue copper models.

In this work, several quinquedentate ligands with a thio group were synthesized by condensation of bis(2-aminoethyl) sulfide (abbreviated as aes) or 2-aminoethyl 3-aminopropyl sulfide(aps) and 2-pyridinecarbaldehyde-(pca) or salicylaldehyde(sal). Copper(II) complexes of these sulfur-containing ligands were prepared and the effects of sulfur coordination at an equatorial or an axial position on absorption and ESR spectra were comparatively studied.

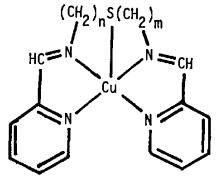

n=2, m=3 Cu(pca=aps=pca)
n=2, n=2 Cu(pca=aes=pca)

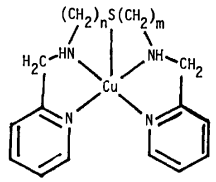

n=2, m=3 Cu(pca-aps-pca)
n=2, n=2 Cu(pca-aes-pca)

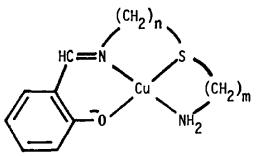

n=2, m=3 or n=3, m=2
Cu(sal=aps)

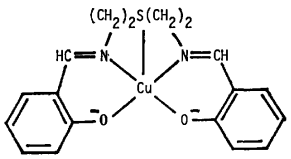

Cu(sap=aes=sal)

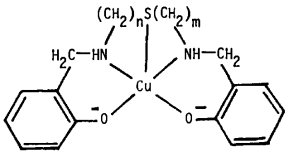

n=2, m=3 Cu(sal-aps-sal)
n=2, n=2 Cu(sal-aes-sal)

Experimental

Materials. Copper(II) perchlorate hexahydrate and salicylaldehyde were purchased from Nakarai Chemicals Ltd., *N*-(2-bromoethyl)phthalimide from Wako Chemicals Ltd., *N*-(3-bromopropyl)phthalimide from Aldrich, and 2-pyridinecarbaldehyde was obtained from Merck AG and distilled. All other reagents used were of the highest grade commercially available.

Preparation of Complexes. Cu(pca=aps=pca): Sulfur-containing diamine, aps, was prepared according to Amundsen *et al.*[6] To this was added twice amounts of pca in aqueous ethanol to give the 2 : 1 pca : aps Schiff base, which was treated with $Cu(ClO_4)_2 \cdot 6H_2O$, and was allowed to stand at room temperature. Blue crystals were isolated as perchlorate, and was recrystallized from H_2O–EtOH. Found: C, 35.79; H, 3.48; N, 9.81%. Calcd for $CuC_{17}H_{20}N_4S(ClO_4)_2$: C, 35.52; H, 3.51; N, 9.75%.

Cu(pca=aes=pca), Cu(sal=aps) and Cu(sal=aes=sal): These complexes were synthesized by the same method as Cu(pca=aps=pca). Found: C, 34.43; H, 3.44; N, 10.35%. Calcd for $CuC_{16}H_{18}N_4S(ClO_4)_2$(Cu(pca=aes=pca)): C, 34.26; H, 3.23; N, 9.99%. Found: C, 35.79; H. 4.17; N, 6.95%. Calcd for $CuC_{12}H_{17}N_2OS(ClO_4)$ (Cu(sal=aps)): C, 36.00; H, 4.28; N, 7.00%. Found: C, 42.94; H, 3.90; N, 5.62%. Calcd for $CuC_{18}H_{18}N_2O_2S \cdot 2H_2O \cdot 2/3\ NaClO_4$ (Cu-(sal=aes=sal)) C, 42.59; H, 4.37: N, 5.62%. The results of elemental analysis for Cu(sal=aes=sal) was only explainable

by assuming the presence of some coprecipitated $NaClO_4$, which was hardly removed. The product was, however, used for the spectroscopic and ESR measurements without further treatment, since there was no fear of serious effect.

Cu(pca=aps=pca): The condensed product of pca and aps in ethanol was reduced with $NaBH_4$ untill the yellow color of the Schiff base faded out, and the excess of $NaBH_4$ was treated with HCl. After filtration, the filtrate was mixed with $Cu(ClO_4)_2 \cdot 6H_2O$ to give blue crystals. Recrystallization was performed once from aqueous ethanol. Found: C, 27.90; H, 4.16; N, 7.52%. Calcd for $CuC_{17}H_{24}N_4S(ClO_4)_2 \cdot 7H_2O$: C, 27.64; H, 4.23; N, 7.58%.

Cu(pca-aes-pca), Cu(sal=aps=sal), and Cu(sal=aes=pca): These complexes were prepared by the same method as described for Cu(pca=aps=pca). Found: C, 33.58; H, 3.96; N, 9.84%. Calcd for $CuC_{16}H_{22}N_4S(ClO_4)_2$(Cu(pca=aes=pca)): C, 34.02; H, 3.93; N, 9.92%. Found: C, 45.53; H, 5.42; N, 5.52%. Calcd for $CuC_{17}H_{24}N_2O_2S \cdot 2H_2O \cdot 1/2NaClO_4$(Cu(sal=aps=sal)): 45.16; H, 5.59; N, 5.55%. Found: C, 37.49; H, 4.06; N, 4.98%. Calcd for $CuC_{18}H_{22}N_2O_2S \cdot 2H_2O \cdot NaClO_4$(Cu(sal=aes=sal)): C, 37.17; H, 4.51; N, 4.82%.

Spectral Measurements and Instruments. Absorption spectra were recorded on 1 cm- or 1 mm-path length cell in the range 260—1100 nm with a Hitachi 323 spectrophotometer at room temperature. Electron spin resonance (ESR) spectra of copper complexes were recorded using a JEOL JES-FE1X instrument at 77 K. Magnetic field was calibrated on a Mn(II) in MnO(ΔH_{3-4}=8.69 mT) and g values were calibrated based on Li-TCNQ(g=2.0025). *N,N*-dimethylformamide was used as solvent.

Results

Absorption spectra of pca-containing complexes exhibited the splitted d-d bands, indicating the successful formations of five-coordinate complexes. Charge transfer bands arising from thio group appeared at 315—340 nm in most cases (Fig. 1). Although the complex Cu(pca=aes=pca) did not exhibit an apparent peak in this region, molar absorptivity of this complex was observed to be five times larger than those of the complexes which have no sulfide ligand (*i.e.* Cu(pca=pda=pca), where pda represents 1,5-pentanediamine). Another charge transfer peak was observed at 462 nm, though it was not certain whether or not the peak arose from charge transfer of thio group to copper. This was because of the fact that pca Schiff base complexes devoid of thio group occasionally exhibited a peak in this region.

ESR parameters and absorption spectral data of each complex are tabulated in Table 1. Cu(pca=aps=pca), Cu(pca-aps-pca), and Cu(pca-aes-pca) have similar spin Hamiltonian parameters: $g_{//}$ values are in the range 2.17—2.21 and $-A_{//}$ values of 16.7—17.1($\times 10^{-4}$) cm^{-1}. The prominently lowered $g_{//}$ values and $-A_{//}$ values indicate that the electron density around the copper(II) ion is appreciably reduced because of the sulfur donation in an equatorial position, since these complexes are five coordinate as clearly indicated in the splitting of d-d bands. On the other hand, Cu(pca=aes=pca) exhibited a larger $g_{//}$ value, suggesting a formation of entirely different donor setting around the copper(II) ion. The weaker contribution of sulfur donation on ESR spectrum seems to be due to the binding of the soft group at an apical position.[7] The

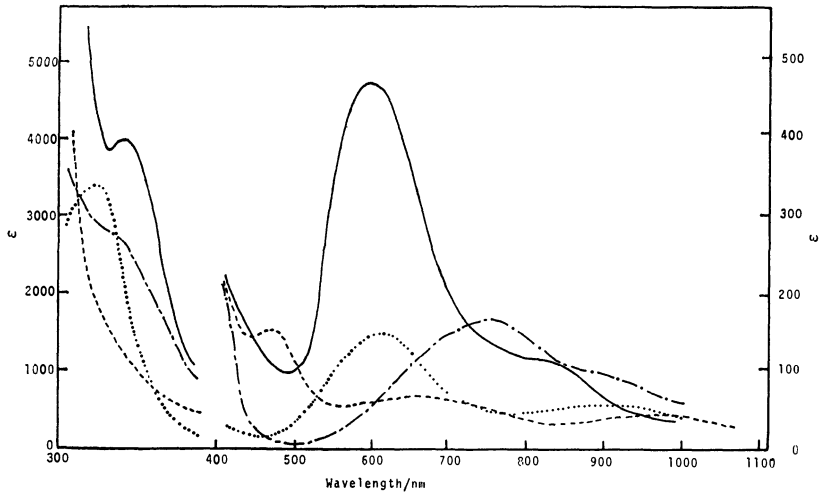

Fig. 1. Absorption spectra of Cu(pca=aps=pca) (——) Cu(pca=aps=pca) (—·—), Cu(pca=aes=pca) (------), and Cu(pca=aes=pca)(·····).

TABLE 1. ESR PARAMETERS AND ABSORPTION SPECTRAL DATA FOR THE COPPER(II) COMPLEXES

Complex	ESR parameters			Absorption spectral data λ_{max}/nm, ε		
	$g_{//}$	$g_{\perp}$	$-A_{//} \times 10^4$ / cm^{-1}	CT band	d-d band	
Cu(pca=aps=pca)	2.17	2.08	17.1	343 (4000)	604 (437)	830 (114)
Cu(pca-aps-pca)	2.20	2.06	17.0	335 (2730)	737 (163)	920 (98)
Cu(pca=aes=pca)	2.27	2.06	16.9	462 (153)	665 (69)	995 (43)
Cu(pca-aes-pca)	2.21	2.06	16.7	315 (3350)	610 (142)	870 (58)

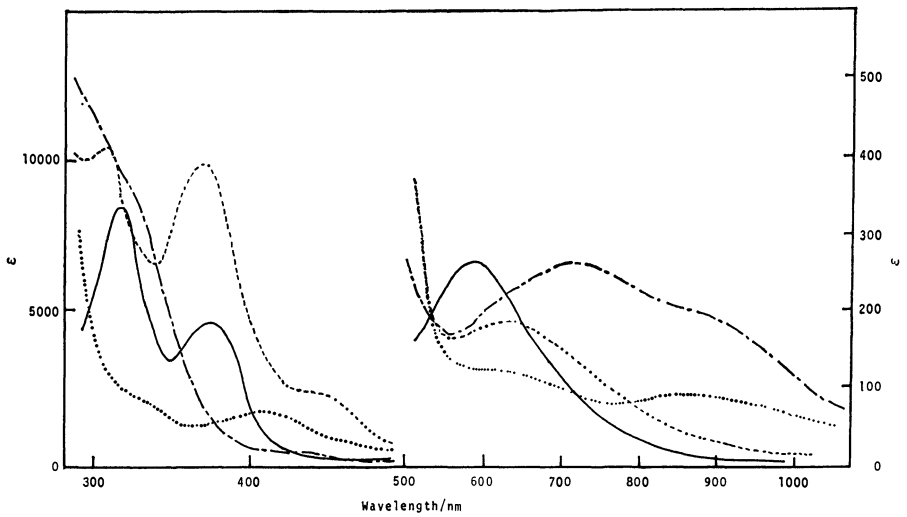

Fig. 2. Absorption spectra of Cu(sal=aps) (——), Cu(sal=aps=sal) (—·—), Cu(sal=aes=sal) (------), and Cu(sal=aes=sal) (·····).

obscured charge transfer band around 350 nm also would favor this interpretation. Copper(II) complex of the Schiff base of salicylaldehyde and aps, Cu(sal=aps=sal), was not isolated as quinquedentate complex but was as a quadridentate planar complex Cu(sal=aps) which contained N_2OS donor set, in spite of being employed twice amount of sal for preparation. The complex exhibited a symmetrical sharp d-d absorption at 584 nm and a charge transfer band at 316 nm (Fig. 2). In line with this, the use of *N*-(2-aminoethyl)-3-aminopropylamine(aea) in place of aps also gave highly square planar quadridentate complex, Cu(sal=aea). The symmetrical d-d absorption appeared in a similar region at 563 nm, but no peak was found in 300—400 nm, indicating that the peaks appeared in this region in figures are charge transfer bands due to sulfur group to copper. In contrast with the above, the reduced Schiff base complex, Cu(sal=aps=sal) afforded the quinquedentate form, exhibiting the splitted d-d bands at 720 and 910 nm. The absorption bands at 320 (shoulder) and 440 nm might be the sulfur to copper(II) charge transfer bands. The former would be attributed to $S(\sigma)\rightarrow Cu$ and the latter to $S(\pi)\rightarrow Cu$.[8] Although Cu(sal=aes=sal) did not exhibit the clearly splitted d-d bands, the rather broader d-d band would imply a formation of square-pyramidal copper(II) complex. Charge transfer bands were clearly observed at 304 and 450 nm. The reduced Schiff base complex, Cu(sal=aes=sal), also gave distinctly splitted d-d bands at 600 and 865 nm and charge transfer bands at *ca.* 330 and 405 nm.

The effect of coordination of the thio group in an equatorial position has been recognized in the smaller $-A_{//}$ values (Table 2). The pronounced instance is the difference in the $-A_{//}$ values of 17.9 and 19.8($\times 10^{-4}$) cm^{-1} for Cu(sal=aps) and Cu(sal=aea), respectively. The similar coordination effect of the thio group can be realized also in the pair Cu(sal=aes=sal) and Cu(sal=aes=sal). The $-A_{//}$ value for Cu(sal=aes=sal) increases *ca.* 1×10^{-4} cm^{-1}, suggesting that the thio group occupies an axial position in this complex similarly to the case of Cu(pca=aes=pca).

Discussion

Of eight complexes, which were tried to prepare in this work, quinquedentate complexes with N_4S or N_2O_2S donor set were isolated and characterized to display apparently splitted d-d transition bands or a broader d-d absorption band. Charge transfer bands of sulfur to copper were disclosed to appear at 300—350 nm and occasionally at 400—500 nm. The band at 300—350 nm was very clear when the sulfur occupies an equatorial position. As for the reason it may be considered that $p(\sigma)$ orbital of sulfur and $d_{x^2-y^2}$ orbital of copper(II) well overlap each other, hence strong charge transfer will occur between these orbitals. On the other hand, overlapping of $p(\pi)$ and $d_{x^2-y^2}$ orbitals can be attributed only through a torsion of these orbitals. Accordingly, the band at 400—500 nm is occasionally

Table 2. ESR parameters and absorption spectral data for the copper (II) complexes

Complex	ESR parameters			Absorption spectral data λ_{max}/nm, ε			
	$g_{//}$	$g_{\perp}$	$-A_{//}\times 10^4$ / cm^{-1}	CT band		d-d band	
Cu(sal=aps)	2.20	2.05	17.9	316 (8740)		584 (176)	
Cu(sal=aps=sal)	2.20	2.05	18.1	320_{sh} (9390)	440 (426)	720 (250)	910 (173)
Cu(sal=aes=sal)	2.21	2.06	17.8	304 (10200)	450 (2260)	639 (184)	
Cu(sal=aes=sal)	2.23	2.05	18.7	330 (2170)	405 (1750)	600 (126)	865 (92)

absent itself or is not very clear even if it appeared. When the sulfur atom binds copper(II) at an axial position, charge transfer from sulfur to copper might be permitted between either $p(\pi)$ and $d_{x^2-y^2}$ or $p(\sigma)$ and d_{z^2} orbitals. These transitions might appear at 330—350 nm and possibly even at 405—460 nm. The difference in the position of sulfur donor sensitively affects the ESR spin Hamiltonian parameters. When the sulfur occupies an equatorial position, both $g_{//}$ and $-A_{//}$ values will appreciably decrease, because the covalent character of Cu–S bond may weaken the electron density of central metal ion.[9] On the other hand, binding of sulfur at an axial position only lowers $-A_{//}$ value a little as compared with those of ordinary tetragonal copper(II) complexes. The parameter, $g_{//}$, does not seem sensitively reflect the sulfur donation in the axial position. The similar effect of soft donor ligation at an axial position of copper(II) has been reported in some cases.[7,8]

The d-d absorptions of non-blue coppers including those of multi-copper oxidases have been observed in the region of 600—1000 nm.[10-13] The presence of charge transfer bands at 314 and 450 nm has been reported for galactose oxidase[2] and in the range 300—500 nm for amine oxidase.[3] In addition, non-blue coppers of multi-copper oxidases have been considered to have a close relation to the absorptions in the regions.[10-13] These bands, even though not all of them, can be attributed to the charge transfer bands of sulfur to copper as described above. Some investigators reported that a SH group participates in the catalytic cycle of galactose oxidase[14] and amine oxidase,[15] although it is not certain whether or not the SH groups are coordinated to copper. If a sulfido group is coordinated to copper(II) ion, it must occupy an axial position, since the ESR parameters of non-blue coppers in enzymes do not suggest the binding of the SH group in an equatorial position. ESR parameters, $g_{//}$ and $-A_{//}$, of non-blue coppers were reported as 2.27 and 18.7×10^{-4} cm^{-1}, 2.29 and 16.9×10^{-4} cm^{-1}, 2.25 and 19×10^{-4} cm^{-1}, 2.21 and 20×10^{-4} cm^{-1}, and 2.22 and 19×10^{-4} cm^{-1} for galactose oxidase, amine oxidase, ceruloplasmine, ascorbate oxidase and laccase, respectively.[17]

The non-blue coppers are not considered to alter the valence state in the course of the catalytic cycles differing from blue coppers, though Hamilton *et al.*[18] considered bivalent state of copper is not active in galactose oxidase. At any rate, coordination chemistry of non-blue coppers does not seem favorable to the alteration of valence state of copper(II).[19,20] The axial sulfur, if it really exists, might be considered to supply electrons *via* copper(II) ion to molecular oxygen.

This work was supported by the Ministry of Education, Science and Culture, Japan through Grants-in-Aid for Special Project Research (No. 511311) and Science Research (No. 443012).

References

1) B. Reinhammar, "Advances in Inorganic Biochemistry," ed by G. L. Eichhorn and L. G. Marzili, Elsevier, North-Holland (1979), Chap. 3.
2) L. Cleveland, R. E. Coffman, P. Coon, and L. Davis, *Biochemistry*, **14**, 1108 (1975).
3) S. Suzuki, T. Sakurai, A. Nakahara, T. Oda, M. Manabe, and T. Okuyama, *FEBS Lett.*, **116**, 17 (1980).
4) R. D. Bereman and D. Shields, *Inorg. Chem.*, **18**, 946 (1979).
5) R. D. Bereman and D. Schields, *J. Inorg. Nucl. Chem.*, **42**, 989 (1980).
6) A. Amundsen, J. Whelan, and B. Bosnich, *J. Am. Chem. Soc.*, **99**, 6730 (1977).
7) R. S. Giordano, R. D. Bereman, D. J. Kosman, and M. J. Ettinger, *J. Am. Chem. Soc.*, **96**, 1023 (1974).
8) V. M. Minskowski, J. A. Thich, R. Solomon, and H. J. Schugar, *J. Am. Chem. Soc.*, **98**, 8344 (1976).
9) Y. Sugiura, *Inorg. Chem.*, **17**, 2176 (1978).
10) L. Marpurgo, A. Desideri, G. Rotilio, and B. Mondovi, *FEBS Lett.*, **113**, 153 (1980).
11) B. Reinhammar and Y. Oda, *J. Inorg. Biochem.*, **11**, 115 (1979).
12) L. Morpurgo, M. T. Grasiani, A. Finazzi-Argo, G. Rotilo, and B. Mondovi, *Biochem. J.*, **187**, 361 (1980).
13) D. M. Dooley, J. Rawlings, J. H. Dawson, P. J. Stephens L.-E. Andereasson, B. G. Malmström, and H. B. Gray, *J. Am. Chem. Soc.*, **101**, 5038 (1979).
14) D. Kosman, M. J. Ettinger, R. E. Weiner, and E. J. Massaro, *Arch. Biochem. Biophys.*, **165**, 456 (1974).
15) R. H. Suva and R. H. Abeles, *Biochemistry*, **17**, 3538 (1978).
16) H. Kumagai, H. Uchida, and H. Yamada, *J. Biol. Chem.*, **254**, 10913 (1979).
17) J. Peisach and W. E. Blumberg, *Arch. Biochem. Biophys.*, **165**, 691 (1974).
18) G. Hamilton, P. K. Adolf, J. de Jersey, G. C. DuBois, G. R. Dyrkacz, and R. D. Hamilton., *J. Am. Chem. Soc.*, **100**, 1899 (1978).
19) T. Sakurai, J. Hongo, A. Nakahara, and Y. Nakao, *Inorg. Chim. Acta*, **46**, 205 (1980).
20) M. E. Winkler and R. D. Bereman, *J. Am. Chem. Soc.*, **102**, 6244 (1980).

  Bull. Chem. Soc. Jpn., 54, 2317—2322 (1981)

Solubility Isotherms of Systems Containing Optically Active Tris(ethylenediamine)cobalt(III) Ion. II.[1] Reciprocal Salt-pairs, (Λ-$[Co(en)_3]^{3+}$, Δ-$[Co(en)_3]^{3+}$)-(I^-, (R,R)-$C_4H_4O_6^{2-}$), at 25 °C

Akira Fuyuhiro,* Kazuaki Yamanari, and Yoichi Shimura

Department of Chemistry, Faculty of Science, Osaka University, Toyonaka, Osaka 560

(Received February 3, 1981)

A four-component solubility isotherm consisting of (Λ-$[Co(en)_3]^{3+}$, Δ-$[Co(en)_3]^{3+}$)-(I^-, (R,R)-$C_4H_4O_6^{2-}$)-H_2O was determined at 25 °C. It was found that four double salts *rac*-$[Co(en)_3]I_3\cdot H_2O$, Λ-$[Co(en)_3]I(d\text{-}C_4H_4O_6)\cdot 2H_2O$, Λ-$[Co(en)_3]_{0.48}\cdot\Delta$-$[Co(en)_3]_{0.52}(d\text{-}C_4H_4O_6)_{1.5}\cdot 5H_2O$, and Δ-$[Co(en)_3]I(d\text{-}C_4H_4O_6)\cdot nH_2O$ exist, six invariant points appearing. Application of this phase diagram to practical optical resolution is discussed in comparison with a system containing Br^-. Some models of phase diagram for effective optical resolution in reciprocal salt-pairs are proposed.

In a previous paper,[1] we reported on the determination of the solubility isotherm of reciprocal salt-pairs of the system (Λ-$[Co(en)_3]^{3+}$, Δ-$[Co(en)_3]^{3+}$)-(Br^-, d-H_2tart^{2-}) at 25 °C (d-H_2tart^{2-}=(R,R)-$C_4H_4O_6^{2-}$), which revealed the region of the well-known diastereomer Λ-$[Co(en)_3]Br(d\text{-}H_2tart)\cdot 5H_2O$, establishing excellent optical resolution of $[Co(en)_3]^{3+}$. On the other hand, the system containing I^- instead of Br^- has not been hitherto used for optical resolution. Thus, it is desirable to confirm the existence of a diastereomer Λ-$[Co(en)_3]I(d\text{-}H_2tart)\cdot nH_2O$, the extent of region it occupies, whether optical resolution of $[Co(en)_3]^{3+}$ is possible, and what kind of solid exists in the region corresponding to that of gelatinous precipitate in the system of Br^-.

In order to clarify these questions, the solubility isotherm of reciprocal salt-pairs (Λ-$[Co(en)_3]^{3+}$, Δ-$[Co(en)_3]^{3+}$)-(I^-, d-H_2tart^{2-}) was determined at 25 °C and the solubility of Λ- and *rac*-$[Co(en)_3]I_3$, and Λ- and Δ-$[Co(en)_3]I(d\text{-}H_2tart)$ was measured in the range 5—60 °C. The isotherm is discussed as regards fundamental models of optical resolution in reciprocal salt-pairs.

Experimental

Materials. *$[Co(en)_3]I_3\cdot H_2O$*: The Λ-, Δ-, and *rac*-$[Co(en)_3]I_3\cdot H_2O$ were obtained by the method of Broomhead *et al.*[2] Found: C, 11.29; H, 4.06; N, 13.16%. Calcd for Λ-$[Co(en)_3]I_3\cdot H_2O$: C, 11.30; H, 4.11; N, 13.17%. Found: C, 11.36; H, 4.06; N, 13.12%. Calcd for Δ-$[Co(en)_3]I_3\cdot H_2O$: C, 11.30; H, 4.11; N, 13.17%. Found: C, 11.31; H, 4.12; N, 13.13%. Calcd for *rac*-$[Co(en)_3]I_3\cdot H_2O$: C, 11.30; H, 4.11; N, 13.17%.

$[Co(en)_3](d\text{-}H_2tart)_{1.5}\cdot nH_2O$: The Λ- and Δ-$[Co(en)_3](d\text{-}H_2tart)_{1.5}\cdot nH_2O$ and the Λ-$[Co(en)_3]_{0.48}\cdot\Delta$-$[Co(en)_3]_{0.52}(d\text{-}H_2tart)_{1.5}\cdot 5H_2O$ diastereomers were the same as reported.[1]

$[Co(en)_3]I(d\text{-}H_2tart)\cdot nH_2O$: The Λ- and Δ-$[Co(en)_3]I(d\text{-}H_2tart)\cdot nH_2O$ diastereomers were prepared by mixing solutions of Λ-$[Co(en)_3]I_3$ and Λ-$[Co(en)_3](d\text{-}H_2tart)_{1.5}$, and Δ-$[Co(en)_3]I_3$ and Δ-$[Co(en)_3](d\text{-}H_2tart)_{1.5}$, respectively, in a 1 : 2 mole ratio. Found: C, 21.85; H, 5.85; N, 15.34%. Calcd for Λ-$[Co(en)_3]I(d\text{-}H_2tart)\cdot 2H_2O$: C, 21.83; H, 5.86; N, 15.27%. Found: C, 21.40; H, 5.88; N, 14.78%. Calcd for Δ-$[Co(en)_3]I(d\text{-}H_2tart)\cdot 2.5H_2O$: C, 21.48; H, 5.95; N, 15.03%.

Measurements. The solubility in water was determined in molality.[1] Since the CD intensity of $[Co(en)_3]^{3+}$ is affected by coexisting d-H_2tart^{2-}, the CD spectra of $[Co(en)_3]^{3+}$ were measured under calibrated conditions in HBr solution. The concentration of I^- was determined by titration with a $AgNO_3$ solution. The solid phases were identified by elemental analysis, absorption and CD spectra. Optical densities were measured with a JASCO UVIDEC-1 spectrophotometer and CD with a JASCO MOE-1 spectropolarimeter.

Results and Discussion

The solubility data are given in Tables 1 and 2, and Figs. 1—5. A saturated solution is expressed as a point defined by summing up the position vectors of the solubility of the component salt(s) contained.[3]

Binary Systems between 5 and 60 °C. As regards the binary solubility of the complexes (Table 1), the solubility ratio of *rac*-$[Co(en)_3]I_3$/Λ-$[Co(en)_3]I_3$ is 0.362 (5 °C) and 0.312 (60 °C), not being so small as in the corresponding bromide (0.173 (5 °C) and 0.294 (60 °C)). The ratio indicates[4] that the iodide as well as bromide are not spontaneously resolvable. This is also evident from the ternary system (Fig. 1). The Λ-$[Co(en)_3]I(d\text{-}H_2tart)$ diastereomer is more soluble below 28 °C than Λ-$[Co(en)_3]Br(d\text{-}H_2tart)$, which is unusual since a metal complex bromide is generally more soluble than the corresponding iodide. On the other hand, the

Table 1. Solubility of $[Co(en)_3]^{3+}$ salts in water (molality m/mol kg^{-1} of anhydrous salt)

T/°C	No. of salt[a]			
	(1)	(2)	(3)	(4)
5	0.0321	0.0886	0.0633	0.0886
10	0.0394	0.110	0.0795	0.114
15	0.0488	0.136	0.103	0.148
20	0.0589	0.167	0.123	0.192
25	0.0720	0.208	0.148	0.248
30	0.0865	0.249	0.179	0.319
35	0.103	0.302	0.215	0.422
40	0.123	0.367	0.258	0.542
45	0.145	0.439	0.307	0.696
50	0.173	0.538	0.376	0.905
55	0.203	0.646	0.445	1.10
60	0.242	0.775	0.532	1.35

a) (1): *rac*-$[Co(en)_3]I_3\cdot H_2O$, (2): Λ-$[Co(en)_3]I_3\cdot H_2O$, (3): Λ-$[Co(en)_3]I(d\text{-}H_2tart)\cdot 2H_2O$, (4): Δ-$[Co(en)_3]I(d\text{-}H_2tart)\cdot nH_2O$, n=4—5.

Table 2. Equilibrium of (Λ-$[Co(en)_3]^{3+}$, Δ-$[Co(en)_3]^{3+}$)-(I^-,d-H_2tart^{2-})-H_2O system at 25 °C

In liquid phases, solubility is presented in molality m of the component ions. Abbreviations are as follows: Λ-$[Co(en)_3]^{3+}=\Lambda^{3+}$, Δ-$[Co(en)_3]^{3+}=\Delta^{3+}$, Λ-$[Co(en)_3]I_3\cdot H_2O=\Lambda I_3$, Δ-$[Co(en)_3]I_3\cdot H_2O=\Delta I_3$, *rac*-$[Co(en)_3]I_3\cdot H_2O=\Lambda\Delta I_6$, Λ-$[Co(en)_3]I(d\text{-}H_2tart)\cdot 2H_2O=\Lambda I$ (tart), Λ-$[Co(en)_3]I(d\text{-}H_2tart)\cdot H_2O=[\Lambda I$ (tart)], Δ-$[Co(en)_3]I(d\text{-}H_2tart)\cdot nH_2O$ (n=4—5)$=\Delta I$(tart), Λ-$[Co(en)_3](d\text{-}H_2tart)_{1.5}\cdot nH_2O$ ($n\gtrsim 7$)$=\Lambda(tart)_{1.5}$, Δ-$[Co(en)_3](d\text{-}H_2tart)_{1.5}\cdot nH_2O$ ($n\simeq 8$)$=\Delta(tart)_{1.5}$, Λ-$[Co(en)_3]_{0.48}\cdot\Delta$-$[Co(en)_3]_{0.52}(d\text{-}H_2tart)_{1.5}\cdot 5H_2O=(\Lambda,\ \Delta)(tart)_{1.5}$. *; metastable state. Paste=a paste-like substance (composition unknown).

a)	b)	Liquid phase[c] $m/10^{-1}$ mol kg^{-1} Λ^{3+}	Δ^{3+}	I^-	Solid phase
A	2	2.08 (±0.05)		6.24 (±0.15)	ΛI_3
E_3	2	0.360 (±0.003)	0.360 (±0.003)	2.16 (±0.02)	$\Lambda\Delta I_6$
E_3 ↕ E_1	3	0.484 0.609 0.775 0.962 1.39 1.71	0.272 0.177 0.101 0.056 0.01 0.01	2.27 2.35 2.63 3.05 4.20 5.16	$\Lambda\Delta I_6$
E_1	3	2.08 (±0.03)	0.00	6.24 (±0.08)	ΛI_3 +$\Lambda\Delta I_6$
E_3 ↕ E_2	3	0.251 0.147 0.074 0.02 0.01	0.512 0.663 0.873 1.16 1.72	2.29 2.43 2.84 3.55 5.19	$\Lambda\Delta I_6$
E_2	3	0.00	2.08 (±0.03)	6.24 (±0.08)	ΔI_3 +$\Lambda\Delta I_6$
B	2		2.08 (±0.05)	6.24 (±0.15)	ΔI_3
D ↕ H_1	3	1.64 1.68 1.86 1.89 1.99 2.06 2.20		0.31 0.37 0.61 0.64 0.75 0.84 1.03	$\Lambda(tart)_{1.5}$
H_1	3	2.29 (±0.02)		1.16 (±0.05)	$\Lambda(tart)_{1.5}$ +ΛI(tart)
H_1 ↕ H_3	3	2.19 2.03 1.96 1.83 1.69 1.63 1.54		1.15 1.18 1.22 1.26 1.34 1.37 1.44	ΛI(tart)
H_3	2	1.48 (±0.02)		1.48 (±0.02)	ΛI(tart)
H_3 ↕ H_2	3	1.41 1.37 1.35 1.38 1.52 1.62 1.84 2.25 2.40 2.61		1.63 1.79 2.00 2.37 2.95 3.40 4.06 5.30 5.78 6.38	ΛI(tart)
H_2	3	2.83 (±0.05)		7.05 (±0.06)	ΛI(tart) +ΛI_3
A ↕ H_2	3	2.22 2.42 2.55 2.65		6.39 6.65 6.74 6.88	ΛI_3
H_1 ↕ H_4*	3	2.40* 2.58* 2.61* 2.84*		1.30* 1.53* 1.56* 1.86*	$\Lambda(tart)_{1.5}$*
H_4*	3	3.10* (±0.03)		2.17* (±0.03)	$\Lambda(tart)_{1.5}$* +Paste*
H_5*	3	3.08* (±0.04)		2.98* (±0.01)	$[\Lambda I(tart)]$* +Paste*
H_5* ↕ H_6*	3	3.02* 2.97* 2.90* 2.83* 2.78* 2.79* 2.99* 3.18* 3.29* 3.40* 3.56* 3.59* 3.75* 3.83*		3.01* 3.08* 3.27* 3.44* 3.72* 4.14* 5.23* 6.00* 6.40* 6.56* 7.30* 7.24* 7.82* 7.95*	$[\Lambda I(tart)]$*
H_6*	3	3.94* (±0.02)		8.33* (±0.07)	$[\Lambda I(tart)]$* +ΛI_3*
H_2 ↕ H_6*	3	3.12* 3.26* 3.43* 3.84*		7.36* 7.52* 7.79* 8.15*	ΛI_3*
E_1 ↕ P_1	4	2.46 2.59 2.67	0.00 0.00 0.00	6.67 6.78 6.86	ΛI_3 +$\Lambda\Delta I_6$
P_1	4	2.87 (±0.09)	0.00	7.11 (±0.07)	ΛI_3 +$\Lambda\Delta I_6$ +ΛI(tart)
P_1 ↕ P_4	4	2.61 2.46 2.22 1.77 1.54 1.42 1.37 1.36 1.34 1.33 1.36 1.35 1.36 1.36 1.37 1.37 1.40 1.42	0.00 0.00 0.02 0.06 0.15 0.27 0.38 0.44 0.54 0.76 0.85 0.89 1.00 1.02 1.22 1.24 1.39 1.60	6.52 6.01 5.28 3.98 3.33 3.07 2.99 2.98 2.97 3.04 3.08 3.09 3.13 3.17 3.27 3.29 3.36 3.50	$\Lambda\Delta I_6$ +ΛI(tart)
P_4	4	1.43 (±0.01)	1.70 (±0.02)	3.55 (±0.04)	$\Lambda\Delta I_6$ +ΛI(tart) +(Λ,Δ)-$(tart)_{1.5}$

TABLE 2. (Continued)

a)	b)	Liquid phase[c] $m/10^{-1}$ mol kg^{-1} A^{3+}	Δ^{3+}	I^-	Solid phase
G_1 ↕ P_2	4	1.62	0.21	0.20	$(A,\Delta)(tart)_{1.5}$ $+A(tart)_{1.5}$
		1.75	0.22	0.36	
		1.75	0.22	0.39	
		1.84	0.23	0.51	
		1.86	0.23	0.55	
H_1 ↕ P_2	4	2.29	0.05	1.16	$A(tart)_{1.5}$ $+\Delta I(tart)$
		2.32	0.07	1.17	
		2.34	0.15	1.20	
		2.42	0.27	1.26	
P_2	4	2.41 (±0.02)	0.30 (±0.01)	1.27 (±0.01)	$(A,\Delta)(tart)_{1.5}$ $+A(tart)_{1.5}$ $+\Delta I(tart)$
P_2 ↕ P_4	4	2.32	0.32	1.30	$(A,\Delta)(tart)_{1.5}$ $+\Delta I(tart)$
		2.16	0.35	1.35	
		2.08	0.36	1.40	
		2.00	0.39	1.44	
		1.84	0.45	1.55	
		1.67	0.59	1.79	
		1.53	0.82	2.15	
		1.47	1.08	2.60	
		1.45	1.25	2.87	
C ↕ F_1	3		3.21	0.19	$\Delta(tart)_{1.5}$
			3.44	0.40	
			3.73	0.72	
			4.04	1.04	
			4.38	1.39	
F_1	3		4.87 (±0.02)	1.92 (±0.02)	$\Delta(tart)_{1.5}$ $+\Delta I(tart)$
F_1 ↕ F_3	3		4.83	1.90	$\Delta I(tart)$
			4.49	1.93	
			4.44	1.93	
			4.09	1.96	
			3.76	1.99	
			3.41	2.08	
			3.08	2.14	
			2.72	2.31	
F_3	2		2.48 (±0.01)	2.48 (±0.01)	$\Delta I(tart)$
F_3 ↕ F_2	3		2.41	2.66	$\Delta I(tart)$
			2.33	2.84	
			2.32	3.01	
			2.29	3.38	
			2.34	3.78	
			2.43	4.18	
			2.57	4.81	
			2.74	5.32	
			2.84	5.67	
			2.90	5.89	
			3.10	6.49	
			3.25	6.99	
			3.42	7.44	
F_2	3		3.58 (±0.05)	7.91 (±0.11)	$\Delta I(tart)$ $+\Delta I_3$
B ↕ F_2	3		2.23	6.46	ΔI_3
			2.52	6.76	
			2.81	7.09	
			3.12	7.39	
			3.50	7.81	
E_2 ↕ P_3	4	0.00	2.37	6.54	ΔI_3 $+A\Delta I_6$
		0.00	2.70	6.88	
		0.00	3.01	7.28	
P_3	4	0.00	3.63 (±0.02)	7.95 (±0.06)	ΔI_3 $+A\Delta I_6$ $+\Delta I(tart)$
P_3 ↕ P_5	4	0.00	3.53	7.78	$A\Delta I_6$ $+\Delta I(tart)$
		0.00	3.34	7.11	
		0.00	3.09	6.45	
		0.00	3.05	6.38	
		0.03	2.74	5.35	
		0.03	2.69	5.24	
		0.04	2.63	5.06	
		0.06	2.56	4.83	
		0.08	2.50	4.56	
		0.10	2.42	4.32	
		0.16	2.38	4.13	
		0.21	2.37	4.01	
		0.27	2.35	3.89	
		0.36	2.33	3.83	
		0.49	2.34	3.78	
		0.65	2.38	3.76	
		0.85	2.45	3.83	
P_5	4	1.01 (±0.01)	2.50 (±0.02)	3.89 (±0.02)	$(A,\Delta)(tart)_{1.5}$ $+A\Delta I_6$ $+\Delta I(tart)$
G_2 ↕ P_6	4	0.10	3.34	0.33	$(A,\Delta)(tart)_{1.5}$ $+\Delta(tart)_{1.5}$
		0.11	3.76	0.71	
		0.11	4.01	0.98	
		0.11	4.30	1.27	
P_6	4	0.13 (±0.02)	4.97 (±0.06)	1.98 (±0.05)	$(A,\Delta)(tart)_{1.5}$ $+\Delta(tart)_{1.5}$ $+\Delta I(tart)$
P_6 ↕ P_5	4	0.17	4.37	2.02	$(A,\Delta)(tart)_{1.5}$ $+\Delta I(tart)$
		0.19	4.23	2.05	
		0.19	4.10	2.09	
		0.19	4.07	2.08	
		0.22	3.97	2.11	
		0.24	3.82	2.14	
		0.23	3.77	2.15	
		0.26	3.45	2.22	
		0.30	3.33	2.29	
		0.38	3.11	2.46	
		0.43	2.85	2.60	
		0.48	2.76	2.71	
		0.53	2.73	2.82	
		0.60	2.67	2.96	
		0.69	2.57	3.20	
		0.78	2.54	3.25	
		0.94	2.51	3.76	
P_4 ↕ P_5	4	1.27	1.69	3.24	$(A,\Delta)(tart)_{1.5}$ $+A\Delta I_6$
		1.23	1.77	3.27	
		1.19	1.82	3.29	
		1.16	1.90	3.31	
		1.11	1.95	3.31	
		1.06	2.05	3.37	
		1.02	2.13	3.42	

a) Positions of points shown in Figs. 1—5. b) Number of components. c) Reported data for C, D, G_1, G_2, $D \leftrightarrow G_1$, and $G_1 \leftrightarrow G_2$[1] are not shown. Values in parentheses are estimated errors and calculated from twice the standard deviations of measurements repeated 3—11 times.

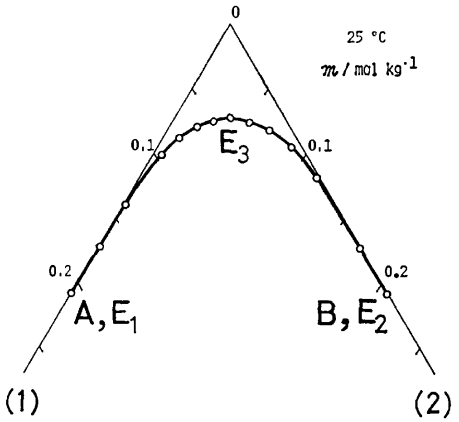

Fig. 1. Solubility isotherm of the ternary system, *Λ*-[Co(en)$_3$]I$_3$(1)–*Λ*-[Co(en)$_3$]I$_3$(2)–H$_2$O, at 25 °C. Solubility is presented in molality *m* of anhydrous salt.

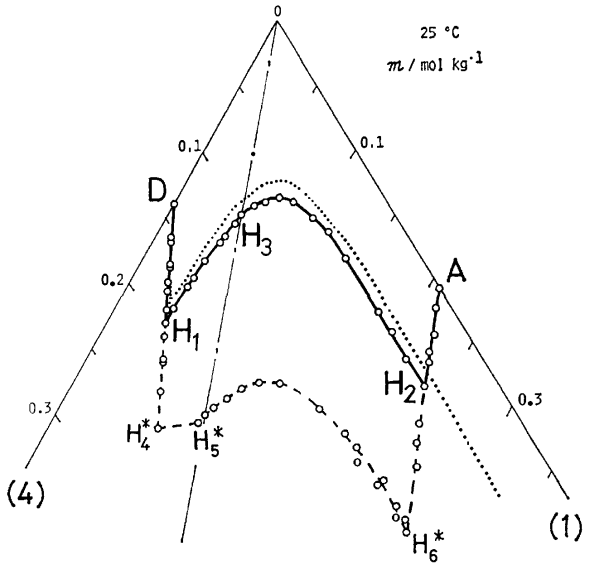

Fig. 2. Solubility isotherm of the ternary system, *Λ*-[Co(en)$_3$] (*d*-H$_2$tart)$_{1.5}$(4)–*Λ*-[Co(en)$_3$]I$_3$(1)–H$_2$O, at 25 °C. Solubility is presented in molality *m* of anhydrous salt. ----- and *: metastable state, ·····: the corresponding system of Br$^-$ at 25 °C (*Λ*-[Co(en)$_3$] (*d*-H$_2$tart)$_{1.5}$(4)–*Λ*-[Co(en)$_3$]Br$_3$(1)–H$_2$O).

solubility of *Δ*-[Co(en)$_3$]I(*d*-H$_2$tart) cannot be compared with that of *Δ*-[Co(en)$_3$]Br(*d*-H$_2$tart) because of the formation of gelatinous precipitate in the latter diastereomer. The solubility ratio of *Δ*-[Co(en)$_3$]I(*d*-H$_2$tart)/*Λ*-[Co(en)$_3$]I(*d*-H$_2$tart) is 1.40 (5 °C) and 2.54 60 °C).

Ternary System Λ-[*Co(en)*$_3$]*I*$_3$–Δ-[*Co(en)*$_3$]*I*$_3$–*H*$_2$*O*. This system at 25 °C (Fig. 1) is similar to the corresponding system of Br$^-$. The central solid phase is the racemic compound *Λ*-[Co(en)$_3$]·*Δ*-[Co(en)$_3$]I$_6$·2H$_2$O= *rac*-[Co(en)$_3$]I$_3$·H$_2$O, which occupies such a wide region ($E_1E_3E_2$) that the invariant points E_1 and E_2 exist nearly on the side axes. The solubility of racemic iodide at 25 °C (0.0720 mol kg^{-1} (E_3)) is lower than that of racemic bromide (0.178 mol kg^{-1}). The difference is considerably responsible for optical resolution in the four-component system described below.

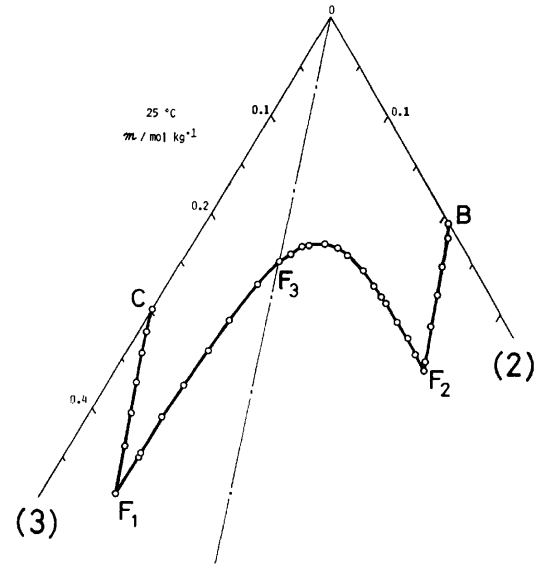

Fig. 3. Solubility isotherm of the ternary system, *Δ*-[Co(en)$_3$] (*d*-H$_2$tart)$_{1.5}$(3)–*Δ*-[Co(en)$_3$] I$_3$(2) – H$_2$O, at 25 °C. Solubility is presented in molality *m* of anhydrous salt.

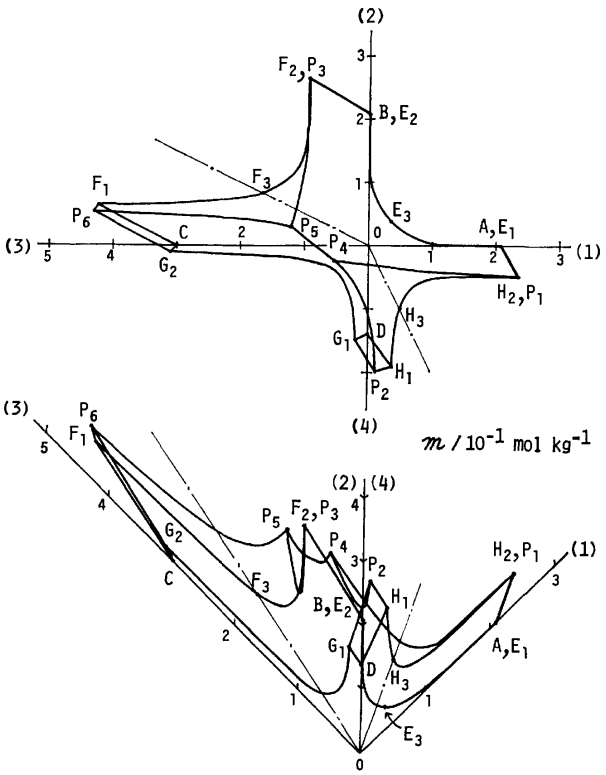

Fig. 4. The plane projection (upper) and the side elevation of solubility isotherm of the system, (*Λ*-[Co(en)$_3$]$^{3+}$, *Δ*-[Co(en)$_3$]$^{3+}$)–(I$^-$, *d*-H$_2$tart^{2-})–H$_2$O, at 25 °C. Solubility is presented in molality *m* of anhydrous salt. (1): *Λ*-[Co(en)$_3$]I$_3$, (2): *Δ*-[Co(en)$_3$]I$_3$, (3): *Δ*-[Co(en)$_3$](*d*-H$_2$tart)$_{1.5}$, (4): *Λ*-[Co(en)$_3$](*d*-H$_2$tart)$_{1.5}$.

Ternary System Λ-[*Co(en)*$_3$](d-*H*$_2$*tart)*$_{1.5}$–Λ-[*Co(en)*$_3$]*I*$_3$–*H*$_2$*O*. This system consists of only *Λ*-salts (Fig. 2). The region $H_1H_3H_2$ shows a diastereomer of double salt *Λ*-[Co(en)$_3$]I(*d*-H$_2$tart)·2H$_2$O, its isotherm being

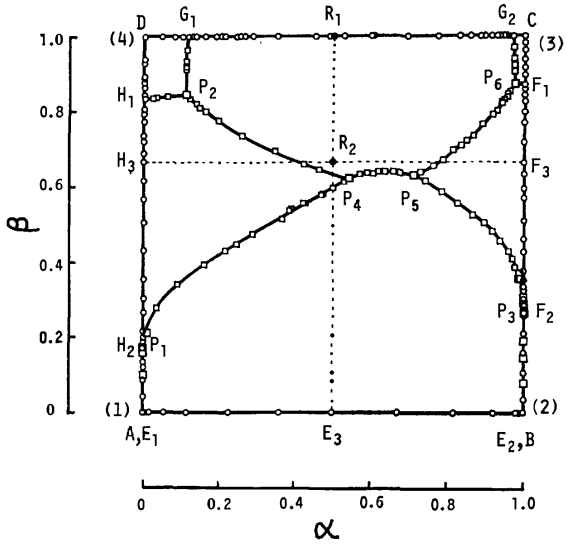

Fig. 5. The clinographic projection of solubility isotherm of the system, (Λ-$[Co(en)_3]^{3+}$, Δ-$[Co(en)_3]^{3+}$)–(I^-, d-H_2tart^{2-})–H_2O, at 25 °C.
α: mole fraction of Δ-$[Co(en)_3]^{3+}$ to all the cations, β: mole fraction of (d-$H_2tart)_{1.5}^{3-}$ to $\{(I_3)^{3-}+(d\text{-}H_2tart)_{1.5}^{3-}\}$, (1): Λ-$[Co(en)_3]I_3$, (2): Δ-$[Co(en)_3]I_3$, (3): Δ-$[Co(en)_3](d\text{-}H_2tart)_{1.5}$, (4): Λ-$[Co(en)_3](d\text{-}H_2tart)_{1.5}$, □: solubilities of four-components, ○: solubilities of two- or three-componts.

located a little lower than that of bromide double salt Λ-$[Co(en)_3]Br(d\text{-}H_2tart)\cdot 5H_2O$. The binary solubility of Λ-$[Co(en)_3]I(d\text{-}H_2tart)$ (H_3, m=0.148 mol kg^{-1} at 25 °C) is larger than that of Λ-$[Co(en)_3]Br(d\text{-}H_2tart)$ (m=0.135 mol kg^{-1}). The line AH_2 appears in a region different from that for the corresponding bromide double salt because of the solubility difference between Λ-$[Co(en)_3]Br_3$ and Λ-$[Co(en)_3]I_3$.

Some metastable states were measured in the system containing I^-; the supersaturated solutions coexist with the metastable solids, Λ-$[Co(en)_3](d\text{-}H_2tart)_{1.5}\cdot nH_2O$ on H_1H_4* and Λ-$[Co(en)_3]I_3\cdot H_2O$ on H_2H_6*. The composition of a paste-like solid phase on H_4*H_5* is unknown. The line H_5*H_6* expresses the metastable isotherm for Λ-$[Co(en)_3]I(d\text{-}H_2tart)\cdot H_2O$. However, this monohydrated diastereomer did not appear as a stable solid in the binary system at 5—60 °C (Table 1). On the other hand, the corresponding bromide double salt Λ-$[Co(en)_3]Br(d\text{-}H_2tart)$ exists as a monohydrated solid phase above 47 °C.

Ternary System Δ-$[Co(en)_3](d\text{-}H_2tart)_{1.5}$–$\Delta$-$[Co(en)_3]I_3$–$H_2O$. In this system (Fig. 3), which differs entirely from the corresponding bromide system where the central part of the isotherms is blank owing to the appearance of a gelatinous substance, the isothermal line $F_1F_3F_2$, on which a saturated solution is in equilibrium with the solid Λ-$[Co(en)_3]I(d\text{-}H_2tart)\cdot nH_2O$ can be measured. Point F_3 denotes the binary solubility of Λ-$[Co(en)_3]I(d\text{-}H_2tart)$.

The Solubility Isotherm of Reciprocal Salt-pairs, (Λ-$[Co(en)_3]^{3+}$, Δ-$[Co(en)_3]^{3+}$)–(I^-, d-H_2tart^{2-})–H_2O.
The ternary systems described above constitute a part of the system of reciprocal salt-pairs. This four-component body was projected on three planes,[3] the plane projection and the side elevation (Fig. 4), and the clinographic projection (Fig. 5). The upper side in Fig. 5 represents the ternary system, Λ-$[Co(en)_3](d\text{-}H_2tart)_{1.5}$–$\Lambda$-$[Co(en)_3](d\text{-}H_2tart)_{1.5}$–$H_2O$, being common between two systems of X^-=Br^- and I^-, (Λ-$[Co(en)_3]^{3+}$, Λ-$[Co(en)_3]^{3+}$)–(X^-, d-H_2tart^{2-})–H_2O. Eight solid phases appear, the composition of each phase corresponding to the following solid: A=Λ-$[Co(en)_3]I_3\cdot H_2O$, B=Λ-$[Co(en)_3]I_3\cdot H_2O$, C=Λ-$[Co(en)_3](d\text{-}H_2tart)_{1.5}\cdot nH_2O$, D=$\Lambda$-$[Co(en)_3](d\text{-}H_2tart)_{1.5}\cdot nH_2O$, E_3=*rac*-$[Co(en)_3]I_3\cdot H_2O$, F_3=Λ-$[Co(en)_3]I(d\text{-}H_2tart)\cdot nH_2O$, (close of R_1)=Λ-$[Co(en)_3]_{0.48}\cdot\Lambda$-$[Co(en)_3]_{0.52}(d\text{-}H_2tart)_{1.5}\cdot 5H_2O$, and H_3=Λ-$[Co(en)_3]I(d\text{-}H_2tart)\cdot 2H_2O$. The present system essentially resembles the corresponding bromide system except for two aspects: (a) appearance of the region of Λ-$[Co(en)_3]I(d\text{-}H_2tart)\cdot nH_2O$, $P_3F_2F_3F_1P_6P_5P_3$, though in the bromide system the corresponding region could not be measured because of the formation of the gelatinous precipitate, and (b) a different combination of phase boundaries. If the gelatinous precipitate in the bromide system is assumed to be a solid phase, the regions of Λ-$[Co(en)_3]Br(d\text{-}H_2tart)\cdot 5H_2O$ and the gelatinous precipitate coexist on the boundary line. On the other hand, the corresponding regions of Λ-$[Co(en)_3]I(d\text{-}H_2tart)\cdot 2H_2O$ ($H_1H_3H_2P_1P_4P_2H_1$) and Λ-$[Co(en)_3]I(d\text{-}H_2tart)\cdot nH_2O$ do not coexist, and the regions of *rac*-$[Co(en)_3]I_3\cdot H_2O$ ($E_1E_3E_2P_3P_5P_4P_1E_1$) and Λ-$[Co(en)_3]_{0.48}\cdot\Lambda$-$[Co(en)_3]_{0.52}(d\text{-}H_2tart)_{1.5}\cdot 5H_2O$ ($G_1P_2P_4P_5P_6G_2R_1G_1$) coexist on the boundary P_4P_5. Since Λ-$[Co(en)_3]Br(d\text{-}H_2tart)\cdot 5H_2O$ and Λ-$[Co(en)_3]I(d\text{-}H_2tart)\cdot 2H_2O$ have almost the same solubility (H_3) and the upper side of the iodide system is the same as that of the bromide system, the positions of H_1 and P_2 or the lines H_1P_2 and G_1P_2 are almost the same as the corresponding points or lines in the bromide system. The line P_2P_4 is located at almost the same position as in the bromide system on the clinographic projection. However, the location of the line P_1P_4, on which *rac*-$[Co(en)_3]X_3\cdot nH_2O$ and Λ-$[Co(en)_3]X(d\text{-}H_2tart)\cdot nH_2O$ (X=Br and I) coexist, differs in the two systems. This results from the solubility difference between *rac*-$[Co(en)_3]Br_3$ and *rac*-$[Co(en)_3]I_3$ (E_3), irrespective of a similar solubility for Λ-$[Co(en)_3]Br(d\text{-}H_2tart)$ and Λ-$[Co(en)_3]I(d\text{-}H_2tart)$ (H_3).

Application to Optical Resolution. The line of α=0.5 (R_1E_3) in Fig. 5 is a "racemic line" where the concentrations of Λ-$[Co(en)_3]^{3+}$ and Λ-$[Co(en)_3]^{3+}$ are equal. If a region of a diastereomer containing only one enantiomer spreads across the "racemic line," such an isotherm can be used for perfect optical resolution. In the present system at 25 °C, the region of Λ-$[Co(en)_3]I(d\text{-}H_2tart)\cdot 2H_2O$ spreads across the "racemic line" and the system can be used for optical resolution. However, the useful region is too narrow to be used effectively.

Let us consider the following case of optical resolution of *rac*-$[Co(en)_3]X_3$ (X=Br or I) by the addition of x mol of $Ag_2(d\text{-}H_2tart)$ at 25 °C ($0\leqq x\leqq 1.5$).

$$rac\text{-}[Co(en)_3]X_3 + xAg_2(d\text{-}H_2tart) \longrightarrow$$
$$rac\text{-}[Co(en)_3]^{3+} + (3-2x)X^- + xd\text{-}H_2tart^{2-} + AgX\downarrow$$

In the case of $x=1$ (R_2 in Fig. 5) the first precipitate is Λ-$[Co(en)_3]_{0.48}$·Δ-$[Co(en)_3]_{0.52}$(d-$H_2tart)_{1.5}$·$5H_2O$, not Λ-$[Co(en)_3]X$(d-H_2tart)·nH_2O. Optical resolution is successful in the range $0.43<x<0.97$ in the bromide system.[1] Similarly in the case of iodide system optical resolution will be accomplished only in the range $0.89<x<0.95$. The maximum yield corresponding to P_4 will become only 15.7% for Λ-$[Co(en)_3]^{3+}$ (7.8% for *rac*-$[Co(en)_3]^{3+}$).

Thus, the solubility difference between Λ-$[Co(en)_3]I$-(d-H_2tart) and Δ-$[Co(en)_3]I$(d-H_2tart) is not directly related to whether optical resolution is successful or not.

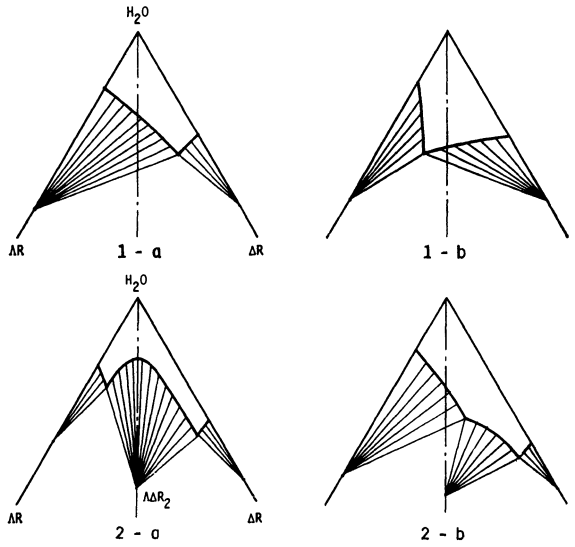

Fig. 6. Models of solubility isotherm of the ternary system ΛR–ΔR–H_2O for optical resolution.
Λ^+ and Δ^+:a pair of enantiomers, R^-: a resolving agent.

Models of Phase Diagram for Optical Resolution. The simplest phase diagram applicable to optical resolution is the ternary system ΛR–ΔR–H_2O shown in Fig. 6, where ΛR is the less soluble diastereomer. Model **1-a** can be used for optical resolution and involves the practical examples Λ-$[Co(ox)(en)_2]$(d-H_3tart)·Δ-[Co-(ox)$(en)_2$](d-H_3tart)–H_2O and Λ-$[Co(ox)(en)_2]$·Δ-[Co-(edta)]–Δ-$[Co(ox)(en)_2]$·Δ-[Co(edta)]–H_2O.[5] Model **1-b** can also be available, and the diastereomer obtained is the more soluble ΔR and not the less soluble ΛR. Model **2-a** can not be used because of the formation of pseudoracemate $\Lambda\Delta R_2$ in the central part. In model **2-b** optical resolution is possible in spite of the formation of the pseudoracemate. Such a case is exemplified by the system Λ-$[Co(ox)(en)_2]$(d-bcs)–Δ-$[Co(ox)(en)_2]$(d-bcs)–H_2O at a temperature below 19 °C (d-bcs^-= (1*R*,3*S*,4*S*,7*R*)-$C_{10}H_{14}OBrSO_3^-$).[6] If we assume that **2-b** is a special case, the possibility of optical resolution of the ternary system depends upon whether the pseudoracemate $\Lambda\Delta R_2$ exists or not, and not on the solubility difference between the pair of diastereomers ΛR and ΔR.

Figure 7 shows several representative models of clinographic projections for the systems of reciprocal salt-pairs effective for optical resolution, (Λ^+, Δ^+)–(X^-, R^-)–H_2O. Effective optical resolution requires that the region of a diastereomer (ΛR, for example) spreads across the "racemic line." Model **3** without any double salt is effective for optical resolution. The upper side of **3** corresponds to the ternary system of **1-a**, introduction of a fourth ion X^- not being important. In **4** there exist two effective diastereomers ΛR and Λ_2XR which include the opposite enantiomer to each other. The upper side of **5** corresponds to **2-b** but the introduction of X^- makes the optical resolution possible: the ΛR diastereomer will be obtained in the coexistence of X^-. Similarly, in model **6** optical resolution is unsuccessful in the absence of X^-, and the effective diastereomer is a double salt Λ_2XR. The systems (Λ-$[Co(en)_3]^{3+}$, Δ-$[Co(en)_3]^{3+}$)–(X^-, d-H_2tart^{2-})–H_2O, X^-=Br^- and I^-, belong to a variety of **6**. Two kinds of diastereomers ΛR and Λ_2XR can be utilized in **7**.

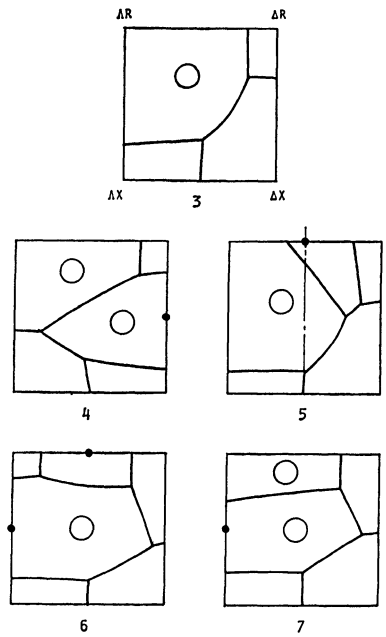

Fig. 7. Models of clinographic projection of solubility isotherm of the system (Λ^+, Δ^+)–(X^-, R^-)–H_2O for effective optical resolution.
Λ^+ and Δ^+: a pair of enantiomers, X^-: a optically inactive ion, R^-: a resolving agent, ○: the region of effective diasteromer for optical resolution, ●: double salt.

References

1) Part I of this series: A. Fuyuhiro, K. Yamanari, and Y. Shimura, *Bull. Chem. Soc. Jpn.*, **53**, 3577 (1980).
2) J. A. Broomhead, F. P. Dwyer, and J. W. Hogarth, *Inorg. Synth.*, **6**, 186 (1960).
3) A. Fuyuhiro, K. Yamanari, and Y. Shimura, *Bull. Chem. Soc. Jpn.*, **52**, 90 (1979).
4) K. Yamanari, J. Hidaka, and Y. Shimura, *Bull. Chem. Soc. Jpn.*, **46**, 3724 (1973).
5) Y. Shimura and K. Tsutsui, *Bull. Chem. Soc. Jpn.*, **50**, 145 (1977).
6) A. Fuyuhiro, K. Yamanari, and Y. Shimura, *Bull. Chem. Soc. Jpn.*, **52**, 1420 (1979).

The Enantioface-differentiating (Asymmetric) Hydrogenation of the C=O Double Bond with Modified Raney Nickel. XXXVI. The Development of Modified Nickel Catalysts with High Enantioface-differentiating Abilities

Tadao HARADA,* Mihoko YAMAMOTO, Shinji ONAKA, Motomasa IMAIDA, Hiroshi OZAKI, Akira TAI, and Yoshiharu IZUMI

Division of Organic Chemistry, Institute for Protein Research, Osaka University, Yamada-oka, Suita, Osaka 565

(Received September 4, 1980)

Various types of modified nickel catalysts were prepared and their enantioface-differentiating (asymmetric) abilities were examined. It was found that the presence of aluminum or related metal compounds in the catalyst was unfavorable for the effective enantioface-differentiating catalyst. The modification with a solution containing tartaric acid and inorganic salt gave a high enantioface-differentiating ability to Raney nickel and reduced nickel catalyst. Among the modified nickel catalysts examined, the Raney nickel modified with tartaric acid and sodium bromide gave the best result with respect to the hydrogenation activity and enantioface-differentiating ability (optical yield 88%). NaBr adsorbed on Raney nickel was found to inhibit the nonenantioface-differentiating hydrogenation.

An asymmetrically modified Raney nickel catalyst (MRNi) is easily prepared by soaking Raney nickel catalyst (RNi) in a solution of an optically active substance.[1] This is the most suitable catalyst for the enantioface-differentiating (asymmetric) hydrogenation because of its high hydrogenation activity and its preparative convenience. Our research group has been continuing the studies to improve the enantioface-differentiating ability (e.d.a.) of MRNi.

Recently, we succeeded in obtaining an improved MRNi with a sufficient e.d.a.[2] The improved catalyst can be prepared by the modification of RNi with a solution containing tartaric acid (TA) and NaBr (TA–NaBr–MRNi). An optical yield of near 90% was attained in the hydrogenation of methyl acetoacetate (MAA) to methyl 3-hydroxybutyrate (MHB) over this catalyst.

This paper will present our approach leading to the development of TA–NaBr–MRNi and the role of adsorbed NaBr in the enantioface-differentiating rocess.

Results and Discussion

TA–MNi and TA–NaBr–MHNi. Asymmetrically modified nickel catalysts (MNi) can be prepared from many kinds of nickel catalysts.[3] The e.d.a.'s of various TA–MNi's are listed in Table 1. The degrees of e.d.a.'s were evaluated by the optical yields (%) of the hydrogenation of MAA to MHB.

The use of the activated nickel prepared by the liquid phase reaction (Entries 1—5) resulted in poor optical yields (below 44%), while the use of the catalyst activated by a dry process (Entries 6—9) resulted in high optical yields (55—82%).

It is well known that Raney type catalysts (Entries 1—3) and Urushibara catalyst (Entry 4) contain some amounts of impurities (Al, Mg, Si, Zn, or derivatives of their cations). The rather poor results listed in Entries 1—4 could be considered to be caused by existence of these impurities in the catalyst. When RNi was modified with a solution containing TA and $NaAlO_2$, the resulting TA–MRNi (Entry 5) showed a lower e.d.a. than that of the conventional TA–MRNi (Entry 1). From the facts mentioned above, it can be concluded that the uses of nickel catalysts containing either Al, Mg, Si, Zn, or related metal compounds are not desirable for obtaining TA–MNi with high e.d.a.

The activated nickels prepared by thermal decomposi-

Table 1. Enantioface-differentiating hydrogenations of MAA over various types of TA–MNi's

No.	Source of activated Ni	Modifying conditions		Reaction conditions					Degree of e.d.a.[a]
		pH	Temp/°C	Amount of MNi/g	MAA ml	Solvent ml	AcOH ml	Temp °C	
1	Ni–Al alloy	5.0	100	0.6	17.5			60	44
2	Ni–Mg alloy	5.0	100	0.6	17.5			60	6
3	Ni–Si alloy	5.0	100	0.6	17.5			60	44
4	Urushibara Ni–A	4.1	85	1.0	11.5	THF/23	0.2	100	4
5	Ni–Al alloy	5.0[b]	100	0.6	17.5			60	30
6	$Ni(HCO_2)_2 2H_2O$	5.0	100	0.6	17.5			100	55
7	NiO	5.0	100	0.6	17.5			100	59
8	NiO	4.1	85	0.8	11.5	THF/23	0.2	100	65—82
9	$Ni(CO)_4$[c]	4.1	85	0.6	11.5	THF/23	0.2	85	58—75

a) Degree of e.d.a. was evaluated by optical yield (%) of hydrogenation of MAA over MNi. b) The pH of modifying solution was adjusted with $NaAlO_2$ instead of NaOH. c) The Ni powder prepared from $Ni(CO)_4$ was supplied by Metal Foil and Powder MFG Co..

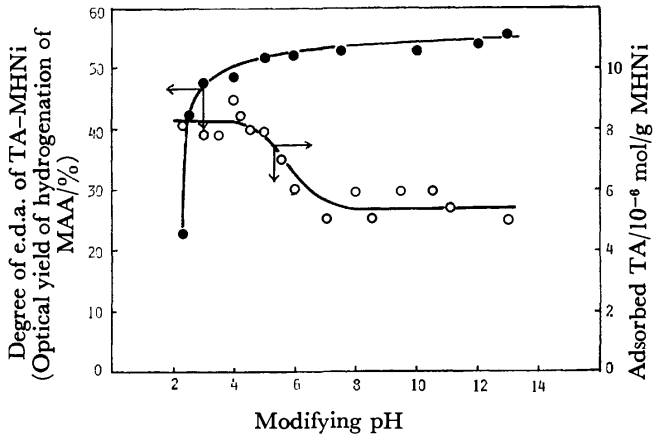

Fig. 1. Relationship between modifying pH and degree of e.d.a. of TA–MHNi(optical yield of hydrogenation of MAA over TA–MHNi) or amount of adsorbed TA. HNi was prepared from NiO supplied by Wako Pure Chemical Industries, Ltd. Amount of HNi: 0.8 g. Modification: at 0 °C for 1 h. Hydrogenation :MAA (17.5 ml) was subjected to hydrogenation at 100 °C.

tion of nickel formate, by hydrogenolysis of nickel oxide (HNi), and by decomposition of nickel carbonyl gave TA–MNi's with rather high e.d.a.'s. Among the catalysts examined, HNi modified with TA (TA–MHNi) gave the best result with respect to the e.d.a.

It was known that the e.d.a. of TA–MRNi was strongly affected by the modifying pH.[4] Thus, the relation between the modifying pH and the e.d.a. of TA–MHNi was examined in order to find out the optimal modifying pH. The results are shown in Fig. 1. Figure 1 also shows the relation between the modifying pH and the amount of TA adsorbed on HNi. The e.d.a. of TA–MHNi was found to increase steeply with increasing pH and settle down at a constant value at the pH range from 3 to 13. The adsorbed amount of TA at below pH 4 is greater than that at above pH 4. Thus, the poor e.d.a. of TA–MHNi at below pH 3 cannot be explained on the basis of the amount of adsorbed TA. It is reasonable to assume that the difference between the e.d.a. at below pH 3 and that at the pH range from 3 to 13 results from the difference in the adsorption mode of TA.[5] The counter ions of adsorbed TA are expected to be Ni^{2+} and H^+ in the pH region intrinsic to the solution of the free TA and to be Na^+ under neutral and basic conditions.

The e.d.a. of TA–MHNi was found to be sensitive to the preparative variations and purity of NiO. That is, differences in the manufacturer and the lot number of NiO caused a significant difference in the e.d.a. of TA–MHNi (Table 2). There was a relation between the colour of NiO powder and the e.d.a. of the resulting TA–MHNi. In general the light green NiO powder tended to give TA–MHNi with high e.d.a., while the dark green one tended to give TA–MHNi with low e.d.a.

Table 2. Enantioface-differentiating hydrogenation of MAA over TA–MHNi

NiO		$[\alpha]_D^{20}$ of the product	Degree of e.d.a.[a]
Manufacturer	Lot No.		
Wako Pure Chemical Industries, Ltd.	LDJ 1657	−18.60	81
Wako Pure Chemical Industries, Ltd.	117-1	−15.51	68
Nihon Kagaku Sangyo, Co., Ltd.		−16.15	70
Mitsuwa Pure Chemicals, Ltd.	34491	−17.30	79

Amount of HNi: 0.8 g. Modification: at pH 4, 100 °C for 1 h. Hydrogenation: MAA (11.5 ml) in THF (23 ml) and AcOH (0.2 ml) was subjected to hydrogenation with each catalyst at 120 °C. a) Optical yield (%) of hydrogenation of MAA over TA–MHNi.

Table 3. Enantioface-differentiating hydrogenation of MAA over TA–MHNi on support

Support	$[\alpha]_D^{20}$ of the product	Degree of e.d.a.[c]
Kieselguhr[a]		
Shimalite SP-17	−12.39	54
Shimalite SP-25	−10.09	44
Shimalite SP-35	−8.48	37
Shimalite SP-55	−8.61	38
Activated alumina[b]		
Woelm acidic	−15.33	67
W 200 basic	−15.53	68
W 200 neutral	−15.55	68
TiO_2	−16.07	70
ZrO_2	−14.46	63

Weight ratio of Ni to support=50 to 50. Amount of supported Ni: 1.2 g. Modification: at pH 4.1, 85 °C for 1 h. Hydrogenation conditions were the same as those described in Footnote of Table 2 except for the hydrogenation temperature (85 °C). a) Kieselguhr was supplied by Wako Pure Chemical Industries, Ltd. b) Activated alumina was supplied by ICN Woelm Laboratories, Inc. c) Optical yield (%) of hydrogenation of MAA over TA–MNi.

Orito and his coworkers reported that Ni–Pd catalyst supported on kieselguhr gave an excellent catalyst for the enantioface-differentiating hydrogenation of MAA to MHB.[6] More than 90% of the optical yield was reported when the catalyst was modified with TA. We also prepared HNi's supported on various kinds of supports and the effects of supports were examined. As found in Table 3, no significant increase of e.d.a. was attained by the uses of nickel catalysts supported on kieselguhr, TiO_2, ZrO_2, and Al_2O_3. The e.d.a. of TA–MHNi supported on kieselguhr was observed to be affected by the sort of kieselguhr. Kieselguhrs well purified by acid or/and alkali washing (Shimalite SP-25, -35, and -55) gave TA–MHNi's with lower e.d.a.'s than that of unpurified one (Shimalite SP-17). It is reasonable to assume that minor components in kieselguhr are dissolved into the modifying solution and some of them serve as supplementary modifying reagents to increase the e.d.a.

We have often noticed that small amounts of impurities in the supplied water used for the modification

Table 4. Enantioface-differentiating hydrogenation of MAA over TA–inorganic salt–MHNi

Inorganic salt in the modifying solution (g)	$[\alpha]_D^{20}$ of the product	Degree of e.d.a.[a)]
None	−16.85	73
NaI (1.0×10^{-3})	−18.34	80
NaBr (20)	−19.75	86
NaCl (10)	−17.83	78

Amount of HNi: 0.8 g. Modification: at pH 4.0, 100 °C for 1 h. Hydrogenation: MAA (11.5 ml) in methyl propionate (23 ml) and AcOH (0.2 ml) was subjected to hydrogenation at 100 °C. a) Optical yield (%) of hydrogenation of MAA over MHNi.

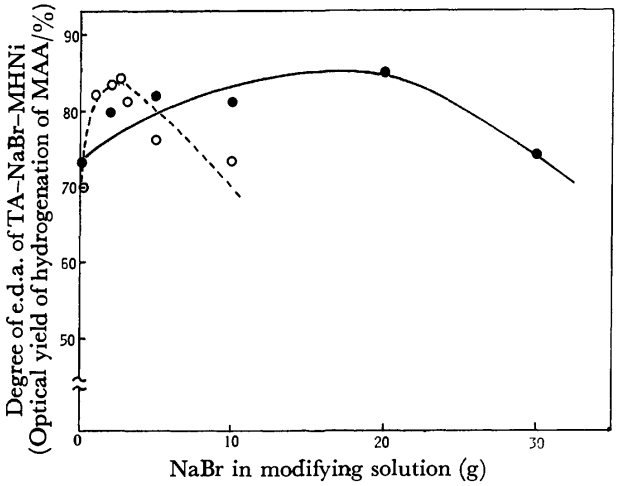

Fig. 2. Relationship between amount of NaBr in modifying solution and degree of e.d.a. of TA–NaBr–MHNi (optical yield of hydrogenation of MAA over TA–NaBr–MHNi).
TA–NaBr–MHNi: NiO was supplied by Wako Pure Chemical Industries, Ltd. (—●—) or Nihon Kagaku Sangyo, Co., Ltd. (—○—). Modification: at pH 4, 100 °C for 1 h. Hydrogenation was carried out under the same conditions as those described in footnote of Table 2.

process affected significantly the e.d.a. of the resulting catalyst. This finding led us to the idea that investigation of supplementary compounds in the modifying solution would enable us to develop a more effective enantioface-differentiating catalyst.

In the course of studies on the effect of supplementary modifying reagents on the e.d.a. of MHNi, it was found that the use of some kinds of inorganic salts increased the e.d.a. (Table 4). Among inorganic salts examined, NaBr was the best supplementary compound in giving a high e.d.a. As shown in Fig. 2, the e.d.a. of TA–NaBr–MHNi increased with the amount of NaBr in the modifying solution, reached a maximum value, and then decreased. The optimal amount of NaBr in the modifying solution was affected by the sort of NiO sample. Under the optimal conditions, TA–NaBr–MHNi showed a sufficient e.d.a. (optical yield, 86%). However, the main disadvantage of TA–NaBr–MHNi is the lack of high hydrogenating activity. The hydrogenation of MAA over TA–MHNi had to be performed at above 100 °C. Under these conditions, the yield of MHB can never be satisfactory because of the formation of by-products (*e.g.*, methyl 3-(3-hydroxybutyryloxy) butyrate). Thus, the preparation of an aluminum free catalyst with high hydrogenating activity was strongly required.

In this regard, our investigation attempted to develop a procedure for elimination of aluminum from the RNi surface in order to prepare a highly active and aluminium free catalyst.

Acid-treated RNi (RNi–A). Aluminium easily dissolves into water by the reaction with hydroxy acids to give highly water soluble products (aluminium chelates). Therefore, the selective elimination of aluminium from RNi was expected, when RNi was treated with a large amount of aqueous solution of hydroxy acid such as TA or glycolic acid (GA) under acidic conditions at a high temperature. A significant decrease of aluminium content was observed on this treatment (from 6% of Al content of the conventional RNi to less than 3% of Al content of GA-treated RNi (RNi–A (GA)) or TA-treated RNi (RNi–A (TA)).[7] Since the corrosion of nickel also took place during this treatment, the surface state of the resulting catalyst was no longer the same as that of RNi.

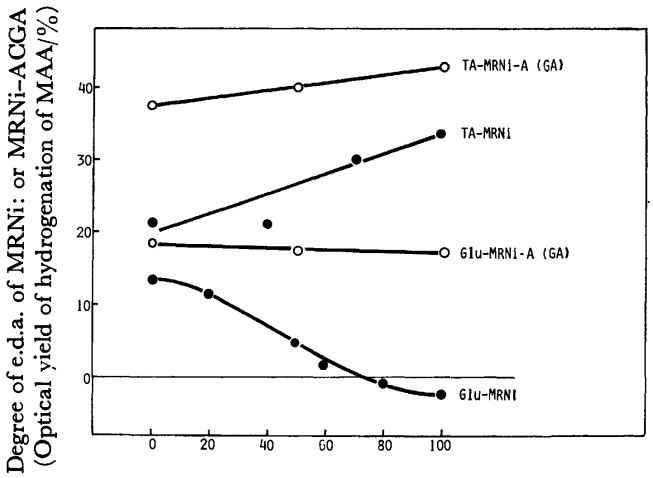

Fig. 3. Relationship between modifying temperature and degree of e.d.a. of MRNi (optical yield of hydrogenation of MAA over MRNi) or MRNi–A (GA). Amount of RNi or RNi–A (GA): 0.6 g. Modification: at pH 5 for 1.5 h. Hydrogenation: MAA (17.5 ml) was subjected to hydrogenation at 60 °C.

Figure 3 shows the e.d.a. of RNi–A (GA) modified with glutamic acid (Glu–MRNi–A (GA)) or TA–MRNi–A (GA), together with the e.d.a. of the conventional Glu–MRNi or TA–MRNi.[8] The e.d.a. of Glu– or TA–MRNi–A (GA) was higher than that of RNi modified with the same modifying reagent. The e.d.a. of MRNi–A (GA) was not affected by the modifying temperature, while that of the conventional MRNi changed significantly with the change in the modifying temperature. The results indicated that the GA-treatment gave a well stabilized and favorable catalyst

TABLE 5. EFFECT OF TA-TREATMENT ON e.d.a. OF TA-MRNi

Catalyst	Modifying conditions		$[\alpha]_D^{20}$ of the product	Degree of e.d.a.[a]
	pH	Temp/°C		
RNi-A (TA)	5.0	0	−14.23	62
RNi	5.0	0	−9.05	40
RNi	3.2	100	−8.99	39

Amount of catalyst: 0.8 g. Hydrogenation conditions were the same as those described in the Footnote of Table 4. a) Optical yield (%) of hydrogenation of MAA.

for the enantioface-differentiating hydrogenation. The hydrogenating activity of RNi-A (GA) was found to be high enough to carry out the hydrogenation of MAA at 60 °C.

The treatment with TA instead of GA functions as acid-treatment as well as modification. Table 5 shows the e.d.a. of TA-MRNi-A (TA) prepared in the following sequence: TA-treatment at 100 °C→water-washing→TA-modification at pH 5, 0 °C. It can be seen that the TA-treatment resulted in a significant increase of e.d.a. The hydrogenation over TA-MRNi-A (TA) was completed in 3—5 h at 100 °C, while the hydrogenation over TA-MHNi required 10—15 h to be completed at the same temperature. The TA- or GA-treatment of RNi was found to be effective for improvement of the e.d.a. of MRNi without sacrificing the hydrogenating activity. The nature of this catalyst was also found to be very close to that of HNi. It was expected that the TA-NaBr modification of RNi-A gave a catalyst with higher e.d.a. than that of TA-MRNi-A. With this expectation, RNi-A (TA) was modified with an aqueous solution containing TA and NaBr at pH 5.0, 0 °C. The resulting catalyst (TA-NaBr-MRNi-A) exhibited a high e.d.a. (optical yield 82%) and a high hydrogenating activity.

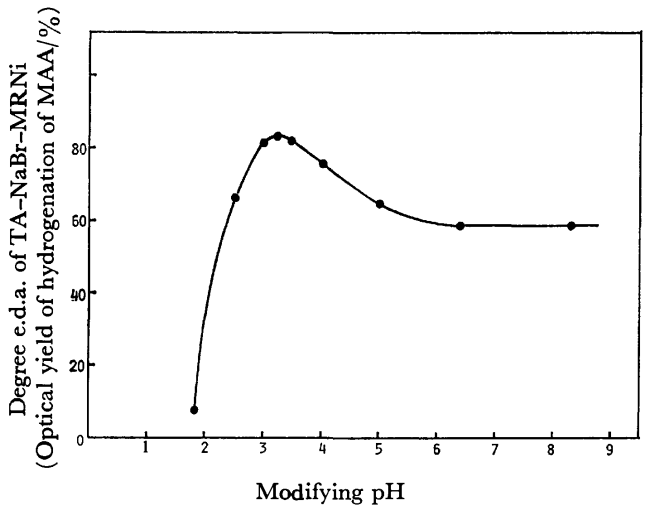

Fig. 4. Relationship between modifying pH and degree of e.d.a. of TA-NaBr-MRNi (optical yield of hydrogenation of MAA).
RNi (0.8 g) was modified with a solution containing TA (1 g) and NaBr (10 g) at 100 °C. The hydrogenation of MAA was carried out under the same conditions as those described in footnote of Table 4.

TA-NaBr-MRNi. In order to prepare TA-NaBr-MRNi-A directly from the conventional RNi, we treated RNi with an acidic aqueous solution containing TA and NaBr at 100 °C. The e.d.a. of TA-NaBr-MRNi thus obtained was examined by the enantioface-differentiating hydrogenation of MAA to MHB.

Figure 4 shows the relationship between the modifying pH and the e.d.a. of TA-NaBr-MRNi. The modification at pH 1.8 resulted in a low e.d.a. and low hydrogenating activity. The modification at pH 3.0—3.5 gave the best result with respect to the e.d.a. (optical yield 83%). The RNi modified with a mixture of TA and NaBr at above pH 3.5 exhibited a lower e.d.a. than that of RNi modified at pH 3.0—3.5 with the same modifying reagents.

Further improvement of e.d.a. was attained when the modification procedure was repeated. Thus, RNi treated three times with a solution containing TA and NaBr at pH 3.2, 100 °C, gave a catalyst with the highest e.d.a. The optical yield of the hydrogenation of MAA to MHB reached 88%. Table 6 shows e.d.a.'s of the catalysts prepared by repeated modifications together with the amount of Al^{3+} and Ni^{2+} eliminated from RNi by repeated modifications.

TABLE 6. AMOUNTS OF IONS ELIMINATED BY MULTI-MODIFICATIONS AND e.d.a. OF MULTI-MODIFIED RNi

Times of modification	Amounts of eliminated ions		Degree of e.d.a.[a]
	Ni^{2+}(mg)	Al^{3+}(mg)	
1	137	27	83
2	257	30	86
3	368	32	88

RNi (0.8 g) was modified with an aqueous solution of TA (1 g) and NaBr (10 g) at pH 3.2, 100 °C. Hydrogenation conditions were the same as those described in the Footnote of Table 4. a) Optical yield (%) of hydrogenation of MAA over MRNi.

As can be seen in Table 6, only a small amount of Al^{3+} was found in the modifying solution at the second and third steps. This fact indicates that most of the aluminium and its derivatives on the catalyst surface were eliminated by a single treatment of RNi with TA and NaBr at pH 3.2, 100 °C.

Figure 5 shows the relationship between the amount of NaBr in the modifying solution (pH 3.0, 4.0, or 5.0) and the e.d.a. of the resulting catalyst. The optimal amount of NaBr was affected by the modifying pH. In our research, increasing the modifying pH value tended to increase the optimal amount of NaBr. The use of an excess amount of NaBr resulted in a remarkable decrease of the e.d.a. The e.d.a. of TA-NaBr-MRNi prepared under the optimal amount of NaBr at each modifying pH increased in the following order: pH 5<pH 4< pH 3.

The effects of various kinds of inorganic salts on the e.d.a. of MRNi were examined with the intention of

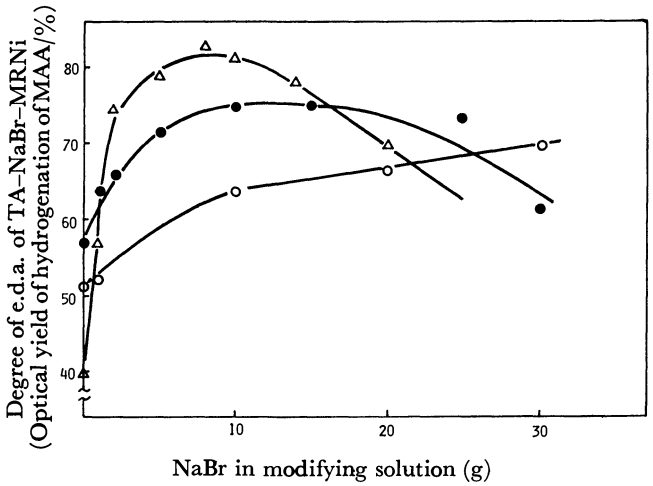

Fig. 5. Relationship between amount of NaBr in modifying solution and degree of e.d.a. of TA–NaBr–MRNi (optical yield of hydrogenation of MAA over TA–NaBr–MRNi).
Amount of RNi: 0.8 g. Modifying pH: at pH 3.0 (—△—), pH 4.0 (—●—), and pH 5.0 (—○—). Modifying temperature: at 100 °C.
The hydrogenation was carried out under the same conditions as those described in Foothnote of Table 4.

Table 7. Enantioface-differentiating hydrogenation of MAA over TA–inorganic salt–MRNi

Inorganic salt in the modifying solution(g)	$[\alpha]_D^{20}$ of the product	Degree of e.d.a.[a)]
None	−8.99	39
NaBr (10)	−19.07	83
NaF (3)	−13.95	61
NaCl (10)	−16.55	72
NaI (5×10^{-4})	−11.74	51
Na_2SO_4(10)	−12.95	56
$NaH_2PO_4\cdot2H_2O$ (1)	−8.19	36
$NaNO_3$ (0.1)	−12.17	53
$NiBr_2$ (1)	−14.36	63
$LiBr\cdot H_2O$ (10)	−14.25	62

Amount of RNi: 0.8 g. Modification: at pH 3.2, 100 °C for 1 h. Hydrogenation conditions were the same as those described in the footnote in Table 4. a) Optical yield (%) of hydrogenation of MAA over MRNi.

finding out the best compound to use as the supplementary modifying reagent. The modification was carried out with a mixture of TA and inorganic salt at the optimal modifing pH (pH 3.2) deduced from the results shown in Figs. 4 and 5. Table 7 shows the e.d.a.'s of TA–inorganic salt–MRNi's together with e.d.a. of TA–MRNi. In general the enhancements of the e.d.a.'s were observed by the addition of inorganic salt. The results shown in Table 7 indicate that the kinds of cations in the supplementary modifying reagents affect the e.d.a.'s of the resulting catalysts like the kinds of anions do. These results are in accord with the fact that there are large effects of the alkali ions on the e.d.a. of TA–MRNi.[4)] In the case of NaI, a large amount of NaI in the modifying solution resulted in the loss of the hydrogenating activity of the catalyst. Among inorganic salts examined, NaBr was found to be the most effective inorganic salt in giving TA–inorganic salt–MRNi with high e.d.a.

From the results described in this section, it turned out that the modification of RNi with TA and NaBr under acidic conditions gave TA–NaBr–MRNi with a rather higher e.d.a. than that of TA–NaBr–MRNi–A. This simple preparative method of TA–NaBr–MRNi is easily applicable for large scale production.

Role of NaBr Adsorbed on RNi. The preceding section dealt with the preparative method of TA–NaBr–MRNi for practical purposes. As can be seen in Fig. 5, the e.d.a. of the catalyst was very much affected by the modifying pH, modifying temperature, and the amount of NaBr in the modifying solution. RNi is an unstable catalyst and the e.d.a. of the resulting MRNi is very sensitive to the modifying conditions whereas RNi–A is a well stabilized one (Fig. 3). Thus, the complicated results shown in Fig. 5 may be caused, at least in part, by the unstability of RNi. Apart from the practical purposes, it is necessary to use a stabilized catalyst such as RNi–A for the studies on the role of adsorbed NaBr in improvement of the e.d.a.

In this regard, the catalysts used for this experiment were prepared from RNi–A under mild modifying conditions. TA–MRNi–A and TA–NaBr–MRNi–A for this experiment were prepared as follows: RNi was pretreated with an aqueous solution of TA at pH 3.2, 100 °C and then modified with a solution of TA or that of TA and NaBr at pH 5, 0 °C. The surface states of TA–MRNi–A and TA–NaBr–MRNi–A can be considered to be similar to that of RNi–A. The e.d.a.'s of these types of the catalysts were high and comparable to those of TA–MRNi and TA–NaBr–MRNi prepared in one step at pH 3.2, 100 °C.

Figure 6 shows the relationship between the amount of NaBr in the modifying solutions and the amount of adsorbed NaBr or TA. The addition of the first small amount of NaBr in the modifying solution resulted in a noticeable decrease of adsorbed TA. However, no further decrease of adsorbed TA was observed with the further addition of NaBr in the modifying solution.

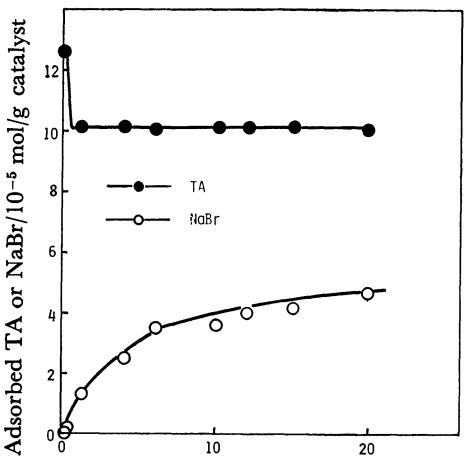

Fig. 6. Relationship between amount of NaBr in modifying solution and amount of adsorbed TA or NaBr.
Catalyst: a 1 g portion of RNi–A (TA). Modification: at pH 5, 0 °C for 1 h.

On the other hand, the amount of adsorbed NaBr increased with the amount of NaBr in the modifying solution. These results can be explained well on the basis of the idea that there are at least two types of areas on RNi-A: one (area-I) prefers to adsorb TA, and the other (area-II) prefers to adsorb NaBr. The increment of adsorbed TA in the absence of NaBr in the modifying solution (Fig. 6; at the point of NaBr=0) may be caused by the adsorption of TA on area-II. On hydrogenation over TA–NaBr–MRNi-A, the enantioface-differentiating hydrogenation may take place over area-I with the aid of adsorbed TA and the non-enantioface-differentiating hydrogenation may take place over area-II. The e.d.a. of TA–MRNi-A was on the line of TA–NaBr–MRNi-A, as will be seen in Fig. 7. This finding suggests that optically active MHB can not be produced over area-II, even when TA was adsorbed on this area.

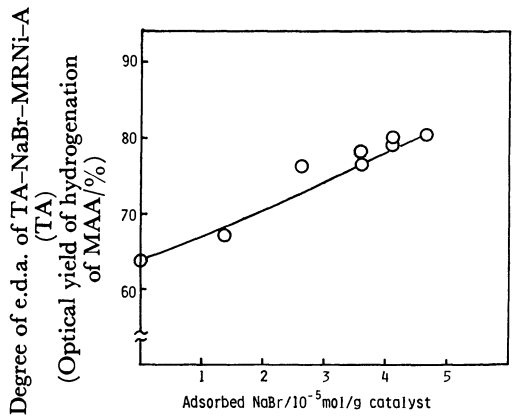

Fig. 7. Relationship between amount of adsorbed NaBr and degree of e.d.a. of TA–NaBr–MRNi-A (TA) (optical yield(%) of hydrogenation of MAA).
Amount of catalyst and modifying conditions were same as those described in Footnote of Fig. 6. The hydrogenation was carried out under the same conditions as those described in Footnote of Table 4.

Figure 7 shows the relationship between the adsorbed amount of NaBr and the e.d.a. of the catalyst. The e.d.a. increased monotonously with the amount of adsorbed NaBr. When the fact that the amount of adsorbed TA is constant under the experimental conditions is taken into account, it is reasonable to assume that the amounts of the optically active MHB produced are not changed by the increase of NaBr adsorbed on the catalyst. The enhancement of the e.d.a. with the amount of adsorbed NaBr results from the decrease of racemic MHB produced over unmodified area-II, because of the deactivation of area-II by the adsorption of NaBr.

In order to compare the hydrogenating activities of TA–MRNi-A and TA–NaBr–MRNi-A, the rates of hydrogenations of acetone over these two catalysts were compared. The time courses of the hydrogenation is shown in Fig. 8. The hydrogenation over TA–NaBr–MRNi-A was found to proceed more slowly than that over TA–MRNi-A. This finding is consistent with the above ideas that NaBr is adsorbed on a different area (area-II) from that (area-I) on which TA is adsorbed

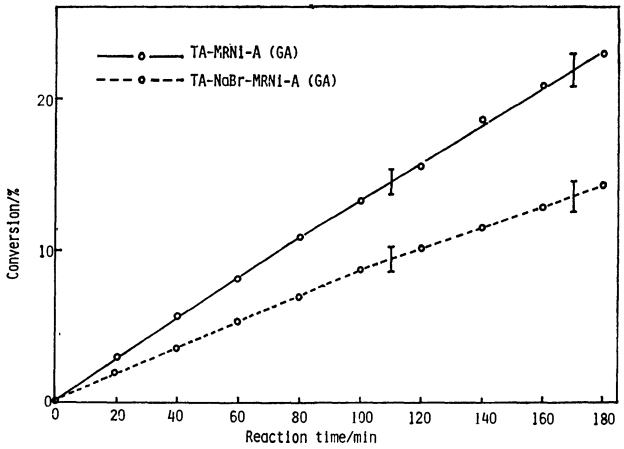

Fig. 8. Time courses of hydrogenation of acetone.
Modifying solution: TA (2 g) or TA (2 g)+NaBr (20 g) were dissolved in deionized water (200 ml). Modification: at pH 5, 0 °C for 1 h.

and that the adsorbed NaBr reduces the formation of MHB over area-II.

The areas occupied by TA, MAA, and TA···MAA complex can be assumed to be $2—4\times10^{-19}$, $2—4\times10^{-19}$, and $4—8\times10^{-19}$ m²/molecule, respectively, which are the silhouette areas of their CPK models. The areas are variable, depending on the adsorption modes of these molecules, and cannot be determined unequivocally at the present stage. When the results of adsorption studies by Welch *et al.*[9] are taken into account, these molecules are too large to cover the parts of small pores and capillaries in the catalyst. Thus, it is difficult to evaluate the e.d.a. of TA–NaBr–MRNi-A simply based on the surface area measured with the BET method and the amounts of adsorbed TA and NaBr.

Although the concepts of areas-I and -II are not directly related to the real surface area of the catalyst, they are informative for understanding the surface state of the catalyst under working conditions.

As a whole, it can be concluded that NaBr adsorbed on RNi inhibits the non-enantioface-differentiating hydrogenation to improve the e.d.a. of TA–MRNi.

Experimental

The optical rotations and visible spectra were measured with a Perkin-Elmer 241 Polarimeter and Hitachi 124 Spectrophotometer, respectively.

Raney Nickel Catalyst. The Ni–Al alloy (Ni/Al=42/58) was leached by adding it portion by poriton to 20 ml of a 20% aqueous solution of NaOH. The Ni–Si alloy (Ni/Si=50/50) was also leached by adding it to 30 ml of a 20% aqueous solution of NaOH. The resulting suspension was kept at 100 °C for 1 h. After removal of the alkaline solution by decantation, the catalyst was washed 15 times with 30 ml portions of deionized water. The Ni–Mg alloy (Ni/Mg=50/50) was leached, using 300 ml of a 3% aqueous solution of tartaric acid. The resulting suspension was kept at room temperature for 45 min. The catalyst was washed 15 times with 30 ml portions of deionized water.

Unless otherwise stated the Ni–Al alloy was used as the Raney alloy in this study.

Reduced Nickel Catalyst. Greenish NiO was reduced for 1 h at 350 °C under a hydrogen stream of 8 l/h.

Catalyst from Nickel Formate. Well-dried nickel formate prepared from nickel chloride and sodium formate was thermally decomposed at 250—300 °C under a pressure of 20—25 mmHg for 1 h.

Urushibara Nickel-A. This was prepared by the procedure of Urushibara *et al.*[10]

Supported Nickel Catalyst. The various types of supported nickel catalysts (weight ratio of Ni to support=50/50) were prepared by a precipitation method. $Ni(NO_3)_2 \cdot 6H_2O$ and the corresponding quatity of kieselguhr, activated alumina, TiO_2, or ZrO_2 were mixed in deionized water. Into the suspension was added dropwise an aqueous solution of Na_2CO_3 with vigorous stirring. After the end of addition of Na_2CO_3, stirring was continued for 1 h. The precipitate was collected by filtration and washed 3 times with water. The residue was dried at 110 °C for 24 h and pulverized in a mortar. The powder was heated to 500 °C and allowed to stand for 3 h at this temperature. The supported NiO thus obtained was reduced for 1 h at 350 °C under a hydrogen stream (8 l/h) just before the modification.

GA-treated Raney Nickel Catalyst. After treatment of RNi (0.8 g) with 100 ml of a 1% aqueous solution of GA at pH 3.2, 100 °C for 1 h, the catalyst was washed 3 times with 30 ml portions of water. Subsequently, the catalyst was treated with 30 ml of 1 M NaOH at 100 °C for 1 h and washed 15 times with 30 ml portions of water.

TA-treated Raney Nickel Catalyst. RNi (0.8 g) was treated with TA under the same conditions as above. The resulting catalyst was washed 3 times with 30 ml portions of water and then subjected to the modification with TA or TA+NaBr.

Modifying Solution. *1)*: TA (1 g) or TA (1 g) and an appropriate amount of inorganic salt were dissolved in deionized water (100 ml), and the pH of the solution was adjusted with 1 M NaOH (the amount of inorganic salt and the value of pH were specified in the text in each case).

2): (*S*)-Glutamic acid (1 g) was dissolved in deionized water (100 ml), and the pH of the solution was adjusted to pH 5 with 1 M NaOH.

Modification. The nickel catalyst was soaked in the modifying solution for 1 h under the conditions stated in the table in the text. After removal of the solution by decantation, the modified catalyst was washed successively with a 10 ml portion of water, two 50 ml portions of methanol, and a 25 ml portion of the reaction solvent.

Hydrogenation of MAA. The hydrogenation of MAA was carried out in a 100 ml autoclave under 110—130 kg/cm² of initial hydrogen pressure at the specified temperature. After removal of the catalyst, fractional distillation gave MHB. The optical purity of the product was calculated based on the value of $[\alpha]_D^{20}=22.95$ (neat) for optically pure MHB.

Optically Pure MHB. The quinine salt of 3-hydroxybutyric acid, obtained by hydrolysis of MHB ($[\alpha]_D^{20}$ −19.50 (neat)), was recrystallized five times from water.[11] Decomposition of the quinine salt and esterification of the free acid with diazomethane gave (*R*)-(−)-MHB with $[\alpha]_D^{20}$ −22.95 (neat) (the observed value (l=1 dm); α_D^{20} −24.23 (neat), and the specific gravity; $d_{20}=1.056^{6}$). Optically pure (*S*)-(+)-MHB was obtained from MHB ($[\alpha]_D^{20}$ +19.50 (neat)) in the same procedure as described above, except for the use of acetone as the solvent for recrystallization.[11] The value of $[\alpha]_D^{20}$ of (*S*)-isomer was $[\alpha]_D^{20}$ +22.77 (neat) (the observed value (l=1 dm); α_D^{20} +24.05 (neat)).

Determinations of Ni^{2+} and Al^{3+} in the Modifying Solution. The combined Ni^{2+} and Al^{3+} content in the modifying solution was determined by the EDTA titration method at pH 3.0—3.3, 95—100 °C, using Cu-PAN as the indicator.[12] The Ni^{2+} content in the solution was determined by the EDTA titration method at pH 10—12, using murexide as the indicator and triethanolamine as the masking reagent for Al^{3+}.[12] The difference between these two determinations represented the Al^{3+} content in the modifying solution.

Determination of TA Adsorbed on the Catalyst. A 1 g portion of MRNi-A (TA) or a 10 g portion of TA-MHNi was suspended in 25 ml of 1 M NaOH solution at 100 °C for 1 h. The supernatant was collected by decantation and the remaining catalyst was washed with four 15 ml portions of water. After combination of the supernatant and the washings, the solution was acidified with 10 ml of 1.5 M H_2SO_4 and then was made up to 100 ml with water. The amount of TA was determined colorimetrically by the method reported by G. R. Christian.[13]

Determination of NaBr Adsorbed on the Catalyst. The amount of NaBr adsorbed on the catalyst was determined by Volhard's titrimetric method.[14] A 1 g portion of TA-NaBr-MRNi-A (TA) was decomposed with 15 ml of 60% HNO_3 in the presence of a known amount of $AgNO_3$. The resulting solution was back-titrated with NH_4SCN.

Hydrogenation of Acetone. A 1.6 g portion of RNi-A (GA) was modified with TA or TA+NaBr and then washed successively with a 20 ml portion of water, two 100 ml portions of methanol, and a 50 ml portion of acetone. After removal of the solution by decantation, the modified catalyst suspended in acetone (30 ml) was introduced into an autoclave (100 ml capacity). The hydrogenation of acetone was conducted under 90 kg/cm² of initial hydrogen pressure at 28 °C. The conversion of acetone to 2-propanol was calculated based on the depression of hydrogen pressure.

The authors wish to express their thanks to Nihon Kagaku Sangyo Co., Ltd. and Wako Pure Chemical Industries, Ltd. for their gifts of NiO samples. The present work was supported in part by a Grant-in-Aid for Scientific Research No. 403531 from the Ministry of Education, Science and Culture.

References

1) Part XXXV of this series: K. Ito, T. Harada, and A. Tai, *Bull. Chem. Soc. Jpn.*, **53**, 3367 (1980).
2) T. Harada and Y. Izumi, *Chem. Lett.*, **1978**, 1195.
3) T. Harada, S. Onaka, A. Tai, and Y. Izumi, *Chem. Lett.*, **1977**, 1131.
4) Y. Izumi, S. Tatsumi, and M. Imaida, *Bull. Chem. Soc. Jpn.*, **39**, 2223 (1966); T. Tanabe, K. Okuda, and Y. Izumi, *ibid*, **46**, 514 (1973).
5) T. Harada, *Bull. Chem. Soc. Jpn.*, **48**, 3236 (1975); **53**, 1019 (1980).
6) Y. Orito, S. Niwa, and S. Imai, *Yuki Gosei Kagaku Kyokai Shi*, **35**, 753 (1977) and references therein,.
7) T. Harada, A. Tai, M. Yamamoto, H. Ozaki, and Y. Izumi, *Proc. 7th Int. Congr. Catal.*, Tokyo (1980), pp. 364—375
8) Y. Izumi, M. Imaida, H. Fukawa, and S. Akabori, *Bull. Chem. Soc. Jpn.*, **36**, 21, 155 (1963).
9) C. M. Welch, H. A. Smith, and J. B. Cole, *J. Phys. Chem.*, **65**, 705 (1961).
10) Y. Urushibara, S. Nishimura, and H. Uehara, *Bull. Chem. Soc. Jpn.*, **28**, 446 (1955).
11) H. T. Clarke, *J. Org. Chem.*, **24**, 1610 (1959).
12) K. Ueno, "Kireito-tekiteiho," 2nd ed, Nankodo, Tokyo, pp. 250, 358—360.
13) G. D. Christian, *Talanta*, **16**, 255 (1969).
14) M. B. Stschigol, *Z. Anal. Chem.*, **91**, 182 (1932); S. Takagi, "Teiryobunseki No Jikken To Keisan," Kyoritsu Shuppan Co. Ltd., Tokyo (1949), Vol. 2, p. 222.

Oxygenation of Aromatic Vinyl Ethers. A Noticeable Formation of Epoxides and Reaction Mechanism

Tatsuya KANNO, Motoyuki HISAOKA, Hirochika SAKURAGI,* and Katsumi TOKUMARU
Department of Chemistry, The University of Tsukuba, Sakura-mura, Ibaraki 305
(Received September 8, 1980)

cis-β-Alkoxystyrenes such as *cis*-β-methoxy-, *cis*-β-ethoxy-, and *cis*-β-isopropoxystyrene were autoxidized as neat at room temperature in the dark even in the absence of any radical generator. UV-irradiation and the use of a radical generator facilitated the oxygenation of these olefins. These oxidations afforded the corresponding epoxides or their derivatives in considerable yields as well as carbonyl compounds resulting from oxidative cleavage of the double bonds. The mechanisms for these oxidations are proposed to involve free-radical chain pathways and charge-transfer complexes between the olefins and oxygen which play an important role in the initiation steps.

Autoxidation of olefins usually affords allylic hydroperoxides, carbonyl compounds formed by cleavage of the double bond, and the remaining polyperoxide residues, but scarcely gives epoxides.[1-4] Dye-sensitized photooxygenation of olefins affords, through singlet oxygen mechanism, hydroperoxides, endoperoxides, and dioxetanes which are often converted into carbonyl compounds, and the formation of epoxides is also only a minor path.[5] However, Shimizu and Bartlett showed that epoxides arose efficiently when biacetyl or benzil was employed as a sensitizer on photooxidation of olefins.[6] Previously we observed that direct irradiation of β-alkoxystyrenes under oxygen led to an oxidative cleavage of the double bond *via* a different pathway from singlet oxygen mechanism.[7] During the course of the investigation, we have found the following noticeable facts: (1) *cis*-β-methoxystyrene (**1a**) as neat or in concentrated solution is sensitive to oxygen at room temperature in the dark even in the absence of any radical generator, while this olefin is not reactive with oxygen in dilute solution at room temperature or as neat at 0 °C in the dark; (2) UV-irradiation of the olefin without dye sensitizer accelerated the oxygenation in dilute solution at room temperature and also as neat at 0 °C; (3) a radical generator effected the autoxidation of the olefin at 50 °C; (4) all these ways of oxygenation of the olefin led to nearly the same distribution of the products, the corresponding epoxide and carbonyl compounds (benzaldehyde and methyl formate). This work was undertaken to investigate the nature of these oxygenations under photochemical and/or thermal conditions using alkoxystyrenes (**1**), 2-methoxy-1,1-diphenylethylene (**2**), 2-phenylpropene (**3**), and 2-methyl-1,1-diphenylpropene (**4**) as substrates. The results are described in detail and the possible reaction mechanism is discussed below.

Results and Discussion

Oxidation Products. *1) Autoxidation in the Absence of Radical Generator in the Dark*: *cis*-β-Methoxy- (**1a**), *cis*-β-ethoxy-(**1b**), and *cis*-β-isopropoxy-styrene (**1c**) were found to be sensitive to molecular oxygen as neat and in concentrated solution (*ca.* 50 vol%) even in the absence of any radical generator at room temperature in the dark. Thus, a highly purified specimen of neat **1a** (432 mg, 3.16 mmol) was stirred overnight under oxygen atmosphere at room temperature in the dark until **1a** was almost consumed. The NMR, GLPC, and chemical examination of the reaction mixture showed the formation of *trans*-2-methoxy-3-phenyloxirane (**5a**, 28%), benzaldehyde (47%), and methyl formate (8%). Likewise, **1b** and **1c** were autoxidized to benzaldehyde and alkyl formates; however, the corresponding epoxides and their isolable derivatives were not detected among the products. The results are summarized in Table 1. At 0 °C the olefins were not oxidized. When dissolved in solvents such as benzene, acetonitrile, and methanol (*ca.* 0.5 mol/dm³), the olefins were scarcely consumed by stirring under oxygen at room temperature for several hours.

2) Photooxidation: To conduct oxygenation effectively, **1a**, **1b**, **1c**, 2-methoxy-1,1-diphenylethylene (**2**), 2-phenylpropene (**3**), and 2-methyl-1,1-diphenylpropene (**4**) were irradiated as neat or in solution under oxygen atmosphere with a high pressure mercury lamp, and the products were determined as summarized in Table 2.

Direct irradiation of **1a**, **1b**, and **1c** under oxygen afforded the corresponding epoxides or their derivatives depending upon the substituents and the solvents employed in addition to benzaldehyde and methyl, ethyl, and isopropyl formate, respectively. In a typical run employing a neat olefin, **1a** (100 mg, 0.75 mmol) was irradiated in a stream of oxygen for 4 h with a 400-W high pressure mercury lamp through a Pyrex wall at room temperature until **1a** was almost completely consumed as revealed by NMR spectra. The NMR, GLPC, and chemical examination of the reaction mixture showed the formation of benzaldehyde (47%), benzoic acid (6%), and *trans*-2-methoxy-3-phenyloxirane (**5a**, 9%). The epoxide was isolated by pre-

Table 1. Yield of autoxidation products of *cis*-β-alkoxystyrenes in the dark at room temperature[a] (mol/mol olefin consumed)

Alkoxystyrene	Products		
	HCO_2R	PhCHO	PhCH–CHOR (O)
PhCH=CHOMe	0.08[b]	0.47	0.28[b]
PhCH=CHOEt	0.35[c]	0.57	—
PhCH=CHO^{i}Pr	0.37[d]	0.50	—

a) No radical initiator was used. b) R=Me. c) R=Et. d) R=^{i}Pr.

Table 2. Yield of oxygenation products on irradiation of alkoxystyrenes and alkylstyrenes at room temperature (mol/mol olefin consumed)

Substrate	Solvent	Products		
		PhCHO	PhCH–CHOR (O)	PhCH–CHOR (OH, OMe)
cis-PhCH=CHOMe	—	0.53[c]	0.09[e]	
	PhH	0.13[c]		
	MeCN	0.20[c]		
	MeOH	0.55[d]		0.27[e]
cis-PhCH=CHOEt	—	0.55[c]		
	PhH	0.55[c]		
	MeCN	0.55[c]		
	MeOH	0.42[d]		0.38[i]
cis-PhCH=CHO^{i}Pr	—	0.87[c]		
	PhH	0.74[c]		
	MeCN	0.67[c]		
	MeOH	0.51[d]		0.38[j]
		Ph_2CO	Ph_2C—CHOMe (O)	Ph_2C–CH$(OMe)_2$ (OH)
Ph_2C=CHOMe	PhH	0.10	0.35	
	MeCN	0.10	0.36	
	MeOH	0.02		0.57
		PhRCO	PhRC—CR′$_2$ (O)	
PhMeC=CH_2[a]	—	0.60[e]	0.05[e,g]	
Ph_2C=CMe_2[b]	—	0.36[f]	0.15[f,h]	

a) Conversion, 18%. b) Conversion, 29%. c) A sum of benzaldehyde and benzoic acid. d) A sum of benzaldehyde and its dimethyl acetal. e) R=Me. f) R=Ph. g) R′=H. h) R′=Me. i) R=Et. j) R=^{i}Pr.

parative GLPC and its *trans*-configuration was confirmed by its NMR spectrum.[8] On treatment of the reaction mixture with deuterated water, NMR signals due to the epoxide instantaneously disappeared because of its high sensitivity to moisture.

A control experiment showed that an authentic specimen of the *trans*-epoxide was recovered unchanged after being left under the reaction conditions, which rules out the possibility that benzaldehyde and the formate ester would be produced through decomposition of the epoxide formed as an intermediate. Photooxidation of **1b** and **1c** likewise afforded the corresponding oxidative cleavage products; however, the corresponding epoxides and their isolable derivatives were not detected among the reaction products (Table 2).

Irradiation of **1a**, **1b**, and **1c** as neat under oxygen at 0 °C also afforded benzaldehyde and the corresponding alkyl formates. Epoxide **5a** was also formed in the case of **1a**. The product distributions were very similar to those in the reaction at room temperature.

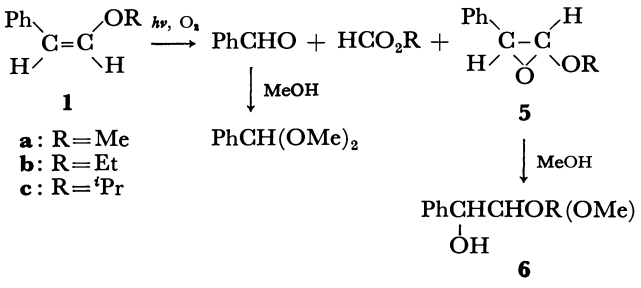

1

a: R=Me
b: R=Et
c: R=^{i}Pr

5

6

It is noticeable that the photooxidation of **1a**, **1b**, and **1c** in methanol gave 2-alkoxy-2-methoxy-1-phenylethanols (**6**) in considerable yields in addition to the cleavage products, benzaldehyde and its dimethyl acetal (Table 2). The resulting 2,2-dimethoxy- (**6a**), 2-ethoxy-2-methoxy- (**6b**), and 2-isopropoxy-2-methoxy-1-phenylethanol (**6c**) were isolated from the reaction mixtures by preparative GLPC and identified by NMR spectra. Formation of these products is reasonably accounted for by polar addition of the solvent methanol to the epoxides once formed as intermediates under the reaction conditions as confirmed by irradiation of **5a** in methanol under oxygen atmosphere yielding **6a**. These results indicate that the photooxidation of **1b** and **1c** also gives the corresponding epoxides which nevertheless seem too unstable to be isolated. Their instability is in keeping with the facts that these epoxides could not be prepared under similar conditions to those employed for the preparation of **5a**, and that **5a** was extremely sensitive to water.

The use of benzene and acetonitrile as solvent on photooxidation of **1a**, **1b**, and **1c** gave only the cleavage products regardless of the alkoxyl substituents and the polarity of the solvents employed (Table 2).

Likewise, photooxidation of **2** in benzene and acetonitrile gave the corresponding epoxide (**7**) together with the oxidative cleavage products, benzophenone and methyl formate. In methanol 2,2-dimethoxy-1,1-diphenylethanol (**8**) was obtained instead of the epoxide (Table 2). The epoxide (**7**) and alcohol (**8**) were isolated

by preparative GLPC and characterized by comparison of their IR and NMR spectra with those of authentic specimens.

$$\underset{\mathbf{2}}{Ph_2C{=}CHOMe} \xrightarrow{h\nu,\ O_2} Ph_2C{=}O + HCO_2Me + \underset{\mathbf{7}}{Ph_2C(O)CHOMe} \xrightarrow{MeOH} \underset{\mathbf{8}}{Ph_2C(OH)CH(OMe)_2}$$

Photooxidation of 2-phenylpropene (**3**)[9] and 2-methyl-1,1-diphenylpropene (**4**) led to the formation of the oxidative cleavage products and the corresponding epoxides (Table 2), although their oxidation proceeded much more slowly than that of **1**.

$$\underset{\mathbf{3}:\ R=Me,\ R'=H;\ \mathbf{4}:\ R=Ph,\ R'=Me}{PhRC{=}CR'_2} \xrightarrow{h\nu,\ O_2} PhRC{=}O + O{=}CR'_2 + \underset{\mathbf{9}:\ R=Me,\ R'=H;\ \mathbf{10}:\ R=Ph,\ R'=Me}{PhRC(O)CR'_2}$$

3) Autoxidation in the Presence of Radical Generator: To investigate the mechanism for the oxygenation of these olefins their autoxidation with a radical initiator was carried out. Autoxidation of neat β-alkoxystyrenes (**1**) with azobisisobutyronitrile (AIBN) as an initiator at 50 °C afforded the same products as did the photooxidation; benzaldehyde and alkyl formates were produced along with epoxide **5a** from **1a**. To examine the effect of oxygen pressure on the product yields autoxidation of **1a** (1 mmol) containing AIBN (0.02 mmol) was carried out at 50 °C for 5.5 h under varying partial pressures of oxygen diluted with nitrogen in a total pressure of 760 Torr (1 Torr=133.322 Pa). The yields of benzaldehyde and the epoxide were determined by GLPC as depicted in Fig. 1, which shows that the yield of the epoxide increased with decreasing oxygen pressure and that the maximum yield (about 60%) was attained at nearly 40 Torr of the partial pressure of oxygen.

Mechanisms for Oxygenations. When **1**'s were stirred as neat under oxygen in the presence of hydroquinone, the well-known radical inhibitor, at room temperature, the olefins were recovered unchanged. Hydroquinone also inhibited the photooxygenation of **1**'s as neat or in benzene solution. Addition of 1,4-diazabicyclo[2.2.2]octane (DABCO) also inhibited autoxidation of **1a** at room temperature without a radical generator and at 50 °C in the presence of AIBN. Since it has been shown that oxidation by singlet oxygen is inhibited by DABCO but usually not by hydroquinone,[10] these results indicate that free singlet oxygen plays no role in the present oxygenation, and the production of the *trans*-epoxide from **1a** requires a stepwise mechanism by way of a freely rotating intermediate.

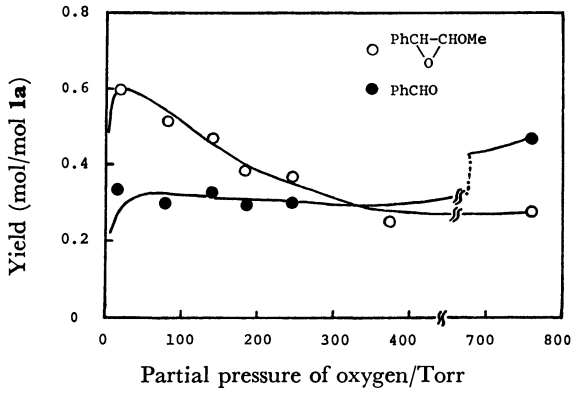

Fig. 1. Effect of oxygen pressure on the yield of autoxidation products of *cis*-β-methoxystyrene (**1a**).

Actually, the products from the oxygenations of **1**'s are different from those resulting from their dye-sensitized photooxygenation, which gave neither epoxides nor their derivatives. Thus, Methylene Blue-sensitized photooxygenation of *trans*-β-ethoxystyrene in dichloromethane was reported to give benzaldehyde and ethyl formate,[11] and recently it was demonstrated that the use of diacenaphtho[1,2-*b* : 1′,2′-*d*]thiophene as sensitizer on photooxygenation of *cis*- and *trans*-β-methoxystyrene at −78 °C led to 1,4-cycloaddition of singlet oxygen across the side chain β-carbon and the *ortho*-carbon of the aromatic ring, and that the *cis*-isomer reacted much more rapidly than the *trans*-isomer under the same conditions.[12] Also, the direct photooxygenation of **2** gave the completely different products from 3-phenyl-2,3-dihydrobenzofuran-2-one (**11**) which was reported to arise on dye-sensitized photooxygenation of **2** through 1,4-cycloaddition of singlet oxygen.[13]

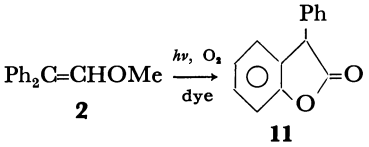

Furthermore, treatment of a mixture of **1a** and 1-methylcyclohexene or 2,3-dimethyl-2-butene, which is known to be highly susceptible to singlet oxygen, with oxygen in the absence of an initiator in the dark at room temperature resulted in exclusive oxidation of **1a** accompanied by nearly quantitative recovery of the added olefin.

These findings, therefore, strongly indicate that the direct photooxygenation of **1**'s as well as their autoxidation in the presence and absence of an initiator involves triplet molecular oxygen without intervention of singlet oxygen.

The effect of oxygen pressure on the yield of the epoxide, combined with the product distribution and the effects of the additives, strongly suggests that the autoxidation of the present olefins in the dark proceeds through a mechanism similar to that proposed previously by Mayo for autoxidation of styrene and related olefins.[1] In Mayo's mechanism, alternating addition of styrene molecules and molecular oxygen results in copolymeric radicals, which finally either afford polymeric peroxides or undergo scission to benzaldehyde, formaldehyde, and phenyloxirane (*cf.* Scheme 1); the yields of these products are changed with the partial pressure of oxygen.

In the present work, however, it is remarkable that

epoxide **5a** was produced in a moderate yield, for example, *ca.* 30%, even at 760 Torr oxygen pressure, and the maximum yield, *ca.* 60%, was attained at a lower oxygen pressure, *ca.* 40 Torr. This is in contrast to the autoxidation of styrene which afforded phenyloxirane in a very low yield (1%) at 760 Torr oxygen pressure and increased its yield to the maximum value (27%) at a very low partial pressure of oxygen (1 Torr).[14]

Comparison of the present photooxygenation with the autoxidation in the product distribution and the behavior toward inhibitors mentioned above indicates that the photooxygenation mechanism is quite similar to that of the autoxidation except for the initiation steps. According to Scheme 1 described below, the intermediate benzylic radicals (**12**) will add to oxygen to give peroxyl radicals (**13**) (rate constant: k_0) or undergo intramolecular substitution on the peroxide linkage to afford the epoxide and alkoxyl radicals (**14**) (rate constant: k_1). Peroxyl radicals **13** give, through bimolecular interaction, alkoxyl radicals (**15**). Alkoxyl radicals **14** and **15** undergo scission into carbonyl compounds or again react with the olefin to give the benzylic radicals.

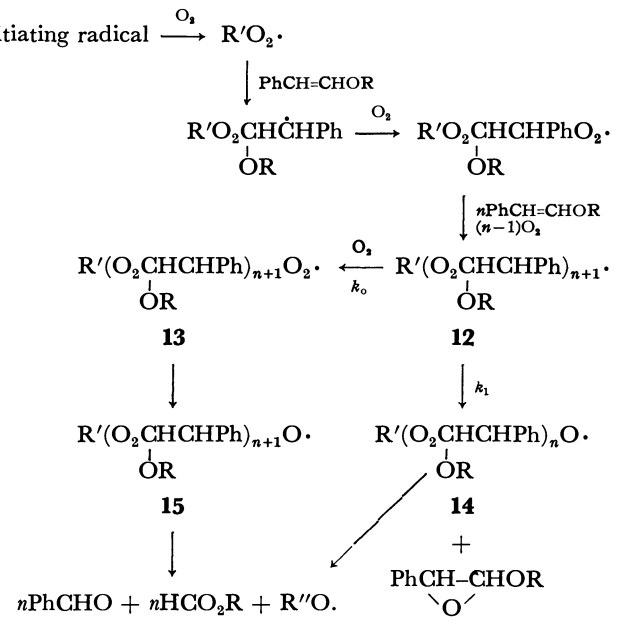

Scheme 1.

No production of polymeric peroxides together with efficient production of the epoxide in the oxidation of **1a** shows that benzylic radicals **12** resulting from **1a**, compared with the corresponding benzylic radicals arising from styrene, more facilely undergo the intramolecular substitution on the peroxide linkage in preference to growing up to polymeric matters.

Formation of Complexes between the Olefins and Oxygen. In order to get insight into the mechanism for the initiation of the free-radical chain oxidation of the alkoxystyrenes, particularly in the absence of any initiator, spectroscopic examination was carried out for the possible formation of charge-transfer complexes between these olefins and oxygen in view of the fact that several aromatic compounds form charge-transfer complexes with oxygen.[15–17] When a stream of oxygen was passed into a cyclohexane solution of **1a** at 0 °C, a new broad band appeared at 305—400 nm with the maximum at 307 nm. When argon was bubbled through the solution, this new band completely disappeared. When the measurements were carried out at 23 °C, the new band decreased in intensity to one-fourth by bubbling with argon. These facts indicate reversible formation of a charge-transfer complex between **1a** and oxygen. Styrene was reported to develop a similar absorption band, when a neat sample was saturated with oxygen at atmospheric pressure, at 305—350 nm with the maximum at 310 nm, which was shifted to shorter wavelengths by dilution with a solvent.[15]

In order to evaluate electron donating abilities of the olefins, their charge-transfer interaction with tetracyanoethylene (TCNE) was investigated. When **1a** or styrene was dissolved with TCNE in dichloromethane, charge-transfer bands appeared. The association constant, K, and extinction coefficient of the complex, ε_{CT}, were determined from concentration dependence of the optical density of the complex according to Benesi-Hildebrand's equation,[18]

$$C_0/A = 1/K\varepsilon_{CT}D_0 + 1/\varepsilon_{CT},$$

where C_0 and D_0 are the initial concentrations of the acceptor and donor, respectively, and A is the absorbance for unit cell path length. The results for **1a**/TCNE and styrene/TCNE are listed in Table 3.

The results for styrene/TCNE accord with those reported by Cooper *et al.*[19] Comparison of **1a** with styrene in the wavelength of the absorption maximum, λ_{CT}, and the association constant, K, shows that **1a** is a stronger donor to give a more stable charge-transfer complex than styrene.

The energy of the charge-transfer transition for the complexes formed by a series of donors with the same acceptor is related to the donor ionization potential, I_D:[19,20]

$$h\nu_{CT} = aI_D + b,$$

where a and b are constant. When the values of a and b

Table 3. Characteristics of charge-transfer complexes between tetracyanoethylene and styrene derivatives in dichloromethane at 23 °C

Donor	Absorption maximum λ_{CT}/nm	λ_{CT}/eV	ε_{CT}	Association constant K/mol^{-1} dm^3	Ionization potential I_D/eV	Free energy change ΔG/kcal mol^{-1}
cis-PhCH=CHOMe	610	2.03	1250	1.38	7.70,[a] 7.54[b]	−0.19
$PhCH=CH_2$	480	2.56	1330	0.60	8.34,[a] 8.40[b]	0.30

a) Values evaluated from the equation by Farrell and Newton.[20] b) Adiabatic values from photoelectron spectra of *cis*-β-methoxystyrene[21] and styrene.[22]

proposed by Farrel and Newton[20] for substituted benzene/TCNE complexes are used, the relationship is expressed by

$$h\nu_{CT} = 0.82I_D - 4.28 \text{ (eV)}.$$

This relationship leads to a much lower value of the ionization potential for **1a**, 7.70 eV, than for styrene, 8.34 eV,[19] which are in reasonable agreement with the values observed by photoelectron spectroscopy, 7.54 for **1a**[21] and 8.40 eV for styrene.[22] This result is in keeping with a fact that **1a** exhibits a much lower oxidation potential (1.00 V) than styrene (>1.95 V).[21,23]

As described above, **1a** forms the charge-transfer complex with oxygen more efficiently than styrene. Therefore, it is not unreasonable to suppose that the charge-transfer complex plays an important role in generating free radicals both thermally and on ultraviolet irradiation to initiate the radical chain oxidation.[24]

Experimental

The IR and UV spectra were recorded on a Hitachi 215 infrared spectrometer and a JASCO UVIDEC-1 spectrophotometer, respectively. The NMR spectra were recorded on a Hitachi R-24 and a JEOL JNM-MH-100 spectrometer. Gas-liquid phase chromatographic analysis was performed on a Hitachi 163 and a Shimadzu GC-4CM-PF gas chromatograph equipped with a flame ionization detector, and a Hitachi 023 gas chromatograph was used for preparative purposes.

Materials. *cis*-β-Methoxystyrene (**1a**),[25] *cis*-β-ethoxystyrene (**1b**),[26] and *cis*-β-isopropoxystyrene (**1c**) were prepared by heating phenylacetylene with potassium hydroxide in the corresponding alcohols.

cis-β-Isopropoxystyrene (**1c**), bp 58 °C/2 Torr (1 Torr= 133.322 Pa); IR (liq): 2975, 1650 cm^{-1}; NMR (CCl_4): δ 1.31 (d, 6H), 3.94 (septet, 1H), 5.06 (d, J=7.0 Hz, 1H), 6.04 (d, J=7.0 Hz, 1H), and 6.9—7.5 (m, 5H); Found: C, 81.05; H, 8.64%. Calcd for $C_{11}H_{14}O$: C, 81.43; H, 8.69%.

2-Methoxy-1,1-diphenylethylene (**2**)[27] and 2-methyl-1,1-diphenylpropene (**4**)[28] were prepared by the Wittig reactions employing benzophenone. *trans*-2-Methoxy-3-phenyloxirane (**5a**)[29] and 3-methoxy-2,2-diphenyloxirane (**7**) were prepared from reactions of 2-chloro-2-phenylethanal and 2-chloro-2,2-diphenylethanal with sodium methoxide, respectively, according to the method reported by Kirrmann *et al.*[29] The latter epoxide was irradiated in methanol to give 2,2-dimethoxy-1,1-diphenylethanol (**8**).

3-Methoxy-2,2-diphenyloxirane (**7**), mp 49—51 °C; NMR (CCl_4): δ 3.30 (s, 3H), 4.55 (s, 1H), and 7.1—7.3 (m, 10H).

2,2-Dimethoxy-1,1-diphenylethanol (**8**), bp 140 °C/1 Torr; NMR (CCl_4): δ 2.91 (s, 1H), 3.25 (s, 6H), 4.48 (s, 1H), and 7.1—7.4 (m, 10H); Found: C, 74.56; H, 7.05%. Calcd for $C_{16}H_{18}O_3$: C, 74.39; H, 7.02%.

On treatment of 2-chloro-2-phenylethanal with sodium ethoxide and sodium isopropoxide, epoxides could not be isolated. Epoxidation of **1b** and **1c** with *m*-chloroperoxybenzoic acid[30] or *N*-bromosuccinimide/sodium hydroxide[30] was also unsuccessful. 2-Methyl-2-phenyloxirane (**9**)[31] and 2,2-dimethyl-3,3-diphenyloxirane (**10**)[32] were prepared by epoxidation of 2-phenylpropene (**3**) and **4** with *m*-chloroperoxybenzoic acid, respectively.

Photooxidation of Olefins. Typical procedures are described below for *cis*-β-methoxystyrene (**1a**).

Without Solvent. Liquid **1a** (100 mg, 0.75 mmol) in a Pyrex tube was irradiated in an oxygen stream with a 400-W high pressure mercury lamp for 4 h at room temperature. GLPC and NMR analyses of the reaction mixture showed almost complete consumption of **1a** and the formation of benzaldehyde (47%), benzoic acid (6%), methyl formate, and *trans*-2-methoxy-3-phenyloxirane (**5a**, 9%). The product distribution was determined by GLPC using internal standards and authentic reference materials on Polypropylene glycol 4025 (5%) and diethylene glycol succinate polyester–H_3PO_4 (5%) columns at 130 and 180 °C, respectively. The epoxide was isolated from the reaction mixture by preparative GLPC on polyethylene glycol (10%) at 150 °C and identified by comparing its IR and NMR spectra with those of an authentic sample. On addition of D_2O to the reaction mixture, signals due to the epoxide disappeared instantaneously in the NMR spectrum.

Liquid **1a** (134 mg, 1 mmol) was irradiated similarly under oxygen atmosphere at 0 °C for 4 h. GLPC and NMR analyses of the reaction mixture showed the formation of benzaldehyde, epoxide **5a**, and methyl formate. The product distribution was found to be very similar to that in the reaction at room temperature.

In Methanol. A solution of **1a** (56 mg, 0.42 mmol) in methanol (1 ml) was irradiated in a Pyrex tube under oxygen atmosphere with a 400-W high pressure mercury lamp for 4 h at room temperature. After almost all the solvent was removed by rotary evaporation, the reaction mixture was subjected to GLPC analysis, which revealed the formation of benzaldehyde (trace), dimethoxyphenylmethane (51%), benzoic acid (5%), and 2,2-dimethoxy-1-phenylethanol (**6a**, 27%). The product **6a** was isolated from the reaction mixture by preparative GLPC, and identified by comparing its IR and NMR spectra with those of an authentic sample,[33] which was prepared by irradiation of **5a** in methanol; NMR (CCl_4): δ 2.50 (s, 1H, exchangeable with D_2O), 3.15 (s, 3H), 4.05 (d, J=6 Hz, 1H), 4.60 (d, J=6 Hz, 1H), and 7.0—7.2 (m, 5H).

2-Ethoxy-2-methoxy-1-phenylethanol (**6b**) and 2-isopropoxy-2-methoxy-1-phenylethanol (**6c**) were similarly isolated from the photooxidation mixtures of *cis*-β-ethoxystyrene (**1b**) and *cis*-β-isopropoxystyrene (**1c**) in methanol, respectively. The structures were determined by comparing their NMR spectra with that of **6a**. The NMR spectra showed that each of the ethanols consisted of two stereoisomers.

2-Ethoxy-2-methoxy-1-phenylethanol (**6b**), bp 76 °C/1 Torr; NMR(CCl_4): δ 0.92 and 1.13 (t, J=6 Hz, 3H), 3.29 and 3.09 (s, 3H), 3.3—3.8 (m, 2H), 4.09 (broad s, 1H), 4.18 (d, J= 6.5 Hz, 1H), 4.47 (d, J=6.5 Hz, 1H), and 7.0—7.4 (m, 5H); Found: C, 67.00; H, 7.88%. Calcd for $C_{11}H_{16}O_3$: C, 67.32; H, 8.21%.

2-Isopropoxy-2-methoxy-1-phenylethanol (**6c**), bp 84 °C/1 Torr; NMR(CCl_4): δ 0.65—1.25 (m, 6H), 3.0 (broad s, 1H), 3.11 and 3.36 (s, 3H), 3.50 and 3.82 (m, 1H), 4.25 (d, J=6 Hz, 1H), 4.43 (d, J=6 Hz, 1H), and 7.0—7.4 (m, 5H); Found: C, 68.41; H, 8.61%. Calcd for $C_{12}H_{18}O_3$: C, 68.54; H, 8.62%.

2,2-Dimethoxy-1,1-diphenylethanol (**8**) was isolated similarly from the reaction mixture of 2-methoxy-1,1-diphenylethylene (**2**) in methanol. The structure was determined by comparing its NMR spectrum with that of an authentic sample.

In Benzene and Acetonitrile. Photooxidation was performed in a similar way to that in methanol. The reaction mixtures were, after rotary evaporation, analyzed quantitatively by GLPC.

3-Methoxy-2,2-diphenyloxirane (**7**) was isolated from the reaction mixture in benzene by preparative GLPC and

identified by comparison of its IR and NMR spectra with those of an authentic sample.

Autoxidation of cis-*β*-*Methoxystyrene (**1a**) in the Dark without Initiator.* Neat **1a** (432 mg, 3.16 mmol) was stirred overnight at room temperature under oxygen atmosphere in the dark. GLPC analysis of the reaction mixture revealed almost complete consumption of **1a** and the formation of benzaldehyde (47%), benzoic acid, methyl formate (8%), and **5a** (28%).

A solution of **1a** (134 mg, 1.0 mmol) in methanol (2 ml) was stirred for 10 h under oxygen at room temperature in the dark. GLPC analysis of the reaction mixture showed a quite low consumption of **1a** and the formation of trace amounts of benzaldehyde and **6a**.

*Effect of Oxygen Pressure on the Product Yields in Autoxidation of **1a**.* Neat **1a** (134 mg, 1.0 mmol) containing azobisisobutyronitrile (6.8 mg, 0.04 mmol) was stirred at 50 °C for 5.5 h in the dark under an atmosphere of varying partial pressures of oxygen (760—40 Torr) diluted with nitrogen (760 Torr in the total pressure). The yields of benzaldehyde and **5a** were determined by GLPC as shown in Fig. 1.

Effects of Hydroquinone, Diazabicyclo[2.2.2]octane (DABCO), and Olefins on the Oxygenations of β-Alkoxystyrenes. As an example, a solution of **1a** (134 mg, 1.0 mmol) and hydroquinone (11 mg, 0.1 mmol) in benzene (2 ml) was irradiated under oxygen atmosphere for 6 h at room temperature in a Pyrex tube with a 400-W high pressure mercury lamp. No consumption of **1a** was confirmed by GLPC analysis.

Neat **1a** (134 mg, 1.0 mmol) was stirred overnight with hydroquinone (11 mg, 0.1 mmol) at room temperature under oxygen atmosphere in the dark. GLPC analysis of the sample revealed almost no consumption of **1a** and the formation of no oxidation products. Neat **1b** and **1c** were also not consumed under similar conditions.

Neat **1a** (134 mg, 1.0 mmol) was similarly stirred with DABCO (11 mg, 0.1 mmol) instead of hydroquinone under oxygen. The olefin was almost completely recovered as revealed by GLPC analysis.

Neat **1a** (134 mg, 1.0 mmol) was stirred overnight with azobisisobutyronitrile (16 mg, 0.1 mmol) and DABCO (11 mg, 0.1 mmol) under oxygen at 50 °C. GLPC analysis of the sample showed almost no consumption of **1a**.

Neat **1a** (134 mg, 1.0 mmol) was stirred for 6 h with 2,3-dimethyl-2-butene or 1-methylcyclohexene (0.5 mmol) under oxygen at room temperature in the dark. NMR and GLPC analyses of the reaction mixture showed the formation of benzaldehyde, methyl formate, and **5a** and almost no consumption of the butene or the cyclohexene.

Charge-Transfer (C-T) Absorption Spectra of Sytrene Derivatives. C-T Spectra with Molecular Oxygen. Samples of **1a** (neat or 0.3 mol/dm^3 in cyclohexane) were placed in a sample cell and a reference cell, and a stream of oxygen was passed for several minutes through the sample in the sample cell. Spectra were measured at 0 and 23 °C. Immediately after a spectrum was recorded, argon was passed through the sample and a spectrum was again measured. The band observed under oxygen atmosphere completely disappeared at 0 °C by argon bubbling; however, at 23 °C the band remained at one-fourth of the intensity under oxygen atmosphere.

C-T Spectra with Tetracyanoethylene (TCNE). Solutions of the C-T complexes were prepared immediately before measurements by mixing dichloromethane solutions of TCNE (0.01 mol/dm^3) with solutions of **1a** (0.23—0.34 mol/dm^3) or styrene (3.7—8.0 mol/dm^3) in the same solvent. The spectra were measured at 23 °C by a conventional method using a Hitachi 200-20 spectrophotometer. In a reference cell was placed a dichloromethane solution of a donor at the same concentration as in a sample cell.

References

1) F. R. Mayo, A. A. Miller, and G. A. Russell, *J. Am. Chem. Soc.*, **80**, 2500 (1958); F. R. Mayo, *Acc. Chem. Res.*, **1**, 193 (1968), and references cited therein. Some olefins such as cyclooctene[2] and 2,4,4-trimethyl-1-pentene[3,4] were reported to give the corresponding epoxides in exceptionally high yields.

2) D. E. Van Sickle, F. R. Mayo, and R. M. Arluck, *J. Am. Chem. Soc.*, **87**, 4824 (1965).

3) E. J. Gasson, A. F. Millidge, G. R. Primavesi, W. Webster, and D. P. Young, *J. Chem. Soc.*, **1954**, 2161.

4) F. R. Mayo, *J. Am. Chem. Soc.*, **80**, 2497 (1958).

5) "Singlet Oxygen," ed by H. H. Wasserman and R. W. Murray, Academic Press, New York, N. Y. (1979); M. Matsumoto and K. Kondo, *J. Synth. Org. Chem.*, **35**, 188 (1977); C. W. Jefford and A. F. Boschung, *Helv. Chim. Acta*, **57**, 2257 (1974).

6) N. Shimizu and P. D. Bartlett, *J. Am. Chem. Soc.*, **98**, 4193 (1976). Also see, P. D. Bartlett and M. E. Landis, *ibid.*, **99**, 3033 (1977).

7) H. Sakuragi, K. Tokumaru, and O. Simamura, Symposium on Photochemistry, Tokyo (1967). Abstracts of Papers, p. 83.

8) J. M. Lehn and J. J. Riehl, *Mol. Phys.*, **8**, 33 (1964).

9) Autoxidation of **3** was reported to afford acetophenone and an epoxide: H. Hock and M. Siebert, *Chem. Ber.*, **87**, 546 (1954); F. R. Mayo and A. A. Miller, *J. Am. Chem. Soc.*, **80**, 2480 (1958).

10) C. S. Foote, "Singlet Oxygen," ed by H. H. Wasserman and R. W. Murray, Academic Press, New York, N. Y. (1979), p. 139.

11) G. Rio and J. Berthelot, *Bull. Soc. Chim. Fr.*, **1969**, 3609.

12) D. Lerdal and C. S. Foote, *Tetrahedron Lett.*, **1978**, 3227. Also see, M. Matsumoto, S. Dobashi, and K. Kondo, *ibid.*, **1977**, 2329; **1977**, 3361.

13) C. S. Foote, S. Mazur, P. A. Burns, and D. Lerdal, *J. Am. Chem. Soc.*, **95**, 586 (1973).

14) F. R. Mayo, *J. Am. Chem. Soc.*, **80**, 2465 (1958).

15) D. F. Evans, *J. Chem. Soc.*, **1953**, 345.

16) H. Tsubomura and R. S. Mulliken, *J. Am. Chem. Soc.*, **82**, 5966 (1960).

17) V. I. Stenberg, R. D. Olson, C. T. Wang, and N. Kulevsky, *J. Org. Chem.*, **32**, 3227 (1967); V. I. Stenberg, C. T. Wang, and N. Kulevsky, *ibid.*, **35**, 1774 (1970).

18) H. A. Benesi and J. H. Hildebrand, *J. Am. Chem. Soc.*, **71**, 2703 (1949); L. J. Andrews and R. M. Keefer, *ibid.*, **74**, 458 (1952); R. E. Merrifield and W. D. Phillips, *ibid.*, **80**, 2778 (1958).

19) A. R. Cooper, C. W. P. Crowne, and P. G. Farrell, *Trans. Faraday Soc.*, **62**, 18 (1966).

20) P. G. Farrell and J. Newton, *J. Phys. Chem.*, **69**, 3506 (1965).

21) T. Kanno, T. Oguchi, H. Sakuragi, K. Tokumaru, and T. Kobayashi, *Denki Kagaku*, **49**, 134 (1981).

22) J. P. Maier and D. W. Turner, *J. Chem. Soc., Faraday Trans. 2*, **69**, 196 (1973).

23) The oxidation potentials were determined by means of cyclic voltammetry in acetonitrile using a Ag/Ag$^+$ (0.1 mol/dm^3) electrode as a reference electrode and 0.1 mol/dm^3 tetraethylammonium perchlorate as supporting electrolyte.

24) Participation of the charge-transfer complexes of ethers with oxygen was described to initiate their photochemical oxidation.[17]

25) K. Auwers, *Chem. Ber.*, **44**, 3514 (1911).
26) J. U. Nef, *Justus Liebigs Ann. Chem.*, **308**, 264 (1899).
27) G. Wittig and M. Schlosser, *Chem. Ber.*, **94**, 1373 (1961).
28) A. Brodhag and C. R. Hauser, *J. Am. Chem. Soc.*, **77**, 3024 (1955).
29) A. Kirrmann, R. Muths, and J.-J. Riehl, *Bull. Soc. Chim. Fr.*, **1958**, 1469.
30) R. Filler, B. R. Camara, and S. M. Naqvi, *J. Am. Chem. Soc.*, **81**, 658 (1959).
31) S. Danilow and E. V. Danilowa, *Chem. Ber.*, **60**, 1050 (1927).
32) H. Böhme, *Org. Synth.*, Coll. Vol. III, 619 (1955).
33) S. H. Pine and J. Cheney, *J. Org. Chem.*, **40**, 870 (1975).

Iminodimagnesium Reagents. Condensation Reaction with Ketones. Direct Preparation of Anils and a Hydrazone of Xanthone

Masao Ōkubo,* Saeko Hayashi, Mayumi Matsunaga, and Yumiko Uematsu

Department of Chemistry, Faculty of Science and Engineering, Saga University, Honjō-machi, Saga 840

(Received September 26, 1980)

The condensation reaction of ketones with iminodimagnesium reagents ($RN(MgBr)_2$) derived from various primary amines as well as 1,1-disubstituted hydrazines was investigated. *N*-Arylimines and 1-methyl-1-phenylhydrazones of diaryl ketones were prepared, their yields being affected by the electronic and positional effects of substituents of reagent and substrate. Direct preparation of some anils of xanthone and its 1-methyl-1-phenylhydrazone was achieved by use of the corresponding iminodimagnesium reagents.

Aryliminodimagnesium reagents ($ArN(MgBr)_2$, aryl-IDMg) derived from methoxy-substituted anilines were reported recently[1] to be condensed with benzophenones and fluorenone (Scheme 1, R=*o*- and *p*-$MeOC_6H_4$; R^1 and R^2=aryl).

$$R\text{-}NH_2 + 2EtMgBr \longrightarrow R\text{-}N(MgBr)_2 + 2EtH\uparrow$$

$$R\text{-}N(MgBr)_2 + O{=}C\begin{matrix}R^1\\R^2\end{matrix} \longrightarrow R\text{-}N{=}C\begin{matrix}R^1\\R^2\end{matrix}$$

Scheme 1.

No extensive studies have been carried out on reagents of this type.[2,3] In order to find the characteristics of IDMg reaction with ketones, we carried out the reaction of diaryl ketones and acetophenone with IDMg reagents derived from arylamines and alkylamines as well as 1,1-disubstituted hydrazines, the results being reported in this paper. Xanthone, which is unreactive towards "carbonyl reagents," gives condensation products by this method.

Results and Discussion

All the experiments 1—24 were carried out in tetrahydrofuran (THF) under nitrogen atmosphere, with use of equimolar amounts of ketones and IDMg reagents except for 11 and 12. Product yields are given in Tables 1—3. The reaction time at room temperature and at 55—60 °C were not optimized and the molar ratio of reagents with ketones was fixed; the yields indicate the reactivity of both components used in individual experiments.

Effect of Alkyl Group of Reagents and Substrates. Applicability of the method to the condensation of alkylamine with benzophenone and to that of arylamine with enolizable ketone has been studied.

When benzophenone was treated with *t*-butyl-IDMg at 50 °C for 2 h, 25% yield of *N*-benzhydrylidene-*t*-butylamine **1** was detected by NMR of the product mixture obtained after quenching with aqueous ammonium chloride. When the same ketone was treated with less hindered isobutyl-IDMg at room temperature for 192 h, the yield of the corresponding imine **2** estimated by NMR after quenching with absolute methanol was *ca.* 50%. A by-product, diphenylmethanol, was formed in *ca.* 50% yield. Since **1** and **2** undergo hydrolysis easily, their isolation by column chromatography was difficult even by use of silica gel dried at 120 °C for 2 h.

An attempt to condense acetophenone with *p*-methylphenyl-IDMg by heating at 60 °C for 5 h was unsuccessful. Even by quenching with absolute methanol, TLC of the product mixture shows the presence of only trace amounts of *N*-(α-methylbenzylidene)-*p*-methylaniline **3** and the aldol condensation product, 1,3-diphenyl-2-buten-1-one: formation of the latter is reasonable since similar basic anilinomagnesium reagents (PhN(R)MgBr, R=H and Me)[4] were used as catalyst for the aldol condensation. An authentic sample of **3** was also hydrolyzed during the treatment with silica gel.

The easily hydrolyzable nature of ketimines **1**—**3** can be ascribed to the insufficient conjugation system as compared with those having three aryl groups around the >C=N– groups (*vide infra*). The results indicate that the method is not suitable for preparing ketimines from alkylamines and enolizable ketones; the reported method using a Lewis acid, $TiCl_4$,[5] is preferable. In the following experiments, aryl-IDMg and diaryl ketones were used.

Aryl-IDMg and Diaryl Ketones. Electronic as well as positional effects of substituents of aryl-IDMg and those of diaryl ketone were examined (Table 1).

m-Methoxyphenyl-IDMg gives anil **4** in moderate yield in the reaction with a 2-methyl-substituted benzophenone; *o*-methylphenyl-IDMg, however, gives anil **5** in poor yield in the reaction with the same ketone. Sterically much hindered 2,4,6-trimethylphenyl-IDMg does not undergo condensation with unhindered 4-methylbenzophenone, but does with planar and less hindered fluorenone; the yield of **7** is low.

p-Chlorophenyl-IDMg, which is less reactive due to the electron-attracting effect of the substituent, can be condensed with a 2-methyl-substituted benzophenone, the yield of **8** being moderate. The IDMg reagent derived from 2-aminopyridine, which is also less reactive due to chelation of the ring nitrogen atom to the Mg atom, gives no condensation product with 2-methylbenzophenone, but does with fluorenone.

Formation of by-products, diarylmethanols, should originate from the initially formed ketyl radicals, which abstract hydrogen from the solvent molecule when the subsequent addition process is slow. The initial formation of ketyl radicals due to electron-transfer from Grignard reagent to benzophenones was discussed.[6]

Aryl-IDMg and 2-Methoxybenzophenones. Condensation of phenyl-IDMg with 2-methoxybenzophenone was accompanied by replacement of the *o*-methoxyl

Table 1. Effect of substituents on the reaction of $ArN(MgBr)_2$ with benzophenones and fluorenone

Anil No.	$ArN(MgBr)_2$ Ar	Ar^1–CO–Ar^2 Ar^1	Ar^2	Yield of the anil/%[a]	By-product
4	3-$MeOC_6H_4$	2-MeC_6H_4	4-MeC_6H_4	57	
5	2-MeC_6H_4	2-MeC_6H_4	4-MeC_6H_4	20	Ar^1Ar^2CHOH
6	2,4,6-$Me_3C_6H_2$	C_6H_5	4-MeC_6H_4	0	$PhAr^2CHOH$
7	2,4,6-$Me_3C_6H_2$	Flu.[b]		11	
8	4-ClC_6H_4	2-MeC_6H_4	4-MeC_6H_4	34	
9	2-Pyridyl	2-MeC_6H_4	C_6H_5	0	$Ar^1PhCHOH$
10	2-Pyridyl	Flu.[b]		54	
11	4-MeC_6H_4[c]	2-$MeOC_6H_4$	4-MeC_6H_4	25	
12	4-MeC_6H_4[c]	2-$MeOC_6H_4$	4-MeC_6H_4	20	

a) Heated at 55 °C for 10—20 h. b) Fluorenone. c) Reaction conditions are given in the text. d) Reagent containing metallic Mg was used.

group, leading to the formation of 2-anilino-substituted anil (Scheme 2, R^3 and R^4=H).[1] However, the "normal" anil **11** (Table 1) was obtained by treating 2-methoxy-4′-methylbenzophenone with five molar equivalents of *p*-methylphenyl-IDMg at 55 °C for 10 h: **11** was recovered unchanged after treatment with three molar equivalents of the reagent at 55 °C for 6 h.

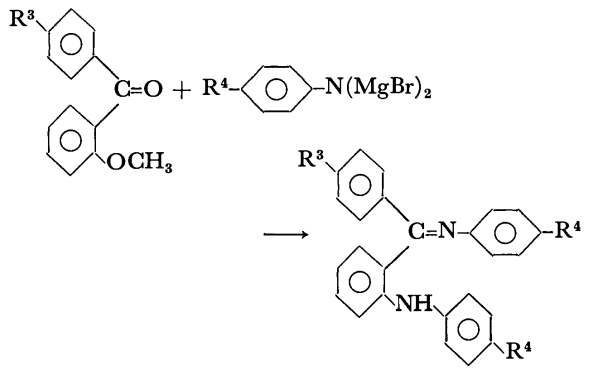

Scheme 2.

In the reaction carried out in order to examine the effect of equimolar excess of metallic magnesium, the condensation-replacement product **12** was obtained (Scheme 2, R^3 and R^4=Me) in 20% yield. The metal dissolved smoothly with intense purple coloration due to the formation of ketyl radicals developed from the metal surface. The condensation-replacement reaction[1] is thus due to the accidental presence of excess metallic magnesium after the preparation of EtMgBr.

The high radical concentration caused by the efficient electron-donor, metallic magnesium, is one reason for the methoxyl replacement. Similar methoxyl replacement in Grignard reaction *via* electron-transfer process was discussed.[7]

Aryl-IDMg and Xanthone. Xanthone does not undergo condensation with hydroxylamine and phenylhydrazine owing to the electron-releasing resonance effect of the ethereal oxygen atom. So far the oxime and the hydrazone have been obtained after the conversion of ketone into more reactive thioketone.[8] The anil was obtained indirectly from 2,2′-dihydroxybenzophenone by strong heating with aniline.[9] The nonreactivity

Table 2. Reaction of $ArN(MgBr)_2$ with xanthone

Anil No.	$ArN(MgBr)_2$ Ar	Yield of the anil/%[a]
13	4-MeC_6H_4	86
14	2-MeC_6H_4	0
15	4-$MeOC_6H_4$	53
16	3-$MeOC_6H_4$	50
17	4-ClC_6H_4	0
18	2-Pyridyl	0

a) Heated at 55—60 °C for 10—20 h.

of xanthone towards amino-functional reagents and its normal reactivity towards Grignard reagents[10] led us to examine the reaction with IDMg (Table 2).

The ketone can be condensed satisfactorily with *p*-methyl-, *p*- and *m*-methoxyphenyl-IDMg giving anils **13**, **15**, and **16** after heating for more than 10 h. No anil **13** was formed after heating of the reaction mixture for 2 h in contrast with the moderate yields of benzophenone anils by heating for only 30 min.[1] IDMg reagents derived from *o*-methyl- and *p*-chloroaniline as well as 2-aminopyridine, less reactive in the reaction with benzophenones, gave no expected products.

In spite of the lower reactivity, anils of xanthone have been prepared directly for the first time.

IDMg Reagents Derived from 1,1-Disubstituted Hydrazines and Diaryl Ketones. The IDMg reagent derived from 1-methyl-1-phenylhydrazine was found to be useful (Table 3): diaryl ketones including xanthone give excellent yields of the hydrazones **19**, **21**, and **24** after heating for a short time except much hindered 2,3,5,6-tetramethylbenzophenone which was recovered unchanged.

The reagent derived from 1,1-dimethylhydrazine is not effective, which resembles the results obtained with

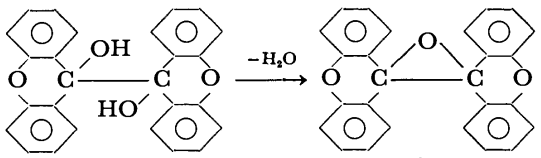

Scheme 3.

Table 3. Reaction of IDMg reagents derived from 1,1-disubstituted hydrazines withdiaryl ketones

Hydrazone No.	$R_2'N-N(MgBr)_2$ R	R′	$Ar^1-CO-Ar^2$ Ar^1	Ar^2	Yield of the hydrazone/%	By-product
19	Ph	Me	Xan.[a]		93[c]	
20	Me	Me	Xan.[a]		0[c]	Epoxide **25**
21	Ph	Me	4-MeC_6H_4	C_6H_5	87[c]	
22	Me	Me	4-MeC_6H_4	C_6H_5	0[c]	$Ar^1PhCHOH$
23	Ph	Me	Dur.[b]	C_6H_5	0[d]	
24	Ph	Me	2-MeC_6H_4	2-MeC_6H_4	78[e]	

a) Xanthone. b) 2,3,5,6-Me_4C_6H. c) Heated at 55 °C for 1 h. d) Heated at 55 °C for 8 h. e) Heated at 55 °C for 5 h.

use of the reagents derived from alkylamines. By-products should be derived from the ketyl radicals. The epoxide **25** isolated from the reaction mixture with xanthone indicates the intermediate formation of the corresponding pinacol (Scheme 3).[11]

Characteristics of IDMg Reaction with Ketones. Taking the previous results[1] into account, characteristics of the reaction can be summarized as follows.

i) Arylamines, 1-methyl-1-phenylhydrazine, and diaryl ketones are favorable components, but not alkylamines, 1,1-dimethylhydrazine and enolizable ketones,

ii) Steric hindrance effect caused by *o*-methyl group of diaryl ketone is overcome when the IDMg reagent is unhindered, and *vice versa*,

iii) Strongly electron-donating methoxyl group, unfavorable to Lewis acid catalyzed condensation, is favorable to the IDMg method,[1]

iv) Xanthone gives anils when reactive aryl-IDMg reagents are used,

v) IDMg reagent derived from 1-methyl-1-phenylhydrazine gives excellent yields of hydrazones of diaryl ketones including xanthone, and

vi) Initial electron-transfer from IDMg reagent to ketones is suggested.

Experimental

Melting points are uncorrected.

Materials. Commercial *t*-butylamine, isobutylamine, all the anilines, 2-aminopyridine, acetophenone, benzophenone, 4-methylbenzophenone, fluorenone, xanthone, 1,1-dimethylhydrazine, and 1-methyl-1-phenylhydrazine were used. 2-Methyl- and 2,4′-dimethylbenzophenone were prepared by the Friedel-Crafts method. 2-Methoxy-4′-methylbenzophenone (mp 64—65 °C) was prepared by the addition of 4-methylphenylmagnesium bromide to 2-methoxybenzaldehyde followed by chromium(VI) oxide oxidation in acetic acid. 2,2′-Dimethylbenzophenone (mp 72 °C) was prepared by treatment of 2-methylbenzoyl chloride with 2-methylphenylmagnesium bromide. Authentic sample of *N*-(α-methylbenzylidene)-*p*-methylaniline **3** was prepared according to the reported method.[12]

Procedures. A typical procedure for IDMg reaction was described.[1] All the experiments were carried out using 5—10 mmol of reagents and substrates in 40—50 ml THF: reaction conditions and yields of isolated products are given in the text and in Tables 1—3.

Column chromatography (Wakogel C-200, petroleum benzine–benzene–diethyl ether = 10 : 1 : 1) was applied to the isolation of products except **13** and **19**: all the condensation products were eluted faster than the unreacted ketones. The isolated crystalline products were recrystallized from ethanol.

Products. Presence of diarylmethanols in product mixtures was confirmed by TLC as well as the NMR signal at 5.4—5.7 ppm characteristic of their benzylic protons.

The NMR spectrum of epoxide **25** (8.48—8.52 (4H, m) and 7.12—7.92 (12H, m)) resembles closely that of xanthone. The IR spectrum, resembling also that of the ketone, has another absorption band at 1070 cm^{-1} assignable to ν(C–O–C) vibration. Found: C, 83.02; H, 4.29; O, 12.69%. Calcd for $C_{26}H_{16}O_3$: C, 82.97; H, 4.25; O, 12.76%.

Imine, anil or hydrazone, melting point, NMR data, and result of elemental analysis are as follows: Imine **2**: an oil; NMR (CCl_4): δ=7.18—7.98 (10H, m), 3.16 (2H, d), 2.00 (1H, m), 0.97 (6H, d). Found: C, 85.95; H, 7.98; N, 5.98%. Calcd for $C_{17}H_{19}N$: C, 86.07; H, 8.02; N, 5.90%. Anil **4**: an oil; NMR (CCl_4): δ=6.22—7.74 (12H, m), 3.42 (3H, s), 2.24 (3H, s), 2.00 (3H, s). Found: C, 83.90; H, 6.60; N, 4.39%. Calcd for $C_{22}H_{21}NO$: C, 83.81, H. 6.66; N, 4.44%. Anil **5**: an oil; NMR (CCl_4): δ=6.16—7.72 (12H, m), 2.34 (3H, s), 2.26 (3H, s), 2.00 (3H, s). Found: C, 88.36; H, 6.97; N, 4.61%. Calcd for $C_{22}H_{21}N$: C, 88.29, H, 7.02, N, 4.68%. Anil **7**: mp 159—162 °C; NMR ($CDCl_3$): δ= 6.75—8.32 (10H, m), 2.35 (3H, s), 2.00 (6H, s). Found: C, 88.92; H, 6.36; N, 4.76%. Calcd for $C_{22}H_{19}N$: C, 88.88; H, 6.39; N, 4.71%. Anil **8**: mp 104—105 °C; NMR (CCl_4): δ=6.65—7.80 (12H, m), 2.38 (3H, s), 2.02 (3H, s). Found: C, 79.01; H, 5.59; N, 4.40%. Calcd for $C_{21}H_{18}ClN$: C, 78.87; H, 5.63; N, 4.38%. Anil **10**: mp 79—80.5 °C; NMR (CCl_4): δ=6.18—8.52 (12H, m). Found: C, 84.40; H, 4.64; N, 11.00%. Calcd for $C_{18}H_{12}N_2$: C, 84.37; H, 4.68; N, 10.93%. Anil **11**: mp 129—131 °C; NMR (CCl_4): δ= 6.44—7.64 (12H, m), 3.56 (3H, s), 2.36 (3H, s), 2.18 (3H, s). Found: C, 84.01; H, 6.70; N, 4.48%. Calcd for $C_{22}H_{21}NO$: C, 83.81; H, 6.66; N, 4.44%. Anil **12**: an oil; NMR (CCl_4): δ=6.24—7.34 (16H, m), 3.90 (1H, broad s), 2.24 (6H, s), 2.14 (3H, s). Found: C, 85.99; H, 6.76; N, 7.25%. Calcd for $C_{28}H_{26}N_2$: C, 86.15, H, 6.66; N, 7.18%. Anil **13**: mp 111—112.5 °C; NMR ($CDCl_3$): δ=6.76—8.65 (12H, m), 2.36 (3H, s). Found: C, 84.18; H, 5.28; N, 4.93%. Calcd for $C_{20}H_{15}NO$: C, 84.21; H, 5.26; N, 4.91%. Anil **15**: mp 151—153 °C; NMR ($CDCl_3$): δ=6.72—8.64 (12H, m), 3.58 (3H, s). Found: C, 79.71; H, 5.00; N, 4.70%. Calcd for $C_{20}H_{15}NO_2$: C, 79.73; H, 4.98; N, 4.65%. Anil **16**: mp 88—90.5 °C; NMR ($CDCl_3$): δ=6.40—8.44 (12H, m), 3.78 (3H, s). Found: C, 79.68; H, 5.01; N, 4.68%. Calcd for $C_{20}H_{15}NO_2$: C, 79.73; H, 4.98; N, 4.65%. Hydrazone **19**: mp 138—139 °C; NMR ($CDCl_3$): δ=6.90—8.96 (13H, m), 3.16 (3H, s). Found: C, 80.15; H, 5.40; N, 9.40%. Calcd for $C_{20}H_{16}$-

N_2O: C, 80.00; H, 5.33, N, 9.33%. Hydrazone **21**: an oil; NMR (CCl_4): δ=6.68—7.60 (14H, m), 2.92 (3H, d), 2.44 (3H, d). Found: C, 84.10; H, 6.70; N, 9.25%. Calcd for $C_{21}H_{20}N_2$: C, 84.00; H, 6.66; N, 9.33%. Hydrazone **24**: an oil: NMR (CCl_4): δ=6.66—7.44 (13H, m), 2.84 (3H, s), 2.40 (3H, s), 2.06 (3H, s). Found: C, 84.12; H, 6.96; N, 9.01%. Calcd for $C_{22}H_{22}N_2$: C, 84.07; H, 7.00; N, 8.91%.

References

1) M. Ōkubo and S. Ueda, *Bull. Chem. Soc. Jpn.*, **53**, 281 (1980).
2) E. W. Abel and G. R. Wiley, *J. Chem. Soc.*, **1964**, 1528; D. R. M. Walton, *J. Chem. Soc., C*, **1966**, 1707.
3) P. A. Petynin and V. V. Boltov, *Zh. Org. Khim.*, **9**, 836 (1973); *Chem. Abstr.*, **79**, 53130 (1973).
4) A. T. Nielsen, C. Gibbons, and G. A. Zimmerman, *J. Am. Chem. Soc.*, **73**, 4696 (1951); W. D. Garden and F. D. Gunstone, *J. Chem. Soc.*, **1952**, 2650; and references cited therein.
5) H. Weingarten, J. P. Chupp, and W. A. White, *J. Org. Chem.*, **32**, 3246 (1967); I. Moretti and G. Torre, *Synthesis*, **1970**, 141.
6) M. Ōkubo, *Bull. Chem. Soc. Jpn.*, **48**, 2057 (1975).
7) M. Ōkubo, *Bull. Chem. Soc. Jpn.*, **50**, 2379 (1977).
8) C. Graebe and P. Roeder, *Ber.*, **32**, 1689 (1899).
9) A. Schoenberg and W. Urban, *J. Chem. Soc.*, **1935**, 530.
10) M. Gomberg and L. H. Cone, *Justus Liebigs Ann. Chem.*, **370**, 142 (1909); R. L. Shriner and C. N. Wolf. *J. Am. Chem. Soc.*, **73**, 891 (1951).
11) E. C. Ashby, H. M. Neumann, F. W. Walker, J. Laemmle, and L.-C. Chao, *J. Am. Chem. Soc.*, **95**, 3330 (1973).
12) G. Reddelien, *Ber.*, **43**, 2476 (1910).

  Bull. Chem. Soc. Jpn., 54, 2341—2344 (1981)

The Adsorption of Nucleic Acid Bases by Raney-nickel, -cobalt, and -copper

Keisuke MITA,* Kazuhiko HOTTA, and Shoji WATANABE
Osaka Municipal Technical Research Institute, Ogimachi, Kita-ku, Osaka 530
(Received October 18, 1980)

The order of the relative affinity of adenine (A), guanine (G), cytosine (C), thymine (T), and uracil (U) to Raney-nickel, Raney-cobalt and Raney-copper was determined in an alkaline solution by means of a column-chromatographic method. These bases could be placed in these orders: G>A>C>U>T for Raney-nickel, G>C>A>T~U for Raney-cobalt, and A~G~C>T~U for Raney-copper. It was also found that these Raney-metals could be placed in the following order as to ability to distinguish those bases: Raney-nickel≫Raney-cobalt> Raney-copper.

It has been well known that metallic nickel powder can induce lung cancer.[1,2] Some investigators consider that the interaction between DNA and the nickel ion leached from metallic nickel is directly responsible for producing cancer.[1,3] The reactions of nucleic acids, nucleotides, nucleosides, or bases with the nickel ion have, therefore, been studied by many workers.[2,4,5] Although it has been known that the nickel ion interacts with both nucleic acid bases and phosphate portions in DNA, there have been few reports concerning the precise interaction sites of nucleic acids with the nickel ion.

In the present work, we determined the order of the relative affinities of adenine, guanine, cytosine, thymine, and uracil for metallic nickel, cobalt, and copper by means of a column-chromatographic method and tried to estimate the interaction sites of nucleic acid with the metal ions. Raney-nickel (R-Ni), Raney-cobalt (R-Co), and Raney-copper (R-Cu) were used as the metals because of their high surface area and well-known surface properties.[6,7]

Experimental

R-Ni (Ni: 2.5 g), R-Co (Co: 10 g), and R-Cu (Cu: 10 g) were prepared from commercial Raney metal–aluminium alloys (Al/metal: 50 atom%) by leaching out the aluminium with a 13% sodium hydroxide solution for 1 h at 70, 50, and 50 °C respectively. After washing with distilled water, each sample was packed in a 1-cm-diameter column, which was fitted at the bottom with a cotton to retain the sample, to a height of approximately 5, 20, or 20 cm respectively. A 0.2 mol dm^{-3} sodium hydroxide solution containing two or three kinds of bases at 2.0 mmol dm^{-3} was allowed to flow into the column at a rate of 10 ml/h. The effluent was collected by fraction collecter. The concentration of each base in the effluent fractions could then be determined by using the absorption spectra of the fractions and by solving Eq. 1:

$$\begin{aligned}
\frac{A_\alpha}{A_\alpha}x + \frac{B_\alpha}{B_\beta}y + \frac{C_\alpha}{C_\gamma}z &= S_\alpha\,, \\
\frac{A_\beta}{A_\alpha}x + \frac{B_\beta}{B_\beta}y + \frac{C_\beta}{C_\gamma}z &= S_\beta\,, \\
\frac{A_\gamma}{A_\alpha}x + \frac{B_\gamma}{B_\beta}y + \frac{C_\gamma}{C_\gamma}z &= S_\gamma\,,
\end{aligned} \tag{1}$$

where A_α, A_β, and A_γ are the absorbances of a 0.1 mol dm^{-3} H_2SO_4 or 0.1 mol dm^{-3} NaOH standard solution containing known quantities of base-A at the maximum absorption wavelengths of base-A (α), base-B (β), and base-C (γ) respectively. Moreover B_α, B_β, and B_γ are the absorbances of base-B, and C_α, C_β, and C_γ, those of base-C at the wavelengths of α, β, γ respectively. S_α, S_β, and S_γ are the absorbances of the standard solutions containing a known quantity of the effluent fraction at the wavelengths of α, β, and γ, while x, y, and z are the concentrations of base-A, base-B, and base-C respectively in the fraction.

The uncertainty of the method is determined by mixing these bases in different known proportions and by estimating the base contents in the mixtures by means of Eq. 1. The experimental conditions are shown in Table 1.

Results and Discussion

It has been known that the fraction of the metallic surface is in the range of 55—85% for conventional preparations of Raney-metals, and the residual fraction is considered to be alumina.[7] In order to examine whether or not the nucleic-acid bases can be absorbed by alumina, a 0.2 mol dm^{-3} sodium hydroxide solution containing these bases was allowed to flow into a column packed with γ-alumina. Since the adsorption of these bases by γ-alumina could not be observed, the possibility of adsorption by alumina on Raney-metals can be disregarded.

In the present work, Raney-cobalt or Raney-copper column is packed with an amount four times that of the

Table 1. Experimental conditions

Bases A	Bases B	Bases C	Standard solution	Wavelength/nm α	Wavelength/nm β	Wavelength/nm γ	Uncertainties %
Guanine,	Uracil,	Cytosine	0.2 mol dm^{-3} H_2SO_4	248,	260,	276	5
Adenine,	Guanine,	Thymine	0.2 mol dm^{-3} NaOH	269,	274,	291	20
Guanine,	Adenine,	Cytosine	0.2 mol dm^{-3} H_2SO_4	248,	262.5,	276	5
Adenine,	Cytosine		0.2 mol dm^{-3} H_2SO_4	262.5,	276		5
Uracil,	Thymine		0.2 mol dm^{-3} NaOH	284,	291		20

Raney-nickel column, because the amount of the bases adsorbed at saturation for R-Ni is about four times those of R-Co and R-Cu. Therefore, it can be considered that the effluent volume/time·metallic surface area is nearly same in each column.

Figures 1—3 show the breakthrough curves of a guanine-uracil-cytosine mixture for R-Ni, R-Co, and R-Cu respectively. It can be seen from Figs. 1 and 2 that the relative affinities of these three bases for R-Ni and R-Co can be placed in this order: guanine>cytosine >uracil. In the case of R-Cu, on the other hand, the relative affinities of these bases can be placed in this order: guanine~cytosine>uracil, because the breakthrough curves exhibit no differences between guanine and cytosine, as is shown in Fig. 3. By comparing the breakthrough curves in Figs. 1—3 with each other, it can be seen that these Raney-metals can be placed

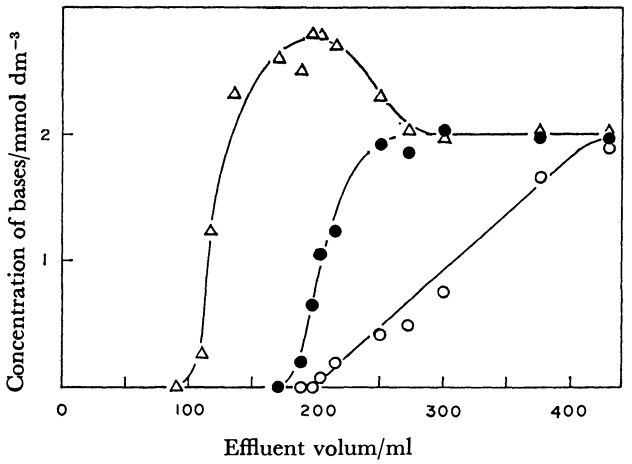

Fig. 1. Breakthrough curves on R-Ni for 0.2 mol dm^{-3} NaOH solution containing guanine (○), cytosine (●) and uracil (△) at the concentration of 2 mmol dm^{-3} respectively.
R-Ni: 2.5 g as nickel, column: 1.0×5 cm, flow rate: 10 ml/h.

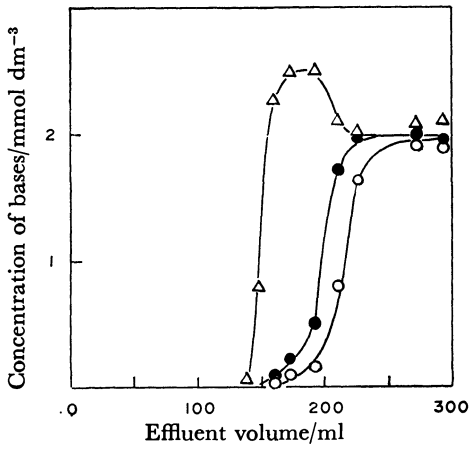

Fig. 2. Breakthrough curves on R-Co for 0.2 mol dm^{-3} NaOH solution containing guanine (○), cytosine (●) and uracil (△) at the concentration of 2 mmol dm^{-3} respectively.
R-Co: 10 g as cobalt, column: 1.0×20 cm, flow rate: 10 ml/h.

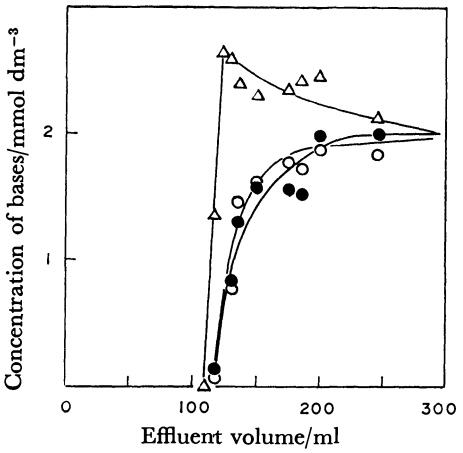

Fig. 3. Breakthrough curves on R-Cu for 0.2 mol dm^{-3} NaOH solution containing guanine (○), cytosine (●) and uracil (△) at the concentration of 2 mmol dm^{-3} respectively.
R-Cu: 10 g as cupper, column: 1.0×20 cm, flow rate: 10 ml/h.

in the following order of ability to distinguish these bases: R-Ni>R-Co>R-Cu.

The breakthrough curves of a guanine-adenine-thymine mixture for R-Ni, R-Co, and R-Cu were found to give patterns similar to Figs. 1—3 respectively. It was shown from the breakthrough curves that, among these three bases, thymine exhibits the weakest affinities for Raney-metals. From these results and Figs. 1—3, it appeared that these five bases can be classified into two groups, one of which exhibits relatively strong affinities (guanine, adenine, and cytosine) for Raney-metals, while the other exhibits relatively weak affinities (uracil and thymine).

Figures 4—6 show the breakthrough curves of a guanine-adenine-cytosine mixture for R-Ni, R-Co, and R-Cu respectively. It appears from Fig. 4 that the relative affinities of these three bases for R-Ni can be placed in this order: guanine>adenine>cytosine. On the other hand, it can be seen from Fig. 5 that the relative affinities of these bases for R-Co can be placed in this order: guanine>cytosine>adenine. It may be noted that a reversed order of adenine and cytosine is observed for R-Co. This difference between R-Ni and R-Co was also confirmed by the breakthrough curves of the cytosine-adenine mixture, as shown in Fig. 7. In the case of R-Cu, however, no differences in these three bases could be detected, as is shown in Fig. 6.

Figure 8 shows the breakthrough curves of a uracil-thymine mixture for R-Ni, R-Co, and R-Cu. It appears that the relative affinities of these two bases can be placed in this order: uracil>thymine for R-Ni, while in the case of R-Co and R-Cu no differences between the relative affinities of these two bases was observed within the limits of experimental error.

In conclusion, the present experiment has made it obvious that the relative affinities of these five bases can be placed in these orders: guanine>adenine> cytosine>uracil>thymine for R-Ni, guanine>cytosine> adenine>thymine~uracil for R-Co, and adenine~ guanine~cytosine>thymine~uracil for R-Cu. It is

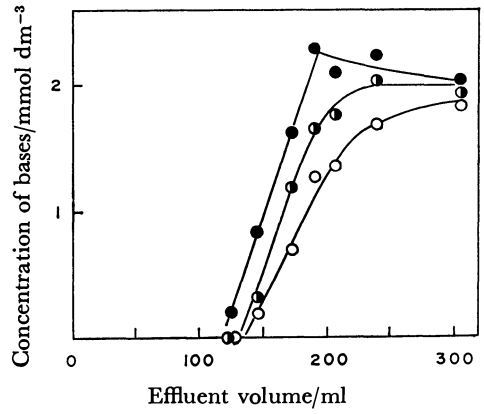

Fig. 4. Breakthrough curves on R-Ni for 0.2 mol dm^{-3} NaOH solution containing adenine (◑), guanine (○) and cytosine (●) at the concentration of 2 mmol dm^{-3} respectively.
R-Ni: 2.5 g as nickel, column: 1.0×5 cm, flow rate: 10 ml/h.

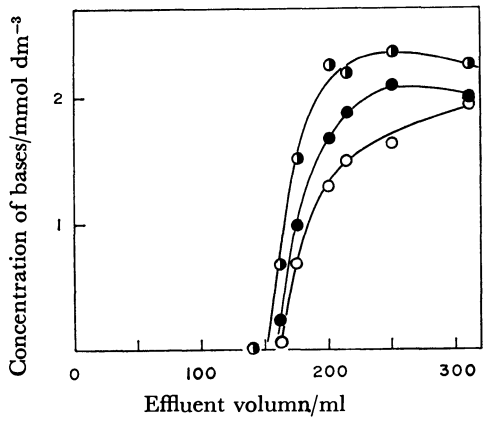

Fig. 5. Breakthrough curves on R-Co for 0.2 mol dm^{-3} NaOH solution containing adenine (◑), guanine (○) and cytosine (●) at the concentration of 2 mmol dm^{-3} respectively.
R-Co: 10 g as cobalt, column: 1.0×20 cm, flow rate: 10 ml/h.

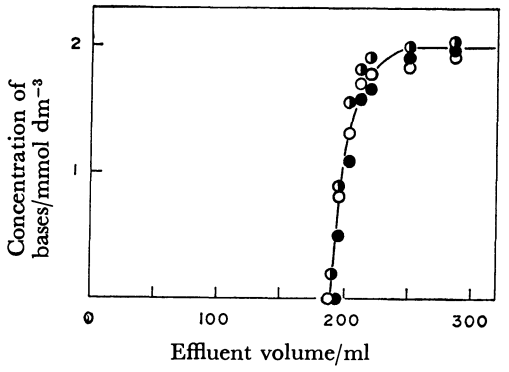

Fig. 6. Breakthrough curves on R-Cu for 0.2 mol dm^{-3} NaOH solution containing adenine (◑), guanine (○) and cytosine (●) at the concentration of 2 mmol dm^{-3} respectively.
R-Cu: 10 g as cupper, column: 1.0×20 cm, flow rate: 10 ml/h.

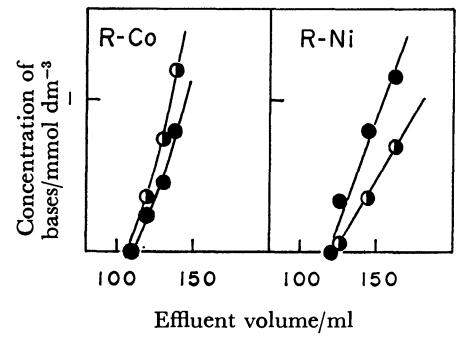

Fig. 7. Breakthrough curves on R-Ni and R-Co for 0.2 mol dm^{-3} NaOH solution containing adenine (◑) and cytosine (●) at the concentration of 2 mmol dm^{-3} respectively.
R-Ni: 2.5 g as niekel, 1.0×5 cm column, R-Co: 10 g as cobalt, 1.0×20 cm column, flow rate: 10 ml/h.

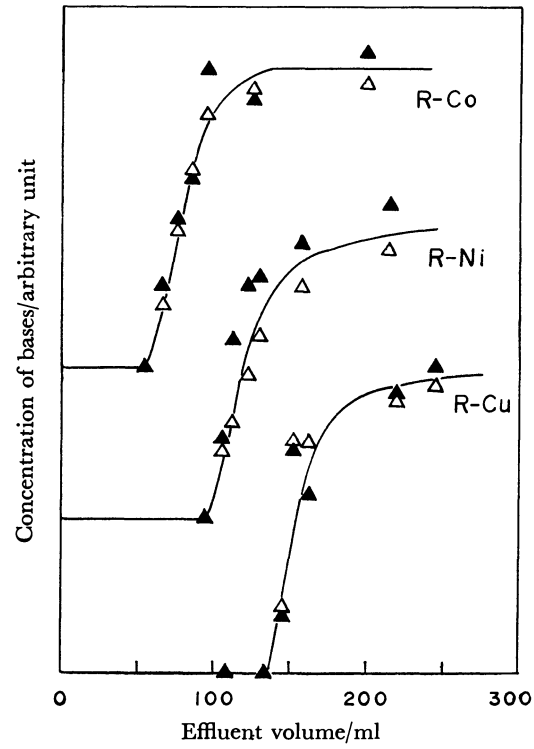

Fig. 8. Breakthrough curves on R-Ni, R-Co, and R-Cu for 0.2 mol dm^{-3} NaOH solution containing thymine (▲) and uracil (△) at the concentration of 2 mmol dm^{-3} respectively.
R-Ni: 2.5 g as nickel, R-Co: 10 g as cobalt, R-Cu: 10 g as cupper, flow rate: 10 ml/h.

also obvious that the ability of Raney-metals to distinguish these bases can be placed in this order: R-Ni> R-Co>R-Cu.

It has been reported that Cu(II),[8-13] Mn(II),[14,15] and Co(II)[14] ions bind mainly to guanine among the bases in nucleic acids. It has also been reported that the antitumor *cis*-dichlorodiammineplatinum(II) complex indicates a preferential binding to guanine,[16-20] followed by adenine[18,21] in DNA. It has also been established that the Ni^{2+}–AMP complex is far more stable than Co^{2+}–AMP complex.[22] On the other hand,

the formation of a stable Co^{2+}–CMP complex has been reported.[23,24] Such similarities of behavior between Raney-metals and their metal ions may suggest that the order of the relative affinities of these bases for the nickel ion is similar to that for Raney-nickel. It would also be interesting to determine whether or not the large ability of Raney-nickel to distinguish these bases is reflected by that of the nickel ion.

References

1) National Research Council, "Medical and Biological Effects of Environmental Pollutants: Nickel," National Academy of Science, Washington, D. C. (1975).
2) Y. Yamane, "Bioinorganic Chemistry," ed by H. Tanaka, A. Nakahara, and S. Fukui, Kagakudojin, Kyoto (1974), p. 265.
3) A. Furst, *Geol. Soc. Am.*, **123**, 109 (1971).
4) R. M. Izatt, J. J. Christensen, and J. H. Rytting, *Chem. Rev.*, **71**, 439 (1971).
5) S. Suzuki, A. Yamada, and K. Akasaka, "Biological Systems as Viewed from Coordination Chemistry and Their Models," ed by the Chemical Society of Japan, Gakkai Shuppan Center, Tokyo (1978), p. 131.
6) T. Kubomatsu, *Bulletin of the Osaka Municipal Technical Research Institute*, **34**, 1 (1962).
7) J. R. Anderson, "Structure of Metallic Catalysts," Academic Press, London (1975), p. 228.
8) Ch. Zimmer, G. Luck, H. Fritzshe, and H. Triebel, *Biopolymers*, **10**, 441 (1971).
9) G. L. Eichhorn and Y. A. Shin, *J. Am. Chem. Soc.*, **90**, 7323 (1968).
10) H. Richard, J. P. Schreiber, and M. Daune, *Biopolymers*, **12**, 1 (1973).
11) Ch. Zimmer, G. Luck, and H. Triebel, *Biopolymers*, **13**, 425 (1974).
12) P. Clark and G. L. Eichhorn, *Biochemistry*, **13**, 5098 (1974).
13) D. C. Liebe and J. E. Stuehr, *Biopolymers*, **11**, 145, 167 (1972).
14) A. Jack, J. E. Lander, D. Rhodes, R. S. Brown, and A. Klung, *J. Mol. Biol.*, **111**, 315 (1977).
15) J. A. Anderson, G. P. P. Kuntz, H. H. Evans, and T. J. Swift, *Biochemistry*, **10**, 4368 (1971).
16) A. B. Robins, *Chem. Biol. Interact.*, **6**, 35 (1973).
17) P. J. Stone, A. D. Kelman, and F. M. Sinex, *Nature (London)*, **251**, 736 (1974).
18) L. L. Munchausen and R. O. Rahn, *Biochim. Biophys. Acta*, **414**, 242 (1975).
19) J. P. Macquet and T. Theophanides, *Biopolymers*, **14**, 781 (1975).
20) J. P. Macquet and J. L. Butour, *Eur. J. Biochem.*, **83**, 375 (1978).
21) S. Mansy, G. Y. H. Chu, R. E. Duncan, and R. S. Tobias, *J. Am. Chem. Soc.*, **100**, 607 (1978).
22) C. M. Frey and J. E. Stuehr, *J. Am. Chem. Soc.*, **94**, 8898 (1972).
23) M. Ogawa and T. Sakaguchi, *Yakugaku Zasshi*, **92**, 1166 (1972).
24) G. R. Clark and J. D. Orbell, *J. Chem. Soc., Chem. Commun.*, **1975**, 697.

Reaction of Organic Tin(II) Compound with Carbonyl Compound

Ikuko WAKESHIMA* and Ichiro KIJIMA

Department of Industrial Chemistry, Faculty of Engineering, Science University of Tokyo, Kagurazaka, Shinjuku-ku, Tokyo 162

(Received October 22, 1980)

The reactions of organic tin(II) compounds bearing Sn–OC bonds with carbonyl compounds, C_6H_5COR (R=C_6H_5CO, C_6H_5, and H) and *p*-benzoquinone, have been investigated. The tin(II) compound reacted with benzil and *p*-benzoquinone to yield the corresponding oxidative addition products. However, the oxidative addition reaction did not occur in benzophenone and benzaldehyde.

We have reported the preparation of organic tin(II) compounds having a high volatility and an excellent solubility toward organic solvents.[1] The chemical behavior of the tin(II) compounds[2–5] has been studied by several research groups: for example, we reported on the reactions of the tin(II) compounds with alkyl halides and heterocumulenes.[2] We describe here a further study on the reactivity of tin(II) compounds, $Sn(OR)_2$, (R=$(CH_3)_2NCH_2CH_2$–, C_2H_5–, *o*-$C_2H_5OCOC_6H_4$–, $CH_3\overset{|}{C}$=$CHCOCH_3$, and $CH_3\overset{|}{C}$=$CHCO_2C_2H_5$), with carbonyl compounds such as benzil, benzophenone, benzaldehyde, and *p*-benzoquinone; the structural analogy of the tin(II) compound with a carbene is important here.

Results and Discussion

The reaction of bis(2-dimethylaminoethoxo)tin(II) (**1**) with benzil in refluxing THF for 6 h afforded yellow powders in 46% yield. The structure of the product was determined as bis(2-dimethylaminoethoxo)(1,2-diphenyl-1,2-ethenediolato)tin(IV), on the bases of the elemental analysis ($C_{22}H_{30}N_2O_4Sn$), the IR spectrum which has no band attributable to $\nu_{C=O}$ (1655 cm^{-1}), and the formation of 1,2-diphenylvinylene dibenzoate when the product was treated with benzoyl chloride. The structure was also supported by its hydrolyzate: on hydrolysis, the product gave benzoin, which appeared to be formed by a rapid tautomerization of the unsaturated glycol, 1,2-diphenyl-1,2-ethenediol.

These facts suggest that compound (**1**) can be oxidized by benzil to a tetravalent tin compound, as shown in Eq. 1:

$$Sn\left(OCH_2CH_2N\begin{matrix}CH_3\\CH_3\end{matrix}\right)_2 + C_6H_5COCOC_6H_5 \longrightarrow \left(\begin{matrix}CH_3\\CH_3\end{matrix}NCH_2CH_2O\right)_2 Sn\begin{matrix}O\text{-}C\\O\text{-}C\end{matrix}\begin{matrix}C_6H_5\\C_6H_6\end{matrix} \quad (1)$$

The reaction proceeded more readily in THF and ethyl alcohol than in benzene (see Table 1).

The reaction of various organic tin(II) compounds with benzil was also examined in THF. The results, as summarized in Table 2, reveal that i) organic tin(II) compounds containing Sn–OC bond are more effective reducing agents for benzil than tin(II) chloride, which is a polymer of intermolecularly coordinated Cl→Sn bond; ii) in the organic tin(II) compounds, the oxidative addition reaction of **1** is the best for benzil, while that of diphenoxotin(II) (**4**) is the worst; iii) the reactivity of alkoxotin(II) compounds (**1** and **2**) is superior that of the conjugated chelate tin(II) compounds (**3**, **5**, and **6**); and finally; iv) the reaction of the monomeric tin(II) compounds (**1** and **3**) proceeds far more readily than that of the corresponding associated tin(II) compounds (**2** and **4**).

From these facts, it may be concluded that the migration of 5s electrons on the tin(II) atom in the intermediate (a), as indicated in Eq. 2, play an important role in the reaction with benzil and that, of the organic tin(II) compounds, the monomeric organic tin(II) compound bearing an electron releasing group behaves most effectively toward benzil.

Table 1. Solvent effect on the reaction[a] of bis(2-dimethylaminoethoxo)tin(II) with benzil

Solvents	Hydrolyzate	
	Yield/%[b]	P[c]
Benzene	90	1.03
Ethyl alcohol	91	1.62
Tetrahydrofuran	95	1.76

a) Reaction conditions: [$Sn(OR)_2$]/[benzil]=1, time: 6 h; temp: benzene 80 °C, ethyl alcohol 78 °C, THF 67—68 °C. b) Based on the weight of benzil used in the reaction. c) Proportion ([benzoin]/[benzil]) of benzoin the hydrolyzate.

Table 2. Hydrolyzates of products from the reaction[a] of various organic tin (II) compounds with benzil in THF

$Sn(OR)_2$ R	Hydrolyzates	
	Yield/%[b]	P[c]
$(CH_3)_2NCH_2CH_2$-(**1**)	95	1.76
C_2H_5-(**2**)[d]	87	0.72
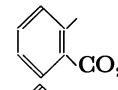 (**3**)	87	0.41
 (**4**)	80	0.09
$CH_3\overset{|}{C}$=$CHCOCH_3$ (**5**)	83	0.14
$CH_3\overset{|}{C}$=$CHCO_2C_2H_5$ (**6**)	81	0.15
$SnCl_2$	86	0.03

a) Reaction conditions: [$Sn(OR)_2$]/[benzil]=1, time; 6 h, temp; 67—68 °C. b) Based on the weight of benzil used in the reaction. c) Proportion ([benzoin]/[benzil]) of benzoin in the hydrolyzate. d)Associated in nature.

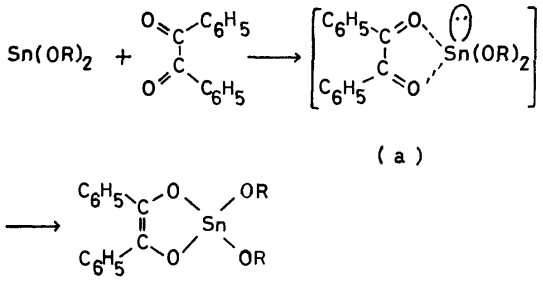

(a) (2)

Compound **2** reacted unsatisfactorily with benzaldehyde in THF at 68—69 °C to give only traces of cinnamaldehyde and benzyl alcohol. Although the reaction was conducted under drastic conditions (no solvent, at 145±5 °C) for 3 h, there was no increase in the yields of cinnamaldehyde and benzyl alcohol. Therefore, it seems that the reaction of compound **2** with benzaldehyde proceeds neither through the oxidative addition reaction (Eq. 1) nor through the intermolecular oxidative coupling reaction (Eq. 3), but rather in a way similar to the Meerwein-Pondorf reaction, as shown in Eqs. 4 and 5:

$$Sn(OC_2H_5)_2 + 2\ C_6H_5CHO \not\longrightarrow (C_2H_5O)_2Sn(O\text{-}CH(C_6H_5)\text{-}O\text{-}CH(C_6H_5)) \quad (3)$$

$$Sn(OC_2H_5)_2 + C_6H_5CHO \longrightarrow (C_2H_5O)Sn(OCH_2C_6H_5) + CH_3CHO \quad (4)$$

$$C_6H_5CHO + CH_3CHO \xrightarrow[H_2O]{Sn(OC_2H_5)_2} C_6H_5CH{=}CHCHO. \quad (5)$$

Compound **1** did not react at all with benzophenone in THF at 67 °C after 6 h.

The reaction of **1** and **5** with *p*-benzoquinone in benzene were investigated. As indicated in Table 3, it was found that each reaction readily gave the corresponding oxidative addition products in excellent yields.

The products were only soluble in common organic solvents with great dificulty and decomposed at high temperature. No chracteristic absorption band of *p*-benzoquinone presented itself. Therefore, the oxidative addition product is considered to be a polymer, as shown below:

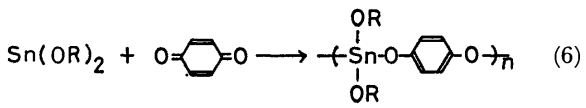

(6)

R=$-CH_2CH_2N(CH_3)_2$, $CH_3C(CH_3)$=CHCOCH$_3$.

Although **5** was a less effective reducing agent for benzil, the reaction with *p*-benzoquinone took place easily to afford the oxidative addition compound. Therefore, it seems that the possibility of the oxidative addition reaction of organic tin(II) compounds depends greatly on the half-wave potentials of the carbonyl compounds: *p*-benzoquinone, benzil, benzaldehyde, and benzophenone have half-wave potentials of −0.146(2), −0.27(2), −0.94(1), and −0.94(1) SCE, respectively. The parenthesized-figure indicates the number of electrons involved in the reaction.

Experimental

All reactions were carried out in a nitrogen atmosphere dried with liquid nitrogen. The melting and boiling points are uncorrected. IR spectra were recorded with a Hitachi EPI-S2 spectrometer, and mass spectra were taken on Hitachi RMU-7 model double-focusing spectrometer. The CHN elemental analyses were carried out with a Yanagimoto MT-2 CHN corder. Gas chromatography was performed on a Yanagimoto model GCG-2, using SE-30 column.

Tin content was determined by chelate titration with M/100 EDTA aqueous solution. Benzil was determined by the redox titration with a chromous sulfate solution.[6] *p*-Benzoquinone was purified by sublimating a commercial extra-pure grade at 70—80 °C/20 mmHg (1 mmHg=133.322 Pa) just prior to use. Benzaldehyde and benzophenone were purified by distillation before use.

Reaction of Organic Tin(II) Compounds with Benzil in a 1 : 1 Molar Ratio. Benzil (50 mmol) was added to a solution or a suspension of organic tin(II) compound (50 mmol) in 100 ml of solvent. After the mixture was refluxed for 6 h, the reaction mixture was evaporated to dryness under reduced pressure. The residue was hydrolyzed with 100 ml of water (5 ml)–benzene (80 ml)–acetone(15 ml) solution. After separating the resulting solids by filtration, the solid was extracted with acetone in a Soxhlet extractor in order to obtain the benzoin. Subsequently, the mother liquor was combined with the extract and distilled *in vacuo* at a temperature below 155 °C (bath temperature) to isolate the hydrolyzate. Bp 118—138 °C/0.3 mmHg. The results are shown in Tables 1 and 2.

Isolation of Bis(2-dimethylaminoethoxo)(1,2-diphenyl-1,2-ethenediolato)tin(IV): Compound **1** (14.7 g, 50 mmol) and benzil (10.5 g, 50 mmol) were dissolved in 53 ml of THF. The mixture was heated at 68 °C for 6 h. Yellow powders precipitated during the reaction were filtered off, washed with THF, and dried: yield 12.0 g (47.5%). Found: C, 52.31; H, 6.01; N, 5.45; Sn, 23.05%. Calcd for $C_{22}H_{30}N_2O_4Sn$: C, 52.30; H, 5.94; N, 5.54; Sn, 23.62%. *m/e*: 505 (M^+). Mp 154 °C (dec).

Isolation of 1,2-Diphenylvinylene Dibenzoate: Benzoyl chloride (44.9 g, 106 mmol) was added drop by drop to the reaction mixture of **1** (7.3 g, 24.9 mmol) and benzil (5.2 g, 24.7 mmol) at 30—40 °C. After being warmed for 1 h, it was allowed to stand for 2 d at room temperature and then hydrolyzed with 100 ml of 9% hydrochloric acid. The resulting solids were

Table 3. Reaction with *p*-benzoquinone

Sn(OR)$_2$ R	Reaction conditions: Molar ratio [Quinone]/[Sn]	Reaction conditions: Time h	Products: Yield %	Products: Mp (dec) °C	Products: Sn Found(Calcd) (%)	Products: IR ν/cm^{-1}
$(CH_3)_2NCH_2CH_2-$	1	3	100	220	28.98(29.45)	1220
$CH_3C(CH_3)$=CHCOCH$_3$	1	5	95	245	27.69(27.93)	1210

isolated and extracted with diisopropyl ether. The ether solution was washed with 5% sodium carbonate aqueous solution, then with water, and evaporated to dryness. After removing the unreacted benzil under a reduced pressure, the residue was recrystallized from benzene–hexane (1/1 volume ratio) solution, giving 2.5 g of 1,2-diphenylvinylene dibenzoate with mp 156—158 °C (lit,[7] 158 °C); white powder. Found: C, 78.85; H, 4.68%. Calcd for $C_{28}H_{20}O_4$: C, 79.98, H, 4.79%. IR (KBr disk): $\nu_{C=O}$ 1720 cm^{-1}; ν_{C-O} 1082 cm^{-1}.

Reaction with p-*Benzoquinone.* A solution of 1.95 g (18 mmol) of *p*-benzoquinone in 37 ml of benzene was added drop by drop to **1** (5.31 g, 18 mmol) in benzene (20 ml) at 22—24 °C and then the solution was refluxed with stirring in an oil bath for 2 h. The precipitated solids were isolated by filtration, washed with benzene, and dried. Yield 7.25 g (100%).

The reaction of compound **5** was also carried out in a similar way.

Reaction with Benzaldehyde. Compound **2** (8.4 g, 40 mmol) and benzaldehyde (48.9 g, 461 mmol) were heated at 66 °C for 11 h. After filtrating the reaction mixture, traces of ethyl alcohol and cinnamaldehyde from the mother liquor were detected by gas chromatography. The residue in the filtrating flask was hydrolyzed with an aqueous diisopropyl ether. The solvent was removed by distillation; a trace of benzyl alcohol was found in the distillation flask.

The reaction under drastic conditions (no solvent, reaction temperature 145±5 °C, reaction time 3 h) was performed in a similar way. The presence of acetaldehyde, ethyl alcohol, cinnamaldehyde, and benzyl alcohol was confirmed by gas chromatography.

Reaction with Benzophenone. The mixture of **1** (16.2 g, 54.9 mmol) and benzophenone (10.3 g, 56.5 mmol) in 55 ml of THF was refluxed for 6 h. No decrease in Sn^{2+}% was observed. After removal of THF under a reduced pressure, the residue was hydrolyzed with 100 ml of water (15 ml)–benzene (80 ml)–acetone (15 ml) solution. The resultant solids were filtered off and then the mother liquor was evaporated to dryness. The solids were distilled *in vacuo*; 10 g of benzophenone (bp 153 °C/1 mmHg) was recovered.

The present work was partially supported by a Grant-in-Aid for Scientific Research No 555348 from the Ministry of Education, Science and Culture.

References

1) I. Wakeshima and I. Kijima, *Chem. Lett.*, **1972**, 325.
2) I. Wakeshima and I. Kijima, *J. Organomet. Chem.*, **76**, 37 (1974); I. Wakeshima, H. Suzuki, and I. Kijima, *Bull. Chem. Soc. Jpn.*, **48**, 1069 (1975); I. Wakeshima, Y. Saitoh, and I. Kijima, *ibid.*, **51**, 3549 (1978).
3) P. G. Harrison and J. J. Zuckerman, *Inorg. Nucl. Chem. Lett.*, **5**, 545 (1969); *J. Chem. Soc., D*, **1969**, 321.
4) A. B. Cornwell and P. G. Harrison, *J. Chem. Soc., Dalton Trans.*, **1975**, 1486, 2017.
5) K. D. Bos, R. J. Bulten, and J. G. Noltes, *J. Organomet. Chem.*, **99**, 397 (1975); *Inorg. Nucl. Chem. Lett.*, **9**, 961 (1973).
6) J. P. Tandon, *Z. Anal. Chem.*, **167**, 184 (1959).
7) W. E. Bachmann, *J. Am. Chem. Soc.*, **53**, 2762 (1931).

Synthesis of β-Substituted Tetramethyltetraazacyclotetradecatetraene and Its Metal(II) Complexes

Takao TOKUMITSU* and Takayuki HAYASHI

Department of Chemistry, Faculty of Science, Yamaguchi University, Yoshida, Yamaguchi 753

(Received October 27, 1980)

N,N'-Bis(1-methyl-3-thioxo-1-butenyl)ethylenediamine (**3**) was prepared by the reaction of *N,N'*-bis(1-methyl-3-oxo-1-butenyl)ethylenediamine with phosphorus pentasulfide in pyridine. The reaction of **3** with ethylenediamine gave 5,7,12,14-tetramethyl-1,4,8,11-tetraazacyclotetradeca-4,6,11,13-tetraene (**4**) in a 46% yield. The reactivity of the β positions of **4** and its metal(II) complexes (M=Cu, Ni, Pd) toward various electrophilic reagents was explored, and some β,β'-bissubstituted tetraaza macrocyclic compounds (substituent=Cl, $SC_6H_4NO_2$(o), N_2Ph) and their metal complexes were prepared, respectively. The former also reacted with metal(II) acetates to afford the same metal complexes.

The preparations and reactivities of tetraaza macrocycles and their metal complexes containing enamino imines conjugated systems have attracted considerable attention as models for natural tetraaza macrocycles, such as porphyrins and corrins. It is also interesting to elucidate the reactivity of the β positions of their macrocyclic ligands and metal complexes. Fischer *et al.*[1] have reported that the β positions of 5,14-dihydrodibenzo[*b,i*][5,9,14,18]tetraaza[14]annulene (**1**) react with *p*-chlorobenzenediazonium salt to give a 7,16-bis(*p*-chlorophenylazo)substituted derivative. The reaction of **1** with ethyl 1-chloro-3,3-dicyanopropenoate has also been found to yield a 7,16-bis(ethoxycarbonyl)-substituted derivative.[2] While nickel(II) complex of **1** reacted with bromine to give an octabromo derivative substituted into benzene nuclei.[2] Holm *et al.*[3] have found that some β,β'-bisphenylated macrocycles are prepared by the reaction of 4-phenyl-1,2-dithiolium salt with diamine. Jäger[4] has also reported the template synthesis of some macrocyclic metal complexes with COR or COOR groups at the β positions. This cyclization appears dependent on the presence of a carbonyl-containing group.[5] The macrocycle, 5,7,12,14-tetramethyl-1,4,8,11-tetraazacyclotetradeca-4,6,11,13-tetraene (**4**), without the substituents at the β positions has been prepared by the reaction of ethylenediamine with 4-amino-2-ethyl-2-oxonia-3-pentene[3b,5] and/or *N,N'*-bis(1-methyl-3-thioxo-1-butenyl)ethylenediamine (**3**), which is prepared from *N,N'*-bis(3-ethyl-3-oxonia-1-methyl-1-butenyl)ethylenediamine and sodium hydrogensulfide.[3a,6] In all these preparations, triethyloxonium tetrafluoroborate is required as a catalyst, and the yield is generally low.

We synthesized **4** without using the specific and expensive catalyst, and elucidated the electrophilic substitution reactivity of the β positions of the free ligand, **4**, and its metal(II) complexes (**6**).

Results and Discussion

The compound, **3**, was synthesized by means of reaction of *N,N'*-bis(1-methyl-3-oxo-1-butenyl)ethylenediamine (**2**) with phosphorous pentasulfide in pyridine in a 34% yield. The macrocycle, **4**, was obtained in the highest yield (46%) when **3** was refluxed with an equimolar amount of ethylenediamine in benzene for 24 h. By these reactions, **4** could be synthesized without using the expensive and specific catalyst.

The macrocycle, **4**, reacted with *N*-chlorosuccinimide (NCS) of 2.2 molar ratio at 5 °C in the dark under a nitrogen atmosphere to give 6,13-dichloro-5,7,12,14-tetramethyl-1,4,8,11-tetraazacyclotetradeca-4,6,11,13-tetraene (**5a**) in a 25% yield; the addition of 4.4 molar ratio gave 6,6,13,13-tetrachloro-5,7,12,14-tetramethyl-1,4,8,11-tetraazacyclotetradeca-4,7,11,14-tetraene (**8**) in a 42% yield. Under these conditions, it is considered that the reactions proceed by an ionic mechanism. Their structure was established by analytical and spectral data. That is to say, the NMR spectrum of **5a** showed the same pattern as that of **4**, except that absorption of –CH= protons in the vicinity of 4.5 ppm was missing. That of **8** also lacked the absorptions for –CH= and NH protons, and the protons of four CH_3 and four

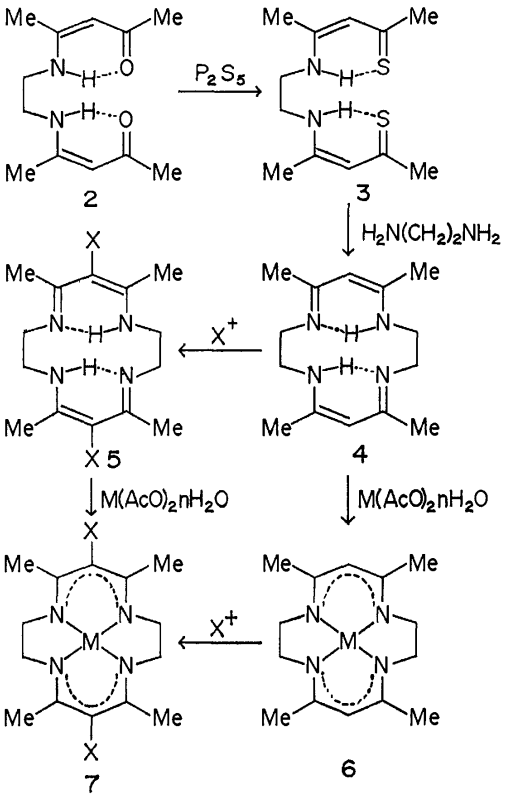

a: X=Cl, **b**: X=$SC_6H_4NO_2$(*o*)
c: X=N_2Ph, **d**: X=COPh
M: Cu, Ni, Pd

Table 1. Melting points and analytical data of the products

Compound	Mp/°C	Found (%)				Calcd (%)			
		C	H	N	Cl or S	C	H	N	Cl or S
5a	178—179	52.91	7.07	17.56	22.27	53.00	6.99	17.66	22.35
5b	224	56.02	5.39	14.96	11.42	56.29	5.45	15.15	11.56
5c	218—219	68.22	7.04	24.27		68.39	7.26	24.54	
6Pd	310—312	47.81	6.26	15.90		47.67	6.28	15.88	
7bCu	194	50.53	4.50	13.75	10.24	50.68	4.58	13.64	10.40
7bNi	198	51.03	4.52	13.61	10.41	51.08	4.61	13.74	10.49
7bPd	204—205	47.50	4.30	12.58	9.60	47.38	4.28	12.75	9.73
7cCu	277—278	60.34	5.78	21.40		60.27	5.83	21.62	
7cNi	275—276	60.83	5.79	21.83		60.84	5.89	21.83	
7cPd	271—272	55.59	5.31	19.76		55.67	5.39	19.97	
7dNi	250—251	56.59	5.71	10.92		56.53	5.89	10.91	
7dPd	267—268	60.02	5.23	9.98		59.95	5.39	9.98	
8	154	43.52	5.15	14.29	36.47	43.54	5.22	14.50	36.72

Table 2. Spectral data of the products

Compound	IR[a] $\tilde{\nu}$/cm^{-1}				NMR[b] δ				UV[c] λ_{max}/nm($10^{-3}\varepsilon$)
	νNH or νC=O	νC=C+ νC=N	δNH or $\nu_{as}NO_2$	$\nu_s NO_2$	CH_3	CH_2–CH_2	X	NH	
4	3200	1620	1568[c]		1.88(s)	3.45(s)	4.51(s)	11.5[d]	297(33.2)[e]
5a	3200	1607	1560[c]		2.13(s)	3.58(s)		11.7[d]	252(2.4), 308[sh](17.2), 317(21.8), 350(4.7)[e]
5b	3200	1590	1565 1515	1337[c]	2.18(s)	3.60(s)	7.4—8.3(m)	13.2[d]	307(20.7), 381(8.0)
5c	3200	1586	1576[c]		2.20(s)	3.50(s)	7.1—7.5(m)	—[f),g)]	296(14.5), 335(26.5), 375(29.2), 420[sh](17.6)
6Pd		1554			2.01(s)	3.53(s)	4.70(s)		282(9.9), 300[sh](7.2), 346(4.6), 367[sh](4.8), 395(6.0), 412(6.3), 459(0.9), 488(1.0)
7bCu		1563	1517	1331					271[sh](30.0), 335(17.6), 382[sh](10.6), 470[sh](2.4), 570(0.6)
7bNi		1561	1518	1340	2.16(s)	3.23(s)	7.1—8.2(m)		281(32.8), 386(14.0), 470(2.2), 560[sh](1.4)
7bPd		1563	1515	1322	2.30(s)	3.65(s)	7.2—8.3(m)		275[sh](29.2), 388(15.0), 480(1.7)
7cCu		1560							290[sh](4.6), 349(21.8), 400[sh](25.0), 465(40.0), 560[sh](2.6)
7cNi		1553			—	—	—[h]		296[sh](13.0), 373(21.6), 485(40.0)
7cPd		1571			—	—	—[h]		288[sh](6.0), 387(17.8), 489(39.0)
7dNi	1625	1537			1.83(s)	3.35(s)	7.5—8.1(m)		280(18.4), 396(9.0), 420(8.9), 445[sh](7.8), 550[sh](1.6)
7dPd	1626	1539			1.93(s)	3.60(s)	7.5—8.1(m)		280(13.0), 408(9.5), 418[sh](9.3), 440[sh](8.0)

a) KBr. b) $CDCl_3$. c) $CHCl_3$. d) Center of broad signal. e) EtOH. f) DMSO-d_6. g) Not observed. h) Could not be detected because of slight solubility in solvents. s: Singlet. m: Multiplet. sh: Shoulder.

–CH_2– were equivalent and appeared as singlets. The IR spectrum in 1600 cm^{-1} region of **8** showed only one strong absorption at 1660 cm^{-1}, which was assigned to νC=N.[7] The mass spectrum showed the parent ion peak at *m/e* 384, and the UV spectrum exhibited an absorption maximum at 250 nm (ε, 580). This shows that **8** does not have a conjugated system. Compound **8** may be formed by Cl^+ attacking at the 6- and 13-

positions of **5a**, followed by the elimination of NH protons, analogously to the gem-dibromination of the β position of 1,4-diazepines.[8] The melting points, analytical data, and spectral data for the products are presented in Tables 1 and 2.

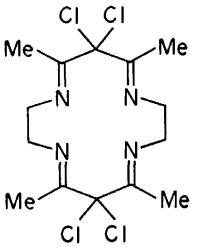

8

The reaction of **4** with *o*-nitrobenzenesulfenyl chloride in acetonitrile in the presence of triethylamine gave 5,7,12,14-tetramethyl-6,13-bis(2-nitrophenylthio)-1,4,8,-11-tetraazacyclotetradeca-4,6,11,13-tetraene ((**5b**) in a 25% yield. The NMR spectrum showed multiplet absorption for aromatic protons of 8H amount, and the IR spectrum showed strong absorptions at 1515 and 1337 cm^{-1}, which were assigned to $\nu_{as}NO_2$ and ν_sNO_2, respectively.

Compound **4** also reacted with benzenediazonium salt to give 5,7,12,14-tetramethyl-6,13-bis(phenylazo)-1,4,8,11-tetraazacyclotetradeca-4,6,11,14-tetraene(**5c**) in a 61% yield. Because this material is slightly soluble in $CDCl_3$, DMSO-d_6, pyridine-d_5, *etc.*, the NMR signal of NH protons of **5c** could not be detected. However, the IR spectrum showed a weak absorption centered at 3200 cm^{-1}, which was assigned to the intramolecular hydrogen bonded νNH, and showed no absorptions for the non-conjugated νC=N in the region of 1640—1690 cm^{-1}.[1,7] In contrast with the coupling product of **1**, which appears to exist as a hydrazo tautomer,[1] these results suggest that **5c** exists in a chelated azo form.

The metal(II) complexes, **6** (M=Cu, Ni, Pd), of **4** reacted with *o*-nitrobenzenesulfenyl chloride in the presence of pyridine to give 6,13-bis(2-nitrophenylthio)-substituted metal complexes (**7b**) in 83% (M=Ni) and 61% (M=Pd) yield, respectively, and **6** (M=Cu) gave decomposition products.

The reaction of **6** (M=Cu, Ni, Pd) with benzenediazonium salt also gave 6,13-bis(phenylazo)-substituted metal complexes (**7c**) in 53% (M=Cu), 97% (M=Ni) and 89% (M=Pd) yield, respectively.

The reaction of **6** (M=Ni, Pd) with benzoyl chloride in the presence of pyridine gave 6,13-dibenzoyl-substituted metal complexes (**7d**) in 57% (M=Ni) and 62% (M=Pd) yield, respectively, and **6** (M=Cu) also gave decomposition products. The structure of **7d** (M=Ni, Pd) was established as follows: the IR spectrum showed νC=O at 1625 and 1626 cm^{-1}, and NMR spectrum showed multiplet absorptions for 10H aromatic protons at 7.5—8.5 ppm; there was no absorption of the methine protons.

The free ligands, **5b** and **5c**, reacted with the metal(II) acetates (M=Cu, Ni, Pd) in DMF and/or DMSO to yield the corresponding metal complexes **7b** and **7c** in 79—90% yield, respectively. The complexation of **5a** gave decomposition products. The structures of these products were confirmed by direct comparison of the spectral data with the corresponding products derived from **6b** and **6c** and mixed examination. The **7b** (M=Cu), which could not be obtained by the reaction of **6** (M=Cu) with *o*-nitrobenzenesulfenyl chloride, was easily obtained by the reaction of **5b** with copper acetate in a 81% yield.

Attempts to synthesize other β,β'-disubstituted derivatives of **4** and **6** such as 6,13-dinitro-, 6,13-dibromo-, 6,13-diiodo-, 6,13-diformyl-, and 6,13-dithiocyano-derivatives were all unsuccessful, and **4** and **6** gave decomposition products, respectively. It thus appears that the substrates or products are unstable under these reaction conditions.

It is considered that the electrophilic reactivity of the β positions of the free ligand, **4**, and its metal(II) complexes, **6**, which are stabilized by the delocalization of π-electrons, may be attributed to their meneidic or regenerative character, as well as that of enamino ketones,[9] vinamidines and its salts[10] and the metal complexes of β-diketones.[11]

The IR spectra for the free ligands, **5a**, **5b**, and **5c**, show a broad absorption at 3200 cm^{-1} and a strong absorption at 1560—1576 cm^{-1} which are associated with νNH and δNH by the shift to lower frequencies owing to the replacement of active protons by deuterium ions. A strong absorption observed in the range of 1586—1607 cm^{-1} may be assigned to the νC=C+νC=N, which shift into the range of 1553—1571 cm^{-1} upon complex formation. The νC=O of the β-substituents and the νC=C+νC=N for the chelate rings of **7d** (M=Ni, Pd) are observed in both lower frequencies at 1625 or 1626 cm^{-1} and at 1537 or 1539 cm^{-1}, respectively. This seems to indicate that the β,β'-dicarbonyl groups have highly conjugated with the chelate rings.

The NMR spectra for the free ligands, **5a**, **5b**, and **5c**, show a broad signal of NH protons at 11.7 and 13.2 ppm except **5c**, and a sharp singlet of N–CH_2– and C–CH_3 at 3.50—3.60 ppm and at 2.13—2.20 ppm, respectively. The signals of the N–CH_2– and the C–CH_3 for the metal complexes also are sharp singlets. These results, together with the results from the IR spectra, have shown that these free ligands exist in an intramolecular hydrogen bonded chelate structure, which seems to be symmetric structure delocalized of π-electrons through the enamino imine conjugation[12] analogous to their metal complexes.

The visible and UV spectra of the free ligands, **5a**, **5b**, and **5c**, display two—four absorption bands in the range of 250—420 nm. The spectral features for these metal complexes are more complicated, and **7b** and **7c** (M=Cu, Ni, Pd) exhibit one or two new absorption peaks in the range of 466—570 nm, which may be assigned to π-π^* transitions within a ligand molecule and/or charge-transfer transitions. **7d** (M=Ni, Pd) also exhibit two or three similar absorption peaks in the range of 418—550 nm.

Experimental

The Schiff base, *N,N'*-bis(1-methyl-3-oxo-1-butenyl)ethylenediamine (**2**) was prepared according to the method of Martell *et al.*[13] The IR, NMR, and UV spectra were

recorded with JASCO IRG, Hitachi R24B, and Hitachi 124 spectrometers respectively. The mass spectra were determined with a JEOL JMS-D100 mass spectrometer. All the melting points are uncorrected.

Preparation of **3**: To a solution of **2** (22.4 g, 0.1 mol) in pyridine (50 ml) was slowly added powdered phosphorus pentasulfide at room temperature. The reaction mixture was stirred for 5 h, and then poured into 2 l of water. The mixture was neutralized by sodium hydrogencarbonate and filtrated. The residue was recrystallized with ethanol to give 8.8 g (34%) of **3**; mp 152—153 °C. Found: C, 56.15; H, 8.05; N, 10.77; S, 24.75%.

Preparation of **4**: A solution containing **3** (5.1 g, 20 mmol) and ethylenediamine (1.2 g, 20 mmol) in benzene (120 ml) was refluxed for 24 h. Removal of solvent, addition of ethanol, filtration, and recrystallization from ethanol gave 2.3 g (46%) of **4**; mp 223—224 °C (lit,[5] mp 226—228 °C, yield 15%).

Reaction of **4** *with NCS*: To a soution of **4** (1.24 g, 5 mmol) in chloroform (10 ml) was added NCS (1.5 g, 11 mmol) under a nitrogen atmosphere in the dark at 5 °C and stirred for 1 h. The resulting succinimide was removed by filtration, and the filtrate was evaporated to dryness under reduced pressure. The residual solid was recrystallized with ethanol to give 0.4 g (25%) of **5a**; MS *m/e*: 316 (M^+). The melting points, analytical data, and spectral data for the products were tabulated in Tables 1 and 2. The addition of 3.0 g (22 mmol) of NCS gave **8** in a 42% yield (from EtOH); MS *m/e*: 384 (M^+).

Preparation of **5b**: To a solution of **4** (2.5 g, 10 mmol) and triethylamine (3.0 g, 30 mmol) in acetonitrile (100 ml) was slowly added a solution of *o*-nitrobenzenesulfenyl chloride (4.2 g, 22 mmol) in acetonitrile (30 ml) under a nitrogen atmosphere, and then refluxed with stirring for 3 h. The reaction mixture was poured into water, and the resulting precipitation was separated by filtration. The products were isolated by column chromatography on silica gel ($CHCl_3$) to give 1.4 g (25%) of **5b**; MS *m/e*: 554 (M^+).

Preparation of **5c**: To 30 ml of a solution, neutralized by sodium acetate, containing 11 mmol of benzenediazonium chloride, was added a diluted acetic acid solution containing 1.2 g (5 mmol) of **4** with stirring at 5 °C. This mixture was then stirred for 2 h at this temperature and for 2 h at room temperature. The reaction mixture was poured into water, and filtrated. The collected solid was recrystallized with DMF to give 1.4 g (61%) of **5c** as yellow powder; MS *m/e*: 456 (M^+).

Preparation of the Metal(II) Complexes, **6**, *of* **4**: Copper(II) and nickel (II) complexes of **4** were synthesized by the method of Holm *et al.*[5] Palladium(II) complex was synthesized by the reaction of equimolar amounts of palladium acetate and **4** in hot ethanol; yield 74% (from $CHCl_3$).

General Procedure for the Reaction of **6** *with* o-*Nitrobenzenesulfenyl Chloride*: To a solution of **6** (5 mmol) and pyridine (11 mmol) in chloroform (150 ml) was added *o*-nitrobenzenesulfenyl chloride (11 mmol) under a nitrogen atmosphere at room temperature, and refluxed for 4 h. The reaction mixture was evaporated *in vacuo*, and recrystallization of the residue from solvent afforded the corresponding **7b**. **7b** (M=Ni): yield 83% (from benzene). **7b** (M=Pd): yield 61% (from $CHCl_3$–EtOH).

General Procedure for the Reaction of **6** *with Benzenediazonium Salt*: To an aqueous solution (100 ml) containing benzenediazonium chloride (11 mmol) and neutralized with sodium acetate, was slowly added a diluted acetic acid solution (80 ml) of **6** (5 mmol) at 5 °C; the mixture was then stirred at room temperature for 2—3 h. The reaction mixture was poured into water, and the resulting precipitate was removed by filtration and washed with ethanol. The product was purified by stirring with about 20 times of DMF. **7c** (M=Cu): yield 53%. **7c** (M=Ni): yield 97%. **7c** (M=Pd): yield 89%.

General Procedure for the Reaction of **6** *with Benzoyl Chloride*: To a solution of **6** (2 mmol) and pyridine (4.4 mmol) in dichloromethane (100 ml) was added benzoyl chloride (4.4 mmol) at room temperature, and the mixture was refluxed for 4 h. After removal of the solvent, the residue was recrystallized. **7d** (M=Ni): yield 57% (from $CHCl_3$–EtOH). **7d** (M=Pd): yield 62% (from $CHCl_3$).

Complexation of **5**: The free ligands, **5**, reacted with the metal(II) acetates of a small excess in DMF and/or DMSO for 15 min at 120 °C to give the corresponding metal complexes **7**. **7b** (M=Cu): yield 81% (from DMF). **7b** (M=Ni): yield 98% (from benzene). **7b** (M=Pd): yield 81% (from $CHCl_3$–EtOH). **7c** (M=Cu): yield 90%. **7c** (M=Ni): yield 88%. **7c** (M=Pd): yield 79%. The complexations of **5a** gave decomposition products.

Other Electrophilic Substitutions: The compounds, **4** and **6**, reacted with acetic anhydride and nitric acid or copper nitrate, *N*-bromosuccinimide, *N*-iodosuccinimide, bromine, Vilsmeier reagent, thiocyanogen, *etc.*, to give products which decomposed during the reactions or the separations.

References

1) D. P. Fisher, F. C. McElroy, D. J. Macero, and J. C. Dabrowiak, *Inorg. Nucl. Chem. Lett.*, **12**, 4351 (1976).

2) H. Hiller, P. Dimroth, and H. Pfitzner, *Ann. Chem.*, **717**, 137 (1968).

3) a) S. C. Tang, S. Koch, G. N. Weinstein, R. W. Lane, and R. H. Holm, *Inorg. Chem.*, **12**, 2589 (1973); b) S. C. Tang, G. N. Weinstein, and R. H. Holm, *J. Am. Chem. Soc.*, **95** 613 (1973).

4) E. Jäger, *Z. Chem.*, **4**, 437 (1964); **8**, 30, 470 (1968); *Z. Anorg. Allg. Chem.*, **364**, 177 (1969).

5) T. J. Truex and R. H. Holm, *J. Am. Chem. Soc.*, **93**, 285 (1971); **94**, 4529 (1972).

6) R. M. C. Wein and S. C. Cumming, *Inorg. Nucl. Chem. Lett.*, **9**, 43 (1973).

7) L. J. Bellamy, "The Infrared Spectra of Complex Molecules," Wiley, New York (1958), p. 49.

8) A. M. Gorringe, D. Lloyd, F. I. Wasson, D. R. Marshall, and P. A. Duffield, *J. Chem. Soc., C*, **1969**, 1449.

9) G. H. Alt, "Enamines: Synthesis, Structure, and Reactions," ed by A. G. Cook, Marcell Dekker, New York (1956), p. 135; T. Tokumitsu and T. Hayashi, *Nippon Kagaku Kaishi*, **1973**, 2152; **1977**, 1388; **1978**, 1267.

10) D. Lloyd and H. McNab, *Angew. Chem. Int. Ed. Engl.*, **15**, 459 (1976).

11) J. P. Collman, *Angew. Chem.*, **77**, 154 (1965).

12) P. Goldstein and K. N. Trueblood, *Acta Crystallogr.*, **23**, 148 (1967).

13) P. J. McCarthy, R. J. Hovey, K. Ueno, and A. E. Martell, *J. Am. Chem. Soc.*, **77**, 5820 (1955).

Photochemical Reactions of Aromatic Compounds. XXXVI.[1] The Photoreactions of Anthracene with Some Selected Tertiary Aromatic Amines in Polar Media

Masahide YASUDA, Chyongjin PAC,* and Hiroshi SAKURAI

The Institute of Scientific and Industrial Research, Osaka University, Suita, Osaka 565

(Received October 31, 1979)

The photoreaction of anthracene with *N,N*-dimethylaniline in acetonitrile gave 9-(*p*-dimethylaminophenyl)-9,10-dihydroanthracene in a good yield, along with 9,10-dihydroanthracene and 9,9′,10,10′-tetrahydro-9,9′-bianthryl. This photoreaction was found to depend on the polarity of the solvent as well as on its protic or aprotic nature. With *N,N*-dimethyl-*m*-toluidine, a similar 1 : 1 adduct was obtained, while the reduced anthracenes were mainly formed in the photoreactions with *N,N*-dimethyl-*o*- and *p*-toluidines. The mechanisms were discussed in terms of the dissociation into the ion radicals as well as their reactivities.

The arene–amine systems are typical electron acceptor-donor pairs for exciplex formation[2] and photochemical electron-transfer reactions.[3] The photoreactions of such systems usually afford adducts of arenes with amines and reduced arenes,[3-7] depending on the structures of the amines as well as on the polarity of solvent. In a previous paper,[4] we reported that the photoreaction of anthracene (A) with *N,N*-dimethylaniline (DMA) in acetonitrile gives mainly 9-(*p*-dimethylaminophenyl)-9,10-dihydroanthracene (**3a**), along with the reduced anthracenes (**1** and **2**) while the irradiation of a benzene solution results in the exclusive dimerization of A. In this paper, we wish to report on the photoreactions of A with some selected tertiary aromatic amines in polar media.

Results

Photoreactions of A with the Tertiary Amines in Acetonitrile. The irradiation was carried out for dry acetonitrile solutions in a Pyrex vessel, using a high-pressure mercury lamp at room temperature. Table 1 lists the isolated yields of the products. The hydrocarbon products (**1**, **2**, and **4**) are known compounds and were unambiguously identified by direct comparison with respective authentic samples. The structures of **3a** and **3c** were indicated by their elemental composition and their spectral properties. For example, the ^{1}H NMR spectrum of **3a** consisted of a sharp singlet at δ 2.75 (N–CH_3), a broad doublet at δ 3.88 (C_{10}–H_2), a broad triplet at δ 5.1 (C_9–H), an A_2B_2 signal at δ 6.7 (*p*-C_6H_4–), and a multiplet at δ 7.2 (other aromatic protons), strongly supporting the structure assigned. When a *p*-cymene solution of **3a** was refluxed over 5% Pd–C, 9-(*p*-dimethylaminophenyl)anthracene, which is a known compound,[8] was obtained in a 90% yield.

Table 1. Product distribution in the photoreactions of anthracene with the tertiary aromatic amines in acetonitrile

Amines	Isolated yields/%			
	1	**2**	**3**	**4**
DMA	8	20	70	0
o-DMT	54	32	trace	0
m-DMT	16	25	60	0
p-DMT	72	21	0	0

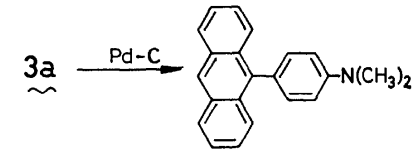

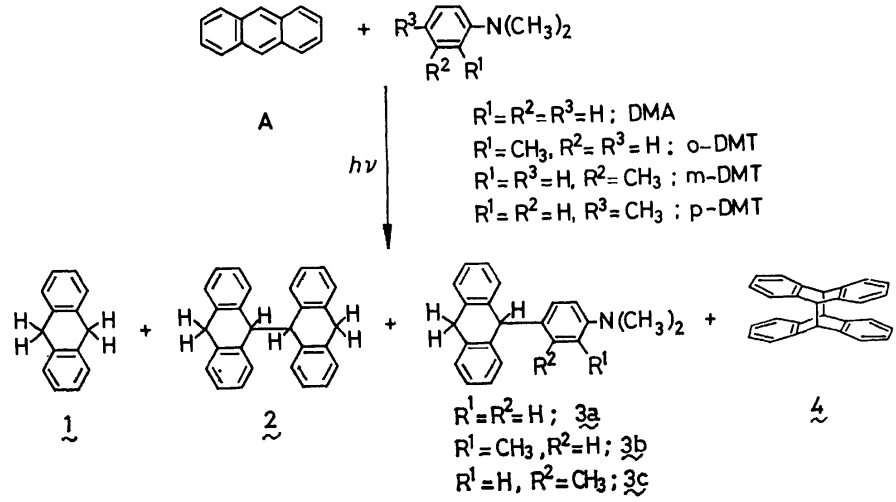

Scheme 1.

It is notable that the photoreaction with DMA and *m*-DMT mainly gave the adducts (**3a** and **3c**), whereas **1** and **2** are the exclusive products with *o*- and *p*-DMT. In the case of *o*-DMT, the formation of **3b** was indicated by the ^{1}H NMR spectrum of a mixture, which showed a sharp singlet at δ 2.15, a sharp singlet at δ 2.52, a broad doublet at δ 3.87, and a very broad singlet at δ 5.12 in an area ratio of *ca.* 3 : 6 : 2 : 1. However, its formation was too small for an unambiguous determination of the structure to be made. On the other hand, no adduct of A with *p*-DMT was isolated.

Table 2. Solvent effect on the photoreactions of anthracene with *N*,*N*-dimethylaniline and *N*,*N*-dimethyl-*p*-toluidine

	Solvents	Isolated yields/%			
		1	**2**	**3**	**4**
DMA	C_6H_6	0	0	0	100
	Et_2O	2	10	trace	85
	EtOH	45	20	30	0
	MeCN	8	20	70	0
p-DMT	EtOH	46	50	—	0
	MeCN–EtOH (9 : 1)	52	47	—	0
	MeCN	72	21	—	0

Solvent Effects on the Photoreactions of A with DMA and p-*DMT.* The photoreaction with DMA depends not only on the polarity of the solvent, but also on its protic or aprotic nature, as is shown in Table 2. The formation of **4** was exclusive in benzene and predominant in diethyl ether, while the combined yields of **1**, **2**, and **3a** were over 90% in such highly polar solvents as acetonitrile and ethanol. The formation of **3a** is favored in acetonitrile, which is a typical, aprotic polar solvent. On the other hand, **1** and **2** are mainly formed in ethanol. Moreover, it was found that the photoreaction with *p*-DMT in acetonitrile affords **1** in a good yield. Ethanol diminished the yields of **1**, though the combined yields of **1** and **2** were invariably high.

Discussion

Aromatic hydrocarbon–tertiary aromatic amine pairs have been extensively investigated as typical exciplex-formation systems and have been well established to dissociate into the ion radicals in polar media.[2,9] Therefore, the observed effect of solvent polarity can be interpreted in terms of a complete electron transfer from DMA to the excited singlet state of A (^{1}A*). Scheme 2 delineates the mechanistic reaction pathways; ^{1}[A·DMA]* and A$^-$····DMA^{+}· represent the exciplex and the ion pair respectively.

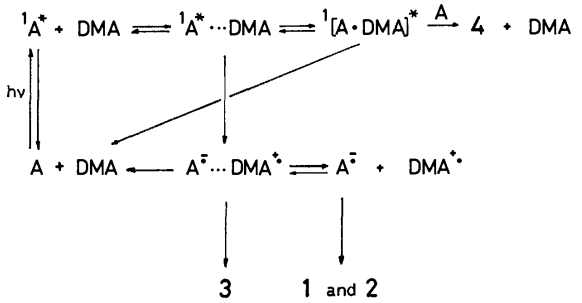

Scheme 2.

In a benzene solution, ^{1}A* forms the exciplex with DMA at the diffusion-controlled limit without any dissociation into the ion radicals.[9] Saltiel and his co-workers have demonstrated that the photodimerization of A in benzene in the presence of DMA proceeds *via* an interaction of the exciplex with A, probably involving a termolecular exciplex, ^{1}[A·A·DMA]*.[10] This mechanism holds for the present photoreaction in benzene since ^{1}A* is completely quenched by DMA under the conditions employed.

Although the photodimerization is still dominant in diethyl ether, the formation of **1** and **2** is notable, perhaps suggesting the occurrence of a partial dissociation into the ion radicals in this solvent; the pyrene–DMA pair is known to dissociate into the ion radicals upon the photoexcitation in moderately polar solvents.[11] In acetonitrile and ethanol, the ionic-dissociation process evidently overcomes the exciplex formation as well as other chemical and physical pathways from the exciplex, thus leading to the complete lack of the photodimerization. In other words, the photoreactions in these solvents are closely related with the chemistry of the ion radicals.

In this regard, it should be noted that the formation of **3a** is more favored in acetonitrile than in ethanol. Since ethanol is a good proton donor for anion radicals, the free anion radical of A and probably also A$^-$· in the ion pair are easily protonated in ethanol.[12] On the other hand, such a rapid protonation of A$^-$· can not be expected in acetonitrile, since possible proton donors in this solvent may be impurities involving water. This argument may lead to the conclusion that the ion pair is a precursor of the formation of **3a**; a radical-coupling reaction between A$^-$· and DMA$^+$· may compete with the charge neutralization between them. The protonation of A$^-$· in the ion pair should result in the loss of the Coulombic force binding the ion pair. As a result, the radical pair, ·AH···DMA$^+$·, will rapidly diffuse out from the solvent cage, thus making a radical-coupling reaction less possible.

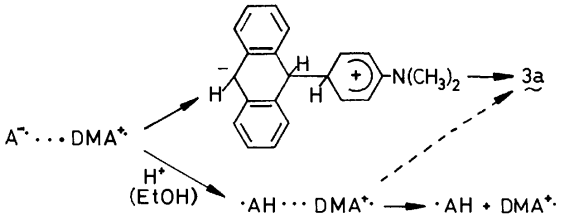

Although a similar mechanism operates for the formation of **3b** and **3c**, the photoreaction with *o*-DMT clearly indicates that the structures of the aromatic amines also affect the reaction courses from the ion pair. It is well known that DMA has a coplanar structure between the dimethylamino group and the benzene ring in the solid state;[13] the structure in solution would again be coplanar, or almost so. This might also be

true for *m*-DMT and *p*-DMT. Therefore, odd electrons of the cation radicals would populate the benzene ring, perhaps largely at the ortho and para positions. Thus, the cation radical of DMA and *m*-DMT can undergo the radical-coupling reaction with $A^{-}\cdot$ at the para position, where the steric hindrance is much less.

On the other hand, coplanarity seems to be largely lost in the case of *o*-DMT because of steric hindrance by the ortho methyl group. Therefore, the spin density of odd electrons on the benzene ring of *o*-$DMT^{+}\cdot$ would be much lower than that of the cation radicals of DMA and *m*-DMT, leading to a lower reactivity of *o*-$DMT^{+}\cdot$ at the benzene ring toward the radical-coupling reaction.

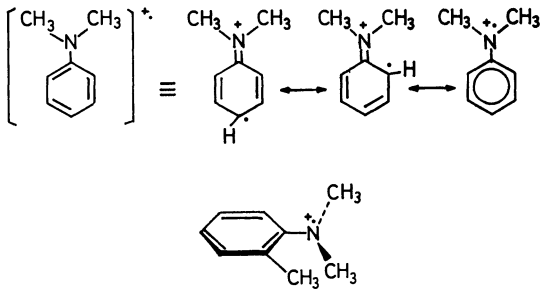

In the case of *p*-$DMT^{+}\cdot$, the para position is blocked by the methyl group and the ortho position is sterically hindered for the radical-coupling reaction. In the cases of *o*- and *p*-DMT, therefore, the escape of the ion radicals from the solvent cage would predominate.

The formation of **1** and **2** evidently arises from the disproportionation and dimerization of $A^{-}\cdot$ and/or ·AH. In protic media, the precursor is certainly ·AH, whereas both ($A^{-}\cdot$) and (·AH) exist in acetonitrile. In the photoreaction with *p*-DMT, as a solvent acetonitrile is more suitable for the formation of **1** than is ethanol. It should be noted that the presence of 10 vol% ethanol in acetonitrile lowered the yields of **1**. Therefore, it may be suggested that $A^{-}\cdot$ predominantly undergo disproportionation, whereas both disproportionation and dimerization occur with ·AH in a *ca.* 1 : 1 ratio.

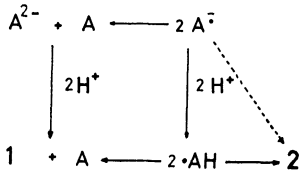

Since the photoreaction with *p*-DMT in acetonitrile gave **1** in a relatively high yield, the *p*-DMT–acetonitrile pair can be expected to be a favorable reaction system for the photo-Birch reduction of aromatic hydrocarbons. Therefore, the photo-Birch reduction of phenanthrene was attempted, using the *p*-DMT–acetonitrile system; 9,10-dihydrophenanthrene was thus obtained in an 86% yield.

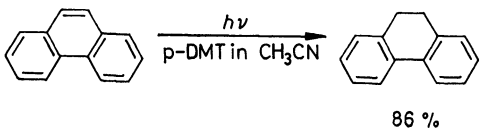

86 %

Experimental

The melting points were determined on a Yanagimoto hot stage and are uncorrected. The ^{1}H NMR spectra were measured on a JEOL JNM-PS-100 spectrometer, with tetramethylsilane as the internal standard. The IR spectra were taken on a Shimadzu IR-400 spectrometer, and the mass spectra, on a Hitachi RMU-6E. The UV spectra were measured on a Hitachi 124 spectrometer. The GLC was carried out on a Shimadzu GC-3BF apparatus using a column of SE-30 (5% on Celite 545, 0.75 m).

Materials. Spectral-grade acetonitrile was distilled three times over P_2O_5 and then twice over CaH_2 before use. The ethanol was distilled over CaH_2 and then over C_2H_5ONa before use. The diethyl ether was distilled over $LiAlH_4$. The benzene was washed three times with concentrated sulfuric acid, with a saturated sodium hydrogencarbonate solution, and three times with water, and was then distilled over P_2O_5. The tertiary aromatic amines (Tokyo Kasei) were distilled *in vacuo* before use. The anthracene (Nakarai Chemicals) was recrystallized five times from a mixture of benzene–ethanol and then sublimed. The phenanthrene was recrystallized three times from ethanol and then sublimed.

Photoreaction of Anthracene with the Amines. General Procedure: The experimental procedures used for the irradiation and isolation of the products were essentially identical in all the runs. A solution (150 ml) containing anthracene (0.5 g, 2.8 mmol) and an amine (5 g, 37 mmol) in a Pyrex vessel was bubbled with a nitrogen stream for 20 min and then irradiated with an Eikosha PIH-300 high-pressure mercury lamp under cooling with water. Except in the case of the benzene solution, the anthracene was not completely dissolved before the irradiation. The progress of the reaction was followed by GLC, and it was confirmed that the irradiation for 24 h resulted in the complete consumption of anthracene. During the irradiation, solids different from anthracene were precipitated except for a few cases where the yields of **2** or **4** are low (see Tables 1 and 2). The filtration of the solids gave **2** or **4**. After the removal of the solvent from the filtrate, vacuum distillation gave the starting amine (4—4.5 g). The remaining semisolids were dissolved into a minimal volume of benzene and then chromatographed on silica gel (Merck, 70—230 mesh). Elution with hexane and then with 10% benzene in hexane gave a mixture of **1** and **2**, to which hot hexane was then added; the filtration of the insoluble solids gave **2** while the evaporation of the filtrate left almost pure **1**. Further elution with a 1 : 1 benzene–hexane mixture gave **3a**—**c**. Tables 1 and 2 summarize the isolated yields of the photoproducts.

The **1** (mp 108 °C) was recrystallized from methanol and was identical to commercially available 9,10-dihydroanthracene (Tokyo Kasei) in all respects. The **2** (mp 245—246 °C) was recrystallized from benzene and identified as 9,9′,10,10′-tetrahydro-9,9′-bianthryl by direct comparison with an authentic sample prepared according to the known method.[14]

The **3a** was recrystallized from a benzene–ethanol mixture; mp 148—149.5 °C; UV (CH_3CN): $\lambda(\varepsilon)=266$ (2.3×10^4) and 306 nm (2.6×10^3); IR (KBr): 3000 (w), 2900 (w), 1610, 1520, 1470, 1450, 1350, 1230, 1200, 1190, 1160, 1060, 1040, 945, 865, 830, 800, 735, and 710 cm^{-1}; MS: 299 (M^{+}, 36%), 178 (40%), and 121 (100%); ^{1}H NMR ($CDCl_3$): δ 2.75 (s, 6H), 3.88 (br d, $J=2$ Hz, 2H), 5.10 (br t, $J=2$ Hz, 1H), 6.45—7.05 (A_2B_2q, $J=9$ Hz, 4H), and 7.06—7.40 (m, 8H); Found: C, 88.52; H, 7.12; N, 4.44%. Calcd for $C_{22}H_{21}N$: C, 88.25; H, 7.07; N, 4.68%.

The **3c** had a mp of 134—135.5 °C (from benzene–ethanol);

UV (CH_3CN): $\lambda(\varepsilon)=263$ (2.3×10^4) and 306 nm (2.6×10^3); IR (KBr): 3030 (w), 3000 (w), 2900—2820 (br, w), 2790, 1605, 1560, 1510, 1470, 1440, 1420, 1360, 1290, 1225, 1200, 1170, 1125, 1095, 1060, 960, 840, 830 (sh), 810, 800, 760, and 740 cm^{-1}; MS: 313 (M^+, 50%), 178 (43%), and 135 (100%); ^1H NMR ($CDCl_3$): δ 2.03 (s, 3H), 2.90 (s, 6H), 4.08 (br d, $J=3$ Hz, 2H), 5.20 (br t, $J=3$ Hz, 1H), 6.45—6.60 (m, 1H), 6.62 (br s, 1H), 6.90—7.41 (m, 9H); Found: C, 88.30; H, 7.41; N, 4.48%. Calcd for $C_{23}H_{23}N$: C, 88.13; H, 7.40; N, 4.47%.

Aromatization of ***3a*** *to 9-(*p*-Dimethylaminophenyl)anthracene.* A *p*-cymene solution (4 ml) containing **3a** (0.1 g) and 5% Pd–C (0.1 g) was bubbled with a nitrogen stream for 20 min and then refluxed for 1.5 h. After the filtration of the Pd–C, evaporation left yellow-green solids (90 mg). Recrystallization from benzene gave pure 9-(*p*-dimethylaminophenyl)-anthracene; mp 252—253 °C (lit,[8] 258 °C); Found: C, 88.62; H, 6.40; N, 4.83%. Calcd for $C_{22}H_{19}N$: C, 88.85; H, 6.44; N, 4.71%.

Photo-Birch Reduction of Phenanthrene with p-*DMT.* An acetonitrile solution (150 ml) containing phenanthrene (0.5 g, 2.8 mmol) and *p*-DMT (5 g, 37 mmol) was irradiated for 24 h; the complete consumption of phenanthrene was confirmed by GLC. After the removal of the solvent, 200 ml of diethyl ether was added to the remaining oil. The ether solution was washed with 150 ml of dilute hydrochloric acid (1 mol dm^{-3}) and three times with brine, and then dried ($MgSO_4$). The evaporation of the ether left an oil, which was then distilled *in vacuo* to give an oil (432 mg, bp 183—184 °C/25 mmHg†). This oil, which was confirmed by GLC to consist of only one component, was identical to commercially available 9,10-dihydrophenanthrene in all respects. To the hydrochloric acid solution sodium hydrogencarbonate was added until the solution became alkaline to litmus. The oil separated was extracted with three 50-ml portions of diethyl ether. The ether layer was dried ($MgSO_4$), evaporated, and then distilled *in vacuo* to give 4.0 g of *p*-DMT.

† 1 mmHg=133.322 Pa.

This work was supported by a Grant-in-Aid for Scientific Research No. 447067 from the Ministry of Education, Science and Culture.

References

1) Part XXXV: M. Yasuda, C. Pac, and H. Sakurai, *J. Org. Chem.*, **46**, 788 (1981).
2) J. B. Birks, "Photophysics of Aromatic Molecules," Wiley-Interscience, New York, N. Y. (1970).
3) R. S. Davidson, in "Molecular Association," ed by R. Foster, Academic Press, London (1975), Vol. 1; S. G. Cohen, A. Parora, and G. H. Parsons, Jr., *Chem. Rev.*, **73**, 141 (1973).
4) C. Pac and H. Sakurai, *Tetrahedron Lett.*, **1969**, 3829.
5) M. Ballas, D. Bryce-Smith, M. T. Clarke, A. Gilbert, G. Klunkin, S. Krestonosich, C. Mannig, and S. Wilson, *J. Chem. Soc., Perkin Trans. 1*, **1977**, 2571, and the references cited therein.
6) J. A. Barltrop, *Pure Appl. Chem.*, **33**, 179 (1973).
7) M. Ohashi, K. Miyake, and K. Tsujimoto, *Bull. Chem. Soc. Jpn.*, **53**, 1683 (1980), and the references cited therein.
8) E. de Barnett, J. W. Cook, and M. A. Matthews, *Recl. Trav. Chim. Pays-Bas*, **44**, 217 (1925).
9) N. Mataga and M. Ottolenghi, in "Molecular Association," ed by R. Foster, Academic Press, London (1979), Vol. 2; A. Weller, *Pure Appl. Chem.*, **16**, 115 (1968).
10) J. Saltiel, D. E. Townsend, B. D. Watson, P. Schannon, and S. L. Finson, *J. Am. Chem. Soc.*, **99**, 884 (1977). See also N. C. Yang, D. M. Schold, and B. Kim, *ibid.*, **98**, 6587 (1976).
11) H. Masuhara, T. Hino, and N. Mataga, *J. Phys. Chem.*, **79**, 994 (1975).
12) S. Arai and L. M. Dorfman, *J. Chem. Phys.*, **41**, 2190 (1964); S. Arai, E. L. Tremba, J. R. Brandon, and L. M. Dorfman, *Can. J. Chem.*, **45**, 119 (1967).
13) M. Van Meerssche and G. Leroy, *Bull. Soc. Chim. Belges.*, **69**, 204 (1960).
14) H. J. S. Winkler and H. Winkler, *J. Org. Chem.*, **32**, 1695 (1967).

CIDNP Studies of the Thermal Decomposition of Arylazo Aryl Sulfones

Masato YOSHIDA,* Naoki FURUTA, and Michio KOBAYASHI

Department of Chemistry, Faculty of Science, Tokyo Metropolitan University, Fukazawa, Setagaya-ku, Tokyo 158

(Received November 4, 1980)

^{1}H-and ^{13}C-CIDNP spectra were obtained during the thermal decomposition of several arylazo aryl sulfones (Ar–N=N–SO_2–Ar') in tetrachloroethylene or 1,1,2,2-tetrachloroethane at 100 °C. An enhanced absorption from the C_1 of the starting material, azo sulfone, was observed; this indicates that the decomposition of azo sulfone proceeds by means of one-bond fission. The formation of sulfones ($ArSO_2Ar'$) and sulfinic esters (ArO(SO)Ar') as recombination products in a solvent cage was established from the signs of polarization (enhanced absorption or emission).

Arylazo aryl sulfones (**1**) decompose unimolecularly when they are heated in neutral or weakly basic media;[1] the generation of an aryl and sulfonyl radical pair has been proposed on the basis of kinetics,[2] product studies,[3] or the spin trapping of free radicals generated from the arylazo aryl sulfones.[4] In the case of aliphatic azo

$$\mathrm{Ar{-}N{=}N{-}S{-}Ar' \longrightarrow Ar\cdot + N_2 + Ar'S\cdot} \quad (1)$$

compounds such as α,α'-azobisisobutyronitrile, solvent-cage products of the geminate radical pair are the main products. On the other hand, the homolysis of arylazo aryl sulfones gives the expected cage product, sulfones ($ArSO_2Ar'$), in only a small yield. These sulfones may be either cage-recombination products or products of the induced decomposition of the azo sulfones by aryl radicals. We have, therefore, studied the ^{1}H-and ^{13}C-CIDNP spectra (chemically induced dynamic nuclear polarization) observed during the thermolysis of several arylazo aryl sulfones in order to clarify the details of the reaction mechanism; the results will be presented in this paper.

Results and Discussion

The thermal decomposition of arylazo aryl sulfones (**1a—g**) was carried out in tetrachloroethylene or 1,1,2,2-tetrachloroethane.

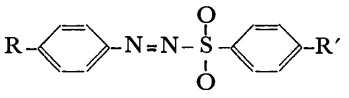

	1a	**1b**	**1c**	**1d**	**1e**	**1f**	**1g**	**1a**-d_3
R	H	Me	Cl	NO_2	NMe_2	H	H	D(2,6-D_2)
R'	Me	Me	Me	Me	Me	H	Cl	Me

Decomposition of Azo Sulfones in Tetrachloroethylene. The rate of the decomposition of **1a** in tetrachloroethylene was determined by following the evolution of the nitrogen gas by the method described in Ref. 2. The reaction was first-order in **1a**, and the rate constant was calculated to be 6.10×10^{-4} s^{-1} (90.8 °C). This value is comparable to those in ethylbenzene, chlorobenzene, or nitrobenzene.[2] The decomposition products of **1a** are shown in Table 1.

When the ^{1}H-NMR spectra of **1a—d** and **1f—g** were observed at 100 °C, strong CIDNP signals appeared in the field of the aromatic-proton region for about 15 min. No CIDNP signal was, though, observed in the field of the methyl-proton region. Since **1e** is rather stable and decomposes very slowly at 100 °C,[1] no CIDNP signal could be observed. To prevent the acid-catalyzed heterolysis of **1**, the ^{1}H-NMR spectra were observed in the presence of 2 mol of triethylamine per mol of azo sulfones. The CIDNP spectrum of **1a** under these conditions is shown in Fig. 1. Enhanced absorption signals were observed in the field of δ 7.89—7.72 and 7.10, and strong emission signals were observed at δ 7.30 and 7.20. The intensity of the CIDNP

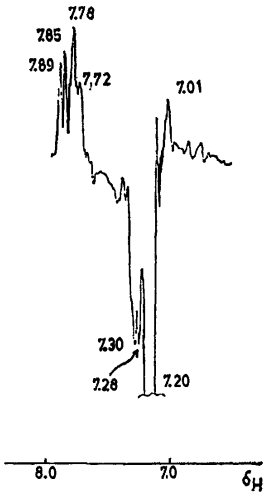

Fig. 1. ^{1}H-CIDNP spectrum in the thermal decomposition of **1a** in the presence of triethylamine in tetrachloroethylene at 100 °C.

Table 1. Products of thermal decomposition of **1a** in tetrachloroethylene

Product	Yield/mol%	Product	Yield/mol%
$PhCCl{=}CCl_2$	21.9	*p*-$CH_3C_6H_4SO_2Cl$	16.9
PhCl	6.1	*p*-$CH_3C_6H_4SO_2Ph$	6.5
PhH	4.9	*p*-$CH_3C_6H_4SO_2OPh$	27.7
Ph–N=N–Ph	3.5	*p*-$CH_3C_6H_4SO_2SC_6H_4CH_3$-*p*	14.1
		p-$CH_3C_6H_4SO_3H$	*ca.* 20

signal at δ 7.20 was very high when triethylamine was added. The ^{1}H-NMR spectrum of 2,4,6-trideuteriophenylazo *p*-tolyl sulfone (**1a**-d_3) at 100 °C was also observed. The enhanced absorption at δ 7.89—7.72 and the emission of δ 7.30 observed in **1a** disappeared, while an enhanced absorption appeared at δ 7.31. The strong emission at δ 7.20 was still observed with **1a**-d_3. From the results described above, and by comparison with the chemical shift of the authentic samples, some signals were assigned as is shown below:

Enhanced absorption	at δ 7.89 —7.72	*o*-H of the phenyl group of phenyl p-tolyl sulfone(**2a**)
Emission	at δ 7.30	*o*-H of α,β,β-trichlorostyrene
Emission	at δ 7.20	Benzene

The assignment of the ^{13}C-CIDNP signals can be expected to be easier than that of the ^{1}H-CIDNP signals, so the ^{13}C-NMR spectrum of **1a** at 100 °C was observed. CIDNP signals were also obtained in the field of the aromatic region for more than 20 min. The intensity of the CIDNP signals as a whole increased when pyridine was added to prevent acid-catalyzed heterolysis. The observed CIDNP spectrum of **1a** in the presence of pyridine is shown in Fig. 2, while the chemical shifts and assignments of the CIDNP signals are tabulated in Table 2. The signals were assigned by comparison with the chemical shifts of the authentic samples of the products, shown in Table 2.

Table 2. ^{13}C-CIDNP data for thermal decompositin of **1a**[a)]

No.[b)]	Chemical shift[c)]	Polarization	Assignment[d)]
1	153.2	A	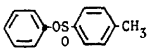
2	152.3	E	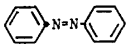
3	149.2	A	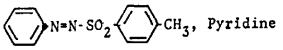 Pyridine
4	142.6	E	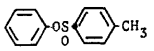
5	142.3	A	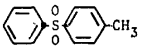
6	139.1	E	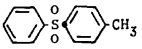
7	136.7	E	Not assigned
8	135.0	E	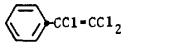
9	134.6		Pyridine
10	122.5		Pyridine
11	119.7		Solvent
12	157.7	A	

a) Pulse interval, 3 s; accumulation, 20; spectral width, 2.5 KHz; data memory, 4K, and pulse width, 9 μs (45° pulse). b) Signal number shown in Fig. 2. c) Ppm from internal TMS. d) • shows polarized carbons.

On the basis of the CIDNP data, the following conclusions could be drawn:

1) As has been mentioned before, azo sulfones decompose unimolecularly. Mechanistically, there may be two possible decomposition modes: one is the one-bond fission to give an aryldiazenyl sulfonyl radical pair (Eq. 2), while the other is the two-bond fission to give an aryl radical, a sulfonyl radical, and nitrogen simultaneously (Eq. 3). The observation of the enhanced

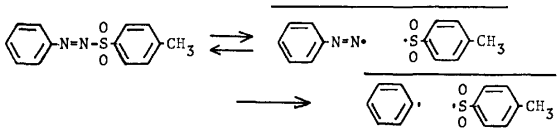

(2)

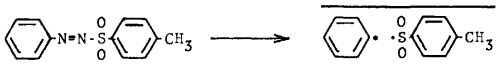

(3)

absorption of the C_1 of **1a** itself indicates that the decomposition of **1a** is reversible, and so it must take place by means of one-bond fission. The sign in the net polarization (Γ_{ne}), as calculated according to Kaptein's rule[5)] agrees with the observed mode:

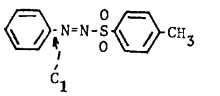

	μ	ε	Δg	a	Γ_{ne}	obsd
C_1	−	+	−	+[6)]	+	A

$g<2.0010$[7)](Ph-N=N•); 2.0041[8)](•$SO_2C_6H_4CH_3$-*p*)

2) If one assumes that the sulfone (**2a**) obtained from the decomposition of **1a** is the cage product, the sign in the net polarization (Γ_{ne}), as calculated according to Kaptein's rule, again agrees with the observed mode:

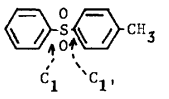

	μ	ε	Δg	a	Γ_{ne}	obsd
C_1	−	+	−	+[9)]	+	A
$C_{1'}$	−	+	+	+[10)]	−	E

$g=2.00234$[11)](Ph•)

The observation of the CIDNP signals of sulfone (**2a**) and the coincidence of the signs mentioned above indicate that **2a** is the cage product from the phenyl *p*-toluenesulfonyl singlet-radical pair.

3) As is shown in Table 1, phenyl *p*-toluenesulfinate (**3a**) was not detected among the decomposition products of **1a**. In the ^{13}C-CIDNP spectra of **1a** shown in Fig. 2, however, the emission and enhanced absorption signals of this sulfinic ester (**3a**) were observed for 2.5—3.5 min. Also, the sign of the net polarization (Γ_{ne}), as calculated according to Kaptein's rule, agrees with the observed results if one assumes that **3a** is the cage product:

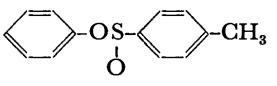

	μ	ε	Δg	a	Γ_{ne}	obsd
C_1	−	+	−	+	+	A
$C_{1'}$	−	+	+	+	−	E

Since **3a** is unstable,[12)] it could not be isolated as a product of the decomposition of **1a**. The ^{13}C-CIDNP study described here shows that not only the sulfone (**2a**), but also the sulfinic ester (**3a**) is generated as the

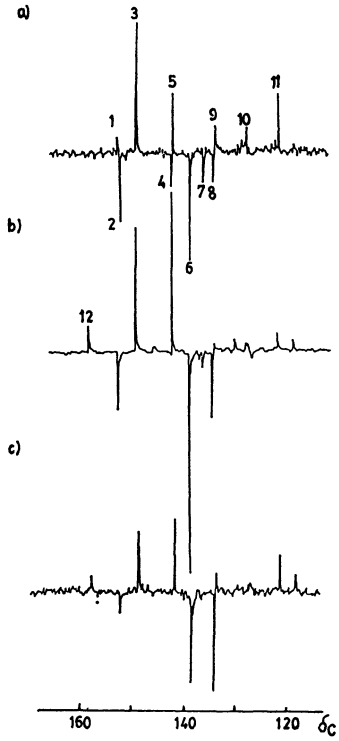

Fig. 2. ^{13}C-CIDNP spectra in the thermal decomposition of **1a** in the presence of pyridine in tetrachloroethylene.
After a) 2.5—3.5, b) 8—9, and c) 20—21 min heating of **1a** in NMR probe at 100 °C.

cage product from the phenyl *p*-toluenesulfonyl radical

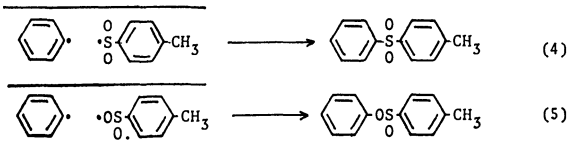

pair. These findings clearly establish that the sulfonyl radical is ambident and acts as either an S- or O-centered radical.

Scavenged products of the escaped phenyl radical in which polarization is maintained should show emission signals (memory effect). The formation of α,β,β-trichlorostyrene (**4**), azobenzene (**5a**), and benzene can be explained by the following mechanism:

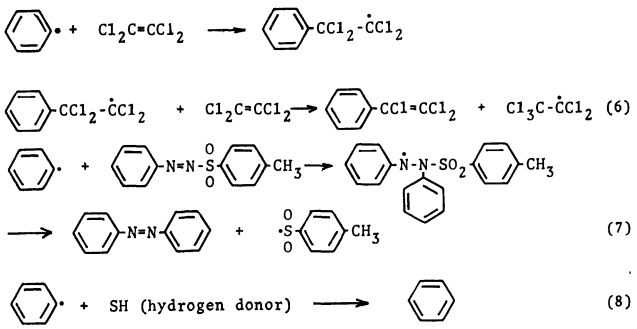

Scheme 1.

These reaction mechanisms are supported by the following experimental findings:

(i) When a large amount of the azo sulfone (**1a**) was present at the beginning of the decomposition, the intensity of the CIDNP signal of azobenzene (**5a**) was very strong, but toward the end of the reaction it decreased. On the other hand, the intensity of the CIDNP of α,β,β-trichlorostyrene (**4**) increased toward the end of the reaction.

(ii) When the ^{13}C-NMR spectrum of a mixture of **1a** and **1c** was measured at 100 °C, the CIDNP signal of 4-chloroazobenzene (4-ClC_6H_4–N=N–Ph **5b**) also appeared. This shows that the escaped phenyl radical attacks both **1a** and **1c**. As has been mentioned before, the rate of the decomposition of **1a** was first-order in **1a**, but a high concentration of azo sulfone at the beginning of the decomposition may favor the induced decomposition (Eq. 7).

(iii) The intensity of the emission of the benzene proton (δ 7.20) was strengthened in the presence of triethylamine. This shows that the escaped phenyl radical abstracts hydrogen from the *N*-ethyl group in the presence of triethylamine.

In conclusion, ^{1}H-and ^{13}C-CIDNP studies support the idea that the thermal decomposition of **1a** in a solvent cage occurred according to Scheme 2 and that the reaction mechanism of the escaped phenyl radicals is explained by Scheme 1.

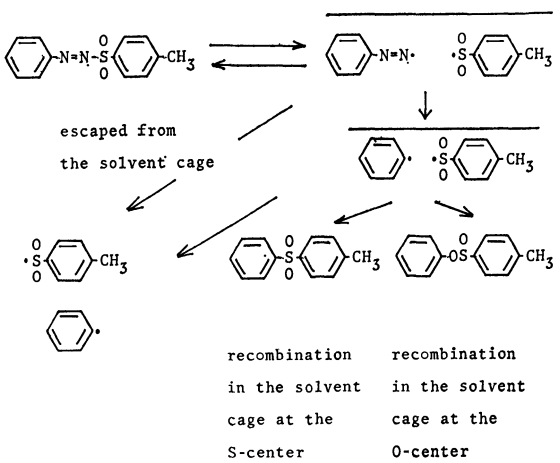

Scheme 2.

Decomposition of Azo Sulfones in 1,1,2,2-Tetrachloroethane. The decomposition of azo sulfone in 1,1,2,2-tetrachloroethane, which may act as a hydrogen donor, was also studied. The rate of the decomposition of **1a** at 90.1 °C was determined by measuring the amount of nitrogen gas by the method described in Ref. 2. It followed a first-order rate equation in **1a** at the beginning of the reaction and they increased toward the end of the reaction. This may be explained by the acid-catalyzed ionic decomposition due to the formation of sulfinic or sulfonic acid. The decomposition products of **1a**, as summarized in Table 3, show that the products and their yields in 1,1,2,2-tetrachloroethane were different from those in tetrachloroethylene.

When the ^{1}H-NMR of **1a** was measured in 1,1,2,2-tetrachloroethane at 100 °C, a strong emission signal was observed at δ 7.29, just as in tetrachloroethylene.

Table 3. Products of thermal decomposition of **1a** in 1,1,2,2-tetrachloroethane

Product	Yield/mol%	Product	Yield/mol%
PhH	36.0	$PhSO_2C_6H_4CH_3$-*p*	8.1
PhCl	14.8	*p*-$CH_3C_6H_4SO_2Cl$	9.6
Cl_2C=CHCl	17.3	*p*-$CH_3C_6H_4SO_2OPh$	18.5
Ph–N=N–Ph	1.3	*p*-$CH_3C_6H_4SO_2SC_6H_4CH_3$-*p*	12.6
		p-$CH_3C_6H_4SO_3H$	*ca.* 20

In the presence of 2 mol of triethylamine per mol of azo sulfone, the intensity of the emission signal at δ 7.29 increased, but not so markedly as in the case of tetrachloroethylene. These CIDNP signals were assigned to benzene. The escaped phenyl radical mainly abstracts hydrogen from the solvent, since the solvent is the hydrogen donor.

Experimental

The ^{1}H-NMR spectra were taken with a Hitachi R-20B spectrometer. The ^{13}C-NMR spectra were taken with a JEOL Fx-60 FT-NMR spectrometer.

Materials. All the arylazo aryl sulfones except **1e** were prepared from the substituted benzenediazonium chlorides and sodium salts of the substituted benzenesulfinic acid.[1] Compound **1e** was prepared from *p*-dimethylaminobenzenediazonium tetrafluoroborate and sodium *p*-toluenesulfinate in water.

Products of Thermal Decomposition of 1a. After the decomposition was complete, the reaction mixture was washed with a 5% aqueous solution of sodium carbonate. The benzene, chlorobenzene, and trichloroethylene were then determined by gas chromatography. The other products listed in Table 1 or 3 were separated by column chromatography on Florisil. Each product was identified by means of its mp, IR, and ^{1}H-NMR spectra. The sodium carbonate extracts were concentrated under reduced pressures and made weakly acidic by the addition of hydrochloric acid, and the *p*-toluenesulfonic acid in the solution was precipitated as its *S*-benzylisothiuronium salt.

CIDNP Spectra. A solution of azo sulfone (*ca.* 0.2 mol/l) in tetrachloroethylene or 1,1,2,2-tetrachloroethane was inserted in a NMR probe which had been heated at 100 °C, and the ^{1}H-NMR or ^{13}C-NMR was measured.

References

1) M. Kojima, H. Minato, and Kobayashi, *Bull. Chem. Soc. Jpn.*, **45**, 2032 (1972).
2) M. Kobayashi, H. Minato, M. Kojima, and N. Kamigata, *Bull. Chem. Soc. Jpn.*, **44**, 2501 (1971).
3) M. Kobayashi, S. Fujii, and H. Minato, *Bull. Chem. Soc. Jpn.*, **45**, 2039 (1972).
4) M. Kobayashi, E. Akiyama, H. Minato, and N. Kito, *Bull. Chem. Soc. Jpn.*, **47**, 1504 (1974).
5) R. Kaptein and J. Osterhoff, *Chem. Phys. Lett.*, **4**, 195, 214 (1969).
6) K.-G. Seifert and F. Gerhalt, *Tetrahedron Lett.*, **1974**, 829.
7) J. Brokken Zijp and H. van de Bogaert, *Tetrahedron Lett.*, **1974**, 249.
8) M. McMillan and W. A. Waters, *J. Chem. Soc., B*, **1966**, 422.
9) J. A. Pople, D. L. Beveridge, and P. A. Dobosh, *J. Am. Chem. Soc.*, **90**, 4201 (1968).
10) When the ^{13}C-NMR spectrum of the mixture of *p*-toluenesulfonyl iodide and phenylazotriphenylmethane in tetrachloroethylene was observed at 100 °C, enhanced absorption signals from the C_1 of *p*-tolyl triphenylmethyl sulfone were obtained. In this case sulfone should be formed by the encounter of free radicals. Therefore, the sign of the hyperfine splitting constant for the C_1 of the sulfonyl radical is estimated to be negative; M. Yoshida, A. Yano, and M. Kobayashi, 40th National Meeting of the Chemical Society of Japan, Fukuoka, October 1979.
11) P. H. Kasai, P. A. Clark, and E. B. Whipple, *J. Am. Chem. Soc.*, **92**, 2640 (1970).
12) A. H. Wragg, J. S. McFadyen, and T. S. Stevens, *J. Chem. Soc.*, **1958**, 3603.

Proton Equilibria of 5-Dimethylamino-1-naphthalenesulfonyl Group Conjugated to Bovine Serum Albumin. II. Neighboring Effects in Urea and Guanidinium Chloride Solutions

Nobuo IKUTA,† Eisaku NOMURA, Joichi KOGA,* and Nobuhiko KUROKI

Department of Applied Chemistry, University of Osaka Prefecture, Mozu-Umemachi, Sakai, Osaka 591

(Received November 18, 1980)

Protonation to the fluorescent probe, 5-dimethylamino-1-naphthalenesulfonyl group, which had been conjugated to bovine serum albumin, was investigated in aqueous solutions of urea and guanidinium chloride. pK values not less than those of the free probe were present even in the positive range of net charge on the protein at high concentration of the denaturants. This was interpreted in terms of the electrostatic and nonpolar effects based on short-range interaction between the probe and its neighboring residues. These effects were substantiated by the reduction of the disulfide bonds in the protein and by the variation of the dielectric constant of the local environment surrounding the probe.

Studies on the acid-base equilibria of optical probe-protein conjugates have been carried out in order to clarify the short-range interaction among the constituent residues.[1-6] A report was given on the acid-base equilibria of the fluorescent probe, 5-dimethylamino-1-naphthalenesulfonyl group (DNS) conjugated to bovine serum albumin (BSA) with various degrees of conjugation.[6] It was found that the apparent dissociation constant, K_a, of the dimethylamino moiety of the DNS–BSA conjugates with less than 1.0 mol of the probe per mol of the protein changes according to the conformational change by acid denaturation. However, the pK_a values of the DNS conjugates at various pH were less than the theoretical values estimated from the Debye-Hückel electrostatic shielding effect on the surface of the protein. The deviation might be ascribed in part to the effect of the nonpolar environment surrounding the probe owing to its hydrophobicity in the basic form.

In order to evaluate the effect of the nonpolar environment, the behavior of the pK_a values of the DNS conjugate was studied at various concentrations of denaturants, such as urea and guanidinium chloride (GuHCl). The denaturants interact strongly with peptide backbone,[7,8] enhancing the solubility of nonpolar groups either by altering the bulk properties of the solvent or through more localized effect.[7,9,10] The former weakens interpeptide hydrogen bonds, the latter reducing hydrophobic interactions. Thus, the denaturation on urea or GuHCl makes the conformational state of the protein less compact and simultaneously, brings about the lowering in hydrophobicity or non-polarity inside the protein. We might expect that the change in the pK_a value is influenced by only the charge of the protein at high concentrations of the denaturants.

The results of the variation of pK_a values at such high concentrations of the denaturants show that the negatively charged groups are present in the neighborhood of the probe in the positive range of the net charge of the protein. The neighboring effect due to the electrostatic interaction is maintained by the disulfide bonds in the protein even in the denaturant solutions.

† Present address: Osaka Municipal Technical Research Institute, Kita-ku, Osaka 530.

Experimental

Materials. The DNS–BSA conjugate used in this experiment was prepared as described previously[6] and contained less than 1.0 mol of the probe per mol of the protein. Such a degree of conjugation has no influence on the conformation of the protein.[6] The reductive cleavage of the disulfide bonds of the DNS–BSA conjugate in 6 M (1 M= 1 mol dm^{-3}). urea or GuHCl solution were accomplished by dithiothreitol (DL-*threo*-1,4-dimercapto-2,3-butanediol) and iodoacetamide according to the procedure of Bewley *et al.*[11] Water was deionized and then distilled. Urea and GuHCl were recrystallized from methanol–water solution. Electrolytes of reagent grade were used without further purification.

Fluorescent Measurements. Solutions of the DNS–BSA conjugate with 1.1×10^{-5} M of the protein were prepared by taking requiste amounts of a stock solution of the DNS–BSA conjugate, solid urea or GuHCl, and water in volumetric flasks. Measurements of the pH and fluorescent spectra of the solutions were carried out as reported[6] with the excitation wavelength taken at 340 nm where only the probe in the basic form absorbs light. In order to obtain the true emission spectra, the measured emission spectra were corrected by using the known emission spectrum of quinine sulfate as a standard.[12]

Potentiometric Titration. Potentiometric titration was carried out in order to determine the number, $\bar{Z}_H$, of proton bound to the protein. The solution of BSA with an appropriate concentration of the denaturants was dialyzed for 48 h against the same concentration of CO_2-free denaturant solution at 25 °C. The protein concentration was in the range 10^{-4} M, about 10 times that for the fluorescent measurements for obtaining the accurate values of $\bar{Z}_H$. Titration of 30 mL (1 L=1 dm^3) of prepared solutions was carried out under nitrogen atmosphere at 25 °C with a Hitachi-Horiba F-7AD pH meter equipped with a Hitachi-Horiba 6326-05C combination electrode. Titrant, 0.5 M HCl, was added with a Mitamura Riken Mechanical Buret (syringe type; a minimum volume of readings, 2.5 μL). The solvent containing the corresponding denaturant was titrated in the same way. No difference in titration curves between the unconjugated and conjugated proteins could be detected in the case of 0.01 M NaCl, 6 M GuHCl, and 8 M urea; the unconjugated protein was employed in the other cases.

Results and Discussion

Fluorescence of DNS Conjugate. The fluorescence

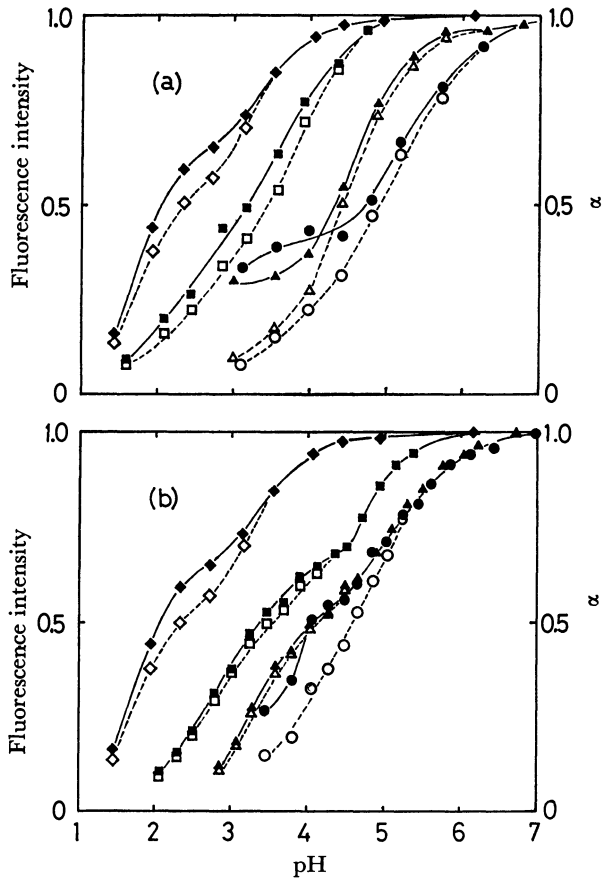

Fig. 1. Variation of fluorescence intensity (open symbols) and fraction in the basic form (closed symbols) of the DNS–BSA conjugate as a function of pH in denaturant solutions. (a) Concentration of urea: 8 M (○, ●), 4 M (△, ▲), 2 M (□, ■), and 0 M (◇, ◆). (b) Concentration of CuHCl: 6 M (○, ●), 4 M (△, ▲), 2 M (□, ■), and 0 M (◇, ◆). Fluorescence intensity is defined by taking a maximum in the intensities measured at each concentration of the denaturants as 1.0. α is calculated with Eq. 2.

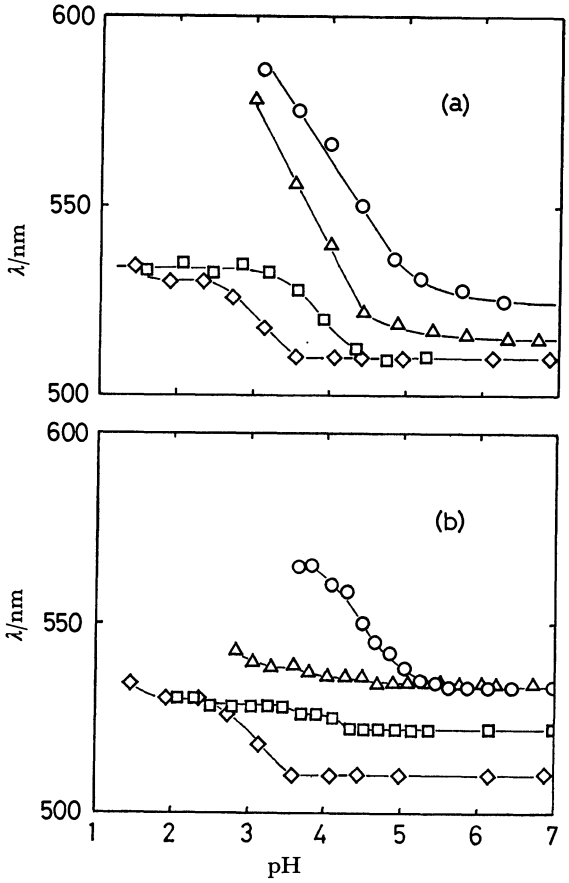

Fig. 2. Plots of peak wavelength of the fluorescence of the DNS–BSA conjugate against pH of the denaturant solutions. (a) Concentration of urea: 8 M (○), 4 M (△), 2 M (□), 0 M (◇). (b) Concentration of GuHCl: 6 M (○), 4 M (△), 2 M (□), 0 M (◇).

intensities of the DNS–BSA conjugate obtained at different concentrations of urea and GuHCl are shown as a function of pH in Figs. 1(a) and 1(b), respectively. In the absence of denaturants the 0.01 M NaCl solution was employed. A maximum in all the fluorescence intensities measured at each denaturant concentration is arbitrarily assigned the numerical value of 1.0 on the ordinates in the figures. Each sigmoid curves can be ascribed in part to the acid-base equilibrium of the conjugated probe since the protonation of the probe quenches the fluorescence, only the probe in the basic form giving the fluorescence.[16]

The peak wavelengths corresponding to the fluorescence in the solutions of urea and GuHCl are also shown in Figs. 2(a) and 2(b), respectively. The peak shifts progressively to higher wavelengths both with an increase of the denaturant concentration and with a decrease of the pH value, reaching 590 nm for the most acidic solution of 8 M urea and 6 M GuHCl. The shift is closely dependent on the change of the polarity of the environment surrounding the probe. Similar shifts in peak wavelength was observed in the fluorescence of DNS–amino acid conjugates in various organic solvents.[13–15] This type of change in the fluorescence with change of solvent polarity has been explained theoretically in terms of the differences in solvent interaction energies of the ground and excited states arising from differences in the polarities or dielectric constants of the states.[13,14] Thus, with increase in the dielectric constant of the organic solvent the peak shifts to higher wavelength, the quantum yield of the fluorescence decreasing. Variation of the peak wavelength and quantum yield with the dielectric constant of solvent was reported by Abe *et al.* for the fluorescence of three DNS–amino acid conjugate, *viz.* DNS–L-alanine, DNS–L-leucine, and DNS–L-phenylalanine, in various organic solvents.[15]

pK_a *Values in Denaturant Solutions.* The relative fluorescence intensities (Fig. 1) change not only with quenching by the protonation of the probe but also with the change in quantum yield of the probe in the basic form.[16] The relative fluorescence intensity, F, should be corrected in order to calculate the true fraction, α, of the probe in the basic form.

Since the fluorescence observed arises from the basic form,[16] F can be related to the quantum yield, Φ, and the concentration, C, of the basic form:

$$F \propto I_0 \varepsilon C \Phi,$$

where I_0 is the strength of the incident beam, and ε the molar absorption coefficient of the basic form at 340 nm. Factors ε and I_0 are constant, while C is dependent upon the degree of the protonation to the probe, Φ changing with the peak wavelength, λ, of the fluorescence measured at each pH value of a denaturant solution. When the fluorescence at different pH values of the solution give the peak wavelengths, λ_1 and λ_2, the relation between the relative fluorescence intensities, $F(\lambda_1)$ and $F(\lambda_2)$, can be written as

$$\frac{F(\lambda_1)}{F(\lambda_2)} = \frac{C_1\Phi(\lambda_1)}{C_2\Phi(\lambda_2)}, \quad (1)$$

where $\Phi(\lambda_1)$ and $\Phi(\lambda_2)$ are the quantum yields giving the corresponding wavelengths, and C_1 and C_2 the respective molarities of the probe in the basic form existing in the solution with the different pH values. If $F(\lambda_2)$ is taken as the fluorescence intensity in the case where all the probe becomes the basic form, α is equal to C_1/C_2, so that

$$\alpha = \frac{F(\lambda_1)\Phi(\lambda_2)}{F(\lambda_2)\Phi(\lambda_1)}. \quad (2)$$

When λ_1 is equal to λ_2, the α value is equal to the ratio $F(\lambda_1)/F(\lambda_2)$. Then, the relative intensity of $F(\lambda_1)$ is identical with the α value if $F(\lambda_2)$ is taken as 1.0 (Fig. 1).

Since the peak wavelength was shifted, $\Phi(\lambda_1)/\Phi(\lambda_2)$ was evaluated from the results obtained by Abe *et al.*[15] The α values calculated by Eq. 2 are shown by closed symbols in Figs. 1(a) and 1(b). The maximum of all the measured fluorescence intensities is taken as the α value of 1.0. The apparent dissociation can be calculated from the α and pH values by the following Henderson-Hasselbalch equation:

$$pK_a = pH - \log\frac{\alpha}{1-\alpha}. \quad (3)$$

The pK_a values in urea and GuHCl solutions are shown as a function of pH in Figs. 3(a) and 3(b), respectively.

Neighboring Effect on pK_a. The pK_a values determined at each pH value increased with an increase in concentrations of the denaturants, suggesting that the probe inside the protein is exposed to the solvent according to the concentration of the denaturants which weaken the hydrophobic interaction between the probe and the nonpolar residues. In the absence of the hydrophobic interaction, the shift of pK_a from the logarithm of the reciprocal of dissociation constant, pK_0, of the free probe can be attributed to the electrostatic interaction between the probe and the charged residues. Taking only the long-range electrostatic effect of the protein based on the Debye-Hückel theory into account,[17] the pK_a values in the range of positive net charge of the protein might be less than the pK_0 values.

The pK_0 values were determined for 1.0×10^{-5} M of DNS-glycine conjugate as a model of the free probe in the corresponding solution: 3.94 in 0.01 M NaCl; 3.93, 4.00, and 4.17 in 2, 4, and 8 M urea; 3.99, 4.00, and 3.99 in 2, 4, and 6 M GuHCl, respectively. The results show that the dissociation constant gives about 4.0 in pH units, either in the presence or in the absence of the denaturants. The value of 4.0 is shown by a dashed line in Fig. 3.

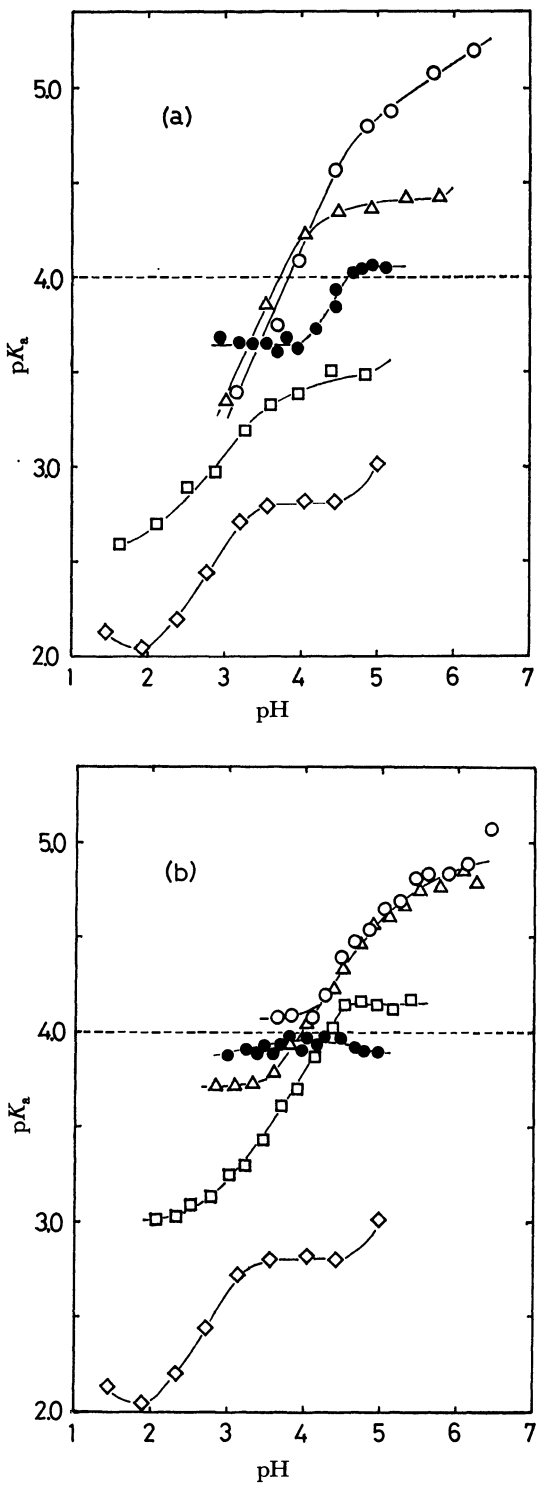

Fig. 3. Apparent pK_a values as a function of pH in the solution of urea (a) and GuHCl (b). Open symbols are obtained for the DNS-BSA conjugate with disulfide bonds at the same concentration of the denaturants as those in Fig. 2. Closed circles are obtained for the DNS-BSA conjugate with disulfide bonds ruptured by the reduction at 6 M of urea (a) and of GuHCl (b).

The pK_a values are not less than the pK_0 values under high concentration of the denaturants. This can be at least anticipated to involve a contribution of the electrostatic effect of negatively charged residues

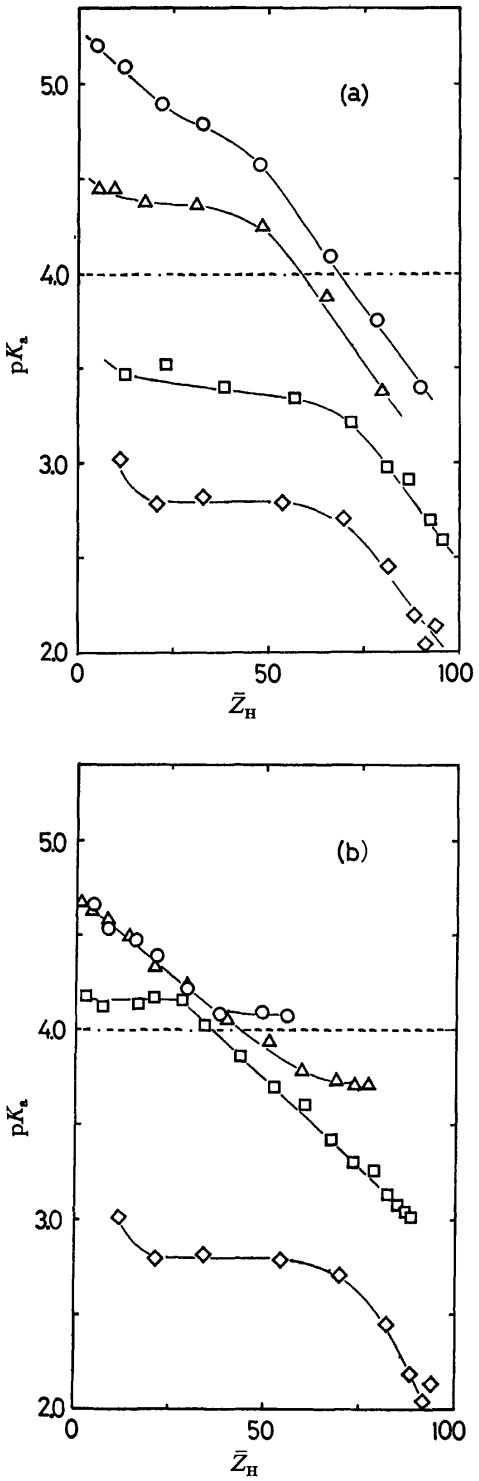

Fig. 4. Apparent pK_a values as a function of $\bar{Z}_H$ in the solutions of urea (a) and GuHCl (b). Symbols are the same as in Fig. 2.

on the acid-base equilibrium of the probe, since the positively charged residues apparently weaken the basic properties of the probe. If we assume that the electrostatic effect is attributable to only the long-range electrostatic interaction, the phenomenon should appear in the range of negative net charge of the protein. The net charge, $\bar{Z}_H$, from the isoelectric point, p*I*, of the protein was determined at various pH in each denaturant solution. The p*I* values were 5.3 in 0.01 M NaCl; 6.4, 6.6, and 7.0 in 2, 4, and 8 M urea; 5.3, 5.3, and 5.6 in 2, 4, and 6 M GuHCl. The pK_a values are plotted in Fig. 4 as a function of $\bar{Z}_H$ instead of pH. The pK_a values not less than the pK_o values are observed even in the range of positive $\bar{Z}_H$ values. This makes it impossible to account for the acid-base equilibrium at the high concentration of the denaturants in terms of the long-range electrostatic interaction. A possible explanation for the observed behavior may be the contribution of the short-range electrostatic interaction between the probe and the negatively charged residues situated in the neighborhood of the probe.

Variation of pK_a *in Reduction of Disulfide Bonds.* Proteins denatured by urea and GuHCl exist as random coils, but the transition to the denatured state is often incomplete even at the highest denaturant concentrations, especially when the native conformation is stabilized by disulfide bonds.[18] It is possible that the local structures surrounding the disulfide bonds maintain the structure of the native protein even in the concentrated denaturant solution. Since a molecule of BSA has seventeen of cystine with a disulfide group as seen from the complete data for the primary structure of BSA reported by Brown,[19] the fixed structures around such disulfide bonds might contribute largely to the neighboring effect on the acid-base equilibrium of the probe.

For the sake of confirmation, the disulfide bonds in the DNS–BSA conjugate were subjected to reductive cleavage by dithiothreitol in 6 M of urea or GuHCl solutions. The pK_a values for the DNS–BSA conjugate with the reduced disulfide bonds were determined in these denaturant solutions (Fig. 3). The values do not exceed the pK_o values in the denaturant solutions, *i.e.*, 4.17 in 8 M urea and 3.99 in 6 M GuHCl in the range of pH measured. The results showing that the neighboring effect disappears with the reduction of the protein suggest that the disulfide bonds play a significant role for fixing the relative situation of the probe and the ionized residues even in the denaturant solutions.

The change of pK_a against pH in the case of the reduced protein was not so remarkable as that in the case of unreduced one. $\bar{Z}_H$ values for the reduced protein were not dentermined, the pK_a values for the reduced DNS–BSA conjugate being less than those for the unreduced one in lower pH range. This suggests that the acid-base equilibrium of the probe is affected remarkably by the positively charged residues, as well as negatively charged residues, according to the dissociation of the ionizable group surrounding the probe.

Dielectric Constant of the Environment Surrounding the Probe. Appearance of the electrostatic neighboring effect is manifested by the lowering of the hydrophobicity around the probe. However, the hydrophobicity should also affect the shift of pK_a as the nonpolar neighboring effect. Since the denaturants weaken the hydrophobic interaction between the nonpolar residues, the local environment surrounding probe might have a solvent-like polarity with a high dielectric constant.

The change of such a local environment can be recognized as that of the medium in which the probe

exist. The nonpolar neighboring effect might be related to the medium effect in organic-water solvents. If a neutral species in the basic form, B^0, which gives a pK_0 value in water exists in a medium with a dielectric constant, D, the pK_a value in the medium can be written as

$$pK_a - pK_0 = \frac{e^2}{2.3rkT}\left(\frac{1}{D_w}-\frac{1}{D}\right), \quad (4)$$

where e, k, and D_w are proton charge, Boltzman constant, and dielectric constant of water, respectively, and r is the mean radius of the ions which forms HB^+ and X^- in the protonation of B^0 by an acid, HX, if these ions are regarded as rigid spheres. The relation is derived from Born's model to account for the medium effect theoretically.[20] Equation 4 shows that the shift of pK_a from pK_0 is proportional to $(1/D_w - 1/D)$.

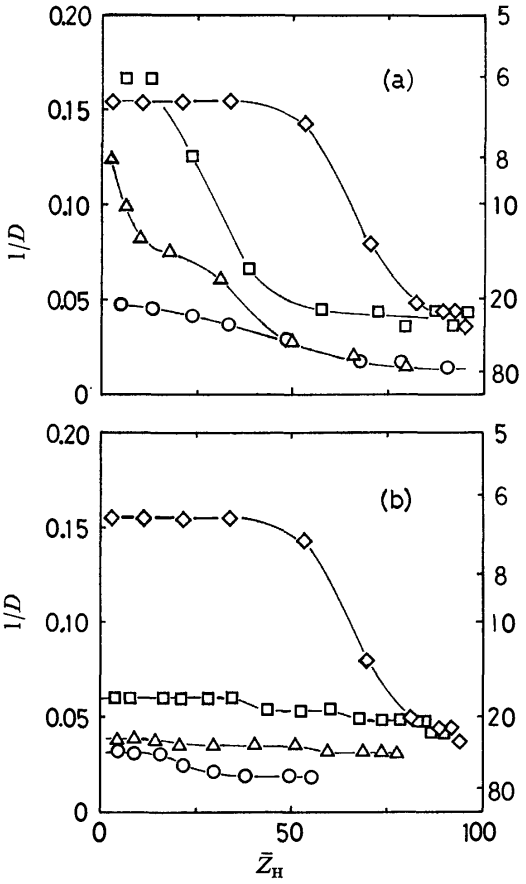

Fig. 5. Plots of the reciprocal of dielectric constant surrounding DNS as a function of $\bar{Z}_H$ in the solutions of urea (a) and GuHCl (b). Symbols are the same as in Fig. 2.

The dielectric constant of the local environment surrounding the probe was estimated by the peak wavelength of the fluorescence of the probe from the data for the fluorescence of DNS–amino acid conjugates in organic solutions.[15] The $1/D$ values estimated are shown as a function of $\bar{Z}_H$ in Fig. 5. In urea solution the $1/D$ values in the lower $\bar{Z}_H$ range decrease remarkably with an increase of the concentration of urea (Fig. 5(a)). This suggests that the nonpolar or medium effects appear in the absence of urea, especially in the lower $\bar{Z}_H$ range. The fact that the pK_a values in 0.01 M NaCl are almost constant in such a range of $\bar{Z}_H$ can be attributed to the nonpolar effect rather than the electrostatic effect. The nonpolar environment is unlikely to give rise to the presence of the electrostatic neighboring effect.

On the other hand, for higher $\bar{Z}_H$ values, the $1/D$ values approach the reciprocal of the dielectric constant of water (=0.0125), either in the presence or in the absence of urea. Thus, the nonpolar effect on pK_a can be ignored at the highest $\bar{Z}_H$ value. The shift of pK_a at such a $\bar{Z}_H$ value might be attributed to the long-range or short-range electrostatic effects. The pK_a values in aqueous solutions in the absence of the denaturants were less than those estimated from the Linderstrøm-Lang equation, especially when the protein formed an expanded state by the protonation.[6] The result can also be interpreted in terms of the short-range electrostatic interaction between the probe and the positively charged residues. The interaction might be caused by the disulfide bonds, similar to the electrostatic interaction between the probe and negatively charged residues in the presence of the denaturants.

In GuHCl solution (Fig. 5(b)), the $1/D$ values behave like those in urea solutions but give a low constant value even in 2 M of GuHCl solution. This is ascribed to the difference of the two denaturants; urea is a neutral molecule and GuHCl is a salt species. In a GuHCl solution with a high ionic strength, it is likely that the neighboring effect is due to the electrostatic interaction rather than the nonpolar interaction as compared with urea solutions.

The following conclusion is made. (1) The shift of pK_a from pK_0 is mainly attributed to the neighboring effects between the probe and its surrounding residues in the case of the unreduced protein. (2) The neighboring effects are attributed to the electrostatic and nonpolar interactions: The former effect is due chiefly to the exposure of the probe to the solvent-like environment by the protonation on the protein or by the denaturants employed, the latter to the probe being buried in the nonpolar environment.

The present work was partially supported by a Grant-in-Aid for Development Research from the Ministry of Education, Science and Culture.

References

1) G. Weber, *Biochem. J.*, **51**, 155 (1952).
2) I. M. Klotz and J. Ayers, *J. Am. Chem. Soc.*, **79**, 4078 (1957).
3) I. M. Klotz and H. A. Fiess, *Biochim. Biophys. Acta*, **38**, 57 (1960).
4) P. A. Frey, F. C. Kokesh, and F. H. Westheimer, *J. Am. Chem. Soc.*, **93**, 7266 (1971).
5) U. P. Strauss and G. Vesnaver, *J. Phys. Chem.*, **79**, 1558 (1975).
6) N. Ikuta, J. Koga, and N. Kuroki, *Bull. Chem. Soc. Jpn.*, **54**, 228 (1981).
7) Y. Nozaki and C. Tanford, *J. Biol. Chem.*, **238**, 4074 (1963).
8) D. R. Robinson and W. P. Jencks, *J. Am. Chem. Soc.*, **87**, 2462 (1965).

9) W. Bruning and A. Holtzer, *J. Am. Chem. Soc.*, **83**, 4865 (1961).
10) D. B. Wetlaufer, S. K. Malik, L. Stoller, and R. L. Coffin, *J. Am. Chem. Soc.*, **86**, 508 (1964).
11) T. A. Bewley, J. S. Dixon, and C. H. Li, *Biochim. Biophys. Acta*, **154**, 420 (1968).
12) R. J. Argauer and C. E. White, *Anal. Chem.*, **36**, 368 (1964).
13) R. F. Chen, *Arch. Biochem. Biophys.*, **120**, 609 (1967).
14) E. Lippert, *Z. Eletrochem.*, **61**, 962 (1967).
15) I. Abe, J. Koga, and N. Kuroki, *Nippon Kagaku Kaishi*, **1975**, 879.
16) Since the probe in the acidic form absorbs no light at excited wavelength of 340 nm,[6] the fluorescent quantum yield of the probe in the acidic form can be taken as zero.
17) C. Tanford, *Adv. Protein Chem.*, **17**, 69 (1963).
18) C. Tanford, *Adv. Protein Chem.*, **23**, 120 (1969).
19) J. R. Brown, *Fed. Proc.*, **35**, 2141 (1976).
20) E. J. King, "Acid-Base Equilibria," in "The international Encyclopedia of Physical Chemistry and Chemical Physics," 1st ed, ed by E. A. Guggenheim *et al.*, Pergamon Press, Oxford (1965), Vol. 4, Chap. 11, pp. 248—279.

Epicubebol and Related Sesquiterpenoids from the Brown Alga *Dictyopteris divaricata*[1]

Minoru Suzuki, Nobuhiko Kowata, and Etsuro Kurosawa*

Department of Chemistry, Faculty of Science, Hokkaido University, Sapporo 060

(Received December 25, 1980)

Epicubebol has been isolated from the methanol extracts of the brown alga *Dictyopteris divaricata* as the major constituent. Cadinane-type sesquiterpenes, cubebenes, δ-cadinene, cubenol, and epicubenol, as well as two sesquiterpene methyl ethers as minor constituents have also been obtained from the extracts.

Recently many interesting secondary metabolites such as diterpenes[2,3] and sesquiterpene-substituted hydroquinones[4] have been obtained from the brown algae of the family Dictyotaceae. This prompted us to reinvestigate the constituents of the brown alga *Dictyopteris divaricata* (Okam.) Okamura ("Ezoyahazu" in Japanese) in this family.[5] We wish to report the isolation and structures of several cadinane-type sesquiterpenoids from this alga.

The neutral methanol extracts, obtained from freshly collected algae, were fractionated by column chromatography over neutral alumina. The fraction eluted with hexane gave a mixture of sesquiterpene hydrocarbons consisting of (−)-α-cubebene (**7**),[6] (−)-β-cubebene (**8**),[6] (+)-δ-cadinene (**9**), and other hydrocarbons. The fraction eluted with benzene was subjected to a combination of column and thin-layer chromatography over silica gel to yield compounds **3**, **4**, **5**, and **6** as minor components. The fraction eluted with ether was subjected to repeated thin-layer chromatography to give compound **1** as the major component.

Compound **1**, colorless oil, $[\alpha]_D^{21}$ −42°, was analyzed for $C_{15}H_{26}O$ by mass spectroscopy *m/e* 222 (M^+). Its IR spectrum showed hydroxyl absorption at ν_{max} 3380 cm^{-1}, and its ^1H NMR spectrum signals due to two cyclopropane protons at δ 0.35 and 0.77 (each 1H, m), a tertiary methyl group at 1.25 (3H, s), and three secondary methyl groups at 0.90, 0.93, and 0.99 (each 3H, d, J=7 Hz), two of which being ascribable to the isopropyl group on the basis of the base peak at *m/e* 161 [$M^+-H_2O-CH(CH_3)_2$] in the mass spectrum of **1**. The tertiary nature of the hydroxyl group was shown by its resistance to acetylation with acetic anhydride in pyridine and by the presence of a quaternary carbon at δ 80.0 ppm in the ^{13}C NMR spectrum. Since the ^{13}C NMR spectrum indicates no sp^2 carbon, compound **1**, having three degrees of unsaturation, should be a tricyclic sesquiterpene alcohol including a cyclopropane ring.

Treatment of **1** with $SOCl_2$ in CH_2Cl_2–pyridine at −7—−9 °C gave (−)-α-cubebene (**7**), (−)-β-cubebene (**8**), and (+)-δ-cadinene (**9**) in a low yield. On the other hand, treatment with TsOH in benzene at room temperature afforded (+)-δ-cadinene (**9**) as a major product and (−)-zonarene (**10**)[7] as a minor one. This indicates that compound **1** is cubebol (**2**), previously isolated from the oil of cubeb *Piper cubeba* L.,[8,9] or epicubebol (**1**) synthesized from (−)-α-cubebene (**7**) by oxymercuration-demercuration reaction.[9] Comparison of the spectral data show **1** to be identical with epicubebol (**1**). Isolation of epicubebol (**1**) as a natural product seems to have been carried out for the first time.

Compounds **3** and **4** were found to be identical with epicubenol (**3**) and cubenol (**4**), respectively, which have also been isolated from the cubeb oil,[10] by comparison of spectral data. **3** and **4** were derived from **1** on treatment with TsOH in benzene and also with dil HCl in dioxane–water[11] (see Experimental).

Compound **6**, $C_{16}H_{28}O$ (*m/e* 236; M^+), $[\alpha]_D^{24}$ −23°, displayed a ^1H NMR spectrum very similar to that of epicubebol (**1**) except for the signal due to the methoxyl group at δ 3.13 (3H, s), suggesting that **6** would be the methyl ether derivative of **1**. Spectral similarity between compounds **5** and **6** indicates that **5** would be the stereoisomer at C-4 of **6**, *viz.* the methyl ether derivative of cubebol (**2**). This was confirmed by the following reaction. Treatment of **1** with methanol containing a catalytic amount of H_2SO_4 at room temperature resulted in the formation of **5** (13%) and **6** (13%), suggesting that these methyl ethers are artifacts which were generated during the course of extraction. Thus, extraction of the alga was performed with ether instead

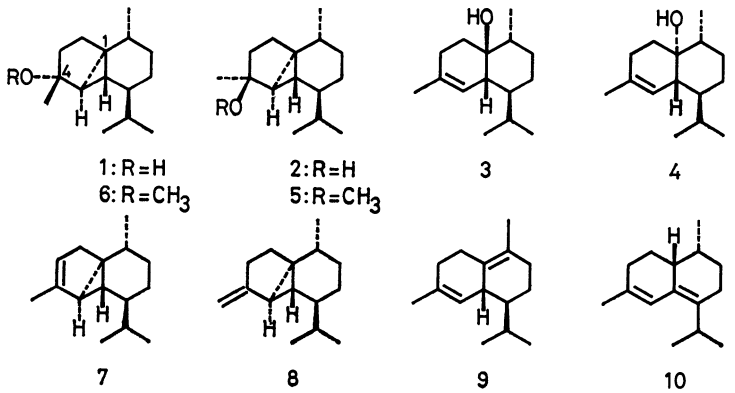

of methanol, no methyl ether derivatives, **5** and **6**, being obtained from the ether extracts as expected.

In previous studies,[5] no epicubebol (**1**), which exists as the major component of the extracts in the present study, was isolated. In contrast, no dictyopterols, dictyopterone, δ-cadinol, and other sesquiterpenes except for (−)-α-cubebene[12] could be detected in the present study. The difference in the results between the present and the previous studies seems to depend mainly upon the isolation procedure. In the previous studies, after distillation of the extracts with steam, fractional distillation was employed for fractionation of the neutral components, whereas we have treated the extracts at low temperature (below 35 °C) and further with rapid column and thin-layer chromatography. On heating at *ca.* 130 °C, epicubebol (**1**) gave (−)-α-cubebene, (−)-β-cubebene, and (+)-δ-cadinene together with (−)-*trans*-calamenene. By prolonged contact with silica gel, **1** turned into (+)-δ-cadinene, (−)-zonarene, and other hydrocarbons.

Recently 4,10-epoxymuurolane, which appears to be derived from epicubebol, has been isolated from the brown alga *Dilophus fasciola* together with several cadinane-type sesquiterpenes.[13]

It is interesting that the marine alga produces epicubebol (**1**) instead of cubebol (**2**) which has been isolated from the terrestrial plant.

Experimental

IR spectra were measured on a JASCO A-102 spectrometer and ^{1}H NMR spectra on a JEOL JNM-PS-100 spectrophotometer, TMS being used as an internal reference in CCl_4. The ^{13}C NMR spectrum was obtained with a Bruker SXP4-100 spectrophotometer in $CDCl_3$. The optical rotations were measured in $CHCl_3$. Aluminum oxide (Merck, activity II—III) and silica gel (Merck, Kieselgel 60, 70—230 mesh) were used for column chromatography. Silica gel (Merck, Kieselgel GF_{254} (Type 60)) was used for preparative thin-layer chromatography (PTLC).

Isolation. *Dictyopteris divaricata* was collected at Oshoro Bay, Hokkaido, during the months April—August 1980. No distinct difference was observed between the extracts in each collection. Half-dried alga (2.2 kg), collected in April, was extracted with methanol, and the resulting solution was concentrated under reduced pressure. The residue was percolated with ether, and the ether solution was shaken with 5% $NaHCO_3$ and saturated brine, and then dried over anhydrous Na_2SO_4. After evaporation of the solvent, a neutral oil (104 g) was obtained. This was fractionated by column chromatography over neutral alumina. Elution with hexane gave a mixture of sesquiterpene hydrocarbons from which (−)-α-cubebene (**7**) (0.04% of the neutral oil), (−)-β-cubebene (**8**) (1%), and (+)-δ-cadinene (**9**) (0.8%) were detected by comparison of the retention times in GLC with those of authentic samples. Elution with benzene gave an oily substance which was subjected to a combination of silica-gel column and PTLC to yield **3** (0.1%), **4** (0.02%), **5** (1.5%), and **6** (1.5%) (in order of decreasing porality) along with an unidentified alcohol. Elution with ether gave a mixture of alcohols which was repeatedly chromatographed on PTLC to yield **1** (13%) together with phytols, cholesterol, and at least two unidentified alcohols.

1: Colorless oil; $[\alpha]_D^{21}$ −42° (*c* 1.54); IR, ν_{max} (film) 3380, 1370, 1180, 1110, and 910 cm^{-1}; ^{1}H NMR, δ 0.35, 0.77 (each 1H, m), 0.90, 0.93, 0.99 (each 3H, d, J=7 Hz) and 1.25 (3H, s); ^{13}C NMR, δ 80.8 (s), 44.6 (d), 39.9 (d), 36.6 (t), 34.9 (s), 33.6 (d), 31.8 (d), 30.2 (t), 29.8 (t), 27.0 (t), 25.3 (d), 25.0 (q), 20.0 (q), 19.8 (q), and 19.1 (q); MS, *m/e* (relative intensity) 222 (12), 207 (83), 204 (9), and 161 (100). The IR (film and CCl_4) and ^{1}H NMR ($CDCl_3$) spectra were consistent with those of epicubebol.

3: Colorless oil; $[\alpha]_D^{25}$ −96° (*c* 0.94); The spectral properties were identical with those reported [10] for epicubenol.

4: Colorless oil; $[\alpha]_D^{20}$ −33° (*c* 0.13); The spectral properties were identical with those reported[10] for cubenol.

5: Colorless oil; $[\alpha]_D^{23}$ −82° (*c* 1.36); IR, ν_{max} (film) 1370, 1310, 1205, 1140, 1070, and 885 cm^{-1}; ^{1}H NMR, δ 0.74 (1H, m), 0.91 (6H, d, J=6 Hz), 0.96 (3H, d, J=6 Hz), 1.14 (3H, s), and 3.14 (3H, s); MS, *m/e* 236 (1), 221 (69), 204 (18), 161 (65), and 41 (100).

6: Colorless oil; $[\alpha]_D^{24}$ −23° (*c* 0.60); IR, ν_{max} (film) 1370, 1110, 1090, 1075, and 865 cm^{-1}; ^{1}H NMR, δ 0.35 (1H, m), 0.90, 0.94, 0.96 (each 3H, d, J=7 Hz), 1.21 (3H, s), and 3.13 (3H, s); MS, *m/e* 236 (1), 221 (100), 204 (8), and 161 (57).

*Dehydration of **1** with Thionyl Chloride.* A solution of **1** (107 mg) and thionyl chloride (0.04 ml) in dry dichloromethane (6 ml) and pyridine (1 ml) was allowed to stand at −7—−9 °C for 5 min. The mixture was then poured into ice-cooled water and extracted with ether. The ether solution was washed with saturated brine and dried over anhydrous Na_2SO_4. A residual substance obtained after removal of the solvent was chromatographed on alumina column. Elution with hexane gave a mixture of hydrocarbon (20 mg), GLC of which revealed that the mixture consists of (−)-α-cubebene (**7**) (20%), (−)-β-cubebene (**8**) (1.5%), (+)-δ-cadinene (**9**) (40%), and other hydrocarbons. Elution with ether gave unreacted **1** (25 mg).

*Dehydration of **1** with p-Toluenesulfonic Acid.* A solution of **1** (97 mg) and *p*-toluenesulfonic acid (2 mg) in benzene (5 ml) was stirred at room temperature for 30 min. After evaporation of benzene, the residual oily products were subjected to column chromatography on alumina. Elution with hexane gave a mixture of hydrocarbons (87 mg) consisting of (+)-δ-cadinene (**9**) (70%) and (−)-zonarene (**10**) (1%). Purification of (+)-δ-cadinene was carried out by preparative GLC. **10** was identified as (−)-zonarene by comparison of the retention time in GLC with that of an authentic sample. Elution with ether gave a mixture of alcohols which was further chromatographed on PTLC to afford epicubenol (**3**) (4 mg), cubenol (**4**) (2 mg), and **1** (1 mg).

*Conversion of **1** into **3** and **4**.* A small amount of dil HCl was added to a solution of **1** (97 mg) in dioxane (6 ml) and water (2.5 ml), and the mixture was allowed to stand at room temperature for 30 h. Water was added and extraction was carried out with ether. The ether solution was washed with saturated brine, dried over anhydrous Na_2SO_4, and evaporated to give an oily residue. The residue was chromatographed on alumina column. Fraction eluted with ether was further subjected to repeated PTLC to give epicubenol (**3**) (11 mg), cubenol (**4**) (4 mg), and **1** (24 mg) along with unidentified alcoholic compounds and ketonic compounds.

*Methanolysis of **1**.* A solution of **1** (65 mg) and a catalytic amount of concd H_2SO_4 in methanol (20 ml) was allowed to stand at room temperature for 2 h with continuous stirring. The mixture was then concentrated *in vacuo*. Water was added and extraction was carried out with ether. The ether solution was washed with 5% $NaHCO_3$ and saturated brine, and then dried over anhydrous Na_2SO_4. After evaporation of the solvent, the residual oil was chromatographed on silica-gel column to give **5** (9 mg), **6** (9 mg), and **1** (44 mg).

*Thermal Reaction of **1**.* **1** (100 mg) was placed in a flask

fitted with condenser which was immersed in an oil bath maintained at 130 °C under nitrogen atmosphere. After 5 h the reaction products were separated by column chromatography over alumina to yield a hydrocarbon fraction (54 mg) which was further subjected to preparative GLC to give (−)-α-cubebene (**7**) (21 mg), (−)-β-cubebene (**8**) (11 mg), (+)-δ-cadinene (**9**) (11 mg), and (−)-*trans*-calamenene (4 mg). The structure of *trans*-calamenene was identified by comparison of the IR and ^{1}H NMR spectra with reported[14] for calamenene. Unchanged **1** (33 mg) was recovered.

The authors are grateful to Prof. Akira Yoshikoshi, Tohoku University, for the spectral data of cubebenes, cubebol, and epicubebol, and also to Mr. Nobuyasu Enoki, Hokkaido University, for providing (−)-zonarene and its spectral data.

References

1) Part 43 of "Constituents of Marine Plants." Part 42: T. Suzuki, H. Kikuchi, and E. Kurosawa, *Chem. Lett.*, **1980**, 1267.

2) W. Fenical, "Marine Natural Products; Chemical and Biological Perspectives," ed by P. J. Scheuer, Academic Press, New York (1978), Vol. 2, p. 173.

3) S. L. Fernandes, S. Y. Kamat, and S. K. Paknikar, *Tetrahedron Lett.*, **1980**, 2244 and references cited therein; V. Amico, G. Oriente, M. Piattelli, C. Tringali, E. Fattorusso, S. Magno, and L. Mayol, *Tetrahedron*, **36**, 1409 (1980) and references cited therein; M. Ochi, M. Watanabe, I. Miura, M. Taniguchi, and T. Tokoroyama, *Chem. Lett.*, **1980**, 1229; M. Ochi, M. Watanabe, M. Kido, Y. Ichikawa, I. Miura, and T. Tokoroyama, *ibid*,. **1980**, 1233.

4) M. Ochi, H. Kotsuki, S. Inoue, M. Taniguchi, and T. Tokoroyama, *Chem. Lett.*, **1979**, 831 and references cited therein.

5) T. Irie, K. Yamamoto, and T. Masamune, *Bull. Chem. Soc. Jpn.*, **37**, 1053 (1964); E. Kurosawa, M. Izawa, K. Yamamoto, T. Masamune, and T. Irie, *ibid.*, **39**, 2509 (1966).

6) Y. Ohta, T. Sakai, and Y. Hirose, *Tetrahedron Lett.*, **1966**, 6365.

7) W. Fenical, J. J. Sims, R. M. Wing, and P. C. Radlick, *Phytochemistry*, **11**, 1161 (1972); N. H. Andersen, D. D. Syrdal, B. M. Lawrence, S. J. Terhune, and J. W. Hogg, *ibid.*, **12**, 827 (1973); M. Iguchi, M. Niwa, and S. Yamamura, *Bull. Chem. Soc. Jpn.*, **46**, 2920 (1973).

8) F. Vonášek, V. Herout, and F. Šorm, *Coll. Czech. Chem. Comm.*, **25**, 919 (1960).

9) A. Tanaka, R. Tanaka, H. Uda, and A. Yoshikoshi, *J. Chem. Soc., Perkin Trans. 1*, **1972**, 1721.

10) Y. Ohta and Y. Hirose, *Tetrahedron Lett.*, **1967**, 2073.

11) Y. Ohta, K. Ohara, and Y. Hirose, *Tetrahedron Lett.* **1968**, 4181.

12) The previous report[5a] on the isolation of '(−)-copaene' was in error and further examination showed that '(−)-copaene' should be revised to (−)-α-cubebene.

13) V. Amico, G. Oriente, M. Piattelli, C. Tringali, E. Fattorusso, S. Magno, and L. Mayol, *Experientia*, **35**, 450 (1979).

14) B. N. Joshi, R. Seshadri, K. K. Chakravarti, and S. C. Bhattacharyya, *Tetrahedron*, **20**, 2911 (1964); N. H. Andersen, D. D. Syrdal, and C. Graham, *Tetrahedron Lett.*, **1972**, 905.

  Bull. Chem. Soc. Jpn., 54, 2369—2373 (1981)

Oxidative Cleavage Reaction of 3-Substituted Indoles Catalyzed by CuCl–Pyridine Complex under Oxygen

Jiro Tsuji,* Hiroaki Kezuka, Hiroshi Takayanagi, and Keiji Yamamoto

Department of Chemical Engineering, Tokyo Institute of Technology, Meguro-ku, Tokyo 152

(Received January 20, 1981)

Oxidative cleavage of 3-methylindole using a catalytic amount of copper(II) salts with added pyridine under an oxygen atmosphere was studied. Smooth cleavage of 3-methylindole took place to give 2-formamidoacetophenone in 73—80% yield, whereas exclusive formation of a hydrate compound derived from 3,3′-dimethyl-3,3′-bi-3*H*-indole resulted under anaerobic conditions. Clean oxidative cleavage of *N*-acetyltryptamine, methyl 3-indolylacetate, and methyl 2-acetamido-3-(3-indolyl)propionate was also achieved, constituting a mimic of tryptophan-2,3-dioxygenase.

We have reported the oxidative cleavage reaction of catechol and phenol using CuCl–pyridine complex under oxygen to give methyl *cis,cis*-muconate in high yields as a non-enzymic model for pyrocatechase.[1]

As an extension of our studies on the metal salt-catalyzed liquid-phase oxidation, which includes oxidative cleavage of *o*-phenylenediamine to *cis,cis*-mucononitrile,[2] oxidation of various olefins to carbonyl compounds,[3] and facile oxidative conversion of acid hydrazides to the corresponding acids,[4] we attempted an oxidative cleavage of an indole ring as a non-enzymic model for tryptophan-2,3-dioxygenase. Although indole derivatives related to tryptophan are fairly sensitive to oxidation, controlled oxidation to give rise to the cleavage of the indole ring is rather limited.[5] We have recently disclosed clean oxidative cleavage of 3-methylindole catalyzed by CuCl–pyridine complex under oxygen.[6] There has been reported an independent study on the oxidative cleavage of 2- and 3-substituted indoles using a CuCl–pyridine–O_2 system.[7]

Tryptophandioxygenase is an important enzyme which selectively cleaves the indole ring of tryptophan and several studies on its model reaction have been reported. Photosensitized oxygenation of tryptophan and related indole derivatives gave the cleaved product.[8,9] Nishinaga reported a successful oxidative cleavage of various indole derivatives using cobalt-Schiff base complexes as catalyst to give 2-formamidoacetophenone derivatives in high yields.[10] Manganese phthalocyanine-catalyzed oxidative cleavage of 3-methylindole gave similar results.[11] More recently, copper-Schiff base complex-catalyzed oxidation of tryptophan has been reported.[12]

In this paper we describe the oxidative cleavage reaction of several 3-substituted indoles under the optimum conditions so far examined using CuCl–pyridine complex under oxygen.

Results and Discussion

Catalytic Oxidation Using Copper(II) Salts. 3-Methylindole: Oxidative cleavage reaction of 3-methylindole using various copper(II) salts as a catalyst under an oxygen atmosphere was studied. Although copper(II) salts such as copper(II) acetate and methoxide did act as a catalyst effectively in the presence of oxygen, copper(I) chloride was principally used in order to compare the catalytic behavior for the oxidative cleavage of 3-methylindole with that for catechol oxidation.

Prior to the reaction, copper(I) chloride dissolved in pyridine–dichloromethane was oxidized until oxygen absorption ceased. Usually about one-fourth mole of oxygen per mole copper(I) used was found to be absorbed, substantiating the equation:[1d]

$$2\,CuCl + 1/2\,O_2 \xrightarrow{\text{pyridine}} CuCl_2 \cdot CuO.$$

Results of screening of the reaction conditions indicated that an added pyridine is crucial and that the choice of solvent has a considerable effect on the reaction rate and the yield of the cleaved product, dichloromethane being satisfactory. Also relative amounts of pyridine to the solvent seem to be important.

The reaction proceeded smoothly at ambient temperature (15—20 °C) with absorption of additional oxygen during the course of 3—6 h. Under the best conditions so far examined, 2-formamidoacetophenone was obtained in 73—80% yield. Results are summarized in Table 1.

It is of interest to note that overall oxygen uptake roughly parallels yields of the cleaved product, except for entries **1a** and **1b**, regardless of the molar ratios of the substrate to catalyst in the range of 3.3 to 0.5.

Under the same conditions as entry **1f** 2,3-dimethylindole underwent oxidative cleavage to form 2-acetamidoacetophenone in 50% yield.

As is discussed below, intervention of a 3*H*-indol-3-yl radical, which is formed by facile one electron transfer from 3-methylindole to Cu(II) species followed by deprotonation, is likely responsible for the subsequent oxygenation to result in the cleavage of the indole ring. Thus, the most effective species for the oxidative cleavage of 3-methylindole would be Cu(II) ion coordinated with pyridine, which is, in turn, able to transfer molecular oxygen effectively to the intermediate 3*H*-indol-3-yl radical.

3-Substituted Indoles. Oxidative cleavage of *N*-acetyltryptamine, methyl 3-indolylacetate, and methyl 2-acetamido-3-(3-indolyl)propionate was carried out under the conditions aforementioned.

These reactions were found to be rather sluggish and the latter two substrates underwent cleavage with relatively low conversions as compared with 3-methylindole even after 24 h of reaction period. All results obtained are summarized in Table 2.

A few points deserve comments. Steric demand of R

Table 1. Copper(II)-catalyzed oxidation of 3-methylindole to 2-formamidoacetophenone under oxygen[a)]

Entry	Cu(II) salt (mmol)	Pyridine (ml)	Solvent (ml)	O_2 Uptake[b)] (mmol)	Yield[c)] %
1a	CuCl, 0.3	20	—	(1.5)	13
1b	0.5	0 (DBU, 1.0)	CH_2Cl_2(20)	(2.9)	8
1c	0.3	0 (DMF, 1.0)	CH_2Cl_2(15)	0.6	32
1d	0.3	0.5	PhMe(20)	0.84	45
1e	0.5	0.5	$CHCl_3$(20)	1.2	56
1f	0.5	0.5	CH_2Cl_2(20)	1.6	73
1g	2.0	2.0	CH_2Cl_2(20)	1.4	72
2	$Cu(OAc)_2$, 0.5	0.5	CH_2Cl_2(20)	1.6	81
3	$Cu(OMe)_2$,0.5	0.5	CH_2Cl_2(20)	—	55

a) 3-Methylindole (1.0 mmol) dissolved in a given solvent (10 ml) was added to the copper(II) catalyst solution (*ca.* 10 ml) under oxygen, and oxidized at ambient temperature in 3—6 h. b) Overall oxygen uptake. c) Isolated by column chromatography.

Table 2. Oxidative cleavage of 3-substituted indoles catalyzed by CuCl–pyridine complex under oxygen[a)]

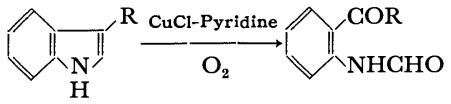

R	O_2 Uptake (mmol)	Conversion %	Yield[b)] %	Mp °C
CH_2CH_2NHAc	1.6	100	68	117—118 (117—119)[10)]
CH_2CO_2Me	—	79	48	40 (44)[7)]
CH_2CHCO_2Me NHAc	1.2	68	57	160—162 (syrup)[7,10)]

a) Substrate (1.0 mmol) and copper(I) chloride (0.5 mmol) in pyridine (0.5 ml) and dichloromethane (20 ml) were used. b) Based on the conversion.

Table 3. Oxidative cleavage of 3-methylindole to 2-formamidoacetophenone under anaerobic conditions[a)]

Cu(II) salt	Pyridine (ml)	Yield %	Recovery %
$CuCl_2$	4.0	34	14
$Cu(OAc)_2 \cdot H_2O$	4.0	48	29
$Cu(OAc)_2$	4.0	67	9
$Cu(OAc)_2$	0.65	63	12
$Cu(OMe)_2$[b)]	2.0	0 (dimer,[c)] 80)	19
$[CuCl_2 \cdot CuO]$[d)]	2.0	0 (dimer,[c)] 59)	16

a) 3-Methylindole (1.0 mmol), Cu(II) salt (4.0 mmol) in dichloromethane (25 ml) with added pyridine under argon. Stirred at room temperature for 4 d. b) Prepared *in situ* from anhydrous MeOLi and $CuCl_2$ in dry THF. c) Hydrate compound (II) (R=Me) derived from 3,3′-dimethyl-3,3′-bi-3*H*-indole (III) (R=Me). Duplicated results. d) Pretreated CuCl with requisite amounts of oxygen:

$$2CuCl + 1/2O_2 \xrightarrow{py} CuCl_2 \cdot CuO \quad (cf.\ \text{Ref. 1}).$$

groups at the 3-position apparently affects the reaction rate, reflecting low conversions of the cleavage. The same is true for cobalt-salen complex-catalyzed oxidative cleavage of these 3-substituted indoles.[10)] Cobalt complex-catalyzed oxidation of methyl 3-indolylacetate in methanol resulted in a side chain oxidation rather than a ring cleavage, whereas the present copper complex-catalyzed reaction afforded methyl 2-formamidobenzoylacetate in 48% yield.

Generally, yields of the cleaved products attained under the present reaction conditions are much superior to those reported,[7)] using CuCl–pyridine–O_2 system without dichloromethane. Selecting simply a solvent, one can improve significantly the yield of oxidative cleavage of 3-substituted indoles, as is seen from Table 1 with respect to 3-methylindole.

Cu(II) as an Oxidant. 3-Methylindole was treated with excess copper(II) salts (4 equiv.) with added pyridine in dichloromethane solution at room temperature under an argon atmosphere. TLC monitoring of the reaction mixture revealed that very slow cleavage took place to give 2-formamidoacetophenone as a sole product in moderate yields with recovery of appreciable amounts of the starting 3-methylindole even after four days. Results obtained are given in Table 3. Although the reaction rate was found to be much slower than that found under oxygen as mentioned above, it is obvious that both copper(II) chloride and acetate are capable of initiating selective cleavage of 3-methylindole.

The most striking, however, is the fact that no cleaved product was obtained when copper(II) methoxide, prepared *in situ* from copper(II) chloride and two equivalents of anhydrous lithium methoxide in tetrahydrofuran (THF), was used as an oxidant. The results are confirmed by duplicated runs. Similar results were also obtained with a dichloromethane solution of copper(I) chloride with added pyridine, which was allowed to absorb a requisite amount of oxygen, followed by purging excess oxygen thoroughly with argon (see Experimental).

The sole product obtained in these two sets of reactions was white crystalline material which had exactly the same melting point after recrystallization from chloroform as well as analytical data as one previously obtained by Dobeneck[13)] in the oxidation of 3-methylindole with iron(III) chloride, and characterized as an ether (I). Acid catalyzed dimerization of 3-methylindole occurs readily, but the resulting dimer has indoline-

indole moieties joined at their 2-positions,[14] while radical dimerization of 3-substituted indoles has been suggested without any structure characterization.[15]

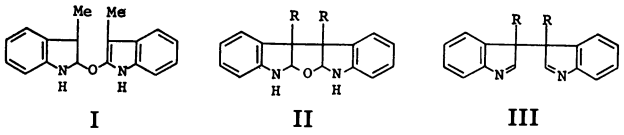

I II III

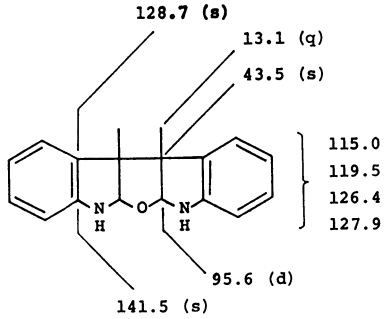

Fig. 1. ^{13}C NMR Data for II (R=Me), δ/ppm (OFR splitting are given in parentheses).

However, the structure (I) assigned by Dobeneck[13] was now found to be erroneous. ^1H and ^{13}C NMR (Data given in Fig. 1) as well as MS data of the products prepared by using either Cu(II) or Fe(III) salt indicate a symmetric structure of compound (II) (R=Me), which is obtained as one diastereomer and is most probably derived from addition of water to a rather unstable 3,3′-dimethyl-3,3′-bi-3*H*-indole III (R=Me). III is a 3*H*-indole-3*H*-indole dimer, the dimeric bond being formed at 3-position in the 3*H*-indole moiety.

It has been reported that such oxidants as potassium hexacyanoferrate(III) and manganese oxide are insufficient for radical generation from indolic nitrogen. Successful oxidative dimerization of indolylmagnesium halides with iron(III) chloride has already been described[16] to form intermediate III (R=CH_2CH_2-NHMe).

It appears to be difficult to account for exactly why the two reaction paths were observed in the course of oxidation of 3-methylindole using four different copper(II) salts under apparent anaerobic conditions. However, the exclusive formation of a dimer (III) (R=Me), which is trapped as compound (II) (R=Me), from 3-methylindole in certain cases may now be rationalized by the following scheme.

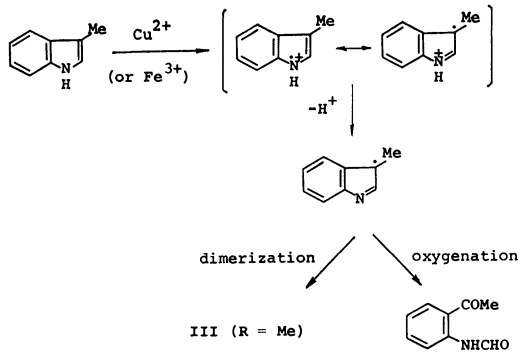

Facile one electron transfer from 3-methylindole at the nitrogen atom to copper(II) (as well as to iron(III)) followed by deprotonation gives an intermediate 3*H*-indol-3-yl radical, which may or may not coordinate to the copper species. The radical undergoes either dimerization under rigorous anaerobic conditions, if any, to give III or oxygenation with oxygen presumably adsorbed on certain copper salts present in the reaction mixture to afford selectively 2-formamidoacetophenone.[17] The scheme is consonant with the fact that attempted reaction of 1,3-dimethylindole under oxygen resulted in complete recovery of the starting material. It is confirmed that 3-ethylindole also formed the corresponding dimeric compound (II) (R=Et). However, the significant role of the anionic ligands of copper(II) species is still unclear at present.

Experimental

Apparatus. For the present oxidative cleavage reactions was throughout used a three-neck, round-bottomed 50 ml flask equipped with a magnetic stirrer, a Hershberg dropping funnel, a serum cap, and a three-way stopcock which was connected either with an oxygen gas buret or with an argon balloon.

Copper(II) Salts. $CuCl_2$ and $Cu(OAc)_2 \cdot H_2O$ were used as received. Anhydrous $Cu(OAc)_2$ commercially available was dried *in vacuo* prior to use. $Cu(OMe)_2$ was prepared *in situ* by the following procedure. A brown suspension of $CuCl_2$ (0.588 g, 4.2 mmol) and LiOMe (0.34 g, 8.6 mmol) in THF (20 ml) was stirred for 1 h under argon. The reaction mixture turned green was evaporated to dryness *in vacuo* and used in dichloromethane for the oxidation immediately. For "Cu reagent," CuCl–pyridine–O_2 system, a typical run is as follows. A clear green solution of CuCl (0.398 g, 4.0 mmol) dissolved under argon in dichloromethane (20 ml) and pyridine (2 ml) was exposed to oxygen with stirring. Oxygen uptake (about 1 mmol) ceased within 1 h, during which time the solution turned to a dark green suspension. The "Cu reagent" thus prepared was used either under oxygen for cleavage reactions or after purging excess oxygen with argon for anaerobic reactions.

Catalytic Oxidative Cleavage of 3-Methylindole. Using "Cu reagent," the following is the best procedure; "Cu reagent" was prepared as above using CuCl (0.050 g, 0.5 mmol), dichloromethane (10 ml), and pyridine (0.5 ml). Into the dropping funnel was placed a solution of 3-methylindole (0.131 g, 1 mmol) in dichloromethane (10 ml). The solution was added dropwise to the "Cu reagent" under oxygen over 1 h. After additional 1.48 mmol of oxygen was absorbed within 4 h, the reaction mixture was hydrolyzed with 40 ml of 3 mol dm^{-3} HCl. The organic layer was separated and aqueous layer was extracted with dichloromethane. The combined organic layer was washed with brine three times and dried over $MgSO_4$. The dichloromethane was removed by evaporation and the residue was purified by column chromatography (silica gel, dichloromethane as eluent) to give 2-formamidoacetophenone in 73% yield: mp 77—78 °C (lit,[10] mp 79—80 °C); ^1H NMR ($CDCl_3$) δ 2.64 (s, 3H), 6.94—8.01 (m, 3H), 8.35—8.87 (m, 2H), and 11.51 (s, broad, 1H); IR (KBr) 3250, 2890, 1690, and 1660 cm^{-1}.

Similarly, a solution of 2,3-dimethylindole (0.022 g, 0.15 mmol) in dichloromethane (2.0 ml) was added dropwise to

the "Cu reagent" prepared from CuCl (0.009 g, 0.09 mmol) and pyridine (0.8 ml) dissolved in dichloromethane (2.0 ml) under oxygen atmosphere. Oxygen uptake ceased within 4 h, and the reaction mixture was worked up as above. Purification of the product by column chromatography gave 2-acetamidoacetophenone in 50% yield: mp 73—75 °C (lit,[18] mp 74—75 °C); ^{1}H NMR ($CDCl_3$) δ 2.20 (s, 3H), 2.63 (s, 3H), 6.85—7.94 (m, 3H), 8.56—8.78 (m, 1H), and 11.61 (s, broad, 1H); IR (KBr) 3250, 1690, and 1655 cm^{-1}.

$Cu(OAc)_2$ (0.09 g, 0.5 mmol) was dissolved in a solution of dichloromethane (10 ml) and pyridine (0.5 ml) under oxygen. In a similar manner as above, the solution of 3-methylindole (0.131 g, 1 mmol) in dichloromethane (10 ml) was added for 1 h. The mixture was stirred for 6 h, during which time slow absorption of oxygen (1.6 mmol) was observed. The reaction mixture was worked up as usual and 2-formamidoacetophenone was obtained in 81% yield.

$Cu(OMe)_2$ was prepared as above using $CuCl_2$ (0.060 g, 0.44 mmol) and LiOMe (0.033 g, 0.87 mmol). The oxidative cleavage of 3-methylindole (0.117 g, 0.89 mmol) under oxygen provided 2-formamidoacetophenone in 55% yield.

Oxidative Cleavage of 3-Substituted Indoles. Oxidation of *N*-acetyltryptamine (0.218 g, 1 mmol) with the "Cu reagent" was carried out under oxygen atmosphere. Stirring was continued for 22 h. Usual workup provided 2-(3-acetamidopropionyl)formanilide in 68% yield: mp 117—118 °C; NMR ($CDCl_3$) δ 1.94 (s, 3H), 2.96—3.78 (m, 4H), 6.38—6.78 (m, 1H), 6.88—7.93 (m, 3H), 8.26—8.79 (m, 2H), and 11.32 (s, broad, 1H); IR (KBr) 3330, 2920, 1675, and 1645 cm^{-1}.

Oxidation of methyl 2-acetamido-3-(3-indolyl)propionate (0.260 g, 1 mmol) with the "Cu reagent" under oxygen provided methyl 2-acetamido-3-(2-formamidobenzoyl)propionate in 57% yield (based on 68% conversion): mp 160—162 °C (hexane–CH_2Cl_2); NMR ($CDCl_3$) δ 2.01 (s, 3H), 3.74 (s, 3H), 4.74—5.09 (m, 1H), 6.42—6.78 (m, 1H), 6.98—8.01 (m, 3H), 8.34—8.90 (m, 2H), and 11.36 (s, broad, 1H); IR (KBr) 3260, 2950, 1755, 1695, and 1655 cm^{-1}. Found: C, 57.78; H, 5.58; N, 8.94%; Calcd for $C_{14}H_{16}N_2O_4$: C, 57.53; H, 5.52; N, 9.58%. MS *m/e* (rel intensity) 292 (3) (M^+); 167 (37), 149 (100), 148 (42), 71 (40), 57 (70), 43 (52), 41 (41).

Oxidation of methyl 3-indolylacetate (0.175 g, 1 mmol) as above with the "Cu reagent" gave methyl (2-formamidobenzoyl)acetate in 48% yield (based on the 79% conversion): mp 40 °C; NMR ($CDCl_3$) δ 3.76 (s, 3H), 4.06 (s, 2H), 7.01—7.99 (m, 3H), 8.47—8.98 (m, 2H), and 11.37 (s, broad, 1H); IR (KBr) 3280, 1725, 1690, and 1600 cm^{-1}.

Cu as an Oxidant. $CuCl_2$ (0.538 g, 4 mmol) was dessolved in a solution of dichloromethane (20 ml) and pyridine (2 ml). As in the case of catalytic oxidative reaction but under argon atmosphere, the solution of 3-methylindole (0.131 g, 1 mmol) in dichloromethane (5 ml) was added dropwise for 1 h. Stirring was continued for 4 d. Work up of the reaction mixture as usual, afforded 2-formamidoacetophenone in 34% yield.

Oxidation of 3-methylindole (0.131 g, 1 mmol) as above with $Cu(OAc)_2 \cdot H_2O$ (0.799 g, 4 mmol) or anhydrous $Cu(OAc)_2$ (0.727 g, 4 mmol) after 4 d afforded 2-formamidoacetophenone in 48 and 67% yields, respectively.

Oxidation of 3-methylindole was carried out under argon for 4 d with $Cu(OMe)_2$ prepared *in situ* described as above. Purification of the product by column chromatography (silica gel, dichloromethane as eluent) gave compound (II) (R=Me) which was thought to consist of two diastereomers: mp 165—167 °C. Recrystallization from chloroform afforded one diastereomer as white crystals: mp 202—204 °C; ^{1}H NMR ($CDCl_3$) δ 1.32 (s, 6H), 4.94 (s, 2H), and 6.45—7.35 (m, 10H); ^{13}C NMR ($CDCl_3$) data are given in Fig. 1; IR (KBr) 3400, 3350, 2960, 1605, 1475, 1295, 1265, 1090, 1050, 885, 805, 755, and 745 cm^{-1}. Found: C, 77.40; H, 6.41; N, 10.06%. Calcd for $C_{18}H_{18}N_2O$: C, 77.67; H, 6.52; N, 10.06%; MS *m/e* (rel intensity) 278 (6) (M^+), 263 (19), 261 (19), 260 (84), 259 (28), 246 (21), 245 (100), 232 (41), 217 (15), and 130 (16).

Compound (II) (R=Me) was dissolved in MeOH containing HCl. After the solution was warmed for 10 min, 3-methylindole and 3-methyl-2-indolinone were obtained. *N,N'*-Dimethyl derivative of II (R=Me) is known to undergo similar cleavage reaction.[19]

Oxidation of 3-Methylindole with $FeCl_3$ and Et_2NH. Oxidation of 3-methylindole (0.508 g, 3.9 mmol) with $FeCl_3$ (1.32 g, 8 mmol), Et_2NH (2.1 ml, 20 mmol), and Et_2O (26 ml) according to Dobeneck's[13] procedure afforded the same product which was obtained by the oxidation with $Cu(OMe)_2$ or "Cu reagent" as an oxidant. Yield 32%.

Oxidation of 3-Ethylindole with $Cu(OMe)_2$. Oxidation of 3-ethylindole (0.145 g, 1 mmol) with $Cu(OMe)_2$ under argon provided compound (II) (R=Et) in 50% yield which was also found to be a mixture of two diastereomeric isomers mp 41—54 °C; ^{1}H NMR ($CDCl_3$) δ 0.68 (t, J=7 Hz, 3H), 1.79 (q, J=7 Hz, 2H), 5.31 (5.02) (s, 1H), and 6.42—7.50 (m, 5H); ^{13}C NMR ($CDCl_3$) Compound (IIa) (R=Et): δ 9.5, 22.1, 47.4, 98.3, 109.5, 118.5, 127.4, 128.0, 129.5, and 149.4; Compound (IIb) (R=Et): δ 8.8, 23.8, 43.5, 95.4, 115.2, 119.0, 126.4, 127.8, 128.1, and 142.6; IR (KBr) 3380, 2960, 1605, 1480, 1260, and 740 cm^{-1}; MS *m/e* (rel intensity) 306 (5) (M^+), 277 (30), 259 (17), 162 (20), 161 (18), 146 (36), 145 (26), 132 (19), and 130 (100).

The authors thank Mr. Y. Nakamura for ^{13}C NMR measurements, and Prof. T. Hino for informing us of his early work on indole derivatives.

References

1) a) J. Tsuji and H. Takayanagi, *J. Am. Chem. Soc.*, **96**, 7349 (1974); b) J. Tsuji, H. Takayanagi, and I. Sakai, *Tetrahedron Lett.*, **1975**, 1245; c) J. Tsuji and H. Takayanagi, *ibid.*, **1976**, 1365; d) J. Tsuji and H. Takayanagi, *Tetrahedron*, **34**, 641 (1978).

2) T. Kajimoto and J. Tsuji, *Synth. Commun.*, **2**, 181 (1972); T. Kajimoto, H. Takahashi, and J. Tsuji, *J. Org. Chem.*, **41**, 1389 (1976); J. Tsuji and H. Takayanagi, *Org. Synth.*, **57**, (1977).

3) J. Tsuji, I. Shimizu, and K. Yamamoto, *Tetrahedron Lett.*, **1976**, 2975.

4) J. Tsuji, S. Hayakawa, and H. Takayanagi, *Chem. Lett.*, **1975**, 437; J. Tsuji, T. Nagashima, N. T. Qui, and H. Takayanagi, *Tetrahedron*, **36**, 1311 (1980).

5) W. A. Remers and R. K. Brown, "Indoles," Partn I in "Heterocyclic Compounds," ed by W. J. Houlihan, Wiley Interscience (1972).

6) J. Tsuji and H. Takayanagi, *Chem. Lett.*, **1980**, 65; J. Tsuji, Report on Biomimetic Model Reactions Mediated by Metal Ions, Grant-in-Aid from the Ministry of Education.

7) H. Yukimasa, H. Sawai, and T. Takizawa, *Chem. Pharm. Bull.*, **27**, 651 (1979).

8) W. E. Savige, *Aust. J. Chem.*, **24**, 1285 (1971).

9) I. Saito, M. Imuta, and T. Matsuura, *Chem. Lett.*, **1972**, 1173, 1192.

10) A. Nishinaga, *Chem. Lett.*, **1975**, 273.

11) K. Uchida, M. Soma, S. Naito, T. Onishi, and K. Tamaru, *Chem. Lett.*, **1978**, 471.

12) Y. Tatsuno, A. Yamada, M. Kudo, and S. Otsuka, 40th National Meeting of the Chemical Soeiety of Japan,

October 1979, Abstr. III, p. 519.
13) H. von Dobeneck, and W. Lehnerer, *Chem. Ber.*, **90**, 161 (1957).
14) a) G. F. Smith and A. G. Walters, *J. Chem. Soc.*, **1961**, 940; b) R. L. Hinman and E. R. Shull, *J. Org. Chem.*, **26**, 2339 (1961).
15) T. Hino and M. Nakagawa, "Tryptophan, Kagaku-Zokan 85," ed by K. Narita, F. Sakiyama, and M. Tokushige, Tokyo Kagaku Dojin, Tokyo (1980), Chap. 5.
16) E. S. Hall, F. McCapra, and S. T. Scott, *Tetrahedron*, **23**, 4131 (1967).
17) **Note added.** After submission of this paper, there appeared a pertinent communication which dealt with the mechanism(s) for the decomposition of 3-(hydroperoxy)-3*H*-indoles: S. Muto and T. C. Bruice, *J. Am. Chem. Soc.*, **102**, 7379 (1980), and references cites therein.
18) L. J. Dolby and D. L. Booth, *J. Am. Chem. Soc.*, **88**, 1049 (1966).
19) T. Hino, *Chem. Pharm. Bull.*, **9**, 989 (1961).

The Pschorr Cyclization of Aromatic Amines with *t*-Butyl Thionitrate in Nonaqueous Media

Shigeru OAE,* Kazuyuki IIDA, Kōichi SHINHAMA, and Toshikazu TAKATA
Department of Chemistry, The University of Tsukuba, Sakura-mura, Ibaraki 305

(Received January 23, 1981)

The Pschorr cyclization of various arylamines with *t*-butyl thionitrate under nonaqueous conditions gave the corresponding cyclic products in moderate yields. The same reaction was also found to proceed readily with *p*-toluenesulfonyl nitrite at room temperature. Treatment of *o*-aminophenyl allyl ether or sulfide with *t*-butyl thionitrate resulted in the intramolecular Meerwein arylation to the olefinic bond affording 3-chlorochroman or -thiochroman, though the yield was low. The plausible mechanism of the Pschorr cyclization with *t*-butyl thionitrate is discussed.

During the course of our study on oxidation of aliphatic and aromatic thiols, disulfides and sulfinic acids with N_2O_4, the corresponding thionitrites, thionitrates and sulfonyl nitrites have been found to be the key intermediates, which are also very useful in synthetic reactions. Namely, diazotization reaction of aromatic amines,[1] nitrosation of secondary amines, and sulfenylation of carbanion[2] are readily promoted in good yields in nonaqueous reaction media. These are remarkably effective reagents for diazotization of aromatic amines due partly to the relatively weak S–N bond as compared to O–N bond of alkyl nitrite. The Gomberg-Bachmann reaction which is used for synthesis of biphenyl from aromatic diazonium salt, has also been carried out using the thionitrates.[1] Thus, various aromatic amines have been allowed to react with the thionitrate in aromatic solvents such as benzene affording biphenyl derivatives in good yields.

While all these reactions we have studied are intermolecular coupling of two aromatic rings, we now have applied the reaction to an intramolecular reaction, *i.e.* the Pschorr cyclization,[3] which is known to be an effective reaction for one-step synthesis of cyclic compounds, used often for syntheses of natural products.[4,5] This paper deals mainly with the Pschorr cyclization of various aromatic amines with *t*-butyl thionitrate, together with the intramolecular Meerwein arylation to give cyclic products.

Results and Discussion

When various aromatic amines bearing two aromatic rings (**1**) such as 2-aminobenzophenone (**1a**, 1.0 mmol) were treated with *t*-butyl thionitrate (**2**, 1.5 mmol) without solvent at 160 °C for 0.5 h the corresponding cyclization product (**3**) was obtained as the main product. *t*-Butyl thionitrate (**2**) was in turn converted to *S*-*t*-butyl 2-methylpropane-2-thiosulfonate (**4**) during

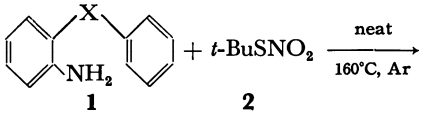

1 **2**

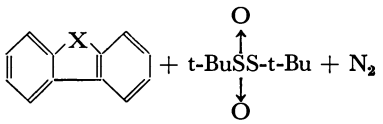

3 **4**

the cyclization. Other unidentified products were in the form of tar or resin. Generally, the Pschorr reaction is known to be accompanied with a few side reactions such as reduction of diazonium ion which produces arene, reductive coupling which affords symmetrical biphenyls, halogenation and phenol formation.[3] Therefore, the yield of the cyclized product in the usual Pschorr reaction is generally low.[3] In this reaction, a small amount of the reduced product, *i. e.* benzophenone, was also obtained, however formation of phenol and reductive coupling derivatives were not observed in this reaction in nonaqueous media.

The Pschorr cyclization of several aromatic amines which possess different bridging group of X in (**1**) with *t*-butyl thionitrate (**2**) has been examined and the yields of the corresponding cyclic products are listed in Table 1. Since the Pschorr reaction is an intramolecular condensation reaction, the ready access of the two reaction centers in the ground state is considered to be quite important for successful cyclization. Namely, the two carbon atoms that are eventually linked together would preferably be in a close vicinity with each other. The most favorable bridging group (X, **1**) is the rigid ethylenic linkage of ethyl (*E*)-2,3-diphenylpropenate (**1g**), which would assume a planar structure by conjugation between the two aromatic rings through an ethylenic group, thus placing the two reaction centers of two aromatic rings in a close vicinity. In fact, ethyl (*E*)-2,3-diphenylpropenate (**1g**) gave ethyl 9-phenanthrenecarboxylate (**3g**) as the main cyclic product in a very good yield in the Pschorr reaction with *t*-butyl thionitrate (**2**). In the case of ether (**1b**) and sulfide (**1c**, **1d**, **1e**), the yield of cyclized products were rather low. Contribution of the following *o*-quinonoid structure (**5**)

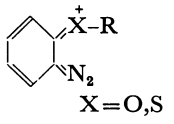

5

in the ground state of the diazonium salts of both the ether (**1b**) and sulfide (**1c**, **1d**, **1e**) may be partly responsible not only for the low yields of the desired products but also for the undesired resin-forming side reactions, while the distant two reaction centers would not favor the recombination.[3] When 2-aminodiphenylamine (**1f**) was treated with the thionitrate, 1-phenylbenzotriazole (**3f**) instead of carbazol, a desired product,

TABLE 1. THE PSCHORR CYCLIZATION OF VARIOUS AMINES (**1**) WITH *t*-BUTYL THIONITRATE (**2**)

Entry	Amine **1**	Product **3**	Yield/%[a]
1	**a** 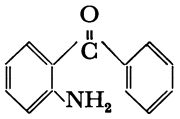	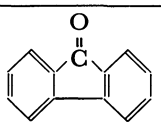	34[b]
2	**b** 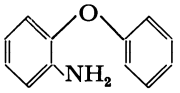	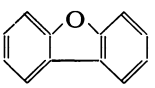	5[b]
3	**c** 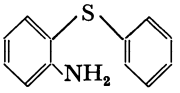	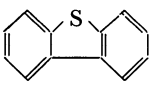	16[b]
4	**d** 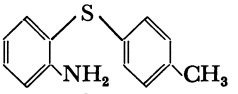	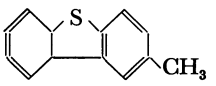	20
5	**e** 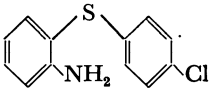	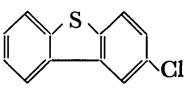	17
6	**f** 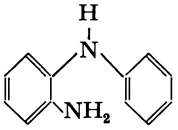	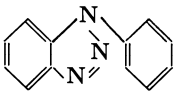	26
7	**g** 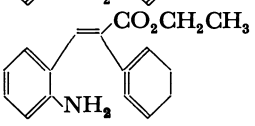	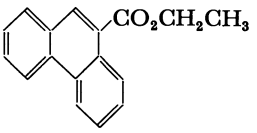	70
8	**h** 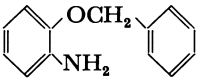	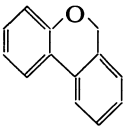	21
9	**i** 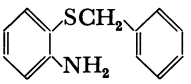	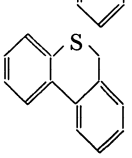	10

a) Isolated yield. b) Yield by GLC.

was obtained. The same result was obtained in the ordinary Pschorr cyclization with nitrous acid in an aqueous media.[3]

In searching the optimum reaction conditions, several runs were carried out (see Table 2). Although the cyclization is an intramolecular reaction, the reaction without solvent was found to offer higher yield of cyclization at higher temperatures, however the best yield of cyclic product was attained in the reaction in DMSO. The Pschorr reaction with nitrous acid in aqueous media is usually carried out in the presence of copper[3] or copper(I) oxide.[7] However when copper or copper(I) oxide was added into our reaction system, the cyclic adduct, fluorenone (**3a**), was not obtained but a complex mixture was obtained.

Meanwhile, the Pschorr reaction of *o*-substituted aromatic amines was also found to proceed smoothly with *p*-toluenesulfonyl nitrite (**6**), which has been shown by us to be a new still more powerful nitrosating agent in certain cases, was used instead of *t*-butyl thionitrate.[1] Namely, aromatic amine (**1**, 1.0 mmol) was treated with three equivalents of *p*-toluenesulfonyl nitrite (**6**, 3.0 mmol) at room temperature for 1—2 h in dry acetonitrile under argon atmosphere. In this case, the reaction was carried out at room temperature instead

TABLE 2. THE PSCHORR CYCLIZATION OF 2-AMINOBENZOPHENONE (**1a**) WITH *t*-BUTYL THIONITRATE (**2**)

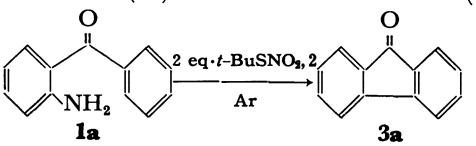

1a **3a**

Entry	Solvent	Temp/°C	Time/h	Yield/%[a]
1	Neat	r.t.	6.0	Trace
2	Neat	120	0.5	15
3	Neat	160	0.5	34
4	CH_3CN	r.t.	2.0	28
5	$(Bu)_2O$	120	4.0	27
6	DMSO	160	1.0	43
7	DMSO Cu or Cu_2O[b]	160	1.0	c)
8	HMPA	160	1.0	Trace

a) Yield by GLC. b) 1.7 Equiv./mol of substrate. c) Complex mixture.

TABLE 3. THE PSCHORR CYCLIZATION OF AMINES (**1a**, **1c**, **1h**) WITH *p*-TOLUENESULFONYL NITRITE (**6**)

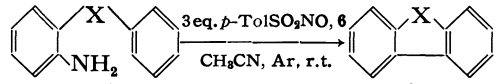

1 **3**

	Amine **1**, X	Yield/%[a]
1a	X=>C=O	49
1c	–S–	16
1h	–OCH_2–	Trace

a) Yield by GLC.

of higher temperatures at which reaction was performed with *t*-butyl thionitrate, since *p*-toluenesulfonyl nitrite (**6**) decomposes at a higher temperature. However the yield of the cyclic adduct was relatively higher than that in the reaction with *t*-butyl thionitrate (see Table 3).

As to the mechanism of the Pschorr cyclization, there are two conceivable pathways, *i. e.* ionic and homolytic paths.[6-8] While thermal decomposition of diazonium salts in acidic media has been believed to take place *via* the ionic process, the reaction has been considered to proceed *via* the homolytic pathway, when the counter anion of diazonium ion is a good reducing agent or the reaction is catalyzed by copper. Since the sulfenate anion derived from the thionitrate (**2**) is considered to be a good reducing agent, while a large amount of tarry material is formed in the reaction, we propose the following free-radical mechanism for this reaction (Scheme 1). The gas evolved in the Gomberg-Bachmann

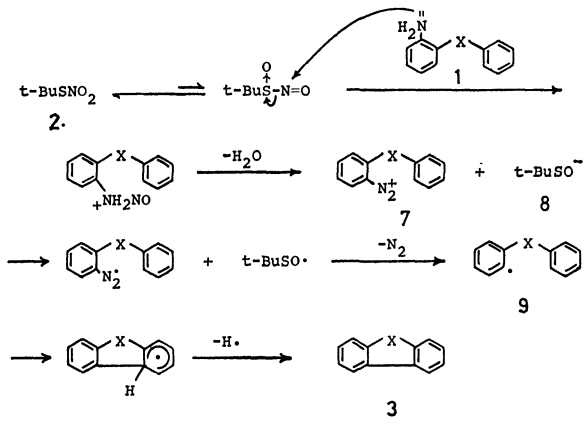

Scheme 1.

reaction of arylamines with aromatic hydrocarbon using *t*-butyl thionitrate[1] was analyzed as N_2 gas by mass spectrometry upon conducting the reaction carefully in a degassed anhydrous system. Therefore, the Pschorr cyclization of aromatic amine with *t*-butyl thionitrate is considered to be initiated by the nucleophilic attack of aromatic amine to nitrogen atom of *t*-butyl thionitrate, like in the aqueous Pschorr reaction. The diazonium ion (**7**) formed after the dehydration may be reduced to the diazo radical by sulfenate anion (**8**), a good reducing agent, which upon release of N_2 gas, gives aryl radical (**9**) that undergoes intramolecular coupling to afford cyclic product (**3**) after hydrogen abstraction. Besides the intramolecular cyclization there may be some intermolecular arylation or a similar side reaction which may be responsible for the formation of much unidentified tarry materials.

Meanwhile, the reaction of diazonium halides derived from aromatic amines with olefinic compound in the presence of copper salt is known as the Meerwein arylation reaction.[9] The Meerwein arylation to olefinic compounds has been found to take place with *t*-butyl thionitrate and addition products were obtained in moderate yields.[1] When an aromatic amine which possesses allyloxy or allylthio group (**10**) at the ortho position was treated with 1.4 equivalent of *t*-butyl

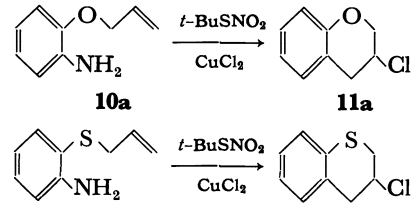

thionitrate (**2**) in the presence of copper(II) chloride in dry acetonitrile at room temperature, the cyclization product (**11**) was obtained as the result of the intramolecular Meerwein arylation despite the lack of any electron-withdrawing substituent on the vinyl group to enhance the Meerwein addition of aryl group. This may be the first example of the intramolecular Meerwein arylation to afford heterocyclic compounds.

Thus, we may conclude that the Pschorr cyclization of *o*-aminophenyl derivatives proceeds quite well with *t*-butyl thionitrate in nonaqueous media and the reaction is useful especially for ring closure reactions of such compounds as *cis*-stilbene or its ester derivatives which are relatively unstable under acidic conditions used in the usual Pschorr cyclization with nitrous acid in strong acids.

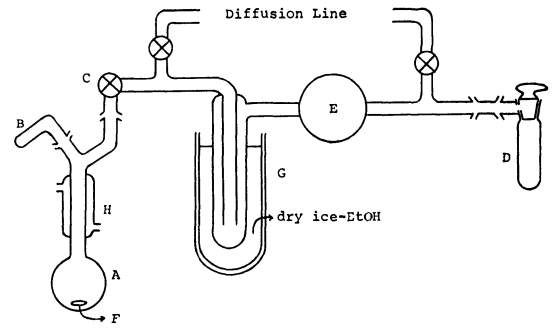

A: Reaction flask, B: bent tube, C: stopcock, D: gas sampler, E: teppler pump, F: magnetic stirrer bar, G: trap, H: water cooler,

Fig. 1. Apparatus for analysis of the gas evolved in the Gomberg-Bachemann reaction with *t*-butyl thionitrate.

Experimental

General. All melting points were taken on a Yanako instrument and were uncorrected. IR spectra were taken on a Hitachi 260-50 spectrometer. NMR spectra were recorded with a Hitachi Perkin-Elmer R-20 spectrometer in $CDCl_3$ using TMS as the internal standard. Mass spectra were

taken with a Hitachi RMU-6MG mass spectrometer. Shimadzu GC-6A instrument was used for gas chromatography using N_2 gas as a carrier gas. Elemental analyses were carried out by the Chemical Analysis Center at this University.

*t-Butyl Thionitrate (**2**) and p-Toluenesulfonyl Nitrite (**6**).* These title compounds were prepared from the corresponding thiol and sulfinic acid with dinitrogen tetraoxide, according to the methods reported earlier.[1]

*Preparation of Ethers (**1b**, **1h**, and **10a**) and Sulfides (**1c**, **1d**, and **1e**).* 2-Nitrodiphenyl ethers and sulfides were prepared by the reaction of *o*-chloronitrobenzene with alkaline salts of desired alcohols or thiols in the presence of a catalytic amount of tetrabutylammonium bromide as a phase transfer catalyst.[10] The yields of the ethers and sufides were nearly 90%. The nitro compound was reduced by the Fe–HCl system,[11] yielding the amine in *ca.* 80% yield.

*2-Aminodiphenyl Ether (**1b**)*: Colorless crystals; mp 44—45 °C (from benzene–hexane) (lit,[12] 43—44 °C); NMR ($CDCl_3$) δ 3.65 (b, 2H, NH_2), 6.46—7.49 (m, 9H, ArH).

*2-Aminodiphenyl Sulfide (**1c**)*: Colorless crystals; mp 41 °C (from benzene–hexane) (lit,[13] 41—42 °C); NMR ($CDCl_3$) δ 4.18 (b, 2H, NH_2), 6.51—7.86 (m, 9H, ArH).

*2-Aminophenyl p-Tolyl Sulfide (**1d**)*: Colorless crystals; mp 47 °C (from hexane–ether) (lit,[14] 48.5—49.0 °C); NMR ($CDCl_3$) δ 2.22 (s, 3H, CH_3), 4.15 (b, 2H, NH_2), 6.52—7.53 (m, 8H, ArH).

*2-Aminophenyl 4-Chlorophenyl Sulfide (**1e**)*: Colorless crystals; mp 33 °C (from ether), bp 194 °C (bath temp)/4 mmHg† (lit,[15] bp 164—166 °C/0.45 mmHg); NMR ($CDCl_3$) δ 4.20 (b, 2H, NH_2), 6.57—7.59 (m, 8H, ArH).

*2-Aminophenyl Benzyl Ether (**1h**)*: Colorless crystals; mp 38 °C (from ether) (lit,[16] 39—40 °C); NMR ($CDCl_3$) δ 3.90 (b, 2H, NH_2), 5.60 (s, 2H, CH_2), 6.63—7.58 (m, 9H, ArH); IR (KBr) 3900 and 3730 (NH_2), 1600, 1210, 724 cm^{-1}.

*2-Aminophenyl Allyl Ether (**10a**)*: Pale yellow oil; bp 136 °C (bath temp)/4 mmHg (lit,[17] bp 129—130 °C/10 mmHg); NMR ($CDCl_3$) δ 3.74 (s, 2H, NH_2), 4.34—4.55 (m, 2H, CH_2), 5.05—5.51 (m, 2H, $=CH_2$), 5.70—6.30 (m, 1H, CH), 6.33—6.93 (m, 4H, ArH); IR (neat) 3890 and 3700 (NH_2), 3100 (=CH), 1600, 1210, 730 cm^{-1}.

*2-Aminodiphenylamine (**1f**).* Commercially available 2-nitrodiphenylamine was reduced by the same system of Fe–HCl.[11] Yield *ca.* 80%. Colorless crystals; mp 80 °C (from hexane) (lit,[18] 78—80 °C); NMR ($CDCl_3$) δ 3.36 (b, 2H, NH_2), 5.10 (b, 1H, NH), 6.51—7.34 (m, 9H, ArH).

*2-Aminobenzophenone (**1a**).* Commercially available compound (Tokyo Kasei Kogyo Co.) was used.

*Ethyl (E)-3-(2-Aminophenyl)-2-phenylpropenate (**1g**).* (*E*)-3-(2-nitrophenyl)-2-phenylpropenic acid was obtained by the Perkin condensation using *o*-nitrobenzaldehyde and phenylacetic acid,[19] and then esterified in ethanol. The nitro compound was reduced to the amino compound by the Fe–HCl system.[11] Yellow crystals; mp 96—97 °C (from benzene–hexane); NMR ($CDCl_3$) δ 1.19 (t, J=6.9 Hz, 3H, CH_3), 3.80 (b, 2H, NH_2), 4.27 (q, J=6.9 Hz, 2H, CH_2), 6.24—7.53 (m, 9H, ArH), 7.82 (s, 1H, =CH); IR (KBr) 3800 and 3690 (NH_2), 1680 (C=O), 1620 (C=C), 1520, 1240, 700 cm^{-1}; Found: C, 76.28; H, 6.38; N, 5.15%. Calcd for $C_{17}H_{17}NO_2$: C, 76.38; H, 6.41; N, 5.23%.

*Preparation of Sulfides (**1i** and **10b**).* *o*-Nitrobenzenethiol was treated with benzyl bromide or allyl bromide, giving the corresponding sulfides in *ca.* 90% yields by the usual method.[20] The nitro compounds then were reduced by the Fe–HCl system.[11]

*2-Aminophenyl Benzyl Sulfide (**1i**)*: Colorless crystals; mp 45 °C (from benzene–hexane) (lit,[16] 45 °C); NMR ($CDCl_3$) δ 3.87 (s, 2H, CH_2), 4.24 (b, 2H, NH_2), 6.44—7.40 (m, 9H, ArH); IR (KBr) 3860 and 3670 (NH_2), 1595, 1440, 695 cm^{-1}.

*2-Aminophenyl Allyl Sulfide (**10b**)*: Pale yellow oil; bp 135—138 °C (bath temp)/4 mmHg (lit,[21] bp 120 °C/4 mmHg); NMR ($CDCl_3$) δ 3.34 (d, J=6.4 Hz, 2H, CH_2), 4.27 (s, 2H, NH_2), 4.69—5.12 (m, 2H, $=CH_2$), 5.48—6.22 (m, 1H, =CH), 6.46—7.43 (m, 4H, AtH); IR (neat) 3880 and 3680 (NH_2), 3100 (=CH), 1595, 1465, 740 cm^{-1}.

*The Pschorr Cyclization of Amines (**1**) with t-Butyl Thionitrate (**2**).* *t*-Butyl thionitrate (**2**, 1.5 mmol) was added with syringe to melted 2-aminobenzophenone (**1a**, 1.0 mmol) at 160 °C under argon. Vigorous reaction occurred and gas evolved. After heating and stirring the mixture at the same temperature for 0.5 h, the mixture was cooled and a portion of the mixture was subjected to GLC to determine the yield. Fluorenone (**3a**) was identified by comparing the GLC and TLC with those of authentic samples, and the yields were determined by GLC. Other compounds (**3d**—**3i**) were isolated by preparative TLC or column chromatography (silica gel, eluent: benzene–hexane=1 : 6) and recrystallized from adequate solvent.

*2-Methyldibenzothiophene (**3d**)*: Colorless crystals; mp 86 °C (from ethanol) (lit,[22] 88—89 °C); NMR ($CDCl_3$) δ 2.59 (s, 3H, CH_3), 7.20—8.20 (m, 7H, ArH).

*2-Chlorodibenzothiophene (**3e**)*: Colorless crystals; mp 125—126 °C (from ethanol) (lit,[23] 113—114 °C); IR (KBr) 1420, 1089, 755, 725 cm^{-1}; MS (70 eV) *m/e* (rel intensity) 220 (38%, M^++2), 218 (100%, M^+), 183 (14%, $C_6H_4SC_6H_3^+$).

*1-Phenylbenzotriazole (**3f**)*: Colorless crystals; mp 85—87 °C (lit,[18] 89—90 °C); IR (KBr) 1592, 1494, 1055, 745 cm^{-1}; MS (70 eV) *m/e* (rel intensity) 195 (23%, M^+), 167 (100%, $C_6H_4N^+C_6H_5$), 77 (25%, $C_6H_5^+$).

*Ethyl 9-Phenanthrenecarboxylate (**3g**)*: Coloress crystals; mp 58—59 °C (from ethanol) (lit,[23] 61 °C); NHR ($CDCl_3$) δ 1.64 (t, J=7.1 Hz, 3H, CH_3), 4.48 (q, J=7.1 Hz, 3H, CH_2), 7.42—8.97 (m, 9H, ArH); IR (KBr) 1700, (C=O), 1440, 1290, 1240, 1030 cm^{-1}; MS (70 eV) *m/e* (rel intensity) 250 (100%, M^+), 205 (99%, $C_{14}H_9C{\equiv}O^+$), 177 (54%, $C_{14}H_9^+$).

*6H-Dibenzo[b, d]pyran (**3h**)*: Oil; NMR ($CDCl_3$) δ 5.07 (s, 2H, CH_2) (lit,[25] δ 5.07, s), 6.84—7.81 (m, 8H, ArH); MS (70 eV) *m/e* (rel intensity) 182 (74%, M^+), 181 (100%, $C_6H_4O^+CHC_6H_4$).

*6H-Dibenzo[b, d]thiopyran (**3i**)*: Colorless crystals; mp 73—74 °C (lit,[26] 75.5 °C); MS (70 eV) *m/e* (rel intensity) 198 (91%, M^+), 197 (100%, $C_6H_4S^+CHC_6H_4$).

*The Pschorr Cyclization of Amines (**1a**, **1b**, and **1h**) with p-Toluenesulfonyl Nitrite (**6**).* A mixture of 2-aminobenzophenone (**1a**, 1.0 mmol) and dry acetonitrile (5 ml) was added onto *p*-toluensulfonyl nitrite (**6**, 3.0 mmol) under argon. Evolution of the gas was observed. Then the solution was stirred for 1 h at room temperature. The cyclic products were identified by comparison of the GLC and TLC with those of authentic samples, and yields were determined by GLC.

*The Intramolecular Meerwein Arylation of Amines (**10a** and **10b**) with t-Butyl Thionitrate (**2**) and Copper (II) Chloride.* *t*-Butyl thionitrate (**2**, 1.4 mmol) was added slowly to the solution of 2-aminophenyl allyl ether (**10a**, 1.0 mmol) and well-dried anhydrous copper (II) chloride (1.2 mmol) in dry acetonitrile (10 ml) under argon with vigorous stirring at room temperature. The solution was stirred further for 1 h. Then cyclic product, 3-chlorochroman (**11a**), was directly isolated by column chromatography (silica gel, eluent: hexane).

*3-Chlorochroman (**11a**)*: Pale yellow oil; NMR ($CDCl_3$) δ 3.43—3.90 (m, 3H, CH_2 and CH), 4.29—4.71 (m, 2H, OCH_2), 6.67—7.35 (m, 4H, ArH); MS (70 eV) *m/e* (rel intensity) 200

† 1 mmHg=133.322 Pa.

13%, $M^+ +2$), 168 (38%, M^+), 119 (100%, $[C_7H_5{=}O]CH_2^+$), 91 (31%, $C_6H_5CH_2^+$); Found: C, 63.65; H, 5.45%. Calcd for C_9H_9ClO: C, 64.10; H, 5.38%.

*3-Chlorothiochroman (**11b**)*: Pale yellow oil; NMR ($CDCl_3$) δ 3.16—3.75 (m, 5H, CH_2, CH and SCH_2), 6.97—7.27 (m, 4H, ArH); MS (70 eV) *m/e* (rel intensity) 186 (11%, $M^+ +2$), 184 (27%, M^+), 135 (100%, $[C_7H_5{=}S]CH_2^+$), 91 (14%, $C_6H_5CH_2^+$); Found: C, 58.51; H, 4.92%, Calcd for C_9H_9ClS: C, 58.53; H, 4.91%.

Determination of Gas Evolved in The Gomberg-Bachmann Reaction of p-*Chloroaniline with* t-*Butyl Thionitrate.* A mixture of *t*-butyl thionitrate (1.4 mmol) in dry benzene (1 ml) was placed in the flask A of the special apparatus shown in Fig. 1, freezed with liquid nitrogen bath and degassed three times using the vacuum line. After the stopcock C was closed, solid *p*-chloroaniline (0.7 mmol) was added from bent tube B, then the mixture was stirred and heated at 80 °C with an oil bath for 5 h. The gas evolved was pumped into the gas sampler D by teppler pump E. The gas obtained was introduced into the mass spectrometer for identification.

References

1) S. Oae, K. Shinhama, and Y. H. Kim, *Bull. Chem. Soc. Jpn.*, **53**, 1065, 2023 (1980).
2) K. Shinhama, Y. H. Kim, and S. Oae, *Bull. Chem. Soc. Jpn.*, **53**, 1771 (1980).
3) D. F. DeTar, *Org. React.*, **9**, 409 (1957).
4) T. Kametani, T. Sugahara, and K. Fukumoto, *Tetrahedron*, **27**, 5367 (1971).
5) M. C. Cava, I. Noguchi, and K. T. Buck, *J. Org. Chem.*, **38**, 2394 (1973).
6) R. A. Abramovitch, *Adv. Free Radical Chem.*, **2**, 87 (1967).
7) A. H. Lewin and T. Cohen, *J. Org. Chem.*, **32**, 3844 (1967).
8) F. F. Gadallah, A. A. Cantu, and R. M. Elofson, *J. Org. Chem.*, **38**, 2386 (1973).
9) C. S. Rondestvendt, Jr., *Org. React.*, **11**, 189 (1960).
10) C. M. Starks and C. Liotta, "Phase Transfer Catalysis," Academic Press, New York (1978), Chap. 4, p. 128.
11) *Org. Synth.*, Coll. Vol. 2, 160 (1943).
12) H. I. Jones and A. N. Cook, *J. Am. Chem. Soc.*, **38**, 1534 (1916).
13) D. F. DeTar and S. V. Sagmanli, *J. Am. Chem. Soc.*, **72**, 965 (1950).
14) H. Gilman and H. S. Broadbent, *J. Am. Chem. Soc.*, **69**, 2053 (1947).
15) A. Burger and J. Stanmyer, *J. Org. Chem.*, **21**, 1382 (1956).
16) A. Sieglitz and H. Koch, *Ber.*, **58**, 78 (1925).
17) J. Braun and O. Braunsdort, *Ber.*, **54**, 702 (1921).
18) M. Schöpff, *Ber.*, **23**, 1839 (1890).
19) *Org. Synth.*, Coll. Vol. 4, 730 (1963).
20) B. R. Wagner and H. D. Zook, "Synthetic Organic Chemistry," Jonh Wiley and Sons, Inc., New York (1953), Chap. 32, p. 787.
21) L. K. Mushkalo, *Ukr. Khim. Zh.*, **23**, 642 (1957).
22) H. Gilman and G. R. Wilder, *J. Org. Chem.*, **22**, 523 (1957).
23) "Beilsteins Handbuch der Organischen Chemie," *II*, 10, 17.
24) R. Pschorr and J. Schöter, *Ber.*, **35**, 2726 (1902).
25) J. P. Devlin, *Can. J. Chem.*, **53**, 343 (1975).
26) A. Lüttringhaus and A. Kolb, *Z. Naturforsch.*, **16b**, 762 (1961).

Branched-chain Sugars. XXIV. Synthesis of Methyl 6-Deoxy-3-*C*-methyl-β-D-gulopyranoside (Methyl β-Virenoside)[1]

Namgi HONG, Ken-ichi SATO, and Juji YOSHIMURA*

Laboratory of Chemistry for Natural Products, Faculty of Science, Tokyo Institute of Technology, Nagatsuta, Midori-ku, Yokohama 277

(Received February 7, 1981)

Methyl 6-deoxy-3-*C*-methyl-β-D-gulopyranoside (methyl β-virenoside) was prepared from D-galactose. An attempted synthesis of the virenoside by the inversion at *C*-4 of methyl 6-deoxy-3-*C*-methyl-α-D-allopyranoside was unsuccessful.

Virenose is a new naturally occuring branched-chain sugar found as a component of the antitumor antibiotic virenomycin produced by *Actiomyces virens* sp. nov.[2] Kulyaeva and her coworkers have reported the isolation of virenose as a methyl glycoside and established its absolute configuration as methyl 6-deoxy-3-*C*-methyl-β-D-gulopyranoside (**1**) from NMR, MS, and IR spectral data, and $[M]^{cupra\ A,B}$ rotational values.[3]

It is one of the most common branched-chain sugars, 6-deoxy-3-*C*-methylhexoses.[4] For the introduction of *C*-methyl branching, it is known that the reaction of methylmagnesium iodide and methyl 4,6-*O*-benzylidene-2-deoxy-α-D-*threo*-[5] and -α-D-*erythro*-hexopyranosid-3-uloses,[6] and methyl 4,6-*O*-benzylidene-α-D-*ribo*-hexopyranosid-3-ulose[7] gave the corresponding branched-chain sugars having the desired configuration at *C*-3 position. This paper describes the synthesis of **1** from methyl 2-*O*-benzoyl-4,6-*O*-benzylidene-α-D-*xylo*-hexopyranosid-3-ulose obtained from D-galactose,[8] though another synthesis *via* the configurational inversion at *C*-4 of methyl 2,3-di-*O*-benzyl-6-deoxy-3-*C*-methyl-4-*O*-(methylsulfonyl)-α-D-allopyranoside (**6**) derived from D-glucose was unsuccessful.

Results and Discussion

Methyl 4,6-*O*-benzylidene-3-*C*-methyl-α-D-allopyranoside[7] obtained from D-glucose through five steps conversions was converted into the corresponding 2,3-di-*O*-benzyl derivative (**2**) in 78% yield by treating with sodium hydride and benzyl bromide in dimethyl sulfoxide. The benzylidene group of **2** was removed by refluxing in 70% acetic acid to produce **3** in 78% yield. Monotosylation of **3** in pyridine gave the corresponding 6-*O*-tosylate (**4**) in 80% yield. Reduction of **4** in tetrahydrofuran with lithium aluminium hydride gave methyl 2,3-di-*O*-benzyl-6-deoxy-3-*C*-methyl-α-D-allopyranoside (**5**) in 65% yield.

For the inversion of the configuration at *C*-4 of **5**, oxidation-reduction method was tried at first. Oxidation of **5** with dimethyl sulfoxide and trifluoroacetic anhydride gave the corresponding 4-ulose (**7**) in 78% yield. However, reduction of **7** with sodium borohydride gave only **5**. Because the conformation of **7** is deduced to be *C*1, the above result is attributed to the steric hindrance of the axial benzyloxy group at *C*-3. As the second procedure, the S_N2 inversion at *C*-4 was tried. Usual mesylation of **5** gave the corresponding 4-*O*-mesylate (**6**) in 83% yield. Unfortunately, all attempts for the conversion of **6** into the 4-*O*-benzoyl derivative (**9**) of

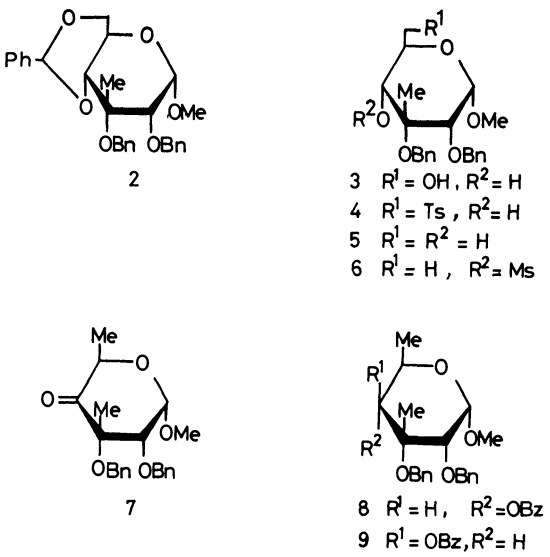

Fig. 1.

D-*gulo* configuration by treatment with sodium benzoate were failed. Treatment of **6** in hexamethylphosphoric triamide at 180 °C for 24 h gave an ester exchange product, methyl 4-*O*-benzoyl-2,3-di-*O*-benzyl-3-*C*-methyl-α-D-allopyranoside (**8**) in 30% yield, which is identical with that obtained by benzoylation of **5**.

On the other hand, oxidation of methyl 2-*O*-benzoyl-4,6-*O*-benzylidene-α-D-galactopyranoside[9] with dimethyl sulfoxide and trifluoroacetic anhydride in dichloromethane gave the corresponding 3-ulose (**10**) in 80% yield. Reaction of **10** in benzene with methylmagnesium iodide gave predominantly one compound (**11**), which was separated by column chromatography from a trace of the corresponding 3-epimer in 85% yield. This result indicates that the Grignard reagent attacks the carbonyl function from the equatorial side as was in the case of the corresponding 2-deoxy-3-ulose.[5] Treatment of **11** with acetone in the presence of anhydrous copper(II) sulfate and catalytic amount of sulfuric acid gave the 2,3-*O*-isopropylidene derivative (**12**) in high yield, indicating the presence of *cis*-hydroxyl groups in **11**.

Reaction of **11** with *N*-bromosuccinimide in carbon tetrachloride in the presence of excess barium carbonate afforded methyl 4-*O*-benzoyl-6-bromo-6-deoxy-3-*C*-methyl-α-D-gulopyranoside (**13**) in 75% yield. The reduction of **13** in benzene with tributylstannane in the presence of α,α'-azobisisobutyronitrile gave the corresponding 6-deoxy derivative (**14**) in 70% yield. Base-catalyzed removal of the 4-*O*-benzoyl group of **14** gave

Table 1. Physical constants of **1** and **16**

	Mp/°C	$[\alpha]_D$/° (in $CHCl_3$)	^1H NMR parameters					
			H-1 ($J_{1,2}$)	H-2	H-4 ($J_{4,5}$)	H-5 ($J_{5,6}$)	H-6	Other protons
1	134—135	−30	4.41d (8.0)	3.39d	3.26d (1.2)	4.22q (6.5)	1.28d	1.40(CMe), 3.54(OMe), 2.52(OH)
Reported **1**[a)]	131	−39	4.31d (7.5)	3.31d	3.16d (1.2)	4.12q (6.0)	1.24d	1.39(CMe)
16	140—141	−24	4.58d (8.0)	4.81d	4.80d (1.2)	4.23q (6.5)	1.14d	1.12(CMe), 3.54(OMe), 2.14(2×OAc)
Reported **16**	140	−27						

a) The NMR spectrum was recorded with a Hitachi R-20A (60 MHz) spectrometer.

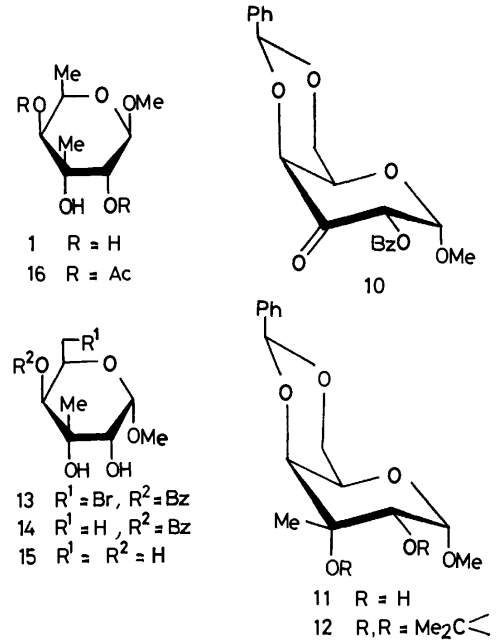

Fig. 2.

the de-*O*-benzoylated product (**15**) in 65% yield. Anomerization of **15** in methanol with cationic ion-exchanger IR-120 by refluxing for 20 h gave crystalline methyl β-D-virenoside (**1**) in 80% yield. The physical constants of **1** are in good agreement with those reported[2)] (Table 1). The usual acetylation of **1** gave the corresponding 2,4-diacetate (**16**).

Experimental

All the melting points are uncorrected. The solutions were evaporated under reduced pressure at a bath temperature not exceeding 45 °C. Specific rotations were measured in a 0.5-dm tube with a Carl Zeiss LEP-Al polarimeter by the use of chloroform as the solvent. The IR spectra were recorded with a Hitachi Model EPI-G2 spectrometer. The NMR spectra were taken with a JEOL PS-100 spectrometer using tetramethylsilane as an internal standard in deuteriochloroform unless otherwise stated. Chemical shifts and coupling constants were recorded in δ and Hz units and IR frequencies in cm^{-1}.

*Methyl 2,3-Di-*O*-benzyl-4,6-*O*-benzylidene-3-*C*-methyl-α-*D*-allopyranoside (2).* To a suspension of sodium hydride (0.5 g, 20.8 mmol) and methyl 4,6-*O*-benzylidene-3-*C*-methyl-α-D-allopyranoside (2 g, 6.75 mmol) in dry dimethyl sulfoxide (15 ml) was added gradually benzyl chloride (1.7 g, 13.4 mmol). The mixture was then heated for 1 h at 70 °C on a water-bath, poured into ice water, and then extracted with chloroform. The extract was washed with water, dried with anhydrous magnesium sulfate, and evaporated to give a syrup that was purified on a preparative TLC (benzene–ethyl acetate 10 : 1) to give a colorless syrup (2.5 g, 78%). $[\alpha]_D^{13}$ +58° (*c* 0.4), NMR: 7.1—7.3 (3×Ph; m), 5.40 (PhCH; s), 4.96 and 4.69 (2×$PhCH_2$; each s), 4.72 and 3.32 (H-1 and H-2; each d, $J_{1,2}$=4.0), 4.60—4.18 (H-6 and H-6′; m), 3.60 (H-5; m), 3.30 (H-4; d, $J_{4,5}$=8.0), 3.42 (OMe), 1.46 (CMe). Found: C, 72.96; H, 6.68%. Calcd for $C_{29}H_{32}O_6$: C, 73.10; H, 6.72%.

*Methyl 2,3-Di-*O*-benzyl-3-*C*-methyl-α-*D*-allopyranoside (3).* A solution of **2** (1.2 g, 2.5 mmol) in 70% acetic acid (4 ml) was kept for 10 h at room temperature, evaporated, and the residue was purified on a preparative TLC (toluene–chloroform–methanol 4 : 4 : 1) to give a syrup in 80% (0.78 g) yield. $[\alpha]_D^{13}$ +41.4° (*c* 0.6); NMR: 7.32 (Ph; s), 5.20—4.48 (2×$PhCH_2$; m, J=10.5), 4.77 and 3.35 (H-1 and H-2; each d, $J_{1,2}$=4.0), 3.30 (H-4; d, $J_{4,5}$=10.0), 3.7—3.9 (H-5, H-6, and H-6′; m), 3.41 (OMe), 2.2 and 2.45 (2×OH; each broad s), 1.48 (CMe). Found: C, 68.23; H, 7.31%. Calcd for $C_{22}H_{28}O_6$: C, 68.04; H, 7.21%.

*Methyl 2,3-Di-*O*-benzyl-3-*C*-methyl-6-*O*-(p-tolysulfonyl)-α-*D*-allopyranoside (4).* Reaction of **3** (5 g, 12.8 mmol) in dry pyridine (20 ml) with *p*-toluenesulfonyl chloride (2.7 g, 14.2 mmol) at room temperature overnight and usual work-up of the reaction mixture gave **4** (5.2 g, 75%) as a syrup. $[\alpha]_D^{13}$ +41° (*c* 1.5); NMR: 7.32 (Ph; m), 5.16—4.44 (2×$PhCH_2$; m. J=10.5), 4.73 and 3.32 (H-1 and H-2; each d, $J_{1,2}$=4.0), 3.33 (H-4; d, $J_{4,5}$=10.0), 4.0—4.4 (H-5, H-6, and H-6′; m), 3.38 (OMe), 2.41 (PhMe), 1.46 (CMe). Found: C, 64.32; H, 6.34%. Calcd for $C_{29}H_{34}O_8S$: C, 64.20; H, 6.27%.

*Methyl 2,3-Di-*O*-benzyl-6-deoxy-3-*C*-methyl-α-*D*-allopyranoside (5).* Lithium aluminium hydride (1.0 g, 32.5 mmol) was gradually added to a solution of **4** (4 g, 7.4 mmol) in dry tetrahydrofuran (100 ml), and the mixture was boiled for 6 h. A small amount of ethyl acetate and water were successively added to the reaction mixture, and the precipitate formed was filtered and washed with ether. The filtrate and washings were evaporated to a syrup, which was purified on a preparative TLC (benzene–ethyl acetate 10 : 1) to give syrupy **5** (1.78 g, 65%). $[\alpha]_D^{12}$ +43.6° (*c* 1.0); NMR: 7.32 (Ph; m), 5.10—4.80 ($PhCH_2$×2; m, J=10.5), 4.71 and 3.34 (H-1 and H-2; each d, $J_{1,2}$=4.0), 2.93 (H-4; dd, $J_{4,5}$=10.0, $J_{4,OH}$=12.0), 3.40 (OMe), 1.44 (CMe), 2.35 (OH; d), 1.20 (H-6; d). Found: C, 70.55; H, 7.32%. Calcd for $C_{22}H_{28}O_5$: C, 70.96; H, 7.52%.

*Methyl 2,3-Di-*O*-benzyl-6-deoxy-3-*C*-methyl-4-*O*-(methylsulfo-*

nyl)-α-D-allopyranoside (6). Methanesulfonyl chloride (0.6 g, 5.2 mmol) was added to a solution of **5** (1 g, 2.7 mmol) in dry pyridine (5 ml) cooled in an ice-water bath. The resulting solution was kept for 12 h at room temperature, poured into water, and then extracted with chloroform. The extracts were washed with saturated aqueous sodium hydrogencarbonate and water. Evaporation of the dried extract gave a syrupy **6** (1 g, 83%), $[\alpha]_D^{13}$ +79.5° (*c* 0.9); NMR: 7.36 (Ph; s), 5.10—4.56 ($PhCH_2\times2$; m, J=10.5), 4.68 and 3.31 (H-1 and H-2; each d, $J_{1,2}$=4.0), 4.19 (H-4; d, $J_{4,5}$=10.0), 4.45 (H-5; oct, $J_{5,6}$=6.0), 3.40 (OMe), 2.99 (Ms), 1.48 (CMe), 1.25 (H-6; d). Found: C, 61.62; H, 6.61%. Calcd for $C_{23}H_{30}O_7S$: C, 61.33; H, 6.66%.

Methyl 4-O-Benzoyl-2,3-di-O-benzyl-6-deoxy-3-C-methyl-α-D-allopyranoside (8). *i)* : A solution of **5** (0.6 g, 1.32 mmol) and sodium benzoate (0.38 g, 2.6 mmol) in hexamethylphosphoric triamide (6 ml) was heated at 180 °C for 24 h, filtered, and then poured into water. The resulting solution was extracted with chloroform. The extract was washed with water and evaporated. The residue was extracted with ether again, and the usual work-up of the extract gave a syrup (0.42 g) which was purified on a preparative TLC (toluene–ethyl acetate 16 : 1) to give **8** (0.18 g, 30%) as a syrup. $[\alpha]_D^{14}$ +26.9° (*c* 0.5); NMR: 8.10—7.8 and 7.50—7.30 ($2\times$Ph; m), 5.52 (H-5; m, $J_{5,6}$=6.0), 4.4—4.8 ($2\times PhCH_2$; m), 4.90 and 3.68 (H-1 and H-2; each d, $J_{1,2}$=4.0), 3.87 (H-4; d, $J_{4,5}$=6.0), 3.48 (OMe), 1.52 (CMe), 1.47 (H-6; d). Found: C, 73.25; H, 6.78%. Calcd for $C_{29}H_{32}O_6$: C, 73.11; H, 6.72%.

ii) : To a solution of **5** (0.1 g, 0.27 mmol) in dry pyridine (5 ml) was added benzoyl chloride (0.1 g, 0.7 mmol), and the usual work-up after 10 h gave **8** (0.9 g, 71%) identical with that obtained above.

Methyl 2,3-Di-O-benzyl-6-deoxy-3-C-methyl-α-D-ribo-hexopyranosid-4-ulose (7). To a solution of dry dimethyl sulfoxide (0.5 g, 6.4 mmol) and dry dichloromethane (2 ml) was added successively trifluoroacetic anhydride (0.54 g, 4.0 mmol) in dichloromethane (2 ml) with stirring during 10 min at −78 °C, and then a solution of **6** (0.5 g, 1.34 mmol) in dichloromethane (2 ml). The reaction mixture was stirred at −78 °C for 20 min, neutralized with triethylamine (4 ml), and extracted with chlorofolm. The extract was washed with water, and then evaporate to give a syrup which was chromatographed on a silica-gel column (toluene–ethyl acetate 16 : 1) to afford **7** (0.38 g, 78%). $[\alpha]_D^{14}$ +101° (*c* 0.4). IR: 1740 (C=O); NMR: 7.4—7.2 ($2\times$Ph; m), 4.9—4.5 ($PhCH_2$; m), 4.80 and 3.59 (H-1 and H-2; each d, $J_{1,2}$=4.0), 4.50 (H-5; q, $J_{5,6}$=6.0), 1.20 (H-6; d), 3.51 (OMe), 1.51 (CMe). Found: C, 71.77; H, 7.21%. Calcd for $C_{22}H_{26}O_5$: C, 71.35; H, 7.02%.

Methyl 4,6-O-Benzylidene-2-O-benzoyl-α-D-xylo-hexopyranosid-3-ulose (10). A similar oxidation of **7** to that of **5** gave the corresponding 3-ulose (**10**) in 80% yield. $[\alpha]_D^{27}$ +142° (*c* 1.8); IR: 1730 (C=O); NMR 7.8—8.2 and 7.2—7.6 ($2\times$Ph; m), 5.59 (PhCH), 6.1 and 5.36 (H-1 and H-2; each d, $J_{1,2}$=3.8), 4.54 (H-4; d, $J_{4,5}$=1.5), 3.97 (H-5; m), 4.15 (H-6′; dd, $J_{5,6}$=2.0), 4.42 (H-6; dd, $J_{6,6'}$=13, $J_{5,6}$=1.5), 3.48 (OMe). Found: C, 65.65; H, 5.42%. Calcd for $C_{21}H_{20}O_7$: C, 65.62; H, 5.21%.

Methyl 4,6-O-Benzylidene-3-C-methyl-α-D-gulopyranoside (11). To a suspension of magnesium turning (4.5 g, 185 mmol) in dry ether (150 ml) was added methyl iodide (25 g, 176 mmol) dropwise with stirring at room temperature. After 20 min, **10** (15 g, 39 mmol) was added to the Grignard solution with the aid of a small amount of benzene. After stirring for 6 h, the reaction mixture was worked up in the usual way to give a syrupy **11** in 85% (10.1 g) yields. $[\alpha]_D^{28}$ +102° (*c* 1.0); NMR: 7.2—7.52 (Ph; m), 5.50 (PhCH), 4.86 (H-1; d, $J_{1,2}$=3.8), 3.78 (H-2; dd, $J_{2,OH}$=12.0), 3.77 (H-4; s), 3.90 (H-5; broad s), 4.30 (H-6; dd, $J_{6,6'}$=13, $J_{5,6}$=2.0), 4.04 (H-6′; dd, $J_{5,6'}$=2.0), 3.3 (3-OH), 3.46 (OMe), 2.64 (2-OH; d), 1.35 (CMe). Found: C, 60.75; H, 6.64%. Calcd for $C_{15}H_{20}O_6$: C, 60.81; H, 6.76%.

Methyl 4,6-O-Benzylidene-3-C-methyl-2,3-O-isopropylidene-α-D-gulopyranoside (12). A suspension of **11** (0.38 g, 1.28 mmol) and copper(II) sulfate (0.4 g, 2.5 mmol) in dry acetone (2 ml) containing catalytic amount of sulfuric acid was stirred for 12 h, filtered, and then evaporated to dryness. The residue was extracted with chloroform, and the usual work-up of the extract gave a syrup which was purified on a TLC (benzene–acetone 5 : 1) to give pure **12** as a syrup (0.35 g, 81%). $[\alpha]_D^{26}$ +8.6° (*c* 0.6); NMR: 7.5—7.2 (Ph; m), 5.50 (PhCH), 5.18 and 3.71 (H-1 and H-2; each d, $J_{1,2}$=1.2), 4.18 (H-4; s), 4.0 (H-5; m), 4.34 (H-6; dd, $J_{6,6'}$=12.2, $J_{5,6}$=2.0), 3.92 (H-6′; dd, $J_{5,6'}$=2.0), 3.62 (OMe), 1.46, 1.50 and 1.52 ($3\times$CMe; each s). Found: C, 64.31; H, 7.33%. Calcd for $C_{18}H_{24}O_6$: C, 64.28; H, 7.14%.

Methyl 4-O-Benzoyl-6-bromo-6-deoxy-3-C-methyl-α-D-gulopyranoside (13). A suspension of **11** (8 g, 0.028 mol), *N*-bromosuccinimide (8.96 g, 0.05 mol), and barium carbonate (8.8 g, 0.04 mol) in dry carbon tetrachloride (150 ml) was boiled for 7 h, filtered, and the filtrate was worked up in the usual way to give **13** as a syrup in 75% (8.5 g) yield. $[\alpha]_D^{27}$ +120.7° (*c* 1.8); NMR: 7.9—8.1 and 7.3—7.5 (PhCO; m), 4.92 and 3.79 (H-1 and H-2; each d, $J_{1,2}$=3.8), 5.26 (H-4; s), 4.46 (H-5; dd, $J_{5,6'}$=8.0, $J_{5,6}$=4.0), 3.44 (H-6′; dd, $J_{6,6'}$=11.0), 3.26 (H-6; dd), 3.54 (OMe), 1.26 (CMe). Found: C, 48.31; H, 5.20%. Calcd for $C_{15}H_{19}O_6Br$: C, 48.00; H, 5.06%.

Methyl 4-O-Benzoyl-6-deoxy-3-C-methyl-α-D-gulopyranoside (14). To a solution of **13** (5 g, 0.013 mol) in anhydrous benzene (100 ml) was added tributylstannane (7.5 g, 0.025 mol) and catalytic amount of α,α′-azobisisobutyronitrile. The mixture was refluxed for 15 h, concentrated and the tin compound in the residue was removed on a silica gel column using hexane as the eluent. Thereafter, the elution with benzene–acetone (10 : 1) gave syrupy **14** in 70% (2.7 g) yield, which was crystallized from ethyl acetate. Mp 133—134 °C, $[\alpha]_D^{28}$ +142° (*c* 1.0); NMR: 8.0—8.16 and 7.30—7.60 (PhCO; m), 4.87 (H-1: d, $J_{1,2}$=4.0), 3.78 (H-2; dd, $J_{2,OH}$=12.0), 5.12 (H-4; s), 4.41 (H-5; q, $J_{5,6}$=6.0), 3.84 (OH-3; s), 3.52 (OMe), 2.40 (OH-2; d), 1.25 (CMe), 1.17 (H-6; d). Found: C, 60.64; H, 6.89%. Calcd for $C_{15}H_{20}O_6$: C, 60.81; H, 6.76%.

Methyl 6-Deoxy-3-C-methyl-α-D-gluopyranoside (15). A solution of **14** (1.5 g, 5 mmol) and sodium (0.4 g, 17 mmol) in dry methanol (60 ml) was refluxed for 4 h, and concentrated to dryness. The residue was extracted several times with dichloromethane, and the usual work-up of the extract gave **15** as a syrup in 65% yield. $[\alpha]_D^{27}$ +123° (*c* 0.3); NMR (CD_3OD): 4.79 and 3.58 (H-1 and H-2; each d, $J_{1,2}$=4.0), 4.25 (H-5; q, $J_{5,6}$=6.0), 3.13 (H-4; s), 3.48 (OMe), 1.26 (CMe), 1.17 (H-6; d). Found: C, 49.85; H, 7.29%. Calcd for $C_8H_{16}O_5$: C, 49.99; H, 8.39%.

Methyl 6-Deoxy-3-C-methyl-β-D-gulopyranoside (Methyl β-D-Virenoside) (1). A suspension of **15** (0.3 g, 1.6 mmol) and cationic resin (IR-120, 1.5 g) in dry methanol (40 ml) was refluxed for 24 h. The anomerization could be monitored by TLC. The reaction mixture was filtered, and the filtrate was evaporated. The residual syrup was purified on a preparative TLC (chloroform–methanol 4 : 1) to give **1** in 80% (0.24 g) yield, which was crystallized from hexane–chloroform. Found: C, 49.74; H, 8.24%. Calcd for $C_8H_{16}O_5$: C, 49.99; H, 8.39%.

Methyl 2,4-Di-O-acetyl-6-deoxy-3-C-methyl-β-D-gulopyranoside

(16). Acetylation of **1** (30 mg, 0.16 mmol) with acetic anhydride in pyridine for 24 h at room temperature, and the usual work-up of the mixture and purification of the product by a preparative TLC (benzene–aceton 5 : 1) gave **16** in 82% (25 mg) yield, which was recrystallized from methanol. Found: C, 52.27; H, 7.34%. Calcd for $C_{12}H_{20}O_7$: C, 52.16; H, 7.30%.

References

1) Part XXIII: M. Matsuzawa, K. Sato, T. Yasumori, and J. Yoshimura, submitted to this Bulletin.

2) M. G. Brazhnikova, M. K. Kudinova, V. V. Kulyaeva, N. P. Potapova, and V. I. Ponomalenko, *Antibiotiki*, **11**, 967 (1977).

3) V. V. Kulyaeva, M. K. Kudinova, N. P. Potapova, L. M. Rubasheva, M. G. Brazhnikova, B. V. Rosynoi, and A. R. Bekker, *Bioorg. Khim.*, **4**, 1087 (1978).

4) H. Grisebach and R. Schmid, *Angew. Chem.*, **84**, 192 (1972).

5) G. B. Howarth, W. A. Szarek, and J. K. N. Jones, *Carbohydr. Res.*, **7**, 284 (1968).

6) B. Flaherty, S. Nahar, W. G. Overrend and N. R. Williams, *J. Chem. Soc., Perkin Trans. 1*, **1973**, 632.

7) F. A. Carey and K. O. Hodgson, *Carbohydr. Res.*, **12**, 463 (1970).

8) J. Yoshimura, N. Hong, and K. Sato, *Chem. Lett.*, **1980**, 1131.

9) W. Szeja, *Synthesis*, **1979**, 821.

Restricted Rotation Involving the Tetrahedral Carbon. XXXIX. 9-(2-Methoxy-1-methylethyl)triptycene Derivatives[1]

Masahiko Suzuki, Gaku Yamamoto, Hiromi Kikuchi, and Michinori Ōki*

Department of Chemistry, Faculty of Science, The University of Tokyo, Bunkyo-ku, Tokyo 113

(Received February 20, 1981)

9-(2-Methoxy-1-methylethyl)triptycenes were prepared from 9-(2-methoxy-1-methylethyl)anthracene and corresponding benzynes to examine the feasibility of isolating rotational isomers of 9-isopropyltriptycene derivatives at room temperature. They afforded crystalline *ap* forms which underwent internal rotation with activation energies of *ca.* 23 kcal/mol. 9-(2-Acetoxy-1-methylethyl)-1,2,3,4-tetrachlorotriptycene gave similar results. Based on the results, the barrier to rotation of 9-isopropyl-1,2,3,4-tetrabromotriptycene was reexamined to show that it must be corrected as 23.5 kcal/mol at 175 °C.

Stable rotamers of triptycene derivatives carrying a *t*-alkyl group in 9-position have been isolated at room temperature.[2] It is also possible to isolate rotamers of a compound carrying a primary alkyl group in 9-position of triptycene at room temperature, if it carries three substituents in three peri-positions which are close to the alkyl group.[3] To date, however, no rotamers have been isolated of compounds which carry a *s*-alkyl group in 9-position of triptycene. The possibility of the isolation has long been suggested because 9-isopropyltriptycenes were shown to have barriers to rotation of more than 23 kcal/mol (1 cal=4.18 J):[4] it is suggested that if the barrier is over 23 kcal/mol, the rotamer is stable at room temperature.[5]

The problem for isolating the rotamers of 9-isopropyltriptycene is that they exist as a pair of enantiomers and a diastereomeric *ap* form is not found for the steric reasons: it is necessary to resolve the racemate into enantiomers. Although a functionality for the resolution

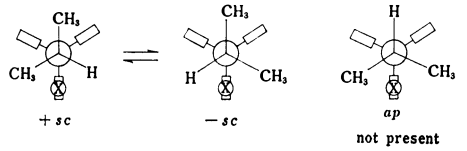

may be introduced into these compounds, the similar results may be obtained by modifying the isopropyl group, because modifying a methyl of the isopropyl group should produce diastereomers, if the rotation in question is slow, which should be separable by ordinary physical methods. Thus we introduced a methoxyl or an acetoxyl group to one of the methyls of the isopropyl group. This paper reports the results of such an investigation.

There is a problem of naming the stereochemistry of these comformations, as discussed elsewhere,[1] because the conformations involve a chiral center. However, we should like to use *ap* and *sc* as designated for simplicity of the discussion: although, in principle, there is another *sc* form in which a methyl and an $ROCH_2$ group flank the substituted benzeno bridge, in practice that conformation is nonexistent for the steric reasons because

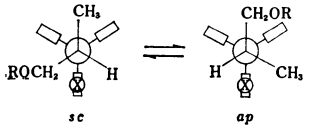

it is a substituted derivative of the *ap* conformation of 9-isopropyltriptycenes.

The compounds examined in this study were prepared in the following way. Anthrone was alkylated with methyl 2-bromopropionate in the presence of a base and the resulted ester (**1**) was reduced with sodium tetrahydridoborate to corresponding alcohols which were dehydrated with hydrochloric acid to produce an anthracene-ester (**2**). The ester was reduced with lithium tetrahydridoaluminate to afford the corresponding alcohol (**3**). The alcohol was methylated with sodium hydride and methyl iodide. Treatment of the methyl ether (**4**) with tetrahalobenzynes afforded desired triptycenes (**5** and **6**). Treatment of the methyl ether (**4**) with *p*-benzoquinone followed by enolization of the adduct and then methylation gave a 1,4-dimethoxytriptycene (**7**). Acetylation of the alcohol (**3**) followed by treatment with tetrachlorobenzyne afforded 1,2,3,4-tetrachloro-9-(2-acetoxy-1-methylethyl)triptycene (**8**).

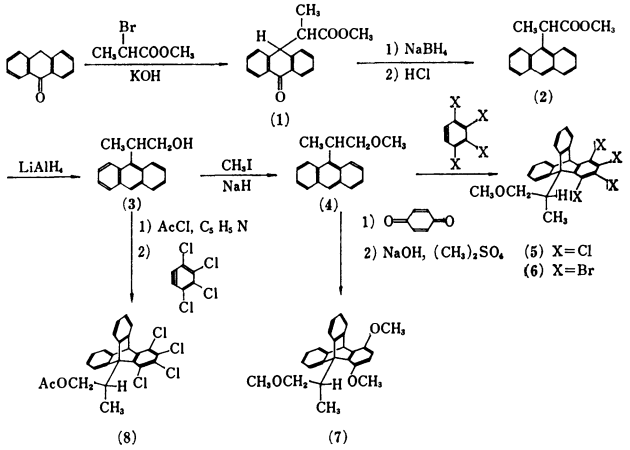

Experimental

10-(1-Methoxycarbonylethyl)anthrone (1). To a mixture of 35 g (0.18 mol) of anthrone and 29 g (0.174 mol) of methyl 2-bromopropionate in 200 mL of methanol was added with stirring a solution of 10 g (0.179 mol) of potassium hydroxide in 150 mL of methanol during a 3 h period at room temperature under a nitrogen atmosphere. Insoluble anthrone was filtered off and the filtrate was concentrated. The residue was taken up in dichloromethane and the solution was washed with water, aqueous ammonium chloride, and then water. The solution was dried over magnesium sulfate

and evaporated to give 42 g (86%) of an oil which was directly used for the next preparation. ^{1}H NMR ($CDCl_3$, δ): 0.63 (3H, d, J=7.5 Hz), 2.91 (1H, dq, J=7.5, 4.5 Hz), 3.70 (3H, s), 4.83 (1H, d, J=4.5 Hz), 7.2—7.7 (6H, m), 8.1$_5$—8.4 (2H, m).

9-(1-Methoxycarbonylethyl)anthracene (2). To a solution of 35 g (0.125 mol) of 10-(1-methoxycarbonylethyl)anthrone in 500 mL of methanol was added 35 g (0.925 mol) of sodium tetrahydridoborate with ice-cooling and the mixture was allowed to stand for 15 min. The mixture was treated with ice and dilute hydrochloric acid and extracted with dichloromethane. The extract was washed and evaporated. The residue was taken up in 300 mL of benzene and the solution was shaken with 300 mL of concentrated hydrochloric acid for 10 min. The benzene layer was separated, washed, and dried. Evaporation of the solvent afforded 31 g (94%) of the desired compound. Recrystallization from acetone–pentane gave a pure sample, mp 117—119 °C. Found: C, 81.69; H, 5.83%. Calcd for $C_{18}H_{16}O_2$: C, 81.79; H, 6.10%. ^{1}H NMR ($CDCl_3$, δ): 1.80 (3H, d, J=7 Hz), 3.54 (3H, s), 5.10 (1H, q, J=7 Hz), 7.3—7.6 (4H, m), 7.8—8.3 (4H, m), 8.38 (1H, s).

9-(2-Hydroxy-1-methylethyl)anthracene (3). A solution of 227 mg (0.86 mmol) of 9-(1-methoxycarbonylethyl)anthracene in 20 mL of dry ether was added to a slurry of 65.3 mg (1.72 mmol) of lithium tetrahydridoaluminate in 30 mL of dry ether and the mixture was stirred for 30 min at room temperature. The excess of the hydride was decomposed with ethyl acetate. The whole was treated with dilute hydrochloric acid and the ether layer was washed with aqueous sodium hydrogencarbonate and then with water, and dried over magnesium sulfate. Evaporation of ether afforded an oil in 192 mg (96.5%) yield. The crude product was directly used for the next reaction. ^{1}H NMR ($CDCl_3$, δ): 1.69 (3H, d, J=7 Hz), 4.24 (2H, br d, J=7 Hz), 4.3—4.7 (1H, m), 7.0—7.6 (4H, m), 7.8—8.1 (2H, m), 8.1—8.5 (3H, m).

9-(2-Methoxy-1-methylethyl)anthracene (4). A mixture of 0.32 g (13 mmol) of sodium hydride, 621 mg (2.64 mmol) of 9-(2-hydroxy-1-methylethyl)anthracene and 10 mL of tetrahydrofuran was stirred for 30 min at room temperature. To the mixture was added 1.6 mL (26 mmol) of methyl iodide and the whole was stirred overnight. The excess of the hydride was decomposed with ethanol and then with water and the mixture was extracted with ether. The ethereal extract was washed with dilute hydrochloric acid and then with aqueous sodium hydrogencarbonate and dried over magnesium sulfate. After evaporation of the solvent, the residue was chromatographed on silica gel, dichloromethane–hexane (1 : 3) being used as an eluent. The desired product was obtained in 429 mg (65%) yield. The product was directly used for the next reaction. ^{1}H NMR ($CDCl_3$, δ): 1.70 (3H, d, J=7.2 Hz), 3.27 (3H, s), 3.77 (1H, dd, J=5.1, 9.0 Hz), 4.11 (1H, dd, J=8.6, 9.0 Hz), 4.35—4.80 (1H, m), 7.0—7.5 (4H, m), 7.7—8.0 (2H, m), 8.1—8.5 (3H, m).

1,2,3,4-Tetrachloro-9-(2-methoxy-1-methylethyl)triptycene (5). To a boiling solution of 429 mg (1.72 mmol) of **4** and 0.9 mL of isopentyl nitrite in 10 mL of dichloromethane was added 1.18 g (4.29 mmol) of tetrachloroanthranilic acid[6] in 10 mL of acetone in 1 h under a nitrogen atmosphere. The mixture was heated for another hour. Insoluble materials were filtered off and the filtrate was evaporated. The residue was submitted to silica gel chromatography and eluted with hexane–dichloromethane (1 : 1). A mixture of the desired material and the starting material (6 : 4) was obtained. Treatment of the mixture with the benzyne was repeated. An eluted fraction from silica gel was recrystallized from tetrahydrofuran–hexane to give 198 mg (25%) of the desired compound, mp 190—192 °C. Found: C, 62.03; H, 3.72; Cl, 30.28%. Calcd for $C_{24}H_{18}OCl_4$: C, 62.09; H, 3.91; Cl, 30.55%. When the crystals of the compound were dissolved in chloroform-*d* at low temperatures, the ^{1}H NMR signals could be attributed to the *ap* conformation (δ): 1.97 (3H, d, J=7.2 Hz), 3.45 (3H, s), 3.8—4.6 (3H, m), 5.94 (1H, s), 6.7—7.9 (8H, m). On standing at room temperature, the solution exhibited a set of NMR signals which could be attributed to the *sc* conformation of which signals were obtained by subtracting those due to the *ap* conformation from those of the mixture. *sc* ($CDCl_3$, δ): 1.78 (3H, d, J=7.2 Hz), 3.48 (3H, s), 3.8—4.6 (3H, m), 5.94 (1H, s), 6.7—7.9 (8H, m).

1,2,3,4-Tetrabromo-9-(2-methoxy-1-methylethyl)triptycene (6). To a boiling solution of 1.10 g (4.40 mmol) of **4** and 2.1 mL of isopentyl nitrite in 20 mL of dichloromethane was added 5.5 g (12.1 mmol) of tetrabromoanthranilic acid[7] in 20 mL of acetone in 30 min. The mixture was heated for another hour and filtered. The filtrate was concentrated and the residue was chromatographed as above. The obtained crystals were recrystallized from acetone–pentane to give the desired product, mp 220—222 °C, in 818 mg (29%) yield. Found: C, 44.98; H, 2.83; Br, 50.29%. Calcd for $C_{24}H_{18}OBr_4$: C, 44.89, H, 2.83; Br, 49.79%. The following ^{1}H NMR data ($CDCl_3$, δ) were obtained as were described for **5**. *ap*: 1.93 (3H, d, J=7.2 Hz), 3.41 (3H. s), 3.8—4.7 (3H, m), 5.97 (1H, s), 6.8—7.9 (8H, m). *sc*: 1.74 (3H, d, J=6.3 Hz), 3.48 (3H, s), 3.8—4.7 (3H, m), 5.97 (1H, s), 6.8—7.9 (8H, m).

1,4-Dimethoxy-9-(2-methoxy-1-methylethyl)triptycene (7). A solution of 1.47 g of **4** and 0.95 g of *p*-benzoquinone in 8 mL of acetonitrile was heated overnight under reflux. The acetonitrile and the benzoquinone were washed off with hot water. The residue was treated with a small portion of aqueous sodium hydroxide and then with a small portion of dimethyl sulfate. The process was repeated several times to use a total of 0.75 g of sodium hydroxide in 5 mL of water and 1 mL of dimethyl sulfate. After one night, the mixture was poured into water and the mixture was extracted with benzene. The benzene solution was dried and evaporated. The residue was chromatographed on silica gel, using eluents from hexane–dichloromethane (1 : 1) to dichloromethane. Some fractions were taken up in pentane–dichloromethane to remove anthraquinone as an insoluble material. The desired product, mp 218—220 °C, crystallized out on addition of pentane. Yield was 741 mg (32.6%). Found: C, 80.66; H, 6.61%. Calcd for $C_{26}H_{24}O_3$: C, 80.80; H, 6.78%. The crystals of this compound, on dissolution in chloroform-*d* at −40 °C, gave ^{1}H NMR signals of the almost pure *ap*-form but the isomerization was much faster than other compounds. From these results, the crystals may be assumed to be composed of the pure *ap*-forms. The following ^{1}H NMR data ($CDCl_3$, δ) were obtained as described for other compounds. *ap*: 1.88 (3H, d, J=6.3 Hz), 3.41 (3H, s), 3.63 (3H, s), 3.72 (3H, s), 3.9—4.2 (3H, m), 5.77 (1H, s), 6.42 (2H, s), 6.8—7.8 (8H, m). *sc*: 1.79 (3H, d, J=6.3 Hz), 3.46 (3H, s), 3.67 (3H, s), 3.72 (3H, s), 3.9—4.2 (3H, m), 5.77 (1H, s), 6.42 (2H, s), 6.8—7.8 (8H, m).

9-(2-Acetoxy-1-methylethyl)-1,2,3,4-tetrachlorotriptycene (8). A solution of 1.154 g (4.89 mmol) of **3** in 50 mL of benzene was mixed with 0.8 mL of pyridine and 0.5 mL of acetyl chloride. The mixture was treated, after 10 min, with ethanol and then with water. The aqueous layer was removed and the organic layer was washed with dilute hydrochloric acid and then with aqueous sodium hydrogencarbonate. Evaporation of the solvent and chromatography of the residue on silica gel, using dichloromethane–hexane (1 : 1), afforded a yellow oil of 9-(2-acetoxy-1-methylethyl)anthracene in

1.349 g (99.3%) yield. ^{1}H NMR ($CDCl_3$, δ): 1.72 (3H, d, J=7.2 Hz), 1.97 (3H, s), 4.4—5.1 (3H, m), 7.1—7.6 (4H, m), 7.8—8.1 (2H, m), 8.2—8.5 (3H, m).

A solution of the acetate (1.349 g or 4.85 mmol) and 2.6 mL of isopentyl nitrite in 20 mL of dichloromethane was treated with 4.00 g (14.6 mmol) of tetrachloroanthranilic acid in 30 mL of acetone as described in the preparation of **5**. The single treatment with the benzyne afforded 404.8 mg (17%) of the desired compound, mp 218—220 °C, on recrystallization from acetone–hexane after chromatography. Found: C, 61.14; H, 3.45; Cl, 28.86%. Calcd for $C_{25}H_{18}O_2Cl_4$: C, 61.00; H, 3.69; Cl, 28.81%. The following ^{1}H NMR data ($CDCl_3$, δ) were obtained as described above. *ap*: 1.96 (3H, d, J=6.3 Hz), 2.24 (3H, s), 4.3—5.2 (3H, m), 5.94 (1H, s), 6.9—7.8 (8H, m). *sc*: 1.76 (3H, d, J=6.3 Hz), 2.11 (3H, s), 4.3—5.2 (3H, m), 5.94 (1H, s), 6.9—7.8 (8H, m).

^{1}H NMR Spectra and Kinetic Data. ^{1}H NMR spectra were obtained on a Hitachi R-20B spectrometer equipped with a temperature variation accessory and operating at 60 MHz.

Rates of isomerization at room temperature were obtained by observing the change of ^{1}H NMR spectra as chloroform-*d* solutions in a probe of the NMR spectrometer. Temperatures were read directly by a thermocouple. The data were treated as the first order reversible reaction. Dynamic NMR spectra were obtained as hexachlorobutadiene solutions and the line shapes were simulated with the use of the modified Binsch program.[8] The temperature was calibrated with the use of the chemical shift differences of the protons of ethylene glycol. Some selected rate constants ($ap \rightarrow sc, s^{-1}$) are given below (numericals in parentheses are temperatures in °C). **5**: 0.82 (116.7), 1.23 (122.7), 1.67 (125.8), **6**: 0.80 (116.6), 1.32 (123.7), 1.76 (127.3), **7**: 0.76 (114.5), 1.22 (120.3), 1.61 (124.0), **8**: 0.52 (126.0), 0.61 (129.2), 0.93 (133.9), 1.33 (138.0).

These data were put into the Eyring equation and the kinetic parameters were obtained.

Results and Discussion

Assignment of Conformations. Assignment of conformations poses a difficult problem. We have succeeded in assigning conformations of ethenoanthracene derivatives by looking at aromatic proton signals of NMR spectra[2] but this method is apparently not applicable to the present case. The only differences are found in chemical shifts of protons due to methyl groups in the 9-substituents. One of the possibilities which give a solution to the problem is to utilize the chemical shifts of the methyl protons. In triptycene derivatives which carry a *t*-butyl group in the 9-position, the two methyl groups which are close to a peri-subsituent (usually a halogen) give a ^{1}H NMR signal at a lower magnetic field than that which is *ap* to the substituent.[9] This is reasonable if we assume van der Waals shift because the two groups are in a congested state. It is also true for other tertiary alkyl groups: methyls in an *ap* conformation which possesses the methyls $\pm sc$ to the peri-substituent give ^{1}H NMR signals at a lower field which corresponds to one of the methyls, that gives its signal at a lower magnetic field, in $\pm sc$ conformations.[10] If these generalities are applicable to the present case, then a conformation which gives the methyl signal at a lower field than another must be *ap*. However, since the steric requirements of a *t*-alkyl and a *s*-alkyl group are so different that the deformation of the molecules in question may differ to some extent. Indeed, 1,2,3,4,5,6,7,8-octachloro-9-isopropyltriptycene in which both methyl groups in the isopropyl are flanked by a tetrachlorobenzo and a benzo groups give a methyl signal at a higher magnetic field: it corresponds to a higher one of the two methyls in 1,2,3,4-tetrachloro-9-isopropyltriptycene.[4] We may have to wait to draw a definite conclusion until direct unambiguous evidence such as X-ray crystallography is obtained. We tentatively assign here, therefore, that, by taking advantage of the analogy from the *t*-alkyl compounds, it is the *ap* conformation that gives methyl proton signals at a relatively low magnetic field. Then the crystalline forms which we obtain by recrystallization are *ap* and those which appear on dissolution are *sc*.

Rotational Barriers. Rates of rotation at room temperature, as examined by the classical method, and free energies of activation are given in Table 1. Every compound examined was, at least, almost pure *ap* form

Table 1. Rates of rotation ($ap \rightarrow sc$) and equilibrium constants of 9-[2-methoxy(or acetoxy)-1-methylethyl]triptycenes

Compound	Substituents		Temp	$\Delta G^{\ddagger}$	$k \times 10^4$	K
	Bridgehead	Peri	K	kcal/mol	s^{-1}	(*sp*/*ap*)
5	$CH_3OCH_2CH(CH_3)$	Cl	306	23.5	1.03	0.40
6	$CH_3OCH_2CH(CH_3)$	Br	307	23.4	1.52	0.28
7	$CH_3OCH_2CH(CH_3)$	OCH_3	306			0.65
8	$AcOCH_2CH(CH_3)$	Cl	305	23.2	1.49	0.64

Table 2. Kinetic parameters for rotation ($ap \rightarrow sc$) obtained by total line shape analysis

Compound	$\frac{K}{(sc/ap)}$(Temp/°C)	$\Delta H^{\ddagger}$ kcal/mol	$\Delta S^{\ddagger}$ e.u.	$\Delta G^{\ddagger}_{298}$ kcal/mol
5	0.56 (126)	22.9±2.4	−0.7±6.2	23.1
6	0.41 (132)	24.1±1.7	2.2±4.4	23.4
7	0.96 (124)	22.2±0.4	−2.3±1.1	22.9
8	0.56 (138)	25.7±1.9	3.9±4.5	24.5

soon after the dissolution in chloroform-*d*. The dimethoxy compound (**7**) was no exception but it isomerized fast at room temperature. Thus, although it was possible to isolate *ap* isomers, we had to abandon isolation of *sc* isomers at room temperature.

As expected from a minute difference in structures, compounds **5** and **8** exhibit similar barriers to rotation. The barriers observed are in good agreement with those obtained by dynamic NMR study of 9-isopropyltriptycenes except the bromo compound (**6**): the barriers to rotation of 9-isopropyl compounds have been reported to be 23.6 ± 1.9, 25.5 ± 2.3, and >26 kcal/mol for compounds carrying a methoxyl, chloro, and bromo group in the peri-position, respectively.[4] Disagreement of the data obtained prompted us to reexamine the barrier to rotation of 1,2,3,4-tetrabromo-9-isopropyltriptycene. We found that the coalescence temperature of the methyl signals of the isopropyl group in the ^{1}H NMR spectrum was 175 °C instead of >200 °C as reported. From the coalescence temperature and the chemical shift difference, the free energy of activation for rotation was calculated to be 23.5 kcal/mol, which is in accordance with the data investigated here. Probably some accidental mishaps caused errors in reading the temperature in the literature.

The results obtained by the dynamic NMR study are given in Table 2. They are generally in good agreement with the data obtained by the classical method. Although the barriers to rotation of these compounds might be considered similar from the free energies of activation at 298 K, yet we can point out that the methoxy compound (**7**) has a lower barrier. The tendency is usually more revealing in the rate constants than the free energies but the difference is obscure in the rate constants obtained by the line shape analysis (see Experimental section). Rather the difference is definite in the rates of rotation at ambient temperatures (Table 1). If we can take the difference between the bromo (**6**) and the chloro compound (**5**) significant, the chloro compound does exhibit a higher barrier to rotation.

We have recently reported that the barriers to rotation in triptycene systems having a *t*-alkyl group show an interesting trend. Namely, in [1-cyano(or methoxycarbonyl)-1-methylethyl]triptycene series, barriers to rotation are higher if that compound carries no substituent in the peri-position[11] than those carrying a substituent in the peri-position.[10] Investigation of a series of 1-substituted 9-(2-phenyl-1,1-dimethylethyl)-triptycenes has revealed that there is a maximum barrier to rotation when the 1-substituent is medium-sized.[12] Thus the results reported here supplement that there is a same trend in the triptycene series which carries a *s*-alkyl group. The only difference is that, whereas the maximum barrier to rotation in the *t*-alkyl series has been observed at the substituent of a methoxyl or a fluoro, it is a chloro (and a bromo) in the case presented here. This shift must be caused by the fact that congestedness in molecules is much more severe in the *t*-alkyl compounds than in the *s*-alkyl compounds in the ground state.

We wish to thank the Ministry of Education, Science and Culture for a Grant-in-Aid for Fundamental Scientific Research which supported this work.

References

1) Part XXXVIII: T. Mori and M. Ōki, *Bull. Chem. Soc. Jpn.*, **54**, 1199 (1981).
2) G. Yamamoto and M. Ōki, *J. Chem. Soc., Chem. Commun.*, **1974**, 67; *Bull. Chem. Soc. Jpn.*, **48**, 3686 (1975).
3) G. Yamamoto and M. Ōki, *Angew. Chem. Int. Ed. Engl.*, **17**, 518 (1978).
4) F. Suzuki, M. Ōki, and H. Nakanishi, *Bull. Chem. Soc. Jpn.*, **47**, 3114 (1974).
5) H. Kessler, *Angew. Chem. Int. Ed. Engl.*, **9**, 219 (1970).
6) V. Villiger and L. Blangey, *Ber.*, **42**, 3549 (1909).
7) H. Heaney, K. G. Mason, and J. M. Stechley, *J. Chem. Soc.*, **1971**, 567.
8) G. Binsch, *Topics in Stercochemistry*, **3**, 97 (1968).
9) S. Seki, T. Morinaga, H. Kikuchi, T. Mitsuhashi, G. Yamamoto, and M. Ōki, *Bull. Chem. Soc. Jpn.*, **54**, 1465 (1981).
10) S. Otsuka, T. Mitsuhashi, and M. Ōki, *Bull. Chem. Soc. Jpn.*, **52**, 3663 (1979).
11) S. Otsuka, G. Yamamoto, T. Mitsuhashi, and M. Ōki, *Bull. Chem. Soc. Jpn.*, **53**, 2095 (1980).
12) G. Yamamoto, M. Suzuki, and M. Ōki, *Angew. Chem. Int. Ed. Engl.*, in press.

The Reaction of 2,4,6-Triphenyl-1,3-oxazinylium Perchlorate with Amino Compounds

Isao SHIBUYA

National Chemical Laboratory for Industry, Yatabe, Ibaraki 305

(Received October 27, 1980)

The reaction of 2,4,6-triphenyl-1,3-oxazinylium perchlorate with various kinds of amino compounds was studied. Primary amines and semicarbazides gave pyrimidinium perchlorates. *o*-Phenylenediamine, *o*-aminobenzamide, and *o*-aminothiophenol afforded 2,4-diphenyl-1,5-benzodiazepine, 2-phenyl-4-hydroxyquinazoline, and 2-phenyl-1,3-benzothiazole respectively. Benzoylhydrazine, 4-pyridinecarbohydrazide, and 4-phenylthiosemicarbazide all led to pyrazoline derivatives. *N,N*-Dimethylhydrazine yielded two chain products competitively, while *N,N'*-dimethylhydrazine gave 1,2-dimethyl-3,5-diphenyl-1,2,4-triazolylium and 1,2-dimethyl-3,5-diphenylpyrazolylium perchlorate competitively. It was thus shown that 2,4,6-triphenyl-1,3-oxazinylium perchlorate reacts with amino compounds in a complicated fashion to afford various heterocyclic compounds and other derivatives.

It has been reported that pyrylium salts react with various kinds of amino compounds to afford numerous derivatives.[1] 1,3-Oxazinylium salts, the *N*-analogs of pyrylium salts, can also be expected to give many derivatives when treated with amino compounds; however, their behavior has not yet been studied so closely. A 1,3-oxazinylium cation may be supposed to be reactive with nucleophiles at the 2-, 4-, and 6-positions. Since the 1,3-oxazinylium ring is unsymmetrical, its 2- and 6-positions are not equal to each other. This suggests that the cation behaves toward nucleophiles in a more complicated fashion than does a pyrylium cation. On the other hand, it has been known that carbanions derived from active methylenes, enamines, or ethyl diazoacetate always attack at the 6-position of the 2,4,6-triphenyl-1,3-oxazinylium cation to afford pyridine, butadiene, or 1,3-oxazepine derivatives.[2,3] In this study, the reaction of 2,4,6-triphenyl-1,3-oxazinylium perchlorate (**1**) with various kinds of amino compounds, such as primary amines, disubstituted hydrazines, hydrazides, and semicarbazides, was attempted; consequently, some interesting results were obtained.

Results and Discussion

The starting material, **1**, was obtained by the reaction of 2,4,6-triphenyl-4*H*-1,3-oxazine with trityl perchlorate.[4]

Primary Amines and Semicarbazides. It has been reported that the reaction of 2,4,6-triphenylpyrylium salt (**2**) with primary amines gives 1-substituted 2,4,6-triphenylpyridinium salt (**3**).[5] On the other hand, upon refluxing with aniline, methylamine, semicarbazide, 4-phenylsemicarbazide, the glycine ethyl ester, or *O*-methylhydroxylamine in dioxane–triethylamine, **1** afforded 1-substituted 2,4,6-triphenylpyrimidinium perchlorate (**4a**—**f**), which correspond to **3**. These data are summarized in Table 1. For the formation of **4a**—**f**, two probable reaction courses were postulated, as is shown in Scheme 1. In order to determine the real reaction course, **1** was treated with aniline under mild conditions to isolate a white powder of **5** (63%). **5** was regarded as the intermediate of the above reaction, because **5** gave **4a** almost quantitatively upon treatment with perchloric acid in acetic anhydride. In its IR spectrum, the presence of the absorption at 1681 cm^{-1}, assigned to C=O stretching, suggested that **5** is

TABLE 1. 1-SUBSTITUTED 2,4,6-TRIPHENYLPYRIMIDINIUM PERCHLORATE (**4a**—**h**)

Compd 4	Substituent	Mp(dc) °C	Yield %	Found (Calcd) (%) C	H	N	Cl	λ_{max}/nm (log ε)	IR(KBr) $\tilde{\nu}$/cm^{-1}
a	Ph–	>300	64	69.25 (69.35)	4.33 (4.37)	5.80 (5.78)	7.32 (7.31)	324 (4.51)	1607, 1584, 1527, 1381, 1080.
b	Me–	200.8	21	65.15 (65.33)	4.58 (4.53)	6.65 (6.62)	8.25 (8.38)	319 (4.51)	1607, 1595, 1540, 1391, 1086.
c	NH_2CONH–	230.3	37	59.39 (59.17)	4.14 (4.10)	11.95 (12.00)	7.80 (7.59)	323 (4.46)	3400—3200, 1677, 1590, 1539, 1393, 1104.
d	PhNHCONH–	230.1	42	63.89 (64.15)	4.23 (4.27)	10.47 (10.32)	6.46 (6.53)	325 (4.46)	3300, 1719, 1606, 1591, 1536, 1393, 1120.
e	$EtOCOCH_2$–	204.5	43	63.26 (63.10)	4.69 (4.68)	5.75 (5.66)	7.08 (7.16)	327 (4.46)	1743, 1609, 1590, 1543, 1397, 1256, 1085.
f	CH_3O–	241.1	35	62.92 (62.95)	4.32 (4.36)	6.46 (6.38)	8.29 (8.08)	320 (4.37)	2960, 1602, 1590, 1543, 1389, 1086.
g	*o*-HOC_6H_4–	>300	62	66.91 (67.14)	4.25 (4.23)	5.67 (5.59)	6.84 (7.08)	325 (4.50)	3260, 1603, 1587, 1530, 1390, 1100.
h	$(CH_3)_2N$–	191.1	46	63.75 (63.51)	4.96 (5.33)	9.38 (9.26)	7.93 (7.81)	320 (4.39)	1606, 1590, 1534, 1390, 1080.

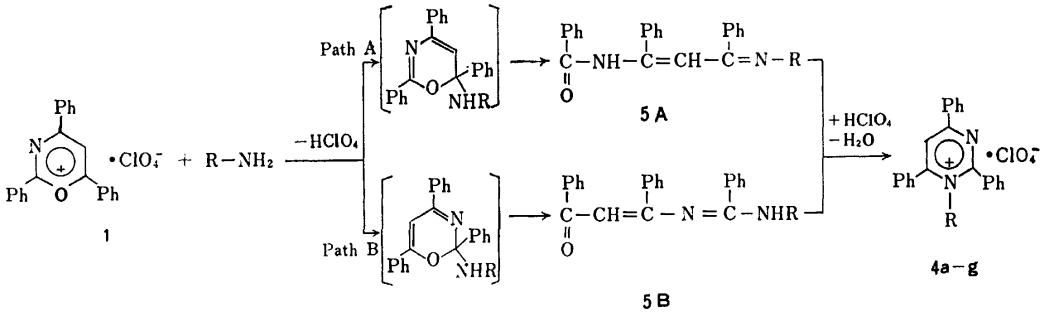

4a: R=Ph–, **4b**: R=Me–, **4c**: R=NH_2CONH–, **4d**: R=PhNHCONH–, **4e**: R=$EtOCOCH_2$–, **4f**: R=CH_3O–, **4g**: R=*o*-HOC_6H_4.

Scheme 1.

one of the two chain compounds (**5A** and **5B**; R=C_6H_5) in Scheme 1. According to ^{13}C NMR spectrum, the absorption assigned to a benzoyl carbon (*δ ca.* 190) was absent, whereas a carbamoyl carbon (*δ* 166.03 or 165.04) was present. The structure of **5** was thus determined to be **5A**; in addition, it was inferred that the reaction of **1** with these primary amines and semicarbazides takes Path A in Scheme 1 to afford **4a—f**.

o-Substituted Anilines. The reaction of *o*-aminophenol, *o*-phenylenediamine, *o*-aminobenzamide, or *o*-aminothiophenol with **1** under the same conditions as above gave 1-(*o*-hydroxyphenyl)-2,4,6-triphenylpyrimidinium perchlorate (**4g**, 62%), 2,4-diphenyl-1,5-benzodiazepine (**6**, 80%), 2-phenyl-4-hydroxyquinazoline (**7**, 32%), or 2-phenyl-1,3-benzothiazole (**8**, 68%) respectively. The data of **4g** are also listed in Table 1; **6**, **7**, and **8** were identified by direct comparison with authentic samples.[6-8] These facts suggest that, in

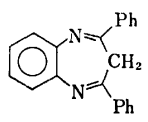

6

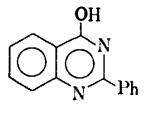

7

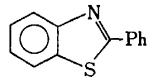

8

the formation of **6**, the reaction was initiated by the attack of *o*-phenylenediamine at the 6-position of the oxazinylium cation, while *o*-aminobenzamide and *o*-aminothiophenol attacked the 2-position of the cation to produce **7** and **8**. It was thus found that these anilines, which have active hydrogen at their ortho-positions, behave in a complicated fashion toward **1**, and produce derivatives with different structures.

Benzoylhydrazine, 4-Pyridinecarbohydrazide, and 4-Phenylthiosemicarbazide. On treatment with these reagents, **1** gave **9a—c** in 50, 32, and 40% yields respectively. Their ^1H NMR spectra had two characteristic absorptions, at *δ* 3.61—3.80, and 4.02—4.74, which were assigned to a pyrazolinic methylene with a geminal coupling constant (J=18 Hz),[9] while their IR spectra have three common absorptions, at 3280—3340 (N–H), 1665—1686 (C=O), and 1520—1530 cm^{-1} (C=N). These data suggested that **9a—c** have the same skeletal structure. The ^{13}C NMR spectrum of **9a**, as determined by means of the ^1H-off-resonance method, showed the presence of a methylene (*δ* 48.23), a quarternary (*δ* 82.26), and two carbamoyl carbons (*δ* 167.71, 154.17). These spectral results and analytical data confirmed that **9a** is 1-benzoyl-3,5-diphenyl-5-benzoylamino-2-pyrazoline, and that both **9b** and **9c** are also pyrazoline derivatives. The mechanism for the formation of **9a—c** was demonstrated to be as is shown in Scheme 2; this mechanism is similar to that of the reaction of **2** with hydroxylamine or phenylhydrazine which gives oxazoline or pyrazoline compounds.[9,10]

N,N-Dimethylhydrazine. When treated with this reagent under mild conditions, **1** gave a main product, **10** (49%), and also a small amount of **11** (9%) competitively. The analytical data showed that both **10** and **11** are adducts of the anion of this reagent and the oxazinylium cation. The M^+ value was observed at *m/e* 369, though their MS spectra were quite different from each other. Their ^{13}C NMR spectra showed that **10** has a benzoyl carbon (*δ* 190.28), whereas **11** has a carbamoyl carbon (*δ* 165.47). Their IR and UV spectra were also different from each ether. When treated with dilute perchloric acid, **10** easily afforded 1-dimethylamino-2,4,6-triphenylpyrimidinium perchlorate (**4h**); however, **11** afforded no pyrimidinium salt, even upon treatment with 70% perchloric acid. On

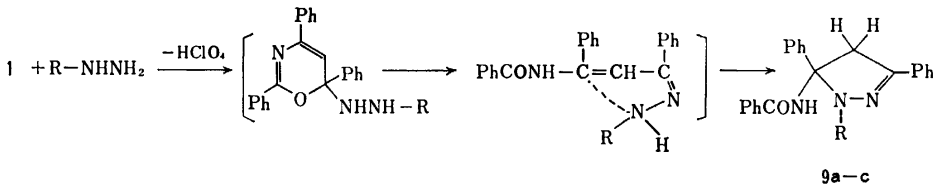

9a: R=–COPh, **9b**: R=–CO–  ·$HClO_4$, **9c**: R=–CSNHPh.

Scheme 2.

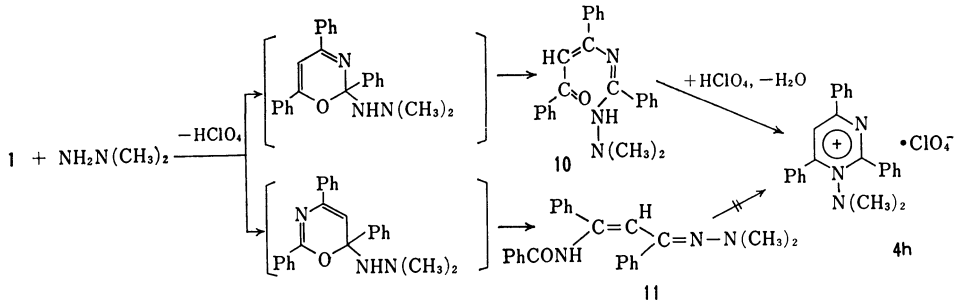

Scheme 3.

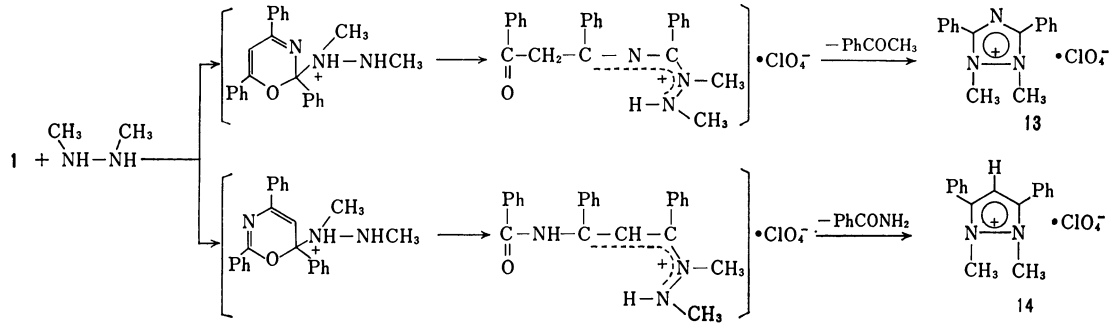

Scheme 4.

the basis of these results, it seems certain that the reaction course to produce them takes the paths shown in Scheme 3.

N,N'-*Dimethylhydrazine.* On treatment with this reagent, **1** gave **12** in a good yield. The analytical results of **12** agreed almost entirely with 1,2-dimethyl-3,5-diphenyl-1,2,4-triazolylium perchlorate (**13**), but its IR and ^{1}H NMR spectra suggested that **12** was a mixture of **13** and 1,2-dimethyl-3,5-diphenylpyrazolylium perchlorate (**14**). Pure samples of **13** and **14** were obtained by the reaction of this reagent with 3,5-diphenyl-1,2,4-dithiazolylium and with 3,5-diphenyl-1,2-dithiolylium salt respectively.[11,12] The constituent ratio of **13** and **14** in **12** was estimated to be 3 : 1 by the use of the integral ratio of the signals at δ 4.24 (**13**, 18.5) and 4.12 (**14**, 6.0) in the ^{1}H NMR spectrum of **12**. Therefore, the reaction of **1** with this reagent proceeds as is shown in Scheme 4, and yields **13** and **14** competitively.

Hence, it is proved that 2,4,6-triphenyl-1,3-oxazinylium perchlorate reacts with amino compounds not only at the 6-position, but also at the 2-position, and that the reaction produce various heterocyclic compounds and other derivatives.

Experimental

The melting points of all the products were measured in a capillary tube with a Mettler FPl apparatus at the rate of 2 °C/min. The IR spectra were measured in KBr pellets with a JASCO-403G spectrometer. The UV spectra were recorded on a Hitachi 200-10 instrument in an ethanol solution, while the MS spectra were recorded on a Hitachi RMU6E spectrometer with a direct inlet at 70 eV. The ^{1}H and ^{13}C NMR spectra were obtained with a Varian FT-80 instrument, using tetramethylsilane as the internal standard.

*1-Substituted 2,4,6-Triphenylpyrimidinium Perchlorate (**4a**—**g**).* Into a solution of aniline, methylamine hydrochloride, semicarbazide hydrochloride, 4-phenylsemicarbazide, glycine ethyl ester hydrochloride, *O*-methylhydroxylamine hydrochloride, or *o*-aminophenol (1.5 mmol) and triethylamine (0.3 ml) in dioxane (2 ml), **1** (0.42 g, 1 mmol) was stirred at room temperature for 10 min, after which the mixture was refluxed for 1 h. The solvent was then distilled out under reduced pressure. The resulting residue was washed with 1 mol dm^{-3} perchloric acid (5 ml) and then recrystallized from ethanol to give pyrimidinium perchlorates (**4a**—**g**). Their data are listed in Table 1.

*Reaction of **1** with Aniline under Mild Conditions.* Into a solution of aniline (0.14 g, 1.5 mmol) and triethylamine (0.3 ml) in dioxane (2 ml), **1** (0.42 g, 1 mmol) was stirred at room temperature and then the mixture was allowed to stand for 5 d. The mixture was poured into dilute perchloric acid, and the resulting precipitate was recrystallized from methanol to give 0.25 g (63%) of **5**; mp 172.5 °C. IR, 1681, 1622, 1544, 1479, and 1296 cm^{-1}; ^{13}C NMR (HMPA-d_{18}), δ 122.10, 127.15—131.03, 135.07, 138.41, 143.42, 165.04, and 166.03. Found: C, 83.33; H, 5.49; N, 6.83%. Calcd for $C_{28}H_{22}N_2O$; C, 83.46; H, 5.51; N, 6.69%.

*Conversion of **5** to 1,2,4,6-Tetraphenylpyrimidinium Perchlorate (**4a**).* Into a solution of **5** (0.30 g) in acetic anhydride (2 ml), 70% perchloric acid (4 drops) was stirred at room temperature, after which the mixture was allowed to stand overnight. The mixture was poured into ether, and the resulting precipitate was collected by filtration and washed with ether to give a white powder of **4a** (0.34 g, 94%).

*Reaction of **1** with o-Substituted Anilines.* *o*-Phenylenediamine, *o*-aminobenzamide, and *o*-aminothiophenol (1.5 mmol) were treated with **1** (1 mmol) by the same procedure as was used in the preparation of **4a**—**g**. The resulting residues were washed with dilute perchloric acid and recrystallized from methanol to give **6** (0.24 g, 80%), **7** (0.07 g, 32%), and **8** (0.14 g, 68%) respectively. The IR spectrum of each of them could be completely superimposed on that of the

corresponding authentic samples.[6-8]

*1-Substituted 3,5-Diphenyl-5-benzoylamino-2-pyrazolines (**9a**—**c**).* Benzoylhydrazine, 4-pyridinecarbohydrazide, and 4-phenylthiosemicarbazide (1.5 mmol) were treated with **1** (1 mmol) by the same procedure as was used in the preparation of **4a**—**g**. The resulting residues were recrystallized from methanol, ethanol, or acetonitrile to yield **9a** (0.22 g, 50%), **9b** (0.17 g, 32%), or **9c** (0.19 g, 40%) respectively. Their data are shown below.

9a: mp, 165.8 °C; IR, 3280, 1667, 1640, 1530, 1447, 1416, and 1338 cm^{-1}; UV, λ_{max} (ε) 293 nm (21400); ^1H NMR ($CDCl_3$), δ 3.64 (d, J=18), 4.74 (d, J=18), 7.22—8.40, ^{13}C NMR ($CDCl_3$), δ 48.23 (-CH_2-), 82.26 (-$\dot{C}$-), 124.07, 126.89—134.46, 142.39, 154.17, and 167.71. MS, *m/e* 445 (M^+), 324 ([M−$PhCONH_2$]$^+$), 295, 220, 121 ([$PhCONH_2$]$^+$), and 105 ($PhCO^+$). Found: C, 78.24; H, 5.23; N, 9.53%. Calcd for $C_{29}H_{23}N_3O_2$; C, 78.24; H, 5.20; N, 9.43%.

9b: mp, 231.2 °C; IR, 3300—3050, 1665, 1651, 1520, 1480, 1432, 1345, and 1100 cm^{-1}; UV, λ_{max} (ε) 321 nm (29900); ^1H NMR (C_5D_5N), δ 3.61 (d, J=18), and 4.47 (d, J=18). Found: C, 61.39; H, 4.23; N, 10.50; Cl, 6.63%. Calcd for $C_{28}H_{23}N_4O_6Cl$; C, 61.49; H, 4.24; N, 10.24; Cl, 6.48%.

9c: mp, 164.7 °C; IR, 3340, 1686, 1523, 1487, 1450, and 1327 cm^{-1}; UV, λ_{max} (ε) 280 nm (21500); ^1H NMR (C_5D_5N), δ 3.80 (d, J=18), 3.84 (*s*), and 4.02 (d, J=18); ^{13}C NMR (DMF-d_7), δ 50.46 (-CH_2-), 83.67 (-$\dot{C}$-), 124.93, 127.87—132.46, 139.50, 143.73, 152.58, 167.31, and 173.89; MS, *m/e* 476 (M^+), 220, 135, 121, and 105. Found: C, 73.17; H, 5.13; N, 11.68; S, 6.65%. Calcd for $C_{29}H_{24}N_4SO$; C, 73.08; H, 5.07; N, 11.75; S, 6.72%.

Reaction of N,N-*Dimethylhydrazine with **1**.* Into a solution of *N,N*-dimethylhydrazine (0.10 g, 1.6 mmol) and triethylamine (0.3 ml) in dioxane (2 ml), **1** (1 mmol) was stirred at room temperature. After the mixture had been allowed to stand for 5 d, it was poured into water and the resulting precipitate was purified by preparative thin-layer chlomatography (silica gel; benzene–acetic acid, 50 : 1) to give orange-yellow needles of **10** (0.18 g, 49%) and pale yellow granules of **11** (0.03 g, 9%). Their data are shown below.

10: mp, 152.6 °C (ethanol); IR, 3060—2780, 1592, 1560, 1537, 1494, 1325, 1306, and 1295 cm^{-1}; UV, λ_{max} (ε) 257 (15900), and 367 nm (14200); ^1H NMR ($CDCl_3$), δ 2.76 (s, 6H), 6.18 (s, 1H), 6.90—8.14 (m, 16H); ^{13}C NMR ($CDCl_3$), δ 46.74 (-CH_3), 99.31 (=CH-), 127.62—139.56, 153.06, 158.26, and 190.26; MS, *m/e* 369 (M^+), 310, 264 ([M−PhCO]$^+$), and 105. Found: C, 78.13; H, 6.30; N, 11.37%. Calcd for $C_{24}H_{23}N_3O$; C, 78.02; H, 6.27; N, 11.37%.

11: mp, 150.1 °C (ethanol); IR, 3060—2780, 1670, 1618, 1498, 1478, 1310, 1298, and 1272 cm^{-1}; UV, λ_{max} (ε) 248 (44200), and 299 nm (sh, 28400); ^1H NMR ($CDCl_3$), δ 2.88 (s, 6H), 6.16 (s, 1H), 7.30—8.12 (m, 15H), and 10.90 (s, 1H); ^{13}C NMR ($CDCl_3$), δ 47.54 (CH_3-), 112.13 (=CH-), and 127.19—138.30, 143.17, 156.69, 165.47; MS, *m/e* 369 (M^+), 248 ([M−$PhCONH_2$]$^+$), 105, and 104. Found: C, 77.95; H, 6.27; N, 11.51%. Calcd for $C_{24}H_{23}N_3O$; C, 78.02; H, 6.27; N, 11.37%.

*Conversion of **10** into 1-Dimethylamino-2,4,6-triphenylpyrimidinium Perchlorate (**4h**).* Into a solution of **10** (0.37 g, 1 mmol) in acetonitrile (2 ml), 1 mol dm^{-3} perchloric acid (2 ml) was stirred after which the mixture was allowed to stand at 0—5 °C overnight. The precipitate was collected by filtration and washed with ether to give **4h** (0.43 g) almost quatitatively. The data of **4h** are shown in Table 1.

*Reaction of **1** with* N,N′-*Dimethylhydrazine.* Into a solution of *N,N′*-dimethylhydrazine dihydrochloride (0.20 g, 1.5 mmol) in 2 mol dm^{-3} MeONa–MeOH (2 ml), **1** (1 mmol) was stirred at room temperature for 10 min, and then the mixture was refluxed for 1 h. The reaction mixture was poured into dilute perchloric acid. The resulting precipitate was collected by filtration and recrystallized from methanol to give **12** (0.27 g). IR, 1544, 1487, 1453, 1420, 1111, 1090, 740, 717, and 691 cm^{-1}; ^1H NMR (DMSO-d_6), δ 3.36, 4.12, 4.24, 7.32, 7.62—8.02. Found: C, 55.32; H, 4.61; N, 11.86; Cl, 10.13%.

*1,2-Dimethyl-3,5-diphenyl-1,2,4-triazolylium Perchlorate (**13**) and 1,2-Dimethyl-3,5-diphenylpyrazolylium Perchlorate (**14**).* *N,N′*-Dimethylhydrazine dihydrochloride (1.5 mmol) was treated with 1 mmol of 3,5-diphenyl-1,2,4-dithiazolylium salt[11] or 3,5-diphenyl-1,2-dithiolylium salt[12] by the same procedure as above. Their data are shown below.

13: yield 25%, mp 152.0 °C (methanol); IR, 1606, 1544, 1485, 1450, 1418, 1392, 1115, 1087, 742, 718, 693 cm^{-1}; ^1H NMR (DMSO-d_6), δ 3.38, 4.24, and 7.62—8.02. Found: C, 54.85; H, 4.59; N, 12.14; Cl, 10.12%. Calcd for $C_{16}H_{16}N_3ClO_4$: C, 54.94; H, 4.61; N, 12.01; Cl, 10.12%.

14: yield 46%; mp, 187.4 °C (methanol); IR, 3120, 1565, 1494, 1476, 1434, 1396, 1111, 1092, 766, and 693 cm^{-1}; ^1H NMR (DMSO-d_6), δ 3.38, 4.12, 7.34, and 7.72. Found: C, 58.55; H, 4.87; N, 8.17; Cl, 10.14%. Calcd for $C_{17}H_{17}N_2ClO_4$; C, 58.55; H, 4.91; N, 8.03; Cl, 10.16%.

References

1) A. T. Balaban and C. D. Nenitzescu, *Justus Liebigs Ann. Chem.*, **625**, 74 (1959); R. M. Anker and A. H. Cook, *J. Chem. Soc.*, **1946**, 117; O. Buchardt, C. L. Pedersen, U. Svanholm, A. M. Dufield, and A. T. Balaban, *Acta Chem. Scand.*, **23**, 3125 (1969).

2) I. Shibuya and M. Kurabayashi, *Bull. Chem. Soc. Jpn.*, **48**, 73 (1975).

3) R. R. Schmidt, *Synthesis*, **1972**, 333; **1974**, 187.

4) R. R. Schmidt, *Chem. Ber.*, **98**, 334 (1965).

5) R. Lobard and A. Kress, *Bull. Soc. Chim. Fr.*, **1960**, 1528.

6) J. A. Bartrop, C. G. Richards, D. M. Russel, and G. Ruback, *J. Chem. Soc.*, **1959**, 1132.

7) B. Powlewski, *Chem. Ber.*, **36**, 2385 (1903).

8) A. W. Hofmann, *Chem. Ber.*, **12**, 2360 (1879).

9) A. T. Balaban, *Tetrahedron*, **24**, 5059 (1968).

10) Ph. L. Kumler, C. L. Pedersen, and O. Buchardt, *Acta Chem. Scand.*, **22**, 2719 (1968).

11) I. Shibuya, *Nippon Kagaku Kaishi*, **1979**, 389.

12) I. Shibuya, *Bull. Chem. Soc. Jpn.*, **52**, 1235 (1979).

  Bull. Chem. Soc. Jpn., 54, 2391—2394 (1981)

The Oxidation of 3,3-Diphenyl-2-propenoic Acid with Manganese(III) Acetate

Kazu KUROSAWA* and Tsuyoshi TSUJITA

Department of Chemistry, Faculty of Science, Kumamoto University, Kurokami 2-39-1, Kumamoto 860

(Received November 8, 1980)

The oxidation of 3,3-diphenyl-2-propenoic acid with manganese(III) acetate in boiling acetic acid gave 3,3-diphenyl-2-propenyl acetate, 4-acetoxymethyl-5,5-diphenyltetrahydro-2-furanone, 3,3-diphenyl-2-propenal, 5,5-diphenyl-2,5-dihydro-2-furanone, 4-acetoxy-5,5-diphenyltetrahydro-2-furanone, benzophenone, and 2-oxo-5,5-diphenyltetrahydro-4-furancarboxylic acid. The reaction pathways are discussed.

In a previous report[1] we described the oxidation of (*E*)-2,3-diphenyl-2-propenoic acids with manganese(III) acetate. The results were explained in terms of the formation of an acyloxy radical, a vinyl radical, and a vinyl cation from (*E*)-2,3-diphenyl-2-propenoic acid and the subsequent reactions of these intermediates (Scheme 1). We have now examined the oxidation of 3,3-diphenyl-2-propenoic acid (**1**) with manganese(III) acetate; the results will be described in this paper.

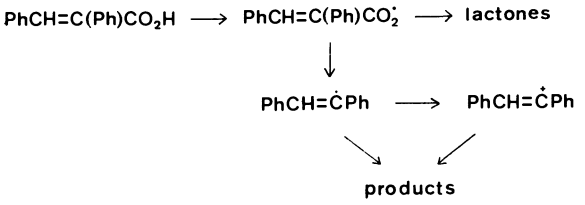

Scheme 1.

When 3,3-diphenyl-2-propenoic acid (**1**) was oxidized with manganese(III) acetate in the molar ratios of 1 : 3, 1 : 4, and 1 : 6 in boiling acetic acid, 3,3-diphenyl-2-propenyl acetate (**2**), 4-acetoxymethyl-5,5-diphenyltetrahydro-2-furanone (**3**), 3,3-diphenyl-2-propenal (**4**), 4-acetoxy-5,5-diphenyltetrahydro-2-furanone (**5**), 5,5-diphenyl-2,5-dihydro-2-furanone (**6**), and benzophenone (**7**) were obtained. When the oxidation was conducted in acetic acid containing acetic anhydride, 2-oxo-5,5-diphenyltetrahydro-4-furancarboxylic acid (**8**) was obtained, along with other products (**2**—**4**, and **6**), but **5** and **7** were not obtained. The results are summarized in Table 1. The structures of the products were determined by means of a study of their IR, NMR, and MS spectra, by elemental analyses, and by comparison with authentic samples.

3,3-Diphenyl-2-propenyl acetate (**2**) was obtained in the oxidation; the yield first increased with the increase in the molar ratio of the oxidant to the substrate, and then it decreased, suggesting that **2** could be further oxidized. In fact, the oxidation of **2**, prepared separately (Scheme 2), with manganese(III) acetate gave Compounds **3**, **4**, and **7** (Entry 8), **3** being the main product. The fact that only a small amount of **7** was formed from **2** indicates that **7** in Entries 1, 3, and 5 was not mainly formed *via* **2**. It seemed that the reaction of **1** with manganese(III) acetate would give an acyloxy radical (**A**), which then decomposed to a 2,2-diphenylethenyl radical (**B**), and that the latter reacted with the carboxymethyl radical formed from manganese(III) acetate to give 4,4-diphenyl-3-butenoic acid (**9**) (Scheme

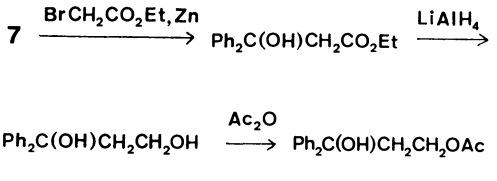

Scheme 2.

Table 1. The reaction of 3,3-diphenyl-2-propenoic acid (**1**) and related compounds with manganese(III) acetate in boiling acetic acid containing acetic anhydride

Entry	Substrate	Molar ratio of substrate : oxidant : Ac_2O	Time / min	Recovered substrate / %	Yield/%[a]							
					2	**3**	**4**	**5**	**6**	**7**	**8**	**11**
1	**1**	1 : 3 : 0	240	30	13	3	4	<1	1	19		
2	**1**	1 : 3 : 50	10	26	9	21	2		<1		8	
3	**1**	1 : 4 : 0	360	17	18	22	<1	<1	2	18		
4	**1**	1 : 4 : 50	13	2	4	35	2		<1		9	
5	**1**	1 : 6 : 0	420	9	14	36	4		3	18		
6	**1**	1 : 6 : 50	20			45					10	
7	**1**[b]	1 : 2 : 50	30	13	7	7					19	
8	**2**	1 : 2 : 0	600	17		58	4			4		
9	**2**	1 : 2 : 50	10	9		89						
10	**8**	1 : 2 : 0	150	32	30	25						
11	**9**	1 : 2 : 0	30		48		<1			<1		
12	**10**	1 : 3 : 6	60	9	4					9		71

a) The yields are based on the amount of the substrate used. b) **1** was pre-treated with excess acetyl chloride before the reaction.

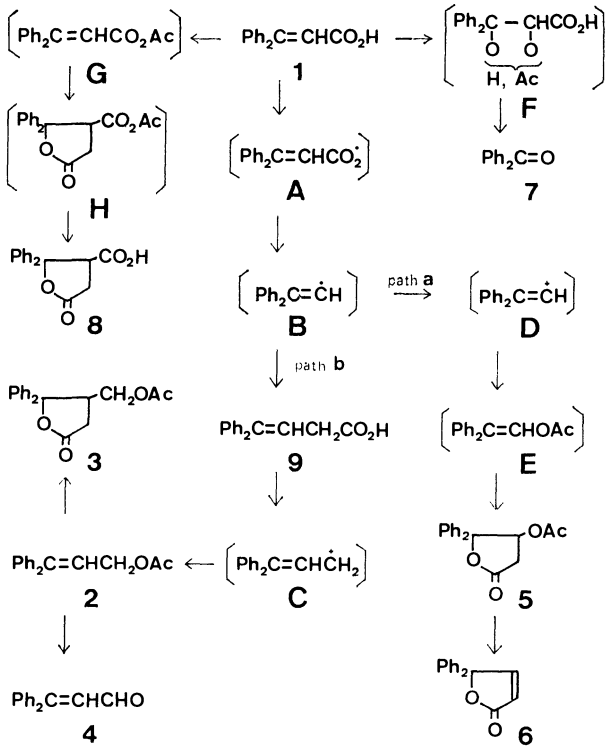

Scheme 3.

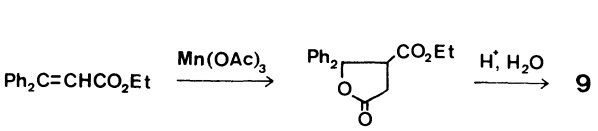

Scheme 4.

3, Path b). However, **9** could not be found in the products. Therefore, **9** was synthesized separately (Scheme 4) and treated with manganese(III) acetate. As a result, **2** was obtained as a single product (Entry 11), showing that **9** is a possible precursor of **2**.

4-Acetoxymethyl-5,5-diphenyltetrahydro-2-furanone (**3**) was obtained as the main product in the oxidation of **1** with manganese(III) acetate in Entries 2—6; the yield increased much with the increase in the oxidant. The oxidation of **2** with manganese(III) acetate in acetic acid containing acetic anhydride gave **3** almost exclusively (Entry 9).

Benzophenone (**7**) was obtained in a fairly large quantity, although it could not be separated from **2** because they have the same R_f values on TLC. However, on HLC it clearly showed two peaks corresponding to those of authentic samples. It is also interesting to note that benzophenone (**7**) was not formed in the reactions of **1** and **2** when acetic anhydride was added. It is known that the yield of lactones increases in the reaction of olefins with mangenese(III) acetate with a lowering of the water content in the reaction mixture.[2] It seems possible to assume that there are pathways which afford a hydroxy acetate like **F** and then **7** in the oxidation of **1** and **2**, and that these pathways do not operate under anhydrous conditions. It has been reported that the cleavage of the double

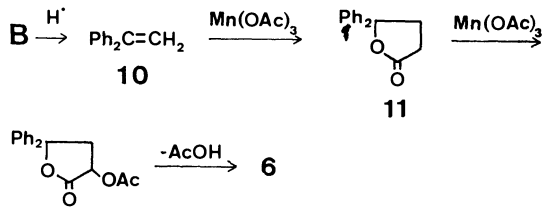

Scheme 5.

bond of chalcones in the oxidation with manganese(III) acetate gave a benzaldehyde,[3] although the reaction pathway was not shown.

As another interesting feature of the reaction, it gave 5,5-diphenyl-2,5-dihydro-2-furanone (**6**) in very low yields (Entries 1, 3, and 5). We oxidized **2**, **8**, and **9**, but none of them gave the lactone (**6**). It seemed possible that acetoxylation of 5,5-diphenyltetrahydro-2-furanone (**11**), followed by decomposition, might give the lactone (**6**), as is shown in Scheme 5. The oxidation of 1,1-diphenylethylene (**10**) with manganese(III) acetate gave **11** as the major product, together with **2** and **7** in minor quantitities (Entry 12), but it did not give **6**. The formation of **2** from **10** can be explained as follows. The addition of a carboxymethyl radical to **10** gives a radical, **I**, which then loses a hydrogen radical to yield **9** and then **2** (Scheme 6). One of the minor

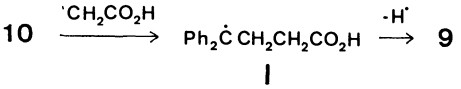

Scheme 6.

fractions isolated from the reaction of **1** with manganese(III) acetate in acetic acid showed a peak at $\delta=1.69$ corresponding to an acetoxyl group. The purification of the fraction by repeated TLC failed to give a pure compound, but the NMR spectrum showed three aliphatic protons, at $\delta=2.45$ (1H, dd, $J=2.5$ and 18.0 Hz), $\delta=2.72$ (1H, $J=6.0$ and 18.0 Hz), and $\delta=6.25$ (1H, dd, $J=2.5$ and 6.0 Hz). Since the chemical shift ($\delta=1.69$) for the acetoxyl group is higher than the normal one ($\delta=2$), and since the J value of 18.0 Hz for methylene protons adjacent to a carbonyl function is comparable to those of cyclic compounds, the structure of this compound must be 4-acetoxy-5,5-diphenyltetrahydro-2-furanone (**5**). When the fraction was heated in acetic acid under reflux, it gave **6**. Thus, it is most probable that **6** was formed from **5**.

3,3-Diphenyl-2-propenal (**4**) was obtained as a minor product which might have been formed from **2** by further oxidation with manganese(III) acetate and hydrolysis during the work-up.

The formation of 2-oxo-5,5-diphenyltetrahydro-4-furancarboxylic acid (**8**) in the reaction containing acetic anhydride seems to indicate that **1** forms an anhydride with acetic anhydride and then reacts with the carboxymethyl radical. The reaction of **1** which had been pretreated with acetyl chloride gave **8** in a much improved yield (Entry 7). Since the reaction of **8** with manganese(III) acetate gave **2** and **3** (Entry 10), therefore, it seems that **8** could be decarboxylated to give **9** which

yielded **2** and **3**. However, **8** cannot be a real precursor for **2** and the other compounds in the oxidation of **1**, because if **8** were first formed and then oxidized to **2**, **3**, and **4** during the prolonged reaction time in the reaction in acetic acid, the total yield of **2**, **3**, **4**, and **8** should be roughly equal to that in the reaction in acetic acid containing acetic anhydride. However, this was not the case. For example, the total yield (20%) of **2**, **3**, **4**, and **8** in Entry 1 was less than that (40%) in Entry 2. The above possible reaction pathways are summarized in Scheme 3.

Experimental

All the 60 MHz ^{1}H NMR spectra were recorded with a Hitachi R-24 spectrometer, while the 100 MHz ^{1}H NMR spectrum was taken on a JEOL MH-100 spectrometer, with TMS as the internal standard. The IR spectra were recorded for the chloroform solution with a JASCO IRA-1 grating spectrometer, while the MS spectra were taken with JMS-01 SG-2 and Hitachi M-80 plus M-003 instruments. Liquid chromatography (HLC) was carried out with a Mitsubishi ALTEX 310/330 instrument, eluting with 60% aqueous methanol using a HY-ODS-SU column 4.6 mm in diameter and 250 mm in length. The melting points were determined on a Yanagimoto micro-melting point apparatus and were not corrected.

Materials. The 3,3-Diphenyl-2-propenoic acid (**1**) was prepared by the standard procedure[4] from benzophenone. The ethyl 3,3-diphenyl-2-propenoate[5] was prepared by the dehydration of ethyl 3-hydroxy-3,3-diphenylpropanoate[4] with thionyl chloride in pyridine.

3-Acetoxy-1,1-diphenyl-1-propanol. To ethyl 3-hydroxy-3,3-diphenylpropanoate (1.95 g) in anhydrous diethyl ether (100 ml), we added lithium aluminium hydride (80 mg), after which the mixture was stirred at 0 °C for 14 h. After the addition of 1 M (1 M = 1 mol dm^{-3}) sulfuric acid (50 ml), the reaction mixture was extracted with diethyl ether. The combined ethereal extract was washed with a saturated solution of sodium chloride and then evaporated. The resulting 1,1-diphenyl-1,3-propanediol was treated with a mixture of acetic anhydride (5 ml) and pyridine (10 ml) at room temperature for 17 h. The reaction mixture was poured into iced water, and the precipitate was collected and recrystallized from light petroleum to give 3-acetoxy-1,1-diphenyl-1-propanol (1.80 g, 92%), mp 84—85 °C; IR 1740 (OAc) and 3560 cm^{-1} (OH); NMR ($CDCl_3$) δ=1.88 (3H, s, OAc), 2.61 (2H, t, J=7.0 Hz, $-CH_2-$), 2.79 (1H, s, OH), 4.16 (2H, t, J=7.0 Hz, $-CH_2-$), and 7.1—7.6 (10H, m, 2×Ph). Found: C, 75.48; H, 6.49%. Calcd for $C_{17}H_{18}O_3$: C, 75.53; H, 6.71%.

3,3-Diphenyl-2-propenyl Acetate (2). A solution of 3-acetoxy-1,1-diphenyl-1-propanol (1.40 g) in pyridine (10 ml) was treated with thionyl chloride (1.24 g) at 0 °C for 19 h. The reaction mixture was poured into 1 M sulfuric acid (100 ml) and then extracted with benzene (50 ml). The benzene layer was washed with 1 M sulfuric acid (30 ml) and then evaporated, giving **2** (1.21 g, 86%). The analytical sample was distilled under reduced pressure; bp 150—155 °C (bath temp)/0.1 mmHg (1 mmHg = 133.322 Pa); IR 1738 cm^{-1} (OAc); NMR (CCl_4) δ=1.97 (3H, s, OAc), 4.54 (2H, d, J=7.0 Hz, $-CH_2-$), 6.15 (1H, t, J=7.0 Hz, >CH–), and 7.2 (10H, m, 2×Ph); MS *m/e* 252.1187 (Calcd for $C_{17}H_{16}O_2$: 252.1150) (59%, M$^+$), 209 (61%), 192 (100%), and 103 (82%).

Ethyl 2-Oxo-5,5-diphenyltetrahydro-4-furancarboxylate. A mixture of ethyl 3,3-diphenyl-2-propenoate (504 mg), manganese(III) acetate dihydrate[6] (1.61 g), acetic acid (20 ml), and acetic anhydride (3 ml) was heated under reflux for 43 min. The reaction mixture was poured into water (50 ml), and the precipitate was collected. Recrystallization from ethanol gave ethyl 2-oxo-5,5-diphenyltetrahydro-4-carboxylate (513 mg, 90%); mp 147—148 °C; IR 1742 (COOEt) and 1780 cm^{-1} (lactone); NMR ($CDCl_3$) δ=0.92 (3H, t, J=7.0 Hz, $-CH_3$), 2.71 (1H, dd, J=8.5 and 18.0 Hz, –CH–), 3.02 (1H, dd, J=4.5 and 18.0 Hz, –CH–), 3.75 (2H, m, $-CH_2-$), 4.20 (1H, dd, J=8.5 and 4.5 Hz, –CH–), and 7.2—7.8 (10H, m, 2×Ph). Found: C, 73.40; H, 5.65%. Calcd for $C_{19}H_{18}O_4$: C, 73.53; H, 5.85.

4,4-Diphenyl-3-butenoic Acid (9). A mixture of ethyl 2-oxo-5,5-diphenyltetrahydro-4-furancarboxylate (572 mg), 3 M hydrochloric acid (100 ml), and ethanol (100 ml) was heated under reflux for 21 h. After the removal of the ethanol and the hydrochloric acid, the resulting mixture was extracted with benzene; then the benzene solution was extracted with a saturated sodium hydrogencarbonate solution. The aqueous solution was separated and acidified with concd hydrochloric acid. The precipitate was collected and recrystallized from a mixture of carbon tetrachloride–light petroleum to give 4,4-diphenyl-3-butenoic acid (115 mg, 25%); mp 109—111 °C; IR 1725 (COOH) and 2400—3400 cm^{-1} (COOH); NMR ($(CD_3)_2SO$) δ=3.06 (2H, d, J=8.0 Hz, $-CH_2-$), 6.26 (1H, t, J=8.0 Hz, =CH–), and 7.3 (10H, m, 2×Ph); MS *m/e* 238.1008 (Calcd for $C_{16}H_{14}O_2$: 238.0994) (66%, M$^+$), 193 (85%), 178 (53%), and 115 (100%).

Oxidations of 3,3-Diphenyl-2-propenoic Acid (1), 3,3-Diphenyl-2-propenyl Acetate (2), 2-Oxo-5,5-diphenyltetrahydro-4-furancarboxylic Acid (8), 4,4-Diphenyl-3-butenoic Acid (9), and 1,1-Diphenylethylene (10). The general procedure for the oxidation of 3,3-diphenyl-2-propenoic acid (**1**) and the other compounds (**2**, **8**, **9**, and **10**) was as follows. A mixture of the substrate (2 mmol), manganese(III) acetate dihydrate (4—12 mmol), acetic acid (30 ml), and acetic anhydride (when it was needed) (10 ml) was heated under reflux until the dark color of Mn(III) ion disappeared (the time is shown in Table 1). After the removal of the acetic acid, 1 M sulfuric acid (30 ml) was added to the mixture, which was then extracted with benzene (30 ml). The benzene solution was washed with aqueous sodium hydrogencarbonate and evaporated under reduced pressure. The products were separated on TLC (Wakogel B 10), with chloroform as the developing solvent, and then recrystallized. The aqueous sodium hydrogencarbonate solution was acidified with concd hydrochloric acid and extracted with chloroform, which gave acidic products. The yields are summarized in Table 1.

Oxidation Products. *3,3-Diphenyl-2-propenyl Acetate (2)*: Liquid (this was identical with an authentic sample).

4-Acetoxymethyl-5,5-diphenyltetrahydro-2-furanone (3): Mp 119—120 °C (EtOH); IR 1752 (OAc) and 1780 cm^{-1} (lactone); NMR (C_6H_6) δ (100 MHz) = 1.60 (3H, s, OAc), 2.12 (2H, d, J=6.0 Hz, $-CH_2-$), 3.16 (1H, m, –CH–), 3.40 (1H, dd, J= 8.0 and 11.5 Hz, –CH–), and 3.94 (1H, dd, J=4.5 and 11.5 Hz, –CH–). Found: C, 73.39; H, 5.97%. Calcd for $C_{19}H_{18}O_4$: C, 73.53; H, 5.85%.

3,3-Diphenyl-2-propenal (4): Liquid (lit,[7] mp 44 °C); IR 1680 cm^{-1} (CHO); NMR ($CDCl_3$) δ=6.56 (1H, d, J=9.0 Hz, =CH–) 7.35 (10H, m, 2×Ph), and 9.49 (1H, d, J=9.0 Hz, CHO); MS *m/e* 208.0896 (Calcd for $C_{15}H_{12}O$: 208.0888) (100%, M$^+$), 207 (99%), 178 (39%), 165 (22%), 152 (14%), 131 (19%), and 102 (38%).

4-Acetoxy-5,5-diphenyltetrahydro-2-furanone (5): Liquid (this compound was obtained as a mixture; its NMR data are given in the text).

5,5-Diphenyl-2,5-dihydro-2-furanone (6): Mp 128—128.5 °C

(EtOH) (lit,[8] mp 131—131.5 °C); IR 1680 (C=C) and 1770 cm^{-1} (lactone); NMR ($CDCl_3$) δ=6.11 (1H, d, J=6.0 Hz, =CH–), 7.26 (10H, m, 2×Ph), and 7.87 (1H, d, J=6.0 Hz, =CH–); MS *m/e* 236 (41%, M^+), 131 (100%), 105 (83%), and 77 (69%).

Benzophenone (7): This was obtained as a mixture of **2** and **7**; it was found by HLC to be identical with authentic samples. The yields were estimated from the NMR spectrum.

2-Oxo-5,5-diphenyltetrahydro-4-furancarboxylic Acid (8): Mp 191—192 °C (CCl_4); IR 1740 (COOH) and 1780 cm^{-1} (lactone); NMR ($(CD_3)_2SO$) δ=2.78 (2H, m, $-CH_2-$), 4.29 (1H, dd, –CH–) (AB_2 system, J_{AB}=6.3 Hz), and 7.1—7.8 (10H, m, 2×Ph); MS *m/e* 282 (5%, M^+), 238 (5%), 183 (100%), 105 (50%), and 77 (20%). Found: C, 72.01; H, 4.89%. Calcd for $C_{17}H_{14}O_4$: C, 72.33; H, 5.00%.

5,5-Diphenyltetrahydro-2-furanone (11): Mp 90 °C (EtOH) (lit,[9] mp 90 °C); IR 1778 cm^{-1} (lactone); NMR (CCl_4) δ= 2.2—3.0 (4H, m, $-CH_2-CH_2-$), and 7.25 (10H, m, 2×Ph).

We wish to thank Professor Hideto Shosenji of the Department of Synthetic Chemistry, Faculty of Technology, Kumamoto University, for his measurement of the 100 MHz ^1H NMR spectrum, and Dr. Shinzaburo Hishida of the Hitachi Co. Ltd., Katsuda, and Mr. Shuichi Ueda at the Taiho Pharmaceutical Co. Ltd., Tokushima, for their measurements of the MS spectra. We also wish to thank Professor John F. W. McOmie for his helpful discussion and for reading the manuscript.

References

1) K. Oishi and K. Kurosawa, *Bull. Chem. Soc. Jpn.*, **53**, 179 (1980).
2) E. I. Heiba, R. M. Dessau, and P. C. Rodewald, *J. Am. Chem. Soc.*, **96**, 7977 (1974).
3) K. Kurosawa and J. Higuchi, *Bull. Chem. Soc. Jpn.*, **45**, 1132 (1972).
4) H. Rupe and E. Busolt, *Ber.*, **40**, 4537 (1907).
5) H. Rupe, *Justus Liebigs Ann. Chem.*, **395**, 136 (1913).
6) P. J. Andrulis Jr., M. J. S. Dewar, R. Dietz, and R. L. Hunt, *J. Am. Chem. Soc.*, **88**, 5473 (1966).
7) E. P. Kohler and R. G. Larsen, *J. Am. Chem. Soc.*, **57**, 1448 (1935).
8) P. M. M. van Haard, L. Thijs, and B. Zwanenburg, *Tetrahedron Lett.*, **1975**, 803.
9) R. E. Lutz, *J. Am. Chem. Soc.*, **49**, 1106 (1927).

  Bull. Chem. Soc. Jpn., 54, 2395—2398 (1981)

Configuration and Conformation of the Photoisomers of *N*-[*p*-(Dimethylamino)benzylidene]anilines

Masato YOSHIDA* and Michio KOBAYASHI

Department of Chemistry, Faculty of Science, Tokyo Metropolitan University, Fukazawa, Setagaya-ku, Tokyo 158

(Received December 5, 1980)

The UV, ^{1}H-NMR, and ^{13}C-NMR spectra of the photoisomers produced by irradiation of *N*-[*p*-(dimethylamino)benzylidene]anilines at low temperature have been studied. The results suggested that the photoisomers have Z structures and the imino benzene rings are twisted around the Ar–N axis out of Ar–CH=N plane due to the steric repulsion between the two rings.

N-Benzylideneanilines (Ar'CH=NAr) are formally related to stilbenes (Ar'CH=CHAr) and azobenzenes (Ar'N=NAr), but differ from the latter in that *Z* (cis) isomers have not yet been isolated. The possibility of the existence of *E*-*Z* isomerism in *N*-benzylideneanilines has interested chemists for many decades. It was reported that the irradiation of a solution of (*E*)-*N*-benzylideneaniline at 200 K converts it reversibly into a photoisomer with a different UV absorption.[1] We investigated the photoisomerism of many substituted *N*-benzylideneanilines (*p*-R'-C_6H_4CH=NC_6H_4-R-*p*) by the measurement of UV spectra, and found that various *N*-benzylideneanilines are converted into their photoisomers upon irradiation by a high pressure mercury lamp at 77 K (liq. N_2) or 200 K (Dry Ice–EtOH or Dry Ice–acetone).[2] Recently, ^{1}H-NMR spectroscopy has been applied to the problem of configuration of the photoisomers of *N*-benzylideneanilines.[3,4] In this paper we report UV, ^{1}H-NMR, and ^{13}C-NMR spectra of the photoisomers of *N*-[*p*-(dimethylamino)benzylidene]-aniline and its methyl or dimethyl derivatives produced by photoirradiation, and discuss the configuration and conformation of the photoisomers. *N*-[*p*-(Dimethylamino)benzylidene]aniline and its methyl or dimethyl derivatives were chosen for this study because they have strong absorption maxima at wavelengths greater than 300 nm, and are most easily converted to the photoisomers.

Results and Discussion

The UV spectra of the following three compounds and their photoisomers produced by photoirradiation at 77 K in M. P. (methylcyclohexane–isopentane 1 : 1) matrix are shown in Fig. 1. When *E*-**1**—*E*-**3** were

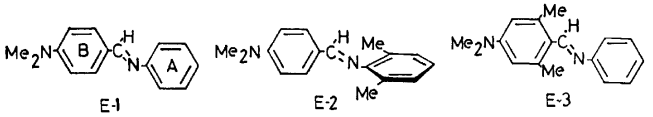

irradiated at the wavelength corresponding to the longest wavelength absorption maxima, they were converted to their photoisomers; these also absorbed the light and reverted to *E* forms. Therefore, the photoequilibrium between the photoisomer and the *E* form depends upon the wavelength of the light used. In order to determine the characteristics of the UV spectra of these isomers, it is desirable to have almost 100% conversion to photoisomers. This could be achieved by

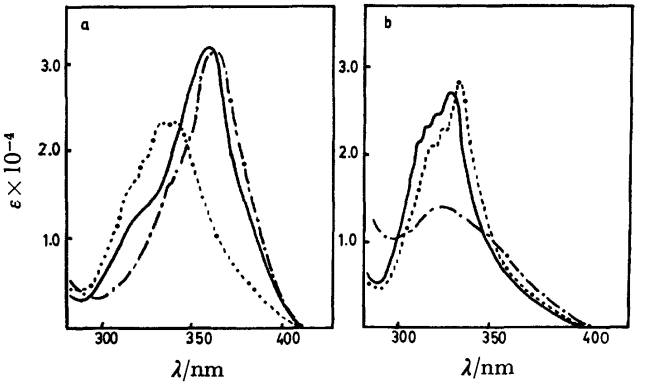

Fig. 1. The UV spectra of (a) *E*-**1** (——), *E*-**2** (- - -), and *E*-**3** (—·—), and (b) their photoisomers in methylcyclohexane–isopentane 1 : 1 at 77 K.

choosing monochromatic light of 366 nm for irradiation.

Compound *E*-**1** was shown to have a planar structure from the UV spectra.[5] As described in our previous paper, the UV spectrum of *E*-**2** is quite similar to that of *N*-[*p*-(dimethylamino)benzylidene]-*t*-butylamine, and so we conclude that the UV absorption band of *E*-**2** shown in Fig. 1a is due to the conjugated system of the benzylidene benzene ring (ring B) and C=N group, with little contribution from the imino benzene ring (ring A).[2] The UV spectrum of *E*-**3** is similar to that of *E*-**1**, so it should also have a planar structure. In the photoisomers, the UV spectrum of **1** is quite similar to that of **2**, but different from that of **3** (Fig. 1b). And the UV spectra of the photoisomers of **1** and **2** are almost the same as that of *E*-**2**. These features of the photoisomers of *N*-[*p*-(dimethylamino)benzylidene]anilines can be explained by the structure of the photoisomers proposed in Fig. 2. The photoisomer of **1** has *Z*-configuration and ring A is greatly twisted around the Ar–N axis; ring B and CH=N group compose a conjugated system with little contribution from ring A. The conformation of ring A of the photoisomer of **2** is the

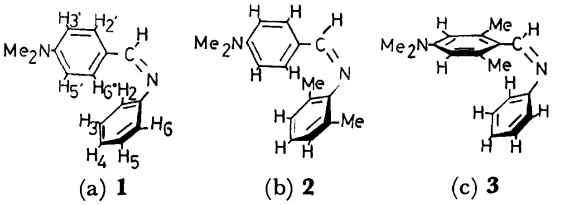

(a) **1** (b) **2** (c) **3**

Fig. 2. The proposed structures for the photoisomers of (a) **1**, (b) **2**, and (c) **3**.

Table 1. ^{1}H-NMR chemical shifts of **1**, **4**, and their photoisomers[a)]

	1	Photoisomer of **1**	$\Delta\delta$[b)]	**4**	Photoisomer of **4**	$\Delta\delta$[c)]
H_α	8.41	8.21	0.20	8.63	8.53	0.10
$H_{2'}$	7.85[d)]	7.09[d)]	0.76			
$H_{6'}$	7.85[d)]	7.09[d)]	0.76	8.03[e)]	6.65[e)]	1.38
$H_{3'}$	6.84[d)]	6.59[d)]	0.25	6.64	6.63	0.01
$H_{5'}$	6.84[d)]	6.59[d)]	0.25	6.71[e)]	6.20[e)]	0.51
$H_{2,6}$	*ca.* 7.4	f)		*ca.* 7.3	*ca.* 6.8	
$H_{3,5}$	7.44	7.42	0.02	7.42	7.32	0.10
H_4	*ca.* 7.4	f)		f)	f)	

a) In ppm downfield from internal TMS. b) $\Delta\delta=\delta$ of **1**$-\delta$ of the photoisomer of **1**. c) $\Delta\delta=\delta$ of **4**$-\delta$ of the photoisomer of **4**. d) $J_{H_{5'},H_{6'}}=J_{H_{3'},H_{2'}}=8.79$ Hz (AA′BB′ quartet). e) $J_{H_{3'},H_{2'}}=8.79$ Hz (AA′BB′ quartet). f) These chemical shifts could not be determined since the signals were multiplet.

same as that of the photoisomer of **1**, because the 2- and 6-methyl groups on ring A do not act as steric hindrances. On the other hand, ring B of the photoisomer of **3** is twisted due to the steric repulsion between the 2- and 6-methyl groups on ring B and ring A.

As shown in our previous paper, the UV spectra of the photoisomers of *p*-substituted *N*-benzylideneanilines (*p*-R′-C_6H_4CH=NC_6H_4-R-*p*) do not vary with the substituents R but with the substituents R′, and are quite similar to those of corresponding *N*-benzylidene-2,6-dimethylanilines (*p*-R′-C_6H_4CH=NC_6H_2-Me_2-2,6-R-4). These results support the idea that the photoisomers of *N*-benzylideneanilines have the structure shown in Fig. 2a.

^{1}H-NMR chemical shifts of *E*-**1** and (*E*)-*N*-(4-dimethylamino-2-methylbenzylidene)aniline (**4**) and their photoisomers were also studied. The aromatic protons of these compounds were assigned by comparison with ^{1}H-NMR chemical shifts of **1**-2,4,6-d_3, **4**-2,4,6-d_3, and **4**-2,4,6,3′,5′-d_5 and their photoisomers. The chemical shifts are summarized in Table 1.

$H_{2'}$ and $H_{6'}$ of the photoisomer of **1** resonate at a field higher than those of *E*-**1**. The significant change in $H_{2'}$ and $H_{6'}$ (0.76 ppm) can be ascribed to the diamagnetic shielding by ring A, since $H_{2'}$ or $H_{6'}$ in photoisomer is located above ring A, as shown in Fig. 2a. In **1** or its photoisomer, the signals of $H_{2'}$, $H_{6'}$, $H_{3'}$, and $H_{5'}$ are AA′BB′ type quartets. This shows that ring B freely rotates around the Ar–C bond within the NMR time scale, although this ring lies in the plane common to the C=N bond most of the time (Eq. 1). Therefore, the upfield shifts observed in $\delta_{H_{5'}}$ and $\delta_{H_{3'}}$ in **1** upon irradiation must be the average of the shifts of the $H_{6'}$, affected by the diamagnetic shielding from the ring A, and of $H_{2'}$, little affected by such shielding. If the rotation of ring B around the Ar–C bond could be restricted, the real upfield shift in $H_{6'}$ upon irradiation should be observed. So the NMR spectra of (*E*)-*N*-(4-dimethylamino-2-methylbenzylidene)aniline and its photoisomer were investigated. In the photoisomer of **4** the 2-methyl group should be situated far from ring A and thus should avoid the steric repulsion of the methyl group and ring A, as shown in Eq. 2. A large upfield shift of 1.38 ppm upon irradiation was observed in $H_{6'}$. This is approximately twice that observed in the $H_{2'}$ and $H_{6'}$ in **1** (0.76 ppm), in accordance with our

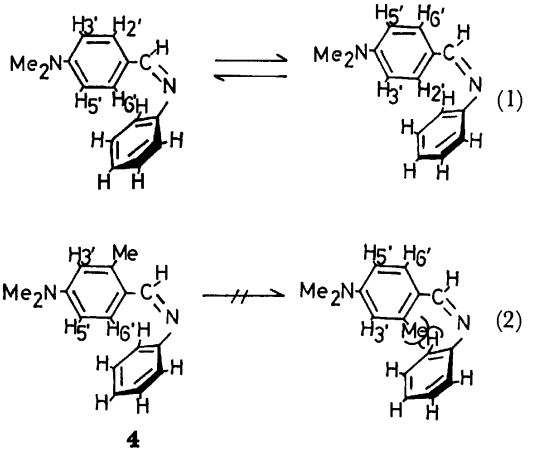

4

expectation. The upfield shift in $H_{5'}$ (0.51 ppm) is also about two times that observed in the $H_{3'}$ and $H_{5'}$ in **1** (0.25 ppm). The fact that $H_{5'}$ is not equivalent to $H_{3'}$ shows the restriction of the rotation.

If one assumes that the ring A is twisted around the Ar–N axis by 90° and that ring B and CH=N group are on the same plane, the theoretical shielding effect on $H_{6'}$ according to the ring currents model proposed by Johnson and Boby[6)] is more than 4 ppm (ρ(Å)=0.79, z(Å)=1.46; ρ and z are two components of the radius vector from the center of shielding ring A to $H_{6'}$. ρ lies in the plane of ring A and z is the component along the hexad axis.). This theoretical value is quite different from the observed one (1.38 ppm). However, the shielding on $H_{6'}$ from ring A is sensitive to the dihedral angle of the Ar–C axis (θ_C). For example, the theoretical shielding is about 2 ppm at $\theta_C=30°$ (ρ(Å)=1.52, z(Å)=1.60) and about 0.5 ppm at $\theta_C=45°$ (ρ(Å)=2.01, z(Å)=1.80). So it is reasonable to assume a little twist of ring B, although ring B is conjugated with C=N.

From the results obtained by the studies with UV and ^{1}H-NMR, the following conclusions may be drawn about the configuration and conformation of the photoisomers of *N*-[*p*-(dimethylamino)benzylidene]-anilines.

1) The photoisomer of *N*-[*p*-(dimethylamino)benzylidene]aniline has *Z*-configuration and is stable only below 200 K; consequently, it has not been isolated.

2) For the steric repulsion of two rings in *Z*-configuration, ring A is twisted greatly around Ar–N axis, so

Table 2. ^{13}C-NMR chemical shifts of **1**, **2**, and their photoisomers[a)]

Position of aromatic ring	*E*-**1**	*Z*-**1**	*E*-**2**	*Z*-**2**
C-2,6	121.5	118 2	b)	b)
C-3,5	129.7	130 2	128.5	128.7
C-4	125.6	123.0	123.5	122.6
C-2′,6′	130.9	133.0	130.5	131.7
C-3′,5′	111.8	111.2	111.8	111.6

a) In ppm downfield from internal TMS. b) δ_{C-1}, $\delta_{C-1'}$, $\delta_{C-4'}$, and $\delta_{C-\alpha}$ in **1** and **2**, and $\delta_{C-2,6}$ in **2** could not be determined because of their long spin-lattice relaxation times.

that ring A does not conjugate with C=N; but the twist of ring B around Ar–C axis is small enough to allow conjugation with C=N.

Such ease of twist of ring A in (*Z*)-*N*-[*p*-(dimethylamino)benzylidene]aniline may be ascribed to the energy gain by delocalization of the N lone pair electrons to ring A upon the twist of the ring, as shown in Eq. 3. In order to investigate the electron density of ring A, we determined ^{13}C-NMR chemical shifts of *E*- and *Z*-**1**, and *E*- and *Z*-**2**; the results are summarized in Table 2.

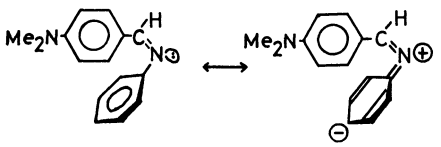
(3)

δ_{C-4} of *Z*-**1** resonates at a field higher than that of *E*-**1** by 2.6 ppm, while there is no difference in the δ_{C-4} of 2 between *E* and *Z* forms. The δ_{C-4} of *Z*-**1** is also similar to those of *Z*-**2** and *E*-**2**. $\delta_{C-2,6}$ of *Z*-**1** resonates at a field higher than that of *E*-**1** by 3.3 ppm while $\delta_{C-3,5}$ of *Z*-**1** is similar to that of *E*-**1**. Ring A of *E*-**2**, *Z*-**1**, and *Z*-**2** are greatly twisted around the Ar–N axis, as stated before, and the twist of ring A causes the upfield shifts of $\delta_{C-2,6}$ and δ_{C-4}. In order to find the reason of the upfield shift of δ_{C-4} by the twist of ring A, ^{13}C-NMR chemical shifts of *N*-benzylideneanilines with various dihedral angles (θ_N) around the Ar–N axis were determined (Table 3). An X-ray diffraction study has shown that ring A in **6** is twisted about 50° around the Ar–N axis.[7)] The smaller extinction coefficients in **8** and **9** compared with that of **6** have been ascribed to the greater twist of ring A around the Ar–N axis, because of the steric hindrance involving methyl groups and ortho or alpha hydrogens.[8)] The extinction coefficent of **7** is not much different from that of **6**, and this suggests that the extents of twist of ring A are similar in **6** and **7**. This is reasonable because the methyl group of **7** can be situated far from the methine hydrogen and no interaction between them may take place. The higher field resonance in C-4 of **5** than that of benzene (δ=128.5) should be due to the resonance shown in Eq. 4. Twisting of ring A around the Ar–N axis is expected to decrease such resonance, and downfield shifts of the C-4 signals should be expected. However, δ_{C-4} values of **8** and **9**, in which ring A is twisted around the Ar–N axis, are observed at a much higher field than that in **5** ($\delta_{C-4}(\mathbf{5})-\delta_{C-4}(\mathbf{8})$=2.19, and $\delta_{C-4}(\mathbf{5})-\delta_{C-4}(\mathbf{9})$= 2.61). This difference cannot be ascribed to the electron-donating effect of the methyl groups. Because methyl substituents do not affect $\delta_{C\text{-meta}}$ greatly[9)] and also δ_{C-4} value in **7** is similar to that of **6**. The finding that δ_{C-4} of **9** possessing α-methyl group is similar to that of **8** possessing methyl groups at **2** and **6** positions on ring A suggests that the twist of ring A around the Ar–N axis causes the upfield shifts observed in **8** and **9**. The upfield shifts actually observed for the C-4 signals of **8** and **9**, in comparison with that of **5**, indicate the existence of the delocalization of N-lone pair electrons to ring A by the resonance shown in Eq. 5. In **8** or **9**, the resonance shown in Eq. 4 should not be possible and the resonance shown in Eq. 5 must be important. The greater electron density on C-4 of **8** and **9** in comparison with that of **5**, which is reflected in the ^{13}C-NMR chemical shift, suggests that the increased contribution of resonance (5) outweighs the decreased contribution of resonance (4). In **6** or **7**, in which ring A is twisted by about 50°, the chemical shift of C-4 is about the same as that of **5**. These results indicate that increased contribution of resonance (4) is approximately equal to the decreased contribution of resonance (5). So we have clarified that the upfield shifts of δ_{C-4} of *N*-benzylideneanilines by the twist of ring A were caused by the delocalization of the N-lone pair to ring A.

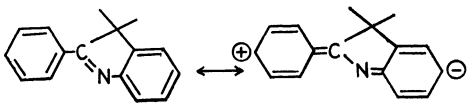
(4)

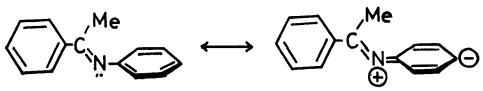
(5)

Table 3. ^{13}C-NMR chemical shifts and UV data of *N*-benzylideneanilines

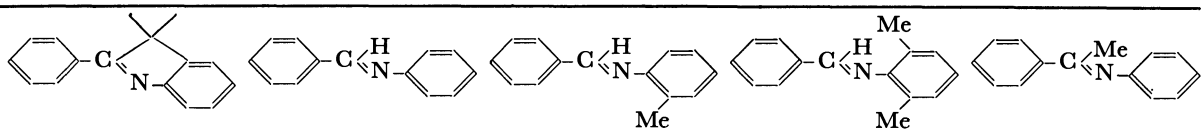

	5	**6**	**7**	**8**	**9**
δ_{C-4}[a)]	125.7	125.8	125.6	123.5	123.1
λ_{max}/nm	309[b)]	314[c)]	325[c)]	331[c)]	320[c)]
ε	16600	6940	4230	1740	1840

a) Chemical shifts of the other carbons of these compounds have been reported in our previous paper : M. Yoshida, H. Minato, and M. Kobayashi, *Chem. Lett.*, **1976**, 1097. b) Ref. 5. c) Ref. 8.

The steric repulsion of the two rings in (*Z*)-*N*-[*p*-(dimethylamino)benzylidene]aniline should be decreased by the preferential twist of ring A around Ar–N axis, because the twist of ring A is energetically more favorable than that of ring B for the stabilization by the delocalization of N-lone pair to ring A. The delocalization of the N-lone pair was reflected in the ^{13}C-NMR chemical shifts of *Z*-**1** and *Z*-**2**.

Experimental

UV spectra were taken with a Hitachi EPS-3T spectrometer. ^{1}H- and ^{13}C-NMR spectra were taken with a JEOL Fx-60 FT-NMR spectrometer.

UV spectra at low temperatures were measured in a sample cell cooled to 77 K with liquid nitrogen in a quartz Dewar bottle. As a solvent, M. P. (methylcyclohexane–isopentane 1 : 1) was used. For volume contraction, a correction factor of 0.8 was used.[10]

An acetone-d_6 solution ($\approx 10^{-3}$ mol dm^{-3}) of an *N*-benzylideneaniline in a Pyrex tube (10 mm) was cooled in a Dry Ice–acetone bath and irradiated through a quartz Dewar bottle with a 500 W high pressure mercury lamp until about 100% isomerization was attained. Then ^{1}H-NMR spectrum of the photoisomer of an *N*-benzylideneaniline was immediately determined at 198 K. Since this photoisomerization is complete only in dilute concentrations, spectra were determined by use of a Fourier transform NMR spectrometer (accumulation 100—500).

The ^{13}C-NMR spectrum of the photoisomer of an *N*-benzylideneaniline was determined in a similar way (Concentration of the solution, 10^{-2} mol dm^{-3}; pulse flipping angle, 60°; sampling time, 900 ms; data points, 4096; accumulation, 5000; pulse interval, 1 s).

N-[*p*-(Dimethylamino)benzylidene]anilines were prepared by heating mixtures of corresponding aldehydes and amines. Samples were purified by repeated recrystallization. The details were described in our previous papers.[3] (Melting points in °C: **1**, 99—101; **2**, 41—43; **3**, 84.5—85.5; **4**, 83—85.)

References

1) E. Fisher and Y. Frei, *J. Chem. Phys.*, **27**, 808 (1959).
2) M. Kobayashi, M. Yoshida, and H. Minato, *Chem. Lett.*, **1976**, 185.
3) M. Kobayashi, M. Yoshida, and H. Minato, *J. Org. Chem.*, **41**, 3322, (1976).
4) K. Maeda and E. Fisher, *Isr. J. Chem.*, **16**, 294 (1977); K. Maeda, K. A. Musuzkat, and S. Sharafi-Ozeri, *J. Chem. Soc., Perkin Trans. 2*, **1980**, 1282.
5) D. Skrabal, J. Steiger, and H. Zollinger, *Helv. Chim. Acta*, **58**, 800 (1975).
6) C. E. Johnson, Jr., and F. A. Bovey, *J. Chem. Phys.*, **29**, 1012 (1958).
7) H. B. Bürgi and J. D. Dunitz, *Helv. Chim. Acta*, **54**, 1225 (1971).
8) W. F. Smith, *Tetrahedron*, **19**, 445 (1963).
9) G. C. Levy and G. L. Nelson, "Carbon-13 Nuclear Magnetic Resonance for Organic Chemists," Interscience, New York (1972), p. 81.
10) A. Kuboyama, R. Yamazaki, and S. Matsuzaki, *Bull. Chem. Soc. Jpn.*, **42**, 10 (1969).

Spectroscopic Studies of Surfactant Solubility. III. Side-chain Effects of Phosphatidyl Compounds in Chloroform Solutions

Mitsuyo OKAZAKI, Ichiro HARA, Yumiko K. TSUTSUI,† and Tsunetake FUJIYAMA*,††

Laboratory of Chemistry, the Department of General Education, Tokyo Medical and Dental University, Ichikawa 272
†*Department of Chemistry, Faculty of Science, Tokyo Metropolitan University, Setagaya-ku, Tokyo 158*
††*Institute for Molecular Science, Myodaiji, Okazaki 444*

(Received July 28, 1980)

The infrared spectra of phosphatidyl and related compounds were studied with respect to their side-chain effects on solubility. It was clarified that the existence of a hydrogen-bonding between chloroform and a phosphate group is essential for these phosphatidyl compounds to form stable solutions in chloroform. The existence of double alkyl-chains and acyloxyl groups is clarified to be very useful for those compounds to have a strong solvent-phobic character without losing their solubility in solvents. The role of a choline moiety was also clarified. The details of the analysis of the infrared intensity were also described. It was emphasized that the intensity enhancement due to hydrogen-bond formation can be quantitatively related to the enthalpy change due to hydrogen-bond formation.

In our previous publications,[1-3] the infrared spectra of some water-soluble surfactants have been reported. On the basis of the quantitative analysis of the absorption intensity, it has been shown that molecules that dissolve in chloroform form a complex with several solvent-chloroform molecules. The bonding between a surfactant and the solvent chloroform has been shown to be of the hydrogen-bond type.

The present study concerns itself with a further study of the solubilities, in chloroform, of the molecules which have a phosphate group:

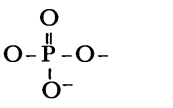

by the use of the infrared spectra and solubility data. Our special interest lies in the solubility of the phosphatidyl compounds, which have this structure:

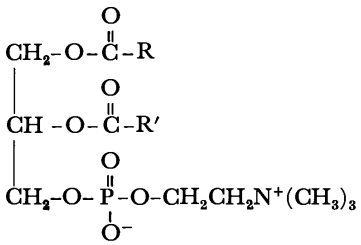

with respect to:

1) the role of a phosphate group (a polar group),
2) the role of a choline moiety (an end group),
3) the role of an acyloxyl group, and
4) the role of double alkyl chains,

to the solubilities in chloroform. We focus our attention on the infrared-absorption band of chloroform-*d*, which is related to the hydrogen bonding between chloroform-*d* and a phosphate group. If we can get quantitative knowledge about the hydrogen bonding between chloroform-*d* and a phosphate group, we can relieve the effects of the other moieties on the solubilities.

Experimental

Meterials. The chloroform-*d* was purchased from Merck and Co., Ltd., and was dried over zeorite A-3. The chloroform was purchased from Wako Pure Chemical Industries, Ltd., and was dried over zeorite A-3 after eliminating the ethanol by column chromatography on alumina. The samples used in this study were both synthesized and natural products. The purities of these samples were checked by means of thin-layer chromatography. The samples are (with the abbreviations in parentheses): (**1**) propylphosphorylcholine (C_3PC), (**2**) butylphosphorylcholine (C_4PC), (**3**) pentylphosphorylcholine (C_5PC), (**4**) heptylphosphorylcholine (C_7PC), (**5**) decylphosphorylcholine (C_{10}PC), (**6**) tetradecylphosphorylcholine (C_{14}PC), (**7**) octadecylphosphorylcholine (C_{18}PC), (**8**) *rac*-1,2-dipalmitoylglycerol-3-phosphorylcholine (DL-di-$C_{16:0}$PC), (**9**) palmitoylglycerolphosphorylcholine ($C_{16:0}$-g-PC), (**10**) 1,2-dioctadecanoylglycerol-3-phosphorylcholine (L-di-$C_{8:0}$PC), (**11**) *rac*-1,2-dilauroylglycerol-3-phosphorylcholine (DL-di-$C_{12:0}$PC), (**12**) 1,2-dilinoleoylglycerol-3-phosphorylcholine (L-di-$C_{18:2}$PC), (**13**) 1,3-dipalmitoylglycerol-2-phosphorylcholine (di-$C_{16:0}$-β-PC), (**14**) *rac*-1-palmitoylglycerol-3-phosphorylcholine (DL-$C_{16:0}$-lyso-PC), (**15**) spingomyelin from beef brain (beef brain $C_{21:0,3}$, or spm.), (**16**) phosphatidylcholine from soy beans (soybean PC, or L-di-$C_{17.5:1.4}$PC), (**17**) *rac*-1,2-dipalmitoylglycerol-3-phosphoryl-*N*,*N*-dimethylethanolamine (DL-di-$C_{16:0}$diMePE), (**18**) *rac*-1,2-dipalmitoylglycerol-3-phosphoryl-*N*-methylethanolamine (DL-di-$C_{16:0}$MePE), (**19**) phosphatidylethanolamine from pig brain (pig PE, or L-di-$C_{19.5:2.1}$PE), and (**20**) phosphatidylserine from pig brain (pig PS, or L-di-$C_{18.9:1.6}$PS).

Absorption Measurements. The absorption spectra were recorded with a JASCO IR-G grating spectrometer at a resolution of 1 cm^{-1}. The spectra of chloroform-*d* solutions containing the acceptor in the concentration range from 0 to 0.5 M were measured with a KBr cell having a thickness of about 0.1 mm. The thickness of the sample cell was checked by the interference-fringe method.

Sample solutions containing various amounts of the solute molecule were prepared in a dry-box just before measurements by weighing the solute and chloroform-*d* in the sample flask. Since all of the solutes are very hygroscopic, they were dried over P_2O_5 under a reduced pressure at 60 °C for more than two days. The elimination of water from the sample solution was confirmed by observing the infrared spectra in the region of 2000—4000 cm^{-1}.

All the measurements were done at 20±2 °C, and the absorption spectra of the C-D stretcing vibration for the frequency region of 2000—2500 cm^{-1} were measured with a resolution of 1 cm^{-1} and a scanning speed of 33.3 cm^{-1}/min. The absorption due to chloroform-*d* was eliminated, when

necessary, by the use of a variable-pathlength cell on the reference side. The thickness of the variable cell was adjusted so that the absorption band of chloroform-*d* at 2254 cm^{-1} disappeared completely.

Measurement of Physical Constants. The refractive index and the specific gravity of the solution were measured, with an Abbe refractometer and a picnometer respectively, at the same time as the absorption measurements.

The solubility was determined by a weight method. A sample was weighed in an NMR tube with a radius of 5 mm after having been dried over P_2O_5 under reduced pressure for 2 d. After dried chloroform-*d* has been added and the tube had beed sealed, the solubility was determined by weighing the sealed tube.

Results and Discussion

Infrared Spectra of Chloroform Solution. All the molecules studied in the resent work have a phosphate group and show high solubilities in chloroform. As these substances are hardly soluble at all in nonpolar solvents and only slightly soluble in non-hydrogen-bonding polar solvents, the solubilities in chloroform suggest the existence of strong hydrogen-bonding between the solute and solvent molecules. Actually, the infrared spectra of chloroform-*d* show remarkable changes in the fundamental bands of chloroform-*d*. The ν_1 vibration (the C-D stretching) changes its frequency about -20 to -50 cm^{-1} from that of pure liquid chloroform-*d*, that is, 2254 cm^{-1}. We will hereafter designate the ν_1 band occurring at 2254 cm^{-1} as an F-band.

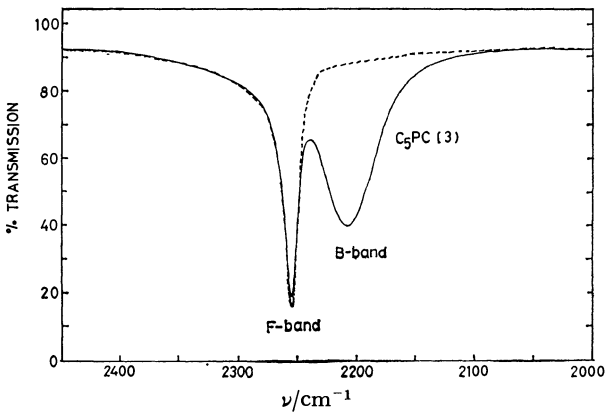

Fig. 1. Infrared spectra of C-D stretching vibration of chloroform-*d*: - - -pure liquid chloroform-*d*, ——C_5PC solution.

Figure 1 shows a typical example of the C-D stretching vibration spectra of the chloroform-*d* solution. The band at 2207 cm^{-1} is related with the chloroform-*d* molecule, which forms a hydrogen bonding with a phosphate group. We will hereafter designate this band as a B-band. For the molecules which have hydrogen-bonding sites other than a phosphate group, on the other hand, additional bands whose frequencies are higher than that of the B-band are observed. Figure 2 shows the spectra corresponding to those molecules which have an acyloxyl group in addition to a phosphate group. The reference spectra for a chloroform-*d*–methyl palmitate system is also shown in Fig. 2 in order to clarify the location of the absorption band due to the hydrogen-bond formation between chloroform and an acyloxyl group. Figure 3 shows the spectra corresponding to a group of molecules which have an acyloxyl group and a double bond in addition to a phosphate group. The spectra for a chloroform-*d* solution of methyl oleate and methyl linoleate are also shown as reference spectra in order to show the location of the additional bands which are related with the hydrogen bonding between chloroform and an acyloxyl group or between chloroform and a double bond. Figure 4 shows the spectra corresponding to a group of molecules which have a hydroxyl group in addition to phosphate and acyloxyl groups and a double bond. The spectrum for a chloroform-*d* solution of 1-pentanol is also included

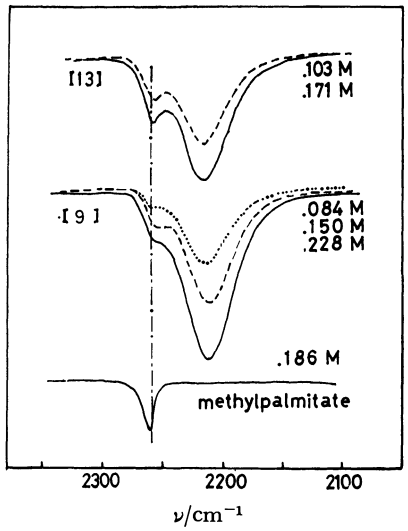

Fig. 2. Infrared spectra of C-D stretching vibration of chlrorform-*d* (solutions of these molecules having an acyloxyl group, (**9**) and (**13**)).

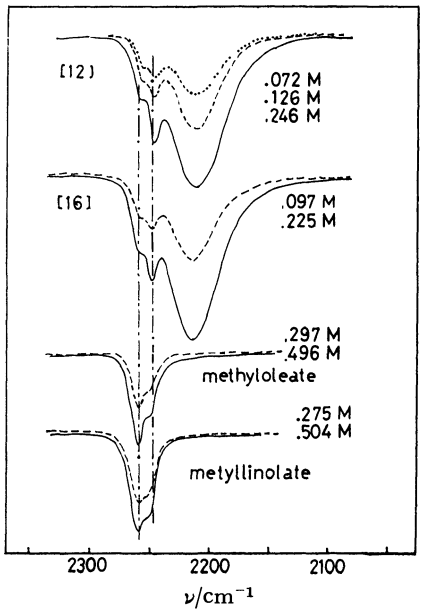

Fig. 3. Infrared spectra of C-D stretching vibration of chloroform-*d* (solutions of these molecules having a double bond and an acyloxyl group, (**12**) and (**16**)).

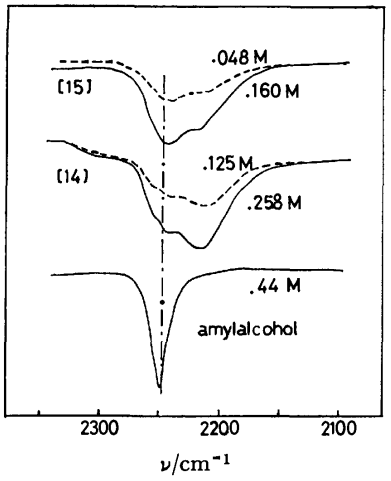

Fig. 4. Infrared spectra of C-D stretching vibration of chloroform-*d* (solutions of these molecules having a double bond, an acyloxyl group, and a hydroxyl group).

Table 1. Spectroscopic information on B-bands andsolubilities

Substance	$\nu^\circ-\nu$ / cm^{-1}	$\Delta\nu_{1/2}$ / cm^{-1}	Solubility(20 °C) / mol l^{-1}
(1) C_3PC	47—47.5	45	0.06*[a]
(2) C_4PC	47	45	0.15*[a]
(3) C_5PC	47	45	2.0
(4) C_7PC	46.5	45	1.6
(5) C_{10}PC	46	45	1.5
(6) C_{14}PC	46	44.5	1.2
(7) C_{18}PC	45.5	44—45	0.9
(8) DL-Di-$C_{16:0}$PC	39.5	42	0.7
(9) $C_{16:0}$-g-PC	43	42.5	1.0
(10) L-Di-$C_{8:0}$PC	42	45	1.0
(11) DL-Di-$C_{12:0}$PC	41.5	41.5	0.9
(12) L-Di-$C_{18:2}$PC	42.5	45	0.8
(13) Di-$C_{16:0}$-β-PC	39.5	42	0.6
(14) DL-$C_{16:0}$lyso-PC	39	48	0.4
(15) Beef brain $C_{21:0,3}$(spm)	37—40	≈45	0.15
(16) L-Di-$C_{17.5.11.4}$PC	42.5	41	>0.6
(17) DL-Di-$C_{16:0}$diMePE	30	42.5	0.21
(18) DL-Di-$C_{16:0}$MePE	23	40	0.20
(19) Pig PE	≈20	30	>0.16
(20) Pig PS	≈10	Not observed	>0.16

a) * Phase separation (see the text).

in Fig. 4 as a reference. Attention must be paid for the fact that, in the spectra of Figs. 2—4, the F-bands are completely cancelled out when pure liquid chloroform-*d* is put in the reference side of the spectrometer.

The half-band width, $\Delta\nu_{1/2}$, and the frequency shift, $\nu^\circ-\nu$, for a B-band are listed in Table 1, where ν° is the maximum absorption frequency of the F-band. For the sake of simplicity, we do not describe in detail the spectral information for any of these hydrogen-bonding bands other than the B-bands.

Determination of Absolute Intensities. In order to determine the absolute intensities, the absorption spectra for F- and B-bands of chloroform-*d* solutions containing various amounts of the solute molecule were measured in each system. We will here begin by considering the spectra which are composed of one F-band and one B-band only, that is, the spectra for those molecules which have only one phosphate group.

The relative intensities of the F- and B-bands are defined as

$$I_f = \frac{1}{l}\int_{\text{band (F)}} \ln(I_0/I)\mathrm{d}(\ln\nu) \qquad (1)$$

and

$$I_b = \frac{1}{l}\int_{\text{band (B)}} \ln(I_0/I)\mathrm{d}(\ln\nu)$$

where the subscripts b and f refer to the bonded and free states (or to the B- and F-bands) respectively. The integration covers the entire band area.

The molar concentration of chloroform-*d* in the solution

$$C_{CDCl_3} = C_f + C_b \qquad (2)$$

was determined from the observed weight concentration and the density of the solution. After being corrected for the local-field effect,[4] the relative intensities, I_f and I_b, are reduced to the values at the molar concentration of pure liquid chloroform-*d*, $C^\circ_{CDCl_3}=12.30$ M, thus:

$$I_f^* = f_d f_c I_f$$
$$I_b^* = f_d f_c I_b \qquad (3)$$

and

$$f_c = 12.30/C_{CDCl_3}$$
$$f_d = 9n_D/(n_D^2+2)^2, \qquad (4)$$

where n_D is the refractive index of the solution.

Now the absolute intensities, Γ_f and Γ_b, are defined as:

$$C_b^*\Gamma_b = I_b^*$$
$$C_f^*\Gamma_f = I_f^* \qquad (5)$$

and

$$(C_f^*+C_b^*) = f_c(C_f+C_b) = C^\circ_{CDCl_3}. \qquad (6)$$

Equations 5 and 6 give the relation:

$$\frac{I_f^*}{\Gamma_f} + \frac{I_b^*}{\Gamma_b} = C^\circ_{CDCl_3} \qquad (7)$$

or

$$I_b^* = -(\Gamma_b/\Gamma_f)I_f^* + \Gamma_b C^\circ_{CDCl_3}.$$

By plotting I_b^* against I_f^* at a series of concentrations, a straight line with a slope of $-(\Gamma_f/\Gamma_b)$ is generated as long as the absolute intensities, Γ_f and Γ_b, are constant over the concentration range employed. The extrapolated I_f^* value at $I_b^*=0$ corresponds to the Γ_f value for pure liquid chloroform-*d*, and may be compared with the Γ_f^* value directly observed for pure liquid chloroform-*d*.

The above procedure can be expanded for the case where a solute molecule has many hydrogen-bonding sites. If we focus our attention especially on the B-band, *i. e.*, the hydrogen-bonded absorption band which is related with a phosphate group, Eqs. 6 and 7 are modified to:

$$C_f^* + C_b^* + \sum_n \frac{I_{bn}^*}{\Gamma_{bn}} = C^\circ_{CDCl_3} \qquad (8)$$

or

$$\frac{I_f^*}{\Gamma_f} + \frac{I_b^*}{\Gamma_b} + \sum_n \frac{I_{bn}^*}{\Gamma_{bn}} = C^\circ_{CDCl_3}, \qquad (9)$$

where the subscript bn refers to the bonded states which are related with these sites other than a phosphate group. If we assume a complete association of the

(1 : 1) type for the hydrogen-bonding between chloroform and these sites,[5] the third term on the left-hand side of Eq. 8 or 9 can be expressed as:

$$\sum_n C^*_{bn} = nC_s f_c, \tag{10}$$

where n is the number of hydrogen-bonding sites other than a phosphate group, and C_s, the concentration of the solute. Thus, Eq. 9 is reduced to:

$$\frac{I^*_f}{\Gamma_f} + \frac{I^*_b}{\Gamma_b} = C^\circ_{CDCl_3} - nC_s f_c = C^\circ_{CDCl_3}\left(\frac{C_{CDCl_3} - nC_s}{C_{CDCl_3}}\right). \tag{11}$$

Eq. 11 indicates that this relation holds:

$$\frac{I^{**}_f}{\Gamma_f} + \frac{I^{**}_b}{\Gamma_b} = C^\circ_{CDCl_3} \tag{12}$$

if we define I^{**}_f and I^{**}_b as:

$$I^{**}_f = f'_c I^*_f = f'_c f_c f_d I_f$$
$$I^{**}_b = f'_c I^*_b = f'_c f_c f_d I_b \tag{13}$$

and:

$$f'_c = \frac{C_{CDCl_3}}{C_{CDCl_3} - nC_s}. \tag{14}$$

In Fig. 5, the plots of I^*_b *vs.* I^*_f (or I^{**}_b *vs.* I^{**}_f) for C_5PC (or $C_{16:0}$-g-PC) are shown. It can be seen from the figures that a linear relationship exists between I^*_b and I^*_f (or I^{**}_b and I^{**}_f). Consequently, the validity of Lambert-Beer's law was verified in these concentration ranges. It can also be seen from the figures that the extrapolated I^*_f (or I^{**}_f) values at $I^*_b=0$ (or $I^{**}_b=0$) are almost the same for these systems. For the chloroform-*d*–C_3PC system, for example, Γ_f and Γ_b were 106 and 2268 cm²/mol respectively. The absolute intensities observed by this method are summarized in Table 2. The values of Γ_f are fairly identical for all the systems. It must be added here that the beautiful linear relationship between I^{**}_b and I^{**}_f of Fig. 5b (for $C_{16:0}$-g-PC) confirms the validity of the assumption used in the derivation of

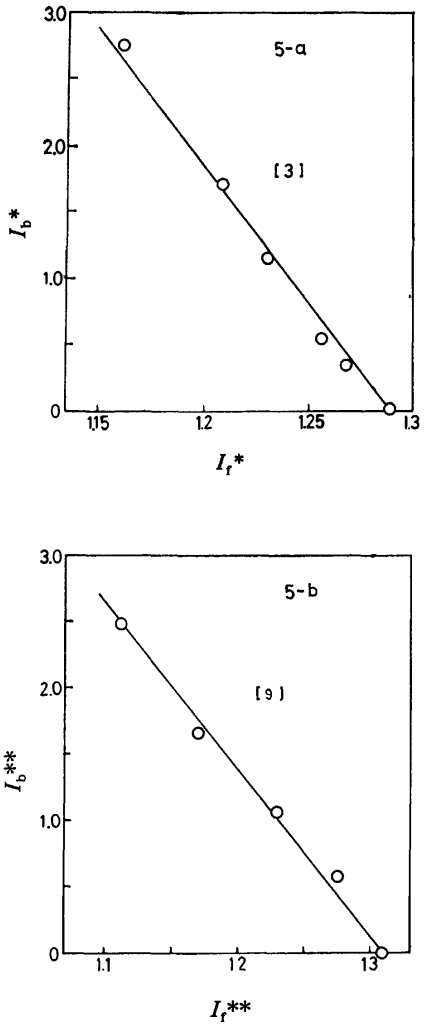

Fig. 5. (a) I_b^* *vs.* I_f^* plot for the chloroform-*d*–C_5PC system. (b) I_b^{**} *vs.* I_f^{**} plot for the chloroform-*d*–(**9**) system.

TABLE 2. CALCULATED PARAMETERS AND ABSOLUTE INTENSITIES

	Γ_f/cm² mol⁻¹	Γ_b/cm² mol⁻¹	n_s	$\sqrt{\Gamma_b} - \sqrt{\Gamma_f}$	E_s
(**1**) C_3PC	106	2268	2.8—3.1	37.3	110
(**2**) C_4PC	106	2226	3.1—3.3	36.9	118
(**3**) C_5PC	105	2205	2.7—3.4	36.7	112
(**4**) C_7PC	105	2006	3.0—3.4	34.5	110
(**5**) C_{10}PC	108	1944	3.0—3.6	33.4	111
(**6**) C_{14}PC	106	1688	3.7—4.0	30.8	118
(**7**) C_{18}PC	104	1460	3.6—4.2	29.3	109
(**8**) DL-Di-$C_{16:0}$PC	107	920	5.8—6.7	20.0	125
(**9**) $C_{16:0}$-g-PC	107	1305	4.8—5.1	25.8	127
(**10**) L-Di-$C_{8:0}$PC	105	1050	5.8—6.3	22.2	134
(**11**) DL-Di-$C_{12:0}$PC	105	1008	6.4—6.6	21.5	139
(**12**) L-Di-$C_{18:2}$PC	106	977	6.1—6.7	21.0	134
(**13**) Di-$C_{16:0}$-β-CP	105	966	6.0—6.2	20.8	127
(**14**) DL-$C_{16:0}$lyso-PC	105	861	3.8—4.2	19.1	76
(**15**) Beef brain $C_{21:0,3}$(spm)	107	578	7.4—7.8	13.7	104
(**16**) L-Di-$C_{17,5:1,4}$PC	107	984	6.1—6.6	21.0	133
(**17**) DL-Di-$C_{16:0}$diMePE	106	837	6.5—7.1	18.6	126
(**18**) DL-Di-$C_{16:0}$MePE	106	742	5.1—5.8	17.0	92
(**19**) Pig PE	105	420	1.5	10.3	15
(**20**) Pig PS	106	350	1.5	8.4	13

Eq. 10.

Determination of the Solvation Number for a Phosphate Group. At a low concentration of the proton acceptor, the phosphate groups of all the acceptor molecules are considered to be bonding to chloroform-*d* molecules.[6] Therefore, the ratio of the concentration, C_b, of the bonded chloroform-*d* to the concentration, C_s, of the solute, C_b/C_s, corresponds to the number of the chloroform-*d* molecule attached to one phosphate group. Using the observed Γ_b value, C_b is determined as:

$$C_b = f_d I_b/\Gamma_b. \quad (15)$$

As C_s is known, the C_b/C_s ratio can easily be determined. We call this ratio the solvation number, n_s, for a phosphate group. The calculated results for n_s are summarized in Table 2. As an example, the detailed data for the C_3PC system are shown in Table 3. The solvation number obtained in this case is 2.8—3.1 (see n_s of Table 2). Therefore, it is concluded that about three chloroform-*d* molecules and one C_3PC (or one phosphate group in C_3PC) form a complex molecule in solution.

Table 3. Relative intensities of the C-D stretching vibrations of the chloroform-*d*–C_3PC system (n_D is the refractive index, and *d* is the specific gravity of this solution)

Sample No.	Wt% of C_3PC	n_D	*d*	I_f^*	I_b^*
1	0	1.4470	1.48	1.300	0
2	0.337	1.4476	1.478	1.293	0.142
3	0.504	1.4474	1.476	1.287	0.215
4	0.676	1.4475	1.475	1.282	0.274
5	0.808	1.4476	1.474	1.284	0.340
6	0.990	1.4477	1.473	1.281	0.392

Spectroscopic Informations and Solubility Parameter. It has been established that there exists a considerable correlation between the frequency shift, $\nu^\circ-\nu$, and the intensity enhancement, Γ_b/Γ_f, due to hydrogen-bond formation, so long as the type of hydrogen-bonding is not very different.[7] We prefer, for the reason described in the Appendix, a $(\sqrt{\Gamma_b}-\sqrt{\Gamma_f})$ value as an appropriate intensity enhancement parameter to a (Γ_b/Γ_f) value. In Fig. 6, the observed $(\sqrt{\Gamma_b}-\sqrt{\Gamma_f})$ values are plotted against the $(\nu^\circ-\nu)$ values. Obviously, the observed data points fall on two different lines, indicating that the (**1**)—(**16**) group is related with a similar type of hydrogen bonding. Actually, the (**1**)—(**16**) molecules all have a choline moiety, while the (**17**)—(**20**) molecules have either a 2-(dimethylamino)ethanol, 2-(methylamino)ethanol, a 2-aminoethanol, or a serine moiety instead. Thus, the nature of the hydrogen bonding between chloroform-*d* and a phosphate group is dependent on the number of methyl groups attached to an amino group. The (**18**), (**17**), and (**8**) molecules are typical examples of those molecules having mono-, di-, and trimethylamino groups respectively.

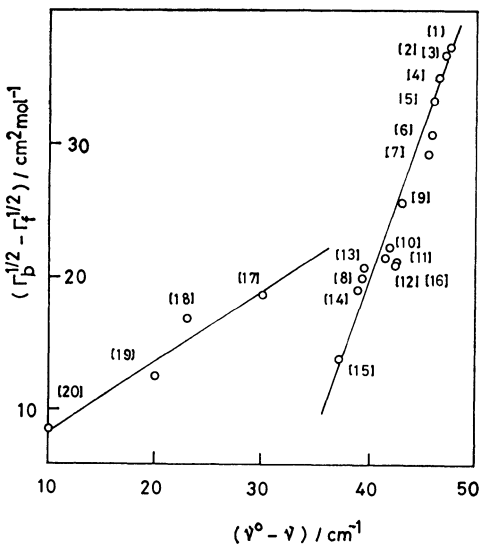

Fig. 6. $(\Gamma_b-\Gamma_f)$ *vs.* $(\nu^\circ-\nu)$ plot for the chloroform-*d* solutions of the molecules (**1**)—(**20**).

Table 2 shows the absolute intensities and the solvation numbers observed for various acceptor molecules. It may be seen from Table 2 that several solvent molecules attach to a phosphate group by forming a strong hydrogen bond. For a series of alkyl phosphorylcholines ((**1**)—(**7**)), for example, the absolute intensity of the B-band, Γ_b, is largest for C_3PC. As the intensity enhancement originates from the hydrogen-bond formation, the intensity difference, $(\sqrt{\Gamma_b}-\sqrt{\Gamma_f})$, can represent the strength of the hydrogen bonding between chloroform-*d* and a phosphate group. Therefore, the product:

$$E_s = \bar{n}_s \cdot (\sqrt{\Gamma_b} - \sqrt{\Gamma_f}), \quad (16)$$

where $\bar{n}_s$ is a mean solvation number, is an appropriate estimate of the stabilization energy of one acceptor molecule through hydrogen-bond formation with a chloroform-*d* molecule in solution. We call this product, E_s, a spectroscopic solubility parameter.

The last column of Table 2 shows the calculated E_s values. The results indicate that the E_s value takes almost identical values for those molecules which have this group:

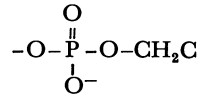

Hereafter, we will designate this group (PC) and call it the PC-group. For all the molecules which have a PC-group, the stabilization energies due to the hydrogen bonding between chloroform-*d* and a phosphate group are almost the same. In case a weak hydrogen bond is formed (*i. e.*, a small Γ_b), a larger number of solvent molecules are attached to a phosphate group. In case a strong hydrogen bond is formed, on the other hand, only a few solvent molecules are attached to a phosphate group. As is shown in the Appendix, $E_s=100$ is equivalent to an enthalpy change of about 2.5 kcal/mol. Therefore, the existence of a phosphate group is essential for these molecules to give a solubility in chloroform.

Side-chain Effects on Solubilities. By comparing the solubility values given in Table 1 and the E_s values of Table 2, a few important conclusions can be drawn as to the effects of the side chains and the molecular

structure on the solubilities.

First, let us compare the solubility data for the (**8**), (**17**), (**18**), (**19**), and (**20**) molecules, whose molecular structures are:

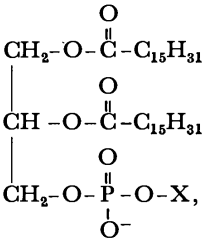

where X is:

(**8**) $-(CH_2)_2N^+(CH_3)_3$ (2-(trimethylammonio)ethyl),

(**17**) $-(CH_2)_2N^+H(CH_3)_2$ (2-(dimethylammonio)ethyl),

(**18**) $-(CH_2)_2N^+H_2(CH_3)$ (2-(methylammonio)ethyl),

(**19**) $-(CH_2)_2N^+H_3$ (2-ammonioethyl),

or (**20**) $-(CH_2)-CH(COO^-)-N^+H_3$ (serine).

As has been described in the preceding paragraph, the stregth and the nature of the hydrogen bonding between chloroform and a phosphate group are quite different for these molecules (see Fig. 6). The observed solubility decreases in magnitude in this order;

$$(8) > (17) > (18) > (19),\ (20).$$

The spectroscopic information shows that both the solvation number and the strength of the hydrogen bonding between chloroform and a phosphate group decrease in this order, resulting in a rapid decrease in the spectroscopic solubility parameter. This rapid decrease in the E_s value may arise from the intramolecular hydrogen-bond formation between a N–H group and a phosphate group.[8] If the hydrogen atoms of the NH_3 group are replaced by methyl radicals, this type of hydrogen-bond cannot be formed (see the structures of (**19**) and (**20**)). It must be added that the slight solubility of the (**19**) and (**20**) molecules arises from the existence of the unsaturated bonds. The corresponding synthesized sample (*rac*-1,2-dipalmitoylglycerol-3-phosphorylethanolamine or *rac*-1,2-dipalmitoylglycerol-3-phosphorylethanolserine) is insoluble in chloroform, so the spectroscopic study could not be performed. Anyway, the end group, X, must be a 2-(trimethylammonio)ethyl group in order to show a high solubility in chloroform. The (**8**) molecule will be used as the reference sample in the following discussion.

Secondly, let us compare the (**1**)—(**7**) molecules, whose molecular structures are:

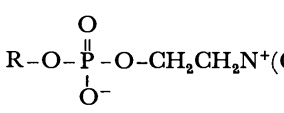

where R is an alkyl chain. The solubility decreases with the increase in chain-length ((**3**)—(**7**)). Although the strength of hydrogen bonding between chloroform and a phosphate group decreases with the increase in the chain length, the solvation number increases at the same time, thus keeping the spectroscopic solubility parameter almost constant for all the molecules. Therefore, the gradual increase in solubility with the increase in the chain-length may be ascribed to the solvent-phobic character of the alkyl chains. In fact, the solubilities of *n*-$C_{20}H_{41}$PC and *n*-$C_{22}H_{45}$PC are observed to be about 0.002 mol/l at room temperature. The abnormal solubility values for the (**1**) and (**2**) molecules will be referred to in a later paragraph in view of the mixing state of these alkylphosphorylcholines and chloroform.

Thirdly, let us compare the (**8**) and (**9**) molecules, whose molecular structures are:

(**8**)

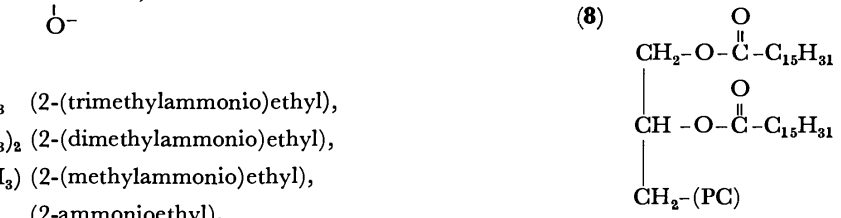

and (**9**)

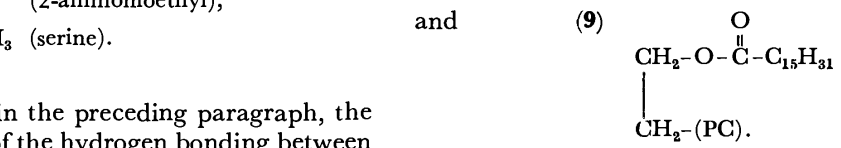

On passing from a single alkyl-chain to double chains, the solubility decreases from 1.0 to 0.7 mol/l. This change is not so much as is expected for a long-chain alkylphosphorylcholine, probably because the effect of the alkyl chains is compensated for by the stabilization energy due to hydrogen bonding between the chloroform and an acyloxyl group. Again, the solubility parameters, E_s, are almost the same for these two molecules. An acyloxyl group plays a role in the solubility in chloroform second in importance only to a phosphate group.

Fourthly, let us compare the (**10**), (**11**), and (**12**) molecules with the (**8**) molecule. The molecular structures of these molecules are;

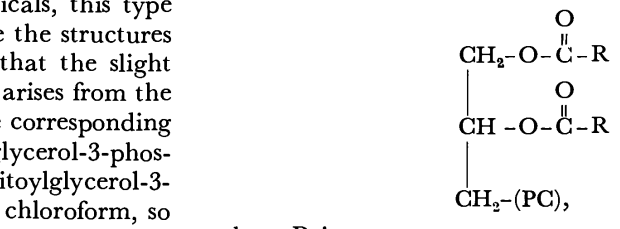

where R is:

(**8**) $-C_{15}H_{31}$,

(**10**) $-C_7H_5$,

(**11**) $-C_{11}H_{23}$,

or: (**12**) $-(CH_2)_3-(CH_2-CH=CH)_2-(CH_2)_7CH_3$.

The solubilities of these molecules do not change so much with the change in the alkyl chain length as is seen for a series of alkylphosphorylcholines. Here again, the solubility-parameter values are almost constant. It must be emphasized that these molecules are distinguished from the long-chain alkylphosphorylcholines by having two long chains. That is to say, this type of molecule can have long alkyl chains without losing their solubilities in chloroform. The existence of the long alkyl chains might increase the solvent-phobic character of these molecules. The variety of alkyl chains might produce the variety of the characters of

these molecules in solutions.

Lastly, let us compare the (**13**), (**14**), and (**15**) molecules with the (**8**) molecule. The structures of these molecules are:

(**8**)

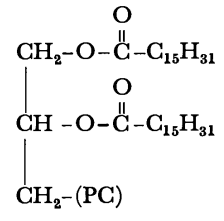

(**13**)

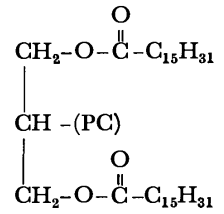

(**14**)

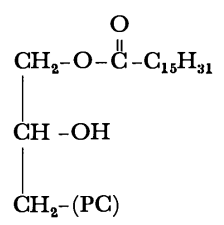

and

(**15**)

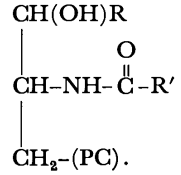

The (**14**) and (**15**) molecules are specified as having a hydroxyl group and/or an imino group. In these molecules, the hydrogen-bonding sites are expected to be deactivated because of the intramolecular hydrogen-bond formation between a phosphate group and the hydroxyl or imino group. If the intramolecular hydrogen-bond is formed, the solvation number, n_s, can be expected to decrease. In fact, the observed solvation number is quite small for the (**14**) molecule in comparison with the (**8**) molecule. Probably, the phosphate group and hydroxyl group from an intramolecular hydrogen bond. This situation is reflected in the low solubility value observed for the (**14**) molecule. In the case of the (**15**) molecule, on the other hand, the n_s value is observed to be slightly larger than that of the (**8**) molecule. This suggests that the intramolecular hydrogen bond is not formed in this molecule. As the strength of the hydrogen bonding between a phosphate group and solvent molecules is relatively small (see the $(\sqrt{\Gamma_b}-\sqrt{\Gamma_f})$ value), the resultant E_s value is relatively small, although the solvation number is relatively large. This situation might be responsible for the observed low solubility value.

The (**13**) molecule is an isomer of the (**8**) molecule. As can naturally be expected, the spectroscopic and physical parameters are quite similar in these two molecules, because the polar group and the side-chain groups are essentially the same. The positional difference of a PC-group does not change the solubility and the spectroscopic solubility parameter very much.

Mixing States of Alkylphosphorylcholines. In the preceding, we have left C_3PC and C_4PC out of our discussion in considering the effects of the alkyl chains on the solubilities for a series of alkylphosphorylcholines, although C_3PC and C_4PC have very low solubilities in chloroform (see Table 1). The (**3**)—(**7**) molecules dissolve into chloroform homogeneously so long as the solute concentration is lower than the solubilities. In the cases of C_3PC and C_4PC, however, their chloroform solutions separate into two solution phases if the solute concentrations exceed the solubility values of Table 1. The upper layers are relatively solute-rich solutions, while the lower layers are chloroform-rich solutions.

The concentration of the lower layers are 0.06 and 0.15 mol/l for C_3PC and C_4PC respectively. The spectroscopic information in Tables 1 and 2 was obtained for these lower layers, because the upper layers were so viscous and seemed unstable.

Taking the observed Γ_b and n_s values into account, we may explain those phenomena as follows. The C_3PC (or C_4PC) molecule forms a very stable complex molecule which is composed of one C_3PC (or C_4PC) and three chloroform molecules. The hydrogen bonding between chloroform molecules and a phosphate group is so strong that the complex molecule is precipitated as it is when the solute concentration exceeds 0.06 (or 0.15) mol/l. The sudden increase in solubility on passing from C_4PC to C_5PC may, therefore, suggest some kind of aggregate formation in the chloroform solutions of the (**3**)—(**7**) molecules. This aggregate formation may not correspond to micelle formation in the usual sense, because the critical solution temperature (CST) could not be observed for these solutions. Perhaps this aggregate has a structure analogous to that which has been clarified to be composed of a few solute molecules doubly solvated by chloroform molecules.[9] It must be emphasized that CST was observed for the alkylphosphorylcholines with longer chains, like *n*-$C_{20}H_{41}PC$ or *n*-$C_{22}H_{45}PC$ at about 40 °C. The mixing states of alkylphosphorylcholines, especially those of short alkyl chains, suggest ideas for future work into the problem.

Concluding Discussion. The main conclusions drawn from the above discussion are:

1) The hydrogen-bonding between chloroform and a phosphate group is the main factor in determining the solubility. The stabilization energy due to this type of hydrogen bonding is almost the same for all the molecules studied. When a weak hydrogen-bond is formed, a large number of solvent molecules are attached to the phosphate group, and *vice versa*. This situation may be helpful for the stabilization of those solutions in which the number of solvated molecules changes from time to time.

2) The hydrogen bonding between chloroform and an acyloxyl group may contribute to the stabilization of a long-chain molecule in a chloroform solution. With the help of the acyloxyl group, these molecules can exhibit various solvent-phobic characters when the long alkyl chains are changed without losing their solubility

in the solvent.

3) The existence of the double chains is also helpful in enabling these molecules to have a strong solvent-phobicity without losing their solubility.

4) The existence of any groups which can form intramolecular hydrogen bonding with a phosphate group can lower the solubilities of these solute molecules. A hydroxyl group is a good example of this.

Appendix. Derivation of Intensity Enhancement Parameter.

We will describe the relation between the intensity-enhancement parameter, $(\sqrt{\Gamma_b}-\sqrt{\Gamma_f})$, and the excess enthalpy, $-\Delta H$, originating from hydrogen-bond formation.

Tsubomura[10] proposes that, in a hydrogen-bonded system like

$$\text{A}\text{——}\text{H}\cdots\text{B},$$

where A and B refer, respectively, to an acid and a base, the intensity change of the A–H stretching vibration is to be attributed to charge-transfer forms in the wave function. It is assumed that the wave function of the ground state of the complex may be expressed by this formula:

$$\Psi = c_1\Psi_1 + c_2\Psi_2, \tag{A1}$$

where c_1 and c_2 are constants normalized to unity, $c_1^2+c_2^2=1$, and Ψ_1 and Ψ_2 are the wave functions associated with the following resonance structure:

Structure 1: A——H B covalent A–H bond

Structure 2: A^- H——B^+ covalent H–B bond. (with charge transfer)

Therefore, the dipole moment, p, of the hydrogen-bonded system is:

$$p = \langle\Psi|p|\Psi\rangle \simeq p_1 + c_2^2 p_2, \tag{A2}$$

where p_1 and p_2 refer to the dipole moments corresponding to Structures 1 and 2 respectively. The derivative of p with respect to the normal coordinate, Q, which corresponds to the A–H stretching vibration, is:

$$\left(\frac{\partial p}{\partial Q}\right) = \left(\frac{\partial p_1}{\partial Q}\right) + 2c_2 p_2\left(\frac{\partial c_2}{\partial Q}\right) \tag{A3}$$

with these definition of the absolute intensities, Γ_f and Γ_b, of the A–H stretching vibration:

$$\Gamma_f = \left(\frac{N_0\pi}{3c^2\omega}\right)\left(\frac{\partial p_1}{\partial Q}\right)^2,$$

$$\Gamma_b = \left(\frac{N_0\pi}{3c^2\omega}\right)\left(\frac{\partial p_2}{\partial Q}\right)^2. \tag{A4}$$

Eq. A3 is reduced to:

$$\sqrt{\Gamma_b} - \sqrt{\Gamma_f} = \sqrt{\frac{N_0\pi}{3c^2\omega}}\,2c_2 p_2\left(\frac{\partial c_2}{\partial Q}\right). \tag{A5}$$

Based upon the same model and the same order of approximation, the stabilization energy due to hydrogen-bond formation is calculated to be:[11]

$$-\Delta H = c_2 W_{12} - \Delta H_0, \tag{A6}$$

where W_{12} is a resonance energy term, $\langle\Phi_1|\tilde{H}|\Phi_2\rangle$ ($\tilde{H}$ being a Hamilton operator), and $-\Delta H_0$ is a stabilization energy due to an interaction other than hydrogen bonding. If $-\Delta H_0$ is ralatively small, as is usually the case for ordinaty intermolecular interactions, Eq. A6 becomes:

$$-\Delta H = c_2 W_{12} \tag{A7}$$

combination of Eqs. A5 and A7 leads to this relation:

$$\sqrt{\Gamma_b} - \sqrt{\Gamma_f} = -\left(\frac{2N_0\pi}{3c^2\omega}\right)^{1/2}\frac{p_2}{W_{12}}\left(\frac{\partial c_2}{\partial Q}\right)\Delta H, \tag{A8}$$

where N_0 is the Avogadro constant; c, the velocity of light, and ω the frequency of light.

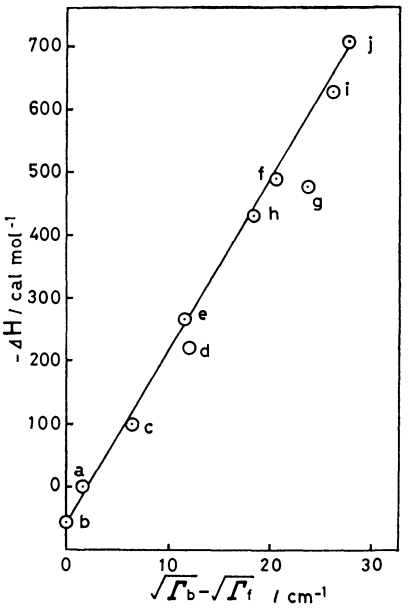

Fig. A1. $-\Delta H$ *vs.* $(\sqrt{\Gamma_b}-\sqrt{\Gamma_f})$ plot for the chloroform-*d* solutions of: (a) chloroform-*d*, (b) carbon tetrachloride, (c) benzene, (d) *p*-xylene, (e) 1,2,4-trichlorobenzene, (f) ethyl acetate, (g) acetone, (h) dibutyl ether, (i) diethyl ether, (j) diisopropyl ether.

In Fig. A1, the observed excess enthalpy values for chloroform solutions of various acceptors are plotted against the observed intensity difference values, $\sqrt{\Gamma_b}-\sqrt{\Gamma_f}$. Attention should be paid to the fact that the absolute intensity of the C–D stretching vibration of a carbon tetrachloride solution was chosen as Γ_f in this case. Obviously, a fine linear relation holds between the $-\Delta H$ and $(\sqrt{\Gamma_b}-\sqrt{\Gamma_f})$ values. Thus, we can safely conclude that the coefficient of the right-hand side of Eq. A8 is almost constant for a hydrogen bonding of a similar type. Conversely, it is very desirable to use the $(\sqrt{\Gamma_b}-\sqrt{\Gamma_f})$ value as a good estimate of the stabilization energy due to hydrogen-bond formation.

Incidentally, the E_s value defined by Eq. 16 can be converted into the excess enthalpy value. It may be seen from Fig. A1 that $E_s=100/\text{cm}^{-1}$ is equivalent to $-\Delta H=2.5$ kcal/mol.

References

1) M. Okazaki, I. Hara, and T. Fujiyama, *J. Phys. Chem.*, **80**, 64 (1976).

2) M. Okazaki, I. Hara, and T. Fujiyama, *J. Phys. Chem.*, **80**, 1586 (1976).

3) M. Okazaki, I. Hara, and T. Fujiyama, *Chem. Phys. Lipids*, **17**, 28 (1976).

4) S. R. Polo and M. K. Wilson, *J. Chem. Phys.*, **23**, 2376 (1955).

5) Actually the complete association may not be realized in solution studies. The errors due to this assumption, however, do not spoil the conclusions drawn in this report.

6) It is ascertained that the C-D stretching band corresponding to the free state completely disappears at saturation.
7) See for example, G. C. Pimentel and A. L. McClellan, "The Hydrogen Bond," W. H. Freemen and Company, New York (1960).
8) T. O. Henderson, T. Glonek, and T. C. Myers, *Biochemistry*, **13**, 623 (1974).
9) T. Kato and T. Fujiyama, *Bull. Chem. Soc. Jpn.*, **51**, 1328 (1978).
10) H. Tsubomura, *J. Chem. Phys.*, **24**, 927 (1956).
11) H. Ratajczak and W. J. Orville-Thomas, *J. Chem. Phys.*, **58**, 911 (1973).

The Crystal Structure of the Charge-transfer Complex of Dibenzotetrathiafulvalene-Tetracyanoquinodimethane, DBTTF-TCNQ

Hayao KOBAYASHI* and Jyuzo NAKAYAMA†

Department of Chemistry, Faculty of Science, Toho University, Funabashi, Chiba 274

† *Department of Chemistry, Faculty of Science and Engineering, Saitama University, Urawa, Saitama 333*

(Received September 29, 1980)

The crystal of the charge-transfer complex of dibenzotetrathiafulvalene-7,7,8,8-tetracyanoquinodimethane, DBTTF-TCNQ, belongs to the triclinic system; $a=10.309(8)$, $b=8.281(2)$, $c=7.727(3)$ Å, $\alpha=110.03(4)$, $\beta=109.80(4)$, $\gamma=72.05(3)°$, space group $P\bar{1}$ with $Z=1$. The structure has been determined by the X-ray method. DBTTF and TCNQ stack alternately along [011] to form mixed columns; this phenomenon is responsible for the low electrical conductivity of DBTTF-TCNQ. The intermolecular distance between DBTTF and TCNQ is 3.303 Å. The charge-transfer complexes of DBTTF with TNB, TCNE, DDQ, and fluoro-TCNQ were examined by means of X-ray photographs. It is shown that the DDQ complex, exhibiting a high conductivity, has segregated uniform columns of donors and acceptors, such as were not found in the other complexes.

Since the discovery of the metallic conductivity of the organic compound, TTF-TCNQ (tetrathiafulvalene-tetracyanoquinodimethane), by Ferrais, Cowan, Walatka, and Perlstein, and by Coleman, Cohen, Sandman, Yamagishi, Garito, and Heeger in 1973,[1] many high-conducting organic materials have been reported. Recently, Jerome, Mazaud, Ribault, and Bechgaard have discovered an organic superconductor.[2]

High conductivity is associated with a crystal structure in which the planar donor and/or acceptor molecules are stacked to form columns.[3] Unlike TTF-TCNQ, however, DBTTF-TCNQ is insulating ($\sigma_{R.T.}\approx10^{-6}$ $(\Omega\,cm)^{-1}$ [4]). This paper will report the crystal and molecular structure of DBTTF-TCNQ and the molecular arrangements in the crystals of several DBTTF complexes.

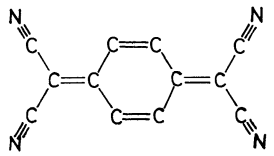

TCNQ

7,7,8,8-Tetracyanoquinodimethane [2,2′-(2,5-Cyclohexadiene-1,4-diylidene)bis(propanedinitrile)]

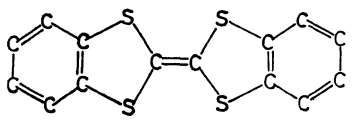

DBTTF

Dibenzotetrathiafulvalene [2-(1,3-Benzodithiol-2-ylidene)-1,3-benzodithiole]

Experimental

Black lath-like crystals of DBTTF-TCNQ were prepared by a diffusion method, acetonitrile solutions of the two compounds being used. The lattice constants as determined by a Rigaku automated four-circle diffractometer are listed in Table 1. The crystals belongs to the triclinic system. The intensity data were collected with monochromated Mo K_α radiation by the ω-2θ scan technique up to $2\theta=60°$. The reflections were scanned at the rate of 4° min^{-1} in 2θ. Three standard reflections were measured after every 50 reflections. No significant intensity variation was observed during the course of the experiment. The crystal used had approximate dimensions of $0.3\times0.3\times0.06$ mm. No corrections for absorption and extinction were made.

Table 1. Crystal data of DBTTF-TCNQ

Formula	$(C_{14}H_8S_4)(C_{12}H_4N_4)$	$F.W.=508.7$
Monoclinic	Space group $P\bar{1}$	
$a=10.309(8)$ Å	$b=8.281(2)$ Å	$c=7.727(3)$ Å
$\alpha=110.03(4)°$	$\beta=109.80(4)°$	$\gamma=72.05(3)°$
$V=573.7$ Å^3		
$D_c=1.474$ g cm^{-3}	$D_m=1.473$ g cm^{-3} (flotation method)	
$Z=1$	μ(Mo $K\alpha$)$=4.273$ cm^{-1}	

Solution and Refinement of the Structure. The structure was solved by the heavy-atom method. Patterson maps were computed on the basis of 1415 independent reflections of $|F_o|\geqq3\sigma$. A refinement of the structure was performed by the block-diagonal, least-squares method. Anisotropic temperature factors were used for non-hydrogen atoms, whiel isotropic ones were used for the hydrogen atoms found by the difference Fourier synthesis. The final R value was 0.089. The weighting scheme used was: $\omega=1/[a+b|F_o|+c|F_o|^2]$ for $|F_o|\geqq6.19$ (absolute scale), $a=12.37$, $b=1.0$, $c=0.015$; $\omega=0.1$ otherwise. The atomic scattering factors were taken from

Table 2. Final atomic parameters

(Values for fractional coordinates are multiplied by 10^4.)

Atom	x	y	z	B_{eq}/Å^2 a)
S(1)	1684 (3)	1415 (4)	924 (4)	8.9
S(2)	619 (3)	−118 (3)	2963 (3)	12.5
N(1)	2429 (12)	5386 (15)	1430 (14)	19.0
N(2)	4011 (11)	7356 (16)	8200 (15)	18.7
C(1)	517 (11)	265 (13)	809 (13)	11.7
C(2)	2600 (9)	1500 (12)	3309 (13)	9.8
C(3)	2090 (11)	797 (13)	4280 (14)	13.1
C(4)	3753 (11)	2301 (14)	4220 (16)	14.5
C(5)	4394 (11)	2288 (14)	6154 (16)	15.0
C(6)	3907 (12)	1554 (15)	7080 (16)	15.0
C(7)	2737 (12)	780 (14)	6167 (15)	14.7
C(8)	74 (10)	4638 (12)	6689 (13)	9.7
C(9)	952 (9)	5806 (12)	4874 (12)	9.0
C(10)	1090 (8)	5436 (11)	6631 (12)	8.1
C(11)	2177 (9)	5917 (12)	8240 (13)	9.7
C(12)	2300 (11)	5607 (13)	5 (14)	11.7
C(13)	3167 (11)	6726 (15)	8216 (14)	14.1

a) Equivalent isotropic temperature factor as defined by H. C. Hamilton (*Acta Crystallogr.*, **12**, 609 (1959)).

"International Tables for X-Ray Crystallography."[5] The final atomic parameters are presented in Table 2.††

Results and Discussion

Arrangement of Molecules. The crystal structure is shown in Fig. 1. The planar π-electron donors (DBTTF) and acceptors (TCNQ) stack alternately to form mixed columns along [011] (Fig. 2). The least-squares planes,

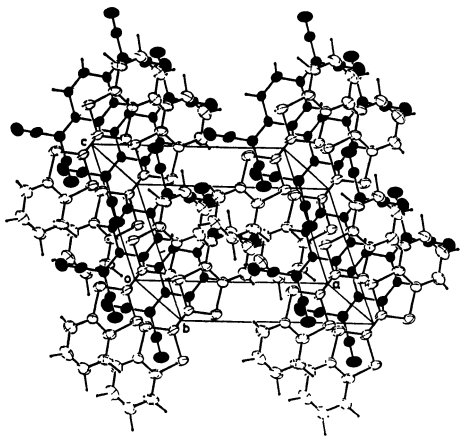

Fig. 1. Three-dimensional structure of DBTTF–TCNQ.

TABLE 3. LEAST-SQUARES PLANES AND DEVIATIONS (Å). (In each of the equations of the planes X, Y, and Z are coordinates (Å) referred to the a, b, and c crystal axes respectively.)

DBTTF molecular plane

$0.4781X-0.6482Y-0.1959Z=0.0$

S(1)	0.066	S(2)	0.078	C(1)	0.003	C(2)	0.021
C(3)	0.044	C(4)	−0.001	C(5)	−0.035	C(6)	−0.029
C(7)	−0.009						

TCNQ molecular plane

$0.4324X-0.6842(Y-b/2)-0.1791(Z-c/2)=0.0$

N(1)	−0.006	N(2)	0.014	C(8)	0.014	C(9)	−0.012
C(10)	0.016	C(11)	0.012	C(12)	−0.009	C(13)	−0.018

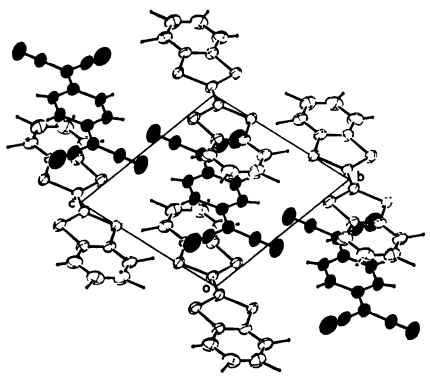

Fig. 2. The projection of the structure.

†† A list of the observed and calculated structure factors and tables of the anisotropic thermal parameters for the non-hydrogen atoms and the atomic parameters for the hydrogen atoms are kept as Document No. 8133 at the Chemical Society of Japan.

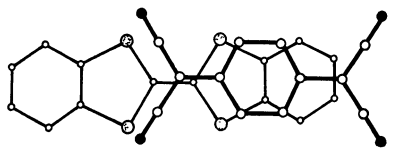

Fig. 3. Projection of DBTTF onto the plane of TCNQ.

as calculated through the DBTTF and TCNQ moieties, are listed in Table 3. The dihedral angle between these two planes is about 3.0°. TCNQ is almost planar: the largest deviation of the atoms from the TCNQ plane is 0.02 Å. DBTTF is slightly one-planar: the dihedral angle between the plane of the ethylenetetrathio group and that of the *o*-phenylene group is about 3°. The short intermolecular distance of 3.303 Å and the mode of intermolecular overlap suggest that the charge-transfer interaction is important. Figure 3 shows the projection of DBTTF onto the TCNQ plane. The charge-transfer interaction requires a large overlap integral between the electron-donating and -accepting orbitals.[6,7] Since the highest occupied molecular orbital of DBTTF and the lowest unocuupied molecular orbital of TCNQ are of different symmetries with respect to inversion (B_{1u}(DBTTF), B_{2g}(TCNQ)),[8] the direct overlap is unfavorable in DBTTF–TCNQ. This may be the reason why DBTTF is shifted from the position just above TCNQ.

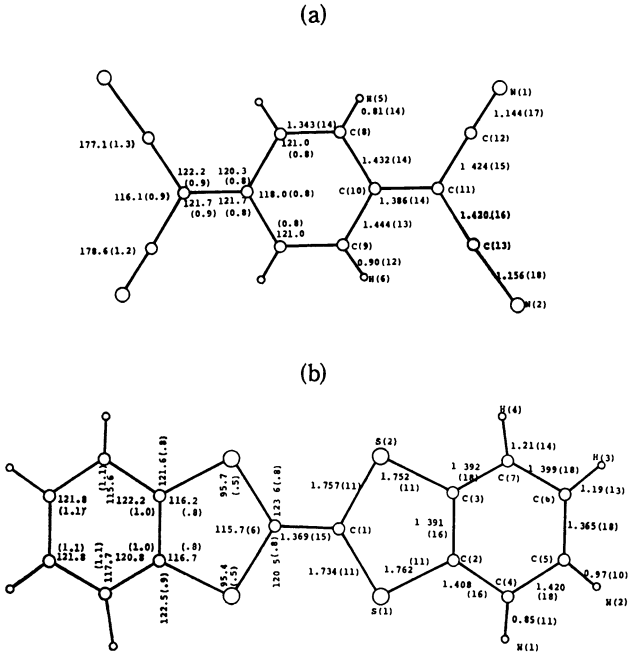

Fig. 4. Bond lengths and angles (e.s.d.'s in parentheses). (a): TCNQ, (b): DBTTF.

Molecular Geometry. The bond lengths and angles are shown in Fig. 4. It is well-known that the bond lengths of TCNQ depend on the size of the negative charge of the molecule ($TCNQ^{-\rho}$).[9,10] In Table 4, the bond lengths of TCNQ in DBTTF–TCNQ are compared with those of TCNQ° (neutral molecule)[11] and $TCNQ^{-}$ (alkali-TCNQ).[12] The averaged bond lengths

TABLE 4. COMPARISON OF AVERAGE BOND LENGTHS (Å)
(The values are averaged by assuming D_{2h} symmetry. The distances are not corrected for rigid-body motions.)

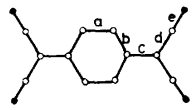

	Ref.	*a*	*b*	*c*	*d*	*e*
TCNQ°	11	1.344	1.443	1.373	1.436	1.138
$TCNQ^-$	12	1.358	1.422	1.410	1.416	1.155
$TCNQ^{-0.59}$	13, 17	1.356	1.433	1.402	1.423	1.151
TCNQ	This work	1.343	1.438	1.386	1.422	1.150

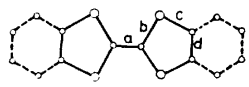

	Ref.	*a*	*b*	c	*d*
TTF°	15	1.349	1.757	1.730	1.314
TTF^+	16	1.404	1.713	1.725	1.306
$TTF^{+0.59}$	13, 17	1.369	1.743	1.736	1.323
DBTTF	This work	1.369	1.746	1.757	1.391

of TCNQ in the present complex resemble those of TCNQ° rather than those of $TCNQ^-$. If we assume that the bond length (l) and the formal charge (ρ) are linearly related, ρ can be estimated to be $|l_i(\rho)-l_i(0)|/|l_i(1)-l_i(0)|$ (i=a,b,..(Table 4)), where $l_i(\rho)$ is the bond length of $TCNQ^{-\rho}$. The values of ρ were calculated for TTF–TCNQ[13] in order to confirm the validity of this assumption; the terminal C–N bond was not used. The mean value of ρ (0.6) is consistent with the degree of charge transfer determined by X-ray diffuse-scattering experiments (ρ=0.59[14]). For TCNQ in the present complex, the mean value of ρ is 0.25, which indicates that DBTTF–TCNQ is a non-ionic complex.

The bond lengths of the TTF skeleton in DBTTF are compared with those of TTF°, TTF^+, and $TTF^{+0.59}$ in Table 4. No simple correlation between l and ρ, as in TCNQ, is observed. The *a* bond tends to elongate, while the *b* bond tends to contract, with an increase in the positive charge on TTF. This change accords with the variation in bond orders estimated on the basis of the wave function of TTF.[8] The lengths of the *a* and *b* of DBTTF are intermediate between those of TTF° and TTF^+. The *d* length of TTF is approximately equal to the length of typical C=C double bonds. The *d* bond of DBTTF is much longer, however, its length is almost equal to the C–C bond length of the benzene molecule. In addition, the *c* bond of DBTTF is fairly long. Consequently, DBTTF may be regarded as a "composite molecule" comprised of ethylenetetrathio and *o*-phenylene groups.

Molecular Arrangements in Some DBTTF Complexes. Many charge-transfer complexes containing TTF and/or TCNQ (or their analogues) exhibit high electrical conductivities.[18,19] Some of them are regarded as "organic metals." High-conducting complexes hitherto known crystallize in segregated uniform stacks, in which donors and acceptors stack separately to form parallel columns. As has been described in the preceding section, the molecular arrangement in DBTTF–TCNQ differs from those in organic metals. The mixed-column structure of DBTTF–TCNQ well interprets the low conductivity ($\sigma_{R.T.}\approx10^{-6}$ $(\Omega\ cm)^{-1}$).[4]

Besides DBTTF–TCNQ, several DBTTF complexes were prepared in order to examine the relationship between the structure and the conductive properties. The acceptors used were tetracyanoethylene (TCNE), 1,3,5-trinitrobenzene (TNB), 2,3-dichloro-5,6-dicyano-*p*-benzoquinone (DDQ), and 2,2'-(2-fluoro-2,5-cyclohexadiene-1,4-diylidene)bis(propanedinitrile) (TCNQ(F)). The preliminary crystal data are: DBTTF–TCNE, monoclinic, $P2_1/c$, a=6.92, b=6.61, c=20.81 Å, β=99.6°; DBTTF–TNB, monoclinic, $P2_1/c$, a=7.44, b=13.91, c=14.47 Å, β=90.1°. The crystal habits and the diffraction patterns of these black crystals suggest that donors and acceptors stack alternately to form mixed columns and that the columns in DBTTF–TCNE and DBTTF–TNB are parallel to the b and a axes respectively. The crystal of DBTTF–TCNQ(F) has a lattice period of about 9.3 Å along the needle axis, indicating that this crystal also does not have segregated uniform columns. The electrical conductivities of these DBTTF complexes are very low ($\sigma_{R.T.}<10^{-4}$ $(\Omega\ cm)^{-1}$).[20] In contrast, DBTTF–DDQ is highly conducting ($\sigma_{R.T.}\approx$ 70 $(\Omega\ cm)^{-1}$).[20] Oscillation photographs around the needle axis show a lattice spacing of about 3.7 Å, indicative of segregated uniform columns of DDQ and DBTTF.

The authors are grateful to Dr. G. Saito for his gift of TCNQ(F).

References

1) J. Ferraris, D. O. Cowan, V. V. Walatka, Jr., and J. H. Perlstein, *J. Am. Chem. Soc.*, **95**, 948 (1973); L. B. Coleman, M. J. Cohen, D. J. Sandman, F. G. Yamagishi, A. F. Garito, and A. J. Heeger, *Solid State Commun.*, **12**, 1125 (1973).

2) D. Jerome, A. Mazaud, M. Ribault, and K. Bechgaard, *J. Phys. Lett.* **41**, 95 (1980).

3) I. F. Shchegolev, *Phys. Status Solidi, A*, **12**, 9 (1972); J. J. Andre, A. Bieber, and F. Gautier, *Ann. Phys.*, **1976**, 145; T. J. Kistenmacher, "Synthesis and Properties of Low-Dimensional Materials (Annals of the New York Academy of Sciences, Vol. 313)," ed by J. S. Miller and A. J. Epstein, The New York Academy of Sciences, New York (1978), pp. 333—342.

4) G. S. Bajwa, K. D. Berlin, and H. A. Pohl, *J. Org. Chem.*, **41**, 145 (1976).

5) "International Tables for X-Ray Crystallography," Kynoch Press, Birmingham, (1974), Vol. IV.

6) J. B. Torrance, J. J. Mayerrle, V. Y. Lee, and K. Bechaard, *J. Am. Chem. Soc.*, **101**, 4747 (1979).

7) H. Kuroda, I. Ikemoto, and H. Akamatu, *Bull. Chem. Soc. Jpn.*, **39**, 1842 (1966); H. Kuroda, T. Amano, I. Ikemoto, and H. Akamatu, *J. Am. Chem. Soc.*, **89**, 6056 (1967).

8) A. J. Berinsky, J. F. Carolan, and L. Weiler, *Solid State Commun.*, **15**, 795 (1974); D. L. Coffen, J. Q. Chambers, D. R. Williams, P. E. Garrett, and N. D. Canfield, *J. Am. Chem. Soc.*, **93**, 2258 (1971).

9) C. J. Fritchie and P. Arthur *Acta Crystallogr.*, **21**, 1939 (1966); T. Sundaresan and S. C. Wallwork, *Acta Crystallogr., Sect. B*, **28**, 491 (1972); P. S. Flandrois and D. Chasseau, *Acta Crystallogr., Sect. B*, **33**, 2744 (1977); P. Coppens and T. N. G. Row, "Synthesis and Properties of Low-Dimensional Materials (Annals of the New York Academy of Science, Vol. 313)," ed by J. S. Miller and A. J. Epstein, New York Academy

of Sciences, New York (1978), pp. 244—255.
10) H. Kobayashi, T. Danno, and Y. Saito, *Acta Crystallogr., Sect. B*, **29**, 2693 (1973).
11) R. E. Long, R. A. Sparks, and K. N. Trueblood, *Acta Crystallogr.*, **18**, 932 (1965).
12) M. Konno and Y. Saito, *Acta Crystallogr., Sect. B*, **31**, 2007 (1975); H. Kobayashi, to be published; T. Sundaresan and S. C. Wallwork, *Acta Crystallogr., Sect. B*, **28**, 2474 (1972).
13) T. J. Kistenmacher, T. E. Phillips, and D. O. Cowan, *Acta Crystallogr., Sect. B*, **30**, 763 (1974).
14) S. Kagoshima, H. Anzai, K. Kajimura, and T. Ishiguro, *J. Phys. Soc. Jpn.*, **39**, 1143 (1975); R. Comes," Chemistry and Physics of One-Dimensional Metals," ed by H. J. Keller, Plenum Press, New York and London (1977), pp. 315—339; R. Comes and G. Shirane, "Highly Conducting One-Dimensional Solids," ed by J. T. Devreese, R. P. Evrard, and V. E. van Doren, Plenum Press, New York and London (1979).
15) W. F. Cooper, N. C. Kenny, J. W. Edmonds, A. Nagel, F. Wudl, and P. Coppens, *J. Chem. Soc., Chem. Commun.*, **1971**, 889.
16) K. Yakushi, S. Nishimura, T. Sugano, H. Kuroda, and I. Ikemoto, *Acta Crystallogr., Sect. B*, **36**, 358 (1980).
17) A. J. Schultz, G. D. Stuky, R. H. Blessing, and P. Coppens, *J. Am. Chem. Soc.*, **98**, 3194 (1976).
18) A. F. Garito and A. J. Heeger, *Acc. Chem. Res.*, **7**, 232 (1974); K. Bechgaard, C. S. Jacobsen, K. Mortensen, H. J. Pedersen, and N. Thorup, *Solid State Commun.*, **33**, 1119 (1980).
19) G. Saito and J. P. Ferraris, *Bull. Chem. Soc. Jpn.*, **53**, 2141 (1980).
20) H. Kobayashi, T. Yamamoto, T. Danno, and J. Nakayama, Paper Presented at the Symposium on Molecular Structure, Tokyo, Japan (1979), p. 22.

The Initial Sintering of Alkaline Earth Oxides in Water Vapor and Hydrogen Gas

Tomoyasu Ito,* Masato Fujita, Masahiro Watanabe, and Taneki Tokuda
Department of Chemistry, Faculty of Science, Tokyo Metropolitan University, Setagaya-ku, Tokyo 158
(Received October 15, 1980)

The initial sintering (crystallite growth and surface-area diminution) of freely dispersed powders was studied. For MgO in H_2O vapor, the sintering rate at 1073 K was directly proportional to the water-vapor pressure, P_{H_2O}, in the range of 27—2700 Pa, and the apparent activation energy, E, for the sintering was 137 kJ mol^{-1}. These facts lead to the conclusion that, in this system, the surface migration of O^{2-} caused by the repetition of the adsorption-desorption cycle of the H_2O molecule is rate-determining step for the sintering. For CaO in H_2O vapor, the rate-determining step appears to be migration on and/or near the surface of a cation vacancy produced by the H_2O adsorption, judging upon the facts that the sintering rate at 873 K was proportional to $P_{H_2O}^{0.34}$ in the range of 11—1600 Pa and that E was 79.4 kJ mol^{-1}. For MgO in H_2 gas, the sintering rate at 1123 K was approximately proportional to the hydrogen pressure in the range of 3.3—66.5 kPa and E was 310 kJ mol^{-1}, indicating that the sintering in H_2 was caused by H_2O vapor formed upon the desorption of the surface hydroxyl groups which had been produced by a heterolytic dissociative adsorption of H_2.

Imperfections on the surface of polycrystalline oxide powders are known to have some remarkable effects on their adsorption behavior and catalytic nature. The properties and degrees of imperfections are controlled by the calcination conditions of the oxides. One of the most significant conditions is the atmosphere. Previously we have studied the initial sintering in 2.7 kPa water vapor of MgO powders originating from magnesium oxalate and reported a marked acceleration effect of H_2O vapor.[1] A similar enhanced sintering for MgO in H_2O vapor has been reported by several workers: (1) Anderson *et al.*[2] studied initial sintering at a relatively high temperature (1323 K) and suggested an adsorption-desorption cycle mechanism, but they did no kinetic analysis of their sintering data; (2) Razouk *et al.*[3] reported mainly changes in the micropore structure of MgO powders with sintering, and (3) Aihara *et al.*[4] studied changes in the crystallite size of MgO powders with sintering in 100-kPa H_2O vapor and proposed an enhanced surface-diffusion mechanism. However, none of these studies has given clear evidence for the proposed mechanisms. A systematic investigation of initial sintering under strictly controlled experimental conditions seems to be necessary in order to clarify its mechanism.

In this paper, the initial sintering (which means the surface-area diminution and/or crystallite growth in the present study) of freely dispersed MgO powders was studied under various H_2O pressures, and the mechanism of enhanced sintering was clarified by a kinetic analysis of the data on the pressure dependence of the sintering rate. A similar sintering study for CaO was carried out and compared with the case for MgO. Since a hydrogen molecule may be expected to produce a water molecule upon adsorption on the oxide surface at high temperatures, the sintering of MgO was also studied in a hydrogen atmosphere.

Experimental

The processes for the sintering measurements were: (1) powders of 0.1-g magnesium oxalate dihydrate (0.33-g calcium hydroxide for CaO) in a Pt crucible mounted in a silica vessel were decomposed at 723 K (523 K for CaO) for 16 h under evacuation; then the resulting oxide was slowly heated to 1073 or 1123 K (873 K for CaO) and maintained at this temperature for 16 h under evacuation (this corresponds to sintering time= 0); (2) after cooling, the specific surface area was measured *in situ*; (3) after the sample had again been heated rapidly to the sintering temperature, H_2O vapor or H_2 gas was admitted into the sintering vessel and the sintering was carried out in a closed system for a prescribed duration; (4) then Processes (2) and (3) were repeated, and the surface-area-diminution curves were obtained, and (5) finally, the crystallite size of sintered powders was measured by means of an X-ray diffractometer. For MgO in H_2O vapor, an alternative method was used, a batch process consisting of the measurements of the surface area and crystallite size for each sintering run.

The hydrogen (Takachiho Chemicals, purity of 99.99% or more) was predried through a trap at 77 K. The specific surface area was measured by the BET method of oxygen adsorption at 77 K. For several samples, the distribution curve of the micropores smaller than 30 nm in diameter was obtained by the Cranston and Inkley method.[5] For the determination of the crystallite size, the (420) and (220) diffraction lines were used for MgO and CaO respectively. The crystallite size obtained by this method was somewhat larger ($<$10%) than that obtained by means of an electron micrograph.[1] For some samples, a volumetric adsorption amount of H_2 at the temperature used in the sintering was measured using a Pirani gauge. The equilibrium pressures in the adsorption study were around 10 Pa, much lower than that in the sintering study. Because a large part of the adsorption was completed within 5 min, this 5-min value is assumed to be an equilibrium-adsorption amount.

The magnesium oxalate dihydrate was prepared by two methods. The first batch (designated by MO-6) was prepared by a reaction of magnesium nitrate with ammonium oxalate, and the second batch (designated by MO-9), by a reaction of magnesium sulfate with ammonium oxalate. The magnesium oxalate dihydrate used was MO-6 unless otherwise stated in the text. The calcium hydroxide was prepared by burning calcium oxalate in air and by subsequent hydration with water free from carbon dioxide. The impurities, as determined by an atomic-absorption spectrometer, were as follows (weight ppm): MO-6: Mn=1.3, Fe$<$6.6; MO-9: Mn=4.6, Fe$<$8.6; $Ca(OH)_2$: Na=9.3, K$<$10, Mg=54. The emission spectra showed Ca in a concentration of 4—180 ppm in MO-6.

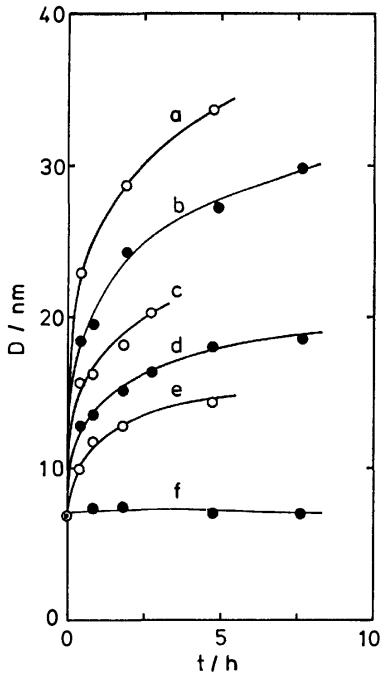

Fig. 1. Crystallite growth of MgO powders sintered at 1073 K in water vapor.
Pressure of water vapor/Pa: 2700 (a), 610 (b), 130 (c), 53 (d), 27 (e), and $<10^{-3}$ (*in vacuo*) (f).

Results

MgO in H_2O Vapor. The crystallite growth curves at 1073 K are shown in Fig. 1. The magnesium oxide powders before sintering had a crystallite size of about 7 nm. No appreciable growth occurred under evacuation ($<10^{-3}$ Pa), but water vapor exhibited remarkable positive effects for the growth rate. It has been established[1,4] that a crystallite growth rate is empirically expressed by:

$$\frac{dD}{dt} = \frac{k'_D}{D^{n'}}, \tag{1}$$

or by its integrated form:

$$D^n - D_0^n = k_D t, \tag{2}$$

where D is the crystallite size (D_0 is D at $t=0$), t is the sintering time, n ($=n'+1$) is a constant determined experimentally, and k_D [$=k_D'(n'+1)$] is the rate constant

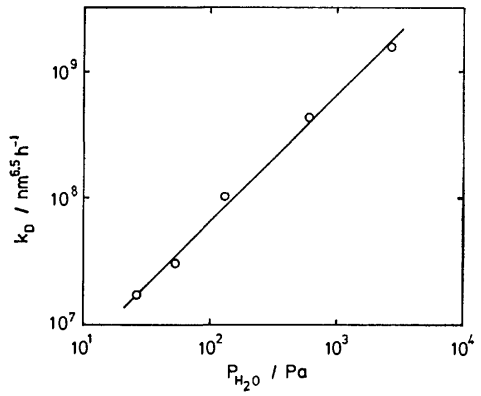

Fig. 2. Water vapor pressure dependence of crystallite growth rate constant at 1073 K for MgO powders.

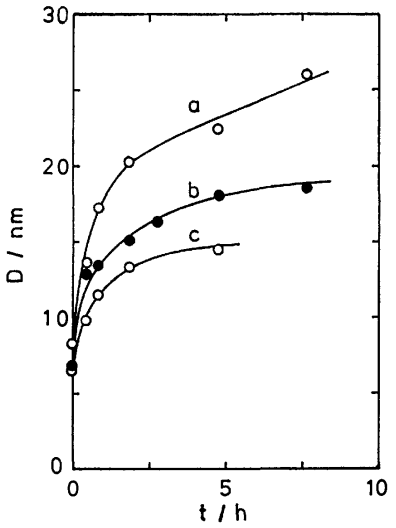

Fig. 3. Crystallite growth of MgO powders sintered in water vapor of 53 Pa.
Sintering temperature/K: 1173 (a), 1073 (b), and 973 (c).

for crystallite growth. The curves in Fig. 1 were well fitted to Eq. 2 if an appropriate value of n was given. Therefore, the rate constants calculated by Eq. 2 were used for a quantitative comparison of the sintering rate, although this equation has no important physical meaning. In Fig. 2 the pressure dependence of k_D is shown ($n=6.5$); the resultant straight line with a slope of 1.0 means that k_D is directly proportional to the water-vapor pressure, P_{H_2O}. Crystallite growth curves at various temperatures are shown in Fig. 3. The rate constants calculated by Eq. 2 gave an apparent activation energy for the crystallite growth of 137 kJ mol^{-1} which agrees with that obtained by Aihara *et al.*[4]

If the secondary agglomeration between crystallites is ignored, an ideal specific surface area, S_x, as calculated from the observed crystallite size, is expressed by:

$$S_x = \frac{6}{\rho} \cdot \frac{1}{D}, \tag{3}$$

where ρ is the density of the sample. For the MgO powders sintered in water vapor, the observed specific surface area, S, was roughly proportional to the inverse of the crystallite size observed, and the degree of the secondary agglomeration scarcely changed at all during the sintering ($S/S_x=0.55$—0.65). These facts indicate that the surface-area reduction was a direct consequence of the crystallite growth. Therefore, an equation similar to Eq. 2 is also applicable to the surface-area diminution:

$$S^m - S_0^m = k_s t, \tag{4}$$

where m ($\approx -n$) is a constant determined experimentally, S_0 is S at $t=0$, and k_s is the rate constant for the surface-area decrease. The temperature dependence of k_s gave an apparent activation energy of 131 kJ mol^{-1}, which is in good agreement with that for k_D.

The micropore distributions are shown in Fig. 4 for several samples sintered at 1073 K for 2 h. No samples had micropores below 1.5 nm in diameter. As the sintering proceeded, micropores with smaller diameters disappeared preferentially and larger ones grew. The

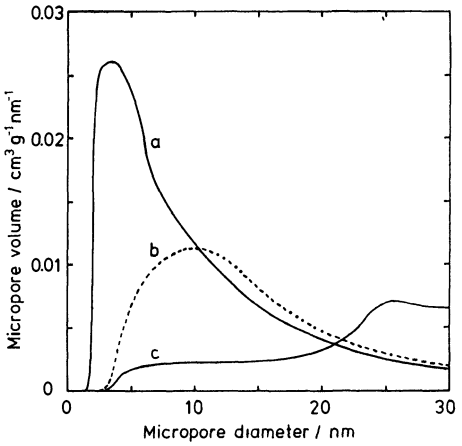

Fig. 4. Micropore distribution of MgO powders sintered at 1073 K for 2 h in water vapor.
Pressure of water vapor/Pa: $<10^{-3}$ (*in vacuo*) (a), 27 (b), and 2700 (c).

Table 1. Micropores of MgO powders sintered at 1073 K for 2 h in water vapor

P_{H_2O} / Pa	Total volume of micropore / $cm^3\ g^{-1}$	Diameter of micropore at maximum distribution/nm	Specific surface area / $m^2\ g^{-1}$
$<10^{-3}$ (*in vacuo*)	0.265	3.5	165.2
27	0.178	10	62.3
2700	0.090	25	26.2

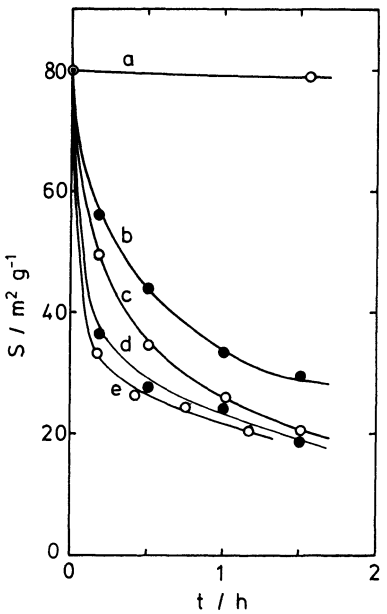

Fig. 5. Surface area decrease of CaO powders sintered at 873 K in water vapor.
Pressure of water vapor/Pa: $<10^{-3}$ (*in vacuo*) (a), 11 (b), 110 (c), 610 (d), and 1600 (e).

resultant micropore volumes are summarized in Table 1.

CaO in H_2O Vapor. The surface area decreases upon the sintering in various P_{H_2O} values at 873 K are shown in Fig. 5. Calcium oxide powders, before sintering, had a specific surface area of about 80 $m^2\ g^{-1}$; this area decreased little during sintering under evacuation. On the other hand, H_2O vapor accelerated the sintering for CaO, which was more remarkable than for MgO. Although there is some scatter, a value of $m=-3.2$ nearly satisfied Eq. 4 for this sintering system. It can be found from Fig. 6 that k_s is proportional to $P_{H_2O}^{0.34}$ in the range of 11—1600 Pa. Figure 7 illustrates the reduction of S at various sintering temperatures for $P_{H_2O}=610$ Pa. The apparent activation energy as estimated by Eq. 4 was 79.4 kJ mol^{-1}, which is smaller than that for MgO in H_2O vapor. The values of S/S_x were in the range of 0.5—0.6 for all the samples, and no important changes in the secondary agglomeration were observed during the sintering process. The micropore distributions for three samples sintered to different extents are shown in Fig. 8. No samples had micropores below 2.5 nm in diameter. As the sintering proceeded, micropores with smaller diameters rapidly disappeared,

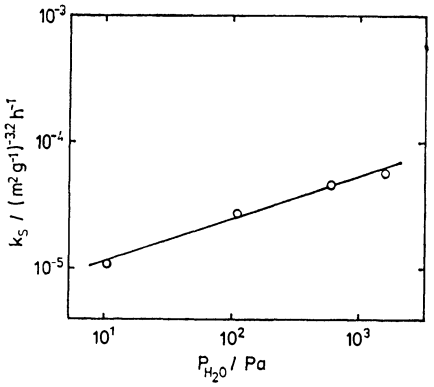

Fig. 6. Water vapor pressure dependence of sintering rate constant at 873 K for the surface area diminution of CaO powders.

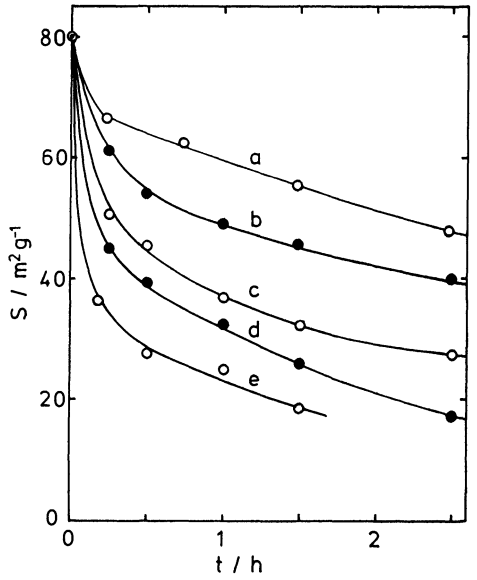

Fig. 7. Surface area diminution of CaO powders sintered in water vapor of 610 Pa.
Sintering temperature/K: 673 (a), 723 (b), 773 (c), 823 (d), and 873 (e).

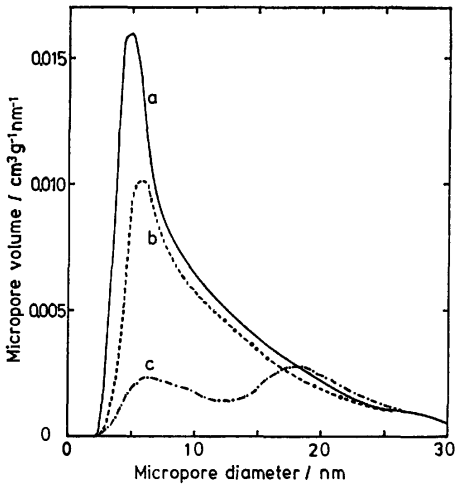

Fig. 8. Micropore distribution of CaO powders sintered in water vapor.
Sintering conditions (temperature/K—pressure/Pa—time/h): 873—$<10^{-3}$ (*in vacuo*)—0 (a), 673—610—2.5 (b), and 873—1600—1.2 (c).

TABLE 2. MICROPORES OF CaO POWDERS SINTERED IN WATER VAPOR

Sintering condition[a)]	Total volume of micropore / $cm^3\ g^{-1}$	Diameter of micropore at maximum distribution/nm	Specific surface area / $m^2\ g^{-1}$
873—$<10^{-3}$—0	0.131	5	80.0
673—610—2.5	0.097	6	48.1
873—1600—1.2	0.052	6, 18	18.0

a) Temperature/K—P_{H_2O}/Pa—time/h.

as in the case of MgO. The micropore volumes are summarized in Table 2.

MgO in H_2 Gas. Figure 9 shows the change of S in an H_2 atmosphere at 1123 K. Hydrogen evidently increased the sintering rate, but its efficiency was far less than that of H_2O. A value of -6.0 for m in Eq. 4 gave the best fit for all the observed data. The pressure dependence of k_s is shown in Fig. 10; the slope of the straight line obtained was 0.9. The sintering-rate constants observed at three temperatures (1023, 1073, and 1123 K) in 33.3 kPa H_2 gave an apparent activation energy of 310 kJ mol^{-1}, more than twice that in an H_2O atmosphere.

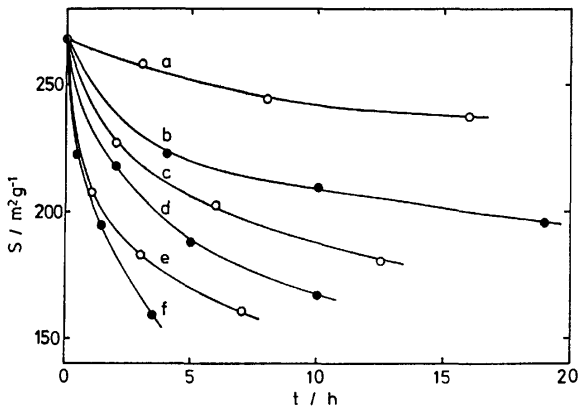

Fig. 9. Surface area decrease of MgO powders sintered at 1123 K in hydrogen gas.
Hydrogen pressure/kPa: $<10^{-3}$ (*in vacuo*) (a), 3.3 (b), 5.3 (c), 13.3 (d), 33.3 (e), and 66.5 (f).

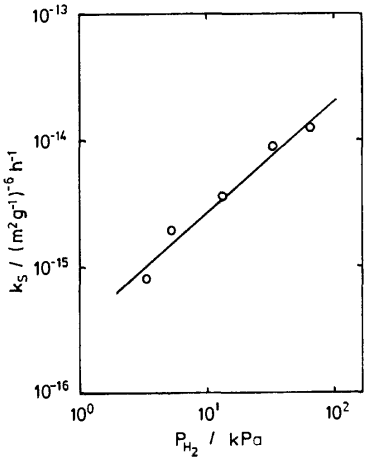

Fig. 10. Hydrogen pressure dependence of sintering rate constant at 1123 K for the surface area diminution of MgO powders.

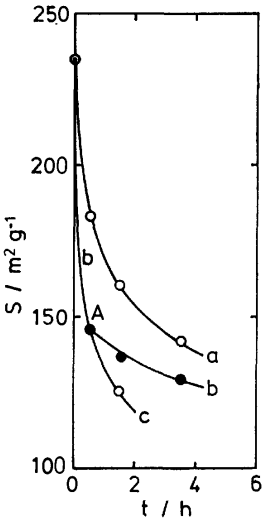

Fig. 11. Effect of Pre-oxidation on surface area decrease of MgO powders (MO-9 origin) sintered at 1123 K in hydrogen gas of 20 kPa.
Pretreatment: (a) no oxidation (normal sintering), (b) 1 h evacuation after oxidation by 13.3 kPa oxygen gas for 1 h at 1123 K, and (c) 1 h evacuation after re-oxidation at point A in curve (b).

If the sample was oxidized by O_2 before sintering, an unusual sintering behavior was observed. Figure 11 shows the sintering of MgO (MO-9 origin) at 1123 K in a 20 kPa H_2 atmosphere. Curve (a) illustrates a normal sintering (namely, without O_2 pretreatment), while Curve (b) shows the sintering of the sample pretreated by 13.3 kPa O_2 at 1123 K for 1 h and a subsequent outgassing for 1 h. In this case, the rate constant in the first run (before Point A) was about 4 times larger than that after the second, the latter being of a magnitude comparable to that of Curve (a). If the

sample was reoxidized at Point A, a faster rate was also observed in the second run, as is shown by Curve (c). The amounts of H_2 adsorbed at 1123 K on MgO (MO-9 origin) with a specific surface area of 210 $m^2\,g^{-1}$ were 14.1, 1.2, and 13.1×10^{18} molecule g^{-1} after oxidation for 1 h followed by evacuation for 1 h, evacuation for 1 h after the first H_2 adsorption, and reoxidation after the second H_2 adsorption respectively. It is, therefore, understandable that the sintering rate depends on the adsorption amount. Similar behavior was also observed for MgO prepared from MO-6, though the sintering rates were different between MO-9 and MO-6.

Discussion

Sintering Mechanism in H_2O Vapor. Because no appreciable sintering occurred in a vacuum, it can easily be understood that the enhanced sintering in H_2O vapor was caused by the adsorption effect. Unfortunately, we have little information on the chemisorption of H_2O on alkaline earth oxides at high temperatures. Previously we reported an IR study of H_2O adsorbed on MgO, revealing that only hydroxyl groups (two types, namely, free and hydrogen-bonded OH^-) were present at 773 K, while physisorbed molecules coexisted below 673 K.[6] This suggests that the species adsorbed on MgO in the present study are also hydroxyl groups. The adsorption amounts (in terms of the apparent surface coverage) thus far reported are 0.15[7] (in 0.8 kPa H_2O vapor at 923 K) and <0.005[2] (in 0.6 kPa at 1273 K). The expected coverages on MgO in the present case, typically carried out at 1073 K, may, therefore, be of the order of 0.01—0.02. For CaO, the adsorbed species may also be hydroxyl groups, but the adsorption amounts appear to be considerably larger than for MgO because of its stronger interaction with a water molecule and because of the lower temperature used for the sintering.

Possible sintering mechanisms include: (1) a diffusion mechanism (surface, grain-boundary, and bulk); (2) a viscous-flow mechanism; (3) an evaporation-condensation mechanism, and (4) an adsorption-induced space-charge mechanism. Furthermore, we must consider (5) the adsorption-desorption-cycle mechanism (anion-exchange mechanism) proposed by Anderson *et al.*,[2] because the free surface of the powders used is relatively large. This mechanism gives a mode of transport for a surface O^{2-} ion through the process by which, upon the desorption of an H_2O molecule, an oxygen ion from the surface may be removed in the desorbing H_2O molecule, leaving the O^{2-} of the original H_2O in an adjacent position on the surface. Of the five possibilities mentioned above, Mechanisms (3) and (4) can be disregarded because of the too low vapor pressure and because of no generation of a new space charge respectively. Mechanisms (1) and (2) both depend on an equilibrium amount of H_2O adsorbed on the oxide under the present experimental conditions [in Mechanism (1), the rate is proportional to the adsorbed amounts to the first power, and in (2), to the second power], and Mechanism (5) depends on the frequency of the adsorption-desorption cycle of H_2O molecules under a dynamic adsorption equilibrium. Therefore, we will consider these two cases in more detail.

In the first case, a sintering rate constant, k, is proportional to the equilibrium adsorption amount, v, to the first or the second power. Because an H_2O molecule can be assumed to be adsorbed on a cation-anion pair site (designated by S) on the surface and results in the formation of OH^-, the adsorption equilibrium near the surface is expressed by:[8]

$$S + H_2O \overset{K_1}{\rightleftharpoons} 2\,OH^- + V_M, \tag{5}$$

where V_M is the cation vacancy and K_1 is an equilibrium constant. From Eq. 5,

$$v \equiv [V_M] = \frac{1}{2}[OH^-] = \left\{\frac{K_1}{4}\cdot[S]\cdot P_{H_2O}\right\}^{1/3}. \tag{6}$$

On the other hand, v can also be expressed by:

$$v = [S]_0 - [S] = [S]_0\theta, \tag{7}$$

where θ is the (apparent) surface coverage and where the subscript 0 refers to a state before the adsorption. By substituting Eq. 7 into Eq. 6 and by differentiating its logarithmic form, we obtain:

$$\frac{d\ln v}{d\ln P_{H_2O}} = \frac{1}{3}\cdot\frac{3-3\theta}{3-2\theta}. \tag{8}$$

If k is proportional to v [Mechanism (1)], then

$$l \equiv \frac{d\ln k}{d\ln P_{H_2O}} = \frac{1}{3}\cdot\frac{3-3\theta}{3-2\theta}, \tag{9}$$

that is, k is proportional to $P_{H_2O}^{l}$ at a coverage of θ. If k is proportional to v^2 [Mechanism (2)], then

$$l = \frac{2}{3}\cdot\frac{3-3\theta}{3-2\theta}. \tag{10}$$

In the second case, k is proportional to the frequency, R, of the adsorption-desorption cycle. When the absolute-rate theory is applied, R depends on where the rate-determining step is. If, for example, an adsorption process is rate-determining, the following two reaction schemes are possible:

$$\left.\begin{aligned} &H_2O + S \overset{K_2}{\rightleftharpoons} I \\ &I \xrightarrow{k_2} 2\,OH^- + V_M, \end{aligned}\right\} \tag{11}$$

and

$$\left.\begin{aligned} &H_2O + S \overset{K_3}{\rightleftharpoons} 2\,I \\ &I \xrightarrow{k_3} OH^- + \frac{1}{2}V_M, \end{aligned}\right\} \tag{12}$$

where I designates an activated complex and where k_i and K_i are the rate constant and the equilibrium constant respectively. The former corresponds to an undissociated activated complex, and R is expressed by:

$$R = k_2\cdot[I] = k_2\cdot K_2\cdot[S]\cdot P_{H_2O}, \tag{13}$$

while the latter corresponds to a dissociated activated complex:

$$R = 2k_3\cdot[I] = 2\,k_3\cdot K_3^{1/2}\cdot[S]^{1/2}\cdot P_{H_2O}^{1/2}. \tag{14}$$

A further examination of other cases (*e. g.*, the presence of a pre-adsorption equilibrium, and the desorption process being a rate-determining step) revealed that either Eq. 13 or 14 is applicable to every case (except for

the constants in them). Therefore, the frequency of the adsorption-desorption cycle is expressed by either:

$$\left.\begin{aligned} R &= c \cdot [S] \cdot P_{H_2O} \\ \text{or} \\ R &= c \cdot [S]^{1/2} \cdot P_{H_2O}^{1/2}, \end{aligned}\right\} \quad (15)$$

where c is a constant. In a manner similar to the first case, we can obtain final expressions corresponding to the two cases in Eq. 15:

$$l = \frac{3-3\theta}{3-2\theta} \quad (16)$$

$$l = \frac{1}{2} \cdot \frac{3-3\theta}{3-2\theta}. \quad (17)$$

Figure 12 shows the values of l in Eqs. 9, 10, 16, and 17. Now we can compare the observed data with the calculated values.

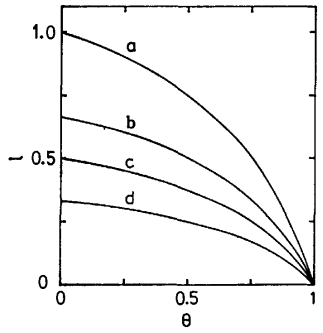

Fig. 12. Dependence of sintering rate constant on apparent surface coverage.
(a): Eq. 16 [mechanism (5)], (b): Eq. 10 [mechanism (2)], (c): Eq. 17 [mechanism (5)], and (d): Eq. 9 [mechanism (1)].

MgO in H_2O Vapor. The experimental facts were that l equals 1 in the P_{H_2O} range of 27—2700 Pa at 1073 K and that the apparent activation energy of the crystallite growth is 137 kJ mol^{-1}. It may be found from Fig. 12 that l becomes 1 only when $\theta \approx 0$ in Eq. 16. As has been described previously, $\theta \approx 0$ (say, $\theta < 0.1$) was fulfilled in the present case. It may be concluded, therefore, that, for MgO in H_2O vapor, an anion-exchange mechanism is operative and that surface O^{2-} ions move on the surface by repeating the adsorption-desorption cycle of H_2O molecules. The measurement of the isotopic-exchange-reaction rate of oxygen atoms between H_2O and surface O^{2-} at high temperatures can afford useful information, but we could not succeed in its measurement because of the too rapid exchange rate and because of the peculiar nature of H_2O vapor. We can see, however, on the basis of simple gas kinetics, that each adsorbing center of the oxide surface is subjected to a collision with an H_2O molecule $\approx 10^5$ times per second under typical sintering conditions and that the time of residence of an H_2O molecule at the surface is sufficient for the molecule to interact with the surface.[2] On the other hand, the cations may easily move on or near the surface by the diffusion of the V_M formed.

There are no micropores with diameters $<$1.5 nm in any sample (Fig. 4). Therefore, the sintering by the anion-exchange mechanism is thought to proceed mainly, not through condensation between two surface OH^- ions of adjacent crystallites in a micropore, thus forming an oxygen bridge between the crystallites and to form a closed micropore, but through condensation between two adjacent OH^- ions on a crystallite, thus leading to an enhanced surface mobility which causes the disappearance of smaller crystallites and the growth of larger ones. This picture is in accord with the finding that S/S_x did not change appreciably during the sintering.

Eastman *et al.*[8] and Mackenzie *et al.*[9] suggested an association of two OH^- and V_M in Eq. 5 and the formation of a complex such as $2OH^- \cdot V_M$. However, this seems not to be valid in the present case considering the two facts that: (1) a completely linear relationship between k and P_{H_2O} holds, even for $P_{H_2O} < 100$ Pa (Fig. 2), and (2) for the CaO sintering, k is proportional to $P_{H_2O}^{0.34}$, suggesting non-association between adsorbed species, even though much more OH^- and V_M are present compared to the case of MgO.

CaO in H_2O Vapor. It was found experimentally that l equals 0.34 in the P_{H_2O} range of 11—1600 Pa at 873 K and that the apparent activation energy for k is 79.4 kJ mol^{-1}. From Fig. 12, $l = 0.34$ is possible in the four cases; namely, $\theta \approx 0$ in Eq. 9, $\theta \approx 0.75$ in Eq. 10, $\theta \approx 0.85$ in Eq. 16, and $\theta \approx 0.6$ in Eq. 17. However, it seems to be impossible, unless $\theta \approx 0$ or 1, that a constant value of l is maintained during about a 150-fold change in P_{H_2O} (11—1600 Pa). Thus, Eqs. 10, 16, and 17 can be excluded, and only the case of $\theta \approx 0$ in Eq. 9 is applicable; that is, the sintering proceeds through a diffusion mechanism ($\theta \approx 0$ suggests that the adsorbed species are present not only on the surface, but also beneath the surface). We must then determine which of the adsorbed species, V_M or OH^-, is concerned with the rate-determining step. It may be possible for an anion on the surface to migrate by means of an anion-exchange mechanism, by analogy with MgO, and a cation in CaO is less movable than one in MgO because of the larger cation size and heavier atomic mass. Therefore, we suggest that V_M is the rate-determining species and that it moves on and/or near the surface layer.

Let us now look at the apparent activation energy of the sintering rate. If the above mechanism is assumed to be valid, k is expressed by:

$$k = k_d \cdot [V_M], \quad (18)$$

where k_d is a diffusion coefficient of V_M. By substituting Eq. 6 into Eq. 18, assuming P_{H_2O}=constant and [S]= constant (because of $\theta \approx 0$), and differentiating by temperature, T, the logarithmic form of a resultant equation, we obtain:

$$\frac{d \ln k}{dT} = \frac{d \ln k_d}{dT} + \frac{1}{3} \cdot \frac{d \ln K_1}{dT}. \quad (19)$$

Using an Arrhenius equation and a van't Hoff equation, we then obtain:

$$E = E_d - \frac{Q}{3}, \quad (20)$$

where E is the apparent activation energy for the sintering rate, E_d is the activation energy for the diffusion of V_M, and Q is the heat of the adsorption of Eq. 5. Unfortunately, there are no appropriate values for E_d and Q. However, if we are allowed to use, as E_d, the value of 118 kJ mol^{-1} of the activation energy for Ca^{2+} bulk-diffusion at 1273—1673 K[10] and, as Q, the 96 kJ mol^{-1} of the heat of the dissociation reaction,[11] $Ca(OH)_2 \rightleftharpoons CaO + H_2O$, then we obtain E=86 kJ mol^{-1}. On and/or near the surface, E_d and Q are probably smaller than those in bulk, but the resultant E as a difference between them may be expected to be not far from the observed value of 79.4 kJ mol^{-1}. This suggests the validity of the concepts that, for CaO in H_2O vapor, a diffusion of V_M on and/or near the surface is rate-determining and that the anion easily migrates on the surface by means of an anion-exchange mechanism.

Sintering Mechanism in H_2. It has been established that H_2 is adsorbed on MgO at high temperatures, and that the higher the temperature, the more the adsorption amount.[12-14] The adsorbed species have been identified as hydroxyl groups by Lisachenko *et al.*[12] Therefore, the desorption from the heated sample under a dynamic adsorption equilibrium can produce an H_2O molecule from two adsorbed OH^-.[12,14] If the resultant pressure of H_2O vapor present in the 10 kPa H_2 atmosphere reaches only 0.1 Pa, it is possible to explain the observed sintering shown in Fig. 9. Unfortunately, we failed to confirm, by the use of a mass-spectrometer, the presence of water vapor in a large excess of H_2 or D_2 gas after the sintering because of its too small quantity, the presence of background peaks, the easy adsorption of water vapor onto the wall, *etc.* However, as has previously been described, the amount of H_2 adsorbed on MgO at 1123 K was 1.2×10^{18} molecule g^{-1} even for the second run, which corresponds to an H_2O partial pressure of 100 Pa if all the adsorbed species are assumed to be desorbed as H_2O molecules. Therefore, it is very possible that the actual partial pressure of H_2O in H_2 reaches 0.1 Pa. Below we will discuss the sintering mechanism based upon the view that the initial sintering in H_2 is caused by the H_2O molecules formed.

It was found experimentally for MgO in H_2 gas that l equals 0.9 in the H_2 pressure range of 3.3—66.5 kPa at 1123 K and that the apparent activation energy for the sintering is quite large, 310 kJ mol^{-1}. The formation of hydroxyl groups upon the H_2 adsorption may be possible through: (1) the reduction of trace amounts ($<$100 ppm) of the transition elements present; (2) a reaction with an O^- ion[15] present on the activated surface; (3) the reduction of Mg^{2+}, and (4) the heterolytic dissociation of H_2 into H^+ and H^-. Mechanisms (1)—(3) are, however, unimportant in the present case because of the disagreements with the actual concentrations and/or with the actual pressure dependences. Therefore, we will consider Mechanism (4) in some detail. Unfortunately, the direct observation of a Mg–H (possibly Mg^{2+}–H^-) stretching frequency by means of the IR spectra is very difficult at the temperatures used in the sintering study. However, recently Coluccia *et al.*[16] reported on the IR spectra upon the H_2 adsorption at room temperature on MgO activated at high temperatures, and proved the formation of O–H and Mg–H bonds. According to our temperature-programed desorption study,[17] these adsorbed species remain on the surface up to around 700 K, even under a high vacuum. Thus, a similar adsorption scheme appears to be possible for the present sintering experiment. This adsorption equilibrium is expressed by:

$$\left.\begin{aligned} H_2 + O^{2-} &\overset{K_4}{\rightleftharpoons} OH^- + H^- + V_M \\ 2\,OH^- + V_M &\overset{K_5}{\rightleftharpoons} H_2O + O^{2-}. \end{aligned}\right\} \quad (21)$$

Therefore,

$$P_{H_2O} = K_4 \cdot K_5 \cdot \frac{[OH^-]}{[H^-]} \cdot P_{H_2}, \quad (22)$$

where P_{H_2O} and P_{H_2} are the partial pressures of H_2O and H_2 respectively. Equation 22 shows that, unless the change in P_{H_2} is large, P_{H_2O} is approximately proportional to P_{H_2}. This agrees with the experimental facts, for the sintering rate in H_2O vapor is simply proportional to P_{H_2O}, as has been mentioned previously. The activation energy of the sintering for this mechanism is expected to be larger than that in a pure H_2O vapor by the heat of reaction necessary for Eq. 21. Though qualitative, this can explain the observed results (137 kJ mol^{-1} for H_2O and 310 kJ mol^{-1} for H_2). It may be concluded, therefore, that the enhanced sintering in H_2 gas proceeds by means of an anion-exchange mechanism caused by H_2O vapor which has been produced upon the heterolytic dissociative adsorption of H_2 on the surface at a high temperature (Eq. 21).

Prior to the sintering, the MgO sample was usually preevacuated at 1123 K for a long time without oxidation. On the other hand, the sample preoxidized at 1123 K exhibited a remarkable sintering upon the first H_2 admission (Fig. 11). This is explicable by considering that each adsorption equilibrium of the four possible mechanisms on OH^- formation described above was shifted to the oxidation side and subsequent admission of H_2 produced more H_2O vapor than usual.

Guilliatt *et al.*[18] carried out a crystallite-growth study of MgO in the H_2 atmosphere of, not a closed, but a flowing system, and found no substantial effectiveness of an H_2 gas for sintering. On the other hand, in the closed (static) system used in the present study, some remarkable effects were observed. One must pay much attention to these differences in the experimental conditions upon the measurements of various properties of solids, such as their sintering behavior and electric conductivity.

References

1) T. Ito and T. Tokuda, *Nippon Kagaku Kaishi*, **1974**, 248.
2) P. J. Anderson and P. L. Morgan, *Trans. Faraday Soc.*, **60**, 930 (1964).
3) R. I. Razouk, R. Sh. Mikhail, and J. Ragai, *J. Appl. Chem. Biotechnol.*, **23**, 51 (1973).
4) K. Aihara and A. C. D. Chaklader, *Acta Metall.*, **23**, 855 (1975).
5) R. W. Cranston and F. A. Inkley, "Adv. in Catalysis," Academic Press, New York (1957), Vol. 9, p. 143.
6) T. Ito, K. Kanehori, and T. Tokuda, *Z. Phys. Chem., N. F.*, **103**, 203 (1976).

7) A. G. Oblad, S. W. Weller, and G. A. Mills, Proc. 2nd Int. Congr. Surface Activity, London (1957), Vol. 2, 309.
8) P. F. Eastman and I. B. Cutler, *J. Am. Ceram. Soc.*, **49**, 526 (1966).
9) K. J. D. Mackenzie and P. J. Melling, *Trans. J. Brit. Ceram. Soc.*, **73**, 23 (1974).
10) V. Kumer and Y. P. Gupta, *J. Phys. Chem. Solids*, **30**, 677 (1969).
11) J. A. C. Samms and B. E. Evans, *J. Appl. Chem.*, **18**, 5 (1968).
12) A. A. Lisachenko and V. N. Filimonov, *Dokl. Akad. Nauk SSSR*, **177**, 391 (1967); A. A. Lisachenko and F. I. Vilesov, *Kinet. Katal.*, **13**, 749 (1972).
13) D. Cordischi, R. L. Nelson, and A. J. Tench, *Trans. Faraday Soc.*, **65**, 2740 (1969).
14) K. V. Topchieva, A. Yu. Loginov, and T. M. Semenkina, *Vestn. Mosk. Univ., Khim.*, **16**, 276 (1975).
15) R. Martens, H. Gentsch, and F. Freund, *J. Catal.*, **44**, 366 (1976).
16) S. Coluccia and A. J. Tench, Preprints of 7th Int. Congr. Catalysis, Tokyo (1980), B35.
17) T. Ito, T. Sekino, N. Moriai, and T. Tokuda, *J. Chem. Soc., Faraday Trans. 1*, in press.
18) I. F. Guilliatt and N. H. Brett, *J. Chem. Soc., Faraday Trans. 1*, **68**, 429 (1972).

Molecular Conformations of 4-Aminomethyl-1-cyclohexanecarboxylic Acids in Aqueous Solution

Mikirô YANAKA,* Satoru ENOMOTO, Yoshio INOUE,† and Riichirô CHÛJÔ†

Tokyo Research Laboratory, Kureha Chemical Industry Co., Ltd., Hyakunin-cho, Shinjuku-ku, Tokyo 160

† *Department of Polymer Chemistry, Tokyo Institute of Technology, Ookayama, Meguro-ku, Tokyo 152*

(Received December 4, 1980)

The structures of *cis*- and *trans*-4-aminomethyl-1-cyclohexanecarboxylic acids were studied by proton and carbon-13 NMR, and by semiempirical molecular orbital methods (CNDO/2 and MNDO). Both isomers exist in zwitter ionic forms in aqueous solution. It was found that the most stable conformations for them are all staggered forms: the diequatorial conformer in the *trans* form and the axial carboxyl group in the *cis* form. These preferred conformers are similar to those in crystalline states. In these conformers the deformation is very small in the cyclohexane ring of the *trans* form. The atomic distance between the nitrogen of amino group and the carbon of carboxyl group in the preferred conformer of *trans* form is 0.65 nm and that in *cis* form is 0.55 nm. This distance of 0.65 nm will play an important role in the antifibrinolytic effect.

There are two geometrical isomers, *i.e.*, *trans* and *cis* isomers, in 4-aminomethyl-1-cyclohexanecarboxylic acid. The *trans* one (TAMCHA) is used as an orally active antifibrinolytic drug and its modified compounds are synthetic protease inhibitors,[1] while the biological activity of the *cis* one (CAMCHA) is quite weak.[2]

According to the study of Mangyo[3] on the relationship between the structures of various ω-amino carboxylic acids and their biological activities, their antifibrinolytic activities depend on the atomic distances between the nitrogen of amino group and the carbon of carboxyl group, and on the isoelectric point.

Conformations of the *trans* isomer[4] and hydrogen halide salts of both isomers[5] were studied by crystallography; however, the biologically active conformation in aqueous solution was not expected to be similar to that in the solid state. In this paper we report the conformations of both isomers in aqueous solutions determined by NMR; we seek some clues to the difference in their biological activities.

Experimental

Samples and Reagents. All reagents and solvents used in this research were analytical grade and were used without further purification. TAMCHA and CAMCHA were prepared from ethyl *p*-(acetamidomethyl)benzoate.[6] The nitrates of Eu(III), Pr(III), Nd(III), Gd(III), and La(III) with purity more than 99.9% were purchased from Wako Chemical Co. They were used as NMR shift and/or relaxation reagents.

NMR Measurements. The proton NMR spectra of TAMCHA and CAMCHA were observed on a Varian EM-360A (60 MHz) spectrometer using a frequency-sweep mode and a JEOL FX-100 spectrometer operating at 99.6 MHz using Fourier transform (FT) mode. Their carbon-13 NMR spectra were observed on a JEOL-PS-100 spectrometer linked with a PFT-100 FT system at 25.14 MHz and a JEOL FX-100 spectrometer operating at 25.05 MHz using FT mode. The probe temperature was kept at 30 °C. Sodium 3-(trimethylsilyl)propionate-2,2,3,3-d_4 (TSP-d_4) was used as an external reference for determinations of proton and carbon-13 chemical shifts. Data were accumulated in an attached computer using 1000 Hz and 5000 Hz sweep widths for proton and carbon-13, respectively, in 8192 points (resolution: 0.2 Hz for proton and 1.2 Hz for carbon-13).

The lanthanoid induced shifts were observed with TAMCHA in D_2O solution by a successive dilution method.[7,8] The initial concentration of TAMCHA was 0.05 M (1 M=1 mol dm^{-3}) for the measurements with Eu(III), Pr(III), Nd(III), and La(III); the molar ratio (ρ) of each lanthanoid ion to the substrate was kept at a fixed value (1.0). The perturbed proton relaxation times were obtained from Gd(III) solution.[9,10] Small amounts of Gd(III) nitrate solution were added successively to the 0.20 M solution of TAMCHA. The concentration of Gd(III) was varied from 5.81 to 118.50 μM at intervals of 5—20 μM; 2-methyl-2-propanol (*ca.* 20 mM) was used as an internal standard. Proton spin-lattice relaxation times (^{1}H-T_1) were measured by the inversion-recovery method using a standard 180 °-t-90 ° pulse sequence, where t is the time in seconds between the 180 ° and 90 ° pulses. The 90 ° pulse recycle times were chosen to be at least five times the longest ^{1}H-T_1 time to be measured. Samples for ^{1}H-T_1 measurement were thoroughly deoxygenated with nitrogen in order to prevent any paramagnetic effect of oxygen molecules on T_1 values.

Data Analysis and MO Calculations. The computer programs "NMR-LAOCN-4A"[11] and "FINITE"[12] were applied to analyze the proton NMR chemical shifts in TAMCHA. The electronic densities and the total energies of TAMCHA and CAMCHA were calculated by CNDO/2[13] and MNDO.[14]

Results and Discussion

Assignments. Structures and notations of each atom of TAMCHA and CAMCHA are shown in Fig. 1. 100-MHz proton NMR spectra of both isomers are shown in Fig. 2. Their carbon-13 NMR titration curves are shown in Fig. 3.

Most carbon signals of both isomers were easily assigned by the aid of the off-resonance proton decoupling technique. Carbon pairs (C_2,C_6) and (C_3,C_5) in the spectrum of CAMCHA were assigned, as shown in Fig. 3, from the consideration of the gamma effect.[15]

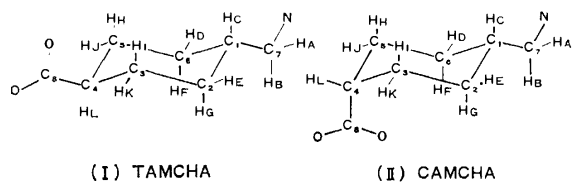

(I) TAMCHA (II) CAMCHA

Fig. 1. Structures and notation of each atom of TAMCHA (I) and CAMCHA (II).

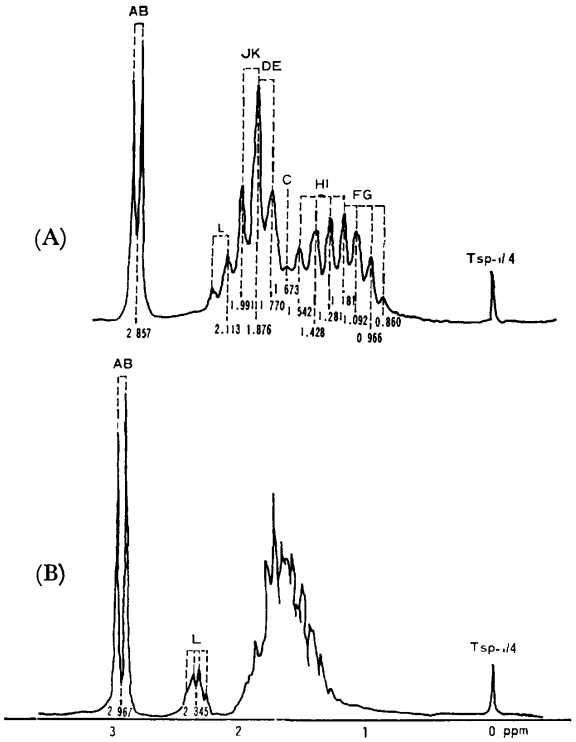

Fig. 2. The 100 MHz-proton FT NMR spectra of AMCHA at 30 °C.
(A): TAMCHA in D_2O (1%(W/V), at pH 7.40),
(B): CAMCHA in D_2O (1%(W/V), at pH 7.20).

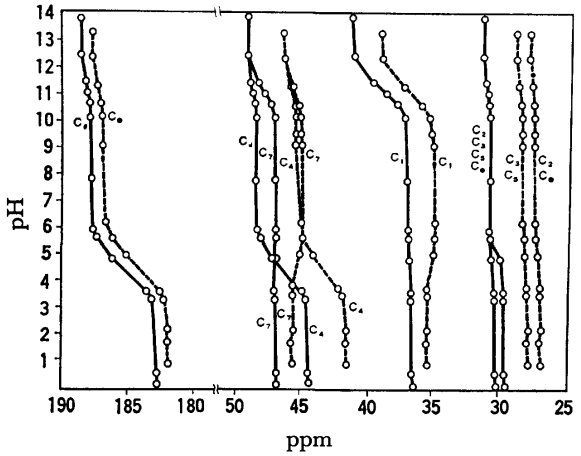

Fig. 3. The pH dependence of the carbon-13 chemical shifts of AMCHA in 15% (W/V) D_2O solution at 30 °C.
——: TAMCHA, ----: CAMCHA.

In the proton NMR spectra of TAMCHA and CAMCHA, the H_A and H_B protons were observed at 2.85 and 2.96 ppm, respectively; they showed a doublet structure due to spin coupling with the H_C proton. The triplet-like signal at 2.11 ppm in TAMCHA and the quartet-like signal at 2.34 ppm in CAMCHA were assigned to the H_L proton because of the selectively proton decoupled carbon-13 NMR spectra and the titration curves of proton NMR shown in Fig. 4. The H_L proton signal of CAMCHA appeared at lower field (by 0.1—0.2 ppm) than that of TAMCHA. An anisotropic effect[16] of the carbon-carbon bond suggest

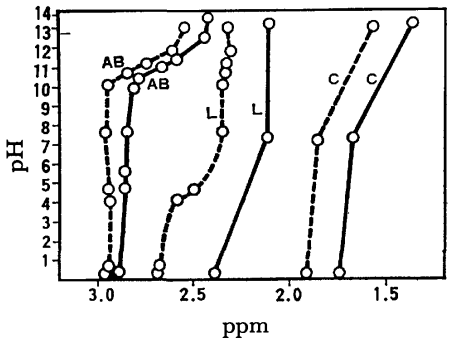

Fig. 4. The pH dependence of the proton chemical shifts of AMCHA in 1% (W/V) D_2O solution at 30 °C.
——: TAMCHA, ----: CAMCHA.
See Fig. 1 about AB, L, C.

that the H_L proton is equatorial and the carboxyl group is axial in CAMCHA.

The signal at 1.67 ppm in TAMCHA was assigned to the H_C proton by the homo-decoupling technique. Other protons of TAMCHA were assigned, as shown in Fig. 2, because of the lanthanoid-induced shift, which produced a fine signal separation while keeping the original spectral pattern.

In the case of CAMCHA, the multiplicity of the H_L proton signals varied on the addition of shift reagent. This trend would suggest some conformational change (such as chair-chair inversion). The assignments of other proton signals were difficult at this stage.

Spin Coupling Constants of TAMCHA. Observed vicinal spin coupling constants are listed in Table 1. $^3J_{AB,C}$ is the representative of $^3J_{A,C}$ and $^3J_{B,C}$ because there is no chemical shift difference between H_A and H_B. Similar notations hereafter are used with similar meanings. Five values among them, *i.e.*, $^3J_{AB,C}$, $^3J_{DE,HI}$, $^3J_{FG,HI}$, $^3J_{HI,L}$, and $^3J_{JK,L}$ were estimated from the 100 MHz proton NMR of TAMCHA to be approximately 6.7, 2.0, 11.0, 11.5, and 3—4 Hz, respectively. The homo-decoupling technique reduced the Pr(III) shifted spectrum to a five-spin system. Refined values of $^3J_{HI,L}$ and $^3J_{JK,L}$ were obtained as 12.04 and 2.49 Hz, respectively, by a computer simulation.[11]

Cyclohexane Ring Conformation of TAMCHA. To clarify whether the observed vicinal coupling constants correspond to those of the chair form, the finite perturbation theory[12] (INDO approximation) was applied. Simple model compounds which are supposed to include some parts of the chair form and of the boat form of the TAMCHA molecule were chosen and calculated. Results are shown in Table 2, in which J_g, J_t, J_c, and J_s denote vicinal coupling constants between two protons in *gauche*, *trans*, *cis*, and *skew* positions, respectively. With α-amino acids, the experimental value of J_g was 2.60 Hz and that of J_t was 13.56 Hz;[17] similar values were also obtained in calculation.

Qualitative results suggest that the observed values were those of the chair form.

Aminomethyl Group Conformation. Three conformers around the C_1–C_7 bond were possible in the aminomethyl group of TAMCHA and CAMCHA. The Newman projections of the possible conformers are

TABLE 1. THE OBSERVED VICINAL SPIN COUPLING CONSTANTS OF TAMCHA IN AQUEOUS SOLUTION AT 30 °C AND pH 7.40

Proton[a]	Dihedral angle[b] Chair form	Dihedral angle[b] Boat form	Notation[c]	Obsd value / Hz
C A and/or B			$^3J_{AB,C}$	6.7
C D and/or E	g	g g	$^3J_{C,DE}$	
C F and/or G	t	t g	$^3J_{C,FG}$	
D and/or E H and/or I	g	c c	$^3J_{DE,HI}$	2.0
D and/or E J and/or K	g	s s	$^3J_{DE,JK}$	
F and/or G H and/or I	t	s s	$^3J_{FG,HI}$	11.0
F and/or G J and/or K	g	c c	$^3J_{FG,JK}$	
L H and/or I	t	g t	$^3J_{HI,L}$	11.5(12.0$_4$[d])
L J and/or K	g	g g	$^3J_{JK,L}$	3—4 (2.4$_9$[d])

a) See Fig. 1. b) g, t, c, and s denote *gauche*, *trans*, *cis*, and *skew*, respectively. c) See text. d) Refined value obtained by a computer simulation.[11]

TABLE 2. THE CALCULATED[a] VICINAL COUPLING CONSTANTS OF THE MODEL COMPOUNDS OF TAMCHA

	Calcd value/Hz		Calcd value/Hz
(I)	$^3J_{I,E}=2.2_2$ (J_g)[b]	(IV)	$^3J_{I,E}=9.7_5$ (J_c)
	$^3J_{I,G}=13.5_4$ (J_t)		$^3J_{I,G}=4.4_1$ (J_s)
	$^3J_{I,L}=13.8_6$ (J_t)		$^3J_{I,L}=2.1_1$ (J_g)
	$^3J_{K,E}=2.3_3$ (J_g)		$^3J_{K,E}=4.4_1$ (J_s)
	$^3J_{K,G}=2.2_2$ (J_g)		$^3J_{K,G}=9.7_5$ (J_c)
	$^3J_{K,L}=2.4_6$(J_g)		$^3J_{K,L}=2.1_1$ (J_g)
(II)	$^3J_{A,C}=2.3_2$ (J_g)	(V)	$^3J_{I,E}=9.7_5$ (J_c)
	$^3J_{B,C}=13.8_4$ (J_t)		$^3J_{I,G}=4.4_1$ (J_s)
	$^3J_{C,D}=2.3_8$ (J_g)		$^3J_{I,L}=13.9_8$ (J_t)
	$^3J_{C,E}=2.3_4$ (J_g)		$^3J_{K,E}=4.4_1$ (J_s)
	$^3J_{C,F}=13.6_7$ (J_t)		$^3J_{K,G}=9.7_5$ (J_c)
	$^3J_{C,G}=13.7_2$ (J_t)		$^3J_{K,L}=2.7_5$ (J_g)
(III)	$^3J_{L,H}=14.3_0$ (J_t)	(VI)	
	$^3J_{L,I}=13.6_7$ (J_t)		
	$^3J_{L,J}=2.3_2$ (J_g)		
	$^3J_{L,K}=2.1_6$ (J_g)		

a) Calculations were carried out by the finite perturbation theory[12] (INDO approximation). The geometrical parameters for calculations are shown in (VI). The bond angles were assumed as a tetrahedral about sp^3 atom and 120.0° about sp^2 atom. b) J_g, J_t, J_c and J_s denote vicinal coupling constants between two protons in *gauche*, *trans*, *cis*, and *skew* positions, respectively.

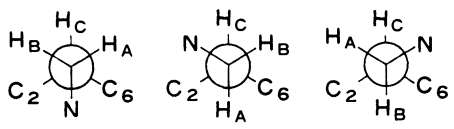

Fig. 5. The possible conformers about the C_1–C_7 bond of AMCHA.

shown in Fig. 5. In solutions TAMCHA and CAMCHA exist as a mixture of these rapidly interconverting rotational isomers. By assuming that J_t, the coupling constant between two hydrogens in the *trans* position with respect to each other, and J_g, the coupling constant between *gauche* hydrogens, are constant for all three isomers, observed vicinal coupling constants $J_{C,A}$ and $J_{C,B}$ are given by

$$J_{C,A} = P_a J_g + P_b J_t + P_c J_g \quad (1)$$

$$J_{C,B} = P_a J_g + P_b J_g + P_c J_t \quad (2)$$

$$P_a + P_b + P_c = 1, \quad (3)$$

where P_a, P_b, and P_c are the populations of the conformers a, b, and c. Strictly speaking, P_b would not be equal to P_c because of a small amount of rotation in the carboxyl group around the C_4–C_8 bond. But because spin-spin coupling is induced through this bond and the carboxyl group is far from the C_1–C_7 bond, P_b can be assumed to be equal to P_c. The fact that only one J value was observed in the present study suggested that $J_{C,A}$ could be equal to $J_{C,B}$ (A_2X spin system assumption). P_a, P_b, and P_c were calculated from Eqs. 1, 2, and 3 with the values J_t(13.84 Hz) and J_g(2.32 Hz) obtained from the model compound (II). P_a and P_b (equal to P_c) are estimated to be 0.240 and 0.380 in TAMCHA

(J_{obsd} was 6.7 Hz); the values in CAMCHA are 0.170 and 0.415 (J_{obsd} was 7.1 Hz). The following equilibrium would be described by either an equilibrium constant K or a free energy ΔG:

$$P_b(=P_c) \rightleftharpoons P_a;\ K = P_a/P_b;\ \Delta G = -RT\ln K.$$

The values of K are 0.632 and 0.410, and the ΔG values (at 30 °C) are 1.159 and 2.248 kJ mol^{-1} in TAMCHA and CAMCHA, respectively.

Table 3. The observed relaxation and shift ratios for TAMCHA

^1H[a]	Relaxation ratio	Shift ratio		
	Gd(III)	Eu(III)	Nd(III)	Pr(III)
L	1.00	1.00	1.00	1.00
JK	0.89	0.69	0.59	0.61
HI	0.54	0.40	0.54	0.59
C	0.21	0.19	0.13	—[b]
DE	0.18	0.24	0.25	—[b]
FG	0.17	0.29	0.32	—[b]
AB	0.01	0.12	0.15	0.15

a) See Fig. 1. b) Observation was difficult due to the overlapping of other signals.

Relative Relaxation Rate and Relative Induced Shift. To confirm the above results, NMR observations were carried out with additions of shift and/or relaxation reagents. The relative values of the relaxation rate in the presence of Gd(III) are listed in Table 3 with respect to relaxation rate of H_L. Values of paramagnetically induced shift by Eu(III), Nd(III), and Pr(III) are also listed in Table 3, where the shift of H_L is chosen as a reference. These were values obtained after the subtraction of complex formation shifts, which were determined by an addition of diamagnetic La(III). The relative induced shift depends on the inter-atomic vector between the lanthanoid ion and the i-th nucleus (r_i^{-3}) and the angle between this vector and the principal axes of symmetry of the complex,[18] while the relative relaxation rate is approximately proportional to the (r_i^{-6}) term.[9,10,19] Roughly speaking, the conformation obtained from the shift and/or relaxation reagent experiments is consistent with the above results. There remain small discrepancies between them. The calculated atomic distance between Gd(III) and ^1H based on the geometry,[8,20] shown in the footnote in Table 4, are listed in Table 4. The observed relative relaxation rate and the calculated values of r_i suggest that a small deformation was produced in the cyclohexane ring, especially at the bond angles of C_2–C_3–C_4 and C_4–C_5–C_6 or the bond angle of C_8–C_4–H_L.

Table 4. The calculated atomic distance between Gd(III) and ^1H

^1H	L	H,I,J,K	F,G	C	D,E	A	B
r_{Ln-^1H}/nm[a]	0.595	0.607	0.801	0.810	0.826	0.997	1.018

a) The geometrical parameters for calculation are given below. As shown in Table 3, the ratios of shifts of different nuclear resonances were found to be independent of the lanthanoid ion; the lanthanoid ion was assumed to be located on the bisector of the O–C–O angle.[8,20]

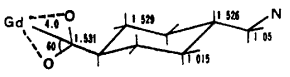

The small deformation in the cyclohexane ring could also be illustrated by the R-value.[21] The relationship between the torsional angle (ϕ) and the R-value in a ring compound is given by

$$R = J_{trans}/J_{cis} \quad (4)$$

$$\cos\phi = (3/(2+4R))^{1/2}, \quad (5)$$

where J_{trans} and J_{cis} are the vicinal coupling constants between two protons in *trans* and *cis* positions, respectively. The R-value of C_3–C_4 bond (or C_4–C_5 bond) of TAMCHA was found to be 4.83 from the refined values listed in Table 1, and the torsional angle about C_3–C_4 bond (or C_4–C_5 bond) was calculated to be 68 degrees from Eq. 5.

Protonation. Lowering of pH values caused the downfield shifts of all proton signals and the upfield shifts of all carbon signals (except the signals of C_1 and C_7). These shifts were observed at pK_1 corresponding to protonation of carboxyl group; they might be accounted for by the changes of the net charges which are produced by the protonation of amino group.[22] Each carbon-hydrogen bond is polarized to C^-–H^+ structure by this protonation and the electron on the hydrogen atom is transmitted onto the positively charged nitrogen atom through the carbon skeleton.

Table 5. Total electron densities of each atom in AMCHA calculated by the CNDO/2 method

	TAMCHA		CAMCHA[a]	
	Neutral	Cation	Neutral	Cation
C_1	3.9777	3.9833	3.9822	3.9848
C_2	3.9961	3.9876*[b]	3.9995	3.9912*
C_3	3.9830	3.9831	3.9790	3.9790
C_4	4.0288	4.0315	4.0311	4.0318
C_5	3.9807	3.9767*	3.9881	3.9827*
C_6	3.9928	3.9967	4.0021	4.0068
C_7	3.9111	3.9246	3.9071	3.9355
C_8	3.6042	3.5984*	3.5988	3.6065
H_A	1.0262	0.9484	1.0291	0.9487
H_B	1.0087	0.9447	1.0095	0.9447
H_C	1.0004	0.9828	1.0001	0.9827
H_D	1.0000	1.0247*	0.9990	1.0223*
H_E	1.0048	0.9899	1.0017	0.9863
H_F	0.9978	0.9843	0.9828	0.9687
H_G	0.9991	0.9845	0.9944	0.9803
H_H	0.9946	0.9842	1.0021	0.9910
H_I	0.9893	0.9779	0.9985	0.9860
H_J	1.0056	0.9821	1.0028	0.9785
H_K	1.0036	0.9764	0.9966	0.9698
H_L	0.9860	0.9767	0.9790	0.9547

a) The geometrical parameters of CAMCHA for calculation were as follows. b) See text.

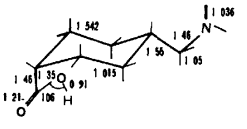

The downfield shifts of the proton signals are due to the decreases in the total charge densities on the protons and the upfield shifts of the carbon signals are the increases in the total charge densities on the carbons. To estimate quantitatively these polarization effects, the electron densities were calculated by the CNDO/2 method; the results are shown in Table 5. The difference of the net charge on each atom between the neutral molecules and the cationic ones give the qualitative explanation for the protonation shifts, except for the few atoms marked with asterisks.

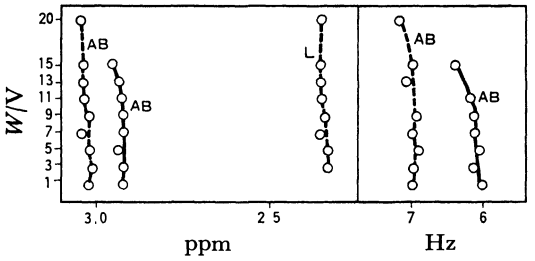

Fig. 6. The concentration dependence of the proton chemical shifts (left) and the proton coupling constants (right) of AMCHA in D_2O solution at 30 °C and 60 MHz.
——: TAMCHA, ----: CAMCHA.
See Fig. 1 about AB, L.

Association. The dependences of the chemical shifts and the coupling constants on the concentration are shown in Fig. 6. A strong hydrogen bond is formed between the solute and the solvent D_2O,[23] and no association of the solute molecules occurred in solutions with the concentration below *ca.* 9% (*ca.* 5.73 mM). The titration curves of carbon-13 chemical shifts (Fig. 3) were drawn at the concentration of 15%, where the association can take place. Small shifts were observed with C_4 and C_8 of TAMCHA and CAMCHA at pK_2 (the protonation of amino group) and the C_1 and C_7 chemical shifts of CAMCHA showed some anormaly in the acidic region.

Semiempirical Molecular Orbital Calculations. To estimate the most stable conformation of TAMCHA and CAMCHA, the conformational energies were calculated by the semiempirical molecular orbital method. The changes of the conformational energies which were caused by the rotations of the aminomethyl group and the carboxyl group were calculated by the CNDO/2 method, based on the assumption that the cyclohexane ring conformations were chair forms free from strain. The calculation was carried out by changing the rotational angle around the C_4–C_8 bond at 30-degree intervals, keeping the N atom *trans* to the position of C_2 to find out the smallest conformational energy value; then the rotational angle around the C_1–C_7 bond was changed at 30- or 60-degree intervals, keeping the carboxyl group fixed. The results are shown in Fig. 7 where the minimum of energy is put to zero as a standard. The curves of the electronic energies were related smoothly with the change of rotational angles, while abnormal changes were observed in the curves of the total energies, in which the contributions of the

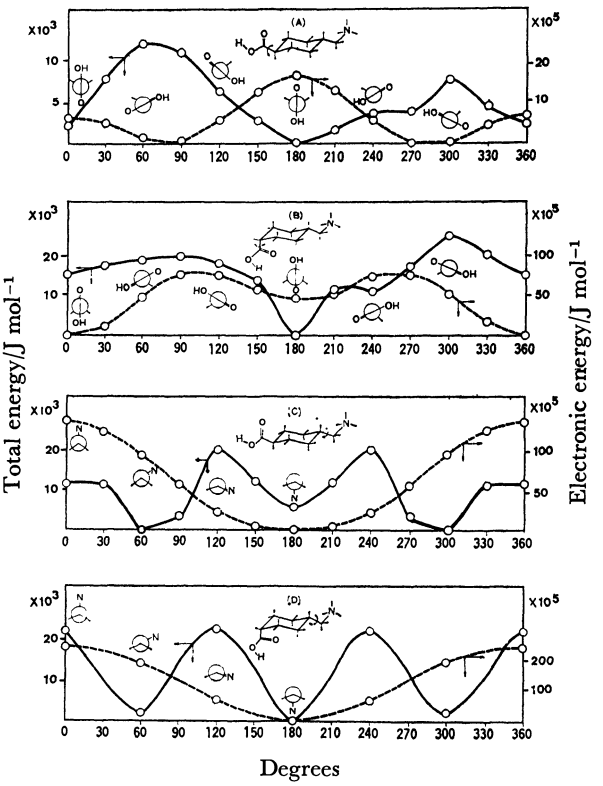

Fig. 7. Relative electronic energies and total energies on the rotational angle about (A) C_4–C_8 bond of TAMCHA, (B) C_4–C_8 bond of CAMCHA, (C) C_1–C_7 bond of TAMCHA, and (D) C_1–C_7 bond of CAMCHA varied respectively and calculated by the CNDO/2 method.
——: Total energies, ----: Electronic energies.

core-core repulsion energies to the electronic energies are taken into account. The CNDO/2 method is inadequate to estimate the energy differences among the conformers.[24] As shown in Table 6, the conformer (IV) was more unstable than that (V) in the calculation of CAMCHA, but this result is inconsistent with the experimental result of the proton NMR. The energies of the conformers were, therefore, calculated by the MNDO method[25,26] at the energy minimum points of the CNDO/2 method. The results are, in this calculation, consistent with proton NMR results.

The energy difference between the diaxial and the diequatorial conformers was also calculated. The results showed the conformer (III) was less stable than (I) by 130.42 kJ mol^{-1} (Table 6), and no equilibrium among them was expected. In the case of CAMCHA, the chair-chair inversion conformer (VI) was more stable than (IV) by 44.617 kJ mol^{-1}. The most probable conformer (IV) would be changed to the conformer (VI) by an addition of the shift reagent. This seems to correspond to the change of the spin-coupling pattern in the proton NMR spectrum due to an addition of the shift reagent.

The Atomic Distance (r_{N-C}) between the Nitrogen of Amino Group and the Carbon of Carboxyl Group. The r_{N-C} was a function of the rotation around the C_1–C_7 bond (aminomethyl group rotation). Mangyo related the

Table 6. The calculated relative conformational energies of AMCHA by the CNDO/2 and MNDO methods, and the atomic distances between N and C_8 (r_{N-C_8})

Conformer	Relative total energy/kJ mol^{-1}			r_{N-C_8}
	CNDO/2	MNDO	NMR[a)]	nm
(I) 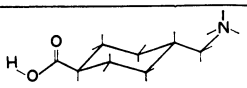	0	0	0	0.658
(II) 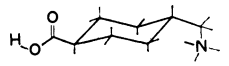	+5.759	+22.782	+1.159	0.610
(III) 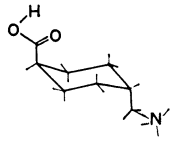	+1.821	+130.42	—	0.556
(IV) 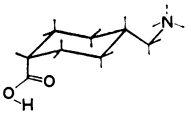	0	0	0	0.555
(V) 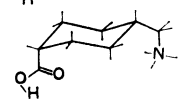	−2.269	+3.587	+2.248	0.437
(VI) 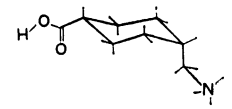	+22.271	−44.617	—	0.551

a) Our proton NMR results.

antifibrinolytic activities of ω-amino carboxylic acids with the distances of r_{N-C}, and concluded that the distance of 0.65 nm is the most active, from the comparison between molecular models with all staggered form and with diequatorial conformation.[3)]

This paper has shown that the most stable conformer of TAMCHA in aqueous solution is the conformer (I) in which the deformation is very small in the cyclohexane ring, that it is a similar conformer to that in the crystal, and that the distance of r_{N-C} is 0.65 nm. CAMCHA exists in aqueous solution as the conformer (IV) in which r_{N-C} is 0.55 nm and does not agree with that value. 6-Aminohexanoic acid is another antifibrinolytic drug and the r_{N-C} of the active conformation is also thought to be the same value of conformer (I). The antifibrinolytic drug is said to interact with plasminogen or plasmine and the distance r_{N-C} of these drugs will play an important role in the antifibrinolytic effect.

The authors wish to express their thanks to Messrs. Atsushi Tomonaga and Hiroshi Chuman of this laboratory for their helpful discussions.

References

1) S. Okamoto and U. Okamoto, *Keio J. Med.*, **11**, 105 (1962); S. Oshiba and S. Okamoto, *ibid.*, **11**, 117 (1962); B. Melander, G. Gliniecki, B. Granstrand, and G. Hanshoff, *Acta Pharmacol. Toxicol.*, **22**, 340 (1965); S. Fujii and M. Hirano, *Taisha*, **14**, 1087 (1977); J. L. G. Nilsson and P. Stenberg, *Acta Pharm. Suecica*, **7**, 441 (1970).

2) Y. Abiko and M. Iwamoto, *Biochim. Biophys. Acta*, **214**, 411 (1970).

3) M. Mangyo, *Seikagaku*, **36**, 735 (1963).

4) S. Kadoya, F. Hanazaki, and Y. Iitaka, *Acta Crystallogr.*, **21**, 38 (1966); P. Groth and O. Hassel, *Acta Chem. Scand.*, **19**, 1709 (1965).

5) P. Groth, *Acta Chem. Scand.*, **22**, 143 (1968).

6) T. Naito, A. Okano, S. Kadoya, T. Miki, M. Inaoka, R. Moroi, and M. Shimizu, *Chem. Pharm. Bull.*, **16**, 728 (1968).

7) F. Inagaki, S. Takahashi, M. Tasumi, and T. Miyazawa, *Bull. Chem. Soc. Jpn.*, **48**, 853 (1975).

8) F. Inagaki, S. Takahashi, M. Tasumi, and T. Miyazawa, *Bull. Chem. Soc. Jpn.*, **48**, 1590 (1975).

9) F. Inagaki, S. Takahashi, M. Tasumi, and T. Miyazawa, *Bull. Chem. Soc. Jpn.*, **49**, 611 (1976).

10) F. Inagaki, M. Tasumi, and T. Miyazawa, *J. Chem. Soc., Perkin Trans. 2*, **1976**, 167.

11) J. A. Musso, =232, NMR-LAOCN-4A (Q. C. P. E.); J. A. Musso and A. Isaia, *J. Chim. Phys.*, **66**, 1676 (1969); S. M. Castellano and A. A. Bothner-By, *J. Chem. Phys.*, **41**, 3863 (1964); R. C. Ferguson and D. W. Marquardt, *ibid.*, **41**, 2087 (1964).

12) N. S. Ostlund, =224, FINITE (Q. C. P. E.); J. A. Pople, J. W. McIver, Jr., and N. S. Ostlund, *J. Chem. Phys.*, **49**, 2960 (1968); J. A. Pople, J. W. McIver, Jr., and N. S. Ostlund, *ibid.*, **49**, 2965 (1968); G. E. Maciel, J. W. McIver, Jr., N. S. Ostlund, and J. A. Pople, *J. Am. Chem. Soc.*, **92**, 4497 (1970).

13) J. A. Pople and D. L. Beveridge, "Approximate Molecular Orbital Theory," McGraw-Hill, New York, N. Y. (1970).

14) W. Thiel, =353, MNDO (Q.C. P. E.).

15) D. K. Dalling and D. M. Grant, *J. Am. Chem. Soc.*, **89**, 6612 (1967); **94**, 5318 (1972); **95**, 3718 (1973); **96**, 5318 (1974).

16) A. A. Bothner-By and C. Naar-Colins, *Ann. New York Acad. Sci.*, **70**, 833 (1958).

17) K. G. R. Pachler, *Spectrochimica Acta*, **20**, 581 (1964); M. Karplus, *J. Chem. Phys.*, **30**, 11 (1959).

18) H. M. McConnel and R. E. Robertson, *J. Chem. Phys.*, **29**, 1361 (1958).
19) C. D. Barry, J. A. Glasel, R. J. P. Williams, and A. V. Xaver, *J. Mol. Biol.*, **84**, 471 (1974).
20) B. A. Levine, J. M. Thornton, and R. J. P. Williams, *J. Chem. Soc., Chem. Commun.*, **1974**, 669.
21) J. B. Lambert, H. F. Shurvell, L. Verbit, R. G. Cooks, and G. H. Stout, "Organic Structural Analysis," Macmillan Publishing Co., Inc. (1976).
22) I. Morishima, K. Yoshikawa, K. Okada, T. Yonezawa, and K. Goto, *J. Am. Chem. Soc.*, **95**, 165 (1973).
23) G. Kotowycz and R. U. Lemieux, *Chem. Rev.*, **73**, 669 (1973).
24) K. Tanaka, H. Akutsu, Y. Ozaki, Y. Kyogoku, and K. Tomita, *Bull. Chem. Soc. Jpn.*, **51**, 2654 (1978).
25) M. J. S. Dewar and W. Thiel, *J. Am. Chem. Soc.*, **99**, 4899 (1977).
26) M. J. S. Dewar and W. Thiel, *J. Am. Chem. Soc.*, **99**, 4907 (1977).

On the Extractability of Univalent Cation as Dibenzo-18-crown-6 Complexes with Picrate Ion

Yuko HASEGAWA,* Hiroji WAKABAYASHI, Manabu SAKUMA, and Tatsuya SEKINE
Department of Chemistry, Science University of Tokyo, Kagurazaka, Shinjuku-ku, Tokyo 162
(Received December 18, 1980)

The solvent extractions of alkali metal(I) with dibenzo-18-crown-6 (the nomenclature recommended by IUPAC is 2,3,11,12-dibenzo-1,4,7,10,13,16-hexaoxacyclooctadeca-2,11-diene) as the picrate into chloroform and benzene were studied at 25°C and compared with those of other univalent ions. The extraction constants of the metal ions ($K_{ex0}=[ME^+A^-]_{org}[M^+]^{-1}[E]_{org}^{-1}[A^-]^{-1}$), are in the sequence of $Tl^+\simeq K^+>Rb^+>NH_4^+\geq Ag^+>Cs^+>Na^+$, but the extraction constants of the metal complexes ($K_{ex}=[ME^+A^-]_{org}\times[ME^+]^{-1}[A^-]^{-1}$) are $NH_4^+\simeq Tl^+\simeq Rb^+\simeq K^+>Cs^+\simeq Ag^+>Na^+$.

The effects of the ionic size, the diluent, and the counter ion on the solvent extraction of univalent metal ions as cyclic polyether complexes were studied previously[1-5] and also recently.[6-10]

Although some early studies[4,11] pointed out that the extraction of metal ions with crown ethers is closely connected with the extractability of the complexes formed, not much has been reported about the extraction of metal ions with crown ethers in connection with the extractability of the complex formed in aqueous solutions. The present work was undertaken in order to learn the relation between the extraction of metal ions and the extractability of the complex. For this purpose, the extraction of alkali dibenzo-18-crown-6 (DBC) complexes with picrate ion was studied and the results were compared with those of thallium(I),[8] silver(I) and ammonium ions.[10]

Experimental

All of the procedures were performed at 25±0.5 °C, as done previously.[8,10] A seven milliliter portion of an aqueous solution containing lithium picrate and one of the alkali metal ions was equilibrated in a stoppered glass tube with an equal volume of chloroform or benzene containing DBC. The concentrations of the metal ions which were back-extracted from the organic phase into 0.1 mol dm^{-3} perchloric acid and that in the equilibrated aqueous phase were determined by flamephotometry. In the cases of sodium(I) and potassium(I), blank tests were necessary to correct the measured concentration of the back-extracts. The distribution ratio, D, was defined as:

$$D=\frac{\text{the total concentration of M(I) in the organic phase}}{\text{the total concentration of M(I) in the aqueous phase}}.$$

Results and Discussion

The statistical treatment was reported previously.[8,10] The extraction constants for the cation and the complex are defined as (here E is DBC and A^- picrate ion):

$$K_{ex0}=[ME^+A^-]_{org}[M^+]^{-1}[E]_{org}^{-1}[A^-]^{-1}, \quad (1)$$

$$K_{ex}=[ME^+A^-]_{org}[ME^+]^{-1}[A^-]^{-1}. \quad (2)$$

When $[M^+]\gg[ME^+]$, the distribution ratio can be written as

$$D=[ME^+A^-]_{org}/[M^+]=K_{ex0}[E]_{org}[A^-] \text{ and } K_{ex}\beta_1[E][A^-], \quad (3)$$

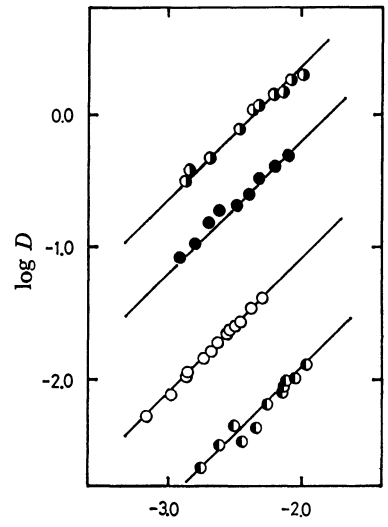

Fig. 1. Distribution ratio K^+ (◑), Rb^+ (●), Cs^+ (○), and Na^+ (◐) as a function of DBC concentration in benzene. The picrate concentration was 1×10^{-2} mol dm^{-3}. The solid lines were calculated using K_{ex0} values in Table 1.

where $\beta_1=[ME^+][M^+]^{-1}[E]^{-1}$. Then $K_{ex}=K_{ex0}K_d\beta_1^{-1}$ where $K_d=[E]_{org}/[E]$.

Figure 1 shows the distribution ratio of alkali metal ions in the benzene system as a function of the DBC concentration and Fig. 2 shows those in the chloroform system; the slope of the curves is always unity in these figures. The slope was also found to be unity for the curves obtained as a function of the picrate concentration at a constant DBC concentration. These results show that the stoichiometry in the extracted species in the organic phase should be 1 : 1 : 1 with respect to the metal ion, DBC, and picrate anion. Thus no correction for Eq. 3 due to the dissociation of the complexes was necessary. The extraction constants K_{ex0} and K_{ex} calculated from these data are listed in Table 1, together with those previously reported. Figure 3 shows the correlation of the values of log K_{ex0} and log K_{ex} with the ionic diameters of the cations.

When these metal ions are extracted with DBC, the more stable the complexes, the better the extraction which is expected. The marked difference in the extraction of the metal ions which is seen from the

Table 1. Summary of constants for univalent metals

	Na^+	K^+	Rb^+	Cs^+	Ag^+[10]	Tl^+[8]	NH_4^+[10]
Diameter/nm[12]	0.19	0.27	0.29	0.33	0.25	0.29	0.29
log $K_{ex0}(C_6H_6)$	2.1	4.4	3.8	2.9	3.6	4.5	3.6
log K_{ex} (C_6H_6)	3.8	5.6	5.6	5.0	5.1	5.9	6.2
log $K_{ex0}(CHCl_3)$	2.1	4.6	4.2	3.2	3.3	4.7	3.7
log K_{ex} $(CHCl_3)$	4.8	6.8	7.0	6.3	5.8	7.1	7.3
log β_1[12]	1.2	1.7	1.1	0.8	1.4	1.5	*ca.* 0.3

log K_d: 2.9(C_6H_6),[5] 3.9($CHCl_3$).[10]

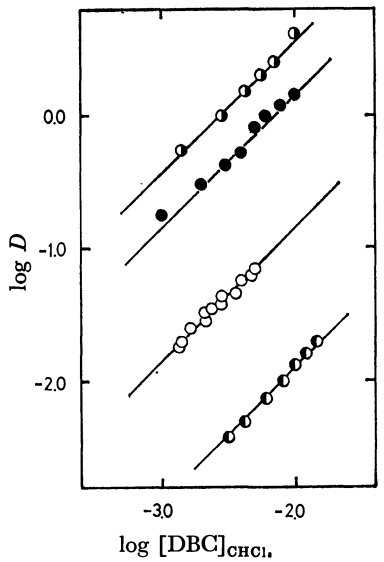

Fig. 2. Distribution ratio of K^+ (◑), Rb^+ (●), Cs^+ (○), and Na^+ (◐) as a function of DBC concentration in chloroform. The picrate concentration was 1×10^{-2} mol dm^{-3}. The solid lines were calculated using K_{ex0} values in Table 1.

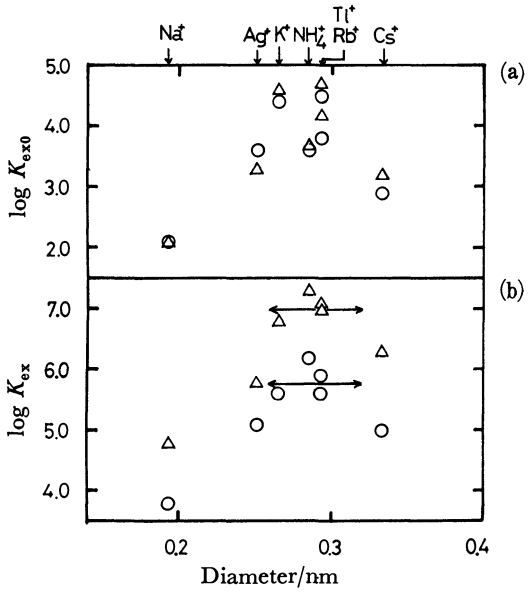

Fig. 3. Extraction constants of univalent metal ions (a) and the complexes (b) with DBC *vs.* the diameters of the ions in benzene system (○), and in chloroform (△). The arrow lines show the hole size of DBC.[2]

values of K_{ex0} in Table 1 should primarily be caused by the difference in the stability of the complexes formed in the aqueous phase. However, the extraction of the metal ions should also be affected by the extractability of the complexes. This property is represented by K_{ex} in Eq. 2. The factors affecting the extractability include:

i) Larger ion-pairs should be extracted better for otherwise identical systems. This hydrophobic tendency, however, is similar for the ion-pairs in the present study because the crown ether is always DBC and the counter-ion picrate.

ii) Stronger attractions of water molecules to the complex should cause poorer extraction. The poorer extractions of sodium(I), silver(I), and caesium(I) complexes, as seen from the K_{ex} values in Table 1, may be attributed to stronger hydrations of them (most probably of the central metal ion). The sodium(I) complex is especially poorly extracted. At present, the authors can not make any reasonable explanation for this markedly strong hydration, although Frensdorff[2] also pointed out that the extractability of sodium-dicyclohexyl-18-crown-6 complex is almost two decades lower than that of potassium complex, when the anion was picrate and the solvent was dichloromethane.

The hydration of a metal ion should be reduced by complexation with crown ethers.[3,4,11] When the size of the central metal ion is larger than the hole, the ion may project over the polyether ring. In such a case, the hydration should be stronger than that of a central metal ion fitting better with the crown ether, for example, potassium(I) for DBC. The lower K_{ex} value of the caesium(I)–DBC complex may be explained by this type of stronger hydration and thus both the instability and the stronger hydration of the caesium(I)–complex should cause the poorer extraction of caesium(I) (represented by K_{ex0}). Hydration of extracted crown ether complexes of alkali metal in nitrobenzene was previously reported.[13] The present authors have no clear explanation for these high K_{ex} values of the ammonium complex, which is much less stable than the other complexes. One possible reason for this may be inaccuracy of the stability constant of the ammonium–DBC complex which was used for the estimation of the K_{ex} values; this value was noted to be somewhat inaccurate.[12]

iii) The extraction of the free crown ether is better into chloroform than into benzene. This may be explained in terms of stronger interactions of the former diluent molecules with DBC. The same tendency is also observed among the metal–DBC complexes and

the diluent effect is somewhat larger with the complexes than with the reagent, except for sodium and silver. The relatively better extraction of the silver complex into benzene than the other metal complexes was explained in terms of the stronger interactions of benzene with the central silver ion due to the π-electrons.[10]

References

1) C. J. Pedersen, *Fed. Proc.* **27**, 1305 (1968).

2) H. K. Frensdorff, *J. Am. Chem. Soc.*, **93**, 4684 (1971); **93**, 600 (1971).

3) J. Rais, M. Kyrš and L. Kadlecová, Proc. Int. Solvent Extraction Conf., **2**, 1705 (1974); J. Rais and P. Selucky, *Radiochem. Radioanal. Lett.*, **6**, 257 (1971).

4) P. R. Danesi, H. Meider-Gorican, R. Chiarizia, and G. Scibona, *J. Inorg. Nucl. Chem.*, **37**, 1479 (1975).

5) A. Sadakane, T. Iwachido, and K. Tôei, *Bull. Chem. Soc. Jpn.*, **48**, 60 (1975).

6) Y. Marcus and L. E. Asher, *J. Phys. Chem.*, **82**, 1246 (1978).

7) M. Jawaid and F. Ingman, *Talanta*, **25**, 91 (1978).

8) T. Sekine, H. Wakabayashi, and Y. Hasegawa, *Bull. Chem. Soc. Jpn.*, **51**, 645 (1978).

9) Y. Takeda and H. Goto, *Bull. Chem. Soc. Jpn.*, **52**, 1920 (1979); Y. Takeda, *ibid.*, **53**, 2393 (1980).

10) Y. Hasegawa, N. Iizima, and T. Sekine, *J. Inorg. Nucl. Chem.*, **43**, 633 (1981); Y. Hasegawa *et al.*, unpublished data.

11) G. Eisenman, S. M. Ciani, and G. Szabo, *Fed. Proc.*, **27**, 1289. (1968): G. Eisenman, S. Ciani, and G. Szabo, *J. Membr. Biol.*, **1**, 294 (1969).

12) E. Shchori, N. Nae, and J. Jagur-Grodzinski, *J. Chem. Soc., Dalton Trans.*, **1975**, 2381.

13) T. Iwachido, M. Kimura, and K. Tôei, *Chem. Lett.* **1976**, 1101.

Liquid Crystal Formation in Binary Systems. III.[1] Effect of the Central Double Bond Linkage on the Induction of Nematic Liquid Crystals

Kotaro ARAYA and Yoshio MATSUNAGA*

Department of Chemistry, Faculty of Science, Hokkaido University, Sapporo 060

(Received December 18, 1980)

The effect of central double bond linkage on the induction of liquid crystals has been examined employing eight binary mixtures of potentially mesomorphic electron donors and acceptors of the type 4-X-C_6H_4-Z-C_6H_4-OC_2H_5-4. The central linkage Z is -N=N-, -CH=N-, or -CH=CH- group. The terminal substituent X is a dimethylamino group in the donor compounds and a nitro group in the acceptor compounds. A stable nematic liquid crystal is observable with the systems of azo-azo and azo-azomethine compounds. When the acceptor is the nitro derivative of stilbene, a 2 : 3 molecular complex is formed and no liquid crystal can be found, irrespective of whether the partner is an azo or azomethine compound. The latent induction of nematic liquid crystals in these combinations has been proved by studies on the phase diagrams of the pseudo-binary systems with a reference nematogen, azoxydianisole. The nematic liquid crystal-isotropic liquid transition temperatures of both the component compounds and the equimolar mixtures depend on the central double bond linkage: the order is -CH=CH-$>$-N=N-$>$-CH=N-. On the other hand, the order of -N=N- and -CH=N- groups is reversed in the extent of the induction of nematic liquid crystals.

In an earlier paper of this series, we reported that nematic and smectic liquid crystals can be induced by mixing of electron donors and acceptors of the type 4-X-C_6H_4-CH=N-C_6H_4-Y-4.[1] The donor molecules with a dimethylamino group as X or Y and the acceptor molecules with a nitro group as X or Y were employed in that work. The remaining terminal substituents were selected from short alkoxyl groups. The component compounds themselves were designed to be not mesomorphic. Nevertheless, they should be considered potentially mesomorphic because a liquid crystal of variable composition appears in the mixtures. The extrapolation of the observed liquid crystal-isotropic liquid transition curve to 0 mol% or 100 mol% gives a finite temperature. In other words, the strength of orientational cohesive forces in the molten component compound is not sufficient to produce a liquid crystal where the long axes of the molecules are essentially parallel. The induction or the enhancement of the thermal stability of liquid crystals in the above-mentioned mixtures was found to be maximum at a mole ratio of 1 : 1. The molecular arrangement characteristic of liquid crystals in the mixture was supposed to be achieved by supplementing the orientational cohesive forces with an electron donor-acceptor interaction. This sort of intermolecular interaction is well known to produce the alignment of the planar component molecules in ordinary crystals.

The above-mentioned Schiff bases belong to the class of compounds of the least complex structure for mesogens: that is,

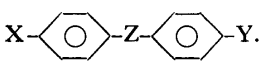

The variation of the nematic liquid crystal-isotropic liquid (N-I) transition temperatures of such single compounds with the nature of central double bond linkage Z is known to be fairly regular. The efficiency for central linkages in promoting N-I transition temperature was concluded by Knaak *et al.* to decrease in the order:

-CH=CH-$>$-N=N-$>$-CH=N-.[2]

We took up two azobenzenes and a stilbene in order to find out how the induction of liquid crystals in binary systems is affected by the central linkages. The terminal substituents other than dimethylamino and nitro groups in the present work were limited to the ethoxyl group. Only with this alkoxyl group did the induced nematic liquid crystals appear as stable single phases in the binary systems which comprise Schiff bases.[1]

Experimental

Materials. 4-Dimethylamino-4′-ethoxyazobenzene (DMAEA) was prepared by the method described by Vorländer and Wolferts: *p*-phenetidine was diazotized and coupled with *N,N*-dimethylaniline dissolved in acetic acid.[3] The supercooled melt was reported to be transformed into a liquid crystal, but neither the transition temperature nor the kind of the phase was given by them. 4-Ethoxy-4′-nitroazobenzene (ENA) was obtained by boiling 4-hydroxy-4′-nitroazobenzene in ethanolic solution with ethyl bromide and sodium ethoxide for about 1 h.[4] 4-Ethoxy-4′-nitrostilbene (ENS) was synthesized by the condensation reaction between *p*-nitrophenylacetic acid and *p*-ethoxybenzaldehyde in the presence of a small amount of piperidine. This is analogous to the preparation of the methoxy compound given by Pfeiffer.[5] The Schiff bases (azomethine compounds) were made by the condensation between *p*-X-benzaldehyde and *p*-Y-aniline. In contrast to the azobenzene and stilbene, these molecules are asymmetric and will be represented by their substituents (X, Y). Binary mixtures were prepared by the procedure given in our previous paper.[1]

Measurements. The calorimetric measurement and examination of the texture were carried out as described in our earlier work.[1]

Results and Discussion

Component Compounds. The melting points and N-I transition temperatures of the component compounds are listed in Table 1. It must be noted that the former values are higher than the latter in all the cases. The transition temperatures in this table have been deduced by the extrapolation of the N-I transition curves observed in the binary systems with mesomorphic

Table 1. Melting points (T_m) and nematic liquid crystal-isotropic liquid transition temperatures (T_t) of the component compounds

Compound	T_m/°C	T_t/°C
4-(Dimethylamino)-4′-ethoxyazobenzene	151.5[a]	117
4-Ethoxy-4′-nitroazobenzene	157[b]	110
4-Ethoxy-4′-nitrostilbene	145	115
N-[4-(Dimethylamino)benzylidene]-4-ethoxyaniline	147[c]	97.5
N-(4-Ethoxybenzylidene)-4-(dimethylamino)aniline	138	102
N-(4-Nitrobenzylidene)-4-ethoxyaniline	122[d]	85
N-(4-Ethoxybenzylidene)-4-nitroaniline	114[e]	90

a) 151 °C according to Vorländer and Wolferts (Ref. 3). b) 155 °C according to Baly *et al.* (Ref. 4). c) 147.3 °C according to Dave and Lohar (Ref. 6). d) 123.5 °C according to Dave and Lohar (Ref. 6). e) 121 °C according to Malthete *et al.* (Ref. 7).

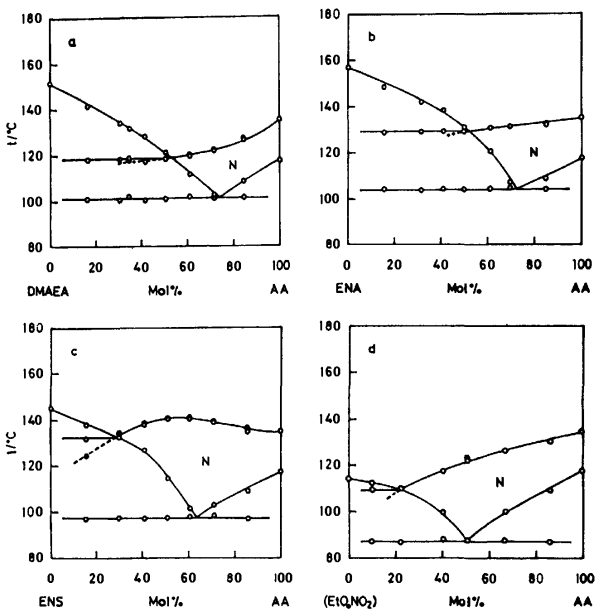

Fig. 1. Phase diagrams of (a) the 4-(dimethylamino)-4′-ethoxyazobenzene–azoxydianisole, (b) 4-ethoxy-4′-nitroazobenzene–azoxydianisole, (c) 4-ethoxy-4′-nitrostibene–azoxydianisole, and (d) *N*-(4-ethoxybenzylidene)-4-nitroaniline–azoxydianisole systems.

azoxydianisole (AA). This reference mesogen exhibits a nematic liquid crystal which is stable between 117.5 and 135°C. The phase diagrams of the systems with DMAEA, ENA, ENS, and (EtO, NO_2) are presented in Fig. 1. The open and shaded circles show the transitions recorded on the calorimetric curves during the processes of heating and cooling respectively. The phase appearing below the transitions, indicated solely by shaded circles, is metastable. When the azobenzene has an electron-donating dimethylamino group, the N-I transition curve is slightly concave upwards (see Fig. 1a). The eutectic point in this system is located at 101 °C and 74 mol% of AA. The enantiotropic N-I transition curve meets the freezing point curve of the azobenzene at 118.5 °C and 53 mol% of AA. The transition to a nematic liquid crystal of the supercooled melt could be observed down to 35 mol% of AA. At this composition, the curve is almost horizontal. As mentioned above, Vorländer and Wolferts noted that a liquid crystal can be formed when the melt of DMAEA is sufficiently supercooled. We failed to observe this; however, the latent N-I transition temperature of DMAEA is located at about 117 °C, if we judge by the extrapolation of the transition curve.

When an electron-withdrawing nitro group is attached to one of the component molecules, the N-I transition curve tends to be convex upwards (see Figs. 1b, c, and d). The extrapolation to 0 mol% of AA gives about 110 °C for the latent transition temperature of ENA, 115 °C for that of ENS, and 90 °C for that of (EtO, NO_2). The phase diagram of the (NO_2, EtO)–AA system can be reproduced from the data given by Dave and Lohar.[6] The N-I transition temperatures, therefore, can be arranged in the following order:

$$\text{DMAEA} > (\text{EtO}, \text{Me}_2\text{N}) > (\text{Me}_2\text{N}, \text{EtO})$$

and

$$\text{ENS} > \text{ENA} > (\text{EtO}, \text{NO}_2) > (\text{NO}_2, \text{EtO}),$$

in agreement with the general order reported by Knaak *et al.*[2] The nonideality of the N-I transition curve is very remarkable in the ENS–AA system (see Fig. 1c). The transition at 50 mol% of AA deviates by about 16 °C from the line joining the transition temperatures of the component compounds. The degree of nonideality of the transition curve, which is the extent of the induction of liquid crystal at 50 mol% of AA, occurs in the following order:

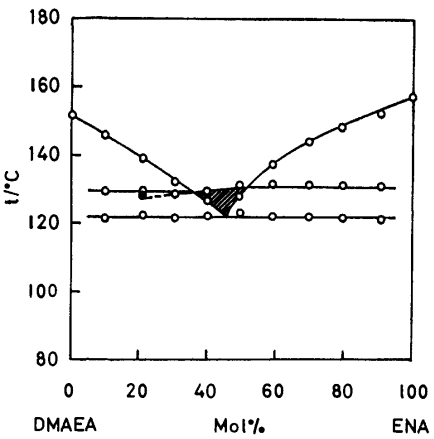

Fig. 2. Phase diagram of the 4-(dimethylamino)-4′-ethoxyazobenzene–4-ethoxy-4′-nitroazobenzene system. In the hatched area, the nematic liquid crystal is stable as a single phase.

$$ENS \simeq (NO_2, EtO) > (EtO, NO_2) > ENA.$$

The attractive interaction with AA is probably of the electron donor-acceptor type, as will be discussed later.

Systems with the Azobenzenes. The phase diagram of the DMAEA–ENA system is of the eutectic type, as is shown in Fig. 2. The eutectic point is found at 122 °C and 46 mol% of ENA. A nematic liquid crystal remains a single phase in the composition range from 36 to 52 mol% of ENA. The maximum transition temperature is 131.5 °C, observed at 60 mol%. Equilibrium diagrams such as the above have been reported by Lohar for the systems consisting of two Schiff bases: namely, (MeO, EtO) mixed with (NO_2, EtO), (Me_2N, EtO), or (MeCO, Me).[8] In his first system, the N-I transition curve is markedly convex upwards, suggesting the electron donor-acceptor interaction between the molecules of different kinds. On the other hand, the observed transitions vary more or less linearly with the composition in the remaining two systems. As the eutectic point is lowered with respect to the curve connecting the latent transition temperatures of the component compounds, a nematic liquid crystal is observable in these mixtures. Because of the strong tendency of the azobenzenes to crystallize, the transition curve observed in Fig. 2 is so short that one cannot say whether it is straight or curved. Considering the latent N-I transition temperatures given in Table 1, one can conclude that the nematic liquid crystal is induced as much as 18 °C by mixing. If there were no stability enhancement, the liquid crystal in this system would be metastable in the entire composition range.

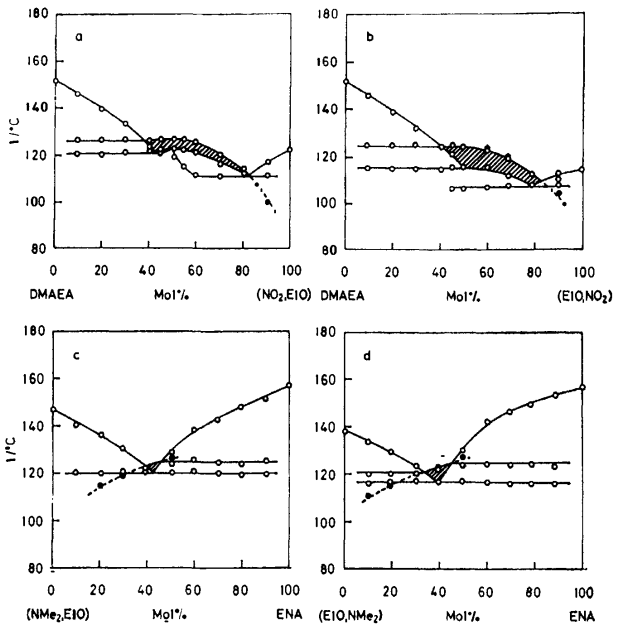

Fig. 3. Phase diagrams of (a) the 4-(dimethylamino)-4′-ethoxyazobenzene–*N*-(4-nitrobenzylidene)-4-ethoxyaniline, (b) 4-(dimethylamino)-4′-ethoxyazobenzene–*N*-(4-ethoxybenzylidene)-4-nitroaniline, (c) *N*-[4-(dimethylamino) benzylidene]-4-ethoxyaniline–4-ethoxy-4′-nitroazobenzene, and (d) *N*-(4-ethoxybenzylidene)-4-(dimethylamino)aniline–4-ethoxy-4′-nitroazobenzene systems. As to the hatched area, see the caption of Fig. 2.

The combination of DMAEA with (NO_2, EtO) or (EtO, NO_2) gives the diagram shown as Fig. 3a or b. The former system involves a congruently melting 1 : 1 molecular complex. The eutectic points are at 120.5°C and 42.5 mol% and at 111 °C and 82 mol% of the Schiff base. The molecular complex melts at 123 °C. The nematic liquid crystal appears as a stable single phase in the hatched area above the freezing point curve of the molecular complex. The area covers the composition range from 38 to 83 mol% of (NO_2, EtO). The maximum N-I transition temperature is located at 127 °C and 50 mol%. This temperature is higher by 26 °C than the mean value of the latent transition temperatures of the component compounds.

As is shown in Fig. 3b, a molecular complex is also formed in the system with (EtO, NO_2), but it is obviously less stable than that mentioned above. A peritectic point appears at 115 °C and 50 mol% and a eutectic point at 107 °C and 79 mol% of (EtO, NO_2). At the former temperature, the molecular complex decomposes, leaving the solid azobenzene and the melt of a 1 : 1 mole ratio. The composition of the solid molecular complex is not 1 : 1 mole ratio but possibly 3 : 2 or 2 : 1. A single phase nematic liquid crystal appears in the composition range from 41 to 83 mol% of the Schiff base. The maximum temperature is 124 °C. The extent of the induction is estimated to be 21 °C.

The (Me_2N, EtO)–ENA and (EtO, Me_2N)–ENA systems yield no solid molecular complex (see Figs. 3c and d). The eutectic points are located at 120 °C and 42.5 mol% and at 117 °C and 39 mol% of ENA respectively. The nematic liquid crystal is stable as a single phase in a very limited area. In the former system, the composition range is only from 39 to 46 mol% and in the latter from 33 to 45 mol% of ENA. The N-I transitions at 50 mol% occur at 126 and 127 °C respectively. The stability of the liquid crystal is enhanced by 22 °C in the former system and by 21 °C in the latter. These values are a little bit larger than the 18 °C found with the system comprising only the azobenzenes. In Fig. 3c, a horizontal transition line is supposed to exist; this extends from the point of intersection between the N-I transition curve and the freezing point curve of the Schiff base. However, no peak due to this transition could be recorded because of overlapping with a much larger peak at the eutectic temperature.

Systems with 4-Ethoxy-4′-nitrostilbene. When the stilbene is the acceptor in binary systems, a stable 2 : 3 molecular complex is formed in all the examined systems and no liquid crystal is observable (see Figs. 4a, b, and c). The regions of existence of the solid molecular complexes (the composition difference between the two eutectic points) are as follows: 69 mol% with DMAEA, 74.5 mol% with (Me_2N, EtO), and 82 mol% with (EtO, Me_2N). The stability of solid molecular complex may be considered to increase in this order. While the stilbene is yellow and (Me_2N, EtO) is pale yellow, the molecular complex is orange, suggesting the appearance of a charge-transfer absorption band. On the other hand, the color change by the molecular complex formation is hardly noticeable when the orange-colored

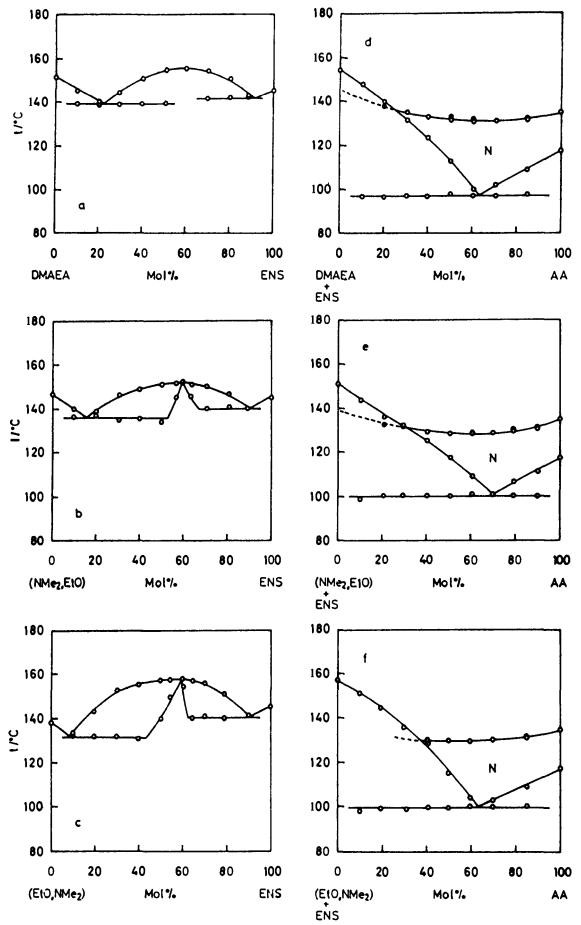

Fig. 4. Phase diagrams of (a) the 4-(dimethylamino)-4′-ethoxyazobenzene–4-ethoxy-4′-nitrostilbene, (b) *N*-[4-(dimethylamino)benzylidene]-4-ethoxyaniline–4-ethoxy-4′-nitrostilbene, and (c) *N*-(4-ethoxybenzylidene)-4-(dimethylamino)aniline–4-ethoxy-4′-nitrostilbene systems, (d) the system consisting of azoxydianisole and the equimolar mixture of 4-(dimethylamino)-4′-ethoxyazobenzene and 4-ethoxy-4′-nitrostilbene, (e) the system consisting of azoxydianisole and the equimolar mixture of *N*-[4-(dimethylamino)benzylidene]-4-ethoxyaniline and 4-ethoxy-4′-nitrostilbene, and (f) the system consisting of azoxydianisole and the equimolar mixture of *N*-(4-ethoxybenzylidene(-4-(dimethylamino)-aniline and 4-ethoxy-4′-nitrostilbene.

azobenzene is one of the components.

It seemed highly likely that the transition of the melt to a metastable nematic liquid crystal is overshadowed by the strong tendency to form a solid molecular complex; therefore, a study on the phase diagram of pseudo-binary system comprising AA and the mixture of the component compounds was undertaken. We employed equimolar mixtures instead of the solid molecular complexes because the nematic liquid crystal of the former composition is expected to be more stabilized than that of the latter composition. Such features are exemplified by the DMAEA–(EtO, NO_2) system presented in Fig. 3b. The diagrams of the pseudo-binary systems are displayed in Figs, 4d, e, and f. The latent induction of nematic liquid crystals is clearly proved in all three. The N-I transition temperature in the mixture of DMAEA and ENS is estimated by the extrapolation of the transition curve to 0 mol% of AA to be 145 °C. The deviation from the mean value of the latent transition temperatures of DMAEA and ENS is 29 °C. The induction of a nematic liquid crystal is even larger in the (Me_2N, EtO)–ENS and (EtO, Me_2N)–ENS systems: namely, 33 and 32 °C respectively.

The N-I transition temperature at 50 mol% and the extent of the induction are summarized in Table 2. For a given electron donor, the temperature varies with electron acceptor in the following order:

$$\text{ENS} > \text{ENA} > (NO_2, \text{EtO}) > (\text{EtO}, NO_2).$$

With a given acceptor, DMAEA gives a higher transition temperature than the Schiff bases do. These results conform to the order of the latent N-I transition temperatures of the component compounds; therefore, they conform also to the order of central double bond linkages reported by Knaak *et al.*[2] Of as great importance as the N-I transition temperatures, however, are the extents of the induction of nematic liquid crystals. In contrast to the transition temperature themselves, the extents of the induction are found more pronounced with the Schiff bases than with the azobenzenes: that is,

$$(Me_2N, \text{EtO}) \simeq (\text{EtO}, Me_2N) > \text{DMAEA}.$$

As to the electron acceptors, the order is consistently

$$\text{ENS} > (NO_2, \text{EtO}) > (\text{EtO}, NO_2) > \text{ENA}.$$

The coincidence between the latter series and the order of the induction of nematic liquid crystals in the systems with AA supports our proposition that AA acts as an electron donor in the examined mixtures. In summary, the order of the induction efficiency of central double bond linkages may be

$$\text{-CH=CH-} > \text{-CH=N-} > \text{-N=N-}.$$

It must be emphasized that the above order agrees

Table 2. Nematic liquid crystal-isotropic liquid transition temperature at 50 mol% and the deviation from the mean value of the transition temperatures of the component compounds
(The latter values are in parentheses)

Acceptor	Donor			
	DMAEA	(Me_2N, EtO)	(EtO, Me_2N)	AA
ENA	131 (18)	126 (22)	127 (21)	129 (6.5)
ENS	145 (29)	139 (33)	140 (32)	141 (16)
(NO_2,EtO)	127 (26)	123 (32)[a]	124 (31)[a]	125.5 (15.5)
(EtO, NO_2)	124 (21)	121 (27)[a]	119 (23)[a]	121.5 (9)

a) Taken from Ref. 1.

with that of the tendency of formation of solid molecular complexes in the systems studied here. As we see in Fig. 4, a stable molecular complex is formed in all the systems containing ENS as one of the components. Comparison of Fig. 2 with Figs. 3a and b undoubtedly leads to the conclusion that the tendency to form a solid molecular complex is higher with the Schiff base than with the azobenzene. Indeed, examining the effect of terminal alkoxyl groups in Schiff base molecules, we have found that the extent of the induction of nematic liquid crystals in binary systems is qualitatively related to the tendency of formation of solid molecular complexes.[1)]

The authors wish to express their sincere thanks to Mr. Nobuhiko Miyajima for the preparation of some component compounds. The present work was partly supported by a Grant-in-Aid for Scientific Research from the Ministry of Education, Science, and Culture (No. 543001).

References

1) Part II: K. Araya and Y. Matsunaga, *Bull. Chem. Soc Jpn.*, **53**, 3079 (1980).
2) L. E. Knaak, H. M. Rosenberg, and M. P. Servé, *Mol. Cryst. Liq. Cryst.*, **17**, 171 (1972).
3) D. Vorländer and E. Wolferts, *Ber.*, **56**, 1229 (1923).
4) E. C. C. Baly, W. B. Tuck, and E. G. Marsden, *J. Chem. Soc.*, **97**, 1494 (1910).
5) P. Pfeiffer, *Ber.*, **48**, 1777 (1915).
6) J. S. Dave and J. M. Lohar, *J. Chem. Soc., A*, **1967**, 1473.
7) J. Malthete, J. Billard, J. Canceill, J. Gabard, and J. Jacques, *J. Phys. (Paris), Colloq.*, **37**, C3-1 (1976).
8) J. M. Lohar, *J. Phys. (Paris), Colloq.*, **36**, C1-393 (1975).

Molecular Structure of Bromotrichloromethane as Determined by Gas Electron Diffraction

Shigehiro KONAKA,* Kiyo YAMAGATA, and Masao KIMURA*

Department of Chemistry, Faculty of Science, Hokkaido University, Sapporo 060

(Received December 18, 1980)

The molecular structure of $CBrCl_3$ has been determined by gas electron diffraction to be as follows: r_g(C–Cl) = $1.765_4(1_7)$ Å, r_g(C–Br) = 1.944(4) Å, and $\angle$ClCCl = $109.7_4(1_3)°$.† The mean amplitudes have been fixed at the calculated values in the data analysis. The result has been compared with the structures of related halomethanes.

The molecular structures of halomethanes have been investigated extensively,[1] but modern structural data are relatively few for halomethanes containing different halogen atoms.[2] Recently, precise structures of HCBrClF,[3] CF_3Cl,[4] CF_3Br, and CF_3I[4,5] have been reported. The C–F bond lengths of CF_3X molecules decrease with increasing electronegativity of atom X(X=H, I, Br, Cl, and F),[4] while the bond angles show only a slight and unsystematic change in value from H to F.[5] A more distinct change in value of bond angles is found for CCl_3X molecules (X=H, Cl, and F).[2] The molecular structure of bromotrichloromethane was determined only by the visual method of gas electron diffraction;[6,7] no accurate geometry of $CBrCl_3$ is available. The present study has been undertaken to supplement the structural data of halomethanes and to compare the structure of $CBrCl_3$ with the geometries of related halomethanes.

Experimental

A sample with the stated purity of at least 99% was obtained from Nakarai Chemical Co., Ltd. and used without further purification. Diffraction patterns were recorded on Kodak electron image plates using an electron diffraction unit[8] equipped with an r^3-sector at two camera distances, 109.3 and 244.3 mm. Experimental conditions were as follows: accelerating voltage, about 39 kV; sample pressure, 20 Torr; vacuum pressure during experiment, $(5-9)\times10^{-5}$ Torr; nozzle temperature, about 18 °C; beam currents, 0.15 and 0.23 μA; exposure times, about 3 and 1 min for the short and long camera distances respectively. The electron wave length was determined from the diffraction patterns of carbon disulfide taken in the same sequence of exposures. The drift of the accelerating voltage was monitored throughout the experiments by measuring the voltage drop of the standard resistance in a high-voltage source.[9] The drift of the wave length during each experimental sequence was confirmed to be less than 0.01%. The number of plates used for data analysis was four and five for the short and long camera distances respectively.

Calculation of Mean Amplitudes

A radial distribution curve obtained from long camera data is shown in Fig. 1. The overlap of C–Cl and C–Br peaks and that of Cl···Cl and Cl···Br peaks indicate difficulty in the precise determination of experimental mean amplitudes. In the data analysis, the mean amplitudes were fixed at the calculated values. Quadratic force constants are needed for the calculation of the mean amplitudes. Zietlow *et al.* reported a quadratic force field for $CBrCl_3$ based on the fundamental frequencies observed for the liquid phase.[10] Recently Clark *et al.*[11] reported the fundamental frequencies for the gas phase which are significantly different from those for the liquid. The force field given by Zietlow

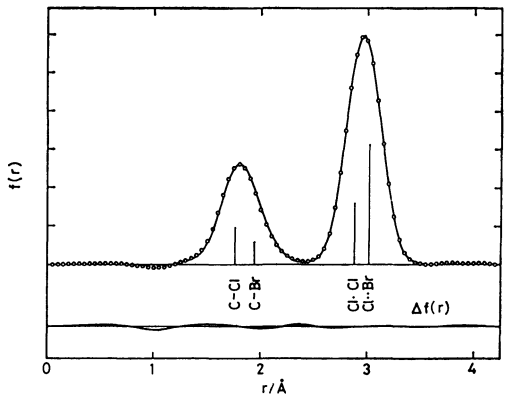

Fig. 1. Experimental (open circles) and theoretical (solid curve) radial distribution curves for $CBrCl_3$; $\Delta f(r) = f(r)^{obsd} - f(r)^{calcd}$. A damping factor, $\exp(-0.0075\,s^2)$, was used.

TABLE 1. F_s-MATRIX ELEMENTS OF $CBrCl_3$[a] (in md/Å units)

		Zietlow *et al.*[b]	Present
A_1 species	F_{11}	4.073	4.073
	F_{12}	0.182	0.166
	F_{13}	0.654	0.600
	F_{22}	0.374	0.376
	F_{23}	−0.379	−0.370
	F_{33}	2.898	2.898
E species	F_{44}	3.150	3.198
	F_{45}	−0.360	−0.343
	F_{46}	0.361	0.355
	F_{55}	0.344	0.345
	F_{56}	−0.043	−0.040
	F_{66}	0.377	0.349

a) The force constants are expressed in the symmetry coordinates defined in Ref. 12, except for the neglect of deviations from tetrahedral bond angles. b) Transformed from the internal coordinate force constants gven in Ref. 10.

† Throughout this paper 1 Å = 10^{-10} m and 1 Torr ≈ 133.3 Pa are used.

TABLE 2. CALCULATION OF THE MEAN AMPLITUDES, THE STRETCHINGS DUE TO PERPENDICULAR THERMAL VIBRATIONS, AND THE CENTRIFUGAL STRETCHINGS FOR $CBrCl_3$[a] (in 10^{-4} Å)

	C–Cl	C–Br	Cl···Cl	Cl···Br
l	517	530	689	695
$(\langle\Delta x^2\rangle+\langle\Delta y^2\rangle)/2r$	30	20	17	9
δr_{cent}	3	6	5	8

a) Calculated at 291 K.

et al. was then modified in the present study to reproduce the gas-phase frequencies. The force constants thus obtained in the symmetry coordinates are listed in Table 1 together with Zietlow's values rewritten in the symmetry coordinates. Although there is some arbitrariness in the choice of the force field, the above force constants are sufficient for our purpose, since the mean amplitudes are not sensitive to force constants chosen as long as they reproduce the vibrational frequencies correctly.[13] In Table 2 are listed the calculated values of the mean amplitudes, along with the stretchings due to the perpendicular thermal vibration and the centrifugal stretchings δr_{cent} to be used for shrinkage correction.[14,15]

Data Analysis

Optical densities measured at an interval of 1/3 mm on each photographic plate were converted to intensities.[9] The intensities were corrected for the imperfection of the sector shape and leveled by the theoretical background. Reduced molecular scattering intensities, $sM(s)$, were obtained by drawing a smooth background through the leveled intensities, then the background was revised by applying the non-negativity criterion to radial distribution curves calculated from $sM(s)$ and the drawing procedure was repeated. Data from the two camera distances covered the s-ranges of 2.8 and 17.4 $Å^{-1}$ and 6.0 and 37.4 $Å^{-1}$. The elastic and inelastic scattering factors were taken from the literature.[16] The asymmetry parameters, κ, for C–Cl and C–Br were estimated from the formula[17]

$$\kappa \simeq \frac{a}{6} l^4,$$

where the Morse parameter, a, was assumed to be 2 $Å^{-1}$. The asymmetry parameters for the non-bonded atom pairs were assumed to be zero. The parameters adjusted by the least-squares analysis of $sM(s)$ constrained to C_{3v} symmetry were r_a(C–Cl), r_a(C–Br), ∠ClCBr, and the index of resolution.[18] A conventional diagonal weight matrix was used.[9]

The observed values of $sM(s)$ and the best fit curve for one plate from each camera distance are shown in Fig. 2.[19] The parameter values obtained from each camera-distance data are listed in Table 3; these data converted to the thermal average structure are listed in Table 4 together with the weighted averages. The limits of error for the parameter values were estimated from 2.6 times the larger of the random standard deviations, σ_1 and σ_2, and the systematic errors. The errors in the scale factor were estimated to be 0.05% and 0.06% for the short and long camera distance data respectively. The systematic errors originating from the uncertainties of the anharmonicity parameters and those of correction values for the sector shape were also taken into consideration.[9] Other details of the analytical procedures are described elsewhere.[9] The experimental errors are smaller for the long distance data than for the short distance data. The agreement between the two data is satisfactory. The weighted average is given as the final result of the present work.

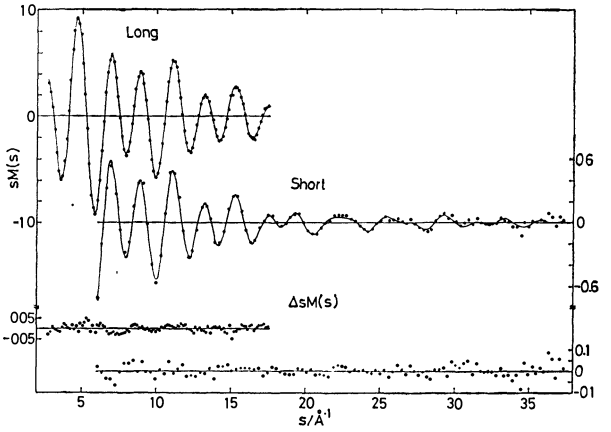

Fig. 2. Experimental (dots) and theoretical (solid curve) molecular intensities for $CBrCl_3$; $\Delta sM(s) = sM(s)^{obsd} - sM(s)^{calcd}$.

TABLE 3. RESULTS OF THE LEAST-SQUARES ANALYSIS[a] (in Å and degree units)

		Average	σ_1[b]	σ_2[b]
Short	r_a(C–Cl)	1.7638	0.0010	0.0005
	r_a(C–Br)	1.9442	0.0032	0.0025
	∠ClCBr[c]	109.27	0.10	0.09
	R[d]	0.19_8		
Long	r_a(C–Cl)	1.7639	0.0005	0.0006
	r_a(C–Br)	1.9423	0.0015	0.0016
	∠ClCBr[c]	109.18	0.05	0.04
	R[d]	0.05_4		

a) Indices of resolution are 0.86—0.88 and 0.92—0.97 for the short and long camera distance data, respectively. b) For the definitions of σ_1 and σ_2, see Ref. 20. c) Defined in the r_a structure. d) $R=\{\sum_i w_i(\Delta sM(s)_i)^2/\sum_i w_i(sM(s)_i^{obsd})^2\}^{1/2}$ where $\Delta sM(s)_i = sM(s)_i^{obsd} - sM(s)_i^{calcd}$.

TABLE 4. MOLECULAR PARAMETERS OF BROMOTRICHLOROMETHANE[a] (in Å and degree units)

Parameter	Short	Long	Weighted average
r_g(C–Cl)	$1.765_3(3_0)$	$1.765_4(2_0)$	$1.765_4(1_7)$
r_g(C–Br)	$1.945_6(8_4)$	$1.943_7(4_5)$	1.944(4)
∠ClCBr[b]	$109.2_7(2_7)$	$109.1_8(1_4)$	$109.2_0(1_3)$
∠ClCCl[b]			$109.7_4(1_3)$

a) The numbers in parentheses represent the estimated limits of error attached to the last significant digits. b) Bond angles defined in the r_a structure.

Discussion

The bond lengths of $CBrCl_3$ are compared with those of tetrahalomethanes in Fig. 3. Only modern structural data are collected here. The data for CF_3X(X=Cl, Br, I) and CF_4 are taken from Typke *et al.*[4] and Fink *et al.*'s[21] papers respectively and those for $CFCl_3$ from the Landolt-Börnstein table.[2] The structures of CCl_4 and CBr_4 have been determined in our laboratory.[22,23] Carbon-halogen bond lengths, r(C–W), in tetrahalomethanes, CWXYZ, are plotted against the sums of electronegativity values†† for the other halogen atoms, X, Y, and Z. In general, the carbon-halogen bond length decreases with an increase in the sum of the electronegativity values. This trend is in accordance with a prediction given by the valence-shell electron-pair repulsion (VSEPR) theory.[25] According to this theory, replacement of neighboring atoms by more electronegative ones shortens the bond length of interest. However, the trend of change in bond lengths is reversed to that expected by the VSEPR theory for CBr_4 and $CBrCl_3$ and for $CBrCl_3$ and CCl_4. This shows that factors governing the geometry of halomethanes are not so simple as those for most inorganic molecules.

The values of ∠ClCCl for related halomethanes are compared in Table 5. As stated before, the bond angle of the CCl_3 group changes considerably with substituents in contrast with that of the CF_3 group. It is noted that the ClCCl angle of $CBrCl_3$ is slightly larger than the tetrahedral angle. This is also inconsistent with the VSEPR theory.

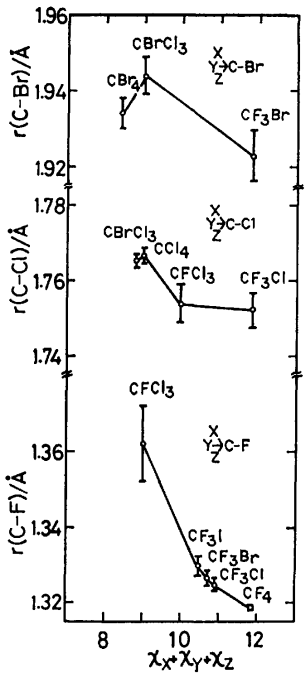

Fig. 3. Plots of carbon-halogen bond lengths of tetrahalomethanes *versus* the sums of electronegativities of adjacent halogen atoms.

†† Electronegativities were taken from Ref. 24.

Table 5. Comparison of ∠ClCCl (in degrees)

	Obsd	Calcd[a]	Calcd[b]
CCl_4	109.5	109.5	109.5
$CBrCl_3$	$109.7_4(1_3)$	110.4	110.5
$CFCl_3$	111(1)[c]	111.4	111.5
$CHCl_3$	111.3(2)[c]	112.0	112.0

a) Molecular mechanics calculation given in Ref. 26 b) Given by molecular mechanics calculation with experimental bond lengths. c) Taken from Ref. 2.

Dashevskii calculated the bond angles of halomethanes by means of molecular mechanics.[26] As shown in Table 5, column 3, his results are in fair agreement with the experimental values. In his calculation, the nonbonded atom potential of a 6-exp type was adopted and the same elastic constant was used for all the bond angles, while the bond lengths were fixed at the following values: C–H 1.10, C–F 1.34, C–Cl 1.77 and C–Br 1.93 Å. The experimental bond lengths differ from the assumed values by as much as 0.02 Å and accordingly a different choice of bond lengths may change the result. Thus, the bond angles were recalculated with the experimental bond lengths, but the change is small, as is shown in Table 5, column 4. The agreement between calculation and experiment suggests that the steric effect is an important factor governing the bond angles of trichloromethanes.

The authors wish to thank Dr. Koichi Tamagawa for his helpful discussions. The numerical computations were carried out on a HITAC M180 of the Hokkaido University Computing Center.

References

1) L. E. Sutton, "Tables of Interatomic Distances and Configuration in Molecules and Ions," The Chemical Society, London (1958) and Supplement (1965).
2) Landolt-Börnstein, New Series, Vol. II/7 (Structure Data of Free Polyatomic Molecules).
3) E. J. Jacob, *J. Mol. Struct.*, **52**, 63 (1979).
4) V. Typke, M. Dakkouri, and H. Oberhammer, *J. Mol. Struct.*, **44**, 85 (1978).
5) A. P. Cox, G. Duxbury, J. A. Hardy, and Y. Kawashima, *J. Chem. Soc., Faraday Trans. 2*, **76**, 339 (1980).
6) P. Capron and M. de Hemptine, *Ann. Soc. Sci. Brux.*, **56**, 342 (1936).
7) Y. Morino and M. Kimura, *Nippon Kagaku Zasshi*, **68**, 77 (1947).
8) Y. Murata, K. Kuchitsu, and M. Kimura, *Jpn. J. Appl. Phys.*, **9**, 591 (1970).
9) S. Konaka and M. Kimura, *Bull. Chem. Soc. Jpn.*, **43**, 1693 (1970).
10) J. P. Zietlow, F. F. Cleveland, and A. G. Meister, *J. Chem. Phys.*, **18**, 1076 (1950).
11) R. J. H. Clark and O. H. Ellestad, *J. Mol. Spectrosc.*, **56**, 386 (1975).
12) J. Aldous and I. M. Mills, *Spectrochim. Acta*, **18**, 1073 (1962).
13) H. L. Sellers and L. Schäfer, *J. Mol. Struct.*, **51**, 117 (1979).
14) K. Kuchitsu and S. Konaka, *J. Chem. Phys.*, **45**, 4342 (1966).

15) K. Kuchitsu and S. J. Cyvin, "Molecular Structures and Vibrations," ed by S. J. Cyvin, Elsevier, Amsterdam (1972), Chap. 12.
16) R. A. Bonham and L. Schäfer, "International Tables for X-Ray Crystallography," ed by J. A. Ibers and W. C. Hamilton, Kynoch Press, Birmingham (1974), Vol. 4.
17) K. Kuchitsu, *Bull. Chem. Soc. Jpn.*, **40**, 498, 505 (1966).
18) For the definitions of r_a, r_g, and r_α, see, *e.g.*, Ref. 2, p. 5 and Ref. 15.
19) The numerical experimental data on the leveled total intensity, the background, and the correlation matrix have been deposited with the Chemical Society of Japan (Document No. 8137).
20) Y. Morino, K. Kuchitsu, and Y. Murata, *Acta Crystallogr.*, **18**, 549 (1965).
21) M. Fink, C. W. Schmiedekamp, and D. Gregory, *J. Chem. Phys.*, **71**, 5238 (1979).
22) K. Suzuki, Y. Todo, and M. Kimura, 35th National Meeting of the Chemical Society of Japan, Sapporo, August 1976.
23) K. Tamagawa and M. Kimura, Symposium on Molecular Structure, Sapporo, August 1977.
24) W. Gordy and W. J. O. Thomas, *J. Chem. Phys.*, **24**, 439 (1956).
25) R. J. Gillespie, *J. Chem. Educ.*, **40**, 295 (1963); **47**, 18 (1970).
26) V. G. Dashevskii, *Zh. Strukt. Khim.*, **11**, 912 (1970).

  Bull. Chem. Soc. Jpn., 54, 2439—2443 (1981)

UV Absorption Studies of the Pyrolysis of Butane in Shock Waves

Tohru KOIKE* and Kihei MORINAGA

Department of Chemistry, National Defense Academy, Hashirimizu, Yokosuka 239

(Received December 19, 1980)

The UV absorption measurements at 216 nm were carried out for three shock-heated mixtures, 1, 2, and 2.8% n-C_4H_{10} diluted in Ar, in the temperature range of 1290—1610 K and at about half atmospheric pressures. From the initial absorption rise, which can be attributed to the CH_3 growth, the rate constant of the reaction, n-$C_4H_{10}=CH_3+n$-C_3H_7, was evaluated as $k_2=8.9\times10^{13}\exp(-71.9\,\text{kcal}/RT)$ (s^{-1}). A computer modeling using a 44-reaction mechanism including the k_2 value so evaluated could reproduce the absorption early in the reaction and in the temperature range of 1420—1610 K with a reasonable value.

The pyrolysis of butane has mainly been studied at lower temperatures using a flow tube[1-3] and a wall-less reactor.[4] The basic idea for the pyrolysis at low temperatures is almost established, and the features of the reaction are explainable through a free-radical mechanism of the Rice-Herzfeld type.[3,4]

At high temperatures, however, only a few studies of the pyrolysis have been reported.[5-7] Recently, shock-tube studies using TOF mass spectroscopy for the pyrolysis have been carried out and the observed concentration profiles of several species have been subjected to a computer modeling.[7] The results of the computer modeling at high temperatures were not as satisfactory as those in the low temperature region where the modeling results tolerably concurred with the observed profiles.[8,9]

The pyrolysis of n-C_4H_{10} has two channels for the initiation reaction:

$$n\text{-}C_4H_{10} = 2C_2H_5, \quad (1)$$

$$n\text{-}C_4H_{10} = CH_3 + n\text{-}C_3H_7. \quad (2)$$

Because of the fall-off effect, the rate constants of these unimolecular reactions at high temperatures may not accord with the values obtained by extrapolations of the rate constants at low temperatures. Therefore, it is desirable to measure the k values directly; this may be one of the most important steps in clarifying the reaction mechanism of the n-C_4H_{10} pyrolysis at high temperatures.

Recently, the absorption measurement at 216 nm of the CH_3 profile has been proved to be a useful method for studying the alkane pyrolysis. However, the measurement has thus far been applied only to the CH_4 and C_2H_6 pyrolysis[10] and the CH_3 recombination.[11]

In this study, we will estimate the k value of Reaction (2) by measuring the absorption profile at 216 nm in the n-C_4H_{10} pyrolysis. The k_2 value thus obtained is incorporated into a reaction mechanism of the pyrolysis, and the absorption profile at the early stage of the reaction is elucidated by computer modeling.

Experimental

The shock tube and the optical system used in this study have been described in a preceding paper.[12] The D_2-lamp of 30 W used before was replaced by a 200 W high-power one (Hanau, D200F) so as to gain much larger signals.

The gases used were 99.8% pure n-C_4H_{10} purchased from the Takachiho Co. and 99.999% pure Ar from the Nippon Sanso Co. The test gas compositions, n-C_4H_{10}/Ar, were 1/99, 2/98, and 2.8/97.2, while the starting pressure of the test gas was always 20 Torr (1 Torr=133.322 Pa). It was confirmed that no emission from the shocked test gas was observed.

The computer modeling for the observed absorption profiles was done using the flow model of the laminar-boundary-layer growth with limiting separation.[13]

Results and Discussion

A sample oscillogram of 216 nm light attenuation through the shocked gas is shown in Fig. 1. This oscillogram is a typical one for the present studies; *i.e.*, the absorption increases gradually right after the shock arrival at the observation window. Since no absorption has been reported for CH_4 and C_2H_6 at 216 nm,[14] n-C_4H_{10} was also expected to have no absorption band in this wavelength region.

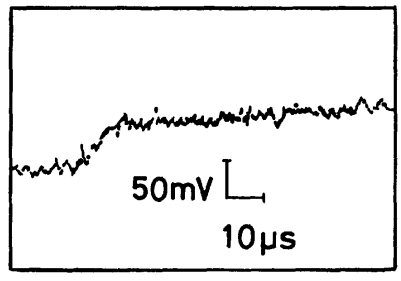

Fig. 1. A representative oscillogram for 2% n-C_4H_{10} in Ar mixture, $P_1=20$ Torr, and $T_2=1436$ K.

The absorption measurement of C_2H_5 in this wavelength range has been reported;[15] the absorptivity at 216 nm is at least 30 times smaller than that of CH_3. The effect of n-C_3H_7 on the measured absorption was assumed to be negligibly small. The validity of this assumption will be confirmed below by a computer modeling; the steady [n-C_3H_7] modeled is about 4 orders of magnitude less than the [CH_3]. Therefore, it is reasonable to assume that the absorption early in the reaction is entirely due to CH_3.

The primary reactions of the CH_3 radical at the early stage of the reaction are:

$$CH_3 + n\text{-}C_4H_{10} = CH_4 + n\text{-}C_4H_9, \quad (5)$$

$$= CH_4 + s\text{-}C_4H_9, \quad (6)$$

$$s\text{-}C_4H_9 = CH_3 + C_3H_6, \quad (11)$$

$$n\text{-}C_3H_7 = CH_3 + C_2H_4. \quad (24)$$

The methyl radical produced by Reaction 2 decreases as a result of metathetical reactions (5) and (6). The unimolecular decompositions of the radicals thus produced, Reactions 11 and 24, also give CH_3. At a very early time in the reaction, for example, lab. time of 0.2 μs, only Reactions 2 and 24 are important for evaluating the CH_3 profile; this can be confirmed by comparing the value of the rate of each reaction obtained by the computer modeling to be discussed later. The steady state assumption for n-C_3H_7 leads to the following expression of CH_3 production:

$$k_2 = (\mathrm{d}[CH_3]/\mathrm{d}t)_{t\to 0}/(2[n\text{-}C_4H_{10}]_0)$$

where t=particle time and $[n\text{-}C_4H_{10}]_0$ is the shock-front concentration of n-C_4H_{10}. To evaluate the k_2 value using the above equation, it is necessary to estimate the absorptivity of CH_3, which correlates the measured absorption to $[CH_3]$. We adopted the absorptivities reported by Tsuboi[10] and Glänzer *et al.*[11]

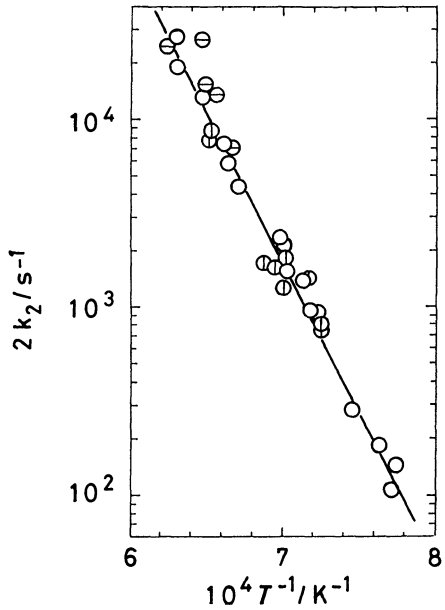

Fig. 2. Arrhenius plots for k_2. The symbols used are as follows.
⊖: For 1% n-C_4H_{10} in Ar, ⓘ: for 2% n-C_4H_{10} in Ar, and ○: for 2.8% n-C_4H_{10} in Ar.
The line shows a least squares fitting for the data points.

The k_2 values thus obtained are shown *vs.* $10^4/T$ in Fig. 2. A least-squares calculation for the relation provided the following Arrhenius expression:

$$k_2 = 8.9\times 10^{13} \exp(-71.9\ \mathrm{kcal}/RT) \quad (s^{-1}).$$
$$(1\ \mathrm{kcal} = 4.184\ \mathrm{kJ})$$

The rate constants of the metathetical reactions are reported to show deviations from the Arrhenius plots, and the actual values of the rate constants at high temperatures are larger than those extrapolated from the k values measured at low temperatures.[2] It is also well known that the k value of the metathetical reaction decreases with an increase in the structual complexity of the radicals accompanying the reaction.[3] At an early time in the n-C_4H_{10} pyrolysis, [H] is much smaller than $[CH_3]$ and $[C_2H_5]$. Therefore, it is expected that the value of k[R], where k and [R] are the rate constant and the concentration of the radical in the metathetical reaction respectively, will change depending on both the temperature and the reaction time. As for the unimolecular decompositions of the radical, the rate constant may be in the fall-off range under the present experimental conditions.

To elucidate the roles of these metathetical reactions and unimolecular decompositions of the radicals in the n-C_4H_{10} pyrolysis, a computer modeling was carried out for the initial stage of the reaction. The absorption at the lab. time of 10 μs, A_{10}, defined as $A_{10}=\ln(I_0/I_{10})$ where I_0 and I_{10} are the incident-light intensity and the transmitted intensity at the time respectively, is calculated and plotted in Fig. 3.

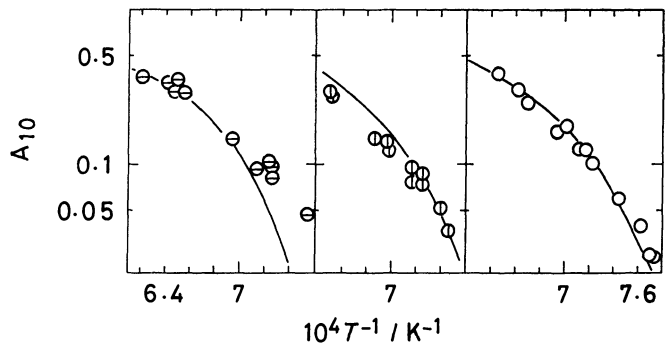

Fig. 3. The relation between A_{10} and $10^4/T$.
The symbols used are the same as those in Fig. 2.
The lines show modeled A_{10} for the three mixtures.

Table 1 shows the final reaction mechanism of the n-C_4H_{10} pyrolysis assumed in this study. The reaction mechanism consists of 44 reactions with the maximum value of the rate larger than 10^{-7} (mol cm^{-3} s^{-1}) during the initial reaction period (10 μs). The rate constant of each reaction was taken from several sources except in a few cases. The k_{-1} value, the rate constant of the reverse reaction (−1), was estimated from the geometric mean rule using the following equation:

$$k_{-1} = k_{18}^2/(4k_{-31}[M]).$$

The k_{-31} value was evaluated from $k_{-31}=k_{31}/K_{31}$, where K_{31} is the equilibrium constant and [M]=density. The k values of the metathetical reactions, (3)—(8), were taken from those in the proposed reaction mechanism.[2,3] Each butyl radical has two channels for the decomposition. One of them is to H and butene, Reactions 9 and 10. The others are Reactions 11 and 12, which obey the β-bond breaking rule;[16] n-C_4H_9 decomposes to C_2H_4 and C_2H_5 and s-C_4H_9 to CH_3 and C_3H_6. Reactions 13—17 are primary steps in the butene pyrolysis. The k values adopted for Reactions 9—14 and 17 are those reported for the high pressure limit. Since these radical decompositions are expected to have different sensitivity spectra for the modeled A_{10} value, while their k values could be corrected for the fall-off with a similar factor, we left the k values of radical decompositions at the values shown in Table 1. In the reactions of the C_3 species, 18—30, their k values are taken mainly from

Table 1. Reaction mechanism and rate constants
$k=A\exp(-E/RT)$ (cm, mol, s, and kcal units)

	Reaction	log A	E	Ref.
1)	n-$C_4H_{10}=C_2H_5+C_2H_5$	$k_{-1}=10^{12.1}$		See text
2)	n-$C_4H_{10}=CH_3+n$-C_3H_7	13.9	71.9	This work
3)	C_2H_5+n-$C_4H_{10}=C_2H_6+n$-C_4H_9	14.0	22.8	3)
4)	C_2H_5+n-$C_4H_{10}=C_2H_6+s$-C_4H_9	13.5	20.1	3)
5)	CH_3+n-$C_4H_{10}=CH_4+n$-C_4H_9	14.7	20.9	3)
6)	CH_3+n-$C_4H_{10}=CH_4+s$-C_4H_9	14.7	18.2	3)
7)	$H+n$-$C_4H_{10}=H_2+n$-C_4H_9	15.1	16.7	3)
8)	$H+n$-$C_4H_{10}=H_2+s$-C_4H_9	15.0	14.0	3)
9)	n-$C_4H_9=C_4H_8(1)$*$+H$	14.4	38.0	a)
10)	s-$C_4H_9=C_4H_8(2)$*$+H$	14.4	37.5	a)
11)	s-$C_4H_9=CH_3+C_3H_6$	14.2	33.9	a)
12)	n-$C_4H_9=C_2H_4+C_2H_5$	13.6	29.0	a)
13)	$C_4H_8(1)=CH_3+C_3H_5$	16.9	73.0	b)
14)	$C_4H_8(2)=CH_3+C_3H_5$	16.0	80.0	c)
15)	$H+C_4H_8(1)=H_2+C_4H_7$	13.7	39.0	9)
16)	$H+C_4H_8(2)=H_2+C_4H_7$	13.7	38.0	9)
17)	$C_4H_7=C_2H_4+C_2H_3$	14.0	37.0	9)
18)	$CH_3+C_2H_5=C_3H_8$	12.9	0.0	17)
19)	$CH_3+C_3H_8=CH_4+i$-C_3H_7	12.6	10.3	d)
20)	$CH_3+C_3H_8=CH_4+n$-C_3H_7	12.6	10.3	d)
21)	$H+C_3H_8=H_2+i$-C_3H_7	13.8	8.0	e)
22)	$H+C_3H_8=H_2+n$-C_3H_7	13.8	8.0	e)
23)	i-$C_3H_7=C_2H_4+CH_3$	12.0	34.5	a)
24)	n-$C_3H_7=C_2H_4+CH_3$	13.8	33.2	a)
25)	i-$C_3H_7=H+C_3H_6$	14.3	41.3	a)
26)	n-$C_3H_7=H+C_3H_6$	13.8	38.0	a)
27)	$C_3H_6+M=C_2H_3+CH_3+M$**	18.0	74.0	24)
28)	$C_3H_6=H+C_3H_5$	13.0	78.0	f)
29)	$H+C_3H_6=H_2+C_3H_5$	10.1	1.5	g)
30)	$C_3H_5=H+C_3H_4$	13.6	70.0	g)
31)	$C_2H_6+M=CH_3+CH_3+M$	111.3—25.26 log T	160.0	18)
32)	$C_2H_6+H=C_2H_5+H_2$	14.1	9.4	h)
33)	$C_2H_5+M=C_2H_4+H+M$	15.3	30.1	18)
34)	$CH_3+CH_3=C_2H_5+H$	14.9	26.6	10, 19)
35)	$CH_3+CH_3=C_2H_4+H_2$	16.0	32.0	10, 19)
36)	$C_2H_5+H=C_2H_4+H_2$	12.3	0.0	h)
37)	$CH_4+M=CH_3+H+M$	17.5	90.6	i)
38)	$CH_4+H=CH_3+H_2$	14.9	15.1	j)
39)	$C_2H_4+H=C_2H_3+H_2$	15.7	22.9	k)
40)	$C_2H_3+M=C_2H_2+H+M$	15.3	30.1	l)
41)	$CH_3+C_2H_5=CH_4+C_2H_4$	11.7	0.0	See text
42)	$C_2H_5+C_2H_5=C_2H_4+C_2H_6$	11.7	0.0	See text
43)	$CH_3+C_2H_4=CH_4+C_2H_3$	11.0	0.0	Assumed
44)	n-$C_4H_9=s$-C_4H_9	17.7	41.0	21)

a) S. W. Benson and H. E. O'Neal, "Nat. Stand. Ref. Data Ser.," NBS, No. 21 (1970). b) T. Kunugi, T. Sakai, K. Soma, and Y. Sakai, *Ind. Eng. Chem. Fundam.*, **9**, 314 (1970). c) P. Jeffers and S. H. Bauer, *Int. J. Chem. Kinet.*, **6**, 763 (1974). d) A. Lifshitz and M. Franklach, *J. Phys. Chem.*, **79**, 686 (1975). e) A. F. Trotman-Dickenson and G. S. Milne, "Nat. Stand. Ref. Data Ser.," NBS, No. 9 (1967). f) K. J. Laidler and B. W. Wojciechowski, *Proc. R. Soc. London, Ser. A*, **259**, 257 (1960). g) A. Amano and M. Uchiyama, *J. Phys. Chem.*, **67**, 1242 (1963). h) P. Camilleri, R. M. Marshall, and J. H. Purnell, *J. Chem. Soc., Faraday Trans. 1*, **70**, 1434 (1974). i) W. C. Gardiner, Jr., T. Koike, and T. Tanzawa, in preparation. j) Th. Just and P. Roth, *Ber. Bunsenges. Phys. Chem.*, **79**, 682 (1975). k) Th. Just, P. Roth, and R. Damm, "16th Int. Symp. Combust.," The Combustion Institute, Pittsburgh (1977), p. 961. l) S. W. Benson and G. R. Haugen, *J. Phys. Chem.*, **71**, 1735 (1967). * $C_4H_8(1)$=1-butene and $C_4H_8(2)$=2-butene. ** [M]=$(4.0\pm0.3)\times10^{-6}$ (mol cm^{-3}).

those determined in the C_3H_8 pyrolysis study in shock waves.[17] The k values of Reactions 31—40 are also taken form those derived in the C_2H_6 pyrolysis study in shock waves.[18] In Reactions 31—40, the k values of the two channels of CH_3+CH_3 into C_2H_5+H and $C_2H_4+H_2$ were determined recently.[10,19] Thus, the reaction mechanism in Table 1 has three channels for CH_3+CH_3, Reactions, —31, 34, and 35. The dispropor-

tionations, (41)—(43), which have only a minor effect on the modeling results, were included and their k values were assumed to be around 10^{11}; the ratios, k_{-1}/k_{42} and k_{18}/k_{41}, are expected to be larger than 1.[20] In comparison with the reaction mechanisms of the C_2H_6 and C_3H_8 previously reported,[17,18] it is characteristic of the 44-reaction mechanism that the isomerization reaction of C_4H_9, Reaction 44, is included.[21]

Our original computer program was devised to calculate the concentration of each species. To compare directly the computer modeling results with the A_{10} values shown in Fig. 3, the concentration of each species was converted to the absorption, A, in the program according to this equation:

$$A = \sum A_i = \sum C_i a_i d,$$

where A_i, C_i, and a_i are the absorption, the concentration, and the absorptivity of a species subscribed i respectively, and where d=optical path length (=7.2 cm). At 216 nm, the species which have large absorptivities are CH_3, C_3H_6, C_2H_4, and C_2H_2. The absorptivity of CH_3 was taken from the values previously reported[10,11] and was expressed by a 4th-order polynominal fit for the temperature. The absorptivity of the other three species were measured from the absorption at the shock front for mixtures diluted in Ar.[12,22] The following expressions of the absorptivity-temperature relation, together with that for CH_3, were incorporated in the computer program:

$$\log a(C_2H_4) = -3430/T + 6.66,^{12}$$
$$\log a(C_2H_2) = -1829/T + 5.88,^{12}$$
$$\log a(C_3H_6) = -3662/T + 8.15.^{22}$$

The lines in Fig. 3 show the A_{10} values for the three mixtures modeled using the reaction mechanism shown in Table 1. We noticed the following disagreements in the two mixtures, though the lines almost went through the data points. In the 1% mixture, the modeled A_{10} value is smaller than the measured value at temperatures lower than 1400 K. The effect of the secondary reactions on the A_{10} value may be negligibly small under the present experimental conditions. Therefore, it is probable that the k_1 and/or k_2 values used are not appropriate to the modeling of the A_{10} value at these low temperatures. The k_2 values shown in Fig. 2 seem to be on a straight line at temperatures as low as 1290 K. However, the light attenuations due to the absorption measured at these low temperatures are small, and the k_2 value evaluated may have much larger data-reading errors than those at high temperatures. As for the k_1 value used, it can be adjusted so as to reproduce the experimental A_{10} value. No further fitting of the modeled A_{10} value to the measured value by adjusting these k values was done because Reactions (1) and (2) have a similar sensitivity for the A_{10}. In the 2% mixture, the modeled A_{10} is slightly larger than the measured one at high temperatures. However, we do not have any clear-cut explanations for the disagreement because almost the same sensitivity spectra were obtained for the 2 and 2.8% mixtures; a nice agreement between the two values is shown in Fig. 3 for the 2.8% mixture.

In the 2.8% mixture, the contributions to the modeled absorption are CH_3; 90%, C_3H_6; 6%, and C_2H_4; 3% at 1300 K and CH_3; 60%, C_3H_6; 27%, and C_2H_4; 12% at 1550 K, and it is found that the effect of C_2H_2 on the A_{10} value is negligible under the present experimental conditions. Thus, it is clear that, with an increase in the temperature, the products by the pyrolysis have much influence on the A_{10} value.

No further modeling for the reported experimental results[5-7] and for the absorption after 10 μs measured in this study were done. Propylene is one of the primary products in the n-C_4H_{10} pyrolysis, but the reaction mechanism of the C_3H_6 pyrolysis at high temperature has not yet been determined.[23] The reaction mechanism proposed by Burcat[24] is not satisfactory in explaining the experimental results measured by means of a 3.39-μm He-Ne laser absorption; that experiment was carried out under conditions similar to the present ones.[23] Since C_3H_6 is subjected to further decomposition as the reaction proceeds at these high temperatures, the ambiguity of the reaction mechanism may give an erroneous result for the modeled product distribution. Moreover, preliminary experimental results[22] by means of the absorption at 216 nm indicate that a large absorption by an unidentified product was measured in the C_3H_6 pyrolysis.

References

1) D. D. Hughes, R. M. Marshall, and J. H. Purnell, *J. Chem. Soc., Faraday Trans. 1*, **70**, 594 (1974).
2) P. D. Pacey and J. H. Purnell, *Int. J. Chem. Kinet.*, **4**, 657 (1972).
3) D. R. Powers and W. H. Corcoran, *Ind. Eng. Chem., Fundam.*, **13**, 351 (1974).
4) G. L. Pratt and D. Rogers, *J. Chem. Soc., Faraday Trans. 1*, **75**, 2688 (1979).
5) T. P. Izod, G. B. Kistiakowsky, and S. Matsuda, *J. Chem. Phys.*, **56**, 1377 (1972).
6) Y. Yoshida, W. Hirose, M. Kitazaki, and F. Kagano, *Proc. 11th Shock Tube Symp.*, Univ. of Washington Press, Seattle (1977), p. 358.
7) K. Fritz and H. Grönig, *Proc. 11th Shock Tube Symp.*, Univ. of Washington Press, Seattle (1977), p. 383.
8) D. L. Allara and D. Edelson, *Int. J. Chem. Kinet.*, **7**, 479 (1975).
9) K. M. Sundaram and G. F. Froment, *Ind. Eng. Chem., Fundam.*, **17**, 174 (1978).
10) T. Tsuboi, *Jpn. J. Appl. Phys.*, **17**, 709 (1978).
11) K. Glänzer, M. Quack, and J. Troe, *16th Int. Symp. Combust.*, The Combustion Institute, Pittsburgh (1977), p. 949.
12) T. Koike and K. Morinaga, *Bull. Chem. Soc. Jpn.*, in press.
13) W. C. Gardiner, Jr., B. F. Walker, and C. B. Wakefield, "Shock Waves in Chemistry," ed by A. Lifshitz, Dekker, New York (1980), Chap. 1.
14) G. Hertzberg, "Molecular Spectra and Molecular Structure," D. Van Nostrand, N. Y. (1966), Vol. 3.
15) D. A. Parkers and C. P. Quinn, *J. Chem. Soc., Faraday Trans. 1*, **72**, 1952 (1976).
16) D. A. Leathard and J. H. Purnell, *Ann. Rev. Phys. Chem.*, **21**, 197 (1970).
17) T. Koike and W. C. Gardiner, Jr., *J. Phys. Chem.*, **84**, 2005 (1980).
18) D. B. Olson, T. Tanzawa, and W. C. Gardiner, Jr.,

Int. J. Chem. Kinet., **11**, 23 (1979).
19) K. A. Bhaskaran, P. Frank, and Th. Just, *Proc. 12th Shock Tube Symp.*, Hebrew Univ. Press, Jerusalem (1980), in press.
20) S. W. Benson, *Adv. Photochem.*, **2**, 1 (1964).
21) M. C. Lin and M. H. Back, *Can. J. Chem.*, **44**, 2369 (1966).
22) T. Koike and K. Morinaga, unpublished results.
23) T. Koike and W. C. Gardiner, Jr., in preparation.
24) A. Burcat, *Fuel.*, **54**, 87 (1975).

The Determination of the Chemical Diffusion Coefficient of n-Type AgBr by Means of a D.c. Polarization Cell

Jun SASAKI,* Junichiro MIZUSAKI,* Shigeru YAMAUCHI, and Kazuo FUEKI

Department of Industrial Chemistry, Faculty of Engineering, The University of Tokyo, Hongo, Bunkyo-ku, Tokyo 113

(Received December 23, 1980)

The electronic conductivity of AgBr and the chemical diffusion coefficient of n-type AgBr were measured by means of a d.c. polarization cell, ⊖ Ag/AgBr/inert electrode ⊕, in the temperature range from 325 °C to 400 °C. In order to suppress the electrolysis of AgBr, a platinum plate was used instead of carbon as the inert anode. The chemical diffusion coefficient, $\tilde{D}$, was determined by two methods. One was the intermediate probe method (IP method) whereby the relaxation of the voltage between the Ag reversible electrode and the Pt intermediate probe, inserted into the middle of AgBr, was followed after an abrupt change in the polarization voltage. The other was the open-circuit method (OC method) whereby the terminal voltage of the cell was followed after the circuit of the cell had been opened. The electronic conductivity in the steady state was independent of the nature of the inert electrodes (Pt or C), provided that the inert electrode was completely sealed. However, it took more time for the cell with a carbon electrode to reach the steady state than that with a platinum one. The chemical diffusion coefficient, $\tilde{D}$, determined by the IP method for the Ag/AgBr/Pt cell agreed with that for the Ag/AgBr/C cell. The chemical diffusion coefficient, $\tilde{D}$, determined by the OC method for the Ag/AgBr/Pt cell agreed with that obtained by the IP method. The chemical diffusion coefficients determined by these methods were expressed by

$$\tilde{D} = 3.0 \times 10^3 \exp\left(\frac{-89.0\ \mathrm{kJ\ mol^{-1}}}{RT}\right) / \mathrm{cm^2\ s^{-1}}.$$

No chemical diffusion coefficient can be obtained by the OC method for the Ag/AgBr/C cell, because of the slow diffusion of the Br_2 gas produced by the electrolysis of AgBr from the carbon electrode.

Since the application of the d.c. polarization technique to the investigation of solid ionic conductors by Hebb[1] and Wagner,[2] the method has been used widely to determine the electronic conductivities or chemical diffusion coefficients of halides of silver and copper.[3–19] Mizusaki *et al.*,[7–10] for instance, investigated silver halides by using the following cell:

$$\mathrm{Ag/AgX(X = Cl, Br, I)/C.} \qquad (1)$$

Using the improved cell configuration shown in Fig. 1(a) (A-type cell), they found several important facts as follows:

(i) One can determine the chemical potential profile in AgX under d.c. polarization by measuring the voltage between the Ag electrode and the Pt probes inserted into AgX. The chemical potential profile obtained experimentally agrees with that expected from Wagner's theory.[2]

(ii) In order to obtain the electronic conductivity, the inert electrode (ion-blocking electrode) must be completely sealed.

(iii) The chemical diffusion coefficient, $\tilde{D}$, in AgX can be determined from the relaxation of the voltage between the Ag electrode and the Pt probe inserted into AgX after an abrupt change in the voltage applied to the cell.

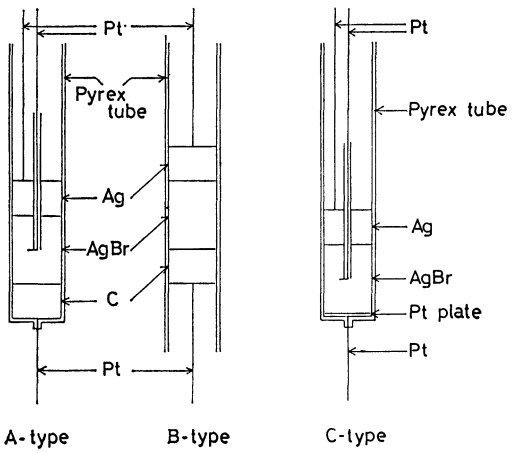

Fig. 1. Configurations of d.c. polarization cell.

The methods for the determination of the chemical diffusion coefficient by using the d.c. polarization cell[6,9,11–17] were classified as follows:

(i)[6,11–15] The method whereby the current is measured with the passage of time after the abrupt change in the polarization potential applied to the cell. (voltage step-transient current method; TC method).

(ii)[9] The method whereby the potential difference between the reversible (reference) electrode and the probe inserted into the sample is measured with the passage of time after a change in the polarization potential (voltage step-intermediate probe method; IP method).

(iii)[16,17] The method whereby the voltage of the cell is followed after the cell circuit has been opened (open circuit method; OC method).

Raleigh[18,19] measured the time change in the current by the TC method using the Ag/AgBr/Pt (or C) cell; he found that the current-time curve involved several time constants. The current was interpreted by the super-imposition of the current due to the charging of the double layer of the AgBr/Pt interface, the current due to the redistribution of electronic carriers within AgBr (chemical diffusion), and the electrolytic current of AgBr. It seems to be difficult, however, to measure these currents separately. Therefore, the TC method is not appropriate for determining the chemical diffusion coefficient.

The IP method has the advantage of measuring the

change in the chemical potential profile directly. However, the influence of the electronic current flowing during the relaxation on the mass transfer caused by the chemical diffusion is not clear. From this point of view, the OC method is considered to be superior to the IP method, because the transient current does not flow during the chemical relaxation.

Weiss[16] determined $\tilde{D}$ in AgBr by means of the OC method using the cell shown in Fig. 1(b) (B-type cell). Since the carbon electrode was exposed to the inert atmosphere, it was doubtful that the decay of the open-circuit voltage gave the correct value of $\tilde{D}$.[9] Even if an A-type cell is used, the Br_2 gas produced by the electrolysis of AgBr diffuses and is absorbed by the carbon electrode. Therefore, the decay of the open-circuit voltage may be supposed not to correspond to the chemical diffusion in AgBr because of the influence of the slow diffusion of Br_2 gas in the carbon electrode. In order to eliminate the influence of Br_2-gas diffusion in the carbon electrode, platinum should be used instead of carbon as follows:

$$\ominus \text{ Ag/AgBr/Pt } \oplus. \qquad \text{(II)}$$

Moreover, the cell configuration shown in Fig. 1(c) (C-type cell) should be used.

The present work aims to determine the electronic conductivity by the d.c. polarization method, and $\tilde{D}$ by means of the IP method and the OC method.

Experimental

Circuit and Measurement Procedure. Figure 2 shows a schematic diagram of the experimental circuit. The polarization voltage was applied by means of a potentiostat. The current was determined by measuring the *IR* drop which appeared between the two ends of a standard resistance, R_s, connected with the cell in series. The potential difference $E(X=L/2)$ between the Ag electrode and Pt probe inserted into AgBr and the open-circulit voltage were recorded by means of a voltage follower with high input impedance.

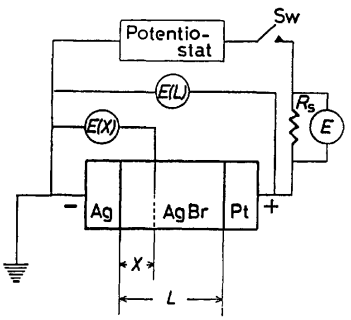

Fig. 2. Schematic diagram of experimental circuit.

IP Method: After the steady state under the applied voltage, E_1, had been attained, a second voltage, E_2, was suddenly applied to the cell by means of a function generator. The time changs in $E(X=L/2)$ and the current were recorded.

OC Method: After the steady state under the applied voltage, $E(L)$, has been attained, the circuit was opened and the time change in $E(L)$ was recorded.

The experiment was carried out in the temperature range from 325 to 400 °C. A polarization voltage below 300 mV was applied. Under these experimental conditions, the electronic conduction of AgBr was of the n-type.

Samples and Cell Configurations. Rod-like single crystals of AgBr were prepared from the powder material of a 99.999% purity by means of the Bridgman method. The rod thus obtained was cut into disks 10 mm in diameter.

Figure 3 shows the construction of the cell. The surface of a platinum plate with platinum-lead wire was polished with 1 μm of alumina abrasive powder and then cleaned with an alkali cleaning solution. The platinum plate was then carefully sealed in a Pyrex tube so that no vacant spaces remained between the Pyrex tube and the platinum plate.

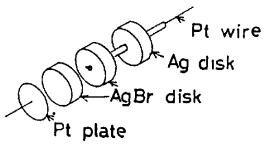

Fig. 3. Cell and samples.

Two AgBr disks of the same size were prepared. A hole 1.2 mm in diameter was drilled in the center of one AgBr disk for inserting the Pt probe. A platinum wire was insulated by means of a mullite tube 1.2 mm in diameter, its tip placed at the center of the interface of two AgBr disks. The surface of each AgBr disk was polished with 1 μm of alumina abrasive powder and cleaned by the use of an ultrasonic cleaner. The cell was constructed in a Pyrex tube 10 mm in inner diameter and was pressed with a slight pressure so that the side surface of the AgBr disk was assured of a good contact with the inside wall of the Pyrex tube as a result of the plastic deformation of AgBr at high temperatures. Thus, a good sealing of the ion-blocking electrode could be obtained.

In the present study, two types of cells, the A-type cell and the C-type cell shown in Fig. 1, were employed. The A-type cell was constructed in a way essentially similar to the C-type cell.

Results and Discussion

Electronic Conductivity. Under the steady state of d.c. polarization, the electronic current flowing in the cell (I) or (II) is represented by:[2,8,10]

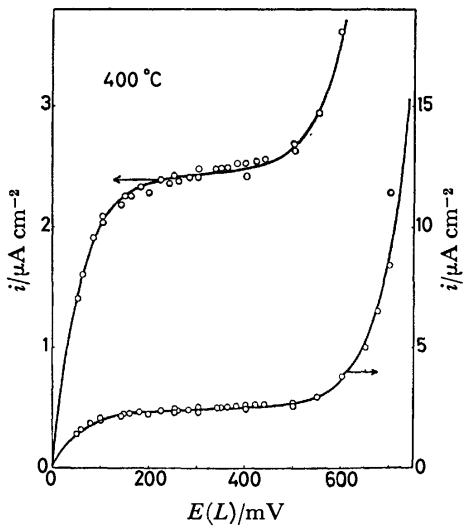

Fig. 4. Plot of i *vs.* $E(L)$ for C-type cell.

$$\frac{iFL}{RT} = \sigma_e^\circ\left[1 - \exp\left(-\frac{E(L)F}{RT}\right)\right] + \sigma_h^\circ\left[\exp\left(\frac{E(L)F}{RT}\right) - 1\right], \quad (1)$$

where L is the thickness of the electrolyte, $E(L)$ is the applied voltage, i is the current density, and σ_e° and σ_h° are the electronic conductivities due to electrons and holes in AgBr in equilibrium with Ag respectively.

Figure 4 shows the plots of i *vs.* $E(L)$ for the C-type cell at 400 °C. By dividing both sides of Eq. 1 by $\exp(E(L)F/RT)-1$, we obtain:[20]

$$\frac{iFL}{RT}\frac{1}{\exp\left(\frac{E(L)F}{RT}\right) - 1} = \sigma_e^\circ \exp\left(-\frac{E(L)F}{RT}\right) + \sigma_h^\circ. \quad (2)$$

From the gradient of the plot of Eq. 2, σ_e° can be determined. Similarly, σ_h° can be determined from the gradient of the plot of the following equation:[20]

$$\frac{iFL}{RT}\frac{1}{1 - \exp\left(-\frac{E(L)F}{RT}\right)} = \sigma_e^\circ + \sigma_h^\circ \exp\left(\frac{E(L)F}{RT}\right). \quad (3)$$

Figure 5 shows the plot of Eq. 2, with a good linear relationship. From the slope of the plot, σ_e° was determined. Similarly, σ_h° was determined from the plot of Eq. 3.

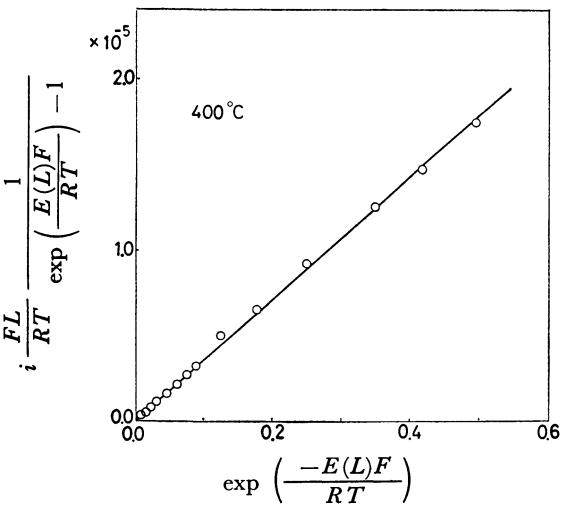

Fig. 5. Plot of $i\frac{FL}{RT}\frac{1}{\exp\left(\frac{E(L)F}{RT}\right)-1}$ *vs.* $\exp\left(\frac{-E(L)F}{RT}\right)$ for C-type cell.

According to Mizusaki *et al.*,[8,10] we can calculate σ_e and σ_h as functions of the chemical potential of bromine. The results are shown in Fig. 6. The broken line indicates the results obtained by Mizusaki *et al.*[8] using the A-type cell. The two sets of results are in good agreement, within the limit of experimental error.

The chemical potential profiles under a steady state were also measured for the C-type cell. The results were in good agreement with those obtained by Mizusaki *et al.*[7] Therefore, it may be concluded that the chemical potential profiles can be well interpreted on the basis

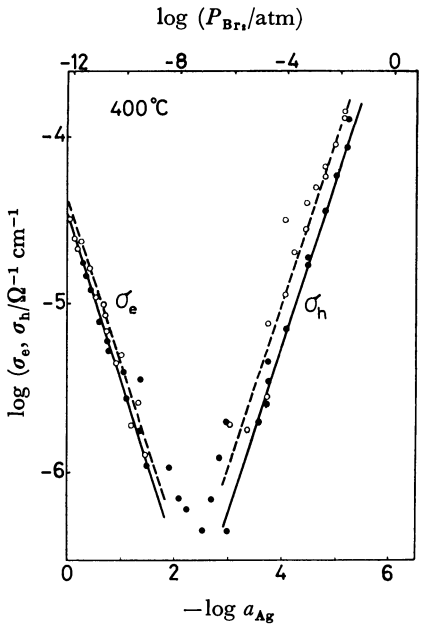

Fig. 6. Plots of σ_e and σ_h *vs.* $-\log a_{Ag}$ for A and C-type cell.
----: Mizusaki *et al.*[8] (A-type cell), ——: this work (C-type cell).

of Wagner's theory[2] and that the same results are obtained under a steady state, whether an A-type cell or a C-type cell is used.

Chemical Diffusion Coefficient. Unlike aqueous electrolyte solutions, solid electrolytes have an electronic conductivity more or less. Therefore, they should be dealt with by the theory on mixed conductors.

According to Ilschner,[3] silver bromide shows n-type conduction under a low polarization potential and at the temperatures studied. Therefore, the silver bromide can be represented by $Ag_{1+\delta}Br$ ($\delta>0$). Mizusaki *et al.*[7] found that δ in silver bromide is distributed linearly under a steady state, as is schematically shown in Fig. 7 (a). The distribution of δ is represented by the following equation:

$$\frac{\delta(X) - \delta^\circ}{\delta(L) - \delta^\circ} = \frac{X}{L}, \quad (4)$$

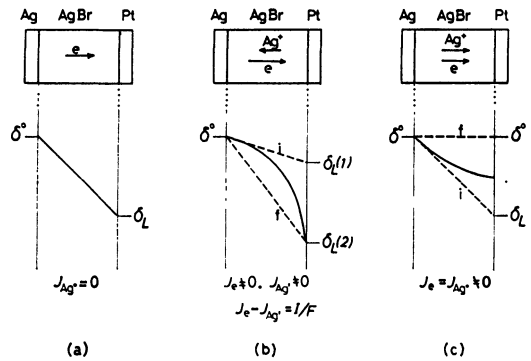

Fig. 7. Schematic diagram of δ profiles.
(a): Steady state, (b): voltage step, (c): open circuit.
i: Initial steady state, t: transient state, f: final steady state.

where $\delta(X)$ denotes δ in $Ag_{1+\delta}Br$ at the distance, X, from the Ag/AgBr interface, L is the thickness of the silver bromide sample, and δ° is δ in $Ag_{1+\delta}Br$ equilibrated with Ag.

Voltage-step Method: After the steady state has been attained under the voltage applied, $E_1(L)$, a second voltage, $E_2(L)$, larger than $E_1(L)$ is abruptly applied to the cell. The chemical potential of silver at the AgBr/inert electrode is immediately fixed to that corresponding to $E_2(L)$. The gradient of the electrical field is compensated for quickly by the motion of the major carrier Ag^+ ions, and the electrochemical potential of the Ag^+ ion becomes uniform throughout the silver bromide. The profile of δ in $Ag_{1+\delta}Br$ changes with the time as is schematically shown in Fig. 7(b). The relaxation process (redistribution of δ) proceeds by means of the counter diffusion of Ag^+ ions and electrons, and the rate is determined exclusively by the diffusion of excess silver atoms. Therefore, the relaxation of δ can be expressed by this equation:

$$\frac{\partial\delta}{\partial t} = \tilde{D}\frac{\partial^2\delta}{\partial X^2}, \tag{5}$$

where $\tilde{D}$ denotes the chemical diffusion coefficient in n-type AgBr. The chemical diffusion coefficient, $\tilde{D}$, is determined by solving Eq. 5 analytically with the following boundary conditions:

$$\frac{\delta(X,0)-\delta^\circ}{\delta(L,0)-\delta^\circ} = \frac{X}{L} \qquad t=0, \tag{6}$$

$$\delta(L,t) = \delta^\circ \exp\left(-\frac{E_1(L)F}{RT}\right) \qquad t<0, \tag{7}$$

$$\delta(L,t) = \delta^\circ \exp\left(-\frac{E_2(L)F}{RT}\right) \qquad t\geqslant 0, \tag{8}$$

$$\delta(0,t) = \delta^\circ, \tag{9}$$

where $\delta(X,t)$ denotes the value of δ at a position X apart from the Ag/AgBr interface and at a time t. When t is sufficiently large, the solution of Eq. 5 at $X=L/2$ is:[9]

$$\frac{\delta(L/2,\infty)-\delta(L/2,t)}{\delta(L/2,\infty)-\delta(L/2.0)} = \frac{4}{\pi}\exp\left(-\frac{D\pi^2 t}{L^2}\right). \tag{10}$$

The nonstoichiometry $\delta(X)$ is related to $E(X)$ by means of this equation:

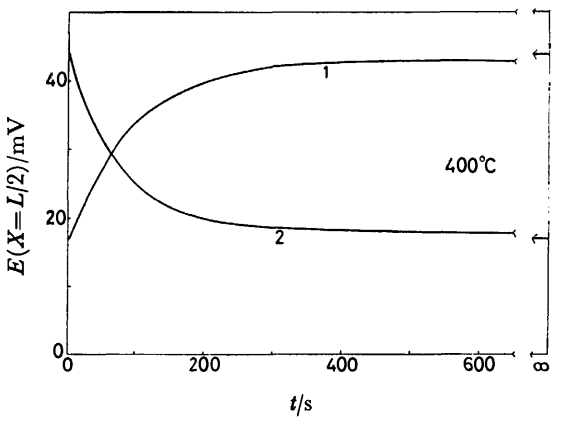

Fig. 8. Time change of $E(L/2)$ for C-type cell.
1: $E(L)$, 40 mV 200 mV, 2: $E(L)$, 200 mV 40 mV.

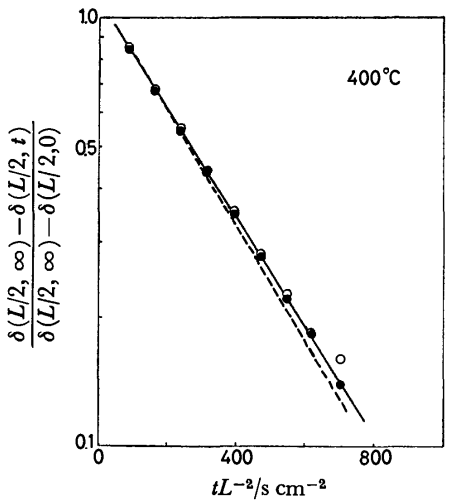

Fig. 9. Plots of $\frac{\delta(L/2,\infty)-\delta(L/2,t)}{\delta(L/2,\infty)-\delta(L/2,0)}$ *vs.* tL^{-2}.
●: $E(L)$, 40 mV→200 mV, ○: $E(L)$, 200 mV→40 mV, ——: this work (C-type cell), -----: Mizusaki *et al.*[9] (A-type cell).

$$\delta(X) = \delta^\circ \exp\left(-\frac{E(X)F}{RT}\right). \tag{11}$$

The time change in $\delta(L/2)$ is calculated from the change in $E(L/2)$.

Figure 8 shows the time change in $E(L/2)$ for the C-type cell. $\tilde{D}$ is determined from the slope of the plot of $\log[\{\delta(L/2,\infty)-\delta(L/2,t)\}/\{\delta(L/2,\infty)-\delta(L/2,0)\}]$ *vs.* tL^{-2}. Figure 9 shows the plot. In the figure, the results of the A-type cell are also given. A good agreement is seen between the $\tilde{D}$ values obtained using both types of cells. The results clearly indicate that the IP method gives the same $\tilde{D}$ values, regardless of the nature of the inert electrode.

Open-circuit Method: In the case of the voltage-step method, the electronic current is driven not by the electrical field, but by the concentration gradient of the electrons. The ionic current due to silver ions is not equal to the electronic current ($J_e - J_{Ag^+} \neq 0$) during the relaxation, as is shown in Fig. 7(b). The difference is observed as the current flowing in the external circuit, and it does not correspond to the flux of mass transport due to the relaxation.

In the case of the OC method, the relaxation proceeeds by means of the ambipolar diffusion of silver ions and electrons, because no net current flows in the external circuit. Therefore, the same diffusion situation as in the metal oxidation is set up in this method.

By solving Eq. 5 with the following boundary conditions:

$$\frac{\delta(X,0)-\delta^\circ}{\delta(L,0)-\delta^\circ} = \frac{X}{L} \qquad t=0 \tag{12}$$

$$\frac{\partial(L,t)}{\partial X} = 0 \qquad t<0 \tag{13}$$

$$\delta(0,t) = \delta^\circ \qquad t\geqslant 0 \tag{14}$$

we obtain:

$$\frac{\delta^\circ - \delta(L,t)}{\delta^\circ - \delta(L,0)} = \frac{8}{\pi^2}\exp\left(\frac{\tilde{D}\pi^2 t}{4L^2}\right) \quad (15)$$

for a sufficiently large t. The time change in $\delta(L,t)$ is calculated from $E(L,t)$ by using Eq. 11.

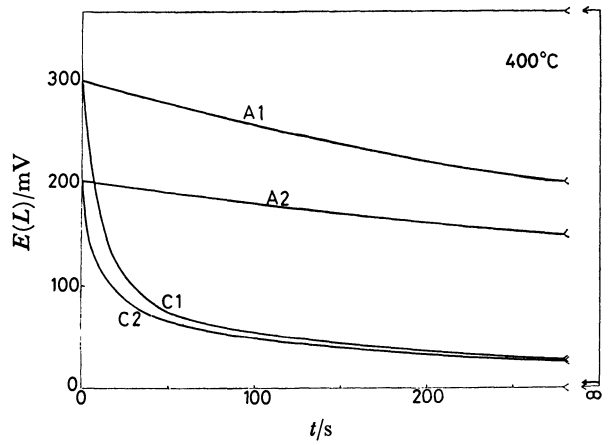

Fig. 10. Time change of $E(L)$ for A and C-type cell.
A1: $E(L)=300$ mV (A-type cell), A2: $E(L)=200$ mV (A-type cell), C1: $E(L)=300$ mV (C-type cell), C2: $E(L)=200$ mV (C-type cell).

Accordingly, $\tilde{D}$ is determined from the slopes of the plot of $\log[\{\delta^\circ-\delta(L,t)\}/\{\delta^\circ-\delta(L,0)\}]$ *vs.* tL^{-2}. Figure 10 shows the time change in the open-circuit voltage $E(L,t)$. As can be seen from the figure, the decay of $E(L,t)$ for the A-type cell is very slow and the reproducibility is poor. On the other hand, the time change in $E(L,t)$ for the C-type cell is reproducible.

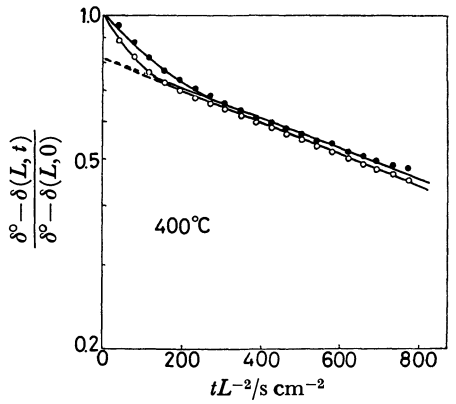

Fig. 11. Plots of $\frac{\delta^\circ-\delta(L,t)}{\delta^\circ-\delta(L,0)}$ *vs.* tL^{-2} for C-type cell.
●: $E(L,0)=300$ mV, ○: $E(L,0)=200$ mV.

Figure 11 gives the plots for determining $\tilde{D}$. This figure shows that $\tilde{D}$ is independent of the voltage applied before opening the circuit. Therefore, $\tilde{D}$ in n-type AgBr may be supposed to be independent of δ. From the decay in $E(L,t)$ for the A-type cell, we can not determine the $\tilde{D}$, for the plot of $\log[\{\delta^\circ-\delta(L,t)\}/\{\delta^\circ-\delta(L,0)\}]$ *vs.* tL^{-2} is curved.

Figure 12 shows the plots of $\log[\{\delta^\circ-\delta(L,t)\}/\{\delta^\circ-\delta(L,0)\}]$ *vs.* tL^{-2} for the C-type cell. As can be seen from the figure, $\tilde{D}$ is independent of the thickness of AgBr. Therefore, it may be concluded that the decay of $E(L,t)$ for the cell is due to the relaxation of δ within AgBr.

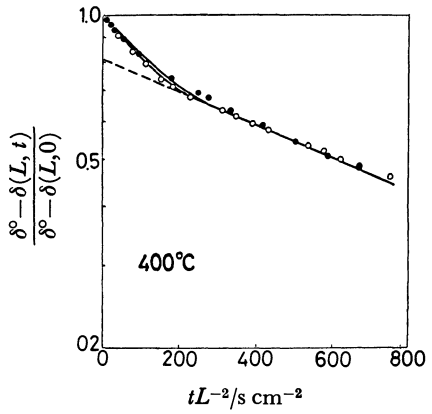

Fig. 12. Plots of $\frac{\delta^\circ-\delta(L,t)}{\delta^\circ-\delta(L,0)}$ *vs.* tL^{-2} for C-type cell.
●: $L=0.84$ cm, ○: $L=0.51$ cm.

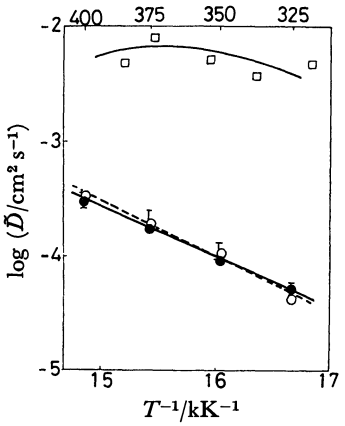

Fig. 13. Arrhenius plots of $\tilde{D}$.
□: B-type cell be Weiss[16] (OC method), I : A-type cell by Mizusaki *et al.*[9] (IP method), —●—: C-type cell in this work (IP method), --○--: C-type cell in this work (OC method).

Figure 13 gives the Arrhenius plot for $\tilde{D}$ of n-type AgBr. The chemical diffusion coefficient, $\tilde{D}$, determined by the IP method using the A and C-type cells and that determined by the OC method using the C-type cell are in good agreement. Therefore, the electronic current driven by the concentration gradient does not affect the mass transfer due to the chemical relaxation. However, $\tilde{D}$ can not be determined by the OC method when the A-type cell is used. This may be due to the diffusion and absorption of the Br_2 gas produced by the electrolysis of AgBr in the carbon electrode.

Weiss'[16] data obtained by the OC method using the B-type cell is one order of magnitude larger than the other data. In his experiment, the carbon electrode was exposed to an inert atmosphere, and bromine gas was supposed to be liberated at the AgBr/C interface by the electrolysis of AgBr. Therefore, larger $\tilde{D}$ values were obtained.

From these results, it seems that the OC method can be used provided that the inert electrode does not absorb or does not react with the electrolysis product. Platinum and gold seem to be appropriate as inert electrodes for the OC method. However, at a high polarization potential (for example, above 777 mV for Ag/AgBr/Pt cell at 400 °C), platinum bromide are produced at the AgBr/Pt interface.[21] Although gold does not react with bromine at a high polarization potential, the formation of a solid solution with AgBr must be taken into account.

References

1) M. H. Hebb, *J. Chem. Phys.*, **20**, 185 (1952).
2) C. Wagner, *Proc. C. I. T. C. E.*, **7**, 361 (1955).
3) B. Ilschner, *J. Chem. Phys.*, **28**, 1109 (1958).
4) D. O. Raleigh, *J. Phys. Chem. Solids.*, **26**, 329 (1965).
5) Y. I. van der Meulen and F. A. Kröger, *J. Electrochem. Soc.*, **117**, 69 (1970).
6) A. V. Joshi and J. B. Wagner, Jr., *J. Electrochem. Soc.*, **122**, 1071 (1975).
7) J. Mizusaki, K. Fueki, and T. Mukaibo, *Bull. Chem. Soc. Jpn.*, **48**, 428 (1975).
8) J. Mizusaki, K. Fueki, and T. Mukaibo, *Bull. Chem. Soc. Jpn.*, **51**, 692 (1978).
9) J. Mizusaki, K. Fueki, and T. Mukaibo, *Bull. Chem. Soc. Jpn.*, **52**, 1890 (1979).
10) J. Mizusaki and K. Fueki, *Rev. Chim. Miner.*, **17**, 356 (1980).
11) K. Weiss, *Electrochim. Acta*, **16**, 201 (1971).
12) A. V. Joshi, "Fast Ion Transport in Solids," ed by W. van Gool, North Holland Pudlishing Co., (1973), p. 173.
13) D. O. Raleigh, *J. Electrochem. Soc.*, **114**, 493 (1967).
14) D. O. Raleigh and H. R. Crowe, *J. Electrochem. Soc.*, **116**, 40 (1969).
15) J. Goldman and J. B. Wagner, Jr., *J. Electrochem. Soc.*, **121**, 1318 (1974).
16) K. Weiss, *Z. Phys. Chem. N. F.*, **59**, 242 (1968).
17) J. B. Wagner, Jr., "Electrode Processes on Solid State Ionics," ed by M. Kleitz, Reidel Publ. Co., (1976), p. 185.
18) D. O. Raleigh, *J. Phys. Chem.*, **71**, 1785 (1967).
19) D. O. Raleigh, "Advances in Electroanalytical Chemistry," Vol. 6, ed by A. J. Bard, M. Dekker, (1973), p. 87.
20) J. W. Patterson, E. C. Borgen, and R. A. Rapp, *J. Electrochem. Soc.*, **114**, 752 (1967).
21) W. L. Worrell and J. Hladik, "Physics of Electrolytes," ed by J. Hladik, Academic Press, London-New York (1972), p. 747.

Visible Light-induced Oxidation of Ascorbic Acid and Formation of Hydrogen Peroxide

Yoshimi KURIMURA,* Hiroshi YOKOTA, and Yuko MURAKI
Department of Chemistry, Ibaraki University, Mito 310
(Received December 23, 1980)

Photosensitized oxidation of ascorbic acid and the formation of hydrogen peroxide using tris(2,2'-bipyridine)-ruthenium(II), $Ru(bpy)_3^{2+}$, proceed simultaneously in oxygen containing an aqueous solution of ascorbic acid with the illumination of visible light. The mechanism of the reaction has been suggested from the rate dependence on the solute concentrations and from quenching experiments. The charge separation could be achieved as the result of scavenging $Ru(bpy)_3^{3+}$, which is formed by the reaction of the lowest excited state species of $Ru(bpy)_3^{2+}$ with O_2.

The luminescence quenching of $Ru(bpy)_3^{2+}$ by various substances is a subject of much current interest.[1-12] The lowest excited state of $Ru(bpy)_3^{2+}$, $*Ru(bpy)_3^{2+}$, is able to react with an electron-transfer reagent.[13,14] The oxidative and reductive quenchings of $Ru(bpy)_3^{2+}$ give $Ru(bpy)_3^{3+}$ as a strong oxidant and $Ru(bpy)_3^{+}$ as a strong reductant, respectively. In most photosystems the utilization of the redox properties of photo-generated $Ru(bpy)_3^{3+}$ or $Ru(bpy)_3^{+}$ is prevented because of fast back-electron-transfer reactions.[12]

The ability of $*Ru(bpy)_3^{2+}$ to act as an electron donor or acceptor has been utilized in several prototype models of solar energy conversion.[15-18] Hydrogen evolution by water splitting with the irradiation of visible light has been extensively studied.[19,20] However, relatively little attention has been paid to the productions of superoxide ion,[21,22] and hydrogen peroxide[22] in the reaction of $*Ru(bpy)_3^{2+}$ with molecular oxygen. The reductions of O_2 to O_2^- and H_2O_2 are both up-hill reactions, *e. g.*, the standard free energy changes for the production of O_2^- and H_2O_2 from O_2 are 129 kJ mol^{-1} ($E_0'(O_2/O_2^-) = -0.32$ V)[23] and 274 kJ mol^{-1} ($E_0(O_2/H_2O_2) = -0.68$ V),[23] respectively. The excited state of $Ru(bpy)_3^{2+}$ is rapidly quenched by O_2 to produce O_2^-: the quenching rate constants obtained were 3.3×10^9 M^{-1} s^{-1} [24] and 3.7×10^9 M^{-1} s^{-1} [25] (1 M = 1 mol dm^{-3}) in neutral aqueous solution and 3.0×10^9 M^{-1} s^{-1} in 0.5 M HCl.[22] Fast back-reaction of the $Ru(bpy)_3^{3+}$ with O_2^-, however, occurs and the production of hydrogen peroxide could not be observed in the $Ru(bpy)_3^{2+}/O_2$ system.

We found that hydrogen peroxide was formed in the solution containing oxygen, using ascorbate ion as a scavenger of $Ru(bpy)_3^{3+}$. So we have investigated the mechanism of visible-light induced formation of hydrogen peroxide in the $Ru(bpy)_3^{2+}$/ascorbic acid/O_2 system.

Experimental

$[Ru(bpy)_3]Cl_2\cdot6H_2O$ was prepared according to the literature method[26] and recrystallized twice from water. Ascorbic acid from Kanto Kagaku was used without further purification.

The ionic strength of the irradiated samples were maintained at 0.2 by sodium chloride. The hydrogen ion concentration was adjusted by acetate buffers. An oxygen- or air-saturated aqueous solution containing $Ru(bpy)_3^{2+}$ and ascorbic acid in a cylindrical glass cell (40-mm diameter and 15-mm thickness) with a glass cap was liluminated by a 150 W tungsten lamp with a UV cut-off filter (Kenko, Skylight L-40, UV) at 25±0.2 °C.

The irradiation sample (2 ml) was poured into a column (10-mm diameter and 30-mm length) of cation-exchange resins (Dowex 50 W, X-8, 100—200 mesh, the hydrogen form), followed by washing with water. The concentrations of hydrogen peroxide[27] and dehydroascorbic acid[28] in the eluant were determined by a colorimetric method. The absorption spectra were observed with a Hitachi Model 320 spectrophotometer.

The quenching experiments were carried out by using a Shimadzu Model RF-500 spectrofluorometer at 25±0.1 °C. For the luminescence experiments, the excitation was carried out at 455 nm. If necessary, dissolved oxygen in the samples was removed by flushing nitrogen gas, which was passed through an alkanine pyrogallol solution. The concentration of the dissolved oxygen in the solutions was adjusted by saturations of air and pure oxygen under atmospheric pressure at 25±0.2 °C.

Results

In the air- and oxygen-saturated solutions containing $Ru(bpy)_3^{2+}$ and ascorbic acid (AH_2) at pH 3.1—5.5, the formation reaction of hydrogen peroxide and the oxidation reaction of ascorbic acid proceeded simultaneously with the illumination of visible light, while the absorption spectrum of the solution in the visible

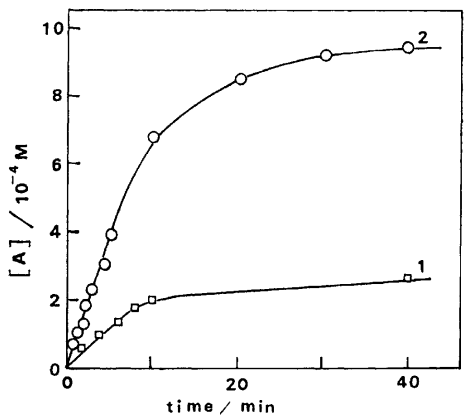

Fig. 1. Plots of [A] *vs.* time in $Ru(bpy)_3^{2+}/AH_2$ solutions at pH 4.6 and 25 °C.
$[Ru(bpy)_3^{2+}] = 1.0\times10^{-4}$ M, $[AH_2]_T = 1.0\times10^{-3}$ M,
1: air-saturated solution, 2: O_2-saturated solution.

region was unchanged during 1 h illumination. These results show that the $Ru(bpy)_3^{2+}$ photosensitized production of hydrogen peroxide occurs in the $Ru(bpy)_3^{2+}/AH_2/O_2$ system.

The plots of the concentration of dehydroascorbic acid (A) against the illumination time in oxygen-saturated and air-saturated solutions are shown in Fig. 1. The oxidation rates of ascorbic acid to dehydroascorbic acid, d[A]/dt, were determined from the slopes of [A] *vs.* time plots. The saturation of [A] *vs.* time curves is seen in Fig. 1 as the result of consumption of the dissolved oxygen in the solutions.

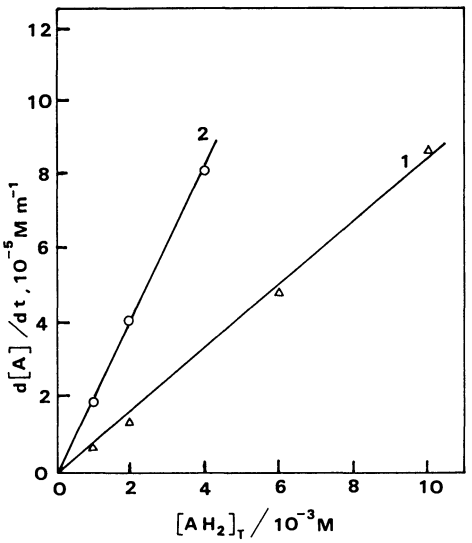

Fig. 2. Dependence of rate on ascorbic acid concentration in air-saturated (1) and O_2-saturated (2) solutions at pH 4.6 and 25 °C.
$[Ru(bpy)_3^{2+}]=1.0\times10^{-4}$ M.

The dependence of the rate on the total concentration of ascorbic acid, $[AH_2]_T$, is shown in Fig. 2. The oxidation rate of ascorbic acid was found to be proportional to the ascorbic acid concentration in the lower concentration region of the acid at a given pH.

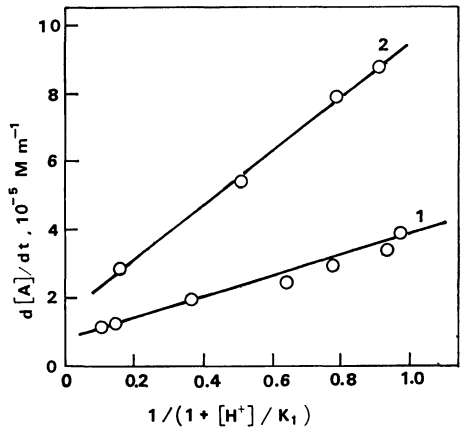

Fig. 3. Plots of d[A]/dt *vs.* $1/(1+[H^+]/K_1)$ in air-saturated (1) and O_2-saturated (2) solutions at 25 °C.
$[Ru(bpy)_3^{2+}]=1.0\times10^{-4}$ M, $[AH_2]_T=1.0\times10^{-3}$ M.

In Fig. 3 the rates are plotted as a function of $1/(1+K_1/[H^+])$ where K_1 is the dissociation constant of Reaction 1: the value of $1/(1+K_1/[H^+])$ is proportional to the concentration of ascorbate monoanion, $[AH^-]$. Under the conditions employed, Reaction 2 can be neglected. The acid dissociation constants of

$$AH_2 \overset{K_1}{\rightleftharpoons} AH^- + H^+ \quad (1)$$

$$AH^- \overset{K_2}{\rightleftharpoons} A^{2-} + H^+ \quad (2)$$

Reactions 1 and 2 are reported to be $K_1=9.16\times10^{-5}$ M and $K_2=4.57\times10^{-12}$ M at 25 °C, respectively.[29]

The rate is also dependent on the concentration of the dissolved oxygen: the ratios of the rates in the oxygen-saturated and air-saturated solutions range from 2.4 to 2.6 (Fig. 3).

The values of product distribution, $[H_2O_2]/[A]$, in the illuminated solutions under various conditions are shown in Table 1. This table shows that the observed $[H_2O_2]/[A]$ ratio are around 0.6.

Table 1. Product distributions in the irradiated solutions[a]

pH	$\frac{[H_2O_2]}{10^{-4}\,M}$	$\frac{[A]}{10^{-4}\,M}$	$\frac{[H_2O_2]}{[A]}$	Sat. gas
3.5[b]	1.86	2.68	0.69	Air
3.6[c]	1.14	1.79	0.64	Air
4.5[c]	1.66	2.61	0.64	Air
5.4[c]	1.32	2.13	0.62	Air
3.3[c]	4.18	8.34	0.50	Oxygen
4.1[e]	4.20	7.99	0.53	Oxygen
4.6[c]	5.68	9.85	0.58	Oxygen
5.0[c]	4.88	8.23	0.59	Oxygen

a) 1.0×10^{-3} M AH_2, 1.0×10^{-4} M $Ru(bpy)_3^{2+}$, μ= 0.2, 25 °C. b) Illumination time 25 min. c) Illumination time 10 min. d) Illumination time 60 min. e) Illumination time 30 min.

By the determination of the concentration of ascorbic acid or hydrogen peroxide in the solutions at pH 5.5 and 25 °C, it was observed that a) the oxidation reaction of ascorbic acid by dissolved oxygen in the O_2-saturated solution can be neglected compared with the photosensitized oxidation of ascorbic acid and b) no appreciable

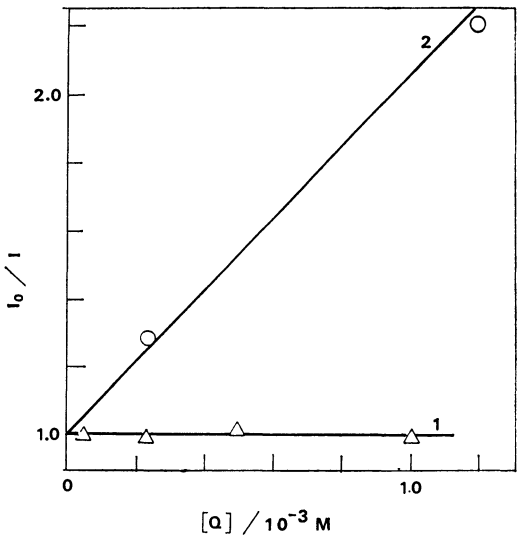

Fig. 4. Stern-Volmer plots at pH 4.6 and 25 °C.
1: Q; ascorbic acid, 2: Q; oxygen.

decomposition of hydrogen peroxide occurred during 30 min illumination of an oxygen-saturated solution containing 2.0×10^{-4} M $Ru(bpy)_3^{2+}$ and 1.0×10^{-3} M H_2O_2.

The luminescence quenching studies were carried out in $Ru(bpy)_3^{2+}/O_2$ and deaerated $Ru(bpy)_3^{2+}$/ascorbic acid solutions at pH 4.6. The Stern-Volmer plots for these systems are shown in Fig. 4. From the results shown in this figure, we conclude that the predominant species that reacts with $*Ru(bpy)_3^{2+}$ is the dissolved oxygen. The Stern-Volmer constant estimated from slope 2 in Fig. 4 was 1900 M^{-1} and the quenching rate constant, k_q, for $*Ru(bpy)_3^{2+}$ by O_2 was 3.2×10^9 $M^{-1}\,s^{-1}$ at 25 °C, since the excited state life time of $*Ru(bpy)_3^{2+}$ is known to be 6.0×10^{-7} s.[30]

Discussion

The rate profiles shown in Figs. 1 to 3 indicate that the rates depend on the concentrations of ascorbic acid and O_2 and that the reactive species of the acid is the ascorbate anion, AH^-. The results of the quenching experiments (Fig. 4) show that the reaction of $*Ru(bpy)_3^{2+}$ with AH^- can be ignored compared with that of $*Ru(bpy)_3^{2+}$ with O_2 under the conditions employed.

The proposed reaction mechanism responsible for the experimental results is given by Reactions 3 to 13.

$$Ru(bpy)_3^{2+} \xrightarrow{h\nu} *Ru(bpy)_3^{2+} \quad (3)$$

The $*Ru(bpy)_3^{2+}$ reacts with O_2 to give a superoxide ion. At low pH the superoxide ion becomes an HO_2 radical. The scavanging reaction of $Ru(bpy)_3^{3+}$ by ascorbate anion competes for the back-electron-transfer reaction.

$$*Ru(bpy)_3^{2+} + O_2 \longrightarrow Ru(bpy)_3^{3+} + O_2^- \quad (4)$$

$$O_2^- + H^+ \rightleftharpoons HO_2 \qquad pK\,4.8^{31} \quad (5)$$

$$Ru(bpy)_3^{3+} + AH^- \rightleftharpoons Ru(bpy)_3^{2+} + AH\cdot \quad (6)$$

$$Ru(bpy)_3^{3+} + O_2^-(\text{or } HO_2) \longrightarrow Ru(bpy)_3^{2+} + O_2(\text{or } O_2 + H^+), \quad (7)$$

where AH· is the ascorbic acid radical. The superoxide ion and HO_2 radical oxidize the ascorbic acid.[29] When the concentration of ascorbic acid is low, the disproportionation reactions of O_2^- and HO_2 occur.[32,33] The HO_2 radical is, presumably, decomposed by Reactions 12 and 13.[29] The rate constant of Reaction 13 was estimated to be 8×10^7 $M^{-1}\,s^{-1}$ in the pH range 2.5—4.0.[34]

$$AH^- + O_2^- + 2H^+ \longrightarrow AH\cdot + H_2O_2 \quad (8)$$

$$AH_2 + HO_2 \rightleftharpoons AH\cdot + H_2O_2 \quad (9)$$

$$O_2^- + O_2^- + 2H^+ \longrightarrow H_2O_2 + O_2 \quad (10)$$

$$HO_2 + HO_2 \longrightarrow H_2O_2 + O_2 \quad (11)$$

$$AH\cdot + O_2 \longrightarrow A + HO_2 \quad (12)$$

$$AH\cdot + AH\cdot \longrightarrow A + AH_2 \quad (13)$$

The rate constants for the forward reaction, k_{14} (Eq. 14), and backward reaction, k_{15} (Eq. 15), were determined by means of flash photolysis by Creutz and Sutin[35] to be $k_{14}=2\times10^7$ $M^{-1}\,s^{-1}$ and $k_{15}=1\times10^9$ $M^{-1}\,s^{-1}$ at 25 °C.

$$*Ru(bpy)_3^{2+} + AH^- \xrightarrow{k_{14}} Ru(bpy)_3^{3+} + AH\cdot \quad (14)$$

$$Ru(bpy)_3^{2+}\,AH\cdot \xrightarrow{k_{15}} Ru(bpy)_3^{3+} + AH^- \quad (15)$$

By assuming the competition between Reactions 4 and 14 the fraction of $*Ru(bpy)_3^{2+}$ molecules scavenged by AH^-, f, is given by:

$$f=\frac{1}{1+k_4[O_2]/k_{14}[AH^-]}. \quad (16)$$

Using $k_4=3.2\times10^9$ $M^{-1}\,s^{-1}$ and $k_{14}=2\times10^7$ $M^{-1}\,s^{-1}$,[34] we can derive $f<0.03$ in the air-saturated solution and $f<0.006$ in the O_2-saturated solution under the conditions employed. The results seem to support the contention that the reaction of $*Ru(bpy)_3^{2+}$ with AH^- could be essentially ignored.

The luminescence quenching efficiency of $*Ru(bpy)_3^{2+}$ by O_2 and thus the rate would increase with an increase in the concentration of O_2. The ratio of the amounts of $*Ru(bpy)_3^{2+}$ being oxidized to $Ru(bpy)_3^{3+}$ by Reaction 4 in the oxygen- and air-saturated solutions would correspond to $(I_0-I_{O_2})/(I_0-I_{air})$ where I_0, I_{O_2}, and I_{air} are the relative luminescence intensities in the deaerated, oxygen-saturated, and air-saturated $Ru(bpy)_3^{2+}$ solutions, respectively. The ratio was estimated to be about 2.8 from the results shown in Fig. 4. The ratio of the rates in O_2-saturated and air-saturated solutions, $(d[A]/dt)_{O_2}/(d[A]/dt)_{air}=2.6$, is essentially in agreement with the value of $(I_0-I_{O_2})/(I_0-I_{air})$.

Dependence of the rate on $[AH_2]_T$ (Fig. 3) would account for the competition between Reactions 6 and 7 for $Ru(bpy)_3^{3+}$. A linear dependence of the rate on $[AH_2]_T$ at lower $[AH_2]_T$ indicates that the rate of Reaction 7 increases almost linearly with $[AH^-]$. The relatively small increase in the rate in the higher concentration region of ascorbic acid is attributable to that $k_7[O_2^-]$ or $k_7'[HO_2]$, where k_7 and k_7' are the rate constants of $Ru(bpy)_3^{3+}$ with O_2^- and $Ru(bpy)_3^{3+}$ with HO_2 respectively, is not so much different from $k_8[AH^-]$. When the concentration of the ascorbic acid becomes high enough for scavenging $Ru(bpy)_3^{3+}$, the rate would not depend on $[AH_2]_T$ any longer.

According to Reactions 3 to 13, the stoichiometric ratio of $[H_2O_2]/[A]$ should be about unity, whereas the observed product distributions (Table 1) show that the ratio was 0.5—0.7. This lower value of the observed ratio is probably attributable to the chain decomposition reaction of H_2O_2.[32] Such cahin reactions would occur when the concentration of H_2O_2 becomes high enough for HO_2 to react with H_2O_2 instead of with ascorbic

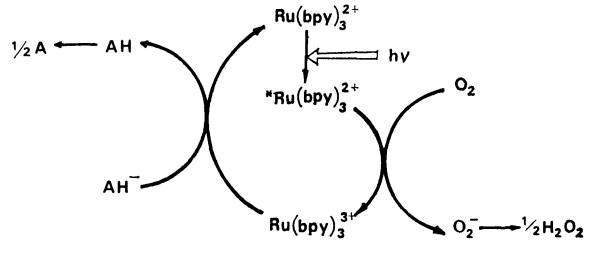

Fig. 5. Schematic representation of the photosensitized reaction.

acid (Eqs. 8 and 9) or with itself (Eqs. 10 and 11).

$$HO_2 + H_2O_2 \longrightarrow H_2O + O_2 + OH \quad (17)$$

$$H_2O_2 + OH \longrightarrow H_2O + HO_2 \quad (18)$$

Similar chain decomposition reactions would occur for O_2^- instead of HO_2. The reactions of OH radical with ascorbic acid and $Ru(bpy)_3^{2+}$ have to be considered.

The main features of the $Ru(bpy)_3^{2+}$ photosensitized reaction are illustrated schematically in Fig. 5. The ratio of the rate of the electron-transfer reaction (Eq. 4) to that of the back-electron-transfer reaction (Eq. 7) would determine the efficiency of the charge-separation of the reaction of $Ru(bpy)_3^{2+}$ with O_2 and thus that of the photosensitized reaction under study.

References

1) C. T. Lin and N. Sutin, *J. Phys. Chem.*, **80**, 97 (1976).
2) J. N. Demas and A. W. Adamson, *J. Am. Chem. Soc.*, **95**, 5159 (1973).
3) H. D. Gafney and A. W. Adamson, *J. Am. Chem. Soc.*, **94**, 8238 (1972).
4) P. Natarajan and J. F. Endicott, *J. Phys. Chem.*, **77**, 971 (1973).
5) P. Natarajan and J. F. Endicott, *J. Phys. Chem.*, **77**, 1823 (1973).
6) C. R. Bock, T. J. Meyer, and D. G. Whitten, *J. Am. Chem. Soc.*, **96**, 4710 (1974).
7) G. Navon and N. Sutin, *Inorg. Chem.*, **13**, 2159 (1974).
8) C. R. Bock, T. J. Meyer, and D. G. Whitten, *J. Am. Chem. Soc.*, **97**, 2909 (1975).
9) G. L. Gaines, Jr., *J. Phys. Chem.*, **83**, 3088 (1979).
10) K. Chandrasekaran and P. Natarajan, *Inorg. Chem.*, **19**, 1714 (1980).
11) R. H. Schmehl and D. G. Whitten, *J. Am. Chem. Soc.*, **102**, 1938 (1980).
12) A. Beronier and T. J. Meyer, *Inorg. Chem.*, **19**, 2912 (1980).
13) V. Balzani, F. Bolletta, M. T. Gandolfi, and M. Maestri, *Top. Curr. Chem.*, **75**, 1 (1978).
14) T. J. Meyer, *Isr. J. Chem.*, **15**, 200 (1977).
15) C. Creutz and N. Sutin, *Proc. Natl. Acad. Sci. U.S.A.*, **72**, 2858 (1975).
16) R. Ballardini, G. Varani, F. Scandola, and V. Balzani, *J. Am. Chem. Soc.*, **98**, 7432 (1976).
17) C. M. Brown, B. S. Brunschwig, C. Creutz, J. F. Endicott, and N. Sutin, *J. Am. Chem. Soc.*, **101**, 1298 (1979).
18) G. M. Brown, S. F. Chan, C. Creutz, and N. Sutin, *J. Am. Chem. Soc.*, **101**, 7638 (1979).
19) K. Kalyanasundram, J. Kiwi, and M. Grätzel, *Helv. Chim. Acta*, **61**, 2720 (1978).
20) K. Kalyanasundaram and M. Grätzel, *Angew. Chem. Int. Ed. Engl.*, **18**, 701 (1979).
21) C. P. Anderson, D. J. Salmon, T. J. Mayer, and R. C. Young, *J. Am. Chem. Soc.*, **99**, 1980 (1977).
22) Y. Kurimura and R. Onimura, *Inorg. Chem.*, **19**, 3516 (1980).
23) P. George, "Oxidases and Related Redox Systems," ed by T. E. King, H. S. Mason, and M. Morison, Wiley, New York (1965), p. 3.
24) C. Tung and N. Sutin, *J. Phys. Chen.*, **80**, 97 (1975).
25) D. Meisel, W. A. Mulac, and J. Rabani, *J. Phys. Chem.*, **81**, 1449 (1977).
26) R. A. Palmer snd T. S. Piper, *Inorg. Chem.*, **5**, 864 (1966).
27) E. B. Sandell, "Colorimetric Determinations of Traces of Metals," 2nd ed, Interscience, New York (1950), p. 572.
28) J. H. Roe, "Method of Biochemical Analysis," Interscience Publ. Inc., New York (1954), Vol. I, p. 115.
29) M. M. T. Khan and A. E. Martell, *J. Am. Chem. Soc.*, **89**, 7104 (1967).
30) C. T. Lin and N. Sutin, *J. Phys. Chem.*, **80**, 97 (1976).
31) D. Meisel and G. Czapski, *J. Phys. Chem.*, **79**, 1503 (1975).
32) A. O. Allen, "Radiation Chemistry of Water and Aqueous Solutions," Van Nostrand, Princeton (1961).
33) E. J. Hart and M. S. Matheson, *Discuss. Faraday Soc.*, **12**, 169 (1952).
34) B. H. J. Bielski, D. A. Comstock, and R. A. Brown, *J. Am. Chem. Soc.*, **93**, 5624 (1971).
35) C. Creutz, N. Sutin, and B. S. Brunschwig, *J. Am. Chem. Soc.*, **101**, 297 (1979).

An Electron Spin Resonance Study of the Phosphorescent Triplet State of Poly(vinylnaphthalene)s

Jiro HIGUCHI,* Mikio YAGI, Juichiro SAITO, and Midori TAKANASHI

Department of Chemistry, Faculty of Engineering, Yokohama National University, Hodogaya-ku, Yokohama 240

(Received February 14, 1981)

The electron spin resonance (ESR) of poly(1-vinylnaphthalene) and poly(2-vinylnaphthalene) in their phosphorescent triplet states is studied in glassy solutions and in plastic hosts. The zero-field splitting parameters thus obtained are discussed in comparison with those of 1- and 2-methylnaphthalene. Through the ESR measurement, the possibility of detecting the triplet energy transfer through the naphthyl groups is examined.

The lowest triplet state of vinyl polymers with aromatic groups attached has been investigated mainly in connection with their intramolecular energy transfer through aromatic chromophores, by measuring the delayed fluorescence and phosphorescence spectra at low temperatures.[1] Nevertheless, comparatively little attention has been paid to studies of their electron spin resonance (ESR), especially for synthetic polymers. If the naphthyl groups are attached to polymeric chains, their fairly strong phosphorescent ESR signals may be expected to be observed in rigid glasses, judging from those of the naphthalene molecule. In the present work, therefore, ESR studies of poly(1-vinylnaphthalene) (P1-VN) and poly(2-vinylnaphthalene) (P2-VN) in their lowest triplet states are taken up as typical examples of such works.

Experimental

The P1-VN and P2-VN were purchased from Polysciences, Inc., and were purified repeatedly by dissolving in tetrahydrofuran and by precipitation with methanol (after a purification, the molecular weights of P1-VN and P2-VN were $M_w=3.4\times10^3$ and $M_n=2.0\times10^3$, and $M_w=1.93\times10^4$ and $M_n=9.2\times10^3$, respectively). The 1-methylnaphthalene (1-MN) and 2-methylnaphthalene (2-MN) were obtained from Tokyo Kasei Co. and were used without further purification, because the ESR signals of the other molecules could not be detected. The ESR spectra were observed in 2-methyltetrahydrofuran (MTHF) glasses. As the plastic host of these polymers, stretched atactic polystyrene (PS) film was used, because it is very hard for isotactic PS to form transparent films from either a toluene or a 1,3,5-trimethylbenzene solution. By evaporating the toluene from a solution containing a 50 : 1 (*w*/*w*) mixture of PS and a sample in a glass vessel on a hot plate, a transparent film was obtained on the glass. Then the film was stretched at 80 °C. The films thus obtained had about 200% of stretch in the stretched direction.

The details of the ESR experiment are exactly the same as in our previous works,[2,3] except for the use of an additional apparatus of JES-UCT-2AX variable-temperature adapter and a JES-VT-3 variable-temperature controller when the measurements were carried out at temperatures above 77 K.

Results and Discussion

In comparison with the ESR spectrum of the naphthalene molecule, the line shapes for P1-VN and P2-VN resemble each other closely, but their intensities are relatively weak in MTHF glasses at 77 K. The zero-field splitting (ZFS) parameters obtained under the same conditions are listed in Table 1. For the naphthalene molecule, the coordinate axes were taken as follows: the x axis is parallel to the longest direction of the molecule, and the y axis is perpendicular to it in the molecular plane, while the z axis is perpendicular to the molecular plane. The directions of the magnetic principal axes of the PVN and MN molecules were assumed not to deviate largely from those of the naphthalene molecule, although they could not be determined in the present work. The results for the ZFS parameters may be summarized as follows: for naphthalene and 1- and 2-MN, the present values are slightly different from those obtained in EPA glasses by Yamanashi and Bowers.[5] (1) The D and $|E|$ values of 1-MN are both smaller than the respective values of 2-MN, although such a relation is completely reversed in the latter work. (2) Similarly, the D and $|E|$ values of P1-VN are both smaller than the corresponding values of P2-VN. (3) Each D value of these polymers is smaller than that of the corresponding MN, while such differences are hardly found at all for the E values.

These relations can reasonably be explained in terms of the spin distributions of these molecules, except for the E values described in (3). That is, since, in the naphthalene molecule, the spin density at the 2 position of the carbon atom is smaller than that at the 1 position, the spin delocalization from the naphthyl group in 2-naphthyl substituents is smaller than that in 1-

Table 1. Zero-field splitting parameters in the phosphorescent triplet states (cm^{-1})[a]

Molecule	$\|X\|$	$\|Y\|$	$\|Z\|$	$\|D\|$	$\|E\|$	D^*[b]	D^*[c]
Naphthalene	0.0489	0.0181	0.0669	0.1004	0.0154	0.1039	0.1040
1-Methylnaphthalene	0.0472	0.0180	0.0652	0.0978	0.0146	0.1012	0.1008
2-Methylnaphthalene	0.0478	0.0179	0.0657	0.0986	0.0150	0.1020	0.1022
Poly(1-vinylnaphthalene)	0.0469	0.0177	0.0643	0.0967	0.0146	0.1000	0.0992
Poly(2-vinylnaphthalene)	0.0476	0.0177	0.0653	0.0980	0.0150	0.1014	0.1031

a) Observed in MTHF glasses at 77 K. b) $D^*=(D^2+3E^2)^{1/2}$. c) Obtained from the observed resonance field of the $\Delta m=\pm2$ transition with Kottis-Lefebvre's correction.[4]

naphthyl ones. Also, such spin delocalization may generally be larger for P1- and P2-VN than for the corresponding MN molecule. The above elucidation is actually based on the hyperconjugation-type consideration. On the other hand, the results of (3) may possibly be interpreted as being caused by the influence of the triplet-energy transfer which occurs slightly through the naphthyl groups at 77 K. The intramolecular triplet-energy transfer through naphthyl groups has been demonstrated by Cozzens and Fox for P1-VN in a THF: diethyl ether (1 : 1) glass at 77 K through the measurements of the delayed fluorescence due to triplet-triplet annihilation.[6] In P1- and P2-VN, therefore, the triplet exciton may mainly move along the polymer chain if the normal axes of naphthyl groups are locally aligned on this direction. In that case, only the D value of PVN slightly decreases from that of the corresponding MN, while the E value is hardly changed.

Until now, the intramolecular triplet-energy transfer through naphthyl groups has been optically studied in P1-VN[6-8] and P2-VN.[8-11] In the present work, the possibility of detecting such a triplet exciton was examined from the change in the ESR line shapes at different temperatures where the rates of triplet-energy transfer may be appreciably changed. Generally, the use of glassy solutions does not permit the detection of the phosphorescent ESR signals at temperatures where the host glass is not rigid. For observing the line shapes over a fairly wide range of temperature, therefore, a stretched PS film was used as a host.

The ZFS parameters obtained in the PS films at 77 K are slightly smaller than those in MTHF glasses, although the line shapes become rather broad. With a rise in the temperature, the intensity of each peak with the $\Delta m=\pm 1$ transition decreases and the line shapes become broad. The peak intensities for P2-VN are quite weak as compared with those of P1-VN. Therefore, further experiments were carried out for only P1-VN and its reference compound of 1-MN. The signals of the $\Delta m=\pm 1$ transition observed at 77 K barely showed a little anisotropy due to the directions of the stretched film against the applied magnetic field. Because of the lowering of the peak intensities, it may be impossible to deduce some meaningful information from its detection at higher temperatures. Actually, its Z peaks could not be detected near 160 K.

On the other hand, it is possible to detect the triplet ESR signal of P1-VN with the $\Delta m=\pm 2$ transition with an appreciable deformation of line shape at a temperature not higher than 160 K. Figure 1 shows the ESR spectra of the $\Delta m=\pm 2$ transition for P1-VN and 1-MN in stretched PS films at 77 K and 160 K. It may be noted here that these samples all contain roughly the same amount of naphthyl groups. For P1-VN, the line shape observed at 160 K becomes fairly broad as compared with that at 77 K, while that of 1-MN is hardly changed over the temperature range studied. This may suggest that some intramolecular triplet-energy transfer through naphthyl groups in the same polymer chain occurs for P1-VN, for the distances between adjacent naphthyl groups along a polymer chain are fairly small as compared with those of separated molecules. Such a consideration may generally support the interpretation of observation (3) described above. At 160 K, the D^* values of P1-VN and 1-MN were also obtained according to Kottis-Lefebvre's correction.[4] They are each 0.002 cm^{-1} smaller than that of the corresponding molecule observed at 77 K. In addition to the effect of triplet-energy transfer in P1-VN, the lowering of D^* values may be partly attributed to the motion of naphthyl groups in the host polymer.[12]

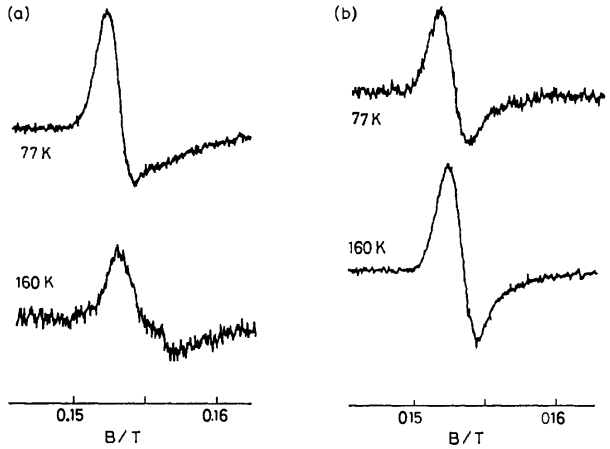

Fig. 1. ESR spectra of the $\Delta m=\pm 2$ transitions for the phosphorescent triplet states of poly(1-vinylnaphthalene) (a) and 1-methylnaphthalene (b) in stretched polystyrene films.

Several years ago, Avakian *et al.*[9] studied the magnetic-field modulation of delayed fluorescence for P2-VN in a THF: diethyl ether (1 : 1) glass at 77 K. In comparison with the fluorescence intensity calculated by assuming that the D value is nearly equal to that of naphthalene and $E=0$, they deduced tendencies for the normal axes of naphthyl groups to be locally aligned approximately parallel to one another and for the naphthyl planes to have orientations tending to an average of the in-plane components. The last part of their assumption is evidently different from our value of $E\neq 0$. Compared with the present results, their interpretation may overestimate the triplet-energy transfer for P2-VN at 77 K, although the steric hindrance between the naphthyl group and the polymer chain is rather small as compared with the case of P1-VN.

In the present work, the host polymer consists of stretched atactic PS films without perfect ordering. Although the isotactic polymers were used, PS and P1-VN have different molecular symmetries, with threefold and fourfold screw axes respectively.[13,14] Therefore, the present selection of guest and host polymers may not always be suitable if we are to expect even the partial ordering of guest molecules. Under these circumstances, a more detailed analysis of the observed spectra could not actually be carried out. Also, the characterization of the molecular weight or polymerization degree of the polymers may possibly be meaningless unless the aforementioned points are improved.

The authors wish to thank Professor Minoru Kinoshita, The University of Tokyo, for his helpful

discussions, and Dr. Shimpei Hashimoto, Japan Synthetic Rubber Co., Ltd., for his kind communications. They also wish to thank Professor Shigeo Tazuke and Mr. Sumio Okano, Tokyo Institute of Technology, for their measurements of the molecular weight of PVN, and Dr. Takashi Nogami, Osaka University, for donating the Pl-VN at the preliminary step of the present work. The present work was partially supported by a Grant-in-Aid for Scientific Research No. 347005 from the Ministry of Education, Science and Culture.

References

1) For a review, see, for example, A. C. Somersall and J. E. Guillet, *J. Macromol. Sci., Rev. Macromol. Chem.*, **C13**, 135 (1975).
2) M. Yagi and J. Higuchi, *Chem. Phys. Lett.*, **72**, 135 (1980).
3) J. Higuchi, M. Yagi, T. Iwaki, M. Bunden, K. Tanigaki, and T. Ito, *Bull. Chem. Soc. Jpn.*, **53**, 890 (1980).
4) P. Kottis and R. Lefebvre, *J. Chem. Phys.*, **39**, 393 (1963).
5) B. S. Yamanashi and K. W. Bowers, *J. Magn. Reson.*, **3**, 109 (1971).
6) R. F. Cozzens and R. B. Fox, *J. Chem. Phys.*, **50**, 1532 (1969).
7) R. B. Fox and R. F. Cozzens, *Macromolecules*, **2**, 181 (1969); R. B. Fox, T. R. Price, and R. F. Cozzens, *J. Chem. Phys.*, **54**, 79 (1971).
8) R. B. Fox, T. R. Price, R. F. Cozzens, and J. R. McDonald, *J. Chem. Phys.*, **57**, 2284 (1972).
9) P. Avakian, R. P. Groff, A. Suna, and H. N. Cripps, *Chem. Phys. Lett.*, **32**, 466 (1975).
10) N. F. Pasch and S. E. Webber, *Chem. Phys.*, **16**, 361 (1976).
11) R. V. Bensasson, J. C. Ronfard-Haret, E. J. Land, and S. E. Webber, *Chem. Phys. Lett.*, **68**, 438 (1979).
12) F. B. Bramwell, M. E. Laterza, and M. L. Spinner, *J. Chem. Phys.*, **62**, 4184 (1975).
13) G. Natta, P. Corradini, and I. W. Bassi, *Nuovo Cimento Soc. Ital. Fis., Supplemento*, **15**, 68 (1960).
14) P. Corradini and P. Ganis, *Nuovo Cimento Soc. Ital. Fis., Supplemento*, **15**, 104 (1960).

  Bull. Chem. Soc. Jpn., 54, 2457—2465 (1981)

X-Ray Structures of Di-μ-oxo, μ-Oxo-μ-thio-, and Di-μ-thio-μ-[(*R*)-propylenediaminetetraacetato]-bis[oxomolybdate(V)] Ions

Akinobu KOJIMA, Shun'ichiro OOI,* Yoichi SASAKI,** Kimiko Z. SUZUKI,** Kazuo SAITO,** and Hisao KUROYA***

Department of Chemistry, Faculty of Science, Osaka City University, Sumiyoshi-ku, Osaka 558
***Department of Chemistry, Faculty of Science, Tohoku University, Aoba, Aramaki, Sendai 980*

(Received November 19, 1980)

The crystal structures of $Na_2[Mo_2O_4(R\text{-pdta})]\cdot 3H_2O$ (**1**), $Na_2[Mo_2O_3S(R\text{-pdta})]\cdot 4H_2O$ (**2**), and $Na_2[Mo_2O_2S_2(R\text{-pdta})]\cdot 4H_2O$ (**3**) have been determined from diffractometer data collected by the use of Mo $K\alpha$ radiation. The structures of **1**, **2**, and **3** were refined by the least-squares method to R 0.064, 0.040, and 0.058 for 1370, 2794, and 2141 nonzero reflections respectively. Each Mo^V ion has a distorted octahedral coordination, and the two coordination octahedra share a common edge to form a binuclear complex. Two terminal oxo ligands are *cis* to the bridging oxide or sulfide. The R-pdta^{4-} ligand bridges two Mo^V ions, yielding a Mo–N–CH_2–CH(CH_3)–N–Mo ring with an equatorial methyl group, the N and carboxyl O atoms occupying the axial (*trans* to the terminal O) and equatorial positions respectively. A specific distortion of the donor-atom disposition is observed, which is represented as the twist (Δ) of the terminal O–O edges in the O(L$_b$)Mo(L$_b$)Mo portion about the axis passing through the mid-points of the O–O edges (Δ denotes the absolute disposition of two skew edges or bonds), and as the twist (Δ) of Mo–N bonds about the Mo–Mo axis. The O=Mo bonds of the O=Mo–Mo=O segment in **1** twist in Δ, but those in **2** and **3** are virtually parallel. The distortion of donor-atom disposition is discussed on the basis of the strain due to chelate-ring formation.

Few studies have been reported on the structure-circular dichroism (CD) correlation for molybdenum complexes, despite the rapid and extensive development of molybdenum chemistry.[1] Four of the present authors (K. Z. S., Y. S., S. O., and K. S.) have previously measured the CD spectra of a number of the binuclear Mo(V) complexes in solution and in crystalline state and have found, from a comparison of the spectral features with the X-ray structure, that the signs of the CD bands in the 26000—33000 cm^{-1} region are related to the distortion of the two coordination polyhedra about the Mo–Mo axis.[2] The present work has been conducted to provide structural data for this investigation. The structural details of $Na_2[Mo_2O_4(R\text{-pdta})]\cdot 3H_2O$ (**1**), $Na_2[Mo_2O_3S(R\text{-pdta})]\cdot 4H_2O$ (**2**), and $Na_2[Mo_2O_2S_2(R\text{-pdta})]\cdot 4H_2O$ (**3**) (R-pdta^{4-}, (R)-propylenediaminetetraacetate) will now be reported, thus providing the first example of the crystal structure of a complete series of binuclear Mo(V) complexes with three kinds of bridging structures and a common ligand.

Experimental

The preparation of the compounds was described elsewhere.[2] All three compounds are red-brown in color. The crystal data are shown in Table 1, where the experimental details are also given. The Laue symmetries and approximate unit-cell dimensions were determined from Weissenberg photographs. The cell dimensions were refined by the least-squares analyses of 15, 31, and 24θ values, as measured on a Philips four-circle diffractometer, for **1**, **2**, and **3** respectively.

The intensities were measured on the diffractometer using graphite-monochromated Mo $K\alpha$ radiation, and corrected for the Lp factor, but not for absorption. The backgrounds were measured on each side of the scan range. The intensities of three standard reflections were monitored every 4 h for each of the three compounds, but they showed no appreciable decay.

The crystal structure was solved by the heavy-atom technique. The positional and thermal parameters were refined by the least-squares method. The minimized function was $\sum w(F_o-|F_c|)^2$. Weights were assigned as $w=p$ for $F_o<F_{min}$, $w=1.0$ for $F_{min}\leq F_o\leq F_{max}$, and $w=(F_{max}/F_o)^2$ for $F_o>F_{max}$. The p, F_{max}, and F_{max} for each compound are as follows:

	p	F_{min}	F_{max}
1	0.1	16.9	42.3
2	0.6	7.8	31.2
3	0.7	9.5	35.6

No attempt was made to locate the H atoms. The atomic scattering factors, with corrections for anomalous dispersions of Mo^0 and S, were taken from Ref. 3. The absolute crystal structure was determined on the basis of the configuration of the asymmetric carbon atom. The atomic coordinate are given in Table 2. The F_o-F_c table and the anisotropic thermal parameters for heavy atoms are preserved by the Chemical Society of Japan (Document No. 8136). All computations were performed by means of a FACOM 230-60 computer at Osaka City University using programs in the UNICS.[4]

Results and Discussion

Crystal Structure. Figures 1 and 2 show the crystal structures of **1** and **2**. Compound **3** is isostructural with **2**. In **2** and **3** the complex anion is surrounded by 6 Na^+ ions, which are in contact with the O(O=C) atoms of the COO portions at distances of 2.30—2.55 Å. Although the cation disposition around the complex anion in **1** is somewhat different from those in **2** and **3**, the 6 Na^+ ions also lie in the vicinities of the O(O=C) atoms.

*** Present address: Department of Chemistry, Okayama University of Science, 1-1, Ridai-cho, Okayama 700.

TABLE 1. CRYSTAL DATA AND INTENSITY DATA COLLECTION

	1	2	3
Crystal system	Monoclinic	Triclinic	Triclinic
Space group	$P2_1$	P1	P1
a/Å	23.215(6)	11.438(3)	11.450(5)
b/Å	7.105(2)	7.401(2)	7.416(2)
c/Å	6.714(2)	6.563(2)	6.675(2)
α/°		89.54(2)	89.26(6)
β/°	99.66(3)	97.04(2)	95.90(3)
γ/°		90.82(2)	90.74(5)
U/Å^3	1091.8(5)	551.4(3)	563.7(3)
D_m/g cm^{-3}	1.98	2.08	2.06
D_c/g cm^{-3}	2.00	2.09	2.09
Z	2	1	1
μ(Mo $K\alpha$)/cm^{-1}	12.5	13.3	13.9
Crystal size/mm^3	0.1×0.1×0.1	0.24×0.12×0.19	0.11×0.08×0.15
Scan type	$\omega-2\theta$	ω	$\omega-2\theta$
Scan speed (ω/°s^{-1})	0.017	0.024	0.008
Scan range (ω/°)	(0.8+0.2 tan θ)	(1.7+0.2 tan θ)	(1.5+0.2 tan θ)
Background count/s^{-1}	20	20	20
$2\theta_{max}$/°	55.0	60.0	55.0
Reflections measured	$\pm h, +k, +l$	$\pm h, \pm k +l$	$\pm h, \pm k, +l$
No. of unique data ($F_o^2>2\sigma(F_o^2)$)	1370	2974	2141
R	0.064	0.040	0.058
R′(=$[\sum w\Delta^2/\sum wF_o^2]^{1/2}$	0.081	0.047	0.072

TABLE 2a. POSITIONAL AND THERMAL PARAMETERS FOR 1

	x	y	z	U/Å^2
Mo(1)	0.2019(1)	−0.0130(4)	−0.0674(2)	0.0230[a]
Mo(2)	0.3094(1)	0.0 (5)	0.0841(2)	0.0253[a]
O(1)	0.1936(6)	0.184(3)	−0.208(2)	0.033(3)
O(2)	0.1454(6)	−0.153(2)	−0.300(2)	0.031(3)
O(3)	0.1211(6)	0.045(2)	0.030(2)	0.030(3)
O(4)	0.0693(6)	−0.338(2)	−0.378(2)	0.031(3)
O(5)	0.0519(6)	−0.034(3)	0.201(2)	0.041(4)
O(6)	0.3283(7)	0.190(3)	−0.040(3)	0.043(4)
O(7)	0.3643(7)	0.091(3)	0.350(2)	0.041(4)
O(8)	0.3831(7)	−0.157(3)	0.048(2)	0.039(4)
O(9)	0.4243(6)	0.023(3)	0.631(2)	0.046(4)
O(10)	0.4434(8)	−0.397(3)	0.116(3)	0.058(5)
O(11)	0.2409(5)	0.060(2)	0.199(2)	0.024(3)
O(12)	0.2670(6)	−0.164(2)	−0.117(2)	0.026(3)
N(1)	0.1714(7)	−0.301(3)	0.088(2)	0.021(3)
N(2)	0.3154(7)	−0.269(3)	0.323(3)	0.023(4)
C(1)	0.1123(8)	−0.291(3)	−0.270(3)	0.020(4)
C(2)	0.1374(9)	−0.408(3)	−0.082(3)	0.030(5)
C(3)	0.0992(9)	−0.067(3)	0.146(3)	0.031(5)
C(4)	0.1326(9)	−0.233(3)	0.226(3)	0.026(5)
C(5)	0.3823(7)	−0.014(5)	0.503(2)	0.024(4)
C(6)	0.3482(10)	−0.200(4)	0.523(4)	0.039(6)
C(7)	0.3973(9)	−0.314(4)	0.124(3)	0.027(4)
C(8)	0.3535(9)	−0.412(4)	0.240(3)	0.035(5)
C(9)	0.2194(8)	−0.434(3)	0.187(3)	0.024(4)
C(10)	0.2596(8)	−0.358(3)	0.370(3)	0.026(4)
C(11)	0.2710(9)	−0.520(6)	0.518(3)	0.044(5)
Na(1)	−0.0029(4)	0.424(1)	0.517(1)	0.034(2)
Na(2)	0.4782(4)	−0.082(2)	−0.066(2)	0.044(2)
O_w(1)	0.0607(7)	0.181(3)	−0.349(3)	0.043(4)
O_w(2)	0.4768(9)	0.170(4)	0.208(4)	0.075(7)
O_w(3)	0.0294(8)	0.378(3)	0.185(3)	0.054(5)

a) Equivalent isotropic mean-square amplitude (W. C. Hamilton, *Acta Crystallogr.*, **12**, 609 (1959)).

TABLE 2b. POSITIONAL AND THERMAL PARAMETERS FOR 2

	x	y	z	U/Å^2
Mo(1)	−0.2276(1)	0.0788(1)	−0.0390(1)	0.0214[a]
Mo(2)	0.0 (1)	0.0 (1)	0.0 (1)	0.0200[a]
S	−0.1323(2)	−0.0498(2)	−0.2934(3)	0.0281[a]
O_x	−0.0905(5)	0.1753(7)	0.1322(8)	0.029(1)
O(1)	−0.2809(5)	−0.0961(8)	0.0912(9)	0.034(1)
O(2)	−0.3370(6)	0.2525(9)	0.1117(10)	0.038(1)
O(3)	−0.3747(5)	0.0963(8)	−0.2689(9)	0.031(1)
O(4)	−0.4539(6)	0.4929(9)	0.0813(11)	0.041(1)
O(5)	−0.4860(5)	0.2499(8)	−0.5042(10)	0.035(1)
O(6)	−0.0017(5)	−0.1911(8)	0.1388(9)	0.032(1)
O(7)	0.1394(5)	−0.1104(7)	−0.1467(8)	0.027(1)
O(8)	0.1459(5)	0.1169(8)	0.1720(9)	0.031(1)
O(9)	0.2795(6)	−0.0813(9)	−0.3506(10)	0.040(1)
O(10)	0.2824(6)	0.3261(9)	0.2473(10)	0.039(1)
N(1)	−0.2187(5)	0.3751(8)	−0.2033(9)	0.023(1)
N(2)	0.0750(5)	0.2519(8)	−0.2075(9)	0.022(1)
C(1)	−0.3655(7)	0.4107(11)	0.0452(12)	0.030(2)
C(2)	−0.2784(8)	0.5041(13)	−0.0783(15)	0.038(2)
C(3)	−0.3923(7)	0.2298(10)	−0.3934(12)	0.028(1)
C(4)	−0.2877(7)	0.3555(11)	−0.4087(13)	0.032(2)
C(5)	0.1937(7)	−0.0199(10)	−0.2761(12)	0.028(1)
C(6)	0.1459(8)	0.1595(12)	−0.3514(13)	0.033(2)
C(7)	0.1992(6)	0.2643(10)	0.1334(11)	0.026(1)
C(8)	0.1528(7)	0.3663(12)	−0.0617(13)	0.034(2)
C(9)	−0.0992(7)	0.4615(10)	−0.2182(12)	0.029(1)
C(10)	−0.0152(8)	0.3645(9)	−0.3424(10)	0.022(1)
C(11)	0.0428(8)	0.5090(13)	−0.4676(15)	0.038(2)
Na(1)	0.4306(3)	0.5291(4)	0.3544(5)	0.029(1)
Na(2)	0.3751(3)	0.0254(5)	0.3636(6)	0.037(1)
O_w(1)	−0.4399(7)	−0.1963(10)	0.4154(11)	0.047(2)
O_w(2)	0.4313(9)	0.0642(14)	0.0293(16)	0.075(3)
O_w(3)	0.3865(7)	−0.4174(11)	−0.3001(13)	0.055(2)
O_w(4)	0.2810(6)	−0.2527(10)	0.2214(11)	0.046(2)

a) Equivalent isotropic mean-square amplitude.

Table 2c. Positional and thermal parameters for **3**

	x	*y*	*z*	*U*/Å²
Mo(1)	−0.6204(1)	0.5399(2)	−0.5274(2)	0.0186[a]
Mo(2)	−0.3800(1)	0.4600(2)	−0.4720(2)	0.0151[a]
S(1)	−0.4807(3)	0.6558(5)	−0.2896(5)	0.0246[a]
S(2)	−0.5087(3)	0.4183(5)	−0.7621(5)	0.0196[a]
O(1)	−0.6777(10)	0.3585(15)	−0.4140(17)	0.029(2)
O(2)	−0.7455(9)	0.7083(14)	−0.4121(16)	0.029(2)
O(3)	−0.7518(10)	0.5533(16)	−0.7709(17)	0.025(2)
O(4)	−0.8505(10)	0.9583(15)	−0.4233(17)	0.041(2)
O(5)	−0.8605(12)	0.7198(19)	−0.9956(21)	0.028(3)
O(6)	−0.3851(10)	0.2586(15)	−0.3458(17)	0.027(2)
O(7)	−0.2423(9)	0.3572(14)	−0.6304(16)	0.024(2)
O(8)	−0.2312(9)	0.5681(14)	−0.3092(16)	0.022(2)
O(9)	−0.1014(11)	0.3904(18)	−0.8292(19)	0.037(3)
O(10)	−0.1002(10)	0.7834(16)	−0.2256(18)	0.032(3)
N(1)	−0.6020(11)	0.8424(17)	−0.6786(19)	0.022(2)
N(2)	−0.3067(10)	0.7188(15)	−0.6741(17)	0.017(2)
C(1)	−0.7654(12)	0.8753(19)	−0.4611(21)	0.024(3)
C(2)	−0.6688(14)	0.9673(22)	−0.5615(24)	0.031(3)
C(3)	−0.7681(13)	0.6936(21)	−0.8864(23)	0.020(3)
C(4)	−0.6680(15)	0.8285(23)	−0.8883(26)	0.027(3)
C(5)	−0.1858(13)	0.4505(20)	−0.7496(22)	0.023(3)
C(6)	−0.2309(13)	0.6349(21)	−0.8122(23)	0.024(3)
C(7)	−0.1825(13)	0.7239(21)	−0.3398(23)	0.024(3)
C(8)	−0.2310(13)	0.8320(21)	−0.5233(23)	0.024(3)
C(9)	−0.4844(14)	0.9300(21)	−0.6889(24)	0.026(3)
C(10)	−0.3944(12)	0.8334(19)	−0.8041(21)	0.019(3)
C(11)	−0.3305(14)	0.9815(22)	−0.9255(24)	0.027(3)
Na(1)	−0.9546(6)	0.9898(8)	−0.1335(10)	0.027(1)
Na(2)	−0.0045(6)	0.4902(10)	−0.1132(11)	0.035(2)
$O_w(1)$	−0.8227(13)	0.2649(20)	−0.0774(22)	0.044(3)
$O_w(2)$	−0.9560(16)	0.5063(26)	−0.4462(29)	0.067(5)
$O_w(3)$	−0.0055(14)	0.0447(23)	−0.7906(25)	0.054(4)
$O_w(4)$	−0.1026(13)	0.2052(19)	−0.2493(22)	0.043(3)

a) Equivalent isotropic mean-square amplitude.

Although no H atoms were located in the structure analyses, some possible hydrogen bonds, inferred from the interatomic distances and angles, are listed in Table 3. All the H atoms of $O_w(1)$, $O_w(2)$, and $O_w(3)$ in **2** and **3**, and those of $O_w(2)$ and $O_w(3)$ in **1**, seem to participate in O–H···O(carboxylate) hydrogen bonding, while one of the H atoms of $O_w(4)$ in **2** and **3** and that of $O_w(1)$ in **1** do not seem to be involved in the hydrogen bonding.

The O atom of Mo=O is generally distant from the Na^+ ions. The $O_w(1)$ atoms in **2** and **3** are located at distances of 3.04(1) and 3.00(2) Å respectively from O(1)(O=Mo), and one of the H atoms of $O_w(1)$ seems to be in contact with the O(1). The O(1) in **2** and **3** also has a short contact with the $C(2)H_2$ group of the adjacent anion at $(x, 1+y, z)$, the O(1)···C(2) distances being 3.17(2) and 3.08(3) Å respectively. However, the O(1)···H(CH_2) distances, calculated on the assumption of C–H=1.05 Å, are 2.57 and 2.70 Å even in **3**. No such contacts are found in **1**.

In **1**—**3**, however, there are no remarkable short distances indicative of a strong interaction; accordingly, the interatomic interaction seems to produce no significant deformation of the complex anion.

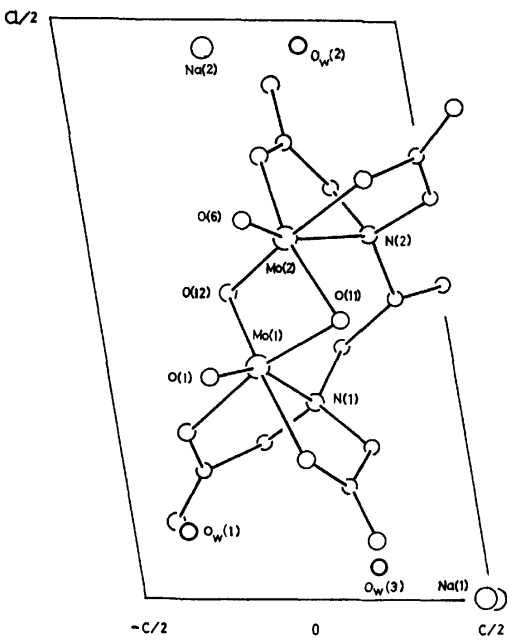

Fig. 1. The crystal structure of $Na_2[Mo_2O_4(R\text{-pdta})]\cdot 3H_2O$ viewed down the b axis.

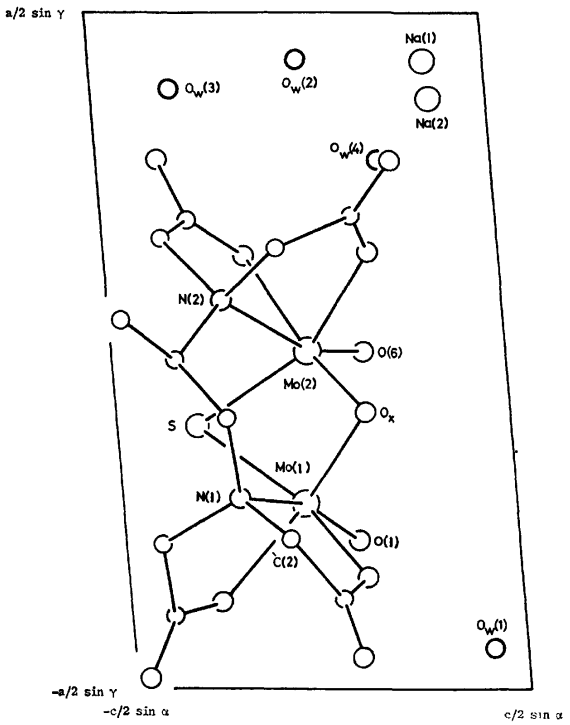

Fig. 2. The crystal structure of $Na_2[Mo_2O_3S(R\text{-pdta})]\cdot 4H_2O$ viewed down the b axis.

Structure of the Binuclear Complex Anion. Figure 3 shows a perspective view of the binuclear complex anion in **1**. As the three complex anions have configurations similar to one another, a common atom numbering was used for all three, as is shown in figure, except for the bridging atoms. The projections and elevations of the anions are given in Fig. 4. Table 3 lists the interatomic distances and bond angles. The corresponding bond lengths agree well within the experimental

TABLE 3. INTERATOMIC DISTANCES AND ANGLES[a)]

Bond length (l)

	1 l/Å	2 l/Å	3 l/Å
Mo(1)–O(1)	1.68(2)	1.691(6)	1.70(1)
O(2)	2.11(1)	2.135(7)	2.12(1)
O(3)	2.13(1)	2.124(5)	2.10(1)
N(1)	2.45(2)	2.440(6)	2.47(1)
$L_b(1)$	1.94(1)	2.318(2)	2.318(4)
$L_b(2)$	1.93(2)	1.946(5)	2.301(4)
Mo(2)–O(6)	1.68(2)	1.676(6)	1.71(1)
O(7)	2.11(2)	2.134(6)	2.14(1)
O(8)	2.09(2)	2.080(5)	2.08(1)
N(2)	2.49(2)	2.501(6)	2.52(1)
$L_b(1)$	1.93(1)	2.329(2)	2.331(3)
$L_b(2)$	1.92(1)	1.943(6)	2.299(4)
Mo(1)–Mo(2)	2.533(2)	2.656(1)	2.808(2)
O(1)···O(6)	3.14(2)	3.255(8)	3.42(2)
N(1)···N(2)	3.46(3)	3.495(9)	3.51(2)
$L_b(1)$···$L_b(2)$	2.79(2)	3.246(6)	3.613(5)
O(2)–C(1)	1.28(3)	1.277(10)	1.29(2)
O(4)–C(1)	1.18(2)	1.234(11)	1.21(2)
N(1)–C(2)	1.48(3)	1.488(12)	1.49(2)
C(1)–C(2)	1.54(3)	1.514(13)	1.51(2)
O(3)–C(3)	1.28(3)	1.279(9)	1.29(2)
O(5)–C(3)	1.24(3)	1.231(9)	1.24(2)
N(1)–C(4)	1.48(3)	1.484(10)	1.53(2)
C(3)–C(4)	1.46(3)	1.516(11)	1.51(2)
O(7)–C(5)	1.28(3)	1.288(10)	1.27(2)
O(9)–C(5)	1.22(2)	1.240(11)	1.24(2)
N(2)–C(6)	1.51(3)	1.492(11)	1.48(2)
C(5)–C(6)	1.56(4)	1.498(11)	1.51(2)
O(8)–C(7)	1.25(3)	1.280(9)	1.30(2)
O(10)–C(7)	1.23(3)	1.223(9)	1.23(2)
N(2)–C(8)	1.51(3)	1.487(10)	1.51(2)
C(7)–C(8)	1.55(3)	1.523(11)	1.52(2)
N(1)–C(9)	1.53(3)	1.514(10)	1.50(2)
N(2)–C(10)	1.52(3)	1.527(9)	1.52(2)
C(9)–C(10)	1.51(3)	1.522(11)	1.54(2)
C(10)–C(11)	1.54(4)	1.534(12)	1.58(2)
C(6)···C(11)	2.89(4)	2.914(13)	2.89(2)
C(8)···C(11)	2.99(3)	2.996(12)	3.01(2)

Short contact

A	B	1 l/Å	2 l/Å	3 l/Å
Na(1)···	$O_w(1)$	2.35(2)^{III}	2.503(8)^{IV}	2.53(2)^{II}
		2.43(2)^{XII}		
	$O_w(3)$	2.49(2)	2.418(9)^{VI}	2.46(2)^{IX}
	$O_w(4)$		2.446(8)^{II}	2.40(2)^{VIII}
	O(4)	2.40(2)^{VI}	2.370(8)^{I}	2.39(2)
		2.49(2)^{XII}		
	O(5)	2.39(2)^{XIV}	2.416(7)^{V}	2.41(2)^{III}
	O(10)		2.297(7)	2.29(1)^{X}
Na(2)···	$O_w(1)$		2.681(9)^{I}	2.67(2)^{I}
	$O_w(2)$	2.57(3)	2.372(12)	2.35(2)^{I}
		2.34(3)^{XV}		
	$O_w(4)$		2.446(8)	2.51(2)
	O(5)		2.377(8)^{V}	2.43(2)^{V}
	O(8)	2.51(2)		
	O(9)	2.32(2)^{XI}	2.404(8)^{III}	2.39(2)^{III}
	O(10)	2.31(3)^{XIII}	2.548(7)	2.52(1)
		2.74(3)		

A	B	1 l/Å	2 l/Å	3 l/Å
$O_w(1)$···	O(3)	2.86(2)	3.031(10)^{III}	3.02(2)^{III}
	O(1)		3.041(10)	3.00(2)
$O_w(2)$···	O(2)		2.969(13)	2.81(2)
	O(7)	2.98(3)		
	O(9)		3.056(12)	3.03(2)^{X}
	O(10)	3.12(3)^{XIII}		
$O_w(3)$···	O(4)		2.990(11)^{VII}	2.95(2)^{VII}
	O(5)	2.97(3)		
		3.00(3)^{XII}		
	O(9)		2.785(11)	2.80(2)
$O_w(4)$···	O(7)		2.937(9)	3.07(2)

Roman numeral superscripts refer to the position of the B atom in the respective A···B contacts: I $1+x, y, z$; II $x, 1+y, z$; III $x, y, 1+z$; IV $1+x, 1+y, z$; V $1+x, y, 1+z$; VI $x, 1+y, 1+z$; VII $1+x, y-1, z$; VIII $x-1, 1+y, z$; IX $x-1, 1+y, 1+z$; X $x-1, y, z$; XI $x, y, z-1$; XII $-x, (1/2)+y, -z$; XIII $1-x, (1/2)+y, -z$; XIV $-x, (1/2)+y, 1-z$; XV $1-x, -(1/2)+y, -z$.

Bond angle (ϕ)

	1 ϕ/°	2 ϕ/°	3 ϕ/°
O(1)–Mo(1)–O(2)	88.9(7)	87.9(3)	90.1(5)
O(1)–Mo(1)–O(3)	89.3(7)	96.1(3)	95.9(5)
O(1)–Mo(1)–$L_b(1)$	106.7(7)	105.9(2)	104.6(4)
O(1)–Mo(1)–$L_b(2)$	112.6(7)	107.1(3)	105.0(4)
O(1)–Mo(1)–N(1)	156.8(6)	159.3(3)	161.0(5)
N(1)–Mo(1)–O(2)	74.4(6)	73.4(2)	72.2(4)
N(1)–Mo(1)–O(3)	72.5(6)	72.5(2)	74.1(4)
N(1)–Mo(1)–$L_b(1)$	87.5(6)	90.7(2)	90.7(3)
N(1)–Mo(1)–$L_b(2)$	84.3(6)	81.9(2)	82.1(3)
O(2)–Mo(1)–O(3)	81.3(6)	80.3(2)	78.2(4)
$L_b(1)$–Mo(1)–$L_b(2)$	92.8(6)	98.8(2)	102.9(1)
Mo(2)–Mo(1)–O(1)	101.9(5)	100.6(2)	100.8(4)
Mo(2)–Mo(1)–N(1)	101.3(4)	99.1(1)	97.4(3)
O(6)–Mo(2)–O(7)	90.1(7)	88.3(3)	89.2(5)
O(6)–Mo(2)–O(8)	94.8(8)	96.3(2)	98.1(5)
O(6)–Mo(2)–$L_b(1)$	108.8(8)	105.6(2)	104.0(4)
O(6)–Mo(2)–$L_b(2)$	106.4(7)	106.5(3)	104.6(4)
O(6)–Mo(2)–N(2)	161.1(6)	160.0(2)	161.2(5)
N(2)–Mo(2)–O(7)	74.4(6)	73.9(2)	73.2(4)
N(2)–Mo(2)–O(8)	72.9(6)	71.9(2)	72.1(4)
N(2)–Mo(2)–$L_b(1)$	82.7(6)	84.0(1)	82.7(3)
N(2)–Mo(2)–$L_b(2)$	87.4(6)	88.9(2)	90.7(3)
O(7)–Mo(2)–O(8)	82.8(6)	79.3(2)	78.1(4)
$L_b(1)$–Mo(2)–$L_b(2)$	93.1(6)	98.5(2)	102.6(1)
Mo(1)–Mo(2)–O(6)	98.7(5)	99.9(2)	100.0(4)
Mo(1)–Mo(2)–N(2)	100.1(4)	100.0(1)	98.0(3)
Mo(1)–$L_b(1)$–Mo(2)	82.0(5)	69.7(1)	74.3(1)
Mo(1)–$L_b(2)$–Mo(2)	82.4(6)	86.1(2)	75.3(1)
Mo(1)–O(2)–C(1)	124(1)	123.0(6)	126(1)
Mo(1)–N(1)–C(2)	105(1)	107.0(5)	107(1)
O(2)–C(1)–O(4)	126(2)	125.4(8)	125(1)
O(2)–C(1)–C(2)	113(2)	115.5(7)	115(1)
O(4)–C(1)–C(2)	121(2)	119.0(8)	121(1)
N(1)–C(2)–C(1)	115(2)	112.4(7)	113(1)
Mo(1)–O(3)–C(3)	122(1)	123.7(5)	123(1)
Mo(1)–N(1)–C(4)	104(1)	105.5(4)	105(1)
O(3)–C(3)–O(5)	122(2)	122.3(7)	123(2)
O(3)–C(3)–C(4)	119(2)	116.1(6)	118(1)

	1	2	3
	ϕ/°	ϕ/°	ϕ/°
O(5)–C(3)–C(4)	119(2)	121.4(7)	120(1)
N(1)–C(4)–C(3)	112(2)	109.6(6)	110(1)
C(2)–N(1)–C(4)	110(2)	109.6(6)	107(1)
Mo(2)–O(7)–C(5)	124(2)	122.8(5)	124(1)
Mo(2)–N(2)–C(6)	107(1)	104.2(4)	105(1)
O(7)–C(5)–O(9)	124(3)	122.2(7)	123(1)
O(7)–C(5)–C(6)	118(2)	118.8(7)	118(1)
O(9)–C(5)–C(6)	119(2)	118.8(7)	119(1)
N(2)–C(6)–C(5)	113(2)	114.4(7)	115(1)
Mo(2)–O(8)–C(7)	126(2)	127.4(5)	127(1)
Mo(2)–N(2)–C(8)	105(1)	106.5(4)	105(1)
O(8)–C(7)–O(10)	125(2)	122.9(7)	122(1)
O(8)–C(7)–C(8)	117(2)	117.2(6)	118(1)
O(10)–C(7)–C(8)	117(2)	119.9(7)	121(1)
N(2)–C(8)–C(7)	111(2)	112.5(6)	113(1)
C(6)–N(2)–C(8)	108(2)	110.2(6)	109(1)
Mo(1)–N(1)–C(9)	117(1)	118.7(4)	121(1)
Mo(2)–N(2)–C(10)	120(1)	117.9(4)	119(1)
N(1)–C(9)–C(10)	116(2)	118.0(6)	118(1)
N(2)–C(10)–C(9)	114(2)	112.4(6)	115(1)
C(9)–C(10)–C(11)	106(2)	107.2(6)	107(1)
N(2)–C(10)–C(11)	113(2)	112.5(6)	111(1)

a) $L_b(1)$ and $L_b(2)$stand for O(11) and O(12) in **1**, S and O_x in **2**, and for S(2) and S(1) in **3**.

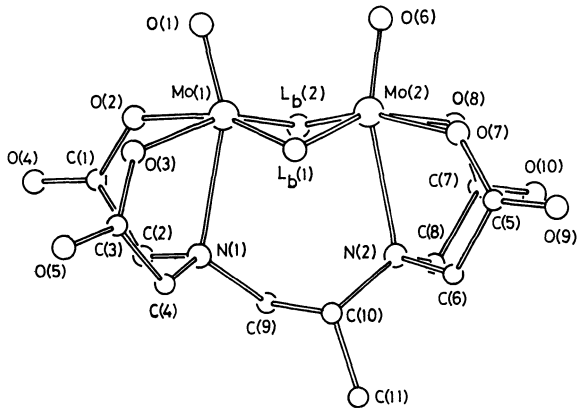

Fig. 3. A perspective view of $[Mo_2O_4(R\text{-pdta})]^{2-}$ anion with atom numbering. The same numbering is used for $[Mo_2O_3S(R\text{-pdta})]^{2-}$ and $[Mo_2O_2S_2(R\text{-pdta})]^{2-}$ anions. The $L_b(1)$ and $L_b(2)$ stand for O(11) and O(12) in $[Mo_2O_4(R\text{-pdta})]^{2-}$, S and O_x in $[Mo_2O_3S(R\text{-pdta})]^{2-}$, and S(2) and S(1) in $[Mo_2O_2S_2(R\text{-pdta})]^{2-}$.

error in the three complexes, except for those in which L_b atoms are concerned (L_b, bridging ligand).

Structure of the $Mo_2O_2L_{b2}$ Core: The geometry and dimensions of $Mo_2O_2L_{b2}$ core are not much different from those of the corresponding core in the other binuclear Mo(V) complexes.[5,6] Each Mo atom has a very distorted octahedral coordination. The deviation of the Mo atom from the mean plane defined by two O(carboxylate) and two L_b atoms is in the range of 0.35—0.37 Å, irrespective of the kind of bridging ligand (Table 4).

The Mo–Mo distance increases in the order of **1**, **2**, and **3**. The distance in **1** is slightly shorter than those so far found in Mo_2O_4 cores (2.541—2.580 Å),[5] while that in **2** is comparable to that in $[Mo_2O_3S(S_2CNPr_2)_2]$ (2.673(3) Å).[7] The Mo–Mo bond in **3** is comparable in length to that in $Cs_2[Mo_2O_2S_2(edta)]\cdot 2H_2O$ (2.799 (1) Å),[8] but shorter than those in the other complexes with a $Mo_2O_2S_2$ core.[6] Although the Mo–Mo=O(1) and Mo–Mo=O(6) bond angles in **2** and **3** are nearly equal, they are significantly different from each other in **1**.

The Mo–S bond length in **3** ranges from 2.299 to 2.331(3) Å. The Mo–S(1) distances are longer than the Mo–S(2) distances; concomitantly, the Mo–S(2)–Mo angle is 1.0° larger than the Mo–S(1)–Mo angle. However, the average value of the Mo–S bond length (2.312 Å) is comparable to that of the edta complex (2.294(1) Å).[8] The Mo–S–Mo angle in **2** is smaller by *ca.* 5° than any of the corresponding angles in the $Mo_2O_2S_2$ cores of other complexes.[6] The Mo–O–Mo angles in **1** are normal and close to those in $[Mo_2O_4(H_2PO_2)_2(bpy)_2]$ (82.5°, 82.9(5)°),[9] but the Mo–O–Mo angle in **2** is greater by 4° than those in **1**. The two L_b–Mo–L_b angles in each complex agree well with each other, and increase in the order of **1**, **2**, and **3**.

The interplanar angle between the two MoL_{b2} planes is 145.4° in **1**, comparable to that in the bpy complex (143°),[9] but smaller than that in $Na_2[Mo_2O_4(R\text{-cys})_2]\cdot 5H_2O$ (151°).[10] The angle increases with the elongation of the Mo–Mo bond (Table 4), and that in **3** is nearly equal to that in the edta complex (152.3°).[8] The two Mo=O bonds in **1** are twisted in a Δ configuration with an O=Mo–Mo=O torsion angle of 5.4(8)°, whereas those in **2** and **3** are virtually parallel (Δ or Λ is used to designate the chirality of two skew edges or bonds, according to the definition given in our previous paper[2]).

Structure of the Chelate Ring: The Mo(1)–N bond in

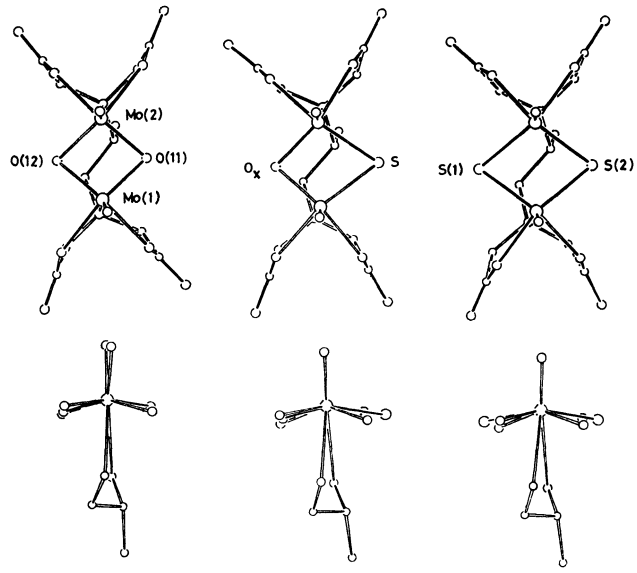

Fig. 4. The projection (top) on [O(2), O(3), O(7), O(8)] plane and the elevation (bottom) viewed along Mo(1)→Mo(2) vector, for each of the three complex anions: $[Mo_2O_4(R\text{-pdta})]^{2-}$ (left), $[Mo_2O_3S(R\text{-pdta})]^{2-}$ (middle), and $[Mo_2O_2S_2(R\text{-pdta})]^{2-}$ (right). The glycinato rings are not drawn in the elevation for clarity. The Mo–L_b bond is shown by solid line in the elevation.

Table 4. Deviations (d) of atoms from mean planes, interplanar angles (ϕ), and torsion angles (τ)[a)]

Plane	Atom	1 d/Å	2 d/Å	3 d/Å
	Mo(1)	0.353(8)	0.362(3)	0.370(4)
	O(2)	0.047(17)	0.080(7)	0.065(11)
[O(2),O(3),L_b(1),L_b(2)]	O(3)	−0.048(15)	−0.078(6)	−0.067(12)
	L_b(1)	0.048(15)	0.066(2)	0.047(4)
	L_b(2)	−0.047(16)	−0.068(6)	−0.047(4)
	Mo(2)	0.364(9)	0.365(3)	0.371(4)
	O(7)	0.055(19)	0.080(5)	0.092(11)
[O(7),O(8),L_b(1),L_b(2)]	O(8)	−0.058(19)	−0.091(6)	−0.097(10)
	L_b(1)	−0.054(15)	−0.066(2)	−0.067(4)
	L_b(2)	0.057(16)	0.077(6)	0.072(4)
	Mo(1)	0.055(3)	0.094(1)	0.114(1)
	Mo(2)	−0.054(3)	−0.093(1)	−0.112(1)
	N(1)	−0.040(18)	−0.072(6)	−0.091(13)
[Mo(1),Mo(2),N(1),N(2)]	N(2)	0.040(18)	0.070(6)	0.090(12)
	C(9)	−0.490(27)	−0.434(14)	−0.432(27)
	C(10)	0.416(28)	0.516(12)	0.508(24)
	C(11)	0.430(43)	0.627(17)	0.639(30)

Interplanar angle between [Mo(1),L_b(1),L_b(2)] and [Mo(2),L_b(1),L_b(2)] planes

	ϕ/°
1	145.4°
2	149.6°
3	153.4°

Torsion angle

Segment	1 τ/°	2 τ/°	3 τ/°
N(1)–C(9)–C(10)–N(2)	−94(2)	−98(1)	−96(2)
N(1)–Mo(1)–Mo(2)–N(2)	−5.4(6)	−9.1(2)	−10.8(4)
O(2)···O(3)···O(7)···O(8)	−8.6(7)	−11.5(2)	−10.4(5)
O(2)···O(3)···L_b(1)···L_b(2)	−4.0(6)	−5.7(2)	−4.6(4)
O(8)···O(7)···L_b(1)···L_b(2)	−4.5(7)	−5.8(2)	−6.1(3)
O(1)–Mo(1)–Mo(2)–O(6)	−5.4(8)	−0.2(3)	0.2(6)

a) The sign of the torsion angle in the A–B–C–D segment is negative if the direction of the rotation which superimposes the A–B bond on the C–D bond is counterclockwise.

every pdta complex is significantly shorter than the Mo(2)–N bond, whose N atom is nearer to the methyl group than that of the Mo(1)–N. The Mo–Mo–N bond angle decreases in the sequence of **1**, **2**, and **3**. The decrement along the sequence is 3.9° in Mo(2)–Mo(1)–N, but 2.1° in Mo(1)–Mo(2)–N; the replacement of the bridging ligands has a greater influence on the Mo–Mo–N bond angle containing an N atom more distant from the methyl group.

The propylenediamine portion of the ligand takes a λ gauche conformation. The methyl group is equatorial with respect to the 6-membered Mo(1)–N(1)–C(9)–C(10)–N(2)–Mo(2) ring. The N···N distance and N–C–C–N torsion angle are in the 3.46—3.51 Å and 94—98° range respectively, and are thus relatively insensitive to the kind of bridging ligand. The torsion angle is much larger than that in the usual 5-membered chelate ring of propylenediamine.[11] The N–Mo–Mo–N frame is not planar, but the two terminal bonds are twisted in a Δ configuration (Fig. 4) and the torsion angle ranges from 5.4° in **1** to 10.8° in **3**. The bond angles in the 6-membered ring indicate the presence of considerable strain: the Mo–N–C and N–C–C angles are considerably larger than the tetrahedral angle and rather near to the trigonal one, except for the C(9)–C(10)–N(2) angle. The methyl group is in short contact with the C(6)H_2 and C(8)H_2 groups. The mean value of the C(11)···C(6) distance is 0.1 Å shorter than that of C(11)···C(8).

The O(carboxylate)–Mo–O(carboxylate) angle diminishes along the 1-2-3 sequence. This arises from the repulsion between the ligating carboxylate O atoms and the bridging atoms, as is indicated by the contact distances of O···O_b (2.74—2.88 Å) and O···S (2.954—3.176 Å).

The Mo–N–C–C–O glycinato rings have a highly puckered structure. The two rings, linked to a common Mo, have an enantiomeric conformation. The glycinato ring has some strain, as is indicated by the bond angle. The Mo(2)–O(8)–C(7) angles are larger than 126°, while the Mo(2)–O(7)–C(5), Mo(1)–O(2)–C(1), and Mo(1)–O(3)–C(3) angles are 122—126°. The C(2)–C(1)–O(2) angles (113—116°) are significantly smaller than 120°, though the other C–C–O(carboxylate) angles

are 116—119°. The N(1)–C(2)–C(1) and N(2)–C(6)–C(5) angles show a significant deviation from 109.5°, but N(1)–C(4)–C(3) and N(2)–C(8)–C(7) do not. All the other bond angles are normal.

As has been described above, there is a slight but significant difference between the corresponding bond lengths and angles around the two Mo's in the dimer. The difference is systematic for the three complexes, despite the difference in crystal packing. This inequivalence of the Mo's is thought to result from the methyl group disposed unsymmetrically in relation to the Mo(1) and Mo(2).

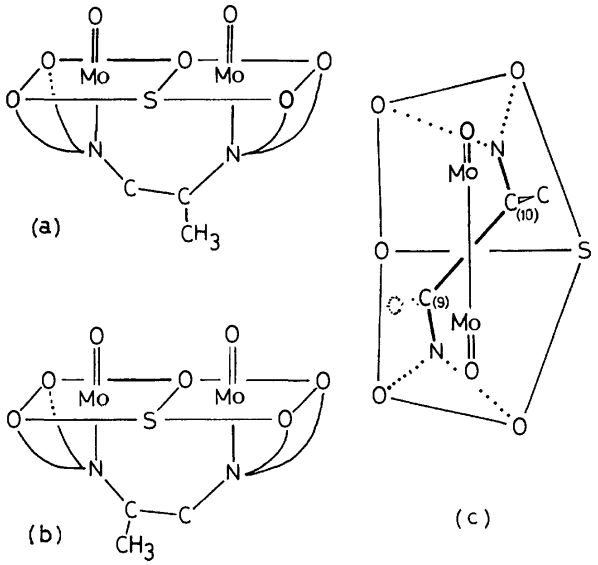

Fig. 5. The two isomers for $[Mo_2O_3S(R\text{-pdta})]^{2-}$ anion. (a) Isomer (1), (b) isomer (2), and (c) the projection of the isomer (1) showing schematically the disposition of the ethylenediamine moiety relative to the Mo_2O_3S core (the methyl carbon shown by dotted letter corresponds to that in the approximated structure of the isomer (2)).

Geometrical Isomerism of $[Mo_2O_3S(R\text{-pdta})]^{2-}$. Figures 5(a) and (b) show two geometrical isomers for this anion. The structure shown in Fig. 4 (middle) corresponds to the (1) isomer, which was selectively obtained by the method of preparation described in Ref. 2. The (1) isomer differs from (2) in the disposition of the methyl group with respect to the Mo_2O_3S core. The structure of the (2) isomer may be approximated by a structure obtained by exchanging C(10)–CH_3 for equatorial C(9)–H in the (1) isomer. Figure 5(c) shows schematically the projection of the (1) isomer. The atom arrangement is unsymmetric with respect to the Mo–Mo line because of the difference between the Mo–O_b and Mo–S distances; accordingly, the ligating $pdta^{4-}$ is bent out of the Mo–Mo line. This gives rise to a difference between the conformational energies of the (1) and (2) isomers. In the approximated structure for the (2) isomer, the $CH_3\cdots C(2)$ and $CH_3\cdots C(4)$ contact distances are estimated to be 2.72 and 2.91 Å respectively. These values are significantly smaller than those of the corresponding short contacts in the (1) isomer, although the atom overcrowding in the approximated structure may be alleviated to some extent in the actual structure of the (2) isomer. Such an unfavorable ligand structure may be responsible for low abundance of the (2) isomer in solution.

Distortion of Donor-atom Disposition. The CD signs of the binuclear Mo(V) complexes of the dissymmetric ligand in the 26000—33000 cm^{-1} region are not directly related to the configuration of asymmetric carbon in the ligand.[2] A closer investigation of the X-ray structures of the eight dissymmetric Mo(V) complexes led us to the conclusion that the asymmetric factor responsible for the sign of the crystalline CD spectra in this region is, in the first approximation, the dissymmetric distortion of the donor-atom disposition. The distortion can be represented by; i) a twist of the X–Y and X′–Y′ edges about the axis parallel to the Mo–Mo axis (Fig. 6), ii) a twist of Mo=O_t and Mo=O'_t about the Mo–Mo axis, and iii) a twist of Mo–Z and Mo–Z′ about the Mo–Mo axis. The third twist is thought to be less important for the optical activity in view of the fact that the Mo–Z(Z′) distance is longer than the other Mo–donor distances in the dimer.[2]

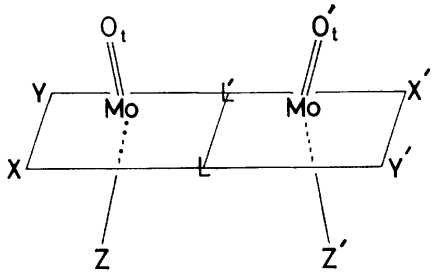

Fig. 6. The idealized corrdination framework for the binuclear Mo(V) complex.

Such a distortion should arise from the strain characteristic of the coordinating ligand. If there were no chelate rings, 2 Mo, O_t, O'_t, Z, and Z′ would lie on one plane[12] (Fig. 6). When the donor atoms of *R*-$pdta^{4-}$ occupy the X, Y, Z, X′, Y′, and Z′ coordination sites, the *R*-propylenediamine moiety takes a λ skew conformation to make C–CH_3 equatorial; accordingly the $N\langle^{C}_{C}C$ portion cannot be symmetric with respect to the [2Mo,O_t,O'_t,Z,Z′] plane of the idealized coordination framework (Fig. 6). Each NC_3 portion rotates counterclockwise about the Mo→N vector, from the symmetric position with respect to the [2Mo,O_t,O'_t,Z,Z′] plane until the N–C–C–N torsion angle becomes 94—98° as in the structures of **1**—**3**. Such a rotation brings about the upper shift of Y(Y′) and the down shift of X(X′), making the X–Y edge (X′–Y′) slant against L–L′ in the Δ configuration. The strain in the glycinato and *R*-propylenediamine rings may be alleviated by the displacement of the N atoms from the [2Mo,O_t,O'_t,Z,Z′] plane, thus twisting the N–Mo–Mo–N in the Δ configuration.

The O(1)···O(2) and O(6)···O(7) distances in the three complexes are shorter than the O(1)···O(3) and O(6)···O(8) distances (Table 5). The former distances

TABLE 5. SOME EDGE LENGTHS (l/Å) IN THE COORDINATION OCTAHEDRA OF BINUCLEAR Mo(V) COMPLEXES

	$O_t\cdots X$	$O'_t\cdots X'$	X or X'	$O_t\cdots Y$	$O'_t\cdots Y'$	Y or Y'	Ref.
$Na_2[Mo_2O_4(R\text{-pdta})]\cdot 3H_2O$	2.70(2)	2.79(3)	O	2.67(2)	2.71(2)	O	This work
$Na_2[Mo_2O_3S(R\text{-pdta})]\cdot 4H_2O$	2.852(8)	2.810(8)	O	2.674(9)	2.674(8)	O	This work
$Na_2[Mo_2O_2S_2(R\text{-pdta})]\cdot 4H_2O$	2.83(2)	2.88(2)	O	2.72(2)	2.72(2)	O	This work
$[Mo_2O_2S_2(S\text{-hist})_2]\cdot 1.5H_2O$	2.71(1)	2.85(1)	N	2.83(1)	2.83(1)	N	12
$Na_2[Mo_2O_4(R\text{-cys})_2]\cdot 5H_2O$	2.89(2)	2.88(2)	N	3.13(2)	3.12(2)	S	10
$Na_2[Mo_2O_2S_2(R\text{-cys})_2]\cdot 2H_2O$	2.86(2)	2.93(4)	N	3.08(4)	3.16(3)	S	13

are in the 2.67—2.72 Å range, and thus substantially invariable for all three complexes. This indicates that the O(1) and O(6) atoms are in short contact with the O(2) and O(7) atoms respectively; hence, the direction of the Mo=O(1) and Mo=O(6) bonds depends on the positions of the O(2) and O(7) atoms. Since the ligation of R-pdta^{4-} displaces the X and Y by 0.09—0.16 Å from the [X,Y,L,L'] plane of the idealized framework (Table 4), the O_t moves so as to keep the contact distance constant, resulting in the Δ twist of the O=Mo–Mo=O segment. The displacements of O'_t, X', and Y' from the idealized positions are similar to those of the unprimed sites and give rise to the enlargement of the O=Mo–Mo=O torsion angle.

The Mo=O bonds are virtually parallel to each other in **2** and **3**. The Mo–Mo distance and the interplanar angle between the [Mo,L_b(1),L_b(2)] planes in these complexes are significantly larger than the corresponding ones in **1**, while the N···N distance, the Mo–Mo=O bond angle, and the deviation of Mo from the equatorial plane are not different from those in **1**. On the basis of these structural features, the idealized framework for **3** can be derived from that for **1** in the following way; i) the elongation of the Mo–Mo, $O_t\cdots O'_t$, X···Y', and Y···X' distances by 0.28 Å along the Mo–Mo axis, followed by ii) the enlargement of the [Mo,L,L'] interplanar angle by 8.0°. In the derived framework, X and Y (as well as X' and Y') are calculated to lie 0.13 Å below the equatorial plane of the intermediate framework obtained by the i) operation. However, the Y(Y') shifts 0.14 Å (average) upward upon the ligation of R-pdta^{4-} (Table 4). Consequently, the atom at the Y(Y') site may be regarded as lying on the equatorial plane of the intermediate framework, in contact with $O_t(O'_t)$ without repelling it, thus making the Mo=O_t bonds nearly parallel to each other in **3**. The inherent low symmetry of the Mo_2O_3S core may have some additional influence on the donor-atom disposition in **2**.

That the twist in the O=Mo–Mo=O segment is solely found in **1**, but not in **2** and **3**, weakens the basis of the interpretation of the twist. However, the interpretation is substantiated by the following analysis of the twist of O=Mo–Mo=O in $[Mo_2O_2S_2(S\text{-hist})_2]\cdot 1.5H_2O$[13] (**4**) (hist$^-$=histidinate), $Na_2[Mo_2O_4(R\text{-cys})_2]\cdot 5H_2O$[10] (**5**), and $Na_2[Mo_2O_2S_2(R\text{-cys})_2]\cdot 2H_2O$[14] (**6**) (cys^{2-}= cysteinate), which were utilized for the investigation of the CD-structure correlation in the Mo(V) dimer.[2] These complexes have a common framework (shown in Fig. 7) and have no bridge like that of the propylenediamine moiety in **1**—**3**. The torsion angle and the

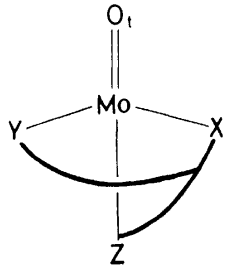

Fig. 7. A sketch of chelate ring in the half of the Mo(V) dimer with terdentate S-hist$^-$ or R-cys^{2-} ligand.

configuration of the distortion were described in Ref. 2 (torsion angle in O_t=Mo–Mo=O'_t (θ_1) and that for the X–Y and Y'–X' edges (ξ) in the respective complexes are as follows: **4** θ_1=2.5°(Δ), ξ=4.5°(Δ); **5** θ_1=4.0°(Δ), ξ=0.1°(Δ); **6** θ_1=4.7°(Δ), ξ=0.2°(Δ); the ξ values for **5** and **6** are meaningless in view of the experimental errors).

Each of the **4**—**6** complexes has an approximate twofold axis passing the mid-point between the Mo's across the XYX'Y' plane. Figure 7 shows a sketch of this type of complex as viewed along the Mo–Mo axis. The three ligating atoms, S, N, and O of R-cys^{2-}, and N(ring), N, and O of S-hist$^-$, are located in a clockwise fashion in this order (Y, X, and Z) when the Mo atom is looked at from the asymmetric carbon of the coordinating R-cys^{2-} and S-hist$^-$. The chelate ring spanning X and Z sites is 5-membered, irrespective of the kind of ligand. Table 5 lists the distances between O_t and atoms at the X and Y sites. These distances are somewhat shorter than those to be expected from the van der Waals radii of the two atoms; therefore, the O_t atom must be in contact with atoms at the X and Y sites. The formation of a 5-membered ring between X and Z shifts X toward Z and makes O_t distant from X. In order to make the interatomic interaction optimal, O_t shifts toward X, and in turn Y approaches O_t. Such shifts lead to, as a whole, a rotation of the O_tXY triangle about its center. The rotations of the O_tXY and O'_tX'Y' triangles compatible with the symmetry of the dimer must have resulted in the twist in O_t=Mo–Mo=O'_t, as well as in that of the X–Y and Y'–X' edges. Since Mo–S(Y) is *ca.* 0.3 Å longer than Mo–N(X), the rotation of Mo–Y(S) and that of Mo–X'(N) in opposite directions about the Mo–Mo axis, giving a torsion angle of 4—5° in O_t=Mo–Mo=O'_t, seems to give the negligible twist of the X–Y and Y'–X' edges in **5** and **6**.

The distortion of the coordination framework in the binuclear Mo(V) complexes, **1**—**6**, is thus explainable

on the basis of the strain due to chelate-ring formation. The *Λ* twist in **1** and the negligible twist in **2** and **3** for the O=Mo–Mo=O segment may be taken to be intrinsic for the respective complex, and not ascribable to crystal packing.

References

1) E. I. Stiefel, *Prog. Inorg. Chem.*, **22**, 1 (1976).
2) K. Z. Suzuki, Y. Sasaki, S. Ooi, and K. Saito, *Bull. Chem. Soc. Jpn.*, **53**, 1288 (1980).
3) "International Tables for X-Ray Crystallography," Kynoch Press, Birmingham (1974), Vol. IV, pp. 71, 148.
4) "The Universal Crystallographic Computation Program System," The Crystallographic Society of Japan (1969).
5) B. Spivack and Z. Dori, *Coord. Chem. Rev.*, **17**, 99 (1975), and the references cited therein.
6) G. Bunzey and J. H. Enemark, *Inorg. Chem.*, **17**, 682 (1978), and the references cited therein.
7) T. Dirand-Colin, M. Schappacher, L. Ricard, and R. Weiss, *J. Less-Common Met.*, **54**, 91 (1977).
8) B. Spivack and Z. Dori, *J. Chem. Soc., Dalton Trans.*, **1973**, 1173.
9) B. M. Gatehouse and E. K. Nunn, *Acta Crystallogr., Sect. B*, **32**, 2627 (1976).
10) J. R. Knox and C. K. Prout, *Acta Crystallogr., Sect. B*, **25**, 1857 (1969).
11) H. Iwasaki and Y. Saito, *Bull. Chem. Soc. Jpn.*, **39**, 92 (1966).
12) B. Jezowska-Trzebiatowska, T. Glowiak, M. F. Rudolf, M. Sabat, and J. Sabat, *Russ. J. Inorg. Chem.*, **22**, 1590 (1977).
13) B. Spivack and Z. Dori, *J. Chem. Soc., Dalton Trans.*, **1975**, 1077.
14) D. H. Brown and J. A. D. Jeffreys, *J. Chem. Soc., Dalton Trans.*, **1973**, 732.

Studies on Characteristics of Electron Capture Responses. V. Estimation of Electron Attachment Mechanisms from Carrier Gas Flow-rate Dependence of Electron Capture Coefficients

Masahiro TAKEUCHI

Tokyo Metropolitan Research Laboratory of Public Health, Hyakunincho, Shinjuku-ku, Tokyo 160

(Received December 6, 1980)

The electron capture coefficients, K, defined by Wentworth *et al.* were measured for several samples in various carrier gas flow-rates, F, by a pulse sampled electron capture detector (ECD). The carrier gas flow-rate dependence of K, *i.e.*, the plot of K *versus* F, is discussed from the viewpoint of the kinetic theory. The results reveal that the flow-rate dependence of K can be used for estimating the electron attachment mechanisms.

In their early studies on the responses of the ECD, Wentworth *et al.*[1-4] theorized about the electron attachment mechanisms on the basis of kinetic derivations using steady-state approximations. According to their theory, the electron attachment phenomena can be classified into four different mechanisms which can be determined from the temperature dependence of K, *i. e.*, the plot of $\ln KT^{3/2}$ *versus* $1/T$.

The author reported[5] that the carrier gas flow-rate dependence of K[6] was also closely related to the electron attachment mechanisms: The values of K for samples undergoing a non-dissociative electron capture reaction were little affected by the flow-rate, those for samples undergoing a dissociative electron capture reaction increased significantly with increasing the flow-rate, and those for samples undergoing an electron capture reaction through an anion radical intermediate were little affected with the flow-rate at lower temperatures, but the values increased gradually with increasing the flow-rate at higher temperatures. In the present paper, these relations have been discussed from the viewpoint of the kinetic theory proposed by Wentworth *et al.*

Experimental

Apparatus and Samples. A Shimadzu GC-5A gas chromatograph equipped with a pulse sampled ECD was used. The ECD was of co-axial geometry and contained a 10 mCi ^{63}Ni radioactive source. Pulses were supplied with a DuMont 404 pulse generator. The pulse conditions were set up as follows in order to collect all of the electrons formed during a pulse period and to assure a steady-state for kinetic equations derived from the reactions postulated within the ECD: the pulse period, 2000 μs; the pulse width, 2.0 μs; the pulse amplitude, 30 V. An analog device was used for the calculation of K from the equation:

$$Kn = \frac{F}{S}\int \frac{I_b - I_e}{I_e}\,dX, \qquad (1)$$

where n is the number of moles injected, F is the carrier gas flow-rate in l/min, S is the chart speed in cm/min, X is the chart distance in cm, I_b is the base current due to pure carrier gas, and I_e is the current in the presence of electron capturing vapor. Practically, K was obtained from the slope of the n *versus* peak area plot under constant conditions of F and S, and corrected in the same manner as in the proceeding paper.[5] The carrier gas used (Nihon Sanso, A Grade) was specified to contain more than 99.9995% of nitrogen and less than 0.5 ppm of oxygen. Before being introduced into the system, the gas was passed through a Molecular Sieve 13X filter and an oxygen scrubber (Alltech, Oxy-Trap). The flow-rate was measured at the exit end of the system with a bubble flow meter and a stopwatch. Peak areas were calculated with a Spectra-Physics Autolab System IV integrator. Two different kinds of chromatographic columns were used. One was a 1 m×3 mm i.d. glass column packed with 2% Silicone OV-17 on Chromosorb W (80—100 mesh), and the other was a 1 m×3 mm i.d. glass column packed with 2% Silicone OV-275 on Chromosorb W (60—80 mesh). The ECD temperature was measured with a thermometer inserted into the detector oven rather than with the thermocouple provided.

The samples used in the present study were commercially available reagents. Solutions of the samples were prepared to give suitable peak heights, *i.e.*, $(I_b - I_e)/I_e = 1$—4.[7]

Results and Discussion

Figures 1, 2, and 3 show the flow-rate dependences of K for nitrobenzene, acetophenone, and Aldrin. The flow-rate dependences of K for these samples are quite different. The values of K for nitrobenzene are constant, *i. e.*, not affected with the flow-rate at all, those for acetophenone decrease in nearly inverse proportion to the increase of the flow-rate, and those for Aldrin increase in nearly direct proportion to the increase of the flow-rate. The differences among these samples are explained below.

According to Wentworth *et al.*,[2] K is represented in the form of Eq. 2 by using the rate constants attached to Eqs. 3—6:

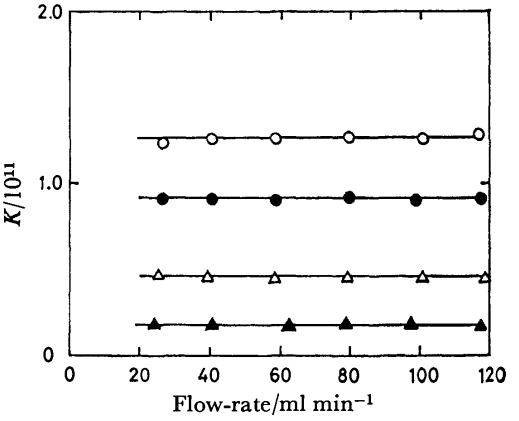

Fig. 1. Carrier gas flow-rate dependence of K for nitrobenzene at 200 °C (○), 240 °C (●), 280 °C (△), and 320 °C (▲).

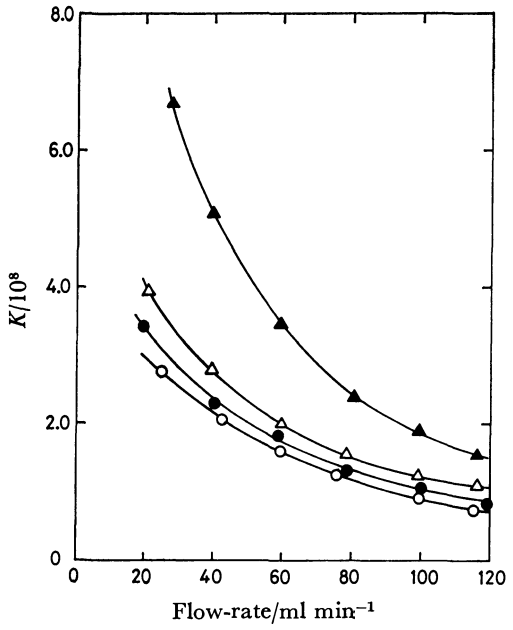

Fig. 2. Carrier gas flow-rate dependence of K for acetophenone at 200 °C (○), 240 °C (●), 280 °C (△), and 320 °C (▲).

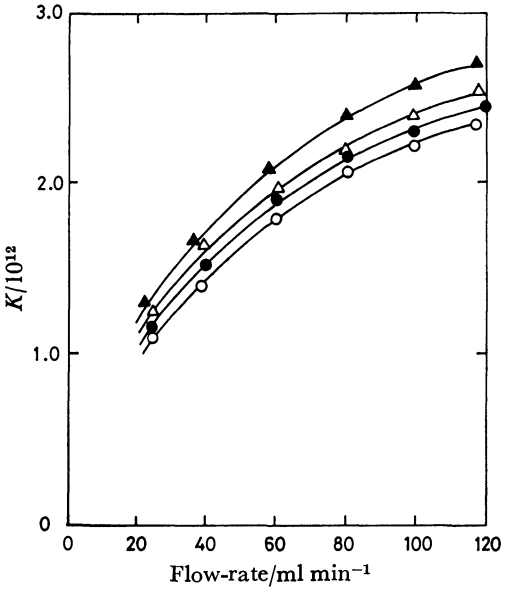

Fig. 3. Carrier gas flow-rate dependence of K for Aldrin at 200 °C (○), 240 °C (●), 280 °C (△), and 320 °C (▲).

$$K = \frac{k_{12}}{k_N + k_R} + \frac{k_1 k_2}{(k_N + k_R)\Sigma k} + \frac{(k_{N1} + k_{R1})k_1}{(k_N + k_R)\Sigma k}, \quad (2)$$

where $k_N+k_R=k'_N[P^+]+k'_R[R\cdot]$, $k_{N1}+k_{R1}=k'_{R1}[P^+]+k_{R1}[R\cdot]$,
and $\Sigma k=k_{-1}+k_2+k_{N1}+k_{R1}$.

$$AB + e^- \xrightarrow{k_{12}} A\cdot + B^- \quad (3)$$

$$AB + e^- \underset{k_{-1}}{\overset{k_1}{\rightleftharpoons}} AB^- \xrightarrow{k_{N1}+k_{R1}} AB \quad (4)$$

$$AB^- \xrightarrow{k_2} A\cdot + B^-$$

$$P^+ + e^- \xrightarrow{k'_N} R\cdot \quad (5)$$

$$R\cdot + e^- \xrightarrow{k'_R} R^-, \quad (6)$$

where AB is an electron capturing molecule, AB^- is a negative ion, A· and B^- are fragments of dissociation, and P^+ and R· are symbols to designate any of the positive ions and radicals.

It can be seen that K is a sum of three terms, and that the first term of Eq. 2 corresponds to the situation in which Eq. 3 predominates. Such a situation, however, is considered to be the same as the situation where $k_2 \gg k_{-1}+k_{N1}+k_{R1}$ is satisfied in Eq. 4 to which the second and the third terms in Eq. 2 correspond. Consequently, the first term of Eq. 2 can be abbreviated.

Hence,

$$K = \frac{k_1(k_2 + k_{N1} + k_{R1})}{(k_N + k_R)\Sigma k}. \quad (7)$$

Equation 7 can be further simplified as follows, according to the relative magnitude of each rate constant in Σk.

(I) When $k_{N1}+k_{R1} \gg k_{-1}+k_2$, the expression for K becomes

$$K = \frac{k_1}{k_N + k_R}. \quad (8)$$

In this situation, K is not affected by the flow-rate. In other words, K for a given sample is constant at any flow-rate. A typical sample belonging to this group is nitrobenzene (Fig. 1).

(II) When $k_{-1} \gg k_2+k_{N1}+k_{R1}$, the expression for K becomes

$$K = \frac{k_2 + k_{N1} + k_{R1}}{k_N + k_R} \times \frac{k_1}{k_{-1}}. \quad (9)$$

The part of k_1/k_{-1} of Eq. 9 is equal to the equilibrium constant, K_{eq}, of the reaction between AB and an electron in Eq. 4. The concentration of AB^- is negligible in comparison with that of AB in Eq. 4, since K_{eq} is very small in this situation. Therefore, K_{eq} is expressed in the form of Eq. 10 by using the ionization efficiency, p, and the initial concentration of AB, a:

$$K_{eq} = \frac{k_1}{k_{-1}} = \frac{[AB^-]}{[AB][e^-]} = \frac{p}{a(1-p)}. \quad (10)$$

On the other hand, p is expressed in the form of Eq. 11:[8]

$$p = \frac{c}{c + F}, \quad (11)$$

where c is a constant, and F is the carrier gas flow-rate. Combination of Eqs. 10 and 11 gives

$$K_{eq} = \frac{k_1}{k_{-1}} = \frac{c}{a} \times \frac{1}{F}. \quad (12)$$

Equation 12 means that K_{eq} is in inverse proportion to the carrier gas flow-rate. Therefore, if the part of $(k_2+k_{N1}+k_{R1})/(k_N+k_R)$ is not affected by the carrier gas flow-rate, K expressed by Eq. 9 will also be in inverse proportion to the flow-rate. A typical sample satisfying Situation II is acetophenone (Fig. 2). Another sample belonging to this group was benzonitrile. The flow-rate dependence of K for benzonitrile was similar to that for acetophenone.

(III) When $k_2 \gg k_{-1}+k_{N1}+k_{R1}$, the expression for K becomes

$$K = \frac{k_1}{k_N + k_R}.$$

The values of K in this situation are expected to be constant in any flow-rate, since K is expressed in the same form as in Situation I. In practice, however, K is approximately proportional to the flow-rate. This is because a molecule AB dissociates spontaneously to give A· and B^- on entering into the ECD. Under such a situation, the ECD is considered to be coulometric in response and to act as a mass-sensitive detector.[9-11] Therefore, the values of K calculated from Eq. 1, which is derived by assuming that the ECD is concentration-sensitive,[9,10] are not kept constant but become proportional to the flow-rate. Aldrin is a typical sample which satisfies Situation III (Fig. 3). In fact, Aldrin has a very small activation energy for dissociation, which is calculated from the slope of the ln $KT^{3/2}$ *versus* $1/T$ plot shown in Fig. 4 and the gas constant ($-\text{slope} \times R$). Consequently, all of the molecules of Aldrin dissociate within the ECD. Therefore, it is reasonable that the ECD acts as a mass-sensitive device rather than a concentration-sensitive one, for detection of Aldrin. Other samples belonging to this group were *p,p'*-DDE, *p,p'*-DDT, and γ-BHC. Their flow-rate dependences of K were similar to that for Aldrin.

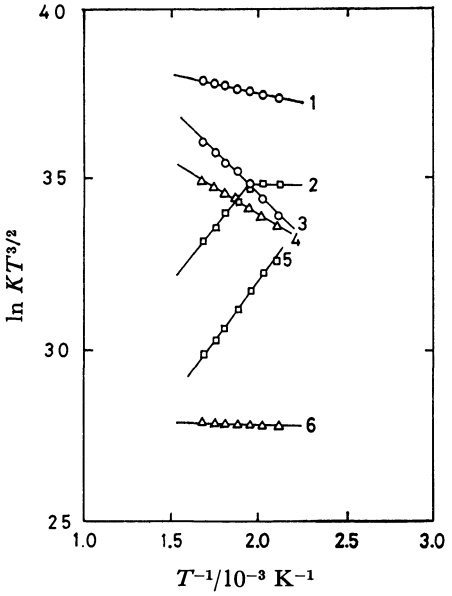

Fig. 4. Temperature dependence of K for Aldrin (1), nitrobenzene (2), 1,2,4-trichlorobenzene (3), dodecyl bromide (4), azulene (5), and acetophenone (6).

On the basis of the flow-rate dependence of K for the three situations described above, those shown in Fig. 5—7 can be considered as follows:

In the case of azulene (Fig. 5), the values of K are not affected at all by the flow-rate at lower temperatures, but decrease slightly with increasing the flow-rate at higher temperatures. Therefore, it is likely that $k_{N1}+k_{R1} \gg k_{-1}+k_2$, *i. e.*, Situation I, is satisfied at lower temperatures, but $k_{-1}+k_2$ becomes almost equal to $k_{N1}+k_{R1}$ at higher temperatures, since k_{-1} becomes larger with the rise of temperature. Although acetophenone,

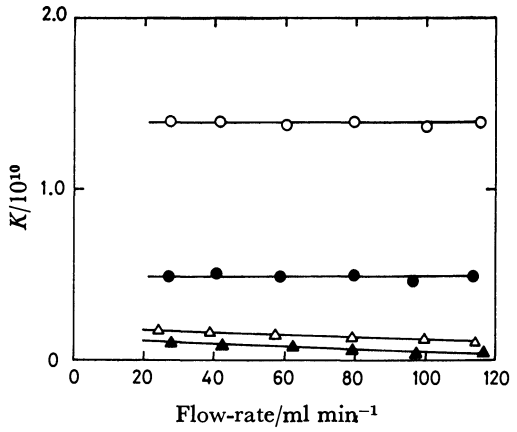

Fig. 5. Carrier gas flow-rate dependence of K for azulene at 200 °C (○), 240 °C (●), 280 °C (△), and 320 °C (▲).

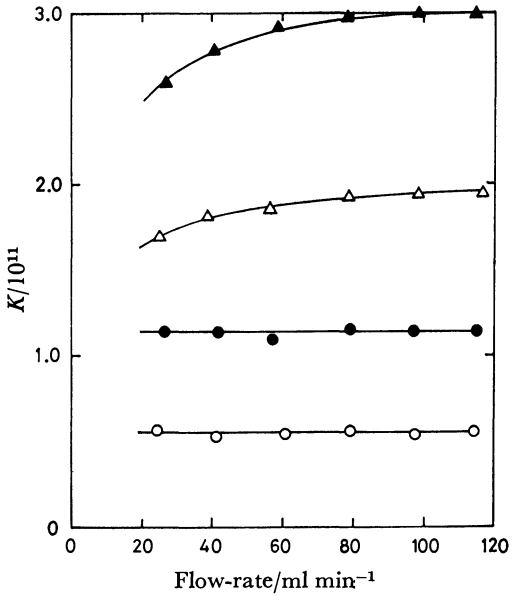

Fig. 6. Carrier gas flow-rate dependence of K for 1,2,4-trichlorobenzene at 200 °C (○), 240 °C (●), 280 °C (△), and 320 °C (▲).

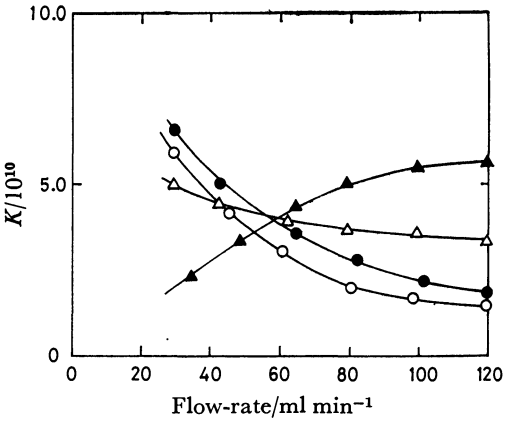

Fig. 7. Carrier gas flow-rate dependence of K for dodecyl bromide at 200 °C (○), 240 °C (●), 280 °C (△), and 320 °C (▲).

nitrobenzene, and azulene are all regarded as non-dissociative samples from the plots of ln $KT^{3/2}$ *versus* $1/T$, *i. e.*, a positive slope at higher temperatures and/or a negative slope nearly zero at lower temperatures (Fig. 4), the flow-rate dependences of K show that they are not necessarily in the same situation. This is owing to the difference of the electron affinities: 5.5, 14.7, and 15.2 kcal/mol, for benzonitrile, azulene, and nitrobenzene, respectively.[4,12]

In the case of 1,2,4-trichlorobenzene (Fig. 6), the values of K are constant at lower temperatures, but increased gradually with increasing the flow-rate at higher temperatures. Therefore, the electron capture reaction of 1,2,4-trichlorobenzene occurs non-dissociatively under Situation I, *i. e.*, $k_{N1}+k_{R1} \gg k_{-1}+k_2$, at lower temperatures, but dissociatively under Situation III, *i. e.*, $k_2 \gg k_{-1}+k_{N1}+k_{R1}$, at higher temperatures. Although 1,2,4-trichlorobenzene apparently belongs to the dissociative sample, considering the plot of ln $KT^{3/2}$ *versus* $1/T$ (Fig. 4), it is really a sample which dissociates through an anion radical intermediate.[5,12-14]

In the case of dodecyl bromide (Fig. 7), which is regarded as one of the dissociative samples from the negative slope of the ln $KT^{3/2}$ *versus* $1/T$ plot, the values of K decrease with increasing the flow-rate at lower temperatures, but increase at higher temperatures. This flow-rate dependence of K suggests that the electron capture reaction of dodecyl bromide occurs under Situation II, *i. e.*, $k_{-1} \gg k_2+k_{N1}+k_{R1}$, at lower temperatures, but occurs under Situation III, *i. e.*, $k_2 \gg k_{-1}+k_{N1}+k_{R1}$, at higher temperatures. The change from Situation II to III with the rise of temperature reveals that the dissociative electron capture reaction of dodecyl bromide proceeds by a mechanism similar to bimolecular nucleophilic substitution (S_N2), as shown in Fig. 8. This mechanism is supported by Kojima *et al.*,[15] who have concluded on the basis of the activation energy that the electron capture reaction of alkyl halide is a kind of S_N2.

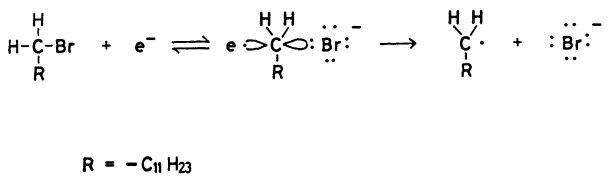

R = $-C_{11}H_{23}$

Fig. 8. Electron attachment mechanism of dodecyl bromide.

Conclusion

The carrier gas flow-rate dependence of K was considered from the viewpoint of the kinetic theory proposed by Wentworth *et al.* The results revealed that the electron capture reaction could be divided into three situations by the relative magnitude of the rate constants of elementary reactions postulated within the ECD, and that each situation is related to the carrier gas flow-rate:

(I) When $k_{N1}+k_{R1} \gg k_{-1}+k_2$, K is not affected by the flow-rate.

(II) When $k_{-1} \gg k_2+k_{N1}+k_{R1}$, K is inversely proportional to the flow-rate.

(III) When $k_2 \gg k_{-1}+k_{N1}+k_{R1}$, K is approximately proportional to the flow-rate.

The author wishes to express his thanks to Emeritus Professor Shun Araki and Professor Shigetaka Suzuki, Tokyo Metropolitan University, for their encouragement and advice.

References

1) W. E. Wentworth, E. Chen, and J. E. Lovelock, *J. Phys. Chem.*, **70**, 445 (1966).

2) W. E. Wentworth, R. S. Becker, and R. Tung, *J. Phys. Chem.*, **71**, 1652 (1967).

3) W. E. Wentworth, E. Chen, and J. C. Steelhammer, *J. Phys. Chem.*, **72**, 2671 (1968).

4) W. E. Wentworth and E. Chen, *J. Gas Chromatogr.*, **5**, 170 (1967).

5) M. Takeuchi, *Bull. Chem. Soc. Jpn.*, **53**, 2829 (1980).

6) Devaux and Guiochon first reported that the response factors, which are correspond to K in this paper, depend on the flow-rate in a complex manner; P. Devaux and G. Guiochon, *J. Chromatogr. Sci.*, **5**, 341 (1967). Afterwards, Van de Wiel and Tommassen insisted that the flow-rate dependence of K was caused by oxygen contaminating the carrier gas used; H. J. Van de Wiel and P. Tommassen, *J. Chromatogr.*, **71**, 1 (1972). The author observed, however, the flow-rate dependence of K even when there was little or no oxygen in the carrier gas.

7) The *n versus* peak height plot of Eq. 1 was linear to as high as approximately 90% of detector saturation, *i.e.*, $(I_b-I_e)/I_e=10$; M. Takeuchi, *Nippon Kagaku Kaishi*, **1979**, 229.

8) J. E. Lovelock, R. J. Maggs, and E. R. Adlard, *Anal. Chem.*, **43**, 1962 (1971).

9) I. Halász, *Anal. Chem.*, **36**, 1428 (1964).

10) L. S. Ettre, *J. Chromatogr. Sci.*, **16**, 396 (1978).

11) W. A. Aue and S. Kapila, *J. Chromatogr. Sci.*, **11**, 255 (1973).

12) M. Satouchi and T. Kojima, *Bunseki Kagaku*, **25**, 764 (1976).

13) I. Dzidic, D. I. Carroll, R. N. Stilwell, and E. C. Horning, *Anal. Chem.*, **47**, 1305 (1975).

14) E. P. Grimsrud and S. H. Kim, *Anal. Chem.*, **51**, 537 (1979).

15) T. Kojima, Y. Tanaka, and M. Satouchi, *Anal. Chem.*, **48**, 1760 (1976).

Kinetic Studies of Fast Equilibrium by Means of High-performance Liquid Chromatography. II. Ligand Exchange of *N,N*-Disubstituted Dithiocarbamate Chelates of Ni(II)

Masataka MORIYASU* and Yohei HASHIMOTO

Kobe Women's College of Pharmacy, Motoyamakita-machi, Higashinada-ku, Kobe 658

(Received December 11, 1980)

The equilibrium of the ligand exchange of labile Ni(II) dialkyldithiocarbamate chelates ($MA_2+B \rightleftharpoons MAB+A$, $MAB+B \rightleftharpoons MB_2+A$, $K_1=[MAB][A]/[MA_2][B]$, $K_2=[MB_2][A]/[MAB][B]$) has been investigated by means of high-perfromance liquid chromatography, two solutions of MA_2 and B being mixed and then equilibrated. The equilibrium constants, K_1 and K_2, have been determined by measuring the concentrations of each complex, including the kinetically unstable ternary complex in the equilibrium state. The ratio of the stability constants of the two Ni(II) chelates, which is equal to K_1K_2, has been calculated. The following series of increasing stability constants has been found for the alkyl substituents in chloroform; tetramethylene<dimethyl<pentamethylene<diethyl<hexamethylene<dipropyl<dibutyl. The rate of ligand exchange has been investigated by mixing very dilute MA_2 and B and by injecting the mixture into HPLC after the lapse of a certain time. The rate of ligand exchange is slow when low initial concentrations of MA_2 and B are chosen. The rate of ligand exchange is more than ten times faster than that of ternary complex formation.

In our previous studies[1,2] the equilibrium of the labile ternary-complex formation of *N,N*-disubstituted dithiocarbamate chelates of Ni(II) and Cu(II) was investigated by means of high-performance liquid chromatography (HPLC). The labile ternary complex, which is formed by mixing two solutions of the corresponding binary complexes, undergoes disproportionation as soon as it is separated from binary complexes in the column. The separation process of HPLC is so rapid that it might compete with the progress of disproportionation during the course of chromatography. In HPLC there are some factors serving to retard disproportionation in the column: (1) Each species is diluted rapidly in the column, suppressing the disproportionation which can be anticipated to occur by means of the bimolecular collisional process of two binary complexes. (2) The rate of disproprotionation can be controlled by a suitable choice of initial concentrations of two binary complexes, disproprotionation being slow when the initial concentrations are low. (3) The control of the column temperature will be effective, disproportionation being retarded when the column temperature is kept low. By the combination of these factors, disproportionation during chromatography is retarded effectively, and chromatograms obtained directly indicate the concentrations of each species before chromatography. Thus, it becomes possible to trace quite fast bimolecular reactions by means of HPLC. In our previou studies, the equilibrium constants and rate constants of labile ternary complex formation of *N,N*-disubstituted dithiocarbamate chelates of Ni(II) and Cu(II) were determined in this way. The present article shows that HPLC can also be applied to the kinetic investigation of ligand exchange in solution. We have chosen Ni(II) chelates because the rate of the ligand exchange of Ni(II) chelates is moderately fast and so the determination of the kinetic characteristics can be carried out by means of HPLC.

Experimental

Reagents. Sodium salts of *N,N*-disubstituted dithiocarbamates were prepared and purified as has been reported previously.[2] Diethylammonium salt of diethyldithiocarbamic acid was purchased commercially (Nakarai Chemicals, Ltd.). Dipropylammonium salt of dipropyldithiocarbamic acid was prepared as follows. In a 500-cm^3 of flask, 0.2 mol of dipropylamine dissolved in 100 cm^3 of hexane was placed. The flask was cooled in an ice bath, and then 0.1 mol of carbon disulfide in 100 cm^3 of hexane was stirred in, drop by drop. A voluminous white product was gradually precipitated. After having been washed with hexane, the product was dried in a vacuum desiccator. This product was found to be >98% pure when the content was determined to be Ni(II) chelates by colorimetry. It was used without further purification, because recrystallization from water gave worse results as a result of the formation of disulfide compounds (mainly *N,N,N',N'*-tetrapropylthiuram disulfide) on heating.

The concentration of the Ni(II) standard solution (0.01 mol dm^{-3} $NiCl_2$) was determined to be Ni(II) diethyldithiocarbamate by colorimetry. All the solvent used for the eluent were saturated with water before use, as had been reported previously.[2]

Apparatus. The apparatus used in this study was identical with that used in our previous reports.[1-3]

Procedure. The metal chelates were prepared by mixing the Ni(II) standard solution and the sodium salts of the corresponding dialkyldithiocarbamic acids. The metal chelates produced were extracted with chloroform under the condition of a complete extraction (pH 4.0 acetate buffer). The chloroform layer was washed with a 1% sodium hydrocarbonate solution four times to remove the residual free ligands in chloroform. Thus, solutions of each metal chelate (0.5 to 1.0×10^{-3} mol dm^{-3}) were prepared. These solutions were stable for at least three weaks when stored in a refrigerator. Solutions of dialkylammonium salts of dialkyldithiocarbamic acids were prepared by dissolving the corresponding salts in chloroform. These solutions were newly prepared before use, for they were not very stable and disulfide-degradation compounds were gradually produced on storage. The contents of these solutions were determined after the formation of Ni(II) chelates as will be shown in the following section.

For the determination of the equilibrium constants and rate constants, each solution was thermostated at 25 °C. All the measurements were carried out at least three times.

Theoretical

HPLC Analysis of Equilibrium of Ternary-complex Formation. The HPLC method for the analysis of a fast equilibrium in solution is, in principle, a conventional one. When two labile binary complexes, MA_2 and MB_2, are mixed in the absence of excess free ligands, the following ternary-complex formation will be equilibrated promptly.

$$MA_2 + MB_2 \underset{k_-}{\overset{k}{\rightleftharpoons}} 2MAB, \quad (1)$$

$$K = [MAB]^2/[MA_2][MB_2]. \quad (2)$$

When the separation speed of HPLC is so fast that the disproportionation of the kinetically unstable ternary complex MAB is negligible during the course of chromatography, K can be determined by measuring the peak heights of each chelate that appears on the chromatograms.

The rate constants, k and k_-, will be determined as follows assuming a simple bimolecular rate equation. When two dilute solutions of MA_2 and MB_2 are mixed, a ternary complex, MAB, is gradually produced according to the following equation:

$$\frac{d[MAB]}{dt} = k[MA_2][MB_2] - k_-[MAB]^2. \quad (3)$$

Taking the initial concentrations of MA_2 and MB_2 to be a_0 and b_0 respectively, we obtain:

$$\frac{dx}{dt} = k(a_0-x/2)(b_0-x/2)-k_-x^2$$

$$= -(kx^2/4)(4/K-1) - (kx/2)(a_0+b_0)+a_0b_0k, \quad (4)$$

where x is the concentration of MAB. We obtain the following equations by integrating Eq. 4:

$$k = -[2/(a_0+b_0)t] \ln [1-(a_0+b_0)x/2a_0b_0], \quad (5)$$
$$(K=4.0)$$

$$k = (2/m_0t)\left[\ln \frac{\left(\frac{a_0+b_0+m_0}{1-K/4}-x\right)}{\left(\frac{a_0+b_0-m_0}{1-K/4}-x\right)} + \ln\left(\frac{a_0+b_0-m_0}{a_0+b_0+m_0}\right)\right], \quad (6)$$
$$(K\neq 4.0)$$

where $m_0=\sqrt{(a_0+b_0)^2-4a_0b_0(1-4/K)}$. Thus, the two rate constants k and k_- can be determined from Eqs. 5 and 6.

HPLC Analysis of the Equilibrium of Ligand Exchange and Determination of the Relative Stability Constants of Metal Chelates. When the free ligand B is added to a solution containing only one kind of binary complex, MA_2, the following ligand exchange will occur in the mixture:

$$MA_2 + B \underset{k_{-1}}{\overset{k_1}{\rightleftharpoons}} MAB + A, \quad (7)$$

$$MAB + B \underset{k_{-2}}{\overset{k_2}{\rightleftharpoons}} MB_2 + A, \quad (8)$$

$$K_1 = [MAB][A]/[MA_2][B], \quad (9)$$

$$K_2 = [MB_2][A]/[MAB][B]. \quad (10)$$

From Eqs. 2, 9, and 10, it follows that:

$$K_1/K_2 = [MAB]^2/[MA_2][MB_2] = K. \quad (11)$$

The product of the two equilibrium constants, K_1K_2, is the ratio of the stability constants of the two binary complexes as is shown below:

$$K_1K_2 = [MB_2][A]^2/[MA_2][B]^2 = \beta_{MB_2}/\beta_{MA_2}, \quad (12)$$

$$\beta_{MA_2} = [MA_2]/[M][A]^2, \quad (13)$$

$$\beta_{MB_2} = [MB_2]/[M][B]^2. \quad (14)$$

These equilibrium constants will be determined if the equilibrium concentrations of each species are determined by HPLC. The rate constants of the ligand exchange can also be obtained by observing the change in the chromatogram patterns after mixing two solutions of MA_2 and B. It should be noted here that, being different from equilibrium constants, the two rate constants k_1 and k_2 vary independently of each other. This complicates the determination of these characteristics. When the initial concentration of MA_2 ($=a$) is much larger than that of B($=b$), the formation of MB_2 in the equilibrium state can be neglected. In this case, we can neglect the equilibrium shown in Eq. 8, and the following equation is obtained if the rate of ligand exchange can be expressed by a simple bimolecular-rate equation including $[MA_2]$ and [B]:

$$\frac{dx}{dt} = k_1(a-x)(b-x)-k_{-1}x^2$$

$$= k_1(1-1/K_1)x^2 - (a+b)k_1x + abk_1. \quad (15)$$

Equation 15 can then be integrated to give:

$$k_1 = -[1/(a+b)t]\ln[1-(a+b)x/ab] \quad K_1=1.0, \quad (16)$$

$$k_1 = (1/mt)\left[\ln \frac{\left(\frac{a+b+m}{2(1-1/K_1)}-x\right)}{\left(\frac{a+b-m}{2(1-1/K_1)}-x\right)} + \ln\left(\frac{a+b-m}{a+b+m}\right)\right], \quad (17)$$
$$K_1\neq 1.0$$

where $m=\sqrt{(a+b)^2-4ab(1-1/K_1)}$.

Results and Discussion

Equilibrium Constants of Ligand Exchange and the Relative Stability of Ni(II) Chelates. Some examples of chromatograms for determining the equilibrium constants, K_1 and K_2, are shown in Fig. 1. Here, for A and B we have chosen $(CH_2)_6NCSS^-$ and $(C_3H_7)_2NCSS^-$ respectively. Standard solutions of MA_2 and MB_2 were diluted with chloroform to various concentrations, and 5-μl portions of these solutions were injected into the column (Figs. 1(a) and (b)). Linear calibration graphs were obtained for MA_2 and MB_2 within a wide range of sample amounts. Then solutions of MA_2 and MB_2 were mixed so that the initial concentrations were equivalent ($=a_0$). In the mixture, the ternary-complex MAB was gradually formed, and after it had stood for some time, equilibrium was attained. The equilibrium concentrations of MA_2, MB_2, and MAB are $a_0/2$, $a_0/2$, and a_0 respectively, because the ternary-complex formation in this case is known to be controlled by a statistical factor ($K=4.0$).[1,2] Then the equilibrated solution was diluted to various concentrations, and these portions were injected into the column (Fig. 1(c)). Calibration graphs of MAB, which were also linear, were obtained in this way.

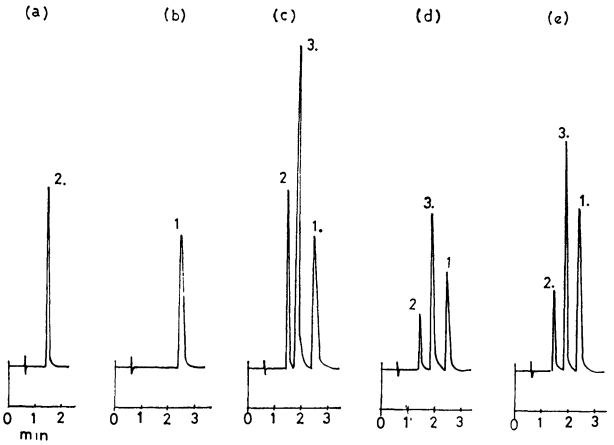

Fig. 1. Chromatogram patterns of the mixture of Ni-$[(CH_2)_6NCSS]_2$ and $(C_3H_7)_2NCSS^-$.
Column: Shodex silipak (4 mm × 15 cm). Eluent: hexane: ethyl acetate = 100 : 8 (water saturated). Flow rate: 2.5 cm³/min. Detector: 325 nm. Sample size: 5 μl. Sample: (a) 0.25 mmol dm^{-3} $Ni[(C_3H_7)_2NCSS]_2$ (=NiB_2) in chloroform; (b) 0.25 mmol dm^{-3} $Ni[(CH_2)_6NCSS]_2$ (=NiA_2) in chloroform; (c) 0.50 mmol dm^{-3} NiA_2+0.50 mmol dm^{-3} NiB_2 in chloroform. Equilibrium concentrations of NiA_2, NiB_2, and NiAB were 0.25, 0.25, and 0.50 mmol dm^{-3}, respectively;[2] (d) 0.50 mmol dm^{-3} NiA_2+b ($=0.58_0$) mmol dm^{-3} B in chloroform. Equibrium concentrations of NiA_2, NiB_2, and NiAB were determined to be 0.18_5, 0.077_3, and 0.24_4 mmol dm^{-3}, respectively. Total concentration of Ni(II) was calculated to be 0.50_5 mmol dm^{-3}. (a=0.50 mmol dm^{-3}); (e) Solution of (d) and aqueous $NiCl_2$ solution were mixed, and the mixture was shaken vigorously for about 20 s. After standing for some time the chloroform layer was supplied to HPLC. Equilibrium concentrations of NiA_2, NiB_2, and NiAB were 0.31_0 0.11_1, and 0.35_8 mmol dm^3, respectively. Thus concentration of b was calculated to be $0.11_1\times2+0.35_8=0.58_0$ mmol dm^{-3}. Total concentration of A was $0.31_0\times2+0.35_8=0.97_8$ ($2a$=1.00 mmol dm^{-3}).
1: NiA_2, 2: NiB_2, 3: NiAB.

Two solutions of MA_2 and B, whose initial concentrations were a and b, were then mixed at 25 °C. When a and b were relatively large (about 1×10^{-3} mol dm^{-3}), the equilibrium of ligand exchange occurred almost instantaneously after mixing. The equilibrated solution was divided into two parts, and a 5-μl portion of one part (Soln A) was supplied to HPLC (Fig. 1(d). Peaks corresponding to MA_2, MB_2 and MAB appeared on the chromatograms. Since free dithiocarbamates have no absorption at 325 nm, peaks of the free ligands, A and B, did not appear on the chromatograms. Injection into the column should be carried out within 10 min after mixing, otherwise, some errors were observed due to the gradual decomposition of the free ligands (probably attributable to the formation of disulfide compounds). The total concentration of Ni(II) of MA_2, MB_2, and MAB in the equilibrium state was equal to the initial concentration of MA_2($=a$), within the limit of experimental error as is shown in Fig. 1. Thus, the concentrations of MA_2, MB_2, and MAB in the equilibrium state were determined. The concentration of the free ligand A was calculated by means of this equation: $[A]=2a-2[MA_2]-[MAB]$. The concentration of the free ligand B was determined as follows: to the residual part of the equilibrated solution mentioned above, an aqueous nickel chloride solution was added, after with the mixture was shaken vigorously for about 20 s. Thus, free ligand residing in chloroform reacted with Ni(II) to form metal chelates, which were then extracted into chloroform quantitatively. Then the solution (Soln B) was supplied to HPLC (Fig. 1(e)). The total concentration of B was thus determined, and the concentration of [B] in Eqs. 9 and 10 was calculated. Here, the total concentration of the A ligand in Soln B should be equal to $2a$: this was confirmed as is shown in Fig. 1(e). Now, since the concentrations of [MA_2], [MB_2], [MAB], [A], and [B] in Eqs. 9 and 10 were determined, K_1 and K_2, and, therefore, K and K' could be calculated.

With similar procedures, the K_1 and K_2 for the system composed of other Ni(II) dialkyldithiocarbamates and dipropylammonium salt of dipropyldithiocarbamic acid were determined. The results are summarized in Table 1. The K_1/K_2 ratio, which are equal to the equilibrium constants of ternary-complex formation, were always

Table 1. Equilibrium constants of ligand exchange and relative stability constants of Ni(II) dithiocarbamate chelates

$NiA_2 + B \rightleftharpoons NiAB + A$, $K_1=[NiAB][A]/[NiA_2][B]$
$NiAB + B \rightleftharpoons NiB_2 + A$, $K_2=[NiB_2][A]/[NiAB][B]$
$NiA_2 + NiB_2 \rightleftharpoons 2NiAB$, $K=[NiAB]^2/[NiA_2][NiB_2]$.

A	K_1	K_2	$K_1K_2=\beta_{MB_2}/\beta_{MA_2}$	$K_1/K_2=K$	Retention time/min			Eluent
					MA_2	MAB	MB_2	
$(CH_3)_2NCSS^-$	6.1 ±0.15	1.8 ±0.2	11.1 ±2.1	3.4±0.7	3.4	1.8	1.1	A
$(C_2H_5)_2NCSS^-$	3.3 ±0.2	0.77±0.04	2.5 ±0.3	4.3±0.5	2.4	1.8	1.4	B
$(C_4H)_2NCSS^-$	1.43±0.13	0.32±0.03	0.46±0.09	4.5±0.8	1.4	1.7	2.2	C
$(CH_2)_4NCSS^-$	12.7±1.2	3.4 ±0.3	43.7 ±8.0	3.7±0.8	2.5	1.6	1.1	A
$(CH_2)_5NCSS^-$	4.6±0.4	1.1 ±0.1	5.1 ±0.9	4.1±0.4	3.3	2.1	1.4	B
$(CH_2)_6NCSS^-$	2.8±0.2	0.67±0.05	1.8 ±0.25	4.1±0.5	2.4	1.8	1.4	B

B: $(C_3H_7)_2NCSS^-$, in chloroform, 25 °C, Chromatographic conditions: column: Shodex silipak (4 mm × 15 cm), eluent: hexane: ethyl acetate (water saturated) = 100 : 15(A), 100 : 8 (B), 100 : 3.5(C), flow rate: 2.5 cm³/min, detector: 325 nm, sample size: 5 μl.

equal to 4 within the limit of experimental error, as was predicted by the results of our previous reports.[1,2] The ratios of the stability constants ($\beta_{MB_2}/\beta_{MA_2}=K_1K_2$) shown in Table 1 suggest that the following order of increasing stability constants was found for alkyl substituents: tetramethylene<dimethyl<pentamethylene<diethyl<hexamethylene<dipropyl<dibutyl. It is well known that the introduction of an alkyl group into chelate reagents has a tendency to stabilize the chelates formed, because the alkyl group shows electron-donating effect, and therefore, the acidity of the chelate reagents is decreased. It seems that the present results can be well interpreted in terms of such electron-donating effects of the alkyl group. The stability constants of dithiocarbamate chelates, including Ni(II) chelates, were investigated by Scharfe *et al.*,[4] and the following order of increasing stability constants was indicated for Ni(II) chelates: diethyl<tetramethylene<pentamethylene<hexamethylene. The discrepancy between their results and the present one with respect to the relationship between cyclic and acyclic alkyl substituents might be interpreted in terms of the difference in the solvent. Janssen[5] scrutinized the stability constants of Cu(II) dialkyldithiocarbamate chelates in a mixed solution of water : ethanol by the spectroscopic method. His results on the order of stability constants as to alkyl substituents were identical with those of our present work.

Rate of Ligand Exchange. There remains some difficulties in the determination of the rate constants of ligand exchange. (1) When the concentrations of MA_2 and B were relatively large, ligand exchange was equilibrated instantaneously after mixing. In order to decrease the rate of ligand exchange enough for determination by HPLC, the initial concentrations of MA_2 and B should be chosen so as to be of the order 10^{-6} mol dm^{-3}, close to the detection limit of the UV detector. (2) If the concentrations of MA_2 and B were chosen to be close to each other, the two steps of ligand exchange shown in Eqs. 7 and 8 should occur simultaneously. This will complicate the determination of the rate constants because k_1 and k_2 vary independently. Therefore, the two solutions of MA_2 and B should be mixed so that only the first step of ligand exchange occurs predominantly ($[MA_2]\gg[B]$). Too much excess of MA_2, however, is not favorable because the rate of ligand exchange increases with the increase of $[MA_2]$. Thus, the concentration range of a and b suitable for kinetic study is narrow, and a large error is inevitable.

For the determination of the rate constants of ligand exchange, two dilute solutions of $Ni[(C_2H_5)_2NCSS]_2$ (=MA_2) and $(C_3H_7)_2NCSSC_3H_7NH$ (=B), were mixed at 25 °C. The mixed solution was left to stand for 15 s, 35 s, 2 min, and 5 min, and then a portion of the mixture was submitted to HPLC. Figure 2 illustrates the change in the chromatograms. Measurements for each were made four times. With the lapse of time, the peak of MAB rose, while that of MA_2 fell. Since the initial concentration of MA_2 was chosen to be considerably larger than that of B, the peak of MB_2 did not appear on the chromatograms, the second step of ligand exchange shown in Eq. 8 being negligible.

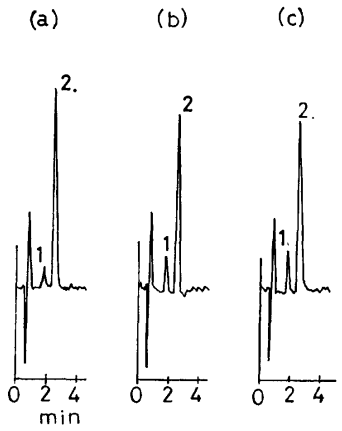

Fig.. 2 Change of chromatogram patterns by ligand exchange. Column: Shodex silipak (4 mm × 15 cm). Eluent: hexane : ethyl acetate=100 : 8 (water saturated). Flow rate: 2.5 cm^3/min. Detector: 325 nm. Sample size: 200 μl (in chloroform: ethyl acetate: hexane=1 : 1 : 8). Sample: 5.0×10^{-6} mol dm^{-3} $Ni[(C_2H_5)_2NCSS]_2$ (=MA_2)+7.9×10^{-7} mmol dm^{-3} $(C_3H_7)_2NCSS^-$ (=B). (a) After mixing 15 s, (b) 35 s, (c) 3 min (equilibrium).
1: NiAB, 2: NiA_2.

The equilibrium was attained within 2 min, as shown by the fact that the chromatograms of the solutions after mixing for 2 and 5 min were identical. The time required to attain equilibrium was approximately inversely proportional to the product of the initial concentrations of MA_2 and B. From these results, the rate constants k_1 and k_{-1} in Eq. 7 can be calculated in terms of Eq. 17 if ligand exchange occurs by means of a bimolecular process. The simple bimolecular mechanism in ligand exchange does not seem to be conclusively proved, however, because of the relatively large experimental error and also because of the following reason. The kinetic study of the ligand exchange of square-planer Pt(II) complexes has been investigated by many workers, and it has been established that the ligand exchange of monodentate ligand proceeds by means of a two-path mechanism, including a five-coordinate intermediate[6] in an aqueous solution. In such cases, the rate of ligand exchange, R, is expressed by the following two-term rate law: ($MA_3X+Y\rightarrow MA_3Y+X$, $R=k[MA_3X]+k'[MA_3X][Y]$). A similar mechanism has been suggested for Ni(II) complexes.[7] Therefore, it seems probable that the rate of ligand exchange of Ni(II) dithiocarbamates might be expressed by a similar two-term rate law, though the present experiments were carried out in a nonaqueous solvent and the ligands involved were bidentate. It can be safely concluded at present that the bimolecular collisional process is predominant, even though the rate equation of ligand exchange is expressed by a two-term rate law or other more complicated equations.[8] If we assume that the simple bimolecular process is valid, the rate constants, k_1 and k_{-1}, in Fig. 2 can be calculated in terms of Eq. 17, because all the variables, K_1, a, b, and x, are known. Thus, k_1 and k_{-1} were calculated to be $(8.3\pm2.4)\times10^3$ mol dm^{-3} s^{-1} and $(2.4\pm0.7)\times10^3$ mol dm^{-3} s^{-1} respectively. The rate constant of ternary-

complex formation between $Ni[(C_2H_5)_2NCSS]_2$ and $Ni[(C_3H_7)_2NCSS]_2$ is $(2.4\pm0.2)\times10^2$ mol dm^{-3} s^{-1}, as was shown in our previous report.[2] The present results show that the rate of ligand exchange is more than ten times faster than that of ternary-complex formation. Considering that the ligand exchange of Ni(II) chelates is so fast that equilibrium is attained promptly at room temperature,[9] the present results seem reasonable.

References

1) M. Moriyasu and Y. Hashimoto, *Chem. Lett.*, **1980**, 117.
2) M. Moriyasu and Y. Hashimoto, *Bull. Chem. Soc. Jpn.*, **53**, 3590 (1980).
3) M. Moriyasu and Y. Hashimoto, *Anal. Lett.*, **A11**, 593 (1978).
4) R. R. Scharfe, V. S. Sastri, and C. L. Chakrabarti, *Anal. Chem.*, **45**, 413 (1973).
5) M. Janssen, *Recl. Trav. Chim. Pays-Bas*, **75**, 1411 (1956); **76**. 827 (1957).
6) For example, U. Belluco, L. Cattalini, F. Basolo, R. G, Pearson, and A. Turco, *J. Am. Chem. Soc.*, **87**, 241 (1951).
7) a) F. Basolo, J. Chatt, H. B. Gray, P. G. Pearson, and B. L. Shaw, *J. Chem. Soc.*, **1961**, 2207; b) R. K. Murmann, *Inorg. Chem.*, **2**, 116 (1963).
8) P. G. Pearson and D. A. Sweigart, *Inorg. Chem.*, **9**, 1167 (1970).
9) a) A. W. Adamson, J. P. Welker, and M. Volpe, *J. Am. Chem. Soc.*, **72**, 4030 (1950); b) F. A. Long, *ibid.*, **73**, 537 (1951).

  Bull. Chem. Soc. Jpn., 54, 2475—2481 (1981)

Electrode Kinetics of the Redox Couples of Co(III/II) Complexes with Ethylenediamine-*N*-acetate, Iminodiacetate, and Diethylenetriamine

Takeo Ohsaka, Noboru Oyama, Shuichiro Yamaguchi, and Hiroaki Matsuda*

Department of Electronic Chemistry, Graduate School at Nagatsuta, Tokyo Institute of Technology, Nagatsuta, Midori-ku, Yokohama 227

(Received December 27, 1980)

The electrochemical kinetic parameters of $Co(edma)_2^{+/0}$ (edma: ethylenediamine-*N*-acetate), $Co(ida)_2^{-/2-}$ iminodiacetate), $Co(dien)_2^{3+/2+}$ (dien: diethylenetriamine), $Co(1,2\text{-pn})_3^{3+/2+}$ (1,2-pn: 1,2-propanediamine), and $Co(gly)_3^{0/1-}$ (gly: glycinate) redox couples were determined by d.c. and normal pulse polarographic measurements as well as galvanostatic double pulse measurements. A difference in the evaluated kinetic parameters for the geometric isomers, *trans*(*O*)- and *cis*(*O*)-$Co(edma)_2^{+/0}$ and *trans*(*N*)- and *cis*(*N*)-$Co(ida)_2^{-/2-}$ couples, was recognized. The values of the standard rate constant for the bis forms with dien, edma, and ida were reduced with increase in the number of replacement of amino groups in dien by carboxyl groups. The standard rate constants of the redox couples of Co(III/II) complexes with a series of bi- and tridentate polyamines and aminocarboxylates increase in proportion to the number of nitrogen donor atoms involved in the ligands.

The relationship between the structure of metal complexes and their electrochemical reactivity has been the research subject of electrochemists for the past three decades.[1] Attempts were made to correlate the structure of Co(III) complexes with their polarographic half-wave potentials or to their reduction rates. The Co(III) complexes with a wide variety of unidentate ligands and their geometric isomers with mixed ligands were used for this purpose.

As regards Co(III) complexes with multidentate ligands, however, only a few papers have been reported. Bond *et al.*[2] found that the half-wave potentials for the reduction of three geometric isomers of $Co(dien)_2^{3+}$ (dien=diethylenetriamine) in acetone solvent slightly differ from each other. Gouzerh[3] reported that the half-wave potentials of *cis*(*N*)- and *trans*(*N*)-$Co(ida)_2^{-/2-}$ (ida=iminodiacetate) redox couples are 0.16 and 0.05 V *vs.* SCE, respectively. Recently, Rader and Mcmillin[4] proposed that the electrolytic reductions of *cis*(*N*)- and *trans*(*N*)-$Co(ida)_2^-$ isomers are reversible and irreversible, respectively, and that the *cis*(*N*) configuration is favored in the Co(II) system. However, no attempt has been made to evaluate the electrochemical kinetic parameters. Systematic examination of the redox behavior of a series of similar metal complexes containing multidentate ligands has not been reported so far.

We have attempted to measure the electrochemical kinetic parameters of $Co(dien)_2^{3+/2+}$, $Co(edma)_2^{+/0}$ (edma=ethylenediamine-*N*-acetate) and $Co(ida)_2^{-/2-}$ redox couples. Discussion was made on the relative effects of amino and carboxyl groups on the electrode kinetics, where dien, edma, and ida are chosen as typical tridentate ligands, which make the five-membered chelate ring with metal ion and contain the amino, imino, and/or carboxyl groups as the donating groups. The difference in the redox behavior of the geometric isomers was also examined. In order to confirm the results obtained for tridentate ligands we have determined the kinetic parameters of $Co(1,2\text{-pn})_3^{3+/2+}$ (1,2-pn=1,2-propanediamine) and $Co(gly)_3^{0/1-}$ (gly=glycinate) redox couples.

Experimental

Reagents. *trans*-(*O*)-$Co(edma)_2^+$ and *cis*(*O*)-$Co(edma)_2^+$ were prepared according to the method of Fujii *et al.*[5] *cis*-Complexes obtained, however, contained an appreciable amount of *trans*-form. A *trans*-form free product was obtained by the following procedure utilizing the fact that the *trans*-form is soluble in a concentrated sodium perchlorate solution but not the *cis*-form: the initial product was dissolved in a saturated $NaClO_4$ solution, and the *cis*-complex precipitated was filtered, decanted with cold water and methanol, and dried. *cis*(*N*)-$Co(ida)_2^-$,[6] *trans*(*N*)-$Co(ida)_2^-$,[6] $Co(dien)_2^{3+}$,[7] $Co(1,2\text{-pn})_3^{3+}$,[8] *mer*-$Co(gly)_3^0$,[9] and *fac*-$Co(gly)_3^0$,[9] were synthesized by the standard procedures, where the following abbreviations were used: edma, $NH_2CH_2CH_2NHCH_2COO^-$; ida, $NH(CH_2COO^-)_2$; dien, $NH_2CH_2CH_2NHCH_2CH_2NH_2$; 1,2-pn, $NH_2CH_2CH(CH_3)NH_2$; gly, $NH_2CH_2COO^-$. Results of the elementary analysis for each species are as follows:

trans(*O*)-$[Co(edma)_2]Cl\cdot 2H_2O$	Found (%)	H(6.27), C(26.39), N(15 35), Cl(9.96),
	Calcd (%)	H(6.08), C(26.32), N(15.36), Cl(9.72)
cis(*O*)-$[Co(edma)_2]ClO_4$	Found	H(4.65), C(24.01), N(14.20), Cl(8.97),
	Calcd	H(4.62), C(24.47), N(14.26), Cl(9 02)
trans(*N*)-$K[Co(ida)_2]\cdot 2H_2O$	Found	H(3.86), C(23.73), N(7.00)
	Calcd	H(3.56), C(24.24), N(7.06)
cis(*N*)-$K[Co(ida)_2]\cdot 5/2H_2O$	Found	H(3.48), C(23.79), N(6.94)
	Calcd	H(3.73), C(23.71), N(6.91)
mer-$[Co(dien)_2]Cl_3\cdot 2H_2O$	Found	H(7.41), C(24.32), N(21.30) Cl(24.40)
	Calcd	H(7.41), C(23.57), N(20.61) Cl(26.09)
$[Co(1,2\text{-pn})_3]Cl_3\cdot 2H_2O$	Found	H(7.70), C(23.12), N(20 97), Cl(26.22)
	Calcd	H(8 08), C(25.51), N(19.83), Cl(25.10)
mer-$[Co(gly)_3]\cdot 2H_2O$	Found	H(5.11), C(23.30), N(13 60)
	Calcd	H(5 08), C(22.73), N(13.25)
fac-$[Co(gly)_3]\cdot H_2O$	Found	H(4.77), C(23.88), N(13.98)
	Calcd	H(4.72), C(24.09), N(14.04)

Ethylenediamine-*N*-acetic acid dihydrochloride dihydrate (Hedma·2HCl·2H_2O), diethylenetriamine (dien), and iminodiacetic acid were prepared and/or purified by the methods described in the previous paper.[10] 1,2-Propanediamine diperchlorate was prepared from perchloric acid and 1,2-propanediamine and then purified by recrystallization three times from water. Other chemicals were of reagent grade. All solutions were prepared with triply distilled water.

Apparatus. An apparatus containing d.c. and pulse polarographic modes constructed in our laboratory was employed, the polarograms being recorded with a X-Y recorder (Riken Denshi Co., Model F-42Cp, Tokyo). The electrolytic cell was designed to measure pH values accurately.[10] A digital pH/mV meter (Orion Research, Model 801) and a glass electrode (Beckman, No. 40495) were used for pH measurements. The dropping mercury electrode (DME) with the following characteristics was used: flow rate of mercury $m=0.45$ mg s^{-1}, the drop time $\tau=4.5$ s at the height of mercury head $h=72.0$ cm in 1 M $NaClO_4$ solution (1 M= 1 mol dm^{-3}). The test solution was deaerated with argon gas before each measurement of the current-voltage curves. All measurements were performed in a paraffin oil thermostat at 25.0±0.1 °C. Potentials were measured and recorded with respect to a saturated calomel reference electrode (SCE).

Results

D.c. and Normal Pulse Polarographic Measurements of trans*(O)- and* cis*(O)-Co(edma)$_2^{+/0}$ Couples.* A solution in which the bis-form of Co(II) complexes with respect to edma is predominantly present was used for the sake of convenience. The mechanism of the electrode processes might be as follows:

$$\begin{array}{ccc} cis(O)\text{-Co(edma)}_2^{+} & \underset{\alpha_c(cis),\ k_0(cis)}{\overset{+e}{\rightleftharpoons}} & cis(O)\text{-Co(edma)}_2^{0} \\ \Big\updownarrow & & \Big\updownarrow \\ trans(O)\text{-Co(edma)}_2^{+} & \underset{\alpha_c(trans),\ k_0(trans)}{\overset{+e}{\rightleftharpoons}} & trans(O)\text{-Co(edma)}_2^{0}, \end{array} \quad (1)$$

where α_c denotes the cathodic transfer coefficient and k_0 the standard rate constant of the charge transfer process.

D.c. polarographic current-potential curves of *cis(O)*- and *trans(O)*-Co(edma)$_2^+$ in 1.0 M NaCl solution were measured in the pH range 8.3—9.7 and the quasi-reversible one-electron reduction waves with diffusion-controlled limiting currents were observed for both species. The reversible half-wave potential $E_{1/2}^r$ was determined by means of extrapolation,[11] the values obtained being given in Table 1. The difference in the values of $E_{1/2}^r$ of the *cis*- and the *trans*-forms exceeds 10 mV, being independent of the drop time in the range 3—6 s. This suggests that within the d.c. polarographic time scale the Co(II) species produced by the reduction at the electrode remain in the same geometric form as the Co(III) species, although the Co(II) species are labile, and the standard potential of the *cis*-Co(III/II) couple is *ca.* 10 mV more negative than that of *trans*-Co(III/II) couple. Thus in the analysis of d.c. and pulse polarographic waves it is not necessary to consider any effects of geometric configuration changes at the state of Co(II) complex.

The electrochemical kinetic parameters were evaluated from the analysis of normal pulse polarograms.

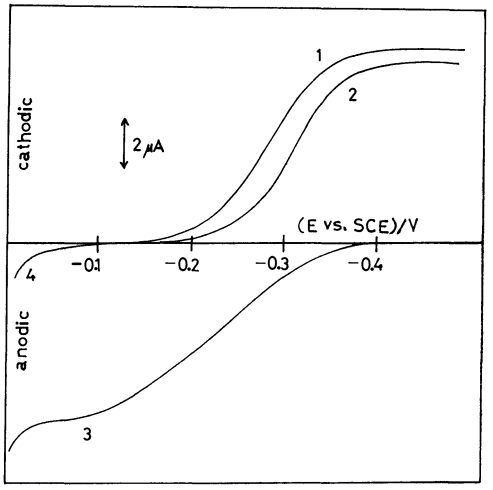

Fig. 1. Typical normal pulse polarograms of the Co(edma)$_2^{+/0}$ couple in 1.0 M NaCl solution.
(1): Reduction wave of 1.0 mM *trans* (*O*)-Co(edma)$_2^+$, (2): reduction wave of 1.0 mM *cis*(*O*)-Co(edma)$_2^+$, (3): oxidation wave of 1.0 mM Co(edma)$_2^0$, (4): residual current.
Concentration of Hedma=20 mM, pH=8.3 and sampling time $\tau_s=34.5$ ms.

Figure 1 shows typical normal pulse polarograms for the reduction of the *cis(O)*- and the *trans(O)*-Co(edma)$_2^+$ complexes as well as the oxidation of Co(edma)$_2^0$ complex. The half-wave potential of reduction waves shifted to cathodic direction with decreasing sampling time, τ_s, and their limiting current was diffusion-controlled, as proved from the fact that the product of the limiting current and $\tau_s^{1/2}$ is always constant.

The current-potential relationship for normal pulse polarograms of the simple electrode process, Ox+$ne \rightleftarrows$ Red, is given by[12]

$$E = E^* - \frac{2.303RT}{\alpha_c nF} \log \left\{ x \left[\frac{1.75 + x^2(1+\exp\zeta)^2}{1 - x(1+\exp\zeta)} \right]^{1/2} \right\} \quad (2)$$

with

$$E^* = E_{1/2}^r + \frac{2.303RT}{\alpha_c nF} \log \left\{ \frac{4}{\sqrt{3}} \frac{k_0\sqrt{\tau_s}}{\sqrt{D}} \right\}, \quad (3)$$

$$x = i/(i_d)_{Cott}, \quad (4)$$

$$\zeta = (nF/RT)(E - E_{1/2}^r), \quad (5)$$

$$D = D_{Ox}^{1-\alpha_c} D_{Red}^{\alpha_c}, \quad (6)$$

where $(i_d)_{Cott}$ denotes the diffusion current expressed by the Cottrel equation, i the normal pulse polarographic current, E the electrode potential, τ_s the sampling time, D_{Ox} and D_{Red} are the diffusion coefficients of Ox and Red, respectively, the other symbols having their usual meanings. The log-plots of the normal pulse polarograms, in which the log-term on r.h.s. of Eq. 2 is plotted against E, gave straight lines for the reduction of *cis(O)*- and *trans(O)*-Co(edma)$_2^+$ (Fig. 2). The straight lines have constant slopes for the *cis(O)*- and *trans(O)*-species, respectively, within experimental errors. The cathodic transfer coefficients were evaluated from their reciprocal slopes. The value of E^* was obtained from the intersects of these lines with the zero-line. The plots of E^* against log τ_s, shown in Fig. 3, give straight lines, their slopes also enabling us to evaluate the transfer

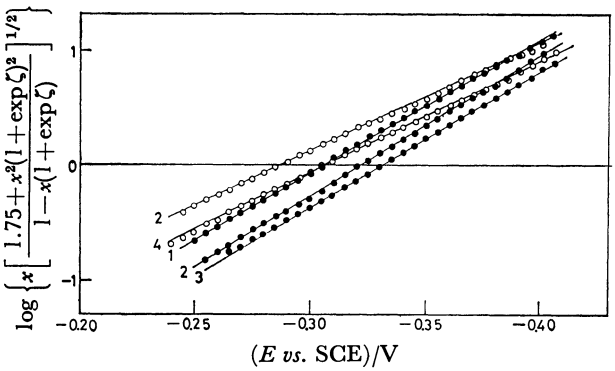

Fig. 2. Representative results for the plots of $\log\left[x\left\{\frac{1.75+x^2(1+\exp\zeta)^2}{1-x(1+\exp\zeta)}\right\}^{1/2}\right]$ *vs.* E for the reduction of 1.0 mM *cis*(*O*)- and *trans*(*O*)-Co(edma)$_2^+$.
(●): *cis*(*O*)-Species and (○): *trans*(*O*)-species. Sampling time τ_s=(1) 24.1 ms, (2) 8.7 ms, (3) 5.9 ms, and (4) 3.1 ms. Other conditions are same as in Fig. 1.

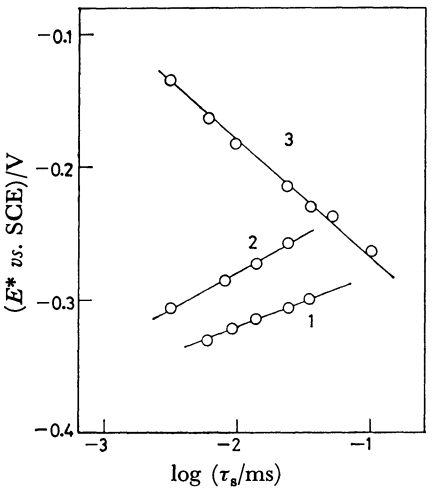

Fig. 3. Plots of E^* against log τ_s for the Co(edma)$_2^{+/0}$ couple.
(1): Reduction of *cis*(*O*)-Co(edma)$_2^+$, (2): reduction of *trans*(*O*)-Co(edma)$_2^+$, and (3): oxidation of Co(edma)$_2^0$. Other conditions are the same as in Fig. 1.

coefficients, as can be seen from Eq. 3. The cathodic transfer coefficients evaluated from the reciprocal slopes of the plots given in Figs. 2 and 3 are in good agreement with each other; they are 0.70 and 0.57 for the *cis*- and the *trans*-forms, respectively. The standard rate constants of charge transfer processes, k_0, were evaluated by means of Eq. 3. The values obtained are given in Table 1, where the values of diffusion coefficients used (6.2×10^{-6} and 7.3×10^{-6} cm^2 s^{-1} for the *cis*- and *trans*-forms, respectively) were obtained from the cathodic limiting currents of d.c. polarograms by using the Ilkovic equation or from those of normal pulse polarograms by using the Cottrell equation. We find that the standard rate constants for the reduction of the Co(III) complexes are in the order: *trans*(*O*)>*cis*(*O*).

The d.c. polarogram for the oxidation of the Co(edma)$_2^0$ complex shows the quasi-reversible nature (Fig. 4), its reversible half-wave potential being obtained as 0.281 ± 0.001 V *vs.* SCE by means of extrapolation.[11]

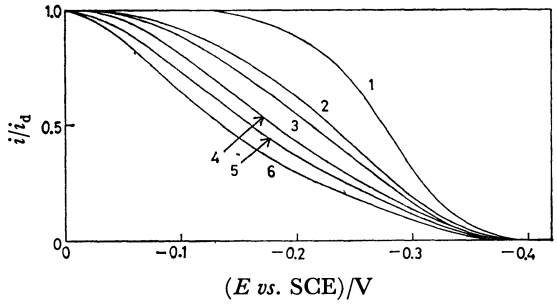

Fig. 4. Normalized d.c. and normal pulse polarograms for the oxidation of Co(edma)$_2^0$ in 1.0 M NaCl solution.
(1) D. c. polarogram at the drop time τ=4.0 s, (2) normal pulse polarograms at the sampling time τ_s= 52.4 ms, (3) 24.1 ms, (4) 8.7 ms, (5) 5.9 ms, and (6) 3.1 ms. Other conditions are the same as in Fig. 1.

The half-wave potential of the normal pulse polarograms shifts to the anodic direction as the sampling time is reduced (Fig. 4), their limiting current being diffusion-controlled. At the sampling times below 30 ms the limiting currents of the oxidation wave start to overlap with the dissolution-wave of mercury. Thus, the current was measured as the difference between the total current and the residual current as measured in the solution containing no Co(II) ion at the same potential. The relevant electrochemical kinetic parameters for the oxidation of the Co(edma)$_2^0$ complex were evaluated according to the same procedure as mentioned for the reduction of Co(III) complex and are summarized in Table 1, where the value of diffusion coefficient used was 5.9×10^{-6} cm^2 s^{-1}.

At present we have no means to decide what form of the geometrical isomer of Co(edma)$_2^0$ complex is predominantly present in the bulk of solution. However, the following indicates that the predominant species at equilibrium is the *cis*(*O*)-form: (1) The value of the reversible half-wave potential obtained from the d.c. polarographic oxidation wave is in good agreement with that of the reduction wave of *cis*(*O*)-Co(edma)$_2^+$ complex, and (2) agreement between the standard rate constants determined from the oxidation wave of Co(II) complex and the reduction wave for the *cis*(*O*)-form of Co(III)

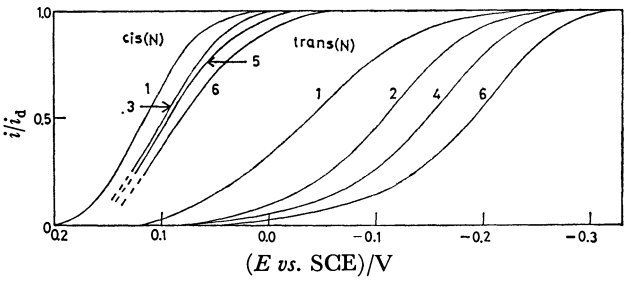

Fig. 5. Normalized d.c. and normal pulse polarograms for the reduction of 1.0 mM *cis*(*N*)-Co(ida)$_2^-$ in 1.0 M KNO_3 solution.
(1) D. c. polarogram at τ=4.2 s, (2) normal pulse polarograms at τ_s=75.0 ms, (3) 24.1 ms, (4) 14.0 ms, (5) 8.7 ms, and (6) 3.1 ms. Concentration of H_2ida= 10 mM and pH=8.3.

complex is quite good, the sum of their transfer coefficients being equal to unity.

D.c. and Normal Pulse Polarographic Measurements of trans-*(*N*)- and* cis*(*N*)-Co(ida)$_2^{-/2-}$ Couples.* Figure 5 shows the d.c. and normal pulse polarograms for reduction of *trans(N)*- and *cis(N)*-Co(ida)$_2^-$ complexes under the conditions in which the bis-species exists predominantly in the state of Co(II). In the case of the *cis*-species the current was measured carefully as the difference between the total and residual currents since the reduction current of the complex at the foot of the wave overlapped with the dissolution current of mercury. The log-plot of d.c. polarogram for the *cis*-species give a straight line with the reciprocal slope of 58 mV, corresponding to the reversible wave, whereas the log-plot of the *trans*-species indicates that the electrode reaction is quasi-reversible (close to irreversible) (Fig. 6).

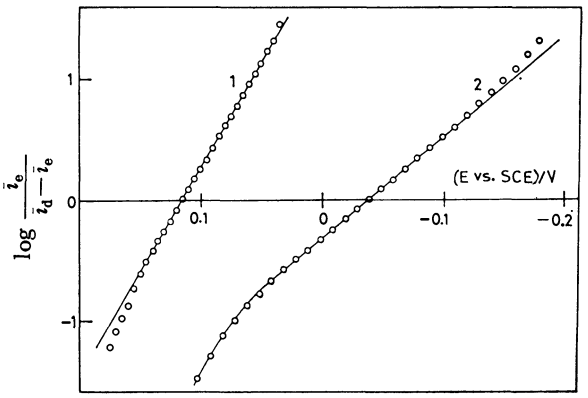

Fig. 6. D. c. polarographic log-plots for the reduction of *cis(N)*- and *trans(N)*-Co(ida)$_2^-$.
(1): *cis(N)* and (2) *trans(N)*.

In order to evaluate the kinetic parameters of reduction for the Co(III) complex, it is necessary to know the isomer form of Co(II) complex produced by reduction. Rader and Mcmillin[4] proposed that the reduced product of *trans(N)*-Co(ida)$_2^-$ isomerizes to the corresponding *cis*-isomer and that *cis(N)*-Co(ida)$_2^-$ is formed at the electrode upon reoxidation, as judged from the assignment of UV-vis. absorption spectra of bulk electrolysis product. They also stated that the isomerization reaction may proceed rapidly. However, our detailed examination of the isomerization kinetics using the anodic normal pulse measurements with cathodic pre-electrolysis of the *cis(N)*- and *trans(N)*-Co(ida)$_2^-$ gave no support for the *rapid* isomerization. The overlap of the polarogram of anodic reaction for the Co(II) species with the dissolution current of mercury was a main obstacle against detailed analysis. That the formation of the *cis*-form does not proceed in a quantitative way within d.c. and pulse polarographic timescales is suggested also by the disagreement between the reversible half-wave potentials for the reduction of the *cis*- and *trans*-Co(III) complexes (Table 1). At any rate, the *cis(N)*-configuration is favored at equilibrium for the state of Co(II).[4] Therefore, *cis(N)*-Co(ida)$_2^-$ keeps preferably the *cis(N)*-configuration after being reduced at the electrode, whereas the reduced product of *trans(N)*-Co(ida)$_2^-$ may gradually be isomerized to the *cis(N)*-form. Even if the isomerization process might proceed rapidly, the electrochemical kinetic parameters of *trans(N)*-Co(ida)$_2^-$ can be evaluated with sufficient accuracy, since the electrode reaction of *trans(N)*-form is d.c. polarographically quasi-reversibe (close to irreversible) and thus pulse-polarographically irreversible, so that the potential-shift due to the follow-up isomerization reaction may be negligibly small.

The kinetic parameters of the *cis(N)*- and *trans(N)*-Co(ida)$_2^-$ complexes were evaluated by means of the same method as described in the previous section. The reduction half-wave potentials for the *cis*- and *trans*-forms shifted to cathodic direction as the sampling time was reduced (Fig. 5) and their limiting currents were diffusion-controlled.

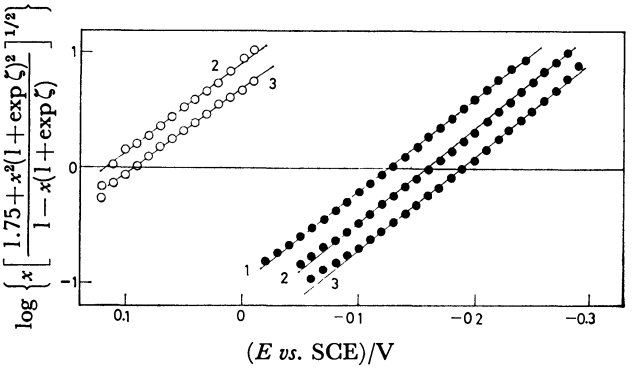

Fig. 7. Representative plots of $\log\left[x\left\{\frac{1.75+x^2(1+\exp\zeta)^2}{1-x(1+\exp\zeta)}\right\}^{1/2}\right]$ *vs.* E for the reduction of 1.0 mM *cis(N)*- and *trans(N)*-Co(ida)$_2^-$.
(○): *cis(O)*-Species and (●): *trans(O)*-species.
τ_s=(1) 34.0 ms, (2) 8.7 ms, and (3) 3.1 ms. Other conditions are the same as in Fig. 5.

The log-plots afford a set of straight lines at the different sampling times (Fig. 7). The cathodic transfer coefficients were obtained from the reciprocal slopes of these lines as follows: $\alpha_c(trans)=0.47\pm0.02$ and $\alpha_c(cis)=0.46\pm0.04$. The standard rate constants evaluated from the values of E^* are summarized in Table 1. Magnitude difference in these two values amounts to several tens. The diffusion coefficients used to evaluate the kinetic parameters were 5.6×10^{-6} and 6.8×10^{-6} cm^2 s^{-1} for the *cis*- and *trans*-forms, respectively, as determined from cathodic limiting currents of normal pulse polarograms.

Galvanostatic Double Pulse Measurements of Co(dien)$_2^{3+/2+}$ Couples. Although the Co(dien)$_2^{3+}$ complex has three geometric isomers, meridional(*mer*), symmetrical facial(*s-fac*), and unsymmetrical facial(*u-fac*), the *mer*-Co(dien)$_2^{3+}$ species which can easily be synthesized was chosen as a typical species of the Co(III) complex with polyamine ligand. D.c. polarographic reduction wave showed a reversible nature and its half-wave potential was constant at −0.448 V *vs.* SCE in the presence of a large excess of dien at pH above 8.5. The rate of charge transfer processes for the Co(dien)$_2^{3+/2+}$ couple was very rapid, so that their kinetic parameters

could not be evaluated even by the normal pulse polarographic technique. We therefore used the galvanostatic double pulse method with polarographic generation of reactant(g.d.p.p. method),[13] which has been recognized to be one of the most powerful techniques for very fast charge transfer processes. The analysis of experimental results was performed by using Eqs. 16 and 18 of Ref. 13. The experimental plots of the overpotential η_h *vs.* square root of the first pulse width $\sqrt{t_1}$ and of the exchange current density i_0 *vs.* applied d.c. potential E are shown in Figs. 8 and 9, respectively, in accordance with Eqs. 16 and 18 of Ref. 13, respectively. The theoretical slope was calculated by use of the diffusion coefficient of 4.4×10^{-6} cm^2 s^{-1} obtained from the d.c. polarographic limiting current (Fig. 8). The standard rate constant and the cathodic transfer coefficient obtained are given in Table 1.

Electrochemical Kinetic Parameters of Co(1,2-pn)$_3^{3+/2+}$ and mer-*Co(gly)$_3^{0/1-}$ Couples.* For the sake of comparison, the kinetic parameters for the reduction of the Co(1,2-pn)$_3^{3+}$ complex were also evaluated by the g.d.p.p. measurement (Table 1). The Co(1,2-pn)$_3^{3+}$ has two geometric isomers, *mer* and *fac*, with respect to methyl group but the product synthesized according to Ref. 8

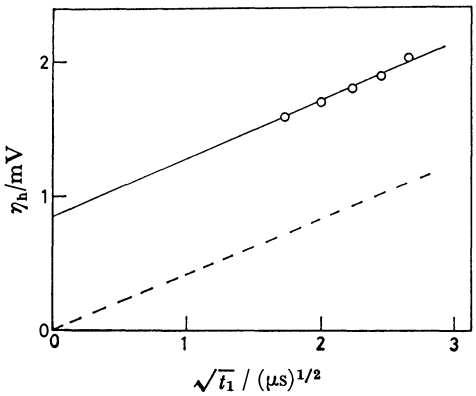

Fig. 8. A plot of the overpotential η_h *vs.* square root of first-pulse width $\sqrt{t_1}$ at the reversible half-wave potential of the *mer*-Co(dien)$_2^{3+/2+}$ couple in the g.d.p.p. measurement.
Solution composition: 1.0 mM *mer*-Co(dien)$_2^{3+}$, 0.10 M dien and 1.0 M $NaClO_4$ (pH=10.7). The dotted line indicates the theoretical slope.

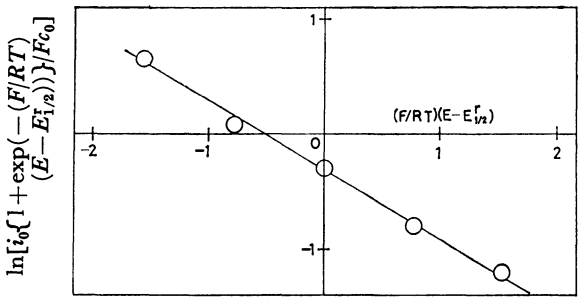

Fig. 9. A plot of ln $[i_0\{1+\exp(-(F/RT)(E-E^r_{1/2}))\}/Fc_0]$ *vs.* $(F/RT)(E-E^r_{1/2})$ for the Co(dien)$_2^{3+/2+}$ couple.

may be a mixture of two isomers. However, d.c. polarogram of the reduction of the synthesized complex showed only a single reversible reduction wave at −0.465 V *vs.* SCE. We thus used the synthesized product recrystallized without separation of the isomers.

In contrast to the electrochemical behavior of the polyamine complexes, the rate of reduction of *mer*-Co(gly)$_3^0$ was very slow and the reduction wave was d.c. polarographically irreversible. Thus, the log-plot of normal pulse polarograms gave only the cathodic transfer coefficient and the cathodic rate constant at $E=0$, *i. e.*, at the potential of SCE. According to Hin-Fat and Higginson,[17] the standard potential of the Co(gly)$_3^{0/1-}$ couple is -0.06 ± 0.01 V *vs.* SCE. If we use this value, we can calculate the standard rate constant of this couple, which is also given in Table 1 together with the cathodic rate constant at $E=0$.

No electrochemical measurements for *fac*-Co(gly)$_3^{0/1-}$ couple were performed since the *fac*-Co(gly)$_3^0$ species is insoluble in aqueous solutions containing 1 M supporting electrolytes.

Discussion

On the basis of the kinetic parameters summarized in Table 1, we can find some correlation between the electrochemical reactivity of Co(III/II) complexes and their structure.

(1) For the reduction of Co(III) complexes, six coordination sites of which are occupied by amines of similar ligands, the standard rate constant, k_0, increases

Table 1. Reversible half-wave potentials and kinetic parameters of the electron transfer reactions of Co(III/II) redox couples in 1.0 M supporting electrolytes at 25 °C

Redox system	($E^r_{1/2}$ *vs.* SCE)/V	k_0/cm s^{-1}	α_c	Medium
mer-Co(dien)$_2^{3+/2+}$	−0.448	$(7.8\pm0.1)\times10^{-1}$ [a]	0.66±0.05	0.1 M dien, $NaClO_4$
cis(*O*)-Co(edma)$_2^{1+/0}$	−0.279	$(3.4\pm0.1)\times10^{-3}$ [b]	0.70±0.02	0.02 M Hedma, NaCl
trans(*O*)-Co(edma)$_2^{1+/0}$	−0.267	$(8.5\pm0.1)\times10^{-3}$ [b]	0.58±0.02	0.02 M Hedma, NaCl
trans(*O*)-Co(edma)$_2^{1+/0}$	−0.263	$(8.5\pm0.1)\times10^{-3}$ [b]	0.59±0.02	0.02 M Hedma, $NaClO_4$
Co(edma)$_2^{0/1+}$	−0.281	$(3.0\pm0.1)\times10^{-3}$ [b]	0.31±0.02 [c]	0.02 M Hedma, NaCl
cis(*N*)-Co(ida)$_2^{1-/2-}$	0.115	$(1.1\pm0.2)\times10^{-2}$ [b]	0.46±0.04	0.01 M H_2ida, KNO_3
trans(*N*)-Co(ida)$_2^{1-/2-}$	0.027	$(4.0\pm0.1)\times10^{-4}$ [b]	0.47±0.02	0.01 M H_2ida, KNO_3
Co(1,2-pn)$_3^{3+/2+}$	−0.465	$(6.2\pm0.1)\times10^{-1}$ [a]	0.68±0.05	0.1 M 1,2-pn, $NaClO_4$
mer-Co(gly)$_3^{0/1-}$	−0.06±0.01 [e]	$(3.0\pm0.1)\times10^{-5}$ [b,d] $(9\pm2)\times10^{-5}$ [b]	0.51±0.02	0.05 M gly, $NaClO_4$

a) Galvanostatic double pulse method. b) Normal pulse polarographic method. c) Anodic transfer coefficient (α_a). d) Cathodic rate constant at the potential of SCE($E=0$). e) Ref. 17.

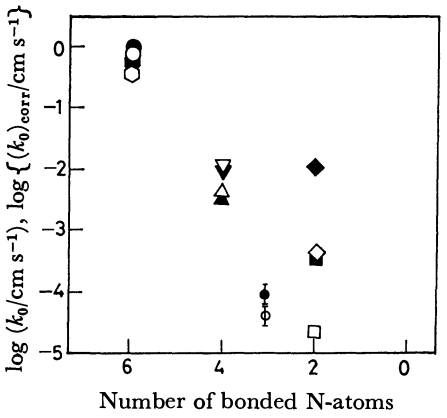

Fig. 10. Correlation between the standard rate constants and the number of bonded nitrogen donor atoms.
(●, ○): *mer*-Co(dien)$_2^{3+/2+}$, (⬢, ⬡): Co(1,2-pn)$_3^{3+/2+}$, (▼, ▽): *trans*(*O*)-Co(edma)$_2^{+/0}$, (▲, △): *cis*(*O*)-Co(edma)$_2^{+/0}$, (◆, ◇): *cis*(*N*)-Co(ida)$_2^{-/2-}$, (■, □): *trans*(*N*)-Co(ida)$_2^{-/2-}$, and (⧫, ⧫): *mer*-Co(gly)$_3^{0/1-}$.
The solid and open symbols denote the measured values, k_0, and the values corrected by the Frumkin theory, $(k_0)_{corr}$, respectively.

in the order: Co(dien)$_2^{3+/2+}$>Co(1,2-pn)$_3^{3+/2+}$, Co(en)$_3^{3+/2+}$ (en: ethylenediamine)[14]>Co(NH$_3$)$_6^{3+/2+}$.[15,16] This order is the same as that of the number of coordination sites involved in the ligand, *i. e.*, tridentate> bidentate>unidentate.

(2) Increase in the number of replacement of amino groups in dien by carboxyl groups reduces the values of k_0. The values of k_0 increase in the order: Co(dien)$_2^{3+/2+}$ >Co(edma)$_2^{+/0}$>Co(ida)$_2^{-/2-}$ (Fig. 10). The complex species studied have a different number of charges, the difference between their reversible half-wave potentials amounting to *ca.* 500 mV, so that the ϕ_2-potential at the outer Helmholtz plane may affect the kinetics of electrode reactions concerned. The open symbols in Fig. 10 express the values of the standard rate constant corrected for the double layer effect by means of the Frumkin theory,[18] in which the values of ϕ_2 were taken from Russell's Tables.[19] We find that for the present series of the redox couples of Co(III/II) complexes with bi- and tridentate polyamines and aminocarboxylates the logarithms of the corrected values, $(k_0)_{corr}$, increase

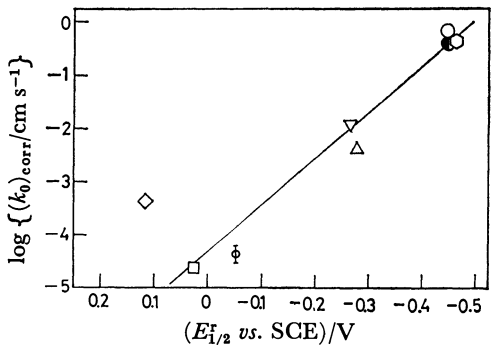

Fig. 11. Linear relationship between $\log(k_0)_{corr}$ and $E_{1/2}^r$.
(◐): Co(en)$_3^{3+/2+}$. Other symbols are the same as in Fig. 10.

in proportion to the number of nitrogen donor atoms involved in the ligand.

(3) Oyama *et al.*[20-22] showed that the linear relation between the logarithms of cathodic rate constants and the corresponding standard potentials holds for the Cd(II) and Pb(II) complexes with EDTA and related compounds. It is of interest to see if such a correlation prevails for the present series of Co(III/II) redox couples. Log $(k_0)_{corr}$ is plotted against the reversible half-wave potential $E_{1/2}^r$ in Fig. 11. We see linear correlation, except for the *cis*(*N*)-Co(ida)$_2^{-/2-}$ couple whose reversible half-wave potential is unusually positive. As can be seen from Table 1, the values of $E_{1/2}^r$ are also proportional to the number of the nitrogen donor atoms involved in the ligand, so that the linear correlation given in Fig. 11 could be attributed to that of Fig. 10.

(4) The difference of the kinetic parameters for the geometric isomers is obvious from the data in Table 1.

The authors wish to express their sincere thanks to Prof. S. Aoyagui and Dr. H. Mizota for allowing them to use their apparatus for the g.d.p.p. method. This work was partially supported by a Grant-in-Aid for Scientific Research No. 247065 from the Ministry of Education, Science and Culture.

References

1) A. A. Vlcek, "Progress in Polarography," ed by P. Zuman and I. M. Kolthoff, Interscience, New York (1962), Vol. 1, p. 269; *Electrochim. Acta*, **13**, 1063 (1968); N. Maki, *Kagaku*, **14**, 632 (1959); **16**, 202 (1961).
2) A. M. Bond, F. P. Keene, N. W. Rumble, G. H. Searle and M. R. Snow, *Inorg. Chem.*, **17**, 2847 (1978).
3) P. Gouzerh, *J. Chim. Phys. Phys.-Chim. Biol.*, **68**, 758 (1971).
4) R. A. Rader and D. R. Mcmillin, *Inorg. Chem.*, **18**, 545 (1979).
5) Y. Fujii, E. Kyuno, and R. Tsuchiya, *Bull. Chem. Soc. Jpn.*, **43**, 786 (1970).
6) J. Hidaka, Y. Shimura, and R. Tsuchida, *Bull. Chem. Soc. Jpn.*, **35**, 567 (1962).
7) F. R. Keene and G. H. Searle, *J. Chem. Soc., D*, **1970**, 784.
8) M. Kojima, Y. Yoshikawa, and K. Yamasaki, *Inorg. Nucl. Chem. Lett.*, **9**, 689 (1973).
9) M. Mori, M. Shibata, E. Kyuno, and M. Kanaya, *Bull. Chem. Soc. Jpn.*, **34**, 1837 (1961).
10) T. Ohsaka, N. Oyama, and H. Matsuda, *Bull. Chem. Soc. Jpn.*, **53**, 3601 (1980).
11) H. Matsuda, Y. Ayabe, and K. Adachi, *Ber. Bunsenges. Phys. Chem.*, **67**, 593 (1963); H. Matsuda, Tokyo Kogyo Shikensho Hokoku, **61**, 315 (1966).
12) H. Matsuda, *Bull. Chem. Soc. Jpn.*, **53**, 3439 (1980).
13) H. Mizota, H. Matsuda, Y. Kanzaki, and S. Aoyagui, *J. Electroanal. Chem.*, **45**, 385 (1973).
14) H. Mizota, S. Aoyagui, and H. Matsuda, *J. Electroanal. Chem.*, **87**, 173 (1978).
15) L. N. Klatt and W. J. Blaedel, *Anal. Chem.*, **39**, 1065 (1967).
16) H. Bartelt and S. Landazury, *J. Electroanal. Chem.*, **22**, 105 (1969).
17) L. Hin-Fat and W. C. E. Higginson, *J. Chem. Soc., A*,

1967, 298.
18) A. N. Frumkin, *Z. Phys. Chem.*, **164**, 121 (1933).
19) C. D. Russell, *J. Electroanal. Chem.*, **6**, 486 (1963).
20) N. Oyama and H. Matsuda, *J. Electroanal. Chem.*, **78**, 89 (1977).
21) N. Oyama and H. Matsuda, *J. Electroanal. Chem.*, **78**, 103 (1977).
22) N. Oyama, T. Shirato, and H. Matsuda, *J. Electroanal. Chem.*, **81**, 67 (1977).

An Alternative Display of Potentiostatic Measurements. I. Instrumental Design and Verification of Modified Pulse Polarograph

Yoshikiyo KATO,* Yoshio ANZAI,† Akifumi YAMADA, and Nobuyuki TANAKA
Department of Chemistry, Faculty of Science, Tohoku University, Sendai 980
(Received January 5, 1981)

A modified instrument for the potentiostatic method (modified pulse polarograph) has been developed, which uses techniques of the time-to-voltage converter. The modified pulse mode and the modified differential pulse mode have been tested as tools for quantitative analysis. The determination of kinetic parameters of electrode reactions is presented, together with the characteristics of the modified pulse polarograph.

Modern polarographic methods, especially normal and differential pulse techniques, have been widely used in trace analysis.[1-23] An advantage of using commercial instruments of pulse polarography is in the high signal-to-noise ratio (S/N): the averaging of current signal is synchronized to the a.c. power line. Although signal averagings of this type produce high S/N ratio, available sampling times are restricted, and current-potential curves are slightly distorted.[7]

Recently, the authors have developed a new polarographic technique. The method records the time instead of current or potential and has been successfully introduced in constant-current electrolysis.[24-26] The measurement and the recording of the time have been carried out by the time-to-voltage converter. Introduction of the time-to-voltage converter produces high S/N ratios without sacrifice of the frequency response of the data sampling circuit.

Previously, the authors reported a modified potentiostatic method. This method is based on the measurement of time required to reach a constant sampling current in the potentiostatic method.[27,28] The fundamental concept and the determination of kinetic parameters were reported. However, the complete system has not been developed. The measurement of time was carried out descretely, using a comparator and a digital counter.[27]

In this report, instrumental designs of a modified pulse polarograph, characteristics of modified pulse polarography (MPP), and some applications in the electrode kinetics are presented. The use of the time-to-voltage converter is indispensable to realize the full advantages of the modified potentiostatic method. The development of the modified pulse polarograph simplified the measurement of the instantaneous time-potential-current relation without limitations of sampling time and without distortion of data, attempts at the modified differential pulse polarography (MDPP) are also reported.

Experimental

A three-electrode cell equipped with a saturated calomel reference electrode (SCE: Yanagimoto MR-P_2-05-1), a platinum wire electrode (counter electrode) and a dropping mercury electrode (DME: Yanagimoto Type-C) was used; synchronization of DME was done by a electro-mechanical knocker (Fuso Solenoid).

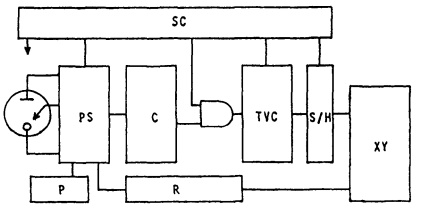

Fig. 1. The block diagram of the modified pulse polarograph. (PS: potentiostat, C: comparator, TVC: time-to-voltage converter, S/H: sample and hold circuit, P: potentiometer, R: ramp generator, SC: sequence controller, XY: x-y recorder).

$[Co(NH_3)_6]Cl_3$ was prepared according to the literature[29] and identified by elemental analysis. The solution was deaerated with pure nitrogen and kept under nitrogen atmosphere. The temperature of the solution was kept constant at 25.0±0.1 °C. All solutions were prepared in twice distilled water; all chemicals were analytical grade.

Apparatus

A new modified pulse polarograph was designed for this study. The polarograms were recorded with this instrument using a Rikadenshi RW-11 x-y recorder. The block diagram and the electronic circuit of the modified pulse polarograph are shown in Figs. 1 and 2. The modified pulse polarograph is constructed with a three-electrode-type potentiostat (PS), comparator (C), time-to-voltage converter (TVC), sample-and-hold

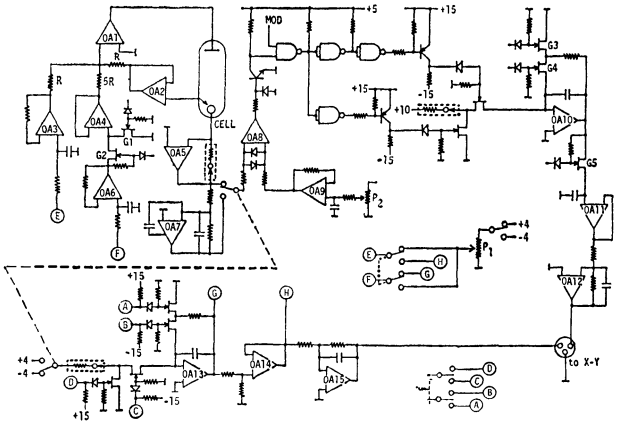

Fig. 2. The electronic circuit of the modified pulse polarograph.

† Present address: Kikakushitsu Kikakuka, Nihon Recruit Center, 8-4-17, Ginza, Chuo-ku, Tokyo 104.

circuit (S/H), and ramp generator (R). The procedure for measurements is controlled by a sequence controller (SC). When a mercury drop begins to grow, it is held at the initial potential E_i set by the potentiometer P_1 (In differential mode, the drop is held at the potential set by the ramp generater.). After the lapse of a preset time period t_w(0.5—11 s), the sequence controller turns the gate G1 off and the gate G2 on. The potentiostat is then connected to the ramp generator, which provides the step voltage ΔE (In the differential mode the step voltage ΔE is provided by the potentiometer P_1.). Simultaneously, the time-to-voltage converter is turned to the ready state by gates G-3 and G-4.

The current signal resulting from potential relaxation (E_i to $E_i+\Delta E$) is fed to a high-speed comparator OA-8. The slice level of the comparator (*i. e.* the constant sampling current, i_s) is set by the potentiometer P_2. The output of the comparater is connected to the gates of the time-to-voltage converter. After 1 s of t_w, the gates G-1 and G-2 are turned to the former state and the DME knocker is started. Simultaneously, gate G-5 stores the output of the TVC in the sample-and-hold circuit (OA-11). Then, gates G-3 and G-4 reset the TVC. The measurement cycle is completed and the sequence is repeated. The values of t are displayed on an x-y recorder as a function of E. The time chart and the relationships between control signals and FET gates are shown in Fig. 3.

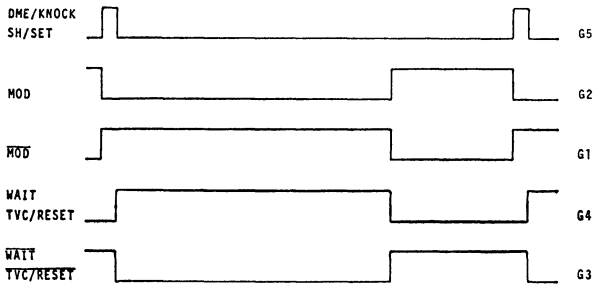

Fig. 3. The time chart of the control sequences and their connection with FET-gates.

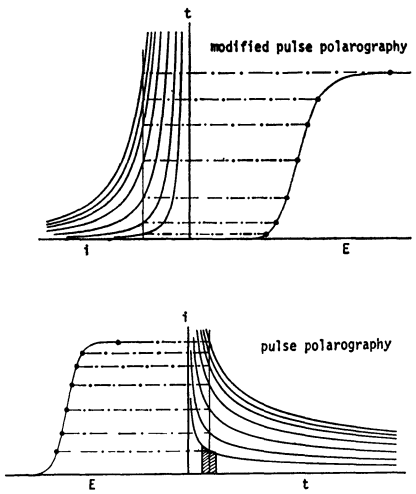

Fig. 4. The relations of current-time curves and the modified pulse and/or the normal pulse polarogram.

The principle of MPP is schematically shown in Fig. 4 together with that of pulse polarography. In MPP, the time required to reach a constant sampling current i_s in potentiostatic measurements is recorded versus the potential. Therefore, the modified pulse polarogram gives the instantaneous time-potential-current relation. On the other hand, in the pulse polarography, the average current in the sampling period is recorded *versus* the potential.

Results and Discussion

System Evaluation. To evaluate the function of the system, modified pulse polarograms of a reversible and an irreversible electrode reactions were measured. Potential-time relations of reversible and irreversible electrode processes were also tested for the case of cathodic reduction, when only the oxidant is present in the solution.

Reversible Case: The potential-time relationships of modified pulse mode are given by

$$E = E_o - \frac{RT}{(\alpha_a+\alpha_c)nF} \ln \sqrt{\frac{D_O}{D_R}} + \frac{RT}{(\alpha_a+\alpha_c)} \ln \frac{\sqrt{t_{diff}}-\sqrt{t}}{\sqrt{t}}, \quad (1)$$

for a reversible electrode process.[27,28] Here E is the electrode potential; E_o, the formal potential; α the transfer coefficient; D, the diffusion coefficient; t, the time; t_{diff}, the time at potentials controlled by diffusion; and R, T and F have their usual meanings. The subscripts a and c indicate the anodic and the cathodic processes, and O and R the oxidant and the reductant.

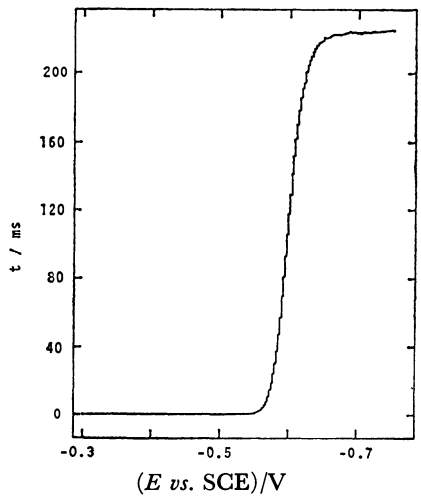

Fig. 5. An example of modified pulse polarogram. (1 mM $Cd(NO_3)_2$†† in 1 M $NaNO_3$ containing 2 μM LEO, i_s=10 μA, t_w=2 s, m=1.063 mg s^{-1}).

The modified pulse polarogram of cadmium ion is shown in Fig. 5 as an example of a reversible process. Equation 1 shows the linear relation between E and $\ln\{(\sqrt{t_{diff}}-\sqrt{t})/\sqrt{t}\}$. Such plots of the Cd(II)/Cd(Hg) system are shown in Fig. 6. The data points lie very close to the least-square line drawn through them. Furthermore, the slope of the least-square line is almost

†† 1 M=1 mol dm^{-3}.

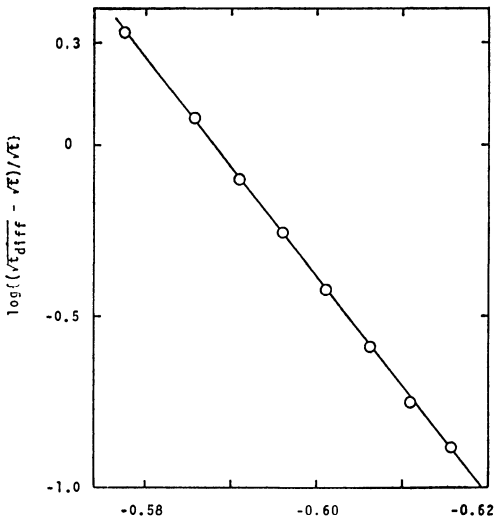

Fig. 6. The plots of $\log\{(\sqrt{t_{diff}}-\sqrt{t})/\sqrt{t}\}$ *vs.* E. (1 mM $Cd(NO_3)_2$ in 1 M $NaNO_3$ containing 2 μM LEO $i_s=30$ μA, $t_w=4$ s, $m=0.6656$ mg s^{-1}).

equal to RT/nF.

The time at potentials controlled by diffusion, t_{diff}, is represented as

$$\sqrt{t_{diff}} = \frac{nFA\sqrt{D_O}c_O^\circ}{\sqrt{\pi}\,i_d} \qquad (2)$$

for both the reversible and the irreversible processes, where A is the electrode area at t_w; c_O°, the concentration of the bulk of the solution and i_d, the diffusion current.

Equation 2 shows the linear relation between $\sqrt{t_{diff}}$ and c_O° or $1/i_d$. In this report, the time data are corrected for the effect of the expansion of DME during measurements. The correcting factor of the time data is

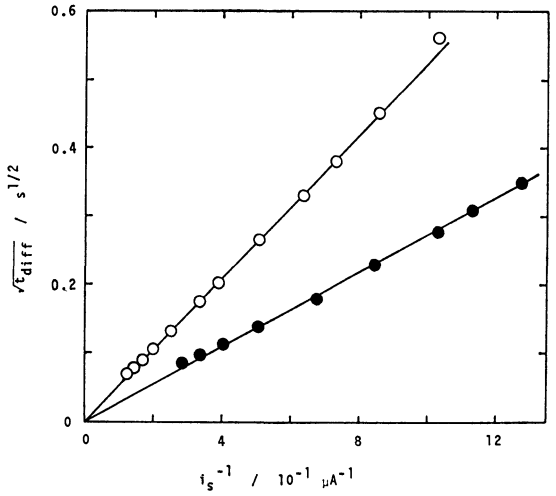

Fig. 8. The plots of $\sqrt{t_{diff}}$ *vs.* reciprocal of i_d. (○: 0.8 mM $Cd(NO_3)_2$ in 1 M $NaNO_3$, $t_w=4$ s, $m=0.6656$ mg s^{-1}; ●: 1 mM $[Co(NH_3)_6]Cl_3$ in 0.9 M $NaNO_3$ containing 0.1 M acetate buffer (pH 5.0) and 2 μM LEO, $t_w=3$ s, $m=1.05$ mg s^{-1}).

$1/(1-t/t_w)^{2/3}$ which is the reciprocal of relative surface area at t_w+t. The linear relations between $\sqrt{t_{diff}}$ and c_O° or reciprocal of i_d were tested for the reduction of Cd(II) and $[Co(NH_3)_6]^{3+}$. The plots of $\sqrt{t_{diff}}$ *versus* c_O° and $\sqrt{t_{diff}}$ *versus* $1/i_d$ are shown in Figs. 7 and 8, respectively. Those plots gave excellent linear relations up to 300 ms of the t_{diff} values, indicating that the instrument works satisfactorily.

Irreversible Case: The potential time relations for an irreversible electrode process are given by[27,28]

$$E = E_o + \frac{RT}{2\alpha_c nF}\ln\frac{16t_{diff}(k_s)^2}{3D_O} - \frac{RT}{2\alpha_c nF}\ln\frac{1.75+t/t_{diff}}{1-\sqrt{t}/\sqrt{t_{diff}}}, \qquad (3)$$

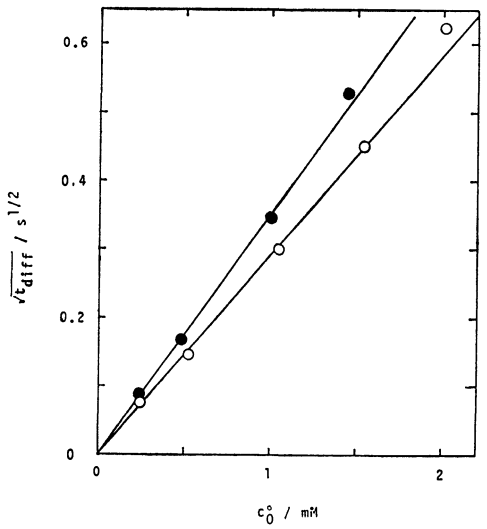

Fig. 7. The plots of $\sqrt{t_{diff}}$ *vs.* the bulk concentration. (●: $[Co(NH_3)_6]Cl_3$ in 0.9 M $NaNO_3$ containing 0.1 M acetate buffer (pH 5.0) and 2 μM LEO, $i_s=8$ μA, $t_w=3$ s, $m=1.05$ mg s^{-1}; ○: $Cd(NO_3)_2$ in 1 M $NaNO_3$ containing 2 μM LEO, $i_s=15$ μA, $t_w=2$ s, $m=0.6656$ mg s^{-1}).

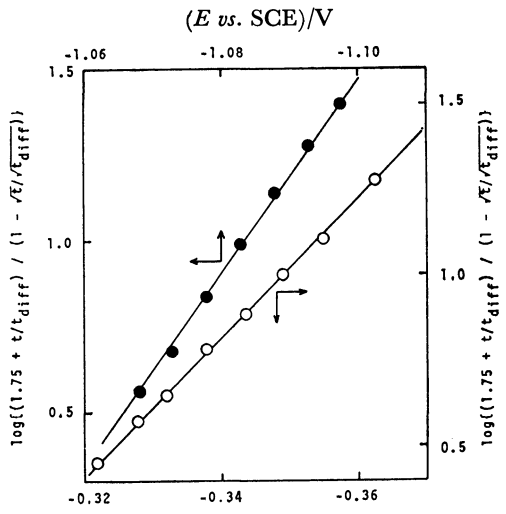

Fig. 9. The plots of $\log\{(1.75+t/t_{diff})/(1-\sqrt{t}/\sqrt{t_{diff}})\}$ *vs.* E. (○: 1 mM $[Co(NH_3)_6]Cl_3$ in 0.9 M $NaNO_3$ containing 0.1 M acetate buffer (pH 5.0) and 2 μM LEO, $i_s=8$ μA; ●: 1 mM $NiCl_2$ in 0.1 M KCl containing 2 μM LEO, $i_s=18$ μA; $t_w=3$ s, $m=1.05$ mg s^{-1}).

where, k_s is the formal standard rate constant. The linear relation of E and $\ln\{(1.75+t/t_{diff})/(1-\sqrt{t}/\sqrt{t_{diff}})\}$ has been tested for the reduction waves of $[Co(NH_3)_6]^{3+}$ and Ni(II). These plots, shown in Fig. 9, gave good linear relations.

The above mentioned results of the system evaluation for reversible and irreversible cases were quite satisfactory. The logarithmic plots shown in Fig. 6 can be utilized for the diagnostic criteria of reversibility. The working curve, $\sqrt{t_{diff}}$ *versus* c_0°, will give a fundamental concept of quantitative analysis.

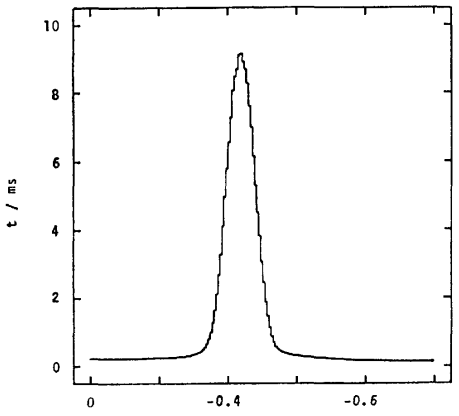

Fig. 10. A display of modified differential pulse polarogram of 600 μM $TlNO_3$ in 1 M KNO_3. (i_s=3.0 μA, t_w=6 s, m=0.539 mg s^{-1}, ΔE=100 mV).

Modified Differential Pulse Polarography. A new method, modified differential pulse polarography, has been successfully introduced. The measurement is carried out by measuring the time required to reach a constant sampling current; the principle of electrolytic method of MDPP is similar to that of the differential pulse polarography. Characteristics of modified differential pulse polarogram were studied using Tl(I)/Tl(Hg) and Cd(II)/Cd(Hg) systems. Figure 10 shows a modified differential pulse polarogram of 600 μM $TlNO_3$ in 1 M KNO_3. The slope of the log-log plots of peak-height and bulk concentration was 2.0. The empirical relation between the peak height t_p of modified differential pulse polarogram and the bulk concentration can be written as

$$\sqrt{t_p} = p \cdot c_0^\circ. \quad (4)$$

Here, p is the proportionality constant. The plots of

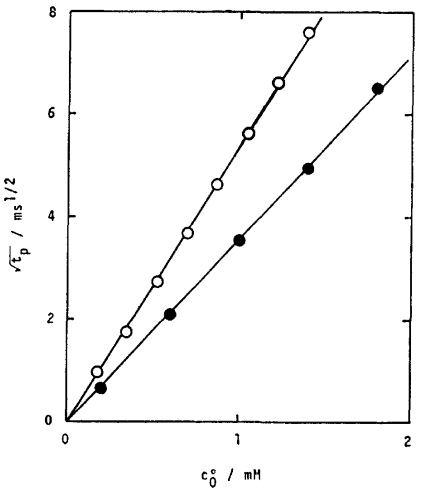

Fig. 11. The plots of $\sqrt{t_p}$ *vs.* the bulk concentration. (●: $TlNO_3$ in 1 M $NaNO_3$, t_w=6 s, ΔE=100 mV, ○: $Cd(NO_3)_2$ in 1 M $NaNO_3$, t_w=6 s, ΔE=100 mV, m=0.539 mg s^{-1}).

$\sqrt{t_p}$ *vs.* c_0° of Tl(I)/Tl(Hg) and Cd(II)/Cd(Hg) systems are shown in Fig. 11. The data points gave a good straight line which through the origin. These plots can be utilized as the working curve of quantitative analysis.

The theoretical treatment of modified differential pulse polarography will be discussed elsewhere.

Application to the Determination of Kinetic Parameters. Kinetic parameters of electrode reactions can be determined from the following relations:[27,28]

$$\frac{\sqrt{t}}{\sqrt{t_{diff}}} \frac{1+\sqrt{D_O/D_R}\gamma}{1-(c_R^\circ/c_O^\circ)\gamma} = \sqrt{\pi}\lambda\sqrt{t}\exp(\lambda^2 t)\mathrm{erfc}(\lambda\sqrt{t}), \quad (5)$$

$$\gamma = \frac{k_a}{k_c} = \exp[(\alpha_a+\alpha_c)(E-E_o)nF/RT], \quad (6)$$

$$k_c = \frac{\sqrt{D_O}}{1+\sqrt{D_O/D_R}\gamma}. \quad (8)$$

Introducing the values of $\alpha_c+\alpha_a$ and E_o from the references,[27,28] the value of γ in Eq. 6 can be calculated. Since the value of $\sqrt{t/t_{diff}}$ is measurable, the left hand side of Eq. 5 is calculated from experimental data. Then, the parameter λ can be obtained at various potentials. In these calculations, the function $\phi(\lambda\sqrt{t})$ and the inverse function of $\phi(\lambda\sqrt{t})$ can be calculated by a computer.[30,31]

The rate constants k_a and k_c are calculated from

Table 1. Kinetic parameters of electrode reactions obtained at 25.0 °C

(E_o *vs.* SCE)/V	α_c	α_a	k_s/cm s^{-1}	Ref.
$Zn(NO_3)_2$ in 0.3 M $NaNO_3$ +1 mM $HClO_4$+2 μ M LEO				
−0.999	0.31	0.63	8.4×10^{-3}	This work
−0.998	0.32	0.62	8.7×10^{-3}	27, 28
$Cu(NO_3)_2$ in 1 M $NaNO_3$+5 mM HNO_3+0.001% PAA				
0.022	0.23	0.73	2.2×10^{-2}	This work
0.022	0.24	0.73	2.9×10^{-2}	27, 28
$[Co(NH_3)_6]Cl_3$ in 0.9 M $NaNO_3$+0.1 M acetate buffer				
−0.250	0.58	0.42	1.5×10^{-3}	This work
−0.249	0.71	0.29	1.9×10^{-3}	27, 28

Eqs. 6 and 7 using the value of λ obtained above. The kinetic parameters are determined from the relations

$$k_a = k_s \exp\left\{\frac{\alpha_a nF}{RT}(E-E_0)\right\}, \quad (8)$$

$$k_c = k_s \exp\left\{\frac{-\alpha_c nF}{RT}(E-E_0)\right\}, \quad (9)$$

using a least square method.[27,28,30,31] Kinetic parameters of the electrode reactions of Cu^{2+}, Zn^{2+}, and $[Co(NH_3)_6]^{3+}$ were determined. The obtained values of k_s, E_0, and α_c are listed together with literature values in Table 1. The results are in good agreement with the literature values.

In conclusion, it should be mentioned that the modified pulse polarograph developed has advantages in the easy measurement of the instantaneous potential-current-time relationship.

The research was carried out by a Grant-in-Aid from the Ministry of Education, Science and Culture. A part of the work was supported by Scientific Grant No. 472570091668.

The authors wish to thank Mr. Tokio Ohoto for his help throughout the experiment.

References

1) G. C. Barker and A. W. Gardner, *At. Energ. Res. Establ. AERE Harwell C/R*, 2297 (1958).
2) G. C. Barker and A. W. Gardner, *Fresenius' Z. Anal. Chem.*, **173**, 79 (1960).
3) E. P. Parry and R. A. Osteryoung, *Anal. Chem.*, **36**, 1366 (1964).
4) E. P. Parry and R. A. Osteryoung, *Anal. Chem.*, **37**, 1634 (1965).
5) G. D. Christian, *J. Electroanal. Chem.*, **22**, 333 (1969).
6) H. E. Keller and R. A. Osteryoung, *Anal. Chem.*, **43**, 342 (1971).
7) J. H. Christie, J. Osteryoung, and R. A. Osteryoung, *Anal. Chem.*, **45**, 210 (1973).
8) N. Klein and Ch. Yarnitzky, *J. Electroanal. Chem.*, **61**, 1 (1975).
9) R. Kalvoda and A. Trojanek, *J. Electroanal. Chem.*, **75**, 151 (1977).
10) V. I. Boduy, I. V. Kotlova, and U. S. Lyapilov, *Zavod. Lab.*, **28**, 1042 (1963).
11) J. H. Christie and R. A. Osteryoung, *J. Electroanal. Chem.*, **49**, 301 (1974).
12) A. A. A. M. Brinkman and J. M. Los, *J. Electroanal. Chem.*, **7**, 171 (1964).
13) A. W. Fonds, A. A. A. M. Brinkman, and J. M. Los, *J. Electroanal. Chem.*, **14**, 43 (1967).
14) A. A. A. M. Brinkman and J. M. Los, *J. Electroanal. Chem.*, **14**, 269 (1967).
15) K. B. Oldham, *Anal. Chem.*, **40**, 1024 (1968).
16) J. P. van Dieren, B. G. W. Kaars, J. M. Los, and B. J. C. Wetsema, *J. Electroanal. Chem.*, **68**, 129 (1976).
17) J. H. Christie, L. L. Jackson, and R. A. Osteryoung, *Anal. Chem.*, **48**, 561 (1976).
18) J. H. Christie, L. L. Jackson, and R. A. Osteryoung, *Anal. Chem.*, **48**, 242 (1976).
19) M. Krizan, H. Schmidtpott, and H. Strehlow, *J. Electroanal. Chem.*, **80**, 345 (1977).
20) M. Krizan, *J. Electroanal. Chem.*, **80**, 337 (1977).
21) C. Peker, H. Herlem, and J. Bodoz-Lambling, *Fresenius' Z. Anal. Chem.*, **224**, 204 (1967).
22) A. Lagrou and F. Verbeek, *J. Electroanal. Chem.*, **19**, 413 (1968).
23) E. Timmerman and F. Verbeek, *J. Electroanal., Chem.* **12**, 158 (1966).
24) Y. Kato, A. Yamada, N. Yoshida, K. Unoura, and N. Tanaka, *Rev. Polarog. (Kyoto)*, **23**, 62 (1977).
25) Y. Kato, A. Yamada, N. Yoshida, K. Unoura, and N. Tanaka, *ACS/CSJ Chemical Congress*, ANAL-74 (1979).
26) Y. Kato, A. Yamada, N. Yoshida, K. Unoura, and N. Tanaka, *Bull. Chem. Soc. Jpn.*, **54**, 175 (1981).
27) N. Tanaka, A. Kitani, A. Yamada, and K. Sasaki, *Sci. Repts. Tohoku Univ. Ser. I*, **55**, 201 (1972).
28) N. Tanaka, A. Kitani, A. Yamada, and K. Sasaki, *Electrochim. Acta*, **18**, 675 (1973).
29) J. Bjerrum and J. P. MacReynolds, *Inorg. Synth.*, **2**, 216 (1946).
30) A. Yamada, and N. Tanaka, *Sci. Repts. Tohoku Univ. Ser. I.*, **53**, 110 (1970).
31) A. Yamada and N. Tanaka, *Anal. Chem.*, **45**, 167 (1973).

Sorption Behavior of Low Molecular Weight Organic Vapors on β-Cyclodextrin Polyurethane Resins

Yoshikazu MIZOBUCHI, Minoru TANAKA, Yoshihiro KAWAGUCHI, and Toshiyuki SHONO*

Department of Applied Chemistry, Faculty of Engineering, Osaka University, Yamada-oka, Suita, Osaka 565

(Received January 24, 1981)

The sorption behavior of low molecular weight organic vapors on β-cyclodextrin polyurethane resins was estimated from desorption or breakthrough experiments and compared with that on the commercially available resins. Temperature-programmed desorption patterns show that the β-cyclodextrin resins interact strongly with benzene vapor in a nitrogen or air stream. This strong interaction presumably results from the hydrophobic interaction of benzene with the β-cyclodextrin cavity. From the breakthrough experiments using the gas stripping method, it was found that the resin prepared by reacting β-cyclodextrin with 1,3-bis(isocyanatomethyl)cyclohexane, β-H6XDI-P-6.0-M, retains the polar volatile organic compounds more than Amberlite XAD-7 does.

Because of the relatively low concentrations of organic contaminants in ambient air or in water, most methods for the measurement of these contaminants require a concentration step before the actual analysis.[1-3] Several commercially available porous polymer beads (*i. e.*, Tenax GC,[4,5] Porapak Q,[6] and Amberlite XAD-2[7]) and graphitized carbon black[8] are used widely to collect organic contaminants. The polarity of monomers brings about some selectivity[9] in sorbing organic compounds to the porous polymer beads: the more polar the monomer is, the more strongly the polymer beads interact with polar organic compounds. A series of the Amberlite XAD resins, for example, are capable of collecting a variety of organic compounds. The Amberlite XAD resins and related ones are hydrophobic in nature and have energetically homogeneous sorption sites. Therefore, the selectivity of these resins in collecting organic compounds cannot be expected to be strong. In order to strengthen the selectivity mentioned above, it is necessary to introduce specific sorption sites into a resin.

We are interested in finding organic sorbents that will be able to collect organic compounds in environments selectively. It is well known that cyclodextrins form stable inclusion complexes with specific organic compounds. The polyurethane resins containing cyclodextrin units were prepared by cross-linking cyclodextrins with diisocyanates.[10] The interactions of these polyurethane resins with low molecular weight organic vapors were investigated by gas chromatography in a dry nitrogen carrier gas. It was found that the cyclodextrin resins exhibit large retention times for the compounds containing π-electrons or hetero atoms (such as benzene, pyridine, and ethyl methyl ketone).

In this work, the preliminary sorption behavior of β-cyclodextrin polyurethane resins is investigated and compared with that of Porapak Q, Tenax GC, or Amberlite XAD-7 in order to evaluate the possibility of using these cyclodextrin resins as sorbents to collect organic vapors. The isothermal and temperature-programmed desorption patterns and the breakthrough times were studied for several low molecular weight organic compounds.

Experimental

Materials. β-Cyclodextrin was obtained from Hayashibara Biochemical Laboratories, 1,3-bis(isocyanatomethyl)-cyclohexane and 1,3-bis(isocyanatomethyl)benzene from Takeda Chemical Industries, and all other chemicals from Wako.

The preparation of β-cyclodextrin polyurethane resins was described in detail in our previous paper.[10] The β-cyclodextrin polyurethane resins obtained were granulated to a particle size of 177—250 μm with an agate mortar, sieved, and used as sorbents.

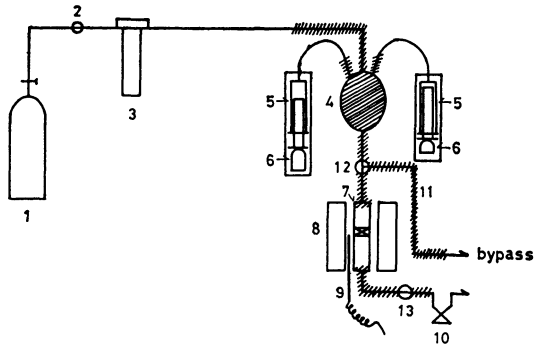

Fig. 1. Apparatus for adsorption behavior studies.
1: Nitrogen gas cylinder, 2: bellows valve, 3: flow meter, 4: mixing vessel, 5: syringe, 6: syringe drive, 7: adsorption tube, 8: furnace, 9: thermocouple, 10: gas sampler, 11: heater, 12: 3-way cock, 13: 2-way cock.

Apparatus. The apparatus utilized for the studies of adsorption behavior of the resins is shown schematically in Fig. 1. This apparatus was constructed in our laboratory and equipped with an automatic temperature-programming device. The nitrogen stream flowing through the path was controlled to 100 ml/min by a bellows valve. The flow rate was measured with an orifice flow meter. One or two adsorbates (model organic compounds) were introduced into an adsorption tube at a known, continuous, reproducible rate using one or more syringe pumps (Adzuma Model MF-2). As the adsorbate(s) vaporized from the syringe tip(s) inserted into the mixing vessel (60 ml) heated with a heater, it was swept into the flowing nitrogen stream. Thus, a constant stream containing the gaseous adsorbate(s) with a constant concentration was provided; the stream was introduced into the glass adsorption tube (25×2 cm i.d.) with a sintered glass filter. Each resin (*ca.* 2 g) was dry-packed into the tube and preconditioned at 180 °C for 1 h in a pure nitrogen stream at 100 ml/min. The nitrogen gas containing the adsorbate(s) was collected in a gas sampler (1.2—1.5 ml), and the concentration of adsorbate(s) was determined by gas chromatography with a thermal conductivity detector (Shimadzu Model

GC-3BT gas chromatograph). The chromatographic column packed with Porapak Q (2 m×3 mm i.d.) or with 10% DNP on Chromosorb W (3 m×3 mm i.d.) was used.

After the resin in the tube was equilibrated with the adsorbate(s)-nitrogen mixture at 102 °C, the asdorbate(s) vapor was completely removed from the mixing vessel through a 3-way cock (by-pass). Then, the 3-way cock was positioned again so that the pure nitrogen stream (at 100 ml/min) passed through the adsorption tube, and the adsorbate(s) taken up by the resin was desorbed at 102 °C for 2 h. Then, the desorption temperature was programmed at 3.1 °C/min to 170 °C. The desorbed adsorbate(s)-nitrogen mixture was periodically collected in a gas sampler and analyzed by gas chromatography.

The measurements of breakthrough time were carried out by replacing nitrogen gas cylinder in Fig. 1 with an air bag containing the adsorbate(s) and by directly introducing the sample gas in the air bag with a pump into a FID (flame ionization detector in a Shimadzu Model GC-3BF gas chromatograph) through the adsorption tube. The sample-air flow rate was 20 ml/min and the resin weight in the tube was 1 g.

The total adsorption capacities of adsorbates on the resins were measured with a Shimadzu Model ADS-1B sorptograph with the automatic temperature-programming device connected to a Shimadzu Model GC-3BT gas chromatograph.

All chromatograms were recorded on a Shimadzu Model R-101 recorder; peak areas were measured by a Shimadzu Chromatopac E-1A integrator.

Results and Discussion

Preliminary Uptake Studies. Initially, the total amounts of organic vapors taken up by the resins were estimated from the desorption peak area measured with the sorptograph. As listed in Table 1, the β-cyclodextrin polyurethane resin, β-HDI-P-5.5-M, gives larger uptake values for the organic vapors than the polyurethane resin containing no cyclodextrin units, BDOL-HDI-P-M, does. This result suggests that the β-cyclodextrin units in the resin interact strongly with the organic vapors.

The amount of benzene vapor taken up by each resin was compared. Porapak Q has the greatest uptake of benzene at 55 °C. On the other hand, at 150 °C Porapak Q takes up less than the resins containing β-cyclodextrin units do. The uptake amount of benzene for the β-cyclodextrin resin at 55 °C varies apparently with the diisocyanate used. The amount of benzene taken up by each β-cyclodextrin resin decreases with increasing adsorption temperature and reaches a constant, nearly equal value at 150 °C; this result strongly suggests that the β-cyclodextrin cavities in the resins take part in the adsorption of benzene molecules.

Sorption Behavior of β-Cyclodextrin Polyurethane Resins for Benzene Vapor. As one approach to the actual application of the β-cyclodextrin resins, it is of value to investigate their sorption behavior for one given organic vapor (benzene in this work) co-existing with another one. The resin was equilibrated with the 0.004% benzene–0.055% cyclohexane–nitrogen flow at 102 °C. After benzene and cyclohexane which had been taken up were desorbed for 2 h by the pure nitrogen stream at the same temperature, the desorption temperature was programmed at 3.1 °C/min to 170 °C. Figure 2

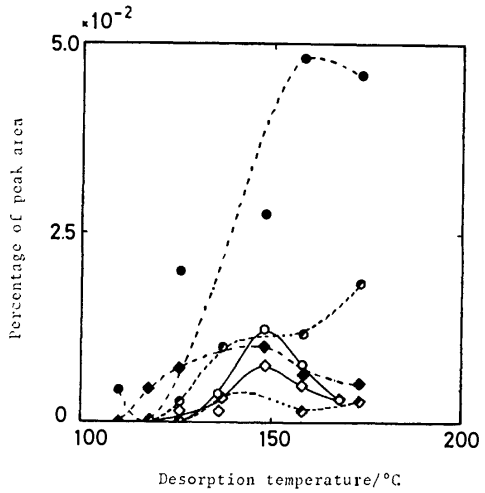

Fig. 2. Desorption of benzene and cyclohexane on β-cyclodextrin polyurethane resins.
——: β-HDI-P-5.5-A, -•-•-: β-H6XDI-P-6.0-M,
----: β-XDI-P-5.8-A.
○●◐: Benzene, ◇◆◈: cyclohexane.
0.004% benzene–0.055% cyclohexane–N_2.

shows the temperature-programmed desorption patterns thus obtained. The amount of benzene desorbed is larger than that of cyclohexane. Considering that there is a much lower concentration of benzene than of cyclohexane in the benzene–cyclohexane–nitrogen flow, we interpret these results as indicating that the β-cyclodextrin resins collect the benzene vapor much better than the cyclohexane one. β-XDI-P-5.8-A gives desorption patterns different from those on either β-HDI-P-5.5-A or β-H6XDI-P-6.0-M; this is presumably due to the lower thermal stability of β-XDI-P-5.8-A. Thermally, the β-H6XDI-P-6.0-M resin is the most stable of the three β-cyclodextrin resins. Therefore,

Table 1. Total adsorption capacities for organic vapors

Resin	mg Benzene/g Resin		mg Cyclohexane/g Resin		mg Ethyl alcohol/g Resin	
	55 °C	150 °C	55 °C	150 °C	55 °C	150 °C
β-HDI-P-5.5-M	107	30	68	40	111	48
β-H6XDI-P-6.0-M	72	32				
β-XDI-P-5.8-A	58	27				
BDOL-HDI-P-M	48	5	38	1	21	0.5
Tenax GC	59	1				
Porapak Q	213	18				

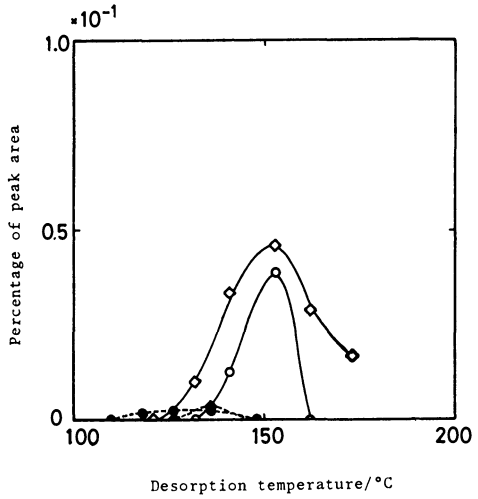

Fig. 3. Desorption of benzene and ethyl methyl ketone on β-H6XDI-P-6.0-M and Porapak Q.
——: β-H6XDI-P-6.0-M, ----: Posapak Q. ○●: Benzene, ◇◆: ethyl methyl ketone.
0.013% benzene–0.12% ethyl methyl ketone–N_2 (β-H6XDI-P-6.0-M), 0.016% benzene–0.074% ethyl methyl ketone–N_2 (Porapak Q).

β-H6XDI-P-6.0-M was investigated in further experiments.

Figure 3 shows the temperature-programmed desorption peaks of benzene and ethyl methyl ketone on both β-H6XDI-P-6.0-M and Porapak Q. β-H6XDI-P-6.0-M gives large peaks of benzene and ethyl methyl ketone. Considering the concentrations of both adsorbates, the benzene peak area is very large compared with that of ethyl methyl ketone. On the other hand, Porapak Q gives only small peaks of both adsorbates; BDOL-HDI-P-M shows no desorption peaks at all in the temperature-programmed experiments.

It is interesting to investigate whether one adsorbate on the resin is replaced by the other or not. Figure 4 clearly shows that ethyl methyl ketone on β-H6XDI-P-6.0-M is replaced by benzene. First, the 0.16% ethyl methyl ketone–nitrogen flow was passed for 1 h through the tube containing the resin to saturate the adsorption sites completely with ethyl methyl ketone; next, the 0.006% benzene–0.06% ethyl methyl ketone–nitrogen flow was passed for 3 h. A large desorption peak of benzene appears when the desorption temperature is programmed at 3.1 °C/min from 102 °C. Similarly, the 0.08% benzene–nitrogen flow was passed for 1 h and then the 0.5% benzene–0.05% ethyl methyl ketone–nitrogen flow was passed for 3 h. The desorption peak of ethyl methyl ketone is minute in comparison with that of benzene.

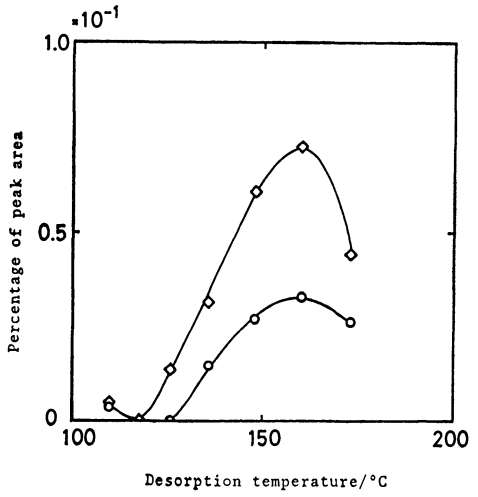

Fig. 4. Replacement of ethyl methyl ketone with benzene on β-H6XDI-P-6.0-M.
○: Benzene, ◇: ethyl methyl ketone.
Adsorption system: 0.16% ethyl methyl ketone–N_2 (1 h), 0.06% ethyl methyl ketone–0.006% benzene–N_2 (3 h).

These results strongly suggest that the β-cyclodextrin polyurethane resin is selectively adsorptive for benzene vapor. Both desorption peaks have the maxima at *ca.* 150 °C; this result supports the contention that the cyclodextrin cavities in the resin take part in the interaction with the adsorbate molecules, as described previously.[10]

Breakthrough Studies. All the experiments cited to this point were carried out with samples prepared by introducing one or two organic compounds into a dry nitrogen flow. Practical samples, however, will contain many different compounds including water. It is thus especially important to study the effect of co-existing water.

First, the 0.4% benzene–air stream containing 0.4% ethyl methyl ketone or 1.76% water as a concomitant was used to obtain the breakthrough profiles for β-H6XDI-P-6.0-M. Co-existing water or ethyl methyl ketone does not affect the breakthrough time (26 min). In the case of 0.4% ethyl methyl ketone–air stream, the breakthrough time is 66 min. It decreases to 45 min, when 0.04% benzene is added to the 0.4% ethyl methyl ketone–air stream. This result is reasonably interpreted as follows. Ethyl methyl ketone is adsorbed on the β-cyclodextrin resin by both the hydrophobic and hydrogen-bonding interactions, while benzene is taken up almost by the hydrophobic one. This is supported by the fact that BDOL-HDI-P-M interacts strongly with the compounds capable of forming hydrogen-bonding.[10] The decrease in the breakthrough time with increasing benzene concentration in the ethyl methyl ketone–air stream seems to result from the strong, selective occupation of the hydrophobic adsorption sites by benzene.

Second, the mixing vessel in Fig. 1 was replaced with a gas stripping vessel in order to perform the breakthrough experiments by a gas stripping method; this is generally a highly sensitive method for collecting volatile organic compounds in water.[11] A stream of nitrogen at 50 ml/min stripped 150 ml of sample solution at 25 °C. After the concentration of stripped organic compound in the gas coming out of the vessel reached a constant value, the sorption tube containing 2 g of a resin was connected to the stripping vessel, and the breakthrough curve was obtained by flame ionization gas chromatography. The breakthrough profiles were well-defined S-shaped curves.

Table 2 shows the breakthrough times on β-H6XDI-

Table 2. Breakthrough times (min) on β-H6XDI-P-6.0-M and amberlite XAD-7

Compound	β-H6XDI-P-6.0-M		Amberlite XAD-7	
	50 °C	100 °C	50 °C	100 °C
Methyl alcohol[a)]	32	5	7.5	0.8
Ethyl alcohol[a)]	123	17	28	3
Acetone[b)]	70	19	39	3.6
Ethyl methyl ketone[b)]	121	53	103	12
Benzene[c)]	12	10.5	72	9
Water[d)]	30	5	5	0

Concentration of solute: a) 4 ml/l. b) 1 ml/l. c) 0.1 ml/l. d) Measured by gas chromatography with a thermal conductivity detector.

P-6.0-M and Amberlite XAD-7 at sorption temperatures of 50 and 100 °C. At both temperatures, β-H6XDI-P-6.0-M gives a larger breakthrough time for each polar solute expect for benzene than XAD-7 does, while the reverse is observed for nonpolar benzene at 50 °C. The greater retention of the polar compounds on β-H6XDI-P-6.0-M presumably results from the much stronger affinity of this resin for water: the distribution of the polar compounds into the water layer retained on β-H6XDI-P-6.0-M plays an important role in their greater retention, compared with the XAD-7 resin. It is unusual that benzene breakthrough on β-H6XDI-P-6.0-M varies little with the sorption temperature in the range of 50—100 °C. Supposedly, a large amount of water on the resin surface also brings about the small breakthrough time of 12 min for benzene at 50 °C: nonpolar benzene must penetrate through the water layer to reach the hydrophobic sorption site of the resin. Amberlite XAD-7, on the other hand, is hydrophobic in nature and retains much less water than β-H6XDI-P-6.0-M does. Therefore, nonpolar benzene is taken up more strongly by the XAD-7 resin.

In summary, it is found from this preliminary work that the β-cyclodextrin polyurethane resins exhibit a strong interaction with benzene vapor in the nitrogen or air stream. Also, in the gas stripping method, the β-H6XDI-P-6.0-M resin retains the polar volatile organic compounds more greatly than Amberlite XAD-7 (used widely to collect them) does; this results indicates the possibility of using the β-cyclodextrin polyurethane resins as sorbents to collect polar volatile organic compounds.

This work was partially supported by a Grant-in-Aid for Scientific Research from the Ministry of Education, Science and Culture.

References

1) G. Holzer, H. Shanfield, A. Zlatkis, W. Bertsch, P. Juarez, H. Mayfield, and H. M. Liebich, *J. Chromatogr.*, **142**, 755 (1977).
2) W. Bertsch, R. C. Chang, and A. Zlatkis, *J. Chromatogr. Sci.*, **12**, 175 (1974).
3) P. Ciccioli, G. Bertoni, E. Brancaleoni, R. Fratarcangeli, and F. Bruner, *J. Chromatogr.*, **126**, 757 (1976).
4) R. H. Brown and C. J. Purnell, *J. Chromatogr.*, **178**, 79 (1979).
5) J. M. Daemen, W. Dankelman, and M. E. Hendriks, *J. Chromatogr. Sci.*, **13**, 79 (1975).
6) C. V. Madjar, M. F. Gonnord, F. Benchah, and G. Guiochon, *J. Chromatogr. Sci.*, **16**, 190 (1978).
7) R. Sydor and D. J. Pietrzyk, *Anal. Chem.*, **50**, 1842 (1978).
8) A. Raymond and G. Guiochon, *J. Chromatogr. Sci.*, **13**, 173 (1975).
9) L. D. Butler and M. F. Burke, *J. Chromatogr. Sci.*, **14**, 177 (1976).
10) Y. Mizobuchi, M. Tanaka, and T. Shono, *J. Chromatogr.*, **194**, 153 (1980).
11) P. K. Kuo, E. S. K. Chian, F. B. Dewalle, and J. H. Kim, *Anal. Chem.*, **49**, 1023 (1977).

The Oxidation Products of Tetracyanoferrate(II) Chelates with Optically Active 1,2-Diamines : Tetracyano(1,2-diamine)ferrate(III)s and Tetracyano(1,2-diimine)ferrate(II)s

Masafumi GOTO,* Michihiro TAKESHITA, and Tomoya SAKAI

Faculty of Pharmaceutical Sciences, Nagoya City University, Mizuho-ku, Nagoya 467

(Received January 31, 1981)

Optically active diamagnetic title complexes were oxidized with hydrogen peroxide under acidic and basic aqueous conditions. The corresponding low-spin tetracyano(diamine)ferrate(III) complexes with (*R*)-1,2-propanediamine, (1*R*,2*R*)-1,2-cyclopentanediamine, and (1*R*,2*R*)-1,2-cyclohexanediamine as diamines formed under acidic conditions and were characterized with several spectral measurements including the CD spectra. Each CD spectrum showed a moderate positive Cotton effect at *ca.* 24700 cm^{-1} and was assigned to a d-d transition. However a ligand oxidation took place, yielding tetracyano(1,2-diimine)ferrate(II) complexes under neutral and basic conditions; their electronic and ^{1}H- and ^{13}C-NMR spectra are also reported.

Diamagnetic and low-spin Fe^{II} and Fe^{III} complexes with a simple ligand system have been scarcely investigated. Tetracyanoferrate(II) chelates of 1,2-diamines are diamagnetic as a result of the strong ligand field produced by cyano groups and have been well characterized.[1,2] The diamagnetic complexes are oxidized with various oxidizing agents to yield metal-oxidized tetracyano(1,2-diamine)ferrate(III) and ligand-oxidized tetracyano(1,2-diimine)ferrate(II) depending on the reaction conditions.[1] Optically active Fe^{III} chelates can be expected to be prepared from the corresponding Fe^{II} chelates with optically active diamines, such as (*R*)-1,2-propanediamine(*R*-pn), (1*R*,2*R*)-1,2-cyclopentanediamine(*R*-cptn), and (1*R*,2*R*)-1,2-cyclohexanediamine(*R*-chxn), under acidic conditions. The chemistry of cyanoammineferrate(III)s has not been fully investigated except for pentacyanoferrate(III)s.[3] Their electronic spectra are still ambiguous because of their many allowed electronic transitions. Hexacyanoferrate(III) and several pentacyano complexes with OH_2, NH_3, $As(C_6H_5)_3$, NCS^-, and $P(C_6H_5)_3$ have been investigated with magnetic circular dichroism spectra as well as electronic spectra.[4] The CD spectra of tetracyano(*R*-diamine)ferrate(III)s will provide unique information on the nature of the electronic transitions.

The other product is ligand-oxidized tetracyano(1,2-diimine)ferrate(II); it has been characterized by visible and ^{1}H-NMR spectroscopies.[1] The diimines examined up to the present bear substituents at the nitrogen atoms(*e. g.*, 1,10-phenanthroline and *N,N'*-dimethyl-2,3-butanediimine), but this dehydrogenation yields diimines which have no substituents at the nitrogens. The dehydrogenation of amines coordinated to transition-metal ions has been reported with Cu^{II},[5] Ni^{II},[6] Ru^{II},[7] Co^{II},[8] and Fe^{II},[9] and it is generally accepted that a higher oxidation state of transition-metal ions is responsible for the reaction.[10] Tetracyano(1,2-ethanediamine)ferrate(III) undergoes a spontaneous metal reduction, yielding a mixture of ligand-oxidized and ligand-intact Fe^{II} chelates, in basic solutions.

This paper will deal with the preparation and some spectral properties of these complexes.

Experimental

Materials. 1,4-Dimethyl-1,4-diazabicyclo[2,2,2]octanediium diiodide(dimethyldabconium iodide) was prepared according to the method of Oae *et al.*[11] $Na_2[Fe(CN)_4(R\text{-pn})]\cdot 0.5NaClO_4\cdot 0.5H_2O$,[2] $Na_2[Fe(CN)_4(R\text{-cptn})]\cdot 0.5NaClO_4\cdot 0.5H_2O$,[12] and $Na_2[Fe(CN)_4(R\text{-chxn})]\cdot 0.5NaClO_4\cdot 0.5H_2O$[2] were prepared according to the methods reported previously. $Na[Fe(CN)_4(en)]\cdot 3H_2O$ and dimethyldabconium tetracyano(1,2-ethanediimine)ferrate(II) were prepared according to the method of Goedken.[1] *cis*-1,2-Cyclohexanediamine was separated from a commercially available mixture of 1,2-cyclohexanediamines(Tokyo Kasei) according to the method of Kidani and Saito.[13]

Preparation of Complexes. *Na[Fe(CN)$_4$(R-pn)]·H$_2$O.* The corresponding diamagnetic Fe^{II} chelate, $Na_2[Fe(CN)_4(R\text{-pn})]\cdot 0.5NaClO_4\cdot 0.5H_2O$ (3.5 g, 0.01 mol), was dissolved in a mixture of acetic acid (1 cm^3), ethanol (20 cm^3), and water (6 cm^3) at 0 °C. Into the mixture, 30% aqueous hydrogen peroxide (1.5 cm^3) was then stirred in small portions. The resultant mixture was filtered after 5 min at 0 °C to remove the undissolved green materials. Ethanol (20 cm^3) and ether were added to the filtrate until the solution became turbid. The mixture was then allowed to stand in a refrigerator overnight. The pale yellow crystals thus separated were collected on a filter, washed with absolute ethanol and subsequently with ether, and dried *in vacuo*. Yield, 2.3 g (84%). Found: C, 30.16; H, 4.47; N, 30.43%. Calcd for $Na[Fe(CN)_4(C_3H_{10}N_2)]\cdot H_2O$: C, 30.55; H, 5.10; N, 30.56%.

Na[Fe(CN)$_4$(R-cptn)]·2H$_2$O. In a mixture of acetic acid (1 cm^3) and ethanol (10 cm^3), $Na_2[Fe(CN)_4(R\text{-cptn})]\cdot 0.5NaClO_4\cdot 0.5H_2O$ (1.5 g, 4 mmol) was suspended: after the mixture had been cooled to 0 °C, 2 M (1 M=1 mol dm^{-3}) perchloric acid (2 cm^3) and water (1 cm^3) were added to dissolve the complex. A portion of aqueous hydrogen peroxide (30%, 0.3 cm^3) was then stirred into the mixture. To the resultant mixture, ether (3 cm^3) was added, and the mixture was filtered at 0 °C. A mixture of ethanol (10 cm^3) and ether (10 cm^3) was added to the filtrate, and the mixture was allowed to stand at −15 °C overnight. The separated crystals were collected on a filter, washed with ether, and dried *in vacuo*. Yield, 1.5 g (quantitative).

This substance was dissolved in a mixture of 2 M $HClO_4$ (0.65 cm^3) and ethanol (5.35 cm^3) at 0 °C, after which the mixture was filtered. Ether (5 cm^3) was added, and the mixture was allowed to stand overnight at −15 °C. The crystals thus separated were collected on a filter, washed with ether, and dried *in vacuo*. Yield, 160 mg (12%).

Found: C, 34.41; H, 5.31; N, 26.41%. Calcd for $Na[Fe(CN)_4(C_5H_{12}N_2)]\cdot 2H_2O$: C, 33.87; H, 5.05; N, 26.34%.

$Na[Fe(CN)_4$(R-chxn)$]\cdot 3H_2O$. Into a solution of $Na_2[Fe(CN)_4(R\text{-chxn})]\cdot 0.5NaClO_4\cdot 0.5H_2O$ (3.0 g, 7.7 mmol) in a mixture of acetic acid (3 cm³), ethanol (30 cm³), and water (3 cm³) in an ice–water bath, 15% aqueous hydrogen peroxide (6 cm³) was stirred, drop by drop, at 0 °C. A mixture of methanol (10 cm³), acetic acid (4 cm³), and ether (30 cm³) was added to the yellow mixture until the mixture became turbid. The mixture then allowed to stand at −15 °C overnight. The yellow crystals thus separated were collected on a filter, washed with ice-cold ethanol and subsequently with ether, and stored *in vacuo*. Yield, 2.0 g (74%).

These were recrystallized by adding ether to a solution of the crude product in a mixture of acetic acid, water, and ethanol (1:2:15) until the solution became turbid. This procedure was carried out at 0 °C. The pale yellow needles thus separated were collected on a filter, washed with ethanol and subsequently with ether, and dried *in vacuo*. Found: C, 34.45; H, 5.62; N, 23.60%. Calcd for $Na[Fe(CN)_4(C_6H_{14}N_2)]\cdot 3H_2O$: C, 34.04; H, 5.62; N, 23.60%.

*Sodium Tetracyano(*cis-*1,2-cyclohexanediamine)ferrate(II) Dihydrate.* A methanol solution (40 cm³) of *cis*-1,2-cyclohexanediamine(*cis*-chxn) (22.8 g, 0.2 mol) was vigorously stirred into a methanol solution (200 cm³) of iron(II) perchlorate hexahydrate (35.2 g, 0.098 mol) under nitrogen at 0 °C, followed by the addition of aqueous sodium cyanide (19.1 g, 0.39 mol) in 80 cm³ of water. The resultant yellow brown solution was concentrated to near dryness under reduced pressure below 40 °C. To the oily residue, ethanol (200 cm³) was added, and a yellow precipitate was collected on a filter, washed with ethanol and subsequently with ether, and dried *in vacuo*. Found: C, 34.20; H, 4.36; N, 23.84%. Calcd for $Na_2[Fe(CN)_4(C_6H_{14}N_2)]\cdot 2H_2O$: C, 33.72; H, 5.09; N, 23.59%.

$Na[Fe(CN)_4$(cis-chxn)$]\cdot 0.5NaClO_4\cdot H_2O$. In a mixture of concentrated $HClO_4$ (3 cm³), methanol (20 cm³), and water (4 cm³), $Na_2[Fe(CN)_4(cis\text{-chxn})]\cdot 2H_2O$ (3.9 g, 0.011 mol) was dissolved, and the mixture was cooled to 0 °C. Concentrated aqueous hydrogen peroxide (30%, 1.4 cm³) was then stirred, drop by drop, into the mixture. A mixture of 1-propanol (40 cm³) and diisopropyl ether (20 cm³) was added to the mixture. The crystals thus separated were collected on a filter. Yield, 3.9 g (70%).

The crude product was dissolved in a mixture of 2 M $HClO_4$ (3 cm³) and ethanol (20 cm³), and the undissolved materials were filtered off. A mixture of ethanol (35 cm³) and diisopropyl ether (25 cm³) was added, and the mixture was allowed to stand at −15 °C overnight. The crystals thus separated were collected on a filter, washed with ether, and dried *in vacuo*. Found: C, 31.77; H, 4.83; N, 21.55%. Calcd for $Na[Fe(CN)_4(C_6H_{14}N_2)]\cdot 0.5NaClO_4\cdot H_2O$: C, 31.91; H, 4.29; N, 22.33%.

Dimethyldabconium Tetracyano(1,2-propanediimine)ferrate(II) Trihydrate, $[C_8H_{18}N_2][Fe(CN)_4$(o-pn)$]\cdot 3H_2O$. The designations of the diimines formed by dehydrogenation are abbreviated by adding the prefix *o-* to the corresponding diamines, as is shown in Table 1 (*vide infra*). Into an aqueous solution of $Na_2[Fe(CN)_4(R\text{-pn})]\cdot 0.5NaClO_4\cdot 5H_2O$ (2.25 g, 6.5 mmol) in 10 cm³ of water, 2 M hydrogen peroxide (18 cm³) was stirred, drop by drop, at 40 °C. The resultant deep red solution was concentrated with a rotatory evaporator. A red residue was dissolved in 10 cm³ of water, and dimethyldabconium iodide (2.6 g) was added to the solution. Ethanol (200 cm³) was added until the solution became turbid, after which the mixture was allowed to stand in a refrigerator overnight. The red crystals thus separated were collected on a filter and washed with ethanol and subsequently with ether. Found: C, 42.03; H, 6.44; N, 26.69%. Calcd for $[C_8H_{18}N_2][Fe(CN)_4(C_3H_6N_2)]\cdot 3H_2O$: C, 42.26; H, 7.09; N, 26.29%.

Dimethyldabconium Tetracyano(1,2-cyclopentanediimine)ferrate(II) Hemi(sodium perchlorate), $[C_8H_{18}N_2][Fe(CN)_4$(o-cptn)$]\text{-}0.5NaClO_4$. Into an aqueous solution of $Na_2[Fe(CN)_4(R\text{-cptn})]\cdot 0.5NaClO_4\cdot 0.5H_2O$ (1.0 g, 2.7 mmol) in 10 cm³ of water, 1 M hydrogen peroxide (17 cm³) was stirred, drop by drop, at 40 °C, the pH of the mixture being kept at 10.5 by adding 1 M aqueous NaOH. The resultant intense red solution was concentrated with a rotatory evaporator. The red residue was dissolved in 4 cm³ of water, and the mixture was filtered to remove brown precipitates. To the filtrate, dimethyldabconium iodide (1.0 g) was added, and then ethanol (6 cm³) was added. The blue precipitates thus separated were removed by filtration, and another 30-cm³ portion of ethanol was added to the filtrate. The mixture was allowed to stand in a refrigerator overnight. The purple crystals thus separated were collected on a filter and washed with ethanol and subsequently with ether. Found: C, 43.88; H, 6.00; N, 24.17%. Calcd for $[C_8H_{18}N_2][Fe(CN)_4(C_5H_8N_2)]\cdot 0.5NaClO_4$: C, 44.43; H, 5.70; N, 24.39%.

Dimethyldabconium Tetracyano(1,2-cyclohexanediimine)ferrate(II) Tetrahydrate, $[C_8H_{18}N_2][Fe(CN)_4$(o-chxn)$]\cdot 4H_2O$. To an aqueous solution of $Na_2[Fe(CN)_4(R\text{-chxn})]\cdot 0.5NaClO_4\cdot 0.5H_2O$ (2.0 g, 5.06 mmol) in 10 cm³ of water, 2 M hydrogen peroxide (20 cm³) was added, drop by drop, at 48 °C. The resultant intensely red solution was concentrated with a rotatory evaporator. The red residue was dissolved in 8 cm³ of water, after which dimethyldabconium iodide (2 g) and then ethanol (18 cm³) were added. The red crystals thus separated were collected on a filter and washed with ethanol and subsequently with ether.

The crude product was dissolved in 3 cm³ of water, and a 30-cm³ portion of absolute ethanol was added. The red crystals thus separated were collected and dried *in vacuo*. Found: C, 44.63; H, 7.25; N, 23.30%. Calcd for $[C_8H_{18}N_2][Fe(CN)_4(C_6H_{10}N_2)]\cdot 4H_2O$: C, 44.63; H, 7.49; N, 22.13%.

Physical Measurements. The electronic spectra of 10^{-3} M hydrochloric acid solutions of tetracyano(diamine)ferrate(III)s and aqueous solutions of Fe^{II} complexes were recorded with a Shimadzu UV-210A spectrophotometer. The CD spectra were measured with a JASCO J-40 recording polarimeter. The ^{1}H-NMR were recorded with a JEOL JNM-MH-100 spectrometer using D_2O solutions and sodium 2,2-dimethyl-2-silapentane-5-sulfonate (DSS) as the internal standard. The ^{13}C-NMR were recorded with a JEOL FX-100 spectrometer using a D_2O solution and dioxane as the internal standard (67.4 ppm). The infrared spectra were measured with a JASCO IRA-2 spectrophotometer using Nujol mulls. The magnetic susceptibilities were measured with a Shimadzu magnetic balance.

Results and Discussion

Tetracyano(*cis*-1,2-cyclohexanediamine)ferrate(II) showed a typical electronic spectrum of tetracyano(1,2-diamine)ferrate(II) chelates:[2] $\tilde{\nu}_{max}(\varepsilon_{max})$=25400(439), 31800(*ca.* 450), 43100(8600), and 46200 cm^{-1}(9430).

Tetracyano(1,2-diamine)ferrate(III) Chelates. Diamagnetic tetracyano(1,2-diamine)ferrate(II) chelates with C-substituted 1,2-diamines, *R*-pn, *R*-cptn, *R*-chxn, and *cis*-chxn, yield two types of oxidation products with hydrogen peroxide, depending on the acidity of the reaction medium, as tetracyano(1,2-ethanediamine)-

ferrate(II).[1]

In an acidic solution, oxidation took place at the central metal ion, yielding the corresponding Fe^{III} chelates at 0 °C. The chelates with *R*-pn, *R*-cptn, and *R*-chxn were prepared with acetic acid as an acid, but that with *cis*-chxn was prepared with perchloric acid as an acid because a successive oxidation to the diimine chelate occurred with acetic acid. These were isolated as sodium salts in pale yellow crystals. These complexes tend to undergo disproportionation at room temperature with atmospheric moisture and so were kept in a refrigerator under a vacuum. The magnetic susceptibilities of the crystals were measured with a magnetic balance by means of the Faraday method at room temperature. The values of the mole magnetic moments were 2.3, 2.4, and 2.4 BM for the *R*-pn, *R*-cptn, and *R*-chxn respectively. These values are in accordance with the low-spin Fe^{III} complexes. These complexes are stable in an acidic solution. The IR spectra contained sharp C≡N stretchings at 2120 cm^{-1}, higher by 80 cm^{-1} than those of the corresponding Fe^{II} chelates.[2] The higher wave numbers of the C≡N stretching absorptions are compatible with the smaller contribution of the back donation from Fe^{III} to coordinated C≡N than from Fe^{II}. The IR absorptions are almost the same as those of the corresponding Co^{III} chelates, as is shown in Fig. 1. These complexes exhibit well-separated ^1H- and ^{13}C-NMR: preliminary results have previously reported.[14] The results are consistent with the bidentate coordination of these diamines.

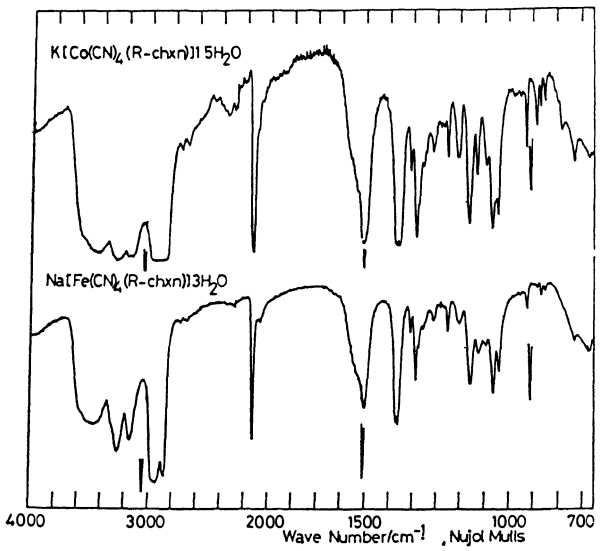

Fig. 1. Infrared spectrum of $K[Co(CN)_4(R\text{-chxn})]\cdot 1.5H_2O$[2] and $Na[Fe(CN)_4(R\text{-chxn})]\cdot 3H_2O$.

The electronic and CD spectra of these complexes in 10^{-3} M HCl are shown in Fig. 2. The CD spectra of these chelates are similar to each other and reflect the conformation of five-membered chelate rings, because the diamines may be expected to coordinate in the λ conformation. These optically active diamines, *R*-pn, *R*-cptn, and *R*-chxn, have been reported to coordinate to Fe^{II}, forming chelate rings of the λ conformation.[2,12]

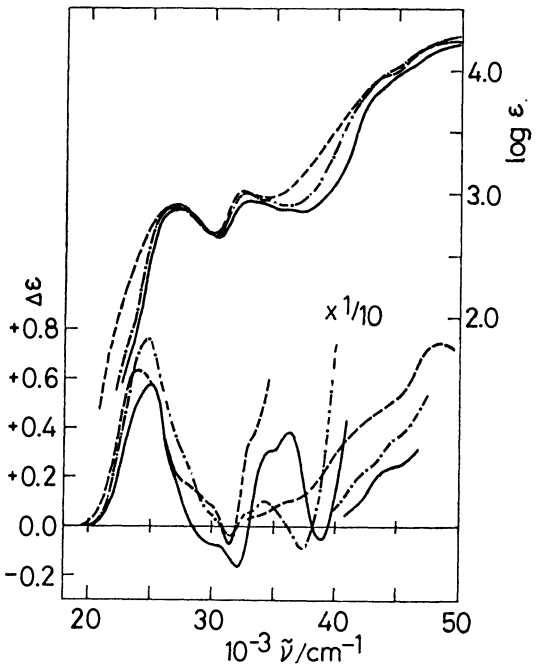

Fig. 2. Electronic and CD spectra of $[Fe(CN)_4(diamine)]^-$ in 10^{-3} M hydrochloric acid. diamine: *R*-pn, ——; *R*-cptn, – – –; *R*-chxn, -·-·-.

A large number of measurements and interpretations of the electronic spectra of $[Fe(CN)_6]^{3-}$ and several pentacyanoferrate(III) complexes have been reported.[4] The electronic configurations of these complexes are low-spin d^5, *i. e.*, $(t_{2g})^5$. The electronic transitions of these complexes are expected to arise from (i) ligand-to-metal charge transfer (LMCT), (ii) metal-to-ligand charge transfer (MLCT), and (iii) d-d transition. McCaffery and Gale assigned electronic absorptions with the aid of the magnetic circular dichroism spectra.[4] The absorptions with d-d transitions are partially hidden by LMCT bands, but are located at 29800, $E_g''(^2T_{2g})\rightarrow U_g'(^2T_{1g})$, 30200$\rightarrow E_g''(^2A_{2g})$, and 33200 $cm^{-1}\rightarrow U_g'(^2E_g)$. The remaining bands below 40000 cm^{-1} originate from LMCT, 25500($^2T_{2g}\rightarrow{}^2T_{1u}(\pi)$), 32700($\rightarrow{}^2T_{2u}(\pi)$), and 40000 cm^{-1} ($\rightarrow{}^2T_{2u}(\sigma)$). They also measured several pentacyanoferrate(III) complexes, but did not assign the d-d transitions. Furthermore, complexes with ligands which have lone pairs of relatively high energies, such as triphenylphosphine and azido, show intense absorptions in the visible region. These absorptions are assigned to the LMCT bands arising from the ligand σ bond to the t_{2g} orbital. From this band, the energy difference between the ligand lone pair and the metal t_{2g} orbital are estimated: *e. g.*, 26600 cm^{-1} for NH_3.

The electronic transitions of $Na[Fe(CN)_4(R\text{-diamine})]^-$ are composed of d-d, LMCT, and MLCT transitions. The electronic spectra show moderate bands at 27000 and 30000—35000 cm^{-1} of ε of *ca.* 800. In this region, d-d and LMCT bands are to be expected if the LMCT band of $NH_3\rightarrow t_{2g}$ retains its energy. The maxima of the electronic spectra in the visible region, 27000 cm^{-1}, seem to arise from CT bands, for the molar-absorption coefficient of 800 is large for a d-d transition. The maxima of the CD spectra are located

at *ca.* 24700 cm^{-1} and correspond to a shoulder of each absorption spectrum. The corresponding d-d transitions of $Na_2[Fe(CN)_4(R\text{-diamine})]^{2-}$ have a minor negative component at 23300 and a positive component at 26000 cm^{-1} for the *R*-pn and the *R*-chxn complexes and a positive component at 25200 cm^{-1} for the *R*-cptn complex. The magnitudes of the major CD components decreased in the order of; *R*-cptn>*R*-chxn>*R*-pn as the ligands. The analogous CD components have been observed for isoelectronic Co^{III} chelates at 25000 and 28700 cm^{-1} for *R*-pn and *R*-chxn as *R*-diamines.[2] The wave numbers and magnitudes of the positive CD components for $[Fe(CN)_4(R\text{-diamine})]^-$ suggest that this component corresponds to the d-d transitions. Two transitions are expected for the first absorption band ($^2T_{2g}\rightarrow{}^2T_{1g}$ parentage) of the $(t_{2g})^5$ configuration, but the energy difference between these bands should be smaller than for the $(t_{2g})^6$ configuration because the interelectron repulsion in the highest t_{2g} orbitals is absent for the d^5 configuration. The minor components appearing in diamagnetic Fe^{II} and Co^{III} chelates will be hidden for the d^5 configuration.

At least four CD components are observed in the region between 31000 and 38000 cm^{-1}. These CD components exhibit similar features for the *R*-pn and *R*-chxn complexes: *i. e.*, negative, positive, positive, and negative components in the order of their energies, and they resemble the MCD components of $[Fe(CN)_6]^{3-}$.[4] The probable origin of these CD components is the charge transfer from the coordinated C≡N to the t_{2g} orbital. Each CD component of the *R*-chxn chelate appears at an energy lower by 2000 cm^{-1} than the corresponding component of the *R*-pn chelate. Since the absolute energy level of coordineated C≡N is expected to be little affected by the structure of 1,2-diamine, this difference represents the difference in energy levels in the t_{2g} orbitals of these Fe^{III} chelates. The large fixed ligand, *R*-chxn, tends to lower d-orbitals. Large positive CD components dominate in the region between 33000 and 37000 cm^{-1} for the *R*-cptn chelate. Similar enhancements of positive CD components in the region of charge-transfer bands have been observed for dianionobis[(1*R*,2*R*)-1,2-cyclopentanediamine]cobalt(III) complexes;[12] they may be due to the strained structure of this ligand.

The remaining electronic bands and CD components, which appear at energies higher than 40000 cm^{-1}, have large absorption coefficients and large CD magnitudes. Two electronic bands and at least three CD components are recognized. MLCT bands are to be expected in this region. Positive CD components appear for $[Fe(CN)_4(R\text{-diamine})]^{2-}$ and $[Co(CN)_4(R\text{-diamine})]^-$ with *R*-pn and *R*-chxn. The invariance of the signs of the CD components on a change in the central metal ions suggests that these bands may be ascribed to the charge transfer from coordinated amine to e_g orbitals; the dependency of the magnitude of the CD components on the structure of 1,2-diamines supports this assignment.

Tetracyano(1,2-diimine)ferrate(II) Chelates. In a neutral or basic solution, the yellow solution of tetracyano(*R*-diamine)ferrate(II) turned an intense red on the addition of a slight excess of hydrogen peroxide at 40 to 50 °C. Tetracyano(1,2-diimine)ferrate(II)s were isolated as dimethyldabconium salts. This cation is almost the same size as the chelate anions, has a bivalent charge, and facilitates the crystallization of soluble-complex anions.[15] The structural identifications are confirmed by the electronic spectra and the ^1H- and ^{13}C-NMR spectra. Each ^1H- and ^{13}C-signal appeared in the normal region for the D_2O solution, indicating that these complexes are diamagnetic Fe^{II} complexes. The results are shown in Table 1, along with the abbreviations and structures of the 1,2-diimines.

Table 1. ^1H- and ^{13}C-NMR of $[Fe(CN)_4(1,2\text{-diimine})]^{2-}$ in D_2O and abbreviations of 1,2-diimines

1,2-Diimine	^1H-Chemical shift[a]/ppm	^{13}C-Chemical shift[b]/ppm
o-en	8.50[c]	166.8
o-pn	8.42,2.48	**1**,[d] 169.1; **2**, 175.1; **3**, 22.3
o-cptn	**2**, 2.71; **3**, 2.35	**1**, 185.6; **2**, 31.5; **3**, 25.3
o-chxn	**2**, 2.90; **3**, 1.87	**1**, 176.8; **2**, 33.8; **3**, 22.6

a) DSS=0.00 ppm. b) Dioxane=67.4 ppm. c) Ref. 1. d) The number denotes the assignment of the corresponding nucleus shown in the structure below.

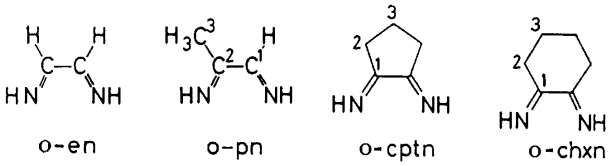

More reliable identifications can be obtained on the basis of the ^{13}C-NMR spectra. The parent material, $[Fe(CN)_4(o\text{-en})]^{2-}$, showed a single resonance at 166.8 ppm. All the 1,2-diimine chelates studied showed signals in the region between 166 and 186 ppm. These are assigned to azomethine carbons. The chemical shifts of the *o*-pn and *o*-chxn chelates showed that an alkyl substituent at the azomethine carbon cause a downfield shift of 9 ppm. The azomethine carbon of the *o*-cptn chelate resonates at a magnetic field lower by 8.8 ppm than that of the *o*-chxn chelate. The steric effect of the cyclopentane ring exerted on the chelate ring causes it to deform from a plane structure, and the conjugation of the diimine is reduced.

The electronic spectra of Fe^{II} complexes with 1,2-diimines have been studied extensively, and a characteristic intense band between 450 and 600 nm has been assigned to an electron-transfer band($t_{2g}\rightarrow$ligand).[16] The tetracyano(1,2-diimine)ferrate(II) has simple structures for the Fe^{II} 1,2-diimine chromophore. The electronic spectra of $[Fe(CN)_4(o\text{-pn})]^{2-}$, $[Fe(CN)_4(o\text{-chxn})]^{2-}$, and $[Fe(CN)_4(o\text{-cptn})]^{2-}$ in water are shown

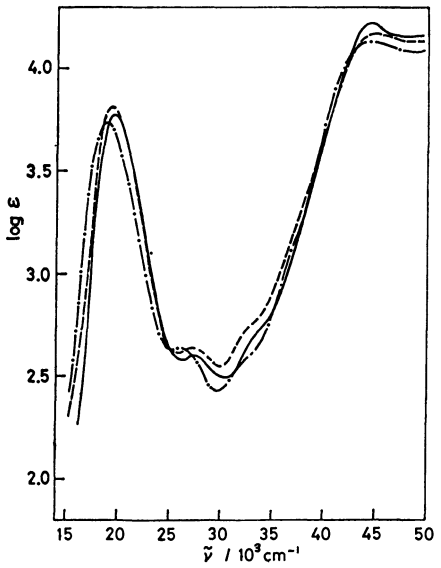

Fig. 3. Electronic spectra of $[Fe(CN)_4(diimine)]^{2-}$ in water.
Diimine: *o*-pn, ——; *o*-cptn, —·—; *o*-chxn, – – –.

in Fig. 3. A sharp absorption appeared at 19400 and at 18700 cm^{-1} for the former two and the latter complexes respectively. Weak absorptions at 30300 and 33300 cm^{-1} are assigned to d-d transitions, based on the results of tris(1,2-diimine)iron(II).[17] The first absorption band ($^1A_{1g} \rightarrow {}^1T_{1g}$) moved to an energy higher by 4700 cm^{-1} than that for $[Fe(CN)_4(diamine)]^{2-}$. This is in agreement with the difference in the spectrochemical series between 1,2-diimine and 1,2-diamine.

The present work was partially supported by a Grant-in-Aid for Scientific Research from the Ministry of Education, Science and Culture.

References

1) V. L. Goedken, *J. Chem. Soc., Chem. Commun.*, **1972**, 207.
2) M. Goto, M. Takeshita, and T. Sakai, *J. Chem. Soc., Chem. Commun.*, **1976**, 1054; *Inorg. Chem.*, **17**, 314 (1978).
3) A. G. Sharpe, "The Chemistry of Cyano Complexes of the Transition Metals," Academic Press, London (1976), p. 126.
4) R. Gale and A. J. McCaffery, *J. Chem. Soc., Dalton, Trans.*, **1973**, 1344, and the references cited therein.
5) D. C. Olson and J. Vasilevskis, *Inorg. Chem.*, **10**, 463 (1971).
6) E. K. Barefield and M. T. Mocella, *J. Am. Chem. Soc.*, **97**, 4238 (1975), and the references cited therein.
7) F. R. Keene, D. J. Salmon, and T. J. Meyer, *J. Am. Chem. Soc.*, **98**, 1884 (1976), and the references cited therein.
8) S. C. Tang and R. H. Holm, *J. Am. Chem. Soc.*, **97**, 3359 (1975).
9) V. L. Goedken and D. H. Busch, *J. Am. Chem. Soc.*, **94**, 7355 (1971).
10) C. J. Hipp and D. H. Busch, "Coordination Chemistry," American Chemical Society, Washington, D. C. (1978), Vol. 2, p. 435.
11) S. Oae, B. Hovarth, C. Zalut, and R. Harris, *J. Org. Chem.*, **24**, 1348 (1959).
12) M. Goto, M. Takeshita, and T. Sakai, *Bull. Chem. Soc. Jpn.*, **52**, 2589 (1979).
13) R. Saito and Y. Kidani, *Chem. Lett.*, **1976**, 123.
14) M. Goto, M. Takeshita, and T. Sakai, *Chem. Lett.*, **1980**, 1081.
15) G. G. Christoph and V. L. Goedken, *J. Am. Chem. Soc.*, **95**, 3869 (1973).
16) P. Krumholz, *Struct. Bonding*, **9**, 139 (1971).
17) T. Ito and N. Tanaka, *J. Inorg. Nucl. Chem.*, **32**, 155 (1970).

Kinetics of the Oxidation of Ethylenediaminetetraacetato and *N*-(2-Hydroxyethyl)ethylenediamine-*N*,*N*′,*N*′-triacetato Complexes of Cobalt(II) by Hydrogen Peroxide in Aqueous Acidic Medium

Pradyot BANERJEE* and Mahesh P. PUJARI

Department of Inorganic Chemistry, Indian Association for the Cultivation of Science, Jadavpur, Calcutta-700 032, India

(Received August 15, 1980)

Kinetics of the oxidation of Co(II) complexes, $Co(edta)^{2-}$ and $Co(hedta)^{-}$ [H_4edta=ethylenediaminetetraacetic acid and H_3hedta=*N*-(2-hydroxyethyl)ethylenediamine-*N*,*N*′,*N*′-triacetic acid] have been studied in aqueous acidic medium (pH 3.6—4.8) at 30—60 °C. The reactions were shown to exhibit second-order kinetics, first-order in each of the reactants. In the pH range studied, the rates of reaction showed inverse $[H^+]$ dependence which could be accounted for in terms of the acid-base equilibrium $H_2O_2 \overset{K_a}{\rightleftharpoons} HO_2^- + H^+$. Applying the limiting conditions $[H^+] \gg K_a$, $[H_2O_2] \gg [HO_2^-]$, the rate-law is given by $d[Co^{III}\text{-}L]/dt = 2\{k_{H_2O_2} + k_{HO_2^-} K_a [H^+]^{-1}\} [Co^{II}\text{-}L] [H_2O_2]$ where L denotes the general form of the ligand in either case. At 30 °C (*I*, 0.5 mol dm^{-3}), values obtained are $k_{H_2O_2} = (5.6 \pm 0.3) \times 10^{-5}$ mol^{-1} dm^3 s^{-1}, $k_{HO_2^-} = (5.4 \pm 0.3) \times 10^2$ mol^{-1} dm^3 s^{-1} for the $Co(edta)^{2-}$ complex and $k_{H_2O_2} = (4.5 \pm 0.4) \times 10^{-5}$ mol^{-1} dm^3 s^{-1}, $k_{HO_2^-} = (5.1 \pm 0.5) \times 10^2$ mol^{-1} dm^3 s^{-1} for the $Co(hedta)^{-}$ complex. The corresponding activation parameters are $\Delta H^* = (71 \pm 8)$ kJ mol^{-1}, $\Delta S^* = -(92 \pm 23)$ J K^{-1} mol^{-1} ($Co(edta)^{2-}$ system) and $\Delta H^* = (89 \pm 2)$ kJ mol^{-1} and $\Delta S^* = -(36 \pm 4)$ J K^{-1} mol^{-1} ($Co(hedta)^{-}$ system).

Redox reactions of hydrogen peroxide have been studied earlier by a number of workers.[1] In view of the resemblance of hydrogen peroxide reactions with the biologically relevant reactions of catalase and peroxidase,[2,3] peroxide reactions are of topical interest. The present kinetic study of the oxidation reactions of $Co^{II}(edta)^{2-}$ and $Co^{II}(hedta)^{-}$[H_4edta= ethylenediaminetetraacetic acid and H_3hedta=*N*-(2-hydroxyethyl)ethylenediamine-*N*,*N*′,*N*′-triacetic acid] with hydrogen peroxide was carried out because of the general interest in redox reactions of hydrogen peroxide, and also due to the fact that marked differences in the reactivity between various coordination complexes with hydrogen peroxide are generally observed.

Experimental

Materials. The Co^{II}–edta solution was prepared by adding a little excess (≈10%) of the requisite amount of Na_2H_2edta to the Co(II) solution. Preparation of Co^{II}–hedta and buffers has been described elsewhere.[4] Stabilizer-free hydrogen peroxide (BDH) was distilled under vacuum, and its concentration was checked by titration with standard $KMnO_4$. Ionic strength of the solutions were adjusted with KNO_3. All chemicals were of reagent grade.

Measurements. pH measurements were done with a Beckman digital pH meter (4500) and a Pye-Unicam recording spectrophotometer (SP8-150) was used for the measurements of absorption spectra. Kinetics were followed on a Hilger Uvispek machine as mentioned earlier.[4]

Results

Kinetics of the Oxidation of Co^{II}–edta and Co^{II}–hedta with H_2O_2. When aqueous solutions of the Co(II) complexes were mixed with that of hydrogen peroxide, intense coloration developed slowly. No rapid reaction as revealed by spectral features was observed.

The stoichiometry of the reactions corresponding to the slow change was determined as follows. Solutions containing the Co(II) complexes of concentration greater than twice the concentration of hydrogen peroxide (in each case) were kept at 50 °C for 24 h, and the amounts of Co(III) product formed were estimated from the ε_{max} values at 380 and 535 nm for the Co^{III}–edta complex, and at 380 and 550 nm for Co^{III}–hedta complex. One mole of the oxidant was consumed per two moles of the Co(II) complexes. Under our experimental conditions (pH 3.6—4.8), Co(III) complexes are formed quantitatively. Spectral data reveal that the product of oxidation for the Co^{II}–hedta complex is not the sexidentate species Co(hedta), but the quinquedentate species, $Co(hedta)H_2O$. Earlier studies[4] carried out by us on the oxidation of Co^{II}–hedta by peroxodisulfate ion show the formation of the identical species. Sulfab[5] also claims the formation of the quinquedentate species in course of the oxidation studies of Co^{II}–hedta with periodate in the pH range 4.0—4.8. Kinetics of both the reaction systems were studied at 30—60 °C using large excess of hydrogen peroxide over the Co(II) complexes. The conventional first-order plots log $(A_\infty - A_t)$ *vs.* time(t) are linear for at least three half-lives of the reactions. This shows that the oxidation reactions are first-order dependent on the Co(II) complex concentration. Plots of k_{obsd} *vs.* $[H_2O_2]$ gave good straight lines passing through zero. This shows that the reactions are also first-order with respect to the oxidant (Fig. 1). The rate-law for the oxidation of Co^{II}–edta and Co^{II}–hedta by H_2O_2 is thus represented by Eq. 1:

$$\frac{d[Co^{III}\text{-}L]}{dt} = 2k[Co^{II}\text{-}L][H_2O_2], \quad (1)$$

where L is the abbreviated form of the ligand in each case (the charges for the complexes have been omitted for brevity) and k is the second-order rate constant. Values of k determined from the slopes of plots of the type shown in Fig. 1 for both the systems are shown in Table 1. ΔH^* and ΔS^* values obtained from least-squares fit to Eyring equation are also shown in Table 1.

The effect of pH on the redox reactions was also

investigated in the range 3.6—4.8 (at a fixed peroxide concentration). Both the complexes exhibited an inverse $[H^+]$ dependence which indicates the occurrence of an acid-base equilibrium. It is well-known that hydrogen peroxide is a weak acid, dissociation of which is governed by an equilibrium of the type,

$$H_2O_2 \overset{K_a}{\rightleftharpoons} HO_2^- + H^+. \quad (2)$$

($K_a = 2.6\times10^{-12}$ mol dm^{-3} at 30 °C[6])

Under the present conditions of kinetic study where $[H^+] \gg K_a$, the predominant reacting species is obviously molecular hydrogen peroxide ($[HO_2^-] \ll [H_2O_2]$). The second-order rate constant (defined by $k_{obsd}/2[H_2O_2]$) is therefore given by:

$$k = k_{H_2O_2} + k_{HO_2^-}K_a[H^+]^{-1}, \quad (3)$$

where $k_{H_2O_2}$ and $k_{HO_2^-}$ denote the rate contributions due to hydrogen peroxide and hydrogen peroxide ion respectively. Values of $k_{H_2O_2}$ and $k_{HO_2^-}$ can be extracted from plots of k *vs.* $K_a[H^+]^{-1}$. Such plots (at 30 °C) gave excellent linearity with slopes and intercepts (Fig. 2), and the computed values are listed in Table 2. The reactivity of HO_2^- is $\approx 10^7$ times

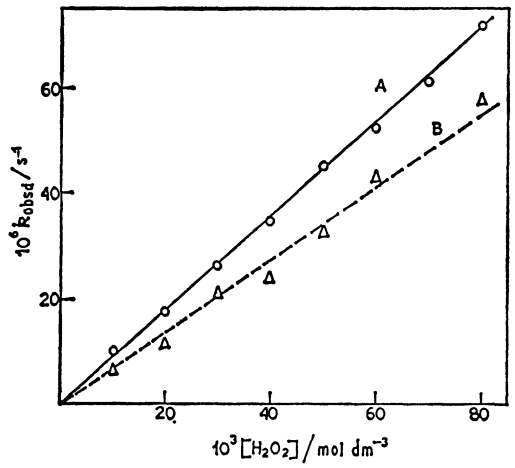

Fig. 1. k_{obsd} *vs.* $[H_2O_2]$ plot at 50 °C.
[Complex]: 0.001 mol dm^{-3}, I: 0.5 mol dm^{-3}, pH: 4.0. A: Co^{II}–edta (○), B: Co^{II}–hedta (△).

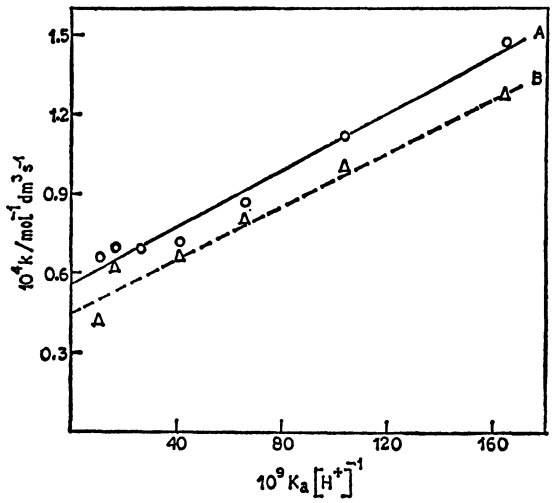

Fig. 2. Plot of k *vs.* $K_a[H^+]^{-1}$ at 30 °C.
[Complex]: 0.001 mol dm^{-3}, $[H_2O_2]$: 0.08 mol dm^{-3}, I: 0.5 mol dm^{-3}. A: Co^{II}–edta (○), B: Co^{II}–hedta (△).

Table 1. Rate constants[a] and activation parameters for the oxidation of Co^{II}–edta and Co^{II}–hedta with H_2O_2

Complex ion[b]	Temp/°C[c]	k / 10^{-4} mol^{-1} dm^3 s^{-1}	ΔH^* / kJ mol^{-1}	ΔS^* / J K^{-1} mol^{-1}
$Co^{II}(edta)^{2-}$	40	1.61±0.05	71±8	−92±23
	50	4.48±0.1		
		4.45±0.28[d]		
	60	8.74±0.26		
$Co^{II}(hedta)^-$	40	1.15±0.01	89±2	−36± 4
	50	3.40±0.3		
		4·08±0.06[d]		
	60	9.53±0.25		

a) pH, 4.0 (NaOAc+HOAc); I, 0.5 mol dm^{-3} (KNO_3+NaOAc). b) Kinetics were followed at 535 nm for the $Co^{II}(edta)^{2-}$ complex. For $Co^{II}(hedta)^-$, these were measured at 550 nm. For the evaluation of k, six to eight sets of experiments at various hydrogen peroxide concentrations were carried out. The k_{obsd} value for each set is again obtained as the average of two or three repetition which were within ±3%. c) Temperature control was within ±0.1 °C in the thermostatic bath. d) pH, 4.0; I, 1.0 mol dm^{-3}.

Table 2. Kinetic parameters[a] obtained from pH variation studies on the oxidation of $Co^{II}(edta)^{2-}$ and $Co^{II}(hedta)^-$ by hydrogen peroxide

Complex ion	$k_{H_2O_2}$ / 10^{-5} mol^{-1} dm^3 s^{-1}	$k_{HO_2^-}$ / 10^2 mol^{-1} dm^3 s^{-1}	$k_{HO_2^-}/k_{H_2O_2}$
$Co(edta)^{2-}$	5.6±0.3	5.4±0.3	9.6×10^6
$Co(hedta)^-$	4.5±0.4	5.1±0.5	11.3×10^6

a) Temp, 30 °C; I, 0.5 mol dm^{-3}; $[H_2O_2]$, 0.08 mol dm^{-3}. Values have been obtained by linear regression analysis of the data and errors shown are standard deviations.

higher than that of H_2O_2 in either case.

Discussion

In most of the reactions of hydrogen peroxide studied earlier one-electron oxidation and formation of radicals are observed.[7] On the basis of our experimental data, it is quite reasonable to believe that the present reaction systems follow the general scheme (Eqs. 4—6) in which H_2O_2 and HO_2^- are both involved in bimolecular rate-determining steps with $Co^{II}L$,

$$Co^{II}L + H_2O_2 \xrightarrow[k_{H_2O_2}]{\text{slow}} Co^{III}L + OH^- + OH\cdot, \quad (4)$$

$$Co^{II}L + OH\cdot \xrightarrow{\text{fast}} Co^{III}L + OH^-, \quad (5)$$

$$Co^{II}L + HO_2^- \xrightarrow{k_{HO_2^-}} \text{Products}. \quad (6)$$

The free radical mechanism, namely (4)—(5) is well supported by experimental evidences gathered over the last few years[8-10] (specially using the ESR technique[1]). The electron transfer step expressed in Eq. 6 could be followed by a precursor equilibrium between the substrate and HO_2^-. The criterion for such an equilibrium under the present conditions must be that it is significantly small. Furthermore, the equilibrium must be obtained fairly rapidly compared to the intramolecular electron transfer step, else saturation of the pseudo-first-order rate constant would have been observed at high concentration of hydrogen peroxide. Sutin[11] has also put forward evidence for an HO_2^- path in course of kinetic studies of the reaction of chromium(II) cyanide complexes with hydrogen peroxide in aqueous solution. The rate-determining intramolecular electron transfer is preceded by an association step as:

$$Cr(CN)_5H_2O^{3-} + HO_2^- \overset{K_a}{\rightleftharpoons} [\text{Complex}]^{3-} + CN^-, \quad (7)$$

$$[\text{Complex}]^{3-} \xrightarrow{k} \text{Products}. \quad (8)$$

Yalman[12] has studied the electron transfer reaction of Co^{II}–edta with hydrogen peroxide in the pH range 6.5—8.5 by manometric, spectrophotometric, and polarographic techniques. A peroxodicobalt(III, III) intermediate, (edta)CoOOCo(edta)$^{4-}$ having an intense band in the ultraviolet region is claimed to be formed, the formation of which is supported by polarographic measurements. In the present study where the pH has been kept below 4.8, no spectral evidence could be gathered for the formation of any intermediate species. However, our earlier studies[4] on the electron transfer reaction of Co^{II}–hedta with peroxodisulfate ion present the opportunity for detection of an intermediate which is believed to be a mononuclear Co^{III} complex containing the oxidant (in part) in the inner-sphere.

The reactivity of the two complexes towards peroxide oxidation is more or less the same (the Co^{II}–edta complex reacting little faster than the Co^{II}–hedta complex). However, a fairly large difference in the entropy of activation (Table 1) is found for the two reaction systems which may originate from the difference in charge on the Co(II) complexes. Positively charged complexes reacting with HO_2^- are expected to have the least negative entropies of activation due to charge neutralization in the transition state leading to desolvation. Neutral and negatively charged complexes will have more negative entropies because of developing charge in the transition state.[13] The activation energies for these reactions are considerably lower than the value of 140 kJ required for the symmetrical fission of the peroxide bond[1] and may be rationalized as a stabilization of the activated complexes caused by partial transfer of electrons from the metal ion to a 'generating' hydroxyl radical ion.

References

1) J. O. Edwards, "Peroxide Reaction Mechanisms," Interscience, New York (1961).
2) L. E. Bennett, "Progress in Inorganic Chemistry," ed by S. J. Lippard, Interscience, New York (1973), Vol. 18, p. 1.
3) S. B. Brown, P. Jones, and A. Suggett, "Progress in Inorganic Chemistry," ed by J. O. Edwards, Interscience, New York (1970), Vol. 13, p. 159.
4) P. Banerjee and M. P. Pujari, *Transition Met. Chem.*, **6**, 47 (1981).
5) A. A. A. Khaleq and Y. Sulfab, *Proc. 2nd Int. Symp. on the Mechanism of Reactions in Solution*, University of Kent, (1979), p. 283.
6) S. S. Mohammad and T. N. Rao, *J. Chem. Soc.*, **1957**, 1077.
7) P. B. Chock, R. B. K. Dewar, J. Halpern, and L-Y. Wong, *J. Am. Chem. Soc.*, **91**, 82 (1969).
8) L. B. Anderson and R. A. Plane, *Inorg. Chem.*, **3**, 1470 (1964).
9) G. Czapski, *J. Phys. Chem.*, **75**, 2957 (1971).
10) G. Czapski, A. Samuni, and D. Meisel, *J. Phys. Chem.*, **75**, 3271 (1971).
11) G. Davies, N. Sutin, and K. D. Watkins, *J. Am. Chem. Soc.*, **92**, 1892 (1970).
12) R. G. Yalman, *J. Phys. Chem.*, **65**, 556 (1961).
13) R. W. Hay and P. Banerjee, *J. Inorg. Biochem.*, **14**, 147 (1981).

Circular Dichroism of Chromium(III) Complexes. VI. Preparation, Optical Resolution, and Circular Dichroism Spectra of (Amino acidato)bis(ethylenediamine)chromium(III) Complexes

Sumio KAIZAKI* and Mieko ITO

Department of Chemistry, Faculty of Science, Nara Women's University, Nara 630

(Received November 7, 1980)

Three (amino acidato)bis(ethylenediamine)chromium(III) complexes were prepared and resolved into their optically active isomers, their absorption and circular dichroism spectra being measured in the spin-forbidden and spin-allowed d-d transition regions. The amino acids used were glycine, L-alanine, and L-phenylalanine, the latter two yielding pairs of diastereomeric, not enantiomeric, isomers in their complexes. The configurational and vicinal CD curves were obtained from the observed CD of each pair of diastereomers. The additivity of configurational and vicinal contributions to the optical activity in the whole region of the d-d transitions was substantiated. The configurational and vicinal CD peaks in the spin-forbidden band region were assigned in connection with those in the first spin-allowed band region.

In contrast to the large number of corresponding Co(III) complexes, only a limited number of Cr(III) complexes containing optically active amino acid chelates are known.[1-3] No complex such as $[Cr(am)(N)_4]^{2+}$ (am=amino acid anion) has been prepared, but this type of Cr(III) complex is fundamental for spectroscopic and stereochemical studies on (amino acidato) chromium(III) complexes as for analogous Co(III) complexes on the basis of their chiro-optical spectra.[4-7] With use of two ethylenediamines as $(N)_4$ ligands, circular dichroism(CD) spectra of the complexes with optically active amino acids might be separated into the configurational contribution due to the chiral arrangement of three chelate rings around a central Cr(III) ion and the vicinal one due to the chirality around optically active amino acidato ligands as in Co(III) complexes.[5-7] For such Cr(III) complexes, the vicinal CD curves in the spin-forbidden transitions might reveal the split components of the excited states as found for the CD in the first band region of Co(III) complexes.[5-7] The electronic doublet states would be clarified for the Cr(III) complexes of the present type as has been revealed for the so-called praseo type complexes[8] and in more detail than for the tris-chelate complexes.[9]

This paper deals with the preparation and optical resolution of $[Cr(am)(en)_2]^{2+}$, where am refers to glycine anion(gly), L-alanine anion(L-ala), and L-phenylalanine anion(L-phala), and with their absorption and CD spectra in the d-d transition region. The absolute configuration and additivity of the configurational and vicinal CD curves of these complexes are discussed. The configurational and vicinal CD peaks in the spin-forbidden transition region are elucidated in relation with those in the first spin-allowed transition region by means of the relations[8-9] between the rotational strengths for the spin-forbidden transitions and those for the first spin-allowed transitions.

Experimental

Preparation of the Complexes. *1)* *$[Cr(gly)(en)_2]Cl_2 \cdot 0.5H_2O$*: A solution of 1.0 g of *cis*-$[CrCl_2(en)_2]Cl \cdot H_2O$ in 4 cm^3 of water was heated at 80 °C. To the resulting red solution in which the species may be *cis*-$[CrCl(en)_2(H_2O)]^{2+}$ was added 0.3 g of glycine at room temperature. After the pH of the mixture had been adjusted to 8—9 with a 2 mol dm^{-3} potassium hydroxide solution, the solution was warmed at 35 °C for a few hours; when the coloration of the solution turned reddish orange. To this was added a large excess of potassium iodide. On cooling the solution in an ice bath, orange powder was precipitated. This was filtered and washed with methanol and ether. Another crop of the crude complex was obtained from the filtrate by adding methanol. The crude product was purified as follows. An aqueous solution of the obtained powder was poured into an SP-Sephadex C-25 column (ϕ3.5 cm×30 cm), and the adsorbed complex was eluted with a 0.2 mol dm^{-3} sodium chloride solution at 5 °C in the dark. A yellow orange eluate showing absorption maxima at 478 nm and 359.5 nm was collected. The eluate was reloaded on a short column of SP-Sephadex C-25 after dilution with cold water at 5 °C, and the adsorbed complex on the Sephadex was washed thoroughly with a 0.05 mol dm^{-3} lithium chloride solution. After elution of the adsorbed complex with a 3 mol dm^{-3} lithium chloride solution, the concentrated solution obtained was evaporated to dryness by means of freeze drying. The orange powder contaminated with a large amount of lithium chloride was dissolved completely in a small amount of ethanol. A large excess of ether was added, yellow orange powder being obtained. This was filtered and washed thoroughly with ethanol. Pure chloride was obtained by recrystallization from cold water and ethanol. Found: C, 20.94; H, 6.74; N, 20.60%. Calcd for $[Cr(gly)(en)_2]Cl_2 \cdot 0.5H_2O$: C, 20.75; H, 6.67; N, 20.57%.

2) *$(+)_{589}$- and $(-)_{589}$-$[Cr(gly)(en)_2]^{2+}$*: An aqueous solution of $[Cr(gly)(en)_2]Cl_2 \cdot 0.5H_2O$ was adsorbed on an SP-Sephadex C-25 column, and the charged complex was eluted with a 0.1 mol dm^{-3} aqueous solution of sodium $(+)_{589}$-tartratoantimonate(III) at a rate of 0.3 cm^3/min at 5 °C in the dark. Equal amounts of two bands, $(+)_{589}$- and $(-)_{589}$-isomers, were eluted separately. Each eluate was reloaded on a short column of SP-Sephadex C-25 after dilution with cold water. Each adsorbed complex was eluted with a 3 mol dm^{-3} lithium chloride solution, the eluates being stored for CD measurements. Isolation of these complexes was unsuccessful. Based on the quantitative analysis of the Cr^{3+} content in these solutions, the absorption spectra of the concentrated solutions coincided in position and intensity with those of the unresolved $[Cr(gly)(en)_2]Cl_2 \cdot 0.5H_2O$ in water.

3) *$(\Delta\Lambda)$-$[Cr(L\text{-}ala)(en)_2]^{2+}$*: This complex ion was prepared by the same method as for the glycinato complex in *1)*. However, it was not isolated owing to decomposition during the course of isolation.

4) $(+)_{589}$- *and* $(-)_{589}$-*[Cr(L-ala)(en)$_2$]$^{2+}$*: After the reaction of *cis*-[$CrCl_2(en)_2$]$Cl\cdot H_2O$ with L-alanine in water as described in *1)*, the mixture was poured into an SP-Sephadex C-25 column (ϕ4 cm×50 cm). The adsorbed band was eluted with a 0.2 mol dm^{-3} sodium chloride solution at 5 °C in the dark. Of six separate bands, the fourth eluted yellow orange band showed a similar absorption spectrum to that of [Cr(gly)$(en)_2$]$^{2+}$. The dilute aqueous solution of this eluate was resorbed on a column of SP-Sephadex C-25 and the adsorbed complex was resolved into diastereomers by elution with a 0.1 mol dm^{-3} aqueous solution of sodium $(+)_{589}$-tartratoantimonato(III) at a rate of 0.3 cm^3/min at 5 °C in the dark. Two bands were separated: the first and the second bands being $(+)_{589}$- and $(-)_{589}$-diastereomers, respectively. $(+)_{589}$- and $(-)_{589}$-isomers are found to be formed in the ratio 48:52. Each eluate was concentrated by the same procedure as given in *2)*.

5) $(\Delta\Lambda)$-*[Cr(L-phala)(en)$_2$]I_2*: The iodide of this complex was obtained as needle-like crystals by the same method as for the glycinato complex. Recrystallization was carried out from a small amount of water and methanol. Found: C, 26.28; H, 4.52; N, 11.73%. Calcd for [Cr(L-phala)-$(en)_2]I_2$: C, 26.46; H, 4.44; N, 11.87%.

6) $(+)_{589}$- *and* $(-)_{589}$-*[Cr(L-phala)(en)$_2$]$^{2+}$*: Two diastereomers of the L-phenylalaninato complex were obtained by SP-Sephadex column chromatography of the mixture after the reaction as in the case of the L-alaninato complexes in *4)*. The faster and slower eluates of two separate bands were $(+)_{589}$- and $(-)_{589}$-isomers, respectively, their formation ratio being *ca.* 3 : 2.

Measurements. Absorption spectra were obtained on a Shimadzu UV-200S spectrophotometer, and CD spectra on a JASCO MOE-1 spectropolarimeter. The quantitative absorption spectra of the unresolved glycinato and L-phenylalaninato complexes were measured on the basis of their elemental analytical results. The molar absorption coefficients of the L-alaninato complex were determined on the basis of quantitative analysis of the Cr^{3+} content in sample solutions, since this complex could not be isolated. The values of the molar absorption coefficients (ε=86.06 mol^{-1} dm^3 cm^{-1} at 478 nm and ε=71.68 mol^{-1} dm^3 cm^{-1} at 359.5 nm) obtained by this method seem reasonable in comparison with those of the other amino acidato complexes: ε=87.05 at 478 nm and 76.65 mol^{-1} dm^3 cm^{-1} at 359.5 nm for the glycinato complex, and ε=86.72 at 478 nm and 72.42 mol^{-1} dm^3 cm^{-1} at 359.5 nm for the L-phenylalaninato complex. The CD measurements of the present optically active complexes were performed by using the sample solutions in *ca.* 2 mol dm^{-3} lithium chloride solutions in which the Cr^{3+} content was determined by quantitative analysis and/or the molar absorption coefficients of the first absorption band. In the latter case, it is assumed that each diastereomer of the L-alaninato and L-phenylalaninato complexes has equal molar absorption coefficients, since those of diastereomers of [Co$(ox)_2$(L-ala)]$^{2-}$, [7] [Co$(mal)_2$(L-phala)]$^{2-}$, [7] and [Cr-(L-ala)$(en)_2]^{2+}$ [5] have been found to be equal.

Chemical Analysis. Chromium content was determined by spectrophotometric analysis of CrO_4^{2-} at 372 nm after oxidation of the complexes with hot alkaline hydrogen peroxide.

Results and Discussion

Absorption and Circular Dichroism Spectra. The first and second absorption band maxima of the three amino acidato complexes coincide with each other (Fig. 1). The positions agree with those predicted from the rule of average environment[10] or Yamatera's rule[11] by using the first and second band positions for $[Cr(en)_3]^{3+}$ and $[Cr(ox)_3]^{3-}$.

The CD spectra of the complexes give only one component in the first band region and two components with opposite signs in the second band region (Figs. 1 and 2). The CD intensities of these complexes are comparable to those of tris-chelate

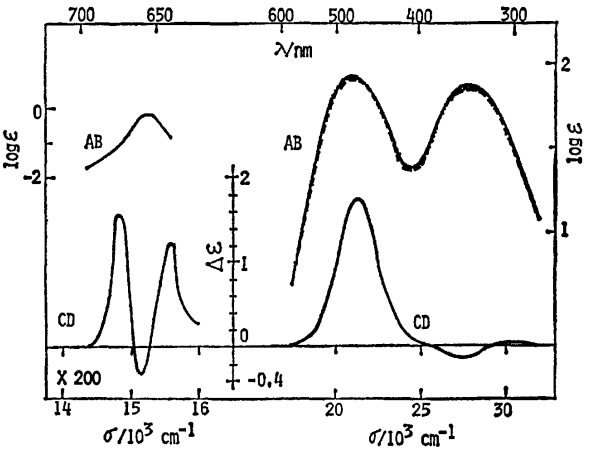

Fig. 1. Absorption curves (upper) of [Cr(gly)$(en)_2]^{2+}$ (——), [Cr(L-ala)$(en)_2]^{2+}$ (----), and [Cr(L-phala)-$(en)_2]^{2+}$ (·····); observed CD curves (lower) of $(+)_{589}$-[Cr(gly)$(en)_2]^{2+}$.

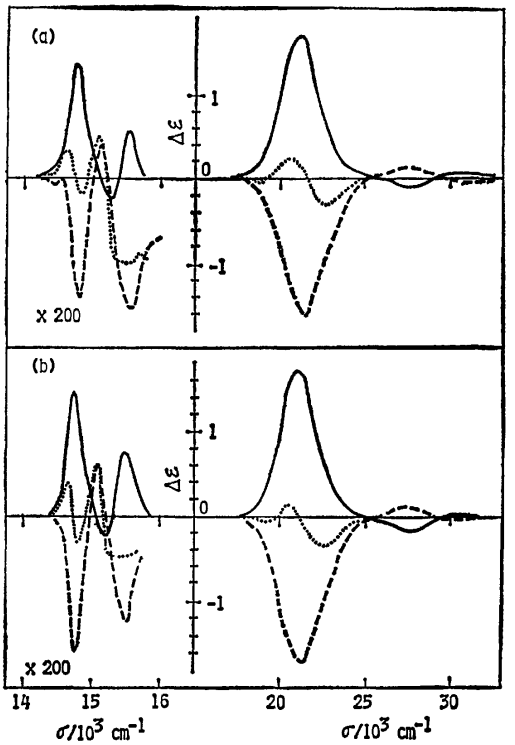

Fig. 2. (a) CD curves of $(+)_{589}$-[Cr(L-ala)$(en)_2]^{2+}$ (——) and $(-)_{589}$-[Cr(L-ala)$(en)_2]^{2+}$ (----), and calculated vicinal CD curve ($2\Delta\varepsilon$(L)) of [Cr(L-ala)-$(en)_2]^{2+}$ (·····). (b) CD curves of $(+)_{589}$-[Cr(L-phala)$(en)_2]^{2+}$ (——) and $(-)_{589}$-[Cr(L-phala)$(en)_2]^{2+}$ (----), and calculated vicinal CD curve ($2\Delta\varepsilon$(L)) of [Cr(L-phala)$(en)_2]^{2+}$ (·····).

complexes such as $(+)_{589}$-$[Cr(en)_3]^{3+}$ and $(+)_{589}$-$[Cr(ox)(en)_2]^{+}$.[9] This confirms the chelation of amino acidato ligands in the complexes. Since the faster eluted $(+)_{589}$-isomers of these complexes exhibit a positive CD band in the first band region, they are assigned to a Λ absolute configuration. Thus, the slower eluted $(-)_{589}$-isomers with a negative CD band in this region take a Λ configuration. The elution order is the same as that found for the corresponding Co(III) complex with glycine anion.[12] A preliminary experiment of the optical resolution for the trimethylenediamine complex, $[Cr(gly)(tn)_2]^{2+}$, indicates that the faster eluted band on SP-Sephadex column chromatography exhibits a negative CD band in the first band region and is assigned to a Λ configuration. The inversion of the elution order for the ethylenediamine and trimethylenediamine complexes is also found for the corresponding Co(III) complexes.[12b]

It has been revealed for several Co(III) complexes[5-7] that the configurational and vicinal contributions are separable and almost additive on the CD curves in the spin-allowed d-d absorption band region. However, there is no application of the additivity rule to the CD of chromium(III) complexes in both the spin-forbidden and spin-allowed band regions. The vicinal CD due to one coordinated optically active amino acidato ligand, $\Delta\varepsilon$(L), and the configurational CD, $\Delta\varepsilon(\Lambda)$ or $\Delta\varepsilon(\Lambda)$, have been calculated by applying the following relations to the observed CD curves, $\Delta\varepsilon(\Lambda_L)$ and $\Delta\varepsilon(\Lambda_L)$, of Λ- and Λ-$[Cr(am)(en)_2]^{2+}$.

$$\Delta\varepsilon(\text{L}) = 1/2\{\Delta\varepsilon(\Lambda_L) + \Delta\varepsilon(\Lambda_L)\}$$
$$\Delta\varepsilon(\Lambda) = 1/2\{\Delta\varepsilon(\Lambda_L) - \Delta\varepsilon(\Lambda_L)\}$$
$$\Delta\varepsilon(\Lambda) + \Delta\varepsilon(\Lambda) = 0$$

The calculated configurational curves from the CD data of each diastereomer of the L-alaninato and L-phenylalaninato complexes agree with the observed curve of the glycinato complex, $(+)_{589}$-$[Cr(gly)(en)_2]^{2+}$, in the lower frequency spin-forbidden band region as well as in the first and second spin-allowed band regions (Fig. 3). The configurational CD in the spin-forbidden band region is similar in appearance to that of $(+)_{589}$-$[Cr(en)_3]^{3+}$,[9] but the half-bandwidths of the complexes are approximately twice as wide as that of $(+)_{589}$-$[Cr(en)_3]^{3+}$.[9] Assuming pseudo D_3 symmetry for the present complexes as for $[Cr(ox)(en)_2]^{+}$,[9] one positive configurational CD component in the first spin-allowed band region is due to the $^4E(^4T_{2g})$ state. Then, three CD peaks of the configurational curves in the spin-forbidden band region are assigned to the $^2E(^2E_g)$, $^2A_2(^2T_{1g})$, and $^2E(^2T_{1g})$ states from the lower frequency side according to the theoretical relation of the rotational strengths for these d-d transitions.[9]

The calculated vicinal CD curves of the L-alaninato and L-phenylalaninato complexes in the first band region give three components, (−), (+), and (−) from the lower frequency side (Fig. 2). This CD

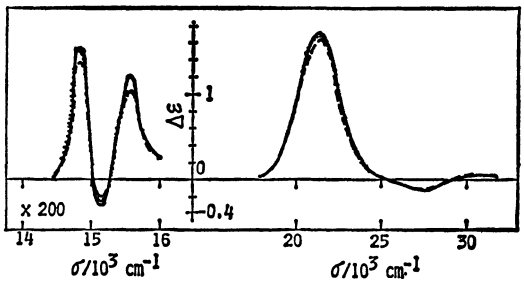

Fig. 3. Calculated configurational CD curves of [Cr(L-ala)$(en)_2]^{2+}$ (----) and $[Cr(L\text{-phala})(en)_2]^{2+}$ (……), and observed CD curve of $(+)_{589}$-$[Cr(gly)(en)_2]^{2+}$ (——).

Table 1. CD data of $[Cr(am)(en)_2]^{2+}$ complexes
(Wave numbers are given in 10^3 cm^{-1}.)

Observed CD extrema of $(+)_{589}$- and $(-)_{589}$-$[Cr(am)(en)_2]^{2+}$				
$(+)_{589}$-(gly)	$(+)_{589}$-(L-ala)	$(-)_{589}$-(L-ala)	$(+)_{589}$-(L-phala)	$(-)_{589}$-(L-phala)
$\sigma(\Delta\varepsilon)$	$\sigma(\Delta\varepsilon)$	$\sigma(\Delta\varepsilon)$	$\sigma(\Delta\varepsilon)$	$\sigma(\Delta\varepsilon)$
14.81(+7.77[a])	14.77(+6.64[a])	14.79(−7.09[a])	14.75(+7.25[a])	14.78(−7.96[a])
15.15(−1.58[a])	15.28(−1.25[a])	15.12(+1.96[a])	15.20(−1.18[a])	15.09(+3.03[a])
15.58(+6.04[a])	15.57(+2.70[a])	15.56(−7.70[a])	15.52(+3.85[a])	15.53(−6.07[a])
21.46(+1.91)	21.15(+1.65)	21.46(−1.63)	21.10(+1.70)	21.42(−1.71)
27.55(−0.16)	27.70(−0.12)	27.47(+0.11)	27.62(−0.16)	27.47(+0.10)
30.45(+0.04)	30.40(+0.04)	30.40(−0.02)	30.53(+0.03)	30.40(−0.03)

Obtained configurational CD extrema			Obtained vicinal CD extrema		
Λ-(L-ala) $\sigma(\Delta\varepsilon)$	Λ-(L-phala) $\sigma(\Delta\varepsilon)$	Assignment(D_3)	(L-ala) $\sigma(\Delta\varepsilon)$	(L-phala) $\sigma(\Delta\varepsilon)$	Assinment(D_4)
14.79(+6.81[a])	14.77(+7.58[a])	$^2E(^2E_g)$	14.60(+0.83[a])	14.64(+1.00[a])	$^2A_1(^2E_g)$
15.15(−1.40[a])	15.13(−1.66[a])	$^2A_2(^2T_{1g})$	14.84(−0.50[a])	14.81(−0.74[a])	$^2B_1(^2E_g)$
15.58(+5.20[a])	15.53(+4.96[a])	$^2E(^2T_{1g})$	15.11(+1.19[a])	15.06(+1.55[a])	$^2A_2(^2T_{1g})$
21.46(+1.62)	21.28(+1.70)	$^4E(^4T_{2g})$	15.60(−2.53[a])	15.35(−1.30[a])	$^2E(^2T_{1g})$
27.62(−0.12)	27.62(−0.13)		18.45(−0.013)	19.01(−0.031)	$^4E(^4T_{2g})$
30.49(+0.03)	30.49(+0.03)		20.58(+0.105)	20.49(+0.080)	
			22.72(−0.168)	22.67(−0.165)	$^4B_2(^4T_{2g})$

a) CD intensities are multiplied by 10^3.

behavior is similar to that of the corresponding Co(III) complexes[5] except their CD intensities. In the spin-forbidden band region, the vicinal CD curves exhibit four components with alternate signs; (+), (−), (+), and (−) from the lower frequency side. The intensity ratios between the configurational and vicinal CD components in the first spin-allowed band region are found to be almost equal to those between the configurational and vicinal CD ones on the lowest frequency side of the spin-forbidden band region (Table 1). This suggests that the intensity borrowing mechanism of the spin-forbidden transitions *via* spin-orbit coupling for the rotational strengths due to the vicinal effect is also operative and valid as in the case of the configurational effect. Of the four vicinal CD components in the spin-forbidden band region, two components on the lower frequency side, (+) and (−), are covered under the band envelope of the configurational CD component on the lowest frequency side in this region; *e.g.*, (+) one for $(+)_{589}$-$[Cr(gly)(en)_2]^{2+}$ (Fig. 2). Thus, the two peaks correspond to the splitting components of the configurational CD peak, which was previously assigned to the $^2E(^2E_g)$ state. The remaining vicinal components, (+) and (−), might correspond to the central $^2A_2(^2T_{1g})$ and the highest frequency $^2E(^2T_{1g})$ configurational CD bands, respectively, in view of the positions of their CD peaks. The large splitting interval of *ca.* 250 cm^{-1} obtained for the $^2E(^2E_g)$ state is comparable to those observed for such tetragonal complexes as $[CrX(NH_3)_5]^{n+}$ type.[13] The splitting interval of the $^2E(^2E_g)$ state for tris(ethylenediamine)chromium(III) complex has been found to be *ca.* 18 cm^{-1}.[14] Assuming that the present complexes belong effectively to holohedrized tetragonal (D_4) symmetry,[15] two vicinal CD peaks on the lower frequency side of the first band, (−) and (+), might be due to the splitting components of the ^4E state, and the remaining negative highest frequency peak to the $^4B_2$ one. The total rotational strength for the $^4E \leftarrow {}^4B_1$ transition in a tetragonal (D_4) field seems to be given by the sum of those for two individual transitions in a lower symmetry field. Thus, the signs of the rotational strengths for the $^4E \leftarrow$ and $^4B_2 \leftarrow {}^4B_1$ transitions are positive and negative, respectively, since the positive component of the ^4E state is much larger than the negative one (Fig. 2 and Table 1). On the basis of the theoretical relation between the rotational strengths for the spin-allowed and magnetic dipole allowed transitions and those for the spin-forbidden transitions of tetragonal Cr(III) complexes (Ref. 8, Table 2 third column), four vicinal CD peaks in the spin-forbidden band region are assigned as follows. Since the rotational strengths for the $^2A_1$, $^2A_2 \leftarrow {}^4B_1$ transitions should have the same signs as those for the $^4E \leftarrow {}^4B_1$ transition, two positive peaks are assigned to the $^2A_1$ and $^2A_2$ states from the lower frequency side. Two remaining negative peaks might be due to the $^2B_1$ and ^2E one from the lower frequency side, the rotational strengths of which are expected to have the same signs as those of the $^4B_2$ state (Table 1). It seems plausible that the orbitally nondegenerate $^2A_2(D_4)$ and the degenerate $^2E(D_4)$ components for the vicinal CD correspond to the nondegenerate $^2A_2(D_3)$ and degenerate $^2E(D_3)$ ones for the configurational CD, respectively.

The authors wish to thank Prof. Yoichi Shimura, Osaka University, and members of his laboratory for their aid in obtaining the circular dichroism spectra. The present work was partially supported by a Grant-in-Aid for Scientific Research from the Ministry of Education, Science and Culture. Some preliminary work was carried out by Miss Misako Nishio.

References

1) R. D. Gillard, S. H. Laurie, D. C. Price, D. A. Phipps, and C. F. Weick, *J. Chem. Soc., Dalton Trans.*, **1974**, 1385.
2) H. Oki, *Bull. Chem. Soc. Jpn.*, **50**, 680 (1977).
3) S. S. Minor, G. Witte, and G. W. Everett, Jr., *Inorg. Chem.*, **15**, 2052 (1976).
4) Y. Shimura, *Bull. Chem. Soc. Jpn.*, **31**, 315 (1958).
5) C. T. Liu and B. E. Douglas, *Inorg. Chem.*, **3**, 1356 (1964); S. K. Hall and B. E. Douglas, *ibid.*, **8**, 372 (1969).
6) N. Matsuoka, J. Hidaka, and Y. Shimura, *Inorg. Chem.*, **9**, 719 (1970); *Bull. Chem. Soc. Jpn.*, **45**, 2491 (1972).
7) K. Yamasaki, J. Hidaka, and Y. Shimura, *Bull. Chem. Soc. Jpn.*, **42**, 119 (1969).
8) S. Kaizaki and Y. Shimura, *Bull. Chem. Soc. Jpn.*, **48**, 3611 (1975).
9) S. Kaizaki, J. Hidaka, and Y. Shimura, *Inorg. Chem.*, **12**, 142 (1973).
10) C. K. Jørgensen, "Absorption Spectra and Chemical Bonding in Complexes," Pergamon Press, Oxford (1962).
11) H. Yamatera, *Bull. Chem. Soc. Jpn.*, **31**, 95 (1958).
12) a) M. Kojima, H. Takayanagi, and J. Fujita, *Bull. Chem. Soc. Jpn.*, **50**, 1891 (1977); b) H. Yoneda, S. Yamasaki, and K. Maruyama, *Proc. 26th Symposium on Coodination Chemistry*, Sapporo, Japan, August 1976, p. 234.
13) C. D. Flint and A. P. Matthews, *J. Chem. Soc., Faraday Trans, 2*, **69**, 419 (1973).
14) I. B. Trabjerg and C. J. Ballhausen, *Mol. Phys.*, **20**, 811 (1971).
15) C. E. Schäffer, *Pure Appl. Chem.*, **24**, 361 (1970).

Formation of Micelles of Acylcarnitines in Glycerol

Lavinel G. Ionescu*,† and Daniel S. Fung

Department of Chemistry and Chemical Engineering, University of Detroit, Detroit, Michigan, U.S.A. 48221

†*Laboratório de Química de Superícies, Departmento de Química, Universidade Federal de Santa Catarina, Florianópolis, S. C., Brazil 88000*

(Received August 5, 1980)

Acylcarnitine chlorides form micelles in water and polyprotic solvents such as glycerol, ethylene glycol; 1,3-propanediol and 1,4-butanediol. The effect of the acyl chain on the formation of micelles was studied for compounds with chain lengths of 2 to 16 carbon atoms. The critical micellar concentration in glycerol was determined at 25 °C by means of difference spectroscopy using phenol as a probe. The acylcarnitine chlorides with chains containing less than 8 C atoms do not form micelles in glycerol. The critical micellar concentration varies from 0.060 mol dm^{-3} for octanoylcarnitine to 0.011 mol dm^{-3} for palmitoylcarnitine. The free energy of micellization, ΔG°_{mic}, varies linearly with chain length in the range of -6.95 kJ mol^{-1} to -11.2 kJ mol^{-1}. The "hydrophobic" or "solvophobic" effect was more pronounced in water than in glycerol and the free energy change per metylene group was -2.89 kJ mol^{-1} and -0.75 kJ mol^{-1}, respectively. The formation of micelles of acylcarnitine chlorides in glycerol is important in terms of the metabolism of fatty acids and their transport across biological membranes.

The principal pathway for the oxidation of fatty acids is generally considered to be β-oxidation. Several enzymes, known collectively as the fatty acid oxidase complex, are found in the mitochondrion closely associated with the enzymes of the respiratory chain. These catalyze the oxidation of fatty acids to acetyl-S-CoA, the system being coupled with the phosphorylation of ADP to ATP. Although the oxidation of fatty acids occurs inside the mitochondrion, the long chain fatty acids in the cytoplasm cannot pass through the mitochondrial membrane, unless they are enzymatically combined with carnitine to form a fattyacylcarnitine complex.

Long chain acylcarnitines are known to form micelles in water.[1,2] The critical micellar concentration (CMC) decreases by an order of magnitude as the alkyl chain length increases by units of two carbon atoms. The aggregation number of long chain acylcarnitines in water slightly increases concomitant with the increment in alkyl chain length.

In comparison with the amount of work done on the properties of surface active agents in water, the chemistry of surfactants in mixed aqueous solvents and nonaqueous solvents is a rather limited field. As part of a systematic study of the process of micellization[3-5] and the use of micelles as simple membrane models,[6] we have decided to search for micelle formation also in nonaqueous protic solvents such as glycerol, ethylene glycol; 1,2-propanediol and 1,4-butanediol. These solvents are very much like water and are known to form micelles with the nonionic detergent polyethylene glycol *p-t*-nonylphenyl ether, NPE_9 (Igepal CO-630) with an average of nine oxyethylene residues in the poly(oxyethylene) chain. The critical micellar concentration of Igepal CO-630 varies from 1.01×10^{-6} mol dm^{-3} in water to 1.55×10^{-2} mol dm^{-3} in 1,4-butanediol and the free energy of micellization, ΔG°_{mic}, ranges from -34.3 to -10.5 kJ mol^{-1} for the same solvents.[7] In general, the process of micellization appears to be thermodynamically favored and is similar to micelle formation in water. The main interaction responsible for micellization is of a hydrophobic type, not unique to water, but found in many other solvents. It is most pronounced in water and glycerol. This interaction is often given by the name "solvophobic" and its exact nature is hard to explain in terms of hydrogen bonding, OH groups, dielectric constant or other parameters.

Glycerol and ethylene glycol form intra- and intermolecular hydrogen bonds,[8,9] although they are much less strong than those in water. Both have been used widely in protein conformation studies and as simple membrane simulators. These dense liquids approximate portions of membranes in terms of the anhydrous environment that they provide. Glycerol has been applied as a viscous agent in the construction of a medium having a viscosity closer to the intracellular environment in the study of the allosteric enzyme glycogen phosphorylase b.[10] Reactivation effects by glycerol and ethylene glycol of inactivated δ-aminolevulic acid synthetase were observed. It was suggested that the protein conformation around the pyridoxal 5'-phosphate binding site of synthetase was stabilized by the polyprotic alcohols.[11]

Materials and Methods

Acylcarnitine chlorides have the generalized structure given below. The compounds studied ranged from acetylcarnitine chloride (n=0) to palmitoylcarnitine chloride (n=14) and differed in the chain

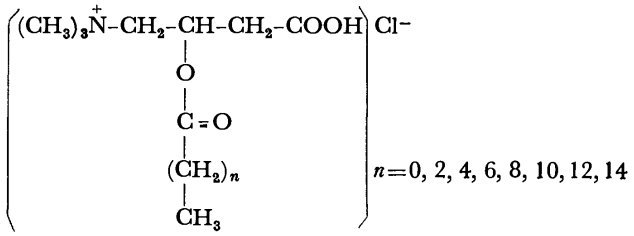

length of the fatty acid by units of two carbon atoms. They were prepared in our laboratory according to the method of Ziegler, Bruckner and Binon.[12] The synthesis essentially involved the preparation of the acyl chlorides from the corresponding acids by means of thionyl chloride, followed by reaction of the acyl

chloride with carnitine employing trichloroacetic acid as the solvent. The acylcarnitines were subsequently recrystallized from isopropyl alcohol and dried over P_2O_5 under high vacuum. Acetyl chloride and trichloroacetic acid (reagent grade) were obtained from Allied Chemical Company. Butanoic, hexanoic, octanoic, decanoic, lauric, myristic, palmitic acid, and *dl*-carnitine hydrochloride were of the highest quality available and were purchased from Aldrich Chemical Co. Thionyl chloride and phenol were of reagent grade and were supplied by Fisher Scientific Co. Glycerol (reagent grade) was purchased from Eastman Organic Chemicals and used without any further purification.

In the original experiments, the CMC was determined by surface tensiometry and only lauroylcarnitine chloride was used. The surface tension measurements were performed at 25 °C with a Du Nouy Tensiometer Model No. 70547 or a Fisher Surface Tensiomat Model 21. Both instruments were calibrated before use. Solutions of lauroylcarnitine chloride in glycerol ranging 1×10^{-9} to 0.1 mol dm^{-3} were prepared. Ten milliliter aliquots of solution in a glass dish with a diameter of 6 cm were used for the measurements. The first determination in a given series was the measurement of the surface tension of deionized distilled water, followed by pure glycerol at 25 °C. Subsequent measurements were of the various surfactant solutions in order of increasing concentration. By plotting the surface tension versus the concentration or the logarithm of the concentration of the surfactant solution, a curve with a sharp initial drop and subsequent levelling off was obtained. The first concentration at which the levelling off took place was taken as the critical micellar concentration.[3,4] Typical results obtained are illustrated in Fig. 1.

Because of the experimental difficulties encountered in the measurement of the surface tension of the viscous glycerol solutions, an alternate method using phenol as a probe for micelle formation was employed for the determination of the CMC. This is essentially a difference spectrophotometric technique developed by Ray and Némethy[13,14] The absolute absorption spectrum of 5.0×10^{-4} mol dm^{-3} phenol in glycerol was recorded with a Beckman Model 24 Spectrophotometer. Phenol has a well-defined λ_{max} at 272 nm. The difference spectra were determined with the same intrument using an expanded absorbance scale (0—0.1, 0—0.25, or 0—0.5). A solution of 5.0×10^{-4} mol dm^{-3} phenol in glycerol was placed in the reference cuvette. The sample cuvette contained a solution of the same concentration of phenol in glycerol and varying amounts of the corresponding acylcarnitine chloride. The spectra of the solutions were measured from 240 to 350 nm. The difference absorption spectra were determined for all the acylcarnitine chlorides mentioned above, namely, acetyl-, butyryl-, hexanoyl-, octanoyl-, decanoyl-, lauroyl-, myristoyl-, and palmitoylcarnitine chloride.

In general fifteen to twenty solutions of the surfactants were measured. These solutions were prepared by diluting stock solutions of acylcarnitines containing 5.0×10^{-4} mol dm^{-3} phenol in glycerol with glycerol containing the same amount of phenol. All the spectra were determined at 25 °C. A plot of the change in absorption at 272 nm, ΔA, *versus* the concentration or the logarithm of the concentration of surfactant gave a curve with a definite break at the CMC. Linear plots were taken as an indication that micelle formation did not take place. Figure 2 gives some typical experimental results obtained for lauroylcarnitine chloride.

Results and Discussion

A summary of the critical micellar concentrations and the free energies of micellization of acylcarnitine chlorides is given in Table 1. As can be seen, octanoylcarnitine chloride is the shortest acylcarnitine that forms micelles in glycerol. The value obtained for the CMC of lauroylcarnitine chloride by surface tension measurements was also 0.030 mol dm^{-3} and thus the agreement between the two different techniques was within experimental error. The CMC decreases with increasing carbon chain length, but the effect is much less pronounced in glycerol than in water.

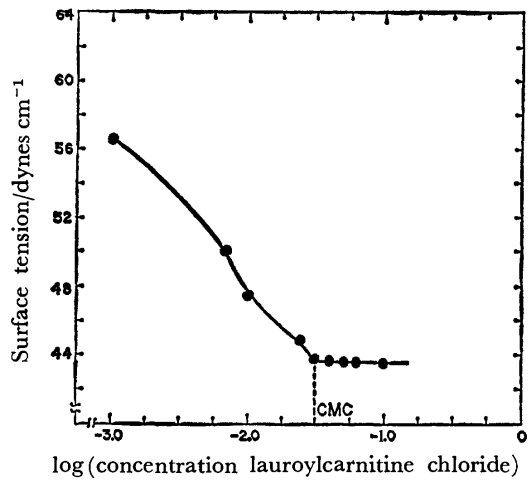

Fig. 1. Plot of surface tension *versus* the logarithm of the concentration of lauroylcarnitine chloride in glycerol at 25 °C.

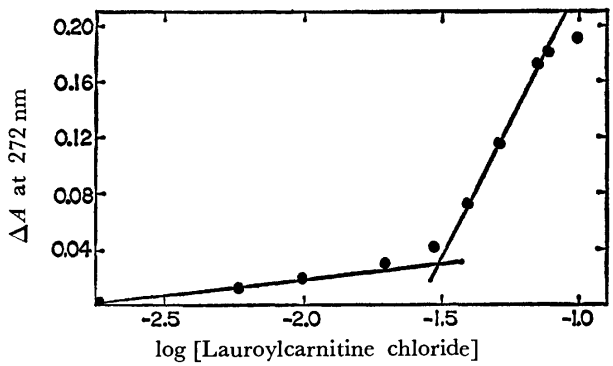

Fig. 2. Dependence of absorbance difference (ΔA) of phenol on the logarithm of the concentration of lauroylcarnitine chloride in glycerol at 25 °C.

Table 1. Critical micellar concentration and free energy of micellization for acylcarnitine chlorides in glycerol at 25 °C

Acylcarnitine chloride	Critical micellar concentration / mol dm^{-3}	ΔG°_m / kJ mol^{-1}
Acetyl-	None	—
Butyryl-	None	—
Hexanoyl-	None	—
Octanoyl-	0.060	−6.95
Decanoyl-	0.050	−7.45
Lauroyl-	0.030	−8.66
Myristoyl-	0.020	−9.67
Palmitoyl-	0.011	−11.2

The formation of normal micelles in nonaqueous polar solvents is of particular interest because in addition to providing novel insights into the process of micellization, it may lead to a better understanding of the interactions that take place between surfactant molecules and the solvent. For micelles in water, the process of micellization is generally explained by means of the hydrophobic interactions between the surfactant and water. "Hydrophobic interactions" is in many ways a convenient term that is used to describe an entire array of inter- and intramolecular interactions involved in micellization and in a certain way the term disguises our ignorance about the actual molecular dynamic processes that take place.

In general, the formation of micelles in water is assumed to take place by the association of the hydrophobic parts of the surfactant molecules and the repulsion of water of solvation from their immediate environment. The thermodynamics of micelle formation has been discussed and treated extensively in the literature.[15,16] One approach assumes that the process of micellization involves the formation of a distinct micellar phase at the CMC and that the concentration of monomers in solution is constant, once micelles are formed. Then, the standard free energy of micellization, ΔG°_{mic}, is given by Eq. 1 to a good

$$\Delta G^\circ_{mic} = RT \ln \mathrm{CMC} \quad (1)$$

approximation. If one postulates that the aggregation number and the degree of ionization of the surfactant are temperature independent, the standard enthalpy (ΔH°_{mic}) and entropy (ΔS°_{mic}) can be evaluated by the temperature dependence of the CMC and the relationship given by Eq. 2.

$$\Delta G^\circ_{mic} = \Delta H^\circ_{mic} - T\Delta S^\circ_{mic} \quad (2)$$

The over-all process of micellization involves a decrease in the free energy of the system. According to Eq. 2, ΔG°_{mic} is the result of enthalpy and entropy contributions. For aqueous solutions, micellization is generally regarded as an entropy directed process and the preponderant contribution of the entropy term is explained by the disordering of the water structure and the breakup of the "Frank-Evans microcrystals" by the surfactant molecules.

The type of interactions involved in the formation of micelles in polar solvents other than water are called "solvophobic." The understanding of "solvophobic interactions" and micellization in nonaqueous media is considerably more nebulous. The driving force for micellization is less for such systems and the more positive ΔG°_m is usually believed to be primarily due to a decrease of the entropic contribution.[7,18] Few solvent systems are as highly ordered and as strongly hydrogen-bonded as water.

As has already been mentioned, the study of nonaqueous micellar systems is of importance also in terms of the understanding of membranes. In fact, the first dynamic membrane model, precursor of the current fluid mosaic or liquid crystal model, was a micelle.[17] In the over-all analysis of solvent-surfactant interactions it is desirable to sort out hydrogen bonding, solvation and the "solvophobic effect." However, the understanding and clear differentiation of these processes in certain systems may prove to be quite a formidable task.

We have attempted to quantify the solvophobic effect in water and glycerol by varying the chain length of the acylcarnitine surfactants. The free energies of micellization of these surfactants at 25 °C have been calculated for water and glycerol and are shown in Fig. 3. The values for water have been calculated from the experimental results of Yalkowsky and Zografi.[1] A simple analysis of the results indicates that the formation of micelles of acylcarnitine chlorides is thermodynamically more favored in water than in glycerol.

The change in ΔG°_{mic} for a given solvent as a function of chain length provides information about the nature of the interaction of the $-CH_2-$ groups with the given solvent and can be interpreted as the solvophobic effect. One can quantify such an interaction by determining the slope of the plots of ΔG°_{mic} *versus* chain length. Large breaks or deviations from linearity in such plots should be indicative of unusual interactions. The data in Fig. 3 illustrates a linear behavior for both solvents, but the slope is considerably steeper for water than for glycerol. The free energy

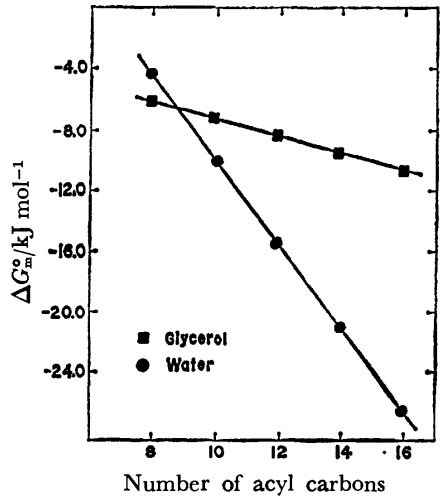

Fig. 3. Dependence of the free energy of micellization (ΔG°_m) on the acyl chain length of acylcarnitine chlorides in water and glycerol at 25 °C.

change per methylene group in water is -2.89 kJ mol^{-1} and in glycerol is -0.75 kJ/mol. The value obtained for water is in agreement with that commonly reported in the literature,[16] while the result for glycerol agrees well with -0.75 kJ mol^{-1} determined by Ray and Némethy for the polyether NPE_9 in ethylene glycol.[18] The solvophobic effect is thus considerably more pronounced in water and shows about the same change in going from water to glycerol and from water to ethylene glycol.

Preliminary experiments performed in our laboratory indicate that lauroylcarnitine chloride forms micelles also in ethylene glycol; 1,3-propanediol and 1,4-butanediol. All these solvents are similar to water in the sense that they form hydrogen bonds and are polar in nature. Glycerol and ethylene glycol form intra and inter hydrogen bonds, although they are much less strong than those in water.[8,9]

The experimental results clearly indicate that the long chain acylcarnitine chlorides, *i.e.*, octanoyl-, decanoyl-, lauroyl-, myristoyl-, and palmitoylcarnitine chloride form micelles in glycerol in addition to water. The shorter chain acylcarnitines do not form micellar aggregates in either of the two solvents. The results may be of biochemical interest for several reasons. It is well known that short chain fatty acids move freely in non-complexed form across membranes. Longer fatty acids, on the other hand, are known to cross the mitochondrial membrane in the form of acylcarnitine complexes. Glycerol has been widely used in protein conformation studies and as a simple membrane simulator. Its viscous nature and anhydrous environment may approximate portions of membranes.[19,20] In addition, the relationship between micelles and the liquid crystal membrane model has already been pointed out. The present work has shown that long chain alkanoylcarnitines form charged colloidal aggregates or micelles in an anhydrous environment akin to that of biological membranes. It would appear reasonable to suggest that micelles may play a role in the transport of long chain acylcarnitines across membranes.

The author (LGI) gratefully acknowledges financial support received from CNPq-National Research Council of Brazil (Grants Nos. 1111.5713/78 and 40.2548/79).

References

1) S. H. Yalkowsky and G. Zografi, *J. Pharm. Sci.*, **59**, 798 (1970).
2) S. H. Yalkowsky and G. Zografi, *J. Colloid Interface Sci.*, **34**, 525 (1970).
3) L. G. Ionescu, T. Tokuhiro, B. J. Czerniawski and E. S. Smith, "Solution Chemistry of Surfactants," ed by K. L. Mittal, Plenum Press, New York (1979), p. 487.
4) L. G. Ionescu, T. Tokuhiro, and B. J. Czerniawski, *Bull. Chem. Soc. Jpn.*, **52**, 922 (1979).
5) T. Tokuhiro, L. G. Ionescu, and D. S. Fung, *J. Chem. Soc., Faraday Trans. 2*, **75**, 975 (1979).
6) L. G. Ionescu and J. K. Tsang, *Rev. Roum. Biochim.*, **15**, 211 (1978).
7) A. Ray, *Nature*, **231**, 313 (1971).
8) M. Ueda, T. Urahata, A. Katyam, and N. Kuroki, *Seni Gakkaishi*, **32**, T 301 (1976).
9) J. L. Beaudoin, *J. Chim. Phys.*, **74**, 268 (1977).
10) S. Damjanovich, B. Somogyi, and J. Bot, *Stud. Biophys.*, **59**, 229 (1976).
11) T. Yubisui, M. Takeshita, and Y. Yoneyama, *Experientia*, **32**, 3989 (1976).
12) H. J. Ziegler, P. Bruckner, and F. Binon, *J. Org. Chem.* **32**, 3989 (1967).
13) A. Ray and G. Némethy, *J. Phys. Chem.*, **75**, 804 (1971).
14) G. Némethy and A. Ray, *J. Phys. Chem.*, **77**, 64 (1973).
15) D. G. Hall, *Trans. Faraday Soc.*, **66**, 1351 (1970).
16) N. Muller, "Reaction Kinetics in Micelles," ed by E. H. Cordes, Plenum Press, New York (1973), p. 1.
17) A. A. Benson, *J. Am. Oil Chem. Soc.*, **43**, 265 (1966).
18) A. Ray and G. Némethy, *J. Phys. Chem.*, **75**, 809 (1971).
19) A. Ray, *J. Am. Chem. Soc.*, **91**, 6511 (1969).
20) H. J. Sage and S. J. Singer, *Biochemistry*, **1**, 305 (1962).

Peroxomonophosphoric Acid Oxidations. VI.[1] Kinetics and Mechanism of Oxidation of 3-Aminopyridine

Surendra Nath MAHAPATRO, Abhina Kumar PANDA, and Ganesh Prasad PANIGRAHI*

Department of Chemistry, Berhampur University-760007, Orissa, India

(Received October 3, 1980)

The oxidation of 3-aminopyridine to 3,3′-azoxypyridine by peroxomonophosphoric acid (PMPA) is a total second order reaction: first order each in peroxomonophosphoric acid and 3-aminopyridine at constant acidity. The observed pH-rate profile has been rationalized invoking various PMPA species, protonated and unprotonated forms of 3-aminopyridine as the reactive species and their reactivities have been estimated. Interestingly, 2-aminopyridine is not oxidized in the pH-range where the oxidation of 3-aminopyridine is facile.

The oxidation of primary aromatic amines by peroxidic reagents have received considerable attention.[2,3] A general feature of these oxidations is the formation of a tetrahedral intermediate involving nucleophilic attack by the amine lone pair on the electrophilic peroxo bond which undergoes oxidative decomposition to phenylhydroxylamine. Further oxidation of the hydroxylamine derivative leads to nitroso and eventually to the nitro group (Eq. 1).

$$Ar\text{-}NH_2 \rightarrow Ar\text{-}NHOH \rightarrow Ar\text{-}NO \rightarrow Ar\text{-}NO_2 \quad (1)$$

Bimolecular condensation between the products and unreacted amine may also lead to azoxy and azo compounds (Eqs. 2a and 2b).

$$Ar\text{-}NHOH + Ar\text{-}NO \rightarrow Ar\text{-}\overset{\overset{O}{\uparrow}}{N}{=}N\text{-}Ar \quad (2a)$$

$$Ar\text{-}N{=}O + Ar\text{-}NH_2 \rightarrow Ar\text{-}N{=}N\text{-}Ar \quad (2b)$$

We have recently reported that in the oxidation of anthranilic acid,[1] Eq. 2a is the major route leading to 2,2′-azoxybenzenedicarboxylic acid.

In our search for similar systems, we have found that 3-aminopyridine is oxidized to 3,3′-azoxypyridine essentially in quantitative yields.[4] Interestingly 2-aminopyridine did not undergo any oxidation in the pH range where the oxidation of 3-aminopyridine was facile. We wish to report the salient kinetic features of this oxidation.

Experimental

PMPA was prepared by the acid hydrolysis of $K_4P_2O_8$[5-8] (Eq. 3).

$$H_4P_2O_8 + H_2O \rightarrow H_3PO_5 + H_3PO_4 \quad (3)$$

The rate of hydrolysis Eq. 3 is about two orders of magnitude higher than the hydrolysis of H_3PO_5 to H_2O_2 (Eq. 4).

$$H_3PO_5 + H_2O \rightarrow H_2O_2 + H_3PO_4 \quad (4)$$

In the entire range of this study, the total amount of H_2O_2 was never more than 2% and H_2O_2 under our experimental conditions did not oxidize 3-aminopyridine in independent runs.

$NaClO_4$ was used to maintain constant ionic strength. $HClO_4$ (Baker analyzed 60%), KH_2PO_4, Na_2HPO_4, NaOH, potassium hydrogen phthalate were used to maintain pH which was measured using a Systronics digital pH-meter 335. 3-Aminopyridine (Aldrich 99%) was recrystallized from ethanol mp 157 °C (lit, 158 °C). The kinetics was followed by measuring the rate of disappearance of PMPA which was estimated by iodometry at pH 4—5 with a drop of ammonium molybdate solution.[1] All the reported rate constants, computed by the usual method, are reproducible to within ±5%. k_{obsd} (second order rate constant) is calculated by dividing pseudo-first order rate constant with respect to PMPA disappearance by the substrate concentration. Least squares analysis of the rate laws were done by a DCM Microsystem 1121.

Stoichiometry. A clean stoichiometry of 3-aminopyridine: PMPA (1:1.5) was observed at several pH's in the range 0—7. 3,3′-Azoxypyridine has been characterized as the only product of this oxidation and has already been reported.[4]

Results and Discussion

The oxidation of 3-aminopyridine by peroxomonophosphoric acid (PMPA) in aqueous acid medium at 308 K with different initial concentrations of PMPA and 3-aminopyridine (Table 1) enabled us to write the rate equation at constant acidity;

Table 1. Pseudo first order rate constants and second order rate constants for the oxidation of 3-aminopyridine at 308 K, μ=0.4 mol dm^{-3} at pH 1.3

[PMPA]×10^4 / mol dm^{-3}	[3-Aminopyridine]×10^3 / mol dm^{-3}	Pseudo first order rate constant×10^4 / s^{-1}	k_{obsd}×10^3 / dm^3 mol^{-1} s^{-1}
4.90	2.57	0.383	14.9
4.99	5.50	0.7206	13.1
5.41	11.6	1.486	12.8
21.40	11.1	1.376	12.4
49.64	11.1	—	11.8[a]
96.24	11.1	—	10.8[a]
4.81	25.7	3.01	11.7

a) k_{obsd} calculated directly from second order rate expression.

TABLE 2. EFFECT OF ADDED SUBSTANCES AND ACIDITY ON THE OXIDATION RATE AT 308 K

pH	[3-Aminopyridine] $\times 10^3$ / mol dm^{-3}	[PMPA] $\times 10^4$ / mol dm^{-3}	$k_{obsd} \times 10^3$ / dm^3 mol^{-1} s^{-1}
0.0	10.3	4.78	56.2
0.3	10.3	5.19	47.3
0.7	10.7	5.21	33.4
1.0	10.7	4.51	25.7
1.3	11.6	5.41	12.8
1.73	21.2	4.78	10.15
2.63	21.2	5.07	2.12
3.00	10.7	4.19	0.896
3.20	10.7	4.01	0.908
3.71	23.5	4.74	1.22
4.15	22.3	4.74	1.67
4.46	21.2	4.86	2.21
4.53	22.0	4.60	2.30
4.76	22.0	3.90	2.73
5.01	21.2	5.01	3.90
5.27	22.0	4.60	4.45
5.72	21.0	4.54	4.52
6.04	21.0	4.84	4.95
6.47	21.0	4.74	3.51
7.02	20.7	4.79	0.835
1.3	5.31	3.91	12.8[a]
1.3	5.31	4.50	13.8[b]
1.3	22.2	4.56	11.6[c]
1.3	20.8	4.70	13.6[d]
1.3	20.8	4.96	13.05[e]

a) $\mu = 0.25$ mol dm^{-3}. b) $\mu = 0.8$ mol dm^{-3}. c) [Acrylamide] $= 2.31 \times 10^{-2}$ mol dm^{-3}. d) [Ag$^+$] $= 4.8 \times 10^{-4}$ mol dm^{-3}. e) [Cu^{2+}] $= 5.34 \times 10^{-4}$ mol dm^{-3}.

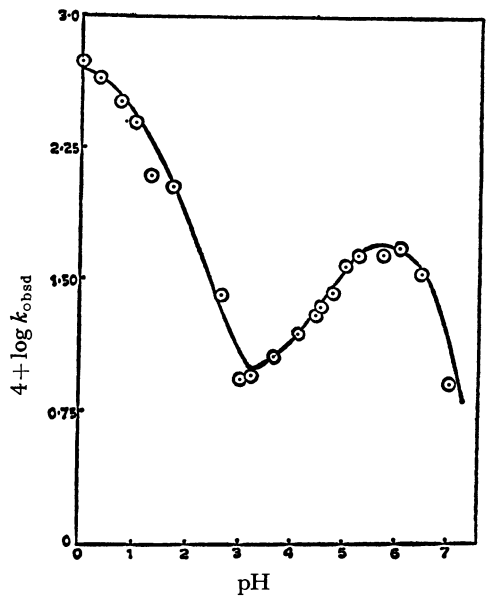

Fig. 1. Plot of log k_{obsd} *vs.* pH.
⊙: Experimental points. —: Theoretical line.

$$\text{Rate} = k_{obsd}[\text{3-Aminopyridine}]_t[\text{PMPA}]_t,$$

where k_{obsd} is the second order rate constant and 't' denotes total concentration.

The influence of acidity on the oxidation rate are presented in Table 2 and shown in Fig. 1 (log k_{obsd} *versus* pH). The pH-rate profile clearly reflects the involvement of various PMPA species and protonated and unprotonated forms of 3-aminopyridine (Eqs. 5, 6, and 7).

$$H_3PO_5 \overset{K_1}{\rightleftharpoons} H_2PO_5^- + H^+, \quad K_1 = 8.0 \times 10^{-2} \qquad (5)^{8)}$$

$$H_2PO_5^- \overset{K_2}{\rightleftharpoons} HPO_5^{2-} + H^+, \quad K_2 = 4.2 \times 10^{-6} \qquad (6)^{8)}$$

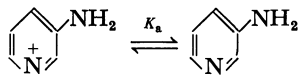

$$\overset{K_a}{\rightleftharpoons} + H^+, \quad K_a = 1.047 \times 10^{-6} \qquad (7)^{3)}$$

(BH$^+$) (B)

Reaction in the pH Range 0—3. In the pH range 0—3, the rate of oxidation goes on decreasing with the increase in pH *i.e.* with the decreasing electrophilic character of PMPA species.[9] The pK_a of 3-aminopyridine (5.98) suggests that whole of 3-aminopyridine (B) exists as BH$^+$ and PMPA exists as H_3PO_5 and $H_2PO_5^-$ in this pH range. Hence, the steps of the oxidation can be written as

$$BH^+ + H_3PO_5 \xrightarrow{k_1} \text{Products} \qquad (8)$$

$$BH^+ + H_2PO_5^- \xrightarrow{k_2} \text{Products}. \qquad (9)$$

Hence,

$$\text{Rate} = -\frac{d[\text{PMPA}]_t}{dt} = k_1[BH^+][H_3PO_5] + k_2[BH^+][H_2PO_5^-]. \qquad (9a)$$

But

$$[PMPA]_t = [H_3PO_5] + [H_2PO_5^-]. \quad (9b)$$

From Eqs. 9b and 5, we get

$$[H_3PO_5] = \frac{[H^+]}{K_1+[H^+]}[PMPA]_t \quad (9c)$$

and

$$[H_2PO_5^-] = \frac{K_1}{K_1+[H^+]}[PMPA]_t. \quad (9d)$$

Substituting Eqs. 9c and 9d in Eq. 9a, we get

$$-\frac{d[PMPA]_t}{dt} = \frac{k_1[H^+]+k_2K_1}{K_1+[H^+]}[BH^+][PMPA]_t, \quad (9e)$$

where

$$k_{obsd} = \frac{k_1[H^+]+k_2K_1}{K_1+[H^+]}. \quad (10)$$

Least squares analysis of the above equation gave us the values of k_1 and k_2 which are collected in Table 3. The correspondence between the k_{obsd} and k_{cald} based on the values of k_1 and k_2 is very good (Fig. 1).

TABLE 3. RATE CONSTANTS IN $dm^3\,mol^{-1}\,s^{-1}\times10^2$

k_1	k_2	k_3	$\left(\frac{k_4K_a}{K_2}+k_5\right)$	$\approx k_4$	k_6
5.28	0.068	0.098	4.50	18	0.05

Reaction in the pH Range 3—7. In this pH region, a bell shaped curve is observed. PMPA exists as $H_2PO_5^-$ and HPO_5^{2-} and 3-aminopyridine exists as BH^+ and B.

Therefore, the reaction steps are postulated as

$$BH^+ + H_2PO_5^- \xrightarrow{k_3} \text{Products} \quad (11)$$

$$B + H_2PO_5^- \xrightarrow{k_4} \text{Products} \quad (12)$$

$$BH^+ + HPO_5^{2-} \xrightarrow{k_5} \text{Products} \quad (13)$$

$$B + HPO_5^{2-} \xrightarrow{k_6} \text{Products}. \quad (14)$$

Equations 11—14 lead us to the rate law

$$-\frac{d[PMPA]_t}{dt} = k_3[BH^+][H_2PO_5^-] + k_4[B][H_2PO_5^-] + k_5[BH^+][HPO_5^{2-}] + k_6[B][HPO_5^{2-}]. \quad (14a)$$

But $$[B]_t = [BH^+] + [B]. \quad (14b)$$

From Eqs. 7 and 14b, we get

$$[BH^+] = \frac{[H^+]}{K_a+[H^+]}[B]_t \quad (14c)$$

and

$$[B] = \frac{K_a}{K_a+[H^+]}[B]_t. \quad (14d)$$

Now,

$$[PMPA]_t = [H_2PO_5^-] + [HPO_5^{2-}]. \quad (14e)$$

From Eqs. 6 and 14e, we get

$$[H_2PO_5^-] = \frac{[H^+]}{K_2+[H^+]}[PMPA]_t \quad (14f)$$

and

$$[HPO_5^{2-}] = \frac{K_2}{K_2+[H^+]}[PMPA]_t. \quad (14g)$$

Substituting Eqs. 14c, 14d, 14f, and 14g in 14a, we get

$$-\frac{d[PMPA]_t}{dt} = \frac{k_3[H^+]^2+\left(\frac{k_4K_a}{K_2}+k_5\right)K_2[H^+]+k_6K_aK_2}{(K_a+[H^+])(K_2+[H^+])} \times [B]_t[PMPA]_t, \quad (14h)$$

where

$$k_{obsd} = \frac{k_3[H^+]^2+\left(\frac{k_4K_a}{K_2}+k_5\right)K_2[H^+]+k_6K_aK_2}{(K_a+[H^+])(K_2+[H^+])}. \quad (15)$$

A least squares analysis of Eq. 15 was done and values of k_3, (k_4K_a/K_2+k_5) and k_6 were obtained (Table 3). These values were used to obtain k_{calcd} which showed excellent agreement with experimental points (Fig. 1).

It is gratifying that the values of k_2 (Eq. 9) and k_3 (Eq. 11), obtained by two different rate expressions Eq. 10 and Eq. 15 are of the same order of magnitude and provide credence to the steps envisaged.

Activation Energy and Entropy. The second order rate constants at 308, 313, 318, and 323 K and at $[H^+]=0.05$ mol dm^{-3} were 1.28×10^{-2}, 1.63×10^{-2}, 2.18×10^{-2}, and 2.73×10^{-2} $dm^3\,mol^{-1}\,s^{-1}$ respectively. The energy of activation from a plot of log k_{obsd} against $1/T$ was 41.8 kJ mol^{-1}. ΔH^* and ΔS^* were estimated to be 39.5 kJ mol^{-1} and -153 J K^{-1} mol^{-1} respectively.

Mechanism. That the rate limiting step involves nucleophilic attack of the amino nitrogen on the electrophilic peroxo oxygen is evident from the following facts.

(1) No oxidation is observed above pH 7. The order of decreasing electrophilicity of the various PMPA species is $H_3PO_5>H_2PO_5^->HPO_5^{2-}>PO_5^{3-}$. At pH $\approx$7 HPO_5^{2-} is about 90%.

(2) The insensitivity of the rates to added acrylamide, Cu^{2+}, Ag^+ points to the polar nature of these oxidations without the mediation of free radical intermediates.

(3) The reactivity of H_3PO_5 (k_1) is about two orders of magnitude higher than that of $H_2PO_5^-$ (k_2), Table 3.

(4) The facile oxidation of 3-aminopyridine stands in sharp contrast to the total unreactivity of 2-aminopyridine. The reason most probably lies in the nucleophilicity of the $-NH_2$ nitrogen. The 3-NH_2 group is not conjugated with the pyridine nitrogen and thus the nitrogen lone pair is not delocalized into the heterocyclic ring.

Thus the nucleophilicity of the NH_2 group in 3-aminopyridine is fully alive. In 2-aminopyridine there are contributing structures like

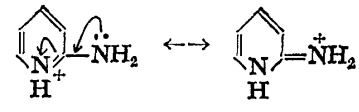

and this reduces the nucleophilicity of 2-NH_2 group to a great extent.[3] In the pH range 0—5 the pyridine nitrogen is protonated which enhances the meso-

meric interaction of the $-NH_2$ group. Above pH 5, we have both B and BH^+ and B is decidedly more nucleophilic than BH^+. We have seen a very slow oxidation of 2-aminopyridine above pH 5.

In the oxidation of anthranilic acid,[1] it is the unprotonated amine which is the reactive species as the rate decreased at higher acidities. The oxidation of 3-aminopyridine provides altogether a different situation. The pK_a of 3-aminopyridine is 5.98 and this refers to the protonation of the tertiary pyridine nitrogen and the 3-NH_2 group is unprotonated. One could in principle protonate it and this obviously requires still higher acidities than presently used in this kinetic study. Our pH-rate profile at still higher acidities could possibly have shown such a decreasing trend which is a reflection of the 3-NH_2 protonation. But our attempts to see that presented serious experimental problems in the estimation of PMPA iodometrically.

Reactivity of Amine and Peroxo Acid.

1) It is seen that the reactivity of H_3PO_5 is two orders of magnitude higher than that of $H_2PO_5^-$ which has been attributed to electrophilicity difference.

2) The peak in the pH region 3—7 is significant which calls for an explanation. In this range, 3-aminopyridine exists as B and BH^+. In BH^+ the tertiary nitrogen becomes tetrahedral on protonation, the delocalized positive charge experiences a field effect due to the NH_2 lone pair which makes the NH_2 of BH^+ less nucleophilic than that of B.

3) The value of (k_4K_a/K_2+k_5) is of the order of 10^{-2}, and k_5 should be very less than k_6 as explained above.

Hence, $(k_4K_a/K_2+k_5)\approx k_4K_a/K_2$.

Using values of K_a, K_2, a rough estimate of k_4 has been obtained (Table 3). Thus it is seen that B is about two orders of magnitude higher in reactivity than BH^+.

References

1) Part V: G. P. Panigrahi and A. K. Panda, *Bull. Chem. Soc. Jpn.*, **54**, 1554 (1981).

2) E. J. Behrman and J. O. Edwards, "Progress in Physical Organic Chemistry," ed by A. Streitwieser, Jr., and R. W. Taft, Interscience, New York (1967), p. 110.

3) G. Chuchani, "The Chemistry of the Amino group," ed by Saul Patai, Interscience, New York (1968).

4) S. N. Mahapatro, G. P. Panigrahi, and A. K. Panda, *Curr. Sci.*, **49**, 227 (1980).

5) M. M. Crutchfield, "Peroxodiphosphoric acid in Peroxide Reaction Mechanisms," ed by J. O. Edwards, Interscience, New York (1961), p. 41.

6) D. H. Fortnum, C. J. Battaglia, S. R. Cohen, and J. O. Edwards, *J. Am. Chem. Soc.*, **82**, 778 (1960).

7) C. J. Battaglia and J. O. Edwards, *Inorg. Chem.*, **4**, 552 (1965).

8) F. Secco and M. Venturini, *J. Chem. Soc., Dalton Trans.*, **1976**, 1410.

9) Y. Ogata, K. Tomizawa, and T. Morikawa, *J. Org. Chem.*, **44**, 352 (1979).

Electrochemical Formation of 1,3,5-Trinaphthylbenzene Tri- and Tetraanions

Tetsuo SAJI* and Shigeru AOYAGUI

Department of Electronic Chemistry, Graduate School at Nagatsuta, Tokyo Institute of Technology, Nagatsuta, Midori-ku, Yokohama 227

(Received January 20, 1981)

Synopsis. Each of the cyclic voltammograms of tri(1-naphthyl)benzene and tri(2-naphthyl)benzene in 1,2-dimethoxyethane at −50 °C exhibits four reversible one-electron reduction steps; this may be evidence for the successive formation of the mono-, di-, tri-, and tetraanions of these hydrocarbons. The degeneracy of their π^*-orbitals can account for the formation of the tri- and tetraanions.

We reported recently a well-defined cyclic voltammogram for the reduction of decacyclene in 1,2-dimethoxyethane (DME).[1] It exhibited four reversible one-electron steps, showing a successive formation of the mono-, di-, tri-, and tetraanions of considerable stability. The formation of the tetraanion was ascribed to the lowest π^*-orbitals of decacyclene degenerating two-fold due to the molecular symmetry of C_{3h}. The only hydrocarbon tetraanions ever reported except decacyclene^{4-} have been bicyclooctatetraene^{4-} [2] and benzo[1,2: 4,5]dicyclooctane^{4-}.[3] This note deals with the voltammograms of trianphthylbenzenes, which provide further examples of hydrocarbon tetraanions.

1,3,5-Tri(1-naphthyl)benzene (I) and 1,3,5-tri(2-naphthyl)benzene (II) were prepared by the trimerization of acetylnaphthalene[4] and identified on the basis of the melting point and IR spectrum.

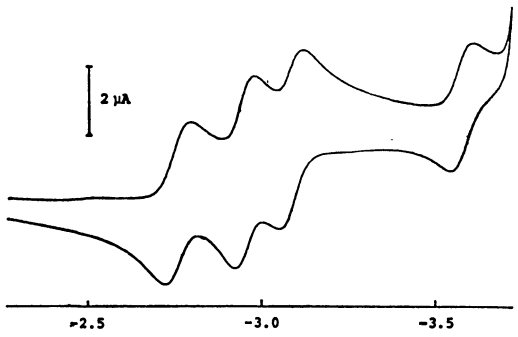

[*E vs.* (Ag/AgNO$_3$)]/V

Fig. 1. Cyclic voltammogram of 0.5 mmol dm^{-3} 1,3,5-tri(β-naphthyl)benzene in 0.2 mol dm^{-1} TBAP–DME at −50 °C. Scan rate 0.1 V s^{-1}.

Figure 1 shows a cyclic voltammogram for 0.5 mmol dm^{-3} of II in 0.2 mol dm^{-3} tetrabutylammonium perchlorate (TBAP)–DME obtained with a scan rate of 0.1 V s^{-1} at −50 °C. It exhibits four reduction steps. They were all reversible one-electron transfer steps, according to the reversibility criteria of the peak separation and the peak current ratio. The ultimate current rise overlapped the reversal peak of the fourth step at −40 °C and 0.1 V s^{-1}; this step was not observed at all at room temperature and 0.1 V s^{-1}, while the first three steps remained reversible. Similar voltammograms were obtained for I. Table 1 lists the reversible half-wave potentials and the peak separations for these compounds, together with the first reduction half-wave potential for naphthalene obtained under the same experimental conditions. The residual resistance of the solution between the reference electrode and the working electrode due to incomplete compensation of the ohmic resistance may account for the peak separations greater than the theoretical separation, 43 mV at −50 °C.

A SCF MO calculation of the π-orbital energies of these substances was made by assuming that the angle between the molecular planes of naphthalene and benzene was 26° for I and 20° for II.[5] Thus the lowest π^*-orbital is two-fold degenerate and the next higher orbital differs from it by only 0.2 eV in II and 0.1 eV in I; a similar situation exists in tris(2,2′-bipyridine) complexes of transition metals[6] of D_{3d} molecular symmetry. If these orbitals are three-fold degenerate, the appearance of the voltammograms for the trinaphthylbenzenes would be very similar to that for tris(bipyridine) complexes. Comparison may better be made with the voltammogram of tris(4,7-diphenyl-1,10-phenanthroline)iron(II),[7] which exhibits two sets of three neighbouring reduction steps; these results lead to the supposition that the penta- and hexaanions of the trinaphthylbenzenes may be formed at potentials between −3.7 and −4 V *vs.* Ag/AgNO$_3$, though such highly negative potentials could not be realized.

The half-wave potentials of the first steps of tri-

Table 1. Cyclic voltammetric data for the reduction of 1,3,5-trinaphthylbenzenes and naphthalene in 0.2 mol dm^{-3} TBAP-DME at −50 °C
Scan rate 0.1 V s^{-1}.

Substance		Reduction step			
		1st	2nd	3rd	4th
1,3,5-Tri(1-naphthyl)benzene	A[a]	−2.81	−3.02	−3.15	−3.64
	B[b]	65	65	65	70
1,3,5-Tri(2-naphthyl)benzene	A	−2.76	−2.95	−3.08	−3.58
	B	60	65	70	70
Naphthalene	A	−3.09			

a) A: Reversible half-wave [potential *vs.* (Ag/AgNO$_3$)]/V. b) B: Peak separation/mV(±5 mV).

naphthylbenzenes are more positive by about 0.3 V than the half-wave potential of naphthalene, which means that the lowest π^*-orbital of each trinaphthylbenzene is more stabilized than that of naphthalene.

References

1) T. Saji and S. Aoyagui, *J. Electroanal. Chem.*, **102**, 139 (1979).

2) L. A. Paquette, G. D. Ewing, and S. G. Traynor, *J. Am. Chem. Soc.*, **98**, 279 (1976).

3) L. A. Paquette, G. D. Ewing, S. G. Traynor, and J. M. Gardlik, *J. Am. Chem. Soc.*, **99**, 6115 (1977).

4) D. B. Clapp and A. A. Morton, *J. Am. Chem. Soc.*, **58**, 2172 (1936).

5) R. J. W. Le Fevre, A. Sundaram, and K. M. S. Sundaram, *J. Chem. Soc.*, **1963**, 3180.

6) T. Saji and S. Aoyagui, *J. Electroanal. Chem.*, **108**, 223 (1980).

7) T. Saji, T. Fukai, and S. Aoyagui, *J. Electroanal. Chem.*, **66**, 81 (1975).

The Measurement of the Solubility of Metallic Mercury in Hydrocarbons by Means of the Cold-vapor Atomic Absorption Method

Shoichi Okouchi* and Sokichi Sasaki

Chemical Laboratory, Faculty of Engineering, Hosei University, Kajino, Koganei, Tokyo 184

(Received April 24, 1980)

Synopsis. The metallic mercury solubility in hydrocarbons (pentane, hexane, heptane, and octane) was determined in the temperature range from 5 to 40 °C by the cold-vapor atomic absorption method. The results, for pentane at 25 °C, were found to agree well with Kuntz's result obtained by means of the ultraviolet absorption method, while those for hexane, heptane, and octane were found to agree well with Spencer's results, which were obtained using a radioactivetracer technique in the above temperature range. The liquid-liquid distribution constant for metallic mercury between the above hydrocarbons and water was measured at 25 °C, and in each case was found to be equal to the ratio of the independent solubility in the hydrocarbon and in water.

The solubility of metallic mercury in water has been studied by many researchers. Early measurements of the solubility of mercury were made by means of the amalgamation[1] or electrodeposition[2] of the dissolved mercury. More recently, the measurements have been made using the radioactive tracer Hg^{203},[3,4] atomic absorption spectrometry,[5,6] and neutron-activation analysis.[7] Mercury solubility in hydrocarbons was studied by Spencer[4] and by Kuntz.[8] Spencer determined the solubility of mercury in hexane, heptane, and octane using a radioactive technique in the temperature range from 0 to 40 °C. Kuntz determined the solubility of mercury in pentane at 25 °C by combining optical data with a known mercury-solubility value.

In this work the mercury solubility in the above hydrocarbons was determined by the cold-vapor atomic absorption method. The liquid-liquid distribution constant of metallic mercury between these hydrocarbons and water was also investigated.

Experimental

All the chemicals used were of an analytical reagent grade. The hydrocarbon solvents (pentane, hexane, heptane, and octane) were purified by passing them through activated alumina, and by distilling. The metallic mercury was purified in the usual manner.[5]

The solubility experiments were conducted by shaking each hydrocarbon solvent with a drop of metallic mercury in a constant-temperature water bath, controlled to within ±0.1 °C. It was found that the mercury concentration was constant after about 24 h of shaking and thereafter remained constant over a period of several days. A solution of 0.5 cm^3 equilibrated was analyzed by the cold-vapor atomic absorption method, consisting of tin(II) chloride reduction, nitrogen bubbling (at a flow rate of 1.5 $dm^3\ min^{-1}$), and passing through a magnesium-perchlorate tube for mercury-vapor drying. The mercury concentration was determined from the area under the atomic absorption peak at 253.7 nm. A calibration curve was constructed by analysing a series of standard solutions from 0.1 to 1.5 ng of mercury in 100 cm^3 of water with the addition of 0.5 cm^3 of hydrocarbon. No effects of the amount of hydrocarbon added in the range from 0.1 to 1.0 cm^3 and of the type of the hydrocarbon on the calibration curve were seen. Also, Fujii[9] has reported on the basis of the cold-vapor atomic absorption method, that these hydrocarbons have no effect on mercury analysis. Experiments were carried out in the temperature range from 5 to 40 °C.

Measurements of the liquid-liquid distribution constant of metallic mercury between the hydrocarbons and water were made by dissolving metallic mercury in the hydrocarbon solvents, shaking these solutions at 25 °C with distilled water containing 0.001 mol of phosphinic acid[3] in order to prevent mercury oxidation, and determining the mercury concentrations of both phases.

Results and Discussion

The temperature dependence of the mercury solubility in each hydrocarbon is shown in Fig. 1. The constants, A and B, that were found to satisfy Eq. 1 are shown in Table 1.

$$\text{Log } X = A \text{ Log } T + B, \qquad (1)$$

where X is the mole fraction of the solute and where T is the absolute temperature. The results for pentane at 25 °C were found to agree well with Kuntz's result,[8]

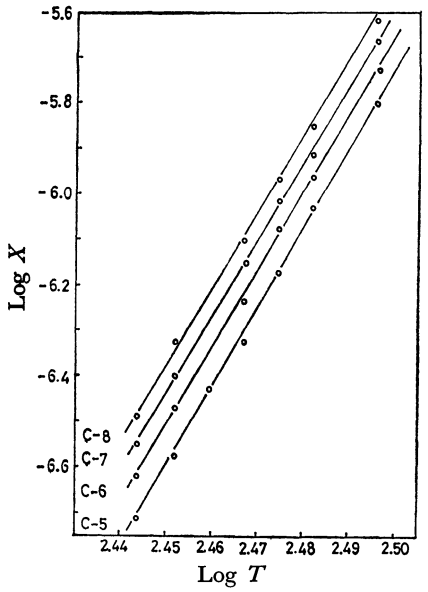

Fig. 1. Temperature dependence of the mercury solubility in hydrocarbons.
C-5: Pentane, C-6: hexane, C-7: heptane, C-8: octane.

Table 1. Constants of Eq. 1

Solvent	A	B
Pentane	17.375	−49.169
Hexane	17.111	−48.432
Heptane	17.250	−48.705
Octane	16.500	−46.800

which was obtained using the ultraviolet-absorption measurements at 256.0 nm, while for hexane, heptane, and octane the results agreed well with those of Spencer,[4] which were obtained using the radioactive tracer Hg^{203} in the temperature range from 5 to 40 °C. The mercury solubility in these hydrocarbons was estimated using the Hildebrand equation for regular solutions.[10] The agreement between the values calculated from the equation and the experimental measurements was a good approximation by an order of magnitude except in the case of water.

The liquid-liquid distribution constant for metallic mercury between each hydrocarbon and water is shown in Table 2. The distribution constant, K, is expressed by Eq. 2:

$$K = [Hg]_{aq}/[Hg]_{hc}, \quad (2)$$

where $[Hg]_{aq}$ and $[Hg]_{hc}$ are the mercury concentrations in the aqueous solution and in the hydrocarbon respectively. Table 2 shows the K values from this work in the first column and those from Moser's work[3] in the second column. The third column shows the values calculated from the ratio of the mercury solubility in the hydrocarbon and water at 25 °C. The mercury solubility in the water used was found to be $(3.0\pm0.1)\times10^{-7}$ mol dm^{-3} at 25 °C in this work, in good agreement with the results of Glew[5] and Enat.[6] The distribution constant was found to be equal to the ratio of the independent mercury solubility in the hydrocarbon and in water.

Table 2. Distribution constants, K, at 25 °C

	Measured	Reference[3]	Calculated
Pentane	0.054	—	0.052
Hexane	0.048	0.048	0.048
Heptane	0.046	—	0.046
Octane	0.046	—	0.045

We gratefully acknowledge the valuable suggestions of Proffesor Yuhbun Tsutsumi, Hosei University.

References

1) H. Reichardt and K. F. Bonhoeffer, *Z. Phys.*, **67**, 780 (1931).
2) A. Stock, F. Cucuel, F. Gerstner, H. Kohle, and H. Lux, *Z. Anorg. Allg. Chem.*, **217**, 241 (1934).
3) H. C. Moser and A. F. Voigt, *J. Am. Chem. Soc.*, **79**, 1837 (1957).
4) J. N. Spencer and A. F. Voigt, *J. Phys. Chem.*, **72**, 464 (1968).
5) D. N. Glew and D. A. Hames, *Can. J. Chem.*, **49**, 3114 (1971).
6) E. Onat, *J. Inorg. Nucl. Chem.*, **36**, 2029 (1974).
7) S. S. Choi and D. G. Tuck, *J. Chem. Soc.*, **1962**, 4080.
8) R. R. Kuntz and G. J. Mains, *J. Phys. Chem.*, **68**, 408 (1964).
9) M. Fujii, K. Moriya, C. Nishihara, J. Minami, and M. Kondo, *Nippon Kohshueiseishi*, **23**, 421 (1976).
10) J. H. Hildebrand and R. L. Scott, "The Solubility of Nonelectrolytes," 3rd ed, Reinhold Publishing Co., New York (1950).

Catalysis by Alkaline Earth Metal Oxides. II. The Mechanism of Ethylene Hydrogenation on Magnesium Oxides

Makoto TEZUKA, Yasunobu INOUE,* and Iwao YASUMORI

Department of Chemistry, Tokyo Institute of Technology, Ookayama, Meguro-ku, Tokyo 152

(Received November 4, 1980)

Synopsis. The kinetic study of ethylene hydrogenation on a thermally activated MgO was carried out. The slow step of the reaction changed from the irreversible addition of a hydrogen atom to adsorbed ethylene in the lower temperature range(373—423 K) to the hydrogenation of an ethyl radical in the higher temperature range (523—673 K).

In a previous paper, we reported the mechanism of ethylene hydrogenation on a thermally activated CaO.[1] The maximum in the reaction rate appeared around a reaction temperature of 340 K. Above this temperature, the kinetic behavior of the reaction resembled those on such transition metals as Ni, Fe, and Pd, whereas, below the temperature, they were rather similar to those on oxides, *e.g.*, ZnO[2] and Cr_2O_3.[3]

Tanabe and his co-workers[4] found that a pretreatment of MgO *in vacuo* at temperatures higher than 1200 K generated the catalytic activity for the hydrogenation of olefins and dienes. In order to establish catalysis by alkaline earth metal oxides, it would be constructive to extend the research into ethylene hydrogenation to other alkaline earth metal oxides. Thus, we undertook the present study to see whether or not the kinetic features described above exist on MgO and then to compare them with the previous results for CaO.

Experimental

Magnesium oxide catalysts were prepared by decomposing $Mg(OH)_2$ of an extra pure grade *in vacuo*. The DTA spectra of $Mg(OH)_2$ showed an endothermic peak in the temperature range of 590—720 K, which was due to H_2O evolution upon the structural rearrangement from trigonal to cubic; this indicated the development of the crystallite structure of MgO by treatment above this temperature range. The oxide thus obtained was subjected to evacuation at 1273 K for 2 h at a pressure lower than 2×10^{-6} Torr (1 Torr=133.3 Pa). Emission spectral analysis showed that the oxide contained Cu (<0.5 ppm), Fe(<0.1), Mn(<10), Si(<80), and Ca(<0.5). The surface area of MgO after the treatment was 118 $m^2\ g^{-1}$. The apparatus, procedure, and reactant gases used were the same as those reported previously.[1] Ethane was the sole product under the present experimental conditions. The repetition of kinetic runs at 523 K decreased the catalytic activity to less than 50% of the initial value, but subsequent evacuation at 1273 K for 2 h recovered the deactivated activity to the original level.

Results and Discussion

As is shown in Fig. 1, the Arrhenius plot of the rate of ethylene hydrogenation on MgO gave rise to a maximum at around 490 K, and the activation energy, E_a, was determined to be 28.5 kJ mol^{-1} in the lower temperature range (373—423 K) and −36.8 kJ mol^{-1} in the higher temperature range (523—673 K). The reaction orders with respect to the pressure of hydrogen, P_h, and ethylene, P_e, were both 1.0 at 623 K, whereas the latter value decreased to nearly zero at 393 K. These variations were similar to those for the same reaction on CaO,[1] but the hydrogen order, 1.0, in the lower temperature range was different from 0.7. Table 1 shows the deuterium distributions in the reaction of ethylene with D_2. At 623 K and in conversions of 28 to 42%, there existed highly-exchanged ethylene ranging from $[D_1]$ to $[D_4]$, and the gaseous composition of H_2, HD, and D_2 nearly reached equilibrium. Ethane contained species from $[D_0]$ to $[D_4]$; the fraction

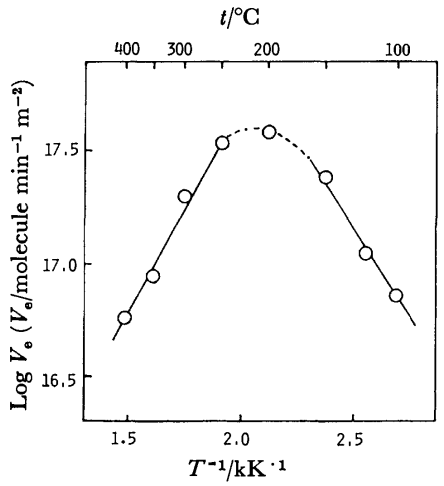

Fig 1. Arrhenius plot of rate in ethylene hydrogenation on MgO.
P_h=20 Torr, P_e=10 Torr.

TABLE 1. DEUTERIUM DISTRIBUTIONS IN THE REACTION OF ETHYLENE WITH D_2 ON MgO

Temp K	Conv. %	Ethylene(%) d_0	d_1	d_2	d_3	d_4	Ethane(%) d_0	d_1	d_2	d_3	d_4	d_5	d_6	H_2	HD (%)	D_2
393	27	96.1	3.9	0	0	0	1.4	6.9	84.4	5.4	1.9	0	0	0	2.8	97.2
	47	83.9	11.4	3.7	1.0	0	0	1.5	87.7	7.7	2.8	0.3	0	0	3.4	96.6
623	28	61.7	28.3	7.9	1.5	0.6	3.3	10.6	65.9	16.8	3.4	0	0	1.8	22.1	76.1
	42	21.5	42.0	26.4	4.8	5.3	1.9	9.0	61.6	20.9	6.4	0.2	0	—	—	—

P_D=20 Torr, P_e=10 Torr.

of ethane [D_2] amounted to about 65%. On the other hand, at 393 K and in similar conversions, small amounts of the deuterium-exchanged ethylene and HD were produced in the gas phase, whereas the fraction of ethane [D_2] was as high as 85%. No isotopic-exchange reaction between ethane and D_2 occurred up to 623 K.

The wide deuterium distributions in the higher temperature range indicated that the hydrogenation proceeds *via* the pathway described by the associative mechanism and that the reaction between the hydrogen atom and the ethyl radical was the rate-determining step, as has been proposed in the case of CaO.[1] Thus, we are able to employ the rate equation obtained before:

$$V_e^h = k_4 K_h K_3 K_e P_h P_e = k^h P_h P_e, \quad (1)$$

where k_4 is the rate constant of the reaction in the rate-determining step. K_e and K_h are the equilibrium constants for the adsorption of ethylene and hydrogen respectively, while K_3 is the equilibrium constant for the surface reaction between the hydrogen atom and the adsorbed ethylene to form the ethyl radical and its reverse reaction. Equation 1 is in agreement with the experimental rate equation.

The drastic fall in the catalytic activity during the course of a reaction at a higher temperature is probably due to the formation of strongly bound surface ethylene species, since the pre-exposure of a fresh catalyst to 10 Torr of ethylene at 523 K caused a decrease in the activity to as low as 15%. The species appears to remain after evacuation at the reaction temperature, but to be removed by evacuation at 1273 K. An analogous poisoning species, presumably polymerized ethylene, was observed in the ethylene hydrogenation on ZnO at 383—673 K.[5]

The reaction in the lower-temperature range provided very small amounts of the deuterium-exchanged ethylene and HD (with scarcely any H_2) in the gas phase, and resulted in the selective formation of ethane-[D_2](≈85%). These findings indicate that the irreversible addition of a hydrogen atom to adsorbed ethylene is a slow step compared to the other steps. When one assumes that the hydrogen atoms adsorbed in a randomly-mixed state participate in the hydrogenation, the reaction order in P_h fails to become larger than 0.5; this contradicts the observed value, 1.0. However, the assumption that the reactive surface hydrogen is a pair of hydrogen atoms on an isolated site leads to the following rate equation:[1]

$$V_e^1 = \frac{k^1 K_e K_h P_h P_e}{(1+K_e P_e + K_h P_h)^2}, \quad (2)$$

where k^1 is the rate constant of the reaction between the hydrogen and adsorbed ethylene. This equation was transformed into the equations having a linear relationship between the $\sqrt{P_e/V_e^1}$ term and P_e or between the $\sqrt{P_h/V_e^1}$ term and P_h in the same way as has been described previously.[1] Figure 2 demonstrates the linearity in their relationships, which gives evidence for the validity of Eq. 2 and, hence, the mechanism proposed. The reaction of 1,3-butadiene with D_2 on MgO was proposed to proceed *via* the attack of a heterolytically split hydrogen atom on the adsorbed butadiene on the isolated sites;[6] this gives support to the assumption employed in deriving Eq. 2. The slightly higher kinetic order in P_h for the ethylene hydorgenation on MgO than for that on CaO suggested the weaker adsorption of hydrogen, in comparison with the ethylene adsorption, on the former oxide.

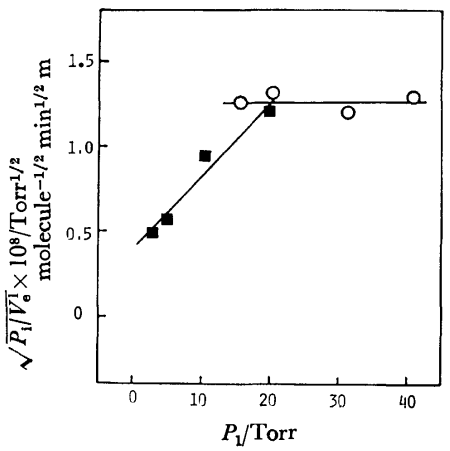

Fig. 2. Plots of $\sqrt{P_1/V_e^1}$ *vs.* P_1.
Reaction temp=393 K, ○: $P_1=P_h$(P_e=10 Torr), ■: $P_1=P_e$(P_h=20 Torr).

There existed a general similarity in the reaction behavior of the ethylene hydrogenation on MgO and CaO; it appears to arise from the common nature of these oxide surfaces. A study of the surface state of thermally-treated alkaline earth metal oxides is in progress using X-ray photoelectron spectroscopy.

References

1) K. Kasama, Y. Inoue, and I. Yasumori, *Bull. Chem. Soc. Jpn.*, **53**, 1842 (1980).
2) W. C. Conner, R. A. Innes, and R. J. Kokes, *J. Am. Chem. Soc.*, **90**, 6858 (1968).
3) R. L. Burwell, Jr., A. B. Littlewood, M. Cardew, G. Pass, and C. T. H. Stoddart, *J. Am. Chem. Soc.*, **82**, 6272 (1960).
4) H. Hattori, Y. Tanaka, and K. Tanabe, *Chem. Lett.*, **1975**, 659; Y. Tanaka, H. Hattori, and K. Tanabe, *ibid.*, **1976**, 37.
5) F. Bozon-Verduraz and S. J. Teichner, *J. Catal.*, **11**, 7 (1968).
6) H. Hattori, Y. Tanaka, and K. Tanabe, *J. Am. Chem. Soc.*, **98**, 4652 (1976).

Electronic Spectra of Some Aromatic Free Radicals

Tatsuo IZUMIDA, Kunihiko INOUE, Shoji NODA,* and Hiroshi YOSHIDA
Faculty of Engineering, Hokkaido University, Kita-ku, Sapporo 060

(Received December 22, 1980)

Synopsis. Electronic spectra are reported for 1-indanyl, 1-tetralyl, and 1-indenyl radicals generated photolytically or radiolytically in rigid matrices; the former two radicals show spectral features similar to those of benzyl radical, whereas the latter radical has a different spectrum because of its non-alternant π electron system.

Aromatic hydrocarbon radicals have been attracting interest as possible intermediates in such reactions as radiolysis of aromatic hydrocarbons,[1] soot formation from combustion,[2] and coal liquefaction.[3] However, there have been very few reports on the observation of the fluorescence spectra of the aromatic free radicals, except for benzyl radical and its methylsubstituted derivatives.[4] We report here for the first time the electronic spectra of 1-indanyl (**1**), 1-tetralyl (1,2,3,4-tetrahydro-1-naphtyl, **2**), and 1-indenyl (**3**) radicals generated photolytically or radiolytically from indan (**4**), indene (**5**), tetralin (1,2,3,4-tetrahydronaphthalene, **6**), and 1,2-dihydronaphthalene (**7**). The electronic spectra will be discussed for α-styryl radical (**8**) generated from phenylacetylene (**9**) also.

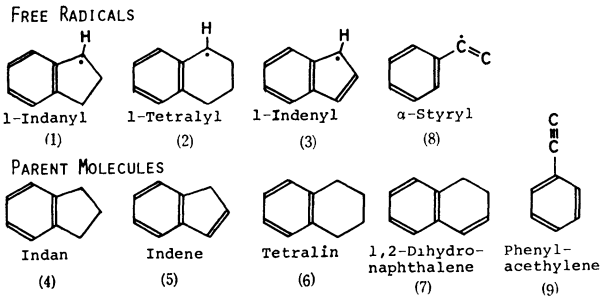

Experimental

4, **5**, **6**, and **9** were vacuum-distilled before use. **7** from Tokyo Kasei Co. (GR grade) and spectrograde ethanol (EtOH) were used as received. 3-Methylhexane (3MHx) was purified as described elsewhere.[5] Solutions of the parent aromatic compounds (about 10 mmol·dm^{-3}) in EtOH or 3MHx were thoroughly degassed by freeze-pump-thaw cycles and sealed in quartz sample tubes (0.4 cm diameter) for optical emission and ESR measurements and in a quartz flat cell (optical path-length of 0.2 cm) for optical absorption measurements. The sample solutions were irradiated at 77 K either with γ-rays from a ^{60}Co source to a dose of 2×10^5 rad or with UV light from a high pressure mercury lamp. Optical emission and excitation spectra of the irradiated samples were recorded with a Hitachi MPF-2A fluorescence spectrophotometer at 77 K. Occasionally, optical absorption and ESR spectra were examined with a Shimadzu MPS-5000 spectrophotometer and a Varian E-109 ESR spectrometer.

Results and Discussion

1-Indanyl and 1-Tetralyl Radicals. The UV-irradiation of **4** and **6** in nonpolar 3MHx matrix gave the emission and excitation spectra shown in Figs. 1A and B. The spectra comprise three excitation bands in visible wavelength region (400—490 nm), near-UV region (300—350 nm), and far-UV region (250—300 nm). The visible excitation band is a mirror image with the emission band. The spectra are attributed to 1-indanyl (**1**) or 1-tetralyl (**2**) radical generated by the photoinduced C–H bond scission in the corresponding parent molecule.

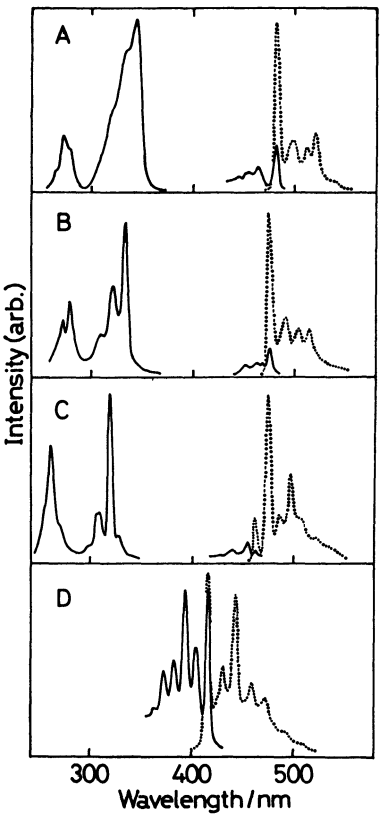

Fig. 1. Emission (·····) and excitation (——) spectra of 1-indanyl (A), 1-tetralyl (B), benzyl (C) and 1-indenyl (D) radicals in 3MHx matrix at 77 K.

When **5** or **7** was γ-irradiated in a polar protic matrix of EtOH, the spectra were essentially the same as Figs. 1A or B. The previous study on the proton transfer to styrene anion gave similar results.[6] These spectra are attributed to **1** or **2**, which result from the electron capture of **5** or **7** followed by the proton transfer from matrix EtOH. The formation of the molecular anions of **5** and **7** was proven by the observation of their absorption spectra which were obtained by γ-irradiating the polar aprotic matrices of 2-methyltetrahydrofuran (MTHF) with **5** and **7**. The absorption spectra of the molecular anions consist of two broad peaks (λ_{max} of 400 and 710 nm for **5**, and 400 and 600 nm for **7**), which are readily bleached with light from an incandescent lamp.

The emission and excitation spectra of benzyl radical generated by UV-irradiation of toluene in the 3MHx matrix are shown for comparison in Fig. 1C. Three excitation bands in the visible, near-UV, and far-UV regions have been assigned to the transitions to $^2A_2$, $^2A_2$, and $^2B_2$ excited states from the $^2B_2$ ground state in the π electron system with C_{2v} symmetry.[7] Both the **1** and **2** radicals, which have the same π electron system, show similar features of the electronic spectra, though a red-shift of the spectra and the removal of the forbidden character of the lowest $^2B_2$—$^2B_2$ transition[8] (comparatively intense 0-0 vibration bands in the visible emission and excitation bands) possibly results from a deviation of the symmetry from C_{2v}. The larger shift observed for **1** may be due to a more constrained structure due to its five-membered ring.

1-Indenyl Radical. The UV-irradiation of **5** in the 3MHx matrix gave two set of emission and excitation spectra generally overlapping each other. The one set was apparently due to **1** mentioned above. The other set could be separated, as shown in Fig. 1D, from the spectra due to **1** by choosing proper wavelengths for excitation and observation. The ESR signal of the same irradiated sample showed a three-line spectrum with a hyperfine separation of 1.2 mT superimposed on a broad spectrum due to 3-methylhexyl radicals and probably due to **1**. The three-line spectrum is assigned to 1-indenyl (**3**) radical on the basis of the hyperfine coupling constants reported by Livingston *et al.*[9] This ESR spectrum and the spectra shown in Fig. 1D slowly disappeared at 77 K, while the emission and excitation spectra of **1** remained unchanged.

The above observations lead to the assignment that the spectra of Fig. 1D is due to **3**. The band origin lies at 415 nm, appreciably shorter than that for benzyl, **1**, and **2** radicals. **3** has a non-alternant π electron system, and it has been suggested that the transition energy to the first excited state is larger.[10] The excited **5** undergoes both the scission of C–H bond giving **3** and the abstraction of H giving **1**; it is not known whether the precursor states for these reactions are the same or not.

α-Styryl Radical. The γ-irradiation of **9** in the MTHF matrix gave the absorption spectrum with maxima at 370 and 533 nm due to the molecular anion of **9**. The irradiation in the EtOH matrix gave the absorption spectrum comprising a visible band with the band origin at 480 nm and a near-UV band with the maximum at 320 nm (no far-UV band could be observed, because of the intense overlapping absorption of the parent molecule). The same near-UV band has been reported previously by Shida and Hamill.[11] This absorption spectrum is very probably due to α-styryl (**8**) radical, because it indicates a π electron system similar to that of benzyl radical.[12] **8** can be generated by the proton transfer to the molecular anion of **9** in the EtOH matrix.

The emission and excitation spectra of **8** were difficult to detect: a weak emission from the irradiated EtOH matrix with **9** was mostly due to α-methylbenzyl radical,[13] probably from impurity styrene contained in **9**. It is unknown why the fluorescence efficiency of **8** is very low compared to that of benzyl radicals, in spite of the fact that both radicals have a similar π electron system. In contrast to the present result, Brocklehurst *et al.* have observed an intense green thermoluminescence spectrum with the band origin at 474 nm upon melting the methylcyclohexane–isopentane mixed solvent containing **9** after γ-irradiating it at 77 K; they have tentatively assigned this luminescence spectrum to **8**.[14]

References

1) S. Noda, M. Ohi, and H. Yoshida, *J. Phys. Chem.*, **84**, 2210 (1980).
2) I. Glassman, "Combusiton," Academic Press (1977), Chap. 8.
3) Y. Sanada, S. Yokoyama, and T. Chiba, *Shokubai*, **22**, 60 (1980).
4) T. Izumida, T. Ichikawa, and H. Yoshida, *J. Phys. Chem.*, **84**, 60 (1980) and references cited in the paper.
5) M. Irie, M. Shimizu, and H. Yoshida, *J. Phys. Chem.*, **80**, 2008 (1976).
6) S. Noda, Y. Fujii, and H. Yoshida, *Bull. Chem. Soc. Jpn.*, **50**, 2226 (1977).
7) J. Baudet and M. Suard, *J. Chim. Phys.*, **67**, 1088 (1972).
8) A. Bromberg, D. M. Friedlich, and A. C. Albrecht, *Chem. Phys.*, **6**, 353 (1974).
9) R. Livingston, H. Zeldes, and M. S. Conradi, *J. Am. Chem. Soc.*, **101**, 4312 (1979).
10) B. Brocklehurst, J. S. Robinson, and D. N. Tawn, *J. Phys. Chem.*, **76**, 3710 (1972).
11) T. Shida and W. H. Hamill, *J. Am. Chem. Soc.*, **88**, 3689 (1966).
12) J. E. Bennett and J. A. Howard, *Chem. Phys. Lett.*, **9**, 460 (1971).
13) T. Saito and H. Yoshida, *Bull. Chem. Soc. Jpn.*, **47**, 3167 (1974).
14) B. Brocklehurst, J. S. Robinson, and D. N. Tawn, *Chem. Phys. Lett.*, **12**, 610 (1972).

X-Ray Photoelectron Spectroscopic Studies of SbSI

Isao IKEMOTO

Research Center for Spectrochemistry, Faculty of Science, The University of Tokyo, Hongo, Bunkyo-ku, Tokyo 113

(Received January 21, 1981)

Synopsis. The binding energies of the core electron peaks suggest that SbSI has more ionic character than covalent character. The valence band spectrum was compared with the calculated density of states. XPS spectra of low temperature ferroelectric phase could not be obtained due to the inhomogeneous spontaneous polarization.

SbSI is the first substance which has been found to be ferroelectrics[1] with semiconductive and photoconductive properties.[2,3] It has a Curie point at 22 °C where it shows first-order phase transition between the high temperature paraelectric phase and the low temperature ferroelectric phase. The crystal structures of the both phases have been analyzed and it has been found that the atomic arrangement is nearly consistent with an ionic model of $Sb^{3+}S^{2-}I^{-}$.[4] However rather short distances among electronegative ions such as sulfurs and iodines suggest that there are tendencies of covalent bond formation.[4] The electronic band structures of SbSI have been calculated using CNDO approximation[5,6] and pseudo-potential method[7] for the ionic and/or covalent models. However more experiments are necessary for more precise calculations.

We measured X-ray photoelectron (XPS) spectra of SbSI and deduced bonding system in SbSI using the binding energies of the core electron peaks. We also compared the XPS valence band with the calculated density of states.[7]

Experimental

X-Ray photoelectron spectra were recorded with a McPherson ESCA 36 Electron Spectrometer, employing Al $K\alpha$ radiation (1486.6 eV). SbSI was kindly supplied by Professor Hideaki Chihara of Osaka University. Samples were single crystals, needle-like along the c axis, but they are not large enough for the measurement. Powdered samples were directly mounted onto Al or Pb plates. Binding energies of photoelectron peaks were calibrated by using the Au $4f_{7/2}$ peak (84.0 eV) of a thin gold film deposited on the sample surface. For the measurement of low temperature ferroelectric phase, samples were cooled with a Dry Ice–ethanol mixture or ice–water mixture.

Results and Discussion

High Temperature Paraelectric Phase. The binding energies of the various core electron peaks are shown in Table 1 with those of related compounds.

The binding energies of iodine peaks in SbSI agree with the corresponding binding energies of iodine peaks in KI. The binding energies of Sb peaks in SbSI are almost same with those of Sb peaks in Sb_2S_3. The binding energy of S peak in SbSI is 1.8 eV smaller than that of S peak in sulfur, and comparing it with the data by Siegbahn *et al.*[8] the state of S in SbSI seems to be S^{2-}. These results show that SbSI has more ionic character than covalent character.

The XPS valence band spectrum of SbSI is shown in Fig. 1 with the density of states obtained by band structure calculation using pseudopotential method.[7] In the calculated density of states, the valence bands separated into five groups and these are interpreted as

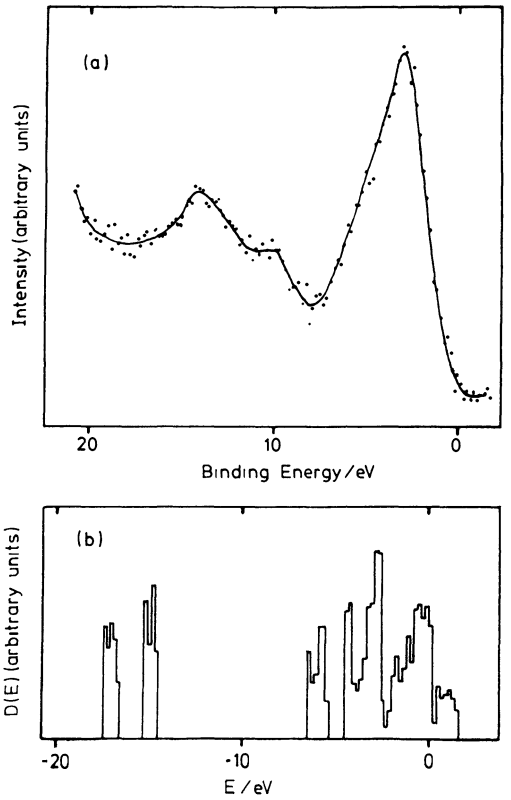

Fig. 1. (a) XPS valence band spectra of SbSI. (b) Calculated density of states of the energy bands of SbSI in the paraelectric phase.[7]

Table 1. Binding energies/eV of SbSI and related compounds

	SbSI	KI	Thiourea	Sulfur	Sb_2S_3[a]	Sb_2S_5[a]
I $3d_{3/2}$	630.3	630.4				
I $3d_{5/2}$	618.8	618.9				
Sb $3d_{3/2}$	538.9				539.0	538.7
Sb $3d_{5/2}$	529.5				529.7	529.4
S 2p	161.2		162.0	163.0		

a) Data from Ref. 9.

the 5s-like bands of I atoms, the 3s-like bands of S atoms, the 5s-like bands of Sb atoms, the 5p-like bands of I atoms, and the 3p-like bands of S atoms as the energy increases. In the XPS spectrum of the valence band region, there are two main bands. On the higher binding energy band, there is a shoulder on the lower binding energy side. The overall shape corresponds well to the calculated density of states, but in the latter the distribution of the density of states is rather broader and the separation between two main bands is also larger than the observed one. Calculated intensities of the bands are rather different from the observed ones, but the difference of the cross section of various levels in XPS must be considered. SbSI has very complicated structure. Therefore, the calculated density of states seems to correspond to the observed XPS valence band rather well.

Low Temperature Ferroelectric Phase. XPS spectra of the ferroelectric phase show very anomalous behavior. When the samples were cooled through the Curie point, each core electron peak showed large shift, sometimes split into two or three peaks or gave a very broad peak. This behavior is similar to that due to large and inhomogeneous charging effect and the reproducible spectra could not be obtained. However when the samples were heated through the Curie point, the normal reproducible spectra of the paraelectric phase could be obtained. Several experiments under various conditions suggested that these behaviors could be explained by the spontaneous polarization which was characteristic of the ferroelectricity. Since samples are powder, the spontaneous polarization is not homogeneous throughout sample surface, then the spectra show the same behavior as that due to the charging effect. Anyway these anomalous behaviors of the XPS spectra are due to the ferroelectric property of SbSI and single crystals must be used to get the true spectra.

The author wishes to express his thanks to Professor Haruo Kuroda, the University of Tokyo for his helpful discussions and Professor Hideaki Chihara for kindly supplying the samples.

References

1) E. Fatuzzo, G. Harbeke, W. J. Merz, R. Nitsche, H. Roetschi and W. Ruppel, *Phys. Rev.*, **127**, 2036 (1962).
2) R. Nitsche and W. J. Merz, *J. Phys. Chem. Solids*, **13**, 154 (1960).
3) T. A. Pikka and V. M. Fridkin, *Fiz. Tverd. Tela (Leningrad)*, **10**, 3378 (1968) [*Sov. Phys.-Solid State*, **10**, 2668 (1969).].
4) A. Kikuchi, Y. Oka, and E. Sawaguchi, *J. Phys. Soc. Jpn.*, **23**, 337 (1967).
5) Y. Yamada and H. Chihara, *J. Phys. Soc. Jpn.*, **21**, 2085 (1966).
6) I. Ya. Nikiforov and A. G. Khasabov, *Fiz. Tverd. Tela (Leningrad)*, **13**, 3589 (1971) [*Sov. Phys.-Solid. State*, **13**, 3030 (1972).].
7) K. Nakao and M. Balkanski, *Phys. Rev. B*, **8**, 5759 (1973).
8) K. Siegbahn, C. Nordling, A. Fahlman, R. Nordberg, K. Hamrin, J. Hedman, G. Johansson, T. Bergmark, S.-E. Karlsson, J. Lindgren, and B. Lindberg, "ESCA-Atomic, Molecular and Solid-State Structure Studied by Means of Electron Spectroscopy," Almgvist and Wiksells, Uppsala (1967).
9) W. E. Morgan, W. J. Stec, and J. R. van Wazer, *Inorg. Chem.*, **12**, 953 (1973).

Highly Active Aluminas for Isomerization of 1-Butene and Hydrogen Exchanges between Ethylene or Cyclopropane and Deuterium

Masahiro UTIYAMA, Hideshi HATTORI, and Kozo TANABE*

Department of Chemistry, Faculty of Science, Hokkaido University, Sapporo 060

(Received February 25, 1981)

Synopsis. Among eleven kinds of aluminas, alumina V prepared from aluminium sulfate with urea exhibited a pronounced activity for the isomerization of 1-butene, while alumina III or II prepared from aluminium nitrate with ammonia or urea showed the highest activities for the exchange reactions between ethylene or cyclopropane and deuterium, respectively.

Alumina is one of the most interesting and useful oxide catalysts for hydrocarbon reactions. The exchange reaction of deuterium between CH_4 and D_2 is known to take place easily over alumina even at room temperature,[1,2] but not over the other oxides such as MgO, CaO, SrO, BaO, La_2O_3, CeO_2, Pr_2O_3, Tb_2O_3, TiO_2, ZnO, and WO_3 below 300 °C of reaction temperature,[3] indicating an anomalously high catalytic activity of alumina compared with the other oxides. However, the catalytic properties of various aluminas for the exchange reaction have been found to change remarkably depending on the preparation method.[4] In order to examine how the activity of alumina is affected by the preparation method and to know what kinds of aluminas are best for particular hydrocarbon reactions, eleven kinds alumina catalysts were prepared by different methods and subjected to the activity test.

Experimental

Various aluminas were prepared from various aluminium compounds by different methods as shown in Table 1. In the case of hydrolysis with ammonia or urea, the final pH was adjusted to 7—8. Precipitation with urea was carried out at ≈90 °C, precipitates of hydroxides being formed gradually in 4 h. Details of precipitation with urea were described previously.[5] The hydroxides of Al_2O_3 V and VI were washed with distilled water until sulfate ions were not detected with barium chloride in the washings. The hydroxide of Al_2O_3 XI was washed with 30 L of distilled water. The hydroxide of Al_2O_3 VII, VIII, and X were washed with 6 L of distilled water. In the latter case, halogen ions remained in the washings. The hydroxides were dried at 120 °C for 20 h and calcined in air at 550 °C. The aluminas which were evacuated at 600 °C for 3 h were used as catalysts. Surface area was determined by applying the BET method to the adsorption isotherm of nitrogen at −196 °C. The structure of aluminas was determined from the powder patterns obtained with a Rigaku Denki Giger flex X-ray diffractometer using filtered Cu K_α radiation.

The exchange reactions between ethylene or cyclopropane and deuterium were carried out at room temperature in a closed recirculation reactor that had a total volume of *ca.* 400 ml. A mixture of 5 Torr of each hydrocarbon and 40 Torr (1 Torr = 133.322 Pa) of D_2 was used. The reaction products were analyzed by a mass spectrometer (Hitachi M-52 type), parent peaks of $m/e=28$—32 and $m/e=42$—48 being used for deuterated ethylene and cyclopropane, respectively. The catalytic activity was expressed by K_ϕ % per unit surface area of catalyst in thefollowing equation.[3]

$$d\phi/dt = K_\phi(\phi_\infty - \phi)/\phi_\infty WS,$$

where ϕ represents the average number of D atoms in 100 molecules of each hydrocarbon in time t, ϕ_∞ for $t=\infty$, W the weight of catalyst, and S specific surface area.

Isomerization of 1-butene was carried out at room temperature in the same reactor as above with 70 Torr of 1-butene. For analysis of the butenes, a 5-m column packed with VZ-7 and thermostated at 0 °C was used. Initial rates of the formation of 2-butenes were taken as the catalytic activity.

Results

Catalytic activities of various aluminas are shown in Table 2, where the activity for the exchange of methane with deuterium was cited from the literature.[4] Al_2O_3 VII which showed the highest activity for the exchange reaction of methane with deuterium did not show high activities for the exchange reaction between ethylene or cyclopropane and D_2 and was almost inactive for the

TABLE 1 PREPARATION METHODS, SURFACE AREA AND STRUCTURES OF ALUMINAS EVACUATED AT 600 °C

Al_2O_3	Preparation		Surface area	Structure
	Starting material	Method	$m^2\ g^{-1}$	
I	Isopropoxide	Hydrolysis	236	γ
II	$Al(NO_3)_3$	Precipitation with urea	110	γ
III	$Al(NO_3)_3$	Precipitation with ammonia	156	γ
IV	$Al(NO_3)_3$	Direct thermal decomposition	135	Amorphous
V	$Al_2(SO_4)_3$	Precipitation with urea	11	Complex, Broad
VI	$Al_2(SO_4)_3$	Precipitation with ammonia	216	γ
VII	$AlCl_3$	Precipitation with urea	147	γ
VIII	$AlCl_3$	Precipitation with ammonia	248	γ
IX	$AlCl_3$	Direct thermal decomposition	103	(χ), Broad
X	$AlBr_3$	Precipitation with urea	173	γ
XI	$NaAlO_2$	Precipitation with CO_2	194	γ

Table 2. Catalytic activities of various aluminas for hydrocarbon reactions at room temperature

Al_2O_3	Exchange reactions[a]			Isomerization of 1-butene	
	CH_4-D_2[b]	C_2H_4-D_2	Cyclo-C_3H_6-D_2	Rate[c]	*cis*/*trans*[d]
I	4.2	7.9	29.0	5.0	4.3
II	2.7	9.1	65.6	2.1	5.4
III	4.1	13.3	49.4	2.7	4.2
IV	0.0	1.7	14.6	10.2	7.4
V	0.0	0.0	0.0[e]	140.6	0.8
VI	1.8	2.4	18.9	5.9	7.4
VII	18.7	3.6	6.0	1.4	3.2
VIII	4.4	3.8	7.0	0.3	3.2
IX	1.0	0.4	2.0	2.9	9.4
X	2.3	10.1	45.7	2.7	4.4
XI	0.0	1.1	9.6	20.0	5.8

a) $10^4 k_\phi$ m^{-2} s^{-1}. b) Cited from Ref. 4. c) 10^2 mmol m^{-2} s^{-1}. d) *cis*-2-Butene/*trans*-2-butene. e) Isomerization to propylene occurs.

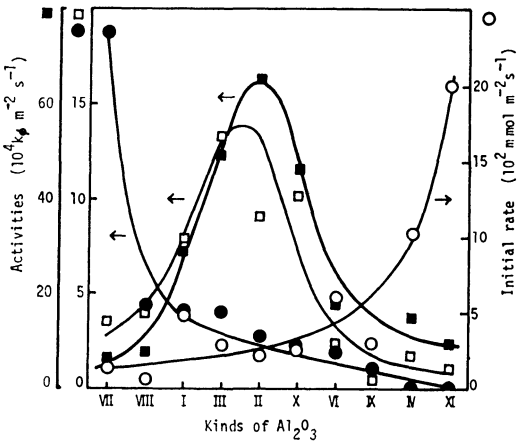

Fig. 1. Activities of various kinds of Al_2O_3 for hydrocarbon reactions. ●; CH_4–D_2, □; C_2H_4–D_2, ■; C_3H_6–D_2, ○; isomerization of 1-butene (Kinds of Al_2O_3 were arranged in decreasing order of the activity for the exchange reaction of CH_4 with D_2).

isomerization of 1-butene. The aluminas which showed the highest activities for the exchange of D_2 with ethylene or cyclopropane and the isomerization of 1-butene were Al_2O_3 III, Al_2O_3 II, and Al_2O_3 V, respectively. Al_2O_3 V exhibited a pronounced activity for the isomerization, but was completely inactive for the exchange reactions. In the case of Al_2O_3 V, the ratio of *cis*-2-butene to *trans*-2-butene is very low (0.8) compared with that of other aluminas. This suggests that the acid sites play an important role for the isomerization of 1-butene.[6] For the exchange reaction of methane with deuterium, the proton abstraction from methane by basic sites is reported to be important.[3,7] However, the activity per unit basic sites of alkaline earth oxides whose basic strength is higher than that of alumina is much lower than that of alumina.[3] The *cis*/*trans* ratio which is sometimes used as an indication of basic property of catalyst[8,9] does not correlate with the exchange activity. Thus, besides basic sites, acidic sites are considered to be important as active sites for exchange reaction to stabilize carbanion intermediates formed by proton abstraction. In the present work, we demonstrate highly active aluminas for the exchange and isomerization reactions and emphasize that the activity of alumina is remarkably controlled by the preparation method.

In order to characterize the activities of various aluminas, the activities for four hydrocarbon reactions were plotted against the eleven kinds of alumina which are arranged in the order of activity for the exchange between methane and deuterium in Fig. 1. The higher the activity for the exchange of methane with deuterium, the lower the activity for the isomerization of 1-butene. On the other hand, the aluminas which are less active for the above two reactions showed the maximum activities for the exchange reaction between ethylene or cyclopropane and deuterium.

References

1) J. G. Larson and W. K. Hall, *J. Phys. Chem.*, **69**, 3080 (1965).
2) B. D. Flockhart, S. S. Uppal, and R. C. Pink, *Trans. Faraday Soc.*, **67**, 513 (1971).
3) M. Utiyama, H. Hattori, and K. Tanabe, *J. Catal.*, **53**, 237 (1978).
4) K. Tanabe, M. Utiyama, and H. Hattori, *Proc. Symp. Sci. Catal. Appl. Ind.*, Fertilizer (Planning & Development) India Ltd., Sindri (1979), p. 453.
5) K. Tanabe, M. Itoh, K. Morishige, and H. Hattori, "Preparation of Catalysts," ed by B. Delmon, P. A. Jacobs, and G. Poncelet, Elsevier, Amsterdam (1976), p. 65.
6) J. W. Hightower and W. K. Hall, *Chem. Eng. Prog.*, **63**, 122 (1967).
7) C. Kemball, *Adv. Catal.*, **11**, 223 (1959).
8) C. C. Chang, W. C. Conner, and R. J. Kokes, *J. Phys. Chem.*, **77**, 1957 (1973).
9) H. Hattori, N. Yoshii, and K. Tanabe, *Proc. Int. Congr. Catal., 5th, 1972*, **10**-233 (1973).

The Crystal and Molecular Structure of 2-Acetoxy-2-methyl[1,3]dioxolo-[4,5-*c*]isoquinoline-5-carbonitrile. A Photoproduct of 1,4-Diacetoxy-2,3-diazidonaphthalene

Yukishige KITANO,* Tamaichi ASHIDA,** and Akira YABE***

Toray Research Center, Inc., Sonoyama, Ohtsu 520

***Faculty of Engineering, Nagoya University, Chikusa-ku, Nagoya 464*

****National Chemical Laboratory for Industry, Yatabe-Higashi 1-1, Tsukuba, Ibaraki 305*

(Received November 19, 1980)

Synopsis. The crystal of the title compound is triclinic, with a space group of $P\bar{1}$ and with two molecules per unit cell with dimensions of $a=8.317$ (2), $b=11.191$ (1), $c=7.731$ (1)Å, $\alpha=105.91$ (1), $\beta=103.76$ (2), and $\gamma=102.60$ (1)°. The fused isoquinoline and dioxolane rings lie on nearly the same plane; the non-hydrogen atoms of the acetoxyl and methyl groups make another plane. These two planes make an angle of 92.0° with each other.

In a series of photolyses of organic azides, it has been reported that 1,4-diacetoxy-2,3-diazidonaphthalene (**1**) gave efficiently an unexpected photoproduct (**3**) *via* α,α′-dicyano-*o*-quinodimethan (**2**) by prolonged photo-irradiation at 77 K in a rigid medium.[1] The structure

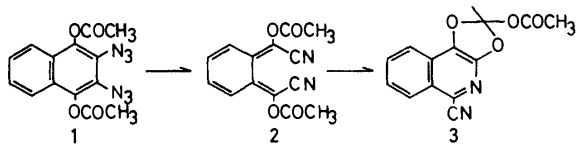

1 2 3

of the product was studied spectroscopically, but could not be established exclusively. The compound, obtained in the form of single crystals, was then submitted to X-ray analysis.

Experimental

Single crystals of the compound were grown by the slow evaporation of an ethanol–dichloromethane solution at room temperature. They were yellow plates tabular on (100), elongated in the *c* direction. The lattice constants were obtained by a least-squares fit of 2θ values of 15 reflections measured on a Rigaku automated four-circle diffractometer.

Crystal Data. $C_{14}H_{10}H_2O_4$, MW=270.24, Mp=146 °C (dec), triclinic, $P\bar{1}$, $a=8.137$ (2), $b=11.191$ (1), $c=7.731$ (1)Å, $\alpha=105.91$ (1), $\beta=103.76$ (2), $\gamma=102.60$ (1)°, $V=640.5$ Å^3, $Z=2$, $d_{obsd}=1.41$, $d_{calcd}=1.402$ g cm^{-3}, μ (for Cu $K\alpha$)=8.95 cm^{-1}.

The intensity data were collected from a crystal having dimensions of $0.3\times0.4\times0.3$ mm. The intensities were recorded in the 2θ-ω scan mode with a speed of 10° (ω) min^{-1} and the range of $(1.0+0.142\tan\theta)$° (ω), graphite-monochromated Cu $K\alpha$ radiation being used. 2270 independent reflections with $2\theta\leq135$° were obtained, of which 2208 were non-zero reflections. The intensities of three reference reflections, periodically remeasured, decreased gradually during data collection. The intensity data were corrected for crystal deterioration and for Lorentz and polarization effects, but no absorption correction was applied.

Structure Determination and Refinement

The structure was solved by the direct method with the MULTAN 78 program,[2] refined by the block-diadonal least-squares procedure with the HBLS V program.[3] In the refinement, the function minimized was $\sum\omega(|F_o|-|F_c|)^2$ with the weight scheme of $\omega=k$ for $F_o=0$, and $\omega=(\sigma^2(F_o)+a|F_o|+b|F_o|^2)^{-1}$ for $F_o\neq0$, where $\sigma(F_o)$ is the standard deviation based on the counting statistics. The final refinement ($k=7.28$, $a=-0.666$, and $b=0.025$) led to the *R*-index ($\sum||F_o|-|F_c||/\sum|F_o|$) of 0.0624 for all the reflections and 0.0610 for the non-zero reflections. The scattering factors were taken from the International Tables for X-Ray Crystallography.[4] The final atomic parameters for the non-hydrogen atoms are given in Table 1.[5]

Table 1. Positional($\times10^4$) and thermal ($\times10^2$) parameters for the non-hydrogen atoms

Atom	*x*	*y*	*z*	B_{eq}/Å^2 a)
C(1)	5267(3)	2399(2)	8348(3)	302
C(2)	3943(3)	1337(2)	8180(3)	309
C(3)	2337(3)	1370(3)	8465(4)	384
C(4)	1142(4)	244(3)	8238(4)	448
C(5)	1526(4)	−957(3)	7767(4)	449
C(6)	3037(4)	−1017(2)	7494(4)	393
C(7)	4326(3)	123(2)	7672(3)	320
C(8)	5931(3)	125(2)	7374(3)	326
C(9)	6768(3)	2268(2)	8044(4)	328
C(10)	6931(3)	4387(2)	8734(4)	344
C(11)	6310(4)	−1100(3)	6796(4)	400
C(12)	8237(3)	5041(3)	12101(4)	381
C(13)	9078(4)	6240(3)	13831(4)	456
C(14)	6663(4)	5070(3)	7300(4)	492
N(1)	7185(3)	1188(2)	7557(3)	353
N(2)	6584(4)	−2069(2)	6333(4)	573
O(1)	5281(2)	3675(2)	8773(3)	337
O(2)	7846(2)	3460(2)	8267(3)	381
O(3)	7876(2)	5351(2)	10515(2)	324
O(4)	7906(3)	3945(2)	12105(3)	569

a) The equivalent isotropic temperature factor defined by W. C. Hamilton (*Acta Crystallogr.*, **12**, 609 (1959)).

Results and Discussion

The bond lengths and angles are shown in Fig. 1, together with the atomic symbols.

All the atoms of the fused heterocyclic ring lie on the same plane; the average deviation of the thirteen ring atoms from the plane is 0.008 Å, with the maximum deviation of 0.017 Å for C(8). The C(11) and N(2) atoms of the cyano group deviate from this plane by 0.069 and 0.118 Å respectively. The non-hydrogen atoms of the acetoxyl and methyl groups bonded to the dioxolane ring also make a plane; the average displace-

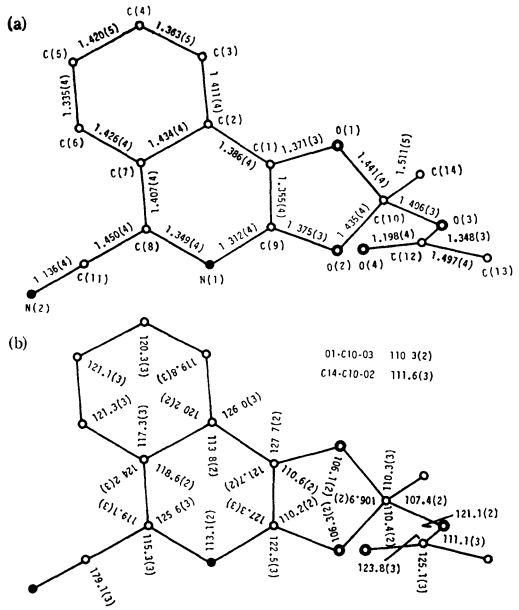

Fig. 1. a) Bond lengths (l/Å) and b) bond angles (ϕ/°) of the compound.

ment of the atoms from the mean plane is 0.030 Å, with the maximum deviation of 0.059 Å for C(13). These two mean planes make an angle of 92.0° with each other.

All the bond lengths and angles are normal. The O(1)–C(10) and O(2)–C(10) bond lengths in the dioxolane ring are in good agreement with the accepted value for the C–O single bond[6] and can well be compared with the corresponding values for the isolated dioxolane ring in 4′-methylsulfonylspiro[1,3-dioxolane-2,4′-piperidine].[7] The somewhat short O(1)–C(1) and O(2)–C(9) lengths can be explained partly in terms of the conjugation of the dioxolane oxygen atoms with the isoquinoline nucleus.

The arrangement of the molecules in the crystals is shown in Fig. 2. The fused heterocyclic rings, approximately parallel to (001), are stacked at intervals of

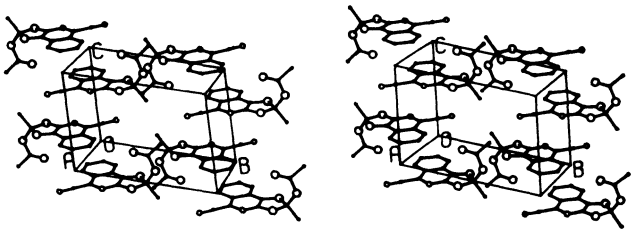

Fig. 2. The arrangement of the molecules in the crystal drawn by the plotter program PLUTO.[8]

3.5 Å along the c axis. The cyano groups of the two molecules around a center of symmetry are antiparallel to each other, leading to favourable dipole-dipole interaction. There are no abnormally short intermolecular contacts.

References

1) A. Yabe, *Bull. Chem. Soc. Jpn.*, **54**, 1176 (1981).

2) P. Main, S. E. Hull, L. Lessinger, G. Germain, J. P. Declercq, and M. M. Woolfson, "MULTAN 78, A System of Computer Programmes for The Automatic Solution of Crystal Structure from X-Ray Diffraction Data," Univ. of York, England, and Louvain, Belgium (1978).

3) T. Ashida, "The Universal Crystallographic Computing System-Osaka," The Computation Center, Osaka University (1973).

4) "International Tables for X-Ray Crystallography," Kynoch Press, Birmingham (1974), Vol. IV, p. 72.

5) The lists of structure factors, anisotropic thermal parameters for the non-hydrogen atoms, atomic parameters for the hydrogen atoms, and the least-squares planes of the molecule are deposited at the office of This Bulletin as Document No. 8139.

6) "International Tables for X-Ray Crystallography," Kynoch Press, Birmingham (1962), Vol. III, p. 276.

7) P. Smith-Verdier, S. Garcia-Blonco, and F. Florencio, *Acta Crystallogr., Sect. B*, **32**, 2006 (1976).

8) S. Motherwell, "PLUTO, A Program for Plotting Molecular and Crystal Structures," Cambridge (1976).

On the Additivity of Molar Volume and Refractivity of Molten $Ca(NO_3)_2 \cdot 3.18H_2O$–KSCN System

Sheik Mahiuddin and Kochi Ismail*

Department of Chemistry, North-Eastern Hill University, Laitumkhrah, Shillong-793 003, India

(Received May 17, 1980)

Synopsis. Densities and refractive indices of $Ca(NO_3)_2 \cdot 3.18H_2O$–KSCN melts have been measured as functions of temperature and composition. Densities, molar volumes, and refractive indices show linear dependence on temperature. Molar volume, intrinsic volume, molar refractivity, and the product of refractive index and molar volume show additivity within ±2% error. The molten $Ca(NO_3)_2 \cdot 3.18H_2O$–KSCN system at ambient temperatures appears to behave like an ideal mixture of molten $Ca(NO_3)_2 \cdot 3.18H_2O$ and supercooled KSCN melt.

Earlier, we have reported the densities, viscosities, and equivalent conductances of molten $Ca(NO_3)_2 \cdot 3.99H_2O$–KSCN systems.[1] In that paper,[1] although we have mentioned about an interesting feature of this system, *i. e.*, its ideal behavior with respect to molar volume, our major emphasis was on the non-Arrhenius temperature dependence of viscosities and equivalent conductances. In order to understand more about the ideal behavior of such a binary system we have reported here the densities and refractive indices of molten $Ca(NO_3)_2 \cdot 3.18H_2O$–KSCN systems as functions of temperature and composition.

Experimental

Reagent grade calcium nitrate tetrahydrate, mp 43.5 °C, was used in the molten state. The exact number of moles of water per mole of calcium nitrate has been determined through EDTA titration method and is found to be 3.18. Potassium thiocyanate was recrystallized twice from double-distilled water. Preparation of samples of $Ca(NO_3)_2 \cdot 3.18H_2O$–KSCN and their density measurements were made as described earlier.[1] The refractive index (±0.1%) measurements were made corresponding to sodium light using the Abbe refractometer.

Results and Discussion

The molar volumes (V) of $Ca(NO_3)_2 \cdot 3.18H_2O$–KSCN melts are calculated from their measured densities and are represented in Table 1 in the form of a linear function

$$V = V_o' + b'T, \tag{1}$$

where V_o' and b' are constants at a particular concentration. As the system under study has an inherent tendency to supercool the temperature dependence of molar volume may also be represented as

$$V = V_o + b'(T - T_o), \tag{2}$$

where T_o is the ideal glass transition temperature and V_o is the intrinsic volume. Comparison of Eqs. 1 and 2 gives that

$$V_o' = V_o - b'T_o. \tag{3}$$

From Fig. 1a it may be noticed that both V_o' and b' vary linearly with mole fraction of KSCN, x_2. Presuming that V_o and T_o vary linearly with concentration,[1] Eq. 3 becomes on substituting the linear concentration dependences of all the terms

$$m_1 = m_2 - m_3T_{o1} + b_1'm_4 - m_3m_4x_2, \tag{4}$$

where m_1, m_2, m_3, and m_4 are the respective slopes of linear variations of V_o', V_o, b', and T_o with x_2. T_{o1} and b_1' are the values of T_o and b', respectively for pure $Ca(NO_3)_2 \cdot 3.18H_2O$ melt. From Eq. 4 it may be understood that the observed constancy of m_1 appears to be explainable only when T_o becomes almost independent of solute concentration. In such

Table 1. Parameters for Eqs. 1 and 6 for the molar volume and refractive index, respectively of $Ca(NO_3)_2 \cdot 3.18H_2O$–KSCN melts

x_2	b' / $cm^3\ mol^{-1}\ K^{-1}$ or k_1	V_o' or k_2 / $cm^3\ mol^{-1}$	σ_1[a] / $cm^3\ mol^{-1}$ or σ_2[a]	V_o[b] / $cm^3\ mol^{-1}$
0.0	0.0675	106.90	0.027	120.81
	(1.0159)	(56.82)	(8×10^{-5})	
0.0265	0.0662	106.00	0.018	119.64
	(0.8917)	(72.14)	(8×10^{-5})	
0.1599	0.0618	97.97	0.022	110.70
	(0.9881)	(56.52)	(1×10^{-4})	
0.3533	0.0544	86.65	0.017	97.86
	(0.9664)	(53.69)	(1×10^{-4})	
0.4499	0.0509	80.81	0.020	91.30
	(0.9567)	(52.00)	(1×10^{-4})	
0.5414	0.0476	75.34	0.015	85.15
	(0.7025)	(72.23)	(1×10^{-4})	
1.0000[c]	(1.1821)	(22.85)	(4×10^{-5})	

Parameters for Eq. 6 (k_1 and k_2) are within the parantheses. a) $\sigma_1 = [\Sigma(V_{obsd} - V_{calcd})^2/N]^{1/2}$ and $\sigma_2 = \Sigma(n_{obsd} - n_{calcd})^2/N]^{1/2}$, N is the number of the data points. b) Intrinsic volume, $V_0 = V_o' + 206b'$. c) Data from Refs. 6 and 7.

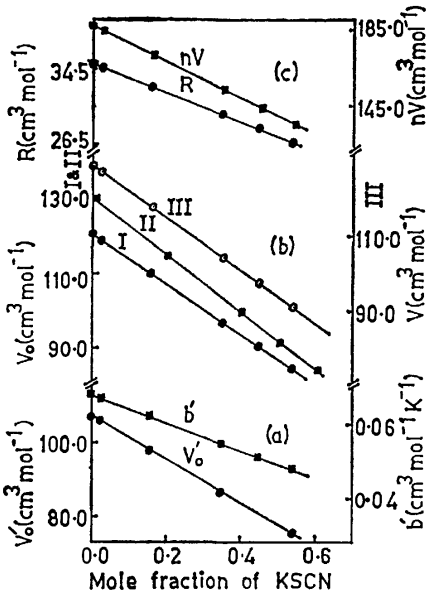

Fig. 1. Variations of (a) V_o' and b', (b) V_o (I-present work; II-Ref 1) and V (at 323 K), and (c) molar refractivity (R) and nV (at 323 K) with concentration for molten $Ca(NO_3)_2 \cdot 3.18H_2O$–KSCN systems.

a case $m_4 \approx 0$ and Eq. 4 reduces to

$$m_1 = m_2 - m_3 T_{o1}. \quad (5)$$

With the knowledge of the reported[1-3] values of T_o for calcium nitrate tetrahydrate, the T_o value for $Ca(NO_3)_2 \cdot 3.18H_2O$ may be considered as nearly equal to 206 K. Substituting this value for T_{o1} and also the values of $m_1 = 59.1$ cm^3 mol^{-1} and $m_3 = 0.037$ cm^3 mol^{-1} K^{-1} obtained from Fig. 1a in Eq. 5, the value of m_2 may be determined which is found to be 66.7 cm^3 mol^{-1}. This value of m_2 is also in agreement with the observed value of the slope of the plot of V_o versus concentration (Fig. 1b), the value of V_o (Table 1) being obtained from Eq. 3 after keeping T_o as 206 K. It is worthy to note that the present extrapolated value of $V_o = 54.0$ cm^3 mol^{-1} for pure KSCN coincides with the value obtained in a similar manner using computed values of V_o from the transport property data of $Ca(NO_3)_2 \cdot 3.99H_2O$–KSCN melts[1] (Fig. 1b). Such an agreement in the V_o value of pure KSCN estimated independently from the molar volume and transport property data appears to envisage that the assumption made regarding the concentration independent nature of T_o is justifiable. Accordingly, the T_o value of pure KSCN may be considered as nearly the same as that of $Ca(NO_3)_2 \cdot 3.18H_2O$ which we have taken as 206 K. This value is closely comparable with the value 203 K for T_o of KSCN computed from its electrical conductance data.[4] Moreover, it has been found that the concentration dependence of V_o predominantly governs the variation of V with x_2 for the $Ca(NO_3)_2 \cdot 3.18H_2O$–KSCN melts. As reported earlier[1] V is found to be additive within ±2% error. The molar volumes of pure KSCN at low temperatures required for testing the additivity of V are estimated from the same linear function for its density above the melting point.[5]

The measured refractive indices (n) of the systems under study also show a linear dependence on temperature. In this case, however, the least-squares fitted values of the intercepts and slopes do not vary linearly with x_2. Therefore, the composition dependence of refractive index has been described in terms of molar refractivity. Molar refractivities show negligible dependence on temperature but vary linearly with x_2 as illustrated with an isotherm at 323 K in Fig. 1c. It may be noted that the extrapolated value of molar refractivity (19.5 cm^3) for pure KSCN at 323 K coincides within ±2% with the value (19.11 cm^3) calculated from the refractive index and density values for molten KSCN obtained after extrapolating the high temperature data[5,6] to 323 K. Therefore, in a mixture of $Ca(NO_3)_2 \cdot 3.18H_2O$ and KSCN the formation of complex ions does not appear to take place.

Furthermore, an attempt to fit the n data to the Gladstone-Dale (G-D) equation,[7] $n = 1 + k/V$, has revealed that the present data fit into a slightly modified G-D equation of the form

$$n = k_1 + k_2/V. \quad (6)$$

The least-squares fitted values of the constants k_1 and k_2 are given in Table 1. Rearranging Eq. 6 and then by substituting the additive behavior of molar volume on the right hand side of the rearranged expression, we obtain

$$nV = A - Bx_2, \quad (7)$$

where $A = n_1V_1$ and $B = n_1V_1 - n_2V_2$. The terms with suffix 1 correspond to $Ca(NO_3)_2 \cdot 3.18H_2O$ and those with 2 to KSCN. In obtaining Eq. 7 k_1 and k_2 are considered to be independent of concentration. The least-squares fitted values of k_1 and k_2 (Table 1), on the other hand, are not exactly independent of concentration, but vary in a non-linear fashion. However, such changes in k_1 and k_2 do not seem to produce much deviation from Eq. 7 as apparent from the linearity of the plot of nV *versus* x_2 (Fig. 1c). It has also been found that the least-squares fitting of nV into Eq. 7 is reasonably good. Therefore, the applicability of the modified G-D equation seems to account for the observed additive nature of the product nV within ±2%.

The financial help from the university to one of us (S.M.) is gratefully acknowledged.

References

1) N. Islam and K. Ismail *J. Phys. Chem.*, **79**, 2180 (1975).
2) C. A. Angell, *J. Phys. Chem.*, **70**, 3988 (1966).
3) C. T. Moynihan, C. R. Smalley, C. A. Angell, and E. J. Sare, *J. Phys. Chem.*, **73**, 2287 (1969).
4) P. Dulieu and P. Claes, *Bull. Soc. Chim. Belg.*, **82**, 639 (1973).
5) D. H. Kerridge, "Advances in Molten Salt Chemistry," ed by J. Braunstein, G. Mamantov, and G. P. Smith, Plenum Press, New York (1975), Vol. III, Chap. 5.
6) H. R. Jindal and G. W. Harrington, *J. Phys. Chem.*, **71**, 1688 (1967).
7) S. S. Kurtz, Jr., and A. Sankin, "Physical Chemistry of the Hydrocarbons," ed by A. Farkas, Academic Press, New York (1953), Vol. II, Chap. 1.

The Halogenation of the *N,N'*-Ethylenebis(5,5,5-trifluoro-4-oxo-2-pentaniminato)nickel(II) Complex and the Reaction Intermediate

Yuki Fujii,* Masaaki Ito, and Kunio Akiyama

Department of Chemistry, Faculty of Science, Ibaraki University, Bunkyo-cho, Mito, Ibaraki 310

(Received October 28, 1980)

Synopsis. [Ni(tfac$_2$en)] reacted with NXS (*N*-chloro- or *N*-bromosuccinimide) in an alcoholic solvent to give the halogenated complexes at the γ-carbon atoms. The reaction intermediate was successfully isolated and was characterized by the use of the ^{1}H-NMR, IR, and AB spectra.

It is well known that the γ-protons of metal β-diketonates[1] and their Schiff-base derivatives[2,3] can be replaced by halogen atoms by the use of NXS. These halogenations have been regarded as examples of the electrophilic substitution reaction of the γ-protons with X^+, and the following reaction mechanism has been proposed:[1]

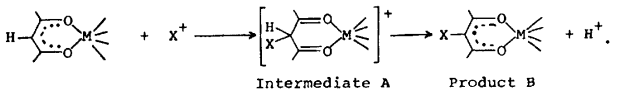

Intermediate A Product B

However, there have been few detailed studies of the reaction mechanism.[4,5]

In the course of our study[6] for the halogenation of Ni(II) complexes of *N,N'*-ethylenebis(β-oxo imine) in an alcoholic solvent, we found that the titled complex, abbreviated as [Ni(tfac$_2$en)],[7] gives a pretty stable reaction intermediate.

Experimental

Chlorination. A methanol solution (100 cm^3) of NCS (1.3 g) was added to a slurry of [Ni(tfac$_2$en)][8] (1.0 g) in methanol (200 cm^3). The mixture was stirred for 10 min at 35 °C to give a homogenious red solution. It was then concentrated to about 30 cm^3 under reduced pressure below 35 °C. When the solution was allowed to stand for 1 h, red crystals were separated out, and were washed with cold methanol. Yield, about 21%. Found: C, 32.04; H, 3.48; N, 5.48%. Calcd for $NiC_{14}H_{18}N_2O_4F_6Cl_2$: C, 32.21, H, 3.48; N, 5.37%. (Complex I).

On the other hand, the red solution obtained above was heated on a water bath for 30 min and then concentrated to about 100 cm^3. When water was added to the solution, a light-green precipitate was separated out. It was subsequently recrystallized from methanol. Yield, about 40%. Found: C, 31.48; H, 2.39; N, 6.24%. Calcd for $NiC_{12}H_{10}N_2O_2F_6Cl_2$: C, 31.48; H, 2.21; N, 6.12%. (Complex II).

When Complex I was allowed to stand in the atomosphere, it gradually decomposed to [Ni(tfac$_2$en)] in the solid state. When water was added to a methanol or DMSO solution of Complex I, it decomposed rapidly to give [Ni(tfac$_2$en)]. However, when the methanol solution of Complex I was heated at about 90 °C, it decomposed to form Complex II.

Bromination. The brominated complexes were obtained by using NBS by a method similar to that for the chloronation. From the red reaction mixture, reddish crystals were separated out in about a 30% yeild. Found: C, 27.38; H, 2.79; N, 4.66%. Calcd for $NiC_{14}H_{18}N_2O_4F_6Br_2$: C, 27.53; H, 2.98; N, 4.59%. (Complex III). When ethanol was used as the solvent, reddish crystals were obtained in about a 60% yield. Found: C, 29.91; H, 3.27; N, 4.52%. Calcd for $NiC_{16}H_{22}N_2O_4F_6Br_2$: C, 30.08; H, 3.48; N, 4.39%. (Complex IV).

When the red reaction mixture was treated by a method similar to that employed for the red solution with NCS, light-green crystals were obtained in about a 80% yield. Found: C, 26.53; H, 1.95; N, 5.33%. Calcd for $NiC_{12}H_{10}N_2O_2F_6Br_2$: C, 26.36; H, 1.95; N, 5.31%. (Complex V).

Results and Discussion

The characterization data are listed in Table 1. It is well known that *N,N'*-ethylenebis(β-oxo iminato)-nickel(II) complexes are diamagnetic and take a square planar structure. Since Complexes II and V are also diamagnetic and show AB spectra similar to that of [Ni(tfac$_2$en)], it is evident that Complexes II and V take the planar structure. In the ^{1}H-NMR spectra of Complexes II and V, no signal which corresponds to the γ-proton is observed. Accordingly, it is clear that they are the halogen-substituted complexes at the γ-carbon atoms. The two strong IR bands at 1500—1600 cm^{-1} for [Ni(tfac$_2$en)] shift to a somewhat lower energy site in Complexes II and V.

Further, the π-π^* transitions at 26.3—28.0 kcm^{-1} for [Ni(tfac$_2$en)] also shift to a somewhat lower energy site in the halogenated complexes II and V. These lower energy shifts of the IR and AB spectra are characteristic of the halogenated complexes at the γ-carbon atom.[1,3,4,9]

Complexes I, III, and IV are also diamagnetic and show the d-d transitions at about 20.8 kcm^{-1} which is characteristic of the square planar Ni(II) complexes. In their ^{1}H-NMR spectra, the signal of the γ-proton is observed at about 4.7 ppm; this position is at a somewhat higher field as compared with that of [Ni(tfac$_2$en)]. This higher field shift may be due to the saturation of the γ-carbon atom upon the addition of the halogen atom to it. Further, Complexes I, III, and IV exhibit the signals corresponding to methoxyl or ethoxyl groups. These groups are thought to be attached to the carbon atom, where the CF_3 group is bonded, and they may stabilize the halogenated intermediate like A. This is because it has been shown for the (trifluoroacetylacetonato)antimony(V)-complex that the complex reacts with water to give a complex in which the hydroxyl group is attached at the carbon atom, where the CF_3 group is bonded, and in which two protons are attached at the γ-carbon atom.[10] The proposed structure for Complexes I, III, and IV is shown in Fig. 1. (Intermediate II). Complexes I, III, and IV exhibit a broad IR band at about 1660 cm^{-1} which can be assigned to the $\nu_{C=N}$ of the C=N group with no conjugation.[11] The π-π^* transitions of these complexes are observed at a higher energy site than those of complexes II and V. This higher energy shift supports the idea that Complexes I, III, and IV take a structure in which the C=N groups do not conjugate with the other group, as is shown in Fig. 1.

Table 1. The characterization data

Complex	^{1}H-NMR spectra δ[a]			Others	IR[g]		AB spectra[h] $\tilde{\nu}$/kcm^{-1} (log ε)		
	γ-CH	CH_2–CH_2	CH_3		$\nu_{C=N}$ cm^{-1}	$\nu_{C=O}$ cm^{-1}	d-d	CT	π-π^*
[Ni(tfac$_2$en)][b]	5.49[2]	3.15[4]	2.02[6][d]		1619	1534	17.5 (1.91)	21.7 (2.34)	26.3 (3.51)[i] 28.0 (3.54)
I[c]	4.67[2]	3.5[e]	2.18[6]	3.84[6] (OCH_3)	1665		20.6 (2.42)		29.7 (3.06)[j]
II[b]		3.37[4]	2.36[6]		1584	1490	17.2 (1.98)	22.2 (2.83)	25.6 (3.49)[i] 26.7 (3.45)
III[c]	4.79[2]	3.5[e]	2.22[6]	3.92[6] (OCH_3)	1655		20.8 (2.41)		28.6 (3.38)[i]
IV[c]	4.81[2]	3.5[e]	2.29[6]	1.55 / 1.43 / 1.31 [6][f] ($OCH_2\underline{CH_3}$)	1660		20.8 (2.48)		27.8 (3.36)[k]
V[b]		3.36[4]	2.41[6]		1573	1488	17.4 (2.06)	22.2 (2.83)	25.6 (3.51)[i] 26.9 (3.47)

a) [ ] represents the number of protons. b) Data in $CDCl_3$. c) Data in DMSO-d_6. d) Ref. 12. e) Overlap with the peak of DMSO. f) Triplet; the $OC\underline{H_2}CH_3$ signal appears at 3.6—3.7 ppm. g) Ref. 13. h) Ref. 14. i) Data in CH_3 OH. j) Data in DMSO. k) Data in acetone.

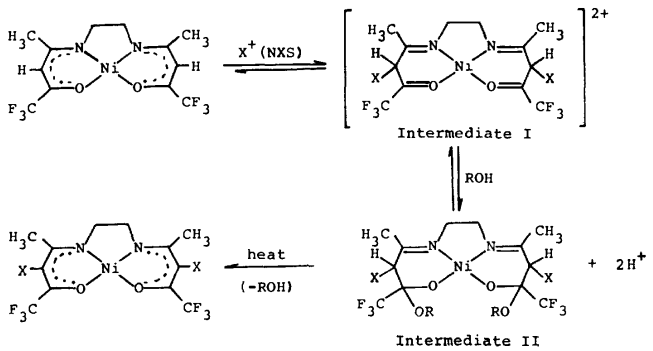

Fig. 1. The reaction scheme and the proposed structure of the reaction intermediate.

The proposed reaction mechanism is also shown in Fig. 1. Since the haloganation of [Ni(tfac$_2$en)] with NXS has also taken place in the presence of 2,6-di-*t*-butylphenol, a kind of radical scavenger, the reaction of NXS can be regarded as the electrophilic attack of the X^+ ion, which is formed by the ionic dissociation of NXS, on the γ-carbon atoms of [Ni(tfac$_2$en)]. Thus, in the first step of the reaction, Intermediate I in Fig. 1 should be formed. This Intermediate I has two positive charges. Further, the electron-withdrawing CF_3 group is attached. Therefore, the carbon atom, where CF_3 group is bonded, should be quite electron-deficient. Therefore, the attack of the alcoholic solvent may occur at the carbon atom to produce Intermediate II. As has been mentioned in the Experimental section, Complexes I, III, and IV decompose to give not only Complexes II or V but also [Ni(tfac$_2$en)]. This fact means that the reverse reaction from Intermediate II to [Ni(tfac$_2$en)] is possible. When water is added to the methanol solutions of Complexes II or IV, [Ni(tfac$_2$en)] is formed quite rapidly. Probably, in the presence of water, the elimination of alcohol from Intermediate II readily occurs upon the attack of the proton which is formed by the dissociation of water to give Intermediate I, and then [Ni(tfac$_2$en)].

The haloganation occurred also in a chloroform solvent. In that case, [Ni(tfac$_2$en)] (reddish brown) turned brown at the initial stage of the reaction, and then it turned to a brownish green with heating. The brown material could not be isolated well. However, when methanol was added to the brown solution, the solution turned to red, and reddish crystals, which correspond to Complex I, could be isolated from the solution. These facts suggest that the brown material may correspond to Intermediate I.

It should be noted that trifluoroacetylacetone, its metal complexes, and its Schiff base ligand itself are not halogenated by NXS.

References

1) J. P. Collman, *Adv. Chem. Ser.*, **37**, 78 (1963); *Angew. Chem.*, **77**, 154 (1965).

2) J. P. Collman and E. T. Kittleman, *Inorg. Chem.*, **1**, 499 (1962).

3) Y. Fujii, *Bull. Chem. Soc. Jpn.*, **43**, 1722 (1970).

4) K. Kuroda, K. Yashitani, K. Kunigita, Y. Kamiiha, and K. Watanabe, *Bull. Chem. Soc. Jpn.*, **49**, 2445 (1976); K. Kuroda, K. Yamaguchi, and N. Yamaoka, *ibid.*, **50**, 535 (1977).

5) T. Nagahara, K. Kasuga, and Y. Yamamoto, The 30th Conference of Coordination Chemistry, Tokyo, October 1980, Abstr. No. 3A14.

6) Y. Fujii, M. Ito, and K. Akiyama, The 22nd Conference of Coordination Chemistry, Osaka, November 1972, Abstr. No. 2A07.

7) It has been confirmed by our X-ray study of [Pd-tfac$_2$en)] that the nitrogen atom of the Shiff-base ligand is bonded at the carbon atom where the CH_3 group is attached (unpublished data).

8) P. J. McCarthy, R. J. Hovey, K. Ueno, and A. E. Martell, *J. Am. Chem. Soc.*, **77**, 5820 (1955).

9) J. P. Collman, R. A. Moss, H. Martz, and C. C. Heidel, *J. Am. Chem. Soc.*, **83**, 531 (1961).

10) F. Ebina, T. Uehiro, T. Iwamoto, A. Ouchi, and Y. Yoshino, *J. Chem. Soc., Chem. Commun.*, **1976**, 245; F. Ebina, A. Ouchi, Y. Yoshino, S. Sato, and Y. Saito, *Acta Crystallogr., Sect. B*, **33**, 3252 (1777); **34**, 1512 (1978).

11) E. K. Barefield, F. V. Lovecchio, N. E. Tokel, E. Ochiai, and D. H. Busch, *Inorg. Chem.*, **11**, 283 (1972).

12) P. J. McCarthy and A. E. Martell, *Inorg. Chem.*, **6**, 781 (1967).

13) K. Ueno, and A. E. Martell, *J. Am. Chem. Soc.*, **59**, 998 (1955).

14) B. Bosnich, *J. Am. Chem. Soc.*, **90**, 627 (1968).

Ligand Dissociation Rate Constants of Tris(4,4′-dimethyl-2,2′-bipyridine)chromium(II) and Tris(5,5′-dimethyl-2,2′-bipyridine)chromium(II) Complexes

Kunio NAKANO, Yoshio NARUSAWA,* and Hiroyuki MOROI

Department of Chemistry, College of Science, Rikkyo University (St. Paul's University), Nishi-Ikebukuro, Toshima-ku, Tokyo 171

(Received December 3, 1980)

Synopsis. Ligand dissociations of tris(4,4′-Me_2bpy)- and tris(5,5′-Me_2bpy)chromium(II) complexes** have been studied by scavenging the ligand with zinc ion according to a stopped-flow method.

The ligand dissociation of $[Cr(bpy)_3]^{2+}$ was first studied by a redox reaction between $[Cr(bpy)_3]^{2+}$ and $[Co(PO_4)(NH_3)_5]$ using a stopped-flow method[1] and subsequently by d.c. polarography,[2,3] while that for a heterogeneous system was studied cyclic voltammetrically.[4,5] Reports were given on the ligand dissociation rate constants obtained from the studies of the oxidation of $[Cr(bpy)_3]^{2+}$ or $[Cr(phen)_3]^{2+}$ with $[Co(NH_3)_6]^{3+}$ by the stopped-flow method.[6,7] Since all the results were obtained by indirect methods, attempts were made to obtain the ligand dissociation rate constants of $[Cr(bpy)_3]^{2+}$ and $[Cr(phen)_3]^{2+}$ directly by the stopped-flow method.[8] Although the ligand dissociation rate constants for a few complexes of 1,10-phenanthroline derivatives ($[Cr(5\text{-Me(phen)})_3]^{2+}$, $[Cr(5\text{-Cl(phen)})_3]^{2+}$ and $[Cr(5\text{-Br(phen)})_3]^{2+}$)*** were measured cyclic voltammetrically,[5] no paper has appeared so far on chromium(II) complexes of 2,2′-bipyridine derivatives. We have studied the ligand dissociations of $[Cr(4,4'\text{-}Me_2bpy)_3]^{2+}$ and $[Cr(5,5'\text{-}Me_2bpy)_3]^{2+}$, and obtained their kinetic and activation parameters.

Experimental

Apparatus. The stopped-flow apparatus for kinetic measurements was the same as reported.[7] Ultraviolet and visible absorption spectra were measured with a Hitachi recording spectrophotometer Type EPS-3T using a quartz cell of 1.0 mm optical path.

Reagents. 4,4′-Me_2bpy and 5,5′-Me_2bpy were synthesized according to the procedure of Sasse and Whittle.[9] The synthesized ligands 4,4′-Me_2bpy and 5,5′-Me_2bpy were checked spectrophotometrically. High purity nitrogen was used after further purification with activated copper columns. All other chemicals were of GR grade and used without purification.

Measurements of Absorption Spectra. The absorption spectra of *ca.* 2 mmol dm^{-3} aqueous solutions of $[Cr(4,4'\text{-}Me_2bpy)_3]^{2+}$ and $[Cr(5,5'\text{-}Me_2bpy)_3]^{2+}$ were measured. Preparation of the sample solution using a vacuum line was carried out as reported previously.[7] Since 4,4′-Me_2bpy and 5,5′-Me_2bpy were hardly soluble in water, not being able to give solutions of the desired concentration, suspensions of these ligands were used. Chromium (II) complex solutions were obtained by mixing anhydrous chromium(II) chloride with their respective suspensions. Absorption spectra of these complexes were measured and found to agree with those reported.[10]

Kinetic Measurements. A solution of $[Cr(4,4'\text{-}Me_2bpy)_3]^{2+}$ or $[Cr(5,5'\text{-}Me_2bpy)_3]^{2+}$ and a zinc chloride solution were mixed with the stopped-flow apparatus, the concentrations of chromium(II) complexes and zinc ion being 2.0 mmol dm^{-3} and 50 mmol dm^{-3}, respectively. The ionic strength for each solution was adjusted to 0.20 mol dm^{-3} by addition of sodium chloride, the pH being adjusted to 5.3 with an acetic acid–sodium acetate buffer solution. Kinetic measurements were performed by observing the absorbance change of the starting chromium(II) complex with time after mixing the solution of the chromium(II) complex with excess zinc ion used as a scavenger. The wavelengths were fixed at 571 nm for $[Cr(4,4'\text{-}Me_2bpy)_3]^{2+}$ and 565 nm for $[Cr(5,5'\text{-}Me_2bpy)_3]^{2+}$. The temperatures for the kinetic measurements were in the range 20—45 °C, the respective temperature being kept constant within ±0.1 °C.

Reaction Analysis. Reaction curves, absorbance *vs.* time, were analyzed by means of

$$\ln[(A_t-A_\infty)/(A_0-A_\infty)] = k_{obsd}\,t, \qquad (1)$$

where A_0, A_t, and A_∞ denote the absorbance of the solution at time $t=0$, t and ∞, respectively, and k_{obsd} is the apparent first-order rate constant.

Results and Discussion

Plots of $\log(A_t-A_\infty)$ *vs.* t show linearity over the whole range of the reaction curves, indicating that the reaction is of first-order type.

The following succesive equilibria seem to hold for both the complex of 4,4′-Me_2bpy and that of 5,5′-Me_2bpy:

Table 1. Rate constants for the ligand dissociation of Cr(II) complexes[a]

Complex	Temp/°C	k_{obsd}/s^{-1}[b]
$[Cr(4,4'\text{-}Me_2bpy)_3]^{2+}$	20.0	0.644±0.005 (7)
	25.0	1.17 ±0.02 (6)
	30.0	2.05 ±0.03 (6)
	35.0	3.60 ±0.04 (8)
	40.0	5.93 ±0.06 (7)
	45.0	9.68 ±0.12 (5)
$[Cr(5,5'\text{-}Me_2bpy)_3]^{2+}$	20.0	0.338±0.002 (6)
	25.0	0.663±0.002 (6)
	30.0	1.22 ±0.01 (6)
	35.0	2.14 ±0.04 (7)
	40.0	3.91 ±0.04 (7)

a) At pH 5.3. b) Number of measurements given in parentheses.

** Ligands, 4,4′-Me_2bpy and 5,5′-Me_2bpy, represent 4,4′-dimethyl-2,2′-bipyridine and 5,5′-dimethyl-2,2′-bipyridine, respectively.

*** The abbreviations "5-Me(phen)," "5-Cl(phen)," and "5-Br(phen)" represent 5-methyl-, 5-chloro-, and 5-bromo-1,10-phenanthroline, respectively.

Table 2. Kinetic and activation parameters of the ligand dissociation for chromium(II) complexes at pH 5.3

Complex	k_{diss}/s^{-1} a)	ΔH^*/kJ mol^{-1}	ΔS^*/J K^{-1} mol^{-1}	Ref.
$[Cr(bpy)_3]^{2+}$	0.390 ±0.003	84.4±1.5	30.6±4.8	8
$[Cr(phen)_3]^{2+}$	0.0643±0.0014	89.0±1.9	30.3±6.3	8
$[Cr(4,4'\text{-}Me_2bpy)_3]^{2+}$	1.17 ±0.02	81.5±1.5	30.1±4.5	b)
$[Cr(5,5'\text{-}Me_2bpy)_3]^{2+}$	0.663±0.002	89.9±1.0	53.5±4.0	b)

a) Values at 25.0 °C. b) This work.

$$[Cr(LL)_3]^{2+}+2H_2O \rightleftharpoons [Cr(H_2O)_2(LL)_2]^{2+}+LL, \quad (2)$$

$$[Cr(H_2O)_2(LL)_2]^{2+}+2H_2O \rightleftharpoons [Cr(H_2O)_4(LL)]^{2+}+LL, \quad (3)$$

$$[Cr(H_2O)_4(LL)]^{2+}+2H_2O \rightleftharpoons [Cr(H_2O)_6]^{2+}+LL, \quad (4)$$

where LL denotes 4,4'-Me_2bpy and 5,5'-Me_2bpy. Since zinc ion rapidly scavenges the free ligand,[11] no reverse reactions need be considered for the equilibria under excess zinc ion. Thus, the ligand dissociation of this system could be observed. The kinetic measurements of the present experiment satisfy the above conditions. Since the molar extinction coefficient of the bis complex is considered to be small, in analogy to $[Cr(bpy)_3]^{2+}$,† the dissociation of the tris to the bis complex can be determined. A first-order reaction was observed over the whole range of each reaction curve, and thus the determination of the first step (Eq. 2) is considered to be rate-determining. It is evident that the observed rate constant k_{obst} represents the rate constant for the ligand dissociation of the tris to bis complex.

The rate constants obtained under various temperatures are given in Table 1, and kinetic and activation parameters in Table 2, along with the previous data.[8] The ligand dissociation rate constants of $[Cr(4,4'\text{-}Me_2bpy)_3]^{2+}$ and $[Cr(5,5'\text{-}Me_2bpy)_3]^{2+}$ are greater than those of $[Cr(bpy)_3]^{2+}$. This seems to correspond to greater rates of $[Cr(5\text{-}Me(phen))_3]^{2+}$, $[Cr(5\text{-}Cl(phen))_3]^{2+}$ and $[Cr(5\text{-}Br(phen))_3]^{2+}$ as compared with $[Cr(phen)_3]^{2+}$.[5] The values of activation entropy ΔS^* for $[Cr(bpy)_3]^{2+}$, $[Cr(phen)_3]^{2+}$, and $[Cr(4,4'\text{-}Me_2bpy)_3]^{2+}$ are *ca.* 30 J K^{-1} mol^{-1}, whereas that for $[Cr(5,5'\text{-}Me_2bpy)_3]^{2+}$ is far greater. The positive activation entropy suggests that the ligand dissociation of the present system proceeds *via* the dissociative mechanism,[12] while the greater value of ΔS^* for $[Cr(5,5'\text{-}Me_2bpy)_3]^{2+}$ suggests the possibility of a different dissociative mechanism.

† In the case of $[Cr(bpy)_3]^{2+}$,[8] the absorbance at the starting point of the reaction is estimated to be 0.833 (concentration, 0.96 mmol dm^{-3}; molar extinction coefficient, 4340 dm^3 mol^{-1} cm^{-1}; cell length, 2 mm). If most of the tris complex was consumed for the formation of the bis complex during the dead-time, the initial absorbance observed would be less than 0.154, since the molar extinction coefficient of the bis complex is 803 dm^3 mol^{-1} cm^{-1}.[8] However, in a typical case, the absorbance for the first observable reaction signal was 0.624, the reaction curve approaching zero. The first-order plot fell on a straight line over the whole range observed. The reaction seems to correspond to the dissociation of the tris to the bis complex, and this step is regarded to be rate-determining.

The authors wish to thank Mr. Teruo Nagaoka and Miss Misa Okamoto for their assistance in absorption spectral measurements, Dr. Yoshio Koike, Kanagawa University, for the samples of 4,4'-dimethyl-2,2'-bipyridine and 5,5'-dimethyl-2,2'-bipyridine, and Prof. Tatsuo Matsuura, Institute for Atomic Energy, Rikkyo University, for use of the stopped-flow apparatus.

References

1) J. P. Candlin, J. Halpern, and D. L. Trimm, *J. Am. Chem. Soc.*, **86**, 1019 (1964).
2) B. R. Baker and B. D. Mehta, *Inorg. Chem.*, **4**, 848 (1965).
3) D. M. Soignet and L. G. Hargis, *Inorg. Chem.*, **11**, 2349 (1972).
4) D. M. Soignet and L. G. Hargis, *Inorg. Chem.*, **11**, 2921 (1972).
5) M. C. Hughes and D. J. Macero, *Inorg. Chem.*, **13**, 2739 (1974).
6) Y. Narusawa, M. Kimura, and K. Nakano, *Bull. Chem. Soc. Jpn.*, **47**, 2017 (1974).
7) Y. Narusawa and K. Nakano, *J. Inorg. Nucl. Chem.*, **42**, 875 (1980).
8) K. Nakano, Y. Narusawa, and M. Tsuchiya, *J. Inorg. Nucl. Chem.*, in press.
9) W. H. F. Sasse and C. P. Whittle, *J. Chem. Soc.*, **1961**, 1347.
10) I. Fujita, T. Yazaki, Y. Torii, and H. Kobayashi, *Bull. Chem. Soc. Jpn.*, **45**, 2156 (1972).
11) R. H. Holyer, C. D. Hubbard, S. F. A. Kettle, and R. G. Wilkins, *Inorg. Chem.*, **4**, 929 (1965).
12) C. H. Langford and H. B. Gray, "Ligand Substitution Processes," Benjamine, New York (1965), p. 11.

Solubility Phase Diagram Containing Racemic Compound of Bis(ethylenediamine)oxalatocobalt(III) Oxalate

Akira FUYUHIRO,* Kazuaki YAMANARI, and Yoichi SHIMURA
Department of Chemistry, Faculty of Science, Osaka University, Toyonaka, Osaka 560
(Received December 20, 1980)

Synopsis. Solubility of *Λ*- and *rac*-$[Co(ox)(en)_2](C_2O_4)_{0.5}$ was measured in water at 5—60 °C, the solubility isotherm of the ternary system, *Λ*-$[Co(ox)(en)_2](C_2O_4)_{0.5}$–*Δ*-$[Co(ox)(en)_2](C_2O_4)_{0.5}$–$H_2O$, being determined at 25 °C. It was found that the oxalate is not spontaneously resolvable and forms the racemic compound, *Λ*-$[Co(ox)(en)_2]$·*Δ*-$[Co(ox)(en)_2](C_2O_4)$·nH_2O.

In 1968 Yamasaki *et al.* reported the spontaneous resolution of bis(ethylenediamine)oxalatocobalt(III) oxalate, $[Co(ox)(en)_2]_2(C_2O_4)\cdot 8H_2O$, which shows hemihedral facets in the crystals.[1] However, the result seemed doubtful considering their method for preparing the oxalate, *i. e.* by the reaction, *trans*-$[CoCl_2(en)_2]Cl + 2H_2C_2O_4 \rightarrow [Co(ox)(en)_2]^+ + 3Cl^- + 4H^+ + C_2O_4^{2-}$. The crystals obtained seem to be chloride known to be spontaneously resolvable, since the solubility of *rac*-$[Co(ox)(en)_2](C_2O_4)_{0.5}$ ($m=0.369$ mol kg^{-1}) is larger than that of *rac*-$[Co(ox)(en)_2]Cl$ ($m=0.118$ mol kg^{-1}) at 25 °C and the molar ratio of counter ions, $Cl^-/(C_2O_4)_{0.5}^-$, is 3/2 even disregarding the association of H^+ and $C_2O_4^{2-}$. Chloride was obtained in our experiments. The hemihedrally distinguishable crystals obtained by Yamasaki *et al.* seem to be $[Co(ox)(en)_2]Cl\cdot 4H_2O$.

In order to confirm whether the spontaneous resolution of oxalate occurs or not, the optically active and the racemic oxalates were prepared and their solubilities in binary and ternary systems were measured.

Experimental

Materials. *$[Co(ox)(en)_2](C_2O_4)_{0.5}\cdot nH_2O$*: The *Λ*-, *Δ*-, and *rac*-$[Co(ox)(en)_2](C_2O_4)_{0.5}\cdot nH_2O$ were obtained from the corresponding chloride and $Ag_2(C_2O_4)$. Found: C, 21.20; H, 6.38; N, 14.09%. Calcd for *Λ*-$[Co(ox)(en)_2](C_2O_4)_{0.5}\cdot 4.5H_2O$: C, 21.44; H, 6.42; N, 14.28%. Found: C, 21.24; H, 6.44; N, 14.13%. Calcd for *Δ*-$[Co(ox)(en)_2](C_2O_4)_{0.5}\cdot 4.5H_2O$: C, 21.44; H, 6.42; N, 14.28%. Found: C, 23.01; H, 5.93; N, 15.33%. Calcd for *rac*-$[Co(ox)(en)_2](C_2O_4)_{0.5}\cdot 3H_2O$: C, 23.02; H, 6.07; N, 15.34%.

Measurements. Solubility in water was determined in molality.[2] The solid phases were identified from elemental analysis, absorption and CD spectra. Optical densities were measured with a JASCO UVIDEC-1 spectrophotometer and CD with a JASCO MOE-1 spectropolarimeter.

Results and Discussion

Binary System. The solubility of *Λ*- and *rac*-$[Co(ox)(en)_2](C_2O_4)_{0.5}$ is given in Table 1. The solubility ratio of racemate/*Λ*-salt is 0.720(5 °C) or 0.340(60 °C). If spontaneous resolution takes place, the ratio should exceed *ca.* $2^{2/3}=1.59$ expected in this type of electrolyte.[3] Thus, the present salt is not spontaneously resolvable. The solubility curve of *Λ*-salt shows an inflection at *ca.* 38 °C, at which the solid phase changes from (4.5—5)-hydrate(below 38 °C) to monohydrate(above 38 °C). However, the trihydrated racemic salt shows no solid phase change at 5—60 °C. This also confirms that the racemic salt exists as a racemic compound.

TABLE 1. SOLUBILITY OF $[Co(ox)(en)_2](C_2O_4)_{0.5}$ IN WATER (molality m/mol kg^{-1} of anhydrous salt)

T/°C	No. of salt[a]		
	(1)	(2)-*α*	(2)-*β*
5	0.170	0.236	
10	0.209	0.342	
15	0.250	0.501	
20	0.302	0.736	
25	0.369	1.07	
30	0.444	1.50	
35	0.537	2.05	
40	0.645		2.56
45	0.769		2.76
50	0.918		3.02
55	1.10		3.38
60	1.29		3.79

a) (1): *rac*-$[Co(ox)(en)_2](C_2O_4)_{0.5}\cdot nH_2O$, $n\simeq 3$, (2): *Λ*-$[Co(ox)(en)_2](C_2O_4)_{0.5}\cdot nH_2O$, $n=4.5$—5(*α*) and $n\simeq 1$(*β*).

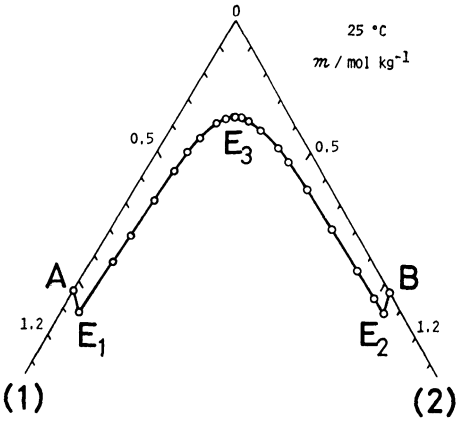

Fig. 1. Solubility isotherm of the ternary system, *Λ*-$[Co(ox)(en)_2](C_2O_4)_{0.5}$ (1)–*Δ*-$[Co(ox)(en)_2](C_2O_4)_{0.5}$ (2)–H_2O, at 25 °C. Solubility is presented in molality m of anhydrous salt.

Ternary System. Figure 1 and Table 2 show the solubility isotherm of the ternary system, *Λ*-$[Co(ox)(en)_2](C_2O_4)_{0.5}$–*Δ*-$[Co(ox)(en)_2](C_2O_4)_{0.5}$–$H_2O$, at 25 °C. As is expected, the isotherm shows the formation of racemic compound, *Λ*-$[Co(ox)(en)_2]$·*Δ*-$[Co(ox)(en)_2]$-

TABLE 2. EQUILIBRIUM OF THE SYSTEM, Λ-[Co(ox)(en)$_2$]-$(C_2O_4)_{0.5}$-Δ-[Co(ox)(en)$_2$]$(C_2O_4)_{0.5}$-H_2O, AT 25 °C
In liquid phases, solubility is presented in molality m of anhydrous salt. Abbreviations: Λ-[Co(ox)(en)$_2$]-$(C_2O_4)_{0.5}\cdot nH_2O$($n$=4.5—5)=$\Lambda$, Δ-[Co(ox)(en)$_2$]$(C_2O_4)_{0.5}\cdot nH_2O$($n$=4.5—5)=$\Delta$, and Λ-[Co(ox)(en)$_2$]·Δ-[Co(ox)(en)$_2$]$(C_2O_4)_{0.5}\cdot nH_2O$($n\simeq 6$)=*rac*.

Positions of points (Fig. 1)	Liquid phase[a] m/mol kg^{-1}		Solid phase
	Λ	Δ	
A	1.07 (±0.01)		Λ
E_1	1.11 (±0.01)	0.06 (±0.01)	Λ+*rac*
E_1 ↕ E_3	0.851 0.745 0.604 0.486 0.402 0.337 0.252 0.216 0.192	0.071 0.077 0.082 0.091 0.098 0.110 0.136 0.157 0.176	*rac*
E_3	0.184 (±0.001)	0.184 (±0.001)	*rac*
E_3 ↕ E_2	0.163 0.144 0.120 0.098 0.090 0.078 0.073 0.067 0.061	0.206 0.239 0.297 0.388 0.448 0.562 0.721 0.885 0.994	*rac*
E_2	0.06 (±0.01)	1.11 (±0.01)	Δ+*rac*
B		1.07 (±0.01)	Δ

a) Values in parentheses are estimated errors and calculated from twice the standard deviations of measurements repeated 5—11 times.

$(C_2O_4)\cdot 6H_2O$=*rac*-[Co(ox)(en)$_2$]$(C_2O_4)_{0.5}\cdot 3H_2O$, whose region spreads widely ($E_1E_3E_2$). It is evident that no spontaneous resolution occurs.[4] Points E_1 and E_2 are the invariant points where two solids (active and racemic salts) coexist.

DTA Analyses. Differential thermal analysis (DTA) of the optically active and the racemic oxalate was carried out under suspended conditions in water at *ca.* 0—100 °C,[5] providing one peak in heating process for each salt. The peak for the optically active salt (38 °C) corresponds to the transition observed in the binary solubility. The racemic salt shows a peak at *ca.* 74 °C at which the solid phase changes from trihydrate-(below 74 °C) to 0.5-hydrate(above 74 °C). However, the transition of racemate does not correspond to the change from the racemic compound to a racemic mixture, because the extrapolated solubility ratio at 74 °C (*ca.* 0.37) in Table 1 does not exceed 1.59, and the active and the racemic salts have different numbers of water of crystallization.

Thus, the optically active oxalate can not be obtained from the racemic solution of [Co(ox)(en)$_2$]$(C_2O_4)_{0.5}$ in equilibrium, *viz.*, the salt is not spontaneously resolvable.

References

1) K. Yamasaki, H. Igarashi, Y. Yoshikawa, and H. Kuroya, *Inorg. Nucl. Chem. Lett.*, **4**, 491 (1968).

2) A. Fuyuhiro, K. Yamanari, and Y. Shimura, *Bull. Chem. Soc. Jpn.*, **52**, 90 (1979).

3) K. Yamanari, J. Hidaka, and Y. Shimura, *Bull. Chem. Soc. Jpn.*, **46**, 3724 (1973). The relations $S_{\Delta\Lambda}<\sqrt[n/(n+1)]{2}\,S_\Delta$ and $S_{\Delta\Lambda}=\sqrt[n/(n+1)]{2}\,S_\Delta$ in Table 1 should be corrected to $S_{\Delta\Lambda}<\sqrt[(n+1)/n]{2}\,S_\Delta$ and $S_{\Delta\Lambda}=\sqrt[(n+1)/n]{2}\,S_\Delta$, respectively.

4) Y. Shimura and K. Tsutsui, *Bull. Chem. Soc. Jpn.*, **50**, 145 (1977).

5) A. Fuyuhiro, K. Yamanari, and Y. Shimura, *Bull. Chem. Soc. Jpn.*, **53**, 3577 (1980).

Extraction of Lead(II) in Aqueous Thiocyanate-Perchlorate Solutions wtih Trioctylphosphine Oxide in Hexane and with 4-Methyl-2-pentanone

Satoshi KUSAKABE and Tatsuya SEKINE*

Department of Chemistry, Science University of Tokyo, Kagurazaka, Shinjuku-ku, Tokyo 162

(Received December 26, 1980)

Synopsis. The stability of lead(II) thiocyanate complexes and the extraction behavior of lead(II) in 1 mol dm^{-3} Na(SCN, ClO_4) were studied. By an extraction method with thenoyltrifluoroacetone, $\log\beta_1=0.49$ was obtained for $PbSCN^+$. The extraction was poor with 4-methyl-2-pentanone but effective with trioctylphosphine oxide in hexane. Not only $Pb(SCN)_2$ but also $Pb(SCN)(ClO_4)$ and $Pb(ClO_4)_2$ were extracted into both of the solvents.

The complex formation equilibria of lead(II) in aqueous 1 mol dm^{-3} Na(SCN,ClO_4) solutions were determined by an extraction method with thenoyltrifluoroacetone (TTA). The extraction equilibria of this metal ion from these ionic media into 4-methyl-2-pentanone (MIBK) and hexane containing trioctylphosphine oxide (TOPO) were studied as follows.

Experimental and Statistical

All of the reagents used were of a reagent grade. Sodium perchlorate was recrystallized from water. The solutions of sodium thiocyanate and sodium perchlorate were standardized by gravimetry. The extractants, TTA and TOPO, were obtained from Dojindo Laboratories in Kumamoto. TOPO and MIBK were purified as described previously.[1,2] A carbon tetrachloride solution containing 0.1 mol dm^{-3} TTA, hexane solutions containing TOPO at various concentrations and MIBK were used as the organic solutions.

All of the experiments were carried out in a thermostated room at 25 °C in a manner essentially similar to that described previously[3] except that the initial metal concentration was 1×10^{-4} mol dm^{-3} and that the metal concentration in the two phases was determined by an atomic absorption method.

In the present paper, the chemical species in the organic phase are denoted by the subscript "org," while the lack of any subscript denotes those in the aqueous phase. The distribution ratio is defined as $D=[Pb(II)]_{org}/[Pb(II)]$. The total concentration of lead(II) in aqueous solution containing thiocyanate ions can be described as:

$$[Pb(II)] = [Pb^{2+}](1 + \sum\beta_i[SCN^-]^i), \quad (1)$$

where β_i is the stability constant of the "i-th" complex.

The TTA extraction can be written as:

$$Pb^{2+} + 2Htta_{(org)} \rightleftarrows Pb(tta)_{2(org)} + 2H^+$$

$$K_{TTA,0} = D_0[H^+]^2[Htta]_{org}^{-2}, \quad (2)$$

where D_0 is the distribution ratio in the absence of thiocyanate ions. If the concentration of TTA in the organic phase and of the hydrogen-ion in the aqueous phase are kept constant, the following equation can be obtained:

$$D/D_0 = 1/(1+\sum\beta_i[SCN^-]^i). \quad (3)$$

The MIBK extraction can be treated as follows. Since it was found that only the $PbSCN^+$ species was the complex in the aqueous phase and that $[Pb(II)]_{org}=[Pb(ClO_4)_2]_{org}+[Pb(SCN)(ClO_4)]_{org}+[Pb(SCN)_2]_{org}$, the distribution ratio is written as:

$$D = (K_{MIBK,0}[ClO_4^-]^2 + K_{MIBK,1}[SCN^-][ClO_4^-] + K_{MIBK,2}[SCN^-]^2)/(1+\beta_1[SCN^-]), \quad (4)$$

where

$$K_{MIBK,n} = [Pb(SCN)_n(ClO_4)_{2-n}]_{org}/([Pb^{2+}][SCN^-]^n[ClO_4^-]^{2-n}). \quad (5)$$

The TOPO(L) extraction was as follows.

$$[Pb(II)]_{org}=[Pb(ClO_4)_2L_4]_{org}+[Pb(SCN)(ClO_4)L_4]_{org}+[Pb(SCN)(ClO_4)L_3]_{org}+[Pb(SCN)_2L_3]_{org}$$

$$D=(K_{ex0,4}[ClO_4^-]^2[L]_{org}^4+K_{ex1,4}[SCN^-][ClO_4^-][L]_{org}^4+K_{ex1,3}[SCN^-][ClO_4^-][L]_{org}^3+K_{ex2,3}[SCN^-]^2[L]_{org}^3)/(1+\beta_1[SCN^-]) \quad (6)$$

where

$$K_{exn,m} = \frac{[Pb(SCN)_n(ClO_4)_{2-n}L_m]_{org}}{[Pb^{2+}][SCN^-]^n[ClO_4^-]^{2-n}[L]_{org}^m} \quad (7)$$

The data were treated by a least squares program in order to find the values of the constant which give the best fit.

Results and Discussion

From the extraction of lead(II) with TTA, the value of $K_{TTA,0}$ in Eq. 2 was obtained to be $10^{-10.60}$. This was valid up to $-\log[H^+]$ 4.0. Figure 1 shows the decrease in the TTA extraction as a function of the thiocyanate concentration in the aqueous phase. By the least squares treatment, the data were found to be explained by assuming only the $PbSCN^+$ species. The value of β_1 determined was $10^{0.49}$.

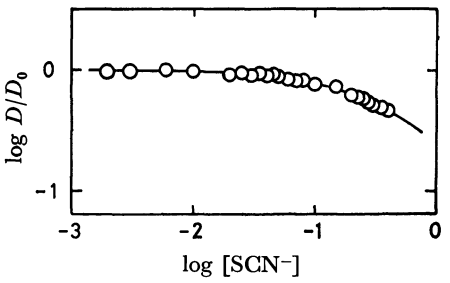

Fig. 1. Decrease in the lead (II) extraction with TTA *vs.* the aqueous thiocyanate concentration. Org. phase; CCl_4 containing 0.1 mol dm^{-3} TTA. Aq. phase; 1 mol dm^{-3} Na (SCN, ClO_4). The solid curve gives; $\log D/D_0=-\log(1+10^{0.49}[SCN^-])$.

The results of the extraction of lead(II) into MIBK are shown by Fig. 2. The extraction constants obtained by the least squares calculation on the basis of Eq. 4 using $\beta_1=10^{0.49}$ are listed in Table 1. The curve is calculated from these constants and Eq. 4.

Figure 2 also shows the extraction curves of lead(II) with TOPO in hexane. The value of $K_{ex0,4}$ was obtained separately from the extraction data from 1 mol dm^{-3} sodium perchlorate solutions as $10^{6.92}$. Using the above β_1 and $K_{ex0,4}$ values, the values of the extraction constants

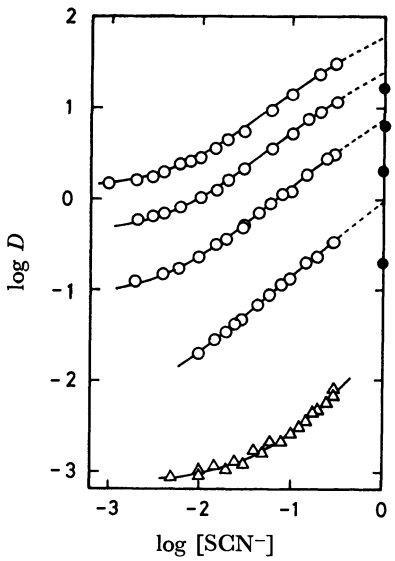

Fig. 2. Extraction curves of lead (II) with 4-methyl-2-pentanone (△) and triocylphosphine oxide in hexane (○) from 1 mol dm^{-3} Na (SCN, ClO_4) solutions. The concentration of TOPO in the organic phase is 0.02, 0.015, 0.01, and 0.005 mol dm^{-3} from top to bottom. The solid curves are calculated ones by means of Eqs. 4 and 6 using the constants in Table 1. The closed circles at 1 mol dm^{-3} thiocyanate indicate the values obtained experimentally (see text).

TABLE 1. SUMMARY OF THE EQUILIBRIUM CONSTANTS[a),b)]

MIBK		TOPO in hexane	
$\log K_{MIBK,0}$	−3.11	$\log K_{ex,0,4}$	6.92
$\log K_{MIBK,1}$	−1.68	$\log K_{ex,1,4}$	8.81
$\log K_{MIBK,2}$	−1.03	$\log K_{ex,1,3}$	6.96
		$\log K_{ex,2,3}$	7.48

a) Stability constant of aqueous complex, $\log \beta_1 = 0.49$.
b) Extraction constant of $Pb(ClO_4)_2$, $Pb(SCN)(ClO_4)_2$, and $Pb(SCN)_2$ species; *cf.* Eqs. 5 and 7.

were determined by means of Eq. 6 also by the least squares method. The best-fit constants are shown in Table 1.

The stability constants of lead(II) thiocyanate have been reported as $\log \beta_1 = 0.20$ and $\log \beta_2 = 0.90$ in 1 mol dm^{-3} $Na(SCN,ClO_4)$[4] and $\log \beta_1 = 0.54$, $\log \beta_2 = 0.88$, $\log \beta_3 \simeq -1$, and $\log \beta_4 = 0.85$ in 2 mol dm^{-3} $Na(SCN, ClO_4)$[5] solutions at 25 °C by polarography. The present β_1 is similar to these literature values, though no higher complexes were found in the present study. The value of β_1 of this metal ion is lower than that for several bivalent transition metals,[6-8] cadmium,[6] mercury(II),[2] and zinc(II).[3]

The MIBK extraction of lead(II) from thiocyanate solutions is poorer than zinc(II),[3] cobalt(II),[7] and mercury(II)[2] but better than nickel(II).[8] The MIBK extraction of lead(II) from 1 mol dm^{-3} $Na(SCN,ClO_4)$ was calculated to be mainly due to $Pb(ClO_4)_2$ and $Pb(SCN)(ClO_4)$ species; the contribution of the $Pb(SCN)_2$ species is rather small up to 0.3 mol dm^{-3} thiocyanate.

It was calculated that under the conditions in Fig. 2, the $Pb(SCN)_2(TOPO)_3$ species is not dominant in the organic phase even at 0.3 mol dm^{-3} thiocyanate. This is due to the instability of the metal thiocyanate and also the high extractability of the lead(II) perchlorate and the mixed thiocyanate. The extraction from sodium thiocyanate solutions containing no perchlorate was poorer than the calculated values, as indicated in Fig. 2. This is due to changes in the activity coefficients of chemical species by the replacement of the anion in the aqueous phase.

The extraction constant of the mixed thiocyanate, $K_{ex1,3}$, is not very much different from that of the dithiocyanate, $K_{ex2,3}$, in Table 1. This evidence, that the extraction of $Pb(SCN)_2$ is rather similar to $Pb(SCN)(ClO_4)$, seems to indicate that the interactions of the second thiocyanate ion with the metal ion are not so strong in the $Pb(SCN)_2$ species. This instability of the dithiocyanate complex should be the reason for its high solvation number, three; it seems to be rather common that if the di-complex of a bivalent metal ion is stable it tends to be extracted as a disolvate.[2,9]

References

1) S. Kusakabe and T. Sekine, *Bull. Chem. Soc. Jpn.*, **53**, 1759 (1980).
2) T. Sekine and T. Ishii, *Bull. Chem. Soc. Jpn.*, **43**, 2422 (1970).
3) H. Moriya and T. Sekine, *Bull. Chem. Soc. Jpn.*, **44**, 3347 (1971).
4) A. C. Gonzalez, T. Mareno, and A. Arevalo, *An. Quim., Ser. A*, **76**, 223 (1980).
5) G. W. Leonard, M. E. Smith, and D. N. Hume, *J. Phys. Chem.*, **60**, 1493 (1956).
6) L. G. Sillén and A. E. Martell, "Stability Constants of Metal-ion Complexes," Spec. Pub., **17**, The Chemical Society, London (1964), p. 116.
7) T. Sekine, R. Murai, and M. Iguchi, *Nippon Kagaku Zasshi*, **92**, 412 (1971).
8) R. Murai, S. Iwahori, and T. Sekine, *Bull. Chem. Soc. Jpn.*, **50**, 1315 (1977).
9) H. Moriya and T. Sekine, *Bull. Chem. Soc. Jpn.*, **45**, 1626 (1972).

Isotope Effects in the *p*-Tolylation of Pyridine

Takeshige NAKABAYASHI,* Toyokazu HORII, Shunichi KAWAMURA, and Yasuo ABE
Radiation Center of Osaka Prefecture, Shinke-cho, Sakai, Osaka 593

(Received October 11, 1980)

Synopsis. *p*-Toluoyl peroxide, *p*-iodotoluene, and di-*p*-tolyl sulfone, sulfoxide, and sulfide were photolyzed in an equimolar pyridine–pyridine-d_5 mixture to give rise to isomeric *p*-tolylpyridines (α, β, and γ) and their deuterated compounds. Isotopic distribution ratios (Y_H/Y_D) in the isomeric products were determined to be slightly larger than unity.

Vidal and coworkers[1] reported that in the phenylation of 4-methylpyridine with benzoyl peroxide (BPO), the deuterium isotope effect (K_H/K_D) at 2-position of the substrate was somewhat large, 3.7, though that at 3-position was 1.0. In order to check the generality of this tendency, isotope effects in arylation of pyridine with various aryl radical sources were determined. We have found previously[2] that *p*-toluoyl peroxide and *p*-iodotoluene, as well as di-*p*-tolyl sulfone, sulfoxide, and sulfide, are photolyzed in pyridine to afford isomeric *p*-tolylpyridines (α, β, and γ, respectively). Here, the isotope effects at the three nuclear positions of pyridine in the free-radical *p*-tolylation with these radical precursors were determined from the isotope distribution ratios (Y_H/Y_D) in the reaction products. The results are summarized in Table 1.

TABLE 1. ISOTOPIC DISTRIBUTION RATIOS (Y_H/Y_D)[a] IN ISOMERIC *p*-TOLYLPYRIDINES PRODUCED IN THE REACTION

Run No.	Compound[b]	*p*-Tolylpyridines		
		α	β	γ
0.015 mol dm^{-3} Solution				
1	$ArSO_2Ar$	1.06	1.15	1.09
2	ArSOAr	1.08	1.20	1.05
3	ArSAr	1.05	1.35	1.12
4	$(ArCO_2)_2$	1.26	1.27	1.10
5	ArI	1.06	1.19	1.17
0.15 mol dm^{-3} Solution				
1′	$ArSO_2Ar$	1.09	1.14	1.08
2′	ArSOAr	1.05	1.18	1.07
3′	ArSAr	1.14	1.45	1.11
4′	$(ArCO_2)_2$	1.30	1.30	1.13
5′	ArI	1.06	1.12	1.12

a) Experimental error is ± 0.05. b) Ar is *p*-tolyl.

As shown in Table 1, only small isotope effects (<1.5) were observed for *p*-tolylation of all positions of pyridine; no case was found in which 2-arylation showed a larger isotope effect than 3-arylation. The difference with the result by Vidal *et al.*[1] appears to depend on the radical sources.

Eliel and coworkers[3] reported that, in the phenylation of benzene-d_6 with the phenyl radical generated from BPO, the isotope effects ($K_H/K_D=1.0$—6.6) vary with the concentrations of BPO used in the reaction. As Table shows, however, the values of Y_H/Y_D in the present reactions were independent of the concentrations of the radical sources used under our conditions.

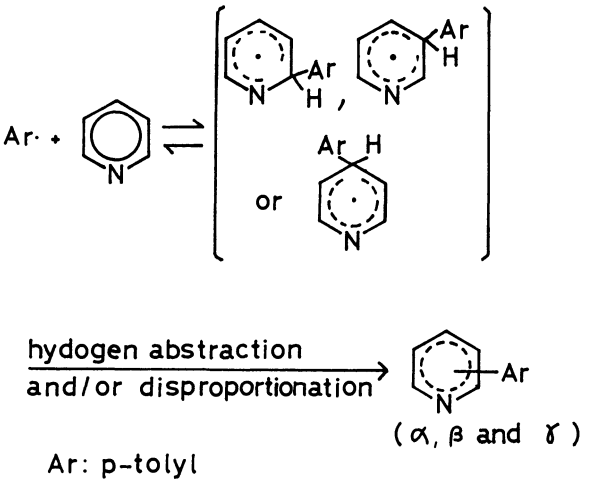

On the basis of the mechanism[3-5] proposed for homolytic arylations of aromatic compounds, it seems reasonable to consider that the product isotope effect is observed in either of the following cases: (1) reversal of the addition of *p*-tolyl radicals on pyridine, or (2), disproportionation and combination between *p*-tolyldihydropyridyl radicals takes place in competition with the production of the *p*-tolylpyridines. In order to check the reversibility of addition of *p*-tolyl radicals to pyridine, the peroxide and the iodide were allowed to react with a small excess of an equimolar pyridine–pyridine-d_5 mixture, and isotopic compositions of the recovered pyridine were compared with those of the starting one. The data in Table 2 reveal that the recovered pyridine was completely unchanged in its isotopic composition within the experimental errors. This finding implies that the values of Y_H/Y_D larger slightly than unity are due to disproportionation and combination between the dihydropyridyl radicals; the disproportionation and combination compete with the hydrogen abstraction from the radical to yield the *p*-tolylpyridines.

TABLE 2. ISOTOPIC COMPOSITIONS OF STARTING[a] AND RECOVERED PYRIDINE-PYRIDINE-d_5 MIXTURE

Run No.[b]	Compound[c]	Pyridine, (% in mol)	Pyridine-d_5, (% in mol)
1	$(ArCO_2)_2$	48.72(48.72)	51.28(51.28)
2	ArI	48.88(48.93)	51.02(51.07)

a) The figures in parentheses indicate those for starting materials. b) In run 1, refluxed for 6 h at boiling point of pyridine. c) Ar is *p*-tolyl.

Table 1 indicates that the values of Y_H/Y_D change with the radical sources to some extent and that in most runs, the values of Y_H/Y_D of β-(*p*-tolyl)pyridines are somewhat larger than those of α- and γ-compounds. The reason for these tendencies is not clear at present.

Experimental

Materials. Commercial available di-*p*-tolyl sulfone and sulfoxide and *p*-iodotoluene were purified by recrystallization and employed for the reaction. *p*-Toluoyl peroxide and authentic *p*-tolylpyridines (α, β, and γ) were prepared and purified by the method[2] reported previously. Di-*p*-tolyl sulfide was prepared by the literature method[6] from reduction of the corresponding sulfoxide with trichlosilane and recrystallized from ethanol (mp 58.5 °C). Pyridine–pyridine-d_5 (isotope purity 99%) were purchased from E. Merck, Darmstadt, and used for the reaction without further purification.

General Procedure for Photolysis of Radical Sources in Pyridine–Pyridine-d_5 *Mixture.* The procedure for the sulfone is described here as a typical run. An equimolar pyridine–pyridine-d_5 mixture was prepared and its isotopic content was determined by GC-MS analysis. In the case of 0.15 mol dm^{-3} solution, 0.3 mmol (74.1 mg) of the sulfone was dissolved in 2 ml of the pyridine mixture. Each solution was placed in a Pyrex cylinder, degassed five times, sealed, and irradiated for 200 h at room temperature with a 400 W medium-pressure mercury arc lamp. After evaporating the excess pyridine under a reduced pressure, the residue was subjected to preparative GLC to collect a mixture of isomeric *p*-tolylpyridines produced. The preparative GLC was done on a 3 mm × 2 m stainless steel column packed with 3% OV-17 on Chromosorb GAW (DMCS), using a JEOL Chromatograph JGC-650. Three isomeric *p*-tolylpyridines were then fractionated from the mixture on a preparative HPLC with THF–hexane (1 : 9 in volume) as a solvent. The instrument used was a Waters Model 6000 A High-Pressure Liquid Chromatograph equipped with a 4 mm × 30 cm column packed with μ-porasil. Each isomeric *p*-tolylpyridine thus separated was identified by comparison of its retention time with that of authentic specimen, and its deuterium content was determined by GC-MS analysis at 70 eV using a Shimadzu-LKB 9000 Gas Chromatograph-Mass Spectrometer equipped with a 3 mm × 2 m glass column packed with 0.5% OV-17 on Chromosorb GAW (DMCS). The values of Y_H/Y_D of isomeric *p*-tolylpyridines were calculated from its parent peak ratios (I_{169}/I_{173}). The parent peak ratios were determined by repeated scans of a range of $m/e=160$ to $m/e=185$. It was ascertained that the parent peak ratios did not change when ionization potentials were changed from 20 to 70 eV.

Isotopic Compositions of Starting and Recovered Pyridine–Pyridine-d_5 *Mixture.* *p*-Toluoyl peroxide (1.35 g, 5 mmol) was added to an equimolar pyridine–pyridine-d_5 (1 g, 12.5 mmol) mixture. The mixture was refluxed at the boiling point of pyridine until evolution of CO_2 gas ceased. The unchanged pyridine was recovered by distillation and subjected to GC-MS analysis by using a small glass vessel in place of the OV-17 column. Its isotopic composition was calculated from the parent peak rations (I_{79}/I_{84}) by the technique mentioned above. *p*-Iodotoluene (2.18 g, 10 mmol) was dissolved in 1 g (12.5 mmol) of the equimolar pyridine–pyridine-d_5 mixture. The solution was placed in a small Pyrex cylinder, degassed, and irradiated for 200 h at room temperature with a 400 W medium-pressure mercury arc lamp. After irradiation, the unchanged pyridine was recovered by distillation and analyzed on the GC-MS. Its isotopic composition was calculated in the way described above. After irradiation for 200 h, GLC analysis indicated that 50% of the initially charged iodide remained unchanged.

References

1) S. Vidal, J. Court, and J. M. Bonnier, *J. Chem. Soc., Perkin Trans. 2*, **1976**, 497.

2) T. Nakabayashi, T. Horii, S. Kawamura, and M. Hamada, *Bull. Chem. Soc. Jpn.*, **50**, 2491 (1977).

3) E. L. Eliel, S. Meyerson, Z. Welvart, and S. H. Wilen, *J. Am. Chem. Soc.*, **82**, 2936 (1960).

4) E. L. Eliel, Z. Welvart, and S. H. Wilen, *J. Org. Chem.*, **23**, 1821 (1958).

5) M. Kobayashi, H. Minato ,and N. Kobori, *Bull. Chem. Soc. Jpn.*, **42**, 2738 (1969).

6) T. H. Chan, A. Melnyk, and D. H. Harpp, *Tetrahedron Lett.*, **1969**, 201.

A Convenient Synthesis of Azuleno[2,1-*b*]thiophene

Kameji YAMANE,* Kunihide FUJIMORI,* and Toru TAKEUCHI
Department of Chemistry, Faculty of Science, Shinshu University, Asahi, Matsumoto 390
(Received December 2, 1980)

Synopsis. Azuleno[2,1-*b*]thiophene and its derivatives were prepared from ethyl 2-chloro-3-formylazulene-1-carboxylate and ethyl mercaptoacetate in a few steps.

Azuleno[2,1-*b*]thiophene, which is a polycyclic aromatic compound containing a heterocycle, is of interest in its physical properties and chemical behavior. The compound and related compounds have so far been prepared by reaction of diethyl 2-chloroazulene-1,3-dicarboxylate with ethyl mercaptoacetate, followed by cyclization, methylation, hydrolysis, decarboxylation, reduction, and dehydration.[1]

We now wish to report a convenient synthesis of the title compound and its derivatives.

When ethyl 2-ethoxycarbonylmethylthio-3-formylazulene-1-carboxylate (**2**) prepared by the reaction of ethyl 2-chloro-3-formylazulene-1-carboxylate (**1**)[2] with ethyl mercaptoacetate was heated with piperidine in EtOH, cyclization occurred to afford the diethyl azuleno[2,1-*b*]thiophene-2,9-dicarboxylate (**3**) in good yield. The conversion of **2** to **3** could also be carried out with basic activated alumina. The compound **3**, on treatment with 100% phosphoric acid at 90 °C, gave ethyl azuleno[2,1-*b*]thiophene-2-carboxylate (**4**). When the ester (**4**) was heated at 150 °C in 100% phosphoric acid, deethoxycarbonylation occurred to give azuleno[2,1-*b*]thiophene (**5**). The compound **5** was also obtained from **4** as follows. Compound **4** was hydrolyzed in ethanolic KOH and the resulting carboxylic acid was heated at 170—180 °C under reduced pressure (2 mmHg†) to yield **5**.

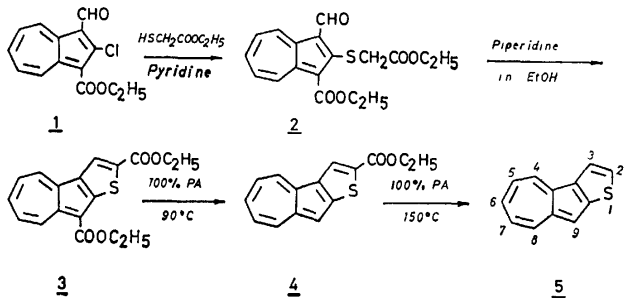

1 2 3 4 5

The spectral data of **2**, **3**, **4**, and **5** are shown in the experimental section.

The NMR vicinal coupling constants indicate that 7-membered rings of **3**, **4**, and **5** exhibit some bond length alternation, similar to the results for benz[*a*]azulene;[3] this behavior is characteristic of polyenes. (Table 1).

TABLE 1. NMR VICINAL COUPLING CONSTANTS OF **3**, **4**, AND **5**

Compound	J_{45}/Hz	J_{78}/Hz	ΔJ/Hz
3	9.0	10.2	1.2
4	9.0	10.2	1.2
5	8.5	10.0	1.5

† 1 mmHg=133.322 Pa.

Experimental

All melting points are uncorrected.

Ethyl 2-Ethoxy Carbonylmethylthio-3-formylazulene-1-carboxylate (**2**). A mixture of ethyl 2-chloro-3-formylazulene-1-carboxylate (51.8 mg), ethyl mercaptoacetate (60 mg), and pyridine (3 ml) was heated at 100 °C on an oil bath for 15 min. After cooling, the reaction mixture was poured into water, acidified with 2 mol dm^{-1} sulfuric acid, and extracted with chloroform. The chloroform layer was dried over anhydrous sodium sulfate and evaporated under reduced pressure. The residue was chromatographed on a silica-gel column with benzene–chloroform (1 : 1). The red effluent was freed from solvent to give **2** (52.4 mg, 76.7%) as red oil, which was used for the next step without further purification.

^{1}H NMR ($CDCl_3$) δ ppm: 1.09 (3H, t, J=7.5 Hz, $SCH_2COOCH_2C\underline{H}_3$), 1.50 (3H, t, J=7.5 Hz, $COOCH_2C\underline{H}_3$), 3.37 (2H, s, $SC\underline{H}_2COOCH_2CH_3$), 4.02 (2H, q, J=7.5 Hz, $SCH_2COOC\underline{H}_2CH_3$), 4.51 (2H, q, J=7.5 Hz, $COOC\underline{H}_2CH_3$), 7.8—8.0 (3H, m, H-5,6,7), 9.4—9.7 (1H, m, H-8 or H-4), 9.8—10.0 (1H, m, H-4 or H-8).

IR ($CDCl_3$): 2992, 1734, 1696, 1652, 1441, 1403, 1195, 647 cm^{-1}.

*Diethyl Azuleno[2,1-*b*]thiophene-2,9-dicarboxylate* (**3**). *a*): Three drops of piperidine were added to a solution of **2** (177.3 mg) in ethanol (17 ml). The mixture was refluxed for 1 h. The reaction mixture was freed from solvent and the residue was chromatographed on a silica-gel column with chloroform. The yellowish brown effluent was evaporated under reduced pressure. The residue was recrystallized from cyclohexane to give **4** (155.6 mg, 92.6%) as yellowish brown needles; mp 136—137 °C.

IR (KBr): 2989, 1695, 1249, 779, 727 cm^{-1}.

ES λ_{max} in cyclohexane ,nm (log ε): 215 (4.27), 252 (4.31), 321 (4.74), 337 (4.80), 348 (4.08), 386 (3.62), 402 (3.80), 409 (3.70), 428 (4.01), 574 (2.45).

^{1}H NMR ($CDCl_3$) δ ppm: 1.44 (3H, t, J=7.0 Hz, 2-$COOCH_2C\underline{H}_3$), 1.51 (3H, t, J=7.0 Hz, 9-$COOCH_2C\underline{H}_3$), 4.40 (2H, q, J=7.0 Hz, 2-$COOC\underline{H}_2CH_3$), 4.43 (2H, q, J=7.0 Hz, 9-$COOC\underline{H}_2CH_3$), 7.2—7.9 (3H, m, H-5,6,7), 8.19 (1H, s, H-3), 8.39 (1H, d, J=9.0 Hz, H-4), 9.43 (1H, d, J=10.2 Hz, H-8).

^{13}C NMR ($CDCl_3$) δ ppm: 14.5 (q), 14.6 (q), 60.3 (t), 61.2 (t), 109.3 (s), 124.6 (d), 128.4 (d), 129.5 (d), 133.6 (d), 133.9 (s), 134.0 (s), 136.4 (d), 137.0 (s), 138.1 (d), 145.2 (s), 153.9 (s), 163.2 (s), 164.1 (s).

Found: C, 65.92; H, 4.85; S, 10.02%. Calcd for $C_{18}H_{16}O_4S$: C, 65.84; H, 4.91; S, 9.76%.

b): Compound **2** (29.9 mg) was dissolved in chloroform and adsorbed on a basic alumina column. After standing overnight, the reaction mixture was eluted with chloroform. From the yellowish brown effluent, **3** was obtained as yellowish brown needles (16 mg, 56.4%); mp 136—137 °C. The IR spectrum was identical with that of a sample prepared by Method *a*) and the mixed melting point was not depressed.

*Ethyl Azuleno[2,1-*b*]thiophene-2-carboxylate* (**4**). A mixture of bis (ethoxycarbonyl) compound (**3**) (121.4 mg) and 100% phosphoric acid (5 ml) was heated at 90 °C for 1 h. After cooling, the reaction mixture was poured into water and extracted with chloroform. The extract was dried, freed

from solvent, and the residue was chromatographed on silica gel. Elution with benzene gave bluish green plates (90 mg, 94.4%); mp 86.5—87.5 °C, which were recrystallized from cyclohexane.

IR (KBr): 2985, 1695, 1510, 1253, 1243, 719 cm^{-1}.

ES λ max in cyclohexane nm (log ε): 216 (4.06), 236 (4.21), 319 (4.82), 332 (4.98), 358 (3.86), 363 (3.56), 376 (3.83), 396 (4.01), 407 (3.65), 420 (4.04), 599 (2.88).

^{1}H NMR ($CDCl_3$) δ ppm: 1.43 (3H, t, J=7.0 Hz, $COOCH_2\underline{CH_3}$), 4.40 (2H, q, J=7.0 Hz, $COO\underline{CH_2}CH_3$), 7.0—7.7 (4H, m, H-5,6,7,9), 8.14 (1H, d, J=10.2 Hz, H-8), 8.33 (1H, dm, J=9.0 Hz, H-4), 8.39 (1H, s, H-3).

^{13}C NMR ($CDCl_3$) δ ppm: 14.5 (q), 61.1 (t), 109.9 (d), 124.5 (d), 125.0 (d), 125.3 (d), 131.5 (d), 132.4 (s), 134.7 (s), 135.8 (d), 135.8 (s), 136.3 (d), 143.8 (s), 152.5 (s), 163.4 (s).

Found: C, 70.25; H, 4.79; S, 12.56%. Calcd for $C_{15}H_{12}O_2S$: C, 70.29; H, 4.72; S, 12.51%.

Azuleno[2,1-b]thiophene (5). *a)*: A mixture of **4** (25 mg) and 100% phosphoric acid was heated at 150 °C for 2 h. After cooling, the reaction mixture was diluted with water and extracted with chloroform. The extract was dried, evaporated under reduced pressure, and the residue was chromatographed on alumina column. From benzene effluent, **5** was obtained as bluish green plates (12 mg, 66.8%); mp 173—174 °C, which were recrystallized from ethanol. The UV spectrum was identical with that of azuleno[2,1-*b*]-thiophene prepared by Matsui *et al.*[1]

^{1}H NMR ($CDCl_3$) δ ppm: 6.9—7.6 (3H, m, H-5,6,7), 7.47 (1H, s, H-9), 7.32 (1H, d, J=5.4 Hz, H-3), 7.69 (1H, d, J=5.4 Hz, H-2), 8.20 (1H, d, J=10.0 Hz, H-8), 8.39 (1H, d, J=8.5 Hz, H-4).

^{13}C NMR ($CDCl_3$) δ ppm: 109.4 (d), 118.6 (d), 122.5 (d), 123.4 (d), 125.5 (d), 131.1 (d), 132.5 (s), 135.7 (d), 136.9 (s), 141.7 (s), 149.7 (s).

b): A mixture of **4** (202 mg), ethanol, and 20% potassium hydroxide aqueous solution was refluxed for 30 min. After removal of the solvent, water was added to the residue. When the solution was made acid with 2 mol dm^{-3} sulfuric acid, a green precipitate separated out. The precipitate was filtered off, washed with a small amount of ethanol to give azuleno-[2,1-*b*]thiophene-2-carboxylic acid as green powder (173 mg, 96.5%); this was used for the next step without further purification.

The carboxylic acid obtained above was heated under reduced pressure (2 mmHg) in a sublimation aparatus. The bluish green crystals was sublimed at 170—180 °C. Recrystallization from ethanol gave bluish green plates (18 mg, 46.1%); mp 173—174 °C. The IR spectrum was identical with that of the sample obtained by Method *a)*, and the mixed melting point was not depressed.

References

1) K. Matsui, *Nippon Kagaku Zasshi*, **82**, 1517, 1520, 1522, 1665 (1961).

2) A. Sato, Doctral Thesis, Tohoku University, Sendai, 1962.

3) D. J. Bertelli and P. Crews, *Tetrahedron*, **26**, 4717 (1970).

A New Synthetic Route to Electrophilic Cyclopropane Derivatives from Olefins

Nariyoshi KAWABATA,* Shinji YANO, Jiro HASHIMOTO, and Jun-ichi YOSHIDA

Department of Chemistry, Faculty of Polytechnic Science, Kyoto Institute of Technology, Matsugasaki, Sakyo-ku, Kyoto 606

(Received January 12, 1981)

Synopsis. 1,1-Bis(alkoxycarbonyl)-, 1-alkoxycarbonyl-1-cyano-, and 1,1-dicyanocyclopropane derivatives were obtained in 10—99% yields by the reaction of $Br_2C(COOR)_2$, $Br_2C(CN)(COOR)$, and $KBr[Br_2C(CN)_2]_4$, respectively, with olefins and Cu_2Br_2 in dimethyl sulfoxide (DMSO).

Recently cyclopropane derivatives activated by two electron-withdrawing substituents such as COOR, COR, and CN at geminal position were found to be useful intermediates in organic synthesis.[1] A number of methods exist for the preparation of these electrophilic cyclopropanes.[2] This paper describes a new synthetic route to electrophilic cyclopropane derivatives from olefins by the reaction with organic *gem*-dihalide and Cu_2Br_2 in dimethyl sulfoxide (DMSO).

The reaction of $Br_2C(COOEt)_2$, $Br_2C(CN)(COOEt)$, and $KBr[Br_2C(CN)_2]_4$ with Cu_2Br_2 in the presence of olefins gave the corresponding 1,1-bis(ethoxycarbonyl)-, 1-cyano-1-ethoxycarbonyl-, and 1,1-dicyanocyclopropane derivatives, respectively, in good yields. Some experimental results are given in Table 1. All products were identified by comparison of their ^1H NMR and IR spectra with those of authentic samples, or showed satisfactory analytical data and expected spectra. GLC analysis of the reaction mixture showed that no isomeric olefins were formed.

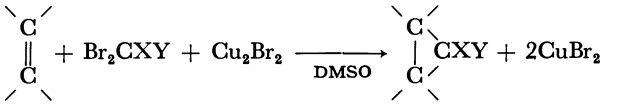

(X, Y=COOEt, CN)

During the course of reaction Cu_2Br_2 was converted into $CuBr_2$, which was isolated as a coordinated complex with two molecules of DMSO, and identified by comparison of its spectral data with those of an authentic

TABLE 1. SYNTHESIS OF ELECTROPHILIC CYCLOPROPANE DERIVATIVES FROM OLEFINS BY THE REACTION WITH ORGANIC *gem*-DIHALIDE AND Cu_2Br_2 IN DMSO

Olefin	Halide	Temp °C	Product	Yield[a] %
Styrene	$Br_2C(COOEt)_2$[b]	28	1,1-Bis(ethoxycarbonyl)-2-phenylcyclopropane	71
		75		68
p-Chlorostyrene		60	1-(*p*-Chlorophenyl)-2,2-bis(ethoxycarbonyl)cyclopropane	77
		30		48
m-Chlorostyrene		60	1-(*m*-Chlorophenyl)-2,2-bis(ethoxycarbonyl)cyclopropane	79
		30		54
m-Trifluoromethylstyrene		60	1,1-Bis(ethoxycarbonyl)-2-(*m*-trifluoromethylphenyl)cyclopropane	71
		30		64
p-Methylstyrene		60	1,1-Bis(ethoxycarbonyl)-2-(*p*-methylphenyl)cyclopropane	24
cis-*β*-Methylstyrene		75	1,1-Bis(ethoxycarbonyl)-2-methyl-3-phenylcyclopropane	10[c]
trans-*β*-Methylstyrene		75		9[d]
1-Octene		75	1,1-Bis(ethoxycarbonyl)-2-hexylcyclopropane	32
cis-Cyclooctene		75	9,9-Bis(ethoxycarbonyl)bicyclo[6.1.0]nonane	10
Acrylonitrile		60	2-Cyano-1,1-bis(ethoxycarbonyl)cyclopropane	39
Ethyl acrylate		70	1,1,2-Tris(ethoxycarbonyl)cyclopropane	17
Styrene	$Br_2C(CN)(COOEt)$[e]	25	1-Cyano-1-ethoxycarbonyl-2-phenylcyclopropane	99[f]
Acrylonitrile		28	1,2-Dicyano-1-ethoxycarbonylcyclopropane	71[g]
cis-Cyclooctene	$Br_2C(CN)(COOEt)$[h]	100	9-Cyano-9-ethoxycarbonylbicyclo[6.1.0]nonane	47
1-Octene		80	1-Cyano-1-ethoxycarbonyl-2-hexylcyclopropane	20
Styrene	$KBr[Br_2C(CN)_2]_4$[i]	22	1,1-Dicyano-2-phenylcyclopropane	67
p-Methylstyrene		30	1,1-Dicyano-2-(*p*-methylphenyl)cyclopropane	39[j]
p-Chlorostyrene		30	1,1-Dicyano-2-(*p*-chlorophenyl)cyclopropane	34[j]
cis-Cyclooctene		50	9,9-Dicyanobicyclo[6.1.0]nonane	21

a) Determined by GLC analysis of the reaction mixture, based on the olefin. b) Reactions were carried out with 4.0 mmol of olefin, 8.0 mmol of $Br_2C(COOEt)_2$, and 9.0 mmol of Cu_2Br_2 in 6.0 ml of DMSO for 2 h. c) A 10 : 90 mixture of *cis* and *trans* isomers obtained. d) A 8 : 92 mixture of *cis* and *trans* isomers obtained. e) Reactions were carried out with 1.0 mmol of olefin, 2.0 mmol of $Br_2C(CN)(COOEt)$, and 2.0 mmol of Cu_2Br_2 in 1.5 ml of DMSO for 2 h. f) A 92 : 8 mixture of E and Z isomers obtained. g) A 60 : 40 mixture of E and Z isomers obtained. h) Reactions were carried out with 0.5 mmol of olefin, 1.0 mmol of $Br_2C(CN)(COOEt)$, and 1.0 mmol of Cu_2Br_2 in 1.0 ml of DMSO for 2 h. i) Reactions were carried out with 0.5 mmol of olefin, 0.25 mmol of $KBr[Br_2C(CN)_2]_4$, and 1.0 mmol of Cu_2Br_2 in 1.0 ml of DMSO for 2 h. j) Determined by isolation using column chromatography, based on the olefin.

material.[3]

The new reaction is useful for the synthesis of electrophilic cyclopropane derivatives from olefins (Table 1). The reaction with $Br_2C(COOEt)_2$ gave cyclopropane derivatives in a non-stereospecific way. A *ca.* 1 : 9 mixture of cis and trans isomers of the corresponding cyclopropane derivatives was obtained from both *cis*- and *trans*-β-methylstyrene. No isomerization of *cis*- and *trans*-β-methylstyrene or of *cis*- and *trans*-1,1-bis-(ethoxycarbonyl)-2-methyl-3-phenylcyclopropane was observed under the experimental conditions. The relative reactivity of substituted styrenes in the reaction with $Br_2C(COOEt)_2$ gave a Hammett ρ-value of −0.1. Thus the reaction was concluded to be weakly electrophilic.

In the reaction with $Br_2C(CN)(COOEt)$, two stereoisomers of the cyclopropane derivatives were obtained from styrene and acrylonitrile, the *E* to *Z* isomer ratio being 92 : 8 and 60 : 40, respectively. The relative configuration was determined on the basis of their ^1H NMR spectra. The *E* : *Z* isomer ratios seemed to reflect the thermodynamic stability of the product. However, GLC analysis of the reaction mixture showed only one peak in the cases with cyclooctene and 1-octene. ^1H NMR spectra of the isolated cyclopropane derivatives did not clearly indicate the presence of stereoisomers.

Experimental

Microanalyses were performed at the Elementary Analyses Center of Kyoto University. ^1H NMR spectra were recorded on a Varian Model T-60A spectrometer in CCl_4 or $CDCl_3$ using Me_4Si as an internal standard. IR spectra were recorded on a Hitachi Model 215 grating spectrophtometer, or a Japan Spectroscopic Co. Model DS-402G spectrophotometer. Mass spectra were obtained on a Hitachi Model RMU-6 mass spectrometer, or on a Japan Electron Optics Lab. Model JMS D-300 mass spectrometer at an ionization potential of 24 eV. GLC analyses were carried out on a Shimadzu GC-4B or GC-4C gas chromatograph.

Materials. $Br_2C(COOEt)_2$,[4] $Br_2C(CN)(COOEt)$,[5] and $KBr[Br_2C(CN)_2]_4$[6] were prepared according to the methods reported. *cis*- and *trans*-β-Methylstyrene, *p*-methylstyrene, *p*-chlorostyrene were prepared as reported.[2] DMSO was purified by distillation under reduced pressure.

Procedure. Olefin, organic *gem*-dihalide and Cu_2Br_2 were allowed to react in DMSO at the prescribed temperature with stirring for 2 h. After the reaction, the organic materials were extracted by hexane, benzene, or ethyl acetate from the reaction mixture. Yields were determined by GLC analysis of the organic layer, and the products were isolated by collection from the organic layer by GLC and analyzed. Some 1,1-dicyanocyclopropane derivatives were thermally unstable. In these cases, products were isolated by column chromatography, yields being determined by means of isolation. Results are given in Table 1.

1,1-Bis(ethoxycarbonyl)cyclopropane derivatives were identified by comparison of their spectral data with those of authentic samples.[2] Spectral data of (*E*)- and (*Z*)-1-cyano-1-ethoxycarbonyl-2-phenylcyclopropane were identical with those of authentic substances.[7] Spectral data of 1,1-dicyano-2-phenylcyclopropane were identical with those of an authentic sample.[8,9] Spectral and elementary analyses of the other electrophilic cyclopropane derivatives are given below.

1,2-Dicyano-1-(ethoxycarbonyl)cyclopropane. n_D^{30} 1.4644. Found: C, 58.37; H, 4.87; N, 16.81%. Calcd for $C_8H_8N_2O_2$: C, 58.53; H, 4.91; N, 17.06%. The *E* isomer: NMR ($CDCl_3$) δ 1.37 (t, J=7.2 Hz, 3H), 1.9—2.2 (m, 2H), 2.54 (d of d, J_{cis} =9.8 Hz and J_{trans}=7.2 Hz, 1H), 4.30 (q, J=7.2 Hz, 2H); $\nu_{C\equiv N}$ (liquid film) 2259 cm^{-1}; $\nu_{C=O}$ (liquid film) 1728 cm^{-1}. The *Z* isomer: NMR ($CDCl_3$) δ 1.38 (t, J=7.2 Hz, 3H), 1.9—2.3 (m, 2H), 2.53 (d of d, J_{cis}=9.8 Hz and J_{trans}=7.2 Hz, 1H), 4.36 (q, J=7.2 Hz, 2H); $\nu_{C\equiv N}$ (liquid film) 2255 cm^{-1}; $\nu_{C=O}$ (liquid film) 1730 cm^{-1}.

9-Cyano-9-(ethoxycarbonyl)bicyclo[6.1.0]nonane. n_D^{30} 1.4879; NMR (CCl_4) δ 1.37 (t, J=7.2 Hz, 3H), 1.0—2.3 (m, 14H), 4.20 (q, J=7.2 Hz, 2H); $\nu_{C\equiv N}$ (liquid film) 2248 cm^{-1}; $\nu_{C=O}$ (liquid film) 1727 cm^{-1}. Found: C, 70.66; H, 8.71; N, 6.16%. Calcd for $C_{13}H_{19}NO_2$: C, 70.56; H, 8.65; N, 6.33%.

1-Cyano-1-ethoxycarbonyl-2-hexylcyclopropane. n_D^{30} 1.4472; NMR (CCl_4) δ 0.91 (t, J=6.0 Hz, 3H), 1.1—1.8 (m, 13H), 1.37 (t, J=6.8 Hz, 3H), 4.23 (q, J=6.8 Hz, 2H); $\nu_{C\equiv N}$ (liquid film) 2238 cm^{-1}; $\nu_{C=O}$ (liquid film) 1728 cm^{-1}. Found: C, 70.03; H, 9.60; N, 6.36%. Calcd for $C_{13}H_{21}NO_2$: C, 69.92; H, 9.48; N, 6.27%.

9,9-Dicyanobicyclo[6.1.0]nonane. Mp 74—75 °C; NMR ($CDCl_3$) δ 0.9—2.4 (m, 14H); $\nu_{C\equiv N}$ (KBr disk) 2250 cm^{-1}. Found: C, 76.01; H, 8.21; N, 16.15%. Calcd for $C_{11}H_{14}N_2$: C, 75.82; H, 8.10; N, 16.08%.

1,1-Dicyano-2-(p-methylphenyl)cyclopropane. n_D^{30} 1.5429; NMR ($CDCl_3$) δ 2.17 (d, J=9.0 Hz, 2H), 2.33 (s, 3H), 3.22 (t, J=9.0 Hz, 1H), 7.11 (s, 4H); $\nu_{C\equiv N}$ (liquid film) 2252 cm^{-1}. Found: C, 79.22; H, 5.49; N, 15.21%. Calcd for $C_{12}H_{10}N_2$: C, 79.10; H, 5.53; N, 15.37%.

1,1-Dicyano-2-(p-chlorophenyl)cyclopropane. Mp 123—125 °C; NMR ($CDCl_3$) δ 2.21 (d, J=9.0 Hz, 2H), 3.24 (t, J= 9.0 Hz, 1H), 7.1—7.4 (m, 4H); $\nu_{C\equiv N}$ (KBr disk) 2256 cm^{-1}. Found: C, 65.09; H, 3.65; N, 13.53; Cl, 17.78%. Calcd for $C_{11}H_7N_2Cl$: C, 65.20; H, 3.48; N, 13.82; Cl, 17.50%.

References

1) S. Danishefsky, *Acc. Chem. Res.*, **12**, 66 (1979).
2) N. Kawabata and M. Tanimoto, *Tetrahedron*, **36**, 3517 (1980) and references cited therein.
3) D. W. Meek, D. K. Straub, and R. S. Drago, *J. Am. Chem. Soc.*, **82**, 6013 (1960).
4) T. Wakui, Y. Otsuji, and E. Imoto, *Nippon Kagaku Kaishi*, **1974**, 1686.
5) D. G. I. Felton, *J. Chem. Soc.*, **1955**, 515.
6) R. A. Carboni, J. Cason, and E. R. Harris, *Org. Synth.*, Coll. Vol. 4, p. 877.
7) E. W. Yankee, B. Spencer, N. E. Howe, and D. J. Cram, *J. Am. Chem. Soc.*, **95**, 4220 (1973).
8) E. Ciganek, *J. Am. Chem. Soc.*, **88**, 1979 (1966).
9) P. Boldt, L. Schulz, and J. Etzemueller, *Chem. Ber.*, **100**, 1281 (1967).

Preparation of (*E*)-1,3,5-Hexatriene and (3*E*, 5*E*)-1,3,5,7-Octatetraene by the Palladium Catalyzed Elimination of Acetic Acid from Allylic Acetates

Keiji YAMAMOTO,* Shigeaki SUZUKI, and Jiro TSUJI

Department of Chemical Engineering, Tokyo Institute of Technology, Meguro-ku, Tokyo 152

(Received January 30, 1981)

Synopsis. Palladium complex-catalyzed elimination of acetic acid from (2*E*,4*E*)-2,4-hexadienyl acetate and (2*E*, 4*E*, 6*E*)-2,4,6-octatrienyl acetate afforded, respectively, the title conjugated polyenes stereoselectively.

Recently, a simple preparative method for terminal conjugated dienes by palladium complex-catalyzed elimination of acetic acid and phenol from easily available allylic acetates and phenyl ethers, has been developed in this laboratory[1] and by Trost *et al.*[2]

The elimination reaction can be explained *via* the formation of a π-allylic palladium complex by oxidative addition of allylic compounds to Pd(0) species. Elimination of acetic acid or phenol is nonstereoselective insofar as each hydrogen α to the π-allylic system in the complex is eliminated, resulting in the formation of a mixture of (*E*)- and (*Z*)-isomers for simple 1,3-dienes.

This method may be of synthetic value for conjugated polyenes as well, especially if stereochemical limitation can be obviated. We wish to present a stereoselective preparation of (*E*)-1,3,5-hexatriene and (3*E*,5*E*)-1,3,5,7-octatetraene by way of the palladium complex-catalyzed elimination. Pyrolytic routes to these polyenes hitherto reported are usually nonstereoselective.

(2*E*,4*E*)-2,4-Hexadienyl acetate (**1**), derived from commercial (2*E*,4*E*)-2,4-hexadien-1-ol (isomeric purity >98%), was heated at reflux in toluene with palladium(II) acetate (1.0 mol%) and excess triphenylphosphine. 1,3,5-Hexatriene[3,4] was obtained by fractional distillation in 87% yield prior to the distillation of acetic acid eliminated. GLC analysis showed the triene to consist of (*E*)- and (*Z*)-isomers at least in a ratio of 97 : 3. IR spectrum of the product indicated characteristic bands of the (*E*)-isomer.

The Diels-Alder adduct of (*E*)-1,3,5-hexatriene with maleic anhydride was prepared for further structural characterization. ^{13}C NMR data for the adduct, 3-vinyl-1,2,3,6-tetrahydrophthalic anhydride[4] (Table 1) indicate high diastereomeric purity which should arise from (*E*)-triene.

On the other hand, the same procedure as above with use of 1-vinyl-3-butenyl acetate (**2**) afforded the triene in 67% yield. GLC analysis revealed isomeric hexatrienes in the ratio 80 : 20. The (*E*)-isomer as a major component was confirmed by IR spectrum. Nonstereoselective elimination of acetic acid from **2** was found to take place. ^{13}C NMR data of the Diels-Alder adduct obtained with this sample are also given in Table 1. Three pairs of signals, which are unambiguously assigned to C_4, C_5, and C_8, respectively, stem from the adduct of the (*Z*)-triene in addition to that of the (*E*)-isomer.

It is noteworthy that the formal 1,ω-elimination of acetic acid from **1** took place as readily as 1,2-elimination to give (*E*)-hexatriene stereoselectively, whereas the 1,2-elimination from **2** gave an *E*/*Z* mixture. The results are related to the fact that the intermediate π-allylic palladium(II) complexes are apt to take *syn* configuration.

As an extension, (2*E*,4*E*,6*E*)-2,4,6-octatrienyl acetate (**3**) was prepared by the Wittig reaction of (ethoxycarbonylmethylene)triphenylphosphorane with (2*E*,4*E*)-2,4-hexadienal followed by lithium aluminium hydride reduction and acetylation. The trienyl acetate **3** was subjected to palladium complex-catalyzed elimination of acetic acid to give white, waxy crystalline (3*E*,5*E*)-1,3,5,7-octatetraene[5] in 48% yield. IR spectrum of the product indicated the *trans* structure.

Experimental

Materials. (2*E*, 4*E*)-2,4-Hexadienyl acetate (**1**)[6] was prepared by acetylation of commercial (2*E*, 4*E*)-2,4-hexadien-1-ol (6.00 g, 60 mmol) with acetic anhydride (11.4 mL, 120 mmol) and excess pyridine in 82% yield, bp 83—84 °C/19 Torr (1 Torr=133.322 Pa). GLC (PEG 20 M 3 m, at 160 °C) analysis indicated the isomeric purity to be >98%.

1-Vinyl-3-butenyl acetate (**2**) was prepared by the method

TABLE 1. ^{13}C NMR DATA FOR 3-VINYL-1,2,3,6-TETRAHYDROPHTHALIC ANHYDRIDE

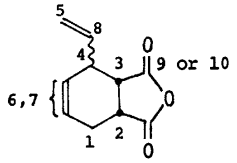

1,3,5-Hexatriene	Chemical shifts, δ/ppm									
	C_1	C_2	C_3	C_4	C_5	C_6	C_7	C_8	C_9	C_{10}
E(Pure)	22.8_4	38.8_4	39.5_1	45.1_8	118.4_8	127.3_4	130.3_4	134.5_0	171.4_3	174.1_3
E/*Z*(Mixture)	22.9_0	38.8_1	39.5_7	45.2_1	118.4_8	127.3_4	130.3_4	134.6_2	171.5_5	174.1_9
				44.5_0	115.7_8			135.8_6		

reported,[3] bp 56—57 °C/18 Torr.

(2E, 4E, 6E)-2,4,6-Octatrienyl Acetate (3). (i) A mixture of (ethoxycarbonylmethylene)triphenylphosphorane (2.93 g, 8.4 mmol) and freshly distilled (2*E*, 4*E*)-2,4-hexadienal (0.81 g, 8.4 mmol) dissolved in dry benzene (20 mL) was heated under argon atmosphere at 60 °C for 3.5 h. Evaporation of the reaction mixture and trituration of the residue with ether follwed by filtration were repeated three times to give phosphine oxide in 98% combined yield. The final filtrate was evaporated to dryness to give crude waxy ethyl (2*E*, 4*E*, 6*E*)-2,4,6-octatrienoate,[7] 1.30 g (93%). (ii) Lithium aluminium hydride reduction of the ester (1.22 g, 7.3 mmol) and acetylation of the resulting crude 2,4,6-octatrien-1-ol[5c] by the conventional procedure yielded **3**, 0.75 g (67%): bp 86—87 °C/3 Torr; ^{1}H NMR (CCl_4) δ 1.76 (t, J=5.6 Hz, MeCH=), 1.96 (s, MeCO), 4.45 (d, J=5.8 Hz, CH_2O), and 5.4—6.3 (m, olefinic protons); IR (neat) 1740 and 1240 cm^{-1}. GLC (PEG 20 M 3 m, at 180 °C) analysis of **3** appeared to cause significant decomposition.

Palladium Complex-catalyzed Elimination from Allylic Acetates. A typical procedure is as follows. A mixture of **1** (5.61 g, 40 mmol), palladium(II) acetate (91 mg, 0.4 mmol), and triphenylphsophine (1.05 g, 4.0 mmol) dissolved in dry toluene (30 mL) was heated at reflux under argon atmosphere. Low-boiling substances formed soon were fractionated through a column packed with glass helices (8×200 mm) until an azeotropic mixture of acetic acid with toluene was distilled. The distillate (bp 78—90 °C) was fractionated again to give a colorless oil, bp 80—83 °C (lit,[3] bp 80.5 °C), 2.42 g (95% purity by NMR, 87% yield) contaminated with a small amount of toluene and acetic acid. GLC (UCON 3 m, at 45 °C) analysis of the triene indicated that a principal peak is accompanied by a small peak, with a little longer retention time, in a ratio of 97 : 3. IR (neat): Characteristic bands of (*E*)-1,3,5-hexatriene are at 1430, 1010, and 940 cm^{-1}; lit,[8] 1429, 1011, and 941 cm^{-1}.

Similarly, 1,3,5-hexatriene was obtained by use of **2** (4.20 g, 30 mmol), bp 78—83 °C, 1.60 g (67%). GLC analysis of the product indicated that the isomeric composition is 4 : 1: IR (neat) 1430, 1010, and 940 cm^{-1} for the (*E*)-isomer, and 1450, 985, and 820 cm^{-1} for the (*Z*)-isomer; lit,[8] 1451, 987, and 818 cm^{-1}.

The acetate **3** (1.05 g, 6.3 mmol) was similarly heated in diethylene glycol diethyl ether (8 mL) in the presence of palladium(II) acetate (1 mol%) with added triphenylphosphine. Fractional distillation under reduced pressure (113 Torr) gave white, way crystalline (3*E*, 5*E*)-1,3,5,7-octatetraene, 0.33 g (48%), bp 89—93 °C/113 Torr, mp 50 °C; ^{1}H NMR (CCl_4) δ 4.90—5.30 (m, 4H) and 6.13 (br s, 6H); IR (CCl_4) 1010 and 900 cm^{-1} for the (*E*, *E*)-configuration.[5b] Octatetraene is rather unstable in the air, giving an insoluble polymeric material.

Diels-Alder Reaction. A mixture of (*E*)-1,3,5-hexatriene (1.40 g, crude fraction, 85% purity) and excess maleic anhydride (3.92 g, 40 mmol) in dioxane (10 mL) was stirred at room temperature for 3 d. After removal of the solvent under reduced pressure, the residue was chromatographed (silica gel, hexane–ethyl acetate, 10 : 1) to give 3-vinyl-1,2,3,6-tetrahydrophthalic anhydride[4] (1.18 g, 40%).

In the case of an isomeric mixture of (*E*)- and (*Z*)-hexatriene obtained by the elimination of **2** (1.12 g, 8.0 mmol), the crude fraction was heated at 60 °C for 2 d with maleic anhydride (2.94 g, 30 mmol) in dioxane under argon. Chromatographic purification as above gave the adduct (0.54 g, 38%).

^{13}C NMR ($CDCl_3$) data for the purified adducts are given in Table 1. Diels-Alder reaction of the tetraene with excess maleic anhydride in toluene at 60 °C under argon afforded a white powder after chromatographic purification in low yield, mp 136—139 °C (lit,[5a] 238—242 °C). No useful assignment of ^{13}C NMR data for the adduct could be made.

The authors thank Mr. Y. Nakamura for ^{13}C NMR measurements and Mr. Y. Kimura for assisting in the experimental work.

References

1) a) J. Tsuji, T. Yamakawa, M. Kaito, and T. Mandai, *Tetrahedron Lett.*, **1978**, 2075; b) T. Mandai, H. Yasuda, M. Kaito, and J. Tsuji, and R. Yamaoka, and H. Fukami, *Tetrahedron*, **35**, 309 (1979).

2) B. M. Trost, T. R. Verhoeven, and J. M. Fortunak, *Tetrahedron Lett.*, **1979**, 2301. For related work, see: R. O. Hutchins, K. Learn, and R. P. Fulton, *ibid.*, **21**, 27 (1980).

3) J. C. H. Hwa and H. Sims, *Org. Synth.*, Coll. Vol. 5, 608 (1973).

4) G. F. Woods and L. H. Schwartzman, *J. Am. Chem. Soc.*, **70**, 3394 (1948); M. S. Schneider and M. Schnaithmann, *ibid.*, **101**, 254 (1979).

5) a) G. F. Woods and L. H. Schwartzman, *J. Am. Chem. Soc.*, **71**, 1396 (1949); b) E. R. Lippincott, W. R. Feairfeller, Jr., and C. E. White, *ibid.*, **81**, 1316 (1959); c) D. F. Evans, *J. Chem. Soc.*, **1961**, 2566.

6) P. Maginiac, *Ann. Chim. (Paris)*, **7**, 445 (1962).

7) V. F. Kucherov, B. G. Kovalev, I. I. Nazarova, and L. A. Yanovskaya, *Izv. Akad. Nauk SSSR, Otdl. Khim. Nauk*, **1960**, 1512 [*Chem. Abstr.*, **55**, 1420d (1961)].

8) J. C. H. Hwa, P. L. DeBenneville, and H. J. Sims, *J. Am. Chem. Soc.*, **82**, 2537 (1960).

Studies on Biologically Active Pteridines. VII.[1] Absolute Configuration of (−)-6-Methyltetrahydropterin Produced by Enzymic Reduction

Sadao MATSUURA* and Takashi SUGIMOTO

Department of Chemistry, College of General Education, Nagoya University, Chikusa-ku, Nagoya 464

(Received February 19, 1981)

Synopsis. The C-6 configuration of (−)-6-methyltetrahydropterin, produced by enzymic reduction of the 7,8-dihydro precursor, is shown to be *S* by a synthesis. Condensation of 2,4-diamino-5-bromo-6-hydroxypyrimidine with (*S*)-1,2-propanediamine gave (*S*)-6-methyltetrahydropterin. Examination of CD spectra of the 6-methyltetrahydropterins from the two origins led to the above conclusion.

The reduction of 7,8-dihydrobiopterin and 7,8-dihydro-6-methylpterin to the 5,6,7,8-tetrahydro derivatives by the action of dihydrofolate reductase is stereospecific and the (−)-tetrahydropterins thus produced are shown to possess the same configuration at the C-6 chiral center.[2,3] (−)-Tetrahydrobiopterin is the natural cofactor for aromatic amino acid hydroxylases, whereas the C-6 diastereoisomeric (+)-tetrahydrobiopterin shows different cofactor characteristics.[3-5] Because of the indispensable contribution of (−)-tetrahydrobiopterin to the biosynthesis of neurotransmitting serotonin and dopamine, the determination of the C-6 configuration is highly desired and has been studied in several ways.[2,3,6,7] In these studies, the C-6 configuration of the enzymically reduced (−)-6-methyltetrahydropterin was shown to be *S* (and then, by analogy, that of (−)-tetrahydrobiopterin to be *R*), by comparison with a tetrahydroquinoxaline or by transformation into a tetrahydrolumazine or a piperazine. This paper describes a straightforward proof for the C-6 configuration of (−)-6-methyltetrahydropterin as *S* by its synthesis.

Since N-5 unsubstituted tetrahydropterins are notoriously unstable to air oxidation, we first attempted to synthesize a N-5 alkylated derivative of 6-methyltetrahydropterin, such as 5,6,8-trimethyl- or 5,8-dibenzyl-6-methyl-tetrahydropterin. In contrast to the ready formation of 5,8-dimethyl-5,6,7,8-tetrahydropterin[8] by condensation of 2,4-diamino-5-bromo-6-hydroxypyrimidine (**1**) with 1,2-bis(methylamino)ethane, an analogous condensation of **1** with 1,2-bis(methylamino)propane or 1,2-bis(benzylamino)ethane gave a very complex mixture, from which we could detect no tetrahydropterins. Heating of **1** with (*S*)-1,2-propanediamine (**2**) at about 115 °C, however, gave 6- and 7-methylpterins as predominant products. These compounds were

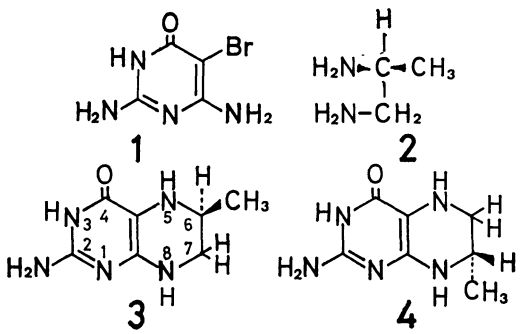

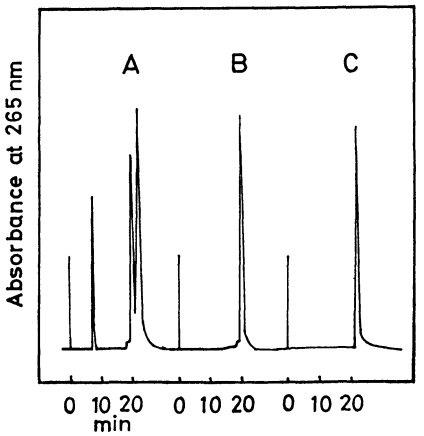

Fig. 1. HPLC of a reaction mixture after CM-Sephadex column separation (A), and authentic (*RS*)-6-methyl- (B) and (*RS*)-7-methyl-tetrahydropterin (C). Column: Whatman Partisil-10 SCX (8.0 mm×250 mm). Eluant, 30 mM† aqueous $NH_4H_2PO_4$ adjusted to pH 3.0 with H_3PO_4. Flow rate 4.0 ml/min.

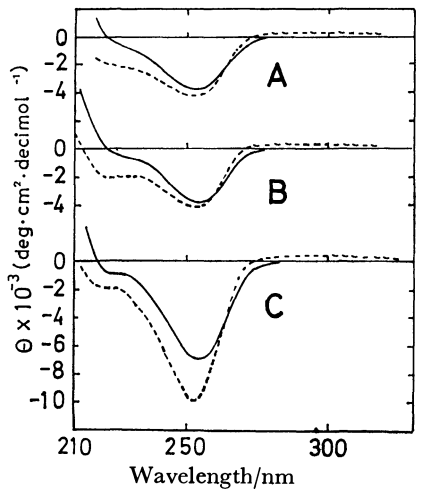

Fig. 2. CD spectra of the enzymically reduced tetrahydro-6-methylpterin[2] (A), synthetic (*S*)-6-methyl- (B), and (*S*)-7-methyl-tetrahydropterin (C). The data were obtained at pH 3.0 (——, monocation) and at H_0 −1.0 (——, dication).

undoubtedly produced by oxidation of the initially formed (*S*)-6-methyl- and (*S*)-7-methyl-5,6,7,8-tetrahydropterins by atmospheric oxygen. This oxidation could be prevented effectively when the condensation was carried out under hydrogen atmosphere. The 6- and 7-methyltetrahydropterins were isolated as a mixture (15% yield, estimated from UV spectra) by chromatography on a Florisil column and subsequently

† 1 M=1 mol dm^{-3}.

on a CM-Sephadex column. Separation of 6- and 7-methyltetrahydropterin from each other was achieved by means of HPLC on a preparative Partisil-10 SCX column (8 mm×250 mm) using an ammonium phosphate buffer (30 mM, pH 3.0) as the solvent. Under the conditions, (*S*)-6-methyl-5,6,7,8-tetrahydropterin (**3**) was eluted a little, but sufficiently, faster than the isomeric (*S*)-7-methyltetrahydropterin (**4**) as shown in Fig. 1. The structure of these compounds were confirmed by comparing their chromatograms (HPLC) and UV spectra with those of the authentic racemates.[9,10]

The CD spectra of (*S*)-6-methyltetrahydropterin (**3**) were found superimposable with those of the enzymatically reduced (−)-6-methyltetrahydropterin[2] as shown in Fig. 2 at two different pH values, *i. e.* pH 3.0 (monocation) and H_0 −1.0 (dication). (*S*)-7-Methyltetrahydropterin (**4**) also showed a negative Cotton effect in CD spectra (Fig. 2) with a trough at a wavelength slightly longer than the isomer (**3**).

The results described here clearly prove that the C-6 configuration of (−)-6-methyltetrahydropterin is *S*, and accordingly that of (−)-tetrahydrobiopterin is *R*, which is consistent with the previous conclusions.[2,3,6,7]

Experimental

The UV spectra were measured on a Shimadzu UV-300 spectrometer, and the CD spectra on a JASCO J-40A recording spectropolarimeter equipped with a JASCO J-PRY data processor. The high-performance liquid chromatography was carried out using a JASCO TRI ROTAR on a Partisil-10 SCX column (8.0 mm×250 mm), which was eluted with a 30 mM ammonium phosphate (pH 3.0) buffer (flow rate 4.0 ml/min) and detected on a JASCO UVIDEC 100-II spectrometer. The retention time was determined by means of a SYSTEM INSTRUMENTS model 500E integrator.

(S)-6-Methyl-5,6,7,8-tetrahydropterin (3) and the *(S)-7-Methyl Isomer (4)*. A mixture of 2,4-diamino-5-bromo-6-hydroxypyrimidine[11] (1.0 g), (*S*)-1,2-propanediamine[12] (4.0 g), and acetic acid (0.7 g) was heated at 115 °C under hydrogen atmosphere for 7 h. The excess amine was removed by distillation under diminished pressure. The residue was dissolved in water (5 ml) and made acid with acetic acid. The solution was fractionated on a Florisil column (20 mm× 80 mm), eluted by 0.3 M acetic acid. The eluate was concentrated to about 10 ml and then passed through a CM-Sephadex column (20 mm×250 mm). The column was washed with water (1000 ml). The tetrahydropterins were eluted gradiently by 0—0.1 M hydrochloric acid (100 ml). The yield of the tetrahydropterins, as a mixture, was estimated to be 15% from the UV absorbance at 265 nm of the pooled eluate. The eluate was concentrated to about 6 ml under reduced pressure. A 0.5 ml aliquot of the concentrate was injected to a preparative Partisil-10 SCX column (8 mm×250 mm) and eluted with the above mentioned ammonium phosphate buffer (4.0 ml/min) to give (*S*)-6-methyltetrahydropterin (retention time 21.5 min) and the (*S*)-7-methyl isomer (retention time 22.7 min). The pooled eluates of each fraction were used for measuring the UV and CD spectra.

References

1) Part VI: S. Matsuura, T. Sugimoto, and T. Nagatsu, *Bull. Chem. Soc. Jpn.*, **54**, 2231 (1981).

2) S. Matsura, T. Sugimoto, H. Hasegawa, S. Imaizumi, and A. Ichiyama, *J. Biochem.*, **87**, 951 (1980).

3) H. Hasegawa, S. Imaizumi, A. Ichiyama, T. Sugimoto, S. Matsuura, K. Oka, T. Kato, T. Nagatsu, and M. Akino, "Chemistry and Biology of Pteridines," ed by Kisliuk and Brown, Elsevier/North Holland, New York (1979), p. 183.

4) S. W. Bailey and J. E. Ayling, *J. Biol. Chem.*, **253**, 1598 (1978).

5) T. Kato, T. Yamaguchi, T. Nagatsu, T. Sugimoto, and S. Matsuura, *Biochim. Biophys. Acta*, **611**, 741 (1980).

6) W. L. F. Armarego, P. Waring, and J. W. Williams, *J. Chem. Soc., Chem. Commun.*, **334** (1980).

7) T. Sugimoto and S. Matsuura, *Bull. Chem. Soc. Jpn.*, **53**, 3388 (1980).

8) W. Ehrenstein, H. Wamhoff, and F. Korte, *Tetrahedron*, **26**, 3993 (1970)

9) J. M. Whiteley and F. M. Huennekens, *Biochemistry*, **6**, 2620 (1967).

10) A. N. Ganguly, P. K. Sengupta, J. H. Bieri, and M. Viscontini, *Helv. Chim. Acta*, **63**, 395 (1980).

10) T. L. V. Ulbricht and C. C. Price, *J. Org. Chem.*, **21**, 567 (1956).

11) S. Schnell and P. Karrer, *Helv. Chim. Acta*, **38**, 2036 (1955).

Preparation of Aryl Hydrazonates and 1,2-Diacylhydrazines by Phase Transfer Catalysis

Ahmad Sami SHAWALI,* Hamdi Mahmoud HASSANEEN,† Richard PAGNI,† and Mourad Sherif SHERIF

Department of Chemistry, Faculty of Science, University of Cairo, Giza, Egypt

†*Department of Chemistry, The University of Tennessee, Knoxville, Tennessee 37916, U.S.A.*

(Received October 21, 1980)

Synopsis. A series of aryl hydrazonates has been prepared in excellent yield (>90%) by phase-transfer-catalysis technique from the corresponding phenol and hydrazonoyl bromides in dichloromethane in the presence of tetrabutylammonium iodide. 1,2-Diacyl derivatives of arylhydrazines were also prepared by the same technique using carboxylic acids in place of phenols.

Recently the phase-transfer-catalysis as a synthetic tool has attracted the attention of several investigators.[1,2] We have extended the application of this technique to the preparation of aryl hydrazonates (**2**) and 1,2-diacylhydrazines (**3**) by the reaction of hydrazonoyl bromides (**1**) with phenols and carboxylic acids, respectively. In both cases tetrabutylammonium iodide was used as the phase transfer catalyst (Scheme 1). Both esters **2** and hydrazides **3** with ortho halogen atom in the *N*-aryl moiety proved useful in synthesis of 4*H*-1,3,4-benzoxadiazine derivatives.[3] The results are given herewith.

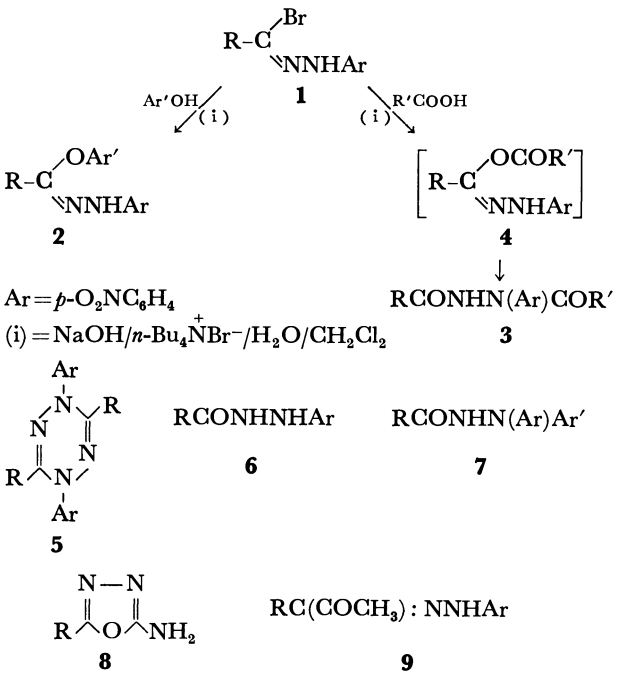

Scheme 1.

Results and Discussion

Treatment of **1** and phenol or naphthol with tetrabutylammonium iodide and sodium hydroxide in dichloromethane at room temperature affords the corresponding aryl hydrazonates (**2**) in 91—96% yields. Previously reported aryl hydrazonates were prepared by treating hydrazonoyl halides (**1**) with sodium phenolates in ethanol[4] or in benzene.[5,6] Alternatively, a mixture of hydrazonoyl halide (**1**) and phenol is treated with triethylamine in benzene[6,7] to give **2**. Reaction of **1** with phenol in the presence of sodium acetate was reported to give **3** (R'=CH_3) instead of **2**.[8] The yield of **2** prepared by either of the foregoing procedures did not exceed 65%. The phase transfer catalysis method described here seems to be more convenient and leads to excellent yields of **2**, eliminating the formation of tetrazines (**5**) or hydrazides (**6**) as competing reaction products. The structures of the esters prepared (Table 1) were confirmed by elemental analysis and spectral data. For example,

TABLE 1. ARYL HYDRAZONATES, **2**

Compound No.	R	Ar	Mp °C	Yield %	Molecular formula (Lit, Mp/°C)	N (%) Found	N (%) Calcd
2a	C_6H_5	C_6H_5	172	93	(172)[4]		
2b	C_6H_5	1-$C_{10}H_7$	201	91	$C_{23}H_{17}N_3O_3$	11.01	10.96
2c	C_6H_5	2-$C_{10}H_7$	179	93	$C_{23}H_{17}N_3O_3$	10.89	10.96
2d	4-$CH_3C_6H_4$	1-$C_{10}H_7$	201	90	$C_{24}H_{19}N_3O_3$	10.51	10.57
2e	4-$CH_3C_6H_4$	2-$C_{10}H_7$	186	95	$C_{24}H_{19}N_3O_3$	10.49	10.57
2f	4-ClC_6H_4	1-$C_{10}H_7$	218	94	$C_{23}H_{16}ClN_3O_3$	10.00	10.05
2g	4-ClC_6H_4	2-$C_{10}H_7$	215	93	$C_{23}H_{16}ClN_3O_3$	9.98	10.05
2h	4-$NO_2C_6H_4$	1-$C_{10}H_7$	205	96	$C_{23}H_{16}N_4O_5$	12.98	13.08
2i	4-$NO_2C_6H_4$	2-$C_{10}H_7$	218	92	$C_{23}H_{16}N_4O_5$	12.93	13.08
2j	CH_3	1-$C_{10}H_7$	167	90	$C_{18}H_{15}N_3O_3$	13.00	13.07
2k	CH_3	2-$C_{10}H_7$	162	94	$C_{18}H_{15}N_3O_3$	12.93	13.07
2l	$(CH_3)_2CH$	1-$C_{10}H_7$	123	94	$C_{20}H_{19}N_3O_3$	11.87	12.02
2m	$(CH_3)_2CH$	2-$C_{10}H_7$	130	91	$C_{20}H_{19}N_3O_3$	12.00	12.02

Table 2. 1,2-Diacyl-1-*p*-nitrophenylhydrazines, **3**

Compound No.	R	R′	Mp °C	Yield %	Molecular formula (Lit, Mp/°C)	N (%) Found	N (%) Calcd
3a	C_6H_5	C_6H_5	169	95	$C_{20}H_{15}N_3O_4$	11.57	11.63
3b	C_6H_5	1-$C_{10}H_7$	210	97	$C_{24}H_{17}N_3O_4$	10.10	10.21
3c	C_6H_5	4-ClC_6H_4	233	93	$C_{20}H_{14}ClN_3O_4$	10.58	10.61
3d	4-$CH_3C_6H_4$	1-$C_{10}H_7$	200	94	$C_{25}H_{19}N_3O_4$	9.90	9.87
3e	4-$CH_3C_6H_4$	4-ClC_6H_4	231	96	$C_{21}H_{16}ClN_3O_4$	10.15	10.25
3f	$(CH_3)_2CH$	C_6H_5	148	97	(148)[16]		
3g	$(CH_3)_2CH$	1-$C_{10}H_7$	163	94	$C_{21}H_{19}N_3O_4$	11.06	11.13
3h	$(CH_3)_2CH$	4-ClC_6H_4	222	95	$C_{17}H_{16}ClN_3O_4$	11.49	11.61
3i	CH_3	C_6H_5	165	97	$C_{15}H_{13}N_3O_4$	14.00	14.04

the infrared spectra of **2** reveal, in each case, two characteristic bands near 1255 and 1070 cm^{-1} assignable to an aryl ether linkage. Their electronic absorption spectra in ethanol are of typical hydrazones. The structures of **2** were also substantiated by the identification of 1,1-diaryl-2-acylhydrazines (**7**) obtained by thermolysis of **2** in xylene.[4,7]

1,2-Diacylhydrazines (**3**) (R′=CH_3) are usually prepared by treatment of hydrazonoyl halides (**1**) with sodium acetate in acetic acid or in water.[9–11] However, this method leads in some cases to hydrolysis product **6** or intramolecular nucleophilic substitution products, for example **8**.[12,13] Ciusa and Mega[14] claimed the formation of **9** by treatment of **1** (R=C_6H_5, Ar=2-Br, 4-$NO_2C_6H_4$) with sodium acetate. We have found that treatment of a mixture of **1** and carboxylic acid with tetrabutylammonium iodide and sodium hydroxide in dichloromethane at room temperature eliminates all such side reactions, giving **3** in yields higher than 93%. In this reaction, the initially formed hydrazonoyl carboxylate **4** undergoes a rapid 1,3-acyl migration to give **3**.[15] All compounds in series **3** exhibit in their infrared spectra two CO bands near 1675 and 1685 cm^{-1} and an NH band near 3250 cm^{-1}. The new 1,2-diacyl-1-aryl hydrazines (**3**) prepared by phase transfer catalysis method are given in Table 2.

Experimental

All melting points are uncorrected. Microanalyses were performed at Galbraith Laboratories, Inc., Knoxville, Tennessee, U. S. A. The IR and UV spectra were recorded on Pye-Unicam spectrophotometers, models SP1000 and SP8000, respectively.

Aldehyde *p*-nitrophenylhydrazones were converted into the corresponding hydrazonoyl bromides (**1**) by reaction with bromine in glacial acetic acid.[4]

Aryl Hydrazonates. As a general procedure a solution of hydrazonoyl bromide (1.6 mmol) in dichloromethane (15 ml) is added to a rapidly stirred solution of the appropriate phenol (2.1 mmol), sodium hydroxide (0.082 g, 2.1 mmol) and tetrabutylammonium iodide (0.022 g, 0.06 mmol) in water (15 ml). The mixture was stirred at room temperature for 1 h and then diluted with chloroform (25 ml). The organic layer was separated and washed successively with 5% sodium hydroxide solution and water, dried with anhydrous sodium sulfate. The solvent was removed and the residue was triturated with methanol. The crude solid formed was collected and crystallized from acetic acid or ethanol to give the corresponding aryl hydrazonates (Table 1).

1,2-Diacyl-1-(p-nitrophenyl)hydrazines (3). General Method: To a rapidly stirred solution of carboxylic acid (1.4 mmol), sodium hydroxide (0.055 g, 1.4 mmol), and tetrabutylammonium iodide (0.011 g, 0.03 mmol) in water (15 ml) was added the appropriate hydrazonoyl bromide (1.3 mmol) in dichloromethane (15 ml) and the mixture was stirred at room temperature for 1 h. The mixture was diluted with chloroform (30 ml) and the organic layer separated, dried with anhydrous sodium sulfate, and evaporated. The crude product was collected, washed with water and crystallized from acetic acid, to give hydrazides **3** in 93—97% yields (Table 2).

References

1) G. W. Gokel and W. P. Weber, "Phase-Transfer-Catalysis in Organic Synthesis," Springer Verlag, Berlin (1977).

2) C. M. Starks and C. Liotta, "Phase-Transfer-Catalysis, Principles and Techniques," Academic Press, New York (1978).

3) A. S. Shawali and C. Parkanyi, *J. Heterocycl. Chem.*, **17**, 833 (1980).

4) A. S. Shawali and H. M. Hassaneen, *Tetrahedron*, **28**, 5903 (1972).

5) A. S. Shawali and M. K. Ahmad, *Bull. Chem. Soc. Jpn.*, **46**, 3625 (1973).

6) A. F. Hegarty, T. A. Kearney, and F. L. Scott, *J. Chem. Soc., Perkin Trans. 2*, **1973**, 1422.

7) A. S. Shawali and H. M. Hassaneen, *Bull. Chem. Soc. Jpn.*, **50**, 2827 (1977).

8) A. S. Shawali, H. M. Hassaneen, and S. Almousawi, *Bull. Chem. Soc. Jpn.*, **51**, 512 (1978).

9) J. M. Burgess and M. S. Gibson, *J. Chem. Soc.*, **1964**, 1500; A. J. Elliott and M. S. Gibson, *J. Chem. Soc., Perkin Trans. 1*, **1972**, 2915.

10) F. D. Chattaway and A. J. Walker, *J. Chem. Soc.*, **1925**, 1687; F. D. Chattaway and A. B. Adamson, *ibid.*, **1930**, 157, 843.

11) A. S. Shawali and A. O. Abdel Hamid, *Bull. Chem. Soc. Jpn.*, **49**, 321 (1976); A. S. Shawali and H. M. Hassaneen, *Indian J. Chem.*, **14B**, 425 (1976).

12) J. Cronin, A. F. Hegarty, P. A. Cashell, and F. L. Soott, *J. Chem. Soc., Perkin Trans. 2*, **1973**, 1708.

13) M. S. Gibson, *Tetrahedron*, **18**, 1377 (1962).

14) R. Ciusa and P. Mega, *Gazz. Chim. Ital.*, **58**, 831 (1928).

15) A. S. Shawali and A. Osman, *Tetrahedron*, **27**, 2517 (1971).

16) A. S. Shawali, H. M. Hassaneen, and N. F. Eweiss, *J. Appl. Chem. Biotechnol.*, **28**, 864 (1978).

The Reaction of Dibenzylthiocarbamoyl Chloride with Sodium Nitrite

Masayuki NAKAJIMA, Rose Ann HERGET, and Jean-Pierre ANSELME*

Department of Chemistry, University of Massachusetts at Boston, Harbor Campus, Boston, MA 02125, U.S.A.

(Received November 12, 1980)

Synopsis. The reaction of dibenzylthiocarbamoyl chloride with sodium nitrite in acetonitrile at room temperature yields *N*-nitrosodibenzylamine, dibenzylcarbamoyl chloride, bis(dibenzylcarbamoyl) disulfide, benzaldehyde, and benzyl isothiocyanate; possible mechanisms for the formation of these products are suggested.

The quantitative formation of *N*-nitrosodibenzylamine (**4**) from the nitrosative decarboxylation of dibenzylcarbamoyl chloride (**5**) with sodium nitrite in acetonitrile was recently reported.[1] In the interest of exploring the use of related systems for the formation of nitrogen-nitrogen bonds, the study of the action of sodium nitrite in dibenzylthiocarbamoyl chloride (**1**) was undertaken.

Although the NMR spectrum of the reaction mixture of equimolar amounts of **1** and sodium nitrite in dry acetonitrile indicated that the reaction was not as clean as that of **5** with sodium nitrite,[1] the presence of benzaldehyde and *N*-nitrosodibenzylamine (**4**) in the crude reaction mixture was established; beside carbonyl bands at 1645, 1675, 1695 cm^{-1}, the IR spectrum displayed absorptions at 2180—2100 cm^{-1} which suggested the presence of a compound with a cumulative bond system. Chromatography of the mixture on silica gel led to the isolation and characterization on benzaldehyde, *N*-nitrosodibenzylamine, dibenzylcarbamoyl chloride (**5**) and the compound which displayed the absorption at 2180—2100 cm^{-1}; in addition an unknown soild, mp 132.5—133 °C, was isolated; its elemental analysis indicated the empirical formula to be $C_{15}H_{14}NOS$; the presence of a carbonyl group,[2] its NMR and mass spectra,[3] established the structure of bis(dibenzylcarbamoyl) disulfide (**8**). The compound displaying the strong absorption at 2180—2100 cm^{-1} was shown to be benzyl isothiocyanate (**6**) by comparison with an authentic sample.[4] Once the identity of the products was established, the reaction was repeated and the yield of each product (except for **8** which was isolated and weighed) was determined by the integration of the NMR spectrum of the crude reaction product.

The formation of **8** may be understood in terms of an oxygen to sulfur migration of the nitroso group of **2**, followed by the loss of nitrogen monoxide from **3** and generation of the carbamoylthio radical (**7**) which could then dimerize to **8**. Although *N*-nitrosodibenzylamine (**4**) may be formed by loss of COS from **2** as anticipated, it could also arise from the action of nitrite ion on **3** and on **5**.[1] However, control experiments showed that **8** did not react either with chloride or nitrite ions. A reaction run with a 1.4 excess of sodium nitrite for four days showed a dramatic increase in the yield of **4** (39%) with a concurrent decrease in the yield of **8** (43%); the yield of **5** was unchanged. The same reaction carried out overnight gave **8** as the major product (63%) with **4** and **5** being formed in only minor amounts. Similarly the formation of **5** could be rationalized by displacement of chloride ion on **3**. Although direct displacement of nitrite ion on **1** may account for the formation of benzyl isothiocyanate (Scheme 2, path a), an alternate path involves **2** as the intermediate which undergoes an internal displacement *via* a six-membered ring transition state leading to benzyl isothiocyanate (**6**) and benzyl nitrite (Scheme 2, path b); the latter compound is known to decompose to benzaldehyde;[5] authentic benzyl nitrite reacted with chloride ion to give benzaldehyde. Scheme 3 summarizes the possible paths leading to the observed products.

Experimental

All mps and bps are uncorrected. Infrared spectra were obtained on a Perkin-Elmer Infracord and NMR spectra were determined on CCl_4 or $CDCl_3$ on a R-24 Hitachi-Perkin Elmer Spectrometer using TMS as an internal standard. Mass spectra were obtained at Chemical Spectrometry Laboratory of Massachusetts Institute of Technology and taken on Varian Mat 44 mass spectrometer. A low energy (50 eV) spectrum was obtained on a Hitachi-Perkin Elmer mass spectrometer model RMU-6L.

Dibenzylthiocarbamoyl Chloride (1). To a solution of 85% (w/w) thiophosgene (10.5 g, 77 mmol) in anhydrous ether (75 ml) at −5 °C, was added a solution of dibenzylamine (30.5 g, 155 mmol) in anhydrous ether (75 ml) with a mechanical stirring. An additional 50 ml of anhydrous ether was added, and the mixture was stirred at ambient temperature overnight. The precipitated dibenzylamine hydrochloride was collected, and the filtrate was evaported to dryness at room temperature *in vacuo*. The solid residue

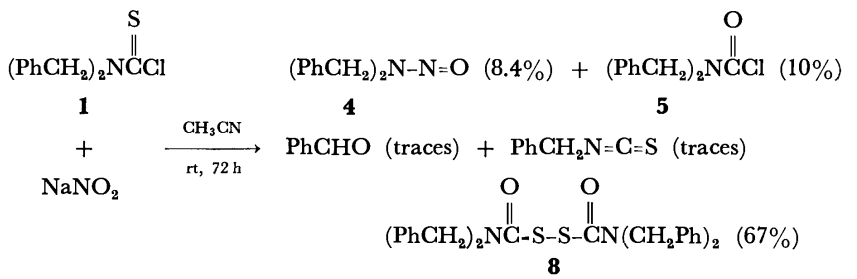

Scheme 1.

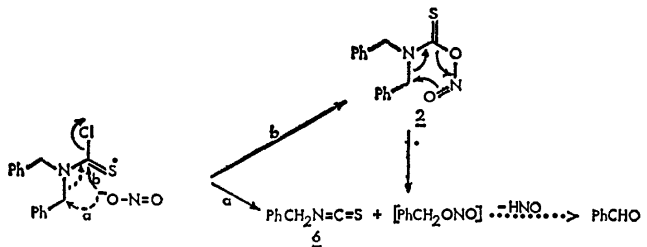

Scheme 2.

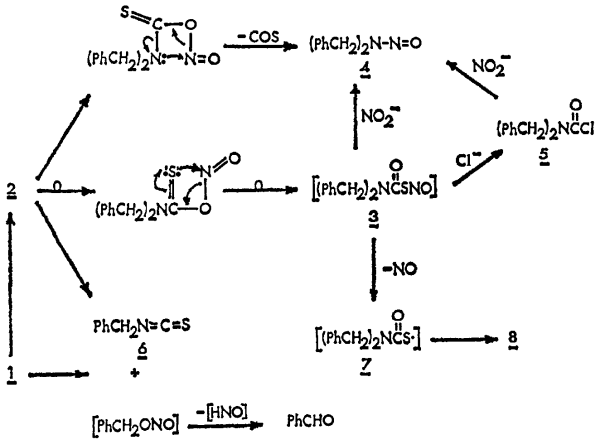

Scheme 3.

was crystallized from chloroform–ligroin mixture to yield 10.6 g (53%) of **1**, mp 43—45 °C, lit,[6] mp 49 °C.

Reactions of ***1*** *with Sodium Nitrite.* A mixture of dibenzylthiocarbamoyl chloride (3.2 g, 12 mmol) and sodium nitrite (1.0 g, 14.5 mmol) in dry acetonitrile (40 ml) was stirred overnight in a flask covered with aluminum foil and connected to a gas bubbler. The insoluble inorganic material was filtered, and the acetonitrile solution was evaporated *in vacuo* to leave a residue, which was deposited on a preparative column chromatography (silica gel mesh 60—200, g). Elution with a mixture of benzene and hexanes (1:2 v/v, 150 ml) gave benzyl isothiocyanate (20 mg) whose IR and NMR spectra were superimposable upon those of an authentic sample.[4,7] Further elution (200 ml) afforded dibenzylcarbamoyl chloride (566 mg, 2.2 mmol, 19%), identical to an authentic sample.[1] Continued elution with the same mixture (100 ml) and with a mixture of benzene and hexanes (1:1 v/v, 100 ml) yielded *N*-nitrosodibenzylamine (**4**, 425 mg, 1.9 mmol, 16%) and trace amounts of benzaldehyde; their structures were established by their spectra data and by addition of authentic samples to the NMR samples. Elution with benzene–hexane (1:1 v/v, 100 ml) and with benzene (200 ml) gave crude bis(dibenzylcarbamoyl) disulfide (797 mg, 1.6 mmol, 31%) mp 130—131.5 °C. The crude disulfide was recrystallized from dichloromethane–hexane mixture to afford colorless crystals, mp 132.5—133 °C. IR (KBr): 1675 cm^{-1} (>C=O); NMR ($CDCl_3$): δ 7.30 (s, ArH, 20H), δ 4.60 (s, $PhCH_2$ 8H); mass spectrum [*m/e*, (relative intensity)]: 512 (very weak),[3] 256 (0.05), 224 (6), 196 (0.3), 91 (100). Found: C, 70.38; H, 5.75; N, 5.33 S, 12.46. Calcd for $C_{30}H_{28}N_2O_2S_2$: C, 70.28; H, 5.50; N, 5.47; S, 12.51.

The reaction was repeated using 11.7 mmol of **1** and 11.7 mmol of sodium nitrite. After overnight stirring, the acetonitrile was evaporated *in vacuo* to leave a solid residue which was stirred with a mixture (20 ml) of ether and petroleum ether (1:3 v/v). The insoluble solid left after the first extraction was stirred with dichloromethane (25 ml×2). Evaporation of dichloromethane from the second extract gave bis(dibenzylcarbamoyl) disulfide (1.97 g, 3.8 mmol, 65%). Evaporation of the solvents from the first extract gave a residue (0.7 g), which was chromatographed on silica gel (mesh 60—200, 20 g). Elution with benzene–hexane mixture (1:1 v/v, 150 ml) gave a mixture of dibenzylcarbamoyl chloride (1.2 mmol, 10%) and *N*-nitrosodibenzylamine (0.1 mmol, 0.8%) whose molar ratio was estimated by the NMR integration under benzyl protons. Continued elution with the same mixture (150 ml) yielded *N*-nitrosodibenzylamine (0.9 mmol, 7.7%). Elution with benzene (200 ml) afforded bis(dibenzylcarbamoyl) disulfide (38 mg, 0.07 mmol, 1.2%).

The same reaction was carried out using 6.2 mmol of dibenzylthiocarbamoyl chloride and 8.7 mmol of sodium nitrite for 4 d. The acetonitrile was evaporated under reduced pressure to give a solid residue. The solid was stirred with ether (25 ml), and the solid left after the first extraction was stirred with dichloromethane (25 ml×2). Evaporation of dichloromethane from the second extract afforded bis(dibenzylcarbamoyl) disulfide (411 mg, 0.8 mmol, 26%). Evaporation of ether from the first extract gave a residue (1.06 g) which was stirred with a mixture (25 ml) of petroleum ether and ether (2:1 v/v) to leave a mixture (322 mg) of the disulfide (0.48 mmol, 15.5%) and *N*-nitrosodibenzylamine (0.34 mmol, 5.5%). The extract was concentrated under reduced pressure to yield a mixture of dibenzylcarbamoyl chloride (0.6 mmol, 10%) and *N*-nitrosodibenzylamine (2.1 mmol, 33%) whose molar ratio was estimated by the NMR integration under benzyl protons.

Control Experiments. Reaction of Bis(dibenzylcarbamoyl) Disulfide with Sodium Chloride: A mixture of the disulfide (200 mg) and sodium chloride (1.0 g) in a mixture of acetonitrile (20 ml) and dichloromethane (5 ml) was stirred at room temperature overnight. Inorganic material was filtered, and filtrate was concentrated on a rotary evaporator to give a quantitative recovery of the disulfide.

Reaction of Bis(dibenzylcarbamoyl) Disulfide with Sodium Nitrite: A mixture of the disulfide (76 mg) and sodium nitrite (1.0 g) in acetonitrile (30 ml) was stirred at room temperature for 3 d. The mixture was filtered, and washed with dichloromethane (50 ml). The acetonitrile filtrate and the dichloromethane solution were combined and concentrated under reduced pressure to afford the unreacted disulfide (66 mg) in 86% recovery.

References

1) M. Nakajima and J. -P. Anselme, *Tetrahedron Lett.*, **1979**, 3831; this is the eighth in a series of papers dealing with *N*-nitrosoamines and related compounds; for previous paper, see M. Nakajima and J. -P. Anselme, *J. Chem. Soc., Chem. Commun.*, **1980**, 796.

2) E. C. Gregg, *J. Am. Chem. Soc.*, **74**, 3691 (1952); L. A. Spurlock and P. E. Newallis, *J. Org. Chem.*, **33**, 2073 (1968).

3) J. Ø. Madsen, S. -O. Lawesson, A. M. Duffield, and C. Djerassi, *J. Org. Chem.*, **32**, 2054 (1967). The parent peak could only be observed at low voltage.

4) W. Schneider, D. Clibbens, G. Hullweck, and W. Steibelt, *Ber.*, **47**, 1248 (1914).

5) A. Baeyer and V. Villiger, *Ber.*, **34**, 755 (1901).

6) E. Lieber, C. N. R. Rao, C. B. Lawyer, and J. P. Trivedi, *Can. J. Chem.*, **41**, 1643 (1963).

7) M. L. Moore and F. S. Crossely, *Org. Synth.*, Coll. Vol. III, 59 (1955).

Properties of Polyelectrolyte Complexes Consisting of [2-(Diethylamino)-ethyl]dextran Hydrochloride, Carboxymethyldextran, and Sodium Dextran Sulfate for Clot Formation *in Vitro*

Yasuo KIKUCHI* and Koji SHIMIZU

Faculty of Engineering, Ōita University, 700-Dannoharu, Ōita 870

(Received July 29, 1980)

Synopsis. A polyelectrolyte complex (PEC) prepared at higher hydrogen ion concentration enhanced the coagulation of blood, whereas PEC prepared at lower hydrogen ion concentration prevented coagulation of blood. This difference sholud be attributed to the difference in the molecular structures of the PEC prepared.

The mixing of oppositely charged polyelectrolytes in solution leads to the formation of a complex.[1] Many reports[2,3] have dealts with the polyelectrolyte interaction between polysaccharides, or between polysaccharide and synthetic macromolecules and their properties. The biomedical characteristics are important in relation to biological systems, membranes, and industrial applications.[4]

We have reported the novel chemical reaction, structure, and properties of polyelectrolyte complexes containing three materials,[5-7] and the clot formation of these polyelectrolyte complex *in vitro*.[5,6] This note deals with the attractive results for clot formation *in vitro* of the novel polyelectrolyte complexes (PEC) consisting of three materials, which have been reported in a previous paper.[7]

Experimental

The materials of [2-(diethylamino)ethyl]dextran hydrochloride (EA), sodium dextran sulfate (DS), and sodium carboxymethyldextran (CMD) and the general experimental procedures, the apparatus and the chemical analyses were the same as those described in the previous paper.[7]

ACD blood samples of O and A type were provided from the Red Cross Hospital Blood Center, Japan and kept in a thermostat at 4—6 °C. The storage time of 0 type ACD blood was 10 d; that of A type ACD blood was 5 d. The ACD blood was prepared by adding the blood to an anticoagulant citrate dextrose solution consisting of sodium citrate, citric acid and dextrose. The blood test was carried out according to the procedure of Imai and Nose[8]: a polymer blend of 80 mg PEC and 320 mg poly (vinyl chloride) in 1-C and 1-D (Table 1 in ref. 8) was pressed (8.5 t/4.9 cm^2) under vacuum for 5 min to make a sample tablet; in series 2—5, the PEC of 5 mg was coated on a sample tablet by pressing (8 t/4.9 cm^2) under vacuum for 5 min after 400 mg poly (vinyl chloride) was pressed (2 t/4.9 cm^2) for 15 s under vacuum.

Experimental conditions and yields in the preparation of PEC, and elementary analyses and composition of PEC, are given in Tables 1 and 2 of the previous paper.[7] As seen in these tables, the hydrogen ion concentration and the mole ratio of mixture solution (DS+CMD) to EA solution in the reaction mixture both played important roles in changing the ratio of the mixture solution to that of EA in the PEC produced. However, all the PEC were found to consist of the three materials, EA, CMD, and DS, by IR spectra, even though precipitates did not form in the reaction mixtures of EA and CMD at higher hydrogen ion concentration of the reaction system (pH$<$2).

The IR spectra and content in CMD of PEC were described in the previous paper.[7] That is, the localized interactions between -OH and $-OSO_3H$ groups in the 1, 2, and 3 series would result from the formation of $-SO_3H$ groups. In other words, the long chains on the three materials having the same dextran ring and the intermolecular hydrogen bonds between OH groups for PEC may be broken at high hydrogen ion concentraiton and consequently bonds will form between $-OSO_3H$ and -OH groups. Furthermore, the carboxy groups in the PEC of 1, 2, and 3 series existed as undissociated -COOH. Actually, the PEC in 4 and 5 series differed appreciably from the PEC in 1 and 2 series in such properties as sulfur content, solubility, and color reaction with Toluidine Blue, as described previously. From those results, the structures of PEC were estimated as follows: the PEC prepared at higher hydrogen ion concentration consisted of both COOH groups and a great number of $-OSO_3H$ groups (4%$>$1%$>$ pH 2 HCl solution of reaction system); the molecular weight of the PEC prepared became smaller because of the breaking of long chains of the materials; those prepared at pH 6.5 or 11.0 were not composed of the -COOH and $-OSO_3H$ groups in PEC; and in addition, the content of CMD in PEC became greater with an increase in hydrogen ion concentration.

The results in three-component solvents show that there is a small region in the solvent composition field where the complex remain in solution to yield a homogenous, transparent, viscous syrup. Phase diagrams were not obtained in the PEC

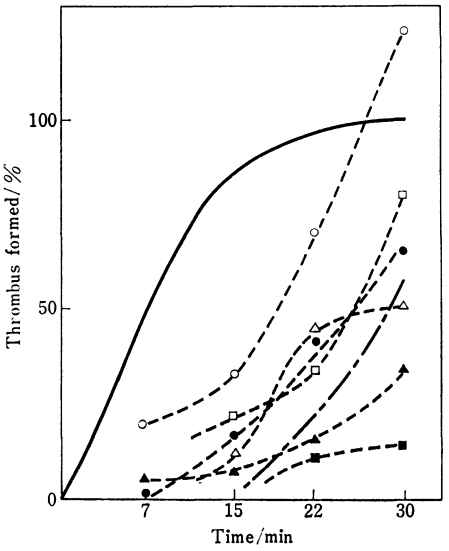

Fig. 1. Percentage of the thrombus formed on polyelectrolyte complexes compared with that on glass after a lapse of 30 min as a criterion.
Storage time of 0 type blood: 10 d, ——: glass, — - —: poly (vinyl chloride). ···□···: 1-C, ···○···: 1-D, ···●···: 2-D, ···▲···: 3-D, ···■···: 4-D, ···△···: 5-C. Sample codes 1-C, 1-D, 2-D, 3-D, 4-D, and 5-C correspond to those in Table 1 in the previous paper.

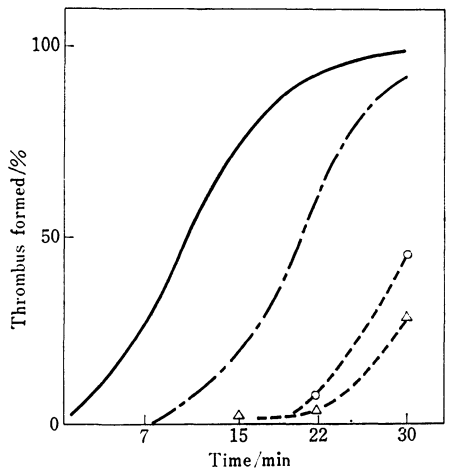

Fig. 2. Percentage of the thrombus formed on polyelectrolyte complexes compared with that on glass after a lapse of 30 min as a criterion.
Storage time of A type blood: 5 d, ——: glass, — — —: poly (vinyl chloride). ···○···: 3-C, ···△···: 5-D. Sample codes 3-C and 5-D correspond to those in Table 1 in the previous paper.

except for 1-C and 1-D, but the PEC in 2-D dissolved partially in the three-component solvent metnioned above. The experimental results in which the PEC in 1 series or 2 series dissolved or partially dissolved in the three-component solvent, and also the colored reaction with Toluidine Blue[7] in PEC, strongly support the difference in the molecular structure according to the experimental conditions of hydrogen ion concentration mentioned above.

Blood tests were performed on PEC (1-C, 1-D, 2-D, 3-C, 3-D, 4-D, 5-C, 5-D) listed in the previous paper[7] by measuring gravimetrically[8] the amount of thrombus formed at appropriate time intervals, after adding $CaCl_2$ solution (0.1 M, 0.02 ml;= 1 mol dm^{-3}) to ACD blood (0.2 ml, O or A type, storage time: 10 or 5 d) which had been in contact with test samples. The blood clotting test by coating on PEC tablet could not be performed on the PEC prepared in 4% hydrochloric acid solution (1-C, 1-D) because of the soaking of blood into the tablet. Therefore, tests were performed on a tablet of polymer blend of PEC and poly(vinyl chloride). A firm clot did not form even after 10 min with PEC of 3, 4, or 5 series except with 1-C, 1-D, and 2-D complexes. It may be noted that the PEC in 3,4, and 5 series suppressed the coagulation of blood considerably. On the other hand, the PEC in 1 series somewhat enhanced the coagulation of blood, as seen in Figs. 1 and 2, considering the amount of poly(vinyl chloride) in a tablet was 4 times as much as the PEC and the amounts of thrombus were larger than that formed on poly (vinyl chloride) tablets. Moreover, it was found that the quantities of the clot on the PEC tablet formed in high hydrogen ion concentration are somewhat greater than those on that formed in lower hydrogen ion concentration, although the contents of DS of PEC in 1, 2, and 3 series were greater than those in 4 and 5 series. Similarly, these experimental results strongly support the difference in molecular structure according to the experimental conditions of hydrogen ion concentration mentioned above. Thus, it has been well confirmed by the experimental results that the difference in the character of coagulation of blood should be attributed to the difference in the molecular structure of PEC prepared as mentioned above.

The likely mechanism of enhancement of coagulation appears to be the following: the factors of coagulation in blood were activated by the interactions of -COOH and $-OSO_3H$ groups with blood in PEC. On the other hand, as seen in the colorimetric reaction of Toluidine Blue, the mechanism of suppression of coagulation may be related to the possibility that negative charges such as $-COO^-$ and $-SO_3^-$ groups exist actively on the surface of PEC.[9]

Finally, it is concluded that the preparation of the described PEC offers an important reservoir of materials whose properties may be tailored according to each requirement.

This work was partially supported by a Grant-in-Aid for Scientic Research from the Ministry of Education, Science and Culture, Japan (1980, No. 455358).

References

1) E. Tsuchida and T. Osada, *Kobunshi*, **22**, 384 (1973).
2) N. Noguchi, *Kobunshi*, **22**, 402 (1973).
3) K. Shinoda and A. Nakajima, Summary of Papers in the 23rd Polymer Symposium, Tokyo, (1974).
4) A. Nakajima, *Kagaku To Kogyo*, **27**, 746 (1974).
5) Y. Kikuchi and Y. Onishi, *Nippon Kagaku Kaishi*, **1979**, 127.
6) Y. Kikuchi and Y. Onishi, *Nippon Kagaku Kaishi*, **1979**, 1101.
7) Y. Kikuchi, K. Hori, and Y. Onishi, *Nippon Kagaku Kaishi*, **1980**, 1157.
8) Y. Imai and Y. Nose, *J. Biomed. Mater. Res.*, **6**, 165 (1972).
9) M. K. Vogel, R. A. Cross, H. J. Bixer, and R. J. Guzman, *J. Macromol. Sci., Chem.*, **A4**, 675 (1970).

Stabilization of Normal Methyl Radicals after γ-Radiolysis at 300 K

Duro A. ODUWOLE* and Barrie WISEALL†

Department of Chemistry, Queen Mary College, Mile End Road, London, El 4NS, England

†*Department of Chemistry, City of London Polytechnic, Jewry Street, London, EC3 2EY, England*

(Received September 16, 1980)

Synopsis. Radiolytically produced normal methyl radicals are stabilized on solid surfaces at room temperature for the first time. The remarkable stability of this species on basic and neutral alumina surfaces at 300 K and in the presence of oxygen makes this system potentially useful as an intermediate in organic synthesis.

Since Turkevich and Fujita[1] first published the stabilization of normal methyl radicals (Me_n, $a \simeq 2.3$ mT) on porous Vycor glass, there have been several investigations of this system.[2-5] Such studies have shown that unlike the photolytically produced Me_n radical, the Me_n radical produced radiolytically at liquid nitrogen temperatures is neither observed at room temperature nor is the radical observed directly after radiolysis at room temperature. No suggestion has been put forward to explain this anomaly. In the course of our studies on the radiolysis of adsorbed species on alumina surfaces we succeeded in stabilizing Me_n radicals directly after radiolysis of adsorbed methyl iodide on basic and neutral alumina at 300 K. The line widths, hyperfine splitting and g values are $\simeq 0.10$ mT, 2.25 ± 0.005 mT and 2.0021 ± 0.0002 respectively, in good agreement with known data for the photolytically produced radical stabilized on other adsorbents.

Chromatographic grades aluminium oxides obtained from Hopkin and William (codes 128400-active basic, 128700-active neutral and 1287.50-acidic), Merck (codes 1076-basic, 1077-neutral and 1078-acidic) British Drug House (code 15139-neutral) and Woelm of Germany (code W200-basic) were used in this investigation; all were specified as γ-alumina and Brockmann activity=1. These oxides were initially heated in oxygen at 680 K and then under vacuum at $\simeq$900 K for 5 h. The samples were given an approximate 2% surface coating of methyl iodide at room temperature and sealed in vitreosil/pyrex ESR cells as generally described by other workers.[1-4] Surfaces given larger MeI coverages gave an unstable broad ESR signal (on radiolysis) having a line width of $\simeq 1.5$ mT and a mean life time of $\simeq 2$ h at room temperature. Samples were mixed thoroughly and were normally given a γ-dose of 250 krad, at room temperature, from a ^{60}Co source, although a dose of 100 krad produced signals having an adequate signal to noise ratio. Irradiation induced defects in the cells were flame annealed from the cavity section before transferring the sample. ESR measurements were made on a Decca X-3 spectrometer, all the hyperfine components of the spectrum being measured with respect to line widths, splittings and intensities.

The Me_n radical thus formed on basic and neutral alumina surfaces was found to be remarkably stable over several months at room temperature and we were able to study its reactivity towards various additives (Table 1). The results are contrary to those observed by Turkevich and Fujita[1] who found that the Me_n radical produced by photolysis of methyl iodide adsorbed on porous Vycor glass at room temperature reacted very rapidly with oxygen and hydrogen.

The decay of the Me_n radical *in vacuo* as a function of temperature (Fig. 1), shows a cascade effect at each temperature with an initial relatively rapid decay followed by a levelling off to a value dependent on the temperature. This result suggests that there is a continuum of activation energies for decay rather than the discrete activation energies proposed by Joppien and Willard.[3] This interpretation is in accord with that of Fujimoto *et al.*[2] who observed such a cascade effect in the decay of photolytically produced Me_n radicals on porous Vycor glass above 77 K.

Measurements of the line widths at liquid nitrogen temperatures showed a generalised broadening effect

Table 1. The effect of additives on the yield of Me_n radicals formed by radiolysis of adsorbed methyl iodide on basic-Al_2O_3 at 300 K

Additive	Me_n Signal intensity/%[c]	
	a)	b)
Oxygen	95	96
Hydrogen	74	81
Water vapour[d]	13	72

a) Additive present during radiolysis. b) Additive introduced after radiolysis. c) Yield of unadulterated sample *in vacuo*=100%. d) These measurements were made at 260 K to compensate for the dielectric loss of H_2O.

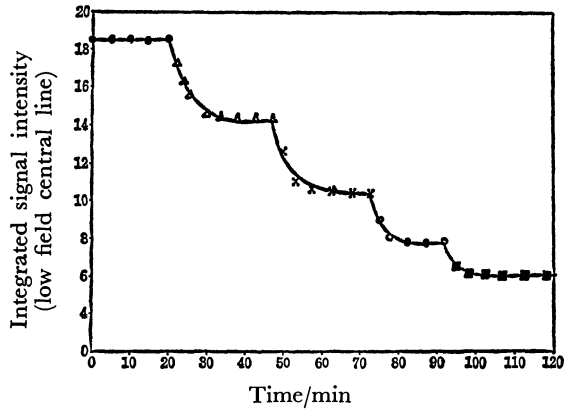

Fig. 1. The decay at elevated temperatures of Me_n radicals radiolytically produced on basic-Al_2O_3 at 300 K.
●: 293 K, △: 323 K, ×: 373 K, ○: 423 K, ■: 473 K.

(of all the component lines) to a value of $\simeq$2.5 mT, suggesting that unlike the Me_n radical trapped on silica gel[5,6] and on porous Vycor glass,[1] the species on alumina is immobilised on the surface.

Failure to observe the radical at room temperature on acidic alumina and other acidic surfaces such as silica gel and porous Vycor glass, suggests that the radical is perturbed under these conditions. Although it is believed that the acidity of the latter surfaces is very much weaker than that of γ-alumina, significantly increased acidity of these surfaces as a result of exposure to ionizing radiation has been reported previously.[7] This irradiation induced acidity may well preclude the stabilization of Me_n radical. A study of these surfaces by the present authors[8] shows that an irradiation induced defect interacts with Me_n radicals stabilized on them at liquid nitrogen temperature to produce line broadening and other secondary effects, and persists to above 300 K; this has a g value of 2.0022 ± 0.0001, suggesting that it may be due to trapped electrons. The absence of such a defect signal on the alumina surfaces would enhance stabilization of the radical.

The above results, showing the remarkable stability of radiolytically produced Me_n radical on alumina surfaces at room temperature and in oxygen, make this system potentially useful as an intermediate in organic synthesis. A more detailed study of the site or mechanism of stabilization of this species and of the effect of other additives on yield is in progress.

References

1) J. Turkevich and Y. Fujita, *Science*, **152**, 1619 (1966).
2) M. Fujimoto, H. D. Gesser, B. Garbutt, and A. Cohen, *Science*, **154**, 381 (1966).
3) P. K. Wong and J. E. Willard, *J. Phys. Chem.*, **72**, 2623 (1968); G. R. Joppien and J. E. Willard, *ibid.*, **78**, 1391 (1974).
4) G. B. Garbutt, H. D. Gesser and M. Fujimoto, *J. Chem. Phys.*, **48**, 4065 (1968); G. B. Garbutt and H. D. Gesser, *Can. J. Chem.*, **48**, 2685 (1970).
5) D. Oduwole, J. D. Barnes, and B. Wiseall, *J. Chem. Soc., Chem. Commun.*, **1978**, 164.
6) C. L. Gardner and E. J. Casey, *Can. J. Chem.*, **46**, 207 (1968).
7) C. Barter and C. D. Wagner, *J. Phys. Chem.*, **68**, 2351 (1964).
8) To be published.

PTFE-bonded Raney Nickel Hydrogen Electrodes in Alkaline Fuel Cells

Tadao KENJO

Department of Applied Science for Energy, Faculty of Engineering, Muroran Institute of Technology, Mizumoto-cho, Muroran 050

(Received September 3, 1980)

Polytetrafluoroethylene (PTFE)-bonded Raney nickel hydrogen electrodes have been prepared and their polarizations have been measured at 62 °C, using 6 M KOH (1 M=1 mol dm^{-3}) as an electrolyte. The electrodes were reproducible in polarization characteristics from electrode to electrode. The polarization resistance was found to be 0.29 Ω cm^2 for the electrode loaded with a 48-mg cm^{-2} catalyst. The limiting current density was 600 mA cm^{-2} for the electrode loaded with a 45.4-mg cm^{-2} catalyst. The influences of the pressure of the press machine and of the PTFE content on the polarizations have been investigated. The polarization resistance decreases with the catalyst loading in the manner to be expected from the reaction mechanism of the gas diffusion through electrolyte film. An experimental evidence for this reaction mechanism has been obtained by measuring the polarization of an electrode of a triple-layered structure containing a silver powder layer.

In most of the Raney nickel electrodes that have thus far been studied, electrolyte penetration into the electrode pores is prevented by the gas pressure applied on the pores from the other side of electrode. To attain a delicate balance between the gas pressure and the capillary force over the whole working area of electrode, a very good uniformity in the pore-size distribution and a careful gas-pressure control are required. Unless the pore sizes are uniform, the hydrogen gas is wasted by bubbling through the large pores, or the working area of catalytic surface is lost by the electrolyte drowning of the small pores. Although the amount of gas wasted by bubbling can be reduced by using a double-layered sintered nickel matrix[1,2] or a finely porous and wettable diaphragm,[3,4] the pore-size uniformity and the control of the gas pressure are still required.

On the other hand, electrodes water-proofed by a repellancy agent do not require such a rigorous pore-size uniformity or such a careful pressure control. However, this type of electrode has rarely been applied to Raney catalysts because the water-proofed metal electrodes have readily suffered from electrolyte drowning at a very low load current and their electrode characteristics have been quite unreproducible.[5]

Polytetrafluoroethylene (PTFE) is the repellancy agent used most frequently because of its good stabilities against heat and electrolytes. The PTFE particles are apt to cross-link with each other when they are milled with the catalyst powder for mixing. The fraction of cross-linked PTFE particles resulting from the mixing process seems to increase with the mixing time and the temperature. The repellancy of electrode and the area of the catalytic surface covered by PTFE, which essentially influence the polarization characteristics, depend not only upon the content of PTFE added, but also upon its cross-linkage. Thus, the polarization characteristics vary with the mixing condition. This is a reason why the PTFE-bonded electrodes are liable to be poorly reproducible. In the present study, the mixing time and the temperature have been kept constant so as to minimize the fluctuations in the polarization data.

The Raney nickel catalysts can be depyrophorized through a slow surface oxidation in air and can be reactivated by a reduction in the hydrogen atmosphere.[6] This permits the Raney catalysts to be handled safely in air for the electrode processing.

Experimental

Preparation of the Catalysts. A melt possessing a mass fraction of 40% Ni (99.95% purity) and 60% Al (99.99% purity) was prepared by means of an induction furnace using an alumina crucible. To avoid the separation of the nickel, the melt was quenched by pouring it into an iron cylinder. The ingot thus obtained was crushed and powdered in a mill to a particle size of less than 37 μm.

The aluminium was leached with a 6 M KOH solution at 40 °C. The Raney nickel thus obtained was washed with water and methyl alcohol alternatively.

Preparation of the Electrodes. A weighed amount of a PTFE dispersion (D-1, Daikin Industrial Company) containing 60% PTFE was added to the Raney catalyst. When the mixture was milled under blowing with a hair-dryer at the room temperature of 20±2 °C for 1 h, it became a paste. This paste was calender-rolled by hand into sheets using spacers 0.1—0.2 mm thick. After having been dried in air overnight, the sheets were boiled in acetone for 2 h to remove the surfactant which had been originally contained in the PTFE dispersion. These sheets were then used as catalyst layers.

Gas-side layers were used to stop the leakage of electrolytes that might occur through the large pores in the catalyst layers. They were prepared by using nickel black powder bound with the PTFE dispersion. Nickel black powder, which had been obtained by heating nickel formate in a hydrogen atmosphere at 250 °C, was milled with the PTFE dispersion in a way similar to that used in the case of Raney nickel. The nickel black sheets obtained by calender-rolling were attached to a stainless steel screen (100 mesh) from both sides and pressed at 200 kg cm^{-2}. The gas-side layer was heated in a nitrogen atmosphere at 380 °C for 15 min to sinter the PTFE particles and to remove the surfactant. The catalyst layers were then attached to the gas-side layer by pressing at pressures ranging from 200 kg cm^{-2} to 1200 kg cm^{-2}. The double-layered electrode thus obtained was heated at 150 °C in a hydrogen atmosphere for 1 h to activate the catalyst.

Measurement of Polarization. The geometrical working area of the electrodes was 7 cm^2. The electrolyte used was a 6 M KOH solution, and it was circulated at a rate of 5 ml min^{-1}. The electrolyte temperature was 62±0.5 °C. The IR voltage drop was eliminated by the current-interruption method.[7]

Results and Discussion

Figure 1 shows plots of the polarization, η, *vs.* the current density, i, for various catalyst loadings. Since they are almost linear up to a polarization of 20 mV, the polarization resistance, ω, which corresponds to the slope can be used as an electrode characteristic. The polarization resistance for the electrode loaded with a 48-mg cm^{-2} catalyst is found to be 0.29 Ω cm^2. It can be compared to the value of 0.31 Ω cm^2 given by Sturm for the supported Raney-Ni-Ti electrodes operated at 60 °C and at a loading of 100 mg cm^{-2}.[8]

The controllable electrode parameters in the present electrode preparation are the PTFE content, the pressure of the press machine, and the catalyst loading. When they are kept constant and a Raney nickel prepared under fixed experimental conditions is used, the performance of electrode should be reproduced. In the present preparative method, however, the thickness of the catalyst layers, which is proportional to the catalyst loading, is scattered from layer to layer beyond the limit required to obtain constant polarization data. To test the reproducibility of performance, therefore, the scattering of data due to the variation in the catalyst loading must be taken into account.

As will be discussed in a later section, the reciprocal polarization resistance, ω^{-1}, for the thin electrode is proportional to the catalyst loading, since the reaction mechanism can be regarded as that of the gas diffusion through the electrolyte film; the current density at a given polarization is proportional to the catalyst loading. The polarization data, therefore, can be normalized to a loading of 1 g cm^{-2} by dividing i by the loading weight in unit of gram. Figure 2 shows the plots thus normalized for various loadings; i_N in the figure refers to the current density divided by the loading. The plots all fall on essentially the same curve. This proves that the electrodes yield reproducible polarization data.

Figure 3 shows the polarization curves as a function of the PTFE content, indicating that the polarization resistance increases with the PTFE content. This is due to an increase in the area of catalytic surface

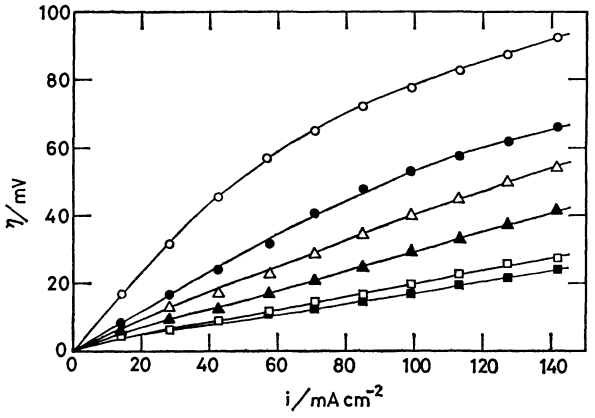

Fig. 1. Polarization curves for PTFE-bonded Raney nickel electrodes.
Catalyst loading ○: 13.5 mg cm^{-2}, ●: 25.9 mg cm^{-2}, △: 37.2 mg cm^{-2}, ▲: 48.0 mg cm^{-2}, □: 64.6 mg cm^{-2}, ■: 125.2 mg cm^{-2}.

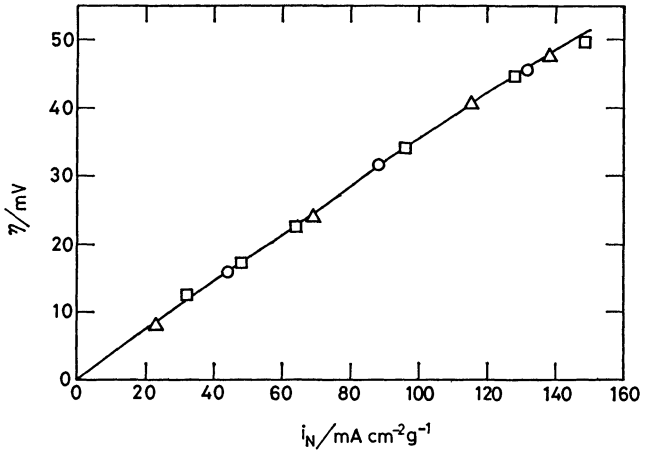

Fig. 2. Reproducibility test in polarization characteristics.
Catalyst loading ○: 13.5 mg cm^{-2}, △: 25.9 mg cm^{-2}, □: 37.2 mg cm^{-2}, current density normalized for catalyst loading.

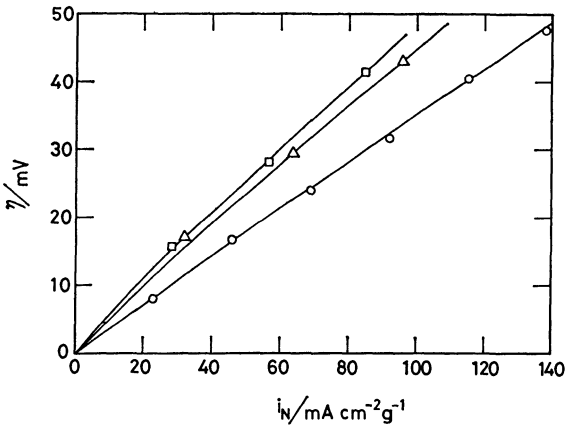

Fig. 3. Influence of PTFE content on the polarization curves.
PTFE content ○: 10.3%, △: 12.8%, □: 18.7%, current density normalized for catalyst loading.

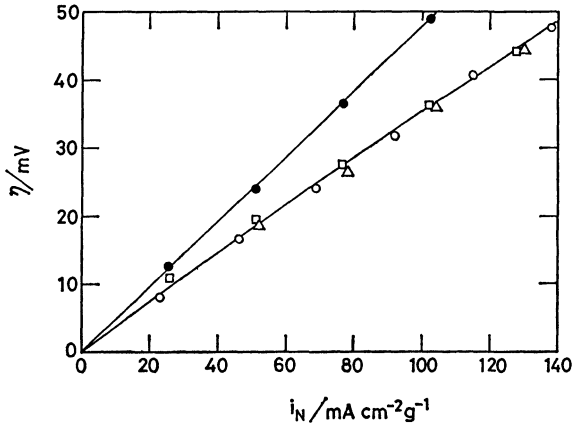

Fig. 4. Influence of the pressure of press machine on the polarization curves.
Pressure △: 210 kg cm^{-2}, ○: 421 kg cm^{-2}, □: 842 kg cm^{-2}, ●: 1260 kg cm^{-2}, current density normalized for catalyst loading.

covered by PTFE.

The pressure of the press machine influences the performance, as is shown in Fig. 4; no significant differences can be observed between the plots in the low-pressure region, and at 1260 kg cm^{-2} the plots deviate markedly. This discrete change is probably due to the calender-rolling, which compacts the catalyst layers as tightly as if they were pressed by the press machine at 842 kg cm^{-2}.

A test piece of electrode was prepared under the preparative conditions of PTFE content=10% and the pressure of press machine=421 kg cm^{-2}. The polarization curve is shown in Fig. 5. A limiting current density of 600 mA cm^{-2} is thus obtained.

Two different mechanisms have been proposed for the porous electrode reactions: a three-phase-boundary zone mechanism and one of the gas diffusion through the electrolyte film.[9] They are two extreme models with regard to the way of the electrolyte penetration into the pores. The first mechanism is based on the assumption that the electrolyte fills the pores up to the boundaries where the gas, electrolyte, and catalyst encounter each other; they are known as the three-phase-boundaries. Most of the load is sustained by the reaction occurring in the very narrow three-phase-boundary zones. It is less likely that the dried area in the pores contributes to sustaining the load by supplying the activated species toward the boundaries through surface diffusion. Hence, one can expect from this model that the polarization resistance is almost independent of the catalyst loading.

The feature of the second mechanism is that the whole catalytic surface of the pores is covered by thin electrolyte films. These films are thin enough to permit the gas molecules to diffuse. The gas molecules are dissolved into the films, and the electrode reaction takes place at the electrolyte-catalyst interface. The whole catalytic surface participates in the electrode reaction. This contrasts with the three-phase-boundary mechanism. The area of the catalytic surface can be enhanced by increasing the catalyst loading. Thus, one can expect that the polarization decreases with the catalyst loading. On the basis of this model, Mund has expressed the polarization resistance, ω, as a function of the catalyst loading, d, in this form;[10]

$$\omega = \sqrt{\rho k}\cdot\coth\sqrt{\rho d^2/k}, \qquad (1)$$

where ρ is the electrolyte resistivity in the catalyst layers, and k, the polarization resistance of the catalysts. When the electrode is so thin that the polarization due to the electrolyte resistivity and the gas diffusibility can be neglected, Eq. 1 can be approximated as $\omega^{-1}\propto d$. This is the case described in the section on the reproducibility test. Figure 6 gives the plots of ω^{-1} *vs.* d for the present electrodes. The plots fall on a curve that is expected from Eq. 1, suggesting that the second mechanism is valid. However, the values for ρ and k are unknown, and a small possibility still remains of the mechanism of the three-phase-boundary zone holding. Further experiments, therefore, are required to judge which mechanism is valid.

For this purpose an electrode of a triple-layered structure containing a sheet of PTFE-bonded silver powder sandwiched by two sheets of a Raney-nickel layer has been prepared. The aim of this electrode is to prevent the activated species in the gas-side layer from diffusing on the surface toward the electrolyte-side layer. The diffusibility of the activated species on the silver surface is probably very small, since the silver powder used is almost inactive as a hydrogen catalyst, as is shown in Fig. 7 (△). Hence, the activated species formed in either of the Raney nickel sheets will not be able to traverse the silver sheet. The three-phase-boundary, if it is the correct mechanism, can be expected to be located in the gas-side Raney nickel layer. In the three-phase-boundary mechanism, the surface diffusion is the only way for the gas-side layer to contribute to sustaining the load. That is prevented by the silver sheet, so that if the

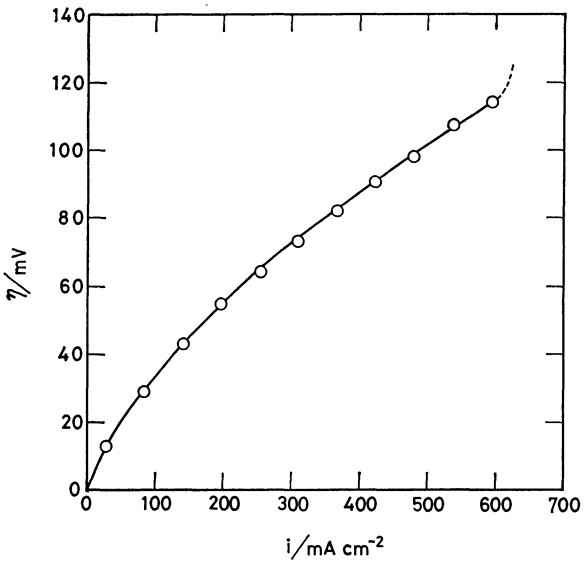

Fig. 5. Polarization curve of PTFE-bonded Raney nickel electrode.
Catalyst loading: 45.4 mg cm^{-2}, PTFE content: 10.4%, the pressure of press machine: 421 kg cm^{-2}.

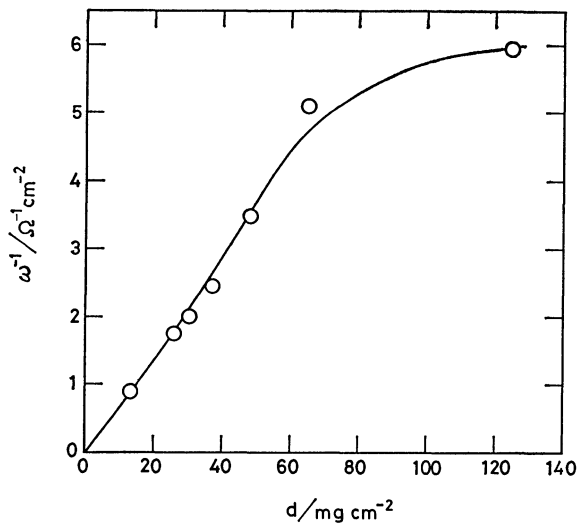

Fig. 6. Reciprocal polarization resistance as a function of catalyst loading at a PTFE content of 10%.

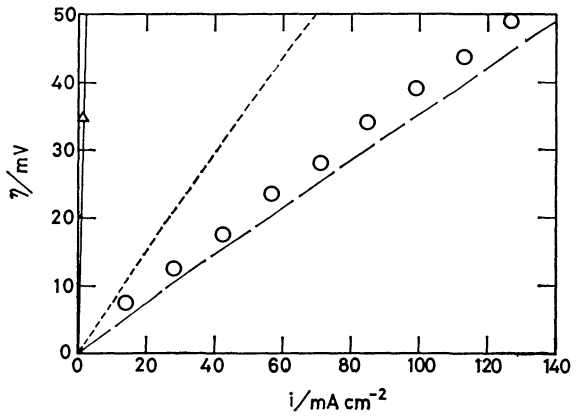

Fig. 7. Polarizations of the triple-layered electrode containing silver catalyst layer.
----: Calculated from the model of three-phase-boundary zone, — — —: calculated from the model of gas diffusion through the electrolyte film, ○: observed, △: electrode loaded with silver catalyst alone.

three-phase-boundary mechanism is valid, this electrode will be as polarized as if it is loaded with the electrolyte-side layer alone.

In the second model, the electrolyte films extend over all three layers so that the two Raney nickel sheets are connected to each other in ionic contact through the films in the silver layer. Therefore, the gas-side catalyst layer shares the load current with the electrolyte-side layer. Thus, the polarization in this case can be expected to be equal to that for a loading of both Raney nickel layers.

The polarization expected for each case can be calculated by using the polarization data in Fig. 2 and the loadings of the electrolyte-side and gas-side layers used. The dotted line and the broken line in Fig. 7 were calculated on the basis of the mechanisms of the three-phase-boundary zone and the electrolyte film respectively. The polarization data observed are closer to the broken line, suggesting that the electrolyte film is more probable.

Another piece of experimental evidence for the electrolyte penetration has been obtained by inserting pieces of filter paper between the layers. The electrode used for this experiment consists of three sheets of Raney nickel layers and a gas-side layer. Three pieces of filter paper were inserted, piece by piece, between adjacent layers. After the measurement of the polarization was over, the filter paper inserted was tested by phenolphthalein to see if it had been wetted by the KOH solution. All the test pieces were found to have been wetted. This experiment indicates that the electrolyte penetrates through all the catalyst layers.

These two experiments lead to the conclusion that the mechanism of the gas diffusion through electrolyte film is valid for the PTFE-bonded Raney nickel electrodes. The role of PTFE is to thin the electrolyte film sufficiently for the diffusion of gas molecules rather than to prevent the electrolyte penetration into the pores.

The present work was partially supported by a Grant-in-Aid from the Saneyoshi Foundation.

References

1) E. Justi, M. Pilkuhn, W. Scheibe, and A. Winsel, "High Drain Hydrogen-Diffusion Electrodes Operating at Ambient Temperature and Low Pressure," Steiner, Wiesbaden (1959).
2) E. Justi and A. Winsel, "Kalte Verbrennung," Steiner, Wiesbaden (1962).
3) F. v. Sturm, H. Nischik, and E. Weidlich, *Ingenieur Digest*, **5** (1966).
4) F. v. Sturm, "Elektrochemishe Stromerzeuzung," Verlag Chemie, Weinheim (1969), p. 109.
5) K. V. Kordesch, "Fuel Cells," ed by W. Mitchell, Jr., Academic Press, London (1963), p. 329.
6) F. v. Sturm and A. Thieleking, German Patent 1542443 (1966).
7) K. V. Kordesch and A. Marko, *J. Electrochem. Soc.*, **107**, 480 (1960).
8) K. Mund, G. Richter, and F. v. Sturm, *J. Electrochem. Soc.*, **124**, 1 (1977).
9) H. A. Liebhafsky, E. J. Cairns, W. T. Grubb, and L. W. Niedrach, "Fuel Cell Systems," American Chemical Society, Washington (1965), p. 116.
10) K. Mund, *Siemens Forsch., Entwichlungs-Ber.*, **4**, 1 (1975).

Isomorphism in the High-temperature Forms of Molecular Complexes between Aromatic Hydrocarbons and Various Electron Acceptors Arising from Molecular Motion

Tamotsu INABE, Yoshio MATSUNAGA,* and Mikiko NANBA
Department of Chemistry, Faculty of Science, Hokkaido University, Sapporo 060
(Received January 12, 1981)

In addition to the six crystalline pyrene complexes reported earlier, the high-temperature forms of the following nineteen 1:1 molecular complexes have been found to be isomorphous to each other; the pyrene complexes with 1,3,5-trinitrobenzene, 2,4,6-trinitrophenol, 4-nitrophthalic anhydride, pyromellitic dianhydride, 5-nitrobenzofuroxan, 4,6-dinitrobenzofuroxan, and benzotrifuroxan, the fluoranthene complexes with 2,4-dinitrophenol, 1,3,5-trinitrobenzene, 2,4,6-trinitrochlorobenzene, 2,4,6-trinitrophenol, 2,4,6-trinitrotoluene, 4-nitrophthalic anhydride, pyromellitic dianhydride, 4,6-dinitrobenzofuroxan, and benzotrifuroxan, and the phenanthrene complexes with 1,3,5-trinitrobenzene, 2,4,6-trinitrophenol, and 4,6-dinitrobenzofuroxan. Furthermore, metastable isomorphous forms were obtained in the process of the solidification of the melt of the following three complexes: fluoranthene-5-nitrobenzofuroxan, phenanthrene-2,4,6-trinitrotoluene, and phenanthrene-4-nitrophthalic anhydride. Rather large entropies of the transitions to these unique high-temperature forms, up to 57 J mol^{-1} K^{-1}, are often comparable with the entropies of melting, 46—67 J mol^{-1} K^{-1}. The isomorphism in these twenty-eight complexes is demonstrated by essentially identical and very simple X-ray diffraction patterns and/or by the formation of continuous solid solutions between pairs of these forms. A trigonal lattice is proposed as the probable structure of these high-temperature forms. A broad-line ^1H NMR study clearly showed that the unusual features of these isomorphous forms are mostly associated with the onset of a large degree of molecular motion at the transition temperatures.

We reported earlier that the crystalline pyrene complexes with 2,4-dinitrofluorobenzene, 2,4-dinitrochlorobenzene, 2,4-dinitrophenol, 2,4-dinitrotoluene, and 2,4,6-trinitrochlorobenzene exhibit polymorphic transitions and become isomorphous to each other above the transition temperatures.[1] Isomorphism in molecular complexes is not unknown; however, the cases so far reported are limited to the complexes of closely related component compounds. For example, the 1,3,5-trinitrobenzene and 2,4,6-trinitrophenol complexes of naphthalene, pyrene, and fluoranthene have each been shown to be isomorphous by Herbstein and Kaftory.[2] This relationship has been established for the crystals stable at room temperature. The phenomenon found by us is apparently different from this kind of isomorphism. Except for the 2,4-dinitrochlorobenzene complex, the transitions are associated with rather large enthalpy and entropy changes: 12—18 kJ mol^{-1} and 37—50 J mol^{-1} K^{-1}, which are of the same order of magnitude as the corresponding values of melting: 18—25 kJ mol^{-1} and 50—59 J mol^{-1} K^{-1} respectively. On the basis of these thermodynamic data, we speculated that the specific interaction between the hydrocarbon molecule and the substituent on the acceptor molecule disappears because of the dynamical averaging of the interaction by a large degree of thermal motion in the high-temperature forms. Later, the onset of such a molecular motion was firmly established by the drastic decreases in the second moments in broad-line ^1H NMR spectra at the transition temperatures.[3] Moreover, the 2,4,6-trinitrotoluene complex was added to the list of this interesting class of molecular complexes. Continuing the search for such complexes, nineteen more complexes have been found to behave similarly. All the complexes studied before are composed of pyrene and one of the derivatives of *m*-dinitrobenzene or 1,3,5-trinitrobenzene; however, we have now succeeded in finding complexes containing hydrocarbons other than pyrene, such as phenanthrene-2,4,6-trinitrophenol and fluoranthene-1,3,5-trinitrobenzene, and also complexes containing an acceptor bearing no nitro group, such as pyrene-pyromellitic dianhydride and fluoranthene-benzotrifuroxan. Thus, the appearance of this kind of isomorphism needs neither a common-component compound nor a close similarity between components. The present paper gives an account of an examination of the thermodynamic data of the transition and melting, the X-ray diffraction pattern, the solid-solution formation, and the broad-line ^1H NMR study of the newly found complexes.

Experimental

Materials. The donors employed were pyrene (Py), fluoranthene (Fl), and phenanthrene (Ph), while the acceptors were 2,4-dinitrophenol (DNP), 1,3,5-trinitrobenzene (TNB), 2,4,6-trinitrochlorobenzene (TNC), 2,4,6-trinitrophenol (TNP), 2,4,6-trinitrotoluene (TNT), 4-nitrophthalic anhydride (NPA), pyromellitic dianhydride (PMDA), 5-nitrobenzofuroxan (NBF), 4,6-dinitrobenzofuroxan (DNBF), and benzotrifuroxan (BTF). Their structural formulas are presented in Fig. 1. The Py, Eastman white label, was recrystallized from xylene. The Ph, Eastman white label, was boiled with maleic anhydride in xylene to remove any anthracene.[4] TNB was prepared, starting from TNT, through 2,4,6-trinitrobenzoic acid.[5] The TNT, Eastman yellow label, was purified by recrystallization from ethanol. The NPA and PMDA were sublimed in a vacuum just before use. The NBF, DNBF, and BTF were prepared following the procedures reported by Bailey and Case.[6] The other reagents obtained from commercial sources were employed without further purification. The complexes were crystallized by mixing the component compounds dissolved in appropriate solvents or by melting mixtures of equimolar amounts of the component compounds.

Measurements. Calorimetric, X-ray, and NMR measurements were carried out as described in our previous

papers.[1,3] Density measurements of four complexes with transition temperatures lower than 60 °C were made using Gay-Lussac pycnometers. A small amount of a detergent had to be added to the water employed as the immersion fluid in order to wet the crystals. Air bubbles trapped by the crystals were eliminated by repeated evacuations and then by leaving the pycnometers overnight under reduced pressure.

Results and Discussion

Thermodynamic Data. The complexes which become isomorphous upon transitions, including the six Py complexes found previously, are summarized in Fig. 1. Solid circles indicate that enantiotropic transitions are observable. On the other hand, broken circles show that the high-temperature forms of these complexes are metastable, as will be described later.

The transition temperatures, melting points, and associated enthalpies and entropies are collected in Table 1. Not only the six Py complexes reported previously by us, but also some other complexes are known to exhibit polymorphic transitions. Casellato *et al.* have located the transitions in the Py–TNB complex at 129 and 215.5 °C with enthalpies of 2.4 and 1.9 kJ mol^{-1} respectively, and the melting point, at 253.3 °C with an enthalpy of 38.5 kJ mol^{-1}.[7] Except for the first transition temperature, our results are in fair agreement with theirs. The transitions in the Py–TNP complex have been reported to occur at 170 and 183.4 °C, with enthalpies of 2.9 and 1.2 kJ mol^{-1} respectively, by Farrell *et al.*[8] The melting point reported by them is 233.4 °C, and the enthalpy is 32.6 kJ mol^{-1}. All our temperatures for this complex are located lower than theirs by about 5 °C. Casellato *et al.* have observed three modifications of the Py–NPA complex.[9] According to them, the I modification crystallized from a solution is transformed into the III modification at 122 °C with an enthalpy of 18 kJ mol^{-1}. The transformation into the III modification from the II obtained by cooling from the melt occurs at 105 °C. The enthalpy of the latter transition was reported to be 11 kJ mol^{-1}. Our enthalpy of the transition at 112.5 °C is a little larger than the former one reported by Casellato *et al.*, but our transition temperature is appreciably lower than theirs. We occasionally observed an additional endothermic peak at 108 °C with samples crystallized from some solvents. This peak could be detected only in the first run of the calorimetric measurements. The Py–NPA complex has been reported to melt at 179.5 °C, with an enthalpy of 24 kJ mol^{-1}, in agreement with our observation. The thermodynamic data for the Py–PMDA complex have been presented by Pelizza *et al.*; the enthalpy for the transition at 174.3 °C is 29 kJ mol^{-1}, while that of the melting at 290.4 °C is 72 kJ mol^{-1}.[10] Our enthalpy values are barely over 40 percent of theirs.

The Fl–TNP complex has been studied by Farrell *et al.*[8] The reported transition temperature, 92.4 °C, and the enthalpy, 13.8 kJ mol^{-1}, agree well with our values. The melting point has been found at 189.2 °C, and the enthalpy, at 24.7 kJ mol^{-1}. The latter is a little larger than the present value.

The Ph–TNB complex has been reported by Kofler to exhibit a transition at 149 °C.[11] Casellato *et al.* have located it at 148.2 °C, with an enthalpy of 12 kJ mol^{-1}, while they located the melting point at 164.6 °C, with an enthalpy of 27 kJ mol^{-1}.[7] Our results in Table 1 generally agree with their values. The transition in the Ph–TNP complex has been noted also by Kofler at 106 °C.[11] The enthalpy has been estimated to be 13 kJ mol^{-1} by one of the present authors, together with an additional transition at 77 °C associated with an enthalpy of 4.6 kJ mol^{-1}.[12,13] Our new determinations well reproduced the previous results. According to Casellato *et al.*, the Ph–NPA complex melts at 96 °C, with an enthalpy of 29 kJ mol^{-1}.[9] Our results are in good agreement with theirs.

With the exception of several complexes, the entropy of transition into the unique high-temperature form is fairly large, up to 57 J mol^{-1} K^{-1}. These values are often comparable with the entropies of melting of these complexes, 46—67 J mol^{-1} K^{-1}. As the sum of all entropies of transition and melting may be supposed to be correlated with the molecular structure, it may agree with the entropy of melting of a complex which is structurally related to the present one but which does not exhibit polymorphic transitions. For example, we observed 102 J mol^{-1} K^{-1} for the Fl–DNT complex, 100 J mol^{-1} K^{-1} for the Fl-3-nitrophthalic anhydride complex, and 101 J mol^{-1} K^{-1} for the 1,10-phenanthroline–TNB complex. These values are reassuringly similar to the sum of the entropies of transition and melting of the present complexes: *e.g.*, 104 J mol^{-1} K^{-1} of the Py–DNF complex. If the latter value is appreciably smaller than the former, the occurrence of low-temperature transitions may be predictable for such a complex.

The ordinary samples of the Fl–NBF, Ph–TNT, and Ph–NPA complexes exhibit no polymorphic transition; however, the metastable high-temperature form appears when the melt is solidified. As the monotropic transition from the supercooled metastable form to the stable one is well separated from the solidification, the enthalpy and entropy associated with the melting of the metastable form could be measured. In Table

D \ A	DNF	DNC	DNP	DNT	TNB	TNC	TNP	TNT	NPA	PMDA	NBF	DNBF	BTF
Py	○	○	○	○	○	○	○	○	○	○	○	○	○
Fl			○		○	○	○	○	○	○	◌	○	○
Ph					○		○	◌	◌			○	

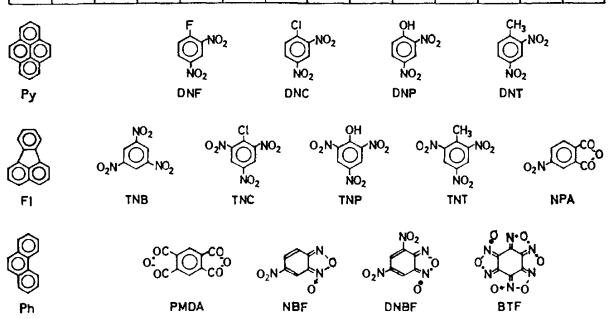

Fig. 1. The molecular complexes which become isomorphous by polymorphic transitions and the structural formulas of the component compounds.

Table 1. Thermodynamic data of molecular complexes
(The values in parentheses are for monotropic transitions.)

Acceptor	Transition			Melting		
	t / °C	$\Delta H^{c)}$ / kJ mol^{-1}	$\Delta S^{c)}$ / J mol^{-1} K^{-1}	t / °C	$\Delta H^{c)}$ / kJ mol^{-1}	$\Delta S^{c)}$ / J mol^{-1} K^{-1}
			Donor: Pyrene			
2,4-Dinitrofluorobenzene[a)]	76.5	18	50	119	21	54
2,4-Dinitrochlorobenzene[a)]	41	2.4	7.5	87	18	50
2,4-Dinitrophenol[a)]	53	13	40	144	25	59
2,4-Dinitrotoluene[a)]	53.5	12	37	92.5	20	54
1,3,5-Trinitrobenzene	138	1.9	4.6	248	35	67
	216	1.5	3.1			
2,4,6-Trinitrochlorobenzene[a)]	79	13	40	154.5	22	50
2,4,6-Trinitrophenol	164.5	3.3	7.5	227	31	62
	178	1.2	2.7			
2,4,6-Trinitrotoluene[b)]	59	12	36	162	22	51
4-Nitrophthalic anhydride	112.5	20	51	177.5	24	54
Pyromellitic dianhydride	170	13	28	290	31	54
5-Nitrobenzofuroxan	89	17	47	147	23	55
4,6-Dinitrobenzofuroxan	130	1.7	4.2		decomp	
	185	1.0	2.1			
Benzotrifuroxan	112	5.4	14		decomp	
			Donor: Fluoranthene			
2,4-Dinitrophenol	57	16	50	92	18	50
1,3,5-Trinitrobenzene	99.5	15	41	205.5	28	59
2,4,6-Trinitrochlorobenzene	54	18	54	121	18	46
2,4,6-Trinitrophenol	93.5	15	42	184.5	21	46
2,4,6-Trinitrotoluene	71	17	50	134	18	46
4-Nitrophthalic anhydride	102	21	57	131.5	18	46
Pyromellitic dianhydride	167	21	48	232	26	52
5-Nitrobenzofuroxan	—	(22)	(59)	92	29	80
4,6-Dinitrobenzofuroxan	82	1.1	3.1		decomp	
	93	12	33			
Benzotrifuroxan	83	5.0	14		decomp	
	86.5	1.3	3.6			
			Donor: Phenanthrene			
1,3,5-Trinitrobenzene	149.5	12	28	165.5	26	61
2,4,6-Trinitrophenol	78	4.6	13	147	22	53
	107	13	33			
2,4,6-Trinitrotoluene	—	(11)	(29)	100	28	75
4-Nitrophthalic anhydride	—	(14)	(37)	97.5	29	78
4,6-Dinitrobenzofuroxan	105.5	8.5	23		decomp	
	121	7.6	19			

a) Taken from Ref. 1. b) Taken from Ref. 3. c) The values are reproducible within 5% when the enthalpies are in the order of 10 kJ mol^{-1}. The errors are twice as large if the enthalpies are about 1 kJ mol^{-1}.

1, the thermodynamic data for the melting of these three complexes are for the stable forms. It is noteworthy that the entropy values of melting, 80 J mol^{-1} K^{-1} for the Fl–NBF, 75 J mol^{-1} K^{-1} for the Ph–TNT, and 78 J mol^{-1} K^{-1} for the Ph–NPA, are definitely larger than those of any other complexes in the table. The enthalpy and entropy associated with the monotropic transition given in Table 1 were estimated by taking the difference between the value for the melting of the stable form and that for the melting of the metastable form.

X-Ray Diffraction Patterns. In Fig. 2, the X-ray diffraction patterns observed at room temperature and above the transition temperature using filtered copper radiation are schematically presented for eight representative complexes. Reflecting the special natures of the donor and acceptor molecules, the room-temperature patterns are not simple and are markedly different from each other. However, the diffraction patterns are remarkably simplified upon the transition. Three or four lines are observable with the high-temperature forms: a strong line appearing between $2\theta_1=11$ and 12°, a weak one near $2\theta_2=20°$, and another strong one between $2\theta_4=26$ and 27°. The patterns of the Ph–TNP complex in its three forms were previously recorded by Koizumi and Matsunaga.[13] It was emphasized that the pattern given by the high-temperature form is very simple.

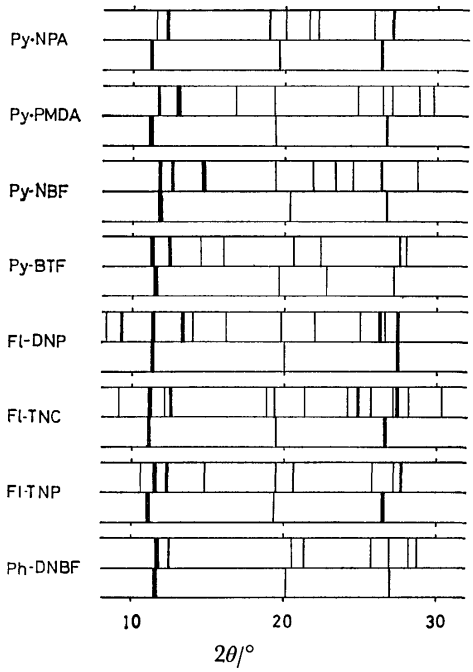

Fig. 2. X-Ray (Cu $K\alpha$ radiation) diffraction patterns of the molecular complexes. The upper pattern for each complex was recorded at room temperature and the lower one above the transition temperature.

Only three lines were found in it, in accordance with the present complexes. For some complexes, a very weak line is detectable near $2\theta_3=23°$, as is exemplified by the Py–BTF complex (see Fig. 2). The general features described here are in good agreement with those obtained for the six Py complexes studied before.

A comparison of the spacings, d_1, d_2, and d_3, which are inversely proportional to $\sin\theta_1$, $\sin\theta_2$, and $\sin\theta_3$ respectively, shows that

$$1/d_1 : 1/d_2 : 1/d_3 = 1 : \sqrt{3} : 2$$

within the limits of error of measurements, for all the complexes examined. On the other hand, the d_4 spacing is not in any simple ratio with the others. This remarkably simple ratio suggests that the lattice in the high-temperature form is hexagonal or trigonal.

With the hope of limiting further the probable structures, the density measurements were carried out for the Py–DNC, Py–DNT, Py–TNT, and Fl–TNC complexes, which can be transformed into the high-temperature forms below 60 °C. The densities measured within a few degrees below and above the transition temperature are summarized in Table 2. Trial

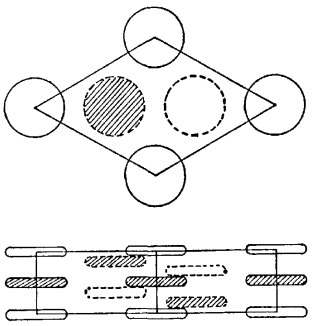

Fig. 3. Proposed structure for the isomorphous high-temperature forms. The molecules located at 000, 2/3 1/3 1/3, and 1/3 2/3 2/3 are different from those located at 0 0 1/2, 2/3 1/3 5/6, and 1/3 2/3 1/6.

shows that the trigonal lattice presented in Fig. 3 well explains the X-ray diffraction patterns and the observed densities and so seems probable. As this lattice must be common to all the complexes listed in Table 1, the shape of the component molecules is entirely ignored in this figure. The indices assigned to the above-mentioned four lines are (110), (300), (220), and (102). Table 2 records also the estimated unit-cell dimensions and the calculated densities. Three molecules of each component are in the cell shown in Fig. 3. The donor and acceptor molecules are stacked alternatively in infinite columns in parallel with the c-axis. The stacking angle may be nil, as the mean separation between the molecular planes is expected to be about 3.5 Å.

Solid-solution Formation. The complete miscibility of a pair of the complexes is a severe test for the isomorphism. To be isomorphous, the high-temperature forms must have the same space group and the same number of molecules per unit cell.[14] The additional requirement to be miscible in all proportions is that the difference in the unit-cell sizes not be too great. The room-temperature forms of the Py–TNB and Py–TNP complexes have been reported to be isomorphous ($P\bar{1}$ and $Z=2$) by Herbstein and Kaftory.[2] Two enantiotropic transitions in the range from room temperature to the melting point are observed with both the complexes: 138 and 216 °C with the TNB complex and 164.5 and 178 °C with the TNP complex. The phase diagram of the pseudo-binary system comprising these two Py complexes given in Fig. 4 clearly shows that each pair of the polymorphs of these two complexes are completely miscible. The combination of the Fl–TNB and Fl–

TABLE 2. DENSITIES MEASURED WITHIN A FEW DEGREES BELOW AND ABOVE THE TRANSITION TEMPERATURE, AND UNIT-CELL DIMENSIONS AND CALCULATED DENSITY OF THE HIGH-TEMPERATURE FORM

Molecular complex	Density / g cm^{-3}		Unit-cell dimensions		Calcd density / g cm^{-3}
	Below Tp	Above Tp	a/Å	c/Å	
Py-DNC	1.414	1.396	15.31	6.99	1.42
Py-DNT	1.350	1.305	15.30	7.03	1.34
Py-TNT	1.450	1.415	15.84	7.03	1.40
Fl-TNC	1.506	1.449	15.80	6.94	1.49

TNP complexes gives similar results. The room-temperature forms are monoclinic ($P2_1/c$, $Z=4$), and the following unit-cell dimensions have been given by Herbstein and Kaftory: $a=8.48$, $b=7.27$, $c=30.35$ Å, $\beta=96°$ for the Fl–TNB complex, and $a=8.68$, $b=7.27$, $c=31.0$ Å, $\beta=96°$ for the Fl–TNP complex, fulfilling the conditions cited above.

The diagrams for the following six systems are illustrated in Fig. 5: Py–(NPA, DNF), Py–(DNF, TNT), (Py, Fl)–TNT, Fl–(TNT, TNP), (Fl, Ph)–TNP, and Ph–(TNP, TNB). These systems were selected so that the two molecular complexes share either a hydrocarbon or an acceptor. Moreover, the neighboring systems share one of the molecular complexes. In all the diagrams, the freezing points of mixtures lie between the melting points of the pure molecular complexes. These results undoubtedly indicate that the solid miscibility between the high-temperature forms is unlimited in all the systems shown in Fig. 5. Thus, we are quite certain that the high-temperature form of the Py–NPA is isomorphous with that of the Fl–TNT complex and also with that of the Ph–TNB complex. Besides the Fl–TNP complex described above, the room-temperature form of the Ph–TNB complex is known to be monoclinic ($P2_1/c$, $Z=4$), and that of the Ph–TNP complex, to be triclinic (P1 or $P\bar{1}$, $Z=2$).[2] Accordingly, a eutectoid system is produced by these two complexes, and the diagram is split by a miscibility gap at room temperature. It may be noticed from Fig. 5 that the formation of substitutional solid solutions based on the parent-complex lattices occurs extensively. The solubility of the Ph–TNP complex into the Ph–TNB complex lattice exceeds 60 mol%, while that in the inverse direction is merely about 20 mol%. The most striking example is found in the diagram involving the Fl–TNT and Fl–TNP complexes, which gives a peritectoid system. The Fl–TNT complex can dissolve the Fl–TNP complex over 80 mol%, and the width of the miscibility gap in this system is as narrow as 3 mol%.

As the high-temperature forms of the Py–DNT and Fl–TNT complexes are isomorphous to each other, the pseudo-binary system gives a continuous solid solution (see Fig. 6). However, it must be noted that the composition of the solid solution is unusually different from the composition of the liquid solution in equilibrium. The equimolar mixture of these two complexes is equally considered to be an equimolar mixture of the Py–TNT and Fl–DNT complexes. As there is no unique high-temperature form appearing in the Fl–DNT complex, the miscibility gap should exist somewhere in the system consisting of the Py–TNT and Fl–DNT complexes. As expected, the diagram of the latter pseudo-binary system (shown in Fig. 6) has a gap extending from 60 to 90 mol% of the Fl–DNT complex. The large temperature difference between the solidus and liquidus near 50 mol% in the other pair of the complexes apparently arises from the wide miscibility gap located close to this composition. Results similar to those presented above may be anticipated for the system consisting of the Fl–TNT and Ph–TNP complexes because of the absence of a transition in the combination of Ph and TNT. Unexpectedly, however, the solidus and liquidus are not so separated as those in the system

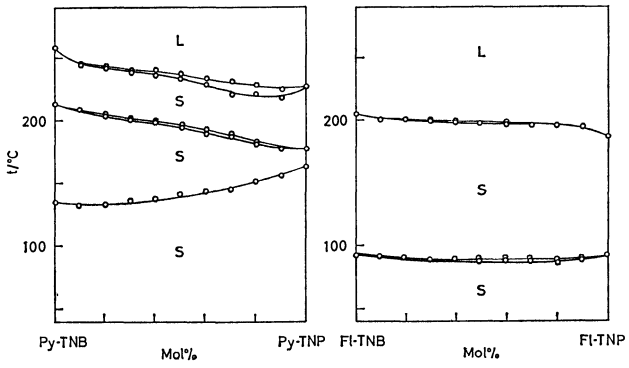

Fig. 4. Phase diagrams for the Py–(TNB, TNP) and Fl–(TNB, TNP) systems.

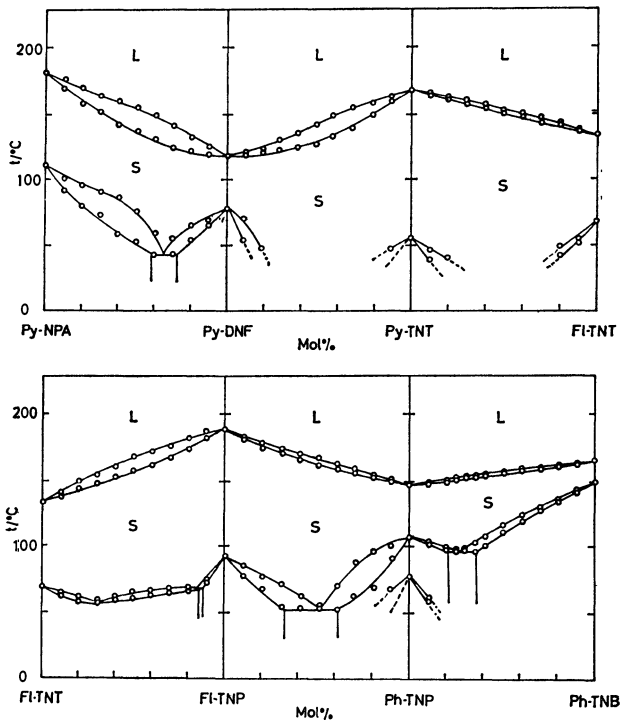

Fig. 5. Phase diagrams for the Py–(NPA, DNF), Py–(DNF, TNT), (Py, Fl)–TNT, Fl–(TNT, TNP), (Fl, Ph)–TNP, and Ph–(TNP, TNB) systems.

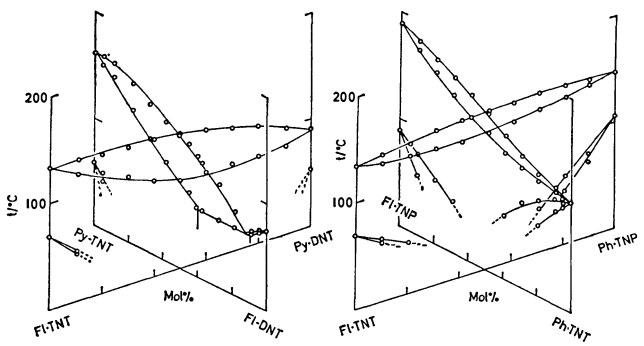

Fig. 6. Phase diagrams for the (Py, Fl)–(DNT, TNT) and (Fl, Ph)–(TNP, TNT) systems.

consisting of the Py–DNT and Fl–TNT complexes. The study of the system of the Fl–TNP and Ph–TNT complexes has revealed the formation of a continuous solid solution (see Fig. 6). The appearance of this phase must be due to the coincidence between the transition and melting points in the latter complex. The metastable polymorphs have also been found for the Fl–NBF and Ph–NPA complexes and have been demonstrated to be completely miscible at high temperatures with the Fl–TNT and Fl–NPA complex respectively (see Fig. 7).

Broad-line ^1H NMR. The second moment, the mean-square width of the resonance line, of the ^1H NMR spectrum is shown in Fig. 8 as a function of the temperature for each of the seven Py complexes. Py is known to have an intramolecular second moment of 3.43 G^2.[15] All the complexes studied here show evidence of molecular motion in the solid state, as indicated by a decrease in the moment. In the case of the TNB complex, the transition to the unique isomorphous form is located at 216 °C, well above the range measurable with our spectrometer. The second moment decreases gradually up to 138 °C and then more sharply above this temperature (see Fig. 8a). The value in the phase stable between 138 and 216 °C is as small as 1 G^2, indicating that some fast motional process exists before the transition to the isomorphous form. This observation is consistent with the small enthalpy and entropy values for the second transition. Similar small changes in the second moment are found for the TNP and DNBF complexes, in which the enthalpy and entropy of the transitions are also comparatively small. There is a large, abrupt drop in the second moment at the transition to the high-temperature forms of the other four complexes, reflecting a significantly larger enthalpy and entropy of the transition.

The PMDA complex is the only one among the complexes studied here for which the crystal structure has been determined. Herbstein and Snyman have made an intensive and comprehensive study of the structure at 110 and 300 K.[16] The NMR spectrum has been measured, and the nature of the molecular motions has been discussed by Fyfe.[15] Our results are essentially the same as his (see Fig. 8d). The moment observed at low temperatures compares very well with 4.8 G^2, the theoretical value for the rigid lattice calculated by means of Van Vleck's formula using the atomic coordinates of the X-ray determination. The reduction in the second moment to 2.3 G^2 by 130 °C has been interpreted by Fyfe in terms of the complete reorientation of the hydrocarbon molecules in their molecular planes. Furthermore, Dunn *et al.* have reported on heat-capacity measurements in the range from 10 to 323 K and have established the growth of orientational disorder over a very considerable temperature range.[17] Unfortunately, the transition located at 170 °C was covered by neither of these works.

Figure 9 shows the second moments of the nine Fl complexes. The intramolecular moment is esti-

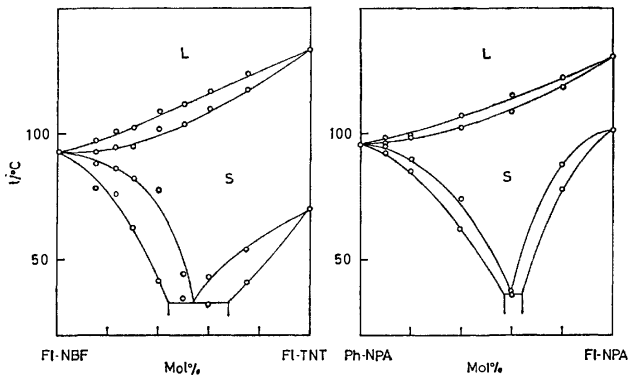

Fig. 7. Phase diagrams for the Fl–(NBF, TNT) and (Ph, Fl)–NPA systems.

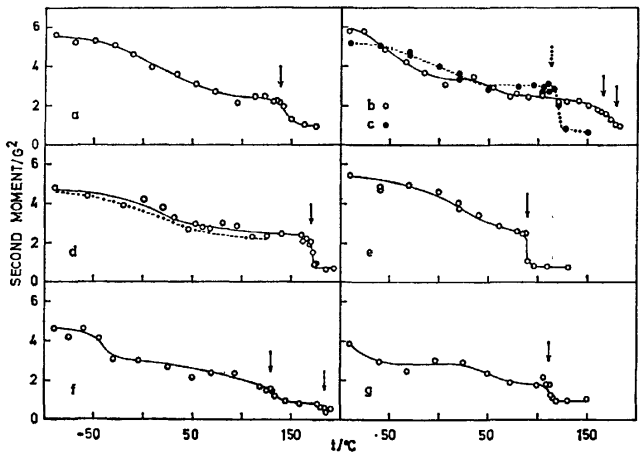

Fig. 8. Second moment values of the proton resonance for the pyrene complexes with a) TNB, b) TNP, c) NPA, d) PMDA, and the result by Fyfe (Ref. 15), e) NBF, f) DNBF, and g) BTF. The vertical arrows indicate the thermodynamic transition temperatures.

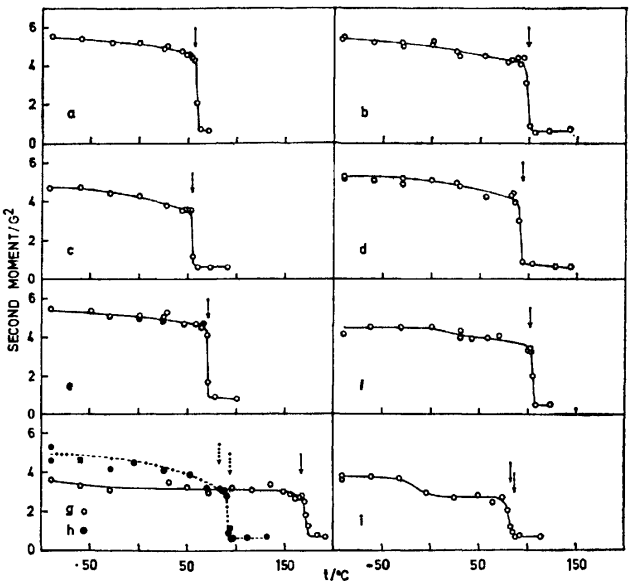

Fig. 9. Second moment values of the proton resonance for the fluoranthene complexes with a) DNP, b) TNB, c) TNC, d) TNP, e) TNT, f) NPA, g) PMDA, h) DNBF, and i) BTF. The vertical arrows indicate the thermodynamic transition temperatures.

mated to be 2.88 G^2 using the atomic coordinates previously reported by Herbstein and Kaftory.[2] The change upon the transition into the isomorphous high-temperature form is drastic except for the BTF complex. In this complex, the reduction occurs by the transition at 83 °C rather than by that at 86.5 °C. The fact that the enthalpy of the former transition is about four times that of the latter may account for this result. The moment is generally not very temperature-dependent below the transition. There is no distinct reduction in the second moment by passing through the transition at 82 °C in the DNBF complex (see Fig. 9h).

The temperature variation in the second moment in the three Ph complexes is shown in Fig. 10. The moment drops abruptly and substantially upon the transition into the isomorphous form, but gradually at the other transitions in the TNP and DNBF complexes. Thus, the thermodynamic transition to the isomorphous form is, in general, accompanied by the abrupt reduction of the second moment. Such a coincidence implies that the molecules are moving fast on an NMR time-scale (40 MHz) above the transition temperature. Although the transition at 105.5 °C in the DNBF complex has a larger enthalpy than that at 121 °C, the change in the second moment is smaller and more gradual, suggesting that the motion initiated by the transition at 105.5 °C is not fast on an NMR time-scale. While the intramolecular moment of the hydrocarbon is calculated to be 4.12 G^2 on the basis of the molecular structure determined by Trotter,[18] the observed moment in the isomorphous form is less than 1 G^2 in every complex. Therefore, the flat hydrocarbon molecules in this phase seem to have a considerable freedom of rotation. The large entropy associated with the transition supports also the onset of such a large degree of molecular motion.

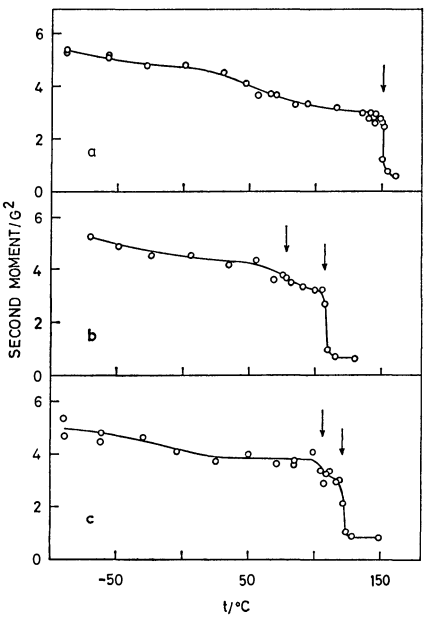

Fig. 10. Second moment values of the proton resonance for the phenanthrene complexes with a) TNB, b) TNP, and c) DNBF. The vertical arrows indicate the thermodynamic transition temperatures.

Benzene is an example which shows line narrowing due to rotation about a single axis.[19] The second moment has been reported to show a slow decrease beginning at about 100 K and ending at about 120 K. Above this temperature, the moment is 0.76 G^2. The entropy of melting is 35.3 J mol^{-1} K^{-1}.[20] Twice this value may be compared with those of our complexes: 46—67 J mol^{-1} K^{-1}. One should remember that this quantity is a measure of the difference in organization between the solid and the melt. As the association of the hydrocarbon and acceptor molecules is likely in the molten complexes,[21] one cannot conclude, on the basis of these entropies, that the acceptor molecules are also mobile in the high-temperature forms. At any rate, the number of hydrogen atoms on the acceptor molecules is so small that the contribution to the second moment may be expected to be appreciably smaller than that due to the hydrocarbon molecules.

General Remarks. The molecular rotation certainly forms an important part of the mechanism for isomorphism reported here. In this connection, the present complexes bear some similarity to plastic crystals, which are composed of globularly shaped molecules. Plastic crystals are of a cubic habit. The transition entropy to this phase is high (about 40 J mol^{-1} K^{-1}) compared with that for melting (less than 20 J mol^{-1} K^{-1}). The largest transition entropy in our complexes to be compared is 59/2 J mol^{-1} K^{-1} for the metastable form of the Fl–NBF complex, while the largest entropy of melting is 67/2 J mol^{-1} K^{-1} for the Py–TNB complex. Clearly, the motion of the flat component molecules in the present complexes is generally more restricted than that of the spherical molecules in plastic crystals; nevertheless, some translational disorder might be also conceivable for the former crystals such as has been reported for the latter.[22] The reactivity for donor- or acceptor-exchange in solids is currently under investigation below and above the transition temperature in order to search for such indications.

The sections of the van der Waals repulsion envelopes of the Py and Fl molecules are drawn in Fig. 11 as Al-Mahdi and Ubbelohde did for a number of aromatic molecules.[23] The two are found to be sufficiently similar and to fit in essentially the same circle. The envelope of the Ph molecule is, of course,

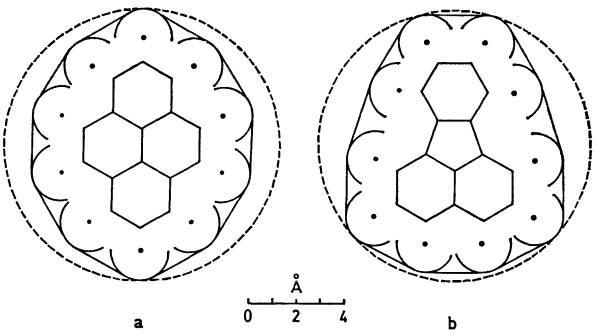

Fig. 11. Sections of van der Waals repulsion envelopes of the pyrene and fluoranthene molecules.

not very different from that of the Py molecule, but of a lower symmetry. If the molecules are rotating in their planes, the columns in the solid complexes of these three hydrocarbons would have cross sections very much alike and would produce unit-cell dimensions close to one another. The ease of the rotation seems to depend on comparatively small differences in the structure of the component molecules. The results summarized in Fig. 1 indicate that the rotation occurs most easily for the Py molecule with a higher symmetry and a little bit less easily for the Fl molecule. In the case of the Ph molecule, the shape of which is farther from a circle than the other two, the rotation is allowed only in limited complexes.

It is apparent that the lattice symmetry proposed in Fig. 3 is incompatible with the symmetry of the constituent molecules. This discrepancy provides one of the reasons for concluding that the molecules, even if not literally rotating, are disordered in orientation. The trigonal lattice is not entirely new for molecular complexes. Some years ago, Dahl found that the crystals of the hexamethylbenzene–hexafluorobenzene (1:1) complex are trigonal ($R\bar{3}m$) at room temperature and are transformed into a triclinic form ($P\bar{1}$) when cooled below 0 °C.[24,25] The lattice constants for the former form are $a=14.596\pm0.012$ Å and $c=7.124\pm0.007$ Å, fairly close to those given in Table 2. The donor and acceptor molecules are stacked alternatively in columns, with some disorder in the stacking sequence, in the trigonal form. No indication has been noted of such a disorder in the low-temperature form.[25] On the basis of thermal-vibration ellipsoids, Dahl postulated that rotation occurs for the hexamethylbenzene molecule not only in the trigonal form, but also in the triclinic form. We have examined the ^1H and ^{19}F NMR spectra of this complex. The second moment in the former spectrum is 11.3 G^2 at −142 °C and gradually decreases to 1.8 G^2 by −65 °C. Similarly, the moment in the latter spectrum shows a decrease from 1.2 to 0.65 G^2 in the same temperature range. The enthalpy associated with the transition located at about −25 °C is as small as 0.7 kJ mol^{-1}; therefore, no change in the second moment may be expected upon this transition.

The proposed lattice suggests that the stacking column acquires an effectively circular cylindrical symmetry. As the minimum distance between the sites for donor and acceptor molecules located in neighboring columns is less than the average of two molecular diameters, the molecules have no room to rotate freely and a change in the orientation requires correlated movements of interlocking molecules. For example, the distance is about 8.9 Å, and the average molecular diameter is about 10.6 Å, in the Py–DNC complex. The ratio of these two quantities, 0.84, fits nicely into the range of the minimum distance between molecular centers divided by the maximum diameter of the molecule, which is found for plastic crystals consisting of globular molecules, 0.81—0.94.[26]

In conclusion, it may be added that the electron acceptors in our complexes are relatively weak ones. The complexes are yellow to orange, and the mean separations between molecular planes are comparatively large, about 3.5 Å. Attempts to find isomorphous high-temperature forms with deeply colored complexes have not met with any success.

The authors wish to express their sincere thanks to Mr. Nobuhiko Miyajima for the preparation of some acceptor compounds; to Mr. Eiji Ochi for recording some X-ray diffraction patterns, and to Dr. Akio Furusaki for his helpful comments on the probable structure of the high-temperature forms. The present work was partly supported by a Grant-in-Aid for Scientific Research No. 543001 from the Ministry of Education, Science and Culture.

References

1) N. Inoue and Y. Matsunaga, *Bull. Chem. Soc. Jpn.*, **51**, 90 (1978).
2) F. H. Herbstein and M. Kaftory, *Acta Crystallogr., Sect. B*, **31**, 60 (1975).
3) T. Inabe, Y. Matsunaga, and Y. Yoshida, *Bull. Chem. Soc. Jpn.*, **52**, 615 (1979).
4) J. Feldman, P. Pantages, and M. Orchin, *J. Am. Chem. Soc.*, **73**, 4341 (1951).
5) H. T. Clarke and W. W. Hartman, *Org. Synth.*, Coll. Vol. I, 541 (1967).
6) A. S. Bailey and J. R. Case, *Tetrahedron*, **3**, 113 (1958).
7) F. Casellato, C. Vecchi, A. Girelli, and P. G. Farrell, *Thermochim. Acta*, **13**, 37 (1975).
8) P. G. Farrell, F. Shahidi, F. Casellato, C. Vecchi, and A. Girelli, *Thermochim. Acta*, **33**, 275 (1979).
9) F. Casellato, C. Vecchi, and A. Girelli, *Thermochim. Acta*, **21**, 195 (1977).
10) F. Pelizza, F. Casellato, and A. Girelli, *Thermochim. Acta*, **4**, 135 (1972).
11) A Kofler, *Z. Elektrochem.*, **50**, 200 (1944).
12) Y. Matsunaga, *Bull. Chem. Soc. Jpn.*, **44**, 2868 (1971).
13) S. Koizumi and Y. Matsunaga, *Bull. Chem. Soc. Jpn.*, **47**, 9 (1974).
14) A. I. Kitaigorodskii, "Organic Chemical Crystallography," Consultant Bureau, New York (1961), pp. 230—240.
15) C. A. Fyfe, *J. Chem. Soc., Faraday Trans. 2*, **70**, 1633 (1974).
16) F. H. Herbstein and J. A. Snyman, *Phil. Trans. R. Soc. London, Ser. A*, **264**, 635 (1969).
17) A. G. Dunn, A. Rahman, and L. A. K. Staveley, *J. Chem. Thermodyn.*, **10**, 787 (1978).
18) J. Trotter, *Acta Crystallogr.*, **16**, 655 (1963).
19) E. A. Andrew and R. G. Eades, *Proc. R. Soc. London, Ser. A*, **218**, 537 (1953).
20) G. D. Oliver, M. Eaton, and H. M. Huffman, *J. Am. Chem. Soc.*, **70**, 1502 (1948).
21) K. Araya, Y. Matsunaga, and E. Ochi, *Bull. Chem. Soc. Jpn.*, **52**, 1264 (1979).
22) J. N. Sherwood, *Bull. Soc. Fr. Minéral. Cristallogr.*, **95**, 253 (1972).
23) A. A. K. Al-Mahdi and A. R. Ubbelohde, *Proc. R. Soc. London, Ser. A*, **220**, 143 (1953).
24) T. Dahl, *Acta Chem. Scand.*, **26**, 1569 (1972).
25) T. Dahl, *Acta Chem. Scand.*, **27**, 995 (1973).
26) M. Postel and J. G. Riess, *J. Phys. Chem.*, **81**, 2634 (1977).

  Bull. Chem. Soc. Jpn., 54, 2565—2568 (1981)

Formation of H(n=4) and CH($A^2\Delta$) by the Electron Impact Dissociation of Benzene, Pyridine, and Pyrazine

Ikuo Tokue* and Masami Ikarashi

Department of Chemistry, Faculty of Science, Niigata University, Ikarashi, Niigata 950-21

(Received January 16, 1981)

Benzene, pyridine, and pyrazine were excited by electron impact (0—70 eV) under low pressure conditions. In the wavelength region of 250—510 nm, emissions from H, CH, C_2, and CN (except for benzene) fragments were observed. Formations of H(n=4) and CH($A^2\Delta$) from benzene, pyridine, and pyrazine were investigated. The appearance potentials for the hydrogen Balmer β emission were determined to be 19.5±1.0 eV in benzene, 19.7±1.0 eV in pyridine, and 19.6±1.0 eV in pyrazine. The appearance potentials for the CH(A-X) emission were also determined to be 12.7±1.0 and 21.4±1.0 eV in benzene, 20.1±1.0 eV in pyridine, and 18.5±1.0 eV in pyrazine. No emissions from the excited parent species of pyridine and pyrazine were observed.

When a relatively large molecule is excited by electron impact, photoemission from small fragments is observed more easily than that from the parent molecule. This is probably because the parent molecule has many degrees of freedom of motion and non-radiative processes become important. However, aromatic molecules are one of the exceptions, where excited parent species give intense fluorescence upon electron impact. The fluorescence ($S_1 \rightarrow S_0$) from benzene by electron impact has been studied extensively.[1-4] On the other hand, nitrogen-heterocycles in the vapor phase hardly emit radiation,[5,6] because radiationless processes among excited states are particularly efficient.

As stressed by Platzman[7] for benzene, neutral excited states having excitation energy in excess of its ionization play an important role in the formation of neutral fragments. Recently, emissions for these neutral fragments from benzene have been studied.[8-10] However, as for large nitrogen-heterocycles such as pyridine and pyrazine, very little is known at this time about the fragments and the mechanism of fragmentation from the excited parent species by electron impact.[11]

The fragmentation of molecules by electron impact has been studied by mass spectrometry, but the information thus obtained has been restricted to relatively large ionic fragments; furthermore, only little has been known about the excited states leading to the ionization.

In the present paper the emission spectra of the fragments produced by electron impact dissociation of benzene, pyridine, and pyrazine are assigned and the appearance potentials for the fragments are determined.

Experimental

Figure 1 shows a schematic drawing of the apparatus, which consists of an electron source, a collision chamber and an optical detection system. The electron source and the collision chamber are evacuated by an oil diffusion pump to about 0.27 mPa, as measured by an ionization gauge. The negative potential from 0 to 70 eV was applied to a tungsten filament (0.1 mm diameter) heated by 3 V d.c. Electrons accelerated and focused by three electrodes were introduced into the collision chamber through an aperture (3 mm diameter). The maximum beam current measured at a Faraday cage (g) was about 0.8 mA at 70 eV. For measurement of the excitation functions electron-beam currents ranging from 10 μA at the threshold to 60 μA at higher energies were used.

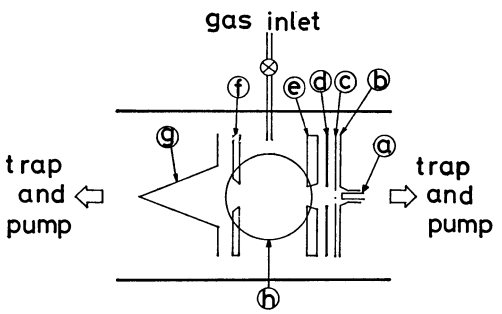

Fig. 1. Schematic diagram of the collision chamber and the electron gun.
a: Tungsten filament, b: repeller electrode, c, d, e, and f: electrodes, g: Faraday cage, h: quartz window.

The sample gases were fed into the collision chamber through a nozzle (1 mm diameter) at a constant pressure controlled by the temperature of the sample holder and a variable leak valve. The sample pressures during the emission measurements, as measured by an ionization gauge, were 5—40 mPa.

A 30 cm Czerny-Turner scanning monochromator equipped with a 1200 Gr/mm grating blazed at 300 nm, an HTV R585 photomultiplier, and an HTV C1230 photon-counter were used. With a slit-width of 200 μm spectral resolution of 0.6 nm (FWHM) was obtained and was used for measurement of the excitation function.

The energy scale for the incident electrons was calibrated using the excitation functions for the (0, 0) band of the N_2-($C^3\Pi$-$B^3\Pi$) emission by Finn *et al.*[12] and the (0, 0) band of the N_2^+($B^2\Sigma$-$X^2\Sigma$) emission by Borst and Zipf.[13] About 5% of nitrogen gas was mixed with the sample gas and their excitation functions were measured simultaneously. A slight discrepancy was observed in the steepness of the excitation function for the N_2(C-B) emission in the threshold region (Fig. 2); it is probably because of the energy spread of about 2 eV in the present experiment.

The samples of benzene, pyridine, and pyrazine were of guaranteed grade from Nakarai Chemicals. Pyridine was fractionally distilled over sodium hydroxide under a stream of nitrogen.[6] Pyrazine was recrystallized from its diethyl ether solution.[14] The samples were degassed by several freeze-pump-thaw cycles just before use.

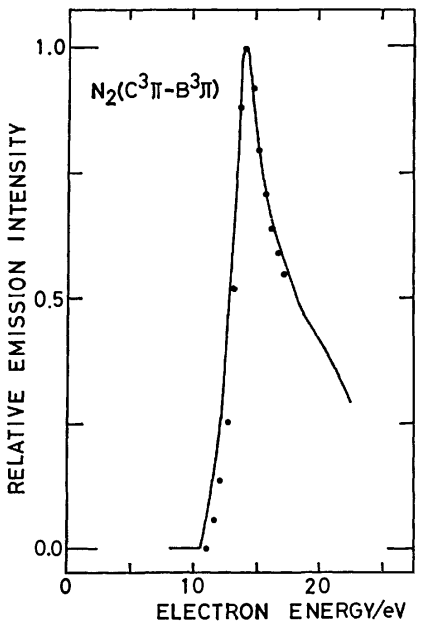

Fig. 2. Excitation functions for the (0,0) band of the N_2(C-B) emission normalized at the peak value. ——: This work, ●●●: Finn *et al.*[12]

Results and Discussion

Emission Spectra. The observed emission spectra by electron impact on benzene are similar to those reported by Smith[1] and Ogawa *et al.*[9] Figure 3 shows the emission spectra obtained from pyridine and pyrazine in the region of 250—510 nm at electron energy of 70 eV. Many sharp bands in these spectra were assigned to the following fragment species; the hydrogen Balmer series (n=4—10→2), the CH($A^2\Delta$-$X^2\Pi$), the C_2($A^3\Pi$-$X^3\Pi$), and the CN($B^2\Sigma$-$X^2\Sigma$) bands.

The photoemission intensities of the hydrogen Balmer β (H_β) and the CH($A^2\Delta$-$X^2\Pi$) band from benzene, pyridine, and pyrazine, and the CN($B^2\Sigma$-$X^2\Sigma$) band from pyridine and pyrazine were found to be proportional to the electron-beam current up to 0.5 mA. In the measurement of the excitation functions, the gas density of the parent molecule in the column of electron-beam (0.4 cm^3) is estimated to be less than 3×10^{12} molecule/cm^3 and is two orders of magnitude lower than the electron density in the collision region, 6×10^{14} electron/s, for a beam current of about 0.1 mA. Such a low gas density was necessary because low-energy electrons formed by ionization can reach the electron collector and affect the Faraday cage current.

Therefore, the H and CH species from benzene, pyridine and pyrazine seem to be formed by fragmentation *via* a single collision, and two-step collisions of the electron with the sample molecule and intermolecular quenching processes seem to be negligible.

As for pyrazine, fluorescence and phosphorescence[15] were expected especially near the excitation threshold. Neverthless, no emission from the parent species was observed even at the sample pressure as high as 47 mPa.

Excitation Functions and Appearance Potentials. Figures 4 and 5 show the excitation functions for the H_β and CH(A-X) emissions from benzene, pyridine, and pyrazine near their thresholds. The electron energy scale for each experiment was calibrated using the well-known thresholds for the N_2(C-B) and N_2^+(B-X) emissions which lie close in energy to the thresholds for the H_β and the CH(A-X) emissions. Although each excitation function near the threshold is broadened by the electron energy distribution of about 2 eV (FWHM), the appearance potential in each excitation function is determined using a linear extrapolation (see Figs. 4 and 5). We estimate that

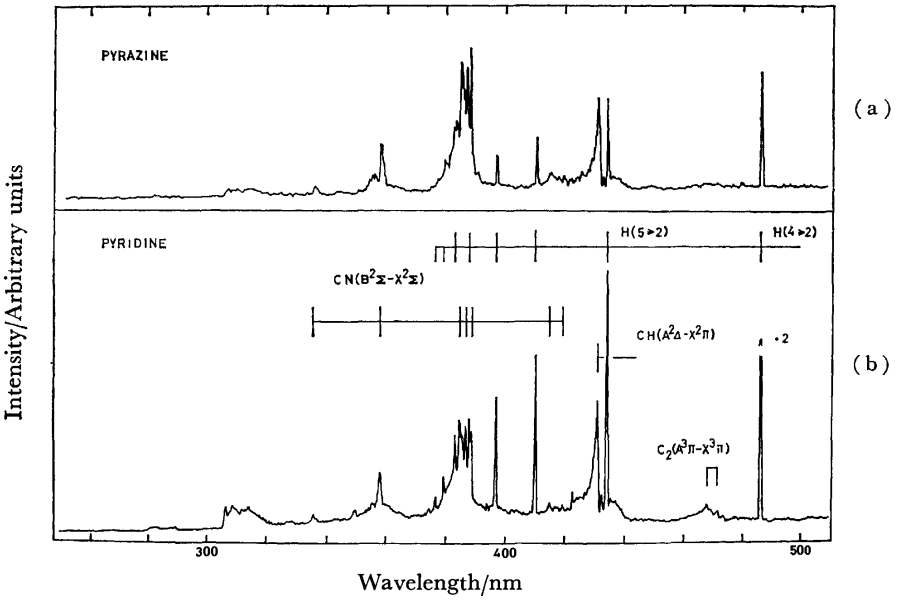

Fig. 3. Emission spectra by electron impact at 70 eV and 0.5 mA. The fragment emission peaks observed are assigned except for the broad peaks near 310 nm. (a): Pyrazine at 16 mPa. (b): Pyridine at 19 mPa.

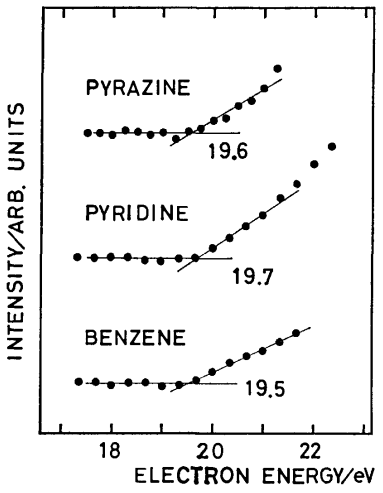

Fig. 4. The excitation functions for H_β from benzene, pyridine, and pyrazine near the thresholds. Typical data are presented. The standard deviation is about twice as large as the diameter of the circles.

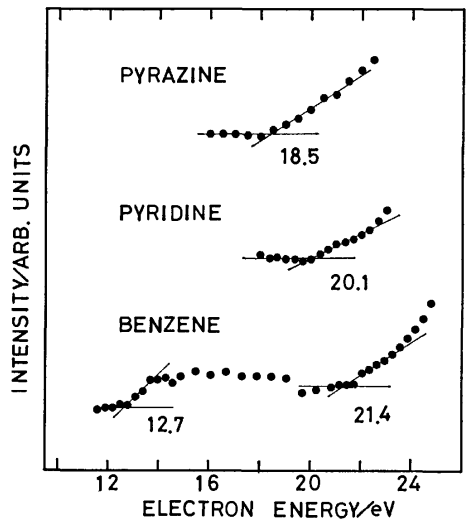

Fig. 5. Same as Fig. 4 for the CH(A-X) emission. The standard deviation is nearly as large as the diameter of the circles.

this calibration is accurate to 1 eV[16] and the random error of each calibrated appearance potential is about 0.4 eV. The appearance potentials thus determined for the H_β and the CH(A-X) emissions are summarized in Table 1 in comparison with previous work.[10]

Formation of H(n=4). The onset for H_β from benzene is found at 19.5±1.0 eV: this value agrees well with 19.3±1.0 eV reported by Beenakker and de Heer.[10] The absence of structure near the threshold indicates that only one state or at most a few states of benzene are involved in the formation of excited hydrogen atoms. By comparison of the observed threshold energy with the dissociation energy of the C–H bond, 4.87 eV,[17] and the excitation energy of H(n=4), 12.7 eV, the following dissociation process, which is reported by Beenakker and de Heer,[10] seems to play an important role in the formation of excited hydrogen atoms.

Table 1. Appearance potentials for the H_β and the $CH(A^2\Delta\text{-}X^2\Pi)$ emissions determined from their excitation functions (in eV)

	H_β		$CH(A^2\Delta\text{-}X^2\Pi)$	
	This work	Beenakker *et al.*[a]	This work	Beenakker *et al.*[a]
Benzene	19.5±1.0	19.3±1.0	12.7±1.0	15.0±1.0
			21.4±1.0	
				29 ±1
Pyridine	19.7±1.0		20.1±1.0	
Pyrazine	19.6±1.0		18.5±1.0	

a) Ref. 10.

$$C_6H_6(19.5\,eV) \longrightarrow C_6H_5(X^2\tilde{A}_1) + H(n=4) + 1.9 \pm 1.0\,eV$$

The onsets for H_β from pyridine and pyrazine are observed at 19.7±1.0 and 19.6±1.0 eV, respectively. A similar consideration on the energy balance with the dissociation energy of the C–H bond, 4.87 eV,[17] because the dissociation energy of the C–H bond of pyridine and pyrazine are not known, leads to the following processes

$$C_5H_5N(19.7\,eV) \longrightarrow C_5H_4N(X) + H(n=4) + 2.1 \pm 1.0\,eV$$

and

$$C_4H_4N_2(19.6\,eV) \longrightarrow C_4H_3N_2(X) + H(n=4) + 2.0 \pm 1.0\,eV.$$

Formation of CH(A). The excitation function for the CH(A-X) emission from benzene indicates some structure and a shallow dip near 20 eV. Hence, several states of benzene seem to be involved in the formation of CH(A), and further, the formation of CH(A) seems to compete with other processes: probably ion formations. The onsets for the CH(A-X) emission from benzene are observed at 12.7±1.0 and 21.4±1.0 eV; the first value is lower than 15.0±1.0 eV obtained by Beenakker and de Heer.[10] The second value, 21.4 eV, is even lower than 29±1 eV reported by Beenakker and de Heer.[10] Comparing the observed excitation function for the CH(A-X) emission with theirs, we conclude that the structure leading to this second appearance potential is different from that reported by Beenakker and de Heer.

Dissociation processes leading to the formation of CH(A) from benzene are still uncertain. Neverthless, if one assumes that the threshold energy consists of the difference between heats of formation of benzene and products[18–20] and the electronic energy of CH(A),[21] the following dissociation processes are considered to occur. Heats of formation and bond dis-

$$C_6H_6 \longrightarrow \text{  } + CH(A^2\Delta) \qquad 14.3\,eV \quad (1)$$

$$\longrightarrow \text{  } + C_2H_2(\tilde{X}) + CH(A^2\Delta) \qquad 22.9\,eV \quad (2)$$

TABLE 2. HEATS OF FORMATION AND BOND DISSOCIATION ENERGIES USED FOR THE CALCULATION OF THRESHOLD ENERGIES

Species	ΔH_f° / kJ mol^{-1}	Ref.	D(R-H) / eV	Ref.
Benzene	82.89±0.54	18	4.87	17
Pyridine	144.56±0.5	18	4.87[a]	
Cyclopentadiene	130.25	18	4.87[a]	
C_2H_2	227.29	19		
HCN	135.5	19		
CH	592.5	19		
$C_3H_3^+$ (Cyclopropenyl ion)	1196.6 ±8[b]	20		

a) The value in benzene is used. b) This is the value of $C_4H_4^+$ (cyclobutadienyl) ion because the formation processes of $C_3H_3^+$ and $C_4H_4^+$ have identical thermochemical thresholds.[20]

sociation energies used for the calculation of the thresholds are summarized in Table 2. Process (1) seems to play an important role in the formation of CH(A) near the first threshold. Dissociation into more than two neutral fragments may happen at an intermediate energy region, 14—22 eV, because $C_4H_4^+$, $C_4H_3^+$, $C_4H_2^+$, and $C_3H_3^+$ ions from benzene are relatively abundant;[22,23] furthermore, dissociations producing only neutral fragments such as CH(A) proceed via so-called super-excited states competing with these ion formations. Process (2) including an ionic byproduct seems to play an important role in the formation of CH(A) near the second threshold. Some processes including $C_5H_5^+$ ion seems to be unimportant because $C_5H_5^+$ ion appears only very weakly or is not observed.[20,22]

The appearance potentials for CH(A) from pyridine and pyrazine are determined to be 20.1±1.0 and 18.5±1.0 eV, respectively. The absence of structures near the thresholds indicates that only one state or at most a few states of pyridine and pyrazine are involved in the formation of CH(A). On the basis of a similar consideration (see Table 2), the following dissociation process from pyridine is considered to occur because $C_3H_3^+$ (cyclopropenyl) ion is relatively abundant in photo-ionization mass spectrometry of pyridine.[20,24] It is impossible to derive dissociation processes from pyrazine because the relevant dissociation energies are not known. Neverthless, processes forming CH(A) from pyrazine presumably include the formation of an ionic fragment and may correspond to the dissociation processes forming CH(A) from benzene with the second threshold and pyridine.

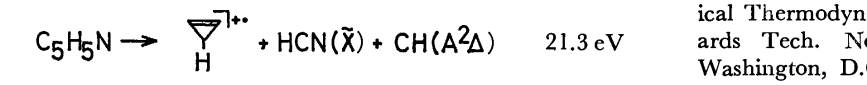

In summary, the appearance potentials for H_β from benzene, pyridine, and pyrazine are nearly equal and H(n=4) may dissociate by a similar mechanism. The two appearance potentials for CH(A) from benzene are found from the structures in the excitation function for the CH(A-X) emission, while no corresponding structures exist near the thresholds of the excitation functions for the CH(A-X) emission from pyridine and pyrazine.

We wish to thank Prof. Kozo Kuchitsu of the University of Tokyo for many valuable comments on the manuscript and useful discussions.

References

1) W. H. Smith, *J. Chem. Phys.*, **54**, 4169 (1971).
2) K. C. Smyth, J. A. Schiavone, and R. S. Freund, *J. Chem. Phys.*, **61**, 1782 (1974).
3) K. C. Smyth, J. A. Schiavone, and R. S. Freund, *J. Chem. Phys.*, **61**, 4747 (1974).
4) C. I. M. Beenakker, F. J. de Heer, and L. J. Oosterhoff, *Chem. Phys. Lett.*, **28**, 320 (1974).
5) A. E. W. Knight and C. S. Parmenter, *Chem. Phys.*, **15**, 85 (1975).
6) I. Yamazaki and H. Baba, *J. Chem. Phys.*, **66**, 5826 (1977).
7) R. L. Platzman, *Radiat. Res.*, **17**, 419 (1962).
8) D. A. Vroom and F. J. de Heer, *J. Chem. Phys.*, **50**, 573 (1969).
9) T. Ogawa, M. Tsuji, M. Toyoda, and N. Ishibashi, *Bull. Chem. Soc. Jpn.*, **46**, 2637 (1973).
10) C. I. M. Beenakker and F. J. de Heer, *Chem. Phys. Lett.*, **29**, 89 (1974).
11) T. Ogawa, M. Toyoda, and N. Ishibashi, *Engineering Sci. Repts. Kyushu Univ.*, **2**, 17 (1980).
12) T. G. Finn, J. F. M. Aarts, and J. P. Doering, *J. Chem. Phys.*, 56, 5632 (1972).
13) W. L. Borst and E. C. Zipf, *Phys. Rev. A*, **1**, 834 (1970).
14) K. Nakamura, *J. Am. Chem. Soc.*, **93**, 3138 (1971).
15) L. M. Logan and I. G. Ross, *J. Chem. Phys.*, **43**, 2903 (1965).
16) K. C. Smyth, J. A. Schiavone, and R. S. Freund, *J. Chem. Phys.*, **62**, 136 (1975).
17) A. S. Rodgers, D. M. Golden, and S. W. Benson, *J. Am. Chem. Soc.*, **89**, 4578 (1967).
18) J. D. Cox and G. Pilcher, "Thermochemistry of Organic and Organometallic Compounds," Academic Press, New York (1970).
19) D. D. Wagman, W. H. Evans, V. B. Parker, I. Halow, S. M. Bailey, and R. H. Schumm, "Selected Values of Chemical Thermodynamic Properties," National Bureau of Standards Tech. Note 270-3, U. S. Govt. Printing Office, Washington, D.C. (1968).
20) H. M. Rosenstock, K. E. McCulloh, and F. P. Lossing, *Int. J. Mass Spectrum. Ion Phys.*, **25**, 327 (1977).
21) G. Herzberg, "Spectra of Diatomic Molecules," 2nd ed, Van Nostrand, Princeton (1950), p. 519.
22) H. Genzel and O. Osberghaus, *Z. Naturforsch., Teil A*, **22**, 331 (1967).
23) K. R. Jennings, *Z. Naturforsch., Teil. A*, **22**, 454 (1967).
24) J. H. D. Eland, J. Berkowitz, H. Schulte, and R. Frey, *Int. J. Mass Spectrum. Ion Phys.*, **28**, 297 (1978).

  Bull. Chem. Soc. Jpn., 54, 2569—2572 (1981)

Formation of Electron-Donor-Acceptor Complex and 1,4-Cycloadduct of Tetracyanoethylene with Styrene and Its α- or β-Substituted Derivatives

Yasuhiro Uosaki, Masaru Nakahara,* and Jiro Osugi

Department of Chemistry, Faculty of Science, Kyoto University, Oiwake-cho, Kitashirakawa, Sakyo-ku, Kyoto 606

(Received February 9, 1981)

EDA-complex formation and 1,4-cycloaddition of tetracyanoethylene (TCNE) with styrene, α-methylstyrene, 1,1-diphenylethylene, *cis*-stilbene, and *trans*-stilbene were studied spectrophotometrically in chloroform at 25 °C. Formation constants of the EDA complexes were found to be in the order, *trans*-stilbene > styrene > α-methylstyrene > *cis*-stilbene > 1,1-diphenylethylene. The difference in the formation constants was discussed in terms of both electronic and steric effects of the donors studied. α-Methylstyrene and 1,1-diphenylethylene underwent thermal cycloaddition to TCNE faster than styrene. It is suggested that some charge separation took place in the transition state. The fact that *trans*- and *cis*-stilbenes do not react with TCNE was explained in terms of the difference in stability of the 1,4-cycloadducts estimated from the 1,4-bislocalization energy obtained by Dewar's perturbation molecular orbital method.

The nature of tetracyanoethylene (TCNE) as a strong acceptor causes a few typical cycloaddition reactions with π-electron donors as well as the EDA (electron-donor-acceptor)-complex formation.[1] When TCNE is mixed with benzene derivatives, electron-rich olefins, and conjugated dienes, it usually yields the EDA complexes only, cyclobutane derivatives (1,2-cycloadducts), and cyclohexene derivatives (1,4-cycloadducts), respectively, under mild conditions.

Styrene has been considered to be nonreactive toward TCNE under mild conditions, although benzylidenemalononitrile and a cycloadduct consisting of two molecules of styrene and one molecule of TCNE were obtained by refluxing in xylene.[2] Recently, however, it was found by the high-pressure quenching method that styrene and its derivatives(D) undergo reversible cycloaddition to TCNE(A) to afford the 1,4-cycloadduct(P) besides the EDA complex.[3,4] The 1,4-cycloaddition reaction illustrated below is of

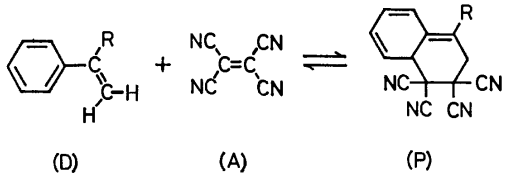

(D) (A) (P)

interest. Styrenes serve as a diene, losing their aromaticity, while they act as a dienophile in the Diels-Alder reaction with anthracenes.[5] In order to get insight into the mechanism of the reaction, a detailed kinetic study has been carried out. It was not clarified in the previous work[4] why neither *cis*- nor *trans*-stilbene provides the 1,4-cycloadduct, despite the fact that ionization potentials of these molecules are lower than those of other styrenes which give the cycloadduct. An interpretation for the unexpected result is given herewith in view of the molecular orbital theory.

The formation constant and molar absorption coefficient of the EDA complex between TCNE and styrene were determined[6-9] without taking into consideration the coexistence of the 1,4-cycloadduct confirmed previously.[3,4] Reliable values of these parameters were obtained in the present study taking into account the 1,4-cycloadduct. Discussion is given on the factors determining the stability of the EDA complexes between TCNE and styrene and its derivatives.

Experimental

Electron donors and TCNE were purified by the method reported.[4] Chloroform as a solvent was purified by the standard method. The boiling points and melting points of all the reagents agree with the values reported.

Stock solutions of the donors and the acceptor were prepared immediately before use. Electronic absorption spectra and their time dependences for kinetic studies were measured with a Shimadzu UV-200S spectrophotometer. Thermostatted water (25 °C) was circulated around a quartz cell and donor and acceptor reservoirs. The temperature was regulated within ±0.1 °C. Under the conditions where the concentration (mol dm^{-3}) of the donor is in large excess, reaction rates were determined by following the increase in the absorbance around 320 nm due to the 1,4-cycloadduct, and equilibrium studies by observing the charge-transfer (CT) band at a longer wavelength. The absorbance due to the EDA complex decreased to a stationary value (not zero) with time except in the case of stilbenes. The time at half-mixing of donor and acceptor solutions was taken as time zero when we get an absorbance of the EDA complex at time zero by extrapolation.

Results and Discussion

EDA Complexes of TCNE with Various Styrene Derivatives. When α-methylstyrene is mixed with TCNE in chloroform, absorption bands due to the EDA complex instantaneously appear in the visible region (Fig. 1b). Similar absorption spectra can be observed in solutions of TCNE and other styrene derivatives. The donor and TCNE have no absorption in this region. The wavelength of the maximum absorption(λ_{max}) is slightly larger in chloroform than that in dichloromethane (Table 1).

The plot of transition energies ($h\nu_{CT}$) of a series of EDA complexes with a fixed acceptor against ionization potential (I_p) of donors generally shows a

Table 1. Spectroscopic properties and formation constants of EDA complexes between TCNE and various styrene derivatives in $CHCl_3$ at 25 °C

Donor	I_p[a] / eV	λ_{max}[b] / nm	ε_{max} / mol^{-1} dm^3 cm^{-1}	K_c / mol^{-1} dm^3
Styrene	8.50	486 (480)	1960±30	0.467±0.010
α-Methylstyrene	8.50	504 (495)	1760±50	0.436±0.013
1,1-Diphenylethylene	8.25	519 (507)	1660±50	0.306±0.011
cis-Stilbene	8.20	541 (528)	1950±110	0.415±0.023
trans-Stilbene	8.00	608 (597)	1880±50	1.16±0.03

a) Ref. 13; 1 eV≈96.48456 kJ/mol. b) Values in parentheses were measured in CH_2Cl_2 from Ref. 4.

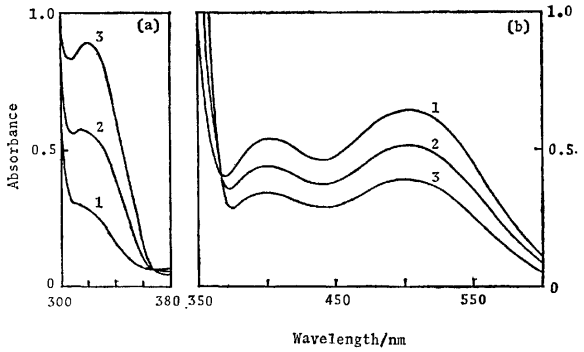

Fig. 1. Time dependence of the electronic spectrum of α-methylstyrene–TCNE system in $CHCl_3$ at 25 °C. (a) 1,4-Cycloadduct ($[D]_0$=0.5 mol dm^{-3}, $[A]_0=2\times10^{-4}$ mol dm^{-3}). (b) EDA complex ($[D]_0$=0.5 mol dm^{-3}, $[A]_0=2\times10^{-3}$ mol dm^{-3}). (1): 10 s after mixing, (2): 1 min, (3): stationary state.

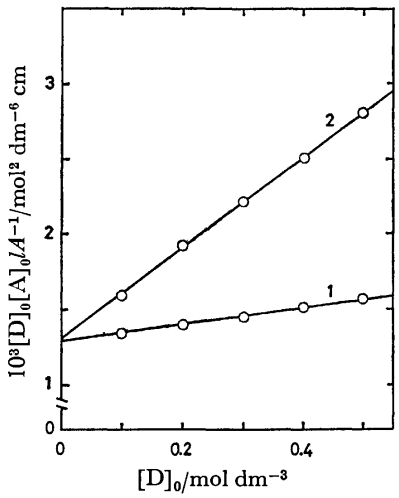

Fig. 2. Scott plots for α-methylstyrene–TCNE system in $CHCl_3$ at 25 °C.
1: t=0, 2: stationary state.

linear relationship.[1b] This was also found to be the case in this study:

$$h\nu_{CT}/\text{eV} = 0.873(I_p/\text{eV}) - 4.89 \quad \text{(in } CHCl_3\text{)} \quad (1)$$

$$h\nu_{CT}/\text{eV} = 0.847(I_p/\text{eV}) - 4.63 \quad \text{(in } CH_2Cl_2\text{)}. \quad (2)$$

The gradients obtained for the TCNE–styrene derivative systems are nearly the same as those obtained for other TCNE–aromatic hydrocarbon systems in the corresponding solvents.[1b] The fact that the gradient is not very far from unity suggests that the resonance interaction between the donors and acceptor is weak; the EDA complexes we have examined are weak ones.

The formation constant(K_c) and molar absorption coefficient (ε_{max}) of the EDA complex at λ_{max} are determined by the Scott equation,[10]

$$\frac{[D]_0[A]_0 l}{A_0} = \frac{1}{K_c\varepsilon_{max}} + \frac{[D]_0}{\varepsilon_{max}}, \quad (3)$$

where $[D]_0$ and $[A]_0$ are the initial concentrations of the donor and acceptor, respectively, A_0 is the absorbance of the EDA complex at λ_{max} at time zero, ε_{max} the molar absorption coefficient at λ_{max}, and l the path length (10 mm). Figure 2 shows a plot of the left-hand side of Eq. 3 against $[D]_0$ for α-methylstyrene–TCNE system. Applying the least-squares method to linear plots like this, we obtain values of K_c and ε_{max} of the complexes as in Table 1, the K_c values being in the sequence, *trans*-stilbene>styrene> α-methylstyrene > *cis*-stilbene > 1,1-diphenylethylene. The sequence of the TCNE complexes is similar to that of the 1,3,5-trinitrobenzene complexes, except for the case of *cis*-stilbene.[11]

In the case of planar molecules like styrene and *trans*-stilbene, the sequence is in accord with the trend that the lower the ionization potential of the electron donors, the larger the formation constant. The trend has been derived theoretically by assuming that CT forces mainly contribute to the stabilization energy of the EDA complex.[9,12] On the other hand, in the case of nonplanar molecules like α-methylstyrene, 1,1-diphenylethylene, and *cis*-stilbene, the result is not in accord with the general trend. Since these three nonplanar styrenes have dihedral angles, *ca.* 30—40°,[13,14] the configuration of the complexes is considered to differ a great deal from that of planar-styrene complexes. The nonplanarity of the electron donors interferes approach of the planar TCNE molecule as a factor of steric hindrance, which is responsible for the formation constant smaller than that expected simply from the electronic effect.

Kinetics of 1,4-Cycloaddition. The absorption band around 320 nm due to the 1,4-cycloadduct increases and the CT-absorption band decreases with time, and finally, they reach stationary values (Fig. 1a). Since the EDA-complex formation and 1,4-cycloaddition take place reversibly, the following reaction scheme in which both reactions proceed successively can be assumed:[15]

$$D + A \overset{K_c}{\rightleftharpoons} \text{EDA complex} \overset{k_1}{\underset{k_{-1}}{\rightleftharpoons}} P \quad (4)$$

where k_1 and k_{-1} are the rate constants of the forward and backward reactions, respectively. Let us carry out a kinetic analysis of the reaction according to Eq. 4. When $[D]_0 \gg [A]_0$, the rate equation for the increase of the 1,4-cycloadduct is

$$\frac{d[P]}{dt} = a - k_{obsd}[P], \quad (5)$$

where the square brackets denote the concentration, t time,

$$a = \frac{k_1 K_c [D]_0 [A]_0}{1 + K_c [D]_0} = k_1 [EDA]_0, \quad (6)$$

and

$$k_{obsd} = \frac{k_1 K_c [D]_0}{1 + K_c [D]_0} + k_{-1}. \quad (7)$$

Integration of Eq. 5 gives the expression for [P] as

$$[P] = \frac{k_1 [EDA]_0 \{1 - \exp(-k_{obsd} t)\}}{k_{obsd}}, \quad (8)$$

since [P]=0 at time zero. Pseudo-first-order rate constant, k_{obsd}, was determined by the Guggenheim plot. Plots of k_{obsd} *vs.* $K_c[D]_0/(1+K_c[D]_0)$ for the styrene- and α-methylstyrene–TCNE systems afford good straight lines as shown in Fig. 3. Values of k_1 and k_{-1} obtained from plots of this kind are given in Table 2, together with those of equilibrium constant between the 1,4-cycloadduct and EDA complex, $K_1(\equiv k_1/k_{-1})$, and overall equilibrium constant $K(\equiv K_c K_1)$. We see from Eq. 7 that the product $k_1 K_c$ is overall second-order rate constant from the reactants to the 1,4-cycloadduct. Table 2 shows that the effect of substitution at the α-position by methyl or phenyl group on $k_1 K_c$ is substantially large, the methyl or phenyl substitution enhancing the reactivity by factors of *ca.* 70 and *ca.* 50, respectively. Though most 1,4-cycloadditions are considered to proceed *via* concerted mechanism, the enhancement of the reaction is too large for a concerted mechanism.[16] Similar enhancement has been observed for 1,2-cycloaddition of TCNE to enol or enethiol ethers in which a dipolar intermediate is considered to be involved.[17,18] Thus the α-substitution effect suggests that some charge separation develops in the transition state of the 1,4-cycloaddition. The marked dependence of the rate on solvent polarity supports this idea.[19]

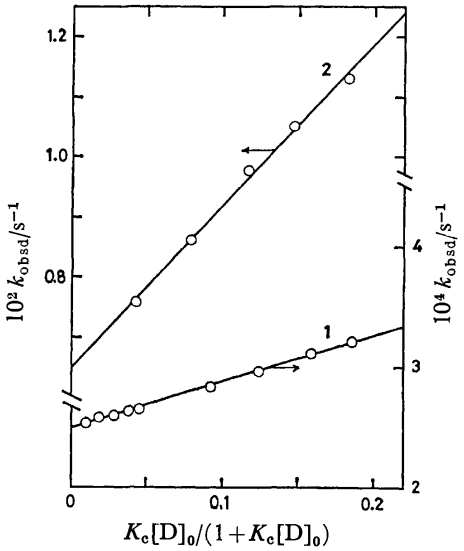

Fig. 3. Plots of k_{obsd} against $K_c[D]_0/(1+K_c[D]_0)$ in $CHCl_3$ at 25 °C.
1: Styrene–TCNE, 2: α-methylstyrene–TCNE.

Equilibria Including 1,4-Cycloadduct. At the stationary state, *i.e.*, $t=\infty$, we obtain

$$[P]_e = \frac{k_1 [EDA]_0}{k_{obsd}}, \quad (9)$$

where $[P]_e$ is the concentration of the 1,4-cycloadduct at the stationary state. By means of the definition $K_1=[P]_e/[EDA]_e$ and Eqs. 6, 7, and 9, we have

$$[EDA]_e = \frac{K_c [D]_0 [A]_0}{1 + (1+K_1) K_c [D]_0}. \quad (10)$$

This can be rewritten as

$$\frac{[D]_0 [A]_0 l}{A_e} = \frac{1}{K_c \varepsilon_{max}} + \frac{(1+K_1)[D]_0}{\varepsilon_{max}}, \quad (11)$$

by means of Beer's relation $[EDA]_e = A_e/\varepsilon_{max}\, l$, where A_e is the absorbance of the EDA complex at λ_{max} at the stationary state. A plot of the left-hand side of Eq. 11 against $[D]_0$ in the α-methylstyrene–TCNE system is also shown in Fig. 2. The two kinds of plots corresponding to Eqs. 3 and 11 should have the same intercept; this is actually the case. The equilibrium constant K_1 is determined from Eq. 11 and the slope of the line 2 in Fig. 2. The value of K_1 obtained from the equilibrium measurement is in accord with that obtained kinetically $(K_1 \equiv k_1/k_{-1})$ within experimental error (Table 2). The agreement indicates that the present analysis is self-consistent.

We can obtain from Eq. 8 a reliable value of the molar absorption coefficient (ε_{320}) of the 1,4-cycloadduct at 320 nm. The values of $\varepsilon_{320}/mol^{-1}\,dm^3\,cm^{-1}$ are $(7.7\pm0.1)\times10^3$, $(5.1\pm0.3)\times10^3$, and $(4.0\pm0.2)\times$

Table 2. Rate and equilibrium constants of the 1,4-cycloaddition between TCNE and various styrene derivatives in $CHCl_3$ at 25 °C

Donor	$10^3 k_1/s^{-1}$	$10^3 k_{-1}/s^{-1}$	K_1	$K/mol^{-1}\,dm^3$
Styrene	0.380±0.012	0.250±0.001	1.52±0.05	0.71±0.04
α-Methylstyrene	26.8±0.6	6.50±0.09	4.12±0.15 (4.29±0.15)[a]	1.80±0.12
1,1-Diphenylethylene	28.9±2.5	8.21±0.12	3.51±0.35	1.07±0.15

a) From the equilibrium measurement.

10^3 for the styrene, α-methylstyrene, and 1,1-diphenylethylene adducts, respectively. The value of ε_{320} for the styrene adduct is slightly larger than that obtained in dichloromethane ($(5.5\pm0.1)\times10^3$).[4] The difference arises from the change of solvents and the neglect of the presence of the EDA complex in the previous treatment.

Tonchéva *et al.* determined K_c and ε_{max} of the TCNE complexes with styrene and α-methylstyrene in 1,2-dichloroethane at 20 °C without noticing the 1,4-cycloadduct, and reported 645 as ε_{max} for styrene and 200 for α-methylstyrene.[7] These values are too small for the TCNE complexes with aromatic hydrocarbons.[1b] The stationary state reaches within 10 minutes in the case of α-methylstyrene–TCNE in chloroform (Table 2). In a more polar solvent, 1,2-dichloroethane, the stationary state is attained faster. The ε_{max} is considered to be $\varepsilon_{max}/(1+K_1)$; ε_{max} and K_1 are shown to be $(3.33\pm0.16)\times10^3$ mol^{-1} dm^3 cm^{-1} and 13.8 under the same condition.[19]

Reactivity of Styrenes. The reactivity of dienes toward TCNE generally increases with the decrease in its ionization potentials, though it is not the diene having lower ionization potential that shows high reactivity in the Diels-Alder reaction. This is also the case for the reaction we examined. Although *trans*- and *cis*-stilbenes have lower ionization potentials than other styrene derivatives, the stilbenes react with TCNE to form only the EDA complex, showing no further reaction such as 1,4-cycloaddition.

The reactivity of styrenes toward TCNE can be examined by the method described by Mok and Nye;[20] the energy of the transition state is considered to depend on the FMO (frontier molecular orbital) interaction energy between reactants and on the stability of the product. The FMO treatment predicts that a diene of lower ionization potential is more reactive on the assumption that other interactions (*e.g.*, van der Waals interactions) are constant within a series of dienes. Since this is contradictory to the experimental results, we should examine the stability of the product. The 1,4-bislocalization energy calculated from Dewar's perturbation molecular orbital method is of great use for a comparison of the stability of the adducts.[21] The 1,4-bislocalization energies computed for three styrenes are given in Table 3, where *para*-localization energies by Brown[22] are included for comparison. It turns out that both parameters have nearly the same value for the donors. We see from the definition of localization energy that a diene of a smaller localization energy, *i.e.*, smaller coefficient of the localization energy, reacts with TCNE to form a stable adduct. For the discussion of reactive sites,[22] the critical value of the localization energy divided by the resonance integral (β) is taken as 3.6 below which reaction takes place. Stilbenes have a larger value than this corresponding to the fact that they are nonreactive toward TCNE (Table 3).

Table 3. 1,4-Bislocalization and *para*-localization energies of three styrenes

Donor	1,4-Bislocalization energy/β	*Para*-localization energy[a]/β
Styrene	3.51	3.44
1,1-Diphenylethylene	3.26	3.34
Stilbene	3.84	3.89

a) Ref. 22.

References

1) For recent reviews see: a) E. M. Kosower, "Progress in Physical Organic Chemistry," ed by S. G. Cohen, A. Streitwieser, Jr., and R. W. Taft, Interscience Publishers, New York (1965), Vol. 3, p. 81; b) R. Foster, "Organic Charge-Transfer Complexes," Academic Press, London (1969); c) A. K. Colter and M. R. J. Dack, "Molecular Complexes," ed by R. Foster, Elek Science, London (1974), Vol. 2, p. 1.
2) J. K. Williams, D. W. Wiley, and B. C. McKusick, *J. Am. Chem. Soc.*, **84**, 2210 (1962).
3) M. Nakahara, Y. Uosaki, M. Sasaki, and J. Osugi, *Rev. Phys. Chem. Jpn.*, **47**, 119 (1977).
4) M. Nakahara, Y. Uosaki, M. Sasaki, and J. Osugi, *Bull. Chem. Soc. Jpn.*, **53**, 3395 (1980).
5) J. Sauer, *Angew. Chem. Int. Ed. Engl.*, **6**, 16 (1967).
6) A. R. Cooper, C. W. P. Crowne, and P. G. Farrell, *Trans. Faraday Soc.*, **62**, 18 (1966).
7) B. Tonchéva, R. Vélichkova, and I. M. Panayotov, *Bull. Soc. Chim. Fr.*, **1974**, 1033.
8) K. Hayashi, P. A. Marchese, S. Munari, and S. Russo, *Chim. Ind. (Milan)*, **56**, 187 (1974).
9) T. Arimoto and J. Osugi, *Rev. Phys. Chem. Jpn.*, **44**, 25 (1974).
10) R. L. Scott, *Recl. Trav. Chim. Pays-Bas*, **75**, 787 (1956).
11) P. H. Emsile, R. Foster, I. Horman, J. W. Morris, and D. W. Twiselton, *J. Chem. Soc., B*, **1969**, 1162.
12) M. J. S. Dewar and C. C. Thompson, Jr., *Tetrahedron, Suppl.*, **7**, 97 (1966).
13) J. P. Maier and D. W. Turner, *J. Chem. Soc., Faraday Trans. 2*, **69**, 196 (1973).
14) H. Suzuki, *Bull. Chem. Soc. Jpn.*, **33**, 619 (1960).
15) For example, there is another scheme in which the complex formation competes with cycloaddition. However, both schemes are indistinguishable kinetically, no means being found for distinction.
16) For a recent review see: J. Sauer and R. Sustmann, *Angew. Chem. Int. Ed. Engl.*, **19**, 779 (1980).
17) R. Huisgen, *Acc. Chem. Res.*, **10**, 117 (1977).
18) T. Okuyama, M. Nakada, K. Toyoshima, and T. Fueno, *J. Org. Chem.*, **43**, 4546 (1978).
19) Y. Uosaki, M. Nakahara, and J. Osugi, unpublished.
20) K. Mok and M. J. Nye, *J. Chem. Soc., Perkin Trans. 1*, **1975**, 1811.
21) M. J. S. Dewar and R. C. Dougherty, "The PMO Theory of Organic Chemistry," Plenum, New York (1975).
22) R. D. Brown, *J. Chem. Soc.*, **1950**, 2730.

  Bull. Chem. Soc. Jpn., 54, 2573—2578 (1981)

Determination of Local Structure and Moving Unit Formed in Binary Solution of *t*-Butyl Alcohol and Water

Nobuyuki Ito,† Tadashi Kato, and Tsunetake Fujiyama*

Institute for Molecular Science, Myodaiji, Okazaki 444

† *Department of Chemistry, Faculty of Science, Tokyo Metropolitan University, Setagaya-ku, Tokyo 158*

(Received February 18, 1981)

The concentration dependences of the mutual diffusion coefficients at 24, 37, and 63 °C were observed for a binary solution of *t*-butyl alcohol (TBA) and water by the use of the light scattering method. The observed concentration dependences of the mutual diffusion coefficients were explained well by postulating the existence of a "moving unit"—a group of molecules which move together for a time much longer than the velocity correlation time. The structure of the moving units which are formed in the solution are $(H_2O)_{11}$TBA at 24 °C and $(H_2O)_{20}$TBA at 63 °C in the concentration range of $0<x_{TBA}<0.1$, where x_{TBA} is the mole fraction of TBA. Taking into account the local structures, which had been determined from the concentration dependences of the mean-square concentration fluctuation values, we could conclude that water molecules form a polyhedron which encages a TBA molecule and that these cages then gather together to form an aggregate. It is essential that these polyhedra do not share their faces with each other in the aggregate. It was also concluded that the number of cages which form an aggregate increases with an increase in the temperature. This suggests the existence of a pseudo-critical temperature for this system. That is to say, the TBA–water solution can separate into two phases under high pressures, a TBA-rich phase and a water-rich phase, in the latter of which almost all the molecules form polyhedra.

In our previous reports,[1,2] the mean-square concentration fluctuation observed by means of the light scattering spectra for TBA–water solution has been reported. From a quantitative analysis of the concentration fluctuation, it has been shown that the local structure of the type $g[(H_2O)_i$TBA$]$ exists in the solution. As the number ratio of TBA to water for this local structure was close to that of the solid clathrate hydrate of TBA,[3] we proposed that this local structure can be a clathrate hydrate-like structure.

It has been established, in the solid clathrate hydrate, that water molecules form polyhedra, each of which encages a guest molecule and that the several polyhedra share one of their faces (we will call this an "associated polyhedron" hereafter). We are interested in whether or not the same sort of associated polyhedra can be formed even in the solution phase, because we can draw another picture for the local structure formed in the solution phase. That is, the polyhedra gather together to form an aggregate without sharing faces with each other (we call this an "aggregated polyhedron" hereafter). The observation of the mean-square concentration fluctuation does not afford information which is accurate enough to judge which picture is correct, that is, whether "associated polyhedron" or "aggregated polyhedron." In addition to the mean-square concentration fluctuation, we have to know the life-time of the local structure in order to solve this problem.[4]

Recently, we have emphasized the importance of the concept of a "moving unit" — a group of molecules which move together for a time much longer than the velocity correlation time — in order to obtain information about the life-time of local structures. A moving unit can be determined by expressing the mutual diffusion coefficient theoretically in terms of the self-diffusion coefficients and the number of moving units.[5,6]

In the present study, we will discuss the above problem on the basis of an analysis of the mutual diffusion coefficients which are obtained from the correlation function of the electric field of Rayleigh light. It will be shown that the aggregated polyhedron picture is preferrable to the associated polyhedron picture. This conclusion will lead us to emphasize the fact that the mixing state of the TBA and water system is governed by a moving unit of the type $(H_2O)_i$TBA. We will also discuss the temperature effect on the mixing state on the basis of the "aggregated polyhedron" picture. It will be suggested that a binary solution of TBA and water may be separated into two phases under high pressure, a TBA-rich phase and a water-rich phase, in the latter of which almost all the water molecules form polyhedra.

Experimental

The light scattering spectrometer used in the present study was designed and constructed in our laboratory. The light source was an Argon ion laser (Spectra-Physics, model 165-09) which produced 0.1—1 W power at 488 nm. The scattering angle, θ, was defined by two pinholes approximately 50 cm apart and 0.5 mm in diameter. The laser beam was focused into a rectangular cell with a path length of 1.5 cm. A scattered light and a local oscillator beam (scattered from the cell walls) were collected onto the surface of a photomultiplier tube (HTV R-374). The photo current was amplified by a factor of about 400 by means of a preamplifier and autocorrelated by a 400-channel correlation and probability analyzer (KANOMAX SAI-43A). The computed time auto-correlation function of the photocurrent was recorded on an X-Y recorder. At the same time, the auto-correlation function was transferred in a digital form from the correlator to a micro-computor (SHARP Mz-80C).

In our previous study,[7] a spectrum analyzer (Takeda Riken, TR-4120S) was used instead of a signal correlator. The signal correlator is superior to the spectrum analyzer for the observation of the current fluctuation in the low-

frequency range (DC≈kHz) in the following respects. First the rate of data collection with the signal correlator is higher than that with the spectrum analyzer by a factor of more than 10^2. Second, we can compare the precision of the data sampling interval, τ. For the signal correlator used in the present work, the precision of τ is about 10^{-4} for the frequency range of DC≈50 kHz. In the case of the spectrum analyzer, on the other hand, the corresponding precision can be estimated from the precision of the observed frequency, $|\Delta f/f|$, because the $|\Delta\tau/\tau| = |\Delta f/f|$ relation holds between these two kinds of precision. The precision of the observed frequency is about 10^{-4} at 50 kHz and about 10^{-2} at 500 Hz. Thus, the signal correlator is more appropriate for the observation of the current fluctuation of the low-frequency signal (DC≈50 kHz). The characteristic frequency of the concentration fluctuation appears in this frequency range.

The time-correlation function of the electric field of Rayleigh light was observed at the temperatures of 24, 37, and 63 °C, with a temperature constancy of ±0.5 °C.

t-Butyl alcohol purchased from the Katayama Chemical Industries Co., Ltd., was used without further purification. Water was distilled after being passed through an ion-exchange resin. The binary mixture of TBA–water was made dust-free by the use of a Nuclepore filter with a pore size of 0.1 μm.

Results and Discussion

Light Scattering Measurement and Mutual Diffusion Coefficient. The time-correlation function of the electric field of the Rayleigh light isotropically scattered from a binary solution is composed approximately from two exponential functions.[8] One corresponds to the scattering due to entropy fluctuation, and the other, to that due to concentration fluctuation. Since the relaxation of the latter is slower than that of the former by a factor of 10^2, these two exponential curves can be identified separately. The correlation function for the concentration fluctuation is expressed as:

$$\frac{\langle \Delta c(\boldsymbol{q}, t)\Delta c(\boldsymbol{q}, 0)\rangle}{\langle \Delta c(\boldsymbol{q}, 0)^2\rangle} = \exp(-q^2Dt) \tag{1}$$

$$\Delta c(\boldsymbol{q}, t) = \int_V (c(\boldsymbol{r}, t) - \langle c\rangle)e^{i\boldsymbol{q}\cdot\boldsymbol{r}}d^3\boldsymbol{r}, \tag{2}$$

where $c(\boldsymbol{r}, t)$ is the concentration at the point $\boldsymbol{r}$ at time t in the scattering volume, V, and where the pointed bracket represents an equilibrium ensemble average. Therefore, we can obtain the mutual diffusion coefficient, D, from the relaxation time of the time correlation function, $\tau_c \equiv 1/q^2D$.

Figure 1 shows a typical example of the observed photocurrent-correlation function, $\langle i(t)i(0)\rangle$, which corresponds to the correlation function of the scattered electric field. The observed correlation function was well expressed by a single exponential function. By plotting $1/\tau_c$ against q^2, the theoretical prediction of the linear dependence of $1/\tau_c$ on q^2 was confirmed. The mutual diffusion coefficients thus obtained are plotted against the mole fraction of TBA in Fig. 2.

The mutual diffusion coefficient for a binary solution composed of A and B components, D, is expressed in terms of the velocity correlation function as:[5]

$$D = QL \tag{3}$$

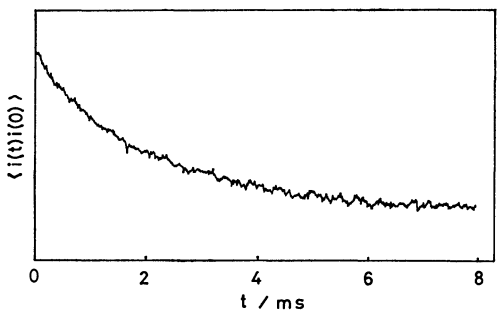

Fig. 1. Typical light scattering photocurrent autocorrelation function observed for TBA–water solution (x_{TBA}=0.13, θ=9.62°).

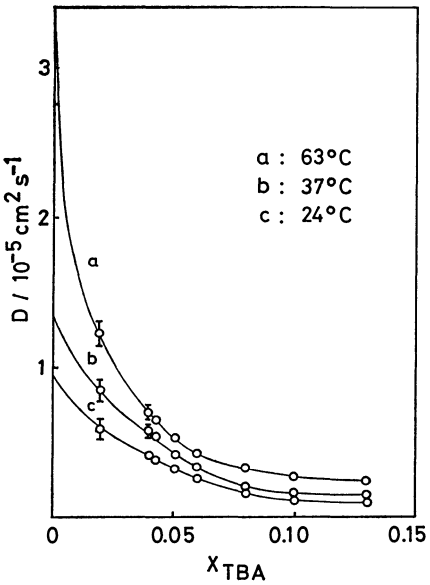

Fig. 2. Concentration dependence of the mutual diffusion coefficient for TBA–water solution at different temperatures.

$$L = L^\circ + (n_A+n_B)x_Ax_B(V_{aa'}+V_{bb'}-2V_{ab}) \quad (a\neq a',\ b\neq b') \tag{4}$$

with

$$Q \equiv x_Ax_B/N\langle(\Delta x_A)^2\rangle \tag{5}$$

$$L^\circ = x_AD_B + x_BD_A \tag{6}$$

$$V_{ij} \equiv \frac{1}{3}\int_0^\infty \langle \boldsymbol{v}_i(t)\boldsymbol{v}_j(0)\rangle dt \quad (i, j=a, a', b, \text{ or } b'), \tag{7}$$

where $\boldsymbol{v}_a(t)$ and $\boldsymbol{v}_b(t)$ are the velocities of an a-th molecule of A and a b-th molecule of B respectively. x_A and x_B are the mole fraction of A and B, and n_A and n_B are the number of A and B molecules respectively. D_A and D_B are the self-diffusion coefficients of the A and B molecules respectively. L is called a kinetic diffusion coefficient. Figure 3 shows the concentration dependence of L for the water(A) and TBA(B) system, where Q is obtained from the observed mean-square concentration fluctuation, $N\langle(\Delta x_A)^2\rangle$, of Fig. 4.[9]

In order to calculate the L° value, the D_A and D_B values must be observed. Figure 5 shows the observed concentration dependences of D_A and D_B which

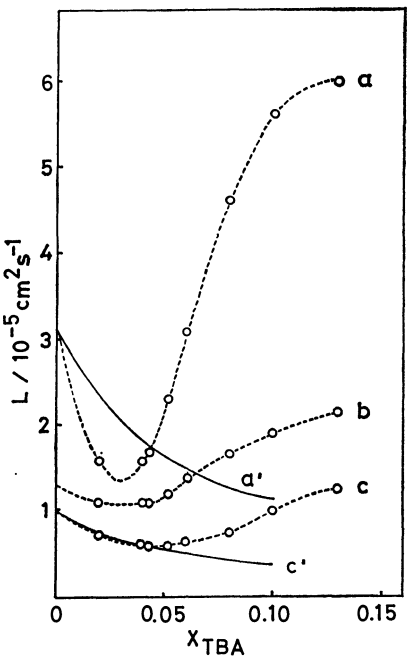

Fig. 3. Concentration dependence of L (curves a, b, and c) and L° (curves a′ and c′); a, a′: 63 °C, b: 37 °C, c, c′: 24 °C (see Eqs. 4—6).

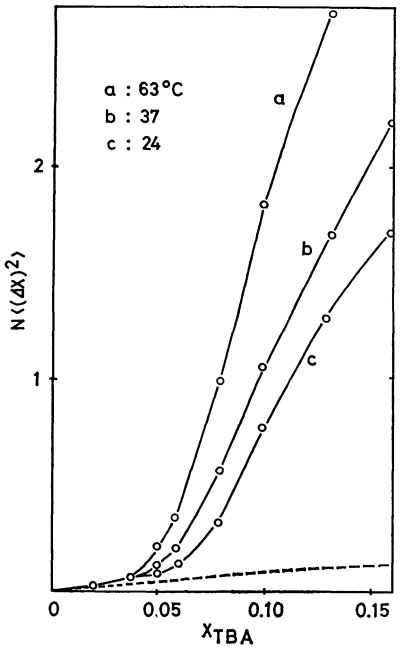

Fig. 4. Concentration dependence of the mean-square concentration fluctuation for TBA–water solution at different temperatures.[2] The dashed line corresponds to the concentration fluctuation expected for an ideal binary solution.

are found in the literature.[10,11] Using these values, we have calculated the D_A and D_B values at 24 and 63 °C according to the following procedure. The temperature dependences of the self-diffusion coefficients, D_s, of pure water (0—55 °C) and TBA for a dilute aqueous solution (4—37 °C) have been reported.[12,13] The plots of $\ln D_s$ against $1/T$ are adequately approximated by straight lines, where T is

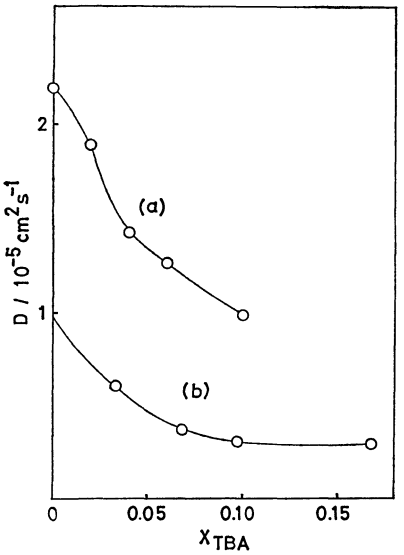

Fig. 5. Concentration dependence of the self-diffusion coefficients of: (a) water at 21 °C, (b) TBA at 25 °C.

the absolute temperature. If we assume that the temperature dependence of the self-diffusion coefficient is independent of the concentration, the D_s values at other temperatures can be estimated from these linear relations.

The concentration dependence of $L°$ thus obtained for 24 and 63 °C are shown in Fig. 3. It may be seen from the figure that $(L\text{-}L°)$ increases with the increase in the temperature in the concentration range of $0.05 < x_{TBA}$. This result indicates that the velocity correlation within the same species is larger for the higher temperature (see Eq. 4).

Analysis of Kinetic Diffusion Coefficient L. In the preceding report,[6] we have obtained the following expression for the kinetic diffusion coefficient, L, for the system composed of the moving units of the A_r, B_s, and gA_lB types:

$$L = M - x_{A_lB} H D_{gA_lB} \tag{8a}$$

and;

$$M = r x_B D_A + s x_A D_B \tag{8b}$$

$$H = l[2g - (x_B/x_A)(gl - r)] - (x_A/x_B)(g - s) \tag{8c}$$

$$x_{A_lB} = (1/2l)\left[x_A + l x_B - \{(x_A + l x_B)^2 - \frac{4Kl}{K+1} x_A x_B\}^{1/2}\right] \tag{8d}$$

$$K = (n_{A_lB}/N')/(n_{A_l}/N')(n_{B_1}/N') \tag{8e}$$

$$N' = n_{A_l} + n_{A_lB} + n_{B_1}, \tag{8f}$$

where D_{gA_lB} is the self-diffusion coefficient of the moving unit, gA_lB. In that preceding report, though, the value of D_{gA_lB} could not be determined uniquely.[6] In the present study, we have determined the parameters included in Eq. 8 in the following way. Table 1 shows the self-diffusion coefficients of pure liquids and the self-diffusion coefficients at an infinite dilution. It may be seen from the table that the ratio of the two diffusion coefficients corresponding to the two different solutes is almost the same for the three solvents. For example, the ratios of the self-diffusion coefficients of acetone and carbon tetrachloride are

Table 1. Self-diffusion coefficients of a few organic substances at an infinite dilution (25 °C)

Solute	Solvent		
	Acetone	Benzene	Carbon tetrachloride
Acetone	4.8* [a]	2.8[b]	1.7[e]
Benzene	4.3[b]	2.2* [a]	1.5[e]
Carbon tetrachloride	3.6[c]	2.0[d]	1.4* [f]

* The self-diffusion coefficient value for the pure liquid.

a) F. A. L. Dullien, *AIChE J.*, **18**, 62 (1972). b) J. Leffler and H. T. Cullinan, *Ind. Eng. Chem. Fundam.*, **9**, 84 (1970). c) P. A. Hardt, D. K. Anderson, R. Ratchbun, B. W. Mar, and A. L. Babb, *J. Phys. Chem.*, **63**, 2059 (1959). d) J. K. Horrocks and E. McLaughlin, *Trans. Faraday Soc.*, **58**, 1357 (1969). e) W. Hayduk and S. C. Cheng, *Chem. Eng. Sci.*, **26**, 635 (1971). f) E. McLaughlin, *Trans. Faraday Soc.*, **55**, 28 (1959); *Quart. Rev.*, **14**, 236 (1960).

almost equal (1.33 in acetone, 1.4 in benzene, and 1.21 in carbon tetrachloride). This fact suggests that the ratio of the self-diffusion coefficients of two different species coexisting in a certain medium is almost constant, even if the physical properties of the medium are changed. Thus, we may assume that the magnitude of D_{gA_lB} is proportional to that of D_{A_r} or D_{B_s}; that is,

$$D_{gA_lB} = D_{B_s}/k_B \tag{9a}$$

or

$$D_{gA_lB} = D_{A_r}/k_A, \tag{9b}$$

where k_A and k_B are constans. On the other hand, the D_A and D_B self-diffusion coefficients have been expressed as:[6]

$$D_A = \frac{(x_A - lx_{A_lB})}{x_A} D_{A_r} + \frac{lx_{A_lB}}{x_A} D_{gA_lB} \tag{10a}$$

$$D_B = \frac{(x_B - x_{A_lB})}{x_B} D_{B_s} + \frac{x_{A_lB}}{x_B} D_{gA_lB}. \tag{10b}$$

By substituting Eqs. 9a and 9b into Eqs. 10b and 10a respectively, we can obtain the expression of D_{gA_lB} in terms of D_A and D_B as:

$$D_{gA_lB} = \frac{x_B}{k_B(x_B - x_{A_lB}) + x_{A_lB}} D_B \tag{11a}$$

or

$$D_{gA_lB} = \frac{x_A}{k_A(x_A - lx_{A_lB}) + lx_{A_lB}} D_A. \tag{11b}$$

By substituting Eq. 11a or 11b into Eq. 8a, we can calculate L by the use of D_A and D_B. In order to obtain the parameters, K, l, r, s, q, and k_A (or k_B), the least-squares method was used.[14] There is no strong reason for having which equation, Eq. 9a or 9b, is more appropriate. However, the better fit between the observed and the theoretical values for the concentration dependences of L could be obtained when we employed Eq. 9a.

Figure 6 shows the concentration dependences of the observed (dots) and the calculated (solid line)

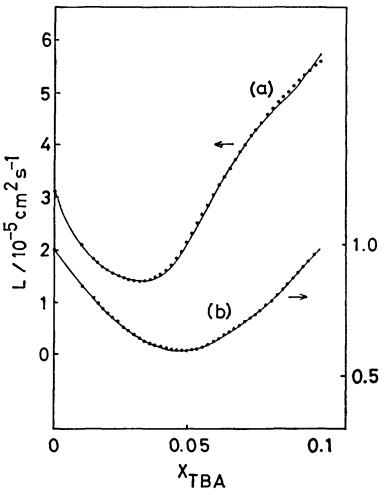

Fig. 6. The observed L values (·····) and the best fit curve (——) calculated from Eqs. 8 and 11a: (a) 63 °C, (b) 24 °C.

L values. For 24 °C, the best-fit parameters are: $K=39.0\pm7.7$, $l=11.1\pm0.3$, $r=6.0\pm0.8$, $s=4.0\pm1.2$, $g=0.9\pm0.03$, and $k_B=2.1\pm1.5$. These results show that the moving units of the $(H_2O)_{11}TBA$, $(H_2O)_6$, and $(TBA)_4$ types coexist in the concentration range of $0<x_{TBA}<0.1$ at 24 °C. For 63 °C, the best-fit parameters are $K=51.0\pm7.1$, $l=20.2\pm0.6$, $r=9.7\pm1.8$, $s=15.6\pm2.3$, $g=0.8\pm0.03$, and $k_B=0.3\pm0.09$. These results indicate the coexistence of the moving units of the $(H_2O)_{20}TBA$, $(H_2O)_{10}$, and $(TBA)_{16}$ types at 63 °C. The value of k_B at 63 °C is much smaller than that at 24 °C. This result seems quite reasonable, because these relations hold;

$$D_{(H_2O)_{11}TBA} \simeq \frac{1}{2} D_{(TBA)_4}$$

and

$$D_{(H_2O)_{20}TBA} \simeq 3D_{(TBA)_{16}}.$$

A self-diffusion coefficient should increase with the decrease in a molecular weight.

Life-time of Local Structure and Mixing State of TBA–Water Solution. In the study of the mean-square concentration fluctuation for the TBA–water system, the existence of local structure of the $g[(H_2O)_lTBA]$, $(H_2O)_r$, and $(TBA)_s$ types has been suggested. In order to compare this result (local structure) with the present result (moving unit), the values of g, l, and s are summarized in Table 2. Hereafter, g, l, r, and s will refer to the parameters related with the local structure, while g^d, l^d, r^d, and s^d will refer to the corresponding parameters related with the moving unit.

In the preceding report,[6] the g^d value was found to be 2—4 at 24 °C when the l^d value was fixed at 20. Based upon this result, we considered that the local structure obtained from the mean-square concentration fluctuation study can also be a moving unit. However, the estimation of the g^d value corresponding to an l^d value other than 20 has not been done. In the present study, the parameter values have been determined uniquely without fixing the

Table 2. The parameter values which characterize the sizes of the local structures and the moving units

Moving unit:

T/°C	l^d	g^d	s^d	r^d
24	11	1	3—5	5—7
63	19—21	1	13—18	8—11

Local structure (data from Ref. 2):

T/°C	l	g[a)]		s	r[b)]
		$x<x^s$	$x^s<x$		
24	15—19	2—3	4—8	4—16	—
63	21—25	2—3	12—22	2—20	—

a) $x^s=0.05$ (mole fraction of TBA). b) The r-value could not be determined uniquely, for the $N\langle(\Delta x)^2\rangle$ value was insensitive to the r-value (see Ref. 2).

l^d value. Therefore, we will be discuss about the moving unit in more detail in comparison with the local structure.

The number ratios of TBA to water molecules which form a moving unit, $g^d[(H_2O)_{l^d}TBA]$, are 1:11 and 1:20 at 24 and 63 °C respectively. It has been known that TBA molecules form a solid clathrate hydrate of the "17 hydrate" structure with water molecules.[3] In this solid clathrate hydrate, the water molecules form polyhedra, each of which encages a guest molecule. As the number ratio of TBA to water molecules in the moving unit is colse to that in the solid clathrate hydrate (1:17), the moving unit is considered to have a polyhedron-like structure.

It can also be seen from Table 2 that the g^d and l^d value are smaller than the g and l values respectively. This difference may be explained as follows. A moving unit is defined as a group of molecules which move together for a time much longer than the velocity-correlation time (10^{-13}—10^{-12} s), while a local structure is defined as an averaged local configuration of molecules, without considering its life-time. If the life-time of the local structure of the $g[(H_2O)_lTBA]$ type is as long as that of the moving unit, the g^d and l^d values should be equal to the g and l values respectively. As g^d and l^d are different from g and l, we can conclude that the life-time of the local structure of the $g[(H_2O)_lTBA]$ type is shorter than that of the moving unit of the $(H_2O)_{l^d}TBA$. In other words, the moving unit is relatively stable. As the g^d value is about 1 in the concentration range of $0<x_{TBA}<0.1$, the local structure determined from the mean-square concentration fluctuation study (*i.e.*, $g[(H_2O)_lTBA]$) can be an aggregate of the moving units of the $(H_2O)_{l^d}TBA$ type. The difference between the local structure and the moving unit has already been pointed out in a previous study of the methanol–carbon tetrachloride system and of the ethanol–carbon tetrachloride system.[5]

Now we can answer the question raised in the introductory paragraph. The above results show that the translational motions of the polyhedra which form a local structure, $g[(H_2O)_lTBA]$, are mutually independent. If an "associated polyhedron" is formed in the solution, the motions of the component polyhedra may be considered to be mutually correlated, because the polyhedra share their faces with each other. Thus, the "aggregated polyhedron" is the more appropriate picture for the mixing state of the TBA–water solution.

The above conclusion is schematically visualized in Fig. 7. In the concentration range of $0<x_{TBA}<0.05$, the water molecules form a polyhedron which encages a TBA molecule and the aggregate of a few polyhedra is dispersed in water. In the concentration range of $0.05<x_{TBA}<0.1$, the aggregate of 4—8 polyhedra is dispersed in TBA. The aggregate of the polyhedra grow larger with the increase in the number of the moving units, $(H_2O)_{l^d}TBA$, formed in the solution.

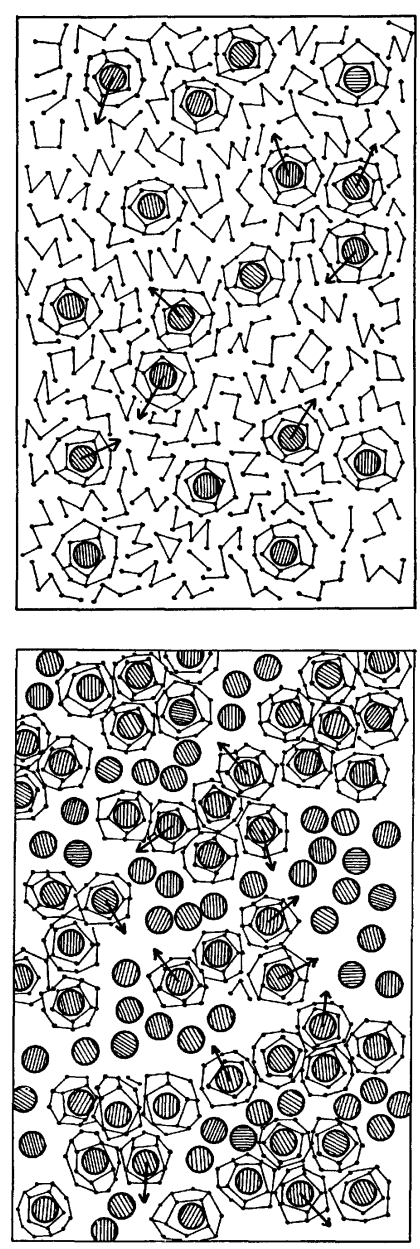

Fig. 7. Mixing state of TBA–water solution for: (a) $x_{TBA}\simeq0.02$, (b) $x_{TBA}\simeq0.09$ (schematic) at 24 °C. (●) and (◍) represent a water and a TBA molecule, respectively.

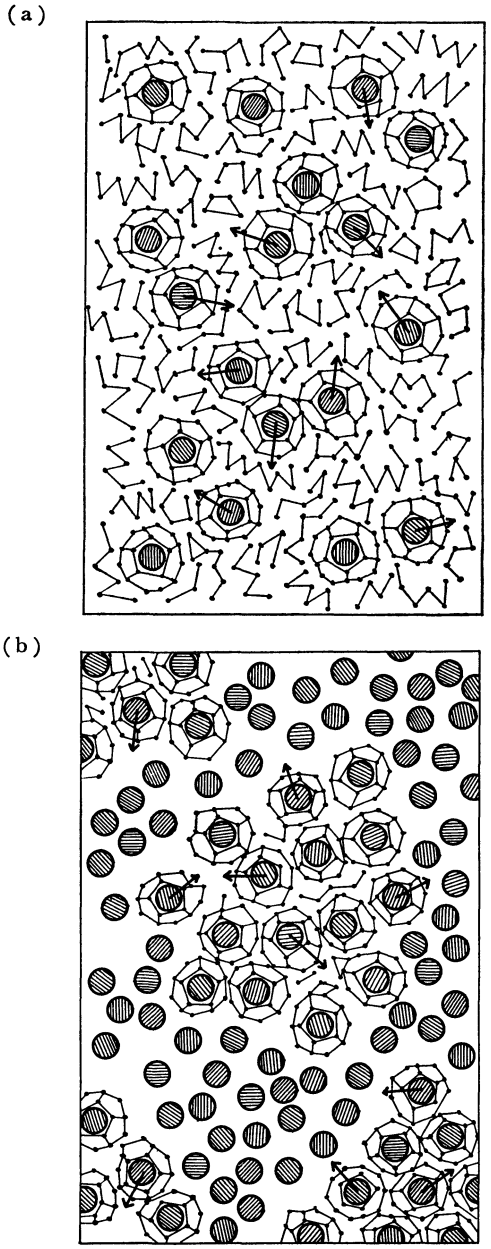

Fig. 8. Mixing state of TBA–water solution for: (a) $x_{TBA} \simeq 0.02$, (b) $x_{TBA} \simeq 0.09$ (schematic) at 63 °C. (●) and (▨) represent a water and a TBA molecule, respectively.

Temperature Effect on Mixing State. Next we will discuss the temperature effect on the mixing state of the TBA–water solution. As can be seen from Table 2, the g and l values increase with the increase of the temperature from 24 °C to 63 °C. The simultaneous increase in g and l brings about rapid increase in the total number of molecules which take part in the formation of the local structure of the $g[(H_2O)_l$-TBA] type. The increase in the l value shows that the number ratio of water to TBA molecules increases with the increase in the temperature. It can also be seen from Table 2 that the l^d value increases with the increase in the temperature, indicating that the polyhedron formed by water molecules becomes larger with an increasing temperature. It is important to emphasize that the g^d value is about 1 at both 24 °C and 63 °C, indicating that the moving unit of the $(H_2O)_{l^d}$TBA type is a relatively stable unit and that these moving units gather together to form a local structure. These situations are visualized in Fig. 8, where the state of mixing at 63 °C is schematically drawn. When we drew Figs. 7 and 8, paying particular attention to the magnitudes of $x_{A_{l^d}B}/x_B$ and $l^d x_{A_{l^d}B}/x_A$, which can be calucluated from Eq. 8d. The former is the number ratio of the moving unit, $(H_2O)_{l^d}$TBA, to all the TBA molecules in the system. The latter is the number ratio of the water molecules which take part in the formation of the moving unit, $(H_2O)_{l^d}$TBA, to all the water molecules in the system. In Figs. 7 and 8, arrows are attached to moving units in order to demonstrate that these units can move independently of one another.

In our previous report,[2] we suggested the existence of a pseudo-critical point for this system. If we compare Fig. 7 with Fig. 8, we can see that the state of mixing at 63 °C ($0.05 < x_{TBA} < 0.1$) is very near to the phase separation into two phases: a water-rich phase and a TBA-rich phase. Moreover, all the water molecules in the water-rich phase may be expected to take part in the formation of polyhedra. Though the phase separation has not been observed at atmospheric pressure for this system, we will probably be able to see this sort of phase separation if we can elevate the temperature of this system under high pressure.

References

1) K. Iwasaki and T. Fujiyama, *J. Phys. Chem.*, **81**, 1908 (1977).
2) K. Iwasaki and T. Fujiyama, *J. Phys. Chem.*, **83**, 463 (1979).
3) D. N. Glew, H. D. Mak, and N. S. Rath, "Hydrogen-Bonded Solvent Systems," ed by A. K. Covington and P. Jones, Taylor and Francis, London (1968); D. W. Davidson, "Water," ed by F. Franks, Plenum Press, New York and London (1973), Vol. 2, Chap. 3.
4) We define the "life time" as the time during which the relative positions of molecules in a local structure change very little.
5) T. Kato, N. Ito, and T. Fujiyama, *Bull. Chem. Soc. Jpn.*, **53**, 2167 (1980).
6) N. Ito, K. Saito, T. Kato, and T. Fujiyama, *Bull. Chem. Soc. Jpn.*, **54**, 991 (1981).
7) N. Ito, T. Kato, and T. Fujiyama, *Bunko Kenkyu*, **29**, 106 (1980).
8) R. D. Mountain and J. M. Deutch, *J. Chem. Phys.*, **50**, 1103 (1969).
9) The presently reported L values at 24 °C are slightly smaller than those reported in Ref. 6 at 25 °C over the entire concentration range. Readers are invited to have more confidence in the present values.
10) F. Franks, J. Ravenhill, P. A. Egelstaff, and D. I. Page, *Proc. R. Soc. London, Ser. A*, **319**, 189 (1970).
11) E. V. Goldammer and M. D. Zeidler, *Ber. Bunsenges. Phys. Chem.*, **73**, 4 (1969).
12) D. A. Johnson and A. L. Babb, *Chem. Rev.*, **56**, 387 (1956).
13) C. M. Gary-bobo and H. W. Weber, *J. Phys. Chem.*, **73**, 1115 (1969).
14) Forty-four data points of L, D_A, and D_B in the concentration range of $0 < x_{TBA} < 0.1$ were used for the least-squares fitting.

  Bull. Chem. Soc. Jpn., 54, 2579—2582 (1981)

Determination of Thermodynamic Properties of Boehmite from its Solubility Data in NaOH Solutions[1)]

Byong-Tae CHANG

Department of Chemistry, Faculty of Science, Korea University, Kodaira, Tokyo 187

(Received February 13, 1981)

Thermodynamic properties of boehmite in alkaline pH range are determined by applying the extended Debye-Hückel theory to its solubility data in NaOH solutions. When $\log(K_s/a_w^2)$, where $K_s=m_H m_{Al}$ and a_w is the activity of the water in NaOH solutions, is plotted against a Debye-Hückel function of ionic strength(I), $I^{1/2}/(1+B_t a_1 I^{1/2})$, at a given temperature, the curve approaches gradually the theoretical Debye-Hückel limiting slope($2A_t$) with decrease in the ionic strength, and at high ionic strength it deviates positively from the straight line. Under the assumption of the same ionic size parameters for OH^- and $Al(OH)_4^-$ ions, the ionic solubility product, $K_s^\circ=a_H a_{Al}/a_w^2$, for boehmite is given by following equations in the temperature range from 80 to 250 °C: $\log K_s^\circ=-2663/T-5.71$ (Case 1) or $\log K_s^\circ=-2764/T-5.45$ (Case 2). From a comparison of the temperature dependences of K_s° for boehmite and gibbsite, a transition temperature between the two alumina hydrates was calculated to be 60±3 °C.

Thermodynamics of Al_2O_3–Na_2O–H_2O system is very important not only for alumina production by the Bayer process, but also for understanding corrosion and passivation of aluminium in water and aqueous geochemistry of aluminous minerals.[2-8)] In the previous paper,[1)] based on the Debye-Hückel theory, a more reasonable method was presented in order to determine thermodynamic properties of alumina hydrates from their solubility data, and was applied to the solubility data of gibbsite, one of alumina trihydrates, in NaOH solutions with success.

The purpose of this paper is to evaluate several thermodynamic properties of boehmite, one of alumina monohydrates, by applying the similar procedure to solubility data of boehmite in NaOH solutions at temperatures up to 300 °C.[2,9)] This problem may be also interesting as a study on the thermodynamics and the Debye-Hückel theory of high temperature aqueous solutions.[10,11)]

Theoretical

One can express a dissolution process of alumina monohydrate and the dissociation of water as follows:

$$AlOOH(s) + 2H_2O(1) = Al(OH)_4^-(1) + H^+(1), \quad (1)$$

$$K_s^\circ = a_{Al}a_H/a_w^2 = K_s\gamma_1^2/a_w^2, \quad (2)$$

$$H_2O(1) = H^+(1) + OH^-(1), \quad (3)$$

$$K_w^\circ = a_H a_{OH}/a_w = K_w\gamma_2^2/a_w, \quad (4)$$

where $K_s=m_{Al}m_H$, $K_w=m_H m_{OH}$, m_i the molality of species i, $\gamma_1^2=\gamma_{Al}\gamma_H$, $\gamma_2^2=\gamma_H\gamma_{OH}$, and a_w the activity of the water in the molar fraction unit. From Eqs. 2 and 4 we can derive a general equation for the alumina monohydrate, introducing a new function, $f(I)$, of ionic strength (I):

$$f(I) = \log(m_{Al}/m_{OH}) + \log(K_w^\circ/a_w)$$
$$= \log K_s^\circ + 2\log(\gamma_2/\gamma_1). \quad (5)$$

It should be noted that, in the case of the monohydrate, $f(I)$ involves a term of a_w, differing from the case of the trihydrate. Evaluation of the a_w values at a given temperature and pressure of sodium aluminate and hydroxide solutions, therefore, become much important together with the solubility data. Russell *et al.* have used the a_w values of corresponding NaOH solutions at 25 °C for the sodium aluminate and hydroxide solutions up to 170 °C without any correction.[2)] Dibrov *et al.* studied in detail the saturated vapor pressure exerted by the sodium aluminate and hydroxide solutions in the wide range of temperatures and concentrations.[12)] In this paper, the a_w values at a given temperature and concentration were calculated by using the vapor pressure data by Dibrov and virial coefficients, B′ and C′ of H_2O(g) by Kell,[13)] that is,

$$a_w = f_1/f_o = \gamma_1^v P_1/\gamma_o^v P_o, \quad (6)$$

$$RT\ln(f_1/P_1) = RT\ln\gamma_1^v = B'P_1 + C'P_1^2, \quad (7)$$

where f_1 and γ_1^v are the fugacity and activity coefficient of H_2O(g), respectively, and a subscript "o" means the pure water.

Figure 1 gives the relationships between $f(I)$ and I obtained from Eq. 5, using the solubility data of boehmite reported by Russell (80—170 °C)[2)] and Bernshtein (250 and 300 °C),[9)] and the a_w values calculated by Eqs. 6 and 7. The K_w° values were quoted from Refs. 14 and 15.

On the other hand, using the following extended

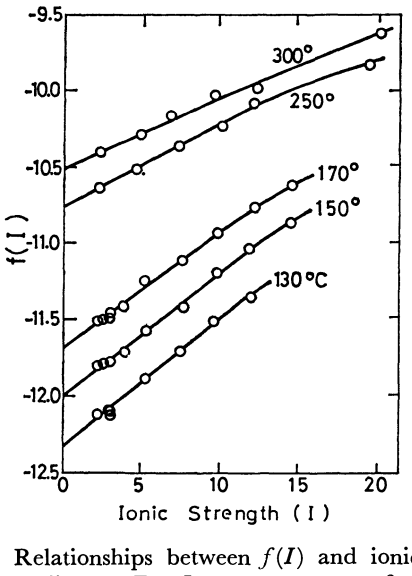

Fig. 1. Relationships between $f(I)$ and ionic strength (I) according to Eq. 5 at temperatures from 130 to 300 °C.

Debye-Hückel equation,

$$\log \gamma_i = -A_t I^{1/2}/(1+B_t a_i I^{1/2}) - c_i I - d_i I^2, \quad (8)$$

the function, $f(I)$, can be expressed by

$$f(I) = \log K_s^\circ + 2A_t I^{1/2}[1/(1+B_t a_1 I^{1/2}) - 1/(1+B_t a_2 I^{1/2})] + CI + DI^2, \quad (9)$$

where A_t is the theoretical Debye-Hückel limiting slope, and B_t, a_1, c_1, d_1, $C=2(c_1-c_2)$ and $D=2(d_1-d_2)$ are adjustable parameters. The problem is to decide the five parameters in Eq. 9 to get the best fit for the data given in Fig. 1.

Results and Discussion

The Case of the Same Ionic Size Parameters. Setting up the same ionic size parameters, that is, $a_1=a_2$, as did May[8] and Smith,[16] Eq. 9 can be simplified into a following equation;

$$f(I) = \log K_s^\circ + CI + DI^2. \quad (10)$$

Table 1 gives the values of $\log K_s^\circ$, C, and D obtained by the least squares method for Eq. 10 in the whole range of ionic strengths (Case 1). Moreover, as being obvious from Fig. 1, there are good linear relationships between $f(I)$ and the ionic strength in the range of low ionic strengths below *ca.* 10, *i.e.*,

$$f(I) = \log K_s^\circ + CI. \quad (11)$$

Table 1 also gives the values of $\log K_s^\circ$ and C for Eq. 11 (Case 2).

Figures 2 and 3 show variations of $\log K_s^\circ$ with the temperature in the case of 1 and 2, respectively. We can observe linear relationships between $\log K_s^\circ$ and $1/T$ in the range of temperature from 80 to 250 °C, which are given by following equations:

$$\log K_s^\circ = -2663/T - 5.71 \text{ (Case 1)}, \quad (12)$$

$$\log K_s^\circ = -2764/T - 5.45 \text{ (Case 2)}. \quad (13)$$

According to Eq. 12 or 13, the value of $\log K_s^\circ$ at 25 °C becomes −14.65 or −14.73, being a little larger than that for gibbsite, −15.18.[1] From the values of $\log K_s^\circ$ at 25 °C for gibbsite and boehmite, the standard Gibbs free energy of following reactions can be calculated as follows:

$$Al(OH)_3 + H_2O = Al(OH)_4^- + H^+, \quad \Delta G_{298}^\circ = 86.61 \text{ kJ}, \quad (14)$$

$$AlOOH + 2H_2O = Al(OH)_4^- + H^+, \quad \Delta G_{298}^\circ = 83.82 \pm 0.23 \text{ kJ}. \quad (15)$$

From the above two equations,

$$Al(OH)_3 = AlOOH + H_2O, \quad \Delta G_{298}^\circ = 2.79 \pm 0.23 \text{ kJ}. \quad (16)$$

This means that gibbsite is more thermodynamically

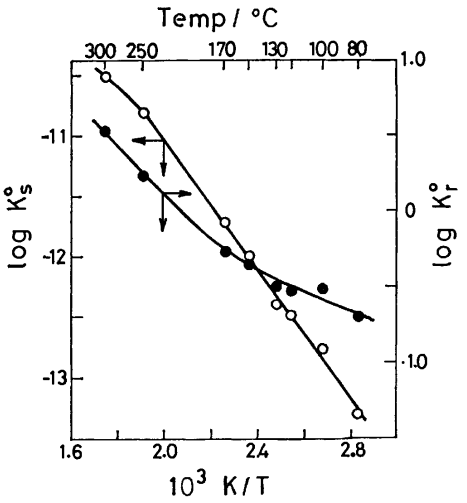

Fig. 2. Temperature dependences of $\log K_s^\circ$ and $\log K_r^\circ$ from 80 to 300 °C for the Case 1.

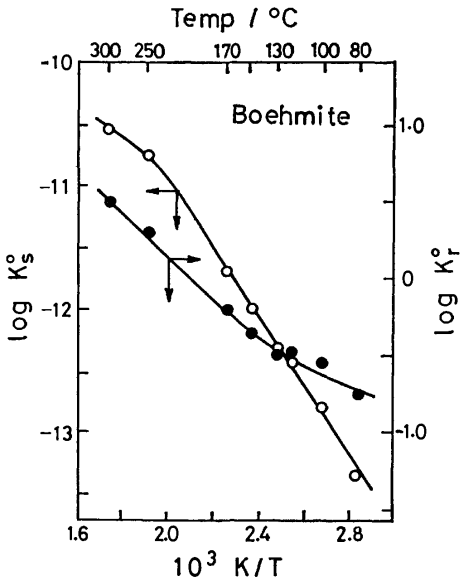

Fig. 3. Temperature dependences of $\log K_s^\circ$ and $\log K_r^\circ$ from 80 to 300 °C for the Case 2.

Table 1. Temperature dependences of K_s°, K_r°, C, and D

No.	Temp °C	Case 1				Case 2		
		$\log K_s^\circ$	$C\times10^2$	$D\times10^3$	$\log K_r^\circ$	$\log K_s^\circ$	$C\times10^2$	$\log K_r^\circ$
1	80	−13.30	1.32	5.61	−0.71	−13.35	4.78	−0.76
2	100	−12.76	1.43	3.24	−0.52	−12.79	3.35	−0.54
3	120	−12.49	8.34	−5.35	−0.53	−12.44	4.99	−0.48
4	130	−12.34	8.41	−0.05	−0.50	−12.34	8.47	−0.50
5	150	−11.99	7.81	0.00	−0.36	−11.99	7.82	−0.36
6	170	−11.73	9.23	−1.19	−0.27	−11.68	7.27	−0.22
7	250	−10.80	6.50	−0.81	0.24	−10.75	4.95	0.30
8	300	−10.51	4.53	−0.12	0.53	−10.53	4.98	0.51

stable than boehmite at 25 °C and 1 atm. From a comparison of the temperature dependences of K_s° for gibbsite and boehmite, a transition temperature between the two alumina hydrates was found to be 60±3 °C. Based on the ΔG_f° value of −915.0 kJ/mol selected as a standard Gibbs free energy of formation for boehmite by Parks,[5] ΔG_f° value for $Al(OH)_4^-$ ion was obtained to be −1305.6 kJ/mol, which agrees well with the value of −1302.5 kJ/mol obtained in the case of gibbsite. A heat of Reaction 1 is equal to be 51.9±0.8 kJ between 80 and 250 °C, using Eqs. 12 and 13.

For a reaction of boehmite with OH^- ion,

$$AlOOH(s) + OH^-(1) + H_2O(1) = Al(OH)_4^-(1) \quad (17$$

$$K_r^\circ = a_{Al}/a_{OH}a_w \quad (18)$$

using Eqs. 2 and 4, K_r° is given by

$$K_r^\circ = K_s^\circ/K_w^\circ. \quad (19)$$

Table 1, and Figs. 2 and 3 also show the values of $\log K_r^\circ$ at various temperatures. They can be expressed approximately as a function of the temperature as follows;

$$\log K_r^\circ = 2217/T + 17.32 \log T - 51.10 \quad \text{(Case 1)}, \quad (20)$$

$$\log K_r^\circ = 1066/T + 11.58 \log T - 33.24 \quad \text{(Case 2)}. \quad (21)$$

It should be noted that the values of C, which usually reflect interactions between ions and solvent, have the magnitude of nearly 0.05 commonly for boehmite and gibbsite[1] in a wide temperature range.

The Case of Different Ionic Size Parameters. In order to evaluate an effect of difference in the ionic size parameters, a_1 and a_2, on magnitudes of K_s°, we assumed conveniently $c_2=0$ and $d_2=0$ for the dissociation of water as well as did in the previous paper.[1] Then, from Eqs. 4 and 8,

$$\log (K_w/a_w) = \log K_w^\circ + 2A_tI^{1/2}/(1+B_ta_2I^{1/2}) \quad (22)$$

using $K_s=m_Hm_{Al}=K_w(m_{Al}/m_{OH})$ and Eq. 22,

$$\log (K_s/a_w^2) = \log (K_w^\circ/a_w) + \log (m_{Al}/m_{OH}) + 2A_tI^{1/2}/(1+B_ta_2I^{1/2}). \quad (23)$$

At a given temperature, K_w°, A_t, and B_t are constant, and so the values of $\log (K_s/a_w^2)$ depend upon (m_{Al}/m_{OH}), a_w, a_2, and I. Figure 4 gives plots of $\log(K_s/a_w^2)$ and $I^{1/2}/(1+1.59I^{1/2})$ at 150 °C with a_1=4.5 Å and various values of a_2 from 3.5 to 6.0 Å. It is obvious from Fig. 4 that the values of $\log (K_s/a_w^2)$ and $\log K_s^\circ$ increase with decrease in the a_2 value.

On the other hand, from Eqs. 2 and 8,

$$\log (K_s/a_w^2) = \log K_s^\circ + 2A_tI^{1/2}/(1+B_ta_1I^{1/2}) + 2c_1I + 2d_1I^2. \quad (24)$$

Figure 4 also shows that the curves approach gradually the theoretical slope, $2A_t=1.38$, as the ionic strength decreases, and deviate positively from the straight line in the range of high ionic strength owing to the last two terms in Eq. 24. The similar tendency was observed at different temperatures up to 300 °C, for example, as shown in Fig. 5. Furthermore, such behaviors are consistent with those of gibbsite in NaOH solutions. Therefore, plots of $\log (K_s/a_w^2)$ *vs.* $I^{1/2}/(1+B_ta_1I^{1/2})$ consist of the straight line in low I range and the positive deviation in high I range, and the latter may be attributed to the formation of complex ion(s) such as $Al_2O(OH)_6^{2-}$ and/or the dehydration of $Al(OH)_4^-$ to $AlO(OH)_2^-$ and AlO_2^- ions.[12] It should be noted that the sodium aluminate and hydroxide solutions show the same behavior according to the extended Debye-Hückel expression in the wide range of temperatures from 40 to 300 °C for the both solid phases of gibbsite and boehmite.

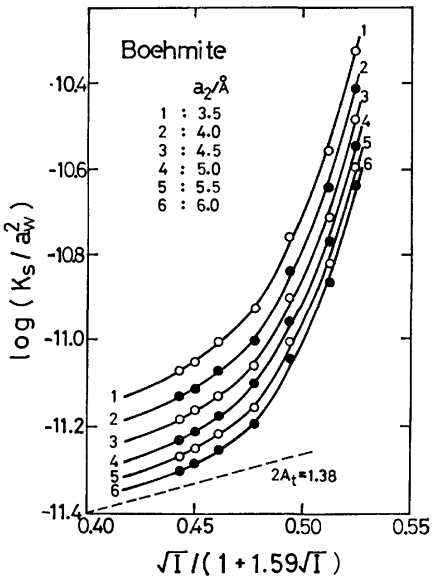

Fig. 4. Plots of $\log(K_s/a_w^2)$ *vs.* $I^{1/2}/(1+1.59I^{1/2})$ at various values of a_2 in the case of a_1=4.5 Å and 150 °C.

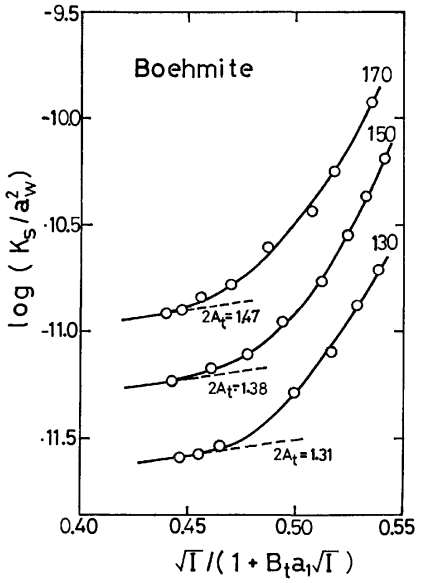

Fig. 5. Plots of $\log(K_s/a_w^2)$ *vs.* $I^{1/2}/(1+B_ta_1I^{1/2})$ at temperatures of 130, 150, and 170 °C in the case of a_1= 4.5 Å and a_2=5.0 Å. A value of B_ta_1 is equal to 1.57, 1.59, and 1.61 at 130, 150, and 170 °C, respectively.

References

1) Thermodynamics of Al_2O_3–Na_2O–H_2O System. Part 3. Part 2: B.-T. Chang, *Bull. Chem. Soc. Jpn.*, **54**, 1960

(1981).
2) A. S. Russell, J. D. Edwards, and C. S. Taylor, *J. Metals*, **7**, 1123 (1955).
3) D. D. MacDonald and P. Butler, *Corros. Sci.*, **13**, 259 (1973).
4) J. A. Kittrick, *Soil Sci. Soc. Am. J.*, **30**, 595 (1966); **44**, 139 (1980).
5) G. A. Parks, *Am. Mineral.*, **57**, 1163 (1972).
6) B. S. Hemingway and R. A. Robie, *Geochim. Cosmochim. Acta*, **41**, 1402 (1977).
7) B. S. Hemingway, R. A. Robie, and J. A. Kittrick, *Geochim. Cosmochim. Acta*, **42**, 1533 (1978).
8) H. M. May, P. A. Helmke, and M. L. Jackson, *Geochim. Cosmochim. Acta*, **43**, 861 (1979).
9) V. A. Bernshtein and E. A. Machenok, *Zhur. Prikl. Khim.*, **34**, 982 (1961).
10) J. W. Cobble, *Science*, **152**, 1479 (1966).
11) T. Okabe, A. Okuwaki, and M.-C. Shieh, *Denki Kagaku*, **39**, 258, 340 (1971).
12) I. A. Dibrov, G. Z. Mal'tsev, and V. P. Mashovets, *Zhur. Prikl. Khim.*, **37**, 1920 (1964).
13) G. S. Kell, G. E. McLaurin, and E. Whalley, *J. Chem. Phys.*, **48**, 3805 (1968).
14) H. S. Harned and B. B. Owen, "The Physical Chemistry of Electrolytic Solutions," 3rd ed, Reinhold, New York (1958), p. 645.
15) J. R. Fisher and H. L. Barnes, *J. Phys. Chem.*, **76**, 90 (1972).
16) R. M. Smith and J. D. Hem, *U. S. Geol. Surv. Water Supply Paper* 1827-D (1972).
17) R. J. Moolaar, J. C. Evans, and C. D. McKeever, *J. Phys. Chem.*, **74**, 3629 (1970).

  Bull. Chem. Soc. Jpn., 54, 2583—2586 (1981)

Pressure and Temperature Dependence of NMR Spin-lattice Relaxation in Plastic 2,2-Dimethylpropanoic Acid

Tooru HASEBE,*,† (the late) Gen SODA, and Hideaki CHIHARA

Department of Chemistry, Faculty of Science, Osaka University, Toyonaka 560

(Received February 23, 1981)

Proton spin-lattice relaxation time T_1 of 2,2-dimethylpropanoic acid in its plastic phase was measured at 10 MHz up to 120 MPa between 268 K and 330 K. A minimum in T_1 appears in the low-pressure region which is due to overall reorientation of molecules. The T_1 minimum value decreases as the pressure increases in a way different from simple-minded prediction. The activation volume, 25 ± 3 cm^3 mol^{-1}, is twice as large as in other plastic crystals when normalized by the molar volume. The pressure dependence of the activation enthalpy is also about twice as large. These can be rationalized by considering associated dimers as the reorienting unit. The phase diagram is given and the volume changes associated with the transition and with the fusion were derived (15.6 and 5.86 cm^3/mol of dimer).

2,2-Dimethylpropanoic acid $(CH_3)_3CCOOH$ has been investigated by various techniques[1—16] because it is a unique plastic crystal having a very small entropy of fusion 6.5 J K^{-1} mol^{-1} (309.7 K) in spite of the molecular polarity.

The NMR studies established the nature of the spin-lattice relaxation in solid as well as in liquid state. Thus, in the low-temperature brittle phase both methyl and t-butyl reorientations are responsible for the T_1 minimum, in the high-temperature plastic phase the overall molecular tumbling governs T_1, and in the liquid phase the self-diffusion is the dominant relaxation mechanism.

Since our previous analysis[7] of T_1 results in the plastic phase was not correct, we decided to carry out additional experiments, particularly about the effect of external pressure on T_1 in the plastic phase. The present paper reports such experimental results and proposes that the dynamical unit for molecular tumbling is probably an associated dimer.

Experimental

Material and T_1 Measurements. 2,2-Dimethylpropanoic acid (reagent grade) from Tokyo Kasei Kogyo Co., Ltd. was subjected to dehydration using Molecular Sieve 4A, vacuum distillation, and degassing by repeated freeze-pump-thaw cycles and then transferred into the pressure vessel *via* a specially designed adapter which will be described.

Proton spin-lattice relaxation time was measured using π-τ-$\pi/2$ pulse sequences with an operating frequency of 10.0 MHz. The working pressure and temperature ranges over which T_1 was measured were between the saturated vapor pressure of the sample and 120 MPa and between 268 K and 330 K, respectively.

Pressure Vessel and Its Operation. Figure 1 is a schematic drawing of the high-pressure NMR vessel (hereafter referred to as the vessel). The vessel was machined from non-magnetic beryllium-copper alloy (Cu 97.57%, Be 1.86%, Co 0.27%, Fe 0.16%, and Ni 0.01%) and was annealed at 570 K for three hours after machining. The ratio of the outside to the inside diameter was nowhere less than 1.9. Hermetic closure of electrical leads was made by using phosphor bronze of cone shape (Fig. 1B) insulated from the body of the vessel with Epoxy putty XD 580 (Japan Ciba-Geigy Co.). At other places (j, k, and l for the lead-wire housing and e and f for the piston), three washers of Teflon, Be–Cu alloy, and lead metal were used in turn from inside to outside to secure pressure-tightness.

The working pressure gauge was a length of manganin wire (B. S. #38) wound round a Teflon bobbin (q) and annealed at 390 K for 17 h *in vacuo*. The gauge was calibrated against the standard Heise gauge up to 200 MPa at the High Pressure Laboratory, Faculty of Engineering Science, Osaka University after several cycles of pressurizing and releasing. The gauge reading was reversible above 100 MPa but showed a small hysteresis effect at lower pressures. The temperature dependence of the electrical resistance was also measured at 0.1 MPa; at other pressures

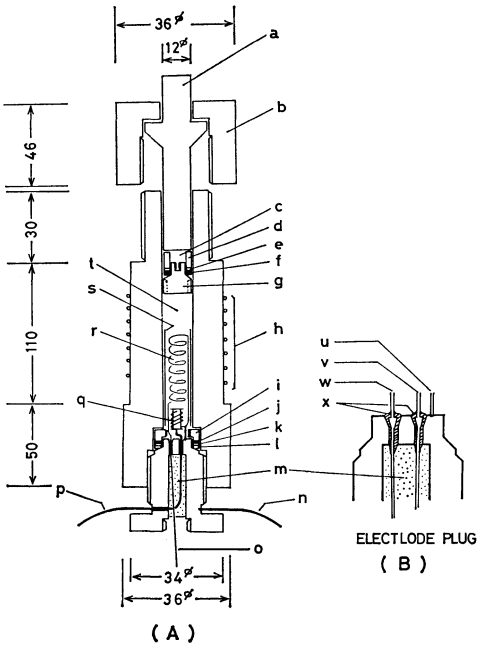

Fig. 1. Pressure vessel.
a: Be–Cu piston plunger, b: Be–Cu clamp, c: unsupported area, d: Be–Cu supporter, e: Be–Cu washer, f: Teflon washer, g: Be–Cu piston, h: heater, i: Be–Cu extractor ring, j: Teflon washer, k: Be–Cu washer, l: Pb washer, m: epoxy resin, n: lead-wire, o: Cu rf lead-wire, p: Cu lead-wire for manganin gauge, q: manganin gauge, r: rf coil, s: Teflon seal, t: sample space, u: electric ground terminal, v: rf lead-wire, w: lead-wire for manganin gauge, x: epoxy putty, All dimensions are given in millimeters.

† Present address: Department of Chemistry, Faculty of Education, Fukushima University, Matsukawa-machi, Fukushima 960-12.

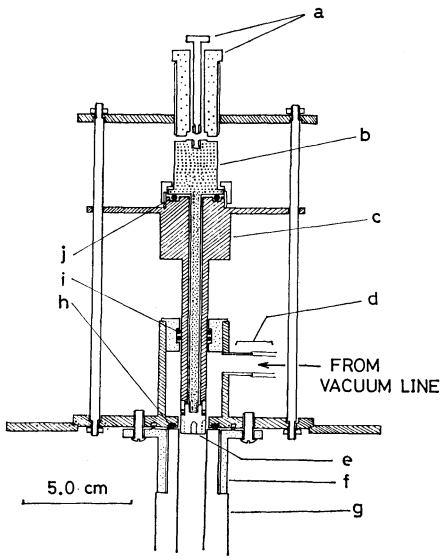

Fig. 2. Pressure vessel and adapter.
a: Brass stopper, b and c: co-axial stainless steel supporter for piston, d: Kovar seal, e: piston, f: brass connector; g: pressure vessel, h—j: fluoro-rubber O-ring.

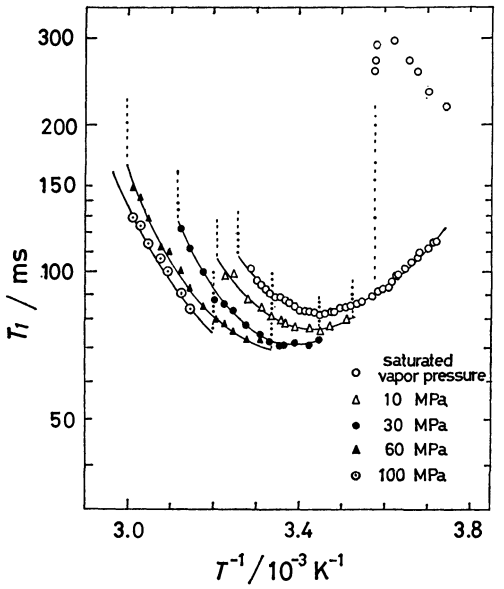

Fig. 3. Temperature dependence of T_1 at various pressures.

we used the pressure coefficient values reported by Wang.[17] The overall uncertainty of the pressure values in the present study was estimated as ± 1.4 MPa.

The temperature of the specimen was controlled by non-inductive winding of KARMA heater (h) (B. S. #36, Driver Harris Co.) and cold nitrogen stream evaporated from the bottom of the Dewar flask in which the vessel was placed. The electrical current through the heater was controlled automatically with a Chromel-P/Constantan thermocouple attached to the outer surface of the vessel as the temperature sensor.

Figure 2 shows the connecting device for distilling the specimen from outside into the vessel. The plunger and the screwed cap (a and b of Fig. 1A) were removed from the top of the vessel and then the body was attached to the connecting device from below (g of Fig. 2). The plug was pulled up with movable supporters b and c to connect the inside of the vessel to the outside vacuum/purification line. The system was made vacuum-tight with a number of fluoride rubber O rings as shown in Fig. 2. When distillation of the specimen is over, the piston (e) was dropped into the vessel using the rods a, b, and c, the vessel was taken off the connecting device, and piston/plunger was pressed and clamped. Because the plastic phase of 2,2-dimethylpropanoic acid is extremely soft for a crystal, we may safely assume that the pressure applied is hydrostatic.

Results and Discussion

Spin-lattice Relaxation Time. The results of experimental determination of T_1 under various pressures are given in Fig. 3. The upper and lower bounds of the existence of the plastic phase of 2,2-dimethylpropanoic acid are indicated by vertical broken lines. The curves in Fig. 3 do not correspond to the results of a continuous run under a given pressure, except the one at the saturated vapor pressure of the specimen, because the pressure inside the vessel changed when the specimen temperature changed. Therefore, the primary results were rearranged to show, in Fig. 3, the temperature dependence of T_1 under a constant pressure. It is seen that the plastic phase is readily undercooled down to about 269 K ($1/T = 3.72 \times 10^{-3}$ K^{-1}), some 10 K below the transition point, giving smooth extrapolation of the T_1 curve under the ordinary pressure.

There is a distinct minimum of T_1 in the plastic phase which has been substantiated as caused by reorientational motion of molecules.[6,7,13] The relaxation rate T_1^{-1} can be expressed in terms of the correlation time τ and the part of second moment M_2 modulated by such molecular motion;[18]

$$T_1^{-1} = C[\{\omega\tau/(1+\omega^2\tau^2)\} + \{4\omega\tau/(1+4\omega^2\tau^2)\}], \quad (1)$$

where

$$C = (2/3)\gamma^2\{M_2(\text{intra}) + M_2(\text{inter})\}, \quad (2)$$

and γ is the gyromagnetic ratio of the proton. The T_1 minimum tends to move to higher temperatures as the pressure is increased although more slowly than the movement of the phase boundaries. Also the minimum value of T_1 decreases as the pressure is increased. This indicates that M_2, particularly M_2-(inter), increases its magnitude upon compression. In the case of fast isotropic reorientation of molecules, M_2(inter), for the fcc lattice is given by

$$M_2(\text{inter}) = 4.14 \times 10^{-2} N_0 a^{-6}, \quad (3)$$

where N_0 is the number of protons per molecule and a is the lattice constant in the units of nanometer. Since M_2(inter) depends on the inverse sixth power of intermolecular proton-proton distances, we would expect that T_1^{-1}(max) changes linearly with the inverse square of the crystal volume. Thus, T_1^{-1}(max) is plotted against $(V_0/V)^2$ in Fig. 4, where V_0 is the crystal volume at the saturated vapor pressure. The volume at other pressures were determined from the distance of travel of the piston plunger into the pressure vessel by compression. The compression was ap-

TABLE 1. THE ENTHALPY OF ACTIVATION ΔH^*, τ_0, T_1(min), AND ITS TEMPERATURE AT DIFFERENT PRESSURES

P/MPa	ΔH^*/kJ mol^{-1}	$\tau_0/10^{-14}$ s	T_1(min)/ms	T/K at T_1(min)
Saturated vapor pressure	32.8±2.0	1.1 ±1.0	82.0±1.0	289.4
10	33.0±2.7	1.2 ±1.0	77.1±1.9	290.7
20	33.4±1.2	1.1 ±1.0	73.0±2.2	292.0
30	35.7±1.3	0.48±0.30	71.6±1.4	294.6
40	37.8±3.0	0.22±0.15	69.8±1.8	296.3
50	38.7±1.7	0.17±0.08	69.1±2.4	297.6

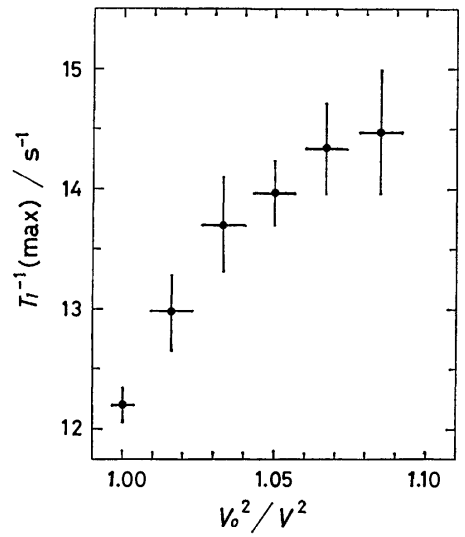

Fig. 4. T_1^{-1}(max) against the square of reduced crystal volume, V_0/V.

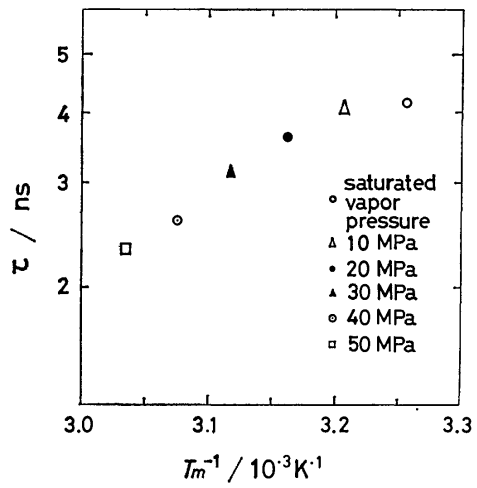

Fig. 5. The correlation time of the overall molecular reorientation at the melting points under different pressures.

parently linear in the pressure increase within the experimental error and it was approximately described by a constant isothermal compressibility $(8\pm2)\times 10^{-4}$ MPa^{-1}. It is seen that T_1^{-1}(max) is not linear in $(V_0/V)^2$ contrary to expectation. The reason is not apparent at present although it is possible that the pressure range studied was not wide enough to cause such a significant volume change that a very meaningful analysis could be made.

The T_1 curves in Fig. 3 were fitted to Eq. 1 assuming the Arrhenius type of activation process

$$\tau = \tau_0 \exp(\Delta G^*/RT), \quad (4)$$

where ΔG^*, the Gibbs energy of activation, is defined by

$$\Delta G^* = \Delta H^* - T\Delta S^*. \quad (5)$$

Since the volume of activation ΔV^* is given by

$$\Delta V^* = (\partial \Delta G^*/\partial P)_T, \quad (6)$$

values of τ derived from the curve fitting may be used to obtain ΔV^* and ΔH^* through the relations,

$$\Delta V^* = RT(\partial \ln \tau/\partial P)_T, \quad (7)$$

and

$$\Delta H^* = R\{\partial \ln \tau/\partial(1/T)\}_P. \quad (8)$$

The value of ΔV^* thus derived was 25 ± 3 cm^3 mol^{-1} between 290 K and 305 K. The magnitude of uncertainty attached to this derived quantity did not permit determination of its dependence on temperature.

The ratio of the volume of activation to the molar volume, $\Delta V^*/V_m$, is 0.24±0.03, considerably larger than for other plastic crystals. Thus, in the case of 2-methyl-2-nitropropane, it is 0.07.[19] In fact, values between 0.04 and 0.08 are more common for this quantity if ΔV^* corresponds to activation of molecular reorientation. Now, if one considers that the plastic phase of 2,2-dimethylpropanoic acid consists of dimeric units in which the two acid molecules are associated with a pair of hydrogen bonds, the ratio $\Delta V^*/V_m$ to be compared would be 0.12 rather than 0.24. However, this value is larger yet than the values for overall molecular reorientation in other plastic organic materials; *e.g.* in cases[20,21] of norbornane, cyclohexane, and 2,2,3,3-tetramethylbutane, they are 0.04, 0.07, and 0.07—0.09, respectively.

The activation enthalpy, ΔH^*, and the value of τ_0 for the overall molecular reorientation under some typical pressure conditions are listed in Table 1. The value of ΔH^* is also much larger than other typical plastic crystals; even a molecule as large as adamantane has a value of only 15 kJ mol^{-1}.[22] The ΔH^* exhibits a pressure dependence with the best slope 0.13 kJ MPa^{-1} mol^{-1} between the saturated vapor pressure of the sample and 50MPa. The slope is also very much larger than the case of adamantane (0.0069 kJ MPa^{-1} mol^{-1}).

Figure 5 shows the correlation time, τ, of the overall molecular reorientation at the melting points under different pressures. In contrast to the behavior of the correlation time for self-diffusion, which assumes

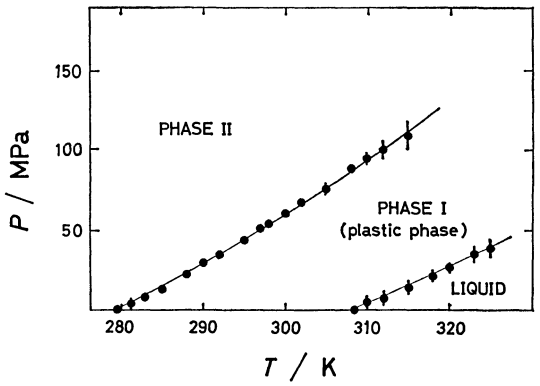

Fig. 6. Phase diagram of 2,2-dimethylpropanoic acid.

an almost constant value at melting points, the correlation time for reorientation decreases as the melting occurs at higher temperatures. This suggests the reorientational motion is not the direct trigger of the fusion phenomenon.

To summarize this subsection, the characteristic quantities, *i.e.* the volume and the enthalpy, of activation for overall molecular reorientation are about twice as large as those for other typical plastic crystals. However, these magnitude can be rationalized if one takes a dimer as the dynamical unit of motion. The molecule would then be not very spherical in shape, which fact explains why T_1 minima can be observed in the temperature region in which the plastic phase exists. This fact also corresponds to much longer correlation time in the plastic solid at its melting points.

Phase Diagram. Figure 6 is the phase diagram obtained by determining the temperature of phase changes from the jumps of the T_1 values. The average slopes of the boundary curves are

$$dP/dT = 3.26 \text{ MPa K}^{-1} \text{ (transition)}$$
$$= 2.22 \text{ MPa K}^{-1} \text{ (fusion)}$$

and show that the two curves become separated further as the pressure increases. The volume changes at these transition points were calculated by use of Clapeyron-Clausius equation from the entropy changes, 25.5 and 6.5 J K^{-1} mol^{-1} at the transition and the melting point, respectively. These were 7.82 and 2.93 cm^3 mol^{-1}, respectively, or 15.6 and 5.86 cm^3/mol of dimer.

It is interesting to note that application of external pressure displaces the region of the existence of the plastic crystal to a higher temperature whereas the T_1 minimum moves more slowly with the result of a shorter correlation time at a higher pressure. This means that although the compression should slow down molecular reorientation, additional thermal energy more than compensates the effect.

The authors would like to express their gratitude to late Professor Naoto Kawai and Dr. Akifumi Onodera for help in developing the high pressure apparatus used in the present study.

References

1) Y. Namba and T. Oda, *Bull. Chem. Soc. Jpn.*, **25**, 225 (1952).
2) S. Kondo and T. Oda, *Bull. Chem. Soc. Jpn.*, **27**, 567 (1954).
3) H. Suga and S. Seki, *J. Phys. Chem. Solids*, **24**, 330 (1963).
4) H. M. Hawthorne and J. N. Sherwood, *Trans. Faraday Soc.*, **66**, 1783 (1970).
5) P. Bladon, N. C. Lockhart, and J. N. Sherwood, *Mol. Phys.*, **20**, 577 (1971).
6) R. L. Jackson and J. H. Strange, *Mol. Phys.*, **22**, 313 (1971).
7) G. Soda and H. Chihara, *Chem. Lett.*, **1972**, 201.
8) G. M. Hood, N. C. Lockhart, and J. N. Sherwood, *J. Chem. Soc., Faraday Trans. 1*, **68**, 736 (1972).
9) M. J. Bird, D. A. Jackson, and J. G. Powles, *Mol. Phys.*, **25**, 1051 (1973).
10) D. Beysens, R. Vacher, G. M. Searby, L. Boyer, and M. Adam, *Rev. Phys. Appl.*, **9**, 465 (1974).
11) P. McKay and J. N. Sherwood, *J. Chem. Soc., Faraday Trans. 1*, **71**, 2331 (1975).
12) L. Kimtys, *Org. Magn. Reson.*, **7**, 179 (1975).
13) S. Albert, H. S. Gutowsky, and J. A. Ripmeester, *J. Chem. Phys.*, **64**, 3277 (1976).
14) L. L. Kimtys, D. W. Aksnes, and T. Gramstad, *Mol. Phys.*, **38**, 993 (1979).
15) M. Brissaud and A. Riviere, *Mol. Cryst. Liq. Cryst.*, **50**, 269 (1979).
16) T. Hasebe, N. Nakamura, and H. Chihara, *Bull. Chem. Soc. Jpn.*, **53**, 896 (1980).
17) C. Wang, *Rev. Sci. Instrum.*, **38**, 24 (1967).
18) N. Bloembergen, E. M. Purcell, and R. V. Pound, *Phys. Rev.*, **73**, 679 (1948).
19) T. Hasebe, (late) G. Soda, and H. Chihara, unpublished.
20) R. Folland, S. M. Ross, and J. H. Strange, *Mol. Phys.*, **26**, 27 (1973).
21) S. M. Ross and J. H. Strange, *J. Chem. Phys.*, **68**, 3078 (1978).
22) N. I. Liu and J. Jonas, *Chem. Phys. Lett.*, **14**, 555 (1972).

  Bull. Chem. Soc. Jpn., 54, 2587—2591 (1981)

Mechanochemical Change in the Solid State and the Solubility of Amobarbital

Akiko IKEKAWA* and Sohachiro HAYAKAWA**

Faculty of Pharmaceutical Sciences, Showa University, Hatanodai, Shinagawa-ku, Tokyo 142

***Department of Applied Physics, Faculty of Science, Tokyo Institute of Technology, Oh-okayama, Meguro-ku, Tokyo 152*

(Received February 23, 1981)

Influence of ball-milling on the X-ray diffraction pattern, the thermal properties, the IR spectra, the particle size distribution and the solubility of amobarbital was investigated. The fraction of crystal I decreased, and the fraction of crystal III and the amorphous part increased at the first stage of ball-milling. The heat of fusion decreased slightly by ball-milling, which was considered to be due to the increase in the fraction of the amorphous part. The melting point lowered by 1—3 °C and the NH and CO absorptions in the IR spectra were influenced by ball-milling, which was considered to be due to the transformation of crystal I into crystal III. The particle size decreased at the first stage of ball-milling. It was considered that the transformation of crystal I into crystal III was remarkable when the particles were broken. The solubility of amobarbital in the KH_2PO_4–Na_2HPO_4 buffer solution with pH of 6.0 increased by ball-milling, which was considered to be due to the increase in the fraction of the amorphous part and crystal III.

The solubility of the slightly soluble powders in the amorphous state is higher than the solubility in the crystal state.[1] The solubility of the powders in the metastable crystal form is also higher than the solubility in the stable crystal form.[2] The solubility of fine particles is larger than the solubility of large particles, as the surface energy of fine particles is larger than the energy of the large particles.[3]

As reported previously, the solubility of amobarbital (5-ethyl-5-isopentylbarbituric acid) increased, the X-ray diffraction intensities decreased and the melting point lowered by the mechanical treatment with the diluent, such as methylcellulose.[4,5] In this paper, amobarbital was ball-milled without the diluent and influence of ball-milling on the physical and chemical properties was investigated in order to clarify the mechanism of solubilization by the mechanical treatment.

Experimental

Commercial powders of amobarbital was of guaranteed grade purchased from Nihon Shinyaku Co. Ten g of the commercial powders was ball-milled under the conditions as referred to the previous paper.[5] Powder II was obtained by recrystallization of amobarbital from the 25 v/v % aqueous ethanol solution, and powder I was obtained by heating powder II at 150 °C for 1 h.[6] Powder III was obtained by freeze-drying the aqueous solution of amobarbital.

The X-ray diffraction measurement was carried out by a JEOL X-ray diffractometer (Model 7E). The differential thermal analysis was made by a thermal analyser (Model DT-20B) of Shimazu Seisakusho. The heat of fusion of amobarbital was measured by a differential scanning calorimeter (Model SC-20) of Shimadzu Seisakusho, using indium as a standard substance. Infrared (IR) spectra of the samples were measured by the Nujol method with a JASCO diffraction granting infrared spectrometer (Model A-2).

The sample was added to the 0.1 w/v % sodium dodecyl sulfate solution saturated with amobarbital in each of the samples, as the solubility varied by ball-milling. The suspension was stirred intensely for 2 min, and irradiated with the supersonic waves for a min. Then, the size distribution of the particles was measured with a micron photosizer (Model SKN 500) of Seishin Kigyo Co. Solubility of amobarbital from various samples in the KH_2PO_4–Na_2HPO_4 buffer solution (pH 6.0, ionic strength 0.08) at 30 °C was obtained from the absorbance at 238 nm as described in the previous paper.[4]

Results and Discussion

X-Ray Diffraction. Mesley reported two polymorphs for amobarbital, that is, crystal II obtained by recrystallization from a 25 v/v % aqueous ethanol solution and crystal I obtained by heating crystal II at 150 °C.[6] It is considered that powder I is composed of crystal I by Mesley and the amorphous part, and that powder II is composed of crystal II by Mesley and the amorphous part. As shown in Fig. 1, the X-ray diffraction pattern for the commercial powders before ball-milling was identical with the pattern for powder I, and the pattern for the ball-milled powders was identical with the pattern for powder III. The pattern for powder III was different from the patterns for powder I and II. The similar pattern as for powder III was obtained for the powders obtained by condensing the vapor from the solution of the fused amobarbital on a cold glassy wall. The pattern for powder III was identical with the pattern for amobarbital crystallized from diethyl ether by Williams.[7] In this paper, the polymorph in powder III is called crystal III. Vizzini *et al.* obtained single crystals of two kinds of polymorphs, I and II, from the same aqueous ethanol solution by slow evaporation at room temperature. They confirmed that the crystal morphology of these two forms were in agreement with those previously reported by Williams. They also found that the melting point of crystal I was lower than the point of crystal II by 4—6 °C.[8] As shown later in this paper, the melting point of powder III was lower than the point of powder I by 2—4 °C, though powder II was transformed into powder I at 150 °C. It is considered that crystal I by Vizzini is identical with crystal III in this paper.

The crystallinity of various kinds of amobaribtal, x_{cr}, was obtained by the Ruland's method.[9] The results are shown in Table 1.

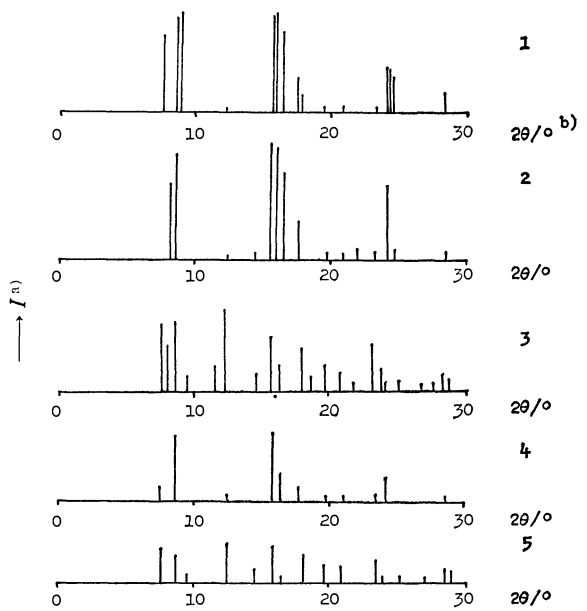

Fig. 1. X-Ray diffraction patterns of various kinds of amobarbital powders.
1: Powder I, 2: powder II, 3: powder III, 4: commercial powders, 5: commercial powders ball-milled for 60 h. a) I is the diffraction intensity. b) 2θ is the angle between the incident X-rays and the scattering X-rays. In this figure, the line broadening is ignored in order to show the difference between the patterns clearly.

TABLE 1. CRYSTALLINITY OF VARIOUS KINDS OF AMOBARBITAL

Sample	bt[a] / h	x_{cr} / %	x_{cr}' / %
Powder I	0	97	—
Powder III	0	77	
Commercial powders	0	87	84
	0.033	85	88
	0.083	84	83
	0.17	84	84
	0.5	84	87
	1	76	74
	3	78	76
	5	76	71
	10	79	78
	20	77	72
	30	76	74
	40	77	75
	60	82	73

a) bt is the ball-milling time.

Hermans *et al.* considered that the coherent scattering was due to the crystal part and that the non-coherent scattering was due to both of the crystal part and the amorphous part. On the basis of this consideration, they obtained the crystallinity of the cellulose fibers.[10] A glassy state was obtained by the rapid cooling of the solution of the fused hexobarbital or phenobarbital, though the state was not obtained for amobarbital. The intensity of the non-coherent scattering for the glassy state of hexobarbital was identical with the intensity for phenobarbital. The mean value of the intensity for these samples was taken as the intensity for the glassy state of amobarbital, assuming that the intensity was independent of the kind of the barbituric acid derivatives. It was confirmed that the kind of the polymorph did not influence the parameters for determining the crystallinity by the Hermans' method, from the results for the glassy state, powder I and III using the values of x_{cr}. The values of the crystallinity by the Hermans' method, x_{cr}', are tabulated in Table 1.

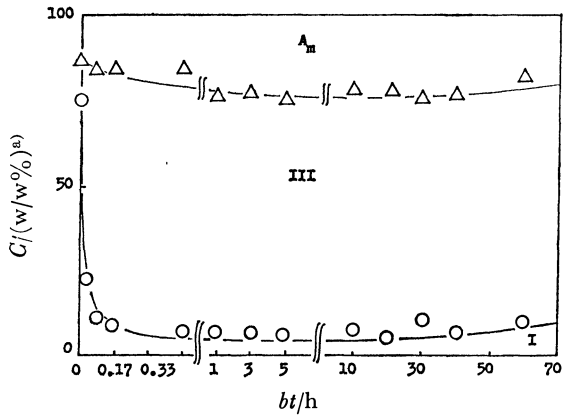

Fig. 2. Influence of ball-milling on the solid state of amobarbital.
○: The content of crystal I, △: the content of the crystal part, I: crystal I, III: crystal III, A_m: amorphous part. a) C is the composition.

The ratio of the intensity of the diffraction lines between 12.4° and 12.7° of 2θ to the intensity between 16.0° and 16.7° of 2θ, R_x, was larger for powder III than for powder I. From the data of R_x and x_{cr} for powder I and III, the fraction of crystal I, III and the amorphous part were obtained for the commercial powders before and after ball-milling. The results are shown in Fig. 2. The fraction of crystal I decreased and that of crystal III increased at the first stage, and the ratio between the fractions was constant after ball-milling for more than 10 min. The fraction of the amorphous part increased at the first stage, but the fraction was approximately constant after ball-milling for more than 1 h.

Thermal Analysis. The melting point of amobarbital lowered by 1—3 °C by ball-milling, as shown in Fig. 3. This phenomenon was already observed after ball-milling for 5 min. The melting point of powder III, 152—154 °C, was 2—4 °C lower than the point of powder I. The lowering of the melting point of amobarbital by ball-milling is considered to be due to the transformation of crystal I into crystal III.

As shown in Table 2, the heat of fusion, ΔH_{obsd}, for powder I and II was larger than the heat for the other samples. It was also shown that ΔH_{obsd} for the commercial powders decreased slightly by ball-milling by the t-test at the probability level of 0.05 and at the freedom of 29. Equation 1 was assumed to be applied, where x_I, x_{III}, and x_a were the fractions of crystal I, III, and the amorphous part and ΔH_I, ΔH_{III}, and ΔH_a were the heat of fusion of crystal

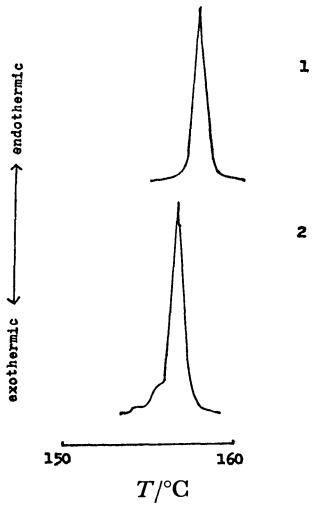

Fig. 3. Influence of ball-milling on DTA thermograms of amobarbital.
The programming speed is 1 °C/min. 1: Commercial powders, 2: commercial powders ball-milled for 60 h.

Table 2. Heat of fusion of various kinds of amobarbital

Sample	$\Delta H_{obsd} \pm \sigma_H$[a] kcal/mol
Powder I	7.0±0.3
Powder II	6.7±0.4
Powder III	6.1±0.5
Commercial powders	6.2±0.5
Commercial powders ball-milled for 60 h	5.7±0.6

a) σ_H is the standard deviation.

I, III, and the amorphous part, respectively.

$$\Delta H_{obsd} = x_I \Delta H_I + x_{III} \Delta H_{III} + x_a \Delta H_a \quad (1)$$

The values of ΔH_I, ΔH_{III}, and ΔH_a, 7.0, 6.9, and 1.2 kcal/mol, respectively were obtained from the data of ΔH_{obsd} and x_{cr} for powder I, the commercial powders before ball-milling and the powders after ball-milling for 60 h. The slight decrease in the heat of fusion of amobarbital by ball-milling is probably due to the decrease in the crystallinity.

IR Spectra. The following facts are confirmed from the study on the IR spectra of various kinds of barbituric acid derivatives by Mesley[6] and the study on the interaction of barbituric acid derivatives with polyethylene glycol by Chang *et al.*[11] The ν-NH absorption band is observed at 3600—3000 cm^{-1} region. The absorption for free NH in the solid state is observed at 3340—3310 cm^{-1} and shifts to the lower frequency by hydrogen bonding. The CO absorption at 1800—1600 cm^{-1} shifts to the lower frequency by hydrogen bonding. The highest frequency band at 1750 cm^{-1} is due to the CO in the 2-position and the other bands are due to the CO in the 4- and 6-position in the spectra of amobarbital. The δ'-NH absorption band at 900—750 cm^{-1} shifts to the higher frequency by hydrogen bonding.

Figure 4 shows the IR spectra of various kinds of amobarbital. In Table 3, $R_{\nu,\nu'}$ is the ratio of the

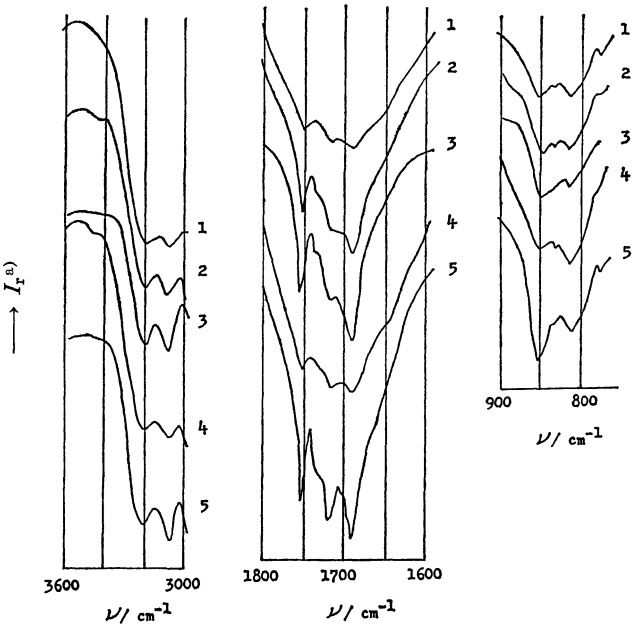

Fig. 4. IR spectra of various kinds of amobarbital powders.
1: Powder I, 2: powder II, 3: powder III, 4: commercial powders, 5: commercial powders ball-milled for 60 h. a) T_r is the transmittance.

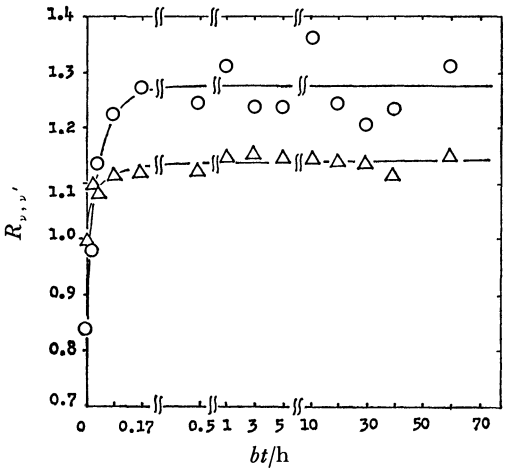

Fig. 5. Influence of ball-milling on IR spectra of amobarbital.
○: $\nu/cm^{-1}=850$; $\nu'/cm^{-1}=815$, △: $\nu/cm^{-1}=3085$; $\nu'/cm^{-1}=3210$.

absorbance at wave number ν to the absorbance at ν' obtained by assuming that the percent transmission at 3450, 2000, 1000, and 700 cm^{-1} are 100. As shown in Fig. 4 and Table 3, the IR spectra of the commercial powders before ball-milling were similar to those of powder I and the spectra of the ball-milled powders were similar to the spectra of powder III. Figure 5 shows the variation in the values of $R_{\nu,\nu'}$ with ball-milling. $R_{\nu,\nu'}$ varied remarkably at the first stage of ball-milling, but the values were nearly constant after ball-milling for more than 10 min. It is considered from the above findings that the variation in the IR spectra of amobarbital with ball-milling is due to the increase in the fraction of the part of

Table 3. Numerical values of $R_{\nu,\nu'} \pm \sigma_R$[a] for various kinds of amobarbital

ν/cm^{-1}	3085	1690	850
ν'/cm^{-1}	3210	1750	815
Powder I	1.06±0.02	1.17±0.09	0.99±0.04
Powder II	1.06±0.01	1.33±0.07	1.04±0.05
Powder III	1.07±0.03	1.42±0.06	1.25±0.06
Commercial powder	1.06±0.01	1.14±0.04	0.84±0.03
Commercial powders ball-milled for 60 h	1.16±0.02	1.32±0.02	1.32±0.01

a) σ_R is the standard deviation.

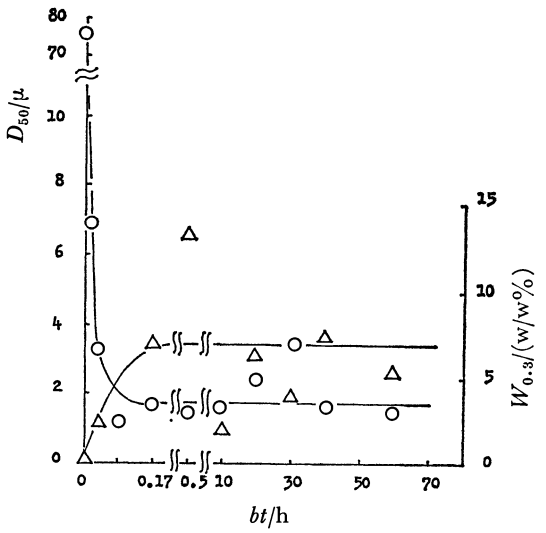

Fig. 6. Decrease in the particle size of amobarbital by ball-milling.
○: D_{50}, △: $W_{0.3}$.

the strong hydrogen bonding between NH and CO, which is probably related to the transformation of crystal I into crystal III.

Particle Size. Figure 6 shows the variation of the particle size of amobarbital with ball-milling. In Fig. 6, D_{50} is the median diameter by weight base and $W_{0.3}$ is the weight fraction of the particles smaller than 0.3 μ in diameter. The value of D_{50} decreased and the value of $W_{0.3}$ increased at the first stage of ball-milling, and these values were nearly constant after ball-milling for more than 10 min. Variation of these values with ball-milling was parallel to the variation of the X-ray diffraction pattern, the IR spectra and the melting point. It is considered that the transformation of crystal I into crystal III is remarkable when the particles are broken.

Solubility. The solubility of amobarbital in the KH_2PO_4–Na_2HPO_4 buffer solution with pH of 6.0 at 30 °C was investigated. The concentration of amobarbital in the filtrate of the suspension in the buffer solution increased at the first stage of dissolution, but the concentration was nearly constant for the dissolution time between 10 min and 2 h. In Fig. 7, c_{2h} is the concentration after shaking for 2 h from the time of the preparation. As shown in Fig. 7 and Table 4, c_{2h} increased by ball-milling.

In the previous paper, the solubility of amobarbital was influenced little by ball-milling with dextran or dextrose, but the solubility increased by 20—30% by ball-milling with methylcellulose only for 10 min.[4] The value of D_{50} for amobarbital ball-milled with methylcellulose for 10 min was larger than the values for amobarbital ball-milled with dextran or dextrose. This finding shows that the decrease in the particle size is not the main factor for the increase in the solubility of amobarbital by ball-milling.

Table 4. Solubility of amobarbital in the KH_2PO_4–Na_2HPO_4 buffer solution in pH of 6.0 at 30 °C

Sample	$c_{2h} \pm \sigma_c$[a] mg/100 ml
Powder I	58.4±1.9
Powder II	64.6±1.6
Powder III	67.4±0.6
Commercial powders	63.4±0.6
Commercial powders ball-milled for 20 h	67.1±1.1
Commercial powders ball-milled for 60 h	65.7±1.1

a) σ_c is the standard deviation.

The variation in c_{2h} with ball-milling was parallel to the variation in the fraction of the amorphous part. Table 4 shows the numerical values of c_{2h} for various samples. The value for the commercial powders before ball-milling was nearly identical with the value for powder I and the value for the ball-milled powders was similar to the value for powder III. If the solid state is equilibrated with the state of solution and ΔH_{obsd} is constant near the melting point, Eq. 2 is applied, where X_2^s is the mole fraction of the solute, R is the gas constant, T is the absolute temperature at the equilibrated state, T_f is the melting point of the solute by absolute temperature and γ is the activity coefficient of the solute.

$$\ln X_2^s = -\frac{\Delta H_{obsd}}{R}\left(\frac{1}{T}-\frac{1}{T_f}\right) - \ln \gamma \qquad (2)$$

The increase in the solubility of amobarbital in the buffer solution by ball-milling can be calculated from Eq. 2, if γ is influenced little by ball-milling. Using the data of ΔH_{obsd} in Table 2 and setting the lowering of the melting point by ball-milling to be 1 °C, the solubility of the ball-milled powders was calculated to be 1.2 times the solubility of the commercial powders, if the solid state obtained by ball-milling was equilibrated with the state of solution. The ratio of

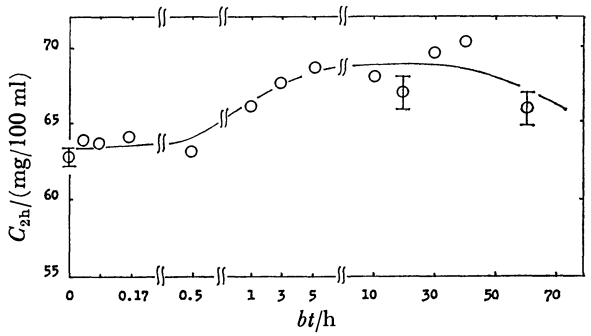

Fig. 7. Influence of ball-milling on solubility of amobarbital in the KH_2PO_4–Na_2HPO_4 buffer solution at 30 °C.

c_{2h} for the ball-milled powders to the value for the commercial powders before ball-milling was approximately 1.1, as shown in Table 4. The above findings show that the increase in the solubility of amobarbital by ball-milling is due to the increase in the fraction of the amorphous part and to the transformation of crystal I into crystal III.

The authors are grateful to Mrs. Mayumi Tobe, one of the members of the Analytical Center of Showa University, for the measurement of the IR spectra.

References

1) J. D. Mullins and T. J. Macek, *J. Am. Pharm. Assoc.*, **49**, 245 (1960).
2) J. K. Dale, U. S. Patent, 2603633 (1952).
3) M. Hori and S. Hayakawa, *Nippon Butsuri Gakkai Shi*, **20**, 396 (1964).
4) N. Kaneniwa, A. Ikekawa, and M. Sumi, *Chem. Pharm. Bull. (Tokyo)*, **26**, 2744 (1978).
5) N. Kaneniwa, A. Ikekawa, and M. Sumi, *Chem. Pharm. Bull. (Tokyo)*, **26**, 2734 (1978).
6) R. J. Mesley, *Spectrochim. Acta, Part A*, **26**, 1427 (1970).
7) P. P. Williams, *Anal. Chem.*, **31**, 140 (1959).
8) B. M. Craven, E. A. Vizzini, *Acta Crystallogr., Sect. B*, **25**, 1993 (1969).
9) W. Ruland, *Acta Crystallogr.*, **14**, 1180 (1961).
10) P. H. Hermans and A. Weidinger, *J. Appl. Phys.*, **19**, 491 (1948).
11) B. L. Chang, N. O. Nuessle, and W. G. Haney, Jr., *J. Pharm. Sci.*, **64**, 1787 (1975).

Effect of Surfactant Micelles on the Rate of Reaction of Tetranitromethane with Hydroxide Ion

Tsuyoshi HARADA, Nagamune NISHIKIDO, Yoshikiyo MOROI,* and Ryohei MATUURA
Department of Chemistry, Faculty of Science, Kyushu University, Higashi-ku, Fukuoka 812

(Received March 2, 1981)

The rates of trinitromethanide anion formation by the reaction of tetranitormethane with hydroxide ion were measured in the presence of anionic, cationic and nonionic surfactant micelles in aqueous solutions. Using the analytical approach which takes into consideration the distribution of hydrophobic reactants among micelles,[1] k_1 (a second-order rate constant on micelles associated with one reactant molecule) and K_1/N(K_1: an association constant of the reactant with micelles having no reactant, N: an aggregation number of surfactant molecule in a micelle) were estimated. The anionic surfactant exhibited no effect on the reaction rate. In the case of cationic surfactants, both k_1 and K_1 values increased not only with alkyl chain length but also with hydrophobicity of the surfactants. In the case of nonionic surfactants, an increase of alkyl chain length with a given oxyethylene unit resulted in an increase in the k_1 values, while an increase of oxyethylene group with the fixed alkyl chain length resulted in an appearance of the maximum k_1 value. From temperature dependence of the reaction rate, a stabilization of the activated complex could be explained by an electrostatic interaction of the complex with the charged micellar surface. It was also found from the analytical approach that the distribution of tetranitromethane among micelles used in the present experiment could be approximated by the Poisson distribution.

Surfactant molecules aggregate to form micelles in aqueous solution above a narrow concentration range which is called the critical micelle concentration (CMC).[2] The hydrophobic groups of surfactant form a core of micelle which is liquid hydrocarbon like in character, while the hydrated polar groups constitute an outer shell of micelle and contact with water. Physico-chemical properties of the micelle-bulk interface and an interior of micelles have been really interested not only from the colloid chemistry itself but also from an application of micelles to other fields of chemistry. Especially, the application to a medium or catalyst for organic reactions has been undertaken since the pioneering work by Duynstee and Grundwald in 1959.[3] Then, for more than a decade many studies have been reported on micelle-catalyzed reactions.[4]

The reactions of tri- and tetranitromethane with hydroxide ion were minutely investigated in both aqueous[5–7] and micellar[8] solutions. However, there have been few systematic studies of the effect of surfactant structures, particularly of nonionic surfactant, on the reaction rate. In the present study, the rates of trinitromethanide anion formation by the reaction of tetranitromethane with hydroxide ion were measured in the presence of various surfactants in aqueous solutions. Hereupon, the dependence of the reaction rate on surfactant structure was systematically investigated. Furthermore, in order to find the relationship of stability of the activated complex with kinds of surfactant structures, a temperature effect on the rate was pursued. In addition, the distribution of tetranitromethane among micelles was also examined by applying the random, Poisson, and Gaussian distributions.

Experimental

Materials. Tetranitromethane (TNM) supplied from Tokyo Kasei Ind. was washed three to five times with 0.8 mol dm^{-3}-H_2SO_4, and subsequently five times with double-distilled water. TNM was recrystallized from water below 10 °C and the supernatant was discarded. After these treatments, no absorption of trinitromethanide anion was found at 350 nm in an aqueous solution of TNM. Anionic surfactant, sodium dodecyl sulfate SDS, was synthesized and purified according to the procedure described previously.[9] Cationic surfactants (decyltrimethylammonium chloride DeTAC, dodecyltrimethylammonium chloride DoTAC, hexadecyltrimethylammonium chloride HTAC, hexadecyltrimethylammonium bromide HTAB, *N*-hexadecylpyridinium chloride HPC, benzylhexadecyldimethylammonium chloride BHAC (all obtained from Tokyo Kasei Ind.)) were recrystallized three times from acetone–ethanol mixture in which the volume fraction of ethanol was below 0.1. Hexadecyltrimethylammonium nitrate HTAN was prepared by refluxing HTAB with an excess of silver nitrate in anhydrous methanol for several hours, and the precipitated silver salts were removed by filtration. The above procedure was repeated twice. The HTAN thus prepared was recrystallized three times from acetone. For all cationic surfactants, small amount of residual solvents on recrystallization were eliminated by heating at 100 °C under reduced pressure for more than ten hours. They were always kept in a desiccator because of their hygroscopicity. All nonionic surfactants, poly(oxyethylene) alkyl ether C_mE_n were a gift from Kao Soap Co. and were used without further purification.[10] The details of these surfactants are given in Table 1 together with their CMCs in pure water and in the reaction systems, which were determined by the plots of surface tension against concentrations. Inorganic salts of reagent grade used for adjusting pH, commercial NH_4Cl, NH_4NO_3, and NH_4Br, were purified by recrystallization from water before use.

Method. The reaction of TNM with hydroxide ion was started by injecting an aliquot of aqueous solution of TNM into alkaline surfactant solutions. The reaction rates were followed spectrophotometrically (Beckman-Toshiba DSB-80) by measuring the rate of trinitromethane anion formation at 350 nm ($\varepsilon\{C(NO_2)_3^-\} = 1.34\times10^4$ dm^3 mol^{-1} cm^{-1}).[8] The temperature was controlled at 30±0.1 °C by circulating water through the equipment. The initial concentration of TNM (*ca.* 5×10^{-5} mol dm^{-3}) in the individual run was estimated from the optical density at 350 nm at infinite time. The pseudo first-order rate constant k^{obsd} was determined from the slope of linear plots of $\log(OD_\infty - OD_t)$ against time in the usual manner, where OD_∞ and OD_t represent the optical density due to trinitromethanide anion at infinite time and time t, repectively. The adjustment of pH was made using an NH_3–NH_4^+ buffer whose

TABLE 1. CMC VALUES OF SURFACTANTS USED IN THE PRESENT STUDY

Surfactant	Abbrev.	CMC/mol dm^{-3} a)	
Cationic		(A)	(B)
$C_{10}H_{21}N^+(CH_3)_3Cl^-$	DeTAC	8.0×10^{-2}	7.7×10^{-2}
$C_{12}H_{25}N^+(CH_3)_3Cl^-$	DoTAC	2.3×10^{-2}	1.7×10^{-2}
$C_{16}H_{33}N^+(CH_3)_3Cl^-$	HTAC	1.3×10^{-3}	9.3×10^{-5}
$C_{16}H_{33}N^+(CH_3)_3Br^-$	HTAB	9.4×10^{-4}	1.0×10^{-4}
$C_{16}H_{33}N^+(CH_3)_3NO_3^-$	HTAN	8.5×10^{-4}	1.0×10^{-4}
$C_{16}H_{33}N^+C_5H_5Cl^-$	HPC	1.0×10^{-3}	8.2×10^{-5}
$C_{16}H_{33}N^+(CH_3)_2CH_2\phi Cl^-$ b)	BHAC	2.5×10^{-4}	1.2×10^{-5}
Nonionic		(C)	(D)
$C_8H_{17}O(C_2H_4O)_6H$	C_8E_6	8.9×10^{-3}	
$C_{10}H_{21}O(C_2H_4O)_6H$	$C_{10}E_6$	7.3×10^{-4}	
$C_{12}H_{25}O(C_2H_4O)_6H$	$C_{12}E_6$	6.7×10^{-5}	6.0×10^{-5}
$C_{12}H_{25}O(C_2H_4O)_{10}H$	$C_{12}E_{10}$	9.0×10^{-5}	9.0×10^{-5}
$C_{12}H_{25}O(C_2H_4O)_{15}H$	$C_{12}E_{15}$	1.3×10^{-4}	1.2×10^{-4}
$C_{12}H_{25}O(C_2H_4O)_{20}H$	$C_{12}E_{20}$	1.8×10^{-4}	1.6×10^{-4}
$C_{12}H_{25}O(C_2H_4O)_{29}H$	$C_{12}E_{29}$	2.6×10^{-4}	2.6×10^{-4}
Anionic			
$C_{12}H_{25}OSO_3^-Na^+$	SDS	8.2×10^{-3}	

a) (A) in pure water at 30 °C, (B) in the reaction system at 30 °C, (C) reference data at 30 °C[23], (D) in pure water at 20 °C. b) ϕ: C_6H_5.

ionic strength was maintained at 0.03; NH_4Cl–aqueous ammonia for anionic and nonionic surfactant solutions, and NH_4X–aqueous ammonia for the micellar solutions of cationic surfactant whose gegenion is X. The pH of the reacting solutions was confirmed not to be changed before and after the reaction.

Results and Discussion

The reaction of TNM with hydroxide ion is represented by:[6]

$$C(NO_2)_4 + OH^- \xrightarrow{k} C(NO_2)_3^- + HNO_3, \quad (1)$$

where k is the second-order rate constant. The reaction rate is expressed by:

$$-[C(NO_2)_4]/dt = k[C(NO_2)_4][OH^-]. \quad (2)$$

Since the pH in each solution is kept constant in an alkaline side by a given buffer, $[OH^-]$ remains constant during the course of reactions. Thus, the reaction obeys the following pseudo first-order kinetics:

$$-d[C(NO_2)_4]/dt = k^{obsd}[C(NO_2)_4] \quad (3)$$

and

$$k = k^{obsd}/[OH^-]. \quad (4)$$

From Eq. 3 we obtain the following relation:

$$OD_\infty - OD_t \propto [C(NO_2)_4]_t = [C(NO_2)_4]_0 \exp(-k^{obsd}t), \quad (5)$$

where $[C(NO_2)_4]_0$ and $[C(NO_2)_4]_t$ represent the concentration of TNM at $t=0$ and t, respectively. The rate constant k^{obsd} increases linearly with hydroxide ion concentration and the linearity is very good. Then, the second-order rate constant k is determined from the slope of linear plots of k^{obsd} against $[OH^-]$ whose linearity is good. The second-order rate constant k thus obtained in the absence of surfactant at 30 °C was calculated to be 0.38 dm^3 mol^{-1} s^{-1}, which seems reasonable compared with 0.52 dm^3 mol^{-1} s^{-1} at 30 °C and at ionic strength of 0.1[8] and with 0.65 dm^3 mol^{-1} s^{-1} at 30 °C and at ionic strength 1.0.[7]

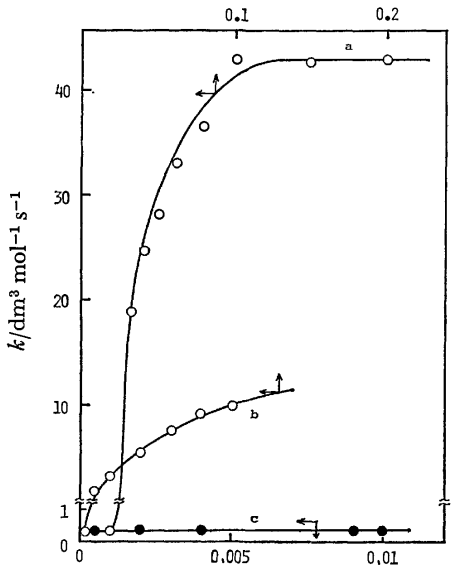

Fig. 1. Effect of surfactant type on the second-order rate constant(k). The variation of k values with surfactant concentrations.
a): DoTAC, b): $C_{12}E_6$, c): SDS.

In the first place, the effect of structure of surfactant on the reaction rate was examined using C_{12} surfactants, DoTAC, SDS, and $C_{12}E_6$ (Fig. 1). SDS had no effect on the reaction rate, while DoTAC and $C_{12}E_6$ brought about an increase in the rate constant with increasing their concentrations.[11–15] From these results, it can be considered that the increase in k

values in the presence of cationic micelles of DoTAC is attributable mainly to the concentration of hydroxide ion in the vicinity of cationic head groups of micelle.

Secondly, in order to understand the above differences on account of surfactant types, further analysis was made using the following reaction mechanism. The reactions take place both in a bulk solution and in micelles. The apparent increase in reaction rate above CMC is mainly due to the presence of micelles. For simplifying the reaction systems, the following assumptions are made; 1) the reactants associate with micelles to form some distribution among micelles and 2) the rate of the association which is of millisecond order is much faster than those of the reactions in both bulk and micellar phases which are of second order. With these assumptions the following reaction scheme which was adopted in the preceeding paper[1] is used to study the present reaction system:

$$\begin{array}{lll} M + R \overset{K_1}{\rightleftharpoons} MR_1 \xrightarrow[OH^-]{k_1} P & & \\ \quad k_b \downarrow OH^- & MR_1 + R \overset{K_2}{\rightleftharpoons} MR_2 \xrightarrow[OH^-]{k_2} P + MR_1 & \\ \quad P & \cdots\cdots\cdots\cdots\cdots\cdots\cdots\cdots\cdots\cdots\cdots\cdots & (6) \\ & MR_{n-1} + R \overset{K_n}{\rightleftharpoons} MR_n \xrightarrow[OH^-]{k_n} P + MR_{n-1}. & \end{array}$$

In the above scheme, M, R, MR_i, and P represent micelle, monomer reactant(TNM), micelle with i reactant molecules, and product(trinitromethanide anion), respectively. K_i is the association constant of monomer reactant with MR_{i-1} micelle, and k_b and k_i are the second-order rate constant in the bulk solution and on the MR_i micelle, respectively. The apparent second-order rate constant for the reaction of TNM with hydroxide ion, k^{app}, is represented in the following way:

$$-d[R_t]/dt = k^{app}[R_t][OH^-]$$
$$= \{k_b[R] + \sum_{i=1}^{n} k_i[MR_i]\}[OH^-], \quad (7)$$

where k^{app} is $k^{obsd}/[OH^-]$ and $[R_t]$ represents the total equivalent concentration of reactant and is given by:

$$[R_t] = [R] + \sum_{i=1}^{n} i[MR_i]. \quad (8)$$

On the other hand, the total micellar concentration $[M_t]$ can be expressed by the following equation:

$$[M_t] = (C_t - CMC)/N, \quad (9)$$

where C_t and N represent the total equivalent surfactant concentration and an aggregation number per micelle, respectively. Eq. 10 or 11 results from the Poisson distribution of reactants,[1]

$$\frac{1}{k^{app}-k_b} = \frac{1}{k_1-k_b} + \frac{N}{K_1(k_1-k_b)} \times \frac{1}{C_t-CMC}, \quad (10)$$

$$\frac{k^{app}-k_b}{k_1-k^{app}} = \frac{K_1}{N} \times (C_t-CMC). \quad (11)$$

In this case the plots of $1/(k^{app}-k_b)$ against $1/(C_t-CMC)$ should be linear, and k_1 and k_1/N values can be determined from the intercept and the slope. At the same time some information on reactant distribution among micelles could be also obtained.[1] The

TABLE 2. SECOND-ORDER RATE CONSTANT (k_1) FOR NITROFORM ANION FORMATION, AND THE ASSOCIATION PARAMETER (K_1/N) AND THE ROUGHLY ESTIMATED ASSOCIATION CONSTANT (K_1) OF TNM WITH THE MICELLES

Surfactant	$k_1 \times 10^{-2}$ / dm^3 mol^{-1} s^{-1}	$K_1/N \times 10^{-1}$ / dm^3 mol^{-1}	$K_1 \times 10^{-2}$ / dm^3 mol^{-1}
Cationic			
DeTAC	0.33	1.17	3
DoTAC	0.56	3.2	12
HTAC	2.28	8.9	54
HTAB	1.76	5.5	44
HTAN	1.27	6.1	48
HPC	1.52	10.9	71
BHAC	2.67	18.3	>150
Nonionic			
C_8E_6	0.044	2.93	9
$C_{10}E_6$	0.104	1.82	17
$C_{12}E_6$	0.171	1.03	48
$C_{12}E_{10}$	0.67	0.70	12
$C_{12}E_{15}$	0.50	0.83	10
$C_{12}E_{20}$	0.289	0.55	4
$C_{12}E_{29}$	0.142	1.60	9

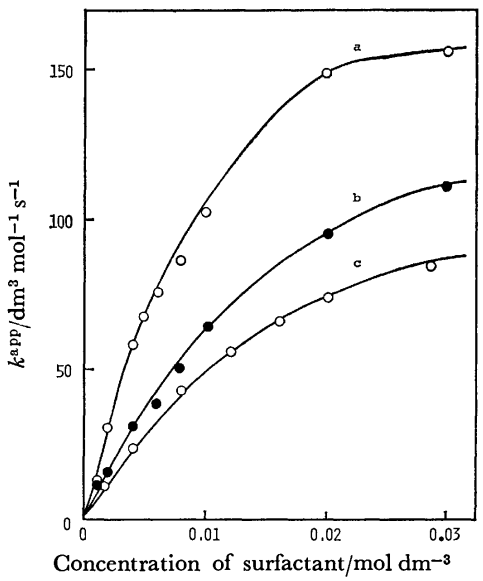

Fig. 2. Effect of the kind of counterion of the cationic surfactants (HTAC(a), HTAB(b), and HTAN(c)) on the apparent second-order rate constant(k^{app}). Plots of k^{app} against the surfactant concentrations.

k_1 values thus obtained are given in Table 2. From the consideration described in the preceeding paper, it can be said that the k_1 value of DoTAC is much larger than that of $C_{12}E_6$ and the reactant distribution is very likely to be the Poisson distribution. Further discussion will be given more in detail in the following sections which describe the effect of the cationic and nonionic surfactants and the temperature effect on the reaction rates.

(1) The Reaction Rates in the Presence of Cationic Surfactants: The k^{app} *vs.* concentration relationship of HTAN, HTAB, and HTAC micelles are plotted in

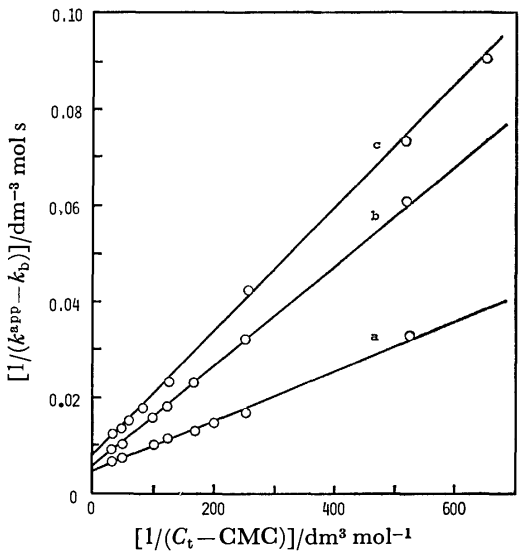

Fig. 3. Determination of the k_1 and K_1/N values from the linearity plots of $1/(k^{app}-k_b)$ against $1/(C_t-CMC)$.
a): HTAC, b): HTAB, c): HTAN.

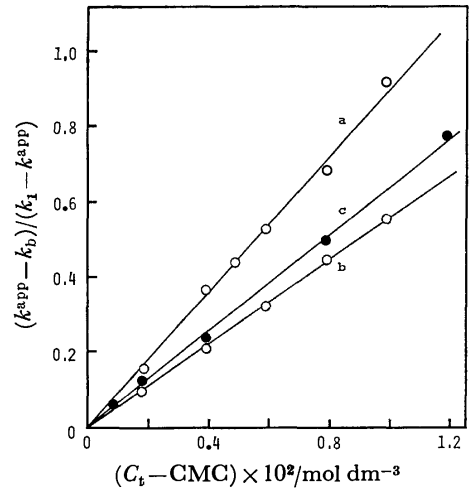

Fig. 4. Determination of the K_1/N vaules from the linearity plots of $(k^{app}-k_b)/(k_1-k^{app})$ against (C_t-CMC).
a): HTAC, b): HTAB, c): HTAN.

Fig. 2 where some differences owing to counterions are clear. In order to make clear a reason for these differences and to take an insight into the reactant distribution, another plots are given in Fig. 3, relating $1/(k^{app}-k_b)$ to $1/(C_t-CMC)$. Judging from the linearity of these plots shown in Fig. 3, the Poisson distribution is well applicable to these reaction systems within experimental error. The k_1 and K_1/N values obtained in this way are given in Table 2. Equation 11 predicts that the plots of $(k^{app}-k_b)/(k_1-k^{app})$ against C_t should be linear and also determine k_1/N values (Fig. 4). The disadvantage of using Eq. 11 is due to a large uncertainty in the value of either numerator or denomenator when k^{app} is nearly equal to k_b or k_1; thus, the useful values are limited to the region of marked increase in k^{app} values. The values of k_1 and K_1/N thus obtained characterize the properties of each micelle.

The k_1 values decrease in the order HTAC>HTAB>HTAN. In these reaction systems, hydroxide ions compete with the surfactant counterions in approaching to charged micellar surface through the electrostatic interaction. In regard to the counterions of surfactants, the hydration radius of the ions decreases in the order $Cl^->Br^->NO^-_3$. That is, the strength of their electrostatic attraction with the charged micelle increases in the order $Cl^-<Br^-<NO^-_3$, which reflects the CMC order (Table 1). In other words, the stronger their electrostatic attraction, the less the electrostatic surface potential of micellar surface. Therefore, it is reasonable to say that the counterions interfere with approach of hydroxide ions to the micellar surface in the order HTAC<HTAB<HTAN. On the other hand, the values of K_1/N decrease slightly in the order HTAC>HTAN>HTAB. For CMC decreases in the order HTAC>HTAB>HTAN, the aggregation number of the micelles may slightly increase in the order HTAC<HTAB<HTAN. Therefore, the large difference is not found in the K_1 values of these cationic surfactants. The K_1 values are about $4—6\times 10^3\ dm^3\ mol^{-1}$.

Next, the effect of the cationic surfactant micelles with different alkyl chain lengths but with the same head group, DeTAC, DoTAC, and HTAC, is examined in order to see the effect of the aggregation number of micelle. The k_1 values (Table 2) increase with increasing alkyl chain length of the surfactants, *i.e.*, with increasing aggregation number of micelle. This increase in the order is mainly due to the increase in electrical surface potential of the micelle in the above order which can be reasoned by analogy of anionic surfactant micelles[16] and partially due to an increase of hydrophobicity of palisade layer of micelle in the above order. Thus, the hydroxide ion concentration of vicinity of the micellar surface is expected to increase with increasing the aggreagation number. The large difference in the k_1 values, however, can not be explained only with the difference in surface potential of the micelles.[16] This must be considered in relation with the K_1/N values. The K_1/N values, on the other hand, increase in the order DeTAC<DoTAC<HTAC, notwithstanding the same order in the aggregation number (*ca.* 36, 50, and 80 for DeTABr, DoTABr, and HTABr, respectively,[17] and these values do not change so much by replacing Br^- by Cl^-; 38 for DoTAC[18]). This means that the K_1 value of TNM for HTAC micelles is about 20 times as large as that of DeTAC. Such a large difference is likely to come from a difference of the location of TNM in the micelles. The roughly estimated K_1 values are given in Table 2. Smaller aggregation number of micelle results in looser palisade layer of micelle, and the hydrophobic reactant is in an innermore part of micelle. Therefore, the effective area for the reactant to sit in micelle becomes less for shorter chain surfactant, which corresponds to a smaller K_1 value. On the other hand, the HTAC micelles have a larger aggregation number as well as a more rigid palisade layer, and the location of TNM must be an outer part of the micelles. This results in a closer contact between TNM and OH^-

ion, a higher value of k_1. The larger effective area thus available for the reactant location leads to larger K_1 value. Thus, the large difference in k_1 values between DeTAC and HTAC results from not only the difference in micellar surface potential term but also the difference of the location of TNM in the micelles.

Finally, in order to confirm the above consideration concerning location site of reactants in micelles, the effect of difference of ionic head groups on the reaction rates was examined using HTAC, HPC, and BHAC micelles. Almost the same aggregation number of HTAC and HPC can be deduced from their CMC values (87 for HPBr). The samller k_1 value of HPC, however, results from a large distance between solubilized TNM and OH^- ion in HPC micelles due to interposition of pyridine ring between them. In the case of BHAC micelle both k_1 and K_1/N values are larger than those of the other micelles in spite of the smaller CMC. This result rests on a more hydrophobic nature of outermost part of the micelle. Therefore, the probability for TNM to sit on an outer part of the micelle increases; this should be the main reason for their increase in BHAC micelles.

From these results, we would like to stress that the reaction rate increase in the presence of cationic surfactant micelles is owing mainly to the hydroxide ion concentration near the cationic micellar surface and that the location of reactants in micelle has a strong influence on the reaction rate.

(2) The Reaction Rates in the Presence of Nonionic Surfactants. As is shown in Fig. 1, the nonionic surfactant also increases the reaction rate. Then, in the first place, an effect of alkylchain length on the reaction rate was examined using the surfactants of C_8E_6, $C_{10}E_6$, and $C_{12}E_6$. The k_1 values increase with increasing alkyl-chain length of the nonionic surfactants, or with increasing aggregation number of micelle, in a similar way as the case of cationic surfactants. On the other hand, the K_1/N values decrease with increasing alkyl-chain length. In the case of nonionic surfactants, the aggregation number of micelle in pure water (30, 100, and 460 at 30 °C for C_8E_6, $C_{10}E_6$, and $C_{12}E_6$, respectively[19]) will remain almost unchanged in the buffer solution of such low ionic strength as 0.03.[19] The roughly estimated K_1 values of these surfactants using the above aggregation number are given in Table 2, too. Contrary to the order of the K_1/N values, the K_1 values thus obtained increase with increasing alkyl-chain length of the surfactants. This increase can also be understood from the view point of an available area of the reactant solubilized. From comparison between cationic and nonionic surfactants with an identical alkylchain length, *e.g.* $C_{10}E_6$ and DeTAC or $C_{12}E_6$ and DoTAC, the k_1 values of the cationic surfactants are almost three times as large as those of nonionic surfactants. On the contrary, the K_1 values of the nonionic surfactants are almost four times as large as those of cationic surfactants, which means that the oxyethylene groups connected with alkyl chain probably constitute a palisade layer of the micelles where the hydrophobic reactant locates.[20] This leads to larger available area in the nonionic surfactant micelles than in the cationic micelles.

TABLE 3. RATE PARAMETERS FOR THE REACTION OF TNM WITH HYDROXIDE ION

Surfactant	ΔG^* / kJ mol^{-1}	ΔH^* / kJ mol^{-1}	ΔS^* / J mol^{-1} K^{-1}
None	76.9	65.6	−37.2
DeTAC	66.5	60.2	−20.9
DoTAC	64.8	59.8	−16.7
HTAC	61.9	57.7	−13.8

Next, to see the effect of an oxyethylene chain length the reaction rates were measured in the presence of nonionic surfactants containing different numbers of oxyethylene unit but with the fixed alkyl-chain length, $C_{12}E_6$, $C_{12}E_{10}$, $C_{12}E_{15}$, $C_{12}E_{20}$, and $C_{12}E_{29}$. The k_1 and K_1/N values obtained from the linearity plots are summarized in Table 2. Concerning the decrease in k_1 values with an increase in oxyethylene unit more than ten, it can be expected that the location of TNM goes into an innermore part of the micelles owing to not only loosening of the palisade layer but also their smaller aggregation number with increasing oxyethylene group. Consequently, a separation between TNM and OH^- comes to increase with an increase in oxyethylene unit. Regarding the K_1/N values, on the other hand, even if the decrease in aggregation number of the micelles with increase of oxyethylene group is taken into account (460, 180, 120, 80, and 60 at 30 °C for $C_{12}E_6$, $C_{12}E_{10}$, $C_{12}E_{15}$, $C_{12}E_{20}$, and $C_{12}E_{29}$, respectively, which were estimated by an interpolation or extrapolation from the aggregation numbers in the literature[19]), the K_1 value of $C_{12}E_6$ is almost five times as large as that of $C_{12}E_{29}$. The roughly estimated K_1 values are given in Table 2. This decrease in K_1 values with increasing oxyethylene group is also likely to result from the loose palisade layer caused by less aggregation number with increase of oxyethylene goup. That is, the area for TNM to sit becomes less with increase of the group. The identical explanation should be applicable to the reaction rates on both cationic and nonionic surfactant micelles.

Concerning the distribution of TNM among micelles, the Poisson distribution could be well approximated for both cationic and nonionic surfactant micelles. Namely, regardless of the kinds of surfactants used, the linearity of the plots of $1/(k^{app}-k_b)$ against $1/(C_t-\mathrm{CMC})$ is very good. We may conclude at this point that the Poisson distribution of TNM among micelles can be applied to the present cationic and nonionic surfactant micelles. In other words, the assumption used for this treatment is suitable for these systems.

(3) Temperature Effect on the Reaction Rates. Finally, a dependency of the reaction rates on temperature was examined both in the absence and presence of micelles. The reaction rates were measured over the temperature range of 20—40 °C, and the surfactants used were DeTAC, DoTAC, and HTAC. The reaction rate determination in the presence of these sur-

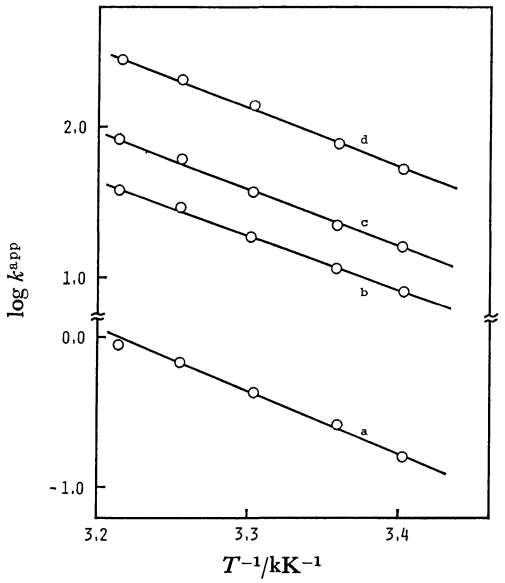

Fig. 5. Arrhenius plots for the reaction of TNM with hydroxide ion.
a): No micelles, b): DeTAC 0.3 mol dm^{-3}, c): DoTAC 0.2 mol dm^{-3}, d): HTAC 0.03 mol dm^{-3}.

factants were made at the higher surfactant concentrations where the second-order rate constant k^{app} is almost equal to the rate constant k_1. The plots of $\log k^{app}$ against $1/T$ gives a straight line as shown in Fig. 5, and then the activation energy E_a can be calculated by the Arrhenius equation. The ΔG^* and ΔH^* values decrease and ΔS^* values increase in the presence of these micelles compared with those in the absence of micelles (Table 3). The transition state of the reaction of TNM with hydroxide ion is represented by:[6]

$$C(NO_2)_4 + OH^- \rightleftharpoons [(NO_2)_3C\text{-}\overset{+}{N}\overset{O^-}{\underset{O}{\diagdown\diagup}}\cdots\cdots OH^-]^- \longrightarrow C(NO_2)_3^- + HNO_3. \quad (12)$$

Therefore, the transition state having a negative charge is electrostatically stabilized by the cationic micelles. In any event, the drastic change of ΔG^* and ΔH^* values could not be found even in the presence of the cationic micelles. This means that the increase in the rate constant in the presence of cationic micelles can be attributed mainly to a local concentration increase of another reactant OH^- ions around the micelles and that the reaction mechanism is not changed much by the presence of these micelles.

References

1) Y. Moroi, *J. Phys. Chem.*, **84**, 2186 (1980).
2) P. Mukerjee and K. J. Mysels, *Natl. Stand. Ref. Data. Ser., Natl. Bur. Stand., No. 36* (1971).
3) E. F. Duynstee and E. Grunwald, *J. Am. Chem. Soc.*, **81**, 4540, 4542 (1959).
4) J. H. Fendler and E. J. Fendler, "Catalysis in Micellar and Macromolecular Systems," Academic Press, New York-San Francisco-London (1975).
5) D. J. Glover, *Tetrahedron*, **19**, 219 (1963).
6) D. J. Glover, *J. Phys. Chem.*, **74**, 21 (1970).
7) S. L. Walters and T. C. Bruice, *J. Am. Chem. Soc.*, **93**, 2269 (1971).
8) J. H. Fendler, *J. Chem. Soc., Perkin Trans. 2*, **1972**, 1041.
9) Y. Moroi, K. Motomura, and R. Matuura, *Bull. Chem. Soc. Jpn.*, **44**, 2078 (1971).
10) N. Nishikido, Y. Moroi, H. Uehara, and R. Matuura, *Bull. Chem. Soc. Jpn.*, **47**, 2634 (1974).
11) M. T. A. Behme, J. G. Fullington, R. Noel, and E. H. Cordes, *J. Am. Chem. Soc.*, **87**, 266 (1965).
12) C. A. Bunton, E. J. Fendler, L. Sepulveda, and K. Yang, *J. Am. Chem. Soc.*, **90**, 5512 (1968).
13) C. A. Bunton, L. Robinson, and L. Sepulveda, *J. Org. Chem.*, **35**, 108 (1970).
14) C. A. Bunton, M. J. Minch, J. Hidalgo, and L. Sepulveda, *J. Am. Chem. Soc.*, **95**, 3262 (1975).
15) T. Kunitake, S. Shinkai, and Y. Okahata, *Bull. Chem. Soc. Jpn.*, **49**, 540 (1976).
16) Y. Moroi, N. Nishikido, H. Uehara, and R. Matuura, *J. Colloid Interface Sci.*, **50**, 254 (1975).
17) H. V. Tartar, *J. Phys. Chem.*, **59**, 1195 (1955).
18) L. M. Kushner, W. D. Hubbard, and R. A. Parker, *J. Research Natl. Bur. Stand.*, **59**, 113 (1957).
19) L. Hsiao, H. N. Dunning, and P. B. Lorenz, *J. Phys. Chem.*, **60**, 657 (1956).
20) N. Nishikido, Y. Moroi, and R. Matuura, *Bull. Chem. Soc. Jpn.*, **48**, 1387 (1975).

Pressure Effect on Rate Constants of Proton-transfer Reactions from 2,4,6-Trinitrotoluene to *N,N,N',N'*-Tetramethylguanidine and 1,8-Diazabicyclo[5.4.0]undec-7-ene in Acetonitrile and Dichloromethane

Naoki Sugimoto, Muneo Sasaki,* and Jiro Osugi
Department of Chemistry, Faculty of Science, Kyoto University, Oiwake-cho, Kitashirakawa, Sakyo-ku, Kyoto 606
(Received March 2, 1981)

Influence of pressure on the rate constants of the proton-transfer reactions between title compounds was studied in acetonitrile and dichloromethane at 25 °C up to 1000 bar by means of a high-pressure stopped-flow method. In the reaction of 2,4,6-trinitrotoluene (TNT) with *N,N,N',N'*-tetramethylguanidine, the volume of activation for the forward reaction ΔV_f^* is -12.7 ± 1.0 cm^3 mol^{-1} in acetonitrile and -19.0 ± 1.5 cm^3 mol^{-1} in dichloromethane. In the reaction of TNT with 1,8-diazabicyclo[5.4.0]undec-7-ene, ΔV_f^* is -9.0 ± 1.0 cm^3 mol^{-1} in acetonitrile and -10.8 ± 1.0 cm^3 mol^{-1} in dichloromethane. These results are discussed in comparison with other proton-transfer reactions.

Proton-transfer reaction in solution has been extensively studied from the theoretical and phenomenological viewpoints.[1-3] Some proton-transfer reactions also have attracted much interest because of occurrence of appreciable tunneling effect.[4] It is known that the proton-transfer reaction between 4-nitrophenylnitromethane (4NPNM) and a base such as amine[4,5] or alkoxide ion,[6] proceeds in a simple way.[7] In the case of the reaction of 2,4,6-trinitrotoluene (TNT) with ethoxide ion in ethanol, two colored compounds are formed.[8] At high concentrations of TNT($\approx10^{-3}$ M; 1 M=1 mol dm^{-3}) and ethoxide ion($\approx10^{-1}$ M) a brown species is formed, which is elucidated to be a type of Meisenheimer complex by Bernasconi.[9] On the other hand at low concentrations of TNT($\approx10^{-5}$ M) and ethoxide ion($\approx10^{-3}$ M), 2,4,6-trinitrobenzyl anion (TNT^-; $\lambda_{max}=514$ nm) is mainly produced by a proton abstraction from the methyl group of TNT.[8,10] Since the reaction with a nonionic base is expected to shift in favor of the proton-transferred state compared with the case of an ionic base, Pruszynski *et al.*[11] have studied the reaction between TNT and *N,N,N',N'*-tetramethylguanidine (TMG) in aprotic solvents, namely acetonitrile and benzonitrile. The reaction in both solvents produces a purple solution due to ion-pair which has the absorption maxima similar to those observed for the reaction of TNT with ethoxide ion in ethanol. Further, they have investigated this reaction in DMF solvent and discussed the relation between kinetic isotope effects and steric effects of solvent.[12]

If we can obtain some informations on the effective mass or volume change accompanied with the proton-transfer reaction, the behavior of the solvent in the vicinity of the reactive site will be made clear. The volume of activation is well known to be a more easily interpretable quantity than the entropy or the energy of activation.[13] There are several works of high-pressure effects on the slow proton-transfer reactions.[14] However, as technical difficulty has restricted the high-pressure investigation on a reaction faster than several seconds, there are only a few reports on high-pressure effects on the fast proton-transfer reactions.[15,16] We reported previously[16] that the proton/deuteron-transfer reactions of 4NPNM+TMG in toluene and dichloromethane were accelerated at high pressure and the kinetic isotope rate ratio reduced from 11.9 at 1 bar to 9.3 at 1000 bar in toluene while it almost unchanged in dichloromethane(10.7±0.2).

In this paper we investigate the proton-transfer reactions between TNT(AH) and TMG(B) in acetonitrile and dichloromethane solvents by means of a high-pressure stopped-flow method up to 1000 bar at 25 °C. The reaction between TNT and 1,8-diazabicyclo[5.4.0]undec-7-ene (DBU) in both solvents is also studied. Such a base was chosen for the reasons that (a) the base nitrogen atom was not protonated in the free base,[7] (b) it was a strong base favorable to proton-transfer reaction, and (c) it was a cyclic amidine suitable for the study of the steric effect.

$$AH + B \underset{k_b}{\overset{k_f}{\rightleftharpoons}} [A]^-[BH]^+_{\text{ion pair}} \quad (1)$$

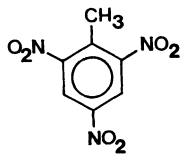

TNT

TMG

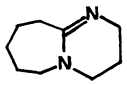

DBU

Experimental

Materials. 2,4,6-Trinitrotoluene (TNT) was purified by repeated crystallization from ethanol with charcoal; mp 81 °C. The purity of TNT was examined by NMR spectrum (methyl protons $\delta=2.75$, benzene ring protons $\delta=8.92$ in the ratio 3:2). *N,N,N',N'*-Tetramethylguanidine (TMG, Nakarai Chemicals Co. Ltd.) was dried with potassium hydroxide and then distilled under a nitrogen atmosphere; bp 161 °C (lit, 161 °C). 1,8-Diazabicyclo[5.4.0]-undec-7-ene(DBU, Nakarai Chemicals Co. Ltd., spectrograde reagent) was dried with potassium hydroxide and then distilled under reduced pressure. The pure DBU was identified by NMR spectrum. Acetonitrile was purified by the method of O'Donell[17] and then distilled over phosphorus pentaoxide; bp 82 °C. Dichloromethane was dried with calcium hydride and then distilled; bp 39.5—40 °C.

Apparatus and Procedure. Absorption spectra were determined by a Shimadzu UV-200S spectrophotometer. Kinetic measurements at 1 bar (1 bar=10^5 Pa) were carried out by a Union Giken RA-401 stopped-flow apparatus. In all measurements at 1 bar, the temperature was kept at 25.0±0.1 °C by circulating thermostated water. At

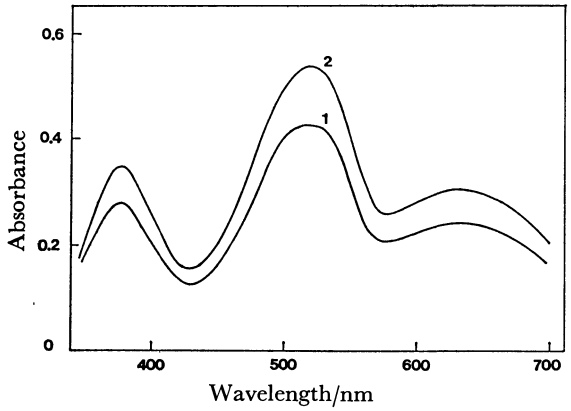

Fig. 1. Visible spectra of the product of the TNT+TMG reaction (1) and of the TNT+DBU reaction (2) in acetonitrile.

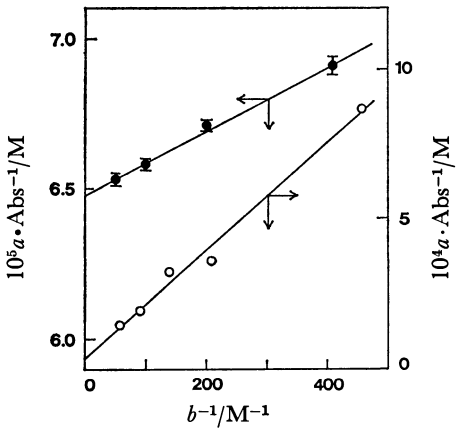

Fig. 2. Plots of a/Abs against reciprocal of DBU concentration in acetonitrile (open circles) and dichloromethane (closed circles) at 25 °C.

high pressure the reaction was followed by means of a high-pressure stopped-flow apparatus; the details were described elsewhere.[18] In high-pressure measurements the temperature was kept at 25.0±0.5 °C by circulating thermostated fluid around the high-pressure vessels.

The following weighed-in concentrations of solutions at 1 bar were freshly prepared every day before use: TNT 0.02—0.03 mM, TMG 2—10 mM in acetonitrile and TNT 0.1—0.3 mM, TMG 5—100 mM in dichloromethane; TNT 0.02—0.06 mM, DBU 2—13 mM in acetonitrile and TNT 0.04—0.08 mM, DBU 3—18 mM in dichloromethane.

The rate of the proton-transfer reactions of TNT with TMG and DBU was determined by monitoring the change of the absorption with time at 520 nm in acetonitrile and at 530 nm in dichloromethane. The increase of the absorbance obeyed first-order kinetics when the base (TMG, DBU) existed in large excess over TNT. The observed rate constant k_{obsd} was determined by the least-squares fitting to the Guggenheim plot.

Results

The reactions of TNT with TMG and DBU within the range of present experimental concentrations give the purple anion. The possibility of reactions other than the proton-transfer was ruled out with reference to the careful examinations of Pruszynski *et al.*[11] and

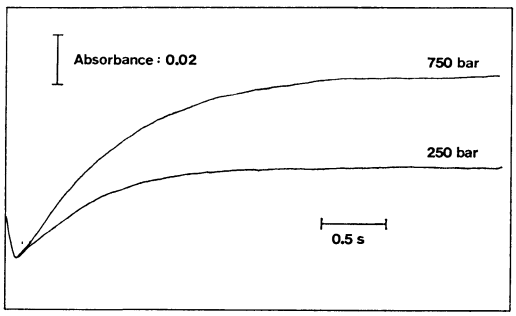

Fig. 3. Typical stopped-flow traces of the TNT+DBU reaction in dichloromethane at 25 °C. The absorbance change was monitored at 530 nm: [TNT]= 3.4×10^{-5} M, [DBU]=2.40×10^{-3} M at 1 bar.

Jarczewski *et al.*[12] The absorption maxima for the ion-pair produced by a proton-transfer from the methyl group of TNT to TMG are around 375, 530, 635 nm in dichloromethane and identical to those observed in acetonitrile (378, 520, 635 nm). The reaction mixtures between TNT and DBU show the absorption maxima at around 375, 530, 635 nm in dichloromethane and 378, 520, 635 nm in acetonitrile; they are very similar to those observed in the reaction between TNT and TMG (Fig. 1), while each reactant is transparent in the visible region.

The equilibrium constant of the TNT+DBU reaction was determined at 25 °C and 1 bar according to the Benesi-Hildebrand equation (2).[19] In this equation, [a] is the initial concentration of TNT, [b] that of the base, K the equilibrium constant, ε the molar absorption coefficient, Abs the absorbance at 520 nm in acetonitrile and 530 nm in dichloromethane at the equilibration. The fact that the plot of Eq. 2 gives a very good straight line as shown in Fig. 2 supports that the product is not separate ions but a contact one, namely ion-pair. Otherwise the plot would be significantly curved and the following would be valid:

$$\frac{[a]}{Abs} = \frac{1}{K\varepsilon}\frac{1}{[b]} + \frac{1}{\varepsilon} \quad (2)$$

$$\frac{[a]}{Abs} = \frac{1}{K\varepsilon^2}\frac{Abs}{[b]} + \frac{1}{\varepsilon}. \quad (3)$$

Therefore, it is concluded that the reaction path between TNT and DBU is simple and the same as that between TNT and TMG as described below.

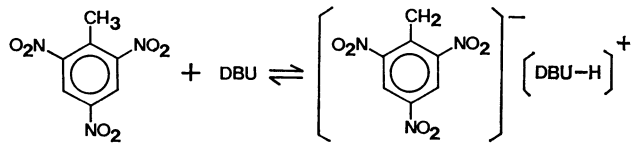

(4)

In Fig. 3 are shown some representative traces of the increase of absorption with time. The stopped-flow trace at each pressure obeyed a first-order kinetic equation. The plot of k_{obsd} against TMG or DBU concentration [b] is of a straight line at each pressure (Figs. 4 and 5), in agreement with Eq. 5.

$$k_{obsd} = k_f[b] + k_b \quad (5)$$

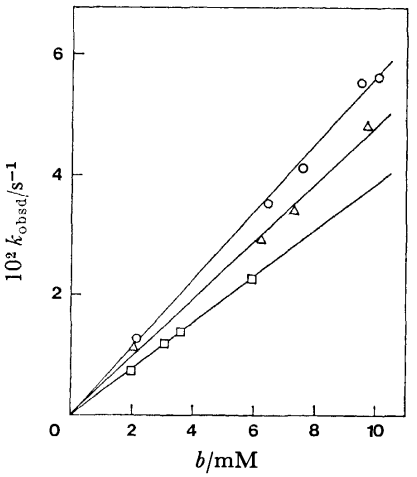

Fig. 4. Dependence of k_{obsd} on TMG concentration in acetonitrile at 25 °C.
□: 1 bar, △: 500 bar, ○: 1000 bar.

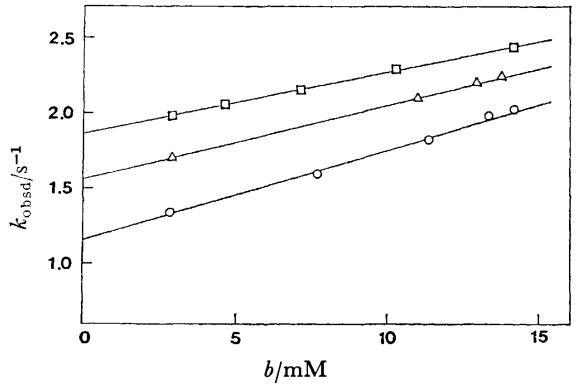

Fig. 5. Dependence of k_{obsd} on DBU concentration in dichloromethane at 25 °C.
□: 1 bar, △: 500 bar, ○: 1000 bar.

In the equation, k_f and k_b are the forward and backward rate constants of the proton-transfer reactions. Since molar concentration unit is convenient to compare the rate constants at various conditions, we corrected the weighed-in concentration at 1 bar for the compression of each solvent to know [b] of molar unit at high pressure. In the plots of Figs. 4 and 5, compression was taken into account on the basis of data of Srinivasan *et al.*[20] for acetonitrile and of Newitt *et al.*[21] for dichloromethane. Thus the values of k_f and k_b were determined from the dependence of k_{obsd} on TMG and DBU concentration by a least-squares method. The values of k_f are given in Table 1. The values of k_b in dichloromethane are given in Table 2, but in acetonitrile they are too small to be reliable and are not recorded. The equilibrium constants K are also evaluated and listed in Table 2.

The volume of activation ΔV^* for either k_f or k_b was determined by

$$\left(\frac{\partial \ln k}{\partial p}\right)_T = -\frac{\Delta V^*}{RT} + \Delta n^* \kappa, \qquad (6)$$

where, κ is the compressibility of the solvent, Δn^* the difference of the number of molecules from the initial to the transition state, T the absolute temperature, and R the gas constant. In the present reaction, the value of Δn^* is -1 for the forward reaction and zero for the backward one. The value of κ at 25 °C were calculated from the literatures.[20,21] The plots of $\ln k_f$ against pressure were almost linear for both systems and both solvents (Figs. 6 and 7). The values of ΔV_f^* are given in Table 3 together with ΔV_b^*.

Table 1. Rate constants k_f ($M^{-1}\,s^{-1}$) at 25 °C

p/bar	(1)[a]		(2)[b]	
	AN[c]	DCM[d]	AN[c]	DCM[d]
1	3.84±0.05	3.13±0.07	204±4	41.8±0.8
250	4.17±0.08	3.71±0.10	220±4	46.9±1.0
500	4.73±0.09	4.58±0.10	230±4	49.2±0.8
750	5.34±0.10	5.19±0.12	238±5	52.4±1.2
1000	5.61±0.14	6.12±0.14	267±6	60.3±1.0

a) k_f of the TNT+TMG reaction. b) k_f of the TNT+DBU reaction. c) Acetonitrile solvent. d) Dichloromethane solvent.

Table 2. Rate constants k_b and equilibrium constants K in dichloromethane at 25 °C

p/bar	k_b/s^{-1}		K[a] $(=k_f/k_b)/M^{-1}$	
	(1)[b]	(2)[c]	(1)[b]	(2)[c]
1	1.53±0.03	1.87±0.03	2.05 (2.0±0.6)[d]	22.4 (24±5)[d]
250	1.31±0.04	1.73±0.04	2.83	27.1
500	1.18±0.03	1.57±0.03	3.88	31.3
750	0.97±0.03	1.39±0.04	5.35	37.7
1000	0.76±0.03	1.15±0.03	8.05	52.4

a) K in acetonitrile at 1 bar and 25 °C is 4100 in the TNT+TMG reaction from Ref. 11 and 6070 in the TNT+DBU reaction from our result. b) The TNT+TMG reaction. c) The TNT+DBU reaction. d) From equilibrium measurement.

Discussion

Equilibrium and Rate Constants at Atmospheric Pressure. In the reaction between TNT and ethoxide ion, Buncel *et al.*[10] found that when first-order rate constants k_{obsd} were plotted against ethoxide ion concentration it was slightly curved. The analysis of these results led them to the conclusion that the brown species other than TNT^- was formed. However, in the reaction between TNT and TMG, Pruszynski *et al.*[11] obtained a linear relation obeying Eq. 5 in both acetonitrile and benzonitrile. In our experiments also, the plots of k_{obsd} against TMG and DBU concentration [b] gave a straight line in acetonitrile and dichloromethane. The equilibrium constants obtained by rate constant ratio $K(=k_f/k_b)$ are well in accord with the direct determination after equilibration by Eq. 2 (Table 2), which strengthens the reliability of the determined rate constants.

The rate constant k_f of TNT+TMG reaction at 25 °C and 1 bar is 3.84±0.05 $M^{-1}\,s^{-1}$ in acetonitrile, which is almost equal to Pruszynski's value (k_f= 4.04±0.12 $M^{-1}\,s^{-1}$), and 3.13±0.07 $M^{-1}\,s^{-1}$ in dichlo-

Table 3. Volumetric data at 25 °C and 1 bar

	(1)[a]		(2)[b]	
	AN[c]	DCM[d]	AN[c]	DCM[d]
ΔV_f^*/cm^3 mol^{-1}	−12.7±1.0	−19.0±1.5	−9.0±1.0	−10.8±1.0
ΔV_b^*/cm^3 mol^{-1}	—	+17.1±1.7	—	+11.9±1.2
ΔV°/cm^3 mol^{-1} [e]	—	−36.1±3.2	—	−22.7±2.2

a) The TNT+TMG reaction. b) The TNT+DBU reaction. c) Acetonitrile solvent. d) Dichloromethane solvent. e) $\Delta V^\circ = \Delta V_f^* - \Delta V_b^*$.

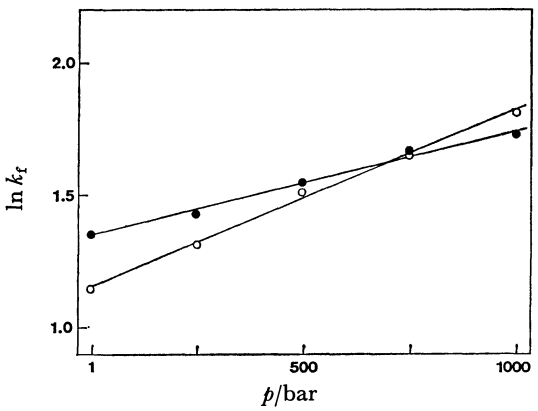

Fig. 6. Pressure dependence of ln k_f of the TNT+TMG reaction in acetonitrile (closed circles) and dichloromethane (open circles).

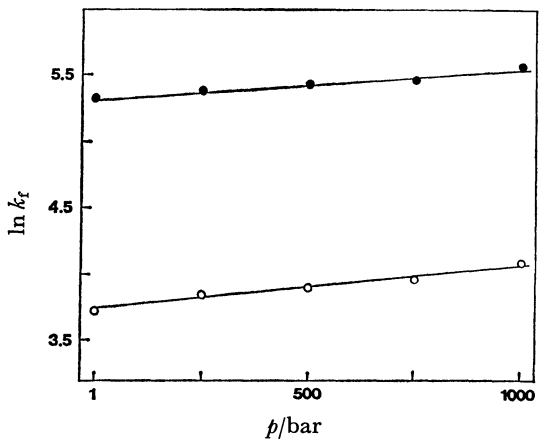

Fig. 7. Pressure dependence of ln k_f of the TNT+DBU reaction in acetonitrile (closed circles) and dichloromethane (open circles).

romethane. In the reaction between TNT and DBU, the value of k_f is 204±4 M^{-1} s^{-1} in acetonitrile and 41.8±0.8 M^{-1} s^{-1} in dichloromethane. In both reactions, the rate constants of the forward reaction in acetonitrile (dielectric constant; ε=36) are larger than those in dichloromethane (ε=8.9). These kinetic behaviors are in accord with the view that each reaction involves the formation of a polar transition state since the polar transition state is, in general, more stabilized in the higher polarity of solvent. Further, the kinetic results for TNT may be compared with those reported for the corresponding reaction of 4NPNM with TMG and DBU.[4,22] The forward rate constant k_f of the reaction of 4NPNM at 25 °C in toluene is larger for DBU (k_f=2.7×10^5 M^{-1} s^{-1}) than for TMG (k_f=2.29×10^3 M^{-1} s^{-1}) by a factor of about 120. While in our results k_f of the reaction of TNT is larger for DBU than for TMG by a factor of about 55 in acetonitrile and 15 in dichloromethane. Thus the explanation on the difference in solvent sensitivity between TMG and DBU is, even qualitatively controversial at present, but it is clear that 4NPNM releases the α-proton more easily than TNT irrespective of solvent or base.

Judging from the results of the reaction with 4NPNM,[22] DBU is a much stronger base: the equilibrium constant K at 25 °C is about 100 times larger than for *N,N*-diethylpentanamidine and about 70 times larger than for *N,N*-diethyldecanamidine. As found in Table 2, K between TNT and DBU is larger than between TNT and TMG: DBU is a much stronger base than TMG especially in less polar solvent. Between TNT and DBU, K at 25 °C and 1 bar is 6070±600 M^{-1} in acetonitrile and 24±5 M^{-1} in dichloromethane (from kinetic measurements, $K=k_f/k_b$ is 5200±400 and 22±4 M^{-1}, respectively). Therefore, the stability of the ion-pair in acetonitrile is higher than that in dichloromethane.

Pressure Effects on Reaction Rates. The volume of activation ΔV^* of chemical reactions in solution are recognized to give very important information about the reaction mechanism and the role of the solvent during activation.[23] ΔV^* mainly consists of two major contributions, one due to the structural change of activation (ΔV_{str}^*), and the other due to the solvation change (ΔV_{solv}^*) on going from the initial to the transition state.[24] In the case of the bond-forming process, ΔV_{str}^* would be negative. When electronic charge is generated during activation, ΔV_{solv}^* will also be negative. The proton-transfer reaction from TNT to TMG and DBU conforms to the above case; in fact, our data result is the negative values of the volume of activation. The volume of activation of the forward reaction ΔV_f^* of TNT+TMG reaction is −12.7±1.0 cm^3 mol^{-1} in acetonitrile and −19.0±1.0 cm^3 mol^{-1} in dichloromethane, and then ΔV_f^* of TNT+DBU reaction is −9.0±1.0, −10.8±1.0 cm^3 mol^{-1}, respectively. Absolute value of ΔV_f^* for TNT+TMG reaction in dichloromethane is a little larger than that of 4NPNM+TMG reaction (−15.3±1.5 cm^3 mol^{-1})[16a] and that of 4NPNM+TMG-d_2 (−14.6±1.7 cm^3 mol^{-1}).[16b]

On the basis of Kirkwood's theory,[25] Eqs. 7 and 8 hold for k and ΔV^*, respectively;

$$\ln k = \ln k_0 + (N_0\Sigma\mu^2/a^3)q, \quad (7)$$

$$\Delta V^* = \Delta V_0^* - (N_0\Sigma\mu^2/a^3)(\partial q/\partial p)_T, \quad (8)$$

where $q=(\varepsilon-1)/(2\varepsilon+1)$, μ and a are dipole moment and radius, respectively, $\sum\mu^2/a^3$ the difference between the initial state and the transition state, and N_0 Avogadro's number. Since the reaction studied here proceeds through a highly polar transition state, the term $\sum\mu^2/a^3$ is expected to be positive. In many cases, though not generally, the larger the q value (the higher dielectric constant) the smaller the $(\partial q/\partial p)_T$ term. Thus, our results that the forward reaction proceeds faster and ΔV_f^* is less negative in the more polar solvent will be qualitatively explained by the above electrostatic solvation-model of an ionogenic reaction: similar tendency is found in many Menschutkin reactions.[26] Hence it is likely that even in the solvent of low polarity such as dichloromethane solvation in the proximity of reaction center, more or less, takes places.

Absolute values of ΔV_f^* for DBU are larger than those for TMG in both solvents. This may be attributed to the steric effect of DBU, that is, the nonplanar seven-membered ring of DBU will prevent solvation in the vicinity of reaction center. ΔV_f^* values in dichloromethane are considerably less negative compared with the volume change of reaction $\Delta V^\circ(=\Delta V_f^*-\Delta V_b^*)$ (Table 3). The transition state is therefore not as highly ionic as the ion-pair.

Further studies of the rate and its kinetic isotope effect in many solvents and other systems at high pressure will reveal the behavior of the solvent in the vicinity of reaction site.

The authors are grateful to Mr. Fujitugu Amita for maintenance of the high-pressure stopped-flow apparatus. The present work was supported by a Grant-in-Aid for Scientific Research No. 454123 from the Ministry of Education, Science and Culture.

References

1) E. F. Caldin, *Chem. Rev.*, **69**, 135 (1969) and the references cited therein.
2) R. P. Bell, "The Proton in Chemistry," 2nd ed, Chapman and Hall, London (1973).
3) E. F. Caldin and V. Gold, "Proton-Transfer Reaction," Chapman and Hall, London (1975).
4) E. F. Caldin and S. Mateo, *J. Chem. Soc., Faraday Trans. 1*, **71**, 1876 (1975).
5) E. F. Caldin, D. M. Parboo, F. A. Walker, and C. J. Wilson, *J. Chem. Soc., Faraday Trans. 1*, **72**, 1856, 2645 (1976).
6) A. Jarczewski, P. Pruszynski, and K. T. Leffek, *Can. J. Chem.*, **53**, 1176 (1975).
7) Rogne pointed out that in the deuteron-transfer reaction between 4NPNM-d_2 and nondeuterated TMG the isotopic exchange scrambling had to be taken into account. O. Rogne, *Acta Chem. Scand. A*, **32**, 559 (1978); J. H. Blanch and O. Rogne, *J. Chem. Soc., Faraday Trans. 1*, **74**, 1254 (1978).
8) E. F. Caldin and G. Long, *Proc. R. Soc. London, Ser. A*, **226**, 263 (1955).
9) C. F. Bernasconi, *J. Org. Chem.*, **36**, 167 (1971).
10) E. Buncel, A. R. Norris, K. E. Russell, and R. Tucker, *J. Am. Chem. Soc.*, **94**, 1646 (1972).
11) P. Pruszynski and A. Jarczewski, *Rocz. Chem.*, **51**, 2171 (1977).
12) A. Jarczewski, P. Pruszynski, and K. T. Leffek, *Can. J. Chem.*, **57**, 669 (1979).
13) W. J. le Noble, *Prog. Phys. Org. Chem.*, **5**, 207 (1967).
14) D. A. Palmer and H. Kelm, *Aust. J. Chem.*, **30**, 1229 (1977); K. R. Brower and H. Hughes, *J. Am. Chem. Soc.*, **100**, 7591 (1978); N. S. Isaacs, K. Javaid, and E. Rannala, *J. Chem. Soc., Parkin Trans. 2*, **1978**, 709; H. Inoue, *Rev. Phys. Chem. Jpn.*, **49**, 95 (1979).
15) C. D. Hubbard, C. J. Wilson, and E. F. Caldin, *J. Am. Chem. Soc.*, **98**, 1870 (1976).
16) a) M. Sasaki, N. Sugimoto, and J. Osugi, *Chem. Lett.*, **1980**, 887; b) N. Sugimoto, M. Sasaki, and J. Osugi, *Bull. Inst. Chem. Res., Kyoto Univ.*, **59**, 1981, in press.
17) J. F. O'Donnell, J. T. Ayers, and C. K. Mann, *Anal. Chem.*, **37**, 1161 (1965).
18) M. Sasaki, F. Amita, and J. Osugi, *Rev. Sci. Instrum.*, **50**, 1104 (1979).
19) H. A. Benesi and J. H. Hildebrand, *J. Am. Chem. Soc.*, **71**, 2703 (1949).
20) K. R. Srinivasan and R. L. Kay, *J. Solution Chem.*, **6**, 357 (1977).
21) D. M. Newitt and K. E. Weale, *J. Chem. Soc.*, **1951**, 3092.
22) E. F. Caldin and O. Rogne, *J. Chem. Soc., Faraday Trans. 1*, **74**, 2065 (1978).
23) T. Asano and W. J. le Noble, *Chem. Rev.*, **78**, 407 (1978) and the literatures cited therein.
24) M. G. Evans and M. Polanyi, *Trans. Faraday Soc.*, **31**, 875 (1935).
25) J. K. Kirkwood, *J. Chem. Phys.*, **2**, 351 (1934).
26) H. Hartmann, H. D. Braner, and G. Rinck, *Z. Phys. Chem.*, **61**, 47 (1967); Y. Kondo, M. Tojima, and N. Tokura, *Bull. Chem. Soc. Jpn.*, **40**, 1408 (1967); Y. Kondo, M. Uchida, and N. Tokura, *ibid.*, **41**, 992 (1968).

Raman Spectra of a Compound under Inversion Motions. II. *N*-Methylpiperazine

Kunio FUKUSHIMA* and Hiromichi TAKAHASHI

Department of Chemistry, Faculty of Science, Shizuoka University, 836 Oya, Shizuoka 422

(Received March 13, 1981)

Raman spectra of *N*-methylpiperazine in proton donors and acceptors were measured. Forms of stable conformers in the donors and the acceptors were studied by comparison of the Raman spectra and normal vibration calculations. A conformational change of the molecule in the donors was found, suggesting the change of valence state of nitrogen atom, which is caused by hydrogen bonding.

One of the present authors reported[1] the conformational change of *N,N'*-dimethylpiperazine, which might be ascribed to suppression of inversion motion at nitrogen by hydrogen bonding. In the present study, the effect of hydrogen bonding on molecular conformation of *N*-methylpiperazine molecule, which has two nitrogen atoms, one bonded by a light atom and the other bonded by a heavier group, was investigated in order to compare the effect by hydrogen bonding on the valence state of nitrogen atoms in different situations.

Experimental

Commercial *N*-methylpiperazine (grade GR, Tokyo Kasei Chemicals Co., Ltd.) distilled under vacuum was used. Raman spectra were measured with a Model R-800T Raman Spectrophotometer (Japan Spectroscopic Co., Ltd.) under excitation with a Spectra Physics argon ion laser (model 165) using 514.5 nm line (300 mW). Depolarization ratio was measured by use of a system consisting of a half-wave plate, a lens and a polarizer. Measured depolarization ratio of the Raman bands of carbon tetrachloride at 459 cm^{-1} (A_1 species) and at 218 cm^{-1} (E species) were 0.007 ± 0.001 and 0.75 ± 0.01, respectively. Liquid samples at room temperature were measured with 0.3 ml Raman cells, while crystal at low temperature was measured with an Oxford-type cryostatt and liquid nitrogen. The experimental results are shown in Tables 1—2 and Figs. 1—2.

Results and Discussion

In the following discussion, refer to Tables 1—2 and Figs. 1—2.

Raman Spectrum Change Associated with Hydrogen Bonding. The three Raman bands of pure liquid at 615 cm^{-1}, 608 cm^{-1}, and 587 cm^{-1} reduce their frequencies by *N*-deuteration as shown in the spectrum of heavy water solution. On the other hand, the band at 339 cm^{-1} shifts to 330 cm^{-1} by an apparently small frequency decrease as the result of both decrease of frequency on *N*-deuteration and increase of frequency by hydration. On the basis of the frequency changes, they are ascribed to the vibrations of –NH– group. Among them, the band at 615 cm^{-1} reduces its intensity both in the benzene and the acetone solutions, where concentration of the species hydrogen-bonded to the nitrogen atom in the group decreases. Therefore, it is assigned to the species, which is hydrogen-bonded to the nitrogen atom, though which might be hydrogen-bonding to other molecule. On the other hand, the band at 587 cm^{-1} increases its intensity in the solutions, being assigned to the species, which is not hydrogen-bonded to the nitrogen atom.

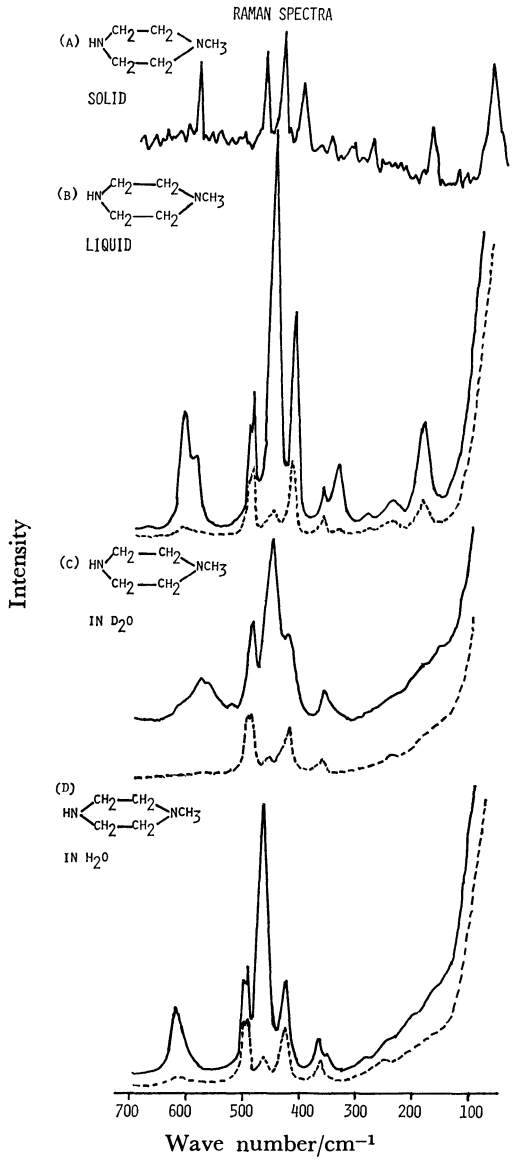

Fig. 1. Raman spectra of *N*-methylpiperazine. (A): Solid at −63 °C, (B): liquid at room temperature, (C): heavy water solution (mole fraction=0.335), (D): aqueous solution (mole fraction=0.335) Solid line: $I_{//}$, dotted line: $I_{\perp}$.

Intensity of the band at 608 cm^{-1} decreases in the acetone solution, in which the species hydrogen-bonding to acetone molecule but not hydrogen-bonded to its nitrogen atom increases. Therefore, it is assigned to the species which is hydrogen-bonded to its nitrogen, but is not hydrogen-bonding to other

TABLE 1. OBSERVED RAMAN SHIFT FREQUENCIES OF *N*-METHYLPIPERAZINE (in cm^{-1})

Liq			C_6H_6 soln		$(CH_3)_2CO$ soln		H_2O soln		CH_3OH soln		D_2O soln		Solid	
ν	I	ρ	ν	I	ν	I	ν	I	ν	I	ν	I	ν	I
1467	34	0.60	1465	32			1472	25	1465	?*	1471	36	1463	32
1447	29	0.60	1442	28	1464	22	1453	22	1446	?*	1452	28	1460	44
1423	11	0.62	1423	sh	1420	13	1426	6	1422	sh	1426	9	1435	53
1397	3	0.54											1389	12
1377	4	0.50	1370	3	1365	4	1379	3	1376	15	1375	5	1370	6
1366	4	0.47	1366	sh									1366	sh
1345	4	0.57					1353	2	1348	5	1335	6	1345	9
1328	7	?	1330	sh	1318	8	1322	8	1317	11	1323	sh	1330	9
1316	11	0.61	1317	10			1307	20	1302	24	1307	27	1316	9
1303	30	0.44	1300	31	1300	17	1298	13	1292	16	1292	16		
													1292	88
1288	20	0.26	1286	19	1284	12	1284	sh						
1275	7	?	1275	sh	1270	4							1270	15
											1248	8		
1197	18	0.56	1194	21	1193	10	1202	13	1194	16	1198	17	1200	9
1187	10	?	1187	sh			1190	7	1183	11	1182	sh	1183	44
1178	9	?	1178	45	1176	6	1178	9					1172	15
							1165	10	1158	13	1160	14		
1155	13	0.52	1152	24			1152	10						
					1144	14			1147	sh	1143	15	1143	41
									1138	14				
1102	9	0.28	1102	sh			1107	8	1101	17*	1100	9	1102	6
1094	7	?	1096	9	1097	6							1094	12
1065	20	0.51	1061	23	1060	16*	1068	16			1063	8	1065	sh
									1058	25				
1053	9	?	1050	sh	1053	sh	1053	7			1050	15	1059	68
1037	11	0.61	1032	13	1030	7	1039	12	1034	?*	1035	15		
													1025	6
1018	9	0.52	*		1010	6	1018	5			1015	7		
1006	7	0.49	*		1000	4	1008	4			1005	5	1010	21
											983	6		
917	14	?	917	sh			910	8					925	29
					900	15								
897	26	0.04	896	41	895	17	895	sh	902	8			900	2
							867	8	872	sh	870	39		
853	10	0.41	850	15	850	5	855	9	857	sh			842	29
									846	9				
839	9	0.45	840	sh	832	6	839	9	830	8	830	sh		
825	7	?	820	sh					819	sh	827	13	825	12
783	100	0.18	780	100			782	100	775	100	780	100	773	100
					727	8								
615	20	0.08	612	sh			616	15	611	16				
608	21	0.07	608	86*	603	12	603	sh	603	sh				
587	13	0.11	585	26	593	13	593	sh	593	sh			592	38
											580	11		
495	19	0.59	490	sh	489	17	496	18	488	14	493	sh		
487	14	0.52	486	23	482	16	490	21	482	16	486	23	475	41
453	70	0.06	448	82	448	47	462	53	458	39	454	41		
440	sh	?	440	sh	439	38					440	sh	444	53
417	38	0.34	414	47	411	29	423	18	418	13	420	19		
													407	29
363	7	0.57	360	6	358	5	363	6	356	4	363	7	360	12
339	8	0.14	333	11	333	9	350	sh					323	9
											330	?		
285	1	0.56	284	1			283	?	278	?	285	?	286	13
244	2	0.75	240	3	252	7	245	?	235	?	245	?	244	6
							200	?						
185	15	0.30	178	10	177	5	190	?			190	?	182	26
													77	50

*: Overlapped by solvent band, ν: shift frequency, I: relative intensity, ρ: depolarization ratio.

TABLE 2. CALCULATED FREQUENCIES OF NON-HYDROGEN-BONDED *N*-METHYLPIPERAZINE COMPARED WITH THE OBSERVED FREQUENCIES (in cm^{-1})

Obsd	ee	e(CH_3)a(H)	aa	a(CH_3)e(H)	Description
			650 (A')	645 (A')	CH_2 rock, CCN def
587 (P)	612 (A')	618 (A')			C(NH)C def
					CCN def
			528 (A'')	529 (A'')	CCN def
			518 (A')	525 (A')	CCN def
487 (P, DP?)	503 (A'')	501 (A'')			CCN def
440 (P)	454 (A')	450 (A')			CNC def, CCN def
			438 (A')	435 (A')	CNC def
417 (P)	420 (A')	421 (A')			CNC def
			403 (A'')	403 (A'')	CNC def
363 (P, DP?)	366 (A'')	367 (A'')			CNC def, CCN def
339 (P)	322 (A')	326 (A')			CNC def, CN tors
			314 (A')	311 (A')	CNC def
244 (DP)	257 (A'')	256 (A'')			CC tors, CCN def
			220 (A'')	221 (A'')	CCN def
185 (P)	193 (A'')	193 (A'')	194 (A'')	194 (A'')	NC tors
	159 (A')	162 (A')			CNC def, CCN def
			133 (A')	131 (A')	CNC def, NC tors

P: Polarized, DP: depolarized, rock: rocking, def: deformation, tors: torsion, ee: diequatorial, aa: diaxial.

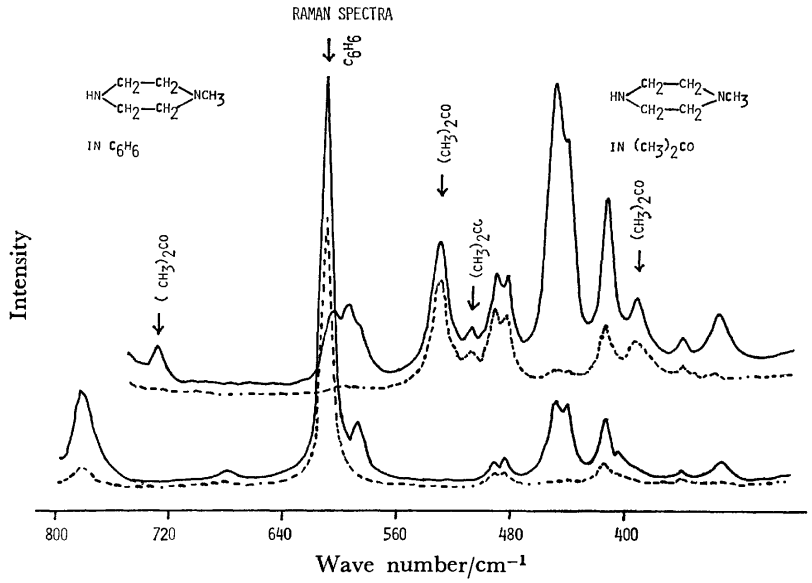

Fig. 2. Raman spectra of *N*-methylpiperazine.
Acetone solution (mole fraction=0.260), benzene solution (mole fraction=0.150).
Solid line: $I_{//}$, dotted line: $I_{\perp}$.

molecule. In the aqueous solution, the band at 587 cm^{-1} becomes weaker, and the band at 615 cm^{-1} becomes intense, so being the case for the methanol solution. Intensity of the band at 339 cm^{-1} increases in the benzene and the acetone solutions, while it decreases in the aqueous and the methanol solutions. So, the band is assigned to a vibration of –NH– group of the species, which is not hydrogen-bonded to nitrogen atom. In the latter solutions, frequency of the band increases to 363 cm^{-1} on hydrogen bonding to nitrogen atom.

These changes indicate that the bands at 587 cm^{-1} and 339 cm^{-1} arising from non-bonded –NH– group increase their frequencies to 615 cm^{-1} or 608 cm^{-1} and 363 cm^{-1} by being hydrogen-bonded to the nitrogen atom.

Frequencies of the bands of pure liquid at 453 cm^{-1}, 440 cm^{-1}, and 363 cm^{-1}, do not change much on *N*-deuteration. The band at 440 cm^{-1} increases its intensity in the benzene and the acetone solutions, while its intensity decreases in the aqueous and the methanol solutions. Therefore, it is attributed to the species which is not hydrogen-bonded to the nitrogen atom of –N(CH_3)– group. The other two bands at 453 cm^{-1} and 363 cm^{-1}, which are intense in the aqueous and the methanol solutions, are attributed to the species hydrogen bonded to the nitrogen atom of –N(CH_3)– group, although the latter band might be overlapped by a band of non-bonded species. Based on these changes, it is concluded that the band at 440 cm^{-1} of non-bonded –N(CH_3)– group increases its frequency to 453 cm^{-1} on the hydrogen bond for-

Table 3. Force constants of *N*-methylpiperazine (in mdyn/Å)

K(N-H)	5.900	H(HCN)(CH_3)	0.272	Y(NH-C)	0.058
K(C-N)	3.017	H(HCH)(CH_3)	0.513	Y(C-C)	0.107
K(C-C)	2.304	F(HNC)	0.313	Y(N(CH_3)-C)	0.062
K(C-H)(CH_2)	4.050	F(CNC)	0.195	Y(CH_3-N)	0·062
K(C-H)(CH_3)	4.437	F(NCC)	0.700	κ(CH_2)	0.030
H(HNC)	0.307	F(HCC)	0.482	κ(CH_3)	−0.010
H(CNC)	0.482	F(HCN)	0.664	t	0.107
H(NCC)	0.300	F(HCH)	0.069	g	−0.025
H(HCC)	0.217	F(HCN)(CH_3)	0.664		
H(HCN)	0.219	F(HCH)(CH_3)	0.173		
H(HCH)	0.363				

K: Stretching force constant, H: angle bending force constant, F: repulsive force constant, Y: internal rotation force constant, κ: intramolecular tension, t: trans coupling force constant, g: gauche coupling force constant.

mation.

Frequency change associated with hydrogen bonding to nitrogen atom in the case of –NH– group ((615−587)/587=0.048, (608−587)/587=0.036; (363−339)/339=0.071) is larger than that of –N(CH_3)– group ((453−440)/440=0.030).

Comparison of the Bands of Non-bonded Species with Normal Vibration Calculation and the Bands of the Solid. The results of normal vibration calculation according to Wilson's GF matrix method[2] by use of the modified Urey-Bradley force field and the force constants in Table 3 are shown in Table 2, compared with the observed frequencies of the non-bonded species. The observed frequencies agree well to the calculated frequencies of ee form or e(CH_3)a(H) (e: equatorial, a: axial), but they are not consistent with those of aa form or a(CH_3)e(H) form. Therefore, it is probable that molecular form of non-bonded species is close to ee form or e(CH_3)a(H) form. As valence state of nitrogen atom is almost sp^3 in the species hydrogen-bonded to the nitrogen atom, the observed frequencies in Table 2 are considered to be due to the molecular form, which is close to but not the same as the form having sp^3 valence state of nitrogen atom. In the solid state, species having similar molecular form persists as frequencies of the non-bonded species are somewhat close to those in the spectrum of the solid in the region below 700 cm^{-1}. From the above discussion, it is concluded that in the liquid state non-bonded *N*-methylpiperazine molecules are in one form close to ee or e(CH_3)a(H) form and that some of normal frequencies of –NH– or –N(CH_3)– group of the form are affected very much by hydrogen bonding to the nitrogen atom of –NH– or –N(CH_3)– group. The frequency changes on hydrogen bonding cannot be explained as the conformational change, ee or e(CH_3)a(H)→aa or a(CH_3)e(H), because the frequency of the polarized band at 339 cm^{-1} decreases and those of the bands at 363 cm^{-1}, 417 cm^{-1}, 440 cm^{-1}, and 587 cm^{-1} all increase in the case of the conformational change, while the observed change is contradictory to the change as shown in Table 2. Therefore, the change may be ascribed to change of valence state of nitrogen atom from the state for the ground state of the normal vibration associated with inversion coordinate to sp^3 type in hydrogen-bonded nitrogen atom.

Interpretation of the Spectrum Change Associated with Hydrogen Bonding. According to the normal vibration calculation, the Raman bands at 339 cm^{-1}, 440 cm^{-1}, and 587 cm^{-1}, which are affected much by hydrogen bonding, correspond to the vibrations to which the symmetrical skeletal deformation modes (A′ species) contribute to a great deal. These modes are related to the coordinates of inversions, ring inversion and inversion at nitrogen. It has been reported for 1,4-dimethylpiperazine and other compounds that rate of inversion at nitrogen is much faster than that of ring inversion and also that the activation energy for inversion at nitrogen of 1,4-dimethylpiperazine is a rather small value of 14 kJ mol^{-1}.[3] Therefore, the potential barrier for inversion at nitrogen is expected to be lower than that for ring inversion. When *N*-methylpiperazine is hydrogen-bonded, inversion at nitrogen may be suppressed and the molecule is likely to be primarily under ring inversion. In that situation, the potential is different from that of inversion motion including inversion at nitrogen especially in the height of potential barrier and the anharmonicity. The change of shape of the potential by hydrogen bonding necessarily accompanies the change of energy levels of normal vibrations associated with inversion coordinates as well as the change of molecular structure for the vibrational ground state. Thus, for the vibrations, to which inversion coordinates contribute, the energy difference between ground state (v=0) and the first excited state (v=1) become different between non-bonded molecule and hydrogen-bonded molecule. The Raman shift frequencies which we observe are related to the transition from the ground state to the first excited state, and therefore, they change considerably by the change of the energy difference of the energy levels.

Difference of frequency change associated with hydrogen bonding to nitrogen atom suggests that potential barrier of inversion at nitrogen of –NH– group is different from that of –N(CH_3)– group.

References

1) K. Fukushima, *Bull. Chem. Soc. Jpn.*, **52**, 2871 (1979).
2) E. B. Wilson, Jr., *J. Chem. Phys.*, **7**, 1047 (1939); **9**, 76 (1941).
3) V. M. Gittins, P. J. Heywood, and E. Wyn-Jones, *J. Chem. Soc., Perkin Trans. 2*, **1975**, 1642.

  Bull. Chem. Soc. Jpn., 54, 2607—2609 (1981)

Pressure Dependence and Cationic Radius Effect of the Glass Transition Temperature in Aqueous Alkali Acetate Solutions

Hitoshi KANNO,* Ichimin SHIROTANI,† and Shigeru MINOMURA†

Department of Chemistry, Meisei University, Hino, Tokyo 191

† *The Institute for Solid State Physics, The University of Tokyo, Roppongi, Minato-ku, Tokyo 106*

(Received March 25, 1981)

The glass transition temperature (T_g) is measured as a function of pressure up to 200 MPa for the aqueous Li, Na, K, Rb, and Cs acetate solutions. The effects of cation radius on the glass transition of these solutions are discussed and some attempts are made to correlate T_g (and associated properties) with r (cation radius).

Glass transition is characterized by a heat absorbing inflection in a DTA trace and affected by many factors.[1] In recent glass formation studies,[2,3] it is shown that glass transition temperature (T_g) is a good diagnostic parameter to represent thermodynamic and transport properties of a supercooled liquid and glass system. In contrast to silicate and borate systems,[4] glass formation studies of aqueous solutions have been still scarce.

As aqueous electrolyte solutions in high concentrations are a very complicated system, defying any simple theoretical treatment, it is of importance, as a first step, to investigate the effects of various factors affecting the magnitude of T_g. Ionic radius of ions (r) is of course an important factor in transport and thermodynamic properties of aqueous solutions.[5] Alkali ions are simple in structure and essentially ionic so that aqueous solutions of alkali salts are a suitable target if only they are glass-forming. It is expected that the effect of pressure on T_g can be an auxilliary diagnostic tool to clarify the structure and thermodynamic properties of concentrated aqueous solutions.

In this work, we have measured the glass transition temperatures of aqueous alkali acetate solutions as a function of pressure and discussed the effects of pressure and cation radius on the glass transition of the solutions.

Experimental

Aqueous solutions of alkali acetates were prepared by dissolving guaranteed grade alkali acetates in distilled water. The concentration was all set to be $R=10$ (R=mol of water/mol of salt). The high pressure DTA cell is essentially the same one as used in the measurements of homogeneous nucleation temperature of emulsified aqueous solutions and water.[6] The sample container used for the high pressure experiment was a 1 mm inner-diameter capillary glass cell, in which an aliquot of sample solution was filled and an alumel-cromel thermocouple junction (Omega-clad 0.02 inch o.d. thermocouples) was inserted. As a pressure transmitting fluid and the reference material, a 1:1 mixture of methylcyclopentane and methylcyclohexane was used because of its low vitrification temperature (below −150 °C at atmospheric pressure).

Vitrification of the sample solution was made at pressure of about 30 MPa by plunging the high pressure cell directly into liquid nitrogen. The overall cooling rate was about 200 K/min. Then the differential and temperature emf's were recorded at a heating rate of about 5 K/min in the temperature range where the glass transition took place Immediately after observing the glass transition, pressure was increased by 20—30 MPa and then the high pressure cell was cooled to liquid nitrogen temperature. This process was repeated up to pressure about 200 MPa.

T_g at atmospheric pressure was also measured with a simple DTA method. The reference material in this case was benzene. Vitrification of the sample solution in a 2 mm diameter Pyrex glass cell was carried out by immersing the cell in liquid nitrogen. The overall cooling rate in this case was about 10^3 K/min. The DTA trace was recorded at a heating rate of about 5 K/min.

Results and Discussion

The T_g values obtained at normal pressure are shown in Fig. 1 together with two insets in which a typical DTA trace and the (T_c/T_g) *vs.* $1/r$ plot are presented (T_c: crystallization temperature). As is already pointed out,[6] T_g for the sodium acetate solution is the maximum among all alkali acetate solutions.

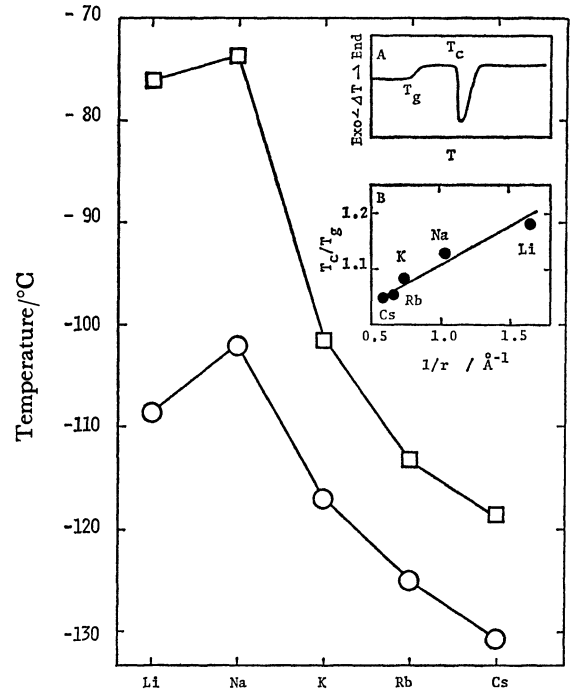

Fig. 1. Glass transition temperature (T_g) and crystallization temperature (T_c) of aqueous alkali acetate solution.
○: Glass transition temperature, □: crystallization temperature. The inset A shows a schematic DTA trace of a glassy sample. The inset B shows the correlation of T_c/T_g with $1/r$.

As acetate anions in these aqueous solutions are common, variation of T_g with a solute can be ascribed to cationic effect. A general trend is the decrease of T_g with the increase in cation radius and is in parallel with the observations for aqueous solutions of lanthanoid chlorides and perchlorates.[7] Kanno and Akama[7] have recently shown that T_g of aqueous rare earth chloride and perchlorate solutions is sensitive to an inner-sphere hydration number of cations. This clearly indicates that the inner-sphere hydration number of cations is one of the key parameters for the magnitude of T_g in aqueous solution. While a smaller ion is expected to have a small number of near neighbor water molecules on account of its small size, it has a greater polarizing power than a larger one, thus accomodating a larger total hydration sphere.[8] As the glass transition takes place at a temperature above which there are relatively rapid translational motions of ions (molecules),[9] a higher T_g is expected for a solution in which ions have a larger hydration sphere. Therefore, the trend of the T_g increase with decreasing ionic radius in these solutions is very reasonable.

The apparent deviation of T_g for the lithium acetate solution from the above-mentioned general trend deserves a special attention because the total hydration sphere of lithium ion should be the largest among all alkali ions. From X-ray diffraction studies of aqueous LiCl and NaCl solutions, the inner-sphere hydration numbers of Li^+ and Na^+ ions are determined to be four although there remains some uncertainty in the case of Na^+ ion.[10] Consequently it is difficult to ascribe the anomalous T_g behavior of the lithium acetate solution to the difference of the inner-sphere hydration number between Li^+ and Na^+.

A plausible explanation, though tentative at the moment, may be resorted to the fact that the electropositivity of lithium ion is rather weak among alkali ions.[11] The lithium ion-water interaction is claimed to be partially covalent.[12] This is simply exemplified by Samoilov's positive and negative hydration concept[13]: the hydration of K^+, Rb^+, and Cs^+ is classified as negative (structure breaker), Na^+ is almost on the borderline between positive and negative hydration and Li^+ is strongly positive (structure marker) in hydration. From T_g's of a vapor-deposited amorphous ice[14,15] and binary mixtures of water and organic compounds,[16] the glass transition temperature of a bulk glassy water is expected to be very near -139 °C. Accordingly, the structure making effect of Li^+ ions should act T_g of a lithium salt solution to become nearer to T_g of a bulk water.

In contrast to the above irregularity, the linear relation between T_c/T_g and $1/r$, shown in the inset of Fig. 1, is interesting. The transport properties of supercooled liquids are well described by the Vogel-Tammann type equation[17]

$$\rho = \rho_0 \exp\left\{\frac{B}{(T-T_0)}\right\}, \qquad (1)$$

where ρ is the transport property such as viscosity, electrical conductivity of supercooled liquid, T_0 is the temperature below which the liquid contains no free volume and is considered to be near T_g, and

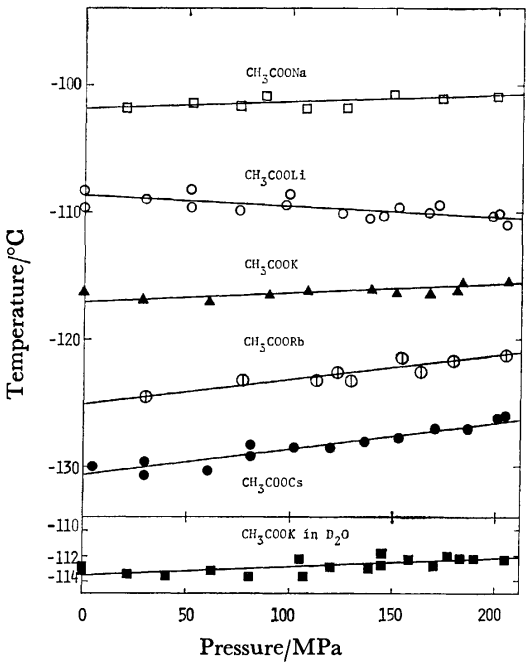

Fig. 2. Pressure dependence of T_g for aqueous alkali acetate solutions ($R=10$).
The (dT_g/dP) values are, CH_3COOLi: -0.85; CH_3COONa: 0.55; CH_3COOK: 0.70; CH_3COORb: 1.91; CH_3COOCs: 2.07; CH_3COOK in D_2O: 0.66 K/kbar (or $\times 10^{-2}$ K/MPa). The estimated error for each (dT_g/dP) is about ± 0.30 K/kbar.

ρ_0 and B are constants. Replacing T_0 with T_g and rearranging Eq. 1, we obtain

$$T_c - T_g \simeq B/\ln(\rho_c/\rho_0), \qquad (2)$$

where ρ_c is ρ at T_c. Therefore, knowing that T_c is one of the corresponding states, the linear relation between T_c/T_g and $1/r$ demonstrates that the transport properties such as viscosity and conductivity of supercooled aqueous alkali acetate solutions are well correlated with ionic radius of alkali ions.

The T_g data at high pressures are presented in Fig. 2. The results for the CH_3COOK solution in D_2O are shown in the bottom inset of Fig. 2. A remarkable point is that the (dT_g/dP) value increases in the order $Li^+<Na^+<K^+<Rb^+<Cs^+$. Another is the negative pressure dependence of T_g for the lithium acetate solution. The latter point is already pointed out by William and Angell.[18] They interpreted this negative pressure dependence as evidence for the failure of the free volume theory for transport properties of liquid. The (dT_g/dP) value obtained in this work is $-0.8_5\pm0.3$ K/kbar (1 kbar=100 MPa), in fair agreement with the value $(-0.6_4\pm0.3)$ by William and Angell.[18]

The (dT_g/dP) *vs.* $1/r$ plot is shown in Fig. 3. We again obtain an approximately linear relation between (dT_g/dP) and $1/r$. Although the glass transition is not an equilibrium phase transition and is still controversial whether it is a kind of second order transition or a kinetic phenomenon due to slow relaxation,[19-21] the applicability of the following thermodynamic relations is often noted at the glass transition[9,22]

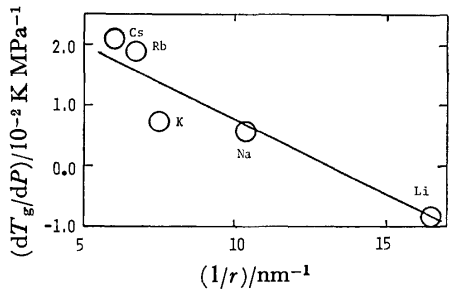

Fig. 3. Correlation of (dT_g/dP) with ionic radius of alkali ion.

$$\frac{dT_g}{dP} \simeq V_g T_g \frac{\Delta\alpha}{\Delta C_p}$$
$$\frac{dT_g}{dP} \simeq \frac{\Delta\kappa}{\Delta\alpha},$$

where $\Delta\alpha$, ΔC_p, and $\Delta\kappa$ are the changes in volume expansion coefficient, constant pressure heat capacity and isothermal compressibility at T_g, and V_g is molar volume of glass. Without experimental data for $\Delta\alpha$, ΔC_p, $\Delta\kappa$, and V_g, it is difficult to single out the factor responsible for the order of the (dT_g/dP) values in alkali acetate solutions. However, knowing that T_g is in the order $Na^+>Li^+>K^+>Rb^+>Cs^+$ and $\Delta\alpha$ can not be a major cause, we infer that V_g and $\Delta\kappa$(or one of them) should be the major factors for the magnitude order of (dT_g/dP) in alkali acetate solutions. This is partially supported by the fact that the partial molal volume of alkali metal ion in an aqueous solution increases in the order $Na^+<Li^+<K^+<Rb^+<Cs^+$ [5] (Note: $T_g(Li)V_{Li}<T_g(Na)V_{Na}$, V_a: partial molal volume for ion **a**) and that it is closely connected with ionic radius of ion. Clearly more data are needed before we can give a more clear-cut interpretation about the sequence of the (dT_g/dP) values.

Finally it is worth mentioning about the isotope effect on T_g at high pressures. The pressure dependence of T_g for the potassium acetate solution in D_2O ($R=10$) is shown in the inset of Fig. 2. The least-square best fit yields $0.6_6\pm0.3$ K/kbar for the slope (dT_g/dP) of the D_2O solution, which is almost identical to the value for the H_2O solution ($dT_g/dP=0.7_0\pm0.3$ K/kbar). This feature is very similar to the isotope effect of melting temperature of water along the melting curve. The difference of melting temperature between H_2O and D_2O is 3.82 °C at normal pressure and changes little with pressure up to 200 MPa.[23]

This work was partially supported by a Research Assistantship (to H. K.) from the Nishina Memorial Foundation.

References

1) W. Kauzmann, *Chem. Rev.*, **43**, 219 (1948).
2) C. A. Angell and E. J. Sare, *J. Chem. Phys.*, **52**, 1058 (1970); C. A. Angell, J. M. Sare, and E. J. Sare, *J. Phys. Chem.*, **82**, 2622 (1978).
3) A. V. Lesikar, *J. Chem. Phys.*, **63**, 2297 (1975); **66**, 4263 (1977); **68**, 3323 (1978).
4) H. Rawson, "Inorganic Glass Forming System," Academic Press, London (1967).
5) F. J. Millero, "Water and Aqueous Solution; Structure, Thermodynamics and Transport Processes," ed by R. A. Horne, Wiley-Interscience, N. Y. (1972), Chap. 13.
6) H. Kanno, R. J. Speedy, and C. A. Angell, *Science*, **189**, 880 (1975); H. Kanno and C. A. Angell, *J. Phys. Chem.*, **81**, 2639 (1977).
7) H. Kanno and Y. Akama, *Chem. Phys. Lett.*, **72**, 181 (1980).
8) F. A. Cotton and G. Wilkinson, "Advanced Inorganic Chemistry," 3rd ed, Interscience Pub. (1972), Chap. 27.
9) J. Wong and C. A. Angell, "Glass:Structure by Spectroscopy," Marcell Dekker, New York (1976), Chap. 1.
10) J. E. Enderby and G. W. Neilson, "Water, A Comprehensive Treatise," ed by F. Franks, Plenum Press (1979) Vol. 6, Chap. 1.
11) Ref. 8, Chap. 6.
12) H. Kistenmacher, H. Popkie, and E. Clementi, *J. Chem. Phys.*, **59**, 5842 (1973).
13) O. Ya. Samoilov, "Structure of Aqueous Electrolyte Solutions and the Hydration of Ions," (translated by D. J. G. Ives), Consultnat Burea, New York (1965).
14) J. A. McMillan and S. C. Los, *Nature*, **206**, 806 (1965).
15) M. Sugisaki, H. Suga, and S. Seki, *Bull. Chem. Soc. Jpn.*, **41**, 2591 (1968).
16) D. H. Rasmussen and A. P. Mackenzie, *J. Phys. Chem.*, **75**, 967 (1971).
17) M. L. Williams, R. F. Landel, and J. D. Ferry, *J. Am. Chem. Soc.*, **77**, 3701 (1955); G. Adam and J. H. Gibbs, *J. Chem. Phys.*, **43**, 139 (1965).
18) E. Williams and C. A. Angell, *J. Phys. Chem.*, **81**, 232 (1977).
19) M. H. Cohen and G. S. Grest, *Phys. Rev. B*, **20**, 1077 (1979).
20) J. N. Cape and L. V. Woodcock, *J. Chem. Phys.*, **72**, 976 (1980).
21) H. Kanno, *J. Non-Cryst. Solids*, **37** 203 (1980).
22) R. O. Davis and G. O. Jones, *Adv. Phys.*, **2**, 370 (1953).
23) P. W. Bridgman, *J. Chem. Phys.*, **3**, 597 (1935).

The Electrical Conductivity of Graphite Filaments and Their Alkali-metal Intercalation Compounds

Mizuka SANO,* Naoki SATO,† Hiroo INOKUCHI,† and Shohei TAMURA††

Department of Materials Science, The University of Electro-Communications, Chofu, Tokyo 182

† *Institute for Molecular Science, Okazaki 444*

†† *The Institute for Solid State Physics, The University of Tokyo, Roppongi, Minato-ku, Tokyo 106*

(Received January 20, 1981)

A bundle of carbon filaments, each about 20 cm in length and 7 μm in diameter, could be grown from purified graphitic material in argon plasma generated in a d.c. arc. The filaments were converted into softer filaments on heat-treatment to 3000—3400 °C. The filaments formed intercalation compounds of potassium, rubidium, and caesium. The electrical resistivities were found to be 1300, 610—660, 23—25, and 28—30 μΩ cm at 300 K for the original filament, the heat-treated filament, and the first stage golden and the second stage dark-blue intercalation compounds of the heat-treated filament, respectively.

Filamentary growth of carbons has been reported to occur when a carbon-rich gas such as carbon monoxide,[1] methane,[2] heptane,[3] and benzene[4] is pyrolyzed in the presence of some solid material, and also when carbons such as graphite[5] and carbon black[6] are heat-treated to temperatures higher than 3000 °C. Haanstra *et al.*[1] have obtained pencil-like carbon columns, 3—6 μm in diameter and about 1 mm long, by pyrolysis of carbon monoxide on a β-SiC crystal. The columns were found to have a conehelical structure; they are stacked from parallel layers of carbon atoms, bent into a cone mantle with a top-angle of about 141°.

Koyama[4] has obtained carbon fibers of a cylindrical scroll structure by pyrolyzing a mixture of benzene and hydrogen on a graphite block abraded with an emery paper. Bacon[5] grew graphite whiskers from a graphite-rod electrode in a d.c. arc under a pressure of 92 atm of argon at 3900 K. They consist of one or more concentric tubes, each in the form of a scroll or rolled-up sheet of graphite layers.

We could grow a bundle of "carbon filaments," each about 20 cm long and 7 μm in diameter, by heating purified graphitic material in argon plasma. Each filament was found to have a smooth surface and a cylindrical shape with circular cross-section of nearly constant diameter over its entire length. Each was composed of three parts: the outer sheath, the inner sheath, and the core.[7] The outher sheath, about 0.7 μm thick, consists mainly of circumferentially oriented graphitic layers; the inner sheath, about 1.4 μm thick, consists mainly of radially oriented graphitic layers. The core, about 2.8 μm in diameter, probably consists of randomly distributed minute crystallites or amorphous material, because it did not show any electron diffraction pattern. The carbon filaments were converted into softer filaments on heat-treatment to 3000—3400 °C.

In this paper we will report the electrical conductivities of these newly obtained carbonaceous filaments as well as of their alkali-metal intercalation compounds. We will discuss the conductivities in relation to their fine crystalline structures inferred not only from the X-ray and electron diffractions but also from the Raman scattering and the magnetoresistance.

Experimental

A piece of grafoil GTA (Union Carbide Co.) was immersed in hot aqua regia for a day and then purified by heating repeatedly to 800 °C for 10 min in a stream of wet chlorine. These processes reduced the concentration of impurities, for example iron, from 80 to less than 8 ppm. Carbon filaments could not be grown from unpurified grafoil. The purified grafoil, supported by a graphite rod between two graphite-rod electrodes, was heated with argon plasma generated in a d.c. arc. When the temperature of plasma exceeded 5000 °C, a bundle of carbon filaments started to grow at the rate of about 1 cm min^{-1} under the nearly atmospheric pressure of argon.

The carbon filaments thus obtained were converted into softer filaments on graphite-resistance heating at 3000 °C, or on high-frequency heating at 3400 °C. The former will be referred to as graphite 30 and the latter as graphite 34 filaments. The diameter of an individual filament was measured by means of scanning electron microscopy.

The intercalation compounds of the filaments with K, Rb, and Cs were prepared by vapor phase reaction in a dual furnace.[8] Their electrical resistivity was measured in the range from 4.2 to 300 K by a four-probe d.c. method in the same way as reported previously.[9] The four-probe contacts with the intercalation compounds were pressure-fixed before the vapor phase reaction.

Graphite 30 and 34 filaments formed lst stage compounds of brilliant golden luster and 2nd stage compounds of dark-blue luster. The X-ray diffraction from the golden compound formed between a graphite filament and Cs, for example, gave sharp spots lying perpendicular to the filament axis and diffuse spots on the axial line. The interlayer distance was determined to be 5.96 Å from the former spots, and the Cs–Cs distance to be 4.92 Å from the latter spots. These values are coincident with those reported for the compound prepared from highly-oriented pyrolytic graphite (abbreviated to HOPG) and Cs.[10] The carbon filaments as grown, on the other hand, did not change their appearance, though their resistivity was reduced by introduction of alkali-metals.

Results and Discussion

The longitudinal resistivities were found to be 1300, 660, and 610 μΩ cm for carbon, graphite 30, and graphite 34 filaments, respectively, at 300 K; these increase monotonously with decreasing temperature down to 4.2 K, as shown in Fig. 1, a—c. The re-

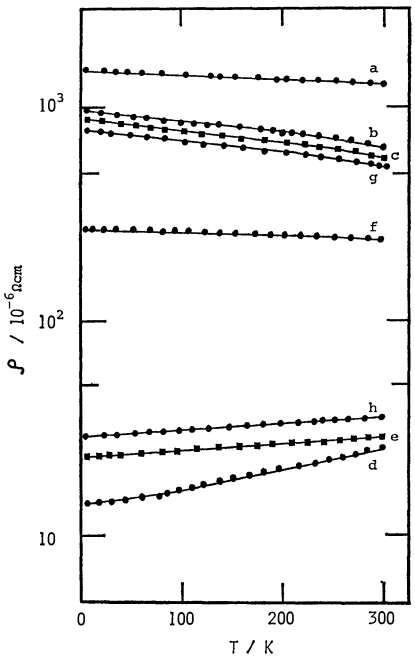

Fig. 1. Temperature dependence of resistivity for filaments.
a: Carbon, b: graphite 30, c: graphite 34, d: K-intercalated graphite (1st), e: K-intercalated graphite (2nd), f: K-intercalated carbon (1st), g: K-intercalated carbon (2nd), and h: K-intercalated graphite (1st) with hydrogen.

sistivity of the graphite filament was found to be lower than that of the carbon filament, but no great difference was found in resistivity between the graphite 30 and 34 filaments. The lower resistivity of the graphite filaments, which were obtained on heat-treatment to 3000—3400 °C, can be ascribed to the preferred alignment of the graphite-type crystallites along the filament axis.

Raman scattering induced by argon-ion laser radiation (488 nm), though it only probed an optical skin depth (<0.1 μm), gave a spectrum of a sharp and intense peak at 1582 cm^{-1} and a tiny and broad peak at 1360 cm^{-1} for the graphite filament. The Raman spectrum for the carbon filament, on the other hand, showed two broad peaks, around 1590 and 1370 cm^{-1}. The former spectrum is quite similar to that found for crudely pulverized natural graphite or for grafoil, and the latter to that of carbon black.[11]

The graphite filament exhibited sharper X-ray diffraction spots and greater intensity contrast between the dark-field (002) or (100) electron-micrograph of the outer sheath and that of the inner sheath, compared with those found for the carbon filament. These results indicate a higher degree of preferred orientation of crystallites in the graphite filament.

The resistivity of HOPG along the basal plane ρ_a has been reported to be 40 μΩ cm at 300 K,[12,13] and to show a slight rise with decreasing temperature down to around 77 K, followed by a rapid descent to 4.2 K. The resistivity along the c-axis, ρ_c has been reported to be about 0.1 Ω cm at 300 K,[12] and to increase with decreasing temperature.[14] The temperature dependence of resistivity observed for the graphite filament is different from that for HOPG, but rather similar to that found for bulk polycrystalline graphite such as grafoil[9] and that of the c-axis resistivity for pyrolytic graphite.[14]

The graphite filament was obtained on heating the carbon filament at a high temperature region where three-dimensional ordering of the layers characteristic to the graphite structure is expected to develop, but some loose aggregates of misoriented crystallites still seem to remain among graphite-type crystallites. The graphite-type crystallites which form the outer and inner sheaths of a filament are preferentially aligned with their basal planes parallel to the filament axis, so charge carriers are expected to move along the basal plane in the direction of the filament axis in each crystallite, the higher basal plane conductivity providing a lower resistivity path along that direction. Hence, the misoriented crystallites and crystalline boundaries seem to determine the value of longitudinal resistivity and to characterize the temperature dependence.

Presumably, some thermally activated process may be included in the conduction through the misoriented crystallites. Indeed, the resistivity exhibited an exponential change with reciprocal temperature in the temperature region above 150 K, and the activation energy was determined to be 0.01 eV for the graphite filament, though it still remains unknown whether this activation energy is related to the semiconducting energy gap or to some hopping process of charge carriers. Graphite whiskers[5] and graphitized carbon fibers[15] have been reported to show an HOPG-like temperature dependence of resistivity.

A preliminary measurement of transverse magnetoresistance ($\Delta\rho/\rho_0$) was carried out on single filaments in the magnetic field up to 120 kOe,††† by using an Intermagnetics MIDIBRUTE 120 superconducting magnet. Electrical contacts of a filament were made with silver paint to four thin gold wires. The magnetoresistance was found to be positive for the carbon filament and to be negative for the graphite filament at 4.2 K in the entire range of magnetic field. Rotation of a single filament around the filament axis, which was oriented perpendicular to the magnetic field, did not change the magnetoresistance.

Soft cokes heat-treated at temperatures lower than 1100 °C have been reported to show a positive magnetoresistance and those heat-treated at 1500 °C to show a negative magnetoresistance at 4.2 K.[16] A number of suggestions have been made as to the origin of the negative magnetoresistance in a wide range of carbons: crystalline size effect,[17] localized spins,[18] a mobility edge,[19] and a dependence of carrier concentration on a magnetic field.[20] It is unknown to which origin the negative magnetoresistance property observed is attributable, but it seems fairly certain that some sort of disordered state is responsible for the property.

The average carrier mobility along the filament axis, $\bar{\mu}$ was estimated to be about 300 $cm^2 V^{-1} s^{-1}$ at 4.2 K for the carbon filament; the following equa-

††† Oe=1000/4π A m^{-1}.

tion[14] was assumed to be applicable to the magnetoresistance observed:

$$\bar{\mu}=\sqrt{2}(\Delta\rho/\rho_0)^{1/2}\times 10^8/H. \quad (1)$$

Graphite filaments formed 1st stage alkali-metal intercalation compounds of such brilliant golden luster as that of HOPG-based compounds. Non-graphitizable carbons have been reported not to form intercalation compounds. This has been attributed to the cross-linking of the graphitic layers.[21] Hence, the graphite filaments in this study seem to have little cross-linking, though three-dimensional ordering of the layers did not develop on heating to 3000—3400 °C. This is the first example of brilliant golden intercalation filaments as far as we know.

The graphite filaments intercalated with K, Rb, or Cs were found to show a greatly reduced resistivity, in the range of 23—25 μΩ cm for the lst stage compounds, and in the range of 28—30 μΩ cm for the 2nd stage compounds, at 300 K. They were also found to be metallic in character, showing a decrease in resistivity with decreasing temperature (Fig. 1, d, e). No difference in resistivity value was found among the potassium, rubidium and caesium compounds.

The lst stage compounds prepared between HOPG and alkali-metals have been reported to possess the basal-plane resistivity in the range of 10—14 μΩ cm at room temperature[22,23] and to show a decreasing resistivity with decreasing temperature. The grafoil-based alkali-metal intercalation compounds showed resistivity values in the same range and a similar temperature dependence.[9]

When the lst stage golden potassium-intercalated filament was heated in a dual furnace under the conditions in which the 4th stage intercalation compound was expected to be prepared,[8] the filament turned black and showed an increase in resistivity. In general, the resistivity was found to decrease monotonously with intercalant concentration.

The carbon filament, on the other hand, provided alkali-metal intercalation compounds of the resistivity of about 240 and 550 μΩ cm at 300 K, when prepared under the same conditions of preparation as those for the lst and the 2nd stage HOPG-based compounds, respectively. The resistivity of these intercalated carbon filaments was found to increase with decreasing temperature (Fig. 1, f, g).

From these observations, it is inferred that an introduction of alkali-metal atoms not only increases the number of conducting carriers in the graphitic layers, but also eliminates some of imperfections present in the pristine graphite filaments. Certainly, the X-ray diffraction from the intercalated graphite filament gave much sharper spots than that from the pristine filament did. The electric anisotropy, ρ_c/ρ_a has been reported to be reduced from 2500 for HOPG to 34 for the intercalated compound,[22] so misorientation of crystallites seems to have less influence on resistivity value after they are intercalated with alkali-metals. The intercalated filaments were unstable in air, so they could not be taken out from a sealed glass tube. Because of the technical difficulties encountered in these reactive filaments, their magnetoresistance have not been measured yet.

A golden potassium-intercalated graphite filament turned blue and its resistivity reached 36 from 25 μΩ cm at 300 K, when hydrogen purified through a heated Pd–Ag thimble was introduced to the intercalated filament. This change is quite similar to that observed for the grafoil-based potassium intercalation compound,[9,24] and can be explained in terms of the formation of a ternary compound.[25]

The authors wish to express their hearty thanks to Professor Yoshihiro Hishiyama of Musashi Institute of Technology, and Drs. Yoichiro Sato and Takaho Tanaka of the National Institute for Research in Inorganic Materials for heat-treating the carbon filaments, and to Dr. Koshiro Toriumi of Institute for Molecular Science for his valuable discussion on the crystal structure of filaments.

References

1) H. B. Haanstra, W. F. Knippenberg, and G. Verspui, *J. Cryst. Growth*, **16**, 71 (1972).
2) L. Meyer, *Z. Kristallogr.*, **109**, 61 (1957).
3) M. Hillert and N. Lange, *Z. Kristallogr.*, **111**, 24 (1958).
4) T. Koyama, *Carbon*, **10**, 757 (1972).
5) R. Bacon, *J. Appl. Phys.*, **31**, 283 (1960).
6) S. Hagiwara and H. Takahashi, *Carbon*, **14**, 86 (1976).
7) T. Okazaki, Y. Kamiya, S. Takahashi, K. Toriumi, and N. Sato, to be published.
8) D. E. Nixon and G. S. Parry, *J. Phys. D*, **1**, 291 (1968).
9) M. Sano and H. Inokuchi, *Chem. Lett.*, **1979**, 405.
10) D. Guerard, P. Lagrange, M. El Makrini, and A. Herold, *Carbon*, **16**, 285 (1978).
11) M. Nakamizo, R. Kammereck, and P. L. Walker, Jr., *Carbon*, **12**, 259 (1974).
12) A. R. Ubbelohde, *Proc. R. Soc. London, Ser. A*, **327**, 289 (1972).
13) L. A. Pendrys, C. Zeller, and F. L. Vogel, *J. Mater. Sci.*, **15**, 2103 (1980).
14) C. A. Klein, *J. Appl. Phys.*, **33**, 3338 (1962).
15) T. Koyama, M. Endo and Y. Hishiyama, *Jpn. J. Appl. Phys.*, **13**, 1933 (1974).
16) Y. Hishiyama, Y. Kaburagi, and A. Ono, *Carbon*, **17**, 265 (1979).
17) S. Fujita, *Carbon*, **6**, 746 (1968).
18) S. Yugo, *J. Phys. Soc. Jpn.*, **34**, 1421 (1973).
19) P. Delhaes, P. de Kepper, and M. Uhlrich, *Philos. Mag.*, **29**, 1301 (1974).
20) K. Yazawa, *J. Phys. Soc. Jpn.*, **26**, 1407 (1969); A. A. Bright, *Carbon*, **17**, 259 (1979).
21) A. Métrot and A. Hérold, *C. R. Acad. Sci., Ser. C*, **264**, 883 (1967).
22) J. J. Murray and A. R. Ubbelohde, *Proc. R. Soc. London, Ser. A*, **312**, 371 (1969).
23) D. Guérard, G. M. T. Foley, M. Zanini, and J. E. Fischer, *Il Nuovo Cimento Soc. Ital. Fis. B*, **38**, 410 (1977).
24) M. Sano, H. Inokuchi, M. Kobayashi, S. Kaneiwa, and I. Tsujikawa, *J. Chem. Phys.*, **72**, 3840 (1980).
25) P. Lagrange and A. Hérold, *Carbon*, **16**, 235 (1978).

  Bull. Chem. Soc. Jpn., 54, 2613—2619 (1981)

Kinetics for Micelle-Monomer Association-Dissociation Reaction of Surfactants with Hydrophobic Counterions

Tohru Inoue,* Masaru Ikeuchi, Takemi Kuroda, and Ryosuke Shimozawa

Department of Chemistry, Faculty of Science, Fukuoka University, Nanakuma, Nishi-ku, Fukuoka 814-01

(Received October 18, 1980)

A pressure-jump technique and a spin label technique were applied to the kinetic investigation of the association-dissociation reactions between monomer and micelle in surfactant solutions of STS, TMTS, TETS, and TPTS.** The rate constants for the reactions were determined at several temperatures by the pressure-jump experiment. The ESR spectra of a spin probe, 5-SAL, solubilized in the micelles were analyzed in terms of the rotational correlation time, τ_c. A linear relationship was found between k_d, the dissociation rate constant, and τ_c^{-1}. This indicates that the dissociation rate depends on the fluidity of the micellar interior, and is in accord with the picture drawn by Aniansson *et al.* for the dissociation process. A qualitative discussion is presented on the activation parameters estimated from the present results according to the scheme presented by Aniansson *et al.*

Kinetics of relaxation processes occuring in micellar solutions have been extensively investigated using fast chemical relaxation techniques. It is established experimentally that in many surfactant solutions at least two relaxation processes exist in well-separated time domains. Kinetic information on the association-dissociation process of the monomer with the micelle is obtained from the fast relaxation time, and that on the micellization-dissolution process is obtained from the slow relaxation time.[1)]

The behavior of the relaxation times associated with these two processes is affected by the counterion;[2-4)] a relaxation study for micellar systems of *N*-alkylpyridinium salts with hydrophobic counterion has been reported by Hoffmann *et al.*[5)] In the present work, the pressure-jump measurements were carried out for the micellar systems of tetradecyl sulfate having several types of tetraalkylammonium ions as counterion; the dissociation and association rate constants of the monomer from and with the micelle were determined from the relaxation data.

Aniansson *et al.*[1)] have treated the dissociation of a surfactant monomer from the micelle as a diffusion process of a monomer in micelle perpendicular to the micellar surface; they derived an expression for the dissociation rate constant in terms of the diffusion coefficient of the leaving monomer and the free energy barrier which a monomer has to overcome to dissociate from the micelle. This model predicts that some correlation will occur between the dissociation rate and the fluidity of the micellar interior. The direct information about the fluidity can be obtained from the ESR spectra of a spin probe solubilized in the micelle. In this work, therefore, ESR measurements were also carried out with the same surfactant systems using 5-SAL (a fatty acid spin label) as a probe. The ESR spectra were analyzed in terms of the rotational correlation time, τ_c, and the relationship between τ_c and dissociation rate constant was examined.

**Abbreviations used in this paper:
STS; sodium tetradecyl sulfate, TMTS; tetramethylammonium tetradecyl sulfate, TETS; tetraethylammonium tetradecyl sulfate, TPTS; tetrapropylammonium tetradecyl sulfate, 5-SAL; 2-tridecyl-2-[3-(carboxyl)propyl]-4,4-dimethyloxazolidin-3-yloxyl

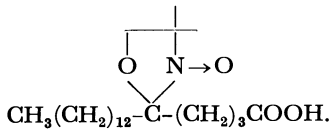

$CH_3(CH_2)_{12}$-C-$(CH_2)_3COOH$.

Experimental

Materials. The surfactants used in this study were prepared by the following procedure.[6)]

STS was prepared by the usual method from tetradecyl alcohol purified by the fractional distillation. This STS was converted to silver tetradecyl sulfate (AgTS) by repeated crystallization in aqueous solution of $AgNO_3$ at about 30 °C followed by repeated recrystallization from water. The content of Ag^+ in AgTS was assayed to be in agreement with the calculated value within 0.5% by titrating ethanolic solution of AgTS with a standard aqueous solution of NaCl, using K_2CrO_4 as an indicator.

TMTS, TETS, and TPTS were prepared by double decomposition of the above mentioned AgTS with tetramethylammonium chloride, tetraethylammonium chloride, and tetrapropylammonium iodide, respectively, in ethanol. These halides were commercial products and purified by recrystallization from ethanol. To AgTS was added a stoichiometric amount of the corresponding halide. The precipitated silver halide was removed by filtration, and a small amount of the reagents was added to the filtrate. This procedure was repeated until no precipitation was observed. The final filtrate was evaporated and the residue was dried *in vacuo*.

The spin label reagent, 5-SAL, was purchased from Syva (Palo Alto, Calif.).

Critical Micelle Concentration (CMC). The CMC's of TMTS, TETS, and TPTS were determined by the conductivity method at different temperatures. The results are summarized in Table 1, together with those of STS.

Relaxation Measurement. The pressure-jump (P-jump) apparatus with conductivity detection was described previously.[4)]

ESR Measurement. ESR spectra were recorded on a JEOL model FEIX ESR spectrometer at room temperature (24±1 °C).

Sample solutions were prepared by the following procedure. A required amount of stock solution of 5-SAL in chloroform was taken into a volumetric flask to give the desired probe/surfactant molar ratio, and the solvent was completely evaporated *in vacuo*. A stock solution of the surfactant was added, and the mixture was then shaken in

the dark overnight to assure the solubilization of the probe in micelle. This surfactant-probe stock solution was diluted to prepare the solution of desired surfactant concentration.

Table 1. Critical micelle concentration (CMC) determined by electroconductivity
(10^{-3} mol dm^{-3})

Surfactant	Temperature/°C			
	10	15	20	25
TMTS	1.36	1.35	1.35	—
TETS	0.96	0.95	0.94	—
TPTS	0.55	0.57	0.59	—
STS	—	—	—	2.10

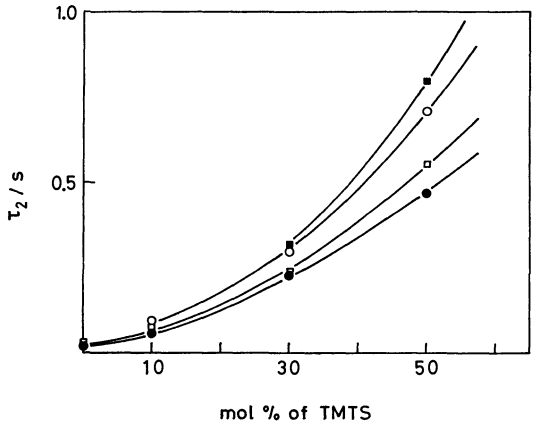

Fig. 1. The slow relaxation time, τ_2, for TMTS–STS mixed system at 25 °C.
Total surfactant concentration (mol dm^{-3}); 2.4×10^{-3} (●), 2.2×10^{-3} (□), 2.0×10^{-3} (○), 1.8×10^{-3} (■).

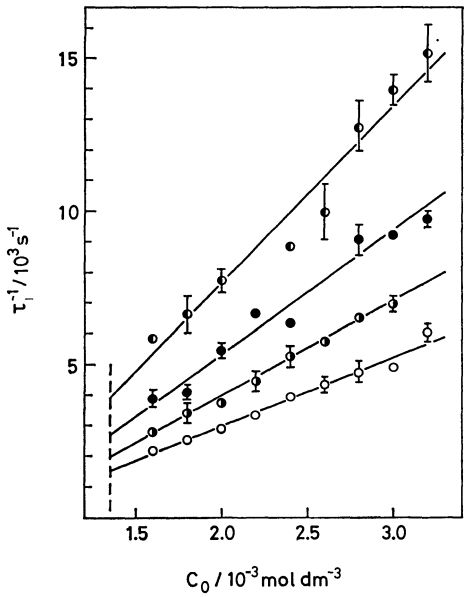

Fig. 2a. Plot of τ_1^{-1} *vs.* total surfactant concentration, C_0, for TMTS at different temperatures.
○: 5 °C, ◑: 10 °C, ●: 15 °C, ◐: 20 °C. Dashed line indicates the CMC. Straight lines represent the best fit of the data by the least-squares method.

Results

Pressure-jump Study. It is usually difficult to observe both of the relaxation processes in micellar solution using a single relaxation technique, because of the restricted time range available for a single apparatus. Fortunately, in the case of STS, two relaxation processes can be observed by the P-jump technique.[1,7,8] However, for the present three surfactant systems, only one of the relaxations could be detected

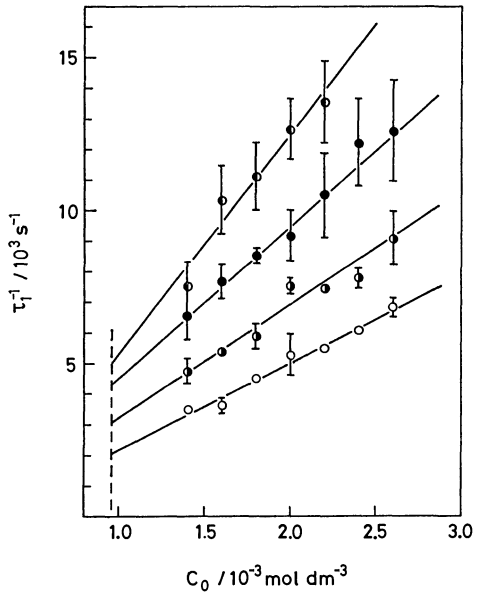

Fig. 2b. Plot of τ_1^{-1} *vs.* total surfactant concentration, C_0, for TETS at different temperatures.
○: 5 °C, ◑: 10 °C, ●: 15 °C, ◐: 20 °C. Dashed line indicates the CMC. Straight lines represent the best fit of the data by the least-squares method.

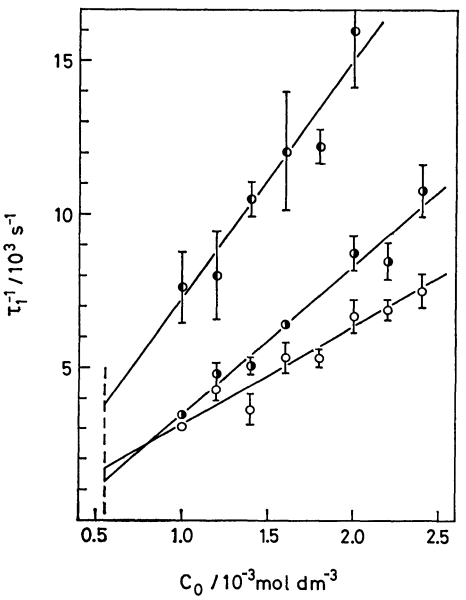

Fig. 2c. Plot of τ_1^{-1} *vs.* total surfactant concentration, C_0, for TPTS at different temperatures.
○: 5 °C, ◑: 10 °C, ◐: 20 °C. Dashed line indicates the CMC. Straight lines represent the best fit of the data by the least-squares method.

TABLE 2. VALUES OF THE KINETIC PARAMETERS FOR TETRADECYL SULFATE WITH VARIOUS COUNTERIONS

	Temp/°C	TMTS	TETS	TPTS	STS[a]
k_d / 10^3 s^{-1}	5	$3.1_1\pm0.1_8$	$2.7_7\pm0.1_9$	$1.7_4\pm0.1_9$	—
	10	$4.1_6\pm0.1_2$	$3.5_4\pm0.3_6$	$2.6_8\pm0.2_5$	—
	15	$5.5_2\pm0.5_3$	$4.7_1\pm0.1_9$	—	—
	20	$7.9_2\pm0.6_9$	$6.8_2\pm0.9_0$	$4.7_3\pm0.6_4$	—
	25	9.8 ±0.5	8.1 ±0.6	6.2 ±0.4	12.1±1.5
k_a / 10^6 mol^{-1} dm^3 s^{-1}	5	0.99	1.2	1.4	—
	10	1.3	1.6	2.1	—
	15	1.8	2.1	—	—
	20	2.5	3.1	3.4	—
	25	3.1	3.7	4.5	2.5
σ^2/m	5	2.1	1.4	1.0	—
	10	2.1	1.2	2.1	—
	15	2.1	1.1	—	—
	20	2.1	1.4	1.3	—
	25	—	—	—	10.8(4.3[b])
E_d/kJ mol^{-1}		41.2±2.5	39.3±3.3	43.0±3.8	31.4±3.8

a) From the data in Ref. 7. b) From the data in Ref. 1.
Errors are standard deviations computed by linear regression analysis.

by P-jump measurement in spite of the identity of the long-chain ion with STS. From the relaxation time range and their concentration dependences, this appears to be the faster of the two processes. In order to confirm this assignment, P-jump measurements were carried out for the systems of TMTS and TETS mixed with STS. In these cases two relaxation processes were observed. The slow relaxation time, τ_2, obtained for TMTS–STS mixed system is plotted in Fig. 1 as a function of the mixing ratio at different surfactant concentration. It is seen from Fig. 1 that τ_2 increases with the fraction of TMTS and finally vanishes beyond the observation limit. A similar result was also obtained for TETS–STS mixed system. Thus, it can be concluded that the slow relaxation process for the present surfactants is too slow to be observed by the P-jump apparatus used in this study, whose effective time range is limited to within about 2 s because of the restricted stability of a high frequency bridge.

The plots of the reciprocal of the fast relaxation time, τ_1^{-1}, against the total surfactant concentration, C_0, are shown in Figs. 2a—c for TMTS, TETS, and TPTS, respectively. τ_1^{-1} increases linearly with C_0 in the measured concentration range.

The fast relaxation process in micellar solution has been assigned to the perturbation of the exchange equilibrium of a monomer between micellar and bulk phases. Some workers have applied the theory developed by Aniansson and Wall[9] for the analysis of the relaxation data.[1-3,5,8] In the previous paper,[10] some contradictions were pointed out in the kinetic parameters deduced from the Aniansson-Wall model, and a modification of the model was proposed to settle the contradictions. According to the modified treatment, the fast relaxation time is expressed by the following equation:

$$\tau_1^{-1} = \frac{mk_d}{\sigma^2} + k_d\frac{C_0-\bar{A}_1}{\bar{A}_1}, \quad (1)$$

where k_d is the dissociation rate constant of a monomer from the micelle, m the average aggregation number of the micelle, σ^2 the variance of the micellar size distribution curve which is assumed to be Gaussian, and $\bar{A}_1$ the equilibrium monomer concentration which may be approximated by the CMC.

According to Eq. 1, k_d and σ^2/m are obtained from the slope and intercept at the CMC of the straight line of τ_1^{-1} *vs.* C_0 plot. Furthermore, the association rate constant of a monomer with the micelle, k_a, is estimated from the following relation:

$$k_a = \frac{\alpha}{1-\alpha}\frac{k_d}{\bar{A}_1}, \quad (2)$$

where α represents the fraction of the surface area occupied by monomers at the micellar surface.

Applying Eqs. 1 and 2 to the present experimental results, the rate constants and σ^2/m value, which is a measure of the relative width of the distribution curve of the aggregation number, were determined. They are summarized in Table 2, together with those for STS. For the evaluation of these parameters, the CMC values listed in Table 1 were used as $\bar{A}_1$, and α was assumed to be 0.3.[10] Some uncertainty is associated with the absolute values of k_a because the exact values of α are not available for the respective surfactants. However, the relative values of k_a listed in Table 2 can be compared for the different surfactants under the following assumptions: (i) α is mostly determined by the type of the amphiphile ion and the aggregation number of the micelle; (ii) the aggregation numbers of the relevant surfactant micelle do not differ so significantly. At 25 °C, the relaxation was too fast to be measured by the P-jump apparatus used in this study. Thus, the values in Table 2 at this temperature, which are listed for comparison with STS, are those extraporated from the temperature dependence of the rate constants (see Fig. 3).

It is seen from Table 2 that k_d values for the present systems are smaller than that for STS and also decrease with increasing hydrophobicity of the counterion. On the other hand, k_a shows the reverse change. Furthermore, σ^2/m values decrease with increasing hydrophobicity of the counterion, although

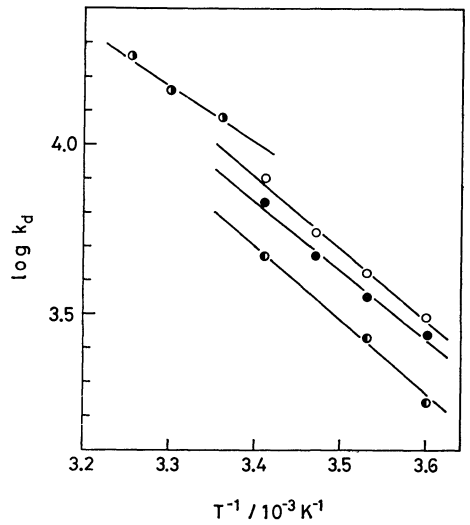

Fig. 3. Plot of log k_d *vs.* T^{-1} for different surfactant systems.
◑: STS, ○: TMTS, ●: TETS, ◐: TPTS. Straight lines represent the best fit of the data by least-squares method.

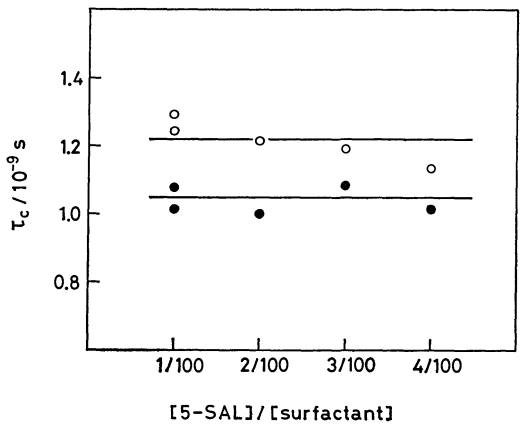

Fig. 4. Plot of τ_c against molar ratio of 5-SAL to surfactant.
●: TMTS, ○: TETS. Surfactant concentration: 1×10^{-2} mol dm^{-3}.

some scatter is seen for TPTS. This means that the micellar size distribution curve becomes narrower for micelles with hydrophobic counterions. The present results on the variation of k_d and σ^2/m are in agreement with those reported by Hoffmann *et al.*[5] for *N*-alkylpyridinium salts having hydrophobic counterion; however, opposite results are obtained for the variation of k_a.

In Fig. 3, the values of log k_d are plotted against $1/T$. The Arrhenius activation energies, E_d, for the dissociation process were determined from the slopes of the straight lines in this figure; these are also listed in Table 2. The E_d values for TMTS, TETS, and TPTS do not differ so significantly, but they are appreciably larger than that for STS.

ESR Study. The ESR spectra of the spin probe, 5-SAL, were analyzed in terms of an effective rotational correlation time, τ_c, which was calculated according to Eq. 3:

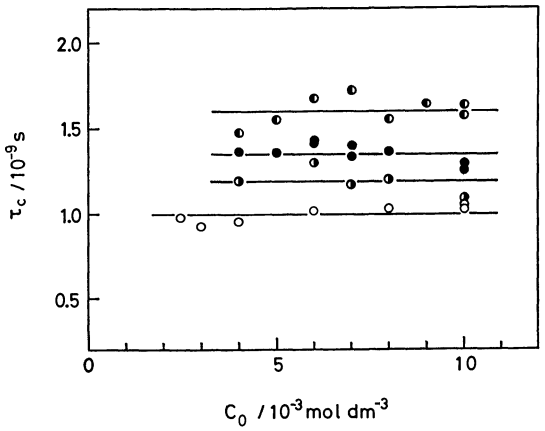

Fig. 5. Plot of τ_c against total surfactant concentration, C_0.
○: STS, ◑: TMTS, ●: TETS, ◐: TPTS. Molar ratio of 5-SAL to surfactant is 1/100.

Table 3. Values of rotational correlation time, τ_c, hyperfine coupling constant, a_N, and degree of counterion association

Surfactant	$\tau_c/10^{-9}$ s	a_N/G	Degree of counterion association
STS	1.00±0.04	15.17±0.04	0.73 (30 °C)
TMTS	1.19±0.07	14.90±0.04	0.79 (20 °C)
TETS	1.35±0.05	14.73±0.06	0.80 (20 °C)
TPTS	1.60±0.07	14.83±0.06	0.82 (20 °C)

$$\tau_c = 6.5\times10^{-10} W_0\left[\left(\frac{h_0}{h_{-1}}\right)^{1/2}+\left(\frac{h_0}{h_{+1}}\right)^{1/2}-2\right], \quad (3)$$

where W_0 is the peak-to-peak width of the center line measured in Gauss, and h_0, h_{+1}, and h_{-1} are the heights of the center, low, and high field spectral lines respectively. This expression has frequently been used to evaluate the degree of motion of probes solubilized in the micelle.[11,12] It is known that Eq. 3 is applicable to a fast isotropic motion of small molecule. The spectra of the spin probe obtained in this study showed a high degree of fast motion, yielding the τ_c values of the order of 10^{-9} s when calculated according to Eq. 3. Furthermore, the patterns of these spectra were similar to those in isotropic media. Thus, it seems reasonable to use Eq. 3 for the present purpose.

Firstly, ESR measurements were carried out for TMTS and TETS by varying the molar ratio of 5-SAL to the surfactant in the range of 1/100 to 4/100 at the fixed total surfactant concentration of 6×10^{-3} mol dm^{-3} and 1×10^{-2} mol dm^{-3}. Under these conditions, the number of the probes solubilized in one micelle is estimated to be about 1 to 5, assuming that the aggregation number of the micelle is approximately 10^2 and that the 5-SAL dissolved in bulk phase is negligibly small compared with that solubilized in the micelle. Figure 4 shows τ_c values plotted against the ratio of the probe to the surfactant. τ_c is almost independent of the ratio. This shows that the state of the micellar interior is not appreciably perturbed by the uptake of the small amounts of the probe.

Secondly, the ESR spectra were measured varying the surfactant concentration at the range above the CMC, keeping the molar ratio of the probe to surfactant constant at 1/100. The values of τ_c obtained with various surfactant systems are shown in Fig. 5 as a function of the total surfactant concentration, C_0. No systematic variations of τ_c with C_0 are seen in Fig. 5. In Table 3 are listed the τ_c values which were averaged over the whole concentration range.

It is seen from Table 3 that τ_c increases with increasing hydrophobicity of the counterion. This means that the degree of motion of the probe in the micelle decreases in the same order. Two main factors may be considered to be responsible for the difference in the degree of motion of the probe; the fluidity of the environment around the probe, and the electrostatic interaction between the negatively charged head group of the probe and the micellar surface charge which is affected by the degree of counterion association. The degree of counterion association was estimated from the counterion concentration dependence of the CMC, and is listed in Table 3. These values are not so different, although a slight regular increase with the hydrophobicity of the counterion is seen. Hence, the difference in τ_c may be mainly attributed to the difference in the fluidity around the solubilized probe.

In Table 3 are also listed the values of the hyperfine coupling constant, a_N, which were determined from the separation between the lines at low and center field in the spectra; these give information about the polarity of the environment around the spin labelled portion. The a_N values for each system were almost independent of both the probe/surfactant ratio and the surfactant concentration. Comparison of STS with other surfactants shows that a_N values for the latter are smaller than that for STS. This indicates that the polarity of the environment around the paramagnetic site becomes smaller for the surfactant with a hydrophobic counterion. For a series of surfactant micelles studied here, the region probed by 5-SAL is considered to be nearly identical, since all the micelle interiors consist of the same long-chain ion, *i.e.*, tetradecyl sulfate ion. Furthermore, the probe used here are considered to be sensing the region relatively close to the surface in the micellar interior, because the probe is the stearic acid derivative spin-labelled at the fifth carbon atom from the carboxyl carbon. Thus, the a_N values in Table 3 show that the tetradecyl sulfate micelles with hydrophobic counterions have fewer water molecules penetrated at the near surface of the micelle interior than STS has; this would be a consequence of the exclusion of water molecules due to the attachment of the hydrophobic counterion. This difference in the extent of water penetration plays a role in the difference in the fluidity at the region probed by 5-SAL.

Discussion

Aniansson *et al.*[1] have treated the dissociation of a monomer from a micelle as a diffusion process of a monomer perpendicular to the micellar surface.

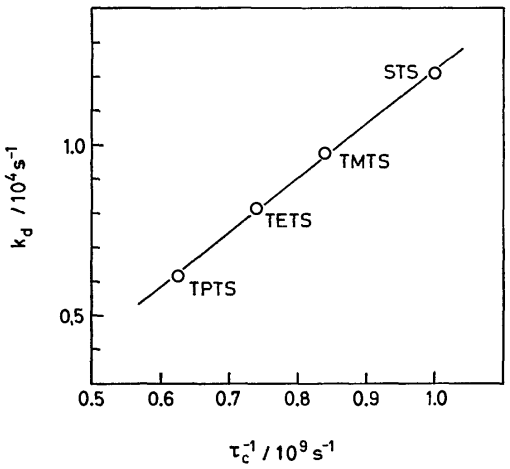

Fig. 6. Relation between dissociation rate constant, k_d, and τ_c^{-1}.
The values of k_d are at 25 °C.

According to their treatment, the dissociation rate constant, k_d, is approximately expressed by Eq. 4:

$$k_d = \frac{D_m}{l^2}\exp(-\Delta G^*/RT), \quad (4)$$

where ΔG^* is the height of the potential barrier corresponding to the activation free energy for the dissociation process, D_m is the diffusion coefficient of a monomer at the potential maximum, and l is the width of the potential maximum region. The main contribution to ΔG^* may arise from the hydrophobic energy, and also from the electrostatic interaction for a charged micelle. Equation 4 can be understood intuitively by noting that D_m/l^2 corresponds to the specific rate constant for the diffusion through the potential maximum, *i.e.*, the number of the molecules transferred through the distance l per unit time, and that $\exp(-\Delta G^*/RT)$ is the probability finding a monomer at an activated state. According to the model postulated by Aniansson *et al.*, the dissociation rate is governed by both ΔG^* and the rate at which a dissociating monomer passes through the potential maximum region.

The diffusion coefficient is proportional to the reciprocal of the viscosity. The viscosity is also reflected in the rotational correlation time of the spin probe, and is proportional to τ_c. Thus, according to the model described above, k_d may be related to τ_c^{-1} through the viscosity, assuming that τ_c well reflects the local viscosity at the region of potential maximum. When k_d was plotted against τ_c^{-1} for the series of surfactant systems studied here, a definite linear relationship was obtained, as is shown in Fig. 6. This indicates that in the series of surfactants the activation free energies, ΔG^*, are almost identical and that the difference in k_d is mainly attributed to the difference in D_m.

For a spherical particle of radius r_1 in a viscous fluid, the value of τ_c is related to the viscosity η by[13]

$$\tau_c = 4\pi\eta r_1^3/3kT. \quad (5)$$

The translational diffusion coefficient of a spherical particle of radius r_2 is related to the viscosity of the

TABLE 4. VALUES OF D_m AND ACTIVATION PARAMETERS FOR THE DISSOCIATION OF A MONOMER FROM A MICELLE ESTIMATED FROM Eqs. 4—6.

Surfactant	D_m / 10^{-7} cm^2 s^{-1}	ΔG^* / kJ mol^{-1}	ΔH^* / kJ mol^{-1}	ΔS^* / J K mol^{-1}
STS	5.6	32.5	11.3	−71
TMTS	4.7	32.6	20.7	−40
TETS	4.1	32.7	18.5	−48
TPTS	3.5	33.0	21.8	−38

medium by the Stokes-Einstein equation, *i.e.*,

$$D = kT/6\pi\eta r_2. \tag{6}$$

Assuming that 5-SAL and tetradecyl sulfate ion are spheres of radius 5 Å (*i.e.*, $r_1=r_2\approx 5$ Å), the values of D_m were estimated from Eqs. 5 and 6 for the present systems. Furthermore, using these D_m values and $l\approx 1$ Å,[1] the value of ΔG^* were estimated from Eq. 4. These values are listed in Table 4. In spite of the rather crude numerical values adopted here, D_m values are in agreement to the order of magnitude with the diffusion coefficient of a different type of spin probe in SDS micelle.[14]

ΔG^* is expressed as

$$\Delta G^* = \Delta H^* - T\Delta S^*, \tag{7}$$

where ΔH^* and ΔS^* are the activation enthalpy and entropy for the dissociation process of a monomer from a micelle. On the other hand, D_m is expressed as Eq. 8, taking into account the temperature dependence of η in Eq. 6, *i.e.*, $\eta=$constant$\cdot\exp(\Delta H_v/RT)$:[15]

$$D_m = TC\exp(-\Delta H_v/RT), \tag{8}$$

where ΔH_v is the viscous enthalpy and C a constant independent of the temperature. Then, from Eqs. 4, 7, and 8, one obtains

$$k_d = \frac{TC}{l^2}\exp(\Delta S^*/R)\exp[-(\Delta H_v+\Delta H^*)/RT]. \tag{9}$$

According to Eq. 9, $\Delta H_v+\Delta H^*$ can be evaluated from the temperature dependence of k_d. The values of $\Delta H_v+\Delta H^*$ for the present surfactant systems were determined from the slope of the $\log k_d$ *vs.* $1/T$ plot in Fig. 3. The values of ΔH^* were evaluated assuming $\Delta H_v\approx 17.6$ kJ mol^{-1} for STS.[1] Furthermore, ΔS^* values were evaluated from Eq. 7. These values of activation parameters are listed in Table 4.

The numerical values in Table 4 might not be good enough for a quantitative discussion, since they were evaluated using rather crude approximations. However, the qualitative discussion given below is reasonable.

As seen in Table 4, the values of ΔS^* are negative for all cases. This implies that the degree of freedom of the system becomes smaller through the activation process. The activated state may be described as a state where the hydrocarbon chain of the dissociating monomer partially leaves the hydrocarbon core of the micelle, while the tail end still remains in this core. Since the freedom of the dissociating monomer chain itself may increase, the observed overall decrease of the freedom may be attributed to the decrease in freedom of water molecules resulting from the formation of an ordered structure around the nonpolar portion of the dissociating monomer. Thus, the negative values of ΔS^* may be interpreted as due to an "iceberg" structure formation of water around the exposed hydrocarbon tail of the escaping monomer.

The absolute values of ΔS^* for TMTS, TETS, and TPTS do not differ significantly, although that for STS is considerably larger than the others. This means that the degree of hydration of the monomer (or degree of "iceberg" formation) at an activated state is larger for STS. This difference in hydration may be interpreted as follows. The properties of water molecules in the vicinity of the micellar surface may be altered from that of the bulk free water by the influence of the counterion present at fairly high concentration. If one assumes that only free water molecules could participate in the formation of the "iceberg" structure, one expects the existence of a water layer which is non-effective for the "iceberg" formation just outside the micellar surface. The thickness of this "non-effective" layer is expected to be larger for a bulky tetraalkylammonium ion than for the sodium ion. Thus, if one assumes, at the activated state, the hydration or "iceberg" formation around the exposed hydrocarbon chain, and also the presence of a thicker water layer which is ineffective for hydration on a micellar surface covered with bulky counterions, then the larger negative ΔS^* for STS could be qualitatively explained.

On the other hand, the values of ΔH^* are positive. This corresponds to the situation in which the energy to break the hydrocarbon contact in the micellar interior is required for activation. This energy may be partly compensated by the heat of hydration which is liberated by the attachment of water molecules to the hydrocarbon chain. Therefore, the ΔH^* value may become smaller when more hydration proceeds through the activation process. Thus, the smaller value of ΔH^* for STS system, compared with those for the others, is also understood on the basis of the difference in the degree of hydration in the activated states.

The contributions from ΔS^* and ΔH^* to the activation free energy are reverse and compensate each other; hence, nearly identical values of ΔG^* are obtained for different surfactant systems. It is considered from the values of ΔS^* and ΔH^* that the water molecules play an important role in the activated state. Furthermore, from the relation between τ_e and a_N, the water molecules present in the probed near-surface region of the micelle may also be responsible for the difference in the fluidity, which is the main factor governing the dissociation rate.

The authors wish to express their thanks to Prof. Magobe Yamamoto, Faculty of Pharmaceutical Sciences, Fukuoka University, for his kind permission and technical advice concerning the measurement of ESR spectra in his laboratory.

References

1) E. A. G. Aniansson, S. N. Wall, M. Almgren, H. Hoffmann, I. Kielmann, W. Ulbricht, R. Zana, J. Lang, and C. Tondre, *J. Phys. Chem.*, **80**, 905 (1976).
2) H. Hoffmann, R. Nagel, G. Platz, and W. Ulbricht, *Colloid Polym. Sci.*, **254**, 812 (1976).
3) W. Baumüller, H. Hoffmann, W. Ulbricht, C. Tondre, and R. Zana, *J. Colloid Interface Sci.*, **64**, 418 (1978).
4) T. Inoue, R. Tashiro, Y. Shibuya, and R. Shimozawa, *J. Phys. Chem.*, **82**, 2037 (1978).
5) H. Hoffmann, H. Nüsslein, and W. Ulbricht, "Micellization, Solubilization, and Microemulsions," ed by K. L. Mittal, Plenum Press, New York (1977), Vol. 1, p. 263.
6) P. Mukerjee and K. J. Mysels, *J. Phys. Chem.*, **62**, 1400 (1958).
7) T. Inoue, Y. Shibuya, and R. Shimozawa, *J. Colloid Interface Sci.*, **65**, 370 (1978).
8) S.-K. Chan, U. Herrmann, W. Ostner, and M. Kahlweit, *Ber. Bunsenges. Phys. Chem.*, **81**, 396 (1977).
9) E. A. G. Aniansson and S. N. Wall, *J. Phys. Chem.*, **78**, 1024 (1974); **79**, 857 (1975).
10) T. Inoue, R. Tashiro, and R. Shimozawa, *Bull. Chem. Soc. Jpn.*, **54**, 971 (1981).
11) A. S. Waggoner, O. H. Griffith, and C. R. Christensen, *Proc. Natl. Acad. Sci. U.S.A.*, **57**, 1198 (1967).
12) S. Schreier, J. R. Ernandes, I. Cuccovia, and H. Chaimovich, *J. Magn. Reson.*, **30**, 283 (1978).
13) A. Carrington and A. D. McLachlan, "Introduction to Magnetic Resonance," Harper & Row, New York (1969), Chap. 11.
14) M. Aizawa, T. Komatsu, and T. Nakagawa, *Bull. Chem. Soc. Jpn.*, **52**, 980 (1979).
15) E. A. Moelwyn-Hughes, "The Chemical Statics and Kinetics of Solutions," Academic Press, New York (1971), Chap. 5.

ESR Spectra and Structure of the Radical Anions of Organo Halosilanes

Akinori HASEGAWA,* Akihiro NAGAYAMA, and Michiro HAYASHI
Department of Chemistry, Faculty of Science, Hiroshima University, Higashi-sendamachi, Naka-ku, Hiroshima 730

(Received December 20, 1980)

The radical anions of ethyl- and vinyl- halosilanes formed in solid matrices of tetramethylsilane and their ESR spectra were investigated to be compared with results obtained from related radical anions. These radical anions have a trigonal bipyramidal structure with two axial and two equatorial positions. Ethyl and methyl groups which are less electronetative than H prefer the equatorial positons. The vinyl group with a single π electron system occupies the equatorial position due to its electron-donating capability, in spite of its larger electronegativity.

We have reported some ESR studies on the radical anions of simple halides whose central atom is a Group IV element; these anions formed in solid matrices of tetramethylsilane (TMS).[1-4] Results for some bromides will be mentioned briefly. In CF_3Br^- radical anions, the three F atoms are equivalent to one another and a large spin density is on the Br atom.[1] It was therefore concluded that the radical anions have C_{3v} symmetry and that the Br atoms are on the symmetry axes. On the other hand, a congeneric SiF_3Br^- radical anion with a central Si atom has larger contributions of spin density on the Br and one F atoms and small contributions on the other two F atoms.[2] This fact led us to the conclusion that the radical anion has trigonal bipyramidal structure with the Br atom and the first F atom in the axial positions and the other two F atoms in the equatorial positions. A similar trigonal bipyramidal structure has also been suggested for SiH_3Br^- radical anion, since hyperfine structure due to the Br and one H nuclei was observed in the ESR spectrum.[3] However, GeH_3Br^- radical anions, which are congeneric to SiH_3Br^-, have been reported to have a structure with C_{3v} symmetry, as in the case of CF_3Br^-, because the hyperfine structure of the Br nucleus in the ESR spectrum is further split by three equivalent H nuclei.[4] Thus, the structure of radical anions is significantly affected by the type of central atom present. Moreover, ESR spectra of methyl-substituted radical anions such as $CH_3SiH_2Br^-$ and $CH_3GeH_2Br^-$ have been investigated in order to confirm the structural difference between trigonal bipyramidal and C_{3v} structures.[5] No substantial change in radical structure resulted from the introduction of methyl groups, and it was therefore concluded that, even in the methyl-substituted radical anions, the silicon-centered radical anions prefer a trigonal bipyramidal structure whereas the germanium-centered radical anions have a local C_{3v} structure. For the silicon-centered radical anions, the methyl groups have been suggested to prefer the equatorial positions to the axial ones of the trigonal bipyramidal structure.

On the basis of these facts, this study was designed. Organo halosilanes $RSiH_2X$ (X=Br or I) containing different kinds of organo group R were prepared; irradiation then produces their radical anions in TMS matrices. Thus we could investigate the effect of substituent groups on radical structure and on the distribution of spin density.

Experimental

Ethylsilane and vinylsilane were prepared by reducing ethyltrichlorosilane and vinyltrichlorosilane (Tokyo Kasei), respectively, with lithium aluminium hydride in dibutyl ether. Ethylbromosilane was prepared by the reaction with mercury(II) bromide[6] and ethyliodosilane with hydrogen iodide in the presence of aluminium triiodide as a catalyst.[7] Vinylbromosilane and vinyliodosilane were similarly obtained.

All of the compounds prepared were isolated and purified by distillation *in vacuo*, and identified from IR spectra.[8]

Solid solutions of tetramethylsilane (Merck) containing 5 mol% of the appropriate silane were irradiated at 77 K with γ-rays to *ca.* 1.5 Mrad in a ^{60}Co γ-source.

ESR spectra were measured at 77 K with an X-band JES-3BSX spectrometer after irradiation.

Results and Discussion

When a solid solution of TMS containing 5 mol% of $C_2H_5SiH_2Br$ was γ-irradiated at 77 K and followed by ESR observations at 77 K, the ESR spectrum shown in Fig. 1 was observed. In addition to the central lines originating from the matrix radical $\cdot CH_2SiMe_3$, one can find an anisotropic spectrum similar to the spectra assigned to the SiH_3Br^-[3] and $CH_3SiH_2Br^-$[5] radical anions, which formed in TMS matrices and have trigonal bipyramidal structures. In accordance with the analyses reported for these radical anions, the observed spectrum is interpreted in terms of hyperfine structure due to one Br ($^{79}Br(I=3/2)50.57\%$, $^{81}Br(I=3/2)49.43\%$) and one H nuclei. The coupling constant of the H nucleus is similar in magnitude to that of H nucleus in an axial position of SiH_3Br^-[3] and to that of the H nucleus which is bonded to the Si atom and possesses an axial position of $CH_3SiH_2Br^-$.[5] Accordingly, the $C_2H_5SiH_2Br^-$ radical anions formed were concluded to have trigonal bipyramidal structure possessing the Br and H atoms with large spin densities in the axial positions and the other H atom and the C_2H_5 group in the equatorial positions.

Similar experiments were also carried out with $C_2H_5SiH_2I$ in a TMS matrix. The observed ESR spectrum was interpreted in terms of hyperfine splittings due to the axial I and H nuclei of trigonal bipyramidal $C_2H_5SiH_2I^-$ radical anions. This result is in contrast to the fact that the radical anions $CH_3SiH_2I^-$ have been assigned to have, exceptionally, a local C_{3v} struc-

TABLE 1. ESR PARAMETERS AND SPIN DENSITIES OF RADICAL ANIONS OF ORGANO HALOSILANES AND HALOSILANES

Radical	g values		Nucleus	Hyperfine couplings		Spin densities		Structure	Reference
	$g_\perp$	$g_{//}$		$A_\perp$/G[a]	$A_{//}$/G[a]	ρ_s	ρ_p		
$C_2H_5SiH_2Br^-$	2.007	2.003	^{79}Br	110	209	0.018	0.145	Tbp[b]	This work
			^{81}Br	118	226	0.018	0.145		
			^1H	39.3	40.8	0.078			
$CH_3SiH_2Br^-$	2.005	2.001	^{79}Br	109	220	0.019	0.160	Tbp	5
			^{81}Br	118	237	0.019	0.160		
			^1H	41.5	45.3	0.084			
SiH_3Br^-	2.004	2.002	^{79}Br	128	254	0.022	0.183	Tbp	3
			^{81}Br	138	274	0.022	0.183		
			^1H	43.4	45.6	0.087			
CH_2=$CHSiH_2Br^-$	2.004	2.003	^{79}Br	117	239	0.020	0.178	Tbp	This work
			^{81}Br	126	258	0.020	0.178		
			^1H	33.7	37.3	0.069			
$C_2H_5SiH_2I^-$	2.022	1.997	^{127}I	142	276	0.026	0.196	Tbp	This work
			^1H	33.4	35.6	0.069			
$CH_3SiH_2I^-$	2.009	1.997	^{127}I	148	276	0.026	0.188	C_{3v}	5
			^1H	20	22	0.041			
SiH_3I^-	2.009	1.994	^{127}I	165	328	0.030	0.238	Tbp	3
			^1H	35.6	35.6	0.070			
CH_2=$CHSiH_2I^-$	2.015	1.992	^{127}I	157	291	0.028	0.196	Tbp	This work
			^1H	31.0	33.4	0.063			

a) 1 G=1×10^{-4} T. b) Tbp means trigonal bipyramidal structure.

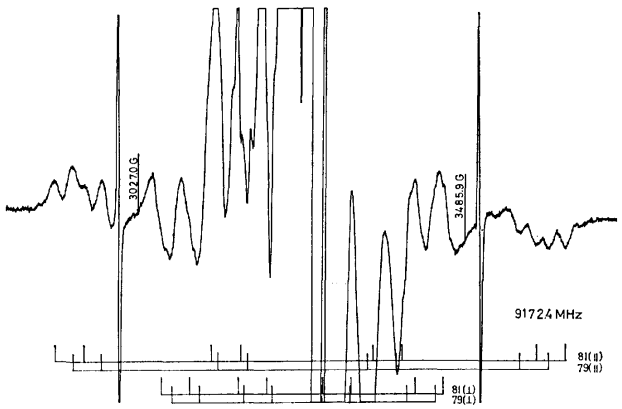

Fig. 1. First derivative ESR spectrum of a γ-irradiated solid solution of 5 mol % ethylbromosilane in tetramethylsilane, recorded at 77 K.
The stick diagrams represent the calculated line positions of the parallel (upper) and the perpendicular (lower) components for $C_2H_5SiH_2{}^{79}Br^-$ and $C_2H_5SiH_2{}^{81}Br^-$ according to the parameters listed in Table 1.

ture rather than a trigonal bipyramidal structure since the ESR spectrum consists of a sextet due to the I nucleus and a 1:2:1 triplet due to three equivalent H nuclei.[5]

Resonance line positions were calculated by a matrix diagonalization program with the ESR parameters listed in Table 1. In accordance with the above analyses, the stick diagrams calculated show good agreement with the observed spectra assigned to $C_2H_5SiH_2Br^-$ and $C_2H_5SiH_2I^-$. Spin densities were obtained by the use of the atomic values of hyperfine coupling constants[9] calculated from Froese's wave functions[10] for comparison with those of related and reported radical anions; the values are listed in Table 1 with ESR parameters. If atomic values calculated recently by Morton and Preston[11] are used, the values become smaller. In Table 1, results for $CH_3SiH_2X^-$[5] and SiH_3X^-[3] (X=Br or I) are given for comparison. Spin densities on the axial H and halogen atoms increase in the order C_2H_5, CH_3, and H for R of $RSiH_2X^-$ (X=Br or I) except for the case $CH_3SiH_2I^-$, where a local C_{3v} structure was suggested.[5] The group electronegativity of each substituent increases in the same order.

Here, it might be of interest to quote results for the SiF_3Br^-[2] and SiH_3Br^-[3] radical anions which have axial Br atoms in their trigonal bipyramidal structure. Since Br is less electronegative than F and more electronegative than H, the less electronegative Br occupies the axial position of SiF_3Br^-. Phosphoranyl radicals are isoelectronic to the silicon-centered radical anions and also have trigonal bipyramidal structures, which are similar to the structure of phosphoranes. Colussi *et al.*[12] have made INDO calculations for phosphoranyl radicals and phosphoranes. According to their results, electron densities (charge densities) in PH_4 and PH_5 are larger in the axial positions than in the equatorial positions. In the cases of PF_4 and PF_5, however, the equatorial positions have higher electron densities than the axial positions. Therefore, when a group which is more electronegative than H is replaced with an H atom of PH_4 or PH_5, the group prefers an axial position with its higher electron density. Coherently, a less electronegative group possesses an axial position with a lower electron density upon the substitution with an F atom of PF_4 or PF_5. The effect of group electronegativity on the preferential occupation of substituents has also been investigated experimentally for phosphoranyl radicals.[13] Similar

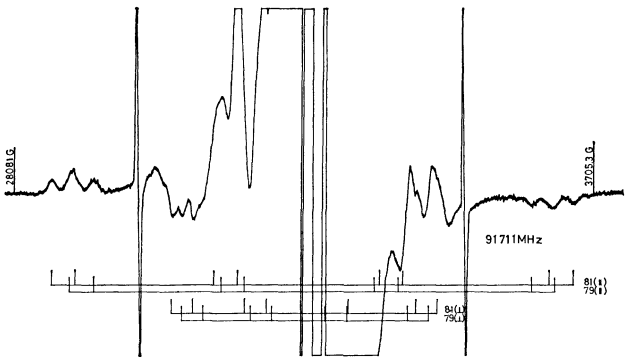

Fig. 2. ESR spectrum of a γ-irradiated solid solution of 5 mol % vinylbromosilane in tetramethylsilane, recorded at 77 K, and the stick diagrams calculated for CH_2=$CHSiH_2{}^{79}Br^-$ and CH_2=$CHSiH_2{}^{81}Br^-$.

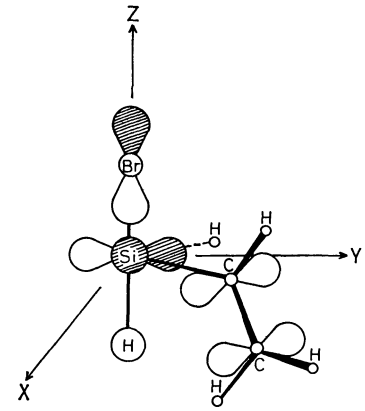

Fig. 3. A structure proposed for CH_2=$CHSiH_2Br^-$. The terminal C atom in the vinyl group is on the upper side or on the lower side of the equatorial plane.

results can be expected for the silicon-centered radical anions which are isoelectronic to phosphoranyl radicals. Accordingly, the axial positions of the Br atom in SiH_3Br^- and SiF_3Br^- are well accepted.

In the case of $RSiH_2X^-$, it is thus reasonable to expect that a group R more electronegative than H takes an axial position and that a less electronegative group R occupies an equatorial position. Indeed, as mentioned above, C_2H_5 and CH_3 groups which are less electronegative than H occupy the equatorial positions of the trigonal bipyramidal $RSiH_2X^-$ radical anions. This result is consistent with the result obtained recently for the radical anions of methylstannanes: that methyl groups prefer the equatorial positions of the trigonal bipyramidal structure.[14]

Since vinyl groups are more electronegative than H and are therefore expected to possess the axial positions of CH_2=$CHSiH_2X^-$ radical anions, a solid solution of TMS containing CH_2=$CHSiH_2Br$ was irradiated. As shown in Fig. 2, the ESR spectrum consists of the anisotropic hyperfine structure of a quartet from one Br atom and a doublet. The doublet may originate from an H atom bonded to the Si atom or from one in the vinyl group. Thus, similar experiments were carried out with CH_2=$CHSiD_2Br$. As a result, the doublet which appeared in the case of CH_2=$CHSiH_2Br$ was removed and the anisotropic quartet spectrum alone was observed. Therefore, the spectrum observed with CH_2=$CHSiH_2Br$ was interpreted to contain hyperfine splittings due to the Br atom and one of the two H atoms bonded to the Si atom. This fact leads us to the conclusion that the CH_2=$CHSiH_2Br^-$ radical anion formed has the vinyl group in the equatorial position of the trigonal bipyramidal structure, although the axial position was the first suggested.

Irrespective of the electronegativity of vinyl group, which is larger than that of H, the value of spin density on the axial Br atom of the CH_2=$CHSiH_2Br^-$ radical anions falls between those obtained for $CH_3SiH_2Br^-$ and SiH_3Br^-, while the value on the axial H atom is smaller than that for $C_2H_5SiH_2Br^-$. Similar trends were obtained between CH_2=$CHSiH_2I^-$ and the related radical anions, although $CH_3SiH_2I^-$ could not be compared because of the different structure.[5] These results may indicate that some other factor than the electronegativity of vinyl groups governs the geometrical and electronic structures of CH_2=$CHSiH_2X^-$ radical anions.

When the effect of substituent groups is considered, electronegativity is important for the inductive effect of σ electrons. However, for the groups with π electrons or nonbonding electron pairs, the more electron attractive for the inductive effect by σ electrons the groups are, the more electron donating are the groups for the π electron mesomeric effect, and the groups behave as π donors. Thus, vinyl groups are considered as electronegative groups and simultaneously as π donors.

As mentioned earlier, the electronic structure of phosphorane PH_5 as well as phosphoranyl radical PH_4 is suggestive of that of the radical anions of halosilane. Therefore, the results for PH_5 derived from extended Hückel calculations by Hoffmann *et al.*[15] may be helpful for the consideration of the effect of substituent groups in organo halosilane radical anions.

Let us first view the interactions arising between the orbitals of PH_5 and a π donor or a π acceptor.[15] For a π donor, interaction I with occupied PH_5 skeleton orbitals and interaction II with phosphorus 3d orbitals were considered, while interaction III with unfilled skeleton orbitals was neglected. I is inherently destabilizing, whereas II is inherently stabilizing, and the interaction I is more important than II. On the other hand, there is only one significant interaction (IV) between the acceptor orbital and the occupied skeletal set. Thus, for an acceptor the site with maximum interaction will be favored (IV is stabilizing), and for a donor the site with maximum interaction will be destabilized (I is a repulsive term).

Axial interactions, e_x and e_y, equatorial interactions, b_1 and b_2, and the relation between their magnitudes, $e_x \simeq e_y \simeq b_1 > b_2$, are shown in the paper by Hoffmann *et al.*[15] According to these results, π acceptors will prefer axial sites in the trigonal bipyramid so as to have the maximum interaction e_x or e_y, while π donors will occupy equatorial positions for b_2 avoiding large interactions. If a substituent has a single π system and is located in the equatorial positions, it will prefer to have its acceptor orbital perpendicular to the equa-

torial plane, having b_1 interaction, or its donor orbital in that plane, having b_2 interaction.

In the light of these results for PH_5, the vinyl group, which has a single π system in $CH_2{=}CHSiH_2X^-$ radical anion may be expected to occupy the equatorial position and to have its donor orbital in the equatorial plane, as shown in Fig. 3. The π donor orbital of the equatorial vinyl group is shown in Fig. 3 with the a_1 antibonding unpaired electron orbital composed of the p orbital of the axial Br, the s orbital of the axial H and the s and p orbitals of the central Si atom.[2-4] This is accordance with the results obtained from the ESR observations described earlier.

In conclusion, the mesomeric effect as well as the inductive effect of substituent group plays an imporant role in the geometrical preference of the substituent groups in the trigonal bipyramidal structure of organo halosilane radical anions.

References

1) A. Hasegawa and F. Williams, *Chem. Phys. Lett.*, **46**, 66 (1977); A. Hasegawa, M. Shiotani, and F. Williams, *Discuss. Faraday Soc.*, **63**, 157 (1978).
2) A. Hasegawa, S. Uchimura, and M. Hayashi, *J. Magn. Reson.*, **38**, 391 (1980).
3) S. Uchimura, A. Hasegawa, and M. Hayashi, *Mol. Phys.*, **38**, 413 (1979).
4) A. Hasegawa, S. Uchimura, and M. Hayashi, *Mol. Phys.*, **40**, 679 (1980).
5) A. Hasegawa, S. Uchimura, and M. Hayashi, *J. Chem. Soc., Perkin Trans. 2*, **1980**, 1690.
6) H. H. Anderson, *J. Am. Chem. Soc.*, **82**, 1323 (1960).
7) H. Emeléus, M. Onyszchuk, and W. Kuchen, *Z. Anorg. Allg. Chem.*, **283**, 74 (1956).
8) J. E. Drake, R. T. Hemmings, and C. Riddle, *J. Chem. Soc., A*, **1970**, 3359; S. G. Frankis, *Spectrochim. Acta*, **22**, 295 (1966).
9) B. A. Goodman and J. B. Raynor, *Adv. Inorg. Chem. Radiochem.*, **13**, 135 (1970).
10) C. Froese, *J. Chem. Phys.*, **45**, 1417 (1966).
11) J. R. Morton and K. F. Preston, *J. Magn. Reson.*, **30**, 577 (1978).
12) A. J. Colussi, J. R. Morton, and K. F. Preston, *J. Phys. Chem.*, **79**, 651 (1975).
13) J. W. Cooper, M. J. Parrott, and B. P. Roberts, *J. Chem. Soc., Perkin Trans. 2*, **1976**, 1154.
14) A. Hasegawa, T. Yamaguchi, and M. Hayashi, *Chem. Lett.*, **1980**, 611.
15) R. Hoffmann, J. M. Howell, and E. L. Muetterties, *J. Am. Chem. Soc.*, **94**, 3047 (1972).

Structural Studies of Fortimicins. IV. The Crystal Structure of Fortamine Sulfate Trihydrate and the Anion Effect on Fortamine Conformation

Noriaki HIRAYAMA,* Kunikatsu SHIRAHATA, Yuji OHASHI,† and Yoshio SASADA†

Tokyo Research Laboratory, Kyowa Hakko Kogyo Co., Ltd., 3-6-6 Asahimachi, Machida, Tokyo 194

† *Laboratory of Chemistry for Natural Products, Tokyo Institute of Technology, Nagatsuta, Midori-ku, Yokohama 227*

(Received January 12, 1981)

The molecular and crystal structure of fortamine sulfate trihydrate, $C_8H_{18}N_2O_4 \cdot H_2SO_4 \cdot 3H_2O$, was determined by X-ray analysis. The space group is $P2_1$ with $a=7.2516(9)$, $b=11.193(1)$, $c=9.022(1)$ Å, $\beta=90.55(2)°$, and $Z=2$. The structure was solved by direct methods, and least-squares refinement using 1679 reflexions led to the final R value of 0.063. The ring conformation of fortamine sulfate is a chair form which corresponds to a chair obtained by inversion of that in the dihydrochloride. This is an extraordinary example of the cyclohexane ring inversion caused by the anion exchange in the crystal. The ring conformation of fortamines in solution and in crystal are compared and discussed.

Fortamine, 1,4-diaminocyclitol, is a component of potent aminocyclitol antibiotics fortimicins.[1] Egan *et al.* have shown that fortamine moiety takes 'B' type conformation in fortimicin B, whereas it takes 'A' type conformation in fortimicin B sulfate and fortimicin A,[2,3] as shown in Fig. 1. The conformation of fortamine moiety in fortimicins is probably related to their biological activity.[2] Therefore, it is quite interesting to deduce the factors which control the conformation of fortamine. From such points of view we have determined the molecular structures of fortamine itself[4] and its dihydrochloride salt[5] by X-ray analysis. The results showed that the conformation of the former is 'B' type, but that of the latter is 'A' type. Although it has been believed that the 'A' type conformation is rather unstable because of the inherent 1,3-diaxial interactions, the latter analysis confirmed that 'A' type conformation could exist in the crystal structure and supported the assignment made by Egan *et al.*[2]

The NMR results, however, revealed that in solution the fortamine rings of fortamine, fortamine dihydrochloride, and fortamine sulfate take essentially the same conformation, *i.e.*, the 'B' type conformation. It means that the ring conformation of fortamine dihydrochloride in the crystal is different from that in solution. This paradoxical observation has prompted us to compare the fortamine ring conformation of the sulfate in the crystal and in solution. In this connection we have undertaken the X-ray analysis of the sulfate. In this paper we will also report on the NMR results of fortamines.

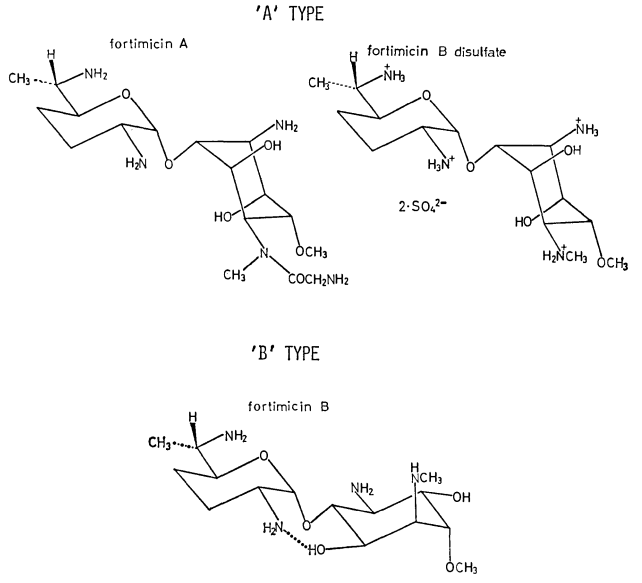

Fig. 1. Structures of fortimicins.

Experimental and Structure Determination

The prismatic crystals of the title compound were grown from a methanol solution. A crystal of $0.4\times0.4\times0.3$ mm³ sealed in a glass capillary was used for data collection on a Rigaku four-circle automated diffractometer with graphite monochromated Mo $K\alpha$ radiation ($\lambda=0.71069$ Å). Preliminary unit-cell dimensions and space group were obtained from photographs. The space group was determined from the systematic absences ($0k0$ for odd k). Accurate cell dimensions were determined by least-squares calculation with 2θ values of 15 high-angle reflexions measured on the diffractometer. Crystal data are summarized in Table 1. All reflexions within the range of $2\theta\leqq55°$ were collected by the use of the ω-2θ scan mode with a scanning rate of $4°(2\theta)$ min^{-1}. Stationary background counts were accumulated for 10 s before and after each scan. Periodic checks of the intensity values of three standard reflexions did not reveal any significant X-ray damage. Any corrections for absorption or extinction were not applied. A total of 1773 independent reflexions were obtained, of which 1679 ($|F_o|>3.0\sigma(|F_o|)$) were considered as observed. The structure was solved by direct methods with MULTAN 78 program.[5] The best set of phases was used to calculate an E map, which gave 13 chemically significant peaks. Other non-hydrogen

Table 1. Crystal data

$C_8H_{18}N_2O_4 \cdot H_2SO_4 \cdot 3H_2O$	$b=11.193(1)$ Å
$F.W.=358.36$	$c=9.022(1)$ Å
$P2_1$	$\beta=90.55(2)°$
$Z=2$	$D_x=1.626$ g cm^{-3}
$a=7.2516(9)$ Å	μ(Mo $K\alpha$) $=2.869$ cm^{-1}

Table 2. Final atomic coordinates with their estimated standard deviations, multiplied by 10^4 for non-hydrogen and 10^3 for hydrogen atoms

Atom	x	y	z	B or B_{eq} / Å^2
C (1)	6432 (8)	3485 (7)	6092 (7)	1.8
C (2)	7703 (9)	4379 (6)	5338 (7)	1.7
C (3)	8081 (8)	4029 (6)	3751 (7)	1.6
C (4)	8786 (9)	2747 (6)	3585 (7)	1.7
C (5)	7534 (9)	1853 (6)	4388 (7)	1.7
C (6)	7172 (9)	2201 (6)	5984 (8)	1.9
C (7)	6486 (12)	4395 (9)	1453 (8)	3.4
C (8)	12106 (9)	3288 (9)	3235 (8)	3.0
N (1)	6257 (8)	3820 (6)	7691 (6)	2.2
N (4)	10743 (7)	2622 (5)	4120 (6)	1.9
O (1)	5829 (7)	1423 (5)	6578 (6)	2.9
O (2)	6985 (6)	5549 (4)	5440 (5)	2.2
O (3)	6346 (6)	4100 (5)	2990 (5)	2.0
O (5)	8390 (7)	711 (4)	4413 (5)	2.5
S	8474 (3)	−1780 (3)	1586 (2)	2.8
OS (1)	6904 (8)	−2010 (7)	679 (6)	4.8
OS (2)	8173 (9)	−1654 (12)	3103 (7)	7.6
OS (3)	9087 (18)	−3165 (12)	1757 (17)	2.0
OS (4)	9973 (25)	−1485 (21)	932 (22)	4.8
OS (5)	10210 (18)	−2063 (13)	917 (16)	2.1
OS (6)	8245 (25)	−334 (12)	1552 (16)	2.6
OS (7)	10038 (26)	−1075 (20)	1074 (24)	5.1
OS (8)	8813 (37)	−2563 (43)	2613 (53)	3.0
OW (1)	498 (1)	−380 (1)	869 (1)	6.4
OW (2)	205 (1)	−426 (1)	90 (1)	7.7
OW (3)	867 (2)	−398 (1)	857 (1)	11.3
HC (1)	495 (10)	351 (8)	569 (8)	3.3
HC (2)	881 (9)	437 (6)	607 (7)	1.8
HC (3)	878 (8)	461 (6)	332 (6)	0.7
HC (4)	875 (12)	256 (9)	249 (10)	4.6
HC (5)	640 (8)	183 (6)	398 (7)	0.9
HC (6)	835 (19)	215 (14)	654 (16)	10.9
HAN (1)	609 (10)	464 (8)	771 (7)	2.8
HBN (1)	706 (14)	391 (11)	821 (12)	7.1
HCN (1)	553 (13)	336 (12)	806 (11)	6.7
HAN (4)	1070 (10)	279 (7)	488 (9)	3.3
HBN (4)	1088 (12)	197 (9)	413 (10)	5.1
HO (1)	617 (8)	110 (6)	687 (6)	1.2
HO (2)	624 (9)	562 (6)	502 (7)	1.5
HO (5)	779 (12)	47 (10)	356 (10)	5.4
HAC (7)	752 (11)	396 (8)	91 (9)	4.0
HBC (7)	509 (17)	440 (14)	78 (14)	10.0
HCC (7)	704 (12)	506 (9)	132 (10)	5.3
HAC (8)	1346 (14)	316 (11)	367 (11)	7.1
HBC (8)	1175 (14)	311 (11)	247 (11)	7.1
HCC (8)	1191 (10)	398 (8)	352 (8)	2.9

atoms were located easily by the subsequent Fourier syntheses. The structural parameters were refined by block-diagonal least-squares methods with a modified HBLS program. The two of sulfate oxygen atoms were considerably disordered and when they were assumed to distribute over six positions with an occupancy of 0.3333, the refinement proceeded successfully. All hydrogen atoms except those of water molecules were located by difference syntheses. Refinement using anisotropic and isotropic thermal parameters for the non-hydrogen and hydrogen atoms, respectively, gave the final R value of 0.063 for 1679 reflexions. The weighting system used in the final stage was $w=(\sigma(|F_o|)^2+(0.015F_o)^2)^{-1}$. Atomic scattering factors were taken from "International Tables for X-Ray Crystallography."[6] The final positional and thermal parameters are given in Table 2. OS(3) to OS(8) denote the sulfate oxygen atoms refined with occupancy of 0.3333. OW denotes the water molecule. The table of observed and calculated structure factors and the list of the anisotropic thermal parameters are kept as Document No. 8144 at the Chemical Society of Japan.

The NMR spectra were measured in D_2O solution by means of an FX100 Model apparatus, JEOL Co., using DSS as the internal standard.

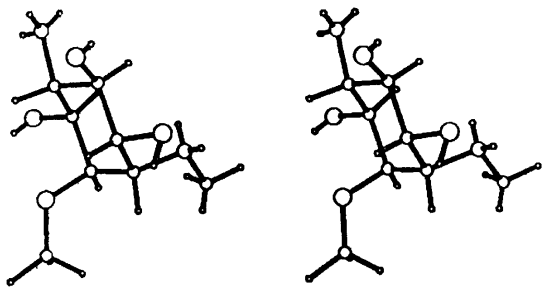

Fig. 2. Stereoscopic drawing of fortamine sulfate.

Table 3. Torsional angles (ϕ/°)

	Fortamine sulfate	Fortamine
C (3)-C (2)-C (1)-C (6)	54.1	53.9
C (4)-C (3)-C (2)-C (1)	−52.8	−56.1
C (5)-C (4)-C (3)-C (2)	51.0	56.3
C (6)-C (5)-C (4)-C (3)	−51.3	−56.4
C (1)-C (6)-C (5)-C (4)	53.4	54.6
C (2)-C (1)-C (6)-C (5)	−54.5	−52.6
O (2)-C (2)-C (1)-N (1)	−59.9	−62.2
O (3)-C (3)-C (2)-O (2)	−60.2	−59.8
N (4)-C (4)-C (3)-O (3)	170.4	173.9
O (5)-C (5)-C (4)-N (4)	−45.8	−60.1
O (1)-C (6)-C (5)-O (5)	−66.8	−57.9
N (1)-C (1)-C (6)-O (1)	65.2	65.2
C (4)-C (3)-O (3)-C (7)	−88.2	−110.1
C (3)-C (4)-N (4)-C (8)	−65.7	−70.9
C (5)-C (4)-N (4)-C (8)	169.7	166.5
C (2)-C (3)-O (3)-C (7)	150.3	129.2

Results

Conformation of the Molecule. The ring conformation of fortamine dication, as shown in Fig. 2, is the 'B' type. The signs of torsional angles listed in Table 3 also represent the 'B' type conformation. The d values[3] of each ring-carbon atoms are as follows; C(1) 0.648, C(2) 0.632, C(3) 0.611, C(4) 0.619, C(5) 0.622, and C(6) 0.644 Å. The average C–C–C–C torsional angle is 52.9° and average d is 0.629 Å. They are quite similar to those of the dihydrochloride, 52.7° and 0.627 Å, respectively and smaller than those

TABLE 4. BOND LENGTHS (l/Å) AND ANGLES (ϕ/°)

C(1)-C(2)	1.524(6)	C(5)-C(4)-N(4)	110.4(3)
C(1)-C(6)	1.538(6)	C(4)-C(5)-O(5)	109.5(3)
C(1)-N(1)	1.497(6)	C(6)-C(5)-O(5)	107.2(3)
C(2)-C(3)	1.512(6)	C(5)-C(6)-O(1)	109.1(4)
C(2)-O(2)	1.413(5)	C(1)-C(6)-O(1)	108.0(4)
C(3)-C(4)	1.532(6)	C(3)-O(3)-C(7)	114.1(4)
C(3)-O(3)	1.430(5)	C(4)-N(4)-C(8)	114.5(4)
O(3)-C(7)	1.430(7)	OS(1)-S-OS(2)	116.8(4)
C(4)-C(5)	1.537(6)	OS(1)-S-OS(3)	95.7(4)
C(4)-N(4)	1.501(6)	OS(1)-S-OS(4)	117.3(7)
N(4)-C(8)	1.478(7)	OS(1)-S-OS(5)	114.8(4)
C(5)-C(6)	1.516(6)	OS(1)-S-OS(6)	95.0(5)
C(5)-O(5)	1.421(5)	OS(1)-S-OS(7)	122.5(6)
C(6)-O(1)	1.416(6)	OS(1)-S-OS(8)	116(2)
S-OS(1)	1.419(6)	OS(2)-S-OS(3)	92.8(5)
S-OS(2)	1.395(8)	OS(2)-S-OS(4)	124.5(7)
S-OS(3)	1.619(10)	OS(2)-S-OS(5)	125.5(5)
S-OS(4)	1.285(14)	OS(2)-S-OS(6)	84.3(5)
S-OS(4)	1.437(9)	OS(2)-S-OS(7)	112.7(7)
S-OS(6)	1.628(11)	OS(2)-S-OS(8)	53(2)
S-OS(7)	1.460(14)	OS(3)-S-OS(4)	93.3(7)
S-OS(8)	1.297(56)	OS(3)-S-OS(5)	65.7(5)
C(1)-C(2)-C(3)	111.7(4)	OS(3)-S-OS(6)	169.0(5)
C(2)-C(3)-C(4)	113.5(4)	OS(3)-S-OS(7)	109.5(7)
C(3)-C(4)-C(5)	111.4(4)	OS(3)-S-OS(8)	40(2)
C(4)-C(5)-C(6)	112.9(4)	OS(4)-S-OS(5)	27.8(7)
C(5)-C(6)-C(1)	111.4(4)	OS(4)-S-OS(6)	79.8(7)
C(6)-C(1)-C(2)	111.8(4)	OS(4)-S-OS(7)	18.7(8)
C(6)-C(1)-N(1)	109.2(4)	OS(4)-S-OS(8)	110(3)
C(2)-C(1)-N(1)	108.9(4)	OS(5)-S-OS(6)	107.5(5)
C(1)-C(2)-O(2)	110.8(4)	OS(5)-S-OS(7)	45.6(7)
C(3)-C(2)-O(2)	111.8(3)	OS(5)-S-OS(8)	89(2)
C(2)-C(3)-O(3)	105.9(3)	OS(6)-S-OS(7)	62.3(7)
C(4)-C(3)-O(3)	107.3(3)	OS(6)-S-OS(8)	135(2)
C(3)-C(4)-N(4)	111.8(3)	OS(7)-S-OS(8)	117(3)

of the free base, 54.9° and 0.655 Å. These values show that the protonation at the nitrogen atoms causes the flattening of the fortamine ring as a whole. While C(1) and C(6) are puckered a little, C(3) and C(4) are flattened a little; the magnitude of puckering or flattening is smaller than that of the dihydrochloride and is almost the same as that of the free base. The smallest exocyclic O(5)–C(5)–C(4)–N(4) torsional angle of −45.8° is due to the intramolecular N(4)–H···O(5) hydrogen bond.

Bond Lengths and Angles. The bond lengths and angles are given in Table 4. The exocyclic C–C bond lengths are 1.512 to 1.538 Å, and the average value of 1.527 Å is essentially equal to those of the free base and the dihydrochloride. The C(2)–O(2) and C(6)–O(1) bond lengths, 1.413 and 1.416 Å, respectively, are significantly shorter than those of fortamine. This shortening is similar to that of the dihydrochloride. The C(1)–N(1), C(4)–N(4), and N(4)–C(8) bond lengths of the sulfate are as long as those of the dihydrochloride. Although the average C–C–C bond angle of 112.1° is the same as that of the dihydrochloride and larger than that of the free base, the scattering

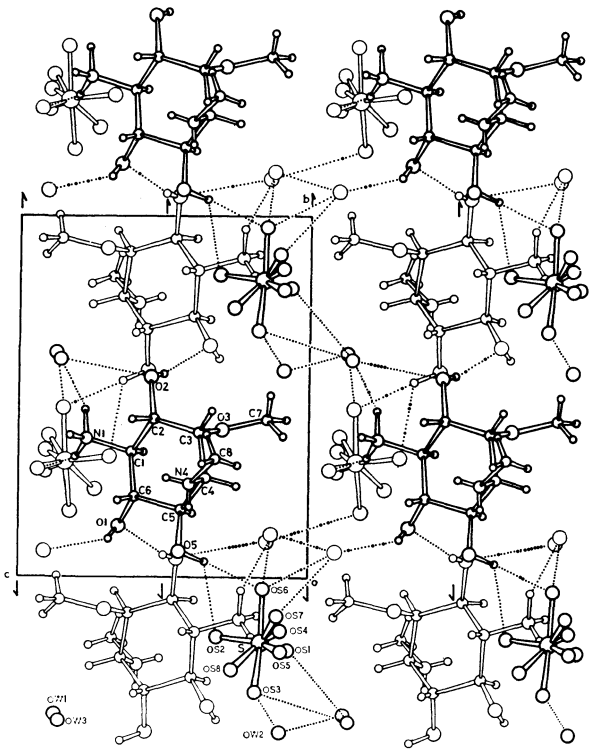

Fig. 3. Crystal structure of fortamine sulfate viewed along the a axis.

of the angles is small, *i.e.*, in the sulfate 111.4 to 113.5°, but in the dihydrochloride 109.7 to 114.3° and in the free base 109.9 to 112.6°. Most of the exocyclic bond angles are similar to those of the free base rather than those of the dihydrochloride. The bond lengths and angles show that the fortamine ring in the sulfate takes almost the same geometry as that of fortamine.

The sulfate oxygen atoms which are not involved in the hydrogen bonds are disordered; hence the relevant bond lengths and angles are distorted. The values are listed in Table 4.

Crystal Structure. The crystal structure viewed along the a axis is shown in Fig. 3. Hydrogen bond lengths and angles are listed in Table 5. Hydrogen bonds are shown by dotted lines in Fig. 3. The molecules linked by the O(2)–H···O(1) hydrogen bonds form helical chains along the b axis. There is no other intermolecular hydrogen bonds between the functional groups. The N(1) atom is hydrogen bonded to the OS(1) atom of the sulfate anion, but there is no sulfate anion sufficiently near the N(4) atom. The positive charge on N(4) may be partially transferred to O(5) through the N(4)–H···O(5) intramolecular hydrogen bond. The O(5) atom is hydrogen bonded to the OS(6) and OS(2) atoms. Therefore the positive charge may be neutralized by these hydrogen bonds. The O(1), O(2), and N(1) atoms are hydrogen bonded to water molecules. There is an extensive hydrogen bond networks between sulfate anion and water molecules.

Conformation in Solution. The NMR parameters of fortamine, its dihydrochloride, and its sulfate are shown in Table 6. The pD of the solution are 11.5, 3.5, and 1.5, respectively. The chemical shifts are

Table 5. Hydrogen bond distances (l/Å) and angles (ϕ/°)

A–H···B	A···B	∠A–H···B
N(4)–H^{I}···O(5)^{I}	2.751(6)	120(4)
O(5)–H^{I}···OS(6)^{I}	2.84(1)	142(10)
O(5)–H^{I}···OS(2)^{I}	2.903(9)	112(6)
O(2)–H^{I}···O(1)^{II}	2.892(5)	162(4)
N(1)–H^{I}···OS(1)^{II}	2.889(7)	152(5)
O(1)–H^{I}···OW(2)^{II}	2.841(7)	143(5)
N(1)–H^{I}···OW(1)^{III}	2.963(7)	151(5)
OS(3)^{I}···OW(2)^{IV}	2.60(1)	
OS(5)^{I}···OW(2)^{IV}	2.80(1)	
OS(6)^{I}···OW(2)^{V}	2.52(1)	
OS(7)^{I}···OW(2)^{V}	3.09(2)	
OW(1)^{I}···OS(1)^{VI}	3.024(8)	
OW(1)^{I}···OW(2)^{VI}	2.972(9)	
OW(3)^{I}···OS(3)^{VI}	3.03(1)	
OS(6)^{I}···OW(1)^{II}	2.91(1)	

Symmetry code

I: (x y z)
II: ($1.0-x$ $0.5+y$ $1.0-z$)
III: (x $1.0+y$ z)
IV: ($-x$ $0.5+y$ $-z$)
V: ($1.0-x$ $0.5+y$ $-z$)
VI: (x y $1.0+z$)

Table 6. 100 MHz ^{1}H-NMR parameters for fortamine free base, dihydrochloride, and sulfate

		Free base	Dihydrochloride	Sulfate
Chemical shifts	H-1	2.80	3.47	3.43
	H-2	3.61	4.19	4.21
	H-3	3.67	3.98	3.97
	H-4	3.11	3.71	3.71
	H-5	3.78	4.19	4.16
	H-6	3.34	3.85	3.87
	OCH_3	3.45	3.48	3.49
	NCH_3	2.38	2.82	2.83
Coupling constants (Hz)	$J_{1,2}$	9.8	7.6	8.1
	$J_{2,3}$	4.4	3.3	3.3
	$J_{3,4}$	3.0	6.0	4.9
	$J_{4,5}$	4.6	4.5	4.9
	$J_{5,6}$	9.8	7.6	8.1
	$J_{6,1}$	9.8	7.6	8.1

expressed in ppm from the internal standard, DSS. The coupling constants are obtained by the first order analysis. The results apparently indicate that the ring conformations of the three are essentially same and they are in the 'B' type.

Discussion

Fortamine sulfate takes the 'B' type conformation in the crystal, whereas the chloride takes the 'A' type. It is interesting to examine the effect of different anions on the fortamine conformation in the crystal. The crystal structure of the dihydrochloride viewed along the b axis is shown in Fig. 4. In the crystal structure all functional groups are involved in intermolecular hydrogen bonds with the chloride anions, the anions locate near the two amino nitrogen atoms, and consequently the fortamine molecules are tightly packed. On the contrary, the fortamine molecules in the sulfate crystal as seen in Fig. 3 are loosely packed and anions are apparently solvated. The difference between the two crystal structures may come mainly from the different valence and the different size of the anions. In the crystal structure of the dihydrochloride, the Cl(1) atom is hydrogen bonded with the two protonated nitrogen atoms, *i.e.*, the N(1) and N(4) atoms. This makes the close packing possible. The sulfate anion, however, is divalent and bulkier than the chloride anion; hence it makes the close packing rather difficult and the structure which could accomodate the solvent molecules is built up.

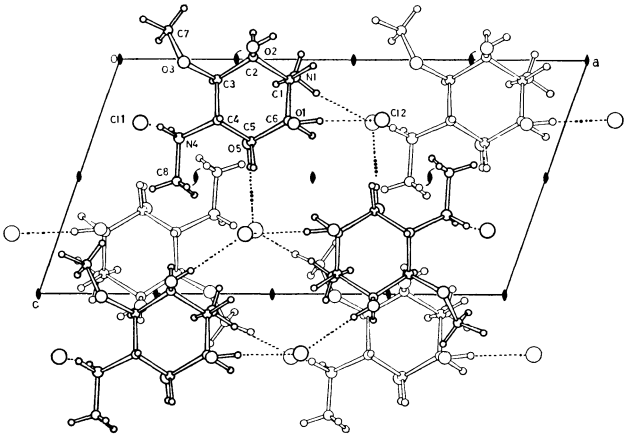

Fig. 4. Crystal structure of fortamine dihydrochloride viewed along the b axis.

The NMR results show that in aqueous solution the fortamine rings of the free base, the dihydrochloride, and the sulfate take essentially the same conformation, *i.e.*, the 'B' type conformation. In solution the anions might be solvated and they could not close to the cations easily; therefore it is conceivable that the environmental condition around the fortamine molecules in aqueous solution is close to that in the sulfate crystal. In the previous paper,[4] the electrostatic repulsion energy in the 'B' type conformation was calculated to be 0.50 kcal/mol higher than that in the 'A' type. Although further studies on the energy of molecular deformation would be required, these results suggest that intramolecular non-bonded interaction or intermolecular interaction must overcome the energy difference and the conformational change can easily occur in the stage of crystallization.

Figure 1 was drawn by TSD:XTAL, which is a computer-graphics interactive modeling programme for the NOVA 3 computer.[7]

References

1) T. Nara, M. Yamamoto, I. Kawamoto, K. Takayama, R. Okachi, S. Takasawa, T. Sato, and S. Sato, *J. Antibiot.*,

30, 533 (1977).

2) R. S. Egan, R. S. Stanaszek, M. Cirovic, S. L. Mueller, J. Tadanier, J. R. Martin, P. Collum, A. W. Goldstein, R. L. De Vault, A. C. Sinclair, E. E. Fager, and L. A. Mitscher, *J. Antibiot.*, **30**, 552 (1977).

3) N. Hirayama, K. Shirahata, Y. Ohashi, and Y. Sasada, *Bull. Chem. Soc. Jpn.*, **53**, 1514 (1980).

4) N. Hirayama, K. Shirahata, Y. Ohashi, and Y. Sasada, *Bull. Chem. Soc. Jpn.*, **53**, 3104 (1980).

5) P. Main, S. E. Hull, L. Lessinger, G. Germain, J. P. Declercq, and M. M. Woolfson, *MULTAN 78. A System of Computer Programs for the Automatic Solution of Crystal Structures from X-Ray Diffraction Data, Univ. of York, England, and Louvain, Belgium* (1978).

6) "International Tables for X-Ray Crystallography," The Kynoch Press, Birmingham (1974), Vol. IV, pp. 72—102.

7) A. Takenaka and Y. Sasada, *J. Cryst. Soc. Jpn.*, **22**, 214 (1980).

  Bull. Chem. Soc. Jpn., 54, 2629—2632 (1981)

The Capillary-tube Isotachophoretic Determination of Sodium(I), Magnesium(II), Calcium(II), Strontium(II), and Barium(II) Using Complex-forming Equilibria between CyDTA and the Metal Ions

Isoshi NUKATSUKA, Mitsuhiko TAGA, and Hitoshi YOSHIDA*

Department of Chemistry, Faculty of Science, Hokkaido University, Sapporo 060

(Received January 5, 1980)

The capillary-tube isotachophoresis technique was used to determine sodium(I), magnesium(II), calcium (II), strontium(II), and barium(II). The complex-forming equilibria between CyDTA and the metal ions were used to expand the differences among their effective mobilities. The mobilities of IIa metal ions decreased with increases in the pH of the leading electrolytes and in the CyDTA concentration in the leading electrolytes. The simultaneous determination of the above five cations could be performed when the pH of the leading electrolyte was adjusted at 5.5 or above. The relative standard deviations were 1.7—2.2% for determining 15.0—25.0 nmol of the cations when the pH of the leading electrolyte was 5.70. Magnesium(II) and calcium(II) ions underwent "enforced isotachophoretic" migration.

It is useful to apply the capillary-tube isotachophoresis technique to the analysis of small amounts of samples which contain several constituents. This method requires only a few μl of the sample solutions.

It is necessary for performing a satisfactory separation that there be enough difference among the effective mobilities of the sample ions. If the difference is not effective enough, we have to expand the difference among the mobilities.

To change the mobilities is to alter the environment of the sample constituents in the leading electrolyte. There are three main methods of doing so:[1] (1) the change in the pH of the leading electrolyte, (2) the replacement of the solvent of the leading electrolyte, and (3) the use of complex-forming equilibria.

In Method (3), various factors, *e.g.*, the kind of complexing agent and the concentration and pH of the leading electrolyte, affect the mobilities of the sample ions and may further complicate the condition. Because of the variation in the mobilities of the sample ions, the separability of the sample ions might be enhanced in some cases.

Although this method is analogous to that which is carried out in zone electrophoresis, adding complexing agents to supporting electrolyte, zone electrophoresis has little quantitative ability, whereas capillary-tube isotachophoresis has a good quantitative ability. This method has been presented in several papers,[2-4] there has, however, been little work in which this method has been applied to the determination of metal ions.

In this paper, we studied the utility of the complex-forming equilibria in determining the metal ions by capillary-tube isotachophoresis. Magnesium(II), calcium(II), strontium(II), and barium(II) were used as sample ions, and CyDTA was added to the leading electrolyte as a complexing agent. The above four cations and sodium(I) were separated and determined simultaneously, and the importance in this method of the choice of the terminating electrolyte was pointed out.

Experimental

Apparatus. Isotachopherograms were recorded with a Capillary-tube Isotachophoretic Analyzer (Shimadzu, model IP-1B, with a potential gradient detector, model PGD-1). The migration current was stabilized at 100 μA. The length of the capillary tube (PTFE, I.D. 0.5 mm) was 20 cm, and the oven temperature was 20 °C. Measurements of pH were made with an expanded-scale pH-meter (Horiba, model F-7ss). 1.0—7.0 μl portions of sample solutions were introduced into the instrument with a micro syringe.

Materials. The 1,2-cyclohexanediamine-*N,N,N',N'*-tetraacetic acid (CyDTA), 2-amino-2-hydroxymethyl-1,3-propanediol (Tris), and Triton X-100 were purchased from the Wako Pure Chemical Industry Co., Ltd. The other chemicals used were of a reagent grade and were dissolved in deionized water.

Sodium(I), Magnesium(II), Calcium(II), Strontium(II), and Barium(II) Solutions: The stock solutions were prepared by dissolving their nitrates in water. The standard solutions containing some or all of the above metal ions were obtained by mixing the stock solutions and then diluting them to the desired concentrations.

NH_4OH Solution: The NH_4OH solution was diluted to give a 1-mol dm^{-3} solution with water.

CyDTA Solution: The CyDTA was dissolved to give a 0.1-mol dm^{-3} solution in 0.4 mol dm^{-3} of an NH_4OH solution.

The leading electrolytes were obtained by mixing the NH_4OH solution and the CyDTA solution, followed by their dilution to the desired concentrations. For adjusting the pH of the leading and terminating electrolytes, acetic acid or succinic acid was used. The compositions of the leading and terminating electrolytes are shown in Table 1.

Results and Discussion

Effect of CyDTA Concentration in the Leading Electrolyte on the PR Value.† Figure 1 shows the relations between the PR values of the metal ions [magnesium-(II), calcium(II), strontium(II), and barium(II)] and the CyDTA concentration in the leading electrolyte. When CyDTA is not added to the leading electrolyte, the order of the PR values *i.e.*, the order of mobilities of the metal ions, was: barium(II)>stron-

† The PR value[4] (potential gradient ratio value) represents the ratio of the potential gradient of the leading ion to that of the sample ion (PG_L/PG_S). Therefore, this corresponds to the ratio of the mobility of the sample ion to that of the leading ion (m_S/m_L).

TABLE 1. ELECTROLYTE SYSTEMS

	Leading electrolyte[a)]		Terminating electrolyte
(I)	0.01 mol dm^{-3} NH_4OH, 0—2 mmol dm^{-3} CyDTA, acetic acid, pH 4.30	(IV)	0.01 mol dm^{-3} Tris, acetic acid, pH 4.40
(II)	0.01 mol dm^{-3} NH_4OH, 1 mmol dm^{-3} CyDTA, acetic acid, pH 4—6	(V)	0·01 mol dm^{-3} β-alanine, acetic acid, pH 4.40
(III)	0.01 mol dm^{-3} NH_4OH, 1 mmol dm^{-3} CyDTA, succinic acid, pH 5.70		

a) 0.1% Triton X-100 was added.

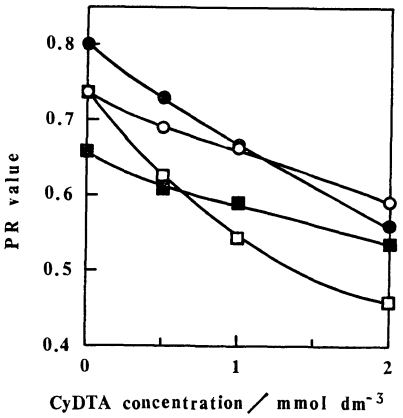

Fig. 1. Relation between the PR value and the concentration of CyDTA in the leading electrolyte.
Electrolyte system: (I) and (IV); ■: Mg^{2+}, □: Ca^{2+}, ○: Sr^{2+}, ●: Ba^{2+}.

tium(II)≈calcium(II)>magnesium(II). It is not possible to separate calcium(II) from strontium(II). When CyDTA was added to the leading electrolyte, the PR value of the metal ions decreased with an increase in the CyDTA concentration. This indicates that the interaction between CyDTA and metal ions increases with an increase in the CyDTA concentration and that it makes possible the mutual separation between the alkaline earths.

The slopes of the curves show that the effect of an increasing CyDTA concentration on the PR value of calcium(II) and barium(II) is greater than on that of magnesium(II) and strontium(II). The variations in the mobilities of the metal ions, which result from the interaction between CyDTA and metal ions, depend on the overall stability constants of the CyDTA complexes.

Comparison of Tris and β-Alanine as Terminating Ions. As is shown in Fig. 2, the PR value of the terminating ion (Tris) became abnormally small with an increase in the pH of the leading electrolyte in the case of calcium(II), which had a rather larger complexing ability than the other IIa elements. Further, the zone length of the metal ions decreased with an increase in the pH of the leading electrolyte, and in the pH region over 5.0, first the calcium(II) ion, and next the magnesium(II) ion were unable to be detected (Fig. 3a), in spite of the fact that the PR values of the metal ions were larger than that of Tris, as is shown in Fig. 4.

On the other hand, when β-alanine was used as the terminating ion, the zone length of the metal

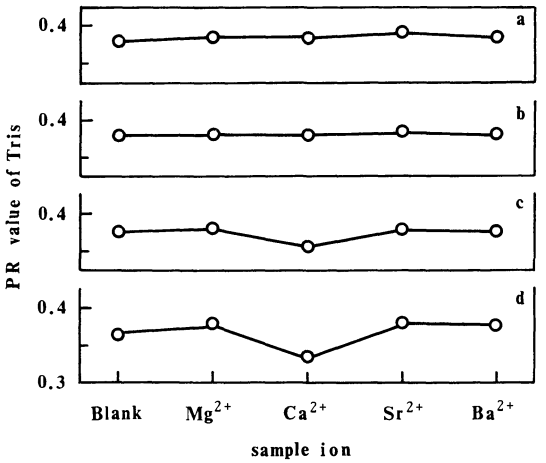

Fig. 2. Effect of pH of the leading electrolyte and sample ions on the PR value of Tris.
Electrolyte system: (II) [a) pH 3.98, b) pH 4.30, c) pH 4.50, d) pH 4.70] and (IV).

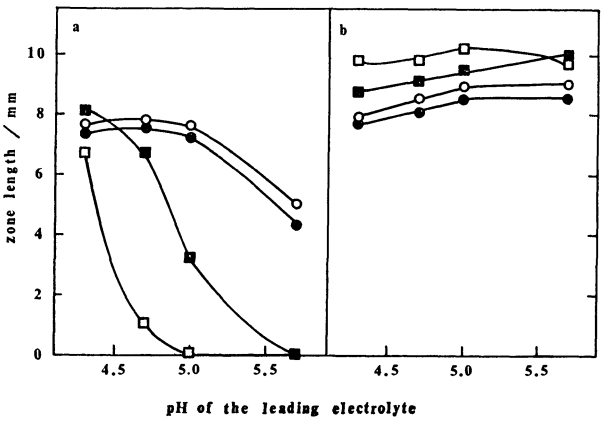

Fig. 3. Effect of terminating ions and pH of the leading electrolyte on the zone length.
Electrolyte system: a) (II) and (IV), b) (II) and (V); migration current: 100 μA; chart speed: 5.0 mm min^{-1}; sample taken: 30 nmol; other symbols are the same as in Fig. 1.

ions varied little, even higher pH's of the leading electrolyte (Fig. 3b).

Protons released from CyDTA by a complexing reaction with sample ions cause the pH of the sample-ion zones to decrease, and the pH of Tris zone is kept near that of the leading electrolyte. Therefore, the pH of the Tris zone seems to be higher than that of the sample-ion zones. In this case, if sample ions are transfered into the Tris zone by diffusion or any

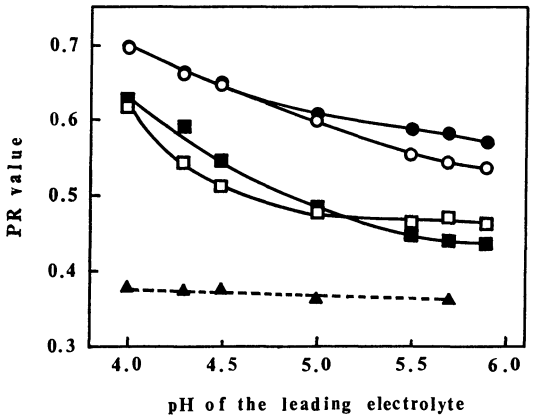

Fig. 4. Relation between the PR value and pH of the leading electrolyte.
Electrolyte system: (II) and (IV) (pH of the leading electrolyte below 4.5) and (V)(above 5.0); ▲: Tris (these values were obtained using electrolyte system (IV) even if pH of the leading electrolyte was above 5.0); other symbols are the same as in Fig. 1.

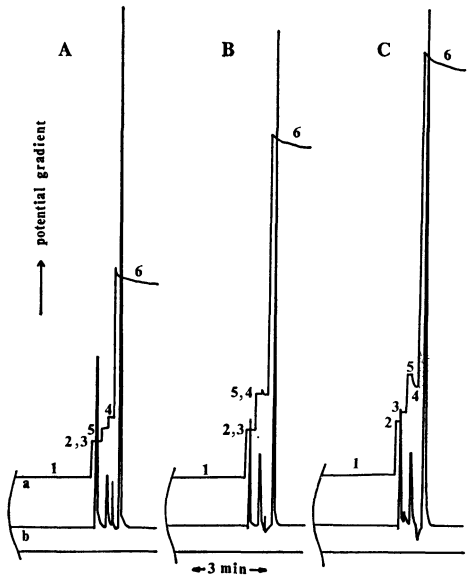

Fig. 5. Isotachopherograms.
Electrolyte system: (II) [(A) pH 4.30, (B) pH 5.00, (C) pH 5.70] and (V); a) potential gradient, b) differential potential gradient; 1) NH_4^+, 2) Ba^{2+}, 3) Sr^{2+}, 4) Ca^{2+}, 5) Mg^{2+}, 6) β-alanine.

other factors, they can not return to their own zones because their effective mobilities are smaller in higher pH zones than in lower pH zones. As a result, the zone lengths of these sample ions decrease and the PR value of Tris becomes smaller to form a mixed zone, as is shown in Figs. 2 and 3a. On the other hand, as β-alanine has a small pK_a value ($pK_{a1}=3.6$), the pH's of this zone decrease, and even if sample ions are transfered into this zone, they can return to their own zones (see Ref. 1).

Consequently, in the IIa metal-ion analysis using complex-forming equilibria, β-alanine should be used as a terminating ion, while Tris can not be applied; nevertheless, the later has a lower effective mobility

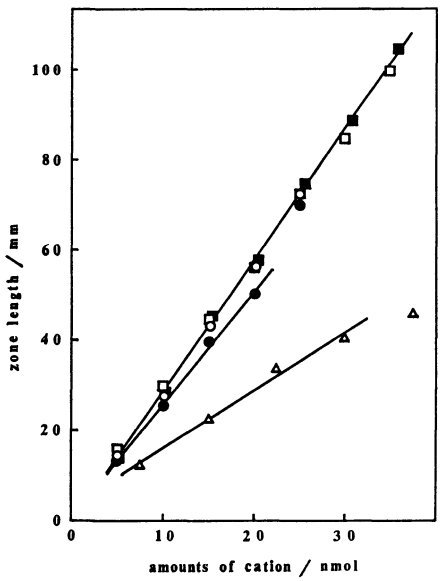

Fig. 6. Calibration curves.
Electrolyte system: (III) and (V); migration current: 100 μA; chart speed: 40 mm min^{-1}; △: Na^+; other symbols are the same as in Fig. 1; the curves of Ca^{2+} and Sr^{2+} were much the same as that of Mg^{2+}.

Table 2. Simultaneous determination of Na(I), Mg(II), Ca(II), Sr(II), and Ba(II) ions

Ion	Taken	Found	Difference	R.S.D.
	nmol	nmol	%	%
Sodium(I)	22.5	22.4	−0.44	2.2
Magnesium(II)	20.4	20.1	−1.5	1.9
Calcium(II)	25.0	25.2	0.80	1.9
Strontium(II)	20.2	19.8	−2.0	1.9
Barium(II)	15.0	15.1	0.67	1.7

The conditions are the same as in Fig. 6.

than IIa metal ions under the complex-forming equilibria.

The PR values of the sample ions are almost the same whether Tris or β-alanine is used as the terminating ion.

Relation between the PR Values and the pH of the Leading Electrolyte. The PR values of the sample ions decreased with an increase in the pH of the leading electrolyte (Fig. 4). The strontium(II) ion and the barium(II) ion were separable at a higher pH of the leading electrolyte; they were, however, not separable at a lower pH of the leading electrolyte. The magnesium(II) ion and the calcium(II) ion were also separable at a higher pH of the leading electrolyte. Four cations of IIa elements could be separated simultaneously when the pH of the leading electrolyte was adjusted to 5.5 or above. The separability of this method was larger in the higher-pH range of the leading electrolyte than in the lower range examined.

Figure 5 shows isotachopherograms of the sample ions at various pH's of the leading electrolytes, indicating that, at pH 5.00 and 5.70, the magnesium(II)

and calcium(II) ions undergo "enforced isotachophoretic"[5] migrations. This phenomenon results from the fact that the magnesium(II)-ion zone has a higher pH than the calcium(II)-ion zone, as is to be expected from the fact that the stability constant of the magnesium(II) ion is smaller than that of the calcium(II) ion.

Simultaneous Determination of Sodium(I), Magnesium(II), Calcium(II), Strontium(II), and Barium(II) Ions. Calibration curves were made by using a mixed solution of 7.5×10^{-3} mol dm^{-3} sodium(I), 5×10^{-3} mol dm^{-3} magnesium(II), calcium(II), strontium(II), and barium(II) nitrates, while varying the sampling volume from 1.0 to 7.0 μl.

For the adjusting pH of the leading electrolyte, succinic acid was used, because the buffer action of succinic acid is greater than that of acetic acid at pH 5.70.

Although the pH of the terminating electrolyte is rather lower than that of the leading electrolyte, in order to decrease the initial potential, it was adjusted to 4.40. The results are shown in Fig. 6. The linear region of the curve of the sodium(I) ion was 7.5—30.0 nmol (1.0—5.0 μl), while that of the barium(II) ion was 5—20.0 nmol (1.0—5.0 μl). When 6.0 μl of the mixture was introduced into the instrument, the sodium(I) ion exceeded the maximum load (about 30 nmol), thus making the zone length of the barium(II) ion (25 nmol) longer. If the amount of the sodium(I) ion is less than the maximum load, the linear region of the calibration curve of the barium(II) ion may be longer.

Table 2 shows the results of the simultaneous determination of the above five cations. The sample solution used was a artificial mixture of 4.5×10^{-3} mol dm^{-3} sodium(I), 4×10^{-3} mol dm^{-3} magnesium(II), 5×10^{-3} mol dm^{-3} calcium(II), 4×10^{-3} mol dm^{-3} strontium(II), and 3×10^{-3} mol dm^{-3} barium(II) nitrates; a 5.0-μl portion of the sample solution was introduced into the instrument.

The relative standard deviations were 1.7—2.2%, and the differences were −2.0—0.80% (mean values of five determinations). The time needed for an analysis was about 16—20 min.

References

1) F. M. Everaerts, J. L. Beckers, and Th. P. E. M. Verheggen, "Isotachophoresis," Elsevier, Amsterdam, Oxford, and New York (1976).

2) P. Boček, I. Miedziak, M. Deml, and J. Janák, *J. Chromatogr.*, **137**, 83 (1977).

3) D. Kaniansky and F. M. Everaerts, *J. Chromatogr.*, **148**, 441 (1978).

4) H. Yoshida, I. Nukatsuka, and S. Hikime, *Bunseki Kagaku*, **28**, 382 (1979).

5) F. E. P. Mikkers, F. M. Everaerts, and J. A. F. Peek, *J. Chromatogr.*, **168**, 317 (1979).

Studies on Room Temperature Phosphorometric and Delayed Fluorometric Analysis. I. Delayed Fluorometric Analysis of Porphyrin Derivatives

Yoshiaki Onoue,* Keizō Hiraki, and Yasuharu Nishikawa
Department of Chemistry, Faculty of Science and Technology, Kinki University, 3-4-1, Kowakae, Higashi-Osaka 577
(Received September 16, 1980)

The spectral characteristics and its application to measurement of porphyrins were investigated by use of room temperature phosphorometry. Certain porphyrin compounds adsorbed on filter paper exhibit intense E-type delayed fluorescence. This could be utilized for the determination of porphyrin derivatives.

Papar and thin layer chromatography have been used for the separation and measurement of porphyrins present in biological and geological materials.[1-5] After chromatography, the porphyrin spots can be easily located on the layer by observing the orange—red fluorescence in ultraviolet radiation. However, quantitative detection of prompt fluorescence of the compounds adsorbed on the layer is tedious, because of the reflection of excitation light and the fluorescence from the support surfaces. This paper describes a new approach to the application of phosphorometric time-resolution of room temperature phosphorometry (RTP).[6,7]

Phosphorometry was usually carried out at 77 K in liquid nitrogen, a low temperature being necessary for maintaining a rigid matrix in order to minimize the effect of intermolecular collisional quenching. Walling and Schulman[8] observed the phosphorescence of various organic compounds adsorbed on filter paper, silica gel, alumina, and polycellulose at room temperature. This method (RTP) has advantages for analysis. No liquid nitrogen, cryogenic equipment, or high purity solvents are required, substances being identified in chromatographic separation without elution. In this article, application of RTP combined with paper chromatography to the analysis of porphyrins is described.

Experimental

Apparatus. Long-life emission was measured with a Hitachi-2A spectrofluorometer with a phosphorescence accessory. The sample holder was designed to fit into the standard MPF-2A phosphoroscope accessory instead of the normal cap and cylinder used for the dewar flask assembly (Fig. 1). The plate of holder was blackened to a dull, non-reflecting finish. A 150-W xenon arc lamp was used as the excitation light source, the signal being detected with a R-446 UR photomultiplier tube. The spectra were recorded on a Hitachi QPD 33 recorder.

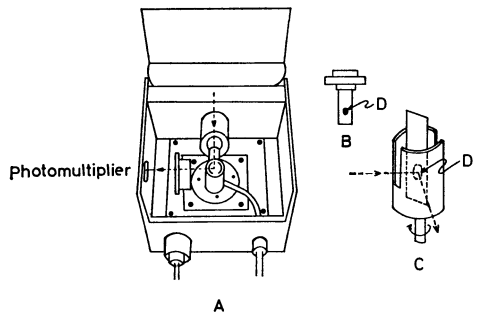

Fig. 1. Schematic diagram of filter paper cell system for room temperature phosphorescence studies.
A: Hitachi MPF-2A phosphoroscope accessory, B: sample holder, C: rotating can assembly, D: sample spot.

Reagents. Magnesium-protoporphyrin IX dimethyl ester (Mg-PPDE) was prepared by refluxing protoporphyrin IX dimethyl ester (Midori jūji Co. Ltd.) and anhydrous magnesium chloride in *N,N*-dimethylformamide.[9] Crude metal chelate was chromatographed on a cellulose column with a light-petroleum : acetone (20 : 3, v/v) eluant. Pure Mg chelate was obtained by recrystallization three times from benzene–chloroform (20 : 1, v/v) solvent. Chlorophyll a and b were extracted from spinach with a mixed solvent, methanol : acetone (1 : 1, v/v). After partial purification by the dioxane method,[10] crude pigments were chromatographed on a glucose column in order to separate chlorophyll a, b, and the other pigments. Chlorophyll c_1 and c_2 were isolated from *Undaria pinnatifida* and *Sargassum racemosum*, respectively, with methanol and acetone according to the Jeffrey method.[11] After being chromatographed, crude chlorophyll c_1 and c_2 were crystallized from pyridine–acetone. All other chemicals were of reagent grade. Toyo No. 51 filter paper was used as a support.

Procedure. The sample solution, four 0.5 μl portions, was allowed to drain slowly from the tip of a microliter syringe when it came into contact with the filter paper. After 1.0 μl of 1 mol dm^{-3} NaOH aqueous solution had been placed on a sample spot, the filter paper was dried for ca. 30 min with an infrared lamp. The samples were then directly mounted on a holder shown in Fig. 1. Since the emission is very sensitive to humidity and temperature, the sample compartment was continuously flushed with warm dried air.

Results and Discussion

As shown in Table 1, porphyrins exhibited a long-life emission (1—100 ms), but no long-life emission was observed for non-ionic porphyrin, Cu-porphyrin chelate and chlorins. The emission was studied for Mg-PPDE.

Spectral Studies of Mg-protoporphyrin IX Dimethyl Ester (Mg-PPDE). The emission spectra of Mg-PPDE adsorbed on the paper are shown in Fig. 2. The spectrum of Mg-PPDE obtained by RTP at 70 °C is almost the same as the usual prompt fluorescence spectra observed in chloroform solution and on filter paper. Phosphorescence of Mg-PPDE in solid solution at liquid nitrogen temperature (77 K) appears in the far red region as compared with the spectrum obtained by RTP. Very weak room tem-

Table 1. Properties of long-life emission from porphyrins adsorbed on filter paper[a)]

Compound	λ excitation nm	λ emission nm
Protoporphyrin IX	415	630
Protoporphyrin IX dimethyl ester	415	630
Mg-protoporphyrin IX dimethyl ester	428	600
Zn-protoporphyrin IX dimethyl ester	420	587
Cu-protoporphyrin IX dimethyl ester	—	—
meso-Tetraphenyl porphinetrisulfonate	465	654
meso-Tetrakis(4-methyl-1-pyridyl)porphyrin	427	650
meso-Tetraphenylporphyrin	—	—
Chlorophyll c_1	430	605
Chlorophyll c_2	430	605
Chlorophyll a	—	—
Chlorophyll b	—	—

a) Measured with phosphoroscope at *ca.* 1000 min^{-1} of rotating can assembly.

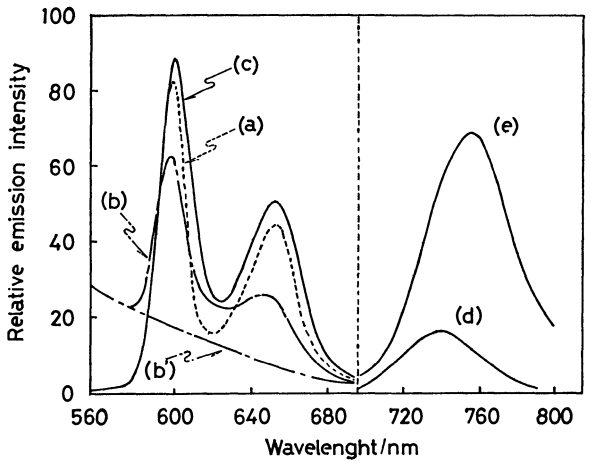

Fig. 2. Spectra of long-life emission from Mg-PPDE adsorbed on filter paper.
(a): Prompt fluorescence; 12 °C in chloroform, (b): prompt fluorescence; 12 °C adsorbed on filter paper, (b'): blank; prompt fluorescence from filter paper at 12 °C, (c): long-life emission; 70 °C adsorbed on filter paper, (d): long-life emission; 20 °C adsorbed on filter paper, (e): phosphorescence; −196 °C in methanol. Intensity scale for (d), (e) is *ca.* 100 times less than for (a)—(c).

perature phosphorescence of Mg-PPDE was also observed when a small amount of sodium iodide was present on the filter paper. The effect of temperature on the intensity of long-life emission is conspicuous. The emission intensity of Mg-PPDE increases with increase in temperature, in contrast to the case of normal prompt fluorescence and phosphorescence (Fig. 3).

Logarithm of the intensity of long-life emission, ln ϕ_e, obtained from the spectra is plotted against $1/T$

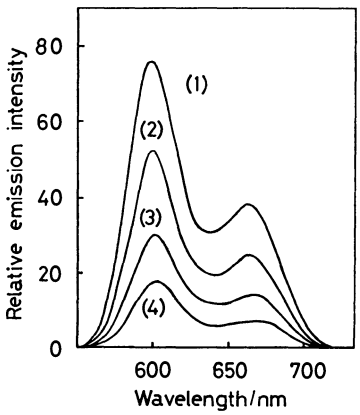

Fig. 3. Effect of temperature on long-life emission of Mg-PPDE (9.6 ng) adsorbed on filter paper.
(1): 72±1 °C, (2): 60±1 °C, (3): 55±2 °C, (4): 40±2 °C.

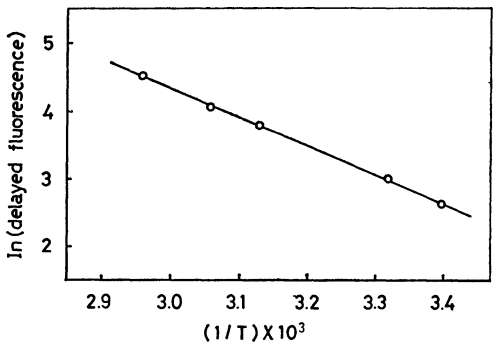

Fig. 4. E-type delayed fluorescence of Mg-PPDE (0.18 μg) adsorbed on filter paper as a function of temperature.

(Fig. 4). The plot is linear. The activation energy calculated from the slope is 0.37 eV, agreeing with the energy difference (0.38 eV) between the maxima of the two emission bands: 600 nm for specific emission, 736 nm for phosphorescence. In room temperature phosphorometry, in most cases, sodium iodide is efficient for increasing the phosphrescence quantum yield.[6)] In this study, however, the intensity of long-life emission decreased drastically in the presence of environmental sodium iodide. The long-life emission of Mg-PPDE could be attributed to E-type delayed fluorescence resulting from the thermal activation of molecules from the lowest triplet state to the first singlet state followed by radiative transition to the ground state.

The relationship between the intensity of E-type delayed fluorescence and the concentration of Mg-PPDE is linear over a wide range of ng—μg. The analytical curve indicates that E-type delayed fluorescence could be applied not only to the identification of porphyrins but also to their determination.

Application of E-type Delayed Fluorescence to Analysis of Chlorophyll c from Algae. Pigments of algae were extracted by freezing the algae fronds at −20 °C for 30 min, immersing the frozen tissue in methanol for 30 s and homogenizing in 100% acetone. Extraction was repeated several times until the cell res-

idue became colourless. The acetone and methanol extracts were separated from the tissue residues by centrifugation, and immediately mixed with diethyl ether. The mixture was shaken with 10% sodium chloride solution to wash out impurities and concentrate the pigments in the ether phase. The ether layer was made up to the designed volume. Two μl of the sample solution was spotted on Toyo No. 51 filter paper with a microsyringe. In applying the sample to the filter paper, care was taken to maintain the spot size (5 mm diameter) as constant as possible, the best reproducibility being attained when spot size was kept constant. The tip of the syringe just touched the filter paper, followed by spotting of four 0.5 μl portions. Each spotting was made at intervals to allow evaporation of the solvent. Chromatography was carried out with light petroleum ether:acetone:1-propanol (90:10:0.4, v/v). After the solvent front had ascended 10 cm, the spots were examined with a ultraviolet mineral light for orange—red fluorescence. Chlorophyll c_1 and c_2 and chlorophyllide having carboxyl side chain did not move from the origin and the spot size of chlorophyll c remained constant, the other pigments being developed. Existence of chlorophyllide, however, gave no influence on emission intensity of chlorophyll c, even when its amount was the same as that of chlorophyll c. After development, 1.0 μl of 1 mol dm^{-3} NaOH aqueous solution was added on the spot of chlorophyll c, and dried for *ca.* 10 min by infrared lamp heating, the emission intensity remaining constant for at least 20 min. The paper strip was mounted on the sample holder, and E-type delayed fluorescence of chlorophyll c was measured by use of rotating can phosphorescence assembly (Ex: 430 nm, Em:605 nm). Chlorophyll c in the concentration range 0.1 ng—μg order could be determined.

Conclusion

E-type delayed fluorescence of porphyrins observed by room temperature phosphorometry can be used for the determination of ng order of porphyrins, and it may be applied to the analysis of porphyrins in biological or geological samples, in combination with paper or thin-layer chromatographic technique.

The authors express their sincere thanks to Professor Tsunenobu Shigematsu (Faculty of General Education, Kinki University), and Professor Masayuki Tabushi (College of Medical Technology, Hirosaki University), for their advice and suggestions. Financial support from the Ministry of Education, Culture and Welfare of Japan, and Kinki University is gratefully acknowledged.

References

1) M. Blumer, *Anal. Chem.*, **28**, 1640 (1956).
2) J. E. Falk, *J. Chromatogr.*, **5**, 277 (1961).
3) S. W. Jeffrey, *Biochem. J.*, **80**, 336 (1961).
4) S. W. Jeffrey, *Biophys. Acta*, **162**, 271 (1968).
5) K. Yanagi and T. Koyama, *Geochem. J.*, **5**, 23 (1971).
6) T. Vo Dinh, E. Lue Yen, and J. D. Winefordner, *Anal. Chem.*, **24**, 146 (1976).
7) R. M. A. von Wandruszka and R. J. Hurtublse, *Anal. Chem.*, **48**, 1784 (1976).
8) E. M. Schulman and C. Walling, *J. Phys. Chem.*, **77**, 902 (1973).
9) A. D. Adler, F. R. Longo, F. Kampas, and J. Kim, *J. Inorg. Nucl. Chem.*, **32**, 2443 (1970).
10) K. Iriyama and N. Ogura, *J. Biochem.*, **76**, 901 (1974).
11) S. W. Jeffrey, *Biochim. Biophys. Acta*, **279**, 15 (1972).

The Electronic Structures of Bis(*cis*-1,2-dicyano-1,2-ethenedithiolato)nickel Complexes

Mitsuru SANO, Hirohiko ADACHI,† and Hideo YAMATERA*

Department of Chemistry, Faculty of Science, Nagoya University, Chikusa-ku, Nagoya 464

† *Department of Nuclear Engineering, Faculty of Engineering, Osaka University, Suita 565*

(Received November 12, 1980)

The core binding energies of N1s and S2s in *cis*-1,2-dicyano-1,2-ethanedithiolate (maleonitriledithiolate, mnt) complexes were measured by means of X-ray photoelectron spectroscopy (XPS), and the energy differences between N1s and S2s, ΔE, were found to be 171.7—172.6 eV throughout the complexes studied. The lowest ΔE value, 171.7 eV, was shown by $[Ni(mnt)_2]^-$. The electronic structures of $[Ni(mnt)_2]^-$ and $[Ni(mnt)_2]^{2-}$ were calculated by the discrete variational Xα method. The XPS measurements and the molecular orbital (MO) calculations provide consistent results that the oxidation state of the nickel atom is +2 for both nickel mnt complexes and that the highest occupied MO is $5b_{3g}$, which is mainly localized on ligands and which holds an unpaired electron in $[Ni(mnt)_2]^-$.

The metal dithiolate compounds have been of great interest to inorganic chemists because of their remarkable oxidation-reduction behavior, including the formation of abnormal valence states of the metal.[1] A typical dithiolate complex is the *cis*-1,2-dicyano-1,2-ethenedithiolate (maleonitriledithiolate, mnt) complex, in which the metal ion has a wide variety of oxidation states. Usually the oxidation state of the metal in an mnt complex is determined so as to satisfy both the stoichiometry and charge of the complex. For example, the formal oxidation state of Ni in $[Ni(mnt)_2]^-$ may be +3, on the assumption that mnt is a dinegative ion. However, the determination of the oxidation state of the metal in such a way is questionable.

There have been extensive studies of the electronic structure of these compounds by Schupack *et al.*,[2] Schmitt *et al.*,[3] Schlapfer *et al.*,[4] and Kobayashi *et al.*[5] The ESR results suggest that the ground state of $[Ni(mnt)_2]^-$ is $^2B_{3g}$, in which the half-filled out-of-plane π molecular orbital (MO) is extensively delocalized over the ligand.[3] Schlapfer *et al.*[4] measured the force constants of dithiolate complexes and estimated that 38% of the unpaired electron in the highest occupied MO of $[Ni(mnt)_2]^-$ is localized on the metal. The X-ray diffraction results of $[Ni(mnt)_2]^-$ have suggested that the ground state is either ^2A_g or $^2B_{3g}$.[5] An X-ray photoelectron spectroscopic (XPS) study of $[M(S_2C_2R_2)]^{0,1-,2-}$ (M=Ni, Pd, and Pt, and R=CN and C_6H_5) has been reported by Grim *et al.*[6] Judging from the absence of satellites and from the line-width of Ni2p XPS, they pointed out that the reduction did not appreciably change the charge on the metal, giving most of the added electronic charge to the ligands. However, there still remain problems in understanding accurately the electronic structure of mnt complexes. A detailed investigation of the electronic structures of these compounds can be expected to explain the results of ESR, IR, XPS, and so on. It has been shown in a previous work[7] that the energy difference between core orbitals gives information about the charge distribution and the electronic structure of metal complexes. The present paper will describe the results of XPS studies of $[M(mnt)_2]^{2-}$ (M=Co, Ni, Cu, and Zn) and $[M(mnt)_2]^-$ (M=Fe and Ni), and also the results of discrete variational (DV) Xα molecular orbital calculations for $[Ni(mnt)_2]^-$ and $[Ni(mnt)_2]^{2-}$. The energy difference between N1s and S2s and the electronic structures of these nickel complexes are then discussed on the basis of the XPS and DV-Xα results.

Experimental

The complexes, $[M(mnt)_2]^{2-}$ (M=Co, Ni, Cu, and Zn) and $[M(mnt)_2]^-$ (M=Fe and Ni), are all well-known and were prepared by standard methods.[8] The X-ray photoelectron spectra were recorded on a JEOL Model JESCA-3A spectrometer. Magnesium $K\alpha_{1,2}$ radiation (1253.6 eV) was used as the X-ray excitation source, and the measurements were carried out at a vacuum of 5×10^{-7} Torr (1 Torr=133.322 Pa) or below. We obtained the difference between the N1s and S2s binding energies by a synchronous measurement. The measurement was repeated several times for each sample, yielding consistent results. The average of the binding-energy difference was determined, by several runs for a given compound, with an accuracy of about ±0.1 eV.

Computational Method

The computational details of the spin-polarized DV-Xα method have been thoroughly described elsewhere.[9] In the Hartree-Fock-Slater model,[10] the exchange-correlation term is given by:

$$X_{xc\uparrow}(1) = -3\alpha[(3/4\pi)\rho_\uparrow(1)]^{1/3},$$

where $\rho_\uparrow$ (1) is the local charge density with up-spin and where α is the exchange-scaling parameter; the value of $\alpha=0.70$ is used for all atoms throughout the present calculation.[11] The spin-polarized DV-Xα self-consistent-charge (SCC) procedure[9] has been performed for both up and down spins. An approximate self-consistent molecular potential is determined from the Mulliken gross orbital populations. The numerical basis functions for up- and down-spin orbitals are obtained with an atom-like potential constructed by spherically averaging the molecular potential around the nucleus for the region inside each atomic sphere. The basis sets, including Ni1s—4p, C and N1s—2p, and S1s—3d, are utilized for the present calculations.

The molecular geometries of the complexes are de-

Table 1. The electron-binding energies (eV) of N1s and S2s for tetrabuthylammonium salts of $[M(S_2C_4N_2)_2]^{n-}$ ($n=2$ or 1) and $Na_2S_2C_4N_2$

	Fe^{3+}	Co^{2+}	Ni*	Ni^{2+}	Cu^{2+}	Zn^{2+}	Na^+
N1s	402.5	401.9	400.5	401.2	401.8	401.7	399.9
S2s	230.4	229.7	228.8	228.8	229.2	229.2	226.9
ΔE	172.1	172.2	171.7	172.4	172.6	172.5	173.0
$Ni2p_{3/2}$			857.3	857.3			
$Ni2p_{1/2}$			874.6	874.6			

Ni*: $[Ni(S_2C_4N_2)_2]^-$.

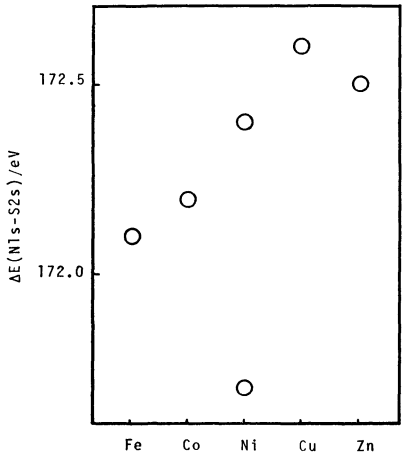

Fig. 1. The correlation between the energy difference, ΔE(N1s−S2s), and the atomic number of the metal in *cis*-1,2-dicyano-1,2-ethenedithiolate complexes.

termined from the experimental results.[5] In the present calculations, the complexes are regarded as having the D_{2h} symmetry.

Results and Discussion

Table 1 shows the N1s and S2s core-binding energies measured for $[M(mnt)_2]^{2-}$ (M=Co, Ni, Cu, and Zn), $[M(mnt)_2]^-$ (M=Fe and Ni), and Na_2mnt. The Ni2p energies are also given for the nickel complexes. Accurate binding energies were not obtained for sulfur $2p_{3/2}$ and $2p_{1/2}$ because of their overlapping. The C1s peaks of the ligand could not be well distinguished from the peaks of various nonequivalent carbon atoms of the tetrabutylammonium ion contained as the counter ion in the sample. The measured values of the binding energies would have to be corrected for the charging and the counter-ion effect, which are hard to evaluate. Thus, the energy differences between them, which are almost free from those effects, are used to give information about the electron distribution in mnt complexes. The energy differences, ΔE, between N1s and S2s is found to be 173.0 eV for the mnt anion and to decrease to 172.6—171.7 eV by coordination to the metal. For a easy comparison of ΔE values between different metal compounds, ΔE is plotted in Fig. 1 against the atomic number of the metal. The observed ΔE value in general increases with an increase in the atomic number (Co(172.2)→Zn(172.5)). An exceptionally low value (171.7) was observed for $[Ni(mnt)_2]^-$, which is of particular interest with regard to its electronic structure. From the core-binding-energy measurements, it is found that: (1) ΔE is decreased by the coordination to the metal, (2) ΔE increases with an increase in the atomic number of the metal, and (3) different ΔE values are obtained for the two nickel complexes.

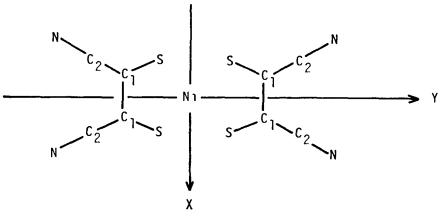

Fig. 2. The structure of mnt and the notations of atoms.

XPS Results and Charge Distributions. First, we will discuss the decrease in ΔE ($=E$(N1s)$-E$(S2s)) by the coordination to the metal in a qualitative way. When the ligand coordinates to the metal ion, electron donation takes place from sulfur to metal. The electron population on sulfur then decreases, which deepens the level of the sulfur core orbital in the first approximation, regardless of the other potentials. The ΔE value of Na_2mnt is eventually larger than those of the metal complexes.

Next, we will discuss the ΔE values of the complexes. The relation between the ΔE value and the charge distribution can be discussed in terms of Siegbahn's equation:[12]

$$E_i = E^\circ_i + k_i q_i + \sum_{i \neq j} q_j / r_{ij}. \quad (1)$$

In this equation, E_i and E°_i are the level energies of the i atom of the complexes studied and that of the reference material; q_i and q_j, the net charge on the i and j atoms respectively, and r_{ij}, the internuclear distance between the i and j atoms. The last term in Eq. 1 represents an interatomic Madelung-type potential. The value of the parameter, k_i depends on the atomic species. Using Eq. 1 and the bond distances previously reported,[5] the binding energies (in eV) for the N1s and S2s can be estimated as follows:

$$E(\text{N1s}) = E^\circ(\text{N1s}) + k_N q_N + 2.60 q_M + 10.78 q_S + 13.21 q_{C1} + 19.76 q_{C2} + 6.28 q_N, \quad (2)$$

$$E(\text{S2s}) = E^\circ(\text{S2s}) + k_S q_S + 6.70 q_M + 12.83 q_S + 19.80 q_{C1} + 13.68 q_{C2} + 10.78 q_N, \quad (3)$$

where the subscripts of q denotes the atomic species

as are shown in Fig. 2. Then, we can evaluate the energy differences between N1s and S2s from the following equation:

$$\Delta E(\mathrm{N1s-S2s}) = \Delta E^{\circ}(\mathrm{N1s-S2s}) + (k_{\mathrm{N}}-4.5)q_{\mathrm{N}} - (k_{\mathrm{S}}+2.05)q_{\mathrm{S}} - 4.10q_{\mathrm{M}} - 6.59q_{\mathrm{Cl}} + 6.08q_{\mathrm{C_2}}. \quad (4)$$

Here, k_{N} is taken as 21.5 according to Siegbahn *et al.*[12] The value of k_{S} is estimated as 21 on the basis of the 2s—3s one-center integral.[13] Thus, the difference in ΔE between the two complexes can be expressed as follows:

$$\Delta(\Delta E) = 17\delta q_{\mathrm{N}} - 23\delta q_{\mathrm{S}} - 4\delta q_{\mathrm{M}} - 7\delta_{\mathrm{Cl}} + 6\delta q_{\mathrm{C_2}}, \quad (5)$$

where δq_{i} is the difference in the effective charge on the i atom between the two complexes. Since the electronegativity of metal increases in going right across the periodic table, the metal net charge gradually decreases, though the value of q_{M} in general remains positive. This negative δq_{M} value causes a positive contribution to $\Delta(\Delta E)$. The less positive metal charge should result in a less negative ligand charge. Since the positive δq_{S} makes a negative contribution to $\Delta(\Delta E)$, opposing the observed trend in ΔE, it is probable that the contribution of δq_{S} is more or less counterbalanced by those of δq_{N}, δq_{C1}, and δq_{C2}.

Finally, the difference in the charge distribution between the two different nickel complexes will be discussed on the basis of the observed ΔE values. The photoelectron spectra show that the nickel $2p_{1/2}$—$2p_{3/2}$ energy separations are almost the same for the two mnt complexes. It has been reported that the splittings of spin-orbit components are often influenced by the oxidation state of the atom, especially for transition-metal ions.[14] If this can be applied to the present case, the almost identical $2p_{1/2}$—$2p_{3/2}$ separations may be taken as reflecting a close resemblance between the nickel electronic states of the two complexes. Thus, the δq_{M} term (with a small coefficient) is assumed to be negligible. Since all the valence electrons existing near the carbon atoms of the mnt^{2-} ligands participate in the bonding, the change in the charge of the complex would have only secondary effects on the charge densities of the carbon atoms. Thus, the δq_{C1} and δq_{C2} terms (with small coefficients) may also be neglected. With these assumptions, Eq. 5 may be approximated by:

$$\Delta(\Delta E) = 17\delta q_{\mathrm{N}} - 23\delta q_{\mathrm{S}}. \quad (6)$$

In the same way, if the difference in charge between the two nickel complexes is attributed to the difference in the nitrogen and sulphur charges, we obtain:

$$1 = 4\delta q_{\mathrm{N}} + 4\delta q_{\mathrm{S}}. \quad (7)$$

With the observed $\Delta(\Delta E)$ value of -0.7 eV ($=\Delta E([\mathrm{Ni(mnt)_2}]^{-}) - \Delta E([\mathrm{Ni(mnt)_2}]^{2-})$). Eqs. 6 and 7 give:

$$\delta q_{\mathrm{S}} = 0.12 \text{ and } \delta q_{\mathrm{N}} = 0.13.$$

In obtaining these values, it was assumed that the charges on Ni, C_1, and C_2 do not appreciably change when an electron is removed from $[\mathrm{Ni(mnt)_2}]^{2-}$. Although there are good reasons for these assumptions, as has been described above, further examination will be made below by reference to the results of the DV-Xα MO calculations.

TABLE 2. THE CORE-ORBITAL ENERGIES (eV) FOR $[\mathrm{Ni(mnt)_2}]^{2-}$ AND $[\mathrm{Ni(mnt)_2}]^{-}$ FROM DV-Xα CALCULATIONS

	$[\mathrm{Ni(mnt)_2}]^{2-}$	$[\mathrm{Ni(mnt)_2}]^{-}$
Ni2p	−827.8	−833.9
N1s	−371.8	−376.8
S_{2s}	−198.5	−204.3

Results of Molecular Orbital Calculations. Next, the results of DV-Xα MO calculations will be discussed in relation to the above XPS results, with particular reference to the electronic structure of $[\mathrm{Ni(mnt)_2}]^{-}$. Table 2 shows the calculated core orbital energies of the two nickel complexes. In order to obtain accurate ionization energies by the Xα method, calculations should be made of Slater's transition state.[10] The values in Table 2 refer to the ground state and do not allow for the relaxation effects on ionization. Thus, they can not be directly compared with the experimental binding energies. However, they may be expected to give a sufficiently good estimate for the $\Delta(\Delta E)$ value, since the relaxation effects are, for the most part, cancelled out in taking the difference between the two complexes. The values of ΔE are found to be 173.3 and 172.5 eV for $[\mathrm{Ni(mnt)_2}]^{2-}$ and $[\mathrm{Ni(mnt)_2}]^{-}$ respectively; thus, their difference, $\Delta(\Delta E)$, is -0.8 eV, in good agreement with the experimental value of -0.7 eV. The differences in the ΔE values on the DV-Xα calculation are 0.3 eV for Ni2p—S2s and 1.1 eV for Ni2p—N1s, which are comparable with the experimental values of 0.0 and 0.7 eV respectively.

The energies and components of the valence orbitals are given for $[\mathrm{Ni(mnt)_2}]^{2-}$ and $[\mathrm{Ni(mnt)_2}]^{-}$ in Table 3. The positive orbital energies for $[\mathrm{Ni(mnt)_2}]^{2-}$ result from the neglect of the Madelung potentials in the present calculation. The highest occupied molecular orbital (HOMO) for both complexes is the out-of-plane π-type $5b_{3g}$ MO, which consists mainly of S3p atomic orbitals with a minor Ni3d component. It is this orbital from which an electron is removed in going from $[\mathrm{Ni(mnt)_2}]^{2-}$ to $[\mathrm{Ni(mnt)_2}]^{-}$. The occupied MO's, whose main component is a metal d orbital, are $4b_{2g}$ (d_{xz}), $20a_g$ ($d_{x^2-y^2}$), $19a_g$ (d_{z^2}), and $4b_{3g}$ (d_{yz}). Therefore, the nickel atoms in both complexes are considered to have the d^8 configuration or the +2 oxidation state. (In spite of the Ni 3d population being slightly less than 50%, $4b_{2g}{}^{\uparrow}$ should be considered to correspond to Ni d_{xz}, since the rest of the d_{xz} population is mainly found in $3b_{2g}$, which is considered to be a ligand orbital.)

Table 4 lists the Mulliken orbital and overlap populations for $[\mathrm{Ni(mnt)_2}]^{2-}$ and $[\mathrm{Ni(mnt)_2}]^{-}$. The Ni net charges are almost the same for $[\mathrm{Ni(mnt)_2}]^{2-}$ (+0.28) and $[\mathrm{Ni(mnt)_2}]^{-}$ (+0.27). A significant mixing is seen between metal and ligand orbitals, and the net charges are greatly different from the formal charge (+2). The net charges on the sulphur and nitrogen atoms slightly increase on going from the binegative to the uninegative ion. The change in

TABLE 3. THE VALENCE-SHELL MO's OF $[Ni(mnt)_2]^{2-}$ AND $[Ni(mnt)_2]^-$

Symmetry	Orbital energy	Orbital populations/%											
		Ni			S			C_1		C_2		N	
		3d	4s	4p	3s	3p	3d	2s	2p	2s	2p	2s	2p
$[Ni(mnt)_2]^{2-}$													
$5b_{3g}$	5.02	28.5				58.3	0.7		7.2		1.2		4.0
$4b_{2g}$	3.87	60.5				12.6	3.5		15.1		0.6		7.5
$20a_g$	3.80	85.4	10.0		0.0	3.8	0.3	0.0	0.3	0.0	0.0	0.0	0.0
$6b_{1u}$	3.59			7.5		59.4	2.8		20.5		0.5		9.2
$19a_g$	3.40	84.9	0.1		2.2	1.8	5.0	0.8	0.4	0.0	0.1	0.0	0.3
$4b_{3g}$	3.05	65.0				14.7	1.5		12.9		0.0		5.9
$16b_{3u}$	3.02			4.5	1.4	90.1	0.7	1.3	0.9	0.0	0.0	0.0	1.0
$3a_u$	2.78					69.3	1.3		19.5		0.0		9.8
$17b_{2u}$	2.50			8.6	0.3	84.3	1.5	0.7	0.2	1.5	1.4	0.0	1.4
$3b_{2g}$	1.96	28.9				58.6	0.5		7.4		0.1		4.5
$14b_{1g}$	1.74	36.6			5.2	54.0	0.4	1.5	2.0	0.0	0.0	0.0	0.2
$18a_g$	1.03	10.9	10.1		5.2	65.8	1.7	0.0	2.6	0.9	1.3	0.3	0.9
$3b_{3g}$	0.83	3.9				20.7	1.2		31.4		8.3		34.3
$5b_{1u}$	0.80			1.7		24.0	0.5		30.0		8.7		34.5
$13b_{1g}$	0.25	12.4			5.1	32.9	2.8	3.3	18.7	1.5	6.0	2.8	14.3
$16b_{2u}$	0.09			0.2	10.9	28.3	2.3	0.9	27.2	0.0	6.2	0.0	24.0
$[Ni(mnt)_2]^-$													
$5b_{3g}\uparrow$	−0.47	17.9				64.3	0.2		11.6		0.7		5.3
$4b_{2g}\downarrow$	−1.61	52.0				23.8	2.6		14.7		0.0		6.8
$6b_{1u}\downarrow$	−1.67			7.7		53.9	3.1		24.4		0.0		10.7
$6b_{1u}\uparrow$	−1.77			7.4		52.4	3.2		25.6		0.0		11.3
$4b_{2g}\uparrow$	−1.82	48.9				28.2	2.2		14.1		0.0		6.6
$20a_g\downarrow$	−1.87	82.5	10.7		0.3	5.8	1.1	0.0	0.4	0.0	0.0	0.0	0.0
$20a_g\uparrow$	−2.14	81.2	10.8		0.3	6.9	0.0	0.0	0.5	0.0	0.0	0.0	0.0
$16b_{3u}\downarrow$	−2.34			4.5	2.1	89.8	0.4	1.3	0.9	0.0	0.0	0.0	0.9
$19a_g\downarrow$	−2.34	80.8	0.1		2.9	3.3	4.2	0.7	4.6	0.0	0.0	0.0	1.4
$3a_u\downarrow$	−2.48					71.8	1.1		17.5		0.1		9.4
$16b_{3u}\uparrow$	−2.49			4.6	2.1	89.7	0.4	1.3	0.9	0.0	0.0	0.0	0.9
$4b_{3g}\downarrow$	−2.55	68.4				6.1	1.6		15.8		0.1		8.0
$3a_u\uparrow$	−2.60					72.8	1.1		16.6		0.2		9.2
$19a_g\uparrow$	−2.62	82.7	0.0		2.9	3.5	3.9	0.7	4.7	0.0	0.0	0.0	1.4
$4b_{3g}\uparrow$	−2.77	68.8				3.7	1.6		16.7		0.3		9.0
$17b_{2u}\downarrow$	−2.99			8.6	0.9	82.8	1.8	0.6	0.4	1.4	1.6	0.2	1.6
$17b_{2u}\uparrow$	−3.13			8.6	0.9	82.6	1.7	0.6	0.5	1.4	1.7	0.2	1.7
$3b_{2g}\downarrow$	−3.56	40.4				49.5	1.0		4.4		0.7		4.0
$3b_{2g}\uparrow$	−3.76	44.4				46.2	1.1		3.6		0.8		3.9
$14b_{1g}\downarrow$	−3.78	32.3			8.4	52.2	0.6	2.0	3.6	0.0	0.2	0.0	0.4
$14b_{1g}\uparrow$	−3.97	31.3			8.8	51.7	0.7	2.1	4.3	0.1	0.3	0.2	0.5
$5b_{1u}\downarrow$	−4.29			2.2		26.3	0.6		21.7		13.6		35.6
$3b_{3g}\downarrow$	−4.29	8.2				22.7	1.3		20.7		13.0		34.0
$5b_{1u}\uparrow$	−4.34			2.3		27.4	0.6		20.0		14.1		35.5
$3b_{3g}\uparrow$	−4.36	10.5				23.6	1.3		18.1		13.4		33.1

sulphur charge is about 0.13, in accordance with the value (0.12) obtained from the XPS results by means of Siegbahn's equation. The change in the N net charge is about 0.10 (0.13), while those in the C_1 and C_2 charges are 0.03 (0.0) and −0.02 (0.0) respectively (the numerals in parentheses being the values obtained or assumed in the preceeding section). By substituting these calculated δq values into Eq. 5, we obtain the $\Delta(\Delta E)$ value of −0.9 eV, in good agreement with the XPS result of −0.7 eV and with the value of −0.8 eV obtained directly from the calculated orbital energies. The good agreements between the calculated and the XPS values demonstrated above add support to our estimate of the charge-density distribution and to our arguments made in the interpretation of the XPS results, including the idea that the electronic state of the nickel ion in $[Ni(mnt)_2]^-$ is very similar to that in $[Ni(mnt)_2]^{2-}$. The spin density on the S atom is calculated to be 0.14, which supports the conclusion from the ESR results

TABLE 4. THE MULLIKEN POPULATIONS FOR $[Ni(mnt)_2]^{2-}$

	$[Ni(mnt)_2]^{2-}$	$[Ni(mnt)_2]^-$		
		Total	Up-spin	Down-spin
Ni 3d	8.549	8.528	4.382	4.146
4s	0.597	0.593	0.295	0.298
4p	0.578	0.608	0.304	0.304
Atomic charge	+0.276	+0.271		
S 3s	1.825	1.827	0.914	0.913
3p	4.166	4.025	2.095	1.930
3d	0.158	0.165	0.082	0.083
Atomic charge	−0.149	−0.017		
C_1 2s	1.056	1.056	0.528	0.529
2p	3.138	3.112	1.565	1.547
Atomic charge	−0.194	−0.168		
C_2 2s	0.904	0.890	0.445	0.445
2p	2.794	2.815	1.407	1.407
Atomic charge	+0.302	+0.295		
N 2s	1.714	1.716	0.858	0.858
2p	3.814	3.713	1.861	1.852
Atomic charge	−0.528	−0.429		
Bond-overlap populations				
Ni-S	0.515	0.530		
S-C_1	0.625	0.659		
C_1-C_2	0.889	0.858		
C_2-N	1.561	1.586		

TABLE 5. THE BOND LENGTHS (Å) AND FORCE CONSTANTS (mdyn/Å) FOR $[Ni(mnt)_2]^{2-}$ AND $[Ni(mnt)_2]^-$ (1 mdyn = 1×10^{-8} N)

	Bond lengths[5]		Force constants[4]	
	$[Ni(mnt)_2]^{2-}$	$[Ni(mnt)_2]^-$	$[Ni(mnt)_2]^{2-}$	$[Ni(mnt)_2]^-$
Ni-S	2.176	2.147	1.27	1.53
S-C_1	1.732	1.727	2.98	3.20
C_1-C_1'	1.360	1.367	5.49	4.99
C_1-C_2	1.428	1.420	3.86	3.48
C_2-N	1.147	1.133		

obtained by Schmitt *et al.*[3] that the $3p_z$ spin population of the S atom is high.

The $5b_{3g}$ MO is shown schematically in Fig. 3 using the results of MO calculation for $[Ni(mnt)_2]^-$. In this MO, the interactions between Ni–S, S–C_1, and C_2–N are antibonding, while those in C_1–C_2 and C_1–C_1' are bonding. This suggests that the removal of one electron from $5b_{3g}$ MO strengthens the Ni–S, S–C_1, and C_2–N bonds, but weakens the C_1–C_2 and C_1–C_1' bond. The changes in the bond overlap populations given in Table 4 are consistent with this MO argument, demonstrating that the bond-overlap population is useful for a qualitative discussion of chemical bonding. The force constants and the bond

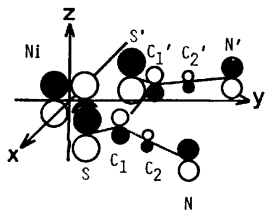

Fig. 3. The $5b_{3g}$ MO with an unpaired electron in $[Ni(S_2C_4N_2)_2]^-$. The black and white circles show positive and negative signs, respectively.

lengths of the two nickel mnt complexes measured by Schlaper *et al.*[4] and Kobayashi *et al.*[5] are given in Table 5. The force constants increase, and the bond lengths decrease, as the bond becomes stronger. Their experimental results are consistent with the calculated bond-overlap populations except for the C_1–C_2 bond. (For this bond, however, their experimental results contradict each other; that is, the force constant increases in spite of the increase in bond length in going from $[Ni(mnt)_2]^{2-}$ to $[Ni(mnt)_2]^-$.)

Conclusion

The XPS measurements have been performed in order to obtain the core binding energies for the N1s and S2s of metal mnt complexes. The DV-Xα MO calculations for two Ni complexes have also been carried out in an attempt to explain the chemical shift and the electronic structure of $[Ni(mnt)_2]^-$. The XPS measurements and the MO calculations provide consistent results that the oxidation state of the nickel atom is +2 for both $[Ni(mnt)_2]^-$ and $[Ni(mnt)_2]^{2-}$. The HOMO is $5b_{3g}$, which is mainly localized on ligands and which holds an unpaired electron in $[Ni(mnt)_2]^-$. This is consistent with other spectroscopic results, such as IR and ESR, and also with the X-ray diffraction data.

The computations reported in this paper have been carried out on the HITAC M-180 computer of the Institute for Molecular Science. This work was supported in part by a Grant-in-Aid for Scientific Research No. 510806 from the Ministry of Education, Science and Culture.

References

1) R. P. Burns and C. A. McAuliffe, *Adv. Inorg. Chem. Radiochem.*, **22**, 303 (1979).
2) S. I. Shupack, E. Billig, R. J. H. Clark, R. Williams, and H. B. Gray, *J. Am. Chem. Soc.*, **86**, 4594 (1964).
3) R. D. Schmitt and A. H. Maki, *J. Am. Chem. Soc.*, **90**, 2288 (1968).
4) C. W. Schlapfer and K. Nakamoto, *Inorg. Chem.*, **14**, 1338 (1975).
5) A. Kobayashi and Y. Sasaki, *Bull. Chem. Soc. Jpn.*, **50**, 2650 (1977).
6) S. O. Grim, L. J. Matienzo, and W. E. Swartz, *Inorg. Chem.*, **13**, 447 (1974).
7) M. Sano and H. Yamatera, *Bull. Chem. Soc. Jpn.*, **54**, 2023 (1981).

8) A. Davison, N. Edestein, R. H. Holm, and A. H. Maki, *Inorg. Chem.*, **2**, 1227 (1963); J. F. Weiher, L. R. Melby, and R. E. Benson, *J. Am. Chem. Soc.*, **86**, 4329 (1964); A. Davison and R. H. Holm, *Inorg. Synth.*, **10**, 8 (1967).
9) H. Adachi, S. Shiokawa, M. Tsukada, C. Satoko, and S. Sugano, *J. Phys. Soc. Jpn.*, **47**, 1528 (1979).
10) For a review of the HFS model, see J. C. Slater, "Quantum Theory of Molecules and Solids," McGraw-Hill (1974), Vol. 4.
11) E. J. Baerends and P. Ros, *Chem. Phys.*, **2**, 52 (1973).
12) K. Siegbahn *et al.*, "ESCA Applied to Free Molecules," North-Holland Pub., Amsterdam-London (1969).
13) According to Siegbahn *et al.*,[12] k_S for S2p is taken as 13.8. By using the same k_S value for S2s, Eq. 4 becomes:

$$\Delta(\Delta E) = 17\delta q_N - 16\delta q_S - 4\delta q_M - 7\delta q_{Cl} - 6\delta q_{C_2} \quad (5')$$

and:

$$\Delta(\Delta E) = 17\delta q_N - 16\delta q_S,$$

in place of Eqs. 5 and 6. With Eq. 7, we obtain $\delta q_S = 0.15$ and $\delta q_N = 0.10$.
14) D. C. Frost, C. A. McDowell, and I. S. Woolsey, *Mol. Phys.*, **27**, 1473 (1974).

A Kinetic Study of the Reactions of Several Cobalt(III) Complexes with Ascorbic Acid

Keiichi TSUKAHARA* and Yasuo YAMAMOTO

Department of Chemistry, Faculty of Science, Shimane University, Nishikawatsucho, Matsue 690

(Received December 1, 1980)

The kinetics of the reactions of $[Co(phen)_3]^{3+}$, $[Co(bpy)_3]^{3+}$, and $[Co(en)(phen)_2]^{3+}$ (phen=1,10-phenanthroline, bpy=2,2′-bipyridine, and en=ethylenediamine) with ascorbic acid (H_2A) have been studied over the temperature range from 17.0 to 35.0 °C, at an ionic strength of 0.10 mol dm^{-3} ($LiClO_4$), and over the pH range from 3.60 to 5.04 (acetate buffer). The $[Co(phen)_3]^{3+}$ and $[Co(bpy)_3]^{3+}$ ions were reduced by both HA^- (k_1 path) and A^{2-} (k_2 path) ions: the second-order rate constants at 25.0 °C are (0.40 ± 0.07) dm^3 mol^{-1} s^{-1} and $(5.8\pm1.1)\times10^6$ dm^3 mol^{-1} s^{-1} for the $[Co(phen)_3]^{3+}$ ion, and (0.13 ± 0.02) dm^3 mol^{-1} s^{-1} and $(2.1\pm0.5)\times10^6$ dm^3 mol^{-1} s^{-1} for the $[Co(bpy)_3]^{3+}$ ion. The $[Co(en)(phen)_2]^{3+}$ ion was reduced only by the A^{2-} ion; $k_2=(1.0\pm0.2)\times10^6$ dm^3 mol^{-1} s^{-1} (25.0 °C). The $[Co(phen)_3]^{3+}$, $[Co(bpy)_3]^{3+}$, and $[Co(en)(phen)_2]^{3+}$ ions were not reduced by H_2A. The activation parameters (ΔH^* and ΔS^*) for the ascorbate reduction of the $[Co(phen)_3]^{3+}$ ion were larger than those of the $[Co(bpy)_3]^{3+}$ ion. This is in contrast to the results of the self-exchange reactions of the $[Co(phen)_3]^{3+/2+}$ and $[Co(bpy)_3]^{3+/2+}$ couples. The mechanisms will be discussed in terms of the activation parameters and the Marcus cross relationships.

The kinetics of the oxidation of ascorbic acid (H_2A) to dehydroascorbic acid (A) by a metal complex have been investigated extensively.[1-5] It has been shown that Cu^{2+} and $[Fe(H_2O)_6]^{3+}$ catalyze the autoxidation of ascorbic acid.[1] The kinetics of the inner-sphere oxidation of ascorbic acid by Cu^{2+} or $[Fe(H_2O)_6]^{3+}$ have been examined,[2,3] as have the outer-sphere oxidations by $[Co(H_2O)_6]^{3+}$,[4] and Fe(III), Ir(IV), and Mo(V).[5] The application of the Marcus theory allowed an estimate of the redox potential and the free energy of activation for the ascorbic acid/radical couple.[5]

Cobalt(III) complexes are very interesting in investigating the electron-transfer reactions because of the problems of the spin-multiplicity change and the ligand-reorganization energy.[6] However, the reactions of cobalt(III) complexes with ascorbic acid have rarely been investigated since Iwasaki[7] reported in 1942 that some cobalt(III) complexes catalyzed the autoxidation of ascorbic acid. As ascorbic acid is a π-donor, ascorbic acid can be expected to interact with cobalt(III) complexes with π-conjugated ligands. We have selected the cobalt(III) complexes ligating 1,10-phenanthroline or 2,2′-bipyridine in order to elucidate the mechanism of the reactions of cobalt(III) complexes with ascorbic acid.

Experimental

Reagents. The $[Co(phen)_3]Cl_3\cdot7H_2O$,[8] $[Co(bpy)_3]Cl_3\cdot3H_2O$,[8] and $[Co(en)_3]Cl_3$[9] complexes were prepared as has been described elsewhere. The perchlorate salts, $[Co(phen)_3](ClO_4)_3\cdot2H_2O$, $[Co(bpy)_3](ClO_4)_3\cdot3H_2O$, and $[Co(en)_3](ClO_4)_3$, were obtained by adding sodium perchlorate to solutions of the chloride complexes. $[Co(en)(phen)_2](ClO_4)_3\cdot2H_2O$,[10] $[Co(en)_2(phen)](ClO_4)_3$,[11] and $Na[Co(edta)]\cdot4H_2O$†,[12] were prepared according to the published procedures. The L-ascorbic acid was supplied by Wako Pure Chemical Industries. The lithium perchlorate, $LiClO_4\cdot3H_2O$, was obtained according to the procedure reported previously.[13] All the solutions used for the measurements were prepared using water obtained by the distillation of alkaline permanganate solutions. A solution of ascorbic acid, partly neutralized with lithium carbonate, was freshly prepared under a nitrogen atmosphere. The acetate buffer solutions were prepared by adding acetic acid to lithium carbonate and purged once with nitrogen gas which had been scrubbed twice with alkaline potassium pyrogallate.

Kinetic Measurements. Solutions containing a cobalt(III) complex, $LiClO_4$, and an acetate buffer were added to an optical cell, which was then sealed with a serum cap. After the solution had been purged with a nitrogen atmosphere for 15 min, the reaction was initiated by the addition of the ascorbic-acid solution by means of a syringe. The change in absorbance with time was followed with a Hitachi 200-20 spectrophotometer. The wavelengths used for the measurements were 350 nm ($[Co(bpy)_3]^{3+}$ and $[Co(en)(phen)_2]^{3+}$), 352 nm ($[Co(en)_2(phen)]^{3+}$), 353 nm ($[Co(phen)_3]^{3+}$), 466 nm ($[Co(en)_3]^{3+}$), and 535 nm ($[Co(edta)]^-$). In order to ensure a pseudo-first order condition, ascorbic acid was in at least a tenfold excess over the cobalt(III) complexes: the initial concentrations of ascorbic acid and the cobalt(III) complexes were $(0.50—1.02)\times10^{-2}$ mol dm^{-3} and $(1.64—5.16)\times10^{-4}$ mol dm^{-3} respectively.

The temperature was kept constant within 0.1 °C at each desired temperature, while the ionic strength (I) was adjusted to 0.1 mol dm^{-3} with lithium perchlorate.

The pH of the solutions was measured by the use of a Hitachi-Horiba F-7 pH meter. The $[H^+]$ was computed from the pH using a value of 0.83 (at 25 °C and I=0.10 mol dm^{-3}) for the activity coefficients of H^+.[14]

Results

In the reactions of $[Co(phen)_3]^{3+}$ and $[Co(bpy)_3]^{3+}$ with ascorbic acid, the absorbance over the range from 300 nm to 400 nm decreased with the time during the course of the reaction. As the dissociations of $[Co(phen)_3]^{2+}$ and $[Co(bpy)_3]^{2+}$ are fast (the rate constants are 0.174 s^{-1} [15] and 0.32 s^{-1} [16] at 25 °C respectively), the reaction corresponds to the absorbance change for the slow steps in the following reactions:

$$[Co(phen)_3]^{3+} \xrightarrow[\text{slow}]{H_2A} [Co(phen)_3]^{2+} \xrightarrow[\text{fast}]{} [Co(phen)_2(H_2O)_2]^{2+} \quad (1)$$

† edta: Ethylenediamine-*N*,*N*,*N*′,*N*′-tetraacetate anion.

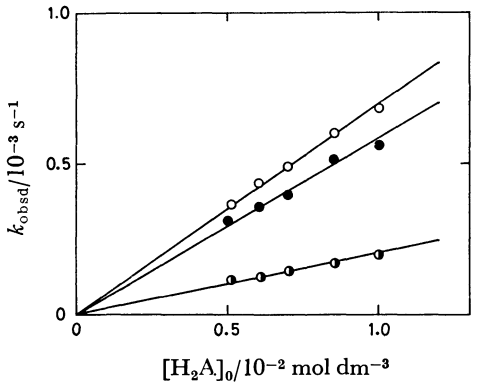

Fig. 1. Plots of k_{obsd} *vs.* $[H_2A]_0$ for the cobalt(III)–ascorbic acid system.
○: $[Co(phen)_3]^{3+}$ at pH 4.53, ●: $[Co(bpy)_3]^{3+}$ at pH 4.83, ◑: $[Co(en)(phen)_2]^{3+}$ at pH 4.83.

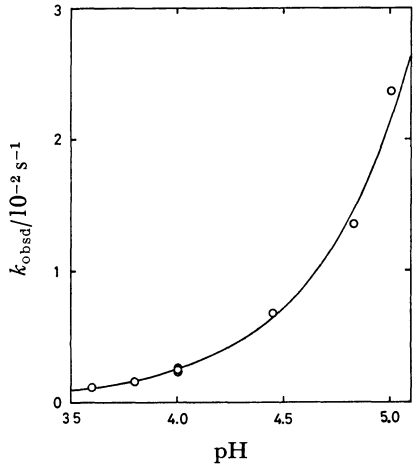

Fig. 2. Plots of k_{obsd} *vs.* pH for the $[Co(phen)_3]^{3+}$–ascorbic acid system.

$$[Co(bpy)_3]^{3+} \xrightarrow[\text{slow}]{H_2A} [Co(bpy)_3]^{2+} \xrightarrow[\text{fast}]{} [Co(bpy)_2(H_2O)_2]^{2+}. \quad (2)$$

Plots of $-\ln(A_t-A_\infty)$ *vs.* the time were linear for at least 85% completion (A_t and A_∞ represent the absorbance at time t and infinity respectively). The observed first-order rate constants (k_{obsd}) obtained from the slope of this straight line show also a linear dependence on the initial concentrations of ascorbic acid (Fig. 1). As the cobalt(III) complexes are one-electron oxidants, ascorbic acid radicals may be formed by the one-electron transfer from the ascorbic acid to the cobalt(III) complexes. Moreover, the dismutation of the ascorbic-acid radicals is very fast.[17] Thus, the rate law was described as follows:

$$-\frac{1}{2}d[Co(III)]/dt = k[Co(III)][H_2A]_0. \quad (3)$$

The second-order rate constants obtained from $k_{obsd}/[H_2A]_0$ increased with a decrease in the acidity (pH 3.60—5.04), as is shown in Fig. 2. The present reaction can, then, be described by this sequence:

$$H_2A \overset{K_1}{\rightleftharpoons} HA^- + H^+ \quad (4)$$

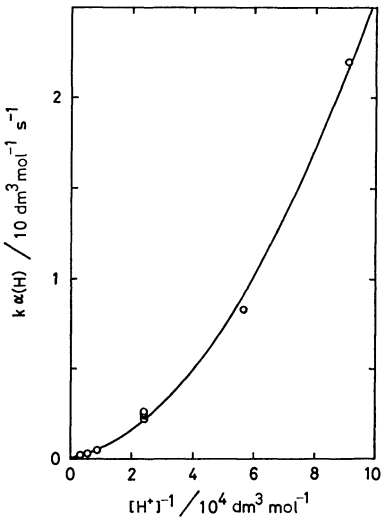

Fig. 3. Plots of $k\alpha(H)$ *vs.* $[H^+]^{-1}$ for the $[Co(phen)_3]^{3+}$–ascorbic acid system at 25.0 °C.

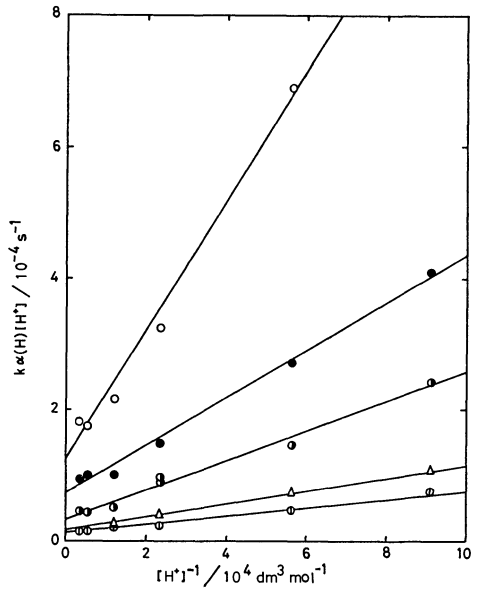

Fig. 4. Plots of $k\alpha(H)[H^+]$ *vs.* $[H^+]^{-1}$ for the $[Co(phen)_3]^{3+}$–ascorbic acid system.
◐: 17.0 °C, △: 21.0 °C, ◑: 25.0 °C, ●: 30.0 °C, ○: 35.0 °C.

$$HA^- \overset{K_2}{\rightleftharpoons} A^{2-} + H^+ \quad (5)$$

$$Co(III) + H_2A \xrightarrow{k_0} \text{radical} + Co(II) \quad (6)$$

$$Co(III) + HA^- \xrightarrow{k_1} \text{radical} + Co(II) \quad (7)$$

$$Co(III) + A^{2-} \xrightarrow{k_2} \text{radical} + Co(II) \quad (8)$$

$$2\,\text{radical} \xrightarrow{\text{fast}} H_nA^{n-2} + A + nH^+, \quad (9)$$

where n is 1 or 2. The above mechanism leads to Eq. 10 for the second-order rate constant:

$$k = \frac{k_0+k_1K_1[H^+]^{-1}+k_2K_1K_2[H^+]^{-2}}{\alpha(H)}, \quad (10)$$

where $\alpha(H)=1+K_1[H^+]^{-1}+K_1K_2[H^+]^{-2}$. As $K_1K_2[H^+]^{-2} \ll 1$ under the present experimental conditions,

Table 1. The rate constants of the reactions of $[Co(phen)_3]^{3+}$, $[Co(bpy)_3]^{3+}$, and $[Co(en)(phen)_2]^{3+}$ with ascorbic acid at $I=0.10$ mol dm^{-3} ($LiClO_4$)[a]

Oxidant	Temp °C	k_1 dm^3 mol^{-1} s^{-1}	$k_2K_1K_2$ 10^{-9} mol dm^{-3} s^{-1}	k_2 10^6 dm^3 mol^{-1} s^{-1}
$[Co(phen)_3]^{3+}$ [b]	17.0	0.22±0.05	0.77±0.35	—
	21.0	0.23±0.01	1.0±0.06	—
	25.0	0.40±0.07	2.4±0.5	5.8±1.1
	30.0	0.60±0.06	4.1±1.1	—
	35.0	0.62±0.09	11±3	—
$[Co(bpy)_3]^{3+}$ [c]	21.0	0.047±0.021	0.59±0.15	—
	25.0	0.13±0.02	0.88±0.23	2.1±0.5
	30.0	0.12±0.04	2.0±0.7	—
	35.0	0.12±0.03	4.2±0.7	—
$[Co(en)(phen)_2]^{3+}$	25.0	≈0	0.42±0.07	1.0±0.2

a) Data were obtained from at least five determinations. b) $\Delta H_1^*(k_1)=(46\pm4)$kJ mol^{-1}, $\Delta S_1^*(k_1)=(-92\pm4)$J K^{-1} mol^{-1}; $\Delta H_2^*(k_2K_1K_2)=(109\pm8)$kJ mol^{-1}, $\Delta S_2^*(k_2K_1K_2)=(-46\pm4)$J K^{-1} mol^{-1}. c) $\Delta H_1^*(k_1)=(38\pm4)$kJ mol^{-1}, $\Delta S_1^*(k_1)=(-140\pm8)$J K^{-1} mol^{-1}; $\Delta H_2^*(k_2K_1K_2)=(80\pm4)$kJ mol^{-1}, $\Delta S_2^*(k_2K_1K_2)=(-160\pm8)$J K^{-1} mol^{-1}.

$\alpha(H)$ can be simplified as $1+K_1[H^+]^{-1}$. The plots of the values of $k\alpha(H)$ *vs.* $[H^+]^{-1}$ gave a quadratic curve (Fig. 3), and the intercept (k_0) was nearly zero. Therefore, the plots of the values of $k\alpha(H)[H^+]$ *vs.* $[H^+]^{-1}$ gave straight lines (Fig. 4). The values of k_1K_1 and $k_2K_1K_2$ are obtained from the intercept and the slope of this straight line respectively. The second-order rate constants, k_1 and k_2, calculated by the use of the values of K_1 and K_2 are listed in Table 1. The values of K_1 at each temperature were estimated from the values at 0.4, 25.0, and 40.0 °C given by Taqui Khan and Martell.[3]

An acetate buffer had little effect on the rate of the reaction of $[Co(phen)_3]^{3+}$ with ascorbic acid (at pH 4.02 and 0.05—0.25 mol dm^{-3} acetate).

For the reaction of $[Co(en)_2(phen)]^{3+}$, $[Co(en)_3]^{3+}$, or $[Co(edta)]^-$, no significant spectral change was observed at 25.0 °C and pH 5.04.

Discussion

The rate constant for the A^{2-} reduction is 10^6 times larger than that for the HA^- reduction. The difference in this reactivity is similar to that in the reactions of cytochrome c-552,[18] Horse Heart cytochrome c,[18] $[Fe(CN)_6]^{3-}$,[19] and Cu^{2+} [20] with ascorbic acid. As the cobalt(III) complexes are substitution-inert, the electron-transfer reaction is considered to occur through an outer-sphere activated complex:

$$Co(III) + HA^- \text{ (or } A^{2-}) \overset{K_{os}}{\rightleftharpoons} [Co(III)^{3+}\cdot HA^-]$$

$$\text{(or } [Co(III)^{3+}\cdot A^{2-}]) \xrightarrow{k_{et}} \text{products,} \qquad (11)$$

where K_{os} and k_{et} are the ion-pair formation constant and the rate constant of the intramolecular electron-transfer respectively. The values of K_{os} can be calculated from the Fuoss equation,[21] where the distance of the closest approach of two ions is 5×10^{-8} cm for the $[Co(phen)_3]^{3+}$ and ascorbate couple; the values of 5.3 and 90 dm^3 mol^{-1} are obtained at 25 °C and $I=0.1$ mol dm^{-3} for the reactions of HA^- and A^{2-} respectively. The large difference in reactivity cannot be elucidated by this small difference in K_{os}. It may, then, be attributed to the intramoleular electron-transfer step if Reaction 11 occurs.

The $[Co(phen)_3]^{3+}$ and $[Co(bpy)_3]^{3+}$ ions were reduced by both HA^- and A^{2-} ions under the present experimental conditions. On the other hand, the $[Co(en)(phen)_2]^{3+}$ ion was reduced only by the A^{2-} ion, and neither the $[Co(en)_2(phen)]^{3+}$ nor the $[Co(en)_3]^{3+}$ ion was reduced by ascorbate ions. These cobalt(III) complexes were not reduced by H_2A. The difference in the reactivities of these reactions may correspond to that of the redox potentials of the complexes (0.391 V for $[Co(phen)_3]^{3+/2+}$, 0.316 V for $[Co(bpy)_3]^{3+/2+}$, and −0.214 V for $[Co(en)_3]^{3+/2+}$),[22] but it cannot be explained why $[Co(edta)]^-$ is not reduced by ascorbic acid in spite of its higher redox potential (0.60 V).

Pelizzetti *et al.*[5] reported on the application of the Marcus theory, which allowed an estimate of the formal reduction potential, $E_{11}^\circ(HA\cdot/HA^-)=0.88$ V, and the intrinsic parameter, $\Delta G_{11}^*(HA\cdot/HA^-)=17$ kJ mol^{-1}. Using these values, we calculated the rate constants of the reactions of $[Co(phen)_3]^{3+}$, $[Co(bpy)_3]^{3+}$, and $[Co(en)_3]^{3+}$ with HA^- from the Marcus cross relationships,[23] neglecting the work terms, which are inferred to be small:[5,24]

$$\Delta G_{12}^* = \lambda(1+\Delta G_{12}^\circ/\lambda)^2/4 \qquad (12)$$

$$k = Z\exp(-\Delta G_{12}^*/RT) \qquad (13)$$

$$\lambda = 2(\Delta G_{11}^* + \Delta G_{22}^*), \qquad (14)$$

where Z is the collision frequency in a solution (10^{11} dm^3 mol^{-1} s^{-1}), where ΔG_{11}^* and ΔG_{22}^* refer to the self-exchange reactions of the reagents, and where ΔG_{12}° is the free-energy change of the reactions. The values calculated at 25 °C are in accord with the observed ones for the reactions of $[Co(phen)_3]^{3+}$ and $[Co(bpy)_3]^{3+}$ (Table 2).

The activation parameters of the reactions of $[Co(phen)_3]^{3+}$ with HA^- and A^{2-} are larger than those of the reactions of $[Co(bpy)_3]^{3+}$: $\Delta\Delta H_1^* = \Delta H_1^*([Co(phen)_3]^{3+}) - \Delta H_1^*([Co(bpy)_3]^{3+}) = 8$ kJ mol^{-1} and $\Delta\Delta S_1^* = \Delta S_1^*([Co(phen)_3]^{3+}) - \Delta S_1^*([Co(bpy)_3]^{3+}) = 48$

TABLE 2. COMPARISON BETWEEN THE OBSERVED RATE CONSTANTS AND THE CALCULATED ONES FROM THE MARCUS CROSS RELATIONSHIPS[a]

Oxidant	k_{22}[b] / $dm^3\ mol^{-1}\ s^{-1}$	ΔG_{22}^{*} / kJ mol^{-1}	E°[c] / V	ΔG_{12}° / kJ mol^{-1}	k_1(calcd) / $dm^3\ mol^{-1}\ s^{-1}$	k_1(obsd) / $dm^3\ mol^{-1}\ s^{-1}$
$[Co(phen)_3]^{3+}$	4.5×10[d]	53	0.391	47	1.4	0.40
$[Co(bpy)_3]^{3+}$	1.8×10[d]	56	0.316	54	0.12	0.13
$[Co(en)_3]^{3+}$	7.7×10^{-5}[e]	86	−0.214	105	3×10^{-10}	—

a) Calculated at 25 °C and $I=0.1$ mol dm^{-3}; $E_{11}^{\circ}(HA\cdot/HA^-)=0.88$ V and $\Delta G_{11}^{*}(HA\cdot/HA^-)=17$ kJ mol^{-1}. b) The rate constant of the self-exchange of the cobalt(III) complex. c) Ref. 22. d) Ref. 25. e) F. P. Dwyer and A. M. Sargeson, *J. Phys. Chem.*, **65**, 1892 (1961).

J K^{-1} mol^{-1} for the HA^- path; $\Delta\Delta H_2^{*}=\Delta H_2^{*}([Co(phen)_3]^{3+}) - \Delta H_2^{*}([Co(bpy)_3]^{3+}) = 29$ kJ mol^{-1} and $\Delta\Delta S_2^{*}=\Delta S_2^{*}([Co(phen)_3]^{3+}) - \Delta S_2^{*}([Co(bpy)_3]^{3+}) = 110$ J K^{-1} mol^{-1} for the A^{2-} path. This is in contrast to the result of the self-exchange reactions of the $[Co(phen)_3]^{3+/2+}$ and $[Co(bpy)_3]^{3+/2+}$ couples, that is, $\Delta\Delta H^{*} = \Delta H^{*}([Co(phen)_3]^{3+}) - \Delta H^{*}([Co(bpy)_3]^{3+}) = -11$ kJ mol^{-1} and $\Delta\Delta S^{*}=\Delta S^{*}([Co(phen)_3]^{3+}) - \Delta S^{*}([Co(bpy)_3]^{3+}) = -30$ J K^{-1} mol^{-1}.[25] This suggests that the mechanism of the reactions of the cobalt(III) complexes with ascorbic acid is different from that of the self-exchange reactions of the complexes, which does not involve a π^*-π^* interaction between ligands of cobalt(II) and cobalt(III).[26] The self-exchange of $[Co(edta)]^{-/2-}$, which has a higher redox potential than these complexes, is very slow;[27] the reaction of $[Co(edta)]^-$ with ascorbic acid is also slow. Extended Hückel π-MO calculations[28] have shown that the lowest π^* orbital energy for phen is higher than that of bpy by about 8 kJ mol^{-1}.

On the basis of the above discussions, it can be thought that the reaction of the cobalt(III) complex with π-accepting ligands with π-donating ascorbic acid is much faster than that of the cobalt(III) complex without π-accepting ligands.

References

1) E. S. G. Barron, R. H. De Meio, and F. Klemperer, *J. Biol. Chem.*, **112**, 625 (1936); H. Schümmer, *Biochem. Z.*, **304**, 1 (1940); K. Shinohara, *Nippon Kagaku Kaishi*, **61**, 803 (1940); A. O. Dekker and R. G. Dickinson, *J. Am. Chem. Soc.*, **62**, 2165 (1940).

2) A. Weissberger and J. E. Lu Valle, *J. Am. Chem. Soc.*, **66**, 700 (1944); H. Nord, *Acta Chem. Scand.*, **9**, 442 (1955); R. G. Grinstead, *J. Am. Chem. Soc.*, **82**, 3464 (1960); S. Udenfriend, C. T. Clar, J. Axelrod, and B. B. Brodie, *J. Biol. Chem.*, **208**, 731, 741 (1954); G. S. Laurence and K. J. Ellis, *J. Chem. Soc., Dalton Trans.*, **1972**, 1667; K. Hayakawa and Y. Hayashi, *J. Nutr. Sci. Vitaminol.*, **23**, 395 (1977).

3) M. M. Taqui Khan and A. E. Martell, *J. Am. Chem. Soc*, **89**, 4176 (1967); **90**, 6011 (1968).

4) R. A. Rickman, R. L. Sorensen, K. O. Watkins, and G. Davies, *Inorg. Chem.*, **16**, 1570 (1977).

5) E. Pelizzetti, E. Mentasti, and E. Pramauro, *Inorg. Chem.*, **15**, 2898 (1976); E. Pelizzetti, E. Mentasti, and C. Baiocchi, *J. Phys. Chem.*, **80**, 2979 (1976); E. Pelizzetti, E. Mentasti, and E. Pramauro, *Inorg. Chem.*, **17**, 1181 (1978).

6) J. F. Endicott and B. Durham, "Coordination Chemistry of Macrocyclic Compounds," ed by G. A. Melson, Plenum Press, New York and London (1979), p. 393.

7) T. Iwasaki, *Nippon Kagaku Kaishi*, **63**, 1743 (1942).

8) N. Maki, *Bull. Chem. Soc. Jpn.*, **42**, 2275 (1969).

9) J. B. Work and J. P. McReynolds, *Inorg. Synth.*, **2**, 221 (1946).

10) L. S. Dollimore and R. D. Gillard, *J. Chem. Soc., Dalton Trans.*, **1975**, 370.

11) R. D. Gillard, R. E. E. Hill, and R. Maskill, *J. Chem. Soc., A*, **1970**, 1447.

12) H. A. Weakliem and J. L. Hoard, *J. Am. Chem. Soc.*, **81**, 549 (1959).

13) H. Ogino, K. Tsukahara, and N. Tanaka, *Inorg. Chem.*, **18**, 1271, 3290 (1979).

14) J. Kielland, *J. Am. Chem. Soc.*, **59**, 1675 (1937).

15) P. Ellis and R. G. Wilkins, *J. Chem. Soc.*, **1959**, 299.

16) R. Davies, M. Green, and A. G. Sykes, *J. Chem. Soc., Dalton Trans.*, **1972**, 1171.

17) I. Yamazaki, H. S. Mason, and L. H. Piette, *Biochim. Biophys. Acta*, **50**, 62 (1961); B. H. J. Bielski, D. A. Comstock, and R. A. Bowen, *J. Am. Chem. Soc.*, **93**, 5624 (1971).

18) H. Kihara, H. Nakatani, K. Hiromi, K. Hon-nami, and T. Oshima, *J. Biochem.*, **83**, 243 (1978).

19) B. Tonomura, H. Nakatani, M. Ohnishi, J. Yamaguchi-Ito, and K. Hiromi, *Anal. Biochem.*, **84**, 370 (1978).

20) K. Hayakawa, S. Minami, and S. Nakamura, *Bull. Chem. Soc. Jpn.*, **46**, 2788 (1973).

21) R. M. Fuoss, *J. Am. Chem. Soc.*, **80**, 5059 (1958).

22) E. L. Yee, R. J. Cave, K. L. Guyer, P. D. Tyma, and M. J. Weaver, *J. Am. Chem. Soc.*, **101**, 1131 (1979).

23) R. A. Marcus, *Ann. Rev. Phys. Chem.*, **15**, 155 (1964).

24) S. Wherland and H. B. Gray, "Biological Aspects of Inorganic Chemistry," ed by A. W. Addison, W. R. Cullen, D. Dolphin, and B. R. James, Wiley, New York (1977), p. 289.

25) H. M. Neumann, quoted in R. Farina and R. G. Wilkins, *Inorg. Chem.*, **7**, 514 (1968).

26) M. Chou, C. Creutz, and N. Sutin, *J. Am. Chem. Soc.*, **99**, 5615 (1977).

27) Y. A. Im and D. H. Busch, *J. Am. Chem. Soc.*, **83**, 3362 (1961).

28) G. N. La Mar, *J. Am. Chem. Soc.*, **94**, 9055 (1972).

The Preparation and Characterization of Dichloromanganese(IV) Schiff Base Complexes

Takayuki MATSUSHITA,* Hiroshi KONO, and Toshiyuki SHONO
Department of Applied Chemistry, Faculty of Engineering, Osaka University, Yamadaoka, Suita, Osaka 565
(Received January 20, 1981)

Some chloromanganese(III) Schiff base complexes react with hydrogen chloride to give deep green complexes with the empirical formula of $MnLCl_2$ or MnL'_2Cl_2, where H_2L denotes quadridentate ligands such as *N,N'*-disalicylideneethylenediamine and its analogs, and where HL' denotes bidentate ligands such as *N*-butylsalicylideneamine and its analogs. These complexes are nonelectrolytes in acetonitrile. Their magnetic moments at room temperature fall within the range of 3.9 to 4.1 BM, and the magnetic susceptibilities obey the Curie-Weiss law with small θ values over the temperature range of 77 to 300 K, indicating that the oxidation state of the manganese ions in these complexes is +IV. The electronic spectra show an intense band around 16000 cm^{-1} which can be assigned to a charge-transfer transition. In the cyclic voltammograms, two cathodic waves are observed at half-peak potentials around +0.9 V and −0.2 V(*vs.* SCE); they can be assigned to the reductions of Mn(IV) to Mn(III) and of Mn(III) to Mn(II) respectively. The probable configurations of the complexes are discussed on the basis of the infrared spectra.

The manganese ion plays an important role in biological redox systems, which are comprised of the oxygen-evolution process of the photosystem II in green plants and the disproportionation of the superoxide ion, O_2^-, by manganese-containing superoxide dismutases. In these systems, the oxidation states of manganese(II), (III), and/or (IV) are believed to be involved.[1] In relation to its function, manganese complexes with higher oxidation states, such as +III and +IV, have been investigated.[2-6] Although manganese(III) complexes with various ligands have thus been synthesized and characterized, few manganese(IV) complexes have been isolated so far, for the manganese(IV) ion is a strong oxidant and its complexes are very unstable.[7,8]

We have found that some chloromanganese(III) Schiff base complexes react with hydrogen chloride to give the corresponding manganese(IV) complexes as deep green crystals. In this paper we will describe the preparation and characterization of a series of novel dichloromanganese(IV) Schiff base complexes.

Experimental

Preparation of Manganese(III) Complexes. The quadridentate Schiff base ligands were prepared by a condensation of the salicylaldehydes with diamines. They were recrystallized from ethanol or appropriate organic solvents. The bidentate Schiff base ligands were prepared by a condensation of the salicylaldehydes with butylamine. The 5-nitro-, 5-bromo-, and 5,6-benzo derivatives were recrystallized from ethanol. All the chloromanganese(III) Schiff base complexes (shown in Fig. 1) were prepared by a modification of the method described in the literature.[9-12] To a methanol solution of a quadridentate Schiff base ligand, an equimolar amount of manganese(III) acetate dihydrate, $Mn(CH_3COO)_3 \cdot 2H_2O$ (a half molar of it when the Schiff-bases were bidentate ligands) was added. The solution was warmed at 60 °C for 1 h, and then a 1.5-molar-fold quantity of lithium chloride over the manganese acetate was added to this solution, which was subsequently further warmed at 60 °C for 1 h. The solution was then concentrated under reduced pressure and cooled. The resulting precipitates were collected on a glass filter, washed with a small volume of water and methanol, and then with ether, and dried *in vacuo*. They were recrystallized from methanol or dichloromethane. The yields were 60—80%. The elemental analyses of the manganese(III) complexes are given in Table 1, along with their magnetic moments measured at room temperature. The magnetic moment of Mn(*N*-Bu-5-NO_2sai)$_2$Cl was found to be lower than those of the other manganese(III) complexes. This may be caused by the magnetic-exchange interaction in this complex.

Preparation of Dichloromanganese(IV) Schiff Base Complexes. Dichloro(N,N'-disalicylideneethylenediaminato)manganese(IV) Dichloromethane Adduct, Mn(salen)$Cl_2 \cdot (CH_2Cl_2)_{0.5}$: Into an acetone solution (200 cm^3) of Mn(salen)Cl·H_2O (0.5 g), a two-molar-fold portion of a methanol solution of HCl over the complex was stirred, drop by drop, at room temperature. The solution turned brown to deep green. After the solution had been filtered, the filtrate was concentrated to about 20 cm^3 under reduced pressure. Anhydrous ether (200 cm^3) was then added to this solution. The resulting green precipitates were collected on a glass filter, washed with ether,

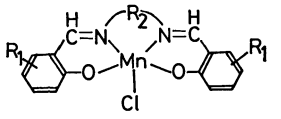

R_1	R_2	L
H	CH_2CH_2	salen
H	C_6H_{10}	salchxn
5-NO_2	CH_2CH_2	5-NO_2salen
5-CH_3	CH_2CH_2	5-Mesalen
5-Br	CH_2CH_2	5-Brsalen
5-Br	$CH(CH_3)CH_2$	5-Brsalpln
5-Br	$CH_2CH_2CH_2$	5-Brsalpn

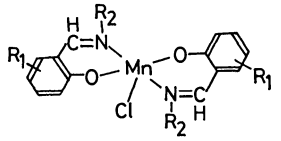

R_1	R_2	L'
H	C_4H_9	*N*-Busai
5-NO_2	C_4H_9	*N*-Bu-5-NO_2sai
5-Br	C_4H_9	*N*-Bu-5-Brsai
5,6-Benzo	C_4H_9	*N*-Bu-5,6-Benzosai

Fig. 1. Manganese(III) Schiff base complexes.

Table 1. Elemental analyses and magnetic moments of manganese(III) complexes

Complex	Found (%)				Calcd (%)				μ_{eff}[a]
	C	H	N	Mn	C	H	N	Mn	BM
Mn(salen)Cl·H_2O	50.61	3.96	7.35	14.28	51.29	4.30	7.48	14.66	4.90
Mn(5-Brsalen)Cl	36.30	2.61	5.20	10.60	37.21	2.73	5.42	10.64	4.88
Mn(5-NO_2salen)Cl	41.00	2.96	11.74	11.60	41.18	3.46	12.00	12.24	5.01
Mn(5-Mesalen)Cl	56.68	4.76	7.28	14.26	56.19	4.72	7.28	14.28	5.02
Mn(salchxn)Cl	57.98	4.82	6.90	13.60	58.48	4.91	6.82	13.37	4.96
Mn(5-Brsalpln)Cl	38.64	2.76	5.59	10.37	38.63	2.67	5.30	10.39	4.88
Mn(5-Brsalpn)Cl·H_2O	37.01	2.91	5.08	9.51	37.36	2.95	5.12	10.05	5.04
Mn(*N*-Busai)$_2$Cl	58.80	6.32	6.21	12.53	59.67	6.37	6.33	12.40	5.03
Mn(*N*-Bu-5-NO_2sai)$_2$Cl	49.53	5.11	10.23	10.37	49.59	4.92	10.51	10.31	4.37
Mn(*N*-Bu-5,6-Benzosai)$_2$Cl	66.33	6.13	4.85	10.10	66.36	5.94	5.16	10.12	4.92
Mn(*N*-Bu-5-Brsai)$_2$Cl	43.77	4.52	4.80	9.17	43.97	4.36	4.66	9.15	5.01

a) Measured at room temperature.

Table 2. Elemental analyses and magnetic moments of manganese(IV) complexes

Complex	Found (%)					Calcd (%)					μ_{eff}[a]
	C	H	N	X	Mn	C	H	N	X	Mn	BM
Mn(salen)Cl_2·$(CH_2Cl_2)_{0.5}$	45.17	3.55	6.49	24.86	12.80	45.60	3.48	6.45	24.47	12.68	3.91
Mn(5-Brsalen)Cl_2	34.82	2.28	5.00	41.99	9.77	34.82	2.56	5.08	41.80	9.95	3.94
Mn(5-NO_2salen)Cl_2	39.97	2.52	11.54	14.26	11.05	39.69	2.91	11.57	14.65	11.35	3.98
Mn(5-Mesalen)Cl_2·$(CH_2Cl_2)_{0.25}$	49.70	4.25	6.28	20.58	12.67	49.66	4.22	6.35	20.08	12.45	3.97
Mn(salchxn)Cl_2·$(CH_2Cl_2)_{0.6}$	49.96	4.21	5.66	22.84	10.90	49.76	4.30	5.69	22.82	11.05	4.04
Mn(5-Brsalpln)Cl_2·$(CH_2Cl_2)_{0.5}$	34.34	2.54	4.66	42.97	9.09	34.66	2.49	4.62	43.88	9.06	4.00
Mn(5-Brsalpn)Cl_2	35.77	2.52	4.82	41.63	9.96	36.21	2.59	4.97	40.91	9.74	4.02
Mn(*N*-Busal)$_2Cl_2$	54.79	5.76	5.70	15.47	12.03	55.24	5.90	5.86	14.87	11.49	4.10
Mn(*N*-Bu-5-NO_2sai)$_2Cl_2$	46.32	4.56	9.85	12.33	9.72	46.49	4.61	9.86	12.48	9.67	3.90
Mn(*N*-Bu-5,6-Benzosai)$_2Cl_2$	62.03	5.60	4.67	12.87	9.39	62.29	5.58	4.87	12.26	9.50	4.07
Mn(*N*-Bu-5-Brsai)$_2Cl_2$	40.95	4.00	4.19	35.22	8.54	41.54	4.12	4.40	36.30	8.64	4.09

a) Measured at room temperature.

and dried *in vacuo*. The solids were recrystallized from dichloromethane to give the above complex as deep green crystals. The yield was *ca.* 30%.

The other dichloromanganese(IV) Schiff base complexes were obtained in a similar manner. The elemental analyses of the manganese(IV) complexes obtained are given in Table 2, together with their magnetic moments measured at room temperature. These deep green complexes are soluble in dichloromethane, acetone, and acetonitrile. The solutions were stable in these solvents if kept without contact with to moisture. They were soluble in donating solvents, such as pyridine, *N*,*N*-dimethylformamide, and methanol, but these solutions gradually turned brown.

Reagents. All the reagents were of a reagent grade. The solvents were purified by refluxing over sodium (ether), calcium chloride (dichloromethane, acetone), or magnesium (methanol), and then distilled. The acetonitrile was distilled twice from diphosphorus pentaoxide prior to use.

Measurements. The UV, VIS, and NIR spectra were obtained from Hitachi EPS-3 and 340 spectrophotometers. The IR spectra were recorded on a Hitachi EPI-215 grating spectrophotometer in the 700 to 4000 cm^{-1} regions and on a Hitachi EPI-L grating spectrophotometer in the 200 to 700 cm^{-1} regions. All the spectra were measured in Nujol mulls or in a KBr disc. The magnetic susceptibilities were measured by the Gouy method at room temperature and by the Faraday method, using a Shimadzu MB 11 apparatus for the temperature range from 77 to 300 K. The conductivities were determined on a Yanagimoto MY-7 conductivity outfit. The cyclic voltammetry was performed with a Yanagimoto P8 polarograph connected with a Yanagimoto P8-PT potentiostat. The working electrode was a platinum-inlay electrode, while the auxiliary electrode was a platinum wire. The reference electrode was a saturated calomel electrode which was inserted in an aqueous solution of 1 M (1 M=1 mol dm^{-3}) KCl in a 100-cm^3 beaker connected with a conventional brown H-type cell by means of a 4% agar-saturated KCl gel bridge. Tetrabutylammonium perchlorate, Bu_4NClO_4, was used as the supporting electrolyte. The dissolved oxygen was removed by passing nitrogen gas through a sample solution for 20 min.

Results and Discussion

Figure 2 shows the spectral changes on the addition of HCl to an acetone solution of Mn(salen)Cl·H_2O in different molar ratios. The spectra change remarkably on the addition of HCl, and a new absorption band appears around 630 nm. Its intensity increases as the molar ratio of HCl to the complex increases to 4. The further addition of HCl leads to the decolorization of the solution, with the formation of white precipitates, which may consist of hydrogen chloride salts of the ligand. This was confirmed by a comparison of the IR spectra of the white

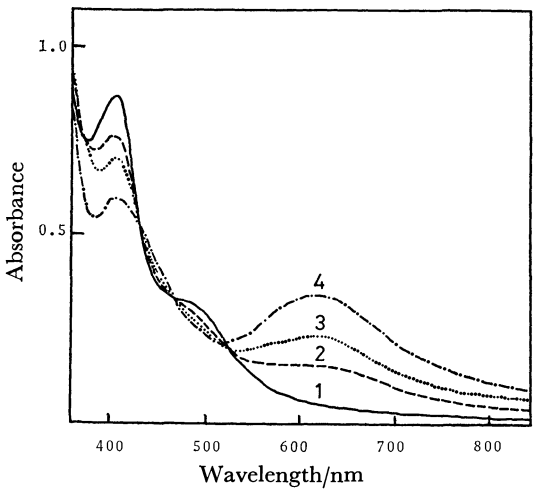

Fig. 2. Spectral changes on the addition of HCl to an acetone solution of 2×10^{-4} M Mn(salen)Cl·H_2O in different molar ratios.
(1): [HCl]/[complex]=0, (2): 1, (3): 2, (4): 4.

precipitates and of the authentic compound obtained by the reaction between salenH_2 and HCl in ether.

The deep green complexes isolated by the reactions between chloromanganese(III) Schiff base complexes and HCl are given in Table 2. Their analytical data are consistent with the empirical formula of $MnLCl_2$ or MnL'_2Cl_2, where L denotes a dianion of quadridentate Schiff base ligands, and L', a monoanion of bidentate Schiff base ligands. Some of them include dichloromethane as a crystalline solvent.

Magnetic Properties. The room-temperature magnetic moments for these complexes (given in Table 2) fall within the range of 3.9 to 4.1 BM, consistent with a calculated spin-only value expected for a complex with a d^3 high-spin configuration. Figure 3 shows the Curie-Weiss plot for Mn(salen)$Cl_2\cdot(CH_2Cl_2)_{0.5}$ over the temperature range from 77 to 300 K. The magnetic susceptibilities obey the Curie-Weiss law, $\chi_A=C/(T+\theta)$. The same behavior was observed for the complexes of Mn(5-Mesalen)$Cl_2\cdot(CH_2Cl_2)_{0.25}$ and Mn(*N*-Bu-5-NO_2sai)$_2Cl_2$. Their Weiss constants are given in Table 3. These values were obtained from an extrapolation of the plot of the reciprocal of the molar susceptibilities, χ_A, against the absolute temperature. These small θ values indicate that there are very small magnetic interactions in these complexes. These results suggest that the oxidation state of the central manganese ion in the complexes is +IV.

Conductivities. The molar conductivities for several manganese(III) and manganese(IV) complexes are summarized in Table 4. These values indicate that they are essentially nonelectrolytes in acetonitrile. The slightly large value observed for the Mn(*N*-Busai)$_2Cl_2$, complex may be caused by its lower solubility in acetonitrile. On the other hand, in methanol the molar conductivity for Mn(salen)Cl·H_2O was found to be 71 S cm^2 mol^{-1}, and that for Mn(salen)$Cl_2\cdot(CH_2Cl_2)_{0.5}$, to be 191 S cm^2 mol^{-1}. These values indicate that both complexes undergo considerable dissociation in methanol.

Electronic Spectra. Figure 4 shows the electronic spectra of Mn(salen)Cl·H_2O and Mn(salen)$Cl_2\cdot(CH_2Cl_2)_{0.5}$ in dichloromethane. In the visible region, the spectrum of the manganese(III) complex shows three absorption bands, at 15600, 20800, and 23800 cm^{-1}. They have been previously assigned to the ligand-field transitions of $d_{xy}\rightarrow d_{x^2-y^2}$ and of d_{yz}, $d_{xz}\rightarrow d_{x^2-y^2}$, and to the charge-transfer transition of $d\pi$(Mn) to π^* (azomethine), respectively.[12,13] On the other hand, the spectrum of the manganese(IV) complex shows two absorption bands, at 15400 and 23000 cm^{-1}. The lower-energy band is very intense compared with that of the manganese(III) complex. Therefore, it seems to be due to a charge-transfer transition.

Moews has reported on the absorption spectrum of $K_2Mn^{IV}Cl_6$ in fluorocarbon grease mulls; it shows two absorption bands, at 15400 (very strong) and 27400 cm^{-1} (strong) in the visible region.[8d] The lower-energy band has been assigned to a charge-transfer

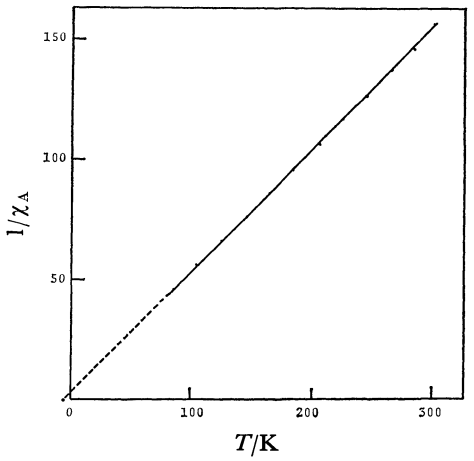

Fig. 3. Curie-Weiss plot for Mn(salen)$Cl_2\cdot(CH_2Cl_2)_{0.5}$.

TABLE 3. WEISS CONSTANTS OF MANGANESE(IV) COMPLEXES

Complex	Weiss constant θ/K
Mn(salen)$Cl_2\cdot(CH_2Cl_2)_{0.5}$	6
Mn(5-Mesalen)$Cl_2\cdot(CH_2Cl_2)_{0.25}$	3
Mn(*N*-Bu-5-NO_2sai)$_2Cl_2$	9

Table 4. MOLAR CONDUCTIVITIES OF MANGANESE(III) AND MANGANESE(IV) COMPLEXES IN ACETONITRILE

Complex	Λ[a] S cm^2 mol^{-1}
Mn^{III}(salen)Cl·H_2O	2.38
Mn^{IV}(salen)$Cl_2\cdot(CH_2Cl_2)_{0.5}$	3.48
Mn^{III}(*N*-Busai)$_2$Cl	8.35
Mn^{IV}(*N*-Busai)$_2Cl_2$	25.28[b]
Mn^{III}(*N*-Bu-5-NO_2sai)$_2$Cl	10.22
Mn^{IV}(*N*-Bu-5-NO_2sai)$_2Cl_2$	3.70

a) Measured at 25 °C. The concentration of the complexes was 10^{-3} M. b) The concentration of the complex was 5×10^{-4} M.

TABLE 5. SPECTROSCOPIC DATA FOR MANGANESE(IV) COMPLEXES

Complex	$\tilde{\nu}_{max}$ / 10^3 cm^{-1} (log ε)[a]		ν(Mn-Cl) / cm^{-1}
Mn(5-Mesalen)$Cl_2\cdot(CH_2Cl_2)_{0.25}$	14.9 (3.60)	22.8 (3.81)	323
Mn(5-Brsalen)Cl_2	15.3 (3.59)	23.1 (3.69)	337
Mn(salchxn)$Cl_2\cdot(CH_2Cl_2)_{0.6}$	15.6 (3.62)	23.7 (3.74)	350
Mn(salen)$Cl_2\cdot(CH_2Cl_2)_{0.5}$	15.4 (3.60)	23.0 (3.78)	341
Mn(5-NO_2salen)Cl_2	16.7 (3.40)	24.4 sh	356
Mn(5-Brsalpln)$Cl_2\cdot(CH_2Cl_2)_{0.5}$	15.3 (3.60)	24.1 (3.78)	339
Mn(5-Brsalpn)Cl_2	14.8 (3.63)	24.1 (3.83)	367
Mn(*N*-Busai)$_2Cl_2$	16.0 (3.52)	22.0 sh	346
Mn(*N*-Bu-5-NO_2sai)$_2Cl_2$	17.2 (3.80)	23.4 sh	359, 342
Mn(*N*-Bu-5-Brsai)$_2Cl_2$	15.5 (3.76)	22.7 sh	333
Mn(*N*-Bu-5,6-Benzosai)$_2Cl_2$	14.6 (3.71)	23.0 sh	334

a) Measured in dichloromethane.

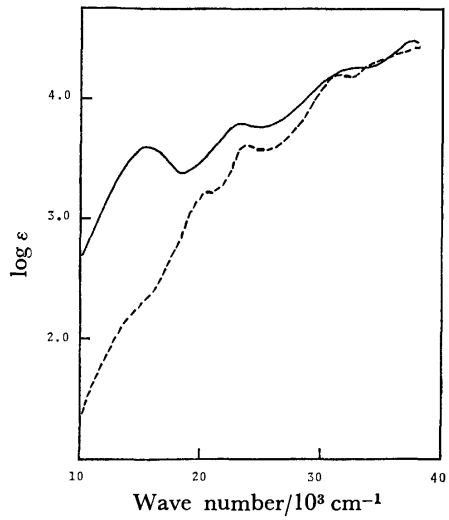

Fig. 4. Electronic spectra in dichloromethane. (——): Mn^{IV}(salen)$Cl_2\cdot(CH_2Cl_2)_{0.5}$, (– – –): Mn^{III}(salen)$Cl\cdot H_2O$.

transition of chlorine to manganese. Later, Jeżowska-Trzbiatowska *et al.*[14] claimed that the absorption spectrum of the same complex in 12 mol dm^{-3} HCl does not agree with that observed by Moews in the intensities of these bands. However, as was pointed out by Moews, hexachloromanganate(IV) salts are rapidly converted to the corresponding aquapentachloromanganate(III) salts on standing in moist air. Therefore, it is uncertain as to whether or not $K_2Mn^{IV}Cl_6$ exists as the $Mn^{IV}Cl_6^{2-}$ ion in 12 mol dm^{-3} HCl.

The spectral data for the manganese(IV) complexes are summarized in Table 5. All the complexes show two intense bands around 16000 and 23000 cm^{-1} in the visible region. It can be seen that the absorption maxima of the lower-energy bands are affected by the Schiff base ligands. In the complexes of the salen type, the absorption maxima are shifted to higher energies in the order of the substituents of 5-Me<5-Br<H<5-NO_2. In the complexes of the *N*-butylsalicylideneamine type, similar shifts are observed in the order of the substituents of 5,6-Benzo<5-Br<H<5-NO_2. Furthermore, the absorption maxima of the

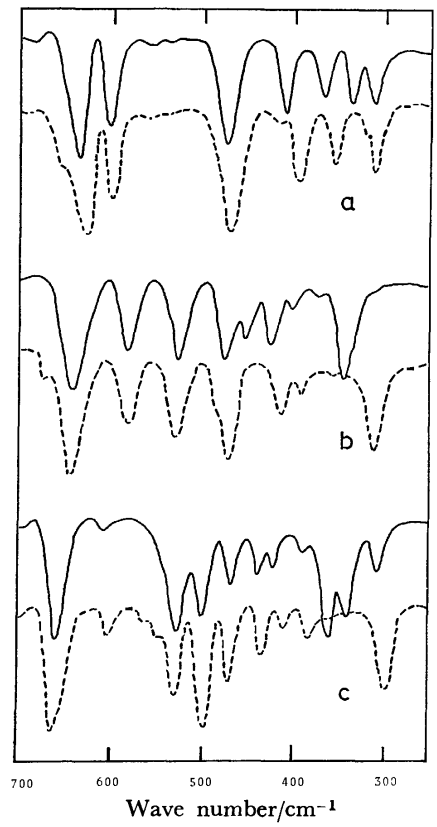

Fig. 5. Infrared spectra (in Nujol mulls). a) (——): Mn^{IV}(salen)$Cl_2\cdot(CH_2Cl_2)_{0.5}$; (– – –): Mn^{III}(salen)$Cl\cdot H_2O$, b) (——): Mn^{IV}(*N*-Busai)$_2Cl_2$; (– – –): Mn^{III}(*N*-Busai)$_2Cl$, c) (——): Mn^{IV}(*N*-Bu-5-NO_2-sai)$_2Cl_2$; (– – –): Mn^{III}(*N*-Bu-5-NO_2sai)$_2Cl$.

former complexes are observed at lower energies than those of the latter complexes. These results imply that the lower-energy bands may be assigned to a charge-transfer transition of Cl(pπ) to Mn(dπ). The absorption bands due to the ligand-field transitions expected for the manganese(IV) complexes may be obscured by these intense bands.

Infrared Spectra. In the region from 4000 to 500 cm^{-1} the infrared spectra of the manganese(IV) complexes are almost the same as those of the cor-

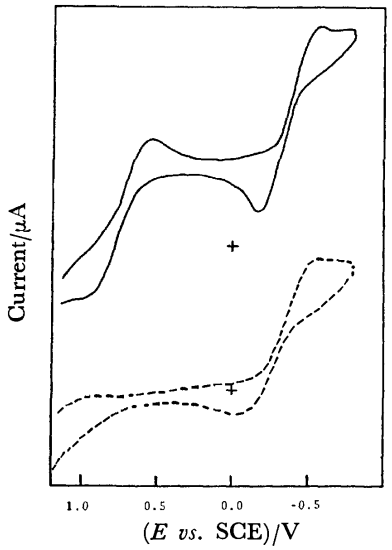

Fig. 6. Current potential curves in acetonitrile. (——): $Mn^{IV}(salen)Cl_2\cdot(CH_2Cl_2)_{0.5}$; (– – –): Mn^{III}-(salen)$Cl\cdot H_2O$.

responding manganese(III) complexes, except around 1290 cm^{-1}, where the absorption band due to ν(C–O) should be observed. This indicates that there is no change in the coordination features of the Schiff base ligands in either manganese(III) or manganese(IV) complexes. In the ν(C–O) region, lower-energy shifts of about 10 cm^{-1} were observed on going from the manganese(III) complexes to the manganese(IV) complexes; they may be caused by the change of the oxidation state of the central manganese ion from +III to +IV. In the region from 200 to 500 cm^{-1}, the spectra of the manganese(IV) complexes show the strong absorption bands at about 340 cm^{-1}, unlike those of the corresponding manganese(III) complexes. Figure 5-a shows the spectra of $Mn^{IV}(salen)Cl_2\cdot(CH_2Cl_2)_{0.5}$ and $Mn^{III}(salen)Cl\cdot H_2O$. The band observed at 341 cm^{-1} for the manganese(IV) complex may be assigned to ν(Mn–Cl). Figure 5-b shows the spectra of Mn^{IV}(*N*-Busai)$_2Cl_2$ and Mn^{III}(*N*-Busai)$_2$Cl. The band observed at 348 cm^{-1} for the manganese(IV) complex may be assigned to ν(Mn–Cl). On the other hand, as is shown in Fig. 5-c, the spectrum of Mn^{IV}(*N*-Bu-5-NO_2sai)$_2Cl_2$ exhibits two strong bands, at 364 and 333 cm^{-1}, which may be assigned to ν(Mn–Cl). The frequencies of the characteristic bands assigned to ν(Mn–Cl) for the manganese(IV) complexes are summarized in Table 5. In the complexes of the salen type, one band assignable to ν(Mn–Cl) was observed, whereas in the Mn^{IV}(*N*-Bu-5-NO_2sai)$_2Cl_2$ complex, two bands were observed. For the octahedral complexes of the MA_4Cl_2 type (A denotes unidentate ligands such as ammonia), one band due to ν(M–Cl) should be observed in the case of a *trans*-configuration, whereas two strong bands should be observed in the case of a *cis*-configuration.[15] These results suggest that the manganese(IV) complexes of the salen type may have a *trans*-octahedral configuration, while in the manganese(IV) complexes of the bidentate Schiff bases, *trans*- and *cis*-octahedral configurations may be probable.

Table 6. Reduction potentials for manganese(IV) complexes

Complex	$E_{p/2}$ *vs.* SCE[a] / V	
	$Mn^{IV}\rightarrow Mn^{III}$	$Mn^{III}\rightarrow Mn^{II}$
$Mn(salen)Cl_2\cdot(CH_2Cl_2)_{0.5}$	0.76	−0.37 (−0.38)[b]
$Mn(5\text{-}Brsalen)Cl_2$	0.85	−0.16 (+0.01)
$Mn(5\text{-}NO_2salen)Cl_2$	0.90	−0.01 (+0.11)
$Mn(5\text{-}Mesalen)Cl_2\cdot(CH_2Cl_2)_{0.25}$	0.85	−0.34 (−0.32)
$Mn(salchxn)Cl_2\cdot(CH_2Cl_2)_{0.6}$	0.83	−0.29 (−0.32)
$Mn(5\text{-}Brsalpln)Cl_2\cdot(CH_2Cl_2)_{0.5}$	1.00	−0.09 (−0.14)
$Mn(5\text{-}Brsalpn)Cl_2$	0.88	−0.05 (−0.02)
Mn(*N*-Busai)$_2Cl_2$	0.84	−0.11 (−0.08)
Mn(*N*-Bu-5-Brsai)$_2Cl_2$	0.94	+0.01 (−0.12)
Mn(*N*-Bu-5-NO_2sai)$_2Cl_2$	0.98	+0.08 (+0.24)

a) Measured in acetonitrile at 25 °C. b) Half-peak potentials observed for the corresponding manganese(III) complexes.

Electrochemical Properties. Figure 6 shows some typical current-potential curves of $Mn^{III}(salen)Cl\cdot H_2O$ and $Mn^{IV}(salen)Cl_2\cdot(CH_2Cl_2)_{0.5}$ measured in acetonitrile. In the manganese(III) complex, one cathodic wave is observed at −0.38 V(*vs.* SCE); it can be assigned to the reduction of Mn(III) to Mn(II). On the other hand, in the manganese(IV) complex, two cathodic waves are observed, at +0.76 and −0.37 V(*vs.* SCE), with similar wave heights; they can be assigned to the reductions of Mn(IV) to Mn(III) and of Mn(III) to Mn(II) respectively. The separations of the peak potentials between the cathodic wave and the corresponding anodic wave for both redox waves are larger than the 57 mV expected for a reversible one-electron redox wave, so these electrode reactions may be irreversible.

All the manganese(IV) complexes show two cathodic waves around +0.85 V and −0.20 V(*vs.* SCE). The half-peak potentials for the reductions of the manganese(IV) complexes are summarized in Table 6, together with those of the corresponding manganese(III) complexes. As has been discussed in connection with the electronic spectra, the potentials for both reductions are also affected by the Schiff base ligands. The reduction potentials are shifted to more positive values upon the introduction of an electron-withdrawing substituent such as the 5-NO_2 group in both types of the complexes. Furthermore, the reduction potentials for the complexes of the *N*-butylsalicylideneamine type are observed at more positive values than those for the complexes of the salen type. These shifts can be explained in terms of the electron density on the central manganese ion in the complexes.

Reactions. These manganese(IV) complexes have reduction potentials high enough to oxidize water. Thus, we have attempted their reactions with water. Figure 7 shows the spectral changes on the addition of water to an acetonitrile solution of $Mn(salen)Cl_2\cdot(CH_2Cl_2)_{0.5}$ in different molar ratios. The

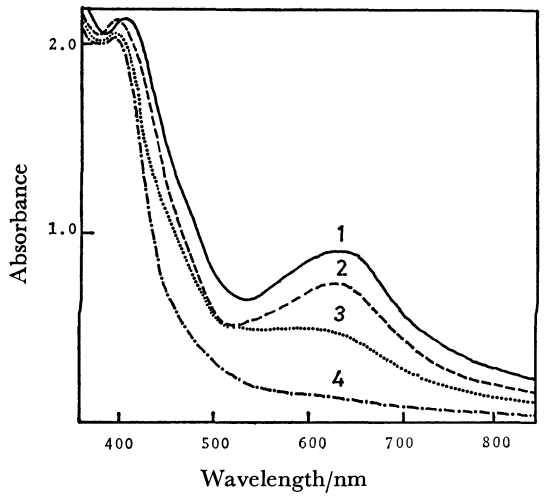

Fig. 7. Spectral changes on the addition of H_2O to an acetonitrile solution of 4×10^{-4} M $Mn(salen)Cl_2\cdot(CH_2Cl_2)_{0.5}$ in different molar ratios.
(1): $[H_2O]/[complex]=0$, (2): 10, (3): 20, (4): 40.

intensity of the characteristic absorption band at 624 nm decreased with an increase in the molar ratio of water to the complex. The final absorption spectrum is almost identical with that of the corresponding manganese(III) complex in the acetonitrile and water mixture, indicating that water reduced the manganese(IV) complex to the manganese(III) complex. We have also succeeded in detecting free "molecular oxygen" liberated during the reactions of the manganese(IV) complexes with water by means of the spectrophotometry of an alkaline pyrogallol solution and a dissolved oxygen probe.[16] The details will be described in the near future.

Some novel dichloromanganese(IV) Schiff base complexes have been prepared and characterized. The higher oxidation state of the manganese ion may be stabilized by charge neutralization with chloride ions. The mechanism for the reaction of the manganese(III) complexes with HCl has not been clarified in this work. However, some experimental evidence suggests that the manganese(IV) complexes may result from a disproportionation of the manganese(III) complexes: manganese(II) compounds are often formed as contaminants in the preparation of the manganese(IV) complexes, and their yields are always 50% or below.

References

1) G. D. Lawrence and D. T. Sawyer, *Coord. Chem. Rev.*, **27**, 173 (1978).
2) I. Tabushi and S. Kojo, *Tetrahedron Lett.*, **1974**, 1577; **1975**, 305.
3) J. K. Howie and D. T. Sawyer, *J. Am. Chem. Soc.*, **98**, 6698 (1976).
4) M. M. Morrison and D. T. Sawyer, *Inorg. Chem.*, **17**, 333 (1978); **17**, 338 (1978).
5) S. R. Cooper, C. C. Dismukes, M. P. Klein, and M. Calvin, *J. Am. Chem. Soc.*, **99**, 6623 (1977); **100**, 7248 (1978).
6) Y. Otsuji, K. Sawada, I. Morishita, Y. Taniguchi, and K. Mizuno, *Chem. Lett.*, **1977**, 983.
7) W. Levason and C. A. McAuliffe, *Coord. Chem. Rev.*, **7**, 353 (1972).
8) a) $[MnCl_2(diphos)_2](ClO_4)_2$: diphos=*o*-phenylenebisdimethylphosphine; L. F. Warren and M. A. Bennett, *Inorg, Chem.*, **15**, 3126 (1976). b) $MnCl_4(bpy)$: bpy=bipyridine; H. A. Goodwin and R. N. Sylva, *Aust. J. Chem.*, **18**, 1743 (1965); **20**, 629 (1967). c) $[Mn(R_2dtc)_3]X$: R_2dtc=alkyldithiocarbamato monoanion and X=BF_4 or ClO_4; A. R. Hendrickson, R. L. Martin, and N. M. Rohde, *Inorg. Chem.*, **13**, 1933 (1974). d) K_2MnCl_6; P. C. Moews Jr., *Inorg. Chem.*, **5**, 5 (1966). e) O=Mn(3-MeOsalen)·MeOH; T. Matsushita, T. Yarino, I. Masuda, T. Shono, and K. Shinra, *Bull. Chem. Soc. Jpn.*, **46**, 1712 (1973).
9) C. P. Prabhakaran and C. C. Patel, *J. Inorg. Nucl. Chem.*, **31**, 3316 (1969).
10) B. C. Sharma and C. C. Patel, *Indian J. Chem.*, **8**, 94 (1970).
11) A. V. Bergen, K. S. Murray, M. J. O'Connor, and B. O. West, *Aust. J. Chem.*, **22**, 39 (1969).
12) L. J. Boucher, *J. Inorg. Nucl. Chem.*, **36**, 531 (1974).
13) L. J. Boucher and D. R. Herrington, *Inorg. Chem.*, **13**, 1105 (1974).
14) B. Jeżowska-Trzebiatowska, S. Wajda, M. Batuka, L. Natkaniec, and W. Wojciechowski, *Inorg. Chim. Acta*, **1**, 205 (1967).
15) K. Nakamoto, "Infrared Spectra of Inorganic and Coordination Compounds," Wiley-Interscience, New York (1970), p. 215.
16) T. Matsushita, M. Fujiwara, and T. Shono, *Chem. Lett.*, **1981**, 631.

Reaction between Aluminium Trichloride and Steam in the Vapor Phase and Properties of the Aluminium Oxide Formed

Yuichi Shoji, Ryoko Matsuzaki, and Yuzo Saeki*

Research Laboratory of Resources Utilization, Tokyo Institute of Technology, 4259, Nagatsuta-cho, Midori-ku, Yokohama 227

(Received February 2, 1981)

The reaction between gaseous $AlCl_3$ and steam, and the products formed were examined by X-ray analysis, TG, DTA, and electron microscopy. The thermal transitions of the Al_2O_3 formed under various conditions were also examined. The reaction between gaseous $AlCl_3$ and steam occurs even at 150 °C and proceeds rapidly above about 400 °C. The product is amorphous Al_2O_3 below 600 °C, amorphous Al_2O_3 containing poorly crystallized γ-Al_2O_3 at 800 °C, γ-Al_2O_3 containing amorphous Al_2O_3 at 900 °C, and γ-Al_2O_3 at 1000 °C. Also, it was observed that the Al_2O_3 formed below 900 °C included a chloride oxide of aluminium, which decomposed in the vicinity of 830 °C to form γ-Al_2O_3 with the evolution of gaseous $AlCl_3$. On heating the amorphous Al_2O_3 formed by the reaction between gaseous $AlCl_3$ and steam, the transition: amorphous $\xrightarrow{ca.\ 700\,^\circ C}$ χ $\xrightarrow{ca.\ 800\,^\circ C}$ κ $\xrightarrow{ca.\ 1000\,^\circ C}$ α occurs; and on heating the γ-Al_2O_3 formed by the same reaction, the transition: γ $\xrightarrow{ca.\ 900\,^\circ C}$ δ $\xrightarrow{ca.\ 1000\,^\circ C}$ θ $\xrightarrow{ca.\ 1000\,^\circ C}$ α occurs.

The reaction of volatile metal chlorides with oxygen or steam has recently become important for the preparation of fine powders of pure metal oxides, because it is possible to carry out the reaction in the vapor phase. To develop a chemical process for preparing fine powders of aluminium oxide (Al_2O_3) by the vapor-phase oxidation of aluminium trichloride ($AlCl_3$), the authors[1] have examined the reaction between $AlCl_3$ and oxygen in the vapor phase and the properties of the Al_2O_3 formed.

There are limited data on the reaction between $AlCl_3$ and steam in the vapor phase. Kato *et al.*[2] have studied the reaction product between gaseous $AlCl_3$ and excess steam at 700—1100 °C and reported that the reaction product is amorphous Al_2O_3 which includes a Cl-containing compound, presumably AlClO, at 700 and 900 °C and δ-Al_2O_3 with or without a small amount of κ-Al_2O_3 at 1100 °C. They have also reported that the amorphous Al_2O_3 crystallizes to κ-Al_2O_3 on heating up to 830 °C in the air and that the δ-Al_2O_3 transforms to α-Al_2O_3 by the heat treatment a 1100 °C in the air.

In this paper, the reaction between gaseous $AlCl_3$ and steam and the product formed have been examined in detail by X-ray analysis, thermogravimetry (TG), differential thermal analysis (DTA), and electron microscopy. The thermal transition of the Al_2O_3 formed under various conditions has also been examined.

Experimental

The $AlCl_3$ used was prepared by the reaction between pure aluminium(Al:99.99%) and chlorine at 400 °C.[1]

A transparent quartz reaction tube (1000 mm length) with an inner concentric tube was used. Gaseous $AlCl_3$ was formed by heating $AlCl_3$ placed in the inner tube at 150 °C, and was carried by a stream of argon (40 cm^3/min) to the reaction zone (27 mm i.d. and 250 mm length) held at a specified temperature. In the meantime, a stream of argon (100 cm^3/min) containing a specified amount of steam was introduced through a separate tube into the reaction zone. The mean flow-rate of the $AlCl_3$ was approximately 3.8 cm^3 Al_2Cl_6(g)/min. The reaction was allowed to proceed for 2 h.

Hydrogen chloride(HCl) formed during the reaction was absorbed in a known amount of 0.1 M† sodium hydroxide (NaOH) solution, and was determined by neutralization titration of the excess NaOH.

The unreacted $AlCl_3$, which was deposited outside the reaction zone together with the reaction product, was separated by heating the mixture in an argon stream at 250 °C. The $AlCl_3$ adsorbed on Al_2O_3 formed was separated by washing the Al_2O_3 with ethanol at boiling point with stirring.[1]

X-Ray analysis of soild product was performed with an X-ray powder diffractometer equipped with a proportional counter, using Ni filtered Cu radiation. TG and DTA were performed in an argon stream and a heating rate of 5 °C/min was employed. The sensitivity of the quartz helix used for TG was approximately 71 mm/g. α-Al_2O_3 was used as a reference for DTA.

Throughout this work, $AlCl_3$ and reaction products were handled in an argon atmosphere or *in vacuo* to prevent any contamination from moisture in the air.

Results and Discussion

Reaction between Gaseous Aluminium Trichloride and Steam. The amounts of HCl formed by the reaction between gaseous $AlCl_3$ and steam(H_2O) at various temperatures were examined. When gaseous $AlCl_3$ and a stream of argon containing excess H_2O (15 vol% H_2O), more than the value calculated as needed to form Al_2O_3 and HCl, was introduced into the reaction zone, a part of the HCl formed by the reaction was dissolved in the unreacted H_2O which condensed outside the heating zone. Aluminium trichloride hexahydrate was also formed from the Al_2O_3 and the HCl. So, the experiments were thus carried out by introducing into the reaction zone a stream of argon containing an amount of H_2O (9, 5, or 2 vol% H_2O) smaller than the calculated value. The reaction temperature above 150 °C was employed, because gaseous $AlCl_3$ was generated by heating $AlCl_3$ at 150 °C. The results are shown in Fig. 1. The broken lines in Fig. 1 show the calculated values of the amount

† 1 M = 1 mol dm^{-3}.

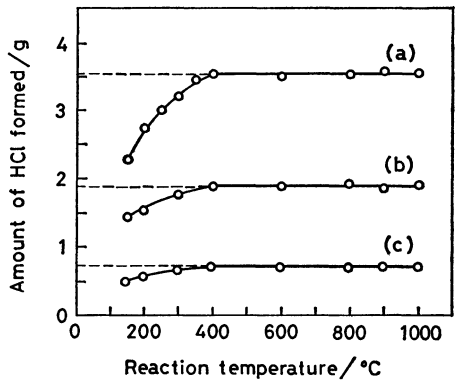

Fig. 1. Amounts of HCl formed by the reaction between gaseous $AlCl_3$ and steam at various temperatures.
Steam content in Ar: (a) 9 vol%, (b) 5 vol%, (c) 2 vol%.

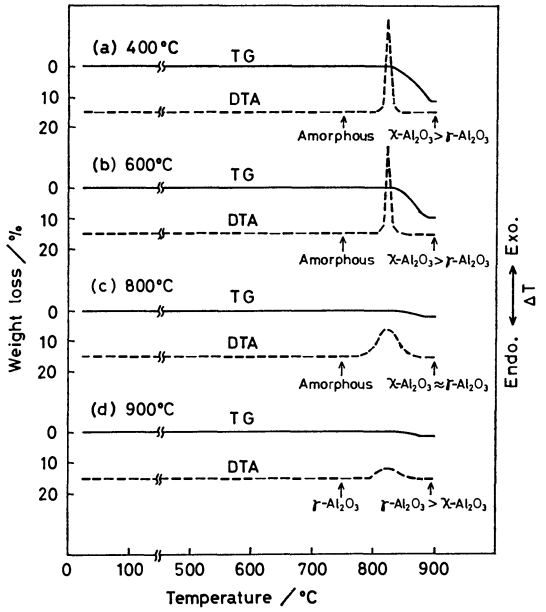

Fig. 2. TG and DTA curves of the products formed by the reaction between gaseous $AlCl_3$ and steam at 400—900 °C.

of HCl, based on the assumption that all the H_2O introduced reacts with gaseous $AlCl_3$ to form HCl.

From the results, the reaction between gaseous $AlCl_3$ and H_2O begins even at 150 °C, and all the H_2O introduced reacts with gaseous $AlCl_3$ above about 400 °C.

To determine the reaction product of gaseous $AlCl_3$ with H_2O, the products formed by introducing a stream of argon containing 9 vol% H_2O at reaction temperatures above 400 °C were examined by X-ray analysis, TG, and DTA.

The X-ray analysis of the reaction products formed at 400 and 600 °C showed no diffraction line. The TG and DTA curves of the products are shown in Figs. 2(a) and (b).

The samples obtained after heating both the products up to 750 °C gave no change in X-ray diffraction pattern (amorphous). The samples obtained after heating up to 900 °C gave diffraction lines corresponding to both χ-Al_2O_3[3,4] and γ-Al_2O_3.[3,5] From these results and the fact that the amorphous Al_2O_3 formed by the reaction between gaseous $AlCl_3$ and oxygen crystallizes to χ-Al_2O_3 in the vicinity of 820 °C with an exothermic effect as previously reported,[1] the exothermic effect observed in the vicinity of 820 °C was considered to be due to the crystallization of amorphous Al_2O_3. During the weight losses in the vicinity of 830 °C which appeared in the TG curves (12% for the product at 400 °C; 10% for the product at 600 °C), it was observed that a white powder was deposited on a cooler part outside the heating zone. The white powder was identified as $AlCl_3$ by chemical analysis. This result and the fact that diffraction lines corresponding to γ-Al_2O_3 in addition to χ-Al_2O_3 based on the crystallization of amorphous Al_2O_3 were observed in both samples obtained after heating up to 900 °C led us to conclude that the products formed by the reaction at 400 and 600 °C were amorphous Al_2O_3 containing a compound which decomposed in the vicinity of 830 °C to form γ-Al_2O_3 with the evolution of gaseous $AlCl_3$. Also, the results of IR spectroscopy confirmed that the reaction products contained neither H_2O nor OH^-. These results indicated that the compound mentioned above was a chloride oxide of aluminium.

The reaction product formed at 800 °C was found to be amorphous by X-ray analysis and its TG and DTA curves are shown in Fig. 2(c). The exothermic effect due to the crystallization of amorphous Al_2O_3 in the vicinity of 820 °C became weak and diffuse. Although the weight loss in the vicinity of 830 °C (3%) was rather small compared with those of the reaction products formed at 400 and 600 °C, the sample obtained after heating up to 900 °C gave diffraction lines corresponding to both χ-Al_2O_3 and γ-Al_2O_3. These results indicated that the reaction product formed at 800 °C was amorphous Al_2O_3 containing poorly crystallized γ-Al_2O_3 and a small amount of the chloride oxide. This estimation was confirmed by the experimental results on the thermal transitions of the Al_2O_3 formed under various conditions, as described later.

The reaction product formed at 900 °C gave diffraction lines corresponding to γ-Al_2O_3. But the DTA curve (Fig. 2(d)) showed a weak exothermic effect due to the crystallization of amorphous Al_2O_3, and the sample obtained after heating up to 900 °C showed diffraction lines corresponding to χ-Al_2O_3 in addition to γ-Al_2O_3. Also, a slight weight loss (1%) due to the thermal decomposition of the chloride oxide was observed. These results indicated that the reaction product formed at 900 °C was γ-Al_2O_3 containing amorphous Al_2O_3 and a small amount of the chloride oxide.

The reaction product formed at 1000 °C gave diffraction lines corresponding to γ-Al_2O_3, and gave no thermal effect in the DTA, and no weight change in the TG. The sample obtained after heating up to 900 °C gave diffraction lines corresponding to γ-Al_2O_3 alone. From these results, the reaction product formed at 1000 °C was found to be γ-Al_2O_3.

The reaction products formed by introducing gaseous

Table 1. Thermal transitions of Al_2O_3 formed at various temperatures

Heating temp °C	Formation temperature of Al_2O_3 and heating atmosphere							
	400 °C		600 °C		800 °C		900 °C	1000 °C
	In argon	In air	In argon	In air	In argon	In air	In argon and air	In argon and air
600	Amorphous		Amorphous		Amorphous		γ	γ
700	χ	χ	χ	χ	χ	χ	$\gamma>\chi$	γ
800	χ, κ, γ	χ, κ	χ, κ, γ	χ, κ	χ, κ, γ	χ, κ, γ	$\gamma>\chi$	γ
900	χ, κ, γ	χ, κ	χ, κ, γ	χ, κ	χ, κ, γ	χ, κ, $\gamma\gg\delta$	$\gamma>\delta$, κ	γ, δ
1000	κ, $\delta>\alpha$	κ, α	κ, $\delta>\alpha$	κ, α	κ, δ, θ, α	κ, δ, θ, α	δ, θ, α	δ, θ, α
1100	α	α	α	α	α	α	$\alpha>\theta$, δ	$\alpha>\theta$, δ
1200	—	—	—	—	—	—	α	$\alpha>\theta$
1300	—	—	—	—	—	—	—	α

Amorphous: amorphous Al_2O_3, χ: χ-Al_2O_3, κ: κ-Al_2O_3,[3,6] γ: γ-Al_2O_3, δ: δ-Al_2O_3,[3,7] α: α-Al_2O_3,[8] θ: θ-Al_2O_3.[9]

$AlCl_3$ and a stream of argon containing 5 vol% H_2O were examined in the manner described above. The results indicated that the reaction product at each temperature was similar to that formed by introducing a stream of argon containing 9 vol% H_2O, described above.

These experimental results show that the reaction between gaseous $AlCl_3$ and H_2O occurs even at 150 °C and proceeds rapidly above about 400 °C. The reaction product formed is amorphous Al_2O_3 at 400—600 °C, amorphous Al_2O_3 containing poorly crystallized γ-Al_2O_3 at 800 °C, γ-Al_2O_3 containing amorphous Al_2O_3 at 900 °C, and γ-Al_2O_3 at 1000 °C. In addition, the Al_2O_3 formed below 900 °C includes the chloride oxide of aluminium, which decomposes in the vicinity of 830 °C to form γ-Al_2O_3 with the evolution of gaseous $AlCl_3$. The amount of the chloride oxide decreased with increasing the reaction temperature, and the formation of the chloride oxide was not observed at 1000 °C.

Kato *et al.*[2] have reported that the products formed by the reaction between gaseous $AlCl_3$ and H_2O at 700 and 900 °C are amorphous and have estimated that the products include a Cl-containing compound, presumably AlClO, from the result that, on heating the products in the air, they lose weight in the vicinity of 800 °C with the evolution of chlorine. In the present work, it was also observed that the Al_2O_3 formed below 900 °C included a chloride oxide of aluminium. The only known chloride oxide of aluminium is AlClO. But, the composition of the chloride oxide formed in these experiments was not evaluated by chemical analysis, because the chloride oxide was included in the Al_2O_3 formed.

As described in the previous report,[1] the reaction between gaseous $AlCl_3$ and oxygen occurs above about 400 °C and proceeds appreciably above about 800 °C. While, the reaction with H_2O was found to proceed rapidly at rather low temperatures. The modification of the Al_2O_3 formed by the reaction with H_2O at each temperature was the same as that of the Al_2O_3 formed by the reaction with oxygen,[1] except that the Al_2O_3 formed by the reaction with oxygen at 800 °C is amorphous Al_2O_3.

The reaction products formed by introducing gaseous $AlCl_3$ and a stream of argon containing 9 or 5 vol% H_2O at various temperatures were examined by electron microscopy. Typical electron micrographs of the Al_2O_3 formed are shown in Fig. 3.

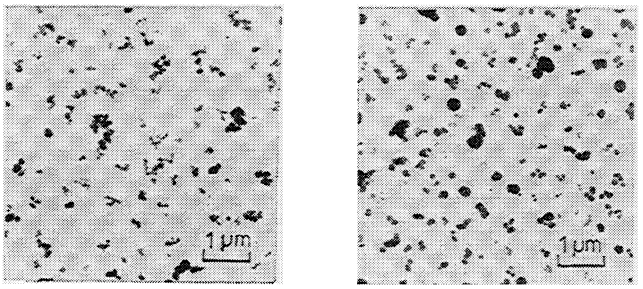

(a) 800°C (b) 1000°C

Fig. 3. Electron micrographs of the Al_2O_3 formed by the reaction between gaseous $AlCl_3$ and steam at 800 and 1000 °C (Steam content in Ar: 9 vol%).

As reported before,[1] the Al_2O_3 formed by the reaction with oxygen is relatively uniform, ultrafine powders with diameters of the order of 1/100 μm. While, the range of particle sizes of the Al_2O_3 formed by the reaction with H_2O was found to be wide, as seen from Fig. 3.

Thermal Transition of the Aluminium Oxide Formed by the Reaction between Gaseous Aluminium Trichloride and Steam. The thermal transitions of the Al_2O_3 formed under various conditions were examined. The samples obtained by heating the Al_2O_3 at a specified temperature for 2 h both in an argon atmosphere and in the air were examined by X-ray analysis.

The results for the Al_2O_3 formed by introducing a stream of argon containing 9 vol% H_2O are shown in Table 1. As examples, the X-ray diffraction patterns of the samples obtained after heating the amorphous Al_2O_3, formed at 400 °C, at various temperatures in an argon atmosphere and after heating the γ-Al_2O_3, formed at 1000 °C, at various temperatures in the air are illustrated in Figs. 4 and 5, respectively.

These experimental results show that, on heating the amorphous Al_2O_3, formed at 400 and 600 °C, both in an argon atmosphere and in the air, the amorphous $\xrightarrow{ca.\ 700\ °C}$ χ $\xrightarrow{ca.\ 800\ °C}$ κ $\xrightarrow{ca.\ 1000\ °C}$ α transition occurs regardless of the heating atmosphere. The γ-Al_2O_3 observed in the samples obtained after heating

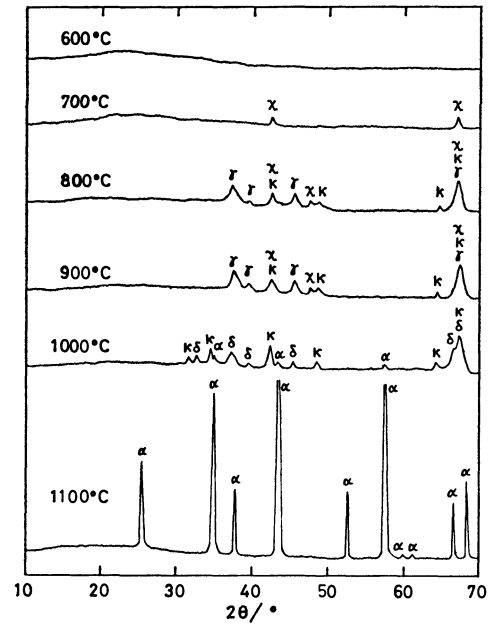

Fig. 4. X-Ray diffraction patterns of the samples obtained after heating the amorphous Al_2O_3, formed at 400 °C, at various temperatures in an argon atmosphere.

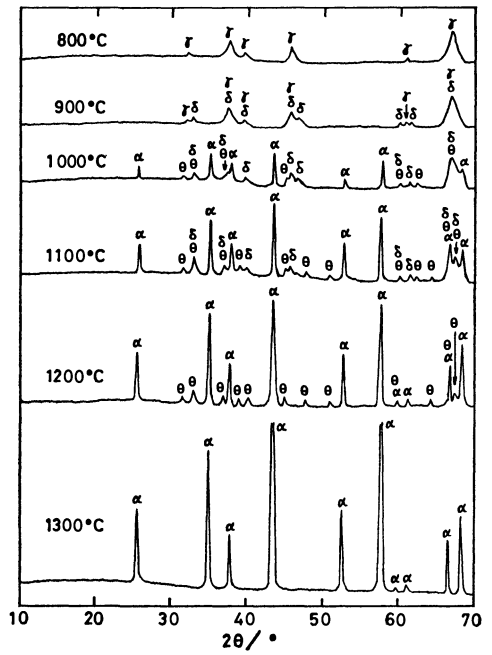

Fig. 5. X-Ray diffraction patterns of the samples obtained after heating the γ-Al_2O_3, formed at 1000 °C, at various temperatures in the air.

at 800 and 900 °C in an argon atmosphere was considered to be due to the decomposition of the chloride oxide, as mentioned before, and the δ-Al_2O_3 observed at 1000 °C was considered to be due to the thermal transition of the γ-Al_2O_3 formed. The samples obtained after heating the amorphous Al_2O_3 in the air gave neither diffraction lines corresponding to γ-Al_2O_3 nor diffraction lines corresponding to δ-Al_2O_3. This fact was considered to indicate that, on heating the chloride oxide in the air, it was oxidized to amorphous Al_2O_3, which transformed in the same manner as the amorphous Al_2O_3 formed by the reaction between gaseous $AlCl_3$ and H_2O.

The result for the γ-Al_2O_3 formed at 1000 °C indicates that, on heating the γ-Al_2O_3, the $\gamma \xrightarrow[\text{ca. 900 °C}]{} \delta \xrightarrow[\text{ca. 1000 °C}]{} \theta \xrightarrow[\text{ca. 1000 °C}]{} \alpha$ transition occurs regardless of the heating atmosphere.

On heating the γ-Al_2O_3 containing amorphous Al_2O_3, formed at 900 °C, and the amorphous Al_2O_3 containing poorly crystallized γ-Al_2O_3, formed at 800 °C, both the amorphous$\rightarrow\chi\rightarrow\kappa\rightarrow\alpha$ and $\gamma\rightarrow\delta\rightarrow\theta\rightarrow\alpha$ transitions occur, as is expected from the above results.

As mentioned above, it was observed that, on heating the Al_2O_3 formed at 800 °C in the air, the $\gamma\rightarrow\delta\rightarrow\theta\rightarrow\alpha$ transition occurred. Also, let us assume that the γ-Al_2O_3 observed in the samples obtained after heating the Al_2O_3 formed at 800 °C both in an argon atmosphere and in the air is due to the thermal decomposition of the chloride oxide included in the Al_2O_3. Then θ-Al_2O_3 should not be observed in the samples obtained after heating at 1000 °C, as seen from the results obtained on heating the amorphous Al_2O_3, formed at 400 and 600 °C, in an argon atmosphere. These results support the estimation, described in the previous paragraph, that the Al_2O_3 formed at 800 °C is amorphous Al_2O_3 containing poorly crystallized γ-Al_2O_3.

The experimental results for the Al_2O_3 formed by introducing a stream of argon containing 5 vol% H_2O were similar to those for the Al_2O_3 formed at 9 vol% H_2O, described above.

These experimental results show that, on heating the amorphous Al_2O_3 formed by the reaction between gaseous $AlCl_3$ and H_2O, the amorphous $\xrightarrow[\text{ca. 700 °C}]{} \chi \xrightarrow[\text{ca. 800 °C}]{} \kappa \xrightarrow[\text{ca. 1000 °C}]{} \alpha$ transition occurs, and on heating the γ-Al_2O_3 formed, the $\gamma \xrightarrow[\text{ca. 900 °C}]{} \delta \xrightarrow[\text{ca. 1000 °C}]{} \theta \xrightarrow[\text{ca. 1000 °C}]{} \alpha$ transition occurs.

As previously reported,[1] on heating the amorphous Al_2O_3 formed by the reaction with oxygen, the amorphous $\xrightarrow[\text{ca. 700 °C}]{} \chi \xrightarrow[\text{ca. 800 °C}]{} \kappa \xrightarrow[\text{ca. 1000 °C}]{} \alpha$ transition occurs. On heating the γ-Al_2O_3 formed, the $\gamma \xrightarrow[\text{ca. 1000 °C}]{} \delta \xrightarrow[\text{ca. 1100 °C}]{} \theta \xrightarrow[\text{ca. 1100 °C}]{} \alpha$ transition occurs. The transition temperatures of $\gamma\rightarrow\delta$, $\delta\rightarrow\theta$, and $\theta\rightarrow\alpha$ on heating the γ-Al_2O_3 formed by the reaction with H_2O are approximately 100 °C lower than those of the γ-Al_2O_3 formed by the reaction with oxygen.

References

1) Y. Shoji, K. Tatsumi, R. Matsuzaki, and Y. Saeki, *Bull. Chem. Soc. Jpn.*, **53**, 269 (1980).
2) A. Kato, S. Kawazoe, and I. Mochida, *Zairyo*, **21**, 540 (1972).
3) K. Funaki and Y. Shimizu, *Denki Kagaku*, **28**, 358 (1960).
4) JCPDS, Powder Diffraction File, 13-373.
5) JCPDS, Powder Diffraction Data Card, 29-63.
6) ASTM, X-Ray Powder Data File, 4-878.
7) JCPDS, Powder Diffraction File, 16-394.
8) ASTM, Powder Diffraction File, 10-173.
9) JCPDS, Powder Diffraction File, 11-517.

  Bull. Chem. Soc. Jpn., 54, 2656—2661 (1981) [Vol. 54, No. 9

Extraction of Bivalent Manganese, Cobalt, Copper, Zinc, and Cadmium from Hydrochloric Acid Solutions by Long-chain Alkyl Quaternary Ammonium Chloride in Various Organic Solvents

Taichi SATO,* Takato NAKAMURA, and Teruo FUJIMATSU

Department of Applied Chemistry, Faculty of Engineering, Shizuoka University, Johoku, Hamamatsu 432

(Received January 20, 1981)

The extraction of bivalent manganese, cobalt, copper, zinc and cadmium from hydrochloric acid solutions by tricaprylmethylammonium chloride (Aliquat-336) has been examined using various diluents such as benzene, chlorobenzene, *o*-dichlorobenzene, toluene, *o*-xylene, *m*-xylene, nitrobenzene, carbon tetrachloride, chloroform, and 1,2-dichloroethane. It was found that by assuming a regular solution, the distribution coefficient and the enthalpy change associated with metal extraction can be expressed in terms of the solubility parameters of Aliquat-336, diluent and the complex formed in the organic phase and their molar volumes. An empirical relation holds between distribution coefficient and the viscosity of diluent.

The influence of diluent on solvent extraction of metal has been studied by a number of researchers who attempted to correlate the distribution of metal between organic and aqueous phases with the physicochemical properties of organic solvent such as dielectric constant,[1,2] dipole moment,[1] and solubility parameter.[3-8] Nevertheless the role of diluent in the extraction process of metal has not been elucidated satisfactorily.

In the extraction of cadmium(II), zinc(II), lead(II), and copper(II) from 2 mol dm^{-3} hydrochloric acid solutions by octadecylbenzyldimethylammonium chloride in various diluents, Leszko and Zaborska[8] suggested that the relationship between the distribution coefficient and the solubility parameter of diluent derived by Vdovenko *et al.*[5] is applicable not to the extraction of lead(II) and copper(II) but to the extraction of cadmium(II) and zinc(II). Studies have been carried out on the extraction of zirconium(IV),[9] vanadium(IV),[10] and uranium(VI)[11] from hydrochloric acid solutions by tricaprylmethylammonium chloride (Aliquat-336, $R_3R'NCl$; R=C_8—C_{10}). In the present work, the extraction of bivalent manganese, cobalt, copper, zinc, and cadmium by Aliquat-336 in various organic solvent has been studied in order to examine the correlation between the distribution coefficient and physicochemical properties of diluent.

Experimental

Reagent. Aliquat-336 (General Mills) purified by washing several times with aqueous sodium chloride solution and hexane[9] was diluted in benzene, chlorobenzene, *o*-dichlorobenzene, toluene, *o*-xylene, *m*-xylene, nitrobenzene, carbon tetrachloride, chloroform, and 1,2-dichloroethane. The concentration of Aliquat-336 in organic solvents was determined by Volhard's method with nitrobenzene. Aqueous solutions of bivalent manganese, cobalt, copper, zinc, and cadmium were prepared by dissolving their chlorides ($MnCl_2\cdot4H_2O$, $CoCl_2\cdot6H_2O$, $CuCl_2\cdot2H_2O$, $ZnCl_2$, and $CdCl_2\cdot2.5H_2O$) in hydrochloric acid. The chemicals used were of analytical reagent grade.

Extraction and Analytical Procedures. Equal volumes (15 ml) of organic and aqueous phases, placed in 50 ml stoppered conical flasks, were shaken for 10 min (preliminary experiments showed that equilibration was complete in 10 min) in a water-bath maintained at the required temperature. The initial concentration of metal chloride in aqueous phase was 0.01 mol dm^{-3}. After equilibrium, the mixture was centrifuged and separated and then the aliquots of both phases were pipetted to determine the distribution coefficient (the ratio of the equilibrium concentration of metal in the organic phase to that in the aqueous phase, D). Manganese, cobalt, copper, and zinc in the organic phase were stripped with 0.1 mol dm^{-3} HCl, and cadmium in the organic phase with 1 mol dm^{-3} HNO_3. The concentration of metal in the aqueous solutions was determined by edta titration using the following indicator: XO (Xylenol Orange) for cobalt,[12] copper,[12] and zinc;[13] BT (Eriochrome Black T) for manganese;[14] Cu–PAN (PAN=1-(2-Pyridylazo)-2-naphthol) for cadmium.[15]

Results and Discussion

Extraction Isotherm. When bivalent manganese, cobalt, copper, zinc, and cadmium are extracted into benzene solution of Aliquat-336 from aqueous solutions of their chlorides at 0.01 mol dm^{-3} containing hydrochloric acid of varying acidity at 20 °C, the extraction efficiency is in the order Cd>Zn>Cu>Co>Mn for [HCl]<5 mol dm^{-3} and Cd>Zn>Co>Cu>Mn for [HCl]>5 mol dm^{-3} (Fig. 1). The distribution coefficient rises with increasing aqueous acidity to a maximum occurring at initial hydrochloric acid concentration of 8, 8, 5, 2, and 1 mol dm^{-3} for manganese, cobalt, copper, zinc, and cadmium, respectively, and then falling again. The shape of the extraction curves is not much influenced by the kind of diluent (Table 1). Thus the extractions are expressed by a reaction similar to that for zirconium(IV),[9] vanadium(IV),[10] and uranium(VI),[11]

$$MCl_4^{2-}(a) + 2R_3R'NCl(o) \rightleftharpoons (R_3R'N)_2MCl_4(o) + 2Cl^-(a), \quad (1)$$

where M=Mn, Co, Cu, Zn, and Cd, (a) and (o) denote aqueous and organic phases, respectively. This is supported by the results for the dependency of distribution coefficient on the extractant concentration and variation of metal concentration in the organic phase as a function of initial aqueous metal concentration at a constant acidity.

The extraction efficiency of Aliquat-336 for bivalent metal depends on the nature of the diluent and is in the following order: for manganese(II) 1,2-$C_2H_4Cl_2$>

Table 1. The distribution coefficient of bivalent manganese, cobalt, copper, zinc, and cadmium in the extraction from hydrochloric acid solutions by Aliquat-336 in various diluents

Metal	$[HCl]_{aq}$ / mol dm^{-3}	Distribution coefficient[a]				
		C_6H_6	$C_6H_5CH_3$	o-$C_6H_4(CH_3)_2$	m-$C_6H_4(CH_3)_2$	C_6H_5Cl
Mn	3	0.050	0.025	0.025	0.033	0.059
	5	0.011	0.059	0.040	0.070	0.17
	7	0.22	0.17	0.13	0.14	0.40
	8	0.25	0.23	0.15	0.17	0·43
Co	3	0.060	0.020	0.068	0.045	0.24
	5	0.68	0.51	0.51	0.58	2.70
	7	5.84	2.49	2.45	2.79	8.80
	8	6.22	2.67	3.00	3.36	8.37
Cu	2	0.18	0.13	0.12	0.097	0.42
	3	0.57	0.43	0.39	0.33	1.12
	5	1.12	0.913	0.908	0.824	2.10
	8	0.492	0.38	0.37	0.35	0.862
Zn	0.05	4.36	3.99	—[b]	3.14	8.55
	0.1	9.27	8.79	—	7.28	18.3
	0.5	130	110	—	75	290
	1	400	290	—	160	480
Cd	0.02	87	55.7	—	49.4	97
	0.1	300	210	—	190	290
	1	280	310	—	270	260
	8	6.70	4.62	—	4.82	7.77

Metal	$[HCl]_{aq}$ / mol dm^{-3}	Distribution coefficient[a]				
		o-$C_6H_4Cl_2$	$C_6H_5NO_2$	$CHCl_3$	CCl_4	1,2-$C_2H_4Cl_2$
Mn	3	0.072	0.710	0.017	0.047	0.14
	5	0.26	0.15	0.040	0.10	1.01
	7	0.61	0.33	0.11	0.19	2.10
	8	0.68	0.36	0.15	0.24	1.39
Co	3	0.44	0.47	0.023	0.090	0.827
	5	4.14	3.67	0.16	0.39	7.02
	7	12.4	6.93	1.19	2.17	10.4
	8	15.9	4.91	1.58	2.63	7.32
Cu	2	0.614	0.49	0.052	0.072	0.57
	3	1.55	1.41	0.064	0.025	1.95
	5	3.17	2.45	0.21	0.765	6.03
	8	1.15	0.750	0.29	0.28	1.35
Zn	0.05	10.4	11.7	0.25	2.54	12.7
	0.1	27.2	25.8	0.36	4.75	36.6
	0.5	310	240	1.90	83	210
	1	600	500	3.46	210	600
Cd	0.02	120	95	0.49	14.8	76
	0.1	310	250	0.925	49.5	250
	1	210	310	1.64	130	200
	8	10.0	6.69	0.756	3.59	10.4

a) The concentration of Aliquat-336 is 0.05 mol dm^{-3} for manganese, cobalt, and zinc, 0.025 mol dm^{-3} for copper and 0.03 mol dm^{-3} for cadmium. b) No datum.

o-$C_6H_4Cl_2$ > $C_6H_5NO_2$ > C_6H_5Cl > C_6H_6 > CCl_4 > m-$C_6H_4(CH_3)_2$ > $C_6H_5CH_3$ > o-$C_6H_4(CH_3)_2$ > $CHCl_3$ from 3 mol dm^{-3} HCl; for cobalt(II) 1,2-$C_2H_4Cl_2$ > $C_6H_5NO_2$ > o-$C_6H_4Cl_2$ > C_6H_5Cl > CCl_4 > o-$C_6H_4(CH_3)_2$ > C_6H_6 > m-$C_6H_4(CH_3)_2$ > $CHCl_3$ > $C_6H_5CH_3$ from 3 mol dm^{-3} HCl; for copper(II) o-$C_6H_4Cl_2$ > 1,2-$C_2H_4Cl_2$ > $C_6H_5NO_2$ > C_6H_5Cl > C_6H_6 > $C_6H_5CH_3$ > o-$C_6H_4(CH_3)_2$ > m-$C_6H_4(CH_3)_2$ > CCl_4 > $CHCl_3$ from 2 mol dm^{-3} HCl; for zinc(II) 1,2-$C_2H_4Cl_2$ > $C_6H_5NO_2$ > o-$C_6H_4Cl_2$ > C_6H_5Cl > C_6H_6 > $C_6H_5CH_3$ > m-$C_6H_4(CH_3)_2$ > CCl_4 > $CHCl_3$ from 0.05 mol dm^{-3} HCl and for cadmium(II) o-$C_6H_4Cl_2$ > C_6H_5Cl > $C_6H_5NO_2$ > C_6H_6 > 1,2-$C_2H_4Cl_2$ > $C_6H_5CH_3$ > m-$C_6H_4(CH_3)_2$ > CCl_4 > $CHCl_3$ from 0.02 mol dm^{-3} HCl. We see that the extraction efficiency of Aliquat-336 in aromatic solvent with electron-accepting radical such as Cl or NO_2 is higher than that with electron-donating one like CH_3, and that chloroform reveals a very poor extraction because of a hydrogen bond-

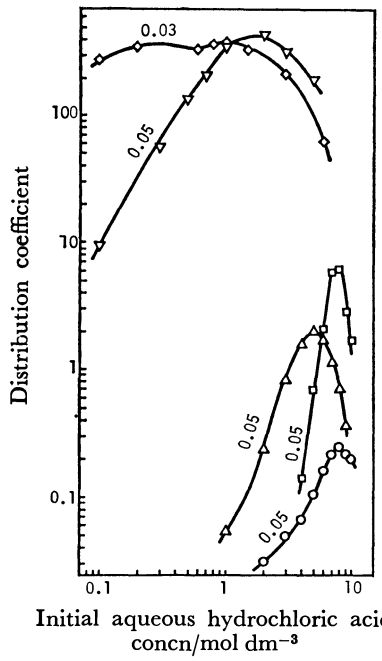

Fig. 1. Extraction of bivalent manganese, cobalt, copper, zinc, and cadmium from hydrochloric acid solutions by Aliquat-336 in benzene (numerals on curves are Aliquat-336 concentrations, mol dm^{-3}; ○ Mn, □ Co, △ Cu, ▽ Zn, ◇ Cd).

ing to extractant. However, no simple relation exists between the distribution coefficient and the dipole moment and dielectric constant of diluent which represent the polarities of molecule and solution, respectively.

Dependence of Distribution Coefficient on Viscosity. The variation of the distribution coefficient for bivalent manganese, cobalt, copper, zinc, and cadmium plotted as a function of the absolute viscosity of diluent, η_d, is given in Fig. 2. The value of η_d are as follows: 0.65, 0,59, 0.81, 0.61, 0.82, 1.23, 2.01, 0.56, 0.97, and 0.80 cp for benzene, toluene, *o*-xylene, *m*-xylene, chlorobenzene, *o*-dichlorobenzene, nitrobenzene, chloroform, carbon tetrachloride, and 1,2-dichloroethane. The distribution coefficients for manganese, cobalt, copper, zinc, and cadmium are indicated by means of the data for the extraction at 3, 3, 2, 0.05, and 0.02 mol dm^{-3}, respectively, in the lowest hydrochloric acid concentrations shown in Table 1. Since the reaction[15]

$$R_3R'NCl(o) + H^+(a) + Cl^-(a) \rightleftharpoons R_3R'NCl\cdot HCl(o) \quad (2)$$

takes place at higher aqueous acidity, the data at low acidity are used to avoid the reduction on the distribution of metal resulting from the competition between reactions (1) and (2).

The distribution coefficient increases with increase in the viscosity of diluent at $\eta_d \leq 1$ cp, but little change occurs at $\eta_d \leq 1$ cp (Fig. 2). In all the extraction systems studied, the distribution coefficient becomes constant as the viscosity of diluent approaches that of water. An empirical correlation is found between the distribution coefficient and the viscosity of diluent in the range $\eta_d \leq 1$ cp:

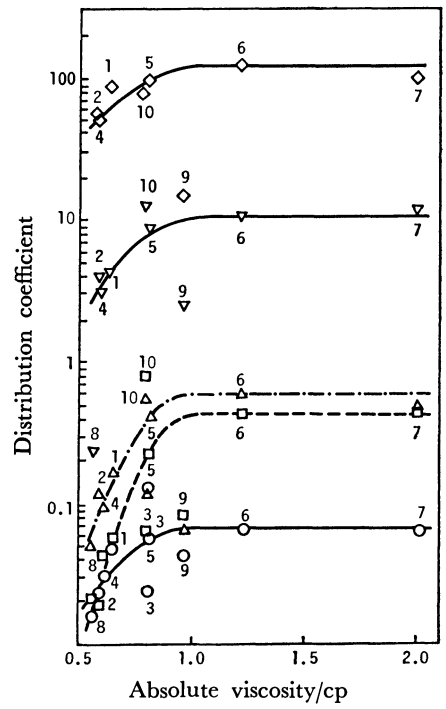

Fig. 2. Dependence of the distribution coefficient on absolute viscosity of diluent (○, □, △, ▽, and, represent the extractions of Mn(II) from 3 mol dm^{-3} HCl soln, Co(II) from 3 mol dm^{-3} HCl soln., Cu(II) from 2 mol dm^{-3} HCl soln, Zn(II) from 0.05 mol dm^{-3} HCl soln, and Cd(II) from 0.02 mol dm^{-3} HCl soln., respectively): 1) benzene, 2) toluene, 3) *o*-xylene, 4) *m*-xylene, 5) chlorobenzene, 6) *o*-dichlorobenzene, 7) nitrobenzene, 8) chloroform, 9) carbon tetrachloride, 10) 1,2-dichloroethane.

$$\log D/D_o = A(\eta_d - 1)^2, \quad (3)$$

where D_o denotes the distribution coefficient for *o*-dichlorobenzene, and A the slope obtained when log D/D_o is plotted against $(\eta_d \leq 1)^2$. Values of the slope calculated by the method of least squares are −2.59, −7.04, −4.93, −2.94, and −2.03 for manganese, cobalt, copper, zinc, and cadmium, respectively.

Effect of Solubility Parameter. From the Hildebrand-Scatchard equation[16] for the excess free energy of a regular solution, formula was worked out by Vdovenko *et al.*[15] for the distribution coefficient in terms of the solubility parameter:

$$\log D = (2/2.3RT)(V_c\delta_c - nV_e\delta_e)\delta_d + \{(nV_e - V_c)/2.3\}(\delta_d^2/RT - 1/V_d) + \text{const}, \quad (4)$$

where V and δ denote molar volume and solubility parameter, respectively, subscripts c, e, and d being the complex formed in the organic phase, extractant and diluent, respectively. Assuming that the composition in aqueous phase and the concentration of extractant in various diluents are constant, and the molar volumes of diluents do not differ from each other, the following relation is derived:

$$\{1/(\delta_d - \delta_s)\}\log(D/D_o) = \{(nV_e - V_c)/2.3RT\}(\delta_d + \delta_s) + 2(V_c\delta_c - nV_e\delta_e)/2.3RT, \quad (5)$$

where the subscript s refers to the diluent chosen as standard

TABLE 2. TEMPERATURE DEPENDENCE OF DISTRIBUTION COEFFICIENT FOR THE EXTRACTION OF BIVALENT MANGANESE, COBALT, COPPER, ZINC, AND CADMIUM FROM HYDROCHLORIC ACID SOLUTION[a] BY ALIQUAT-336[b] IN VARIOUS DILUENTS

Metal	Diluent	Distribution coefficient				Change in enthalpy
		10 °C[c]	20 °C[c]	30 °C[c]	40 °C[c]	kJ mol^{-1}
Mn	C_6H_6	0.0497	0.0498	0.0499	0.0500	0.17
	$C_6H_5CH_3$	0.023	0.025	0.033	0.038	12
	o-$C_6H_4(CH_3)_2$	0.023	0.025	0.034	0.034	9.9
	m-$C_6H_4(CH_3)_2$	0.028	0.033	0.035	0.039	8.3
	C_6H_5Cl	0.044	0.059	0.077	0.10	20
	o-$C_6H_4Cl_2$	0.084	0.072	0.098	0.11	6.3
	$C_6H_5NO_2$	0.037	0.071	0.12	0.17	36
	$CHCl_3$	0.007	0.017	0.034	0.055	50
	CCl_4	0.03	0.047	0.066	0.071	23
	1,2-$C_2H_4Cl_2$	0.15	0.14	0.13	0.13	−3.4
Co	C_6H_6	0.045	0.060	0.090	0.12	24
	$C_6H_5CH_3$	0.015	0.020	0.040	0.070	37
	o-$C_6H_4(CH_3)_2$	0.054	0.068	0.075	0.091	9.3
	m-$C_6H_4(CH_3)_2$	0.035	0.045	0.085	0.090	20
	C_6H_5Cl	0.21	0.24	0.28	0.37	10
	o-$C_6H_4Cl_2$	0.31	0.44	0.60	0.73	23
	$C_6H_5NO_2$	0.60	0.47	0.48	0.57	−1.2
	$CHCl_3$	0.050	0.023	0.015	0.007	−48
	CCl_4	0.080	0.090	0.10	0.13	12
	1,2-$C_2H_4Cl_2$	0.85	0.83	0.77	0.75	−3.0
Cu	C_6H_6	0.13	0.18	0.27	0.22	28
	$C_6H_5CH_3$	0.091	0.13	0.17	0.17	27
	o-$C_6H_4(CH_3)_2$	0.085	0.21	0.15	0.18	23
	m-$C_6H_4(CH_3)_2$	0.069	0.097	0.14	0.14	25
	C_6H_5Cl	0.35	0.42	0.49	0.50	19
	o-$C_6H_5Cl_2$	0.54	0.61	0.72	0.84	17
	$C_6H_5NO_2$	0.55	0.49	0.44	0.40	−12
	$CHCl_3$	0.054	0.052	0.054	0.053	1.9
	CCl_4	0.068	0.072	0.11	0.14	22
	1,2-$C_2H_4Cl_2$	0.85	0.57	0.49	0.32	−3.3
Zn	C_6H_6	4.59	4.36	4.49	4.05	−3.4
	$C_6H_5CH_3$	4.03	3.99	3.76	3.75	−2.2
	m-$C_6H_4(CH_3)_2$	2.80	3.14	3.36	3.49	7.4
	C_6H_5Cl	9.55	8.55	7.83	7.78	−7.1
	o-$C_6H_4Cl_2$	15.3	14.4	13.3	13.2	−4.4
	$C_6H_5NO_2$	18.1	11.7	7.80	5.20	−26
	$CHCl_3$	0.20	0.25	0.29	0.33	8.9
	CCl_4	2.69	2.54	2.26	2.12	−5.6
	1,2-$C_2H_4Cl_2$	16.3	12.7	8.71	5.83	−29
Cd	C_6H_6	100	87	61	46	−21
	$C_6H_5CH_3$	78	55	42.1	29.8	−26
	m-$C_6H_4(CH_3)_2$	68	49	40	31	−20
	C_6H_5Cl	130	97	71	63	−19
	o-$C_6H_4Cl_2$	150	140	140	130	−8.5
	$C_6H_5NO_2$	100	95	62	43	−24
	$CHCl_3$	0.52	0.45	0.48	0.47	−3.7
	CCl_4	23.3	14.8	11.4	8.53	−26
	1,2-$C_2H_4Cl_2$	150	76	41.9	26.1	−47

a) The concentration of hydrochloric acid is 3 mol dm^{-3} for manganese and cobalt, 2 mol dm^{-3} for copper, 0.05 mol dm^{-3} for zinc, and 0.02 mol dm^{-3} for cadmium. b) The concentration of Aliquat-336 is 0.05 mol dm^{-3} for manganese, cobalt, and zinc, 0.025 mol dm^{-3} for copper, and 0.03 mol dm^{-3} for cadmium. c) Temperature of extraction.

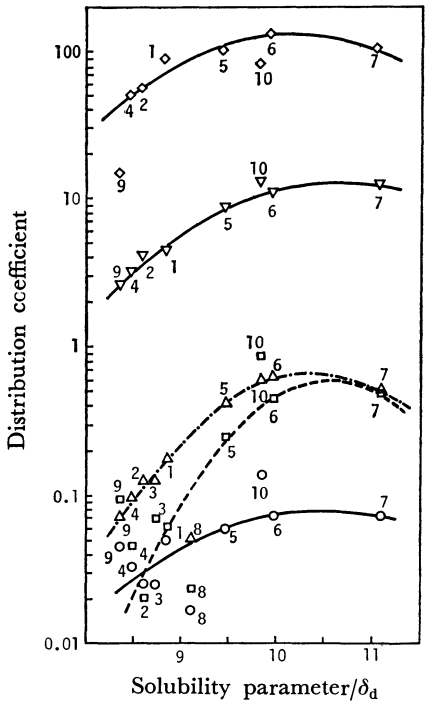

Fig. 3. Dependence of the distribution coefficient on the solubility parameter of diluent (○, □, △, ▽, and ◇ represent the extractions of Mn(II) from 3 mol dm^{-3} HCl soln, Co(II) from 3 mol dm^{-3} HCl soln, Cu(II) from 2 mol dm^{-3} HCl soln, Zn(II) from 0.05 mol dm^{-3} HCl soln, and Cd(II) from 0.02 mol dm^{-3} HCl soln, respectively): 1) benzene, 2) toluene, 3) *o*-xylene, 4) *m*-xylene, 5) chlorobenzene, 6) *o*-dichlorobenzene, 7) nitrobenzene, 8) chloroform, 9) carbon tetrachloride, 10) 1,2-dichloroethane.

In Fig. 3 showing the plots of log D *vs.* δ_d, the curves for manganese, cobalt, copper, zinc, and cadmium are obtained from the values of $(nV_e-V_e)/2.3RT$ as −0.165, −0.510, −0.370, −2.00, and −0.210, respectively, and $2(V_c\delta_c-nV_e\delta_e)/2.3RT$ as 3.45, 10.7, 7.64, 4.22, and 4.27, respectively, which are estimated by Eq. 5 using nitrobenzene as standard. In this case, the values of δ_d are as follows: 9.1, 8.9, 9.0, 8.8, 9.6, 10.0, 10.9, 9.3, 8.7, and 9.9 for benzene, toluene, *o*-xylene, *m*-xylene, chlorobenzene, *o*-dichlorobenzene, nitrobenzene, chloroform, carbon tetrachloride, and 1,2-dichloroethane, respectively. The parabolic dependence of distribution coefficients on the solubility parameter is obtained, suggesting that Eq. 4 gives a good estimate for the value of distribution coefficients in the extraction of these bivalent metals from hydrochloric acid solutions by Aliquat-336. However, since the large deviation from the parabola is observed in the extraction with chloroform, it seems that the negative deviation arises from the non-random interaction due to hydrogen bonding between chloroform and Aliquat-336.

Temperature Effect. The equilibrium constant in reaction (1) and the distribution coefficient are given by

$$K = [(R_3R'N)_2MCl_4][Cl^-]^2/[MCl_4^{2-}][R_3R'NCl]^2 \quad (6)$$

and

$$D = [(R_3R'N)_2MCl_4]/[M^{2+}](1+\Sigma\beta_i[Cl^-]^i), \quad (7)$$

where β_i refers to the overall stability constant in the reaction

$$M^{2+}(a) + iCl^-(a) \rightleftharpoons MCl_i^{(2-i)+}(a). \quad (8)$$

From Eqs. 6 and 7 the following relationship is obtained:

$$K = D(1+\Sigma\beta_i[Cl^-]^i)/\beta_4[Cl^-]^2[R_3R'NCl]^2. \quad (9)$$

By assuming that the values of overall stability constant β_4 and the term $(1+\Sigma\beta_i[Cl^-]^i)$ do not change significantly in the temperature range studied, the change in enthalpy, ΔH, associated with the reaction(1) can be estimated by means of the Van't Hoff equation. The distribution coefficients for bivalent manganese, cobalt, copper, zinc, and cadmium from aqueous hydrochloric acid solutions with solutions of Aliquat-336 in various diluents, measured in the temperature range 10—40 °C, are summarised in Table 2 in comparison with the values of ΔH.

The extraction process of bivalent metals is considered by a Born-Harber type of cycle. The change in enthalpy observed is the sum of five terms which represent enthalpies for dehydration of the species MCl_4^{2-} $(-\Delta H_1)$, for desolvation of $R_3R'NCl$ $(-\Delta H_2)$, for the reaction of MCl_4^{2-} with $R_3R'NCl$ (ΔH_3), for hydration of Cl^- (ΔH_4) and for dissolution of the complex $(R_3R'N)_2MCl_4$ into organic phase (ΔH_5). The magnitude and sign of the change in enthalpy observed depend on the contribution from enthalpies in these processes. The ΔH_1 and ΔH_4 values are correlated with the composition of aqueous acidity, since the water activity decreases with increase in hydrochloric acid concentration, while the ΔH_3 value is independent of the kind of diluent. If the concentration of hydrochloric acid in the aqueous phase remains constant, the change in enthalpy observed is expressed by

$$\Delta H = -2\Delta H_2 + \Delta H_5 + \text{const.} \quad (10)$$

Partial molar enthalpies for dissolution of Aliquat-336 and the complex $(R_3R'N)_2MCl_4$ into organic solvent given by $V_e\phi_d^2(\delta_d-\delta_e)^2$ and $V_c\phi'^2_d(\delta_d-\delta_c)^2$, from regular solution theory,[17] give the equation

$$\Delta H = -2V_e\phi_d^2(\delta_d-\delta_e)^2 + V_c\phi'^2_d(\delta_d-\delta_c)^2 + \text{const}, \quad (11)$$

where ϕ_d and ϕ'_d refer to the volume fraction of diluent. This provides the equation

$$\Delta H = (V_c\phi'^2_d-2V_e\phi_d^2)\delta_d^2 + 2(2V_e\phi_d^2\delta_e-V_c\phi'^2_d\delta_c)\delta_d + \text{const.} \quad (12)$$

We see that when ΔH is plotted against δ_d, its shape depends on the magnitude of the term $(V_c\phi'^2_d-2V_e\phi_d^2)$. For $V_c\phi'^2_d<2V_e\phi_d^2$ or $V_c\phi'^2_d>2V_e\phi_d^2$, the plot should give a parabola with a maximum or minimum at $\delta_d=(V_c\phi'^2_d\delta_c-2V_e\phi_d^2\delta_e)/(V_c\phi'^2_d-2V_e\phi_d^2)$. In contrast, a linear relationship is expected for $V_c\phi'^2_d=2V_e\phi_d^2$. The value of $(V_c\phi'^2_d-2V_e\phi_d^2)$ is determined by means of

$$(\Delta H-\Delta H_s)/(\delta_d-\delta_s) = (V_c\phi'^2_d-2V_e\phi_d^2)(\delta_d+\delta_s) + 2(2V_e\phi_d^2\delta_e-V_c\phi'^2_d\delta_c). \quad (13)$$

The $(V_c\phi'^2_d-2V_e\phi_d^2)$ and $2(2V_e\phi_d^2\delta_e-V_c\phi'^2_d\delta_c)$ are the slope and intercept of the line, respectively, when

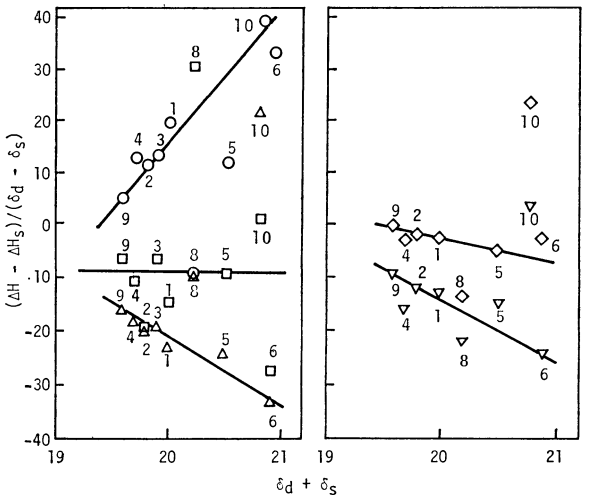

Fig. 4. Correlation between $(\Delta H-\Delta H_s)/(\delta_d-\delta_s)$ and $\delta_d+\delta_s$ for the correlation of bivalent manganese, cobalt, copper, zinc, and cadmium from hydrochloric acid solutions by Aliquat-336 in various diluents (○ Mn, □ Co, △ Cu, ▽ Zn, ◇ Cd): 1) benzene, 2) toluene, 3) *o*-xylene, 4) *m*-xylene, 5) chlorobenzene, 6) *o*-dichlorobenzene, 7) nitrobenzene, 8) chloroform, 9) carbon tetrachloride, 10) 1,2-dichloroethane.

$(\Delta H-\Delta H_s)/(\delta_d-\delta_s)$ is plotted as a function of $(\delta_d+\delta_s)$. The plots for manganese, cobalt, copper, zinc and cadmium show the linear relationship in Fig. 4, although the points for chloroform and 1,2-dichloroethane deviate from the lines in all the cases studied. The values of $(V_e\phi'^2_d-2V_e\phi_d^2)$ obtained indicate that $V_e\phi'^2_d>2V_e\phi_d^2$ is satisfied for manganese (as 6.2), $V_e\phi'^2_d=2V_e\phi_d^2$ for cobalt (as zero), and $V_e\phi'^2_d<2V_e\phi_d^2$ for copper, zinc and cadmium (as −3.1, −2.7, and −3.2, respectively). The plots of ΔH against δ_d confirm that Eq. 12 holds in the enthalpy change for various diluents. This suggests that the change in enthalpy for the extraction of bivalent manganese, cobalt, copper, zinc, and cadmium by Aliquat-336 in various diluents depends on the solubility parameter of diluent, the molar volume of the complex formed in the organic phase and Aliquat-336, and the volume fraction of diluent.

Conclusion

A parabolic dependency of the distribution coefficient on the solubility parameter of diluent is observed in the extraction by Aliquat-336 in organic solvents except chloroform and 1,2-dichloroethane, indicating that Eq. 4 derived from the regular solution theory is satisfied. The enthalpy change associated with metal extraction is also explained by assuming a regular solution. It is concluded that in the extraction of bivalent manganese, cobalt, copper, zinc, and cadmium from hydrochloric acid solutions by Aliquat-336 in various organic solvents, the distribution coefficient depends on the solubility of the complex formed in the organic diluent and the solubility parameter being an important factor for evaluation the distribution coefficient.

Distribution coefficients increase with increase in the viscosity of diluent in the range $\eta_d\leq 1$ cp, and an empirical relation is obtained between the distribution coefficient and the viscosity of diluent. It is found that in the extraction by Aliquat-336 in aromatic solvents, the distribution coefficient in the diluents with electron-accepting radical is higher than that with an electron-donating one.

The authors wish to thank Messrs. Wataru Sangawa, Tadashi Fujishita, and Akihiro Takahashi for their assistance in experiments.

References

1) T. Sato, *J. Inorg. Nucl. Chem.*, **27**, 1399 (1965); **30**, 1065 (1968).
2) O. V. Singh and S. N. Tandon, *J. Inorg. Nucl. Chem.*, **36**, 439 (1974).
3) W. Smulek and S. Siekierski, *J. Inorg. Nucl. Chem.*, **24**, 1651 (1962).
4) S. Siekierski and R. Olszer, *J. Inorg. Nucl. Chem.*, **25**, 1351 (1963).
5) V. M. Vdovenko, T. V. Kovaleva, and M. A. Ryazanov, *Radiokhimiya*, **7**, 133 (1965).
6) H. A. Mottola and H. Freiser, *Talanta*, **13**, 55 (1966).
7) H. M. H. Irving and R. H. Al-Jarrah, *Anal. Chim. Acta*, **63**, 79 (1973).
8) M. Leszko and W. Zaborska, *Rocz. Chim.*, **51**, 1961 (1977).
9) T. Sato and H. Watanabe, *Anal. Chim. Acta*, **49**, 463 (1970).
10) T. Sato, S. Ikoma, and T. Nakamura, *J. Inorg. Nucl. Chem.*, **39**, 395 (1977).
11) T. Sato, *J. Inorg. Nucl. Chem.*, **34**, 3835 (1972).
12) J. Kinnunen and B. Wennerstrand, *Chem. Anal.*, **46**, 92 (1957).
13) J. Körble and R. Pribil, *Chem. Anal.*, **45**, 102 (1956).
14) H. Flaschka, *Mikrochim. Acta*, **39**, 38 (1952).
15) T. Sato, H. Watanabe, and S. Kikuchi, *J. Appl. Chem. Biotechnol.*, **25**, 63 (1975).
16) G. Scatchard, *Chem. Rev.*, **8**, 321 (1931).
17) A. F. M. Barton, *Chem. Rev.*, **75**, 731 (1975).

  Bull. Chem. Soc. Jpn., 54, 2662—2667 (1981) [Vol. 54, No. 9

The Correlation between the Bonding Properties of Ligands and the Irradiation Effects of Gamma-rays on Iron Compounds

Yonezo MAEDA,* Yoshihiro KATSUKI, Tooru MORINAGA, and Yoshimasa TAKASHIMA

Department of Chemistry, Faculty of Science, Kyushu University 33, Higashi-ku, Fukuoka 812

(Received August 5, 1980)

Various iron compounds have been irradiated with gamma-rays of cobalt-60. The foreign-charge states of the irradiated compounds were confirmed by means of Mössbauer spectroscopy. The results showed that high-spin iron(III) compounds with large conjugated molecules and low-spin iron(II) compounds are insensitive to γ-radiations. However, iron(III) compounds with carboxyl groups or reducing ligands and low-spin iron (III) compounds are sensitive to γ-radiations. Further, $FeCl_2 \cdot 4H_2O$ was found to be insensitive to radiation up to a total exposure dose of 10^9 R, in contrast to other ionic iron(II) compounds.

The gamma-ray sensitivity of solid coordination compounds has long been studied[1-6] and studies of the after-effect associated with the EC decay of ^{57}Co have increased in the past several years.[7-11] These after-effects have been attributed to radiolytic self-decomposition in the molecular environment of a decaying atom by low-energy electrons emitted during the Auger cascade, and to the subsequent stabilization of foreign-charge states by virtue of the redox properties of the radicals so produced. We have studied the effect of the electronic state and nature of the ligands on the sensitivity of iron compounds to gamma-ray irradiation by means of Mössbauer spectroscopy.

Experimental

The composition of the samples listed in Tables 1 and 2 was checked by elemental analyses for C, H, and N at the Elemental Analysis Center, Kyushu University. The phosphorus contents were colorimetrically determined with the formation of orthophosphate heteropoly blue using a molybdenum(V)–molybdenum(VI) reagent.[12] The results were in agreement with the calculated values. The metal complexes sealed in a glass tube *in vacuo* were irradiated with gamma-rays of 4000 Ci cobalt-60 in the Gamma-ray Irradiation Laboratory, Kyushu University. The irradiation was carried out at room temperature at a dose rate of 0.35—0.39×10^6 R h^{-1} or 1.17—1.19×10^6 R h^{-1}.

The Mössbauer spectra were measured immediately after the appropriate total exposure dose has been accumulated. Mössbauer measurements were carried out at 80 K with a spectrometer described elsewhere.[13] A cobalt-57 source diffused into a palladium foil was used. The isomer shift, δ_{Fe} was measured relative to the center of the spectrum of an iron foil enriched with ^{57}Fe at 296 K, which was also used as a standard material for the velocity calibration. The infrared spectra of the samples in the potassium bromide region(650—4000 cm^{-1}) were obtained using a Hitachi Grating Infrared Spectrophotometer, type 215.

Results and Discussion

Only the species stabilized during the irradiation of the investigated compounds were determined in the present study, since the Mössbauer measurements were carried out after an elongated irradiation. The Mössbauer parameters measured for the compounds before and after gamma-ray irradiation are listed in Tables 1 and 2. The Mössbauer data in Tables 1 and 2 were calculated using a least-squares method at the Computer Center, Kyushu University.

The compounds studied are classified into three groups in terms of the relation of the irradiation effects, such as the change in the oxidation state of iron with the chemical properties of the ligands, and the results of the Mössbauer spectra of the irradiated complexes are discussed in each case.

Group A. Group A consists of iron(III) compounds for which chemical changes were observed through the use of Mössbauer spectroscopy after irradiation.

A-1: This sub-group includes iron(III) compounds with only monodentate ligands. Compounds $FeCl_3 \cdot 2CH_3OH$, $[Fe(en)_3]Cl_3$ (en: ethylenediamine), $FeCl_3 \cdot$(1,4-dioxane), and $FeCl_3 \cdot dma \cdot 2H_2O$ (dma: *N,N*-dimethylacetamide) were sensitive to radiation. Some Mössbauer spectra of these compounds are shown in Figs. 1—3. New absorption lines due to bivalent iron were observed in the Mössbauer spectra of these compounds after irradiation. The ratio of the absorption area of the new lines to the total absorption area increased with the increase in the exposure dose, as is shown in Figs. 1 and 2. From this behavior

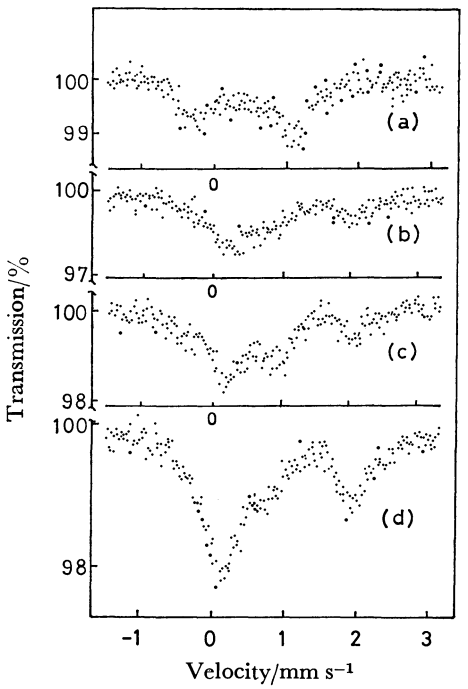

Fig. 1. Mössbauer spectra of $Fe(en)_3Cl_3$, (a) non-irradiated, (b) 4.4×10^8 R, (c) 11×10^8 R, and (d) 27×10^8 R irradiated.

Table 1. The Mössbauer parameters of the compounds before and after irradiation

	Compound	Exposure dose / 10^8 R	δ_{Fe}	ΔE	Γ_1[a]	Γ_2[b]	Remark
A-1	$FeCl_3 \cdot 2CH_3OH$	0	0.46	0.71	0.43	0.46	
		5.7	0.45	0.65	0.45	0.46	
			1.25	2.24	0.28	0.28	New[c]
	$[Fe(en)_3]Cl_3$	0	0.21	1.29	0.69	0.90	
		11	0.19	1.36	0.25	0.51	
			1.07	1.85	0.62	0.35	New
	$FeCl_3 \cdot$ (1,4-dioxane)	0	0.45	1.23	0.44	0.72	
		4.5	0.47	1.23	0.35	0.69	
			1.36	2.59	0.60	0.62	New
	$FeCl_3 \cdot$ dma $\cdot 2H_2O$	0	0.34	0			
		1.6	0.35	0			
			1.13	2.43			
A-2	$FeCl_2$gly(Hgly) $\cdot 7/2H_2O$	0	0.50	0.77	0.35	0.38	
		6.7	0.61	0.65	0.35	0.39	
			1.10	2.33	0.40	0.45	New
	$[Fe_3(HCO_2)_6][Fe(HCO_2)_6] \cdot 8H_2O$	0	0.53	0.86	0.45	0.45	
		9.0	0.51	0.93	0.45	0.46	
			1.32	2.55	0.5[d]	0.6[d]	New
A-3	$Fe(H_2PO_2)_3$	0	0.41	0.15	0.24	0.25	
		5.4	0.42	0.24	0.24	0.24	
			1.25	2.68	0.25	0.25	New
	$Fe_2(HPO_3)_3 \cdot 9H_2O$	0	0.53	0.48	0.28	0.28	
		8.3	0.54	0.42	0.35	0.35	
			1.37	2.27	0.48	0.48	New
A-4	$[Fe(bpy)_2(CN)_2]NO_3$	0	0.04	1.76	0.39	0.39	
		11	0.04	1.71	0.39	0.39	
			0.23	0.62	0.32	0.56	New

a) Full width at half-maximum of the lower energy peak. b) Full width at half-maximum of the higher energy peak. c) New peak due to irradiation. d) The errors are estimated to be ± 0.1 mm s^{-1}. The errors of the other data are ± 0.02 mm s^{-1} or less.

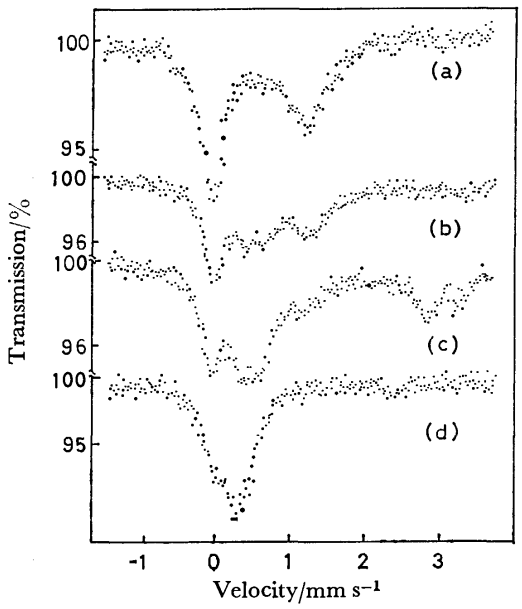

Fig. 2. Mössbauer spectra of $FeCl_3 \cdot$ (1,4-dioxane), (a) non-irradiated, (b) 1.1×10^8 R, (c) 2.5×10^8 R, and (d) 4.5×10^8 R irradiated.

of the ratio, the iron(III) ion in these compounds is confirmed to be reduced to an iron(II) ion under irradiation.

Figure 1 shows the Mössbauer spectra for $[Fe(en)_3]Cl_3$ at successive stages of irradiation. Compound $[Fe(en)_3]Cl_3$ is in a low-spin state. The Mössbauer parameters of the new lines produced by irradiation are as follows: The quadrupole splitting, $\Delta E = 1.85$ mm s^{-1}; the isomer shift, $\delta_{Fe} = 1.07$ mm s^{-1}. These values range among those for high-spin iron(II) compounds. The Mössbauer parameters for $[Fe(en)_3]Cl_2$ have not yet been reported because the compound is very unstable in air. It is very probable, however, that the orbital ground state of $[Fe(en)_3]Cl_2$ is in a high-spin state as a result of the strength of the ligand field of ethylenediamine.[14] The isomer shift of 1.07 mm s^{-1} at 80 K is smaller than that for high-spin hexacoordinated iron(II) compounds. However, the radiolysis of ethylenediamine ligands might have resulted in a smaller coordination number about the central iron atom, thus causing a small value of the isomer shift because of the change in bonding from d^2sp^3 hybridized orbitals to sp^3.

In the IR spectrum of the irradiated $FeCl_3 \cdot 2CH_3OH$, new lines appeared at 2850 and 2900 cm^{-1}; they are assigned to the vibration of the C–H of a formyl group. A characteristic vibration band for the formyl group appears at about 1700 cm^{-1},[15] but this band

TABLE 2. THE MÖSSBAUER PARAMETERS OF THE COMPOUNDS BEFORE AND AFTER IRRADIATION

	Compound	Exposure dose 10^8 R	δ_{Fe}	ΔE	Γ_1	Γ_2
B-1	$FeCl_3(pyrazole)_3$	0	0.50	0	1.09	
		10	0.45	0	1.11	
	$Fe(koj)_3$[a]	0	0.55	0.96	0.35	0.49
		10	0.48	1.01	0.36	0.48
	$[Fe(bpy)_2Cl_2][FeCl_4]$	0	0.40	0	0.45	
			0.44	0.33	0.47	0.47
		10	0.29	0	0.47	
			0.41	0.47	0.44	0.44
	$[Fe(pyridine)_5ClO_4](ClO_4)_2$	0	0.39	0.66	0.65	0.65
		10	0.46	0.76	0.67	0.59
B-2	$[Co(pn)_3][FeCl_6]$	0	0.46	0.26	0.29	0.29
		16	0.47	0.17	0.29	0.29
	$[Co(NH_3)_6][FeCl_6]$	0	0.47	0	0.40	
		12	0.55	0	0.40	
	$Fe_3(OCH_3)_9$	0	0.44	0.37		
		17	0.46	0.42	0.69	0.51
	$FePO_4 \cdot 2H_2O$	0	0.67	0.18	0.25	0.25
		10	0.66	0.18	0.25	0.25
C-1	$Fe(phen)_2Cl_2$	0	1.08	3.26		
		10	1.12	3.30		
	$Fe(H_2PO_2)_2$	0	1.29	2.68	0.26	0.26
		10	1.32	2.73	0.24	0.24
	$FeCl_2 \cdot 4H_2O$	0	1.36	3.12		
		10	1.35	3.12	0.29	0.30
C-2	$[Fe(bpy)_3]Cl_2 \cdot 4H_2O$	0	0.40	0.37	0.31	0.27
		10	0.39	0.35	0.44	0.34
	$Fe(bpy)_2(CN)_2 \cdot 4H_2O$	0	0.19	0.62	0.34	0.34
		10	0.26	0.65	0.36	0.38
	$[Fe(phen)_3](NO_2)_2 \cdot 5H_2O$	0	0.35	0.27	0.26	0.26
		10	0.39	0.27	0.33	0.32
	$Fe(phen)_2(NO_2)_2 \cdot \frac{1}{2}H_2O$	0	0.33	0.42	0.27	0.31
		10	0.34	0.42	0.27	0.32

a) koj: kojate ion.

is obscured because of overlapping with the very strong band at 1600 cm^{-1}. The reduction of iron(III) chloride in a methanol solution has been studied extensively.[16] The production of H_2, CH_2O, CH_4, and glycol has been reported. The following steps are inferred to be involved in the reaction induced by the gamma-ray irradiation of $FeCl_3 \cdot 2CH_3OH$ on the assumption that the radiolysis of $FeCl_3 \cdot 2CH_3OH$ undergoes a series of reactions similar to those of iron-(III) chloride in a methanol solution:[17]

$$CH_3OH \longrightarrow \cdot CH_2OH + \cdot H$$

$$Fe^{3+} + \cdot CH_2OH \longrightarrow Fe^{2+} + HCHO + H^+$$

$$Fe^{3+} + \cdot H \longrightarrow Fe^{2+} + H^+$$

$$Fe^{3+} + Cl^- \longrightarrow Fe^{2+} + Cl.$$

The $Fe_3(OCH_3)_9$ compound was insensitive to radiation, as will be described later. The $\cdot CH_2OH$ radical may be reactive in redox reactions, while CH_3O^- may not.

Figure 2 shows the Mössbauer spectra for irradiated $FeCl_3 \cdot$(1,4-dioxane) at successive stages of irradiation. Iron(II) ions initially reduced by gamma-ray irradiation are oxidized to iron(III) ions upon further irradiation. The total exposure dose of 4.5×10^8 R causes serious damage to this compound, as may be seen in Fig. 2(d). The main decomposition products of dioxane have been reported to be HCHO(G=9.7), HCOO–CH_2–CH_2OH(G=8.5), and H_2(G=1.4).[18]

The compound $FeCl_3 \cdot$dma$\cdot 2H_2O$ was also sensitive to radiation. That is, iron(II) absorption lines were observed in the Mössbauer spectrum of this compound after irradiation. The new bands found in the IR spectrum can be assigned to the formyl, which is known to have absorption in the region from 2800 to 2900 cm^{-1}.

A-2: This sub-group is composed of iron(III) compounds with a carboxyl group. Glycine(Hgly) is comprised of carboxyl and amino groups. The carboxyl group is known to be very sensitive to radiation and to produce reductive radicals, as has been reported by many workers.[19,20] The G values ($Fe^{3+} \rightarrow Fe^{2+}$) for $FeCl_2 \cdot$gly(Hgly)$\cdot 7/2H_2O$ and $[Fe_3(HCO_2)_6]$ $[Fe(HCO_2)_6] \cdot 8H_2O$ were estimated to be about 2.5±

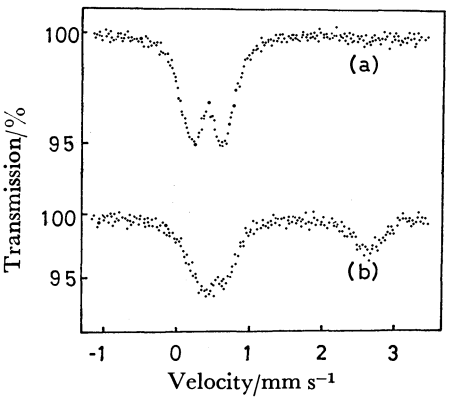

Fig. 3. Mössbauer spectra of (a) non-irradiated and (b) 8.3×10^8 R irradiated $Fe_2(HPO_3)_3\cdot9H_2O$.

0.5 (at a total exposure dose of 6.7×10^8 R) and 3.2± 0.5 (at a total exposure dose of 9.0×10^8 R) respectively from analyses of the Mössbauer spectra using equation:

$$G=\frac{\text{A}_\text{I}\text{(the absorption area of a new peak)}}{\text{A(the total absorption area)}}\times\frac{100}{\text{the absorption energy(eV)}}$$

and assuming that the recoilless fractions of the original peaks and the new peaks are equal, and that an exposure dose of 1 R gives an absorbed dose of 1 rad for these compounds. The initial G values, however, will be larger than these values.

A-3: This sub-group is composed of iron(III) compounds with reducing ligands. The $H_2PO_2^-$ and HPO_3^{2-} ions are considered to be reducing ions. The iron(III) ions in $Fe(H_2PO_2)_3$ and $Fe_2(HPO_3)_3\cdot9H_2O$ were reduced to iron(II) ions under irradiation. The G value of the decomposition for $Fe(H_2PO_2)_3$ is reported to be 3.4±0.4[21] and the main decomposition products after it had been dissolved in water were confirmed chemically to be phosphate and phosphonate ions.[22,23] That is, the P(I) ligand is oxidized to P(III) and P(V) under irradiation. Figure 3 shows the Mössbauer spectra for $Fe_2(HPO_3)_3\cdot9H_2O$ before and after irradiation. The oxidation state of phosphorus of this compound is trivalent, and may be oxidized to P(V) upon irradiation.

A-4: This sub-group is composed of iron(III) compounds with a low-spin state. The Mössbauer parameters of the new lines for irradiated $[Fe(bpy)_2(CN)_2]NO_3$(bpy: 2,2′-bipyridyl) were $\Delta E=0.62$ mm s^{-1}, $\delta_{Fe}=0.23$ mm s^{-1}. These values are similar to those of nonirradiated $Fe(bpy)_2(CN)_2$ ($\Delta E=0.62$ mm s^{-1}, $\delta_{Fe}=0.19$ mm s^{-1}). This similarity of the Mössbauer parameters suggests that the iron(II) ion produced under irradiation has the same coordination structure as the nonirradiated $Fe(bpy)_2(CN)_2$. The iron(III) ion of $[Fe(phen)_3](ClO_4)_3\cdot2H_2O$ has been reported to be reduced to the Fe(II) ion upon irradiation.[4] The iron(III) compounds in a low-spin state may be supposed to be reduced to iron(II) easily upon irradiation, although they contain large conjugated ligands.

Group B. Group B consists of iron(III) compounds in which no change of valence was observed in the Mössbauer spectra. The Mössbauer parameters of these compounds are shown in Table 2. A total exposure dose of 1×10^9 R or more was delivered to the compounds of this group.

B-1: This sub-group is made up of iron(III) compounds with large conjugated ligands. In this group, no reduced iron(II) species were observed in the Mössbauer spectra after irradiation. Iron(III) kojate and $FeCl_3\cdot(pyrazole)_3$ show broad Mössbauer spectra attributable to a relaxation effect. There was no change in the width at the half-maximum in the spectra between before and after irradiation. Although a part of the ligands are initially excited upon irradiation, the excitation energy is considered to be distributed in a short time through the conjugated bonds and delocalized over all of the molecules. Therefore, the fragmentation and the excitation of the molecules due to irradiation may be minimized. Compounds $[Fe(bpy)_2Cl_2][FeCl_4]$ and $[Fe(pyridine)_5ClO_4](ClO_4)_2$ were also insensitive to radiation.

B-2: This sub-group is made up of iron(III) compounds without large conjugated ligands. No influence of radiation was observed in $[Co(pn)_3][FeCl_4]$ (pn: 1,2-propanediamine) and $[Co(NH_3)_6][FeCl_6]$, although the radiolysis of 1,2-propanediamine and ammonia would be expected because iron(II) species are observed in the spectra of irradiated $[Fe(en)_3]Cl_3$. This fact shows that the iron ion is well shielded in $[Co(pn)_3][FeCl_4]$ and $[Co(NH_3)_6][FeCl_6]$ by the large volume of chloride ions from the electrons and the radicals produced upon irradiation.

Each iron atom in $FePO_4\cdot2H_2O$ is surrounded by four oxygen atoms of the PO_4^{3-} ions and two oxygen atoms of the water molecules.[24] The oxygen atoms of the PO_4^{3-} ions, however, coordinate tetrahedrally to the iron atom as the nearest atoms, and the two oxygen atoms of water molecules coordinate to the iron atom as the next nearest atoms. It is concluded that the radicals resulting from the radiolysis of water molecules were not able to react with the central iron(III) atom during the life-time of the radicals because the distance between the iron atom and water molecules is large, or because the iron atom is shielded by the four oxygen atoms of PO_4^{3-} ions from the electrons and the radicals as has been described above. The influence of the radiolysis of water molecules on the redox of the iron atom was not observed for the compounds studied in this paper. One of the reasons for this is that the $G(-H_2O)$ value for the decomposition of the water is as small as 0.1. The $G(-H_2O)$ value is less than 0.01 for the hydrates, whereas for ice it is known to be greater than 0.1.[25]

Compound $Fe_3(OCH_3)_9$ was also insensitive to radiation, although the bond-dissociation energy of methanol is 389 kJ mol^{-1} for $HOCH_2$–H, 383 kJ mol^{-1} for H_3C–OH, and 418 kJ mol^{-1} for CH_3O–H,[26] and the bond-dissociation energies of $HOCH_2$–H and H_3C–OH are lower than that of CH_3O–H. The following reaction of the hydrated electron is known in the pulse radiolysis of a water–methanol solution:[17]

$$e_{aq}^- + CH_3OH \longrightarrow CH_3O^- + H$$

$$e_{aq}^- + CH_3OH \longrightarrow CH_3 + OH^-.$$

In a solid phase, the bare electron produced by ir-

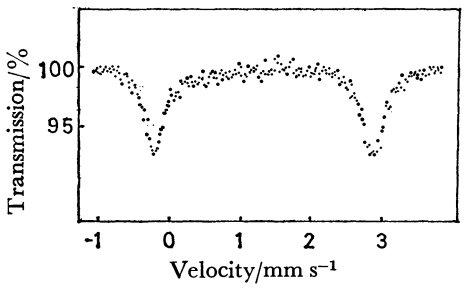

Fig. 4. Mössbauer spectrum of 10×10^8 R irradiated $FeCl_2\cdot4H_2O$.

radiation may take the place of the hydrated electron. Thus, CH_3O^- would not react with electrons and the $G(H_2)$ from $Fe_3(OCH_3)_9$ would be smaller than that from $FeCl_3\cdot2CH_3OH$.

Group C. Generally, high-spin iron(II) compounds, such as $(NH_4)_2Fe(SO_4)_2\cdot6H_2O$ and $FeSO_4\cdot7H_2O$, are easily oxidized to basic iron(III) species upon irradiation.[27] Although the iron(II) ions of both compounds are surrounded by six water molecules, the reducing radicals produced from the decomposition of the water may react with other species, such as NH_4^+ and SO_4^{2-}, by preference, for the Fe(III) ion, the sulfite ion, and hydrogen have been reported to exist as products of decomposition.[28]

Group C consists of iron(II) compounds in which no chemical change was observed through the Mössbauer spectra. The compounds of this group were subjected to a total exposure dose of 1.0×10^9 R or more.

C-1: This sub-group contains high-spin iron(II) compounds in which no change of valence was observed. That is, $Fe(H_2PO_2)_2$ and $FeCl_2\cdot4H_2O$ were insensitive to radiation up to an exposure dose of 1.0×10^9 R.

The $H_2PO_2^-$ anion is a strong reducing ion. The decomposed fractions of $H_2PO_2^-$ in 400 Mrad delivered $Fe(H_2PO_2)_2$ and $Fe(H_2PO_2)_3$ were 5 and 10% respectively.[21] The compounds with a lower valent iron(II) ion and a strong reducing anion, iron (II) oxalate, are also radioresistant.[1] The remarkably high stability upon the irradiation of these compounds must involve the process of the recombination of radicals and electrons due to the absence of a redox reaction between radicals and central metal ions.

Figure 4 shows the Mössbauer spectrum of irradiated $FeCl_2\cdot4H_2O$. This compound contains four water molecules which are arranged around an iron(II) ion.[29] It is easy for the radicals produced from the radiolysis of water molecules to react with an iron(II) ion because water molecules are coordinated directly with the iron(II) ion. Nevertheless, the iron ion of $FeCl_2\cdot4H_2O$ was not oxidized to an iron(III) ion. This suggests that the radicals formed on the radiolysis of H_2O will be inclined to participate in the recombination reaction, as the chloride ion is not easily oxidized or reduced. Kopcewicz *et al.*[30] reported that they observed the Fe_3O_4, $Fe_{1-x}O$, and $FeCl_2\cdot2H_2O$ species, in proton-irradiated $FeCl_2\cdot4H_2O$. The effects observed were interpreted in terms of the "thermal spike" model. Friedt *et al.*[31] reported the emission spectra of $^{57}CoCl_2\cdot X(X=2H_2O$ and $6H_2O)$ to show the existence of two kinds of Fe(III) species and two kinds of Fe(II) species, due to the self-radiolysis of the ligand environment by the low-energy electrons and X-rays emitted during the Auger cascade. As our experimental method has the limitation that only stabilized changes after irradiation can be observed the metastable species with a short lifetime can not be observed in the Mössbauer spectra. Emission experiments, on the other hand, might sometimes show the metastable state. Compound $Fe(bpy)_2Cl_2$, which has a high degree of conjugation, showed no chemical change due to irradiation.

C-2: This sub-group is composed of the low-spin iron(II) compounds. Compounds $[Fe(bpy)_3]Cl_2\cdot4H_2O$, $[Fe(bpy)_2(CN)_2]\cdot4H_2O$, $[Fe(phen)_3](NO_2)_2\cdot5H_2O$-(phen: 1,10-phenanthroline), and $[Fe(phen)_2(NO_2)_2]\cdot1/2H_2O$ were insensitive to radiation, and the oxidation state of iron(III) was not observed in the Mössbauer spectra up to an exposure dose of 1.0×10^9 R.

The electron configurations of high-spin iron(II) and iron(III) ions in octahedral complexes are $t^4_{2g}e^2_g$ and $t^3_{2g}e^2_g$ respectively. The reduction of the iron-(III) ion to the iron(II) ion results in the transfer of an electron from ligands to a t_{2g} orbital of the Fe (III) ion, the rate of which is faster than that to an e_g orbital in an octahedral complex.[32] The situation is the same for iron ions in a low-spin state in an octahedral complex, for the electronic configurations of the low-spin iron(II) and iron(III) ions are t^6_{2g} and t^5_{2g} respectively. However, some of the compounds were highly radioresistant. The high-spin iron(III) compounds with large conjugated ligands and low-spin iron(II) compounds exhibited especially strong radioresistant properties. The fact that the orbital ground states of high-spin iron(III) and low-spin iron (II) ions have more stability than high-spin iron(II) and low-spin iron(III) ions respectively would affect the reaction of electrons and radicals formed under the action of radiation, thus leading to the observed stability of the compounds of both categories upon irradiation.

The width of the Mössbauer spectra of the compounds which were insensitive to radiation became broad, and the spectra showed a little distortion. This means that considerable damage in the coordination structure has taken place under irradiation, although no changes in the valence of the iron ion were detected in the Mössbauer spectra.

References

1) J. M. Friedt and J. Danon, *Radiochim. Acta*, **17**, 173 (1972).
2) H. S. Cheng, S. J. Yeh, and P. K. Cheng, *J. Chinese Chem. Soc.*, **18**, 179 (1971).
3) H. Sano, K. Sato, and H. Iwagami, *Bull. Chem. Soc. Jpn.*, **44**, 2570 (1971).
4) Y. Maeda, H. Ohshio, and Y. Takashima, *Bull. Chem. Soc. Jpn.*, **53**, 179 (1980).
5) H. Sano and H. Iwagami, *J. Chem. Soc., Chem. Commun.*, **1971**, 1637.
6) H. Ohshio, Y. Murakami, G. Mori, and Y. Takashima,

Memoirs of the Faculty of Science, Kyushu University Ser. C, **10**, 239 (1978).
7) G. K. Wertheim and D. N. E. Buchanan, *Chem. Phys. Lett.*, **3**, 87 (1969).
8) T. S. Srivastava and A. Nath, *J. Phys. Chem.*, **80**, 529 (1976).
9) H. Sano and T. Ohnuma, *Bull. Chem. Soc. Jpn.*, **48**, 266 (1975).
10) H. Sano, *J. Radioanal. Chem.*, **36**, 105 (1977).
11) Y. Maeda, H. Ohshio, and Y. Takashima, *Chem. Lett.*, **1980**, 1359.
12) N. Yoza and S. Ohashi, *Bull. Chem. Soc. Jpn.*, **37**, 33 (1964).
13) Y. Maeda and Y. Takashima, *J. Inorg. Nucl. Chem.*, **35**, 1219 (1973).
14) B. N. Figgis, "Introduction to Ligand Field," Interscience Publishers, New York (1966).
15) A. D. Cross, "Practical Infrared Spectroscopy," Butterworth & Co., London (1964)
16) V. Balzani and V. Carassiti, "Photochemistry of Coordination Compounds," Academic Press, London (1970), p. 178.
17) J. H. Baxendale and F. W. Mellows, *J. Am. Chem. Soc.*, **83**, 4720 (1961).
18) M. G. Vacherot, *Bull. Soc. Chim. Fr.*, **1969**, 765.
19) A. Sugimori, *Bull. Chem. Soc. Jpn.*, **39**, 2583 (1966).
20) D. N. E. Buchanan, *J. Inorg. Nucl. Chem.*, **32**, 3531 (1970).
21) Y. Maeda and Y. Takashima, *J. Phys.*, **40**, C2-553 (1979).
22) Y. Maeda, S. Hachitsuka, and Y. Takashima, unpublished results on the irradiation effect for hypophosphoric compounds. These data will be published in the future.
23) F. Kosal and H. Yuksel, *Z. Naturforsch., Teil A*, 30, 1044 (1975).
24) R. Hiriyana and K. Sakurai, *X-Rays*, **5**, 85 (1949).
25) E. R. Johnson, "The Radiation-induced Decomposition of Inorganic Molecular Ions," Gordon and Breach Science Publishers, New York (1970), p. 137.
26) "Kagaku Binran," ed by The Chemical Society of Japan, Maruzen, Tokyo (1975), p. 976.
27) V. P. Gütlich, S. Odar, B. W. Fitzsimmons, and N. E. Erickson, *Radiochim. Acta*, **10**, 147 (1968).
28) E. R. Johnson, *J. Am. Chem. Soc.*, **78**, 5196 (1956).
29) J. Meunier-Piret and M. van Meerssche, *Acta Crystallogr., Sect. B*, **27**, 2329 (1971).
30) M. Kopcewicz, I. Sosnowska, and J. Tatarkiewicz, *Radiat. Eff.* **30**, 207 (1976).
31) J. M. Friedt, G. K. Shenoy, G. Abstreiter, and R. Poinsot, *J. Chem. Phys.*, **59**, 3831 (1973).
32) F. Basolo and R. G. Pearson, "Mechanisms of Inorganic Reactions," 2nd ed, John Wiley & Sons, New York (1967).

The Spectrophotometric Determination of Ethylene Diamine with Phthalaldehyde and 2-Mercaptoethanol

Goro HIHARA,* Hiroshi MIYAMAE, and Miharu NAGATA

Department of Chemistry, Faculty of Science, Josai University, Sakado, Saitama 350

(Received January 16, 1981)

A simple spectrophotometric method has been developed for the determination of ethylenediamine in an aqueous or ethanolic solution. This method is based on the reaction of ethylenediamine with phthalaldehyde and 2-mercaptoethanol, and on the measurement of the absorbance of the yellow-developed solution at 430 nm. Beer's law holds for 0.5—10 μg of ethylenediamine per 1 ml. Secondary and tertiary amines do not interfere with theestimation. Two of the primary amines, diethylenetriamine and triethylenetetramine, interfere with the estimation when present in quantities of more than 10 μg per ml of the sample solutions. 1,3-Propanediamine interferes seriously. The colored compound was found to be composed of ethylenediamine, phthalaldehyde, and 2-mercaptoethanol in a molar ratio of 1:2:1.

Several spectrophotometric methods for the determination of ethylenediamine have already been reported.[1-4] These methods, however, have low sensitivities. Roth[5] developed a highly sensitive fluorophotometric method for amino acids, in which the amino acids were combined with phthalaldehyde and 2-mercaptoethanol in an alkaline medium to grow fluorescent materials. Roth[6] and Svedas *et al.*[7] improved this method so that these products could be detected by a method of spectrophotometric estimation. Simons and Johnson[8] made it clear that this fluorogenic compound was 1-alkylthio-2-alkyl-substituted isoindole by a reaction of propylamine with phthalaldehyde and 2-mercaptoethanol. Moreover, they found that phthalaldehyde reacts only primary amines and not with secondary amines.

The objective of this paper is to examine the effects of various factors on the coloration and to present a spectrophotometric method for ethylenediamine in an aqueous or ethanolic solution.

Experimental

Apparatus. A Hitachi 101 spectrophotometer was used for the measurement of the absorbance, while a Hitachi EPS-3 spectrophotometer was used to estimate the absorption spectra with 10-mm glass cells. For the adjustment of the pH of the buffer solutions, a Toa Denpa HM-5A pH meter was used.

Reagents. Phthalaldehyde of a biochemical grade and ethylenediamine with a 99.5% purity were obtained from Wako Pure Chemical Industries, Ltd. 2-Mercaptoethanol was also obtained with a purity of 98%. The other reagents, except for the secondary and tertiary amines, were of a guaranteed grade.

Buffered Reagent for Coloration. A 0.1 M† solution of sodium tetraborate was adjusted to pH 9.5 with a concentrated NaOH solution. Into 100 ml of this borate buffer solution, 1 ml of an ethanol solution containing 20 mg of phthalaldehyde and 1 ml of an ethanolic solution of 70 mg of 2-mercaptoethanol were then mixed. This reagent was stable for at least two days at room temperature.

Procedure A for the Measurement of Ethylenediamine in an Aqueous Solution. 1.0 ml of an aqueous sample solution containing 0.5—10 μg of ethylenediamine was mixed with 1 ml of ethanol and 3 ml of the buffered reagent, after which the mixture was allowed to stand for 30 min at 26±0.5 °C in a thermostat. Then the absorbance of the solution was measured at 430 nm against the reagent blank.

Procedure B for the Measurement of Ethylenediamine in an Ethanolic Solution. The procedure was the same as in Procedure A, except that 1 ml of pure water was used in place of 1 ml of ethanol.

† 1 M = 1 mol dm^{-3}.

Results and Discussion

Influence of the pH of the Buffered Reagent. One-ml portions of an aqueous solution containing 4.68 μg of ethylenediamine were mixed with 1 ml of distilled water and 3 ml of a buffered reagent, the pH of which was varied in the range of 5—11, the absorption spectrum was then examined. As is shown in Fig. 1, the absorption maximum in every spectrum shifted toward lower wavelength, as the pH of the solution became higher, converging on 430 nm in the pH range of 9—11. The intensity of the absorbance also varied with the change in the pH. It seemed to become highest in the 9—10 pH range. Figure 2

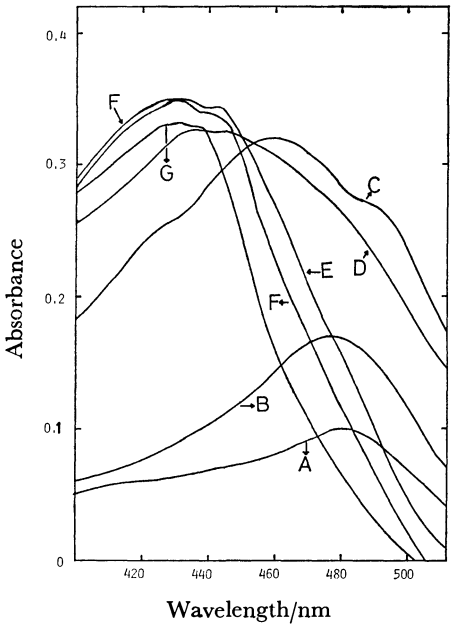

Fig. 1. The absorption curves at the various values of pH.
A: pH 5, B: pH 6, C: pH 7, D: pH 8, E: pH 9, F: pH 10, G: pH 11. KH_2PO_4–Na_2HPO_4 buffer solutions were used in pH 5—8, HCl–$Na_2B_4O_7$ in pH9, and NaOH–$Na_2B_4O_7$ in pH 10 and 11.

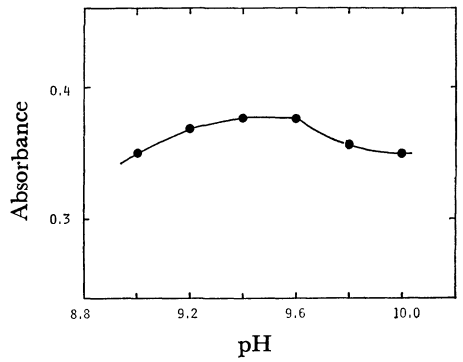

Fig. 2. Effect of pH on the absorbance at 430 nm between pH 9.0 and 10.0. 1 ml of an aqueous solution of ethylenediamine (4.68 μg/ml) was used.

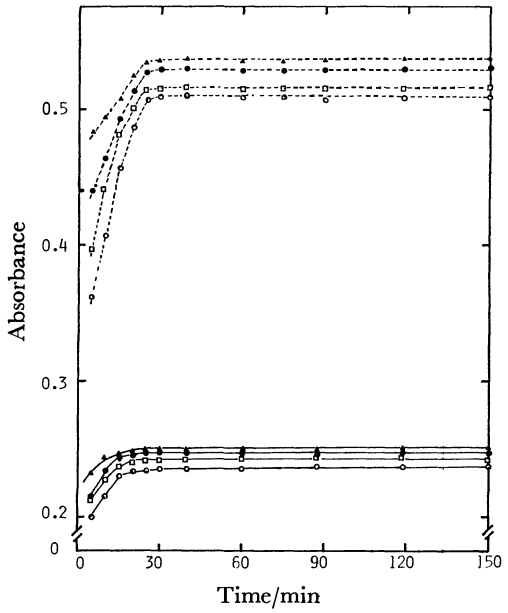

Fig. 3. Influence of temperature and time-dependance of the coloration.
——: Concentration of ethylenediamine 1.56 μg/ml, ···: 3.12 μg/ml, ○: 20 °C, □: 23 °C, ▲: 26 °C, ●: 30 °C.

shows that the absorbance measured at 430 nm attained its maximum value at the pH values of 9.4 and 9.6. Thus, the borate solution of pH 9.5 was used as a buffer in the color reaction throughout this work, and the absorbance was measured at 430 nm.

Influence of Time Delay and Reaction Temperature. After 2-ml portions of the ethylenediamine solution (1.56 and 3.12 μg/ml) had been mixed with 3 ml of the buffered reagent, they were held in a thermostat at various temperatures between 20—30 °C, while the absorbances of the solution were measured at regular time intervals. The results are shown in Fig. 3. The absorbances of every solution attained constancy within 30 min, and thereafter remained unchanged for 150 min regardless of the reaction temperatures. However, the intensities of the absorption were slightly affected by the reaction temperature and showed their maximum at 26 °C.

Influence of Addition of Ethanol and Other Organic Solvents. When 1 ml of distilled water was added instead of 1 ml of ethanol in Procedure A, Beer's law was adopted for the relation of the absorbance *vs.*

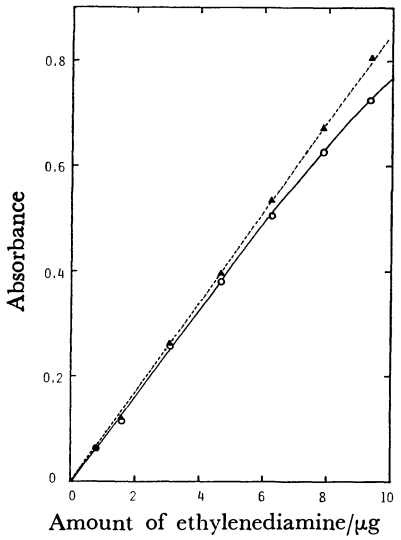

Fig. 4. Calibration curves in the presence and absence of ethanol.
···▲···: Procedure A, —○—: in the absence of ethanol.

Table 1. Effect of coexisting compounds and ions on the absorbance

Compound	Amount taken/μg	Relative value[a] of the absorbance
Propylamine	100	0.92
	10	1.01
Dimethylamine	500	1.01
Triethylamine	1000	1.00
1,3-Propanediamine	80	ppt[b]
	10	1.40
Aniline	500	ppt
	50	0.95
N-Methylaniline	500	1.00
Dien[c]	100	ppt
	10	1.02
Trien[c]	100	ppt
	10	1.02
HMTA[c]	600	0.86
	60	0.99
Pyridine	100	1.00
Pyrazine	500	1.00
Piperazine	600	1.01
Acetonitrile	5000	1.01
Urea	500	1.01
Thiourea	500	1.00
Pb^{2+} (from $Pb(NO_3)_2$)	100	1.02
I^- (from KI)	1000	1.02
NH^+_4 (from NH_4Cl)	10	1.03

a) This value is the ratio of the absorbance with and without the compound listed in the left colum. A 1-ml portion of the ethylenediamine solution(4.68 μg/ml) was chosen. b) ppt means that the precipitate formed when the buffered reagent was added. c) dien, trien, and HMTA represent diethylenetriamine, triethylenetetramine, and hexamethylenetetramine respectively.

the ethylenediamine concentration only in the range of 0.5—5.0 μg of ethylenediamine contents, the absorbance showed a negative deviation from Beer's law at larger concentrations of ethylenediamine as is shown in Fig. 4. In order to improve the linearity in the relation of the absorbance *vs.* the ethylenediamine content, the addition of organic solvents miscible with water was tested. The addition of acetone remarkably reduced the coloration. Methanol and ethanol increased the absorbance, with no fluctuation in the absorption maximum in wavelength. With the addition of 1 ml of ethanol, the linearity was extended up to an ethylenediamine content of 10 μg, as is shown in Fig. 4.

Influence of Active Compounds and Ions. The influence of the addition of several compounds and ions which may interfere with the coloration in the present method was also examined. A 1-ml portion of an aqueous solution of each compound listed in Table 1 was mixed with 1 ml of an aqueous solution of ethylenediamine and 3 ml of the buffered reagent, and the absorbance was estimated at 430 nm. The results of the examination are shown in Table 1. Dimethylamine and trimethylamine did not interfere, and propylamine reduced the absorbance only slightly. This corresponds to the conclusion suggested by Simons *et al.* that phthalaldehyde reacts only with primary amines and not with secondary and tertiary amines. Among the tested compounds, only 1,3-propanediamine interferes significantly.

The Composition of the Product. Simons *et al.* offered the following equation for the reaction of primary amines with phthalaldehyde and 2-mercaptoethanol:

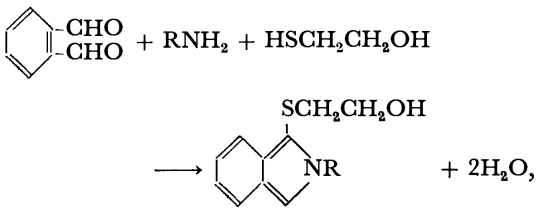

where R is an alkyl group. When ethylenediamine reacts on phthalaldehyde with 2-mercaptoethanol, the product may be supposed to have the structure shown as (I).

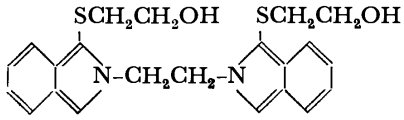

(I)

In order to elucidate the structure of the product, 0.06 g of ethylenediamine (1 mmol) was added to 50 ml of a borate buffer solution (pH 9.5) containing 0.27 g of phthalaldehyde (2 mmol) and 0.16 g of 2-mercaptoethanol (2 mmol). A yellow precipitate formed very soon, it had turned brown within one or two hours after it was separated from the solution. Therefore, the composition of the product only was determined as follows: to 1-ml portions of ethylenediamine solutions (3.12, 6.24, and 9.36 μg/ml), various amounts of a 2-mercaptoethanol aqueous solution (10.9 μg/ml) were added, and then the containers were filled up to 3 ml with pure water. Then 2 ml of a borate-buffer solution (pH 9.5) containing phthalaldehyde (0.2 mg/ml) was added, and the absorbance at 430 nm was estimated after 30 min. The relationships are shown in Fig. 5 between the absorbances and the amounts of 2-mercaptoethanol added. A similar relation is given in Fig. 6, where ethylenedi-

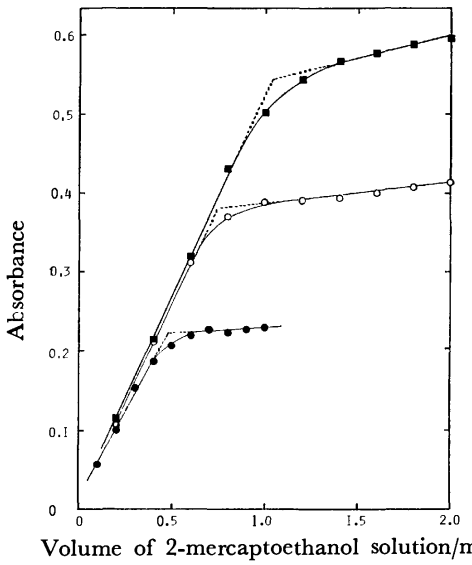

Fig. 5. Relationships between the absorbance and the added amounts of 2-mercaptoethanol solution (10.9 μg/ml) in the presence of excess phthalaldehyde. The solid curves are of the experimental estimation and the dotted lines are the prolongations of the tangential lines. ●: Ethylenediamine 3.12 μg/ml, ○: 6.24 μg/ml, □: 9.36 μg/ml.

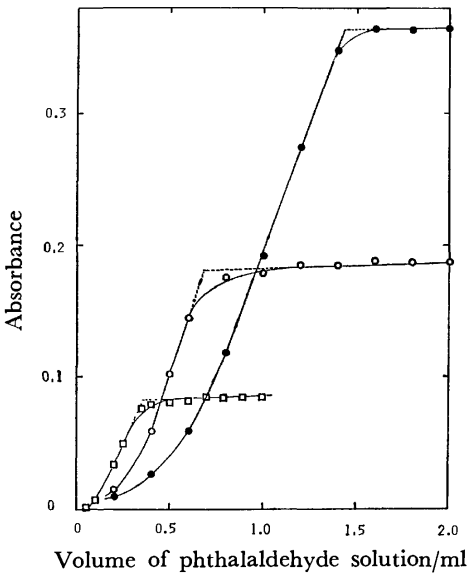

Fig. 6. Relationships between the absorbance and the added volume of an aqueous solution of phthalaldehyde (20.0 μg/ml) in the presence of excess of 2-mercaptoethanol.
Borate buffer solution (pH 9.5) was used containing 2-mercaptoethanol (0.7 mg/ml). □: Ethylenediamine 1.56 μg/ml, ○: ethylenediamine 3.12 μg/ml, ●: ethylenediamine 6.24 μg/ml.

amine reacts with phthalaldehyde in the presence of an excess amount of 2-mercaptoethanol. The absorbances were nearly equal, regardless of the amount of ethylenediamine present, and increased proportionally to a certain point as the amount of 2-mercaptoethanol increased when there was a large excess of phthalaldehyde. On the other hand, in the presence of a large excess of 2-mercaptoethanol, the absorbances increased only a little as the content of phthalaldehyde increased. They began to increase proportionally to the amount of phthalaldehyde after the molar ratio of phthalaldehyde/ethylenediamine became nearly 1:1. This can be explained by assuming that phthalaldehyde reacts with ethylenediamine to give an intermediate product consisting of 1:1 (=phthalaldehyde: ethylenediamine), which does not have the absorption near 430 nm. The intermediate then reacts with one more mole of ethylenediamine to give a final product having its absorption peak at 430 nm. Two tangential lines are drawn per curve in Figs. 5 and 6, one in the range where the absorbances increase linearly with the amount of 2-mercaptoethanol or phthalaldehyde added, and the other in the plateau range where the absorbances become almost constant. These lines were then extended, and the point of intersection was found. These points were 0.35, 0.68, and 1.43 ml of the phthalaldehyde solution when the concentrations of ethylenediamine were 1.56, 3.12, and 6.24 μg/ml respectively. The molar ratios of phthalaldehyde/ethylenediamine were calculated to be 2.01, 1.96, and 2.06 respectively. In Fig. 5 the points of intersection are 0.43, 0.74, and 1.04 ml of a 2-mercaptoethanol solution when the concentrations of ethylenediamine are 3.12, 6.24, and 9.36 μg/ml, and 1.16, 0.99, and 0.93 respectively, in terms of the molar ratio of 2-mercaptoethanol/ethylenediamine. The composition of the product was found to be 1:2:1(ethylenediamine: phthalaldehyde: 2-mercaptoethanol).

Precision. The precision of Procedure A was checked with a sample containing a known amount of ethylenediamine. Based on six determinations, the relative standard deviations were 1.2% at the level of 1.56 μg and 1.0% at 9.36 μg.

This method is less sensitive than the fluorophotometric one reported by Benson and Hare[10] who determined primary amines in the range of picomole. This method is very simple and convenient for use assaying ethylenediamine in an aqueous or ethanolic solution, even in the presence of secondary and tertiary amines.

References

1) J. S. Hanker, M. D. Sulkin, M. Gilman, and A. M. Seligman, *Anal. Chim. Acta*, **28**, 150 (1963).
2) E. I. Kas'yanenko and I. V. Samborskii, *Teoriya i Prakt. Ionnogo Obmena, Akad. Nauk Kaz. SSR, Tr. Resp. Soveshch*, **1962**, 100; *Chem. Abstr.*, **62**, 2242 (1965).
3) T. S. Al-Ghabsha, S. A. Rahim, and A. Townshend, *Anal. Chim. Acta*, **1976**, 85, 189.
4) G. N. Smith and M. G. Swank, *Anal. Chem.*, **32**, 978 (1960).
5) M. Roth, *Anal. Chem.*, **43** 880 (1971).
6) M. Roth, Ger. Offen., 2 102 985(Cl.G0ln), 02 Sep. 1971; Swiss Appl. 17 Feb. 1970; *Chem. Abstr.*, **75** 136846 m (1971).
7) V. Svedas, I. Yu. Galaev, and I. V. Berezin, *Bioorg. Khim.*, **1978**, 4, 19.
8) S. S. Simons, Jr., and D. F. Johnson, *J. Am. Chem. Soc.*, **98**, 7098 (1976).
9) S. S. Simons, Jr., and D. F. Johnson, *J. Chem. Soc., Chem. Commun.*, **1977**, 374.
10) J. R. Benson, and P. E. Hare, *Proc. Natl. Acad. Sci. U.S.A.*, **1975**, 72, 619.

Bis(cyclohexyl isocyanide)palladium(II) Halides and Their Benzene Complexes

Tsunesuke KAJIMOTO,* Yukishige KITANO,** Hidetaka TAKAHASHI, and Jiro TSUJI***

Basic Research Laboratories, Toray Industries, Inc., Tebiro, Kamakura, Kanagawa 248

(Received February 17, 1981)

Bis(cyclohexyl isocyanide)palladium(II) chloride, $PdCl_2(C_6H_{11}NC)_2$ (**1**) was prepared from $PdCl_2$. The configuration of the complex **1** is cis with respect to the isocyanides. The isocyano group in one cyclohexyl isocyanide takes axial conformation to chair form cyclohexyl group, while another takes equatorial conformation. By recrystallization of **1** from benzene bis(cyclohexyl isocyanide)palladium(II) chloride–benzene, $PdCl_2(C_6H_{11}NC)_2(C_6H_6)_2$ (**2**) was prepared. IR spectrum of **2** shows a characteristic absorption at 700 cm^{-1} which is due to the benzene incorporated in the complex. Similar benzene complex was also prepared from $PdBr_2$.

Many benzenoid complexes are known with various transition metals, but a few with palladium.[1] Synthesis of a unique benzene–palladium(II) complex with the formula of $[PdAl_2Cl_7(C_6H_6)]_2$ was reported and its X-ray structural analysis showed that the Pd–Pd system is sandwitched between two benzene rings with each palladium essentially associated with three carbon atoms of each benzene.[2] Formation of an unstable benzene–palladium(I) complex was also reported.[3] In the preceeding paper we reported an insertion reaction of cyclohexyl isocyanide to π-allylpalladium chloride.[4] Palladium halides have been reported to react readily with aryl isocyanides yielding stable complexes, $PdX_2(RNC)_2$.[5] These complexes had been treated with benzene, but benzene complex was not reported to be formed. We obtained bis(cyclohexyl isocyanide)palladium(II) chloride, $PdCl_2(C_6H_{11}NC)_2$(**1**) by the use of cyclohexyl isocyanide in place of aryl isocyanide and found that the complex **1** has a unique structure and gives a new benzene complex, bis(cyclohexyl isocyanide)palladium(II) chloride–benzene, $PdCl_2(C_6H_{11}NC)_2(C_6H_6)$(**2**) by recrystallization from benzene. Similar benzene complex was also prepared from palladium bromide. Details of the reaction and IR spectroscopic analyses of the complexes are presented in this paper.

Results and Discussion

The complex **1** was obtained as white precipitates by the reaction of two molar equivalents of cyclohexyl isocyanide with palladium(II) chloride in benzene, successive concentration and dilution with ethyl ether. Recrystallization of **1** from hot benzene gave a yellow complex **2**, the analysis of which suggested the molecular formula, $PdCl_2(C_6H_{11}NC)_2(C_6H_6)$. On the other hand, recrystallization of **1** from *p*-xylene or toluene gave no complex containing xylene or toluene and the complex **1** was recovered. IR spectra of **1** and **2** are shown in Fig. 1.

$$PdCl_2 + 2C_6H_{11}NC \longrightarrow \underset{\textbf{1}}{cis\text{-}PdCl_2(C_6H_{11}NC)_2} \underset{Et_2O}{\overset{C_6H_6}{\rightleftharpoons}} \underset{\textbf{2}}{PdCl_2(C_6H_{11}NC)_2(C_6H_6)}$$

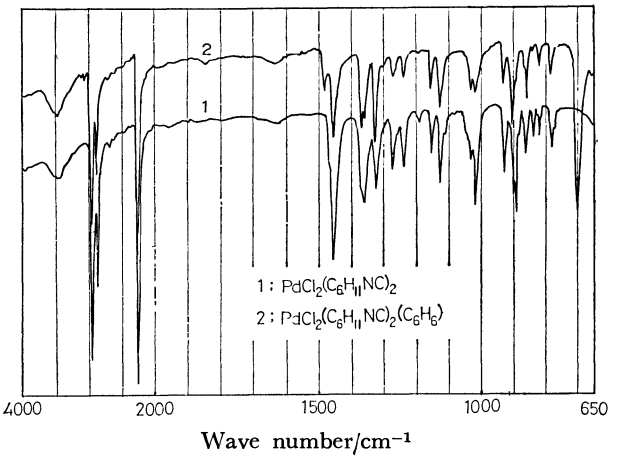

Fig. 1. IR spectra of $PdCl_2(C_6H_{11}NC)_2$ and $PdCl_2(C_6H_{11}NC)_2(C_6H_6)$.

By heating at 95 °C for 15 min, **2** was transformed into **1**, but **2** is fairly stable in air at room temperature and decomposes slowly with liberation of benzene. The complex **2** was also transformed into **1** by treating with ethyl ether. This result was ascertained by IR spectrum and elemental analysis of the complex obtained. The presence of benzene in the ether after contacting with **2** was confirmed by UV spectrum.

The IR spectrum of **2** shows several characteristic absorptions at 700, 1480, 1840, 1985, 3030, and 3075 cm^{-1} which are thought to be originated from the benzene incorporated in the complex. Especially the strong absorption at 700 cm^{-1} is worth noticing. It is well-known that the absorption of out of plane deformation band of benzene proton(ν_{11}) is observed at 672 cm^{-1} in vapor or liquid state, and at 687 cm^{-1} in solid state with free benzene as a stronger and broader absorption.[6] Shifting of the absorption to higher wave length suggests some probable interaction of benzene with palladium in the complex.

Crystallographic analyses of these complexes have been carried out and the crystal data are shown in Table 1. It is noteworthy that the extent of symmetry of **2** is higher than that of **1**. This result also suggests an interaction of benzene with palladium in complex **2**. We could not succeed in obtaining precise X-ray structural analysis of **2** because of its de-

**Present address: Toray Research Center Inc., Sonoyama, Ohtsu 520.

***Present address: Department of Chemical Engineering, Tokyo Institute of Technology, Meguro-ku, Tokyo 152.

Table 1. Crystal data of $PdCl_2(C_6H_{11}NC)_2$ and $PdCl_2(C_6H_{11}NC)_2(C_6H_6)$

	$PdCl_2(C_6H_{11}NC)_2$	$PdCl_2(C_6H_{11}NC)_2(C_6H_6)$
Molecular weight	395.7	471.4
Crystal system	Monoclinic	Tetragonal
Cell parameters	a; 12.299 Å, b; 9.604 Å, c; 17.383 Å, β; 127.59°	a; 17.95 Å, c; 14.12 Å
Unit cell volume	1627.0 Å^3	4549.5 Å^3
Dencity obsd(calcd)	1.605(1.615)	1.3—1.5(1.376)
Z	4	8
Space group	C_{2h}^5-$P2_1/c$(No. 14)	D_{4h}^{12}-$P4_2/nnm$(No. 134)

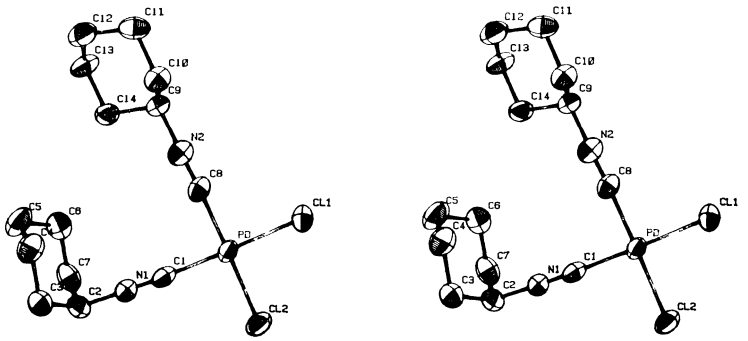

Fig. 2. Stereographic schematic drawing of $PdCl_2(C_6H_{11}NC)_2$.

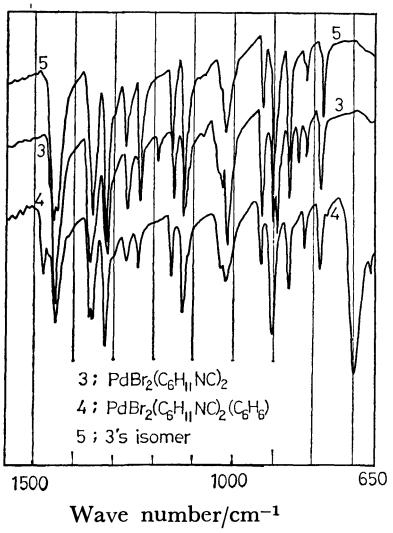

Fig. 3. IR spectra of $PdBr_2(C_6H_{11}NC)_2$, its isomer and $PdBr_2(C_6H_{11}NC)_2(C_6H_6)$.

composition during the diffraction analysis. It is suspected that **2** is five-co-ordinate with a π-bond of benzene, two chlorines and two isocyanides. X-ray structural analysis showed that the complex **1** has the structure shown in Fig. 2. Details of the analysis will be given in a forthcoming paper, but it should be noticed that the configuration of **1** is cis with respect to the isocyanides. Furthermore it is quite interesting that one isocyano group takes equatorial conformation and another isocyano group takes axial conformation to chair form cyclohexyl group.

The reaction of palladium(II) bromide with cyclohexyl isocyanide gave bis(cyclohexyl isocyanide)palladium(II) bromide, $PdBr_2(C_6H_{11}NC)_2$(**3**). By recrystallization of **3** from hot benzene, another benzene complex, bis(cyclohexyl isocyanide)palladium(II) bromide–benzene, $PdBr_2(C_6H_{11}NC)_2(C_6H_6)$(**4**) was obtained. Two kinds of complexes having the same molecular formula; $PdBr_2(C_6H_{11}NC)_2$ and different IR absorptions were obtained from the complex **4**. By washing with ethyl ether, **4** was transformed into **3**, but by heating at 100 °C for 1 h, **4** was transformed into another complex **5**. Recrystallization of **3** from hot *p*-xylene gave the complex **5** too. The complexes **3** and **5** are thought to be stereoisomers, but it is not clear why the two distinct IR absorptions at 860 and 1180 cm^{-1} observed with **3** are not in the spectrum of **5** as shown in Fig. 3.

$$PdBr_2 + 2C_6H_{11}NC \longrightarrow PdBr_2(C_6H_{11}NC)_2 \ (\mathbf{3}) \xrightarrow{p\text{-Xylene}} PdBr_2(C_6H_{11}NC)_2 \ (\mathbf{5})$$

$$\mathbf{3} \underset{Et_2O}{\overset{C_6H_6}{\rightleftarrows}} PdBr_2(C_6H_{11}NC)_2(C_6H_6) \ (\mathbf{4}) \xrightarrow{100\,^\circ C} \mathbf{5}$$

As a related reaction, it was reported that $RuCl_2(C_6H_{11}NC)_2(C_6H_6)$ was formed by the reaction of $[RuCl_2(C_6H_6)]_2$ with cyclohexyl isocyanide, while only $RuCl_2(C_6H_5NC)_4$ was formed with phenyl isocyanide.[7] Formation of benzene complex from $PdCl_2(C_6H_5NC)_2$ is not known as described in the introduction. On the other hand, the benzene complexes were obtained from the cyclohexyl isocyanide complexes. According to these facts cyclohexyl isocyanide rather than phenyl isocyanide is essential as the ligand in order to obtain benzene complexes from palladium halides and ruthenium halides.

Experimental

*Preparation of $PdCl_2(C_6H_{11}NC)_2$ (**1**).* To a benzene solution (100 cm^3) containing palladium chloride (4.5 mmol, 0.80 g) was added cyclohexyl isocyanide (9 mmol, 1.1 cm^3)

with continuous stirring by a magnetic stirrer and the mixture was heated at temperatures between 70 °C and 80 °C to give a yellow solution. After filtration the hot solution to remove the remaining palladium chloride (0.08 g), the filtrate was concentrated under reduced pressure and ethyl ether (100 cm^3) was added to give white precipitates (1.43 g); mp 123 °C.

Found: C, 42.52; H, 5.58; N, 7.14; Cl, 18.17; ash, 27.2%. Calcd for $C_{14}H_{22}N_2Cl_2Pd$: C, 42.51; H, 5.58; N, 7.09; Cl, 17.93; ash, 26.90%.

Preparation of $PdCl_2(C_6H_{11}NC)_2(C_6H_6)$ ***(2)***. $PdCl_2(C_6H_{11}NC)_2$ (0.5 g) was recrystallized from hot benzene (20 cm^3) to give yellow crystals (0.52 g); mp 127—128 °C.

Found: C, 50.67; H, 5.98; N, 6.04; Cl, 15.28; ash, 22.6%. Calcd for $C_{20}H_{28}N_2Cl_2Pd$: C, 50.70; H, 5.97; N, 5.91; Cl, 14.97; ash, 22.47%.

Preparation of $PdBr_2(C_6H_{11}NC)_2$ ***(3)***. To a benzene solution (125 cm^3) containing palladium bromide (5 mmol, 1.33 g) was added cyclohexyl isocyanide (10 mmol, 1.2 cm^3) with stirring and the mixture was heated at temperatures between 70 °C and 80 °C to give a yellow solution. After filtration of the hot solution to remove the remaining palladium bromide, the filtrate was concentrated under reduced pressure and ethyl ether (150 cm^3) was added to give pale yellow crystals (1.81 g); mp 152 °C.

Found: C, 34.71; H, 4.58; N, 5.86; ash, 22.1%. Calcd for $C_{14}H_{22}N_2Br_2Pd$: C, 34.70; H, 4.58; N, 5.78; ash, 21.96%.

Preparation of $PdBr_2(C_6H_{11}NC)_2(C_6H_6)$ ***(4)***. The complex **3** was recrystallized from hot benzene to give yellow crystals; mp 155—160 °C.

Found: C, 42.44; H, 5.02; N, 5.10; Br, 28.52; ash, 19.2%. Calcd for $C_{20}H_{28}N_2Br_2Pd$: C, 42.70; H, 5.01; N, 4.98; Br, 28.42; ash, 18.90%.

Preparation of $PdBr_2(C_6H_{11}NC)_2$ ***(5)***. The complex **4** was treated with ethyl ether and dried under reduced pressure to give pale yellow powder; mp 152 °C.

Found: C, 34.80; H, 4.59; N, 5.86; ash, 22.1%. Calcd for $C_{14}H_{22}N_2Br_2Pd$: C, 34.70; H, 4.58; N, 5.78; ash, 21.96%.

Apparatus. IR spectra were obtained on a Perkin-Elmer 125 spectrometer and Hitachi EPI-S spectrometer in KBr disks, UV spectra on a Varian Cary 14 spectrometer. X-ray spectra were obtained on a Rigakudenki AFC-6A diffractometer.

References

1) W. E. Silverthorn, "Advances in Organometallic Chemistry," ed by F. G. Stone and R. West, Academic Press, New York (1975), Vol. 13, pp. 47—137.

2) G. Allegra, A. Immirzi, and L. Porri, *J. Am. Chem. Soc.*, **87**, 1394 (1965).

3) J. M. Davidson and C. Triggs, *J. Chem. Soc. A*, **1968**, 1324.

4) T. Kajimoto, H. Takahashi, and J. Tsuji, *J. Organomet. Chem.*, **23**, 275 (1970).

5) M. Angoletta, *Ann. Chim. (Italy)*, **45**, 970 (1955).

6) R. D. Mair and D. F. Hornig, *J. Chem. Phys.*, **17**, 1236 (1949).

7) F. Felice and M. Vittorio, *Inorg. Chim. Acta*, **27**(2), L109 (1978).

  Bull. Chem. Soc. Jpn., 54, 2675—2677 (1981)

An Improved Ion-exchanger Colorimetry for the Determination of a Trace Amount of Phosphate

Kiichi MATSUHISA,** Kunio OHZEKI, and Tomihito KAMBARA*

Department of Chemistry, Faculty of Science, Hokkaido University, Sapporo 060

** *Division of Environmental Conservation, Graduate School of Environmental Science, Hokkaido University, Sapporo 060*

(Received March 3, 1981)

A highly sensitive and selective method has been developed for the determination of a trace amount of phosphate. It is based on the concentration of phosphate as the familiar molybdenum blue complex on the coagulated material prepared from finely divided anion and cation exchangers, collection of the mixed resin on a filter paper, and the subsequent measurement of the absorbance of the complex on the resulting thin layer of resin phase. The calibration curve shows a good proportionality in the concentration range of 1 to 6 μg P l^{-1}. The absorbance corresponding to 1 μg P l^{-1} is 0.095. The method is successfully applied to the determination of phosphate in a tap water and a river water.

Ion-exchanger colorimetry[1,2] was developed by Yoshimura *et al.* A colored metal complex is collected by batch method on the ion-exchanger, the size of which is ranging from 200 to 400 mesh. A part of the resin is then transferred into a cell of 0.1 cm in thickness, and the complex on the resin phase is determined colorimetrically. Trace amounts of chromiun(VI)[3] and zinc[4] were determined. The method was also applied to the determination of phosphate.[5] Phosphate was concentrated on the molybdate-loaded ion-exchanger and determined as the molybdenum blue complex.

An improved ion-exchanger colorimetry[6] was reported for the determination of chromium(VI). The method utilizes a mixture of finely divided anion and cation exchangers. Finely divided cation exchanger collects chromium(VI)–diphenylcarbazide complex rapidly by batch method in combination with anion exchanger to form bulky material. The coagulated resin is then separated by filtration and the resulting thin layer of the colored resin on a filter paper is directly subjected to spectrophotometric measurement.

In the present paper, an improved ion-exchanger colorimetry is reported for the determination of phosphate. The molybdenum blue complex is insistently fixed to the coagulated ion-exchangers. A highly sensitive and selective method is developed.

Experimental

Reagents. All reagents used were of analytical reagent grade. Freshly dried potassium dihydrogenphosphate was dissolved into deionized water to give a solution of 50 mg P l^{-1} (1 l=1 dm^3). A solution containing 0.05 μg P ml^{-1} (1 ml=1 cm^3) was prepared fresh daily by dilution of the stock solution. Twenty grams of hexaammonium heptamolybdate tetrahydrate were dissolved and diluted to 500 ml with water. Ascorbic acid solution of 0.1 mol dm^{-3} was made fresh dialy. Potassium antimony tartrate was dissolved into water to give a solution of 1 mg Sb ml^{-1}.

Mixed Reagent A: A 100-ml portion of 2.5 mol dm^{-3} sulfuric acid was mixed with 30 ml of the ammonium molybdata solution.

Mixed Reagent B: A 60-ml portion of 0.1 mol dm^{-3} ascorbic acid was mixed with 10 ml of the potassium antimony tartrate solution.

Dipping Solution: A 5-ml portion of 2.5 mol dm^{-3} sulfuric acid, 6 ml of 0.1 mol dm^{-3} ascorbic acid and 1 ml of potassium antimony tartrate solutions were mixed and diluted to 50 ml with water.

Mixed reagents and the dipping solution were prepared fresh daily and stored in a thermostat kept at 25±1 °C.

Ion-exchange Resins. Macroreticular type Amberlyst 15 and A-27 (both Rohm and Haas Co.) in RSO_3H and $RN(CH_3)_3Cl$ forms, respectively, were used. Suspension of the respective resins was prepared according to the method reported.[7] The stock suspension was stored as required in the thermostat kept at 25±1 °C. The solution was well shaken before being pipetted out. The mutual coagulation of the finely divided anion and cation exchangers was examined as follows. The varying amounts of the anionic resin suspension (ARS) up to 20 ml were separately taken into a 50-ml beaker and diluted to 30 ml with water. A 10-ml portion of 0.25 mol dm^{-3} potassium chloride solution was added to keep the constant ionic strength. A 2.0-ml aliquot of the cationic resin suspension (CRS) was then added and the final volume of the solution was adjusted to 50 ml with water. The mixture was stirred magnetically for 10 min and filtered. The absorbance of filtrate was determined at 500 nm against water.

Apparatus. A Shimadzu UV-140-01 spectrophotometer was used. Filter papers (Toyo Roshi No. 5 A) were cut in 3 cm×6 cm wide strips. A Toyo KG 25 filter holder (Toyo Roshi Co.) was used.

General Procedure. A 50-ml aliquot of the solution containing less than 0.3 μg phosphorus as phosphate was placed in a 100-ml beaker set in a water bath kept at 25± 1 °C. A 6.0-ml portion of the mixed reagent A, 3.0-ml of the mixed reagent B, 6.0 ml of ARS and finally 2.0 ml of CRS were added to the sample solution. The mixture was stirred by means of a magnetic stirrer for 10 min. The resulting coagulated material was collected on one end of the filter strip placed on a holder. A disk of colored resin of the 17-mm diameter and about 0.3 mm in thickness was formed. The filter strip was dipped in the dipping solution for 20 min. It was then fixed on a glass plate fitted to the cell holder. The absorbance of the resin phase was measured at 700 nm against the other end of filter paper.

Another disk of resin was prepared without addition of phosphate. The absorbance corresponding to the reagent blank including the resins was also measured. The net absorbance of the complex on the resin was obtained by the difference.

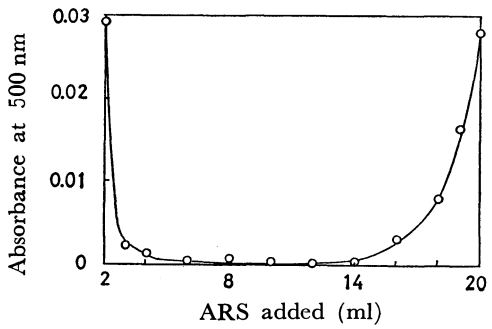

Fig. 1. Coagulation of the suspensions of finely divided cation and anion exchangers (CRS and ARS). A 2-ml portion of CRS was mixed with ARS in 50 ml of 0.05 mol dm^{-3} potassium chloride solution.

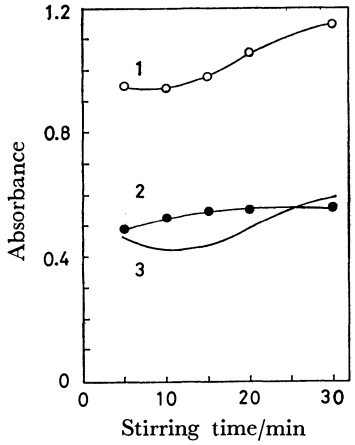

Fig. 2. Effects of shaking time on the fixation of the molybdenum blue compound on the mixed resin from the 50-ml solution containing 0.25 μg P (1), and without addition of P (2). Curve 3 indicates the net absorbance at 700 nm.

Results and Discussion

Ion-exchanger. In the previous works[6-8] Amberlyst 15 and A-26 were used. In this work A-27 was used in place of A-26. The ion-exchange capacities of A-26 and A-27[9] have been reported as 4.4 and 2.6 meq g^{-1}, respectively. The pore radius range of A-26 is 14—22 nm and that of A-27 is 21—120 nm. Amberlyst A-27 is well suited for fixing the bulky anions.

Suspension. The suspension of Amberlyst 15 is slightly brown while that of A-27 is white. The ion-exchange capacities of ARS and CRS were determined by conductometric titration with the standard silver nitrate and sodium hydroxide solutions, respectively. The exchange capacities were 2.54×10^{-3} meq ml^{-1} for ARS and 5.21×10^{-3} meq ml^{-1} for CRS. The anion exchanger is 4—16 ml of ARS was almost completely coagulated with the cation exchanger in 2 ml of CRS (Fig. 1). The resulting mixed resin was easily separated by filtration from the solution. The combination of 2.0 ml of CRS and 6.0 ml of ARS was used throughout the following experiments.

Effect of Temperature. The preliminary experiments revealed that the development of coloration

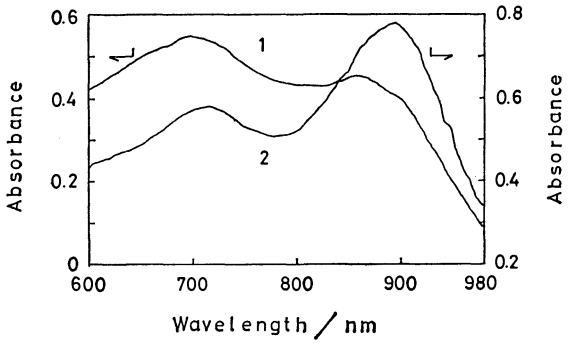

Fig. 3. Absorption curves of the molybdenum blue compound; (1) on the thin layer of mixed resin prepared from 50 ml of solution containing 0.3 μg P as phosphate, and (2) in aqueous solution containing 1 μg P ml^{-1} (1-cm cell).

was seriously affected by the temperature of reaction solution. Hence, all experiments were carried out at a constant temperature of 25 °C.

Shaking Time. During the course of shaking, the anionic molybdenum blue complex is fixed on the anion exchanger, which combines with cation exchanger to form the coagulated material. The effect of shaking time was examined (Fig. 2). The absorbance of sample disk was almost constant in the shaking period of 5—10 min. With a prolonged shaking, the absorbance increased gradually. On the other hand, the blank value increased slowly with increasing shaking time. The net absorbance showed a constant value between 10 to 15 min.

Standing Time. The coagulated resin was filtered with a gentle suction. The resulting thin layer was stored wet in the dipping solution, the composition being determined after many trials. Almost a constant coloration was kept for 10—60 min.

Absorption Curve. The absorption curve of the molybdenum blue in the resin phase was different from that of in the solution (Fig. 3). The maximum at 890 nm in the solution[10] disappered when the complex was fixed on the ion-exchange resin. The complex on the resin has an absorption maximum at 700 nm.[5]

Calibration Curve. A calibration curve showed a proportionality in the concentration range of 1 to 6 ppb (μg l^{-1}) P as phosphate. The mean absorbance of blank value with the standard deviation was 0.535± 0.024 (n=7). The net absorbance for 6 ppb P were 0.550±0.038 (n=8). The variation would be reduced if a temperature could be much more exactly controlled.

Effects of Forein Ions. The effects of arsenate and silicate were examined. The duplicate determinations of 0.2 μg P were carried out in the presence of one of them. The equal amount of As as arsenate gave a relative error of +8.1% and a 5000-fold amount of SiO_2 as silicate showed the deviation of +3.9%.

Analysis. The method was applied to the determination of phosphate in a tap water and a river water (Table 1). The standard addition method together with the original calibration method was applied to the analysis of a tap water. Both plots show-

Table 1. Results of analysis of a tap water for phosphate

Date 1980	Sample volume (ml)	P found (μg)	P in tap water ($\mu g\ l^{-1}$)
05/11	5.0	0.088	17.6
	5.0	0.199[a)]	19.8
	5.0	0.294[b)]	18.8
10/11	5.0	0.099	19.8
	5.0	0.102	20.4
11/11	10.0	0.201	20.1
	10.0	0.203	20.3
14/11	10.0	0.156	15.6
	10.0	0.165	16.5

a) 0.100-μg P was added. b) 0.200-μg P was added.

ed good linearity with the same slope (Fig. 4). This result indicated that the recovery of phosphate as the molybdenum blue complex was quantitative from the sample solution to the mixed resin, although there were many competing ions for the ion-exchange sites. The variation of the phosphate content in the tap water supplied to our laboratory was examined. The water sample was taken freshly each day. As shown in Table 1, no significant variation was found in the period studied.

A river water was filtered through a filter paper (Toyo Roshi No. 5C) as soon as possible. The concentration was found to be 12 ppb P as phosphate. The value increased to 50 ppb P when the filtrate was treated with sulfuric and nitric acids to decompose the organic substances according to JIS method.[11] The considerable amounts of phosphate were found to originate from the organic substances in the river water.

The method was ascertained to be highly selective and sensitive for the determination of phosphate in water samples. Only small amount of sample water was required.

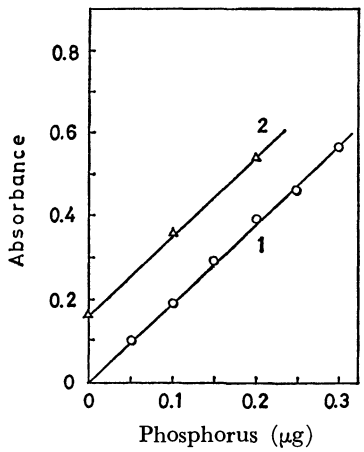

Fig. 4. Calibration curve (1) and the result of the standard addition method (2). Sample amount: 50 ml.

References

1) K. Yoshimura, H. Waki, and S. Ohashi, *Talanta*, **23**, 449 (1976).
2) K. Yoshimura, H. Waki, and S. Ohashi, *Kagaku Zokan*, **78**, 95 (1978).
3) K. Yoshimura and S. Ohashi, *Talanta*, **25**, 103 (1978).
4) K. Yoshimura, H. Waki, and S. Ohashi, *Talanta*, **25**, 579 (1978).
5) T. Tanaka, K. Hiiro, and A. Kawahara, *Bunseki Kagaku*, **28**, 43 (1979).
6) K. Ohzeki, T. Sakuma, and T. Kambara, *Bull. Chem. Soc. Jpn.*, **53**, 2878 (1980).
7) M. Abe, K. Ohzeki, and T. Kambara, *Bull. Chem. Soc. Jpn.*, **51**, 1090 (1978).
8) M. Abe, N. Takei, K. Ohzeki, and T. Kambara, *Bull. Chem. Soc. Jpn.*, **52**, 2574 (1979).
9) K. A. Kun and R. Kunin, *J. Polym. Sci., Part C*, 1457 (1976).
10) J. Murphy and J. P. Riley, *Anal. Chim. Acta*, **27**, 31 (1962).
11) JIS K 0101-1979, "Testing Method for Industrial Water."

Preparation and Electronic Spectra of Dichlorobis(1,10-phenanthroline)-molybdenum(III) and Dichlorobis(2,2′-bipyridine)molybdenum(III) Ions

Tomoji S. Morita, Yoichi Sasaki,* and Kazuo Saito

Department of Chemistry, Faculty of Science, Tohoku University, Aoba, Aramaki, Sendai 980

(Received March 14, 1981)

A preparation method of pure crystalline salts, *cis*-$[MoCl_2(phen)_2]X$ (phen, 1,10-phenanthroline; X^-= Cl^-, Br^-, $CH_3C_6H_4SO_3^-$) and *cis*-$[MoCl_2(bpy)_2]Cl$ (bpy, 2,2′-bipyridine), has been established. They are stable in solid state under oxygen- and moisture-free conditions. They deteriorate within one hour in water at room temperature, but are much more stable in various organic solvents free from oxygen. In the visible region, two absorption peaks were observed in methanol at 21510 cm^{-1} (ε=2570 $dm^3\ mol^{-1}\ cm^{-1}$) and 26740 cm^{-1} (ε=4420 $dm^3\ mol^{-1}\ cm^{-1}$) for the phen complex, and one broad peak at 22820 cm^{-1} (ε=3630 $dm^3\ mol^{-1}\ cm^{-1}$) for the bpy complex, which are assigned to the metal-to-ligand d-π^* charge transfer transition.

The coordination chemistry of molybdenum(III) has been less known as compared with that of chromium(III). Particularly, there are very few well characterized monomeric molybdenum(III) complexes containing amino carboxylates or aliphatic amines.[1,2] While chromium(III) complexes are inert to the oxidation with common oxidants, molybdenum(III) complexes are easily oxidized by air and by a variety of mild oxidants.[1] Nevertheless molybdenum(III) complexes have drawn interest as a counterpart of the well studied chromium(III) chemistry.

2,2′-Bipyridine(bpy) and 1,10-phenanthroline(phen) provide a variety of stable complexes of transition elements in low oxidation states.[3,4] Several monomeric molybdenum(III) complexes have been reported,[5-10] containing one to three 2,2′-bipyridine or 1,10-phenanthroline. However, some of them were not well characterized, and chemical properties of the characterized species are uncertain. Particularly only a few electronic absorption data are available.

We have isolated pure dichlorobis(2,2′-bipyridine)- and dichlorobis(1,10-phenanthroline)molybdenum(III) complexes in crystalline state and observed their electronic absorption spectra in various solvents.

Experimental

Materials. 2,2′-Bipyridine, 1,10-phenanthroline, and *p*-toluenesulfonic acid (Wako pure chemical industries, Ltd.) were used without further purification. Ammonium pentachloroaquamolybdate(III), $(NH_4)_2[MoCl_5(H_2O)]$, was prepared by the known method.[11] Organic solvents except acetone for the spectrometry were dehydrated with Molecular Shieves 4A and used without distillation. Acetone (Dotite spectrosol) was used as received. The concentration of water in these solvents was $(2—20)\times10^{-3}$ mol dm^{-3}.

Preparation of the Complexes. The bis(bpy) and bis(phen) complexes were synthesized by substituting the aromatic ligands for the aqua and the chloro ligands in $[Mo^{III}Cl_5(H_2O)]^{2-}$.

Dichlorobis(1,10-phenanthroline)molybdenum(III) Chloride Tetrahydrate, $[MoCl_2(phen)_2]Cl\cdot4H_2O$: A three-necked round-bottomed flask (1 dm^3) was connected to a dropping funnel and a reflux condenser,[12] the top of which was connected to a manifold for vacuum and nitrogen gas. Aqueous ethanol (40% v/v, 200 cm^3) containing 16 g of 1,10-phenanthroline and 5 g of *p*-toluenesulfonic acid was placed in the flask and the content was stirred with a teflon-coated bar. The whole system was evacuated and nitrogen gas was introduced. The purge cycle was repeated more than ten times. A solution of $(NH_4)_2[MoCl_5(H_2O)]$ (4.3 g) in 1.0 mol dm^{-3} hydrochloric acid (100 cm^3) was prepared in a 300 cm^3 round-bottomed Schlenk tube filled with nitrogen, transfered to the dropping funnel through a transfer tube, and added dropwise (6 h) to the phen solution at 50 °C with stirring. The red mixture was refluxed in an oil bath (*ca.* 100 °C) for 24 h. The color turned deep violet and then dark orange. The solution was allowed to cool slowly and kept in a refrigerator for 24 h. Yellowish orange needles appeared during storage, which were filtered off with a fritted funnel under nitrogen atmosphere, dried under a stream of nitrogen, dried *in vacuo*, and recrystallized from methanol. The deep orange prismatic crystals were washed with diethyl ether and dried *in vacuo*. Yield 2.2 g (35% from $(NH_4)_2[MoCl_5(H_2O)]$). Found: C, 45.94; H, 3.55; N, 8.85; Cl, 16.79%. Calcd for $C_{24}H_{24}N_4O_4Cl_3Mo$: C, 45.41; H, 3.81; N, 8.83; Cl. 16.76%. $[MoCl_2(phen)_2]Cl\cdot4H_2O$ is soluble in water, propylene carbonate, acetonitrile, *N,N*-dimethylformamide, methanol, ethanol, acetone and dichloromethane, slightly soluble in acetic acid, and insoluble in diethyl ether and 1,4-dioxane. The magnetic moment of the solid was 3.20 BM (292 K).

Dichlorobis(1,10-phenanthroline)molybdenum(III) p-Toluenesulfonate Sesquihydrate, $[MoCl_2(phen)_2](CH_3C_6H_4SO_3)\cdot1.5H_2O$: This was prepared similarly to the chloride salt by use of 20 g (instead of 5 g) of *p*-toluenesulfonic acid in aqueous ethanol to obtain large dark orange prismatic crystals. Yield 4.6 g (50% from $(NH_4)_2[MoCl_5(H_2O)]$). Found: C, 51.31; H, 3.65; N, 7.77; Cl, 9.72; S, 4.48%. Calcd for $C_{31}H_{26}N_4O_{4.5}Cl_2SMo$: C, 51.32; H, 3.61; N, 7.72; Cl, 9.77; S, 4.42%.

Dichlorobis(1,10-phenanthroline)molybdenum(III) Bromide Tetrahydrate, $[MoCl_2(phen)_2]Br\cdot4H_2O$: The preparation method was similar to that of the chloride salt except using 1.0 mol dm^{-3} hydrobromic acid in place of 1.0 mol dm^{-3} hydrochloric acid. The solution of $(NH_4)_2[MoCl_5(H_2O)]$ in 1.0 mol dm^{-3} hydrobromic acid (100 cm^3) was stirred for 24 h, and then added to the phen solution. Yield of orange powder, 15%. Found: C, 41.54; H, 2.90; N, 8.94; Cl, 10.32; Br, 11.62%. Calcd for $C_{24}H_{24}N_4O_4BrCl_2Mo$: C, 42.44; H, 3.56; N, 8.25; Cl, 10.44; Br, 11.76%.

Dichlorobis(2,2′-bipyridine)molybdenum(III) Chloride Dihydrate, $[MoCl_2(bpy)_2]Cl\cdot2H_2O$: This was made by a method similar to that for the phen complex chloride. Yield 2.3 g (31% from $(NH_4)_2[MoCl_5(H_2O)]$). Found: C, 43.65; H, 3.56; N, 10.16; Cl, 18.67%. Calcd for $C_{20}H_{20}N_4O_2Cl_3Mo$: C, 43.62; H, 3.66; N, 10.17; Cl, 19.31%. The orange crystals of $[MoCl_2(bpy)_2]Cl\cdot2H_2O$ are soluble in the same solvents as mentioned for $[MoCl_2(phen)_2]Cl\cdot4H_2O$.

Stability of the Complexes. The complex solids are stable under nitrogen atmosphere or *in vacuo* for at least one month, and relatively stable in dry air for at least two

days at room temperature. Their solutions in organic solvents free from oxygen are stable for at least 1 h at room temperature. Aqueous solutions (pH $\approx$7) are very unstable at room temperature even in the absence of oxygen.

Measurements. Ultraviolet and visible absorption spectra were recorded on a Hitachi 330 spectrophotometer under nitrogen atmosphere by the syringe technique.[12] Air was eliminated and nitrogen or argon was introduced into the solvents before measurement. Infrared spectra were recorded on a JASCO IRA-1 and a Hitachi 215 infrared spectrophotometer in KBr disks. The magnetic susceptibility was measured by the Faraday method in the Physics Department of this University at room temperature.

The concentration of water in organic solvents was determined by the Karl Fischer method with a Metrohm Karl Fischer-Automat E547, equipped with a Multi-Dosimat E415 and a Multi-Bürette E485.

Results and Discussion

Preparation. Bis(2,2'-bipyridine) and Bis(1,10-phenanthroline) Complexes: $[MoCl_2(phen)_2]Cl$ was prepared by Du Bois *et al.* from $[Mo^{III}Cl_3(py)_3]$ (py= pyridine) and phen in xylene.[9] The complexes, $[Mo^{III}I_2L_2]X$ (L=bpy, phen; $X^-=I^-$, $B(C_6H_5)_4^-$) were prepared by Westland and Muriithi,[10] by treating MoI_3 and the ligands in tetralin at 160—170 °C for 24 h. When MoI_3 and phen were mixed in benzonitrile at 180 °C for 3 d, $[Mo^{II}I_2(phen)_2]$ was claimed to be formed.[10] The products were reported to be powder, and the formulations were based on analytical data of Mo, and Cl or I alone. No electronic absorption spectrum was reported.

The elemental analysis of the present complexes are consistent with the given formulae. The magnetic moment of $[MoCl_2(phen)_2]Cl\cdot 4H_2O$ (3.20 BM) is similar to those of other monomeric molybdenum(III) complexes.[1] Three salts of the bis(phen) complexes gave almost identical absorption spectra in the visible region in methanol, indicating that all the samples contain the same complex cation. $[MoCl_2(phen)_2]Cl\cdot 4H_2O$ and $[MoCl_2(bpy)_2]Cl\cdot 2H_2O$ gave infrared absorption bands at 325 cm^{-1} and 323 cm^{-1}, respectively, which are assigned to $M^{III}o$–Cl stretching frequency (*cf.* Mo^{III}–Cl stretching frequency at 305 cm^{-1} in $K_3[MoCl_6]$[13,14]).

The bis-chelate complexes were successfully synthesized by the dilution method; *i.e.* $[Mo^{III}Cl_5(H_2O)]^{2-}$ in 1.0 mol dm^{-3} hydrochloric acid slowly added to the ligand solution. The ligand solution contains *p*-toluenesulfonic acid as 'inert' acid (perchloric acid is known to oxidize Mo(III)[11]) to keep reaction mixture acidic and low chloride concentration. The initial red reaction mixture turned violet within twenty minutes and then dark orange within 1 h. The violet color may indicate the formation of an intermediate $[MoCl_4L]^-$ (L=bpy, phen).[8] When the solutions of the ligand and of $[Mo^{III}Cl_5(H_2O)]^{2-}$ were rapidly mixed, a red-violet precipitate was formed, which was first assigned to $[MoL_3]Cl_3$ (L=bpy, phen) by Steele,[5] but later claimed to be $[MoCl_2L_2][MoCl_4L]$, $(LH)[MoCl_4L]$ or their mixture by Marzilli and Buckingham.[8] Our results of elemental analysis (C, H, N, Cl) of the red-violet precipitate fell between the calculated values for the last two formulations. Carmichael *et al.* reported that a similar insoluble salt was obtained by the reaction of molybdenum(III) trichloride or potassium hexachloromolybdate(III) with molten bipyridine.[7] It seems that under the reaction conditions where substantial amounts of $[MoCl_4L]^-$ and $[MoCl_2L_2]^+$ (or LH^+) are present, an insoluble salt between these two ions precipitated.

A large excess of the ligand (more than 8 times of the molybdenum) was also required to obtain the bis complex in high yield. When only 2.5 molar excess of the ligand was used, a red-violet precipitate was formed, which can be $[MoCl_2L_2][MoCl_4L]$. Substantial amount of $[MoCl_2L_2]Cl$ was also obtained from the filtrate.

Attempts to Prepare the Tris-chelate Complexes, $[Mo(bpy)_3]^{3+}$ and $[Mo(phen)_3]^{3+}$: Various attempts by the ligand substitution method were unsuccessful. Prolonged refluxing (1—10 d) of the reaction mixture used for the preparation of the bis-chelate complexes (*vide supra*) always resulted in exclusive formation of the bis-chelate complexes. We thought that the third bpy or phen would not coordinate to molybdenum(III) in a strongly acid medium. Addition of a small amount of 0.5 mol dm^{-3} sodium hydroxide solution free from oxygen to the reaction mixture gave a blue solution even at a pH less than unity. This solution was evaporated to dryness to leave a purple-gray residue which gave an infrared absorption band at 950 cm^{-1}, suggesting the presence of Mo=O bond.[1] When $[MoCl_2(phen)_2]Cl\cdot 4H_2O$ and phen were mixed in ethanol free from oxygen in the Schlenk tube, the color also turned blue within 1 h. When this complex was dissolved in ethanol without phen, the color remained orange for 1 h even in the presence of oxygen. This solution turned black, and then almost colorless after 1 d. No attempt was made for clarifying the oxidation process of the molybdenum(III).

Preparation of $[MoL_3]X_3$ (L=bpy, phen; $X^-=Cl^-$, Br^-, I^-) was reported previously by Steele[5] and Carmichael *et al.*[7] We repeated Carmichael's method,[7] *i.e.* MoI_3 was treated with molten bipyridine, and obtained a black-brown powder, of which the elemental analysis (C, H, N, I) was closer to $[MoI_2(bpy)_2]I$ rather than to $[Mo(bpy)_3]I_3$. Further attempts to obtain crystals of $[MoI_2(bpy)_2]I$ or $[Mo(bpy)_3]I_3$ from the powder were unsuccessful. Thus the hitherto reported "tris-chelate complexes" deserve further experimental evidence for the formulation.

Tris(bpy) and tris(phen) complexes of chromium(III) have not been prepared by the ligand substitution,[15,16] but obtained by the oxidation of the tris-chelate complexes of chromium(II).[16,17] Such an oxidation method cannot be applied to the molybdenum(III) complexes since the corresponding uninuclear molybdenum(II) complexes are not known.

Geometrical Structure. The present complexes, $[MoCl_2L_2]^+$ can occur in *cis* and *trans* forms. The shape of crystals (orange prismatic crystals in the case of $[MoCl_2(phen)_2]Cl\cdot 4H_2O$) of the complex salts and their absorption patterns in solution did not change on further recrystallization from methanol, ethanol or acetonitrile, suggesting no change in the

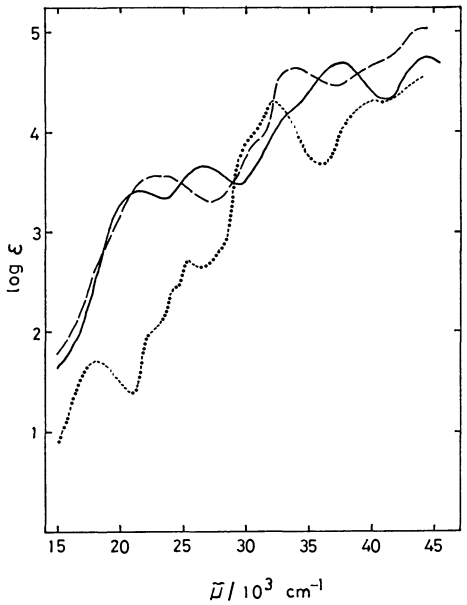

Fig. 1. Absorption spectra of $[MoCl_2(bpy)_2]Cl \cdot 2H_2O$ in methanol (— —), *cis*-$[MoCl_2(phen)_2]Cl \cdot 4H_2O$ in methanol (——) (under nitrogen atmosphere) and *cis*-$[CrCl_2(bpy)_2]Cl$[19] in 1:1 aqueous methanol (----).

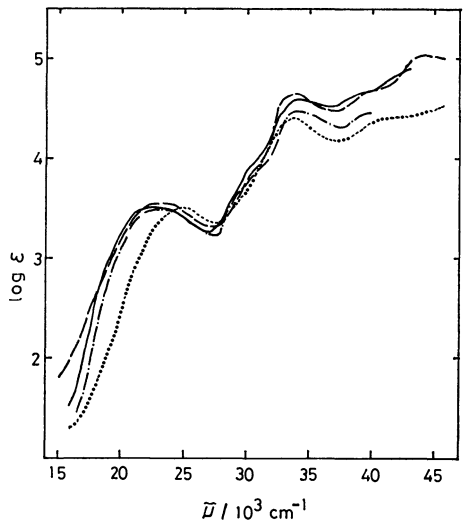

Fig. 2. Absorption spectra of $[MoCl_2(bpy)_2]Cl \cdot 2H_2O$ in dichloromethane (——), in acetonitrile (— —), in methanol (—·—) and 0.1 mol dm^{-3} hydrochloric acid (----) (under nitrogen atmosphere).

geometrical structure of molybdenum complex cation. The X-Ray diffraction method disclosed *cis* structure for $[MoCl_2(phen)_2]Cl \cdot 4H_2O$.[18] No such information is available for the salts of $[MoCl_2(bpy)_2]^+$.

Electronic and infrared absorption spectra did not give straightforward evidence for their geometrical isomerism. Absorption spectral patterns of the two complex cations in the visible region are apparently different from each other (Fig. 1); two peaks for the phen complex and one broad band for the bpy complex in the region from 20000 to 30000 cm^{-1}. However, such a difference cannot be taken as an evidence for different geometrical isomerism of these two complex cations, since the nature of the absorption bands are of charge-transfer type (*vide infra*) and their relation to the geometrical isomers would not be simple. Since all the known geometrical structures of dihalobis(2,2'-bipyridine) type complexes with various metal ions are *cis*,[19-25] we tend to consider that the bpy complex is also of the *cis* form.

Absorption Spectra. The absorption spectra in all the solvents except water changed only very slightly over 100 min at room temperature. Whenever the spectrum (patterns and/or intensity) changed, it was measured for 100 min at ten minutes intervals and the original pattern was estimated by the extrapolation to zero time. The spectrum changed so rapidly in water (pH $\approx$7) that the zero-time spectrum was not obtained. The complex solution in 0.1 mol dm^{-3} hydrochloric acid was relatively stable, and the original absorption spectrum was estimated.

General Features: The absorption curves of the 2,2'-bipyridine and 1,10-phenanthroline complexes are shown in Fig. 1, together with that of *cis*-$[CrCl_2(bpy)_2]^+$.[19] In the visible region (<30000 cm^{-1}), the bpy and the phen complexes of molybdenum(III) have one broad and two distinct peaks, respectively, with extinction coefficients between 2000 and 4000 dm^3 mol^{-1} cm^{-1}. Two or three much stronger absorption peaks ($\log \varepsilon > 4$) are observed in the ultraviolet region (>30000 cm^{-1}). Some of the peaks shift in different solvents, but the overall pattern remains almost unchanged, and the nature of absorption bands is discussed on the basis of the spectra in methanol (Fig. 1, *vide infra*).

Bands in the Ultraviolet Region: The phen complex shows two distinct bands at 44250 cm^{-1} and 37840 cm^{-1}, which are assigned to the intraligand transitions corresponding to the two bands of free 1,10-phenanthroline at 44440 cm^{-1} and 37880 cm^{-1} in methanol. Similarly, bands of the bpy complex at 40000 cm^{-1} and 33900 cm^{-1}, are of intraligand transition nature corresponding to the two bands of free 2,2'-bipyridine at 42550 cm^{-1} and 35570 cm^{-1}. The peaks of free ligand shift to lower energy on coordination to the metal ion, as reported for other metal complexes.[26,27]

Bands in the Visible Region: The bpy complex in methanol gives apparently one very broad maximum at 22800 cm^{-1}, which seems to involve two or more transitions as indicated by the spectra in different solvents (Fig. 2); *i.e.* the bpy complex gives a maximum at 24770 cm^{-1} and no shoulder is appreciable in 0.1 mol dm^{-3} hydrochloric acid, but a prominent shoulder is observed at a lower wave number in a less polar solvent. The phen complex gives two bands at 26740 cm^{-1} and 21510 cm^{-1} in methanol. The shape of the two bands of $[MoCl_2(phen)_2]^+$ did not change in different solvents (Fig. 3).

All these bands have extinction coefficients between 2000 and 4000 dm^3 mol^{-1} cm^{-1}, too strong to be assigned to the d-d transition. The spectral data of the other metal complexes having the same ligand environment are shown in Table 1. The extinction coefficients of the complexes of chromium(III),[19] cobalt(III),[20,21] and rhodium(III)[22,28] are different from those of the complexes of iridium(III),[23,28] iron-

TABLE 1. SPECTRAL DATA OF (a) *cis*-DICHLOROBIS(DIIMINE)TYPE COMPLEXES AND (b) MOLYBDENUM(III) COMPLEXES CONTAINING bpy OR phen IN THE VISIBLE REGION

	Complex	$\tilde{\nu}$/cm^{-1} (ε/dm^3 mol^{-1} cm^{-1})	Assignment	Solvent	Reference
(a)	$[MoCl_2(bpy)_2]^+$	22820 (3630)	d-π*	CH_3OH	This work
	$[MoCl_2(phen)_2]^+$	21510 (2570) 26740 (4420)	d-π*	CH_3OH	This work
	$[CrCl_2(bpy)_2]^+$	18020 (46) 22400^{sh} (100)	d-d	H_2O-CH_3OH (1 : 1)	19
	$[FeCl_2(bpy)_2]$	18870 (1540) 27780 (2700)	d-π*	CH_2Cl_2	24
	$[RuCl_2(bpy)_2]$	18020 (9200) 26460 (9170)	d-π*	CH_2Cl_2	24, 25
	$[OsCl_2(bpy)_2]$	17910 (12000) 26110 (11500)	d-π*	CH_2Cl_2	24, 25
	$[CoCl_2(bpy)_2]^+$	17100 (100) 18300 (125)	d-d	H_2O	21
	$[CoCl_2(phen)_2]^+$	19230 (60) 21650 ($\approx$100)	d-d	H_2O	20
	$[RhCl_2(bpy)_2]^+$	25800^{sh} (110)	d-d	H_2O	22, 28
	$[RhCl_2(phen)_2]^+$	26100^{sh} (110)	d-d	H_2O	22, 28
	$[IrCl_2(bpy)_2]^+$	28570 (2400)	d-π*	H_2O	28, 30
	$[IrCl_2(phen)_2]^+$	27780 (3300)	d-π*	H_2O	23, 31
(b)	$[MoCl_4(bpy)]^-$	18380 (1210)	d-π*	$(CH_3)_2NCHO$	8
	$[MoCl_4(phen)]^-$	18690 (2720)	d-π*	$(CH_3)_2NCHO$	8
	$[MoCl_3(py)(bpy)]$	20330 (1275)	d-π*	$(CH_3)_2NCHO$	8

sh: Shoulder.

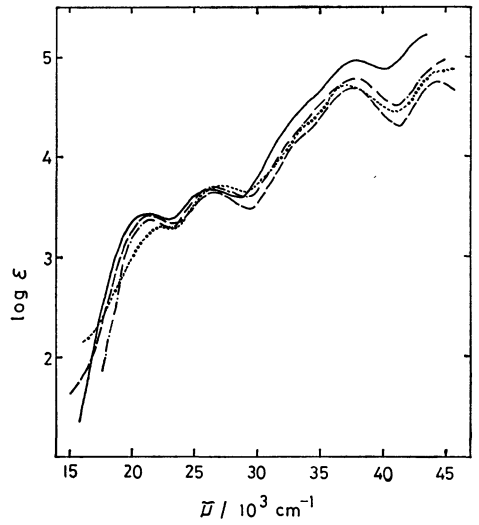

Fig. 3. Absorption spectra of *cis*-$[MoCl_2(phen)_2]Cl \cdot 4H_2O$ in dichloromethane (——), in acetonitrile (— —), in methanol (—·—), and in 0.1 mol dm^{-3} hydrochloric acid (----) (under nitrogen atmosphere).

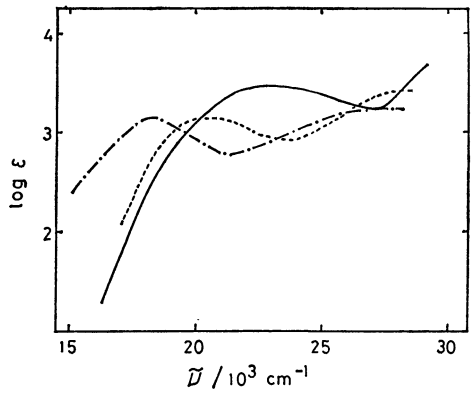

Fig. 4. Absorption spectra in *N*,*N*-dimethylformamide of $[MoCl_2(bpy)_2]^+$ (——), $[MoCl_3(bpy)(py)]$[8] (----), and $[MoCl_4(bpy)]^-$ [8] (—·—) (under nitrogen atmosphere).

(II),[24] ruthenium(II),[24,25] and osmium(II).[24,25] The absorption bands of the former and the latter group of complexes have been assigned to the d-d transitions, and the metal-to-ligand charge transfer (d-π*) transitions, respectively. The extinction coefficient, as well as the ease of oxidation of molybdenum(III) state, suggest that the bands of *cis*-$[MoCl_2(phen)_2]^+$ and $[MoCl_2(bpy)_2]^+$ in the visible region are of the d-π* charge transfer type.

The difference in spectral pattern of d-π* transitions between the bpy and the phen complexes is found in the complexes of other metal ions. The d-π* transitions (near 23000 cm^{-1}) appear as a sharp maximum and a prominent shoulder for $[Ru^{II}(bpy)_3]^{2+}$ and two distinct peaks for $[Ru^{II}(phen)_3]^{2+}$.[29] *cis*-$[Ir^{III}Cl_2(bpy)_2]^+$ shows one maximum near 28000 cm^{-1},[28,30] while *cis*-$[Ir^{III}Cl_2(phen)_2]^+$ shows one maximum and a prominent shoulder.[23,31] Also an appreciable difference is observed between the tris(bpy) and the tris(phen) complexes of iron(II)[32] as well as osmium(II).[33] On the other hand, the difference is very small between *cis*-$[Fe^{II}Cl_2(bpy)_2]$ and *cis*-$[Fe^{II}Cl_2(phen)_2]$.[24,25,34]

Thus the d-π* spectral pattern is not necessarily similar between the bpy and the phen complexes. The difference of the spectral patterns of the present complexes does not contradict our assignment of the d-π* charge transfer transitions.

Comparison with Analogous Molybdenum(III) Complexes in the Visible Region: The absorption bands of (bpyH)-[$MoCl_4$(bpy)] and [$MoCl_3$(bpy)py] in the visible region[8] (Fig. 4) must be of charge-transfer type as judged from their intensity. The absorption peaks give blue shift with decrease in number of chloride ligand. This fact implies that these bands involve the transition from d-orbitals of molybdenum(III) to the ligand π^*-orbital. The increase in number of nitrogen (the decrease in number of chloride) causes the increase in the degree of d-orbital splitting which would increase the gap between the occupied d-orbitals and the ligand π^*-orbitals. The change in overall charge of the complexes can be also responsible for the band shift.[35]

T.S.M. has learned the technique of handling air-sensitive materials from Professor Junnosuke Fujita and his collaborators at Nagoya University (Department of Chemistry), to whom the authors' thanks are due. The authors also would like to thank Professor Toyonobu Asao of Tohoku University (College of General Education) for the measurement of the infrared spectra (Hitachi 215) and Dr. M. Kogi of Tohoku University (Department of Physics) for the measurement of the magnetic moment.

References

1) E. I. Stiefel, *Progr. Inorg. Chem.*, **22**, 1 (1977), and references therein.
2) S. P. Ghosh and K. M. Prasad, *J. Inorg. Nucl. Chem.*, **40**, 1963 (1978).
3) T. Saji and S. Aoyagui, *J. Electroanal. Chem.*, **63**, 405 (1975), and references therein.
4) For example, P. J. Taylor and A. A. Shilt, *Inorg. Chim. Acta*, **5**, 691 (1971).
5) M. C. Steele, *Aust. J. Chem.*, **10**, 489 (1957).
6) E. A. Allen, K. Feenan, and G. W. A. Fowles, *J. Chem. Soc.*, **1965**, 1636.
7) W. M. Carmichael, D. A. Edwards, and R. A. Walton, *J. Chem. Soc., A*, **1966**, 97.
8) P. A. Marzilli and D. A. Buckingham, *Aust. J. Chem.*, **19**, 2259 (1966).
9) D. W. Du Bois, R. T. Iwamoto, and J. Kleinberg, *Inorg. Chem.*, **8**, 815 (1969).
10) A. D. Westland and N. Muriithi, *Inorg. Chem.*, **12**, 2356 (1973).
11) Y. Sasaki and A. G. Sykes, *J. Chem. Soc., Dalton Trans.*, **1975**, 1078. We used $Na_2MoO_4 \cdot 2H_2O$ instead of $H_2MoO_4 \cdot H_2O$ as the starting material.
12) D. F. Shriver, "The Manipulation of Air-Sensitive Compounds," McGraw-Hill, New York (1969) p. 141.
13) B. M. Figgis, J. Lewis, and F. E. Mabbs, *J. Chem. Soc.*, **1961**, 3138.
14) K. Nakamoto, "Infrared Spectra of Inorganic and Coordination Compounds," 2nd ed, John Wiley & Sons, New York (1963).
15) a) P. Pfeiffer and Br. Werdelman, *Z. Anorg. Allg. Chem.*, **263**, 31 (1950); b) F. H. Burstall and R. S. Nyholm, *J. Chem. Soc.*, **1952**, 3750.
16) R. G. Inskeep and J. Bjerrum, *Acta Chem. Scand.*, **15**, 62 (1961).
17) B. R. Baker and B. D. Mehta, *Inorg. Chem.*, **4**, 848 (1965).
18) K. Toriumi, T. S. Morita, and T. Ito, *Acta Crystallogr. Sect. B*, to be published.
19) W. A. Baker, Jr., and M. G. Phillips, *Inorg. Chem.*, **5**, 1042 (1966).
20) M. P. Hancock, J. Josephsen, and C. E. Schäffer, *Acta Chem. Scand.*, **A30**, 79 (1976).
21) A. A. Vlček, *Inorg. Chem.*, **6**, 1425 (1967).
22) D. H. W. Carstens and G. A. Crosby, *J. Mol. Spectrosc.*, **34**, 113 (1970).
23) R. Ballardini, G. Varani, L. Moggi, V. Balzani, K. R. Olson, F. Scandola, and M. Z. Hoffman, *J. Am. Chem. Soc.*, **97**, 728 (1975).
24) J. E. Fergusson and G. M. Harris, *J. Chem. Soc., A*, **1966**, 1293.
25) G. M. Bryant, J. E. Fergusson, and H. K. J. Powell, *Aust. J. Chem.*, **24**, 257 (1971).
26) P. Day and N. J. Sanders, *J. Chem. Soc., A*, **1967**, 1530, 1536, and references therein.
27) I. Hanazaki and S. Nagakura, *Inorg. Chem.*, **8**, 648 (1969).
28) R. D. Gillard and B. T. Heaton, *J. Chem. Soc., A*, **1969**, 451.
29) G. A. Crosby, W. G. Perkins, and D. M. Klassen, *J. Chem. Phys.*, **43**, 1498 (1965).
30) R. J. Watts and G. A. Crosby, *J. Am. Chem. Soc.*, **93**, 3184 (1971).
31) R. Ballardini, G. Varani, L. Moggi, and V. Balzani, *J. Am. Chem. Soc.*, **99**, 6881 (1977).
32) D. H. Busch and J. C. Bailar, Jr., *J. Am. Chem. Soc.*, **78**, 1137 (1956).
33) J. N. Demas and G. A. Crosby, *J. Am. Chem. Soc.*, **93**, 2841 (1971).
34) K. Madeja and E. König, *J. Inorg. Nucl. Chem.*, **25**, 377 (1963).
35) T. Ito, N. Tanaka, I. Hanazaki, and S. Nagakura, *Bull. Chem. Soc. Jpn.*, **42**, 702 (1969).

  Bull. Chem. Soc. Jpn., 54, 2683—2690 (1981)

Preparation, Resolution, and Absorption and Circular Dichroism Spectra of $[Co(en)_n\{NH_2CH_2CH_2P(CH_3)_2\}_{3-n}]^{3+}$ and the Related Complexes, and the Absolute Configuration of $(+)_{589}$-*fac*-$[Co\{NH_2CH_2CH_2P(CH_3)_2\}_3]^{3+}$ Determined by X-Ray Analysis

Isamu KINOSHITA,† Kazuo KASHIWABARA, Junnosuke FUJITA,*
Keiji MATSUMOTO,† and Shun'ichiro OOI†

Department of Chemistry, Faculty of Science, Nagoya University, Chikusa-ku, Nagoya 464
† *Department of Chemistry, Faculty of Science, Osaka City University, Sumiyoshi-ku, Osaka 558*

(Received March 26, 1981)

A series of complexes, $[Co(en)_n\{NH_2CH_2CH_2P(CH_3)_2\}_{3-n}]^{3+}$ (en=ethylenediamine, n=0,1,2) and three bis(ethylenediamine)cobalt(III) complexes of the related ligands, $NH_2CH_2CH_2P(C_6H_5)_2$, (*S*)-$NH_2CH(CH_3)CH_2P(C_6H_5)_2$, and *rac*-$NH_2CH_2CH_2P(C_4H_9)(C_6H_5)$ were prepared and resolved (or separated) into optical isomers, and their absorption and circular dichroism spectra were recorded. The molecular structure and the absolute configuration of $(+)_{589}$-*fac*-$[Co\{NH_2CH_2CH_2P(CH_3)_2\}_3]Br_3\cdot 3H_2O$ were determined by X-ray analysis. The crystals are lemon-yellow, orthorhombic, a=26.501(8), b=9.573(4), c=10.081(5) Å, space group $P2_12_12_1$, z=4. The Co atom is surrounded by 3P and 3N in the facial manner with the average distances of 2.237 and 2.041 Å, respectively. The absolute configuration of the complex ion is Δ. The chelate rings are puckered and chiral to form a pseudo λ gauche conformation.

Most of cobalt(III) complexes of tertiary phosphines so far known are those formed with unsaturated ligands such as dimethylglyoximate or acetylacetonate ions, and no complex with saturated ligands such as ammonia or ethylenediamine seems to be reported.[1] In a previous paper,[2] we have reported that (2-aminoethyl)diphenylphosphine and its related ligands, $NH_2CH(R^1)CH_2PR^2R^3$, give stable bis(acetylacetonato)cobalt(III)-type complexes, forming a five- membered chelate ring. This paper is concerned with preparation, resolution, and absorption and circular dichroism (CD) spectra of a series of complexes, $[Co(en)_n\{NH_2CH_2CH_2P(CH_3)_2\}_{3-n}]^{3+}$ (en=ethylenediamine, n=0, 1, 2), and the related complexes. These diamine–alkylphosphine complexes would be useful for studying ligand field absorption spectra of a cobalt(III)–phosphine complex of which little work has been done, since they have no unsaturated group which often shows strong absorption bands in the region where ligand field absorption bands would arise. The paper also reports the molecular structure and absolute configuration of $(+)_{589}$-*fac*-Δ-$[Co\{NH_2CH_2CH_2P(CH_3)_2\}_3]^{3+}$ determined by the X-ray method.

Experimental

Free aminoalkylphosphines were handled under nitrogen atmosphere until they formed air-stable cobalt(III) complexes. Absorption, CD, and ^1H and ^{13}C NMR spectra were recorded on a Hitachi 323 spectrophotometer, a JASCO J-40 spectropolarimeter, and JEOL JNM-PMX 60 and JNM-FX 100 spectrometers, respectively.

Preparation of Ligands. *(2-Aminoethyl)dimethylphosphine (edmp)*: To liquid ammonia (100 cm³) containing metallic sodium (1.08 g, 0.047 mol) in a 300 cm³ three-necked, round-bottomed flask equipped with a mechanical stirrer and an ammonia gas inlet was added tetramethyldiphosphine[3] (2.88 g, 0.024 mol) with stirring at −78 °C. After 30 min, 2-chloroethylamine hydrochloride (2.74 g, 0.024 mol) was added with small portions, giving a colorless solution. On evaporation of liquid ammonia, a mixture of a white solid and oily edmp was obtained. The edmp was extracted with chloroform (50 cm³). The chloroform was removed *in vacuo* to give transparent, colorless liquid of edmp (1.1 g). It was used for the preparation of complexes without further purification.

(2-Aminoethyl)diphenylphosphine (edpp),[4] *(S)-(2-aminopropyl)-diphenylphosphine (pdpp)*,[2] and racemic[5] and optically active[6] *(2-aminoethyl)butylphenylphosphine (ebpp)* were prepared according to the procedures reported.

Preparation of Complexes. *$[Co(edmp)_3]^{3+}$, $[Co(en)(edmp)_2]^{3+}$, and $[Co(en)_2(edmp)]^{3+}$*: These complexes and the known $[Co(en)_3]^{3+}$ complex were yielded by the reaction of *cis*-$[CoCl_2(en)_2]Cl$ with edmp in *N*,*N*-dimethylformamide (DMF). To a DMF solution (50 cm³) of *cis*-$[CoCl_2(en)_2]Cl$ (285 mg, 1 mmol) was added edmp (105 mg, 3 mmol) with stirring. The resulting blue-green solution was allowed to stirr overnight at room temperature to give a yellow precipitate, which was filtered and dissolved in water. The solution was poured onto a column (ϕ 2.7×80 cm) of SP-Sephadex C-25, and the product adsorbed was eluted with an aqueous 0.4 mol/dm³ NaBr solution. A good separation into four yellow bands was observed. The last orange yellow eluate contained $[Co(en)_3]^{3+}$. Each of the other three eluates was diluted ten times with water and poured again onto a small column of SP-Sephadex C-25. The complex adsorbed was eluted with an aqueous 1 mol/dm³ NaBr solution, and the eluate was concentrated in a vacuum desiccator over P_4O_{10} to give yellow crystals, which were filtered, washed with a small amount of water, and air-dried. The first, second, and third eluates gave racemates of $[Co(edmp)_3]Br_3\cdot 3H_2O$, $[Co(en)(edmp)_2]Br_3\cdot H_2O$, and $[Co(en)_2(edmp)]Br_3\cdot H_2O$, respectively. Although the first two complexes can have geometrical isomers, only one isomer was yielded for each of them, no indication for the presence of other isomers being observed on column chromatography. The total yield of the four complexes including $[Co(en)_3]^{3+}$ was *ca.* 70%, and the formation ratio was *ca.* 8:2:1:7 for $[Co(edmp)_3]^{3+}$: $[Co(en)(edmp)_2]^{3+}$: $[Co(en)_2(edmp)]^{3+}$: $[C(en)_3]^{3+}$.

The racemates were resolved by SP-Sephadex column chromatography. Each racemate charged on the top of a column (ϕ 2.7×80 cm) of SP-Sephadex C-25 was eluted with an aqueous 0.2 mol/dm³ sodium $(+)_{589}$-tartratoantimonate(III) solution. A good separation between enantiomers was observed. In the case of $[Co(edmp)_3]^{3+}$ lemon-yellow crystals of optically active $[Co(edmp)_3]Br_3\cdot 3H_2O$ were obtained by the same method as that for the racemate,

TABLE 1. ANALYTICAL DATA OF THE NEW COMPLEXES

Complex	C (%) Found(Calcd)	H (%) Found(Calcd)	N (%) Found(Calcd)
$[Co\{NH_2CH_2CH_2P(CH_3)_2\}_3]Br_3\cdot 3H_2O$	21.08(21.57)	6.28(6.35)	6.28(6.29)
Λ-$[Co\{NH_2CH_2CH_2P(CH_3)_2\}_3]Br_3\cdot 3H_2O$	21.24(21.57)	6.24(6.35)	6.22(6.29)
$[Co(en)\{NH_2CH_2CH_2P(CH_3)_2\}_2]Br_3\cdot H_2O$	20.14(20.46)	5.77(5.83)	9.29(9.54)
$[Co(en)_2\{NH_2CH_2CH_2P(CH_3)_2\}]Br_3\cdot 2H_2O$	17.55(17.73)	5.53(5.58)	12.80(12.92)
$[Co(en)_2\{NH_2CH_2CH_2P(C_6H_5)_2\}]Br_3\cdot 2H_2O$	31.37(31.60)	5.20(5.30)	10.15(10.24)
Λ-$[Co(en)_2\{(S)$-$NH_2CH(CH_3)CH_2P(C_5H_5)_2\}]Br_3\cdot 2H_2O$	32.50(32.69)	5.36(5.48)	9.77(10.03)
Λ-$[Co(en)_2\{(R)$-$NH_2CH_2CH_2P(C_4H_9)(C_6H_5)\}]Br_3\cdot 4NaBr$	18.59(18.48)	3.67(3.49)	6.77(6.74)
$[Co(en)_2\{rac$-$NH_2CH_2CH_2P(C_4H_9)(C_6H_5)\}]Br_3\cdot 2H_2O$(Band II)	29.03(28.94)	5.55(6.07)	10.40(10.54)

en: $NH_2CH_2CH_2NH_2$.

The enantiomer obtained from the faster moving band showed negative rotation at 589 nm (Λ-isomer). In the cases of $[Co(en)(edmp)_2]^{3+}$ and $[Co(en)_2(edmp)]^{3+}$, however, the enantiomers were not isolated because of small amounts, and the CD spectra were obtained by the following method. Each eluate of the enantiomers was diluted with water and poured onto a small column of SP-Sephadex C-25. After washing the column with 0.05 mol/dm^3 hydrochloric acid, the enantiomer was eluted with 1 mol/dm^3 hydrochloric acid. The eluate was evaporated to dryness under reduced pressure, and the residue was dissolved in water. On addition of $K_3[Co(CN)_6]$, a yellow precipitate was obtained. It was filtered, washed with water, and then mixed with Dowex 1×8 anion exchange resin in the bromide form and a small amount of water. The mixture was stirred for a few hours and filtered. The filtrate which contains the complex bromide was used for CD measurement, and its concentration was determined from ε values of the racemate. In all the resolutions, the Λ isomers were always eluted faster than their antipodes.

$[Co(en)_2(edpp)]^{3+}$. A DMF solution (50 cm^3) containing *cis*-$[CoCl_2(en)_2]Cl$ (363 mg) and edpp (292 mg) was stirred overnight at room temperature. The resulting brown solution was poured into 1 dm^3 of water to give a precipitate, which was filtered off. The filtrate was poured onto a column (ϕ 2.7×80 cm) of SP-Sephadex C-25, and the product adsorbed was eluted with an aqueous 0.2 mol/dm^3 Na_2SO_4 solution. Many bands were observed. The first and second orange yellow eluates contained $[Co(en)_3]^{3+}$ and $[Co(en)_2(edpp)]^{3+}$, respectively. The second eluate was evaporated to dryness under reduced pressure, and the complex was extracted with methanol. The extract was diluted with water and poured onto a column (ϕ 2.7×80 cm) of SP-Sephadex C-25. By elution with an aqueous 0.2 mol/dm^3 sodium $(+)_{589}$-tartratoantimonate(III) solution, two bands corresponding to a pair of enantiomers were obtained. Each eluate was diluted with water, poured again onto a small column of SP-Sephadex C-25, and the enantiomer adsorbed was eluted with an aqueous 1 mol/dm^3 NaBr solution. On concentration *in vacuo*, the eluate gave orange yellow crystals of optically active $[Co(en)_2(edpp)]Br_3\cdot 2H_2O$, which were collected and washed with a small amount of water. Yield: 30 mg for each enantiomer.

*$[Co(en)_2$(S-*pdpp*$)]^{+}$.* This complex was prepared by a method similar to that for the edpp complex using *S*-pdpp (242 mg) and *cis*-$[CoCl_2(en)_2]Cl$ (285 mg). A pair of diastereomers were separated by similar column chromatography using an aqueous 0.2 mol/dm^3 sodium $(+)_{589}$-tartratoantimonate(III) solution as an eluent. Yellow crystals of Λ-$[Co(en)_2(S$-pdpp$)]Br_3\cdot 2H_2O$ (55 mg) were isolated by a method similar to that for the edpp complex, but another diastereomer was not isolated because of a very small amount.

*$[Co(en)_2$(rac-*ebpp*$)]^{3+}$.* Four isomers of this complex were obtained by a method similar to that for the edpp complex, using *rac*-ebpp (252 mg) and *cis*-$[CoCl_2(en)_2]Cl$ (343 mg). By elution with an aqueous 0.2 mol/dm^3 Na_2SO_4 solution, the orange yellow band of $[Co(en)_3]^{3+}$ and two yellow bands, I and II were eluted in succession. Bands I and II correspond to a pair of racemates, $\Lambda(R)$ and $\Lambda(S)$, and $\Lambda(S)$ and $\Lambda(R)$ isomers, respectively. The former racemate was resolved by the same column chromatographic method as that for the edpp complex. Yellow crystals of Λ-$[Co(en)_2(R$-ebpp$)]Br_3\cdot 4NaBr$ (8 mg) were obtained from the faster moving eluate. However, the yield of the latter racemate was poor, and thus the complex was isolated as the racemate, $[Co(en)_2(rac$-ebpp$)]Br_3\cdot 2H_2O$ (3.9 mg). The CD spectrum was determined by a method similar to that for the en-edmp complexes without isolating the active complex, the $\Lambda(S)$ isomer being eluted faster.

Analytical data of the new complexes are given in Table 1.

Structure Determination of $(+)_{589}$-$[Co(edmp)_3]Br_3\cdot 3H_2O$. Crystal data: orthorhombic, a=26.501(8), b=9.573(4), c=10.081(5) Å, U=2557.5(15), D_m=1.73, D_c=1.73 g cm^{-3}, Z=4, μ(Mo $K\alpha$)=58.3 cm^{-1}, λ(Mo $K\alpha$)=0.7107 Å, space group $P2_12_12_1$. The Laue symmetry, space group extinctions, and approximate unit-cell dimensions were obtained from Weissenberg photographs. The unit-cell dimensions were refined by the least squares analysis of 38θ values automatically centered on a Phillips PW 1100 diffractometer by the use of Mo $K\alpha$ radiation. The intensity data (2θ=52°) were collected on the diffractometer using Graphite-monochromated Mo $K\alpha$ radiation. The specimen size was 0.17×0.18×0.28 mm^3. The ω-2θ scan mode was employed. The scan range was $(0.7+0.2\tan\theta)°$, and the scan speed, 0.025 °/s. The background was counted for half of the scan time as each end of the scan range. During the data collection, the intensities of 3 standard reflections were monitored every 4 h in order to check the orientation and stability of the crystal. No appreciable decay was observed. A total of 1924 reflections with $I>3\sigma(I)$ were observed and used in the subsequent structure determination and refinement. The observed intensities were corrected for Lorents-polarization and absorption effect, and the relative structure factors were derived.

The crystal structure was solved by the heavy-atom method. The parameters of all the non-hydrogen atoms were refined by the block-diagonal least-squares method, using anisotropic temperature factors for the Br, Co, and P atoms. The final agreement indices, R and $Rw=|W\Delta F^2/WF_o^2|^{1/2}$, were 6.57 and 6.55%, respectively. The function minimized was $\sum W(F_o-|F_c|)^2$, with $W=1/\sigma^2(F_o)$ being used. No attempt was made to locate H atoms. All the parameter shifts in the final cycle refinement were less than 0.5σ. The

Table 2. Positional and thermal parameters with their e.s.d. values in parenthesis

Atom	x	y	z	U/Å^2
Br(1)	0.4930(1)	0.1659(2)	0.5087(2)	a)
Br(2)	0.1268(1)	0.3619(2)	0.0156(2)	a)
Br(3)	0.2295(1)	0.2180(2)	0.5115(2)	a)
Co	0.3633(1)	0.1584(2)	0.0181(2)	a)
P(1)	0.3567(1)	0.1673(4)	0.0008(4)	a)
P(2)	0.4474(1)	0.1377(4)	0.0307(4)	a)
P(3)	0.3664(2)	0.3069(4)	−0.1537(4)	a)
N(1)	0.2859(4)	0.1505(12)	0.0261(11)	0.029(3)
N(2)	0.3643(5)	0.0004(13)	0.1517(13)	0.028(3)
N(3)	0.3551(4)	0.0057(13)	−0.1216(11)	0.024(3)
C(1)	0.2869(6)	0.3548(19)	0.1756(15)	0.039(4)
C(2)	0.2652(6)	0.2147(17)	0.1529(16)	0.039(4)
C(3)	0.3838(6)	0.5011(17)	0.1437(15)	0.033(4)
C(4)	0.3738(6)	0.2827(17)	0.3369(15)	0.038(4)
C(5)	0.4565(6)	−0.0069(17)	0.1498(15)	0.031(4)
C(6)	0.4077(6)	−0.0951(15)	0.1415(13)	0.023(4)
C(7)	0.4872(6)	0.2772(18)	0.0918(17)	0.040(4)
C(8)	0.4813(6)	0.0739(18)	−0.1133(17)	0.040(5)
C(9)	0.3600(5)	0.1891(15)	−0.2991(13)	0.028(4)
C(10)	0.3330(6)	0.0531(16)	−0.2516(14)	0.030(4)
C(11)	0.4217(6)	0.4126(18)	−0.1911(16)	0.037(4)
C(12)	0.3132(6)	0.4350(18)	−0.1732(16)	0.040(5)
O(1)	0.0780(5)	0.2121(16)	0.2793(14)	0.076(5)
O(2)	0.2188(5)	0.2204(15)	0.8283(14)	0.077(4)
O(3)	0.1110(4)	0.0246(12)	0.9469(11)	0.048(3)

a) Anisotropic temperature factors ($\times 10^4$/Å^2) expressed in the form $\exp[-2^2(U_{11}h^2a^{*2}+U_{22}k^2b^{*2}+U_{33}l^2c^{*2}+2U_{12}hka^*b^*+2U_{13}hla^*c^*+2U_{23}klb^*c^*)]$.

Atom	U_{11}	U_{22}	U_{33}	U_{12}	U_{13}	U_{23}
Br(1)	435(9)	435(9)	398(9)	64(85)	−67(9)	21(12)
Br(2)	757(12)	437(10)	416(10)	13(10)	113(12)	−19(11)
Br(3)	529(10)	487(10)	357(9)	−154(9)	5(10)	−3(16)
Co	231(9)	212(9)	165(8)	−5(9)	17(10)	−5(10)
P(1)	281(24)	288(24)	197(18)	15(21)	34(19)	1(19)
P(2)	295(21)	237(20)	221(20)	19(18)	5(18)	−19(20)
P(3)	291(23)	256(23)	183(18)	31(20)	14(20)	37(18)

final difference Fourier map was rather flat and showed no peak of structural significance. The atomic scattering factors were taken from Ref. 7. The real and imaginary parts of the anomalous dispersion correction were applied for the Br, Co, and P atoms. The atomic coordinates and the temperature factors are listed in Table 2. A complete list of observed and calculated structure factors is preserved by the Chemical Society of Japan (Document No. 8146).

The absolute configuration of the complex cation was determined by the anomalous dispersion technique. Table 3 gives the calculated structure amplitudes of several Bijvoet pairs and the observed inequality relationships which were obtained from Weissenberg photographs taken with Cu $K\alpha$ radiation. The observed relationships indicate that the absolute configuration of the complex ion is $\Lambda(\lambda\lambda\lambda)$.

Results and Discussion

Preparation and Properties of the Complexes. The reaction of edmp with *cis*-$[CoCl_2(en)_2]^+$ in the mole ratio of 3:1 in DMF under nitrogen atmosphere gives a series of complexes, $[Co(edmp)_3]^{3+}$, $[Co(en)(edmp)_2]^{3+}$, $[Co(en)_2(edmp)]^{3+}$, and $[Co(en)_3]^{3+}$ in the ratio of 8:2:1:7. The formation ratio of these tris-type complexes varies on changing the mole ratio of the starting materials. The reaction with a large excess of edmp affords almost only $[Co(edmp)_3]^{3+}$. However, the product obtained with an equivalent mole of the ligand involves the blue *trans*-$[CoCl_2(edmp)_2]^+$ complex, which can be isolated.[8] This suggests that the en ligands in *cis*-$[CoCl_2(en)_2]^+$ are easily replaced by edmp without dissociating the chloride ions. The fact that on addition of edmp the DMF solution of *cis*-$[CoCl_2(en)_2]^+$ changes almost instantly from violet to blue-green also implies the rapid formation of *trans*-$[CoCl_2(edmp)_2]^+$ (Experimental). The dichloro complex thus formed will be transformed to the tris en-edmp complexes by substitution reactions with free en or edmp ligands. On the other hand, the other phenyl- and diphenyl-(aminoalkyl)-phosphines form only $[Co(en)_2$(aminoalkylphos-

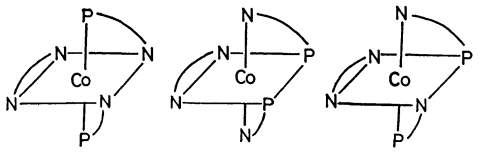

Fig. 1. Three geometrical isomers of $[Co(en)(N\text{-}P)_2]^{3+}$.

phine)]$^{3+}$ by similar reactions with *cis*-$[CoCl_2(en)_2]^+$. Aminoalkylphosphines with a bulky and electron withdrawing phenyl group on the phosphorus atom seem to have weaker affinity than edmp toward the cobalt(III) ion. All the aminoalkylphosphine complexes thus obtained are stable in both the solid state and aqueous solutions.

The $[Co(edmp)_3]^{3+}$ and $[Co(en)(edmp)_2]^{3+}$ complexes have two (*mer* and *fac*) and three (*trans*(P,P), *trans*(N,N), and *trans*(P,N)) possible geometrical isomers, respectively, for the arrangement of P and N atoms of edmp (Fig. 1). However, each complex gives only one isomer by the reactions under the conditions given. The *S*-pdpp complex which has a chiral carbon atom on the chelate ring yields almost one diastereomer stereoselectively, a very small amount of another diastereomer being observed in column chromatography. The *rac*-ebpp ligand has a chiral phosphorus donor atom and its bis-en complex gives a pair of racemates, $\Lambda(R)$ and $\Delta(S)$, and $\Lambda(S)$ and $\Delta(R)$, but there is also a fairly difference between the yields of the racemates. All racemates of the aminoalkylphosphine complexes were resolved completely by the SP-Sephadex column chromatographic method using 0.2 mol/dm^3 sodium $(+)_{589}$-tartratoantimonate(III) as an eluent. The Λ isomers are always eluted faster than the Δ isomers. The isomers are stable to racemization in aqueous solutions.

The Structure of $(+)_{589}$-$[Co(edmp)_3]Br_3\cdot 3H_2O$. A perspective view of the $(+)_{589}$-$[Co(edmp)_3]^{3+}$ ion is shown in Fig. 2. Table 4 gives the interatomic distances and bond angles within the complex ion. The complex ion has approximate C_3 symmetry, and the P atoms are arranged in the facial manner. The absolute configuration is determined to be Δ on the basis of the data given in Table 3. The chelate rings are puckered with a pseudo λ gauche form. The C–C bonds are nearly parallel to the C_3 axis of the complex ion. Thus, the complex ion can be designated as the $lel_3(\Delta(\lambda\lambda\lambda))$ isomer. The average Co–P distance of 2.237 Å is fairly short as compared with those (2.3—2.4 Å) reported for $[CoX(PR_3)(dmg)_2]$-type complexes (R=–C_6H_5, –C_4H_9; dmg=dimethylglyoximate ion).[9] The Co–N distance averages 2.041 Å, which is significantly longer than that of 1.978 Å in $[Co(en)_3]^{3+}$.[10] The elongation of Co–N distances can be attributed to the strong *trans* effect of the donating P atoms. Each ligand forms a five-membered chelate ring with an average P–Co–N angle of 84.8°, which is nearly the same as the average N–Co–N angle of 85.4° in $[Co(en)_3]^{3+}$.[10] The average distances of P–CH_3 and P–CH_2 are 1.827 and 1.859 Å, respectively. The average angle of P–Co–P (94.3°) is fairly larger than that of N–Co–N (85.8°), and the

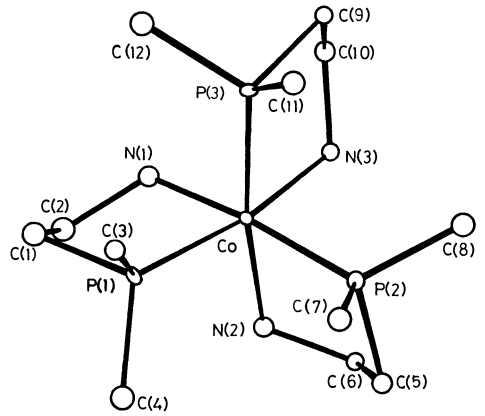

Fig. 2. A perspective view of the $(+)_{589}$-$[Co(edmp)_3]^{3+}$ ion.

TABLE 3. OBSERVED AND CALCULATED INTENSITIES BETWEEN SOME *hkl* AND $\bar{h}kl$ REFLECTIONS

hkl	$\lvert F_c(hkl)\rvert$	$\lvert F_c(\bar{h}kl)\rvert$	Observed
221	85	73	>
321	71	50	>
421	121	127	<
521	222	193	>
131	59	35	>
511	159	171	<
322	124	96	>
323	129	141	<
423	99	110	<

average Co–P–CH_3(//) angle of 122.7° is also larger than the other Co–P–CH_3($\perp$) and Co–P–CH_2 angles as shown in Table 4, where the CH_3(//) and CH_3($\perp$) denote those parallel and perpendicular to the C_3 axis of the complex ion, respectively. Thus the overcrowding due to the facial three CH_3(//) groups is relieved, although the non-bonded C···C distances (3.51—3.62 Å) among these CH_3(//) groups are still shorter than the sum of the van der Waals radius of a methyl group (4 Å). The non-bonded C···C distances between the CH_3($\perp$) and the P–CH_2 are also shorter than 4 Å. Such a crowded structure seems to afford the conformation of the chelate ring differing from the typical gauche form. The dihedral angles of the N–C–C–P moieties are 53.3°, 48.7°, and 44.3°.

The packing mode of the complex ions, bromide ions, and water molecules is illustrated in Fig. 3. Some short interatomic distances outside the complex ions are listed in Table 5. One out of three bromide ions lies approximately on the C_3 axis of the complex ion to form weak N–H···Br hydrogen bonds (3.38—3.56 Å) with three N–H atoms parallel to the C_3 axis in the three facial NH_2 groups. The other N–H groups are also linked by N–H···O or N–H···Br hydrogen bonds.

Absorption and CD Spectra. Absorption spectra of a series of the $[Co(en)_n(edmp)_{3-n}]^{3+}$ complexes are shown in Fig. 4, and the data given in Table 6. With an increase in the number of ligating phosphorus

Table 4. Bond distances (l/Å) and angles (ϕ/°)

Co-P(1)	2.231(5)	P(1)-C(1)	1.869(18)	P(3)-C(9)	1.858(16)	N(3)-C(10)	1.505(20)
Co-P(2)	2.239(4)	P(1)-C(3)	1.810(17)	P(3)-C(11)	1.824(18)		
Co-P(3)	2.242(5)	P(1)-C(4)	1.825(17)	P(3)-C(12)	1.877(17)	C(1)-C(2)	1.479(24)
Co-N(1)	2.055(12)	P(2)-C(5)	1.849(16)			C(5)-C(6)	1.548(22)
Co-N(2)	2.024(13)	P(2)-C(7)	1.809(18)	N(1)-C(2)	1.521(20)	C(9)-C(10)	1.560(22)
Co-N(3)	2.043(12)	P(2)-C(8)	1.816(18)	N(2)-C(6)	1.472(19)		

P(1)-Co-P(2)	96.0(2)	Co-P(1)-C(1)	101.7(6)	C(9)-P(3)-C(12)	104.4(7)
P(1)-Co-P(3)	93.3(2)	Co-P(1)-C(3)	123.2(6)		
P(1)-Co-N(1)	85.5(4)	Co-P(1)-C(4)	115.7(6)	Co-N(1)-C(2)	112.3(9)
P(1)-Co-N(2)	95.8(4)	C(1)-P(1)-C(3)	106.3(8)	Co-N(2)-C(6)	115.4(9)
P(1)-Co-N(3)	169.3(4)	C(1)-P(1)-C(4)	103.6(8)	Co-N(3)-C(10)	115.2(9)
		C(3)-P(1)-C(4)	104.4(8)		
P(2)-Co-P(3)	93.7(2)			N(1)-C(2)-C(1)	110.7(13)
P(2)-Co-N(1)	171.0(4)	Co-P(2)-C(5)	103.5(5)	N(2)-C(6)-C(5)	108.0(12)
P(2)-Co-N(2)	83.4(4)	Co-P(2)-C(7)	122.3(6)	N(3)-C(10)-C(9)	109.8(12)
P(2)-Co-N(3)	94.7(4)	Co-P(2)-C(8)	118.5(6)		
		C(5)-P(2)-C(7)	104.8(8)	P(1)-C(1)-C(2)	105.1(12)
P(3)-Co-N(1)	95.1(4)	C(5)-P(2)-C(8)	101.7(8)	P(2)-C(5)-C(6)	105.3(10)
P(3)-Co-N(2)	170.6(4)	C(7)-P(2)-C(8)	103.4(8)	P(3)-C(9)-C(10)	107.8(10)
P(3)-Co-N(3)	85.7(4)				
		Co-P(3)-C(9)	102.8(5)		
N(1)-Co-N(2)	87.5(5)	Co-P(3)-C(11)	122.7(6)		
N(1)-Co-N(3)	83.9(5)	Co-P(3)-C(12)	118.0(6)		
N(2)-Co-N(3)	85.7(5)	C(9)-P(3)-C(11)	104.3(7)		

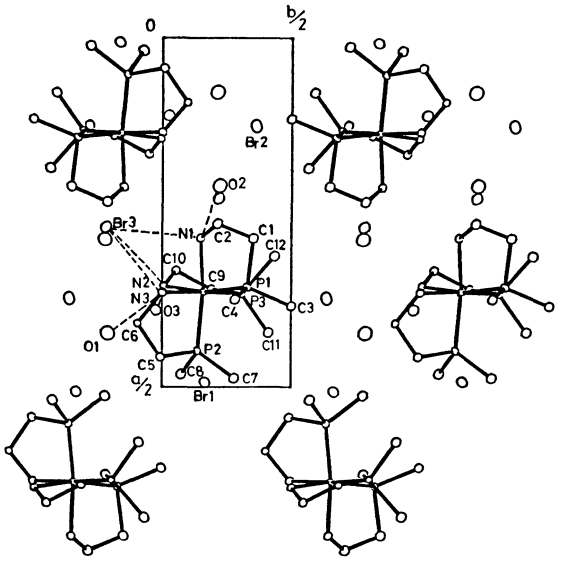

Fig. 3. Projection of the crystal structure along the c axis. Possible hydrogen bonds are indicated by broken lines.

atoms, the first absorption bands are shifted to higher wavenumbers and increase the intensity. The wavenumber difference in the first absorption bands between $[Co(edmp)_3]^{3+}$ and $[Co(en)_3]^{3+}$ amounts to 2300 cm^{-1}, and edmp stands at a fairly higher position than en in the spectrochemical series. The band of $[Co(edmp)_3]^{3+}$ is symmetrical and shows no splitting, which agrees with a pattern expected from Yamatera's rule[11] for a complex with C_3 symmetry (*fac* isomer). The *fac* structure was confirmed by X-ray analysis (*vide ante*). The $[Co(en)_2(edmp)]^{3+}$ complex gives the first absorption band at 22400 cm^{-1}. This value is just an average of those of *fac*-$[Co(edmp)_3]^{3+}$ and $[Co(en)_3]^{3+}$, and also agrees with that expected for one of two components split in the first absorption band.[11] Another component which should be at the same wavenumber as that of the first absorption band of $[Co(en)_3]^{3+}$ would be hidden by this strong component. The first absorption band of $[Co(en)(edmp)_2]^{3+}$ shows the maximum at 23700 cm^{-1} and a shoulder at 21000 cm^{-1}. These values quite agree with those calculated for the *trans*(P,P) isomer according to Yamatera's rule. Thus the complex can be assigned to the *trans*(P,P) isomer. However, the absorption spectrum of this complex is very similar over the whole region to that of $[Co(en)_2(P\text{–}P)]^{3+}$ (P–P=1,2-bis(dimethylphosphino)ethane), which forms necessarily *cis*(P,P) configuration.[12] In general, ligands which exhibit the strong *trans* effect such as a phosphine tend to occupy the *cis* positions to each other in metal complexes.[13] In fact, the $[Co(edmp)_3]^{3+}$ complex yielded only the *fac* isomer, despite its structure seems to be more crowded than

Table 5. Relevant interatomic distances (l/Å)

Br(3)-N(1)	3.555(12)	C(3)-C(7)	3.518(23)
Br(3)-N(2)	3.542(13)	C(7)-C(11)	3.580(24)
Br(3)-N(3)	3.377(12)	C(11)-C(3)	3.621(23)
O(1)-N(3)	2.912(19)	C(1)-C(12)	3.665(25)
O(2)-N(2)	3.420(19)	C(4)-C(5)	4.007(25)
O(3)-N(2)	3.058(17)	C(8)-C(9)	3.877(23)
O(2)-N(1)	2.877(19)		

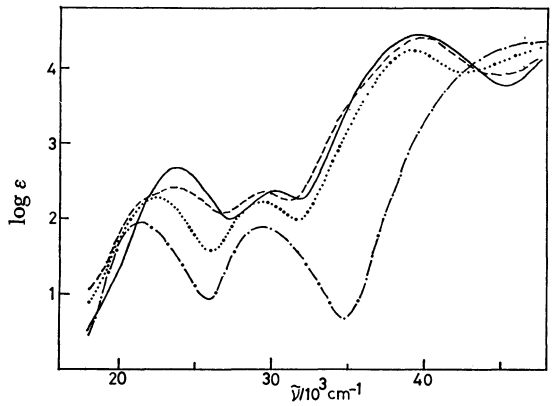

Fig. 4. Absorption spectra of $[Co(edmp)_3]^{3+}$ (——), $[Co(en)(edmp)_2]^{3+}$ (----), $[Co(en)_2(edmp)]^{3+}$ (·····), and $[Co(en)_3]^{3+}$ (—·—·—).

TABLE 6. ABSORPTION(AB) AND CD SPECTRAL DATA

Complex	$\tilde{\nu}^{AB}/10^3$ cm^{-1}(log ε)	$\tilde{\nu}^{CD}/10^3$ cm^{-1}(Δε)
Λ-$[Co(edmp)_3]^{3+}$	23.70(2.68)	22.32(+1.45)
		24.84(−1.57)
	30.18(2.36)	30.03(+0.49)
	39.76(4.42)	37.88(−20.6)
		40.98(+4.74)
		45.00(−9.33)
Λ-$[Co(en)(edmp)_2]^{3+}$	21.4 (2.2)(sh)	20.90(+2.07)
	23.72(2.41)	23.98(−0.89)
	29.43(2.34)	29.41(+0.62)
	39.84(4.38)	37.74(−9.9)
		40.50(+5.4)
		44.84(−14.9)
Λ-$[Co(en)_2(edmp)]^{3+}$	22.46(2.28)	20.47(+1.26)
		23.39(−0.16)
	29.28(2.23)	27.40(+0.36)
	39.22(3.92)	39 (−3.3)(sh)
		46.73(−17.8)
Λ-$[Co(en)_2(edpp)]^{3+}$	21.51(2.53)	19.88(+1.67)
		22.47(−0.91)
	32.63(4.17)	33.67(+10.4)
	44.44(4.39)	38 (+5)(sh)
		41.32(−0.7)
Λ-$[Co(en)_2(S\text{-pdpp})^{3+}$	21.51(2.54)	19.92(+1.80)
		22.30(−1.28)
	32.79(4.15)	34.36(+2.98)
	40.98(4.00)	38 (+4.5)(sh)
	44.50(4.43)	42.37(−3.4)
Λ-$[Co(en)_2(S\text{-ebpp})]^{3+}$	21.90(2.51)	20.16(+1.77)
		22.86(−0.58)
		27.97(+0.51)
	33.56(4.18)	33.22(−8.9)
	41 (4)(sh)	40.82(+0.9)
		43.96(−10.1)
		47.17(−3.7)
Λ-$[Co(en)_2(R\text{-ebpp})]^{3+}$	21.93(2.45)	20.08(+0.96)
		22.62(−1.42)
		28 (+0.6 ((sh)
	33.73(4.05)	34.01(+12.6)
	41 (3.9)(sh)	45.66(−29)

sh: Shoulder.

the *mer* isomer. In column chromatographic resolution using SP-Sephadex C-25 and a sodium $(+)_{589}$-tartratoantimonate(III) solution, the *Λ*-isomers are eluted faster for both $[Co(edmp)_3]^{3+}$ and $[Co(en)(edmp)_2]^{3+}$. For five-membered chelate complexes, it is reported that in complexes with three facial NH_2 groups which can form hydrogen bonds with the $(+)_{589}$-tartratoantimonate(III) ion, a *Λ* isomer is eluted almost always faster than the antipode.[14] For complexes with no such facial NH_2 groups; for example $[Co(en)_2(C_2O_4)]^+$ [14] and $[Co(en)_2(P\text{-}P)]^{3+}$ [12], the elution order is reversed to give a *Λ* isomer as the faster moving enantiomer. The $[Co(en)(edmp)_2]^{3+}$ complex can have the three facial NH_2 groups in only the *trans*(P,N) isomer. These considerations lead to the conclusion that $[Co(en)(edmp)_2]^{3+}$ is the *trans*-(P,N) isomer. This isomer has C_1 symmetry and the two edmp ligands are not in equivalent environment. Thus NMR spectroscopy would give useful information for assigning the structure. However, the ^1H NMR spectrum was too complicated to assign, and no good ^{13}C NMR spectrum was obtained because of the small amount of the complex. Thus the structure of $[Co(en)(edmp)_2]^{3+}$ remains unknown.

In contrast with the first absorption bands, the second absorption bands of the edmp complexes do not show any remarkable shift when en is replaced by edmp. Thus the energy difference between the first and the second absorption bands in the edmp complexes becomes small as compared with that in $[Co(en)_3]^{3+}$. The energy difference between the first and the second absorption bands is expressed by 16B, where *B* is the Racah's parameter of interelectronic repulsion.[15] The *B* value is known to be a measure for representing covalent character of the bond between a ligand and a metal ion, the smaller the value the more the covalent character.[16] The *B* values for *fac*-$[Co(edmp)_3]^{3+}$ and $[Co(en)_3]^{3+}$ are 406 and 506 cm^{-1}, respectively. The value of 406 cm^{-1} is as small as that of $[Co(CN)_6]^{3-}$ (416 cm^{-1}).[17] The coordinate bond between the edmp ligand and the cobalt(III) ion might involve fairly strong covalent character.

The edmp complexes show a strong absorption band around 40000 cm^{-1}, which can be assigned to the charge transfer band from the phosphine group to the cobalt(III) ion. With an increase in the number of ligating phosphorus atoms, these bands increase the intensity, while the absorptions around 46000 cm^{-1} which can be assigned to the charge transfer band from the amine group to the cobalt(III) ion decrease the intensity.

Absorption spectra of $[Co(en)_2(edpp)]^{3+}$ and $[Co(en)_2(ebpp)]^{3+}$ (lst fraction) are compared with that of $[Co(en)_2(edmp)]^{3+}$ in Fig. 5. By replacing the methyl group in edmp by a phenyl group, both the first and the charge transfer absorption bands are shifted progressively to smaller wavenumbers. The shift of the latter bands are particularly noticeable and the second absorption bands are hidden by these bands. The maximum wavenumber of the first absorption band of the edpp complex is nearly the same as that of $[Co(en)_3]^{3+}$.

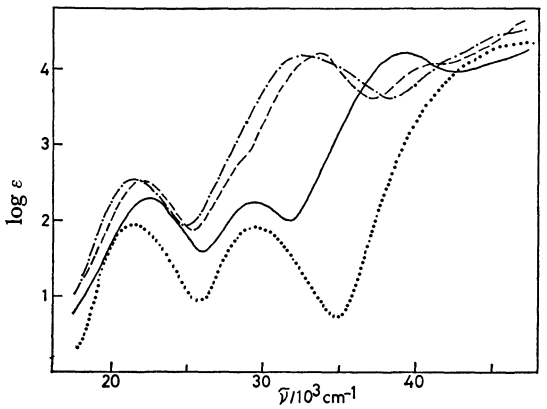

Fig. 5. Absorption spectra of $[Co(en)_2(edmp)]^{3+}$ (——), $[Co(en)_2(ebpp)]^{3+}$ (----), $[Co(en)_2(edpp)]^{3+}$ (—·—), and $[Co(en)_3]^{3+}$ (·····).

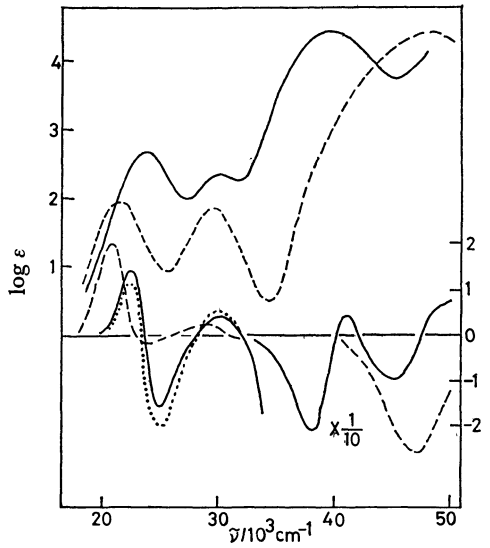

Fig. 6. Absorption and CD spectra of *Λ*-*fac*-$[Co(edmp)_3]^{3+}$ in water (——) and in 0.1 mol/dm³ PO_4^{3-} (·····), and *Λ*-$[Co(en)_3]^{3+}$ in water (----).

The CD spectrum of $(-)_{589}$-*Λ*-*fac*-$[Co(edmp)_3]^{3+}$ is compared with that of *Λ*-$[Co(en)_3]^{3+}$ in Fig. 6. Both complexes show a similar CD pattern in the first absorption band region, although the negative component of *Λ*-*fac*-$[Co(edmp)_3]^{3+}$ is very strong. On addition of phosphate ions, the positive and the negative components are diminished and enhanced, respectively. The same effect is well known to occur in the CD spectrum of *Λ*-$[Co(en)_3]^{3+}$.[17] In the ultraviolet region, a negative and a positive CD band are observed corresponding to each charge transfer band from the phosphine and the amine groups to the cobalt(III) ion. The appearance of the negative CD band in the small wavenumber side in each charge transfer region is the same as cases of tris-diamine complexes in the *Λ* configuration.[18] Thus the CD spectrum of *fac*-$[Co(edmp)_3]^{3+}$ can be understood on the basis of that of $[Co(en)_3]^{3+}$. Figure 7 shows the CD spectra of $[Co(en)_n(edmp)_{3-n}]^{3+}$, all of which are eluted faster on column chromatography. All the complexes can be assigned to *Λ* configuration

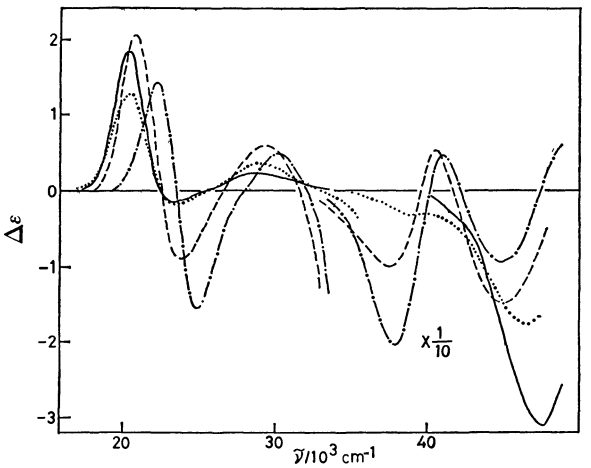

Fig. 7. CD spectra of *Λ*-$[Co(edmp)_3]^{3+}$ (—·—·—), *Λ*-$[Co(en)(edmp)_2]^{3+}$ (----), *Λ*-$[Co(en)_2(edmp)]^{3+}$ (·····), and *Λ*-$[Co(en)_3]^{3+}$ (——).

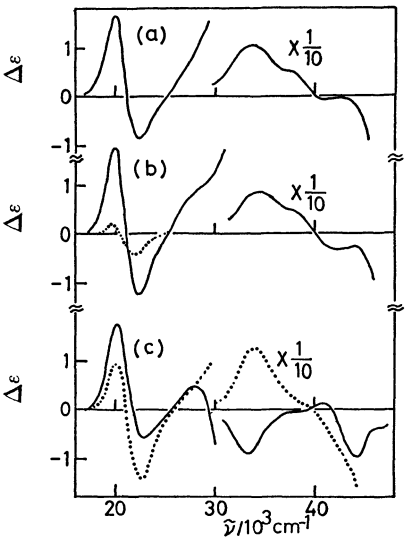

Fig. 8. CD spectra of *Λ*-$[Co(en)_2(N-P)]^{3+}$. N-P: (a) edpp, (b) *S*-pdpp (——) and the vicinal effect curve of *S*-pdpp (·····) (see text), and (c) *R*-ebpp (——) and *S*-ebpp (·····).

from the CD patterns in the first absorption band region. The CD bands corresponding to the charge transfer transitions from the phosphine and the amine groups to the cobalt(III) ion decrease or increase the strength depending on the number of phosphorus or nitrogen donor atoms. In Fig. 8 are shown the CD spectra of $[Co(en)_2(N-P)]^{3+}$ (N–P=edpp, *S*-pdpp, and *S*- and *R*-ebpp). The CD patterns in the first absorption band region are all similar, and these enantiomers can be assigned to *Λ* configuration. However, the CD spectra in the ultraviolet region differ from those of the edmp complexes probably because of the presence of the phenyl group or the chiral phosphorus or carbon atom. The absolute configurations of the phosphorus atoms in the diastereomeric ebpp complexes were assigned by comparing the CD spectra with those of the authentic complexes prepared by use of optically active *S*-ebpp.[6,19]

The *S*-pdpp complex involves a chiral chelate ligand.

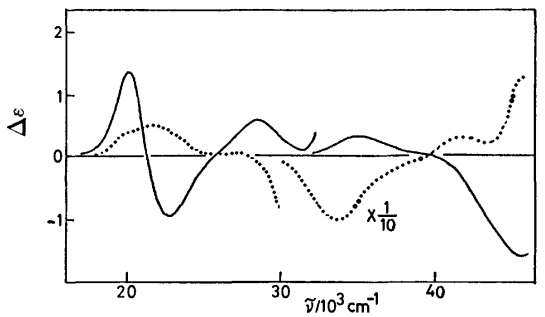

Fig. 9. Configurational(Λ) (——) and vicinal(R) (……) effect CD curves of $[Co(en)_2(ebpp)]^{3+}$.

When the additivity[20] in CD between the configurational and vicinal effects holds in the CD of this complex, the vicinal effect of S-pdpp can be estimated by subtracting the CD spectrum of Λ-$[Co(en)_2(edpp)]^{3+}$ from that of Λ-$[Co(en)_2(S\text{-pdpp})]^{3+}$. The vicinal CD curve thus obtained quite resemble those of (S)-propylenediamine (S-pn) chelate ligands in some S-pn complexes[20-22] (Fig. 8), indicating the same conformational chirality for both S-pdpp and S-pn chelate rings. Thus the S-pdpp chelate ring is assumed to be stabilized in a δ gauche conformation with the equatorial methyl group as seen in the S-pn chelate ring.[23] The ebpp complex has a chiral donating phosphorus atom, and gives a pair of diastereomers, $\Lambda(R)$ and $\Lambda(S)$. These diastereomers show a similar CD pattern in the first absorption band region, but give a CD band with the different sign from each other around 34000 cm^{-1}, where the charge transfer transition between the phosphine group and the cobalt(III) ion arises. From these CD spectra, the configurational (Λ) and vicinal (R) curves are obtained by the usual method[20] (Fig. 9). The configurational CD curve resembles the CD spectra of the other aminoalkylphosphine complexes. The curve in the ultraviolet region seems to be an average of the CD spectra of the edpp and the emdp complexes. The vicinal CD curve shows a positive and a negative peak in the regions of the first and the charge transfer, from the phosphine group to the cobalt(III) ion, bands, respectively. The vicinal effect of chiral phosphorus atoms donating to the cobalt(III) ion is only known for the $[Co(acac)_2(ebpp)]^+$ (acac=acetylacetonate ion).[2] In order to discuss such optical activity, more data will be needed.

This work was partly supported by the Kurata Research Grant of the Kurata Foundation.

References

1) C. A. McAuliffe and W. Levason, "Phosphine, Arsine and Stibine Complexes of the Transition Elements," Elsevier, Amsterdam (1979).
2) K. Kashiwabara, I. Kinoshita, T. Ito, and J. Fujita, *Bull. Chem. Soc. Jpn.*, **54**, 725 (1981).
3) H. Neibergall and B. Langefeld, *Chem. Ber.*, **95**, 64 (1962).
4) K. Issleib and D. Haferberg, *Z. Naturforsch., Teil B*, **20**, 916 (1965).
5) K. Issleib and H. Oehme, *Chem. Ber.*, **100**, 2685 (1967).
6) I. Kinoshita, K. Kashiwabara, and J. Fujita, *Bull. Chem. Soc. Jpn.*, **53**, 3715 (1980).
7) "International Tables for X-Ray Crystallography," Kynoch Press, Birmingham (1974), Vol. IV, pp. 71 and 148.
8) To be published.
9) S. Bruckner and L. Randaccio, *J. Chem. Soc., Dalton Trans.*, **1974**, 1017; N. Bresciani-Pahor, M. Calligaris, and L. Randaccio, *Inorg. Chim. Acta*, **27**, 47 (1978); L. G. Marzilli, L. A. Epps, T. Sorrell, and T. J. Kistenmacher, *J. Am. Chem. Soc.*, **97**, 3351 (1975); W. W. Adams and P. G. Lenhert, *Acta Crystallogr., Sect. B*, **29**, 2412 (1973); P. J. Toscano and L. G. Marzilli, *Inorg. Chem.*, **18**, 421 (1979); L. Randaccio, N. Bresciani-Pahor, P. J. Toscano, and L. G. Marzilli, *J. Am. Chem. Soc.*, **102**, 7373 (1980).
10) M. Iwata, K. Nakatsu, and Y. Saito, *Acta Crystallogr., Sect. B*, **25**, 2562 (1969).
11) H. Yamatera, *Bull. Chem. Soc. Jpn.*, **31**, 95 (1958).
12) T. Ohishi, K. Kashiwabara, and J. Fujita, 30th Conference on Coordination Chemistry, Japan, Tokyo, October 1980, Abstr. No. 2A17.
13) For example, F. Basolo and R. G. Pearson, "Mechanism of Inorganic Reactions," John Wiley & Sons, New York (1967), Chap. 5.
14) H. Nakazawa, C. E. Oh, K. Miyoshi, and H. Yoneda, *Bull. Chem. Soc. Jpn.*, **53**, 273 (1980).
15) Y. Tanabe and S. Sugano, *J. Phys. Soc. Jpn.*, **9**, 753, 766 (1954).
16) C. E. Schaffer and C. K. Jørgensen, *J. Inorg. Nucl. Chem.*, **8**, 143 (1958).
17) R. Larsson, S. F. Mason, and B. J. Norman, *J. Chem. Soc., A*, **1966**, 301; S. F. Norman and B. J. Norman, *ibid.*, **1966**, 307.
18) M. Kojima, H. Yamada, H. Ogino, and J. Fujita, *Bull. Chem. Soc. Jpn.*, **50**, 2325 (1977).
19) I. Kinoshita, K. Kashiwabara, J. Fujita, T. Yamane, H. Ukai, and T. Ashida, *Bull. Chem. Soc. Jpn.*, **52**, 1413 (1979).
20) C. T. Liu and B. E. Douglas, *Inorg. Chem.*, **3**, 1356 (1964).
21) K. Ogino, K. Murano, and J. Fujita, *Inorg. Nucl. Chem. Lett.*, **4**, 35 (1968).
22) K. Kashiwabara and S. Suzuki, *Bull. Chem. Soc. Jpn.*, **49**, 3329 (1976).
23) S. Yano, H. Ito, Y. Koike, J. Fujita, and K. Saito, *Bull. Chem. Soc. Jpn.*, **42**, 3184 (1969).

Isomers of Tris[(*R*)-1-phenyl-1,2-ethanediamine]- and Tris[(*S*)-3,3-dimethyl-1,2-butanediamine]cobalt(III), and the Related Complexes

Masaaki Kojima and Junnosuke Fujita*

Department of Chemistry, Faculty of Science, Nagoya University, Chikusa-ku, Nagoya 464

(Received April 21, 1981)

The $[Co\{(R)\text{-1-phenyl-1,2-ethanediamine}\}_3]^{3+}$ complex yielded all of the four possible isomers, *mer*-$\Lambda(lel_3)$, *mer*-$\Lambda(ob_3)$, *fac*-$\Lambda(lel_3)$, and *fac*-$\Lambda(ob_3)$, while the $[Co\{(S)\text{-3,3-dimethyl-1,2-butanediamine}\}_3]^{3+}$ complex gave only two isomers of *mer*-$\Lambda(lel_3)$ and *fac*-$\Lambda(lel_3)$. Two isomers, $\Lambda(lel_3)$ and $\Delta(ob_3)$ of the $[Co\{(S,S)\text{-2,3-butanediamine}\}_3]^{3+}$ complex were obtained. The formation ratios of these tris(1,2-diamine)cobalt(III) complexes were compared with those of the analogous complexes and discussed. The tetraammine complexes of all those diamines were also prepared. Absorption and circular dichroism spectra of all the complexes were recorded.

Recently Bernth and Larsen[1] isolated three out of four possible isomers of $[Co(R\text{-pen})_3]^{3+}$ (*R*-pen=(*R*)-1-phenyl-1,2-ethanediamine), and reported their circular dichroism (CD) spectra. This paper deals with the isolation and CD spectra of all the isomers. The CD spectrum of one isomer (*mer*-$\Lambda(ob_3)$) reported by Bernth and Larsen differs markedly from that obtained in this study. The present paper also reports the preparation and CD spectra of two isomers of $[Co(S\text{-dmbn})_3]^{3+}$ (*S*-dmbn=(*S*)-3,3-dimethyl-1,2-butanediamine), two isomers of $[Co(SS\text{-2,3-bn})_3]^{3+}$ (*SS*-2,3-bn=(*S,S*)-2,3-butanediamine), and the tetraammine complexes of those diamines. The *R*-pen and *S*-dmbn ligands have a bulky substituent on the carbon atom, and the *SS*-2,3-bn the methyl group on each carbon atom.

Experimental

Ligands. 1-Phenyl-1,2-ethanediamine (pen) was obtained by reducing 2-amino-2-phenylethaneamide which was derived from 2-amino-2-phenylacetic acid (Tokyo Kasei Co.), with $LiAlH_4$ according to the known method,[2] and resolved with (+)-tartaric acid to give *R*-pen by the method of Reihlen *et al.*[3] Optically active *R*-pen was also derived from (−)-(*R*)-2-amino-2-phenylacetic acid (Aldrich Chem. Co.) by the same method. However, the product was not optically pure so that the procedure of resolution given above was necessary.

(+)-(*S*)-3,3-Dimethyl-1,2-butanediamine (*S*-dmbn) was obtained by the method of Hawkins and Peachey.[4] The dihydrochloride salt (*S*-dmbn·2HCl) was used to prepare cobalt(III) complexes.

2,3-Butanediamine (2,3-bn) was prepared by the method of Bailar *et al.*[5] and separated into the *meso* and *racemic* isomers by the method of Billo and Vitiello.[6] The (+)-*SS*-2,3-bn isomer was obtained from the racemate by the method of Dickey *et al.*[7]

mer-Δ- *and* fac-Δ-$[Co(\text{R-}pen)_3]Cl_3\cdot 2.5H_2O$, mer-Λ-$[Co(\text{R-}pen)_3]Cl_3\cdot 3H_2O$, *and* fac-Λ-$[Co(\text{R-}pen)_3]Cl_3\cdot 4H_2O$.
A mixture of $[Co(NH_3)_5(H_2O)](ClO_4)_3$ (0.5 g, 1.1 mmol), *R*-pen (0.68 g, 5 mmol), and active charcoal (0.2 g) in 30 cm³ of water was heated at 60 °C for 5 h, and filtered. The filtrate was diluted with 1 dm³ of water and passed through an SP-Sephadex column ($\phi 2.7\times 3$ cm). The Sephadex charged with the product was placed on the top of an SP-Sephadex column ($\phi 2.7\times 120$ cm). By elution with 0.2 mol/dm³ Na_2SO_4, the orange band separated into four bands, I, II, III, and IV named in the order of elution, which were *mer*-Δ, *fac*-Δ, *mer*-Λ, and *fac*-Λ isomers of $[Co(R\text{-pen})_3]^{3+}$, respectively. Each eluate was diluted with water and poured again on a small column of SP-Sephadex. After the column had been washed with 10^{-2} mol/dm³ HCl (*ca.* 5 dm³), the adsorbed complex was eluted with 1 mol/dm³ HCl. The eluate was concentrated in a vacuum desiccator over P_2O_5 and NaOH to give orange crystals, which were filtered and washed with a small amount of water. The total yield was almost quantitative, and the formation ratio, I:II:III:IV was *ca.* 17:8:4:1. I. Found: C, 46.5; H, 6.6; N, 13.8%. II. Found: C, 46.6; H, 6.7; N, 13.8%. Calcd for $[Co(\text{R-pen})_3]Cl_3\cdot 2.5H_2O$: C, 46.6; H, 6.7; N, 13.6%. III. Found: C, 45.6; H, 6.7; N, 13.6%. Calcd for $[Co(\text{R-pen})_3]Cl_3\cdot 3H_2O$: C, 45.9; H, 6.7; N, 13.4%. IV. Found: C, 44.6; H, 6.3; N, 12.8%. Calcd for $[Co(R\text{-pen})_3]Cl_3\cdot 4H_2O$: C, 44.6; H, 6.9; N, 13.0%.

mer-Λ- *and* fac-Λ-$[Co(\text{S-}dmbn)_3](ClO_4)_3\cdot 3H_2O$. The $[Co(S\text{-dmbn})_3]^{3+}$ complex was prepared and separated into the isomers by a method similar to that for $[Co(R\text{-pen})_3]^{3+}$, using *S*-dmbn which was obtained by neutralizing the dihydrochloride with an aqueous NaOH solution, instead of *R*-pen. Only two isomers, A(*mer*-Λ) and B(*fac*-Λ) were yielded in nearly the same amount, A being eluted faster than B in column chromatography. The isomers were isolated as perchlorates by use of 1.5 mol/dm³ $HClO_4$ instead of 1 mol/dm³ HCl. Yield: *ca.* 40% for each isomer. A. Found: C, 28.8; H, 7.1; N, 11.0%. B. Found: C, 28.5; H, 6.8; N, 11.0%. Calcd for $[Co(\text{S-dmbn})_3](ClO_4)_3\cdot 3H_2O$: C, 28.5; H, 7.2; N, 11.1%.

The $[Co(S\text{-dmbn})_3]^{3+}$ complex was also obtained by mixing a methanol solution (15 cm³) of *trans*-$[CoCl_2(\text{pyridine})_4]Cl\cdot 6H_2O$ (0.59 g, 1 mmol)[8] and a methanol solution (15 cm³) containing *S*-dmbn·2HCl (0.57 g, 3 mmol) and $NaOCH_3$ (0.32 g, 6 mmol). The reaction took place almost instantly to give a yellow solution. It was diluted with water and chromatographed by the same method as the above to give the *mer*-Λ and *fac*-Λ isomers. The formation ratio, *mer*-Λ: *fac*-Λ was 3:1, no Δ isomer being yielded.

Λ-$[Co(\text{SS-}2,3\text{-}bn)_3]Cl_3\cdot 1.5H_2O$ *and* Δ-$[Co(\text{SS-}2,3\text{-}bn)_3]Cl_3\cdot 5H_2O$. Two isomers of $[Co(SS\text{-2,3-bn})_3]^{3+}$ were obtained by a method similar to that for $[Co(R\text{-pen})_3]^{3+}$ using *SS*-2,3-bn instead of *R*-pen. The formation ratio of the $\Lambda(lel_3)$ to the $\Delta(ob_3)$ isomers was *ca.* 10:1. The Λ isomer. Found: C, 31.7; H, 8.6; N, 18.1%. Calcd for $[Co(SS\text{-2,3-bn})_3]Cl_3\cdot 1.5H_2O$: C, 31.7; H, 8.6; N, 18.4%. The Δ isomer. Found: C, 28.0; H, 8.7; N, 16.5%. Calcd for $[Co(SS\text{-2,3-bn})_3]Cl_3\cdot 5H_2O$: C, 27.7; H, 8.9; N, 16.2%.

$[Co(NH_3)_4(\text{R-}pen)](ClO_4)_3\cdot 2H_2O$ *and* $[Co(NH_3)_4(\text{S-}dmbn)](ClO_4)_3$. These complexes were prepared from $[Co(NH_3)_5(H_2O)](ClO_4)_3$ and *R*-pen or *S*-dmbn·2HCl in dimethyl sulfoxide (DMSO) by a method similar to that reported.[9,10] Yield: *ca.* 20% (*R*-pen complex). *ca.* 10% (*S*-dmbn complex). The *R*-pen complex. Found: C, 16.2; H, 4.7; N, 14.1%. Calcd for $[Co(NH_3)_4(R\text{-pen})](ClO_4)_3\cdot 2H_2O$: C, 16.1; H, 4.7; N, 14.1%. The *S*-dmbn complex. Found: C, 13.4; H, 5.1; N, 15.8%. Calcd for $[Co(NH_3)_4$-

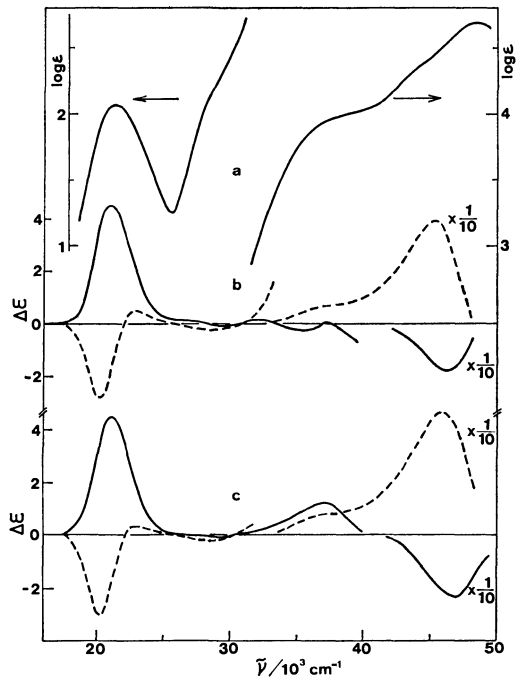

Fig. 1. a: Absorption spectrum of *fac*-*Λ*-[Co(*R*-pen)$_3$]$^{3+}$ (IV). b: CD spectra of *fac*-*Λ*-[Co(*R*-pen)$_3$]$^{3+}$ (IV) (——) and *fac*-*Δ*-[Co(*R*-pen)$_3$]$^{3+}$ (II) (----). c: CD spectra of *mer*-*Λ*-[Co(*R*-pen)$_3$]$^{3+}$ (III) (——) and *mer*-*Δ*-[Co(*R*-pen)$_3$]$^{3+}$ (I) (----).

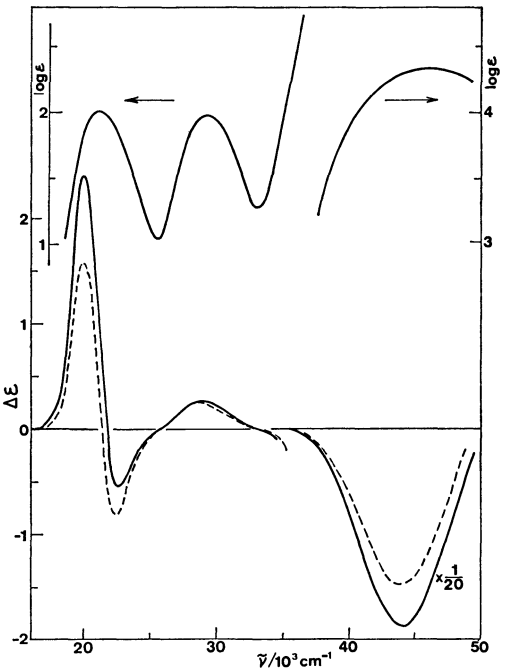

Fig. 2. Absorption spectrum of *mer*-*Λ*-[Co(*S*-dmbn)$_3$]$^{3+}$ (A), and CD spectra of *mer*-*Λ*-[Co(*S*-dmbn)$_3$]$^{3+}$ (A) (——) and *fac*-*Λ*-[Co(*S*-dmbn)$_3$]$^{3+}$ (B) (----).

(*S*-dmbn)](ClO$_4$)$_3$: C, 13.3; H, 5.2; N, 15.8%.

[Co(NH$_3$)$_4$(SS-2,3-bn)](ClO$_4$)$_3$. This complex was prepared by a method similar to that of Mizukami *et al.*[11] for the corresponding (*R*,*R*)-2,4-pentanediamine complex. The method for the above *R*-pen and *S*-dmbn complexes gives a large amount of [Co(*SS*-2,3-bn)$_3$]$^{3+}$ owing to disproportionation. The NH$_4$[Co(SO$_3$)$_2$(NH$_3$)$_2$(*SS*-2,3-bn)] complex (not analyzed) prepared from NH$_4$[Co(SO$_3$)$_2$-(NH$_3$)$_4$][12] and *SS*-2,3-bn was allowed to react with 47% hydrobromic acid to yield *trans*(Br,Br)-[CoBr$_2$(NH$_3$)$_2$(*SS*-2,3-bn)]Br (not analyzed). It was dissolved in liquid ammonia to give an orange solution. A crude complex which remained on evaporation of the liquid ammonia was purified by column chromatography with SP-Sephadex. The complex was isolated as perchlorate by a method similar to that for [Co(*S*-dmbn)$_3$]$^{3+}$. Yield: *ca.* 10%. Found: C, 9.2; H, 4.6; N, 16.7%. Calcd for [Co(NH$_3$)$_4$(*SS*-2,3-bn)] (ClO$_4$)$_3$: C, 9.4; H, 4.7; N, 16.4%.

Equilibrium Studies. Each isomer of *mer*-*Λ*- and *fac*-*Λ*-[Co(*S*-dmbn)$_3$](ClO$_4$)$_3$ was refluxed in water (50 cm^3) in the presence of active charcoal (0.1 g) for 3—8 h. The charcoal was filtered off and the filtrate was subjected to SP-Sephadex column chromatography in order to see the distributions of isomers. The ratio, *mer*-*Λ*:*fac*-*Λ*=1:1 was obtained, no formation of the *Δ* isomer being observed. The *Λ*-[Co(*SS*-2,3-bn)$_3$]Cl$_3$·1.5H$_2$O complex was equilibrated by the same method, giving the ratio, *Λ*:*Δ*=10:1. The ratios for both complexes thus obtained are the same as the respective formation ratios obtained when the complexes were prepared in the presence of active charcoal. Equilibration of [Co(*R*-pen)$_3$]$^{3+}$ by the same method as the above was accompanied with reduction of Co(III) to Co(II).

Measurements. Absorption and CD spectra were recorded on a Hitachi 323 spectrophotometer and a JASCO J-40CS spectropolarimeter, respectively. ^{1}H NMR spectra in DMSO-d_6 solutions and ^{13}C NMR spectra in DMSO solutions were obtained with a JEOL PMX-60 and a JEOL FX-60 spectrometer, respectively.

Results and Discussion

Four isomers (I, II, III, IV) of the [Co(*R*-pen)$_3$]$^{3+}$ complex are easily assigned on the basis of the ^{13}C NMR and CD spectra. II and IV give only one kind of signal for each resonance of the methylene (II, 49.3 ppm; IV, 49.8 ppm) and methine (II, 61.2 ppm; IV 60.4 ppm) carbons, while I and III show more than two signals (unresolved peaks) for each of the corresponding carbons. Thus the former two and the latter two can be assigned to the *fac*(C_3) and *mer*(C_1) configurations, respectively. In the first absorption band region, I and II show a negative main CD band, and III and IV a strong positive CD band (Fig. 1). Thus I, II, III, and IV are assigned to the *mer*-*Δ*, *fac*-*Δ*, *mer*-*Λ*, and *fac*-*Λ* isomers, respectively. The [Co(*S*-dmbn)$_3$]$^{3+}$ complex yielded only two isomers, A and B out of four possible isomers. ^{1}H NMR spectra of A and B exhibit two and one signals, respectively, in the resonance region of the t-butyl group. Both isomers show a similar CD pattern which is characteristic of the *Λ* configuration (Fig. 2). Thus A and B can be assigned to the *mer*-*Λ* and *fac*-*Λ* isomers, respectively.

The *Δ*- and *Λ*-[Co(*R*-pen)$_3$]$^{3+}$, and *Λ*-[Co(*S*-dmbn)$_3$]$^{3+}$ complexes have the *lel*$_3$, *ob*$_3$, and *lel*$_3$ structures, respectively, since the *R*-pen and *S*-dmbn chelate rings should be stabilized in the *λ* and *δ* conformations, respectively, with the phenyl or *t*-butyl group disposed equatorially. For a [Co(1,2-diamine)$_3$]$^{3+}$ complex, the *lel*$_3$ isomer is known to be more stable than the *ob*$_3$ one.[13] The relative amounts of the *lel*$_3$ to the *ob*$_3$

Table 1. Absorption (AB) and CD spectral data

Complex	$\tilde{\nu}^{AB}/10^3$ cm^{-1}(log ε)	$\tilde{\nu}^{CD}/10^3$ cm^{-1}($\Delta\varepsilon$)	Complex	$\tilde{\nu}^{AB}/10^3$ cm^{-1}(log ε)	$\tilde{\nu}^{CD}/10^3$ cm^{-1}($\Delta\varepsilon$)
mer-Δ-$[Co(R\text{-pen})_3]^{3+}$	21.20 (2.10)	20.24 (−2.94)	Δ-$[Co(SS\text{-2,3-bn})_3]^{3+}$	21.51 (1.99)	21.28 (−3.47)
		23.04 (+0.34)		29.63 (1.96)	27.00 (−0.068)
	29.0 (2.2) sh	28.20 (−0.16)			29.24 (+0.94)
	37.0 (3.9) sh				32.05 (−0.29)
	48.50 (4.73)	45.90 (+48)		46.90 (4.49)	41.00 (−0.94)
fac-Δ-$[Co(R\text{-pen})_3]^{3+}$	21.20 (2.06)	20.16 (−2.79)			47.10 (+25.5)
		22.90 (+0.52)	*fac*-Δ-$[Co(R\text{-pn})_3]^{3+}$ [19]	21.39 (2.00)	20.28 (−2.44)
	29.0 (2.1) sh	28.25 (−0.19)			22.83 (+0.75)
	37.0 (4.0) sh			29.50 (1.96)	28.99 (−0.32)
	48.50 (4.75)	45.20 (+39)		47.30 (4.40)	47.00 (+48)
mer-Δ-$[Co(R\text{-pen})_3]^{3+}$	21.20 (2.07)	21.05 (+4.50)	*mer*-Δ-$[Co(R\text{-pn})_3]^{3+}$ [18]	21.39 (1.95)	21.05 (+2.48)
	29.0 (2.1) sh	28.99 (−0.03)		29.40 (1.90)	27.30 (+0.078)
	37.0 (4.0) sh	37.00 (+1.25)			29.30 (−0.031)
	48.50 (4.72)	46.50 (−23)			31.70 (+0.036)
fac-Δ-$[Co(R\text{-pen})_3]^{3+}$	21.20 (2.08)	21.05 (+4.46)		47.00 (4.43)	41.50 (+1.35)
	29.0 (2.3) sh	29.07 (−0.07)			47.20 (−20.1)
		31.25 (+0.14)	$[Co(NH_3)_4(R\text{-pen})]^{3+}$	21.19 (1.89)	19.05 (−0.037)
	37.0 (3.9) sh	35.60 (−0.27)			21.60 (+0.465)
		37.00 (+0.10)		29.8 (1.9) sh	28.20 (−0.007)
	48.50 (4.69)	46.10 (−18)		39.0 (3.6) sh	
mer-Δ-$[Co(S\text{-dmbn})_3]^{3+}$	21.16 (2.02)	20.08 (+2.42)		49.00 (4.59)	46.10 (+5.9)
		22.62 (−0.55)	$[Co(NH_3)_4(S\text{-dmbn})]^{3+}$	21.19 (1.84)	19.53 (+0.037)
	29.28 (1.99)	28.82 (+0.26)			21.65 (−0.386)
	46.50 (4.33)	44.20 (−37.9)		29.46 (1.77)	29.40 (+0.014)
fac-Δ-$[Co(S\text{-dmbn})_3]^{3+}$	21.16 (2.02)	19.96 (+1.57)		50.00 (4.39)	46.90 (−5.54)
		22.37 (−0.82)	$[Co(NH_3)_4(SS\text{-2,3-bn})]^{3+}$	21.28 (1.84)	19.42 (+0.075)
	29.28 (1.99)	28.57 (+0.25)			21.74 (−0.345)
	46.50 (4.34)	43.90 (−29.5)		29.46 (1.77)	29.41 (+0.012)
Δ-$[Co(SS\text{-2,3-bn})_3]^{3+}$	21.51 (2.00)	20.41 (+2.73)		49.60 (4.43)	47.80 (−4.92)
		23.09 (−0.56)	$[Co(NH_3)_4(R\text{-pn})]^{3+}$ [19]	21.19 (1.85)	19.31 (−0.066)
	29.63 (1.97)	28.99 (+0.32)			21.69 (+0.326)
	47.60 (4.45)	46.70 (−41)		29.50 (1.78)	29.15 (−0.02)
				50.30 (4.44)	47.00 (+5.4)

sh: Shoulder.

isomers in equilibrium at 373 K for $[Co(R\text{-pn})_3]^{3+}$ (*R*-pn=(*R*)-1,2-propanediamine),[14] $[Co(SS\text{-2,3-bn})_3]^{3+}$, and $[Co(RR\text{-chxn})_3]^{3+}$ (*RR*-chxn=(*R*,*R*)-*trans*-1,2-cyclohexanediamine)[15] are 8.8:1, 10:1, and 14:1, respectively. In the present study, $[Co(S\text{-dmbn})_3]^{3+}$ yielded only the *lel*$_3$ form by either preparative method and by heating the complex in water with active charcoal (Experimental). The relative stability of the *ob*$_3$ to the *lel*$_3$ isomers seems to decrease as the substituent becomes larger and the number of the substituent increases.

On the other hand, the formation ratio of the *lel*$_3$ to the *ob*$_3$ isomers of $[Co(R\text{-pen})_3]^{3+}$ was 5:1. Although the equilibration study was unsuccessful because of decomposition of the complex, this value can be regarded as that at equilibrium, since the reaction was carried out by prolonged heating in the presence of active charcoal (Experimental). The value of 5:1 indicates that the *ob*$_3$ isomer of $[Co(R\text{-pen})_3]^{3+}$ is fairly stable as compared with those of the other complexes given above, despite the ligand has a bulky phenyl substituent. Bosnich and Harrowfield[16] reported that for the $[Co\{(-)\text{-dpen}\}_3]^{3+}$ complex ((−)-dpen=(−)-1,2-diphenyl-1,2-ethanediamine), in which each chelate ring has two phenyl substituents, the (−)-isomer predominates to the extent of at least 90% over the (+)-isomer at equilibrium. Later Kuroda and Mason[17] determined the absolute configuration of (+)-$[Co\{(-)\text{-dpen}\}_3]^{3+}$ by X-ray analysis to be Λ(*lel*$_3$)-$[Co(SS\text{-dpen})_3]^{3+}$. These reports show that in $[Co(SS\text{-dpen})_3]^{3+}$ the *ob*$_3$ isomer is much more stable than the *lel*$_3$ one. Thus it is concluded that tris-type complexes of 1,2-diamines with phenyl substituents tend to stabilize the *ob*$_3$ isomer, contrary to those of 1,2-diamines with alkyl substituents.

It is known that the *mer* and *fac* isomers of $[Co(R\text{-pn})_3]^{3+}$ with the same absolute configuration give essentially the same CD spectra.[18] The corresponding isomers of $[Co(R\text{-pen})_3]^{3+}$ show a small difference in the CD spectra, but there is a fairly large difference between *mer*- and *fac*-Λ-$[Co(S\text{-dmbn})_3]^{3+}$. In the first absorption band region, the CD patterns of Δ(*lel*$_3$) and Λ(*ob*$_3$) isomers of $[Co(R\text{-pen})_3]^{3+}$ (*mer* and *fac*)

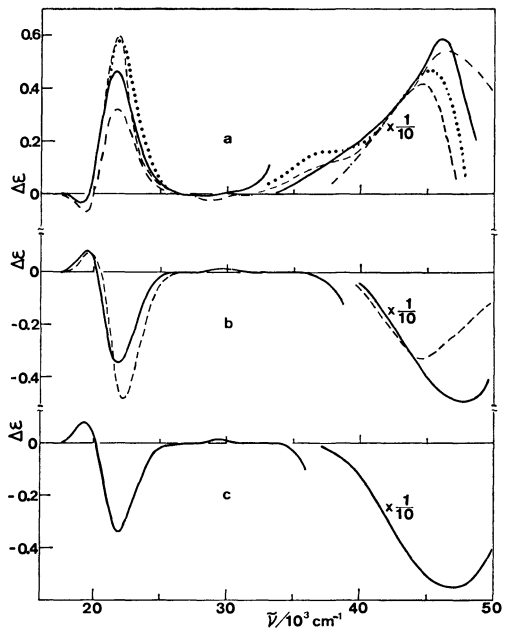

Fig. 3. a: Observed CD spectra of $[Co(NH_3)_4(R\text{-pen})]^{3+}$ (——) and $[Co(NH_3)_4(R\text{-pn})]^{3+}$ (—·—·—), and calculated CD curves, $1/6\{\Delta\varepsilon(fac\text{-}\Lambda\text{-}[Co(R\text{-pen})_3]^{3+}) + \Delta\varepsilon(fac\text{-}\Delta\text{-}[Co(R\text{-pen})_3]^{3+})\}$ (----) and $1/6\{\Delta\varepsilon(mer\text{-}\Lambda\text{-}[Co(R\text{-pen})_3]^{3+}) + \Delta\varepsilon(mer\text{-}\Delta\text{-}[Co(R\text{-pen})_3]^{3+})\}$ (....). b: Observed CD spectrum of $[Co(NH_3)_4(SS\text{-2,3-bn})]^{3+}$ (——) and calculated CD curve, $1/6\{\Delta\varepsilon(\Lambda\text{-}[Co(SS\text{-2,3-bn})_3]^{3+}) + \Delta\varepsilon(\Delta\text{-}[Co\text{-}(SS\text{-2,3-bn})_3]^{3+})\}$ (----). c: CD spectrum of $[Co(NH_3)_4(S\text{-dmbn})]^{3+}$.

quite resemble those of Δ- and Λ-$[Co(R\text{-pn})_3]^{3+}$ (*mer* and *fac*), respectively, although the CD strengths of $\Lambda(ob_3)$ isomers of the *R*-pen complex are much larger than those of the corresponding isomers of the *R*-pn complex (Table 1). The CD strength of *mer*-$\Lambda(ob_3)$-$[Co(R\text{-pen})_3]^{3+}$ reported by Bernth and Larsen[1] is about 2.5 times as small as ours. For tris(1,2-diamine)–cobalt(III) complexes reported so far, the ob_3 isomer gives always stronger CD than does the lel_3 one in the first absorption band region.

The vicinal CD curve of *R*-pen derived from the CD spectra of *fac*-Λ and *fac*-Λ (or *mer*-Λ and *mer*-Λ) isomers of $[Co(R\text{-pen})_3]^{3+}$ is similar to the observed CD spectrum of $[Co(NH_3)_4(R\text{-pen})]^{3+}$ over the whole region (Fig. 3). The CD patterns of $[Co(NH_3)_4(R\text{-pen})]^{3+}$ and $[Co(NH_3)_4(R\text{-pn})]^{3+}$ are very similar in the first absorption band region, although the CD strength of the former is fairly larger than that of the latter. The vicinal CD curve of *SS*-2,3-bn derived from Δ- and Λ-$[Co(SS\text{-2,3-bn})_3]^{3+}$ resembles the observed CD spectrum of $[Co(NH_3)_4(SS\text{-2,3-bn})]^{3+}$. The CD patterns of $[Co(NH_3)_4(SS\text{-2,3-bn})]^{3+}$ and $[Co(NH_3)_4(S\text{-dmbn})]^{3+}$ are almost mirror images of those of the corresponding *R*-pen and *R*-pn complexes. These results indicate that the *R*-pen and *S*-dmbn chelate rings are stabilized in the λ and δ gauche conformations, respectively, and that the vicinal effects of chiral 1,2-diamines in the $[CoN_6]$-type complexes are little dependent on the kind and the number of substituents on skeletal carbon atoms.

This work was partly supported by a Grant-in-Aid for Scientific Research No. 243013 from the Ministry of Education, Science and Culture.

References

1) N. Bernth and E. Larsen, *Acta Chem. Scand., Ser. A*, **32**, 545 (1978).
2) S. Yano, M. Saburi, S. Yoshikawa, and J. Fujita, *Bull. Chem. Soc. Jpn.*, **49**, 101 (1976).
3) H. Reihlen, E. Weinbrenner, and G. V. Hessling, *Ann.*, **494**, 143 (1932).
4) C. J. Hawkins and R. M. Peachey, *Aust. J. Chem.*, **29**, 33 (1976).
5) W. E. Cooley, C. F. Liu, and J. C. Bailar, Jr., *J. Am. Chem. Soc.*, **81**, 4189 (1959).
6) E. J. Billo and J. R. Vitiello, *Inorg. Chim. Acta*, **26**, L10 (1978).
7) F. H. Dickey, W. Fickett, and H. J. Lucas, *J. Am. Chem. Soc.*, **74**, 944 (1952).
8) A. Werner and R. Feenstra, *Ber.*, **39**, 1538 (1906).
9) H. Ogino, *Bull. Chem. Soc. Jpn.*, **50**, 2459 (1977).
10) M. Kojima, M. Fujita, and J. Fujita, *Bull. Chem. Soc. Jpn.*, **50**, 898 (1977).
11) F. Mizukami, H. Ito, J. Fujita, and K. Saito, *Bull. Chem. Soc. Jpn.*, **45**, 2129 (1972).
12) A. Werner and H. Gruger, *Z. Anorg. Allg. Chem.*, **16**, 398 (1898).
13) E. J. Corey and J. C. Bailar, Jr., *J. Am. Chem. Soc.*, **81**, 2620 (1959).
14) S. E. Harnung, S. Kallesoe, A. M. Sargeson, and C. E. Schaffer, *Acta Chem. Scand., Ser. A*, **28**, 385 (1974).
15) S. E. Harnung, B. S. Sørensen, I. Creaser, H. Maegaard, U. Pfenninger, and C. E. Schaffer, *Inorg. Chem.*, **15**, 2123 (1976).
16) B. Bosnich and J. MacB. Harrowfield, *J. Am. Chem. Soc.*, **94**, 3426 (1972).
17) R. Kuroda and S. F. Mason, *J. Chem. Soc., Dalton Trans.*, **1977**, 1016.
18) T. E. MacDermott, *Inorg. Chim. Acta*, **2**, 81 (1968); M. Kojima, Y. Yoshikawa, and K. Yamasaki, *Inorg. Nucl. Chem. Lett.*, **9**, 689 (1973).
19) M. Kojima and J. Fujita, Unpublished data.

  Bull. Chem. Soc. Jpn., 54, 2695—2699 (1981)

Kinetics and Mechanism of Cobalt(II) Incorporation into *meso*-Tetra(4-pyridyl)porphine in Acetic Acid[1)]

Shigenobu Funahashi, Keiji Saito, and Motoharu Tanaka*

Laboratory of Analytical Chemistry, Faculty of Science, Nagoya University, Chikusa-ku, Nagoya 464

(Received April 30, 1981)

The kinetics of reactions of *meso*-tetra(4-pyridyl)porphine (H_2TPyP) with cobalt(II) acetate and cobalt(II) nitrate was studied in acetic acid spectrophotometrically. The rate of cobalt incorporation into H_2TPyP is first-order in H_2TPyP. The conditional first-order rate constants are expressed as follows: for the cobalt(II) acetate system $k_{0(Co)}=K[Co(OAc)_2]_0(1+K[Co(OAc)_2]_0)^{-1}(k_1+k_2[Co(OAc)_2]_0)$, where at 25 °C $K=(5.5\pm2.0)\times10^4$ kg mol^{-1} ($\Delta H=-36\pm15$ kJ mol^{-1}, $\Delta S=-30\pm30$ J mol^{-1} K^{-1}), $k_1=(6.3\pm0.5)\times10^{-5}$ s^{-1} ($\Delta H^*=89\pm8$ kJ mol^{-1}, $\Delta S^*=-27\pm15$ J mol^{-1} K^{-1}), and $k_2=(1.17\pm0.05)\times10^{-1}$ kg mol^{-1} s^{-1} ($\Delta H^*=75\pm3$ kJ mol^{-1}, $\Delta S^*=-11\pm8$ J mol^{-1} K^{-1}); for the cobalt nitrate system $k_{0(Co)}=K_1[Co(NO_3)_2]_0(1+K_1[Co(NO_3)_2]_0)^{-1}(k_1+k_2[Co(NO_3)_2]_0+k_3K_2[Co(NO_3)_2]_0^2)$, where at 25 °C $k_1=(5.1\pm0.5)\times10^{-5}$ s^{-1}, $k_2=(2.0\pm0.1)\times10^{-1}$ kg mol^{-1} s^{-1}, $K_1=(7.2\pm2.0)\times10^4$ kg mol^{-1}, and $k_3K_2=(1.6\pm0.15)\times10^2$ kg^2 mol^{-2} s^{-1}. Formation constants of sitting-atop complexes were determined dynamically. Mechanisms are proposed for metal ion incorporation and some discussions are made on the difference in the reactivities of acetate and nitrate of cobalt(II) in acetic acid.

Metalloporphyrins are ubiquitous in living systems. For understanding the possible role of enzymatic catalysis of a variety of porphyrins related to biologically relevant material and the metalation mechanism from the viewpoint of coordination chemistry, thorough kinetic studies are required. Several reviews of metalloporphyrin formation are available.[2-4)]

Metalloporphyrins in which the metal is bonded to fewer than four nitrogen atoms, sitting-atop complexes, have been considered as models for the initial steps of the metalation of the macrocycle. Such complexes are known for rhenium and technetium,[5)] platinum,[6)] and rhodium.[7,8)] Several examples of mercury complexes have also been formulated.[9-11)]

Recently Hambright,[12)] Krishnamurthy,[13)] and Lavallee[14)] have proposed mechanisms for the formation of metalloporphyrins. Despite the numerous investigations on the formation of metalloporphyrins, many of basic features of the reaction are still conjectural.

We have investigated the rates of reaction of *meso*-tetra(4-pyridyl)porphine with cobalt(II) acetate and cobalt(II) nitrate in acetic acid. Similar measurements have been made in acetic acid/water solutions,[15)] where the nature of the metal ion reactants is often in doubt. We describe the kinetic proof for the existence of a cobalt(II) porphyrin sitting-atop complex. In acetic acid metal salts are all in the undissociated form, since it is a non-dissociating solvent having low dielectric constant ($D=6.18$ at 20 °C).[16)] Thus in this solvent we have no complication arising from the presence of dissociated anions and from ionic strentgh.

Experimental

Reagents. It is very important that all reagents be as dry as possible. Therefore, extreme care was taken in the purification and preparation of all reagents and compounds. Solutions of reagents were prepared in a glove box filled with dried air.

Anhydrous Acetic Acid: The preparation of acetic acid was described previously.[17)] The amount of water in the acetic acid was less than 9×10^{-3} %.

Porphyrin: *meso*-Tetra(4-pyridyl)porphine (Strem Chemicals) was chromatographed on an alumina column by elution with chloroform.

Cobalt(II) Acetate: Thirty grams of cobalt(II) acetate hydrate was refluxed in 300 cm^3 of acetic anhydride for 3 h. After centrifugation the precipitates were washed four times with anhydrous acetic acid. The crystals $(Co(OAc)_2\cdot4HOAc)$ were dried at 120 °C for 3 h to obtain $Co(OAc)_2$. The quantitative change of $Co(OAc)_2\cdot4HOAc$ to $Co(OAc)_2$ was confirmed thermogravimetrically.

Cobalt(II) Nitrate: Reagent grade cobalt(II) nitrate hydrate was recrystallized from distilled water. The hydrate was dissolved in acetic acid. Acetic anhydride equivalent to the water involved was added to the cobalt(II) nitrate solution. Several days were required for complete reaction of water with acetic anhydride. The concentration of cobalt was standardized against EDTA using Methylthymol Blue as indicator.

Ammonium Nitrate: Reagent grade ammonium nitrate was recrystallized from water. The crystals were dried at 120 °C for 3 h under reduced pressure.

Cobalt(II) acetate, ammonium nitrate, and porphyrin solutions were prepared by weighing corresponding crystals. We use molal units (mol kg^{-1}).

Measurements. Spectral measurements were performed on a highly sensitive spectrophotometer (SM401, Union Giken Co., Ltd.). The concentration of water was determined by the Karl-Fisher aquametry. A thermogravimeter (Thermal Analyzer DT-30 Shimadzu) was used to check the thermal stability.

The reactions were followed spectrophotometrically with a Union Giken spectrophotometer with a thermostated cell compartment maintained within ±0.1 °C. All the reactions were carried out in 1.00-cm cells by mixing reactants pre-equilibrated at the reaction temperature. The metalloporphyrin Co-TPyP was made in solution by addition of a large excess of cobalt(II) to H_2TPyP. The absorption spectra as a function of time showed excellent isosbestic points within several hours. The metalloporphyrin tended to precipitate after about 20 h at room temperature. The reaction was followed at 418 nm for the $Co(OAc)_2$ system and at 422 nm for the $Co(NO_3)_2$ system.

Under pseudo-first-order conditions with an excess of total cobalt over porphyrin, reactions were followed and pseudo-first-order rate constants were obtained from the data. Under conditions where the cobalt concentration

is about 10^{-3} mol kg^{-1}, the half-life time of formation of the metalloporphyrin is several tens of minutes. At such higher concentrations of cobalt, the linearity of first-order plot is good and gives the conditional first-order rate constant. The rate constants are obtained by an initial rate method or by the Guggenheim method,[18] which does not require a final absorbance value. Most of conditional first-order rate constants at lower concentration of cobalt were obtained by an initial rate method in order to avoid complications due to the precipitation of metalloporphyrin.

Equilibria. Recently equilibria of aquation for cobalt (II) acetate[19] and cobalt(II) perchlorate[20] in acetic acid have been studied.

$$Co(OAc)_2(HOAc)_4 + nH_2O \overset{\beta_n}{\rightleftharpoons} Co(OAc)_2(H_2O)_n(HOAc)_{4-n}, \quad (1)$$

($\beta_1 = 6.7$ kg mol^{-1}, $\beta_2 = 11$ kg^2 mol^{-2}, $\beta_3 = 28$ kg^3 mol^{-3})

$$Co(HOAc)_6(ClO_4)_2 + nH_2O \overset{\beta_n}{\rightleftharpoons} Co(H_2O)_n(HOAc)_{6-n}(ClO_4)_2, \quad (2)$$

($\beta_1 = 34$ kg mol^{-1}, $\beta_2 = 850$ kg^2 mol^{-2})

where equilibrium constants are given in parentheses. No data have been published for the equilibrium constant for aquation of cobalt(II) nitrate, although, presumably, it would not be much different from that of cobalt(II) perchlorate. Thus in the present systems no appreciable amount of aqua complexes was thought to be present: cobalt(II) acetate is in the form of diacetatotetrasolvatocobalt(II) and cobalt(II) nitrate exists as an ion-pair involving hexasolvatocobalt(II) [$Co(HOAc)_6^{2+}$][$2NO_3^-$] (*vide infra*).

TPyP showed no spectral evidence for protonation in acetic acid: the spectrum of TPyP in acetic acid was the same as that in chloroform. Thus TPyP is entirely in the free base form (H_2TPyP) in acetic acid.

Results

Reaction of H_2TPyP with $Co(OAc)_2$. Values of $k_{0(Co)}$ obtained at constant cobalt(II) acetate concentration (4.80×10^{-4} mol kg^{-1}) and at various concentrations of H_2TPyP (1.88, 2.32, 3.05, 5.37×10^{-6} mol kg^{-1}) were the same ($(1.06 \pm 0.03) \times 10^{-4}$ s^{-1}) within experimental errors. The rate for formation of metalloporphyrin (Co-TPyP) is first order in porphyrin:

$$\frac{d[\text{Co-TPyP}]}{dt} = -\frac{d[H_2\text{TPyP}']}{dt} = k_{0(Co)}[H_2\text{TPyP}'], \quad (3)$$

where $k_{0(Co)}$ is the conditional first-order rate constant involving cobalt concentration and [H_2TPyP'] is the total concentration of porphyrin minus the concentration of metalloporphyrin. The values of $k_{0(Co)}$ at 20.0, 25.0, and 30.0 °C are plotted against initial concentration of cobalt(II) acetate $[Co(OAc)_2]_0$ in Fig. 1. The logarithmic relationship between rate constants and cobalt concentrations is shown in Fig. 2. As apparent from curve A in Fig. 2, at lower and higher cobalt concentration $k_{0(Co)}$ tends to be first order in $[Co(OAc)_2]_0$, while at the intermediate cobalt concentration $k_{0(Co)}$ changes with $[Co(OAc)_2]_0$ to a lesser extent. This kinetic behavior of formation of metalloporphyrin can be formulated by the following equation:

$$H_2\text{TPyP} + Co(OAc)_2 \rightleftharpoons H_2\text{TPyP}\cdots Co(OAc)_2, \ K, \quad (4)$$

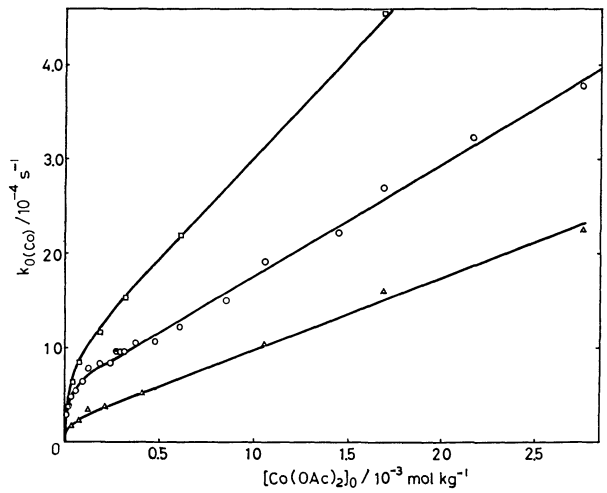

Fig. 1. Cobalt(II) acetate dependence of conditional first-order rate constants for the reaction of *meso*-tetra(4-pyridyl)porphine with cobalt(II) acetate in acetic acid.
△, 20 °C; ○: 25 °C; □, 30 °C.
The solid curves are calculated with the rate constants and formation constants obtained.

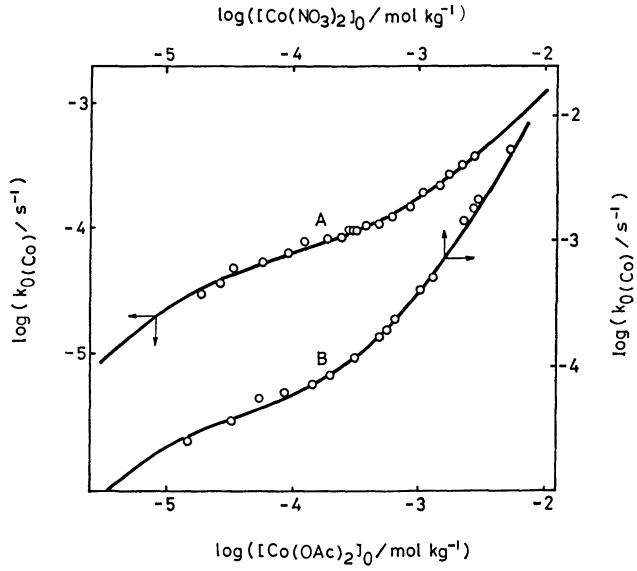

Fig. 2. Relationship between log $k_{0(Co)}$ and logarithmic values of cobalt concentration.
A, TPyP-$Co(OAc)_2$ system at 25 °C; B, TPyP-$Co(NO_3)_2$ system at 25 °C.
The solid curves are calculated with the rate constants and formation constants obtained.

$$SAT \longrightarrow \text{Co-TPyP} + 2HOAc, \qquad k_1 \quad (5)$$

$$SAT + Co(OAc)_2 \longrightarrow \text{Co-TPyP} + Co(OAc)_2 + 2HOAc, \qquad k_2 \quad (6)$$

where H_2TPyP$\cdots Co(OAc)_2$ is an intermediate which may be so-called sitting-atop complex and is denoted as SAT. For simplicity, acetic acid molecules in the reactions are omitted. If one assumes a rapid pre-equilibrium step of Eq. 4 and two parallel rate-determining steps of Eqs. 5 and 6, then an expression for $k_{0(Co)}$ can be derived for this mechanism and it is

Table 1. Rate constants, formation constants, and activation parameters for cobalt incorporation into H_2TPyP

Temp/°C	k_1/s^{-1}	k_2/kg mol^{-1} s^{-1}	K/kg mol^{-1}
	TPyP-$Co(OAc)_2$ system		
20.0	$(3.0\pm0.3)\times10^{-5}$	$(7.36\pm0.15)\times10^{-2}$	$(6.6\pm2.0)\times10^{4}$
25.0	$(6.3\pm0.5)\times10^{-5}$	$(1.17\pm0.05)\times10^{-1}$	$(5.5\pm2.0)\times10^{4}$
30.0	$(1.0\pm0.1)\times10^{-4}$	$(2.11\pm0.10)\times10^{-1}$	$(4.0\pm2.0)\times10^{4}$
	ΔH^*/kJ mol$^{-1}=89\pm8$	ΔH^*/kJ mol$^{-1}=75\pm3$	ΔH/kJ mol$^{-1}=-36\pm15$
	ΔS^*/J mol^{-1} K$^{-1}=-27\pm15$	ΔS^*/J mol^{-1} K$^{-1}=-11\pm8$	ΔS/J mol^{-1} K$^{-1}=-30\pm30$

Temp/°C	k_1/s^{-1}	k_2/kg mol^{-1} s^{-1}	K_1/kg mol^{-1}	k_3K_2/kg^2 mol^{-2} s^{-1}
	TPyP-$Co(NO_3)_2$ system			
25.0	$(5.1\pm0.5)\times10^{-5}$	$(2.0\pm0.1)\times10^{-1}$	$(7.2\pm2.0)\times10^{4}$	$(1.6\pm0.15)\times10^{2}$

given below

$$k_{0(Co)}=\frac{K[Co(OAc)_2]_0}{1+K[Co(OAc)_2]_0}(k_1+k_2[Co(OAc)_2]_0). \quad (7)$$

The experimental rate data fit this expression very well as illustrated in Fig. 1. In Reaction 5, the metal ion in the sitting-atop complex just drops into the porphyrin ring, and Reaction 6 indicates that a second metal is inserted from the opposite side. Values of k_1, k_2, and K were determined by a non-linear least squares method.[21] The rate constants, formation constants, and their corresponding parameters are tabulated in Table 1.

An introduction of 0.5% water into the solvent acetic acid did not affect the rate constants within experimental errors. Errors for estimation of rate constants were within 10%. Since the water concentration of our systems is much less than 0.5%, we believe with confidence that the presence of water, if any, did not affect our results.

Reaction of H_2TPyP with $Co(NO_3)_2$. The relationship between $k_{0(Co)}$ and initial concentration of cobalt(II) nitrate is shown in Fig. 2. The cobalt dependence of $k_{0(Co)}$ at lower concentration of cobalt nitrate is similar to that in the cobalt acetate system. At higher concentration of cobalt nitrate, however, the conditional rate tends to be second-order in cobalt nitrate concentration (see curve B in Fig. 2). The mechanism of the reaction is postulated as follows:

$$H_2TPyP + Co(NO_3)_2 \rightleftharpoons H_2TPyP\cdots Co(NO_3)_2, \quad K_1 \quad (8)$$

$$SAT + Co(NO_3)_2 \rightleftharpoons SAT\cdots Co(NO_3)_2, \quad K_2 \quad (9)$$

$$SAT \longrightarrow Co\text{-}TPyP + 2HNO_3, \quad k_1 \quad (10)$$

$$SAT + Co(NO_3)_2 \longrightarrow Co\text{-}TPyP + Co(NO_3)_2 + 2HNO_3, \quad k_2 \quad (11)$$

$$SAT\cdots Co(NO_3)_2 + Co(NO_3)_2 \longrightarrow Co\text{-}TPyP + 2Co(NO_3)_2 + 2HNO_3, \quad k_3 \quad (12)$$

where $H_2TPyP\cdots Co(NO_3)_2$ is a sitting-atop complex denoted as SAT, and $SAT\cdots Co(NO_3)_2$ is a complex formed by interaction of cobalt with a nitrogen atom of pyridyl groups in porphyrin (*vide infra*). With steps 10, 11, and 12 as rate determining and steps 8 and 9 as rapid preequilibria, Eq. 13 can be readily derived.

$$k_{0(Co)}=\frac{K_1[Co(NO_3)_2]_0}{1+K_1[Co(NO_3)_2]_0+K_1K_2[Co(NO_3)_2]_0^2}\times(k_1+k_2[Co(NO_3)_2]_0+k_3K_2[Co(NO_3)_2]_0^2) \quad (13)$$

Table 2. Effect of ammonium nitrate on the rate for Co-TPyP formation

$10^5[Co(NO_3)_2]_0$ / mol kg^{-1}	$10^4[NH_4NO_3]$ / mol kg^{-1}	$10^5k_{0(Co)}$ / s^{-1}
8.81	0	6.19
8.6	0.84	6.7
8.6	1.2	5.2
8.6	1.37	4.8
14.4	0	7.1
14.4	1.4	6.9
14.4	2.23	6.1
14.4	3.73	5.7
14.4	6.78	5.5

The data obtained indicate that the third term of the denominator in Eq. 13, $K_1K_2[Co(NO_3)_2]_0^2$, is negligible all over the range of cobalt concentrations. As illustrated in Fig. 2, the empirical kinetic data are best described by Eq. 13 without the term $K_1K_2[Co(NO_3)_2]_0^2$. Constants in the TPyP–$Co(NO_3)_2$ system are tabulated in Table 1.

The kinetics of cobalt incorporation into H_2TPyP have been studied in the presence of ammonium nitrate. Conditional first-order rate constants obtained in the presence of ammonium nitrate are summarized in Table 2. Values of $k_{0(Co)}$ tend to decrease only slightly as the concentration of ammonium nitrate increases. Therefore the second order cobalt nitrate dependence is in fact due to the participation of the second cobalt and not of nitrate in the reaction.

Discussion

There have been several studies of the kinetics of metal acetate incorporation into porphyrin molecules in acetic acid.[15,22-25] The kinetic results are discouragingly inconsistent with each other. Choi and Fleisher[15] found the reaction between TPyP and manganese, cobalt, nickel, and copper in glacial acetic acid to be first order in metal in every case. Brisbin and Balahura[25] and Kingham and Brisbin[24] found the reaction between hematoporphyrin and manganese, iron, cobalt, copper, and zinc to be first order in metal and that between hematoporphyrin and nickel to be half order in metal. Brisbin and Richards[23] studied the reaction between protoporphyrin IX di-

methyl ester (Proto-IX-DME) and some first-row transition metals in glacial acetic acid. The reaction appears to be half order in cobalt and nickel and close to half order in copper and shows orders between one-half and one in manganese and zinc.

The results by Choi and Fleischer[15] are inconsistent with ours. Their experiments were conducted over a very narrow range of metal concentrations: $(3—6)\times10^{-3}$ M, and they found the reaction of cobalt(II) acetate with TPyP to be first order with respect to metal.[15] It seems quite likely that if the kinetics were investigated over a wider range of concentration, the simple rate laws would not be found to hold. In fact, it is possible to estimate the first order metal dependence from the range of $(3—6)\times10^{-3}$ M metal concentration from Fig. 1. Moreover, assuming the similar reactivity of cobalt for TPyP and Proto-IX-DME, the decision of about half order in cobalt for the reaction of Proto-IX-DME with $(2—8)\times10^{-4}$ M cobalt is possible, as apparent from Fig. 2. Therefore it is indispensable in these studies to conduct experiments over as wide a concentration range as possible.

The first metal ion forms a SAT complex to deform the porphyrin (Eqs. 4 and 8). This step is not rate-limiting. The metal in the SAT complex just drops into the porphyrin ring (the k_1-path given by Eqs. 5 and 10). It is the k_2-path that a second metal attacks from the opposite side (Eqs. 6 and 11). The two metals in transition state are considered to be on opposite sides of the porphyrin plane according to the crystal structure of several bi-metalloporphyrins.[26] This is also supported by results on the mechanisms of electrophilic exchange between one metal ion and another complexed in a porphyrin molecule.[27,28]

Kinetic studies[28] on the Zn/Cd–TPP (TPP: tetraphenylporphine) and Zn/Hg–TPP systems revealed rate laws of first order in each reactant. Because of their large ionic radii, cadmium and mercury can not fit as well into the plane of the four central porphyrin nitrogen atoms. It is thus considered that Hg–TPP and Cd–TPP complexes have a configuration favorable for the attack by zinc from the back. So these reactions corresponds to the k_2-path in the present systems.

Recently large metallic ions such as mercury(II), cadmium(II), and lead(II) have been found to accelerate the complex formation of manganese(II), cobalt(II), copper(II), and nickel(II) with *meso*-tetra(4-sulfonatophenyl)porphine.[29] A heterobinuclear transition state has been proposed for these systems, and it may be appropriate to postulate a homobinuclear transition state for the present system. Coordination of the first metal ion makes the configuration of porphine favorable for the attack by the second metal ion from the back. At the same time it may facilitate the dissociation of the pyrrole proton in porphine, which seems important in the formation of metalloporphyrins.

If the dissociation of solvent from metal ions were important in the formation of metalloporphyrins, $Co(OAc)_2$ should react faster than $Co(NO_3)_2$, since electron donor ability of acetate is higher than nitrate.[30,31] In this respect it is interesting to observe no appreciable difference in k_1 and k_2 between $Co(OAc)_2$ and $Co(NO_3)_2$ reactions (see Table 1).

In solvent of low dielectric constant such as acetic acid, it is valuable to consider both ionization and dissociation of reactants. Overall dissociation of AB is written as

$$AB \overset{K_I}{\rightleftharpoons} A^+B^- \overset{K_d}{\rightleftharpoons} A^+ + B^-$$

with an overall dissociation constant K_D:

$$K_D = \frac{[A^+]+[B^-]}{[AB]+[A^+B^-]} = \frac{K_I K_d}{1+K_I},$$

where K_I is an ionization constant and K_d is a dissociation constant. Available values of K_D in acetic acid are $10^{-10.1}$ for H_2O,[32] $10^{-10.1}$ for HNO_3,[33] and $10^{-7.56}$ for $Co(OAc)_2$ ($Co(OAc)_2 \rightleftharpoons CoOAc^+ + OAc^-$).[34] K_d can be calculated by an equation of the type derived by Fuoss for ion-pair formation.[35] Unknown K_d values may be predicted, at least to a correct order of magnitude. On this basis, K_d may be estimated to be about 10^{-6} M for all of these 1:1 electrolytes in acetic acid. Therefore in the concentration higher than 10^{-4} M, 1:1 electrolytes exist as undissociated ion-pair. Water, nitric acid, and cobalt acetate[36] are largely unionized, while cobalt nitrate and ammonium nitrate should be to a considerable extent in the form of undissociated ion-pair. The breaking of pyrrole type protons is involved in metalloporphyrin formation reactions. Protons released as reaction proceeds react rapidly with OAc^- and NO_3^- to form HOAc and HNO_3 molecules.

The k_3-path found for the $Co(NO_3)_2$ system is missing in the $Co(OAc)_2$ system. It may arise from the interaction of $Co(NO_3)_2$ with pyridyl nitrogen in TPyP. The interaction should lower the basicity of pyrrole in TPyP through the change of peripheral charge. This may make easy the deprotonation of H_2TPyP and thus the k_3-path requires lower activation energy than the k_2-path. Since $Co(NO_3)_2$ is more electropositive than $Co(OAc)_2$, $Co(NO_3)_2$ is more reactive than $Co(OAc)_2$. Consequently the k_3-path should not be appreciable, if any, for $Co(OAc)_2$ system.

We are grateful to the Japanese Ministry of Education, Science and Culture for support of this work through Grant No. 584023.

References

1) Metal complexes in acetic acid IV. Part III: S. Funahashi, T. Nishimoto, A. Hioki, and M. Tanaka, *Inorg. Chem.*, **20**, 2648 (1981).

2) P. Hambright, "Porphyrins and Metalloporphyrins," ed by K. M. Smith, Elsevier, New York (1975), Chap. 6, pp. 233—278.

3) F. R. Longo, E. M. Brown, W. G. Rau, and A. D. Adler, "The Porphyrins," ed by D. Dolphin, Academic Press, New York (1979), Vol. V, Chap. 10, pp. 459—481.

4) W. Schneider, *Struct. Bonding (Berlin)*, **23**, 123 (1975).

5) M. Tsutsui, C. P. Hrung, D. Ostfeld, T. S. Srivastava, D. L. Cullen, and E. F. Meyer, Jr., *J. Am. Chem. Soc.*, **97**,

3952 (1975).
6) J. P. Macquet, M. M. Millard, and T. Theophanides, *J. Am. Chem. Soc.*, **100**, 4741 (1978).
7) H. Ogoshi, T. Omura, and Z. Yoshida, *J. Am. Chem. Soc.*, **95**, 1666 (1973).
8) E. B. Fleischer and F. Dixon, *Bioinorg. Chem.*, **7**, 129 (1977).
9) M. F. Hudson and K. M. Smith, *J. Chem. Soc., Chem. Commun.*, **1973**, 515.
10) A. Adeyemo and M. Krishnamurthy, *Inorg. Chem.*, **16**, 3355 (1977).
11) H. J. Callot, B. Chevrier, and R. Weiss, *J. Am. Chem. Soc.*, **101**, 7729 (1979).
12) J. Turay and P. Hambright, *Inorg. Chem.*, **19**, 562 (1980).
13) A. N. Thompson and M. Krishnamurthy, *J. Inorg. Nucl. Chem.*, **41**, 1251 (1979).
14) M. J. Bain-Ackerman and D. K. Lavallee, *Inorg. Chem.*, **18**, 3358 (1979).
15) E. I. Choi and E. B. Fleischer, *Inorg. Chem.*, **2**, 94 (1963).
16) W. Dannhauser and R. H. Cole, *J. Am. Chem. Soc.*, **74**, 6105 (1952).
17) S. Funahashi, T. Nishimoto, P. Banerjee, K. Sawada, and M. Tanaka, *Bull. Chem. Soc. Jpn.*, **53**, 1555 (1980).
18) R. G. Wilkins, "The Study of Kinetics and Mechanism of Reactions of Transition Metal Complexes," Allyn and Bacon, Boston (1974), pp. 5 and 13.
19) K. Sawada and M. Tanaka, *J. Inorg. Nucl. Chem.*, **35**, 2455 (1973).
20) K. Sawada, K. Agata, and M. Tanaka, *Inorg. Chim. Acta*, **30**, 127 (1978).
21) T. Nakagawa and Y. Oyanagi, Nagoya Computation Center, Library program SALS (Statistical analysis with least-squares fitting), 1979.
22) J. James and P. Hambright, *Inorg. Chem.*, **12**, 474 (1973).
23) D. A. Brisbin and G. D. Richards, *Inorg. Chem.*, **11**, 2849 (1972).
24) D. J. Kingham and D. A. Brisbin, *Inorg. Chem.*, **9**, 2034 (1970).
25) D. A. Brisbin and R. J. Balahura, *Can. J. Chem.*, **46**, 3431 (1968).
26) D. Ostfeld and M. Tsutsui, *Acc. Chem. Res.*, **7**, 52 (1974).
27) H. Baker, P. Hambright, L. Wagner, and L. Ross, *Inorg. Chem.*, **12**, 2200 (1973).
28) C. Grant, Jr., and P. Hambright, *J. Am. Chem. Soc.*, **91**, 4195 (1969).
29) M. Tabata and M. Tanaka, *Inorg. Chim. Acta Lett*, **40**, X71 (1980); *Anal. Lett.*, **13**, 427 (1980).
30) S. Funahashi and M. Tanaka, *Inorg. Chem.*, **8**, 2159 (1969).
31) M. Tanaka and S. Yamada, *J. Chem. Soc., Chem. Commun.*, **1976**, 178.
32) S. Bruckenstein and I. M. Kolthoff, *J. Am. Chem. Soc.*, **78**, 2974 (1956).
33) W. Poscham and A. Engelbrecht, *Z. Phys. Chem., Leipzig*, **248**, 177 (1971).
34) O. W. Kolling and J. L. Lambert, *Inorg. Chem.*, **3**, 202 (1964).
35) R. M. Fuoss, *J. Am. Chem. Soc.*, **80**, 5059 (1958).
36) C. F. Hendriks, H. C. A. van Beek, and P. M. Heertjes, *Ind. Eng. Chem. Prod. Res. Dev.*, **18**, 43 (1979).

Determination of Ultratrace Zinc by Enzymatic Activity of Carbonic Anhydrase. II. Use of Carbonate Hydro-lyase Activity

Kensei KOBAYASHI, Kitao FUJIWARA, Hiroki HARAGUCHI, and Keiichiro FUWA*

Department of Chemistry, Faculty of Science, The University of Tokyo, Hongo, Bunkyo-ku, Tokyo 113

(Received February 9, 1981)

A method for the determination of trace zinc has been investigated using hydro-lyase activity of carbonic anhydrase. It was proved theoretically and experimentally that the activation rate of the apo-carbonic anhydrase with zinc is proportional to the amount of zinc present in the solution. Hydro-lyase activity was measured electrochemically using sodium hydrogencarbonate as a substrate. The limit of detection was 0.89 ng/ml or 40 pg of zinc, lower than that obtained by the esterase activity method. Application of the present method to the determination of zinc in real samples has been examined in order to evaluate its analytical feasibility.

At the present time, enzymes show high potentiality for utilization in analytical chemistry in terms of their selectivity for substrates and high sensitivity originating from biochemical amplification.[1,2] Actually, the availability of enzyme electrode or enzyme colorimeter is well recognized, especially in clinical and agricultual fields.[3,4] Of the enzymes, metalloenzymes have specific metal ions located at their active centers, which play essential roles in enzymatic activities. The specificity of enzymatic activity to certain metal ions of metalloenzymes indicates the possibility of determination of trace metal ions. Only a few workers have studied the determination of zinc and copper by enzymatic activity of metalloenzymes, such as aminopeptidase,[5] alkaline phosphatase,[6] and polyphenoloxidase (tyrosinase).[7,8]

In a previous paper, we reported on the determination of trace zinc using the esterase activity of carbonic anhydrase, the recovery of the esterase activity of apo-enzyme (a zinc-free enzyme) being monitored by colorimetric technique.[9] The carbonic anhydrase method has a high selectivity to zinc, and is useful for determining trace zinc ion in natural samples such as fruit juices. On the other hand, carbonic anhydrase has another function, *i.e.*, hydration-dehydration catalysis of carbon dioxide (hereafter referred to as "hydro-lyase activity"), which is more essential in biological systems and has a higher turn-over rate than its esterase activity.

In the present investigation, the hydro-lyase activity of carbonic anhydrase was used for the determination of zinc in combination with the electrochemical detection method. We have found an almost linear relationship between the recovery of enzymatic activity and the amount of zinc. Since this method is more sensitive and convenient than the previous one, it was applied to the determination of zinc in natural water.

Theoretical Consideration

Carbonic anhydrase (CA) has one zinc atom at its active center, the atom being essential for its enzymatic activity (All symbols which follow are described in the Appendix.). Under the conditions $[E_a]_0 \gg [Zn]_0$, the equation between metal ion and apo-CA concentration is written as follws:[9]

$$[E] = K[E_a]_0[Zn]_0/(1+K[Zn]_0). \quad (1)$$

Since the relation $K[E_a]_0 \gg 1$ can be assumed, we obtain

$$[E] \simeq [Zn]_0. \quad (2)$$

CA catalyzes the following hydration-dehydration equilibrium,

$$H_2O + CO_2 \underset{A}{\rightleftharpoons} H_2CO_3 \underset{B}{\rightleftharpoons} H^+ + HCO_3^-, \quad (3)$$

where A is the rate-determining step. Thus, Eq. 3 can be written as

$$H_2O + CO_2 \underset{k_{-1}}{\overset{k_1}{\rightleftharpoons}} H^+ + HCO_3^-. \quad (4)$$

When sodium hydrogencarbonate is used as a substrate, the non-enzymatic reaction rate can be expressed as the decrease of hydrogen ion concentration:

$$(d[H^+]/dt)_{non} = k_1[H_2O][CO_2] - k_{-1}[HCO_3^-][H^+]. \quad (5)$$

The reaction rate for the enzymatic process can also be expressed as

$$(d[H^+]/dt)_{enz} = [E](V'_m[HCO_3^-]/K'_m - V_m[CO_2]/K_m)/(1+[HCO_3^-]/K'_m+[CO_2]/K_m). \quad (6)$$

The total reaction rate, $d[H^+]/dt$, is given by the summation of Eqs. 5 and 6. Under the conditions in which the concentration of total carbonate (*i.e.*, $[HCO_3^-]+[CO_2]$) and the initial pH are constant, V'_m, V_m, $[HCO_3^-]$, and $[CO_2]$ are represented as the functions of $[H^+]$. We then have

$$d[H^+]/dt = [E]f([H^+]) + g([H^+]), \quad (7)$$

where $f([H^+])=(d[H^+]/dt)_{enz}/[E]$, and $g([H^+])=(d[H^+]/dt)_{non}$. Here we define τ and τ_0 as the time required for the pH change from pH_A to pH_B, when CA is added and not added, respectively. Then τ and τ_0 can be expressed as follows:

$$\tau = \int_{[H^+]_A}^{[H^+]_B} (dt/d[H^+])d[H^+] = \int_{[H^+]_A}^{[H^+]_B} [1/\{[E]f([H^+])+g([H^+])\}]d[H^+], \quad (8)$$

$$\tau_0 = \int_{[H^+]_A}^{[H^+]_B} \{1/g([H^+])\}d[H^+]. \quad (9)$$

Since the condition $[E]\,f([H^+]) \gg g([H^+])$ is easily satisfied because of the high turn-over rate of carbonic anhydrase, we obtain

$$1/\tau = [E]/\int_{[H^+]_A}^{[H^+]_B} d[H^+]/f([H^+]) + \int_{[H^+]_A}^{[H^+]_B} \{g([H^+])/f^2([H^+])\}d[H^+]/\left\{\int_{[H^+]_A}^{[H^+]_B} d[H^+]/f([H^+])\right\}^2. \quad (10)$$

When we take $1\Big/\int_{[H^+]_B}^{[H^+]_A} d[H^+]/f([H^+])$ as c, and the second term as c', we get

$$1/\tau = c[E] + c', \quad (11)$$

which shows that a plot of $1/\tau$ against [E] is linear. When $[H^+]_B$ is nearly equal to $[H^+]_A$, c' could be approximated to $1/\tau_0$. After all, the following expression is derived from Eqs. 2 and 11:

$$1/\tau = c[Zn]_0 + 1/\tau_0. \quad (12)$$

Namely, the amount of zinc in the solutions can be determined from the plot of $1/\tau$ *vs.* $[Zn]_0$.

Experimental

Chemicals. Bovine carbonic anhydrase C-7500 (EC 4. 2. 1. 1, abbreviation BCA, Sigma Chem. Co.) was used. Buffer (barbital sodium–HCl, abbreviation Veronal) was purified by means of solvent extraction using a 0.001% dithizone–chloroform solution.[11] The substrate, sodium hydrogencarbonate (Wako Pure Chemicals) was of pH measurement grade. Sodium salts of analytical grade were used as anion standards, and metal chlorides (except $Pb(NO_3)_2$ and $FeSO_4(NH_4)_2SO_4$) of analytical grade were used as metal ion standards, both purchased from Wako Pure Chemicals. The distilled water was prepared by a Daiken Sekiei subboiling distiller, zinc content not exceeding 20 pg/ml.[12]

Instruments. A Toa pH meter HM-5B with a glass electrode GS-125C, a pH stat HSM-10A, and a recorder EPR-200A, were used for the measurement of hydro-lyase activity of carbonic anhydrase. A Hitachi 170-50 atomic absorption spectrophotometer with a Jarrel-Ash FLA-100 carbon rod atomizer was used to determine the zinc content in the sample solutions. UV absorption was measured with Shimadzu UV-210A spectrophotometer. All the pH measurements and ultrafiltration were performed in a Thomas Scientific bath circulator TRL-111SP.

Preparation of the Apo-enzyme. A zinc-free enzyme (apo-enzyme) was prepared by a modified method of Hunt *et al.*,[13] which also differs from the previous method.[9] The procedure is as follows: 30 mg BCA was dissolved in 5 ml of 25 mM Veronal buffer (pH 7.0) containing 50 mM 2,6-pyridinedicarboxylic acid (referred to as PDA solution) (1 M=1 mol dm^{-3}). The enzyme was placed in an Amicon Diaflo cell (type 12), and the PDA solution placed in the reservoir was allowed to run through the Amicon UM-10 ultrafiltration membrane for several hours. Zinc concentration of the effluent was monitored by atomic absorption spectrometry. After zinc concentration of the effluent was as low as the original PDA solution and constant, sub-boiling-distilled water was allowed to flow through the ultrafiltration membrane until the UV absorbance of the effluent at 271 nm (due to PDA) was negligible. All the ultrafiltration was done at 0.5 °C. The residue in the cell (apo-BCA solution) was then taken out and filled up to 3 ml as a "stock reagent," and zinc and protein concentrations were measured by atomic absorption and micro-biuret methods,[14] respectively.

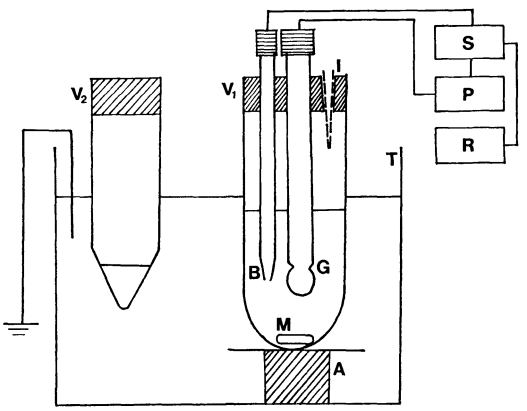

Fig. 1. Reaction vessel for the present method. V_1: Reaction vessel, V_2: incubation vessel, T: thermostatic bath, P: pH meter, S: pH stat, R: recorder, A: acrobat stirrer, M: magnetic spinner, G: glass electrode, B: buret (0.1 M NaOH is contained), I: inlet of reagent.

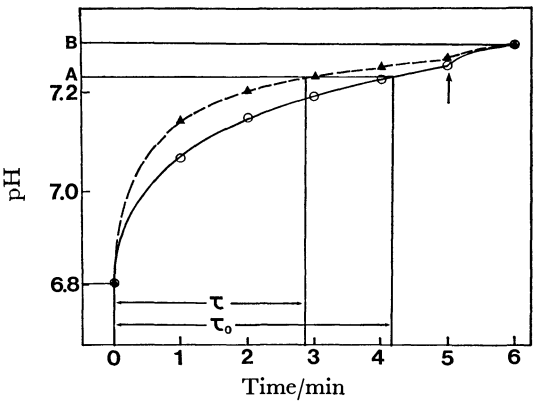

Fig. 2. Time dependence of pH change. ○——○: Without BCA, ▲----▲: with 5 nmol apo-BCA and 230 pg zinc ion, ——→: excess holo-BCA is added, A: $pH_{90\%}$, B: pH_{eq}.

Measurement of Enzymatic Activity. There are some conventional methods for measuring the hydro-lyase activity of BCA,[15,16] where carbon dioxide or sodium hydrogencarbonate is usually used as a substrate, but these are not suitable for zinc-determination. We have used sodium hydrogencarbonate as a substrate, working out a new method to determine zinc. The reaction vessel for this method is shown in Fig. 1. Reaction temperature was maintained at 0.5±0.2 °C.

In order to accelerate the reaction between the apo-enzyme and zinc in the sample, 20 μl of 200 μM apo-BCA solution was pre-incubated with a mixture of 100 μl of the Veronal buffer (pH 6.8) and 100 μl of the sample for 5 min. The mixture was added to the measurement media of 20 ml of the Veronal buffer (pH 6.8). After stirring for 1 min (t=6 min) the substrate solution, 100 μl of 0.65 M sodium hydrogencarbonate, was added to the reaction vessel. The pH change of the mixture resulting from the enzymatic reaction was recorded (Fig. 2). After equilibrium was reached (*ca.* 5 min after mixing the substrate), $[H^+]_{90\%}$ was calculated by the equation

$$[H^+]_{90\%} = \{[H^+]_0 + 9[H^+]_{eq}\}/10. \quad (13)$$

τ is defined as the time required to reach $[H^+]_{90\%}$ (Fig. 2).

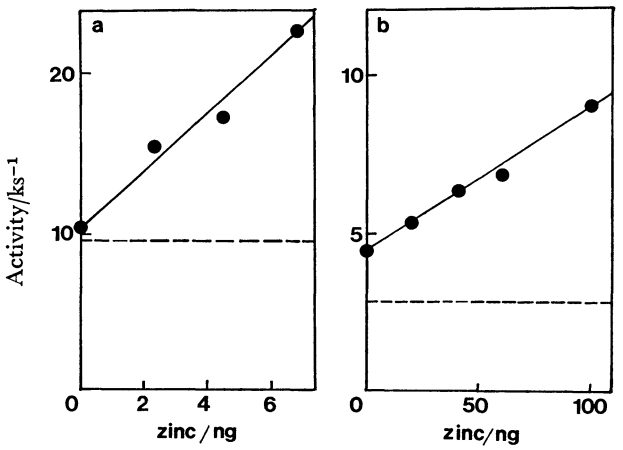

Fig. 3. Calibration curve for zinc measured by hydro-lyase activity of Bovine carbonic anhydrase.
a) Pre-incubation was done. 4.1 ng of apo-BCA and zinc sample were mixed in a separate vessel for 5 min, and added into the reaction vessel. b) No pre-incubation was done. 18 ng of apo-BCA and zinc sample were added directly into the reaction vessel, and kept 5 min before measurement.

Results

Calibration Curve for Zinc. The calibration curve for zinc under the conditions described (see Experimental), is shown in Fig. 3a. The detection limit is 0.89 ng/ml or 40 pg of zinc. The detection limit and dynamic range of the method are dependent on the amount of apo-BCA, the volume of the sample-apo-BCA mixture, and the incubation time in the vessel.

By this method, the dimension of enzymatic activity value is time^{-1} (*i.e.*, reciprocal of τ). When activity becomes high, τ-value becomes smaller, and $1/\tau$ value varies widely. The upper limit of detection is restricted by the deviation of $1/\tau$ value.

Interference of Coexistent Metal Ions. The interferences of the concomitant metal ions under the conditions $\sum_i [M_i^{2+}]_0 \gtrsim [E_a]_0$ are summarized in Table 1. Only Co^{2+} at a concentration equal to that of zinc ion increases the hydro-lyase activity by *ca.* 50%. Other metal ions might interfere with the enzymatic activity, particularly Hg^{2+}. When $\sum_i [M_i^{2+}]_0 \ll [E_a]_0$, the influence of concomitant metal ions is small.

Interference of Coexistent Anions. The interference of the concomitant anions in the present method is given in Table 2. Excess amounts of cyanide and perchlorate ions (100 times more than $[Zn^{2+}]$,) significantly interfere with the analytical results as in the esterase method. On the other hand, thiocyanate and nitrite ions at high level (1000 times in excess of $[Zn^{2+}]$) appear to activate enzymatic activity. If interference of the concomitants occurs. the standard addition method should be employed.

For the determination of zinc in sea water, we studied the influence of 0.5 M NaCl in order to estimate the ppb-level of zinc. No apparent inhibition was observed, the calibration curve for zinc being the same as that without NaCl.

Table 1. Effect of metal ions on hydro-lyase activity of carbonic anhydrase[a)]

Coexistent metal ions	Concentration of coexistent metal ions/ppb				
	10000	1000	100	10	1
Hg^{2+}		10	50	74	96
Co^{2+}			150		
Cu^{2+}	3	16	101		
Fe^{2+}	74	104	101		
Ni^{2+}	45	99	97		
Mn^{2+}	91	96	98		
Cd^{2+}	6	30	100		
Pb^{2+}	22	112	105		

a) The ratio (%) of the enzymatic activities measured with and without coexistent metal ions. Zn^{2+}: 35 pmol (100 ppb) apo-BCA: 140 pmol, incubation time: 5 min.

Table 2. Effect of anions on hydro-lyase activity of BCA[a)]

Anions	Concentration/mM	Activity/%[b)]
CN^-	100	45
	10	57
SCN^-	100	990
	10	228
	1	107
NO_2^-	100	290
	10	126
ClO_4^-	100	43
I^-	100	68
Br^-	100	82
Cl^-	100	106
F^-	100	89
CH_3COO^-	100	90
NO_3^-	100	84

a) Zn^{2+}: 1.5 μM (100 ppb), apo-BCA: 6.0 μM, incubation time: 5 min. b) Ratio (%) of the enzymatic activities measured with and without the anions.

Table 3. Determination of zinc in real samples

Sample	Zinc concentration/(ng/ml)	
	Present method[a)]	Atomic absorption
City water	155	157
Orange juice	131	124

a) apo-BCA: 200 pmol, sample: 20 μl, incubation time: 5 min.

Determination of Zinc in Real Samples. Analytical results for orange juice and city water (Both filtrated with a membrane filter; pore size 0.2 μm) are given in Table 3, together with the amount of zinc in the samples determined by flame atomic absorption spectrometry. The analytical values are in line with those obtained by atomic absorption spectrometry.

Discussion

Consideration for Incubation. The formation reac-

tion between zinc and apo-BCA is

$$E_a + Zn \underset{k_f}{\longrightarrow} E. \quad (14)$$

The k_f value estimated by Henken *et al.*[17] is *ca.* 10^4 $M^{-1}\,s^{-1}$. When $[E_a]_0 \gg [Zn]_0$, the concentration of holo-BCA ([E]) obtained after the incubation for t s is

$$[E] = [Zn]_0\{1-\exp(k_f[E_a]_0 t)\}. \quad (15)$$

By this equation, 1 min is enough to complete the reaction of forming holo-BCA, since $[E_a]_0$ is *ca.* 5 μM by the esterase method.

In the present system, the amount of apo-enzyme needed for analysis is less than that for the esterase method. This is due to the higher activity of BCA in the hydro-lyase reaction than that in the esterase reaction. The use of a less amount of apo-BCA reduces background activity which is due to the contaminant zinc in apo-enzyme. The incubation time in the analytical procedure should be prolonged as can be estimated from Eq. 15. The sample and apo-enzyme were pre-incubated before detection, using a separate vessel so as to increase the net value of $[E_a]_0$ in Eq. 15. The analytical time could be reduced to *ca.* 1% of that in the direct analysis (without pre-incubation (*ca.* 5 min).

No pre-incubation was required for the determination of zinc in high concentration, because τ in Eq. 8 became too small. The calibration curve for zinc in the case of without pre-incubation is shown in Fig. 3b. Here Eq. 2 does not hold, while holo-BCA is approximately proportional to zinc content if incubation time is kept constant (Eq. 15). Employing these two methods (with and without pre-incubation) properly according to the zinc concentration, we could get a wide dynamic range from 40 pg to 100 ng for zinc.

Interference of Coexistent Metal Ions. Several transition metal ions such as copper(II), iron(II), cadmium(II), mercury(II), cobalt(II), and zinc(II) can coordinate to the active center of apo-BCA. Only cobalt-BCA and zinc-BCA have hydro-lyase and esterase activities.[18] Let us assume the following equilibrium between metal ions (M_i^{2+}) and the apo-BCA in solution,

$$E_a + M_i^{2+} \underset{K_i}{\rightleftharpoons} M_i^{2+}\text{-}E_a, \quad (16)$$

$$K_i = [M_i^{2+}\text{-}E_a]/[E_a][M_i^{2+}]. \quad (17)$$

Metal ions interfere with the reaction by sharing the coordination sites of the active center in apo-BCA, inhibiting the association of zinc(II) and apo-BCA. When $\sum_i [M_i^{2+}]_0 \ll [E_a]_0$, the influence of concomitant metal ions is small. Conversely, when $\sum_i [M_i^{2+}]_0 \simeq [E_a]_0$, the influence of metal ions becomes appreciable according to the K_i values which are specific to each concomitant metal ion, M_i^{2+}, as shown by

$$[E] \simeq K_{Zn}[Zn]/\sum_i K_i[M_i^{2+}]. \quad (18)$$

The degree of interference due to the concomitant metal ions is given in Table 1. Generally, interference of metal ions, except mercury(II) ion (for K_{Hg} is not small) and cobalt(II) ion can be neglected when $[M_i^{2+}]_0 < [E_a]_0$. The level of mercury(II) ion or cobalt(II) ion contained in most of the real samples, such as biological samples and sea water, is much lower than that of zinc(II) ion,[19,20] so that the interferences of metal(II) ions can be ignored.

Interference of Coexistent Anions. The effects of the coexisting anions (X^-) on the activity of carbonic anhydrase[21] are based on the fact that the holo-BCA forms 1:1 complexes with monovalent anions which have no enzymatic activity.

$$Zn\text{-}BCA + X_j^- \underset{K_j}{\rightleftharpoons} BCA\text{-}Zn\text{-}X_j^-, \quad (19)$$

where

$$K_j = [BCA\text{-}Zn\text{-}X_j^-]/[Zn\text{-}BCA][X_j^-]. \quad (20)$$

From Eq. 16, we get

$$\alpha = [BCA\text{-}Zn\text{-}X_j^-]/[BCA\text{-}Zn] = [X_j^-]K_j. \quad (21)$$

As compared to the esterase method, samples are more diluted with buffer in the present method, indicating the lowering in α-value (*i.e.*, the interference rate of anions,) and reduction of anion effects.

Application to Zinc Determination in Real Samples. The results shown in Table 2 indicate that the present method can be applied to the determination of zinc in water. The fact that the concentrations of zinc analyzed by the present method are close to those obtained by atomic absorption spectrometry in most of the samples shows that zinc in such samples is dissolved as the reactive form with apo-BCA (exchangeable zinc.) Since the present method is applicable to samples with high salinity, the zinc at the proper concentration in sea water could be directly analyzed by this method.

In the esterase activity method, non-specific esterases in real samples might interfere with the results.[9] By contrast, hydro-lyase activity is specific to carbonic anhydrase, so only its contamination in samples such as serums, should be taken into account. Precision in the present method would thus be better than that in the previous method.

Conclusion

The hydro-lyase method shows promise for determining trace zinc. Carbonic anhydrase has the following characteristics.

1) Reversible dissociation of zinc from protein; zinc-free apo-enzyme has no activities.

2) High specificity to zinc ion as a central metal ion; other than zinc ion, only cobalt(II) ion reactivates apo-enzyme.

3) High biochemical amplification; hydro-lyase activity of carbonic anhydrase has maximum turn-over rate.

4) Linearity between metal concentration and enzyme activity; *i.e.*, only one zinc ion per enzyme.

5) Easy enzymatic assay.

6) An enzyme easily available.

These characteristics, especially 2) and 4), indicate the superiority of carbonic anhydrase over other zinc metalloenzymes for zinc determination.

The present method is superior in selectivity and

sensitivity to the conventional colorimetric method such as the dithizone method.[22] It is possible to determine zinc in a concentrated salt solution, such as sea water, which is one of the most difficult subjects in furnace atomic absorption spectrometry.

This research was supported by Grant-in-Aid for Special Project Research on Trace characterization No. 510804 from the Ministry of Education, Science and Culture.

Appendix

E: Holoenzyme,
E_a: Apo-enzyme,
M_i^{z+}: Metal ion,
X_j^-: Monovalent anion,
K: Stability constant between enzyme protein and zinc,
K_i: Stability constant between enzyme protein and metal ions (M_i^{z+}),
K_j: Stability constant between holoenzyme and monovalent anion (X_j^-),
k_0: Molecular activity of enzyme,
k_1, k_{-1}: Rate constant,
k_f: Formation rate constant,
t: Reaction time,
V_m: Maximum reaction rate of hydration reaction,
V_m': Maximum reaction rate of dehydration reaction,
K_m: Michaelis constant of hydration reaction,
K_m': Michaelis constant of dehydration reaction,
$[]_0$: Concentration at the condition of initial stage,
$[]_{eq}$: Concentration at an equilibrium stage,
$()_{non}$: Value when no enzyme is added,
$()_{enz}$: Value when enzyme is added.

References

1) G. G. Guilbault, "Enzymatic Methods of Analysis," Pergamon Press, Oxford (1970).
2) M. M. Fishman and H. F. Schiff, *Anal. Chem.*, **48**, 322R (1980).
3) L. D. Boweres and P. W. Carr, *Anal. Chem.*, **48**, 544A (1976).
4) Y. Umezawa, *Kagaku No Ryoiki*, **31**, 20 (1977).
5) P. Lehky and E. A. Stein, *Anal. Chim. Acta*, **49**, 366 (1969).
6) A. Townshend, and A. Vaughan, *Talanta*, **17**, 289 (1970).
7) J. V. Stone and A. Townshend, *J. Chem. Soc., Dalton Proc.*, **1973**, 495.
8) B. Mattiasson, H. Nilsson, and B. Olsson, *J. Appl. Biochem.*, **1**, 377 (1979).
9) K. Kobayashi, K. Fujiwara, H. Haraguchi, and K. Fuwa, *Bull. Chem. Soc. Jpn.*, **52**, 1932 (1979).
10) J. C. Kernohan, *Biophys. Biochim. Acta*, **81**, 345 (1964).
11) B. G. Malmström, *Arch. Biochim. Biophys.*, **46**, 345 (1953).
12) T. Harada, K. Fujiwara, and K. Fuwa, *Bunseki Kagaku*, **26**, 877 (1977).
13) J. B. Hunt, M. -J. Rhee, and C. B. Storm, *Anal. Biochem.*, **79**, 614 (1977).
14) R. F. Itzhaki and D. M. Gill, *Anal. Biochem.*, **9**, 401 (1964).
15) E. R. Waygook, "Methods in Enzymology," ed by S. P. Colowick and N. O. Kaplan, Academic Press, New York (1955), Vol. 2, pp. 836—846.
16) K. M. Wilbur and N. G. Anderson, *J. Biol. Chem.*, **176**, 147 (1948).
17) R. W. Henkens and I. M. Sturtevant, *J. Am. Chem. Soc.*, **90**, 669 (1968).
18) J. E. Coleman, *Biochemistry*, **4**, 2644 (1965).
19) E. J. Underwood, "Trace Elements in Human and Animal Nutrition," 3rd ed, Academic Press, New York (1971).
20) S. Okabe, I. Hirota, and K. Shimizu, "Kaiyo No Kagaku," Tokai Daigaku Shuppan-kai, Tokyo (1980), pp. 11—14.
21) Y. Pocker and J. T. Stone, *Biochem. J.*, **40**, 319 (1946).
22) E. B. Sandell, "Colorimetric Determination of Traces of Metals," 3rd ed, Interscience, New York (1959).

  Bull. Chem. Soc. Jpn., 54, 2705—2707 (1981)

The Steric Hindrance of the Stepwise Reaction of *N*-Carboxy α-Amino Acid Anhydride with the α-Amino Acid Ester

Masanao Ōya* and Tomoko Takahashi

Department of Chemistry, College of Technology, Gunma University, Tenjin-cho, Kiryu, Gunma 376

(Received July 21, 1980)

The mechanisms of the reactions of 4-alkyloxazolidinediones (**1**) (*N*-carboxy α-amino acid anhydrides(NCAs)) with α-amino acid benzyl ester *p*-toluenesulfonates (**2**) were investigated in acetonitrile containing triethylamine at low and room temperatures. Two types of reactions were observed: (1) the polymerization of NCAs was initiated with a small amount of **2** to produce polypeptides (**6**), and (2) the dipeptide benzyl esters (**4**) were produced by the stepwise reaction of NCAs with the esters. Both the polymerization and the dipeptide formation (**1**+**2**) seemed to be initiated by the nucleophilic attack of the amino group of the ester on the C-5 carbon of NCAs. The polymerization proceeded when the side chains of the amino acid esters (R^2) were more bulky than those of the NCAs (R^1). On the contrary, dipeptide esters were produced when the side chains of the NCAs (R^1) were more bulky than those of the esters (R^2).

The mechanisms of the polymerization of *N*-carboxy α-amino acid anhydrides (NCAs) are extensively studied. The mechanisms involve the initiation of the polymerizations of the NCAs with amines, sodium alcoholates, inorganic salts such as lithium chloride, and organometallic compounds, followed by propagation reactions.[1-4] In comparison, there is little information on the stepwise reaction of NCAs with compounds having an α-amino group to produce α-amino acid amides or their derivatives. The mechanism of the reaction of the glycine ethyl ester with the NCAs derived from other α-amino acids to produce dipeptide-ethyl esters is regarded as the stepwise reaction of an α-amino group with NCAs.[5] This stepwise reaction does not occur for any α-amino acid esters except for the glycine ester (with NCAs) in anhydrous media, because the polymerization reaction of NCAs occur.[6]

We previously synthesized oligopeptides with regular sequences by the stepwise reaction of α-amino acid sodium salts with NCAs in a water–acetonitrile system.[7] In another previous study, we synthesized dipeptides and cyclodipeptides by the stepwise reaction of α-amino acid benzyl ester *p*-toluenesulfonates with NCAs in anhydrous acetonitrile in the precence of triethylamine.[8] No mechanism of the reaction was discussed in detail, however.

In this paper, the mechanisms of the reactions are discussed with regard to the steric hindrance of the side chains of both α-amino acid esters and NCAs.

Results and Discussion

The reactions of NCAs (**1**) with α-amino acid benzyl-ester *p*-toluenesulfonates (**2**) were carried out in acetonitrile containing triethylamine at low and room temperatures (Eq. 1). The reactions which occured may be classified as the following types: (1) polypeptides were obtained by the polymerization of NCAs initiated with a small amount of the amino acid esters, (2) dipeptide esters were produced by the stepwise reaction of NCAs with the amino acid esters, and (3) both the polypeptides and dipeptide esters were produced by the polymerizations and the stepwise reactions. The results are shown in Table 1.

In the polymerization of γ-benzyl L-glutamate NCA with a primary amine in dioxane, it has been reported that 70% of the initiator (the amine) was involved

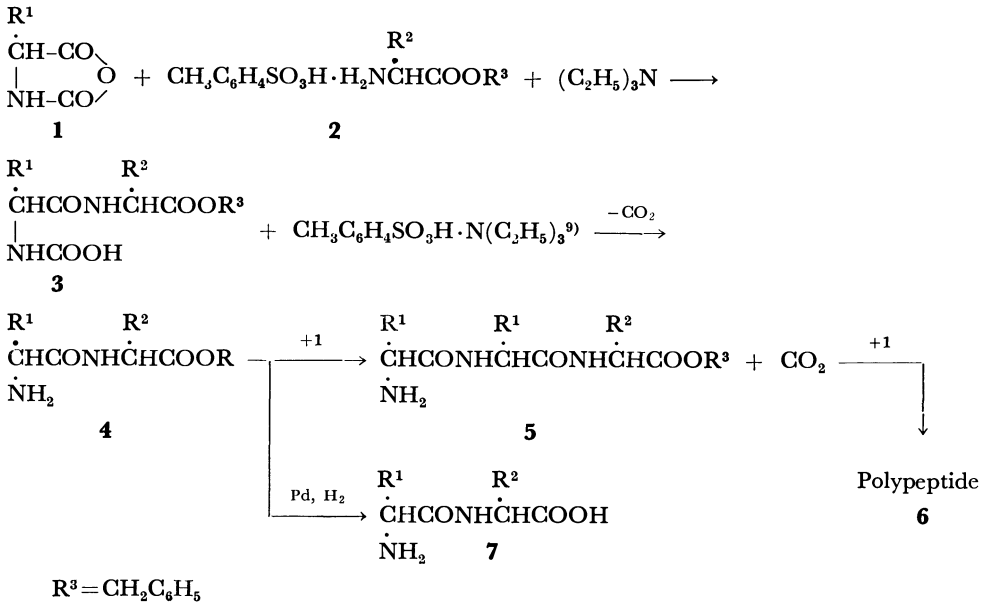

(1)

Table 1. Reaction of NCA with amino acid benzyl ester in acetonitrile

Reactant[a]		Product yield/%			
		Dipeptide (**7**)[b]		Polypeptide (**6**)[c]	
NCA/R^1	Ester/R^2	−20 °C	20 °C	−20 °C	20 °C
H	H	0	0	90	85
	CH_3	0	0	97	97
	$(CH_3)_2CH$	0	0	92	95
	$(CH_3)_2CHCH_2$	0	0	98	99
	$C_6H_5CH_2$	0	0	90	95
CH_3	H	80	80	0	0
	CH_3	20[d]	20[d]	50	55
	$(CH_3)_2CH$	0	0	92	94
	$(CH_3)_2CHCH_2$	0	0	97	98
	$C_6H_5CH_2$	15	15	75	80
$(CH_3)_2CH$	H	80	80	5	0
	CH_3	70	70	8	7
	$(CH_3)_2CH$	80	75	5	5
	$(CH_3)_2CHCH_2$	80	80	10	10
	$C_6H_5CH_2$	0	0	96	90
$(CH_3)_2CHCH_2$	H	75	75	5	0
	CH_3	75	80	5	5
	$(CH_3)_2CH$	10	10	90	90
	$(CH_3)_2CHCH_2$	70	75	5	5
	$C_6H_5CH_2$	0	0	90	90
$C_6H_5CH_2$	H	90	90	0	0
	CH_3	90	90	0	0
	$(CH_3)_2CH$	90	90	0	0
	$(CH_3)_2CHCH_2$	90	90	0	0
	$C_6H_5CH_2$	90	90	0	0

a) L-Amino acid (except for glycine) was used. b) Isolated yields. c) Isolated yields; near reaction yields. d) Isolated yields of mixtures of dipeptides and amino acids.

in the attack on the C-5 carbonyl carbon of the NCA, while the remaining 30% of the amine was involved in the abstraction of the proton attached to the nitrogen of NCA.[3-4] When the polymerization of NCAs was initiated by the proton abstraction, the propagation could not be controlled because of the fast polymerization.

It has been concluded that the reactions of NCAs with amino groups are initiated only by the C-5 attack in acetonitrile.[10] As is shown in Eq. 1, the polymerization of NCAs should not proceed when the reaction of **1** with **2** is faster than that of **4** with **1**. The following mechanism are assumed. (1) Since the carbamic acid (**3**) is stable, the reaction from **3** to **4** should be very slow. (2) The basicity of the amino group of the amino acid ester (**2**) may be stronger than that of the dipeptide and tripeptide esters, so that the reaction of **1** with **2** is predominant compared to that of **1** with **4** or **5**. (3) An unknown mechanism other than (1) and (2) proceeds. As is shown in Table 1, glycine NCA is polymerized by all amino acid esters. Alanine NCA ($R^2=CH_3$) was usually polymerized with amino acid esters, but it produced the alanylglycine benzyl ester in 80% yield when reacted with the glycine ester ($R^2=H$). Valine and leucine NCAs were polymerized when the reactions were carried out with the amino acid esters having side chains more bulky than those of NCAs. Phenylalanine NCA produced the dipeptide esters without the polymerization of NCAs, even when the NCAs were allowed to react with the phenylalanine benzyl ester having the same side chain as that of the NCA.

It is known that a carbamic acid is stable in a basic medium at a low temperature.[5] The decarboxylation reaction from the carbamic acid occurs through the zwitter ion as the temperature increases.[11] If the decarboxylation reactions (**3**→**4**) were influenced by the temperature in Eq. 1, the yields of the polypeptides would also be influenced by the temperature. Table 1 shows, however, that the yields of the polypeptides and dipeptides were not influenced by the rise in temperature from −20 °C to 20 °C. Therefore, the decarboxylation reactions (**3**→**4**) can not be considered to have been influenced by the temperature and has to be the rate-determining step in the reactions.

It has generally been considered that the basicity of the amino group on dipeptides is slightly stronger than that of the corresponding amino acid.[12] This

may be also the case with the basicity of the dipeptide benzyl ester and the corresponding amino acid benzyl esters. If such a consideration could be applied to Eq. 1, the polymerization would proceed in all cases. The polymerization, however, proceeds only when the side chains of the esters are more bulky than that of NCAs. From these results, it is concluded that the steric hindrance of the side chains of both NCAs and esters affected whether the polymerization of NCAs proceeds or whether the stepwise reaction proceeds to produce the dipeptide esters.

Experimental

The α-amino acid benzyl esters[13] and NCAs[10,14] were prepared by the methods reported previously.

Reaction of NCAs (1) with α-Amino Acid Benzyl Esters (2). General Procedure: To the α-amino acid benzyl ester *p*-toluenesulfonate (**2**) (10 mmol) was added NCA (**1**) (10 mmol) in acetonitrile (25 cm^3) containing triethylamine (10 mmol). The mixture was thus stirred for 4 h. When the polypeptide formed by the polymerization of NCA was precipitated, it was separated by filtration and dried *in vacuo* to determine the extent of polymerization. The clear solution of the resulting mixture or the filtrate was distilled *in vacuo* to remove the solvent. The residual oily product was washed with ethyl ether and hydrogenated with palladium black in a mixture of acetic acid, *t*-butyl alcohol, and water. Dipeptide was thus obtained (**7**). When the NCA was partly polymerized, the final product was mixture of amino acid and dipeptide. The isolated polypeptides, dipeptides, and these mixtures, when analyzed on C, H, N, and by means of the NMR and IR spectra, proved identical with independently synthesized authentic specimens.[7,8]

Valylalanine ($R^1=(CH_3)_2CH$, $R^2=CH_3$): ^{1}H-NMR (CF_3COOH): δ 1.2—1.3(d, 6H), 1.6—1.7(d, 3H), 2.1—2.6(m, H), 4.1—4.4(q, H), 4.8—4.9(t, H), 7.3(s, H), 7.7—7.8(d, H). Found: C, 50.77; H, 8.59; N, 14.68%. Calcd for $C_8H_{16}O_3N_2$: C, 51.06; H, 8.51; N, 14.87%.

Further, the polypeptides were analyzed by means of X-ray diffraction measurement.[15]

The residual NCA after finishing the reaction was analyzed by the method of Berger.[16]

References

1) C. H. Bamford, "Polyamino Acids, Polypepeptides, and Proteins," ed by M. A. Stahman, Univ. Wisconsin Press, Madison, Wisconsin (1965), p. 65.
2) C. H. Bamford, A. Elliott, and W. E. Hamby, "Synthetic Polypeptides," Academic Press, New York (1965), p. 62.
3) M. Goodman and U. Aron, *Biopolymers*, **1**, 500 (1963).
4) M. Goodman and H. Huchison, *J. Am. Chem. Soc.*, **87**, 3524 (1965); **88**, 3627 (1966); E. Piggion, M. Tervojevich, and A. Cosani, *ibid.*, **88**, 3630 (1966).
5) J. L. Bailey, *J. Chem. Soc.*, **1950**, 3461.
6) Ōkawa, *Bull. Chem. Soc. Jpn.*, **29**, 486 (1956).
7) Y. Iwakura, K. Uno, M. Ōya, and R. Katakai, *Biopolymers*, **9**, 1419 (1970).
8) M. Ōya and T. Takahashi, *Nippon Nōgei Kagaku Zasshi*, **51**, 259 (1977); T. Takahashi, H. Hoshino, and M. Oya, *ibid.*, **53**, 69 (1979).
9) *p*-Toluenesulfonic acid combined with the α-amino acid ester is separated with triethylamine to produce free amino acid ester.
10) M. Ōya, K. Uno, and Y. Iwakura, "Progress in Polymer Science Japan," ed by K. Uno and S. Onogi, Kodansha, Tokyo (1973), Vol. 6, p. 51.
11) B. R. Brown and D. L. Hamik, *J. Chem. Soc.*, **1949**, 659.
12) A. H. Cook and A. L. Levy, *J. Chem. Soc.*, **1960**, 651.
13) N. Izumiya, T. Katō, M. Ohno, and A. Aoyagi, "Peptide Gosei," Maruzen, Tokyo (1975), pp. 71 and 224.
14) M. Ōya, K. Uno, and Y. Iwakura, *J. Polym. Sci., A-1*, **8**, 1851 (1970).
15) M. Ōya, M. Tomizawa, K. Uno, and Y. Iwakura, *Bull. Chem. Soc. Jpn.*, **43**, 3416 (1970).
16) A. Berger, M. Sela, and E. Katchalski, *Anal. Chem.*, **10**, 1554 (1953).

The Photochemistry of the Host-Guest Complex. V. The Effect of the Sodium Ion on the Photoreaction of Benzil Derivatives with a Crown Ether Moiety

Hideki HIRANO, Katsuyuki KURUMAYA, and Masaru TADA*

Department of Chemistry, School of Science and Engineering, Waseda University, Shinjuku-ku, Tokyo 160

(Received September 8, 1980)

The photolysis of 4′-(2-phenyl-1,2-dioxoethyl)benzo-15-crown-5 in benzene containing 1-dodecanethiol gives benzaldehyde and 4′-formylbenzo-15-crown-5. The formation of the aldehydes was inhibited by the sodium ion, whereas the photolysis of 1-(3,4-dimethoxyphenyl)-2-phenylethanedione was not inhibited by the sodium ion. This inhibition must be due to the decrease in the formation of benzoyl radicals from the triplet excited state of the crown ether derivative. The salt effect was discussed on the basis of the spectral data.

We have been studying the effect of a guest ion on the photoreactivity of crown ether derivatives,[1] and have shown that the formation of a host-guest complex affects the photoreaction in several aspects. In the course of our study of the photoreaction of a host-guest complex, the photoreactivity of benzil derivatives was tested in the presence of a guest cation.[2] In this paper we wish to report the photolyses of 4′-(2-phenyl-1,2-dioxoethyl)benzo-15-crown-5 (**1**) and 1-(3,4-dimethoxyphenyl)-2-phenylethanedione (**2**) in benzene containing 1-dodecanethiol.

The excitation of benzil in hydrogen-donating solvents gives a complex mixture of products,[3] which derives from the ketyl radical[4] formed by hydrogen abstraction by a triplet-excited benzil.[5] However, the excitation of benzil in benzene does not cause a remarkable reaction. This behavior of benzil must be due to the lack of ketyl-radical formation in benzene, a poor hydrogen-donating solvent. Another photochemical process of benzil is the formation of benzoyl radicals by an α-cleavage, but the benzoyl radicals preferentially recombine to regenerate the starting material. In the present study, 1-dodecanethiol was added to the reaction mixture as a scavenger of the benzoyl radicals[6] formed by the α-cleavage of the benzil derivative.

Results and Discussion

Photoreactions of Benzil Derivatives in the Absence or Presence of the Sodium Ion. The irradiation of **1** in deoxygenated benzene–acetonitrile (6:4) containing 1-dodecanethiol gave benzaldehyde (**3**) and 4′-formylbenzo-15-crown-5 (**4**). The irradiation of **2** in the same manner gave benzaldehyde (**3**) and 3,4-dimethoxybenzaldehyde (**5**). All the products were identified by comparison with authentic aldehydes. The starting material in the reaction mixture did not change in the dark. The photolyses of **1** and **2** (2.5×10^{-2} mol dm^{-3}) are sluggish, and only *ca.* 30% of the starting materials disappeared after irradiation for 40 h (see the experimental section for details of the reaction conditions). The sluggishness of the photolyses of **1** and **2** is accounted for by the rapid recombination of benzoyl radicals in a solvent cage. It has been reported that 0.03 mol dm^{-3} of 1-dodecanethiol scavenges the cage-free benzoyl radical formed by the photolysis of 1,2-diphenylethanone.[6] In the present study, we used enough 1-dodecanethiol (0.25 mol dm^{-3}) as the scavenger of benzoyl radicals.

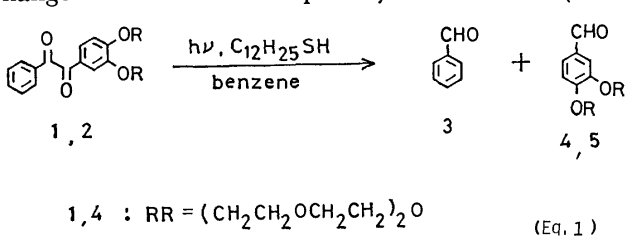

1, 4 : RR = $(CH_2CH_2OCH_2CH_2)_2O$
2, 5 : R = CH_3 (Eq. 1)

The effect of the guest cation on the photoreactivity of the crown ether derivative (**1**) was tested by adding varying amounts of sodium perchlorate. Figure 1 shows the effects of the added sodium perchlorate on the relative quantum yield (ϕ_{rel}) of aldehyde **3** and **4**. The depressing in ϕ_{rel} can not be due to the perchlorate anion, since the addition of tetrabutylammonium perchlorate stimulated ϕ_{rel}. The photolysis of **2** in the presence of sodium perchlorate gave an entirely different result from that of the photolysis of **1**, and the addition of sodium perchlorate increased the formation of aldehyde **3** and **5** (Fig. 2). These results clearly show that the effect

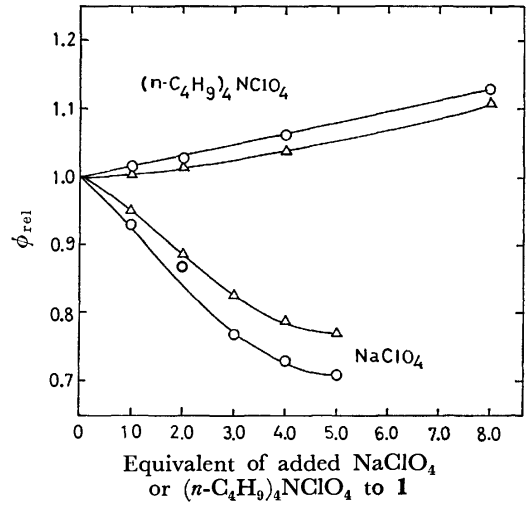

Fig. 1. Relative quantum yield of the formation of benzaldehyde (**3**) (△——△) and 4′-formylbenzo-15-crown-5 (**4**) (○——○) on the photolysis of crown ether derivative (**1**) (2.5×10^{-2} mol dm^{-3}) in the presence of $NaClO_4$ or $(C_4H_9)_4N\cdot ClO_4$.

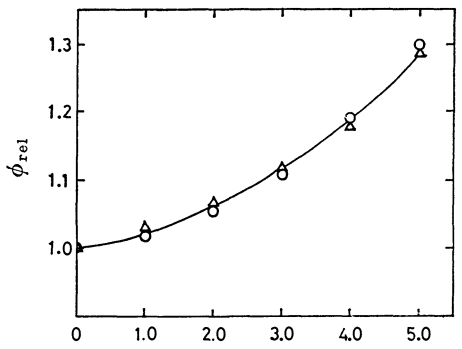

Fig. 2. Relative quantum yield of benzaldehyde (**3**) (△——△) and 3,4-dimethoxybenzaldehyde (**5**) (○——○) on the photolysis of dimethoxy compound (**2**) (2.5×10^{-2} mol dm^{-3}) in the presence of $NaClO_4$.

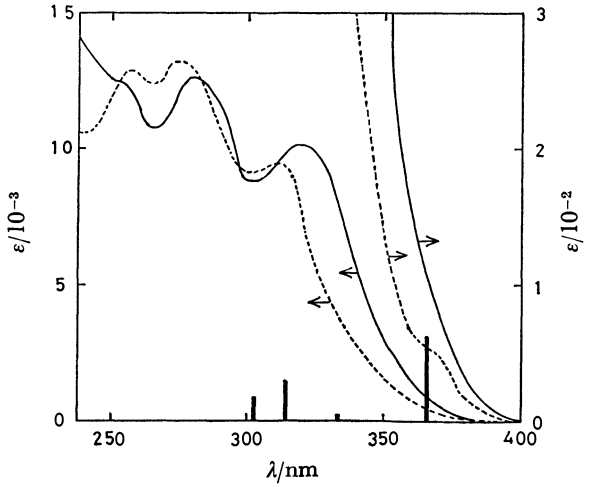

Fig. 3. UV absorption spectra of 4′-(2-phenyl-1,2-dioxoethyl)benzo-15-crown-5 (**1**) (1.00×10^{-4} mol dm^{-3} in acetonitrile) in the absence (——) and presence (·····) of $NaClO_4$ (20 equivalents), and emission lines from a high pressure mercury lamp in 300—400 nm region

of the sodium salt on the photoreactivity of **1** is related to the complex formation between the sodium ion and the crown ether derivative (**1**).

Discussion of the Salt-effect Based on the Spectroscopic Data. The ultraviolet absorption of **1** changes upon the addition of sodium perchlorate due to the formation of a host-guest complex (Fig. 3). The absorption of **2** is essentially the same as that of **1**, but it does not change upon the addition of sodium perchlorate. The formation constant ($K=2.8\times10^3$ mol^{-1} dm^3 in acetonitrile) of the complex between **1** and the sodium ion can be obtained by the analysis of the spectral change by means of the Benesi-Hildebrand equation (Eq. 2),[7] in which **Abs** denotes the absorbance (solution thickness: 1.0 cm) of the mixture of **1** and the sodium ion, while $\Delta\varepsilon$ denotes the difference in the molar absorptivity of **1** and the complex. From Eq. 2 we calculated $\Delta\varepsilon(=674)$ at 366 nm, at which a high-pressure Hg lamp has a strong emission line. The $\Delta\varepsilon$ thus obtained and the molar absorptivity of **1** at 366 nm ($\varepsilon=962$) gave the molar absorptivity of the host-guest complex at 366 nm ($\varepsilon=268$). We photolyzed a 2.5×10^{-2} mol dm^{-3} solution of the crown ether derivative (**1**) in the presence of varying amounts of sodium perchlorate (0.0—1.25×10^{-1} mol dm^{-3}). The absorbance of the reaction solution at 366 nm is calculated to be **Abs**(366)=6.7 (path length: 1.0 cm) when the crown ether derivative (**1**) exists entirely as the complex. This analysis shows that the **Abs** (366 nm) of the reaction mixture must be larger than 5.7, even at a solution thickness of 1.0 mm, and that a 366-nm light is almost completely absorbed by the reaction mixture contained in a Pyrex tube 1 cm in diameter. The reaction mixtures containing varying amounts of the sodium salt, therefore, must absorb the same number of photons under the present conditions. Other emission lines (304, 313, and 334 nm) from the Pyrex-filtered lamp should be completely absorbed by the reaction mixture, since it has large absorption coefficients at these wave lengths (see Fig. 3) and since the number of the excited molecule is

$$\frac{[\mathbf{1}]\cdot[Na^+]}{\mathbf{Abs}} = \frac{[Na^+]}{\Delta\varepsilon} + \frac{1}{\Delta\varepsilon\cdot K} \qquad (2)$$

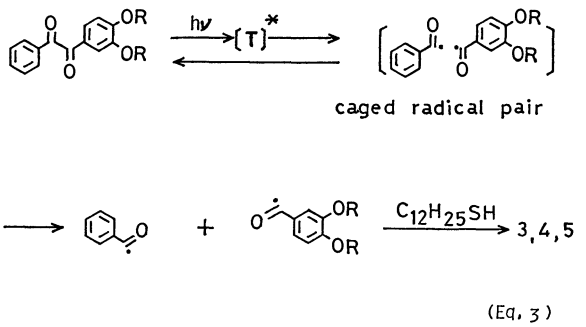

(Eq. 3)

essentially not affected by the existence of the sodium ion.

1-Dodecanethiol is an efficient scavenger of a cage-free benzoyl radical,[6] and the decrease in ϕ_{rel} upon the complex formation with the sodium ion must be due to the retardation of benzoyl-radical formation from the crown ether derivative (**1**).

The phosphorescence from **1** in glassy EPA (1.02×10^{-4} mol dm^{-3}) shows a spectrum with a diffused vibrational structure, presumably from the $^3(n\pi^*)$ or $^3(\pi\pi^*)$ of a considerable mixing with $^3(n\pi^*)$, and the emission neither shifts nor changes its shape on the addition of sodium perchlorate. The intensity of the phosphorescence from **1**, however, diminishes by *ca.* 15% upon the addition of sodium perchlorate (7.05×10^{-4} mol dm^{-3}). The dimethoxy analog (**2**) shows essentially the same phosphorescence spectrum as that of the crown ether derivative (**1**), but the spectrum is not affected by the addition of sodium perchlorate or tetrabutylammonium perchlorate. The lifetime of the emissive state of **1** was determined to be $\tau=54$ ms, and it was not affected by the sodium salt. Since the lifetime of the triplet state of **1** is insensitive to the sodium ion, the decreases in the ϕ_{rel} of the reaction and the phosphorescence intensity can not be attributed to the additional decay process of the triplet state, but must be attributable to the decrease in the quantum yield of the triplet state upon

the complex formation. Decreases in the rate of intersystem crossing are attributable to several factors: (i) an electronic-field perturbation by the added electrolyte, (ii) an external heavy-atom effect, and (iii) the energy gap between the S_1 and T_1 states (ΔE_{ST}). The first two factors can not be important in the present case, however, since another intersystem crossing, $T_1 \rightarrow S_0$, is not affected, as is evidenced by the insensitivity of the lifetime of the phosphorescence to the sodium salt. The energy level of the triplet state (T_1) of **1** does not change upon the complex formation, as is evidenced by the wavelength of the phosphorescence, whereas the complexation of **1** with the sodium ion raises the energy level of the singlet excited state (S_1) of **1**, as is evidenced by the absorption spectrum in acetonitrile; λ_{max}: 319 nm (without Na^+) and λ_{max}: 310 nm (with Na^+). This increase in ΔE_{ST} is one of the most probable factors in retarding the intersystem crossing ($S_1 \rightarrow T_1$) and, hence, the formation of a benzoyl-radical pair from the T_1 state.

It is still uncertain why the relative reactivities of **1** and **2** increase upon the addition of the ammonium perchlorate. Since the addition of sodium perchlorate to the reaction system of **2** (see Fig. 2) increases its photoreactivity, these effects must, however, be related to the perchlorate anion. We must await further studies about other aspects for the solution to this problem.

Experimental

Synthesis of 4′-(2-Phenyl-1,2-dioxoethyl)benzo-15-crown-5 (1). A mixture of benzo-15-crown-5 (2.68 g, 1.0×10^{-2} mol) and phenylacetic acid (2.04 g, 1.5×10^{-2} mol) in 10 cm³ of polyphosphoric acid was stirred for 5 h at 70 °C. After cooling, the mixture was poured into ice water (*ca.* 15 cm³); the new solution was stirred for 1 h to hydrolyze polyphosphoric acid, and the resulting aqueous mixture was extracted by chloroform (20 cm³×3). The evaporation of the extract after successive washing by water and a saturated solution of sodium hydrogencarbonate and drying over magnesium sulfate gave a pale yellow solid. The chromatography of the crude product on an alumina column (1.0(ϕ)×20 cm) (chloroform, 70 cm³), followed by recrystallization from methanol, gave 4′-(2-phenyl-1-oxoethyl)benzo-15-crown-5; 1.62 g (42%). Mp 73.5—74.5 °C; IR(CCl_4): 1660, 1590, 1510, 1425, 1262, and 1130 cm⁻¹; NMR($CDCl_3$): δ 7.50—7.35 (2H, m), 7.14 (5H, m), 6.63 (1H, d, J=8 Hz), 4.02 (2H, s), 3.99 (4H, m), 3.75 (4H, m), and 3.57 (18H, diff. s).

A mixture of 4′-(2-phenyl-1-oxoethyl)benzo-15-crown-5 (1.0 g, 2.6×10^{-3} mol), selenium dioxide (0.35 g, 3.2×10^{-3} mol), dioxane (20 cm³), and water (10 cm³) was refluxed for 15 h, after which the solvent were removed *in vacuo*. Benzene (20 cm³) was then added to the residue, and the mixture was evaporated twice to remove the residual dioxane and water. The solid residue was dissolved in chloroform (20 cm³) and filtered to remove the solid selenium. The filtrate was condensed *in vacuo* after drying over magnesium sulfate to give a pale yellow product. The purification of the product by passing it through a column of alumina (1.0(ϕ)×10 cm, and chloroform 70 cm³) and subsequent recrystallization from methanol gave 4′-(2-phenyl-1,2-dioxoethyl)benzo-15-crown-5 (**1**); 0.78 g, (75%). Mp 110—112 °C; Found: C, 65.85; H, 5.97%. Calcd for $C_{22}H_{24}O_7$: C, 65.99; H, 6.04%. $\lambda_{max}^{CH_3CN}$: (ε) 252 (1.26×10^4), 282 (1.26×10^4), and 318 nm (1.01×10^4); IR($CHCl_3$): 1665, 1595, 1510, 1438, 1280, and 1135 cm⁻¹; NMR($CDCl_3$): δ 7.95(2H, m), 7.52(5H, m), 6.72(1H, d, J=8 Hz), 4.15 (4H, m), 3.75(4H, m), and 3.66(8H, diff. s).

Synthesis of 1-(3,4-Dimethoxyphenyl)-2-phenylethanedione (2). 1-(3,4-Dimethoxyphenyl)-2-phenylethanone was prepared from 1,2-dimethoxybenzene (13.8 g, 1.0×10^{-1} mol) and phenylacetic acid (17.0 g, 1.25×10^{-1} mol) in polyphosphoric acid (100 cm³) by the procedure used for the preparation of 4′-(2-phenyl-1-oxoethyl)benzo-15-crown-5. The crude product was purified by distillation under reduced pressure (230 °C/0.15 mmHg(20.0 Pa)); subsequent recrystallization from methanol gave 20.0 g (78%) of the product. Mp 79—80 °C; IR(CCl_4): 1675, 1590, 1520, 1420, 1152, and 1012 cm⁻¹; NMR($CDCl_3$): δ 7.46(1H, dd, J=8 and 2 Hz), 7.42 (1H, s), 7.18(5H, m), 6.68(1H, d, J=8 Hz), 4.05(2H, s), and 3.77(6H, s).

1-(3,4-Dimethoxyphenyl)-2-phenyl-1-ethanone (12.88 g, 5.0×10^{-2} mol) was oxidized by selenium dioxide (7.0 g, 6.3×10^{-2} mol) in dioxane (70 cm³) and water (30 cm³) by means of the procedure used for the preparation of 4′-(2-phenyl-1,2-dioxoethyl)benzo-15-crown-5 (**1**). The product was purified by recrystallization from methanol to give 12.0 g (89%) of 1-(3,4-dimethoxyphenyl)-2-phenylethanedione (**2**). Mp 111—113 °C; Found: C, 71.42; H, 5.09%. Calcd for $C_{16}H_{14}O_4$: C, 71.10; H, 5.22%. $\lambda_{max}^{CH_3CN}$: (ε) 253(1.28×10^4), 281(1.26×10^4), and 319 nm(1.04×10^4); IR (CCl_4): 1663, 1585, 1512, 1252, and 862 cm⁻¹; NMR (CCl_4): δ 7.90(2H, m), 7.60—7.20(5H, m), 6.75(1H, d, J=8 Hz), and 3.83(6H, s).

Photoreaction of 4′-(2-Phenyl-1,2-dioxoethyl)benzo-15-crown-5 (1) in the Presence of 1-Dodecanethiol. To a solution of **1** (100 mg, 2.5×10^{-4} mol) and 1-dodecanethiol (505 mg, 2.5×10^{-3} mol) in 10 cm³ of a mixed solvent of benzene–acetonitrile (6:4) were added varying amounts of sodium perchlorate (0.0—1.25×10^{-3} mol). The solutions, placed in Pyrex tubes, were dipped in an ultrasonic bath and bubbled with nitrogen from a syringe needle for 10 min. The solutions were then irradiated externally for 40 h with a 450-w high-pressure Hg lamp mounted in a rotary irradiation apparatus (Rikosha RH-400), the distance between the lamp and the reaction tube being *ca.* 5 cm. The reaction mixtures were condensed to *ca.* 3 cm³, a 4-cm³ portion of chloroform was added, and the solutions were dried over magnesium sulfate. After the removal of the drying agent and the precipitated sodium perchlorate, the solutions were condensed to *ca.* 0.5 cm³, and a weighed amount of tetrachloroethane was added as an internal reference for the determination of the relative yields of aldehydes, benzaldehyde, and 4′-formylbenzo-15-crown-5. The results are shown in Fig. 1. Under these conditions about 35% of the starting diketone was photolyzed to give 4′-formylbenzo-15-crown-5 (**4**). The chromatography of the reaction mixture from the photolysis without sodium perchlorate on a column of silica-gel (1.0(ϕ)×10 cm) removed 1-dodecanethiol as a hexane eluate and gave the product mixture as a methanol. 4′-Formylbenzo-15-crown-5 (**4**) was separated from the product mixture by preparative TLC on a silica-gel plate using a mixed solvent of chloroform–methanol (50:7); it was identical with an authentic sample prepared by a previously reported procedure.[8]

Photolysis of 1-(3,4-Dimethoxyphenyl)-2-phenylethanedione (2) in the Presence of 1-Dodecanethiol. 1-(3,4-Dimethoxyphenyl)-2-phenylethanedione (**2**) was photolyzed in the manner used for the photolysis of the crown ether derivative (**1**). The product aldehydes, benzaldehyde, and 3,4-dimethoxybenzaldehyde (**5**), were found to be identical with authentic

samples in terms of GLC results (PEG-20M on Chromosorb W, N_2, 200 °C) and their NMR spectra. Fig. 2 shows the effect of the added sodium perchlorate on the photoreactivity of **2**.

Photolysis of 4'-(2-Phenyl-1,2-dioxoethyl)benzo-15-crown-5 (1) in the Presence of Tetrabutylammonium Perchlorate. A mixture of the crown ether derivative (**1**) (2.5×10^{-2} mol dm^{-3}) and 1-dodecanethiol (2.5×10^{-1} mol dm^{-3}) was photolyzed in the presence of tetrabutylammonium perchlorate (0—8 equivalents) in the same manner as was used for the photolysis in the presence of sodium perchlorate. The results are shown in Fig. 1.

Phosphorescence from 4'-(2-Phenyl-1,2-dioxoethyl)benzo-15-crown-5 (1) and 1-(3,4-Dimethoxyphenyl)-2-phenylethanedione (2). The phosphorescence spectra were measured by means of a Hitachi EPA-4 spectrometer at 77 K in EPA (ether–isopentane–ethanol, 5:5:1). **1** and **2** show phosphorescence spectra similar in wave length (440—600 nm (λ_{max}^{emiss}: 498 nm)) and in intensity. The addition of sodium perchlorate or tetrabutylammonium perchlorate (7 equivalents) to the dimethoxy analog (**2**) did not affect the spectrum. In contrast, the addition of sodium perchlorate to **1** (7 equivalents) gave a spectrum similar in wave length, but decreased the intensity by *ca.* 15%.

References

1) Part IV: A. Suzuki and M. Tada, *Chem. Lett.*, **1980**, 515.

2) M. Tada and H. Hirano, *Tetrahedron Lett.*, **1978**, 5111; M. Tada, A. Suzuki, and H. Hirano, *J. Chem. Soc., Chem. Commun.*, **1979**, 1004; M. Tada, H. Hirano, and A. Suzuki, *Bull. Chem. Soc. Jpn.*, **53**, 2304 (1980).

3) "Advance in Photochemistry," ed by W. A. Noyes, Jr., G. S. Hammond, and J. N. Pitts, Jr., Interscience Publ., New York (1977), Vol. 8.

4) A. Becket, A. D. Osborne, and G. Porter, *Trans. Faraday Soc.*, **60**, 873 (1964).

5) D. L. Bunbury and C. T. Wang, *Can. J. Chem.*, **46**, 1473 (1968).

6) F. D. Lewis and J. G. Magger, *J. Am. Chem. Soc.*, **95**, 5973 (1973).

7) H. A. Benesi and J. H. Hildebrand, *J. Am. Chem. Soc.*, **71**, 2703 (1949).

8) E. M. Hyde, B. L. Shaw, and I. Shepherd, *J. Chem. Soc., Dalton*, **1978**, 1696.

Reaction of Organic Sulfur Compounds with Hyperoxide Anion ($O_2^{\cdot-}$). IV.[1] Evidence for Formation of Peroxysulfur Intermediates: Oxidation of Sulfoxides, Phosphines, and Olefins[2] with Intermediary Peroxysulfur Species

Shigeru OAE,* Toshikazu TAKATA, and Yong Hae KIM†
Department of Chemistry, The University of Tsukuba, Sakura, Ibaraki 305
(Received October 15, 1980)

Formations of peroxy-sulfenate(I), -sulfinate(II), and -sulfonate(III) as intermediates have been confirmed by stripping the peroxy oxygen with three kinds of trapping agents such as sulfoxides, phosphines, and olefins, added in the reaction systems of various organic sulfur compounds with hyperoxide anion ($O_2^{\cdot-}$). These sulfoxides, phosphines, and olefins were inert to $O_2^{\cdot-}$ alone while electrophilic olefins, such as α,β-unsaturated ketones reacted readily with $O_2^{\cdot-}$ to afford the carboxylic acid. Sulfoxides, added into the reaction system of disulfide, thiosulfinic *S*-ester, thiosulfonic *S*-ester, or sulfonyl chloride with $O_2^{\cdot-}$, were found to be oxidized to the sulfones with peroxysulfur intermediates formed *in situ* in the system. Phosphines, added into the reaction system of disuflide or sodium thiolate with $O_2^{\cdot-}$ were also oxidized to the phosphine oxides. Not only stilbene and acenaphthylene but also chalcone and its derivatives, placed in the reactions of sulfonyl chloride, sulfinyl chloride and thiosulfonic *S*-ester with $O_2^{\cdot-}$ were found to be oxidized to the corresponding epoxides. These observations suggest clearly that the intermediary peroxysulfur compounds can act as oxidizing agents which oxidize these trapping agents by the nucleophilic oxygenative oxidation. Similar intermediates were postulated and confirmed in the alkaline autoxidations of thiol and disulfide in which added phosphines and sulfoxides were also found to be oxidized to their oxides. The mechanisms of the reactions of these trapping agents with peroxysulfur intermediates are discussed.

The discovery of superoxide dismutase(SOD) by Fridovich and McCord in 1969[3] has given the considerably vital energies on the investigation of hyperoxide anion radical($O_2^{\cdot-}$), not only in biochemistry but also in organic chemistry.

Since the observation of Valentine and Curtis in which KO_2 can be appreciably dissolved in aprotic solvents, by complexation with crown ethers,[4] has quickly promoted the use of this reagent for many reactions with simple organic substrates, numerous reports dealing with reactions of various organic substrates with "naked" hyperoxide anion have appeared within only five years. However, nobody has looked into the reaction of organic sulfur compounds with $O_2^{\cdot-}$ till we initiated as a part of our works on the oxygenative oxidation of organic sulfur compounds,[5] except some sporadic experiments.[6]

The oxidation with $O_2^{\cdot-}$ may be limited partly due to its relatively weak reactivity. In fact, $O_2^{\cdot-}$ has been called as a moderate reducing agent but a pitifully weak oxidizing agent.[7] However, its reactivity has been seen in oxidation, reduction, nucleophilic substitutions, and also radical reactions.

We reported recently that several organic sulfur compounds are oxidized with $O_2^{\cdot-}$ generated *in situ* from KO_2 and 18-crown-6 to the corresponding sulfinic and sulfonic acids under mild conditions.[5a,b] These organic sulfur compounds are either those which have sulfur–sulfur linkage such as disulfide, thiosulfinic *S*-ester, thiosulfonic *S*-ester, or thiolate and sulfinate, all of which are expected to give peroxy-sulfur compounds such as peroxy-sulfenate(I), -sulfinate(II), and -sulfonate (III) as initial intermediates in the reactions with $O_2^{\cdot-}$. In fact, Berger already postulated the intermediary peroxy-sulfenate(I) and -sulfinate(II) in the autoxidation of thiol to the sulfinic and sulfonic acids in strong alkali media.[8] Since the two reactions give both sulfinic and sulfonic acids and are presumed to involve common intermediates of peroxysulfur species, we have carried out the experiments which would suggest the formation of these peroxysulfur intermediates in the reactions with $O_2^{\cdot-}$, and obtained evidence to support the intermediary formations of these new class of peroxy compounds (I—III) in the reactions of several sulfur compounds with $O_2^{\cdot-}$. Namely, sulfoxides, phosphines, and olefins(which are inert to $O_2^{\cdot-}$ without any one of sulfur substrates) were found to be oxidized to their oxides in the reaction systems of various sulfur compounds with $O_2^{\cdot-}$. Similar results were obtained in the alkaline autoxidations of thiol and disulfide.

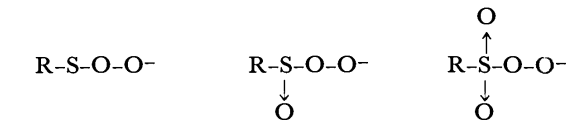

Peroxysulfenate I Peroxysulfinate II Peroxysulfonate III

Results and Discussion

All of the sulfur compounds shown below, *i.e.* **1**, **2**, **3**, **4**, and **5** have been found in our earlier study to be oxidized with $O_2^{\cdot-}$ to afford the corresponding sulfinic and sulfonic acids,[5a,b] while sulfenyl(**6**), sulfinyl(**7**) and sulfonyl(**8**) chlorides have also been found to be oxidized to the corresponding sulfinic and sulfonic acids. When unsymmetrical thiosulfinic and thiosulfonic *S*-esters were treated with KO_2 and 18-crown-6, formation of symmetrical disulfides from only the sulfenyl sulfur side was observed.

Since the peroxysulfur species, formed *in situ* during the reaction of these sulfur compounds with $O_2^{\cdot-}$, are

† Present address: Department of Chemistry, The Korea Advanced Institute of Science, P.O. Box 150, Chongyangyni, Seoul, Korea.

Table 1. Oxidation of sulfoxide

Entry No.	Substrate	Conversion %	Temp °C	Time min	KO_2	Crown	Added sulfoxide	Solvent	Yield of sulfone[a] %
1	*p*-TolSSTol-*p*	95	22	240	(6)[d]	(1)[d]	*p*-TolSMe(2)[d]	CH_3CN	72[b]
2	PhSSTol-p	*ca.* 100	17	10	(5)	(1)	PhSPh(2)	Py	17[c]
3	PhSSPh	89	0	58	(4)	(1)	PhSPh(2)	Py	3[c]
4	*p*-TolSNa	*ca.* 100	25	120	(3)	(0.5)	MeSMe(5)	CH_3CN	93[b]
5	$PhSO_2Na$	80	25	150	(1)	(0.5)	PhSPh(1)	Py	3[c]
6	*p*-TolSCl	*ca.* 100	22	25	(3)	(1/3)	MeSMe(3)	CH_3CN	57[b]
7	*p*-TolSCl	*ca.* 95	25	480	(3)	(1/10)	*p*-ClC_6H_4SMe(1/2)[d]	CH_3CN	46[b] (23)[e]

a) Yield of sulfone based on the substrate. b) Yield by NMR. c) Isolated yield. d) Value in parenthesis is molar ratio. e) Yield calculated on the basis of the sulfoxide added.

believed to have fairly strong nucleophilic oxidizing abilities, sulfoxides, phosphines, and olefins, which are relatively inert to $O_2^{\cdot-}$ alone but reactive with rather strong nucleophilic oxidizing agents, were added into the reaction system of one of these sulfur substrates with $O_2^{\cdot-}$, expecting that these additives would be oxidized to the corresponding oxides. Indeed, while the organic sulfur compounds were all oxidized to the sulfinic and sulfonic acids, added sulfoxides, phosphines, or olefins were also found to be oxidized to the corresponding sulfones, phosphine oxides, or epoxides. The added substrates, *i.e.* **9**, **10**, and **11**, are thus believed to be oxidized by the intermediary peroxysulfur compounds(I—III) formed *in situ* during the reactions of these sulfur compounds with $O_2^{\cdot-}$.

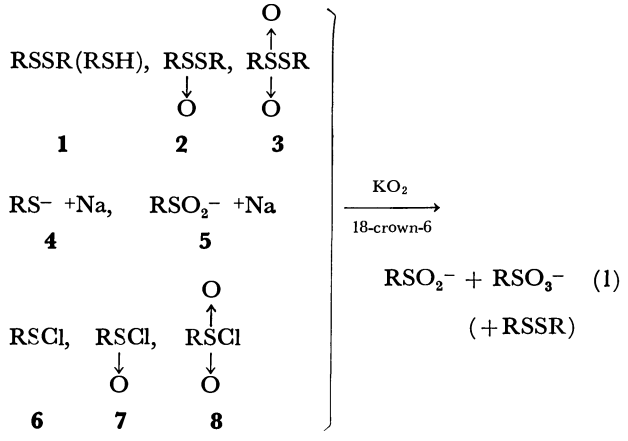

Oxidation of Sulfoxide. As a typical run, a solution of a selected sulfoxide (**9**, 0.5—6 eq.) and an organic sulfur compound (one of **1**—**8**, 1 eq.) in dry pyridine or acetonitrile was added into a heterogeneous solution of KO_2 (1—6 eq., finely powdered) and dry 18-crown-6 (0.5—1.0 eq.) in the same solvent at a set temperature and the resulting mixture was stirred under argon atmosphere. After extraction or filtration, the corresponding sulfone was obtained in the yield shown in Table 1. In the aqueous layer both sulfinic and sulfonic acids were obtained as reported previously.[5a,b] Yield of the sulfone obtained thus was determined by isolation by means of column chromatography on silica gel, or by comparison of the integral ratio of the NMR spectrum of the reaction mixture after evaporation of organic solvent. The sulfones were produced in most cases, except methyl phenyl sulfoxide which was not oxidized in the reaction system of benzenesulfenyl chloride with $O_2^{\cdot-}$ but reduced exothermically to the corresponding sulfide by the sulfenyl chloride in a very short time (≈5 min), like the reduction by sulfinyl chloride.[9] However, the sulfenyl chloride itself was readily oxidized with $O_2^{\cdot-}$ to the corresponding sulfinic and sulfonic acids.

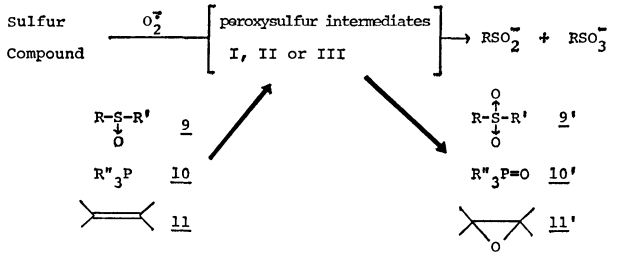

Scheme 1.

TABLE 2. EFFECTS OF SOLVENT, TEMPERATURE, AND SULFOXIDE, AND OTHER EFFECTS

Entry No.	Substrate	Conversion %	Temp °C	Time min	KO_2	Crown	Added sulfoxide	Solvent	Yield of sulfone[a] %
1	PhSSPh	64	25	133	(6)[d]	(1)[d]	PhSPh(2)[d] ↓ O	Py	22[c]
2	*p*-TolSSTol-p	93	21	330	(6)	(1)	PhSPh(2) ↓ O	CH_3CN	57[c]
3	*p*-TolSSTol-*p*	91	21	300	(6)	(1)	PhSPh(2) ↓ O	CH_3CN	56[c]
4	*p*-TolSNa	*ca.* 100	25	270	(3)	(1)	PhSPh(1) ↓ O	Py	4[c]
5	*p*-TolSNa	—	25	120	(5)	(1/2)	MeSMe(5) ↓ O	CH_3CN	93[b]
6	PhSSTol-*p* ↓ O	*ca.* 100	25	35	(5)	(1)	PhSPh(2) ↓ O	Py	32[c]
7	*p*-TolSSTol-*p* ↓ O	*ca.* 100	17	10	(5)	(1)	PhSPh(3) ↓ O	Py	15[c]
8	PhSSTol-*p* ↓ O	*ca.* 100	−25	60	(5)	(1)	PhSPh(2) ↓ O	Py	9[c]
9	PhSSTol-*p* ↓ O	*ca.* 100	−40	90	(5)	(1)	PhSPh(2) ↓ O	Py	4[c]
10	*p*-TolSSTol-*p*	91	21	300	(6)	(1)	PhSPh(2) ↓ O	CH_3CN	54[c]
11	*p*-TolSSTol-*p*	100	20	240	(6)	(1)	*p*-TolSPh(2.3) ↓ O	CH_3CN	56[b]
12	*p*-TolSSTol-*p*	95	22	240	(6)	(1)	*p*-TolSMe(2) ↓ O	CH_3CN	72[b]
13	*p*-TolSSTol-*p*	95	22	264	(6)	(1)	*p*-ClC_6H_4SMe(2) ↓ O	CH_3CN	71[b]
14	*p*-TolSSTol-*p*	95	25	240	(6)	(1)	PhSMe(2) ↓ O	CH_3CN	50[b]
15	*p*-TolSCl ↓ O	*ca.* 100	20	90	(3)	(1/3)	*p*-ClC_6H_4SMe(2) ↓ O	CH_3CN	17[b]
16	*p*-TolSCl ↓ O	*ca.* 100	22	25	(3)	(1/3)	MeSMe(3) ↓ O	CH_3CN	57[b]
17	*p*-TolSSTol-*p*	97	25	300	(6)	(1)	*p*-TolSMe(6) ↓ O	CH_3CN	111[b]

Table notes are same as those in Table 1.

Sulfoxides were shown to be rather inert to O_2^- by Valentine and Curtis who revealed that KO_2 is nicely soluble in DMSO by complexation with perhydrodibenzo-18-crown-6.[4] Effects of solvent, temperature, and added sulfoxide were then investigated. The oxidation of sulfoxides during the reaction of organic sulfur compounds with KO_2 and the crown ether has been found to be affected by both solvent and temperature (entries 1—5, Table 2). Sulfoxides were oxidized in better yields in acetonitrile than in pyridine. Decomposition of $RS(O)_xOO^-$ (x=0—2: I—III) is presumably facilitated in pyridine, while acetonitrile may interact with the peroxysulfur species which might live longer in acetonitrile than in pyridine and hence would be a better nucleophilic oxidizing agent for sulfoxide. However, acetonitrile was found to react with disulfide in the presence of O_2^-, forming bis(arylthio)acetonitrile in the yield of 25—50%.[5b] A radical process shown below (Eqs. 2—4) seems to be responsible for the formation of bis(arylthio)-

acetonitrile, and details of the reaction are under investigation.

$$O_2^{\cdot-} + CH_3CN \longrightarrow HO_2^- + \cdot CH_2CN \quad (2)$$

$$ArSSAr + \cdot CH_2CN \longrightarrow ArSCH_2CN \quad (3)$$

$$ArSCH_2CN \xrightarrow{O_2^{\cdot-}} \xrightarrow{ArSSAr} (ArS)_2CHCN \quad (4)$$

The yield of diphenyl sulfone from the added sulfoxide into the reaction system of **2** with $O_2^{\cdot-}$ increased as the temperature of the reaction was raised (entries 6—9). Change of sulfoxide did not affect much the yield of the corresponding sulfone in the reaction of di-*p*-toly disulfide with $O_2^{\cdot-}$ (entries 10—14). However, in the reaction of *p*-toluenesulfinyl chloride with $O_2^{\cdot-}$, dimethyl sulfone was obtained in a much better yield than methyl *p*-chlorophenyl sulfone (entries 15 and 16). An analogous result was observed in the oxidation of sodium *p*-toluenethiolate(entries 4 and 5), though the conditions of the above two reactions are somewhat different.

Meanwhile, since the yield of the sulfone was calculated based on the amount of the starting organic sulfur compound used, the yield of sulfone more than 100% (111%, entry 17) is not surprizing, as the amount of the added sulfoxide was six equivalent to the organic sulfur compound used. This may mean that more than an equimolar amount of peroxysulfur intermediate(s) is produced from the organic sulfur compound during the reaction. Thus, the yield of the sulfone clearly increased as the amount of the added sulfoxide to the reaction system increased.

Sulfoxide, having *p*-nitrophenyl group, such as *p*-nitrophenyl phenyl and methyl *p*-nitrophenyl sulfoxides, were not oxidized to the sulfones but presumably reacted with $O_2^{\cdot-}$. The reaction mixture turned to reddish brown and no product, even the starting material, was obtained from the organic layer.

Common sulfides such as diethyl, methyl phenyl, and diphenyl sulfides were found not to be oxidized at all under the conditions, as in the reaction with $O_2^{\cdot-}$ which was reported to be unreactive toward sulfides.[10]

In order to reconfirm the facile reaction of sulfoxides and no reactivity of sulfides in these oxidation systems, thianthrene 9-oxide (**12**) was used as the trapping agent, and found to be oxidized to thianthrene 9,9-dioxide(**13**), but not to the 9,10-dioxide(**14**) in the reaction of di-*p*-tolyl disulfide with $O_2^{\cdot-}$ in CH_3CN at 25 °C for 4 h (Eq. 5). This result clearly indicates that the peroxysulfur intermediates formed during the reaction oxidize trivalent sulfinyl function but not divalent sulfenyl function.

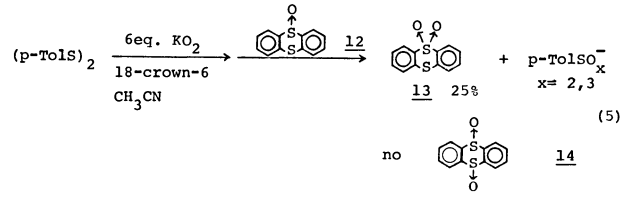

Although oxygenation of sulfide is well-known to be initiated by the electrophilic attack of oxidant on the sulfide, oxygenation of the sulfoxide involves either the initial electrophilic attack of the electrophilic oxidant,[11a] or the nucleophilic attack of nucleophilic oxidant.[11b,c] In general, the anions of peroxy acid and hydroperoxide which are well-known to be powerful α-nucleophiles,[12] have been shown to oxidize sulfoxide through the nucleophilic attack on the trivalent sulfur.[11b,13] Therefore, peroxysulfur intermediates, being α-nucleophiles, would oxidize similarly the sulfoxide by nucleophilic oxidation.[11c]

The yield of the sulfone alone cannot give any difinite information on the effect of substituent in these oxidations of various sulfoxides with the peroxysulfur intermediates (Table 2). Modena *et al.* showed that the electron-withdrawing substituent on sulfoxide accelerates the rate of the oxidation of sulfoxide but could not obtain any clear-cut relationship on the effect of the substituent,[11b] since decomposition of the sulfurane intermediate is also a slow reaction and could become the rate-determining step of the overall reaction. The two successive reaction steps, *i.e.* the nucleophilic attack of acyloxy anion on sulfur atom and the collapse of the sulfurane intermediate, demand the entirely opposite electronic environments. The oxidation of sulfoxide with the peroxysulfur intermediates is considered to proceed similarly. As shown in Eq. 6, sulfoxide would be attacked by one

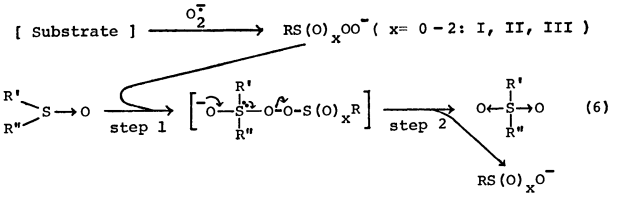

of the peroxysulfur intermediates generated *in situ*, forming incipiently the sulfurane intermediate which collapses to sulfone and $RS(O)_xO^-$ in the subsequent step.

An alternative mechanism which involves radical species of peroxysulfur intermediates in the oxidation of sulfoxide to the sulfone may be postulated. However, this seems to be quite unlikely because of the lack of nucleophilicity of the radical species, as was suggested earlier in the oxidation of dimethyl sulfoxide with *t*-butyl hydroperoxide.[14]

Oxidation of Phosphines. Both triphenyl- and tributylphosphines were also selected as trapping agents. Although these phosphines are known to be oxidized readily to the phosphine oxides with molecular oxygen,[15] both phosphines were quite inert under the present oxidation conditions in pyridine in dry argon atmosphere. The reaction procedure is identical to that in "*Oxidation of Sulfoxide.*" However, when the phosphines are used as trapping agents no oxygenated sulfur compounds could be used as the substrate for the oxidation with $O_2^{\cdot-}$, since the oxygenated sulfur compounds (**2**, **3** *etc.*) are known to be reduced readily with phosphines.[16] In fact, thiosulfinic *S*-ester was very readily reduced to the disulfide with triphenylphosphine in pyridine even at −25 °C. This reduction of thiosulfinic *S*-ester with triphenylphosphine is considered to compete with the reaction of thiosulfinic *S*-ester with $O_2^{\cdot-}$. Therefore,

TABLE 3. OXIDATION OF PHOSPHINES

Entry No.	Substrate	Conversion %	Temp °C	Time min	KO_2	Crown	Added phosphine	Solvent	Yield of product[a] %
1	PhSSPh	60	25	66	(6)	(1)	Ph_3P(1)	Py	Ph_3P=O 17
2	PhSSPh	81	23	300	(6)	(1)	Ph_3P(2)	Py	Ph_3P=O 21
3	PhSSPh	49	21	60	(6)	(1)	Bu_3P(2)	Py	Bu_3P=O Quant.
4	PhSSPh	95	25	240	(6)	(1)	Ph_3P=S(1)	Py	Ph_3P=O 0
5	MeSSMe	—	25	90	(6)	(1)	Ph_3P(1)	Py	Ph_3P=O 6 Ph_3P=S 13
6	BuSSBu	31	25	56	(6)	(1)	Ph_3P(1)	Py	Ph_3P=O 30 Ph_3P=S Trace
7	$PhCH_2SSCH_2Ph$	95	25	30	(6)	(1)	Ph_3P(1)	Py	Ph_3P=O 11 Ph_3P=S 31
8	*p*-TolSNa	*ca.* 100	20	300	(3)	(1/2)	Bu_3P(1)	Py	Bu_3P=O 5
9	*p*-TolSNa	*ca.* 100	25	1380	(5)	(1/2)	Ph_3P(2)	CH_3CN	Ph_3P=O 37

a) Yields were determined by GC.

the disulfide and sodium thiolate were chosen as the substrates in the reaction with $O_2^{\cdot-}$ in the presence of the phosphine to yield the phosphine oxide (Table 3). Yields of the phosphine oxides were determined directly by GC in order to avoid the autoxidation of phosphines. When tributylphosphine was added as a trapping agent of the peroxysulfur intermediate in the oxidation of disulfide with $O_2^{\cdot-}$, a vigorous exothermic reaction took place and the phosphine oxide was formed quantitatively within an hour, during which the conversion of the disulfide to the acids was still incomplete as shown in Table 3 (entry 3). In the oxidation of alkyl disulfide such as dibenzyl disulfide, triphenylphosphine was not only oxidized to the phosphine oxide but also converted to the phosphine sulfide. The phosphine sulfide thus formed along with the phosphine oxide was found to be quite inert to $O_2^{\cdot-}$ and recovered completely when it was added into the reaction system of disulfide with $O_2^{\cdot-}$ (entry 4). Therefore, formation of the phosphine oxide is not derived from the phosphine sulfide which is a simple by-product formed by the nucleophilic attack of the phosphine to the disulfide. Here again, triphenylphosphine was oxidized in a better yield in acetonitrile than in pyridine (entries 8 and 9), suggesting the reaction to proceed *via* an ionic pathway.

Phosphines are known to react with alkyl disulfide in an equilibrium reaction and generally yield the phosphine sulfide and monosulfide.[17] In the reaction of alkyl disulfide with $O_2^{\cdot-}$ in the presence of the phosphine the initial step is also considered to be the formation of alkylthiophosphonium ion which undergoes the Albuzov type reaction to yield the phosphine sulfide, by the nucleophilic attack of thiolate anion (counter anion of the phosphonium salt) on the carbon atom attached to the sulfur atom (Scheme 2). Due to the lack of nucleophilic attack of arenethiolate anion on aromatic carbon, diaryl disulfide did not give any phosphine sulfide (Table 3). Meanwhile, the formation of the phosphine oxide would be rationalized by Scheme 2. While $O_2^{\cdot-}$ can attack directly the disuflide as shown by Scheme 6, $O_2^{\cdot-}$ can attack competitively both sulfur and phosphorous atoms of the

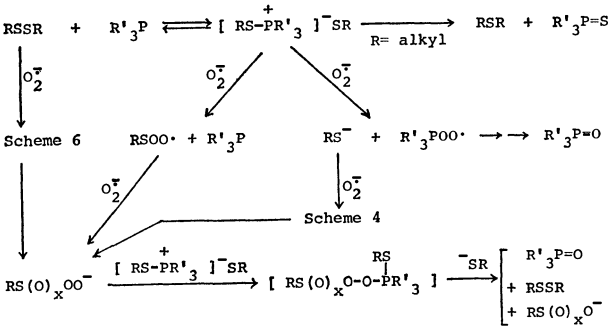

Scheme 2.

phosphonium ion. Although direct attack of $O_2^{\cdot-}$ on phosphorus atom may finally afford phosphine oxide, peroxysulfur species formed during the reaction, being good nucleophiles, may also attack the phosphorus atom of the phosphonium ion to afford an incipient phosphorane intermediate which upon nucleophilic attack of thiolate anion on the sulfur atom can give the phosphine oxide, as shown in Scheme 2. The rapid oxidation of tributylphosphine, therefore, may be due to the shift of the equilibrium between disulfide and the phosphine to right side to form the phosphonium ion which then would preferentially be attacked by $O_2^{\cdot-}$ on the phosphorus atom, to afford tributylphosphine oxide quantitatively before all the disulfide was oxidized to the acids.

Triphenylphosphine was not oxidized quantitatively in the reaction of sodium thiolate with $O_2^{\cdot-}$. The oxidation of triphenylphosphine in the reaction of sodium thiolate with $O_2^{\cdot-}$ seems to be different from that in the reaction of disulfide with $O_2^{\cdot-}$. The initial step is very likely the one electron transfer from thiolate anion to $O_2^{\cdot-}$ in view of the reducing nature of $O_2^{\cdot-}$.[18] Then, the peroxysulfur free radical formed *in situ* may oxidize directly the phosphine as reported in the autoxidation of trialkylphosphines.[15] Another possibility for the oxidation of the phosphine involves the initial reaction of thiyl radical with the phosphine to form arylthiophosphoryl radical, which can react with either $O_2^{\cdot-}$ or $RS(O)_xOO\cdot$ to give a phosphorane

Table 4. Chemical shifts of epoxides (δ, $CDCl_3$, TMS, 27 °C)

	Expoxide	Chemical shift	Lit	Ref.
1	*trans*-Stilbene oxide	3.83	3.88	20
2	*trans*-Chalcone oxide	4.08 4.30 (J=1.7 Hz)	4.06 4.27 (J=1.7 Hz)	21
3	*trans*-4-Bromochalcone oxide	4.03 4.25 (J=1.6 Hz)	3.99 4.19	22
4	*trans*-4-Methoxychalcone oxide	4.02 4·25 (J=1.8 Hz)	3.97 4.23	22
5	Acenaphthylene oxide	4.75	4.56	23

Table 5. Epoxidation of olefin (at 20 °C)[a]

Entry No.	Substrate	Olefin	Time/h	Solvent	Yield/mol%	
					Epoxide[b]	Recovery[b]
1	TsCl	**15**, X=Br	15.5	CH_3CN	85 (66)[c]	Trace (5)[c]
2	TsCl	**15**, X=H	15	CH_3CN	85	8
3	TsCl	**15**, X=OMe	3	CH_3CN	60 (45)[d]	Trace
4	*p*-TolSOCl	**15**, X=H	22.5	Benzene	60	35
5	**18**[f]	**15**, X=H	20.5	CH_3CN	26	58
6	PhCOCl	**15**, X=H	9	CH_3CN	41	49
7	TsCl	**16**	24	Benzene	40 (39)[c]	55
8	PhCOCl	**16**[e]	10	Benzene	30 (20)[c]	20 (15)[c]
9	TsCl	**17**	10	CH_3CN	— (30)[d]	— (70)[d]

a) Molar ratio: olefin:sub.:KO_2:crown=10:5:30:1. b) Yield by HPLC. c) Isolated yield. d) Yield by NMR. e) Molar ratio of PhCOCl/Olefin(**16**)=5/2. f) *p*-$ClC_6H_4S(O)_2SC_6H_4CH_3$-*p*(**18**).

Table 6. Effects of solvent, crown ether, and substrate (at 20 °C)[a]

Entry No.	Substrate	Olefin	Crown	Time/h	Solvent	Yield/%	
						Epoxide[b]	Recovery[b]
1	TsCl	**15**, X=H	(1)	15	CH_3CN	85	8
2	TsCl	**15**, X=H	(1)	20[f]	CH_2Cl_2	65	25
3	TsCl	**15**, X=H	(1)	17	Benzene	39	52
4	TsCl	**15**, X=Br	(1)	15.5	CH_3CN	85 (66)[c]	Trace (5)[c]
5	TsCl	**15**, X=Br	(1)	21	Benzene	35 (25)[c]	50 (48)[c]
6	TsCl	**16**	(1)	24	Benzene	40 (39)[c]	55
7	TsCl	**16**[g]	(1)	3	CH_3CN	Complex mixture	
8	PhCOCl	**16**	(1)	10	Benzene	30 (20)[c]	20 (15)[c]
9	PhCOCl	**16**	(1)	1	CH_3CN	10	20
10	TsCl	**15**, X=H	(0)	22	CH_3CN	75	10
11	TsCl	**15**, X=OMe	(0)	13	Benzene	Trace	95
12	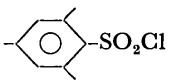	**15**, X=OMe	(1)	11[f]	CH_3CN	— (75)[d]	— (25)[d]
13	Cl_3CSO_2Cl	**15**, X=H	(1)	15.5[f]	CH_3CN	40	55
14	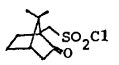	**15**, X=H	(1)	104	CH_3CN	50 (41)[c,e]	35

a) Molar ratio: sub.:olefin:KO_2:crown=10:5:30:1. b) Yiled by HPLC. c) Isolated yield. d) Yield by NMR. e) (+)-*d*-Camphor-10-sulfonyl chloride: $[\alpha]_D^{25}$ +20.9°. f) Reaction at 18 °C. g) Molar ratio of TsCl/Olefin=5/2.

intermediate which then reacts according to Scheme 2(Scheme 2′).

Oxidation of Olefin. Several olefins were found to be readily oxidized to the corresponding epoxides in appreciable yields when these olefins were added into the reaction system of any one of the organic sulfur compounds (**3**, **7**, and **8**) with O_2^-. Since the epoxide formed was sensitive to alkaline media, the reaction mixture was immediately filtrated to remove alkali and the yields of the epoxides were obtained by measuring the NMR spectra of the mixtures, and the epoxides were isolated through column chromatography on silica gel using benzene–hexane mixture as an eluent. In NMR spectra of the epoxides, signals of methine protons of the usual three membered oxyrane ring appear at high fields (Table 4). Olefins used are the following three compounds, *i.e.* chalcone derivatives(**15**), stilbene(**16**), and acenaphthylene(**17**). Both **16** and **17** were quite inert to O_2^- while **15** and its derivatives were found to react with O_2^- as described later. Most epoxides obtained in the reactions were *trans* since the olefins used were also *trans*. However,

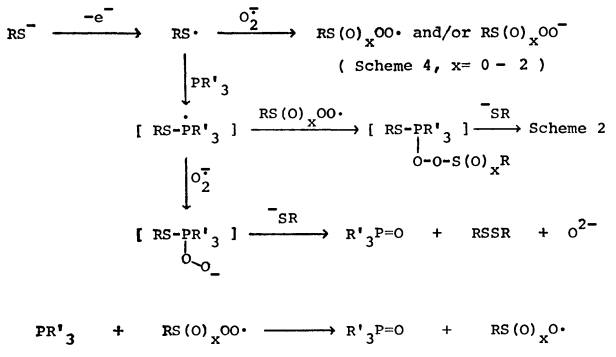

Scheme 2′.

the epoxide obtained from acenaphthylene was apparently *cis* but not *trans*, indicating that all the epoxidations in these systems were found to take place in *cis* fashion. Results obtained are listed in Tables 5 and 6, though the yields are not optimized.

The epoxidation proceeds very little when disulfide (**1**) and thiosulfinic *S*-ester (**2**) were used. Sodium thiolate(**4**) and sulfenyl chloride(**6**), both of which can be oxidized with $O_2^{\cdot-}$, were effective for the epoxidation of none of these olefins, giving complicated reaction mixtures with no epoxide.

Other olefins such as cyclohexene and cinnamonitrile were not oxidized and recovered nearly quantitatively under the conditions, while dibenzoylethylene was very readily oxidized (<1 h) by $O_2^{\cdot-}$ with and without the sulfur compounds to give benzoylformic acid in a good yield as reported previously.[19]

Recently the epoxidation of stilbene, in the reaction system of benzoyl chloride with $O_2^{\cdot-}$, was observed by Hirobe *et al.*[24] We also confirmed the epoxidation of stilbene in the same system (entry 8, Table 5; entries 8 and 9, Table 6). By-products in these reactions are carboxylic acids formed by direct oxidation of olefin and the epoxide with $O_2^{\cdot-}$.

Solvent, crown ether, and substrate also affected the epoxidation (Table 6). Inspection of data in Table 6 reveals that such a polar solvent as acetonitrile is better than dichloromethane or benzene in the epoxidation of chalcones, and the yield of the epoxide increased as the polarity of the solvent increased. However, acetonitrile was not a good solvent in the epoxidation of stilbene since other polar products including benzaldehyde were formed by the cleavage of C–C bond. This was confirmed in both cases using tosyl and benzoyl chlorides. Without crown ether, the yield of the epoxide was rather little in benzene but remained nearly the same in acetonitrile as shown in Table 6 (entries 10 and 11). Even the sterically hindered mesitylene and (+)-*d*-camphor-10-sulfonyl chlorides were also found to be effective in the epoxidation of olefins, however, the yields of the epoxides were relatively low and the rate of the reaction seemed to be slower than that with tosyl chloride. Chalcone epoxide, obtained by the oxidation of chalcone added in the reaction system of (+)-*d*-camphor-10-sulfonyl chloride ($[\alpha]_D^{25}$+20.9°) with $O_2^{\cdot-}$, did not show any optical activity, presumably because the optically active center is so far away from the reaction center.

The yield of stilbene oxide was lower than that of the epoxide from chalcone and its derivatives. Epoxidation of chalcone is known to be initiated by nucleophilic attack of an oxidant such as hydrogen peroxide anion as shown below (Eq. 7).[25] Even stilbene is known to undergo the Michael type addition by the attack of a strong nucleophile in some cases.[26]

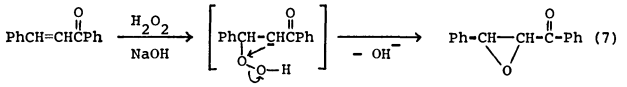

Chalcone, added in the reaction system of disulfide (**1**) with $O_2^{\cdot-}$ in acetonitrile, was not oxidized much, however, upon heating the reaction mixture in the absence of air at 50 °C chalcone decomposed to the corresponding carboxylic acids by the cleavage of C–C bond, as was reported by Rosenthal and Frimer.[27] Chalcone was oxidized in argon atmosphere much more readily without organosulfur compounds than in the presence, revealing that the rate of the reaction of chalcone with $O_2^{\cdot-}$ is appreciably slower than that of the reaction of organic sulfur compound with $O_2^{\cdot-}$. Since the reactions of both sulfinyl and sulfonyl chlorides with $O_2^{\cdot-}$ are considerably faster than that of chalcone with $O_2^{\cdot-}$, the epoxidation is considered to proceed *via* the initial nucleophilic substitution of the chlorides with $O_2^{\cdot-}$ and subsequent one electron transfer to afford the peroxysulfinate(II) and peroxysulfonate (III) which then oxidize olefin to the epoxide as shown in Eq. 8.

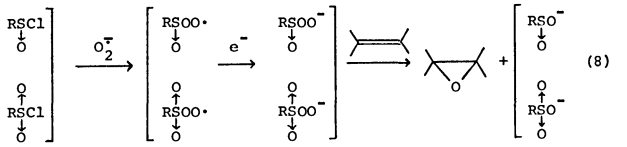

Nucleophilicity of $O_2^{\cdot-}$ has been nicely demonstrated in the reactions of various organic compounds with $O_2^{\cdot-}$,[28] and also in the complete inversion of configuration in the S_N2 reaction of an optically active aliphatic halide with $O_2^{\cdot-}$.[29] While none of the electrophilic olefins used was epoxidized with $O_2^{\cdot-}$ alone in our experiment, some cyclic α,β-unsaturated ketones were shown to be epoxidized with $O_2^{\cdot-}$ though in considerably low yields.[30]

Recently, Grieco and his-coworkers found that common nucleophilic olefins are nicely oxidized to the epoxides with benzeneperoxyseleninic acid which is generated *in situ* from benzeneseleninic acid and hydrogen peroxide,[31] apparently suggesting the formation of analogous intermediary peroxyselenium compound (Eq. 9).

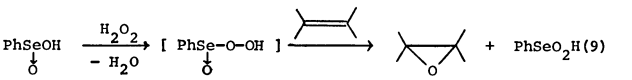

Oxidation Mechanisms of Several Sulfur Compounds with $O_2^{\cdot-}$. We have shown previously that several sulfur compounds (**1**—**8**) are oxidized to the corresponding sulfinic and sulfonic acids,[5a,b] and have suggested that the oxidation proceeds *via* formation of peroxysulfur intermediates (I, II, and III). Now let us consider the mechanisms of oxidations of several these

sulfur compounds with $O_2^{\cdot-}$ to the sulfinic and sulfonic acids.

Oxidation of Sodium Sulfinate with $O_2^{\cdot-}$. Anhydrous sodium arenesulfinate can be oxidized with an equimolar amount of $O_2^{\cdot-}$ to afford mainly the sulfonic acid in pyridine at 25 °C for 2.5 h (Eq. 10).[5b] The

$$\mathrm{RSO_2Na} \xrightarrow[\text{18-crown-6}]{\text{eq. } KO_2} \mathrm{RSO_3^-} \quad (+\mathrm{RSO_2^-}: \text{recovery}) \qquad (10)$$

R = Ph, *p*-Tol; pyridine, 25 °C, 2.5 h; ≈80%; ≈17%

initial step of the reaction would be the electron transfer. The resulting sulfonyl radical is known to be an excellent initiator in the polymerization of vinyl monomers or in the autoxidation of sulfinic acid.[32] Peroxysulfonyl radical, $RS(O)_2OO\cdot$, was also postulated in the photolysis of sulfur dioxide[33] in air and also in the autoxidation of sulfinic acid.[32,34] Thus, the oxidation of arenesulfinate with $O_2^{\cdot-}$ is considered to be initiated by one electron transfer and proceed *via* subsequent coupling of the resulted arenesulfonyl radical with $O_2^{\cdot-}$. The peroxyarenesulfonate(III) formed thus would slowly decompose to the sulfonic acid and molecular oxygen, or oxidize the present sulfinate or added sulfoxide to the sulfonate or the sulfone (Scheme 3).

The one electron transfer process from $O_2^{\cdot-}$ or to $O_2^{\cdot-}$ has been shown to be in operation in several reactions of $O_2^{\cdot-}$.[18] In view of the redox potentials of O_2—$O_2^{\cdot-}$ and $O_2^{\cdot-}$—H_2O_2 at neutral pH being −0.33 and +0.94 V, respectively, this radical anion is considered to act as a reductant in the presence of an electron acceptor and as an oxidant in the presence of an electron donor.[19] In fact, during a series of these experiments, evolution of molecular oxygen was observed by gas-mass spectrometry at the peak height of oxygen (*m/e* 32) along with that of argon (*m/e* 40) used, when the reaction was carried out in argon gas. This observation also seems to support the one electron transfer from $O_2^{\cdot-}$.

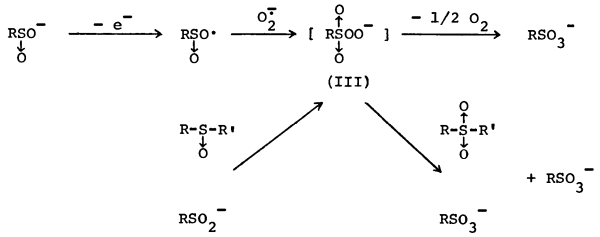

Scheme 3.

Oxidation of Sodium Thiolate with $O_2^{\cdot-}$. Sodium arenethiolate was also found to be oxidized to afford the corresponding sulfinic and sulfonic acids with a small amount of disuflide (Eq. 11).[5b] A similar one

$$\mathrm{RS^-{+}Na} \xrightarrow[\text{18-crown-6, r.t., pyridine, 4 h}]{\text{3eq. } KO_2} \mathrm{RSO_2^-} + \mathrm{RSO_3^-} + \mathrm{RSSR} \qquad (11)$$

≈10%; ≈86%; trace

electron transfer process is important in this oxidation. Recently, Degrand and Lund suggested that radical recombination of thiyl radical and $O_2^{\cdot-}$ gives sulfinate *via* the rearrangement of the peroxysulfenate(I) in

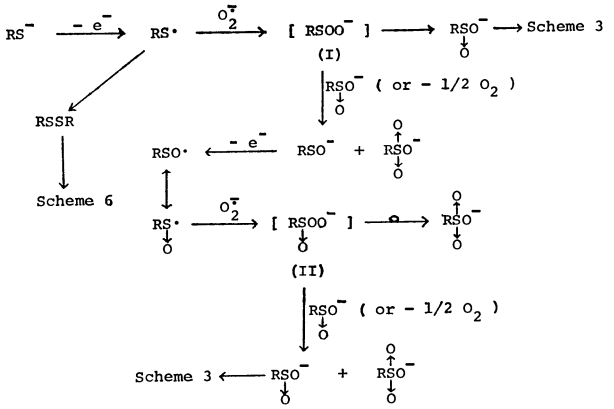

Scheme 4.

the electrochemical synthesis of sulfinic acid from alkyl disulfide and molecular oxygen.[35] As shown in Scheme 4, the thiyl radical thus formed would either dimerize to the disulfide or react with $O_2^{\cdot-}$ to form the incipient peroxysulfenate(I). Recombination of two thiyl radicals has been reported to be very fast ($k = 10^9$—10^{10} M^{-1} s^{-1}).[36] In the reaction of arenethiolate with $O_2^{\cdot-}$ all the intermediates (I—III) can thus be produced and would oxidize the added sulfoxides or the phosphines to the sulfones or the phosphine oxides. Rearrangement of the intermediates(I and II) to the sulfinate and the sulfonate are also conceivable while the degradation of all the intermediates may give both molecular oxygen and the acids (Eq. 12). Peroxysulfur intermediates may also

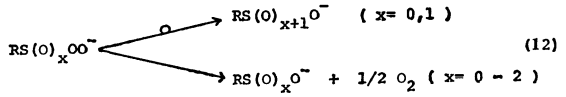

oxidize arenesulfinate directly to the sulfonate since the added trivalent sulfoxide is readily oxidized and the sulfinate is also another trivalent sulfur compound. Formation of a small amount of disulfide should be due to the recombination of the thiyl radicals. A small amount of diaryl disulfide was also obtained in the alkaline autooxidation of arenethiol, in which thiyl radical and $O_2^{\cdot-}$ were considered to be formed *via* one electron transfer.[36b] This oxidation of thiolate with $O_2^{\cdot-}$ required a little longer reaction time than that of sulfinate, in keeping with the suggested mechanism.

Oxidation of Sulfenyl, Sulfinyl, and Sulfonyl Chlorides with $O_2^{\cdot-}$. The reactions of arene-sulfenyl, -sulfinyl, and -sulfonyl chlorides with $O_2^{\cdot-}$ are considered to be initiated by nucleophilic substitution of the chlorides

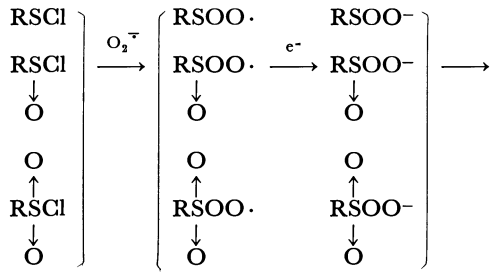

with $O_2^{\cdot-}$. Therefore, these three systems should be the best systems to give three peroxysulfur intermediates cleanly (Eq. 13). These three radicals, RSOO·, RS(O)OO·, and $RS(O)_2OO\cdot$, thus formed readily undergo one electron transfer from $O_2^{\cdot-}$ to form the corresponding peroxysulfur anions, which oxidize sulfoxides and olefins, added into the reaction system. The reaction of a sulfonyl chloride with NaO_2 without crown ether have already been reported to afford the corresponding sulfonate in refluxing benzene.[6a]

Oxidation of Thiol and Disulfide with $O_2^{\cdot-}$. Thiols react very readily with $O_2^{\cdot-}$ at first to afford the disulfides, which are then oxidized with $O_2^{\cdot-}$ to the corresponding sulfinic and sulfonic acids (Eq. 14). The

$$RSH \xrightarrow{O_2^{\cdot-}} RSSR \xrightarrow[\text{18-crown-6, r.t.}\atop\text{pyridine or}\atop\text{acetonitrile}]{\text{6 eq. } KO_2} RSO_2^- + RSO_3^- \qquad (14)$$

$$RSH + O_2^{\cdot-} \longrightarrow RS\cdot + HOO^-(RS^- + HOO\cdot)$$
$$2RS\cdot \longrightarrow RSSR$$
$$HOO^- \longrightarrow 1/2O_2 + HO^-$$

Scheme 5.

initial step of the reaction is the formation of the hydroperoxide anion and the thiyl radical which rapidly coupled to give the disulfide, while hydroperoxide anion may decompose slowly to molecular oxygen and hydroxide anion (Scheme 5).

The reaction of disulfide with $O_2^{\cdot-}$ undoubtedly involves nucleophilic attack of $O_2^{\cdot-}$ on S–S bond. Aromatic disulfide reacts faster than aliphatic disulfide, in keeping with the mechanism involvling the initial nucleophilic attack of $O_2^{\cdot-}$ on disulfide bond. Solvent effect may also support this process.[5b]

The peroxysulfenyl radical formed at the initial stage would undergo one electron transfer or collapse to form I or sulfinyl radical and molecular oxygen, as shown in Scheme 6. The peroxysulfur intermediates can oxidize the added sulfoxides or phosphines to the oxides.

Recently, Hirobe *et al.* reported[24] that two symmetrical disulfides, upon reacting with electrochemically generated $O_2^{\cdot-}$, gave three disulfides involving a new unsymmetrical disulfide in a theoretical ratio of the equilibrium mixture (1:2:1), without any oxidized product. This is quite reasonable if a very small amount of $O_2^{\cdot-}$ (only 1/60 amount of our case) was used. The reaction is considered to generate

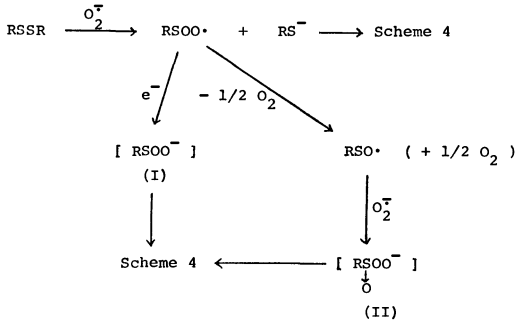

Scheme 6.

the thiyl radical either through the initial one electron transfer from $O_2^{\cdot-}$ to the disulfide or direct S_N2 type displacement of the disulfide with $O_2^{\cdot-}$. The thiyl radical thus formed would scramble the disuflides through S_N2 process rapidly, eventually resulting in the formation of the equilibrium mixture of disulfides.[37] However, when the amount of $O_2^{\cdot-}$ is abundant the initial step should be the nucleophilic reaction of $O_2^{\cdot-}$ on S–S linkage in view of the solvent effect[5b] and the following order of the reactivities, *i.e.* thiosulfinic *S*-ester > thiosulfonic *S*-ester > disulfide.[5b]

Oxidation of Thiosulfinic S-*Ester with* $O_2^{\cdot-}$. Thiosulfinic *S*-ester was found to react with $O_2^{\cdot-}$ more easily than any other sulfur compounds used.[5b] The reaction proceeded readily even at −40 °C within an hour, and not only sulfinic and sulfonic acids but also symmetrical disulfide were obtained (Eq. 15).[5]

$$\underset{\text{O}}{\overset{\downarrow}{\text{RSSR}'}} \xrightarrow[\text{18-crown-6}\atop\text{pyridine, } -40\,^\circ\text{C}\atop\text{within 1 h}]{\text{5 eq. } KO_2} \underset{\text{trace}}{RSO_2^-} + \underset{\approx 48\%}{RSO_3^-} + \underset{\approx 50\%}{R'SSR'} \qquad (15)$$

The symmetrical disulfide was formed in ≈50% yield only from the sulfenyl side and the two acids only from the sulfinyl side, revealing that the nucleophilic attack of $O_2^{\cdot-}$ occurs only on the sulfinyl sulfur of the unsymmetrical thiosulfinic *S*-ester. The predominant formation of the sulfonic acid may indicate that the main reaction path after the attack of $O_2^{\cdot-}$ is the rearrangement of peroxysulfinate(II) to the sulfonate. Therefore, peroxysulfinate(II) would be unstable enough to rearrange to the sulfonate under these conditions, and hence it would not be a good oxidizing agent of sulfoxide, thus yield of the sulfone being rather small (Table 2). Only when the temperature was elevated, the yield of the sulfone gradually increased (Table 2).

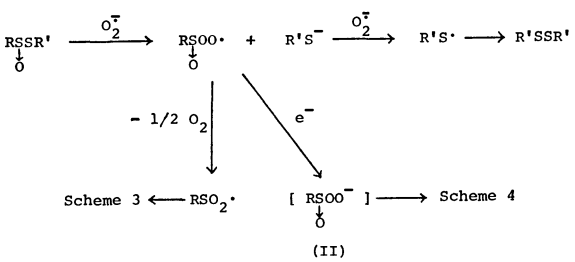

Scheme 7.

Oxidation of Thiosulfonic S-*Ester with* $O_2^{\cdot-}$. In the reaction of unsymmetrical thiosulfonic *S*-ester with $O_2^{\cdot-}$, however, two sulfinic and two sulfonic acids were obtained from both sulfur sides along with a small amount of symmetrical disulfide (*ca.* 25%) from the sulfenyl sulfur side (Eq. 16),[5b] revealing clearly that

$$\begin{array}{c}\text{O}\\\uparrow\\\text{RSSR}'\\\downarrow\\\text{O}\end{array} \xrightarrow[\text{18-crown-6}\atop\text{pyridine, } 0\,^\circ\text{C}\atop\approx 30\text{ min}]{\text{4 eq. } KO_2} \begin{bmatrix}RSO_2^-\\R'SO_2^-\end{bmatrix} + \begin{bmatrix}RSO_3^-\\R'SO_3^-\end{bmatrix} + R'SSR' \qquad (16)$$

the nucleophilic attack of $O_2^{\cdot-}$ occurs at both sulfenyl (a) and sulfonyl (b) sulfur atoms of the thiosulfonic *S*-ester (Scheme 8). The thiolate anion formed in the initial step must be converted to the disulfide by

Table 7. Change of product distribution[a)]

Entry No.	Substrate	Temp/°C	Time/min	Solvent	Additive	Yield/%	Yield/%		
							RSO_2^-	RSO_3^-	RSSR
1	PhSSPh	23	300	Pyridine	—	—	9	68	—
2	PhSSPh	23	300	Pyridine	Ph_3P	26[b)]	29	67	—
3	*p*-TolSSTol-*p*	22	300	CH_3CN	—	—	6	88	—
4	*p*-TolSSTol-*p*	22	300	CH_3CN	PhSPh ↓ O	62[c)]	31	61	—
5	*p*-TolS(O)STol-*p*	18	10	Pyridine	—	—	14	37	50
6	*p*-TolS(O)STol-*p*	17	10	Pyridine	PhSPh ↓ O	17[c)]	24	26	50

a) Molar ratio of substrate:KO_2:crown ether:additive=1:6:1:2 or 1:5:1:2 for disulfide or thiolsulfinate. b) Yield by GC. c) Isolated yield.

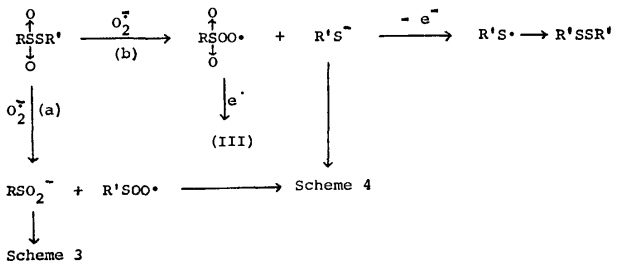

Scheme 8.

rapid recombination of the thiyl radicals after one electron transfer. At *ca.* 0 °C, the sulfinate would not be oxidized any further. The low yield of the sulfone formation from added sulfoxide should be also due to the low reaction temperature.

Both this reaction and that of thiosulfinic *S*-ester clearly involve the initial nucleophilic attack of $O_2^{\cdot-}$ at sulfur atoms of S–S linkage and gave partially the disulfide. A similar nucleophilic substitution(S_N2) on sulfur atom of S–S linkage has been observed in the alkaline hydrolyses of both compounds.[37)]††

Addition of the sulfoxide or the phosphine as a trapping agent into the reaction systems of disulfide and thiosulfinic *S*-ester with $O_2^{\cdot-}$ changed distribution of the products (Table 7). Amount of the sulfinate increased appreciably while that of sulfonate decreased only a little by the additives, very likely due to the two competitive reactions, *i.e.* the reactions of peroxysulfinate(II) with sulfoxides or phosphines to the sulfones or the phosphine oxides and the rearrangement of II to the sulfonate.

Thus, the reactions of these organosulfur compounds each having S–S linkage with $O_2^{\cdot-}$ are another S_N2 processes, like the nucleophilic substitution of alkyl halide or tosylate with $O_2^{\cdot-}$.[39)] This S_N2 mechanism with $O_2^{\cdot-}$ is in good accordance with the order of the reactivities of the three disulfidic species (**2**>**3**>**1**).[5)] This order is identical to that of the reactivities of the three in the alkaline hydrolyses.[38)]

Among a few trapping agents used, dimethyl sulfoxide was found to be the best reagent. Phosphines were not the good trapping agents since they reacted easily with several substrates. Olefins are relatively less reactive while the epoxides formed are usually so reactive that the epoxide itself reacted with various species present in the reaction system.

Since the alkaline autoxidation of thiols and disulfides gives sulfinate and sulfonate, and is expected to involve the peroxysulfur intermediates,[8,40)] a mixture of the sulfoxide or the phosphine (2 mmol), thiol or disulfide (1 mmol) and potassium *t*-butoxide (2 mmol) was treated in pyridine (5 ml) under pure oxygen atmosphere at room temperature for 0.5—11 h. Indeed, the sulfone (≈10.6%) or the phosphine oxide (≈20.2%) was obtained besides the autoxidation products of sulfinic and sulfonic acids[41)] (Scheme 9). Both sulfoxides and phosphines were inert under the conditions without any one of these sulfur compounds. Thus, the mechanism for the autoxidation suggested by Berger[8)] is considered to be identical to that of the reactions of disulfides and other related sulfur compounds with $O_2^{\cdot-}$, involving the common peroxysulfur intermediates (I, II, and/or III).

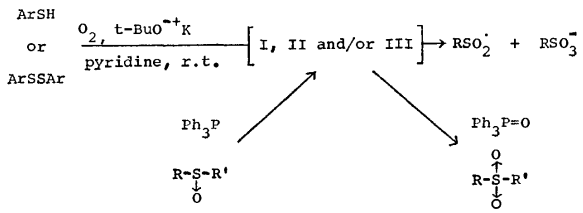

Scheme 9.

Among these peroxysulfur intermediates the peroxysulfenate(I) seems to collapse most readily. The oxidation of sulfoxide with I—III seems to be faster than that of olefin (Tables 1, 2, 5, and 6). The peroxysulfinate(II) is more stable and fairly reactive while only the peroxysulfonate(III) is stable enough to be characterized and hence be utilized for the oxidation of sulfoxide and olefin.

Experimental

General. All the reactions with $O_2^{\cdot-}$ were carried

†† These two reactions can be also conceivable but the second reaction (B) should be minor since amount of $O_2^{\cdot-}$ is considerably large at the initial stage in the reactions of both **2** and **3**.

$$R\text{-}S(O)_x\text{-}S\text{-}R' \xrightarrow{O_2^{\cdot-}} R\text{-}S(O)_xOO\cdot + R'\text{-}S^- \quad (A)$$

$$R\text{-}S(O)_x\text{-}S\text{-}R' + R'\text{-}S^- \longrightarrow RS(O)_x^- + R'SSR' \quad (B)$$

out under dry argon atmosphere.

Melting points were taken on a Yanaco instrument. NMR spectra were recorded on a Hitachi Perkin-Elmer R-20 spectrometer. Gas and liquid chromatographic analyses were carried out with Shimadzu GC-6A and Yanaco L-1030 instruments, respectively. Specific rotations were calculated from the values of optical rotations which were measured by a JASCO DIP-140 polarimeter using a 5 cm quartz cell.

Materials. KO_2 was obtained from Ventron Products. 18-Crown-6 was from Wako Pure Chemical Ind. and used after drying *in vacuo* by heating at 60—70 °C. All the solvents used except for CH_2Cl_2 were purified by distillation and dried with drying agent, as shown in the preceding paper.[5b] Purification of CH_2Cl_2 was performed at first by drying with $CaCl_2$ and then distillation after filtration. Distilled CH_2Cl_2 was stored in dark under N_2 in the presence of $CaCl_2$.

Preparation and purification of all the disulfides, thiosulfinic *S*-esters, thiosulfonic *S*-esters, sodium thiolates, and sodium sulfinates as substrates are reported in our previous paper.[5b]

Extra pure reagent grade triphenyl- and tributylphosphines, *trans*-stilbene and trichloromethanesulfonyl chloride from Wako Pure Chemical Ind. were directly used without any treatment. Tosyl and mesitylene-sulfonyl chlorides from Wako were used after recrystallization from hexane. Benzoyl chloride was purified by distillation and dehydration with $CaCl_2$, and DMSO was purified by distillation and stored under dry nitrogen gas. Diphenyl sulfoxide and acenaphthylene from Tokyo Kasei Kogyo were also used after recrystallyzation. Three chalcone derivatives were all from Aldrich Chemical Company and directly used for the reaction.

Sulfoxides, *i.e.* *p*-chlorophenyl methyl, methyl *p*-tolyl, and methyl phenyl sulfoxides, were prepared by oxidations of the corresponding sulfides with H_2O_2 in AcOH.[42] All the sulfoxides were determined by measuring the absorption peaks at the region of 1040—1060 cm^{-1} in their IR spectra. Thianthrene 9-oxide was prepared by a known method.[43] Benzenesulfenyl chloride was prepared by the reaction of benzenethiol with gaseous chlorine according to a known method.[44] The crude product was purified by distillation (bp 75—79 °C/3.0 Torr (1 Torr=133.322 Pa)). *p*-Toluenesulfinyl chloride was also prepared by the reaction of *p*-toluenethiol with gaseous chlorine in the presence of acetic anhydride.[44] The crude product was purified by distillation (bp 110 °C/2.5 Torr).

(+)-d-Camphor-10-sulfonyl chloride was prepared by treating (+)-*d*-camphor-10-sulfonic acid (from Wako) with PCl_5. To the sulfonic acid (0.5 mol) dissolved in $CHCl_3$ (150 ml) was added slowly solid PCl_5 (0.7—0.9 mol). After slow evolution of HCl gas, the mixture was heated at refluxing temperature for *ca.* 1 h. The resulting clean colorless mixture was washed more than three times with water. Organic layer was dried with $MgSO_4$ and the solvent was evaporated to afford the sulfonyl chloride which was purified by recrystallization from hexane. Yield 72%. IR (KBr, cm^{-1}, S=O) 1365 and 1168. $[\alpha]_D^{25}+20.9°$ (c=4.3, $CHCl_3$) (lit,[45] $[\alpha]_D^{25}+28.8°$ (C=4.2, $CHCl_3$).

Oxygen Trapping Reaction. The amount of KO_2 in the reaction of each substrate was not kept constant and hence is shown in each Table, which also shows reaction time, molar ratio of additives, and solvent used.

Oxidation of Additives Added in The Reaction System with $O_2^{\cdot-}$. The following is a typical run for the "*Oxidation of Sulfoxide.*" A solution of diphenyl sulfoxide (2 mmol) and di-*p*-tolyl disulfide (1 mmol) in dry acetonitrile (5 ml) was added with a syringe into a heterogeneous solution of KO_2 (6 mmol, finely powdered in advance and stored under nitrogen) and dry 18-crown-6 (1 mmol, dried *in vacuo* at 60—70 °C) in the same solvent in a two-necked flask under dry argon atmosphere at 21 °C. The resulting heterogeneous mixture was stirred at the same temperature for 6 h, during which the substrate generally disappears nearly completely. After the consumption of the substrate the reaction mixture was quenched by pouring into excess cold water containing crushed ice. Extraction with $CHCl_3$, drying with $MgSO_4$ and evaporation of $CHCl_3$ gave an oily residue. The residue, containing oxidized sulfone, unreacted sulfoxide, and crown ether, was subjected to column chromatography through silica gel using an eluent of a mixed solvent of hexane:EtOAc:$CHCl_3$=4:1:1. Yield of sulfone was 54% based on the starting disulfide.

When a sulfoxide bearing methyl group was used the yield of the sulfone was directly determined by integration ratio of the NMR spectrum of the crude mixture. The sulfones formed were identified by comparing the melting points or chemical shifts in NMR spectra with those of authentic samples.

Oxidation of phosphines in the reaction system was carried out according to the same procedure as mentioned for sulfoxide. The yield of the phosphine oxide was measured by injecting the reaction mixture directly into GC since the phosphine was actually oxidized in the usual work-up. The phosphine oxide was not produced at all, even if the reaction mixture was injected directly into GC instrument. The phosphine oxides obtained were found to be identical to the authentic samples by comparing the retention times in GC.

Epoxidation of olefin in the reaction system was also carried out similarly. However, the work-up was different, *i.e.* the reaction mixture, after stirring till the disappearance of most of substrate, was stirred further for a few hours. The resulting heterogeneous reaction mixture was filtered and the residue was washed with a large amount of CH_2Cl_2 ($\approx$40 ml). The combined organic layer was subjected to the assay after evaporation of organic solvent. Yield of the epoxide in the residue was sometimes determined by isolation by column chromatography through silica gel using benzene (or benzene–hexane) as an eluent. However, the amount of the epoxide was determined usually by HPLC. In some cases, the yield of the epoxide was directly estimated by measuring the NMR spectrum of the residual mixture. Epoxides thus obtained were identified by comparing the chemical shifts of the methine protons with those of the authentic samples as shown in Table 4.

This research was supported by Toray Science and Technology Prize and Grants for 1980 and Grant-in-Aid for Scientific Research B of the Ministry of Education, Science and Culture for 1980 which are gratefully acknowledged.

References

1) Part III: S. Oae and T. Takata, *Tetrahedron Lett.*, **21**, 3689 (1980).

2) Address correspondence to Department of Chemistry, The Korea Advanced Institute of Science, P.O. Box 150, Chongyangyni, Seoul, Korea.

3) J. M. McCord and I. Fridovich, *J. Biol. Chem.*, **244**, 6049 (1969).

4) J. S. Valentine and A. B. Curtis, *J. Am. Chem. Soc.*, **97**, 224 (1975).
5) a) T. Takata, Y. H. Kim, and S. Oae, *Tetrahedron Lett.*, **1979**, 821; b) S. Oae, T. Takata, and Y. H. Kim, *Tetrahedron*, **37**, 37 (1981); c) S. Oae, and T. Takata, *Tetrahedron Lett.*, **21**, 3689 (1980).
6) a) A. LeBeere and Y. Berguer, *Bull. Soc. Chim. Fr.*, **1966**, 2306; b) J. San Fillippo, Jr., L. J. Romano, C.-I. Chern, and J. S. Valentine, *J. Org. Chem.*, **40**, 1678 (1975).
7) D. T. Sawyer, M. J. Gibian, M. M. Morrison, and E. T. Seo, *J. Am. Chem. Soc.*, **100**, 627 (1978).
8) H. Berger, *Recl. Trav. Chim. Pays-Bas*, **82**, 773 (1963).
9) T. Numata, K. Ikura, Y. Shimano, and S. Oae, *Org. Prep. Proced. Int.*, **8**, 119 (1976).
10) D. Fukushima, Y. H. Kim, T. Iyanagi, and S. Oae, *J. Biochem.*, **83**, 1019 (1978).
11) a) R. Curci, A. Giovine, and G. Modena, *Tetrahedron*, **22**, 1235 (1966); b) R. Curci, F. DiFuria, and G. Modena, *J. Chem. Soc., Perkin Trans. 2*, **1978**, 603, and references cited therein; c) S. Oae and T. Takata, *Tetrahedron Lett.*, **21**, 3213 (1980).
12) R. Curci and J. O. Edwards, "Organic Peroxide," ed by D. Swern, Wiley-Interscience, New York (1970), Vol. I, Chap. 4.
13) Y. Ogata and S. Suyama, *J. Chem. Soc., Perkin Trans. 2*, **1973**, 755.
14) M. J. Gibian and T. Ungerman, *J. Org. Chem.*, **41**, 2500 (1976).
15) S. A. Buchler, *J. Am. Chem. Soc.*, **84**, 3093 (1962).
16) J. F. Carson and F. F. Wong, *J. Org. Chem.*, **26**, 1467 (1961).
17) A. Schönberg, *Ber. Deutsch. Chem. Ges.*, **68**, 163 (1935).
18) For example, E. LeeLuff, *Chem. Soc. Rev.*, **6**, 195 (1977).
19) A. A. Frimer, I. Rosenthal, and S. Hoz, *Tetrahedron Lett.*, **1977**, 4631.
20) "The Aldrich Library of NMR Spectra," (1974), Vol. 4, p. 103.
21) S. Mitsui, Y. Senda, T. Shimodaira, and H. Ichikawa, *Bull. Chem. Soc. Jpn.*, **38**, 1897 (1965).
22) A. B. Turner, R. E. Juts, N. S. McFarlane, and D. W. Boykin, Jr., *J. Org. Chem.*, **36**, 1107 (1971).
23) D. H. Hunter and D. J. Shearing, *J. Am. Chem. Soc.*, **95**, 8333 (1973).
24) T. Nagano, K. Aragane, and M. Hirobe, 6th Symposium on Progress of Reaction and Synthesis, 1979, Abstract p. 114.
25) S. Patai and Z. Rappoport, "The Chemistry of Alkenes," ed by S. Patai, Wiley (1964), Chap. 8, p. 469.
26) S. Oae, "Chemistry of Organic Sulfur Compounds (Japanese)," Kagakudojin, Kyoto (1069); R. Backer and M. J. Spielet, *Chem. Commun.*, **1966**, 757.
27) I. Rosenthal and A. A. Frimer, *Tetrahedron Lett.*, **1976**, 2805.
28) For example, A. A. Frimer and I. Rosenthal, *Tetrahedron Lett.*, **1976**, 2809, and references cited therein.
29) R. A. Johnson and E. G. Nidy, *J. Org. Chem.*, **40**, 1680 (1975).
30) A. A. Frimer and P. Gilinsky, *Tetrahedron Lett.*, **1979**, 4331; I. Saito, T. Otsuki, and T. Matsuura, *Tetrahedron Lett.*, **1979**, 1693; R. Dietz, A. E. J. Forno, B. E. Larcombe, and M. E. Peover, *J. Chem. Soc., B*, **1970**, 816.
31) P. A. Grieco, S. Yokoyama, and M. Nishizawa, *J. Org. Chem.*, **42**, 2034 (1977).
32) A review: C. J. M. Stirling, *Int. J. Sulfur Chem.*, **6**, 277 (1970).
33) B. Graf, *Justus Liebigs Ann. Chem.*, **578**, 50 (1950); B. Bielquist, *Acta Chem. Scand.*, **27**, 3180 (1973).
34) L. Horner and O. H. Basedow, *Justus Liebigs Ann. Chem.*, **612**, 108 (1958).
35) C. Degrand and H. Lund, *Acta Chem. Scand.*, **B33**, 512 (1979).
36) a) M. Z. Hoffman and E. Hayon, *J. Am. Chem. Soc.*, **94**, 7950 (1972); b) T. J. Wallace and A. Shriesheim, *J. Org. Chem.*, **27**, 1514 (1962).
37) W. A. Pryor, "Free Radicals," McGraw-Hill, New York (1966).
38) S. Oae, T. Takata, and Y. H. Kim, *Tetrahedron Lett.*, **1977**, 4219; S. Oae, K. Nomura, Y. Yoshikawa, and W. Tagaki, *Bull. Chem. Soc. Jpn.*, **42**, 2903 (1969).
39) J. S. Fillipo, Jr., C. -I. Chern, and J. S. Valentine, *J. Org. Chem.*, **40**, 1678 (1975).
40) J. P. Danehy and W. E. Hunter, *J. Org. Chem.*, **32**, 2047 (1967).
41) Y. H. Kim, T. Takata, and S. Oae, unpublished results.
42) R. B. Wagner and H. D. Zook, "Synthetic Organic Chemistry," John-Wiley & Sons (1953), p. 801.
43) S. Oae, Y. Ohnishi, S. Kozuka, and W. Tagaki, *Bull. Chem. Soc. Jpn.*, **39**, 364 (1966).
44) G. F. Klivenyi, *Magy. Kem. Foly.*, **64**, 121 (1958); *Chem. Abstr.*, **54**, 16416e (1959).
45) H. J. Backer and H. Kloosterziel, *Recl. Trav. Chim. Pays-Bas*, **73**, 129 (1954).
46) E. L. Eliel and W. J. Frazee, *J. Org. Chem.*, **44**, 3598 (1979).

The Liquid-phase Oxidation of Methylbenzenes by the Cobalt–Copper–Bromide System

Toshihiko OKADA* and Yoshio KAMIYA

Department of Reaction Chemistry, Faculty of Engineering, The University of Tokyo, Hongo, Bunkyo-ku, Tokyo 113

(Received October 30, 1980)

The liquid-phase oxidation of methylbenzenes catalyzed by a catalyst system composed of cobalt(II) and copper(II) acetates and sodium bromide was carried out in acetic acid at 150 °C. The corresponding benzyl acetates and benzaldehydes were obtained in high selectivities in most cases. A nuclear-brominated product, *i.e.*, 3-bromo-4-methoxytoluene was also obtained in the oxidation of *p*-methoxytoluene, which has two different reaction sites, *i.e.*, *o*-positions to the electron-donating methoxyl substituent and the benzyl position. However, the substitution of the bromide ion for the acetate ion in the catalyst system gave satisfactory selectivities for the side-chain oxidation products. In *p*-xylene oxidation, α,α′-diacetoxy-*p*-xylene and *p*-(acetoxymethyl)benzonic acid were also obtained, as well as *p*-methylbenzyl acetate, though their amounts were small. The oxidation of polymethylbenzenes was also carried out.

There have been many reports concerning liquid-phase oxidations catalyzed by transition metal ions.[1] In general, however, primary products (*e.g.*, aldehyde or alchhol) are more sensitive toward oxidation than the starting substrate, and the selective synthesis of alcohols with the liquid-phase oxidation has some limitations.[2] An improved method for the alcohol and glycol synthesis is to use the acetoxylation of them, by which the resulting primary products are restrained toward the secondary oxidation. In acetoxylation, many transition metals are employed as catalysts: palladium(II) acetate for a nuclear[3] and a side-chain acetoxylation of aromatic hydrocarbons,[4] silver(I) acetate for a side-chain acetoxylation,[5] and copper(II) acetate–lithium bromide,[6] and tellurium dioxide–hydrogen bromide[7] for olefens. In a previous report,[8] we have studied the liquid-phase oxidation of toluene catalyzed by a cobalt(II) acetate–sodium bromide catalyst in the presence of copper(II) acetate in acetic acid, we found that benzyl acetate, which is a useful organic intermediate for benzaldehyde and benzyl alcohol synthesis, can be synthesized in one pot.

In the oxidation of toluene catalyzed by the Co–Cu–Br system, the reaction can be considered to proceed through the abstraction of α-hydrogen by bromide atoms (from cobalt(III) bromide or copper(II) bromide), the ligand-transfer of the resulting benzil radical by copper(II) bromide to benzyl bromide, and the replacement of benzyl bromide with the acetate ion to give benzyl acetate.

Here, we wish to report on the liquid-phase oxidation of substituted toluenes and polymethylbenzenes catalyzed by the Co–Cu–Br system as an extension of the study of the oxidative side-chain acetoxylation of aromatic hydrocarbons.

Experimental

General. *p*-Methoxytoluene, *p*-xylene, *p*-chlorotoluene, *p*-*t*-butyltoluene, *p*-nitrotoluene, *etc.*, mesitylene, durene, and hexamethylbenzene were purified by usual methods. When a substrate easily oxidized to the hydroperoxides was used, the substrate was further treated with an active alumina.

Acetic acid, cobalt(II) acetate tetrahydrate, copper(II) acetate monohydrate, and sodium bromide of a reagent grade were used without further purification. The products were identified by means of IR (Shimadzu IR 420) ^{1}H-NMR (Varian EM 360A), and GC-MS (ANELVA TE 600S).

Oxidation Procedure. A 200-ml Ti-made autoclave equipped with a gas inlet, a magnetic-induced stirrer, and a pressure gauge was charged with *ca.* 50 mmol of a substrate, 4 mmol of cobalt(II) acetate, 4 mmol of copper(II) acetate, 28 mmol of sodium bromide, and 60 ml of acetic acid. Then, the autoclave, pressured with air to 40 kg/cm^2 was placed in an electric furnace and heated to 150 °C.

After 1.0 h, the autoclave was cooled with water and vented. Internal standards (chlorobenzene, *p*-bromoanisole, and 1-chloronaphthalene) were then added to the autoclave. The contents were poured into ice water and then extracted with ether.

The extract was washed with water and a saturated sodium carbonate solution, and subsequently dried (sodium sulfate), and the ether was removed on a rotary evaporator. The residue was submitted to GC analysis.

The substituted benzoic acids isolated by the acidification of the combined aqueous solution were determined by the weighing of their quantities or by ^{1}H-NMR analysis. The GC analysis was mainly conducted on a Shimadzu GC-3T gas chromatograph, using a 10% PEG 20 M on Uniport B column operated isothermally at 180 °C.

Results and Discussion

The liquid-phase oxidations of the substituted toluenes were carried out in acetic acid, using cobalt(II) and copper(II) acetates and a sodium bromide system with air. The results are summarized in Table 1. As may be seen from the Table, a corresponding substituted benzyl acetate was obtained as the main product, along with a significant amount of the substituted benzaldehyde. The increase in the electron-donating ability of the substituent on the ring caused the higher conversion, which is roughly accordant with the tendencies on the oxidation of substituted toluenes catalyzed by a cobalt–bromide system[9] and on the bromination with NBS.[10] As compared with the palladium-catalyzed side-chain acetoxylation of methylbenzenes, the Co–Cu–Br catalyzed reaction seems to be more useful because of the lower cost of the catalyst and because of the possibility of a wider application to the acetoxylation of many methylbenzenes (the palladium-catalyzed reactions of

Table 1. Oxidation of substituted toluenes catalyzed by the Co–Cu–Br system

Toluenes	Conversion %	Products (mol%)[a] $ArCH_2OAc$	Products (mol%)[a] ArCHO
O-Chlorotoluene	40	55	27
m-Chlorotoluene	39	63	30
p-Chlorotoluene	60	52	13
p-Nitrotoluene	20	62	22
Toluene	55	54	20
p-*t*-Butyltoluene	74	55	27
p-Methoxytoluene[b]	94	21	13
p-Toluic acid[c]	29	30	12
p-Tolualdehyde[d]	98	0	1
p-Methylbenzyl acetate[e]	82	44	17

Reaction conditions: $[Co(OAc)_2]=[Cu(OAc)_2]=5.7\times10^{-2}$ M,† [NaBr]=0.4 M, [Substrate]=0.7 M, air pressure; 40 kg/cm², 1.0 h, 150 °C. a) Based on the substrate consumed. b) 3-Bromo-4-methoxytoluene (20%) was also obtained. c) The evolution of carbon dioxide was observed. d) The other product was *p*-toluic acid. e) *p*-Tolualdehyde (16%) and *p*-acetoxymethylbenzoic acid (8%) were also obtained, accompanied by *p*-toluic acid (10%).

toulenes bearing substituents such as chloro, nitro, and methyl groups more than two on the ring are very slow[4]). It is noteworthy that the benzaldehyde, as a by-product, can also be obtained in many cases. However, in the *p*-methoxytoluene oxidation, as will be described later in detail, a ring bromination occurred, because 3-bromo-4-methoxytoluene was detected. On the other hand, it is interesting that *p*-acetoxymethylbenzoic acid can be produced, though its yield is low in the oxidation of *p*-toluic acid. The oxidation of *p*-tolualdehyde gave *p*-toluic acid as the sole product, suggesting that the aldehyde group in the catalyst system is more sensitive toward the oxidation. On the other hand, the mechanism in the oxidation by the Co–Cu–Br system has been estimated on the basis of the results of an earlier variable study.[8] It could be considered to proceed through the pathway of the bromination with copper(II) bromides of the benzyl radical, which can be produced from the hydrogen abstraction of benzylic hydrogen by cobalt(III) bromide and/or bromine atoms arising from the rapid reaction of cobalt(II) bromide and the peroxyl radical[9] and from the decomposition of copper(II) bromide,[11] *i.e.*,

$$ArCH_3 \xrightarrow[\text{and/or Br}\cdot]{\text{Co(III)Br}} ArCH_2\cdot \xrightarrow{\text{Cu(II) Br}} ArCH_2Br \xrightarrow{OAc^-} ArCH_2OAc.$$

Although aryl alkyl bromides can usually be detected under the given conditions because of the low substitution rate of aryl alkyl bromide with the acetate ion, aryl alkyl bromide could hardly be detected under the conditions employed here suggesting that the substitution is rapid. Furthermore, the rate of the ligand transfer by copper(II) halides is known to be diffusion-controlled according to the study by

† 1M=1 mol dm^{-3}.

Table 2. Oxidation of *p*-methoxytoluene catalyzed by the Co–Cu system

Sodium salt	*p*-Methoxytoluene conversion/%	Products (mol%)[a] $ArCH_2OAc$	Products (mol%)[a] ArCHO	Products (mol%)[a] [A][b]
None	0	—	—	—
NaBr[c]	26	47	1	49
NaBr[d]	94	21	13	20
NaOAc	44	51	42	—
NaOAc[e]	54	56	26	—

Reaction conditions: $[Co(OAc)_2]=[Cu(OAc)_2]=5.7\times10^{-2}$ M, [Sodium salt]=0.4 M, [*p*-Methoxytoluene]=1.4 M, air pressure; 40 kg/cm², 1.0 h, 150 °C. a) Based on the *p*-methoxytoluene consumed. b) [A] represents 3-bromo-4-methoxy toluene. c) This run was carried out under the conditions: 100 °C, 20 h, air flow. e) Acetic anhydride (5 ml) was added. d) [*p*-Methoxytoluene]=0.7 M.

Kochi.[12] Therefore, the substituents on the ring can be considered to influence the hydrogen abstraction of benzylic hydrogen.

As has been mentioned above, 3-bromo-4-methoxytoluene and *p*-anisic acid were both obtained as by-products in the oxidation of *p*-methoxytoluene. In order to avoid the ring bromination, some experiments were carried out (Table 2). Many works have reported on the ring halogenation of aromatic hydrocarbons with copper(II) halides at high temperatures,[13] and it is a useful method for the halogenation even now. On the other hand, a cobalt(III) acetate and halogen-ion system such as cobalt(III) chloride,[14] has also the ability to effect ring halogenation as well as side-chain halogenation. Accordingly, it appears to be difficult to prevent the ring bromination in the Co–Cu–Br catalyzed oxidation of *p*-methoxytoluene, because the above two systems exist. Indeed, the ratio of the amount of the benzyl acetate to the ring-bromination product at a low conversion shows nearly the same value as at a high conversion (Table 2). The ^{1}H-NMR analysis of the reaction mixture (an ether residue) showed the formation of 3-bromo-4-methoxybenzyl acetate when the conversion of *p*-methoxytoluene was completely achieved. A ring bromination similar to the oxidation of *p*-methoxytoluene was observed in the oxidation of 1-methylnaphthalene, *m*-phenoxytoluene, and mesitylene (*e.g.*, in the oxidation of 1-methylnaphtalene, 4-bromo-1-methylnaphthalene(12%) was obtained, accompanied by 1-naphthaldehyde(18%) and 1-acetoxymethylnaphthalene-(39%) at a 70% conversion of 1-methylnaphthalene). Since *p*-methoxytoluene, having a relatively lower ionization potential, could be supposed to react with cobalt(III) acetate even in the presence of copper(II) acetate, a run with no bromide ion was examined. However, the induction period was found to be very long in the cobalt(II) and copper(II) acetates system. The addition of the acetate ion to the system, however, caused a rapid oxidation, in which satisfactory selectivities for the benzyl acetate and the benzaldehyde were achieved. It is interesting that an unusual selectivity for *p*-anisaldehyde was obtained. Fur-

Table 3. Oxidation of *p*-xylene catalyzed by the Co–Cu–Br system

Run	1	2
p-Xylene(mmol)	41	81
Conversion/%	90	59
Products(mol%)[a]		
p-Tolualdehyde	13	24
p-Methylbenzyl acetate	34	59
p-Acetoxymethylbenzaldehyde	2	5
p-Phthalaldehyde	Trace	0
α,α′-Diacetoxy-*p*-xylene	8	8
p-Toluic acid	28	—[b]
p-Formylbenzoic acid	0	—
Terephthalic acid	0	—
p-Acetoxymethylbenzoic acid	4	—

Reaction conditions: $[Co(OAc)_2]=[Cu(OAc)_2]=5.7\times10^{-2}$ M, [NaBr]=0.4 M, air pressure: 40 kg/cm², 150 °C, 1.0 h. a) Based on the *p*-xylene consumed. b) No determination.

thermore, the addition of acetic anhydride accelerated the oxidation and caused a higher selectivity for the benzyl acetate. Recently, Imamura has reported in detail on the oxidation of *p*-methoxytoluene catalyzed by the addition of cobalt(II) acetate and a small amount of a bromide-ion system to *p*-anisaldehyde, he found that *p*-methoxybenzyl acetate was also obtained under the given conditions.[15] However, our results are somewhat better than their results in the selectivity for *p*-methoxybenzyl acetate. As it is now well established that cobalt(III) acetate can oxidize alkyl aromatics such as toluene by direct electron-transfer, even in the presence of oxygen,[16] the mechanism in the Co–Cu–OAc system can be estimated to be as follows:

$$Co(III) + p\text{-}MeOC_6H_4CH_3 \rightleftharpoons Co(II) + (p\text{-}MeOC_6H_4CH_3)^{+}$$

$$(p\text{-}MeOC_6H_4CH_3)^{+} \longrightarrow p\text{-}MeOC_6H_4CH_2\cdot + H^{+}$$

$$p\text{-}MeOC_6H_4CH_2\cdot + Co(III) \text{ and/or } Cu(II) \longrightarrow p\text{-}MeOC_6H_4CH_2OAc$$

$$p\text{-}MeOC_6H_4CH_2\cdot + O_2 \longrightarrow p\text{-}MeOC_6H_4CH_2OO\cdot \xrightarrow[Co(III)]{} p\text{-}MeOC_6H_4CHO.$$

However, as has previously been reported, it should be mentioned that the oxidizing activity of cobalt(III) acetate was lowered by the binuclear complex formation with copper(II) acetate.[17]

As has been described above, many important oxidation products of *p*-xylene are used as monomers in the polymer industry.[18] α,α′-*p*-Xylene-diol and *p*-hydroxymethylbenzoic acid as well as terephthalic acid are of particular interest.

Thus, we attemped the synthesis of these compounds in the oxidation of *p*-xylene by the Co–Cu–Br system. The results are presented in Table 3. At a low conversion of *p*-xylene, the products are *p*-methylbenzyl acetate and *p*-tolualdehyde, by analogy with the substituted toluene oxidations. On the other hand, at a high conversion, since *p*-xylene has two methyl groups, many products were obtained. It was found that *p*-xylene-α,α′-diol and *p*-acetoxymethylbenzoic acid are obtainable, though small amounts. Thus, the secondary oxidations of *p*-methylbenzyl acetate, *p*-toluic acid, and *p*-tolualdehyde were investigated. As has already been shown in Table 1, although no effort to seek out the optimum conditions for the selective oxidation was made, the expected compounds were obtained in considerable amounts. In the oxidation of *p*-methylbenzyl acetate, *p*-tolualdehyde was also obtained, even at a low conversion (for example, at a 44% conversion, 17% of *p*-tolualdehyde as well as 54% of α,α′-diacetoxy-*p*-xylene and 20% of *p*-acetoxymethylbenzaldehyde were obtained), indicating that the further oxidation of the benzyl acetate can not be ignored in these cases. Under these conditions, the oxidation of benzyl acetate gave benzaldehyde(14%) and benzoic acid(76%) at a 55% conversion of benzyl acetate. Therefore, there appears to be a limitation in the one-step synthesis of α,α′-diacetoxy-*p*-xylene with the oxidation of *p*-xylene. However, the results of the oxidation of *p*-tolualdehyde and *p*-toluic acid indicate that the formation of *p*-acetoxymethylbenzoic acid in the oxidation of *p*-xylene is through the pathway of the secondary oxidation of *p*-methylbenzyl acetate, because of the low rate of *p*-toluic acid oxidation and the high rate of *p*-tolualdehyde oxidation.

Table 4. Oxidation of polymethylbenzenes catalyzed by the Co–Cu–Br system

Substrate	Conversion %	Products (mol%)[a]	
		$ArCH_2OAc$	ArCHO
o-Xylene[b]	89	34	1
p-Xylene[b]	34	34	13
Mesitylene	89	49	11
Durene	98	63	10
Hexamethylbenzene	99	45	8

Reaction conditions: $[Co(OAc)_2]=[Cu(OAc)_2]=5.7\times10^{-2}$ M, [NaBr]=0.4 M, [Substrate]=0.7 M, air pressure; 20 kg/cm², 150 °C, 1.0 h. a) Based on the substrate consumed. b) Air pressure; 40 kg/cm².

Accordingly, it was concluded that two synthetically useful compounds, α,α′-diacetoxy-*p*-xylene and *p*-acetoxymethylbenzoic acid, were obtainable in the oxidation of *p*-methylbenzyl acetate, for the by-products are the precursors of *p*-acetoxymethylbenzoic acid.

$$p\text{-}CH_3C_6H_4CH_2OAc \xrightarrow{Co\text{-}Cu\text{-}Br} p\text{-}AcOCH_2C_6H_4CH_2OAc,\ p\text{-}AcOCH_2C_6H_4COOH$$

$$p\text{-}CH_3C_6H_4CHO \qquad p\text{-}AcOCH_2C_6H_4CHO$$

By-products

$$p\text{-}CH_3C_6H_4COOH \qquad p\text{-}AcOCH_2C_6H_4COOH$$

Finally, the Co–Cu–Br catalyzed oxidations of *o*- and *p*-xylenes, mesitylene, durene, and hexamethylbenzene were conducted. The results are summarized in Table 4. Since these compounds have more

than two methyl groups and low ionization potentials, they were very reactive as compared with the palladium-catalyzed side-chain acetoxylation. In the oxidation of hexamethylbenzene, for example, the products which have more than two oxidized methyl groups were detected, though they could not be completely determined before the whole conversion.

Then, the reaction was controlled by the amount of oxygen charged. As may be seen from Table 4, the monoacetoxylated compounds can be synthesized in high selectivities, even if at a high conversion.

In the oxidation of mesitylene, as has been reported by many workers,[19] the ring bromination occurred, though its amount was not determined.

In conclusion, the Co–Cu–Br system previously reported in the oxidative side-chain acetoxylation of toluene was found to be applicable to the side-chain acetoxylation of substituted toluenes and polymethylbenzenes. In the oxidation of *p*-methoxytoluene, ring bromination also occurred, although the side reaction could be removed by replacing the bromide ion in the catalyst system with the acetate ion.

References

1) A. Saffer and R. S. Barker, U. S. Patent 2833816 (1953); W. F. Brill, *Ind. Eng. Chem.*, **52**, 837 (1960).
2) Japan Kokai Patent 495324 (1974); Japan Kokai Patent 535132 (1978).
3) P. M. Henry, *J. Org. Chem.*, **36**, 1886 (1971); L. Eberson and G. Gonzales, *Acta. Chem. Scand.*, **27**, 1249, 1256 (1973).
4) DI. R. Bryant, J. E. McKeon, and B. C. Ream, *J. Org. Chem.*, **33**, 4123 (1968), **34**, 1106 (1969).
5) D. B. Smith and S. S. Adcock, Brit. Patent 1148863 (1969).
6) P. R. Stapp, *J. Org. Chem.*, **44**, 3216 (1979).
7) German. Offen, 2038781 to Halcon Int. (1971).
8) T. Okada and Y. Kamiya, *Bull. Chem. Soc. Jpn.*, **52**, 3321 (1979).
9) Y. Kamiya, *J. Catal.*, **33**, 480 (1974).
10) W. Offermann and F. Vögtle, *J. Org. Chem.*, **44**, 710 (1979).
11) J. K. Kochi, *J. Am. Chem. Soc.*, **84**, 2121 (1962).
12) J. K. Kochi and R. V. Subramanian, *J. Am. Chem. Soc.*, **87**, 4855 (1965).
13) J. C. Ware and E. E. Borchert, *J. Org. Chem.*, **26**, 2263, 2267 (1961); I. Tanimoto, K. Kushioka, T. Kitagawa, and K. Maruyama, *Bull. Chem. Soc. Jpn.*, **52**, 3586 (1979).
14) E. I. Heiba, R. M. Dessau, and W. J. Kochi, Jr., *J. Am. Chem. Soc.*, **91**, 6830 (1960).
15) J. Imamura, Y. Iwane, H. Minagawa, K. Kizawa, and H. Katagiri, 37th Annual Meeting of the Chemical Society of Japan, Yokohama, April 1978, Abstr., p. 1172.
16) Y. Kamiya and M. Kashima, *J. Catal.*, **25**, 326 (1972).
17) R. Kawai and Y. Kamiya, *Nippon Kagaku Kaishi*, **1974**, 933.
18) G. D. Brindell, L. D. Lillwitz, J. P. Wuskell, and A. P. Dunlop, *Ind. Eng. Chem., Prod. Res., Dev.*, **15**, 83 (1976).
19) E. Baciocchi, C. Rol, and L. Mandolini, *J. Org. Chem.*, **42**, 3682 (1977).

The Synthesis of α-D-Galactopyranosyl and α-D-Mannopyranosyl 2-Amino-2-deoxy-α-D-glucopyranosides and the Conformation of Their Glycoside Linkage[1]

Shinkiti Koto,* Shigeru Inada, and Shonosuke Zen
School of Pharmaceutical Sciences, Kitasato University, Shirokane, Minato-ku, Tokyo 108
(Received November 14, 1980)

A new analog of trehalosamine, α-D-galactopyranosyl 2-amino-2-deoxy-α-D-glucopyranoside, was synthesized by the glycosylation of 2,3,4,6-tetra-*O*-(*p*-chlorobenzyl)-α-D-galactopyranose with 3,4,6-tri-*O*-acetyl-2-deoxy-2-(2,4-dinitroanilino)-α-D-glucopyranosyl bromide, using silver perchlorate and tribenzylamine in benzene, followed by chromatographic separation and the subsequent removal of the protecting groups. Similarly, α-D-mannopyranosyl 2-amino-2-deoxy-α-D-glucopyranoside was synthesized. The conformation of the glycoside linkage of these α,α-disaccharides is discussed in relation to the ^{13}C chemical shifts of their anomeric carbons.

Trehalosamine (**25**)[2] and its analogs[3] are unique antimicrobial aminoglycosides which are 1,1′-linked disaccharides. However, since the synthesis of **25**,[4] only a few non-symmetrical α-glycosyl α-glycosides with an amino group have thus far been synthesized,[5] although the chemical modification of α,α-trehalose has often been performed recently.[6,7] Interestingly, some antibiotics possess the structure of 1,1′-linked glycosyl glycoside.[8] Such circumstances prompted us to synthesize the *galacto* analog (**17**) as well as the *manno* one (**21**) of trehalosamine. After our work had been completed, a synthesis of **21** *via* a different route was described.[9]

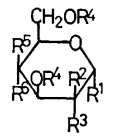

Compound	R^1	R^2	R^3	R^4	R^5	R^6
1	Br	H	NHDp	Ac	H	OAc
2	OH	H	OCb	Cb	OCb	H
3	OH	OCb	H	Cb	H	OCb
4	OH	H	OCb	Cb	H	OCb
5	OH	H	NHDp	Ac	H	OAc

Ac=acetyl, Cb=*p*-chlorobenyl, Dp=2,4-dinitrophenyl.

3,4,6-Tri-*O*-acetyl-2-deoxy-2-(2,4-dinitroanilino)-α-D-glucopyranosyl bromide (**1**),[10] occasionally used for synthesizing various 2-amino-2-deoxy-α-D-glucopyranosides,[11] was chosen to perform the glycosylation of 2,3,4,6-tetra-*O*-(*p*-chlorobenzyl)-α-D-galactopyranose (**2**).[12] The condensation using silver perchlorate[13] and tribenzylamine[14] in benzene at room temperature gave the α,α-form of the 1,1′-linked disaccharide derivative (**6**) as the main product. The chromatography of the reaction mixture gave **6** and three other configurational isomers (**7**, **8**, and **8a**) in yields of 35, 15, 9, and 3% respectively.

The protecting groups of **6** were removed in the order of deacetylation with a dil solution of sodium methoxide in methanol, dedinitrophenylation with a basic resin in aq acetone, and dechlorobenzylation by catalytic hydrogenolysis over palladium black in aq acetic acid, followed by deionization with a basic resin to afford **17** in a 16% yield from **2**. When the other three isomers **7**, **8**, and **8a**, were subjected to the above set of deprotection processes, they were converted into **18**, **19**, and **20** respectively.

The glycosylation of the mannose derivative (**3**) with **1** was next performed similarly to furnish the α,α-linked disaccharide derivative (**9**) in a 31% yield. Again, three isomers (**10**, **11**, and **12**) were separated from the glycosylation mixture. The deprotection of **9** gave the *manno* analog of trehalosamine, **21**, in a 16% yield from **3**.

Table 1. Molecular rotations of α-D-hexosyl α-D-glucosaminides and α-D-hexosyl α-D-glucosides and their per-acetates

Compound	Unprotected	Acetate
α-D-Gal*p* α-D-GlcN*p*	+702	+1225
α-D-Gal*p* α-D-Glc*p*	+711[a]	+1329[a]
α-D-Man*p* α-D-GlcN*p*	+500	+718
α-D-Man*p* α-D-Glc*p*	+569[b]	+786[b]
α-D-Glc*p* α-D-GlcN*p*	+649	+1022
α-D-Glc*p* α-D-Glc*p*	+680[c]	+1100[d]

a) Ref. 5b. b) Ref. 5a. c) G. Birch, *J. Chem. Soc.*, **1965**, 3489. d) C. S. Hudson and J. M. Johnson, *J. Am. Chem. Soc.*, **37**, 2748 (1915).

Table 2. ^1H chemical shifts of anomeric protons of D-hexosyl D-glucosaminides[a]

Compound	Temp[b] °C	H-1		H-1′	
		δ	$J_{1,2}$[c]	δ	$J_{1,2}$
17	22	5.56	3.7	5.62	3.3
18	22	5.09	8.0	5.74	3.0
19	90	5.75	3.2	5.12	8.0
20	80	5.30	8.0	5.26	7.0
21	22	5.53	3.8	5.51	1.5
22	22	4.97	8.3	5.55	1.6
23	22	5.59	3.7	5.27	0.6
24	50	5.21	8.3	5.48	1.0
25	22	5.60	3.8	5.63	3.3
26	90	5.11	8.0	5.72	3.8
27	80	5.80	4.0	5.22	7.0
28	70	5.27	8.0	5.31	7.0

a) Spectra were measured at 100 MHz in D_2O with ext. TMS. b) Measurement temperature. c) Decoupled by saturating the signal of H-2 at δ 3.1—3.2.

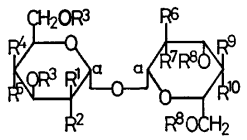

Compound	R^1	R^2	R^3	R^4	R^5	R^6	R^7	R^8	R^9	R^{10}
6	H	NHDp	Ac	H	OAc	OCb	H	Cb	H	OCb
9	H	NHDp	Ac	H	OAc	H	OCb	Cb	OCb	H
13	H	NHDp	Ac	H	OAc	OCb	H	Cb	OCb	H
15	H	NHDp	H	H	OH	H	OCb	Cb	OCb	H
16	H	NHDp	H	H	OH	OCb	H	Cb	OCb	H
17	H	NH_2	H	H	OH	OH	H	H	H	OH
21	H	NH_2	H	H	OH	H	OH	H	OH	H
25	H	NH_2	H	H	OH	OH	H	H	OH	H
29	H	NHAc	Ac	H	OAc	OAc	H	Ac	H	OAc
30	H	NHAc	Ac	H	OAc	H	OAc	Ac	OAc	H
31	H	NH_3Cl	H	H	OH	H	OH	H	OH	H
32	H	OCb	Cb	OCb	H	OCb	H	Cb	H	OCb
33	OCb	H	Cb	H	OCb	H	OCb	Cb	OCb	H

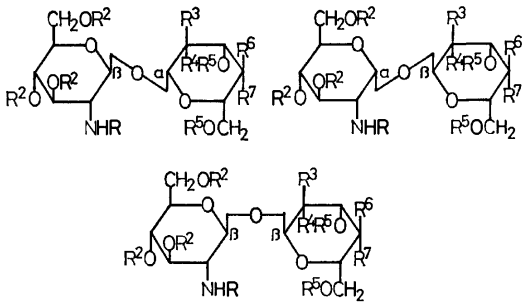

Compound	Anomeric configuration	R^1	R^2	R^3	R^4	R^5	R^6	R^7
7	β α	Dp	Ac	H	OCb	Cb	H	OCb
8	α β	Dp	Ac	H	OCb	Cb	H	OCb
8a	β β	Dp	Ac	H	OCb	Cb	H	OCb
10	β α	Dp	Ac	OCb	H	Cb	OCb	H
11	α β	Dp	Ac	OCb	H	Cb	OCb	H
12	β β	Dp	Ac	OCb	H	Cb	OCb	H
14	β α	Dp	Ac	OCb	H	Cb	OCb	H
13a	α β	Dp	Ac	OCb	H	Cb	OCb	H
14a	β β	Dp	Ac	OCb	H	Cb	OCb	H
18	β α	H	H	H	OH	H	H	OH
19	α β	H	H	H	OH	H	H	OH
20	β β	H	H	H	OH	H	H	OH
22	β α	H	H	OH	H	H	OH	H
23	α β	H	H	OH	H	H	OH	H
24	β β	H	H	OH	H	H	OH	H
26	β α	H	H	OH	H	H	OH	H
27	α β	H	H	OH	H	H	OH	H
28	β β	H	H	OH	H	H	OH	H

Trehalosamine, **25**, was itself similarly synthesized from **1** and the α-glucopyranose derivative (**4**) *via* the afore-mentioned glycosylation.

Synthetically speaking, two facts are worthy of notice: first, even in the case of a configurationally pure α-D-hexopyranose derivative (**2**, **3**, or **4**),[12] all four configurational isomers of the 1,1′-linked heterodisaccharides were always formed in such glycosylation; secondly, small amounts of the self-condensation products of such hexopyranose derivatives were always formed during the reaction.

Based on the magnitude of the specific rotation of hexosyl glucosaminides (**17**—**28**), the structure of the most *dextro*-rotatory α,α-isomers and the most *levo*-rotatory β,β-isomers were readily assigned. The molecular rotations of **17** and **21** and their acetates (**29** and **30**) reasonably coincide with those of the structurally related 1,1′-linked disaccharides and their acetates (Table 1). The anomeric configurations of twelve 1,1′-linked hexosyl glucosaminides were then checked by measuring the ^1H chemical shifts of the anomeric hydrogens (Table 2). The pH-dependent

Table 3. ^{13}C NMR of D-galactosyl D-glucosaminides

Compound	17			18			19			20		
C pD:	8.7	2.3	Δ	8.5	2.2	Δ	8.8	1.9	Δ	8.7	2.3	Δ
1	94.8	91.9	−2.9	104.8	100.7	−4.1	102.1	97.7	−4.4	101.1	97.1	−2.3
2	55.9	54.8		57.9	56.9		56.4	55.1		57.1	56.5	
3	75.1	70.7	−4.4	76.6	73.2	−3.4	75.0	70.6	−4.4	76.5	73.1	−3.4
4	71.2	70.5		70.8	70.6		70.9	70.9		70.8	70.7	
5	73.6	73.7		77.5	77.6		73.6	73.7		77.4	77.6	
6	61.8	61.4		61.9	61.5		61.8	61.4		61.8	61.4	
1′	94.1	94.7		101.6	102.0		104.6	103.9		101.1	101.1	
2′	70.3	69.9		70.3	70.3		72.0	71.9		71.4	71.3	
3′	71.0	70.3		70.3	70.3		74.1	74.2		73.9	73.6	
4′	69.0	68.6		69.5	69.3		69.6	69.6		69.7	69.7	
5′	72.6	73.1		72.9	73.0		76.5	76.7		76.5	76.6	
6′	62.4	62.5		62.3	62.3		62.2	62.1		62.2	62.3	

Table 4. ^{13}C NMR of D-mannosyl D-glucosaminides

Compound	21			22			23			24		
C pD:	8.8	2.7	Δ	8.8	2.3	Δ	9.0	2.0	Δ	8.5	2.0	Δ
1	96.0	92.3	−3.7	104.2	100.0	−4.2	101.6	97.4	−4.2	100.8	97.0	−3.8
2	55.9	54.6		57.6	56.8		56.1	55.0		57.1	56.5	
3	75.3	70.8	−4.5	76.5	73.0	−3.5	74.9	70.9	−4.0	76.4	73.0	−3.4
4	71.0	70.5		70.8	70.7		70.8	70.5		70.7	70.6	
5	74.1	74.2		77.5	77.5		73.8	73.7		77.6	77.6	
6	61.9	61.4		61.9	61.5		61.7	61.4		61.7	61.4	
1′	95.5	96.5		102.6	102.8		101.2	101.2		97.9	97.9	
2′	71.3	71.1		70.8	70.7		71.6	71.8		71.7	71.4	
3′	71.7	71.3		71.3	71.3		74.0	74.1		73.9	73.7	
4′	68.0	67.7		67.7	67.7		67.8	67.6		67.9	67.8	
5′	74.6	75.1		74.7	75.0		77.6	77.6		77.6	77.6	
6′	62.2	62.2		61.9	62.0		62.2	62.1		62.2	62.1	

Table 5. ^{13}C NMR of D-glucosyl D-glucosaminides

Compound	25			26			27			28		
C pD:	9.0	2.7	Δ	8.5	2.0	Δ	8.8	1.8	Δ	8.8	1.7	Δ
1	94.8	91.8	−3.0	105.0	101.9	−3.1	102.1	97.8	−4.3	101.4	97.1	−4.3
2	55.9	54.7		57.8	56.7		56.3	55.1		57.1	56.5	
3	74.9	70.7	−4.2	76.7	73.1	−3.6	74.8	70.9	−3.9	76.8	73.1	−3.7
4	70.8	70.7		70.6	70.5		70.6	70.4		70.8	70.5	
5	73.6	73.7		77.5	77.6		74.2	74.2		77.3	77.2	
6	61.7	61.3		61.8	61.5		61.7	61.4		61.9	61.5	
1′	94.0	94.5		101.4	101.1		104.0	103.4		100.5	100.4	
2′	72.0	71.7		72.5	72.4		74.2	74.2		73.8	73.6	
3′	73.4	73.3		73.8	73.8		77.3	77.4		77.4	77.6	
4′	70.8	70.7		70.6	70.5		70.8	70.5		70.8	70.7	
5′	73.6	73.9		73.8	74.3		76.6	76.7		76.9	76.7	
6′	61.7	61.8		61.5	61.5		61.8	61.7		61.9	61.7	

^{13}C NMR signals[8b,15] (Tables 3, 4, and 5) were quite useful in assigning the signal of C-1[16] of the two anomeric carbons in 1,1′-linked disaccharides, since, at a lower pH, the signal of the C-1 neighboring the carbon bearing amino group moved upfield, while that of C-1′ did not. The differences (Δ) in the value of the pH-dependent ^{13}C chemical shift of C-1 (Tables 3, 4, and 5) are almost constant, regardless of the configurations of C-1 and C-1′ (-3.7 ± 0.2 ppm). The data in Tables 3—5 show that the signal of C-2 was of use in diagnosing the anomeric configuration of glucosaminides (56.1 ± 0.1 ppm for the α-anomers and 57.4 ± 0.1 ppm for the β-anomers), whereas that of C-4′, which is insensitive to the anomeric

Table 6. ^{13}C chemical shifts of anomeric carbons of some D-glycosyl D-glycosides

Compound	Unprotected		Per-*O*-benzyl		Per-*O*-(*p*-chlorobenzyl)
α-D-Glc*p* α-D-Glc*p*	94.4	94.8[a]	94.4	94.26[b]	
α-D-Glc*p* β-D-Glc*p*	101.3 104.0	101.3[a] 104.0[a]	99.4 104.1	99.54[b] 104.27[b]	
β-D-Glc*p* β-D-Glc*p*	100.3	100.7[a]	99.3		
α-D-Gal*p* α-D-Gal*p*	94.4	94.32[b]	93.5	93.54[b]	93.6
α-D-Man*p* α-D-Man*p*	96.4		93.3	93.25[b]	93.4
α-D-Gal*p* α-D-Glc*p*		94.3[c] 94.5[c]			
α-D-Man*p* α-D-Glc*p*		94.6[d] 96.1[d]			

a) Ref. 18. b) Ref. 20. c) Ref. 6b. d) Ref. 6a.

configuration, was good as a probe of the galactopyranosyl (69.5±0.2 ppm) and mannopyranosyl (67.9 ±0.1 ppm) moieties.

One of our aims in the present study was to observe the ^{13}C chemical shifts of the anomeric carbons of 1,1′-linked disaccharides, in which the conformation of the glycoside linkage would be influenced by the *exo*-anomeric effect[17] exterted by both glycoside bonds, C-1–O and C-1′–O. The data in Tables 3—5 show that the ^{13}C chemical shifts of the anomeric carbons of the α,α- and β,β-isomers of 1,1′-linked disaccharides always appear at field above those of the α,β- and β,α-isomers; those up-field shifts are the same in nature with those observed in the cases of α,α- and β,β-trehaloses.[18] Because fully benzylated α,α- and β,β-trehaloses also exhibit such properties[19,20] (Table 6), inter-unit hydrogen-bondings[18] seem hardly responsible for them. Instead, the α,α- and β,β-isomers of trehalose are considered to adopt the conformation in which the dihedral angles of O-5–C-1–O–C-1′ and O-5′–C-1′–O–C-1 are $\approx +60°$ (α,α-isomer) or $\approx -60°$ (β,β-isomer), as is shown in Fig. 1. The fact that such an upfield shielding of the ^{13}C chemical shifts of the anomeric carbons of α,α- and β,β-isomers is observed regardless of the configuration at C-2′ (Tables 3—5) is consistent with the conformation in Fig. 1, where the substituents at C-2 and C-2′ are completely separated from each other. It is, then, conceivable that the *gauche* effect[21] would work on such a conformation so that the ^{13}C chemical shifts of both anomeric carbons, C-1 and C-1′, can be expected to appear at an upper field, as has been observed.

The *galacto* analog of trehalosamine was as active (cylinder plate assay) against the *Escherichia coli* NIHJ strain as, but a little less active against the *Mycobacterium smegmatis* ATCC 607 strain than, trehalosamine, **25**, and its *manno* analog, **21**.

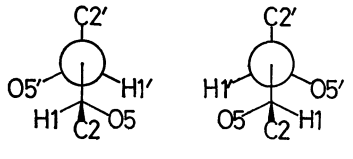

α-D-, α-D- β-D-, β-D-

Fig. 1. Projection formula of anomeric carbons of α-D-hexosyl α-D-glucosaminide and β-D-hexosyl β-D-glucosaminide.

Experimental

General. The melting points were determined by means of a MP-1 melting point apparatus (Yanagimoto). The specific rotations were measured in a jacketed 1-dm cell by means of a DIP-180 automatic polarimeter (Japan Spectroscopic) at 20 °C. The IR spectra were determined by means of a JASCO IRA-1 infrared spectrometer. The ^1H NMR spectra were recorded by a Varian S-60T spectrometer and a JEOL-PS-100 spectrometer. The ^{13}C NMR spectra were recorded by means of JEOL-PS-100 spectrometer equipped with a JEOL-EC-100 computer using a 8-mmϕ tube at 37 °C (noise decoupled; pulse width, 13 μs (45°); repetition, 2 s; frequency range, 5000 Hz; 8 K data points). A PT-3D digital pH/mV meter with a PCE-101S electrode (Toyo Kagaku) was used for the determination of the pD value, deutrium chloride (*ca.* 20% in deuterium oxide) was used as a titrant. Chromatography on silica gel (Kanto Kagaku) was done using a mixture of benzene and butanone (Solvent-BB) or of benzene and ethanol (Solvent-BE). TLC was carried out using silica gel (Merck 7731). Ascending paper chromatography was practiced by the use of Toyo filter paper (No. 50), developed by a solvent system of 1-butanol–pyridine–water–acetic acid (6:4:3:1) and then heated after having been sprayed with ninhydrin in ethanol (0.3%) containing pyridine. Compounds **1**, **2**, **3**, and **4**, as well as silver perchlorate (Alpha) and tribenzylamine (Tokyo Kasei), were kept *in vacuo* over phosphorus pentaoxide before use. All the reactions were conducted at room temperature (20—25 °C), while evaporation was done at 35—40 °C under reduced pressure, unless otherwise stated.

*α-D-Galactopyranosyl 2-Amino-2-deoxy-α-D-glucopyranoside (**17**) and Its Isomers (**18**, **19**, and **20**).* A mixture of **1** (854 mg, 1.6 mmol), **2** (1085 mg, 1.6 mmol), silver perchlorate (331 mg, 1.6 mmol), and tribenzylamine (459 mg, 1.6 mmol) in benzene (8 ml) was vigorously stirred in the dark for 24 h. The resulting mixture was poured onto a column of silica gel (30 g), which was then developed with Solvent-BB (100:1→5:1, gradient, 10-ml fraction). Fraction A (Nos. 12 and 13) gave **32** (43.4 mg, 4.1%), identified with the sample prepared alternatively as below. Fraction B (Nos. 19—30) was a mixture (852.2 mg) of **6** and unchanged **2**. Fraction C (Nos. 31—38) consisted of impure **8** (408.9 mg). Fraction D (Nos. 40—42) was a mixture (414.0 mg) of **7** and **8a**. Fraction E (Nos. 43—46) was 3,4,6-tri-*O*-acetyl-2-deoxy-2-(2,4-dinitroanilino)-α-D-glucopyranose (**5**) (192.6 mg, 25.6%); mp 150—154 °C [lit,[9] mp 154—156 °C].

A portion of Fraction B was purified by means of TLC to give a glass of **6**; $[\alpha]_D +128°$ (*c* 0.7, $CHCl_3$). Found:

C, 55.16; H. 4.56; N, 3.49%. Calcd for $C_{52}H_{51}Cl_4N_3O_{17}$: C, 55.18; H, 4.54; N, 3.71%. The rest of Fraction B was treated with a solution of sodium methoxide in methanol (0.05 M, 25 ml) overnight, followed by neutralization with acetic acid and chromatography (Solvent-BB, 10:1→1:1, gradient), to give unchanged **2** (240.4 mg, 22.2%) and the pure de-*O*-acetate of **6** (563.9 mg, 35% from **2**). This was agitated for 5 h in aq acetone (80%, 50 ml) in which Dowex 1×2 (OH-form, 15 ml) has been suspended. After filtration and evaporation, chromatography using Solvent-BE (10:1→5:1, gradient) gave a colorless mass (388.2 mg). This was hydrogenated over palladium black (390 mg) in acetic acid (10 ml) at 340 kPa overnight. After the removal of the catalyst, followed by concentration, the residue obtained was chromatographed on Dowex 1×2 (OH-form, 20×1ϕ cm, 5-ml fraction) developed with water; each fraction was examined by paper chromatography. Fraction Nos. 10—20 gave a ninhydrin-positive, homogeneous glass of **17** (106.3 mg, 19% from **2**); $[\alpha]_D$+198° (*c* 1.0, H_2O). Found: C, 40.79; H, 6.85; N, 3.79%. Calcd for $C_{12}H_{23}NO_{10}\cdot 0.75H_2O$: C, 40.69; H, 6.96; N, 3.95%.

The treatment of this (14 mg) with a mixture of acetic anhydride (2 ml) and pyridine (2 ml) for 4 d gave the acetate (**29**) (25 mg, 94%); mp 222—223 °C, $[\alpha]_D$+181° (*c* 0.3, $CHCl_3$), IR(KBr)ν: 1745 (OAc), 1645, 1545 (NHAc), NMR ($CDCl_3$, TMS) δ: 2.01 (3H, s, $NHCOCH_3$), 2.03, 2.04, 2.05, 2.09, 2.17 (3H, 6H, 3H, 6H, 3H, $OCOCH_3$), 6.20 (1H, d, J=8.0 Hz, NHAc). Found: C, 49.93; H, 5.95; N, 1.97%. Calcd for $C_{28}H_{39}NO_8$: C, 49.63; H, 5.80; N, 2.07%.

The purification of Fraction C gave **8** (163.0 mg, 9%); mp 79—80 °C, $[\alpha]_D$+70° (*c* 0.9, $CHCl_3$). Found: C, 54.90; H, 4.79; N, 3.98%. Calcd for $C_{52}H_{51}Cl_4N_3O_{17}$: C, 55.18; H, 4.54; N, 3.71%. This was treated with a dil solution of sodium methoxide in methanol and then with Dowex resin in aq acetone and successively hydrogenated to afford glass of **19** (26 mg); $[\alpha]_D$+117° (*c* 0.4, H_2O). Found: C, 41.91; H, 7.03; N, 4.09%. Calcd for $C_{12}H_{23}NO_{10}$: C, 42.23; H, 6.79; N, 4.10%.

A sample of (≈30 mg) of Fraction D was purified by TLC to furnish **7**; mp 74—77 °C, $[\alpha]_D$−11° (*c* 0.9, $CHCl_3$). Found: C, 54.43; H, 4.73; N, 4.18%. Calcd for $C_{52}H_{51}Cl_4N_3O_{17}$: C, 55.18; H, 4.54; N, 3.71%. The rest of Fraction D was treated with a dil solution of sodium methoxide in methanol and chromatographed as described above to furnish the de-*O*-acetate of **7** (238.9 mg, 15% from **2**) and then that of **8a** (52.4 mg, 3% from **2**). The former compound was treated with Dowex resin in aq acetone and then hydrogenated to afford **18** (55.3 mg); $[\alpha]_D$+93° (*c* 0.4, H_2O). Found: C, 40.84; H, 6.92; N, 3.81%. Calcd for $C_{12}H_{23}NO\cdot 0.75H_2O$: C, 40.62; H, 6.96; N, 3.95%. The latter compound was subjected to the same deprotection process to afford **20** (7 mg); $[\alpha]_D$−19° (*c* 0.3, H_2O). Found: C, 41.43; H, 7.02; N, 3.91%. Calcd for $C_{12}H_{23}NO_{10}\cdot 0.5H_2O$: C, 41.14; H, 6.91; N, 4.00%.

*α-D-Mannopyranosyl 2-Amino-2-deoxy-α-D-glucopyranoside (**21**) and Its Isomers (**22**, **23**, and **24**).* A mixture of **1** (854 mg, 1.6 mmol), **3** (1085 mg, 1.6 mmol), silver perchlorate (331 mg, 1.6 mmol), and tribenzylamine (459 mg, 1.6 mmol) in benzene (8 ml) was stirred in the dark for 24 h. The subsequent chromatography of the reaction mixture (silica gel (30 g) and Solvent-BB (100:1→5:1, gradient, 10-ml fraction)) gave five fractions: A (Nos. 17 and 18), B (Nos. 22—29), C (No. 30), D (Nos. 31—35), and E (Nos. 38—41).

Fraction A gave **33** (59.3 mg, 5.5%), which was identified with the sample prepared alternatively as below.

A small portion of Fraction B was purified by TLC to furnish **9**; $[\alpha]_D$+104° (*c* 0.8, $CHCl_3$). Found: C, 55.92; H, 4.91; N, 3.49%. Calcd for $C_{52}H_{51}Cl_4N_3O_{17}$: C, 55.18; H, 4.54; N, 3.71%. The rest of Fraction B was treated with a dil solution of sodium methoxide in methanol, followed by chromatography, to afford unchanged **3** (382.6 mg, 30%) and the yellow de-*O*-acetate of **9** (496.5 mg, 31% from **3**). This was treated with Dowex resin in aq acetone to give a colorless mass of **15** (303.2 mg); mp 149—153 °C, $[\alpha]_D$+53° (*c* 0.2, MeOH). Found: C, 56.38; H, 5.11; N, 1.57%. Calcd for $C_{40}H_{41}Cl_4NO_{10}\cdot H_2O$: C, 56.15; H, 5.06; N, 1.64%. Compound **15** was then hydrogenated and deionized to afford **21** (94.0 mg 16% from **3**); $[\alpha]_D$ +141° (*c* 0.4, H_2O). Found: C, 40.46; H, 6.74; N, 3.91%. Calcd for $C_{12}H_{23}NO_{10}\cdot 0.75H_2O$: C, 40.62; H, 6.96; N, 3.95%.

An aqueous solution of this (32 mg) was acidified with hydrochloric acid (35%) to pH 3 and then freeze-dried to give crystals. Recrystallization from methanol containing acetone afforded needles of **31** (*ca.* 20 mg); mp 194—195 °C (dec), $[\alpha]_D$ +110° (*c* 0.5, H_2O) [lit,[3a] mp 230 °C (dec), $[\alpha]_D^{23}$ +91.3° (*c* 2, H_2O)], NMR (D_2O, ext. TMS) δ: 5.64 (1H, d, J=1.9 Hz, H-1′), 5.90 (1H, d, J=3.8 Hz, H-1′). Found: C, 37.07; H, 6.32; N, 3.37%. Calcd for $C_{12}H_{23}NO_{10}\cdot HCl\cdot 0.5H_2O$: C, 37.26; H, 6.52; N, 3.62%.

The treatment of **9** (22 mg) with pyridine and acetic anhydride afforded octaacetate, **30** (38.2 mg, 87%); mp 90—93 °C, $[\alpha]_D$ +106° (*c* 1.0, $CHCl_3$) [lit,[3a] mp 91.5—93 °C]; IR(KBr)ν: 1745 (OAc), 1660, 1540 (NHAc); NMR ($CDCl_3$, TMS) δ: 1.97 (3H, s, $NHCOCH_3$), 2.03, 2.05, 2.07, 2.08, 2.16 (3H,6H,6H,3H,3H, $OCOCH_3$), 6.25 (1H, d, J=8 Hz, NH). Found: C, 49.49; H, 5.89; N, 1.97%. Calcd for $C_{28}H_{39}NO_{18}$: C, 49.63; H, 5.80; N, 2.07%.

Fraction C was **11** (200.3 mg, 11% from **3**); mp 77—79 °C, $[\alpha]_D$ −1° (*c* 1.0, $CHCl_3$). Found: C, 55.13; H, 4.50; N, 3.61%. Calcd for $C_{52}H_{51}Cl_4N_3O_{17}$: C, 55.18; H, 4.54; N, 3.71%. Removal of the protecting groups from **11** furnished **23** (38.4 mg); $[\alpha]_D$ +71° (*c* 1.0, $CHCl_3$). Found: C, 40.81; H, 6.68; N, 3.89%. Calcd for $C_{12}H_{23}NO_{10}\cdot 0.75H_2O$: C, 40.62; H, 6.96; N, 3.95%.

A portion of Fraction D was purified by means of TLC to give **10**; mp 70—73 °C, $[\alpha]_D$ −49° (*c* 1.0, $CHCl_3$) (Found: C, 55.29; H, 4.03; N, 3.76%. Calcd for $C_{52}H_{51}Cl_4N_3O_{17}$: C, 55.18; H, 4.54; N, 3.71%) and **12**; mp 74—75 °C, $[\alpha]_D$ −55° (*c* 1.0, $CHCl_3$) (Found: C, 54.99; H, 4.40; N, 3.72%. Calcd for $C_{52}H_{51}Cl_4N_3O_{17}$: C, 55.18; H, 4.54; N, 3.71%). The rest of Fraction D was treated with a dil solution of sodium methoxide in methanol, followed by chromatography, to afford the de-*O*-acetate of **10** (394.4 mg, 25% from **3**) first and then that of **12** (54 mg, 3.3% from **3**). These compounds were subsequently subjected to the de-protection processes to give **22** (82.1 mg); $[\alpha]_D$ +34° (*c* 1.0, H_2O) (Found: C, 41.18; H, 6.82; N, 3.90%. Calcd for $C_{12}H_{23}NO_{10}\cdot 0.5H_2O$: C, 41.14; H, 6.91; N, 4.00%) and **24** (9.2 mg), $[\alpha]_D$ −71° (*c* 0.1, H_2O) (Found: C, 39.85, H, 6.61; N, 3.64%. Calcd for $C_{12}H_{23}NO_{10}\cdot H_2O$: C, 40.11; H, 7.01; N, 3.90), respectively.

*α-D-Glucopyranosyl 2-Amino-2-deoxy-α-D-glucopyranoside (**25**) and Its Isomers (**26**, **27**, and **28**).* A mixture of **1** (1068 mg, 2.0 mmol), **4** (1356 mg, 2.0 mmol), silver perchlorate (414 mg, 2.0 mmol), and tribenzylamine (574 mg, 2.0 mmol) in benzene (10.6 ml) was vigorously stirred in the dark for 24 h. Chromatography on silica gel (50 g) with Solvent-BB (100:1→10:1, gradient, 15-ml fraction) gave five fractions: A (Nos. 17—20), B (Nos. 21—31), C (Nos. 32—36), D (Nos. 37—41) and E.

Fraction B (1335 mg) was composed of the fast-moving, major yellow band and unchanged **4**. A sample of Fraction B (≈50 mg) was subjected to TLC (25 mg/20×20×0.05 cm, developed with Solvent-BB (20:1), 15 times) to

give two yellow products, **13a** (minor faster-moving) and **13** (major slower-moving); mp 125—130 °C, $[\alpha]_D$ +112° (*c* 0.9, $CHCl_3$). Found: C, 55.41; H, 4.66; N, 3.76%. Calcd for $C_{52}H_{51}Cl_4N_3O_{17}$: C, 55.18; H, 4.54; N, 3.71%. The rest of Fraction B was treated with a mixture of a methanolic solution of sodium methoxide (0.05 M, 34 ml) and 1,4-dioxane (10 ml), followed by neutralization with acetic acid and chromatography, to give a mixture (717 mg, 36% from **4**) of the de-*O*-acetates of **13** and **13a**. A portion of this was treated with Dowex resin in aq acetone, followed by chromatography (Solvent-BE) and recrystallization from diisopropyl ether containing ethanol, to give **16**; mp 153—156 °C; $[\alpha]_D$ +108° (*c* 0.3, MeOH). Found: C, 56.58; H, 5.09; N, 1.53%. Calcd for $C_{40}H_{41}Cl_4NO_{10}\cdot 0.5H_2O$: C, 56.75; H, 5.00; N, 1.65%. The mixture (*ca.* 650 mg) of the de-*O*-acetates of **13** and **13a** was subjected to the deprotecting processes as described above to afford a free base whose ^{13}C NMR (D_2O) showed the presence of **25** and **27** (*ca.* 3:1). The free base (110 mg) was then dissolved in water (6 ml), and to the mixture 2,4-dinitrofluorobenzene (Wako, 70 mg), sodium hydrogencarbonate (45 mg) and ethanol (3 ml) were added. After this mixture had been stirred for 2 d, a yellow mixture was acidified and evaporated to give a residue which was further treated with pyridine and acetic anhydride. The yellow product (230 mg) composed of two compounds (R_f=0.55 (major) and 0.45, ethyl acetate–1,2-dichloroethane (1:3)) gave a homogeneous faster-moving compound (>126 mg) after preparative TLC. The treatment of this with a dil solution of sodium methoxide in methanol and then Dowex resin in aq acetone, followed by passing it through a little column of the resin, afforded $[\alpha]_D$ +183° (*c* 0.9, H_2O). Found: C, 40.66; H, 6.81; N, 3.87%. Calcd for $C_{12}H_{23}NO_{10}\cdot 0.75H_2O$: C, 40.62; H, 6.96; N, 3.93%.

The treatment of this with acetic anhydride and pyridine gave octaacetate of **25**; mp 98—100 °C, $[\alpha]_D$ +151° (*c* 0.5, $CHCl_3$) [lit, mp 100—102 °C,[1] 99 °C,[3] $[\alpha]_D$ +163.5° ($CHCl_3$),[1] +152° (*c* 1.08, $CHCl_3$, at 25 °C)[3]].

The slower-moving, yellow band obtained by preparative TLC mentioned just above furnished a homogeneous glass (≈45 mg) which was later converted into **27** (15 mg); $[\alpha]_D$ +111° (*c* 0.4, H_2O). Found: C, 41.30; H, 7.19; N, 3.87%. Calcd for $C_{12}H_{23}NO_{10}\cdot 0.5H_2O$: C, 41.14; H, 6.91; N, 4.00%.

Fraction C (352.5 mg) was treated with a dil solution of sodium methoxide in methanol and chromatographed to give the de-*O*-acetate of **14a** (131.7 mg, 6.6% from **4**). This was then converted into **28** (29 mg), $[\alpha]_D$ −43° (*c* 0.3, H_2O). Found: C, 40.92; H, 7.09; N, 4.02%. Calcd for $C_{12}H_{23}NO_{10}\cdot 0.5H_2O$: C, 41.14; H, 6.91; N, 4.00%.

Fraction D was purified by rechromatography to give **14** (581.7 mg, 26% from **4**); mp 73—75 °C, $[\alpha]_D$ −51° (*c* 0.3, $CHCl_3$). Found: C, 55.32; H, 4.81; N, 3.71%. Calcd for $C_{52}H_{51}Cl_4N_3O_{17}$: C, 55.18; H, 4.51; N, 3.71%. Fraction D was subjected to deprotection processes to furnish **26** (87 mg), $[\alpha]_D$ +81° (*c* 0.3, H_2O). Found: C, 40.64; H, 6.79; N, 3.85%. Calcd for $C_{12}H_{23}NO_{10}\cdot 0.75H_2O$: C, 40.62; H, 6.96; N, 3.95%.

*2,3,4,6-Tetra-O-(p-chlorobenzyl)-α-D-galactopyranosyl 2,3,4,6-Tetra-O-(p-chlorobenzyl)-α-D-galactopyranoside (**32**).* A mixture of **2** (136 mg, 0.2 mmol), silver *p*-nitrobenzenesulfonate[20] (62 mg, 0.2 mmol), and diphenyldichlorosilane (21 μl, 0.1 mmol) in dichloromethane (0.7 ml) was stirred at 0 °C in the dark for 6 h. The subsequent chromatography of the reaction mixture using Solvent-BB on silica gel gave **32** (106.6 mg, 79%); $[\alpha]_D$ +81° (*c* 0.8, $CHCl_3$). Found: C, 61.30; H, 4.57%. Calcd for $C_{68}H_{62}Cl_8O_{11}$: C, 61.00; H, 4.64%.

The hydrogenation of **32** in acetic acid in the presence of palladium black gave α-D-galactopyranosyl α-D-galactopyranoside; mp 268—269 °C, $[\alpha]_D$ +211° (*c* 0.5, H_2O) [lit,[18] 264—267 °C, $[\alpha]_D^{20}$ +235° (*c* 0.35, H_2O)].

*2,3,4,6-Tetra-O-(p-chlorobenzyl)-α-D-mannopyranosyl 2,3,4,6-Tetra-O-(p-chlorobenzyl)-α-D-mannopyranoside (**33**).* Compound **3** (136 mg, 0.2 mmol) was similarly condensed to afford **33** (81.2 mg, 60%); $[\alpha]_D$ +21° (*c* 1, $CHCl_3$). Found: C, 60.62; H, 4.57%. Calcd for $C_{68}H_{62}Cl_8O_{11}$: C, 61.00; H, 4.67%.

The hydrogenolysis of **33** in acetic acid in the presence of palladium black furnished α-D-mannopyranosyl α-D-mannopyranoside; mp 245—246 °C, $[\alpha]_D$ +122° (*c* 0.3, H_2O) [lit,[21] mp 240—243 °C, $[\alpha]_D^{20}$ +124° (*c* 1, H_2O)], ^{13}C-NMR (D_2O, ext, TMS) δ: 96.4, 74.6, 71.4, 71.1, 67.8, 62.0.

We are grateful to Professor Satoshi Ōmura and Mr. Rokuro Masuma for their microbial assays.

References

1) Presented at ACS/CSJ Chem. Congr. 1979, Honolulu, CARB 66.

2) F. Arcamone and F. Bizioli, *Gazz. Chim. Ital.*, **87**, 896 (1957).

3) a) M. Uramoto, N. Otake, and H. Yonehara, *J. Antibiot.*, **20A**, 236 (1967); b) H. Naganawa, N. Usui, T. Takita, M. Hamada, K. Maeda, and H. Umezawa, *ibid.*, **27**, 145 (1974); c) L. A. Dolak, T. M. Castle, and A. L. Laborde, *ibid.*, **33**, 690 (1980).

4) S. Umezawa, K. Tatsuta, and R. Muto, *J. Antibiot.*, **20A**, 388 (1967).

5) S. Hanessian and P. Lavalee, *J. Antibiot.*, **25**, 683 (1972); H. H. Baer and A. J. Bell, *Carbohydr. Res.*, **75**, 175 (1979).

6) a) E. Bar-Guilloux, J. Defaye, H. Driguez, and D. Robic, *Carbohydr. Res.*, **45**, 217 (1975); b) J. Defaye, H. Driguez, B. Henrissat, J. Gelas, and E. Bar-Guilloux, *ibid.*, **63**, 41 (1978).

7) A. F. Hadfield, L. Hough, and A. C. Richardson, *Carbohydr. Res.*, **63**, 51 (1978).

8) a) S. O'Connor, L. K. T. Lam, N. D. Jones, and M. O. Chaney, *J. Org. Chem.*, **41**, 2087 (1967); b) R. U. Lemieux and S. Koto, *Abstracts of Papers*, Am. Chem. Soc., 1973, 165, MEDI 022; c) D. E. Dorman, J. W. Paschal, and K. E. Merkel, *J. Am. Chem. Soc.*, **98**, 6885 (1976); d) A. Takatsuki, K. Kawamura, M. Okina, Y. Kodama, T. Ito, and G. Tamura, *Agric. Biol. Chem.*, **41**, 2307 (1977).

9) H. Paulsen and B. Sumfleth, *Chem. Ber.*, **112**, 3203 (1979).

10) P. F. Lloyd and M. Stacey, *Tetrahedron*, **9**, 116 (1960).

11) S. Umezawa and S. Koto, *Bull. Chem. Soc. Jpn.*, **39**, 2014 (1966); W. Meyer zu Reckendorf and N. Wassiliadou-Micheli, *Chem. Ber.*, **103**, 1792 (1970); A. Hasegawa, D. Nishimura, T. Kurokawa, and M. Nakajima, *Agric. Biol. Chem.*, **36**, 1773 (1972); S. Ogawa, Y. Funaki, K. Iwata, and T. Suami, *Bull. Chem. Soc. Jpn.*, **49**, 1975 (1976).

12) S. Koto, S. Inada, N. Morishima, and S. Zen, *Carbohydr. Res.*, **87**, 264 (1980).

13) K. Igarashi, J. Irisawa, and T. Honma, *Carbohydr. Res.*, **39**, 213 (1975).

14) F. J. Kronzer and C. Schuerch, *Carbohydr. Res.*, **33**, 273 (1974).

15) S. Omoto, S. Inouye, M. Kojima, and T. Niida, *J. Antibiot.*, **26**, 717 (1973); K. F. Koch, J. A. Rhoades, E. W. Hagaman, and E. Wenkert, *J. Am. Chem. Soc.*, **96**,

3300 (1974).
16) Unprimed numbers are given to the glucosaminyl moiety, while primed ones are used for the hexosyl moiety. Anomeric oxygen is unnumbered.
17) R. U. Lemieux, A. A. Pavia, J. C. Martin, and K. A. Watanabe, *Can. J. Chem.*, **47**, 4427 (1969); R. U. Lemieux and S. Koto, *Tetrahedron*, **30**, 1933 (1974); R. U. Lemieux, S. Koto, and D. Voisin, "Anomeric Effect, Origin and Consequences," ed by W. A. Szarek and D. Horton, ACS Symp. Ser., **87**, 17 (1979).
18) T. Usui, N. Yamaoka, K. Matsuda, K. Tuzimura, J. Sugiyama, and S. Sato, *J. Chem. Soc., Perkin Trans. 1* **1973**, 2425.
19) S. Koto, S. Inada, and S. Zen, *Chem. Lett.*, **1980**, 403.
20) A. A. Pavia, J. -M. Rocheville, and S. N. Ung, *Carbohydr. Res.*, **79**, 79 (1980).
21) D. G. Gorenstein, *J. Am. Chem. Soc.*, **99**, 2254 (1977).
22) S. Koto, N. Morishima, and S. Zen, *Bull. Chem. Soc. Jpn.*, **52**, 784 (1979).
23) F. Micheel and D. Bormann, *Chem. Ber.*, **93**, 1143 (1960).

Note added in proof: A. A. Pavia, *et al.* describe and discuss about the ^{13}C chemical shifts of the anomeric carbons of the 1,1′-linked glycosyl glycosides in their latest paper (*Nouv. J. Chem.*, **5**, 101 (1981)).

  Bull. Chem. Soc. Jpn., 54, 2735—2738 (1981)

A Novel Ring-closure Reaction between 1,4-Dihydroxyanthraquinone and Diamines Promoted by Copper Ions

Toshio Takei, Masaru Matsuoka,* and Teijiro Kitao

Department of Applied Chemistry, College of Engineering, University of Osaka Prefecture, Sakai, Osaka 591

(Received November 17, 1980)

The reaction of 1,4-dihydroxyanthraquinone(DHAQ, **1**) with various diamines were carried out in the presence of $CuCl_2$. Primary 1,2-ethylenediamines or 1,2-cyclohexanediamine afforded the ring-closure products, 6-hydroxy-1,2,3,4-tetrahydronaphtho[2,3-*f*]quinoxaline-7,12-dione derivatives, in good yields of 70—98%. On the other hand, in the cases of *N*-alkylethylenediamines or 2-(alkylamino)ethanols, the major products were the 2-aminated 1,4-dihydroxyanthraquinones. The direct 2-amination of **1** was greatly inhibited when an alkyl group was introduced to the amino group because of its steric requirement. The role of copper ions, the effect of a steric requirement of the *N*-alkyl substituent of amines, and the effect of the chain length of alkanediamines in the reaction of **1** with amines were studied. It was proposed that the reaction was initiated by the direct 2-amination of **1** *via* the copper complex, followed by the intramolecular nucleophilic substitution of the 2-amino group on the 2-alkylamino substituent to give the ring-closure product.

Aminoanthraquinone derivatives are very important compound as dyes or dye intermediates. A large number of papers and patents have been reported on substitution reactions introducing amino groups into the anthraquinone nucleus,[1] but little is known about the direct amination of the anthraquinone nucleus.

The direct amination of anthraquinone or aminoanthraquinones with hydroxylamine catalyzed by iron sulfate or vanadium pentaoxide has been described, but it produces random substitution products.[2] Hida *et al.*[3] recently reported the direct amination of anthraquinone catalyzed by a rhodium complex to give α-aminoanthraquinones. Recently, the present authors reported[4,5] the metal-promoted direct alkylamination of α-substituted anthraquinones, in which the amination products were obtained in good yields under mild conditions. On the other hand, in the reaction of DHAQ (**1**) with ethylenediamine (ETDA) in the presence of copper ions, a ring-closure product, 6-hydroxy-1,2,3,4-tetrahydronaphtho[2,3-*f*]quinoxaline-7,12-dione (**3a**), was obtained in a quantitative yield at the ambient temperature.[6] Such a metal-promoted direct amination of α-substituted anthraquinones is a useful method for preparing some aminoanthraquinone derivatives.

In this paper, we whish to report on the reaction of **1** with diamines in detail and propose a possible mechanism of this novel ring-closure reaction.

Results and Discussion

In our previous paper,[6] it was reported that the reaction of DHAQ (**1**) with ethylenediamine (ETDA) in the presence of $CuCl_2$ afforded the ring-closure products, 6-hydroxy-1,2,3,4-tetrahydronaphtho[2,3-*f*]-quinoxaline-7,12-dione (**3a**), in a 98% yield at the ambient temperature (Run 1). Without copper ions under atmospheric oxygen, **3a** was obtained in a 47% yield, together with a 15% yield of leucoquinizarin (1,4-dihydro-9,10-dihydroxyanthracene-1,4-dione) and a 9% recovery of **1** (Run 2). The reaction of **1** with ETDA in the presence of CuCl under the conditions without oxygen gave **3a** in a 96.6% yield, together with the deposition of metal copper in a 44.1% yield (Run 3). On the other hand, the reaction of ETDA with quinizarinquinone (1,4,9,10-tetrahydroanthracene-1,4,9,10-tetrone, **4**), which has previously been prepared by the oxidation of **1** with lead tetraacetate,[7] gave **3a** in a 90.7% yield, along with a 1.2% yield of **1** (Run 4). These results suggested that the role of copper ions is the same as in our previous cases of the quantitative 2-butylamination of **1**,[4] that is; the copper ions oxidize **1** to quinizarinquinone (**4**) *via* the copper complex,[8] and the copper ions are reduced to metal copper. Thus, the formation of **3a** was proposed to proceed as follows: the reaction was initiated by the 2-amination of **1** to give **2a**, followed by the ring-closure reaction. The reaction of **1** with 1,3-propanediamine in the presence of $CuCl_2$ did not give the rin -closure product **3b**), but 2-(3-aminopropylamino)-1,4-dihydroxyanthraquinone (**2b**) in a 95% yield (Run 5). The facile ring-closure of **1** with ETDA, but not with 1,3-propanediamine, was proposed to result from the fact that the spontaneous formation of the six-membered ring in **3a** was much more favorable in entropy than that of the seven-membered ring in **3b**. The six-membered ring could be formed by the intramolecular nucleophilic substitution of the 2-aminoethylamino group to the 1-hydroxyl group of **2a**, as is shown in Scheme 1. The reaction of **1** with 1,2-propanediamine (Run 6) or 1,2-cyclohexanediamine (Run 7) gave **3c** or **3d** in a yield of 89.5% or 68.9% respectively, but none of the corresponding **2c** or **2d** was obtained. These results suggested that the ring-closure reaction was not inhibited by the alkyl substituents at the 1 and/or 2-position of ETDA. On the

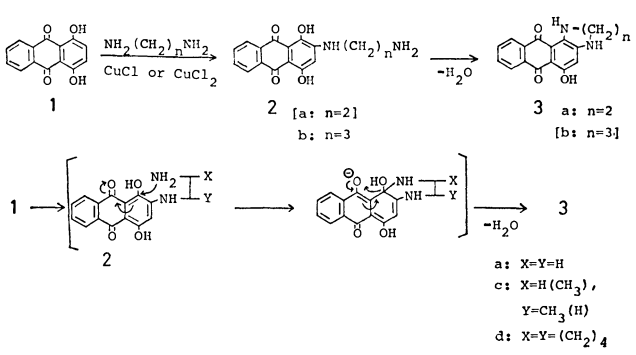

Scheme 1.

Table 1. The reaction of **1** with various diamines[a)]

Run	Diamines	Copper salt	Yield/%		
			1 (Recovered)	**2**	**3**
1	$NH_2(CH_2)_2NH_2$ $n=2$	$CuCl_2$	0	0	98.0
2[b)]	$NH_2(CH_2)_2NH_2$ $n=2$	None	9	0	47.0
3[c)]	$NH_2(CH_2)_2NH_2$ $n=2$	CuCl	0	0	96.6
4[d)]	$NH_2(CH_2)_2NH_2$ $n=2$	None	1.2	0	90.7[e)]
5	$NH_2(CH_2)_3NH_2$ $n=3$	$CuCl_2$	0	95.0	0
6	$NH_2CH(CH_3)CH_2NH_2$ $n=2$	$CuCl_2$	7.6	0	89.5
7	$NH_2CH(CH_2)_4CHNH_2$ $n=2$	$CuCl_2$	28.2	0	68.9
8[f)]	$NH_2(CH_2)_2NHMe$ $n=2$	$CuCl_2$	0	31.4	31.1
9	$NH_2(CH_2)_2NHEt$ $n=2$	$CuCl_2$	0	93.3	3.6

a) Reactant **1**(2.5 mmol) and diamine(12 ml) were stirred with or without copper salts(5.0 mmol) in pyridine (6 ml) at 30 °C for 6 h. Unless otherwise noted, the reaction was carried out under atmospheric oxygen. b) Leucoquinizarin was obtained in a 15% yield. c) Reaction was carried out under reduced pressure without oxygen. Metal copper was obtained in a 44.1% yield. d) Quinizarinquinone (**4**) was used as the reactant instead of **1**. e) The instability of **4** as a reactant caused a decrease in the yield of **3a**, and a 1.2% yield of **1**, which is the reduced product of **4**, was obtained. f) A complex mixture of compounds(246 mg) was obtained, but these compounds were not identified.

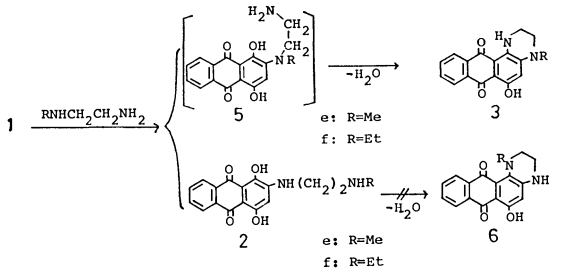

Scheme 2.

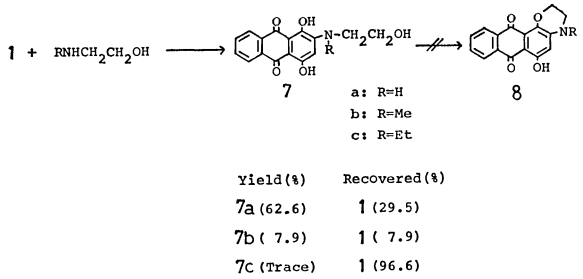

Scheme 3.

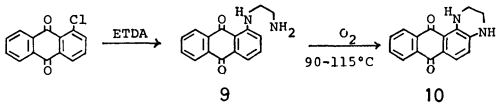

Scheme 4.[9)]

other hand, the *N*-alkyl substituent of ETDA markedly inhibited both the 2-amination and the ring-closure reaction. The reaction of **1** with *N*-methylethylenediamine gave **3e** in a 31% yield, together with **2e** in a 31% yield (Run 8). The yield of **3e** was greatly decreased in comparison with that of **3a** (Run 1). The reactions of **1** with various diamines are summarized in Table 1. As is shown in Scheme 2, the formation of **5e** and **2e** should compete on the 2-amination of **1** with *N*-methylethylenediamine. On the other hand, the formation of **5e** was much more unfavorable than that of **2e** because of the steric hindrance of the *N*-methyl group; the **5e** intermediate could be easily cyclized to give **3e**, and no **5e** was obtained. On the other hand, **2e** could not give the ring-closure product (**6e**) because of the steric hindrance of the *N*-methyl group. Another example of the steric hindrance was observed in the reaction of **1** with *N*-ethylethylenediamine (Run 9). The ring-closure product (**3f**) *via* **5f** was obtained only in a 3.6% yield, while **2f** was obtained in a 93.3% yield. The competitive 2-amination of **1** with *N*-ethylethylenediamine was obviously much more likely to give **2f** than **5f**, and only a small amount of **3f** was obtained. Compound **2f** could not be converted to **6f** because of the steric hindrance under these conditions, just as in the case of **2e**. Under the more severe conditions of 95—100 °C for 96 h, **2f** afforded **3a**, the deethylation product of **6f**, in a 19.7% yield, along with a 61% recovery of **2f**, but no **6f** was obtained. A similar steric hindrance of the *N*-alkyl group of amines in the 2-amination of **1** was also observed in the case of the reaction of **1** with 2-(alkylamino)ethanols (Scheme 3). The yield of **7** was markedly decreased with the increase in the size of *N*-alkyl substituents, and none of the ring-closure product (**8**) was obtained.

From these results, together with our previous results obtained from the reactions of **1** with various amines,[4)] another possibility of ring-closure reaction (shown in Scheme 4) was excluded; it had been reported in the case of the reaction of 1-chloroanthraquinone with ETDA under atmospheric oxygen at 90—115 °C.[9)] In this reaction, α-amination took place first, followed by direct β-amination at a higher temperature.

On the basis of the experimental results described above, together with previous results,[4)] the mechanism of this ring-closure reaction of **1** with ETDA was

$$\mathbf{1} + \text{ETDA(excess)} \longrightarrow \text{Dianion} \quad (1)$$

$$\left.\begin{array}{l}\text{Dianion} + \text{CuCl}_2(\text{CuCl}_2:\mathbf{1}=2:1) \longrightarrow \\ \qquad 2:1\ \text{Copper(II) complex[I]} \\ \text{Dianion} + \text{CuCl}_2(\text{CuCl}_2:\mathbf{1}=1:1) \longrightarrow \\ \qquad 1:1\ \text{Copper(II) complex[II]} \\ \text{Dianion} + \text{CuCl(CuCl}:\mathbf{1}=2:1) \longrightarrow \\ \qquad 2:1\ \text{Copper(I) complex[III]}\end{array}\right\} \quad (2)$$

$$\text{Copper complex}^{8)} \left\{\begin{array}{l}\text{[I]} \longrightarrow \mathbf{4} + 2\text{Cu}^+ \\ \text{[II]} \longrightarrow \mathbf{4} + \text{Cu}^0 \\ \text{[III]} \longrightarrow \mathbf{4} + 2\text{Cu}^0\end{array}\right\} \quad (3)$$

$$\mathbf{1} + \text{O}_2 \longrightarrow \mathbf{4}\ \text{(without copper salt)} \quad (4)$$

$$\mathbf{1} \longrightarrow \mathbf{4} + \text{Leucoquinizarin (without copper salt and/or O}_2\text{)} \quad (5)$$

$$\mathbf{4} + \text{ETDA} \longrightarrow \mathbf{2a} \quad (6)$$

$$\mathbf{2a} \xrightarrow[-\text{H}_2\text{O}]{} \mathbf{3a} \quad (7)$$

Scheme 5.

proposed to be as is shown in Scheme 5. The formation of dianion was proved by the color change of the reaction mixture from orange to violet (λ_{max} 566, 606 nm) after the addition of excess amines (Eq. 1). The formation of the copper complex (Eq. 2) and the redox system of the copper complex (Eq. 3) have previously been reported in the cases of the reactions of **1** with amines in our previous paper;[4] the deposition of metal copper, the effect of the atmosphere (with or without O_2), the effect of the molar ratio of copper salts, and the effect of the kind of copper salt were there discussed in detail. Without copper salts, atmospheric oxygen oxidized **1** to **4** (Eq. 4), and/or **1** spontaneously disproportionated to **4** and leucoquinizarin (Eq. 5), and 47% of **3a** was obtained, together with 15% of leucoquinizarin (Run 2). Similar results (48% yield) were obtained in the 2-amination of **1** with butylamine under the same conditions.[4] When the reaction was carried out without either O_2 or copper salts, none of the oxidizing agent was present, **1** spontaneously disproportionated to **4** and leucoquinizarin (Eq. 5), and the yield of the 2-aminated product was reduced from 48.1% to 13.1%.[4] Without copper salt, leucoquinizarin was also obtained in a 15% yield (Run 2). The Michael-type addition of ETDA to **1** give rise to **2a** (Eq. 6). The intramolecular substitution of the 2-aminoethylamino group with the 1-hydroxyl group of **2a** gives rise to the ring-closure product **3a** (Eq. 7).

Experimental

The melting points are uncorrected. The visible spectra were measured using a Hitachi EPS-3T spectrophotometer. The ^{1}H-NMR spectra were recorded on a Hitachi Perkin Elmer Model R-20 spectrometer, with TMS as the internal standard. The elemental analyses were recorded on a Yanaco CHN recorder, MT-2. Column chromatography was carried out on silica gel (Wakogel C-300), using benzene as the eluent. The structural assignment of the products were done by means of their NMR, Mass spectra, and elemental analyses.

Materials. 1,4-Dihydroxyanthraquinone(**1**) was supplied by the Mitsubishi Chemical Industry, Inc., and was purified by column chromatography, using benzene as an eluent, followed by recrystallization from benzene. The metal salts, amines, and solvents were of a reagent grade and were used without further purification.

*Reaction of **1** with Various Diamines.* A typical example of the reaction is shown below: *N*-ethylethylenediamine (12 ml, 135 mmol) was added into a mixture of **1** (0.6 g, 2.5 mmol), pyridine (6 ml), and $CuCl_2$ (0.63 g, 5.0 mmol), after which the mixture was stirred under atmospheric oxygen for 5 h at room temperature and then poured into a solution of concd HCl (40 ml) and water (100 ml). The separated products were filtered, washed with water, dried, and extracted with benzene. The extract was concentrated and separated by column chromatography, using benzene as the eluent, to give **3f** (28 mg, 3.6%), which was then recrystallized from 1-butanol. The residue was washed with benzene several times to give the HCl salt of **2f** (845 mg, 93.3%).

The reactions of **1** with other diamines were carried out in the same way.

In the reaction of **1** with 1,2-cyclohexanediamine(Run 7), two isomeric compounds of **3d** were obtained; they were identified on the basis of their ^{1}H-NMR spectra. Similar compounds had previously been reported by Koeliker *et al.*[9] in the reaction of 1-chloroanthraquinone with 1,2-cyclohexanediamine.

*Reaction of **1** with 2-(Alkylamino)ethanols.* A typical example of the reaction is shown below: 2-aminoethanol (12 ml, 200 mmol) was added to a mixture of **1** (0.6 g, 2.5 mmol), pyridine (6 ml), and $CuCl_2$ (0.673 g, 5.0 mmol), after which the mixture was stirred under atmospheric oxygen at room temperature for 5 h. The mixture was then poured into water and the separated products were filtered, washed with water, and dried. The residue was boiled in an aqueous solution of oxalic acid and filtered, washed with water, dried, and chromatographed using a mixture of benzene–methanol (95:5) as the eluent to give **1** (177 mg 29.5%) and **7d** (468 mg 62.2%).

The reactions of **1** with other 2-(alkylamino)ethanol were carried out in the same way.

Characterization and Identification of Products. Compounds **2b** and **3a** were already reported in our previous paper.[6]

3c: Mp 227—229 °C (1-butanol); UV, λ_{max} (benzene) (ε) 585 (18800), 543 (18000), 509^s nm (9400); ^{1}H-NMR (DMSO-d_6): δ 1.25 (3H d) 6.02 (1H s), 7.52—8.15 (4H, m), 7.86 (1H, broad), 10.34 (1H, broad), 15.20 (1H, s); MS, *m/e* (rel intensity): 294 (M^+, 46), 293 (3), 279 (58), 262 (100).

*4-N-Benzoyl Derivative of **3c***: Mp 179—180 °C (methanol); UV, λ_{max} (benzene) (ε) 596 (14900), 552 (15200), 521^s nm (9200); Found: C, 72.37; H, 4.64; N, 6.87%. Calcd for $C_{24}H_{18}N_2O_4$: C, 72.35; H, 4.55; N, 7.03%; ^{1}H-NMR ($CDCl_3$): δ 1.35 (3H, dd), 3.32—4.34 (3H, m), 6.47 (1H, s), 7.35 (5H, m), 7.64 (2H, m), 8.18 (2H, m), 10.52 (1H, broad), 13.43 (1H, s).

3d: Mp 181—181.5 °C (benzene); UV, λ_{max} (benzene) (ε) 586 (18300), 544 (17500), 510^s nm (9000); Found: C, 71.75; H, 5.51; N, 8.18%. Calcd for $C_{20}H_{18}N_2O_3$: C, 71.84; H, 5.43; N, 8.38%; ^{1}H-NMR ($CDCl_3$): δ 1.10—2.20 (8H, m), 3.00 (1H, broad), 3.60 (1H, broad), 4.84 (1H, broad), 6.04 (1H, s), 7.54 (2H, m), 8.14 (2H, m), 10.24 (1H, broad), 14.84 (1H, s); MS, *m/e* (rel intensity): 334 (M^+, 100), 333 (10).

2e: UV, λ_{max} (methanol) 532^s, 502 nm.

2'-N-Benzoyl Derivative of ***2e***: Mp 207—208 °C (methanol); UV, λ_{max} (benzene) (ε) 514 (11700), 545^{s} nm (8900); Found: C, 69.51; H, 5.02; N, 7.05%. Calcd for $C_{24}H_{20}N_2O_5$: C, 69.22; H, 4.84; N, 6.73%; ^{1}H-NMR ($CDCl_3$): δ 3.02 (3H, s), 3.29—4.03 (4H, m), 6.03 (1H, s), 7.32 (5H, s), 7.63 (2H, m), 8.08 (1H, broad), 8.15 (2H, m), 13.73 (1H, s), 14.03 (1H, s); IR (KBr), ν_{CO} 1610 cm^{-1}; MS, *m/e* (rel intensity): 416 (M$^+$, 9), 281 (100), 268 (88), 239 (45).

3e: Mp 213—214 °C (1-butanol); UV, λ_{max} (benzene) (ε) 584 (23100), 543 (21900), 508^{s} nm (11100); Found: C, 69.14; H, 4.94; N, 9.32%. Calcd for $C_{17}H_{14}N_2O_3$: C, 69.38; H, 4.79; N, 9.52%; ^{1}H-NMR ($CDCl_3$): δ 2.98 (3H, s), 3.40 (4H, m), 5.84 (1H, s), 7.54 (2H, m), 8.10 (2H, m), 10.65 (1H, broad), 14.95 (1H, s); MS, *m/e* (rel intensity): 294 (M$^+$, 100), 293 (90), 279 (16), 262 (92).

2f: UV, λ_{max} (methanol) 542^{s}, 512 nm.

2'-N-Benzoyl Derivative of ***2f***: Mp 209—210 °C (methanol); UV, λ_{max} (benzene) (ε) 513 (12900), 545^{s} nm (9700); Found: C, 70.23; H, 5.32; N, 6.73. Calcd for $C_{25}H_{22}N_2O_5$: C, 69.76; H, 5.15; N, 6.51%; ^{1}H-NMR ($CDCl_3$): δ 1.14 (3H, t), 3.06—3.92 (6H, m), 6.02 (1H, s), 7.28 (5H, m), 7.63 (2H, m), 8.01 (1H, s), 8.24 (2H, m), 13.53 (1H, broad), 13.83 (1H, s); IR (KBr): ν_{CO} 1615 cm^{-1}; MS, *m/e* (rel intensity): 430 (M$^+$, 27), 281 (100), 268 (58), 239 (66).

3f: Mp 190—190.5 °C; UV λ_{max} (benzene) (ε) 588 (25000), 546 (23400), 511^{s} nm (11800); Found: C, 69.78; H, 5.19; N, 8.83%. Calcd for $C_{18}H_{16}N_2O_3$: C, 70.12; H, 5.28; N, 9.09%; ^{1}H-NMR ($CDCl_3$): δ 1.22 (3H, t), 3.13—3.65) (6H, m), 6.01 (1H, s), 7.55 (2H, m), 8.15 (2H, m), 10.72 (1H, broad), 14.97 (1H, s); MS, *m/e* (rel intensity): 308 (M$^+$, 100), 307 (56), 293 (30), 279 (16).

7a: Mp 263—264 °C (1-butanol); UV, λ_{max} (benzene) (ε) 544^{s} (9000), 512 nm (11700); Found: C, 64.08; H, 4.28; N, 4.45%. Calcd for $C_{16}H_{13}NO_5$: C, 64.21; H, 4.38; N, 4.68%; MS, *m/e* (rel intensity): 299 (M$^+$, 38), 281 (13), 268 (100).

7b: Mp 138.5—140 °C (1-butanol); UV, λ_{max} (benzene) (ε) 532 nm (11200); Found: C, 64.71; H, 4.91; N, 4.36%. Calcd for $C_{17}H_{15}NO_5$: C, 65.17; H, 4.83; N, 4.47%; MS, *m/e* (rel intensity): 313 (M$^+$, 20), 295 (54), 282 (100).

This work was supported in part by a Grant-in-Aid for Scientific Research from the Ministry of Education, Science and Culture.

References

1) K. Venkataraman, "The Chemistry of Synthetic Dyes," Academic Press, New York (1952), II, p. 803; (1970), III, p. 391.
2) A. C. Robson and S. Coffey, *J. Chem. Soc.*, **1954**, 2372.
3) K. Mita, T. Yamagishi, and M. Hida, *Nippon Kagaku Kaishi*, **1980**, 1855.
4) M. Matsuoka, K. Yoshida, Y. Makino, and T. Kitao, *Dyes and Pigments*, **1**, 27 (1980).
5) K. Yoshida, M. Matsuoka, Y. Yamashita, and T. Kitao, *Bull. Chem. Soc. Jpn.*, **53**, 2552 (1980).
6) M. Matsuoka, Y. Makino, T. Takei, and T. Kitao, *Chem. Lett.*, **1980**, 743.
7) O. Dimroth, O. Friedmann, and H. Kaemmerer, *Ber.*, **53**, 481 (1920).
8) The details of the structure of the copper complexes were previously reported in another of our article.[4]
9) H. P. Koelliker and P. Caveng, *Chimia*, **20**, 281 (1966).

  Bull. Chem. Soc. Jpn., 54, 2739—2746 (1981)

Pseudo-sugars. VII. Synthesis of Pseudo-hexopyranose Derivatives with α- and β-Gluco Configurations[1]

Seiichiro OGAWA,* Tatsushi TOYOKUNI, Takashi KONDOH, Yoshihisa HATTORI, Shinichi IWASAKI, Masaru SUETSUGU, and Tetsuo SUAMI

Department of Applied Chemistry, Faculty of Engineering, Keio University, Hiyoshi, Kohoku-ku, Yokohama 223

(Received December 3, 1980)

Several derivatives of pseudo-hexopyranose (5-hydroxymethyl-1,2,3,4-cyclohexanetetrol) with α-gluco, (1,2,4/3,5), and β-gluco, (1,3,5/2,4), configurations were synthesized starting from the compounds obtained by *cis*-hydroxylation and oxyamination of DL-di-*O*-acetyl-(1,3/2)-3-bromomethyl-5-cyclohexene-1,2-diol. The ^{1}H NMR chemical shifts of the acetyl methyl protons of the several acetyl derivatives of *N*-(*p*-tolylsulfonyl)-pseudo-glucosamines are discussed.

In connection with the preceding paper of this series,[2] the synthesis of pseudo-hexopyranose (5-hydroxymethyl-1,2,3,4-cyclohexanetetrol) derivatives having α- and β-gluco configurations are described. It has been hoped that pseudo-sugars, biologically interesting analogs, *e.g.* of glucose, galactose, and mannose, will be accepted by some enzymes or biological systems in place of corresponding true sugars, and may have useful biological properties.[3] On the other hand, pseudo-amino sugars related to 2-amino-2-deoxy-, 6-amino-6-deoxy-, and 2,6-diamino-2,6-dideoxy-D-glucose, components of some clinically important amino sugar antibiotics,[4] are also expected to be useful for study on a structure-activity relationship of the antibiotics.

In the present study, *cis*-hydroxylation and oxyamination reactions of the unsaturated derivatives (**3** and **4**) of pseudo-hexopyranoses were carried out.

Debromination of DL-di-*O*-acetyl-(1,3/2,4,6)-3,4-dibromo-6-bromomethyl-1,2-cyclohexanediol (**1**)[5] with an excess of zinc dust in acetic acid at 70 °C for 10 min gave DL-di-*O*-acetyl-(1,3/2)-3-bromomethyl-5-cyclohexene-1,2-diol (**3**) in 92% yield. The ^{1}H NMR spectrum of **3** showed the signals for two acetoxyl groups as singlets at δ 2.01 and 2.03, and those for the H-2 and H-6 protons as a triplet of doublets (J= 3, 7.5, and 7.5 Hz) and a broad doublet (J=*ca.* 11 Hz) at δ 5.02 and 5.77, respectively. Treatment of **1** with 4 molar equivalent of sodium benzoate in 80% aqueous ethanol under reflux for 2 d gave the 7-*O*-benzoate (**2**) in 66% yield. The structure was confirmed by the ^{1}H NMR spectrum that showed the down-field shift of the signal for the C-7 methylene group resulting from the replacement of the bromine atom by a benzoyloxyl group. Compound **2** was debrominated similarly with zinc dust to give DL-di-*O*-acetyl-(1,3/2)-3-benzoyloxymethyl-5-cyclohexene-1,2-diol (**4**) in 70% yield, which was also obtained from **3** by treatment with sodium benzoate in refluxing aqueous 2-methoxyethanol for 5 h. The above results confirmed the proposed structures of **3** and **4**. These olefins may be considered as the pseudo-glycal derivatives, versatile intermediates, for the preparation of pseudo-sugar derivatives.

Oxidation of **3** with osmium tetraoxide and hydrogen peroxide in *t*-butyl alcohol, followed by acetylation with acetic anhydride in pyridine, gave mainly a crystalline DL-tetra-*O*-acetyl-(1,2,4/3,5)-5-bromomethyl-1,2,3,4-cyclohexanetetrol (**6**) in 37% yield, together with a small proportion of a sirupy DL-*trans*-2,4-diacetoxy-5-bromomethyl-2-cyclohexanone (**5**), which was isolated in 7.5% yield by chromatography on silica gel. The structure of **5** was tentatively assigned by the elemental analysis and ^{1}H NMR spectral data, the latter of which showed the presence of two acetoxyl groups (δ 2.15 and 2.22) and an olefinic proton (doublet, J=2.5 Hz, δ 6.47), and the remarkable down-field shift of the signal (broad doublet, δ 2.72) for the C-7 methylene protons. In the ^{1}H NMR spectrum of **6**, the signals for H-1, H-2, H-3,

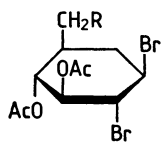

	R
1	Br
2	OBz

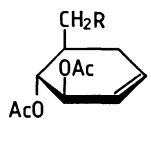

	R
3	Br
4	OBz

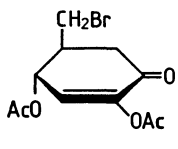

5

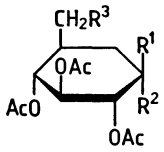

	R¹	R²	R³
6	H	OAc	Br
7	H	OAc	OAc
8	H	OAc	N_3
9	H	OAc	NHAc
10	H	OAc	H
11	OAc	H	OAc
12	OAc	H	Br
13	OAc	H	N_3
14	OAc	H	NHAc
15	OAc	H	H

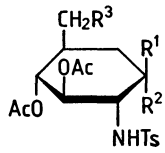

	R¹	R²	R³
16	H	OH	Br
17	H	OAc	Br
18	H	OH	OBz
19	H	OAc	OBz
20	H	OH	OAc
21	H	OAc	OAc
22	H	OH	N_3
23	H	OH	NHAc
24	H	OAc	NHAc
25	H	OH	H
26	H	OMs	Br
27	H	OMs	N_3
28	N_3	H	N_3
29	H	OMs	NHAc
30	NHAc	H	NHAc
31	H	H	NHAc
32	OAc	H	OAc

and H-4 protons appeared as a quartet (J=3.5 Hz), a doublet of doublets (J=3.5 and 10.5 Hz), a triplet (J=10.5 Hz), and a triplet (J=10.5 Hz) at δ 5.39, 4.87, 5.23, and 4.94, respectively, which indicated the equatorial-axial-axial-axial conformations for H-1, H-2, H-3, and H-4, being consistent with the assigned structure. Treatment of **6** with an excess of sodium acetate in refluxing aqueous 2-methoxyethanol, followed by conventional acetylation, gave DL-penta-*O*-acetyl-(1,2,4/3,5)-5-hydroxymethyl-1,2,3,4-cyclohexanetetrol (pseudo-α-DL-glucopyranose) (**7**)[6] in 70% yield. Similar treatment of **6** with sodium azide gave the corresponding C-7 azido derivative (**8**) in 80% yield, which was subsequently converted to the acetamide (**9**) in 31% yield[7] by hydrogenation in ethanol containing acetic anhydride in the presence of Raney nickel T-4.[8] Hydrogenolysis of **6** in ethyl acetate with Raney nickel and Amberlite IR-45 (OH^-) gave the 7-deoxy compound (**10**) in 70% yield. The ^{1}H NMR spectra of **6**—**9** substantially resemble one another in the region for ring protons, except for signals for the exocyclic methylene groups carrying the different functions.

In order to synthesize the same series of compounds with the β-gluco configurations, DL-tetra-*O*-acetyl-(1,3,5/2,4)-5-bromomethyl-1,2,3,4-cyclohexanetetrol (**12**) was prepared, in 91% yield, by treatment of the corresponding C-7 acetate (**11**)[9] with 10% hydrogen bromide in acetic acid in a sealed tube at 80 °C overnight. The corresponding C-7 azido (**13**), acetamido (**14**), and deoxy derivatives (**15**) were obtained analogously starting from **12** in appropriate yields. The structures were confirmed similarly by the ^{1}H NMR spectral data.

Next, several carbocyclic analogs of glucosamine derivatives were synthesized from **3** and **4**. Treatment of **3** with osmium tetroxide and chloramine T in chloroform–water (1:1) in the presence of triethylbenzylammonium chloride at 60 °C for 40 h, (essentially the procedure of Sharpless and his coworkers)[10] gave a mixture of at least four products. The major product was easily separated by crystallization from ethanol–ether to give DL-3,4-di-*O*-acetyl-(1,2,4/3,5)-5-bromomethyl-2-(*p*-toluenesulfonamido)-1,3,4-cyclohexanetriol (**16**) in 31% isolated yield, which was further characterized as the triacetate (**17**).[11] In the ^{1}H NMR spectrum of **17**, the signals for H-2, H-3, and H-4 protons appeared as a triplet of doublets (J=3, 11, and 11 Hz), a triplet (J=11 Hz), and a triplet (J=11 Hz) at δ 3.49, 5.09, and 4.88, respectively. Upon deuteration, a doublet (J=11 Hz, δ 5.42) due to the amido proton disappeared and the H-2 signal changed to a doublet of doublets (J=3 and 11Hz). Therefore, the conformations of H-1, H-2, and H-3 were shown to be equatorial-axial-axial, supporting the structure assigned above. Similar *cis*-oxyamination of **4** gave mainly the pseudo-glucosamine derivative (**18**) in 30% yield, which was converted to triacetate (**19**). The structure of **18** could be correlated to that of **16** by comparison of the ^{1}H NMR spectral data.[12]

Treatment of **16** with sodium acetate in refluxing aqueous 2-methoxyethanol gave its triacetate (**20**) in 57% yield, which was further acetylated to give the tetraacetate (**21**). The ^{1}H NMR spectrum of **20** resembled that of **16** in the region for ring protons, apart from that the signal for the C-7 methylene protons was shifted down field.

Azidolysis of **16** with sodium azide in *N*,*N*-dimethylformamide (DMF) at 80 °C for 2 h gave the azido derivative (**22**) in 90% yield, which was converted to the corresponding acetamide (**23**) in 57% yield. Tetra-*N*,*O*-acetyl derivative (**24**) was prepared. Hydrogenolysis of **16** gave the C-7 debromo compound (**25**) in 82% yield. The ^{1}H NMR spectra of **22**—**25** were all consistent with the assigned structures.

On the other hand, to obtain the derivatives having the β-gluco configuration, an inversion of the C-1 configuration was attempted by a direct substitution reaction of the 1-*O*-methanesulfonate (**26**) of **16**. Thus, **26** was prepared in 69% yield by treatment of **16** with an excess of methanesulfonyl chloride in pyridine. Azidolysis of **26** with 1.5 molar equivalent of sodium azide in DMF at 80 °C for 2 h gave preferentially the C-7 azido derivative (**27**) in 68% yield. While, on treatment with 5 molar equivalent of sodium azide at 85 °C for a prolonged period (20 h), the diazido derivative (**28**) was obtained mainly in 71% yield. Hydrogenation of **27** and **28** followed by acetylation gave the corresponding acetamide (**29**) and diacetamide (**30**) in 65 and 66% yields, respectively. As the side product of the hydrogenation of **28**, DL-1,2-di-*O*-acetyl-(1,3/2,6)-3-acetamidomethyl-6-(*p*-toluenesulfonamido)-1,2-cyclohexanediol (**31**) was isolated in 18% yield, which might arise from the elimination of the C-4 azido group under slightly basic conditions.

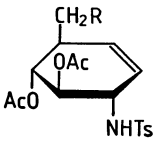

R

33 OAc

34 NHAc

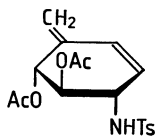

35

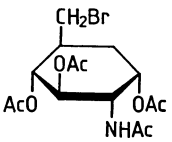

36

Reaction of **26** with an excess of sodium acetate in DMF at 80 °C for 20 h gave a mixture of products from which DL-tetra-*O*-acetyl-(1,3,5/2,4)-5-hydroxymethyl-2-(*p*-toluenesulfonamido)-1,3,4-cyclohexanetriol (**32**), DL-1,2-di-*O*-acetyl-(1,3/2,6)-3-hydroxymethyl-6-(*p*-toluenesulfonamido)-4-cyclohexene-1,2-diol (**33**), and DL-1,2-di-*O*-acetyl-(1/2,6)-3-methylene-6-(*p*-toluenesulfonamido)-4-cyclohexene-1,2-diol (**35**) were isolated in 10, 28, and 7% yields, respectively, by chromatography on silica gel. The structures were determined by the elemental analysis and ^{1}H NMR spectral data. The ^{1}H NMR spectrum of **32** in chloroform-*d* showed the signal for the H-2 proton as a quartet (J=10 Hz) at δ 3.65, which changed to a triplet upon deuteration, indicating the *trans*-diaxial arrangement of H-1 and H-2. The structure of **33** was assigned by the appearance of two-proton singlet at δ 5.50 attributable to two olefinic protons. In the spectrum of **35**, the signals for the exocyclic methylene protons appeared as a broad singlet at δ 4.96

Table 1. Chemical shifts of acetyl methyl protons[a)]

Compound	1-OAc	3-OAc	4-OAc	7-OAc
16		1.62	2.00	
17	2.06	1.76	1.99	
18		1.64	1.97	
19	2.10	1.78	1.98	
20		1.60	1.97	2.02
21	2.05	1.72	1.97	2.01
22		1.61	2.01	
25		1.60	1.97	
26		1.66	2.01	
27		1.60	2.00	
32	1.71[b)]	1.79[b)]	1.97	2.03

a) Taken at 90 MHz in $CDCl_3$ with reference to TMS. Chemical shifts are given in terms of δ-values. b) Assignments may be reversed.

and 5.06.[13)]

The elimination occurred predominantly in the reaction of **29** with sodium acetate in DMF giving rise to DL-1,2-di-*O*-acetyl-(1,3/2,6)-3-acetamidomethyl-6-(*p*-toluenesulfonamido)-4-cyclohexene-1,2-diol (**34**) in 59% yield. The ^1H NMR spectrum showed the signals for two olefinic protons as two triplets of doublets (J=2, 2, and 12 Hz) at δ 5.34 (H-4) and 5.57 (H-5).

The olefins **33**, **34**, and **35** thus obtained may be good precursors for preparation of branched-chain amino- and diaminocyclitols. Removal of the *N*-(*p*-tolylsulfonyl) group can usually be performed by the influence of sodium in liquid ammonia. Alternatively, on treatment with 20% hydrogen bromide in acetic acid in a sealed tube at 70 °C overnight, **16** gave the corresponding tri-*O*-acetyl amine hydrobromide, which was successively acetylated to the peracetyl derivative (**36**) in 69% yield. This procedure may be used for a small scale deprotection of *N*-(*p*-tolylsulfonyl) derivatives.

We are studying to prepare glycosides of **20** and **22**, which would provide the pseudo analogs of antibiotic trehalosamine and its related compounds.[14)]

Assignment of Acetyl Methyl Protons of N-(p-*Tolylsulfonyl) Derivatives of Pseudo-glucosamine.* Comparison of the ^1H NMR spectra of **16**, **17**, **20**, and **21** allowed to assign all the signals due to the acetyl methyl protons (Table 1). The appreciable up-field shift of the signal for the C-3 equatorial acetoxyl group is observed (at least 0.20 ppm), which may be attributed to a shielding effect by the aromatic ring of the C-2 equatorial *p*-toluenesulfonamido group being in the position perpendicular to the acetyl methyl protons.[15,16a)] Whereas, the C-1 axial acetoxyl group resonates slightly up-shifted by *ca.* 0.10 ppm in the region of δ 2.05—2.10.[16)] These results are consistent with the structure of **32**, in which the presence of two equatorial acetoxyl groups at C-1 and C-3 may be supported by appearance of two up-shifted acetyl signals.

The *N*-(*p*-tolylsulfonyl) derivative (**37**) of validamine was prepared[17)] in order to see the shielding effect of the axially oriented *p*-toluenesulfonamido function. The ^1H NMR spectrum of **37** revealed the acetyl signals as two singlets at δ 1.79 and 2.00 in a ratio of 1:3, while, those of the peracetyl derivative (**38**)[9)]

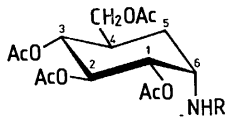

37 R = Ts
38 R = Ac

showed three singlets at δ 1.99, 2.01, and 2.03 in a ratio of 1:2:2. Therefore, the C-1 acetoxymethyl-signal seems to be shifted to higher field by at least 0.20 ppm due to the C-6 axail *p*-toluenesulfonamido group.

Experimental

Melting points were determined on a Büchi 510 capillary melting point apparatus and are uncorrected. Solutions were concentrated below 50 °C under reduced pressure. Catalytic hydrogenations were carried out in a Parr shaker type apparatus in the initial hydrogen pressure of 3.4 kg/cm² at ambient temperature. Unless otherwise noted, ^1H NMR spectra were taken on a Varian EM-390 (90 MHz) spectrometer in chloroform-*d* ($CDCl_3$) or dimethyl-d_6 sulfoxide (DMSO-d_6) with reference to tetramethylsilane as an internal standard. The peak positions are given in terms of δ-values and values given for coupling constants are of first-order. TLC was performed on precoated silica gel 60 F-254 plaques (Merck, Darmstadt; 0.25 mm thickness). The silica gel used for a column chromatography was Wakogel C-300 (Wako Pure Chemical Industries, Ltd.).

DL-*Di-O-acetyl-(1,3/2,4,6)-3,4-dibromo-6-benzoyloxymethyl-1,2-cyclohexanediol (2).* A mixture of DL-di-*O*-acetyl-(1,3/2,4,6)-3,4-dibromo-6-bromomethyl-1,2-cyclohexanediol (**1**, 2 g),[4)] sodium benzoate (2.56 g, 4 molar equivalent), and 80% aqueous ethanol (50 ml) was refluxed for 2 d. The reaction mixture was allowed to stand in a refrigerator overnight, and the resulting crystals were collected by filtration. Recrystallization from ethanol gave **2** (1.44 g, 66%) as colorless plates: mp 154—155 °C. ^1H NMR ($CDCl_3$, 60 MHz)[18)] δ 1.96 (3H, s) and 2.03 (3H, s) (OAc), 3.80—4.30 (4H, m, H-3, H-4, and $C\underline{H}_2OBz$), 4.70—5.35 (2H, m, H-1 and H-2), 7.05—7.90 (5H, m, phenyl).

Found: C, 44.00; H, 4.15; Br, 32.52%. Calcd for $C_{18}H_{20}Br_6$: C, 43.93; H, 4.10; Br, 32.47%.

DL-*Di-O-acetyl-(1,3/2)-3-bromomethyl-5-cyclohexene-1,2-diol (3).* To a solution of **1** (10 g) in acetic acid (70 ml) was added zinc dust (5.76 g) in three portions at 70 °C. The reaction mixture was stirred vigorously at 70 °C for 10 min and then cooled immediately, and the white precipitates and an excess of zinc dust were removed by filtration. The filtrate was concentrated to give a sirup which crystallized from ethanol–water to give **3** (5.96 g, 92%) as plates: mp 83—84 °C. ^1H NMR ($CDCl_3$) δ 2.01 (3H, s) and 2.03 (3H, s) (OAc), 3.19—3.52 (2H, m, $C\underline{H}_2Br$), 5.02 (1H, td, J=3, 7.5, and 7.5 Hz, H-2), 5.29—5.53 (2H, m, H-1 and H-5), 5.63—5.91 (1H, broad d, J=*ca.* 11 Hz, H-6).

Found: C, 45.16; H, 5.04; Br, 27.70%. Calcd for $C_{11}H_{15}BrO_4$: C, 45.37; H, 5.20; Br, 27.44%.

DL-*Di-O-acetyl-(1,3/2)-3-benzoyloxymethyl-5-cyclohexene-1,2-diol (4).* *a)* A stirred suspension of **2** (1 g) and zinc dust (0.53 g) in acetic acid (10 ml) was heated at 70 °C for 0.5 h. After cooling, the reaction mixture was processed as described for the preparation of **3**. The crystalline product was recrystallized from ethanol to give **4** (0.47 g, 70%)

as prisms: mp 75—76.5 °C. ^{1}H NMR ($CDCl_3$) δ 2.02 (6H, s, two OAc), 4.22 (1H, dd, J=5.3 and 12 Hz, H-7), 4.40 (1H, dd, J=4.2 and 12 Hz, H-7'), 5.25 (1H, dd, J=7.7 and 10.5 Hz, H-2), 5.40—5.66 (2H, m, H-1 and H-5), 5.69—5.99 (1H, broad d, J=*ca.* 11 Hz, H-6), 7.34—7.60 (2H, m) and 7.93—8.12 (2H, m) (phenyl).

Found: C, 64.82; H, 6.09%. Calcd for $C_{18}H_{20}O_6$: C, 65.05; H, 6.07%.

b) A mixture of **3** (1.5 g) and sodium benzoate (1.5 g, 2 molar equivalent) in 80% aqueous 2-methoxyethanol (30 ml) was refluxed for 5 h. Then the mixture was concentrated to dryness and the residue was treated with acetic anhydride (10 ml) and pyridine (10 ml) at amibient temperature overnight. An insoluble material was removed by filtration and the filtrate was concentrated. The residue was dissolved in chloroform (20 ml) and passed through a short column of alumina. The filtrate and washings were combined and concentrated. Recrystallization of the residue from ethanol–hexane gave **4** (1.15 g, 67%) as prisms: mp 75—76 °C. This compound was identical with the compound obtained from **2**.

*Oxidation of **3** with Osmium Tetroxide.* *a)* To a solution of **3** (4.37 g) in *t*-butyl alcohol (75 ml) and 35% hydrogen peroxide (15 ml) was added a solution of osmium tetroxide (0.16 g) in *t*-butyl alcohol (15 ml), and the mixture was kept at 30 °C for 24 h under dark. At that time, TLC indicated the disappearance of **3** and the formation of three components (R_f 0.45, 0.38, and 0.34) in 1:1 2-butanone–toluene. The reaction mixture was concentrated and the residue was treated with acetic anhydride and pyridine in usual way. Evaporation of the excess reagent gave a sirup, which was crystallized from ethanol to give DL-tetra-*O*-acetyl-(1,2,4/3,5)-5-bromomethyl-1,2,3,4-cyclohexanetetrol (**6**, 2.24 g, 36.5%). Recrystallization from ethanol gave an analytical sample: mp 137—138 °C. ^{1}H NMR ($CDCl_3$) δ 1.98 (3H, s), 2.00 (3H, s), 2.06 (3H, s), and 2.12 (3H, s) (OAc), 3.34 (2H, d, J=4.5 Hz, C$\underline{H}_2$Br), 4.87 (1H, dd, J=3.5 and 10.5 Hz, H-2), 4.94 (1H, t, J=10.5 Hz, H-4), 5.23 (1H, t, J=10.5 Hz, H-3), 5.39 (1H, q, J=3.5 Hz, H-1).

Found: C, 43.79; H, 5.18; Br, 19.74%. Calcd for $C_{15}H_{21}BrO_8$: C, 44.02; H, 5.17; Br, 19.53%.

The mother liquor from **6** was concentrated and the sirupy residue (2.3 g) was chromatographed on a silica-gel column (40 g) with 1:6 2-butanone–toluene as an eluent. The fractions containing the faster moving component were collected and concentrated to give DL-*trans*-2,4-diacetoxy-5-bromomethyl-2-cyclohexenone (**5**, 0.34 g, 7.5%) as a chromatographically homogeneous sirup. ^{1}H NMR ($CDCl_3$, 60 MHz)[18] δ 2.15 (3H, s) and 2.22 (3H, s) (OAc), 2.72 (2H, broad d, J=2.5 Hz, ring methylene), 3.50 (2H, broad d, J=2.5 Hz, C$\underline{H}_2$Br), 5.70 (1H, symmetric m, H-4), 6.47 (1H, d, J=2.5 Hz, H-3).

Found: C, 43.14; H, 4.50; Br, 26.34%. Calcd for $C_{11}H_{13}BrO_5$: C, 43.30; H, 4.29; Br, 26.19%.

b) To a mixture of **3** (4 g), 35% hydrogen peroxide (15 ml), and *t*-butyl alcohol (75 ml) was added a solution of osmium tetroxide (0.2 g) in *t*-butyl alcohol (40 ml) and the reaction mixture was stirred at 25 °C overnight. The mixture was processed similarly as described in *a)* and the product directly crystallized from ethanol to give **6** (2.6 g, 46%) as prisms: mp 137—138 °C.

DL-*Penta*-O-*acetyl*-*(1,2,4/3,5)*-*5*-*hydroxymethyl*-*1,2,3,4*-*cyclohexanetetrol* (**7**). A mixture of **6** (0.82 g), anhydrous sodium acetate (0.49 g), and 90% aqueous 2-methoxyethanol (20 ml) was refluxed for 20 h. The reaction mixture was concentrated and the residue was treated with acetic anhydride and pyridine in the usual way. The reaction mixture was filtered and the filtrate was concentrated. The residue was triturated with chloroform and the suspension was passed through a short column of alumina. The filtrate was concentrated and the residue was crystallized from ethanol–ether to give **7** (0.32 h, 42%) as needles mp 110—111 °C. ^{1}H NMR ($CDCl_3$) δ 1.99 (3H, s) 2.00 (3H, s), 2.03 (3H, s), 2.05 (3H, s), and 2.13 (3H, s) (OAc), 3.86 (1H, dd, J=3.5 and 11 Hz, H-7), 4.11 (1H, dd, J=4.5 and 11 Hz, H-7'), 4.89 (1H, dd, J=3 and 10.5 Hz, H-2), 4.99 (1H, dd, J=9 and 10.5 Hz, H-4), 5.39 (1H, t, J=10.5 Hz, H-3), 5.41 (1H, q, J=3 Hz, H-1).

Found C, 52.65; H, 6.18%. Calcd for $C_{17}H_{24}O_{10}$: C, 52.57; H, 6.23%.

DL-*Tetra*-O-*acetyl*-*(1,2,4/3,5)*-*5*-*azidomethyl*-*1,2,3,4*-*cyclohexanetetrol* (**8**). A mixture of **6** (0.82 g), sodium azide (0.78 g), and 90% aqueous 2-methoxyethanol (20 ml) was refluxed for 20 h. The reaction mixture was concentrated and the residue was treated with acetic anhydride and pyridine in usual way. The reaction mixture was processed as described for the preparation of **7** to give crystals which were recrystallized from ethanol–ether to give **8** (0.55 g, 74%) as prisms: mp 85—86 °C. ^{1}H NMR ($CDCl_3$, 60 MHz)[18] δ 2.00 (6H, s), 2.07 (3H, s), and 2.13 (3H, s) (OAc), 3.27—3.35 (2H, m, CH_2N_3), 4.85 (1H, dd, J=3 and 9.5 Hz, H-2), 4.92 (1H, broad t, J=9.5 Hz, H-4), 5.38 (1H, broad t, J=9.5 Hz, H-3), 5.45 (1H, q, J=3 Hz, H-1).

Found: C, 48.77; H, 5.81; N, 11.53%. Calcd for $C_{15}H_{21}N_3O_8$: C, 48.52; H, 5.70; N, 11.32%.

DL-*Tetra*-O-*acetyl*-*(1,2,4/3,5)*-*5*-*acetamidomethyl*-*1,2,3,4*-*cyclohexanetetrol* (**9**). A solution of **8** (0.3 g) in ethanol (10 ml) containing acetic anhydride (0.4 ml) was hydrogenated in the presence of Raney nickel T-4[8] overnight. The catalyst was removed by filtration and the filtrate was concentrated. The product was purified by passage through a short column of alumina with chloroform. The filtrate was concentrated and the residue was crystallized from ethanol–ether to give **9** (0.10 g, 31%) as needles: mp 150—151 °C. ^{1}H NMR ($CDCl_3$, 60 MHz)[18] δ 1.99 (9H, s) and 2.08 (6H, s) (NAc and OAc), 3.33—3.95 (2H, m, C$\underline{H}_2$NHAc), 4.78 (1H, broad t, J=9.5 Hz, H-4), 4.84 (1H, dd, J=3 and 9.5 Hz, H-2), 5.33 (1H, q, J=3 Hz, H-1), 5.40 (1H, broad t, J=9.5 Hz, H-3), 6.07 (1H, t, J=5.5 Hz, N$\underline{H}$).

Found: C, 52.87; H, 6.49; N, 3.65%. Calcd for $C_{17}H_{25}NO_9$: C, 52.71; H, 6.51; N, 3.62%.

DL-*Tetra*-O-*acetyl*-*(1,2,4/3,5)*-*5*-*methyl*-*1,2,3,4*-*cyclohexanetetrol* (**10**). A solution of **6** (0.8 g) in ethyl acetate (10 ml) was hydrogenated in the presence of Raney nickel T-4 (one spoonful) and Amberlite IR-45 (OH^-) (5 ml) overnight. The catalyst and the resin were removed by filtration and the filtrate was concentrated. The residue was crystallized from ethanol to give **10** (0.45 g, 70%) as plates: mp 137—138 °C. ^{1}H NMR ($CDCl_3$) δ 0.93 (3H, d, J=6 Hz, methyl), 1.98 (6H, s), 2.03 (3H, s), and 2.10 (3H, s) (OAc), 4.71 (1H, t, J=10.5 Hz, H-4), 4.87 (1H, dd, J=3 and 10.5 Hz, H-2), 5.30 (1H, t, J=10.5 Hz, H-3), 5.31 (1H, q, J=3 Hz H-1).

Found: C 54.82; H, 6.69%. Calcd for $C_{15}H_{22}O_8$: C, 54.54: H, 6.71%.

DL-*Tetra*-O-*acetyl*-*(1,3,5/2,4)*-*5*-*bromomethyl*-*1,2,3,4*-*cyclohexanetetrol* (**12**). A mixture of DL-penta-*O*-acetyl-(1,3,5/2,4)-5-hydroxymethyl-1,2,3,4-cyclohexanetetrol (**11**, 1.0 g)[9] and 10% hydrogen bromide in acetic acid (4.5 ml) was heated in a sealed tube at 80 °C for 16 h. The reaction mixture was poured into ice–water (40 ml) and the precipitates were collected by filtration. Recrystallization from ethanol gave **12** (0.88 g, 83%) as plates: mp 128—129.5 °C. ^{1}H NMR ($CDCl_3$, 60 MHz)[18] δ 1.98 (3H, s), 2.00 (3H,

s), 2.03 (3H, s), and 2.06 (3H, s) (OAc), 3.38 (1H, broad d, J=4 Hz, C$\underline{H}_2$Br), 4.8—5.2 (4H, m, H-1, H-2, H-3, and H-4).

Found: C, 44.20; H, 5.19; Br, 19.67%. Calcd for $C_{15}H_{21}BrO_8$: C, 44.03; H, 5.17; Br, 19.52%.

DL-*Tetra*-O-*acetyl*-*(1,3,5/2,4)*-*5*-*azidomethyl*-*1,2,3,4*-*cyclohexanatetrol* (**13**). A mixture of **12** (0.2 g), sodium azide (0.06 g), and 90% aqueous *N,N*-dimethylformamide (DMF) (5 ml) was stirred at 80 °C for 7 h. The reaction mixture was concentrated and the residue was processed as described for the preparation of **8**. The crude product was recrystallized from ethanol to give **13** (0.16 g, 85%) as prisms: mp 101—102 °C. ^{1}H NMR ($CDCl_3$) δ 1.97 (3H, s), 1.99 (3H, s), 2.02 (3H, s), and 2.03 (3H, s) (OAc), 3.22 (1H, dd, J=6 and 13 Hz, H-7), 3.39 (1H, dd, J=5 and 13 Hz, H-7′), 4.67—5.20 (4H m, H-1, H-2, H-3, and H-4).

Found: C, 48.61; H, 5.71; N, 11.28%. Calcd for $C_{15}H_{21}N_3O_8$: C, 48.52; H, 5.70; N, 11.32%.

DL-*Tetra*-O-*acetyl*-*(1,3,5/2,4)*-*5*-*acetamidomethyl*-*1,2,3,4*-*cyclohexanetetrol* (**14**). A solution of **13** (0.10 g) in ethanol (20 ml) was hydrogenated in the presence of Raney nickel T-4 (one spoonful) overnight. The catalyst was removed by filtration and the filtrate was concentrated. The residue was acetylated in the usual way. The product was crystallized from ethanol to give **14** (60 mg, 58%) as needles: mp 210—211 °C. ^{1}H NMR ($CDCl_3$) δ 1.97 (12H, s) and 2.06 (3H, s) (NAc and OAc), 2.75 (1H, td, J=5, 5, and 14 Hz, H-7, changes to a doublet of doublets with 5 and 14 Hz splittings on deuteration), 3.69 (1H, ddd, J=3, 8, and 14 Hz, H-7′, changes to a doublet of doublets with 3 and 14 Hz splittings on deuteration), 4.63—5.16 (4H, m, H-1, H-2, H-3, and H-4), 5.99 (1H, broad dd, J=5 and 8 Hz, N$\underline{H}$, disappears on deuteration).

Found: C, 52.80; H, 6.46; N, 3.50%. Calcd for $C_{17}H_{25}NO_9$: C, 52.71; H, 6.51; N, 3.62%.

DL-*Tetra*-O-*acetyl*-*(1,3,5/2,4)*-*5*-*methyl*-*1,2,3,4*-*cyclohexanetetrol* (**15**). A solution of **12** (0.2 g) in ethyl acetate (15 ml) was hydrogenated as described for the preparation of **10**. The product was recrystallized from ethanol to give **15** (0.13 g, 82%) as prisms: mp 110—111 °C. ^{1}H NMR ($CDCl_3$) δ 0.94 (3H, d, J=6 Hz, methyl), 1.12—2.02 (3H, m, H-5, H-6, and H-6′), 1.97 (3H, s), 1.98 (3H, s), 2.00 (3H, s), and 2.02 (3H, s) (OAc), 4.59—5.17 (4H, m, H-1, H-2, H-3, and H-4).

Found: C, 54.41; H, 6.69%. Calcd for $C_{15}H_{22}O_8$: C, 54.54; H, 6.71%.

DL-*3,4-Di*-O-*acetyl*-*(1,2,4/3,5)*-*2*-*(*p-*toluenesulfonamido)*-*5*-*bromomethyl*-*1,3,4*-*cyclohexanetriol* (**16**). To a solution of **3** (1.5 g, 5.2 mmol) in chloroform (25 ml) was added a solution of osmium tetroxide in *t*-butyl alcohol (2.6 ml, 0.052 mmol), chloramine T (trihydrate) (1.82 g), triethylbenzylammonium chloride (0.06 g), and water (25 ml). The mixture was stirred at 60 °C for 40 h. At that time, TLC indicated the formation of the major (R_f 0.64) and three minor components (R_f 0.60, 0.49, and 0.45), together with a trace of **3** (R_f 0.85) in 1:8 ethanol–toluene. Sodium hydrogensulfite (1.5 g) was added to the mixture and it was refluxed for 5 h. Chloroform (50 ml) was added to the cooled mixture, and the organic layer was separated, washed successively with 1% aqueous sodium hydroxide and brine, and dried over anhydrous sodium sulfate. Evaporation of the solvent gave a sirup from which the major product was crystallized out on addition of ethanol. Recrystallization from ethanol gave **16** (0.76 g, 31%) as prisms: mp 196—197 °C. ^{1}H NMR ($CDCl_3$) δ 1.62 (3H, s) and 2.00 (3H, s) (OAc), 2.42 (3H, s, tosyl methyl), 3.01 (1H, d, J=4 Hz, O$\underline{H}$, disappears on deuteration), 3.18—3.51 (1H, m, H-2), 3.32 (2H, d, J=4 Hz, C$\underline{H}_2$Br), 4.07—4.26 (1H, m, H-1), 4.86 (1H, J=10 Hz, H-4), 5.09 (1H, t, J=10 Hz, H-3), 5.62 (1H, d, J=8 Hz, N$\underline{H}$, disappears on deuteration), 7.28 (2H, d) and 7.75 (2H, d) (J=9 Hz, phenyl).

Found: C, 44.94; H, 5.04; N, 2.78%. Calcd for $C_{18}H_{24}BrNO_7S$: C, 45.20; H, 5.06; N, 2.93%.

Acetylation of **16** (0.1 g) in the usual way gave the triacetate (**17**), which was recrystallized from ethanol to give an analytical sample (0.07 g, 66%) as prisms: mp 192—193 °C. ^{1}H NMR ($CDCl_3$) δ 1.76 (3H, s), 1.99 (3H, s), and 2.06 (3H, s) (OAc), 2.40 (3H, s, tosyl methyl), 3.29 (2H, d, J=3 Hz, C$\underline{H}_2$Br), 3.49 (1H, ddd, J=3, 9, and 11 Hz, H-2, changes to a doublet of doublets with 3 and 11 Hz splittings on deuteration), 4.88 (1H, t, J=11 Hz, H-4), 5.09 (1H, t, J=11 Hz, H-3), 7.42 (2H, d) and 7.69 (2H, d) (J=9 Hz, phenyl).

Found: C, 45.96; H, 5.07; N, 2.46%. Calcd for $C_{20}H_{26}BrNO_8S$: C, 46.16; H, 5.04; N, 2.69%.

DL-*3,4-Di*-O-*acetyl*-*(1,2,4/3,5)*-*5*-*benzoyloxymethyl*-*2*-*(*p-*toluenesulfonamido)*-*1,3,4*-*cyclohexanetriol* (**18**). To a solution of **4** (2 g, 6 mmol) in chloroform (30 ml) was added a solution of osmium tetroxide in *t*-butyl alcohol (4.5 ml, 0.09 mmol), chloramine T (trihydrate) (2.1 g), benzyltriethylammonium chloride (0.07 g), and water (30 ml), and the mixture was heated at 60 °C under stirring for 2 d. At that time, TLC indicated the formation of one major (R_f 0.45) and one minor products (R_f 0.28), together with **4** (R_f 0.75) in 1:10 ethanol–toluene. The reaction mixture was processed as described for the preparation of **16**. The crude product was purified by passage through a short column of caoline and silica gel with chloroform. Recrystallization from toluene gave **18** (0.93 g, 30%) as prisms: mp 150—152 °C. ^{1}H NMR ($CDCl_3$) δ 1.64 (3H, s), 1.97 (3H, s) (OAc), 2.38 (3H, s, tosyl methyl), 3.41 (1H, dd, J=2.5 and 10 Hz, H-2), 4.99 (1H, t, J=9 Hz, H-4), 5.17 (1H, t, J=9 Hz, H-3), 5.85 (1H d J=9 Hz N$\underline{H}$), 7.18—8.13 (9H, m, phenyl).

Found: C, 57.74; H, 5.70; N, 2.55; S, 6.15%. Calcd for $C_{25}H_{29}NO_9S$: C, 57.79; H, 5.63; N, 2.70; S, 6.17%.

Compound **18** was converted into the triacetate (**19**) by the conventional manner. An analytical sample was obtained by recrystallization from ethanol: mp 200—201 °C. ^{1}H NMR ($CDCl_3$) δ 1.78 (3H, s), 1.98 (3H, s), and 2.10 (3H, s) (OAc), 2.40 (3H, s, tosyl methyl), 3.55 (1H, td, J=5, 9, and 9 Hz, H-2), 4.23 (2H, d, J=4 Hz, C$\underline{H}_2$OBz), 4.91—5.20 (3H, m, H-1, H-3, and H-4), 5.28 (1H, d, J=9 Hz, N$\underline{H}$), 7.13—8.13 (9H, m, phenyl).

Found: C, 57.46; H, 5.57; N, 2.36; S, 5.50%. Calcd for $C_{27}H_{31}NO_{10}S$: C, 57.74; H, 5.56; N, 2.49; S, 5.71%.

DL-*3,4,7-Tri*-O-*acetyl*-*(1,2,4/3,5)*-*5*-*hydroxymethyl*-*2*-*(*p-*toluenesulfonamido)*-*1,3,4*-*cyclohexanetriol* (**20**). A mixture of **16** (0.2 g), anhydrous sodium acetate (0.086 g), and DMF (5 ml) was heated at 80 °C for 3 d. The reaction mixture was concentrated and the residue was extracted with hot ethyl acetate (20 ml) and the extracts were washed with water. The solution was dried and concentrated to give crystals which were recrystallized from ethanol to give **20** (0.11 g, 57%) as prisms: mp 174—175 °C. ^{1}H NMR ($CDCl_3$) δ 1.60 (3H, s), 1.97 (3H, s), and 2.02 (3H, s) (OAc), 2.39 (3H, s, tosyl methyl), 3.32 (1H, td, J=3, 9, and 9 Hz, H-2), 3.81 (1H, dd, J=3 and 11 Hz, H-7), 4.05 (1H, dd, J=5 and 11 Hz, H-7′), 4.81 (1H, t, J=10 Hz, H-4), 5.03 (1H, t, J=10 Hz, H-3), 5.64 (1H, d, J=8 Hz, N$\underline{H}$), 7.23 (2H, d) and 7.68 (2H, d) (J=9 Hz, phenyl).

Found: C, 52.23; H, 5.92; N, 3.01; S, 6.76%. Calcd for $C_{20}H_{27}NO_9S$: C, 52.51; H, 5.95; N, 3.06; S, 7.01%.

Compound **20** (75 mg) was converted into the tetraacetate (**21**) by the conventional manner. The product was crystallized from ethanol to give an analytical sample (73 mg, 90%) as prisms: mp 173.5—174.5 °C. ^{1}H NMR ($CDCl_3$) δ 1.72 (3H, s), 1.97 (3H, s), 2.01 (3H, s), and 2.05 (3H, s) (OAc), 2.37 (3H, s, tosyl methyl), 3.47 (1H, dd, J= 3.2 and 10.5 Hz, H-2, on deuteration), 3.73 (1H, dd, J= 3.3 and 11.7 Hz, H-7), 4.02 (1H, dd, J=4.5 and 11.7 Hz, H-7′), 4.65—5.25 (3H, m, H-1, H-3, and H-4), 5.29 (1H, d, J=9 Hz, NH, disappears on deuteration), 7.22 (2H, d) and 7.67 (2H, d) (J=9 Hz, phenyl).

Found: C, 52.61; H, 5.76; N, 2.78; S, 6.53%. Calcd for $C_{22}H_{29}NO_{10}S$: C, 52.90; H, 5.85; N, 2.80; S, 6.42%.

DL-*3,4-Di*-O-*acetyl*-*(1,2,4/3,5)*-5-*azidomethyl*-2-(p-*toluenesulfonamido*)-1,3,4-*cyclohexanetriol* (**22**). A mixture of **16** (0.5 g), sodium azide (0.56 g, 4 molar equiv.), and DMF (10 ml) was heated at 80 °C for 3 h under stirring. The reaction mixture was diluted with water (4 ml) and extracted with ethyl acetate (3×5 ml), and the extracts were washed with water and dried. Evaporation of the solvent gave a crystalline residue which was recrystallized from ethanol to give **22** (0.42 g, 90%) as prisms: mp 185—186 °C. ^{1}H NMR ($CDCl_3$) δ 1.61 (3H, s) and 2.01 (3H, s) (OAc), 2.41 (3H, s, tosyl methyl), 3.16—3.47 (3H, m, H-2 and CH_2N_3), 4.02—4.23 (1H, m, H-1), 4.80 (1H, dd, J=11 and 12 Hz, H-4), 5.04 (1H, t, J=11 Hz, H-3), 5.62 (1H, d, J=8 Hz, NH), 7.24 (2H, d) and 7.69 (2H, d) (J=9 Hz, phenyl).

Found: C, 49.10; H, 5.47; N, 12.46; S, 7.04%. Calcd for $C_{18}H_{24}N_4O_7S$: C, 49.08; H, 5.49; N, 12.72; S, 7.28%.

DL-*3,4-Di*-O-*acetyl*-*(1,2,4/3,5)*-5-*acetamidomethyl*-2-(p-*toluenesulfonamido*)-1,3,4-*cyclohexanetriol* (**23**). A solution of **22** (0.25 g) in methanol (15 ml) containing acetic anhydride (0.1 ml) was hydrogenated in the presence of Raney nickel T-4 for 3 d. The catalyst was removed by filtration and the filtrate was concentrated to give crystals which were recrystallized from methanol to give **23** (0.14 g, 57%) as prisms: mp 233.5—234 °C. ^{1}H NMR (DMSO-d_6) δ 1.65 (3H, s), 1.76 (3H, s), and 1.90 (3H, s) (NAc and OAc), 2.32 (3H, s, tosyl methyl), 2.8—3.1 (2H, broad s, CH_2NHAc, changes to a broad doublet with 5 Hz splitting on deuteration), 4.67 (1H, t, J=11 Hz, H-4), 4.91 (1H, t, J= 11 Hz, H-3), 7.32 (2H, d) and 7.67 (2H, d) (J=9 Hz, phenyl).

Found: C, 52.61; H, 6.14; N, 5.87; S, 7.15%. Calcd for $C_{20}H_{28}N_2O_8S$: C, 52.62; H, 6.18; N, 6.14; S, 7.02%.

Compound **23** was converted to triacetate (**24**) in the conventional method. An analytical sample was prepared by recrystallization from ethanol: mp 194—195 °C. ^{1}H NMR ($CDCl_3$) δ 1.83 (3H, s), 1.96 (3H, s), and 2.07 (6H, s) (NAc and OAc), 2.41 (3H, s, tosyl methyl), 2.77 (1H, td, J=5, 5, and 14 Hz, CH_2NHAc, changes to a doublet of doublets with 5 and 14 Hz splittings on deuteration), 3.45 (1H, dd, J=4 and 11 Hz, H-2, on deuteration), 3.62 (1H, dd, J=4 and 14 Hz, H-7′, on deuteration), 4.72 (1H, t, J=11 Hz, H-4), 5.10 (1H, t, J=11 Hz, H-3), 5.51 (1H, d, J=9 Hz, NHTs), 6.02 (1H, dd, J=5 and 8 Hz, NHAc), 7.23 (2H, d) and 7.65 (2H, d) (J=9 Hz, phenyl).

Found: C, 53.16; H, 6.05; N, 5.43; S, 6.13%. Calcd for $C_{22}H_{30}N_2O_9S$: C, 53.00; H, 6.07; N, 5.62; S, 6.43%.

DL-*3,4-Di*-O-*acetyl*-*(1,2,4/3,5)*-2-(p-*toluenesulfonamido*)-5-*methyl*-1,3,4-*cyclohexanetriol* (**25**). A solution of **16** (0.2 g) in ethyl acetate (15 ml) was hydrogenated in the presence of Raney nickel T-4 (one spoonful) and Amberlite IR-45 (OH^-) (3 ml) overnight. The reaction mixture was processed in the usual way. The product was crystallized from ethanol to give **25** (0.14 g, 82%) as plates: mp 179.5—180 °C. ^{1}H NMR ($CDCl_3$) δ 0.88 (3H, d, J=6 Hz, methyl), 1.60 (3H, s) and 1.97 (3H, s) (OAc), 2.39 (3H, s, tosyl methyl), 3.27 (1H, broad d, H-2, changes to a doublet of doublets with 3 and 10 Hz splittings on deuteration), 3.49—4.10 (1H, m, H-1), 4.56 (1H, dd, J=9 and 10 Hz, H-4), 4.99 (1H, t, J=10 Hz, H-3), 5.34—5.80 (1H, m, NH), 7.24 (2H, d) and 7.69 (2H, d) (J=9 Hz, phenyl).

Found: C, 53.89; H, 6.24; N, 3.38; S, 7.78%. Calcd for $C_{18}H_{25}NO_7S$: C, 54.12; H, 6.31; N, 3.51; S, 8.03%.

DL-*3,4-Di*-O-*acetyl*-1-O-*methylsulfonyl*-*(1,2,4/3,5)*-5-*bromomethyl*-2-(p-*toluenesulfonamido*)-1,3,4-*cyclohexanetriol* (**26**). To a solution of **16** (1.0 g) in pyridine (10 ml) was added methanesulfonyl chloride (0.36 g) under ice cooling, and then the reaction mixture was stirred at ambient temperature overnight. The mixture was poured into ice-water (50 ml) and the crystals were collected and dried. Recrystallization from ethanol gave **26** (0.81 g, 69%) as needles: mp 187—188 °C. ^{1}H NMR ($CDCl_3$) δ 1.66 (3H, s) and 2.01 (3H, s) (OAc), 2.40 (3H, s, tosyl methyl), 3.17 (3H s mesyl methyl), 3.25—3.59 (3H, m, H-3 and CH_2Br), 4.71—5.03 (3H, m, H-1, H-2, and H-3), 5.68 (1H, d, J= 8 Hz, NH), 7.26 (2H, d) and 7.68 (2H, d) (J=9 Hz, phenyl).

Found: C, 41.27; H, 4.79; N, 2.61%. Calcd for $C_{19}H_{26}BrNO_9S_2$: C, 41.01; H, 4.71; N, 2.52%.

DL-*3,4-Di*-O-*acetyl*-1-O-*methylsulfonyl*-*(1,2,4/3,5)*-5-*azidomethyl*-2-(p-*toluenesulfonamido*)-1,3,4-*cyclohexanetriol* (**27**). A mixture of **26** (0.39 g), sodium azide (0.05 g, 1.5 molar equiv.), and DMF (10 ml) was stirred at 80 °C for 2 h. The reaction mixture was processed as described for the preparation of **8**. The product was crystallized from ethanol to give **27** (0.22 g, 68%) as plates: mp 173.5—174.5 °C. ^{1}H NMR ($CDCl_3$) δ 1.60 (3H, s) and 2.00 (3H, s) (OAc), 2.40 (3H, s, tosyl methyl), 3.15 (3H, s, mesyl methyl), 3.21—3.60 (3H, m, H-3 and CH_2N_3), 4.66—5.12 (3H, m, H-1, H-2, and H-4), 5.59 (1H, d, J=8 Hz, NH), 7.29 (2H, d) and 7.66 (2H, d) (J=8 Hz, phenyl).

Found: C, 43.85; H, 4.99; N, 10.52; S, 12.48%. Calcd for $C_{19}H_{26}N_4O_9S_2$: C, 44.01; H, 5.05; N, 10.80; S, 12.36%.

DL-*1,2-Di*-O-*acetyl*-*(1,3/2,4,6)*-4-*azido*-6-*azidomethyl*-3-(p-*toluenesulfonamido*)-1,2-*cyclohexanediol* (**28**). A mixture of **26** (0.4 g), sodium azide (0.24 g, 5 molar equivalent), and DMF (10 ml) was stirred at 85 °C for 20 h. The reaction mixture was processed as described for the preparation of **8**. The product was crystallized from ethanol to give **28** (0.24 g, 71%) as prisms: mp 130—131 °C. ^{1}H NMR ($CDCl_3$) δ 1.90 (3H, s) and 2.03 (3H, s) (OAc), 2.39 (3H, s, tosyl methyl), 3.00—3.65 (4H, m, H-3, H-4, and CH_2N_3), 4.85—4.95 (2H, m, H-1 and H-2), 5.41 (1H, d, J=9 Hz, NH), 7.24 (2H, d) and 7.73 (2H, d) (J=8 Hz, phenyl).

Found: C, 46.39; H, 4.95; N, 20.76; S, 6.69%. Calcd for $C_{18}H_{23}N_7O_6S$: C, 46.45; H, 4.98; N, 21.06; S, 6.89%.

DL-*3,4-Di*-O-*acetyl*-1-O-*methylsulfonyl*-*(1,2,4/3,5)*-5-*acetamidomethyl*-2-(p-*toluenesulfonamido*)-1,3,4-*cyclohexanetriol* (**29**). A solution of **27** (0.18 g) in methanol (15 ml) containing acetic anhydride (0.11 ml) was hydrogenated in the presence of Raney nickel T-4 overnight. The product was recrystallized from ethanol to give **29** (0.12 g, 65%) as powder: mp 215—215.5 °C. ^{1}H NMR (DMSO-d_6) δ 1.55 (3H, s), 1.76 (3H, s), and 1.89 (3H, s) (NAc and OAc), 2.38 (3H, s, tosyl methyl), 2.85—3.10 (2H, m, CH_2NHAc), 3.16 (3H, s, mesyl ethyl), 3.59—3.88 (1H, m, H-3), 4.55—5.00 (3H, m, H-1, H-2, and H-4), 7.33 (2H, d) and 7.68 (2H, d) (J= 8 Hz, phenyl), 8.20 (1H, broad s, NH).

Found: C, 46.98; H, 5.63; N, 4.97; S, 11.68%. Calcd for $C_{21}H_{30}N_2O_{10}S_2$: C, 47.18; H, 5.66; N, 5.42; S, 11.99%.

DL-*1,2-Di*-O-*acetyl*-*(1,3/2,4,6)*-4-*acetamido*-6-*acetamidomethyl*-3-(p-*toluenesulfonamido*)-1,2-*cyclohexanediol* (**30**). A solution of **28** (42 mg) in methanol (5 ml) containing acetic

anhydride (0.05 ml) was hydrogenated in the presence of Raney nickel T-4 overnight. At that time, TLC indicated the disappearance of **28** and the formation of a major product along with a minor product. The mixture was fractionated on a silica-gel column with 1:3 ethanol–toluene. The fractions containing the minor product were concentrated to give DL-1,2-di-*O*-acetyl-(1,3/2,6)-3-acetamidomethyl-6-(*p*-toluensulfonamido)-1,2-cyclohexanediol (**31**, 7 mg, 18%) as powder: mp 227.5—228.5 °C. ^{1}H NMR ($CDCl_3$ and D_2O) δ 1.76 (3H, s), 1.97 (3H, s), and 2.03 (3H, s) (NAc and OAc), 2.40 (3H, s, tosyl methyl), 2.72 (1H, dd, J=4 and 14 Hz, H-7), 3.23 (1H, broad dt, J=3, 3, and ca. 9 Hz, H-6), 3.62 (1H, dd, J=3 and 14 Hz, H-7′), 4.52—4.78 (2H, m, H-1 and H-2), 7.25 (2H, d) and 7.67 (2H, d) (J=8 Hz, phenyl).

Found: C, 54.23; H, 6.16; N, 6.05%. Calcd for $C_{20}H_{28}N_2O_7S$: C, 54.53; H, 6.41; N, 6.36%.

The fractions containing the major product gave **30** (29 mg, 66%) as a homogeneous sirup, which solidified on standing. Attempts to crystallize it from several solvents failed. ^{1}H NMR ($CDCl_3$ and D_2O) δ 1.49 (3H, s), 1.87 (3H, s), 1.96 (3H, s) (NAc and OAc), 2.38 (3H, s, tosyl methyl), 2.83 (1H, dd, J=6 and 14 Hz, H-7), 3.32 (1H, dd, J=9 and 11 Hz, H-3), 3.50 (1H, dd, J=3 and 14 Hz, H-7′), 3.90 (1H, ddd, J=4, 11, and 12 Hz, H-4), 4.67 (1H, t, J=9 Hz, H-1), 4.92 (1H, t, J=9 Hz, H-2), 7.22 (2H, d) and 7.67 (2H, d) (J=8 Hz, phenyl).

Found: C, 52.77; H, 6.13; N, 8.13%. Calcd for $C_{22}H_{31}N_3O_8S$: C, 53.12; H, 6.28; N, 8.45%.

*Reaction of **26** with Sodium Acetate.* A mixture of **26** (0.2 g) and anhydrous sodium acetate (0.12 g, 4 molar equiv.) in DMF (5 ml) was stirred at 80 °C for 20 h. At that time, **26** still remained in the mixture. Then the mixture was further heated at 80 °C overnight with addition of sodium acetate (0.06 g, 2 molar equivalent). The reaction mixture was processed as described for the preparation of **27**. The products were fractionated by a silica-gel column with 1:4 2-butanone–toluene. The fractions containing the faster-moving component (R_f 0.48) were concentrated to give DL-1,2-di-*O*-acetyl-(1/2,6)-3-methylene-6-(*p*-toluenesulfonamido)-4-cyclohexene-1,2-diol (**35**, 10 mg, 7%) as crystals: mp 129—130 °C. ^{1}H NMR ($CDCl_3$ and D_2O) δ 1.77 (3H, s) and 2.05 (3H, s) (OAc), 2.40 (3H, s, tosyl methyl), 4.06 (1H broad d, J=8 Hz, H-1), 4.86 (1H, broad d, J=8 Hz, H-1), 4.96 (1H, broad s, H-7), 5.06 (1H, broad s, H-7′), 5.46 (1H, broad d, J=*ca.* 10 Hz, H-5), 5.56 (1H, broad d, J=8 Hz, H-2), 7.23 (2H, d) and 7.68 (2H, d) (J=9 Hz, phenyl).

Found: C, 56.65; H, 5.48; N, 3.48%. Calcd for $C_{18}H_{21}NO_6S$: C, 56.98; H, 5.58; N, 3.69%.

The second fractions (R_f 0.24) gave crystals of DL-1,2,7-tri-*O*-acetyl-(1,3/2,6)-3-hydroxymethyl-6-(*p*-toluenesulfonamido)-4-cyclohexene-1,2-diol (**33**, 44 mg, 28%): mp 156—157 °C. ^{1}H NMR ($CDCl_3$ and D_2O) δ 1.74 (3H, s), 1.99 (3H, s), and 2.02 (3H, s) (OAc), 2.41 (3H, s, tosyl methyl), 3.88 (1H, dd, J=7 and 12 Hz, H-7), 4.06 (1H, dd, J=5 and 12 Hz, H-7′), 4.78—5.28 (3H, m, H-1 and H-2), 5.50 (2H, s, H-4 and H-5), 7.23 (2H, d) and 7.68 (2H, d) (J=8 Hz, phenyl).

Found: C, 54.60; H, 5.72; N, 3.21%. Calcd for $C_{20}H_{25}NO_8S$: C, 54.66; H, 5.73; N, 3.19%.

The third fractions gave DL-tetra-*O*-acetyl-(1,3,5/2,4)-5-hydroxymethyl-2-(*p*-toluenesulfonamido)-1,3,4-cyclohexanetriol (**32**, 15 mg, 10%) as crystals: mp 137—138 °C. Recrystallization from ethanol gave an analytical sample. ^{1}H NMR ($CDCl_3$ and D_2O) δ 1.71 (3H, s), 1.79 (3H, s), 1.97 (3H, s), and 2.03 (3H, s) (OAc), 2.37 (3H, s, tosyl methyl), 3.65 (1H, t, J=10 Hz, H-2), 3.85 (1H, dd, J=2 and 11 Hz, H-7), 4.02 (1H, dd, J=4 and 11 Hz, H-7′), 4.6—5.0 (3H, m, H-1, H-2, and H-4), 7.22 (2H, d) and 7.67 (2H, d) (J=9 Hz, phenyl).

Found: C, 52.70; H, 5.76; N, 2.75%. Calcd for $C_{22}H_{29}NO_{10}S$: C, 52.90; H, 5.85; N, 2.80%.

*Reaction of **29** with Sodium Acetate.* A mixture of **29** (0.12 g), anhydrous sodium acetate (0.055 g, 3 molar equivalent), and DMF (5 ml) was stirred at 80 °C for 2 d. The reaction mixture was concentrated and the residue was taken up in chloroform and filtered. The filtrate was concentrated and the residual product was fractionated on a silica-gel column with 1:4 ethanol–toluene as an eluent. The fractions containing the major product gave crystals of DL-1,2-di-*O*-acetyl-(1,3/2,6)-3-acetamidomethyl-6-(*p*-toluenesulfonamido)-4-cyclohexene-1,2-diol (**34**). Recrystallization from ethanol–ether gave an analytical sample (58 mg, 59%): mp 193.5—194.5 °C. ^{1}H NMR ($CDCl_3$ and D_2O) δ 1.78 (3H, s), 1.92 (3H, s), and 2.02 (3H, s) (NAc and OAc), 2.38 (3H, s, tosyl methyl), 2.90 (1H, dd, J=5 and 14 Hz, H-7), 3.64 (1H, dd, J=4 and 14 Hz, H-7′), 3.99 (1H, broad d, J=8 Hz, H-6), 4.65—5.10 (2H, m, H-1 and H-2), 5.34 (1H, td, J=2, 2, and 12 Hz, H-4), 5.57 (1H, td, J=2, 2, and 12 Hz, H-5), 7.26 (2H, d) and 7.67 (2H, d) (J=8 Hz, phenyl).

Found: C, 54.51; H, 5.96; N, 6.19; S, 7.06%. Calcd for $C_{20}H_{26}N_2O_7S$: C, 54.78; H, 5.98; N, 6.39; S, 7.31%.

*DL-1,3,4-Tri-O-acetyl-(1,2,4/3,5)-2-acetamido-5-bromomethyl-1,3,4-cyclohexanetriol (**36**).* Compound **16** (0.2 g) was heated with 20% hydrogen bromide in acetic acid (3.5 ml) in a sealed tube at 80 °C for 20 h. The mixture was poured into ice–water (50 ml) and, after overnight, the solution was extracted with chloroform (3×10 ml). The extracts were dried and concentrated to give *p*-toluenesulfonic acid (77 mg). The aqueous layer was concentrated to dryness and the residue was treated with acetic anhydride and pyridine in usual way. The product was purified by passage through a short column of alumina with chloroform. Recrystallization from ethanol–ether gave **36** (124 mg, 69%) as needles: mp 177—178 °C. ^{1}H NMR ($CDCl_3$) δ 1.96 (3H, s), 1.98 (3H, s), 2.05 (3H, s), and 2.18 (3H, s) (NAc and OAc), 3.37 (2H, d, J=4.5 Hz, C$\underline{H}_2$Br), 4.21 (1H, td, J=3, 9, and 9 Hz, H-2), 4.82—5.30 (3H, m, H-1, H-3, and H-4), 6.23 (1H, d, J=9 Hz, N$\underline{H}$).

Found: C, 43.94; H, 5.30; N, 3.37; Br, 19.69%. Calcd for $C_{15}H_{22}BrNO_7$: C, 44.13; H, 5.43; N, 3.43; Br, 19.57%.

The authors wish to express their thanks to Mr. Saburo Nakada for elemental analyses.

References

1) The nomenclature is based on the IUPAC-IUB Tentative Cyclitol Nomenclature Rule [*J. Biol. Chem.*, **22**, 5809 (1968)]. Alternatively, according to the proposal of McCasland,[3] 5-hydroxymethyl-1,2,3,4-cyclohexanetetrols are named as pseudo-hexopyranoses. For convenience, all the formulas depict one of the respective enantiomers.

2) For paper VI of this series, see S. Ogawa, M. Ara, T. Kondoh, M. Saitoh, R. Masuda, T. Toyokuni, and T. Suami, *Bull. Chem. Soc. Jpn.*, **53**, 1121 (1980).

3) G. E. McCasland and S. Furuta, *J. Org. Chem.*, **31**, 1516 (1966).

4) S. Umezawa, *Adv. Carbohydr. Chem. Biochem.*, **30**, 111 (1974).

5) S. Ogawa, I. Kasahara, and T. Suami, *Bull. Chem. Soc. Jpn.*, **52**, 118 (1979).

6) Compound **7** was obtained as one of the side products formed by the reaction of DL-tri-*O*-acetyl-(1,3/2,4,6)-4-bromo-6-bromomethyl-1,2,3-cyclohexanetriol with sodium benzoate in aqueous DMF: S. Ogawa, N. Chida, and T. Suami, *Chem. Lett.*, **1980**, 1559.

7) Elimination of the azido group of **8** seemed to occur under the slightly basic conditions, decreasing the yield of **9**.

8) S. Nishimura, *Bull. Chem. Soc. Jpn.*, **32**, 61 (1959).

9) T. Suami, S. Ogawa, K. Nakamoto, and I. Kasahara, *Carbohydr. Res.*, **58**, 240 (1977).

10) K. B. Sharpless, D. W. Patrick, L. K. Truesdale, and S. A. Biller, *J. Am. Chem. Soc.*, **97**, 2305 (1975); K. B. Sharpless, A. O. Chong, and K. Oshima, *J. Org. Chem.*, **41**, 177 (1976).

11) Sharpless reaction has been already extensively studied in the field of carbohydrates: K. Heyns and J. Feldmann, *Tetrahedron Lett.*, **1977**, 2789; I. Dyong, Q. Lam-Chi, G. Schulte, B. Fraser-Reid, and L. Primeau, *Angew. Chem.*, **89**, 565 (1977) and the references cited therein.

12) Attempts to isolate the minor products were not made.

13) The ^{1}H NMR spectra of **33** and **35** were in good accord with those of the corresponding 3-acetates, respectively.[6]

14) F. Arcamone, G. Canevazzi, and M. Ghione, *Giorn. Microbiol.*, **2**, 205 (1956); L. A. Dolak, T. M. Castle, and A. L. Laborde, *J. Antibiot.*, **33**, 690 (1980) and the references cited therein.

15) D. Horton, J. B. Huges, J. S. Jewell, K. D. Philips, and W. N. Turner, *J. Org. Chem.*, **32**, 1073 (1967). When an axial hydroxyl group locates at C-1, the C-2 *p*-toluenesulfonamido group may be fixed by it, presumably, through a hydrogen bonding, in the position favorable for a shielding of the C-3 acetoxymethyl protons.

16) a) F. W. Lichtenthaler, G. Bambach, and P. Emig, *Chem. Ber.*, **102**, 994 (1969); b) F. W. Lichtenthaler and P. Emig, *Carbohydr. Res.*, **7**, 121 (1968). In the ^{1}H NMR spectra in $CDCl_3$, the axial and equatorial acetoxyl groups of aminocyclitols and cyclitols were shown to resonate in the regions of δ 2.10—2.27 and 1.97—2.07, respectively.

17) Compound **37** was prepared from DL-validamine with assistance of Messrs. N. Chida and M. Ohya: mp 152—153 °C. ^{1}H NMR ($CDCl_3$, 90 MHz) δ 1.79 (3H, s) and 2.00 (9H, s) (OAc), 3.62—3.91 (2H, m, H-6 and H-7), 4.03 (1H, dd, J=4.5 and 11.5 Hz, H-7′), 4.75 (1H, dd, J=4.5 and 10.5 Hz, H-1), 4.87 (1H, dd, J=9 and 10.5 Hz, H-3), 5.23 (1H, dd, J=9 and 10.5 Hz, H-2), 5.43 (1H, d, J=4.5 Hz, NH). Found: C, 52.85; H, 5.58; N, 2.49; S, 6.02%. Calcd for $C_{22}H_{29}NO_{10}S$: C, 52.90; H, 5.85; N, 2.80; S, 6.42%.

18) Taken on a Varian EM-360A (60 MHz) spectrometer

Regio- and Stereoselective Cyclopentannulation with Ketones and Propargyl Alcohol Derivatives. Synthesis of *dl*-Nootkatone and *dl*-Muscopyridine

Tamejiro HIYAMA,* Masaki SHINODA, Hiroyuki SAIMOTO, and Hitosi NOZAKI

Department of Industrial Chemistry, Kyoto University, Yoshida, Sakyo-ku, Kyoto 606

(Received January 27, 1981)

A highly regio- and stereoselective five-membered ring annulation involving the acid-treatment of propargyl alcohol dianion adducts of ketones is described. The propargyl alcohol adduct of 2-octanone was converted into 2-methyl-3-pentyl-2-cyclopentenone by treatment with sulfuric acid–methanol (1:1) at 0 °C. As the major product, 1-methylbicyclo[5.3.0]dec-6-en-8-one was produced from 2-methylcycloheptanone. Remarkable regioselective cyclopentannulation was observed in 2-methylcyclohexanone and 2,3-dimethylcyclohexanone wherein 1-methyl- and *trans*-1,2-dimethyl-substituted bicyclo[4.3.0]non-5-en-7-one (BNO) are produced, respectively. With 3-butyn-2-ol, 2-methylcyclohexanone was converted into the *cis*-1,9-dimethyl-substituted BNO. 4-Isopropyl-2-methylcyclohexanone was transformed into an 83—85:17—15 mixture of *c*-3-isopropyl-*r*-1,*c*-9-dimethyl-BNO and its 3-epimer. These results are explained in terms of the conrotatory ring-closure of thermodynamically most favorable hydroxypentadienyl cation intermediates. 3-Methoxycarbonyl-*cis*-1,9-dimethyl-BNO produced from 4-methoxycarbonyl-2-methylcyclohexanone and 3-butyn-2-ol was successfully transformed into *dl*-nootkatone by converting the methoxycarbonyl group into isopropenyl of correct stereochemistry followed by ring enlargement. Cyclopentannulation using propargyl alcohol dianion adducts of 2-cycloalkenones is discussed. Annulation takes place regioselectively to give conjugated dienones, *e.g.*, (*E*)-bicyclo[10.3.0]pentadeca-1(12),2-dien-13-one from 2-cyclododecenone. This product is led to *dl*-muscopyridine by conjugate 1,6-addition of methyl group followed by ring expansion and finally by aromatization with hydroxylamine hydrochloride.

Selective ring-forming reactions are important with respect to construction of fused carbocyclic skeletons. The regio- and stereochemistry of the annulation in particular should be controlled. The Robinson annulation has been extensively studied and is now well-established.[1] The analogous synthetic problem for five-membered ring annulation[2] still remains unsolved in spite of the development of efficient three-carbon annulation process.[3–5] In view of the stereospecificity of electrocyclic reactions, the ring-closure of pentadienyl cation intermediates was utilized.[6] Characteristic procedures have been developed for cyclopentannulation,[7,8] but though highly efficient for simple cyclic ketones, the method[7b] involving dichloroallyllithium–ketone adducts is not applicable to a moderately hindered ketone such as 2-methylcyclohexanone. Having made efforts to elaborate access to 2-substituted cycloalkanones, we have found a process noted briefly by Islam and Raphael[9a] and others[9b,c] which is effective as regards to regio- and stereoselectivity. Details are reported herein.[10]

Cyclopentannulation of 2-Methylcyclohexanones. In order to disclose the regioselectivity of the Raphael process, 2-octanone was allowed to react with the dilithium salt of propargyl alcohol, and the resulting adduct was treated with sulfuric acid–methanol (1:1) at 0 °C to give 2-methyl-3-pentyl-2-cyclopentenone (**1**) as a sole product. Starting with 2-methylcycloheptanone, we obtained **2** as the major product. Thus, the more substituted α-carbon of these ketones is preferentially incorporated into the five-membered ring. This selectivity may be attributed to the thermodynamically most stable intermediates of types A and B, respectively, showing a sharp contrast to the exclusive production of **3** from 2-methylcycloheptanone by the dichloroallyllithium method.[7b]

Remarkable selective annulation was observed in 2-methylcyclohexanone derivatives (Table 1). The propargyl alcohol adduct **5** of 2-methylcyclohexanone (**4**) was cyclized under acidic conditions to give the hexahydroindenone derivative **6** exclusively. The electrocyclic ring-closure of the intermediate C followed by deprotonation should be responsible for selective annulation.

When 3-butyn-2-ol was added to **4** and the adduct **7** treated with sulfuric acid and methanol, *cis*-3,3a-dimethylhexahydroindenone **8** was produced along with its isomer **9**. The stereochemistry of **8** was unambiguously established by transforming **8** into the known octalone **28** (Scheme 1). Thus, dibromomethyllithium[11] was allowed to react with **8**, and the adduct **26** was then treated with 2 mol of butyllithium to give **27**. One methylene unit is selectively insert-

Table 1. Cyclopentannulation of 2-methylcyclohexanone derivatives

Entry	Cyclohexanone	Propargyl alcohol derivative	Adduct (% yield)	Annulated product (% yield)
1	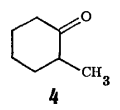 **4**	$CH{\equiv}CCH_2OH$	**5** (88) [a]	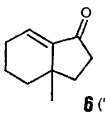 **6** (70)
2		$CH{\equiv}CCHOH$ $\vert$ CH_3	**7** (84) [b]	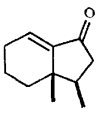 **8** (67) 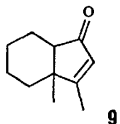 **9** (10)
3	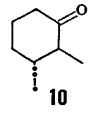 **10**	$CH{\equiv}CCH_2OH$	**11** (89) [c]	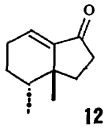 **12** (60)
4	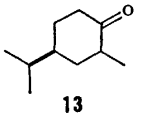 **13**	$CH{\equiv}CCHOH$ $\vert$ CH_3	**14** (87) [b]	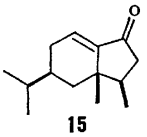 **15** 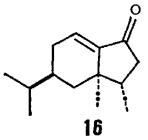 **16** (64% yield, **15** : **16** 83-85:17-15)
5	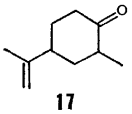 **17**	$CH{\equiv}CCHOH$ $\vert$ CH_3	**18** (71) [b]	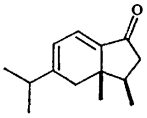 **19** (55)
6	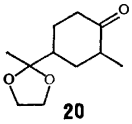 **20**	$CH{\equiv}CCHOH$ $\vert$ CH_3	**21** (84) [d]	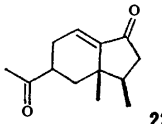 **22** (34)
7	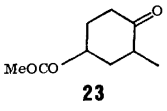 **23**	$CH{\equiv}CCHOH$ $\vert$ CH_3	**24** (86) [e]	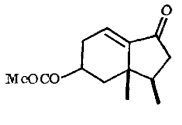 **25** (60)

a) Diastereomer ratio 42:58. Although the compounds were separable, the mixture was used directly for the next annulation. b) Two of the diastereomers were separable, the mixture being used for the subsequent annulation. c) About 1:1 diastereomeric mixture. d) Based on the consumed cyclohexanone. e) Isolated as carboxylic acid.

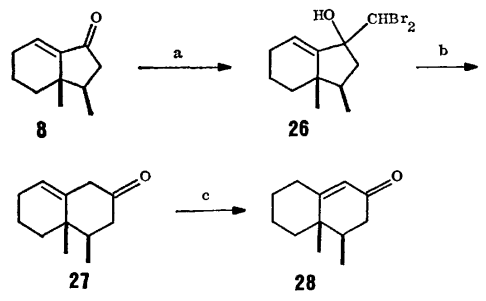

a: $LiCHBr_2$, b: n-BuLi, c: 5% H_2SO_4-THF

Scheme 1.

ed between the carbonyl and olefinic carbon of **8**. Treatment with aqueous sulfuric acid gave **28** having a ^{1}H-NMR absorption at δ 1.08 (singlet for the bridgehead methyl) consistent with the *cis* isomer **28** (*cf.* the *trans* isomer, δ 1.27).[12] The sole formation of **8** is ascribed to the conrotatory ring-closure of the intermediate D wherein the steric interaction between the two methyl groups is most reduced.

Using 2,3-dimethylcyclohexanone and propargyl alcohol, we attempted to cyclize the adduct **11** with sulfuric acid–methanol mixture as above and obtained an intractable mixture of products. The result was improved by converting the diol **11** into a monoacetate with acetic anhydride in pyridine and by employing 2,2,2-trifluoroethanol in place of methanol, a single product **12** being formed whose stereochemistry was established by transformation into the known enol lactone **30**[13] (Scheme 2). The enone moiety of **12** was reduced with lithium in anhydrous ammonia and the resulting enolate was trapped with acetic anhydride to give **29**. Ozonolysis of **29** fol-

lowed by lactone formation with acetic anhydride and sodium acetate gave **30** which exhibited a ^{1}H-NMR absorption at δ 1.20 (singlet for bridgehead methyl) pertinent to the *trans* isomer (*cf.* δ 1.03 for the *cis* isomer).[13]

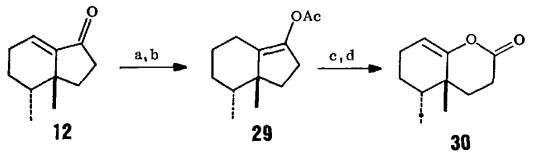

a: Li/NH_3, b: Ac_2O, c: O_3, Me_2S, d: Ac_2O, AcONa

Scheme 2.

Let us consider the factors governing the transformation of **11** into **12**. *A priori*, four intermediates E—H are conceivable precursors for the five-membered ring annulation. The intermediate E or F gives **12** while G or H affords the *cis* isomer of **12**. Examination of molecular models suggests that in G or H severe interaction between the two methyl groups takes place as new C–C bond formation proceeds. However, such an interaction is not crucial in E or F since the two methyl groups are further apart during the course of C–C bond formation. Of the two favorable intermediates E and F, E seems to be the responsible one since the methyl group on the six-membered ring takes a pseudoequatorial position and C–C bond formation takes place from the antiperiplanar direction of a pseudoaxial C–H bond under orbital control.[14]

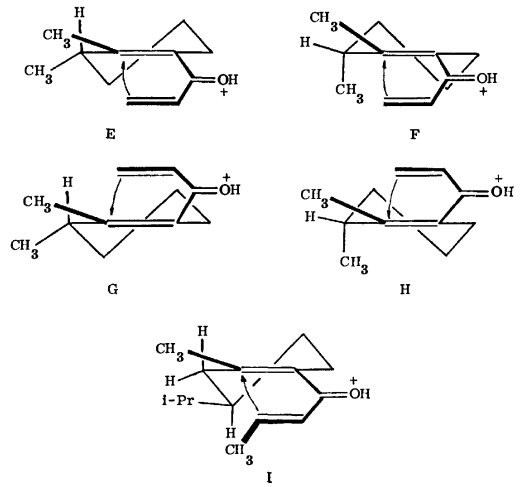

Provided that such orbital control is operative during the course of cyclization, we can take advantage of this effect by starting with 4-isopropyl-2-methylcyclohexanone (**13**) and 3-butyn-2-ol. The intermediate postulated here would be I whose isopropyl group should prefer an equatorial position; C–C bonding should occur from the antiperiplanar direction of the pseudoaxial C–H bond to produce a hexahydroindenone derivative with all *cis* substituents predominantly. This was found to be the case.

Addition of 3-butyn-2-ol to **13** gave an acetylenic diol **14** as a mixture of eight possible diastereomers. Without separation of the diastereomers, **14** was treated with sulfuric acid and methanol (1:1) at 0 °C to afford two products **15** and **16** in a ratio of 83:17 or 85:15 as revealed by ^{1}H-NMR or GLC respectively. The stereochemical outcome was secured by converting the mixture of products into an 82:18 (^{1}H-NMR) mixture of **31** and **32** by the sequence shown in Scheme 3 and by comparison of the retention time on capillary column GLC as well as ^{1}H-NMR spectra with those of each authentic sample. The authentic samples of **31** and **32** were prepared by the hydrogenation of 7-*epi*-nootkatone[15] and nootkatone,[16] respectively, with the aid of the catalyst chlorotris(triphenylphosphine)rhodium(I).

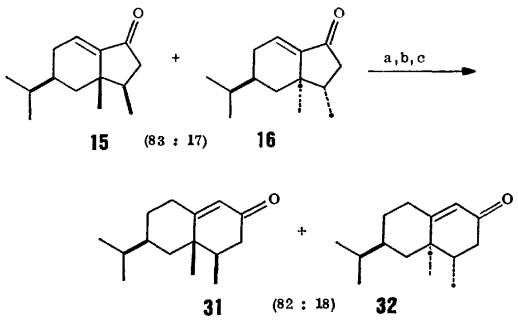

a: $LiCHBr_2$, b: n-BuLi, c: 5% H_2SO_4-THF

Scheme 3.

The results of entries 1—4 in Table 1 can be summarized as follows. A cyclohexanone **33** is converted by attaching a three-carbon unit of **34** into **35** in which the alkyl substituent R^3 on the bridgehead carbon comes invariably *cis* to R^4, *trans* to R^2 and selectively *cis* to R^1.

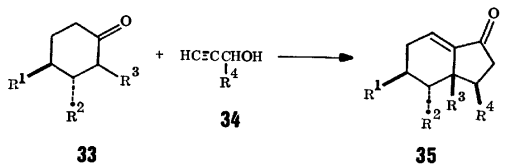

Synthesis of dl-*Nootkatone.* Scheme 3 shows that the annulation process is effective for stereoselective synthesis of an eremophilane-type sesquiterpene. We have applied this process to the synthesis of *dl*-nootkatone,[16,17] a component of the taste and flavor of grapefruit (*Citrus paradisi* Macfayden). Its carbon framework is characterized by the C(7)-epimer of eremophilane, *vis.*, valencane. An attempt using the adduct **18** of **17** and 3-butyn-2-ol resulted in the isomerization of the isopropenyl C=C bond to the conjugated one to give **19**. Taking account of the required epimerization at C(7), we started with **20** and obtained apossible precursor of nootkatone, **22**, in 34% yield. Because of the relative inefficiency of the annulation as well as the difficulty to obtain the starting material in large amount, we abandoned this route.

An ester group is found to be the appropriate functional group equivalent to isopropenyl group. The starting cyclohexanone **23**[18] was synthesized by the Diels-Alder reaction of methyl acrylate and 2-methyl-

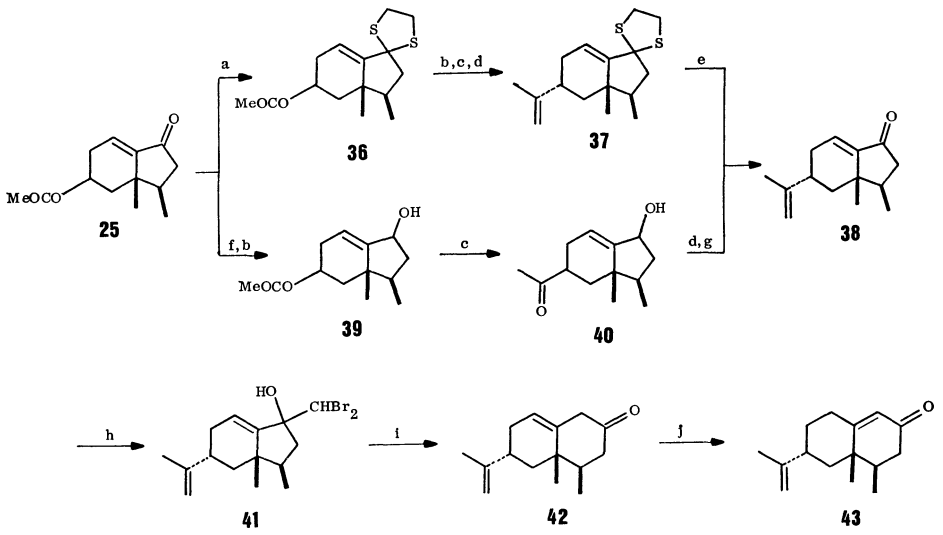

a: $HSCH_2CH_2SH$, BF_3OEt_2, b: KOH, c: MeLi, d: $Ph_3P{=}CH_2$, DMSO, e: i-$C_5H_{11}ONO$, f: $CeCl_3$-$NaBH_4$
g: $PyHClCrO_3$, h: $LiCHBr_2$, i: BuLi, j: 5% H_2SO_4-THF

Scheme 4.

3-trimethylsilyloxybutadiene[19] followed by hydrolysis. Subsequent addition of 3-butyn-2-ol was effected with concomitant hydrolysis of the ester group to give the adduct **24** as a stereoisomeric mixture, which was then treated with sulfuric acid–methanol (1:1) at 50 °C. The annulation product **25** was found to be a 3:2 mixture of epimers as evidenced by GLC and ^{13}C-NMR. Subsequent steps toward the target **43** are illustrated in Scheme 4.

In order to convert the methoxycarbonyl group of **25** into isopropenyl moiety of the correct configuration, we first transformed **25** into the ethylene dithioacetal **36** whose methoxycarbonyl group was transformed into isopropenyl group by standard methods. The final product **37** exhibited a ^1H-NMR spectrum revealing at least 97% stereochemical purity although one of its precursors, the methyl ketone, was a *ca.* 7:3 mixture of epimers. Probably epimerization took place before the Wittig olefiniation to yield a thermodynamically favorable product and/or the thermodynamically favorable isomer reacted more rapidly. Deprotection of the dithioacetal group was accomplished with isopentyl nitrite[20] to give the desired intermediate **38**. The configuration at C(5) turned out to be the correct one (purity >97%) as evidenced by hydrogenation of **38** to **16** with chlorotris(triphenylphosphine)rhodium(I) as a catalyst[16a] and by comparison of the spectrometric and chromatographic feature of **38** with those of the authentic specimen. Although the stereochemical outcome of **38** prepared by this route is acceptable, both formation and removal of the dithioacetal group were relatively inefficient (57% and 48% yield respectively), and hence another route from **25** to **38** was explored.

The enone **25** was reduced with sodium borohydride–cerium(III) chloride[21] in methanol to give an allyl alcohol **39** which was converted into a methyl ketone **40** as above. The Wittig reaction of **40** followed by oxidation with pyridinium chlorochromate gave **38** of >88% stereochemical purity at C(5) in 78% overall yield.

TABLE 2. CYCLOPENTANNULATION OF 2-CYCLOALKENONES

2-Cycloalkenone	Propargyl alcohol adduct (% yield)	Annulated product (% yield)
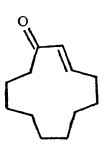 44	**45** (92)	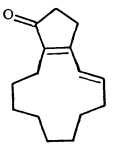 **46**(65)
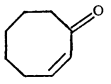 47	**48** (51[a], 76[b])	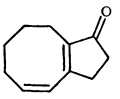 **49**(42)
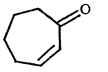 50	**51** (65)	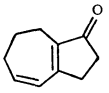 **52**(49)

a) Cyclooctenone (30%) recovered. b) Yield based on the consumed starting enone.

Final ring-enlargement was effected by the β-oxido carbenoid procedure.[11] The hexahydroindenone **38** was allowed to react with dibromomethyllithium at −78 °C to give the adduct **41** which in turn was treated with 3 equivalents of butyllithium at −95 °C for 1.6 h to give an octalone **42**. The IR of **42** showed the presence of a cyclohexanone moiety with no contamination of a conjugated enone. Subsequently, **42** was isomerized to *dl*-nootkatone in 5% sulfuric acid–THF (1:1). The synthetic sample thus prepared was of more than 93% purity and chromatographically and spectrometrically identical with the authentic specimen.[16a]

Cyclopentannulation of 2-Cycloalkenones. Having disclosed the salient feature of the cyclopentannula-

tion using 2-methylcycloalkanones and propargyl alcohol we extended the concept to 2-functionalized cycloalkanones such as 2-phenylthiocyclohexanone, 2-chloro-2-methylcyclohexanone, and 2-propargylcyclohexanone. Although the addition of propargyl alcohol dianion occurred with no trouble, the next acid-catalyzed cyclization turned out futile. We eventually found that 2-cycloalkenones undergo regioselective annulation (Table 2).

2-Cyclododecenone (**44**) was allowed to react with propargyl alcohol and the adduct **45** was treated with a 1:2 mixture of sulfuric acid and methanol at −20 to −3 °C to give the conjugated dienone **46**. The spectral data of **46** (see Experimental) are fully consistent with the given structure. In particular, the configuration of the newly produced C=C bond was found to be (*E*) based on the ^{1}H-NMR and IR spectra. The formation of the conjugated dienone is explained in terms of the conrotatory ring-closure of a heptatrienyl cation J to a vinylcyclopentenyl cation K,[22] since the disrotatory ring-closure of J to a cycloheptadienyl cation L is sterically hindered by the octamethylene chain. It is worthy to note that the C(1) and C(2) solely of **44** are incorporated into the five-membered ring. In this sense the annulation is regioselective.

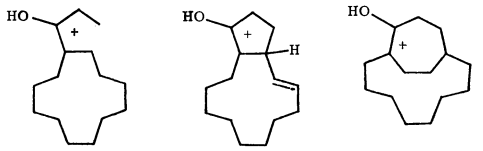

J K L

This two-step annulation was applied to lower homologs (Table 2) with less satisfactory results. The major obstacle was low efficiency in the addition of propargyl alcohol dianion to enones to induce enolization of the enones. The next cyclization is best performed by using the monoacetates of the adducts and by dissolving the monoacetates in sulfuric acid–methanol. Thus, bicyclic conjugated dienones **46**—**52** are now easily available which are otherwise hardly accessible.

Synthesis of dl-*Muscopyridine.* With the dienone **46** in hand, we planned to synthesize *dl*-muscopyridine (**55**).[23] A logical precursor of **55** should be 7-methyl-1,5-cyclopentadecanedione (**54**, Scheme 5). However, the introduction of methyl group into the parent diketone at the desired position is apparently difficult. We anticipated that diketone **54** would be derived from the bicyclic cyclopentenone **53**.

Selective 1,6-conjugated addition of the methyl group across the dienone moiety of **46** was best carried out using methylmagnesium iodide in the presence of copper(I) chloride,[24] **53** being obtained as the sole product. Dimethylcopperlithium turned out futile to give an intractable mixture of products with no trace of the desired one. Subsequent transformation into the diketone **54** was carried out according to the procedure of Gray and Dreiding.[25] Thus, **53** was reduced with sodium borohydride to an allyl alcohol which was then oxidized to an epoxy alcohol with *m*-chloroperoxybenzoic acid. Tosylation followed by solvolysis

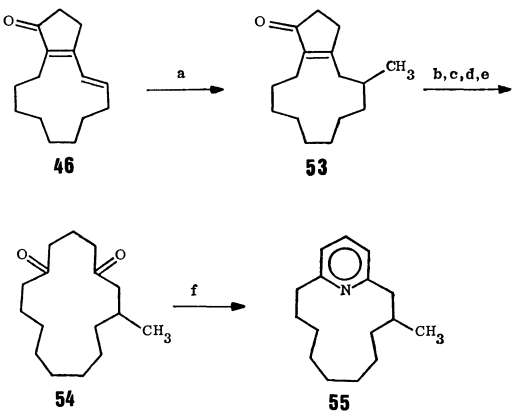

a: CH_3MgI, CuCl, THF, b: $NaBH_4$, c: m-$ClC_6H_4CO_3H$, d: p-$CH_3C_6H_4SO_2Cl$, pyridine, e: aq dioxane, $CaCO_3$, f: $NH_2OH{\cdot}HCl$

Scheme 5.

in aqueous dioxane gave the diketone, which was finally heated with hydroxylamine hydrochloride in ethanol at 160 °C.[26] *dl*-Muscopyridine (**55**) thus prepared exhibited correct spectra.

Experimental

Distillation was carried out by use of Kugelrohr (Büchi) and boiling points were determined by measuring the bath temperature. All temperatures are uncorrected. ^{1}H-NMR spectra (tetramethylsilane as an internal standard) were obtained on a Varian EM 390 spectrometer, chemical shifts being given in ppm unit, ^{13}C-NMR spectra on a Varian CMR-20 spectrometer, IR spectra on a Shimadzu IR-27G spectrometer in neat liquid film unless otherwise stated, MS on a Hitachi RMU-6L spectrometer, exact mass on a JEOL-JMS-D 300 spectrometer and UV on a Hitachi 124 spectrophotometer. Propargyl alcohol was distilled before use. 3-Butyn-2-ol (Tokyo Kasei-Kogyo Co. or Nakarai Chemicals Ltd., 55% aqueous solution) was used. Commercial sulfuric acid (95%) was used for cyclization. Preparative TLC plates (20 cm×20 cm) were prepared with Merck Kiesel-gel PF_{254}. Column chromatography was carried out with silica gel (Wakogel C-100) at atmospheric pressure.

Synthesis of 2-Methyl-3-pentyl-2-cyclopentenone (1) from 2-Octanone. Under a nitrogen atmosphere at −78 °C, butyllithium (1.50 M† hexane solution, 6.0 ml, 9.0 mmol) was added dropwise to a tetrahydrofuran (THF, 15 ml) solution of propargyl alcohol (0.25 g, 4.5 mmol). After stirring for 70 min, 2-octanone (0.39 g, 3.0 mmol) in THF (5 ml) was added and the reaction mixture was warmed to room temperature and stirred for 30 min. Work-up followed by preparative TLC purification (ether, R_f 0.68—0.84) gave 4-methyl-2-decyne-1,4-diol (0.42 g, 75% yield) as a viscous oil. IR: 3324, 1038, 1000 cm^{-1}; ^{1}H-NMR (CCl_4): δ 0.7—1.8 (m, 13H), 1.43 (s, 3H, CH_3), 4.20 (s, 2H, $C\underline{H}_2OH$), 3.9—4.5 (br s, 2H, OH); MS: *m/e* (rel intensity) 169 (M^+-CH_3, 4), 99 (100, $M^+-C_6H_{13}$), 81 (24). Found: C, 71.73; H, 11.22%. Calcd for $C_{11}H_{20}O_2$: C, 71.69; H, 10.94%.

Sulfuric acid (1.5 ml) was added dropwise over a period of 20 min to a methanol solution (1.5 ml) of 4-methyl-2-

† 1 M=1 mol dm^{-3}.

decyne-1,4-diol (172 mg, 0.93 mmol) at 0 °C. After stirring for 1.7 h, the reaction mixture was diluted with ether (10 ml) and neutralized with aqueous sodium hydrogencarbonate solution. The organic phase was separated, and the aqueous phase was extracted thoroughly with ether, the combined ethereal extracts being dried (Na_2SO_4) and concentrated *in vacuo*. Preparative TLC (hexane–ether 1:1, R_f 0.34—0.53) of the residue gave **1**[7b] (90 mg, 58% yield).

Cyclopentannulation of 2-Methylcycloheptanone. Butyllithium (1.81 M hexane solution, 8.3 ml, 15 mmol) was added at −78 °C under a nitrogen atmosphere to propargyl alcohol (0.40 g, 7.1 mmol) in THF (30 ml) in 5 min. The resulting viscous solution was stirred for 1 h and admixed with 2-methylcycloheptanone (0.60 g, 4.8 mmol) in THF (5 ml) during a period of 10 min. Stirring at −78 °C for 3 h, at room temperature for 0.5 h, followed by work-up, gave an oil (1.15 g). Purification by column chromatography (hexane–ether 1:1) gave the desired diol (TLC, hexane–ether 10:3, R_f 0.28, single spot, 0.67 g, 77% yield; 87% based on the consumed ketone) along with the recovered 2-methylcycloheptanone (68 mg, 10% recovery). The diol, mp 68.0—68.1 °C (hexane), showed the following spectra. ^{1}H-NMR (CCl_4): δ 1.08 (d, J=6.0 Hz, 3H, CH_3), 1.2—2.2 (m, 11H, methylenes and methine), 3.95 (br s, 1H, OH), 4.20 (s, 2H, $C\underline{H}_2OH$), 4.60 (br s, 1H, OH); IR: 3340, 1090 cm^{-1}; MS: *m/e* (rel intensity) 182 (M^+, 5), 164 (7), 151 (29), 111 (64), 79 (80), 55 (100). Found: C, 72.54; H, 10.09%. Calcd for $C_{11}H_{18}O_2$: C, 72.49; H, 9.96%.

Sulfuric acid (1.0 ml) was added dropwise over a period of 10 min at 0 °C to a methanol (0.1 ml) solution of the diol (17 mg, 0.093 mmol). The reaction mixture turned dark reddish purple. After 4 h the reaction was quenched by dilution with ether (10 ml) and neutralization with sodium hydrogencarbonate aqueous solution. TLC purification of the crude product (hexane–ether 2:1) gave 1-methylbicyclo[5.3.0]dec-6-en-8-one (**2**) (10.0 mg, 67% yield, R_f 0.41—0.50) and 6-methylbicyclo[5.3.0]dec-1(7)-en-8-one (**3**)[7b] (2.1 mg, 14% yield, R_f 0.22—0.26). Physical properties of **2**: bp 97—103 °C (bath temp)/0.06 Torr††. ^{1}H-NMR (CCl_4): δ 1.11 (s, 3H, CH_3), 1.3—2.8 (m, 12H, methylenes), 6.57 (dd, J=7.0, 5.0 Hz, 1H, olefinic H); IR: 1716, 1643 cm^{-1}; MS: *m/e* (rel intensity) 164 (M^+, 70), 149 (67), 122 (100), 107 (91), 93 (98), 79 (93). Found: C, 80.57; H, 10.08%. Calcd for $C_{11}H_{16}O$: C, 80.44; H, 9.83%.

The regioselectivity of the annulation at 0 °C was dependent on the acidic conditions. Conditions, yield(%), ratio of **2** to **3** were as follows: sulfuric acid–methanol (1:1), 61%, 77:23; sulfuric acid–methanol (1:10), 90, 40:60; sulfuric acid–acetic acid (1:1), 59, 84:16; sulfuric acid–2,2,2-trifluoroethanol (1:1), 55, 75:25; sulfuric acid only, 62, 88:12; sulfuric acid–methanol (1:1) and 1 mol of mercury(II) sulfate, 97%, 82:18.

*Cyclopentannulation of 2-Methylcyclohexanone (**4**) with Propargyl Alcohol.* Propargyl alcohol dianion solution was prepared at −78 °C under a nitrogen atmosphere by adding butyllithium hexane solution (2.0 M, 15.8 ml, 32 mmol) to propargyl alcohol (0.85 g, 15.1 mmol) in THF (40 ml), and stirring for 3 h. Addition of 2-methylcyclohexanone (1.12 g, 10.0 mmol) dissolved in THF (10 ml) followed by stirring at −78 °C for 1 h, at room temperature for 0.5 h, and then work-up gave an oil which was purified by column chromatography to give the adduct **5** (1.48 g, 88% yield) as *ca.* 3:2 diastereomeric mixture (TLC, hexane–ether 1:2, R_f 0.14 and 0.22). ^{1}H-NMR (CCl_4): δ 1.01 (d, J=5.0 Hz, 3H), 1.2—2.2 (m, 9H), 3.67 (br s, 1H), 4.19 (s, 2H), 4.50 (br s, 1H); IR: 3340, 1012, 968 cm^{-1}; MS: *m/e* 168 (M^+). Each diastereomer was separated by careful column chromatography. The less polar isomer: colorless needles, mp 36.2—37.0 °C (hexane). Found: C, 71.29; H, 9.66%. The more polar isomer: bp 126—128 °C (bath temp)/0.06 Torr; Found: C, 71.44; H, 9.71%. The mixture was used for the subsequent cyclization.

Sulfuric acid (1.5 ml) was added dropwise at 0 °C over a period of 15 min to a methanol (1.5 ml) solution of the adduct **5** (162 mg, 0.96 mmol). Stirring for 1.5 h at 0 °C, followed by extractive work-up as before and preparative TLC (dichloromethane), gave 1-methylbicyclo[4.3.0]non-5-en-7-one (**6**) (101 mg, 70% yield, R_f 0.35—0.49). GLC assay of the reaction mixture showed the presence of a trace amount (less than 5%) of the regioisomer corresponding to **3**. Physical properties of **6** are: bp 78—80 °C (bath temp)/0.04 Torr; ^{1}H-NMR (CCl_4): δ 1.08 (s, 3H, CH_3), 1.2—2.5 (m, 10H), 6.37 (t, 1H, J=3.6 Hz); IR: 1716, 1646 cm^{-1}; MS: *m/e* (rel intensity) 151 (M^++1, 8), 150 (M^+, 42), 135 (32), 122 (33), 108 (75), 93 (88), 79 (100). Found: C, 79.69; H, 9.33%. Calcd for $C_{10}H_{14}O$: C, 79.95; H, 9.39%.

Each diastereomer of **5** was separated by preparative TLC and subjected to cyclization under similar conditions. The more polar isomer gave **6** in 66% isolated yield, and the less polar one in 62% isolated yield.

*Annulation of 2-Methylcyclohexanone (**4**) with 3-Butyn-2-ol.* Potassium hydroxide (6.80 g, 121 mmol) was dissolved in 55% aqueous solution (5.7 g, 45 mmol) of 3-butyn-2-ol and the resulting solution was warmed at 40 °C. To this mixture was added dropwise 2-methylcyclohexanone (3.4 g, 30 mmol) over a period of 2 h, and the whole was stirred for 24 h at 40 °C, then diluted with water (10 ml) and extracted with ether (20 ml×4 times). The ethereal extracts were dried with anhydrous sodium sulfate and concentrated *in vacuo*. Column chromatography of the residue (hexane–ether 1:2) gave 1-(3-hydroxy-1-butynyl)-2-methylcyclohexanol (**7**) as a diastereomeric mixture (R_f 0.24 and 0.35 on TLC with hexane–ether 1:2) (4.6 g, 84% yield), bp 110—118 °C (bath temp)/0.08 Torr. ^{1}H-NMR (CCl_4): δ 0.91 (d, J=6.0 Hz, 3H), 1.02 (d, J=6.0 Hz, 3H), 1.1—2.1 (m, 9H), 3.5—4.3 (br s, 2H, OH), 4.3—4.7 (m, 1H, C$\underline{H}$–OH); IR: 3344, 1116, 1062, 1024 cm^{-1}; MS: *m/e* 182 (M^+). Found: C, 72.20; H, 10.15%. Calcd for $C_{11}H_{18}O_2$: C, 72.49; H, 9.96%.

Sulfuric acid (1.0 ml) was added at 0 °C over a period of 10 min to **7** (106 mg, 0.58 mmol) dissolved in methanol (1.0 ml). After 30 min the reaction was stopped by dilution with ether (10 ml) and neutralization with aqueous sodium hydrogencarbonate solution. The ethereal extracts were dried (Na_2SO_4), concentrated *in vacuo* to give an oil (107 mg). Preparative TLC purification (hexane–ether 1:1) gave 1,9-*cis*-dimethylbicyclo[4.3.0]non-5-en-7-one (**8**) (63 mg, 67% yield, R_f 0.58—0.71) and 1,9-dimethylbicyclo-[4.3.0]non-8-en-7-one (**9**) (10 mg, 10% yield, R_f 0.47—0.58). GLC assay of the crude product gave the **8**:**9** ratio to be 86:14. Physical properties of **8** were as follows. Bp 105—112 °C (bath temp)/0.07 Torr; ^{1}H-NMR (CCl_4): δ 0.95 (s, 3H, C–CH_3), 1.07 (d, J=6.0 Hz, 3H, CH–C$\underline{H}_3$), 1.5—2.3 (m, 9H), 6.37 (t, 1H, J=3.0 Hz, olefinic H); IR: 1723, 1653 cm^{-1}; MS: *m/e* (rel intensity) 164 (M^+, 50), 149 (23), 136 (15), 122 (95), 79 (100). Found: C, 80.65; H, 10.04%. Calcd for $C_{11}H_{16}O$: C, 80.44; H, 9.83%. Physical properties of **9**: bp 110—118 °C (bath temp)/0.09 Torr; ^{1}H-NMR (CCl_4): δ 1.23 (s, 3H), 1.0—2.3 (m+d (J=1.7 Hz) at δ 1.99, 12H), 5.70 (q, J=1.7 Hz, 1H); IR: 1700, 1619 cm^{-1}; MS: *m/e* (rel intensity) 164 (M^+, 46), 149

†† 1 Torr=133.322 Pa.

(100), 135 (22), 122 (27). Exact mass, found: *m/e* 164.1213 (M^+). Calcd for $C_{11}H_{16}O$: *m/e* 164.1201.

Transformation of ***8*** *to an Octalone* ***28***. Lithium dicyclohexylamide, prepared by addition of butyllithium (1.81 M hexane solution, 1.70 ml, 3.1 mmol) to a THF (2 ml) solution of dicyclohexylamine (0.56 g, 3.1 mmol) at 0 °C and by stirring the solution at 0 °C for 15 min, was added dropwise over a period of 2.3 h to a mixture of **8** (0.163 g, 1.0 mmol) and dibromomethane (0.37 g, 2.1 mmol) dissolved in THF (3 ml) at −78 °C under an argon atmosphere. The reaction mixture was stirred at −78 °C for 40 min and quenched by adding methanol (1.0 ml) at −78 °C. The reaction mixture was then warmed to room temperature, diluted with water (10 ml) and then treated with 5% hydrochloric acid. The precipitated insoluble material was filtered and washed with ether thoroughly. The aqueous phase of the filtrate was separated from the ethereal one and extracted with ether (20 ml×4 times). The combined ethereal extracts were dried (Na_2SO_4), and concentrated under reduced pressure to give an oil (0.45 g). Preparative TLC purification (benzene) gave the adduct **26** (R_f 0.34—0.46, 0.20 g, 60% yield; 83% yield based on the consumed starting material) along with the recovered **8** (R_f 0.08—0.21, 46 mg). ^{1}H-NMR (CCl_4) of **26**: δ 0.94 (d, J=7.5 Hz, 3H), 1.00 (s, 3H), 1.0—2.7 (m, 9H), 5.63 (t, J=3.3 Hz, 1H), 5.80 (s, 1H, $CHBr_2$); IR: 3440 cm^{-1}.

The adduct **26** (168 mg, 0.50 mmol) was dissolved in THF (4 ml) under an argon atmosphere, and a butyllithium hexane solution (1.83 M, 0.60 ml, 1.1 mmol) was added dropwise over a period of 12 min to the solution cooled at −95 °C. The reaction mixture was stirred at −95 °C for 2 h, then warmed to 0 °C, stirred for 5 min, and quenched with water (10 ml). Ether extraction (20 ml×4 times) followed by drying (Na_2SO_4) and concentration gave a crude product (115 mg) which was purified by preparative TLC (benzene) to give the octalone **27** (R_f 0.32—0.43, 36 mg, 41% yield). IR: 1715 cm^{-1}; ^{1}H-NMR (CCl_4): δ 0.94 (d, J=6.0 Hz, 3H), 1.10 (s, 3H), 1.1—2.5 (m, 9H), 1.73 (d, J=15.6 Hz, 1H), 3.10 (dm, J=15.6 Hz, 1H), 5.3—5.5 (m, 1H); MS: *m/e* (rel intensity) 178 (M^+, 50), 163 (23), 150 (23), 136 (56), 108 (76), 93 (100).

The octalone **27** (15 mg, 0.08 mmol) was dissolved in THF (0.5 ml) and 5% aqueous sulfuric acid (0.5 ml) and stirred for 2 h at room temperature. Work-up and TLC purification (hexane–ether 1:1) gave the octalone **28**[12] (R_f 0.23—0.31, 11 mg, 73% yield). ^{1}H-NMR (CCl_4): δ 0.94 (d, J=6.0 Hz, 3H), 1.08 (s, 3H), 1.1—2.5 (m, 11H), 5.60 (br s, 1H); IR: 3129, 1663, 1614 cm^{-1}; MS: *m/e* (rel intensity) 178 (M^+, 44), 163 (15), 150 (12), 136 (100), 121 (56). The recorded chemical shifts (CCl_4) of **28**:[12] δ 1.08 (s, 3H), and its *trans* isomer δ 1.27 (s, 3H).

*Cyclopentannulation of 2,3-Dimethylcyclohexanone (****10****) with Propargyl Alcohol.* Propargyl alcohol dianion was prepared by adding butyllithium hexane solution (1.92 M, 7.8 ml, 15.0 mmol) to propargyl alcohol (0.39 g, 7.0 mmol) in THF (35 ml) at −78 °C and allowed to react with 2,3-dimethylcyclohexanone (0.57 g, 4.5 mmol) dissolved in THF (10 ml) at −78 °C for 2.5 h, and at room temperature for 40 min. Work-up followed by column chromatography (hexane–ether 1:2) gave 1-(3-hydroxy-1-propynyl)-2,3-dimethylcyclohexanol (**11**) (0.74 g, 89% yield). Bp 118—126 °C (bath temp)/0.06 Torr; ^{1}H-NMR ($CDCl_3$): δ 0.8—1.0 (d, 6H), 1.0—2.3 (m, 8H), 3.08 (s, 2H), 4.26 (s, 2H); IR: 3340, 1008 cm^{-1}; MS: *m/e* (rel intensity) 182 (M^+, trace), 164 (M^+-H_2O, 8), 149 (33), 135 (42), 93 (44), 55 (100). Found: C, 72.42; H, 10.11%. Calcd for $C_{11}H_{18}O_2$: C, 72.49; H, 9.96%.

The diol **11** (0.28 g, 1.5 mmol) was admixed with acetic anhydride (1 ml) and pyridine (0.1 ml) at room temperature for 50 min, all volatile material being evaporated with the aid of a vacuum pump. The residue was dissolved in 2,2,2-trifluoroethanol (1 ml). To the resulting solution was added dropwise at 0 °C a mixture of sulfuric acid (1 ml) and 2,2,2-trifluoroethanol (1 ml). The reaction mixture was stirred overnight and warmed up to room temperature. Work-up gave an oil (0.37 g) which was purified by preparative TLC (benzene–ether 10:1) to give *trans*-1,2-dimethylbicyclo[4.3.0]non-5-en-7-one (**12**) (R_f 0.40—0.52, 150 mg, 60% yield), bp 95—102 °C (bath temp)/0.06 Torr. The homogeneity of the sample was confirmed by GLC assay as well as ^{1}H-NMR assay using shift reagent, Eu(fod)$_3$. ^{1}H-NMR (CCl_4): δ 0.87 (d, J=7.2 Hz, 3H, CH-C$\underline{H}_3$), 1.19 (s, 3H, C-CH_3), 1.2—2.5 (m, 9H), 6.46 (t, J=3.6 Hz, 1H); IR: 1718, 1712, 1654, 1649 cm^{-1}; MS: *m/e* (rel intensity) 165 (M^++1, 11), 164 (M^+, 29), 149 (18), 122 (100), 107 (50), 93 (59), 79 (95). Found: C, 80.59; H, 9.93%. Calcd for $C_{11}H_{16}O$: C, 80.44; H, 9.83%.

Transformation of ***12*** *into* ***30***. Lithium metal (18 mg, 2.6 mmol) was dissolved at −78 °C in anhydrous liquid ammonia (distilled over sodium). To this blue solution was added dropwise the enone **12** (0.21 g, 1.29 mmol) dissolved in THF (12 ml). The blue color vanished at the completion of addition. After 4 min the cooling bath was removed and ammonia was allowed to evaporate over a period of 2 h. The residue was then treated with acetic anhydride (1 ml) in THF (6 ml) and stirred at room temperature for 45 min. Work-up followed by column chromatography (hexane–ether 15:1) gave the enol acetate **29** (178 mg, 66% yield). ^{1}H-NMR (CCl_4): δ 0.95 (d, J=7.0 Hz), 1.18 (s), 2.03 (s, $OCOCH_3$).

The dichloromethane (5 ml) solution of **29** (101 mg, 0.49 mmol) was allowed to react with ozone at −78 °C until the solution turned slightly blue. Quenching with dimethyl sulfide (0.5 ml) at −78 °C, warming to room temperature followed by concentration and purification on preparative TLC plate (hexane–ether 1:1) gave a keto carboxylic acid (R_f 0.05—0.27, 29 mg, 31% yield), IR ($CHCl_3$): 3600—2400, 1710 cm^{-1}.

The keto carboxylic acid (28 mg, 0.14 mmol) was heated with sodium acetate (30 mg, 0.37 mmol) in acetic anhydride (3 ml) at reflux temperature for 2.3 h. Work-up followed by preparative TLC (hexane–ether 1:1, R_f 0.38—0.49) gave the enol lactone **30**[13] (8 mg, 32% yield) having ^{1}H-NMR ($CDCl_3$): δ 0.95 (d, J=6.8 Hz, 3H, CHC$\underline{H}_3$), 1.20 (s, 3H, C-CH_3), 1.2—2.3 (m, 7H), 2.62 (dd, J=8.5, 6.0 Hz, 2H), 5.30 (quintet, J=3.0 Hz, 1H); IR (CCl_4): 1758, 1680, 1132 cm^{-1}; MS: *m/e* 180 (M^+). The reported chemical shift ($CDCl_3$) of **30**:[13] δ 0.96 (d, 3H, J=6.5 Hz), 1.21 (s, 3H), and its *cis* isomer: δ 0.96 (d, 3H, J=6.0 Hz), 1.03 (s, 3H).

*Cyclopentannulation of 4-Isopropyl-2-methylcyclohexanone (****13****) with 3-Butyn-2-ol.* **13** (0.33 g, 2.1 mmol) was added at 40 °C over a period of 2 h to a solution of potassium hydroxide (0.62 g, 11.0 mmol) dissolved in 55% aqueous solution of 3-butyn-2-ol (0.58 g, 4.5 mmol). After 16 h, the reaction mixture was worked up to give an oil (580 mg) which was purified by column chromatography (hexane–ether 1:1) to give 4-isopropyl-1-(3-hydroxy-1-butynyl)-2-methylcyclohexanol (**14**) as a viscous oil (0.42 g, 87% yield). TLC (hexane–ether 1:1) showed roughly two spots at R_f 0.09 and 0.14, but these were not separated. Bp 118—126 °C (bath temp)/0.08 Torr. ^{1}H-NMR (CCl_4): δ 0.87 (d, J=6.0 Hz, 6H, CH(C$\underline{H}_3$)$_2$), 1.02 (d, J=6.0 Hz, 3H, CHC$\underline{H}_3$), 1.1—2.2 (m+d (δ 1.43 J=6.0 Hz), 12H), 3.9—4.3 (br s, 2H, OH),

4.3—4.7 (m, 1H, CH(OH)); IR: 3346, 1120, 1071 cm^{-1}; MS: *m/e* (rel intensity) 224 (M^+, trace), 206 (8), 191 (15), 163 (16), 107 (24), 57 (72), 43 (100). Found: C, 75.18; H, 10.55%. Calcd for $C_{14}H_{24}O_4$: C, 74.95; H, 10.78%.

Sulfuric acid (1.5 ml) was added to a methanol (1.5 ml) solution of **14** (0.34 g, 1.5 mmol) at 0 °C over a period of 15 min and the resulting solution was stirred at 0 °C for 30 min and then worked up to give an oil (0.33 g) which was purified by preparative TLC (hexane–ether 1:1), giving a mixture of 3-isopropyl-*cis*-1,9-dimethylbicyclo[4.3.0]non-5-en-7-one (**15** and **16**) (R_f 0.60—0.71, 196 mg, 64% yield), bp 123—127 °C (bath temp)/0.05 Torr. The ratio of **15** to **16** was estimated by GLC (PEG 20 M, 10% on Celite 545, 2 m, 170 °C, N_2 carrier gas 0.8 kg/cm^2, FID detector) to be 85:15, R_t being 18.4 min and 19.7 min respectively. The ratio was alternatively estimated to be 83:17 by ^{1}H-NMR (CCl_4): δ 0.91 (s, 3H, CCH_3), 0.92 (d, J=6.2 Hz, 6H, $CH(CH_3)_2$), 1.03 (d, J=5.7 Hz, 3H, $CHCH_3$), 1.1—2.4 (m, 9H), 6.36 (t, J=3.3 Hz, 0.17 H), 6.53 (dd, J=7.7, 3.0 Hz, 0.83H). IR: 1715, 1652 cm^{-1}; MS: *m/e* (rel intensity) 206 (M^+, 31), 191 (9), 178 (6), 164 (87), 121 (100). Found: C, 81.55; H, 10.98%. Calcd for $C_{14}H_{22}O$: C, 81.50; H, 10.75%.

*Transformation of a Mixture of **15** and **16** into a Mixture of **31** and **32**.* Lithium dicyclohexylamide generated from butyllithium hexane solution (1.79 M, 2.5 ml, 4.4 mmol) and dicyclohexylamine (0.79 g, 4.4 mmol) in THF (3 ml) at 0 °C was added dropwise at −78 °C over a period of 1.5 h to a mixture of dibromomethane (0.76 g, 4.4 mmol), **15** and **16** (0.36 g, 1.76 mmol) in THF (7 ml) under an argon atmosphere. Stirring was continued for 1.5 h, and the reaction was stopped by addition of methanol (1 ml) at −78 °C. The reaction mixture was then allowed to warm to room temperature and treated with saturated aqueous ammonium chloride solution (20 ml). The precipitated material was filtered off and the filtrate was extracted with ether (20 ml×4 times). The ethereal phase was dried with anhydrous sodium sulfate, and concentrated *in vacuo* to give an oil (1.00 g) which was purified by column chromatography (hexane–benzene 1:1) to give the adduct (R_f 0.47—0.56, 0.45 g, 67% yield; 74% yield based on the consumed starting material) along with the starting material (36 mg, 10%). ^{1}H-NMR (CCl_4) of the adduct: δ 0.91 (d, J=6.0 Hz, 6H), 0.95 (d, J=6.4 Hz, 3H), 1.00 (s, 3H, CCH_3), 1.1—2.7 (m, 9H), 5.76 (s, 1H, $CHBr_2$), 5.6—6.1 (m, 1H); IR: 3435, 1120 cm^{-1}.

Butyllithium hexane solution (1.79 M, 1.40 ml, 2.5 mmol) was added at −95 °C over a period of 20 min to the above adduct (0.39 g, 1.0 mmol) in THF (8 ml) under an argon atmosphere. The reaction mixture was stirred at −95 °C for 1.7 h, at 0 °C for 5 min and then quenched with water (10 ml). Work-up followed by preparative TLC (benzene) gave an octalone (R_f 0.24—0.36, 186 mg, 83% yield). Bp 120—125 °C (bath temp)/0.06 Torr. IR: 1721, 1661 cm^{-1}; ^{1}H-NMR (CCl_4): δ 0.90 (d, J=6.3 Hz, 6H, $CH(CH_3)_2$), 0.91 (d, J=6.3 Hz, 3H, $CHCH_3$), 1.09 (s, 3H, CCH_3), 1.1—2.3 (m, 9H), 2.69 (dm, J=15.0 Hz, 1H, one of C(7) methylene), 3.20 (dm, J=15.0 Hz, 1H, the other of C(7) methylene), 5.3—5.5 (m, 1H); MS: *m/e* (rel intensity) 220 (M^+, 30), 178 (19), 177 (29), 107 (100), 93 (49), 91 (38), 79 (35), 77 (24), 69 (30). Exact mass, found: *m/e* 220.1827 (M^+). Calcd for $C_{15}H_{24}O$: *m/e* 220.1827.

A mixture of the octalone (103 mg, 0.47 mmol), THF (1.5 ml), and 5% sulfuric acid (1.5 ml) was stirred overnight vigorously. Work-up and preparative TLC separation gave a mixture of the conjugated octalones **31** and **32** (R_f 0.55—0.67, 48 mg, 47% yield, 79% yield based on the recovered octalone) along with the starting unconjugated octalone (42 mg, 41%). The bp of **31** and **32**: 121—123 °C (bath temp)/0.06 Torr; ^{1}H-NMR (CCl_4): δ 0.87 (d, J=6.0 Hz, 6H, $CH(CH_3)_2$), 0.97 (d, J=6.0 Hz, 3H, $CHCH_3$), 1.05 (s, 3H, CCH_3), 1.1—2.6 (m, 11H), 5.59 (br s, 0.18 H), 5.65 (br s, 0.82 H); ^{1}H-NMR ($CDCl_3$): δ 5.75 (br s, 0.18H), 5.80 (br s, 0.82H). IR: 3030, 1663, 1627 cm^{-1}; MS: *m/e* (rel intensity) 220 (M^+, 22), 178 (39), 177 (24), 135 (48), 108 (28), 107 (28), 91 (24), 79 (27), 55 (22), 40 (100). Found: C, 81.49; H, 11.23%. Calcd for $C_{15}H_{24}O$: C, 81.76; H, 10.98%.

GLC retention times of these samples (glass capillary column, 30 m×0.3 mm, SF-96 at 180 °C) were 27.4 min and 28.0 min, respectively, identical with those of the authentic samples (*vide infra*).

*An Authentic Sample of 11,12-Dihydro-7-*epi*-nootkatone (**31**).* A mixture of 7-*epi*-nootkatone[15] (43 mg, 0.2 mmol) and chlorotris(triphenylphosphine)rhodium(I) (20 mg) in benzene (2 ml) was stirred under a hydrogen atmosphere at room temperature for 19 h. Concentration followed by preparative TLC (benzene–ether 5:1, R_f 0.40—0.52) gave **31** (35 mg, 81% yield). ^{1}H-NMR (CCl_4): δ 0.86 (d, J=6.3 Hz, 6H, $CH(CH_3)_2$), 0.96 (d, J=6.5 Hz, 3H, $CHCH_3$), 1.046 (s, 3H, CCH_3), 1.1—2.6 (m, 11H), 5.65 (br s, 1H); IR: 1665, 1617 cm^{-1}. A *ca.* 1:1 mixture of 7-*epi*-nootkatone and nootkatone was also hydrogenated under similar conditions to give the corresponding dihydro derivatives of *ca.* 1:1 mixture which showed ^{1}H-NMR (CCl_4) absorptions: two broad singlets at δ 5.59, 5.65, and two singlets at 1.046 and 1.066.

*An Authentic Sample of 11,12-Dihydronootkatone (**32**)*[16a] exhibited ^{1}H-NMR (90 MHz) peaks at δ 5.75 (br s) and 1.066 (s) in $CDCl_3$, and 5.60 (br s) in CCl_4. GLC coinjection experiments revealed an identical R_t to that of the minor product, **32**.

*Cyclopentannulation of 4-Isopropenyl-2-methylcyclohexanone (**17**) with 3-Butyn-2-ol.* **17** (149 mg, 0.98 mmol) was added at 40 °C to a mixture of potassium hydroxide (0.24 g, 4.3 mmol) and 55% aqueous solution of 3-butyn-2-ol (193 mg, 1.50 mmol), and the resulting mixture was stirred at 40 °C overnight. Work-up followed by preparative TLC gave the adduct **18** (154 mg, 71% yield). ^{1}H-NMR (CCl_4): δ 1.01 (d, J=7.2 Hz, 3H), 1.44 (d, J=6.5 Hz, 3H), 1.1—2.3 (m, 8H), 1.71 (s, 3H), 4.1 (br s, 2H, OH), 4.4—4.7 (m+br s at δ 4.63, 2H); IR: 3355, 1642, 1040, 889 cm^{-1}; MS: *m/e* (rel intensity) 222 (M^+, trace), 204 (M^+-H_2O, 6), 189 (13), 107 (51), 79 (42), 55 (56), 43 (100). Exact mass, found: *m/e* 204.1500 (M^+-H_2O). Calcd for $C_{14}H_{20}O$: *m/e* 204.1512 (M^+-H_2O).

Sulfuric acid (0.5 ml) was added at 0 °C to a methanol (0.5 ml) solution of **18** (43 mg, 0.19 mmol) over a period of 15 min. After 30 min the reaction mixture was worked up and the crude product purified by preparative TLC (hexane–ether 1:1, R_f 0.66—0.76) to give 3-isopropyl-*cis*-1,9-dimethylbicyclo[4.3.0]nona-3,5-dien-7-one (**19**) (22 mg, 55% yield). ^{1}H-NMR (CCl_4): δ 0.91 (s, 3H, CH_3), 1.07 (d, J=6.6 Hz, 6H, $CH(CH_3)_2$), 1.09 (d, J=6.6 Hz, 3H, $CHCH_3$), 1.8—2.6 (m, 6H), 5.85 (dm, J=5.4 Hz, 1H), 6.53 (d, J=5.4 Hz, 1H); IR: 1702, 1644, 1574, 835 cm^{-1}; MS: *m/e* (rel intensity) 204 (M^+, 23), 161 (21), 147 (70), 119 (100), 91 (28). Exact mass, found: *m/e* 204.1493 (M^+). Calcd for $C_{14}H_{20}O$: *m/e* 204.1513.

*Cyclopentannulation of 4-(2-Methyl-1,3-dioxolan-2-yl)-2-methylcyclohexanone (**20**) with 3-Butyn-2-ol.* The keto acetal **20**[27] (0.60 g, 3.0 mmol) was added over a period of 2 h to a solution of potassium hydroxide (0.65 g, 11.6 mmol) in 55% aqueous 3-butyn-2-ol (0.64 g, 5.0 mmol) at 40 °C and the resulting mixture was stirred overnight. Work-up

followed by column chromatography (ether) gave the adduct **21** (0.40 g, 48% yield; 84% yield based on the consumed **20**) along with the recovered **20** (0.25 g, 42%). The adduct showed ^{1}H-NMR (CCl_4): δ 1.18 (s, 3H), 0.9—1.3 (m, 6H), 1.3—2.3 (m, 8H), 3.87 (br s, 6H), 4.4—4.7 (m, 1H); IR: 3420, 1038 cm^{-1}; MS: *m/e* (rel intensity) 253 (M^+-CH_3, 4), 87 (100). Exact mass, found: *m/e* 253.1312 (M^+-CH_3). Calcd for $C_{14}H_{21}O_4$: *m/e* 253.1332.

Sulfuric acid (1.0 ml) was added at 0 °C over a period of 15 min to **21** (92 mg, 0.34 mmol) dissolved in methanol (1.0 ml), and the reaction mixture was stirred for 30 min. Work-up followed by preparative TLC (hexane–ether, 1:1, R_f 0.21—0.35) gave 3-acetyl-*cis*-1,9-dimethylbicyclo[4.3.0]-non-5-en-7-one (**22**, 24 mg, 34% yield). Bp 120—128 °C (bath temp)/0.05 Torr. ^{1}H-NMR (CCl_4): δ 0.99 (s, 3H), 1.09 (d, J=6.5 Hz, 3H), 1.1—3.0 (m, 8H), 2.16 (s, 3H), 6.42 (t, J=3.0 Hz, 1H); IR (CH_2Cl_2): 1708, 1654, 1249, 894 cm^{-1}; MS: *m/e* (rel intensity) 206 (M^+, 1), 204 (11), 163 (100), 121 (59). Exact mass, found: *m/e* 206.1324 (M^+). Calcd for $C_{13}H_{18}O_2$: *m/e* 206.1307.

*Synthesis of Methyl 3-Methyl-4-oxocyclohexanecarboxylate (**23**).* A mixture of 2-methyl-3-trimethylsilyloxy-1,3-butadiene[19] (158 mg, 1.0 mmol) and methyl acrylate (175 mg, 2.0 mmol) dissolved in benzene (1 ml) was heated in a sealed tube at 160—180 °C for 4 h. After cooling to room temperature the volatile material was evaporated with a water-aspirator, and the residue was dissolved in 90% methanol (20 ml) containing potassium fluoride (*ca.* 0.2 g). After 4 h the reaction mixture was diluted with water (10 ml) and extracted with ether (20 ml×4 times). The ethereal extracts were dried (Na_2SO_4) and concentrated *in vacuo* to give a crude product (172 mg) which was purified by preparative TLC. The desired product **23**[18] at R_f 0.10—0.23 weighed 134 mg, 78% yield.

A large scale synthesis was carried out by using the diene (15.5 g, 0.10 mol), methyl acrylate (17.2 g, 0.20 mol) in benzene (10 ml) at 184—191 °C for 4 h and by hydrolyzing the resulting enol silyl ether with 20% acetic acid (30 ml) and methanol (30 ml) at room temperature for 1 h. The product (13.1 g, 77% yield) was collected by distillation at 140—142 °C/18 Torr. ^{1}H-NMR (CCl_4): δ 0.99 (d, J= 6.0 Hz, 3H), 1.1—2.9 (m, 8H), 3.66 (s, 3H); IR: 1735, 1710, 1195 cm^{-1}; (Found: C, 63.42; H, 8.26%).

*Synthesis of 3-Methoxycarbonyl-*cis*-1,9-dimethylbicyclo[4.3.0]non-5-en-7-one (**25**).* The keto ester **23** (0.39 g, 2.3 mmol) was added at 40 °C over a period of 1 h to potassium hydroxide (0.84 g, 14.9 mmol) dissolved in 55% aqueous solution (0.67 g, 5.3 mmol) of 3-butyn-2-ol and the mixture was allowed to react overnight. Dilution with water (10 ml), acidification with 10% hydrochloric acid, extraction with ether (20 ml×4 times), followed by drying (Na_2SO_4), and concentration gave a viscous oil (0.68 g) which was purified by column chromatography (ether) to give 4-hydroxy-4-(3-hydroxy-1-butynyl)-3-methylcyclohexanecarboxylic acid (**24**) (0.45 g, 86% yield). IR: 3650—2400, 1704 cm^{-1}; ^{1}H-NMR ($CDCl_3$): δ 1.0—1.2 (d, 3H, $CHC\underline{H}_3$), 1.2—2.7 (m+2d (δ 1.43 and 1.47 each J=6.0 Hz), 11H), 4.4—4.9 (m, 3H, $\underline{H}O-C\underline{H}$ and OH). No peak due to the carboxyl group was observable. However, treatment of **24** with diazomethane gave the methyl ester (δ 3.68, s).

A large scale experiment using **23** (7.3 g, 43 mmol), potassium hydroxide (13.5 g, 0.24 mol) and 55% aqueous solution 3-butyn-2-ol (10.4 g, 82 mmol), afforded 8.9 g of **24** (91% yield).

Sulfuric acid (0.3 ml) was added at room temperature to **24** (24 mg, 0.11 mmol) dissolved in methanol (0.3 ml). The mixture was then heated at 50 °C for 30 min. Work-up followed by preparative TLC (hexane–ether 1:1, R_f 0.27—0.41) gave 3-methoxycarbonyl-*cis*-1,9-dimethylbicyclo-[4.3.0]non-5-en-7-one (**25**) (15 mg, 60% yield), bp 139—145 °C (bath temp)/0.05 Torr. ^{1}H-NMR (CCl_4): δ 0.84 and 0.98 (2s, 3H, CCH_3), 1.07, 1.09 (2d, J=6.0 Hz, 3H), 1.1—2.9 (m, 8H), 3.83 (s, 3H, CH_3COO), 6.3—6.6 (m, 1H). ^{13}C-NMR ($CDCl_3$) showed two peaks at δ 128.72 and 129.09 ($\underline{C}H_3O\underline{C}O$), with the ratio 1.9:1. IR: 1735, 1719, 1654, 1200 cm^{-1}; MS: *m/e* (rel intensity) 222 (M^+, 23), 207 (12), 180 (14), 163 (39), 121 (100), 93 (57), 77 (24). Found: C, 70.15; H, 8.40%. Calcd for $C_{15}H_{18}O_3$: C, 70.24; H, 8.16%.

A large scale experiment using **24** (8.9 g), methanol (25 ml), sulfuric acid (25 ml) resulted in 49% yield (4.3 g) of **25**.

Synthesis of t-*3-Isopropenyl-*r-*1,*c*-9-dimethylbicyclo[4.3.0]non-5-en-7-one (**38**).* A methanol (2 ml) solution of sodium borohydride (76 mg, 2.0 mmol) was added at room temperature to a mixture of **25** (0.45 g, 2.0 mmol) and cerium-(III) chloride heptahydrate (0.30 g, 0.80 mmol) in methanol (5 ml). After 20 min the reaction mixture was worked up to give a crude allyl alcohol **39** (0.50 g), which was dissolved in methanol (5 ml), treated with potassium hydroxide (0.23 g, 4.1 mmol) in water (5 ml) at room temperature and heated at 80 °C for 30 min. The reaction mixture was acidified with 5% hydrochloric acid and then extracted with ethyl acetate. The crude product thus obtained was dissolved in ether (5 ml) and methyllithium (1.14 M ether solution, 7.9 ml, 9.0 mmol) was added at 0 °C under an argon atmosphere and allowed to react for 2 h. Work-up followed by column chromatography (hexane–ethyl acetate 2:1) gave **40** (0.20 g, 49% yield, 97% yield based on the recovered **39**) along with **39** (0.21 g, 50%). The methyl ketone **40** showed IR: 3210, 1705 cm^{-1}; ^{1}H-NMR (CCl_4): δ 0.7—1.0 (m, 6H), 1.0—2.9 (m, 8H), 2.15 (s, 3H), 3.4—3.8 (br s, 1H), 4.2—4.7 (m, 1H), 5.5—5.7 (m, 1H).

Sodium hydride (50% in oil, 0.24 g, 5.0 mmol) was added to DMSO (2 ml) under an argon atmosphere and heated at 80 °C for 30 min. The resulting solution was cooled with a water bath and admixed with a DMSO (2 ml) solution of triphenylmethylphosphonium bromide (2.7 g, 4.8 mmol). After 15 min **40** (0.25 g, 1.20 mmol) in DMSO (5 ml) was added to the resulting red solution. After 1 h the reaction mixture was worked up. The crude product was dissolved in dichloromethane (2 ml) and added to pyridinium chlorochromate (1.33 g, 5.0 mmol) in dichloromethane (5 ml) at room temperature and allowed to react for 1. 5h. Work-up and preparative TLC purification (hexane–ether 1:1) gave **38** (0.20 g, 80% yield), bp 128—135 °C (bath temp)/0.3 Torr. ^{1}H-NMR (CCl_4): δ 1.00 (s, 3H, CCH_3), 1.07, 1.10 (2d, J=6.0 Hz, 3H, $CHC\underline{H}_3$), 1.5—2.7 (m, 8H), 1.76 (s, 3H, $C\underline{H}_3C=CH_2$), 4.72 (br s, 2H, $CH_2=C$), 6.39 (t, J=3.6 Hz, 0.88H), 6.53 (m, 0.12 H); IR: 3086, 1718, 1654, 886 cm^{-1}; MS: *m/e* (rel intensity) 204 (M^+, 61), 189 (31), 161 (28), 147 (41), 136 (30), 133 (32), 119 (100), 105 (50), 93 (53), 91 (48), 77 (43). Found: C, 82.21; H, 9.73%. Calcd for $C_{14}H_{20}O$: C, 82.30; H, 9.87%.

*Alternative Route from **25** to **38**.* A mixture of **25** (0.68 g, 3.0 mmol), 1,2-ethanedithiol (0.43 g, 4.5 mmol), chloroform (10 ml) and boron trifluoride etherate (40 mg) was stirred at room temperature under an argon atmosphere. After 16 h boron trifluoride ethereate catalyst (5 drops, *ca.* 50 mg) was added and the reaction mixture was stirred for 24 h. Work-up followed by preparative TLC (hexane–ether 3:1) gave **36** (R_f 0.64—0.76, 0.51 g, 57% yield). ^{1}H-NMR (CCl_4): δ 0.8—1.1 (m, 6H), 1.1—3.0 (m, 8H), 3.0—3.5 (m, 4H, SCH_2CH_2S), 3.65 (s, 3H, CH_3OCO), 5.9—6.2

(m, 1H); IR: 1728, 1195, 1167 cm^{-1}; MS: *m/e* 298 (M^+).

A mixture of **36** (126 mg, 0.42 mmol), methanol (2 ml), potassium hydroxide (53 mg, 0.95 mmol) dissolved in water (2 ml) was heated to reflux for 1 h. The reaction mixture was extracted once with ether and acidified with 10% hydrochloric acid. Extractive work-up with ether (20 ml×4 times) gave the carboxylic acid (120 mg) which was dissolved in ether (2 ml) at 0 °C. To this solution was added methyllithium (1.66 M ether solution, 0.76 ml, 1.26 mmol) over a period of 5 min and the resulting solution was stirred at 0 °C for 4.5 h. Work-up followed by preparative TLC (hexane–ether 2:1) gave the corresponding methyl ketone (78 mg, 66% yield). IR: 1707 cm^{-1}; ^{1}H-NMR (CCl_4, * refers to the major isomer): δ 0.79, 0.97 (s, 3H, CCH_3), 0.93*, 0.97 (d, J=7.0*, 7.5 Hz respectively, 3H), 1.1—2.9 (m, 8H), 2.13*, 2.10 (s, 3H, CH_3CO), 3.0—3.5 (m, 4H, SCH_2CH_2S), 5.97 (t, J=3.0 Hz, 0.29 H), 6.06* (dd, J=6.0, 3.0 Hz, 0.71 H); MS: *m/e* 282 (M^+).

The methyl ketone (73 mg, 0.26 mmol) was allowed to react with triphenylphosphonium methylide (0.52 mmol) in DMSO (7 ml) at room temperature for 2.3 h. Work-up followed by preparative TLC (hexane–ether 5:1) gave the corresponding isopropenyl derivative **37** (69 mg, 96% yield). ^{1}H-NMR (CCl_4): δ 0.91 (d, J=6.0 Hz, 3H), 0.97 (s, 3H, CCH_3), 1.0—2.7 (m, 8H), 1.73 (s, 3H, CH_3C=), 3.0—3.5 (m, 4H, SCH_2CH_2S), 4.67 (br s, 2H, CH_2=C), 5.96 (t, J=3.6 Hz, 1H). Careful examination of the olefinic region confirmed purity >97%. IR: 3090, 1642, 887 cm^{-1}; MS: *m/e* 280 (M^+).

Hydrolysis of the dithioacetal group was carried out by mixing **37** (40 mg, 0.14 mmol) in dichloromethane (1 ml) with isopentyl nitrite (19 mg, 0.16 mmol) and 30 min after with water (9 mg, 0.5 mmol). After 1.5 h isopentyl nitrite (0.5 ml) was added to complete the reaction and the entire mixture was stirred for 14.3 h. Work-up and preparative TLC purification (hexane–ether 1:1) gave the key intermediate **38** (14 mg, 48% yield) having the correct spectra. ^{1}H-NMR (CCl_4) gave olefinic absorption at δ 6.41 (t, J=3.6 Hz, 1H) only, thus indicating the purity higher than 97%.

Synthesis of dl-*Nootkatone.* A THF (2 ml)–hexane (1.6 ml) solution of lithium dicyclohexylamide (2.6 mmol) was added dropwise at −78 °C over a period of 2 h to **38** (88% purity) (177 mg, 0.87 mmol), dibromomethane (0.31 g, 1.77 mmol) dissolved in THF (5 ml) under an argon atmosphere, and the reaction mixture was stirred for 1 h, and then quenched with methanol (1.0 ml) at −78 °C. Work-up and preparative TLC (benzene) gave the adduct **41** (198 mg, 60% yield; 84% yield based on the consumed **38**) along with the recovered **38** (50 mg, 28%). ^{1}H-NMR (CCl_4): δ 0.98 (d, J=4.5 Hz, 3H, $CHC\underline{H}_3$), 1.07 (s, 3H, CCH_3), 1.1—2.7 (m, 8H), 1.74 (s, 3H, $C\underline{H}_3$-C=), 4.69 (s, 2H, CH_2=C), 5.66 (t, J=3.6 Hz, 1H), 5.81 (s, 1H, $CHBr_2$); IR: 3450, 3085, 1643, 888 cm^{-1}; MS: *m/e* 205 (M^+-CHBr_2).

A butyllithium hexane solution (1.57 M, 0.94 ml, 1.47 mmol) was added over a period of 20 min to the adduct **41** (185 mg, 0.49 mmol) in THF (10 ml) at −95 °C under an argon atmosphere. Stirring was continued at −95 °C for 100 min, and then at room temperature for 5 min. Work-up and preparative TLC (benzene) gave *t*-8-isopropenyl-*r*-5,*c*-6-dimethylbicyclo[4.4.0]dec-10(1)-en-3-one (**42**) (89 mg, 83% yield). ^{1}H-NMR (CCl_4): δ 0.97 (d, J=6.5 Hz, 3H, CH-C$\underline{H}_3$), 1.17 (s, 3H, CCH_3), 1.1—2.5 (m+s (δ 1.75), 11H), 2.73 d, J=16.5 Hz, 1H), 3.10 (dm, J=16.5 Hz, 1H), 4.70 (br s, 2H, CH_2=C), 5.3—5.5 (m, 1H); IR: 3090, 1721, 1644, 887 cm^{-1}; MS: *m/e* 218 (M^+).

The octalone **42** (78 mg, 0.36 mmol) was stirred at room temperature in THF (3 ml) and 5% sulfuric acid (3 ml) for 4 h. Work-up followed by preparative TLC (hexane–ethyl acetate 5:1) gave *dl*-nootkatone (**43**) (45 mg, 58% yield; 74% yield based on the recovered **42** (17 mg, 22%)). The synthesized sample had IR absorptions at 3080, 1671, 1619, 887 cm^{-1}, and ^{1}H-NMR (CCl_4) at δ 0.97 (d, J=6.5 Hz, 3H), 1.13 (s, 3H), 1.1—2.6 (m, 10H), 4.67 (s, 2H), 5.61 (s, 1H) identical exactly with the spectra of the authentic specimen. Careful integration around δ 5.9—5.5 revealed that the sample has purity higher than 93%. The 7-*epi*-nootkatone should give a peak at δ 5.68.[15]

*Cyclopentannulation of 2-Cyclododecenone (**44**).* A butyllithium hexane solution (1.49 M, 8.8 ml, 13.1 mmol) was added dropwise at −78 °C to a THF (90 ml) solution of propargyl alcohol (0.37 g, 6.5 mmol) under an argon atmosphere, and the reaction mixture was stirred for 2 h. To this solution was added a THF (5 ml) solution of 2-cyclododecenone (0.78 g, 4.4 mmol) over 8 min, and the whole was stirred at −78 °C for 2 h, then allowed to warm to room temperature and stirred for 16 min. Work-up followed by column chromatography (hexane–ethyl acetate 2:1 to 1:1) gave 1-(3-hydroxy-1-propynyl)-2-cyclododecenol (**45**) (0.95 g, 92% yield) as colorless needles, mp 71.5—72.5 °C (hexane–dichloromethane, *ca.* 2:1). ^{1}H-NMR (CCl_4): δ 1.0—2.3 (m, 18H), 2.93 (br s, 2H), 4.22 (s, 2H), 5.40 (d, J=16.1 Hz, 1H), 5.80 (dt, J=16.1, 6.3 Hz, 1H); IR: 3300, 785, 760 cm^{-1}; MS: *m/e* (rel intensity): 236 (M^+, 1), 218 (30), 205 (13), 187 (11), 175 (11), 161 (16), 147 (21), 125 (47), 117 (100), 95 (100), 91 (87), 79 (63), 67 (53), 55 (89). Found: C, 76.24; H, 10.46%. Calcd for $C_{15}H_{24}O_2$: C, 76.22; H, 10.24%.

The adduct **45** (1.20 g, 5.1 mmol) was dissolved in methanol (80 ml) and cooled at −20 °C. To this solution was added sulfuric acid (40 ml) over a period of 40 min. The resulting mixture was stirred for 14 h, being allowed to warm to room temperature. The reaction mixture was diluted successively with ether (100 ml) and satd. aq sodium chloride solution (100 ml), and shaken vigorously. The ethereal layer was separated, neutralized with aq sodium hydrogencarbonate solution, dried with anhydrous sodium sulfate and concentrated. The residue purified by column chromatography (hexane–ethyl acetate 5:1) gave *trans*-bicyclo-[10.3.0]pentadeca-1(12),2-dien-13-one (**46**) (0.72 g, 65% yield) as a colorless needles, mp 87—87.5 °C (hexane–dichloromethane *ca.* 1:1). ^{1}H-NMR (CCl_4): δ 0.8—1.9 (m, 12H), 2.1—2.4 (m, 6H), 2.4—2.7 (m, 2H), 6.17 (dt, J=16.5, 4.5 Hz, 1H), 6.68 (d, J=16.5 Hz, 1H); IR (CCl_4): 1693, 1643, 1596, 972 cm^{-1}; UV (EtOH); λ_{max} 281 nm (log ε 4.3); MS: *m/e* (rel intensity) 218 (M^+, 38), 203 (4), 189 (6), 175 (8), 161 (10), 147 (17), 133 (100), 122 (35), 105 (17), 91 (33). Found: C, 82.37; H, 9.8%. Calcd for $C_{15}H_{22}O$: C, 82.51; H, 10.16%.

*3-Methylbicyclo[10.3.0]pentadec-1(12)-en-13-one (**53**).* A methylmagnesium iodide ether solution (4.6 ml, 3.7 mmol), THF (10 ml) and then copper(I) chloride (29 mg, 0.29 mmol) were added successively at 0 °C over a period of 11 min to a THF (5 ml) solution of the dienone **46** (0.40 g, 1.83 mmol) and copper(I) chloride (14 mg, 0.14 mmol) under an argon atmosphere. The mixture was stirred for 1.4 h, treated with ice–hydrochloric acid mixture and then extracted successively with ether and ethyl acetate. The combined organic phase was dried (Na_2SO_4), concentrated *in vacuo*, and the residue was purified by preparative TLC (hexane–ethyl acetate 3:1) to give **53** (0.29 g, R_f 0.6—0.68, 68% yield; 74% yield based on the consumed **46**) along with the recovered dienone **46** (28 mg, R_f 0.55—0.60). Bp 157—159 °C (bath temp)/0.04 Torr. ^{1}H-NMR

(CCl_4): δ 0.9—3.0 (m+d (δ 1.08, J=6.6 Hz), 26H); IR: 1692, 1630 cm^{-1}; MS: *m/e* (rel intensity) 234 (M^+, 100), 219 (60), 191 (28), 177 (52), 163 (73), 149 (63), 135 (52), 121 (34), 110 (45), 79 (45), 155 (59). Found: C, 81.70; H, 11.45%. Calcd for $C_{16}H_{26}O$: C, 81.99; H, 11.18%.

*7-Methylcyclopentadecane-1,5-dione (**54**).* Sodium borohydride (0.56 g, 14.7 mmol) was added portionwise at 0 °C to the cyclopentenone **53** (0.29 g, 1.25 mmol) dissolved in a 5:1 mixture of methanol and water (17 ml) and the reaction mixture was stirred for 2.5 h. Work-up gave an allyl alcohol (0.32 g) which was dissolved in dichloromethane (14 ml) and treated at 0 °C with *m*-chloroperoxybenzoic acid (0.26 g, 1.5 mmol) dissolved in dichloromethane (14 ml). The reaction mixture was stirred at 0 °C for 1.2 h, quenched with satd. aq sodium sulfite solution and neutralized with aq satd. sodium hydrogencarbonate solution. Extraction with dichloromethane followed by concentration gave an epoxy alcohol (0.34 g) which was dissolved in pyridine (4 ml) and treated with *p*-toluenesulfonyl chloride (0.36 g, 1.87 mmol) at 0 °C under an argon atmosphere, and the whole was left at 0 °C for 21 h, then poured into 2 M hydrochloric acid solution, and extracted with ether. The usual work-up gave a crude epoxy tosylate (0.47 g) which was dissolved in a 3:2 mixture of dioxane–water (10 ml) and heated at reflux in the presence of calcium carbonate (185 mg, 1.85 mmol) for 24 h. Work-up followed by preparative TLC (hexane–ethyl acetate 2.5:1) afforded the desired diketone **54** (0.22 g, R_f 0.47—0.60, 71% overall yield). Bp 156—158 °C (bath temp)/0.05 Torr, ^{1}H-NMR (CCl_4): δ 0.8—2.9 (m+d (δ 0.91, J=5.7 Hz), 28H); IR: 1709 cm^{-1}; MS: *m/e* (rel intensity) 252 (M^+, 24), 195 (15), 167 (22), 128 (39), 97 (54), 69 (42), 55 (100). Found: C, 76.00; H, 11.39%. Calcd for $C_{16}H_{28}O_2$: C, 76.14; H, 11.18%.

dl-*Muscopyridine (**55**).* A mixture of the diketone (**54**) (90 mg, 0.36 mmol), ethanol (20 ml), and hydroxylamine hydrochloride (0.55 g, 0.79 mmol) was heated under an argon atmosphere at 150—160 °C in an autoclave (capacity 100 ml) for 17.6 h. After cooling the reaction mixture was taken in ether, and the ethereal solution was washed with aq satd. hydrogencarbonate solution, then dried (Na_2SO_4), and concentrated. The residue was purified by preparative TLC (hexane–ethyl acetate 5:1) to give *dl*-muscopyridine (**55**) (54 mg, R_f 0.65—0.75, 65% yield). The synthetic sample exhibited the following spectra identical with those of the authentic chiral specimen. ^{1}H-NMR (CCl_4): δ 0.6—2.3 (m+d (δ 1.11, J=7.5 Hz), 18H), 2.3—3.0 (m, 4H), 6.83 (d, J=7.8 Hz, 2H), 7.42 (t, J=7.8 Hz, 1H), IR: 3065, 1589, 1575, 1453, 763, 743 cm^{-1}; MS: *m/e* (rel intensity) 231 (M^+, 88), 188 (38), 160 (41), 147 (31), 146 (41), 134 (59), 133 (34), 120 (100), 107 (97).

*Cyclopentannulation of 2-Cyclooctenone (**47**).* A butyllithium hexane solution (1.49 M, 20.1 ml, 30.0 mmol) was added to a THF (170 ml) solution of propargyl alcohol (0.84 g, 15.0 mmol) at −78 °C under an argon atmosphere, and the reaction mixture was stirred for 2.7 h. The solution was warmed to −55 °C, and to this was added a THF (6 ml) solution of 2-cyclooctenone (**47**) (1.24 g, 10.0 mmol) over a period of 10 min. The reaction mixture was stirred for 10.7 h, and warmed to 20 °C. Work-up gave an oil (2.2 g) which was purified by column chromatography to give 1-(3-hydroxy-1-propynyl)-2-cycloocten-1-ol (**48**) (0.92 g, 51% yield; 76% yield based on the consumed enone **47**) along with the recovered **47** (0.37 g, 30%). Physical properties of **48**: bp 170—173 °C (bath temp)/0.07 Torr; ^{1}H-NMR (CCl_4): δ 1.2—2.8 (m, 10H), 3.17 (br s, 2H), 4.24 (s, 2H), 5.25—5.7 (m, 2H); IR: 3350, 1063, 1035, 708 cm^{-1}; MS: *m/e* (rel intensity) 180 (M^+, 2), 106 (51), 91 (100), 77 (51), 55 (60). Found: C, 73.55; H, 8.95%. Calcd for $C_{11}H_{16}O_2$: C, 73.30; H, 8.95%.

The adduct **48** (68 mg, 0.38 mmol) was stirred with acetic anhydride (0.5 ml) and pyridine (0.05 ml) at room temperature for 1 h. All the volatile material was evaporated *in vacuo*. The residue was dissolved in methanol (1 ml) and to this was added sulfuric acid (1 ml) dropwise at −15 °C over a period of 10 min. The solution was stirred for 25 min, and warmed up to −5 °C. Work-up followed by preparative TLC (hexane–ethyl acetate 2:1) gave bicyclo[6.3.0]undeca-1(8),2-dien-9-one (**49**) (26 mg, 42% yield). Bp 114—118 °C (bath temp)/0.08 Torr; ^{1}H-NMR (CCl_4): δ 1.3—1.9 (m, 4H), 1.9—2.7 (m, 8H), 5.7—6.4 (m, 2H); IR: 1693, 1620, 741 cm^{-1}; MS: *m/e* (rel intensity) 162 (M^+, 100), 133 (87), 115 (56), 91 (77). Found: C, 81.65; H, 8.98%. Calcd for $C_{11}H_{14}O$: C, 81.44; H, 8.70%.

*Cyclopentannulation of 2-Cycloheptenone (**50**).* Butyllithium (1.49 M hexane solution, 8.4 ml, 12.5 mmol) was added dropwise to a THF (70 ml) solution of propargyl alcohol (0.35 g, 6.3 mmol) at −78 °C under an argon atmosphere and the resulting solution was stirred for 4.5 h and warmed to −25 °C. At this temperature 2-cycloheptenone (**50**) (0.46 g, 4.2 mmol) dissolved in THF (5 ml) was added in 3 min and the reaction mixture was stirred for 15 h and allowed to warm to room temperature. Work-up followed by column chromatography (hexane–ethyl acetate 1:1) gave 1-(3-hydroxy-1-propynyl)-2-cyclohepten-1-ol (**51**) (0.45 g, 65% yield); bp 169—172 °C (bath temp)/0.07 Torr; ^{1}H-NMR (CCl_4): δ 1.2—2.9 (m, 8H), 4.29 (s, 2H), 4.42 (br s, 2H), 5.7—5.9 (m, 2H); IR: 3330, 1072, 1015, 686 cm^{-1}; MS: *m/e* (rel intensity) 166 (M^+, 14), 148 (24), 119 (43), 115 (48), 98 (33), 92 (43), 91 (100), 79 (52), 78 (48), 77 (52), 47 (43), 65 (43), 55 (67). Found: C, 72.06; H, 8.78%. Calcd for $C_{10}H_{14}O_2$: C, 72.26; H, 8.49%.

The diol **51** (68 mg, 0.41 mmol) was stirred with acetic anhydride (0.5 ml) and pyridine (0.05 ml) at room temperature for 1.5 h. The volatile material was evaporated off and the residue was dissolved in methanol (4 ml). To the solution was added sulfuric acid (2 ml) at −15 °C over a period of 5 min. Stirring was continued for 2.5 h and the reaction mixture was diluted with dichloromethane (5 ml), poured onto crushed ice (*ca.* 10 g), and the extracted with dichloromethane. The usual work-up followed by preparative TLC (hexane–ethyl acetate 2:1) gave bicyclo[5.3.0]deca-1(7),2-dien-8-one (**52**) (30 mg, 49% yield); bp 124—126 °C (bath temp)/0.06 Torr; ^{1}H-NMR (CCl_4): δ 1.7—2.1 (m, 2H), 2.2—2.7 (m, 8H), 5.90 (d, J=11.6 Hz, 1H), 6.20 (dt, J=11.6, 5.0 Hz, 1H); IR: 1689, 1639, 1607, 726 cm^{-1}; MS: *m/e* (rel intensity) 148 (M^+, 65), 133 (26), 116 (58), 115 (65), 92 (35), 91 (100), 79 (25), 78 (35), 77 (25), 65 (21). Found: *m/e* 148.0876 (M^+). Calcd for $C_{10}H_{12}O$: *m/e* 148.0888.

This work was financially supported by the Ministry of Education, Science and Culture (Grant-in-Aid Nos. 311702, 375462, 411102, and 475665).

References

1) M. E. Jung, *Tetrahedron*, **32**, 3 (1976); J. d'Angelo, *ibid.*, **32**, 2979 (1976); R. E. Gawley, *Synthesis*, **1976**, 777.
2) R. A. Ellison, *Synthesis*, **1973**, 397.
3) B. M. Trost and D. E. Keeley, *J. Am. Chem. Soc.*, **98**, 248 (1976).
4) Y. Hayakawa, K. Yokoyama, and R. Noyori, *J. Am. Chem. Soc.*, **100**, 1799 (1978).

5) M. Miyashita, T. Yanami, and A. Yoshikoshi, *J. Am. Chem. Soc.*, **98**, 4679 (1976).
6) R. B. Woodward and R. Hoffmann, "The Conservation of Orbital Symmetry," Verlag Chemie GmbH, Weinheim-Berchstr., Germany (1970), p. 58; T. S. Sorensen and A. Rauk, "Pericyclic Reactions," ed by A. P. Marchand and R. E. Lehr, Academic Press, New York (1977), Vol. 2, p. 31.
7) a) S. Hirano, S. Takagi, T. Hiyama, and H. Nozaki, *Bull. Chem. Soc. Jpn.*, **53**, 169 (1980); b) T. Hiyama, M. Shinoda, M. Tsukanaka, and H. Nozaki, *ibid.*, **53**, 1010 (1980).
8) R. M. Jacobson, G. P. Lahm, and J. W. Clader, *J. Org. Chem.*, **45**, 395 (1980); L. A. Paquette, W. E. Fristad, D. S. Dime, and T. R. Bailey, *ibid.*, **45**, 3017 (1980); F. Cooke, R. Moerck, J. Schwindeman, and P. Magnus, *ibid.*, **45**, 1046 (1980).
9) a) A. M. Islam and R. A. Raphael, *J. Chem. Soc.*, **1953**, 2247; b) M. Karpf and A. S. Dreiding, *Helv. Chim. Acta*, **59**, 1226 (1976); c) M. Baumann, W. Hoffmann, and N. Müller, *Tetrahedron Lett.*, **1976**, 3585.
10) Preliminary reports: a) T. Hiyama, M. Shinoda, and H. Nozaki, *J. Am. Chem. Soc.*, **101**, 1599 (1979); b) *Tetrahedron Lett.*, **1979**, 3529; c) H. Saimoto, T. Hiyama, and H. Nozaki, *ibid.*, **1980**, 3897.
11) H. Taguchi, H. Yamamoto, and H. Nozaki, *Bull. Chem. Soc. Jpn.*, **50**, 1588, 1592 (1977).
12) C. J. V. Scanio and R. M. Starrett, *J. Am. Chem. Soc.*, **93**, 1539 (1971).
13) E. Piers, R. W. Britton, and W. de Waal, *Can. J. Chem.*, **47**, 4307 (1969).
14) C. L. Liotta, *Tetrahedron Lett.*, **1975**, 519.
15) Y. Takagi, Y. Nakahara, and M. Matsui, *Tetrahedron*, **34**, 517 (1978).
16) a) H. C. Odom (jun.) and A. R. Pinder, *J. Chem. Soc., Perkin Trans. 1*, **1972**, 2193. We are indebted to Prof. Pinder for the supply of a sample of *dl*-nootkatone; b) G. L. K. Hunter and W. B. Brogden, Jr., *J. Food Sci.*, **30**, 876 (1965); c) M. Pesaro, G. Bozzato, and P. Schudel, *J. Chem. Soc., Chem. Commun.*, **1968**, 1152; d) J. A. Marshall and R. A. Ruden, *J. Org. Chem.*, **36**, 594 (1971); e) A. Van Der Gen, L. M. Van Der Linde, J. G. Witteveen, and H. Boelens, *Recl. Trav. Chim. Pays-Bas*, **90**, 1034, 1045 (1971); f) T. Yanami, M. Miyashita, and A. Yoshikoshi, *J. Org. Chem.*, **45**, 607 (1980); g) R. E. Berry, C. J. Wagner, Jr., and M. G. Moshonas, *J. Food Sci.*, **32**, 75 (1967) and references cited therein.
17) K. P. Dastur, *J. Am. Chem. Soc.*, **96**, 2605 (1974); F. Näf, R. Decorzant, and W. Thommen, *Helv. Chim. Acta*, **62**, 114 (1979).
18) T. Miki, M. Ineoka, Y. Isoda, and J. Okano, Japan Patent, 7633902 (1976); *Chem. Abstr.*, **86**, P-170953f (1977).
19) C. Girard and J.-M. Conia, *J. Chem. Res.*, **1978**, (S) 182, (M) 2351.
20) K. Fuji, K. Ichikawa, and E. Fujita, *Tetrahedron Lett.*, **1978**, 3561.
21) J.-L. Luche, L. Rodriguez-Hahn, and P. Crabbé, *J. Chem. Soc., Chem. Commun.*, **1978**, 601.
22) Similar ring closure of heptatrienyl cations to five-membered rings is observed: R. Noyori, Y. Ohnishi, and M. Kato, *J. Am. Chem. Soc.*, **94**, 5105 (1972).
23) a) H. Schniz, L. Ruzicka, U. Geyer, and V. Prelog, *Helv. Chim. Acta*, **29**, 1524 (1946); b) K. Biemann, G. Büchi, and B. H. Walker, *J. Am. Chem. Soc.*, **79**, 5558 (1957). The reference citation[10c] was inappropriate with respect to the structure determination which was actually carried out by Biemann, Büchi and Walker (*loc. cit.*) on the basis of total synthesis. The ETH group[23a] carried out isolation and gave brief information on its structure; c) K. Tamao, S. Kodama, T. Nakatsuka, Y. Kiso, and M. Kumada, *J. Am. Chem. Soc.*, **97**, 4405 (1975).
24) N. W. Atwater, R. H. Bible, Jr., E. A. Brown, R. R. Burtner, J. S. Mihina, L. N. Nysted, and P. B. Sollman, *J. Org. Chem.*, **26**, 3077 (1961); J. A. Campbell and J. C. Babcock, *J. Am. Chem. Soc.*, **81**, 4069 (1959).
25) R. W. Gray and A. S. Dreiding, *Helv. Chim. Acta*, **60**, 1969 (1977).
26) S. Fujita and H. Nozaki, *Bull. Chem. Soc. Jpn.*, **44**, 2827 (1971); *Yuki Gosei Kagaku Kyokai Shi*, **30**, 679 (1972).
27) G. Büchi and J. E. Powell, Jr., *J. Am. Chem. Soc.*, **89**, 4559 (1967).

  Bull. Chem. Soc. Jpn., 54, 2759—2762 (1981)

Synthesis of Oligoinosinates with 2′–5′ Internucleotide Linkage in Aqueous Solution Using Pb^{2+} Ion

Hiroaki SAWAI* and Masaji OHNO

Faculty of Pharmaceutical Sciences, The University of Tokyo, Hongo, Bunkyo-ku, Tokyo 113

(Received January 28, 1981)

Oligoinosinates up to a pentamer were synthesized by the polymerization of inosine-5′-phosphorimidazolide in aqueous solution using Pb^{2+} ion. 2′–5′ Internucleotide linkage was preferentially formed. The yields of the 2′–5′ linked dimer, trimer, and tetramer were 14.8, 4.5, and 1.6%, respectively. A small amount of linkage isomers of oligoinosinates with 3′–5′ linkage was obtained. The products were characterized by sequential enzyme tests.

Recently 2′–5′ linked oligoadenylate ($pppA^{2'}p^{5'}A^{2'}p^{5'}A$) was isolated from interferon-treated cell and has attracted widespread interest because of its strong biological activity and unusual structure.[1-3] The availability of various oligonucleotides with 2′–5′ linkage would facilitate further study of their biological action. As a part of our program in the synthetic approach to oligonucleotides, attention was focused on the selective synthesis of short chained oligonucleotides containing 2′–5′ linkage without using any protecting group.

Reports were given on the synthesis of 2′–5′ linked oligoadenylates from adenosine-5′-phosphorimidazolide in aqueous solution using Pb^{2+} ion.[4,5] The method employs no protecting group, various oligoadenylates being obtained in the one step reaction. We have attempted the synthesis of other homooligonucleotides with 2′–5′ linkage by a similar procedure.[6] This paper describes the oligoinosinates synthesis from inosine·5′·phosphorimidazolide in aqueous solution using Pb^{2+} ion. The products were separated by ion exchange column chromatography and characterized by sequential enzyme and alkaline digestion.

Results and Discussion

Inosine-5′-phosphorimidazolide (ImpI) was prepared from inosine-5′-monophosphate (pI) and imidazole using di-2-pyridyl disulfide and triphenylphosphine as a condensing agent. Phosphorimidazolide bond is labile, hydrolyzing in aqueous solution spontaneously in the absence of divalent metal ion catalyst. The Pb^{2+} ion promoted the internucleotide linkage formation from ImpI. Addition of lead nitrate to a neutral aqueous solution of ImpI caused precipitation, suggesting formation of Pb^{2+}–ImpI complex. The ImpI was allowed to react in a neutral aqueous mixture for 3 d with stirring in the presence of the Pb^{2+} ion for polymerization. Treatment of the reaction mixture with *N*·(2-hydroxyethyl)-ethylenediamine-*N*,*N*′,*N*′·triacetic acid trisodium (Versenol) buffer turned the mixture homogeneous. The Pb^{2+} ion formed a complex with Versenol completely. The formation of the oligoinosinates and Pb^{2+}–Versenol complex was checked by high pressure liquid chromatography (HPLC). The products were separated on a QAE·Sephadex A·25 anion exchange column. The separated products were further purified by paper chromatography when necessary. The elution pattern obtained on column chromatography is shown in Fig. 1. The composition and the yields of the products are given in Table 1 along with the hyperchromicity of the main products.

Oligoinosinates up to a pentamer were formed in addition to the hydrolyzed product pI. The internucleotide linkage formation took place as the following Scheme 1. The 2′–5′ internucleotide linkage was preferentially formed in the reaction.

The oligoinosinates thus obtained were characterized by enzymatic tests, paper chromatography and HPLC. The 2′–5′ internucleotide linkage is not degraded

Table 1. Oligoinosinates obtained from ImpI

Peak No.	ODU_{248}	h[a]	Structure identification	Yield/%[b]
1	36		I	1.0
2	12		3′,5′-Cyclic IMP	0.3
3	231		ImpI	5.5
4	1558		pI	41
5	72		ImpIpI	1.0
			-pIpI- (2′–5′, 2′–5′)	0.9[c]
6	51		IppI	1.3[c]
7+8	770		-pIpI- (2′–5′, 3′–5′)	1.8[c]
		1.04	-pIpI- (3′–5′, 3′–5′)	5.0
		1.08	$pI^{2'}p^{5'}I$	14.8
9	130	1.06	$pI^{3'}p^{5'}I$	2.6
			$IppI^{2'}p^{5'}I$	0.6[c]
10	146	1.15	$pI^{2'}p^{5'}I^{2'}p^{5'}I$	4.5
11	116	1.18	$pI^{2'}p^{5'}I^{3'}p^{5'}I$	2.6
			Unidentified	0.8[c]
12	66	1.15	$pI^{3'}p^{5'}I^{2'}p^{5'}I$	1.5
			Unidentified	0.5[c]
13	120	1.15	$pI^{3'}p^{5'}I^{3'}p^{5'}I$	1.6
		1.20	$pI^{2'}p^{5'}I^{2'}p^{5'}I^{2'}p^{5'}I$	1.5
			Unidentified	0.4[c]
14	33	1.24	$pI^{2'}p^{5'}I^{3'}p^{5'}I^{2'}p^{5'}I$	0.7
			$pI^{2'}p^{5'}I^{2'}p^{5'}I^{3'}p^{5'}I$	0.4
15	30		$(pI)_4$ (Mixtures of isomers)	0.8[c]
16	72	1.31	$pI^{2'}p^{5'}I^{2'}p^{5'}I^{2'}p^{5'}I^{2'}p^{5'}I$	0.6
			$(pI)_4$ and $(pI)_5$ (Mixture of isomers)	1.3[c]

a) Hyperchromicity calculated from alkaline hydrolysis. b) Yield obtained from UV_{248} after allowing for hyperchromicity of each oligoinosinate. Total ODU_{248} of starting ImpI is 3800 (0.31 mmol). c) Hyperchromicity correction was not carried out.

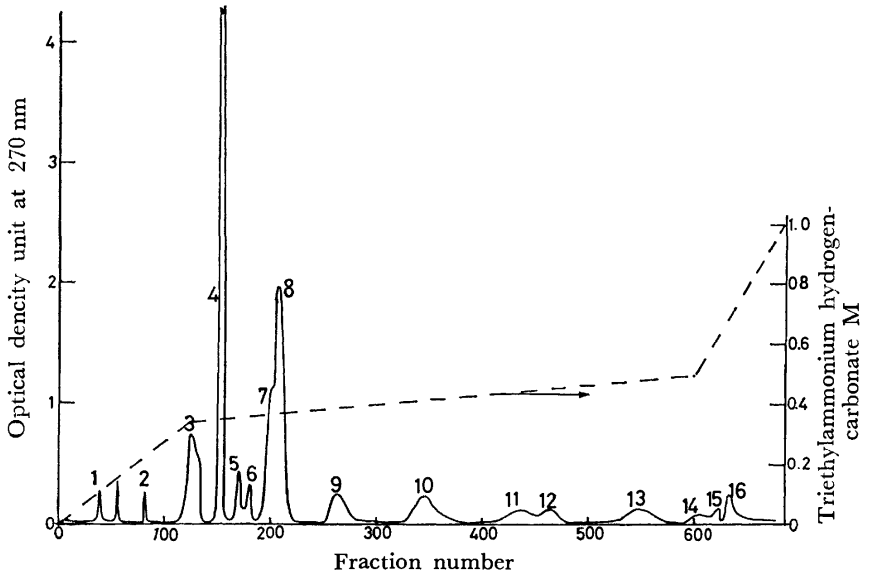

Fig. 1. Chromatography of the oligoinosinates on a QAE-Sephadex A-25 (hydrogen carbonate) column. A linear gradient of triethylammonium hydrogencarbonate was used for elution (dotted line). The characterization of the several peaks is listed in Table 1.

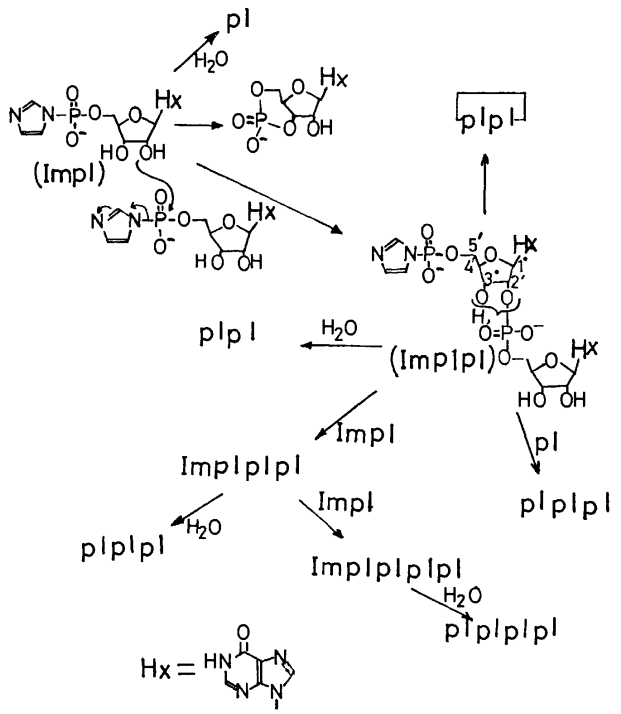

Scheme 1.

with nuclease P_1 (N. P_1) and ribonuclease T_2, while 3′–5′ linkage is degraded. Both 2′–5′ and 3′–5′ internucleotide linkages are hydrolyzed with venom phosphodiesterase (VPD) and by alkaline digestion. Thus, the internucleotide linkage and the chain length of the oligoinosinates were determined by sequential enzyme digestion using bacterial alkaline phosphatase (BAP), N. P_1, and VPD and by alkaline hydrolysis.

The 2′–5′ linked dimer, 5′-phosphoinosinyl-[2′–5′]-inosine ($pI^{2'}p^{5'}I$) and the trimer, 5′-phosphoinosinyl-[2′–5′]-inosinyl-[2′–5′]-inosine ($pI^{2'}p^{5'}I^{2'}p^{5'}I$) were degraded with the enzymes as follows. Digestion of $pI^{2'}p^{5'}I$ with BAP gave inosinyl-[2′–5′]-inosine. $pI^{2'}p^{5'}I$ and $I^{2'}p^{5'}I$ were insensitive to N. P_1. On the other hand, alkaline hydrolysis of $pI^{2'}p^{5'}I$ yielded to inosine (I) and inosine-2′(3′),5′-diphosphate (pIp), and $I^{2'}p^{5'}I$ to I and inosine-2′(3′)-monophosphate (Ip). $I^{2'}p^{5'}I$ was degraded with VPD to I and pI. The tetramer ($pI^{2'}p^{5'}I^{2'}p^{5'}I^{2'}p^{5'}I$) and pentamer ($pI^{2'}p^{5'}\cdot I^{2'}p^{5'}I^{2'}p^{5'}I^{2'}p^{5'}I$) were degraded in a similar way. The yields of the 2′–5′ linked dimer, trimer, tetramer, and pentamer were 14.8, 4.5, 1.5, and 0.5%, respectively.

$$pI^{2'}p^{5'}I \xrightarrow{\text{N. P}_1} \not\rightarrow$$

$$pI^{2'}p^{5'}I \xrightarrow{\text{NaOH}} pIp + I \quad (1:1)$$

$$pI^{2'}p^{5'}I \xrightarrow{\text{BAP}} I^{2'}p^{5'}I \xrightarrow{\text{N. P}_1} \not\rightarrow$$

$$I^{2'}p^{5'}I \xrightarrow{\text{NaOH}} Ip + I \quad (1:1)$$

$$I^{2'}p^{5'}I \xrightarrow{\text{VPD}} I + pI \quad (1:1)$$

$$pI^{2'}p^{5'}I^{2'}p^{5'}I \xrightarrow{\text{N. P}_1} \not\rightarrow$$

$$pI^{2'}p^{5'}I^{2'}p^{5'}I \xrightarrow{\text{NaOH}} pIp + Ip + I \quad (1:1:1)$$

$$pI^{2'}p^{5'}I^{2'}p^{5'}I \xrightarrow{\text{BAP}} I^{2'}p^{5'}I^{2'}p^{5'}I \xrightarrow{\text{N. P}_1} \not\rightarrow$$

$$I^{2'}p^{5'}I^{2'}p^{5'}I \xrightarrow{\text{NaOH}} Ip + I \quad (2:1)$$

$$I^{2'}p^{5'}I^{2'}p^{5'}I \xrightarrow{\text{VPD}} I + pI \quad (1:2)$$

The 3′–5′ linked dimer, 5′-phosphoinosinyl-[3′–5′]-inosine ($pI^{3'}p^{5'}I$), and the trimer, 5′-phosphoinosinyl-[3′–5′]-inosinyl-[3′–5′]-inosine ($pI^{3'}p^{5'}I^{3'}p^{5'}I$), were isolated in 2.6 and 1.4% yield, respectively. These compounds were hydrolyzed by the enzymes as illustrated below.

$$pI^{3'}p^{5'}I \xrightarrow{N.P_1} pI$$

$$pI^{3'}p^{5'}I \xrightarrow{BAP} I^{3'}p^{5'}I \xrightarrow{N.P_1} I + pI \ (1:1)$$

$$I^{3'}p^{5'}I \xrightarrow{NaOH} Ip + I \ (1:1)$$

$$pI^{3'}p^{5'}I^{3'}p^{5'}I \xrightarrow{N.P_1} pI$$

$$pI^{3'}p^{5'}I^{3'}p^{5'}I \xrightarrow{BAP} I^{3'}p^{5'}I^{3'}p^{5'}I \xrightarrow{N.P_1} I + pI \ (1:2)$$

$$I^{3'}p^{5'}I^{3'}p^{5'}I \xrightarrow{NaOH} Ip + I \ (2:1)$$

Two linkage isomers, $pI^{3'}p^{5'}I^{2'}p^{5'}I$ and $pI^{2'}p^{5'}I^{3'}p^{5'}I$, were present in peaks 11 and 12, respectively. Their characterization was accomplished by the following enzyme digestion.

$$pI^{3'}p^{5'}I^{2'}p^{5'}I \xrightarrow{N.P_1} pI + pI^{2'}p^{5'}I \ (1:1)$$

$$pI^{3'}p^{5'}I^{2'}p^{5'}I \xrightarrow{BAP}$$

$$I^{3'}p^{5'}I^{2'}p^{5'}I \xrightarrow{N.P_1} I + pI^{2'}p^{5'}I \ (1:1)$$

$$\downarrow NaOH$$

$$pIp + I \ (1:1)$$

$$pI^{2'}p^{5'}I^{3'}p^{5'}I \xrightarrow{N.P_1} pI^{2'}p^{5'}I + pI \ (1:1)$$

$$pI^{2'}p^{5'}I^{3'}p^{5'}I \xrightarrow{BAP}$$

$$I^{2'}p^{5'}I^{3'}p^{5'}I \xrightarrow{N.P_1} I^{2'}p^{5'}I + pI \ (1:1)$$

$$\downarrow NaOH$$

$$Ip + I \ (1:1)$$

Two tetramers containing one 3′–5′ and two 2′–5′ internucleotide linkages in a different position, $pI^{2'}p^{5'}I^{3'}p^{5'}I^{2'}p^{5'}I$ and $pI^{2'}p^{5'}I^{2'}p^{5'}I^{3'}p^{5'}I$, were isolated in a small amount. They were degraded with the enzymes as follows.

$$pI^{2'}p^{5'}I^{3'}p^{5'}I^{2'}p^{5'}I \xrightarrow{N.P_1} pI^{2'}p^{5'}I$$

$$pI^{2'}p^{5'}I^{3'}p^{5'}I^{2'}p^{5'}I \xrightarrow{BAP}$$

$$I^{2'}p^{5'}I^{3'}p^{5'}I^{2'}p^{5'}I \xrightarrow{N.P_1} I^{2'}p^{5'}I + pI^{2'}p^{5'}I \ (1:1)$$

$$pI^{2'}p^{5'}I^{2'}p^{5'}I^{3'}p^{5'}I \xrightarrow{N.P_1} pI + pI^{2'}p^{5'}I^{2'}p^{5'}I$$

$$pI^{2'}p^{5'}I^{2'}p^{5'}I^{3'}p^{5'}I \xrightarrow{BAP}$$

$$I^{2'}p^{5'}I^{2'}p^{5'}I^{3'}p^{5'}I \xrightarrow{N.P_1} I^{2'}p^{5'}I^{2'}p^{5'}I + pI \ (1:1)$$

$$\downarrow NaOH$$

$$Ip + I \ (2:1)$$

Linkage isomers of the tetramer and pentamer were present in peaks 15 and 16 in a small amount. They remain unidentified.

Contrary to the oligoadenylate formation,[5] appreciable amounts of cyclic diinosinates were obtained in peaks 6 and 7. They were characterized by resistance to BAP and by their chromatographic mobilities. The internucleotide linkage of the cyclic diinosinates was determined by susceptibility to N. P_1. N. P_1 degraded 3′–5′, 3′–5′, and 3′–5′, 2′–5′ linked isomers to pI and $pI^{2'}p^{5'}I$, respectively. 2′–5′,2′–5′ Linked cyclic diinosinate was insensitive to N. P_1, being degraded to pI with VPD. The degradation rate of the cyclic diinosinates with the enzymes was lower than that of the linear dimer. Of the three linkage isomers, the 3′–5′, 3′–5′ linked cyclic diinosinate was predominant. A molecular model indicates that the cyclic dinucleotide prefers 3′–5′ linkage to 2′–5′ linkage conformationally.

The side products containing pyrophosphate bond were characterized as 5,5′-diinosine diphosphate (IppI) and 5′-inosine-5′-inosinyl-[2′–5′]-inosine diphosphate ($IppI^{2'}p^{5'}I$) by resistance to BAP and mobility on paper chromatograms. Both IppI and $IppI^{2'}p^{5'}I$ were degraded with VPD giving pI. Alkaline hydrolysis of $IppI^{2'}p^{5'}I$ followed by incubation with BAP gave IppI.

Peaks 1, 2, 3, and 4 were identified as I, 3′,5′-cyclic IMP, ImpI, and pI, respectively, by comparison of paper chromatogram mobility and HPLC with those of authentic samples.

The selective formation of 2′–5′ linked oligoinosinates was established in this polymerization reaction. Yield and regioselectivity of internucleotide linkage were lower than those for the oligoadenylates.[5] This procedure employs no protecting group, condensation reaction taking place in an aqueous solution. It provides a simple preparative method for the 2′–5′ linked oligoinosinates, though the yield is not satisfactory.

Experimental

Materials. Inosine-5′-monophosphate sodium salt (Yamasa) and commercial imidazole, triethylamine, triphenylphosphine, Versenol trisodium salt, and lead nitrate were used. Di-2-pyridyl disulfide was prepared by a modification of the procedure of Jones and Katrizky.[7] Inosine-5′-phosphorimidazolide was prepared from pI and imidazole using triphenylphosphine and di-2-pyridyl disulfide as a condensing agent in a similar way to that of Lohrmann and Orgel.[8] Bacterial alkaline phosphatase, (BAPF) and venom phosphodiesterase (VPD) from Worthington, nuclease P_1 (N. P_1) from Yamasa and QAE-Sephadex A-25 from Pharmacia Fine Chemicals were used.

Paper Chromatography and HPLC. Paper chromatography was carried out by a descending technique on Whatman 3MM paper. The solvent systems were (**1**), 1-propanol–concentrated ammonia–water (55:10:35 v/v), and (**2**), saturated ammonium sulfate–0.1 M sodium acetate (pH 6.5)–2-propanol (79:19:2 v/v). R_f values of various oligoinosinates are given in Table 2.

HPLC was performed with a Hitachi 538 apparatus using a RPC-5 column (4 mmϕ × 25 cm). RPC-5 was prepared according to the method of Pearson *et al.*[9] The elution of the HPLC column was carried out with a linear gradient of aqueous $NaClO_4$ solution (H_2O–0.025 M $NaClO_4$) containing 0.0025 M Tris-acetate buffer (pH 7.5). The compounds were monitored by UV absorption at 260 nm.

Preparation of Oligoinosinate. Lead nitrate solution (0.25 M 0.3 ml) was added to a 5.7 ml aqueous solution of ImpI (150 mg, 3800 optical density unit at 248 nm, 0.3 mmol) containing 0.2 M imidazole buffer at pH 7.0 with stirring. White precipitates were formed. The solution was kept at 20 °C for 3 d with stirring. The reaction mixture was treated with 0.5 ml of 0.25 M Versenol buffer to complex the Pb^{2+} ion. A small portion (10 μl)

TABLE 2. R_f VALUES OF THE COMPOUNDS

Compound	R_f values relative to pI	
	Solvent 1	Solvent 2
I	1.57	0.80
3′,5′-Cyclic IMP	1.43	0.87
ImpI	1.56	
pI	1.00	1.00
IppI	0.91	0.86
ImpIpI	1.12	
[pIpI] - [3′–5′, 3′–5′ / 3′–5′, 2′–5′ / 2′–5′, 2′–5′]	1.05	0.30—0.50
$pI^{2'}p^{5'}I$	0.78	0.92
$pI^{3'}p^{5'}I$	0.76	0.81
$I^{2'}p^{5'}I$	1.17	
$I^{3'}p^{5'}I$	1.14	
$IppI^{2'}p^{5'}I$	0.60	0.80
$pI^{2'}p^{5'}I^{2'}p^{5'}I$	0.53	0.83
$pI^{2'}p^{5'}I^{3'}p^{5'}I$	0.48	0.77
$pI^{3'}p^{5'}I^{2'}p^{5'}I$	0.50	0.75
$pI^{3'}p^{5'}I^{3'}p^{5'}I$	0.49	0.64
$pI^{2'}p^{5'}I^{2'}p^{5'}I^{2'}p^{5'}I$	0.37	0.79
$pI^{2'}p^{5'}I^{3'}p^{5'}I^{2'}p^{5'}I$	0.35	0.67
$pI^{2'}p^{5'}I^{2'}p^{5'}I^{2'}p^{5'}I^{2'}p^{5'}I$	0.23	0.64

of the resulting homogeneous solution was analyzed with HPLC. The bulk of the solution was applied to the top of a QAE-Sephadex A-25 (hydrogencarbonate form) column, 25 mmϕ × 36 cm. After washing with water, elution was carried out by a stepwise linear gradient of triethylammonium hydrogencarbonate buffer (pH 7.5); (1) H_2O (0.75 l)–1/3 M (0.75 l); (2) 1/3 M (3 l)–1/2 M (3 l); 1/2 M (1 l)–1 M (1 l). *Ca.* 14 ml fractions were collected every 10 min. UV absorption of each fraction was measured at 270 nm. The fractions containing the UV absorbing compound were pooled and evaporated *in vacuo* below 30 °C. The excess of triethylammonium hydrogencarbonate was removed by repeated evaporation after addition of water. UV absorption of the oligoinosinates was measured at 248 nm. The yield was calculated from ODU_{248} after allowing for the hyperchromicity of each oligoinosinate. The hyperchromicity was obtained by the ratio of UV absorption at 248 nm after and before alkaline hydrolysis of the oligoinosinate.

Characterization of Products. Characterization of the products was carried out by means of sequential enzymes and alkaline digestion. The structure was confirmed by comparing the paper chromatograms and HPLC with those of authentic samples. The separated products were subjected to paper chromatography in solvent systems **1** and **2**. The UV active spot on the paper developed with system **1** was eluted with water, and then incubated with BAP. The incubated mixture was chromatographed on the paper using system **1**. The spot on the paper was elute with water. The eluate was evaporated *in vacuo* and incubated with N. P_1. The mixture was analyzed with HPLC, and applied to paper chromatography in system **1**. The UV absorbing spot was eluted with water and divided into two portions. One was digested with VPD and the other was degraded in a 0.5 M alkaline solution. The digested solution was analyzed with HPLC. The molar ratio of inosine and inosine nucleotides was determined with HPLC.

Digestion of the Products with Enzymes. Digestion with BAP was carried out by incubating a mixture of 0.5—1.5 μmol of nucleotidic material in a 50 μl solution containing 0.1 M Tris-HCl (pH 8.05), 0.001 M $MgCl_2$ and 0.1 unit of enzyme, at 37 °C for 2.5 h. The mixture was spotted directly on a Whatman 3MM paper and developed in system **1**.

Degradation with N. P_1 was performed at 37 °C for 2.5 h in a mixture (50 μl) containing the nucleotidic material (0.5—1.5 μmol), 0.006 M Veronal-acetate buffer (pH 5.75) and an enzyme solution (5 μg in 5 μl).

Degradation with VPD was carried out at 37 °C for 2.5 h in a mixture (50 μl) containing the substrate (0.2—0.4 μmol), 0.01 M Tris-acetate (pH 8.8), 0.01 M $MgCl_2$ and enzyme solution (0.01 unit).

Alkaline hydrolysis was carried out at room temperature for 1 d in a mixture (50 μl) containing the substrate (0.2—0.5 μmol) in a 0.5 M NaOH solution.

References

1) I. M. Kerr and R. E. Brown, *Proc. Natl. Acad. Sci. U.S.A.*, **75**, 256 (1978).
2) L. A. Ball and C. White, *Proc. Natl. Acad. Sci. U.S.A.*, **75**, 1167 (1978).
3) C. Baglioni, *Cell*, **17**, 255 (1979).
4) H. Sawai, *J. Am. Chem. Soc.*, **98**, 7037 (1976).
5) H. Sawai, T. Shibata, and M. Ohno, *Tetrahedron*, **37**, 481 (1981).
6) H. Sawai and M. Ohno, *Chem. Pharm. Bull.*, in press.
7) R. A. Jones and A. R. Katrizky, *J. Chem. Soc.*, **1958**, 3610.
8) R. Lohrmann and L. E. Orgel, *Tetrahedron*, **34**, 853 (1978).
9) R. L. Pearson, J. F. Weiss, and A. D. Kelmers, *Biochim. Biophys. Acta*, **228**, 770 (1971).

  Bull. Chem. Soc. Jpn., 54, 2763—2769 (1981)

The Biosynthesis of Monoterpenoids in Higher Plants. The Biosynthetic Pathway Leading to the Monoterpenoids from Amino Acids with a Carbon-skeleton Similar to Mevalonic Acid

Keiji TANGE†

Department of Chemistry, Faculty of Science, Hiroshima University, Higashisenda-machi, Naka-ku, Hiroshima 730

(Received January 31, 1981)

Radioisotopically labeled L-leucine, L-valine, DL-alanine, sodium acetate, and DL-mevalonic acid were incorporated into linalool by the intact plant of *Cinnamomum camphora* Sieb. var. *linalooliferum* Fujita and into geraniol and citronellol by that of *Pelargonium roseum* Bourbon. The uptake of leucine and valine resulted in the preferential location of the radioactivity on the 3,3-dimethylallyl pyrophosphate-derived moiety of these acyclic monoterpenoids, whereas the uptake of alanine resulted in the preferential location on the isopentenyl pyrophosphate-derived moiety, much as in the cases of mevalonic acid and sodium acetate. A biosynthetic pathway leading to the monoterpenoids from the amino acids is discussed.

The biosynthesis of monoterpenoids is believed to involve the conversion of mevalonic acid (MVA)[1] into isopentenyl pyrophosphate (IPP)[1] and 3,3-dimethylallyl pyrophosphate (DMAPP),[1] followed by the condensation of IPP with DMAPP directed toward the formation of monoterpenoids.[2] The predominant location of the radioactivity on the IPP-derived moiety has been observed for the biosynthesis of monoterpenoids from MVA-2-^{14}C by the leaves of higher plants,[3–6] in contrast to the equal distribution in the IPP- and DMAPP-derived moieties of squalene and triterpenoids biosynthesized from MVA-2-^{14}C by *Pisum sativum*.[7] The unbalanced distribution of the labeling in the monoterpenoids has been explained in terms of the operation of several factors, which involve the participation of some other pathway or intermediates in the DMAPP formation. No incorporation, or only a slight one, of leucine and valine into monoterpenoids by higher plants has been reported,[3,8,9] but the biosynthetic pathway of steroids from leucine *via* MVA has been established in animal tissues,[10–13] and it is highly probable that such a pathway takes part in higher plants, also.

We have performed the feeding experiments of radioisotopically labeled leucine, valine, and alanine into linalool (**1**) with the intact plant of *Cinnamomum camphora* Sieb. var. *linalooliferum* Fujita, and into geraniol (**2**) and citronellol (**3**) with that of *Pelargonium roseum* Bourbon, and then compared the distribution of the radioactivity originating from these precursors in the IPP- and DMAPP-derived moieties of the monoterpenoids with its distribution in the moieties of the monoterpenoids biosynthesized from ^{14}C-labeled MVA and acetate. The results have been partly outlined in the preliminary communications.[14–17] We here wish to report, *en bloc*, details of the results.

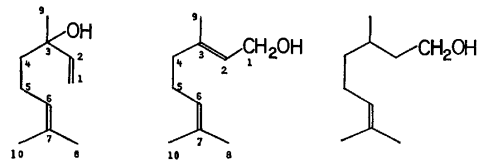

1 2 3

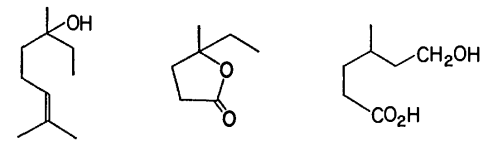

4 5 6

† Present address: Imabari-kita High School, Miyashita-cho, Imabari, Ehime 794.

Results

*The Incorporation of the Radioisotopically Labeled Precursors into Linalool (**1**), Geraniol (**2**), and Citronellol (**3**).* Feeding experiments were carried out on sprigs of *C. camphora* and *P. roseum*. The radioisotopically labeled precursors used for the incorporation were L-leucine-U-^{14}C,[18] L-valine-U-^{14}C, DL-alanine-2-^{14}C, sodium acetate-2-^{14}C, and DL-mevalonic-2-^{14}C acid. A phosphate-buffered solution (pH 7 4) of each precursor was fed through the cut stem to the leaves of the plants. The leaves and stems were subsequently steam-distilled to give an essential oil, which was then subjected to preparative TLC to isolate **1** from *C. camphora* and **2** and **3** from *P. roseum*. The radioactivities of **1**, **2**, and **3** were measured in Bray's scintillation solvent[19] with a liquid scintillation spectrometer; they are shown in Tables 1 and 2. Leucine and valine were incorporated into **1**, **2**, and **3** in the range of 0.0002—0.0055%. The incorporation of alanine into these monoterpenoids was at a considerably high level (0.014—0.076%), whereas that of acetate was at a low level (0.004—0.027%).

*The Distribution of Radioactivity in Linalool (**1**) Biosynthesized from ^{14}C-Labeled Leucine, Valine, and MVA by* C. camphora. Linalool (**1**), biosynthesized from leucine-U-^{14}C, valine-U-^{14}C, and MVA-2-^{14}C, was subjected to degradation to determine the labeling pattern. The radioactive linalool (**1**) isolated was hydrogenated in the presence of platinum dioxide to give 1,2-dihydrolinalool (**4**), which was subsequently degraded to 4-methyl-4-hexanolide (**5**) containing the C-1—C-6 and C-9 carbon atoms of **1**, and to acetone containing the C-7, C-8, and C-10 carbon atoms of **1**, by permanganate-periodate oxidation.[20] The hexanolide (**5**) and acetone were then converted to the *S*-benzylthiouronium salt[21] and the thiosemicarbazone

TABLE 1. INCORPORATION OF THE RADIOISOTOPICALLY LABELED PRECURSORS INTO LINALOOL (**1**) BY *C. camphora*

Exptl No.	Precursors[a] (mCi)	Feeding time[b] h	Season	Sp. act.[c] dpm/mmol	Incorp. %
1	Leu-U-^{14}C (0.02)	24	April	1.40×10^{2}	0.0010
2	Leu-U-^{14}C (0.025)	24	May	1.70×10^{2}	0.0040
3	Val-U-^{14}C (0.01)	24	July	7.52×10^{2}	0.0055
4	Val-U-^{14}C (0.005)	12	Oct.	5.92×10^{2}	0.0015
5	Val-U-^{14}C (0.02)	24	Oct.	2.72×10^{2}	0.0015
6	Ala-2-^{14}C (0.05)	24	June	1.86×10^{4}	0.076
7	Ala-2-^{14}C (0.02)	24	July	3.00×10^{3}	0.026
8	NaOAc-2-^{14}C (0.12)	24	June	1.10×10^{4}	0.0043
9	NaOAc-2-^{14}C (0.12)	24	July	3.76×10^{4}	0.0075
10	MVA-2-^{14}C (0.10)	24	June	4.39×10^{3}	0.022[d]
11	MVA-2-^{14}C (0.04)	24	July	3.15×10^{3}	0.086[d]

a) Leu-U-^{14}C, Val-U-^{14}C, Ala-2-^{14}C, NaOAc-2-^{14}C, and MVA-2-^{14}C denote L-Leucine-U-^{14}C, L-valine-U-^{14}C, DL-alanine-2-^{14}C, sodium acetate-2-^{14}C, and DL-mevalonic-2-^{14}C acid respectively. b) Metabolic period after uptake of tracer. c) Values cannot be compared among different batches of incorporations, since different quantities of the carrier and/or the tracer are used. Sp. act. denotes specific radioactivity. d) Calculated as the only (3*R*)-enantiomer of a racemic mixture of the substrate participates in the formation of **1**.

TABLE 2. INCORPORATION OF THE RADIOISOTOPICALLY LABELED PRECURSORS INTO GERANIOL (**2**) AND CITRONELLOL (**3**) BY *P. roseum*

Exptl No.	Precursors[a] (mCi)	Feeding time[b] h	Season	Geraniol (**2**)		Citronellol (**3**)	
				Sp. act.[c] dpm/mmol	Incorp. %	Sp. act.[c] dpm/mmol	Incorp. %
12	Leu-U-^{14}C (0.01)	12	Oct.	5.34×10^{3}	0.0011	8.50×10^{2}	0.0002
13	Leu-U-^{14}C (0.07)	24	Oct.	1.13×10^{4}	0.0028	5.15×10^{3}	0.0017
14	Leu-U-^{14}C (0.01)	72	Oct.	1.20×10^{4}	0.0036	1.40×10^{4}	0.0032
15	Val-U-^{14}C (0.05)	24	Oct.	3.10×10^{4}	0.0009	2.84×10^{3}	0.0009
16	Ala-2-^{14}C (0.03)	24	Aug.	3.86×10^{5}	0.024	1.85×10^{4}	0.014
17	NaOAc-2-^{14}C (0.083)	12	July	5.67×10^{5}	0.016	1.48×10^{5}	0.0060
18	NaOAc-2-^{14}C (0.083)	24	July	1.11×10^{6}	0.027	2.15×10^{5}	0.0091
19	MVA-2-^{14}C (0.02)	24	Aug.	1.12×10^{4}	0.010[d]	4.76×10^{3}	0.0054[d]
20	MVA-2-^{14}C (0.02)	24	Sep.	1.53×10^{4}	0.016[d]	1.59×10^{4}	0.018[d]

a), b), and c) Refer to a), b), and c) in Table 1 respectively. d) Calculated as the only (3*R*)-enantiomer of a racemic mixture of the substrate participates in the formation of **2** and **3**.

TABLE 3. RADIOACTIVITY IN LINALOOL (**1**) AND ITS DEGRADATION PRODUCTS AFTER UPTAKE OF L-LEUCINE-U-^{14}C, L-VALINE-U-^{14}C, AND DL-MEVALONIC-2-^{14}C ACID

Compound (carbons originating from **1**)	Specific radioactivity, dpm/mmol				
	Exptl 1[a] (Leu-U-^{14}C)[b]	Exptl 2 (Leu-U-^{14}C)	Exptl 3 (Val-U-^{14}C)	Exptl 5 (Val-2-^{14}C)	Exptl 11 (MVA-2-^{14}C)
Linalool[a] (**1**) (C-1—C-10)	1.40×10^{2}	1.70×10^{2}	7.52×10^{2}	2.72×10^{2}	3.15×10^{3}
Hexanolide (**5**) (C-1—C-6 and C-9)	7.37×10	8.40×10	4.36×10^{2}	1.69×10^{2}	2.05×10^{3}
Acetone (C-7, C-8, and C-10)	7.01×10	8.62×10	3.17×10^{2}	1.06×10^{2}	9.50×10^{2}

a) "Exptl No." correspond to the numbers in Table 1. b) Refer to a) in Table 1.

derivative respectively; these products were purified to a constant specific radioactivity by recrystallization. Table 3 shows the radioactivities of these degradation products. In the uptake of leucine-U-^{14}C and valine-U-^{14}C, the atoms of their tracer element are uniformly located on all the carbon atoms of DMAPP and IPP; therefore, the 5/3 of the total radioactivity of acetone resides on the DMAPP-derived moiety (C-5—C-8 and C-10), and the radioactivity of the IPP-derived moiety (C-1—C-4 and C-9) must be the difference between the radioactivity of **5** and 2/3 that of acetone. On the other hand, it has been established that the C-4 and C-8 carbon atoms of the monoterpenoids are labeled with the tracer from MVA-2-^{14}C.[22,23] In this

Table 4. The distribution of radioactivity in the IPP- and the DMAPP-derived moieties of linalool (**1**), geraniol (**2**), and citronellol (**3**) biosynthesized from the radioisotopically labeled precursors

Exptl No.[a]	Compound	Precursors[b]	Distribution/%	
			IPP-M.[c]	DMAPP-M.[c]
1	Linalool (**1**)	Leu-U-^{14}C	19	81
2		Leu-U-^{14}C	16	84
3		Val-U-^{14}C	30	70
5		Val-U-^{14}C	36	64
6		Ala-2-^{14}C	57	43
7		Ala-2-^{14}C	56	44
8		NaOAc-2-^{14}C	51	49
11		MVA-2-^{14}C	68	32
13	Geraniol (**2**)	Leu-U-^{14}C	23	72
15		Val-U-^{14}C	16	84
16		Ala-2-^{14}C	64	36
18		NaOAc-2-^{14}C	65	35
19		MVA-2-^{14}C	75	25
13	Citronellol (**3**)	Leu-U-^{14}C	17	83
15		Val-U-^{14}C	12	88
16		Ala-2-^{14}C	63	37
18		NaOAc-2-^{14}C	58	42
19		MVA-2-^{14}C	80	20

a) "Exptl No." correspond to the numbers in Tables 1 and 2. b) Refer to a) in Table 1. c) IPP-M. and DMAPP-M. denote the IPP- and DMAPP-derived moieties respectively.

case, therefore, all the radioactivity located on the DMAPP- and IPP-derived moieties would appear in acetone and **5**.

On the basis of the radioactivity of acetone and **5**, the distributions of radioactivity in the IPP- and DMAPP-derived moieties of **1** were determined by proportional allotment; they are shown in Table 4. The DMAPP-derived moiety of **1** was labeled with 81—84% of the total radioactivity incorporated into **1** in the administration of leucine-U-^{14}C and with 64—70% of it in the case of valine-U-^{14}C, whereas the DMAPP-derived moiety of **1** biosynthesized from MVA-2-^{14}C was labeled with less than 32% of the total activity.

In order to confirm the contrasted localization of the radioactivity on the IPP- and DMAPP-derived moieties between the incorporations of leucine and mevalonate, a mixture of leucine-4,5-^{3}H and MVA-2-^{14}C was fed to the plant to give a ^{3}H- and ^{14}C-labeled sample of **1**. The linalool (**1**) was then degraded to levulinic acid and acetone in the same manner as above. The tracer originating from leucine-4,5-^{3}H would be located on the C-4 and C-9 and the C-8 and C-10 carbon atoms; the former pair of carbon atoms constitutes a part of the IPP-derived moiety, and the latter, a part of the DMAPP-derived moiety. On the other hand, the tracer originating from MVA-2-^{14}C is located at the C-4 and the C-8 carbon atoms, which reside on the IPP- and DMAPP-derived moieties respectively. In the incorporation of the mixture of ^{3}H-labeled leucine and ^{14}C-labeled MVA, therefore, all the radioactivities located on the DMAPP- and IPP-derived moieties would appear in molecules of acetone and levulinic acid respectively. The distributions of the radioactivity of these tracers and the ^{3}H/^{14}C ratio of the radioactivity in molecules of the degradation products are shown in Table 5. Although the ^{3}H/^{14}C ratio in the whole molecule of **1** was 0.77, the ratios in the IPP- and DMAPP-derived moieties were 0.45 and 1.18 respectively. This fact indicates that the distribution of ^{3}H originating from leucine was greater in the DMAPP-derived moiety than in the IPP-derived moiety, whereas the distribution of ^{14}C originating from MVA was greater in the IPP-derived moiety than in the DMAPP-derived moiety. Thus, the experiment of the simultaneous feeding of ^{3}H-labeled leucine and ^{14}C-labeled MVA has firmly established the occurrence of the contrasted unbalanced distribution of radioactivity in the IPP- and DMAPP-derived moieties of the monoterpenoids when leucine and MVA are separately incorporated into the monoterpenoids.[3-6,14-17]

Table 5. Radioactivity in linalool (**1**) and its degradation products after uptake of a mixture of dl-leucine-4,5-^{3}H and dl-MVA-2-^{14}C to *C. camphora*

Compound (carbons originating from **1**)	Specific radioactivity		^{3}H/^{14}C ratio
	^{3}H dpm/mmol	^{14}C dpm/mmol	
Linalool (**1**) (C-1—C-10)	2.18×10^{3}	2.85×10^{3}	0.77
Levulinic acid (C-3—C-6 and C-9)	0.74×10^{3}	1.66×10^{3}	0.45
Acetone (C-7, C-8, and C-10)	1.43×10^{3}	1.21×10^{3}	1.18

*The Distribution of Radioactivity in Geraniol (**2**) and Citronellol (**3**) Biosynthesized from ^{14}C-Labeled Leucine, Valine, and MVA.* Radioactive samples of geraniol (**2**) and citronellol (**3**), resulting from the uptake of leucine-U-^{14}C, valine-U-^{14}C, and MVA-2-^{14}C, were subjected to permanganate-periodate oxidation. Geraniol (**2**) was degraded to levulinic acid containing the C-3—C-6 and C-9 carbon atoms and to acetone containing the C-7, C-8, and C-10 carbon atoms. Citronellol (**3**) was degraded to 6-hydroxy-4-methylhexanoic acid (**6**) containing the C-1—C-6 and C-9 carbon atoms and to acetone containing the C-7, C-8, and C-10 carbon atoms. The radioactivities of these compounds are listed in Tables 6 and 7. The distribution of the radioactivity of the ^{14}C-tracer in the IPP- and DMAPP-derived moieties of **2** and **3** were determined by the proportional allotment in the same manner as in the case of **1**; they are shown in Table 4. The uptake of the radioisotopically labeled amino acids resulted in the location of 72—88% of the total radioactivities on the DMAPP-derived moiety, whereas the predominant radioactivity resided on the IPP-derived moiety in the uptake of the ^{14}C-labeled MVA.

*The Distribution of Radioactivity in Linalool (**1**), Geraniol (**2**), and Citronellol (**3**) Biosynthesized from ^{14}C-Labeled Alanine, Acetate, and MVA.* The distribution of radioactivity in the IPP- and DMAPP-derived moieties of **1**, **2**, and **3**, biosynthesized from alanine-2-^{14}C,

TABLE 6. RADIOACTIVITY IN GERANIOL (2) AND ITS DEGRADATION PRODUCTS AFTER UPTAKE OF THE RADIOISOTOPICALLY LABELED PRECURSORS

Compound (carbons originating from **2**)	Specific radioactivity, dpm/mmol				
	Exptl 13[a] (Leu-U-^{14}C)[b]	Exptl 15 (Val-U-^{14}C)	Exptl 16 (Ala-2-^{14}C)	Exptl 18 (NaOAc-2-^{14}C)	Exptl 19 (MVA-2-^{14}C)
Geraniol (**2**) (C-1—C-10)	1.84×10^3	3.76×10^2	2.95×10^3	9.71×10^4	1.24×10^3
Levulinic acid (C-3—C-6 and C-9)	8.32×10^2	1.86×10^2	1.48×10^3	5.31×10^4	9.33×10^2
Acetone (C-7, C-8, and C-10)	7.89×10^2	1.90×10^2	5.27×10^2	2.25×10^4	3.08×10^2

a) "Exptl No." correspond to the numbers in Table 2. b) Refer to a) in Table 1.

TABLE 7. RADIOACTIVITY IN CITRONELLOL (3) AND ITS DEGRADATION PRODUCTS AFTER UPTAKE OF THE RADIOISOTOPICALLY LABELED PRECURSORS

Compound (carbons originating from **3**)	Specific radioactivity, dpm/mmol				
	Exptl 13[a] (Leu-U-^{14}C)[b]	Exptl 15 (Val-U-^{14}C)	Exptl 16 (Ala-2-^{14}C)	Exptl 18 (NaOAc-2-^{14}C)	Exptl 19 (MVA-2-^{14}C)
Citronellol (**3**) (C-1—C-10)	1.25×10^3	1.77×10^3	1.03×10^3	1.45×10^4	1.52×10^2
6-Hydroxy-4-methylhexanoic acid (**6**) (C-1—C-6 and C-9)	6.27×10^2	9.38×10^2	8.40×10^2	1.01×10^4	1.12×10^2
Acetone (C-7, C-8, and C-10)	6.20×10^2	8.36×10^2	1.90×10^2	3.97×10^3	3.08×10

a) "Exptl No." correspond to the numbers in Table 2. b) Refer to a) in Table 1.

TABLE 8. RADIOACTIVITY IN LINALOOL (1) AND ITS DEGRADATION PRODUCTS AFTER UPTAKE OF DL-ALANINE-2-^{14}C, SODIUM ACETATE-2-^{14}C, AND DL-MEVALONIC-2-^{14}C ACID

Compound (carbons originating from **1**)	Specific radioactivity, dpm/mmol			
	Exptl 6[a] (Ala-2-^{14}C)[b]	Exptl 7 (Ala-2-^{14}C)	Exptl 8 (NaOAc-2-^{14}C)	Exptl 10 (MVA-2-^{14}C)
Linalool (**1**) (C-1—C-10)	4.25×10^3	4.46×10^3	1.10×10^4	4.39×10^4
4-Methyl-4-hexanolide (**5**) (C-1—C-6 and C-9)	—	3.25×10^3	—	2.68×10^4
Formaldehyde (C-1)	9.37×10^2	—	3.78×10^2	1.37×10^3
Levulinic acid (C-3—C-6 and C-9)	2.53×10^3	—	4.90×10^3	2.85×10^4
Iodoform (C-9)	2.67×10	—	—	9.70×10^2
Succinic acid (C-3—C-6)	2.35×10^3	—	—	2.77×10^4
Acetone (C-7, C-8, and C-10)	1.10×10^3	9.90×10^2	3.21×10^3	1.70×10^4
Iodoform (C-8 and/or C-10)	—	—	—	8.07×10^3

a) "Exptl No." correspond to the numbers in Table 1. b) Refer to a) in Table 1.

acetate-2-^{14}C, and MVA-2-^{14}C, was determined by subjecting them to degradation as follows. The oxidation of **1** with permanganate-periodate gave levulinic acid, acetone, and formaldehyde, which contain the C-3—C-6 and C-9 carbon atoms, the C-7, C-8, and C-10 carbon atoms, and the C-1 carbon atom respectively. A part of the sample of levulinic acid was further degraded by an iodoform reaction to iodoform containing the C-9 carbon atom and to succinic acid containing the C-3—C-6 carbon atoms. Also, **1** was, on partial hydrogenation, converted to 1,2-dihydrolinalool (**4**), which was then degraded to 4-methyl-4-hexanolide (**5**) and acetone by permanganate-periodate oxidation. Table 8 shows the radioactivities of **1** and these degradation products. By oxidation with this reagent, geraniol (**2**) was degraded to levulinic acid and acetone, and citronellol (**3**), to 6-hydroxy-4-methylhexanoic acid (**6**) and acetone. The radioactivities of **2** and **3** and the degradation products are shown in Tables 6 and 7.

Table 8 indicates that 22% of the radioactivity due to the tracer originating from alanine-2-^{14}C is located on the C-1 carbon atom of **1** and 26% on the portion composed of the C-7, C-8, and C-10 carbon atoms, while the C-9 carbon atom is unlabeled. These results indicate that the tracer from alanine-2-^{14}C resides on the C-1, C-3, C-5, and C-7 carbon atoms. Tables 6 and 7 indicate that the labeling pattern of

2 and **3** is the same as that of **1**. In the uptake of alanine-2-^{14}C, therefore, the radioactivity of the DMAPP-derived moiety (C-5—C-8 and C-10) of **1**, **2**, and **3** is double that of acetone. On the other hand, the radioactivity of the IPP-derived moiety (C-1—C-4 and C-9) of **1** and **2** was evaluated by doubling the difference between the radioactivities of levulinic acid and acetone; in addition, the radioactivity of the IPP moiety of **1** was evaluated by deducting the radioactivity of acetone from that of 4-methyl-4-hexanolide (**5**). With respect to **3**, the radioactivity of its IPP-derived moiety was evaluated by deducting the radioactivity of acetone from that of 6-hydroxy-4-methylhexanoic acid (**6**). In the uptake of acetate-2-^{14}C, it has been well established that the tracer resides on the C-2, C-4, C-6, and C-8—C-10 carbon atoms of the acyclic monoterpenoids.[24-27] Taking this labeling pattern into consideration, the distribution of radioactivity in the IPP- and DMAPP-derived moieties of **1**, **2**, and **3** was evaluated by the proportional allotment of the radioactivities of acetone and levulinic acid in a manner similar to that described above.

On the basis of the specific radioactivities of the IPP- and DMAPP-derived moieties determined as above, the distribution of radioactivity in these moieties was evaluated; it is shown in Table 4. The incorporation of ^{14}C-labeled alanine and acetate into geraniol (**2**) and citronellol (**3**) resulted in the preferential location of radioactivity on the IPP-derived moiety, similarly to the incorporation of ^{14}C-labeled MVA, but in opposition to the incorporation of ^{14}C-labeled leucine and valine. The localization of radioactivity in linalool (**1**) biosynthesized from ^{14}C-labeled alanine was predominant on its IPP-derived moiety, but when **1** was biosynthesized from ^{14}C-labeled acetate, the imbalance of the distribution of radioactivity on the IPP- and DMAPP-derived moieties was very small.

Discussion

The previous reports[3,9] described that leucine and valine are not precursors for the monoterpenoid biosynthesis in higher plants because of their negligible incorporation into monoterpenoids. However, it has been found that the radioisotopically labeled leucine and valine are surely incorporated into monoterpenoids, though the incorporation is at a low level, as is shown in Tables 1 and 2. The low incorporation of the amino acids may be explained in terms of the operation of several factors: (i) the radioactivity of the amino acids is scattered into other metabolites rather than the monoterpenoids, (ii) there is a great pool of the amino acids, so that their radioactivity is diluted, and (iii) the low permeation of the amino acids into the biosynthetic site of monoterpenoids causes the low incorporation.

The DMAPP-derived moiety of the monoterpenoids, **1**, **2**, and **3**, biosynthesized from leucine-U-^{14}C and valine-U-^{14}C was labeled with more than 64% of the incorporated tracers, whereas this moiety of the monoterpenoids biosynthesized from MVA-2-^{14}C contained less than 32% of the tracers, as is shown in Table 4. If the monoterpenoids are biosynthesized from the amino acids *via* MVA, the distribution pattern will be similar to the pattern in the monoterpenoids biosynthesized from MVA-2-^{14}C. This indicates that, although leucine and valine have a carbon-skeleton similar to that of MVA, these amino acids are incorporated into the monoterpenoids, not *via* MVA, but by an alternate route. On the other hand, the distribution pattern in the monoterpenoids biosynthesized from alanine-2-^{14}C was similar to that in the monoterpenoids biosynthesized from MVA-2-^{14}C and acetate-2-^{14}C. This indicates that alanine is incorporated into the monoterpenoids by a route *via* MVA. Thus, it is likely that administered leucine and valine participate in the biosynthesis of the monoterpenoids by their direct conversion to DMAPP through an alternate route rather than through the mevalonate pathway, whereas administered alanine is first metabolized to acetyl-CoA, which then constructs preferentially the IPP-derived moiety of the monoterpenoids *via* MVA.

Experimental

The radioisotopically labeled monoterpenoids and their degradation products were purified to a constant specific radioactivity by a combination of preparative TLC and/or repeated recrystallization of the crystalline derivatives in every case that these could be prepared. The melting points and spectral data of all the products agreed with those of authentic samples.[22,23] The TLC analyses were carried out using silica-gel plates (Kieselgel 60 G; 0.25 mm thick) and the following five kinds of solvents: (i) hexane/EtOAc=9/1, (ii) hexane/EtOAc=4/1, (iii) hexane/EtOAc=1/1, (iv) $CHCl_3$, and (V) MeOH/acetone/formic acid=70/10/1. Spots on the plates were visualized by vaniline-H_2SO_4 spraying and subsequent heating to 120 °C. The preparative TLC was performed on silica-gel plates (Kieselgel 60 G; 0.75 mm thick) or on 3% $AgNO_3$–silica-gel plates (Kieselgel 60 G; 0.75 mm thick) with the above-described solvents. The GLC analyses were performed on an instrument equipped with FID and a glass column (2.0 m×3 mm) packed with either 2% OV-17, 15% DEGS, or 10% PEG-20M on Chromosorb W (80—100 mesh). The radioactivity was measured on a liquid-scintillation spectrometer using Bray's scintillation solvent.[19] The counting error was within 2%.

Plant Materials and Labeled Precursors. The leaves of *Cinnamomum camphora* Sieb. var. *linalooliferum* Fujita, which had been grown outdoors on the campus of Hiroshima University, produced an essential oil containing up to 90% (wt) of linalool (**1**) in August. The linalool (**1**) isolated showed $[\alpha]_D^{25}$ −19.3° (*c* 13.3, $CHCl_3$) and n_D^{25} 1.4603. Each top branch used for the feeding experiments was *ca.* 10 cm in length and *ca.* 5 g in fresh wt. The leaves of *Pelargonium roseum* Bourbon, which had been wintered indoors and grown outdoors from spring to autumn, produced an essential oil containing 35—40% of geraniol (**2**) and 25—30% of citronellol (**3**) in August. The isolated geraniol (**2**) and citronellol (**3**) showed n_D^{25} values of 1.4760 and 1.4551 respectively. Each top branch of the plant used for feeding experiments was *ca.* 15 cm long and *ca.* 10 g in fresh wt.

DL-Mevalonic-2-^{14}C acid (MVA-2-^{14}C) (7.16 mCi/mmol), L-leucine-U-^{14}C (Leu-U-^{14}C) (251 mCi/mmol), L-valine-U-^{14}C (Val-U-^{14}C) (225 mCi/mmol), DL-alanine-2-^{14}C (Ala-2-^{14}C) (12 mCi/mmol), and sodium acetate-2-^{14}C (58 mCi/

mmol) used for the feeding experiments were products of the Daiichi Pure Chemicals Co., Ltd., Tokyo.

Administration of the Labeled Precursors and Isolation of the Radioisotopically Labeled Monoterpenoids. The labeled precursor, dissolved in a phosphate-buffered solution (0.5 cm^3; pH 7.4), was fed to the fresh cuttings (50 g in total wt) through their cut-stem in a glass tube, and then distilled water was soaked into the cuttings several times to complete the uptake of the labeled precursor. At the end of the metabolic periods shown in Tables 1 and 2, the cuttings were steam-distilled. The distillate was extracted with four 50-cm^3 portions of ether. The combined ether layer was washed with two 50-cm^3 portions of a 5% sodium hydrogencarbonate solution and water, and then dried over anhydrous sodium sulfate. The removal of the solvent from the ether layer at temperature below 40 °C afforded a crude essential oil. The essential oil (0.6—1.0 g) obtained from *C. camphora* was subjected to preparative TLC with solvent (i) to give linalool (**1**), which was then further purified by TLC. The essential oil (0.15—0.2 g) obtained from *P. roseum* was separated on $AgNO_3$–silica-gel plates with solvent (ii) to give geraniol (**2**) and citronellol (**3**), which were subsequently further purified by TLC with silica-gel plates and solvent (i). The homogeneity of these monoterpene alcohols was confirmed by GLC analyses using a 2% OV-17 column at 100 °C, a 15% DEGS column at 120 °C, and a 10% PEG 20 M column at 120—180 °C, in addition to the examination of the constant specific radioactivity.

For time-course studies of the incorporation of the tracers into the monoterpene alcohols, each precursor was fed to the cuttings of the plant in the same manner as above, and then the cuttings were steam-distilled at appropriate time intervals to give the essential oil. This oil was subjected to isolation of the monoterpene alcohol in the same way as above.

Degradation of Linalool (1). Following the reported procedure of the $KMnO_4$–$NaIO_4$ oxidation,[20] a suspension of linalool (**1**) (350 mg) in a solution of $NaIO_4 \cdot H_2O$ (2.6 g) in water (260 cm^3) was stirred for 10 min at room temp. The mixture was neutralized with sodium carbonate under cooling to 0—10 °C. To the neutralized solution, $KMnO_4$ (250 mg) dissolved in water (15 cm^3) was added drop by drop, and, after which, the mixture was stirred overnight below 10 °C. The mixture, after the reduction of the remaining oxidant with sodium hydrogensulfite, was steam-distilled. The distillate (5 cm^3) was divided into two portions. One portion (2.5 cm^3) was treated with thiosemicarbazide as usual to give acetone thiosemicarbazone (64 mg), which was then purified by a combination of preparative TLC with silica gel and solvent (iii) and repeated recrystallizations; it showed mp and mixed mp 179.0—179.5 °C. The other portion (2.5 cm^3) was added to a solution of dimedone in water to give the bisdimedone derivative of formaldehyde (23 mg; mp and mixed mp 187—188 °C).[28]

The steam-distillation residue was concentrated to 100 cm^3, acidified with diluted H_2SO_4, and extracted, after the reduction of the remaining oxidant with sodium hydrogensulfite, with ether using a liquid-liquid continuous extractor to give an acidic product. This acidic product was subjected to preparative TLC with silica gel and solvent (v) to give levulinic acid (79 mg). This acid, on methylation with CH_2N_2, was converted to methyl levulinate (75 mg), which was subsequently further purified by TLC with silica gel and solvent (ii). The purified levulinate was divided into two portions. One portion (25 mg) was treated with an aqueous solution of thiosemicarbazide to give methyl levulinate thiosemicarbazone (38 mg; mp and mixed mp 140—141 °C). The other portion (25 mg) was subjected to hypoiodite oxidation to give iodoform (17 mg; mp and mixed mp 119—120 °C) and succinic acid (7 mg; mp and mixed mp 186—188 °C). The radioactivities of these products are shown in Tables 5 and 8.

Degradation of Geraniol (2). Radioactive geraniol (**2**) (20 mg) isolated was diluted with the carrier (280 mg) and then degraded to acetone and levulinic acid with $KMnO_4$–$NaIO_4$ in the same manner as above. The acetone was converted to the thiosemicarbazone derivative (72 mg; mp and mixed mp 179—180 °C). The levulinic acid (110 mg) was converted to methyl levulinate (86 mg), which was then transformed to the thiosemicarbazone derivative (116 mg; mp and mixed mp 140—141 °C). Table 6 shows the radioactivities of geraniol and these products.

Degradation of Citronellol (3). Radioactive citronellol (**3**) (20 mg) isolated was diluted with the carrier (300 mg) and degraded to acetone and 4-methyl-6-hydroxyhexanoic acid (**6**) by $KMnO_4$–$NaIO_4$ oxidation in the same manner as above. The acetone was converted to the thiosemicarbazone derivative (68 mg; mp and mixed mp 179—180 °C). The 4-methyl-6-hydroxyhexanoic acid (**6**)[22] [110 mg; IR (liq.) 3500—2900 and 1710 cm^{-1} (COOH)] was, on treatment with CH_2N_2, converted to its methyl ester [IR (liq.) 3450 (OH) and 1741 cm^{-1} (ester C=O); ^{1}H-NMR δ=0.93 (3H, d, J=5.8 Hz, CH_3), 2.33 (2H, bt, J=6.0 Hz, $-\underline{CH_2}-COOCH_3$), 3.65 (3H, s, $COOCH_3$), and 3.67 (2H, t, J=6.1 Hz, $-\underline{CH_2}OH$); MS (70 eV), m/z (rel intensity), 160 (M^+, 22), 142 (12), 129 (23), 87 (88), 74 (83), 69 (84), 55 (100), 43 (73), and 41 (95)]. The specific radioactivities of citronellol and the degradation products are shown in Table 7.

Degradation of Dihydrolinalool (4). Purified, radioactive linalool (**1**) (350 mg), dissolved in absolute MeOH (3 cm^3), was selectively hydrogenated in the presence of Adams PtO_2 (4 mg). The purification of the reaction mixture by preparative TLC, using $AgNO_3$–silica-gel plates and solvent (i), gave 1,2-dihydrolinalool (**4**) (300 mg), which was then subjected to $KMnO_4$–$NaIO_4$ oxidation as described above. The reaction mixture was steam-distilled. The distillate (5 cm^3) was divided into two portions. One portion (2.5 cm^3) was treated with an aqueous solution of thiosemicarbazide as usual to give acetone thiosemicarbazone (105 mg; mp and mixed mp 179—180 °C). Another portion (2.5 cm^3) was subjected to hypoiodite oxidation to give iodoform (80 mg; mp and mixed mp 119—120 °C). On the other hand, a steam-distillation residue was concentrated to 100 cm^3, acidified with 5% HCl, and extracted with ether to give 4-methyl-4-hexanolide (**5**)[23] [80 mg; IR (liq.) 1765 (C=O of γ-lactone) and 1238 and 1161 cm^{-1} (C–O of the lactone); ^{1}H-NMR ($CDCl_3$) δ=0.97 (3H, t, J=7.0 Hz, CH_3), 1.38 (3H, s, CH_3), and 1.73 (2H, q, J=7.0 Hz, $-CH_2-$)]. The hexanolide (**5**), dissolved in EtOH (1 cm^3), was refluxed with 1 M† NaOH (1.5 cm^3) for 1 h. To this reaction mixture, after neutralization, we added *S*-benzylthiouronium urea (160 mg) dissolved in EtOH (1 cm^3) to give the *S*-benzylthiouronium salt (150 mg; mp 132—133 °C). The radioactivities of linalool and its degradation products are shown in Tables 3 and 8.

The author wishes to express his thanks to Professor Takayuki Suga for his continuing guidance and encouragement, to Dr. Toshifumi Hirata for his useful discussions, and to Messrs. Yoshitaka Nakao and Hitoshi Okita for their co-work in the experiment. The author also would like to thank the Takasago

† 1 M=1 mol dm^{-3}.

Perfumery Co., Ltd., for a gift of the samples of linalool, geraniol, and citronellol, and the Soda Perfumery Co., Ltd., for a gift of the plants of *C. camphora* and *P. roseum*.

References

1) According to the IUPAC Nomenclature, mevalonic acid, isopentenyl, and 3,3-dimethylallyl are represented as 3,5-dihydroxy-3-methylpentanoic acid, 3-methyl-3-butenyl, and 3-methyl-2-butenyl respectively.

2) J. H. Richards and J. B. Hendrickson, "The Biosynthesis of Steroids, Terpenes, and Acetogenins," Benjamin, New York, N. Y. (1964), p. 173, and the references cited therein.

3) D. V. Banthorpe, B. V. Charlwood, and M. J. O. Francis, *Chem. Rev.*, **72**, 115 (1975), and the related papers cited therein.

4) T. Suga, T. Shishibori, K. Kotera, and R. Fujii, *Chem. Lett.*, **1972**, 533.

5) T. Suga and T. Shishibori, *Chem. Lett.*, **1972**, 1093.

6) D. V. Banthorpe and G. N. J. Le Patourel, *Biochem. J.*, **130**, 1055 (1972).

7) C. Croteau and W. D. Loomis, *Phytochemistry*, **12**, 1957 (1973), and the related papers cited therein.

8) W. D. Loomis, "Terpenoids in Plants," ed by J. B. Pridham, Academic Press, New York, N. Y. (1967), p. 59.

9) K. G. Allen, D. V. Banthorpe, B. V. Charlwood, O. Ekundayo, and J. Mann, *Phytochemistry*, **15**, 101 (1976).

10) M. J. Coon, *J. Biol. Chem.*, **187**, 71 (1950).

11) F. Lynen, *Proc. Intern. Symp. Enzyme Chem., Tokyo-Kyoto*, **1957**, 57.

12) A. del Campillo-Camphbell, E. E. Dekker, and M. J. Coon, *Biochim. Biophys. Acta*, **31**, 290 (1959).

13) H. Hily, J. Knappe, E. Ringelmann, and F. Lynen, *Biochem. Z.*, **329**, 476 (1958).

14) T. Suga, T. Hirata, T. Shishibori, and K. Tange, *Chem. Lett.*, **1974**, 189.

15) T. Suga, T. Hirata, and K. Tange, *Chem. Let.*, **1975**, 131.

16) T. Suga, T. Hirata, and K. Tange, *Chem. Lett.*, **1975**, 243.

17) K. Tange, T. Hirata, and T. Suga, *Chem. Lett.*, **1979**, 269.

18) U denotes uniformity. Leucine-U-^{14}C, for example, indicates that all the carbon atoms of leucine are uniformly labeled with ^{14}C.

19) G. A. Bray, *Analyst. Biochem.*, **1**, 279 (1960).

20) T. Suga and E. von Rudloff, *J. Sci. Hiroshima Univ.*, A-II, **34**, 69 (1970).

21) C-T. Chang, *Formosan Sci.*, **16**, 127 (1962); *Chem. Abstr.*, **59**, 3873a (1963).

22) T. Suga and T. Shishibori, *Bull. Chem. Soc. Jpn.*, **46**, 3545 (1973).

23) T. Suga, T. Shishibori, and M. Bukeo, *Bull. Chem. Soc. Jpn.*, **45**, 1480 (1972).

24) A. R. Guseva and V. A. Paseshnichenko, *Biokhimiya*, **31**, 988 (1966); *Chem. Abstr.*, **66**, 8844b (1967).

25) M. J. O. Francis and M. O'Connel, *Phytochemistry*, **8**, 1705 (1969).

26) D. V. Banthorpe and A. Wirz-Justice, *J. Chem. Soc., C*, **1969**, 541.

27) D. V. Banthorpe, O. Ekundayo, J. Mann, and K. W. Turnbull, *Phytochemistry*, **14**, 707 (1975).

28) E. C. Horning and M. G. Horning, *J. Org. Chem.*, **11**, 95 (1946).

Synthesis of 7-Alkylidene-5-oxadispiro[2.0.4.4]dodecan-6-ones

Kiyomi KAKIUCHI,* Takehito YONEI, Yoshito TOBE, and Yoshinobu ODAIRA
Department of Petroleum Chemistry, Faculty of Engineering, Osaka University, Suita, Osaka 565
(Received February 9, 1981)

7-Alkylidene-5-oxadispiro[2.0.4.4]dodecan-6-ones, having a cyclopropane ring, were synthesized by the α-alkylidenation of easily available 5-oxadispiro[2.0.4.4]dodecan-6-one. Also, α-alkylidene-γ-butyrolactones, containing an additional hydroxyl group, were prepared. The screening of the biological activities of these γ-lactones gave the interesting results. For instance, α-isopropylidene-γ-lactone exhibited the antiarrhythmia activity *in vivo*.

Recently, α-methylene-γ-butyrolactones have been the subject of extensive research because a large number of sesquiterpene lactones, containing α-methylene-γ-butyrolactone moiety, have been shown to exhibit marked antitumor, cytotoxic, and other biological activities attributed to this moiety.[1a,b] The biological activities of these lactones are apparently driven from significant chemical affinity of this moiety for the thiol groups of sulfhydryl enzymes.[1c-f] In particular, interest in α-methylene-γ-butyrolactones as medical agents has been stimulated by the possibility that some of these might show enough selective toxicity against neoplastic cells to be of the therapeutic value as anticancer agents.[1b,c,g] Although the enone component is essential for the biological activities, there are additional factors which may enhance these properties. These enhancement factors include the presence of some substituents such as hydroxyl group or epoxy ring which may facilitate the addition of sulfide anion or proton transfer at some intermediate stage in the addition involving the thiol groups of enzymes.[1a,h] On the other hand, it has been well known that some natural products, having a cyclopropane ring, display remarkable biological activities.[2] For example, illudin S, containing a spiro cyclopropane ring, is well examined about antitumor activity.[2b] Previously, we reported on the synthesis of 5-oxadispiro-[2.0.4.4]dodecan-6-one (**3**) (γ-lactone), containing a spiro cyclopropane ring, by the acid catalyzed or thermally induced cyclobutyl-cyclopropylcarbinyl rearrangement of 2-oxatricyclo[4.4.2.0^{1,6}]dodecan-3-one (**2**) (δ-lactone).[3] From the above point of view, the γ-lactone **3** may be advantageously taken as a useful intermediate for the synthesis of a new type of α-alkylidene-γ-butyrolactones. As part of the studies on the structure-biochemical activity relationship,[4] we wish to describe here the synthesis of several 7-alkylidene-5-oxadispiro[2.0.4.4]dodecan-6-ones (**4a**—**h**) from the γ-lactone **3** and the interesting results on the screening of the biological activities of the α-alkylidene-γ-lactones *in vivo*.

Results and Discussion

Propellalactone **2** was prepared by the Baeyer-Villiger oxidation of tricyclo[4.3.2.0^{1,6}]undecan-7-one (**1**), easily derived from the photocycloaddition of bicyclo[4.3.0]non-1(6)-en-7-one to ethylene as described previously.[6] In practice, however, the reaction mixture after the above oxidation without isolation of propellalactone **2** was heated at 50 °C for 1 d and then refluxed gently for 1 h to give a 78:22 ratio of dispiro-γ-lactone **3** and propellalactone **2** in 80% yield. The γ-lactone **3** was readily isolated from the reaction mixture by column chromatography on silica gel (Scheme 1).

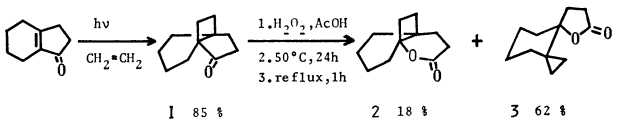

1 85 % 2 18 % 3 62 %

Scheme 1.

α-Alkylidenation of the γ-lactone **3** was carried out according to the usual method[7] comprised of α-hydroxyalkylation and subsequent dehydration as shown in Scheme 2. To a solution of lithium diisopropylamide (LDA) in anhydrous tetrahydrofuran (THF) at −78 °C was slowly added a solution of the γ-lactone **3** in anhydrous THF and hexamethylphosphoric triamide (HMPT). After stirring at −78 °C for 30 min, the carbonyl compound was added and the mixture was stirred for 2 h. In the case of α-hydroxymethylation, gaseous formaldehyde was passed into the reaction mixture at −20 °C under nitrogen stream. In every case, α-hydroxyalkylation proceeded smoothly to afford the desired products in 80—100% yields. The crude products of α-hydroxyalkyl-γ-lactones were subjected to the next reaction without isolation. Next, the dehydration of the α-hydroxyalkyl-γ-lactones was carried out by means of two methods, depending upon the type of the hydroxyl group. Namely, when the hydroxyl group was primary or secondary, a solution of the alcohol in dry pyridine was treated with methanesulfonyl (Ms) chloride at 5 °C for 9 h, and the obtainable mesylate was dissolved in dry benzene containing 1.4 equivalent of 1,8-diazabicyclo[5.4.0]undec-7-ene (DBU) and then stirred at room temperature for 6 h (method A).[7b] On the other hand, when the hydroxyl group was tertiary, thionyl chloride was added to a solution of the alcohol in dry pyridine and dry dichloromethane and the reaction mixture was stirred at 0 °C for 30 min and then at room temperature for 4 h (method B).[8] After usual work-up, the crude product of 7-alkylidene-5-oxadispiro[2.0.4.4]dodecan-6-ones (**4a**—**f**) was obtained and purified by column chromatography on silica gel. The use of aldehydes as the carbonyl compound in the α-hydroxyalkylation resulted in the formation of *E*/*Z* stereoisomers of the γ-lactones (**4b**—**e**). They were, however, separated successfully by the careful chromatography. The results are summarized in Table 1.

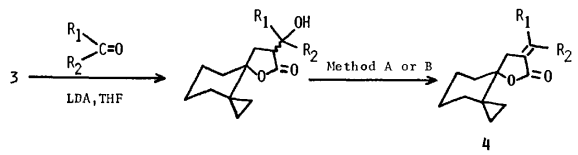

Method A: 1. MsCl, Pyridine, 2. DBU, PhH.
Method B: $SOCl_2$, Pyridine, CH_2Cl_2.

Scheme 2.

TABLE 1. SYNTHESIS OF α-ALKYLIDENE-γ-BUTYROLACTONES

Carbonyl compd	α-Alkylidene-γ-butyrolactone	R_1	R_2		Yield/%[a]
Formaldehyde	**4a**	H	H		77[b]
Acetaldehyde	**4b**	CH_3	H	(*E*)	54
	4c	H	CH_3	(*Z*)	7
Propionaldehyde	**4d**	C_2H_5	H	(*E*)	30
	4e	H	C_2H_5	(*Z*)	20
Acetone	**4f**	CH_3	CH_3		52

a) Isolated yield based on **3**. b) Determined by ^1H NMR analysis.

It was easy to establish the stereochemistry around the olefinic part of the γ-lactones **4b**—**e** by the comparison of the ^1H NMR chemical shifts of the vinyl protons of **4b**—**e** with those of α-alkylidene-γ-butyrolactones described in literature.[9] The chemical shifts of the olefinic protons (6.57 and 6.11 ppm for *E* and *Z* isomers, respectively) were the most remarkable point to descriminate between the geometrical isomers of α-ethylidene-γ-lactones (**4b**) and (**4c**). Similarly, the observed values of the olefinic protons (6.48 and 6.00 ppm) of α-propylidene-γ-lactones (**4d**) and (**4e**) distinguished one from the other.

Furthermore, we tried to synthesize the α-alkylidene-γ-lactones having a hydroxyl group which was expected to enhance the reactivity of the conjugated lactone toward biological nucleophiles as mentioned earlier. The tetrahydropyran-2-yl (THP) ether of hydroxyacetone (**5**) was used for α-hydroxyalkylation of the γ-lactone **3**. Dehydration by the method B gave the mixture of *E*/*Z* isomers of the THP–ether (**6**), which was treated with 60% aqueous acetic acid at 45 °C for 3 h. After usual work-up followed by purification by column chromatography on silica gel, (*E*)- and (*Z*)-α-(2-hydroxy-1-methylethylidene)-γ-lactones (**4g**) and (**4h**) were obtained in 9% and 31% overall yields from the γ-lactone **3**, respectively (Scheme 3). The distinction in stereochemistry between two isomers was accomplished by the comparison of the chemical shifts of the methyl groups in ^1H NMR spectra (2.16 and 1.90 ppm for *E* and *Z* isomers, respectively) with those of α-isopropylidene-γ-lactone (**4f**), since the methyl groups of **4f** located in *syn*- and *anti*-positions toward the carbonyl group show resonances at 2.20 and 1.84 ppm, respectively.

The screening of biological activities of a series of the present α-alkylidene-γ-butyrolactones **4a**, **4b**, **4d**—**f**, and **4h** gave attractive results. Concerning the antitumor activity of these γ-lactones against Sarcoma 180 A *in vivo*, all of them were less active than the famous antitumor antibiotic, Mitomycin C. Interestingly, the other biological activities of these γ-lactones *in vivo*, however, were found out: the antihistamine activity of (*E*)-α-propylidene-γ-lactone **4d**, the antihistamine and the anticholine activities of (*Z*)-α-propylidene-γ-lactone **4e**, the antiarrhythmia activity of α-isopropylidene-γ-lactone **4f**, and the platelet aggregation inhibition activity of (*Z*)-α-(2-hydroxy-1-methylethylidene)-γ-lactone **4h**.

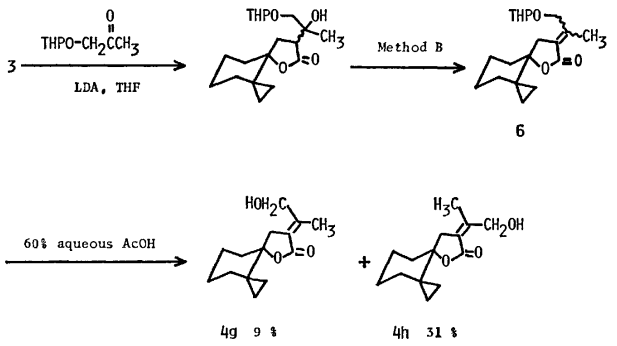

Scheme 3.

In this way, 7-alkylidene-5-oxadispiro[2.0.4.4]dodecan-7-ones **4a**—**h**, having a spiro cyclopropane ring, were synthesized and the interesting results relating to the biological activities of these lactones were given.

Experimental

All melting and boiling points are uncorrected. IR spectra were recorded with a JASCO IR-G spectrometer as liquid film unless otherwise stated. ^1H NMR spectra were obtained on a JEOL JNM-PS-100 instrument using Me_4Si as an internal standard and CCl_4 as a solvent. Mass spectra were measured with a Hitachi RMU-6E spectrometer. Analytical GLC was carried out on a Hitachi 163 gas chromatograph and preparative GLC separation was conducted on a Varian Aerograph 920 gas chromatograph.

Acetaldehyde, propionaldehyde, and hydroxyacetone were distilled prior to use. Acetone was distilled from potassium carbonate before use. Tricyclo[4.3.2.$0^{1,6}$]undecan-7-one (**1**) was prepared in 85% yield by the photocycloaddition of bicyclo[4.3.0]non-1(6)-en-7-one[10] to ethylene in ether (0.4 M†) at −70 °C as described previously.[6]

5-Oxadispiro[2.0.4.4]dodecan-6-one (3). To a solution of 40.7 g (0.248 mol) of **1** in 500 ml of acetic acid was added 20-fold excess of 30% aqueous hydrogen peroxide. The mixture was stirred at room temperature for 7 d and at 50 °C for 1 d, then at gentle reflux for 1 h. The solution was poured into water and extracted with ether. The ethereal extracts were washed with saturated sodium carbonate (Na_2CO_3) solution, brine, and dried over anhydrous sodium sulfate (Na_2SO_4). The solvent was evaporated *in vacuo* to give 35.7 g of 2-oxatricyclo[4.4.2.$0^{1,6}$]dodecan-3-one (**2**) and γ-lactone **3** in a ratio 22:78 (by GLC analysis) (80%). The γ-lactone **3** was isolated by column chromatography (SiO_2, 8% ether–petroleum ether). Spectral and analytical data were already described.[3b]

General Procedure for Synthesis of α-Alkylidene-γ-butyrolactones (4a—f). *α-Hydroxyalkylation*: A solution of diisopropylamine (2 mmol) in dry THF (1.5 ml) cooled to −78 °C was treated dropwise with butyllithium (1.5 mmol) in hexane under nitrogen atmosphere. After stirring at −78 °C for 1 h, a solution of the γ-lactone **3** (1 mmol) in dry THF (0.2 ml) and dry HMPT (0.1 ml) was added dropwise *via* a

† 1 M = 1 mol dm^{-3}.

syringe. After addition was complete, stirring was continued at −78 °C for 30 min, then a carbonyl compound (1 mmol) was added *via* a syringe and the mixture was stirred for 2 h. The reaction was quenched by saturated ammonium chloride solution and the mixture was extracted with ether. The organic extracts were washed with 5% HCl, saturated sodium hydrogencarbonate ($NaHCO_3$) solution, brine, and dried (Na_2SO_4). The solvent was removed *in vacuo* to give the crude alcohol product.

Dehydration: *Method A.* The above alcohol (1 mmol) was dissolved in dry pyridine (2 ml) and treated at 0—5 °C with methanesulfonyl chloride (3 mmol). After stirring at 5 °C for 9 h, an ice-water was added and the mixture was extracted with ether. The ethereal extracts were washed with 5% HCl, saturated $NaHCO_3$ solution, and brine. After drying (Na_2SO_4), the solvent was evaporated under reduced pressure to give the crude mesylate. The crude mesylate (1 mmol) was dissolved in dry benzene (2.0 ml) containing DBU (1.4 mmol) and the mixture was stirred at room temperature for 6 h. Water was added and the product was extracted with ether. The organic layer was washed with 5% HCl, saturated $NaHCO_3$ solution, and brine. After drying (Na_2SO_4), the solvent was removed *in vacuo* leaving the crude α-alkylidene-γ-lactones.

Method B. Thionyl chloride (1.2 mmol) was added dropwise to a solution of the crude alcohol (1 mmol) in dry pyridine (0.5 ml) and dry CH_2Cl_2 (1.5 ml). The reaction mixture was stirred at 0 °C for 30 min and then at room temperature for 4 h. After addition of a few pieces of ice, the mixture was extracted with CH_2Cl_2. The extracts were washed with 5% HCl, water, and dried (Na_2SO_4). The solvent was evaporated under reduced pressure to give the crude α-alkylidene-γ-lactones. Analytical samples of the γ-lactones were obtained by preparative GLC.

*7-Methylene-5-oxadispiro[2.0.4.4]dodecan-6-one (**4a**).* The reaction of **3** (829 mg, 4.6 mmol) and formaldehyde, generated by depolymerization of paraformaldehyde (3.5 g) at 160 °C (bath temperature) and passed into the reaction mixture at −20 °C under nitrogen stream, gave the crude α-hydroxymethyl-γ-lactone (873 mg, 90%: IR 3450, 1750 cm^{-1}). Dehydration of the alcohol by method A (the mesylate: IR 1750, 1350, 1160 cm^{-1}) gave α-methylene-γ-lactone **4a** (684 mg). Overall yield based on **3** was 77% (determined by ^1H NMR analysis). **4a**: IR 3050, 1750, 1660 cm^{-1}; NMR δ 0.10—1.00 (m, 4H), 1.23—2.00 (m, 8H), 2.68 (t, J=2.8 Hz, 2H), 5.50 (t, J=2.6 Hz, 1H), 6.10 (t, J=2.6 Hz, 1H); MS *m/e* 192 (M^+). Found: C, 74.59; H, 8.56%. Calcd for $C_{12}H_{16}O_2$: C, 74.97; H, 8.39%.

*(E)- and (Z)-7-Ethylidene-5-oxadispiro[2.0.4.4]dodecan-6-one (**4b**) and (**4c**).* The reaction of **3** (5.7 g, 31.6 mmol) and acetaldehyde (1.4 g, 31.6 mmol) gave the crude α-(1-hydroxyethyl)-γ-lactone (7.3 g, quantitatively: IR 3450, 1740 cm^{-1}). Dehydration of the alcohol by method A (the mesylate: IR 1750, 1350, 1160 cm^{-1}) gave the mixture of *E*-isomer **4b** and *Z*-isomer **4c** which were separated by column chromatography (SiO_2, 3% ether–petroleum ether). **4b** (54% from **3**): IR 3050, 1750, 1670 cm^{-1}; NMR δ 0.10—1.00 (m, 4H), 1.12—2.04 (m, 11H), 2.55 (m, 2H), 6.57 (m, 1H); MS *m/e* 206 (M^+). Found: C, 75.43; H, 8.76%. Calcd for $C_{13}H_{18}O_2$: C, 75.69; H, 8.80%. **4c** (7% from **3**): IR 3050, 1740, 1660 cm^{-1}; NMR δ 0.10—1.00 (m, 4H), 1.12—2.00 (m, 8H), 2.10 (m, 3H), 2.62 (m, 2H), 6.11 (m, 1H); MS *m/e* 206 (M^+). Found: C, 75.37; H, 8.89%. Calcd for $C_{13}H_{18}O_2$: C, 75.69; H, 8.80%.

*(E)- and (Z)-7-Propylidene-5-oxadispiro[2.0.4.4]dodecan-6-one (**4d**) and (**4e**).* The reaction of **3** (6.0 g, 33.3 mmol) and propionaldehyde (2.3 g, 33.3 mmol) gave the crude α-(1-hydroxypropyl)-γ-lactone (6.4 g, 80%: IR 3450, 1740 cm^{-1}). Dehydration of the alcohol by method A (the mesylate: IR 1740, 1350, 1160 cm^{-1}) gave the mixture of *E*-isomer **4d** and *Z*-isomer **4e** which were separated by column chromatography (SiO_2, 3% ether–petroleum ether). **4d** (30% from **3**): IR 3050, 1740, 1670 cm^{-1}; NMR δ 0.10—1.00 (m, 4H), 1.10 (t, 3H), 1.28—2.00 (m, 8H), 2.18 (m, 2H), 2.56 (m, 2H), 6.48 (m, 1H); MS *m/e* 220 (M^+). Found: C, 76.03; H, 9.21%. Calcd for $C_{14}H_{20}O_2$: C, 76.32; H, 9.15%. **4e** (20% from **3**): IR 3050, 1735, 1660 cm^{-1}; NMR δ 0.10—1.00 (m, 4H), 1.03 (t, 3H), 1.16—2.00 (m, 8H), 2.64 (m, 4H), 6.00 (m, 1H); MS *m/e* 220 (M^+). Found: C, 76.14; H, 9.24%. Calcd for $C_{14}H_{20}O_2$: C, 76.32; H, 9.15%.

*7-Isopropylidene-5-oxadispiro[2.0.4.4]dodecan-6-one (**4f**).* The reaction of **3** (5.0 g, 27.8 mmol) and acetone (1.6 g, 27.8 mmol) gave the crude α-(1-hydroxy-1-methylethyl)-γ-lactone (6.4 g, 97%: IR 3450, 1735 cm^{-1}). Dehydration of the alcohol by method B gave the crude α-isopropylidene-γ-lactone **4f** which was purified by column chromatography (SiO_2, 5% ether–petroleum ether) to afford 3.2 g of **4f** (52% from **3**): mp 70—71 °C (recrystallized from petroleum ether); IR (KBr) 3050, 1730, 1650 cm^{-1}; NMR δ 0.10—1.00 (m, 4H), 1.15—1.80 (m, 8H), 1.84 (m, 3H), 2.20 (m, 3H), 2.58 (m, 2H); MS *m/e* 220 (M^+). Found: C, 76.11; H, 9.28%. Calcd for $C_{14}H_{20}O_2$: C, 76.32; H, 9.15%.

*Tetrahydropyran-2-yl Acetonyl Ether (**5**).* A solution of hydroxyacetone (10 g, 0.135 mol) in 200 ml of dry CH_2Cl_2 containing 1.0 g of *p*-toluenesulfonic acid was treated at 0 °C with 3,4-dihydro-2*H*-pyran (13.6 g, 0.162 mol). After stirring at 0 °C for 3.5 h, the reaction was quenched by the addition of saturated $NaHCO_3$ solution and the mixture was extracted with CH_2Cl_2. The organic layer was washed with water, dried (Na_2SO_4), and concentrated *in vacuo* leaving the crude THP-ether **5**. Column chromatography (SiO_2, 20% ether–petroleum ether) followed by distillation gave 12.0 g of pure **5** in 57% yield: bp 64—66 °C/267 Pa; IR 1710, 1110, 1060, 1010 cm^{-1}; NMR δ 1.36—2.00 (m, 6H), 2.10 (s, 3H), 3.52 (m, 1H), 3.80 (m, 1H), 4.00 (m, 2H), 4.58 (t, 1H); MS *m/e* 156 (M^+−2). Found: C, 60.56; H, 8.99%. Calcd for $C_8H_{14}O_3$: C, 60.74; H, 8.92%.

*(E)- and (Z)-7-(2-hydroxyisopropylidene)-5-oxadispiro[2.0.4.4]dodecan-6-one (**4g**) and (**4h**).* The reaction of **3** (6.0 g 33.3 mmol) and **5** (5.3 g, 33.3 mmol) gave the crude alcohol (11.2 g, quantitatively: IR 3450, 1750, 1010 cm^{-1}). Dehydration of the alcohol by method B afforded the crude THP-ether (**6**) (10.1 g, 95% from **3**: IR 3050, 1720, 1650, 1010 cm^{-1}). The above ether **6** was dissolved in 100 ml of 60% aqueous acetic acid and the solution was stirred at 45 °C for 3 h. The reaction mixture was neutralized with saturated $NaHCO_3$ solution and the mixture was extracted with CH_2Cl_2. The organic layer was washed with water, dried (Na_2SO_4), and concentrated *in vacuo* leaving the mixture of *E*-isomer **4g** and *Z*-isomer **4h**. Separation by column chromatography (SiO_2, 20% ether–petroleum ether) gave 0.7 g of **4g** and 2.4 g of **4h** (9% and 31% from **3**, respectively). **4g**: IR 3400, 3050, 1730, 1650 cm^{-1}; NMR δ 0.10—0.90 (m, 4H), 1.08—2.04 (m, 8H), 2.16 (m, 3H), 2.64 (m, 2H), 2.74 (broad s, 1H), 4.10 (s, 2H); MS *m/e* 236 (M^+). Found: C, 70.94; H, 8.58%. Calcd for $C_{14}H_{20}O_3$: C, 71.16; H, 8.53%. **4h**: IR 3400, 3050, 1720, 1650 cm^{-1}; NMR δ 0.10—0.95 (m, 4H), 1.08—1.85 (m, 8H), 1.90 (m, 3H), 2.62 (m, 2H), 3.48 (broad s, 1H), 4.36 (s, 2H); MS *m/e* 236 (M^+). Found: C, 70.95; H, 8.57%. Calcd for $C_{14}H_{20}O_3$: C, 71.16; H, 8.53%.

We thank the Kyowa Hakko Co., Ltd for the

screening of the biological activities.

References

1) a) E. Rodriguez, G. H. N. Towers, and J. C. Mitchell, *Phytochemistry*, **15**, 1573 (1976); b) K. H. Lee, E. S. Huang, C. Piantadosi, J. S. Pagano, and T. A. Geissman, *Cancer Res.*, **31**, 1649 (1971); c) S. M. Kupchan, D. C. Fessler, M. A. Eakin, and T. J. Giacobbe, *Science*, **168**, 376 (1970); d) E. E. van Tamelen and S. R. Bach, *J. Am. Chem. Soc.*, **77**, 4683 (1955); e) A. Rosowsky, N. Papathanasopoulos, H. Lazarus, G. E. Foley, and E. J. Modest, *J. Med. Chem.*, **17**, 672 (1974); f) V. Nair and A. K. Sinhababu, *J. Org. Chem.*, **45**, 1893 (1980); g) R. L. Hanson, H. A. Lardy, and S. M. Kupchan, *Science*, **168**, 378 (1970); h) S. M. Kupchan, M. A. Eakin, and A. M. Thomas, *J. Med. Chem.*, **14**, 1147 (1971).

2) a) T. Tsuji and S. Nishida, *Gendai Kagaku*, **97**, 33 (1979); b) K. Nakanishi, M. Ohashi, M. Tada, and Y. Yamada, *Tetrahedron*, **21**, 1231 (1965).

3) a) Y. Tobe, K. Kakiuchi, Y. Kawakami, Y. Sakai, K. Kimura, and Y. Odaira, *Chem. Lett.*, **1978**, 1027; b) K. Kakiuchi, Y. Tobe, and Y. Odaira, *J. Org. Chem.*, **45**, 729 (1980).

4) Also, we already reported the synthesis of 1,6-dioxadispiro[2.0.4.4]dodecan-7-one (**7**), having a spiro epoxy ring, which is a useful intermediate for the synthesis of α-alkylidene-γ-butyrolactones.[5]

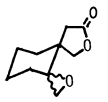

7

5) K. Kakiuchi, Y. Hiramatsu, Y. Tobe, and Y. Odaira, *Bull. Chem. Soc. Jpn.*, **53**, 1779 (1980).

6) Y. Tobe, A. Doi, K. Kimura, and Y. Odaira, *Bull. Chem. Soc. Jpn.*, **52**, 639 (1979).

7) a) P. A. Grieco and K. Hiroi, *J. Chem. Soc., Chem. Commun.*, **1972**, 1317; b) P. A. Grieco, J. A. Noguez, Y. Masaki, K. Hiroi, M. Nishizawa, A. Rosowsky, S. Oppenheim, and H. Lazarus, *J. Med. Chem.*, **20**, 71 (1977); c) P. A. Grieco, M. Nishizawa, T. Oguri, S. D. Burke, and N. Marinovic, *J. Am. Chem. Soc.*, **99**, 5773 (1977); d) I. Matsuda, S. Murata, and Y. Izumi, *Bull. Chem. Soc. Jpn.*, **52**, 2389 (1979).

8) S. Torii, K. Uneyama, and K. Okamoto, *Bull. Chem. Soc. Jpn.*, **51**, 3590 (1978).

9) K. Tanaka, H. Uneme, N. Yamagishi, R. Tanikaga, and A. Kaji, *Bull. Chem. Soc. Jpn.*, **53**, 2910 (1980).

10) S. Dev, *J. Indian Chem. Soc.*, **34**, 169 (1957).

Dynamic NMR as a Nondestructive Method for the Determination of Rates of Dissociation. III. Ionic Dissociation of α-Chlorodibenzyl Sulfide[1)]

Atsushi Shimizu, Yoshitaka Sakamaki, Kazufumi Azuma, Hiroshi Kihara, Nobuo Nakamura, and Michinori Ōki*

Department of Chemistry, Faculty of Science, The University of Tokyo, Hongo, Bunkyo-ku, Tokyo 113

(Received February 10, 1981)

Rates of dissociation of α-chlorodibenzyl sulfide have been determined by dynamic NMR technique. Examination of the rates at various concentrations of chloroform-*d* solutions has confirmed that the rates are not dependent on concentration, thus establishing that the NMR measurement affords data of unimolecular dissociation. The salt effect seems to be very small since addition of tetraethylammonium bromide hardly affects the rates of dissociation. Rates of dissociation in *o*-dichlorobenzene are smaller than in chloroform-*d*. The main contribution to the decrease in rates is given by the increase in enthalpy of activation, indicating that the hydrogen-bonding ability of chloroform is favorable for ionic dissociation.

Ionization of organic halides is an important process, since it is regarded as the first and rate-determining step in S_N1 type reactions.[2)] Winstein *et al.* were able to analyze the dissociation process into at least three steps: formation of intimate ion pair, solvent-separated ion pair, and free ions.[3)] In solvolytic reactions, any of the ionic species can produce products depending on concentration,[4)] making it difficult to study the earlier stages of ionization by solvolysis.

$$RX \rightleftharpoons R^+X^- \rightleftharpoons R^+ /\!/ X^- \rightleftharpoons R^+ + X^-$$

products products products

Various methods have been worked out in order to clarify the early stages. One is the exchange of a halogen (or a sulfonyloxyl) group which is labeled by an isotope.[5,6)] However, it has a handicap intrinsically in that the rates are measured in the presence of salts, giving rise to the salt effect. Other methods involve racemization of an optically active halide (or sulfonate)[7)] or scrambling or retention of oxygen-18 isotopes in carboxylates[8)] and sulfonates.[9)] These techniques apparently require optical resolution of the substrate and preparation of the isotopically labeled compounds. If a facile method is available, it would help clarify the initial stages of ionization of organic halide to a considerable extent.

We have found that easily ionizable compounds such as 2-chloro-1,3,5-trithiane exhibit a drastic change in line shapes of their NMR spectra, indicating the ionization process of the compounds.[10)] The method has been applied to substituted α-chlorodibenzyl sulfide to show that it is possible to extend the method to ionic dissociation if the compound in question carries diastereotopic protons and a chiral center which is lost on ionization.[11)]

Since the process was followed by the coalescence temperature method[12)] of NMR spectroscopy, only the free energies of activation have been available. Kinetic data at various temperatures would enable us to get further insight into the early stages of ionization; most of earlier works provided kinetic data only at a certain temperature. The concentration *ca.* 0.5 mol L^{-1} utilized in the routine measurements of ^1H NMR spectroscopy might be too high to observe S_N1 type ionization; in the classical methods a lower concentration was used. It is necessary to examine the usual concentration in NMR measurements as regards S_N1 reactions.

We have carried out dynamic NMR measurements of α-chlorodibenzyl sulfide solutions in various concentrations. The line shapes were simulated and activation parameters, ΔH^* and ΔS^*, were obtained. This paper reports the results. The effects of the salts added as well as the solvents on ionic dissociation are discussed.

Experimental

Materials and Solutions. α-Chlorodibenzyl sulfide was prepared by the chlorination of dibenzyl sulfide with *N*-chlorosuccinimide.[11)] Chloroform-*d* or *o*-dichlorobenzene was dried over Molecular Sieves 4A and solutions were prepared in a dry box desiccated with diphosphorus pentaoxide. The solutions were made directly by weighing the sample and the solvent. The concentrations were calculated by using the density of the solvent. Substance to be added to chloroform-*d* solutions was carefully dried either in a vacuum or by means of Molecular Sieves.

^1H NMR Measurements. The spectra were obtained on a Hitachi R-20B spectrometer equipped with a temperature variation accessory for solutions with high concentration, and on a JEOL FX-60 spectrometer equipped with a temperature variation accessory and FT-facilities for solutions with low concentration. Both instruments were operated at 60 MHz. The temperature of the solution was determined by the chemical shift differences of methanol and ethylene glycol protons, at low and high temperatures, respectively, when not directly read by a thermocouple.

Acquisition and Processing of Data. The ^1H NMR spectral line shapes were simulated with a modified Binsch program,[13)] the process being treated as an AB⇌BA exchange. $\Delta\delta_{AB}$ and J_{AB} were obtained by simulating the spectra at temperatures low enough where the rate of exchange is considered to be zero. They were treated as constant throughout the temperature range examined. The T_2 values were obtained from the half band widths of the methine proton signals at given temperatures. The calculated spectra were compared with the observed by visual fitting. The rates of proton spin exchange thus obtained were put into the Eyring equation and activation parameters, ΔH^* and ΔS^*, were obtained.

The free energies of activation for the spin exchange at the coalescence temperatures were obtained by putting the observed data into[14)]

$$k_c = \frac{\pi}{\sqrt{2}}\sqrt{6J_{AB}^2 + \Delta\delta_{AB}^2}. \quad (1)$$

Table 1. AB proton exchange in α-chlorodibenzyl sulfide in chloroform-*d*: ^{1}H NMR spectral data at 60 MHz and kinetic parameters

	Run 1	Run 2	Run 3	Run 4
Concentration/mol L^{-1}	0.267	0.195	0.116	0.0190
$\Delta\delta_{AB}$/Hz	9.49	9.39	8.97	9.26
J_{AB}/Hz	13.80	13.20	13.20	13.66
ΔH^*/kcal mol^{-1}	6.8±1.0	6.8±0.6	6.8±0.1	6.8±0.6
ΔS^*/e.u.	−29.8±3.2	−28.9±2.0	−29.7±0.3	−30.1±2.0
ΔG_c^*/kcal mol^{-1} a)	15.5	15.3	15.4	15.4
ΔG_c^*/kcal mol^{-1} b)	16.0	15.6	15.9	16.1
T_c/°C	37	32	34	36
k_c/s^{-1} a)	78.0	74.8	74.5	77.1

a) Obtained by the coalescence temperature method. b) Calculated from the enthalpy and the entropy of activation.

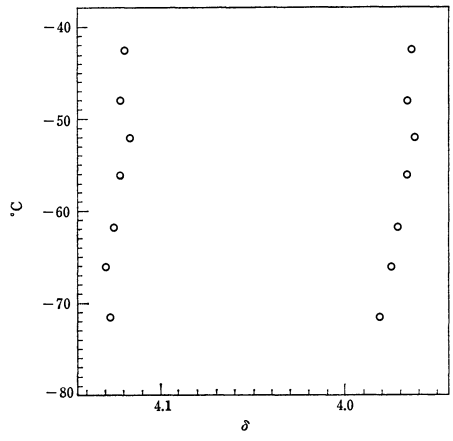

Fig. 1. Chemical shifts of A and B protons of α-chlorodibenzyl sulfide in chloroform-*d* at various temperatures.

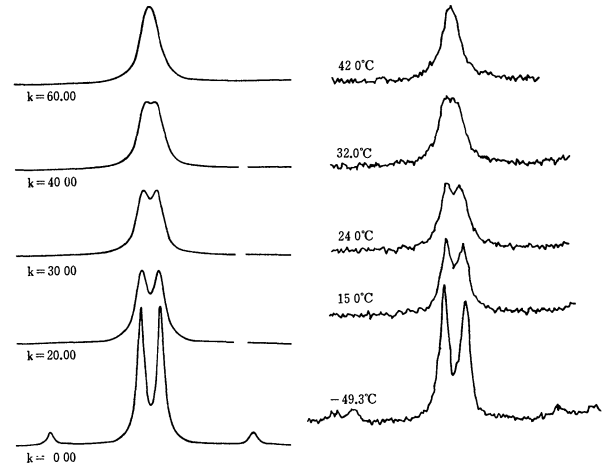

Fig. 2. Calculated and observed AB parts of the spectra of α-chlorodibenzyl sulfide in chloroform-*d* at the concentration of 0.195 mol L^{-1}. The signals outside of the AB are due to impurities.

Results and Discussion

Since the diastereotopic protons in α-chlorodibenzyl sulfide is connected to the chiral center *via* two single bonds, there are various conformations possible in solution. The distribution of the conformations and consequently chemical shift difference might change with temperature. This is serious in total line shape analysis, since the chemical shift difference cannot be directly read from the line shapes at near-by coalescence temperatures. The difficulty is usually overcome by assuming the linearity of the change in the chemical shift difference due to temperature. We have measured the chemical shift differences at various temperature by observing the spectra at a temperature where the exchange of proton spins is slow, and also at several lower temperatures. The results are shown in Fig. 1. We see that the chemical shifts change with temperature. The difference in chemical shifts between protons A and B remains almost constant, enabling us to assume that the chemical shift differences are constant througout the temperature range examined. Coupling constants of the AB protons were invariant as well.

The agreement between the calculated and the observed spectra is satisfactory. A set of typical data is given in Fig. 2. The data obtained with chloroform-*d* solutions are summarized in Table 1. The kinetic parameters obtained with various concentrations agree within the error limit, although the concentrations have been changed by an order of magnitude. The calculated free energies of activation from the enthalpies and entropies of activation, obtained by line shape analyses, are in good agreement with those obtained by the coalescence temperature method. This may be taken as evidence that the line shape analysis affords reliable data since the principles of the two methods differ.

The activation parameters are independent of concentration. It is assumed in the NMR theory of exchange of proton spins that the process is unimolecular. If the reaction is multimolecular, its treatment would be as follows. If the actual reaction is of *n*-th order, the rates of the reaction is expressed by

$$v = k[x]^n. \quad (2)$$

Since, in the NMR treatment, the reaction is taken to be of the first order, the rate expression becomes

$$v = k[x]^{n-1}[x] = k'[x]. \quad (3)$$

Putting the k' value into the Eyring equation, we obtain

Table 2. AB proton exchange in α-chlorodibenzyl sulfide in *o*-dichlorobenzene: ^{1}H NMR spectral data at 60 MHz and kinetic parameters

	Run 5	Run 6	Run 7
Concentration/mol L^{-1}	0.214	0.197	0.167
$\Delta\delta_{AB}$/Hz	10.15	10.39	10.15
J_{AB}/Hz	13.2	13.2	13.2
ΔH^*/kcal mol^{-1}	10.6±1.0	8.1±0.4	9.1±0.9
ΔS^*/e.u.	−22.0±2.7	−29.8±1.1	−24.4±4.7
ΔG_c^*/kcal mol^{-1} a)	18.4	19.1	17.4
ΔG_c^*/kcal mol^{-1} b)	18.7	19.4	17.4
T_c/°C	92.5	105.3	96.0
k_c/s^{-1}	75.3	75.4	75.3

a) Obtained by the coalescence temperature method. b) Calculated from the enthalpy and the entropy of activation.

$$\ln\frac{k'}{T} = \frac{\Delta H^*}{R}\times\frac{1}{T} + \ln[x]^{n-1} + \frac{\Delta S^*}{R} + \ln\frac{k_B}{h}. \quad (4)$$

Thus correct ΔH^* can be obtained from the slope of the straight line by the plot. However, the intercept contains a $\ln[x]^{n-1}$ term, indicating that if the reaction is not unimolecular but multimolecular, the apparent ΔS^* should change with concentration. Since the actual values of ΔS^* are invariant throughout the concentration range examined, the constancy assures that we are measuring the unimolecular dissociation process of the α-halo sulfide.

The enthalpy of activation is very small whereas the entropy of activation is very large negative (Table 1). Easily ionizable organic halides give very large negative entropy of activation for solvolysis. For example, triphenylmethyl chloride gives ΔH^* 12.5 kcal mol^{-1} (1 cal=4.18 J) and ΔS^* −17 e.u. (1 e.u.= 4.18 J K^{-1} mol^{-1}) in aqueous acetone.[15] The entropy of activation for the exchange of chloride ion between an ammonium salt and triphenylmethyl chloride is even larger: ΔH^* and ΔS^* are 12.4 kcal mol^{-1} and −39 e.u. at 50 °C, respectively.[6] It is suggested that a large negative entropy of activation is associated with an ionization process in a medium of low dielectric constant.[16] The loss of freedom in motion of solvent molecules by ionization should cause the phenomenon.

The present results are the consequence of racemization of the compound which should be derived by the motion of ionic species. If the ion pair collapses from the side where the chloride ion departs, it does not cause racemization: it is not observed as the exchange of proton spins and the situation is apparent from Eq. 5.

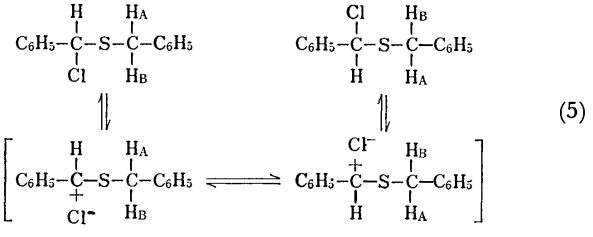

(5)

Instead, either the rotation of the planar cation or the motion of chloride ion from one side to another of the cation plane is necessary to cause racemization, *i.e.* exchange of AB proton spins. This motion requires some freedom of the ionic species. This process does not seem possible in the intimate ion pair as suggested by Winstein and Robinson[17] for the attack by a solvent molecule, but it is possible in a loose, solvent-separated ion pair. It is not clear whether the formation of the intimate ion pair is the rate determining step of the observed change: the second step, intervention of solvent molecule(s), might be the rate determining as well. However, the above discussion indicates that the solvent-separated ion pairs are formed in nonpolar solvents like chloroform.

As a preliminary test of the salt effect on the ionization in this system, tetraethylammonium bromide was added. A solution containing 0.115 mol L^{-1} of α-chlorodibenzyl sulfide and 0.112 mol L^{-1} of the salt in chloroform-*d* showed the coalescence of the signals AB due to the methylene protons at 32.2 °C which differ little from those in Table 1. Since lowering in solution temperature caused precipitation of the salt, it was not possible to obtain the chemical shift difference and the coupling constant of the AB protons for calculation of the free energy of activation at the coalescence temperature. By using the data of Run 2, Table 1, which are not considered to be affected much by the salt added, the rate constant at 32.2 °C is calculated to be 74.8 s^{-1}. The presence or absence of the salt effect should be discussed carefully,[4] but the results suggest that the salt effect[18] is practically absent, since high concentration of the salt should affect the rates of ionization to some extent.[19] The salt effect is larger in less polar media.[20] Winstein *et al.* suggested that it is mostly caused by ion pairs in less polar media because the concentration of free ions is too low.[21] Although sodium tetraethylaluminate becomes solvent-separated ion pairs in benzene on addition of polar solvents,[22] it is not possible to utilize this in our case. However, it is almost certain that there are solvent-separated ion pairs in our system because of the low polarity of the medium. Further elaboration to fill the gap between the solvents, such as acetone and diethyl ether used by Winstein *et al.*,[20] and chloroform is apparently needed.

Pyridine reacts almost instantaneously with chloride to form a salt on addition to a solution in chloroform, but we could detect no ^{1}H NMR signals attributable

to α-bromodibenzyl sulfide which could be formed by exchange of the anion, after leaving a solution of tetraethylammonium bromide and α-chlorodibenzyl sulfide in chloroform to stand overnight. Swain and Kreevoy[6] found that the chloride-exchange could occur in benzene with measurable rates.

In order to examine the solvent effect on the enthalpy and entropy of activation for ionization, *o*-dichlorobenzene was used as a solvent. The results are given in Table 2. The dissociation of the halide in *o*-dichlorobenzene is slower in this solvent than in chloroform.[11] The main factor which decreases the rates of dissociation is the enthalpy term. Entropy of activation is large negative, the absolute value decreasing to some extent.

The larger enthalpy of activation indicates that the ionic species are less stabilized by the solvation of *o*-dichlorobenzene than by that of chloroform. This is contrary to expectation from the dielectric constants; 4.81 and 9.93 for chloroform and *o*-dichlorobenzene, respectively. Donor numbers and acceptor numbers are often used for the ionic species,[23] but they are unknown for these solvents except for the acceptor number of chloroform. *Z* values[24] may be useful because they are obtained from the UV spectra of salts (ion pairs) in various solvents; 63.2 and 60.0 for chloroform and *o*-dichlorobenzene, respectively. The Z values correspond to energy (kcal mol^{-1}) of the light absorbed by the ion pairs and ions and the difference is correlated with the difference in energy of the ground and the excited states,[25] not being directly connected with the freedom of ion pairs. Nonetheless, among other solvent parameters the *Z* values give best results for correlating the rates of dissociation of α-chlorodibenzyl sulfide in the two solvents. From the microscopic stand point, chloroform, which is capable of forming hydrogen bond,[26] can stabilize anions[27] and this ability is responsible for the observed results. The observed decrease in the enthalpy of activation should include this stabilization.

Conclusion. Dynamic NMR technique has been used for the investigation of ionic dissociation of α-chlorodibenzyl sulfide, which has a pair of diastereotopic protons; their diastereotopicity is lost on ionization. The process involves the ionization of the halide into intimate ion pairs and then solvent-separated ion pairs. Racemization may take place at this stage and the racemized solvent-separated ion pairs lose the solvent molecule(s) to give racemized intimate ion pairs which then collapse into the inverted covalent species.

$$RX \rightleftharpoons R^+X^- \rightleftharpoons R^+ /\!/ X^- \rightleftharpoons X^- /\!/ R^+ \rightleftharpoons X^-R^+ \rightleftharpoons XR$$

In this technique we do not have to see the presence of ionic species. The usual dynamic NMR technique makes use of the coalescence of the two signals ascribable to the respective species to estimate the rates of exchange. Kessler *et al.* investigated the rates of ionization of triarylmethyl derivatives by observing both the covalent and ionic species.[28] The rates of dissociation are obtained in relatively nonpolar solvents. The rates of ionization can be obtained at various temperatures without prior optical resolution of the substrate, affording activation parameters of ionization. The technique affords information on unimolecular dissociation at concentration of *ca.* 0.2 mol L^{-1}, which gives insight into the early stages of the S_N1 reactions.

The only shortcoming of this technique is that the substrate should possess diastereotopic protons whose diastereotopicity is lost on ionization. This may limit utilization of the technique to some extent and may require modification of a molecule which is conveniently studied by the classical method. The rates of exchange of proton spins should be 10^0—10^{-5} s^{-1} as in the usual dynamic NMR technique.[29] This will not hamper the usefulness of the technique because this kind of limitation is always present for other techniques as well. It is difficult to obtain reliable data by the classical method if the rates exceed 10^{-3} s^{-1}. The compound we used is very easily ionizable, thus reacting with atmospheric moisture. Although this may cause some errors, but it is the main reason why we were able to carry out the studies in relatively nonpolar aprotic solvents.

It is not possible to identify by this method how much of the solvent-separated ion pairs return to the covalent species without racemization, but this is unavoidable in the ionization of organic halides. Combination with isotopic labeling and subsequent observation of scrambling will afford useful data in this context.

The work was carried out with a Grant-in-Aid for Scientific Research from the Ministry of Education, Science and Culture.

References

1) Preceding paper: M. Ōki, Y. Yoshioka, H. Kihara, and N. Nakamura, *Chem. Lett.*, **1980**, 1625.

2) C. K. Ingold, "Structure and Mechanism in Organic Chemistry," Cornell University Press, Ithaca (1953), pp. 306—418.

3) S. Winstein, E. Clippinger, A. H. Fainberg, and G. C. Robinson, *J. Am. Chem. Soc.*, **76**, 2597 (1954); S. Winstein, B. Appel, R. Baker, and A. Diaz, *Chem. Soc. (London), Spec. Publ.*, **19**, 109 (1965).

4) D. J. Raber, J. M. Harris, and P. v. R. Schleyer, "Ions and Ion Pairs in Solvolytic Reactions," in "Ions and Ion Pairs in Organic Reactions," ed by M. Szwarc, John-Wiley, New York (1974), Vol. 2, pp. 247—374.

5) S. Winstein, E. Clippinger, A. H. Fainberg, R. Heck, and G. C. Robinson, *J. Am. Chem. Soc.*, **78**, 328 (1956); P. B. D. de la Mare, D. M. Hall and E. Maugher, *Recl. Trav. Chim. Pay-Bas*, **87**, 1394 (1968).

6) C. G. Swain and M. M. Kreevoy, *J. Am. Chem. Soc.*, **77**, 1122 (1955).

7) S. Winstein, A. Ledwith, and M. Hojo, *Tetrahedron Lett.*, **1961**, 341; Ref. 5b.

8) H. L. Goering and J. F. Levy, *Tetrahedron Lett.*, **1961**, 644; *J. Am. Chem. Soc.*, **84**, 3853 (1962).

9) H. L. Goering and B. E. Jones, *J. Am. Chem. Soc.*, **102**, 1628 (1980) and papers cited therein.

10) K. Arai and M. Ōki, *Tetrahedron Lett.*, **1975**, 2183; *Bull. Chem. Soc. Jpn.*, **49**, 553 (1976).

11) K. Arai and M. Ōki, *Bull. Chem. Soc. Jpn.*, **50**, 175 (1977).
12) J. A. Pople, W. G. Schneider, and H. J. Bernstein, "High Resolution Nuclear Magnetic Resonance," McGraw-Hill, New York (1959), p. 218; J. W. Emsley, J. Feeney, and C. H. Sutcliff, "High Resolution Nuclear Magnetic Resonance Spectroscopy," Pergamon Press, Oxford (1965), p. 481.
13) G. Binsch, *Topics Stereochem.*, **3**, 87 (1970).
14) M. Ōki, H. Iwamura, and N. Hayakawa, *Bull. Chem. Soc. Jpn.*, **36**, 1542 (1963); **37**, 1865 (1964); R. J. Kurland, M. B. Rubin, and W. B. Wise, *J. Chem. Phys.*, **40**, 2426 (1964).
15) C. G. Swain and C. B. Scott, *J. Am. Chem. Soc.*, **75**, 246 (1953).
16) A. A. Frost and R. G. Pearson, "Kinetics and Mechanisms," John-Wiley, New York (1953), p. 127.
17) S. Winstein and G. C. Robinson, *J. Am. Chem. Soc.*, **80**, 169 (1958).
18) L. C. Bateman, M. G. Church, E. D. Hughes, C. K. Ingold, and N. A. Taher, *J. Chem. Soc.*, **1940**, 979.
19) A. H. Fainberg and S. Winstein, *J. Am. Chem. Soc.*, **78**, 2763 (1956).
20) S. Winstein, S. Smith, and D. Darwish, *J. Am. Chem. Soc.*, **81**, 5511 (1959).
21) S. Winstein, P. E. Klinediensk, and G. C. Robinson, *J. Am. Chem. Soc.*, **83**, 885 (1961).
22) N. Ahmad and M. C. Day, *J. Am. Chem. Soc.*, **99**, 941 (1977).
23) V. Gutman, "The Donor-Acceptor Approach to Molecular Interactions," Plenum Press, New York (1978), pp. 17—33.
24) C. Reichardt, "Solvent Effects in Organic Chemistry," Verlag Chemie, Weinheim (1979), pp. 237—250.
25) E. M. Kosower, "An Introduction to Physical Organic Chemistry," John-Wiley, New York (1968), pp. 260—263 and pp. 293—302. See also J. W. Larsen, A. G. Edwards, and P. Dobi, *J. Am. Chem. Soc.*, **102**, 6780 (1980).
26) G. C. Pimentel and A. L. McCllelan, "The Hydrogen Bond," W. H. Freeman, San Francisco (1960), p. 197.
27) S. Y. Lam, C. Louis, and R. L. Benoit, *J. Am. Chem. Soc.*, **98**, 1156 (1976).
28) M. Feigel, H. Kessler, and A. Walter, *Chem. Ber.*, **111**, 2947 (1978) and earlier papers.
29) L. M. Jackman and A. Cotton, "Dynamic Nuclear Magnetic Resonance Spectroscopy," Academic Press, New York (1975).

5-Amino-1-vinyl-4,5-dihydro-1*H*-1,2,3-triazoles as a Source of 1-Amino-2-aza-1,3-butadiene[1)]

Yujiro NOMURA,* Yoshito TAKEUCHI, Shuji TOMODA, and Masato M. ITO
Department of Chemistry, College of General Education, The University of Tokyo, Komaba, Meguro-ku, Tokyo 153
(Received February 19, 1981)

Thermolysis of 4,4-dimethyl-1-(1-phenylvinyl)-5-(1-pyrrolidinyl)-4,5-dihydro-1*H*-1,2,3-triazole gave 2-methyl-*N*-(1-phenylvinyl)-1-(1-pyrrolidinyl)-1-propanimine, which reacted as a 2-azabutadiene with electron-deficient dienophiles to afford the corresponding [4+2] cycloadducts. Reactivity and regioselectivity of the cycloaddition reactions were rationalized with the frontier molecular orbital treatment.

In the numerous examples cummulated previously for the Diels-Alder type [4+2] cycloaddition reaction of heterodienes[2)] the cases of 2-aza-1,3-butadienes are few, and in most of the few cases the azadiene system is a part of the ring system.[3)] To the best of our knowledge, three examples have been reported concerning the [4+2] cycloaddition reaction of *acyclic* 2-azabutadienes. Aue and Thomas have trapped methyl *N*-isopropenylacetimidate formed by thermolysis of 2-methoxy-4,4-dimethyl-1-azetine with dimethyl acetylenedicarboxylate (DMAD) (Eq. 1).[4)] Ghosez

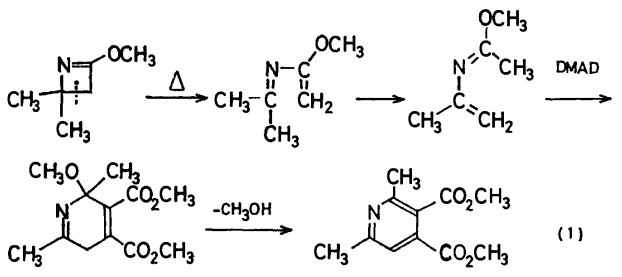

(1)

and coworkers have reported the [4+2] cycloaddition reaction of N^2-isopropenyl-N^1,N^1-dimethylformamidine formed by thermolysis of 3-dimethylamino-2,2-dimethyl-2*H*-azirine with electron-deficient dienophiles (Eq. 2).[5)] On the other hand, Taylor and coworkers have

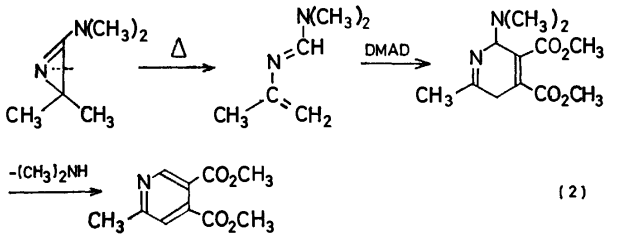

(2)

reported that the reaction of N^1,N^1-diethyl-N^2-(1-propenyl)benzamidine with DMAD gave N^1,N^1-diethyl-N^2-[2,3-bis(methoxycarbonyl)-1,3-pentadienyl]benzamidine *via* [2+2] cycloaddition reaction and that no [4+2] adduct was formed (Eq. 3).[6)]

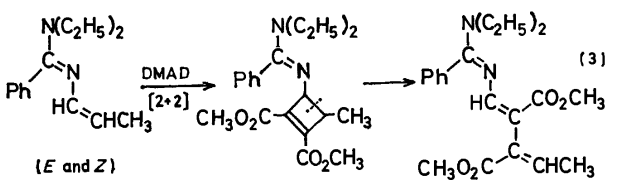

(3)

In the course of our studies on the reaction of 5-amino-1-vinyl-4,5-dihydro-1*H*-1,2,3-triazoles (**1**), which were prepared by the 1,3-dipolar cycloaddition reaction of vinyl azides with enamines,[7)] we noticed that the N^2-vinylamidine (**2**) formed by thermolysis of **1a** acted as a 2-aza-1,3-butadiene to form the [4+2] cycloadduct with some dienophiles.

Results and Discussion

*Thermolysis of 4,4-Dimethyl-1-(1-phenylvinyl)-5-(1-pyrrolidinyl)-4,5-dihydro-1*H*-1,2,3-triazole (**1a**).* 4,4-Dimethyl-1-(1-phenylvinyl)-5-(1-pyrrolidinyl)-4,5-dihydro-1*H*-1,2,3-triazole (**1a**) was thermolyzed at 80 °C in DMSO-d_6 for 22 h in a sealed NMR tube. The NMR spectra of the solution showed that 2-methyl-*N*-(1-phenylvinyl)-1-(1-pyrrolidinyl)-1-propanimine (**2**) was formed in quantitative yield (Eq. 4).

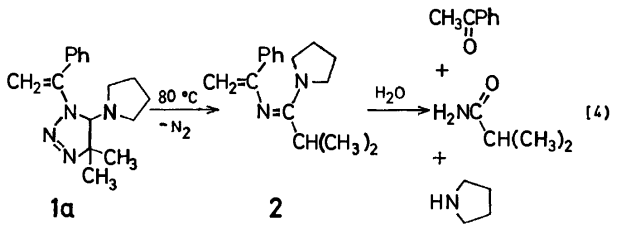

(4)

Since **2** was rapidly hydrolyzed into acetophenone and isobutyramide upon exposure to air, the isolation in pure form or combustion analysis of **2** was unsuccessful.

Table 1 collects the ^{1}H and ^{13}C NMR data pertinent to the structural confirmation of **2**. In addition to a phenyl and 1-pyrrolidinyl group, the presence of newly formed isopropyl group was indicated in its characteristic ^{1}H NMR peak pattern (a doublet at δ 1.04 and a septet at δ 3.01). The two low field singlets were assigned to the terminal olefinic protons at C-5. The structure was further supported by the ^{13}C NMR spectra. The presence of three singlets at low field, one of which corresponds to the *ipso* carbon of the phenyl group, and a triplet at δ 93.0 suggested a trisubstituted 2-aza-1,3-butadiene skeleton. The location of the three substituents was appropriately explained by the hydrolysis products, acetophenone and isobutyramide.

In other solvents (cyclohexane, benzene, diglyme, *etc.*) the amidine **2** was formed in much lower yields accompanied by 2,2-dimethyl-5-phenyl-2*H*-pyrrole (**3a**) (Scheme 1). The compound **3a** was separated with alumina column chromatography, and its structure was determined by spectral and analytical results.

TABLE 1. NMR SPECTRAL DATA OF 2-METHYL-*N*-(1-PHENYLVINYL)-1-(1-PYRROLIDINYL)-1-PROPANIMINE (**2**) (in DMSO-d_6)

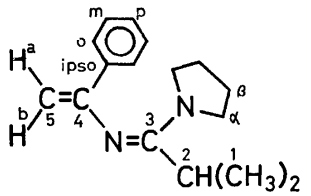

^{1}H NMR			Assignment	^{13}C NMR	
δ	Appearance (J/Hz)	Area		δ	Appearance[a]
1.04	d (J=7)	6H	1	19.7	q
1.6—2.0	m	4H	β	24.8	t
3.01	sep (J=7)	1H	2	29.9	d
3.2—3.7	m	4H	α	47.4	t
4.34	s	1H	H^b	93.0	t
4.94	s	1H	H^a 5		
7.2—7.7	m	5H	*o*	125.2	d
			p	127.2	d
			m	127.8	d
			ipso	139.8	s
			3[b]	152.7	s
			4[b]	159.4	s

a) Splitting pattern determined by off-resonance decoupling. b) May be reversed.

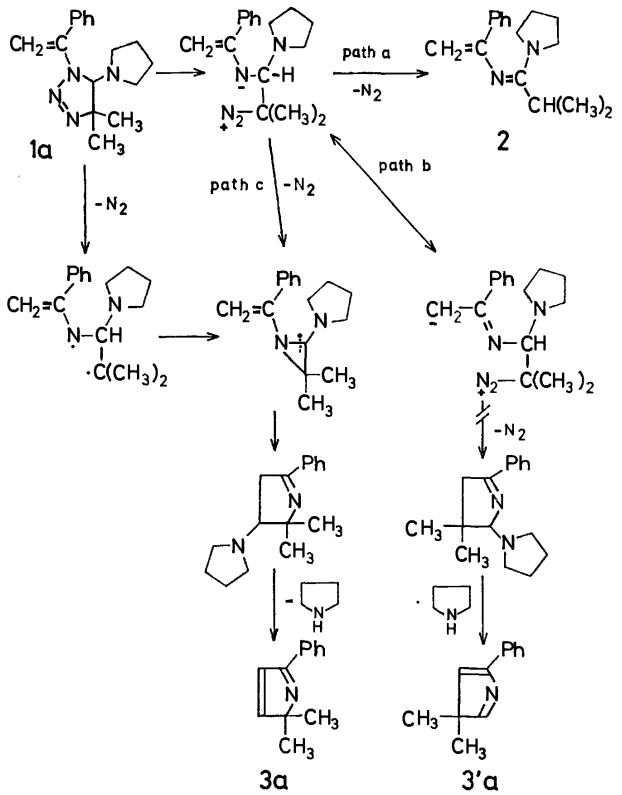

Scheme 1. Formation of the N^2-vinylamidine (**2**) and the 2*H*-pyrrole (**3a**) by thermolysis of the vinyltriazoline (**1a**).

In ^{1}H NMR the singlet at δ 1.45 corresponds to the two methyl groups and the doublet at δ 6.73 (J= 4.5 Hz) corresponds to the proton at C-4. In ^{13}C NMR the two doublets at δ 162.6 and 123.1 correspond to the C-3 and C-4 of the 2*H*-pyrrole ring, and the singlets at δ 169.6 and 79.5 correspond to the C-5 and C-2 of the pyrrole ring, respectively.[8a] The alternative structure of the 3*H*-pyrrole (**3'a**) is eliminated because the signal at δ 79.5 should be assigned to the quaternary sp^3 carbon adjacent to one nitrogen atom.[8b]

The formation of the N^2-vinylamidine (**2**) and the 2*H*-pyrrole (**3a**) was most simply explained by the tentative routes shown in Scheme 1. In the thermolysis of 5-amino-4,5-dihydro-1*H*-1,2,3-triazoles, it is generally accepted that the heterolytic cleavage of the bond between N-1 and N-2 occurs first,[9-11] and that the loss of nitrogen followed by 1,2-hydride (or carbanion) shift gives amidines.[10-12] In the present case the N^2-vinylamidine (**2**) would be formed *via* the similar path (path a). Since the ring closure *via* path b would lead to the 3*H*-pyrrole (**3'a**), which was not actually formed, the 2*H*-pyrrole (**3a**) should be formed *via* another path. A plausible path involves the formation of aziridine, followed by the subsequent ring conversion to the pyrroline and elimination of pyrrolidine to the 2*H*-pyrrole (**3a**) (path c).[12] The homolytic extrusion of nitrogen from **1a** can also lead to the aziridine as was the case of thermolysis and photolysis of other 4,5-dihydro-1*H*-1,2,3-triazoles.[13] The fact that **3a** was not formed by thermolysis in DMSO but was formed in the less polar solvents may be suggestive of the homolytic mechanism for the aziridine formation (and the heterolytic one for the amidine), although no example of homolytic extrusion of nitrogen by thermolysis of 5-amino-4,5-dihydro-1*H*-1,2,3-triazoles has been reported.

Thermolysis of Other Vinyltriazolines. In contrast with the quantitative formation of the N^2-vinylamidine (**2**) from **1a** in DMSO, 4-ethyl-1-(1-phenylvinyl)-5-

(1-pyrrolidinyl)-4,5-dihydro-1*H*-1,2,3-triazole (**1b**) was stable at 80 °C. Thermolysis at 100 °C in DMSO-d_6, diglyme-d_{14}, or pyridine-d_5 caused decomposition with evolution of nitrogen, but the NMR spectra of the resulting solution showed that neither amidine nor pyrrole was formed.

Thermolysis of 7a-morpholino-1-(1-phenylvinyl)-3a,4,5,6,7,7a-hexahydro-1*H*-1,2,3-benzotriazole (**1c**) also gave neither amidine nor pyrrole. Chromatographic separation of the reaction mixture gave faint yellow oil, whose spectral data were identical with those of previously reported 1-(1-phenylvinyl)-4,5,6,7-tetrahydro-1*H*-1,2,3-benzotriazole (**4**; 36% yield) (Eq. 5).[7]

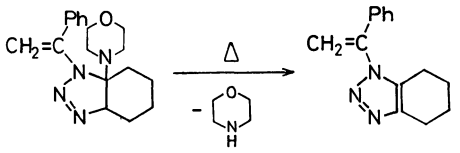

(5)

1c **4**

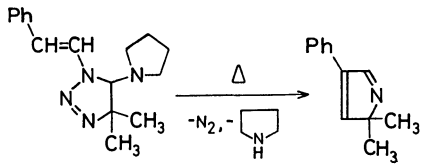

(6)

1d **3d**

Thermolysis of 4,4-dimethyl-5-(1-pyrrolidinyl)-1-styryl-4,5-dihydro-1*H*-1,2,3-triazole (**1d**) was carried out at 80 °C in DMSO and in benzene to give the corresponding 2,2-dimethyl-4-phenyl-2*H*-pyrrole (**3d**) in 38 and 80% yields, respectively (Eq. 6). No amidine was detected in the crude solution. The 2*H*-pyrrole (**3d**) seems to be formed *via* aziridine as in the case of **3a**.

These results were in sharp contrast with the Fusco's results of thermolysis of 1-aryl-5-amino-1,2,3-triazolines, in which the corresponding N^2-arylamidines were the sole products.[10-12]

[4+2] Cycloaddition Reaction of the 2-Aza-1,3-butadiene (2). In order to examine the reactivity of 2-methyl-*N*-(1-phenylvinyl)-1-(1-pyrrolidinyl)-1-propanimine (**2**) as a 2-aza-1,3-butadiene, **2** prepared by heating **1a** in DMSO at 80 °C for 1 d was allowed to react with an appropriate dienophile (**5**) at room temperature.

The results were summarized in Scheme 2 and Table 2. In the case of some electron-deficient dienophiles (**5a—d**, and DMAD), the corresponding dihydropyridines (**6**) and pyridines (**7**) were formed at room temperature for 1—5 d, but reaction with *p*-benzoquinone (**5e**) or *N*-phenylmaleimide (**5f**) gave only polymeric substances. With 3,4-dihydro-2*H*-pyran (**5g**), an olefin with a π-donating group, no reaction occurred even at 110 °C and **5g** remained unchanged.

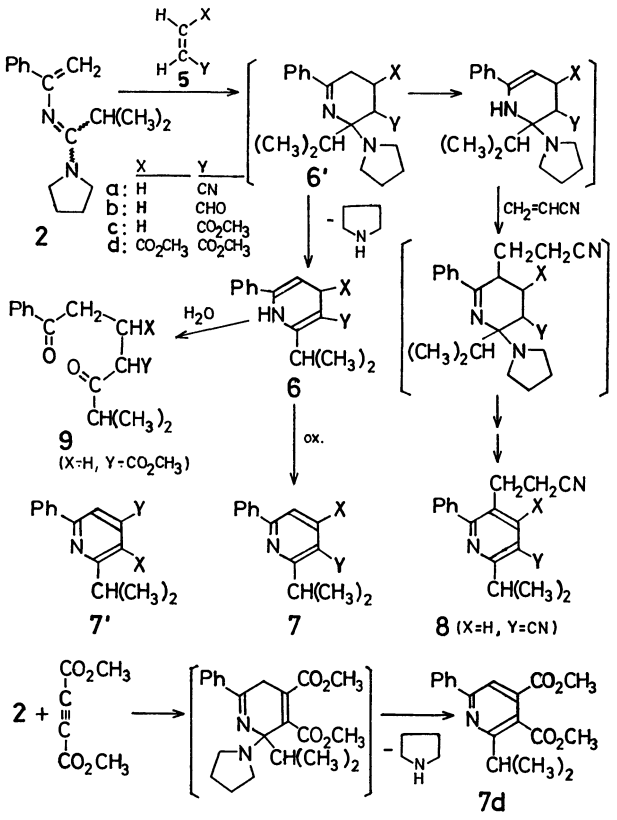

Scheme 2. Cycloaddition reaction of the 2-azabutadiene (**2**) with electron-deficient dienophiles.

In the case of the reaction with acrylonitrile (**5a**) or acrylaldehyde (**5b**), the initially formed dihydropyridine (**6a,b**) was gradually oxidized to the pyridine (**7a,b**) upon exposure to air. In the case of **5a**, the reaction at 80 °C for 36 h or at room temperature for 30 d gave the 1:2 adduct **8** besides **6a** and **7a**. In the case of methyl acrylate (**5c**), dihydropyridine was not isolated but considerable amount of methyl 2-isobutyryl-5-oxo-5-phenylpentanoate (**9**) was isolated. The dioxo ester **9** was identified by spectral comparison with the authentic sample prepared according to the route shown in Eq. 7.

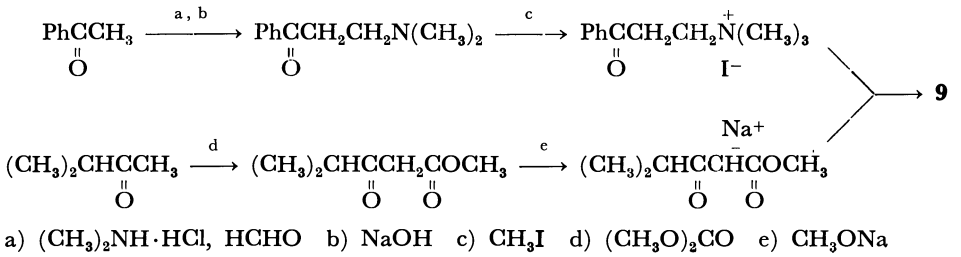

(7)

a) $(CH_3)_2NH\cdot HCl$, HCHO b) NaOH c) CH_3I d) $(CH_3O)_2CO$ e) CH_3ONa

TABLE 2. REACTION OF **2** WITH DIENOPHILES IN DMSO[a)]

Dienophile	X	Y	Molar ratio (**5**/**1a**)	Reaction time/d	Yield/% of products			
					6	**7**	**8**	**9**
5a	H	CN	2.0	2	37	25	—	—
			2.0	30	16	7	24	—
			2.0	1.5[b)]	—	13	10	—
5b	H	CHO	1.3	3	24	22	—	—
5c	H	CO_2CH_3	1.1	5	—	21	—	24
			1.1	5	—	44	—	—[c)]
5d	CO_2CH_3	CO_2CH_3	2.1	2	—	11	—	—
			2.1	2	—	23	—	—[e)]
5e	-COCH=CHCO-		1.1	2	—	—	—	—[d)]
5f	-CONPhCO-		1.0	2	—	—	—	—[d)]
5g	$-O(CH_2)_3-$		1.8	3[e)]	—	—	—	—
DMAD	CO_2CH_3	CO_2CH_3	2.1	1	—	37	—	—

a) Carried out at room temperature, unless otherwise noted. b) Carried out at 80 °C. c) Initial crude products were oxidized with *p*-benzoquinone prior to work up. d) Only polymeric products were formed. e) Carried out at 80—110 °C, but dienophile remained unchanged.

A plausible mechanism for the formation of these products was depicted in Scheme 2. The [4+2] cycloaddition reaction of **2** with a dienophile would give the cyclic imine intermediate **6'**, which is deaminated to the dihydropyridine **6**. The Michael addition of acrylonitrile to the isomeric enamine form of **6'a** would lead to **8**.[14)] Formation of **9** would indicate the initial formation of dihydropyridine **6c**, which was hydrolyzed into **9** on silica gel. This was prevented by oxidation of **6c** to **7c** with *p*-benzoquinone prior to work up.

An intriguing aspect of these cycloaddition reactions involving **5a**—**c** is the formation of only one of the possible regioisomers. Two regioisomeric structures **7** and **7'** were expected, but only **7** was actually formed in all cases. In the case of **7a**, for instance, the two doublets at δ 7.68 and 7.92 in ^{1}H NMR spectra can be assigned to the two adjacent pyridine ring protons at C-5 and C-4. The large coupling constant between these protons (8 Hz) precluded the possibility of isomer **7'a** in which only a small *meta* coupling should be observed. This assignment was further supported by the general observation that the coupling constant between 4-H and 5(or 3)-H is the largest (about 8 Hz) in ordinary pyridine derivatives.[15)] These structural assignments were further confirmed by ^{13}C NMR data (see Experimental).

Taylor and coworkers suggested that the preference of [2+2] to [4+2] cycloaddition in the case of N^1,N^1-diethyl-N^2-(1-propenyl)benzamidine (Eq. 3) could be caused by the inaccessibility of the *s-cis* conformation in the 2-aza-1,3-butadiene system.[6)] In the present case *s-cis* conformation is not sterically unfavorable due to the presence of phenyl group at 3-position of the 2-aza-1,3-butadiene system of **2**, so that the preference of the [4+2] cycloaddition is in accord with the Taylor's postulate. But further experimental results about the cycloaddition reactions of various 2-aza-1,3-butadienes are necessary to examine the validity of his postulate. Useful synthetic methods of 2-aza-1,3-butadienes are awaited.

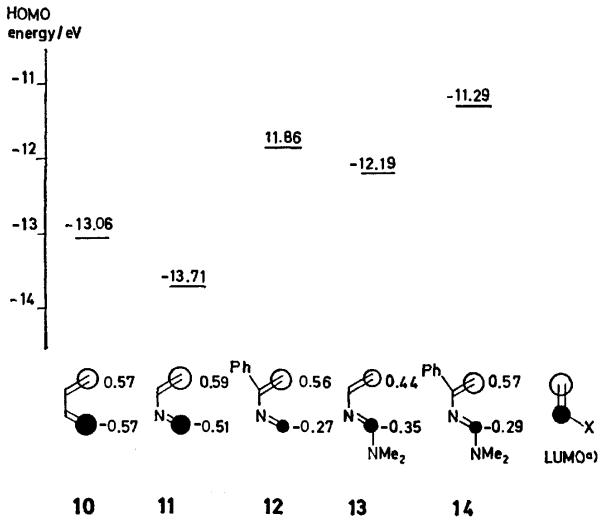

Fig. 1. Energies and coefficients of HOMO of 2-azabutadienes estimated with CNDO/2 method.
a) LUMO of a typical electron-deficient dienophile.

Frontier Molecular Orbital Treatment. Frontier molecular orbital treatment was successfully applied to rationalize the reactivity and regioselectivity of cycloaddition reactions such as Diels-Alder reactions and 1,3-dipolar cycloaddition reactions.[16)] We found that this treatment also rationalized the rather high reactivity and high regioselectivity in the [4+2] cycloaddition reactions of the 2-aza-1,3-butadiene (**2**).

Frontier orbital energies and coefficients of various 2-azabutadienes were estimated with CNDO/2 method (Fig. 1).

In Diels-Alder reaction with electron-deficient dienophiles, the interaction between HOMO (highest occupied molecular orbital) of the diene and LUMO (lowest unoccupied molecular orbital) of the dienophile is important.[16)] As shown in Fig. 1, the HOMO of 2-azabutadiene (**11**) is lower than that of butadiene (**10**), suggesting the lower reactivity of **11** compared with **10**. However, the HOMO of 3-phenyl-2-aza-

butadiene (**12**) or 1-amino-2-azabutadiene (**13**) is raised by their substituents (phenyl and amino groups), so that the HOMO of the 2-azabutadiene **14** (a model of **2**) is much higher in energy than that of **10** or **11**. The higher energy of HOMO would increase the interaction with LUMO of dienophiles, resulting the rather high reactivity in cycloaddition reaction of **2** with electron-deficient dienophiles.

On the other hand, the LUMO of enol ethers is higher in energy so that the interaction would be too small to cause the reaction with **2** in spite of the high energy of HOMO of **2**.

The magnitude of coefficients of HOMO of 2-azabutadienes were also in accord with the observed regioselectivity in the reactions of non-symmetrical dienophiles (**5a**—**c**). The coefficient of HOMO of **11** was larger at 4-position than at 1-position, and this trend was enhanced by the substitution of the phenyl and amino groups (**12**, **13**). Consequently the coefficients of HOMO of **14** was much larger at 4-position than at 1-position, so that the high regioselectivity in the [4+2] cycloaddition reaction of **2** would be induced.

Experimental

General. Melting points were determined on a Mitamura Riken hot-stage melting point apparatus and were uncorrected. Infrared spectra were determined on a JASCO DS-403G grating infrared spectrophotometer. Nuclear magnetic resonance spectra were determined on a JEOL MH-100, FX-90Q, and Varian FT-80A NMR spectrometer (splitting pattern in ^{13}C NMR data was obtained by off-resonance decoupling). Ultraviolet spectra were determined on a Hitachi EPS-3T recording spectrophotometer. Mass spectra were determined on a Hitachi RMU-6MG mass spectrometer. The vinyltriazolines (**1**) were prepared by the previously described method.[7] Solvents were distilled under anhydrous conditions before use.

*Thermolysis of 4,4-Dimethyl-1-(1-phenylvinyl)-5-(1-pyrrolidinyl)-4,5-dihydro-1*H*-1,2,3-triazole (**1a**).* *Method A*: In 0.5 ml of an appropriate solvent was dissolved 71—118 mg (0.26—0.44 mmol) of **1a** with 3.8—5.7 mg of 2,2,3,3-tetramethylbutane as an internal standard in a 5 mm diameter NMR sample tube. The tube was then sealed *in vacuo*, and was heated in an 80 °C bath until **1a** was completely consumed.

Method B: In 100 ml of an appropriate solvent was dissolved 1.0 g (3.7 mmol) of **1a** and the solution was heated to reflux under nitrogen until **1a** was completely consumed.

In Dimethyl-d_6 *Sulfoxide (DMSO-*d_6*, Method A)*: Thermolysis of **1a** was carried out in DMSO-d_6 at 80 °C for 22 h. NMR spectra of the resulting solution showed that 2-methyl-*N*-(1-phenylvinyl)-1-(1-pyrrolidinyl)-1-propanimine (**2**) (see Table 1) was formed in quantitative yield.

In Toluene (Method B): Thermolysis of **1a** (1.0 g, 3.7 mmol) was carried out in refluxing toluene (110 °C) for 75 min. Removal of the solvent *in vacuo* gave 700 mg of the residue, whose ^{1}H NMR spectra showed the existence of **2** and 2,2-dimethyl-5-phenyl-2*H*-pyrrole (**3a**) in 6:7 ratio. Chromatographic separation of 220 mg of the residue afforded 40 mg (28% yield) of acetophenone and 62 mg (37% yield) of **3a**, respectively. Analytically pure sample of **3a** was obtained by distillation with the Kugelrohr apparatus at 55 °C/3 mmHg†: mp 19—20 °C; MS *m/e* 171 (M^+); IR (neat) 1605, 1446, 1358, 1198, 1020, 760, and 694 cm^{-1}; UV_{max} (methanol) 212.5 (ε, 12000), 217.5 (12000), and 249 nm (10000); ^{1}H NMR ($CDCl_3$) δ 1.45 (6H, s), 6.73 (1H, d, J=4.5 Hz), 7.3—7.5 (4H, m), and 7.8—8.0 (2H, m); ^{13}C NMR ($CDCl_3$) δ 23.4 (q), 79.5 (s), 123.1 (d), 127.6 (d), 128.6 (d), 130.2 (d), 134.3 (s), 162.6 (d), and 169.6 (s, C=N).

Found: C, 84.04; H, 7.63; N, 8.27%. Calcd for $C_{12}H_{13}N$: C, 84.17; H, 7.65; N, 8.18%.

The rest of the residue (480 mg) was left at room temperature for 3 d. Then 1 ml of diethyl ether was added, and the precipitates of isobutyramide was collected by filtration and washed three times with 1 ml of diethyl ether (yield, 30 mg, 14%).

In Toluene-d_8 *(Method A)*: Thermolysis of **1a** was carried out in toluene-d_8 at 80 °C for 21 h. The ^{1}H NMR spectra of the resulting solution showed the formation of **2** and **3a** in 58 and 23% yields, respectively.

In Diglyme-d_{14} *(Method A)*: Thermolysis of **1a** was carried out in diglyme-d_{14} at 80 °C for 20 h. The ^{1}H NMR spectra of the resulting solution showed the formation of **2** and **3a** in 31 and 8% yields, respectively.

In Benzene (Method B): Thermolysis of **1a** was carried out in refluxing benzene (80 °C) for 1 d. The ^{1}H NMR spectra of the residue after removal of the solvent showed the formation of **2** and **3a** in 42 and 11% yields, respectively.

In Cyclohexane (Method B): Thermolysis of **1a** was carried out in refluxing cyclohexane (80 °C) for 1 d. The ^{1}H NMR spectra of the residue after removal of the solvent showed the formation of **2** and **3a** in 50 and 20% yields, respectively.

*Thermolysis of 7a-Morpholino-1-(1-phenylvinyl)-3a,4,5,6,7,7a-hexahydro-1*H*-1,2,3-benzotriazole (**1c**).* Toluene (20 ml) solution of **1c** (92 mg, 0.29 mmol) was heated to reflux for 16 h under nitrogen until **1c** was completely consumed. The toluene was removed *in vacuo* at room temperature. The ^{1}H NMR spectra of the residue showed that no N^2-vinylamidine was formed. Chromatographic separation of the residue through silica-gel column eluting with diethyl ether gave 1-(1-phenylvinyl)-4,5,6,7-tetrahydro-1*H*-1,2,3-benzotriazole (**4**)[7] in 36% yield.

*Thermolysis of 4,4-Dimethyl-5-(1-pyrrolidinyl)-1-styryl-4,5-dihydro-1*H*-1,2,3-triazole (**1d**).* *In DMSO-*d_6: The DMSO-d_6 (0.5 ml) solution of **1d** (0.16 g, 0.60 mmol) was heated at 80 °C according to Method A for 2 d. The ^{1}H NMR spectra of the resulting solution showed that N^2-vinylamidine was not formed. Diethyl ether (50 ml) was added to the solution, and the ether solution was washed four times with water (50 ml) and once with saturated aqueous solution of sodium chloride (50 ml) and dried over anhydrous magnesium sulfate. The ether was removed *in vacuo* and the residue was purified with silica gel preparative thin layer chromatography (Merck Art. 7747) developing with dichloromethane to give 38 mg (38% yield) of 2,2-dimethyl-4-phenyl-2*H*-pyrrole (**3d**). Analytically pure sample was obtained by distillation with the Kugelrohr apparatus at 65 °C/4 mmHg): mp 16.5—17.5 °C; MS *m/e* 171 (M^+); IR (neat) 1620, 1600, 1530, 1490, 1450, 925, 765, and 695 cm^{-1}; UV_{max} (methanol) 224 (ε, 15000), 268 (5000), 287 (sh), and 296 nm (sh); ^{1}H NMR ($CDCl_3$) δ 1.43 (6H, s), 7.4—7.8 (6H, m), and 8.55 (1H, s); ^{13}C NMR ($CDCl_3$) δ 23.2 (q), 80.3 (s), 126.3 (d), 128.1 (d), 128.8 (d), 132.4 (s), 138.1 (s), 153.6 (d), and 161.3 (d, C=N).

Found: C, 84.04; H, 7.65; N, 8.10%. Calcd for $C_{12}H_{13}N$: C, 84.17; H, 7.65; N, 8.18%.

In Benzene: The benzene (40 ml) solution of **1d** (0.68 g, 2.5 mmol) was heated to reflux for 42 h under nitrogen

† 1 mmHg≈133.322 Pa.

until **1d** was completely consumed. After removal of the benzene *in vacuo*, the residue was purified with alumina dry column chromatography (Woelm 04511) eluting with dichloromethane to give 0.35 g (80% yield) of **3d**.

Cycloaddition Reaction of 2 with Dienophiles. Method A: The N^2-vinylamidine (**2**) was prepared by heating the DMSO solution of the vinyltriazoline (**1a**, 1.0 g, 3.7 mmol) at 80 °C for 24 h under nitrogen atmosphere. After it was cooled to room temperature, an appropriate dienophile (molar ratio described in Table 2) was added to the solution with a micro syringe, and the solution was stirred at room temperature for 1—5 d. Then diethyl ether (50 ml) was added, and the ether layer was washed four times with water (50 ml) and once with saturated aqueous solution of sodium chloride (50 ml) successively, and dried over anhydrous magnesium sulfate. After removal of the ether *in vacuo*, the residue was purified with silica gel dry column chromatography (Woelm 04526, eluting with hexane–dichloromethane (1:1)) and/or with silica gel preparative thin layer chromatography (developing with dichloromethane).

Method B: The reaction procedure and the method of purification were similar to Method A, but *p*-benzoquinone (0.40 g, 3.7 mmol) was added to the DMSO solution in order to oxidize the initial products after the cycloaddition was completed.

Reaction with Acrylonitrile (5a): (*i*) Reaction of **2** with 2.0 molar amount of **5a** according to Method A for 2 d gave 3-cyano-1,4-dihydro-2-isopropyl-6-phenylpyridine (**6a**) and 3-cyano-2-isopropyl-6-phenylpyridine (**7a**) in 37 and 25% yields, respectively. Analytically pure samples of **6a** and **7a** were obtained respectively by recrystallization from methanol as colorless crystals: 3-cyano-1,4-dihydro-2-isopropyl-6-phenylpyridine (**6a**): mp 107—108 °C; MS *m/e* 224 (M^+); IR (KBr) 3330 (N–H), 2270 (C≡N), 1665 (C=C), 1610, 1495, 1290, 1110, 760, and 705 cm^{-1}; UV_{max} (methanol) 243 (ε 14000) and 335 nm (3000); ^1H NMR ($CDCl_3$) δ 2.21 (6H, d, J=7 Hz), 3.15 (1H, septet, J=7 Hz), 3.26 (2H, d, J=3.5 Hz), 4.90 (1H, td, J=3.5 and 1.7 Hz), 5.4 (1H, NH), and 7.32 (5H, C_6H_5).

Found: C, 80.19; H, 7.16; N, 12.20%. Calcd for $C_{15}H_{16}N_2$: C, 80.32; H, 7.19; N, 12.49%.

3-Cyano-2-isopropyl-6-phenylpyridine (**7a**): mp 75.5—76.5 °C; MS *m/e* 222 (M^+); IR (KBr) 2305 (C≡N), 1580, 1445, 1380, 860, 840, 770, and 695 cm^{-1}; UV_{max} (methanol) 260 (sh), 266 (ε, 15000), and 297 nm (20000); ^1H NMR ($CDCl_3$) δ 1.47 (6H, d, J=7 Hz), 3.64 (1H, septet, J=7 Hz), 7.4—7.6 (3H, m), 7.68 (1H, d, J=8 Hz), 7.92 (1H, d, J=8 Hz), and 8.0—8.2 (2H, m); ^{13}C NMR ($CDCl_3$) δ 21.7 (q), 34.8 (d), 105.8 (s), 116.9 (d), 117.1 (s, C≡N), 127.3 (d), 128.8 (d), 130.3 (d), 137.7 (s), 140.9 (d), 158.9 (s), and 169.1 (s).

Found: C, 80.96; H, 6.59; N, 12.69%. Calcd for $C_{15}H_{14}N_2$: C. 81.05; H, 6.35; N, 12.60%.

(*ii*) Reaction of **2** with 2.0 molar amount of **5a** according to Method A for 30 d gave **6a**, **7a**, and 3-cyano-5-(2-cyanoethyl)-2-isopropyl-6-phenylpyridine (**8**) in 16, 7, and 24% yields, respectively. Analytically pure sample of **8** was obtained by recrystallization from methanol as colorless crystals: mp 111.5—112 °C; MS *m/e* 275 (M^+); IR (KBr) 2235 (C≡N), 2230 (C≡N), 1590, 1435, 1070, 980, 785, 750, 715, and 700 cm^{-1}; UV_{max} (ethanol) 254 (ε, 10100) and 289 nm (10300); ^1H NMR ($CDCl_3$) δ 1.38 (6H, d, J=6.5 Hz), 2.24 (2H, t, J=7.5 Hz), 3.11 (2H, t, J=7.5 Hz), 3.58 (1H, septet, J=6.5 Hz), 7.48 (5H, C_6H_5), and 7.81 (1H, s). ^{13}C NMR ($CDCl_3$) δ 17.5 (t), 21.7 (q), 27.6 (t), 34.5 (d), 106.4 (s), 116.8 (s, C≡N), 118.4 (s, C≡N), 128.6 (s), 128.8 (d), 128.9 (s), 129.1 (d), 138.8 (s), 141.5 (d), 161.6 (s), and 167.7 (s).

Found: C, 78.50; H, 6.52; N, 15.11%. Calcd for $C_{18}H_{17}N_3$: C, 78.52; H, 6.22; N, 15.26%.

(*iii*) The vinyltriazoline (**1a**, 0.87 g, 3.2 mmol) and **5a** (0.34 g, 6.4 mmol) was dissolved in DMSO (20 ml) and stirred at 80 °C for 36 h under nitrogen atmosphere. After removal of excess **5a** and DMSO *in vacuo* at about 60 °C, the residue was dissolved in dichloromethane (50 ml) and the solution was washed with water (3×50 ml) and saturated aqueous solution of sodium chloride (50 ml) successively, and was dried over anhydrous magnesium sulfate. After removal of the solvent, the residue was purified according to Method A to give 90 mg of **7a** (13% yield) and 0.18 g of **8** (20% yield).

Reaction with Acrylaldehyde (5b): Reaction of **2** with 1.3 molar amount of **5b** according to Method A for 3 d gave 1,4-dihydro-2-isopropyl-6-phenylnicotinaldehyde (**6b**) and 2-isopropyl-6-phenylnicotinaldehyde (**7b**) in 24 and 22% yields, respectively. Analytically pure sample of **6b** was obtained by recrystallization from benzene as faint yellow crystals: mp 105—106.5 °C; MS *m/e* 227 (M^+); IR (KBr) 3230 (N–H), 1680 (C=C), 1595, 1505, 1390, 1365, 1290, 1240, 1110, 765, and 700 cm^{-1}; ^1H NMR ($CDCl_3$) δ 1.28 (6H, d, J=7.5 Hz), 3.17 (2H, d, J=3 Hz), 3.60 (1H, septet, J=7.5 Hz), 5.11, (1H, m), 5.81 (1H, NH), 7.34 (5H, C_6H_5), and 9.83 (1H, s, CHO).

Found: C, 79.21; H, 7.58; N, 6.21%. Calcd for $C_{15}H_{17}NO$: C, 79.26; H, 7.54; N, 6.16%.

The compound **7b** was obtained as colorless oil: MS *m/e* 225 (M^+); IR (CH_2Cl_2) 1685 (C=O), 1580, and 1370 cm^{-1}; ^1H NMR ($CDCl_3$) δ 1.44 (6H, d, J=7 Hz), 3.97 (1H, septet, J=7 Hz), 7.4—7.7 (3H, m), 7.77 (1H, d, J=8.5 Hz), 8.1—8.4 (3H, m), and 10.50 (1H, s, CHO). *p*-Nitrophenylhydrazone of **7b**: mp 248.5—249.5 °C.

Found: C, 70.12; H, 5.33; N, 15.60%. Calcd for $C_{21}H_{20}N_4O_2$: C, 69.98; H, 5.59; N, 15.55%.

Reaction with Methyl Acrylate (5c): (*i*) Reaction of **2** with 1.1 molar amount of **5c** according to Method A for 5 d gave methyl 2-isopropyl-6-phenylnicotinate (**7c**) and methyl 2-isobutyryl-5-oxo-5-phenylpentanoate (**9**) in 21 and 24% yields, respectively. Analytically pure sample of **7c** was obtained by recrystallization from methanol as colorless crystals: mp 88.5—89.5 °C; MS *m/e* 255 (M^+); IR (KBr) 1720 (C=O), 1580, 1270, 1080, 760, and 688 cm^{-1}; ^1H NMR ($CDCl_3$) δ 1.42 (6H, d, J=7 Hz), 3.92 (3H, s), 4.02 (1H, septet, J=7 Hz), 7.3—7.5 (3H, m), 7.52 (1H, d, J=7.5 Hz), and 8.0—8.2 (3H, m); ^{13}C NMR ($CDCl_3$) δ 22.4 (q), 32.6 (d), 52.2 (q, OCH_3), 116.8 (d), 123.1 (s), 127.4 (d), 128.8 (d), 129.8 (d), 138.3 (s), 139.3 (d), 158.4 (s), and 167.3 (s).

Found: C, 75.45; H, 6.81; N, 5.70%. Calcd for $C_{16}H_{17}NO_2$: C, 75.27; H, 6.71; N, 5.99%.

The dioxo ester **9** was obtained as faint yellow oil: IR (neat) 1740 (C=O), 1710 (C=O), 1680 (C=O), 1595, 1580, 1450, 755, and 695 cm^{-1}; ^1H NMR ($CDCl_3$) δ 1.13 (3H, d, J=6 Hz), 1.17 (3H, d, J=6 Hz), 2.28 (2H, q, J=7 Hz), 2.89 (1H, septet, J=6 Hz), 3.07 (2H, t, J=7 Hz), 3.74 (3H, s), 3.91 (1H, t, J=7 Hz), 7.3—7.6 (3H, m), and 7.8—8.1 (2H, m).

(*ii*) Reaction of **2** with 1.1 molar amount of **5c** according to Method B for 5 d gave **7c** in 44% yield.

Reaction with Dimethyl Maleate (5d): (*i*) Reaction of **2** with 2.1 molar amount of **5d** according to Method A for 2 d gave dimethyl 2-isopropyl-6-phenylpyridine-3,4-dicarboxylate (**7d**) in 11% yield. Analytically pure sample was obtained by recrystallization from methanol as colorless crystals: mp 75.5—76.5 °C; MS *m/e* 313 (M^+); IR (KBr)

1730 (C=O), 1580, 1330, 1275, 1250, 1085, 990, 755, 740, and 690 cm^{-1}; ^1H NMR ($CDCl_3$) δ 1.40 (6H, d, $J=7$ Hz), 3.09 (1H, septet, $J=7$ Hz), 3.92 (3H, s), 3.95 (3H, s), 7.3—7.5 (3H, m), 7.9—8.1 (3H, m); ^{13}C NMR ($CDCl_3$) δ 22.5 (q), 33.8 (d), 52.7 (q, OCH_3), 52.9 (q, OCH_3), 116.7 (d), 125.8 (s), 127.1 (d), 128.8 (d), 136.6 (s), 138.2 (s), 157.9 (s), 164.3 (s, C=O), 165.5 (s), and 168.9 (s).

Found: C, 69.16; H, 6.11; N, 4.52%. Calcd for $C_{18}H_{19}NO_4$: C, 69.00; H, 6.11; N, 4.47%.

(*ii*) Reaction of **2** with 2.1 molar amount of **5d** according to Method B for 2 d gave **7d** in 23% yield.

Reaction with Dimethyl Acetylenedicarboxylate (DMAD): Reaction of **2** with 2.1 molar amount of DMAD according to Method A for 1 d gave **7d** in 37% yield.

*Synthesis of an Authentic Sample of Methyl 2-isobutyryl-5-oxo-5-phenylpentanoate (**9**).* Methyl 4-methyl-3-oxopentanoate was prepared from 3-methyl-2-butanone and dimethyl carbonate according to Corey's method.[17] 3-Dimethylamino-1-phenyl-1-propanone was prepared from acetophenone, formaldehyde, and dimethylamine hydrochloride by Mannich reaction,[18] quaternized with methyl iodide, and it was condensed with the 3-oxo ester in methanol at 0 °C by means of sodium methoxide.[19] The dioxo ester **9** formed was purified with alumina (Woelm 04511) dry column chromatography eluting with hexane–dichloromethane (1:1). Its IR and ^1H NMR spectra were identical with the dioxo ester formed in the reaction of **2** with methyl acrylate (**5c**). Analytically pure sample was obtained by distillation with the Kugelrohr apparatus at 140 °C/0.1 mmHg.

Found: C, 69.58; H, 7.51%. Calcd for $C_{16}H_{20}O_4$: C, 69.55; H, 7.29%.

Method for CNDO/2 Calculation. The CNDO/2 calculation programme used was made by Professor Nozomu Ebara and members in his laboratory of College of General Education of The University of Tokyo, based mainly on the Pople's method.[20] Calculation was carried out at The Computer Center of The University of Tokyo.

References

1) For a preliminary report, see Y. Nomura, Y. Takeuchi, S. Tomoda, and M. M. Ito, *Chem. Lett.*, **1979**, 187.

2) a) Reviews: G. Desimoni and G. Tacconi, *Chem. Rev.*, **75**, 651 (1975); b) G. Desimoni, P. Righetti, G. Tacconi, and A. Vigliani, *Gazz. Chim. Ital.*, **107**, 91 (1977); G. Desimoni, P. P. Righetti, E. Selva, and G. Tacconi, *Tetrahedron*, **33**, 2829 (1977); G. Jenner, H. Abdi-Oskoui, and J. Rimmelin, *Bull. Soc. Chim. Fr.*, **1977**, 983; K. B. Lipkowitz and B. P. Mundy, *Tetrahedron Lett.*, **1977**, 3417; S, Sommer and U. Schubert, *Angew. Chem. Int. Ed. Engl.*, **18**, 696 (1979); L.-F. Tietze, G. von Kiedrowski, K. Harms, W. Clegg, and G. Sheldick, *ibid.*, **19**, 134 (1980).

3) B. Burg, W. Dittmar, H. Reim, A. Steigel, and J. Sauer, *Tetrahedron Lett.*, **1975**, 2897; H, Reim, A Steigel, and J. Sauer, *ibid.*, **1975**, 2901; A. Robert, M. Baudy, A. Foucaud, L. Golic, and B. Stanovnik, *Tetrahedron*, **34**, 3525 (1978); I. Hasan and F. W. Fowler, *J. Am. Chem. Soc.*, **100**, 6696 (1978); P. H. Daniels, J. L. Wong, J. L. Atwood, L. G. Canada, and R. D. Rogers, *J. Org. Chem.*, **45**, 435 (1980); Y. Nomura, M. Kimura, Y. Takeuchi, and S. Tomoda, *Chem. Lett.*, **1978**, 267.

4) D. H. Aue and D. Thomas, *J. Org. Chem.*, **40**, 1349 (1975).

5) A. Demoulin, H. Gorissen, A.-M. Hesbain-Frisque, and L. Ghosez, *J. Am. Chem. Soc.*, **97**, 4409 (1975).

6) S. D. Worley, K. G. Taylor, B. Venugopalan, and M. S. Clark, Jr., *Tetrahedron*, **34**, 833 (1978).

7) Y. Nomura, Y. Takeuchi, S. Tomoda, and M. M. Ito, *Bull. Chem. Soc. Jpn.*, **54**, 261 (1981).

8) a) In the case of 2,2,3,4,5-pentachloro-2*H*-pyrrole, it is reported that the ^{13}C NMR chemical shift of C-3 and C-5 is 26 and 38 ppm low-fielded compared to that of C-4, respectively: P. H. Daniels and J. L. Wong, *J. Org. Chem.*, **45**, 435 (1980). b) It is reported that the ^{13}C NMR chemical shift of the C-5 of cyclopentadiene is δ 42.2 (Y. K. Grishin, N. M. Sergeyer, and Y. A. Ustyryuk, *Org. Magn. Reson.*, **4**, 377 (1972)). The low field shift of the C-5 as large as 37 ppm is unlikely unless it is attached to a hetero atom such as nitrogen.

9) R. Fusco, G. Bianchetti, D. Pocar, and R. Ugo, *Chem. Ber.*, **96**, 802 (1963); J, Kučera and Z. Arnold, *Tetrahedron Lett.*, **1966**, 1109; F, Texier and J. Bourgois, *J. Heterocycl. Chem.*, **12**, 505 (1975); D. Pocar, L. M. L. Rossi, and P. Trimarco, *ibid.*, **16**, 925 (1979).

10) R. Fusco, G. Bianchetti, and D. Pocar, *Gazz. Chim. Ital.*, **91**, 933 (1961).

11) R. Fusco, G. Bianchetti, D. Pocar, and R. Ugo, *Gazz. Chim. Ital.*, **95**, 1220 (1965); D. Pocar and P. Trimarco, *J. Chem. Soc., Perkin Trans. 1*, **1976**, 622; P. Dalla Croce and R. Stradi, *Tetrahedron*, **33**, 865 (1977).

12) The results suggestive of aziridine intermediate have been reported recently: L. Citerio, M. L. Saccarello, and R. Stradi, *Synthesis*, **1979**, 305.

13) a) G. Szeimes and R. Huisgen, *Chem. Ber.*, **99**, 491 (1966); b) P. Scheiner, *J. Am. Chem. Soc.*, **88**, 4739 (1966); M. S. Ouali, M. Vaultier, and R. Carrié, *Bull. Soc. Chim. Fr.*, **1979**, 633.

14) Reaction of 3,4,5,6-tetrahydropyridine as an enamine has been reported: Y. Nomura, T. Bando, Y. Takeuchi, and S. Tomoda, *Tetrahedron Lett.*, **1979**, 3453.

15) M. Hansen and H. J. Jacobsen, *J. Magn. Reson.*, **10**, 74 (1973); W. Brügel, *Z. Electrochem.*, **66**, 159 (1962).

16) a) K. N. Houk, *J. Am. Chem. Soc.*, **94**, 8953 (1972); K. N. Houk, J. Sims, C. R. Watts, and I. J. Luskus, *ibid.*, **95**, 7301 (1973); b) K. N. Houk, "Application of Frontier Orbital Theory to Pericyclic Reactions," in "Pericyclic Reactions," Academic Press, New York (1977), Vol. 2.

17) E. J. Corey, R. B. Mitra, and H. Udo, *J. Am. Chem. Soc.*, **86**, 485 (1964).

18) C. Mannich and G. Heilner, *Ber.*, **55**, 356 (1922).

19) E. C. du Feu, F. J. McQuillin, and R. Robinson, *J. Chem. Soc.*, **1937**, 53.

20) J. A. Pople and D. L. Beveridge, "Approximate Molecular Orbital Theory," McGraw-Hill, New York (1970).

The Structures of Rabdosianin A, B, and C, Three New Diterpenoids from *Rabdosia shikokianus* Hara

Masamitsu Ochi,* Mitsuyuki Okamura, Hiyoshizo Kotsuki, Iwao Miura,†
Isao Kubo,†† and Takashi Kubota†††

Faculty of Science, Kochi University, Akebono-cho, Kochi 780

† *Laboratories of Natural Products Chemistry, Otsuka Pharmaceutical Co. Ltd., Kawauchi-cho, Tokushima 771-01*

†† *Division of Entomology and Parasitology, College of Natural Resources, University of California, Berkeley, California 94720*

††† *School of Medicine, Kinki University, Sayama-cho, Osaka 589*

(Received March 2, 1981)

Three new bitter diterpenoids, rabdosianin A, B, and C, have been isolated from the leaves of *Rabdosia shikokianus* Hara, and their structures, determined by spectroscopic and chemical methods. Complete assignments of the ^{1}H and ^{13}C NMR data are described.

The isolation of four diterpenoids: oridonin (**1**),[1] shikokianin (**2**),[1] shikokianidin (**3**),[2] and shikodonin (**4**),[3] from the leaves of *Rabdosia shikokianus* Hara[4] has already been reported. Further investigation of the bitter principles from this plant has led to the isolation of five additional diterpenoids: effusanin B (**5**),[5] longikaurin E (**6**),[6] and three new *ent*-kaurenoids. In this paper, we will deal with the isolation and structures of these new compounds, designated as rabdosianin A, B, andC.

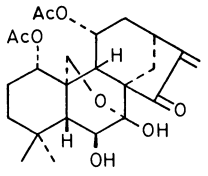

2

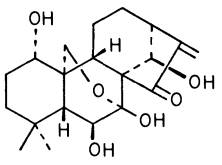

1

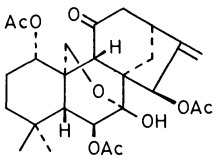

3

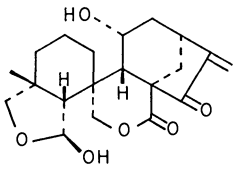

4

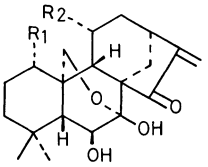

5 R_1=OAc, R_2=H
6 R_1=H, R_2=OAc

Rabdosianin A (**7**), $C_{26}H_{36}O_9$, mp 150—153 °C, $[\alpha]_D^{20}$ −50° (*c* 0.21, $CHCl_3$), was isolated as white needles in 0.053% yield from the ether extract of the dried leaves by extensive column chromatography. It had IR absorptions indicative of hydroxyl (3540, 3440), acetoxyl (1740, 1235), and *exo*-methylene (1660 and 902 cm^{-1}) groups. The ^{1}H NMR spectrum at 400 MHz showed signals due to two tertiary methyl groups at δ 1.08 and 1.14, three acetyl groups at δ 1.94, 2.10, and 2.11, one secondary hydroxyl group at δ 2.48 (d, J=2.4 Hz), one tertiary hydroxyl group at δ 3.17, one methine proton on an oxygenated carbon atom at δ 3.96 (dd, J=7.8 and 2.4 Hz), one ether type methylene group at δ 4.12 (dd, J=8.9 and 1.0 Hz) and 4.50 (dd, J=8.9 and 1.6 Hz), three methine protons attached to carbon atoms bearing an acetoxyl group at δ 4.82 (dd, J=4.1 and 3.5 Hz), 4.87 (dd, J=10.7 and 4.6 Hz), and 5.63 (dd, J=1.9 and 1.0 Hz), and one terminal methylene group at δ 4.86 (br s) and 5.03 (dd, J=1.9 and 1.0 Hz). In addition, extensive ^{1}H NMDR studies, summarized in Table 1, revealed the presence of the partial structures (**A**) and (**B**), the latter showing the following long-range couplings: $J_{H_5,H_{20b}}$=1.6 Hz, $J_{H_9,H_{20a}}$=1.0 Hz, $J_{H_{13},H_{17a}}$=1.9 Hz, $J_{H_{13},H_{17b}}$=1.0 Hz, $J_{H_{15},H_{17a}}$=1.0 Hz, and $J_{H_{15},H_{17b}}$=1.9 Hz.

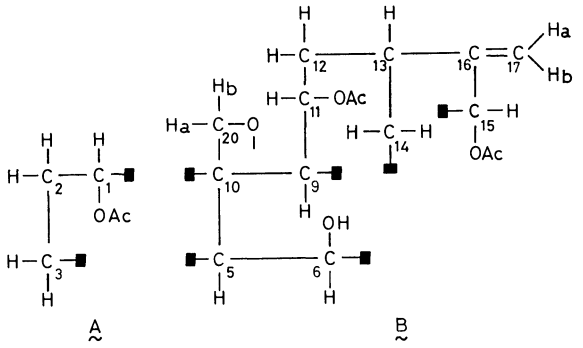

A B

The spectral data and the analogy with the congeners isolated from *Rabdosia* species[1,2] suggested the structure **7** for rabdosianin A. The proposed structure was also supported by the ^{13}C NMR data at 100 MHz (Table 2), which showed the presence of one hemiacetal group (δ 96.5), four methylene groups, three methine groups, and three quaternary carbon atoms. The α-configuration of two acetoxyl groups at C_1 and C_{11} was evident from the J values of H_1 and H_{11} signals. Namely, the large axial-axial coupling (J=10.7 Hz) and the small axial-equatorial coupling (J=4.6 Hz) of the former signal indicated the axial nature of the corresponding proton. Hence, the acetoxyl group at C_1 must be α-oriented. The small J values of the latter signal ($J_{H_9,H_{11}}$=4.1 Hz, $J_{H_{11},H_{12\beta}}$= 3.5 Hz, and $J_{H_{11},H_{12\alpha}}\approx$0 Hz) revealed that the di-

Table 1. ^{1}H NMR spectra at 400 MHz of rabdosianin A (**7**), B (**10**), and C (**12**)[a]

	7	**10**	**12**
$H_{1\alpha}$			1.87 (ddd, 13.0, 1.9, 1.9)
$H_{1\beta}$	4.87 (dd, 10.7, 4.6)	4.89 (dd, 11.5, 5.0)	1.43 (m)
$H_{2\alpha}$	1.39 (m)	*ca.* 1.40 (m)	*ca.* 1.55 (m)
$H_{2\beta}$	1.77 (m)	1.81 (m)	*ca.* 1.55 (m)
$H_{3\alpha}$	1.37 (br d, 12.4)	*ca.* 1.45 (m)	*ca.* 1.55 (m)
$H_{3\beta}$	1.45 (ddd, 12.4, 10.0, 3.0)	*ca.* 1.40 (m)	*ca.* 1.20 (m)
H_5	1.68 (dd, 7.8, 1.6)	1.96 (dd, 8.4, 1.9)	1.38 (dd, 4.6, 1.1)
H_6	3.96 (dd, 7.8, 2.4)	5.33 (d, 8.4)	5.17 (d, 4.6)
H_9	2.15 (dd, 4.1, 1.0)	2.19 (dd, 3.8, 1.2)	2.26 (dd, 2.4, 2.2)
H_{11}	4.82 (dd, 4.1, 3.5)	4.82 (dd, 4.1, 3.8)	
$H_{12\alpha}$	2.31 (dd, 15.7, 9.5)	2.32 (dd, 15.7, 9.2)	3.11 (m)
$H_{12\beta}$	1.65 (dd, 15.7, 3.5)	1.62 (dd, 15.7, 4.1)	3.13 (m)
H_{13}	2.65 (dddd, 9.5, 4.3, 1.9, 1.0)	2.64 (dddd, 9.2, 4.9, 1.4, 0.8)	2.94 (dddd, 4.6, 4.4, 1.0, 1.0)
$H_{14\alpha}$	2.49 (d, 12.4)	2.47 (d, 12.4)	2.20 (d, 12.4)
$H_{14\beta}$	1.63 (dd, 12.4, 4.3)	1.72 (dd, 12.4, 4.9)	1.63 (dd, 12.4, 4.6)
H_{15}	5.63 (dd, 1.9, 1.0)	5.66 (dd, 2.4, 2.2)	4.53 (ddd, 1.9, 1.9, 1.1)
H_{17a}	4.86 (br s)	4.91 (dd, 2.2, 1.4)	5.18 (br s)
H_{17b}	5.03 (dd, 1.9, 1.0)	5.05 (dd, 2.4, 2.2)	5.25 (br s)
H_{20a}	4.12 (dd, 8.9, 1.0)	4.16 (dd, 9.5, 1.2)	4.03 (dd, 9.5, 2.2)
H_{20b}	4.50 (dd, 8.9, 1.6)	4.55 (dd, 9.5, 1.9)	4.16 (dd, 9.5, 1.1)
Me_{18}	1.08 (s)	0.89 (s)	0.85 (s)
Me_{19}	1.14 (s)	1.16 (s)	1.14 (s)
6-OH[b]	2.48 (d, 2.4)		
7-OH[b]	3.17 (s)	3.43 (s)	3.19 (s)
15-OH[b]			3.30 (d, 1.9)
OAc	2.11, 2.10, 1.94	2.16, 2.09, 2.06, 1.94	2.18

a) The spectra were determined at 25 °C in $CDCl_3$ solutions with TMS as an internal standard. Multiplicity and J values (in Hz) are in parentheses. b) These signals disappeared on addition of D_2O.

hedral angles between H_9 and H_{11}, and H_{11} and $H_{12\beta}$, are both close to 45°, and that between H_{11} and $H_{12\alpha}$ is roughly 90°. Thus, the acetoxyl group at C_{11} is α-oriented.

The catalytic hydrogenation of **7** afforded a dihydro compound (**8**), $C_{26}H_{38}O_9$, mp 252—253 °C, as the major product. Since the hydrogenation of the C_{16} double bond is assumed to occur from the less hindered α-side, the newly introduced secondary methyl group must be β-oriented.[2] The ^{1}H NMR spectrum of **8** displayed a signal of H_{15} as a doublet at δ 5.20 (J=10.4 Hz), the large J value of which defined the configuration of the acetoxyl group at C_{15} as β.[2] The β-configuration for the secondary hydroxyl group at C_6 is common to all *ent*-kaurenoids from *Rabdosia* species which have the same functional groups in the B-ring as **7**.

Finally, the structure was confirmed by the chemical correlation of **7** with **2**. Thus, the partial hydrolysis of **7** with methanol–0.1 M (1M=1 mol dm^{-3}) sodium hydroxide solution (1:1) gave a triol (**9**), $C_{24}H_{34}O_8$, mp 254—256 °C, which was found to be identical with the compound derived from **2** by the reduction with sodium borohydride.

Rabdosianin B (**10**), $C_{28}H_{38}O_{10}$, mp 215 °C (dec), $[\alpha]_D^{20}$ −70° (c 0.39, $CHCl_3$), was isolated as colorless prisms in 0.004% yield and exhibited spectral data quite similar to those of **7**, except for the following

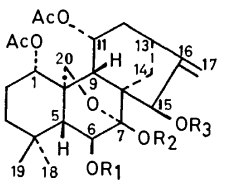

7 R_1=R_2=H, R_3=Ac
9 R_1=R_2=R_3=H
10 R_1=R_3=Ac, R_2=H
11 R_1=R_2=R_3=Ac

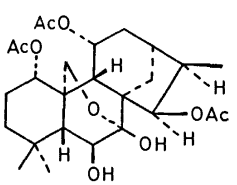

8

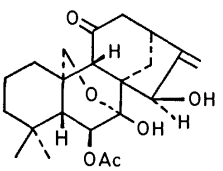

12

observation: the IR spectrum did not show the presence of a secondary hydroxyl group and, instead, the ^{1}H NMR spectrum (Table 1) revealed the signals due to four acetoxyl groups, one more than those of **7**. These facts, and the appearance of the H_6 signal at a lower field (δ 5.33) as a doublet (J=8.4 Hz) suggested that an acetoxyl group took the place of the secondary hydroxyl group at C_6 of **7**. From the evidence outlined above and the pertinent ^{13}C NMR data (Table 2), we assigned the structure **10**

Table 2. ^{13}C chemical shifts of rabdosianin A (**7**), B (**10**), and C (**12**)[a)]

Carbon	7	10	12
1	76.9 d	76.7 d	41.1 t
2	25.3 t	25.2 t	18.5 t
3	38.9 t	38.7 t	41.4 t
4	33.4 s	33.5 s	33.9 s
5	53.5 d	52.5 d	53.3 d
6	74.1 d	75.7 d	74.1 d
7	96.5 s	95.9 s	96.1 s
8	50.7 s	50.6 s	50.9 s
9	48.4 d	48.4 d	58.3 d
10	40.7 s	41.1 s	37.6 s
11	69.6 d	69.5 d	199.0 s
12	39.9 t	39.9 t	50.3 t
13	35.1 d	35.4 d	37.7 d
14	26.7 t	26.7 t	29.8 t
15	74.9 d	75.2 d	75.2 d
16	157.0 s	157.1 s	151.6 s
17	109.5 t	110.0 t	109.6 t
18	22.6 q	22.7 q	21.5 q
19	33.8 q	33.5 q	32.1 q
20	65.5 t	65.4 t	68.1 t
$\underline{C}OCH_3$	171.7 s	173.8 s	170.2 s
	170.8 s	170.8 s	
	170.0 s	170.5 s	
		170.1 s	
$CO\underline{C}H_3$	22.2 q	22.3 q	21.5 q
	21.9 q	22.1 q	
	21.8 q	22.0 q	
		21.3 q	

a) The spectra were measured at 100.61 MHz in $CDCl_3$ solutions and the shifts are given in ppm (δ) relative to the internal TMS. Assignments were made by off-resonance and selective proton-noise decouping technique.

for rabdosianin B.

Final confirmation of the structure was achieved by the chemical correlation of **10** with **7**. The acetylation of **10** with acetic anhydride–boron trifluoride etherate gave a pentaacetate (**11**), $C_{30}H_{40}O_{11}$, mp 182—183 °C, which was also obtained by a similar treatment from **7**.

Rabdosianin C (**12**), $C_{22}H_{30}O_6$, mp 222—225 °C, $[\alpha]_D^{20}$ −170° (*c* 0.15, $CHCl_3$), was obtained as colorless flakes in 0.003% yield and showed IR absorptions attributable to hydroxyl (3520, 3320), carbonyl (1755), and *exo*-methylene (3080, 1660, and 905 cm^{-1}) groups. The ^1H NMR spectrum exhibited signals due to two tertiary methyl groups at δ 0.85 and 1.14, one acetyl group at δ 2.18, one tertiary hydroxyl group at δ 3.19, one secondary hydroxyl group at δ 3.30 (d, J=1.9 Hz), one ether type methylene group at δ 4.03 (dd, J=9.5 and 2.2 Hz) and 4.16 (dd, J=9.5 and 1.1 Hz), one methine proton on an oxygenated carbon atom at δ 4.53 (ddd, J=1.9, 1.9, and 1.1 Hz), one methine proton attached to a carbon atom bearing an acetoxyl group at δ 5.17 (d, J=4.6 Hz), and one terminal methylene group at δ 5.18 and 5.25 (each br s). The ^{13}C NMR data (Table 2) revealed the presence of one acetal group (δ 96.1) and one ketonic carbon atom (δ 199.0) together with five methylene groups, three methine groups, and three quaternary carbon atoms. In addition, the presence of the partial structure (**C**) was revealed by extensive ^1H NMDR studies, the results of which are tabulated in Table 1. A long-range coupling across a ketonic group ($J_{H_9,H_{12\beta}}$=2.4 Hz) was observed in this system. Thus, all of the ten oxygen atoms in **12** can be characterized by the functional groups in the partial sturcture (**C**) and a hemiacetal group.

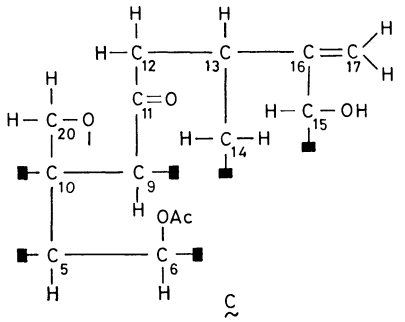

From the aforementioned data, it would be quite reasonable to assign the *ent*-kaurenoid structure for rabdosianin C, in which the partial structure (**C**) would form the B, C, and D-rings. Observation of about 10% N. O. E. on H_{15}, upon irradiation of $H_{14\beta}$, defined the configuration of the secondary hydroxyl group at C_{15} as β. The magnitude of the coupling constant between H_6 and H_5 (J=4.6 Hz) indicated that the acetoxyl group at C_6 is β-oriented.[2)] From this evidence, we propose the structure **12** for rabdosianin C.

Experimental

All mps were determined on a Mitamura micro melting point apparatus and are uncorrected. The IR spectra were recorded on a JASCO model IRA-1 spectrophotometer. The ^1H and ^{13}C NMR spectra were taken on a Bruker WH-400 instrument in $CDCl_3$ solutions with TMS as an internal standard unless otherwise stated. A Union Gikken apparatus, model PM-101, was used for the measurement of the rotations.

Isolation. The dried leaves (5.2 kg) of *Rabdosia shikokianus* Hara were extracted with ether (50 l). The ether solution was treated with activated charcoal (50 g) and evaporated to dryness. The residue (210 g) was subjected to chromatography over silicic acid (1.5 kg) eluting with $CHCl_3$–MeOH mixtures, with MeOH increasing from 0 to 10%. Elution with 2% MeOH in $CHCl_3$ gave a fraction (15 g) which was rechromatographed over silicic acid (300 g), using 40% ethyl acetate in petroleum ether as eluent, to yield rabdosianin C (**12**) (115 mg) and B (**10**) (250 mg). The material (28 g) which was eluted with 5% MeOH in $CHCl_3$ was rechromatographed over silicic acid (600 g), using 50% ethyl acetate in petroleum ether as eluent, to give effusanin B (**5**) (203 mg) and longikaurin E (**6**) (71 mg). The material (22 g) eluted with 10% MeOH in $CHCl_3$ was rechromatographed over silicic acid (600 g), using 70% ethyl acetate in petroleum ether as eluent, to afford rabdosianin A (**7**) (2.70 g).

Rabdosianin A (7). The crude material was recrystallized from ether to give fine needles (1.60 g), mp 150—153 °C; $[\alpha]_D^{20}$ −50° (*c* 0.21, $CHCl_3$); IR (Nujol) 3540, 3440, 1740, 1660, 1235, and 902 cm^{-1}; ^1H NMR (see Table 1); ^{13}C NMR (see Table 2); MS *m/e* 492 (M^+), 450, 432 (M^+—AcOH), 390, 372 (M^+—2AcOH), 330, and 312 (M^+—3AcOH). Found: C, 62.91; H, 7.21%. Calcd for $C_{26}H_{36}O_9$: C, 63.40; H, 7.37%.

Rabdosianin B (10). The crude solid was recrystallized from ether to yield colorless prisms (156 mg), mp 215 °C (dec); $[\alpha]_D^{20}$ −70° (*c* 0.39, $CHCl_3$); IR (Nujol) 3530, 3080, 1740, 1720, 1660, 1240, and 895 cm^{-1}; ^1H NMR (see Table 1); ^{13}C NMR (see Table 2); MS *m/e* 534 (M^+), 474 (M^+—AcOH), 432, 414 (M^+—2AcOH), 372, 354 (M^+—3AcOH), 312, and 294 (M^+—4AcOH). Found: C, 62.52; H, 7.06%. Calcd for $C_{28}H_{38}O_{10}$: C, 62.91; H, 7.17%.

Rabdosianin C (12). The crude substance was recrystallized from EtOH to afford colorless flakes (75 mg), mp 222—225 °C; $[\alpha]_D^{20}$ −170° (*c* 0.15, $CHCl_3$); IR (Nujol) 3520, 3320, 3080, 1755, 1660, 1245, and 905 cm^{-1}; ^1H NMR (see Table 1); ^{13}C NMR (see Table 2); MS *m/e* 372 (M^+—H_2O), 330 (M^+—AcOH), 312, 284, and 266. Found: C, 67.58; H, 7.79%. Calcd for $C_{22}H_{30}O_6$: C, 67.67; H, 7.74%.

Hydrogenation of **7**. **7** (100 mg) and 10% Pd–C (40 mg) were stirred in EtOH (10 ml) under a hydrogen atmosphere at room temperature for 16 h. The catalyst was removed by filtration, and the filtrate was evaporated. The residue was subjected to chromatography over silicic acid (10 g). Elution with ether gave dihydrorabdosianin A (**8**) (50 mg) which was recrystallized from aqueous MeOH to yield colorless plates (30 mg), mp 252—253 °C; IR (Nujol) 3570, 3460, 1740, 1735, 1720, and 1255 cm^{-1}; ^1H NMR δ 0.75 (3H, d, J=7.6 Hz, 17-Me), 1.05 and 1.12 (3H each, s, 18- and 19-Me), 1.95, 2.06, and 2.09 (3H each, s, 3Ac), 2.30 (1H, d, J=2.1 Hz, 6-OH), 2.87 (1H, s, 7-OH), 3.87 (1H, dd, J=7.3 and 2.1 Hz, H_6), 4.10 (1H, br d, J=8.9 Hz, H_{20a}), 4.51 (1H, dd, J=8.9 and 1.5 Hz, H_{20b}), 4.81 (1H, dd, J=3.6 and 3.4 Hz, H_{11}), 4.87 (1H, dd, J=10.7 and 4.6 Hz, H_1), and 5.20 (1H, d, J=10.4 Hz, H_{15}). Found: C, 63.08; H, 7.57%. Calcd for $C_{26}H_{38}O_9$: C, 63.14; H, 7.75%.

Partial Hydrolysis of **7**. A solution of **7** (150 mg) in MeOH (30 ml) and 0.1 M NaOH solution (30 ml) was allowed to stand in a refrigerator for 14 h to yield a crystalline precipitate (50 mg). The crude precipitate was recrystallized from EtOH to give a triol (**9**) as fine needles (33 mg), mp 254—256 °C; $[\alpha]_D^{20}$ +2° (*c* 0.11, $CHCl_3$); IR (Nujol) 3470, 3390, 1735, 1255, and 890 cm^{-1}; ^1H NMR (C_5D_5N) δ 1.14 and 1.24 (3H each, s, 18- and 19-Me), 2.09 and 2.13 (3H each, s, 2Ac), 4.31 (1H, dd, J=8.9 and 1.0 Hz, H_{20a}), 4.40 (1H, dd, J=7.6 and 4.3 Hz, H_6), 4.85 (1H, dd, J=8.9 and 1.4 Hz, H_{20b}), 5.07 (1H, ddd, J=3.0, 2.7, and 1.0 Hz, H_{15}), 5.11 (1H, dd, J=11.3 and 5.6 Hz, H_1), 5.15 (1H, br s, H_{17a}), 5.17 (1H, dd, J=5.4 and 4.6 Hz, H_{11}), 5.48 (1H, br s, H_{17b}), 6.65 (1H, d, J=3.0 Hz, 15-OH), 8.03 (1H, s, 7-OH), and 8.26 (1H, d, J=4.3 Hz, 6-OH); MS *m/e* 450 (M^+), 432 (M^+—H_2O), 390 (M^+—AcOH), 372, and 330 (M^+—2AcOH). Found: C, 63.62; H, 7.47%. Calcd for $C_{24}H_{34}O_8$: C, 63.98; H, 7.61%.

Reduction of **2** *with* $NaBH_4$. To a solution of **2** (100 mg) in MeOH (4 ml) and THF (4 ml) were added excess amounts of $NaBH_4$ (40 mg) with ice cooling. The mixture was stirred for 8 h at 0 °C. The solution was then concentrated, diluted with water (10 ml), and extracted with ethyl acetate. The organic layer was washed with water, dried over Na_2SO_4, and evaporated to dryness. The residue was recrystallized from EtOH to afford a triol (62 mg) which was identified by mixed mp, IR, and ^1H NMR comparison with **9**.

Acetylation of **10**. To a solution of **10** (50 mg) in acetic anhydride (6 ml) was added one drop of BF_3–etherate at −60 °C; the mixture was kept for 3 h below −20 °C, then poured into ice–water and extracted with $CHCl_3$. The $CHCl_3$ layer was washed with water, dried over Na_2SO_4, and evaporated to dryness. The residue was crystallized from ether–petroleum ether to yield a pentaacetate (**11**) as colorless prisms (33 mg), mp 182—183 °C; IR (Nujol) 1740, 1720, and 1235 cm^{-1}; ^1H NMR δ 1.94, 1.97, 1.99, 2.03, and 2.23 (3H each, s, 5Ac); MS *m/e* 516 (M^+—AcOH), 474, 456 (M^+—2AcOH), 432, 414, 396 (M^+—3AcOH), 372, 354, 336 (M^+—4AcOH), 312, 294, and 281. Found: C, 62.79; H, 6.92%. Calcd for $C_{30}H_{40}O_{11}$: C, 62.48; H, 6.99%. **11** was also obtained by the treatment of **7** with acetic anhydride and BF_3–etherate in a similar manner to that described.

We are grateful to Mr. Hideo Mori, Laboratories of Natural Products Chemistry, Otsuka Pharmaceutical Co. Ltd., for recording the mass spectra.

References

1) T. Kubota and I. Kubo, *Bull. Chem. Soc. Jpn.*, **42**, 1778 (1969).
2) T. Isobe, T. Kamikawa, I. Kubo, and T. Kubota, *Bull. Chem. Soc. Jpn.*, **46**, 583 (1973).
3) I. Kubo, M. J. Pettei, K. Hirotsu, H. Tsuji, and T. Kubota, *J. Am. Chem. Soc.*, **100**, 628 (1978).
4) The taxon of this genus was previously recognized as *Isodon*. (*cf.* H. Hata, *J. Jpn. Bot.*, **47**, 193 (1972)).
5) T. Fujita, Y. Takeda, T. Shingu, and A. Ueno, *Chem. Lett.*, **1980**, 1635.
6) T. Fujita, Y. Takeda, and T. Shingu, *Heterocycles*, **16**, 227 (1981).

Chiroptical Properties of 10,11-Dihydro-5,10-methano-5*H*-dibenzo[*a*,*d*]cycloheptene Derivatives

Sanji HAGISHITA* and Kaoru KURIYAMA

Shionogi Research Laboratories, Shionogi & Co. Ltd., Fukushima-ku, Osaka 553

(Received April 4, 1981)

The titled compounds have been prepared from (+)-(9*R*,10*R*)-dimethyl 11-oxo-9,10-dihydro-9,10-ethanoanthracene-1,5-dicarboxylate. Their absolute configurations were determined by chemical reaction, and by IR and CD spectra. Although the CD spectra of **2** and **3** (R=NH_2) were expected to show an antipodal pattern from analysis of the simple coupling mechanism, they showed approximately the same magnitude of the positive Cotton effect in both regions of the ^1L_b and ^1L_a benzenoid transitions. Their CD spectra were calculated by the point-dipole exciton treatment and by the π-SCF approximation using the dipole velocity procedure with and without the charge transfer transition between the aromatic chromophores. Thus, the electric transition dipole moment should not be treated as a point dipole at any place and the rotational strength should be calculated by the dipole velocity procedure since a local magnetic transition dipole moment was produced perpendicular to the benzene ring in the region of the ^1L_b transition. The charge transfer transition can not be neglected in the calculation of the MO, though it does not cause the alteration of the sequence of the coupling mode.

In our previous report,[1] we pointed out that the chiroptical properties of C_2-symmetrical (+)-2,6-disubstituted 9,10-dihydro-9,10-ethanoanthracene (DEA) **1** should not be analyzed with a dipole-dipole coupling mechanism,[2] but should be calculated with the dipole velocity method using the molecular orbital calculations, which take into consideration an electron exchange effect between the two aromatic chromophores. Mixing of the charge transfer transition may change the sequence of the A- and B-coupling mode of local transitions into the opposite one and thus result in wrong assignment of the configuration.

In order to estimate the limitation of the electron exchange effect in changing the energy sequence, we synthesized optically active 10,11-dihydro-5,10-methano-5*H*-dibenzo[*a*,*d*]cycloheptene (DMDC) derivatives. They have two aromatic chromophores linked with ethylene and methylene chains and are rigid in conformation. Thus they would have a smaller electron exchange effect than DEA.

The skeletons of compounds **2** and **3** are antipodal to each other but they are not antipodes owing to the substituents at the 1,6- and 4,9-positions. But if the substituents are the same in both compounds and the direction of the electric transition dipole moment of the aromatic chromophores does not change, the CD curves of the two compounds can be expected to be quasi mirror images of each other from a simple coupling mechanism. Therefore the deviation from the antipodal pattern of their CD spectra may be a key to clarify the following factors; the contributions of the charge transfer effect, and a local magnetic transition moment produced perpendicular to the plane of the benzene ring, and a treatment of the electric transition dipole moment as a point dipole, and selection of its position (Fig. 1).[1,3]

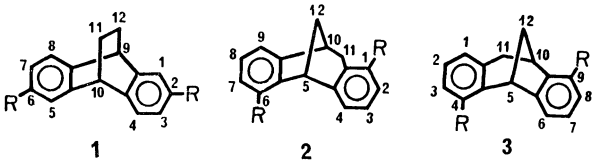

Fig. 1.

Synthesis. (+)-Dimethyl 12-oxo-DEA-1,5-dicarboxylate, (+)-**4b**, with an absolute configuration determined by us to be 9*R*,10*R*,**,[4] was reduced with sodium borohydride to give a 1:2 mixture of the diols, (+)-**7b** and (+)-**8b**, with a configuration determined by analysis of the NMR spectra of their acetates, (+)-**5b** and (+)-**6b**. The minor product (+)-**7b** was isolated by conversion into the *p*-nitrobenzoyl derivative (+)-**9b** and reduced to the triol (+)-**15b**. Its IR spectrum showed the band attributable to the intramolecular hydrogen bonding at 3483 cm^{-1}, CH_2OH/OH for the dilute chloroform solution, 1.495 mmol/l. Then an *endo*-configuration could be assigned to (+)-**15b** from the model consideration. The solvolysis of the tosylate **11b** took place by Wagner-Meerwein rearrangement giving the rearranged compound, (+)-**17b**, together with less than 5% of other rearranged DMDC, (+)-**18b**. The former could be purified by conversion into the alcohol (+)-**19b**, followed by TLC. The latter was obtained from the crude alcohol (+)-**8b** by the same procedure. The acetate group was assigned the *exo*-configuration in both rearranged products (+)-**17b** and (+)-**18b** by analysis of the NMR spectra.[5] The triol (+)-**21b** obtained from the former acetate showed intramolecular hydrogen bonding at 3439 cm^{-1}, CH_2OH/OH. On the other hand, (+)-**22b** from the latter acetate lacked the corresponding absorption. Thus, from both the NMR and IR spectra, the configurations of the rearranged products (+)-**17b** and (+)-**18b** were assigned as shown in Scheme 1 and coincided with the stereochemical outcome reported by Cristol *et al.*, that is, solvolysis rearrangement brought about migration of the *anti*- to the leaving group.[6] Since the configuration at C-10 of DEA does not change by the rearrangement, the configuration at C-5 of DMDC must possess the (*R*)-configuration. The absolute configurations of (+)-**17b** and (+)-**18b** can therefore be assigned as being (5*R*,10*R*) and (5*R*,10*S*), respectively.

Hydrogenolysis of the hydroxy diesters (+)-**19b** and

** The notation of the absolute configuration of (+)-1,5-disubstituted 11-oxo-DEA in Ref. 4 should be 9*R*,10*R*.

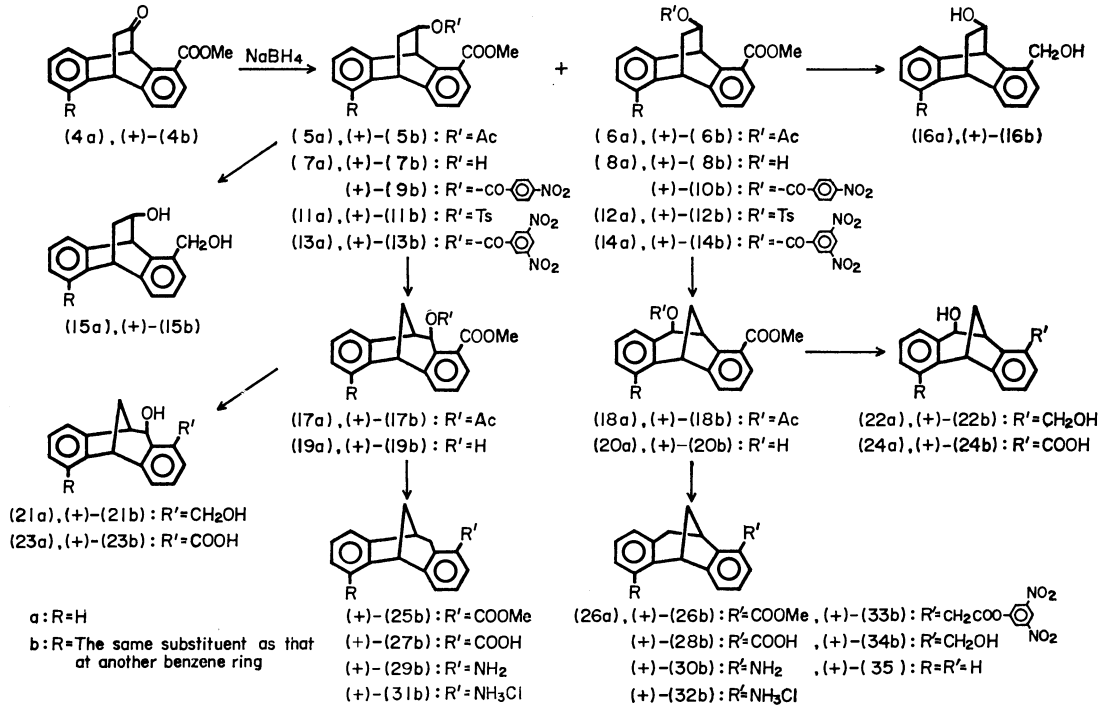

Scheme 1.

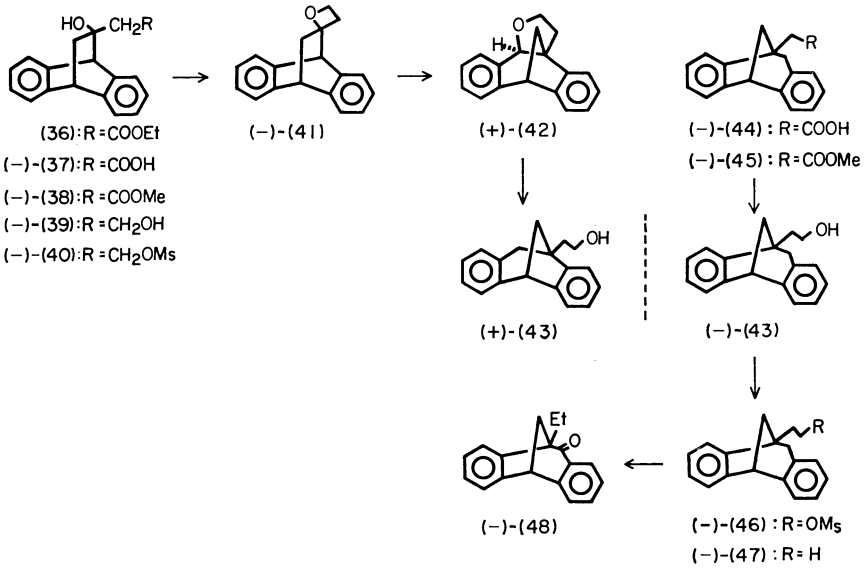

Scheme 2.

(+)-**20b** furnished the desired DMDC compounds (+)-**25b** and (+)-**26b** with absolute configurations of 10*S*,5*R* and 10*R*,5*R*, respectively. Other DMDC derivatives (+)-**27b**—**34b** and (+)-**35** could be prepared according to Scheme 1. The same procedure was applied to (±)-methyl 12-oxo-DEA-1-carboxylate **4a**.

11-Hydroxy-DEA-11-acetic acid,*** **37** was resolved with cinchonidine to the (−)-isomer, and (−)-oxetane (−)-**41** was obtained from (−)-**37** as shown in Scheme 2 according to literature[7] cited for the racemate. Rearrangement of the (−)-oxetane (−)-**41** of 94.4% optical purity took place at once with a catalytic amount of *p*-toluenesulfonic acid to give (+)-**42** in quantitative yield. The rearrangement occurred at the asymmetric center. Then in order to determine the optical yield of the reaction, the enantiomer of the hydrogenolyzed alcohol (−)-**43**, was prepared by a different route from optically pure (−)-DMDC-10-acetic acid, (−)-**44** which was obtained from cinchonidine salt. Comparing the optical rotations, $[\alpha]_D$ +180.0° and $[\alpha]_D$ −190.6°, the optical purity of 94.4% was obtained for the alcohol (+)-**43** and was the same as that of the starting carboxylic acid (−)-**37**. Therefore the rearrangement is a completely stereoselective process.

In the NMR spectrum of the rearranged compound

*** This was obtained from the ethyl ester[7] and was very sensitive to acid.

TABLE 1. UV AND CD SPECTRA OF DMDC DERIVATIVES

Compound	UV		CD		Solvent
	λ_{nm}	ε	λ_{nm}	$\Delta\varepsilon$	
(+)-**35**	277	2170	277	+3.80	Cyclohexane
	270	1820	269	+2.85	
	263	1160	262 sh	+1.11	
	256	743	254	+0.676	
	231 sh	6350	231	+12.5	
	222 sh	11800	224	+10.3	
			216 sh	+5.63	
			210	−18.0	
			197 sh	+37.0	
	195!	48900	190	+75.6	
(+)-**30b**	291	3230	293	+9.24	MeOH
	231 sh	19900	238 sh	+29.9	
	213	36000	217	+97.5	
	204	41400	201	−117.	
(+)-**32b**	274	1590	275	−0.755	MeOH-HCl
			272	+1.39	
	266	1540	263	+2.17	
			256 sh	+1.72	
	220 sh	11600	224	+18.8	
	202 sh	36400	197	+60.3	
(+)-**26b**	298	4690	299	+11.6	Cyclohexane
	292	4950	294	+11.6	
			258	−4.73	
			237 sh	+25.6	
	230	20400	217	+91.2	
	210 sh	40500	201	+114.	
	202	54500			
(+)-**28b**	291	4140	295	+10.0	MeOH
			256	−2.90	
	226	20200	214	+90.3	
	210	36800			
	202	42200	197	−83.3	
(+)-**34b**	279	1720	275 sh	+0.991	MeOH
	271	1530	266	+1.92	
	263	1080	259 sh	+1.32	
	235 sh	5490	230	+20.0	
	223 sh	14700	210	+45.8	
	196	47900	195!	0	
(+)-**29b**	289	3340	290	+7.99	MeOH
	231 sh	18100	240	+32.4	
	213 sh	38900	221	−34.3	
	203	44500	201	+17.0	
			195!	0	
(+)-**31b**	274	1630	274	−3.67	MeOH-HCl
	266	1480	268	−1.83	
	260 sh	1190	248	+0.042	
	225 sh	4060	230	−13.0	
	210 sh	24100	211 sh	+30.3	
			202	+41.9	
			196!	0	
(+)-**25b**	299	4630	298	+8.42	Cyclohexane
	292	4580			
	230	18700	237	+32.9	
	209 sh	10100	218	−36.1	
	202	13100	209	+53.9	
			200	−18.7	
(+)-**27b**	294	3130	297	+5.56	MeOH
	228 sh	13100	235	+16.7	
			218	−25.8	
	201	34500	209	+34.5	
			198	−21.1	
(+)-**22b**	280	1310	280	+4.76	MeOH
	272	1150	273	+2.49	
			232 sh	+15.7	
	211	27400	211	+49.2	
	196	47600	195!	−54.1	
(+)-**19b**	293	3860	294	+4.76	CH_3CN
			279	+7.91	
	227 sh	20100	236	+16.9	
			221	−18.6	
	207 sh	37000	211	+32.4	
	200	54000			
(+)-**21b**	279	1010	280	−8.03	MeOH
	270	1060	274	−3.64	
			266	+0.855	
			259	+0.670	
			241	−0.893	
	214 sh	26200	215	+22.6	
	195!	40500	193!	−37.7	
(+)-**42**	276	1900	276	+5.74	Hexane
	269	1630	269	+3.17	
	263	1120	256	−0.114	
	255 sh	649	230	+14.4	
	211 sh	26900	211	−18.2	
	204.5sh	32800	190	+57.1	
(−)-**43**	276	2110	276	−3.58	MeOH
	269	1810	269	−2.81	
	263	1190	263 sh	−1.56	
	256 sh	753	254 sh	−0.836	
	229 sh	7230	231	−13.9	
	221 sh	12000	224	−10.3	
	203	37500	217	−8.09	
			211	+6.72	
			195!	−39.1	
(−)-**44**	276	4020	275	−2.77	MeOH
	268.5	3490	268	−2.36	
	262	2350	262 sh	−1.28	
	256 sh	1570	253 sh	−0.074	
	230 sh	13900	229	−13.1	
	221 sh	23700	223 sh	−10.4	
	194	92700	216	−10.1	
(−)-**45**	276	4070	275	−2.91	Hexane
	269	3480	268	−2.42	
	262	2230	262 sh	−1.44	
	229 sh	15900	229	−12.9	
	221 sh	24800	222 sh	−9.15	

Table 1. (continued)

Compound	UV λ_{nm}	UV ε	CD λ_{nm}	CD $\Delta\varepsilon$	Solvent
	202 sh	75300	214	−12.4	
			209	+9.72	
	195 sh	98500	196	−33.6	
(−)-**46**	276	4070	275	−2.92	Hexane
	269	3480	268	−2.42	
	262	2230	262 sh	−1.44	
	256 sh	1390			
	229 sh	15900	229	−12.9	
	221 sh	24800	222 sh	−9.15	
	202 sh	75300	214	+9.72	
	195 sh	98500	196	−33.6	
(−)-**47**	276	2170	276	−3.79	Hexane
	269	1830	269	−2.88	
	263	1150	262 sh	−1.40	
	256 sh	674			
	230 sh	7000	229	−13.2	
	221 sh	12100	223 sh	−10.8	
	203 sh	36700	215	−10.3	
			210	+12.0	
			197 sh	−30.9	
			189	−72.1	
(−)-**48**	377	184	375	−3.06	Hexane
	358	395	357.5	−6.18	
	342.5	389	341	−5.76	
	328	251	326	−3.09	
	303	987	314	−1.18	
	293.5	1000	300 sh	+3.48	
	275.5	2090	293	+4.97	
	266 sh	2580	275	−8.61	
	257 sh	4140	267	−12.0	
	247 sh	7970	258	−13.5	
	239	12900	244 sh	+7.55	
	233	13800	238 sh	+33.9	
	217 sh	23400	232	+38.2	
	211	26200	212	−31.8	
			201	+57.6	
			187	−38.8	

sh; Shoulder, !; lowest recorded value, not a maximum.

(+)-**42** in benzene-d_6, the signal at the C-11 proton appeared in lower field than other methylene and bridgehead protons and exhibited W-letter long-range coupling, J=1.0 Hz, with the C-12 *exo*-proton. This led us to decide upon an α-configuration for the hydrogen at C-11.

(−)-10-Ethyl-DMDC (−)-**47** was prepared from the (−)-alcohol, (−)-**43**, and showed an almost antipodal CD spectrum to (+)-**35**, (Fig. 2). Since the ethyl group at the bridgehead did not have a significant effect on the CD spectrum, the absolute configuration of (−)-**47** assigned was 5*R*,10*S*. This assignment was also supported by the negative Cotton effect attributable to the n-π^* transition of (−)-**48** (Table 1), since Tatemitsu *et al.*[8] have reported that in the structurally similar compound (+)-**49**, the contribution of β,γ-unsaturation is predominant and that of α,β-unsaturation is negligibly small in this region of the CD spectrum (Fig. 3).

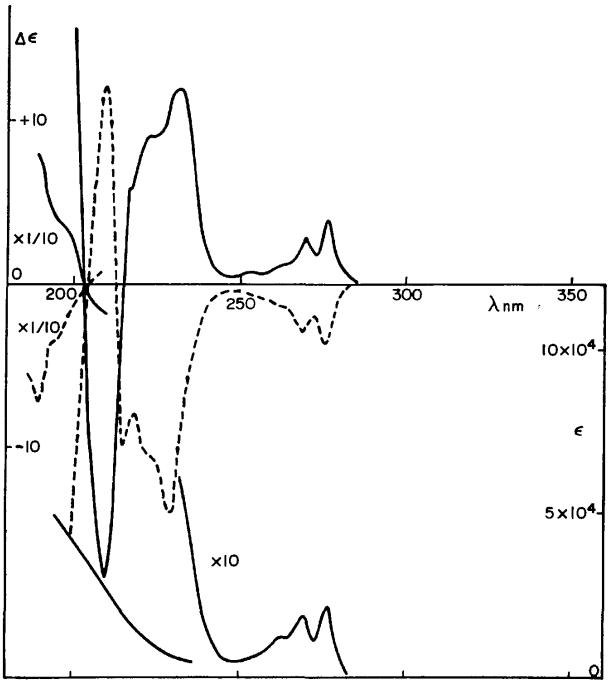

Fig. 2. UV and CD spectra of (+)-**35**, (——), and CD spectrum of (−)-**47**, (- - -).

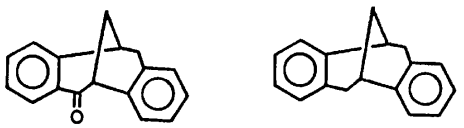

(+)-**49** (+)-**50**

Fig. 3.

Results and Discussion

Figure 4 shows temperature-dependent CD spectra of (−)-**47** in M.I.† Though the vibrational structure became fine for the ^1L_b transition with a decrease in temperature, the rotational strengths, -5.18×10^{-40} cgs at 25 °C, -5.08×10^{-40} cgs at −68 °C, and -5.16×10^{-40} cgs at −190 °C, were invariable within the experimental error. The DMDC skeleton proved to be rigid in conformation, as was expected from the model consideration.

Table 1 shows the UV and CD spectra. (+)-DMDC, (+)-**35**, did not exhibit the couplet pattern but did show a positive Cotton effect with fine structure in the region of the ^1L_b transition. We tried to apply the sector rule[9] to (+)-**35**, assuming the presence of two chromophores with CD spectra that were merely additive. Figure 5 shows two projections along the C_2-axis of the A and B benzene chromophores. In projection A, the rule predicts a negative CD within the ^1L_b band, while projection B predicts that contributions from the second benzene ring should be strongly positive. As they have op-

† Methylcyclohexane isopentane, 4:1,

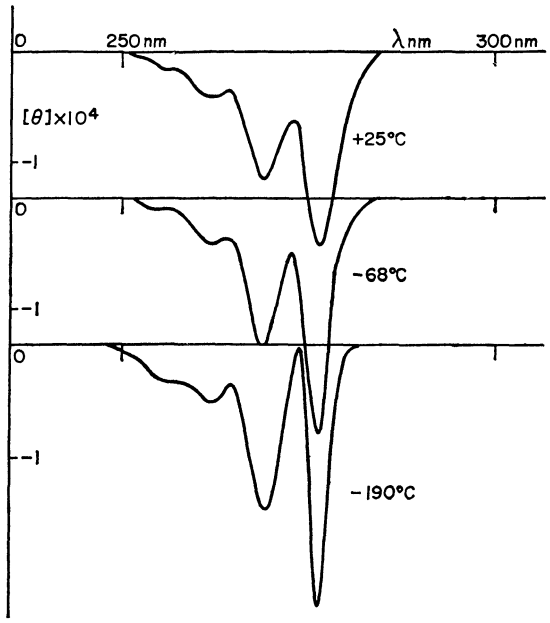

Fig. 4. Temperature-dependent CD spectra of (−)-**47**.

posite signs, a small positive value is expected and this agrees with the measurements.

In the 210—231 nm region, four Cotton effects were detected, three positive CD band followed by one negative CD band at shorter wavelength, with the last two CD bands looking like a couplet. Compound (−)-**50**, with two benzene rings linked with two ethylene chains, has been reported to have four Cotton effects in the 214—226 nm region.[8] Presumably, the couplet centered around 224 nm of (−)-**50** corresponds to the couplet at about 213 nm of (+)-**35** by the nature of the transition, owing to the similarity of the couplet pattern. In this region, besides the ^1L_a transition, the charge transfer transition between two aromatic chromophores are predicted to play an important role, and the positive CD bands at 231 and 224 nm of (+)-**35** and the negative CD bands at 218 and 214 nm of (−)-**50** seem to be assignable to the charge transfer transition by nature. The energy sequences seem likely to displace each other in (+)-**35** and (−)-**50** by their geometrical change.

In the ^1B transition region, two positive Cotton effects were observed but not the couplet pattern.

Compounds (−)-**43**—(−)-**47** have the opposite configuration in the DMDC skeleton to (+)-**35** and showed almost antipodal CD spectra to that of (+)-**35**, though their couplet was clearer in the region of 222—210 nm. Thus the substituent at the bridgehead has only a minor effect on the CD spectrum of DMDC.

Compound (+)-**42** showed a larger magnitude of the positive Cotton effect in the ^1L_b transition than (+)-**35** and only two Cotton effects were observed in the region of 221—230 nm, unlike the case of (+)-**35**. The tetrahydrofuran ring seems to produce little strain on the DMDC skeleton from model inspection. From another point of view, one of the aromatic chromophores is perturbed by oxygen of the ring or

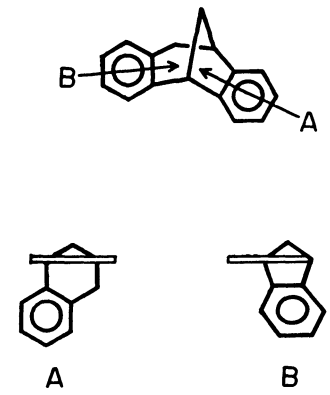

Fig. 5. Stereoformula of (+)-**35** and projection diagrams in the directions A and B.

the ring itself, though the sector rule[9] could not predict their contributions because the oxygen is situated in the negative sector while the ring is in the positive one. The contribution of the hydroxyl group at C-11 to the ^1L_b band CD was found to be positive from comparison of the CD spectra of (+)-**22b** with that of (+)-**34b**. Though this disagrees with the sector rule, it may suggest the predominance of the effect of the oxygen rather than the tetrahydrofuran ring in (+)-**42**.

Compounds (+)-**29b** and (+)-**31b** are antipodal to compounds (+)-**30b** and (+)-**32b** in the skeleton itself, respectively. The substituents, NH_2 or NH_3Cl do not change the direction of electric transition dipole moment of the aromatic chromophores. We would expect from the simple exciton coupling mechanism that they show CD spectra antipodal to each other. In fact, compounds (+)-**29b** and (+)-**30b** showed oppositely signed CD spectra in the wavelength region shorter than 230 nm. However, they showed almost the same magnitude of the positive Cotton effects in the region of the ^1L_b and ^1L_a transition. On the other hand, compounds (+)-**31b** and (+)-**32b** showed antipodal CD spectra in the region of the ^1L_b and ^1L_a transitions but the same signed Cotton effects in the shorter wavelength region.

Compounds (+)-**31b** and (+)-**32b** are not suitable for detailed treatments of the chiroptical properties, because of the uncertainty of the molecular orbitals of the chromophores or the direction of the transition dipoles. Therefore we will later describe the results of theoretical treatments of the optical activity of (+)-**29b** and (+)-**30b**.

In spite of the (+)-DMDC skeleton being rigid in conformation as previously described, the CD spectra of (+)-**25b** and (+)-**26b** were found to vary with temperature as shown in Table 2. For (+)-**25b**, assuming the equilibrium between two conformers, we estimated the free energy difference (ΔG^0) and the $\Delta\varepsilon$ values of two conformers by a simple method described by Moscowitz *et al.*[10]: $\Delta G^0 = 1.0$ kcal/mol; 298 nm ($\Delta\varepsilon$, +11.9 and −7.64); 235 nm ($\Delta\varepsilon$, +31.3 and −6.15).

With compound (+)-**26b**, the magnitude also increased for positive Cotton effects at 295—298 nm and at 230 nm and the negative Cotton effect at 254—

Table 2. Temperature dependent CD spectra of (+)-**25b** and (+)-**26b**

25 °C		−68 °C		−190 °C	
λ_{nm}	$\Delta\varepsilon$	λ_{nm}	$\Delta\varepsilon$	λ_{nm}	$\Delta\varepsilon$
(+)-**25b** in E. P. A.					
297	+8.94	298	+10.4	299	+11.8
260.5	+1.02	260.5	+0.40	260	−0.58
235	+25.7	235.5	+28.4	236	+31.2
227	0	227	0	227	0
(+)-**26b** in E. P. A.					
296.5	+7.97	295	+13.3	298	+13.8
257	−1.90	255	−5.06	254	−9.79
230 sh	+87.3	230	−87.9	230	+90.9
215	+136.	215.5	+135.	216	+138.

E. P. A.=Ether-isopentane-ethanol 5:5:2.

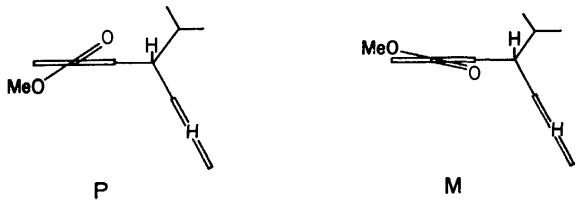

Fig. 6. Projective diagram of the rotamers P and M from the methoxycarbonyl group.

257 nm with the decrease in temperature. But the change could not be analyzed by assuming it to be an equilibrium between two kinds of species.

The methoxycarbonyl group at C-6 of (+)-**25b** and those at C-4 and C-19 of (+)-**26b** are not coplanar with the benzene ring judging from the steric interaction with the bridgehead proton (Fig. 6). But that at C-1 of (+)-**25b** can be coplanar with the benzene ring. Therefore, we deduced that (+)-**25b** had two rotamers. On the other hand, (+)-**26b** had more than two rotamers and showed complex temperature-dependent CD spectra.

The sign of the Cotton effect of the conjugation band in the 270 nm region is correlated with chirality of the conjugated system in some lactonic aromatic compounds, the absolute configurations of which have been determined. The P (right-handed) and M (left-handed) helicity produced positive and negative Cotton effects, respectively, as found with lycorenine alkaloids[11] (Table 3), ochracin derivatives[12] and dihydroisocoumarin compounds.[13]

This empirical rule predicts that the rotamer P will show a positive Cotton effect and the rotamer M, a negative one. Rotamer P would be more stable than rotamer M owing to an additional steric interaction of the methoxycarbonyl group with the proton at C-4. The experimental results of (+)-**25b** support the preference of the rotamer P.

A methoxycarbonyl group will change the direction of the electric transition dipole moment of the benzenoid chromophore, if it is fixed. But the CD spectra of (+)-**25b** and (+)-**26b** are quite similar to those of (+)-**29b** and (+)-**30b**, respectively. This may indicate that the CD spectra of DMDC are not altered very much by the minor change of direction of the local electric transition dipole moment.

Theoretical Consideration. For insight into the contribution of various factors to the chiroptical properties of (+)-**29b** and (+)-**30b**, we tried the following calculations.

1) The rotational strength was obtained by a coupling theory[14] using a point dipole approximation located at the center of the benzene ring. The local transition energy and intensity were taken from the experimental value of the four transitions of 5-aminotetralin.††,4) Structural parameters required for the calculation were derived from idealized geometry as follows: aromatic C-alkyl C bond length=1.52 Å, aromatic C–C=1.40 Å, alkyl C–C=1.54 Å, C–N=1.38 Å, C_{1l}–C_{1a}–C_{4a} and C_{1a}–C_{4a}–C_5 bond angles=122°, C_5–C_{5a}–C_9 and C_{5a}–C_{9a}–C_{10}=110°, and atoms C_5, C_{4a}, C_{1a}, C_{11}, and C_{10} in a plane.

2) The point dipole moment was displaced from the center of the benzene ring according to the calculation by the dipole velocity procedure[15] as follows: ^1L_b, −0.093 Å; ^1L_a, 0.375 Å; ^1B_b, −0.050 Å and ^1B_a, −0.038 Å toward the nitrogen atom.

3) The calculation of the molecular orbital and the rotational strength was as described in Ref. 1. The resonance energies between the two aromatic chromophores were evaluated by proportion to the overlap integrals.

4) All of the charge transfer (c.t.) transitions were neglected in calculating the rotational strength in the above treatment, though the MO contained the c.t. transition.

5) All of the c.t. transitions were neglected in obtaining the MO, and the rotational strength was calculated as in method 3.

Figure 7 shows the results of the calculations by methods 1—5. The CD spectra calculated by method 1 are completely antipodal to each other for (+)-**29b** and (+)-**30b**. The displacement of the point dipole moment does not seem to improve the rotational strength. Thus the disagreement between the calculated and the observed CD spectra may be caused by the assumption of the local electric transition dipole moment as a point dipole and the neglect of the c.t. transition. The results calculated by method 3 reproduce the qualitative features of the CD spectra quite well, with the exception of the transition energy (Figs. 7 and 8). The shift, *ca.* 10 nm, is mainly caused by the direct use of the value of the π-SCF-MO of aniline as a local transition energy. Even if the contribution of the c.t. transition is neglected in calculating the rotational strength by the same MO in method 4, the difference from the results by method 3 is not very large. This similarity indicates that the rotational strength is mainly produced by the coupling of the local transition dipole moments and not very much by the c.t. transition.

When the c.t. transition is completely neglected in obtaining the MO, by method 5, the calculated CD spectra do not reproduce the experimental one. Though the couplet pattern around 230 nm in method

†† The unit should be corrected to 10^{19} cgs in Ref. 4.

TABLE 3. UV AND CD SPECTRA OF LYCORENINE ALKALOIDS

Compound	UV		CD		Solvent	Chirality
	λ_{nm}	ε	λ_{nm}	$\Delta\varepsilon$		
51	307	7040	275	−4.67	MeOH	M
	269	6050	254	+0.97		
	227	28700	232	−16.8		
51 HCl	306	4720	275	−4.79	MeOH	M
	269	4270	252	+4.21		
	227	20400	230	−6.67		
52	307	5330	275	−5.30	MeOH	M
	270	4050	252	+1.62		
	227.5	21400	232	−11.5		
52 HCl	305	6190	275	−4.21	MeOH	M
	270	5790	255	+3.67		
	227	27000	232	−9.58		
53	302	5230	310	−0.91	MeOH	M
	268	8650	273	−6.93		
	277	18300	250	+4.96		
			230	−9.82		
54	307	4550	311	−2.52	MeOH	M
	269	4100	272.5	−4.12		
	227	16800	250	+2.20		
			236	−1.12		
55	306	5150	310	−2.29	MeOH	M
	268	4920	273	−3.24		
	226	21100				
56	306	5420	305	−1.16	MeOH	P
	268	5450	271.5	+4.52		
	225.5	19500	245	−2.63		
			229.5	+6.97		

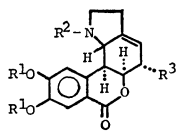

51: R^1=-CH_2-, R^2=CH_3, R^3=OH
52: R^1=-CH_2-, R^2=CH_3, R^3=OAc
53: R^1=CH_3, R^2=CH_3, R^3=H

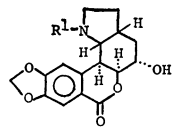

54: R^1=CN
55: R^1=CH_3

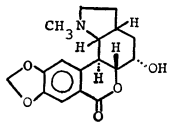

56

5 is shared by six transitions in method 3, the sequence of the coupling mode does not change and method 3 gives good agreement with the experimental results in this region. Thus the c.t. transition must be taken into consideration in the calculation of the MO.

In method 5, the local electric transition dipole moment is not assumed to be a point dipole and the rotational strength is calculated by the dipole velocity method.

Also, in method 5 a local magnetic transition dipole moment is produced perpendicular to the benzene ring,[16] which distinguishes this method from methods 1 and 2. The result from method 5 agrees better with the experimental one than those from methods 1 and 2, especially in the region of the ^1L_b transition. This indicates that the induced magnetic transition dipole moment can not be neglected in the transition of small rotational strength.

In summary, the electric transition dipole moment should not treated as a point dipole at any place and the rotational strength should be calculated with a dipole velocity method. The c.t. transition continues

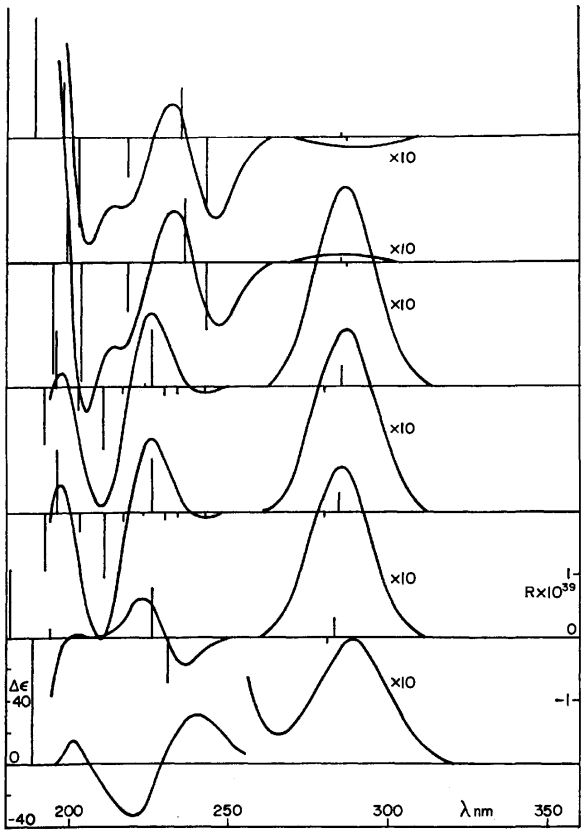

Fig. 7. CD spectra of (+)-**29b**. The theoretical spectra refer to calculations by methods 1 to 5 from the top. The experimental spectrum in cyclohexane is at the bottom.

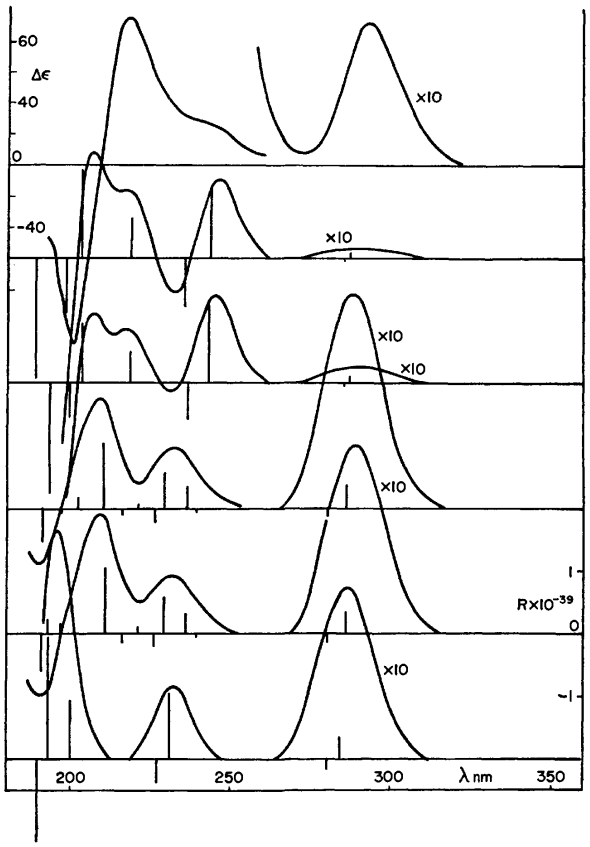

Fig. 8. CD spectra of (+)-**30b**. The experimental spectrum in cyclohexane is at the top. The theoretical spectra refer to calculations by methods 1—5 from the upper part.

to function in the chiroptical properties of the DMDC compounds and can not be neglected in the calculation of the MO, though it does not cause alteration of the coupling mode sequence. The rotational strength is mainly produced by the coupling of the local electric transition dipole moments without much contribution from the c.t. transition.

Experimental

IR spectra were recorded on a JASCO-DS-402G grating spectrophotometer. Optical rotations were determined with a Perkin-Elmer Model 141 polarimeter using a 1-dm microcell. Circular dichroism curves were obtained using a JASCO Model J-40C spectropolarimeter. ^{1}H NMR spectra were measured with a Varian A56/60 D spectrometer using tetramethylsilane as an internal standard. UV spectra were obtained with a Hitachi Model 323 spectrometer.

*Methyl 12-Hydroxy-DEA-1-carboxylate (**7a**) and (**8a**).* $NaBH_4$ (0.42 g) was added in small portions to a solution of methyl 12-oxo-DEA-1-carboxylate (**4a**) (1.03 g) in dry diglyme (20 ml) with ice cooling. The mixture was stirred for 3 h and dilute HCl was added dropwise at 0 °C. The mixture was extracted with ether. The solution was washed with water, dried (Na_2SO_4) and concentrated *in vacuo* to 1.05 g.

A small portion of the residue (53 mg) treated with acetic anhydride and pyridine gave the acetate. Its NMR showed it to be a 1:2 mixture of the epimers.

*(+)-Dimethyl 12-Hydroxy-DEA-1,5-dicarboxylate [(+)-(**7b**) and (+)-(**8b**)].* Dimethyl 12-oxo-DEA-1,5-dicarboxylate [(+)-(**4b**)] (10.1 g) was reduced as above to obtain the desired mixture, 11.0 g.

*Methyl 12-(3,5-Dinitrobenzoyloxy)-DEA-1-carboxylate (**13a**).* 3,5-Dinitrobenzoyl chloride (3.0 g) was added to a solution of a mixture of the alcohols **7a** and **8a** (1.0 g) in pyridine (15 ml) with ice cooling. The mixture was stirred for 1 h and allowed to stand overnight, poured into water and allowed to stand for 1 h. The mixture was extracted with chloroform. The solution was washed with dilute HCl, water, aqueous Na_2CO_3, and water, then dried (Na_2SO_4) and concentrated *in vacuo*. The oily residue was crystallized from benzene–ether and recrystallized twice from the same solvent, giving a colorless powder (113 mg): mp 216—217 °C; IR (Nujol) 1735, 1713, 1340 cm^{-1}; NMR ($CDCl_3$) δ 1.72 (1H, ddd, J=3, 3, 14 Hz), 2.59 (1H, ddd, J=3, 8, 14 Hz), 3.88 (3H, s), 4.45 (1H, t, J=3 Hz), 5.49 (1H, m), 6.02 (1H, d, J=2 Hz), 7.1—7.9 (7H, m), 8.90 (2H, d, J=2 Hz), 9.13 (1H, t, J=2 Hz). Found: C, 63.65; H, 3.75; N, 5.78%. Calcd for $C_{25}H_{18}N_2O_8$: C, 63.29; H, 3.82; N, 5.90%.

The epimer could not be isolated in pure form.

*(+)- and (±)-Dimethyl 11-(3,5-Dinitrobenzoyloxy)-DEA-1,5-dicarboxylate [(+)- and (±)-(**13a**) and (**13b**)].* The (+)- and (±)-alcohols (+)- and (±)-**7b** and **8b** were treated as above but both of the products could not be crystallized. The NMR spectrum showed a mixture of *ca.* 1:2 of the epimers.

*(+)-Dimethyl 11-(4-Nitrobenzoyloxy)-DEA-1,5-dicarboxylate [(+)-(**9b**)].* The (+)-alcohol (+)-**7b** and (+)-**8b**

(11.0 g) was treated with *p*-nitrobenzoyl chloride in the same manner as above. The residue was crystallized and recrystallized from ether, giving colorless prisms (1.5 g): mp 189—191 °C (racemic mp 189—190 °C) $[\alpha]_D^{21}$ +246.3°± 3.5° (*c* 0.709, $CHCl_3$); $\Delta\varepsilon$ +0.065 (333 nm), −0.036 (312), +7.12 (290), +15.9$_{sh}$ (235), +20.9$_{sh}$ (219), +26.6 (208); IR (Nujol) 1715, 1526, 1280 cm^{-1}; NMR ($CDCl_3$) δ 1.72 (1H, ddd, J=3, 3, 13 Hz), 2.52 (1H, ddd, J=13, 9, 3 Hz), 3.78 (3H, s), 4.96 (3H, s), 5.46 (1H, ddd, J=10, 3, 3 Hz), 5.78 (1H, t, J=3 Hz), 6.02 (1H, d, J=3 Hz), 7.0—8.4 (10H, m). Found: C, 66.27; H, 4.31; N, 2.81%. Calcd for $C_{27}H_{21}NO_8$: C, 66.53; H, 4.34; N, 2.87%.

The epimer could not be purified.

(+)-Dimethyl endo-*11-hydroxy-DEA-1,5-dicarboxylate [(+)-(**7b**)]*. A suspension of the (+)-ester (+)-**9b** (1.5 g) in a solution of sodium methoxide in methanol [Na metal (0.05 g) and methanol (25 mg)] was heated under reflux for 18 h and concentrated *in vacuo*. Water was added. The mixture was extracted with ethyl acetate. The solution was washed with water, dried (Na_2SO_4), and concentrated *in vacuo*. The residue was chromatographed on thick silica gel plate [Merck, pre-coated plate; benzene–ethyl acetate (3:1)]. The residue (0.7 g) could not be crystallized (racemic mp 142—145 °C).

(+)-Dimethyl exo-*11-hydroxy-DEA-1,5-dicarboxylate [(+)-(**8b**)]*. The crude ester (+)-**10b**, obtained from the mother liquor, was treated as above and gave the crude product (5.5 g).

Methyl endo-*12-hydroxy-DEA-1-carboxylate (**7a**)*. The ester **13a** was treated as above and gave an oily product.

Methyl exo-*12-hydroxy-DEA-1-carboxylate (**8a**)*. *1)* The crude ester **14a**, obtained from the mother liquor was treated as above and gave an oily product. *2)* A mixture of the ester **14a** (657 mg), obtained from the mother liquor, in a solution of 5% KOH in methanol (12 ml) was heated under reflux for 2 h, poured into water, acidified with dilute HCl and extracted with ether. The solution was washed with water, dried (Na_2SO_4) and concentrated *in vacuo*. The crystalline residue could not be fractionally recrystallized and was heated under reflux in methanol (20 ml) and concentrated H_2SO_4 (1 ml) for 15 h. The mixture was poured into water and extracted with ether. The solution was washed with water, dried (Na_2SO_4), and concentrated *in vacuo*. The residue was chromatographed on alumina (23 g, Merck, grade *2)* in benzene to obtain methyl 3,5-dinitrobenzoate and in ethyl acetate to obtain the oily product **8a** (402 mg).

*(±)- and (+)-Dimethyl 11-Acetoxy-DMDC-1,6-dicarboxylate [(±) (**17b**) and (+)-(**17b**)]*. A solution of *p*-toluenesulfonyl chloride (0.9 g) in pyridine (8 ml) was added dropwise to a solution of the alcohol (±) **7b** (0.45 g) in pyridine (15 ml) at −5—−7 °C over a period of 1.5 h. The mixture was allowed to stand at 4 °C for 40 h, poured into ice water and extracted with ether. The solution was washed with dilute HCl and water, dried (Na_2SO_4), and concentrated *in vacuo*.

A solution of the crude tosylate (0.423 g) in a solution of anhydrous sodium acetate (0.5 g) in glacial acetic acid (20 ml) was heated at 105 °C for 3 d, concentrated *in vacuo* and dissolved in a mixture of ether and aqueous $NaHCO_3$. The organic phases were washed with water, dried (Na_2SO_4), and concentrated *in vacuo*. The NMR spectrum of the crude product was contaminated with less than 5% of dimethyl 11-acetoxy-DMDC-4,9-dicarboxylate (**18b**). The residue was crystallized from hexane and recrystallized from ether, giving a powder (152 mg): mp 173—175 °C; IR (Nujol) 1743, 1722 cm^{-1}; NMR ($CDCl_3$) δ 2.06 (3H, s), 2.40 (2H, m), 3.63 (2H, m), 3.75 (3H, m), 3.89 (3H, m), 4.90 (1H, m), 6.29 (1H, d, J=2 Hz), 7.0—7.4 (2H, m), 7.6—7.9 (4H, m). Found: C, 69.29; H, 5.29%. Calcd for $C_{22}H_{20}O_6$: C, 69.46; H, 5.30%.

The (+)-isomer (+)-**17b** could not be crystallized.

*(+)-Dimethyl 11-Acetoxy-DMDC-4,9-dicarboxylate [(+)-(**18b**)]*. The alcohol (+)-**8b** (5.5 g) was treated as above and gave an oily product (4.1 g).

*Methyl 11-Acetoxy-DMDC-1-carboxylate (**17a**)*. The alcohol **7a** (0.3 g) gave an oily product **17a** by the same treatment.

*Methyl 11-Acetoxy-DMDC-9-carboxylate (**18a**)*. The alcohol **8a** (0.402 g) gave the rearranged compound **18a** (0.286 g).

*(+)-Dimethyl 11-Hydroxy-DMDC-1,6-dicarboxylate [(+)-(**19b**)]*. The crude acetate (+)-**17b** obtained above was treated as in the solvolysis of **9b** and gave the crude product, which was chromatographed on thin silica gel plate [Merck, pre-coated; benzene–ethyl acetate (2:1)] and gave an oily material: $[\alpha]_D^{26}$ +310.4°±5.5° (*c* 0.714, $CHCl_3$); IR ($CHCl_3$) 3465, 1714 cm^{-1}; NMR ($CDCl_3$) δ 2.2—2.9 (2H, m), 3.68 (1H, broad s), 3.83 (3H, s), 3.90 (3H, s), 4.88 (1H, broad s), 4.91 (1H, d, J=4 Hz), 6.9—7.9 (6H, m).

*(+)-Dimethyl 11-Hydroxy-DMDC-4,9-dicarboxylate [(+)-(**20b**)]*. Oil, $[\alpha]_D^{22}$ +433.5°±9.9° (*c* 0.480, MeOH); IR ($CHCl_3$) 3610, 1717 cm^{-1}; NMR ($CDCl_3$) δ 2.43 (2H, m), 3.90 (3H, s), 3.95 (3H, s), 4.16 (1H, broad s), 4.85 (1H, d, J=2 Hz), 4.98 (1H, broad s), 6.9—7.9 (6H, m); (racemic compound, mp 152—153 °C).

*Methyl 11-Hydroxy-DMDC-1-carboxylate (**19a**)*. Oil; IR (film) 3480, 1700 cm^{-1}; NMR ($CDCl_3$) δ 2.2—2.8 (2H, m), 3.65 (1H, m), 3.78 (1H, s), 3.94 (1H, m), 4.88 (1H, d, J=3 Hz), 6.9—7.5 (1H, m), 7.71 (1H, dd, J=7, 2 Hz).

*Methyl 11-Hydroxy-DMDC-9-carboxylate (**20a**)*. Mp 159—161 °C; IR (Nujol) 3503, 1698, 1024, 1012 cm^{-1}; NMR ($CDCl_3$) δ 2.40 (2H, m), 3.89 (3H, s), 3.90 (1H, s), 4.17 (1H, m), 4.82 (1H, d, J=2 Hz), 6.9—7.5 (6H, m), 7.72 (1H, dd, J=7.2 Hz). Found: C, 76.77; H, 5.64%. Calcd for $C_{18}H_{16}O_3$: C, 77.12; H, 5.75%.

1-Hydroxymethyl-endo-*12-hydroxy-DEA and 1-Hydroxymethyl*-exo-*1-hydroxy-DEA [(**15a**) and (**16a**)]*. A solution of the keto ester **4a** (193 mg) in dry tetrahydrofuran (5 ml) was added to a slurry of $LiAlH_4$ (100 mg) in tetrahydrofuran (5 ml) with ice cooling. This mixture was heated under reflux for 2 h. Excess $LiAlH_4$ was decomposed with a solution of methanol in ether then dilute HCl with ice cooling. The organic phase was separated and the aqueous phase was extracted with ether. The combined organic phases were washed with water, dried (Na_2SO_4), and concentrated *in vacuo*. The oily residue was chromatographed on thin silica gel plate [Merck, pre-coated; benzene–ethyl acetate (1:3)].

Fraction 1, 54.3 mg, was recrystallized from benzene: mp 169—170 °C; IR ($CHCl_3$) 3611, 3482 cm^{-1} (8.565×10^{-3} M/l); NMR ($CDCl_3$) δ 1.36 (1H, ddd, J=3, 3, 13 Hz), 2.28 (1H, ddd, J=3, 9, 13 Hz), 4.30 (1H, t, J=3 Hz), 4.30 (1H, m), 4.52 (1H, d, J=12 Hz), 4.80 (1H, d, J=3 Hz), 5.01 (1H, d, J=11 Hz), 7.0—7.5 (7H, m), Found: C, 80.45; H, 6.30%. Calcd for $C_{17}H_{16}O_2$: C, 80.93; H, 6.39%.

Fraction 2, 76.1 mg, was recrystallized from benzene: mp 142—143 °C; IR ($CHCl_3$) 3606, 3576 cm^{-1} (7.525×10^{-3} M/l); NMR ($CDCl_3$) δ 1.30 (1H, ddd, J=3, 3, 13 Hz), 2.21 (1H, ddd, J=3, 9, 13 Hz), 4.10 (1H, m), 4.20 (1H, t, J=3 Hz), 4.66 (3H, d, J=3 Hz), 6.9—7.4 (7H, m). Found: C, 81.89; H, 6.47%. Calcd for $C_{17}H_{16}O_2\cdot1/2C_6H_6$: C, 82.44; H, 6.57%.

Reduction of the diesters **5a** and **6a** gave the same product.

(+)-11-Hydroxy-1,6-bis(hydroxymethyl)-DMDC [*(+)-(**21b**)*]. The ester (+)-**19b** (80 mg) was reduced as described above and recrystallized from ethyl acetate: mp 194—196 °C, (31.6 mg), $[\alpha]_D^{22}$ +47.9°±1.6° (*c* 0.553, MeOH); IR ($CHCl_3$) 3595, 3439 cm^{-1} (a supernatant of 3.09 mg/5 ml); NMR (CD_3OD) δ 2.1—2.8 (2H, m), 3.47 (1H, broad s), 4.78 (1H, m), 4.44 (1H, d, J=13 Hz), 4.60 (2H, s), 4.78 (1H, d, J=13 Hz), 4.82 (s), 6.9—7.4 (6H, m). Found: C, 76.04; H, 6.44%. Calcd for $C_{18}H_{18}O_3$: C, 76.57; H, 6.43%.

(+)-11-Hydroxy-4,9-bis(hydroxymethyl)-DMDC [*(+)-(**22b**)*]. The ester (+)-**20b** (101 mg) was reduced as described above to give a powder (24.5 mg): mp 155—156 °C, $[\alpha]_D^{22}$ +357.8°±7.0° (*c* 0.573, MeOH); IR ($CHCl_3$) 3603 cm^{-1} (supernatant of 3.26 mg/5 ml); NMR (CD_3OD) δ 2.42 (2H, m), 3.62 (1H, broad s), 4.35 (1H, broad s), 4.65 (2H, s), 6.8—7.4 (6H, m). Found: C, 76.34; H, 6.53%. Calcd for $C_{18}H_{18}O_3$: C, 76.57; H, 6.43%.

*11-Hydroxy-1-hydroxymethyl-DMDC (**21a**).* The ester **19a** (87 mg) was reduced in the same manner to give a powder (48 mg): mp 155 °C; IR ($CHCl_3$) 3590, 3440 cm^{-1} (8.52×10^{-3} M/l); NMR ($CDCl_3$) δ 2.2—2.7 (2H, m), 3.52 (1H, broad s), 3.93 (1H, m), 4.23 (1H, d, J=12 Hz), 4.64 (1H, d, J=12 Hz), 4.80 (1H, d, J=2 Hz), 6.9—7.5 (7H, m). Found: C, 80.65; H, 6.51%. Calcd for $C_{17}H_{16}O_2$: C, 80.93; H, 6.39%.

*11-Hydroxy-9-hydroxymethyl-DMDC (**22a**).* The ester **20a** (24 mg) was reduced as described above to give a powder (6.5 mg): mp 129—130 °C; IR ($CHCl_3$) 3604 cm^{-1} (8.53×10^{-3} M/l); NMR ($CDCl_3$) δ 2.40 (2H, m), 3.63 (1H, m), 3.87 (1H, t, J=2 Hz), 4.62 (2H, s), 4.72 (1H, d, J=2 Hz), 6.9—7.3 (7H, m). Found: C, 80.78; H, 6.34%. Calcd for $C_{17}H_{16}O_2$: C, 80.93; H, 6.39%.

(+)-Dimethyl DMDC-4,9-dicarboxylate [*(+)-(**26b**)*]. A mixture of the hydroxy ester (+)-**20b** (2.8 g), 30% palladium charcoal (0.9 g) and a few drops of 70% perchloric acid in methanol (130 ml) was stirred in a hydrogen atmosphere for 6 d. The catalyst was filtered then washed with methanol. The filtrate was concentrated *in vacuo*. The residue was dissolved in dichloromethane, washed with water, dried (Na_2SO_4), and concentrated *in vacuo*. The residue was distilled at 220 °C (bath temperature) at 0.05 mmHg through a short-path distillation apparatus and gave a viscous oil (2.4 g).

A solution of the (+)-diester (2.25 g) in a solution of 5% KOH in methanol (60 ml) was heated under reflux for 2 h and concentrated to the half volume *in vacuo*. Ice-cold dilute HCl was added. The crystals were collected by filtration, washed with water and dissolved in ethyl acetate. The solution was washed with water, dried (Na_2SO_4), and concentrated *in vacuo*. The residue was recrystallized from acetone, ethyl acetate then methanol and gave (+)-**28b**: mp 258—262 °C, $[\alpha]_D^{21}$ +575.4°±9.4° (*c* 0.349, MeOH); IR (Nujol) 1692 cm^{-1}; NMR (CD_3OD) δ 2.00 (1H, d, J=11 Hz), 2.42 (1H, ddd, J=11, 6, 1 Hz), 2.84 (1H, dd, J=4 Hz), 3.33 (1H, dd, J=18, 6 Hz), 4.18 (1H, broad t, J=4 Hz), 4.98 (1H, d, J=4 Hz), 6.9—7.8 (6H, m). Found: C, 73.37; H, 4.91%. Calcd for $C_{18}H_{14}O_4$: C, 73.46; H, 4.79%.

The (+)-dicarboxylic acid (55.3 mg) was esterified with excess diazomethane to give the diester (60 mg), which was crystallized from hexane: mp 92.5—93.5 °C; $[\alpha]_D^{21}$ +547.4°±9.6° (*c* 0.327, $CHCl_3$); IR ($CHCl_3$) 1716 cm^{-1}; NMR ($CDCl_3$) δ 2.04 (1H, d, J=13 Hz), 2.46 (1H, ddd, J=10, 6, 1 Hz), 2.92 (1H, dd, J=16, 1 Hz), 3.38 (1H, dd, J=16, 5 Hz), 3.88 (3H, s), 3.93 (3H, s), 4.15 (1H, broad t, J=4 Hz), 4.91 (1H, d, 5 Hz), 6.9—7.8 (6H, m), Found: C, 73.84; H, 5.49%. Calcd for $C_{20}H_{18}O_4$: C, 74.51; H, 5.63%.

(+)-Dimethyl DMDC-1,6-dicarboxylate [*(+)-(**25b**)*]. The same hydrogenolysis was carried out on the alcohol (+)-**19b** (110 mg) giving the desired product (44 mg): mp 113 °C; $[\alpha]_D^{22}$ +315.3°±2.0° (*c* 0.275, $CHCl_3$); IR (film) 1719 cm^{-1}; NMR ($CDCl_3$) δ 1.9—2.8 (2H, m), 2.9—3.3 (1H, m), 3.3—3.7 (2H, m), 3.77 (3H, s), 3.90 (3H, s), 4.82 (1H, d, J=5 Hz), 6.9—7.9 (6H, m). Found: C, 74.65; H, 5.57%. Calcd for $C_{20}H_{18}O_4$: C, 74.51; H, 5.63%.

*Methyl DMDC-9-carboxylate (**26a**).* The acetate **20a** (238 mg) was hydrogenolyzed according to the procedure cited above and gave prisms (53.3 mg): mp 80—81 °C; IR 1713 cm^{-1}; NMR ($CDCl_3$) δ 2.12 (1H, d, J=13 Hz), 2.47 (1H, broad dd, J=13, 6 Hz), 2.85 (1H, d, J=16 Hz), 3.32 (1H, dd, J=16, 6 Hz), 6.8—7.3 (6H, m), 7.73 (1H, dd, J=8, 2 Hz). Found: C, 81.43; H, 5.97%. Calcd for $C_{18}H_{16}O_2$: C, 81.79; H, 6.10%.

(+)-DMDC-1,6-dicarboxylic Acid [*(+)-(**27b**)*]. Mp 259—260 °C; $[\alpha]_D^{22}$ ±315.3°±5.7° (*c* 0.347, MeOH).

(+)-1,6-Diamino-DMDC [*(+)-(**29b**)*]. NaN_3 (1.11 g) was added in small portions to a solution of the (+)-dicarboxylic acid [(+)-(**27b**)] (612 mg) in concentrated H_2SO_4 (33 ml) at 40—45 °C over a period of 1 h with vigorous stirring. The mixture was then heated at 50 °C for 6 h, allowed to stand overnight, poured onto ice, made alkaline with 40% aqueous NaOH and extracted with benzene. The solution was washed with water, dried (Na_2SO_4), and concentrated *in vacuo*. The crystalline residue was recrystallized from benzene and gave prisms (368 mg) (74.9%): mp 178—179 °C; $[\alpha]_D^{22}$ +736.1°±11.4° (*c* 0.357, MeOH); IR (Nujol) 3355 cm^{-1}; NMR ($CDCl_3$) δ 1.97 (1H, d, J=10 Hz), 2.41 (1H, dd, J=5, 10 Hz), 2.63 (1H, d, J=14 Hz), 3.12 (1H, dd, J=5, 14 Hz), 3.31 (1H, d, J=4 Hz), 3.51 (4H, s), 3.90 (1H, d, J=5 Hz), 6.2—7.4 (6H, m). Found: C, 81.29; H, 6.76; N, 11.78%. Calcd for $C_{16}H_{16}N_2$: C, 81.32; H, 6.82; N, 11.85%.

(+)-4,9-Diamino-DMDC [*(+)-(**30b**)*]. The (+)-dicarboxylic acid [(+)-(**28b**)] (45 mg) was treated as above and gave prisms (21.5 mg): mp 224—225 °C; $[\alpha]_D^{23}$ +212.9°±4.1° (*c* 0.364, $CHCl_3$); IR (Nujol) 3465, 3375 cm^{-1}; NMR ($CDCl_3$–a drop of CD_3OD) δ 2.07 (1H, d, J=11 Hz), 2.42 (1H, dd, J=5, 11 Hz), 2.66 (1H, dd, J=5, 16 Hz), 3.15 (1H, dd, J=5, 16 Hz), 3.5 (1H, m), 3.81 (1H, d, J=5 Hz), 6.3—7.3 (6H, m). Found: C, 80.99; H, 6.66; N, 12.04%. Calcd for $C_{16}H_{16}N_2$: C, 81.32; H, 6.82; N, 11.85%.

*1,5-bis(hydroxymethyl)-11-*endo*-hydroxy-DEA (**15b**).* A solution of the ester **9b** (99 mg) in dry tetrahydrofuran (3 ml) was added to a slurry of $LiAlH_4$ (0.1 g) in tetrahydrofuran (3 ml) with cooling in ice. The mixture was then heated under reflux for 2 h and treated as usual. The residue was chromatographed on thin silica gel plate [Merck, pre-coated plate; ethyl acetate] and recrystallized from chloroform, giving a powder (31.2 mg): mp 153—154 °C; IR ($CHCl_3$) 3607, 3484 cm^{-1} (1.495 M/l); NMR (CD_3OD) δ 1.33 (1H, ddd, J=3, 3, 13 Hz), 2.22 (1H, ddd, J=3, 9, 13 Hz), 4.13 (1H, m), 4.5—4.8 (m), 6.8—7.4 (6H, m). Found: C, 75.67; H, 5.41%. Calcd for $C_{18}H_{18}O_4$: C, 76.57; H, 6.43%.

(+)-4,9-Bis(hydroxymethyl)-DMDC [*(+)-(**34b**)*]. The (+)-diester (+)-**26b** (91 mg) was reduced as above. The product could not be crystallized and was converted into the bis(3,5-dinitrobenzoyl) ester according to the above procedure, giving crystals (109 mg): mp 176—178 °C; $[\alpha]_D^{22}$ +179.8°±2.5° (*c* 0.511, $CHCl_3$); IR (Nujol) 1720, 1550,

1288 cm^{-1}; NMR ($CDCl_3$) δ 2.20 (1H, d, J=11 Hz), 2.64 (1H, dd, J=5, 11 Hz), 2.86 (1H, d, J=16 Hz), 3.43 (1H, dd, J=5, 16 Hz), 3.78 (1H, m), 4.42 (1H, m), 5.55 (1H, s), 5.57 (1H, d, J=12 Hz), 5.82 (1H, d, J=12 Hz), 6.9—7.4 (6H, m), 9.1—9.3 (6H, m). Found: C, 58.63; H, 3.54; N, 8.18%. Calcd for $C_{32}H_{22}N_4O_{12}$: C, 58.72; H, 3.39; N, 8.56%.

The ester was hydrolyzed with a 5% KOH solution in methanol by refluxing for 3 h giving an oily residue: $[\alpha]_D^{23}$ +407.5°±6.1° (c 0.402, MeOH); NMR ($CDCl_3$) δ 2.06 (1H, d, J=11 Hz), 2.48 (1H, dd, J=11Hz), 2.77 (1H, d, J=16 Hz), 3.28 (1H, dd, J=16, 5 Hz), 3.63 (1H, m), 4.34 (1H, d, J=5 Hz), 4.68 (2H, s), 4.80 (2H, s), 6.8—7.3 (6H, m). Found: C, 79.96; H, 6.79%. Calcd for $C_{16}H_{18}O_2$: C, 79.31; H, 7.49%.

*(+)-11-Hydroxy-DMDC-4,9-dicarboxylic Acid (**24b**).* A crude rearranged compound **18b** (4.1 g) was hydrolyzed with a solution of 5% KOH in methanol (60 ml) by heating under reflux for 3 h. The product could not be purified by recrystallization and was esterified with methanol in the presence of concentrated H_2SO_4 by heating under reflux for 16 h. The crude ester was chromatographed on a thick silica gel plate [Merck, pre-coated plate; benzene–ethyl acetate (5:2)]. The residue was crystallized from benzene–hexane giving a powder (1.0 g): mp 152—153 °C. Found: C, 71.32; H, 5.51%. Calcd for $C_{20}H_{18}O_5$: C, 70.99; H, 5.36%.

The ester was hydrolyzed as above. Mp 286 °C (dec); IR (Nujol) 1692 cm^{-1}; NMR (CD_3OD) δ 2.30 (2H, m), 4.32 (2H, broad s), 5.00 (1H, broad s), 6.9—7.9 (6H, m). Found: C, 70.22; H, 4.72%. Calcd for $C_{18}H_{14}O_5$: C, 69.67; H, 4.55%.

*(+)-DMDC [(+)-(**35**)].* A mixture of the (+)-dicaboxylic acid [(+)-(**28b**)] (163 mg), copper chromite (220 mg) and quinoline, which was distilled over copper chromite, was heated under reflux for 1.5 h, poured into water and extracted with ether. The solution was washed with dilute HCl, aqueous $NaHCO_3$ and water, dried (Na_2SO_4) and concentrated *in vacuo*. The residue was chromatographed on thin silica gel plate [Merck, pre-coated; hexane] and distilled at 140 °C (bath temperature) at 0.05 mmHg (1mmHg=133.322 Pa). $[\alpha]_D^{23}$ +206.5°±2.0° (c 0.3056, $CHCl_3$); IR (film) 750 cm^{-1}; NMR ($CDCl_3$) δ 2.08 (1H, d, J=11 Hz), 3.23 (1H, dd, J=15, 5 Hz), 3.46 (1H, m), 3.85 (1H, d, J=4 Hz), 7.8—7.4 (8H, m). Found: C, 92.92; H, 6.61%. Calcd for $C_{16}H_{14}$: C, 93.16; H, 6.84%.

*Ethyl 11-Hydroxy-DEA-11-acetate (**36**).* The procedure used was a modification of a reported method.[7] A solution of 11-oxo-DEA (10.3 g) and ethyl bromoacetate (10 ml) in dry tetrahydrofuran (70 ml) was added dropwise to a mixture of activated Zn powder (20 g) in tetrahydrofuran (80 ml) with vigorous stirring at refluxing temperature. The reaction was started by addition of a small piece of iodine. After completion of the addition, the mixture was heated for 1 h. Activated Zn powder (20 g) and a small piece of iodine was added together. The mixture was again heated for 30 min. A solution of ethyl bromoacetate (2 ml) in tetrahydrofuran (5 ml) and activated Zn powder (20 g) were added. Heating of the solution was continued for 1 h. Acetic acid (20 ml) was added with cooling in ice then water was added. The organic phase was separated and the aqueous phase was extracted with ether. The combined organic phases were washed with dilute NH_4OH and water, dried (Na_2SO_4) and concentrated *in vacuo*. The oily residue was crystallized from ether giving colorless crystals, 9.8 g (68.0%). All of the physicochemical properties were identical with those of the authentic samples.

*11-Hydroxy-DEA-11-acetic Acid (**37**).* A solution of the ester **36** (1.0 g) in 5% KOH solution of methanol (20 ml) was heated under reflux for 2 h then poured into ice-cold dilute HCl (1.8 ml of concentrated HCl in 80 ml of ice water). The mixture was extracted with ethyl acetate. The solution was washed with water, dried (Na_2SO_4) and concentrated *in vacuo*. The crystalline residue, 0.877 g (96.4%), was washed with ether. Mp 211 °C.

*Optical Resolution of the Carboxylic Acid **37**.* A solution of the acid **37** (0.877 g) in methanol (5 ml) was added to a solution of cinchonidine (0.925 g) in methanol (10 ml). The solvent was changed to ethyl acetate. The crystals were collected by filtration and recrystallized from methanol four times to give a pure diastereomer (0.34 g): $[\alpha]_D^{25}$ −89.5°±1.7° (c 0.784, MeOH).

The salt was shaken with ethyl acetate and dilute HCl. The organic phase was separated and the aqueous phase was extracted with ethyl acetate. The combined organic phases were washed with water, dried (Na_2SO_4), and concentrated *in vacuo*. The residue was crystallized from methanol–water giving crystals (0.15 g): mp 139—140 °C, 158—159 °C (dimorphism), $[\alpha]_D^{27}$ −21.6°±0.6° (c 1.060, MeOH); IR (Nujol) 3330, 1708 cm^{-1}. Found: C, 75.83; H, 6.04%. Calcd for $C_{18}H_{16}O_3 \cdot 1/2H_2O$: C, 74.72; H, 5.92%.

*(−)-Methyl 11-Hydroxy-DEA-11-acetate [(−)-(**38**)].* A solution of the (−)-carboxylic acid (−)-**37** (0.685 g) in ether (10 ml) was added to a solution of excess diazomethane in ether. The solution was allowed to stand at 5 °C for 30 min and concentrated *in vacuo*. The crystalline residue was recrystallized from ether–hexane giving crystals (0.707 g): mp 117—118 °C; IR (Nujol) 3520, 3490, 1726, 1715 cm^{-1}; $[\alpha]_D^{24}$ +15.2°±0.5° (c 1.246, $CHCl_3$), CD $\Delta\varepsilon$ −0.175 (272.5 nm), +0.04 (270), −0.10 (267), +0.09 (262), +5.33 (232) (94.4% optical purity). Found: C, 77.82; H, 6.42%. Calcd for $C_{19}H_{18}O_3$: C, 77.53; H, 6.16%.

*(−)-11-Hydroxy-11-(2-hydroxymethyl)-DEA [(−)-(**39**)].* The (−)-ester (−)-**38** was reduced with $LiAlH_4$ by the same method reported for the reduction of the racemic ethyl ester **36**.[7] Mp 131—132 °C; $[\alpha]_D^{24}$ −21.4°±0.6° (c 1.027, MeOH), CD $\Delta\varepsilon$ −0.118 (273 nm), +0.023 (270), +0.052 (266), +6.33 (231), −7.78 (213) (94.4% optical purity).

*(−)-Monomesylate [(−)-(**40**)] of (−)-11-Hydroxy-11-(2-hydroxyethyl)-DEA.* The optically active compound (0.427 g, 95.3%) was synthesized from (−)-**39** (0.347 g) by the same procedure cited for the racemic compound.[7] The oily residue was used for the next preparation without further purification.

*(−)-Spiro[9,10-dihydro-9,10-ethanoanthracene-11,2′-oxetane] [(−)-(**41**)].* The optically active compound was also prepared by the same method cited for the racemic one. Mp 136—138 °C, $[\alpha]_D^{24}$ −67.0°±1.0° (c 1.119, $CHCl_3$), CD $\Delta\varepsilon$ +0.03 (276.5 nm), −0.16 (273), +0.087 (269.5), −0.12 (266), +0.056 (263), +2.20 (228) (94.4% optical purity).

*2,3,3a,12b-Tetrahydro-3a,8-methano-8H-dibenzo[3,4:6,7]cyclohepta[b]furan [(+)-(**42**)].* 1) The (−)-oxetane (−)-**41** (9.51 mg) was dissolved in chloroform (1 ml) containing *p*-toluenesulfonic acid (10 mg). After 3 min, $[\alpha]_D^{24}$ +145.8°±2.0°. The value did not change after 6 h.

2) The (−)-oxetane (−)-**41** (0.15 g) was dissolved in a solution of *p*-toluenesulfonic acid (0.1 g) in chloroform (10 ml). The solution was shaken for 10 min, washed with aqueous $NaHCO_3$ and water, dried (Na_2SO_4) and concentrated *in vacuo*. The oily residue (0.137 g) was distilled at 180 °C (bath temp) at 0.4 mmHg through a short path distillation apparatus. $[\alpha]_D^{24}$ +132.2°±3.6° (c 0.481, $CHCl_3$).

*(+)-10-(2-Hydroxyethyl)-DMDC [(+)-(**43**)].* A

mixture of the rearranged material (+)-**42** (63 mg, 94.4% e.e.), 30% palladium charcoal (0.4 g), a drop of 70% perchloric acid, and ethanol (4 ml) was stirred in a hydrogen atmosphere for 5 d. The catalyst was removed by filtration. The filtrate was concentrated *in vacuo*. The residue was chromatographed on florisil (5 g) in dichloromethane and crystallized from ether. Mp 131—134 °C; $[\alpha]_D^{25}$ +180.0° ±2.6° (*c* 0.845, MeOH).

*DMDC-10-Acetic Acid (**44**).* A Jones' reagent was added to a solution of the alcohol **39** (3.3 g) in acetone (50 ml) with cooling in ice until the characteristic brown color persisted. After 10 min, the mixture was diluted with water and extracted with ether. The solution was washed with water, dried (Na_2SO_4), and concentrated *in vacuo*. The oily residue was crystallized from benzene–hexane giving a powder, 2.5 g (71.7%): mp 155—156 °C; IR (Nujol) 1700 cm^{-1}. Found: C, 82.70; H, 6.21%. Calcd for $C_{18}H_{16}O_2$: C, 81.79; H, 6.10%.

*Optical Resolution of **44**.* Cinchonidine (2.60 g) was added to a solution of the carboxylic acid **44** (2.33 g) in methanol (40 ml). The mixture was warmed to a clean solution then allowed to stand at room temperature overnight. The crystals were collected by filtration and recrystallized from methanol three times to give the pure diastereomer (1.25 g): $[\alpha]_D^{24}$ −163.8°±5.6° (*c* 0.469, MeOH).

The salt was shaken with dilute HCl and ether. The organic phase was separated and the aqueous phase was extracted with ether. The combined organic phases were washed with water, dried (Na_2SO_4), and concentrated *in vacuo*. The oily residue, 0.578 g, could not be crystallized. $[\alpha]_D^{24}$ −170.0°±1.6° (*c* 1.329, MeOH).

*(−)-Methyl DMDC-10-Acetate [(−)-(**45**)].* A solution of the (−)-carboxylic acid (−)-**44** (0.157 g) in ether (3 ml) was added dropwise to a solution of excess diazomethane in ether with ice cooling. The mixture was stirred for 30 min and concentrated *in vacuo*. The residue was distilled at 200 °C (bath temperature) at 0.4 mmHg giving a viscous oil, 0.162 g (98.0%): $[\alpha]_D^{23}$ −158.4°±2.4° (*c* 0.826, $CHCl_3$); IR (film) 1738 cm^{-1}. Found: C, 81.82; H, 6.48%. Calcd for $C_{19}H_{18}O_2$: C, 81.99; H, 6.52%.

*(−)-1-(2-Hydroxyethyl)-DMDC [(−)-(**43**)].* The ester (−)-**45** (0.148 g) was reduced with $LiAlH_4$ as for (−)-**38**. The residue was distilled at 180 °C at 0.4 mmHg. The distillate (0.113 g) crystallized quickly and then was recrystallized from ether giving a powder (0.088 g): mp 133—134 °C; $[\alpha]_D^{23}$ −190.6°±3.1° (*c* 0.745, MeOH). Found: C, 86.51; H, 7.25%. Calcd for $C_{18}H_{18}O$: C, 86.36; H, 7.25%.

*Mesylate (−)-**46** of (−)-1-(β-Hydroxyethyl)-DMDC.* (−)-**43** (0.341 g) was mesylated as usual. The residue crystallized on standing and was used for the next preparation.

*(−)-10-Ethyl-DMDC [(−)-(**47**)].* A solution of the (−)-mesylate (−)-**46** (0.40 g) in dry tetrahydrofuran (5 ml) was added to a slurry of $LiAlH_4$ (0.3 g) in tetrahydrofuran (10 ml) with ice cooling. The mixture was then heated under reflux for 6 h. Excess $LiAlH_4$ was decomposed with a solution of methanol in ether then dilute HCl with ice cooling. The mixture was extracted with ether. The solution was washed with water, dried (Na_2SO_4), and concentrated *in vacuo*. The residue was chromatographed on alumina (Merck grade 2, 7 g) in hexane. The elute was recrystallized from hexane: mp 81—82 °C, $[\alpha]_D^{25}$ −187.1°±2.0° (*c* 1.150, $CHCl_3$) (0.175 g); IR (Nujol) 755 cm^{-1}; NMR ($CDCl_3$) δ 1.00 (3H, t, *J*=7.0 Hz), 1.7—2.1 (2H, m), 2.34 (1H, ddd, *J*=1, 5, 10 Hz), 2.50 (1H, dd, *J*=1, 16 Hz), 3.10 (1H, d, *J*=16 Hz), 3.92 (1H, d, *J*=5 Hz), 6.8—7.3 (8H, m). Found: C, 92.47; H, 7.70%. Calcd for $C_{18}H_{18}$: C, 92.26; H, 7.74%.

*Oxidation of (−)-10-Ethyl-DMDC [(−)-(**47**)].* A mixture of the (−)-hydrocarbon (−)-**47** (0.325 g), *N*-bromosuccinimide (0.3 g), *m*-chloroperbenzoic acid (10 mg), and dry carbon tetrachloride (10 ml) was heated under reflux for 8 h. After cooling, the mixture was filtered and the solid was washed with carbon tetrachloride. The filtrate was concentrated *in vacuo*. The residue was chromatographed on thin silica gel plate [Merck, pre-coated plate; benzene]. The fraction of the larger R_f value was recrystallized from ether giving colorless crystals (62.5 mg): $[\alpha]_D^{25}$ 0°, $[\alpha]_{365}^{25}$ 0° (*c* 0.727, $CHCl_3$): mp 173—175 °C; IR (Nujol) 810, 770, 753 cm^{-1}; NMR ($CDCl_3$) δ 1.41 (3H, d, t, *J*=7, 1 Hz), 2.31 (2H, m), 4.40 (1H, t, *J*=3 Hz), 4.63 (1H, s), 5.56 (1H, m), 6.9—7.4 (8H, m). Found: C, 92.45; H, 6.82%. Calcd for $C_{18}H_{16}$: C, 93.05; H, 6.94%. The fraction with the smaller R_f value was recrystallized from hexane and gave (−)-**48** (46.4 mg): mp 130—134 °C; $[\alpha]_D^{23}$ −111.0° ±1.7° (*c* 0.928, $CHCl_3$); IR 1687, 763 cm^{-1}; δ ($CDCl_3$) 0.95 (3H, t, *J*=7 Hz), 1.87 (1H, q, *J*=7 Hz), 2.45 (1H, q, *J*=7 Hz), 2.72 (2H, d, *J*=3 Hz), 4.17 (1H, t, *J*=3 Hz), 6.9—7.4 (7H, m), 7.8—8.0 (1H, m). Found: C, 86.87; H, 6.49%. Calcd for $C_{18}H_{16}O$: C, 87.06; H, 6.49%.

We thank Dr. Kazuo Tori for the NMR measurement, Mr. Mamoru Takasuka for the IR measurements, and Mr. Tatsuo Iwata for assistance in performing the variable-temperature CD measurement.

References

1) S. Hagishita and K. Kuriyama, *Tetrahedron*, **28**, 1435 (1972).
2) J. A. Schellman, *Acc. Chem. Res.*, **1**, 1448 (1968); R. Grinter and S. F. Mason, *Trans. Faraday Soc.*, **60**, 274 (1964); S. F. Mason and G. W. Vane, *J. Chem. Soc., B*, **1966**, 370.
3) S. Hagishita and K. Kuriyama, *Bull. Chem. Soc. Jpn.*, **44**, 617 (1971).
4) S. Hagishita and K. Kuriyama, *J. Chem. Soc., Perkin Trans. 2*, **1978**, 59.
5) S. J. Cristol, J. R. Mohrig, and D. E. Plorde, *J. Org. Chem.*, **30**, 1956 (1965).
6) S. J. Cristol, F. P. Parungo, and D. E. Plorde, *J. Am. Chem. Soc.*, **87**, 2870 (1965); S. J. Cristol and M. C. Kochansky, *J. Org. Chem.*, **40**, 2171 (1975) and references cited therein.
7) P. F. Hudrlik, A. M. Hudrlik, and C.-N. Wan, *J. Org. Chem.*, **40**, 1116 (1975).
8) H. Tatemitsu, F. Ogura, Y. Nakagawa, K. Naemura, and M. Nakazaki, *Bull. Chem. Soc. Jpn.*, **48**, 2473 (1975).
9) J. A. Schellman, *J. Chem. Phys.*, **44**, 55 (1966); G. Snatzke and P. C. Ho, *Tetrahedron*, **27**, 3645 (1971); K. Kuriyama, T. Iwata, M. Moriyama, K. Kotera, Y. Hamada, R. Mitsui, and K. Takeda, *J. Chem. Soc., B*, **1967**, 46.
10) A. Moscowitz, K. Wellman, and C. Djerassi, *J. Am. Chem. Soc.*, **85**, 3515 (1963).
11) K. Kotera, Y. Hamada, and R. Nakane, *Tetrahedron*, **24**, 759 (1968), we thank Dr. Hamada for giving us the samples.
12) H. Arakawa, *Bull. Chem. Soc. Jpn.*, **41**, 2541 (1968).
13) T. R. Govindachari, S. J. Patankar, and N. Viswanathan, *Phytochemistry*, **10**, 1603 (1971).
14) B. Bosnich, *Acc. Chem. Res.*, **2**, 266 (1969).
15) S. F. Mason, *J. Chem. Soc., Chem. Commun.*, **1973**, 239.
16) D. J. Caldwell and H. Eyring, *Ann. Rev. Chem.*, **15**, 281 (1964); A. Moscowitz, A. Rosenberg, and A .E. Hansen, *J. Am. Chem. Soc.*, **87**, 1813 (1965).

Electronic Properties and π-π^* Absorption Spectrum of 2-Pyridone

Akira FUJIMOTO, Kozo INUZUKA,* and Ryuichi SHIBA
Department of Applied Science, Faculty of Technology, Tokyo Denki University, Kanda, Chiyoda-ku, Tokyo 101
(Received April 28, 1980)

The IR and UV absorption spectra as well as the Raman spectra of monomer and dimer of 2-pyridone were studied. The molecular weight of 2-pyridone in benzene and dimethyl sulfoxide was determined in order to examine the association. 2-Pyridone in nonpolar solvents shows two types of carbonyl stretching vibration bands due to the coexistence of the monomer and dimer. The highest wavelength UV absorption of 2-pyridone in isooctane (2,2,4-trimethylpentane) is ascribed to π-π^* electronic transitions of the monomer and dimer. The dimer absorption band appears at a higher wavenumber than that of the monomer by *ca.* 830 cm^{-1}. The dimer band corresponds to the π-π^* transition from the ground ^1A_g state to the excited ^1B_u state. No π-π^* transition absorption from the ground ^1A_g state to the excited ^1A_g state could be observed because of the g-g Laporte forbiddance in the transition under an assumption of the molecular C_{2h} symmetry.

Equilibrium between the monomer and dimer of 2-pyridone, investigated by ultrasonic[1] and dipole moment[2] measurements, is attained in certain solvents. As regards the solvent effect on the absorption and fluorescence spectra of 1-methyl-2-pyridone, the π-π^* absorption spectra were found to shift toward short-wavelengths on the hydrogen-bonding formation of 1-methyl-2-pyridone with ethanol, this being attributed to the decrease of dipole moment in the excited states.[3]

We have observed the C=O stretching vibration bands and π-π^* absorption bands of 2-pyridone, the band assignment for the monomer and dimer of 2-pyridone being made from the results for 1-methyl-2-pyridone.[3]

Experimental

2-Pyridone was recrystallized several times from ethanol and sublimed *in vacuo* at *ca.* 120 °C. 1-Methyl-2-pyridone was purified in the same way as described previously.[3] Purification of benzene, dioxane, isooctane (2,2,4-trimethylpentane), chloroform, and ethanol was carried out by conventional methods.[4] Dimethyl sulfoxide (DMSO) was dried over a calcium chloride-calcium hydride mixture and distilled in a stream of nitrogen. The distilled DMSO was further dehydrated with a mixture of calcium hydride and molecular sieves 3A. The dehydrated DMSO was distilled at 56—57 °C in a nitrogen atmosphere of 667 Pa.

Measurement of IR and UV absorption spectra were carried out with the spectrophotometers reported.[3] The molecular weight of 2-pyridone was measured in benzene and DMSO solvents with a modified Shibayama freezing point depression equipment (SS-50_c-KM). The measurement was carried out six times, the concentration of 2-pyridone being in the range 10^{-3}—10^{-2} mol dm^{-3}. The errors inherent to the measurement were $\pm 0.1\%$.

Methods of Calculation and Molecular Models

The dipole moments, π-bond orders, and charge densities of 2-pyridone and 1-methyl-2-pyridone in the ground state were calculated by the CNDO/2 method using the parameter given by Pople, Santry, and Segal.[5,6] The values of the bond distance and bond angle of 2-pyridone measured by Penfold[7] were used. The data were also used for the ring framework of 1-methyl-2-pyridone. For the methyl group the following values were used:

C-N: 1.48 Å, C-H: 1.096 Å, ∠HCH: 109°28′.

The P-P-P SCF-MO-CI method[8,9] was employed for calculated molecular properties such as the π-π^* transition energies, π-π^* transition oscillator strengths, π-charge densities, and π-bond orders in the lower excited states, and π-dipole moments of the monomer of 2-pyridone in the lower excited and ground states. The following empirical parameters were used:

Atom, μ	I_μ/eV	A_μ/eV
C	11.42	0.58
-NH-	27.50	11.20
=O	17.30	2.60

The value −2.50 eV was taken for all the resonance integrals of 2-pyridone. The Mataga-Nishimoto approximation[10] was used for the calculation of two-center Coulomb integrals. All singly excited configuration interactions were taken into account for the monomer.

Results and Discussion

Electronic Properties in the Ground State. The charge densities and π-bond orders of the two compounds calculated by the CNDO/2 method are given in Fig. 1. There is little difference in the charge density distributions of 2-pyridone and 1-methyl-2-pyridone except for the charge density on each nitrogen atom. The π-bond orders of the two molecules are also similar to each other.

The calculated dipole moments of 2-pyridone and 1-methyl-2-pyridone are 4.385 and 4.305 D, respectively. The observed dipole moments[2] of the latter molecule are 4.04 D in benzene and 4.07 D in dioxane. It seems that the dipole moment of 1-methyl-2-pyridone is independent of solvent. The calculated value (4.305 D) of 1-methyl-2-pyridone is in fairly good agreement with the observed values. The calculation shows that the dipole moment of 2-pyridone is close to that of 1-methyl-2-pyridone. However, the observed dipole moment of 2-pyridone is 1.73 D in benzene and 2.94 D in dioxane,[2] showing that the dipole moment of 2-pyridone changes with solvent. A large discrepancy between the values of the calculated and observed dipole moments and the dependence of the values

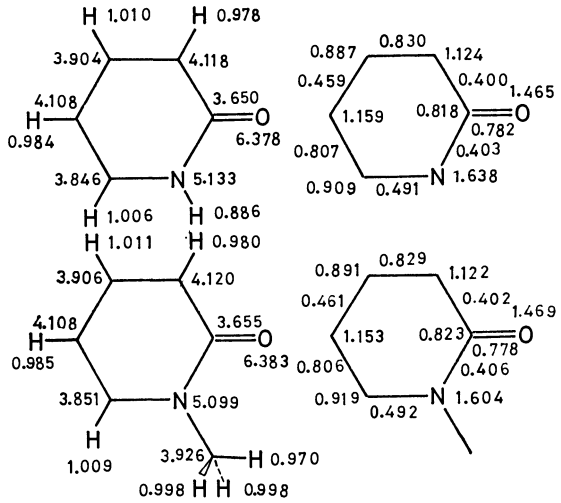

Fig. 1. Several molecular properties of 2-pyridone and 1-methyl-2-pyridone calculated by the CNDO/2 method; the total charge densities of valence electron, π-charge densities, and π-bond orders in the ground state.

of dipole moment on solvents are due to the coexistence of 2-pyridone dimer in such solutions.[1,2]

On the other hand, the IR absorption spectra of 2-pyridone and 1-methyl-2-pyridone were measured both in benzene and dioxane. The spectra in the range 1650—1700 cm^{-1} are shown in Fig. 2. 2-Pyridone shows two strong bands and 1-methyl-2-pyridone only one. The 1667 cm^{-1} IR band of 1-methyl-2-pyridone in carbon tetrachloride was assigned to the C=O stretching vibration on the basis of the band intensity and frequency-shift to the low frequency side taking place on addition of ethanol to carbon tetrachloride solution of 1-methyl-2-pyridone (Fig. 1, Ref. 3). The two bands of 2-pyridone are related to the C=O stretching vibrations of monomer and dimer as seen from their intensities and band positions. The higher-frequency band of 2-pyridone was assigned to the C=O stretching vibration of the monomer and the other to that of the dimer. The C=O stretching frequency of the monomer of 2-pyridone is thus higher than that of 1-methyl-2-pyridone. This is in line with the calculated π-bond orders of the carbonyl groups of 2-pyridone and 1-methyl-2-pyridone (Fig. 1). The IR band intensity of the monomer relative to that of the dimer increases with change of solvent from benzene to dioxane. On the assumption that the molar absorption coefficient of the C=O group of the dimer is approximately equal to that of the monomer, we conclude that the concentration of dimer is higher than that of monomer in benzene, and *vice versa* in dioxane. This is in line with the change of dipole moments observed in these solvents.[2] For the sake of comparison we have measured the bands of 2-pyridone in the range 1650—1700 cm^{-1} in isooctane and chloroform. The result in each case is similar to that of benzene (Figs. 2(1), (3), and (6)).

When the dimer of 2-pyridone belongs to the point group of the C_{2h} symmetry, its 66 normal vibrations are grouped into the following four species.

$$\Gamma = 23A_g + 10B_g + 11A_u + 22B_u$$

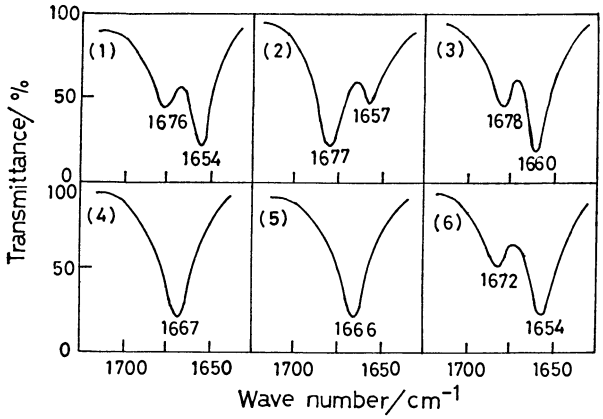

Fig. 2. The IR C=O absorption bands of 2-pyridone (1.2×10^{-2} mol dm^{-3}) and 1-methyl-2-pyridone (1.1×10^{-2} mol dm^{-3}) in various solvents:
(1) 2-Pyridone in benzene, (2) 2-pyridone in dioxane, (3) 2-pyridone in isooctane, (4) 1-methyl-2-pyridone in benzene, (5) 1-methyl-2-pyridone in dioxane, (6) 2-pyridone in chloroform. A cell of 0.5 mm path length was used.

Table 1. IR and Raman spectra of 2-pyridone

IR[a,b] (cm^{-1})	Raman[a,c] (cm^{-1})
1672 s	
1654 s	
	1625 w
1616 s	
1540 w	1539 m
1468 m	1462 m
1438 m	
1375 w	1374 m
	1256 s
1152 m	1153 w
1095 w	1096 w
	1008 w
990 m	988 w
903 w	
875 w	
840 w	841 s
	613 m
557 m	549 m
	460 w
	387 w

a) s, Strong; m, medium; w, weak. b) 4.6×10^{-2} mol dm^{-3} in chloroform, c) 1 mol dm^{-3} in chloroform.

The vibrations with species A_g and B_u belong to the in-plane vibration and the others to the out-of-plane vibration. The vibrations with species A_g and B_g are Raman-active, the others being infrared-active.

In order to ascertain whether the dimer belongs to the point group of C_{2h} or not, we measured the Raman spectrum of 2-pyridone† in chloroform. The results are given in Table 1. Both the IR band at 1654 cm^{-1} and the Raman band at 1625 cm^{-1} were assigned to the stretching vibration of the C=O groups of the dimer, the former being strong and the latter

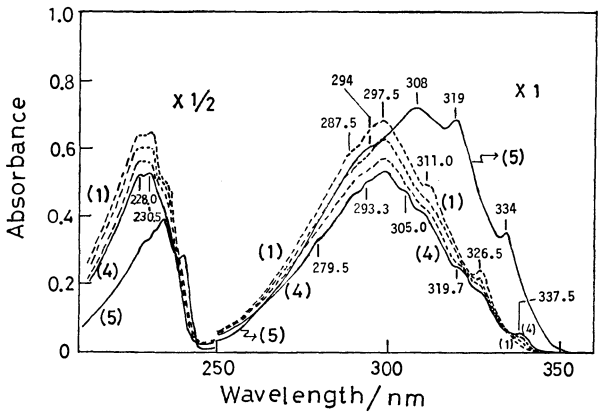

Fig. 3. The UV absorption spectra of 2-pyridone in isooctane solution with UV absorption spectrum of 1-methyl-2-pyridone in isooctane solution: (1) 1.68×10^{-3} mol dm^{-3} 2-pyridone, 1 mm cell, (2) 1.68×10^{-4} mol dm^{-3} 2-pyridone, 10 mm cell, (3) 3.36×10^{-5} mol dm^{-3} 2-pyridone, 50 mm cell, (4) 1.68×10^{-5} mol dm^{-3} 2-pyridone, 100 mm cell, (5) 1.0×10^{-4} mol dm^{-3} 1-methyl-2-pyridone, 10 mm cell.

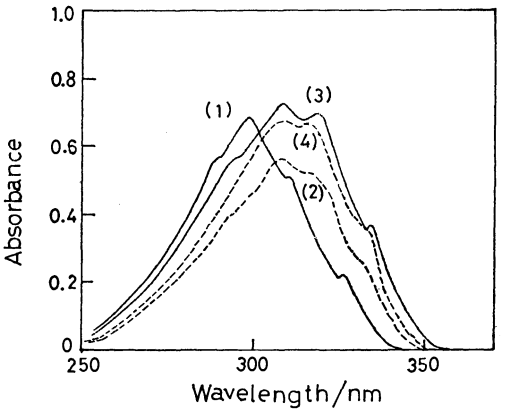

Fig. 4. The UV absorption spectra of 2-pyridone (1.6×10^{-3} mol dm^{-3}) and 1-methyl-2-pyridone (1.0×10^{-3} mol dm^{-3}): (1) 2-pyridone in isooctane, (2) 2-pyridone in DMSO, (3) 1-methyl-2-pyridone in isooctane, (4) 1-methyl-2-pyridone in DMSO. A cell of 1 mm path length was used.

weak. If the 2-pyridone dimer has the C_{2h} symmetry, the former should be assigned to the B_u species and the latter to the A_g species. No band was found in the Raman spectrum near 1672 cm^{-1} at which the carbonyl stretching band of the monomer was observed in the IR spectrum. The C=O band of the monomer might be too weak to be observed in the Raman spectrum, since the concentration of monomer is smaller than that of the dimer in chloroform. The 2-pyridone dimer seems to belong to the point group of C_{2h}. The fact that the dipole moment of 2-pyridone decreases with the change of solvent from dioxane to benzene also seems to support the interpretation that the 2-pyridone dimer belongs to the point group of C_{2h}.

π-π^* Absorption Spectrum of 2-Pyridone. The UV spectrum of 2-pyridone in isooctane in the concentration range 10^{-5}—10^{-3} mol dm^{-3} is shown in Fig. 3. In spectrum (1), the first π-π^* absorption system of 2-pyridone in the range 355—250 nm consists mainly of four vibrational bands. The first one appears at 326.5 nm, the second at 311.0 nm, the third at 297.5 nm corresponding to the band maximum, and the fourth at near 288 nm. Let us call these vibrational bands band system A. The concentration of 2-pyridone in spectrum (4) is 10^{-2} times lower than that of 2-pyridone in spectrum (1). In spectrum (4) band system A appears clearly, the other vibrational bands being observed at 337.5, 319.7, 305.0, 293.3, and 279.5 nm. Let us call these new vibrational bands band system B.

On the other hand, the first π-π^* absorption system of 1-methyl-2-pyridone shows the vibrational bands at 334, 319, 308, and 294 nm (Fig. 3(5)). The vibrational band at 308 nm is the band maximum of this system. The four bands seem to be related with the respective vibrational bands of 2-pyridone in isooctane, *i.e.*, the bands at 337.5, 319.7, 305.0, and 293.3 nm. The absorption spectra of 2-pyridone and 1-methyl-2-pyridone may be expected to be similar in their spectral features, since the π-charge densities and π-bond orders of 2-pyridone and 1-methyl-2-pyridone calculated by the CNDO/2 method are approximately equal to each other (Fig. 1). Good correspondence is seen between band system B of 2-pyridone and the vibrational bands of the first π-π^* absorption of 1-methyl-2-pyridone (Fig. 3).

In order to confirm which of the two molecular species of 2-pyridone is responsible for the appearance of band system B, we measured the absorption spectra of 2-pyridone and 1-methyl-2-pyridone in DMSO (Fig. 4). Each vibrational band position/intensity of 1-methyl-2-pyridone in isooctane solution is close to that in DMSO solution. The vibrational band features of 2-pyridone in DMSO are close to those of band system B (spectrum (4), Fig. 3). For the sake of comparison the molecular weight of 2-pyridone was determined by means of freezing point depression, benzene and DMSO being used as solvent. The observed values in benzene and DMSO are 217.1 and 96.3, respectively. The former is 2.28 times greater than the calculated molecular weight 95.1 and the latter almost equal to it, suggesting that 2-pyridone exists mainly as a dimer in the benzene soild solution although some associated complexes larger than a dimer may be formed, while 2-pyridone exists mainly as a monomer in the DMSO solid solution. The UV spectrum of 2-pyridone in DMSO is related to the monomer species of 2-pyridone. Band system B may be due to the monomer species, since its vibrational band position is close to that of 2-pyridone in DMSO (spectrum (4), Fig. 3). Band system A may thus be ascribed to the dimer species (Fig. 3). The band at 305.0 nm seems to be the maximum of the monomer band (Fig. 4). The energy difference of the maxima of the monomer and dimer

† The measurement, made at the laboratory of Prof. M. Ito, Tohoku University, was carried out in chloroform since the solubility of 2-pyridone in carbon tetrachloride is low.

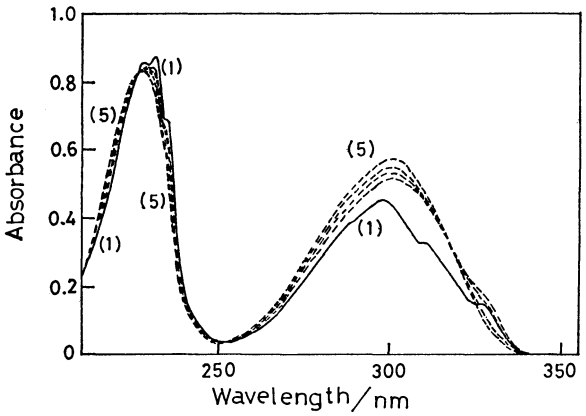

Fig. 5. The UV absorption spectra of 2-pyridone in isooctane-ethanol mixed solvents at room temperature.
Concentration of 2-pyridone: 2.19×10^{-4} mol dm^{-3}.
Concentrations of ethanol (mol dm^{-3}): (1) 0, (2) 7.0×10^{-2}, (3) 1.5×10^{-1}, (4) 5.0×10^{-1}, (5) 2.0.

absorptions is *ca.* 830 cm^{-1}.

The second π-π^* absorption system of 2-pyridone appears near 230 nm (Fig. 3). The concentration effect on the system is not so clear as the first one. As shown in spectrum (4) of Fig. 3, the band maximum of the second system apparently splits into two (228.0 and 230.5 nm), although a similar splitting is also observed in spectrum (1). The splitting energy is *ca.* 480 cm^{-1}.

The UV spectrum of 2-pyridone changes with a change in the concentration of ethanol (Fig. 5). The band maximum of the first π-π^* absorption system shifts toward longer-wavelengths with increase in the amount of ethanol, the second π-π^* absorption system, *e.g.*, the peak at 228.0 nm, shifting toward shorter-wavelengths accompanied by intensity decrease. When ethanol is added to an isooctane solution of 2-pyridone, the shift direction of the first band is opposite that of the first band of 1-methyl-2-pyridone.[3]

The π-π^* transition of the monomer is related to the excited state of A′ symmetry under the point group of the symmetry C_s, and that of dimer to the excited states of the A_g and B_u symmetries under the point group of the C_{2h} symmetry. Transition from the ground to the excited A_g state of the dimer is symmetry-forbidden, whereas transition to the excited B_u state is allowed by the dipole selection rule. Dimer formation gives rise to the paired excited states essentially based on the monomer electronic state. One of the states is lower in energy than the original monomer state and the other is higher if there is no remarkable difference between the solvent effects on the two molecular species. We have tentatively assigned the vibrational band at 337.5 nm to the 0-0 band of the first π-π^* absorption band of the 2-pyridone monomer, since the vibrational band at 337.5 nm is a member of system B which appears in DMSO solution. 2-Pyridone exists in DMSO almost as a monomer. The observed band maximum of the 2-pyridone dimer at 297.5 nm seems to correspond to the second π-π^* absorption band of the dimer with

Table 2. Calculated transition energies (E), oscillator strength (f), and π-dipole moments (μ) of the singlet π,π^* excited states of 2-pyridone monomer with π-dipole moment in the ground state

State	E/eV	λ/nm	f	μ/D	λ_{obsd}/nm
G	0	0	0	4.680	
1	4.022	308	0.257	2.502	305.0
2	5.356	231	0.334	2.492	
3	6.590	188	0.194	2.966	
4	6.703	185	0.664	4.905	

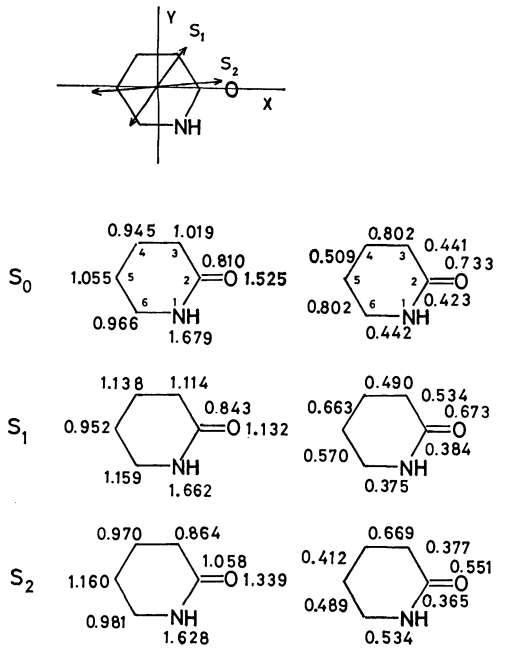

Fig. 6. The calculated π-charge densities and π-bond orders of 2-pyridone in S_0, S_1, and S_2. These calculations are based on the P-P-P SCF-MO-CI method. The uppermost drawing of this figure denotes the direction and the magnitude of the predicted dipole moments.

the B_u symmetry which is produced by the splitting of the monomer states on the formation of the dimer. The first π-π^* absorption band of the dimer would thus correspond to the electronic transition to the ^1A_g state. However, it might be difficult to observe the first π-π^* absorption band of the dimer due to the symmetry-forbidden band by a dipole selection rule. It is hard to decide which of the peaks at 230.5 and 228.0 nm in the second absorption band belongs to the vibrational band of the dimer; one belongs to the peak of the monomer band and the other to that of the dimer as judged by the experimental results.

The transition energies, oscillator strengths and π-dipole moments in the excited states calculated by the P-P-P SCF-MO-CI method for the monomer of 2-pyridone are given in Table 2. The π-dipole moment of the monomer is larger in the ground state than in the excited states except for the fourth-excited state. The calculated results suggest that the first

and second π-π^* absorption bands of the 2-pyridone monomer might move toward the shorter-wavelength side on the hydrogen-bonding formation with ethanol. This might be reasonable from the solvent effect on the absorption and fluorescence spectra of 1-methyl-2-pyridone.[3] However, the first absorption band maximum of the 2-pyridone–ethanol system shifts to the longer-wavelength side (Fig. 5). This is opposite the shift of the first absorption band of the 1-methyl-2-pyridone–ethanol system, the band maximum of the 2-pyridone–ethanol complex being located at a longer-wavelength than that of the 2-pyridone dimer, and the former at a shorter-wavelength side than the band maximum of the monomer. Addition of ethanol to the isooctane solution of 2-pyridone disturbs the equilibrium between the monomer and dimer of 2-pyridone. The hydrogen-bonded monomer of 2-pyridone with ethanol may increase and the dimer may decrease in concentration with an increase of ethanol. Thus, the band maximum of 2-pyridone moves to the longer-wavelength side, but the shift of the band maximum depends on the concentration of the dimer, monomer, and monomer–ethanol complex.

The directions of transition moment for the first and second excited states, π-charge densities, and π-bond orders calculated by the P-P-P. SCF-MO-CI method for the ground and excited states of the 2-pyridone monomer are shown in Fig. 6. There is a large difference in the π-bond order and π-charge density of the ground and first excited states. The calculated π-bond orders suggest that there is a large change in bond length between the ground and first-excited states, which is similar to the result for polyenals. A large deformation of the ring framework between the ground and first excited states may give rise to the band broadening of 2-pyridone (Fig. 3) as shown in polyenal[11] and fulvene spectra.[12]

The photochemical dimerization property[13] of 2-pyridone in the first-excited state can be attributed to an increase in π-charge density at the C_3 and C_6 atoms and in π-bond order between the C_4 and C_5 atoms.

The authors are grateful to Prof. M. Ito, Tohoku University, for his cooperation in the measurement of the Raman spectrum of 2-pyridone and for his valuable suggestions. The work was supported by grants from the Tokyo Denki University Research Fund. One of the authors (K. I) acknowledges the assistance of the staff of Tokyo Denki University Computing Center.

References

1) G. G. Hammes and A. C. Park, *J. Am. Chem. Soc.*, **91**, 956 (1969).
2) M. H. Krackov, C. M. Lee, and H. G. Mautner, *J. Am. Chem. Soc.*, **87**, 892 (1965).
3) A. Fujimoto and K. Inuzuka, *Bull. Chem. Soc. Jpn.*, **52**, 1816 (1979).
4) J. A. Riddick and E. E. Toops, "Organic Solvents, Physical Properties and Methods of Purification," Interscience Publishers, Inc., New York (1955).
5) J. A. Pople, D. P. Santry, and G. A. Segal, *J. Chem. Phys.*, **43**, 129 (1965).
6) J. A. Pople and G. A. Segal, *J. Chem. Phys.*, **43**, 136 (1965); **44**, 3289 (1966).
7) B. R. Penfold, *Acta Crystallogr.*, **6**, 591 (1953).
8) R. Pariser and R. G. Parr, *J. Chem. Phys.*, **21**, 466, 767 (1953).
9) J. A. Pople, *Trans. Faraday Soc.*, **49**, 1375 (1953).
10) N. Mataga and K. Nishimoto, *Z. Phys. Chem.*, **13**, 140 (1957).
11) E. R. Blout and M. Fields, *J. Am. Chem. Soc.*, **70**, 189 (1948).
12) Kekulé Symposium, "Theoretical Organic Chemistry," Butterworths Scientific Publications, London (1959), p. 35.
13) E. C. Taylor, R. O. Kan, and W. W. Paudler, *J. Am. Chem. Soc.*, **83**, 4484 (1961).

The Correlation between the Electron-capture Detector Response and the Chemical Structure for Polychlorinated Biphenyls†

Yukikazu HATTORI,* Yoshio KUGE, and Masao NAKAMOTO
Environmental Pollution Control Center of Osaka Prefecture,
1-3-62, Nakamichi, Higashinari-ku, Osaka, Osaka 537
(Received November 12, 1980)

The relative sensitivities of an electron-capture detector for various polychlorinated biphenyls were measured at different temperatures. Generally, the sensitivities of these compounds become larger as the number of the chloro substituent increases. The temperature dependence of the electron-capture coefficients(K) for these compounds was also determined. These results show that the electron-capture reactions of polychlorinated biphenyls containing less than four chlorine atoms proceed dissociatively, while for four chlorine atoms the reactions proceed either dissociatively or non-dissociatively. For more than five chlorine atoms, the reactions almost always proceed non-dissociatively.

The electron-capture detector (ECD) which exhibits a highly sensitive response to various organic compounds containing halogen, oxygen, and sulfur atoms is used for the analyses of environmental pollutants. Many reports about ECD sensitivities for various compounds have been published,[1-4] but the temperature dependence of the sensitivity has not been considered in these studies.

Wentworth *et al.*[5-7] and Kojima *et al.*[8-11] studied the electron-capture phenomena by using the pulse-sampling technique. From the temperature dependence of the electron-capture coefficient (K) for various compounds, the activation energies and electron affinities were calculated. The present authors[12-15] have also previously studied the ECD sensitivities and the temperature dependence for various environmental pollutants using the D.C. mode.

In this work, the ECD sensitivities and the temperature dependence for various polychlorinated biphenyl (PCB) isomers were determined. The correlation between the ECD response and the chemical structure for these compounds was also studied.

Experimental

Apparatus and Materials. A Varian aerograph, 2100-type gas chromatograph with an ECD (^{63}Ni, 8.5 mCi) was used in this experiment. The applied voltage was supplied using the D.C. mode. A glass column (2 mmϕ × 1.8 m) was packed with Gaschrom Q (100—120 mesh) coated with 2% Silicone OV-1. The extra pure nitrogen gas (Teikoku Sanso Co., Ltd.) used as a carrier gas was purified by passing it through two tubes (20 cm) packed with Molecular Sieve 5A and an Oxy-trap tube (Alltech Associate Co., Ltd., 4002 type); the flow rate was 30 cm^3/min. The injector temperature was kept at 200 °C. The column temperature was set at 150 °C (1—3 chlorinated biphenyls) and at 180 °C (4—6 chlorinated biphenyls). The detector temperature was varied from 210 °C to 340 °C.

The PCB isomers (Analytical Standard, Analab Co., Ltd.), hexachlorobenzene (HCB) (special grade from Wako Pure Chemical Co., Ltd.) and pentachlorobenzene (PTCB) (guranteed grade from Tokyo Chemical Co., Ltd.) were used without further purification. All the substances were used as hexane (pesticide analytical grade from Wako Pure Chemical Co., Ltd.) solutions and were checked by gas chromatography.

Procedure. The relative sensitivity (*R.S.*) was calculated from the relative peak area per mole of the compound, using HCB as a standard. The relative retention time (*R.R.T.*) was obtained at a column temperature of 150 or 180 °C by using HCB as a standard. The sample size was chosen so as to keep the peak area within a linear range on the calibration curve. The K values, the electron affinities (EA'), and the *R.S.* values were calculated by the method reported in a previous paper.[12] The temperature dependence of the K values was shown by plotting the logarithm values of K or $KT^{3/2}$ against $1/T$, where T was the absolute temperature of the detector cell, which had been predetermined by inserting a Fe-Constantan thermocouple into a vacant ECD cell.

Results and Discussion

Relative Sensitivities of ECD and Relative Retention Times for PCBs. For various PCBs containing 1—6 chlorine atoms, the *R.S.*s of ECD at the detector temperatures of 230 °C, 290 °C and 320 °C and the *R.R.T.*s are tabulated in Table 1. The *R.S.*s of PCBs ordinarily become larger as the number of chloro substituents increases. These results agreed with the reports by Zitko *et al.*[16] and Gregory *et al.*[17] The *R.S.* of PCBs containing the same number of chlorine atoms are not equal, but they depend upon the position of the chlorine substituents. The *R.S.*s of monochlorinated biphenyls (Cl-PCB) were in the order of: 2-chlorobiphenyl>4-chlorobiphenyl>3-chlorobiphenyl; the *R.S.* of 3-chlorobiphenyl was especially small. The *R.S.*s of dichlorinated biphenyls (2Cl-PCB) were in the order of: 4,4′-dichlorobiphenyl> 3,3′-dichlorobiphenyl > 2,2′-dichlorobiphenyl. These orders of the *R.S.*s for mono- and dichlorobiphenyls are in accordance with the report by Gregory *et al.*[17] The *R.S.*s of tri- and tetrachlorobiphenyl were increased by one order of magnitude over those of dichlorobiphenyls. Among the pentachlorobiphenyls, the ECD sensitivity of 2,3,4,5,6-pentachlorobiphenyl was the highest. This compound has five chloro substituents and one phenyl substituent on a benzene ring. The *R.S.* of the compound was on the same level as that of pentachlorobenzene. The *R.S.* value of 2,2′3,5′6-pentachlorobiphenyl, which has three chloro substituents on the 2- or 6- position, was the

† This report constitutes part IV of "The Correlation between Electron-capture Detector Response and the Chemical Structure."

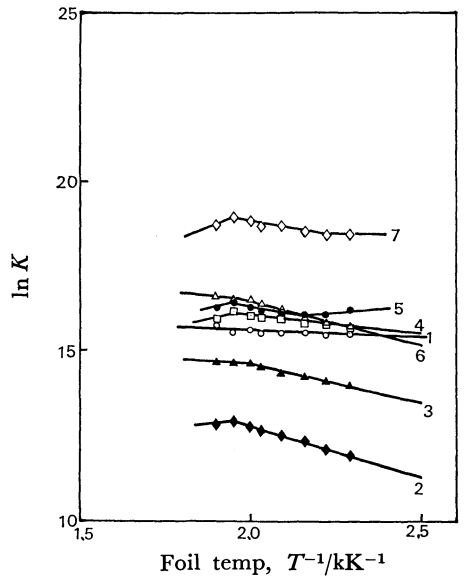

Fig. 1. Temperature dependence of K values measured at a column temperature of 150 °C.
1; 2-Chlorobiphenyl, 2; 3-chlorobiphenyl, 3; 4-chlorobiphnyl, 4; 2,2′-dichlorobiphenyl, 5; 3,3′-dichlorobiphenyl, 6; 4,4′-dichlorobiphenyl, 7; 2,3′,5-trichlorobiphenyl.

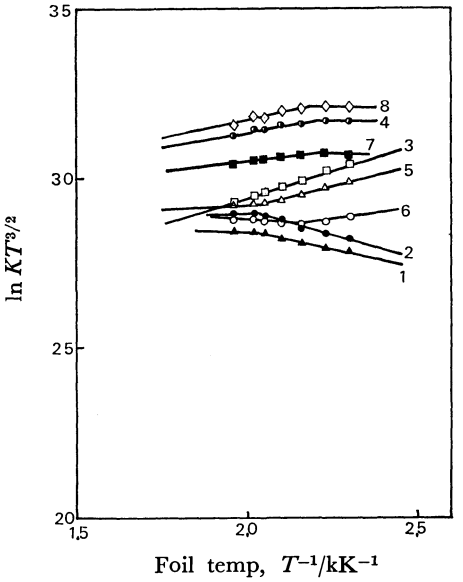

Fig. 2(a). Temperature dependence of K values measured at a column temperature of 180 °C.
1; 2,2′,4,5′-tetrachlorobiphenyl, 2; 2,2′,3,3′-tetrachlorobiphenyl, 3; 2,3′,4′,5-tetrachlorobiphenyl, 4; 2,3,4,5,6-pentachlorobiphenyl, 5; 2,2′,3′,4,5-pentachlorobiphenyl, 6; 2,2′,3,5′,6-pentachlorobiphenyl, 7; 2,2′,3,4,4′,5′-hexachlorobiphenyl, 8; hexachlorobenzene.

smallest.

As the number of chloro substituents increases, the *R.R.T.* value of PCB become larger, much as with the *R.S.* values of PCB. As to the PCB containing the same number of chlorine atoms, when the compound has fewer chlorine atoms on the 2- or 6- position, the value of *R.R.T.* is larger than those of the other compounds.

The Temperature Dependence of the ECD Response for PCBs. The temperature dependence of the K values of PCBs was examined in order to obtain some information about the electron-capture reactions of PCBs. Figures 1, 2(a), and 2(b) show the temperature dependence of the K values of the PCB isomers. The values of electron affinities (EA') and/or the activation energies (E^*) were calculated; they are tabulated in Table 2. The K values of the PCBs which contain fewer chloro substituents, such as mono-, di-, and trichlorinated biphenyls, become larger as the detector temperature increases. Therefore, the reaction of these PCBs appears proceeds dissociatively. The E^* values of Cl–PCBs were in the order of: 3-chlorobiphenyl>4-chlorobiphenyl>2-chlorobiphenyl. This order seems to be consistent with the degree of difficulty in eliminating chloro substituents. On the other hand, the *R.S.*s of Cl–PCB were in the order of: 2-chlorobiphenyl>4-chlorobiphenyl>3-chlorobiphenyl; this order agrees with that of the ease of eliminating chloro substituents. However, the order of the E^* values of 2Cl-PCBs was 4,4′-dichlorobiphenyl>3,3′-dichlorobiphenyl>2,2′-dichlorobiphenyl, the same as that of the *R.S.*s.

The temperature dependence of the K values of tetra-, penta-, and hexachlorinated biphenyl are shown in Figs. 2(a) and (b). The K values of 2,2′,3,3′-, 2,2′,4,5′-, and 2,2′,3,5′-tetrachlorobiphenyl become

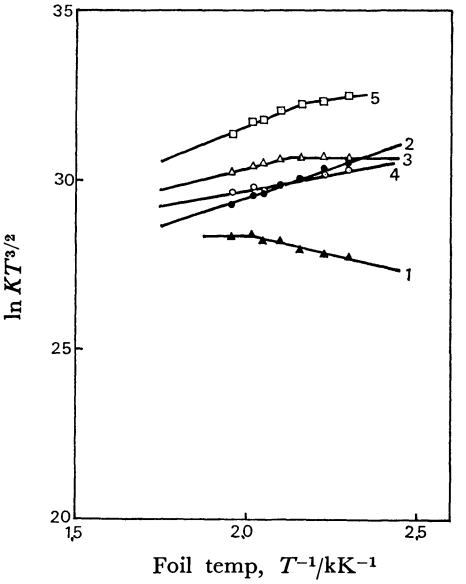

Fig. 2(b). Temperature dependence of K values measured at a column temperature of 180 °C.
1; 2,2′,3,5′-tetrachlorobiphenyl, 2; 2,2′,4,5,5′-pentachlorobiphenyl, 3; 2,2′,3,3′,4,4′-hexachlorobiphenyl, 4; 2,2′,3,4,5′-pentachlorobiphenyl, 5; pentachlorobenzene.

larger as the detector temperature increases; therefore, the EC reactions of these tetrachlorinated biphenyls seem to proceed dissociatively. On the contrary, the K value of 2,3′,4′,5-tetrachlorobiphenyl become smaller as the detector temperature increases, so the EC reaction of this PCB isomer seems to proceed non-dissociatively. From Fig. 1, the EC reaction of 2,3′,5-trichlorobiphenyl seems to proceed dissociatively. The

Table 1. Relative sensitivities for relative retention times of polychlorinated biphenyls

Compound	Relative sens (320 °C)	Relative sens (290 °C)	Relative sens (230 °C)	Relative retention time
2-Chlorobiphenyl[a)]	1.00×10^{-3}	1.30×10^{-3}	9.47×10^{-4}	0.42
3-Chlorobiphenyl[a)]	1.03×10^{-4}	7.78×10^{-5}	3.44×10^{-5}	0.55
4-Chlorobiphenyl[a)]	5.31×10^{-4}	4.73×10^{-4}	2.49×10^{-4}	0.57
2,2′-Dichlorobiphenyl[a)]	2.43×10^{-3}	2.02×10^{-3}	1.25×10^{-3}	0.67
3,3′-Dichlorobiphenyl[a)]	3.22×10^{-3}	2.52×10^{-3}	1.75×10^{-3}	1.22
4,4′-Dichlorobiphenyl[a)]	3.68×10^{-3}	3.02×10^{-3}	1.41×10^{-3}	1.32
2,3′,5-Trichlorobiphenyl[a)]	4.16×10^{-2}	3.24×10^{-2}	1.46×10^{-2}	1.77
2,2′,3,3′-Trichlorobiphenyl[b)]	7.50×10^{-2}	5.47×10^{-2}	2.42×10^{-2}	2.70
2,2′,3,5′-Tetrachlorobiphenyl[b)]	4.21×10^{-2}	2.91×10^{-2}	1.44×10^{-2}	2.37
2,2′,4,5′-Tetrachlorobiphenyl[b)]	4.59×10^{-2}	3.46×10^{-2}	1.57×10^{-2}	2.15
2,3′,4′,5-Tetrachlorobiphenyl[b)]	1.03×10^{-1}	1.03×10^{-1}	1.36×10^{-1}	3.13
2,2′,3,5′,6-Pentachlorobiphenyl[b)]	6.53×10^{-2}	4.86×10^{-2}	3.39×10^{-2}	3.23
2,2′,3′,4,5-Pentachlorobiphenyl[b)]	1.03×10^{-1}	8.71×10^{-2}	8.95×10^{-2}	4.41
2,3,4,5,6-Pentachlorobiphenyl[b)]	7.64×10^{-1}	7.05×10^{-1}	6.50×10^{-1}	4.57
2,2′,3,4,5′-Pentachlorobiphenyl[b)]	1.52×10^{-1}	1.24×10^{-1}	1.30×10^{-1}	4.54
2,2′,3,3′,4,4′-Hexachlorobiphenyl[b)]	2.85×10^{-1}	2.74×10^{-1}	2.40×10^{-1}	9.93
2,2′,3,4,4′,5′-Hexachlorobiphenyl[b)]	3.10×10^{-1}	2.91×10^{-1}	2.52×10^{-1}	8.43
Pentachlorobenzene[b)]	7.69×10^{-1}	9.14×10^{-1}	1.16	7.29
Hexachlorobenzene[a),b)]	1.00	1.00	1.00	1.00

a) The values of the relative sens. and the relative retention time for the compounds marked a) were measured at a column temperature of 150 °C. b) The values of the relative sens. and the relative retention time for the compounds marked b) were measured at a column temperature of 180 °C.

Table 2. Apparent electron affinities (EA') and activation energies (E^*) for polychlorinated biphenyls

Compound	E^* / kJ mol^{-1}	EA' / kJ mol^{-1}
2-Chlorobiphenyl	3.9 (526—436)	
3-Chlorobiphenyl	25.2 (512—436)	
4-Chlorobiphenyl	16.0 (496—436)	
2,2′-Dichlorobiphenyl	10.2 (512—436)	
3,3′-Dichlorobiphenyl	14.1 (512—464)	
4,4′-Dichlorobiphenyl	21.4 (512—436)	
2,3′,5-Trichlorobiphenyl	12.2 (499—450)	
2,2′,3,3′-Tetrachlorobiphenyl	17.9 (496—435)	
2,2′,3,5′-Tetrachlorobiphenyl	13.7 (510—435)	
2,2′,4,5′-Tetrachlorobiphenyl	12.4 (496—435)	
2,3′,4′,5-Tetrachlorobiphenyl		27.1 (510—435)
2,2′,3,5′,6-Pentachlorobiphenyl	1.7 (510—463)	16.6 (463—435)
2,2′,3′4,5-Pentachlorobiphenyl	6.5 (510—489)	
	22.6 (489—435)	
2,2′,4,5,5′-Pentachlorobiphenyl		31.5 (510—435)
2,3,4,5,6-Pentachlorobiphenyl		12.2 (510—436)
2,2′,3,4,5′-Pentachlorobiphenyl		15.7 (510—435)
2,2′,3,3′,4,4′-Hexachlorobiphenyl		17.5 (510—476)
2,2′,3,4,4′,5′-Hexachlorobiphenyl		8.2 (510—449)
Pentachlorobenzene		30.5 (510—463)
Hexachlorobenzene		13.0 (510—463)

The values of E^* and EA' for the compounds were determined at the ranges of detector temperatures(K) which are shown in parentheses.

EC reaction of 2,2′,3,5′-tetrachlorobiphenyl(2,2′3′,5-tetrachlorobiphenyl), with one more chloro substituent added on the 2′-position to 2,3′,5-trichlorobiphenyl, is of the dissociative-reaction type, but 2,3′,4′,5-tetrachlorobiphenyl, with one more chloro substituent added on the 4′-position to 2,3′,5-trichlorobiphenyl, is of the non-dissociative-reaction type.

These phenomena can be explained in the following way. The latter compound is able to form a stable negative ion by catching an electron, and so the EC reaction proceeds non-dissociatively, but it is difficult for the former compound, containing more chloro substituents on the 2- or 2′-position, to form a stable negative molecular ion because of steric hindrance. The EC reactions of penta- and hexachlorinated biphenyls seem to proceed non-dissociatively. These are of the same reaction type as the PTCB, HCB, and BHC isomers which contain five six chloro substituents. These compounds seems to be able to form stable negative ions by catching electrons.

Karasek[18] studied the EC reaction of PCB compounds by means of plasma chromatography. He reported that the peaks corresponding to PCB-ion complexes appeared in negative plasmagrams for tetra- to decachlorobiphenyl compounds. On the other hand, as to mono- and dichlorobiphenyl compounds, no peak corresponding to the negative PCB-ion complex was observed in negative plasmagram; only positive-ion peaks corresponding to the PCB molecule with an added water molecule introduced into the carrier gas were observed. These phenomena are considered to show that these higher-chlorinated biphenyl compounds form stable negative ions, while lower-chlorinated biphenyl compounds do not. This supports our experimental results. Therefore, it is considered that the EC reactions of lower-chlorinated biphenyls proceed dissociatively, while those of higher-chlorinated biphenyls proceed non-dissociatively.

References

1) J. E. Lovelock, "Gas Chromatography," ed by N. Brenner, Academic Press, New York and London (1962), p. 219.
2) W. L. Zielinski, Jr., and L. Fishbein, *J. Chromatogr.*, **28**, 293 (1967).
3) W. L. Zielinski, Jr., L. Fishbein, and R. O. Thomas, *J. Chromatogr.*, **30**, 77 (1967).
4) W. L. Zielinski, Jr., L. Fishbein, and L. Martin, Jr., *J. Gas Chromatogr.*, **5**, 552 (1967).
5) W. E. Wentworth, E. Chen, and J. E. Lovelock, *J. Phys. Chem.*, **70**, 445 (1966).
6) W. E. Wentworth and E. Chen, *J. Gaschromatogr.*, **5**, 170 (1967).
7) W. E. Wentworth, L. W. Kao, and R. S. Becker, *J. Phys. Chem.*, **79**, 1161 (1975).
8) M. Satouchi and T. Kojima, *Anal. Lett.*, **5**, 931 (1972).
9) T. Kojima and M. Satouchi, *Bunsekikagaku*, **22**, 1428 (1973).
10) M. Satouchi and T. Kojima, *Bunsekikagaku*, **25**, 764 (1976).
11) T. Kojima, Y. Tanaka, and M. Satouchi, *Anal. Chem.*, **48**, 1760 (1976).
12) Y. Hattori, Y. Kuge, and S. Nakagawa, *Bull. Chem. Soc. Jpn.*, **51**, 2249 (1978).
13) Y. Hattori, Y. Kuge, and S. Asada, *Nippon Kagaku Kaishi*, **1978**, 1102.
14) Y. Kuge, Y. Hattori, A. Asada, and S. Yamada, *Chem. Lett.*, **1979**, 208.
15) Y. Hattori, Y. Kuge, and S. Asada, *Bull. Chem. Soc. Jpn.*, **53**, 1435 (1980).
16) V. Zitko, O. Hutzinger, and S. Safe, *Bull. Environ. Contam. Toxicol.*, **6**, 160 (1971).
17) N. L. Gregory, *J. Chem. Soc., B*, **1968**, 295.
18) F. W. Karasek, *Anal. Chem.*, **43**, 1982 (1971).

NOTES

Bull. Chem. Soc. Jpn., 54, 2811—2812 (1981)

Molecular Deformation Caused by Hydrogen Bonding. 1,3-Dimethylurea

Kunio FUKUSHIMA* and Takeshi KAWAI

Department of Chemistry, Faculty of Science, Shizuoka University, 836 Oya, Shizuoka 422

(Received October 16, 1980)

Synopsis. Raman spectra of 1,3-dimethylurea were measured for the crystalline state, acetone (proton acceptor) solution and water and methanol (proton donors) solutions. Remarkable differences were observed among the spectra of the aqueous solution and those of the acetone solution and the crystal. The difference is interpreted as due to the molecular deformation caused by hydrogen bonding.

Urea dissolves almost freely into water to form a solution similar to an ideal solution.[1] It is expected that the interaction of urea molecule with water molecules in an aqueous solution is strong enough to cause deformation of some parts of molecules associated with a change of the valence state of nitrogen atom (sp^2 state→sp^3 type state) by hydrogen bonding to the atom. This deformation in aqueous solutions, if it exists, may be found most effectively by Raman spectroscopy. A recent unpublished study of Raman spectra of urea in aqueous solutions by one of the present authors suggested the presence of the deformation, but the experimental results were not clear enough to be certain about it. In the present study, a related molecule, 1,3-dimethylurea, which is expected to show considerable frequency changes of its skeletal deformation vibrations associated with molecular deformation, was examined by Raman spectroscopy.

Experimental

Commercial 1,3-dimethylurea (grade EP, wako Chemicals Co., Ltd.) was used for preparation of the sample solutions: aqueous solution (x=0.065); acetone solution (x=0.096); methanol solution (x=0.176); water-heavy water solution (x=0.151, x_{D_2O}=0.412, x_{H_2O}=0.437), heavy water solution of 1,3-dimethylurea-d_2 (x=0.113), where x denotes mol fraction of 1,3-dimethylurea or 1,3-dimethylurea-d_2. The heavy water was purchased from Merck Co., Ltd. (99.75%). Raman spectra were recorded on a Model 800T Raman Spectrophotometer (Japan Spectroscopic Co., Ltd.) using the excitation line of 514.5 nm (300 mW) of a Spectra Physics argon ion laser (model 165). Spectra of solutions were obtained by use of 0.3 ml Raman cells, while those of the crystal were obtained with a sample disc. The spectra were obtained under four time accumulations and with the resolution of 5 cm^{-1}.

Results and Discussion

In the following discussion, refer to Table 1 and Fig. 1. Observed Raman bands of crystalline 1,3-dimethylurea are consistent with previous works.[2-4] These bands persist in the spectrum of the compound in acetone (proton acceptor), while a new band having lower intensity appears at 875 cm^{-1}. Since the Raman bands of the crystal of 1,3-dimethylurea in the region below 1000 cm^{-1} are due to skeletal vibrations,[3] the presence of the band at 875 cm^{-1} suggests

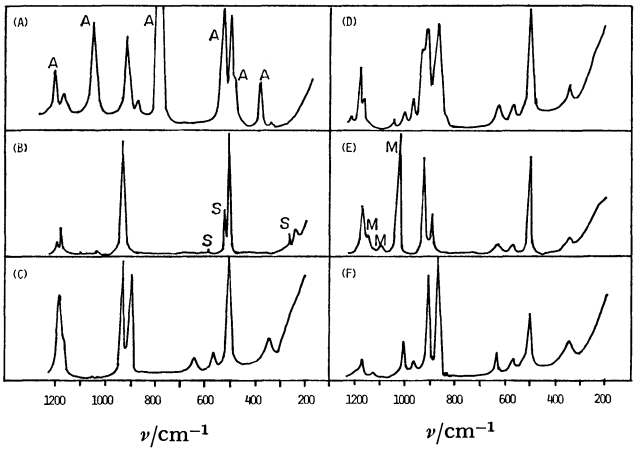

Fig. 1. Raman spectra ($I_{//}$) of 1,3-dimethylurea and 1,3-dimethylurea-d_2.
(A) Acetone solution, A: acetone band, (B) crystal, s: spontaneous emission line, (C) aqueous solution, (D) water–heavy water solution, (E) methanol solution, M: methanol band, (F) 1,3-dimethylurea-d_2 in heavy water.

that another species, having a molecular skeleton different from that in the crystal, is generated in the solution. However, the abundance of the species is very low, because the relative intensity of the band is very weak. For the aqueous solution, a very intense band at 891 cm^{-1} and three other bands at 353 cm^{-1}, 573 cm^{-1}, and 643 cm^{-1} appear, and the same is the case for the methanol solution. Moreover, it was confirmed that the relative intensities of the four bands increase as the mol fraction of water or methanol (proton donor) in the solutions increases. Considering the remarkable spectrum change associated with solution, these four bands may be due to molecules deformed by being hydrogen bonded or due to the skeletal vibrations of non-deformed molecules, which include NH deformation modes and, therefore, are expected to change their frequencies considerably by hydrogen bond formation. The latter explanation is not reasonable, because the spectra of 1,3-dimethylurea in water–heavy water solution show that the frequencies of these four bands do not change much by N-deuteration. The band at 891 cm^{-1} forms a pair with the band of the crystal at 932 cm^{-1}, which is assigned to a coupled vibration of the CH_3–N stretching mode and the CH_3 rocking mode.[3] The band at 643 cm^{-1} and 573 cm^{-1} exist in the spectra of aqueous solutions instead of the band of the crystal at 510 cm^{-1}, which is assigned to a skeletal deformation vibration of the CH_3–NH–CO–N skeleton.[3] The band at 353 cm^{-1} forms a pair with the band of the crystal at 244 cm^{-1}, which is assigned to a skel-

Table 1. Observed shift frequencies of raman bands of 1,3-dimethylurea and 1,3-dimethylurea-d_2 (in cm^{-1})

Crystal		Aq soln			Acetone soln			Methanol soln			H_2O-D_2O soln			1,3-dmu-d_2 in D_2O		
ν	I	ν	I	ρ	ν	I	ρ	ν	I	ρ	ν	I	ρ	ν	I	ρ
244	6	?	sh	?	?	sh	?	?	sh	?	?	sh	?			
		353	15	0.16	343	6	0.50	348	9	0.20	350	16	0.32	350	8	0.15
510	100	510	100	0.14	506	100	0.31	506	100	0.14	504	100	0.18	503	51	0.13
		573	12	0.29				572	5	0	572	13	0.30	570	7	0.30
		643	11	0.15				640	6	0	635	17	0.17	635	17	0.14
											840	sh	?	840	3	?
		891	86	0.04	875	20	0.31	890	42	0.42	870	85	0.06	870	100	0.04
932	93	930	99	0.05	924	76	0.07	926	95	0.04	915	82	0.06	910	83	0.04
											925	sh	?			
											968	25	0.14	968	14	0.12
											1007	10	0	1008	30	0
1043	2	1033	1	?				1035*	?	?	1044	5	0.14			
		1052	1	?							1055	sh	?			
														1130	5	0.30
		1161	11	0.14				1155*	5	0.40						
1179	22	1176	68	0.06	1175	31	0	1175*	47	0.33	1175	52	0.10	1175	17	0.09
1195	11	?	sh	?	?	sh	?	?	sh	?	?	sh	?			
														1210	5	0.10

ν: Shift frequency below 1220 cm^{-1}, I: relative intensity, ρ: depolarization ratio, *: overlapped by solvent band, 1,3-dmu-d_2: 1,3-Dimethylurea-d_2.

etal vibration of CH_3–NH–C skeleton.[3] Thus, these four bands are interpreted as generated by deformation of the CH_3–NH–C skeleton. Therefore, it is most probable that 1,3-dimethylurea undergoes molecular deformation when it acts as a proton acceptor at its nitrogen atom. But the presence of the band at 875 cm^{-1} in the spectrum of acetone (proton acceptor) solution seems to be contradictory with our explanation, even though it is very weak. However, this band may be ascribed to the molecules whose CH_3–NH–C skeletons are deformed by the N–H..N hydrogen bonding between 1,3-dimethylurea molecules.

References

1) H. D. Ellerton and P. J. Dunlop, *J. Phys. Chem.* **70**, 1831 (1966).
2) C. N. R. Rao, G. C. Chaturvedi, and R. K. Gosavi, *J. Molecular Spectroscopy* **28**, 526 (1968).
3) Y. Mido and H. Murata, *Bull. Chem. Soc. Jpn.*, **42**, 3372 (1969).
4) K. Ravindranath, V. Balasubramanian, and K. V. Ramiah, *Indian J. Pure Appl. Phys.*, **14**, 58 (1976).

The Far-infrared Absorption Intensities and the Dipole Moments of Acetone and Dimethyl Sulfoxide in Solutions

Yusei OHKUBO* and Masao KIMURA

Department of Chemistry, Faculty of Science, Hokkaido University, Sapporo 060

(Received November 12, 1980)

Synopsis. The effective dipole moments of acetone and dimethyl sulfoxide in nonpolar solutions were obtained from the far-infrared absorption intensities on the basis of an extended Onsager model with an eccentric point dipole.

Dipolar molecules in the liquid phase have absorptions in the far-infrared region[1-5] due to the rotational motion of the molecules and the temporary dipole moments induced by collision. However, the collision-induced absorption is generally much weaker than the dipolar absorption.[6] If the far-infrared absorption is attributed solely to the rotational motion of the molecule, the effective dipole moment can be obtained using Gordon's sum rule[7] after correcting for the internal-field effect.[8,9] In a previous study of CH_3I, $CHCl_3$, CH_2Cl_2, and CH_3CN in solutions,[5] the far-infrared absorption intensities were explained successfully by taking into account the internal-field effect and the internal moment[10] based upon Onsager's model. In the present study, far-infrared absorption intensities were measured for acetone and dimethyl sulfoxide (DMSO) in dilute C_6H_6, CCl_4, C_2Cl_4, and n-C_6H_{14} solutions. The observed intensities, however, cannot be interpreted by the same model as was employed in the previous study. Therefore, the model for the reaction field has been extended to a model with an eccentric dipole-location.

Experimental

The far-infrared spectra were measured at room temperature by means of an apparatus described previously.[5] Solutions were prepared from spectroscopic-grade reagents except for the deuterated compounds, which were already more than 99.6% pure when obtained from CEA and Merck. The concentration range was 0.06—0.17 M.

Results and Discussion

The absorption coefficients, $\sigma(\nu)$, of the solutes in nonpolar solvents are given by:

$$\sigma(\nu) = (1/\rho l)\ln(T_0/T)_\nu, \quad (1)$$

where ρ is the concentration (molecules cm^{-3}); l, the sample thickness (cm), and T_0 and T, the transmittances of the solvent and the solution respectively. The observed results are shown in Fig. 1, where the fine broken lines indicate the spectra profiles assumed in order to obtain the intensities, $A=\int\sigma(\nu)d\nu$. The value of A for each solution was determined by measurements at four concentrations. The results obeyed Beer's law. The A values were estimated, from the fluctuation of the four measurements, to be within ±3%. The systematic errors are due mainly to uncertainties in the assumed curves. The area of the assumed portion is 3—4% of the total area. Thus, the total experimental errors in A were estimated to be ±5% at most.

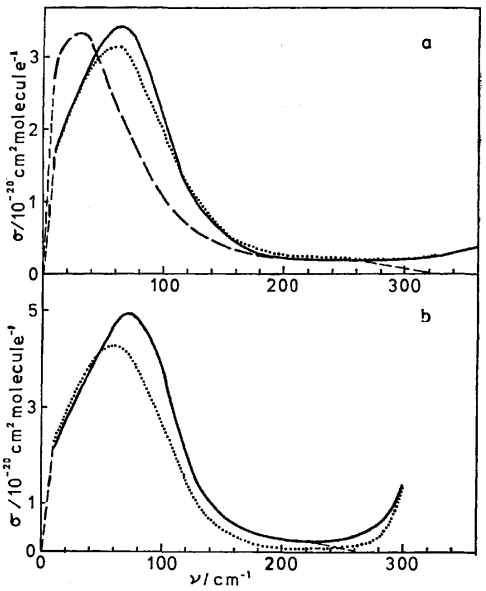

Fig. 1. a) Far-infrared absorption bands of $(CH_3)_2CO$ dissolved in CCl_4(——), in C_6H_6(……), and n-C_6H_{14} (----). b) Far-infrared absorption bands of $(CH_3)_2SO$ dissolved in CCl_4(——), and in C_6H_6(……).

The intensities, as corrected for the internal field effect, A_c, are given as:[8,9]

$$A_c = xA, \quad x = n_s\{[(n/n_s)^2+2]/(n^2+2)\}^2, \quad (2)$$

where n and n_s are the refractive indices of the solute and the solvent respectively. For C_{2v} symmetric molecules, Gordon's sum rule is expressed by:[7]

$$A_c = (\pi\mu^2/3c^2)(1/I_x+1/I_y), \quad (3)$$

where c is the velocity of light; μ, the effective dipole moment taken along the z axis, and I_x and I_y, the moments of inertia about the x and y axes respectively. The μ values, μ_I, obtained from Eq. 3 are shown in the fourth column of Table 1, together with the values of the moments of inertia and the permanent dipole moments in the gas phase, μ_0. The μ_I values for the H-compounds are in good agreement with those for the D-compounds, which have different moments of inertia. Furthermore, the μ_I values are about 10—30% larger than the μ_0 values for all the solutions.

In Onsager's model, the internal moment, μ^*_I, is expressed as:[10,11]

$$\mu^*_I = \mu_0(n^2+2)(2\varepsilon+1)/3(2\varepsilon+n^2), \quad (4)$$

where ε is the dielectric constant of the uniform medium and can be replaced by n_s^2 to a good approximation. The μ^*_I values calculated from μ_0 are listed in the fifth column of Table 1. However, the μ_I

Table 1. Observed intensities and dipole moments[a)]

Solute	Solvent	A	μ_I	μ^*_I	μ_{II}	μ^*_{II}	μ_0	I[b)]
		10^{-19} cm mol^{-1}	D					10^{-40} g cm^2
$(CH_3)_2CO$	C_6H_6	34.6	3.6_5	3.2_6	3.4_8	3.4_2	2.93[c)]	$I_x=82.56$, $I_y=170.9$
	CCl_4	35.8	3.7_2	3.2_4	3.5_6	3.3_8		
	C_2Cl_4	33.1	3.5_7	3.2_6	3.4_0	3.4_2		
	n-C_6H_{14}	29.5	3.4_1	3.1_9	3.2_8	3.3_1		
$(CD_3)_2CO$	CCl_4	30.0	3.7_5	3.2_4	3.5_8	3.3_8		$I_x=99.09$, $I_y=209.2$
$(CH_3)_2SO$	C_6H_6	40.6	4.4_3	4.5_5	4.1_6	4.8_5	3.96[c)]	$I_x=119.3$, $I_y=198.9$
	CCl_4	51.1	5.0_0	4.5_1	4.7_1	4.7_9		
$(CD_3)_2SO$	C_6H_6	35.6	4.5_1	4.5_5	4.2_3	4.8_5		$I_x=139.2$, $I_y=241.0$
	CCl_4	43.4	5.0_1	4.5_1	4.7_2	4.7_9		

a) I: The simple Onsager model; II: The eccentric dipole model. b) Calculated from the rotational constants taken from Ref. 12. c) Ref. 13.

values are larger by about 10% or more than the μ^*_I values except for that of DMSO in the C_6H_6 solutions. Onsager's model was extended to a model with an ellipsoidal cavity and an eccentric point dipole.[11] It turned out that, in nonpolar solvents, the magnitude of the reaction-field effect was almost independent of the cavity shape, but was significantly dependent on the position of the dipole in the cavity. For a molecule with an eccentric point dipole in a spherical cavity, the internal-field correction factor, x, and the internal moment, μ^*, are given by:[11]

$$x = n_s[3\varepsilon/(2\varepsilon+1)(1-f\cdot\alpha)]^{-2}, \quad (5)$$

$$\mu^* = \mu_0/(1-f\cdot\alpha), \quad (6)$$

where:

$$f = (1/a^3)\sum_{m=1}^{\infty}[m^2(m+1)(\varepsilon-1)/(m+m\varepsilon+\varepsilon)](s/a)^{2m-2}, \quad (7)$$

and where α is the average polarizability of the molecule, a is the radius of the cavity, and s is the distance from the center of the cavity to the point dipole. The parameter, s/a, is a measure of the eccentricity of the position of the dipole. α and a are related in a good approximation by:[10]

$$\alpha = a^3(n^2-1)/(n^2+2). \quad (8)$$

If $s=0$, Eqs. 5 and 6 reduce to Eqs. 2 and 4. The μ and μ^* values thus calculated with $s/a=0.3$, μ_{II} and μ^*_{II}, are shown in Table 1. There is no other means to confirm the propriety of the s/a value. However, a good agreement between μ_{II} and μ^*_{II} is obtained except for the C_6H_6 solutions of DMSO. For acetone, the internal moments are the least in the hexane solutions and almost the same in the other solutions, reflecting the dielectric constants of the solvents. Unlike as in the results for acetone, the μ_{II} value in the C_6H_6 solutions of DMSO is distinctly smaller not only than that in the CCl_4 solutions, but also than the μ^*_{II} value. There seems to exist a short-range ordering of C_6H_6 molecules around a DMSO molecule, such as the alignment of benzene rings perpendicular to the direction of the dipole moment of DMSO. The reaction field becomes weak because the axial polarizability of benzene molecules is smaller than the average polarizability, and so a μ_{II} value smaller than the μ^*_{II} value is obtained.

The authors wish to thank Dr. Shun-ichi Ikawa for his valuable suggestions and discussions.

References

1) P. Datta and G. M. Barrow, *J. Chem. Phys.*, **43**, 2137 (1965).
2) M. Davies, G. W. F. Pardoe, J. Chamberlain, and H. A. Gebbie, *Trans. Faraday Soc.*, **66**, 273 (1970).
3) M. W. Evans, *Spectrochim. Acta, Part A*, **30**, 79 (1974).
4) Y. Ohkubo, S. Ikawa, and M. Kimura, *Chem. Phys. Lett.*, **43**, 138 (1976).
5) K. Sato, Y. Ohkubo, T. Moritsu, S. Ikawa, and M. Kimura, *Bull. Chem. Soc. Jpn.*, **51**, 2493 (1978).
6) K. Fujiwara, S. Ikawa, and M. Kimura, *Bull. Chem. Soc. Jpn.*, **52**, 227 (1979).
7) R. G. Gordon, *J. Chem. Phys.*, **38**, 1724 (1963).
8) W. C. Mallard and J. W. Straley, *J. Chem. Phys.*, **27**, 877 (1957).
9) W. B. Person, *J. Chem. Phys.*, **28**, 319 (1958).
10) H. Fröhlich, "Theory of Dielectrics," 2nd ed, Oxford University Press, London (1960).
11) C. J. F. Böttcher, "Theory of Electoric Polarization," 2nd ed, Elsevier, Amsterdam (1973).
12) Landort-Börnstein, "Numerical Data and Functional Relationships," New Series, II/4, Springer, Berlin (1967).
13) A. L. McClellan, "Tables of Experimental Dipole Moments," Rahara Enterprises, El Cerrito, Cal. (1974), Vol. 2.

Effects of β-Cyclodextrin on Fluorescence Quenching of Sodium 1-Pyrenesulfonate by Aniline in Aqueous Media

Harumichi KOBASHI,* Masatoshi TAKAHASHI, Yasuyoshi MURAMATSU, and Toshifumi MORITA

Department of Chemistry, Faculty of Engineering, Gunma University, Kiryu, Gunma 376

(Received December 24, 1980)

Synopsis. β-Cyclodextrin added to the fluorescence quenching system of the title compounds has two effect, depression on dynamic quenching and binding between the fluorescer and quencher causing rapid quenching.

Catalytic actions of cyclodextrins on various chemical reactions are well known.[1] Inclusion effects on excited state properties of organic molecules, such as fluorescence enhancement, have been investigated by several workers,[2] but studies of the effects on intermolecular interactions from photophysical view points are still scarce.[3]

This paper gives results of addition effects of β-cyclodextrin (CD) on fluorescence quenching of sodium 1-pyrenesulfonate (PS) by aniline (A) in aqueous solutions. It is concluded that CD acts as a mediator for ground state association between the fluorescer and the quencher as well as acting as a retarder for dynamic quenching. Immediately after this work had been completed, a similar effect of CD was reported by Kano *et al.*[4] for fluorescence quenching of pyrene and PS by diethylamine. The enhancement of the quenching induced by CD was very small because of a higher ionization potential of the aliphatic amine (8.51 eV) than that of the aromatic amine (7.68 eV) we used. A more efficient quenching induced by such association together with retardation for the dynamic quenching has been revealed from a general consideration of the intensities and lifetimes of fluorescence consisting of two components.

Experimental

After measurements of absorption and fluorescence spectra, fluorescence lifetimes were measured with a Hitachi time resolved photometer and an apparatus for ns flash photolysis.[5] All measurements were carried out at 22 °C unless otherwise stated. Concentrations of CD and A were $\leq 1.0\times10^{-2}$ and $\leq 6.0\times10^{-3}$ M (1 M=1 mol dm^{-3}), respectively. The PS was fixed at 2.0×10^{-5} M. Degassed solutions of these concentrations were stable.

Results and Discussion

The absorption and fluorescence spectra of PS alone agreed with those obtained by Klein *et al.*[6] Addition of CD caused a slight red shift in the L_a absorption band. This shift, similar to that in micellar systems[6,7] originates from the hydrophobic property of a central void of CD. It gives an evidence for inclusion by CD.

In order to study the inclusion further, the difference absorption spectra between PS with and without CD were measured (Fig. 1). With an increase in the amount of CD the positive (d_+) and negative (d_-) absorptions increase their amplitudes. No changes

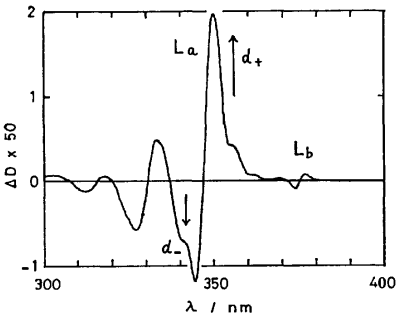

Fig. 1. Difference Spectrum of PS+CD against PS in aqueous solution at 15 °C.
[PS]=2.0×10^{-5} M, [CD]=6.0×10^{-3} M.

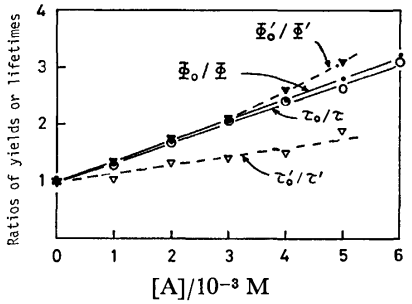

Fig. 2. Stern-Volmer plots for fluorescence yields and life-times of PS in the absence and presence of CD.
[PS]=2.0×10^{-5} M, [CD]=1.0×10^{-2} M.

were observed in positions and shapes of the absorption bands. This indicates that PS included by CD has a characteristic absorption differing from that of the free PS. The separation of wavelength between d_- and d_+ of the maximum amplitudes are ≈460 cm^{-1} for the L_a band and ≈180 cm^{-1} for the L_b band, respectively. The dependence of d_+ and d_- on [CD] was analyzed by means of a modified Ketelaar equation, $a/d_\pm = 1/(b^n K\varepsilon_\lambda) + 1/\varepsilon_\lambda$, where a and b are the initial concentrations of PS and CD, respectively, K is the association constant between PS and CD, ε_λ the difference of molar extinction coefficients between complexed PS and free PS at a wavelength λ, $d_\pm$ denotes d_+ or d_-, and n is the number of CD concerning the complex formation. The equation with $n=1$ corresponds to the observed dependence, the K value for the 1:1 complex between PS and CD being obtained to be 46±9 M^{-1} at 15 °C.

Fluorescence spectra with and without CD are very similar, their quantum yields being almost the same. The Stern-Volmer plots for the fluorescence quenching by A are shown in Fig. 2. In the case with no CD, both plots of Φ_0/Φ and τ_0/τ, where Φ_0/Φ and τ_0/τ have their usual meanings, are in good agreement with each other. The quenching rate con-

Table 1. Lifetimes and quenching constants and rate constants for the system with and without CD

	τ_0/ns	K_{sv}/M^{-1}		$k_q/10^9\ M^{-1}\ s^{-1}$	
		a	b	a	b
Without CD	79±1	377±6	347±11	4.7±0.1	4.4±0.1
With CD	76±1	381±13	175±23	5.0±0.2	2.3±0.3

a) Obtained from the plots for Φ_0/Φ and Φ'_0/Φ'. b) Obtained from the plots for τ_0/τ and τ'_0/τ'.

stants (k_q) were obtained to be $4.7\times10^9\ M^{-1}\ s^{-1}$ from the Φ_0/Φ plot and $4.4\times10^9\ M^{-1}\ s^{-1}$ from the τ_0/τ plot. In the case with CD, however, each plot for Φ'_0/Φ' and τ'_0/τ' (the prime is used to distinguish the quantities from those in the former case) splits with increase in A. The difference in the Stern-Volmer constants (K_{SV}) estimated approximately from Φ'_0/Φ' and τ'_0/τ' is larger than that given by Kano *et al.*[4] For the purpose of comparison apparent quenching parameters and lifetimes in the presence and absence of CD are given in Table 1.

The τ'_0 and τ' have been calculated according to the statistical definition of the lifetime, $\tau_s=\int_0^\infty t\phi(t)\mathrm{d}t\Big/\int_0^\infty \phi(t)\mathrm{d}t$, where $\phi(t)$ is an observed decay function of the fluorescence. The decay function in the absence of the quencher is nearly exponential in both cases with and without CD. This might be due to a slight change between the fluorescence lifetimes of the free and the complexed PS. However, the non-exponential feature of the decay in the presence of CD becomes remarkable with increase of quencher. This indicates that at least these two kinds of fluorescers, the free PS and the (PS···CD) complex, are quenched by A with a different rate. Since the complex (the long life component) decays more slowly than the free PS, the excited PS in the complex has been protected to some extent from quenching. When the decay is non-exponential it is not correct to regard the discrepancy between Φ'_0/Φ' and τ'_0/τ' (Fig. 2) as being due to the static quenching. In the present case the following consideration may be possible. Since the inclusion rate constants (k_a) in the ground state are of an order less than $10^7\ M^{-1}\ s^{-1}$ in many cases,[1b] the excited state equilibrium between PS and the complex would not be attained within the lifetime ($k_a\tau_0[CD]\ll1$ for $\tau_0=79$ ns and $[CD]=10^{-2}$ M). The excited species might decay independently of each other. If the observed decay functions can be expressed approximately by $\phi'(t)=A\ \exp(-\alpha' t)+B\ \exp(-\beta' t)$ and $\phi'_0(t)=C\ \exp(\alpha'_0 t)$ in the presence and absence of the quencher, respectively, we have

$$\frac{\Phi'_0}{\Phi'}=\frac{\int_0^\infty \phi'_0(t)\mathrm{d}t/C}{\int_0^\infty \phi'(t)\mathrm{d}t/(A+B)}=\frac{\alpha'}{\alpha'_0}\cdot\frac{A+B}{A+(\alpha'/\beta')B},\qquad(1)$$

$$\frac{\tau'_0}{\tau'}=\frac{\int_0^\infty t\phi'_0(t)\mathrm{d}t\Big/\int_0^\infty \phi'_0(t)\mathrm{d}t}{\int_0^\infty t\phi'(t)\mathrm{d}t\Big/\int_0^\infty \phi'(t)\mathrm{d}t}=\frac{\alpha'}{\alpha'_0}\cdot\frac{A+(\alpha'/\beta')B}{A+(\alpha'/\beta')^2B},\qquad(2)$$

where α' and β' denote the rate parameters of the free and the complexed PS depending on [A], respectively, and α'_0 the one observed at [A]=0. A, B, and C are coefficients depending on [CD] and excitation wavelength. Since we can put $\alpha'=\alpha$, $\alpha'_0\approx\alpha_0$, $\alpha'>\beta'$, and $\alpha/\alpha_0=\Phi_0/\Phi=\tau_0/\tau$, the relations, $\tau'_0/\tau'<\tau_0/\tau$ (Eq. 3), $\tau'_0/\tau'<\Phi'_0/\Phi'$ (Eq. 4), and $\Phi'_0/\Phi'<\Phi_0/\Phi$ (Eq. 5), are obtained from Eqs. 1 and 2 at a certain concentration of the quencher. We see from Fig. 2 that Eqs. 3 and 4 fit the observed results, but not Eq. 5. The results obtained from fluorescence intensity give the relation, $\Phi'_0/\Phi'\gtrsim\Phi_0/\Phi$. There is a discrepancy between the yield (Φ') obtained by the intensity measurements and the one calculated from the decay functions, the former being smaller than the latter. This suggests that there exists an additional quenching so rapid that it is impossible to detect by decay experiments. It would be reasonable to take into account the ground state association between the fluorescer and the quencher induced by CD, because such quenching occurs only with the coexistence of CD. A 1:1:1 complex among PS, CD, and A is plausible as suggested by Kano *et al.*[4] Such a three component complex has also been suggested by Hamai in the system of 2-methoxynaphthalene and *p*-dicyanobenzene in the presence of CD.[8]

The effects of CD on the intermolecular quenching are summarized as follows. (1) Inclusion of the fluorescer and the quencher[9] depresses the dynamic quenching by diffusive collision. (2) Mutual association of the quenching pairs mediated by CD gives rise to rapid quenching. The second effect appears to be important as one of catalytic functions of CD in relation to the association between biological substances under a very low concentration.

The authors are grateful to Mr. Noriaki Ikeda and Prof. Noboru Mataga, Osaka University for their advice and the supply of purified PS.

References

1) M. L. Bender and M. Komiyama, "Cyclodextrin Chemistry," Reactivity and Structure Concepts in Organic Chemistry 6, Springer-Verlag (1978); J. H. Fendler and E. J. Fendler, "Catalysis in Micellar and Macromolecular Systems," Academic Press, New York (1975).

2) T. Kinoshita, F. Iinuma, and A. Tsuji, *Chem. Pharm. Bull.*, **22**, 2413 (1974); H. Kondo, H. Nakatani, and K. Hiromi, *J. Biochem.*, **79**, 393 (1976).

3) H. E. Edwards and J. K. Thomas, *Carbohydr. Res.*, **65**, 173 (1978); Y. Muramatsu, M. Takahashi, H. Kobashi, and T. Morita, The 41st National Meeting of the Chemical Society of Japan, Osaka, April 1980, Abstr. No. 3E12.

4) K. Kano, I. Takenoshita, and T. Ogawa, *Chem. Lett.*, **1980**, 1035.

5) H. Kobashi, H. Gyoda, and T. Morita, *Bull. Chem. Soc. Jpn.*, **50**, 1731 (1977).

6) U. K. A. Klein, D. J. Miller, and M. Hauser, *Spectrochim. Acta, Part A*, **32**, 379 (1976).

7) T. F. Hunter and A. I. Younis, *J. Chem. Soc., Faraday Trans. 1*, **75**, 550 (1979).

8) S. Hamai, Symposium on Molecular Structure, Fukuoka, October 1980, Abstr. No. 3B09.

9) Dissociation constant of the (A···CD) complex has been estimated to be 2×10^{-2} M. M. Hoshino, M. Imamura, K. Ikehara, and Y. Hama, Symposium on Photochemistry, Tokyo, December 1979, Abstr. No. AII-204.

A Photoelectrochemical Study of Polyacetylene, $(CH)_x$

Toshihiro YAMASE,* Hideo HARADA, Tsuneo IKAWA, Sakuji IKEDA, and Hideki SHIRAKAWA†

Research Laboratory of Resources Utilization, Tokyo Institute of Technology, 4259 Nagatsuta, Midori-ku, Yokohama 227

† *Institute of Materials Science, University of Tsukuba, Sakura-mura, Ibaraki* 305

(Received January 14, 1981)

Synopsis. The photoelectrochemical behavior of *p*-type semiconducting *trans*-$(CH)_x$ film in the presence of *N,N'*-dimethyl-4,4'-bipyridinium as the solution species is described. The spectral response of the photocurrent shows a mismatch with the absorption spectrum, and the quantum yield ($\approx 10^{-3}$) of the charge flow is extremely low. It is assumed that $(CH)_x$ film has a high trap density and that the lifetime of the photogenerated hole is limited by trapping and recombination in the space-charge region.

In recent years, there has been a considerable interest in the electrical and optical properties of polyacetylene, $(CH)_x$, film as a new class of semiconducting material.[1-6] A $(CH)_x$-sodium polysulfide solution photovoltaic cell has been fabricated as an active photoelectrode for a photoelectrochemical cell.[7] Although Chen *et al.* mentioned that the $(CH)_x$ photocathode exhibited significant photoresponse with an open circuit voltage, $V_{oc} \approx 0.3$ V, and a short circuit current, $I_{sc} \approx 40$ μA/cm², under illumination of approximately 1 sun,[7] the photoresponse ($V_{oc} \approx 60$ mV, $I_{sc} \approx 1$ μA/cm²) in our work was very low. These results suggest that, in order to use the $(CH)_x$ as an active photoelectrode for a photoelectrochemical cell, it is of primary importance to characterize its general photoelectrochemical behavior before any modification experiments are performed. The studies reported here concern the basic photoelectrochemical properties of the *trans*-$(CH)_x$ film in the presence of *N,N'*-dimethyl-4,4'-bipyridinium (MV^{2+}) as the solution species.

Experimental

The preparation of the *trans*-$(CH)_x$ film has been described elsewhere.[8] The film was about 0.1 mm thick. The conductivity of the film was found to be about 10^{-6} Ω^{-1} cm^{-1}, as determined by the standard four-probe van der Pauw technique.[9] The ohmic contact with a thin copper sheet was obtained by the use of Electrodag on the shiny side of the $(CH)_x$ film. The preparation of the $(CH)_x$ working electrode was done according to Chen's method.[7]

Photocurrent measurements were performed under potentiostatic conditions with a home-made potentiostat.

The light source used in the study of the photoelectrochemical effect was a 100-W high-pressure mercury lamp with a glass filter ($\lambda \leq 430$ nm cut-off). A water filter with a 10-cm optical pathlength as a heat-absorbing filter was employed. Chemical actinometry for 436-nm-wavelength light, obtained by combination with a KL-43 filter, was carried out using the potassium ferrioxalate system. The measurement of the action spectrum of the photocurrent was done by the lock-in (NF Model LI-574) technique using a modulation of the light beam with 8 Hz. As a light source in this case, a Xe 500-W lamp was used, while a grating monochrometer (Nikon G-250) was employed for the wavelength selection.

Reagent-grade chemicals were used without further purification. All the solutions were deoxygenated for at least 30 min with purified nitrogen before each experiment. All the experiments were carried out with the solution under nitrogen without stirring.

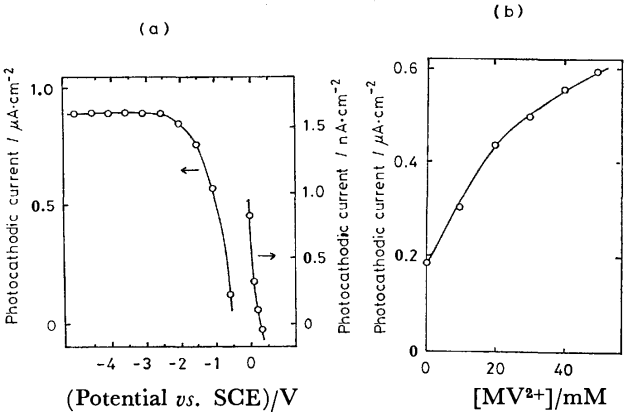

Fig. 1. (a) Steady-state photocurrent *vs.* electrode potential for 20 mM MV^{2+} in 1 M KCl (pH 5) at *trans*-$(CH)_x$ electrode; (b) Steady-state photocurrent as a function of concentration of MV^{2+} (1 M KCl, pH 5, $U_{SCE} = -1.0$ V).

Results and Discussion

Cyclic-voltammetric curve revealed that the $(CH)_x$ film did not react with MV^{2+} in the dark at all. Figures 1(a) and (b) show the steady-state photocurrent-voltage characteristic and the dependence of the signal on the MV^{2+} concentration respectively. The results can be qualitatively explained in terms of the p-type semiconducting properties of the $(CH)_x$ film. The cathodic photocurrent indicates that MV^{2+} acts as a primary acceptor of the electron as the minority carrier ejected from the $(CH)_x$ into the solution and can be attributed to the reduction of MV^{2+} to the purple $MV^{\cdot+}$, as evidenced by the blue-purple color streaming from the $(CH)_x$ film surface at $U_{SCE} \leq -1.5$ V. This fact suggests that the lower edge of the $(CH)_x$ conduction band is positioned at energies above the standard redox potential (−0.7 V *vs.* SCE) of $MV^{2+}/MV^{\cdot+}$.[10] Figure 1(b) shows the observation of the signal in the absence of MV^{2+} as well. The electron acceptor in this case remains unidentified, but dissolved oxygen gas as an impurity is a possible candidate, because O_2 can mediate the transfer of the conduction-band electron across the $(CH)_x$ film-solution interface. The onset potential ($U_{SCE} \approx 0.4$ V) of the photocurrent, which approximately corresponded to the flat-band potential for the $(CH)_x$ electrode, was almost independent of the solution pH (1—13), and the signal decreased with the solution acidity when U_{SCE} was kept constant. When a solution containing sodium polysulfide (20 mM as Na_2S_2) and 1 M (mol dm^{-3}) KCl at pH 11.6 was used,[7] the photo-

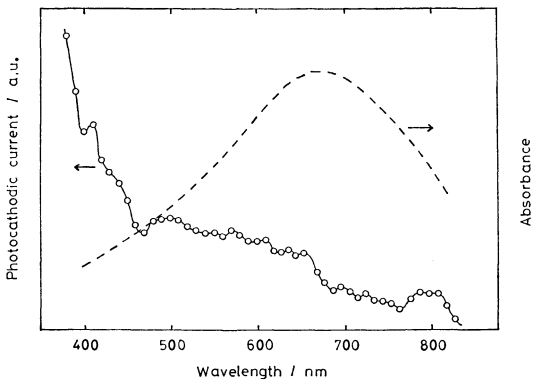

Fig. 2. Spectral response (in arbitrary units) of *trans*-$(CH)_x$ electrode in 20 mM MV^{2+}+1 M KCl aqueous solution (pH 5).
Dashed curve indicates absorption spectrum of *trans*-$(CH)_x$ with about 1 μm in thickness.

current was lower (≈0.27 μA/cm² at $U_{SCE}=-1.0$ V) than that of the 20 mM MV^{2+} system at pH 5 (≈0.45 μA/cm² at $U_{SCE}=-1.0$ V). This lower photocurrent may be mainly caused by an absorbance of the polysulfide solution used, and we may conclude that, in the polysulfide electrolyte, $(CH)_x$ does not exhibit the significant photoresponse previously reported.[7]

In Figure 2 the spectral response of the $(CH)_x$ electrode is shown. The data on the vertical axis were obtained by dividing the photocurrent at a certain wavelength by the number of photons incident on the electrode. It can be seen that the spectral response of the photocurrent shows a mismatch with the absorption spectrum of the $(CH)_x$ film, which exhibits an absorption maximum at 670 nm.[11] Similar behavior has been observed for the solid-state $(CH)_x$ Schottky junction.[12] The threshold of the photocurrent response is observed at about 830 nm (≈1.5 eV), in agreement with the direct-band gap calculated from the optical studies of the $(CH)_x$ film.[1] The anticorrelation between the action and the absorption spectrum indicates that the light absorbed on the front suface of the $(CH)_x$ film is not effective in creating free-charge carriers. In effect, most holes generated on the front surface are not long-lived enough to diffuse into the space-charge layer, while holes generated within the bulk have a finite probability of transiting the space-charge layer to be registered as carriers in the external circuit. The rate of charge generation at a certain distance, x, from the front surface is proportional to $\exp(-kx)$, where k is the absorption coefficient of the $(CH)_x$ film (for example, $k_{670}\approx 2\times 10^5$ cm^{-1} [1]). Detailed studies of the photovoltaic response for *p*-$(CH)_x$: *n*-CdS heterojunction have implied the existence of a meta-stable trapping state 0.9 eV below the conduction band of the $(CH)_x$ film.[6] Therefore, the anticorrelation may be explained by assuming that the $(CH)_x$ film has an excessively high trap density; if the penetration depth of the light ($\lambda\leq 600$ nm) is large, the trapping of the photogenerated holes may be insignificant compared to the case of about a 670 nm-wavelength light corresponding to the absorption maximum of the $(CH)_x$ film. The quantum yield of the charge flow under the 436-nm-light irradiation was extremely low, being 1×10^{-3} at $U_{SCE}=-1.0$ V in the 20 mM MV^{2+} +1 M KCl aqueous solution (pH 5). Furthermore, the light-intensity dependence of the photocurrent varied with the applied potential; the light-intensity exponent for the photocurrent was less than unity and increased from 0.8 to 0.9 as $-U_{SCE}$ increased from 0.5 to 3.0 V. These results may be related to the recombination or trapping of the photogenerated holes in the bulk of the $(CH)_x$ film, which arises from the high trap density and which well limits the photocurrent to a significant level, if we consider that an increase in the electric field in the space-charge layer would cause the photogenerated holes to have an increasing chance of transiting the space-charge layer before being trapped.[13]

References

1) C. K. Chiang, C. R. Fincher, Jr., Y. W. Park, A. J. Heeger, H. Shirakawa, E. J. Louis, S. C. Gau, and A. G. MacDiarmid, *Phys. Rev. Lett.*, **39**, 1098 (1977).
2) C. K. Chiang, Y. W. Park, A. J. Heeger, H. Shirakawa, E. J. Louis, and A. G. MacDiarmid, *J. Chem. Phys.*, **69**, 5098 (1978).
3) C. R. Fincher, Jr., M. Ozaki, M. Tanaka, D. Peebles, L. Lauchlan, A. J. Heeger, and A. G. MacDiarmid, *Phys. Rev. B*, **20**, 1589 (1979).
4) Y. W. Park, A. Denestein, C. K. Chiang, A. J. Heeger, and A. G. MacDiarmid, *Solid State Commun.*, **29**, 747 (1979).
5) M. Ozaki, D. L. Peebles, B. R. Weinberger, C. K. Chiang, S. C. Gau, A. J. Heeger, and A. G. MacDiarmid, *Appl. Phys. Lett.*, **35**, 83 (1979).
6) M. Ozaki, D. L. Peebles, B. R. Weinberger, A. J. Heeger, and A. G. MacDiarmid, *J. Appl. Phys.*, **51**, 4252 (1980).
7) S. N. Chen, A. J. Heeger, Z. Kiss, A. G. MacDiarmid, S. C. Gau, and D. L. Peebles, *Appl. Phys. Lett.*, **36**, 96 (1980).
8) T. Ito, H. Shirakawa, and S. Ikeda, *J. Polym. Sci., Polym. Chem. Ed.*, **12**, 11 (1974).
9) L. J. van der Pauw, *Philips Tech. Rev.*, **20**, 220 (1958); J. Lange, *J. Appl. Phys.*, **35**, 2659 (1964).
10) S. Hunig, J. Gross, and W. Schenk, *Justus Liebigs Ann. Chem.*, **1**, 324 (1973).
11) H. Shirakawa, T. Ito, and S. Ikeda, *Polym. J.*, **4**, 460 (1973).
12) T. Tani, P. M. Grant, W. D. Gill, G. B. Street, and T. C. Clarke, *Solid State Commun.*, **33**, 499 (1980).
13) The AsF_5-doped *trans*-$(CH)_x$ film with 8.4×10^{-3} Ω^{-1} cm^{-1} exhibited 5×10^{16} and 2.5×10^{18} cm^{-3} as the ionized acceptor concentration (N_A) and the trap density (N_T), respectively.[14] Accordingly, it may be reasonable to assume $N_A\approx 10^{15}$ cm^{-3} for the present $(CH)_x$ film with 10^{-6} Ω^{-1} cm^{-1}. Then, about 10^4 Å as the space-charge layer width under the band bending of about 1 eV can be calculated, when $\varepsilon\approx 10$ is taken as the dielectric constant. In this case, most of the absorption maximum-photons ($k_{670}\approx 2\times 10^5$ cm^{-1}) incident on the $(CH)_x$ film would be absorbed within 10^3 Å of the front surface, and most of the photogenerated holes would be not long-lived enough to transit the space-charge layer with a 10^4 Å width, due to the trapping by the high-trap density (probably $N_T>2.5\times 10^{18}$ cm^{-3}). This may lead to the absence of any parallel effect for the photocurrent signal, as is shown in Fig. 2.
14) H. Shirakawa and T. Tani, *Kotai Butsuri*, **14**, 435 (1979).

Prediction of Adsorption Isotherms of Organic Compounds from Water on Activated Carbons

Ikuo ABE,* Katsumi HAYASHI, and Mutsuo KITAGAWA**
Osaka Municipal Technical Research Institute, Ogimachi, Kita-ku, Osaka 530
***Society for Activated Carbon Research, Ogimachi, Kita-ku, Osaka 530*
(Received January 22, 1981)

Synopsis. An adsorption equation is postulated for predicting the adsorption isotherms of organic compounds from water on activated carbons.

It is known that the prediction of adsorption isotherms for a given adsorbent from the physical properties of the adsorbate is important for adsorbent-adsorbate interaction. For gas-phase adsorption, Dubinin[1] showed that the physical constants such as molar volume and parachor are useful for predicting the isotherms. Reucroft *et al.*[2] studied the relationship between the adsorbability and physical constants and concluded that the molecular refraction gives a good correlation. In liquid-phase adsorption, Abe *et al.*[3] have calculated partition coefficient of 93 organic compounds between the solution and the adsorbed phases at an infinite dilution and examined the correlation with various physical constants. We present the following adsorption equation for predicting the adsorption isotherms of organic compounds from water on activated carbons in terms of a physical constant.

$$\log X = \alpha\Phi + \beta + \gamma \log C, \quad (1)$$

where X is the weight of solute adsorbed (mg/g), C the equilibrium concentration of the solute (mg/l), and α, β, γ are constants. The constant Φ represents the adsorbability of the adsorbate and is independent of the nature of adsorbent. We have tried to replace the Φ value with a physical constant such as molecular refraction or parachor.

Equation 1 was applied to the adsorption isotherms of 22 aliphatic monofunctional compounds from water on an activated carbon at 25 °C,[4] the data of 122 plots being given to a HITAC 10—II computer to determine the α, β, γ values by means of multiple regression analysis. The constants and statistic analysis for several physical constants are given in Table 1. High correlation coefficients have been obtained for molecular refraction and parachor. The result resembles that in gas-phase adsorption. Standard deviations, the t values in the Student test and the overall goodness of fit expressed by means of the F values indicate that Eq. 1 in which the Φ value is replaced with molecular refraction or parachor provides a satisfactory approximation. Figure 1 shows a plot of log X observed *vs.* log X calculated by means of

$$\log X_{\text{calcd}} = 0.08111R - 1.230 + 0.4895 \log C. \quad (2)$$

We see from Fig. 1 that the molecular refraction gives a good prediction of the isotherms as shown by

$$\log X_{\text{obsd}} = 0.99998 \log X_{\text{calcd}} - 0.000066. \quad (3)$$

(r=0.9685, s=0.09400, F=1018, t=42.63)

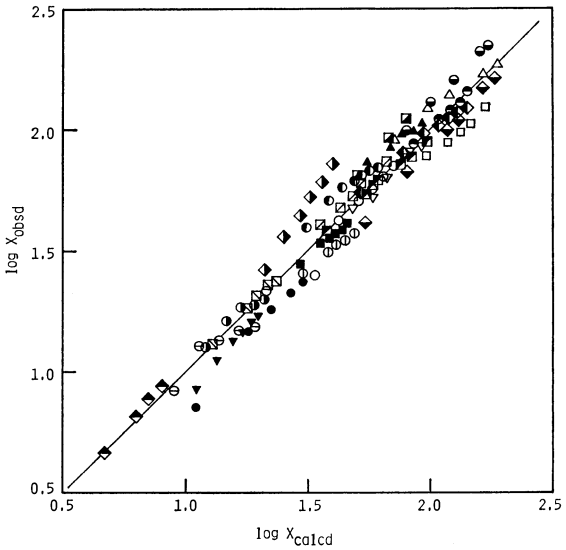

Fig. 1. Prediction of adsorption isotherms of 22 aliphatic monofunctional compounds from water on an activated carbon.
●: 1-Propanol, ○: 1-butanol, ◓: 1-pentanol, ◒: 1-hexanol, ◑: propionic acid, ◐: butyric acid, ▲: valeric acid, △: hexanoic acid, ▼: acetone, ■: 2-butanone, ▽: 2-pentanone □: 2-Hexanone, ⓘ: diethyl ether, ◆: dipropyl ether, ▧: methyl acetate, ◰: ethyl acetate, ◩: propyl acetate, ◈: butyl acetate, ◆: acetaldehyde, ⊖: propionaldehyde, ◈: butyraldehyde, ◪: valeraldehyde.

TABLE 1. MULTIPLE REGRESSION ANALYSIS FOR THE $\log X = \alpha\Phi + \beta + \gamma \log C$ EQUATION

Physical constant	Φ	α	β	γ	Multiple correlation coefficient r	Standard deviation s	Statistical test F	$t(\Phi)$	$t(\log C)$
Molecular refraction	R	0.08111	−1.230	0.4895	0.9685	0.09438	901.5	40.88	17.17
Parachor	P	0.009448	−1.445	0.5007	0.9671	0.09651	859.5	39.91	17.05
Molar-attraction constant	ΣF	0.002779	−1.683	0.4335	0.9337	0.1358	404.6	27.30	10.73
Molecular weight	M	0.02290	−1.146	0.4383	0.9198	0.1489	326.8	24.51	9.806
Molar volume	V	0.02067	−1.356	0.4704	0.9181	0.1397	300.5	23.61	10.69

$F(2, 60; 0.001)=7.76$, $t(60, 0.001)=3.460$.

Table 2. Multiple regression analysis for the $\log X=\alpha R+\beta+\gamma \log C$ equation

Activated carbon	α	β	γ	Number of data n	Multiple correlation coefficient r	Standard deviation s	Statistical test F	$t(R)$	$t(\log C)$
[A]	0.08407	−1.390	0.5461	12	0.9910	0.05971	247.3	22.22	7.506
[B]	0.06397	−0.4797	0.4312	13	0.9949	0.03543	487.6	31.21	11.14
[C]	0.06214	−0.4509	0.3823	13	0.9845	0.06103	157.7	17.76	5.590
[D]	0.07344	−1.328	0.5220	12	0.9650	0.09909	60.89	10.78	3.580
[E]	0.08439	−1.147	0.5137	13	0.9957	0.03989	578.4	33.53	11.64
[F]	0.07755	−1.117	0.5126	13	0.9948	0.04184	481.1	30.93	10.35
[G]	0.07095	−0.5225	0.4074	13	0.9943	0.04018	435.7	29.45	10.13
[H]	0.07318	−0.6517	0.4354	13	0.9921	0.04866	312.8	24.95	8.780
[I]	0.07232	−0.5587	0.4037	13	0.9893	0.05616	229.2	21.33	7.224
[J]	0.06798	−0.6728	0.4283	13	0.9905	0.05137	259.1	22.76	7.525
[K]	0.07390	−0.8544	0.4377	13	0.9932	0.04627	363.9	26.88	8.275
[L]	0.05782	−0.3705	0.4229	12	0.9858	0.05011	155.6	17.62	7.429
[M]	0.06805	−0.8374	0.4562	13	0.9887	0.05636	218.0	20.88	6.896
[N]	0.07847	−1.185	0.5622	13	0.9908	0.05577	267.6	23.07	8.514
[O]	0.08109	−0.9335	0.4906	13	0.9966	0.03400	724.5	37.58	13.70
[P]	0.07351	−0.9372	0.4527	13	0.9946	0.04128	459.9	30.28	9.383
[Q]	0.07543	−1.178	0.5277	13	0.9911	0.05439	275.9	23.48	8.019
[R]	0.07846	−1.050	0.5501	13	0.9933	0.04675	370.4	27.11	10.43
[S]	0.06239	−0.4707	0.4220	13	0.9977	0.05411	200.3	20.00	7.082
[T]	0.06926	−0.8454	0.5206	13	0.9836	0.06853	149.2	17.26	6.775

$F(2, 9; 0.001)=16.4$, $t(9, 0.001)=4.781$, $t(9, 0.01)=3.250$.

In order to examine whether Eq. 1 is applicable to the other activated carbons with different adsorption capacities, the adsorption experiments were carried out for 20 different activated carbons and 7 aliphatic monofunctional compounds (1-pentanol, butyric acid, hexanoic acid, 2-butanone, 2-pentanone, methyl acetate, butyl acetate). The results of multiple regression analysis for Eq. 1 with molecular refraction are given in Table 2. The high muliple correlation coefficients indicate that Eq. 1 is applicable to all the carbons.

If the α, β, and γ constants for a given activated carbon are determined from the adsorption data of several compounds, the adsorption isotherms of many other aliphatic monofunctional compounds can be predicted from only the molecular refraction constant.

References

1) M. M. Dubinin, *Chem. Rev.*, **60**, 235 (1960).
2) P. J. Reucroft, W. H. Simpson, and L. A. Jonas, *J. Phys. Chem.*, **75**, 3526 (1971).
3) I. Abe, K. Hayashi, M. Kitagawa, and T. Urahata, *Bull. Chem. Soc. Jpn.*, **53**, 1199 (1980).
4) I. Abe, K. Hayashi, M. Kitagawa, and T. Urahata, *Bull. Chem. Soc. Jpn.*, **52**, 1899 (1979).

The Measurement of the Distribution Equilibrium Constant of Metallic Mercury for $Hg_{(aq)} \rightleftharpoons Hg_{(gas)}$

Shoichi Okouchi* and Sokichi Sasaki

Chemical Laboratory, Faculty of Engineering, Hosei University, Kajino, Koganei, Tokyo 184

(Received May 10, 1980)

Synopsis. The gas-aqueous distribution equilibrium constant of mercury(0) was determined in the temperature range from 5 to 45 °C. The experiment was made by volatilizing metallic mercury dissolved in water to the gas phase, which was connected with the absorption cell in a cold-vapor atomic absorption spectrophotometer, and by measuring the absorbance under gas-aqueous distribution equilibrium conditions. The distribution equilibrium constant, $[Hg]_{gas}/[Hg]_{aq}$, was found, *e.g.*, to be 0.40 ± 0.02 at 25 °C. The effect of the concentration of NaCl on the distribution equilibrium constant was measured at 25 °C. The salting-out effect was found to be expressed by the Setschenow equation, and the salting-out coefficient was found to be 0.105.

The behavior of mercury in an environment is interesting, although rather complicated and still not entirely explainable. The most distinct difference between mercury and the other metals is the high vapor pressure of mercury, so that the mercury volatilizes[1,2] from water surfaces, such as seas and rivers, to the atmosphere. The most important factor[3] in the mercury volatilization is the gas-aqueous distribution equilibrium constant of mercury, although the distribution equilibrium constant has not yet been measured, to our knowledge.

In this work, the distribution equilibrium constant was measured by volatilizing metallic mercury dissolved in water to the gas phase, which was connected with the absorption cell in a cold-vapor atomic absorption spectrophotometer.

Experimental

Doubly distilled water was used throughout this work. All the chemicals were of an analytical reagent grade. Analytical-grade metallic mercury was further purified in the usual manner.[4]

By shaking the distilled water containing a few drops of the purified metallic mercury and 0.001 mol dm^{-3} of phosphinic acid[5,6] as a reducing agent to prevent the mercury oxidation, the mercury was dissolved in the water. The solution with the dissolved free mercury was prepared in the vessel shown in Fig. 1, and stirred by means of a magnetic stirrer. The mercury in the solution was equilibrated with the gas phase,[7,8] which was connected with the absorption cell in a cold-vapor atomic absorption spectrophotometer (Hiranuma, HG-1). The absorbance became constant under the gas-aqueous distribution equilibrium conditions of mercury (first equilibrium conditions). The absorbance at equilibrium was measured, the stirring was stopped, and then the mercury vapor in the gas phase was swept by nitrogen gas into a ($KMnO_4+H_2SO_4$) absorber without disturbing the aqueous phase. When the absorbance had returned to zero level (base line), the same procedure was repeated and a second absorbance was measured (second equilibrium conditions). The variation in the absorbance with the time is shown in Fig. 2. The experiment was made in the temperature range from 5 to 45 °C, the precision of the temperature in the aqueous and the gas phases being ±0.1 °C and ±0.5 °C respectively.

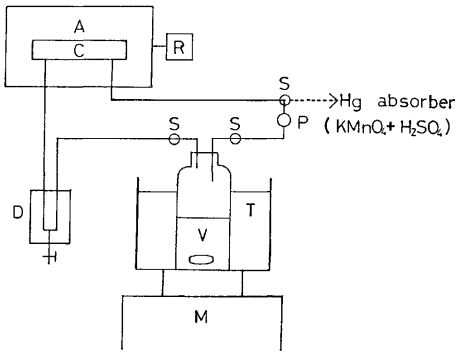

Fig. 1. Schematic diagram of apparatus.
A: Atomic absorption spectrophotometer, C: absorption cell, D: cold trap, M: magnetic stirrer, P: pump, R: recorder, S: stopcock, T: thermostat, V: mercury solution.

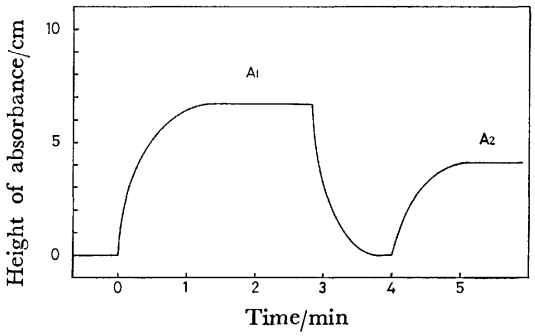

Fig. 2. Variation in absorbance with time at 25 °C. $[Hg]_0 = 1.32 \times 10^{-8}$ mol dm^{-3}, $V_L = 250$ cm^3, $V_G = 395$ cm^3.

Results and Discussion

The distribution equilibrium constant, K, for $Hg_{(aq)} \rightleftharpoons Hg_{(gas)}$ is expressed as follows:

$$K = [Hg]_{gas}/[Hg]_{aq}, \quad (1)$$

where $[Hg]_{gas}$ and $[Hg]_{aq}$ are the mercury concentrations in the gas and aqueous phases respectively. Assuming that $[Hg]_0$ is an initial mercury concentration, V_G and V_L are the volumes in the gas and aqueous phases respectively under the first equilibrium conditions:

$$K = \frac{[Hg]_{gas\,1}\, V_L}{[Hg]_0\, V_L - [Hg]_{gas\,1}\, V_G} \quad (2)$$

and under the second equilibrium conditions:

$$K = \frac{[Hg]_{gas\,2}\, V_L}{[Hg]_0\, V_L - \{[Hg]_{gas\,1} + [Hg]_{gas\,2}\} V_G}, \quad (3)$$

where the subscript numbers 1 and 2 indicate the

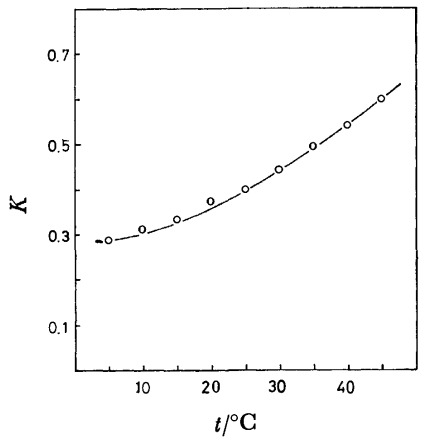

Fig. 3. Temperature dependence of K.

first and the second equilibrium conditions respectively. The relation between the mercury concentration in the gas phase and the absorbance is expressed as follows:

$$[\mathrm{Hg}]_{\mathrm{gas}\,1} = A_1\,a$$
$$[\mathrm{Hg}]_{\mathrm{gas}\,2} = A_2\,a, \qquad (4)$$

where a is the mercury concentration in the gas phase per unit absorbance; it indicates a constant value if the temperature and the operating conditions of the spectrophotometer are fixed. Therefore, from Eqs. 2, 3, and 4, Eq. 5 is obtained:

$$K = \frac{A_1 - A_2}{A_2} \times \frac{V_L}{V_G}. \qquad (5)$$

The distribution equilibrium constant, K, can be determined by measuring the absorbances, A_1 and A_2, under the gas-aqueous equilibrium conditions. In case of Fig. 2, A_1=6.7 cm** and A_2=4.1 cm** were measured. Therefore, the value of K=0.40 was calculated from Eq. 5. The value of K obtained at 25 °C is found to be 0.40±0.02 by measurements in the various cases of V_1 from 100 to 500 cm^3 and of $[\mathrm{Hg}]_0$ from (0.35 to 1.64)×10^{-8} mol dm^{-3}. The constant was found to be unaffected by the reducing-agent concentrations of phosphinic acid between 0.0005 and 0.02 mol dm^{-3}.

The standard Gibbs energies of the formation and the solution for the mercury element at 25 °C are 31.853[9] and 39 K J/mol[10] respectively. Using these values, K=0.74 is calculated. Compared with the K measured in this work, the calculated value is larger, though the ±2 K J/mol differences of $\Delta G°$ give about a 5-fold change of K in the calculating method of the free-energy change. The calculation of K by using the mercury solubility in water previously reported gives K=0.79 with Pariaud's data (1.3×10^{-7} mol dm^{-3})[11] and K=0.34 with Moser's data (3.0×10^{-7} mol dm^{-3}).[5] According to recent solubility studies,[4,12,13] the latter value is preferable. The distribution equilibrium constant in this work is reasonable in view of the above discussion and the dilution of the mercury. The temperature dependence of K is shown in Fig. 3.

** The absorbances, A_1 and A_2, were expressed by the height of the absorbance (cm) on the recorder chart in the cold-vapor atomic absorption spectrophotometer.

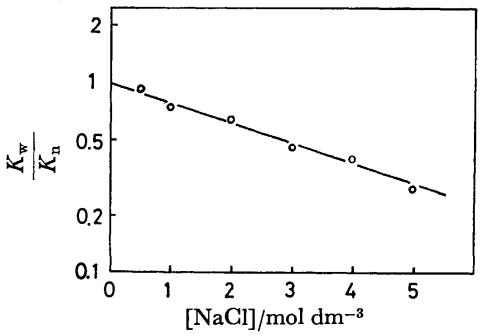

Fig. 4. Salting-out effect at 25 °C.
K_w:K for water (0.40), K_n:K for NaCl solution.

Instead of distilled water, sodium chloride solutions were used under the same distribution equilibrium experiments. The effect of the concentration of NaCl on the distribution equilibrium constant is shown in Fig. 4. A salting-out effect was observed; it could be explained by the Setshenow equation[14] for an aqueous electrolyte solution. The salting-out coefficient was found to be 0.105 at 25 °C.

Conclusion

The distribution equilibrium constant of metallic mercury between the aqueous and the gas phases was determined in the temperature range from 5 to 45 °C by using a cold-vapor atomic absorption spectrophotometer and the equation derived from the material balance of the mercury.

The effect of the concentration of NaCl on the distribution equilibrium constant was investigated at 25 °C, and the salting-out coefficient was determined in the concentration range from 0 to 5 mol dm^{-3}.

We gratefully acknowledge the valuable suggestions of Professor Yuhbun Tsutsumi, Hosei University.

References

1) S. Kitamura, M. Kondo, Y. Takizawa, M. Fujii, and M. Fujiki, "Suigin," Kodanshya, Tokyo (1976), p. 258.
2) J. D. Hem, Geological Survey Prof. Paper 713, 19 (1970).
3) S. Okouchi, Y. Itakura, and S. Sasaki, *Nippon Kagaku Kaishi*, 1263 (1979).
4) D. N. Glew and D. A. Hames, *Can. J. Chem.*, **49**, 3114 (1971).
5) H. C. Moser and A. F. Voigt, *J. Am. Chem. Soc.*, **79**, 1837 (1957).
6) J. N. Spencer and A. F. Voigt, *J. Phys. Chem.*, **72**, 464 (1968).
7) Y. Umesaki and K. Iwamoto, *Jpn. Analyst*, **20**, 173 (1971).
8) T. Kamata, Y. Hayashi, T. Kumamaru, and Y. Yamamoto, *Jpn. Analyst*, **22**, 1481 (1973).
9) Chemical Society of Japan, "Kagaku Binran Kisohen (II)," Maruzen, Tokyo (1975), p. 958.
10) J. Ö. Hill, G. Ojelund, and I. Wadsö, *J. Chem. Thermodynamics*, **1**, 111 (1969).
11) J. C. Pariaud and P. Archinard, *Bull. Soc. Chim. Fr.*, **1952**, 454.
12) S. S. Choi and D. G. Tuck, *J. Chem. Soc.*, **1962**, 4080.
13) E. Onat, *J. Inorg. Nucl. Chem.*, **36**, 2029 (1974).
14) A. Yasunishi, *Kagaku Kogaku Ronbunshu*, **4**, 185 (1978).

Isomers of the Diamminebis(trimethylenediamine)cobalt(III) Complex

Mitsuru SANO, Miho FUJITA,† Ken-ichi SASAKI, Yuzo YOSHIKAWA, and Hideo YAMATERA*

Department of Chemistry, Faculty of Science, Nagoya University, Chikusa-ku, Nagoya 464

†*Department of Chemistry, Nagoya City University, Mizuho-ku, Nagoya 467*

(Received January 5, 1981)

Synopsis. The isomers of $[Co(NH_3)_2(tn)_2]^{3+}$ were separated by recycling chromatography. The CD spectra of cis isomers were obtained and are compared with the spectra of the corresponding tris complexes. The magnitude of CD intensity of bisdiamine complex is roughly one-third of the corresponding trisdiamine complex.

A number of studies have been made on the stereochemistry of cobalt(III) complexes with five-membered diamine chelate rings. However, this has not been the case for those complexes including six-membered diamine chelate rings, probably because many of their isomers can be hardly separated and/or resolved.

The circular dichroism (CD) intensity of cobalt(III) complexes with six-membered diamine chelate rings is known to be much weaker than the corresponding cobalt(III) complexes with five-membered rings. The purpose of the present work was to separate *cis*-$[Co(NH_3)_2(tn)_2]^{3+}$, which had not yet been separated, to resolve it into antipodes, and to assign the configuration by comparing their CD spectra with those of known $[Co(NH_3)_2(diamine)_2]^{3+}$- and $[Co(diamine)_3]^{3+}$-type complexes (diamine=en, tn, and RR-ptn**).

Experimental

To about 10 ml of liquid ammonia cooled in a Dry Ice–acetone bath was added 350 mg of *trans*-$[CoCl_2(tn)_2]Cl$ prepared according to the literature.[1] The mixture was stirred for one hour and allowed to stand overnight, while the temperature of the solution gradually increased up to room temperature and finally all the solvent ammonia evaporated.

The orange-red product obtained as residue was subjected to recycling chromatography[2,3] on an SP-Sephadex column (4.1 dia.×96 cm) using an aqueous 0.18 M (1 M= 1 mol dm^{-3}) sodium $(+)_{589}$-tartrate solution as eluent. The flow rate of elution was about 2.0 ml per minute. The elution after the sixth recycling gave two well-separated bands, which are denoted by A and B in the order of effluence (Fig. 1a).

The CD spectral measurements of each fraction of the effluent showed that the complex contained in the B band was partially resolved. The combined solution of B-band fractions was rechromatographed on the same column with a different eluent, 0.15 M sodium $(+)_{589}$-tartratoantimonate(III) solution. The elution after the tenth recycling resulted in two well-separated bands, B-I and B-II, with an area ratio of about 1:1 (Fig. 1b). The notations, A, B-I, and B-II, will hereafter be used to designate the isomer contained in each band.

The chlorides of A, B-I, and B-II were obtained from the eluates of the corresponding bands with the method described previously.[4] Found for the isomer A: C, 19.62; H, 7.65; N, 22.61%. Found for the isomer B-I: C, 19.32; H, 7.65; N, 22.61%. Calcd for $[Co(NH_3)_2(tn)_2]Cl_3 \cdot H_2O$: C, 19.72; H, 7.72; N, 22.99%.

** Ethylenediamine, trimethylenediamine, and (2*R*,4*R*)-2,4-pentanediamine, respectively.

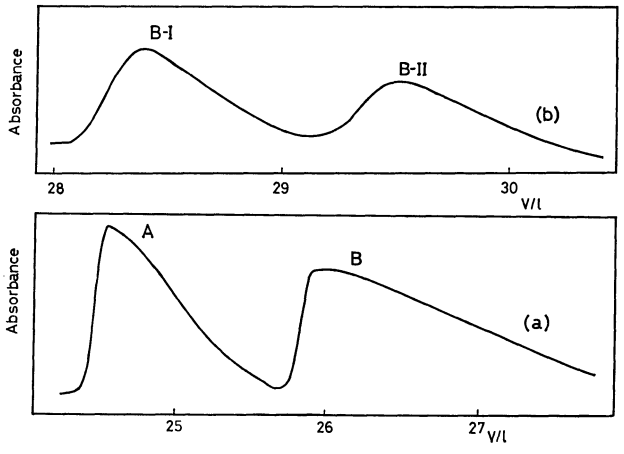

Fig. 1. The elution curves of the recycling chromatography of (a) $[Co(NH_3)_2(tn)_2]^{3+}$ by the 0.18 M sodium $(+)_{589}$-tartrate and (b) *cis*-$[Co(NH_3)_2(tn)_2]^{3+}$ by the 0.15 M sodium $(+)_{589}$-tartratoantimonate(III).

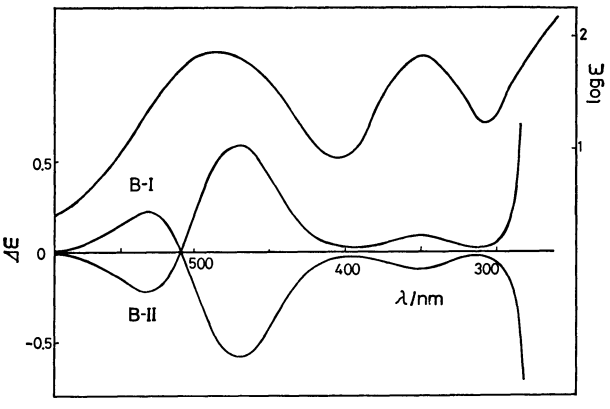

Fig. 2. Visible absorption and CD spectra of isomers of *cis*-$[Co(NH_3)_2(tn)_2]^{3+}$.

The ^{13}C NMR spectra were obtained with a JEOL JNM FX-60 spectrometer, using dioxane as an external reference. Absorption spectra were recorded on a Hitachi EPS-3T spectrophotometer and CD curves on a JASCO J-20 spectrophotometer.

Results and Discussion

The ^{13}C NMR spectra of $[Co(NH_3)_2(tn)_2]Cl_3$ isomers have a broader signal at 25.5 ppm and a more intense signal at 39—40 ppm, the latter being split into two peaks for the B isomer. The signals, in the order mentioned, are assigned to β- and α-methylene carbons according to the literature.[5]

The α-methylene carbon atoms are all equivalent in the trans complex, but are divided into two groups in the *cis* complex. Therefore, the A and B isomers

Table 1. CD intensities of bis- and tris-diamine complexes

Diamine	Λ-$[Co(NH_3)_2(diamine)_2]^{3+}$		Λ-$[Co(diamine)_3]^{3+}$		$\frac{\Delta\varepsilon_{bis}}{\Delta\varepsilon_{tris}}$
	$\Delta\varepsilon_{bis}$	(λ/nm)	$\Delta\varepsilon_{tris}$	(λ/nm)	
en	+0.42	(492) [a]	+1.89	(493) [a]	0.22
	−0.04	(430)	−0.166	(428)	0.24
	+0.056	(356)	+0.25	(351)	
tn	+0.024	(531) [b]	+0.081	(535) [c]	0.30
	−0.064	(473)	−0.0165	(478.5)	0.39
	−0.011	(352)	−0.020	(357)	
RR-ptn [e]	+1.01	(482) [d]	+3.22	(482) [d]	0.31
	+0.031	(362)	−0.31	(352)	

a) Ref. 8. b) Present work. c) Ref. 6. d) Ref. 9. e) This ligand holds the *ob* form of chelate rings in both the bis and tris complexes.

are assigned to the trans and cis isomers of $[Co(NH_3)_2(tn)_2]^{3+}$, respectively. These assignments are supported also from the fact that the B isomer has been resolved into catoptromers, as described below.

The CD spectra of the B-I and B-II isomers are shown in Fig. 2 with the absorption spectrum of *cis* (B) isomer. Their CD spectra are enantiomeric to each other and resemble those of Λ- and Δ-$[Co(en)_3]^{3+}$, respectively, in their Cotton effects and their shapes.[6] Thus, the B-I and B-II isomers are the optical antipodes of pure *cis*-$[Co(NH_3)_2(tn)_2]^{3+}$, and were assigned to the Λ and Δ forms, respectively.

Table 1 shows the maximum CD intensities and positions in the first and second absorption region of the Λ-$[Co(NH_3)_2(diamine)_2]^{3+}$ and $[Co(diamine)_3]^{3+}$ spectra. The CD spectra of each bisdiamine and the corresponding trisdiamine complex are similar to each other with respect to peak positions and signs, as mentioned above for the tn complexes.

If the number of chelate rings contributes to CD intensity of a bisdiamine complex, the intensity would be expected to be two-thirds of that of the corresponding trisdiamine complex. However, as seen from the last column of Table 1, the observed ratio is roughly one-third or less, particularly with regard to the dominant CD peaks in the first absorption region. Therefore, the number of asymmetric pairs of chelate rings is considered to be more important in determining the CD intensity at least in the first absorption region of the spectra of $[Co(NH_3)_2(diamine)_2]^{3+}$ and $[Co(diamine)_3]^{3+}$, in which the diamine forms either five-membered or six-membered chelate ring. This is consistent with the previous results for the CD intensity of $[Co(en)_x(tn)_y(tmd)_z]^{3+}$ isomers.[7]

References

1) J. C. Bailar, Jr., and J. B. Work, *J. Am. Chem. Soc.*, **68**, 232 (1946).
2) J. Killander, *Biochim. Biophys. Acta*, **93**, 1 (1964).
3) M. Sano, K. Sasaki, Y. Yoshikawa, and H. Yamatera, unpublished work.
4) M. Fujita, Y. Yoshikawa, and H. Yamatera, *Bull. Chem. Soc. Jpn.*, **50**, 3209 (1977).
5) J. B. Stothers, "Carbon-13 NMR Spectroscopy," Academic Press, New York and London (1972), Chap. 5.
6) M. Fujita, Y. Yoshikawa, and H. Yamatera, *J. Chem. Soc., Chem. Commun.*, **1975**, 941.
7) M. Kojima, M. Fujita, H. Ogino, and J. Fujita, *Bull. Chem. Soc. Jpn.*, **50**, 2325 (1977).
8) A. J. McCaffery, S. F. Mason, and B. J. Norman, *J. Chem. Soc., A*, **1965**, 5094.
9) M. Kojima, M. Fujita, and J. Fujita, *Bull. Chem. Soc. Jpn.*, **50**, 898 (1977).

The Synthesis of Purpurosamine B Derivatives

Yutaka HONDA and Tetsuo SUAMI*

Department of Applied Chemistry, Faculty of Engineering, Keio University, Hiyoshi, Kohoku-ku, Yokohama 223

(Received June 7, 1980)

Synopsis. Purpurosamine B and its 6-epimer have been found in antibiotic gentamicin C_2 and fortimicin A respectively. Methyl 2,6-di-*N*-acetyl-α-purpurosaminide B and its corresponding 6-epimer have been synthesized from methyl 2-acetamido-2,3,4-trideoxy-α-D-*erythro*-hexodialdo-1,5-pyranoside.

In a continuation of preceding papers,[1,2] the synthesis of methyl 2,6-di-*N*-acetyl-α-purpurosaminide B (**6**) and its 6-epimer (**8**) will be described in the present paper. The nitromethane addition of methyl 2-acetamido-2,3,4-trideoxy-α-D-*erythro*-hexodialdo-1,5-pyranoside[2] (**1**) gave a mixture of two diastereomers, methyl 2-acetamido-2,3,4,7-tetradeoxy-7-nitro-α-D-*ribo*- and -β-L-*lyxo*-heptopyranosides, in a yield of 49%. The catalytic hydrogenation of the mixture, followed by treatment with benzyloxycarbonyl chloride in pyridine afforded 7-benzyloxycarbonylamino derivatives in a yield of 69%. The mesylation of the derivatives gave a mixture of 6-*O*-mesyl derivatives (**2**) in a yield of 89%.

Compound **2** was converted to aziridine derivatives by treatment with sodium isopropoxide. When the derivatives reacted with benzyloxycarbonyl chloride in dioxane and subsequently treated with HCl in dioxane, methyl 2-acetamido-6-(benzyloxycarbonylamino)-7-chloro-2,3,4,6,7-pentadeoxy-α-D-*ribo*-heptopyranoside (**3**) and the corresponding β-L-*lyxo* derivative (**4**) were obtained in 23 and 35% yields respectively.

The dehalogenation of **3** with tributylstannane gave methyl 2-acetamido-6-(benzyloxycarbonylamino)-2,3,4,6,7-pentadeoxy-α-D-*ribo*-heptopyranoside (**5**) in a yield of 84%; this was then converted to methyl 2,6-di-*N*-acetyl-α-purpurosaminide B (**6**), which was found to be identical with an authentic sample.[3]

Analogous reaction sequences of **4** gave methyl 2,6-di-*N*-acetyl-6-*epi*-α-purpurosaminide B (**8**).

Experimental[4]

A Mixture of Methyl 2-Acetamido-7-(benzyloxycarbonylamino)-2,3,4,7-tetradeoxy-6-O-mesyl-α-D-ribo- and -β-L-lyxo-heptopyranosides (2). A 1.34-g portion of methyl 2-acetamido-2,3,4-trideoxy-α-D-*erythro*-hexodialdo-1,5-pyranoside[2] (**1**) was treated with nitromethane (0.62 ml) in the presence of sodium methoxide at an ambient temperature for 40 h, as has been described in the preceding paper,[2] without recrystallization, to give 845 mg (49%) of a mixture of the two diastereomers.

The product was catalytically hydrogenated and subsequently treated with benzyloxycarbonyl chloride to give 805 mg (69%) of 7-*N*-benzyloxycarbonyl derivatives. The derivatives were mesylated analogously to the method described in the preceding paper[2] to give 872 mg (89%) of **2**: mp 123—126 °C.

Found: C, 51.25; H, 6.27; N, 6.34; S, 6.90%. Calcd for $C_{19}H_{28}N_2SO_8$: C, 51.34; H, 6.35; N, 6.30; S, 7.21%.

Methyl 2-Acetamido-6-(benzyloxycarbonylamino)-7-chloro-2,3,4,6,7-pentadeoxy-α-D-ribo-heptopyranoside (3) and -β-L-lyxo-heptopyranoside (4). To a solution of sodium isopropoxide (0.11 g of Na in 10 ml of isopropyl alcohol) in dioxane (5 ml), **2** (780 mg) was added, and the mixture was heated under reflux for 2 h. The solution was then concentrated, and benzyloxycarbonyl chloride (1.4 ml of 30% toluene solution) was added to a solution of the residue in dioxane (10 ml). After 3 h, dioxane (5 ml) containing 3% HCl was added to the mixture. After 1 h, the mixture was neutralized with Amberlite IRA-400(OH^-) and concentrated. The residue was purified on a silica-gel column using 3:2 (v/v) 2-butanone–toluene. Fractions homogeneous on TLC (R_f 0.43) in the same solvent were combined and concentrated. The residue was recrystallized from $CHCl_3$–

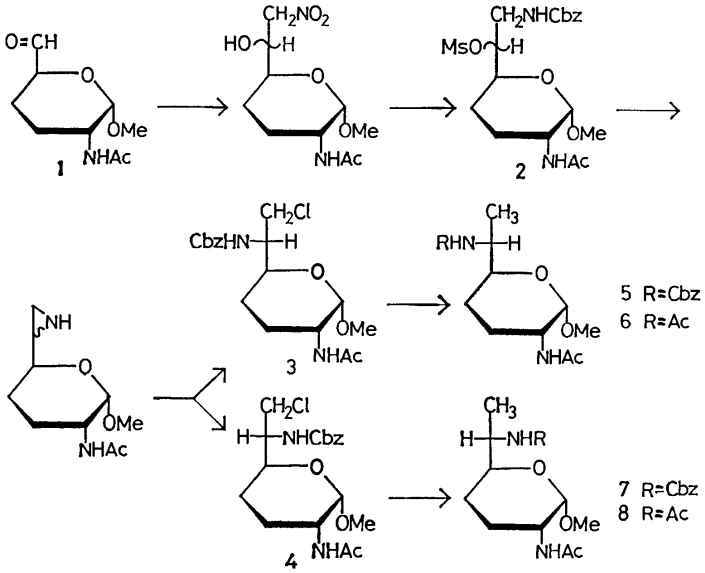

Scheme 1.

ether to give 139 mg (23%) of **3**: mp 196—197 °C; $[\alpha]_D^{20}$ +76.7° (*c* 0.43, $CHCl_3$); ^1H NMR ($CDCl_3$) δ 1.98 (s, 3, NAc), 3.42 (s, 3, OCH_3), 4.59 (d, 1, J=3.4 Hz, H-1), 5.78 (d, 1, J=8.5 Hz, NH-2).

Found: C, 56.36; H, 6.47; N, 7.18; Cl, 9.00%. Calcd for $C_{18}H_{25}N_2ClO_5$: C, 56.17; H, 6.55; N, 7.28; Cl, 9.21%.

Fractions homogeneous on TLC (R_f 0.46) were combined and concentrated, and the residue was recrystallized from ether to give 211 mg (35%) of **4**: mp 145—146 °C; $[\alpha]_D^{20}$ +59.3° (*c* 1.03, $CHCl_3$); ^1H NMR ($CDCl_3$) δ 1.97 (s, 3, NAc), 3.40 (s, 3, OCH_3), 4.59 (d, 1, J=3.4 Hz, H-1), 5.66 (d, 1, J=10 Hz, NH-2).

Found: C, 55.90; H, 6.50; N, 7.47; Cl, 9.45%. Calcd for $C_{18}H_{25}N_2ClO_5$: C, 56.17; H, 6.55; N, 7.28; Cl, 9.21%.

*Methyl 2-Acetamido-6-(benzyloxycarbonylamino)-2,3,4,6,7-pentadeoxy-α-*D*-ribo-heptopyranoside (**5**).* To a solution of **3** (74 mg) in dioxane (5 ml), tributylstannane (1.0 ml) and a small amount of α,α′-azobisisobutyronitrile were added under a N_2 atmosphere. After 7 h at 80 °C, the mixture was concentrated and the residue was purified on a silica-gel column using 3:2 (v/v) 2-butanone–toluene to give 56 mg (84%) of **5**: mp 195—196 °C; $[\alpha]_D^{20}$ +98.4° (*c* 0.95, $CHCl_3$); ^1H NMR ($CDCl_3$) δ 1.97 (s, 3, NAc), 3.31 (s, 3, OCH_3), 4.59 (d, 1, J=3.2 Hz, H-1), 5.00 (d, 1, NH-6), 5.68 (d, 1, J=10 Hz, NH-2).

Found: C, 61.53; H, 7.42; N, 7.93%. Calcd for $C_{18}H_{26}N_2O_5$: C, 61.69; H, 7.48; N, 8.00%.

*Methyl 2,6-Diacetamido-2,3,4,6,7-pentadeoxy-α-*D*-ribo-heptopyranoside (Methyl 2,6-Di-*N*-acetyl-α-purpurosaminide B) (**6**).* Compound **5** (48 mg) was hydrogenated in methanol (10 ml) in the presence of Pd black under a H_2 atmosphere for 48 h. The product was acetylated with acetic anhydride in methanol to give 24 mg (69%) of **6**: mp 261—262 °C; $[\alpha]_D^{20}$ +185.7° (*c* 0.7, methanol); ^1H NMR ($CDCl_3$–CD_3OD) δ 1.15 (d, 3, J=6.7 Hz, CH_3), 1.99 (s, 6, 2 NAc), 3.41 (s, 3, OCH_3), 4.67 (d, 1, J=3.1 Hz, H-1). The IR spectrum of **6** was superimposable on that of an authentic sample.[3] (Found: C, 55.71; H, 8.44; N, 10.76%). Lit,:[3] mp 261—262 °C; $[\alpha]_D^{20}$ +195°.

*Methyl 2-Acetamido-6-(benzyloxycarbonylamino)-2,3,4,6,7-pentadeoxy-β-*L*-lyxo-heptopyranoside (**7**).* Compound **4** (100 mg) was treated with tributylstannane (0.5 ml) as has been described above to give 82 mg (90%) of **7**: mp 163—164 °C; $[\alpha]_D^{20}$ +55.6° (*c* 0.99, $CHCl_3$); ^1H NMR ($CDCl_3$) δ 1.21 (d, 3, J=6.7 Hz, CH_3), 1.96 (s, 3, NAc), 3.36 (s, 3, OCH_3), 4.59 (d, 1, J=3.2 Hz, H-1), 5.00 (d, 1, NH-6), 5.64 (d, 1, J=9.0 Hz, NH-2).

Found: C, 61.83; H, 7.35; N, 7.94%. Calcd for $C_{18}H_{26}N_2O_5$: C, 61.69; H, 7.48; N, 8.00%.

*Methyl 2,6-Diacetamido-2,3,4,6,7-pentadeoxy-β-*L*-lyxo-heptopyranoside (Methyl 2,6-Di-*N*-acetyl-6-epi-α-purpurosaminide B) (**8**).* Compound **7** (50 mg) was hydrogenated and subsequently acetylated as has been described above to give 33 mg (88%) of **8**: mp 212—213 °C; $[\alpha]_D^{20}$ +62.5° (*c* 0.99, methanol). The ^1H NMR and IR spectra of **8** were superimposable on those of an authentic sample.[2]

References

1) T. Suami, Y. Honda, and T. Kato, *Chem. Lett.*, **1978**, 1125.

2) T. Suami, Y. Honda, T. Kato, M. Masu, and K. Matsuzawa, *Bull. Chem. Soc. Jpn.*, **53**, 1372 (1980).

3) The identification of methyl 2,6-di-*N*-acetyl-α-purpurosaminide B has been performed by Dr. P. J. L. Daniels, Research Division, Schering Plough Co., Bloomfield, N. J., 07003, U. S. A., to whom the authors' thanks are due.

4) The general methods used in the present work have been described in the preceding paper.[2]

Photochemical Isomerization of 6,7-Dicyano- and 6,7-Bis(methoxycarbonyl)-3-phenylsulfonyl-(2,4-*exo*)-3-azatricyclo[3.2.1.$0^{2,4}$]oct-6-ene

Katsumi UMANO,* Hiroto KOURA, and Hiroo INOUE

Department of Applied Chemistry, College of Engineering, University of Osaka Prefecture, Mozu-Umemachi, Sakai, Osaka 591

(Received November 4, 1980)

Synopsis. The photochemical reactions of 6,7-bis(methoxycarbonyl)- and 6,7-dicyano-3-phenylsulfonyl-(2,4-exo)-3-azatricyclo[3.2.1.$0^{2,4}$]oct-6-ene afford the corresponding tetracyclic compounds (**3b** and **3c**) by the skeletal isomerization, but those of their endo isomers do not result in the formation of **3b** and **3c**.

Recently we have reported that 3-phenylsulfonyl-(2,4-*exo*)-3-azatricyclo[3.2.1.$0^{2,4}$]oct-6-enes **1a—c** undergo thermal rearrangement to afford the corresponding 2-phenylsulfonyl-2-azabicyclo[3.2.1]oct-3,6-dienes in high yields under moderate conditions.[1] Our interest in the reactivity of these tricyclic aziridines prompted us to examine the photochemical isomerization of compounds **1a—c** and their endo isomers **2a—c**. The photochemical isomerization of tricyclo[3.2.1.-$0^{2,4}$]oct-6-enes[2] and their 3-oxa[3] and 3-aza[4] analogs has been known to afford tetracyclo[3.3.0.$0^{2,8}$.$0^{4,6}$]-octanes by a $[2\pi+2\sigma]$ cycloaddition pathway. Herein, we wish to report several results on the photochemical reaction of the tricyclic aziridines.

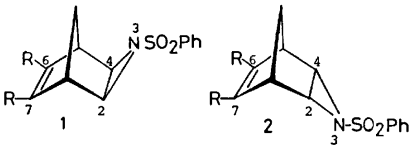

(a; R = H, b; R = CO_2Me, c; R = CN)

A solution of compounds **1a—c** and **2a—c** in acetonitrile was degassed in a Pyrex or quartz tube and irradiated with a high-pressure mercury lamp (300 W); the products were isolated in the usual manner. The results are summarized in Table 1. The irradiation of the unsubstituted *exo* and *endo* compounds **1a** and **2a** afforded no tetracyclic product. On the other hand, the 6,7-disubstituted *exo* compounds **1b** and **1c** were converted into the corresponding tetracyclic compounds **3b** and **3c** together with an unidentifiable polymeric material, as Table 1 shows.

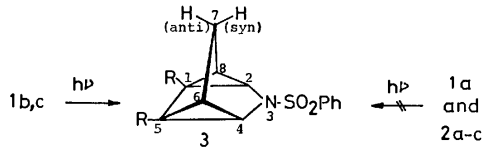

(b; R = CO_2Me, c; R = CN)

The cyano and methoxycarbonyl groups made possible the intramolecular photocyclization of the *exo* tricyclic aziridines, although in the thermal rearrangements of **1a—c** such substituents caused a decrease in their reactivity.[1] Furthermore, the cyano group brought about a higher yield of a tetracyclic compound than that in the case of the methoxycarbonyl group. The use of a quartz tube as a reaction vessel or a low-pressure mercury lamp as a light source resulted in the increase of the amount of the polymeric material produced.

TABLE 1. THE YIELDS OF THE TETRACYCLIC COMPOUNDS IN THE PHOTOCHEMICAL REACTIONS OF AZIRIDINES **1a—c** AND **2a—c**[a]

Compound	Tube[b]	Time/h	Yield/%	Recovery/%
1b	P	96	11	56
1b	Q	12	24	41
2b	P	96	0	96
2b	Q	12	0	53
1c	P	96	76	5
1c	Q	6	54	0
2c	P	96	0	78
2c	Q	6	0	64

a) Solvent: acetonitrile. Concentration of compound: 6.1×10^{-2} mol/l (Pyrex) and 1.3×10^{-1} mol/l (quartz). In the cases of **1a** and **2a**, the tetracyclic compounds were not obtained at all. The unreacted **1a** (*ca.* 90%) was isolated as 2-phenylsulfonyl-2-azabicyclo[3.2.1]oct-3,6-diene, which was produced by the thermal rearrangement on silica gel chromatography. The compound **2a** was recovered in *ca.* 90% yield. b) P= Pyrex and Q=quartz.

Contrary to the results in the cases of the *exo* compounds **1b** and **1c**, it was found that the 6,7-disubstituted *endo* compounds **2b** and **2c** undergo no isomerization under the similar conditions, as Table 1 shows. Thus, this result demonstrates that the bent C_2–C_4 bond directed toward the *endo* side is necessary for the photochemical isomerization of the tricyclic aziridines. A similar phenomenon has been observed in the thermal reactions of **1a—c** and **2a—c** described previously.[1]

Experimental

Melting points were uncorrected. Acetonitrile was distilled under nitrogen from CaH_2. IR, ^{1}H- and ^{13}C-NMR, and mass spectra were obtained on a Hitachi 216 grating infrared spectrometer, a Hitachi R-24A spectrometer, a JEOL FX 90Q Fourier transform NMR spectrometer, and a Hitachi RMU-6E mass spectrometer, respectively.

Material. The compounds, **1a—c** and **2b,c**, were prepared by the reactions of the corresponding norbornadienes with benzenesulfonyl azide. The ^{1}H-NMR, IR, and mass spectral data of their compounds are summarized in Table 2. The **2a** was prepared according to the methods described in the literature.[5]

General Procedure for Photochemical Reaction. All reactions were performed similarly in a pyrex or quartz tube (72 cm^3 total capacity). A reaction tube was charged with 0.61—0.65 mmol of **1a—c** and **2a—c** and 5—10 ml of dry

Table 2. Spectral data of compounds **1a—c** and **2b,c**

Compound	IR (KBr) ν/cm^{-1}	^{1}H-NMR (δ, $CDCl_3$)	MS m/e(M^+)
1a	1345(ν_{SO_2})	7.38—8.11(m, 5H, aromatic), 6.35(t, 2H, J=1.6 Hz, 6-H, 7-H), 3.17(s, 2H, 2-H, 4-H), 3.00(m, 2H, 1-H, 5-H), 1.16(d, 1H, J=8.3 Hz, 8-Hs), 1.72(d, 1H, J=8.3 Hz, 8-Ha)	247
1b	1740(ν_{CO}) 1345(ν_{SO_2})	7.30—8.00(m, 5H, aromatic), 3.80(s, 6H, OCH_3), 3.45(brs, 4H, 1-H, 2-H, 4-H, 5-H), 1.83(d, 1H, J=8.7 Hz, 8-Hs), 1.41(d, 1H, J=8.7 Hz, 8-Ha)	363
2b	1730(ν_{CO}) 1325(ν_{SO_2})	7.40—8.00(m, 5H, aromatic), 3.72(brs, 2H, 2-H, 4-H), 3.66(s, 6H, OCH_3), 3.38(m, 2H, 1-H, 5-H), 1.98(brs, 2H, 8-CH_2)	363
1c	2240(ν_{CN}) 1335(ν_{SO_2})	7.46—8.16(m, 5H, aromatic), 3.50(brs, 2H, 1-H, 5-H), 3.43(s, 2H, 2-H, 4-H), 2.03(d, 1H, J=10.7 Hz, 8-Hs), 1.55(d, 1H, J=10.7 Hz, 8-Ha)	297
2c	2230(ν_{CN}) 1325(ν_{SO_2})	7.50—8.30(m, 5H, aromatic), 3.81(m, 2H, 2-H, 4-H), 3.45(m, 2H, 1-H, 5-H), 2.15(s, 2H, 8-CH_2)	297

a) The spectra were measured at 60 MHz.

Table 3. Spectral data of compounds **3b,c**

Compound	IR (KBr) ν/cm^{-1}	^{1}H-NMR (δ)[a]	^{13}C-NMR (δ)[b,c]
3b	1725(ν_{CO}) 1320(ν_{SO_2})	$CDCl_3$: 7.30—8.00(m, 5H, aromatic), 4.12(d, 2H, J=9.0 Hz, 2-H, 4-H), 3.53(s, 6H, OCH_3), 2.22(m, 2H, 6-H, 8-H), 1.98(m, 1H, 7-H_{antl}), 1.70(d, 1H, J=13 Hz, 7-H_{syn})	$CDCl_3$: 167(s, C=O), 54(d, 2-C, 4-C), 52(q, OCH_3), 36(s, 1-C, 5-C), 32(d, 6-C, 8-C), 23(t, 7-C)
3c	2230(ν_{CN}) 1320(ν_{SO_2})	DMSO-d_6: 7.40—8.05(m, 5H, aromatic), 4.56(d, 2H, J=9.0 Hz, 2-H, 4-H), 2.36(m, 2H, 6-H, 8-H), 1.94(m, 1H, 7-H_{antl}), 1.52(d, 1H, J=13.0 Hz, 7-H_{syn})	DMSO-d_6: 115(s, CN), 54 (d, 2-C, 4-C), 31(d, 6-C, 8-C), 23(t, 7-C), 21(s, 1-C, 5-C)

a) The spectra were measured at 90 MHz. b) Splitting patterns were obtained by off-resonance decoupling. c) Signals of aromatic protons are omitted.

acetonitrile. After the air in the tube was replaced by argon by a freezing method, the tube was sealed and irradiated for a definite time at an equidistant (5 cm) location from a 300 W mercury lamp. After the removal of acetonitrile *in vacuo*, the residue was chromatographed on silica gel. The **3b** and **3c** were eluted with (12:1) benzene–acetone, **3b** was recrystallized from ethanol to give colorless prisms, and **3c** from chloroform to give needles. **3b**: 120—122 °C; MS *m/e* 363 (M^+). Found: C, 55.90; H, 4.74; N, 4.01%. Calcd for $C_{17}H_{17}NO_6S$: C, 56.19; H, 4.68; N, 3.86%. **3c**: 197—199 °C; MS *m/e* 297 (M^+). Found: C, 60.55; H, 3.67; N, 14.40%. Calcd for $C_{15}H_{11}N_3O_2S$: C, 60.61; H, 3.70; N, 14.14%. The ^{1}H- and ^{13}C-NMR and IR spectral data of their compounds are summarized in Table 3.

References

1) K. Umano, H. Taniguchi, H. Inoue, and E. Imoto, *Tetrahedron Lett.*, **1979**, 247.
2) P. K. Freeman, D. G. Kuper, and V. N. M. Rao, *Tetrahedron Lett.*, **1965**, 3301.
3) H. Prinzbach and M. Klaus, *Angew. Chem. Int. Ed. Engl.*, **8**, 276 (1969).
4) M. Klaus and H. Prinzbach, *Angew. Chem. Int. Ed. Engl.*, **10**, 273 (1971).
5) A. C. Oehlschlager and L. H. Zalkow, *Can. J. Chem.*, **47**, 461 (1969).

The Photochemical Reaction of Benzo[c]cinnoline. IV. Comments on the Mechanism of 2,2′-Diaminobiphenyl Formation

Hiroyasu Inoue,* Yukimi Hiroshima, Toshihiko Sakai, Tadamitsu Sakurai, and Norio Fukuda

Department of Applied Chemistry, Faculty of Technology, Kanagawa University, Kanagawa-ku, Yokohama 221

(Received November 20, 1980)

Synopsis. In order to determine the mechanism of 2,2′-diaminobiphenyl formation from benzo[*c*]cinnoline, effect of aldehyde on the reaction was examined. It is proposed that ethanal, which was generated from ethanol in the initial photoreduction, formed an adduct with 5,6-dihydrobenzo[*c*]cinnoline, and that the resulting adduct participated in the subsequent photo-induced 2,2′-diaminobiphenyl formation.

Photochemical reactions of benzo[*c*]cinnoline (hereafter referred to as BCC) show a dependence on excitation wavelengths and solvents. In a previous paper,[1] BCC found to give 2,2′-diaminobiphenyl (referred to as DAB) under irradiation of light of wavelength longer than 400 nm in an acidic aqueous ethanol. In the DAB formation, 5,6-dihydroBCC, which is monoprotonated in the acidic solution, is initially produced as an intermediate. On the other hand, when 2-propanol is used in the place of ethanol, the visible light irradiation does not afford DAB, although the photoreduction to 5,6-dihydroBCC occurs.[2] Therefore, there is a distinct difference in the DAB formation between these alcohols. Such solvent dependence is a problem to be solved.

Protonated 5,6-dihydroBCC itself can not be excited electronically by visible light; it has been shown that the excitation of 5,6-dihydroBCC with ultraviolet light causes the photoelimination to afford carbazole in an acidic 2-propanol as well as in an acidic ethanol.[3]

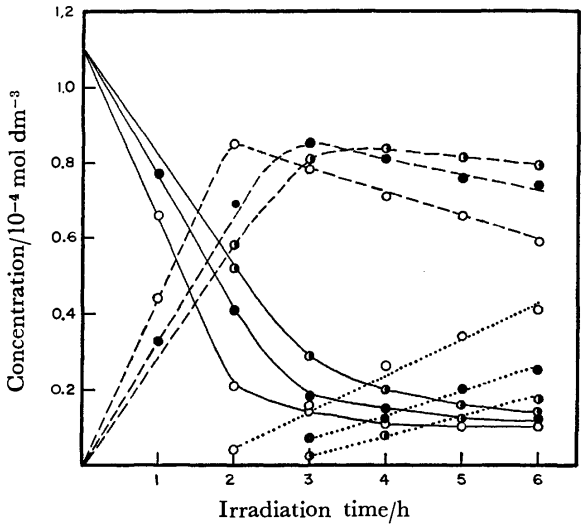

Fig. 1. Rate of the reaction under the visible light irradiation upon a 3.6 mol dm^{-3} HCl ethanol solution of BCC (1.1×10^{-4} mol dm^{-3}).
Concentrations of BCC(——), 5,6-dihydroBCC(- - -), and DAB(·····). Relative light intensity; ○: 3.1; ●: 1.6; ◑: 1.0.

The present paper is concerned with the mechanism of the photo-induced DAB formation from 5,6-dihydroBCC.

Experimental

BCC and 2-propanol were the same as those used previously.[2] Aldehydes used here were ethanal, propanal, butanal, and 2-methylpropanal and were purified by distillation.

A 500 W high pressure mercury arc lamp (Ushio USH-500), with a glass filter (Corning CS-3—73), which cut off light of wavelength shorter than 400 nm, was used as a visible light source. The quantitative conversion of BCC (5.0×10^{-5} mol dm^{-3}) into 5,6-dihydroBCC was attained by the visible light irradiation for 3 h upon an acidic (4 mol dm^{-3} HCl) 2-propanol solution of BCC. In order to examine the effects of some added compounds, further irradiation were carried out in the same manner after the addition of additives into the reactant solution. All irradiations were carried out at room temperature under nitrogen. The intensity of incident light was determined by actinometry, using a potassium trioxalatoferrate(III) solution.

Results and Discussion

Figure 1 shows the rates of reaction under the visible light irradiation upon a 3.6 mol dm^{-3} HCl aqueous ethanol solution of BCC (1.1×10^{-4} mol dm^{-3}). The concentrations of BCC, 5,6-dihydroBCC, and 2,2′-diaminobiphenyl were determined spectrophotometrically as reported earlier.[1] The DAB formation was initiated after about 80% of the initial amount of BCC was converted into 5,6-dihydroBCC, irrespective of light intensities. Moreover, as seen from Fig. 1, the amount of DAB produced is related linearly to the irradiation time, and is dependent on light intensities. Since 5,6-dihydroBCC itself has no absorption in the visible region, these results suggest that a certain species, which can be excited electronically with the visible light, may play an essential role in the subsequent DAB formation.

Effects of aldehyde and ketone on the reaction were examined, because these compounds were generally produced from primary and secondary alcohols, respectively, in photo-induced hydrogen abstraction reactions by substrates.[4,5] When ethanal was added into an acidic 2-propanol solution of 5,6-dihydroBCC prepared previously[2] and the irradiation was allowed to continue, the DAB formation was observed without the induction period. On the other hand, acetone was shown to have no effect on the reaction. Therefore, the solvent dependence of the photo-induced DAB formation can be interpreted in terms of the

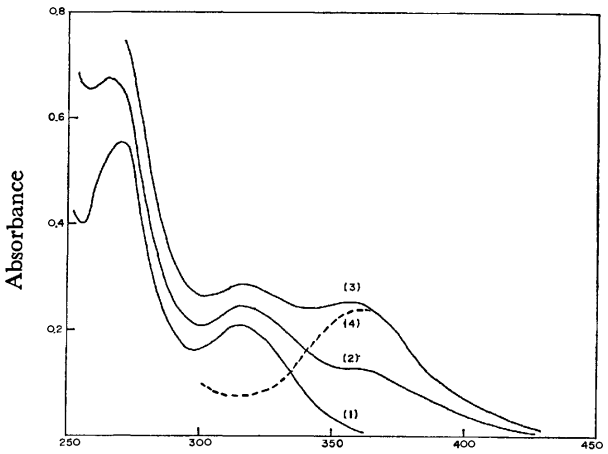

Fig. 2. Spectral change caused by the addition of butanal into an acidic 2-propanol solution of 5,6-dihydroBCC(5.0×10^{-5} mol dm^{-3}).
Concentration of butanal; (1): 0 mol dm^{-3}, (2): 2.2×10^{-3} mol dm^{-3}, (3): 8.9×10^{-3} mol dm^{-3}, (4): difference spectrum (3)—(1).

difference of the products from alcohols in the initial photoreduction.

Figure 2 shows the spectral change caused by the addition of butanal into an acidic 2-propanol solution of 5,6-dihydroBCC. As seen from this figure, a new absorption band appears around 360 nm on the addition of the aldehyde, thus indicating that there is interaction between 5,6-dihydroBCC and the aldehyde giving a certain species. The resulting species can absorb the irradiation light. On the other hand, no spectral change was observed when acetone was added.

The species formed is so unstable that it gives BCC quantitatively after being allowed to stand for several hours under nitrogen, although 5,6-dihydroBCC itself is relatively stable in the acidic solution. Here it should be noted that this aldehyde is known to form an adduct with amine, and the resulting adduct (carbinolamine) is usually unstable.[6-8] In the present case, therefore, the following equilibrium can be considered to be established, and the adduct may participate in the DAB formation through the visible light absorption. The adduct converts spontaneously

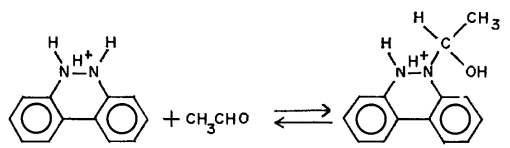

5*H*-6-(1-Hydroxyethyl)-benzo[*c*]cinnoline

to BCC, as described above. This conversion may be expected to be accompanied by the generation of a primary alcohol, RCH_2OH. In order to detect the alcohol generated from the adduct, an acidic tetrahydrofuran solution of 5,6-dihydroBCC in concentration of 1.2×10^{-1} mol dm^{-3} was prepared using $LiAlH_4$ as reported earlier.[2] Propanal was added into the 5,6-dihydroBCC solution to form the adduct,[9] and then the solution was allowed to stand for enough time for the conversion of the adduct to BCC. Gas chromatography showed that propanol was present in the tetrahydrofuran solution.

Table 1. Equilibrium constants (K) of the adduct formation and rates of the conversion of BCC into DAB[a]

Aldehyde[b]	K/mol dm^{-3} at 21 °C	DAB produced (%)
Ethanal	322	67
Butanal	243	39
Propanal	110	31
2-Methylpropanal	25	14

a) Initial concentration of BCC: 2.0×10^{-5} mol dm^{-3}, Irradiation time: 30 min. b) Concentration of aldehyde: 4.0×10^{-4} mol dm^{-3}.

For several aldehydes the same new absorption band was observed around 360 nm. The alkyl groups in the aldehydes did not affect the position of the band. The equilibrium constants for the adduct formation were determined by applying the Benesi-Hildebrand equation.[10] The results are presented in Table 1, in which the rates of the DAB formation are also shown. The equilibrium constant is dependent on the alkyl groups in the aldehydes. The observed correlation between the equilibrium constant and the product yield indicates that the carbinolamine adduct serves as a precursor of DAB.

References

1) Part I of this series: H. Inoue, T. Sakurai, and F. Tanaka, *Bull. Chem. Soc. Jpn.*, **48**, 924 (1975).
2) Part II of this series: H. Inoue, Y. Hiroshima, and N. Makita, *Bull. Chem. Soc. Jpn.*, **52**, 351 (1979).
3) Part III of this series: H. Inoue, Y. Hiroshima, and K. Miyazaki, *Bull. Chem. Soc. Jpn.*, **52**, 664 (1979).
4) B. Atkinson and M. Di, *Trans. Faraday Soc.*, **54**, 1331 (1958).
5) J. N. Pitts, Jr., R. L. Letsinger, R. P. Taylor, J. M. Patterson, G. Recktenwald, and R. B. Martin, *J. Am. Chem. Soc.*, **81**, 1068 (1959).
6) O. H. Whealer, "The Chemistry of the Carbonyl Group," ed by S. Patai, Intersci. Pub., (1966), p. 529.
7) P. Y. Sollenberger and R. B. Martin, "The Chemistry of the Amino Group," ed by S. Patai, Intersci, Pub., (1968), p. 367.
8) Y. Ogata and A. Kawasaki, "The chemistry of the carbonyl group," ed by J. Zabiky, Intersci. Pub., (1970), Vol. 2, p. 42.
9) The absorption spectrum of the adduct thus obtained is similar to the difference spectrum shown in Fig. 2(4).
10) H. A. Benesi and J. H. Hildebrand, *J. Am. Chem. Soc.*, **71** 2703 (1949).

Synthesis of 2-Substituted 1,3-Butadienes by Cross-coupling Reaction of 2-(1,3-Butadienyl)magnesium Chloride with Alkyl or Aryl Iodides

Sadaaki NUNOMOTO,* Yuhsuke KAWAKAMI,** and Yuya YAMASHITA**

Faculty of Chemical Engineering, Toyama Technical College, Hongo, Toyama 930

***Department of Synthetic Chemistry, Faculty of Engineering, Nagoya University, Chikusa-ku, Nagoya 464*

(Received January 12, 1981)

Synopsis. The cross-coupling reactions of 2-(1,3-butadienyl)magnesium chloride (1) with aryl and alkyl iodides were investigated in the presence of transition metal catalysts. Tetrakis(triphenylphosphine)palladium(0) catalyzes the cross-coupling reactions of **1** with aryl iodides, and copper(I) iodide catalyzes the reaction with alkyl iodides. These cross-coupling reactions offer convenient routes for the synthesis of 2-substituted 1,3-butadienes.

It has been reported that the cross-coupling reactions of Grignard reagents with allyl or alkenyl halides occurred in the presence of nickel or palladium complexes under mild conditions.[1-5]

Allyl Grignard reagent was reported to be alkylated by alkyl iodides or tosylates in the presence of copper(I) iodide.[6,7]

The authors carried out the synthesis of 2-substituted 1,3-butadienes by the cross-coupling reactions of **1** with aryl iodides in benzene–tetrahydrofuran (THF) catalyzed by tetrakis(triphenylphosphine)palladium(O) (**4**) or alkyl iodides in THF by copper(I) iodide (**5**) (Eqs. 1 and 2), and wish to report the results.

$$\underset{\text{MgCl}}{\underset{|}{\text{CH}_2{=}\text{CH}{-}\text{C}{=}\text{CH}_2}} + \text{ArI} \xrightarrow[\text{C}_6\text{H}_6\text{-THF}]{\text{Pd(pph}_3)_4} \underset{\text{Ar}}{\underset{|}{\text{CH}_2{=}\text{CH}{-}\text{C}{=}\text{CH}_2}} \quad (1)$$

1 **2**

$$\underset{\text{MgCl}}{\underset{|}{\text{CH}_2{=}\text{CH}{-}\text{C}{=}\text{CH}_2}} + \text{RI} \xrightarrow[-30\,^\circ\text{C, THF}]{\text{CuI}} \underset{\text{R}}{\underset{|}{\text{CH}_2{=}\text{CH}{-}\text{C}{=}\text{CH}_2}} \quad (2)$$

1 **3**

The results of cross-coupling reactions of **1** with iodobenzene are shown in Table 1. Only **4** is highly active among the transition metal complex catalysts examined, and 2-phenyl-1,3-butadiene (**2**) was obtained in increasing yield with an increase in the amount of the catalyst. Nickel(II) acetylacetonate was inactive for the reaction. As **4** showed a high activity, the cross-coupling reactions of **1** with aryl and alkyl halides were investigated in the presence of **4**. However, **4** was not an effective catalyst for the cross-coupling reaction of **1** with bromobenzene, alkyl iodide, or iodocyclohexane, as shown in Table 2.

Only aryl iodides gave the cross-coupling products

Table 1. The effects of catalysts on the cross-coupling reaction of **1** with iodobenzene in C_6H_6/THF (50:100 ml)[a]

No.	Catalyst	Catalyst amount / mol%	Cross-coupling product **2** Yield/%
1	$Ni(acac)_2$	2	0
2	$Ni(pph_3)_4$	2	Polymerized
3	$Pd(OCOCH_3)_2$	6	**5**
4	$Pd(pph_3)_4$	1	40
5	$Pd(pph_3)_4$	2	55
6	$Pd(pph_3)_4$	3	75
7	$Pd(pph_3)_4$	4	90

a) $[RMgX]_0$: 1.0 mol/l, $[RMgX]:[C_6H_5I]=1:1$ molar ratio.

Table 2. Preparation of 2-substituted 1,3-butadienes by the cross-coupling reactions of **1** with aryl and alkyl halides in C_6H_6/THF using **4**[a]

No.	ArX	Catalyst amount / mol%	Cross-coupling product **2** Yield/%	Bp/°C (mmHg)
8	C_6H_5Cl	4	0	
9	C_6H_5Br	4	0	
10	c-$C_6H_{11}I$	3	0	
11	p-BrC_6H_4I	3	Polymerized[b]	
12	p-$CH_3OC_6H_4I$	3	50	66—69 (3)
13	1-$C_{10}H_7I$	3	40	122—126 (3)
6	C_6H_5I	3	75	62—65 (20)
14	p-$CH_3C_6H_4I$	3	56	60—64 (5)
15	$C_6H_5CH_2I$	3	71	71—75 (5)

a) $[RMgX]_0$: 1.0 mol/l, $[RMgX]:[ArX]=1:1$ molar ratio. b) 2-(*p*-Bromophenyl)-1,3-butadiene was separated by preparative GLC, and was identified by MS and NMR spectra.

Table 3. Preparation of butadiene derivatives from **1** and alkyl halides catalyzed by **5**[a]

No.	RX	CuI / mol%	Cross-coupling product **3** Yield/%	Bp/°C (mmHg)
16	C_6H_5Br	20	0	
17	C_6H_5I	20	0	
18	c-$C_6H_{11}I$	20	5	
19	n-$C_6H_{13}CHICH_3$	20	0	
20	n-$C_8H_{17}Cl$	20	0	
21	n-$C_8H_{17}Br$	20	5	
22	n-$C_6H_{13}I$	20	60	75—79 (20)
23	n-$C_8H_{17}I$	10	45	74—77 (3)
24	n-$C_8H_{17}I$	20	67	
25	n-$C_{10}H_{21}I$	20	68	95—99 (5)
26	n-$C_{16}H_{33}I$	20	40	155—160 (2)
27	$ClCH_2CH_2CH_2I$	20	30[b]	62—66 (30)

a) $[RMgX]_0$: 1.0 mol/l, $[RMgX]:[RX]=1:1$ molar ratio, solvent: THF. b) The product, 2-(3-chloropropyl)-1,3-butadiene was identified by MS and NMR spectra.

in reasonably good yield. In order to overcome the low activity of **4** in the reaction, **5**, which is known to form an ate complex with a Grignard reagent, was used as a catalyst and the results with aryl and alkyl halides are shown in Table 3.

Although **5** was not active for iodobenzene, iodocyclohexane, or alkyl bromides, reasonable yields could be obtained with linear alkyl iodides, giving 2-alkyl-1,3-butadienes. These selectivities can be applied to the chemoselective cross-coupling reaction (Table 2 No. 11 and Table 3 No. 27) for the synthesis of functionalized 1,3-butadienes.

Experimental

Reagents. **1** was prepared as described in the previous report.[8] **4** and **5** were prepared by the procedures described elsewhere.[9,10]

*Cross-coupling Reaction of **1** with Aryl Iodides.* To a mixture of an aryl iodide (0.1 mol), **4** (1—3 mol% to an aryl iodide) and dry benzene (50 ml) in a 300 ml four-necked flask, **1** (0.1 mol) in THF (100 ml) was added dropwise with stirring under nitrogen atmosphere.

An exothermic reaction occurred during the addition, and the color of the contents gradually changed from yellowish green to black. After the completion of the addition, stirring was continued for 30 min at the refluxing temperature of the reaction system.

The organic layer was separated after hydrolyzing with 6 mol dm^{-3}-HCl, and the aqueous layer was extracted with two portions of diethyl ether (80 ml). The combined organic layer was washed first with 5% aqueous sodium hydrogencarbonate, then with water, then dried (Na_2SO_4) and distilled.

*Cross-coupling Reaction of **1** with Alkyl Iodides.* To a mixture of an alkyl iodide (0.1 mol), 5 (10—20 mol% to an alkyl iodide) and THF (50 ml) in a 300 ml four-necked flask cooled to −30 °C, **1** was added dropwise with stirring under nitrogen atmosphere.

The color of the contents gradually changed from light yellow to black. After the completion of the addition, stirring was continued for 2 h at 0 °C. The products were isolated by the work-up used for aryl iodides. The reaction products were identified by comparing their IR and NMR spectra with the reported data.

References

1) A. S. Kende, L. S. Liebeskind, and D. M. Braitsch, *Tetrahedron Lett.*, **1975**, 3375.
2) H. P. Dang and G. Linstrumelle, *Tetrahedron Lett.*, **1978**, 191.
3) F. D. Boumechal, R. Lorne, and G. Linstrumelle, *Tetrahedron Lett.*, **1977**, 1181.
4) K. Tamao, K. Sumitani, Y. Kiso, M. Zembayashi, A. Fujioka, S. Kodama, I. Nakajima, A. Minato, and M. Kumada, *Bull. Chem. Soc. Jpn.*, **49**, 1958 (1976).
5) S. Murahashi, M. Yamamura, K. Yanagisawa, N. Mita, and K. Kondo, *J. Org. Chem.*, **44**, 2408 (1979).
6) C. R. Johnson and G. A. Dutra, *J. Am. Chem. Soc.*, **95**, 7777 (1973).
7) F. D. Boumechal and G. Linstrumelle, *Tetrahedron Lett.*, **1976**, 3223 (1976).
8) S. Nunomoto and Y. Yamashita, *J. Org. Chem.*, **44**, 4788 (1979).
9) D. R. Coulson, *Inorg. Synth.*, **13**, 121 (1972).
10) G. B. Kauffman and R. P. Pinnell, *Inorg. Synth.*, **6**, 3 (1960).

Facile Dehydrogenative Dimerization of Indolizine Derivatives

Akikazu KAKEHI,* Suketaka ITO, Akihiro HAMAGUCHI, and Tsutomu OKANO

Department of Industrial Chemistry, Faculty of Engineering, Shinshu University, Wakasato, Nagano 380

(Received January 28, 1981)

Synopsis. Treatment of 3-unsubstituted indolizines with a dehydrogenating agent such as palladium on carbon in refluxing xylene gave the corresponding 3,3′-biindolizine derivatives in 19—74% yields.

It is well known that indolizines react smoothly at the 3-position with various electrophiles, as observed, for example, in the cycloaddition and the Michael addition with electron-poor olefins[1-3] and substitution with diazonium salts[4] or an acylating agent.[5] In order to study nitrogen-bridged heterocycles, a method for direct functionalization of indolizine derivatives was required. Attempts to obtain the corresponding adducts by the reactions of an indolizine with electron-poor olefins such as diethyl fumarate and ethyl cinnamate under various conditions were unsuccessful. However, in the reaction in the presence of a dehydrogenating agent, an unexpected product, *i.e.* a dimer of the indolizine was obtained. In this note we wish to report a facile dehydrogenative dimerization of some 3-unsubstituted indolizine derivatives and the structural assignment of the resulting biindolizines.

When the reaction of 1-methylindolizine (**1a**) with diethyl fumarate or ethyl cinnamate was carried out in refluxing xylene in the presence of palladium on carbon (Pd/C), a product (**2a**, pale yellow needles), mp 144—145 °C, was separated as the only isolable compound. Elementary analysis (Table 1), and the mass spectrum (M^+ 260) of the product show that **2a** is a bimolecular dehydrogenative coupling product from **1a**. The same product (**2a**) was also formed by the reaction of **1a** with Pd/C in the absence of the olefin in 38% yield. In order to confirm the generality of this reaction, we carried out the reactions of some indolizines with Pd/C. As expected, the corresponding pale yellow products (**2b—e**) were formed from 2-phenyl- (**1b**), 1-methyl-2-phenyl- (**1c**), 1-ethyl-2-phenyl- (**1d**), and 1,2-diphenyl-indolizine (**1e**), respectively. Elementary analyses and mass spectra (Table 1) of **2b—e** were also in accord with the expected structures. The site of the coupling in these biindolizines (**2a—e**) was determined mainly by means of their NMR spectral data (Table 2): For example, the NMR spectrum of **2a** exhibited signals at δ 6.40 (2H, dt, J=7.0, 7.0, and 1.5 Hz, 6-H and 6′-H), 6.71 (2H, br t, J=9.0 and 7.0 Hz, 7-H and 7′-H), 7.46 (2H, br d, J=9.0 Hz, 8-H and 8′-H), and 7.72 (2H, br d, J=7.0 Hz, 5-H and 5′-H) due to the protons on the pyridine rings, and at δ 2.43 (6H, s, 1-Me and 1′-Me) and 6.86 (2H, s, 2-H and 2′-H) due to the methyl groups and the protons on the pyrrole rings. As compared with the original 1-methylindolizine (**1a**),[6] in particular, the disappearance of the 3- and 3′-protons and the absence of the coupling of the 2- and 2′-protons (δ 6.86, singlet) in **2a** are ultimate evidences that **2a** is 3,3′-biindolizine derivative. Furthermore, distinct symmetrical structures of **2a—e** were also suggested by their IR spectra in which only a few weakened absorption bands appear in contrast with those of **1a—e**. From these results we conclude the structures of **2a—e** to be 3,3′-biindolizines.

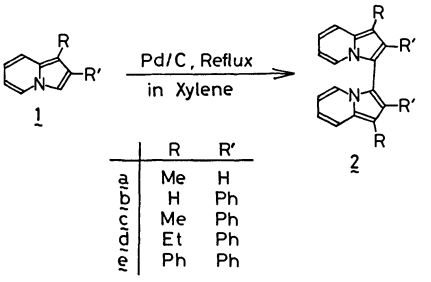

Scheme 1.

Similar reactions of aromatic substrates by the action of palladium(II) compounds[7,8] are well established, but that with Pd(O) as described above is unprecedent. The dehydrogenative dimerization with Pd/C is of interest and high synthetic value because of its simplicity and low cost, though the yields were not satisfactory.

Experimental

Melting points were measured with a Yanagimoto micromelting point apparatus and are uncorrected. Microanalysis was carried out in a Perkin-Elmer 240 Elemental Analyzer. NMR spectra were determined with a Varian EM360A NMR spectrometer in deuteriochloroform with tetramethylsilan as an internal standard, chemical shifts being expressed in terms of δ, mass spectra with a JEOL LMS-01SG-2 mass spectrometer with a JEC-6 spectrocom-

TABLE 1. DATA OF 3,3′-BIINDOLIZINE DERIVATIVES

Compd No.	Yield %	Mp/°C	ν/cm^{-1}(KBr)			M^+	Formula	Calcd (%)			Found (%)		
								C	H	N	C	H	N
2a	38	144—145	1436	1420	732	260	$C_{18}H_{16}N_2$	83.04	6.20	10.76	82.91	6.30	10.70
2b	19	169—171	1600	1449	1336	384	$C_{28}H_{20}N_2$	87.47	5.24	7.29	87.29	5.31	7.26
2c	35	244—246	1595	1435	1336	412	$C_{30}H_{24}N_2$	87.34	5.87	6.79	87.39	5.98	6.63
2d	38	194—196	1596	1437	1339	440	$C_{32}H_{28}N_2$	87.23	6.41	6.36	86.94	6.53	6.26
2e	74	230—231	1598	1520	1340	536	$C_{40}H_{28}N_2$	89.52	5.26	5.22	89.33	5.52	5.14

Table 2. Proton NMR spectra of 3,3′-biindolizine derivatives

2a	2.43(6H, s, 1-Me and 1′-Me), 6.40(2H. dt, J=7.0, 7.0, and 1.5 Hz, 6-H and 6′-H), 6.71(2H, br t, J=9.0 and 7.0 Hz, 7-H and 7′-H), 6.86(2H, s, 2-H and 2′-H), 7.46(2H, br d, J=9.0 Hz, 8-H and 8′-H), and 7.72(2H, br d, J=7.0 Hz, 5-H and 5′-H).
2b	6.34(2H, dt, J=7.0, 7.0, and 1.5 Hz, 6-H and 6′-H), 6.80(2H, br t, J=9.0 and 7.0 Hz, 7-H and 7′-H), 7.03(2H, s, 1-H and 1′-H), and 7.1—7.7(14H, m, 2-Ph, 2′-Ph, 5-H, 5′-H, 8-H, and 8′-H).
2c	2.44(6H, s, 1-Me and 1′-Me), 6.40(2H, dt, J=7.0, 7.0, and 1.5 Hz, 6-H and 6′-H), and 6.6—7.7(16H, m, 2-Ph, 2′-Ph, 5-H, 5′-H, 7-H, 7′-H, 8-H, and 8′-H).
2d	1.19(6H, t, J=7.0 Hz, 2 $CH_2C\underline{H}_3$), 2.88(4H, q, J=7.0 Hz, 2 $C\underline{H}_2CH_3$), 6.40(2H, dt, J=7.0, 7.0, and 1.5 Hz, 6-H and 6′-H), and 6.6—7.7(16H, m, 2-Ph, 2′-Ph, 5-H, 5′-H, 7-H, 7′-H, 8-H, and 8′-H).
2e	6.3—8.1(28H, m).

puter attached, and IR spectra with a Hitachi 260—10 Infrared spectrophotometer.

Materials. Indolizines (**1b—2e**) were synthesized by the Tschitschibabin reaction of the corresponding 1-phenacylpyridinium bromides.[9-11] 1-Methylindolizine (**1a**)[12] was prepared in overall 45% yield by the reaction of 1-(ethoxycarbonylmethyl)-2-ethylpyridinium bromide with ethyl (ethoxymethylene)cyanoacetate in ethanol in the presence of potassium carbonate at 40—50 °C followed by acidic hydrolysis of the resulting ethyl 1-methylindolizine-3-carboxylate.

Preparation of 3,3′-Biindolizines (2a—e). General Method. A mixture of indolizine (2 mmol), palladium on carbon (5%, 0.8—1.0 g), and dry xylene (50 ml) was heated under reflux in a 100 ml round flask equipped with a condenser for 20—25 h and then cooled. Insoluble substances were removed from the reaction solution by filtration and the filtrate was concentrated at reduced pressure. The residue was separated carefully by column chromatography (alumina) using hexane and then ether as eluents. Recrystallization several times from ether–hexane gave the corresponding 3,3′-biindolizine derivatives as pale yellow needles (**2a**) or prisms (**2b—e**).

Similar treatment of the parent indolizine with Pd/C did not afford the expected 3,3′-biindolizine because of its instability.

These results and some properties of **2a—e** are given in Tables 1 and 2.

References

1) A. Galbraith, T. Small, R. A. Barnes, and V. Boekelheide, *J. Am. Chem. Soc.*, **83**, 453 (1961).
2) S. Ikeda, S. Kajigaeshi, and S. Kanemasa, *Chem. Lett.*, **1976**, 367.
3) T. Uchida and K. Matsumoto, *Chem. Lett.*, **1980**, 149.
4) J. Bailey, *Chem. Abstr.*, **71**, 92638f (1969).
5) V. Boekelheide and R. J. Windgassen Jr., *J. Am. Chem. Soc.*, **81**. 1456 (1959).
6) δ 2.27 (3H, s, 1-Me), 6.16 (1H, dt, J=7.0, 7.0, and 1.5 Hz, 6-H), 6.40 (1H, br t, J=9.0 and 7.0 Hz, 7-H), 6.52 (1H, d, J=2.5 Hz, 2-H), 7.06 (1H, d, J=2.5 Hz, 3-H), 7.17 (1H, br d, J=9.0 Hz, 8-H), and 7.06 (1H, d, J=7.0 Hz, 5-H).
7) R. van Helden and G. Verberg, *Rec. Trav. Chim. Pays-Bas*, **84**, 1263 (1965).
8) J. Davidson and C. Triggs, *Chem. Ind. (London)*, **1966**, 457.
9) E. T. Borrows, D. O. Holland, and J. Kenyon, *J. Chem. Soc.*, **1946**, 1069.
10) E. A. Kochethova, *Zh. Obsch. Khim.*, **33**, 1201 (1963).
11) P. A. Barrett, *J. Chem. Soc., C*, **1958**, 325.
12) P. A. Barrett and K. A. Chalmers, *J. Chem. Soc., C*, **1958**, 338.

An Improved Oxidation Method of Pyridoxine

Masaaki IWATA

The Institute of Physical and Chemical Research, Wako, Saitama 351

(Received January 28, 1981)

Synopsis. Manganese dioxide oxidation in the presence of primary amine was found to be an efficient oxidation system for pyridoxine.

Prevalent method to synthesize pyridoxal and its congeners from the corresponding pyridoxines has been carried out by use of "active" manganese dioxide as an effective oxidant in aqueous solution of restricted pH ranges or in chloroform.[1] The efficiency of the oxidation method seems to depend on activity of manganese dioxide, which is reported to be dependent on the preparation method,[2] and on solvent choice and reaction temperature which are proved to affect product yield as much as or more than the activity of manganese dioxide.[2,3]

In connection with our study directed toward devised molecular construction from pyridoxine to pyridinophanes with pyridoxal-like activity,[4] it was inevitably required to develop a new oxidation system by use of manganese dioxide.[5] With those above in mind and through several attempts employing pyridoxine (**1**) as a substrate model, we eventually found

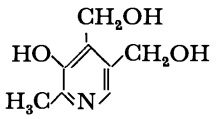

1

a new oxidation system by use of manganese dioxide[7] in the presence of amine. The present method has been successfully applied to pyridinophane congeners without exception or reduction in yield.[4]

The fundamental reaction system consisted of **1**, manganese dioxide,[7] and an amine in the molar ratio of 1:10:2 in benzene. Pyridine was added to dissolve **1**. The mixture was heated under reflux with azeotropic removal of the resulting water. The resulting imine was subjected to transimination for isolation (path A). For the purpose of comparison of amine effect on the reaction, path C was examined as well.

$$\mathbf{1} \xrightarrow[R'\text{-}NH_2]{MnO_2} \underset{\mathbf{2}}{R\text{-}CH{=}N\text{-}R'} \xrightarrow{R''\text{-}NH_2} \underset{\mathbf{3}}{R\text{-}CH{=}N\text{-}R''} \quad \text{(path A)}$$

$$\mathbf{1} \xrightarrow[R''\text{-}NH_2]{MnO_2} \underset{\mathbf{3}}{R\text{-}CH{=}N\text{-}R''} \quad \text{(path B)}$$

$$\mathbf{1} \xrightarrow{MnO_2} \underset{\mathbf{4}}{R\text{-}CHO} \xrightarrow{R''\text{-}NH_2} \underset{\mathbf{3}}{R\text{-}CH{=}N\text{-}R''} \quad \text{(path C)}$$

R′=$-CH_2CH_2NH_2$, $-CH_3\cdot HCl$, or $-CH_2CH_2CH_2N(CH_3)_2$
R″=$-C_6H_4$-*p*-$OC_2H_5\cdot HCl$

The results obtained are listed in Table 1. Each primary amine has a positive effect on the oxidation. Especially, 3-(dimethylamino)propylamine was the most effective of amines used.

Although we have no substantial evidence for the bimolecular oxidation mechanism,[9] the primary amino group might participate in the oxidation process by forming a transient manganese dioxide complex. The previous work on the oxidation of β-amino alcohols[10] could be mechanistically related to the present work.

The present method will provide "an oxidant substitute" for "active" manganese dioxide and, thus, seems to be a useful tool for the synthesis of unstable aldehydes, protected directly by coexisting primary amine to form a relatively stable Schiff base during oxidation.

Experimental

The melting point is uncorrected. The IR spectra were recorded on a Shimadzu IR-27 instrument. The UV spectra were measured with Hitachi 124 spectrophotometer. The ^{1}H-NMR spectra were recorded on a Varian HA-100D apparatus, with TMS as the internal standard and the chemical shift and coupling constant were represented by δ and Hz, respectively. Merck silica gel 60 (Art. 7734, 0.063—0.20 mm) was used for the column chromatography and Wakogel B-5 FM (Wako Pure Chem. Co., Ltd.) for analytical thin layer chromatography. The elemental analyses were performed by this Institute. All the reagents used were commercially available and employed without further purification.

Oxidation Method. The mixture consisting of **1**, manganese dioxide,[7] and an amine in the molar ratio of 1:10:2 in benzene (150 ml/g of **1**) was heated under reflux for the mentioned time with azeotropic removal of the resulting

Table 1. Manganese dioxide oxidation of pyridoxine accompanied by schiff base formation

Reaction path	Initial amine	Reaction time/min	Amine used for isolatn	Treated time/min	Product	Yield[a]/%
C	—	120	EAN[b]	10	**3**	14
C	TEA[c]	120	EAN	10	**3**	26
B	EAN	130	—	—	**3**	57
A	EDA[d]	60	EAN	15	**3**	57
A	MA[e]	30	EAN	10	**3**	59
A	DAPA[f]	50	EAN	10	**3**	75

a) Isolated yield. b) *p*-Ethoxyaniline hydrochloride. c) Triethylamine. d) Ethylenediamine. e) Methylamine hydrochloride. f) 3-(Dimethylamino)propylamine.

water by the Dean-Stark apparatus until no more water came out. Pyridine was mixed to dissolve **1** up to fifty volume percent of benzene. The reaction mixture was then filtered, while hot, through celite (No. 545) to remove excess amount of manganese dioxide and the resulting manganese oxide, washed several times with hot pyridine. The combined filtrate was treated, after removal of the solvents under reduced pressure, with one of the following ways.

For transimination[8] (path A), the residue was dissolved into small amount of benzene–ethyl acetate (1:1 v/v), and equal weight of *p*-ethoxyaniline hydrochloride to the amine initially used was mixed, followed by addition of equal volume of water to the organic layer. By magnetic stirring, immediately, the brown solution resulted in orange-red precipitate which was recrystallized from methanol after collection by filtration. Spectral data supported that the orange red crystals are 4-(*p*-ethoxyphenyliminomethyl)-5-hydroxy-6-methylpyridine-3-methanol (**3**); mp 211—212.5 °C (decomp), needles. Found: C, 66.62; H, 6.35, N, 9.66%. Calcd for $C_{16}H_{20}O_3N_2$: C, 66.64; H, 6.99; N, 9.72%. UV (EtOH): λ_{max} (ε) 210 (19200), 224 (sh, 17700), 253 (sh, 8400), 297 (sh, 7100), 305 (sh, 7500), 350 (14700), 366 (15000), and 384 (sh, 11800) nm. UV (EtOH–0.1 M NaOH): λ_{max} (ε) 239 (18800), 310 (7000), and 410 (3400) nm. ^{1}H-NMR (DMSO-d_6): 1.34 (3H, t, J=7.0, OCH_2–$C\underline{H}_3$), 2.41 (3H, s, $C\underline{H}_3$ on the pyridine ring), 4.07 (2H, q, J=7.0, $OC\underline{H}_2CH_3$), 4.75 (2H, broad d, J=5.0, $C\underline{H}_2$–OH on the pyridine ring), 5.38 (1H, broad t, J=5.0, CH_2–$O\underline{H}$), 7.10 and 7.46 (2H each, d, J=9.0, protons on the benzene ring), 7.83 (1H, s, proton on the pyridine ring), 9.10 (1H, s, –$C\underline{H}$=N–), and 15.10 (1H, broad s, phenolic proton on the pyridine ring). IR (KBr disc): ν_{C-O-C} 1250; $\nu_{C=N}$ 1615; ν_s 1500, 1406, 1385, 1298, 1020, and 818; ν_m 1582, 1475, 1310, 1265, 1198, 1163, 1118, 1019, 860, 789, 572, and 535 cm^{-1}.

For direct isolation of **3** (path B), the residue was triturated with benzene. The precipitate was collected by filtration and recrystallized from methanol.

For (indirect) Schiff base (**3**) formation (path C), the residue was dissolved into *ca.* 20 ml of benzene followed by addition of equal weight of *p*-ethoxyaniline hydrochloride to **1** and the mixture was stirred for the mentioned time. **3** was isolated by silica gel chromatography eluted with chloroform–methanol (9 : 1 v/v).

The author would like to express appreciation to Dr. Haruo Homma and his staff for elemental analyses, to Dr. Jun Uzawa and Mrs. Tamiko Chijimatsu for ^{1}H-NMR measurement, and to Drs. Sakae Emoto and Hiroyoshi Kuzuhara for encouragement through this work.

References

1) a) D. Heyl, *J. Am. Chem. Soc.*, **70**, 3434 (1948); b) A. N. Wilson and S. A. Harris, *ibid.*, **73**, 4693 (1951); c) W. Korytnyk, S. C. Srivastava, N. Angelino, P. G. G. Potti, and B. Paul, *J. Med. Chem.*, **16**, 1096 (1973); d) R. H. Wiley and G. Irick, *J. Med. Pharm. Chem.*, **5**, 49 (1962); *Chem. Abstr.*, **57**, 12424f (1962).

2) R. M. Evans, *Q. Rev. Chem. Soc.*, **13**, 61 (1959); A. J. Fatiadi, *Synthesis*, **1976**, 65 and 133.

3) R. J. Gritter and T. J. Wallace, *J. Org. Chem.*, **24**, 1051 (1959).

4) M. Iwata, H. Kuzuhara, and S. Emoto, *Chem. Lett.*, **1976**, 983; H. Kuzuhara, M. Iwata, and S. Emoto, *J. Am. Chem. Soc.*, **99**, 4173 (1977); M. Iwata and H. Kuzuhara, *Chem. Lett.*, **1981**, 5.

5) Under the conditions described in Ref. 1a—c with active manganese dioxide newly prepared according to the method of Attenburrow *et al.*,[6] any of modified compounds with pyridoxine-like functionality afforded insufficient yield (less than 16%).

6) J. Attenburrow, A. F. B. Cameron, J. H. Chapman, R. M. Evans, B. A. Hems, A. B. A. Jasen, and T. Walker, *J. Chem. Soc.*, **1952**, 1094.

7) Commercially available, supplied by Junsei Chem. Co., Ltd. (Tokyo).

8) The transimination occurred quantitatively; for the essence of this reaction, see E. H. Cordes and W. P. Jencks, *J. Am. Chem. Soc.*, **84**, 826 (1962).

9) O. H. Wheeler, *Chem. Ind. (London)*, **1965**, 1769.

10) L. Birkofer and L. Erlenbach, *Chem. Ber.*, **91**, 2383 (1958).

A Simple Regioselective Partial Hydrolysis of Di-*O*-isopropylidene Monosaccharides with Copper(II) Ion

Masaaki IWATA* and Hiroshi OHRUI

The Institute of Physical and Chemical Research, Wako, Saitama 351

(Received January 30, 1981)

Synopsis. Copper(II) ion was found to be effective for regioselective removal of the 5,6-O-isopropylidene group of α-D-mannose and α-D-glucose derivatives in alcohols at ambient temperature.

In connection with a series of reactions promoted by copper(II) ion in organic solvent,[1] a convenient method was developed for the preparation of 1-*O*-benzoyl-2,3-*O*-isopropylidene-α-D-mannofuranose (**3**), benzyl 2,3-*O*-isopropylidene-α-D-mannofuranoside (**4**), 3-*O*-benzoyl-1,2-*O*-isopropylidene-α-D-glucofuranose (**6**), and 6-*O*-benzoyl-1,2-*O*-isopropylidene-α-D-glucofuranose (**7**) from the corresponding diisopropylidene monosaccharides.

Monoisopropylidene-D-mannose and -D-glucose are useful starting materials for the preparation of numerous derivatives and chiral natural products.[2] Monoisopropylidene derivatives of monosaccharides are usually prepared from the corresponding diisopropylidene derivatives by preferential partial hydrolysis of the more acid labile 5,6-*O*-isopropylidene group. Methods reported so far[3] have employed acetic acid or mineral acids as promoters, thus making it necessary to control pH, temperature, and/or reaction time, and evaporate a large quantity of solvent occasionally giving rise to further hydrolysis. The present method is easy, giving quantitative yield under mild conditions and not requiring certain manipulation required in other procedures.

The 5,6-*O*-isopropylidene group was regioselectively hydrolyzed by stirring a mixture of 1-*O*-benzoyl-2,3:5,6-di-*O*-isopropylidene-α-D-mannofuranose (**1**), benzyl 2,3:5,6-di-*O*-isopropylidene-α-D-mannofuranoside (**2**), or 3-*O*-benzoyl-1,2:5,6-di-*O*-isopropylidene-α-D-glucofuranose (**5**) and five molar equivalents[4] of copper(II) chloride dihydrate in ethanol or 2-propanol[5] at room temperature to give **3**, **4**, or **6** in 97, 99, or 99% yields, respectively, after neutralization by sodium hydrogencarbonate. The prolonged reaction time and scale-up of the preparation from 0.5 to 40 g can be achieved without reduction in the yield.

Interestingly, however, when the reaction mixture of **5** was neutralized by sodium carbonate, the product was solely 6-*O*-benzoyl-1,2-*O*-isopropylidene-α-D-glucofuranose (**7**). On the other hand, when an ethanol solution of **6** was stirred in the presence of 1 M—Na_2CO_3 at room temperature for 10—30 min, quantitative transformation of **6** into **7** was observed by measurement of the specific rotation change before and after the reaction.[6] Thus, it was confirmed that the benzoyl group is labilized and easily migrates to the C_6-position by subtle pH change.[7]

The β-anomer of **2** was more acid-sensitive than **2**. When a mixture of the β-anomer of **2** and a molar equivalent[9] of copper(II) chloride dihydrate in 2-propanol was stirred at room temperature for 44 h, silica gel chromatographic separation ($CHCl_3$–MeOH 9:1 v/v) of the product after work-up provided benzyl 2,3-*O*-isopropylidene-β-D-mannofuranoside (**8**) in 30% yield, benzyl β-D-mannofuranoside (**9**) in 12% yield, and benzyl 5,6-*O*-isopropylidene-β-D-mannofuranoside (**10**) in 20% yield, along with 34% recovery of the starting diisopropylidenemannoside. The formation of **10** was rationalized by the isopropylidenation of **9** with liberated acetone *in situ*.[10]

The copper(II)-ion promoted partial hydrolysis was inhibited in the presence of pyridine; thus, a copper complex of sugar may be a possible intermediate in this reaction which could be supported by other circumstantial evidence.[4,5]

Experimental

Merck silica gel 60 (Art. 7734, 0.063—0.20 mm) was used for the column chromatography and Wakogel B-5 FM (Wako Pure Chem. Co., Ltd.), for the analytical TLC. TLC plates were visualized by spraying *p*-methoxybenzaldehyde–concd sulfuric acid–methanol (5:10:85 v/v) followed by heating. The optical rotations were measured with Perkin-Elmer model 241 MC polarimeter. The IR spectra were recorded on a Shimadzu IR 27 instrument. Elemental analyses were carried out in this Institute. The mp is uncorrected.

*Preparation of 1-O-Benzoyl-2,3-O-isopropylidene-α-D-mannofuranose (**3**).* A mixture of 20 g (0.055 mol) of **1** and 48 g (0.28 mol) of copper(II) chloride dihydrate in 500 ml of ethanol was magnetically stirred at room temperature for 14 h (overnight). The reaction was terminated by addition of 48 g of sodium hydrogencarbonate crystals and the mixture was stirred (mostly for 0.5—1 h) until no more carbon dioxide was evolved. Then 100 ml of water was added, further amount of carbon dioxide being evolved, and the mixture was diluted with 400 ml of water to promote precipitation. The pale blue precipitate was filtered off through celite (No. 545). The filtrate was extracted with *ca.* 500 ml of chloroform and dried over $MgSO_4$ followed by filtration. After removal of the solvent, the residue was chromatographed on a silica gel column eluted with chloroform and then with chloroform–methanol (9:1 v/v) to give 17.2 g (97% yield based on **1**, colorless amorphous powder) of **3**; $[\alpha]_D^{20}$ 37.4° (*c* 0.968, $CHCl_3$) (lit,[11] $[\alpha]_D^{20}$ 52.5° (*c* 1.7, ethanol); IR (KBr disc) $\nu_{C=O}$ 1724 cm^{-1}.

*Preparation of Benzyl 2,3-O-Isopropylidene-α-D-mannofuranoside (**4**).* A mixture of 40.54 g (0.116 mol) of **2** and 98.7 g (0.58 mol) of copper(II) chloride dehydrate in 400 ml of 2-propanol was stirred overnight (*ca.* 14 h). A similar work-up to that for **1** afforded 35.5 g (99% yield, syrup) of **4**; $[\alpha]_D^{30}$ 71.1° (*c* 0.771, $CHCl_3$) (lit,[12] mp 60—61 °C, $[\alpha]_D^{30}$ 90° (*c* 1, $CHCl_3$)).

*Preparation of 3-O-Benzoyl-1,2-O-isopropylidene-α-D-glucofuranose (**6**).* A mixture of 0.5 g (1.37 mmol) of **5** and 1.2 g (7 mmol) of copper(II) chloride dihydrate in 20 ml of ethanol was stirred overnight (*ca.* 15 h). The reaction mixture was neutralized with 1.2 g of sodium hydrogencarbonate followed by a similar work-up to that for **1** to

give 0.441 g (99% yield) of **6** (syrup); $[\alpha]_D^{25}$ −26.5° (*c* 0.941, ethanol) (lit,[3d] −26° (ethanol); lit,[13] −26.5° (*c* 0.859, ethanol)).

Preparation of 6-O-Benzoyl-1,2-O-isopropylidene-α-D-glucofuranose (7). A mixture of 0.5 g (1.37 mmol) of **5** and 1.2 g (7 mmol) of copper(II) chloride dihydrate in 20 ml of ethanol was stirred at room temperature for 19 h followed by neutralization with 1.2 g of sodium carbonate. A similar work-up to that for **1** afforded 0.43 g (97% yield) of **7**; recryst. from ethanol (minor)–chloroform (major); mp 195—196 °C (lit,[7] 195—197 °C); $[\alpha]_D^{26.5}$ 4.71° (*c* 0.488, ethanol) (lit,[8] 7.4° (*c* 0.535, ethanol)).

The authors are grateful to Dr. Haruo Homma and his staff for carrying out elemental analyses, and to Drs. Hiroyoshi Kuzuhara and Masajiro Kawana for their valuable discussions.

References

1) M. Iwata and S. Emoto, *Chem. Lett.*, **1974**, 759, 959; M. Iwata, H. Kuzuhara, and S. Emoto, *ibid.*, **1976**, 17; M. Iwata and S. Emoto, *Bull. Chem. Soc. Jpn.*, **49**, 1369 (1976).

2) W. A. Szabo and H. T. Lee, *Aldrichimica Acta.* **13**, 13 (1980).

3) E. Fischer, *Ber.*, **28**, 2496 (1895); J. C. Irvine and J. L. A. MacDonald, *J. Chem. Soc.*, **107**, 1701 (1915); O. Svanberg and K. Sjöberg, *Ber.*, **56**, 863 (1923); H. Ohle and E. Dickhauser, *ibid.*, **58**, 2601 (1925); K. Freudenberg, W. Dürr, and H. v. Hochstetter, *ibid.*, **61**, 1735 (1928); H. W. Coles, L. D. Goodhue, and R. M. Hixon, *J. Am. Chem. Soc.*, **51**, 523 (1929); A. S. Meyer and T. Reichstein, *Helv. Chim. Acta*, **29**, 139 (1946); F. Blindenbacher and T. Reichstein, *ibid.*, **31**, 1669 (1948). C. L. Mehltretter, B. H. Alexander, R. L. Mellies, and C. E. Rist, *J. Am. Chem. Soc.*, **73**, 2424 (1951); S. G. Land, *Acta Chim. Scand.*, **8**, 866 (1954); R. E. Gramera, A. Park, and R. L. Whistler, *J. Org. Chem.*, **28**, 3230 (1963).

4) The molar ratio was not optimized. However, it was found by changing the ratio of copper(II) ion quantity to diisopropylidene monosaccharide that when one molar equivalent of copper(II) ion is used in ethanol at room temperature, **2** is obtained in 79% yield in 46 h along with 20% recovery of **1**. When two molar equivalents of copper(II) ion was employed under the same conditions, **2** was obtained in 85% yield with 14% recovery of **1** in 43 h.

5) Qualitatively, the relative reaction rate was greater in ethanol than in 2-propanol. Aprotic solvents such as benzene, dioxane, *N,N*-dimethylformamide, and dimethyl sulfoxide were found to be unsuitable for the hydrolysis due to insolubility of copper(II) ion or the formation of copper(II) ion–solvent complex.

6) When the reaction mixture was divided into two equal parts and neutralized by sodium hydrogencarbonate and sodium carbonate, respectively, both chloroform extracts showed $[\alpha]_D^{25}$ −23° (*c* 1.12, ethanol) (lit,[3d] −26° (*c* 0.94 ethanol)) and 1.3° (*c* 0.547, ethanol) (lit,[8] 7.4° (*c* 0.535, ethanol)), respectively.

7) The migration of the acetyl group in a glucose derivative from C_3 to C_6 induced by ammonium hydroxide (pH *ca.* 9) has been reported by K. Josephson, *Justus Liebigs Ann. Chem.*, **472**, 217 (1929).

8) E. Fischer and H. Noth, *Ber.*, **51**, 321 (1918).

9) When molar ratio of copper(II) ion was increased up to five, yield of **8** decreased and that of **9** increased. When the β-anomer of **2** was hydrolyzed by 90% acetic acid at around 50 °C for 1 h, **9** was obtained quantitatively.

10) When **9** was acetonated in acetone in the presence of one molar equivalent of copper(II) chloride dihydrate at room temperature, **9** was lost in 2 h accompanied by the formation of **10** and the diisopropylidenemannoside in equal ratio on TLC, **10** being converted into the diisopropylidenemannoside in 18 h.

11) H. Ohrui and S. Emoto, *Tetrahedron Lett.*, **1975**, 2765.

12) J. S. Brimacobe, F. Hunedy, and L. C. N. Tucker, *J. Chem. Soc., C*, **1968**, 1381.

13) P. Brigl and H. Grünner, *Ber.*, **66**, 1977 (1933).

The Synthesis of Phenyl Carboxylates from *p*-Bromophenol and Carboxylic Acids

Shizunobu HASHIMOTO and Isao FURUKAWA*
Department of Applied Chemistry, Doshisha University, Karasuma-imadegawa, Kamigyo-ku, Kyoto 602
(Received February 2, 1981)

Synopsis. The reaction of *p*-bromophenol with carboxylic acids in the presence of triphenylphosphine and triethylamine proceeded at a high temperature, with the elimination of hydrogen bromide, to give phenyl carboxylates and small amounts of *p*-bromophenyl carboxylates.

We have recently reported that the direct esterification of phenols (ArOH) with carboxylic acids proceeds easily at room temperature by the use of both triphenylphosphine and carbon tetrachloride as dehydrating agents in the presence of triethylamine, giving only the corresponding aryl carboxylates (RCOOAr) such as *p*-bromophenyl benzoate from *p*-bromophenol and benzoic acid in a high yield.[1] From our further investigation into the esterification of *p*-bromophenol, we have found that the esterification in the presence of triphenylphosphine and triethylamine gives phenyl carboxylates, with the elimination of hydrogen bromide:

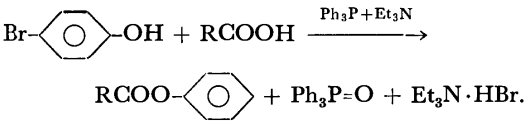

The results are shown in Table 1. The reaction proceeds at a high temperature to give, simultaneously, phenyl carboxylate and small amounts of *p*-bromophenyl carboxylates. The yield of the phenyl carboxylates increased with an increase in the reaction temperature, but the yield of *p*-bromophenyl carboxylates decreased conversely. A black-colored, tarry product was produced in the absence of triethylamine, and the use of pyridine instead of triethylamine gave phenyl carboxylate in a poor yield. Also, the esterification with carboxylic acid having a nitro group resulted in the formation of a tarry product in contrast to the expected ester.

It is concluded that the esterification of *p*-bromophenol with carboxylic acids in the presence of triphenylphosphine and triethylamine proceeds through the process shown in the following scheme:

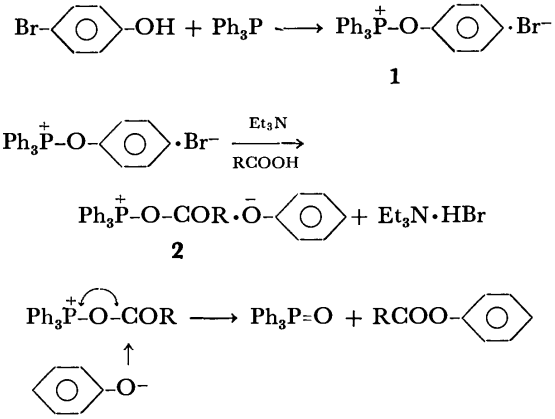

It has been reported by Hoffmann that the phosphonium salt (**1**) assumed as an intermediate is formed by the elimination of bromine from *p*-bromophenol with triphenylphosphine at a high temperature.[2] The resulting salt **1** is converted to acyloxytriphenyl-

TABLE 1. PHENYL AND *p*-BROMOPHENYL CARBOXYLATES[a]

RCOOH R	Reaction temp °C	Phenyl esters Yield %	Mp °C	IR(ν/cm^{-1}) C=O	IR C-O	MS(m/e) M+	*p*-Bromophenyl esters Yield %	Mp °C	IR C=O	IR C-O	MS M+
CH_3	200	50	82—83/10[b]	1770	1230	136	0				
CH_3	170	46	84—86/12[b]	1770	1230	136	13	122—124/11[b]	1770	1230	214
CH_3[c]	200			Tarry product was formed							
$CH_3CH_2CH_2$	200	62	106—108/8[b]	1770	1205	164	4	—	1770	1205	242
C_6H_5	200	84	70—72	1725	1265	198	0				
C_6H_5	170	62	71—72	1725	1265	198	12	104—106	1740	1260	276
C_6H_5[d]	170	9	70—73	1725	1265	198	21	105—106	1740	1260	276
p-ClC_6H_4	200	64	100—102	1735	1280	232	0				
p-ClC_6H_4	170	54	101—103	1735	1280	232	4	100—104	1750	1270	310
o-ClC_6H_4	200	40	37—38	1735	1280	232	0				
p-$CH_3C_6H_4$	200	75	71—73	1735	1275	212	14	95—97	1740	1270	290
p-$CH_3OC_6H_4$	200	62	67—69	1730	1275	228	5	103—105	1730	1270	306
p-$NO_2C_6H_4$	200			Tarry product was formed							
$C_6H_5CH=CH$	200	58	74—76	1730	1205	224	5	111—114	1750	1215	302

a) Reaction time: 4 h. b) Bp: °C/Torr (1 Torr = 133.322 Pa). c) In the absence of triethylamine. d) Pyridine was used instead of triethylamine.

phosphonium phenoxide (**2**) by the nucleophilic attack of the acyloxy anion onto the phosphorus atom of **1**, followed by the attack of the phenoxy anion onto the carbonyl carbon of **2**, giving phenyl carboxylate with the elimination of triphenylphosphine oxide. Otherwise, it is considered that the formation of *p*-bromophenyl carboxylate is by the attack of *p*-bromophenol on **2**.

Experimental

All the melting and boiling points are uncorrected. All the chemicals used were of an analytical reagent-grade. The thin-layer chromotography (TLC) was performed on Merck's silica gel 60 (70—230 mesh). The IR spectra were recorded in KBr on a Shimadzu IR-27C spectrometer, and the MS, on a Hitachi RM-50GC spectrometer with 60 eV.

General Procedure. A mixture of triphenylphosphine (5.5 mmol), triethylamine (5.5 mmol), carboxylic acid (5.5 mmol), and *p*-bromophenol (5.0 mmol) was heated at 200 °C for 4 h in the absence of a solvent. After hexane has been poured into the resulting mixture, the insoluble triphenylphosphine oxide and triethylamine hydrobromide were filtered off. The filtrate was washed with an aqueous sodium hydroxide solution, dried over anhydrous sodium sulfate, and concentrated, thus giving an ester. The pure ester was obtained by recrystallization from hexane or methanol, or by chromatography on silica gel, and was determined by infrared and mass-spectral analysis.

References

1) S. Hashimoto and I. Furukawa, *Bull. Chem. Soc. Jpn.*, **54**, 2227 (1981).
2) H. Hoffmann, L. Horner, H. G. Wippel, and D. Michael, *Chem. Ber.*, **95**, 523 (1962).

Effects of Crown Ethers on the Critical Micelle Concentration and the Micellar Catalysis of Sodium and Potassium Dodecyl Sulfates in Aqueous Solutions

Manabu Senō, Tomiyuki Namba, and Hideo Kise*

Institute of Industrial Science, The University of Tokyo, 7-22-1 Roppongi, Minato-ku, Tokyo 106

(Received February 12, 1981)

Synopsis. The catalytic micellar effects of potassium dodecyl sulfate on the hydrolysis of trimethyl orthobenzoate were found to be much retarded by 15-crown-5 or 18-crown-6.

It has been reported that complex-forming crown ethers lower the critical micelle concentration and increase the partial molal volumes and compressibilities of sodium decanoate in aqueous solutions.[1] The results have been interpreted in terms of the formation and association of Na^+–crown ether complexes with micelles, reducing the repulsion between the ionic groups at the micelle surface.

This article describes the effects of crown ethers on the critical micelle concentration (cmc) of sodium dodecyl sulfate (SDS) and potassium dodecyl sulfate (PDS) in aqueous solutions, and their effects on the rate of hydrolysis of methyl orthobenzoate in the PDS micellar systems.

When 15-crown-5 or 18-crown-6 was added to an aqueous SDS or PDS solution, an appreciable decrease in the specific conductivity of the solution was observed, and, as summarized in Table 1, the cmc, which was determined by the plot of conductivity against surfactant concentration, was found to decrease. The apparent enhancement of the micelle formation by the crown ethers is quite similar to that of sodium decanoate.[1] The magnitude of the decrease in cmc seems to have a correlation with the association constant of the crown ethers with alkali metal ions of the surfactants as shown in Table 1. 18-Crown-6 has higher association constants both with K^+ and Na^+ and gives lower cmc of PDS and SDS than 15-crown-5. The plot of cmc against the ratio of 18-crown-6 to PDS is shown in Fig. 1.

It is known that organic compounds often increase the cmc of surfactants, as is the case of urea in an aqueous SDS solution.[2] The effects of crown ethers described above may be the consequence of the formation of crown ether–metal ion complexes and their incorporation into the micelles, which leads to the decrease in the electrostatic repulsion between the anionic head groups of the micelles.

Table 1. Critical micelle concentration of SDS and PDS in the absence and presence of equimolar amounts of crown ethers

Surfactant	Crown ether	Cmc/mM 35 °C	Cmc/mM 23 °C	Association const (log K) of crown ether[a]
SDS	None	8.0	8.1	—
	15-Crown-5	6.7	7.2	0.70(Na^+)
	18-Crown-6	6.6	6.7	0.80(Na^+)
PDS	None	8.0		—
	15-Crown-5	6.5		0.74(K^+)
	18-Crown-6	4.1		2.03(K^+)

a) From Ref. 4 (at 25 °C).

A kinetic study was made to clarify the effects of crown ethers on the hydrolysis of methyl orthobenzoate in aqueous PDS solutions. The hydrolysis was followed by the change in absorbance of the product methyl benzoate at 228 nm at 35 °C and pH 3.41, which was adjusted by acetic acid. As shown in Fig. 2, the first order rate constant in PDS solution in the absence of crown ethers increases markedly above cmc. In the presence of a crown ether, however, the rate enhancement by the surfactant micelle is much decreased; 18-crown-6 has a larger inhibitory effect than 15-crown-5. Since the effects of crown ethers on the hydrolysis rate below cmc are small

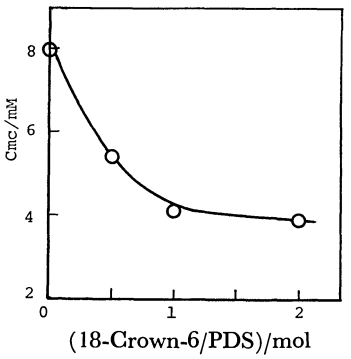

Fig. 1. The effect of 18-crown-6 on the cmc of PDS in aqueous solutions.

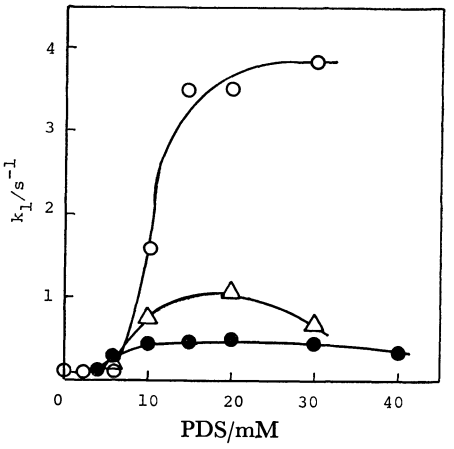

Fig. 2. First order rate constant for the hydrolysis of trimethyl orthobenzoate in the absence and presence of equimolar crown ethers (35 °C, pH 3.41). ○: PDS only, △: PDS-15-crown-5, ●: PDS-18-crown-6.

(first order rate constants are 0.052 and 0.054 s^{-1} for PDS concentrations of 2.0 and 4.0 mM, respectively, while those for PDS-18-crown-6 systems are 0.052 and 0.064 s^{-1} at the same concentrations, respectively), the rate retardation is obviously the consequence of the change of the nature of the micelles.

The reaction is considered to proceed by general acid catalysis, involving the proton transfer to the substrate followed by the formation of a carbenium ion by the elimination of methyl alcohol as shown in Scheme 1.[3] The catalytic effects of anionic micelles have been interpreted by the solubilization of the substrate in the Stern layer of the micelle where the proton concentration is higher than in the bulk water phase. The rate retardation by the crown ethers may be interpreted by the decrease in the charge density and hence the lower hydrogen ion concentrations on the surface of the micelles as implied by the decrease in the cmc by the addition of the crown ethers. A larger inhibitory effect of 18-crown-6 which has stronger complex-forming ability than 15-crown-5 seems to support the above consideration.

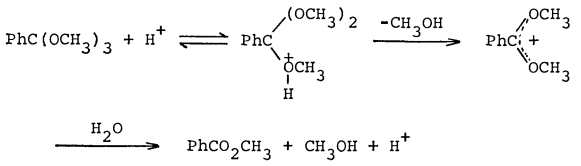

Scheme 1.

Since the complexation with crown ethers is considered to enhance the hydrophobic nature of potassium ion, the inclusion of the complexes into the micelle is likely to occur in the present systems, which would result in the decrease in the fraction of micelle charge.

It is interesting to note that, as shown in Fig. 2, in the presence of the crown ethers, the hydrolysis rate decreases at higher concentrations of the surfactant–crown ethers. Since no maximum rate is observed in the absence of the crown ethers, the interaction of the free crown ethers with hydroxonium ions may be responsible for the rate retardation.

The formation of crown ether–metal ion complexes and their interaction with micelles described above may serve as an experimental model system of biological ionophore-mediated metal ion-protein interactions.

References

1) E. Vikingstad and J. Bakken, *J. Colloid Interface Sci.*, **74**, 8 (1980).

2) M. F. Emerson and A. Holtzer, *J. Phys. Chem.*, **71**, 3320 (1967); M. J. Shick, *ibid.*, **68**, 3585 (1964).

3) J. H. Fendler and E. J. Fendler, "Catalysis in Micellar and Macromolecular Systems," Academic Press, New York (1975), p. 120.

4) M. Hiraoka, "Crown Compounds," Kodansha Scientific, Tokyo (1978), p. 112.

Chlorination of Acetylenes with Sulfuryl Chloride

Sakae UEMURA,* Chiaki MASAKI,** Akio TOSHIMITSU, and Seiji SAWADA**

Institute for Chemical Research, Kyoto University, Uji, Kyoto 611

***Department of Chemistry, Kyoto University of Education, Kyoto 612*

(Received March 9, 1981)

Synopsis. The reactions of some acetylenes with sulfuryl chloride in benzene and carbon tetrachloride at the reflux temperature afford the corresponding (*E*)- and (*Z*)-dichloroalkenes in good to moderate yields *via* homolytic pathway. The kinetically controlled isomer ratios(*E*/*Z*) depended very much on the kind of acetylenes employed; *i.e.*, 93/7 for 1-octyne to 14/86 for 3,3-dimethyl-1-phenyl-1-butyne in benzene.

Sulfuryl chloride has long been known to chlorinate olefin homolytically, both chlorine atoms and chlorosulfonyl radicals acting as chain carriers.[1] To our knowledge, however, the application to acetylenes seems to be so far limited only to divinylacetylene,[2] 2-butyne,[3] and phenylpropiolic acid and its methyl ester.[4] In the last case where sulfuryl chloride itself was used as solvent, the products were the complex mixture and, interestingly, the stereoisomeric ratios (*E*:*Z*) of the produced dichloroalkenes (one of the main products) were 1:4 and 4:1 for the acid and its methyl ester, respectively. Since a systematic study on the stereoisomeric ratios in radical chlorination of acetylenes has been reported only for (dichloroiodo)-benzene,[5] we undertook the chlorination of some acetylenes with sulfuryl chloride in nonpolar solvent to know whether the reaction proceeds homolytically and what the isomer ratios of dichloroalkenes are. As one of a series of our studies of halogenation of acetylenes by molecular halogen and metal halides,[6] we wish here to describe the details of the reaction.

Results and Discussion

The reactions of some acetylenes with equimolar amount of sulfuryl chloride in carbon tetrachloride or benzene at the reflux temperature gave a mixture of the corresponding *E*- and *Z*-dichloroalkenes in good to moderate yields [Scheme (1)]. Typical results are shown in Table 1 together with the reported isomer

$$\mathrm{R{-}C{\equiv}C{-}R' + SO_2Cl_2 \longrightarrow}$$

(1)

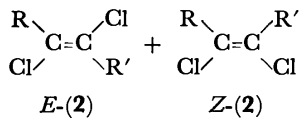

E-(**2**) *Z*-(**2**) (1)

ratios of the chlorination with $PhICl_2$ and of thermodynamic equilibrium. A use of excess sulfuryl chloride resulted in an increase of tetrachloroalkanes with a slight increase of (**2**), the isomer ratio being almost constant. As exemplified from the product yield in the table, the reactions proceeded more smoothly in benzene than in carbon tetrachloride, the isomer ratio being nearly the same in both solvents. Since prolonged reaction time had little effect on the isomer ratios of the products, the reactions must be almost entirely kinetically controlled. We confirmed independently that interconversion between the isomers of (**2**; R=Ph, R′=H or Me) did not occur in both solvents at the reflux temperature for 1—2 h in the presence of 1 equiv. of sulfuryl chloride. The observed kinetically controlled ratio is much different with the ratio of thermodynamic equilibrium and slightly different with the one of radical chlorination using $PhICl_2$. In the case of (**1**; R=Ph, R′=*t*-Bu) the *Z*-isomer was the major product, as has been observed in the chlorination with several chlorinating agents such as Cl_2,[6b] $CuCl_2$,[6a] and $SbCl_5$.[6d]

In order to know whether the reaction is homolytic, we have carried out the chlorination of (**1**; R=Ph, R′=H or Me) in the presence of a radical scavenger such as *t*-butylcatechol or phenol and found that the product yield decreased profoundly and the isomer ratio of *E*/*Z* became low. For example, *E*- and *Z*-(**2**; R=Ph, R′=H) were obtained from (**1**; R=Ph, R′=H) in a yield of 11% (*E*/*Z*=76/24) and 17% (*E*/*Z*=63/37) in chloroform (0.5 mmol of *t*-butylcatechol added) and in benzene (0.2 mmol of the catechol added) at reflux for 2 h, respectively. Similarly, the yield of (**2**) in the reaction of (**1**; R=Ph, R′=Me) in benzene at reflux for 2 h decreased to 27% (*E*/*Z*=66/34) by addition of 0.2 mmol of the catechol. On the other hand, when the reaction of (**1**; R=Ph, R′=H) in carbon tetrachloride was carried out by the addition of benzoyl peroxide, a radical initiator, the product yield of (**2**) increased to 58% from 34% without it. This finding also supports the radical nature of the reaction. An ionic chlorination of (**1**; R=Ph, R′=H or Me) with chlorine gas has been reported to give (**2**) in a ratio (*E*/*Z*) of 51/49 or 67/33 respectively. Therefore, a slight increase for the *Z*-isomer in the isomer ratio obtained in the presence of the radical inhibitor may be explained by assuming that this radical chlorination is slightly accompanied with an ionic one with chlorine which may be formed by dissociation of sulfuryl chloride. In fact, when the chlorination of (**2**; R=Ph, R′=Me) with sulfuryl chloride in benzene was carried out at 30 °C for 30 min under UV irradiation, *E*- and *Z*-(**2**; R=Ph, R′=Me) were obtained in a yield of 20%, *E*/*Z* being 91/9. Under similar conditions without irradiation almost no products were obtained. This fact shows that under completely radical condition the formation of the *E*-isomer is much favored.

Considering from the proposed mechanism for olefin chlorination with sulfuryl chloride,[1] the reaction scheme for the chlorination of phenyl-substituted acetylene seems to be as that shown in Scheme 2 where both chlorine atom and chlorosulfonyl radical act as chain carriers (R· may be derived from organic peroxides). The *E*/*Z* isomer ratio of (**2**) may be determined by the step of sulfuryl chloride attack on the intermediate linear α-phenylvinyl radical [A][7] where

Table 1. Chlorination of acetylenes with sulfuryl chloride[a)]

1 R	1 R′	Time h	Yield of 2 %	Isomer ratio (E : Z) This work[b)]	PhICl$_2$[c)]	d)
CCl_4 solvent						
Ph	H	2	34	83 : 17	70 : 30	14 : 86
Ph	H	65	46	84 : 16		
Ph	Me	2	46	87 : 13	51 : 49	54 : 46
Ph	Me	15	68	85 : 15		
Ph	Et	2	37	79 : 21	57 : 43	44 : 56
Ph	Et	15	54	73 : 27		
Ph	*t*-Bu	2	46	14 : 86		
Ph	*t*-Bu	15	49	13 : 87		
Ph	Ph	2	9	55 : 45	76 : 24	28 : 72
Ph	Ph	21	36	56 : 44		
Hexyl	H	2	10	98 : 2	94 : 6	53 : 47
Hexyl	H	20	38	92 : 8		
Benzene solvent						
Ph	H	2	75	85 : 15		
Ph	Me	2	85	84 : 16		
Ph	Et	2	97	75 : 25		
Ph	*t*-Bu	2	87	14 : 86		
Ph	Ph	2	69	57 : 43		
Hexyl	H	2	23	93 : 7		

a) Carried out at reflux temperature (78 °C for CCl_4 and 81 °C for benzene) with **1** (2 mmol), SO_2Cl_2 (2 mmol), and solvent (4 ml). b) Determined by GLC. c) Ref. 5. d) The ratio of thermodynamic equilibrium; Ref. 5.

$$\left.\begin{array}{l} R\cdot + SO_2Cl_2 \longrightarrow RCl + SO_2Cl\cdot \\ SO_2Cl\cdot \longrightarrow SO_2 + Cl\cdot \\ SO_2Cl_2 \xrightarrow{h\nu} SO_2Cl\cdot + Cl\cdot \\ Cl\cdot + (\mathbf{1};\ R=Ph) \longrightarrow Ph\text{-}\dot{C}\text{=}C(Cl)(R') \quad [A] \\ \downarrow \\ Ph\text{-}\dot{C}\text{=}C(Cl)(R') + SO_2Cl_2 \longrightarrow (\mathbf{2};\ R=Ph) + SO_2Cl\cdot \end{array}\right\} \quad (2)$$

the attack by sulfuryl chloride should occur in the plane containing both Cl and R groups.[6b)] When R is sterically smaller than Cl (like H or Me), the *E*-isomer would be favored, while the *Z*-isomer should be the major one when R is a large substituent like *t*-Bu. This assumption is consistent with the experimental results.

Experimental

1-Phenyl-1-alkynes and authentic samples of (**2**) for GLC analyses were prepared as previously described.[6a)] Phenylacetylene, diphenylacetylene, 1-octyne, and other organic materials were commercial products and used without further purification. Sulfuryl chloride was distilled before use. The GLC analyses were carried out on Shimadzu 4BMPF apparatus using EGSS-X(1 or 3 m)-Chromosorb-W columns (N_2 as the carrier gas); the *E*-isomer has a shorter retention time than the *Z*-isomer in all cases except (**2**; R=R′=Ph). The internal standards were ethyl cinnamate for (**2**; R=Ph, R′=H, alkyl, Ph) and *cis*-1,2-dichlorocyclohexane for (**2**; R=*n*-C_6H_{13}, R′=H). The NMR spectra were recorded with a Varian EM-360 and a JEOL JNM-MH-100 apparatus using CCl_4 solvent (TMS as an internal standard). The UV irradiations were carried out with a high-pressure mercury lamp(Ushio UM-103).

References

1) a) M. S. Kharasch and H. C. Brown, *J. Am. Chem. Soc.*, **61**, 2142, 3432 (1939); b) H. C. Brown, *Ind. Eng. Chem.*, **36**, 785 (1944); c) D. C. Nonhebel and J. C. Walton, "Free-radical Chemistry," Cambridge Univ. Press, Cambridge (1974), p. 189.

2) W. S. Calcott and A. S. Carter, U. S. 1, 896, 160 (1933).

3) I. V. Smirnow-Zamkov and N. A. Kostromina, *Chem. Abstr.*, **50**, 9302c (1956).

4) W. N. Lok and A. D. Ward, *Aust. J. Chem.*, **31**, 605 (1978).

5) A. Debon, S. Masson, and A. Thuillier, *Bull. Soc. Chim. Fr.*, **1976**, 2493.

6) a) S. Uemura, A. Onoe, and M. Okano, *J. Chem. Soc., Chem. Commun.*, **1975**, 925; S. Uemura, H. Okazaki, A. Onoe, and M. Okano, *J. Chem. Soc., Perkin Trans. 1*, **1977**, 676; b) S. Uemura, H. Okazaki, and M. Okano, *ibid.*, **1978**, 1278; c) S. Uemura, H. Okazaki, M. Okano, S. Sawada, A. Okada, and K. Kuwabara, *Bull. Chem. Soc. Jpn.*, **51**, 1911 (1978); d) S. Uemura, A. Onoe, and M. Okano, *J. Chem. Soc., Chem. Commun.*, **1976**, 145; S. Uemura, H. Okazaki, A. Onoe, and M. Okano, *J. Chem. Soc., Perkin Trans. 1*, **1979**, 548; e) S. Uemura, H. Miyoshi, and M. Okano, *Chem. Lett.*, **1979**, 1357.

7) See for example, Ref. 1c pp. 90—92.

Wittig Reaction of 1,3-Benzodithiol-2-ylidenetriphenylphosphorane with Carbon Disulfide

Juzo NAKAYAMA,* Sanae MARUYAMA, and Masamatsu HOSHINO
Department of Chemistry, Faculty of Science, Saitama University, Urawa, Saitama 338

(Received March 10, 1981)

Synopsis. 1,3-Benzodithiol-2-ylidenetriphenylphosphorane reacted with carbon disulfide to give 1,3-benzodithiole-2-thione, dibenzotetrathiafulvalene, and an unidentified crystalline red compound in addition to triphenylphosphine sulfide. The same products were also obtained by treatment of 1,3-benzodithiol-2-ylthiocarbonyl chloride with base.

Recent findings concerning the highly-conductive charge transfer salt of tetrathiafulvalene (TTF) with tetracyanoquinodimethan (TCNQ) have created a wide and extensive interest in the design of organic donors and acceptors.[1] Thus, the syntheses of compounds of types **1**[2] and **2**[3] have appeared recently; in compounds **1**, TTF system is extended by insertion of a quinonoid unit and compound **2** is isoelectronic with TCNQ. In this connection, the synthesis of organic donor like **3** is of current interest. We report here some findings found during the attempted synthesis of **3**.

There are abundant examples of dimerization of thioketenes which yield 1,3-dithietans.[4] Therefore, dimerization of the thioketene **4**, which would be produced by the Wittig reaction of carbon disulfide with 1,3-benzodithiol-2-ylidenetriphenylphosphorane (**5**) (conveniently obtainable by treatment of **6** with butyllithium),[5] was chosen as our synthetic strategy to **3**.

A stirred suspension of **6** in tetrahydrofuran was treated with a slight excess of butyllithium and then carbon disulfide was added at −78 °C. The mixture was gradually warmed to room temperature and then refluxed. Chromatographic purifications gave 1,3-benzodithiole-2-thione (**7**) (9—25%), dibenzotetrathiafulvalene (**8**) (15—20%), and a red crystalline compound **9** (5—9%) in addition to triphenylphosphine sulfide (44—65%). The reaction was repeated several times and gave reproducible results. Although the occurrence of triphenylphosphine sulfide is suggestive of the formation of the expected thioketene **4**, no products, which correspond to the dimer of **4**, were isolated. The red compound **9** has a molecular formula of $C_{15}H_8S_5$ on the basis of mass spectrum and elemental analysis (a tentative structure is given in the Experimental section).

The use of compound **10**[5] instead of **6** gave an intractable mixture.

As to the mechanism of the formation of **7** and **8**, initial formation of **7** from **5** and carbon disulfide followed by reaction of **7** and **5** which yields **8**, was ruled out since control experiment showed that compound **7** is unreactive toward **5**.

Attempted trapping of **4** with amine was fruitless. The Wittig reagent **5**, prepared as above, was allowed to react with carbon disulfide and then a solution of *p*-toluidine in tetrahydrofuran was added at −78 °C. Workup of the mixture by column chromatography did not give the expected adduct **11**, but afforded compounds **7**, **8**, and **9** in decreased yields. The result indicates that either the final products, **7**, **8**, and **9**, are produced by a mechanism which does not involve **4** as the intermediate or **4** fails to react with *p*-toluidine and is readily converted to the final products under the conditions.

Generation of **4** by other method was next tried. 1,3-Benzodithiole (**12**) was lithiated by butyllithium[6] and allowed to react with thiophosgene at −78 °C, and then the resulting **13** was dehydrochlorinated by triethylamine. Purification of the mixture by column chromatography yielded **7** (2%), **8** (28%), and **9** (2%). The use of DBU as the base gave a similar result. The formation of the same products, **7**, **8**, and **9**, by two different reactions is strongly suggestive of the presence of the common intermediate **4**.

One of possibilities as to the mechanism of the formation of the final products is the decomposition of **4** to the carbene **14** and carbon monosulfide since **14**, generated by addition of carbon disulfide to benzyne, is known to give **8** by dimerization and **7** by an uncertain mechanism.[7]

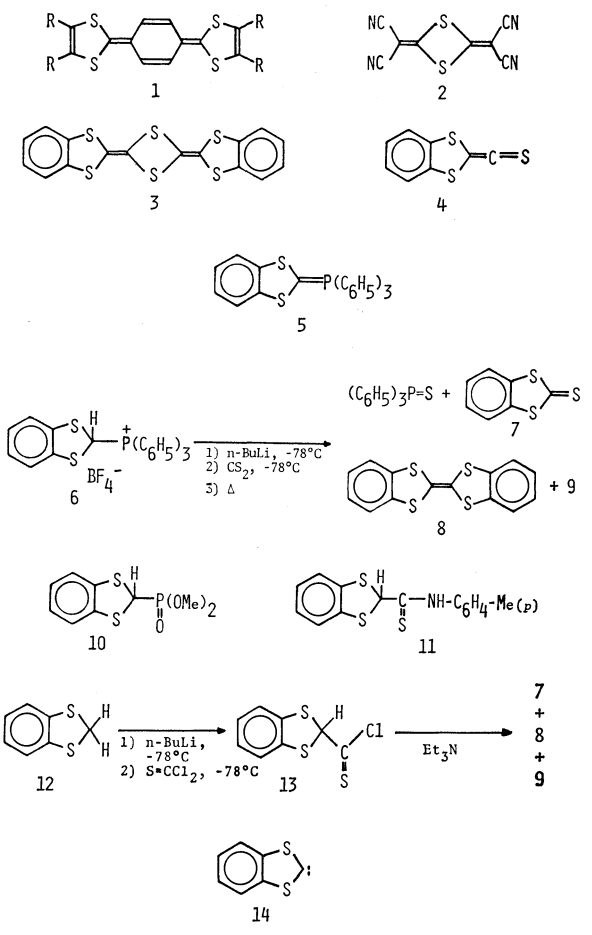

Experimental

Reaction of 1,3-Benzodithiol-2-ylidenetriphenylphosphorane (5) with Carbon Disulfide. To a stirred suspension of 4.02 g (8 mmol) of **6**[5] in 200 ml of anhydrous tetrahydrofuran (THF) was added a 15% solution of butyllithium in hexane (6.0 ml, 9.2 mmol) under nitrogen at −78 °C. After stirring of 1.5 h, 0.76 g (10 mmol) of carbon disulfide in 7 ml of THF was added at −78 °C. The mixture was stirred for 0.5 h at −78 °C, gradually warmed to room temperature, and then refluxed for 2 h. The solvent was removed under reduced pressure and the residue was extracted with 200 ml of dichloromethane, washed with water, dried on sodium sulfate, and evaporated. The resulting reddish brown mass was chromatographed on a silica-gel column (Merck, Art 7734, 100 g). Elution with carbon tetrachloride gave 0.26 g (21.5%) of dibenzotetrathiafulvalene (**8**), mp 244—246 °C (lit,[8] mp 235—236 °C), 0.36 g (24.5%) of 1,3-benzodithiole-2-thione (**7**), mp 165—166 °C (lit,[9] mp 164 °C), and 82 mg (6%) of a dark red compound (**9**), mp 220—221 °C (from benzene). Elution of the column with benzene gave 1.03 g (44%) of triphenylphosphine sulfide, mp 158—159 °C.

The reaction was repeated several times and the yields of **7**, **8**, and **9** varied in the range of 15—25%, 9—25%, and 5—9%, respectively.

The red compound **9** has the following properties: ^{1}H NMR (CS_2) δ 5.94—6.35 (complex m); UV ($CHCl_3$) λ_{max} (log ε) 242 (4.4), 261sh (4.3), 287sh (4.0), 383 (3.7), and 480 nm (4.3); IR (KBr) 1450, 1380, 1270, 990, 960, and 740 cm^{-1}; MS *m/e* 348 ($C_{15}H_8S_5$, M^+, 100%), 304 (M^+—CS), 283, 208, 196, 164, 152, 120, 108, 96, and 69. Found: C, 51.68; H, 2.31; S, 45.79%. Calcd for $C_{15}H_8S_5$: C, 51.74; H, 2,32; S, 45.95%.

When compound **9** was heated at 200—220 °C for 2 h without solvent, it was converted into a mixture of compounds **7** and **8**. Attempted reduction with sodium borohydride resulted in the decolorization of **9**.

On the basis of these results, the following tentative structure was given for **9**.

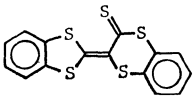

Attempted Reaction of 5 with 7. To a stirred solution of **5**, prepared from 1.51 g (3 mmol) of **6** as described above, was added a solution of 0.55 g (3 mmol) of **7** in 25 ml of THF at −78 °C. The mixture was stirred for 0.5 h at −78 °C, gradually warmed to room temperature, and then refluxed for 3 h. Chromatographic purification gave 23 mg (5%) of **8** and a nearly quantitative yield of **7**.

When a solution of **5**, prepared at −78 °C in THF, was gradually warmed and then refluxed without any additive, a 10% yield of **8** was obtained.

It is therefore concluded that **8**, formed by attempted reaction of **5** with **7**, is produced by decomposition of **5**, but not by reaction of **5** with **7**, and thus the phosphorane **5** is unreactive toward **7**.

Attempted Trapping of 4 by p-Toluidine. The phosphorane **5**, prepared from 1.51 g (3 mmol) of **6** in THF, was allowed to react with carbon disulfide (0.28 g, 3.75 mmol) at −78 °C. After stirring of 2 h, a solution of *p*-toluidine (0.32 g, 3 mmol) in THF (5 ml) was added at −78 °C under nitrogen. The mixture was stirred for 2 h at −78 °C and then gradually warmed to room temperature. Chromatographic purification gave 43 mg (2.8%) of **8**, 23 mg (1.3%) of **7**, 82 mg (4.7%) of **9**, and 0.57 g (64%) of triphenylphosphine sulfide. *p*-Toluidine was recovered nearly quantitatively.

Attempted Generation of 4 from 1,3-Benzodithiole (12). Compound **12** was conveniently prepared by reduction of 1,3-benzodithiolylium tetrafluoroborate[10] with sodium borohydride in THF. A 15% solution of butyllithium in hexane (7.8 ml, 12 mmol) was added through a syringe to a stirred solution of **12** (1.54 g, 10 mmol) in THF (120 ml) under nitrogen at −78 °C.[6] Stirring was continued for 2 h and then a solution of thiophosgene (1.15 g, 10 mmol) in THF (1 ml) was added all at once. The mixture was stirred for 1 h at −78 °C and then 2 ml of triethylamine was added. After 0.5 h of stirring, the mixture was warmed to room temperature and then evaporated. The resulting dark red residue was extracted with dichloromethane (200 ml), washed with water, dried, and evaporated. Chromatographic purification of the residue gave 0.42 g (28%) of **8**, 40 mg (2%) of **7**, and 30 mg (2%) of **9**.

The use of DBU as the base instead of triethylamine yielded **7** (3%), **8** (0.3%), and **9** (4%).

References

1) A. F. Garito and A. J. Heeger, *Acc. Chem. Res.*, **7**, 232 (1974); M. Narita and C. U. Pittman, Jr., *Synthesis*, **1976**, 489.

2) Y. Ueno, M. Bahry, and M. Okawara, *Tetrahedron Lett.*, **1977**, 4607; Y, Ueno, A. Nakayama, and M. Okawara, *J. Chem. Soc., Chem. Commun.*, **1978**, 74; M. V. Lakshmikantham and M. P. Cava, *J. Org. Chem.*, **43**, 82 (1978); M. Sato, M. V. Lakshmikantham, M. P. Cava, and A. F. Garito, *ibid.*, **43**, 2085 (1978).

3) N. F. Haley, *J. Chem. Soc., Chem. Commun.*, **1977**, 207.

4) *Organic Compounds of Sulphur, Selenium, and Tellurium*, **1**, 196 (1970); **2**, 220 (1973); **3**, 244 (1975); **4**, 135 (1977); **5**, 131 (1979).

5) K. Ishikawa, K. Akiba, and N. Inamoto, *Tetrahedron Lett.*, **1976**, 3695.

6) D. Seebach, K. H. Geib, A. K. Beck, B. Graf, and H. Daum, *Chem. Ber.*, **105**, 3280 (1972).

7) E. K. Fields and S. Meyerson, *Tetrahedron Lett.*, **1970**, 629; *Int. J. Sulfur Chem. (C)*, **1971**, 51; J, Nakayama, *J. Chem. Soc., Perkin Trans. 1*, **1975**, 525.

8) J. Nakayama, *Synthesis*, **1975**, 168.

9) S. Hünig and E. Fleckenstein, *Ann. Chem.*, **738**, 192 (1970).

10) J. Nakayama, K. Fujiwara, and M. Hoshino, *Bull. Chem. Soc. Jpn.*, **49**, 3567 (1976).

A Mild and Convenient Procedure for Conversion of Aromatic Compounds into Their Iodides Using Ammonium Hexanitratocerate(IV)

Takashi SUGIYAMA

Institute for Chemical Research, Kyoto University, Uji, Kyoto 611

(Received March 12, 1981)

Synopsis. Polymethylbenzenes, polymethoxybenzenes, and naphthalene are iodinated with tetrabutylammonium iodide, alkali metal iodides, or molecular iodine in the presence of ammonium hexanitratocerate(IV). Ammonium hexanitratocerate(IV) behaves as a catalyst in the latter system, whereas it is a reagent in the fomer two.

Although there are some reports on direct iodination of aromatic compounds, it presents rather complicated problems; molecular iodine is the least reactive of the halogens in aromatic substitution; the reaction is reversible and hydrogen iodide produced in the reaction must be removed to allow the reaction to be completed.[1)]

During the course of a study on one-electron-transfer reaction, the author found a novel and regioselective iodination of aromatic compounds using ammonium hexanitratocerate(IV) (CAN), a potential one electron oxidizing agent.

The results from iodination of some polymethylbenzenes are summarized in Table 1.

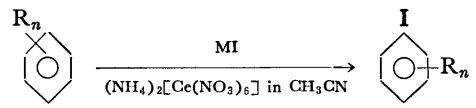

$R=CH_3$ ($n=2$, 3, 4, 6) or OCH_3 ($n=1$, 2, 3)
$M=n\text{-}Bu_4N$, Li, Na, K, I

There are two remarkable feautures in the present iodination. First, the reaction takes place only on the aromatic ring. It is noteworthy that, even hexamethylbenzene affords iodopentamethylbenzene as the sole iodinated product. This is a marked contrast with the oxidation of polymethylbenzenes promoted by CAN in acetic acid where the reaction on side-chains are predominated.[2)] Secondary, the iodination proceeds with ortho-para orientation with respect to methyl substituents. In particular, the result from *o*-xylene shows that para substitution occurs in preference to ortho substitution (the ortho:para-ratio being 1:6).

The present reaction proceeds under mild conditions. The yield, however, decreases as the number of methyl groups increases probably because of some side reactions.

Alkali metal iodides and molecular iodine as well as tetrabutylammonium iodide can be used as iodinating agents (Table 2).

In the case of iodination with molecular iodine, 0.5 mmol of iodine for 1.0 mmol of substrate is enough to complete the reaction in 80% yield based on aromatics. In general, one-half part of the molecule is discarded when molecular iodine is used as an iodinating agent. However, this economical disadvantage is overcome in the present reaction.

The substrate can be extended to polymethoxybenzenes and fused-ring aromatic as shown in Table 3. Evidentry, as the number of methoxyl groups attached on benzene ring increases, the reactant is consumed more rapidly. However, the yield of iodinated compounds are not parallel with the number of methoxyl groups.

Attempts to iodinate aromatic compounds bearing an electron-withdrawing substituent such as nitro- and chlorobenzenes, were unsuccessful, and these unchanged reactants were recovered from the reaction mixture. On the other hand, phenols and anilines were not iodinated, although they were consumed completely.

Among several possible reaction mechanisms, the author favors the one which involves the reaction of aromatic compound with a cationic halogen species, which is produced by the interaction between the halogen source and CAN. The argument is based on the facts that; (1) the only aromatics bearing electron donating substituents react with halogen species, (2) the iodination shows an ortho-para orientation, and (3) the reaction occurs only on an aromatic ring.

TABLE 1. IODINATION OF POLYMETHYLBENZENES WITH n-Bu_4NI

Substrate	Product	Conversion/%	Yield/%[a)]
m-Xylene		100	71 (75)
o-Xylene	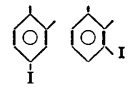	95	69 (75)
1,2,3-Trimethylbenzene[b)]		86	74 (77)
Mesitylene		100	70 (83)
1,2,4,5-Tetramethylbenzene		98	— (21)
1,2,4,5-Tetramethylbenzene[c)]		92	56 (60)
1,2,3,5-Tetramethylbenzene[b)]		100	54 (60)
Hexamethylbenzene[b)]		100	— (16)
Hexamethylbenzene[c)]		95	— (17)

a) Isolated yield based on the substrates used. Numerical values in parentheses are the yields determined by GLC. b) Time: 48 h. c) At room temperature for 10 d.

Table 2. Iodination of polymethylbenzenes with alkali metal iodide or molecular iodine

Substrate	Iodinating agent[a)]	Time h	Conversion %	Yield[b)] %
Mesitylene	LiI	24	100	65 (77)
Mesitylene	NaI	24	18	15 (18)
Mesitylene	KI	24	96	48 (57)
m-Xylene	I_2	24	100	68 (80)
Mesitylene	I_2	24	100	86 (90)
1,2,3-Trimethylbenzene	I_2	24	85	58 (64)
1,2,4,5-Tetramethylbenzene	I_2	168	100	33 (35)
1,2,3,5-Tetramethylbenzene	I_2	48	100	58 (67)
Hexamethylbenzene	I_2	168	100	— (16)

a) MI: 8.0 mmol, CAN: 8.0 mmol, or I_2: 2.0 mmol, CAN: 2.0 mmol. b) Isolated yield based on the substrates used. Numerical values in parentheses are the yields determined by GLC.

Table 3. Iodination of methoxybenzenes and naphthalene with *n*-Bu_4NI

Substrate Compound	mmol	*n*-Bu_4NI mmol	CAN mmol	Temp °C	Time h	Product	Conversion %	Yield[a)] %
Methoxybenzene	4.2	14.4	14.4	60	48	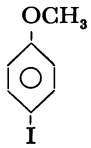	100	84 (87)
o-Dimethoxybenzene	4.0	12.0	12.0	60	48	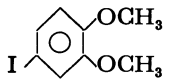	93	72 (77)
m-Dimethoxybenzene	3.3	4.0	4.0	r. t.	24	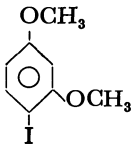	85	78 (80)
1,3,5-Trimethoxybenzene	3.8	7.6	7.6	r. t.	1	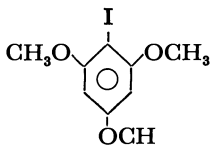	100	87 (90)
Naphthalene	0.5	1.0	1.0	60	48	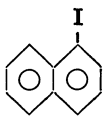	91	— (45)

a) Isolated yield based on the substrates used. Numerical values in parentheses are the yields determined by GLC.

Experimental

General Procedure. Into a solution of 4.0 mmol of an aromatic compound and 4.0 mmol of tetrabutylammonium iodide in 40 ml of acetonitrile was added a solution of 8.0 mmol of CAN (dried at 90—100 °C for 2 h) in 40 ml of acetonitrile. The mixture was stirred for 24 h at 60 °C, poured into 80 ml of water, and extracted with benzene (4×30 ml). The combined benzene layers were treated with sodium thiosulfate, washed with water, dried over $CaCl_2$, and the benzene was removed, carefully, under reduced pressure. The residue was purified by distillation, column chromatography (Woelm Akt I: hexane–benzene), and/or preparative gas chromatography (10% silicon OV-17). The isolated product was weighed and identified by comparing their IR, MS, and ^{1}H-NMR spectra with those of corresponding authentic samples. Elemental analyses also gave satisfactory results. The yield was, also, determined by analytical gas chromatography.

The author thanks Professor S. Oka and Dr. A. Ohno for useful discussions.

References

1) P. B. D. De La Mare and J. H. Ridd, "Aromatic Substitution Nitration and Halogenation," Butterworths Scientific Publications (1959), p. 110.

2) E. Bacciocchi, L. Mandolini, and C. Rol, *Tetrahedron Lett.*, **1976**, 3346; E. Bacciocchi, C. Rol, and L. Mandoliin, *J. Org. Chem.*, **42**, 3682 (1977).

Reaction of μ-Peroxo Complexes of Palladium with Alcohols, Amines, and Thiols

Ryuichi SUGIMOTO, Hajime EIKAWA, Hiroharu SUZUKI,* Yoshihiko MORO-OKA,* and Tsuneo IKAWA
Research Laboratory of Resources Utilization, Tokyo Institute of Technology, Nagatsuta 4259, Midori-ku, Yokohama 227
(Received March 18, 1981)

Synopsis. Reactions of μ-peroxo complexes of palladium with alcohols, amines, and thiols proceed at room temperature to afford hydrogen peroxide and alkoxo-, amido-, and alkylthio-bridged complexes of palladium, respectively.

In the previous papers we reported a novel preparation method of μ-peroxo complexes of palladium, platinum and rhodium having olefinic ligands *via* an anion exchange reaction of μ,μ'-dihalo complexes with potassium superoxide in dichloromethane and suggested that μ-peroxo ligand in the complexes behaved as a base and did not participate in the oxygenation of the olefinic ligands.[1-3] Such basic nature of dioxygen ligands was also reported for the mononuclear peroxo complexes of transition metal elements.[4-6] Important role of the basic nature of the coordinated dioxygen of the cobalt Schiff base complex was demonstrated by Nishinaga *et al.* in the catalytic oxidation of substituted phenols.[7] In the present investigation, reactions of μ-peroxo ligand with a series of alcohols, amines, and thiols have been examined in order to clarify the nature of μ-peroxo complexes of palladium.

Results and Discussion

Reactions of dioxygen complexes **1** with alcohols, thiols and amines were carried out in dry benzene at room temperature under dry nitrogen atmosphere. Treatment of **1a** with methanol gave μ,μ'-bis(methoxo) complex **2a-Me** in a 50% yield accompained with liberation of hydrogen peroxide. Formation of hydrogen peroxide was confirmed by the iodometry. Methoxy-bridged complex **2d-Me** was prepared in a similar manner. Methoxy-bridged complexes **2a-Me**

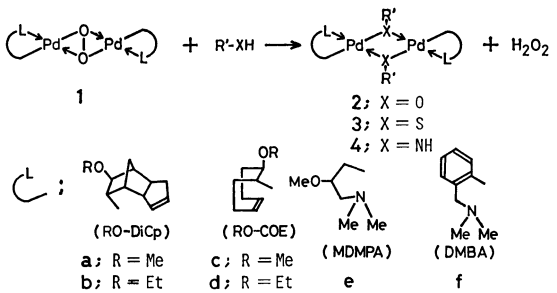

and **2d-Me** were unstable in benzene solution and decomposed immediately with heating at 30—40 °C to deposit metallic palladium. Even in the solid state, they decomposed after standing for one day at ambient temperature under dry nitrogen atmosphere. Ethoxy-bridged complexes **2a-Et** and **2c-Et** were also prepared by the reaction of **1** with ethanol. It was found that they were less stable than the corresponding methoxy-bridged ones. Further attempts to prepare the alkoxy-bridged complexes of bulky alcohols were resulted in vain. The starting μ-peroxo complex was recovered in the reaction of **1a** with 2-propanol (pK_a 18) or *t*-butyl alcohol (pK_a 19) at room temperature. Decomposition of complex **1a** in *t*-butyl alcohol proceeded giving a cyclic diene **6** at higher reaction temperatures (40—60 °C). Abstraction of proton from such alcohols is well supported by the fact that **1a** is basic enough to abstract active hydrogen from acetone (pK_a 20). Steric repulsion between Me-DiCp ligand and bulky alkoxo groups may force the β-elimination of Pd–H from a coordinatively unsaturated intermediate **5**. Yoshida *et al.* reported that treatment of $[Ni(CCl{=}CCl_2)(\mu\text{-}OMe)(PPh_3)]_2$ in alkaline solution gave $[Ni(CCl{=}CCl_2)(\mu\text{-}OH)(PPh_3)]_2$ *via* an anion exchange reaction.[8] In the present work, the bridging methoxy group was readily exchanged with ethoxy group by treatment of **2a-Me** with a large excess of ethanol in benzene at room temperature, and *vice versa*.

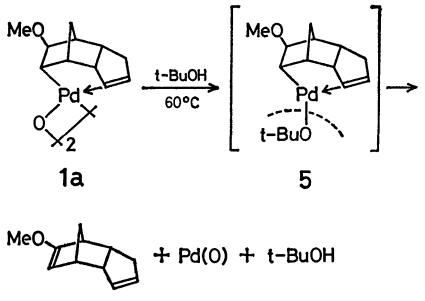

μ-Peroxo complexes also reacted with thiols to yield the corresponding alkylthio-bridged complexes. Alkylthio-bridged complex **3a-Et** was obtained by the dropwise addition of a diluted solution of ethanethiol to a rigorously stirred solution of **1a** in benzene. Analogous alkylthio complex **3e-Et** and phenylthio-bridged complexes **3a-Ph** and **3f-Ph** were prepared similarly. All these alkylthio-bridged complexes were stable sufficiently so that decomposition was not observed after standing for several months without special care. The reaction of the μ-peroxo complexes with benzylamine or acrylamide also gave the corresponding amido-bridged complex **4** and hydrogen peroxide at room temperature. A similar reaction of mononuclear peroxo complex of platinum with phenylenediamine was previously studied by Pizzotti *et al.* and they reported that the reaction afforded an amido complex with hydrogen peroxide.[9] Since an ordinary μ-peroxo complex does not react with compounds hav-

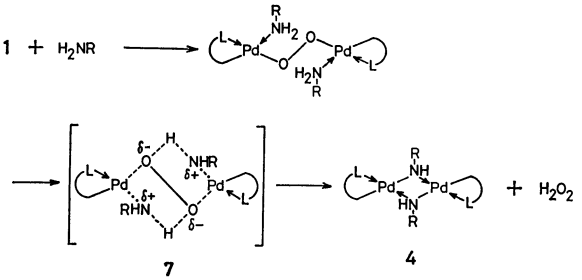

Scheme 1.

Table 1. Reactions of dioxygen complexes **1** with alcohols, thiols, and amines

Dioxygen complex	RXH (X=O, S, NH)	Product[a]	Yield %	Mp °C	Found (Calcd) (%) C	H	N	S
[(MeO-DiCp)PdO]$_2$	MeOH	[(MeO-DiCp)PdOMe]$_2$	50	155	47.81 (47.94)	6.02 (6.03)		
[(MeO-DiCp)PdO]$_2$	EtOH	[(MeO-DiCp)PdOEt]$_2$	28	180	49.76 (49.76)	6.21 (6.37)		
[(MeO-COE)PdO]$_2$	EtOH	[(MeO-COE)PdOEt]$_2$	81	130	45.83 (45.45)	7.19 (6.94)		
[(EtO-COE)PdO]$_2$	MeOH	[(EtO-COE)PdOMe]$_2$	47	140	45.07 (45.45)	7.15 (6.94)		
[(MeO-DiCp)PdO$_2$	EtSH	[(MeO-DiCp)PdSEt]$_2$	58	114	47.45 (47.21)	6.22 (6.09)		8.35 (9.69)
[(MeO-DiCP)PdO]$_2$	PhSH	[(MeO-DiCp)PdSPh]$_2$	41	105	50.71 (50.78)	5.70 (5.68)		8.80 (9.04)
[(DMBA)PdO]$_2$	EtSH	[(DMBA)PdSEt]$_2$	22	161—163	42.90 (43.79)	5.50 (5.68)	4.42 (4.46)	11.42 (10.63)
[(MDMPA)PdO]$_2$	PhSH	[(MDMPA)PdSPh]$_2$	66	197—203	51.33 (51.51)	4.40 (4.90)	3.67 (4.00)	8.80 (9.17)
[(MeO-COE)PdO]$_2$	$PhCH_2NH_2$	[(MeO-COE)PdNHCH$_2$Ph]$_2$	67	135	53.81 (54.63)	6.06 (6.59)	4.61 (3.98)	
[(MeO-COE)PdO]$_2$	CH_2=CHCONH$_2$	[(MeO-COE)Pd(CH_2=CHCONH)]$_2$	64	62	45.26 (45.66)	6.24 (6.07)	4.10 (4.40)	

a) For all products, satisfactory ^{1}H-NMR and IR spectra were obtained.

ing pK_a values higher than 20, the reaction observed in this strudy is not explicable by the direct interaction of the coordinated dioxygen with amines. A zwitter ionic transition state **7** resulted from the coordination of amine to the μ-peroxo complex may assist the abstraction of proton to form amido-bridged complex **4** and hydrogen peroxide.

Experimental

General. All reactions were run under a pressure of dry nitrogen. ^{1}H-NMR spectra were determined in $CDCl_3$ on a Hitachi R-24B instrument. Chemical shifts are reported in the δ unit, parts per million (ppm) downfield from tetramethylsilane and coupling constants are reported in hertz. Melting points were obtained on a Yanagimoto MP-apparatus and are uncorrected.

Diethyl ether and benzene for the solvent were distilled from sodium benzophenone ketyl. Pentane was distilled from sodium. Dichloromethane was purified by washing with water and dried over calcium hydride and then distilled from phosphorous pentoxide under a pressure of dry nitrogen. Methanol and ethanol were distilled from magnesium turnings. Isopropanol and *t*-butyl alcohol were dried over molecular sieve 3A and distilled prior to use. Benzylamine was dried over potassium hydroxide pellets. Acrylamide, ethanethiol, and thiophenol were used without further purification. Dioxygen complexes (**1a**—**f**) were prepared according to the procedure reported previously.[1-3]

*Reaction of **1a** with Methanol.* To a solution of 0.176 g (0.38 mmol) of **1a** in 5 cm^3 of dry benzene was added 0.2 cm^3 of dry methanol followed by 3 cm^3 of dry diethyl ether at room temperature. The solution was stirred for a few minutes and was allowed to stand for 20 h in a refrigerator. Pale yellow prisms precipitated in the solution were collected by suction and washed with dry pentane, then dried *in vacuo* to give 0.115 g (50%) of di-μ-methoxybis(8-*exo*-methoxytricyclo[5.2.1.0^{2,6}]dec-3-en-9-yl)dipalladium. Mp (dec.) 155 °C; IR (KBr) ν(C–O) 1082, 1053 (bridging) cm^{-1}; NMR ($CDCl_3$) δ 3.18 (6H, s, OCH_3), 3.40 (6H, s, OCH_3), 5.16 (2H, m, olefinic), 5.63 (2H, m, olefinic); Mol wt (cryoscopy in benzene) calcd 600.8, found 645.

In a similar procedure, alkoxo-bridged complexes were prepared and characterized. Yields, mps, and results of elemental analyses are summarized in Table 1.

*Reaction of **1a** with Ethanethiol.* To a suspension of 0.329 g (0.58 mmol) of **1a** in 25 cm^3 of dry diethyl ether was added dropwise 1.63 cm^3 of a solution of ethanethiol in benzene (0.7 mmol/cm^3). The solution was stirred for 6 h at room temperature. The resulting orange solution was filtered and filtrate was dried in vacuo to give red powder. Recrystallization from a mixed solvent of benzene, diethyl ether and pentane (1:1:1 vol ratio) gave di-μ-ethylthiobis(8-*exo*-methoxytricyclo[5.2.1.0^{2,6}]dec-3-en-9-yl)dipalladium (**3a-Et**) as yellowish orange prisms (0.259 g, 58%). Mp (dec.) 114 °C; IR (KBr) ν(C–S) 1250, ν(C–O) 1080 cm^{-1}; NMR ($CDCl_3$) δ 1.41 (6H, t, J=7, S–CH_2–CH_3), 2.53 (4H, q, J=7, S–CH_2–), 3.26 (6H, s, OCH_3), 5.87 (2H, m, olefinic), 6.35 (2H, m, olefinic).

*Reaction of **1c** with Benzylamine.* To a suspension of 0.174 g (0.33 mmol) of **1c** in 25 cm^3 of dry diethyl ether was added slowly 1.4 cm^3 of a solution of benzylamine in benzene (0.47 mmol/cm^3). The solution was stirred for 10 h at ambient temperature. The resulting yellow solution was filtered and the filtrate was concentrated under a reduced pressure. Addition of dry pentane and storage in a refrigerator for 40 h yielded di-μ-benzylaminobis(8-*exo*-methoxy-4-cyclooctenyl)dipalladium (**4c-Bz**) as pale yellow precipitates (0.152 g, 67%). Mp (dec.) 135 °C; IR (KBr) ν(N–H) 3450, ν(C–O) 1090 cm^{-1}. NMR ($CDCl_3$) δ 3.10 (3H, s, OCH_3), 4.13 (2H, d, Ph–CH_2–), 5.25 (2H, br, olefinic), 7.0—7.5 (5H, aromatic). Mol wt (cryoscopy in benzene) Calcd 702.8; Found 714.

References

1) H. Suzuki, K. Mizutani, Y. Moro-oka, and T. Ikawa, *J. Am. Chem. Soc.*, **101**, 748 (1979).

2) P. J. Chung, H. Suzuki, Y. Moro-oka, and T. Ikawa, *Chem. Lett.*, **1980**, 63.

3) F. Sakurai, H. Suzuki, Y. Moro-oka, and T. Ikawa, *J. Am. Chem. Soc.*, **102**, 1749 (1980).

4) S. Muto, H. Ogata, and Y. Kamiya, *Chem. Lett.*, **1975**, 809.

5) S. Muto, K. Tasaka, and Y. Kamiya, *Bull. Chem. Soc. Jpn.*, **50**, 2493 (1977).

6) S. L. Regen and G. M. Whitesides, *J. Organomet. Chem.*, **59**, 293 (1973).

7) A. Nishinaga and T. Matsuura, *Chem. Commun.*, **1973**, 9; A. Nishinaga, T. Tojo, and T. Matsuura, *ibid.*, **1974**, 809; A. Nishinaga and H. Tomita, *J. Mol. Cat.*, **7**, 179 (1980).

8) T. Yoshida, T. Okano, and S. Otsuka, *J. Chem. Soc., Dalton Trans.*, **1976**, 993.

9) M. Pizzotti, S. Cenini, and G. L. Monica, *Inorg. Chim. Acta*, **33**, 161 (1978).

The Reaction of 2-Methylfuran with Methyl Acrylate. Unusual Formation of 1,1′-Bis(5-methyl-2-furyl)ethane and Methyl 3,3′-Bis(5-methyl-2-furyl)propionate

Osamu MARUYAMA, Yuzo FUJIWARA,* and Hiroshi TANIGUCHI

Department of Applied Chemistry, Faculty of Engineering, Kyushu University, Higashi-ku, Fukuoka 812

(Received March 23, 1981)

Synopsis. The reaction of 2-methylfuran with methyl acrylate in the presence of $Pd(OAc)_2$ gave unusual products such as 1,1′-bis(5-methyl-2-furyl)ethane (22%) and methyl 3,3′-bis(5-methyl-2-furyl)propionate (10%) along with the usual aromatic substitution product. This is a marked contrast to the reaction of furan with olefins.

In our previous paper we reported the palladium-assisted one-step alkenylation reactions of heterocycles.[1,2] These reactions afford both the 2-mono- and 2,5-dialkenylated products when the five-membered aromatic heterocycles such as furan, thiophene, or pyrrole are allowed to react with olefins. In subsequent related studies, we attempted 2-methylfuran to react with methyl acrylate, and obtained some unusual products such as 1,1′-bis(5-methyl-2-furyl)-ethane (**2**) and methyl 3,3′-bis(5-methyl-2-furyl)propionate (**3**).

The reaction of 2-methylfuran with methyl acrylate was carried out with stirring at 100 °C for 8 h. After the usual work-up, there were obtained 27%[3] of methyl 3-(5-methyl-2-furyl)acrylate (**1**), the usual aromatic substitution product, 22% of **2** of which identity was proved by comparison of NMR and IR spectra with those of an authentic sample prepared from 2-methylfuran and acetaldehyde,[4] 10% of **3**, and 5% of 5-methyl-2-furyl acetate (**4**). The formation of **2** and **3** in considerable amounts is of particular interest since no such products are obtained in the case of unsubstituted five-membered heterocycles.[1,2]

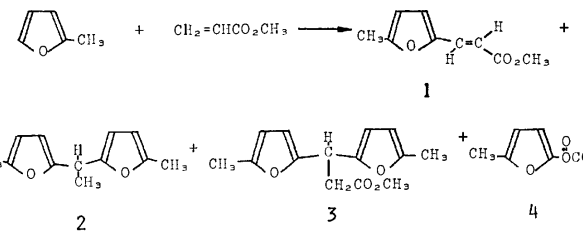

The formation of **2** and **3** may be explained in the following way (Scheme 1). First, palladium(II) attackes at the 5-position of 2-methylfuran electrophilically to give a furyl-Pd σ complex **5**. Then **5** adds to methyl acrylate affording a σ complex **6**. Elimination of a PdH species gives **1**. Then the furyl-Pd σ complex adds to **1** giving an intermediate complex **7**. Elimination of HPdOAc from **7** gives an olefin **8** which may be transformed into **2** and **3** by hydrogenation[5] and/or decarboxylation.[6] In the case of furan, Pd(II) can attack further at the 5-position of the furan ring of **9** to produce a furyl-Pd σ complex **10** which reacts with the olefin yielding the dialkenylated products.[1,2] However, in the present case, there is no reactive 5-position available since the 5-position is occupied with a methyl group.

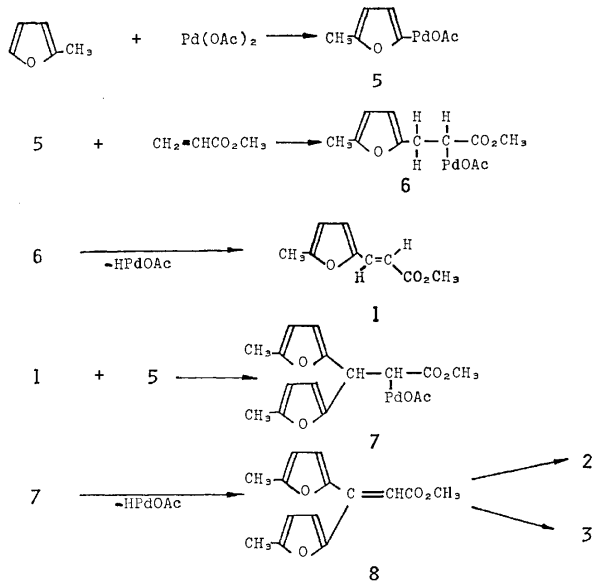

Scheme 1.

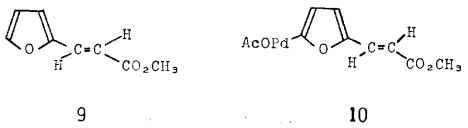

Experimental

NMR spectra were obtained with a Hitachi R-24S spectrometer using Me_4Si as an internal standard. Materials used were prepared and purified as described already.[2]

Reaction of 2-Methylfuran with Methyl Acrylate. The reaction was performed with stirring at reflux for 8 h using 2-methylfuran (2 mmol), methyl acrylate (2 mmol), palladium(II) acetate (2 mmol), dioxane (20 ml), and acetic acid (5 ml). After work-up as described already,[2] the residue was chromatographed on a column of silica gel. Elution with hexane–ether (9:1) yielded **2** (22% yield) which was assigned by comparison of the IR and NMR spectra with those of an authentic sample prepared from 2-methylfuran and acetaldehyde.[4] **2**: bp 130 °C/15 mmHg†; IR (neat) 2960, 1562, 1015, and 790 cm^{-1}; NMR (CCl_4) δ 1.50 (d, 3H, J=7 Hz), 2.23 (s, 6H), 3.84 (q, 1H, J=7 Hz), and 5.69 (4H). Further elution gave a 1:5 mixture of **3** and **1**. The products were isolated by preparative glc (OV-17, 0.5 m, 118 °C). **1**: 27% yield; IR (Nujol) 1724 and 974 cm^{-1}; NMR ($CDCl_3$) δ 2.36 (s, 3H), 3.81 (s, 3H), 6.0—6.7 (3H), and 7.44 (d, 1H, J=17 Hz). **3**: 10% yield; IR (neat) 1725 cm^{-1}; NMR ($CDCl_3$) δ 2.22 (s, 6H), 2.91 (d, 2H, J=8 Hz), 3.60 (s, 3H), 4.48 (t, 1H, J=9 Hz), and 5.7—6.0 (m, 4H). Further elution with hexane–ether (3:2)

† 1 mmHg≈133.322 Pa

gave 5-methyl-2-furyl acetate (**4**). **4**: 5% yield; IR (neat) 1770 cm^{-1}; NMR ($CDCl_3$) δ 1.84 (s, 3H), 2.07 (s, 3H), 6.20 (d, 1H, J=6 Hz), and 7.17 (d, 1H, J=6 Hz).

References

1) O. Maruyama, M. Yoshidomi, Y. Fujiwara, and H. Taniguchi, *Chem. Lett.*, **1979**, 1229.
2) Y. Fujiwara, O. Maruyama, M. Yoshidomi, and H. Taniguchi, *J. Org. Chem.*, **46**, 851 (1981).
3) Yields are all based on palladium acetate.
4) D. S. P. Effax and A. P. Dunlop, *J. Org. Chem.*, **30**, 1317 (1965).
5) H. Tanaka, Y. Fujiwara, I. Moritani, and S. Teranishi, *Bull. Chem. Soc. Jpn.*, **48**, 3372 (1975).
6) K. Yamamura, *J. Org. Chem.*, **43**, 724 (1978).

Possibility of the Intramolecularity of Triazene Rearrangement[1)]

Yoshiro OGATA,* Yoshiaki NAKAGAWA, and Morio INAISHI
Department of Applied Chemistry, Faculty of Engineering, Nagoya University, Chikusa-ku, Nagoya 464

(Received September 29, 1980)

Synopsis. The mechanism for the ortho-rearrangement of diaryltriazenes still remains equivocal. An interesting result suggesting an intramolecular nature of the triazene rearrangement was obtained on the basis of the effect of concentration of added *N,N*-dimethylaniline in the ortho-rearrangement of 1,3-bis(4-methylphenyl)triazene (**1**). The ortho/para ratio for the rearrangement of 1,3-diphenyltriazene (**4**) tends to increase with an increase of the viscosity. The results are discussed on the basis of increasing nucleophilicity of free amine by H-bonding with dimethylaniline and favoring ortho-migration with viscosity, respectively.

It is known that acid-catalyzed rearrangement of 1,3-diphenyltriazene to *p*-aminoazobenzene, accompanied by a small amount of *o*-isomer[2)] (Eq. 2), is intermolecular based on the trap of intermediary diazonium ion with phenols and dialkylanilines.[3)] However, as to the ortho-rearrangement at least, the possibility of intramolecular mechanism cannot be excluded.

Berezovskii *et al.*[4)] suggested that the ortho-rearrangement has an intramolecular character based on analogous yields for the rearrangement of 1,3-bis(3,4-dimethylphenyl)triazene in *p*-toluidine and in chlorobenzene, but their evidence is not definitive.

We attempted to clarify the mechanism of triazene rearrangement by the examination of the effects of the addition of *N,N*-dimethylaniline as a trapping agent for the intermediary diazonium ion during the rearrangement and also of the solvent effect on the ortho/para ratio of 1,3-diphenyltriazene. The results suggest the partial intramolecularity of the rearrangement.

Results and Discussion

Effect of N,N-*Dimethylaniline on 1,3-Bis(4-methylphenyl)-triazene Rearrangement.* 1,3-Bis(4-methylphenyl)-triazene (**1**) was rearranged in acidic ethanol, affording 2-amino-5,4′-dimethylazobenzene (**2**). In the presence of *N,N*-dimethylaniline (DMA) as a scavenger of diazonium ion, **1** gave 4-dimethylamino-4′-methylazobenzene (**3**) as well as the rearrangement product **2**.

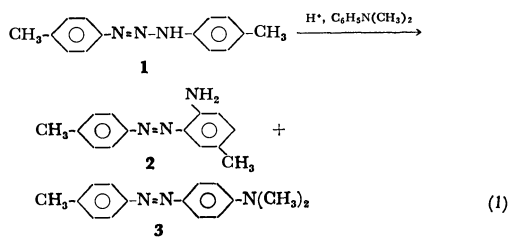

(1)

A plot of the reciprocal of the initial concentration of added DMA ($1/[DMA]_0$) *vs.* a ratio of the yields of **2** to **3** (**2/3**) is shown in Fig. 1.

Assuming this rearrangement to be completely intermolecular, the ratio (**2/3**) must be zero, when

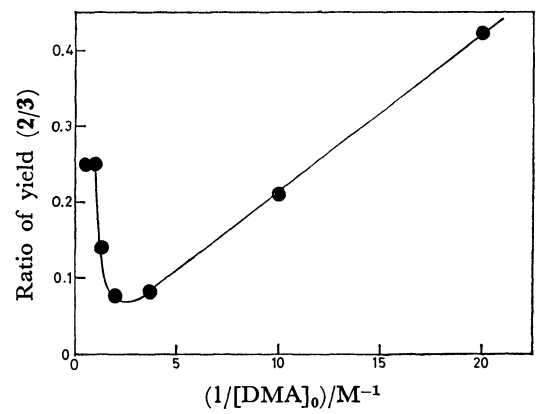

Fig. 1. Effect of *N,N*-dimethylaniline on the rearrangement of **1** in ethanol at room temperature. The initial concentrations of reagents were: $[\mathbf{1}]_0$= 0.05 M, $[HCl]_0$=0.011 M.

$[DMA]_0$ is extrapolated to infinity. As shown in Fig. 1, the ratio decreases really until $[DMA]_0$ of 0.75 M (1 M=1 mol dm^{-3}), but with increasing $[DMA]_0$ over 0.75 M, the ratio increases to 0.25, which suggests an increase of intramolecular nature of the rearrangement at very high concentration of DMA.

The Goldschmidt mechanism[5)] in which protonated triazene reacts with anilines might explain the observed plot of the **2/3** ratio *vs.* $1/[DMA]_0$ (Fig. 1), but the mechanism requires that the analogous DMA-catalyses should operate with both rearrangement and DMA-coupling at high $[DMA]_0$. Hence the higher ratio of **2/3** at low $1/[DMA]_0$ cannot be explained.

The increase of intramolecular nature by increasing $[DMA]_0$ may be caused by increasing the nucleophilicity of $ArNH_2$ of intermediary $[ArNH_2 \cdot N\equiv \overset{+}{N}Ar]$ *via* hydrogen bonding $Ar\overset{\delta-}{N}H\cdots H\cdots \overset{\delta+}{N}Me_2Ph$. The diazo coupling reaction takes place between diazonium ion and free amine[6)] which exist in neutral and even weakly acidic media. In fact, the yield of **2** for the rearrangement of **1** ($[\mathbf{1}]_0$=0.05 M) in ethanol with $[HCl]_0$=0.005 M (37%) in the absence of DMA was found to be higher than those with $[HCl]_0$=

Table 1. Effect of *N,N*-dimethylaniline (DMA) on the rearrangement of 1,3-bis(4-methylphenyl)-triazene (**1**) in ethanol at room temperature[a)]

$[\mathbf{1}]_0$ (M)	$[DMA]_0$ (M)	Yield/%		Ratio of yields
		2	**3**	**2/3**
0.051	0	23	—	—
0.045	0.050	19	48	0.39
0.046	0.10	13	65	0.21
0.046	0.27	3.7	45	0.083
0.045	0.52	3.4	44	0.077
0.046	0.75	8.1	58	0.14
0.048	1.0	11	48	0.25
0.045	2.0	14	57	0.25

a) Initial concentration; $[HCl]_0$=0.011 M. Products other than **2** and **3** were toluene and *p*-toluene formed by decomposition.

Table 2. Solvent effect on the rearrangement of 1,3-diphenyltriazene (**4**)[a] and 1,3-bis(4-methylphenyl)triazene (**1**)[b]

Solvent	Viscosity/cp		Dielectric constant	Rearr. of 4 Yield[c]/%		Ratio of yields	Rearr. of 1 Yield/%
	At 30 °C	At 30 °C	at 25 °C	5	6	6/5	2
Methanol	0.51		32.6	64	5.8	0.09	5
Ethanol	0.99	1.46	24.3	75	8.2	0.11	21
Propanol	1.72	2.89	19.7	74	—[e]	—	32
2-Propanol	1.77	3.26	18.3	73	10	0.14	33
1-Butanol	2.27	3.87	17.7	75	12	0.16	4[f]
2-Butanol	3.18	—	16.6	55	—[e]	—	33
t-Butyl alcohol	3.32	—	12.5	61	14	0.23	34
DG[d]	30[g]	—	31.7[h]	18	1.8[i]	0.10	3

a) Initial concentration; $[4]_0=0.051$—0.052 M, $[HCl]_0=0.0054$ M. Reaction temp.; 30 °C. b) Initial concentration; $[1]_0=0.046$—0.051 M, $[HCl]_0=0.011$ M. Reaction temp.; room temp. c) Duplicates gave similar results on the trend with viscosity effect, so that the average yields were shown here. d) Diethylene glycol. e) These yields could not be estimated because of the overlapping of the HPLC peaks of **6** and unknown product. f) A large amount of **1** was recovered. g) At 25 °C. h) At 20 °C. i) This yield was estimated after concentration of the solution of products by evaporating the solvent. However, the yield for DG is low because of the decomposition of triazene giving aniline and benzene (GLC analysis) so that the data are little reliable.

0.01 M (25%) and 0.02 M (15%). Ethanol, as in the case of HCl, may deactivate $ArNH_2$ by hydrogen bonding. The increase of nucleophilicity of $ArNH_2$ lowers the selectivity and raises the *o*/*p* ratio.

Solvent Effect in 1,3-Diphenyltriazene Rearrangement. 1,3-Diphenyltriazene (**4**) gives *p*- (**5**) and *o*-aminoazobenzene (**6**).[2] As shown in Table 2, satisfactory yields of rearrangement products were obtained except with 1-butanol and diethylene glycol. We expected that the ortho-rearrangement may occur *via* intramolecular process, especially in viscous solvents. Hence, **4** was rearranged in various solvents under

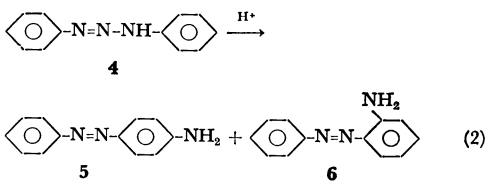

(2)

acidic conditions. The effect of viscosity on the ratio of ortho/para-was examined by estimating the ratio of the yields of ortho *vs.* para (**6**/**5**) (Table 2).

The ratio, **6**/**5**, or the trend for ortho migration tends to increase slightly with increasing viscosity of the solvent in going from methanol to *t*-butyl alcohol. The same tendency was also observed with the rearrangement of **1**, where the yield of **2** increased in going from methanol to **2**-propanol (Table 2).

This tendency for the ratio **6**/**5** and yields of **2** suggests that the triazene rearrangement has at least a partial contribution of intramolecularity. The increase of the ratio **6**/**5** and the yield of **2** may be caused by an increase of viscosity. In the reaction of diethylene glycol, the decomposition of triazene to aniline and benzene is remarkable; the yields of rearrangement products are so poor. Also the yield of rearrangement of **1** in 1-butanol was poor, a considerable amount of **1** being recovered.

Experimental

Melting points were measured by a Yanagimoto micro melting point apparatus and uncorrected. NMR spectra were recorded on a Hitachi R-24B NMR spectrometer using Me_4Si as an internal standard. The HPLC analysis was performed with a Yanagimoto L-1030 high pressure liquid chromatograph.

Materials. Triazenes were prepared from corresponding anilines by the method of Hartman *et al*;[7] 1,3-diphenyltriazene: mp 95—97.5 °C (lit,[7] 94—96 °C); NMR (CCl_4) δ 7.3 (m, 10H, ArH), 9.9 (s, 1H, NH); UV (EtOH) λ_{max} 353 nm (ε 1.98×10^4), 294 nm (0.74×10^4), 236 nm (1.69×10^4). 1,3-bis(4-methylphenyl)triazene: mp 119—120 °C (lit,[8] 118 °C); NMR (CCl_4) δ 2.28 (s, 6H, CH_3), 7.1 (dd, 8H, ArH), 9.5 (s, 1H, NH); UV (EtOH) λ_{max} 357 nm (ε 2.03×10^4), 292 nm (1.02×10^4), 238 nm (1.73×10^4). Solvents were of commercial guaranteed grade and purified by fractional distillation.

Effect of N,N-*Dimethylaniline on the Rearrangement of 1,3-Bis(4-methylphenyl)triazene (1).* An ethanolic solution (10 ml) of **1** (0.05 M) and *N*,*N*-dimethylaniline containing HCl (0.011 M) was allowed to stand at room temperature for 3 d, until **1** was consumed. One ml of the resulting solution was pipetted out and ethanol was added for dilution to a suitable concentration for HPLC analysis. The HPLC analysis was performed under the following conditions using Yanaco SA-I as a packing. A carrier solvent of hexane/THF (9 1 in vol.) was used at a flow rate of 40 ml/h. The products were identified by HPLC peaks in comparison with the authentic specimens.

Solvent Effect in 1,3-Diphenyltriazene (4) Rearrangement. Various solutions (10 ml) of **4** (0.05 M) containing HCl (0.005 M) were allowed to stand at 30 °C in a thermostat for 2 d, until **4** was consumed. In a similar manner as above, the products were identified and estimated by HPLC under the following conditions. Yanaco SA-I was used as a packing, and hexane/THF (7/3) was used at a flow rate of 90 ml/h. Products from propanol and 2-butanol contained a small amount of unknown product, which showed UV peaks (334 nm) different from *o*-aminoazobenzene, 4-(phenyldiazoamino)azobenzene (C_6H_5–N=N–NH–C_6H_4–N=N–C_6H_5) and *p*-[*p*-(phenylazo)phenylazoaniline (C_6H_5–N=N–C_6H_4–N=N–$C_6H_4NH_2$).

References

1) Contribution No. 274.
2) F. H. Witt, *Ber.*, **46**, 2557 (1913).
3) E. Noelting and F. Binder, *Ber.*, **20**, 3004 (1887).
4) V. M. Berezovskii and L. S. Tul'chinskaya, *J. Gen. Chem. U.S.S.R.*, **31**, 3371 (1961).
5) C. K. Ingold, "Structure and Mechanism in Organic Chemistry," 2nd ed, Cornell University Press, Ithaca (1969), p. 897.
6) H. Zollinger, *Chem. Rev.*, **51**, 347 (1952).
7) W. W. Hartman and J. B. Dickey, *Org. Synth.*, Coll. Vol. II, 163 (1943).
8) D. F. Day, T. W. Campbell, and G. M. Coppinger, *J. Am. Chem. Soc.*, **73**, 4687 (1951).

Cyclodehydrogenation of 3-Cinnamoyltropolones with 2,3-Dichloro-5,6-dicyanobenzoquinone

Kimiaki IMAFUKU* and Kazuko YAMAGUCHI†

Department of Chemistry, Faculty of Science, Kumamoto University, Kurokami, Kumamoto 860

(Received April 15, 1981)

Synopsis. 3-Cinnamoyltropolone and 3-(3-methoxycinnamoyl)tropolone were oxidized with 2,3-dichloro-5,6-dicyanobenzoquinone to give 2-phenyl- and 2-(3-methoxyphenyl)-4,9-dihydrocyclohepta[*b*]pyran-4,9-diones, while 2′- and/or 4′-methoxy-substituted 3-cinnamoyltropolones gave 2-arylmethylene-2*H*-3,8-dihydrocyclohepta[*b*]furan-3,8-diones.

2,3-Dichloro-5,6-dicyanobenzoquinone (DDQ) is recently used for synthetic organic chemistry as a dehydrogenating or cyclodehydrogenating agent.[1a-c] In connection with our studies on cyclization reactions of 3-cinnamoyltropolones,[2-4] which have a 2′-hydroxychalcone-like structure, we have been interested in the use of DDQ for their cyclization reaction. Little is known about the DDQ cyclization of 2′-hydroxychalcones except for 2′-hydroxy-5′-prenyl-4,4′-diphenylchalcone, which gave the corresponding flavone.[5]

A mixture of 3-cinnamoyltropolones (**1a—i**) (1 mmol) and DDQ (2 mmol) in dry benzene was refluxed for 20 h. Thus, the reactions of 3-cinnamoyltropolone (**1a**) and 3-(3-methoxycinnamoyl)tropolone (**1c**) gave flavone-like compounds, 2-aryl-4,9-dihydrocyclohepta[*b*]pyran-4,9-diones, while the other 3-cinnamoyltropolones (**1b**, **d—i**) which have the methoxyl group at 2′- and/or 4′-position gave selectively aurone-like compounds, 2-arylmethylene-2*H*-3,8-dihydrocyclohepta[*b*]furan-3,8-diones (**3b**, **d—i**). Each of the products was identified with comparison of its mp and IR and NMR spectra with those of the product from selenium dioxide oxidation[2] and alkaline hydrogen peroxide oxidation[3] of the corresponding 3-cinnamoyltropolones. The results are summarized in Table 1.

These results show that the DDQ is a useful cyclodehydrogenating reagent of 3-cinnamoyltropolones. This reaction might be extended to the oxidative cyclization of 2′-hydroxychalcones.

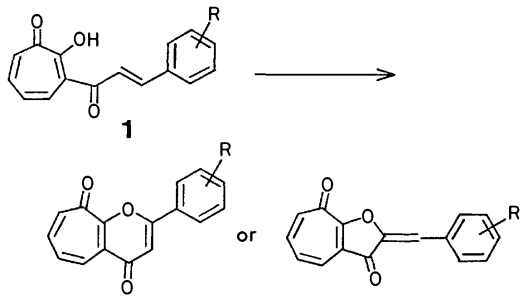

a R=H **b** R=2-OCH_3
c R=3-OCH_3 **d** R=4-OCH_3
e R=2,3-$(OCH_3)_2$
f R=2,4-$(OCH_3)_2$
g R=3,4-$(OCH_3)_2$
h R=2,3,4-$(OCH_3)_3$
i R=3,4-(OCH_2O)

Scheme 1.

Experimental

Measurement. The melting points were determined with a Yanagimoto melting-point measuring apparatus and are uncorrected. The IR spectra were taken on a JASCO IRA-1 spectrophotometer. The NMR spectra were recorded with a Hitachi R-24 spectrometer (60 MHz).

*Oxidative Cyclization of 3-Cinnamoyltropolones (**1a—i**).* A mixture of 3-cinnamoyltropolone (**1a—i**) (1 mmol, 252—343 mg) and DDQ (2 mmol, 454 mg) in dry benzene (20 ml) was refluxed for 20 h. The reaction mixture was poured into a saturated sodium carbonate solution (100 ml) and extracted with chloroform. The extract was washed with water, dried over anhydrous sodium sulfate, and brought to dryness by evaporation of the solvent. The residue was recrystallized from benzene to afford 2-aryl-4,9-dihydro-

TABLE 1. CYCLODEHYDROGENATION OF 3-CINNAMOYLTROPOLONES

	R	Product	Yield %	Mp °C	(Lit, mp)	Ref.
a	H	**2a**	46	200—202	(201—202)	2
b	2-OCH_3	**3b**	44	262—265	(261—262)	3
c	3-OCH_3	**2c**	43	212—213	(212—214)	2
d	4-OCH_3	**3d**	53	225—227	(227—228)	3
e	2,3-$(OCH_3)_2$	**3e**	38	225—226	(225—226)	3
f	2,4-$(OCH_3)_2$	**3f**	42	231—232	(231—233)	3
g	3,4-$(OCH_3)_2$	**3g**	39	282—284	(285—286)	3
h	2,3,4-$(OCH_3)_3$	**3h**	36	184—185	(183—184)	3
i	3,4-(OCH_2O)	**3i**	46	277—278	(279—280)	3

† Present address: Tokyo Office, USAC Electronic Industry Co., Ltd., Shinkawa, Chuo-ku, Tokyo 104.

cyclohepta[*b*]pyran-4,9-dione (**2a**, **c**) or 2-arylmethylene-2*H*-3,8-dihydrocyclohepta[*b*]furan-3,8-dione (**3b**, **d**—**i**).

References

1) a) H. -D. Becker, "The Chemistry of Quinoid Compounds," ed by S. Patai, John Wiley & Sons, Inc., New York (1974), p. 335; b) T. Kinoshita and T. Tokuyama, "Shin Jikken Kagaku Koza," Maruzen, Tokyo (1976), Vol. 15, p. 844; c) A. B. Turner, "Synthetic Reagents," ed by J. S. Pizey, Ellis Horwood Ltd., Sussex (1977), Vol. 3, p. 193.

2) K. Imafuku, A. Yamane, and H. Matsumura, *Yuki Gosei Kagaku Kyokai Shi*, **38**, 308 (1980).

3) K. Yamaguchi, K. Imafuku, and H. Matsumura, *Yuki Gosei Kagaku Kyokai Shi*, **38**, 998 (1980).

4) K. Imafuku, K. Suezaki, and H. Matsumura, *Heterocycles*, **16**, 637 (1981).

5) A. C. Jain, R. C. Gupta, and R. Khazanchi, *Tetrahedron*, **35**, 413 (1979).

Use of Propagators in the Hückel Model. III. Stability and Reactivity

Takayuki Ohmae, Kiyoshi Nishikawa, Kisaburo Deguchi, and Shigeyuki Aono*
Department of Chemistry, Faculty of Science, Kanazawa University, Marunouchi, Kanazawa 920
(Received December 20, 1980)

The propagator approach is applied to the problems of chemical reactivity and stability. Subjects discussed are the ring closure and opening reactions, the Diels-Alder reaction and sigmatropic reaction for reactivity; the aromaticity, two ring compounds (such as naphthalene and azulene), and benzenoid hydrocarbons (such as anthracene and phenanthrene) for stability. Results are given in analytical formulas.

The Hückel model or the tight-binding approximation is of great use because of its mathematical simplicity in analysis of molecular electronic states and chemical reactivities. Coulson and Longuet-Higgins[1] emphasized that once the Hückel determinant is given for a system all its physical properties are derived by making analysis of the determinant, not *via* wave functions as has been done in the usual theories. The charge density, bond order and total energy are expressed by the corresponding contour integrals closely related to the Hückel determinant. The perturbation theory has been developed in terms of mutual polarizability, which are also given by similar expressions. They applied their theory to the conjugated molecules and successfully derived many rules. Recent trials of Hosoya *et al.*[2] with topological aspects seem to be inherently related to the treatment of Coulson and Longuet-Higgins.

On the other hand Fukui[3] discussed chemical reactivity and stability in view of frontier electron. In this theory, the specified orbitals called LUMO and HOMO play dominant roles in the chemical reactions, and their mutual phases qualitatively decide whether the reaction takes place or not. The last is known as the Woodward-Hoffmann rule.[4]

In the first paper[5] of this series, the Hückel theory is reformulated in terms of propagators. This is a Green's function version of Coulson's work, and has merit of giving results beyond the elementary perturbation theory. Our theory is not so easy as the usual LCAO theory, but sometimes successfully reveals physical concepts hidden in the latter. The bond order between the r-th and s-th sites, $q(r,s)$ is usually inferred to the overlap charge or the charge density at the bond. This might not be feasible if the r-th and s-th sites are far from each other. By use of a propagator the bond order is defined by

$$q(r, s) = \frac{1}{2\pi i}\int_c dz G(r, s; z). \quad (1)$$

What this means is as follows: consider the probability amplitude which an electron at the r-th site transfers to the s-th site in any one-electron state. If we sum up such amplitude with respect to the levels occupied in the ground state, the result is $q(r, s)$. Moreover, $q(r, s)$ is divided into the contributions arising from several independent paths.[6] The bond order between the nearest sites in benzene is composed of two components which refer the shorter and longer paths in a way from the one site to the other.

Any chemical bond produced by the chemical reaction under consideration is due to the propagations of interactions. Thus the bond order plays a leading role in the following investigations, showing quantitatively what kind of route of propagation is important.

Interaction Energy

In order to investigate the stability condition in the ground state and the chemical reactivity, *i.e.*, selection of the reaction path of the chemical reaction, we derive the expression of energy stabilization due to perturbation. In the case of reactivity, we estimate the stabilization energy due to perturbation at some point along the reaction path, then at the corresponding point along the other path. Comparing these two, we can decide which one is favorable. Calculations will be performed following those in I, but are limited to the second order with respect to the perturbation. This suffices for the present case.

The total energy of the system is

$$E = \mathrm{Tr}\frac{1}{2\pi i}\int_c dz\, z\mathbf{G}(z), \quad (2)$$

where $\mathbf{G}$ is the matrix of Green's function represented by the site indices, z the energy parameter and Tr the trace with respect to the site indices. Integration contour c is the so-called Coulson contour shown in Fig. 1. Note that the integration in Eq. 2 includes the spin sum.

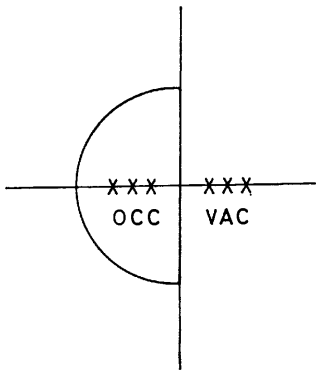

Fig. 1. Coulson's contour.

Let us consider the perturbation $\mathbf{v}$, which is a matrix represented by the site indices. The interaction energy caused by the perturbation is

$$\Delta E = \mathrm{Tr}\frac{1}{2\pi i}\int_c dz\, z[\mathbf{G}_0\mathbf{v}\mathbf{G}_0+\mathbf{G}_0\mathbf{v}\mathbf{G}_0\mathbf{v}\mathbf{G}_0+\cdots]$$
$$= \mathrm{Tr}\frac{1}{2\pi i}\int_c dz\, z\mathbf{G}_0\sum_n(\mathbf{v}\mathbf{G}_0)^n$$
$$= \sum_n\frac{1}{n}\mathrm{Tr}\frac{1}{2\pi i}\int_c dz(\mathbf{G}_0\mathbf{v})^n. \quad (3)$$

The final result is as follows:

$$\frac{1}{2}\mathrm{Tr}\frac{1}{2\pi i}\int_c dz\mathbf{G}_0\mathbf{v}\mathbf{G}_0\mathbf{v}$$
$$=\frac{1}{2}\mathrm{Tr}\frac{1}{2\pi i}\int_c dz\frac{1}{z-\mathbf{H}_0}\mathbf{v}\frac{1}{z-\mathbf{H}_0}\mathbf{v}$$
$$=\frac{1}{2}\mathrm{Tr}\frac{1}{2\pi i}\int_c dz\, z\left[\frac{1}{(z-\mathbf{H}_0)^2}\mathbf{v}\frac{1}{z-\mathbf{H}_0}\mathbf{v}\right.$$
$$\left.+\frac{1}{z-\mathbf{H}_0}\mathbf{v}\frac{1}{(z-\mathbf{H}_0)^2}\mathbf{v}\right]$$
$$= \mathrm{Tr}\frac{1}{2\pi i}\int_c dz\, z\frac{1}{z-\mathbf{H}_0}\mathbf{v}\frac{1}{z-\mathbf{H}_0}\mathbf{v}\frac{1}{z-\mathbf{H}_0}$$
$$= \mathrm{Tr}\frac{1}{2\pi i}\int_c dz\, z\mathbf{G}_0\mathbf{v}\mathbf{G}_0\mathbf{v}\mathbf{G}_0, \quad (4)$$

where the second equality arises from the partial integration and the third one from the permutation invariability in Tr.

Illustrative Example Provided that the perturbation is applied to the site a, say $v_{aa}=\varepsilon$, it follows that

$$\Delta E = \sum_n\frac{1}{n}\frac{1}{2\pi i}\int_c dz[G_0(a)\varepsilon]^n$$
$$= \frac{1}{2\pi i}\int_c dz\ln(1-G_0(a)\varepsilon)^{-1} \quad (5a)$$
$$\simeq \frac{1}{2\pi i}\int_c dz\, G_0(a)\varepsilon+\frac{1}{2}\frac{1}{2\pi i}\int_c dz\, G_0(a)^2\varepsilon^2$$
$$\equiv q(a)\varepsilon+\frac{1}{2}\Pi_{a,a}\varepsilon^2. \quad (5b)$$

Here $q(a)$ is the charge density at the a-th site and $\Pi_{a,a}$ is the atom-atom polarizability defined by Coulson and Longuet-Higgins.[1)]

Ring Closure and Ring Opening

Let us first consider the ring closure reaction of conjugated chain. Figure 2a shows the transition state where the chain begins the ring closure reaction. The arrows at both ends stand for the basis functions, $2p\pi$ together with the phases. Note that we can put the phases in this way without loss of generality. We need not worry about one-electron state, *i.e.*, the shape of MO and its energy.

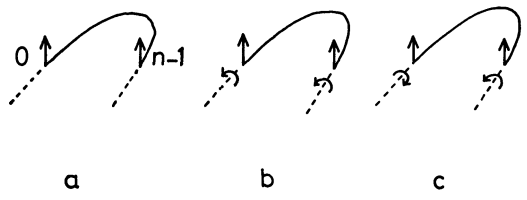

Fig. 2. Ring closure reaction.
a: Transition state, b: con-rotatory, c: dis-rotatory.

For the sake of simplicity, let us consider the case in which the chain is composed of n sites and n electrons. If the ring closure begins in the con-rotatory mode or in the dis-rotatory mode, the interaction arises between sites 0-th and (n-1)-th.

$$v_{0,n-1}=v_{n-1,0}=v\begin{cases}\text{positive for the con-rotatory}\\ \text{negative for the dis-rotatory.}\end{cases} \quad (6)$$

The extra energy due to this is given by Eq. 3. If one mode works to stabilize the system, *i.e.*, $\Delta E<0$, we can choose this mode as the desired reaction path.

Let us consider the ring opening reaction. The σ-bond in the transition state slightly rotates (Fig. 3a) in a con-rotatory mode (Fig. 3b) or in the dis-rotatory mode (Fig. 3c) to yield a small fraction of π-bond. The extra energy due to this determines which mode is preferable. Since the perturbation energy arising in these motion is classified entirely in the same way as that of ring closure reaction, *i.e.*, as Eq. 6, we see that the mathematical procedures are the same, *viz.*, if in any system the con-rotatory mode is desirable for the ring closure reaction, the same mode is also desirable for the ring opening reaction for the system in which transition state is similar to that of the previous system.

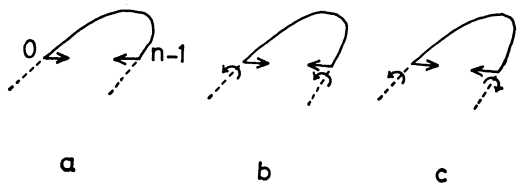

Fig. 3. Ring opening reaction.
a: Transition state, b: con-rotatory, c: dis-rotatory.

In both cases, the extra energy ΔE in Eq. 3 due to perturbation to the second order is

$$\Delta E = \frac{1}{2\pi i}\int_c dz[G_n(0,n-1)v_{n-1,0}+G_n(n-1,0)v_{0,n-1}]$$
$$+\frac{1}{2}\frac{1}{2\pi i}\int_c dz[G_n(0,n-1)v_{n-1,0}G_n(0,n-1)v_{n-1,0}$$
$$+G_n(n-1,0)v_{0,n-1}G(n-1,0)v_{0,n-1}]$$
$$+\frac{1}{2}\frac{1}{2\pi i}\int_c dz[G_n(0)v_{0,n-1}G_n(n-1)v_{n-1,0}$$
$$+G_n(n-1)v_{n-1,0}G_n(0)v_{0,n-1}] \quad (7a)$$
$$= \frac{1}{2\pi i}\int_c dz[2vG_n(0,n-1)+v^2G_n(0,n-1)G(n-1,0)$$
$$+v^2G_n(0)G_n(n-1)]. \quad (7b)$$

Each term in Eq. 7b, shown in detail in Eq. 7a, has its own structure: the first order term indicates a path going round the system once, the path indicated by the second terms in Eq. 7a goes round the system twice, and the final second order term corresponds to the interaction going back and forth between the ends. Let us examine each term in detail.

The matrix elements of Green's function in Eq. 7a are given in the second paper[7)] of this series, as

$$G_n(0) = G_n(n-1) = \frac{\sin n\theta}{\sin(n+1)\theta}, \tag{8}$$

$$G_n(0, n-1) = G_n(n-1, 0) = \frac{\sin\theta}{\sin(n+1)\theta}, \tag{9}$$

$$z = 2\cos\theta. \tag{10}$$

If we map the Coulson contour in z-plane onto θ-plane by means of the relation (10), the contour in θ-plane turns round twice the corresponding points in z-plane. This is why we introduced the factor, 1/2.[7]

As an example, let us take the system with n sites and n electrons, n being even. The first order energy in Eq. 7b is

$$\Delta E^{(1)} = -4\frac{1}{4\pi i}\int_c d\theta \frac{\sin^2\theta}{\sin(n+1)\theta} v. \tag{11}$$

The poles of the propagator are given by

$$\theta_r = \frac{\pi r}{n+1}, \quad r = \pm 1, \pm 2, \cdots, \pm(n+1), \tag{12}$$

in which the single particle states from $r=\pm 1$ to $r=\pm n/2$ are doubly occupied. The result of calculation is

$$\begin{aligned}\Delta E^{(1)} &= -\frac{8v}{(n+1)}\sum_{r=1}^{n/2}(-1)^r \sin^2\theta_r \\ &= -\frac{4v}{(n+1)}\left\{\sum_{r=1}^{n/2}(-1)^r + 1/2 \right. \\ &\quad \left. + \frac{(-1)^{n/2}}{2}\sec\pi/(n+1)\right\}. \end{aligned} \tag{13}$$

The second order energy arising from the path going round the system twice is

$$\begin{aligned}\Delta E^{(2,q)} &= -2\frac{1}{4\pi i}\int_c d\theta \frac{\sin^3\theta}{\sin^2(n+1)\theta}\frac{v^2}{\beta} \\ &= \frac{-3}{2(n+1)^2}\left\{\operatorname{cosec}\pi/2(n+1)\right. \\ &\quad \left. + \operatorname{cosec} 3\pi/2(n+1)\right\}\frac{v^2}{\beta}. \end{aligned} \tag{14}$$

The resonance integral β which was scaled to unity in evaluating G, is recovered by dimensional analysis. The resonance integral β is negative. Another second order term is

$$\begin{aligned}\Delta E^{(2,c)} &= -2\frac{1}{4\pi i}\int_c d\theta \frac{\sin\theta\sin^2 n\theta}{\sin^2(n+1)\theta}\frac{v^2}{\beta} \\ &= \frac{(2n-1)}{2(n+1)^2}\left\{\operatorname{cosec}\pi/2(n+1)\right. \\ &\quad \left. + \operatorname{cosec} 3\pi/2(n+1)\right\}\frac{v^2}{\beta}. \end{aligned} \tag{15}$$

Thus we get

$$\begin{aligned}\Delta E &= \Delta E^{(1)} + \Delta E^{(2,q)} + \Delta E^{(2,c)} \\ &= \frac{-4}{n+1}\left\{\sum_{r=1}^{n/2}(-1)^r + 1/2 + \frac{(-1)^{n/2}}{2}\sec\pi/(n+1)\right\}v \\ &\quad + \frac{n-2}{(n+1)^2}\left\{\operatorname{cosec}\pi/2(n+1) + \operatorname{cosec} 3\pi/2(n+1)\right\}\frac{v^2}{\beta}. \end{aligned} \tag{16}$$

Due to the fact that $n>2$ in the actual molecules the second order terms in Eqs. 16 and 20 are negative, irrespective of the sign of v. The second order term has nothing to do with the determination of the reaction path, except for slight stabilization of the system as regards energy. The first order term should dominantly affect the progress of the reaction. The reaction proceeds if the quantity in the curly bracket has the same sign as that of v in the first order term.

Let us examine the case with odd n sites and n electrons. In this case, the single particle states, $r=\pm 1$ to $\pm(n-1)/2$, are doubly occupied and those with $n=\pm(n+1)/2$ are singly occupied. The spin summation should be carefully done. Terms corresponding to the previous ones are

$$\Delta E^{(1)} = \frac{-4}{n+1}\left\{\sum_{r=1}^{(n+1)/2}(-1)^r + \frac{1}{2} - \frac{(-1)^{(n+1)/2}}{2}\right\}v = 0, \tag{17}$$

$$\Delta E^{(2,q)} = \frac{-3}{2(n+1)^2}\left\{\cot\frac{\pi}{2(n+1)} + \cot\frac{3\pi}{2(n+1)}\right\}\frac{v^2}{\beta}, \tag{18}$$

$$\Delta E^{(2,c)} = \frac{2n-1}{2(n+1)^2}\left\{\cot\frac{\pi}{2(n+1)} + \cot\frac{3\pi}{2(n+1)}\right\}\frac{v^2}{\beta}. \tag{19}$$

Thus

$$\begin{aligned}\Delta E &= \Delta E^{(1)} + \Delta E^{(2,q)} + \Delta E^{(2,c)} \\ &= \frac{n-2}{(n+1)^2}\left\{\cot\frac{\pi}{2(n+1)} + \cot\frac{3\pi}{2(n+1)}\right\}\frac{v^2}{\beta}. \end{aligned} \tag{20}$$

The first order term vanished identically, the second order term having a similar character as previous ones.

Since the first order term predominantly affects the electrocyclic interaction, we will reexamine this more carefully. Denote the number of sites by n, which is even or odd, and the number of electrons by M, which is less than $2n$. Let us investigate the cases where M is $4m$, $4m+2$, $4m+1$, and $4m+3$.

(i) $M = 4m$

$$\begin{aligned}\Delta E^{(1)} &= -\frac{8v}{n+1}\sum_{r=1}^{2m}(-1)^r \sin^2\theta_r \\ &= \frac{4v}{n+1}\sum_{r=1}^{2m}(-1)^r \cos 2\pi r/(n+1) \\ &= -\frac{2v}{n+1}\left\{1 - \frac{\cos(4m+1)\pi/(n+1)}{\cos\pi/(n+1)}\right\}. \end{aligned} \tag{21a}$$

Note that

$$1 - \frac{\cos(4m+1)\pi/(n+1)}{\cos\pi/(n+1)} > 0. \tag{21b}$$

(ii) $M=4m+2$ Similar calculation yields

$$\Delta E^{(1)} = \frac{2v}{n+1}\left\{1 - \frac{\cos(4m+3)\pi/(n+1)}{\cos\pi/(n+1)}\right\}. \tag{22a}$$

Note that

$$1 - \frac{\cos(4m+3)\pi/(n+1)}{\cos\pi/(n+1)} > 0. \tag{22b}$$

(iii) $M = 4m+1$

$$\begin{aligned}\Delta E^{(1)} &= \frac{v}{(n+1)\cos\pi/(n+1)} \\ &\quad \times [\cos(4m+1)\pi/(n+1) - \cos(4m+3)\pi/(n+1)] \\ &= \frac{2v}{n+1}\tan\pi/(n+1)\sin(4m+2)\pi(n+1). \end{aligned} \tag{23a}$$

Note that $\tan\pi/(n+1)>0$, but

$$\sin(4m+2)\pi/(n+1)\begin{cases} >0 & \text{for } 1 < M < n \\ =0 & \text{for } M = n \\ <0 & \text{for } n < M < 2n. \end{cases} \tag{23b}$$

$(iv) M = 4m+3$

$$\Delta E^{(1)} = \frac{-2v}{n+1} \tan \pi/(n+1) \sin(4m+4)\pi/(n+1) \quad (24a)$$

with

$$\sin(4m+4)\pi/(n+1) \begin{cases} >0 & \text{for } 1 < M < n \\ =0 & \text{for } M = n \\ <0 & \text{for } n < M < 2n. \end{cases} \quad (24b)$$

It is desirable to clarify the fact that in the ring closure and ring opening reactions, it is not the number of sites but the number of electrons which control the reactivity of these reactions.[8] The results obtained are summarized in Table 1.

Table 1. Conditions for $\Delta E^{(1)} < 0$

M[a]	[b]	Sign of v	Reaction path[c]
$4m$		+	con
$4m+2$		−	dis
	$0<M<n$	−	dis
$4m+1$	$M=n$		
	$n<M<2n$	+	con
	$0<M<n$	+	con
$4m+3$	$M=n$		
	$n<M<2n$	−	dis

a) Number of electrons. b) Relation between M and the number of sites, n. c) con: con-rotatory, dis: dis-rotatory.

In order to confirm the previous general results the details of small systems are given in Table 2. Care should be taken on signs of $\Delta E^{(1)}$ and $\Delta E^{(2)}$, remembering that β is negative. Our predictions as to whether the reactions is con-rotatory or dis-rotatory are made only from the first order term, $\Delta E^{(1)}$. Agreements with those from the Woodward-Hoffmann rule are almost satisfactory. For cases written as non-selective or that indicating disagreements between two predictions, there has been no experimental result,[4] so far we are aware of.

Diels-Alder Reaction

The simplest Diels-Alder reaction is shown in Fig. 4. As transition states for this sort of reaction, we adopt two types (Fig. 5a). In both models, the phases of basic orbitals can be chosen, without a loss of generality, such that the perturbing interactions are negative (attractive).

Let us investigate the case in which two interactions

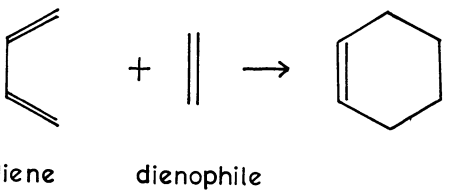

Fig. 4.

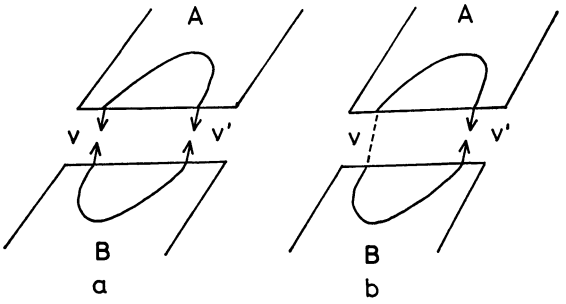

Fig. 5. Diels-Alder reaction.
a: Two interactions, b: single interaction.

v and v' coexist (Fig. 5a). We will show that this is not acceptable. For the sake of simplicity, we assume that the combining two species A and B are the same consisting of n sites and n electrons.

The extra energy due to perturbation Eq. 3, up to the second order is

$$\begin{aligned} \Delta E &= (v^2+v'^2)\frac{1}{2\pi i}\int_c dz\, G_n(0) G_n(n-1) \\ &\quad + 2vv' \frac{1}{2\pi i}\int_c dz\, G_n^2(0, n-1) \\ &= (v^2+v'^2)\frac{-2}{4\pi i}\int_c d\theta \frac{\sin\theta \sin^2 n\theta}{\sin^2(n+1)\theta} \\ &\quad + 2vv' \frac{-2}{4\pi i}\int_c d\theta \frac{\sin^3\theta}{\sin^2(n+1)\theta}. \end{aligned} \quad (25)$$

Calculations are carried out in a similar way to that for the second order terms $\Delta E^{(2)}$.

If n is even, the levels up to $n/2$ are doubly occupied, so that

$$\begin{aligned} \Delta E = \frac{1}{2(n+1)^2\beta} &[\operatorname{cosec} \pi/2(n+1) + \operatorname{cosec} 3\pi/2(n+1)] \\ &\times [(2n-1)(v^2+v'^2) - 6vv'], \end{aligned} \quad (26a)$$

Table 2. Ring closure and ring opening reaction

n[a]	M[b]	Species	$\Delta E^{(1)}$	$\Delta E^{(2)}$	Prediction	W-H rule[c]
	2	+ion	v	$\sqrt{2}v^2/8\beta$	dis	dis
3	3	neutral	0	$\sqrt{2}v^2/8\beta$	non-selective	con
	4	−ion	$-v$	$\sqrt{2}v^2/8\beta$	con	con
	3	+ion	$(5-3\sqrt{5})v/10$	$3\sqrt{5}v^2/25\beta$	con	con
4	4	neutral	$-\sqrt{5}v/5$	$4\sqrt{5}v^2/25\beta$	con	con
	5	−ion	$(5-3\sqrt{5}v/10$	$3\sqrt{5}v^2/25\beta$	con	dis
	4	+ion	$-2v/3$	$(3+\sqrt{3})v^2/12\beta$	con	con
5	5	neutral	0	$(3+\sqrt{3})v^2/12\beta$	non-selecitve	dis
	6	−ion	$2v/3$	$(3+\sqrt{3})v^2/12\beta$	dis	dis

a) Number of sites. b) Number of electrons. c) Predictions from the Woodward-Hoffmann rule.

and for $v=v'$

$$\Delta E = \frac{2(n-2)}{(n+1)^2}[\text{cosec}\,\pi/2(n+1) + \text{cosec}\,3\pi/2(n+1)]\frac{v^2}{\beta}. \tag{26b}$$

By means of dimensional analysis, we write explicitly β put to unity in evaluating propagators of the original system.

If n is odd, the levels up to $(n-1)/2$ are doubly occupied and the $(n+1)/2$-th is singly occupied, thus

$$\Delta E = \frac{1}{2(n+1)^2\beta}[\cot\pi/2(n+1) + \cot 3\pi/2(n+1)] \times [(2n-1)(v^2+v'^2) - 6vv']. \tag{27a}$$

For $v=v'$ we have

$$\Delta E = \frac{2(n-2)}{(n+1)^2}[\cot\pi/2(n+1) + \cot 3\pi/2(n+1)]\frac{v^2}{\beta}. \tag{27b}$$

Since β is negative, ΔE given by Eqs. 26b and 27b are negative, indicating that the Diels-Alder reaction is possible if two species are like those given in Fig. 5a. The result shows that the combined system is more stable than the original, not explaining the selection rule of Diels-Alder reaction.

Let us consider the model in Fig. 5b. Simultaneous interactions considered in Fig. 5a hardly seem to happen, instead a two step process like Fig. 5b is more probable. In the first step, A and B combine, due to v, yielding a long chain. In the second step, the chain starts the ring closure interaction due to the v' interaction. Note that in this model v' has always negative sign.

If we assume that the first step is rate-determining, the rules investigated for the ring closure reaction can be applied. Only the cases with negative v in Table 1 are allowed:

1) The case $M=4m$ is forbidden.
2) The case $M=4m+2$ is allowed.
3) For the case $M=4m+1$
   if $0<M<n$, the reaction is allowed,
   if $n<M<2n$, the reaction is forbidden,
   where n is the number of sites.
4) For the case of $M=4m+3$
   if $0<M<n$, the reaction is forbidden,
   if $n<M<2n$, the reaction is allowed.

The Cope and Claisen rearrangements are also treated in a similar way.

Sigmatropic Reaction

Let us consider the reaction shown in Fig. 6. This has been pointed out by Berson[9] as an example that the Woodward-Hoffman rule does not hold exactly. The Woodward-Hoffmann rule suggests the reaction path shown in Fig. 6a rather than that in Fig. 6b. In view of symmetry, the highest occupied orbital of the allyl type radical is described by displaying the phases of the atomic orbitals of both ends.

As has been done in the Diels-Alder reaction, we make use of the models shown in Figs. 7a and 7b for the transition states in Figs. 6a and 6b, respectively. v_a and v_b are examined since v_a' and v_b' have no significant contribution. The interactions, v_a and v_b are split

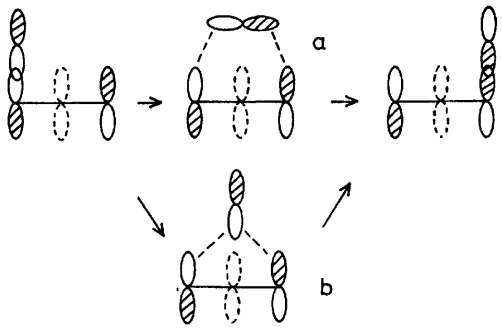

Fig. 6. Sigmatropic reaction.
The highest occupied orbital of the allyl type radical is described by displaying the phases of the atomic orbitals at the both ends.

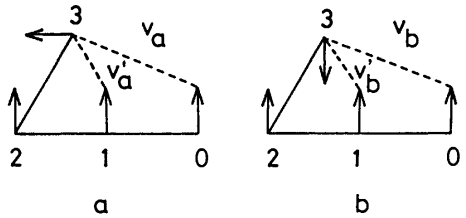

Fig. 7. Models for the transition states of the sigmatropic reaction.
Figures 7a and 7b correspond to the Figs. 6a and 6b respectively, but here arrows indicate the phases of the basic atomic orbitals.

into σ- and π-components, the parallel or perpendicular components with respect to the binding axis. Both components of v_a are positive, v_a being repulsive. The σ-component of v_b is negative and the π-one is positive. The migrating radical in the reaction is the methyl type one. This suggests that if we consider the steric effect, the methyl type radical might migrate above the allyl radical considerably nearer in the case of Fig. 7b than in the case of Fig. 7a. If this is the case, it is possible that the π-component becomes predominant and v_b is repulsive. Thus i) $v_a>0$, ii) $v_b>0$, if the migrating radical moves considerably close to the allyl radical.

For the cases of Figs. 7a and 7b, we obtain ΔE in Eq. 3 in the first order approximation;

$$\Delta E = \text{Tr}\frac{1}{2\pi i}\int_c dz\,\mathbf{Gv} = 2\left\{\frac{v_a}{2\pi i}\int_c dz\,G_4(0,3) + \frac{v_a'}{2\pi i}\int_c dz\,G_4(1,3)\right\}, \tag{28}$$

for the cases of Fig. 7a. Replacing v_a and v_a' by v_b and v_b', respectively, we get the expression for Fig. 7b. $G_4(0,3)$ is the 0-3 matrix element of the chain propagator with four sites. In Eq. 28, the second integral is the bond order between the starred sites of the conjugated chain, vanishing identically. The remaining term gives

$$\Delta E_a(\Delta E_b) = \frac{2\sqrt{5}}{5}v_a(v_b),\ v_a(v_b) > 0. \tag{29}$$

The reaction mechanism infers the first case in Table 1, in other words, the formation of the Möbius ring

presented in the next section. Accordingly our theory explains the possibility of two reaction paths.

Aromaticity

Let us examine the stability conditions in the ground state of the conjugated systems. The question what aromaticity is has been discussed for a long time. We consider it as a problem of energy stabilization when the conjugated chain becomes a ring by connection of both ends.[10]

Let the interaction between two ends be v. The following conclusions are obtained from Table 1.

A. The ring with the negative v or the Hückel ring is more stable than the original chain, under the conditions where

i) $M=4m+2$
ii) $M=4m+1$ and $0<M<n$
iii) $M=4m+3$ and $n<M<2n$,

where n is the number of sites.

B. The ring with positive v or the Möbius ring is preferable under the conditions that

i) $M=4m$
ii) $M=4m+1$ and $n<M<2n$
iii) $M=4m+3$ and $0<M<n$.

Naphthalene and Azulene

The stability of compounds consisting of two rings is of interest. Naphthalene and azulene are well-known examples. Two ring compounds consisting of ten atoms are presented (Fig. 8).

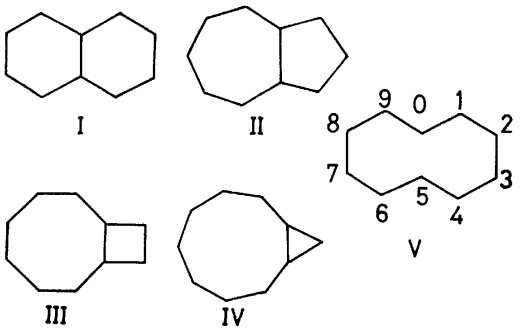

Fig. 8. Two ring compounds (I—IV) composed of cyclodecapentaene (V).

Compounds I—IV are derived from various perturbations put in cyclodekapentaene V as follows:

$$v' = \begin{cases} v'_{05} \text{ for I} \\ v'_{04} \text{ for II} \\ v'_{03} \text{ for III} \\ v'_{02} \text{ for IV.} \end{cases} \tag{30}$$

The stabilization energies in these cases are mainly due to the first order term:

$$\left.\begin{matrix} \Delta E(\mathrm{I}) \\ \Delta E(\mathrm{II}) \\ \Delta E(\mathrm{III}) \\ \Delta E(\mathrm{IV}) \end{matrix}\right\} = 2v' \frac{1}{2\pi i}\int_c dz \begin{Bmatrix} G_{10}(0,5) \\ G_{10}(0,4) \\ G_{10}(0,3) \\ G_{10}(0,2) \end{Bmatrix} = 2v' \begin{Bmatrix} q_{10}(0,5) \\ q_{10}(0,4) \\ q_{10}(0,3) \\ q_{10}(0,2). \end{Bmatrix} \tag{31}$$

The problems are reduced to the evaluation of the corresponding bond orders. The bond order $q_n(0, k)$ in this case is

$$q_n(0,k) = \frac{2}{n}\frac{\sin(k\pi/2)}{\sin(k\pi/n)}, \tag{32}$$

from which it follows that

$$\begin{aligned} q_{10}(0,5) &= 1/5 \\ q_{10}(0,4) &= 0 \\ p_{10}(0,3) &= -(\sqrt{5}-1)/5 \\ q_{10}(0,2) &= 0. \end{aligned} \tag{33}$$

Naphthalene is the most stable, azulene and IV next, III being the most unstable.

Anthracene and Phenanthrene

In order to clarify the distinction between anthracene and phenanthrene in view of stabilization, a simple method has been worked out for generalization to larger benzenoid hydrocarbons.

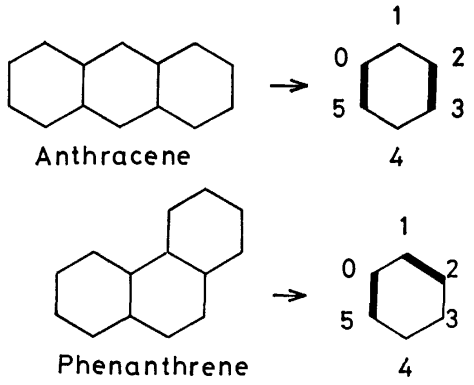

Fig. 9.

We rewrite anthracene and phenanthrene, as in Fig. 9, by means of structures with bold bonds which indicate the adjacent benzene rings in each compound. Anthracene is considered as a fictitious benzene in which the 0-5 and 2-3 bonds have the effective resonance integrals, β_{eff}, instead of the original β. If we put

$$v = \beta_{\mathrm{eff}} - \beta, \tag{34}$$

and use Eq. 3 up to the second order, ΔE for anthracene is given by

$$\begin{aligned} \Delta E_{\mathrm{A}} = \frac{1}{2\pi i}\int_c dz \{ & 2v[G(0,5)+G(2,3)]+v^2[G(0)G(5) \\ & +G(2)G(3)+G(0,5)G(5,0) \\ & +G(2,3)G(3,2)]+2v^2[G(0,2)G(3,5) \\ & +G(0,3)G(2,5)]\}. \end{aligned} \tag{35}$$

In a similar way, ΔE for phenanthrene is given by

$$\begin{aligned} \Delta E_{\mathrm{P}} = \int_c dz \{ & 2v[G(0,5)+G(1,2)]+v^2[G(0)G(5) \\ & +G(1)G(2)+G(0,5)G(5,0) \\ & +G(1,2)G(2,1)]+2v^2[G(0,1)G(2,5) \\ & +G(0,2)G(1,5)]\}. \end{aligned} \tag{36}$$

The difference between ΔE_A and ΔE_P arises from the second order terms,

$$\Delta E_A - \Delta E_P = \frac{1}{2\pi i}\int_c dz\, 2v^2[G(0,2)G(3,5)+G(0,3)G(2,5) - G(0,1)G(2,5)-G(0,2)G(1,5)]. \quad (37)$$

It is instructive to trace the routes indicated by combining propagators and v of Eq. 37. We can easily evaluate this and find

$$\Delta E_A - \Delta E_P = -(0.17+0.35)v^2/\beta = -0.25v^2/\beta. \quad (38)$$

Because of the negative sign of β, the value of Eq. 38 is positive, with a small magnitude. Thus phenanthrene should be more stable than anthracene. This is in line with the observation. The result is independent of the sign of v. Generalization to a larger system is straigtforward (Fig. 10).

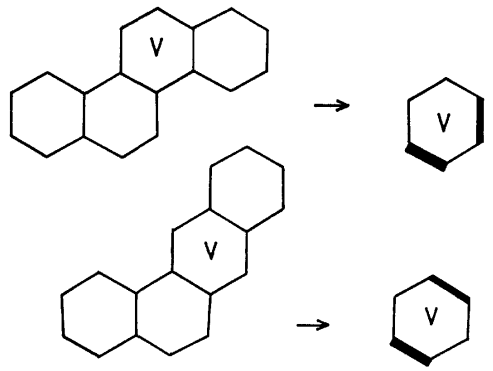

Fig. 10. Shorthand display of the benzenoid.

β_{eff} in Eq. 34 is interpreted as an average of the operator, $|s><\beta_{st}<t|$, with respect to the ground state of the system in question,

$$|0> = \prod_i^{\text{occ}} |i>. \quad (39)$$

Namely

$$\beta_{\text{st:eff}} = \beta_{\text{st}} \sum_i <s|i><i|t> = \beta_{\text{st}} \frac{1}{2\pi i}\int_c dz\, G(s,t;z). \quad (40)$$

This relation reproduces the original β_{st} in the diatomic chain. Using Eq. 40 in the benzene ring, we obtain

$$\beta_{\text{eff}} = 0.667\beta. \quad (41)$$

This is in line with the fact that in anthracene or phenanthrene, the corresponding bond length is slightly greater than that of benzene.

Concluding Remarks

Propagator theory has been successfully applied to the problems of chemical reactivity and stability. No use was made of wave functions or LCAO coefficients. Even if the concept of orbital is established, the orbital is not a physical quantity. The final result should be presented only in terms of the coupling constants in the Hamiltonian. In this respect our theory is nearer to that of Coulson than that of Fukui and Woodward-Hoffmann.

References

1) C. A. Coulson and H. C. Longuet-Higgins, *Proc. R. Soc. London, Ser. A*, **191**, 39 (1947); **192**, 16 (1947).
2) H. Hosoya, K. Hosoi, and I. Gutman, *Theor. Chim. Acta (Berl.)*, **38**, 37 (1957).
3) K. Fukui, "Chemical Reactions and Electron Orbital," (in Japanese), Maruzen, Tokyo (1976).
4) R. B. Woodward and R. Hoffmann, "The Conservation of Orbital Symmetry," Academic Press (1970).
5) S. Aono and K. Nishikawa, *Bull. Chem. Soc. Jpn.*, **53**, 3418 (1980), referred to as I.
6) E. N. Economou, "Green's Function in Quantum Physics," Springer-Verlag (1979).
7) S. Aono, T. Ohmae, and K. Nishikawa, *Bull. Chem. Soc. Jpn.*, **54**, 1645 (1981).
8) K. Fukui and H. Fujimoto, *Bull. Chem. Soc. Jpn.*, **39**, 2116 (1966); **40**, 2018 (1967).
9) J. A. Berson and L. Salem, *J. Am. Chem. Soc.*, **94**, 8917 (1972); J. A. Berson, *Acc. Chem. Res.*, **5**, 406 (1972).
10) M. J. S. Dewar, *J. Am. Chem. Soc.*, **74**, 3341, 3345 (1952).

Electron Spin-Spin Interaction in Excited Triplet States of Aromatic Hydrocarbons with a Trigonal Symmetry Axis

Jiro Higuchi

Department of Chemistry, Faculty of Engineering, Yokohama National University, Hodogaya-ku, Yokohama 240

(Received December 20, 1980)

Zero-field splitting (ZFS) parameters of benzene, triphenylene, and coronene molecules in their lowest and second excited triplet states are calculated from the electron spin-spin interaction using semi-empirical self-consistent-field π-electron molecular orbitals. The results show that in obtaining a good agreement of the evaluated ZFS parameters with the experimental values the selection of the basis functions in LCAO-MO's with zero-differential overlap is actually important. The ZFS parameters in some distorted structures are also calculated.

Since the detection of electron spin resonance (ESR) signals for the phosphorescent naphthalene molecule by Hutchison and Mangum,[1] many theoretical works on the zero-field splittings (ZFS) of aromatic molecules in their triplet states have been carried out with various degrees of approximations.[2-8] Nevertheless, the progress in such a calculation has essentially been slow in spite of the development in the theory of electronic structures of molecules. For large molecules, *ab initio* studies have scarcely been done except a work of benzene by Langhoff, Davidson, and Kern.[3] On the other hand, semi-empirical calculations have usually been concerned with the explanation of experimental values without careful reexamination of points in question. In most of these works, the electron spin-spin interactions were evaluated by using Slater-type or Gaussian-type atomic orbitals (AO's) as the AO bases and adopting the zero differential overlap (ZDO) approximation. The spin-orbit interactions were ignored in expecting their minor influence.[9]

As the basis functions of semi-empirical LCAO-MO's cannot pertinently be approximated by AO's of the corresponding free atoms, these calculations usually include some adjustable parameters although they are not always explicitly specified. That is, for obtaining a good agreement between the calculated values and the experimental ones, many works employed one of the following modifications: (1) use of partly adjusted values of spin-spin interaction integrals;[4] (2) use of adjusted orbital exponent of Slater-type 2p AO;[6,7] (3) inclusion of unsuitable approximation in exchange-type spin-spin interaction integrals,[8] and so on. In these works, the meanings of modified points were not distinctly explained.

With the recent development of accurate measurements in magnetic resonance experiments, detailed experimental data on the phosphorescent triplet states of aromatic molecules have been accumulated using methods such as conventional ESR and the optically detected magnetic resonance. From the standpoint of theoretical calculation, however, instructive information on ZFS parameters is still insufficient in discussing the values evaluated, except the case of benzene.[3,5] Under these circumstances, it may be desirable to reexamine the semi-empirical calculations of ZFS parameters on the basis of the works of benzene. Besides, there are many interesting experiments on the lowest triplet states of aromatic molecules with trigonal symmetry.[10-16] For these molecules, a relatively simple approximation with only Coulomb-type spin-spin interaction integrals is fairly satisfactory, since the other integrals have minor influence upon the ZFS parameters when the E value is very small.[5] Especially for benzene, the ratios among coefficients of AO's in the π-electron LCAO-MO's are uniquely determined from only the molecular symmetry and the calculated ZFS parameters may not largely be affected by the selection of semi-empirical parameters. In the present work, therefore, ZFS parameters of benzene, triphenylene, and coronene in the lowest and second excited triplet states were evaluated from the electron spin-spin interactions:

$$\begin{aligned}\mathcal{H}_{ss} &= \frac{\mu_0 g^2\beta^2}{4\pi}\left[\frac{(\boldsymbol{s}_1\cdot\boldsymbol{s}_2)}{r_{12}^3}-\frac{3(\boldsymbol{s}_1\cdot\boldsymbol{r}_{12})(\boldsymbol{s}_2\cdot\boldsymbol{r}_{12})}{r_{12}^5}\right]\\ &= \frac{\mu_0 g^2\beta^2}{8\pi}\left[s_x^2\left(\frac{r_{12}^2-3x_{12}^2}{r_{12}^5}\right)+s_y^2\left(\frac{r_{12}^2-3y_{12}^2}{r_{12}^5}\right)\right.\\ &\quad + s_z^2\left(\frac{r_{12}^2-3z_{12}^2}{r_{12}^5}\right)-(s_ys_z+s_zs_y)\frac{3y_{12}z_{12}}{r_{12}^5}\\ &\quad \left.-(s_zs_x+s_xs_z)\frac{3z_{12}x_{12}}{r_{12}^5}-(s_xs_y+s_ys_x)\frac{3x_{12}y_{12}}{r_{12}^5}\right] \qquad (1)\end{aligned}$$

(μ_0: vacuum permeability; $\boldsymbol{S}=\boldsymbol{s}_1+\boldsymbol{s}_2$: total spin)

using a standard and simple approximation with only Coulomb-type integrals.[8,17] In terms of the principal magnetic axes shown in Figs. 1—3, the ZFS parameters can be expressed as

$$D = \frac{3\mu_0 g^2\beta^2}{16\pi hc}\left\langle\frac{r_{12}^2-3z_{12}^2}{r_{12}^5}\right\rangle \qquad (2)$$

$$E = \frac{3\mu_0 g^2\beta^2}{16\pi hc}\left\langle\frac{y_{12}^2-x_{12}^2}{r_{12}^5}\right\rangle. \qquad (3)$$

Calculation

The wavefunctions (WF's) used were constructed from Pariser-Parr-Pople-type (PPP) LCAO-MO's[18,19] by including configurations arising from all the single excitations relative to the ground state. ZFS parameters were calculated by adopting one of the following three kinds of treatments:

(A) The basis AO used was a double-zeta SCF-AO of carbon atom by Clementi.[20] This treatment corresponds to the conventional standard calculations except the used AO instead of a single Slater-type AO (STAO). A similar work with all the spin-spin interaction integrals evaluated with single STAO's has been carried out for benzene and naphthalene by Godfrey,

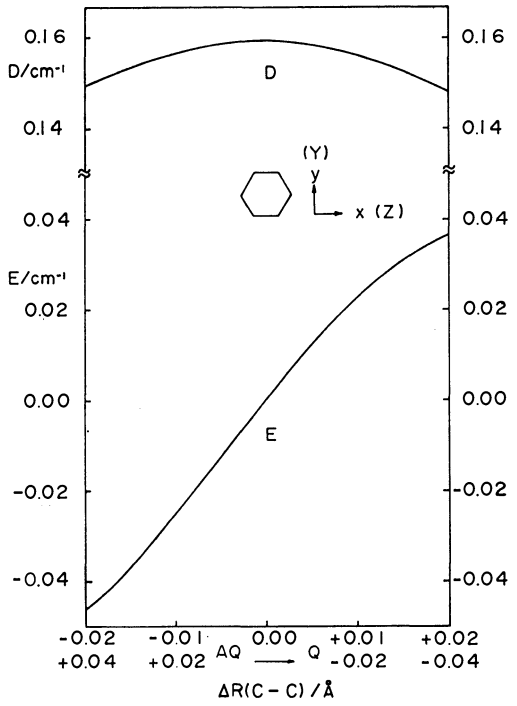

Fig. 1. Variation of the calculated zero-field splitting parameters of benzene with antiquinonoidal (AQ) and quinonoidal (Q) forms. The lower and the upper value in ΔR(C–C) are the change of length in two C–C bonds which are parallel to the x axis and that for the other four C–C bonds, respectively. The axis system for D_{2h} symmetry is indicated in parentheses.

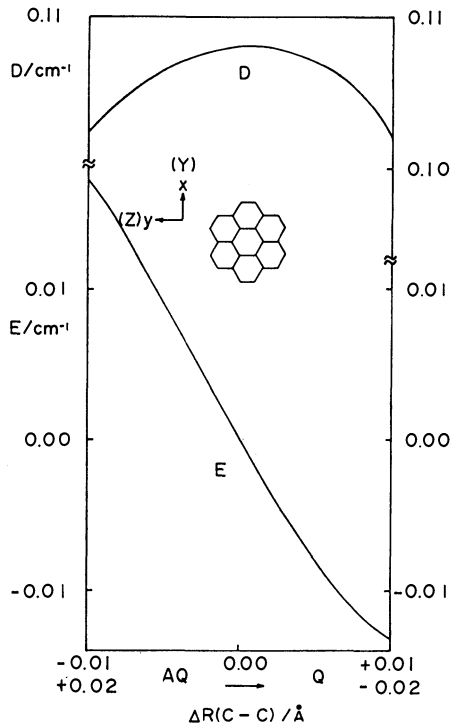

Fig. 3. Variation of the calculated zero-field splitting parameters of coronene with antiquinonoidal (AQ) and quinonoidal (Q) forms. The lower and the upper value in ΔR(C–C) are the change of length in C–C bonds which are parallel to the y axis and that for the other C–C bonds, respectively. The axis system for D_{2h} symmetry is indicated in parentheses.

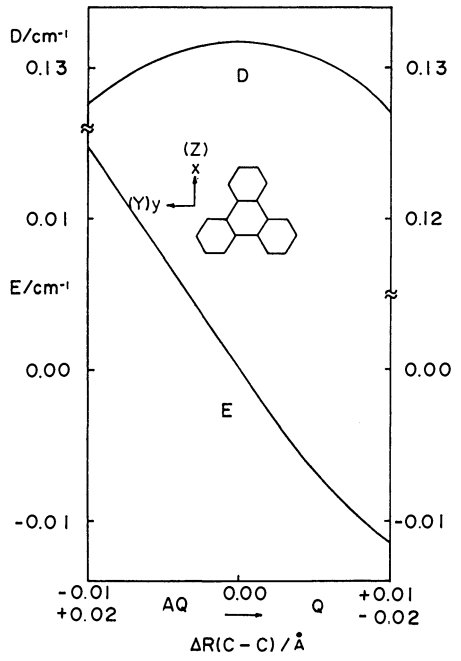

Fig. 2. Variation of the calculated zero-field splitting parameters of triphenylene with antiquinonoidal (AQ) and quinonoidal (Q) forms. The lower and the upper value in ΔR(C–C) are the change of length in C–C bonds which are parallel to the y axis and that for the other C–C bonds, respectively. The axis system for C_{2v} symmetry is indicated in parentheses.

Kern, and Karplus.[5]

(B) The basis AO used was an adjusted single STAO, the orbital exponent of which was chosen to give the experimental D value of benzene [D=0.1593 cm^{-1}].[12] The value of δ=1.5055 thus obtained is considerably different from that of Capello-Pullman's improved AO (δ=1.37)[6] which was determined from the SCF-AO of carbon atom. In any case, such AO's should not generally be better than the double-zeta AO used in Treatment (A).

(C) Since the usual AO's χ_p's do not satisfy the orthogonal relation in the PPP LCAO-MO's, approximate orthogonalized AO's were taken as the basis functions. In reality, the calculation was carried out as described below. As the AO bases of PPP MO's should essentially be different from the usual AO's χ_p's in the valence state of constituent atoms, the following orthogonalized AO's ϕ_p's proposed by Löwdin[21] may be chosen as one of suitable bases:

$$\boldsymbol{\phi} = \boldsymbol{\chi}(\boldsymbol{1}+\boldsymbol{S})^{-1/2}, \tag{4}$$

where $\boldsymbol{S}$ is a matrix with elements

$$S_{pq} = \int \chi_p^* \chi_q d\tau - \delta_{pq}. \tag{5}$$

Since the π-electron MO's of benzene are essentially unique as described above, the PPP MO's taking the orthogonalized AO's ϕ_p's as the bases are exactly identical with those in which the nonorthogonality between the AO's χ_p's is strictly included.[22] For

alternant hydrocarbons, the PPP MO's with basis functions of the orthogonalized AO's ϕ_p's may semi-empirically be good approximations of the SCF-MO's with inclusion of all overlap integrals as pointed out by Parr,[22] although this relation should not exactly be valid. In Treatment (C), the ZFS parameters were simply calculated by using LCAO-MO's which the coefficients of AO's χ_p's are in the same ratios as those of the PPP MO's, and by including the nonorthogonality between the nearest neighboring AO's χ_p's, as a first step of approximation with orthogonalized AO's. In this case, the overlap integrals were evaluated by using the aforementioned double-zeta AO's.[20]

In the present work, molecular structures of benzene, triphenylene, and coronene were assumed to be planar with symmetry D_{6h}, D_{3h}, and D_{6h}, respectively.[23-25] Since triphenylene and coronene are deformed in crystals,[24-26] structures with symmetry C_{2v} and D_{2h}, respectively, were taken as typical examples of such conformations. The internuclear distances and bond angles used were obtained by averaging the observed values in each ground state[23-26] for each equivalent bond and angle. A similar study was carried out by assuming hypothetical structures with which all the benzene rings involved are the same size as in the ground state of benzene. As the observed E values are nonzero for these molecules,[10,12-15] the influence of distortion from hexagonal or trigonal symmetry upon the ZFS parameters was also examined for conformations in which the benzene rings of the system are all antiquinonoidal (AQ) or all quinonoidal (Q) forms. Such a calculation was carried out under the following assumptions: (i) the sum of the six nearest C–C bond lengths of each benzene ring and all the bond angles are unchanged from those of the ground state with symmetry D_{6h}, D_{3h}, and D_{6h} for benzene, triphenylene, and coronene, respectively; (ii) the changes of the lengths in a pair of parallel C–C bonds [ΔR(C–C)] are taken to be identical with each other and twice as large as the change in each of the other four C–C bond lengths [$-\Delta R$(C–C)/2]. The coordinate system used for ZFS parameters of each molecule is indicated by small letters in Figs. 1—3.

When the SCF π-electron MO's were calculated for each ground state with the PPP approximation,[18,19] the Coulomb integrals were evaluated by using Ohno-Klopman-type (OK) approximation:[27]

$$J_{pq} = e^2/(k^2a^2+r_{pq}^2)^{1/2}, \quad (6)$$

where $a=e^2/(I_p-A_p)$, $I_p(C)=11.16$ eV, $A_p(C)=0.03$ eV[28] and r_{pq} is an internuclear distance between atoms p and q. The parameter k is chosen as 1.0 and 0.7[29] for electron repulsion and electron-core attraction integrals, respectively. The resonance integrals were evaluated by adopting Wolfsberg-Helmholz-type approximation[30] in which β_{cc} for benzene was assumed to be -2.60 eV[31] and the overlap integrals were calculated by using the double-zeta AO by Clementi.[19]

Results and Discussion

For the lowest triplet state of benzene with symmetry D_{6h}, the D value in Treatment (A) is fairly small [$D=0.1341$ cm^{-1}], while a rather larger value is obtained, if a single STAO with conventional orbital exponent of $\delta=1.59$ (or 1.625) is used [$D=0.1770$ (or 0.1842) cm^{-1} with the present approximation and 0.1671 cm^{-1} with all the spin-spin interaction integrals[5]]. Also, if one use Capello-Pullman's improved STAO with $\delta=1.37$,[6] the D value becomes 0.1295 cm^{-1} still smaller than that obtained in Treatment (A). Further, a fairly good agreement with the observed value cannot be obtained, if only the C–C distances are varied within their permissible limits of the bond lengths. In Treatment (C), however, the evaluated D value [0.1594 cm^{-1}] is very close to the experimental one, in spite of the fact that orthogonalized AO's used were not strictly obtained.

For triphenylene and coronene, the D and E values by Treatment (C) are surprisingly close to those by Treatment (B) and in fair agreement with the experimental values as compared with the case of Treatment (A). These results are listed in Table 1. For the cases where the structures for the lowest triplet states were changed

Table 1. Calculated lowest excited triplet state energies and zero-field splitting parameters[a]

	E_T/eV	Treatment (A)		Treatment (B)		Treatment (C)		Experimental		
		D/cm^{-1}	E/cm^{-1}	D/cm^{-1}	E/cm^{-1}	D/cm^{-1}	E/cm^{-1}	E_T/eV	D/cm^{-1}	E/cm^{-1}
Benzene										
(D_{6h})	3.872	0.1341	0.0000	0.1593	0.0000	0.1594	0.0000	3.65[c]	0.1593[d]	0.0091[d]
	[2.672]	[0.1358]	[0.0000]	[0.1593]	[0.0000]	—	—		0.1593[d]	0.0115[d]
Triphenylene										
(D_{3h})	3.194	0.1125	0.0000	0.1337	0.0000	0.1318	0.0000			
	[2.210]	[0.1164]	[0.0000]	[0.1367]	[0.0000]	—	—	2.86[e]	0.1367[e]	0.0026[e]
(C_{2v})	3.185	0.1117	0.0034	0.1328	0.0037	0.1309	0.0041			
(Benz)[b]	3.155	0.1110	0.0000	0.1319	0.0000	0.1305	0.0000			
Coronene										
(D_{6h})	2.585	0.0920	0.0000	0.1094	0.0000	0.1081	0.0000			
	[1.754]	[0.0963]	[0.0000]	[0.1131]	[0.0000]	—	—	2.40[f]	0.0967[f]	0.0030[f]
(D_{2h})	2.737	0.0930	−0.0046	0.1108	−0.0050	0.1096	−0.0057			
(Benz)[b]	2.581	0.0897	0.0000	0.1066	0.0000	0.1062	0.0000			

a) Values in brackets were calculated with NM approximation. b) (Benz) means a structure with which all the benzene rings are the same size as in the ground state of benzene. c) Paper cited in Ref. 29. d) Ref. 12. e) Ref. 14. f) Ref. 15.

from hexagonal and/or trigonal symmetry, therefore, only the ZFS parameters obtained in Treatment (C) are shown in Figs. 1-3.

In general, the D-type spin-spin interaction integrals except the Coulomb-type ones are relatively small compared with those of the E-type ones.[5] Since such integrals were disregarded here, the D values obtained may possibly be more reliable than the E values. Comparing with the observed E value, the calculated E value of benzene shown in Fig. 1 is relatively large at a distorted structure where the change of bond lengths from the equilibrium ones are nearly the same as those obtained by the SCF-MO-CI calculation.[4,32] This result is quite similar with those of the previous works.[4,5] Under the present circumstances, therefore, the quantitative estimation of the distorted structures in crystals is actually difficult from the calculated ZFS parameters, even if all the spin-spin interaction integrals were included.[3,5]

As can be seen in Figs. 2 and 3, the change of the ZFS parameters of triphenylene and coronene with the molecular distortion have a similar trend with that of benzene, although the influence on the E value is fairly small compared with the case of benzene. The calculated E value of triphenylene assuming the aforementioned C_{2v} structure in a crystal is not much different from the observed value. On the other hand, the experimental E value of coronene changes slightly according to the host crystal,[15,16] as is seen in benzene.[12,13] This makes it very difficult to infer whether the intramolecular pseudo-Jahn-Teller instability significantly affects the E value or not.

As a preliminary step, the ZFS parameters of these molecules were also calculated by using Nishimoto-Mataga-type (NM) two-center integrals:[33]

$$J_{pq} = e^2/(ka+r_{pq}). \quad (7)$$

In this case, Treatments (A) and (B) were adopted by using the traditional parameters: $I_p(C)=11.22$ eV, $A_p(C)=0.62$ eV,[34] and $\beta_{cc}(\text{Benzene})=-2.39$ eV.[18] As given in Table 1,[35] the OK approximation does not always give a better result for the ZFS parameters than the NM one, while the former formula may yield better electronic energies for the triplet state rather than the latter one.[31] Actually, the present results with the use of OK approximation are in general satisfactory compared with the previous works on these molecules used various different treatments.[36]

For the second excited triplet state of these molecules, the ZFS parameters were similarly calculated as is given in Table 2. These values may have some theoretical interest, although the experimental values have not yet been available. The E value of benzene might apparently be zero because of its D_{6h} symmetry and can be obtained to be zero using complex WF's of $\Psi(^3E_{1u\pm})=2^{-1/2}[\Psi(^3B_{1u})\pm i\Psi(^3B_{2u})]$.[37] However, if the real WF's of $\Psi(^3B_{1u})$ and $\Psi(^3B_{2u})$ were separately used as the limit forms of D_{2h} symmetery, the E values so obtained are negative and positive, respectively, as given in Table 2 and both the ZFS levels obtained are still degenerate. This might appear the fact that each of such real WF's does not seemingly satisfy the condition of symmetry D_{6h}. For D_{2h} structures which are slightly deformed from D_{6h}, the influence of the off-diagonal element of $\langle\Psi(^3B_{1u})|-2x_{12}y_{12}/r_{12}^5|\Psi(^3B_{2u})\rangle$ upon E values should be considerable if the separation between the $^3B_{1u}$ and $^3B_{2u}$ states is the same order as their E values. Similar results were obtained by using real WF's of $\Psi(^3B_2)$ and $\Psi(^3A_1)$ for triphenylene[38] and those of $\Psi(^3B_{2u})$ and $\Psi(^3B_{1u})$ for coronene[39] (see Table 2). With the OK approximation, the $^3E_{1u}$ state of coronene is calculated to be located slightly lower than the $^3B_{2u}$ state. Because of the perturbation from this state, the D value becomes fairly small as compared with that obtained with the NM approximation where the $^3B_{2u}$ state is not much close to the $^3E_{1u}$ state. This is a rather different type of interaction than the above-mentioned slightly deformed case. To examine these points, further studies are necessary from the viewpoint of both theory and experiment. In near future, it is hoped to observe fine structures of the second excited triplet state using some new refined technique.

In previous studies, ZFS parameters were evaluated by using various treatments which do not always give

Table 2. Calculated second excited triplet state energies and zero-field splitting parameters[a]

	E_T/eV	Treatment (A)		Treatment (B)		Treatment (C)		Experimental		
		D/cm^{-1}	E/cm^{-1}[b]	D/cm^{-1}	E/cm^{-1}[b]	D/cm^{-1}	E/cm^{-1}[b]	E_T/eV	D/cm^{-1}	E/cm^{-1}
Benzene										
(D_{6h})	4.896	0.0625	0.0000(±0.0742)	0.0685	0.0000(±0.0793)	0.0696	0.0000(±0.0826)	4.58[d]	—	—
	[4.063]	[0.0625]	[0.0000(±0.0741)]	[0.0680]	[0.0000(±0.0785)]	—	—			
Triphenylene										
(D_{3h})	3.835	0.0965	0.0000(∓0.0076)	0.1128	0.0000(∓0.0083)	0.1159	0.0000(∓0.0115)			
	[2.846]	[0.1151]	[0.0000(∓0.0160)]	[0.1340]	[0.0000(∓0.0171)]	—	—			
(C_{2h})	3.887	0.0998	−0.0074	0.1168	−0.0081	0.1206	−0.0111	3.38[e]	—	—
	3.780	0.0952	0.0131	0.1112	0.0143	0.1138	0.0178			
(Benz)[c]	3.804	0.0951	0.0000(∓0.0125)	0.1111	0.0000(∓0.0136)	0.1146	0.0000(∓0.0172)			
Coronene										
(D_{6h})	3.299	0.0375	0.0000(∓0.0383)	0.0419	0.0000(∓0.0410)	0.0429	0.0000(∓0.0440)			
	[2.529]	[0.0957]	[0.0000(∓0.0404)]	[0.1110]	[0.0000(∓0.0430)]	—	—			
(D_{3h})	3.433	0.0388	−0.0360	0.0431	−0.0385	0.0439	−0.0404	—	—	—
	3.442	0.0373	0.0445	0.0416	0.0476	0.0424	0.0517			
(Benz)[c]	3.284	0.0389	0.0000(∓0.0383)	0.0435	0.0000(∓0.0410)	0.0450	0.0000(∓0.0445)			

a) Values in brackets were calculated with NM approximation. b) Values in parentheses calculated by using the real WF's in stead of the corresponding complexWF's. c) (Benz) means a structure with which all the benzene rings are the same size as in the ground state of benzene. d) Paper cited in Ref. 29. e) Ref. 14.

a satisfactory D value for benzene without some modifications. Concerning this point, however, no detailed explanation was made in such publications, except a paper in which the effect of overlap integrals was non-empirically pointed out.[3] In the present work, such a difficulty is partly reduced by using the approximate orthogonalized AO's which are given by a linear combination of SCF-AO's. Although the present work includes various points to be improved such as spin-spin interaction integrals, orthogonalized AO's, configuration interactions, and so on, the general trend for the calculated D value should not significantly be changed. In view of these facts, the present results may show the fact that for evaluating physical constants such as ZFS parameters using semi-empirical LCAO-MO's with ZDO approximation their basis functions should carefully be chosen without use of the usual AO's.

This work was undertaken in collaborating with Professor M. Kinoshita, The University of Tokyo, in connection with the work on the triplet state of triphenylene.[14] At several stages, the author is indebted to him for his suggestion and discussions. The author also wished to thank Professor Y. Gondo, Kyushu University, for informing the error in a formula of spin-spin interaction integrals appeared in Ref. 17, and Dr. S. Iwata, The Institute of Physical and Chemical Research, for his helpful suggestion. The numerical calculations were carried out on HITAC 8700/8800 at Computer Centre, The University of Tokyo.

References

1) C. A. Hutchison, Jr., and B. W. Mangum, *J. Chem. Phys.*, **34**, 908 (1961).
2) S. P. McGlynn, T. Azumi, and M. Kinoshita, "Molecular Spectroscopy of the Triplet State," Prentice-Hall, Inc., Englewood Cliffs, New Jersey (1969), p. 329; S. R. Langhoff and C. W. Kern, "Applications of Electronic Structure Theory," ed by H. F. Schaefer, III, Plenum Press, New York (1977), p. 381.
3) S. R. Langhoff, E. R. Davidson, and C. W. Kern, *J. Chem. Phys.*, **63**, 4800 (1975).
4) M. S. de Groot and J. H. van der Waals, *Mol. Phys.*, **6**, 545 (1963); J. H. van der Waals and G. ter Maten, *ibid.*, **8**, 301 (1964).
5) M. Godfrey, C. W. Kern, and M. Karplus, *J. Chem. Phys.*, **44**, 4459, (1966).
6) D. Capello and A. Pullman, *Theor. Chim. Acta*, **8**, 383 (1967).
7) J. Zuclich, *J. Chem. Phys.*, **52**, 3592 (1970).
8) Y. Gondo and A. H. Maki, *J. Chem. Phys.*, **50**, 3270, 3638 (1969); Y. Gondo and Y. Kanda, *Bull. Chem. Soc. Jpn.*, **43**, 3943 (1970).
9) D. S. McClure, *J. Chem. Phys.*, **20**, 682 (1952); M. Mizushima and S. Koide, *ibid.*, **20**, 765 (1952).
10) M. S. de Groot, I. A. M. Hesselmann, and J. H. van der Waals, *Mol. Phys.*, **13**, 583 (1967); **16**, 45 (1969).
11) J. H. van der Waals, A. M. D. Berghuis, and M. S. de Groot, *Mol. Phys.*, **13**, 301 (1967); **21**, 497 (1971).
12) Ph. J. Vergragt and J. H. van der Waals, *Chem. Phys. Lett.*, **36**, 283 (1975); **42**, 193 (1976).
13) Ph. J. Vergragt and J. H. van der Waals, *Mol. Phys.*, **33**, 1507 (1977).
14) N. Nishi, K. Matsui, M. Kinoshita, and J. Higuchi, *Mol. Phys.*, **38**, 1 (1979).
15) K. Ohno, N. Nishi, M. Kinoshita, and H. Inokuchi, *Chem. Phys. Lett.*, **33**, 293 (1975).
16) A. M. Merle, M. Lamotte, S. Risemberg, C. Hauw, J. Gaultier, and J. Ph. Grivet, *Chem. Phys.*, **22**, 207 (1977).
17) S. A. Boorstein and M. Gouterman, *J. Chem. Phys.*, **41**, 2776 (1964).
18) R. Pariser and R. G. Parr, *J. Chem. Phys.*, **21**, 466, 767 (1953).
19) J. A. Pople, *Trans, Faraday Soc.*, **49**, 1375 (1953).
20) E. Clementi, "Tables of Atomic Functions" [supplement to *IBM J. Res. Develop.*, **9**, 2 (1965)] Table 45-01.
21) P.-O. Löwdin, *J. Chem. Phys.*, **18**, 365 (1950).
22) R. G. Parr, *J. Chem. Phys*, **33**, 1184 (1960).
23) A. Langseth and B. P. Stoicheff, *Can. J. Phys.*, **34**, 350 (1956).
24) F. R. Ahmed and J. Trotter, *Acta Crystallogr.*, **16**, 503 (1963).
25) J. M. Robertson and J. G. White, *J. Chem. Soc.*, **1945** 607.
26) J. K. Fawcett and J. Trotter, *Proc. R. Soc. London, Ser. A*, **289**, 366 (1966).
27) K. Ohno, *Theor. Chim. Acta*, **2**, 219 (1964); G. Klopman, *J. Am. Chem. Soc.*, **86**, 4550 (1964); **87**, 3300 (1965).
28) J. Hinze and H. H. Jaffé, *J. Am. Chem. Soc.*, **84**, 540 (1962).
29) It may be noted that with $k=0.7$ for the electron-core attraction integrals the calculated lowest three triplet states of naphthalene are located to be the same ordering as its experiment [J. B. Birks, L. G. Christophorous, and R. H. Huebner, *Nature*, **217**, 809 (1968)]. For benzene, no appreciable change in the calculated values is found when the core-attraction integrals with $k=1.0$ are used instead of those with $k=0.7$.
30) M. Wolfsberg and L. Helmholz, *J. Chem. Phys.*, **20**, 837 (1952).
31) K. Schulten, I. Ohmine, and M. Karplus, *J. Chem. Phys.*, **64**, 4422 (1976).
32) Y. Fujimura, H. Yamaguchi, and T. Nakajima, *Bull. Chem. Soc. Jpn.*, **45**, 384 (1972).
33) K. Nishimoto and N. Mataga, *Z. Phys. Chem. (Frankfurt am Main)*, **12**, 335 (1957).
34) G. Pilcher and H. A. Skinner, *J. Inorg. Chem.*, **24**, 937 (1962).
35) With the NM approximation, the value of δ determined in Treatment (B) is 1.4955.
36) S. A. Boorstein and M. Gouterman, *J. Chem. Phys.*, **39**, 2443 (1963); Y.-N. Chiu, *ibid.*, **39**, 2736 (1963); J. H. van der Waals and G. ter Maten, *Mol. Phys.*, **8**, 301 (1964); Y. Gondo and Y. Kanda, *Bull. Chem. Soc. Jpn.*, **43**, 3943 (1970).
37) For the states indicated in real WF's, the axis system is chosen for D_{2h} symmetry as shown in parentheses in Fig. 1.
38) For the states indicated in real WF's, the axis system is chosen for C_{2v} symmetry as shown in parentheses in Fig. 2.
39) For the states indicated in real WF's, the axis system is chosen for D_{2h} symmetry as shown in parentheses in Fig. 3.

  Bull. Chem. Soc. Jpn., 54, 2869—2871 (1981)

The Formation of Amino Acids by the Reactions of Singlet NH with Several Carboxylic Acids

Shigeru TSUNASHIMA,* Takashi KITAMURA, and Shin SATO

Department of Applied Physics, Tokyo Institute of Technology, Ookayama, Meguro-ku, Tokyo 152

(Received February 3, 1981)

The photolysis of hydrogen azide was studied in liquid acetic acid, propionic acid, and isobutyric acid at room temperature. The formation of amino acids was confirmed by the color reactions with ninhydrin and with chromotropic acid and by the NMR spectra. From the propionic acid, α- and β-alanine were formed in the ratio of 1.5. In the case of isobutyric acid, α- and β-aminoisobutyric acids were formed in the ratio of about 5. These results are explained by the insertion reaction of NH($a^1\Delta$) into the C–H bonds of carboxylic acids.

The formation of NH($a^1\Delta$) has been observed in the photolysis of hydrogen azide with light of wavelengths between 250 and 320 nm.[1] Since NH radicals are isoelectronic with O or CH_2 radicals, it is expected that the reactions of the singlet NH radicals are similar to those of O(^{1}D) and $CH_2(^1A_1)$. Recently, we photolyzed hydrogen azide in liquid paraffin at the temperature of Dry Ice–methanol and found the formation of amines: ethylamine from the ethane solution, propyl- and isopropylamine from the propane solution, and isobutyl- and *t*-butylamine from the isobutane solution.[2,3] These amine formations were explained by the insertion reaction of the singlet NH into the C–H bonds of paraffins.

If the singlet NH inserts into the C–H bonds of hydrocarbons, the singlet NH will insert into the C–H bonds of carboxylic acid to form amino acids. The formation of amino acids on the primitive earth is an interesting problem in the study of prebiotic molecular evolution. The formation of singlet NH has been found in the discharge and vacuum ultraviolet photolysis of ammonia.[4] Since ammonia is known to have been an important component of the primordial atmosphere, the insertion reaction of the singlet NH into the C–H bonds of carboxylic acid, if it occurred, might have been important for the formation of amino acids on the primitive earth.

For these reasons, the photolysis of hydrogen azide was studied in liquid propionic acid, as was shown in a previous letter, and the formation of α- and β-alanine was observed.[5] The present paper will report the details of the previous letter, together with new results obtained with acetic acid and isobutyric acid.

Experimental

The methods of the preparation and purification of hydrogen azide have already been described.[2,3] Acetic acid, propionic acid, and isobutyric acid (Tokyo Kasei Co.) were used after distillation *in vacuo*.

The reaction cell was a Pyrex tube, 10 mm o.d., in which about 2 cm^3 of carboxylic acid and a small amount of hydrogen azide were introduced *in vacuo*. A medium pressure mercury lamp (Toshiba HP 400) was used to illuminate the reaction cell through a transparent quartz Dewar flask filled with distilled water. Since a Pyrex tube was used as a reaction cell, the effective wavelengths absorbed by hydrogen azide were limited within about 280—320 nm.

After the irradiation, non-condensable products at −196 °C were collected with a Toepler pump and their amount was measured with a gas burette. Unreacted hydrogen azide and carboxylic acid were evacuated *in vacuo* at about 50—90 °C. The residue in the cell was dissolved in water and subjected to the analysis by color reactions.[6] A D_2O solution of the residue was analyzed with an NMR spectrometer (JEOL FX 100). The NMR spectra were compared with those obtained with D_2O solutions of glycine, α- and β-alanine, and α- and β-aminoisobutyric acid (Tokyo Kasei Co.). To measure the amount of the products, a known amount of maleic acid was added to the NMR sample, and the integrated intensities were compared.

Results

The non-condensable product at −196 °C was nitrogen. The mass spectrometric analysis showed neither methane nor hydrogen. The yield of nitrogen increased with the increase in the concentration of hydrogen azide and in the irradiation time.

When the solvent was evacuated together with unreacted hydrogen azide, a white solid was left on the

Table 1. The ratios of the yields of amino acids to that of nitrogen in the photolysis of hydrogen azide in carboxylic acids

$[HN_3]$ / mol dm^{-3}	Irradiaton time/h	α/N_2	β/N_2	β/α
CH_3COOH				
0.10	4	0.21	—	—
0.10	3	0.19	—	—
0.10	2	0.21	—	—
0.05	4	0.22	—	—
0.05	2	0.22	—	—
	Mean	0.21±0.02		
CH_3CH_2COOH				
0.10	3	0.19	0.25	1.3
0.10	2	0.13	0.21	1.6
0.10	1	0.20	0.32	1.6
0.05	3	0.11	0.18	1.6
0.05	2	0.16	0.24	1.5
	Mean	0.16±0.04	0.24±0.05	1.5±0.1
$(CH_3)_2CHCOOH$				
0.10	4	0.082	0.47	5.7
0.10	3	0.091	0.44	4.8
0.10	2	0.083	0.41	4.9
0.05	5	0.079	0.40	5.1
0.05	3	0.083	0.38	4.6
	Mean	0.084±0.005	0.42±0.04	5.0±0.4

wall of the reaction cell in the cases of acetic acid and propionic acid. In the case of isobutyric acid, the residue was a yellowish liquid. When methanol was added to this liquid, the white solid remained undissolved. The white solid was soluble in water.

In the case of acetic acid solution, the formation of glycine was confirmed by the color reactions with ninhydrin and with chromotropic acid. The color observed for the products agreed well with that observed with an authentic glycine.

The D_2O solution of the residue was subjected to the NMR analysis. The NMR spectra of the products coincided with those obtained with a mixture of amino acids and the reactant acid: glycine with acetic acid, α- and β-alanine with propionic acid, and α- and β-aminoisobutyric acid with isobutyric acid. An attempt to eliminate the reactant acid from the products was not successful. The ratios of the yield of amino acid to that of nitrogen are summarized in Table 1, as functions of the concentration of hydrogen azide and of the irradiation time.

Discussion

As shown in Table 1, the ratios of the yield of amino acid to that of nitrogen were independent of the changes in the concentration of hydrogen azide and in the irradiation time for every case examined. The trend observed is similar to that observed in the photolysis of hydrogen azide in liquid ethylene or propene at the temperature of Dry Ice–methanol.[7] The following mechanism can be considered to explain the results:

$$NH_3 + h\nu \rightarrow NH(a^1\Delta) + N_2 \quad (1)$$

$$NH(a^1\Delta) + CA \rightarrow \text{Amino acids} \quad (2)$$

$$\rightarrow NH(X^3\Sigma^-) + CA \quad (3)$$

$$NH(X^3\Sigma^-) + NH_3 \rightarrow NH_2 + N_3 \quad (4)$$

$$NH_2 + HN_3 \rightarrow NH_3 + N_3 \quad (5)$$

$$2\,N_3 \rightarrow 3\,N_2, \quad (6)$$

where CA is carboxylic acid. Reaction 2 is the insertion reaction of the singlet NH into the C–H bond of carboxylic acid. In the cases of propionic acid and isobutyric acid, α- and β-amino acids are formed, which correspond to the two types of the C–H bonds involved in the carboxylic acid. As shown in Table 1, the β/α ratios in alanine and in aminoisobutyric acid produced were 1.5 and 5.0 respectively; these are very close to the ratios of the numbers of the C–H bonds in the two types. These results agree well with the assumption that the amino acids are formed by the insertion reaction.

Reaction 3 is the quenching of the singlet NH by carboxylic acid. In the above mechanism, the triplet NH is assumed to abstract a hydrogen atom from hydrogen azide. The triplet NH might abstract a hydrogen atom from carboxylic acid:

$$NH(X^3\Sigma^-) + CA \rightarrow NH_2 + R. \quad (7)$$

When the resultant radical, R, was assumed to abstract a hydrogen atom from hydrogen azide:

$$R + HN_3 \rightarrow CA + N_3. \quad (8)$$

Reaction 7 followed by Reaction 8 is indistinguishable from Reaction 4.

In the present experiment, ammonia could not be analyzed, since it was difficult to isolate it from the reactant. If ammonia is formed, an ammonium salt will be formed by the reactions with acid. The ammonium salt may be evacuated together with the reactant and/or will give $RCOO^-$ in the D_2O solution. Thus the NMR spectra of the ammonium salt in D_2O are the same as those of the reactant acid.

According to the above mechanism, (1)—(6), the quantum yields of amino acid (ϕ_a) and of nitrogen (ϕ_n) should have the following relation:

$$\phi_n = 4 - 3\phi_a. \quad (9)$$

Using the values of relative yields (ϕ_a/ϕ_n) shown in Table 1, the quantum yields of amino acid formation can be calculated. The results are shown in Table 2. As are shown in Table 2, the quantum yield of amino acid increased with an increase in the number of C–H bonds in the reactant acid.

TABLE 2. THE QUANTUM YIELDS OF AMINO ACID FORMATION

Reactant	α-Amino acid	β-Amino acid	Total
CH_3COOH	0.52	—	0.52
CH_3CH_2COOH	0.29	0.43	0.72
$(CH_3)_2CHCOOH$	0.13	0.67	0.80

Miller found the formation of amino acids in the electric discharge of a mixture of methane, ammonia, hydrogen, and water.[8] This mixture is considered to be the primordial atmosphere of earth. He considered that α-amino acids are formed by the hydrolysis of cyanohydrin:

$$RCHO + NH_3 + HCN \rightarrow RCH(NH_2)CN + H_2O \quad (10)$$

$$RCH(NH_2)CN + 2H_2O \rightarrow RCH(NH_2)COOH + NH_3. \quad (11)$$

For the formation of β-alanine, he assumed acrylonitrile as the intermediate:

$$CH_2{=}CHCN + NH_3 \rightarrow NH_2CH_2CH_2CN \quad (12)$$

$$NH_2CH_2CH_2CN + 2H_2O \rightarrow NH_2CH_2CH_2COOH + NH_3. \quad (13)$$

Miller also found the formation of carboxylic acids such as formic acid, acetic acid, and propionic acid.[8] Since it is known that the singlet NH radicals are formed in the electric discharge of ammonia,[9] the insertion reaction of the singlet NH into the C–H bond of carboxylic acid might explain the formation of amino acids in Miller's study.

The present study suggests a new possibility of the prebiotic synthesis of amino acids on the primordial earth.

The authers are much obliged to Professors Takeshi Nakai and Yoshihiko Morooka of Tokyo Institute of Technology for the NMR measurements.

References

1) A. P. Baronavski, R. G. Miller, and J. R. McDonald, *Chem. Phys.*, **30**, 119 (1978).

2) S. Tsunashima, M. Hotta, and S. Sato, *Chem. Phys.*

Lett., **64**, 435 (1979).
3) S. Tsunashima, J. Hamada, M. Hotta, and S. Sato, *Bull. Chem. Soc. Jpn.*, **53**, 2443 (1980).
4) H. Okabe, "Photochemistry of Small Molecules," John Wiley and Sons, New York (1978).
5) S. Sato, T. Kitamura, and S. Tsunashima, *Chem. Lett.*, **1980** 687.
6) B. Alexander, G. Landwehr, and A. M. Seligman, *J. Biol. Chem.*, **160**, 51 (1945).
7) T. Kitamura, S. Tsunashima, and S. Sato, *Bull. Chem. Soc. Jpn.*, **54**, 55 (1981).
8) S. L. Miller, *J. Am. Chem. Soc.*, **77**, 2351 (1955).
9) M. McCarty, Jr., and G. W. Robinson, *J. Am. Chem. Soc.*, **81**, 4472 (1959).

Temperature Dependence of the Rate Constants of H and D-Atom Additions to C_2H_4, C_2H_3D, C_2D_4, C_2H_2, and C_2D_2

Ko-ichi SUGAWARA, Kiyoshi OKAZAKI, and Shin SATO*

Department of Applied Physics, Tokyo Institute of Technology, Ookayama, Meguro-ku, Tokyo 152

(Received February 7, 1981)

The high pressure limiting rate constants of H and D-atom additions to C_2H_4, C_2H_3D, C_2D_4, C_2H_2, and C_2D_2 have been measured in the temperature range from 206 to 461 K by means of the pulse radiolysis-resonance absorption method. Practically no isotope effects due to the deuteration of ethylene and acetylene could be observed. The rate constants were compared with those calculated by the activated complex theory using the potential energy surfaces provided by the *ab initio* calculations. Concerning the isotope effects, very poor agreement was obtained between theory and experiment. This seems to suggest that the assumptions on which the activated complex theory is based have to be reconsidered when it is applied to such reactions as $H+C_2H_4 \rightarrow C_2H_5$ and $H+C_2H_2 \rightarrow C_2H_3$.

The reaction of H-atoms with ethylene has been extensively studied for the last 50 years.[1] The following reaction mechanism is now established:

$$H + C_2H_4 \rightleftharpoons C_2H_5^* \xrightarrow{+M} C_2H_5. \quad (1)$$

Here M stands for the third body for the deactivation of the energized ethyl radicals, $C_2H_5^*$. When H_2 is used as the third body, 200 Torr (1 Torr=133.3 Pa) is probably high enough to suppress the decomposition of $C_2H_5^*$.[2] The reaction of H-atoms with acetylene has also been studied for many years and a similar reaction mechanism has been proposed:

$$H + C_2H_2 \rightleftharpoons C_2H_3^* \xrightarrow{+M} C_2H_3. \quad (2)$$

Recently, we studied the unimolecular decomposition of $C_2H_3^*$[3] and showed that 500 Torr of He is high enough to suppress the decomposition of $C_2H_3^*$. If H_2 is used, 300 Torr may be high enough. In the present paper, we report the high pressure limiting rate constants of these addition reactions in the temperature range 206—461 K. Such measurements were made by Lee *et al.* on the reaction $H+C_2H_4 \rightarrow C_2H_5$[4] and by Payne and Stief on the reaction $H+C_2H_2 \rightarrow C_2H_3$.[5]

Since these addition reactions are relatively simple, the *ab initio* calculations have been carried out for drawing the potential energy surfaces.[6-9] Nagase and Kern predicted the structure of the activated complex for the $H+C_2H_2$ reaction[6] and Nagase *et al.* for the $H+C_2H_4$ reaction.[9] Using this calculated potential energy surface, Nagase *et al.* predicted the kinetic isotope effects in the $H+C_2H_4$ reaction on the basis of the activated complex theory (ACT). We therefore extended our measurement to the reactions with D-atoms and to those with isotopic ethylenes and acetylene, C_2H_3D, C_2D_4, and C_2D_2. A short communication on the $H+C_2H_4$ reaction has already been published.[10]

The kinetic isotope effect is one of the key points when the rate theory of chemical reactions is discussed. The potential energy surfaces calculated for any reactions are not accurate enough to estimate the absolute rate constants;[11] an error of 0.1 kcal/mol (1 kcal=4.184 kJ) introduces a crucial effect on the estimation of the rate constant. For the discussion on the isotope effect, however, such an accurate potential energy surface is not considered necessary.

Experimental

The details of the apparatus and experimental procedures were given in previous papers.[2,12]

The main modification of the apparatus is that the temperature of the reaction system can be controlled in the range from 200 to 500 K. The temperatures lower than room temperature were obtained by letting chilled nitrogen gas flow in a box made of Styroform which surrounds the cell. Higher temperatures were attained by winding the cell with flexible insulated heating tapes. The gas temperature was measured with an accuracy of ±2 K with a copper-constantan thermocouple at the center of the cell prior to each pulse irradiation. Because of the small capacity of the reaction cell and of the simple technique of temperature control, some temperature deviation during a series of measurements (2—3 h) could not be avoided; however, since the rate measurement is finished within 0.1 s, the temperature fluctuation during each measurement may be ignored.

The H_2, D_2 (Takachiho Shoji Co.), and He (Nihon Helium Co.) were used after having been passed through traps filled with molecular sive 4A at 77 K. The C_2H_4, C_2H_2 (Takachiho Shoji Co.), C_2H_3D, C_2D_4, and C_2D_2 (Merck Sharp and Dohme, Canada Ltd.) were used as received. The nominal purities of the last three compounds are 98, 99, and 99%, respectively; these values have been confirmed by gas chromatographic and mass spectrometric analyses.

Results

With a system containing only H_2 or D_2, a very slow decay of H or D-atoms was observed at every temperature. The decay rate increased from 2 to 10 s^{-1} with increasing temperature. This decay may be attributable to the diffusion of the atoms from the optical path. In the presence of a small amount of ethylene or acetylene, the decay of H or D-atoms was far more rapid (10^2—10^4 s^{-1}). A typical oscillogram is shown in Fig. 1. The mixture of 0.212 Torr† C_2D_2 and 595 Torr D_2 was irradiated at 273 K. The lower figure is the first order decay plot of the optical density at 121.6 nm against the reaction time. From this first order decay plot, we can calculate a bimolecular rate constant. All data thus obtained for the reaction of $D+C_2D_2$ are listed in Table 1. When the average of rate constants in each group of measurements is estimated, the deviation due to a small difference of temperature is corrected by using the following formula:

† 1 Torr ≈ 133.322 Pa.

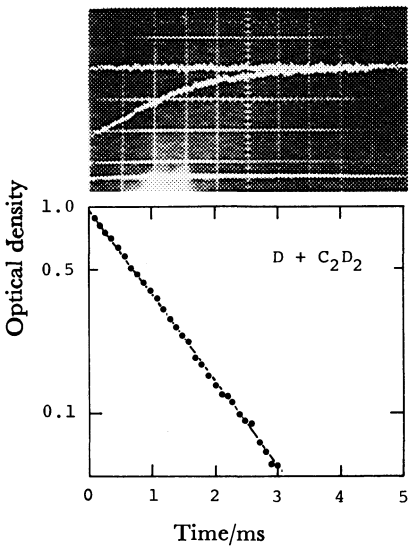

Fig. 1. The oscillogram for the decay of D-atoms in the system of 0.212 Torr C_2D_2 and 595 Torr D_2 at 273 K.

$$k(T+\Delta T) = k(T)[1+(E/R)(\Delta T/T^2)].$$

Here, $k(T)$ is the rate constant at temperature T, E is the activation energy, and R is the gas constant. For the reaction with ethylene, E was assumed to be 2.2

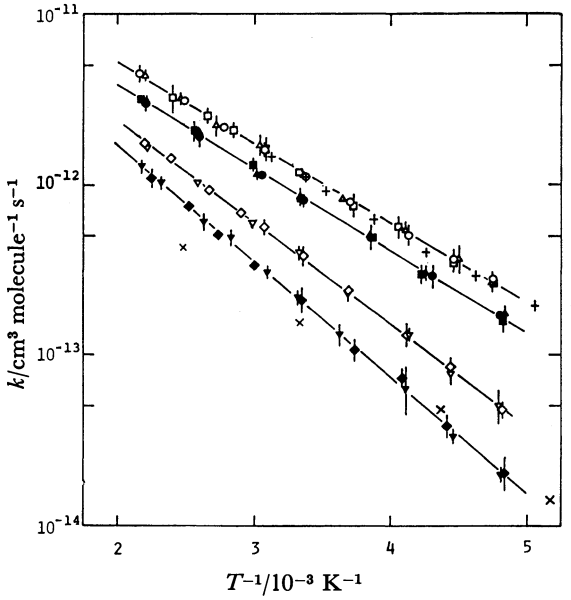

Fig. 2. The Arrhenius plots for the reactions: (○), H+C_2H_4; (△), H+C_2H_3D; (□), H+C_2D_4; (●), D+C_2H_4; (▲), D+C_2H_3D; (■), D+C_2D_4; (◇), H+C_2H_2; (▽), H+C_2D_2; (◆), D+C_2H_2; (▼), D+C_2D_2; (+), the results of Lee *et al.* for H+C_2H_4; (×), the results of Payne and Stief for H+C_2H_2.

Table 1. Rate measurements on the reaction of D atoms with C_2D_2
Uncertainties are 2σ.

C_2D_2 / mTorr	D_2/Torr	T/K	k_{dr} / 10^3 s^{-1}	k / 10^{-13} cm s^{-1}	C_2D_2 / mTorr	D_2/Torr	T/K	k_{dr} / 10^3 s^{-1}	k / 10^{-13} cm s^{-1}
55	607	452	1.48	12.6	237	758	294	1.64	2.11
138	616	450	3.83	12.9	470	532	298	3.07	2.02
359	615	452	8.80	11.5	476	521	298	3.09	2.01
775	615	452	20.9	12.6	616	528	298	4.55	2.28
		av. 452		12.5±1.4[a)]	899	597	299	5.98	2.06
46	595	427	1.11	10.7			av. 297		2.10±0.27
89	600	427	2.02	10.1	43	593	272	2.22	1.45
279	605	425	5.95	9.38	212	595	273	9.97	1.33
691	606	427	14.9	9.54	512	469	275	22.5	1.24
		av. 427		9.97±1.11	833	545	273	32.3	1.26
48	570	379	0.825	6.76			av. 273		1.32±0.25
102	580	375	1.46	5.55	39	550	243	1.15	0.740
454	570	375	7.02	6.00	190	732	237	4.09	0.528
		av. 376		6.07±0.93	498	780	243	10.1	0.509
68	568	352	0.920	4.95	792	545	243	19.4	0.616
107	563	352	1.27	4.32			av. 242		0.603±0.184
189	566	352	2.66	5.13	36	507	223	0.486	0.311
293	562	352	3.58	4.46	97	505	222	1.31	0.310
515	563	350	6.84	4.82	194	786	225	2.93	0.352
		av. 352		4.76±0.70	481	494	223	7.07	0.340
92	541	322	0.830	3.01	775	510	220	9.77	0.287
118	537	318	1.04	2.89	1083	510	223	15.2	0.323
293	538	322	2.56	2.91			av. 223		0.323±0.022
591	540	322	5.66	3.20	35	500	210	0.338	0.210
859	540	322	8.02	3.11	109	490	207	0.940	0.185
		av. 321		3.01±0.22	295	485	205	2.56	0.184
201	520	298	1.33	2.04	778	480	207	7.10	0.196
234	650	294	1.66	2.17			av. 207		0.192±0.012

a) Before averaging, the correction for temperature is made. See the text for the details.

TABLE 2. RATE CONSTANTS OF H OR D-ATOMS WITH C_2H_4, C_2H_3D, C_2D_4, C_2H_2, OR C_2D_2
Uncertainties are 2σ.

Reaction	T/K	$k/10^{-13}$ cm^3 molecule^{-1} s^{-1}	Reaction	T/K	$k/10^{-13}$ cm^3 molecule^{-1} s^{-1}
$H+C_2H_4$	461	44.2±5.2		299	8.62±1.12
	401	31.2±1.8		259	5.06±0.32
	360	21.9±1.3		234	3.14±0.46
	325	16.4±1.6		206	1.73±0.24
	297	11.4±0.9	$D+C_2D_4$	457	30.8±2.6
	270	7.94±0.68		392	20.5±3.2
	242	5.06±0.54		333	12.8±1.0
	224	3.66±0.56		298	8.18±0.47
	211	2.84±0.54		257	4.81±0.37
$H+C_2H_3D$	451	43.0±5.0		235	2.97±0.47
	411	31.3±3.1		206	1.55±0.22
	368	22.3±3.7	$H+C_2H_2$	451	17.9±0.6
	329	17.4±3.1		415	14.5±1.2
	297	11.6±1.0		374	9.58±1.29
	275	8.27±0.49		343	6.85±0.84
	243	5.48±0.85		326	5.63±0.62
	221	3.59±0.77		297	3.79±0.37
	210	2.71±0.46		270	2.40±0.14
$H+C_2D_4$	455	43.7±1.7		242	1.28±0.20
	411	31.3±7.4		225	0.846±0.127
	373	24.3±2.9		207	0.477±0.045
	348	20.3±1.9	$H+C_2D_2$	448	16.2±0.4
	321	16.0±2.6		385	10.2±0.6
	298	11.4±0.9		331	5.86±0.35
	269	7.39±1.01		298	3.82±0.49
	245	5.54±0.98		270	2.25±0.28
	223	3.40±0.15		241	1.28±0.09
	209	2.59±0.11		224	0.759±0.129
$D+C_2H_4$	453	30.2±3.2		208	0.485±0.117
	384	19.4±2.7	$D+C_2H_2$	443	10.9±1.3
	327	11.5±0.9		394	7.58±0.50
	298	8.19±0.74		364	5.10±0.24
	260	4.91±0.95		327	3.35±0.23
	232	2.96±0.50		297	2.07±0.46
	208	1.70±0.10		267	1.08±0.22
$D+C_2H_3D$	449	30.6±3.0		244	0.774±0.099
	382	20.3±1.4		226	0.384±0.059
	331	12.0±1.4		206	0.202±0.402

kcal/mol, and for acetylene, 3.0 kcal/mol was used.

For the other nine reactions, similar measurements and calculations were carried out. The rate constants thus obtained are summarized in Table 2 and in Fig. 2 in the form of an Arrhenius plot, together with the results of Lee *et al.* and Payne and Stief. The results of Lee *et al.* are in good agreement with the present ones, while those of Payne and Stief on the $H+C_2H_2$ reaction are in serious disagreement with ours. This discrepancy will be discussed later.

At high temperatures, the total pressure used might not be high enough to obtain the high pressure limiting rate constant. Figure 3 shows the result of this check.

Table 3 summarizes the Arrhenius parameters calculated from Fig. 2 by the least-squares method, in which the weights resulting both from the experimental errors and from the calculation of the logarithms of

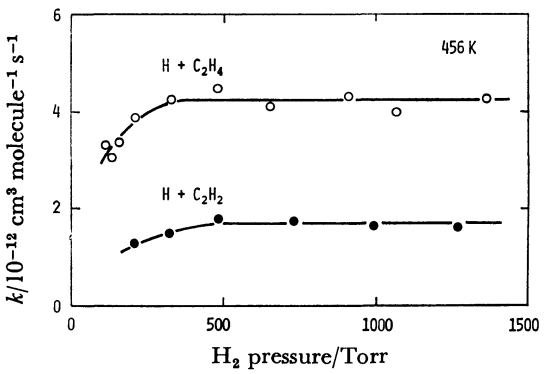

Fig. 3. The pressure dependence of the rate constants for the reactions, $H+C_2H_4$ and $H+C_2H_2$, at 456 K.

TABLE 3. ARRHENIUS PARAMETERS OBTAINED: $A/10^{-11}$ cm^3 molecule^{-1} s^{-1} AND E/cal mol^{-1}
Uncertainties are 2 σ.

	H-Atom addition		D-Atom addition	
	A	E	A	E
C_2H_4	4.70±0.49	2178±58	3.36±0.15	2186±23
C_2H_3D	4.43±0.76	2153±100	3.57±0.34	2193±56
C_2D_4	4.57±0.49	2160±51	3.55±0.43	2216±71
C_2H_2	3.80±0.20	2731±35	3.44±0.61	3023±117
C_2D_2	3.17±0.20	2643±47	4.39±0.31	3184±36

rate constants are included. This calculating method was recently discussed by Cvetanovic *et al.*[13] In the previous communication,[10] we did not use this procedure. The Arrhenius parameters reported in the previous communication should be read as those shown in Table 3 of this paper, although the discrepancy is not substantial. It should be noted in this table that practically no isotope effects due to the deuteration of ethylene and acetylene could be observed.

Discussion

Effect of Product Radicals on the Decay of Atoms. One of the most difficult problems in the present experiment is whether or not the produced ethyl or vinyl radicals affect the measurement of the decay of the reacting atoms. It is established that, if the concentration of hydrogen atoms is higher than or comparable to that of the reactant, ethylene or acetylene, the produced ethyl or vinyl radicals participate into the decay of the reacting atoms, and the decay rate of the atoms is thus overestimated.

As Fig. 2 shows, the temperature dependence of the rate constant of the $H+C_2H_4$ reaction obtained is in good agreement with that obtained by Lee *et al.*, but in the case of the $H+C_2H_2$ reaction, the agreement between the present measurement and that by Payne and Stief is very poor; our data is twice as large as theirs at low temperatures and three times larger at high temperatures. This discrepancy has been discussed in a previous paper;[3] its final conclusion was retained because, when the resonance absorption method is used, the concentration of atoms cannot be reduced to lower than 10^{11} cm^{-3}. In the measurement of the rate constant of the $H+C_2H_4$ reaction, Lee *et al.* used the resonance fluorescence method, by which the atomic concentration can be reduced to 10^{10} cm^{-3}. In fact they obtained the rate constants shown in Fig. 2 by using this low concentration of H-atoms.

When we discussed the participation of vinyl radicals in the $H+C_2H_2$ system, the Runge-Kutta integration method was used to estimate the concentration of vinyl radicals. It was concluded that the participation of this radical in the decay of hydrogen atoms is negligibly small at room temperature; however, since the rate constant $k(H+C_2H_2)$ at room temperature is about 3 times slower than $k(H+C_2H_4)$ at room temperature, there remains a small suspicion about the calculation. As is shown in Fig. 2, $k(H+C_2H_2)$ at 400 K is almost in the same order as $k(H+C_2H_4)$ at room temperature; therefore, if the value for k $(H+C_2H_4)$ at room temperature is reliable, the same thing may be said to that for k $(H+C_2H_2)$ at 400 K. On the other hand, all Arrhenius plots obtained in the present experiments are nicely linear. Consequently, we believe that the rate constants obtained here do not suffer from any disturbance due to the participation of product radicals, although we have no proper explanation for the discrepancy between our results and those of Payne and Stief.

The ACT Calculations. In order to calculate the absolute rate constant of an elementary reaction by the ACT, we need the geometrical structure and the normal mode frequencies of the activated complex. For the reactions of $H+C_2H_4$ and $H+C_2H_2$, we have two sets of data for each reaction. The one is that somewhat arbitrarily constructed for the discussion of the uni-

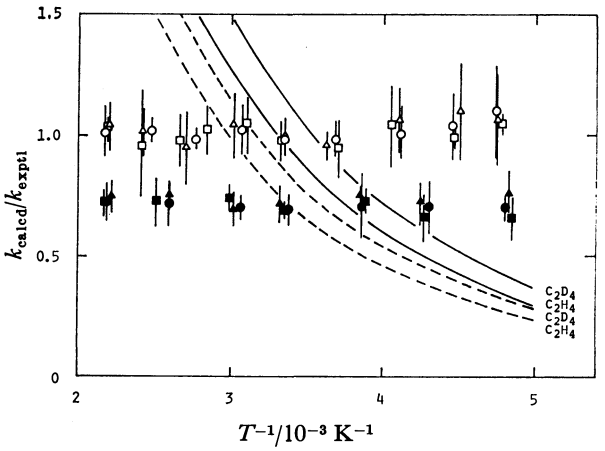

Fig. 4. Comparison of the experimental results with the theoretical calculations, in which the data of Cowfer and Michael are used. For symbols, see the caption of Fig. 2. The experimentally obtained rate constant for the reaction, $H+C_2H_4$, $k_{exptl}=4.7\times10^{-11}\exp(-2.18/RT)$, is taken as the standard. Solid lines for H-atom reactions and dashed lines for the D-atom reactions.

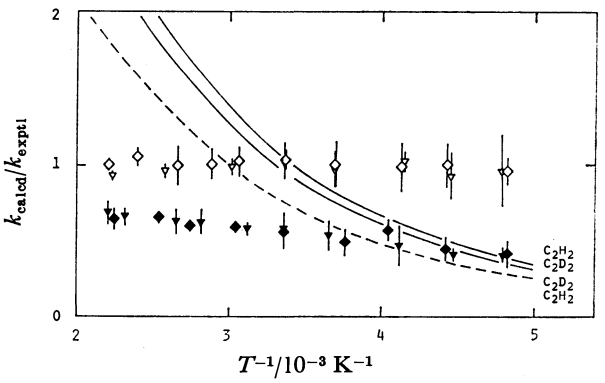

Fig. 5. Comparison of the experimental results with the theoretical calculations, in which the data of Keil *et al.* are used. For symbols, see the caption of Fig. 2. The experimentally obtained rate constant for reaction, $H+C_2H_2$, $k_{exptl}=3.8\times10^{-11}\exp(-2.73/RT)$, is taken as the standard. Solid lines for the H-atom reactions and dashed lines for the D-atom reactions.

molecular decomposition of energized ethyl[14] and vinyl radicals,[15] and the other is the results of the *ab initio* calculations.[6,9]

Figures 4 and 5 compare the experimental results with those calculated by using the parameters estimated for the discussion of the unimolecular decomposition of energized radicals. Here, the experimental rate constants for the $H+C_2H_4$ and $H+C_2H_2$ reactions, $k_{exptl}=4.7\times10^{-11}\exp(-2.18/RT)$ and $k_{exptl}=3.8\times10^{-11}\exp(-2.73/RT)$ respectively, are taken as the standard for each group of reactions, and the k_{calcd}/k_{exptl} ratios are plotted as a function of $1/T$. In these calculations, the barrier heights for the two groups of reactions are adjusted so as to fit the room temperature rate constants for the $H+C_2H_4$ and $H+C_2H_2$ reactions to the experimental ones.

For the convenience of the following discussions, we give the formula used for the calculation of the rate constant:

$$k_{calcd}=\kappa\frac{kT}{h}\frac{F^{\dagger}_{tr}}{F_{atom}F^{1}_{tr}}\frac{f^{\dagger}_{rot}}{f^{1}_{rot}}\frac{f^{\dagger}_{vib}}{f^{1}_{vib}}\exp(-E/RT) \quad (3)$$

$$E=V+\frac{1}{2}\Sigma h\nu_{\dagger}-\frac{1}{2}\Sigma h\nu_{1}. \quad (4)$$

Here V is the barrier height and the other symbols are the same as those appearing in a textbook of reaction kinetics.[16]

In the calculation of the theoretical curves shown in Figs. 4 and 5, the V values are adjusted and found to be 2.83 kcal/mol for the $H+C_2H_4$ reaction and 3.56 kcal/mol for the $H+C_2H_2$ reaction. The transmission coefficient κ is assumed to be unity. As both figures show, the agreement between calculation and experiment is very poor, especially for the temperature dependence.

In the treatment of the unimolecular decomposition of ethyl and vinyl radicals, the activated complexes were assumed to be loose, in order to explain the fall-off pressure.[14,15] In the "loose activated complex," most of the normal mode frequencies are very close to those in the reactants, except for the vibrations newly formed in the activated complex, and their frequencies are considered to be small compared with those in stable compounds. In fact, Cowfer and Michael estimated 120 cm^{-1} for the frequency of the two newly formed vibrations in the activated complex of the $H+C_2H_4$ reaction. The substitution of this value into the vibrational partition function, $f^{\dagger}_{vib}=(1-e^{-h\nu/kT})^{-1}$, gives 2.29 at 300 K. Small vibrational frequencies thus increase the preexponential factor and result in the increase of the adjustable barrier height. This seems to be the main reason for the disagreement between calculation and experiment in Figs. 4 and 5. If the frequencies of the newly formed vibrations in the activated complex could be estimated to be more than 400 cm^{-1} with no effect on the other vibrations, the agreement between calculation and experiment would be much improved.

On the other hand, the recent *ab initio* calculations have suggested that the activated complexes for the reactions of $H+C_2H_4$ and $H+C_2H_2$ have more "tight" structures than those discussed above. The structure

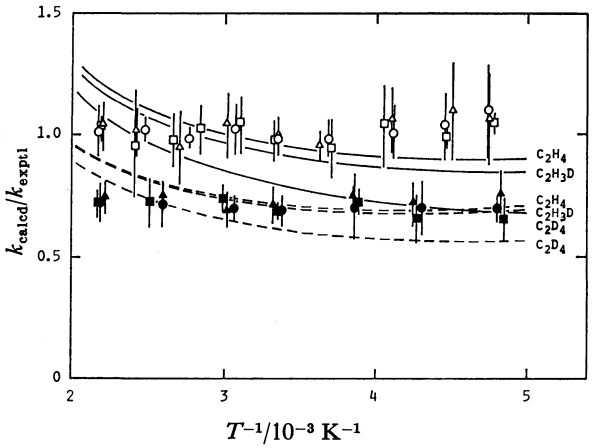

Fig. 6. Comparison of the experimental results with the theoretical calculations, in which the results of the *ab initio* calculations by Nagase *et al.* are used. For the details, see the caption of Fig. 4.

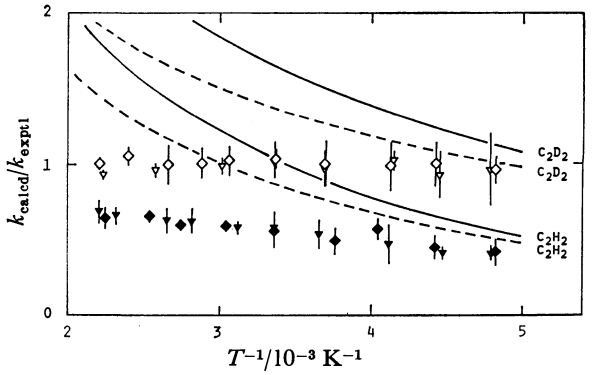

Fig. 7. Comparison of the experimental results with the theoretical calculations, in which the results of the *ab initio* calculations by Nagase and Kern are used. For the details, see the caption of Fig. 5.

and the normal mode frequencies calculated have already been published in previous papers;[3,10] therefore it will not be necessary to restate them. According to these data, the frequencies of the newly formed vibrations in the activated complexes are larger than 400 cm^{-1}, but, along with this increase, other vibrational frequencies are changed and the isotope effects strongly appear. Figures 6 and 7 show the calculated results. In these calculations, the transmission coefficients are estimated by using Wigner's approximation:

$$\kappa=1+\frac{1}{24}(h|\nu|/kT)^2. \quad (5)$$

Here, ν is the imaginary frequency along the reaction coordinate at the top of the barrier. The adjustable V values used in the calculation of the theoretical curves in Figs. 6 and 7 are 2.43 and 2.46 kcal/mol, respectively.

Comparing these figures with Figs. 4 and 5, we can say that the agreement for the temperature dependence between calculation and experiment in Figs. 6 and 7 is better than that in Figs. 4 and 5; however, concerning the isotope effects due to the deuteration of the reactants, C_2H_4 and C_2H_2, the agreement seems to get worse. Another method for the estimation of the transmission

coefficient using an inverted parabola[17] does not improve the situation.

Recently Kupperman and Truhlar developed the generalized transition state theory, in which they stressed that the real activated complex is not necessarily situated on the top of the barrier of the reaction coordinate.[18] This concept was discussed by Horiuchi years ago.[19] This treatment might improve the agreement between the theoretical calculation and experiment; however, as Figs. 6 and 7 show, the isotope effects between C_2H_4 and C_2D_4, and between C_2H_2 and C_2D_2 are so remarkable that filling the gap would be a difficult task.

In 1938, Wigner classified the assumptions on which the ACT is based into three categories:[20] 1) adiabatic condition, 2) quantum effects, and 3) return at the saddle point. The second and third categories have been discussed by many investigators. The transmission coefficient discussed above belongs to the second category. The problem in the third category has been discussed in connection with the trajectory calculation on the atom-diatomic molecule reaction.[21] In the present case, the overshoot of the theoretical curves at high temperatures may be explained by this effect.

Our present impression is that any corrections belonging to the second and third categories cannot improve the agreement between calculation and experiment, especially for the isotope effects due to the deuteration of reactants, and that the first category—adiabatic condition—has to be reconsidered when the ACT is applied to such reactions as $H+C_2H_4$ and $H+C_2H_2$.

References

1) E. W. R. Steacie, "Atomic and Free Radical Reactions," 2nd ed, Reinhold, New York (1954).
2) Y. Ishikawa, M. Yamabe, A. Noda, and S. Sato, *Bull. Chem. Soc. Jpn.*, **51**, 2488 (1978).
3) K. Kowari, K. Sugawara, S. Sato, and S. Nagase, *Bull. Chem. Soc. Jpn.*, **54**, 1222 (1981).
4) J. H. Lee, J. V. Michael, W. A. Payne, and L. J. Stief, *J. Chem. Phys.*, **68**, 1817 (1978).
5) W. A. Payne and L.J. Stief, *J. Chem. Phys.*, **64**, 1150 (1976).
6) S. Nagase and W. Kern, *J. Am. Chem. Soc.*, **101**, 2544 (1979).
7) W. L. Hase, G. Mrowka, and R. J. Brudzynski, *J. Chem. Phys.*, **69**, 3548 (1978).
8) O. Nomura and S. Iwata, *Bull. Chem. Soc. Jpn.*, **53**, 61 (1980).
9) S. Nagase, T. Fueno, and K. Morokuma, *J. Am. Chem. Soc.*, **101**, 5849 (1979).
10) K. Sugawara, K. Okazaki, and S. Sato, *Chem. Phys. Lett.*, **78**, 259 (1981).
11) The potential energy surface for H_3 is exceptional. B. Lin and P. Siegbahn, *J. Chem. Phys.*, **68**, 2457 (1978).
12) Y. Ishikawa and S. Sato, *Bull. Chem. Soc. Jpn.*, **52**, 984 (1979).
13) R. J. Cvetanović, R. P. Overend, and G. Paraskevopoulos, *Int. J. Chem. Kinet.*, **S1**, 249 (1975).
14) J. A. Cowfer and J. V. Michael, *J. Chem. Phys.*, **62**, 3504 (1975).
15) D. G. Keil, K. P. Lynch, J. A. Cowfer, and J. V. Michael, *Int. J. Chem. Kinet.*, **8**, 825 (1976).
16) K. J. Laidler, "Chemical Kinetics," 2nd ed, McGraw-Hill, New York (1965).
17) R. P. Bell, *Trans. Faraday Soc.*, **55**, 1 (1959).
18) The application has made only on the atom-diatomic molecule reactions. B. C. Garrett and D. G. Truhlar, *J. Phys. Chem.*, **83**, 1052 (1979).
19) J. Horiuchi, *Bull. Chem. Soc. Jpn.*, **13**, 210 (1938).
20) E. Wigner, *Trans. Faraday Soc.*, **34**, 29 (1938).
21) S. Chapman, S. M. Hornstein, and W. H. Miller, *J. Am. Chem. Soc.*, **97**, 892 (1975).

On the Continuous Slowing Down Approximation for the Degradation Spectra of Secondary Electrons

Ken-ichi KOWARI and Shin SATO*

Department of Applied Physics, Tokyo Institute of Technology, Ookayama, Meguro-ku, Tokyo 152

(Received February 28, 1981)

The degradation spectra of secondary electrons produced in helium irradiated with high energy electrons have been calculated by two methods. In the first method, the direct integration of the basic formula was carried out and in the second one, the continuous-slowing-down-approximation (CSDA) was used. When the energy of incident electrons is 1 keV (1 eV=9.648×10⁴ J/mol), the second method gave a *G*-value of ionization, 2.17, while the first method gave 2.29. With the decrease in the energy of incident electrons, the CSDA was found to become less reliable. With the incident electrons of 100 eV, the error in the *G*-value of ionization exceeded 15%. The implication of these calculations to the theoretical treatment of the initial process of radiation chemistry is discussed. As an example, the spatial distribution of ion-pairs in γ-irradiated water has been recalculated.

The degradation spectrum of secondary electrons produced in a material irradiated with ionizing radiations is a useful concept for discussing physical and chemical changes induced by these secondary electrons in the material. However, the numerical calculation of the degradation spectrum is not a simple problem, even when all the inelastic collision cross sections of electrons are known. Consequently, the continuous-slowing-down-approximation (CSDA) has often been used for the calculation.

In the previous papers,[1-4] the theoretical estimation of *G*-values of ionization and excitation has been made on many atoms and molecules by using the CSDA. The calculated *G*-values were found to be in fair agreement with those obtained experimentally. However, we were not confident of these calculated *G*-values, partly because of the CSDA.

The accuracy of CSDA has been discussed by many investigators,[5,6] but few numerical checks have been made.[7,8] Klots and Wright carried out Monte Carlo calculations to obtain accurate degradation spectra in some physical model systems and compared them with those calculated under CSDA. Both spectra apparently coincided with each other, but the implication of these calculations to the theoretical treatment of radiation chemistry was not given. The Monte Carlo calculation is very laborious and time-consuming.

The basic formula for the degradation spectrum has been originally proposed by Fano.[9] The numerical calculation of this formula is not a difficult problem, if the energy of incident electrons is not extremely high and if the material consists of simple atoms or molecules.

In the present paper, we will calculate the exact degradation spectra of secondary electrons in helium irradiated with less than 1 keV electrons and estimate the *G*-values of ionization and excitation. These spectra and the *G*-values will be compared with those calculated by using CSDA. Since all the collision cross sections used in the present calculations are obtained by the classical binary-encounter-collision theory, "the exact degradation spectrum" does not mean the true one but the mathematically exact one.

Theory

The basic form of the degradation equation for secondary electrons is expressed as follows:

$$y(T)\int_{E_0}^{T} k(T,E)\,\mathrm{d}E = \int_{E_0}^{\lambda} y(T+E)k(T+E,E)\mathrm{d}E + \int_{2T+I}^{T_0} y(T')k(T',T+I)\,\mathrm{d}T' + S(T). \quad (1)$$

Here, $y(T)$ is the degradation spectrum at the electron energy T, and $k(T, E)$ is the probability per unit path length that an electron of energy T experiences an energy loss between E and $E+\mathrm{d}E$. This probability is the product of the differential cross section by the number density of molecules in the medium. $S(T)$ is the energy distribution of source electrons. In the present calculations, $S(T)=\delta(T_0-T)$. When an electron induces ionization, we cannot distinguish which electron is the incident electron or the electron originally attached to the medium. In the formulation, we define the electron carrying the larger energy after collision to be the incident one; therefore, the upper limit of the integration range of the first term in the right hand side of Eq. 1, λ, is the lesser of T_0-T and $T+I$, where I is the ionization energy, and the lower limit of the second term is $2T+I$. E_0 is the lowest energy loss resulted from the collision.

It is mathematically possible to obtain the degradation spectrum $y(T)$ by numerically solving Eq. 1, if all inelastic collision cross sections are known; however, since the lowest energy loss E_0 is usually much smaller than that of the incident electron T_0, numerous reiterations for integration are necessary and consume a long time for the calculation even by the use of an electronic computer. In the present calculations, the T_0 is limited to 1 keV. If its energy is increased, the calculation time is increased exponentially.

Continuous-slowing-down-approximation. In 1954, Spencer and Fano showed that, if the inelastic collision cross section is proportional to $(\pi e^4/T)(1/E^2)$ and the lowest energy loss E_0 can be assumed to be much smaller than T, the degradation spectrum for the incident particle is expressed as the reciprocal of the stopping power of the medium for that particle.

The exact degradation equation for the incident particle may be written as follows:

$$y_1(T)\int_{E_0}^{T} k(T,E)\mathrm{d}E = \int_{E_0}^{\lambda} y_1(T+E)k(T+E,E)\mathrm{d}E + S(T). \quad (2)$$

This equation is similar to Eq. 1 except for the second term of the right hand side of Eq. 1, the term which corresponds to the generation of new particles. The result of Spencer-Fano's derivation may be expressed as follows:

$$y_1(T) \approx 1/s(T) = \left[\int_{E_0}^{T} k(T,E)E\mathrm{d}E\right]^{-1}, \quad (3)$$

where, $s(T)$ is the stopping power. Now let us consider that the incident particle is an electron, then $y_1(T)$ calculated above corresponds to the degradation spectrum of the incident electron. Once $y_1(T)$ is calculated, the degradation spectrum of the second generation $y_2(T)$ can be calculated as follows:

$$y_2(T) = \frac{N}{s(T)}\int_{T}^{I/2(T_0-T)}\int_{2T_2+I}^{T_0} y_1(T)\sigma(T_1,T_2)\,\mathrm{d}T_1\mathrm{d}T_2. \quad (4)$$

Here, N is the number density of electrons in the medium and $\sigma(T_1, T_2)$ is the cross section for the formation of electrons with energy T_2 in the collision of electrons with energy T_1. A similar equation for the degradation spectrum of the third generation can be constructed:

$$y_3(T) = \frac{N}{s(T)}\int_{T}^{I/4(T_0-3I)}\int_{2T_2+I}^{T_0} y_2(T)\sigma(T_1,T_2)\,\mathrm{d}T_1\mathrm{d}T_2. \quad (5)$$

The degradation spectrum of all electrons is thus calculated by summing up those of all generations:

$$y(T) = \sum_m y_m(T). \quad (6)$$

Collision-cross-section. All the inelastic collision cross sections used in the present calculations are derived by the classical binary-encounter-collision-theory. These cross sections have been fully discussed in a previous paper.[1] For example, $\sigma(T_1, T_2)$ is expressed as follows:

$$\sigma(T_1,T_2) = \frac{\pi e^4}{T_1+I_1+E_1}\left[\frac{1}{(T_2+I_1)^2} + \frac{4E_1}{3(T_2+I_1)^2} + \frac{1}{(T_1-T_2)^2} + \frac{4E_1}{3(T_1-T_2)^3}\right]. \quad (7)$$

Here I_i and E_i are the binding energy and the average kinetic energy of i-th shell.

G-Values of Ionization and Excitation. Once $y(T)$ is obtained, we can calculate the G-values of ionization and excitation.

$$G_n = \frac{1}{100\ T_0}\int_{E_n}^{T_0} Ty(T)Q_n(T)\,\mathrm{d}\ln T. \quad (8)$$

Here Q_n and E_n are the total cross section and the threshold energy for the excitation process n.

Subexcitation Electrons. In order to discuss the behavior of secondary electrons in the medium, the initial energy distribution of subexcitation electrons is indispensable, which can be calculated by using $y(T)$:

$$N(T)_{T<E_0} = \int_{E_0}^{T+I} y(T+E)k(T+E,E)\mathrm{d}E + \int_{2T+I}^{T_0} y(T')k(T',T+I)\mathrm{d}T'. \quad (9)$$

Results and Discussion

The Degradation Spectra near the Energy of Incident Electrons. Figure 1 shows the $y(T)$ near the source energy, 1 keV. The solid line shows the result of the direct integration of Eq. 1 and the dashed line shows the result calculated under the CSDA. Table 1 summarizes necessary in-put data.

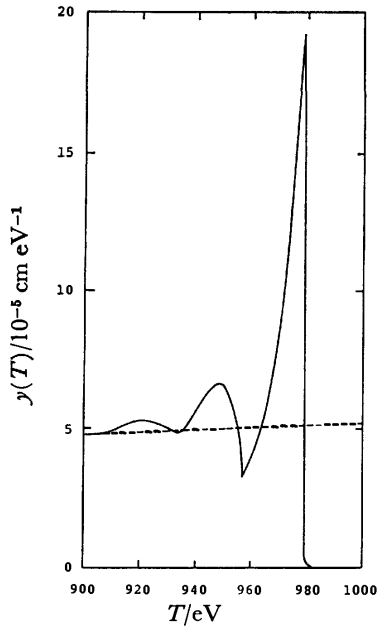

Fig. 1. The degradation spectra of secondary electrons near the energy of incident electrons.
——: Direct integration, – – – –: CSDA calculation.

Table 1. The binding energy (I_i) and the average kinetic energy(E_1) of electrons in helium, and the singlet(E_s) and triplet(E_t) excitation energies of helium in units of eV

I_i	E_1	E_s	E_t
24.581	38.74	21.2	19.8

Since the lowest energy loss accompanying the inelastic collision in helium is the triplet excitation energy, E_t=19.8 eV, no electrons can be produced having energy in the range 980.2 to 999.9 eV. The solid line correctly expresses this transient effect. The oscillations of $y(T)$ for energies near the source energy, which is known as the Lewis effect,[10] is also correctly expressed by the solid line. The spacing between maxima is about 30 eV. On the other hand, the $y(T)$ obtained by using the CSDA does not show such effects. If the detailed structure of $y(T)$ near the source energy is to be included, CSDA cannot be used.

The numerical calculation of such oscillations of $y(T)$ has been carried out by Douthat, who used a different approximate method named SF-2 cord.[6] The general trend of the degradation spectrum he reported is in fair agreement with that obtained here.

The Degradation Spectra and the G-Values of Ionization and Excitation. In Fig. 2 two degradation spectra calculated by the two methods are compared: the solid curve is the result of the direct integration and the dashed one is that calculated under CSDA. Both curves are apparently in good agreement. In the range from 900 to 80 eV, the difference is within a few %, but below 80 eV, the difference increases to about

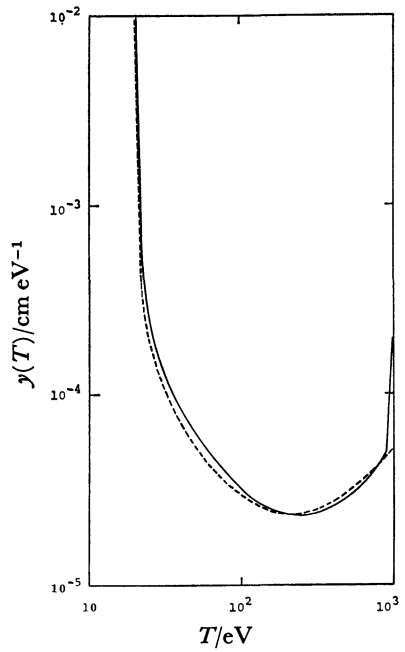

Fig. 2. The degradation spectra of secondary electrons produced in helium irradiated with 1 keV electrons.
——: Direct integration, ----: CSDA calculation.

20%. These calculations depend upon the mesh with which the numerical integration is carried out. For the solid curve, the smallest mesh used was 0.1 eV; with this mesh, the curve obtained was nearly completely converged. For the CSDA calculation, the logarithmic mesh was used; the curve shown in Fig. 2 was obtained with log $(\Delta T/T)=0.01$. With this mesh, the convergion was nearly complete.

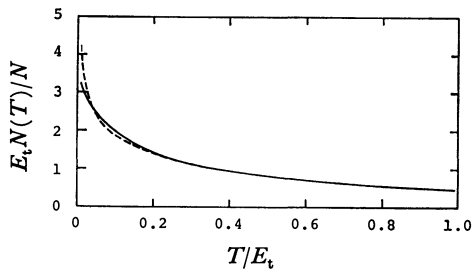

Fig. 3. The initial energy distribution of subexcitation electrons produced in helium irradiated with 1 keV electrons.
——: Direct integration, ----: CSDA calculation.

TABLE 2. THE G-VALUES OF IONIZATION AND SINGLET AND TRIPLET EXCITATIONS CALCULATED BY THE TWO METHODS: DIRECT INTEGRATION (DI) AND THE APPROXIMATE METHOD USING CSDA[a)]

	DI	CSDA
G_{ion}	2.29	2.17
$G_{singlet}$	0.91	0.82
$G_{triplet}$	0.17	0.14

a) Comparison of the calculated G_{ion} with experiment has been made in Ref. 2.

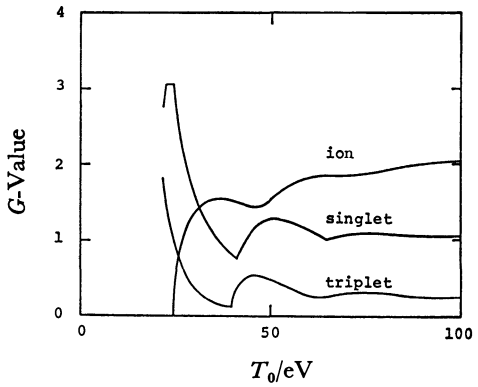

Fig. 4. The source energy dependence of the G-values of ionization and singlet and triplet excitations calculated by the direct integration.

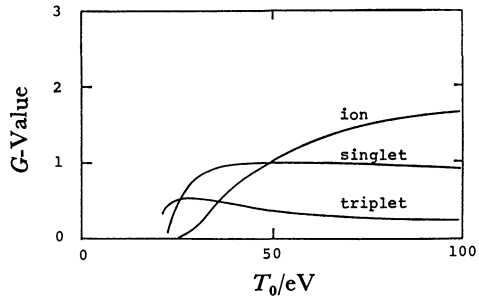

Fig. 5. The source energy dependence of the G-values of ionization and singlet and triplet excitations calculated under the CSDA.

Using these two degradation spectra, we calculated the initial energy distribution of subexcitation electrons and the G-values of ionization and singlet and triplet excitations. The results are shown in Fig. 3 and Table 2. The discrepancy between the CSDA calculation and the direct integration was found in the G-values. The CSDA calculation gave G-values smaller than the direct integration of Eq. 1. This is probably due to the underestimation by the CSDA calculation of $y(T)$ near the threshold energy E_t.

In order to clarify this discrepancy, we calculated the dependence of the G-values of ionization and excitation on the source energy T_0 in the range of 20—100 eV. Figures 4 and 5 show the results. A comparison of these two figures clearly shows that the CSDA calculation underestimates the G-values and that, with the decrease in the source energy, the discrepancy increases. At $T_0=1$ keV, the discrepancy is 6%, while at 100 eV, it increases to 15%.

In a previous paper,[2)] the source energy dependence of the G-values of ionization and excitations of helium was calculated by using the Fowler equation, and curves similar to those in Fig. 4 were obtained. In fact, these two sets of curves coincide exactly with each other. In the actual calculations, the Fowler equation is solved from lower energies, while Eq. 1 is solved from higher energies. The agreement of these sets of curves probably means that the mesh used in these calculations is small enough for the numerical integrations. Incidentally,

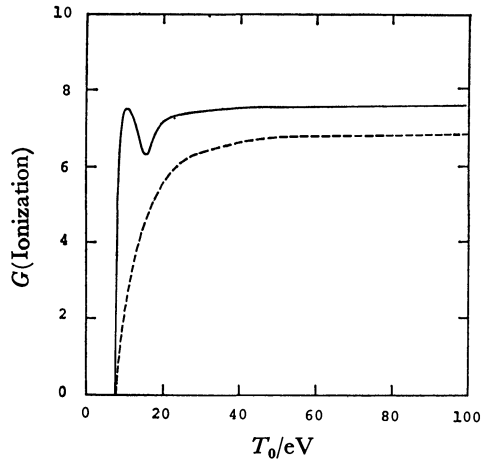

Fig. 6. The source energy dependence of the G-value of ionization in water.
——: Direct integration, ----: CSDA calculation.

it has been proved that the Fowler equation is mathematically equivalent to the Spencer-Fano equation, Eq. 1.[11]

In summary of the above calculations, it may be said that, if the energy of incident electrons is higher than 1 keV, CSDA is accurate enough to estimate the G-value of ionization and excitation; the error limit caused by the use of CSDA is within 6%.

Relative Numbers of Ion-pairs in Different Spurs Generated in the γ-Irradiated Water. In a previous paper,[4] we calculated the spatial distribution of ion-pairs produced in water irradiated with ^{60}Co-γ rays. About 27% of ion-pairs were found to be produced in isolated spurs and another 27% were found in the condensed spurs consisting of more than 100 ion-pairs. In that estimation, we used the source energy dependence of the G-value of ionization calculated under CSDA. As has been discussed above, when the source energy is small, the G-value of ionization is underestimated by the CSDA calculation. We calculated the source energy dependence of the G-value of ionization in water by the direct integration of the Spencer-Fano equation. The result is shown in Fig. 6. By using this result, we recalculated the relative frequencies of spurs in water and the relative numbers of ion-pairs in different spurs. The results are shown in Tables 3 and 4, together with those previously reported. It is noticeable that the agreement between calculation and experiment has been improved.

Table 3. Calculated relative frequencies of spurs in water and relative frequencies of clusters observed in a cloud chamber

Ion-pairs per spur	1	2	3	4	>4
Relative frequency/%	65.7	18.6	6.0	3.1	6.6
(Previously reported)	(73.6)	(11.7)	(5.0)	(3.1)	(6.6)
Ion-pairs per cluster	1	2	3	4	>4
Relative frequency/%					
Source: 25 keV[12]	42.6	22.5	12.4	10.1	12.4
150 keV[13]	60	23	8	4	5
320 keV[13]	62	20	9	4	5

Table 4. Relative numbers of ion-pairs in different spurs

Ion-pairs per spur	Relative number/%	
	(CSDA)	(Corrected)
1	26.8	23.1
2	8.5	13.1
3	5.4	6.3
4	4.5	4.4
5—10	10.9	10.6
11—100	16.5	16.0
>100	27.4	26.5

References

1) S. Sato, K. Okazaki, and S. Ohno, *Bull. Chem. Soc. Jpn.*, **47**, 2174 (1974).
2) K. Okazaki, M. Yamabe, and S. Sato, *Bull. Chem. Soc. Jpn.*, **50**, 1409 (1977).
3) S. Sato, K. Kowari, and K. Okazaki, *Bull. Chem. Soc. Jpn.*, **49**, 933 (1976).
4) K. Kowari and S. Sato, *Bull. Chem. Soc. Jpn.*, **51**, 741 (1978).
5) L. V. Spencer and U. Fano, *Phys. Rev.*, **93**, 1172 (1954).
6) D. A. Douthat, *Radiat. Res.*, **61**, 1 (1975).
7) L. R. Peterson, *Phys. Rev.*, **187**, 105 (1969).
8) C. E. Klots and H. Wright, *Int. J. Radiat. Phys. Chem.*, **2**, 191 (1970).
9) U. Fano, *Phys. Rev.*, **92**, 328 (1953).
10) H. W. Lewis, *Phys. Rev.*, **125**, 937 (1962).
11) A. R. P. Rau, M. Inokuti, and D. A. Douthat, *Phys. Rev., A*, **18**, 971 (1978).
12) C. T. R. Wilson, *Proc. R. Soc. London, Ser. A*, **104**, 1, 192 (1923).
13) W. J. Beekman, *Physica*, **15**, 327 (1949); A. Ore and A. Larsen, *Radiat. Res.*, **21**, 331 (1964).

Spherical Particles and Their Surface Properties. III. Formation of Spherical Particles of Metal Oxides by O_2–H_2 Flame Fusion

Shigeharu KITTAKA* and Tetsuo MORIMOTO**

Department of Chemistry, Faculty of Science, Okayama College of Science, 1-1 Ridaicho, Okayama 700
***Department of Chemistry, Faculty of Science, Okayama University, Tsushima, Okayama 700*

(Received February 16, 1981)

The formation mechanism of spherical particles of various metal oxides through O_2–H_2 flame fusion was investigated. Molten droplets of Al_2O_3 are solidified to form spherical particles having the structure of δ- and θ-Al_2O_3 in the surface layer and α-Al_2O_3 inside. Heat treatment of the spherical particles of Al_2O_3 at temperatures higher than 1573 K gave rise to the transition from δ- and θ-Al_2O_3 to α-Al_2O_3 and made the crystal growth, but no change in the smooth surface structure was observed, contrary to the case of TiO_2 where facetting of the surface occurred on heating. In the cases of NiO and Cr_2O_3, particles bigger than 2—3 μm in diameter are spherical, but smaller ones are apt to form single crystals. With ZnO, SnO_2, and MgO, no spherical particles were formed. It is suggested that amorphous or polymorphous substances easily form spherical particles but monomorphous ones do not. Substances, which can sublime or have higher melting point, do not give pherical particles but only single crystals.

Spherical particles having homogeneous size and smooth surface are important for research on surface and colloidal chemical properties of materials. Recent developments in the preparation of spherical latex particles promoted progress in researches in this field.[1,2] The present authors are interested in the interaction of water molecules with the surface of metal oxides, using samples with a homogeneous surface.[3–6] Recently, we have investigated the surface properties of spherical metal oxides produced by melting the particles in the O_2–H_2 flame,[7,8] as such surfaces may be expected to be homogeneous. It has been found that SiO_2 particles[7] produced by this method have excellent sphericity with smooth surfaces and a dense internal phase. Water adsorption experiments on the SiO_2 particles manifested an improvement of surface homogeneity compared to that of raw Aerosil SiO_2. In the case of TiO_2[8] it has been found that the outer layer of the spherical particles has an anatase structure and the inner part a rutile one; in contrast to SiO_2 there are many cavities inside the particles. Heat treatment of TiO_2 spheres at temperatures higher than 1073 K not only changes the anatase structure in the surface layer into a rutile one, but also promotes facetting of the spherical particle surface and finally splitting of the particles into a few rutile single crystals.

The present paper will deal with high temperature treatment of such metal oxides as SiO_2, TiO_2, SnO_2, Al_2O_3, Cr_2O_3, MgO, NiO, and ZnO in the O_2–H_2 flame and with the formation mechanism of spherical particles.

Experimental

Materials. Two kinds of raw alumina, Al_2O_3-I and Al_2O_3-II were used for the preparation of spherical particles. Al_2O_3-I is the sample pulverized from an α-Al_2O_3 ingot to give a mean particle size of 7 μm. Al_2O_3-II is aluminium oxide-C produced by Degussa; its particles are ultrafine with a particle diameter of about 20 nm; it gives broad X-ray diffraction peaks characteristic of γ-Al_2O_3. MgO powder was produced by Tokyo Electro-Chemical Industry. Both NiO and ZnO were formed by heating each metal oxalate at 873 K in air. Cr_2O_3 was formed by pyrolizing $(NH_4)_2Cr_2O_7$ at 573 K in an N_2 stream. The SnO_2 used was a commercial sample provided by Wako Pure Chemicals. These metal oxide samples were confirmed to contain only one type of crystal structure by X-ray diffraction. In the present work these materials were used without any additional treatment.

Apparatus for Preparing Spherical Particles. The facilities used for the O_2–H_2 flame treatment of metal oxides were the same as those used previously.[7] Metal oxide particles were introduced into the O_2–H_2 flame through the O_2 stream, the flame being generated by burning the mixture of 13 L·min^{-1} O_2 and 20 L·min^{-1} H_2 gases. The temperature of the flame in the furnace was determined to be higher than 2300 K over a 10 cm length from a point 7 cm below the gas nozzle by use of an optical pyrometer together with a siliconit rod. Fused particles were drawn and cooled by pumping through a 3 m duct, which is constructed from duct-1, duct-2, duct-3 of 1 m each (D_1, D_2, and D_3), stainless steel net of 100 mesh (N) and cotten gauze (G). The particles produced were collected at several positions along the flight path.

Examination of Particles. Particles treated in the O_2–H_2 flame were examined by electron microscopic observation by use of a scanning electron microscope JEOL-JSM 35, Au–Pd alloy being deposited in advance on all the samples to avoid the electrification during bonbardment by the electron beam. The particles size distribution histogram was determined by investigating more than 500 particles in electron micrographs. The crystal structure of both the raw and the product particles was established by a powder X-ray diffraction method using Cu $K\alpha$ radiation as well as with a polarizing microscope.

Results and Discussion

Formation of Spherical Al_2O_3 Particles. Figure 1 shows electron micrographs of spherical particles of Al_2O_3-I and Al_2O_3-II. The size of spherical Al_2O_3-I particles captured at any collection point is closely similar to that (6—9 μm) of non-spherical particles of the raw material; this indicates that each raw particle has been sphered individually, *i.e.*, no coalescence has occurred between them. It was also found that no cavity was present in a spherical partcle. On the contrary, spherical particles of Al_2O_3-II were very much larger than raw material particles, *i.e.*, larger than 1 μm (Fig. 1b), indicating the wide particle size distribu-

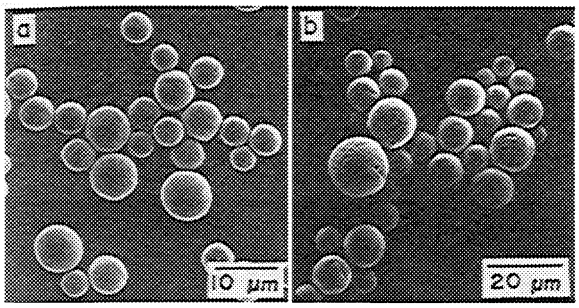

Fig. 1. Scanning electron micrographs for spherical particles of Al_2O_3-I (a) and Al_2O_3-II (b) captured at duct.

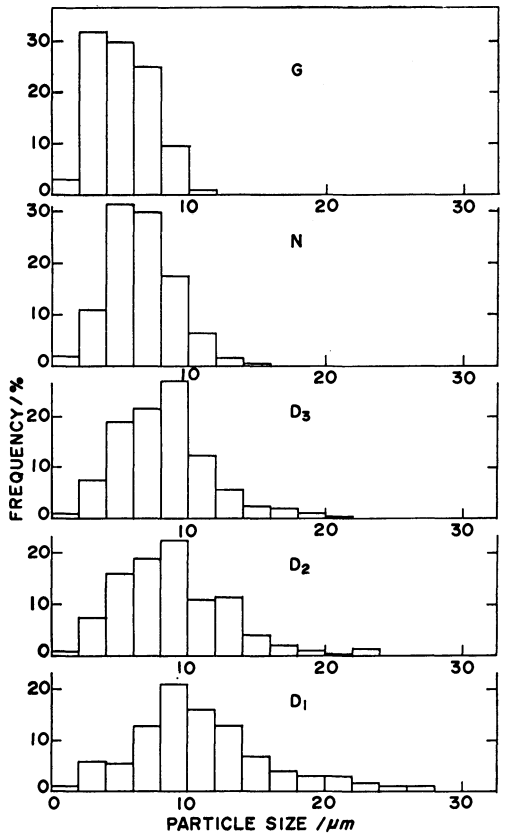

Fig. 2. Dependence of size distribution of Al_2O_3-II spherical particles on the flight distance from the furnace.

tion (Fig. 2). It is also found that the further the collection point, the smaller the mean particle size. Though the Al_2O_3-II particles look perfectly spherical, the inside of the particle is not perfectly fused and has much empty space.

The crystal structure of so formed spherical particles of Al_2O_3-I was examined by X-ray diffraction analysis. Spherical particles formed by passing through O_2–H_2 flame consist of δ- and θ-Al_2O_3, which are stable at lower temperatures, together with small portion of α-Al_2O_3, though the raw material is α-Al_2O_3 (Fig. 3). In the case Al_2O_3-II, these three structures are also observed, but their ratio varies with the collection point of the sample in the duct, α-Al_2O_3 content being much more

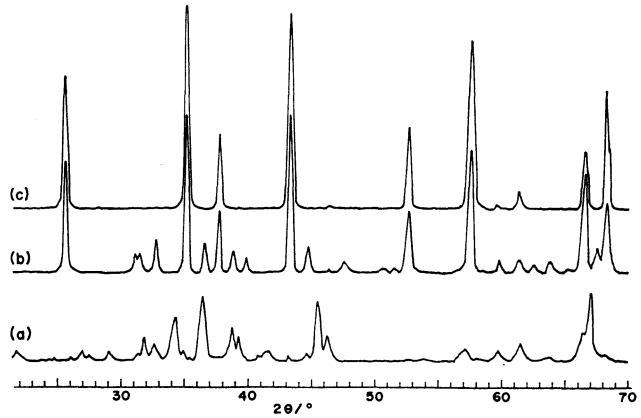

Fig. 3. X-Ray diffraction spectra of spherical Al_2O_3-II particles determined by using the radiation of Cu $K\alpha$.
a: As-grown sample including the crystal structures of α-, δ-, and θ-Al_2O_3, b: 1473 K-treated, α- and θ-Al_2O_3, c: 1573 K-treated, α-Al_2O_3.

than δ- and θ-Al_2O_3 when the particles are collected at duct-1, and less when collected at points far from the furnace, where the ratio of δ-Al_2O_3 to θ-Al_2O_3 was constant throughout the collection points. A similar situation holds also for the sample of TiO_2,[8] where the concentration of rutile exceeds that of anatase in the larger particles. These results can be interpreted as follows. Smaller particles having smaller heat capacity can be quenched so rapidly that crystal forms of δ- and θ-Al_2O_3 appeared in a large amount in the surface layer, while that of α-Al_2O_3 appeared in inner part of particles. On the bigger particles with larger heat capacity the inner part of the spherical particle is rich in α-Al_2O_3.

When the spherical particles of Al_2O_3 are heated for 4 h up to 1373 K, the X-ray diffraction spectrum remains almost unchanged. Upon calcination at 1473 K δ-Al_2O_3 disappeared, θ- and α-Al_2O_3 being left (Fig. 3b). Treatment of the sample at temperatures higher than K led to the complete transition of crystal structure from θ-Al_2O_3 to α-Al_2O_3 (Fig. 3c). Contrary to the TiO_2 particles, however, no facetting of the particle surface was observed upon heat treatment, even at higher temperatures, in spite of the drastic changes in crystal structure. What appeared here was merely a smoothing of the particle surface and charging up of the particle during SEM observation. This might have stemmed from the increased insulation upon dehydration by heat treatment. Polarizing microscope observation of so grown spherical Al_2O_3 particles under crossed nicols showed small spots in a vague back ground, probably because of the polycrystallinity of the particles. After the crystal structures were changed into α-Al_2O_3 by heat treatment, the small spots decreased in number and became brilliant, which indicates that the heated spherical particle has mosaic structure of a few well grown α-Al_2O_3 crystallites, as reported by Nelson *et al.*[9] on Al_2O_3 spheres.

Formation of Spherical Particles of Metal Oxides by Means of O_2–H_2 Flame Treatment. Like SiO_2 and TiO_2 particles, it has been ascertained that spherical particles of Al_2O_3 can be produced through O_2–H_2 flame fusion

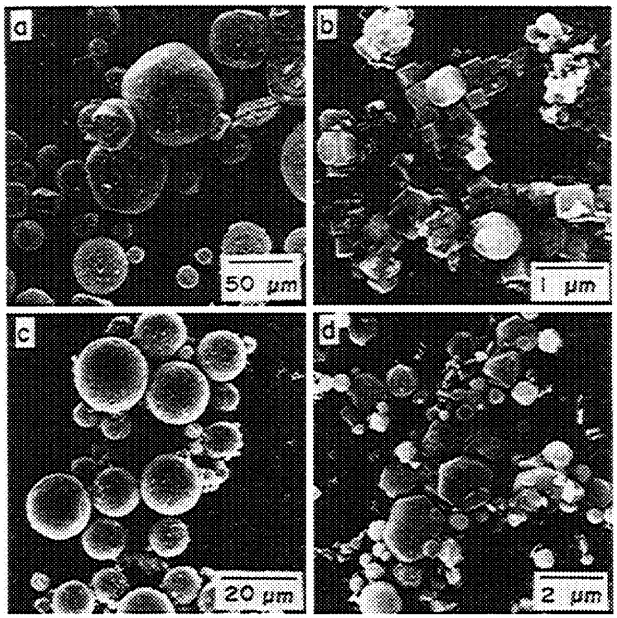

Fig. 4. Scanning electron micrographs for NiO and Cr_2O_3 particles treated through O_2–H_2 flame.
a: NiO at D_1, b: NiO at G, c: Cr_2O_3 at D_1, d: Cr_2O_3 at G.

irrespective of the preparation method of raw materials. However, there are some metal oxide samples that it is difficult or impossible to make spherical. Figure 4 demonstrates electron micrographs for NiO and Cr_2O_3 particles treated in the O_2–H_2 flame. Larger particles of both metal oxides are almost spherical have wrinkles in the surface, but those of NiO having a smooth surface are cubic. With larger particles of NiO, a small amount of contamination by Ni metal was detected by X-ray diffration; this indicates partial dissociation of NiO at higher temperatures. Smaller NiO particles collected on gauze have a characteristic cubic shape; some of them are lacking corners. In the case of Cr_2O_3 particles the shape changed from sphere, through short hexagonal rod, to hexagonal platelet as the size decreased. Inner structure of spheres of metal oxides is similar to that of Al_2O_3 and includes many cavities. It is interesting here that despite the presence of cavities, the NiO particles obtained near the furnace are apt to become cubic. By considering this fact together with the result that apparently spherical having cavities approach the cubic particle by heating at 1473 K (Fig. 5a), it can be understood that a molten NiO particle is apt to take up an ordered arrangement of atoms and to form almost a single crystal sphere. On the other hand, change in the surface structure of Cr_2O_3 spheres upon calcination is very similar to that of TiO_2:[8] heat treatment results in facetting to split a particle into single crystals (Fig. 5b).

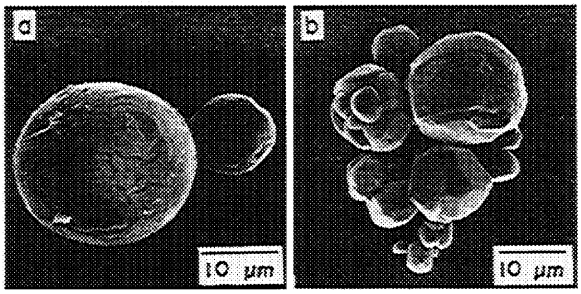

Fig. 5. Scanning electron micrographs for spherical particles of NiO (a) Cr_2O_3 (b) heated at 1573 K for 4 h.

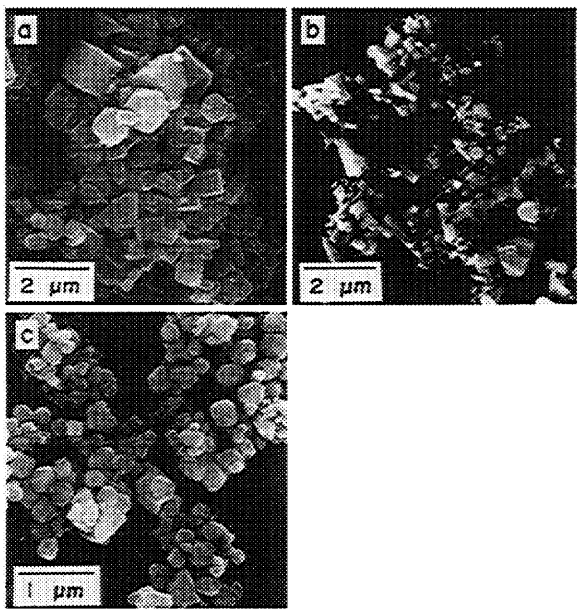

Fig. 6. Scanning electron micrographs for MgO (a), ZnO (b), and SnO_2 (c) particles treated through O_2–H_2 flame and captured at gauze.

When metal oxides such as MgO, ZnO, and SnO_2 were passed through the O_2–H_2 flame, the particles obtained were not spherical but polyhedral, having well defined crystal planes. As shown in Fig. 6, smaller particles collected by gauze are single crystals of each crystal structure of the metal oxides: cubes for MgO, needlelike single crystals with well defined prism planes $(10\bar{1}0)$ for ZnO, similar to those produced by burning Zn metal in air,[4] and polyhedra for SnO_2 in which some particles are octahedral, that is trigonal planes are exposed. Similar particles have been formed by oxidizing SnO vapour at 1423 K in air,[10] where the trigonal face was identified to be the (111) plane by electron diffraction.

As has been discussed above, the possibility whether metal oxide particles formed by the O_2–H_2 flame fusion are spherical or not seems to depend upon the nature of metal oxide. Next, let us consider the reason for this phenomenon on the basis of data shown in Table 1. Using our technique for producing spherical particles, to produce a decrease in the surface free energy of a molten metal oxide particle on sphering, it is necessary that the temperature of the O_2–H_2 flame is higher than the melting point of the sample. With SiO_2, TiO_2, and Al_2O_3, as can be expected from data in Table 1, this condition is found to be satisfied, since spherical particles were obtained.

It would be anticipated that smaller particles would be more easily liquified to give spherical particles than larger ones. With TiO_2 and Al_2O_3, this expectation is

Table 1. Physical properties and sphericity of metal oxides

Metal oxide	$\frac{Mp}{K}$	Crystal structure	Sphericity
Al_2O_3	2320	α-, δ-, θ-Al_2O_3	Yes
TiO_2	2143	Rutile, Anatase	Yes
SiO_2	1883 (quartz)	Amorphous	Yes
NiO	2230	NaCl	Difficult (spheres, single crystallites)
Cr_2O_3	2607 2530 (sublimate)	α-Al_2O_3	Difficult (spheres, single crystallites)
ZnO	2073 (sublimate)	Wurtzite	No (single crystallites)
SnO_2	1898 (sublimate)	Rutile	No (single crystallites)
MgO	3073	NaCl	No (single crystallites)

valid, but with NiO and Cr_2O_3, the inverse is truth. The larger particles are spheres and the smaller ones fine single crystals, though the flame temperature exceeds the melting point. The data in Table 1 lead to a conclusion that one simple rule is involved in the present phenomena. Namely, such metal oxides as SiO_2, TiO_2, and Al_2O_3 which easily form spheres have amorphous or polymorphous structures, while NiO and Cr_2O_3, which have lower ability to produce spheres, are crystallized monomorphously. This interrelationship can be interpreted as follows. First, NiO forms cubic particles not only of the smaller ones but also for the larger ones sedimented in duct 1. Cr_2O_3 particles with fairly large size (4—7 μm) are hexagonal prisms (almost spheres) with about the same length of the diagonal distance and height. That is, these two molten oxides have a strong tendency to form single crystal particles. It is well known that the liquid, at temperatures not much higher than the melting point, is composed of a number of small domains which retain the ordered structures of the solid even below the melting point. In the case of small molten particles of monomorphous metal oxides, it may be considered that the liquid domains of the same quasi-crystal structure unite to control the shape of the particle. Barry *et al.*[11] obtained fine spherical particles of Cr_2O_3 (<0.1 μm) besides hexagonal platelets from CrO_2Cl_2 by the induction plasma torch method. The ease of formation of fine spheres in their experiments seems to differ from that reported here, but this may be explained as follows. They raised the temperature of the furnace to 5000 K which is much higher than that in the present case; the spherical liquid droplets formed would have lost any ordered structure and would be quenched as spherical particles.

Secondly, the molten particles of Al_2O_3 or TiO_2, which are polymorphous, will possibly have a number of domains with different crystal structures just like polycrystalline particles from time to time and from place to place, in contrast to the case of monomorphous oxides. Such a molten particles should be isotropic to form spherical particles due to surface tension. It will easily be understood that the spherical glassy SiO_2 droplet has been solidified as it stands in a liquid state.

ZnO and SnO_2, have sublimation temperatures lower than the flame temperature and therefore no liquid phase is present under our conditions. Thus, it will be reasonable to conclude that particles of these two oxides sublimed to recrystallize as fine single crystallites at relatively lower temperatures. For MgO, the melting point is much higher than the flame temperature; accordingly spherical particles were not formed but the crystal growth of well defined cubic particles proceeded during the O_2–H_2 flame treatment.

References

1) J. W. Goodwin, J. Hearn, C. C. Ho, and R. H. Ottewill, *Br. Polym. J.*, **5**, 347 (1973).
2) W. Norde and J. Lyklema, *J. Colloid Interface Sci.*, **66**, 257 (1978).
3) T. Morimoto, M. Nagao, and J. Imai, *Bull. Chem. Soc. Jpn.*, **44**, 1282 (1971).
4) T. Morimoto and M. Nagao, *J. Phys. Chem.*, **78**, 1116 (1974).
5) S. Kittaka, S. Kanemoto, and T. Morimoto, *J. Chem. Soc., Faraday Trans. 1*, **74**, 676 (1978).
6) S. Kittaka, J. Nishiyama, K. Morishige, and T. Morimoto, *Colloids and Surfaces*, **3**, 51 (1981).
7) T. Morimoto, T. Kadota, H. Yanazawa, and S. Kittaka, *Bull. Chem. Soc. Jpn.*, **53**, 26 (1980).
8) T. Morimoto and S. Kittaka, *J. Colloid Interface Sci.*, **78**, 356 (1980).
9) L. S. Nelson, S. R. Skaggs, and N. L. Richardson, *Laser J.*, March/April, **1971**, 12.
10) K. Morishige, S. Kittaka, and T. Morimoto, *Bull. Chem. Soc. Jpn.*, **53**, 2128 (1980).
11) T. I. Barry, R. K. Bayliss, and L. A. Lay, *J. Mater. Sci.*, **3**, 229 (1968).

Amination of Chloromethylated Polystyrene with Amino Alcohols[1)]

Hiroshi KAWABE

The Institute of Physical and Chemical Research, Wako, Saitama 351

(Received February 19, 1981)

The amination of chloromethylated polystyrene (CMPS) and benzyl chloride (BC) with amino alcohols was investigated kinetically in dioxane, *N,N*-dimethylformamide (DMF), and dimethyl sulfoxide (DMSO). The amination rate was related mainly to the branching structure and partly to the pK of amino alcohols; $\Delta G^{\ddagger}$ and $\Delta H^{\ddagger}$ increased in the following order: 2-aminobutanol<1-amino-2-propanol<2-amino-1-butanol<2-amino-2-methyl-1-propanol<tris(hydroxymethyl)methanamine<triethanolamine. The rate was also related to the polarity of the solvent; $\Delta G^{\ddagger}$ and $\Delta H^{\ddagger}$ decreased in the following order: dioxane>DMF>DMSO. The difference in the amination rate between CMPS and BC is also discussed in terms of the activation parameters. The amination rate of the polymer partly containing quaternary ammonium groups (QCMPS) in DMSO was found to be greater than that of CMPS probably owing to the ion-dipole interaction.

The amination kinetics of chloromethylated polystyrene conforms to a second-order rate equation in many cases. However, there are cases where the rate constant increases or decreases during the course of the amination. The reaction of CMPS with 2-amino-1-butanol (AB), for example, followed second-order kinetics in *N,N*-dimethylformamide (DMF) and dimethyl sulfoxide (DMSO).[2)] However, it exhibited self-acceleration in dioxane.[3)] The reactions of CMPS with various amino alcohols containing a primary amino group in the above-mentioned solvents have been investigated in the present study and the same kinetic behavior as that in the reaction with AB is found. Dragan *et al.*[4)] found a self-accelerating effect in the amination of CMPS with such *N*-(hydroxyalkyl) tertiary amines as 1-dimethylamino-3-propanol and 3-dimethylamino-1-propanol in dioxane and *N,N*-dimethylacetamide. The same kind of acceleration was also observed by Luca *et al.*[5)] in the amination of CMPS with *N,N*-dimethyl-2-hydroxyethylamine and *N,N*-bis-(2-hydroxyethyl)methylamine in DMF. Kawabe[1)] noted an example of self-deceleration in the reaction of CMPS with triethylamine (TEA) in DMSO, although the usual second-order kinetics was observed in the reaction in DMF. The reaction of CMPS with triethanolamine (TEOA) in the present study, however, has been shown to exhibit a different kinetic behavior from that with TEA; it follows the second-order kinetics in DMSO and exhibits the self-acceleration in DMF. The amination of benzyl chloride (BC), a low molecular weight species having a chloromethyl group, follows second-order kinetics in all cases. The author has determined the activation parameters of the aminations of CMPS and BC with a view to discussing the dependence of the reaction rate on the species of the amino alcohols, the solvents, and the chlorides (CMPS or BC). The acid-base equilibria of the polyelectrolytes produced by the reactions of CMPS with the amino alcohols have also been investigated.

Experimental

Materials. The chloromethylated polystyrene (CMPS) was prepared and purified as previously reported;[3,6)] chlorine contents of the samples: 22.38—22.89%, degrees of chloromethylation: 0.979—0.984, and mol wts.: 9.65—11.43×10^4. The (*R*)-2-amino-1-butanol was prepared and purified as previously reported.[3)] The triethanolamine used was of analtical grade. The other amino alcohols, triethylamine (TEA), and benzyl chloride (BC) were of reagent grade. Except for tris(hydroxymethyl)methanamine (TRIS), the amino alcohols, TEA, BC, and the solvents were distilled before use and proved to be pure by their refractive indices.

Kinetic Measurements. In the reactions of CMPS and BC with the amino alcohols in dioxane, the initial concentration of chloromethyl groups (b) was 0.040 mol dm^{-3}, while that of the amino alcohol (a) was 0.8000 mol dm^{-3}. It was not possible to examine the reactions with TRIS in dioxane and DMF because of its insolubility. The author also examined the reactions in DMSO of QCMPS, the chloromethylated polystyrene with half of its chloromethyl groups being converted to quaternary ammonium groups. In practice, CMPS (b=0.040 mol dm^{-3}) was first treated with TEA (a=0.020 mol dm^{-3}) in DMSO at 318 K until 48% of chloromethyl group was converted to quaternary ammonium groups, and QCMPS thus obtained was then aminated with the amino alcohols in DMSO at 318 K on the conditions that the initial concentrations of the remaining chloromethyl groups and amino alcohol were 0.017 and 0.170 mol dm^{-3} respectively. In all the kinetic measurements, temperature was kept constant within ±0.1 K and aliquots of a reaction mixture were removed at appropriate intervals, poured into dilute nitric acid, and titrated potentiometrically with a standard silver nitrated solution (1/10 mol dm^{-3}) to determine the concentration of chloride ions produced by the reaction.

Purification of the Polyelectrolytes Produced by the Reactions of CMPS and the Amino Alcohols. The reaction of CMPS (degree of chloromethylation: 0.979) with amino alcohols was carried out in DMSO until the conversion rose to 99%, and each reaction mixture was dialysed in dilute hydrochloric acid (pH 2.0) and lypophilized. Deionized water was used throughout. The polyelectrolytes produced by the reactions of QCMPS with the amino alcohols were also purified by the same procedure.

Acid-Base Titrations of the Amino Alcohols and the Polyelectrolytes. An aqueous solution containing 0.2—0.5 mmol of an amino alcohol was titrated with a standard hydrochloric acid (0.1006 mol dm^{-3}) to determine the pK_a value of the amino alcohol on the basis of the pH value at the midpoint of the titration curve. The acid-base titrations of the polyelectrolytes were carried out with and without the addition of salt. A 50 ml acidic solution of each purified polyelectrolyte, containing about 0.15 mmol of amino alcohol residues and about 0.30 mmol of hydrogen chloride, was titrated with a standard sodium hydroxide solution (0.1007 mol dm^{-3}). To aother

solution containing the same amount of polyelectrolyte and hydrogen chloride (50 ml) 0.1 mol of sodium chloride and 20 ml of DMSO were added; the mixture was diluted with water to 100 ml and was also titrated with the standard sodium hydroxide solution. The addition of DMSO was intended to avoid the deposition of the polymer in a higher pH range. In the foregoing process, deionized and decarbonized water was used, and nitrogen gas was bubbled through the solution during the titration.

Results and Discussion

The reactions of chloromethylated polystyrene (CMPS) and benzyl chloride (BC) with amino alcohols such as 2-aminoethanol (AE), 1-amino-2-propanol (AP), 2-amino-2-methyl-1-propanol (AMP), tris(hydroxymethyl)methanamine (TRIS), and triethanolamine (TEOA) were investigated in dioxane, *N,N*-dimethylformamide (DMF), and dimethyl sufoxide (DMSO).

Reactions in Dioxane. The reactions of BC with AE and AP in dioxane stopped at low fractional conversions. Since the maximum fractional conversion in the reaction with AE was only 0.1, it was difficult to determine the reaction rate exactly. It was proved, however, that the reaction rates of BC with AP and AMP in dioxane conformed to the following second-order rate equation:

$$kt = \frac{1}{a-b}\ln\frac{b(a-x)}{a(b-x)} = \frac{1}{a-b}\ln\frac{1-\alpha}{1-\beta} \equiv kt, \qquad (1)$$

where a and b are initial concentrations of an amine and the chloromethyl group respectively, while x is the concentration of the chloride ions produced at time t, and $\alpha=x/a$ and $\beta=x/b$. On the other hand, the reactions of CMPS with AE, AP, and AMP, which proceeded nearly to completion, were found to conform to Eq. 2:

$$k = k_0(1+m\beta), \qquad (1)$$

where k is the apparent rate constant obtained by Eq. 1, and where k_0 and m are constants. Kawabe and Yanagita[3] found similar self-acceleration with respect to the reaction of CMPS with 2-amino-1-butanol (AB) in dioxane, and the author attributed such acceleration to the intramolecular hydrogen bonding between the hydroxyl group of the already-aminated neighbor and the chlorine of the chloromethyl group in the transition state.[1] The observed value of m were 2.0 for AE, 1.9 for AP and 0.9 for AMP, whereas the m value for AB was 1.2. The m value decreases in the following order; AE>AP>AB>AMP, and this order conforms to the branching structures of the amino alcohols. Since the m value is a measure of the acceleration, the foregoing suggests that the more complex the branching structure, the more the formation of the hydrogen bond is sterically obstructed.

The k values of BC and the k_0 values of CMPS are listed in Table 1. No further kinetical analysis was performed for the reactions of CMPS with AE and AP because of the deposition of the polymer beyond $\beta=0.5$. The process of the reaction of CMPS with AMP which proceeded in a homogeneous system was found to be represented by Eq. 3:

$$\beta = 1 - A'\exp(-3k_1at) - B'\exp(-k_2at), \qquad (3)$$

where $A'=(k_1-k_2)/(3k_1-k_2)$ and $B'=2k_1/(3k_1-k_2)$. The author[1] found the reaction of CTPS with AB in dioxane to follow closely the same equation. The exact values of k_1 and k_2 are determined by correcting the approximate values of k_1 and k_2 obtained as slopes of the plot of kt against t, which is represented approximately by two lines intersecting at the point corresponding to $\beta=1/3$; the correction of the k_1 and k_2 values was made by means of the repeated computation of the equations:[1]

$$k_2t = -\ln X'/a \equiv \overline{k_2t}$$
$$X' \equiv [(1-\beta)-A'\exp(-3k_1at)]/B' \qquad (4)$$
$$k_1t = -\ln Y'/3a \equiv \overline{k_1t}$$
$$Y' \equiv [(1-\beta)-B'\exp(-k_2at)]/A'. \qquad (5)$$

The observed β values of the reaction of CMPS with AMP fall exactly on the line computed on the basis of Eq. 3 as shown in Fig. 1. This suggests that the self-acceleration in the reaction of CMPS with AMP can be explained by the same mechanism as in the case of the reaction with AB. Table 1 indicates that the k_1 value agrees with the k_0 value (for AMP) with the k_0 values being equal to the k values of BC (for AP and AMP). In Table 1 are also listed the activation energies (E_a) and the frequency factors (A) which are computed by means of the least-squares method on the basis of the equation:

$$\ln k = \ln A - E_a/RT. \qquad (6)$$

The k_0 value decreases and the E_a value increases in the following order: AE, AP, (AB),[1] AMP. Arrhenius plots for the amination of CMPS are shown in Fig. 2, where dotted lines are calculated in accordance with Eq. 6.

Table 1. Amination in dioxane

Amine	Chloride	$k\times10^5$/dm^3 mol^{-1} s^{-1}			E_a / kJ mol^{-1}	log A[a]
		318.2 K	333.2 K	348.2 K		
AE	CMPS, k_0	5.08	12.1	28.2	52.6±0.7	4.336±0.107
AP	BC	3.27	9.17	20.3	56.2±2.0	4.752±0.275
	CMPS, k_0	3.70	8.42	22.2	54.9±2.6	4.558±0.409
AMP	BC	0.408[b]	1.35	4.38	61.0±3.0	4.760±0.474
	CMPS, k_0	0.612	1.60	4.23	59.3±1.2	4.522±0.181
	k_1	0.605	1.54	4.27	59.9±2.0	4.602±0.307
	k_2	1.65	3.60	9.92	55.0±3.6	4.225±0.560

a) A is expressed by dm^3 mol^{-1} s^{-1}. b) The k value at 313.2 K.

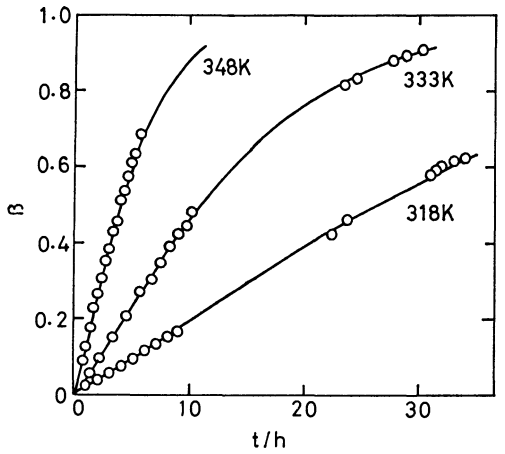

Fig. 1. Amination of CMPS with 2-amino-2-methyl-1-propanol in dioxane.
——: Calculated values, ○: observed values.

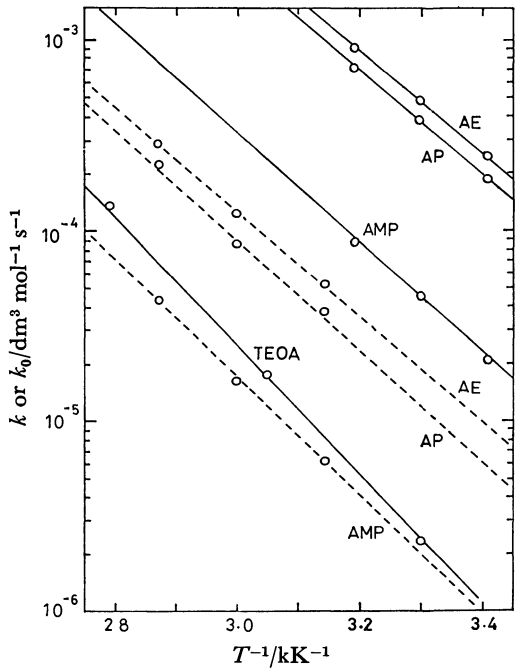

Fig. 2. Arrhenius plots for the aminations of CMPS in dioxane and DMF.
○: Observed values, ----: calculated values in dioxane, ——: calculated values in DMF.

Reactions in DMF and DMSO. The reactions of CMPS, with AE, AP, AMP, and TRIS in DMF and DMSO all comformed to the second-order rate equation, Eq. 1, as in the case of BC. The values of the rate constant (k), E_a and A are tabulated in Tables 2 and 3. Arrhenius plots for the amination of CMPS are shown in Figs. 2 and 3, where solid lines are calculated in accordance with Eq. 6.

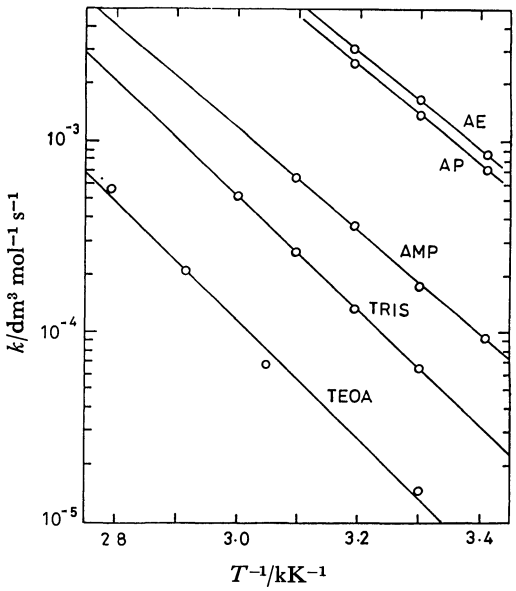

Fig. 3. Arrhenius plots for the amination of CMPS in DMSO.
○: Observed values, ——: calculated values.

The reactions of BC with TEOA in DMF and DMSO and that of CMPS with TEOA in DMSO, all of which proceeded in a homogeneous system, conformed to Eq. 1. The reaction of CMPS with TEOA in DMF exhibited the self-acceleration represented in the form of Eq. 2 up to $\beta=0.5$ with the m value of 0.8. In the process, deposition of the polymer was observed with the progress of the reaction due to cross-linking as reported by Luca *et al.*[7] and Drăgan *et al.*[8] The values of k or k_0, E_a, and A are listed in Table 4. Arrhenius plots for the amination of CMPS are shown in Figs. 2 and 3.

The reaction of CMPS with triethylamine (TEA) was found by the author to follow second-order kinetics in DMF and self-decelerate in DMSO.[1] The difference

Table 2. Amination in DMF

Amine	Chloride	$k\times10^4$/dm^3 mol^{-1} s^{-1}				E_a / kJ mol^{-1}	log A[a]
		293.2 K	303.2 K	313.2 K	323.2 K		
AE	BC	2.53	4.87	9.77		51.5±1.3	5.567±0.217
	CMPS	2.42	4.80	9.05		50.4±0.1	5.363±0.021
AP	BC		4.33	8.43	16.1	54.3±0.5	5.842±0.088
	CMPS	1.82	3.78	7.12		52.1±0.8	5.552±0.139
AMP	BC	0.300	0.635	1.33		56.7±0.5	5.573±0.085
	CMPS	0.205	0.445	0.867		55.0±0.9	5.124±0.150

a) A is expressed by dm^3 mol^{-1} s^{-1}.

Table 3. Amination in DMSO

Amine	Chloride	$k\times10^4$/dm^3 mol^{-1} s^{-1}					$\frac{E_a}{\text{kJ mol}^{-1}}$	log A[a]
		293.2 K	303.2 K	313.2 K	323.2 K	333.2 K		
AE	BC	10.9	21.5	40.2			49.7±0.1	5.898±0.024
	CMPS	8.63	16.6	30.8			48.6±0.1	5.592±0.008
AP	BC	9.85	19.7	37.2			50.7±0.2	6.025±0.027
	CMPS	7.07	13.7	25.7			49.2±0.1	5.619±0.020
AMP	BC	1.42	2.98	5.68			53.0±0.8	5.606±0.134
	CMPS	0.943	1.75	3.62	6.50		51.3±1.0	5.106±0.170
TRIS	BC	0.718	1.51	2.12	5.82		54.6±0.5	5.587±0.084
	CMPS		0.645	1.32	2.63	5.20	58.4±0.5	5.865±0.079

a) A is expressed by dm^3 mol^{-1} s^{-1}.

Table 4. Amination with TEOA in DMF and DMSO

Solvent	Chloride	$k\times10^5$/dm^3 mol^{-1} s^{-1}						$\frac{E_a}{\text{kJ mol}^{-1}}$	log A[a]
		303.2 K	328.2 K	343.2 K	358.2 K	373.2 K	388.2 K		
DMF	BC	0.208	1.24		9.35		54.8	64.3±0.9	5.361±0.145
	CMPS, k_0	0.230	1.77		13.6	35.2	59.8	65.3±1.1	5.625±0.172
DMSO	BC	1.40	7.47	19.5	45.0			57.2±1.0	4.984±0.161
	CMPS	1.48	6.62	21.2	57.3			60.0±2.6	5.454±0.414

a) A is expressed by dm^3 mol^{-1} s^{-1}.

in kinetic behavior between TEOA and TEA, which are both tertiary amines, may be due to the presence of hydroxyl groups in TEOA. The self-acceleration in the reactions of CMPS with amino alcohols in dioxane may be attributed to the formation of the intramolecular hydrogen bond between the hydroxyl group of the already aminated neighbor and the chlorine of the chloromethyl group at the transition state. The formation of the bond does not take place in DMF and DMSO which are much more polar solvents than dioxane. This does not preclude the possibility of the bond formation in DMF in the case of TEOA with three hydroxyl groups. The author suggested that the deceleration during the reaction of CMPS with TEA in DMSO can be ascribed to the electrostatic effect of the quaternary ammonium groups formed in the polymer.[1] In the case of TEOA, pK_a of the quaternary ammonium groups is made to decrease by the hydroxyl groups as described later, so that their electrostatic effect must be insufficient to cause the deceleration.

Reactions of QCMPS in DMSO. The treatment of CMPS with a limited amount of TEOA (equivalent to half the chloromethyl groups) in DMSO yielded the polymer composed of 48 mol% quaternary ammonium groups and 52 mol% chloromethyl groups (QCMPS). QCMPS thus obtained was made to react with the amino alcohols in DMSO at 318 K. The reaction proceeded to completion (β=0.99) in conformity with Eq. 1. The reaction rate constants of QCMPS are compared with those of CMPS in Table 5, which indicates that k of QCMPS (k_{QCMPS}) is two or three times as large as k of CMPS (k_{CMPS}). This may be because the positive charges of the quaternary ammonium groups in QCMPS attract amino alcohol molecules by an ion-dipole interaction thereby increasing the local concentration of amino alcohol and hence increasing the reaction rate.

Table 5. Comparison of amination rate constants, k, in DMSO at 318.2 K between QCMPS and CMPS

Amine	$k\times10^4$/dm^3 mol^{-1} s^{-1}		$\frac{k_{QCMPS}}{k_{CMPS}}$
	QCMPS	CMPS[a]	
AE	74.0	41.3	1.8
AP	66.8	34.5	1.9
AB	18.7	9.25[b]	2.0
AMP	9.20	4.93	1.9
TRIS	5.53	1.87	3.0

a) The k values at 318.2 K computed on the basis of the equation $k=A\exp(-E_a/RT)$, by the use of the E_a and A values given in Table 3. b) E_a=51.08 kJ mol^{-1} and log A=5.350.[2]

Activation Parameters. The activation parameters, ΔH^*, ΔS^*, and ΔG^*, of the reactions of CMPS and BC with the amino alcohols are summarized in Tables 6—8. The difference in ΔG^* between CMPS and BC is generally small. In each solvent, the magnitude of ΔG^* of CMPS or BC depends on the species of amino alcohols, increasing in the following order:

$$\text{AE} < \text{AP} < \text{AB} < \text{AMP} < \text{TRIS} < \text{TEOA}.$$

This order of ΔG^* in each solvent corresponds to the order of ΔH^*; the difference in ΔG^* among the amino alcohols is mainly ascribed to the difference in ΔH^*, since the difference in ΔS^* is slight. It seems that the difference in ΔG^* or ΔH^* is largely due to the structural differences of the amino alcohols in question. Since the pK_a of the amino alcohols composed of monohydric alcohol (AE, PA, AB, and AMP) are similar to each other (refer to the pK_a values in Table 10), the difference in ΔG^* among the amino alcohols is ascribed to the difference in their structures. That is to say, the differ-

TABLE. 6 ACTIVATION PARAMETERS OF THE AMINATION IN DIOXANE AT 298.2 K

Amine	Chloride	$\Delta H^{\ddagger}$ / kJ mol^{-1}	$\Delta S^{\ddagger}$ / J K^{-1}mol^{-1}	$\Delta G^{\ddagger}$ / kJ mol^{-1}
AE	CMPS, k_0	50.1±0.7	−170±2	100.9
AP	BC	53.7±2.0	−162±5	102.1
	CMPS, k_0	52.4±2.6	−166±8	101.9
AB[a)]	BC	53.5±0.4	−169±1	103.9
	CMPS, k_0	54.4±0.3	−168±1	104.5
AMP	BC	58.5±3.0	−162±9	106.8
	CMPS, k_0	56.9±1.2	−167±3	106.6
	k_1	57.4±2.0	−165±6	106.7
	k_2	52.5±3.6	−172±11	103.9

a) The values calculated on the basis of the data in Ref. 3.

TABLE 7. ACTIVATION PARAMETERS OF THE AMINATION IN DMF AT 298.2 K

Amine	Chloride	$\Delta H^{\ddagger}$ / kJ mol^{-1}	$\Delta S^{\ddagger}$ / J K^{-1}mol^{-1}	$\Delta G^{\ddagger}$ / kJ mol^{-1}
AE	BC	49.0±1.3	−147±4	92.7
	CMPS	47.9±0.1	−151±0	92.8
AP	BC	51.0±0.5	−141±2	93.1
	CMPS	49.7±0.8	−147±3	93.5
AB[a)]	BC	53.4±0.2	−144±1	96.4
	CMuS	52.2±1.0	−150±3	96.8
AMP	BC	54.2±0.5	−147±2	97.9
	CMPS	52.6±0.9	−155±3	98.8
TEOA	BC	61.8±0.9	−151±3	106.7
	CMPS, k_0	62.8±1.1	−146±3	106.3

a) The values calculated on the basis of the data in Ref. 2.

TABLE 8. ACTIVATION PARAMETERS OF THE AMINATION IN DMSO AT 298.2 K

Amine	Chloride	$\Delta H^{\ddagger}$ / kJ mol^{-1}	$\Delta S^{\ddagger}$ / J K^{-1}mol^{-1}	$\Delta G^{\ddagger}$ / kJ mol^{-1}
AE	BC	47.3±0.1	−140±1	89.1
	CMPS	46.1±0.0	−146±0	89.7
AP	BC	48.2±0.2	−138±1	89.3
	CMPS	46.8±0.1	−146±0	90.2
AB[a)]	BC	50.0±0.6	−144±2	92.9
	CMPS	48.6±0.7	−151±2	93.6
AMP	BC	50.6±0.8	−146±3	94.1
	CMPS	48.9±1.0	−156±3	95.2
TRIS	BC	52.2±0.5	−146±2	95.8
	CMPS	55.9±0.5	−141±2	98.0
TEOA	BC	54.7±1.0	−158±3	101.8
	CMPS	57.5±2.6	−149±8	101.9

a) The values calculated on the basis of the data in Ref. 2.

ence in the branching structure of the hydroxyalkyl group may produce the difference in the steric hindrance of the benzene ring to the group in the transition state. Kawabe and Yanagita[9] reported on this kind of structural effect on $\Delta G^{\ddagger}$ in regard to the reactions of CMPS and BC with butylamine isomers in DMF; $\Delta G^{\ddagger}$ increases in the following order: butylamine< isobutylamine<*s*-butylamine<*t*-butylamine. The higher $\Delta G^{\ddagger}$ values for TRIS and TEOA may be ascribed not only to their increased steric hindrance but also to their decreased basicity, as indicated by the lower pK_a values (refer to the pK_a values in Table 10). Both $\Delta H^{\ddagger}$ and $\Delta S^{\ddagger}$ values of CMPS are lower than those of BC for the amino alcohols composed of a monohydric alcohol, while the $\Delta H^{\ddagger}$ and $\Delta S^{\ddagger}$ values of CMPS are higher than those of BC for the amino alcohols with three hydroxyl groups, TRIS and TEQA.

Review of Tables 6—8 with respect to the solvent effect on the activation parameters reveals that for each amino alcohols examined, $\Delta G^{\ddagger}$ is higher in dioxane than in DMF due to higher $\Delta H^{\ddagger}$ and lower $\Delta S^{\ddagger}$ in the former. The fact that $\Delta G^{\ddagger}$ is higher in DMF than in DMSO is mainly due to the higher $\Delta H^{\ddagger}$ in the former. The author reported a similar solvent effect for primary alkylamines such as butylamines[9,10] and for amino alcohols such as AB[2] and diethanolamine.[11]

It is to be noted that $\Delta G^{\ddagger}$ is a linear function of the electrostatic factor of the solvent, EF, for the amination of CMPS and BC with AE, AP, AB, and AMP, and the slopes of the lines range (−0.52)—(−0.61); EF is the product of dielectric constant, ε, and dipole moment, μ. It takes on values of 1 for dioxane, 140 for DMF, and 209 for DMSO.[12] The plots of $\Delta G^{\ddagger}$ against the Hildebrand solubility parameter, δ, or against δ^2, are also approximately linear; the δ values were calculated on the basis of the equation, $\delta=[(\Delta H^{v}-RT)\rho/M]^{1/2}$, where ΔH^{v} is the heat of vaporization of a solvent with molecular weight M and density ρ, taken to be 40.3 for dioxane, 49.3 for DMF and 54.4 kJ$^{1/2}$ dm$^{-3/2}$ for DMSO at T=298.2 K.[13] However, the plot of $\Delta G^{\ddagger}$ against $1/\varepsilon$ or $(\varepsilon-1)/(2\varepsilon+1)$ is not linear. These results, in addition to the dependence of the change in $\Delta G^{\ddagger}$ on the change in $\Delta H^{\ddagger}$ and $\Delta S^{\ddagger}$ mentioned above, suggest that the solute-solvent interactions, notably the solvation of the activated complex, are controlling factor of the rate of the amination of CMPS or BC.

Comparison of the activation parameters of CMPS with those of BC in Tables 6—8 shows the polymer effects described below, where the difference in the activation parameters ($\Delta X^{\ddagger}$: $\Delta H^{\ddagger}$, $\Delta S^{\ddagger}$, $\Delta G^{\ddagger}$) between CMPS and BC is represented by $\delta\Delta X^{\ddagger}(=\Delta X_{\mathrm{CMPS}}-\Delta X_{\mathrm{BC}})$:

(1) $\delta\Delta H^{\ddagger}$ are negative for the reactions with the amino alcohols composed of a monohydric alcohol (AE, AP, AB, and AMP) in dioxane, DMF and DMSO ($-\delta\Delta H^{\ddagger}$=1—2 kJ). This is also the case with the reactions with primary, secondary, and tertiary alkylamines such as butylamines,[9,10] diethylamine,[11] and TEA.[1] Negative $\delta\Delta H^{\ddagger}$ values may due to some energetic interactions between the polymer skeleton and the alkyl or hydroxyalkyl group of the amine or amino alcohol molecule at the transition state.

(2) The reactions with the amino alcohols and alkylamines described in paragraph (1) above all exhibit negative values of $\delta\Delta S^{\ddagger}$ in DMF and DMSO ($-T\delta\Delta S^{\ddagger}$=1—3 kJ). In DMF and DMSO, the solvation of the activated complex is an important factor in determining the amination rate of CMPS or BC, and this solvation works to decrease $\Delta G^{\ddagger}$ in DMF and DMSO. The negative value of $\delta\Delta S^{\ddagger}$ in DMF and

DMSO appears to have resulted from the steric hindrance to the solvation in the polymer. This is evident from the results of the author's study[10,14] on the reactions with AB and the butylamines, isobutylamine and *s*-butylamine, in DMF-dioxane binary system, which showed that $T\Delta S^{*solv}$ (ΔS^{*solv}: the entropy of the solvation of the activated complex) of CMPS was lower some 2 kJ than that of BC. The $\delta\Delta G^*$ values of all these reactions in DMF and DMSO are slightly positive, since the $T\delta\Delta S^*$ values are lower than the $\delta\Delta H^*$ values. On the other hand, the $\delta\Delta G^*$ are zero or otherwise slightly on the negative side in dioxane, since its solvation effect is much smaller than that of DMF or DMSO.

(3) The reactions with TEOA and TRIS in DMSO and the one with TEOA in DMF are characterized by the positive values of both $\delta\Delta H^*$ and $\delta\Delta S^*$; the magnitudes of $\delta\Delta H^*$ and $\delta\Delta S^*$ in DMSO are greater than those in DMF. Both amino alcohols contain three hydroxyl groups and it is expected that they are strongly solvated in DMF and DMSO. Considering that both ΔH^* and ΔS^* of CMPS are higher than the respective values of BC, it is quite reasonable to assume that the desolvation is required for the activated complex to form in the polymer.

Elementary Analysis of the Polyelectrolytes. The polymers obtained by the reaction of CMPS with the amino alcohols (AMPS) were dialysed in diluted hydrochloric acid and lypophylized. The composition of AMPS is represented by:

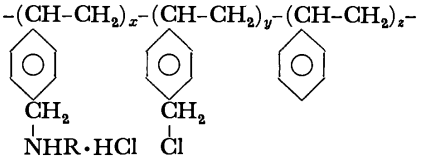

where –NHR represents the amino alcohol residue composed of secondary amino group and the residue is assumed to form monohydrochloride. The reaction of CMPS with TEOA produces the quaternary ammonium chloride residue ($-NR_3Cl$). The mole fractions, x, y, and z, were determined by the following equations:

$$\left.\begin{aligned} x &= r_c r_a \\ y &= r_c(1-r_a) \\ z &= 1-r_c \end{aligned}\right\}, \qquad (7)$$

where r_c is a fractional conversion in the chloromethylation of polystyrene and r_a that in the amination of CMPS. The mole fractions were $x=0.97$, $y=0.01$, and $z=0.02$ for all the AMPS polymers shown in Table 9, in which the data of elementary analysis are listed.

The best agreement of the found and calculated values in Table 9 is shown for the reaction product from TEOA. The agreement is fairly good for the other AMPS polymers, though the found nitrogen content is a little lower than the calculated one for the AMPS polymers from EA and PA. The result suggests that the reaction of CMPS with the amino alcohols scarcely induce such a side reaction as an intramolecular reaction of the chloromethyl groups with the neighboring amino alcohol residues in the polymer.

Acid-Base Equilibria of the Polyelectrolytes. A 50 ml acidic solution of AMPS containing about 0.15 mmol amino alcohol residues was titrated with a standard sodium hydroxide solution (1/10 mol dm^{-3}). The titration curves of the AMPS polymers containing AB, AMP, TRIS, and TEOA residues are shown in Fig. 4. The titration curve of the AMPS polymer containing AB residues in the absence of salt gives an inflection point at a higher pH range, and another inflection point is observed in a lower pH range in the presence of salt (Fig. 4A). The acid-base equilibria of the AB residues are represented by the titration curves in a region between the two inflection points. Similar titration curves were obtained for the AMPS polymers

TABLE. 9 ELEMENTARY ANALYSIS OF THE POLYELECTROLYTES PRODUCED BY THE AMINATION OF CMPS[a,b]

Amine		C(%)	H(%)	N(%)	Cl(%)	O(%)
AE	Found	61.88	6.95	5.40	19.61	6.16
	Calcd	62.21	7.54	6.43	16.47	7.35
AP	Found	64.71	7.43	5.04	17.05	5.76
	Calcd	63.62	7.96	6.05	15.47	6.91
AB	Found	67.91	7.95	5.43	12.50	6.21
	Calcd	64.89	8.31	5.69	14.60	6.50
AMP	Found	66.05	7.22	5.63	14.68	6.43
	Calcd	64.88	8.33	5.74	14.58	6.52
TRIS	Found	61.81	7.06	4.52	11.15	15.47
	Calcd	57.32	7.37	5.08	12.85	17.39
TEOA	Found	60.87	7.60	4.43	11.91	15.18
	Calcd	60.02	8.00	4.57	11.74	15.67

a) The found values are the ones corrected for water contents. b) The calculated values are the ones calculated on the basis of the fractional conversions by means of Eq. 7.

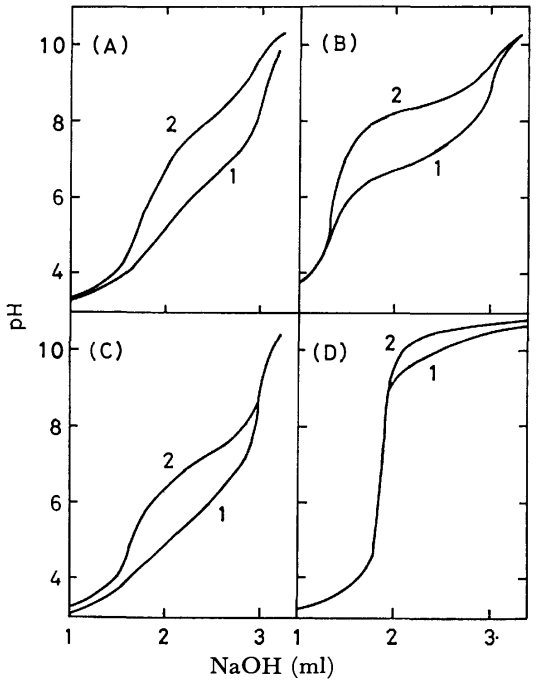

Fig. 4. Titration curves of the polyelectrolytes (AMPS) produced by the amination of CMPS with (A) AB, (B) AMP, (C) TRIS, and (D) TEOA.
Curve 1: In the absence of salt, Curve 2: in the presence of NaCl (1 mol dm^{-3}).

prepared from AE and AP. Since the pK_a of AMP residue is higher than that of AB residue, the titration curve in the absence of salt in Fig. 4B has two inflection points. In contrast, the curve in the presence of salt in Fig. 4C has two inflection points due to the fact that the pK_a of TRIS residue is lower than that of the AB residue. On the other hand, the inflection point does not appear in Fig. 4D in a higher pH range, as expected from the fact that TEOA produces a strong basic quaternary ammonium residue.

The acid-base equilibria of these AMPS polymers, except for the one from TEOA, can be described by the modified Henderson-Hasselbach equation:

$$pH = pK_m - n'(1-\alpha_i)/\alpha_i, \quad (8)$$

where α_i is the degree of dissociation of the conjugated acid of the amino alcohol residue, n' is a constant, and pK_m is the pK_a value at $\alpha_i=0.5$. The results are summarized in Table 10, where the pK_a values of the amino alcohols are also listed. The values of n' were 1.8—2.0 in the absence of salt and 1.5—1.7 in the presence of salt, except for the polymer from AMP (n' was close to unity). The addition of sodium chloride (1 mol dm^{-3} concentration) weakens the electrostatic field effect and pK_m becomes higher ($\Delta pK_m=1.1$—1.6). The difference between the pK_a value of an amino alcohol and the pK_m value of the corresponding AMPS in the presence of the salt becomes smaller in the following order: AE>AP>AB>AMP>TRIS ($\Delta pK=pK_a-pK_m=1.7$—1.2). Since this order is related to the branching structure of the amino alcohol residue, it may be that the branching structure has the shielding effect on the electrostatic interaction or that it lowers the local dielectric constant around the amino group thereby decreasing the effective charge of the the charged group. The reason that the pK_m value of AMPS does not agree with the pK_a value of the corresponding amino alcohol is to certain extent explained by the amino alcohol residue being combined with the benzyl group. pK_a are found in certain cases to decrease by about unity due to the effect of the benzyl group.[15] The pK_m of the TEOA residue is greater than the pK_a value of TEOA, because TEOA combines with the benzyl group to form the strong basic quaternary ammonium group. Neverthless, the pK_a of the TEOA quaternary ammonium residue is lower than that of the TEA quaternary ammonium residue ($pK_m>11$) because of the inductive effect of the hydroxyl groups in the former residue. Table 10 also lists the pK_m values of QAMPS or the amino alcohol residues of the reaction products of QCMPS and the amino alcohols in the presence of salt. They are found to be practically identical with those of AMPS.

TABLE 10. THE pK VALUES OF THE AMINO ALCOHOLS AND THE POLYELECTROLYTES

Aminoalcohol		AMPS		QAMPS
Species	pK_a	(No salt)[a] pK_m	(Salt)[b] pK_m	(Salt)[b] pK_m
AE	9.49	6.63	7.77	7.43
AP	9.43	6.31	7.62	7.20
AB	9.23	6.10	7.73	7.69
AMP	9.69	7.00	8.37	8.21
TRIS	8.15	5.53	6.94	—
TEOA	7.86	>10	>10	—

a) The values in the absence of added salt. b) The values in the presence of 1 mol dm^{-3} sodium chloride.

The author wishes to express his thanks to Dr. Masaya Yanagita for his valuable discussions. He is also grateful to Mr. Yukio Uesugi and Mr. Masayuki Kamiya for their helpful assistance in carrying out the measurements.

References

1) Group Interactions in Polyelectrolytes. XIV. For Part XIII: H. Kawabe, *Bull. Chem. Soc. Jpn.*, **54**, 1914 (1981).
2) H. Kawabe and M. Yanagita, *Bull. Chem. Soc. Jpn.*, **46**, 38 (1973).
3) H. Kawabe and M. Yanagita, *Bull. Chem. Soc. Jpn.*, **44**, 896 (1971).
4) S. Drăgan, I. Petrariu, and M. Dima, *J. Polym. Sci., Polym. Chem. Ed.*, **10**, 3077 (1972).
5) C. Luca, I. Petrariu, and M. Dima, *J. Polm. Sci., Polym. Chem. Ed.*, **17**, 3879 (1979).
6) H. Kawabe and M. Yanagita, *Bull. Chem. Soc. Jpn.*, **41**, 1518 (1968).
7) C. Luca, S. Drăgan, V. Bărboiu, and M. Dima, *J. Polym. Sci., Polym. Chem. Ed.*, **18**, 449 (1980).
8) S. Drăgan, C. Luca, I. Petrrariu, and M. Dima, *J. Polym. Sci., Polym. Chem. Ed.*, **18**, 455 (1980).
9) H. Kawabe and M. Yanagita, *Bull. Chem. Soc. Jpn.*, **46**, 3627 (1973).
10) H. Kawabe, *Bull. Chem. Soc. Jpn.*, **48**, 163 (1975).
11) H. Kawabe, *Bull. Chem. Soc. Jpn.*, **47**, 2936 (1974).
12) M. R. J. Dack, "The Influence of Solvent on Chemical Reactivity," in "Techniques of Chemistry," ed by A. Weissberger, Wiley-Interscience, New York (1976), Vol. 8 ("Solution and Solubilities," ed by M. R. J. Dack), Part II, Chap. 11, p. 100.
13) The δ values were estimated on the basis of published ΔH^v data in J. A. Riddick and W. B. Bunger "Organic Solvents," in "Technique of Chemistry," 3rd ed, ed by A. Weissberger, Wiley-Interscience, New York (1970), Vol. 2.
14) H. Kawabe, *Bull. Chem. Soc. Jpn.*, **49**, 2043 (1976).
15) For instance, the difference of pK_a between methylamine and *N*-methylbenzylamine is nearly unity.

  Bull. Chem. Soc. Jpn., 54, 2893—2897 (1981)

Effect of Pressure on Charge-transfer Spectra and Equilibria in Solutions of Tetracyanoethylene and Styrene Derivatives

Yasuhiro UOSAKI, Masaru NAKAHARA,* Muneo SASAKI, and Jiro OSUGI

Department of Chemistry, Faculty of Science, Kyoto University, Oiwake-cho, Kitashirakawa, Sakyo-ku, Kyoto 606

(Received May 11, 1981)

Charge-transfer spectra of *trans*-stilbene–, *cis*-stilbene–, 1,1-diphenylethylene–, and α-methylstyrene–TCNE mixtures in chloroform and in 1,2-dichloroethane have been measured at high pressures at 25 °C. The spectra shifted to a lower energy (red shift) with increasing pressure, the two bands in each complex shifting almost in parallel to each other. The shifts are qualitatively interpreted by McRae's theory. The spectral changes in intensity with pressure was analyzed taking account of reversible formation of the EDA complex and 1,4-cycloadduct; only the complex was formed in the stilbene systems. Volume changes for the complex formation are in the range of −4 to −7 $cm^3\ mol^{-1}$ and those for the cycloaddtion are in the range of −23 to −30 $cm^3\ mol^{-1}$. The latter slightly increase in magnitude when solvent is changed from chloroform to a more polar solvent, 1,2-dichloroethane.

Disappearance of red color in dichloromethane solution of styrene and tetracyanoethylene (TCNE) was discovered at a high pressure of about 8 kbar (1 bar=0.1 MPa) half a decade ago.[1] The observation has led to finding a new 1,4-cycloaddition between styrene and TCNE with the aid of the quenching method; the electron-donor-acceptor (EDA) complex is transformed to the cycloadduct by the application of pressure.[2,3] Effects of substituents in styrene, solvent polarity, and temperature on the found 1,4-cycloaddition have been investigated to elucidate the reaction mechanism from a kinetic point of view in a series of papers.[4-6] A short paper has been published where effect of pressure on the 1,4-cycloaddition between α-methylstyrene and TCNE in 1,2-dichloroethane is studied.[7] In the present paper, charge-transfer (CT) spectra of *trans*-stilbene–, *cis*-stilbene–, 1,1-diphenylethylene–, and α-methylstyrene–TCNE mixtures in chloroform and in 1,2-dichloroethane have been taken at high pressures and spectral changes in intensity are analyzed by taking account of chemical equilibria involved in each system. The pressure effect allows us to know the volume change accompanying the reversible 1,4-cycloaddition without measuring the partial molal volumes of the reactants and product; in this case, direct density measurements can not be carried out on the product because it is not isolated. The large effect of pressure on the 1,4-cycloaddition is well established here; a decrease of 10—12% in volume accompanies the cycloaddition where two bonds are formed between the component molecules.

Experimental

TCNE, α-methylstyrene, 1,1-diphenylethylene, and *trans*- and *cis*-stilbenes were purified by the method described elsewhere.[3] Solvents were purified by the standard method.

Electronic absorption spectra were recorded on a Shimadzu UV-200S spectrophotometer at 1 bar and on a Union Giken RA-405 spectrophotometer at high pressure. All the other apparatuses and procedures for spectroscopic measurements at high pressure were the same as those in the previous work.[3]

The formation constants for the EDA complex and 1,4-cycloadduct were determined from absorbance of the EDA complex at the first charge-transfer band at each pressure at 25°C. The temperature was regulated to ±0.1 °C and the pressure was measured within ±1%. The concentration of the donor was always much larger than that of TCNE. The concentrations of the donor and the acceptor at high pressure were corrected for compression by using the Tait equation for the solvents.[8]

The partial molal volumes of α-methylstyrene in several solvents were determined by the method described in the previous work.[6]

Results and Discussion

Charge-transfer Spectra. Some typical electronic absorption spectra of the complexes studied here in the visible region are shown in Figs. 1—4 as a function of pressure. Two kinds of intermolecular charge-transfer transitions occur in each complex, while in Figs. 2 and 3, the second transition band lying at a higher energy is markedly obscured by the absorption due to the donor. The band multiplicity can arise from electron donation from the two highest occupied levels in the donor or from electron acceptance at the two lowest unoccupied levels in the acceptor.[9] The latter is not the case in the complexes of TCNE with these styrenes, because the difference in energy between the maxima ($\tilde{\nu}_{max,1}$ and $\tilde{\nu}_{max,2}$) of the first and second bands is dependent on the

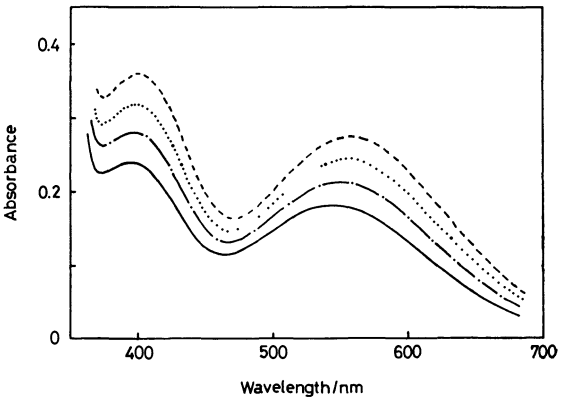

Fig. 1. Absorption spectra of TCNE complex with *cis*-stilbene in chloroform at 25°C at various pressures.
$[D]_0=0.1160$ mol dm^{-3}; $[A]_0=5.184\times10^{-3}$ mol dm^{-3} at 1 bar; $l=0.506$ cm.
——, 1 bar; —·—, 500 bar; ····, 1000 bar; -----, 1500 bar.

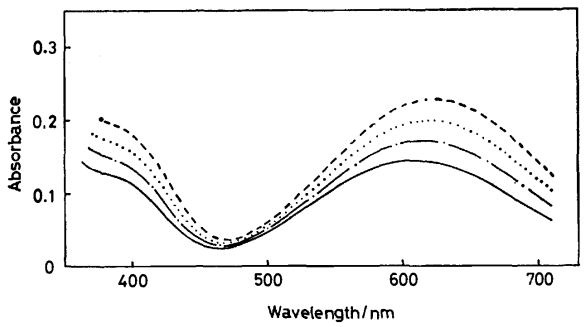

Fig. 2. Absorption spectra of TCNE complex with *trans*-stilbene in chloroform at 25°C at various pressures.
$[D]_0=0.1034$ mol dm^{-3}; $[A]_0=2.436\times10^{-3}$ mol dm^{-3} at 1 bar; $l=0.587$ cm.
——, 1 bar; —·—, 500 bar; ····, 1000 bar; -----, 1500 bar.

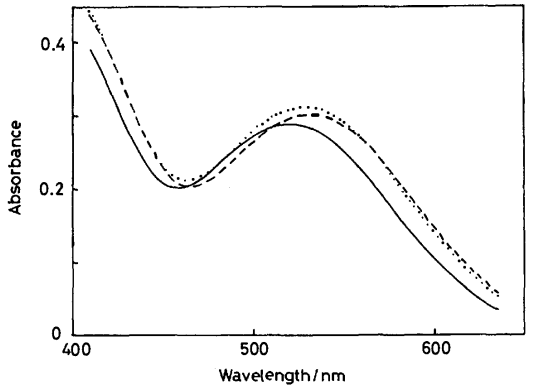

Fig. 3. Absorption spectra of TCNE complex with 1,1-diphenylethylene in chloroform at 25°C at various pressures.
$[D]_0=0.2409$ mol dm^{-3}; $[A]_0=5.184\times10^{-3}$ mol dm^{-3} at 1 bar; $l=0.551$ cm.
——, 1 bar; ····, 1000 bar; ------, 1500 bar.

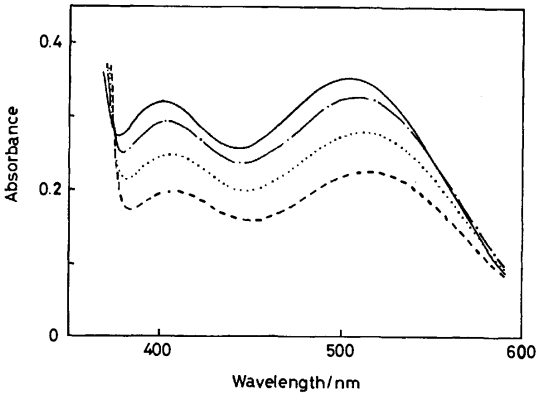

Fig. 4. Absorption spectra of TCNE complex with α-methylstyrene in chloroform at 25°C at various pressures.
$[D]_0=0.3283$ mol dm^{-3}; $[A]_0=4.809\times10^{-3}$ mol dm^{-3} at 1 bar; $l=0.525$ cm.
——, 1 bar; —·—, 500 bar; ····, 1000 bar; -----, 2500 bar.

donors.[10,11] Each band maximum shifts toward a lower energy (red shift) with increasing pressure, as found in other EDA complexes.[12] The frequency shifts between 1 and 1500 bar are in the range of −200 to −400 cm^{-1} kbar^{-1}. Causes for the red shift are pressure-induced increases in the refractive index and dielectric constant of the solvent according to McRae's theory.[13] The excited state much polar than the ground state is stabilized more at higher pressures, and as a result, the energy gap between the ground and excited states is reduced to some extent by pressure. The difference between $\tilde{\nu}_{max,1}$ and $\tilde{\nu}_{max,2}$ is independent of pressure within an experimental uncertainty of 10^2 cm^{-1} as follows; $(\tilde{\nu}_{max,2}-\tilde{\nu}_{max,1})/10^2$ cm^{-1} in chloroform at 1, 500, 1000, and 1500 bar are 68.3, 68.4, 69.4, and 69.8 for the *cis*-stilbene complex and 50.3, 49.7, 50.6, and 50.5 for α-methylstyrene complex, respectively. A similar behavior is found for the biphenyl–TCNE complex, while the two bands of the naphthalene–TCNE complex are reported to behave differently from each other.[14] In that case, existence of isomeric forms of the complex is proposed on the basis of the nonparallel shifts, but the present result of the parallel shifts of the two bands suggest some similarity in polarity between the excited states of the first and second bands.[15]

Spectral Intensities and Chemical Equilibria. An increase, a decrease, and a complicated variation in absorbance with increasing pressure are observed in the solutions of stilbenes (Figs. 1 and 2), α-methylstyrene (Fig. 4), and 1,1-diphenylethylene (Fig. 3), respectively. The increase is due to the formation of the EDA complex promoted by pressure and the decrease is caused by the transformation of the complex to the 1,4-cycloadduct which is promoted by pressure more than the complex formation. Thus, the following reversible reactions,

$$D + A \overset{K_c}{\rightleftharpoons} \text{EDA Complex} \qquad (1)$$

and

$$D + A \overset{K_c}{\rightleftharpoons} \text{EDA Complex} \overset{K_1}{\rightleftharpoons} P \qquad (2)$$

occur in solutions of TCNE with stilbenes and in those with α-methylstyrene and 1,1-diphenylethylene, respectively.[4] Here, D, A, and P denote the donor, the acceptor, and the 1,4-cycloadduct, respectively, and K_c and K_1 are, respectively, expressed by

$$K_c = \frac{[EDA]}{[D][A]} \qquad (3)$$

and

$$K_1 = \frac{[P]}{[EDA]}, \qquad (4)$$

where the square brackets indicate the concentration of each species. The equilibrium constants in Eqs. 3 and 4 can be determined, respectively, by the Scott equations

$$\frac{[D]_0[A]_0 l}{A_e} = \frac{1}{K_c\varepsilon_{max}} + \frac{1}{\varepsilon_{max}}[D]_0 \qquad (5)$$

and

$$\frac{[D]_0[A]_0 l}{A_e} = \frac{1}{K_c\varepsilon_{max}} + \frac{1+K_1}{\varepsilon_{max}}[D]_0, \qquad (6)$$

where $[D]_0$ and $[A]_0$ are the initial concentration of the

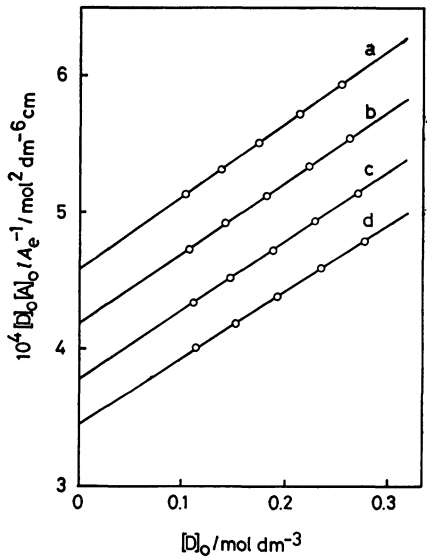

Fig. 5. Scott plots for *trans*-stilbene–TCNE system in chloroform at 25°C at various pressures.
(a), 1 bar; (b), 500 bar; (c), 1000 bar; (d), 1500 bar.

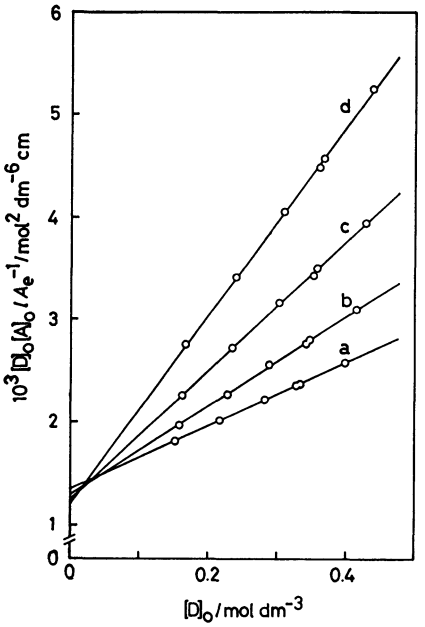

Fig. 6. Scott plots for α-methylstyrene–TCNE system in chloroform at 25°C at various pressures.
(a), 1 bar; (b), 500 bar; (c), 1000 bar; (d), 1500 bar.

Table 1. Formation constants (K_c/mol^{-1} dm^3) of EDA complexes in chloroform at 25 °C at various pressures

Donor	P/bar			
	1	500	1000	1500
trans-Stilbene[a]	1.16	1.23	1.34	1.42
cis-Stilbene[b]	0.415	0.424	0.467	0.493
α-Methylstyrene[c]	0.422	0.443	0.452	0.466
1,1-Diphenylethylene[d]	0.312	0.329	0.353	0.369

a) ε_{max} is 1880, 1940, 1960, and 2040 mol^{-1} dm^3 cm^{-1} at 1, 500, 1000, and 1500 bar, respectively. b) ε_{max} is 1950, 2090,2050, and 2100 mol^{-1} dm^3 cm^{-1} at 1, 500, 1000, and 1500 bar, respectively. c) ε_{max} is taken to be 1760 mol^{-1} dm^3 cm^{-1} from Ref. 4. d) ε_{max} is taken to be 1660 mol^{-1} dm^3 cm^{-1} from Ref. 4.

donor and acceptor, respectively, l is the path length (0.5—0.6 cm), A_e is the equilibrium absorbance at $\tilde{\nu}_{max.1}$, and ε_{max} is the molar absorption coefficient.

When spectra in the *trans*-stilbene–TCNE system like those in Fig. 2 are measured at high pressures over a wide range of $[D]_0$, the left-hand side of Eq. 5 can be plotted against $[D]_0$ as shown in Fig. 5. The plots are linear at each pressure and provide K_c and ε_{max} from their slopes and intercepts (see Eq. 5). Similar plots are obtained in the *cis*-stilbene–TCNE system. The results are summarized in Table 1 as a function of pressure; actually, the formation constants increase with increasing pressure.

Figure 6 illustrates plots of the left-hand side of Eq. 6 against $[D]_0$ for the α-methylstyrene–TCNE system in chloroform; the intercept, $1/(K_c\varepsilon_{max})$ becomes smaller and the slope, $(1+K_1)/\varepsilon_{max}$ becomes larger as pressure increases, both K_c and K_1 increasing with pressure. Similar plots are obtained for the α-methylstyrene–TCNE system in 1,2-dichloroethane and for the 1,1-diphenylethylene–TCNE system in chloroform and in 1,2-dichloroethane. We can not determine the pressure dependence of ε_{max} in the present case where the two kinds of equilibria are involved. Hence, we use the values of ε_{max} at 1 bar[4,6] to determine the values of K_c and K_1 at high pressures. The determined values of K_c and K_1 are listed in Tables 1 and 2 and 3 and 4, respectively. The values of K_c/mol^{-1} dm^3 and K_1 at 1 bar for the α-methylstyrene–TCNE system in chloroform are comparable with those obtained by a kinetic method,[4] 0.436 and 4.12, respectively, and the values in 1,2-dichloroethane with 0.084 and 11.6,[6] respectively. The values of K_c/mol^{-1} dm^3 at 1 bar for the 1,1-diphenylethylene–TCNE system in chloroform is in reasonable agreement with the kinetically determined one, 0.306, whereas the K_1 value is smaller than that determined kinetically, 3.51 for some unknown reason.[4]

Volume Changes for Reactions. Volume change

Table 2. Formation constants (K_c/mol^{-1} dm^3) of EDA complexes in 1, 2-dichloroethane at 25 °C at various pressures

Donor	P/bar					
	1	300	600	900	1200	1500
α-Methylstyrene[a]	0.094	0.097	0.101	0.104	0.117	0.126
1,1-Diphenylethylene[b]	0.072	0.075	0.078	0.081	0.084	0.087

a) ε_{max} is taken to be 3330 mol^{-1} dm^3 cm^{-1} from Ref. 6. b) ε_{max} is taken to be 3000 mol^{-1} dm^3 cm^{-1}.

Table 3. Formation constants (K_1) of 1,4-cycloadducts in chloroform at 25 °C at various pressures

Donor	P/bar			
	1	500	1000	1500
α-Methylstyrene	4.44	6.67	10.0	15.1
1,1-Diphenylethylene	2.15	2.90	4.35	6.11

Table 4. Formation constants (K_1) of 1,4-cycloadducts in 1,2-dichloroethane at 25 °C at various pressures

Donor	P/bar					
	1	300	600	900	1200	1500
α-Methylstyrene	10.8	14.1	18.3	23.2	30.1	39.5
1,1-Diphenylethylene	2.91	4.26	6.08	7.90	10.3	13.1

(ΔV_c) accompanying the EDA-complex formation and that (ΔV_1) for the 1,4-cycloaddition are determined from the thermodynamic relation,

$$\left(\frac{\partial \ln K}{\partial P}\right)_T = -\frac{\Delta V}{RT} + \Delta m \cdot \kappa, \qquad (7)$$

where R, K, P, T, ΔV, Δm, and κ are the gas constant, the equilibrium constant (K_c or K_1), the pressure, the temperature, the volume change (ΔV_c or ΔV_1), the change in the molecular number for the reaction ($\Delta m = -1$ for K_c and 0 for K_1), and the isothermal compressibility of the solvent, respectively. Plots of ln K *vs.* P are linear within the experimental error in every case. Typical plots for α-methylstyrene–TCNE system in chloroform are shown in Fig. 7. The values of ΔV_c and ΔV_1 obtained thus are given in Table 5, where the volume changes, $\Delta V_R = \Delta V_c + \Delta V_1$, for the overall reactions from the donor and the acceptor in the two solvents are included.

The volume changes accompanying the complex formation are in the range of −4 to −7 cm³ mol⁻¹.

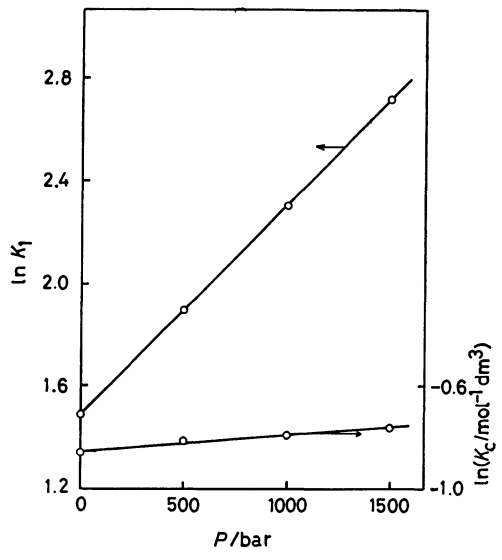

Fig. 7. Plots of ln K *vs.* P for α-methylstyrene–TCNE system in chloroform at 25°C.

Table 5. Volume changes (ΔV_c, ΔV_1, and ΔV_R/cm³ mol⁻¹) in chloroform at 25 °C

Donor	ΔV_c	ΔV_1	ΔV_R
trans-Stilbene	−5.8±1.9	—	—
cis-Stilbene	−5.4±0.5	—	—
α-Methylstyrene	−4.0±0.2	−20±1	−24±1
	(−6.9±0.6)[a]	(−21±1)[a]	(−28±1)[a]
1,1-Diphenylethylene			
	−5.2±0.2	−18±1	−23±1
	(−5.1±0.0)[a]	(−25±1)[a]	(−30±1)[a]

a) In 1,2-dichloroethane.

The relatively small negative values are found also for other TCNE complexes.[12,16] There is no general correlation between ΔV_c and $-RT \ln K_c$ in the series of donors studied here.

The reaction volumes(ΔV_R) for the 1,4-cycloadditions studied in the present work are comparable with those reported so far for many other 1,4-cycloadditions (−30 to −40 cm³ mol⁻¹).[17] The difference (4—7 cm³ mol⁻¹) in ΔV_R between chloroform and 1,2-dichloroethane is probably due to the polarity of the adduct for the following reason. The partial molal volume of α-methylstyrene varies little in the solvent used here; its value at 25 °C is 132.5±0.3, 132.3±0.3, 131.3±0.3, and 130.8±0.1 cm³ mol⁻¹ in 1,2-dichloroethane, dichloromethane, chloroform, and carbon tetrachloride, respectively. The partial molal volume of TCNE sparlingly soluble in these solvents are 107, 107, and 106 cm³ mol⁻¹ in 1,2-dichloroethane, dichloromethane, and carbon tetrachloride, respectively.[6,18] Thus, the partial molal volumes of the donor and the acceptor depend little on solvent polarity in these solvents. It is clarified in the previous paper[6] that the cycloadduct has a relatively large dipole moment as a result of the symmetry breakdown in the TCNE moiety. In consequence, the partial molal volume of the polar adduct is expected to be smaller in 1,2-dichloroethane than in chloroform. If this is the case, the reaction volume becomes larger in magnitude in 1,2-dichloroethane than in chloroform as observed.

References

1) M. Nakahara, Y. Tsuda, M. Sasaki, and J. Osugi, *Chem. Lett.*, **1976**, 731.
2) M. Nakahara, Y. Uosaki, M. Sasaki, and J. Osugi, *Rev. Phys. Chem. Jpn.*, **47**, 119 (1977).
3) M. Nakahara, Y. Uosaki, M. Sasaki, and J. Osugi, *Bull. Chem. Soc. Jpn.*, **53**, 3395 (1980).
4) Y. Uosaki, M. Nakahara, and J. Osugi, *Bull. Chem. Soc. Jpn.*, **54**, 2569(1981).
5) Y. Uosaki, M. Nakahara, and J. Osugi, *Bull. Chem. Soc. Jpn.*, submitted.
6) Y. Uosaki, M. Nakahara, and J. Osugi, *Bull. Chem. Soc. Jpn.*, in press.
7) Y. Uosaki, M. Nakahara, M. Sasaki, and J. Osugi, *Chem. Lett.*, **1979**, 727.
8) D. M. Newitt and K. E. Weale, *J. Chem. Soc.*, **1951**, 3092.
9) R. Foster, "Organic Charge-Transfer Complexes," Academic Press, London (1969).

10) T. Matsuo and H. Aiga, *Bull. Chem. Soc. Jpn.*, **41**, 271 (1968).
11) J. Bendig, B. Dobslaw, D. Kreysig, and J. Sauer, *J. Prakt. Chem.*, **318**, 618 (1976).
12) A. H. Ewald, *Trans. Faraday Soc.*, **64**, 733 (1968).
13) E. G. McRae, *J. Phys. Chem.*, **61**, 562 (1957).
14) J. R. Gott and A. I. Maisch, *J. Chem. Phys.*, **39**, 2229 (1963).
15) When we apply McRae's theory[13] to the two bands under the same conditions, we can expect cancellation of the dispersion term *etc.* and also neglect of the dipole moment of the ground state much smaller than the dipole moment (μ_E) of the excited state. In the present case, therefore, McRae's formula is simplified as

$$\{\tilde{\nu}_{max,2}(P)-\tilde{\nu}_{max,1}(P)\} - \{\tilde{\nu}_{max,2}(1)-\tilde{\nu}_{max,1}(1)\} = -\frac{\mu_{E,2}^2-\mu_{E,1}^2}{hca^3}\cdot\frac{n(P)^2-n(1)^2}{\{2n(P)^2+1\}\{2n(1)^2+1\}},$$

where $n(P)$ is the refractive index of the solvent at pressure P, h is Planck's constant, c is the velocity of light, and a is the effective radius of the complex. The above equation shows that if the left-hand side is zero, $\mu_{E,2}$ is equal to $\mu_{E,1}$.

16) T. Nakayama, *Rev. Phys. Chem. Jpn.*, **49**, 25, (1979).
17) T. Asano and W. J. le Noble, *Chem. Rev.*, **78**, 407 (1978).
18) F. K. Fleischmann and H. Kelm, *Tetrahedron Lett.*, **1973**, 3733.

The DV-Xα MO Study of the Electronic Structures of $[M(CN)_6]^{3-}$ (M=Cr, Mn, Fe, and Co) and $[Fe(CN)_6]^{4-}$

Mitsuru SANO,** Hirohiko ADACHI,† and Hideo YAMATERA*

Department of Chemistry, Faculty of Science, Nagoya University, Chikusa-ku, Nagoya 464
†Department of Nuclear Engineering, Faculty of Engineering, Osaka University, Suita 565

(Received August 5, 1980)

The discrete-variational Xα (DV-Xα) calculations are used for the hexacyano transition-metal complexes, $[M(CN)_6]^{3-}$ (M=Cr, Mn, Fe, and Co) and $[Fe(CN)_6]^{4-}$. The calculated values of the core- and valence-orbital energies can be correlated with the XPS results. The Mulliken populations are presented. The calculated d-d excitation energies are in good agreement with the Δ (ligand-field parameter) values obtained from the spectra.

The Hartree-Fock-Slater (HFS) model[1] has recently been applied to the molecular orbital (MO) calculation of the electronic structures of molecules, clusters, and crystals. Three methods have been developed for the application of this model to the MO calculation: the multiple-scattering Xα (MS-Xα) method,[2] the discrete-variational Xα (DV-Xα) method,[3] and the LCAO-Xα method.[4] The MS-Xα method developed by Johnson and his co-workers seems to be oversimplified for use in the calculation of a metal complex which contains heteropolar covalent bonds. The LCAO-Xα method is an attractive approximation,[5] but it does not seem to meet the present purpose because of the incompatibility of a satisfactory basis set and a reasonable computer time. Most suitable to the present case, therefore, is the DV-Xα method, which has the following advantages: any type of functions, including numerical functions, can be used as the basis functions and as the potential functions, mathematical difficulties are eliminated, and a large system can be calculated in a relatively short computer time. On the other hand, this method is not suitable for the calculation of accurate total energies. The DV-Xα calculations for the ionization and excitation energies have shown an excellent agreement with the experimental results for small molecules[6,7] and metal clusters.[8,9]

However, only a few reports[9,10] have so far appeared concerning the systematical application of the DV-Xα method to a series of transition-metal complexes. It still remains uncertain how far the DV-Xα method can be relied on for the calculation of the orbital energy, the atomic charge, the bond-overlap population, and the d-d excitation energy of a transition-metal complex.

The present study is concerned with the application of the DV-Xα method to a series of hexacyano transition-metal complexes, which have been of special interest for both inorganic and theoretical chemists.[11] Cyanide ions are coordinated to a metal ion with both σ- and π-type bondings, and cyano complexes are typical of the complexes in which the π back-donation of electrons possibly takes place.

The main purpose of the present study is to obtain a deeper understanding of the coordinate bond by comparing the electronic structures of hexacyano complexes. For this purpose, an HFS MO calculation with the numerical-basis DV-Xα method has been made of $[M(CN)_6]^{3-}$ (M=Cr, Mn, Fe, and Co) and $[Fe(CN)_6]^{4-}$. The results are compared with the experimental results in order to confirm their reliability, and comparisons are made between the results for different complexes of the series. A comparison is also made with the recent results of the *ab initio* MO calculation of $[Co(CN)_6]^{3-}$ by Sano *et al.*[12,13]

Computational Method

The computational details of the spin-polarized DV-Xα method and the relation between the DV-Xα treatment and ligand-field theory have been sufficiently described elsewhere.[9]

In the HFS model,[1] the exchange-correlation term is given by:

$$V_{xc}^{\uparrow}(1) = -3\alpha[(3/4\pi)\rho^{\uparrow}(1)]^{1/3}$$

where $\rho^{\uparrow}(1)$ is the local charge density with up-spin and α is the exchange scaling parameter; α=0.70 is used for all atoms throughout the present calculation.[6] The spin-polarized DV-Xα self-consistent-charge (SCC) procedure[9] has been performed for both up and down spins, where an approximate self-consistent molecular potential is determined from the Mulliken gross orbital populations. The up- and down-spin numerical basis functions are generated as the solutions of the atomic HFS equations in which an atom-like potential is constructed by spherically averaging the molecular potential around the nucleus for the region inside each atomic sphere.[8] The basis sets including the metal 1s-4p and C and N 1s-2p are utilized for most of the present calculations.

The molecular geometries for the complexes are taken from the experimental results.[14] In the present calculation, the complexes are regarded as having the O_h symmetry.

Results and Discussion

The MO's of the Cyanide Ion and Its Coordination to a Metal Ion. The eigenvalues and charge distributions calculated for free CN^- are tabulated in Table 1.

The 1σ and 2σ MO's are N1s and C1s orbitals respectively. On the basis of the orbital components and the bond-overlap populations, each orbital may be characterized as follows: 3σ is the N2s-C2s bonding

** Present address: Laboratory of Inorganic Chemistry, Faculty of General Education, Nagoya University, Chikusa-ku, Nagoya 464.

Table 1. Electronic structure of CN^-

Orbital	Energy/eV	Charge distribution/% C 1s	C 2s	C 2p	N 1s	N 2s	N 2p
5σ	2.5		23	39		6	32
1π	1.4			42			58
4σ	−0.6		32	9		24	34
3σ	−11.9		21	12		55	11
2σ	−258.1	100					
1σ	−368.8				100		

Carbon orbital	Orbital population	Nitrogen orbital	Orbital population
1s	2.00	1s	2.00
2s	1.52	2s	1.72
$2p\sigma$	1.21	$2p\sigma$	1.55
$2p\pi$	1.68	$2p\pi$	2.32
Atomic charge	−0.41	Atomic charge	−0.59

C–N	Overlap population
5σ	−0.249
1π	1.110
4σ	0.013
3σ	0.397

orbital, the major part of the population of nonbonding 4σ and that of antibonding 5σ reside at N and C respectively, and 1π is bonding. These features are similar to previous results[12,13] derived from the *ab initio* MO calculation. However, the results of the population analysis in the present calculation (−0.59 on N and −0.41 on C) are in contrast with the previous results (−0.454 on N and −0.546 on C).[13] The present results are more reasonable for the reason that they are consistent with the higher electronegativity of the nitrogen atom. The *ab initio* calculation with double-zeta basis functions sometimes gives unreasonable results for Mulliken populations due to a diffuse component of the double-zeta function extending to the neighboring atom.[15] Thus, one of the merits of the DV-Xα SCC method seems to be that it gives reasonable populations.

In spite of the higher negative charge located on the nitrogen atom, the cyanide ion is coordinated to the metal at the carbon atom. This can be expected from the frontier-electron theory,[16] according to which an electrophilic reaction tends to takes place on the atom that has the highest electron density in the highest occupied MO (HOMO) of the ground state of the nucleophile. The HOMO of the free CN^- ion is 5σ, the population of which is greater on the carbon atom (62%) than on the nitrogen atom (38%); this is consistent with the tendency of CN^- to coordinate at the carbon atom.

Table 2. ΔE(N1s–C1s) from XPS experiments[17] and DV-Xα MO calculation (eV)

	Cr^{3+}	Mn^{3+}	Fe^{3+}	Co^{3+}	Fe^{2+}
DV-Xα	110.0	109.9	109.9	109.6	109.8
Expt	113.6	113.4	113.3	113.2	113.1

Orbital Energies and Ionization Potentials of the Metal Complexes. The core-electron binding energies for N1s and C1s are first discussed. The orbital-energy values calculated by the Xα method cannot be directly compared with the experimental values obtained from X-ray photoelectron spectroscopy (XPS), since the relaxation effect is disregarded in the calculation. However, the relaxation energies for C and N core orbitals do not change appreciably from one cyano complex to another; thus, the relative changes in core levels may be meaningful. In Table 2, the differences between the N1s and C1s orbital energies of the complexes are compared with the corresponding XPS results. The calculated N1s−C1s difference, ΔE(N1s−C1s), decreases from $[Cr(CN)_6]^{3-}$ (110.0 eV) to $[Co(CN)_6]^{3-}$ (109.6 eV) and from $[Fe(CN)_6]^{3-}$ (109.9 eV) to $[Fe(CN)_6]^{4-}$ (109.8 eV), showing a trend similar

Table 3. The energies, symmetries, and populations of the filled outer-shell molecular orbitals of $[Co(CN)_6]^{3-}$

Symmetry	Energy/eV	Population analysis/% Metal orbital 3d	Metal orbital 4s	Metal orbital 4p	Carbon orbital 2s	Carbon orbital 2p	Nitrogen orbital 2s	Nitrogen orbital 2p
$2t_{2g}$	5.34	70.7				1.8		27.5
$8t_{1u}$	4.07			1.3	8.5	33.4	3.1	53.6
$1t_{1g}$	3.99					35.4		64.6
$1t_{2u}$	3.61					41.5		58.5
$7t_{1u}$	2.96			0.0	0.0	22.7	19.8	57.6
$5e_g$	2.83	10.8			0.0	6.4	27.0	55.8
$8a_{1g}$	2.82		0.0		0.0	8.3	30.1	61.8
$1t_{2g}$	2.26	20.5				49.9		29.5
$6t_{1u}$	0.29			6.0	38.8	33.7	11.9	9.4
$4e_g$	0.18	36.3			31.2	20.8	7.2	4.5
$7a_{1g}$	−2.61		9.9		39.6	44.2	6.3	0.0
$3e_g$	−10.68	0.2			19.7	14.7	52.2	13.3
$5t_{1u}$	−10.86			1.7	18.0	15.3	51.2	13.4
$6a_{1g}$	−11.00		3.1		20.9	12.3	49.7	14.0

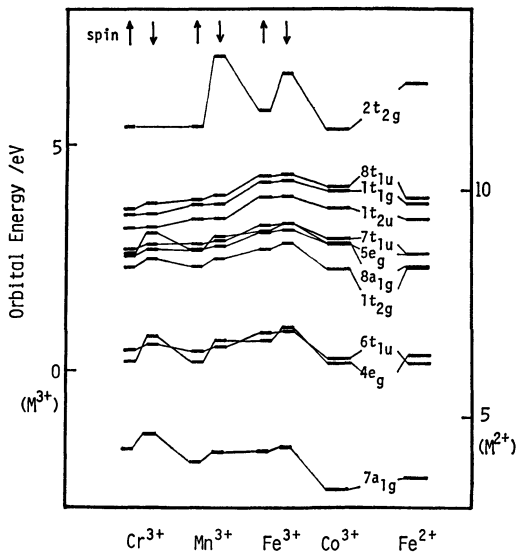

Fig. 1. The occupied valence orbital levels of $[M(CN)_6]^{3-}$ (M=Cr, Mn, Fe, and Co) and $[Fe(CN)_6]^{4-}$.

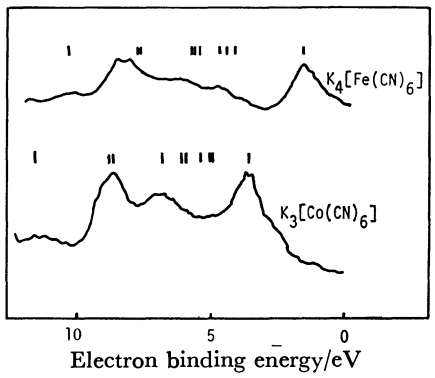

Fig. 2. Valence shell spectra of XPS[20] and orbital energies for $[Fe(CN)_6]^{4-}$ and $[Co(CN)_6]^{3-}$.

to that observed in the XPS data. Detailed discussions of the XPS results have been given elsewhere.[17]

Table 3 shows the energies and symmetries of the filled outer-shell MO's of $[Co(CN)_6]^{3-}$, along with their atomic components. The energies of orbitals with up- and down-spins are schematically shown in Fig. 1 for all the complexes of the series. In all cases, the HOMO is $2t_{2g}$, consisting mainly of metal $d\pi$ with a small contribution of ligand π orbitals. This is different from the previous results of a simple Hartree-Fock (HF) calculation,[12] which showed that $2t_{2g}$ consists mainly of ligand orbitals, but it is consistent with the results of the HF calculation with the ΔSCF procedure,[13] according to which the ionization potential of $2t_{2g}$ (a mainly ligand orbital) is larger than that of $1t_{2g}$ (a mainly metal orbital) and the latter may therefore be regarded as HOMO. The XPS results[19,20] also show that the electron of the smallest binding energy is of a mainly metal-d character, in agreement with the present and the ΔSCF results. Figure 2 shows a comparison of the calculated orbital-energy levels and the XPS spectra of the valence regions of $[Fe(CN)_6]^{4-}$ and $[Co(CN)_6]^{3-}$.[20] For easy comparison, the position of the calculated energy level of $2t_{2g}$ ($d\pi$, HOMO) was arbitrarily taken as the reference to be fitted to the corresponding XPS peak in Fig. 2. The relative positions of the calculated orbital-energy levels appear to show a good correlation with the spectra, in spite of the fact that the reorganization energy is neglected in the calculation. A more detailed discussion, including the calculation by the transition-state method and an estimation of the relative intensities, will be given elsewhere.[21]

In the valence levels, the $6a_{1g}$, $5t_{1u}$, and $3e_g$ MO's of the complexes are predominantly composed of CN^- 3σ orbitals (see Tables 1 and 3). The $7a_{1g}$, $4e_g$, and $6t_{1u}$ MO's are CN^- σ orbitals mixed with metal σ orbitals. The $1t_{2g}$ MO is composed of CN^- π and metal $d\pi$. The $8a_{1g}$, $7t_{1u}$, and $5e_g$ MO's are CN^- σ orbitals located mainly on N. The $1t_{1g}$ and $1t_{2u}$ MO's are CN^- π orbitals, while $8t_{1u}$ MO is predominantly CN^- π orbitals slightly mixed with the metal 4p orbital.

We shall compare the orderings of MO's in the free and coordinated CN^- ions. Although the 5σ orbital

TABLE 4. ATOMIC CHARGES

Metal	Cr^{3+}		Mn^{3+}		Fe^{3+}		Fe^{2+}	Co^{3+}
	up	down	up	down	up	down		
3dσ	0.79	0.49	0.85	0.64	0.91	0.79	1.52	1.89
3dπ	2.75	0.13	2.75	0.98	2.75	1.87	4.99	5.48
4s	0.14	0.10	0.13	0.11	0.12	0.11	0.22	0.26
4p	0.23	0.15	0.24	0.18	0.24	0.21	0.44	0.53
Atomic charge	+1.21		+1.13		+0.98		+0.83	+0.84
Carbon								
2s	0.62	0.66	0.61	0.64	0.60	0.62	1.25	1.20
2pσ	0.56	0.59	0.55	0.58	0.55	0.56	1.12	1.10
2pπ	0.86	0.89	0.87	0.89	0.85	0.87	1.69	1.75
Atomic charge	−0.17		−0.14		−0.05		−0.06	−0.04
Nitrogen								
2s	0.86	0.86	0.86	0.86	0.86	0.86	1.72	1.72
2pσ	0.77	0.77	0.76	0.76	0.76	0.76	1.51	1.50
2pπ	1.19	1.10	1.19	1.13	1.21	1.17	2.51	2.38
Atomic charge	−0.53		−0.55		−0.61		−0.74	−0.60

Table 5. Bond-overlap populations

	Cr^{3+}	Mn^{3+}	Fe^{3+}	Co^{3+}	Fe^{2+}
M–Cπ	0.05	0.05	0.05	0.04	0.08
$1t_{2g}$	0.05	0.06	0.07	0.08	0.06
$2t_{2g}$	0.00	−0.01	−0.02	−0.03	0.03
M–Cσ	0.21	0.23	0.24	0.27	0.23
$4e_g$	0.10	0.12	0.12	0.13	0.11
$5e_g$	0.05	0.04	0.04	0.03	0.06
a_{1g}'s, t_{1u}'s	0.06	0.07	0.08	0.11	0.06
Total M–C	0.25	0.27	0.29	0.30	0.31
C–N σ	0.42	0.43	0.44	0.45	0.43
C–N π	1.10	1.08	1.07	1.07	1.01
Total C–N	1.51	1.50	1.50	1.51	1.44

is the HOMO in the free CN^- ion, the ordering of the σ and π orbitals is reversed by the coordination of CN^- with a metal ion. Thus, the ordering is

$5\sigma > 1\pi > 4\sigma$ in the free CN^- ion

and;

metal $d\pi > \pi(CN^-) > \sigma(CN^-)$ in the complex ion.

Since the cyanide ion is a good σ-electron donor, the 5σ orbital energy is greatly decreased by the bonding interaction with the metal dσ orbital.

Bond-overlap Population and Bond Strength. The calculation has been done by the procedure of SCC. The numerical basis set generated by iterative SCC[8] gave adequate wavefunctions suitable to the Mulliken population analysis. The bond-overlap population and charge distributions thus obtained are given in Tables 4 and 5. The metal-carbon bond strength is related to both the σ- and π-overlap populations for the M–C bond. The σ-bond-overlap populations of the $[M(CN)_6]^{3-}$-type complexes gradually increase with an increase in the atomic number of the metal (from Cr to Co). This is consistent with the tendency for the effective nuclear charge of the metal ion to increase in the order of $Cr^{3+}<Mn^{3+}<Fe^{3+}<Co^{3+}$. The increase in the nuclear charge is only incompletely screened by the increase in the number of metal dπ electrons. Thus, the ligand-to-metal donation of σ electrons is expected to increase with an increase in the atomic number of the metal. On the other hand, the π-bond-overlap population remains almost unchanged, probably because of the counterbalancing effects of the π+dπ bonding and dπ—π antibonding interactions. The total bond-overlap population and, consequently, the M–C-bond strength increase in the order of Cr–C<Mn–C<Fe–C< Co–C. As regards the C–N bond, the bond-overlap population is 1.43 in the free CN^- ion and 1.44—1.51 in the complexes. The C–N-overlap population consists of two components, the σ- and π-overlap populations, which are, respectively, 0.32 and 1.11 in the free CN^- and 0.42—0.45 and 1.07—1.10 in the complexes (except for the Fe^{2+} complex, to be discussed below). The formation of the M–C bond results in a decrease in the antibonding character of 5σ (HOMO) and, consequently, in an increase in the C–N bond-overlap population from 0.32 to 0.42—0.45. This suggests that a stronger metal–carbon σ bond is associated with a stronger C–N σ bond. On the other hand, the formation of metal–ligand π bonds with π back-donation slightly weakens the C–N bond, as is shown by the descrease in the C–N π-overlap population from 1.11 to 1.07—1.10. The σ and π effects partially compensate for each other, resulting in a slight increase in the C–N bond strength. When Fe^{3+} in the hexacyano complex is reduced to Fe^{2+}, an electron is added to the dπ orbital. Thus, in $[Fe(CN)_6]^{4-}$ the π back-donation of iron dπ electrons to the cyanide antibonding π orbitals occurs to a greater extent, resulting in a weakening of the C–N π bond. The increase in the number of dπ electrons will only indirectly affect the Fe–C σ bonding and the C–N σ bonding. Consistent with this argument, Table 5 shows that the π-overlap population decreases from 1.07 to 1.01 and that the σ-overlap population changes very little in going from the Fe^{3+} to the Fe^{2+} complex.

Charge Distribution. The differences in the charge distribution between the free CN^- ion and the CN^- ligand in the complexes are seen mainly in the carbon charges as a result of the σ donation to metal. A fraction (0.3—0.4) of electron flows into the metal ion from each carbon atom, partially neutralizing the positive charge of the metal ion. The 3dσ population increases from 1.28 to 1.89 with the increase in the carbon-to-metal σ donation in going from Cr^{3+} to Co^{3+}. The 3dπ population, of course, increases with the increase in the atomic number. The net population of 3dπ, however, is lower than the formal population, and the deficiency increases from 0.12 to 0.52, showing an increase in the π back-donation with an increase in the atomic number. The population of 4s changes only slightly, while that of 4p increases from 0.38 to 0.53 across the series (due to ligand-to-metal donation). The metal positive charge thus decreases with the increase in the 3dσ population in going from Cr^{3+} to Co^{3+}. On carbon, the C2s and C2pσ populations decrease from 1.28 and 1.15 for $[Cr(CN)_6]^{3-}$ to 1.20 and 1.10 for $[Co(CN)_6]^{3-}$ respectively with an increase in the σ donation from carbon to metal, while the C2pπ population remains approximately constant. As for the nitrogen charge, the population remains unchanged for 2s, slightly decreases for 2pσ, and increases for 2pπ, in going from Cr^{3+} to Co^{3+}. As a result, the negative charge of nitrogen increases from −0.53 to −0.60, in contrast to the

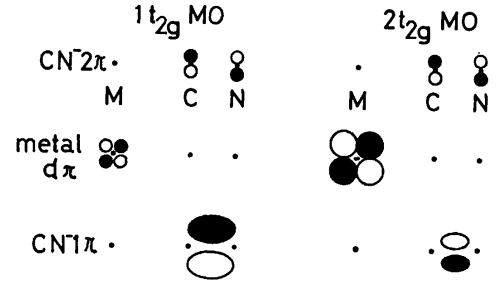

Fig. 3. Orbital interaction of metal dπ and cyanide π orbitals of T_{2g} symmetry. Sizes of circles and ellipses roughly indicate the magnitudes of orbital components. Signs of orbital wavefunctions, namely positive or negative, are shown by white and black area.

decrease in that of carbon from −0.17 to −0.04.

The changes in the cyanide π populations will now be briefly discussed. According to the orbital-mixing rule,[22] the $1t_{2g}$ and $2t_{2g}$ MO's consist of linear combinations of the $(1\pi+2\pi+d\pi)$- and $(d\pi-1\pi+2\pi)$-types respectively. These combinations are schematically summarized in Fig. 3. In the formation of the bonding $1t_{2g}$ MO, the CN^- 1π and 2π amplitudes intensify each other at the carbon atom and compensate for each other at the nitrogen atom to result in increased and decreased populations on the carbon and nitrogen atoms respectively. On the other hand, in the $2t_{2g}$ MO, a compensation and an intensification of the amplitudes occur at the carbon and nitrogen atoms respectively. The mixing of 2π (antibonding cyanide orbital) into $d\pi$ with bonding combination strengthens the M–C bond, but weakens the C–N bond.

In the cyano complexes of Fe^{2+} and Fe^{3+}, the metal charges are +0.83 and +0.98, respectively, and the difference results mainly from different 3d populations. The $3d\sigma$ population for Fe^{3+} (1.70) is greater than that for Fe^{2+} (1.52) in agreement with a greater σ donation to Fe^{3+}, while the difference in the $3d\pi$ population between Fe^{2+} (4.99) and Fe^{3+} (4.62) is much less than unity (or the difference in the formal charge) indicating a greater π back-donation from Fe^{2+}. The charges on the two kinds of iron atoms differ from each other only by 0.15, which is much smaller than the difference in the oxidation number.

As has been shown in previous papers,[12,15] the charge distribution derived from the Mulliken population analysis strongly depends on the basis set of orbitals used in the calculation. Thus, the cobalt charge in $[Co(CN)_6]^{3-}$ was estimated to be +3.138 and +1.301 by two *ab initio* MO calculations with only slightly different basis sets. On the other hand, the atomic charge derived from the analysis of the spatial charge distribution naturally depends on the atomic radius assumed. Our previous analysis[13] gave +0.3 or +2.3 for the cobalt charge in the same complex, depending on the radius: 1.22 Å, in accordance with the results of an X-ray analysis,[23] or 0.95 Å, which is the distance of minimum electron density on the calculated distribution curve. As has previously been discussed,[12,15] the diversity of the calculated charges results from the fact that the allocation of charge to each atom is artificial. Nevertheless, the atomic charges are one of the important clues for elucidating the electronic structure of metal complexes, provided that an appropriate method is used consistently to calculate the charge distributions for the complexes to be compared. In this sense, the present results for charge distribution give useful information on the electronic state of the complexes. The resonable numerical values obtained for atomic charges may indicate that the iterative SCC procedure would give suitable wavefunctions for the purpose of population analysis.

The Excitation Energies. One of the main purposes of the present work is to examine the extent to which the experimental values of the ligand field parameter, Δ, can be reproduced by the DV-Xα SCC scheme. The theory has been thoroughly described by Adachi *et al.*[9] The Δ values are obtained as the weighted averages of the energy differences between the vacant $6e_g$ and occupied $2t_{2g}$ orbitals with the same spin:

$$\Delta = [n^{\uparrow}\{E(6e_g^{\uparrow})-E(2t_{2g}^{\uparrow})\}+n^{\downarrow}\{E(6e_g^{\downarrow}) -E(2t_{2g}^{\downarrow})\}]/(n^{\uparrow}+n^{\downarrow}),$$

where the superscripts $\uparrow$ and $\downarrow$ indicate the up- and down-spins, and n, the occupation number of the $2t_{2g}$ orbital with the designated spin. In Table 6, the calculated Δ values are compared with the experimental values reported by Alexander and Gray.[24]

The agreement is reasonably good if the difficulties associated with the estimation of the experimental Δ values are taken into consideration. For some complexes such as $[Fe(CN)_6]^{3-}$, the d-d bands are not clearly observed due to the overlap of strong charge-transfer bands. The estimation of the Δ values from the observed wavenumbers of the absorption bands may be more or less dependent on the values assumed for Racah's B and C parameters. A good agreement between the calculated and experimental values of Δ for metal fluorides has been reported by Larsson and Connolly,[25] who used the SW-Xα method to obtain the Δ values as the difference between the two d-orbital energies. More careful DV-Xα treatments of the same compounds made by Adachi *et al.*[9] gave an excellent agreement. Along with their results, our present results illustrate the usefulness of the Xα method for the estimation of the Δ values.

The Δ values calculated for the $[M(CN)_6]^{3-}$-type complexes increase with the increase in the atomic number of the metal. Though not fully consistent with the existing experimental data, this trend can be expected from the following reasoning: in going from Cr^{3+} to Co^{3+}, the effective charge of the metal ion increases, the σ donation from CN^- σ to metal $d\sigma$

TABLE 6. CALCULATED VALUES OF THE LIGAND-FIELD PARAMETER, Δ, AND THE EXPERIMENTAL VALUES[24]

Orbital	Cr^{3+}	Mn^{3+}	Fe^{3+}	Co^{3+}	Fe^{2+}	
$6e_g^{\downarrow}$	11.11	10.61	10.43	9.46	16.50	(eV)
$6e_g^{\uparrow}$	8.89	9.17	9.73	9.46	16.50	(eV)
$2t_{2g}^{\downarrow}$	7.71	6.95	6.57	5.35	12.35	(eV)
$2t_{2g}^{\uparrow}$	5.42	5.40	5.76	5.35	12.35	(eV)
Δ (calcd)	28000	30200	31600	33200	33500	(cm^{-1})
Δ (exptl)	26600	34000[a]	34950	34500	33800	(cm^{-1})

a) 30000 cm^{-1} in Ref. 26.

occurs to a greater extent, and metal dσ is more strongly destabilized by the increased antibonding interaction. The π back-donation is small in these complexes; thus, the change in π back-donation makes a minor contribution to the change in the Δ values.

The calculated Δ value for $[Fe(CN)_6]^{4-}$ is greater than that for $[Fe(CN)_6]^{3-}$. This is contrary to the above reasoning, according to which $[Fe(CN)_6]^{4-}$ with Fe^{2+}, with a lower effective charge, would have a lower Δ value. In this case, however, a change in the π back-donation makes a significant contribution to the change of the Δ value. The increase in the stabilization of Fe dπ due to the stronger π-bonding effect overbalances the decrease in the destabilization of Fe dσ due to the weaker σ-antibonding effect in going from the Fe^{3+} to the Fe^{2+} complex. Calculation showed that the σ donation decreased from 42.3% to 37.7%, while the π back-donation increased from 8.5% to 16.8% correspondingly.

Conclusions

The spin-polarized DV-Xα method has been applied to the calculation of the electronic structures of transition-metal cyano complexes. This leads to the following conclusions:

(1) The calculated orbital energies give a good correlation with the XPS results.

(2) The calculated atomic charges and bond-overlap populations due to Mulliken population analysis show a trend that can be satisfactorily elucidated by a qualitative molecular-orbital consideration using the orbital mixing rule.

(3) The Δ value, as expressed by the difference between dσ ($6e_g$) and dπ ($2t_{2g}$) orbital energies, shows a good agreement with the spectroscopic Δ values.

(4) The conclusions described under (1)—(3) suggest that the DV-Xα MO method gives an adequate description of the electronic structures of transition-metal complexes.

The numerical calculations were performed with a HITAC M-180 system at the Computer Center of the Institute for Molecular Science and a FACOM 230-75 system at the Nagoya University Computation Center. The authors are grateful to the staffs of the computer centers for their assistance in the calculation.

References

1) For a review of the Hartree-Fock-Slater model, see J.C. Slater, "Quantum Theory of Molecules and Solids," McGraw-Hill, New York (1974), Vol. 4.

2) K. H. Johnson and F. C. Smith, Jr., "Computational Methods in Band Theory," ed by P. M. Marcus, J. F. Janak, and A. R. Williams, Plenum, New York (1971), p. 337; K, H. Johnson, J. G. Norman, Jr., and J. E. D. Connolly, "Computational Methods for Large Molecules and Localized States in Solids," ed by F. Herman, A. D. McLean, and R. K. Nesbet, Plenum, New York (1973), p. 161; J. C. Slater and K. H. Hohnson, *Phys. Rev. B*, **5**, 844 (1979).

3) D. E. Ellis and G. S. Painter, *Phys. Rev. B*, **2**, 2887 (1970); E. J. Baerends, D. E. Ellis, and P. Ros, *Chem. Phys.*, **2**, 41 (1973).

4) H. Sambe and R. H. Felton, *J. Chem. Phys.*, **62**, 1122 (1975).

5) T. Ziegler and A. Rauk, *Inorg. Chem.*, **18**, 1558 (1979).

6) E. J. Baerends and P. Ros, *Chem. Phys.*, **2**, 52 (1973); **8**, 412 (1975).

7) A. Rosen, D. E. Ellis, H. Adachi, and F. W. Averill, *J. Chem. Phys.*, **65**, 3629 (1976).

8) H. Adachi, M. Tsukada, and C. Satoko, *J. Phys. Soc. Jpn.*, **45**, 875 (1978).

9) H. Adachi, S. Shiokawa, M. Tsukada, C. Satoko, and S. Sugano, *J. Phys. Soc. Jpn.*, **47**, 1528 (1979).

10) E. J. Baerends and P. Ros, *Mol. Phys.*, **30**, 1735 (1975).

11) A. G. Sharpe, "The Chemistry of Cyano Complexes of the Transition Metals," Academic Press, London (1976).

12) M. Sano, Y. Hatano, and H. Yamatera, *Chem. Phys. Lett.*, **60**, 257 (1979).

13) M. Sano, Y. Hatano, H. Kashiwagi, and H. Yamatera, *Bull. Chem. Soc. Jpn.*, **54**, 1523 (1981).

14) S. Jagner, *Acta Chem. Scand., A*, **29**, 255 (1975).

15) M. Sano, Y. Hatano, and H. Yamatera, *Chem. Lett.*, **1979**, 789.

16) H. Fujimoto and K. Fukui, "Chemical Reactivity and Reaction Paths," ed by G. Klopman, John Wiley and Sons, New York (1974), p. 23.

17) M. Sano and H. Yamatera, *Bull. Chem. Soc. Jpn.*, **54**, 2023 (1981).

18) The N1s and C1s binding energies obtained from XPS are influenced by the charging and the Madelung potential. However, these effects are canceled in their difference, E(N1s − C1s), so that a comparison between the experimental and calculated values of ΔE (N1s − C1s) becomes possible.

19) A. Calabrese and R. G. Hayes, *J. Am. Chem. Soc.*, **96**, 5054 (1974).

20) N. G. Vannerberg, *Chem, Scrip.*, **9**, 122 (1976).

21) M. Sano, H. Adachi, and H. Yamatera, to be published.

22) S. Inagaki and K. Fukui, *Chem. Lett.*, **1974**, 509; S. Inagaki, H. Fujimoto, and K. Fukui, *J. Am. Chem. Soc.*, **98**, 4504 (1976).

23) M. Iwata and Y. Saito, *Acta Crystallogr., Sect.B*, **29**, 822 (1973).

24) J. J. Alexander and H. B. Gray, *J. Am. Chem. Soc.*, **90**, 4260 (1968).

25) S. Larson and L. W. D. Connolly, *Chem. Phys. Lett.*, **20**, 323 (1973).

26) I. D. Chawla and M. J. Frank, *J. Inorg. Nucl. Chem.*, **32**, 555 (1970).

Preparation and Analytical Evaluation of Liquid Membrane Electrodes Based on Solid-solvents

Hirokazu HARA, Satoshi OKAZAKI, and Taitiro FUJINAGA*

Department of Chemistry, Faculty of Science, Kyoto University, Sakyo-ku, Kyoto 606

(Received September 16, 1980)

A new type of liquid membrane electrode has been developed in which organic compounds solidified at room temperature were used as solvents of an ion-sensing membrane. The electrode performance of a *p*-toluenesulfonate ion-sensitive electrode was examined and compared with that of a corresponding liquid membrane electrode, no remarkable difference being observed in sensitivity and response time. However, a distinct difference in selectivity was observed between the 1-octadecanol (solid) and 1-decanol (liquid) membranes. The difference was interpreted on the basis of the solvation energy of interfering anions. The effects of ion-pair concentration, membrane thickness, and pH on the electrode potentials of the 1-octadecanol membrane were investigated in comparison to those of the 1-decanol membrane. The electrodes responsive to various anions such as iodide, nitrate, bromide, and chloride were prepared with an 1-octadecanol membrane.

Liquid membrane electrodes (LME) have the advantage of a wide variety in their ion-exchanger as regards solvent extraction systems. However, they have disadvantages in practical use in comparison with solid membrane electrodes. The potentiometric response of LME is liable to be disturbed by hydrostatic pressure or stirring of the sample solution, or its ion-exchanging liquid tends to leak into the sample. In order to overcome these difficulties studies have been made resulting in the development of an LME based on plastic matrices,[1,2] carbon paste,[3] and the solidification of ion-exchanging liquid by addition of naphthalene to a nitrobenzene membrane.[4]

Organic sulfonate selective electrodes were developed by use of a coated wire type electrode.[5] We have developed a *p*-toluenesulfonate selective electrode (solid-solvent membrane electrode, SSME) using organic compounds having a high melting point, which solidify at room temperature. The effects of the membrane components, such as ion-pair concentration, membrane thickness, and pH on the response behavior of SSME with an 1-octadecanol membrane were also studied in comparison to LME with a 1-decanol membrane. The electrode performance of SSME was examined and compared with that of the corresponding LME. A distinct difference in the selectivity patterns between the 1-octadecanol (SSME) and 1-decanol (LME) membranes was observed.

Experimental

Reagents. Reagent grade solid-solvents, 1-octadecanol, 1-docosanol, *m*-dinitrobenzene, 1,2,4,5-tetrachlorobenzene and triphenyl phosphate, and liquid-solvents, 1-octanol, 1-decanol, nitrobenzene, *o*-dichlorobenzene, and tributyl phosphate were used without further purification. An ion-pair of methyltrioctylammonium *p*-toluenesulfonate (TOMA·pTS) was prepared with methyltrioctylammonium chloride (Capriquat, from Dojin Research Laboratories Co.) by the extraction method[5] and recrystallized from ethyl acetate. Capriquat salts of perchlorate, iodide, nitrate, and bromide were similarly prepared. These salts of iodide, nitrate, and bromide are hygroscopic and they were dehydrated under reduced pressure before use. The pH of the sample solution was adjusted with hydrochloric acid or sodium hydroxide solutions.

Preparation of Membranes. An ion-pair was dissolved into solid-solvent molten at elevated Temperature. After cooling at room temperature, the solidified ion-exchanger was ground into powder and pressed on a polished silver disk 1 cm in diameter at *ca.* 300 MPa to form a thin film of ion-sensing membrane. The thickness of the membranes was in the range 0.2—0.4 mm unless otherwise stated. The impedance of these membranes was several mega-ohms.

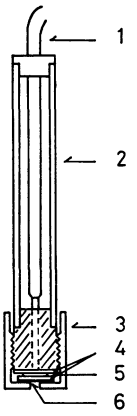

Fig. 1. Configuration of solid-solvent membrane electrode.
(1) Coaxial wire, (2) glass tube, (3) Teflon cap, (4) silver plate, (5) metal for electric conduction, and (6) pressed ion-exchanger.

Electrode Assembly and Potential Measurements. For the potentiometric test of the pressed membranes, SSME was constructed as shown in Fig. 1. For LME, a Corning type liquid membrane electrode was used. The membrane potentials were measured *versus* SCE with an Orion Digital Ionalyzer Model 601 connected to a Matsushita pen recorder Model VP654A.

Results and Discussion

The membrane conditions which affect the electrode response of SSME with an 1-octadecanol membrane responsive to *p*-toluenesulfonate ion (pTS) were investigated in comparison to those of LME with a 1-decanol membrane as follows:

Effect of the Ion-pair Concentration. Dependence of the sensitivity of the SSME on the concentration of the ion-pair is illustrated in Fig. 2. The optimum concen-

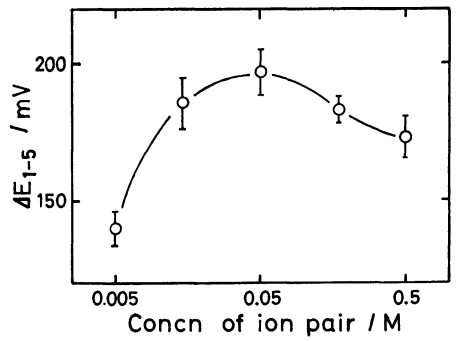

Fig. 2. Effect of ion-pair concentration on the potential difference between 10^{-1} M and 10^{-5} M.
Ion-exchanger: TOMA·pTS in 1-octadecanol (20 mg).
The mean value of four measurements with its standard deviation is given.

tration of the ion-pair is *ca.* 0.05 M†. As in LME,[6] the sensitivity decreased in a very high concentration region due to the elution of the membrane solute. The sensitivity decreased also in low concentration range, the membrane potential becoming unstable below 0.005 M because of the increase of membrane impedance. The potential reproducibility of SSME was not very good, ± 5 mV, in comparison to the conventional liquid membrane electrode.

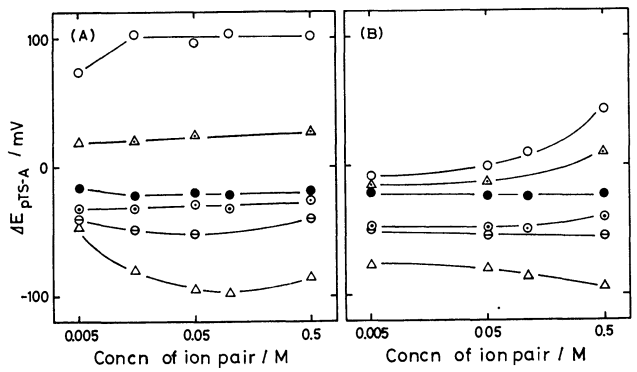

Fig. 3. Effect of ion-pair concentration on SPD of (A) SSME and (B) LME.
Interfering ions: (○) ClO_4^-, (△) I^-, (●) $PhSO_3^-$, (⊙) NO_3^-, (⊖) Br^-, and (△) Cl^-.

The selectivity of SSME changes slightly with the concentration of the ion-pair (Fig. 3A). Selective potential difference (SPD, ΔE_{pTS-A}) was defined in order to study the selectivity characteristic of the membrane as follows. The membrane potentials of 0.01 M objective pTS ion (E_{pTS}) and each interfering anion (E_A) were measured separately. The potential difference, $\Delta E_{pTS-A}=E_{pTS}-E_A$, was used instead of the conventional selectivity factor because of its super-Nernstian responses. The decrease in selectivity at 0.005 M resulted from the poor response to the objective ions. On the other hand, the range of the selectivity of LME widened somewhat with increase in concentration of the ion-pair (Fig. 3B).

† Throughout this paper 1 M=1 mol dm^{-3}.

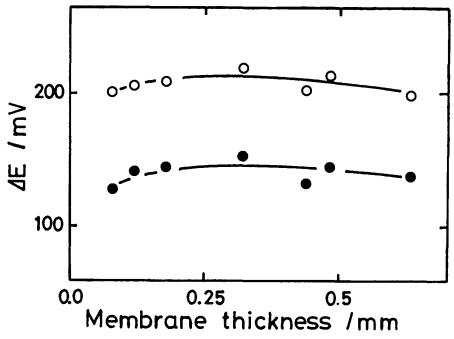

Fig. 4. Effect of membrane thickness on the potential defference between 10^{-1} M and (●) 10^{-4} M or (○)10^{-5} M.
Ion-exchanger: 0.05 M TOMA·pTS in 1-octadecanol.

Effect of the Membrane Thickness. As shown in Fig. 4, the sensitivity of the SSME is not influenced much by the membrane thickness, little effect of the membrane thickness on selectivity and response time being observed.

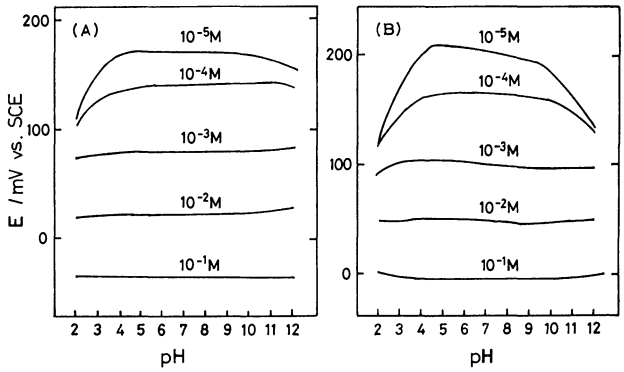

Fig. 5. Effect of pH on the membrane potentials of (A) SSME and (B) LME.
Ion-exchanger: 0.05 M TOMA·pTS in (A) 1-octadecanol and (B) 1-decanol.

Effect of pH. The effects of pH on the membrane potential of SSME (A) and LME (B) were examined (Fig. 5). In the low pH range, the interference of chloride ion could not be ignored in both membranes, the interference of hydroxide ion in an alkaline solution being much larger in LME than in SSME.

Comparison of the Potentiometric Behavior of SSME with That of LME. The response behavior of SSME and LME is summarized in Table 1, four pairs of the pressed membranes and the corresponding liquid membranes being compared. Super-Nernst slopes were observed for both liquid and pressed membranes. This might be attributed to the malfunction of the reference electrode as reported by Moody and Thomas.[7] SSME gave a slightly better result in the linear response ranges in comparison to the corresponding LME except in the case of a pair of 1-alkanols. Since the linear response range of LME depends not only on the membrane solvent but also on the ion-pair species,[6] the most appropriate solvent for a given ion-pair should be selected in order to obtain a highly sensitive electrode. In view of the wide linear response range, 1-decanol

Table 1. Response behavior of *p*-toluenesulfonate ion-sensitive electrodes with (A) liquid membrane and (B) solid-solvent membrane

Solvent	Mp °C	Type of membrane	Slope mV/pa	Limit of linear response/pa	Response time/min at 10^{-2} M	Response time/min at 10^{-4} M
1-Decanol	7	A	64.2	3.8	1.2	4.6
1-Octadecanol	59	B	64.7	3.7	2.0	3.7
Nitrobenzene	6	A	66.1	3.4	1.0	4.1
m-Dinitrobenzene	90	B	62.9	3.6	0.5	3.4
o-Dichlorobenzene	−17	A	63.4	3.4	1.6	2.7
1,2,4,5-Tetrachlorobenzene	140	B	67.1	3.6	0.1	2.5
Tributyl phosphate	−80	A	62.1	3.4	1.6	2.3
Triphenyl phosphate	49	B	67.9	3.7	0.1	2.4

Ion-pair: *ca.* 0.1 M TOMA·pTS, Temp: 25 °C.

was found to be the best liquid-solvent of those tested for a long chain tetraalkylammonium as a counter ion. However, in case of SSME, the linear response range was independent of the kind of solid-solvent used. The sensitivity of SSME seems to be determined mainly by the solubility of the ion-pair.[8] Shorter response time was needed for SSME than the corresponding LME, especially in the high concentration range of pTS^-.

The selectivity characteristics of SSME and LME based on various solvents are shown in Figs. 6 and 7. Hardly any difference was observed among the solid-solvents in the selectivity patterns of SSME (Fig. 6A), while an exceptional pattern was found among LME for 1-decanol membrane (Fig. 6B).

The selectivity patterns of SSME with solid 1-alkanols were compared with those of LME with liquid 1-alkanols (Fig. 7). A distinct difference in patterns was observed. The solvent effects of the solid-solvents on the selectivity pattern were small in contrast to the liquid-solvents examined. The potentials of SSME seem to be governed mainly by the direct ion-exchange reaction at the membrane-solution interface, being hardly affected at all by the inner-membrane phenomena. The selectivity of SSME was anticipated to be

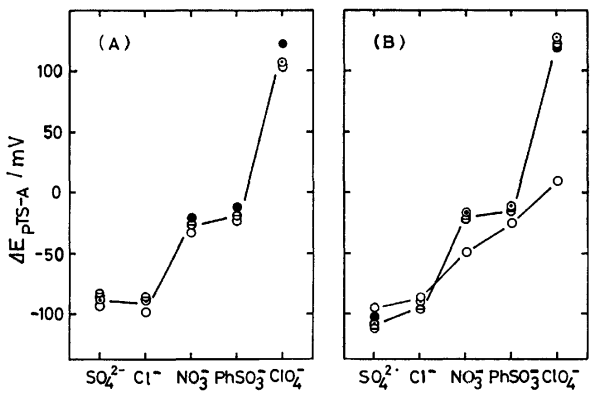

Fig. 6. Selectivity patterns of (A) SSME and (B) LME.
Solvents used for SSME: (●) triphenyl phosphate, (⊙) *m*-dinitrobenzene, (⊖) 1,2,4,5-tetrachlorobenzene, and (○) 1-octadecanol.
Solvents used for LME: (●) tributyl phosphate, (⊙) nitrobenzene, (⊖) *o*-dichlorobenzene, and (○) 1-decanol.

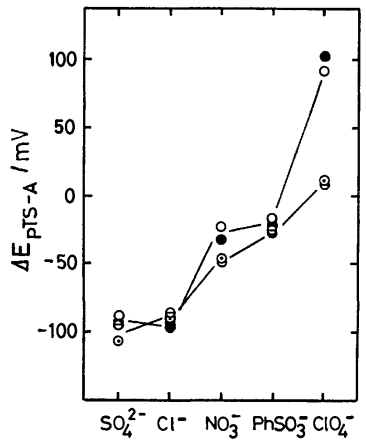

Fig. 7. Selectivity patterns of (●) 1-octadecanol, (○) 1-docosanol, (⊙) 1-octanol, and (⊖) 1-decanol membranes.

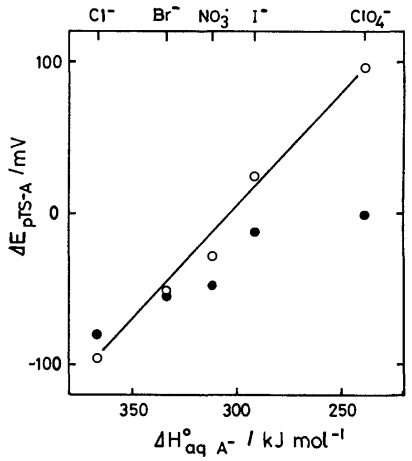

Fig. 8. Relationship between standard hydration enthalpy and SPD. (○) 1-Octadecanol and (●) 1-decanol membranes.

determined mainly by the hydration energy of the interfering ions. A linear relationship is seen between hydration energy and the SPD for an 1-octadecanol membrane, no such correlation being observed for a 1-decanol membrane (Fig. 8). The SPD of the 1-decanol membrane seems to be determined not only by the hydration energy of interfering anions but also

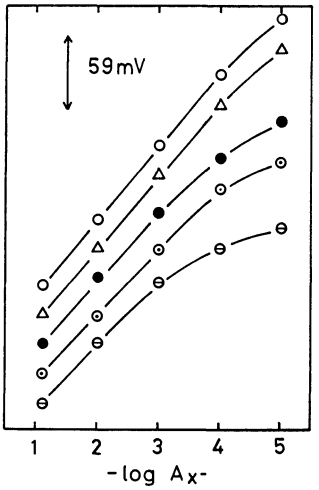

Fig. 9. Calibration curves of solid-solvent membranes. Ion-exchanger: 0.05 M TOMA·X^- in 1-octadecanol (20 mg).
X^-: (○) ClO_4^-, (△) I^-, (●) NO_3^-, (⊙) Br^-, and (⊖) Cl^-.

by the solvation energy in the solvent, as reported by Reinsfelder and Schults for the $Fe(bphen)_3^{2+}$–*t*-pentyl alcohol electrode.[9]

SSMEs Responsive to Other Anions. Figure 9 shows the calibration curves of each electrode sensitive to the respective anions. The sensitivity to ions having a smaller hydration energy is better than that having a larger one.[8,10] SSME with 1-octadecanol membrane has several merits over LME with common aromatic compounds; 1) it is insoluble in water, 2) it does not sublime, and 3) it can be use as the matrix of a coated-wire type electrode in place of the conventional PVC matrix.

An SSME with an inner reference electrode showed reproducibility to be better than ±2 mV. This type of pressed membrane should be *ca.* 0.5 mm thick or else it will break easily. A coated-wire type SSME, prepared by dipping a platinum tip into the extract of the ion-pair in molten 1-octadecanol, also showed good response.

SSME has advantages of both solid and liquid membranes; it shows fast response and can be used as a sensor of a flowing system.[11] The contamination of the sample solution with the eluted solvent from the membrane can be minimized. It is widely applicable to most LME-systems. A highly selective organic sulfonate ion selective electrode with alkylphenol derivative has been developed.[12]

References

1) G. J. Moody, R. B. Oke, and J. D. R. Thomas, *Analyst*, **95**, 910 (1970).
2) H. James, G. Carmack, and H. Freiser, *Anal. Chem.*, **44**, 856 (1972).
3) G. Ali Qureshi and J. Lindquist, *Anal. Chim. Acta*, **67**, 243 (1973).
4) M. Kataoka and T. Kambara, *Bunseki Kagaku*, **23**, 1081 (1974).
5) T. Fujinaga, S. Okazaki, and H. Freiser, *Anal. Chem.*, **46**, 1842 (1974).
6) N. Ishibashi, H. Kohara, and K. Horinouchi, *Talanta*, **20**, 867 (1973).
7) G. J. Moody and J. D. R. Thomas, *Talanta*, **19**, 623 (1972).
8) N. Kamo, N. Hazemoto, and Y. Kobatake, *Talanta*, **24**, 111 (1977).
9) R. E. Reinsfelder and F. A. Schultz, *Anal. Chim. Acta*, **65**, 425 (1973).
10) A. Hulanicki and R. Lewandowski, *Chem. Anal.*, **19**, 53 (1974).
11) E. H. Hansen, A. K. Ghose, and J. Ruzicka, *Analyst*, **102**, 705 (1977).
12) H. Hara, S. Okazaki, and T. Fujinaga, *Bull. Chem. Soc. Jpn.*, **53**, 3610 (1980).

The Decomposition of Hydrogen Iodide and Separation of the Products by the Combination of an Adsorbent with Catalytic Activity and a Temperature-swing Method

Yoshinao Oosawa

National Chemical Laboratory for Industry, Higashi, Yatabe-cho, Tsukuba-gun, Ibaraki 305

(Received October 29, 1980)

The decomposition of hydrogen iodide and the separation of the products by the combination of a column packed with an adsorbent with catalytic activity (platinum-supported active carbon, 2.3 wt%) and a temperature-swing method (450—900 K) are carried out, and the features and the problems of the method are examined. A one-step conversion of hydrogen iodide, 70%, is obtained at 450 K, where the equilibrium conversion is 13%. It is shown that the products of the decomposition of hydrogen iodide containing water are separated from each other.

The decomposition of hydrogen iodide serves as the hydrogen-evolution step in several thermochemical water-splitting cycles,[1-3] including the Magnesium–Iodine cycle[4,5] previously proposed by Kondo *et al.* Suitable catalysts for the catalytic decomposition of hydrogen iodide were searched for,[6] and the kinetic analysis of the reaction over a platinum-supported active carbon catalyst and an active carbon catalyst which had been found effective was carried out.[7] The results showed that hydrogen iodide could be decomposed rapidly enough by the use of those catalysts in the range of comparatively low temperatures (500—700 K) and in the presence of water vapor that might coexist in the actual cycle. However, the equilibrium conversion of hydrogen iodide is low (0.13—0.20 at 450—700 K)[6] when all the components, including the products, are in the gaseous phase. Therefore, the separation of the product mixture into its components, *i.e.*, hydrogen, iodine, undecomposed hydrogen iodide, and water, is necessary. However, iodine and undecomposed hydrogen iodide cannot be separated from each other easily, since iodine readily dissolves in the hydriodic acid formed from hydrogen iodide and water. On the other hand, the amount of undecomposed hydrogen iodide which has to be recirculated should be minimzied in order to increase the thermal efficiency of the whole cycle.

Therefore, from the standpoint of the thermochemical water splitting, the problems in the decomposition of hydrogen iodide can be summarized as follows: the elevation of a one-step coversion, and the development of an effective separation method of the product mixture. Various decomposition-separation methods have been proposed, *i.e.*, methods in which hydrogen iodide is decomposed, when iodine is in the liquid phase[8] or hydrogen iodide is in the liquid phase,[8] a method with porous membrane,[9] a method with MgO,[10] *etc.* However, each method has its own problems. Therefore, the present author considered that the development of a new method was necessary.

Principle

An adsorbent with catalytic activity is prepared by the addition of catalytic activity to an adsorbent which has very different adsorption characteristics toward the reactant, hydrogen iodide, and the products, hydrogen and iodine. Under the conditions that a column packed with the adsorbent with catalytic activity is heated in the temperature range where hydrogen iodide is decomposed rapidly, and that hydrogen iodide is fed in intermittently, there is a possibility that a one-step conversion higher than the equilibrium one can be obtained.

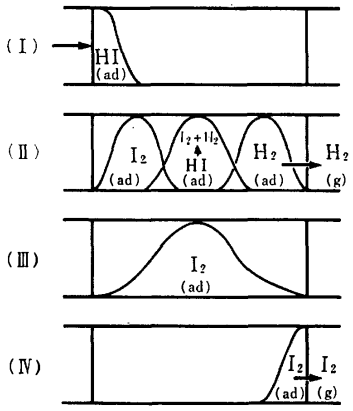

Fig. 1. Conceptual drawing of the decomposition of hydrogen iodide and the separation of the products by the use of a column packed with an adsorbent with catalytic activity.

Figure 1 is the conceptual drawing of the method. As a certain amount of hydrogen iodide fed intermittently proceeds in the column, it decomposes on the surface of the adsorbent, thus forming hydrogen and iodine. If it is hard for the adsorbent to adsorb hydrogen, while it readily adsorbs iodine, the hydrogen formed on the surface of the adsorbent desorbs into the gaseous phase, while the iodine formed remains adsorbed. Since the iodine formed is continuously removed from the reaction system, the undecomposed hydrogen iodide is decomposed further as it proceeds in the column (Figs. 1-I, II). Thus, if the decomposition of hydrogen iodide is rapid enough, a one-step conversion higher than the equilibrium one is obtained. The iodine remaining in the adsorbent is desorbed, and the adsorbent is regenerated (III, IV). In the present method, the one-step conversion of hydrogen iodide will be dependent

on both the catalytic activity of the adsorbent and the difference in the adsorption characteristics of the adsorbent toward hydrogen iodide, hydrogen, and iodine. If a higher one-step conversion is obtained, the thermal efficiency of the whole cycle is expected to become higher, since the amount of the undecomposed hydrogen iodide which has to be recirculated decreases. This method may be divided into two kinds of procedures. One is a procedure in which the decomposition of hydrogen iodide and the desorption of iodine are carried out at a constant temperature (Pressure-swing Method). The other is one in which they are carried out at different temperatures (Temperature-swing Method).

As has been mentioned above, the platinum-supported active carbon catalyst has been found to reveal high catalytic activity for the decomposition of hydrogen iodide. On the other hand, active carbon, which is the support of the catalyst, is known to exhibit markedly different adsorption characteristics toward hydrogen, iodine, and hydrogen iodide.[11,12] Therefore, it seems that it is possible for the platinum-supported active carbon (abbreviated as Pt/C) to behave as the adsorbent with catalytic activity mentioned above. With this in view, the present author has attempted the decomposition of hydrogen iodide and the separation of the products by the combination of a column packed with a Pt/C and a temperature-swing method; he has also examined the features and the problems of the present decomposition-separation method.

Experimental

Materials. The Pt/C's (1.1 wt%, 2.3 wt%) were prepared by an impregnation-calcination method (1000 K, 6 h, in an argon stream) from $H_2PtCl_6 \cdot 6H_2O$ (WAKO, Sp. Gr.) and active carbon (PITTSBURG ACTIVATED CARBON, BPL, 12-30 U. S. Sieve Series). Six grams of the Pt/C (2.3 wt%) was used in each run, unless otherwise stated. One ml of hydriodic acid (WAKO, Sp. Gr., 7.52 mol dm^{-3}, $d=1.70$) was fed in in each run.

Apparatus. Figure 2 shows the experimental apparatus. The inside diameter of the quartz reaction tube (b) was 12 mm. The length of the quartz wool layer (c) was 20 mm, while that of the adsorbent layer (d) was 165 mm.

Procedure. The quartz reaction tube was heated in an argon stream at 900 K for 2—3 h, after which the water, oxygen, and so on adsorbed on the quartz wool and the Pt/C were desorbed. After the reaction tube had been cooled, it was set up and 1 ml of hydriodic acid was added to the quartz-wool layer by means of a transfer pipet from the end. After the Pt/C layer only had been heated at the reaction temperature in an electric furnace, the quartz-wool layer also was moved into the electric furnace. The hydriodic acid contained in the quartz-wool layer was evaporated in an argon stream within 10 (450 K) —0.5 min (900 K) and fed into the Pt/C layer. The step of the iodine desorption followed the step of the decomposition of hydrogen iodide. The flow rate of argon in both the steps was usually 27 ml/min.

Thermogravimetry. The Pt/C (2.3 wt%, 100 mg, ground into a diameter less than 0.3 mm and heated at 1000 K for 6 h in an argon stream) and the samples prepared from the Pt/C by the addition of a certain amount of water, hydriodic acid, or iodine were used in the measurements. The sample containing iodine was prepared by the adsorption of iodine into the Pt/C at 373 K in a glass ampoule. After a reduced-pressure treatment (660 Pa, 30 min) of the samples in the sample chamber, argon was introduced and the samples were analyzed by means of thermogravimetry (CHYO, TRDA3-L). The flow rate of argon was 100 ml/min, while the heating rate was 5 K/min.

Analyses. All the components of the product-gas mixture except for hydrogen and argon were condensed at the back part of the reaction tube or trapped in the scrubber. The hydrogen concentration of the exhaust gas was determined by means of gas-chromatography (YANACO 180G, Molecular Sieve 13A). The amount of hydrogen iodide or iodide, condensed or trapped, was determined by titration.[13,14]

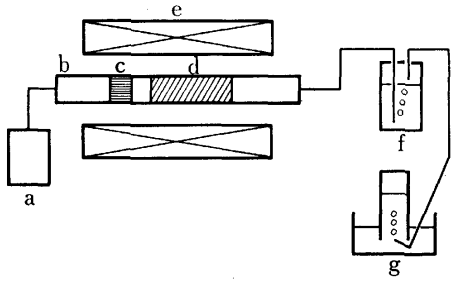

Fig. 2. Schematic drawing of apparatus employed: a, argon bomb; b, quartz reaction tube; c, quartz wool; d, adsorbent with catalytic activity; e, electric furnace; f, scrubber; g, gas reservoir.

Results and Discussion

Thermogravimetry. Figure 3 shows the results of the thermogravimetric analyses of the Pt/C samples. The weight of the Pt/C itself which had been treated at 1000 K remained almost constant up to 1000 K. The water added desorbed almost completely in the pre-measurement operation composed of a reduced-pressure treatment and an argon introduction at room temperature. The iodine added began to desorb around 450 K and finished its desorption at 900 K. In the case of hydriodic acid, about 40% of the weight of the hydriodic acid added was reduced in the pre-measurement operation, after which the residue was reduced in weight in a manner similar to that of the iodine added. The weight loss in the pre-measurement

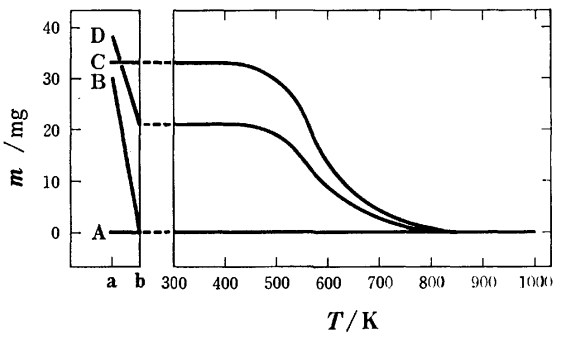

Fig. 3. Thermogravimetric analyses of the Pt/C samples: (a) before and (b) after the pre-treatment; A, Pt/C; B, Pt/C with H_2O; C, Pt/C with I_2; D, Pt/C with HIaq: heating rate, 5 K/min; argon flow rate, 100 ml/min.

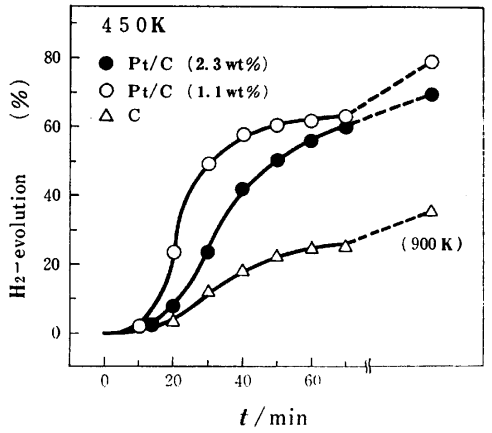

Fig. 4. Influence of the addition of platinum to active carbon on the hydrogen evolution. Six grams of the adsorben twas used. The points above (900 K) corres ponds tothe sum of the amount of hydrogen evolved in the course of the reaction at 450K and that evolved in the hightemperature after-treatment at 900 K for 30 min.

operation was almost equal to the weight of the water contained in the hydriodic acid. This fact suggested the possibility of a selective removal of water from hydriodic acid.

Influence of the Addition of Platinum to Active Carbon on the Hydrogen Evolution. Figure 4 shows the hydrogen evolution (equals the conversion of hydrogen iodide; 100% corresponds to 84 ml (STP) of hydrogen). The points above (900 K) correspond to the sum of the amount of the hydrogen evolved in the course of the reaction at 450 K and that evolved in the high-temperature after-treatment (iodine desorption) at 900 K for 30 min. The amount of hydrogen evolved after the after-treatment was negligibly small, even at 1000 K. The hydrogen evolution obtained with the active carbon itself was remarkably lower than that obtained with the two kinds of Pt/C. This fact indicates that the catalytic activity of the adsorbent is one of the important factors that affect the hydrogen evolution.

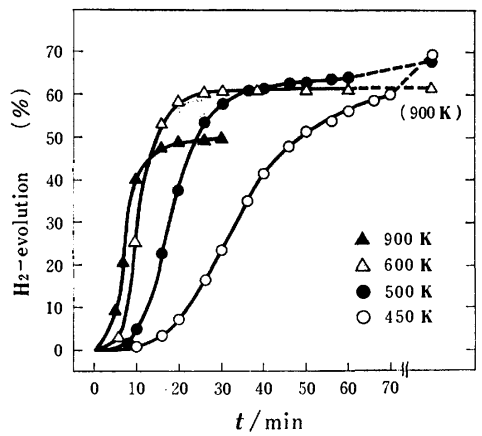

Fig. 5. Influence of the reaction temperature on the hydrogen evolution. The points above (900 K) corresponds to the sum of the amount of hydrogen evolved in the course of the reaction at each temperature and that in the high temperature after-treatment at 900 K for 30 min.

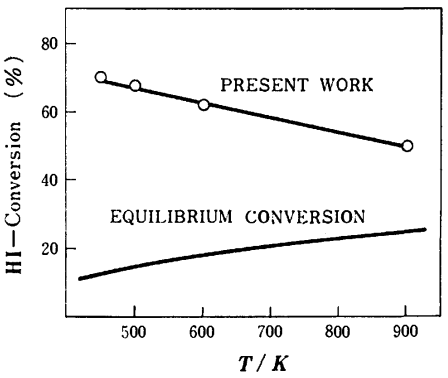

Fig. 6. Comparison of the one-path conversion with the equilibrium one.[6]

Influence of the Reaction Temperature on the Hydrogen Evolution. Figure 5 shows the hydrogen evolution at various temperatures. In the case of the reaction temperature of 900 K, the hydrogen evolution stopped within 30 min. Figure 6 shows that a one-step conversion fairly higher than the equilibrium one was obtained at each temperature. In the temperature region employed in the present experiment, lower temperatures gave higher hydrogen evolutions. This fact may be explained as follows. When the reaction temperature was low, the hydrogen formed was easily desorbed, while the iodine remained adsorbed and the reaction conditions favorable for the elevation of one-step conversion which have been mentioned in the "Principle" section were satisfied. However, as the reaction temperature increased, the desorption of the iodine became easier, as is shown in Figs. 3 and 7. Thus, the removal of the iodine formed from the reaction system by the adsorption became more difficult. Therefore, the one-step conversion decreased as the reaction temperature increased. At higher temperatures, the one-step conversion is expected to approach the equilibrium conversion. However, of course, higher temperatures required a shorter re ction time.

There was a reproducibility for each hydrogen evolution when fresh (not used) Pt/C was used. On the other hand, the hydrogen evolution obtained with a used Pt/C was lower than that obtained with a fresh Pt/C, even if the adsorbates had been fully desorbed from the used Pt/C: for example, the hydrogen evolutions were 61.5% for the first use, 58.6% for the second use, and 54.1% for the third use at 600 K. This fact suggests that the Pt/C gradually deteriorates on repeated runs through the interaction with hydrogen iodide, hydrogen, iodine, and water.

Influence of the Desorption Temperature on the Recoveries of Iodine and Hydrogen Iodide. As Fig. 7 shows, the undecomposed hydrogen iodide began desorbing at 500 K, the iodine formed did so at 600 K, and the total iodine ($HI+I_2$) finished desorption at 900 K. This is in fairly good agreement with the results of the thermogravimetric analyses (Figs. 3-c and d). The maximum temperature available in the thermochemical water splitting is expected to be around 1200 K (High Temperature Gas Cooled Reactor). The fact that the

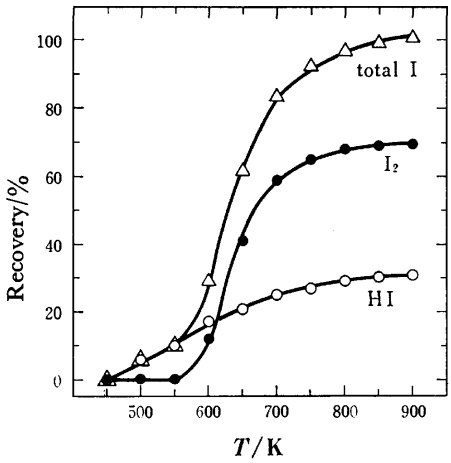

Fig. 7. Influence of the desorption temperature on the recoveries of iodine and hydrogen iodide. Column was kept at each temperature (in the direction of higher temperature) for 30 min: total $I=HI+I_2$.

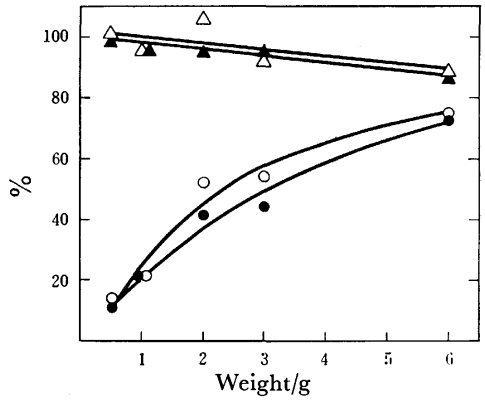

Fig. 8. Influence of the amount of the Pt/C on the hydrogen evolution, the iodine evolution, the total H recovery, and the total I recovery. Each value was obtained in one hour's reaction and thirty minutes' after-treatment at 900 K.
H_2 evolution (○), I_2 evolution (●), total H recovery (△), total I recovery (▲).

iodine desorption, which requires the maximum temperature of this method, is completed around 900 K indicates that this method may be used in the thermochemical water-splitting cycles.

Selective Removal of Water from Hydriodic Acid. As Fig. 7 shows, the undecomposed hydrogen iodide began desorbing around 500 K. On the other hand, a colorless and transparent liquid was already found to condense in the back part of the reaction tube at 450 K. As has been mentioned in the "Thermogravimetry" section, it may be suggested that the liquid was water and that the amount of it corresponded to that of the water contained in the hydriodic acid initially added on the basis of the behavior of the sample D in Fig. 3. The following experiments were carried out in order to confirm this idea. A Teflon tube packed with about 10 g of calcium chloride was attached to the back part of the reaction tube. After 1 ml of hydriodic acid had been added to Part c and the reaction tube had been maintained at 450 K for one hour in an argon stream, the weight of the Teflon tube (kept at room temperature) increased 0.72—0.73 g, with a good reproducibility. The results of titration showed that the total iodine ($HI+I_2$) present in the calcium chloride after the reaction was negligibly small. As no other colorless and transparent liquid except for water and hydriodic acid was included in the system, the liquid was confirmed to be pure water. The amount of 0.72—0.73 g corresponds to 97—98% of the amount of water (0.739 g) contained in 1 ml of the hydriodic acid. On the basis of these experiments, it was found that the water in the hydriodic acid could be removed selectively and almost completely by the use of the Pt/C.

It is well known that active carbon is consumed through the water-gas reaction with water vapor at elevated temperatures. The amounts of hydrogen evolved in the reaction of the Pt/C (2.3 wt%, 6.0 g) with water vapor (0.738 g, corresponding to the amount of the water contained in 1 ml of hydriodic acid) were as follows: 0 mmol(450 K), 0(600 K), 0(700 K), and 0.0982(900 K). On the basis of these results, it is concluded that the consumption of active carbon attributable to the water-gas reaction can be prevented when the water in the hydriodic acid is desorbed at temperatures below 750 K.

Influence of the Amount of the Pt/C on the Hydrogen Evolution. Figure 8 shows the dependence of the hydrogen evolution, the iodine evolution, the total H recovery (H_2+HI), and the total I recovery (I_2+HI) on the amount of the Pt/C. When the amount of the Pt/C was large, a high hydrogen evolution and a high iodine evolution were obtained. On the other hand, the total H recovery and the total I recovery were low in that case, since the time devoted to the desorption was not long enough. As Fig. 7 shows, if enough long time is devoted to the desorption, a total I recovery of almost 100% will be obtained. The optimum amount should be found to obtain a high hydrogen evolution, a high iodine evolution, a high total H recovery, and a high total I recovery, all at the same time.

As has been described above, it was confirmed that a fairly higher one-step conversion of hydrogen iodide than the equilibrium one could be obtained by the combination of the adsorbent with the catalytic activity, namely, the platinum-supported active carbon, and the tempreature-swing method. By the use of this method, the hydrogen formed and almost all the water contained in hydriodic acid could be separated from the product mixture through the operation at 450 K. By removing the water completely from the product mixture, the iodine and the undecomposed hydrogen iodide that desorbs below 900 K can be separated from each other easily. Therefore, the author could show the possibility of the solution of both the subjects mentioned in the introduction; the elevation of the one-step conversion and the development of an effective separation method. However, the method proposed above has two problems which remain unsolved: the rate of the process is low in the temperature region employed; and the process must be driven between the two separated temperatures. It remains necessary to undertake the research

and development of new adsorbents which do not deteriorate, their activation, and that of the pressure-swing method at elevated temperatures, where the rate of the decomposition of hydrogen iodide and the desorption of the adsorbates are high enough, from the standpoint of thermochemical water splitting.

References

1) G. E. Besenbruch, K. H. McCorkle, J. H. Norman, D. R. O'Keefe, J.R. Schuster, and M. Yoshimoto, *Proceedings of the 3rd World Hydrogen Energy Conference (WHEC), Tokyo*, 243 (1980).

2) M. Dokiya, K. Fukuda, T. Kameyama, Y. Kotera, and S. Asakura, *Denki Kagaku*, **45**, 139 (1977).

3) G. De Beni, G. Pierini, G. Spelta, D. van Velzen, and H. Langenkamp, *Proceedings of the 2nd WHEC, Zürich*, 617 (1978).

4) W. Kondo, S. Mizuta, T. Kumagai, Y. Oosawa, Y. Takemori, and K. Fujii, *Proceedings of the 2nd WHEC, Zürich, 909 (1978)*.

5) T. Hakuta, K. Haraya, T. Sako, N. Ito, H. Yoshitome, N. Todo, and J. Kato, *Proceedings of the 3rd WHEC, Tokyo*, 311 (1980).

6) Y. Oosawa, Y. Takemori, and K. Fujii, *Nippon Kagaku Kaishi*, **1980**, 1081.

7) Y. Oosawa, T. Kumagai, S. Mizuta, W. Kondo, Y. Takemori, and K. Fujii, *Bull. Chem. Soc. Jpn.*, **54**, 742 (1981).

8) D. R. O'Keefe and J. H. Norman, *Proceedings of the 3rd WHEC, Tokyo*, 277 (1980).

9) Y. Shindo, K. Obata, T. Hakuta, H. Yoshitome, N. Todo, and J. Kato, *Proceedings of the 3rd WHEC, Tokyo*, 325 (1980).

10) S. Mizuta and T. Kumagai, *Denki Kagaku*, **47**, 105 (1979).

11) "Landort Börnstein Tabellen," 6 Aufl., II Band, 4 Teil, "Kalorishe Zustandsgrössen," Springer Verlag, Berlin (1961).

12) C. L. Mantell, "Industrial Carbon," D. van Nostrand Company, New York (1946).

13) "Treatise on Analytical Chemistry," ed by I. M. Kolthoff and P. J. Elving, John Wiley and Sons, New York (1961), Vol. II, No. 7, p. 369.

14) K. Kodama, "Methods of Quantitative Inorganic Analysis," John Wiley and Sons, New York (1963).

Thermochromism of Metal Chelates with Triphenylmethane Complexons in Aqueous Solutions. IV. Carbon-13 Nuclear Magnetic Resonance Studies of Xylenol Orange (XO) and Its Zinc(II) Complex†

Shoji NAKADA, Tasuku ITO,†† Mutsuo YAMADA, and Masatoshi FUJIMOTO*

Department of Chemistry, Faculty of Science, Hokkaido University, Sapporo 060

††*Institute for Molecular Science, Okazaki 444*

(Received November 25, 1980)

Reversible thermochromism of a Zn(II) complex with 3,3′-bis[bis(carboxymethyl)aminomethyl]-*o*-cresolsulfonphthalein (Xylenol Orange, XO) was studied in D_2O by means of the ^{13}C NMR method with reference to the data of spectrophotometric and temperature-jump measurements. ^{13}C NMR spectra of XO were measured in the pD range between 2.0 and 11.0 and the signals were assigned. π-Electron conjugations in XO and Zn(II)–XO spread on phenol- and quinonoid-rings through the central carbon atom, but the phenyl ring having an SO_3^- substituent is not involved in the π-conjugated system. The temperature- and the pD-dependences of ^{13}C NMR spectra of the Zn(II)–XO complex show that the thermochromism is caused by the temperature-dependence of a protolytic equilibrium of a phenolic hydroxyl group of the Zn(II)–XO complex.

In previous papers, thermochromisms observed for the Cu(II) complexes with triphenylmethane complexons (TPMC), Xylenol Orange (XO),[1] Methylthymol Blue (MTB),[2] and Methylxylenol Blue (MXB),[2] were interpreted in terms of the temperature-dependence of a protolytic equilibrium between a complex species AH having an uncoordinated free phenolic hydroxyl group and a complex species A having a coordinated phenolate group:

$$AH \rightleftharpoons A + H. \quad (1)$$

In the present paper, we aimed at studying thermochromism of metal chelates with TPMC by the ^{13}C NMR method. We chose a diamagnetic Zn(II) complex of XO, which is remarkably thermochromic.[1] The ^1H NMR spectrum of XO[3,4] is too complicated for the present purpose. Since the ^{13}C NMR spectrum of XO has not been reported, the related compounds were also examined for ^{13}C signal assignments of XO.

Experimental

Materials. XO was synthesized by Mannich condensation from *o*-Cresol Red (*o*-CR), iminodiacetic acid (IDA), and formaldehyde.[5] A crude sample of the synthesized XO purified beforehand through a cellulose column was finally purified by means of high-performance liquid chromatography (HPLC).[6] The purified XO was used as a free acid form. Anhydrous zinc(II) chloride[7] was used for the NMR measurements. Zinc(II) perchlorate was used for equilibrium and kinetic measurements. Reagent grade Aurin, Phenol Red (PR), *o*-CR, and IDA were used. The purity of these triphenylmethane derivatives was checked by analytical HPLC with a column of Microbondapak C_{18} (4×300 mm) and water–methanol (50/50, v/v) as a solvent. Deuterium oxide (99.7%), *ca.* 37% DCl in D_2O, and *ca.* 40% NaOD in D_2O were purchased from E. Merck, Ltd.

Measurements. The carbon-13 Fourier transform NMR spectra were measured in D_2O solutions at 25.0 MHz with a JEOL JNM-FX-100/PFT-100 spectrometer at various temperatures. The sample was held in a 5 mm tube. The sample concentration was adjusted to 200 mg cm^{-3} for $ZnCl_2$, 100 mg cm^{-3} for IDA and XO, and 40 mg cm^{-3} for Aurin, *o*-CR, and PR. Dioxane was used as an internal reference. Chemical shifts are expressed by δ as δ(dioxane)=67.4.[8] The spectral width was 5000 Hz covered by 4096 addresses in the Fourier transform spectrum and the pulse width was 6 μs. Pulse repetition times ranged from 1.0 to 4.0 s with delay times of 200 μs. The number of scans ranged from 5000 to 20000.

Details on the equilibrium and kinetic measurements were described in the previous papers.[1,2]

The pD values (= pH-meter readings + 0.40)[9] of D_2O solutions were adjusted with DCl and NaOD, and measured with a Hitachi-Horiba pH-meter Model F-7SS equipped with a micro combined pH electrode. Phthalate and phosphate buffers were used for ^{13}C NMR measurements. Acetate buffers were used for equilibrium and kinetic measurements.

Results and Discussion

^{13}C NMR Spectra of XO and Related Compounds in D_2O. In order to assign ^{13}C signals of XO and Zn(II)–XO, we measured ^{13}C NMR spectra of related compounds of XO, Aurin, PR, *o*-CR, and IDA, at various pD. The structures and the abbreviated nomenclatures of those compounds are shown in Fig. 1. The ^{13}C NMR

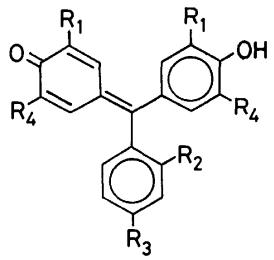

Compound	R_1	R_2	R_3	R_4
Aurin	H	H	OH	H
PR	H	SO_3H	H	H
o-CR	CH_3	SO_3H	H	H
XO	CH_3	SO_3H	H	A[a]

a) $A=CH_2N(CH_2COOH)_2$.

Fig. 1. The structures of the triphenylmethanes.

† Presented in part at the 30th Annual Meeting on Coordination Chemistry, Tokyo, October 9, 1980, Abstracts, p. 382.

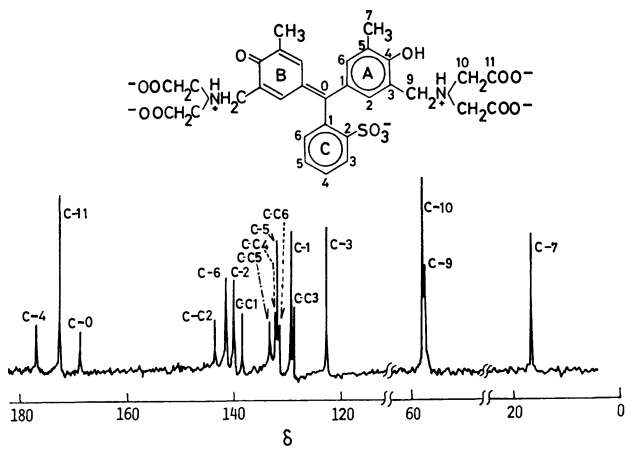

Fig. 2. The ^{13}C NMR spectrum of XO in D_2O at 29°C and pD 6.59.

spectrum of XO is given in Fig. 2.

The central carbon atom of a triphenylmethane skeleton is designated as C-0. The carbon atoms in the A, B, and C ring moieties are designated as C-A*i*, C-B*i*, and C-C*i* ($i=1, 2, \cdots, n$), respectively. In the case of the structural equivalence of the ring moieties, the carbon atoms in these ring moieties are written simply as C-*i*. The ^{13}C signals of the compounds described above were assigned by the peak intensities, the single-frequency off-resonance ^1H decoupling technique, and comparisons of their chemical shifts with those of analogous compounds.[10-12] Data on chemical shifts are summarized in Table 1.

The ^{13}C NMR spectra of Aurin, PR, and *o*-CR show the equivalence between a phenol and a quinonoid ring in neutral and alkaline solutions.[13] Machida *et al.* reported data on the structure of phenolsulfonphthalein dyes, PR, *o*-CR, *etc.*, based on laser-induced Raman spectroscopy. They suggested that phenolsulfonphthalein dyes exist in alkaline solutions as a resonance hybrid of quinonoid and phenolate structures.[14] In the ^{13}C NMR spectra of XO, seventeen peaks were observed in the range of pD 2.0—11.0. This indicates that the A- and the B-ring moieties are equivalent on the NMR time scale irrespective of the existence of a phenolic proton. High intensities of peaks of C-10 and C-11 show the existence of four identical acetate moieties. Ray *et al.* reported that the chemical shifts of the central carbon atom are in the ranges from δ 80 to 82 for para-substituted triphenylmethanols, $(p\text{-}XC_6H_4)_3COH$, and from δ 194 to 212 for the corresponding carbonium ions, $(p\text{-}XC_6H_4)_3C^+$.[15] The central carbon atoms in triphenylmethanols have the tetrahedral configuration, while those in triphenylmethyl cations are reported to be coplanar to the three adjacent ring carbons.[16] For Aurin, PR, *o*-CR, and XO, the signals of C-0 appear in the range from δ 165 to 180, which are comparable to the chemical shifts of C-0 in triphenylmethyl cations.

pD-Dependence of ^{13}C Chemical Shifts for XO. Figure 3 shows plots of values of ^{13}C chemical shifts for seventeen carbon atoms in XO *versus* pD between pD 2.0 and 11.0. C-0, C-1, C-3, C-4, and C-11 undergo significant changes in chemical shifts. Upfield signal shifts for C-0 and C-4, and a small downfield shift for C-10 with an increase in pD observed between pD 2.0 and 4.0 are attributed to the deprotonation at the carboxyl groups. Downfield signal shifts for C-0 and C-4, and an upfield shift for C-1 with an increase in pD observed between pD 5.0 and 8.0 are caused by deprotonation at the phenolic hydroxyl group. Downfield signal shifts for C-3, C-10, and C-11, and an upfield shift for C-0 with an increase in pD observed between pD 9.0 and 11.0 are caused by the deprotonation at $-NH^+-$ groups.[17] For triphenylmethane derivatives, delocalization of charge throughout the π-electron system of the molecule was suggested by Ray *et al.* on the basis of ^{13}C NMR measurements[15] and by

Table 1. ^{13}C chemical shift data for XO and related compounds in D_2O at 29 °C[a,b]

Compound	Aurin	PR	*o*-CR	XO			IDA
	pD=10.63	7.85	9.90	1.99	6.59	11.00	5.92
C-0	179.4(s)	167.6(s)	170.6(s)	166.4(s)	167.3(s)	167.9(s)	
C-1	126.6(s)	123.0(s)	126.4(s)	130.5(s)	129.5(s)	126.5(s)	
C-2	141.7(d)	140.0(d)	140.0(d)	139.1(d)	139.3(d)	139.0(d)	
C-3	121.0(d)	121.9(d)	122.1(d)	121.3(s)	122.2(s)	125.9(s)	
C-4	179.1(s)	176.0(s)	181.6(s)	173.0(s)	175.0(s)	179.6(s)	
C-5			131.2(s)	131.2(s)	131.3(s)	131.4(s)	
C-6			140.2(d)	141.1(d)	140.7(d)	140.3(d)	
C-7			17.2(q)	16.5(q)	16.4(q)	17.0(q)	
C-9				56.1(t)	57.0(t)	57.6(t)	
C-10				55.8(t)	57.5(t)	58.6(t)	49.7(t)
C-11				169.4(s)	171.6(s)	176.7(s)	172.3(s)
C–C1		137.9(s)	138.8(s)	137.3(s)	137.8(s)	138.5(s)	
C–C2		142.7(s)	142.9(s)	142.7(s)	142.8(s)	142.9(s)	
C–C3		128.8(d)	128.9(d)	128.9(d)	128.7(d)	128.6(d)	
C–C4		131.4(d)	131.2(d)	131.5(d)	131.7(d)	131.4(d)	
C–C5		132.2(d)	132.6(d)	132.5(d)	132.9(d)	132.9(d)	
C–C6		130.8(d)	130.5(d)	131.2(d)	131.0(d)	130.7(d)	

a) δ Values; δ(dioxane)=67.4. b) s=Singlet, d=doublet, t=triplet, and q=quartet.

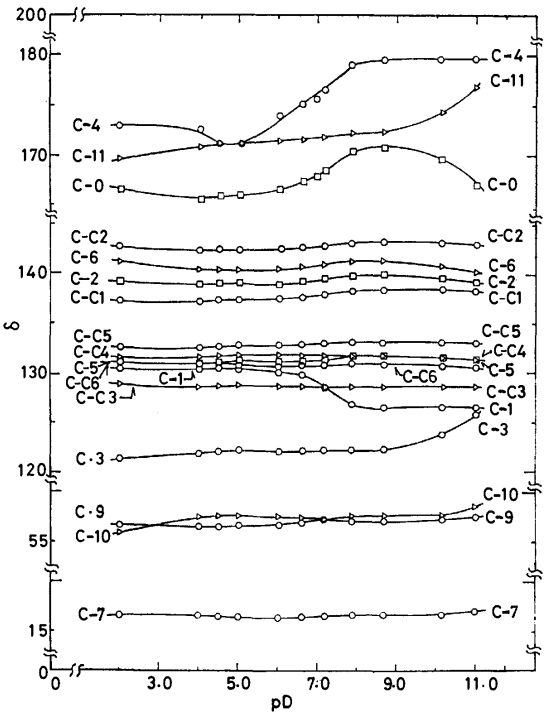

Fig. 3. pD-Dependence of the ^{13}C chemical shifts of XO.

Machida *et al.* from resonance Raman spectroscopic measurements.[14] The large pD-dependence of the chemical shift for C-0 could be explained in terms of the localization-delocalization effect of the π-electron in the molecule.

The chemical shifts of the C-ring carbon atoms were not sensitive to the pD change. In view of this fact, π-electron conjugation in the XO molecule does not spread on the C-ring.

Unexpected distinct pD-dependence of the chemical shift was observed for C-11 in the pD region 9.0—11.0. ^{1}H and ^{13}C chemical shifts are usually influenced by the formation of an intramolecular hydrogen bond.[8] Chapman *et al.* reported in their infrared and ^{1}H NMR studies of ethylenediaminetetraacetic acid and related substances the existence of doubly hydrogen-bonded rings, $-COO^{-}\cdots(NH)^{+}\cdots{}^{-}OOC-$.[19] We infer that the above pD-dependence observed in the chemical shift of C-11 should reflect the existence of such intramolecular hydrogen bonds $-COO^{-}\cdots(NH)^{+}\cdots{}^{-}OOC-$ in XO. A downfield signal shift for C-11 with an increase in pD observed between pD 9.0 and 11.0 would be attributed to the rupture of the hydrogen bonds at the protonated amino groups. Furthermore, a small upfield signal shift for C-4 observed in the pD region 2.5—4.5 would be attributed to the formation of a doubly hydrogen-bonded ring structure, $-COO^{-}\cdots(OH)\cdots{}^{-}OOC-$. Murakami *et al.* suggested the existence of a hydrogen bond between the phenolate oxygen and the proton attached to the amino nitrogen in Semi-Xylenol Orange by spectrophotometric method.[20] However, no pD-dependence was observed in the chemical shift of C-4 for XO in the pD range 9.0—11.0. This result suggests the absence of the hydrogen bond between the phenolate oxygen and the proton attached to the amino nitrogen. From the pD-dependence of chemical shifts of C-0 and C-4, the pK_a value of the phenolic hydroxyl group was determined to be 6.55 at 29 °C. This value is in good agreement with the value derived from the spectrophotometric measurements.[1]

Temperature-dependence of ^{13}C Chemical Shifts for XO. Upon heating a solution of XO buffered at pD 6.93 from 1 to 88 °C, the signals of C-0 and C-4 moved downfield by +0.7 and +1.6 ppm (Table 2). The feature of the temperature-dependence of the chemical shifts of C-0 and C-4 was similar to that of the pD-dependence of the chemical shifts of the same carbon atoms in the pD range 5.0—8.0. Since the pD-dependence of the chemical shifts of C-0 and C-4 is caused by the protonation-deprotonation equilibrium of the phenolic hydroxyl group, we conclude that the temperature-dependence of the chemical shifts for the free ligand XO is also caused by temperature-dependent protonation-deprotonation at the phenolic hydroxyl group.

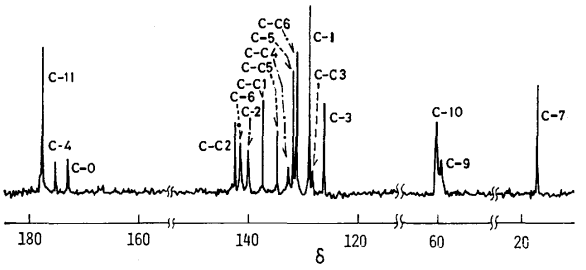

Fig. 4. The ^{13}C NMR spectrum of the Zn(II)–XO in D_2O at 29 °C and at pD 3.88. $[Zn(II)]_0=1.7$ mol dm^{-3}. $[XO]_0=0.17$ mol dm^{-3}.

^{13}C NMR Spectrum of Zn(II)–XO Complex and its pD-Dependence. ^{13}C NMR spectra of Zn(II)–XO complex were measured in the pD range 1.9—5.5 and at 29 °C using D_2O solutions containing a ten-fold excess of Zn(II) ion over the ligand. Figure 4 shows ^{13}C NMR spectrum at pD 3.88. Around pD 2.0 the signals of the carbon atoms, except for the C-ring carbon atoms, were broadened. Seventeen peaks resulting from the predominance of 2 : 1 Zn(II)–XO complex having coordinated carboxylate and amino groups were

Table 2. Chemical shifts of C-0 and C-4 for Zn(II)–XO and free XO[a] at various pD values[b] and temperatures

	T/°C		1	29	88
Zn(II)–XO	pD=3.88[c]	C-0	173.8	174.0	175.5
		C-4	176.9	176.8	180.1
	pD=5.46	C-0		176.0	
		C-4		182.5	
XO	pD=6.93[d]	C-0	167.3	167.6	168.0
		C-4	174.8	175.5	176.4
	pD=8.24	C-0		170.7	
		C-4		179.5	

a) δ Values; δ(dioxane)=67.4. b) At 29 °C. c) Phthalate buffers were used. d) Phosphate buffers were used.

observed at pD 3.88 (Fig. 4). At pD 5.46, more than nineteen peaks were observed, indicating that the formation of 1 : 1 Zn(II)–XO complex is not negligible.[21] Signals of C-0 and C-4 were observed at δ 174.0 and 176.3 at pD 3.88, and δ 176.0 and 182.5 at pD 5.46, respectively (Table 2). Both signals of C-0 and C-4 were shifted to lower fields with an increase in pD of the solution. The features of pD-dependence of chemical shifts of C-0 and C-4 for Zn(II)–XO in the pD range 3.8—5.5 were quite similar to those for the free ligand XO in the pD range 5.0—8.0. Therefore, the pD-dependence of chemical shifts of C-0 and C-4 observed for Zn(II)–XO was ascribed to the deprotonation of a phenolic hydroxyl group accompanied with coordination to the central Zn(II).

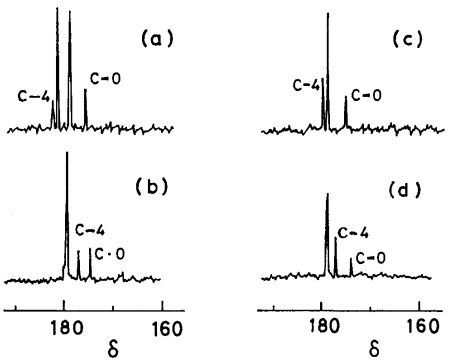

Fig. 5. pD- and temperature-dependence of the chemical shifts of C-0 and C-4 for Zn(II)–XO in D_2O. At 29 °C and at pD 5.46 (a) and 3.88 (b). At pD 3.88 and at 88 (c) and 1 °C (d). Phthalate buffres were used for (c) and (d).

Temperature-dependence of ^{13}C Chemical Shifts for Zn(II)–XO. ^{13}C NMR spectra of Zn(II)–XO were measured at various temperatures in the pD region where remarkable pD-dependences of the chemical shifts of C-0 and C-4 were observed.[22] Signals of C-0 and C-4 moved downfields by +1.7 and +3.2 ppm upon heating a solution of Zn(II)–XO buffered at pD 3.88 from 1 to 88 °C (Table 2). The feature of the temperature-dependences of chemical shifts of C-0 and C-4 (Figs. 5(a) and (b)) was similar to that of the pD-dependences of chemical shifts of the same carbon (Figs. 5(c) and (d)). This fact indicates that the temperature-dependences of the chemical shifts of C-0 and C-4 for Zn(II)–XO is caused by temperature-dependent protonation-deprotonation of a phenolic hydroxyl group in the coordinated ligand.

Spectrophotometric and Temperature-jump Studies. Figure 6 shows the temperature-dependence of the visible absorption spectra of an aqueous solution of Zn(II)–XO at pH 3.97 in the presence of a ten-fold excess of the metal ion over the ligand. The absorption spectrum changes reversibly with a distinct isosbestic point at 492 nm. As the temperature rises the absorbance at 450 nm decreases accompanied with a large increase in the absorbance at 572 nm. The feature of the temperature-dependence of the absorption spectra at a constant pH was quite similar to that of the pH-dependence of the absorption spectra at a constant temperature. These facts clearly indicate that the observed thermochromism of Zn(II)–XO is primarily due to the temperature-dependence of the protolytic equilibrium (1).

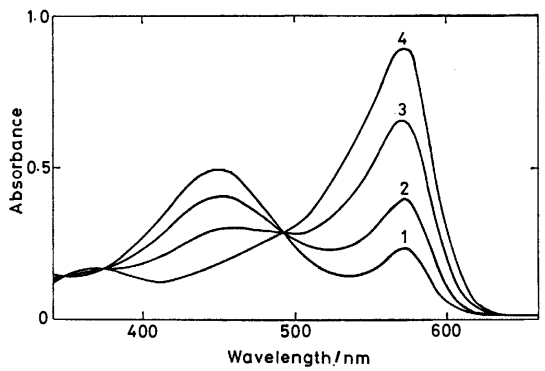

Fig. 6. Temperature-dependence of the absorption spectra of the Zn(II)–XO. At 5 (1), 24 (2), 45 (3), and 69 °C (4). $[Zn(II)]_0=2.0\times10^{-4}$ mol dm^{-3}. $[XO]_0=2.0\times10^{-5}$ mol dm^{-3}. $I=0.1$ mol dm^{-3} ($NaClO_4$). At pH = 3.97 ± 0.02.

Upon heating a solution of Zn(II)–XO complex at pH 3.97 from 15 to 35 °C, the absorbance at 572 nm increased by so large as 40%, whereas the absorbance at 580 nm of the free ligand at pH 6.40, near the pK_a value of the phenolic proton of the free ligand XO, increased only by 19% for the same temperature-rise. The increments in the chemical shifts of C-0 and C-4 for Zn(II)–XO at pD 3.88 were 1.0 and 1.9%, respectively, for temperature-rise from 1 to 88 °C, and those for the free ligand at pD 6.93 were 0.4% and 0.9% for the same temperature-rise.[23] In both spectrophotometric and ^{13}C NMR measurements, the increments of the quantities measured for the Zn(II) complex were twice as large as those for the free ligand upon heating the solutions.

Temperature-jump studies were carried out for Zn(II)–XO. A relaxation signal of an increasing absorbance at 572 nm observed in 5—10 μs region is attributed to the protolytic reaction of a phenolic hydroxyl group. The value of the rate constant for the dissociation of a phenolic proton in the complex was estimated to be 2.3×10^5 s^{-1}. This value was in the same order of magnitude as that for Cu(II)–XO.[1]

Considering the equilibrium and the kinetic data, we concluded that the temperature-dependence of the chemical shifts of C-0 and C-4 for Zn(II)–XO is primarily ascribed to the temperature-dependence of protolytic equilibrium (1).

This work was supported by the Joint Studies Program (1979—1980) of the Institute for Molecular Science.

References

1) S. Nakada, M. Yamada, T. Ito, and M. Fujimoto, *Chem. Lett.*, **1977**, 1243; *Bull. Chem. Soc. Jpn.*, **52**, 766 (1979).
2) S. Nakada, M. Yamada, T. Ito, and M. Fujimoto, *Bull. Chem. Soc. Jpn.*, **53**, 2252 (1980).
3) N. A. Kostromina, L. N. Krashnevskaya, and A. I.

Kirillov, *Ukr. Khim. Zh.*, **43**, 454 (1977).
4) H. Sato and U. Fukazawa, The 37th National Meeting of the Chemical Society of Japan, Tokyo, April 2, 1978, Abstract Vol. 1, p. 179.
5) J. Körbl and R. Přibil, *Chem. Ind. (London)*, **1957**, 233.
6) S. Nakada, M. Yamada. T. Ito, and M. Fujimoto, *Bull. Chem. Soc. Jpn.*, **50**, 1887 (1977).
7) A. R. Pray, *Inorg. Synth.*, Vol. V, 153 (1957).
8) J. B. Stothers, "Carbon-13 NMR Spectroscopy," Academic Press, New York, N. Y. (1972).
9) R. G. Bates, "Determination of pH," 2nd ed, John Wiley and Sons, New York, N. Y. (1973), p. 375.
10) L. F.Johnson and W.C. Jankowski, "Carbon-13 NMR Spectra," John Wiley and Sons, New York, N. Y. (1972).
11) "Selected ^{13}C Nuclear Magnetic Resonance Spectral Data," Vol. 1 and Supplementary Volume No. G4, Thermodynamics Research Center, Texas A and M University (1975 and 1976).
12) E. Breitmaier, G. Haas, and W. Voelter, "Atlas of Carbon-13 NMR Data," IFI/Plenum, Heyden and Son, New York, N. Y. (1975 and 1976).
13) The NMR spectra of Aurin, PR, and *o*-CR were measured in neutral and/or alkaline solutions, since they are only slightly soluble in acidic solutions.
14) K. Machida, H. Lee, and T. Uno, *J. Raman Spectrosc.*, **8**, 172 (1979).
15) G. J. Ray, R. J. Kurland, and A. K. Colter, *Tetrahedron*, **27**, 735 (1971).
16) D. W. A. Sharp and N. Sheppard, *J. Chem. Soc.*, **1957**, 674.
17) It has been reported that deprotonation of the $-NH_3^+$ or –COOH in amino acids usually causes downfield shifts of the signals of the α-, β-, and γ- carbon atoms.[18]
18) E. Breitmaier and W. Voelter, "^{13}C NMR Spectroscopy," 2nd ed, Verlag Chemie, Weinheim (1978), pp. 80—82 and 282.
19) D. Chapman, D. R. Lloyd, and R. H. Prince, *J. Chem. Soc.*, **1963**, 3645.
20) M. Murakami, T. Yoshino, and S. Harasawa, *Talanta*, **14**, 1293 (1967).
21) S. Murakami, K. Ogura, and T. Yoshino, *Bull. Chem. Soc. Jpn.*, **53**, 2228 (1980).
22) Changes in all chemical shift values upon heating unbuffered solutions of both XO and Zn(II)–XO were similar to the changes in chemical shifts with a decrease in pD of the same solutions. At 88 °C the spectrum of an unbuffered XO solution at pD 6.42 showed two new peaks assigned to C-10 and C-11 of free IDA (Table 2) in the same pD region.
23) Increases in ^{13}C chemical shifts were smaller than those expected because of the incomplete buffer action in the solutions. Upon heating from 1 to 75 °C the pH-meter reading decreased from 3.75 to 3.10 for Zn(II)–XO and from 6.51 to 6.06 for the free ligand XO.

Metal Complexes of Peptides. II.[1] Circular Dichroism Spectra and Absolute Configuration of Bis(dipeptidato)cobalt(III) Complexes

Takaji YASUI,* Hiroshi KAWAGUCHI, and Tomoharu AMA

Department of Chemistry, Faculty of Science, Kochi University, Akebono-cho, Kochi 780

(Received December 3, 1980)

Type $[Co(dipeptidato)_2]^-$ complexes (dipeptidato denotes dianions of glycylglycine, -β-alanine, -L-alanine, and -L-leucine, β-alanylglycine and -L-alanine, L-alanylglycine and -β-alanine, L-leucylglycine, and L-prolylglycine) and the complex $[Co(gly\text{-}gly)(L\text{-}pro\text{-}gly)]^-$ were prepared by a method using lead dioxide as an oxidizing agent, and these complexes were separated into two diastereomers or enantiomers by column chromatography. The absolute configurations of the optical isomers were determined on the basis of their circular dichroism patterns in the ligand transition region.

A great number of metal complexes with various peptides have been studied as enzymatic metal complexes.[2-14] However, coordination behaviors of peptides to metal ions are delicately different among metals and peptides. It is very interesting to characterize systematically metal complexes with various peptides. It is well-known that cobalt(III) ion produces stable peptide complexes.[1,3,13-20]

According to X-ray crystallographic studies of bis(glycylglycinato)cobalt(III) complex,[21,22] two glycylglycinates are coordinated to cobalt(III) in the meridional (mer) configuration as terdentate ligand. In our previous studies concerning mixed-ligand complexes containing both dipeptidate and iminodiacetate or *N*-methyliminodiacetate,[1,23] it was demonstrated by ^1H and ^{13}C NMR data that the dipeptidate coordinates to cobalt(III) in mer disposition.

Recently, Boas *et al.*[20] studied several preparative methods for type $[Co(\alpha_1\text{-}\alpha_2)_2]^-$ complexes ($\alpha_1\text{-}\alpha_2$ denotes dianion of dipeptide) and their configurations by ^1H NMR, circular dichroism (CD) spectroscopy in the d-d transition region, and column chromatography.

In the present paper, we will describe the preparation of new type bis(dipeptidato)cobalt(III) complexes containing L-proline or β-alanine residue and discuss their absolute configurations on the basis of absorption and CD spectral data.

Experimental

Ligands. Glycyl-β-alanine (H_2gly-β-ala), β-alanylglycine (H_2β-ala-gly), L-alanyl-β-alanine (H_2L-ala-β-ala), and β-alanyl-L-alanine (H_2β-ala-L-ala) were prepared by the method described in our previous paper.[1] Glycylglycine (H_2gly-gly), glycyl-L-leucine (H_2gly-L-leu), L-leucylglycine (H_2L-leu-gly) were obtained commercially from Protein Research Foundation, glycyl-L-alanine (H_2gly-L-ala) and L-alanylglycine (H_2L-ala-gly) from Fluka Chemical Company, and L-prolylglycine (H_2L-pro-gly) from Sigma Chemical Company. These purchased dipeptides were used without further purification.

Preparation of Complexes. Two Diastereomers of Potassium Bis(L-prolylglycinato)cobaltate(III), K[Co(L-pro-gly)$_2$]: L-Prolylglycine (3.44 g, 0.02 mol) was dissolved in 20 cm^3 of water, and the solution was adjusted to pH 9—9.5 with a 1 M† NaOH solution. An aqueous solution containing cobalt(II) chloride hexahydrate (2.37 g, 0.01 mol) in 10 cm^3 of water was added drop by drop to the above peptide solution, keeping the pH of the solution at *ca.* 9 with a NaOH solution. The mixed solution was oxidized with lead dioxide (5 g) at 40 °C for 1 h with stirring. The resulting solution was filtered to remove insoluble materials, and the purple filtrate was chromatographed on a QAE-Sephadex A-25 column (4.7 cm × 90 cm, Cl^- form). The positively charged and neutral complexes were removed by flushing the column with water. The adsorbed band was separated into violet and purple bands by elution with an 0.05 M KCl solution. Each eluted solution was concentrated to a small volume by a rotary evaporator at 35—40 °C. A large amount of methanol was added to the concentrated solution, and then potassium chloride which deposited was removed by filtration. The filtrate was concentrated again to a few milliliters, and the residual KCl in the solution was removed completely by using a Sephadex G-10 column. The early eluted isomer ($R(C_2)$-K[Co(L-pro-gly)$_2$]·3H_2O) was crystallized by addition of ethanol to the concentrated aqueous solution and by keeping the solution in a refrigerator for a few days. The crystals were filtered and washed with 90% ethanol, 99.5% ethanol, and then acetone. The late eluted isomer ($S(C_2)$-K[Co(L-pro-gly)$_2$]·3.5H_2O) was isolated as needle crystals by addition of acetone to the methanolic solution and by keeping the solution in a refrigerator for a few days. The crystals were filtered and washed with acetone. Both complexes were dried over calcium chloride in a desiccator under reduced pressure.

The diastereomers of other bis(dipeptidato)cobalt(III) complexes with L-alanyl-β-alaninate, β-alanyl-L-alaninate, glycyl-L-leucinate, L-leucylglycinate, glycyl-L-alaninate, or L-alanylglycinate were prepared and separated by the same procedure as that used for the complex K[Co(L-pro-gly)$_2$] described above, except that the pH of the reaction solutions containing the dipeptide ligands with β-alanyl or β-alanine residue was adjusted to 8—8.5. Crystallization of these complexes was carried out from the concentrated aqueous solutions by addition of methanol or acetone.

Two Diastereomers of Potassium(glycylglycinato)(L-prolylglycinato)cobaltate(III), K[Co(gly-gly)(L-pro-gly)]: The preparation and chromatographic separation for the diastereomers of this mixed ligand complex were carried out by the method similar to that used for the complex K[Co(L-pro-gly)$_2$], except that a mixture of glycylglycine (1.32 g, 0.01 mol) and L-prolylglycine (1.72 g, 0.01 mol) was used instead of L-prolylglycine. However, in this case an adsorbed band was separated into five ($[Co(L\text{-}pro\text{-}gly)_2]^-$ ($R(C_2)$-isomer), $[Co(gly\text{-}gly)(L\text{-}pro\text{-}gly)]^-$ ($R(C_2)$-isomer), $[Co(gly\text{-}gly)_2]^-$, $[Co(gly\text{-}gly)(L\text{-}pro\text{-}gly)]^-$ ($S(C_2)$-isomer), and $[Co(L\text{-}pro\text{-}gly)_2]^-$ ($S(C_2)$-isomer)) by continuous development using six QAE-Sephadex columns (4.7 cm × 90 cm, Cl^- form). Two diastereomers (second and forth eluates) of the mixed ligand complex were

† 1 M = 1 mol dm^{-3}.

Table 1. Analytical data of the bis(dipeptidato)cobalt(III) complexes

Complex	Elution order	C(%)		H(%)		N(%)	
		Found	(Calcd)	Found	(Calcd)	Found	(Calcd)
$Ba[Co(gly\text{-}\beta\text{-}ala)_2]_2\cdot 4H_2O$		26.50	(26.58)	4.44	(4.46)	12.22	(12.40)
$K[Co(\beta\text{-}ala\text{-}L\text{-}ala)_2]\cdot 2H_2O$	1	32.23	(32.00)	5.58	(5.37)	12.59	(12.44)
$K[Co(\beta\text{-}ala\text{-}L\text{-}ala)_2]\cdot 4H_2O$	2	29.97	(29.63)	5.61	(5.81)	11.16	(11.52)
$K[Co(L\text{-}ala\text{-}\beta\text{-}ala)_2]\cdot 3H_2O$	1	30.67	(30.77)	5.61	(5.60)	12.07	(11.96)
$K[Co(L\text{-}ala\text{-}\beta\text{-}ala)_2]\cdot 1.5H_2O$	2	32.65	(32.67)	5.22	(5.25)	12.46	(12.69)
$K[Co(L\text{-}pro\text{-}gly)_2]\cdot 3H_2O$	1	33.86	(34.15)	4.92	(5.32)	11.49	(11.38)
$K[Co(L\text{-}pro\text{-}gly)_2]\cdot 3.5H_2O$	2	33.69	(33.54)	5.40	(5.43)	10.76	(11.17)
$K[Co(gly\text{-}gly)(L\text{-}pro\text{-}gly)]\cdot 2.5H_2O$	1	30.02	(29.80)	4.97	(4.77)	12.67	(12.63)
$K[Co(gly\text{-}gly)(L\text{-}pro\text{-}gly)]\cdot 4H_2O$	2	28.14	(28.09)	4.91	(5.14)	12.04	(11.91)

isolated as needle crystals of reddish-purple color.

Barium Bis(glycyl-β-alaninato)cobaltate(III) Tetrahydrate and Potassium Bis(β-alanylglycinato)cobaltate(III) Monohydrate, $Ba[Co(gly\text{-}\beta\text{-}ala)_2)]_2\cdot 4H_2O$ and $K[Co(\beta\text{-}ala\text{-}gly)_2]\cdot H_2O$:[1] These complexes were obtained by the method similar to that used for $K[Co(L\text{-}pro\text{-}gly)_2]$. However, since the potassium salt of bis(glycyl-β-alaninato)cobaltate(III) complex was hygroscopic, it was converted to the barium salt using a small SP-Sephadex C-25 column (Ba^{2+} form).

The analytical data of the newly prepared complexes are listed in Table 1.

Partial Resolution of $[Co(gly\text{-}\beta\text{-}ala)_2]^-$. Racemic $Ba[Co(gly\text{-}\beta\text{-}ala)_2]_2\cdot 4H_2O$ (*ca.* 0.2 g) was dissolved in a small amount of water and loaded on a QAE-Sephadex column (4.7 cm × 90 cm, Cl^- form). An adsorbed band was developed with an 0.1 M L-histidinium chloride solution. After the development had been repeated about twenty-five times using a circulating micropump, the broadened band was eluted fractionally. The first and last fractions exhibited optical rotations of (−) and (+) signs at 589 nm, respectively. Each fraction was concentrated by a rotary evaporator until crystals of L-histidinium chloride appeared. The L-histidinium chloride was removed by filtration, and methanol was added to the filtrate to deposit out the residual L-histidinium chloride. After the removal of L-histidinium chloride, the methanolic solution was evaporated again almost to dryness. The resulting residue was dissolved in a small amount of water and chromatographed to remove completely the L-histidinium chloride and to convert the complex to the potassium salt using a small SP-Sephadex column (K^+ form). The crude complex was purified using a Sephadex G-10 column. The CD spectra of the optically active complexes were measured without isolating them as crystals, and the $\Delta\varepsilon$ values of the complexes were calculated from the absorption spectral data of the racemic complexes. The main CD band in the first absorption region showed negative and positive signs for the two isomers from the first and last fractions, respectively.

Partial resolution of racemic $[Co(\beta\text{-}ala\text{-}gly)_2]^-$ and $[Co(gly\text{-}gly)_2]^-$ was also carried out by the method similar to that used for the complex $[Co(gly\text{-}\beta\text{-}ala)_2]^-$. However, in the case of the complex $[Co(\beta\text{-}ala\text{-}gly)_2]^-$ the $(+)_{589}$- and $(-)_{589}$-isomers were obtained from the first and last fractions, respectively, and the elution order of the enantiomers was opposite to the cases of the complexes $[Co(gly\text{-}\beta\text{-}ala)_2]^-$ and $[Co(gly\text{-}gly)_2]^-$.

Measurements. The absorption and CD spectra were measured by a Hitachi 557-type spectrophotometer and a JASCO J-22 spectropolarimeter, respectively.

Results and Discussion

Boas *et al.*,[20] trying seven preparative methods for type $[Co(dipeptidato)_2]^-$ complexes, adopted the method starting from cobalt(III) hydroxide oxide. In the present study, however, we used the preparative method based on oxidizing cobalt(II) by lead dioxide, which is not included in the above seven methods. The present method is featured by rapid reaction, minor by-products, comparable yields of two diastereomeric complexes, and prevention of the hydrolysis of dipeptide.

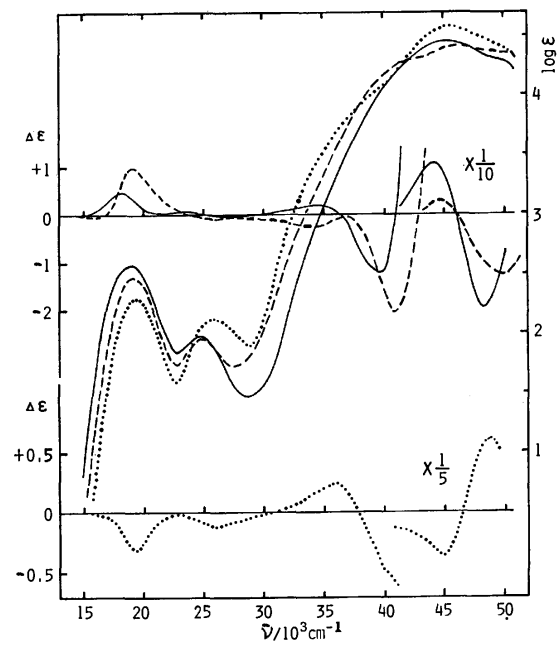

Fig. 1. Absorption (racemate) and CD (last fraction resolved by column chromatography) spectra: $[Co(gly\text{-}gly)_2]^-$ (——), $[Co(gly\text{-}\beta\text{-}ala)_2]^-$ (------), and $[Co(\beta\text{-}ala\text{-}gly)_2]^-$ (····).

Absorption Spectra. Absorption spectral data of the complexes bis(dipeptidato)cobalt(III) examined are summarized in Table 2. These complexes show a slight difference in their spectral behaviors. Figure 1 shows a comparison of absorption curves among the complexes $[Co(gly\text{-}gly)_2]^-$, $[Co(gly\text{-}\beta\text{-}ala)_2]^-$, and $[Co(\beta\text{-}ala\text{-}gly)_2]^-$. The first and second absorption maxima shift to the higher energy side in the order of gly-gly, gly-β-ala,

TABLE 2. ABSORPTION DATA OF M[Co(dipeptidato)$_2$] COMPLEXES

	Complex	Elution order	$\bar{\nu}_{max}$[a] (log ε) d-d Transition 1st band	d-d Transition 2nd band	Ligand transition band	$\varepsilon_I/\varepsilon_{II}$[b]
1	K[Co(gly-gly)$_2$]·1.5H$_2$O		18.94(2.57)	24.69(1.97)	45 25(4 45)	1.30
2	Ba$_{0.5}$[Co(gly-β-ala)$_2$]·2H$_2$O		19.16(2.48)	24.88(1.96)	46.30(4.41)	1.27
3	K[Co(β-ala-gly)$_2$]·H$_2$O		19.38(2.30)	25.84(2.13)	45 46(4 57)	1 08
4	S(C$_2$)-K[Co(gly-L-ala)$_2$]·H$_2$O	1	18.98(2 60)	24.75(1.94)	44 84(4 44)	1 34
5	R(C$_2$)-K[Co(gly-L-ala)$_2$]·2.5H$_2$O	2	18.90(2.59)	24.75(2 07)	45 25(4 48)	1 25
6	S(C$_2$)-K[Co(L-ala-gly)$_2$]·1.5H$_2$O	1	18.98(2.63)	24 88(2 01)	45 45(4 51)	1 31
7	R(C$_2$)-K[Co(L-ala-gly)$_2$]·2.5H$_2$O	2	18.90(2.59)	24.69(2 07)	45 25(4 49)	1 25
8	S(C$_2$)-K[Co(gly-L-leu)$_2$]·3H$_2$O	1	19.23(2.51)	25.51(2 03)	46.51(4.31)	1 24
9	R(C$_2$)-K[Co(gly-L-leu)$_2$]·3.5H$_2$O	2	19.16(2.58)	25.00(2.14)	46 30(4.43)	1.21
10	S(C$_2$)-K[Co(L-leu-gly)$_2$]·5.5H$_2$O	1	19.16(2.63)	25.25(2 02)	46 84(4 50)	1.30
11	R(C$_2$)-K[Co(L-leu-gly)$_2$]·4H$_2$O	2	19.05(2 62)	25 00(2 10)	46 51(4 50)	1 25
12	S(C$_2$)-K[Co(β-ala-L-ala)$_2$]·2H$_2$O	1	19.38(2 27)	26 32(1 99)	45 05(4 50)	1 14
13	R(C$_2$)-K[Co(β-ala-L-ala)$_2$]·4H$_2$O	2	19.31(2 28)	25 97(2 30)	45 05(4 55)	0 99
14	S(C$_2$)-K[Co(L-ala-β-ala)$_2$]·3H$_2$O	1	19 23(2 57)	25 00(2 06)	46 08(4 47)	1 25
15	R(C$_2$)-K[Co(L-ala-β-ala)$_2$]·1.5H$_2$O	2	19.16(2.39)	25 00(1 90)	46 51(4 36)	1 24
16	R(C$_2$)-K[Co(L-pro-gly)$_2$]·3H$_2$O	1	18 25(2 64)	24 10(2 00)	44 25(4 47)	1 32
17	S(C$_2$)-K[Co(L-pro-gly)$_2$]·3.5H$_2$O	2	18.55(2 66)	24 39(2 07)	44 84(4 53)	1.29
18	R(C$_2$)-K[Co(gly-gly)(L-pro-gly)]·2.5H$_2$O	1	18.80(2.56)	24 63(2 04)	44 64(4 47)	1 25
19	S(C$_2$)-K[Co(gly-gly)(L-pro-gly)]·4H$_2$O	2	18.73(2 62)	24 57(2 02)	44 84(4 46)	1.30

a) In the unit of 10^3 cm^{-1}. b) Molar extinction coefficient ratio of the first and second absorption maxima.

and β-ala-gly complexes. Such a shift of the maximum positions may be attributed to a delicate difference in the ligand field strength of coordinated dipeptidates or in the stability of dipeptidato complexes; it follows that the six-membered chelate ring (β-alanyl ring) in the N-terminal side is less strained than the five-membered chelate ring (glycyl ring). The order of the stability of these dipeptidato complexes quite agrees with that established by Nakahara *et al.* for copper(II) complexes of dipeptides[24] and tripeptides[25] containing glycine and/or β-alanine residues.

Difference between the type [Co(β-ala-α_2)$_2$]$^-$ and [Co(α_1-β-ala)$_2$]$^-$ or [Co(α_1-α_2)$_2$]$^-$ (α denotes α-amino acid residue) complexes is also observed in the intensity ratio of the first to second absorption maximum ($\varepsilon_I/\varepsilon_{II}$) (Table 2). It is interesting that the $\varepsilon_I/\varepsilon_{II}$ ratios of the diastereomeric complexes indicate higher values for the early eluted isomers ($S(C_2)$-isomers) than for the late eluted ones ($R(C_2)$-isomers), except for the [Co(L-pro-gly)$_2$]$^-$ complexes.

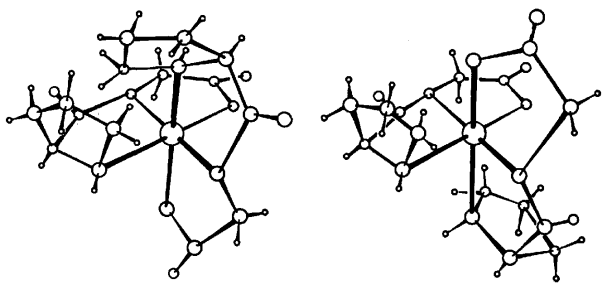

Fig. 2. Possible structures of two diastereomers in [Co(L-pro-gly)$_2$]$^-$ complex.

Figure 2 shows the two diastereomeric structures of the complex [Co(L-pro-gly)$_2$]$^-$. With the notation, proposed by Boas *et al.*[20] for the bis(dipeptidato)cobalt(III) type complexes, applied to the case of complex [Co(L-pro-gly)$_2$]$^-$, a diastereomer assuming the $R(C_2)$ configuration has a larger steric compression between the two pyrrolidine rings in the complex molecule than the other assuming the $S(C_2)$ configuration. As shown in Table 2, the first and second absorption maxima of the early eluted isomer (violet isomer) locate toward the longer wavelength side by as much as 300 and 290 cm^{-1}, respectively, than those of the late eluted isomer (purple isomer). Consequently, it is expected from these spectral behaviors that the former isomer assumes a structure of larger steric compression than the latter isomer, hence the configurations of the early and late eluted isomers can be assigned to R(C$_2$) and S(C$_2$), respectively.

Circular Dichroism Spectra and Absolute Configurations. The CD spectral data of all the complexes are listed in Table 3, and their absolute configurations and the elution order of the diastereomers are shown in Table 2. The CD spectra of the complexes examined may be divided into three band regions in the d-d transition range 15000—30000 cm^{-1}, the charge transfer range 30000—40000 cm^{-1}, and the ligand transition range 40000—50000 cm^{-1}. Figure 3 shows the CD curves of the two pairs of diastereomers in the complexes [Co(L-pro-gly)$_2$]$^-$ and [Co(gly-gly)(L-pro-gly)]$^-$. These diastereomers exhibit quite similar CD patterns in the first and second absorption regions. Therefore, in these cases it is difficult to assign their absolute configurations from their CD patterns only for the d-d transition region. On the other hand, the CD curves of the pair of diastereomers in the range of

TABLE 3. CD DATA OF M[Co(dipeptidato)$_2$] COMPLEXES

Complex	$\bar{\nu}_{ext}$[a] (log ε)				
	1st band region	2nd band region	Charge transfer band region		Ligand transition band region
1[b]	18.18(+0.41)	23.53(+0.04)	34.25(+0.18)	39.53(−1.25)	44.05(+11.00)
		27.32(−0.02)			48.08(−19.70)
2[b]	16.26(−0.012)	25.97(−0.07)	34.25(−0.27)	40.82(−2.07)	44.84(+2.94)
	19.17(+1.00)				50.00(−12.42)
3[b]	19.31(−0.31)	25.97(−0.12)	35.97(+0.23)	*ca.*40.0(−0.45)	44.84(−1.78)
					48.78(+3.00)
4	19.76(−4.127)	24.69(+0.618)	34.48(+0.426)	38.00(−0.350)	43.29(−16.59)
					49.50(+18.32)
5	17.39(+0.299)	25.64(−0.641)	35.34(+0.706)	38.76(+0.965)	47.17(−16.17)
	20.00(−1.911)				
6	19.72(−2.243)	25.84(+0.518)	31.25(+0.050)		43.86(−9.171)
					48.54(+18.66)
7	17.61(+1.857)	24.94(+1.795)	34.97(+2.082)	39.53(−2.588)	43.86(+12.88)
	20.08(−4.260)				48.08(−29.25)
8	19.27(−3.424)	26.32(−0.234)	33.56(+0.501)		42.74(−10.03)
					49.02(+15.81)
9	19.57(−3.035)	25.19(−0.900)	33.11(+0.307)	40.65(−2.479)	43.48(+1.024)
					46.73(−10.24)
10	19.76(−3.047)	25.45(+0.807)	34.22(+0.331)		43.10(−7.921)
					48.31(+13.50)
11	17.39(+1.598)	24.69(+1.612)	34.60(+2.310)	39.37(−2.700)	43.48(+10.67)
	19.80(−5.221)				47.62(−29.65)
12	19.05(−3.847)	25.97(−1.642)	32.47(+0.823)		44.05(−13.02)
	21.37(+0.905)				48.78(+5.923)
13	19.19(−2.273)	25.97(−0.839)	33.67(−0.574)	37.19(+1.146)	44.64(+4.788)
	21.28(+0.441)			40.82(−1.699)	48.31(−8.428)
14	16.53(+0.076)	25.71(+0.827)	33.67(+1.573)	37.59(−1.114)	44.25(−3.714)
	19.69(−5.419)			40.65(+0.801)	49.75(+33.87)
15	18.32(+1.480)	25.13(+0.638)	29.94(−0.120)	41.15(−7.727)	44.84(+13.97)
	20.37(−0.542)				49.75(−35.58)
16	17.27(+3.720)	24.15(+2.811)	29.59(−0.551)	38.46(−1.361)	42.19(+7.061)
	19.49(−3.589)		33.90(+2.015)		46.51(−28.24)
17	17.24(+1.933)	24.69(+1.481)	32.79(+0.174)	38.17(−2.730)	42.92(−16.41)
	19.72(−3.048)				47.17(+25.97)
18	17.67(+1.716)	24.51(+0.825)	29.85(−0.100)	39.06(−2.090)	43.10(+6.844)
	20.00(−1.298)		33.90(+0.721)		47.17(−19.72)
19	17.24(+0.348)	25.00(+0.719)		37.74(−0.777)	43.10(−10.30)
	19.88(−1.610)				47.39(+20.60)

a) In the unit of 10^{-3} cm^{-1}. b) The isomer was obtained from the last fraction when the complex was chromatographed on a QAE-Sephadex C-25 column with an 0.1 M L-histidinium chloride solution.

40000—50000 cm^{-1} show antipodal CD patterns with opposite signs, which may be related to the absolute configurations of the diastereomeric complexes. Namely, in the complex [Co(L-pro-gly)$_2$]$^-$ the CD curve of the early eluted isomer assigned to the R(C$_2$) shows plus and minus peaks at 42190 and 46510 cm^{-1}, respectively, and that of the late eluted isomer assigned to the S(C$_2$) shows minus and plus peaks at 42920 and 47170 cm^{-1}, respectively. Quite similar CD patterns are observed also for the pair of the diastereomers of the complex [Co(gly-gly)(L-pro-gly)]$^-$ (Fig. 3). Therefore, we can assign the early and late eluted isomers the configurations R(C$_2$) and S(C$_2$), respectively.

However, the observed CD spectra of the present diastereomers are produced as a sum of the configurational and vicinal contributions. Figure 4 shows only the configurational CD curves (obtained through subtraction of values for the early eluted diastereomer from those for the late eluted) for the diastereomeric complexes. The configurational CD curves in the d-d transition region exhibit quite similar patterns to each other for the L-ala-gly and L-leu-gly complexes of the gly-L-ala and gly-L-leu complexes, but those of the L-pro-gly, L-ala-β-ala, and β-ala-L-ala complexes do not indicate such a similarity among them. On the other hand, the configurational CD curves in the region of 40000—50000 cm^{-1} show the same patterns (plus and minus signs from the longer wavelength side) for

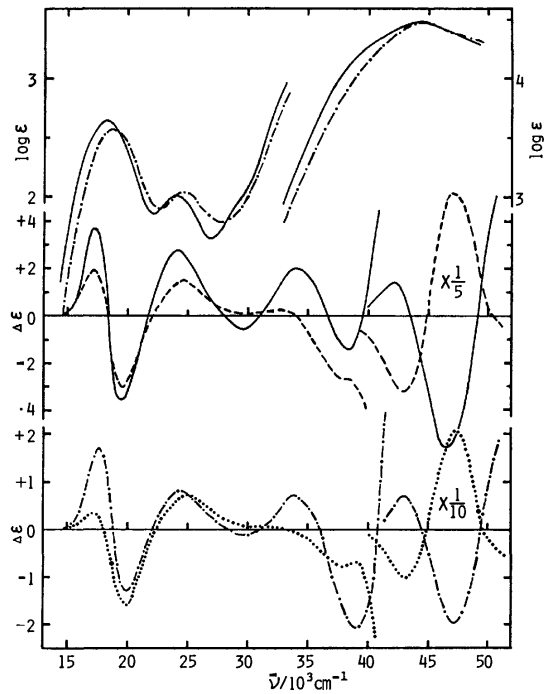

Fig. 3. Absorption and CD spectra of the dipeptidato complexes: early (——) and late (------) eluted diastereomers of [Co(L-pro-gly)$_2$]$^-$; early (·····) and late (·····) eluted diastereomers of [Co(gly-gly)(L-progly)]$^{-1}$.

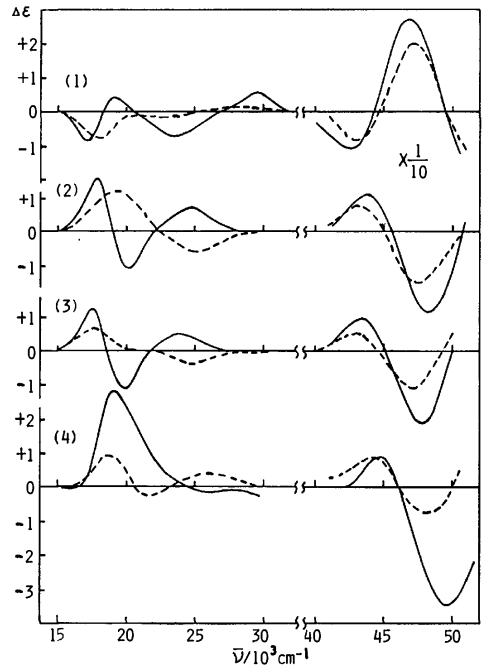

Fig. 4. Configurational CD curves calculated for the dipeptidato complexes: [(late eluted diastereomer)—(early eluted diastereomer)]/2. (1) [Co(L-pro-gly)$_2$]$^-$ (——) and [Co(gly-gly)(L-pro-gly)]$^-$ (------), (2) [Co(L-ala-gly)$_2$]$^-$ (——) and [Co(gly-L-ala)$_2$]$^-$ (------), (3) [Co(L-leu-gly)$_2$]$^-$ (——) and [Co(gly-L-leu)$_2$]$^-$ (------), (4) [Co(L-ala-β-ala)$_2$]$^-$ (——) and [Co(β-ala-L-ala)$_2$]$^-$ (------).

complexes (2)—(4) in Fig. 4. From a comparison of these CD patterns with those of the L-pro-gly and (gly-gly)(L-pro-gly) complexes one can assign the absolute configurations to the paired diastereomers in complexes (2)—(4). Namely, the R(C_2) and S(C_2) configurations can be assigned to the late and early eluted diastereomers of complexes (2)—(4), respectively, as shown in Table 2. These configurational assignments for the gly-L-ala, L-ala-gly, gly-L-leu, and L-leu-gly complexes are quite in agreement with those by Boas *et al.*[20]

An analogous discussion can be made for the complexes [Co(gly-gly)$_2$]$^-$, [Co(gly-β-ala)$_2$]$^-$, and [Co(β-ala-gly)$_2$]$^-$ which were partially resolved by column chromatography[26] using an 0.1 M L-histidinium chloride solution. Figure 1 shows the CD spectra of their first fractions ((+)$_{589}$-[Co(gly-gly)$_2$]$^-$, (+)$_{589}$-[Co(gly-β-ala)$_2$]$^-$, and (—)$_{589}$-[Co(β-ala-gly)$_2$]$^-$). The CD patterns in the ligand transition region exhibit plus and minus signs in the range 40000—50000 cm^{-1} for the gly-gly and gly-β-ala complexes. Therefore, the R(C_2) configuration can be assigned to the first fractions ((+)$_{589}$-isomer) of these complexes. The elution order of the two enantiomers in the complex [Co(gly-gly)$_2$]$^-$ was the same as that Gillard *et al.*[15,20] obtained with a starch column. On the other hand, the first fraction ((—)$_{589}$-isomer) of the complex [Co(β-ala-gly)$_2$]$^-$ shows the CD pattern with opposite (minus and plus) signs which can be assigned to the S(C_2) configuration.

This work was supported by a Grant-in-Aid for Scientific Research No. 343012 from the Ministry of Education, Science and Culture.

References

1) Part 1 of this series: H. Kawaguchi, M. Kanekiyo, T. Ama, and T. Yasui, *Bull. Chem. Soc. Jpn.*, **53**, 3208 (1980).
2) J. B. Gilbert, M. C. Otey, and V. E. Price, *J. Biol. Chem.*, **190**, 377 (1951).
3) E. D. McKenzie, *J. Chem. Soc., A*, **1969**, 1655.
4) E. Kimura, *Inorg. Chem.*, **13**, 951 (1974).
5) F. P. Bossu, E. B. Paniago, D. W. Margerum, S. T. Kirksey, Jr., and J. L. Kurtz, *Inorg. Chem.*, **17**, 1034 (1978).
6) D. W. Appleton, T. P. A. Kruck, and B. Sarkar, *J. Inorg. Biochem.*, **10**, 1 (1978).
7) Y. Nakao and A. Nakahara, *Bull. Chem. Soc. Jpn.*, **51**, 3522 (1978).
8) R. E. Viola, C. R. Hartzell, and J. J. Villafranca, *J. Inorg. Biochem.*, **10**, 293 (1979).
9) H. Lakusta and B. Sarkar, *J. Inorg. Biochem.*, **11**, 303 (1979).
10) S. T. Kirksey, Jr., and D. W. Margerum, *Inorg. Chem.*, **18**, 966 (1979).
11) Y. Sugiura and Y. Mino, *Inorg. Chem.*, **18**, 1335 (1979).
12) T. Sakurai and A. Nakahara, *Inorg. Chem.*, **19**, 847 (1980).
13) R. D. Gillard, E. D. McKenzie, R. Mason, and G. B. Robertson, *Coord. Chem. Rev.*, **1**, 263 (1966).
14) J. P. Collman and E. Kimura, *J. Am. Chem. Soc.*, **89**, 6096 (1967).
15) R. D. Gillard, *Inorg. Chim. Acta Rev.*, **1**, 69 (1967).
16) R. D. Gillard, P. M. Harrison, and E. D. McKenzie, *J. Chem. Soc., A*, **1967**, 618.

17) I. G. Browning, R. D. Gillard, J. R. Lyons, P. R. Mitchell, and D. A. Phipps, *J. Chem. Soc., Dalton Trans.*, **1972**, 1815.
18) L. G. Stadtherr and R. B. Martin, *Inorg. Chem.*, **12**, 1810 (1973).
19) R. D. Gillard and P. R. Mitchell, *J. Chem. Soc., Chem. Commun.*, **1978**, 428.
20) L. V. Boas, C. A. Evans, R. D. Gillard, P. R. Mitchell, and D. A. Phipps, *J. Chem. Soc., Dalton Trans.*, **1979**, 582.
21) R. D. Gillard, E. D. McKenzie, R. Mason, and G. B. Robertson, *Nature*, **1966**, 1347.
22) M. T. Barnet and H. C. Freeman, *J. Chem. Soc., D*, **1970**, 367.
23) H. Kawaguchi, K. Maeda, T. Ama, and T. Yasui, *Chem. Lett.*, **1979**, 1105.
24) O. Yamauchi, Y. Hirano, Y. Nakao, and A. Nakahara, *Can. J. Chem.*, **47**, 3441 (1969).
25) Y. Nakao, H. Ishibashi, and A. Nakahara, *Bull. Chem. Soc. Jpn.*, **43**, 3457 (1970).
26) Y. Yoshikawa and K. Yamasaki, *Coord. Chem. Revs.*, **28**, 205 (1979).

Metal Complexes Coordinating Pyridine Derivatives. III.[1] Stereoselective Formation of Chromium(III) Complexes of Chiral Quadridentate Ligands

Yukihiro YAMAMOTO* and Yoichi SHIMURA

Department of Chemistry, Faculty of Science, Osaka University, Toyonaka, Osaka 560

(Received December 22, 1980)

Dichloro mononuclear and di-μ-hydroxo dinuclear chromium(III) complexes were prepared with the following three ligands, (*S*)-*N*,*N*′-bis(2-pyridylmethyl)propylenediamine (abbrev. *S*-picpn), (*S*,*S*)-*N*,*N*′-bis(2-pyridylmethyl)-2,3-butanediamine (abbrev. *SS*-picbn), and (*S*,*S*)-*N*,*N*′-bis(2-pyridylmethyl)-1,2-cyclohexanediamine (abbrev. *SS*-picchxn). The *SS*-picbn and *SS*-picchxn ligands produce novel *Λ*(*SS*)-*cis*-α diastereomer of dichloro complex, in which the terminal chelate ring is formed by coordination of equatorially-oriented substituent on the secondary nitrogen atom. An explanation from the viewpoint of steric repulsion is given for the stereoselective formation of *Λ*(*SS*) diastereomers for the *cis*-α dichloro complexes of *SS*-picchxn and *SS*-picbn. A similar explanation is also given for stereoselective formation of a limited number of isomers of dinuclear μ-hydroxo complexes of *S*-picpn, *SS*-picbn, and *SS*-picchxn.

In a previous paper,[2] two diastereomers *Δ*(*S*) and *Λ*(*S*) were prepared for a *cis*-α-dichloro or dibromo chromium(III) complex of a quadridentate ligand (*S*)-*N*,*N*′-bis(2-pyridylmethyl)propylenediamine (abbrev. *S*-picpn). In the *Δ*(*S*)-*cis*-α diastereomer, the quadridentate ligand takes the most stable conformation, the aminomethylpyridine chelate ring being formed by coordination of an axially-oriented substituent on the secondary nitrogen atom. This fact was confirmed from the X-ray crystal structure analysis of *Δ*-*cis*-α-[$CrCl_2$(*S*-picpn)]Cl.[3] On the other hand, the *Λ*(*S*)-*cis*-α diastereomer belongs to a rather rare type, in which the terminal chelate ring is formed by coordination of an equatorially-oriented substituent on the secondary nitrogen (Fig. 1). Another example of this type found in literature is a *Δ*-*cis*-α diastereomer of (oxalato or ethylenediamine) {(*R*,*R*)-*N*,*N*′-dimethyl-1,2-cyclohexanediamine(diacetato)}cobalt(III).[4]

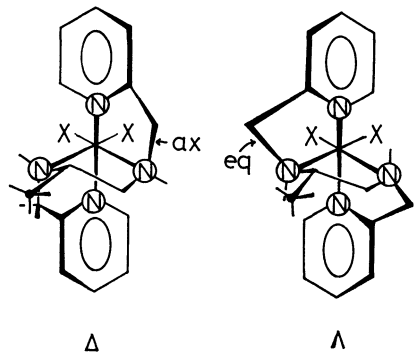

Fig. 1. Two *cis*-α diastereomers of $[CrX_2$(*S*-picpn)]$^+$, "ax" showing the axial orientation of the pyridylmethyl substituent on the secondary nitrogen atoms and "eq" the equatorial orientation.

In this paper, two kinds of chiral ligands, (*R*,*R*)-*N*,*N*′-bis(2-pyridylmethyl)-1,2-cyclohexanediamine (abbrev. *RR*-picchxn) and (*S*,*S*)-*N*,*N*′-bis(2-pyridylmethyl)-2,3-butanediamine (abbrev. *SS*-picbn), were used for preparation of dichloro and di-μ-hydroxo type chromium(III) complexes, turning our attention to the *cis*-α structure. For convenience, the explanation is made in Results and Discussion using *SS*-picchxn, actually *RR*-picchxn being used in Experimental.

Experimental

Ligands. *(S,S)-2,3-Butanediamine*: This was prepared and resolved by the method in the literature.[5] The absolute configuration is considered to be (*S*, *S*) from the literature.[6]

(R,R)-1,2-Cyclohexanediamine: This was resolved by the method in the literature.[7]

The quadridentate ligands *S*-picpn, *SS*-picbn, and *RR*-picchxn were prepared from (*S*)-propylenediamine, (*S*, *S*)-2,3-butanediamine, or (*R*,*R*)-1,2-cyclohexanediamine and 2-pyridinecarbaldehyde by the method of Goodwin and Lions.[8]

Mononuclear Complexes. *Preparation I*: Anhydrous chromium(III) chloride (1.0 g) was suspended in 0.1 cm^3 of dimethyl sulfoxide, the equimolar amount (1.79 g) of *SS*-picbn (1.8 g in the case of *RR*-picchxn) being added slowly with stirring. After thirty minutes, unreacted material was filtered off and the filtered solution was poured onto an SP-Sephadex C-25 column ($\phi 30 \times 700$ mm) and the adsorbed band was eluted with 0.1 mol dm^{-3} NaCl aqueous solution. Three bands were eluted, a purple one (i), a red-violet one (ii), and a violet one (iii). The first band proved to contain only one diastereomer by examining circular dichroism (CD) spectra of the fractions of this band collected with a fraction collector. To the concentrated solution of the eluate was added sodium perchlorate and obtained precipitates were recrystallized from warm water. For the *SS*-picbn complex: Found; C, 38.24; H, 4.56; N, 10.97%. Calcd for $[CrCl_2$(*SS*-picbn)]$ClO_4 \cdot 0.5H_2O = C_{16}H_{22}N_4O_4Cl_3Cr \cdot 0.5H_2O$: C, 38.30; H, 4.62; N, 11.17%. For the *RR*-picchxn complex: Found; C, 41.24; H, 4.68; N, 10.68%. Calcd for $[CrCl_2$(*RR*-picchxn)]$ClO_4 \cdot 0.5H_2O = C_{18}H_{24}N_4O_4Cl_3Cr \cdot 0.5H_2O$: C, 40.96; H, 4.77; H, 10.62%. The band (ii) contained two species but decomposed during the concentration procedure even below 25 °C. The band (iii) seemed to be a di-μ-hydroxo complex, but its yield was very low. In the same way the *S*-picpn dichloro complex has been prepared, both *Δ* and *Λ* diastereomers being isolated.[2]

Preparation II: Chromium shot (0.50 g) was crushed and dissolved in hydrochloric acid under nitrogen atmosphere. the blue solution was evaporated to dryness, to which was added 2.56 g of *SS*-picbn (2.86 g in the case of *RR*-picchxn) in 4 cm^3 of pyridine. While refluxing for ten minutes, a pyridine solution (10 cm^3) of iodine (2.44 g) was added. The deposited product was dissolved in water and passed through the Dowex 1-X8 column (Cl^- form). After concentrating the eluate, 60% perchloric acid was added. The precipitate was recrystallized from hot water. Only one diastereomer was obtained, the CD spectrum being the same as the band

(i) in Preparation I. For the *SS*-picbn complex: Found; C, 38.65; H, 4.57; N, 11.24%. Calcd for $[CrCl_2(SS\text{-picbn})]ClO_4 \cdot 0.5H_2O = C_{16}H_{22}N_4O_4Cl_3Cr \cdot 0.5H_2O$: C, 38.30; H, 4.62; N, 11.17%. For the *RR*-picchxn complex: Found; C, 40.88; H, 4.72; N, 10.54%. Calcd for $[CrCl_2(RR\text{-picchxn})]ClO_4 \cdot 0.5H_2O = C_{18}H_{24}N_4O_4Cl_3Cr \cdot 0.5H_2O$: C, 40.96; H, 4.77; N, 10.62%. This method of preparation gave only the more stable diastereomer (*Λ*) in the case of the *S*-picpn ligand.[2]

Di-μ-hydroxo Dinuclear Complexes. Chromium(III) bromide hexahydrate (2.0 g) was dissolved in 2-methoxyethanol (15 cm^3). After adding zinc powder, *S*-picpn (1.28 g) was added with stirring. After ten minutes, the zinc powder and violet precipitate were filtered off, and the filtrate was poured onto an SP-Sephadex C-25 column ($\phi 30 \times 700$ mm). Eluting with 0.5 mol dm^{-3} NaCl aqueous solution, three bands were obtained, a brown one (i), and two violet ones (ii) and (iii). Pure crystalline product was obtained by concentrating the eluate (ii) and adding an aqueous solution of sodium perchlorate. For the *S*-picpn complex: Found; C, 32.44; H, 4.24; N, 9.95%. Calcd for $[\{Cr(OH)(S\text{-picpn})\}_2](ClO_4)_4 \cdot 3.5H_2O = C_{30}H_{42}N_8O_{18}Cl_4Cr_2 \cdot 3.5H_2O$: C, 32.42; H, 4.44; N, 10.08%. For the *SS*-picbn complex: Found; C, 33.32; H, 4.52; N, 9.59%. Calcd for $[\{Cr(OH)(SS\text{-picbn})\}_2](ClO_4)_4 \cdot 3H_2O = C_{32}H_{46}N_8O_{18}Cl_4Cr_2 \cdot 3H_2O$; C, 33.99; H, 4.64; N, 9.91%. For the *RR*-picchxn complex: Found; C, 35.92; H, 4.83; N, 9.24%. Calcd for $[\{Cr(OH)(RR\text{-picchxn})\}_2](ClO_4)_4 \cdot 4H_2O = C_{36}H_{50}N_8O_{18}Cl_4Cr_2 \cdot 4H_2O$: C, 36.01; H, 4.87; N, 9.33%. The eluate (i) seemed to be a mononuclear species. From (iii) pure crystals could not be obtained in spite of repeated crystallizations. This may be a polynuclear complex.

The dinuclear complex $[\{Cr(OH)(RR\text{-picchxn})\}_2](ClO_4)_4$ was dissolved in concd hydrochloric acid. After 6 d, 30% perchloric acid was added to it and the obtained perchlorate salt was recrystallized from water. Found: C, 40.41; H, 4.68; N, 10.40%. Calcd for $[CrCl_2(RR\text{-picchxn})]ClO_4 \cdot H_2O = C_{18}H_{24}N_4O_4Cl_3Cr \cdot H_2O$: C, 40.28; H, 4.88; N, 10.44%. The CD spectrum of this mononuclear complex was the same as those of the samples prepared in Preparations I and II.

Other Complexes. The dinuclear complexes $[\{Cr(OH)(picen)\}_2](ClO_4)_4$, $[\{Cr(OH)(pma)_2\}_2](ClO_4)_4$ (pma=2-pyridylmethylamine), and *meso*-$[\{Cr(OH)(en)_2\}_2]Cl_4$ were prepared by the methods in the literatures.[9-12]

ΛΛ-trans(py)*trans*(py)-$[\{Cr(OH)(S\text{-pea})_2\}_2]I_4$ (*S*-pea=(*S*)-1-(2-pyridyl)ethylamine) was prepared in a previous paper.[1]

Measurements. The visible and ultraviolet absorption spectra were measured with a Shimadzu UV-200 and a Hitachi 330 spectrophotometer. The CD spectra were measured on a JASCO MOE-1 spectropolarimeter. The dichloro complexes were measured in 0.1 mol dm^{-3} HCl and the dinuclear ones in water.

Results and Discussion

Structure Assignments. The absorption and CD spectra of the mononuclear dichloro complexes of *SS*-picbn and *SS*-picchxn are shown in Fig. 2. The geometries and absolute configurations were determined from the CD spectra in the first d-d absorption band region. As stated in a previous paper,[2] the CD of *Λ-cis-α* complex of chromium(III) or cobalt(III) coordinated with pcen derivative shows a typical (+, −) dispersion pattern from the lower energy side and that of *Λ-cis-α* (−, +), the $|\Delta\varepsilon|$ value at the each extremum being larger than 1.0. From this criterion, the present complexes of *SS*-picbn and *SS*-picchxn are assigned *Λ-cis-α* form. The absorption and CD spectra of di-*μ*-hydroxo dinuclear complexes of *S*-picpn, *SS*-picbn, and *SS*-picchxn are shown in Figs. 3 and 4 together with those of *ΔΔ-trans*(py)*trans*(py)-$[\{Cr(OH)(picen)\}_2](ClO_4)_4$ (picen=*N,N'*-bis(2-pyridylmethyl)ethylenediamine)(each parts linked by two hydroxyl groups take *trans*(py)*trans*(py) structure(cis-α structure)), which takes the *trans*(py)*trans*(py) structure stereoselectively because of the steric hindrance between pyridine rings.[10] The CD curve of *S*-picpn complex is nearly a mirror image to that of the picen complex of *ΔΔ* configuration. Thus the configuration of the *S*-picpn complex is assigned

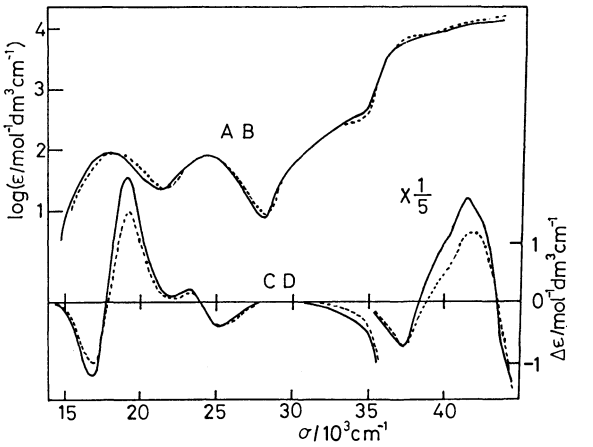

Fig. 2. The absorption (AB) and CD spectra of *Λ-cis-α*-$[CrCl_2(SS\text{-picchxn})]ClO_4$ (——) and *Λ-cis-α*-$[CrCl_2(SS\text{-picbn})]ClO_4$ (------).

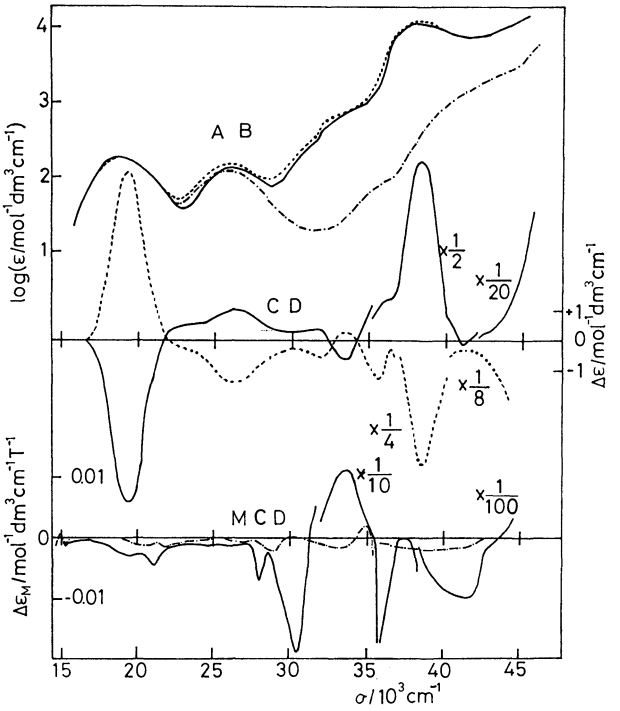

Fig. 3. The absorption (AB) and CD spectra of *ΔΔ-trans*-(py)*trans*(py)$[\{Cr(OH)(picen)\}_2](ClO_4)_4$ (——) and *ΔΔ-trans*(py)*trans*(py)$[\{Cr(OH)(S\text{-picpn})\}_2](ClO_4)_4$ (------). The AB and MCD spectra of *meso*-$[\{Cr(OH)(en)_2\}_2]Cl_4$ (·····) and MCD of *trans*(py)*trans*(py)$[\{Cr(OH)(picen)\}_2](ClO_4)_4$ (——) are also presented.

TABLE 1. THE ABSORPTION AND CD DATA (sh=shoulder)

Complex	Absorption		CD		
	σ_{max}/cm^{-1}	log ε_{max} [a)]	σ_{ext}/cm^{-1}	$\Delta\varepsilon$ [a)]	Assignment
Λ-*cis*-*α*-[$CrCl_2$(*SS*-picbn)]ClO_4 (Fig. 2)	18280	1.96	16980	−1.01	d-d
			19230	+1.49	
	24570	1.92	23310	+0.15	
			25450	−0.44	
			30030	−0.01	py(triplet)
			30490	−0.01	
	34000(sh)	2.45	31060	+0.03	
	36360(sh)	3.85	37370	−7.50	py(^1L_b), CT
			39220(sh)	+1.75	
			42190	+11.2	
			46730	−35.5	
Λ-*cis*-*α*-[$CrCl_2$(*SS*-picchxn)]ClO_4 (Fig. 2)	18080	1.97	16860	−1.21	d-d
			19080	+2.06	
	24390	1.94	23260	+0.22	
			25320	−0.43	
			30770	+0.33	py(triplet)
	34000(sh)	2.5	32150	+0.06	
	36360(sh)	3.63	37310	−7.29	py(^1L_b), CT
			39220(sh)	+5.70	
			41490	−17.0	
			46950	+39.9	
ΛΛ-[{Cr(OH)(*SS*-picbn)}$_2$]$(ClO_4)_4$ (Fig. 4)	18760	2.27	19270	+6.59	d-d
	25910	2.17	26040	−1.54	
	32790(sh)	2.86	31550	−0.46	py(triplet), *μ*-OH
			33110	+0.64	
			35090	−1.06	
	38020	4.14	36100	+2.08	py(^1L_b)
			38170	−15.0	
ΛΛ-[{Cr(OH)(*SS*-picchxn)}$_2$]$(ClO_4)_4$ (Fig. 4)	18980	2.24	19120	+6.59	d-d
	25910	2.17	26040	−1.36	
	32790(sh)	2.82	31550	−0.50	py(triplet), *μ*-OH
			33060	+0.50	
			35090	−1.22	
	38170	4.33	36230	+1.75	py(^1L_b)
			38460	−15.0	
ΛΛ-[{Cr(OH)(*S*-picpn)}$_2$]$(ClO_4)_4$ (Fig. 3)	18870	2.24	19230	+5.61	d-d
	26040	2.21	26600	−1.58	
	32790(sh)	2.83	31750	−0.61	py(triplet), *μ*-OH
			33330	+0.36	
			35590	−1.34	
	38460	4.12	38310	−16.8	py(^1L_b)
ΔΔ-[{Cr(OH)(picen)}$_2$]$(ClO_4)_4$ (Fig. 3)	18800	2.29	19160	−5.39	d-d
	26040	2.16	25910	+1.06	
	32790(sh)	2.80	31750	+0.39	py(triplet), *μ*-OH
			33330	−0.74	
			36230	+3.03	
	38020	4.10	38310	+11.9	py(^1L_b)
			40980	−0.19	
ΔΔ-[{Cr(OH)(pma)$_2$}$_2$]$(ClO_4)_4$	18400	2.29	17090	+0.34	d-d
			19720	−5.38	
	26050	2.06	26600	+1.53	
	32790(sh)	2.76	32260	+0.08	py(triplet), *μ*-OH
			33840	−1.16	
	38000	4.12	36870	−9.02	py(^1L_b)
			39000	+6.3	
ΛΛ-[{Cr(OH)(*S*-pea)$_2$}$_2$]I_4 (Fig. 6)	18500	2.32	17000	−0.27	d-d
			19800	+5.29	
	26450	2.12	26620	−1.75	
	32790(sh)	2.82	32270	−0.25	py(triplet), *μ*-OH
			33950	+1.23	
			35400	−0.40	
	38300	4.21	37330	+16.8	py(^1L_b)
			39100	−1.20	
			41350	+3.50	
	44600	4.73			

a) ε is given in mol^{-1} dm^3 cm^{-1}.

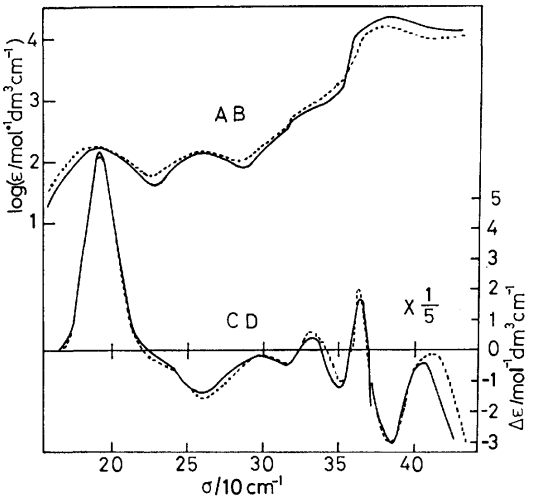

Fig. 4. The absorption (AB) and CD spectra of *ΔΔ-trans*-(py)*trans*(py)-[{Cr(OH)(*SS*-picchxn)}$_2$](ClO$_4$)$_4$ (——) and *ΔΔ-trans*(py)*trans*(py)-[{Cr(OH)(*SS*-picbn)}$_2$]-(ClO$_4$)$_4$ (------).

ΔΔ-trans(py)*trans*(py). From the CD spectra in Fig. 4, the *SS*-picbn and *SS*-picchxn complexes are assigned *ΔΔ-trans*(py)*trans*(py). These assignments are supported by the decomposition experiment of the dinuclear complex into the mononuclear complex. The numerical data for the absorption and CD spectra are collected in Table 1.

Stereoselective Formation of Diastereomers. The *Δ* and *ΔΔ* diastereomers of the mononuclear and dinuclear complexes were prepared, respectively, for the ligands, *S*-picpn, *SS*-picbn, and *SS*-picchxn, in this study. They belong to the type in which the terminal chelate ring are formed by coordination of the equatorially-oriented substituents on the secondary nitrogen atoms (Fig. 1). Both *Δ* and *Λ* diastereomers of *S*-picpn dichloro mononuclear complex were obtained by the method of Preparation I, but only the more stable *Δ* one in Preparation II. On the other hand, only one isomer was obtained in the case of *SS*-picchxn and *SS*-picbn in either method of preparation. In Fig. 5 the two diastereomers, *Δ-cis-α* and *Λ-cis-α* of mononuclear *SS*-picchxn complex are shown. The central chelate ring takes the most stable *δ* conformation for the *SS*-picchxn ligand. In the *Δ* form, there is a steric repulsion between one of the methylene proton (1 in Fig. 5) of the terminal chelate ring and the proton (2 in Fig. 5) attached to the cyclohexane carbon atom adjacent to the asymmetric one. In this form the terminal chelate ring is less strained than that of the *Λ* form. On the other hand, in the *Λ* form there is no such steric repulsion as in the *Δ* form, though the terminal chelate ring in the *Λ* form is more strained than that in *Δ* form. If the steric hindrance predominates, only the *Λ* form will be formed. A preliminary X-ray crystal structure analysis revealed that the *Λ-cis-α*-[CrCl$_2$(*SS*-picchxn)]ClO$_4$ has in fact the terminal chelate rings of equatorially-oriented pyridylmethyl groups on the secondary nitrogen atoms.[13] In the case of *SS*-picbn ligands, the steric repulsion between the methylene proton and the methyl group on the central chelate ring is considered to be similar to the case of *SS*-picchxn ligand. Thus the *Λ* form was actually isolated.

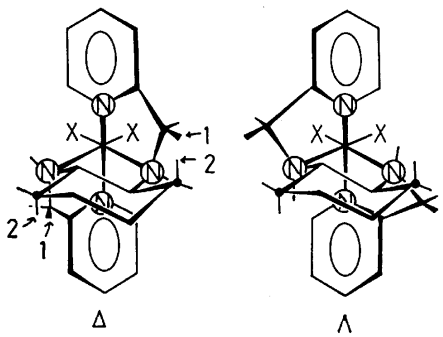

Fig. 5. The two diastereomers of *cis*-α-[CrX$_2$(*SS*-picchxn)]$^+$.

For the dinuclear complexes of *SS*-picchxn and *SS*-picbn, the stereoselective formation of diastereomers can be explained by the same way as in the mononuclear ones. For the *S*-picpn ligand, only the *ΔΔ* form was formed. One more factor must be taken into account. From the X-ray structure analyses of *meso*-[{Cr(OH)-(en)$_2$}$_2$](S$_2$O$_6$)$_2$[14] and racemic [{Cr(OH)(phen)$_2$}$_2$]I$_4$-4H$_2$O[15] (phen=1,10-phenanthroline), the in-plane <NCrN angle of di-*μ*-hydroxo dinuclear complexes is larger than 90° ("in-plane" means that the N atoms are in the plane defined by two chromium and two hydroxo-oxygen atoms). On the other hand, the

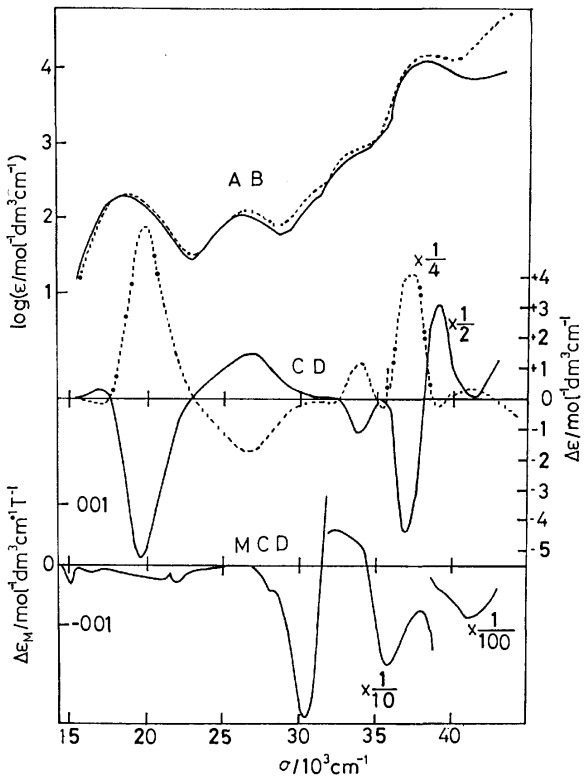

Fig. 6. The absorption (AB), CD and MCD spectra of *ΔΔ-trans*(py)*trans*(py)-[{Cr(OH)(pma)$_2$}$_2$](ClO$_4$)$_4$ (——), and AB and CD spectra of *ΔΔ-trans*(py)*trans*-(py)-[{Cr(OH)(*S*-pea)$_2$}$_2$]I$_4$ (------).

TABLE 2. MCD SPECTRAL DATA (sh=shoulder)

Complex	σ_{ext}/cm^{-1}	$10^2\ \Delta\varepsilon_M$ [a]	Assignment
$[\{Cr(OH)(en)_2\}_2]Cl_4$ (Fig. 3)	14390	−0.38	d-d(doublet)
	14860	+0.08	
	15380	−0.11	
	20830	−0.14	d-d(quartet)
	21880	−0.16	d-d(doublet)
	27030	−0.06	d-d(doublet)
	28900	−0.23	d-d(doublet)?
	29850	+0.04	
	33440	−0.15	
	34840	+0.25	
	38460	−1.67	
$[\{Cr(OH)(pma)_2\}_2](ClO_4)_4$ (Fig. 6)	15040	−0.35	d-d(doublet)
	16390	−0.13	d-d(quartet)
	20410	−0.24	
	21880	−0.32	d-d(doublet)
	28010	−0.42	d-d(doublet)?
	30490	−2.51	py(triplet), μ-OH
	32260	+5.82	
	33330(sh)	+4.91	
	35710	−17	py(^1L_b)
	40820	−88	
$[\{Cr(OH)(picen)_2\}](ClO_4)_4$ (Fig. 3)	14490	−0.14	d-d(doublet)
	14930	−0.14	
	15380	−0.10	
	16390	−0.07	d-d(quartet)
	19230	−0.29	
	21010	−0.46	d-d(doublet)
	24390	−0.14	d-d(quartet)
	26320	−0.13	
	27930	−0.68	d-d(doublet)?
	30300	−1.91	py(triplet), μ-OH
	33670	+12	
	35710	−18	py(^1L_b)
	41670	−100	

a) $\Delta\varepsilon_M$ is given in $mol^{-1}\ dm^3\ cm^{-1}\ T^{-1}$.

∠NCrN angle of the mononuclear complexes is less than 90°. For example, that of *Δ-cis*-α-$[CrCl_2(S\text{-picpn})]^+$ is 83.9°.[3] Accordingly, the central chelate ring of the present dinuclear complexes approaches near planar, and the strain energy becomes not so different between the *ΔΔ* and the *ΛΛ* forms, so the strain of the terminal chelate ring has a less important contribution. ("strain" means the deviation from the picen (=*N,N'*-bis(2-pyridylmethyl)ethylenediamine) chelate rings of the complex $[\{Cr(OH)(picen)\}_2]^{4+}$.) The steric repulsion between the methyl group and the terminal chelate ring is the main factor of the stereoselective formation of diastereomers. Thus only the *ΛΛ* form which has no such steric repulsion is considered to be isolated.

Spectral Properties. A shoulder is observed in the region of 33000—34000 cm^{-1} for the dinuclear complexes, overlapping to the spin-forbidden band[1] or pyridine ring band (Figs. 3 and 4). The CD pattern in this region is identical for all the dinuclear complexes treated here, three (+, −, +) or (−, +, −) bands are observed in 32500—37000 cm^{-1}. The absorption and CD spectra of di-μ-hydroxo dinuclear complexes of bidentate ligands are shown in Fig. 6 in which the same shoulder and CD pattern are also observed for $[\{Cr(OH)(pma)_2\}_2]^{4+}$ and $[\{Cr(OH)(S\text{-pea})_2\}_2]^{4+}$. The MCD spectra in this region are shown for $[\{Cr(OH)(picen)\}_2]^{4+}$ and $[\{Cr(OH)(pma)_2\}_2]^{4+}$ (Figs. 3 and 6). The two complexes show only a large positive MCD band in this region. The mononuclear complexes also display a large positive MCD band in this region.[1] The weak absorption band observed in this region for the di-μ-hydroxo en complex has been assigned tentatively to the weak exchange interaction between the two chromium(III) ions.[16] The MCD spectrum (Fig. 3) shows a small (−, +) dispersion in this region, which is a clear indication of existence of a band. The MCD spectral data are shown in Table 2 for $[\{Cr(OH)(en)_2\}_2]^{4+}$, $[\{Cr(OH)(pma)_2\}_2]^{4+}$, and $[\{Cr(OH)(picen)\}_2]^{4+}$. For the di-μ-hydroxo cobalt(III) complex, a strong band has been observed in the same region and assigned to be a hydroxo-to-cobalt charge transfer band, characteristic of this type complexes.[16] In view of the optical electronegativities of chromium(III) and cobalt(III), 1.9 and 2.3, respectively,[17] the shoulders found for the di-μ-hydroxo chromium(III) complexes seem to be due to some another origin than that for the cobalt(III) complexes.

References

1) Part II of this series: Y. Yamamoto and Y. Shimura, *Bull. Chem. Soc. Jpn.*, in press.
2) Y. Yamamoto and Y. Shimura, *Bull. Chem. Soc. Jpn.*, **53**, 395 (1980).
3) Y. Hata, Y. Yamamoto, and Y. Shimura, *Bull. Chem. Soc. Jpn.*, **54**, 1255 (1981).
4) S. Yoshikawa, M. Asami, M. Inoue, and S. Yano, presented at the 29th Symposium on the Coordination Chemistry, Hamamatsu, 1979, Abstract, No. 1B09.
5) F. H. Dickey, W. Fickett, and H. J. Lucas, *J. Am. Chem. Soc.*, **74**, 944 (1952).
6) B. Bosnich and I. M. Harrowfield, *J. Am. Chem. Soc.*, **94**, 3425 (1972).
7) R. G. Asperger and C. F. Liu., *Inorg. Chem.*, **4**, 1492 (1965).
8) H. A. Goodwin and F. Lions, *J. Am. Chem. Soc.*, **82**, 5021 (1960).
9) K. Michelsen, *Acta Chem. Scand.*, *A*,**30**, 521 (1976).
10) K. Michelsen, *Acta Chem. Scand.*, *A*,**31**, 429 (1977).
11) K. Michelsen, *Acta Chem. Scand.*, *A*,**32**, 847 (1978).
12) J. B. Dubsky, *J. Prakt. Chem.*, **90**, 61 (1914).
13) Y. Yamamoto, Y. Hata, and Y. Shimura, *Chem. Lett.*, in contribution
14) S. J. Cline, R. P. Scaringe, W. E. Hatfield, and D. J. Hodgson, *J. Chem. Soc., Dalton Trans.*, **1977**, 1662.
15) R. P. Scaringe, P. Singh, R. P. Eckberg, W. E. Hatfield, and D. J. Hodgson, *Inorg. Chem.*, **14**, 1127 (1975).
16) J. Springborg and C. E. Schäffer, *Inorg. Synth.*, **18**, 75 (1978).
17) C. K. Jørgensen, "Orbitals in Atoms and Molecules," Academic Press (1962), p. 95.

Studies on the Solvent Extraction of Metal Perchlorates III. Extraction Equilibria of Alkaline Earth Ions with Trioctylphosphine Oxide as Perchlorate and Thiocyanate

Satoshi KUSAKABE and Tatsuya SEKINE*

Department of Chemistry, Science University of Tokyo, Kagurazaka, Shinjuku-ku, Tokyo 162

(Received January 23, 1981)

Solvent extraction of alkaline earth metal ions in 1 mol dm^{-3} sodium perchlorate or thiocyanate aqueous solution with trioctylphosphine oxide (TOPO) in hexane was studied at 25 °C. The extraction in both systems improved in the order: beryllium(II)>calcium(II)>strontium(II)≃magnesium(II)≃barium(II). When the TOPO concentration was the same, the extraction of beryllium or calcium thiocyanate was better than that of the perchlorate, that of magnesium or strontium thiocyanate was nearly similar to that of the perchlorate, while barium perchlorate was extracted better than its thiocyanate. From these results it was concluded that these five perchlorates and strontium and barium thiocyanates were extracted as ion-pairs, $[M(topo)_4]^{2+}(X^-)_2$, ($X^- = ClO_4^-$ or SCN^-), while beryllium thiocyanate was extracted as solvates of noncharged complexes, $M(SCN)_2(topo)_n$, ($n=2$ and 3), and that magnesium and calcium thiocyanates in the organic phase ($n=3$ and 4) should have both ionic and coordinative properties. The poor extraction of magnesium salts was assumed to be due to their strong hydration.

In the previous study, the authors observed that the solvent extraction of alkali metal ions with trioctylphosphine oxide (TOPO) in hexane as perchlorate improved in the order lithium(I)>sodium(I)>potassium(I)>rubidium(I)>caesium(I). This was explained by suggesting that the extraction is mainly dependent on the stability of the TOPO solvates, which is higher when the ionic size is smaller.[1] In the present reseach we studied the solvent extraction of alkaline earth ions as perchlorate and thiocyanate with TOPO in hexane and have considered the effect of possible coordination of these metal ions with the anions on their solvent extraction with solvating type extractants.

Experimental

Materials. The materials were the same as reported previously.[1,2] The beryllium perchlorate stock solution was prepared by dissolving its hydroxide, obtained by precipitation from sulfate solutions. The other alkaline earth stock solutions were prepared by dissolving their chloride in sodium perchlorate or thiocyanate solutions.

The content of beryllium(II) was analyzed by gravimetry of its 2-methyl-8-quinolinolate;[3] that of the other alkaline earths was determined by titration with a standard EDTA or silver nitrate solution.

Procedures. Experiments were carried out in a thermostated room at 25 °C. The metal stock solution and 1 mol dm^{-3} sodium perchlorate or thiocyanate solution were placed in a stoppered glass tube. The initial metal concentration of barium was 5×10^{-3} mol dm^{-3} and that of the other metal ions was 1×10^{-3} mol dm^{-3}. For the experiments with beryllium, the hydrogen-ion concentration was adjusted at 1×10^{-3} mol dm^{-3} by perchloric acid or hydrochloric acid. The same volume of a hexane solution of TOPO was then added and the two solutions were agitated mechanically for half an hour and then centrifuged. A portion of the organic phase was transferred into another glass tube and the metal ions contained were back-extracted into diluted nitric or hydrochloric acid. The concentrations of strontium(II) and barium(II) in this solution and those in the aqueous phase were determined by flame spectrophotometry and those of the other metals by an atomic absorption method.

Statistical. Distribution ratio of the metal, M(II), is defined as

$$D = [M(II)]_{org}/[M(II)], \quad (1)$$

where the subscript "org" denotes the species in the organic phase and the absence of a subscript denotes that in the aqueous phase. The extraction equilibrium of the metal with TOPO can be written as

$$M^{2+} + 2X^- + n\text{topo(org)} \rightleftharpoons MX_2(topo)_n(org)$$

$$K_{ex,n} = [MX_2(topo)_n]_{org}[M^{2+}]^{-1}[X^-]^{-2}[topo]_{org}^{-n}, \quad (2)$$

$$D = \sum K_{ex,n}[topo]_{org}^{n}, \quad (3)$$

where X^- denotes a perchlorate or thiocyanate ion. The concentration of free TOPO in the organic phase is reduced by the solvation of the metal ions and sodium ions co-existing in the organic phase. (Both sodium perchlorate and thiocyanate are extracted as tri-solvates into hexane and the extraction constants $K_{ex,NaX}(=[NaX)topo)_3]_{org}[Na^+]^{-1}[X^-]^{-1}[topo]_{org}^{-3})$ are $10^{1.01}$ and $10^{0.38}$, respectively.[2]) Since the concentration of both sodium ions and X^- in the aqueous phase are nearly equal to 1 mol dm^{-3}, the equilibrium concentration of TOPO can be related to its total concentration by the following equation;

$$\begin{aligned}[topo]_{org,total} &= [topo]_{org} + \sum n[MX_2(topo)_n]_{org} \\ &\quad + 3[NaX(topo)_3]_{org} \\ &= [topo]_{org} + \sum nK_{ex,n}[M^{2+}][topo]_{org}^{n} \\ &\quad + 3K_{ex,NaX}[topo]_{org}^{3}. \end{aligned} \quad (4)$$

The constants which fit best with the experimental data, and the equilibrium TOPO concentration, were calculated using a least squares program.

Results

Figures 1a—c give the extraction curves from 1 mol dm^{-3} $NaClO_4$ and Figs. 2a—c from 1 mol dm^{-3} NaSCN, both as a function of the TOPO concentration in the organic phase at equilibrium. These results may be summarized as follows: (i) The perchlorate extractions of magnesium(II), strontium(II), and barium(II) are nearly the same, that of calcium(II) is about one and half orders better than the extraction of these metal

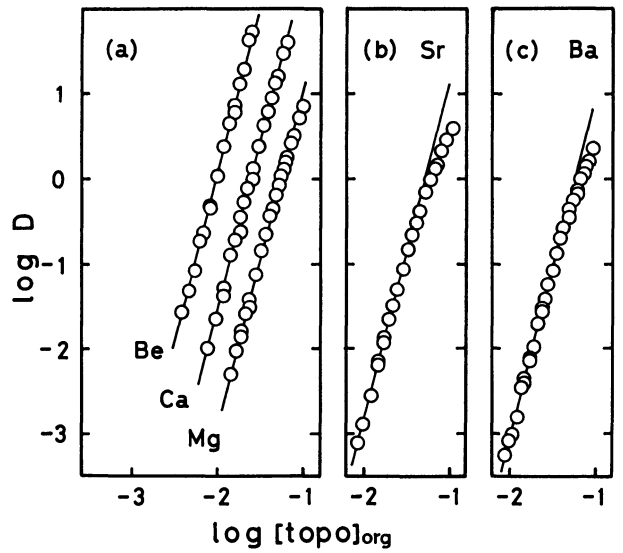

Fig. 1. Extraction of alkaline earth metal ions from 1 mol dm^{-3} $NaClO_4$ with TOPO in hexane. The TOPO concentrations are the values at equilibrium. Some data at higher TOPO concentrations in Figs. b and c were not used for the calculation of the constants (see text). The solid lines were calculated by introducing the constants in Table 1 into Eq. 3.

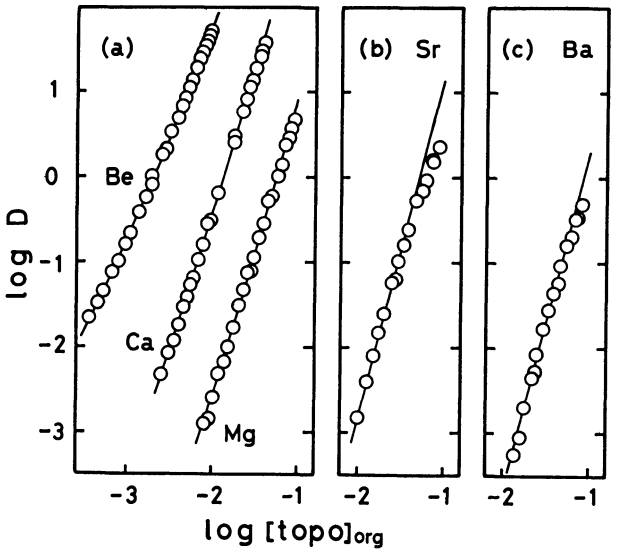

Fig. 2. Extraction of alkaline earth metal ions from 1 mol dm^{-3} NaSCN with TOPO in hexane. The TOPO concentrations are the values at equilibrium . Some data at higher TOPO concentrations in Figs. b and c were not used for the calculation of the constants (see text). The solid lines were calculated by introducing the constants in Table 1 into Eq. 3.

ions and that of beryllium(II) is better still: one and half orders better than calcium(II). (ii) The differences of the extraction curves of the thiocyanates are greater than those of the perchlorates. (iii) The extraction of magnesium(II) and strontium(II) as perchlorate and the thiocyanate is nearly the same. The extraction of barium thiocyanate is somewhat inferior to that of its perchlorate, while the opposite is found with calcium(II). The extraction of beryllium thiocyanate is much better than its perchlorate.

The data were analyzed by using a least squares computer program. As is seen from the figures, the slope of the extraction curve of strontium(II) and barium(II) decreased in the higher TOPO concentration region both in the perchlorate and thiocyanate extraction systems. Since this trend could not be explained stoichiometrically, those data were eliminated from the least squares calculation. Beryllium(II) was reported to form thiocyanate complexes in aqueous solutions[4] and corrections for them are necessary in order to obtain accurate extraction constants from the data in the figures. It is assumed from the stability constants ($\beta_1=10^{-0.16}$ and $\beta_2=10^{-0.60}$ in 4 mol dm^{-3} $NaClO_4$) that the total concentration of the complexes is approximately equivalent to Be^{2+} in the 1 mol dm^{-3} thiocyanate solution. Thus the constants $K_{ex,n}$ obtained in the present study, assuming no complexes in the aqueous phase should be a little lower than the values defined by Eq. 2. The formation of thiocyanate complexes in the aqueous phase of the other alkaline earths should be slight[5] and no correction for that may be necessary.

Solvation of the alkaline earth salts and of the co-extracted sodium perchlorate or thiocyanate should decrease the free TOPO concentration. In the higher concentration region, this was not negligible. For example, in the extraction of barium perchlorate from the 1 mol dm^{-3} $NaClO_4$ medium with 0.14 mol dm^{-3} of initial TOPO in hexane, it is calculated by Eq. 4 by introducing the values in Table 1 that about 20% of this TOPO combines with sodium perchlorate and 10% combines with barium perchlorate. Correction for this decrease in the free TOPO concentration by successive approximation was included in the computer program.

All of the extraction data of the perchlorates were found to be well explained in terms of solvation with four TOPO molecules in the organic phase. The $K_{ex,4}$ values obtained by the least squares calculation are listed in Table 1. In the extraction of thiocyanates, a solvation number of four well explained the data of strontium(II) and barium(II), but two types of solvates

Table 1. Extraction constants[a] of alkaline earth metal perchlorates and thiocyanates with TOPO in hexane at 25°C[b]

Metal	Perchlorate	Thiocyanate		
	log $K_{ex,4}$	log $K_{ex,2}$	log $K_{ex,3}$	log $K_{ex,4}$
Be(II)	8.01±0.20	5.18±0.16	7.73±0.19	
Mg(II)	4.99±0.21		3.32±0.39	4.86±0.41
Ca(II)	6.39±0.17		5.45±0.14	7.12±0.32
Sr(II)[c]	5.13±0.10			5.17±0.18
Ba(II)[c]	4.92±0.13			4.29±0.21

a) The limit of error is 3σ. b) Aq phase: 1 mol dm^{-3} $NaClO_4$ or NaSCN. Org. phase: hexane containing TOPO. c) Some of the data for these ions in the higher TOPO concentration region in Figs. 1b, 1c, 2b, and 2c were eliminated in the calculation of these constants. See text.

were necessary in order to explaine the extraction of the other metal ions; solvation numbers of two and three for beryllium(II) and of three and four for magnesium(II) and calcium(II) were found to give a better fit of the calculated values with the experimental data than only one solvation number. The extraction constants thus computed are listed in Table 1.

Discussion

As is seen from Fig. 1 and Table 1, the solvent extraction of alkaline earth perchlorates with TOPO is much better than that of alkali perchlorates[1] under identical conditions. The solvation number is four in the former extraction, but three in the latter one. The extraction of alkaline earth thiocyanates with TOPO is also much better than that of alkali metals.

The smaller the ionic size, the better the TOPO extraction which was found among the alkali perchlorates.[1] This tendency is also found among the alkaline earth perchlorates, except magnesium(II): the extraction of magnesium(II) is nearly similar to that of barium(II). The extraction order of the alkaline earth thiocyanates is also similar to that of their perchlorates, again except magnesium(II).

If we omit magnesium(II), this extraction order may be explained in terms of the higher ability of solvation with TOPO of smaller ions and of the difference in the nature of the chemical bonds between the anion and the metal ion. The solvation reduces hydrating water and also increases the molar volume of the cation; these effects are favorable for its extraction. A smaller ion tends to form more stable solvates than a larger one, although the former tends to be hydrated more strongly. On the other hand, since the metal ions combine with four molecules of TOPO in their extraction as perchlorates, the molar volumes of the resulting solvates should be rather similar even when the size of the central metal ion is different. For this reason, smaller metal ions are extracted better than larger ones. It is generally true that when the bond between the anion and the metal is coordinative the extraction is better than when it is ionic. The better extraction of beryllium thiocyanate than of its perchlorate indicates that the thiocyanate ions in the extracts coordinate with the central metal ion. The smaller solvation numbers of beryllium thiocyanate with TOPO than of its perchlorate also indicate that the thiocyanate ions occupy the coordination sphere of the metal ion in the extracts. As is seen from the stability of the alkaline earth thiocyanates in the aqueous phase, the coordination with thiocyanate ions should be weaker when the ionic size is larger. The extraction of thiocyanates of strontium(II) and barium(II) is rather similar to their perchlorates. The somewhat poorer extraction of barium thiocyanate than of its perchlorate may indicate that this thiocyanate is essentially an ion-pair; the same tendency was observed in the TOPO extraction of sodium(I)[2] and this was explained in this previous paper in terms of the larger molar size and the less polar nature of the perchlorate ion than of the thiocyanate ion, these factors make the extraction of the ion-pairs containing the former more favorable.

The poorer extraction of magnesium(II), both as perchlorate and thiocyanate, than of calcium(II) seems to suggest a stronger hydration for the magnesium(II) ion than for the calcium(II) ion. The same tendency has been pointed out before: the extraction of magnesium(II) with tributyl phosphate (TBP) as nitrate[6] and as halides[7] was also poorer than calcium(II). This was explained by a higher tendency of hydration of magnesium(II). Similar reasoning was also proposed for the poor extraction of nickel perchlorate and thiocyanate than of cobalt(II).[8] However, in order to continue discussion about this problem, much comparative work on the extractability of magnesium(II) and calcium(II) in several liquid-liquid systems seems to be necessary.

The extraction of ion-pairs into polar solvents is very often better when the metal ion is larger.[9] However, although the extracted perchlorates are ion-pairs in the present study, the magnitude of the extraction is mainly dependent on the ability to form the solvate with TOPO. The tendency of extraction is similar to that of coordination complexes: the smaller the metal ion, the better the extraction.

The differences among the extraction of the alkaline earth thiocyanates are larger than those of their perchlorates. This is especially marked with beryllium(II); the thiocyanate in the organic phase should be coordinative. As is described above, barium thiocyanate in the organic phase may be essentially ion-paired and the other thiocyanates may have both of these characters.

The extraction of alkaline earths as perchlorates[10,11] and thiocyanates[12-15] with TBP has been reported. The observations such as the order of extraction and the solvation numbers of extracts are similar with our results for the extraction with TOPO.

The authors are grateful to Mr. Kenji Ohira for his experimental aid.

References

1) S. Kusakabe and T. Sekine, *Bull. Chem. Soc. Jpn.*, **53**, 2087 (1980).
2) S. Kusakabe and T. Sekine, *Bull. Chem. Soc. Jpn.*, **53**, 1759 (1980).
3) K. Motojima, *Bull. Chem. Soc. Jpn.*, **29**, 29 (1956).
4) T. Sekine, Y. Komatsu, and M. Sakairi, *Bull. Chem. Soc. Jpn.*, **44**, 1480 (1971).
5) L. G. Sillén and A. E. Martell, "Stability Constants," Spec. Pub. No. 17 and 25, The Chemical Society, London (1964 and 1971).
6) A. I. Mikhailichenko, M. A. Klimenko, and V. B. Bulgakova, *Zh. Neorg. Khim.* **16**, 2557 (1971).
7) Yu. M. Glubokov, S. S. Korovin, A. M. Reznik, and T. A. Rasskazova, *Izv. Vyssh. Uchebn. Zaved., Khim. Khim. Tekhnol.*, **14**, 983 (1971).
8) R. Murai, S. Iwahori, and T. Sekine, *Bull. Chem. Soc. Jpn.*, **50**, 1315 (1977).
9) T. Sekine and Y. Hasegawa, "Solvent Extraction Chemistry," Marcel Dekker, New York (1977), p. 141.
10) E. V. Lapitskaya and F. P. Gorbenko, *Radiokhimiya*, **10**, 90 (1968).

11) F. P. Gorbenko and E. V. Lapitskaya, *Anal. Khim. Ekstr. Protsessy*, 40 (1970).
12) C. Rozycki and E. Lachowicz, *Chem. Anal.* (*Warsaw*), **15**, 255 (1970).
13) E. D. Kuchkina, F. P. Gorbenko, and G. V. Litvinova, *Zh. Anal. Khim.*, **28**, 595 (1973).
14) S. Kalyanaraman and S. M. Khopkar, *Anal. Chem.*, **47**, 2041 (1975).
15) L. Kocheva and V. Doichinova, *Dokl. Bolg. Akad. Nauk*, **28**, 1649 (1975).

Determination of Germanium by Atomic Absorption Spectrometry Following Volatile Hydride Generation

Kazuo JIN,*,† Hiroaki TERADA,†† and Mitsuhiko TAGA

Department of Chemistry, Faculty of Science, Hokkaido University, Nishi-8-chome, Kita-ku, Sapporo 060
†Hokkaido Institute of Public Health, Nishi 12-chome, Kita 19-jo, Kita-ku, Sapporo 060
††Iwamizawa College, Hokkaido University of Education, Midorigaoka 2-34, Iwamizawa 068

(Received January 28, 1981)

A sensitive technique for determination of germanium was investigated by atomic absorption spectrometry following volatile hydride generation. Of the three types of hydride generator and atomizer systems tested, direct transfer of the generated hydride into nitrogen–hydrogen flame for atomization was found to be suitable. The sensitivity was enhanced more than 40—60% in phosphoric acid medium as compared to hydrochloric acid, malic acid, or tartaric acid media. Interference of nickel(II), gold(III), and cobalt(II) in hydrochloric acid medium was reduced by adding ethylenediaminetetraacetate as a masking reagent or replacing the acid medium by malic acid. Detection limit and relative standard deviation of ten determinations of 0.5 μg germanium(IV) in 20 ml of 0.20 M** phosphoric acid were 7 ng (S/N=2) and 4.3%, respectively, with 3 ml of 8 w/v % sodium tetrahydroborate solution. The method was applied to the determination of germanium in standard rocks, concentrations of germanium in JB-1 and JG-1 being evaluated as 1.3_1 and 1.3_2 ppm, respectively.

In the determination of germanium by atomic absorption spectrometry (AAS), it is difficult to attain high sensitivity because of production of highly stable oxide species in the flame. Dinitrogen oxide–acetylene flame is often used in combination with solvent extraction. The highest sensitivity so far reported is 0.13 ppm for 1% absorption by means of nebulizer effect.[1] Indirect AAS based on the formation of molybdogermanic acid complex has also been used because of chemical amplification.[2]

Volatile hydride generation technique has been applied to the determination of germanium by AAS,[3–6] but the sensitivity and reproducibility are inferior to those of elements such as arsenic, selenium, and antimony.[3,5] This technique was also extended to plasma emission spectrometry,[7–10] and thermal conductivity detection systems.[11]

Investigation was carried out to find suitable conditions for the determination of germanium by AAS by means of three types of hydride generation and atomization systems. Chapman and Dale[12] suggested the use of dinitrogen oxide–acetylene flame for the atomization following hydride generation. However, it was found that nitrogen–hydrogen (entrained air) flame is suitable when combined with a direct transfer type hydride generator, enabling us to use a large amount of sodium tetrahydroborate as a reductant.

The method was applied to the determination of germanium in rock samples (JB-1 and JG-1). Samples were decomposed with acid mixture; germanium was extracted into carbon tetrachloride from 9 M hydrochloric acid, and then back-extracted into water, the aqueous solutions being subjected to analysis.

Experimental

Apparatus. A Hitachi Model 170-50 type atomic absorption spectrophotometer equipped with deuterium background corrector and germanium hollow-cathode lamp (Hamamatsu TV) were used. Atomic absorption signals were recorded with a Hitachi 056 type recroder, peak height signals being used for the determination. Hydride generator and atomizer systems were used as follows.

I: Collection type hydride generator connected to nitrogen–hydrogen flame. Volatile hydride was generated with Nippon Jarrel-Ash Model ASD-1A and introduced into a nitrogen–hydrogen flame (one slot burner with 10 cm).

II: Direct transfer type hydride generator connected to heated silica tube. The hydride generator system reported by Thompson and Thomerson[5] was slightly modified, the gas being introduced into a heated silica tube (14φ×114 mm) mounted on 10 cm path air–acetylene flame burner.

III: Direct transfer type generator connected to nitrogen-hydrogen flame. A modified Hitachi hydride generator connected to a nitrogen–hydrogen flame system described in a previous paper[13] was used, the dispenser (REBURET) being replaced by another one (HANSEN 500 ml).

Conditions for the nitrogen–hydrogen flame: wavelength 256.1 nm, nitrogen flow rate 8 l min^{-1}, hydrogen flow rate 7 l min^{-1}, height of beam above burner tip 12.5 mm.

Reagents. All the reagents were of analytical grade. Deionized water was distilled twice.

Germanium(IV) stock solution (0.5 mg/ml): 0.360 g of soluble germaniumdioxide prepared by the method of Shimomura *et al.*[14] was dissolved in hot water, cooled, and diluted with water to 500 ml.

Sodium tetrahydroborate solution (8 w/v %): Sodium tetrahydrobolate(powder, Aldrich Chemical Company, Inc) was dissolved in 0.5% sodium hydroxide and filtered with 1 μm glass filter.

Sodium tetrahydroborate tablet (*ca.* 0.13 g $NaBH_4$): Thirty tablets were prepared from 2 g of caoline (Fisher Scientific Co.,) and 4 g of sodium tetrahydroborate by addition of 2.5 ml of 2 M aqueous ammonia.[15] The tablet was wrapped in wafer sheet when added to the I type hydride generation vessel.

Procedure. *I*: Pipet the prescribed volume of sample solution into the reaction vessel, add an appropriate volume of acid and dilute the solution to 20 ml with water. Put a teflon coated spin bar into the vessel and set it up on the hydride generation unit. Pass nitrogen into the vessel for 20 s, turn the four-way stopcock to collection mode. Remove the cap of the reaction vessel, put sodium tetrahydroborate tablet into the vessel and replace the cap immediately. Collect the gas for 30 s, then sweep it to the nitrogen–hydrogen flame.

II: Pipet 1 ml of 8 w/v% sodium tetrahydroborate solution into the reaction vessel and set it up on the hydride

** 1M=1 mol dm^{-3}

generation unit. A plastic syringe containing 1 ml of the sample solution is inserted into the side-arm seal of the vessel. Pass nitrogen through the reaction vessel to replace air with nitrogen for 15-20 s, then inject the sample solution into the reaction vessel and carry the gas into heated silica tube with nitrogen flow rate of 2 l min^{-1}.

III: The procedure reported[13] was carried out with modification: 3 ml of 8 w/v% sodium tetrahydroborate solution was used and nitrogen was passed through the vessel with flow rate of 2 l min^{-1}.

Results and Discussion

Stability of Germanium Hydride. The stability of volatile hydride should be considered at first in the hydride generation method.[4,12,15] The effect of germanium hydride collection time in system I was examined. Figure 1 shows effect of collection time 15—300 s for 5.0 μg of germanium. Collection time 20—300 s causes no fall in sensitivity, showing that germanium hydride is stable during the course of collection. The precision of the method is not improved by altering the collection time to 30—300 s.

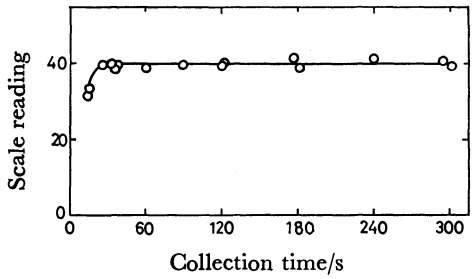

Fig. 1. Effect of collection time on the generation of germanium hydride, in system I.
Ge(IV): 5.0 μg/20 ml, acidity: 0.2 M HCl.

Atomization of Germanium Hydride. A comparison was made between nitrogen-hydrogen and argon-hydrogen flames. The former was found to be superior by *ca.* 20—30% in sensitivity of systems I and III. Sensitivity of the germanium determination by heated silica tube atomization with system II is inferior to that of flame atomization.

Effect of Acids and Acidity. Effect of acids and acidity on the relative sensitivity of germanium determination was investigated by system I for 5.0 μg germanium(IV) and system III for 0.5 μg germanium(IV); the results are shown in Figs. 2 and 3, respectively. Concentration of acids seriously affects peak height of the signals in both types of hydride generator systems, giving maximum peak height at 0.1—0.2 M, at which acids are almost neutralized by the alkaline sodium tetrahydroborate solution. In addition to hydrochloric acid reaction medium used in volatile hydride generation with sodium tetrahydroborate, various acids can be used as reaction media, *i.e.* malic acid, tartaric acid, acetic acid, and oxalic acid (Fig. 2). Nitric acid, sulfuric acid, and phosphoric acid are also useful, but not citric acid (Fig. 2).

In system III, the effect of acid is differs somewhat from that of system I. A large difference in sensitivity

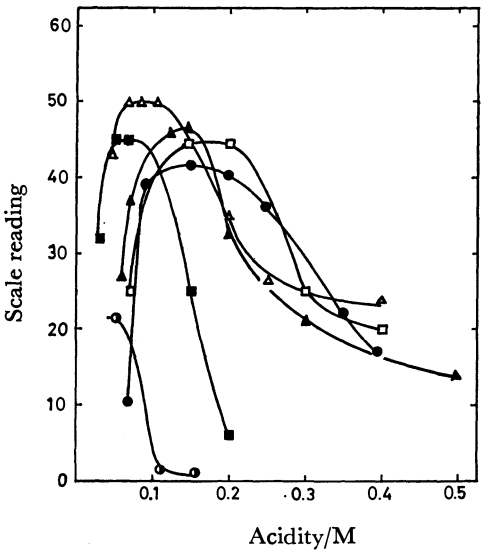

Fig. 2. Effect of acidity on the determination of germanium, in system I.
Ge(IV): 5.0 μg/20 ml, collection: 30 s, —●—: HCl, —△—: malic acid, —▲—: tartaric acid, —□—: acetic acid, —■—: oxalic acid, —◑—: citric acid.

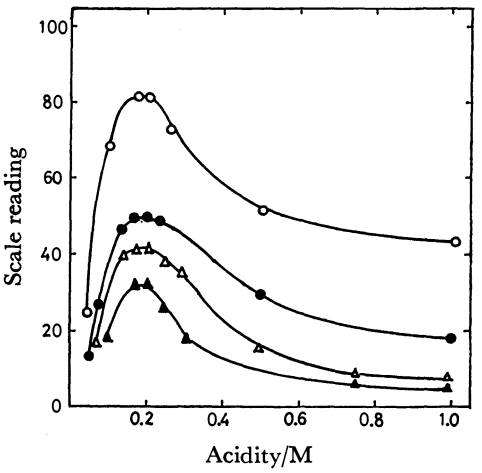

Fig. 3. Effect of acidity on the determination of germanium, in system III.
Ge(IV): 0.5 μg/20 ml, 8 w/v % $NaBH_4$: 3 ml, —○—: H_3PO_4, —●—: HCl, —△—: malic acid, —▲—: tartaric acid.

is observed with use of these acids (Fig. 3). About 40% enhancement in sensitivity is attained in 0.20 M phosphoric acid medium as compared with hydrochloric acid. The difference seems to originate from the change in reaction rate of germanium(IV) to germanium hydride.

The utility of nitric acid is different from the result of Thompson and Pahlavanpour;[10] the results of hydrochloric acid also differ. The peak height does not increase at 2—5 M hydrochloric acid.

Amount of Sodium Tetrahydroborate. In system I, the best sensitivity is attained with 0.13 g of sodium tetrahydroborate. Because of the limitation of the internal gas pressure during the course of collection, more than 0.13 g of the reductant could not be used.

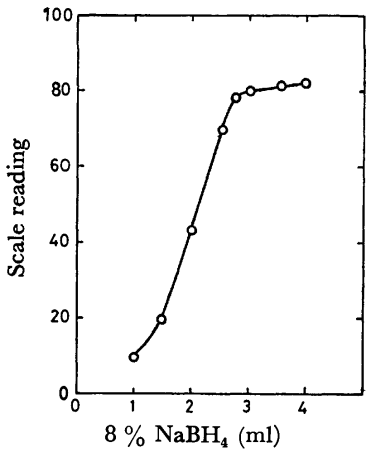

Fig. 4. Effect of the volume of tetrahydroborate solution, in system III.
Ge(IV): 0.5 μg in 20 ml of 0.2 M H_3PO_4.

Effects of the amount of sodium tetrahydroborate on germanium determination examined in system III are shown in Fig. 4, high senistivity being attained with 3—4 ml of 8 w/v% sodium tetrahydroborate solution. A relatively large amount of sodium tetrahydroborate can be treated as compared with system I. However, the use of more than 3.5 ml of 8 w/v% sodium tetrahydroborate solution sometimes caused overflow of the reaction medium. The reductant volume was fixed at 3 ml.

TABLE 1. REPRODUCIBILITY AND DETECTION LIMIT OF THE METHOD

System[a)]	Matrix	RSD[b)] %	Detection limit (S/N=2)
I	0.15 M HCl	8.3[c)]	140 ng/20 ml
	0.1 M Malic acid	7.7[c)]	
II	0.20 M HCl	4.6[d)]	
	0.20 M H_3PO_4	2.7[d)]	200 ng/ml
III	0.20 M HCl	4.5[e)]	10 ng/20 ml
	0.20 M H_3PO_4	4.3[e)]	7 ng/20 ml

a) Described in Experimental. b) Relative standard deviation calculated from ten determinations. c) Germanium taken: 5.0 μg/20 ml. d) Germanium taken: 5.0 μg/ml. e) Germanium taken: 0.5 μg/20 ml.

Precision and Sensitivity. Precision and sensitivity of germanium determination in system I—III were compared. The results are given in Table 1. System I is conventional, but its precision and sensitivity are not so good as that of system III. Precision is improved in system II as compared with system I, but not sensitivity. The highest sensitivity was attained in system III; detection limit of 7 ng/20 ml (=0.35 ppb) is more sensitive than 50 ng/13 ml (=4 ppb) reported by Smith,[6] the highest sensitivity so far reported by AAS.

Influence of Foreign Ions. The influence of various foreign ions on the determination of germanium(IV) (0.5 μg) were examined in system III. The results are shown in Table 2. The ions showing strong suppression in 0.2 M hydrochloric acid medium were paradium(II), nickel(II), gold(III), and cobalt(II). Suppression was also observed in the presence of 50 μg of volatile hydride forming elements such as arsenic(III), antimony(III), and selenium(IV) in the same medium, 250 μg of bismuth(III) not interfering. The interference was not eliminated significantly except selenium(IV) by addition of potassium iodide; coexistence of 100 μg of selenium(IV) was tolerable by addition of 1 ml of 40% potassium iodide solution in hydrochloric acid.

TABLE 2. EFFECTS OF FOREIGN IONS ON THE DETERMINATION OF GERMANIUM
(Results given are percentage changes in absorbance for 0.5 μg of germanium(IV) in systemIII.)

Ion	Added (μg)	Acid reaction matrix[a)] 0.2 M-HCl[b)]	0.2 M-H_3PO_4	0.2 M-H_3PO_4 +EDTA[c)]	0.2 M-Malic acid
Ni(II)	20	−74	−60	0	0
	100	−97	—	0	0
Pd(II)	3	−66	−90	−90	−11
Au(III)	20	−55	−27	0	−19
	60	−70	—	−30	−34
Co(II)	60	−24	0	0	0
	250	−65	0	0	0
Cd(II)	125	−35	−30	−5	−40
Fe(III)	1400	−20	0	0	0
	2800	−37	0	0	0
As(III)	50	−9	−15	−15	−9
Sb(III)	50	−30	−30	−30	—
	250	−50	—	−54	−56
Se(IV)	50	—	−25	−25	—
	125	−31	—	—	−11

a) Volume of test solution, 20 ml; 3 ml of 8 w/v % sodium tetrahydroborate solution was added as a reductant. b) The following are tolerable: Sn(II), Pb(II), Te(IV) (50 μg coexistence); Bi(III)(250 μg coexistence); Hg(II), Ca(II), Mg(II), Mn(II, VII), Ru(III), Mo(VI), V(V), Cr(III, VI), Al(III) (500 μg coexistence); Cl^-, Br^-, NO_3^-, SO_4^{2-}, CH_3COO^-, SiO_3^{2-}, BO_3^{3-}, IO_3^-, ClO_4^-, Na^+, K^+ (2500 μg coexistence). c) 0.25 M EDTA2Na 1 ml was added.

The influence of foreign ions on the determinations in phosphoric acid medium was almost the same as that of hydrochloric acid, but the interference by cobalt(II) and iron(III) is much more reduced than that of hydrochloric acid medium (Table 2).

In malic acid reaction medium, interference caused by nickel(II), gold(III), cobalt(II), zinc(II), or iron(III) is less than that of hydrochloric acid medium as shown in Table 2. Malic acid is superior to other organic acids such as tartaric acid and lactic acid as regards the influence of nickel(II); coexistence of 100 μg of nickel(II) caused no loss of sensitity in 0.2 M malic acid. However, 70% sensitivity suppression took place in 0.2 M tartaric acid, and 95% in 0.2 M ractic acid.

Addition of EDTA to reaction medium is effective for eliminating the interference of nickel(II), gold(III), cadmium(II), and zinc(II) as shown in Table 2. Addition of EDTA to phosphoric acid medium is suitable for the determination of germanium(IV) in

view of sensitivity and influence of foreign ions.

Determination of Germanium in Standard Rocks. The method was applied to the determination of germanium in standard rocks JB-1 and JG-1. Samples were decomposed by the following methods.

Procedure A: Germanium separation process developed by Schneider and Sandell,[16] Onishi,[17] Argollo and Schilling[18] was appleid with a slight modification: Weigh 0.5 g of rock samples in Uniseal decomposition vessel. Add 2 ml of 9 M sulfuric acid, 1 ml of concentrated nitric acid, and 5 ml of 46% hydrogen fluoride. Seal the vessel immediately, put the vessel in air bath for 2 h at 100 °C. After cooling, take off the cap of the decomposition vessel and heat it on a hot plate until fuming of sulfuric acid begins. Transfer the contents into the separation funnel, add 15 ml of 9 M hydrochloric acid and shake for 10 min with an electric shaker. Add 10 ml of carbon tetrachloride and shake for 3 min. Separate each phase and transfer the carbon tetrachloride phase to another separation funnel. Repeat the procedure by adding another 10 ml of carbon tetrachloride into the first separation funnel. Add second carbon tetrachloride phase to previous carbon tetrachloride phase, and wash the phase with 5 ml of hydrochloric acid. Separate each phase, transfer the carbon tetrachloride phase to another separation funnel and add 10 ml of water. Shake for 5 min, then separate each phase. The aqueous solutions were subjected to germanium determination by the proposed method (system III, phosphoric acid matrix). Blank solution was prepared by the same preparation as above. Recovery of germanium was checked by adding standard germanium(IV) solution into Uniseal vessel with sample and carrying out the same procedure described above.

Procedure B: Procedure without germanium separation as in Procedure A was carried out until the decomposition step of the sample in air bath. After cooling the reaction vessel, add 80 ml of 4% boric acid in order to mask excess fluoride ion and transfer the solution to a 100 ml volumetric flask, and add water to the mark. The prescribed volume of the sample solution was subjected to germanium determination by means of standard addition technique (in phosphoric acid containing EDTA). Blank solution was also prepared by the same procedure as above.

The analytical results are given in Table 3. Recovery of 85—95% germanium in Procedure A (both for JB-1 and JG-1) agreed with that of other rock samples.[17] The germanium contents of JB-1 and JG-1 corrected with recovery percent agreed with those by Argollo and Scilling[18] attained by neutron activation analysis. Results obtained by Procedure B were somewhat inaccurate. However, the technique is very simple, rapid, and an average of two or three multiple sample determinations gives almost the same result as that by Procedure A (Table 3). A large discrepancy of germa-

Table 3. Determination of germanium in standard rocks

Sample	Taken (g)	Ge Added (μg)	Pretreatment[a]	Ge Found			Reported (ppm)
				μg[b]	ppm	ppm corrected[c]	
JB-1	0.502		A	0.56_7	1.1_3	1.2_8	0.7[d]
	0.510		A	0.56_0	1.2_7	1.4_4	0.22±0.03[e]
	0.507		A	0.55_0	1.0_8	1.2_3	1.33[f]
	0.502		A	0.50_0	1.2_0	1.3_6	
	0.517		A	0.56_7	1.1_0	1.2_5	
				av.:	1.1_6	1.3_1 (RSD 6.6%)	
	0.517	0.50	A	1.0_5	90%	Recovery[g]	
	0.510	1.00	A	1.4_5	86%	av. 88%	
	0.296		B		1.3		
	0.249		B		1.0	av. 1.2_3 ppm	
	0.138		B		1.4		
JG-1	0.508		A	0.63_3	1.2_5	1.4_4	1.2[d]
	0.510		A	0.58_3	1.1_4	1.3_1	1.7±0.5[e]
	0.513		A	0.58_0	1.1_3	1.3_0	1.32[f]
	0.505		A	0.59_7	1.1_8	1.3_6	
	0.503		A	0.56_0	1.1_1	1.2_8	
	0.503		A	0.53_3	1.0_6	1.2_2	
				av.:	1.1_5	1.3_2 (RSD 5.7%)	
	0.513	0.50	A	1.0_4	90.6%	Recovery	
	0.506	0.50	A	1.0_0	84.2%	av. 87.4%	
	0.180		B		1.5		
	0.228		B		1.3	av. 1.3_3 ppm	
	0.218		B		1.2		

a) Described in the text. b) Mean of two determinations. c) Calculated from recovery test. d) Ref. 19. e) Ref. 18. g) Calculated from average amount of germanium.

nium content is observed in the results of JB-1 between 1.3_3 ppm in this work and 0.22 ± 0.03 ppm by Ohta and Suzuki.[20] They decomposed 2—3 g of the sample at a time, but this seems too much for complete decomposition.

References

1) S. Simomura, H. Sakurai, H. Morita, and Y. Mino, *Anal. Chim. Acta*, **96**, 69 (1978).
2) R. Jakubiec and D. F. Boltz, *Anal. Chem.*, **41**, 78 (1969).
3) E. N. Polloc and S. J. West, *At. Abs. Newslett.*, **12**, 6 (1973).
4) F. J. Fernandez, *At. Abs. Newslett.*, **12**, 93 (1973).
5) K. C. Thompson and D. R. Thomerson, *Analyst*, **99**, 595 (1974).
6) A. E. Smith, *Analyst*, **100**, 300 (1975).
7) R. Nakashima, *Bunseki Kagaku*, **25**, 869 (1976).
8) F. L. Frike, W. D. Robbinse, and J. A. Caruso, *J. Assoc. Off. Anal. Chem.*, **61**, 1118 (1978).
9) W. B. Robbins, J. A. Caruso, and F. L. Fricke, *Analyst*, **104**, 35 (1979).
10) M. Thomson and B. Pahlavanpour, *Anal. Chim. Acta*, **109**, 251 (1979).
11) R. K. Skogerboe and A. P. Bejumuk, *Anal. Chim. Acta*, **94**, 279 (1977).
12) J. E. Chapman and L. S. Dale, *Anal. Chim. Acta*, **111**, 137 (1979).
13) K. Jin, M. Taga, H. Yoshida, and S. Hikime, *Bull. Chem. Soc. Jpn.*, **52**, 2276 (1979).
14) S. Shimomura, H. Sakurai, H. Morita, and Y. Mino, *Anal. Chim. Acta*, **91**, 421 (1977).
15) K. Jin and M. Taga, *Bunseki Kagaku*, **29**, 522 (1980).
16) Wm. A. Schneider, Jr., and E. B. Sandell, *Microchim. Acta*, **1954**, 263.
17) H. Onishi, *Bull. Chem. Soc. Jpn.*, **29**, 686 (1956).
18) R. M. Argollo and J. G. Schilling, *Anal. Chim. Acta*, **96**, 117 (1978).
19) A. Ando, H. Kurasawa, T. Ohmori, and E. Takeda, *Geochem. J.*, **8**, 117 (1978).
20) K. Ohta and M. Suzuki, *Anal. Chim. Acta*, **104**, 293 (1979).

  Bull. Chem. Soc. Jpn., 54, 2939—2942 (1981)

Circular Dichroism Spectra and Absolute Configurations of *cis,cis,cis*-(*C,N,O*)-Dicyanobis(glycinato)cobaltate(III) and Dicyanobis-(β-alaninato)cobaltate(III) Complexes

Shuhei FUJINAMI* and Muraji SHIBATA

Department of Chemistry, Faculty of Science, Kanazawa University, Kanazawa 920

(Received February 9, 1981)

The $[Co(CN)_2(NO)_2]^-$-type complexes (NO: gly^- and β-ala^-), which have *cis,cis,cis* geometry with respect to the donor atoms C, N, and O, have been prepared by a new method, and resolved into their optical antipodes. The CD spectra of the resolved complexes have been measured, and compared with that of $(-)_{589}[Co(CN)_2(ox)(en)]^-$ complex which has the same chromophore with the bis(glycinato) complex. It is found that the optical activity of the *cis,cis,cis*-$[Co(C)_2(N)_2(O)_2]^-$-type complex mainly arises from the arrangement of the donor atoms; the non-ligating atoms of NO ligand make minor contribution to the optical activity.

Recent years have seen dramatic development in CD spectral studies of transition metal complexes, on account of development of theoretical treatment. In particular, many investigations have been carried out on tris(diamine)-type complexes, and the optical rotatory strength of a d-d transition has been connected in detail with the structure of a given complex.[1] Evans *et al.*[2] have calculated the optical activity of $[Co(en)_3]^{3+}$ complex by a molecular orbital method, and obtained good coincidence with the experimental values. Mason and Seal[3] have applied the dynamic coupling model to the complexes of this type, and given numerical evaluations of the optical activities, differentiating between the contribution from donor atoms and that from non-ligating atoms.

In contrast to the above complexes whose absolute configurations are designated with *Λ* and *Δ* notation, a few studies of optically active complexes such as *cis,cis*-$[Co(CN)_2(CO_3)(NH_3)_2]^-$,[4] $[Co(Br)(CN)(NH_3)(tacn)]^+$[5] and $[Co(NO_2)(gly)(tacn)]^+$[6](tacn represents 1,4,7-triazacyclononane), whose absolute configurations cannot be defined in *Λ* and *Δ* notation, have been reported in our laboratory. We have expressed the absolute configurations of those complexes in the *R* and *S* notation proposed by Cahn *et al.*[7] and it has been found that the arrangement of donor atoms plays an important role in the optical activity of these complexes. However, an apparent role of the non-ligating atoms in the chelate rings has not been examined.

On the other hand, the CD spectrum of a $(-)_{589}$-$[Co(CN)_2(ox)(en)]^-$ complex[4] is interesting, because the optical activity of the complex is considered to be derived from two origins; one is due to the arrangement of the donor atoms of the ligands as in the *cis,cis,cis*-$[Co(CN)_2(NH_3)_2(H_2O)_2]^+$,[4] and another due to the helical distribution of the two bidentate ligands. If the deviation of the donor atoms from the octahedral sites due to the chelations does not have a large influence on the optical activity, the contribution to the optical activity from the non-ligating atoms is intimately associated with the "*Λ* or *Δ*" configuration, and that from the donor atoms, with "*R* or *S*" configuration. It is significant to elucidate with contribution is dominant in the complex. In order to clarify this problem, we attempted to prepare a *cis,cis,cis*(*C,N,O*)-$[Co(CN)_2(gly)_2]^-$ complex, whose chromophore was the same as the $[Co(CN)_2(ox)(en)]^-$ complex, and then to resolve it into a pair of enantiomers. The absolute configuration of an enantiomer in the bis(glycinato) complex is represented with either *Δ*(*R*) or *Λ*(*S*). Since the absolute configuration of the $(-)_{589}[Co(CN)_2(ox)(en)]^-$ isomer is known to be *Λ*(*R*),[4] the comparison between the CD spectra of the two dicyano complexes will be helpful to determine the origin of the optical activities of the complexes. We also attempted to determine the absolute configuration of a diastereoisomeric salt $(-)_{589}[Co(ox)(en)_2]\cdot cis,cis,cis(C,N,O)\text{-}(+)^{CD}_{500}[Co(CN)_2(gly)_2]\cdot 3H_2O$ by X-ray analysis, in order to facilitate the analyses of the CD spectra.

There are five possible geometrical isomers for the $[Co(CN)_2(gly)_2]^-$ complex. Poznjak and Pawlowski[8] have isolated three isomers with *cis*(*CN*) geometry, modifying the method devised in our laboratory.[9] In this paper, a new method to prepare the dicyano complex will be reported.

Experimental

Preparation of $[Co(CN)_2(gly)_2]^-$ *Complex.* The complex has been prepared from $[Co(gly)_3]$ by reaction with KCN in the presence of activated charcoal,[8] but this method yields a poor product. We devised a new method: To a cold green solution of the so-called tricarbonato solution ($Co(NO_3)_2\cdot 6H_2O$, 29 g, 0.1 mol scale),[10] potassium cyanide (16.3 g, 0.25 mol) was added, and the mixed solution was stirred for 1 h at room temperature in order to prepare *cis*-$[Co(CN)_2(CO_3)_2]^{3-}$.[11] The solution was slowly neutralized by 30% $HClO_4$ in an ice bath. After the precipitated $KClO_4$ was filtered off, glycine (18.8 g, 0.25 mol) was added to the filtrate. With occasional neutralization by 30% $HClO_4$, the reaction mixture was stirred for 10 h. The dominant species in the solution was considered to be $[Co(CN)_2(gly)(CO_3)]^{2-}$. The solution was adjusted to pH 1 with 30% $HClO_4$, and stirred again for 1 h to complete the acid hydrolysis. The solution was adjusted to pH 9 with 6 mol/dm³ KOH and then the precipitated material was filtered off. The filtrate was stirred for 2 h at 40 °C. The reaction mixture was sufficiently diluted with water (3—4 dm³) and poured onto a column of Dowex 1-X8 resin (Cl^- form, 4×25 cm). By elution with 0.2 mol/dm³ KCl solution, complex species of univalent anion were collected in a fraction . After concentration and removal of the eluent, the filtrate was diluted with 2 dm³ of water and rechromatographed on a column of Dowex 1-X8 (Cl^- form, 4×30 cm). When the adsorbed band was eluted with 0.1

mol/dm³ $CaCl_2$ solution, nine bands were distinguished (labeled A1-A9 in the order of elution). The yellow A4, orange A8 and rose A9 bands were the main products. Hereafter, the notations A1—A9 will be used to designate the isomer contained in each band. A4, A8 and A9 were identified with the *trans(N)-cis(C)*, *cis,cis,cis(C, N, O)*, and *trans(O)-cis(C)* isomers, respectively, on the basis of the absorption spectral data.[8] The other bands contained no dicyano complex species.

Preparation of the $[Co(CN)_2(\beta\text{-}ala)_2]^-$ *Complex.* This complex was prepared in the same way as the bis(glycinato) complex except for the use of β-alanine in the place of glycine. Upon rechromatography, three bands were obtained as univalent species (B1—B3 in the order of elution), by elution with 0.1 mol/dm³ $CaCl_2$ solution, After removal of the eluting agent from each fraction, the counter ions were converted to sodium ions by means of column chromatography. The effluents were concentrated and then kept in a refrigerator. Found for B2: C, 28.54; H, 4.50; N, 16.62%. Found for B3: C, 28.67; H, 4.30; N, 16.89%. Calcd for $Na[Co(CN)_2(\beta\text{-ala})_2]\cdot 1.5H_2O$: C, 28.50; H, 4.48; N, 16.62%. B1 was not a sought complex species.

Resolution. The crystals of *cis,cis,cis(C,N,O)*-$Na[Co(CN)_2(gly)_2]\cdot 2H_2O$ (3.2 g, 0.01 mol) were dissolved in a minimum amount of warm water (60 °C). The solution was mixed with a warm solution of $(-)_{589}[Co(ox)(en)_2](CH_3COO)$, which had been prepared using $(-)_{589}[Co(ox)(en)_2]I$ (1.7 g, 0.005 mol) and CH_3COOAg (0.84 g, 0.005 mol). The mixed solution was mechanically stirred and cooled in an ice bath. The diastereoisomeric salt obtained was recrystallized several times, until the Δε values became constant. Found: C, 24.79; H, 5.41; N, 19.47%. Calcd for $(-)_{589}[Cn(ox)(en)_2]\cdot(+)^{CD}_{500}[Co(CN)_2(gly)_2]\cdot 3H_2O$: C, 24.84; H, 5.21; N, 19.31%.

The *trans(N)-cis(C)*- and *trans(O)-cis(C)*-$[Co(CN)_2(gly)_2]^-$ complexes were resolved into each optical antipodes in a similar way as the *cis,cis,cis(C,N,O)*-$[Co(CN)_2(gly)_2]^-$ complex, by using $(-)_{589}[Co(ox)(en)_2](CH_3COO)$ as resolving agent. The *trans(N)-cis(C)*- (B2) and *cis,cis,cis(C,N,O)*-$[Co(CN)_2(\beta\text{-ala})_2]^-$ (B3) complexes were also resolved by use of $(-)_{589}[Co(NO_2)_2(en)_2](CH_3COO)$.

Measurements. The absorption spectra in aqueous solution were measured with a Hitachi 323 recording spectrophotometer. The CD spectra were recorded on a JASCO J-40C automatic recording spectropolarimeter equipped with a JASCO Model J-DPZ data processor for CD. The less-soluble diastereoisomeric salts obtained were passed through columns of cation exchanger in sodium form, and the effluents were submitted to the measurements of CD spectra. The Δε values were evaluated from the absorption spectral data.

Results and Discussion

Absorption and CD Spectra. Absorption spectral data of the complexes obtained are listed in Table 1. Absorption spectra of the isomers of the bis(glycinato) complex coincided with those of the literature.[8] Therefore, A4 is identified as *trans(N)-cis(C)* isomer, A8 as *cis,cis,cis(C,N,O)* one, and A9 as *trans(O)-cis(C)* one. As for the bis(β-alaninato) complex, B2 exhibited a narrow absorption band in the first absorption band region, and B3 two maxima in the region. By comparison with the spectra of the bis(glycinato) complex, B2 is assignable to *trans(N)-cis(C)* isomer and B3 to *cis,cis,cis(C,N,O)* isomer. As shown in Fig. 1, the absorption spectrum of the *cis, cis,cis(C,N,O)*-bis(glycinato) complex resembles that of the $[Co(CN)_2(ox)(en)]^-$ complex in shape and intensity, that is, two maxima in the first absorption band region have comparable intensity to each other. However, an intense band is observed at a lower frequency in the *cis,cis,cis(C,N,O)*-bis(β-alaninato) complex, and at a higher frequency in the *cis,cis*-$[Co(CN)_2(ox)(NH_3)_2]^-$ complex. These phenomena are considered to be associated with the rigidity of the chelate rings in terms of the vibronic mechanism of an intensity borrowing.[12] The absorption maxima of the bis(β-alaninato) isomers appear at a lower frequency than those of the corresponding bis(glycinato) isomers.

The CD spectral data are also collected in Table 1. The CD spectrum of the *trans(N)-cis(C)*-$[Co(CN)_2(gly)_2]^-$ exhibits a single Cotton peak at the maximum position of the first absorption band. An attempt to isolate an enantiomer of the *trans(N)-cis(C)*-bis(β-

Table 1. Absorption and CD spectral data of the dicyano complexes

Complex	Absorption $\bar{\nu}/10^3$ cm^{-1} (log ε)	CD $\bar{\nu}/10^3$ cm^{-1}(Δε)
A4: *trans(N)-cis(C)*-$(+)^{CD}_{400}[Co(CN)_2(gly)_2]^-$	23.3(2.34)	23.5(+4.09)
	30.9(2.13)	31.0(−0.59)
A8: *cis,cis,cis(C,N,O)*-$(+)^{CD}_{500}[Co(CN)_2(gly)_2]^-$	21.1(2.04)	20.3(+1.28)
	24.4(2.05)	24.7(−1.63)
	30.5(2.16)	*ca.* 28(−0.7)sh
		31.0(+0.08)
		33.0(−0.02)
A9: *trans(O)-cis(C)*-$(+)^{CD}_{500}[Co(CN)_2(gly)_2]^-$	19.2(1.84)	16.8(−0.004)
		18.7(+0.015)
	ca. 26(1.9)sh	*ca.* 25(−0.002)sh
	30.7(2.14)	27.0(−0.003)
B2: *trans(N)-cis(C)*-$(+)^{CD}_{450}[Co(CN)_2(\beta\text{-ala})_2]^-$	23.0(2.42)	22.7(+0.045)
	30.3(2.06)	*ca.* 31(−0.004)sh
B3: *cis,cis,cis(C,N,O)*-$(+)^{CD}_{500}[Co(CN)_2(\beta\text{-ala})_2]^-$	20.7(2.29)	20.4(+1.56)
	23.9(2.12)	24.8(−0.82)
	30.2(2.00)	*ca.* 27(−0.6)sh
		ca. 30(−0.2)sh

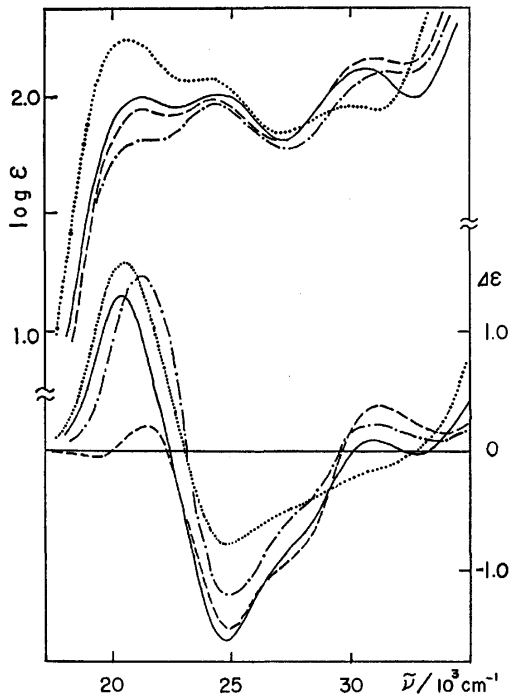

Fig. 1. Visible absorption and CD spectra of;
——: *cis, cis, cis(C, N, O)*-$(+)^{CD}_{500}[Co(CN)_2(gly)_2]^-$,
……: *cis, cis, cis(C, N, O)*-$(+)^{CD}_{500}[Co(CN)_2(\beta\text{-ala})_2]^-$,
– – –: *cis*-$(-)_{589}[Co(CN)_2(ox)(en)]^-$, –·–·–: *cis, cis*-$(+)_{589}$ $[Co(CN)_2(ox)(NH_3)_2]^-$.

alaninato) isomer using $(-)_{589}[Co(ox)(en)_2]^+$ and $(-)_{589}[Co(CO_3)(en)_2]^+$, *etc.* as resolving agents failed. However, when $(-)_{589}[Co(NO_2)_2(en)_2]^+$ was used, an extremely weak Cotton peak with a negative sign was observed at 22700 cm^{-1} for an enantiomer obtained in the form of the less-soluble diastereomer. The *trans(O)-cis*(C)-$[Co(CN)_2(gly)_2]^-$ complex could be resolved by using $(-)_{589}[Co(ox)(en)_2]^+$, however, the optical purity of the diastereoisomeric salt obtained was very low. The CD spectrum of *trans(O)-cis(C)*-$[Co(CN)_2(gly)_2]$ exhibits two extrema with opposite signs in the region of the absorption band at 19200 cm^{-1} which is assigned to $^1A_{1g}\rightarrow{}^1E_g$ in a holohedrized symmetry[13] D_{4h}. A Cotton peak corresponding to $^1A_{1g}\rightarrow{}^1A_{2g}$ is observed as a shoulder at *ca.* 25000 cm^{-1}. As shown in Fig. 1, the CD spectrum of *cis,cis,cis(C,N,O)*-$[Co(CN)_2(gly)_2]^-$ exhibits two extrema with opposite signs in the first absorption band region, and a shoulder, observed at *ca.* 27000 cm^{-1}, is considered to be a splitting component of the second absorption band. The spectra of *cis,cis,cis(C,N,O)*-bis-(β-alaninato) isomer also exhibits two extrema in the first absorption band region; the Cotton peak at the lower frequency is dominant.

Optical Activity of cis,cis,cis-$[Co(C)_2(N)_2(O)_2]^-$ *Complexes.* The CD spectra of *cis,cis*-$[Co(CN)_2(OO)(NH_3)_2]^-$ and *cis*-$[Co(CN)_2(OO)(en)]^-$ complexes (OO: CO_3^{2-} and ox^{2-}) have been reported.[4] The optical activities of the former complexes are mainly derived from the chiral arrangement of three kinds of donor atoms. However, the chirality of the latter complexes are considered to have two origins; one is the arrangement of the donor atoms, and another is a chiral distribution of the chelate rings. The absolute configurations of these dicyano complexes have been predicted in terms of the sign of the Cotton peak observed at the higher frequency in the first absorption band region. For example, the absolute configuration of $(-)_{589}[Co(CN)_2(ox)(en)]^-$ complex, which exhibits three Cotton peaks with alternating signs, has been assigned as shown in Fig. 2, being denoted as $\Lambda(R)$ according to the two origins of the chirality. The *cis,cis,cis(C,N,O)*-$[Co(CN)_2(gly)_2]^-$ complex has also two chiral origins as for *cis*-$[Co(CN)_2(ox)(en)]^-$, however, the absolute configuration is denoted with either $\Lambda(R)$ or $\Lambda(S)$.

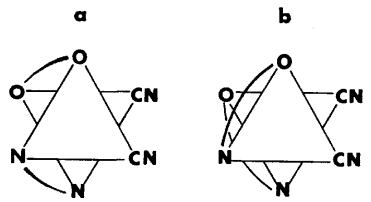

Fig. 2. Absolute configurations of;
a. *cis*-$\Lambda(R)$-$(-)_{589}[Co(CN)_2(ox)(en)]^-$, b. *cis, cis, cis(C, N, O)*-$\Lambda(R)$-$(+)^{500}_{CD}$ $[Co(CN)_2(gly)_2]^-$.

Mason and Seal[3] have applied a dynamic coupling model to the $[Co(en)_3]^{3+}$ and $[Co(tn)_3]^{3+}$ complexes. In their treatment, the contribution to the optical activity from the donor atoms was separated from that of the non-ligating atoms. It is possible to apply such a treatment in the present complexes. If the deviation of the donor atoms from the octahedral sites due to chelations can be disregarded, the contribution from the donor atoms intimately associates with the *R* (or *S*) configuration, while the contribution from the non-ligating atoms associates with the Λ (or Λ) configuration. The CD spectrum of the *cis,cis,cis(C,N,O)*-$(+)^{CD}_{500}[Co(CN)_2(gly)_2]^-$ isomer roughly resembles that of the $(-)_{589}[Co(CN)_2(ox)(en)]^-$ isomer. This suggests that either the donor atoms or the non-ligating atoms mainly contribute to the optical activity of the complexes. The resemblance between the CD spectrum of *cis,cis,cis-(C,N,O)*-$(+)^{CD}_{500}[Co(CN)_2(gly)_2]^-$ and that of *cis,cis-R*$(+)_{589}[Co(CN)_2(ox)(NH_3)_2]^-$ (shown in Fig. 1) suggests the larger contribution from the donor atoms, and predicts the absolute configuration of the bis(glycinato) isomer as $\Lambda(R)$, since the chirality of the *cis,cis*-$[Co(CN)_2(ox)(NH_3)_2]^-$ complex is considered to be derived from the arrangement of the donor atoms.

In order to confirm the above suggestion, an X-ray crystal analysis of $(-)_{589}[Co(ox)(en)_2]\cdot$*cis,cis,cis(C,N,O)*-$(+)^{CD}_{500}[Co(CN)_2(gly)_2]\cdot 3H_2O$ was attempted, and the detailed data will be presented elsewhere. The absolute configuration of the bis(glycinato) isomer was determined as $\Lambda(R)$, as illustrated in Fig. 2. This result shows that the optical activity of the *cis,cis,cis*-$[Co(C)_2(N)_2(O)_2]^-$-type complexes mainly arises from the chiral arrangement of the donor atoms and the non-ligating atoms cause auxiliary optical activity. It is found that the deviation of the donor atoms from the octahedral sites due to the chelations also makes a minor contribution to the optical activity. The results supports the

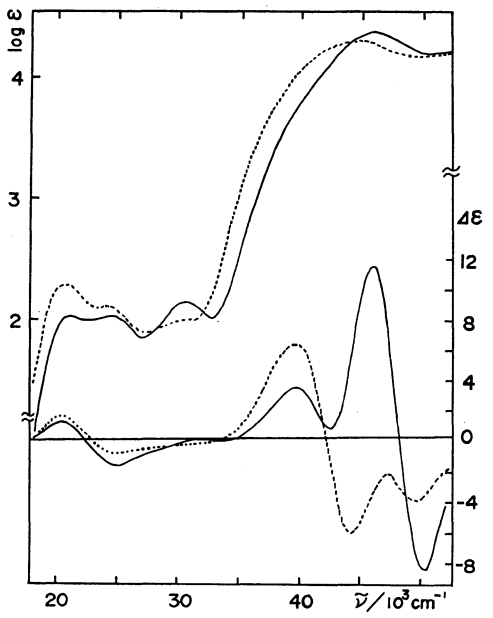

Fig. 3. Visible and ultra-violet absorption and CD spectra of;
——: *cis*, *cis*, *cis*(*C*, *N*, *O*)-(+)$^{CD}_{500}$ [Co(CN)$_2$(gly)$_2$]$^-$,
……: *cis*, *cis*, *cis*(*C*, *N*, *O*)-(+)$^{CD}_{500}$ [Co(CN)$_2$(*β*-ala)$_2$]$^-$.

evaluation of the absolute configurations of the *cis,cis*-[Co(CN)$_2$(OO)(NH$_3$)$_2$]$^-$ and *cis*-[Co(CN)$_2$(OO)(en)]$^-$ complexes reported in the previous paper,[4] by the CD spectral comparison.

At a glance, the results obtained are incompatible with those for the tris(diamine) complexes, where the non-ligating atoms play an important role in the optical activities of the complexes. As to the tris(diamine) complexes, if the existence of the non-ligating atoms and the deviation of the donor atoms from the octahedral sites be disregarded, the distribution of the donor atoms around a metal ion creates no optical activity. On the contrary, as to the *cis,cis,cis*-[Co(C)$_2$(N)$_2$(O)$_2$]$^-$ complexes, such a distribution is considered to generate large optical activity, because the ligand field strengths of the C, N, and O donors are very different from each other.

The isomer (+)$^{CD}_{500}$[Co(CN)$_2$(*β*-ala)$_2$]$^-$ is also assignable to *Δ*(*R*) configuration by comparison with the CD spectrum of the bis(glycinato) complex in the first absorption band region, since the change from gly to *β*-ala chelate rings results in a slight change of the intensities of the Cotton peaks. This is supported by the comparison with the spectra in the ultra-violet region, illustrated in Fig. 3. Since several transitions lie closely in the same region, the CD spectra of the isomers are complicated. However, both isomers exhibit the positive Cotton peaks at *ca.* 40000 cm^{-1} which correspond to the lowest lying allowed-transition.

The authors wish to express thanks to Mr. T. Katahara for his aid in the experiment.

References

1) F. S. Richardson, *Chem. Rev.*, **79**, 17 (1979).
2) R. S. Evans, A. F. Schreiner, and P. J. Hauser, *Inorg. Chem.*, **9**, 2185 (1974).
3) S. F. Mason and R. H. Seal, *Mol. Phys.*, **31**, 755 (1976).
4) T. Ito and M. Shibata, *Inorg. Chem.*, **16**, 108 (1977).
5) S. Shimba, S. Fujinami, and M. Shibata, *Chem. Lett.*, **1979**, 783.
6) S. Shimba, S. Fujinami, and M. Shibata, *Bull. Chem. Soc. Jpn.*, **53**, 2523 (1980).
7) R. S. Cahn. C. K. Ingold, and V. Prelog, *Angew. Chem., Int., Ed. Engl.*, **5**, 385 (1966).
8) V. A. L. Poznjak and V. I. Pawlowski, *Z. Anorg. Allg. Chem.*, **465**, 159 (1980).
9) K. Konya, H. Nishikawa, and M. Shibata, *Inorg. Chem.*, **7**, 1165 (1968).
10) M. Shibata, *Proc. Jpn. Acad.*, **50**, 779 (1974).
11) S. Fujinami and M. Shibata, *Bull. Chem. Soc. Jpn.*, **46**, 3443 (1973).
12) R. Englman, *Mol. Phys.*, **3**, 48 (1960).
13) C. K. Jørgensen, "Modern Aspects of Ligand Field Theory," North-Holland, Amsterdam (1971).

Binuclear Metal Complexes. XL.[1] Synthesis and Magnetic and Spectral Properties of Alkoxo-bridged Copper(II) Complexes with 2-(Alkylthio)ethanols

Masahiro MIKURIYA, Hisashi OKAWA, and Sigeo KIDA*

Department of Chemistry, Faculty of Science, Kyushu University 33, Hakozaki, Higashi-ku, Fukuoka 812

(Received February 12, 1981)

Alkoxo-bridged copper(II) complexes with 2-(alkylthio)ethanols, $Cu(RSCH_2CH_2O)X$ ($R=CH_3$, C_2H_5, n-C_3H_7, i-C_3H_7, s-C_4H_9, t-C_4H_9; X=Br, Cl), have been prepared and characterized by elemental analyses, infrared and electronic spectra and magnetic susceptibilities (80—300 K). Based on the magnetic properties, these complexes were divided into three types, A, B, and C. Type A complexes show a strong antiferromagnetic interaction and exhibit a distinct absorption band characteristic of alkoxo-bridged structure in the 22—24$\times 10^3$ cm^{-1} region. Type B and C complexes follow the Curie-Weiss law. The former complexes show a ferromagnetic behavior, whereas the latter complexes show a weak antiferromagnetism. The results were compared with those of the complexes with 2-(dialkylamino)ethanols, $Cu(R_2NCH_2CH_2O)X$.

A great number of copper(II) complexes with 2-(dialkylamino)ethanols (abbreviated as HR-no) with the general formula Cu(R-no)X were reported and their structures and magnetic properties have been extensively studied.[2-5] However, there has been no study on copper(II) complexes with 2-(alkylthio)ethanols so far. This may partly be due to the poor coordinating ability of both thioether sulfur and alcoholic oxygen atoms.[6] As a continuing project for binuclear copper(II) complexes of sulfur-containing ligands, we recently reported the synthesis, crystal structures and spectral and magnetic properties of alkoxo-bridged copper(II) complexes with tridentate ligands having sulfur, nitrogen and oxygen as donor atoms (SNO and NSO donor sets). The results were discussed in relation to those of the alkoxo-bridged copper(II) complexes with NNO tridentate ligands.[7,8] In this study, we have prepared a series of alkoxo-bridged copper(II) complexes with 2-(alkylthio)ethanols, $Cu(RSCH_2CH_2O)X$ (abbreviated as Cu(R-so)X, $R=CH_3$, C_2H_5, n-C_3H_7, i-C_3H_7, s-C_4H_9, t-C_4H_9; X=Br, Cl), and investigated their magnetic and spectral properties in comparison with those of the complexes with 2-(dialkylamino)ethanols, Cu(R-no)X (Fig. 1).

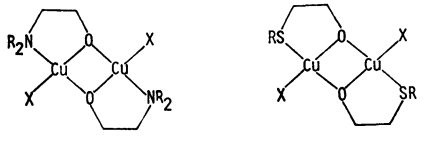

(a) (b)

Fig. 1. Structures of complexes. (a) Cu(R-no)X, (b) Cu(R-so)X.

Experimental

Preparation of the Complexes. The ligands, $RSCH_2CH_2OH$ ($R=CH_3$, C_2H_5, n-C_3H_7, i-C_3H_7, s-C_4H_9, t-C_4H_9), were prepared after the method described in the literature.[9] Preparation of the complexes is exemplified by $Cu(CH_3$-so)Cl. To an absolute ethanol solution of 2-(methylthio)ethanol (370 mg) and triethylamine (143 mg) was added an absolute ethanol solution of copper(II) chloride (135 mg). A dark green precipitate was yielded in the solution. This precipitate was separated by filtration, washed with ethanol and dried *in vacuo* over P_2O_5. Yield: 125 mg.

Table 1. Analytical data of Cu(R-so)X

Complex R	X	Found(Calcd) (%) C	H
CH_3	Cl	19.45(18.95)	3.89(3.71)
C_2H_5	Cl	23.43(23.53)	4.47(4.44)
n-C_3H_7	Cl	27.03(27.52)	5.09(5.08)
i-C_3H_7	Cl	27.62(27.52)	5.18(5.08)
s-C_4H_9	Cl	30.99(31.03)	5.64(5.64)
t-C_4H_9	Cl	30.81(31.03)	5.72(5.64)
CH_3	Br	15.59(15.36)	3.03(3.01)
C_2H_5	Br	19.44(19.32)	3.76(3.65)
n-C_3H_7	Br	22.88(22.86)	4.20(4.22)
i-C_3H_7	Br	22.98(22.86)	4.31(4.22)
s-C_4H_9	Br	25.88(26.05)	4.68(4.74)
t-C_4H_9	Br	25.85(26.05)	4.81(4.74)

The bromides, Cu(R-so)Br, were prepared by a method similar to that for the chlorides except for using copper(II) bromide instead of copper(II) chloride.

Carbon and hydrogen analyses were carried out at the Service Center of Elemental Analysis, Kyushu University. The results of elemental analyses are listed in Table 1.

Measurements. Infrared spectra were measured with a Hitachi Grating Infrared Spectrophotometer Model 215 in the region 4000—650 cm^{-1} on a KBr disk. Electronic spectra were measured with a Shimadzu Multipurpose Spectrophotometer Model MSP-5000 at room temperature. Magnetic susceptibilities were measured by the Faraday method over the range 80—300 K. The apparatus was callibrated by the use of $[Ni(en)_3]S_2O_8$.[10] All the susceptibilities were corrected for the diamagnetism of the constituting atoms by the use of Pascal's constants.[11] Effective magnetic moments were calculated from the equation, $\mu_{eff}=2.828\sqrt{(\chi_A-N\alpha)T}$, where χ_A is atomic magnetic susceptibility and $N\alpha$ is temperature-independent paramagnetism in cgs emu. (1 BM=9.274$\times 10^{-24}$ A m^2, 1 cm^3 mol^{-1} (cgs emu)=$4\pi\times 10^{-6}$ m^3 mol^{-1}.)

Results and Discussion

Infrared spectra of the free ligands show a strong band around 3370 cm^{-1}, which is attributed to the OH stretching vibration. In the case of 2-(methylthio)-ethanol, the OH deformation vibration was assigned

TABLE 2. MAGNETIC DATA OF Cu(R-so)X

Type	Complex R	X	μ_{eff}/BM (T/K)	θ/K	$2J$/cm^{-1}[a]	$N\alpha\times10^6$/cgs emu	P
A	CH_3	Cl	0.60 (293)		−745	57	0
	C_2H_5	Cl	0.50 (298)		−865	41	0.96×10^{-2}
	t-C_4H_9	Cl	0.72 (292)		−665	36	1.7×10^{-2}
	CH_3	Br	0.57 (298)		−780	54	0
	C_2H_5	Br	0.38 (294)		−930	56	0
	s-C_4H_9	Br	0.62 (297)		−735	60	0.78×10^{-2}
	t-C_4H_9	Br	0.56 (298)		−820	47	1.7×10^{-2}
B	i-C_3H_7	Cl	1.85 (294)	13		60	
	n-C_3H_7	Br	1.84 (295)	22		60	
	i-C_3H_7	Br	1.84 (294)	16		60	
C	n-C_3H_7	Cl	1.72 (298)	−55		60	
	s-C_4H_9	Cl	1.70 (298)	−45		60	

a) For all the complexes $g=2.10$ was assumed.

to the band at 1160 or 1010 cm^{-1}.[12] All these bands are absent in the spectra of the copper(II) complexes. This indicates that the alcoholic proton is lost upon complexation.

Based on the temperature dependence of the magnetic susceptibilities, we classified the complexes into three types: type A; complexes whose magnetic behavior can be interpreted in terms of the Bleaney-Bowers equation[13] with considerably large J values, type B; complexes which obey the Curie-Weiss law with positive Weiss constants in the temperature range studied, and type C; complexes which obey the Curie-Weiss law with negative Weiss constants. These types exactly correspond to the types A, B, and C(a) of Nishida and Kida's classification,[5] respectively.

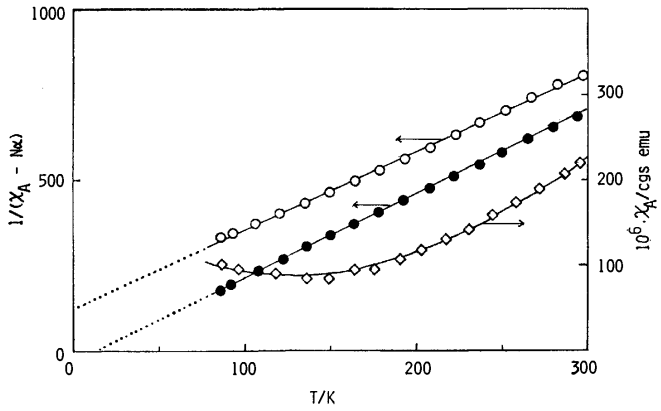

Fig. 2. Temperature dependence of magnetic susceptibilities of Cu(s-C_4H_9-so)Br (type A) (◇), Cu(i-C_3H_7-so)Cl (type B) (●), and Cu(n-C_3H_7-so)Cl (type C) (○). The solid curve was calculated from Eq. 1 using the parameters listed in Table 2.

Type A Complexes. The magnetic moments are very low at room temperature, indicating the existence of a strong antiferromagnetic interaction in these complexes. An example of the temperature dependence of magnetic susceptibilities of type A complexes is shown in Fig. 2. The temperature dependence of magnetic susceptibilities can be interpreted by the modified Bleaney-Bowers equation[14]

$$\chi_A = \frac{Ng^2\beta^2}{3kT}\left[1+\frac{1}{3}\exp(-2J/kT)\right]^{-1}(1-P) + \frac{0.45P}{T} + N\alpha, \quad (1)$$

where χ_A is susceptibility per copper atom, P is the mole fraction of the mononuclear copper(II) impurity, and other symbols have the usual meanings. The second term in Eq. 1 was added to account for the presence of the small amount of a paramagnetic impurity which was found in some samples of type A complexes. The parameters, $-2J$, $N\alpha$, and P were evaluated from the best fit of the experimental data to Eq. 1 and are listed in Table 2. The $-2J$ values, the energy separation between the spin-singlet ground state and the lowest spin-triplet state, is comparable to those of type A complexes of Cu(R-no)X,[4,5] indicating that a strong antiferromagnetic interaction is operating between the copper(II) ions.

The electronic absorption spectra in nujol mull of type A complexes are shown in Fig. 3. The band maxima of the absorption spectra in nujol mull and in 1,2-dichloroethane solutions are given in Table 3. Both spectra display a broad band centered at about 14—15$\times10^3$ cm^{-1} which is attributable to d-d transitions. In the higher frequency region 22—24$\times10^3$ cm^{-1}, a

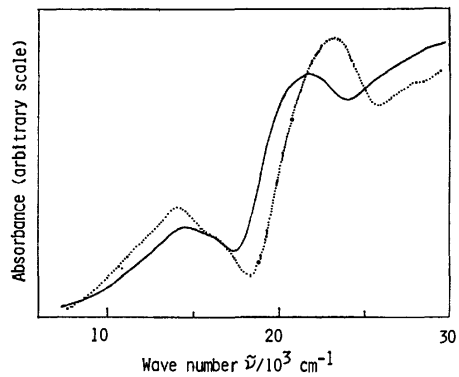

Fig. 3. Mull spectra of Cu(CH_3-so)Br (——) and Cu(C_2H_5-so)Cl (……).

Table 3. Spectral data of Cu(R-so)X

Type	Complex R	Complex X	Mull spectra $\bar{\nu}_{max}/10^3$ cm^{-1}			Solution spectra[a] $\bar{\nu}_{max}/10^3$ cm^{-1}(ε)	
A	CH_3	Cl	13.9	16.1sh	23.8sh[b]		
	C_2H_5	Cl	14.1	16.4sh	23.2	14.5(120)	23.8(1570)
	t-C_4H_9	Cl	13.9		22.7	14.2(99)	23.5(1260)
	CH_3	Br	14.5		21.7	14.5(160)	22.5(1750)
	C_2H_5	Br	14.2	16.3sh	21.8	14.5(160)	22.4(2220)
	s-C_4H_9	Br	14.4		21.8	14.7(190)	22.4(2420)
	t-C_4H_9	Br	14.7		21.7	14.9(240)	22.3(1790)
B	i-C_3H_7	Cl	12.7sh	15.5		14.6(91)	23.7(1490)
	n-C_3H_7	Br	13.0sh	15.3		14.6(160)	22.4(2220)
	i-C_3H_7	Br	12.8sh	15.3		14.6(170)	22.3(2520)
C	n-C_3H_7	Cl		13.9	21.5	14.5(130)	23.8(1700)
	s-C_4H_9	Cl		15.2	22.2sh	14.7(170)	23.6(2200)

a) 1,2-Dichloroethane solution. b) sh=Shoulder.

distinct absorption band with higher intensity ($\log \varepsilon =$ *ca.* 3) was observed. This band should correspond to the band in the 24—25$\times 10^3$ cm^{-1} region observed for type A complexes of Cu(R-no)X,[4,5] and may be assigned to p_π(O)→d(Cu) charge transfer transition.[5] The lowering of the transition energy for Cu(R-so)X relative to that of Cu(R-no)X may be interpreted in terms of lowering of optical electronegativity[15] of copper ion of Cu(R-so)X on the assumption that the energies of p_π electrons of alkoxo oxygen are nearly constant.[7]

Type B Complexes. The room-temperature magnetic moments of type B complexes fall in the range of the value generally observed for mononuclear copper(II) complexes. As shown in Fig. 2, the magnetic susceptibilities of type B complexes follow the Curie-Weiss law, $\chi_A = C/(T-\theta) + N\alpha$, in the temperature range 80—300 K. Since the ground states of these complexes are orbitally nondegenerate, the positive Weiss constants indicate that a ferromagnetic interaction is operative between the copper ions (Table 2), as was so in the case of type B complexes of Cu(R-no)X.[4,5] The X-ray structure analyses showed that type B complexes of Cu(R-no)X have tetranuclear structures with a cubane type Cu_4O_4 core.[3] Therefore, it can be presumed that type B complexes of Cu(R-no)X have similar cubane tetranuclear structures.

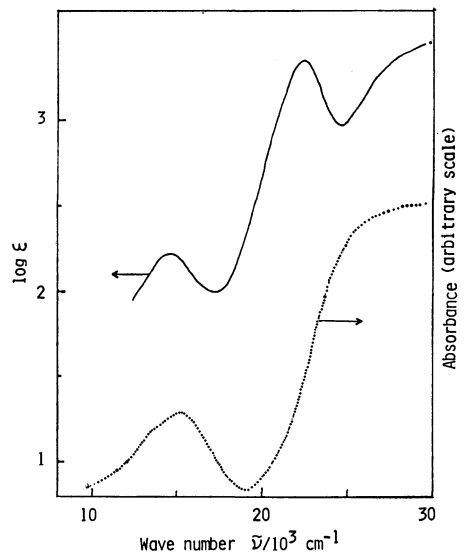

Fig. 4. Absorption spectra of Cu(n-C_3H_7-so)Br in Nujol mull (·····) and in 1,2-dichloroethane solution (——).

As shown in Fig. 4, type B complexes show no distinct absorption band at 22—24$\times 10^3$ cm^{-1} in the nujol mull spectra, whereas in the solution a distinct absorption in that region. This fact suggests that type B complexes are likely to dissociate in solution to form a binuclear species similar to type A complexes.[16]

Type C Complexes. The effective magnetic moments at room temperature of type C complexes are slightly lower than the spin-only value for one unpaired electron per copper atom. The cryomagnetic data follow the Curie-Weiss law with a negative Weiss constant, indicating the existence of a weak antiferromagnetic interaction in this type of complexes (Fig. 2).

The band maxima of the electronic absorption spectra of type C complexes are given in Table 3. In both the solid state and the solution spectra, type C complexes show a distinct absorption band at 22—24$\times 10^3$ cm^{-1}, as observed for type A complexes. These magnetic and spectral properties are similar to those of type C(a) complexes of Cu(R-no)X.[4,5]

References

1) Part XXXIX: M. Nakamura, M. Mikuriya, H. Okawa, and S. Kida, *Bull. Chem. Soc. Jpn.*, **54**, 1825 (1981).

2) D. J. Hodgson, *Prog. Inorg. Chem.*, **19**, 173 (1975); J. A. Bertrand and P. G. Eller, *ibid.*, **21**, 29 (1976); A. Pajunen and M. Lehtonen, *Suom. Kemistil. B*, **44**, 200 (1971); W. Haase, *Chem. Ber.*, **106**, 3132 (1973); R. Mergehenn and W. Haase, *Z. Naturforsch., Teil B*, **30**, 155 (1975); L. Merz and W. Haase, *Acta Crystallogr., Sect. B*, **34**, 2128 (1978); E. D. Estes and D. J. Hodgson, *Inorg. Chem.*, **14**, 334 (1975); N. Matsumoto, I. Ueda, Y. Nishida, and S. Kida, *Bull. Chem. Soc. Jpn.*, **49**, 1308 (1976); R. Mergehenn and W. Haase, *Acta Crystallogr., Sect. B*, **33**, 2734 (1977); A. Pajunen and K. Smolander, *Finn. Chem. Lett.*, **1974**, 99; R. Mergehenn, L. Merz, and W. Haase, *Z. Naturforsch., Teil B*, **30**, 14 (1975); W. Haase, R. Mergehenn, and W. Krell, *ibid.*, **31**, 85 (1976); M. Mikuriya, Y. Nishida,

S. Kida, T. Uechi, and I. Ueda, *Acta Crystallogr., Sect. B*, **33**, 538 (1977).
3) R. Mergehenn, W. Haase, and R. Allmann, *Acta Crystallogr., Sect. B*, **31**, 1847 (1975); R. Mergehenn, L. Merz, and W. Haase, *J. Chem. Soc., Dalton Trans.*, **1980**, 1703.
4) E. Uhlig and K. Staiger, *Z. Anorg. Allg. Chem.*, **346**, 21 (1966); **360**, 39 (1968).
5) Y. Nishida and S. Kida, *J. Inorg. Nucl. Chem.*, **38**, 451 (1976).
6) M. R. Udupa and B. Krebs, *Inorg. Chim. Acta*, **39**, 267 (1980).
7) M. Mikuriya, H. Okawa, and S. Kida, *Inorg. Chim. Acta*, **34**, 13 (1979); **42**, 233 (1980); *Bull. Chem. Soc. Jpn.*, **53**, 2871 (1980).
8) M. Mikuriya, M. Aihara, Y. Nishi, H. Okawa, and S. Kida, *Chem. Lett.*, **1980**, 795; M. Mikuriya, H. Okawa, and S. Kida, *Bull. Chem. Soc. Jpn.*, **53**, 3717 (1980).
9) W. R. Kirner, *J. Am. Chem. Soc.*, **50**, 2446 (1928).
10) N. F. Curtis, *J. Chem. Soc.*, **1961**, 3147.
11) P. W. Selwood, "Magnetochemistry," Interscience Publishers, New York (1956).
12) K. S. Boustany and A. Jacot-Cuillarmod, *Chimia*, **23**, 31 (1969).
13) B. Bleaney and K. D. Bowers, *Proc. R. Soc. London, Ser. A*, **214**, 451 (1952).
14) K. E. Hyde, G. Gordon, G. F. Kokoszka, *J. Inorg. Nucl. Chem.*, **30**, 2155 (1968).
15) C. K. Jørgensen, *Prog. Inorg. Chem.*, **12**, 101 (1970).
16) Y. Nishida, F. Numata, and S. Kida, *Inorg. Chim. Acta*, **11**, 189 (1974).

Preparation and Spectroscopic Studies of Cobalt(III) Complexes Containing Optically Active Seven-membered Chelate Ligands

Masaaki KOJIMA, Ken'ichi MORITA, and Junnosuke FUJITA*

Department of Chemistry, Faculty of Science, Nagoya University, Chikusa-ku, Nagoya 464

(Received April 16, 1981)

New cobalt(III) complexes of the types, *trans*-$[CoCl_2L_2]^+$, $[Co(NH_3)_4L]^{3+}$, *cis*-$[Co(NH_3)_2L_2]^{3+}$, and $[Co(en)_2L]^{3+}$, where L denotes a seven-membered chelate diamine ligand, (*R*)-2-methyl-1,4-butanediamine or *meso*- and (*R* or *S*)-2,5-hexanediamine, have been prepared. The dichloro complexes decompose gradually even in the solid state, and rapidly in methanol. The ammine and ethylenediamine complexes are stable in acidic water, but decompose gradually in neutral water. The absorption and circular dichroism spectra of all the complexes have been recorded in aqueous or acetone solutions. The circular dichroism spectra in the first absorption band region are changed by the addition of sulfate ions, and the variation has been discussed in terms of the structure of isomers and the conformational instability of the seven-membered chelate rings.

A six-membered chelate ring has been shown to be conformationally flexible and to interchange easily its conformation between two forms, the chair and the skew depending on environment. In the previous papers,[1-3] we reported that spectral changes in absorption and circular dichroism (CD) of some 1,3-diamine cobalt(III) complexes caused by the addition of sulfate ions can be interpreted in terms of such conformational instability of six-membered chelate rings.

Studies with molecular models suggest that a seven-membered diamine chelate ring is also conformationally labile and can interchange among some conformers (Fig. 1). In fact, two 1,4-butanediamine (tetramethylenediamine, tmd) chelate rings in *trans*-$[CoCl_2(tmd)_2]Cl\cdot H_2O$ have been shown by X-ray analysis to have different conformations, *skew*(*h*) and *skew*(*v*),[4] while those in *Δ*-$[Co(tmd)_3]Br_3$ have the *λ*-*skew*(*h*) conformation.[5] In [Pd{(*S*)-ornithinato}$_2$], two seven-membered chelate (*N*,*N*) rings are in the *twist-chair* conformation, which can be regarded as the distorted *chair* form.[6] Thus, seven-membered chelate rings are stabilized in various conformations in crystals of metal complexes. In solution, however, these conformations might be changed by different factors such as solvation and ion-pair formation. In order to elucidate the conformation of seven-membered chelate rings in solution, we have prepared cobalt(III) complexes containing tmd, (*R*)-2-methyl-1,4-butanediamine (*R*-mtmd), and 2,5-hexanediamine (dmtmd), and measured their absorption and CD spectra in the absence and presence of sulfate ions.

Experimental

Measurements. Absorption spectra were recorded on a Hitachi 323 spectrophotometer, and CD spectra on JASCO model J-20 and J-40CS spectropolarimeters. Optical rotation at 589 nm were measured with a JASCO DIP-4 polarimeter. All the measurements were made at 25±1 °C.

Preparation. *2-Methyl-1,4-butanediamine(mtmd).* Dimethyl 2-methylbutanedioate prepared by the method of Jeffery and Vogel[7] was dissolved in methanol which had been saturated with ammonia. The solution was stirred for 6 days at room temperature to give 2-methyl-1,4-butanediamide. 2-Methyl-1,4-butanediamine (mtmd) was prepared by reducing the diamide with $LiAlH_4$ in dry tetrahydrofuran (THF). To a suspension of $LiAlH_4$ (11.4 g, 0.3 mol) in dry THF (280 cm^3) was added the diamide (7.6 g, 0.056 mol) in small portions. The mixture was refluxed for 27 h, and then cooled in an ice-bath. A mixture of water–THF (1:1) was added dropwise with vigorous stirring. The slurry was filtered by suction, the residue was extracted with THF (*ca.* 100 cm^3) under reflux for 1 h, and filtered again. The extraction was repeated once more. The combined filtrate and extracts were mixed with hydrochloric acid to adjust the pH to *ca.* 2, and then evaporated to dryness under reduced pressure. The residue was dissolved in a small amount of water, and a concd sodium hydroxide solution was added. The separated amine layer was extracted three times with chloroform. The extracts were dried over potassium hydroxide pellets, and the chloroform was removed under atmospheric pressure. The remaining oily liquid was distilled under reduced pressure. Bp 88—91 °C/5.3 kPa (lit,[8] 172—173 °C/101 kPa). Yield: 10 g. The diamine was also prepared by reducing 1,2-dicyanopropane[9] in ethanol with sodium.[8] The *rac*-diamine thus obtained was resolved by the following method. To a hot ethanol solution (90 cm^3) of (*R*,*R*)-2,3-bis(benzoyloxy)succinic acid monohydrate (10 g, 0.027 mol) was slowly added an ethanol solution (27 cm^3) of *rac*-mtmd (2.8 g, 0.027 mol). White crystals (4.5 g, crude (*R*,*R*)-2,3-bis(benzoyloxy)-succinate) which formed were collected, washed with ethanol, recrystallized seven times from water, and then converted to the dihydrochloride ((+)-mtmd·2HCl) by a method similar to that for (*R*,*R*)-2,4-pentanediamine dihydrochloride.[10] Yield: *ca.* 30%. $[\alpha]=+5.6°$ (*c* 0.01, H_2O). The (+)-isomer is known to have the (*R*) configuration.[11]

2,5-Hexanediamine (dmtmd). This diamine was prepared by reducing 2,5-hexanedione dioxime[12] with sodium in ethanol according to the known method,[13] or with Raney-Ni in water. The dioxime (50 g, 0.35 mol) was dissolved in an aqueous solution (1 dm^3) of sodium hydroxide (150 g, 3.75 mol). To this solution was added Raney-Ni alloy (100 g) in small portions while the solution was vigorously stirred and cooled to keep the reaction temperature between 25 and 30 °C. After the addition had been completed (*ca.* 1.5 h), the mixture was allowed to stand overnight at room temperature. The residual nickel was filtered off and washed with water. The combined filtrate and washings were steam distilled until no further amine was detected. The distillate was acidified with hydrochloric acid (pH *ca.* 2) and evaporated to dryness to give the diamine hydrochloride. The free diamine was obtained from the hydrochloride by extracting and distilling according to a method similar to that for mtmd, for extraction ether being used instead of chloroform. Bp 80 °C/3.3 kPa (lit,[13] 175 °C/101 kPa). Yield: 12 g. The meso and active diamines were obtained by the following method. To a

hot ethanol solution (240 cm^3) of (*R,R*)-2,3-bis(benzoyloxy)-succinic acid monohydrate (24.3 g, 0.065 mol) was added an ethanol solution (70 cm^3) of the diamine (7.5 g, 0.065 mol). The solution was allowed to stand overnight at room temperature. Colorless crystals which formed were filtered, and recrystallized three times from water–ethanol (1:3). Yield: 6.7 g. $[\alpha]=-86.4°$ (*c* 0.033, H_2O). No change in the rotation was observed with further recrystallizations. This product was converted to the dihydrochloride ((+)-dmtmd·2HCl) by a method similar to that for (+)-mtmd·2HCl. Yield: 1.7 g. $[\alpha]=+11.4°$ (*c* 0.051, H_2O). The free diamine prepared from this dihydrochloride showed negative rotation. The *meso*-diamine dihydrochloride was obtained from the most soluble fraction of the (*R,R*)-2,3-bis-(benzoyloxy)succinate salt by a method similar to that for the active diamine.

trans-$[CoCl_2(R\text{-}mtmd)_2]ClO_4$. A mixture of *R*-mtmd·2HCl (2.0 g, 11.4 mmol) and sodium methoxide (1.08 g, 20 mmol) in methanol (15 cm^3) was stirred for *ca.* 1 h. Sodium chloride which deposited was filtered off and washed with a small amount of methanol. The combined filtrate and washings were diluted with dimethyl sulfoxide (DMSO, 200 cm^3). This solution of *R*-mtmd and a DMSO solution (200 cm^3) of $Co(NO_3)_2\cdot 6H_2O$ (1.02 g, 3.5 mmol) were simultaneously added dropwise to vigorously stirred DMSO (500 cm^3). Air was bubbled through the resulting solution for 6 d in the presence of active charcoal (2 g). After removal of the active charcoal, the dark red solution was diluted with 4 dm^3 of 10^{-2} M HCl (1 M=1 mol/dm^3), and passed through a column (ϕ 2.7×7 cm) of SP-Sephadex. The Sephadex charged with the product was placed on the top of a column (ϕ 7×30 cm) of the same resin, and the adsorbed complexes were eluted with 0.2 M Na_2SO_4 adjusted to pH 2 with $HClO_4$. The effluent of the fastest moving violet band, which was presumed from the absorption spectrum to involve $[Co(R\text{-}mtmd)_2(H_2O)_2]^{3+}$, was collected, diluted with water, and passed again through an SP-Sephadex column (ϕ 2.7×5 cm). After the column had been washed with water, the adsorbed band was eluted with 1 M HCl. Perchloric acid (70%, 0.5 cm^3) was added to the eluate, and the solution was concentrated in a vacuum desiccator over P_2O_5 and NaOH to yield green needles. They were filtered and washed with water. Yield: 0.05 g. The complex is unstable even in the solid state, decomposing at room temperature in 2 months. It is much more unstable in solution; a methanol solution became turbid in 5 min, while an acetone solution was stable enough to record absorption and CD spectra, although it decomposed in a day.

trans-$[CoCl_2\{(-)\text{-}dmtmd\}_2]ClO_4\cdot 0.5H_2O$. This complex was prepared from (+)-dmtmd·2HCl (dihydrochloride of (−)-dmtmd) and $Co(NO_3)_2\cdot 6H_2O$ by a method similar to that for the corresponding *R*-mtmd complex. The complex is as unstable as the *R*-mtmd complex.

$[Co(NH_3)_4(tmd)]Cl_3\cdot 1.5H_2O$. This complex was prepared by a method similar to that reported.[14] To a DMSO solution (380 cm^3) of tmd (1.0 g, 11 mmol) was slowly added a DMSO solution (380 cm^3) of $[Co(NH_3)_5(H_2O)](ClO_4)_3$ (5.3 g, 11 mmol). The solution was stirred for 2 days at room temperature. The resulting orange-red solution was diluted with water, adjusted to pH 2 with HCl, and poured onto a column (ϕ 2.7×4 cm) of SP-Sephadex. A small portion of the Sephadex charged with the product was placed on the top of a column (ϕ 2.7×120 cm) of SP-Sephadex, and the adsorbed complexes were eluted with 0.2 M Na_2SO_4 adjusted the pH to 2 with HCl. The column showed several bands. The effluent of the third orange band was diluted ten times with 10^{-2} M HCl and passed again through an SP-Sephadex column (ϕ 2×3 cm). After the column had been washed with 10^{-2} M HCl (10 dm^3), the adsorbed band was eluted with 1 M HCl. The effluent was evaporated to almost dryness in a vacuum desiccator over P_2O_5 and NaOH. Orange crystals which formed by the addition of ethanol were filtered and washed with ethanol. Yield: 0.5 g.

$[Co(NH_3)_4(R\text{- }or\text{ }S\text{-}mtmd)](ClO_4)_3$. This complex was prepared from *rac*-mtmd and $[Co(NH_3)_5(H_2O)](ClO_4)_3$ by a method similar to that for the corresponding tmd complex. The effluent containing $[Co(NH_3)_4(mtmd)]^{3+}$ was diluted with 10^{-2} M HCl, and passed through a column (ϕ 2×3 cm) of SP-Sephadex. The adsorbed band was eluted with 1.5 M $NaClO_4$ adjusted to pH 2 with $HClO_4$. On concentration with a rotary evaporator, the effluent yielded orange crystals, which were collected and washed with ethanol. Yield: 10%. This racemate was resolved by SP-Sephadex column chromatography. The complex (*ca.* 50 mg) adsorbed on a column of SP-Sephadex (ϕ 2.7×120 cm) was eluted with 0.15 M sodium (+)-tartratoantimonate(III). A good separation between the enantiomers was observed. From the fast and the slowly eluted fractions, $[Co(NH_3)_4(S\text{-}mtmd)](ClO_4)_3$ and $[Co(NH_3)_4(R\text{-}mtmd)](ClO_4)_3$ were isolated, respectively, by a method similar to that for the racemate. The assignment of the isomers was made by comparing the CD spectra with that of the complex prepared from the active *R*-mtmd and $[Co(NH_3)_5(H_2O)](ClO_4)_3$.

$[Co(NH_3)_4(meso\text{-}dmtmd)]Cl_3\cdot 2.5H_2O$, $[Co(NH_3)_4\{(+)\text{-}dmtmd\}](ClO_4)_3\cdot H_2O$, *and* $[Co(NH_3)_4\{(-)\text{-}dmtmd\}](ClO_4)_3\cdot H_2O$. These complexes were prepared from a mixture of *meso*- and *rac*-dmtmd and $[Co(NH_3)_5(H_2O)](ClO_4)_3$ by a method similar to that for $[Co(NH_3)_4(tmd)]^{3+}$. By elution with 0.2 M Na_2SO_4 adjusted to pH 2 with HCl, the column showed five bands; orange-red ($[Co(NH_3)_5(H_2O)]^{3+}$), purple ($[Co(NH_3)_5(DMSO)]^{3+}$), yellow-orange ($[Co(NH_3)_6]^{3+}$) and two orange ($[Co(NH_3)_4(dmtmd)]^{3+}$) bands in the order of elution. From the fourth band, $[Co(NH_3)_4(meso\text{-}dmtmd)]Cl_3\cdot 2.5H_2O$ was obtained by the same method as that for the corresponding tmd complex. The complex corresponding to the fifth band ($[Co(NH_3)_4(rac\text{-}dmtmd)]^{3+}$) was resolved into a pair of enantiomers by the same method as that for $[Co(NH_3)_4(mtmd)]^{3+}$. The fast and the slowly moving bands were assigned to the (−)-dmtmd and the (+)-dmtmd complexes, respectively, by comparing their CD spectra with that of the complex prepared by use of (+)-dmtmd·2HCl ((−)-dmtmd). The enantiomers were isolated as perchlorates by a method similar to that for $[Co(NH_3)_4(mtmd)](ClO_4)_3$ using an eluent of 1 M $HClO_4$ instead of 1.5 M $NaClO_4$. Attempts to obtain the crystalline chlorides were unsuccessful.

Λ-$[Co(en)_2(R\text{-}mtmd)](ClO_4)_3\cdot 0.5H_2O$ *and* Δ-$[Co(en)_2(R\text{-}mtmd)](ClO_4)_3\cdot 2H_2O$. To a DMSOsolution (200 cm^3) of *trans*-$[CoCl_2(en)_2]ClO_4$ (0.7 g, 2 mmol) was slowly added a DMSO solution (50 cm^3) of *rac*-mtmd (0.2 g, 2 mmol). The solution was stirred for 2 d at room temperature. The resulting solution was subjected to SP-Sephadex column chromatography by a method similar to that for the corresponding tetraammine complex. By elution with 0.2 M Na_2SO_4 adjusted to pH 2 with HCl, the column showed four bands; two pink (small amount) and two orange (nearly the same amount) bands; M-I and M-II, in the order of elution. M-I and M-II are racemates of a pair of diastereomers, *Λ*(*R*) and *Δ*(*S*), and *Λ*(*S*) and *Δ*(*R*), respectively. The racemates were resolved without isolation by the same method as that for $[Co(NH_3)_4(mtmd)]^{3+}$. The faster eluted enantiomers of M-I and M-II are *Λ*-$[Co(en)_2(R\text{-}mtmd)]^{3+}$ (M-I-1) and *Λ*-$[Co(en)_2(S\text{-}mtmd)]^{3+}$(M-II-1). respectively. The isomers obtained from the slower eluted bands are thus *Δ*-$[Co(en)_2(S\text{-}mtmd)]^{3+}$ (M-I-2) and *Δ*-$[Co(en)_2(R\text{-}mtmd)]^{3+}$ (M-II-2).

The absolute configurations of these isomers were assigned by comparing the CD spectra with those of the isomers prepared by use of active *R*-mtmd which was obtained by neutralizing *R*-mtmd·2HCl with sodium methoxide in methanol. When excess sodium methoxide was used to neutralize the (*R*)-dihydrochloride, *Δ*-[Co(en)$_2$(*R*-mtmd)]$^{3+}$ (M-II-2) was not yielded, giving only *Λ*-[Co(en)$_2$(*R*-mtmd)]$^{3+}$ (M-I-1) stereoselectively. All the isomers were isolated as perchlorates by the same method as that for [Co(NH$_3$)$_4$(mtmd)](ClO$_4$)$_3$·H$_2$O.

Preparation and Resolution of [*Co(en)$_2$(dmtmd)*]$^{3+}$. The isomers of this complex were prepared from dmtmd·2HCl (a mixture of *meso* and *rac* forms)and *trans*-[CoCl$_2$(en)$_2$]ClO$_4$ in *N,N*-dimethylformamide (DMF) by a method similar to that for the corresponding mtmd complex. By elution with 0.2 M Na$_2$SO$_4$ adjusted to pH 2 with HCl, the column gave four bands; orange-yellow ([Co(en)$_3$]$^{3+}$) and three orange bands, D-I, D-II, and D-III named in the order of elution. From the effluent of D-II, *rac*-[Co(en)$_2$(*meso*-dmtmd)]Cl$_3$·1.5H$_2$O was isolated by the same method as that for [Co(NH$_3$)$_4$(tmd)]-Cl$_3$·1.5H$_2$O. In a similar way one racemate (*Λ*-[Co(en)$_2$-{(+)-dmtmd}]$^{3+}$ and *Δ*-[Co(en)$_2${(−)-dmtmd}]$^{3+}$) was isolated as perchlorate from the effluent of D-III. The racemate in D-I (*Λ*-[Co(en)$_2${(−)-dmtmd}]$^{3+}$ and *Δ*-[Co(en)$_2${(+)-dmtmd}]$^{3+}$) was not isolated because of a small amount. The formation ratio of the racemates, D-I: D-II: D-III was 1 : 4 : 2. Each of the racemates was resolved into a pair of enantiomers by the same method as that for [Co(NH$_3$)$_4$-(mtmd)]$^{3+}$. In all cases, the column showed two separate bands (D-I-1, D-I-2, *etc.*), the *Λ* isomer (D-I-1, *etc.*) being eluted faster. The optically active chlorides were obtained by the same method as that for [Co(NH$_3$)$_4$(tmd)]Cl$_3$·1.5H$_2$O. To assign the isomers, the (−)-dmtmd complex was prepared from (+)-dmtmd·2HCl ((−)-dmtmd). A pair of diastereomers, *Λ*(−) and *Δ*(−) corresponding to D-I-1 and D-III-2, respectively, were obtained.

Preparation and Resolution of cis-[*Co(NH$_3$)$_2$(tmd)$_2$*]$^{3+}$. The *trans*-[CoCl$_2$(tmd)$_2$]ClO$_4$[15] complex was dissolved in liquid ammonia to give an orange solution. After evaporation of ammonia, the crude complex remained was dissolved in 10^{-2} M HCl and column-chromatographed by the same method as that for [Co(NH$_3$)$_4$(tmd)]$^{3+}$. The column showed two orange bands. From the slower moving band, *cis*-[Co(NH$_3$)$_2$-(tmd)$_2$](ClO$_4$)$_3$ was obtained by the same method as that for [Co(NH$_3$)$_4$(mtmd)](ClO$_4$)$_3$·H$_2$O. Yield: 70%. The trans isomer (the faster moving band) was not isolated because of the very small amount. The cis isomer was resolved by the same method as that for [Co(NH$_3$)$_4$(mtmd)]$^{3+}$, the (+)-*Δ* isomer being eluted first. The enatiomers were isolated as perchlorates by the method described.

cis-*Δ*-[*Co(NH$_3$)$_2$*{(−)-*dmtmd*}$_2$]*Cl$_3$*·*2H$_2$O*. This complex was prepared from *trans*-[CoCl$_2${(−)-dmtmd}$_2$]ClO$_4$·H$_2$O and liquid ammonia by the same method as that for the corresponding tmd complex, and isolated as chloride by the method described. Yield: 10%. The other diastereomer was not yielded under the conditions given.

Analytical data of the new complexes are given in Table 1.

Results and Discussion

Preparation and Stability of the Complexes. The *trans*-[CoCl$_2$(*R*-mtmd)$_2$]$^+$ and [CoCl$_2${(−)-dmtmd}$_2$]$^+$ complexes were prepared by oxidizing a DMSO solution of the diamine and cobalt(II) ions with air and by treating with hydrochloric acid. The air-oxidation in aqueous solution resulted in only the formation of insoluble cobalt hydroxide. The DMSO solution was prepared by slowly mixing fairly dilute solutions of the reactants in order to avoid the formation of polymeric complexes.[16] The yields are still very poor, *ca.* 3%. The complexes isolated as perchlorate decompose gradually even in the solid state, and rapidly in methanol (Experimental). The *trans*-[CoCl$_2$(*R*-mtmd)$_2$]$^+$ complex can have two geometrical isomers, *trans-trans* and *trans-cis*, by the alignment of the two methyl groups. However, no attempt to separate them was made because of instability of the complex. The tetraammine and bis-(ethylenediamine) complexes of the diamines were prepared from [Co(NH$_3$)$_5$(H$_2$O)]$^{3+}$ and *trans*-[CoCl$_2$-(en)$_2$]$^+$, respectively by mixing with the diamine in a large amount of DMSO or DMF. Such reactions are

Table 1. Analytical data of the new complexes

Complex	C (%) Found(Calcd)	H (%) Found(Calcd)	N (%) Found(Calcd)
trans-[CoCl$_2$(*rac*-mtmd)$_2$]ClO$_4$	27.49(27.70)	6.45(6.51)	12.84(12.92)
trans-[CoCl$_2$(*R*-mtmd)$_2$]ClO$_4$	27.46(27.70)	6.34(6.51)	12.67(12.92)
trans-[CoCl$_2${(−)-dmtmd}$_2$]ClO$_4$·0.5H$_2$O	30.75(30.62)	7.04(7.07)	11.90(11.90)
[Co(NH$_3$)$_4$(tmd)]Cl$_3$·1.5H$_2$O	13.74(13.78)	7.81(7.81)	24.49(24.11)
[Co(NH$_3$)$_4$(*rac*-mtmd)](ClO$_4$)$_3$·H$_2$O	11.08(11.01)	5.16(5.17)	15.47(15.40)
[Co(NH$_3$)$_4$(*R*-mtmd)](ClO$_4$)$_3$	11.55(11.38)	4.84(4.97)	15.60(15.93)
[Co(NH$_3$)$_4$(*meso*-dmtmd)]Cl$_3$·2.5H$_2$O	18.35(18.26)	8.30(8.43)	21.20(21.29)
[Co(NH$_3$)$_4$}(+)-dmtmd}](ClO$_4$)$_3$·H$_2$O	13.29(12.88)	5.09(5.40)	15.01(15.02)
[Co(NH$_3$)$_4$}(−)-dmtmd}](ClO$_4$)$_3$·H$_2$O	12.91(12.88)	5.13(5.40)	14.85(15.02)
Λ-[Co(en)$_2$(*R*-mtmd)](ClO$_4$)$_3$·0.5H$_2$O	18.60(18.36)	5.33(5.31)	13.61(14.28)
Δ-[Co(en)$_2$(*R*-mtmd)](ClO$_4$)$_3$·2H$_2$O	17.88(17.56)	5.51(5.57)	13.16(13.65)
[Co(en)$_2$(*meso*- dmtmd)]Cl$_3$·1.5H$_2$O	28.28(28.02)	8.37(8.23)	19.49(19.60)
Δ-[Co(en)$_2$(*meso*-dmtmd)]Cl$_3$·1.5H$_2$O	28.32(28.02)	8.55(8.23)	19.52(19.60)
Λ-[Co(en)$_2$}(−)-dmtmd}]Cl$_3$·0.5H$_2$O	29.24(29.25)	8.28(8.10)	20.11(20.46)
[Co(en)$_2$(*rac*-dmtmd)](ClO$_4$)$_3$·H$_2$O(D-III)	19.75(19.64)	5.80(5.60)	13.85(13.74)
Δ-[Co(en)$_2$}(−)-dmtmd}]Cl$_3$·1.5H$_2$O	28.14(28.02)	8.38(8.23)	20.21(19.60)
cis-[Co(NH$_3$)$_2$(tmd)$_2$](ClO$_4$)$_3$H$_2$O	16.43(16.41)	5.24(5.51)	14.58(14.35)
cis-Λ-[Co(NH$_3$)$_2$(tmd)$_2$](ClO$_4$)$_3$	16.71(16.93)	5.42(5.33)	14.81(14.80)
cis-Δ-[Co(NH$_3$)$_2$}(−)-dmtmd}$_2$]Cl$_3$·2H$_2$O	30.81(31.23)	9.05(9.09)	17.97(17.57)

known to be useful in obtaining complexes containing a large chelate ring.[16] Similar reactions with 1,2- or 1,3-diamines are usually accompanied by disproportionation to yield complexes of other bis- and tris-diamine than the desired mono-diamine. In the present study, however, the formation of bis or tris(1,4-diamine) complexes are *seldom* observed. These complexes would be unstable because of crowding due to the bulky seven-membered chelate rings. The $[Co(en)_2(R\text{-mtmd})]^{3+}$ complex yielded only the *Λ* isomer when excess sodium methoxide was used for neutralizing *R*-mtmd·2HCl. However, when distilled free *R*-mtmd was used, such selectivity was not observed, forming the *Λ* and *Δ* isomers in nearly the same amount. The di- and tetraammine and bis(ethylenediamine) complexes with the 1,4-diamines are stable in acidic water, but decom-

TABLE 2. ABSORPTION(AB) AND CD SPECTRAL DATA

Complex	$\tilde{\nu}^{AB}/10^{-3}$ cm^{-1} (log ε)	$\tilde{\nu}^{CD}/10^{-3}$ cm^{-1} ($\Delta\varepsilon$)
$[Co(NH_3)_4(tmd)]^{3+}$	20.70(1.83)	
	29.00(1.76)	
	48.20(4.32)	
$[Co(NH_3)_4(R\text{-mtmd})]^{3+}$	20.72(1.83)	21.00(−0.34)
	29.03(1.76)	28.30(+0.014)
	48.20(4.32)	47.50(−8.2)
$[Co(NH_3)_4\{(-)\text{-dmtmd}\}]^{3+}$	20.62(1.90)	20.41(−0.25)
	28.82(1.83)	
	47.62(4.37)	40.50(−0.76)
		46.30(+6.2)
$[Co(NH_3)_4(meso\text{-dmtmd})]^{3+}$	20.45(1.88)	
	28.74(1.83)	
	46.1 (4.3)sh	
	49.50(4.38)	
Λ-$[Co(en)_2(R\text{-mtmd})]^{3+}$	20.96(1.93)	19.75(+1.07)
		22.10(−0.58)
	29.00(1.90)	28.00(+0.15)
	45.70(4.33)	46.30(−30)
Δ-$[Co(en)_2(R\text{-mtmd})]^{3+}$	20.88(1.99)	20.58(−1.22)
	28.99(1.96)	29.20(+0.070)
	45.70(4.40)	45.90(+20)
Δ-$[Co(en)_2\{(-)\text{-dmtmd}\}]^{3+}$	20.83(1.96)	19.88(−1.11)
		22.73(+0.06)
	28.99(1.93)	27.70(−0.12)
	45.20(4.37)	45.90(+24)
Λ-$[Co(en)_2\{(-)\text{-dmtmd}\}]^{3+}$	20.79(2.02)	21.14(+1.09)
	28.90(1.99)	28.74(−0.17)
	45.20(4.36)	46.10(−15)
Δ-$[Co(en)_2(meso\text{-dmtmd})]^{3+}$	20.62(2.03)	20.24(−0.79)
		26.39(−0.022)
	28.65(2.00)	29.50(+0.037)
	45.10(4.39)	45.50(+18)
cis-*Δ*-$[Co(NH_3)_2(tmd)_2]^{3+}$		18.32(−0.034)
	20.33(1.85)	20.88(+0.52)
	28.49(1.81)	27.78(−0.040)
	45.00(4.33)	45.50(+17)
cis-*Δ*-$[Co(NH_3)_2\{(-)\text{-dmtmd}\}_2]^{3+}$		18.87(−0.29)
	20.12(1.93)	21.41(+0.088)
	28.21(1.89)	27.55(−0.067)
	44.10(4.40)	42.00(+3.6)
trans-$[CoCl_2(R\text{-mtmd})_2]^{+}$ [a]	15.58(1.64)	15.67(−1.27)
	20.12(1.49)	20.00(+0.58)
	24.69(1.81)	23.81(+0.21)
trans-$[CoCl_2\{(-)\text{-dmtmd}\}_2]^{+}$ [a]	15.43(1.71)	15.58(+1.43)
	19.80(1.57)	19.69(−1.45)
	24.45(1.89)	25.40(+0.10)
trans-$[CoCl_2(tmd)_2]^{+}$ [a]	15.55(1.67)	
	20.04(1.50)	
	24.57(1.83)	

a) Solvent: acetone, sh: shoulder.

pose gradually in neutral water. Thus, care was taken to maintain solutions acidic in the course of preparation. The chelate coordination of 1,4-diamines in all the complexes is supported by elution behavior in column chromatography.[16]

Absorption and CD Spectra. As seen in Table 2, the first absorption maxima of $[Co(NH_3)_4(R\text{-mtmd})]^{3+}$, $[Co(NH_3)_4(tmd)]^{3+}$, $[Co(NH_3)_4\{(-)\text{-dmtmd}\}]^{3+}$, and $[Co(NH_3)_4(meso\text{-dmtmd})]^{3+}$ appear at 20720, 20700, 20620, and 20450 cm^{-1}, respectively. Thus the order of these 1,4-diamines in the spectrochemical series can be determined as *R*-mtmd$\gtrsim$tmd$>$(−)-dmtmd$>$*meso*-dmtmd. Since the basicities of (−)-dmtmd and *meso*-dmtmd ligands will be similar, the red shift of the first absorption band of the *meso*-dmtmd complex can be attributed to the strained structure of the complex (*vide infra*). It is reported that cobalt(III) complexes with a strained structure show the red shift in the first absorption band.[17] In the ultraviolet region, the *meso*-dmtmd complex shows a shoulder (46100 cm^{-1}) and a strong band (49500 cm^{-1}), which can be assigned to charge transfer transitions from the *meso*-dmtmd and ammonia ligands, respectively to the cobalt(III) ion. No shoulders are observed for the other tetraammine complexes. The appearance of the shoulder in the *meso*-dmtmd complex indicates that there is a fairly large energy difference between those two kinds of charge transfer transitions. For the other complexes, the charge transfer bands from the 1,4-diamines to the cobalt(III) ion might be hidden by that from the ammonia to the cobalt(III) ion owing to small energy differences between them. The $[Co(NH_3)_6]^{3+}$ complex gives the charge transfer band at 51150 cm^{-1}.[18] Thus the strained $[Co(NH_3)_4(meso\text{-dmtmd})]^{3+}$ complex shows the red shift in both the d-d and charge transfer bands.

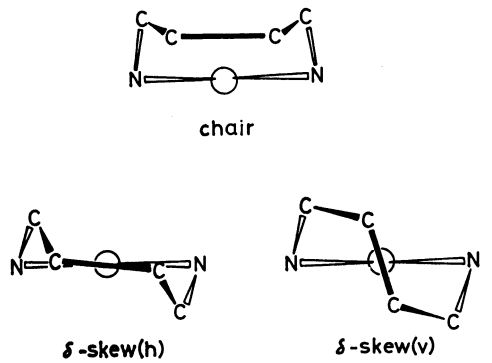

Fig. 1. Possible conformations of a seven-membered 1,4-diamine chelate ring.

Figure 1 shows three typical conformations of a 1,4-diamine chelate ring. Each of the skew conformations is chiral and has its antipode. The chair conformation seems to be unstable because big steric hindrance is involved among the axial hydrogens of 1- and 4-carbon atoms of the 1,4-diamine chelate ring and an apical ligand. However, the *meso*-dmtmd chelate ring might take the chair conformation, since both methyl groups can have equatorial positions in only this form. In any skew conformation one of the two methyl groups is forced to take the axial position. Molecular models indicate that for 1,4-diamine chelate rings, conformations with an axial methyl group do not seem to be plausible. Thus the $[Co(NH_3)_4(meso\text{-dmtmd})]^{3+}$ complex would be strained and shows the red shift in the absorption spectrum. The conformations of the *R*-mtmd and *RR*-dmtmd chelate rings with the equatorial methyl group(s) are either *δ-skew(h)* or *λ-skew(v)*, and *λ-skew(h)* or *λ-skew(v)*, respectively (Figs. 1 and 2).

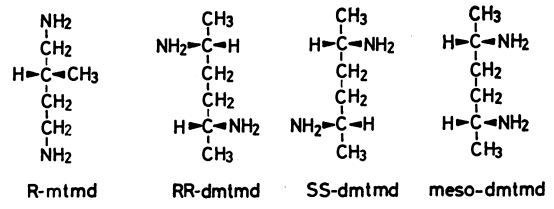

Conformation

Ligand	δ-skew(h)	λ-skew(h)	δ-skew(v)	λ-skew(v)	chair
R-mtmd	e	a	a	e	e(a)
RR-dmtmd	aa	ee	aa	ee	ae
SS-dmtmd	ee	aa	ee	aa	ae
meso-dmtmd	ae	ae	ae	ae	ee(aa)

e: methyl equatorial a: methyl axial

Fig. 2. Absolute configurations of *R*-mtmd and three isomers of dmtmd, and their conformations in chelates.

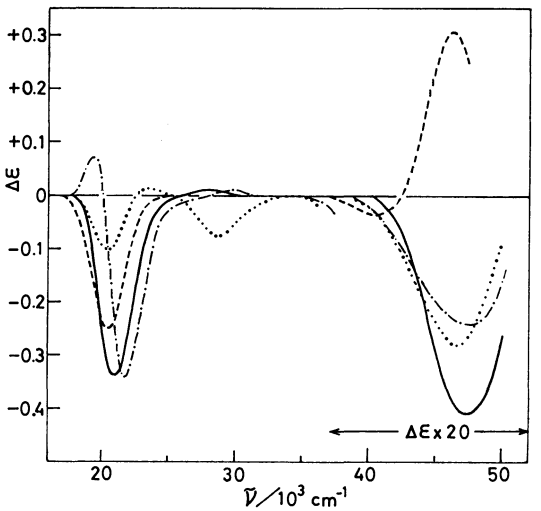

Fig. 3. CD spectra of $[Co(NH_3)_4(diamine)]^{3+}$ in water. Diamine: *R*-mtmd (——), (−)-dmtmd (------), *SS*-2,3-bn (·····), and *SS*-ptn (·····).

Figure 3 compares CD spectra of some tetraamine complexes of a chiral diamine. Except for the (−)-dmtmd complex, all the complexes show negative CD in both the first and the charge transfer absorption band regions. Since the (*S,S*)-2,3-butanediamine (*SS*-2,3-bn)[18] and (*S,S*)-2,4-pentanediamine (*SS*-ptn)[1] chelate rings are stabilized in the *δ-gauche* and *δ-skew* forms, respectively, the *R*-mtmd chelate ring can also be assigned to have the same chirality, *δ-skew(h)*. The *R*-mtmd complex increases the CD strength in the first absorption band region in DMSO ($\Delta\varepsilon=-0.48$ at

21000 cm^{-1}). The same trend is observed for the *SS*-2,3-bn and *SS*-ptn complexes. In the (−)-dmtmd complex, on the other hand, the CD sign in the first absorption band region differs from that in the charge transfer absorption band region. In addition, the complex decreases the CD strength in the first absorption band region in DMSO ($\Delta\varepsilon = -0.18$ at 20300 cm^{-1}), which is opposite to those of the other tetraammine complexes. The results make the assignment for the chirality of the (−)-dmtmd chelate ring difficult. Thus the *trans*-$[CoCl_2\{(-)\text{-dmtmd}\}_2]^+$ complex was prepared and the CD spectrum was compared with those of the related complexes. The relationship between CD patterns and conformational chirality in complexes of this type has also been studied extensively.[10,19]

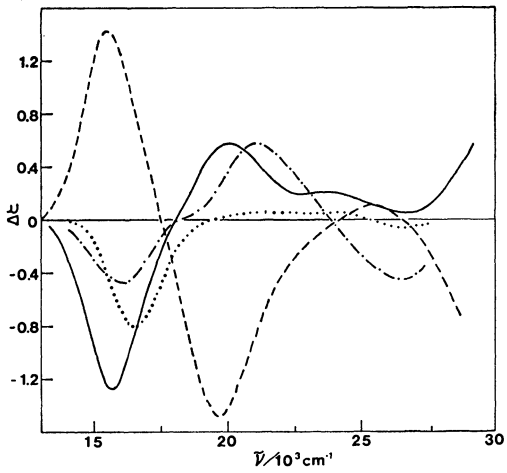

Fig. 4. CD spectra of *trans*-$[CoCl_2(\text{diamine})_2]^+$. Diamine: *R*-mtmd(——, in acetone), (−)-dmtmd (------, in acetone), *SS*-2,3-bn (·····, in methanol), and *SS*-ptn (-·-·-, in methanol).

The *R*-mtmd complex shows a CD pattern similar to those of the *SS*-2,3-bn[10,18] and *SS*-ptn[20] complexes; negative and positive CD bands corresponding to the Ia ($^1E_g \leftarrow {}^1A_{1g}$) and Ib ($^1A_{2g} \leftarrow {}^1A_{1g}$) bands,[21] respectively (Fig. 4). Thus the R-mtmd chelate ring can be assigned to have the *δ-skew(h)* conformation. This assignment agrees with that based on the CD spectrum of the tetraammine complex. On the other hand, the CD pattern of the (−)-dmtmd complex is opposite to those of the other dichloro complexes, indicating the conformation of *λ* chirality. When the *λ*-(−)-dmtmd chelate ring has two equatorial methyl groups, the two chiral carbon atoms are determined to have the (*R*,*R*) configuration, regardless of two kinds of conformations, *skew(h)* or *skew(v)*. This assignment is supported by CD spectra of a pair of diastereomers of $[Co(en)_2\{(-)\text{-dmtmd}\}]^{3+}$ discussed later. The reason why the $[Co(NH_3)_4\{(-)\text{-dmtmd}\}]^{3+}$ complex, in which the chelate ring has *λ* chirality, shows the negative CD band in the first absorption band region is unknown. Similar anomalous CD has been reported for the tetraammine complexes of (*S*,*S*)-1,3-diphenyl-1,3-propanediamine[22] and (*S*)-1,3-butanediamine.[2]

In Fig. 5 are shown CD spectra of M-I-1 and M-II-2

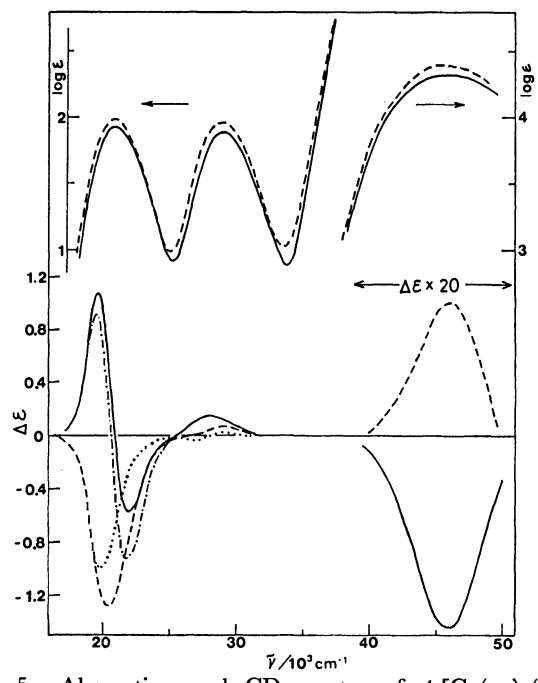

Fig. 5. Absorption and CD spectra of *Λ*-$[Co(en)_2(R\text{-mtmd})]^{3+}$ (M-I-1) in water (——) and in 0.2 mol/dm^3 Na_2SO_4 (·····), and *Δ*-$[Co(en)_2(R\text{-mtmd})]^{3+}$ (M-II-2) in water (------) and in 0.2 mol/dm^3 Na_2SO_4 (·····).

isomers of the $[Co(en)_2(R\text{-mtmd})]^{3+}$ complex in aqueous solutions in the absence or the presence of sulfate ions. The complexes give a typical CD pattern for a tris(diamine) complex, and their absolute configurations can be assigned on the basis of the CD spectra in the first absorption band region; M-I-1 and M-II-2 are assigned to the *Λ*(*R*) and *Δ*(*R*) isomers, respectively. The line connecting 1- and 4-carbon atoms of the *R*-mtmd chelate ring in the *δ-skew(h)* (or *λ-skew(v)*) or *λ-skew(v)* (or *δ-skew(h)*) form is nearly parallel or oblique to the pseudo C_3 axis of the *Λ* (or *Δ*)-$[Co(en)_2(R\text{-mtmd})]^{3+}$ complex, respectively. Thus *Λ* and *Δ* isomers of the *R*-mtmd complex in the *δ-skew(h)* conformation are designated as "*lel*" and "*ob*" isomers, respectively, as in the case of $[Co(en)_3]^{3+}$.[23] The CD patterns of *Λ*- and *Δ*-$[Co(en)_2(R\text{-mtmd})]^{3+}$ in aqueous solutions are characteristic of the "*lel*" and "*ob*" isomers, respectively; the former gives two CD bands with different signs in the first absorption band region, while the latter only one band in this region. Thus the *R*-mtmd chelate rings in these complexes are also stabilized in the *δ-skew(h)* conformation. In the presence of sulfate ions, the *Λ*(*R*) isomer diminishes the CD strength of the major positive component, and complementarily enhances that of the minor component. Such a phenomenon is known to be brought about by an increase in the amount of the lel_3 conformer of a tris(diamine) complex stabilized by ion-association with a sulfate ion.[24] The ion-pair is formed through hydrogen bonding between the three amino protons nearly parallel to the C_3 axis of a tris(diamine) complex and a sulfate ion, and the lel_3 structure affords such amino protons. Thus the *Λ*-$[Co(en)_2(R\text{-mtmd})]^{3+}$ complex will be stabilized in the *Λ*(*δ-gauche*$_2$, *δ-skew(h)*)(lel_3) confor-

mer to increase the amount of δ-diamines in the presence of sulfate ions, and increases the negative CD strength in the first absorption band region. It is known that the vicinal effect of a δ-diamine chelate ring in the $[CoN_6]$-type complex is negative in this region.[25] The Δ-$[Co(en)_2(R\text{-mtmd})]^{3+}$ complex also shows a CD change on addition of sulfate ions, decreasing considerably the negative strength. According to the previous discussion, the decrease in the negative CD strength indicates an increase in the amount of λ-diamines in order to form the $\Delta(lel_3)$ conformer. The complex can afford the lel_3 conformer when the R-mtmd chelate ring forms the λ-*skew*(v) structure, in which the methyl group is disposed equatorially.

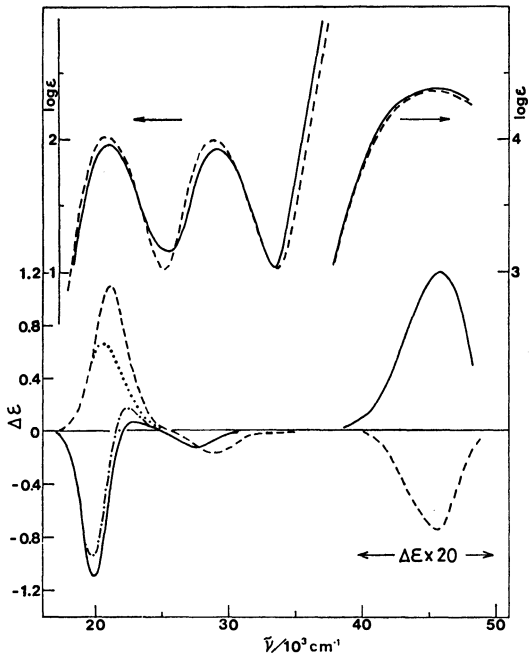

Fig. 6. Absorption and CD spectra of Δ-$[Co(en)_2\{(-)\text{-dmtmd}\}]^{3+}$ (D-III-2) in water (——) and in 0.2 mol/dm³ Na_2SO_4 (·····), and Λ-$[Co(en)_2\{(-)\text{-dmtmd}\}]^{3+}$ (D-I-1) in water (------) and in 0.2 mol/dm³ Na_2SO_4 (·····).

The D-I-1 and D-III-2 isomers of $[Co(en)_2\{(-)\text{-dmtmd}\}]^{3+}$ can be assigned to the Λ and Δ configurations, respectively from the sign of the main CD band in the first absorption band region (Fig. 6). The Λ and Δ isomers show CD patterns characteristic of the "*ob*" and "*lel*" isomers, respectively. This indicates that the (—)-dmtmd ligand has the (R,R) carbon atoms, forming the λ-*skew*(h) or λ-*skew*(v) conformation with the two equatorial methyl groups. The assignment for (—)-dmtmd agrees with that given previously from the CD spectrum of *trans*-$[CoCl_2\{(-)\text{-dmtmd}\}_2]^+$. The CD change for the $\Delta(lel)$ isomer caused by the addition of sulfate ions is characteristic of the "*lel*" isomer, but the magnitude of the change is fairly small as compared with that of $\Lambda(lel)$-$[Co(en)_2(R\text{-mtmd})]^{3+}$. The smaller CD change in the (—)-dmtmd complex seems to be related with difficulty in forming an ion-pair with a sulfate ion. The Δ-$[Co(en)_2\{(-)\text{-dmtmd}\}]^{3+}$ complex can form the lel_3 conformer (λ-*gauche*$_2$, λ-*skew*(h) or λ-*skew*(v)), and provides two sets of three N–H bonds for the ion-pair formation with a sulfate ion. In the lel_3 conformer, however, the two methyl groups on 1- and 4-carbons of the (—)-dmtmd ligand stick out in nearly parallel with the pseudo C_3 axis of the complex ion, and hinder a sulfate ion from approaching the complex ion along this axis. On the other hand, the methyl group on 2-carbon of the R-mtmd complex is disposed far from the pseudo C_3 axis to involve no such hindrance to a sulfate ion. Thus $\Delta(lel)$-$[Co(en)_2\{(-)\text{-dmtmd}\}]^{3+}$ might have weaker affinity in ion-association with sulfate ions than the R-mtmd complex, and shows the smaller CD change in the presence of sulfate ions. On the other hand, the CD change of $\Lambda(ob)$-$[Co(en)_2\{(-)\text{-dmtmd}\}]^{3+}$ in the presence of sulfate ions is as large as that of $\Lambda(ob)$-$[Co(en)_2(R\text{-mtmd})]^{3+}$ (Fig. 6). The two methyl groups in $\Lambda(ob)$-$[Co(en)_2\{(-)\text{-dmtmd}\}]^{3+}$ are disposed far from the pseudo C_3 axis, differing from those in the $\Delta(lel)$-(—)-dmtmd complex. However, the complex should not form the lel_3 conformer, since the conversion of the (—)-dmtmd chelate ring to the *lel* form (δ-*skew*(h or v)) with the two axial methyl groups is very unlikely. The reason for the large CD change is not clear. However, molecular models indicate that the large and flexible (—)-dmtmd chelate ring can form rather easily an intermediate conformation suitable for ion-association with a sulfate ion by a slight distortion from the typical skew form. The $\Lambda(ob)$ isomer comprising such a conformer might form an ion-pair with a sulfate ion to cause the large CD change. The suggestion that the $\Lambda(ob)$ isomer has stronger affinity for a sulfate ion than the $\Delta(lel)$ isomer is supported by the elution order in column chromatography. By elution with 0.2 M Na_2SO_4, the former is eluted faster than the latter (Experimental). In similar column chromatographic separation for a pair of diastereomers, it has been observed that a *lel* isomer is always eluted faster than an *ob* isomer.[26] The $[Co(en)_2(R\text{-mtmd})]^{3+}$ complex in this study is the case. The elution order of such a pair of diastereomeric complexes is reported to depend on the ion-association constant between a complex ion and an anion;[27] a complex with the larger value is eluted faster. In the ion-association between $[Co(R\text{-pn})_3]^{3+}$ (R-pn=(R)-1,2-propanediamine) and a sulfate ion, the constant for the $\Delta(lel_3)$ isomer is larger than that for the $\Lambda(ob_3)$ isomer.[28] Thus the $\Lambda(ob)$ isomer of $[Co(en)_2\{(-)\text{-dmtmd}\}]^{3+}$ which is eluted faster than the other $\Delta(lel)$ isomer should have a larger constant in association with a sulfate ion, and causes a larger CD change than the other isomer does in the presence of sulfate ions.

In Fig. 7 are shown the CD spectra of Δ-$[Co(en)_2(meso\text{-dmtmd})]^{3+}$ (D-II-2) in the absence and presence of sulfate ions, the absolute configuration of which is assigned on the basis of the CD sign in the first absorption band region. In the presence of sulfate ions, the complex shows a CD change as small as that in $\Delta(lel)$-$[Co(en)_2\{(-)\text{-dmtmd}\}]^{3+}$. The small CD change of the *meso*-dmtmd complex would also be attributable to weak association with a sulfate ion as stated for the

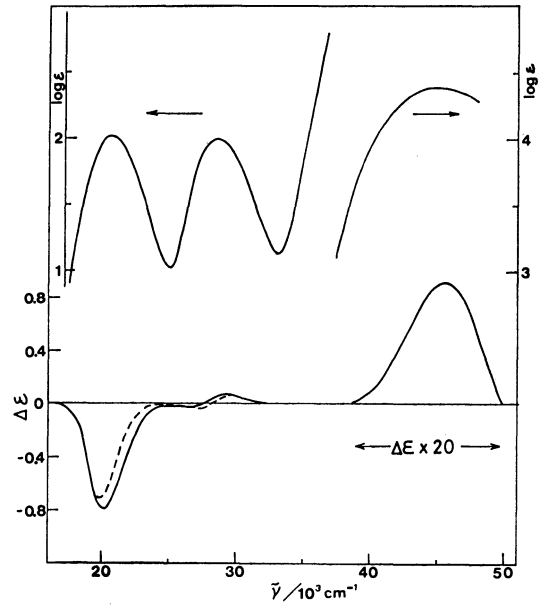

Fig. 7. Absorption and CD spectra of Δ-[Co(en)$_2$(*meso*-dmtmd)]$^{3+}$ (D-II-2) in water (——) and in 0.2 mol/dm^3 Na_2SO_4 (------).

$\Delta(lel)$-(−)-dmtmd complex. When the *meso*-dmtmd chelate ring is in the same chair form as that in the tetraammine complex, one methyl group is disposed near one set of three N–H bonds to hinder the ion-association, but the other methyl group is located away from the other set of three N–H bonds, a sulfate ion being able to approach the complex ion. However, the amino protons of the *meso*-dmtmd ligand are oblique to the C_3 axis of the complex ion, and unfavorable for association of the lel_3-SO_4^{2-} type. The *meso*-dmtmd chelate ring would be less flexible than the (−)-dmtmd chelate one because of the strained structure as stated previously. Thus the [Co(en)$_2$(*meso*-dmtmd)]$^{3+}$ complex would have weak affinity for a sulfate ion to cause the small CD change.

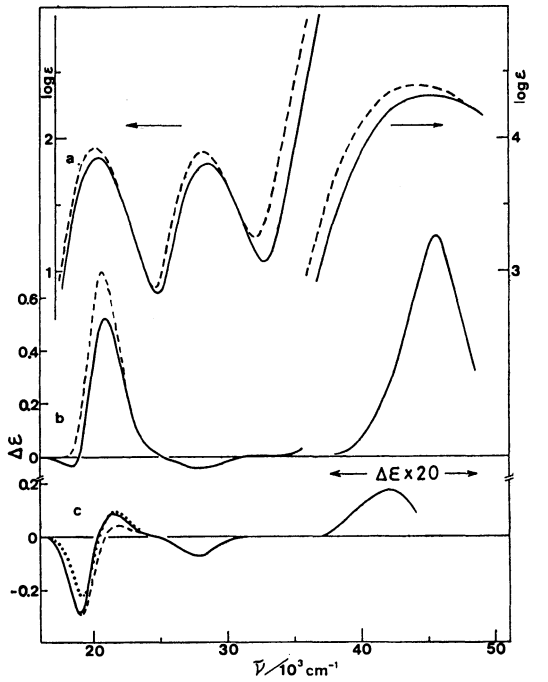

Fig. 8. a. Absorption spectra of *cis*-Δ-[Co(NH$_3$)$_2$(tmd)$_2$]$^{3+}$ (——) and *cis*-Δ-[Co(NH$_3$)$_2${(−)-dmtmd}$_2$]$^{3+}$ (------) in water.
b. CD spectra of *cis*-Δ-[Co(NH$_3$)$_2$(tmd)$_2$]$^{3+}$ in water (——) and in 0.2 mol/dm^3 Na_2SO_4 (------).
c. CD spectra of *cis*-Δ-[Co(NH$_3$)$_2${(−)-dmtmd}$_2$]$^{3+}$ in water (——) and in 0.2 mol/dm^3 Na_2SO_4 (------), and the calculate dCD curve, $2\times\Delta\varepsilon$([Co(NH$_3$)$_4${(−)-dmtmd}]$^{3+}$)$+\Delta\varepsilon$(*cis*-Δ-[Co(NH$_3$)$_2$(tmd)$_2$]$^{3+}$) (·····).

In Fig. 8 are compared CD spectra of the Δ isomers of $(+)_{589}$-[Co(NH$_3$)$_2$(tmd)$_2$]$^{3+}$ and $(-)_{589}$-[Co(NH$_3$)$_2$-{(−)-dmtmd}$_2$]$^{3+}$ in the absence and presence of sulfate ions. The main CD bands of these complexes exhibit different signs in the first absorption band region. The absolute configuration of the tmd complex was assigned from a comparison of CD patterns of Δ-[Co(en)-(tmd)$_2$]$^{3+}$[29] and Δ-[Co(tmd)$_3$]$^{3+}$,[29] and that of the(−)-dmtmd complex was done on the basis of the stereoselective complex formation {$\Delta(lel_2)$}brought about by the ligand of *R,R*-configuration. The $\Lambda(ob_2)$ isomer involves severe steric hindrance between the two chelate ligands. Both Δ isomers of the tmd and (−)-dmtmd complexes show a negative CD component in the small wavenumber side in the first absorption band region, and a strong positive CD band in the ultraviolet region. The features agree with those observed for other related complexes of the Δ configuration. The Δ-[Co(NH$_3$)$_2$-{(−)-dmtmd}$_2$]$^{3+}$ complex involves two chiral sources, the Δ configuration and the *RR*-dmtmd chelate ligand of λ-*skew*(*h* or *v*). When the additive law[25,30] for the configurational and vicinal CD effects holds in the CD spectrum of Δ-[Co(NH$_3$)$_2${(−)-dmtmd}$_2$]$^{3+}$, it can be approximated by the sum of the CD spectrum of Δ-[Co(NH$_3$)$_2$(tmd)$_2$]$^{3+}$ and the curve doubled the CD strength of [Co(NH$_3$)$_4${(−)-dmtmd}]$^{3+}$. The CD curve calculated in the first absorption band region resembles

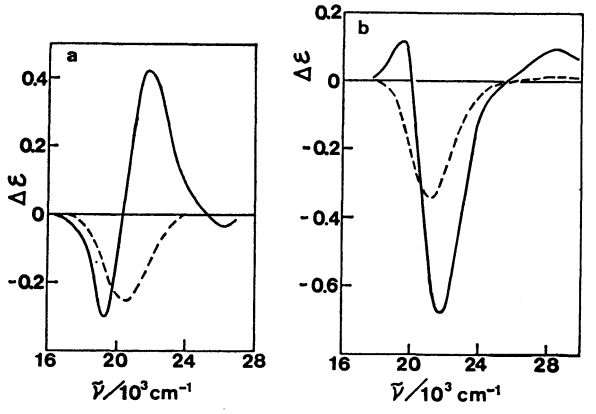

Fig. 9. a. Vicinal effect CD of the (−)-dmtmd ligand. The calculated CD curve, $1/2\{\Delta\varepsilon(\Delta$-[Co(en)$_2${(−)-dmtmd}]$^{3+})$+\Delta\varepsilon(\Delta$-[Co(en)$_2${(−)-dmtmd}]$^{3+})\}$, (——). The observed CD spectrum of [Co(NH$_3$)$_4${(−)-dmtmd}]$^{3+}$ (------).
b. Vicinal effect CD of the *R*-mtmd ligand. The calculated CD curve, $1/2\{\Delta\varepsilon(\Delta$-[Co(en)$_2$(*R*-mtmd)]$^{3+})$ $+\Delta\varepsilon(\Delta$-[Co(en)$_2$(*R*-mtmd)]$^{3+})\}$, (——). The observed CD spectrum of [Co(NH$_3$)$_4$(*R*-mtmd)]$^{3+}$ (------).

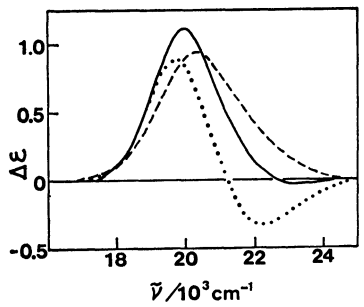

Fig. 10. Configurational effect CD ($\Delta\varepsilon(\Lambda)$) curves. The calculated CD curve, $1/2\{\Delta\varepsilon(\Lambda\text{-}[Co(en)_2(R\text{-mtmd})]^{3+}) - \Delta\varepsilon(\Lambda\text{-}[Co(en)_2(R\text{-mtmd})]^{3+})\}$, (——). The calculated CD curve, $1/2\{\Delta\varepsilon(\Lambda\text{-}[Co(en)_2\{(-)\text{dmtmd}\}]^{3+}) - \Delta\varepsilon(\Lambda\text{-}[Co(en)_2\{(-)\text{-dmtmd}\}]^{3+})\}$, (----). The observed CD spectrum of Λ-$[Co(en)_2(tmd)]^{3+}$(·····).

well the observed CD spectrum (Fig. 8). Thus the strong negative CD of Λ-$[Co(NH_3)_2\{(-)\text{-dmtmd}\}_2]^{3+}$ in the first absorption band region can be attributed to the strong negative vicinal effect of the *RR*-dmtmd chelate ligand.

In the presence of sulfate ions, the tmd complex shows fairly large CD change, but the (−)-dmtmd complex a little change. Such a difference might also be related with a difference in the flexibility and structure of the chelate rings. The more flexible tmd chelate ring would be stabilized in a certain conformation by forming an ion-pair between the complex ion and a sulfate ion. On the other hand, the (−)-dmtmd complex has four methyl groups, which hinder a sulfate ion from approaching the N–H protons of the chelate ligands to cause little change in the conformation of the chelate rings. Thus the complex would show the small CD change in the presence of sulfate ions.

Figures 9 and 10 show the configurational and vicinal effect CD curves obtained by the usual way[30] from CD spectra of the diastereomers of $[Co(en)_2(R\text{-mtmd})]^{3+}$ and $[Co(en)_2\{(-)\text{-dmtmd}\}]^{3+}$. These curves are compared with CD spectra of the related complexes in the Figures. The additive law for the configurational and vicinal effects does not hold among these complexes, although it works among the ammine complexes of tmd and (−)-dmtmd. The lack of the additivity might be related with crowded structures of those tris-chelate-type complexes involving a large seven-membered chelate ring. Some six-membered diamine complexes have also been reported to show lack of the additivity, and it has been interpreted as the results of flexible conformation of a six-membered chelate ring; the conformation of a six-membered chelate ring in one complex would differ from that in the other.[1] The same interpretation can be made on the complexes concerned. The stable conformation of a seven-membered chelate ring in the crowded bis-en complex would differ from that in the much less crowded tetra-ammine complex, and this might cause the lack of the additivity.

This work was partly supported by a Grant-in-Aid for Scientific Research No. 243013 from the Ministry of Education, Science and Culture.

References

1) M. Kojima, M. Fujita, and J. Fujita, *Bull. Chem. Soc. Jpn.*, **50**, 898 (1977).
2) M. Kojima and J. Fujita, *Bull. Chem. Soc. Jpn.*, **50**, 3237 (1977).
3) K. Kashiwabara, M. Kojima, and J. Fujita, *Bull. Chem. Soc. Jpn.*, **52**, 772 (1979).
4) Y. Nakayama, S. Ooi, and H. Kuroya, 30th National Meeting of the Chemical Society of Japan, Osaka, April 1974, Abstr. No. 3D36.
5) S. Sato and Y. Saito, *Acta Crystallogr., Sect. B*, **31**, 1378 (1975).
6) Y. Nakayama, K. Matsumoto, S. Ooi, and H. Kuroya, *J. Chem. Soc. Chem. Commun.*, **1973**, 171.
7) G. H. Jeffery and A. I. Vogel, *J. Chem. Soc.*, **1948**, 658.
8) H. Oldach, *Ber.*, **20**, 1654 (1887); W. Euler, *Ber.*, **28**, 2952 (1895).
9) R. A. Smiley and C. Arnold, *J. Org. Chem.*, **25**, 257 (1960).
10) B. Bosnich and J. MacB. Harrowfield, *J. Am. Chem. Soc.*, **94**, 3426 (1972).
11) K. Feudenberg and W. Hohmann, *Ann.*, **584**, 54 (1953).
12) C. Paal, *Ber.*, **18**, 58 (1885).
13) G. Ciamician and C. U. Zanetti, *Ber.*, **22**, 3176 (1889).
14) H. Ogino, *Bull. Chem. Soc. Jpn.*, **50**, 2459 (1977).
15) J. Fujita and H. Ogino, *Chem. Lett.*, **1974**, 57.
16) H. Ogino and J. Fujita, *Bull. Chem. Soc. Jpn.*, **48**, 1836 (1975).
17) F. Mizukami, H. Ito, J. Fujita, and K. Saito, *Bull. Chem. Soc. Jpn.*, **46**, 2410 (1973).
18) Unpublished data.
19) S. Yano, M. Saburi, S. Yoshikawa, and J. Fujita, *Bull. Chem. Soc. Jpn.*, **49**, 101 (1976).
20) F. Mizukami, H. Ito, J. Fujita, and K. Saito, *Bull. Chem. Soc. Jpn.*, **45**, 2129 (1972).
21) H. Yamatera, *Bull. Chem. Soc. Jpn.*, **31**, 95 (1958).
22) S. Arakawa, K. Kashiwabara, J. Fujita, and K. Saito, *Bull. Chem. Soc. Jpn.*, **50**, 2331 (1977).
23) E. J. Corey and J. C. Bailar, Jr., *J. Am. Chem. Soc.*, **81**, 2620 (1959).
24) R. Larsen, S. F. Mason, and B. J. Norman, *J. Chem. Soc., A*, **1966**, 301; S. F. Mason and B. J. Norman, *ibid.*, **1966**, 307.
25) K. Ogino, K. Murano, and J. Fujita, *Inorg. Nucl. Chem. Lett.*, **4**, 351 (1968).
26) For example, M. Kojima, Y. Yoshikawa, and K. Yamasaki, *Inorg. Nucl. Chem. Lett.*, **1973**, 689.
27) Y. Yoshikawa and K. Yamasaki, *Inorg. Nucl. Chem. Lett.*, **1970**, 523.
28) K. Ogino, *Bull. Chem. Soc. Jpn.*, **42**, 447 (1969).
29) M. Kojima, H. Yamada, H. Ogino, and J. Fujita, *Bull. Chem. Soc. Jpn.*, **50**, 2325 (1977).
30) C. T. Liu and B. E. Douglas, *Inorg. Chem.*, **3**, 1356 (1964).

Pyrolytic Sulfurization Gas Chromatography. IX. Determination of the Atomic Ratio between C, H, O, N, Cl, Br, and I in an Organic Halogen Compound

Tadashi HARA,* Kaoru FUJINAGA, and Fujio OKUI

Department of Chemical Engineering, Faculty of Engineering, Doshisha University, Karasuma Imadegawa, Kamigyo-ku, Kyoto 602

(Received February 20, 1981)

The atomic ratio between C, H, O, N, Cl, Br, and I in an organic halogen compound was obtained satisfactorily by gas chromatography and ion chromatography. At first the atomic ratio between C, H, O, and N was determined simultaneously by PSGC and then the atomic ratio between a halogen atom and C, H, O, and N was obtained by estimating the amount of a halogen atom in the reaction residue and by calculating the weight percent in Eq. 4 by use of a correction factor and peak areas in gas and ion chromatograms.

Pyrolytic sulfurization gas chromatography (PSGC), which was originated by the present authors, has been successfully applied to the simultaneous determination of the atomic ratio between C, H, O, and N in a normal organic compound,[1] a metal organic chelate compound,[2] a polymer,[3] and an organic halogen compound.[4]

The present study has been further carried out with the objective of estimating the atomic ratio between C, H, O, N, and halogen atoms (Cl, Br, and I) (X) in an organic halogen compound. Since X in an organic halogen compound was fixed in the reaction residue as sodium halide (NaX) by PSGC,[4] determination of X in the NaX was separately investigated by (1) gas chromatography after conversion of the halide to hydrogen halide (HX) and (2) ion chromatography after dissolving the halide in water, and the results obtained were compared. In the former, HX was easily identified but its determination was difficult due to the incomplete conversion of the NaX to HX and the decomposition of HX. In the latter, a satisfactory result was obtained by dissolving the reaction residue with an aqueous solution of potassium hydrogen phthalate (KHP), by filtering S and quartz pieces off, and by introducing the filtrate to an ion chromatograph through a Teflon membrane filter. On the basis of the relationship between the peak of hydrogen sulfide (H_2S) in a gas chromatogram and that of halide ions (X^-) in an ion chromatogram for a definite composition of organic halogen compound, the atomic ratio of H to X for an unknown compound was obtained without weighting it.

Experimental

Apparatus and Samples. The same gas chromatograph was used as described in the previous paper. A HITACHI 634A liquid chromatograph fitted with a Wescan model 213 conductivity detector and Vydac 302 IC 4.6 column (250 mm), was operated at the flow rate of 1.7 cm³/min by use of a 0.004 mol/dm³-KHP as an eluent to monitor X^-.

The organic halogen compound samples were of analytical grade.

Procedure. The ampule containing an organic halogen compound, S, and sodium sulfide (Na_2S) was made to react by the previously described procedure.[4] It was placed in a 80 mm long, 4.22 mm i.d., 4.94 mm o.d. Teflon tube, and crushed in a gas sampler, the evolved gases being analyzed in accordance with the previous paper to determine the atomic ratio between C, H, O, and N. The pieces obtained by crushing the ampule was taken out of the sampler and treated with 0.004 mol/dm³-KHP, followed by filtration through a G4 glass filter. The filtrate was passed through a Teflon membrane filter (pore size 0.5 μm) and introduced into an ion chromatograph. According to the present procedure, well-defined and separated peaks were obtained for X^- and they were used for the determination of the atomic ratio between C, H, O, N, and X.

Results and Discussion

Analysis of X^- by Ion Chromatography. A mixed solution consisting of each 5×10^{-4} mol/dm³ sodium chloride, sodium bromide, and sodium iodide was analyzed by ion chromatography under the above-mentioned conditions. As can be seen from Fig. 1, the present procedure gives a satisfactory result for the

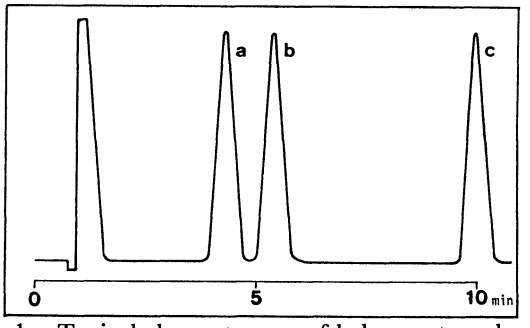

Fig. 1. Typical chromatogram of halogen atoms by the ion chromatography.
a): Cl^-, b) Br^-, c): I^-.
Conditions: Column Vydac 302 IC 4.6 (250 mm); detector conductivity (Wescan model 213); eluent 0.004 mol/dm³-KHP; flow rate 1.7 cm³/min.

Table 1. Precision[a] in the determination of halide ions by ion chromatography

Ions	C.V. (%)
Cl^-	2.133
Br^-	1.203
I^-	1.814

a) 10 runs for the standard solution. (5×10^{-4} mol/dm³-NaCl, -NaBr, -NaI)

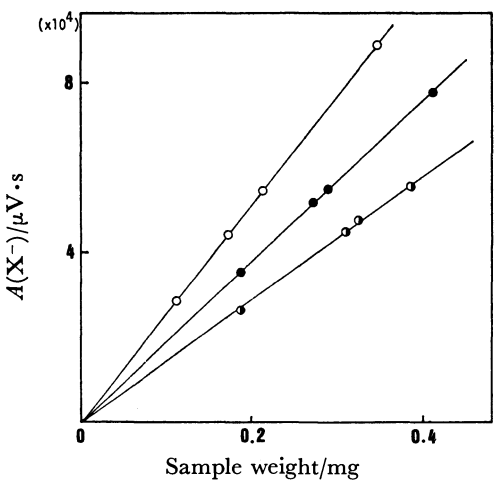

Fig. 2. Relationship between sample weight and $A(X^-)$.
○: *p*-Chlorobenzoic acid, ●: *p*-bromoacetanilide, ◑: *o*-iodobenzoic acid.

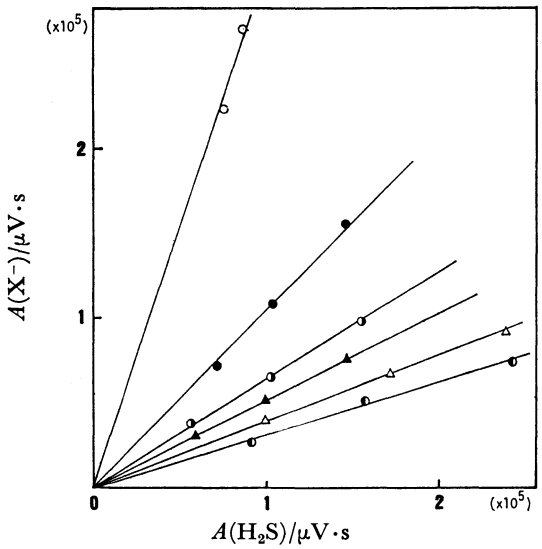

Fig. 3. Relationship between $A(H_2S)$ and $A(X^-)$.
○: 1,2,3,4,5,6-Hexachlorocyclohexane, ●: 1-chloro-2,4-dinitrobenzene, ◐: S-benzylthiouronium chloride, ◑: *p*-chlorobenzoic acid ▲: *p*-bromoacetanilide △: *o*-iodobenzoic acid.

separation of X^-. In order to examine the precision of the present procedure, each 5×10^{-4} mol/dm³ standard solution of X^- was analyzed 10 times and the results were shown in Table 1 by the coefficient of variation (C.V.). The values of C.V. in Table 1 are reasonable ones in comparison with those obtained by an ordinary ion chromatography.

Determination of X by Use of Calibration Curve. Three kinds of organic halogen compounds, that is, 0.112—0.350 mg *p*-chlorobenzoic acid, 0.188—0.416 mg *p*-bromoacetanilide, and 0.188—0.390 mg *o*-iodobenzoic acid were analyzed by the above-mentioned procedure and the relationship between sample weight and peak area in an ion chromatogram were plotted in Fig. 2. Judging from the linearity in Fig. 2, the present procedure is suitable for the determination of X in an organic halogen compound.

To examine the recovery of the present procedure, a definite amount of organic halogen compound was treated by PSGC and the absolute value of X in it was determined using a calibration curve which had been obtained with a standard solution of NaX (Tables 2 and 3). As can be seen from Tables 2 and 3, satisfactory results were obtained for X. This means that both

Table 2. Analytical results of organic halogen compounds by use of a calibration curve

Sample	Weight (mg)	Halogen content			
		Theor. (mg)	Found (mg)	Found (%)	Error (%)
p-Chlorobenzoic acid	0.442	0.100	0.101	22.9	(+0.3)
S-Benzylthiouronium chloride	0.504	0.0881	0.0869	17.2	(−0.3)
1-Chloro-2,4-dinitrobenzene	0.477	0.0835	0.0838	17.6	(+0.1)
1,2,3,4,5,6-Hexachlorocyclohexane	0.289	0.216	0.216	74.7	(0)
α-Bromoisovarerylurea	0.350	0.125	0.127	36.3	(+0.5)
p-Bromoacetanilide	0.386	0.144	0.144	37.3	(0)
1,2,3,4,5,6-Hexabromocyclohexane	0.403	0.347	0.346	85.9	(−0.1)
o-Iodobenzoic acid	0.397	0.203	0.204	51.4	(+0.2)

Table 3. Analytical results of organic halogen compounds by use of a calibration curve

Sample	Weight (mg)	Cl			Br			I		
		Theor. (mg)	Found (mg)	Content (%) [Error]	Theor. (mg)	Found (mg)	Content (%) [Error]	Theor. (mg)	Found (mg)	Content (%) [Error]
p-Chlorophenacyl bromide	0.472	0.0716	0.0696	14.7 [−0.5]	0.162	0.164	34.8 [+0.5]			
5-Chloro-7-iodo-8-quinolinol	0.496	0.0575	0.0560	11.3 [−0.3]				0.206	0.205	41.3 [−0.2]
p-Bromoiodobenzene	0.486				0.137	0.135	27.8 [−0.4]	0.218	0.220	45.3 [+0.4]

TABLE 4. CORRECTION FACTOR OF X⁻

Run No.	Ions	Correction factor[a]	C.V. (%)
1[b]	Cl⁻	0.6765	2.011
2[c]	Br⁻	0.6978	1.818
3[d]	I⁻	0.6407	2.026

a) Average of 10 runs for the standard sample. b) 1-Chloro-2,4-dinitrobenzene. c) α-Bromoisovarerylurea. d) *o*-Iodobenzoic acid.

the fixation of X to the reaction residue by PSGC and the dissolution of NaX from the reaction residue are quantitative.

Calculation of the Atomic Ratio between C, H, O, N, and X. Six kinds of organic halogen compounds were analyzed by the present method, and the relationship between the peak area of H_2S in a gas chromatogram ($A(H_2S)$) and the peak area of X^- in an ion chromatogram ($A(X^-)$) was plotted in Fig. 3. Each relationship gives a straight line. The relationship between $A(H_2S)$ and $A(Cl^-)\times(H/Cl)$, which meant the product of the peak

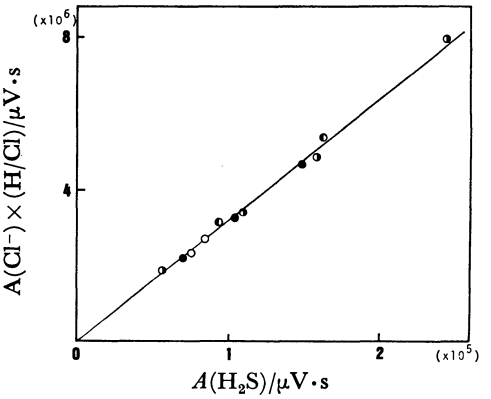

Fig. 4. Relationship between $A(H_2S)$ and $A(Cl^-)\times(H/Cl)$.
○: 1,2,3,4,5,6-Hexachlorocyclohexane, ●: 1-chloro-2,4-dinitrobenzene, ◐: S-benzylthiouronium chloride, ◑: *p*-chlorobenzoic acid.

TABLE 5. ANALYTICAL RESULTS OF ORGANIC HALOGEN COMPOUNDS

Sample	Content[a] (wt %)						
	C	H	O	N	Cl	Br	I
p-Chlorobenzoic acid	53.70	3.22	20.44		22.64		
	53.59	3.26	20.64		22.51		
	(−0.11)	(+0.04)	(+0.20)		(−0.13)		
S-Benzylthiouronium chloride[b]	56.30	6.50		16.42	20.78		
	56.24	6.41		16.46	20.89		
	(−0.06)	(−0.09)		(+0.04)	(+0.11)		
1,2,3,4,5,6-Hexachlorocyclohexane	24.78	2.08			73.14		
	25.09	2.12			72.79		
	(+0.31)	(+0.04)			(−0.35)		
1-Chloro-2,4-dinitrobenzene	35.58	1.49	31.60	13.83	17.50		
	35.91	1.48	31.39	13.82	17.40		
	(+0.33)	(−0.01)	(−0.21)	(−0.01)	(−0.10)		
1,2,3,4,5,6-Hexabromocyclohexane	12.93	1.08				85.99	
	12.60	1.09				86.31	
	(−0.33)	(+0.01)				(+0.32)	
α-Bromoisovarerylurea	32.31	4.97	14.34	12.56		35.82	
	32.55	4.91	14.53	12.50		35.51	
	(+0.24)	(−0.06)	(+0.19)	(−0.06)		(−0.31)	
p-Bromoacetanilide	44.89	3.77	7.47	6.54		37.33	
	45.03	3.71	7.33	6.59		37.35	
	(+0.14)	(−0.07)	(−0.14)	(+0.05)		(+0.02)	
o-Iodobenzoic acid	33.90	2.03	12.90				51.17
	34.12	2.00	12.79				51.09
	(+0.22)	(−0.03)	(−0.11)				(−0.08)
p-Chlorophenacyl bromide	41.16	2.59	6.85		15.18	34.22	
	40.96	2.45	6.76		14.81	35.02	
	(−0.20)	(−0.14)	(−0.09)		(−0.37)	(+0.80)	
5-Chloro-7-iodo-8-quinolinol	35.38	1.65	5.24	4.58	11.60		41.55
	35.80	1.67	5.29	4.62	11.36		41.26
	(+0.42)	(+0.02)	(+0.05)	(+0.04)	(−0.24)		(−0.29)
p-Bromoiodobenzene	25.47	1.43				28.24	44.86
	25.03	1.40				28.14	45.43
	(−0.44)	(−0.03)				(−0.10)	(+0.57)

a) The upperline: theoretical values, the medium line: experimental values, and the lower line: error. b) The sulfur atom was neglected in the composition of the sample since it could not be determined.

area of Cl^- in an ion chromatogram and the atomic ratio of H to Cl in an organic chlorine compound, was plotted in Fig. 4. It was found to give a straight line regardless of the Cl content of the compound. The slope(a) of the straight line in Fig. 4 is shown by Eq.1.

$$a = \left(\frac{H}{Cl}\right) \times \frac{A(Cl^-)}{A(H_2S)} = \text{const.} \quad (1)$$

Equation 1 is rewritten by Eq. 2.

$$\frac{2}{a} = \left(\frac{Cl}{H}\right) \times \frac{2A(H_2S)}{A(Cl^-)} = \text{const.} \quad (2)$$

Equation 2 is also given by Eq. 3 for all halogen atoms.

$$\frac{2}{a} = \left(\frac{H}{X}\right) \times \frac{2A(H_2S)}{A(X^-)} = \text{const.} \quad (3)$$

The form of the $(H/X) \times 2A(H_2S)/A(X^-)$ in Eq. 3 is the same as that of the correction factor[1] which was used for the determination of the atomic ratio between C, H, O, and N. Therefore, the value of Eq. 3 can be replaced by $K(X^-)$ which is used for the determination of the atomic ratio between C, H, O, N, and X. The values of $K(X^-)$ were obtained by analyzing each standard sample (Table 4). They were consistent with a definite value of Eq. 3. Thus the atomic ratio between C, H, O, N, Cl, Br, and I is obtained by Eq. 4.

$$\alpha(wt\%) = \frac{\sum M(\gamma)K(\gamma)A(\gamma)}{\sum M'(\beta)K(\beta)A(\beta)} \times 100 \quad (4)$$

where α: C, H, O, N, Cl, Br, and I, β: the product obtained by the present method, γ: the product containing an element α, $M'(\beta)$: the value obtained by subtracting the amount of S from the formula weight of β, $M(\gamma)$: the formula weight of α in γ, $K(\gamma)$: correction factor of γ, and $A(\gamma)$: peak area of γ.

Determination of the Atomic Ratio between C, H, O, N, and X in an Organic Halogen Compound. Various organic halogen compounds were analyzed by the present method and the atomic ratio between C, H, O, N, and X was calculated by introducing both chromatographic data to Eq. 4 (Table 5). It can be seen from Table 5 that the atomic ratio between C, H, O, N, and X is obtained satisfactorily by the present method in which only one sample is used.

References

1) T. Hara, K. Fujinaga, and K. Tsuji, *Bull. Chem. Soc. Jpn.*, **51**, 1110 (1978).
2) T. Hara, K. Fujinaga, and K. Tsuji, *Bull. Chem. Soc. Jpn.*, **51**, 2951 (1978).
3) T. Hara, K. Fujinaga, F. Okui, and K. Negayama, *Sci. Eng. Rev. Doshisha Univ.*, **21**, 241 (1981).
4) T. Hara, K. Fujinaga, and F. Okui, *Bull. Chem. Soc. Jpn.*, **53**, 1308 (1980).

Formation of Anatase Precipitates Containing Fe(III) by the Air Oxidation at 95 °C of Strongly Acidic Solutions

Masao KIYAMA* and Toshio TAKADA
Institute for Chemical Research, Kyoto University, Uji, Kyoto 611
(Received February 27, 1981)

Strongly acidic titanium(III) chloride solutions containing iron(II) sulfate were subjected to oxidation with air at 95 °C. The products consist of spheres, 0.5—1.0 μm in size, each composed of extremely fine particles, 100—150 Å in size. Fe(III) is incorporated up to about 6% of the total metal ions in the product, in spite of the strongly acidic solution. The products, containing H_2O and SO_4^{2-} besides Fe(III), are dehydrated in the temperature range 100—400 °C and the sulfate decomposition begins at about 750 °C in air. The SO_4^{2-} in the products can be easily removed by washing at room temperature with NaOH solution. No marked differences can be detected in color, magnetic properties, or in growth of the extremely fine particles before and after the dehydration by heat treatment at 500 °C; a change in such physical properties begins to occur at 550 °C. It is concluded that the Fe(III) in the product is interposed between the extremely fine particles, whereas the H_2O and SO_4^{2-} are adsorbed in the spherical polycrystalline particles formed with oxo and hydroxo combination of the extremely fine particles.

Titanium dioxide, TiO_2, can be formed in three kinds of crystalline modifications—brookite, rutile and anatase. Two of the three modifications—precipitates of anatase and rutile, can be prepared by selecting the conditions of hydrolysis of titanium(IV) salts—*i.e.*, kinds and concentrations of the acid anions present in acidic solutions and the hydrolysis temperature.[1-4] Precipitates consisting of any one of the three modifications can be prepared by selecting the conditions for allowing Ti(III) ions gradually to oxidize in an acidic solution at 65—90 °C.[5]

Ti(III) in HCl solution forms a precipitate of brookite or rutile according to the excess HCl concentration or oxidation temperature. Precipitates of brookite or rutile thus formed consist of fine needle-like(a) or extremely fine cubic(b) particles as shown in Fig. 1. The presence of SO_4^{2-} was found to promote the formation of a precipitate of anatase consisting of extremely fine particles, similar to the precipitates of brookite and rutile previously mentioned, as determined by X-ray diffraction examination.[5] Nevertheless, the BET surface area is much less than that of the precipitate of brookite or rutile, the anatase precipitate consisting of relatively large spherical or flat leaf polycrystalline particles as shown in Fig. 1(c). It has been found that in spite of a strongly acidic solution, Fe(III) is partly incorporated into the anatase precipitate in the presence of $FeSO_4$ in the starting solution. A clue to the elucidation of the mechanism of the formation of the polycrystalline particles of anatase would be obtained by clarifying the properties of the polycrystalline particles containing Fe(III).

This paper is an account of the formation of the anatase precipitates containing Fe(III) and the properties of such precipitates.

Experimental

The starting titanium(III) chloride solution (Wako Pure Chemical Industries Ltd.) contained 2.0 M (1 M=1 mol dm^{-3}) $TiCl_3$, 1.6 M $ZnCl_2$, and 1.2 M HCl. To this the required amount of either $FeSO_4 \cdot 7H_2O$ or Na_2SO_4 (analytical grade) was added in various mole ratios of Fe(II) or SO_4^{2-} to Ti(III). Each mixed solution was diluted with water to 3 L (dm^3) in a 4 L flask. The oxidation of the mixed solutions was carried out at 95 °C by bubbling air into them at a constant rate of 200 L/h. The construction of the flask for the air-oxidation experiments has been previously described.[6] After a time lapse of 20 h, Ti(III) ions in the solutions changed completely to Ti(IV) and the solutions, originally colored bluish black, turned to yellowish white suspensions of various hues depending on the Fe(II) concentrations in the starting solutions.

The sedimentation velocities of most oxidation products consiting of anatase particles were extremely fast and they

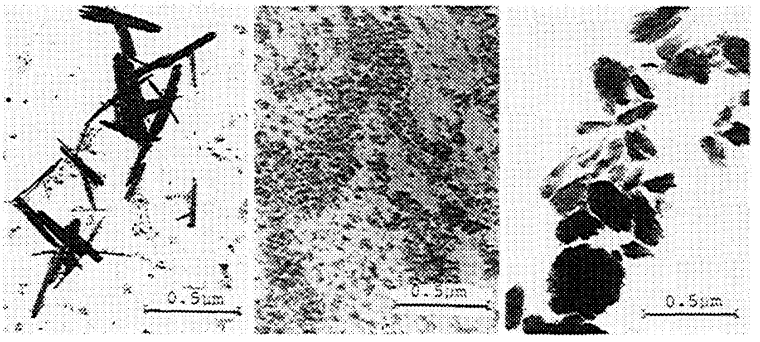

(a) (b) (c)

Fig. 1. Electronmicrographs of rutile (a), brookite (b), and anatase (c) precipitates. Preparation conditions for samples (a), (b), and (c) correspond respectively to those for sample Nos. 4, 6, and 5 shown in Ref. 5.

could easily be separated from the solutions by filtration. After filtration, the products were washed with water, treated with acetone, and then dried in air at 100 °C. All powdery samples thus obtained were examined by X-ray diffraction using Ni filtered Cu $K\alpha$ radiation; some were further examined by electronmicroscopic observation, magnetic measurement using a magnetic torsion balance, BET surface area determination using nitrogen gas, and, thermal and chemical analyses.

The mean size of the extremely fine particles was estimated from the line broadening of the X-ray diffraction peak for the (101) plane of the anatase crystal structure. Thermogravimetry (TG) and differential thermal analysis (DTA) were carried out each with 40 mg samples at a heating rate of 5 °C/min in air using a Shimadzu Dt-TG simultaneous recording apparatus, Model DTG 30 M.

After the samples had been fused with Na_2CO_3 and then dissolved into water, the SO_4^{2-} content was gravimetrically determined as $BaSO_4$. The Cl^- content was determined by nephelometry for a mixture of $AgNO_3$ solution and the solution prepared by the dissolution of the samples in a HF solution by heating. The metal ion contents were determined by atomic absorption after the samples had been dissolved in a mixed solution of HF and HCl.

Results and Discussion

Four typical oxidation products of anatase are given in Table 1. These products were found to consist of spherical particles, 0.5—1.0 μm in size, each composed of a number of extremely fine anatase particles, 100—150 Å in size, as a result of electronmicroscopic and X-ray diffraction examination.

Table 1. Anatase precipitates containing Fe(III)

Sample	Starting solution Concn/mol dm^{-3}		Oxidation product	
	Ti(III)	Fe(II)	Fe(III) content(At%)	S ($m^2 g^{-1}$)
A[a)]	0.166	0		1.34
B	0.166	0.166	1.8	2.17
C	0.166	0.333	4.2	3.49
D	0.083	0.333	5.9	4.34
E[b)]	0.166	0.333	1.3	

a) Sample prepared in the presence of 0.166 mol dm^{-3} Na_2SO_4. b) Rutile prepared by the use of $FeCl_2$ in place of $FeSO_4$.

As evident from the table, the mean size of the polycrystalline particles, as estimated from the BET surface area, slightly decreases with increasing Fe ion content; at the same time, the color changes from white to yellowish white. These samples contained 4—5 wt% SO_4^{2-}, about 10 wt% H_2O and less than 0.1 wt% Cl^-. It is noteworthy that in spite of being products from strongly acidic solutions, these samples contain Fe(III) to the extent of nearly 6% of the total metal ions. However they contained less than 0.02% Zn(II). Increasing the Fe(II) concentration in the starting solution yielded a whitish yellow product containing more than 6% Fe(III). In the whitish yellow products thus prepared, however, extremely fine particles of α-FeO(OH) were intermingled with the anatase particles.

Similar experiments were also conducted using iron(II) chloride in place of the sulfate. Whitish products consisting of rutile particles with or without brookite could be obtained int he absence of SO_4^{2-}. Their sedimentation velocities were extremely slow and the suspended particles could not easily be filtered off. The Fe(III) content was much smaller than would be obtained in the presence of SO_4^{2-} as will be evident from sample E in the table containing less than 0.02 wt% Zn(II).

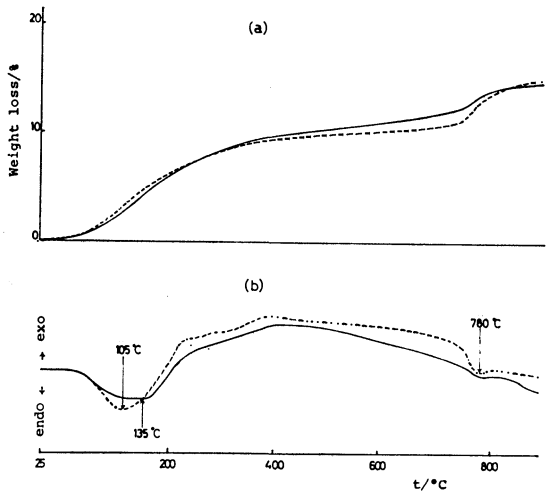

Fig. 2. TG (a) and DTA (b) curves for samples A (——) and D (------).

As shown by the TG and DTA curves in Fig. 2 for samples A and D, these samples are dehydrated in the temperature range 100—400 °C and the sulfate decomposition begins at about 750 °C. The fact that dehydration for the samples takes place continuously from 100°C to temperatures as high as 400 °C indicates that part of the OH^- is interposed between the extremely fine particles. Sample D was divided into several parts and introduced into separate furnaces for heat treatment in air at temperatures between 400 and 750 °C for 20 h. Afterwards they were taken out from the furnaces and allowed to cool to room temperature.

For the sample heat-treated at 500 °C, a decrease in the BET surface area to 3.3 $m^2 g^{-1}$ was observed, but no appreciable differences in color, half broadening of X-ray diffraction peaks and magnetic properties could be detected before and after the dehydration by heat treatment. The samples heat-treated at 550—700 °C became more yellowish and at the same time, their X-ray diffraction peaks became sharper with increasing heat treatment temperature as seen in Fig. 3.

As shown in Fig. 4, no particle growth due to sintering between the spherical polycrystalline particles at 700 °C could be detected, but the BET surface area decreased to 2.2 $m^2 g^{-1}$ because of the decrease in fine projections. The SO_4^{2-} content of this sample still remained at 2.6 wt%. Part of the anatase changes to rutile on heat treatment at 750 °C (Fig. 3(d)).

Magnetic susceptibilities, χ, were measured with the original sample D and its heat treated samples in a

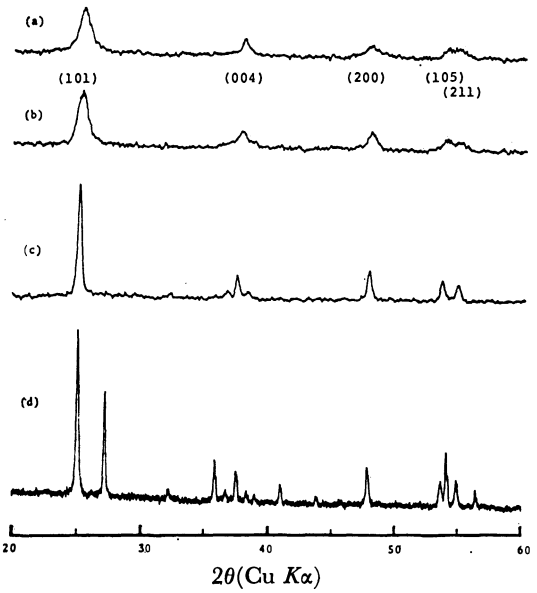

Fig. 3. X-Ray diffraction patterns of the original sample D (a) and its 500 (b), 700 (c), and 750°C (d) heat treated samples.

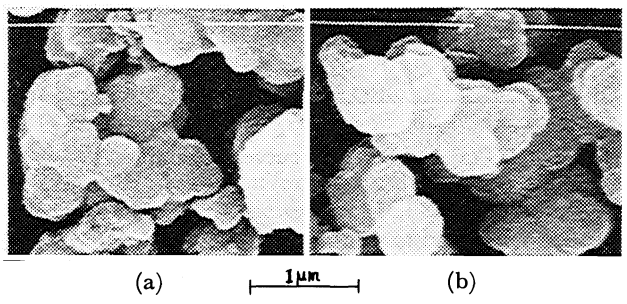

Fig. 4. Scanning electronmicrographs of sample D before (a) and after heat treatment at 700 °C in air.

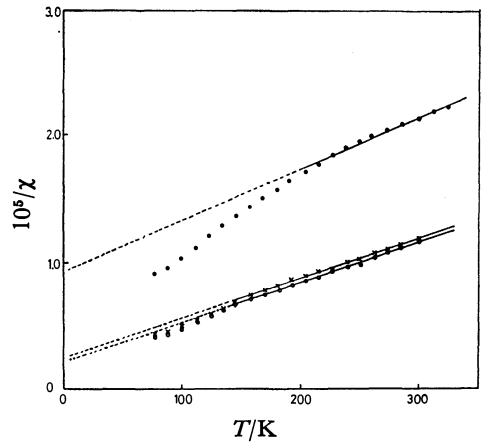

Fig. 5. A plot of reciprocal of magnetic susceptibility, χ emu/g ($4\pi 10^{-3}$ m^3 kg^{-1}), as a function of temperatures T for the original sample D (○) taken after heat treatment in air at 500 (×) and 700 °C (●).

magnetic field range 2—9 kOe (1 Oe=1000/4 π A m^{-1}) at temperatures between 77 and 300 K. No magnetic field dependency of χ could be detected with any of these samples.

Figure 5 is a plot of χ^{-1} of typical samples as a function of T(K). An inspection of these curves readily reveals the following: χ values of sample D on the higher temperature side follow the Curie-Weiss equation

$$\chi = C(T-\theta)^{-1},$$

the paramagnetic Curie temperature θ is −60 K, and the Curie constant C is 31×10^{-4} emu. From the C value, sample D is estimated to contain 4.0 wt% Fe(III) with an effective magnetic moment of 5.9—that is, Fe(III) content is 6.6% in the total metal ions.

No marked differences in the values of C and θ can be observed before and after the heat treatment at 500 °C for sample D. The temperature range to follow the Curie-Weiss equation becomes narrow with the sample heat-treated at 700 °C, and its θ value is −230 K. A shift in θ to the lower temperature side is attributable to the greater magnetic interaction generated between the Fe (III) ions.

To clarify how SO_4^{2-} is intermingled within the polycrystalline particles, the following experiments were conducted. Samples A and D, each weighing 5 g, were immersed in separate 100 mL 1 M NaOH solutions and left at room temperature for 8 h. During this period, ultrasonic dispersion was applied several times, 5 min each time, to each of these suspensions. Precipitates were separated from alkaline solutions by filtration, thoroughly washed with water, treated with acetone, and dried at 100 °C to obtain white and yellowish white samples.

X-Ray diffraction and electron-microscopic examinations of these samples before and after the alkaline treatment, could detect no appreciable differences between the two samples. It was found, however, that the BET surface area increased to 4.0 (sample A) and to 7.9 m^2 g^{-1} (sample D), probably because of chipping of polycrystalline particles due to the ultrasonic dispersion,whereas the SO_4^{2-} content of the samples A and D decreased markedly to 0.38 and to 0.47 wt%, respectively, with the alkaline treatment. From these results, it can be concluded that the major portion of the SO_4^{2-} ions is adsorbed, similar to H_2O, in the polycrystalline particles, without being interposed between extremely fine anatase particles.

It is well known that since titanium(III) chloride solutions are powerful reducing agents, Ti(III) easily reduces Fe(III) in a strongly acidic solution. Accordingly, the oxidation with air of Ti(III) to Ti(IV) must take place before that of Fe(II) to Fe(III). The Ti(IV) in a HCl solution containing SO_4^{2-} will be present as sulfato complexes.[7] It is presumed, therefore, that the Ti(IV) in the strongly acidic solution formed by oxidation generates the polynuclear complexes, each consisting of the oxo, aqua, hydroxo, and sulfato groups where the Ti(IV) concentration is high. These complexes would form extremely fine particles of anatase with the oxo combining as a result of the dissociation by hydrolysis of the H_2O, OH^-, and SO_4^{2-}. The Ti(IV) ions present in the subsurfaces of extremely fine particles will be still combined with SO_4^{2-} besides OH^- and H_2O. With the desorption by further hydrolysis of these SO_4^{2-} and H_2O from the subsurfaces, the formation of polycrystalline particles will take place with oxo and

hydroxo combinings of the extremely fine particles in the absence of Fe(III). The oxidation into Fe(III) would begin to take place after most of the Ti(III) ions have been changed to Ti(IV). The Fe(III) ions formed by oxidation exist as monomers[8] and part of them must exist as hydroxo complexes.

Ramakrishna and Seneratyapa reported as a result of their spectrometric studies, that Fe(III) hydroxo complexes in strongly acidic solutions easily reacted with Ti(IV) hydroxo complexes to form mixed complexes, whose formation was governed by the nature of the dissolved acid anions.[9] This reaction suggests that under the existence of the Fe(III) hydroxo complexes, part of the Ti(IV) combined with H_2O, OH^-, or SO_4^{2-} in the subsurface of each extremely fine particle would be combined with the Fe(III) hydroxo complexes. Each polycrystalline particle, in which the Fe(III) ions are relatively evenly interposed between the extremely fine particles, would be formed and become greater in size with the oxo and hydroxo combination caused during the progress of hydrolysis.

The authors wish to thank Messrs T. Akita, N. Horiishi, and I. Sugano for their help in conducting numerous experiments.

References

1) H. B. Weiser and W. O. Milligan, *J. Phys. Chem.*, **38**, 513 (1934).
2) A. Bowman, *J. Oil Col. Chem. Ass.*, **35**, 314 (1952).
3) J. E. Latty, *J. Appl. Chem.*, **8**, 96 (1958).
4) T. Iida, K. Yamaoka, S. Noziri, and H. Nozaki, *Kogyo Kagaku Zasshi*, **69**, 2087 (1966).
5) M. Kiyama, T. Akita, Y. Tsutsumi, and T. Takada, *Chem. Lett.*, **1972**, 21.
6) M. Kiyama, *Bull. Chem. Soc. Jpn.*, **47**, 1646 (1974).
7) C. F. Baes Jr., and R. E. Mesmer, "The hydrolysis of cations," John Wiley and Sons, New York (1976), p. 151.
8) M. Kiyama and T. Takada, *Bull. Chem. Soc. Jpn.*, **46**, 1680 (1973).
9) R. S. Ramakrishna and D. A. T. A. Seneratyapa, *J. Inorg. Nucl. Chem.*, **39**, 333 (1977).

^{1}H NMR Studies on the Interactions of Acyclic Polyethers with Dimethyltin Dichloride in Aromatic Solvents[1)]

Junzo OTERA,* Tadashi SHIOMI, Kazuhiko MURAKAMI, and Yoshikane KAWASAKI†

Okayama University of Science, Ridai-cho, Okayama 700

†*Department of Petroleum Chemistry, Osaka University, Yamadagaoka, Suita, Osaka 565*

(Received March 2, 1981)

The interactions between various acyclic polyethers, $RO(CH_2CH_2O)_nR'$(R, R'=CH_3, Ph), and dimethyltin dichloride (DMTC) in aromatic solvents have been studied by means of ^{1}H NMR spectroscopy. On the basis of a continuous variation method, the formation of the 1 : 1 complexes between glymes, $CH_3O(CH_2CH_2O)_nCH_3$ (n=2, 3, 4), and DMTC was revealed in benzene. The $^2J(^{119}Sn-CH_3)$ values suggested distorted *trans*-octahedral configurations for these complexes. From the statistical consideration of stability constants, it was found that the coordination occurred virtually through neighboring two oxygen atoms in these complexes. DMTC gave the complexes of both 1 : 1 and 1 : 2 glyme/DMTC stoichiometry with glymes (n=5, 6) in benzene and with all glymes employed here in toluene and 1-chloronaphthalene. Coexistence of 1 : 1 and 1 : 2 species was also encountered for $PhO(CH_2CH_2O)_nCH_3$ (n=3, 4, 5), whereas no appreciable interaction was observed between $PhO(CH_2CH_2O)_nPh$ (n=2, 3, 4) and DMTC. On the basis of these observations, the additional formation of the 1 : 2 complexes was assumed to be caused by the bulkiness of polyethers.

With recent development of the crown ether chemistry, much attention has also been paid on the metal complexes of acyclic polyethers.[2)] Structural analysis of these complexes in the solid state[2)] and their thermodynamic properties in solution[3)] have been extensively studied. However, it is rather limited to elucidate their behavior, especially their configuration, in solution, because metals employed in these studies were mostly inorganic ions. The structure of some fluorenyl metal complexes of polyethylene glycol dimethyl ethers (glymes) in solution has been investigated by means of ^{1}H NMR[4,5)] and optical spectroscopies.[5)] Coordinating abilities of glymes towards the Na^+ ion have been discussed from kinetical point of view using ^{23}Na NMR spectra.[6)] More recently, ^{1}H NMR spectra of metal complexes with polyethers containing aromatic terminal groups have been reported.[7)]

Molecular complexes of methyltin(IV) halides have been studied for a long time, since their configurations in solution can be deduced easily from their ^{1}H NMR spectra.[8)] Therefore, it seems probable that NMR studies on the polyether/methyltin(IV) halides systems afford various informations on these complexes in solution. In addition, methyltin(IV) halides, unlike the naked metal ions studied so far, possess four substituents attached to the central metal atom. Accordingly, the interactions of methyltin(IV) halides with polyethers are expected to be sterically different from those of inorganic metal ions.

In this paper are presented the results of ^{1}H NMR studies on the interactions of various acyclic polyethers, $RO(CH_2CH_2O)_nR'$ (R, R'=CH_3, Ph), with dimethyltin dichloride (DMTC) in some aromatic solvents.

Experimental

Commercially available DMTC was purified by sublimation. DiG, TrG, and TetG[9)] were of reagent grade and distilled from $LiAlH_4$ before use. The preparative methods for PeG,[10)] HeG,[10)] and $PhO(CH_2CH_2O)_nPh$[3)] have been reported.

Preparation of $PhO(CH_2CH_2O)_nCH_3$. n=*2*: The procedure for this compound is as follows;

$$(ClCH_2CH_2)_2O \xrightarrow{+\frac{1}{2}PhONa} Ph(OCH_2CH_2)_2Cl \xrightarrow[+NaI]{+CH_3ONa} PhO(CH_2CH_2O)_2CH_3.$$

To a suspension of NaH (4.8 g, 0.2 mol) in 150 cm^3 of DMF was added phenol (18.8 g, 0.2 mol) in DMF (27 cm^3) with stirring and the mixture was heated at 80 °C for 4 h. After cooling, the mixture was combined with $(ClCH_2CH_2)O$ (57.2 g, 0.4 mol) and heated at 80 °C for 6 h. The reaction mixture was combined with benzene and shaken twice with 0.2 mol dm^{-3} NaOH and with water for several times. The organic layer was dried over sodium sulfate. Evaporation of solvent and distillation gave $Ph(OCH_2CH_2)_2Cl$ (24.4 g, 61%); bp, 104—107 °C (27 Pa). $Ph(OCH_2CH_2)_2Cl$ (24.4 g, 122 mmol) and NaI (33.6 g, 224 mmol) in 100 cm^3 of acetone were heated under reflux for 41 h. After filtration of NaCl and evaporation of acetone, the product was treated with an ether–water mixture. Ether was evaporated and resulting crude $Ph(OCH_2CH_2)_2I$ (29.3 g, 82%) was used in the next reaction without further purification. To 50 cm^3 of methanol was added 1.4 g (60 mmol) of Na and subsequently $Ph(OCH_2CH_2)_2I$ (14.6 g, 50 mmol). The mixture was heated under reflux for 9 h, and combined with water and ether. The organic layer was dried over sodium sulfate and evaporated to leave a yellow oil which was chromatographed on a silica gel column (hexane–ether 10 : 1) to give $PhO(CH_2CH_2O)_2CH_3$ (4.0 g, 41%): ^{1}H NMR (CCl_4) δ=3.23 (s, 3H, CH_3), 3.40—4.07 (m, 8H, CH_2), and 6.58—7.23 (m, 5H, aromatic), high-resolution mass spectrum, 196.2437 (Calcd for $C_{11}H_{16}O_3$, 196.2456).

n=*3*: This compound was prepared by an analogous method for n=2 employing $CH_3OCH_2CH_2ONa$ in place of CH_3ONa: ^{1}H NMR (CCl_4) δ=3.23 (s, 3H, CH_3), 3.43—4.06 (m, 12H, CH_2), and 6.33—7.20 (m, 5H, aromatic), high-resolution mass spectrum, 240.2971 (Calcd for $C_{13}H_{20}O_4$, 240.2986).

n=*4*: This compound was prepared by an analogous method for n=3 employing $(ClCH_2CH_2OCH_2)_2$ in place of $(ClCH_2CH_2)_2O$: ^{1}H NMR (CCl_4) δ=3.23 (s, 3H, CH_3), 3.40—4.07 (m, 16H, CH_2), 6.60—7.20 (m, 5H, aromatic), high-resolution mass spectrum, 284.3511 (Calcd for $C_{15}H_{24}O_5$, 284.3516).

n=*5*: The procedure for this compound is as follows;

$$(HOCH_2CH_2OCH_2CH_2)_2O \xrightarrow{+PBr_3,\ C_5H_5N}$$

$$(BrCH_2CH_2OCH_2CH_2)_2O \xrightarrow{+\frac{1}{2}PhONa} Ph(OCH_2CH_2)_4Br$$

$$\xrightarrow{+CH_3OCH_2CH_2ONa} PhO(CH_2CH_2O)_5CH_3.$$

To 100 cm³ of benzene solution containing PBr_3 (189 g, 0.7 mol) and pyridine (32 g, 0.4 mol), tetraethylene glycol (194 g, 1.0 mol) was added with stirring at 0 °C for a period of 4 h. After completion of addition, the mixture was kept on stirring for 72 h at room temperature and extracted with a benzene–water mixture. Drying and evaporation of the organic layer gave crude $(BrCH_2CH_2OCH_2CH_2)_2O$ (206 g, 76%), which was subjected to the reaction with PhONa (0.38 mol) in 100 cm³ of DMF. After heating at 80 °C for 7 h, the product was poured into a benzene–water mixture. Benznene layer was shaken twice with 0.2 mol dm^{-3} NaOH and with water for several times. Drying and evaporation gave a crude mixture (103 g) of $Ph(OCH_2CH_2)_4Br$ and $PhO(CH_2CH_2O)_4$-Ph in *ca.* 8 : 2 ratio. This mixture (30 g) was treated with $CH_3OCH_2CH_2ONa$ prepared from $CH_3OCH_2CH_2OH$ (20.5 g, 270 mmol) and Na (3.1 g, 135 mmol) and heated at 120 °C for 30 h. Ether and water were added to the reaction product. The organic layer was dried over sodium sulfate and evaporated to yield 19.7 g of an oil. Column chromatography of this oil on silica gel (hexane–ether 5 : 1) gave 2.8 g of pure $PhO(CH_2CH_2O)_5CH_3$: ^1H NMR (CCl_4) δ=3.23 (s, 3H, CH_3), 3.42—4.10 (m, 20H, CH_2), and 6.63—7.22 (m, 5H, aromatic), high-resolution mass spectrum, 328.4011 (calcd for $C_{17}H_{28}O_6$, 328.4046).

Measurements of ^1H NMR spectra were carried out with a Hitachi R-24B spectrometer operating at 60 MHz at 35°C. The chemical shifts (δ) were referred to internal TMS and accurate to $\pm$0.01 ppm. Solvents were purified by standard methods.

Stability constants, K, for the equilibrium (1), $\delta^c(CH_3\text{–Sn})$, and $^2J^c$ ($^{119}Sn\text{–}CH_3$) were calculated by a least-squares method using Eqs. 2 and 3.[11]

$$(CH_3)_2SnCl_2 + Gly \overset{K}{\rightleftharpoons} (CH_3)_2SnCl_2\cdot Gly \quad (1)$$

$$\delta = \delta^\circ + \frac{\delta^c-\delta^\circ}{2}[(r+1+1/A_0K) - \sqrt{(r+1+1/A_0K)^2-4r}] \quad (2)$$

$$J = J^\circ + \frac{J^c-J^\circ}{2}[(r+1+1/A_0K) - \sqrt{(r+1+1/A_0K)^2-4r}]. \quad (3)$$

Gly: glyme.

δ, δ°, and δ^c: values of $\delta(CH_3\text{–Sn})$ for the observed, the uncomplexed, and the 1:1 complexed, respectively.

J, J°, and J^c: values of $^2J(^{119}Sn\text{–}CH_3)$ for the observed, the uncomplexed, and the 1:1 complexed, respectively.

A_0: concentration of DMTC.

r: Gly/DMTC mole ratio.

The calculations were made with a NEAC model 900 computer at the Calculation Center of Osaka University.

Results and Discussion

In Fig. 1 is illustrated the dependence of chemical shifts of methyl protons attached to tin, $\delta(CH_3\text{–Sn})$, on DiG/DMTC mole ratio (r) in some aromatic solvents

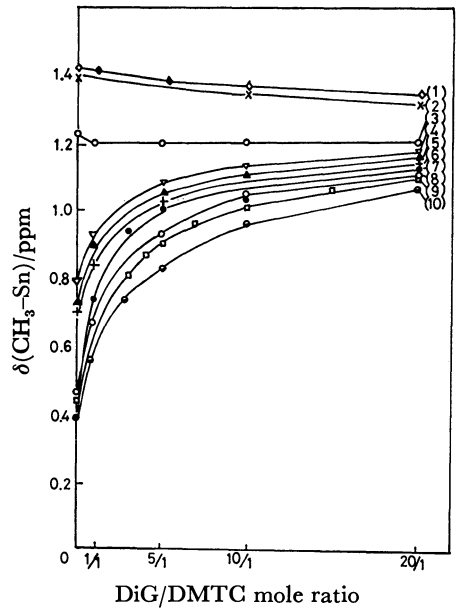

Fig. 1. Dependence of $\delta(CH_3\text{–Sn})$ on DiG/DMTC mole ratio at constant DMTC concentration (0.15 M) in various solvents.
(1): Nitrobenzene, (2): benzonitrile, (3): dichloromethane, (4): bromobenzene, (5): chlorobenzene, (6): anisole, (7): 1-chloronaphthalene, (8): *p*-xylene, (9): toluene, (10): benzene.

and dichloromethane. Marked difference was observed for the change of $\delta(CH_3\text{–Sn})$ among these solvents; the first group giving rise to little change in $\delta(CH_3\text{–Sn})$ with r involves benzonitrile, nitrobenzene, and dichloromethane, the second group affecting some dependence on r involves chlorobenzene, bromobenzene, and anisole, and the third group involves benzene, toluene, *p*-xylene, and 1-chloronaphthalene in which the largest dependence of $\delta(CH_3\text{–Sn})$ on r was observed. In the solvents of the latter two groups, the solvent effect caused by aromatic rings disappeared upon coordination of DiG to tin. This change of $\delta(CH_3\text{–Sn})$ can be a

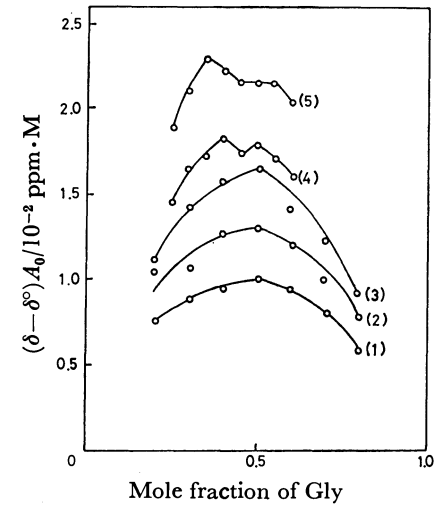

Fig. 2. Job's plot for Gly/DMTC in benzene at total concentration of 0.2 M.
(1): DiG, (2): TrG, (3): TetG, (4): PeG, (5): HexG.

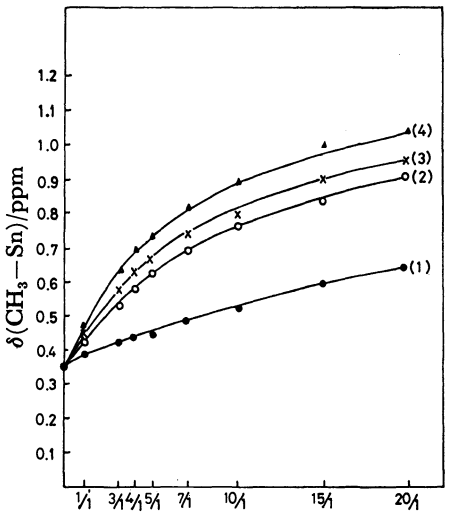

(a) Gly/DMTC mole ratio

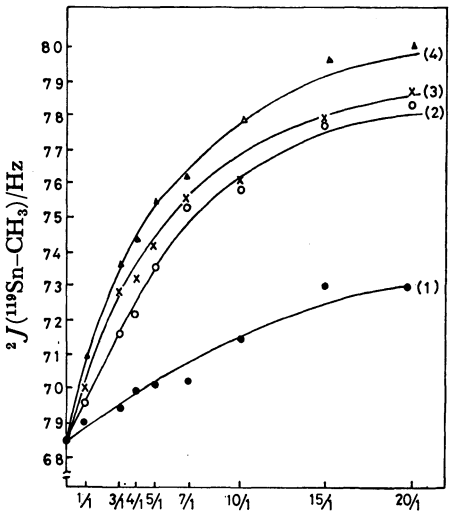

(b) Gly/DMTC mole ratio

Fig. 3. Dependence of $\delta(CH_3–Sn)$ (a) and $^2J(^{119}Sn–CH_3)$ (b) on Gly/DMTC mole ratio at constant DMTC concentration (0.05 M) in benzene.
(1): MoG, (2): DiG, (3): TrG, (4): TetG.

Table 1. Stability constant, K, $\delta^c(CH_3–Sn)$ and $^2J^c(^{119}Sn–CH_3)$ for Gly/DMTC in benzene at 35 °C

	K	δ^c (CH_3–Sn) ppm	$^2J^c(^{119}Sn–CH_3)$ Hz
MoG[a]	0.47±0.11	1.18	85.4
DiG	2.0±0.2	1.20	83.5
TrG	2.9±0.4	1.19	82.0
TetG	3.5±0.5	1.26	83.4

a) MoG was assumed to give 1 : 1 stoichiometry.

good measure for the interactions between glymes and DMTC. Therefore, we have studied, in detail, the ^1H NMR spectra of a series of Gly/DMTC system in benzene, toluene, and 1-chloronaphthalene.

First, the results obtained in benzene will be described. The stoichiometry of complexation was successfully disclosed by the Job's continuous variation method[12] as shown in Fig. 2. While no reliable curve could be drawn in the case of MoG, the evident 1 : 1 stoichiometry was found for DiG, TrG, and TetG. Figure 3 shows plots of $\delta(CH_3–Sn)$ and $^2J(^{119}Sn–CH_3)$ *vs.* r.[13] Stability constants, K, for the equilibrium (1), along with the values of $\delta^c(CH_3–Sn)$ and $^2J^c(^{119}Sn–CH_3)$ calculated by a least squares method using the above data are given in Table 1. The K values reveal a large gap of complexing ability between MoG and DiG. This trend is similar to the results obtained for some alkali metal salts in THF, in which the K value for DiG is larger by 10^2 times than that for MoG.[5a,b] The values of $^2J^c(^{119}Sn–CH_3)$ are comparable to those of *trans*-octahedral dimethyltin(IV) compounds with a slightly bent C–Sn–C moiety such as dimethyltin diacetate[14] and dikojate.[15] Since the benzene solutions containing Gly and DMTC in a 10 : 1 mole ratio at the DMTC concentration of 10^{-4} M (1 M=1 mol dm^{-3}) found to be nonelectrolytes by conductivity measurements indicative of nonionic structures, analogous distorted *trans*-octahedral configurations are suggested for the 1 : 1 complexes formed in this study.[16]

In the glyme complexes of inorganic metal ions, the coordination mode of the oxygen atoms has been the subject of considerable interest. While naked metal ions such as Li^+, Na^+, and K^+ can accommodate four to eight coordinating oxygen atoms on the interaction with glymes,[5,6] DMTC can accept two oxygen atoms at most due to the existence of four substituents. If we assume that all oxygen atoms are equivalent in coordinating ability and the coordination takes place virtually through neighboring two oxygen atoms in our 1 : 1 complexes, the total number of possible coordination modes should be 2, 3, and 4 for DiG, TrG, andTetG, respectively, leading to the increase in K values by the same factors. The observed K values of 2.0, 2.9, and 3.5 for these glymes are almost in accordance with the above statistical consideration.

For the complexes of PeG and HexG, unexpected Job's plots were encountered (Fig. 2). Appearance of two peaks at *ca.* 0.33 and 0.5 in mole fraction of Gly suggests the formation of the 1 : 2 and 1 : 1 complexes[17] as shown in the equilibrium (4).[18] An intramolecular chelation of glyme molecule resulting in a six-coordinate

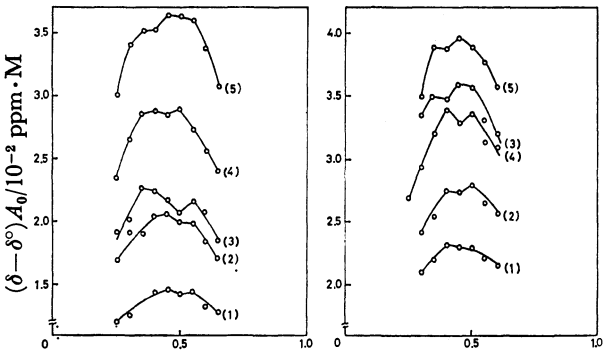

(a) Mole fraction of Gly (b) Mole fraction of Gly

Fig. 4. Job's plot for Gly/DMTC in toluene (a) and 1-chloronaphthalene (b) at total concentration of 0.2 M.
(1): DiG, (2): TrG, (3): TetG, (4): PeG, (5): HexG.

$$2(CH_3)_2SnCl_2 \underset{K_1}{\overset{Gly}{\rightleftharpoons}} [(CH_3)_2SnCl_2]_2\cdot Gly$$

$$\underset{K_2}{\overset{Gly}{\rightleftharpoons}} 2(CH_3)_2SnCl_2\cdot Gly \quad (4)$$

configuration obviously becomes sterically unfavored on increasing chain length of glymes. The additional formation of the 1 : 2 species was found for all glymes in toluene and 1-chloronaphthalene as shown in Fig. 4. On the basis of $(\delta-\delta^\circ)A_0$ values in the Job's plots which are proportional to stability constants,[12] overall stability constants in these solvents seem to be larger than those in benzene for respective glymes.

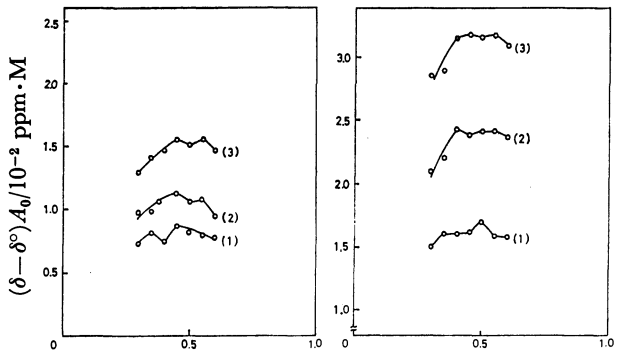

(a) Mole fraction of Gly (b) Mole fraction of Gly

Fig. 5. Job's plot for $PhO(CH_2CH_2O)_nCH_3$/DMTC in benzene (a) 1-chloronaphthalene (b) at total concentration of 0.2 M.
(1): $n=3$, (2): $n=4$, (3): $n=5$.

Steric effect on stoichiometry and complexation was further confirmed with polyethers involving terminal phenoxy groups. As shown in Fig. 5, replacement of one of the methoxy groups in glymes by a bulkier phenoxy group resulted in the coexistence of 1 : 2 and 1 : 1 complexes in both benzene and 1-chloronaphthalene even for lower members of the polyethers. It should be noted that each $PhO(CH_2CH_2O)_nCH_3$ ($n=3$, 4, 5) shows a smaller $(\delta-\delta^\circ)A_0$ value than that of $CH_3O(CH_2CH_2O)_{n-1}CH_3$ and no reliable Job's plot could be obtained for $n=2$. When a series of $PhO(CH_2CH_2O)_nPh$ ($n=2$, 3, 4) was employed, no appreciable interaction was detected in all cases. It is rather unexpected that little interaction was observed even for $PhO(CH_2CH_2O)_4Ph$, since this polyether involves three oxygen atoms linked by ethylene units and accordingly should be equivalent to $CH_3O(CH_2CH_2O)_2CH_3$ or $PhO(CH_2CH_2O)_3CH_3$ in coordinating ability. These observations suggest that the coordination behavior of polyethers towards DMTC is affected to a considerable degree by the bulkiness of the terminal groups.

References

1) For a preliminary communication of this study, see J. Otera, M. Shiigi, and Y. Kawasaki, *Chem. Lett.*, **1980**, 1091.
2) F. Voegtle and E. Weber, *Angew. Chem. Int. Ed.*, **18**, 753 (1979).
3) For example, B. Tuemmler, G. Maass, F. Voegtle, H. Sieger, U. Heimann, and E. Weber, *J. Am. Chem. Soc.*, **101**. 2588 (1979).
4) J. A. Dixon, P. A. Gwinner, and D. C. Lini, *J. Am, Chem. Soc.*, **87**, 1379 (1965).
5) a) L. L. Chan and J. Smid, *J. Am. Chem. Soc.*, **89**, 4547 (1967); b) L. L. Chan, K. H. Wong, and J. Smid, **92**, 1955 (1970); c) U. Takaki and J. Smid, **96**, 2588 (1974).
6) C. Detellier and P. Laszlo, *Helv. Chim. Acta*, **59**, 1333 (1976).
7) a) E. Weber and F. Voegtle, *Tetrahedron Lett.*, **1975**, 2415; b) W. Rasshofer, G. Oepen, and F. Voegtle, *Chem. Ber.*, **111**, 419 (1978).
8) V. S. Petrosyan, N. S. Yashina, and O. A. Reutov, *Adv. Organomet. Chem.*, **14**, 63 (1976).
9) Abbreviation for $CH_3O(CH_2CH_2O)_nCH_3$: MoG, DiG, TrG, TetG, PeG, and HexG for $n=1,2,3,4,5$, and 6, respectively.
10) S. Yanagida, T. Takahashi, and M. Okahara, *Bull. Chem. Soc. Jpn.*, **51**, 1294 (1978).
11) M. Aritomi, H. Hashimoto, and Y. Kawasaki, *J. Organomet. Chem.*, **93**, 181 (1975).
12) K. Roth, M. Grosse, and D. Rewki, *Tetrahedron Lett.*, **1972**, 435.
13) Apparent larger deviation of plots in Fig. 3b than those in Fig. 3a may be due to a expansion of the ordinate (by six times in scale) in the former case, because R_f values calculated as $R_f=\sqrt{\frac{\sum(\text{calcd}-\text{obsd})^2}{\sum(\text{obsd})^2}}$ are 0.5—1.0 for δ values and 0.3—0.6 for J values.
14) Y. Maeda and R. Okawara, *J. Organomet. Chem.*, **10**, 247 (1967).
15) J. Otera, Y. Kawasaki, and T. Tanaka, *Inorg. Chim. Acta*, **1**, 294 (1967).
16) J. Otera, T. Hinoishi, Y. Kawabe, and R. Okawara, *Chem. Lett.*, **1981**, 273.
17) L. I. Katzin and E. Gebert, *J. Am. Chem. Soc.*, **72**, 5455 (1950).
18) Simulation of the concentration dependence involved in the equilibrium consisted of three components has been reported to result in scattering of final values.[19] Our attempts also gave the same results.
19) H. Fujiwara, F. Sakai, and Y. Sasaki, *J. Phys. Chem.*, **83**, 2400 (1979).

The Separation by Means of the Zone-melting Technique and the Spectrofluorometric Determination of Trace Amounts of Anthracene in Phenanthrene

Motohisa FURUSAWA* and Masaki TACHIBANA
Faculty of Engineering, Yamanashi University, Takeda, Kofu 400
(Received December 16, 1980)

Since ordinarily available phenanthrene contains interfering impurities, such as phenanthrenequinone and fluoranthene, it is difficult to determine anthracene by spectrofluorimetry directly. Trace amounts of anthracene in phenanthrene can, however, be selectively separated from the interfering impurities by means of the zone-melting technique, for the distribution coefficient of anthracene in phenanthrene is greater than unity. The anthracene thus separated is spectrofluorometrically measured using xylene as the solvent. The determination limit of anthracene is 0.05 ppm. In a glass tube with an i.d. of 4 mm, 4.0 g of the sample was charged to a length of about 27 cm, and then the zone-pass was repeated 20 times. The molten zones were set to travel at a speed of 100 mm/h under constant stirring. Exactly 2.5 g of the zone-molten sample was cut out and dissolved in 50 ml of xylene. The fluorescence intensity of the solution was measured at 403 nm with excitation at 378 nm. The recovery of anthracene was 95%, with a coefficient of variation of 0.6%. The incompleteness of the recovery was corrected for.

The fluorometric determination of trace amounts of anthracene in phenanthrene has been developed by Parker *et al.*[1] and Iwashima *et al.*[2] These methods, however, are difficult to apply to the determination of anthracene in ordinarily available samples of phenanthrene, for these samples contain interfering impurities, such as fluoranthene and phenanthrenequinone.

In the present paper, the separation of anthracene from the interfering impurities in phenanthrene by means of the zone-melting technique and its spectrofluorometric determination will be described. The distribution coefficient of anthracene in phenanthrene being greater than unity, anthracene is concentrated toward the beginning of the ingot by repeating the zone-melting process. On the contrary, the interfering impurities show an opposite behavior; they are accumulated toward the end of the ingot. Therefore, the anthracene can be separated. The anthracene thus separated is spectrofluorometrically measured, using xylene as the solvent. The determination limit of anthracene is 0.05 ppm.

Experimental

Reagent. Phenanthrene was purified in the following manner. Commercial phenanthrene was fused with maleic anhydride in the presence of chloranil at 170 °C for 1 h to remove the anthracene. After cooling, the solidified product was dissolved in acetone. Phenanthrene crystals were precipitated by the addition of water, collected, and dissolved in benzene. The solution was shaken with 85% sulfuric acid, and then the benzene was evaporated. After this process had been repeated once more, the phenanthrene thus obtained was further purified by repeating the zone refining according to the method of Matsumoto *et al.*[3] and finally by ordinary zone refining.

Apparatus. The fluorometric measurements were carried out using a Hitachi 204 fluorescence spectrophotometer. A 150-W xenon lamp was used as the exciting source. A 10 mm × 10 mm × 45 mm quartz cell was used.

Zone melting was performed using a Shibayama SS-950 high-speed zone refiner. In this apparatus, six zones are produced by six ring heaters placed at equal spacings on the charge, and each zone is set to travel by moving the heater along the charge. After traveling to the distance between the centers of the nearest neighbor zones, the heater assembly returns quickly to its initial position. In this cycle, each molten zone is transferred into its next one. The tube is rotated around its longitudinal axis with a reversal of the rotation direction.

Procedure. In a glass tube with an i.d. of 4 mm, 4.0 g of the sample was charged to a length of about 27 cm, and then the zone-pass was repeated 20 times. The molten zones about 30 mm in length were set to travel at a speed of 100 mm/h. During the travels, the zones were stirred by spinning the glass tube at 1200 rpm with a reversal of the rotation direction at intervals of 1.0 s. Exactly 2.5 g of the zone-molten sample was cut out from the beginning part of the ingot and dissolved in 50 ml of xylene. The fluorescence intensity of the solution was measured at 403 nm, with excitation at 378 nm. An anthracene solution (50 or 500 ng/ml) and xylene were used as the standard and the blank respectively. The quantity of anthracene was determined by using a calibration curve, which had been prepared by measuring the relative fluorescence intensities of anthracene solutions (0—50 or 0—500 ng/ml) containing phenanthrene (50 mg/ml). Since the recovery of anthracene was 95%, the incompleteness of the recovery was corrected for by using the reciprocal of 0.95 as the correction factor.

Results and Discussion

Solvent. Fluorometric methods for the determination of trace amounts of anthracene in phenanthrene[1,2] use ethanol as the solvent, and the lower limit of determination in these methods is approximately 1 ppm. For the determination of more minute amounts of anthracene in phenanthrene, it is desirable to measure the fluorescence intensity of anthracene using a concentrated solution of the sample. For the purpose of dissolving large amounts of phenanthrene, xylene was selected as the solvent.

Fluorescence Spectra. The fluorescence spectra of anthracene and phenanthrene were measured with excitation at 378 nm by means of an apparatus with the same sensitivity. The measurements were made on a

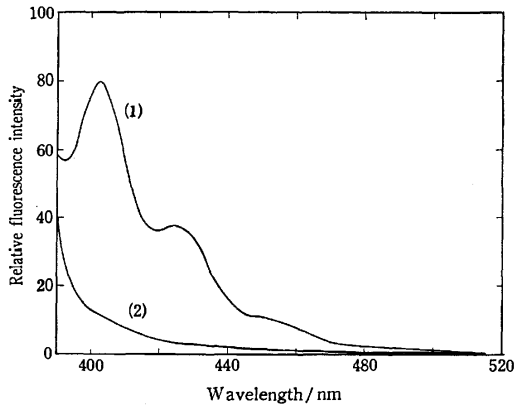

Fig. 1. Fluorescence emission spectra of anthracene and phenanthrene.
Excitation wavelength: 378 nm; solvent: xylene; (1): anthracene (uncorrected), 50 ng/ml; (2): Phenanthrene (uncorrected), 50 mg/ml.

solution containing 50 ng/ml of anthracene and on a concentrated phenanthrene solution containing a concentration 10^6 times as high as that of anthracene. These spectra are shown in Fig. 1. The fluorescence spectrum of anthracene exhibits a maximum at 403 nm. A concentrated solution of phenanthrene shows a weak fluorescence at this characteristic wavelength of anthracene.

Calibration Curves. For the determination of trace amounts of anthracene in phenanthrene, it is necessary to correct for the influence of phenanthrene. The fluorescence intensity of phenanthrene at the characteristic wavelength of anthracene is so weak that it seems to be correctable by using a calibration curve, which can be prepared by measuring the fluorescence intensities of anthracene solutions containing phenanthrene. The sensitivity of the fluorescence spectrophotometer was adjusted by setting the intensity of a standard anthracene solution (50 or 500 ng/ml) at 80 division; then, the relative fluorescence intensities of anthracene solutions (0—50 and 0—500 ng/ml) containing phenanthrene (50 mg/ml) were measured. The resultant calibration curves are shown in Figs. 2(1) and (2). For comparison, the fluorescence intensities of anthracene solutions were also measured in the absence of phenanthrene; the results are illustrated in Figs. 2(3) and (4). As a result of the influence of phenanthrene, the calibration curves shown in Figs. 2(1) and (2) do not intersect at the point of origin, and each gradient shows a slight decrease compared with the corresponding curve of anthracene alone. However, good linear relationships are observed between the fluorescence intensity and the concentration of anthracene. Therefore, the influence of phenanthrene is correctable by using the calibration curve, and anthracene in phenanthrene can be determined over the range from 0.05 to 10 ppm.

Separation of Anthracene. Since ordinarily available phenanthrene contains interfering impurities, such as phenanthrenequinone and fluoranthene, it is necessary to separate anthracene prior to its determination. For this purpose, the separation of anthracene by means of the zone-melting technique was studied. After the zone melting had been performed using phenanthrene samples containing 1.7 and 12.3 ppm of anthracene, each zone-molten ingot was divided into fifteen portions 1.5—2 cm in length, and then the anthracene was spectrofluorometrically measured. The resultant distribution profile of anthracene on the zone-molten ingot is shown in Fig. 3(1). The distribution profiles of phenanthrenequinone and fluoranthene, obtained in a manner similar to that used for anthracene, are shown in Figs. 3(2) and (3). The initial contents of phenanthrenequinone and fluoranthene were 0.1% and 0.2% respectively. The phenanthrenequinone was spectrophotometrically evaluated by employing the absorption at 416 nm, using a mixture of xylene and methanol (1 : 1) as the solvent. The presence of methanol was necessary to avoid a decrease in the absorbance. The fluoranthene was evaluated by measuring the fluores-

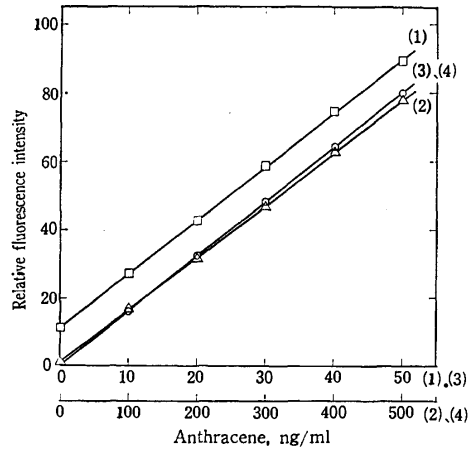

Fig. 2. Calibration curves of anthracene.
(1), (3): As the standard, fluorescence intensity of 50 ng/ml anthracene solution was taken as 80 div.; (2), (4): 500 ng/ml solution was taken as 80 div.; (1), (2): coexistence of phenanthrene, 50 mg/ml; (3), (4): Anthracene alone.

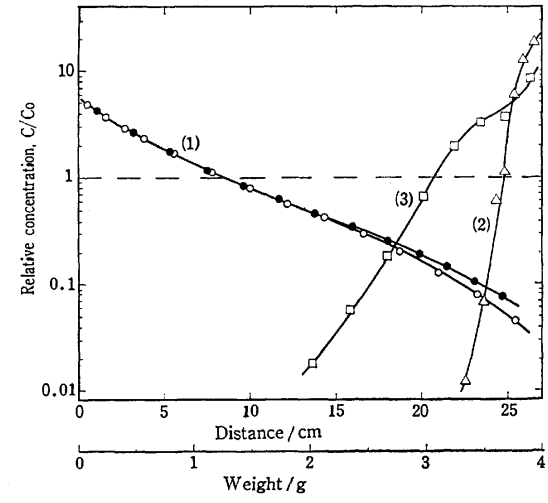

Fig. 3. Concentration profiles for anthracene, phenanthrenequinone and fluoranthene in phenanthrene.
C_0 and C are initial and final contents of the solute; (1): anthracene, ○ $C_0=12.3$ ppm, ● $C_0=1.7$ ppm; (2): phenanthrenequinone, $C_0=0.1\%$; (3): fluoranthene, $C_0=0.2\%$.

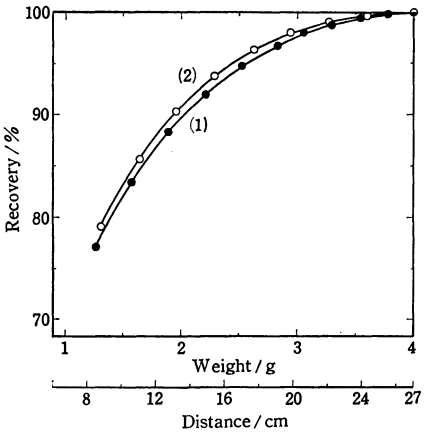

Fig. 4. Recovery profiles for anthracene.
(1): C_0=1.7 ppm; (2): C_0=12.3 ppm.

cence intensity at 460 nm with excitation at 378 nm, using xylene as the solvent. Figure 3 indicates that anthracene is concentrated toward the beginning of the zone-molten ingot, and that both impurities are effectively removed from the beginning, and accumulated toward the end, of the ingot. Therefore, anthracene in phenanthrene can be effectively separated from these interfering impurities.

Recovery of Anthracene. After the zone melting of two phenanthrene samples containing 1.7 and 12.3 ppm of anthracene had been carried out, each zone-molten ingot was divided into 10—12 portions; the quantity of anthracene in each divided ingot was then spectrofluorometrically evaluated. From the results, the relation between the amounts of the ingot cut out from the beginning and the recovery of anthracene were calculated; they are illustrated in Fig. 4. Figures 3 and 4 show that it is the most suitable for the determination of anthracene to use 2.5 g of the sample cut out from the beginning of the ingot. In this case, about 95% of anthracene can be recovered. Under these conditions, the recovery of anthracene was measured more precisely. After the zone melting of the phenanthrene samples had been performed, exactly a 2.5 g portion of each zone-molten ingot was cut out and the quantity of the anthracene was evaluated. The results are shown in Table 1. Table 1 indicates that the recovery is 95%, with a coefficient of variation of 0.6%. Since a reproducible value is obtained, the incompleteness of the recovery can be corrected for by using the reciprocal of 0.95 as the correction factor.

TABLE 1. RECOVERY OF ANTHRACENE

Anthracene added (μg)	Anthracene found (μg)	Recovery %	
7.00	6.6_3	$94._7$	
7.00	6.6_2	$94._6$	
7.00	6.7_3	$96._1$	$\bar{x}=95._1$
13.4	$12._8$	$95._5$	$\sigma=0.61$
17.2	$16._2$	$94._2$	c. v.=0.6%
25.2	$23._9$	$94._8$	
49.2	$47._0$	$95._5$	

Determination of Anthracene in Synthetic Mixtures. The analytical results for anthracene in synthetic mixtures of phenanthrene are shown in Table 2. Each synthetic mixture contains 200 ppm of phenanthrenequinone, carbazole, and fluorene, 100 ppm of acenaphthene, dibenzofuran, and naphthalene, 40 ppm of 9-fluorenone, and 10 ppm of fluoranthene, pyrene, and anthraquinone. Table 2 indicates that the analytical results agree closely with the individual contents of anthracene in synthetic mixtures. Therefore, trace amounts of anthracene in phenanthrene containing impurities can be determined by this proposed method.

Determination of Anthracene in Practical Samples. A commercial sample of phenanthrene containing about 300 ppm of anthracene was purified by treating it with sulfuric acid to remove the anthracene according to the

TABLE 2. ANALYTICAL RESULTS FOR ANTHRACENE IN SYNTHETIC MIXTURES

No.	Content ppm	Relative fluorescence intensity	Found ppm	
1	0.049	17.9	0.05_6	
2	0.102	24.3	0.11_0	
3	0.385	58.2	0.39_4	
4	3.36	40.5	3.3_4	
5	6.29	74.9	6.2_8	
6	0.644	88.7, 88.4	0.65_0, 0.64_7	$\bar{x}=0.64_9$
		89.5, 89.2	0.65_6, 0.65_4	$\sigma=0.0066$
		87.1, 89.1	0.63_6, 0.65_3	c.v.=1.0%

Nos. 1—3,6: as the standard, the fluorescence intensity of a 50 ng/ml anthracene solution in xylene was taken as 80 div.; Nos. 4, 5: a 500 ng/ml anthracene solution was used.

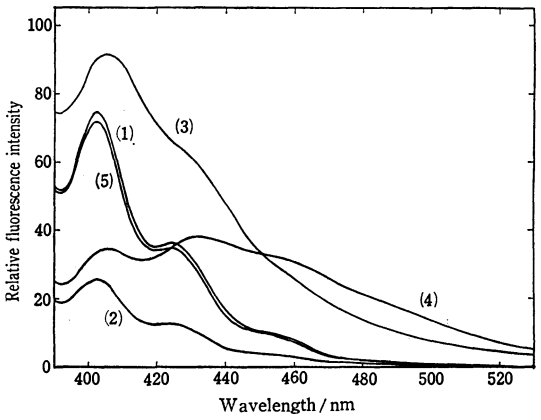

Fig. 5. Comparison of fluorescence emission spectra of practical or zone-molten samples with the spectrum of anthracene containing phenanthrene.
Standard: fluorescence intensity of 1 μg/ml anthracene solution was taken as 80 div; (1), (2): solutions employed for the determination (uncorrected), 50 mg/ml; (3), (4): solutions of practical samples (uncorrected), 100 mg/ml; (5): anthracene solution containing 50 mg/ml of phenanthrene (uncorrected); (1), (3): results of a sample purified with sulfuric acid; (2), (4): results of a sample purified with maleic anhydride and by recrystallization; excitation wavelength: 378 nm; solvent: xylene.

method of Lamey and Maloy.[4] Another commercial phenanthrene containing about 1200 ppm of anthracene was purified by a combination of the treatment with maleic anhydride and recrystallization. Trace amounts of anthracene in the two purified samples were determined by this proposed method. The analytical results were 13 ppm and 4.3 ppm respectively. The fluorescence spectra of the xylene solutions employed for the determination are shown in Figs. 5 (1) and (2). The spectra of the sample solutions were also measured; they are shown in Figs. 5 (3) and (4). The spectrum of an anthracene solution containing phenanthrene is shown in Fig. 5 (5). The shapes of the spectra shown in Figs. 5 (3)—(5) are not identical. However, the shapes of the spectra shown in Figs. 5 (1) and (2) agree closely with that of the spectrum shown in Fig. 5 (5). Therefore, this proposed method can be used in the determination of trace amounts of anthracene in practical samples of phenanthrene.

The authors are indebted to Mrs. Suzuko Kiba and Miss Sumiko Yamada for their technical assistance. The present work was partially supported by a Grant-in-Aid for Scientific Research from the Ministry of Education, Science and Culture.

References

1) C. A. Parker, C. G. Hatchard, and T. A. Joyce, *Analyst*, **90**, 1 (1965).
2) S. Iwashima, T. Sawada, H. Honda, M. Kuramachi, and J. Aoki, *Bunseki Kagaku*, **25**, 29 (1976).
3) T. Matsumoto, M. Sato, S. Hirayama, and S. Uemura, *Bunseki Kagaku*, **21**, 1641 (1972).
4) S. C. Lamey and J. T. Maloy, *Sep. Sci.*, **9**, 391 (1974).

The Preparation and Properties of Ethylenediamine(8-quinolinolato)cobalt(III) Complexes

Yoshihisa YAMAMOTO,* Reiko KATAOKA, Shinji IMAHARA,† and Toshio AMANO††

Faculty of Pharmaceutical Science, Higashi Nippon Gakuen University, Ishikari-Tobetsu, Hokkaido 061-02

(Received March 16, 1981)

Bis(ethylenediamine)(8-quinolinolato)cobalt(III) chloride dihydrate and ethylenediaminebis(8-quinolinolato)-cobalt(III) chloride dihydrate have been isolated and characterized. The ^{1}H-NMR spectrum of the latter complex indicates that the two oxygen atoms of the coordinated 8-quinolinolato ligands are in the cis positions.

Previously, we have reported the preparation and properties of the ammine(8-quinolinolato)cobalt(III) complexes.[1] Among these complexes, the two oxygen atoms of the coordinated 8-quinolinolato ligands of diamminebis(8-quinolinolato)cobalt(III) chloride hydrate were found to be in the *trans* positions.

In the corresponding ethylenediamine complexes which have been obtained in the present research, the two oxygen atoms of the coordinated 8-quinolinolato ligands were found to be in the *cis* positions.

Results and Discussion

Bis(ethylenediamine)(8-quinolinolato)cobalt(III) chloride dihydrate, $[Co(C_9H_6NO)(en)_2]Cl_2\cdot 2H_2O$ (**1**) and ethylenediaminebis(8-quinolinolato)cobalt(III) chloride dihydrate, $[Co(C_9H_6NO)_2(en)]Cl\cdot 2H_2O$ (**2**) have been obtained by the chromatographic separation of the reaction mixture of *trans*- or *cis*-dichlorobis(ethylenediamine)cobalt(III) chloride,[2] Ag_2O and 8-quinolinol. Tris(8-quinolinolato)cobalt(III) complex[3,4] (**3**) and tris(ethylenediamine)cobalt(III) chloride[5] (**4**) are produced as by-products from the reaction mixture. Complex **1** is very soluble in water, soluble in methanol and slightly soluble in ethanol. Complex **2** is soluble in methanol and somewhat soluble in water and ethanol. These complexes are insoluble in most other organic solvents. The corresponding nitrate (**5**) has been prepared from the chloride (**1**) and silver nitrate. Also the corresponding picrate (**6**) has been prepared from the chloride (**2**) and picric acid. The possible geometrical structures of **2** are shown in Fig. 1. The NMR spectra and behavior in chromatography with Dowex 50W-X2[6,7] show that the complex **2** obtained has one of these structures and is not a mixture of isomers.

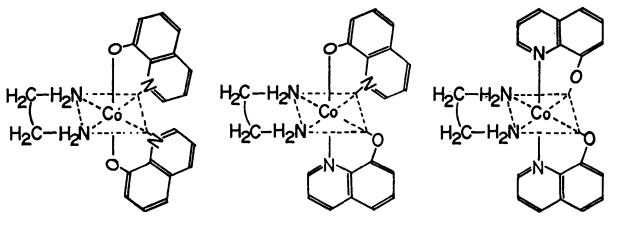

2a 2b 2c

Fig. 1. The possible isomeric structures of $[Co(oxine)_2(en)]Cl\cdot 2H_2O$.

The absorption bands of 8-quinolinolato-metal complexes have already been reported by several researchers.[8-10] The absorption spectra of **1** and **2** have three absorption bands around 324, 338, and 407 nm in methanol. The bands around 407 nm are considered to be charge-transfer bands.[1] These bands shift to 383—388 nm in water.

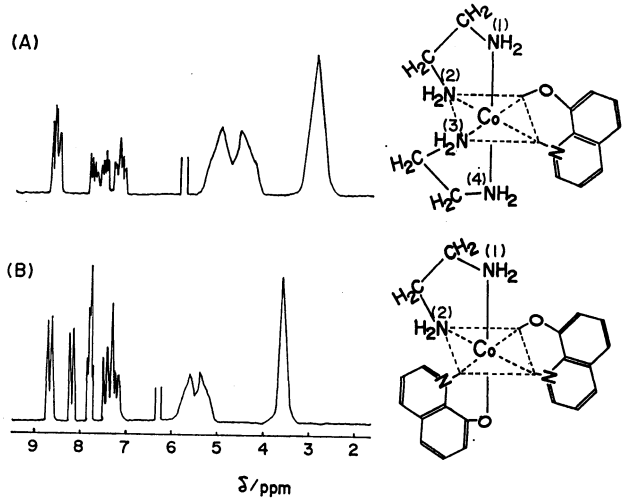

Fig. 2. The ^{1}H-NMR spectra of ethylenediamine-(8-quinolinolato)cobalt(III) chloride.
(A): $[Co(oxine)(en)_2]Cl_2\cdot 2H_2O$ in 1.8 mol dm^{-3} D_2SO_4, (B): $[Co(oxine)_2(en)]Cl\cdot 2H_2O$ in 2.5 mol dm^{-3} D_2SO_4

In the ^{1}H-NMR spectrum of **1** shown in Fig. 2, the signal at 2.92 ppm is assigned to the methylene protons of the coordinated ethylenediamine. The NH_2 protons of that ligand showed two singlet signals in the intensity ratio of 1 : 1. The singlet signal at 4.55 ppm (4H) is assigned to the protons of the two amines of $N(1)H_2$ and $N(4)H_2$ which are *cis*[1] to the coordinated 8-quinolinolato ligand, while the singlet signal at 5.0 ppm (4H) is assigned to the protons of $N(2)H_2$ and $N(3)H_2$ which are *trans* to the coordinated 8-quinolinolato ligand. In

† Present address : Takeda Chemical Industries Ltd., 27 Dosho-machi 2-chome, Higashi-ku, Osaka 541.

†† Present address : Dainippon Pharmaceutical Co., Ltd., 25 Dosho-machi 3-chome, Higashi-ku, Osaka 541.

Table 1. ^{1}H-NMR spectra of ethylenediamine(8-quinolinolato)cobalt(III) complexes

Complex No.	$NH_2CH_2CH_2NH_2$ δ/ppm					8-Quinolinolato δ/ppm	Picrate δ/ppm	Solvent and standard
	CH_2	$N(4)H_2$	$N(1)H_2$	$N(2)H_2$	$N(3)H_2$			
1	2.92 s(8H)	4.55 s(4H)		5.0 s(4H)		7.0—8.7 m(6H)		A-1
5	2.99 s(8H)	4.55 s(4H)		5.0 s(4H)		7.1—8.7 m(6H)		A-1
2	3.54 s(4H)		5.38 s(2H)	5.58 s(2H)		7.1—8.7 m(12H)		B-1
6	2.78 s(4H)		5.31 s(2H)	5.80 s(2H)		7.0—8.4 m(12H)	8.6 s(2H)	C-2
L						6.7—8.7 m		D-2

Solvents: A, 1.8 mol dm^{-3} D_2SO_4; B, 2.5 mol dm^{-3} D_2SO_4; C, DMSO-d_6; D, $CDCl_3$. Standard: 1, internal DSS; 2, internal TMS.

the ^{1}H-NMR spectrum of **2**, the signal (3.54 ppm) at the highest field is assigned to the methylene protons of the coordinated ethylenediamine. The NH_2 protons of that ligand showed two singlet signals in the intensity ratio of 1 : 1. The singlet signal at 5.38 ppm is assigned to the protons of $N(1)H_2$ which are *trans*[11,12] to the oxygen of the coordinated 8-quinolinolato ligand. Another singlet signal at 5.58 ppm is assigned to the protons of $N(2)H_2$ group which are *trans* to the nitrogen of that ligand, which is less electronegative than the 8-quinolinol oxygen. Thus, the structure of **2** is considered to be **2b**. The two oxygen atoms of the coordinated 8-quinolinolato ligands in **2b** are in the *cis* positions in contrast to most of the known cases where the two oxygen atoms of the coordinated 8-quinolinolato ligands in an octahedral configuration are in *trans*[13–15] positions. The diamminebis(8-quinolinolato)cobalt(III) chloride dihydrate, $[Co(C_9H_6NO)_2(NH_3)_2]Cl\cdot H_2O$ (**7**), reported previously,[1] is included among these cases. The complexes of **1**, **2**, **7**, and tetraammine(8-quinolinolato)cobalt(III) chloride monohydrate, $[Co(C_9H_6NO)(NH_3)_4]Cl_2\cdot H_2O$ (**8**),[1] are thermally stable compounds. Concerning decomposition of these complexes, their stabilities are arranged in the following order: **1** (247 °C), **7** (205 °C), **8** (177 °C), **2** (163 °C).

The ethylenediamine complex (**2**) is less stable than the corresponding ammine complex (**7**) and bis(ethylenediamine) complex (**1**). This is probably due to the positions of the two oxygen atoms of the coordinated 8-quinolinolato ligands of **2** in an octahedral configuration; in the ammine complexes, diammine complex **7** is more stable than the tetraammine complex (**8**). Tetraammine(8-quinolinolato)cobalt(III) nitrate, $[Co(C_9H_6NO)(NH_3)_4](NO_3)_2$ (**9**), and diamminebis(8-quinolinolato)cobalt(III) nitrate hydrate, $[Co(C_9H_6NO)_2(NH_3)_2]NO_3\cdot H_2O$ (**10**) have been prepared from the corresponding chloride[1] and silver nitrate. Also tetraammine(8-quinolinolato)cobalt(III) picrate, $[Co(C_9H_6NO)(NH_3)_4](pic)_2$ (**11**) and diamminebis(8-quinolinolato)cobalt(III) picrate, $[Co(C_9H_6NO)_2(NH_3)_2]pic$ (**12**) have been prepared from the corresponding chloride[1] and picric acid. ^{1}H-NMR spectral data of **1**, **2**, **5**, and **6** complexes are listed in Table 1.

In the ^{13}C-NMR spectra of **1** and **2** in D_2O, nine

Table 2. ^{13}C-NMR spectra of the amine(8-quinolinolato)cobalt(III) complexes

Complex No.	$NH_2CH_2CH_2NH_2$ δ/ppm				δ/ppm									Solvent and standard
					C-2	C-3	C-4	C-5	C-6	C-7	C-8	C-9	C-10	
1	44.1	45.0	45.8	46.2	150.3	115.0	141.0	124.1	116.3	131.3	146.2	165.1	131.3	a
2		45.9			148.5	114.7	139.6	123.4	116.2	131.1	145.5	165.3	130.7	a
7					149.1	111.0	138.1	122.7	114.4	129.7	d	166.6	130.2	b
8					150.2	115.2	140.9	124.0	116.6	131.2	146.0	164.8	131.2	a
3					146.1 147.0	111.0 111.2 111.8	137.8 137.9 138.2	121.5 122.1	115.4 116.0 116.3	130.3 130.7 131.1	d	167.2 168.0 169.3	130.3 130.7 131.1	c
L					147.9	110.3	136.1	121.7	117.9	127.7	138.3	152.4	128.6	c

Solvent and standard: a;D_2O, internal dioxane (δ=67.4 ppm). b; DMSO-d_6 (δ=39.5 ppm). c ; $CDCl_3$(δ=77.1 ppm).
L: 8-Quinolinol, d: disappeared.

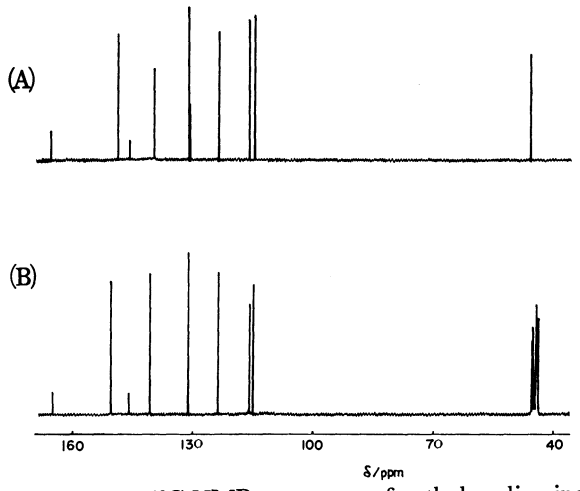

Fig. 3. The ^{13}C-NMR spectra of ethylenediamine-(8-quinolinolato)cobalt(III) chloride.
(A): $[Co(oxine)_2(en)]Cl_2 \cdot 2H_2O$ in D_2O, (B): $[Co(oxine)(en)_2]Cl \cdot 2H_2O$ in D_2O.

signals have been observed for the coordinated 8-quinolinolato ligand in the regions 115—170 ppm. The assignment (Table 2) of that ligand has been tried by the means of a consideration of the assignments of quinoline[16] and 8-quinolinol. The chemical shifts of C-8 of quinoline move to lower field upon the substitution of a hydroxyl group[17] to form 8-quinolinol. The methylene carbons of the coordinated ethylenediamine in **1** have been observed at 44.1, 45.0, 45.8, and 46.2 ppm and those of **2** have been observed at 45.9 ppm as is shown in Fig. 3, but the chemical shifts of the methylene carbons of the coordinated ethylenediamine of **1** are difficult to assign to the individual carbon atom. The methylene carbon signals of **2** overlapped. An X-ray study is expected to give further information as to the structure of **2b** or **2c**.

The complexes **1**, **2**, **5**—**12** are diamgnetic compounds.

Experimental

Measurements. The NMR spectra were recorded with an FX-60 spectrometer (JEOL) for ^{13}C-NMR and R-40 (Hitachi) for ^{1}H-NMR. The visible absorption spectra were recorded with a Shimadzu MPS-5000 recording spectrophotometer. The magnetic susceptibilities were measured by Faraday's method using a magnetic balance (Shimadzu) at room temperature. The electric conductivities of aqueous solutions were determined by the use of a conductometer, CM-30 (Shimadzu) at room temperature.

Preparation of Complexes. Bis(ethylenediamine)(8-quinolinolato)cobalt(III) Chloride Dihydrate (1), and Ethylenediaminebis(8-quinolinolato)cobalt(III) Chloride Dihydrate (2) and Tris(8-quinolinolato)cobalt(III) Complex (3) and Tris(ethylenediamine)cobalt(III) Chloride (4): One hundred cubic centimeters of a methanol solution of 8-quinolinol (4.16 g, 28.66 mmol) were slowly added to 100 cm^3 of an aqueous solution of $[Co(OH)_2(en)_2]^+$, which was prepared from *trans*-$[CoCl_2(en)_2]Cl$ (4.0 g, 14.01 mmol) and Ag_2O which, in turn, was prepared from $AgNO_3$ (4.8 g, 28.26 mmol) and KOH (2.0 g, 35.65 mmol). They were stirred for 2 d at 60 °C. The precipitated yellow complex (**3**) was filtered. The filtrate was concentrated on a rotary evaporator and dried over silica gel. Complex **2** was extracted with dry ethanol from the dried reaction mixture. The purification (removal of **1**) of **2** from the ethanol solution was achieved by column chromatography on alumina. On elution with ethanol–acetone (3 : 1), the first band (complex **2**) was collected and concentrated. Complex **2** was recrystallized from ethanol–ether twice. Complex **1** was extracted with dry methanol from the dried reaction mixture. This complex was recrystallized from water-acetone twice. Complex **4** remaining to the last did not dissolve in dry methanol. Yield: 0.8 g (13.27%) for **1**, 2.9 g (43.23%) for **2**, 1.2 g (17.4%) for **3** and 0.5 g (10.3%) for **4**. Found **1**: C, 36.51; H, 6.19; N, 16.70; Cl, 16.98%. **2**: C, 49.95; H, 5.20; N, 11.39; Cl, 7.41%. Calcd for **1**: $CoC_{13}H_{26}N_5O_3Cl_2$ (M.W. 430.22) C, 36.29; H, 6.09; N, 16.28; Cl, 16.48%. **2**: $CoC_{20}H_{24}N_4O_4Cl$ (M.W. 478.82) C, 50.17; H, 5.05; N, 11.70; Cl, 7.40%. Dec 245—247 °C for **1**, 161—163 °C for **2**. Λ=270 S cm^2 for **1**, 130 S cm^2 for **2** in water. Absorption spectra, 320 nm (ε=910), 335 (1100), and 338 (2400) in water, 271 nm (ε=11000), 324 (1150), 338 ((1250), and 407 (2900) in methanol for **1**, 320 nm (ε=1070), 334 (1370), and 384 (4780) in water, 267 nm (ε=14800), 325 (2400), 339 (2960), and 404 (5730) in methanol for **2**. Color: brick-red for **1**, brown for **2**.

Bis(ethylenediamine)(8-quinolinolato)cobalt(III) Nitrate, $[Co($ 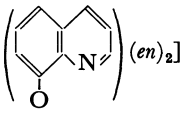 $)(en)_2](NO_3)_2$ (**5**): To an aqueous solution of **1** (0.5 g, 1.16 mmol) was added an aqueous solution of silver nitrate (0.4 g, 2.35 mmol). The mixture was stirred, and the silver chloride precipitated was filtered. The filtrate was concentrated and recrystallized from water twice. Yield: 0.42 g (80.9%). Found: C, 34.91; H, 5.17; N, 21.43%. Calcd for $CoC_{13}H_{22}N_7O_7$ (M.W. 447.30) C, 34.91; H, 4.96; N, 21.92%. Dec 245—249 °C. Absorption spectrum: 322 nm (ε=860), 339 (1050) and 388 (2500) in water. Color: brick-red.

Ethylenediaminebis(8-quinolinolato)cobalt(III) Picrate, $[Co($ 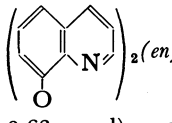 $)_2(en)]pic$ (**6**): An aqueous solution of **2** (0.30 g, 0.63 mmol) was added to a solution of picric acid (0.16 g, 0.7 mmol), the mixture was stirred, and the separated brown complex was filtered and recrystallized from methanol. Yield: 0.29 g (66.2%). Found: C, 48.76; H, 3.92; N, 15.50%. Calcd for $CoC_{26}H_{22}N_7O_9$ (M.W. 635.44) C, 49.14; H, 3.49; N, 15.43%. Dec 156—160 °C Absorption spectrum: 267 nm (ε=18300), 350 sh (15400), 362 (15700), and 393 (15100) in methanol. Color: brown.

Tetraammine(8-quinolinolato)cobalt(III) Nitrate (9). An aqueous solution of silver nitrate (0.90 g, 5.30 mmol) was added to an aqueous solution of tetraammine (8-quinolinolato)-cobalt(III) chloride dihydrate[1] (**8**) (1.0 g, 2.78 mmol). The mixture was stirred, and the precipitated silver chloride was filtered. The filtrate was concentrated and recrystallized from water twice. Yield: 0.92 g (83.7%). Found: C, 27.29; H, 4.87; N, 24.44%. Calcd for $CoC_9H_{18}N_7O_7$(M.W. 395.22) C, 27.35; H, 4.59; N, 24.81%. Dec 163—165 °C. Λ=240 S cm^2 in water. Absorption spectrum: 321 nm (ε=940), 337 (1170), and 384 (2450) in water. ^{1}H-NMR spectrum,[1] δ: 3.36 ppm (s, 6H) for N(4)H$_3$ and N(1)H$_3$, 3.99 (s, 3H) for N(2)H$_3$ and 3.59 (s, 3H) for N(3)H$_3$, 7.24—8.7 (m, 6H) for 8-quinolinol. Color: brown.

Diamminebis(8-quinolinolato)cobalt(III) Nitrate Monohydrate

(10). This complex was prepared from diamminebis-(8-quinolinolato)cobalt(III) chloride hydrate[1] (**7**) (1.0 g, 2.30 mmol) and silver nitrate (0.39 g, 2.30 mmol) according to the method of **9**, and recrystallized from methanol–water (1 : 1) twice. Yield: 0.81 g (76.4%). Found: C, 46.92; H, 4.61; N, 15.39%. Calcd for $CoC_{18}H_{20}N_5O_6$ (M.W. 461.33) C, 46.86; H, 4.37; N, 15.18%. Dec 193—195 °C. Absorption spectrum: 300 nm (ε=3600), 319 (3000), 337 (3100) and 408 (6100) in methanol. ^{1}H-NMR spectrum δ: 3.09 ppm (s, 6H) for NH_3, 7.0—9.1 (m, 12H) for 8-quinolinol. Color: yellowish brown.

Tetraammine(8-quinolinolato)cobalt(III) Picrate (11). An aqueous solution of **8** (0.5 g, 1.39 mmol) was added to a solution of picric acid (0.61 g, 2.65 mmol), the mixture was stirred, and the separated yellowish brown complex was filtered and recrystallized from methanol. Yield: 0.82 g (81.2%). Dec 156—159 °C. Found: C, 34.88; H, 3.09; N, 21.42%. Calcd for $CoC_{21}H_{22}N_{11}O_{15}$ (M.W. 727.41) C, 34.68; H, 3.05; N, 21.18%. Color: yellowish brown.

Diamminebis(8-quinolinolato)cobalt(III) Picrate (12). This complex was prepared from **7** (1 g, 2.30 mmol) and picric acid (0.053 g, 2.31 mmol) according to the method of **11**, and recrystallized from methanol. Yield: 1.1 g (78.6%). Dec 200—203 °C. Found: C, 47.57; H, 3.32; N, 15.97%. Calcd for $CoC_{24}H_{20}N_7O_9$ (M.W. 609.40) C, 47.30; H, 3.31; N, 16.09%. Color: yellow.

References

1) Y. Yamamoto, *Chem. Lett.*, **1980**, 1555.
2) J. C. Bailar. Jr, *Inorg. Synth.*, Coll. Vol. **II**, 222 (1946).
3) H. Kuroya, M. Aimi, and R. Tsuchida, *Nippon Kagaku Kaishi*, **64**, 995 (1943).
4) A. Ablov, *Bull. Soc. Chim.*, **53**, 234 (1933).
5) J. B. Work, *Inorg. Synth.*, Coll. Vol. **II**, 221 (1946).
6) Y. Yamamoto and E. Toyota, *Bull. Chem. Soc. Jpn.*, **52**, 2540 (1979).
7) D. A. Buckingham, M. Dwyer, G. J. Gainsford, V. Janson Ho, L. G. Marzilli, Ward T. Robinson, A. M. Sargeson, and K. R. Turnbull, *Inorg. Chem.*, **14**, 1739 (1975).
8) C. D. Barsode, P. Umapathy, and D. N. Sen, *J. Indian Chem. Soc.*, **54**, 1172 (1977).
9) T. Moller and B. L. Pundsack, *J. Am. Chem. Soc.*, **76**, 617 (1954).
10) K. Sone, *J. Am. Chem. Soc.*, **75**, 5207 (1953).
11) Y. Yamamoto, *Bull. Chem. Soc. Jpn.*, **51**, 2894 (1978).
12) W. L. Jolly, A. D. Jarris, and T. S. Briggs, *Inorg. Chem.*, **4**, 1064 (1965).
13) E. O. Schlemper, *Inorg. Chem.*, **6**, 2012 (1967).
14) J. D. Matthews, N. Singer, and A. G. Swallow, *J. Chem. Soc., A*, **1970**, 2545.
15) B. F. Studd and A. G. Swallow, *J. Chem. Soc., A*, **1968**, 1961.
16) F. Johnson and W. G. Jankowski, "Carbon-13 NMR Spectra, A Collection of Assigned, Coded, and Indexed Spectra," Wiley-Interscience, New York (1972), No. 335.
17) a) G. C. Levy and G. L. Nelson, "Carbon-13 NMR for Organic Chemists," Wiley-Interscience, New York (1972), p. 81, b) G. L. Nelson, G. C. Levy, and J. D. Cargioli, *J. Am. Chem. Soc.*, **94**, 3089 (1972); *J. Chem. Soc., D*, **1971**, 506.

A Facile Reduction of Copper(II) Leading to Formation of Stable Copper(I) Complexes. Redox Properties of Four- and Five-coordinate Copper Complexes

Takeshi SAKURAI,* Masazo KIMURA, and Akitsugu NAKAHARA

Institute of Chemistry, College of General Education, Osaka University, Toyonaka, Osaka 560

(Received March 17, 1981)

Schiff bases derived from 2-pyridinecarbaldehyde and 1,6-hexanediamine or bis(2-aminoethyl) disulfide gave stable Cu(I) complexes instead of Cu(II) complexes by reactions with copper(II) perchlorate. The facile reduction of copper(II) has been discussed on the basis of systematic comparisons of redox and ESR properties of about 20 complexes of similar structures.

In the course of our study on biological coppers[1] and model compounds,[2-4] we found that some Schiff base ligands derived from 2-pyridinecarbaldehyde (pca) and 1,6-hexanediamine (heda) or bis(2-aminoethyl) disulfide (baed) afford stable copper(I) complexes in spite of the use of divalent copper as starting material. We have systematically investigated redox and ESR properties of some four- and five-coordinate copper complexes in order to shed light on this novel phenomenon. Diamines employed in this study to derive Schiff bases with pca were as follows: heda, 1,5-pentanediamine (peda), 1,4-butanediamine (buda), 1,3-propanediamine (prda), 1,2-ethanediamine (etda), baed, bis(2-aminoethyl) sulfide (baes), 2-aminoethyl 3-aminopropyl sulfide (aeps), *N*-(2-aminoethyl)-1,3-propanediamine (aepd), *N*-(2-aminoethyl)-1,2-ethanediamine (aeed), and bis(2-aminoethyl) ether (baee).

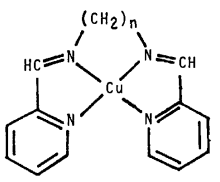

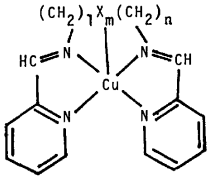

n=6: Cu(pca=heda=pca)
n=5: Cu(pca=peda=pca)
n=4: Cu(pca=buda=pca)
n=3: Cu(pca=prda=pca)

X=S, l=2, m=2, n=2: Cu(pca=baed=pca)
X=S, l=2, m=1, n=2: Cu(pca=baes=pca)
X=S, l=2, m=1, n=3: Cu(pca=aeps=pca)
X=N, l=2, m=1, n=2: Cu(pca=aeed=pca)
X=N, l=2, m=1, n=3: Cu(pca=aepd=pca)
X=O, l=2, m=1, n=2: Cu(pca=baee=pca)

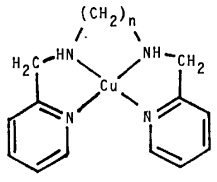

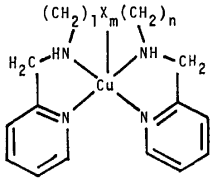

n=6: Cu(pca-heda-pca)
n=5: Cu(pca-peda-pca)
n=4: Cu(pca-buda-pca)
n=3: Cu(pca-prda-pca)
n=2: Cu(pca-etda-pca)

X=S, l=2, m=2, n=2: Cu(pca-baed-pca)
X=S, l=2, m=1, n=2: Cu(pca-baes-pca)
X=S, l=2, m=1, n=3: Cu(pca-aeps-pca)
X=N, l=2, m=1, n=2: Cu(pca-aeed-pca)
X=N, l=2, m=1, n=3: Cu(pca-aepd-pca)

Experimental

Materials. Copper(II) perchlorate hexahydrate, heda, peda, buda, prda, etda, and aeed were purchased from Nakarai Chemicals Ltd., and baed, aeps, and baee from Aldrich. Diamines with single thio group, baes and aeps, were prepared according to literatures.[3,5] All other reagents used were of the highest grade commercially available.

Preparation of Complexes. *Cu^{I}(pca=heda=pca)*:** To a 80 ml of neutral or basic aqueous ethanol (1 : 1 by volume) solution of heda (1.16 g) was added twice as much amount of pca (2.14 g) to give 2 : 1 pca: heda Schiff base, and was treated with 3.71 g of $Cu(ClO_4)_2 \cdot 6H_2O$. A brown complex precipitated very soon. On account of its poor solubility in most solvents, the precipitate was washed by aqueous ethanol instead of being recrystallized. Found: C, 46.57; H, 4.79; N, 12.39; Cu, 13.1%. Calcd for $C_{18}H_{22}N_4Cu(ClO_4) \cdot H_2O$: C, 46.25; H, 5.18; N, 11.99; Cu, 13.6%.

Cu^{I}(pca=baed=pca). This brown complex was prepared by the same method as that in Cu^{I}(pca=heda=pca). Found: C, 36.39; H, 3.55; N, 10.45; Cu, 11.5%. Calcd for $C_{16}H_{18}N_4S_2Cu(ClO_4) \cdot 2H_2O$: C, 36.29; H, 4.19; N, 10.58; Cu, 12.0%.

The other parent copper(II) complexes were prepared according to the methods in previous papers[3,6,7] as diperchlorate except Cu(pca=prda=pca), Cu(pca=baee=pca), Cu(pca-prda-pca) and Cu(pca-heda-pca) which were monochloride monoperchlorate. All these compounds were identified based on elemental analyses and IR spectra.

Measurements. Cyclic voltammetry was performed at 25 °C with a three electrode system consisting of platinum working and auxiliary electrodes and a standard calomel electrode. Voltammograms were generated using a Yanagimoto P-1000 voltammetric analyzer and an NF FG-121G function generator and recorded on a National VP-6421 X-Y recorder for *N,N*-dimethylformamide (DMF) solutions of complexes (*ca.* 5×10^{-3} mol·dm^{-3}, I=0.1 (tetrabutylammonium perchlorate)). $E°$ values were determined as the midpoints between the peak potentials. Absorption spectra were recorded in 1 cm- or 1 mm-path length quartz cell in the range 270—700 nm with a Hitachi 323 spectrophotometer at room temperature. Electron spin resonance spectra of copper(II) complexes were obtained using a JEOL JES-FEIX instrument at 77 K. Infrared spectra were measured using a Hitachi 260-10 grating infrared spectrophotometer by KBr disk method. Copper contents of complexes were determined by a Nippon Jarrell-Ash AA-1 atomic absorption spectrometer. DMF was used as solvent throughout measurements unless otherwise specified. The magnetic susceptibility was determined at room temperature by using a Gouy magnetic apparatus.

** The notation "pca=heda=pca" represents hereafter the 2 : 1 Schiff base derived from pca and heda, and "pca-heda-pca" the aorresponding reduced ligand.

Results and Discussion

Brown copper(I) complex, Cu^{I}(pca=heda=pca), unexpectedly precipitated immediately after addition of $Cu(ClO_4)_2$ to pca=heda=pca in aqueous ethanol, instead of producing green Cu^{II}(pca=heda=pca). Reduction of copper(II) to copper(I) was substantiated not only by elemental analysis but also by ESR and absorption spectroscopy. Copper(II) content was several percent, which was determined by double integration of ESR signals using $Cu(imidazole)_4$ as standard. Addition of H_2O_2 or permission to stand Cu^{I}(pca=heda=pca) in H_2O–DMF for several days presented full copper(II) ESR signal (Fig. 1), and the solution turned green.

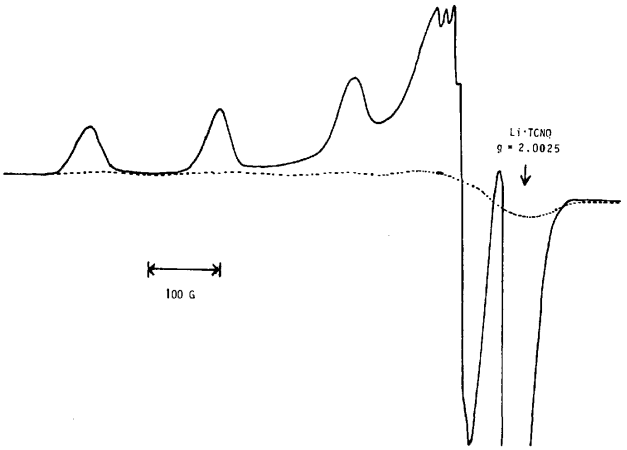

Fig. 1. ESR spectra of isolated Cu(pca=heda=pca) (------) and H_2O_2-treated Cu(pca=heda=pca) (——).

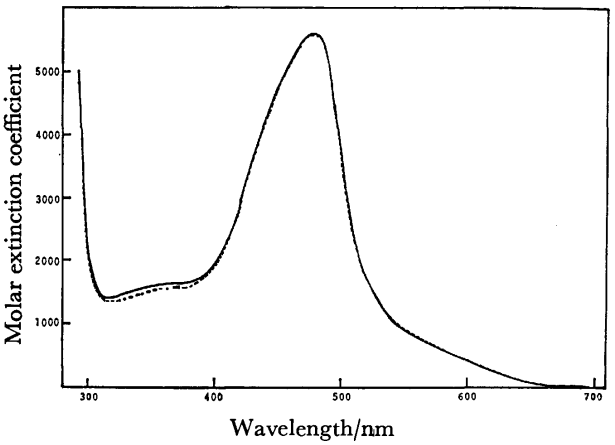

Fig. 2. Absorption spectra of authentic (——) and isolated (------) Cu(pca=heda=pca).

An authentic copper(I) complex solution prepared by using $Cu^{I}(CH_3CN)_4(ClO_4)$ as copper(I) source afforded a quite similar absorption spectrum as that of the isolated Cu(pca=heda=pca) (Fig. 2), exhibiting an intense MLCT band at 478 nm. Magnetic moment per copper atom was calculated from susceptibility to be 0.62 BM ($1\ BM = 9.274 \times 10^{-24}\ A\ m^2$) at room temperature, indicating that paramagnetic copper(II) was really a trivial contaminant. The present quite rapid reduction of copper, which occurs much readily in alkaline medium than in neutral aq ethanol, might be accompanied by generation of 2-pyridinecarboxylic acid from free 2-pyridinecarbaldehyde in the system. In fact, thin layer chromatography on silica gel plate has suggested the formation of 2-pyridinecarboxylic acid in the brown reaction mixture. A green copper(II) complex which was precipitated in acidic solution also gradually turned brown in DMF. Copper does not seem to be reduced by a concomitant oxidation of the coordinated ligand, since the IR spectrum of brown Cu^{I}(pca=heda=pca) is similar to green intact copper(II) complexes providing with various lengths of methylene chain.

In line with this, the quite similar reduction of copper(II) ligated by pca=baed=pca has been observed. However, pure Cu(I) complex has not been isolated: Cu(II) content determined by ESR spectrum was 35% and magnetic moment of this complex was evaluated as 1.55 BM at room temperature. The extremely delicate difference in stabilizing Cu(I) complex of the present kind might be interpreted on the basis of the greater size of sulfur over a methylene group. The dithio group would not bind copper, or if any, the interaction of the dithio group with copper will be rather weak. These examples suggest that the facile reduction of Cu(II) to Cu(I) may occur when providing the ligand with methylene chain of appropriate length. In the case of the present series of complexes, diamines having six methylene groups or equivalent length as half moiety of Schiff base are considered to best suit the condition.

In order to understand this phenomenon, redox potentials of copper have been compared for about 20 copper complexes. $E°$ values and ESR parameters to exhibit properties of parent copper(II) complexes are

Table 1. Redox potentials and ESR parameters of copper complexes

Complex	ESR parameters			
	$E°$ vs.SCE / V	$g_{//}$	$g_{\perp}$	$-A_{//} \times 10^4$ / cm^{-1}
Cu(pca=heda=pca)	+0.13	2.27	2.07	16.5
Cu(pca=peda=pca)	+0.00	2.24	2.07	14.0
Cu(pca=buda=pca)	−0.10	2.22	2.06	15.0
Cu(pca=prda=pca)	−0.08	2.24	2.06	18.4
Cu(pca=baed=pca)	+0.06	2.29	2.05	16.4
Cu(pca=baes=pca)	+0.00	2.27	2.06	16.9
Cu(pca=aeps=pca)	+0.12	2.17	2.08	17.1
Cu(pca=aepd=pca)	−0.16	2.21	2.06	17.8
Cu(pca=aeed=pca)	−0.14	2.22	2.06	18.5
Cu(pca=baee=pca)	−0.02	2.24	2.06	15.4
Cu(pca-heda-pca)	−0.19	2.22	2.06	17.3
Cu(pca-peda-pca)	−0.13	2.23	2.06	14.8
Cu(pca-buda-pca)	−0.25	2.22	2.06	15.5
Cu(pca-prda-pca)	−0.33	2.22	2.05	19.1
Cu(pca-etda-pca)	−0.33	2.23	2.04	17.7
Cu(pca-baed-pca)	−0.25	2.27	2.07	18.2
Cu(pca-baes-pca)	−0.19	2.21	2.06	16.7
Cu(pca-aeps-pca)	+0.01	2.20	2.06	17.0
Cu(pca-aepd-pca)	−0.52	2.20	2.06	18.1
Cu(pca-aeed-pca)	−0.43	2.21	2.06	18.3

tabulated in Table 1. For Cu(pca=heda=pca) and Cu(pca=baed=pca) copper(I) complexes were used for determining $E°$ values since pure green Cu(II) complexes have not been isolated. As clearly seen from Table 1, Cu(pca=heda=pca) and Cu(pca=baed=pca) exhibited higher redox potentials over zero volt. In contrast to this, the analogues with shorter methylene chain lengths exhibited lower $E°$ values. This implies that the former two bear the favorable chain length adaptable to tetrahedral coordination around Cu(I). In addition, the present copper(II) complexes display a trend toward tetrahedral distortion, as visualized in $g_{//}$—$A_{//}$ profile for $Cu(N)_4$-type complexes as described by Peisach and Blumberg.[8]

The single thio group-containing five coordinate Schiff base complexes also exhibited higher redox potentials. These complexes, Cu(pca=baes=pca) and Cu(pca=aeps=pca) also tend to be reduced spontaneously in DMF, although Cu(I) complexes have not yet been isolated. Other five coordinate Schiff base complexes devoid of thio group display lower $E°$ values and favor a copper(II) state. The reduction of Schiff bases prominently lowered $E°$ values (0.2—0.3 V), hence the stabilization of copper(I) state cannot be realized even by pca–heda–pca and pca–baed–pca. Thus it can be considered that the aliphatic amine is not necessarily favorable for stabilizing the copper(I) state.

The present unexpected reduction of copper(II) and stabilization of Cu(I) in the presence of air is anticipated to afford a clue to appreciate the nature of biological coppers and to design model compounds.

This work was supported by the Ministry of Education, Science and Culture through Grants-in-Aid for Special Project Research (No. 511311) and Science Research (No. 50740247).

References

1) S. Suzuki, T. Sakurai, A. Nakahara, O. Oda, T. Manabe, and T. Okuyama, *FEBS Lett.*, **116**, 171 (1980); *J. Biochem.* (*Tokyo*), **90**, 905 (1981).

2) T. Sakurai and A. Nakahara, *Inorg. Chim. Acta*, **55**, 157 (1981).

3) T. Sakurai, S. Suzuki, and A. Nakahara, *Bull. Chem. Soc. Jpn.*, **54**, 2313 (1981).

4) T. Sakurai, J. Hongo, A. Nakahara, and Y. Nakao, *Inorg. Chim. Acta*, **46**, 205 (1980).

5) A. Amundsen, J. Whelan, and B. Bosnich, *J. Am. Chem. Soc.*, **99**, 5730 (1977).

6) J. G. Gibson and D. MacKenzie, *J. Chem. Soc., A*, **1971**, 1666.

7) B. F. Hoskins and F. D. Whillans, *J. Chem. Soc., A*, **1970**, 123.

8) J. Peisach and W. E. Blunberg, *Arch. Biochem. Biophys.*, **165**, 69 (1974).

Binuclear Metal Complexes. XLI.[1] Crystal Structure and Unusual Magnetic Property of Isothiocyanato{2-[2-(dimethylamino)-ethylthio]ethanolato}copper(II)

Masahiro MIKURIYA, Hisashi OKAWA, and Sigeo KIDA*

Department of Chemistry, Faculty of Science, Kyushu University 33, Hakozaki, Higashi-ku, Fukuoka 812

(Received March 27, 1981)

A binuclear copper(II) complex, isothiocyanato{2-[2-(dimethylamino)ethylthio]ethanolato}copper(II), (Cu(CH_3-nso)NCS), was prepared and characterized by elemental analysis, infrared and electronic spectra, magnetic susceptibility (90—300 K), and single-crystal X-ray diffraction. The complex exhibits a band at 25×10^3 cm^{-1} characteristic of alkoxo-bridged structure. The temperature dependence of the magnetic susceptibility is unusual and shows a dramatic change in the temperature range 240—180 K. The magnetic data were fitted to the Bleaney-Browers equation separately in the two temperature ranges ($-2J=535$ cm^{-1} for $300\geq T\geq240$ K; $-2J=595$ cm^{-1} for $170\geq T\geq90$ K).

In the previous paper[2] of this series, we reported the synthesis, structure, spectra, and magnetic properties of binuclear copper(II) complexes with 2-[2-(dialkylamino)ethylthio]ethanols, Cu{$R_2N(CH_2)_2S(CH_2)_2O$}X (abbreviated as Cu(R-nso)X, where R=CH_3, C_2H_5, n-C_3H_7, n-C_4H_9; X=Br, Cl, NO_3). With Cu(CH_3-nso)-Br we found that its crystal consists of discrete binuclear units but that its magnetic susceptibility exhibits a temperature dependence which does not obey the Bleaney-Bowers equation[3] based on a binuclear structure; similar temperature dependence applies also to all the other Cu(R-nso)X but Cu(n-C_4H_9-nso)Cl. In order to elucidate this unusual magnetic behavior, we have continued collecting information on magnetic properties of similar complexes. In the course of this activity, we found that isothiocyanato{2-[2-(dimethylamino)ethylthio]ethanolato}copper(II), Cu(CH_3-nso)-NCS, exhibits a magnetic behavior suggestive of a phase transition between two binuclear structures at 240—180 K. The present investigation was undertaken to characterize Cu(CH_3-nso)NCS by means of elemental analysis, infrared and electronic spectra, magnetic susceptibility, and single-crystal X-ray diffraction, for the purpose of elucidating the unusual magnetic behavior.

Experimental

Preparation of the Complex. 2-[2-(Dimethylamino)ethylthio]ethanol was prepared by the method previously described.[2] To an ethanol solution (50 ml) of 2-[2-(dimethylamino)ethylthio]ethanol (298 mg) and copper(II) acetate monohydrate (200 mg) was added an ethanol solution (10 ml) of potassium thiocyanate (97 mg). On standing overnight, dark green crystals were formed, which were separated by filtration, washed with ethanol and dried *in vacuo* over P_2O_5.

Found: C, 31.16; H, 5.24; N, 10.33%. Calcd for $C_7H_{14}CuN_2OS_2$: C, 31.16; H, 5.23; N, 10.38%.

Measurements. Infrared spectra were measured with a Hitachi Grating Infrared Spectrophotometer Model 215 in the region 4000—650 cm^{-1} on a KBr disk. Electronic spectra were measured with a Shimadzu Multipurpose Spectrophotometer Model MSP-5000 at room temperature. Magnetic susceptibility was measured by the Faraday method in the temperature range from liquid nitrogen temperature to room temperature. The apparatus was calibrated by the use of $[Ni(en)_3]S_2O_3$.[4] The susceptibility was corrected for the diamagnetism of the constituent atoms by the use of Pascal's constants.[5] Effective magnetic moment was calculated from the equation, $\mu_{eff}=2.828\sqrt{(\chi_A-N\alpha)T}$, where χ_A is the atomic magnetic susceptibility and $N\alpha$ is the temperature-independent paramagnetism. For the present complex, $N\alpha$ is assumed to be 60×10^{-6} cgs emu.[6]

X-Ray Crystal Structure Analysis. A crystal with dimensions of 0.19 mm × 0.25 mm × 0.31 mm was used for the X-ray analysis. The unit-cell parameters and intensities were measured on a Rigaku AFC-5 automated four-circle diffractometer with graphite-monochromated Mo $K\alpha$ radiation ($\lambda=0.71069$ Å) at 24 ± 1 °C. The unit-cell parameters were determined by the least-squares refinement based on the 15 reflections in the range of $23<2\theta<33°$.

Crystal Data: $C_{14}H_{28}N_4O_2S_4Cu_2$, F.W.=539.73; monoclinic; $P2_1/a$; $a=10.025(3)$, $b=14.421$ (3), and $c=8.595$ (2) Å; $\beta=110.49$ (2)°; $D_m=1.52$ (by floatation in n-C_6H_{14}–CCl_4); $D_c=1.54$ g cm^{-3}; $Z=2$; μ(Mo $K\alpha$)=21.7 cm^{-1}.

The intensity data were collected by the 2θ-ω scan technique with a scan rate of 8° min^{-1}. For weak reflections the peak scan was repeated up to four times depending on thier intensities. Three standard reflections were monitored every 100 reflections, and their intensities showed a good stability. A total of 2282 reflections with $2\theta<50°$ were collected. The intensity data were corrected for the Lorentz and the polarization effects, but not for absorption. Independent 1605 reflections with $|F_o|>3\sigma(|F_o|)$ were considered as "observed" and were used for the structure analysis.

The systematic absences observed, h odd for $h0l$ and k odd for $0k0$, uniquely define the space group as $P2_1/a$. The structure was solved by the heavy atom method. The position of the copper atom was obtained from a three-dimensional Patterson synthesis. Successive Fourier Synthesis revealed all the nonhydrogen atoms. Refinement was carried out by the block-diagonal least-squares method. Anisotropic thermal parameters being introduced, the block-diagonal least-squares refinement yielded discrepancy factors $R_1=\sum||F_o|-|F_c||/\sum|F_o|=0.068$ and $R_2=[\sum w(|F_o|-|F_c|)^2/\sum w|F_o|^2]^{1/2}=0.103$. In the course of refinement, it became apparent that the carbon atom of the chelate ring, C(4), is subjected to disorder. The carbon atom was divided between two positions with an occupancy factor 0.5 on the basis of a difference Fourier map. Hydrogen atoms were inserted in their calculated positions and included in the refinement. Further refinement with anisotropic thermal parameters for nonhydrogen atoms and isotropic temperature factors for hydrogen atoms gave final values of 0.062 and 0.093 for R_1 and R_2, respectively. In the least-squares refinement the function

minimized was $\sum w(|F_o|-k|F_c|)^2$, and the weighting scheme was $w=(6.0+|F_o|+0.012|F_o|^2)^{-1}$.[7] The final difference Fourier synthesis showed no peaks higher than 0.65 e/Å^3.

The atomic scattering factors for Cu, S, O, N, and C_{val} and the anomalous dispersion corrections, $\Delta f'$ and $\Delta f''$ for Cu and S, were taken from the International Tables for X-Ray Crystallography.[8] For the hydrogen atom, the scattering factors were adopted from the tables of Stewart et al.[9] All the calculations were carried out on the FACOM M-200 computer in the Computer Center of Kyushu University by the use of a local version[10] of the UNICS-II[11] and the ORTEP[12] programs.

Lists of structure factors and anisotropic thermal parameters have been deposited at the Chemical Society of Japan as Document No. 8142. The final positional and thermal parameters with their estimated standard deviations are given in Table 1.

TABLE 1. FRACTIONAL POSITIONAL PARAMETERS ($\times 10^4$) AND THERMAL PARAMETERS OF NON-HYDROGEN ATOMS WITH THEIR ESTIMATED STANDARD DEVIATIONS IN PARENTHESES

Atom	x	y	z	B_{eq}/Å^2
Cu	1386(1)	120(1)	−290(1)	4.7
S(1)	3628(3)	24(2)	1860(4)	7.4
S(2)	2254(3)	1977(2)	−4259(3)	7.8
O	663(6)	−171(4)	1424(7)	6.2
N(1)	1953(7)	−1317(4)	−1029(8)	5.4
N(2)	1906(8)	862(5)	−1872(9)	6.7
C(1)	1492(10)	−477(8)	2993(10)	7.1
C(2)	2961(13)	−130(9)	3519(13)	8.9
C(3)	4026(12)	−1154(10)	1397(17)	11.3
C(4A)	2829(26)	−1784(15)	494(28)	8.6
C(4B)	3402(21)	−1586(16)	−180(28)	8.6
C(5)	823(14)	−1964(7)	−1121(18)	9.7
C(6)	2158(18)	−1296(9)	−2612(16)	11.4
C(7)	2024(8)	1326(5)	−2860(9)	5.1

Results and Discussion

The molecular packing in the unit cell is shown in Fig. 1. As is evident from the packing diagram and the closest interdimer contact (C(4A)–C(7) 3.37(2)Å), the crystal consists of discrete binuclear units.

As shown in Fig. 2, the complex consists essentially of

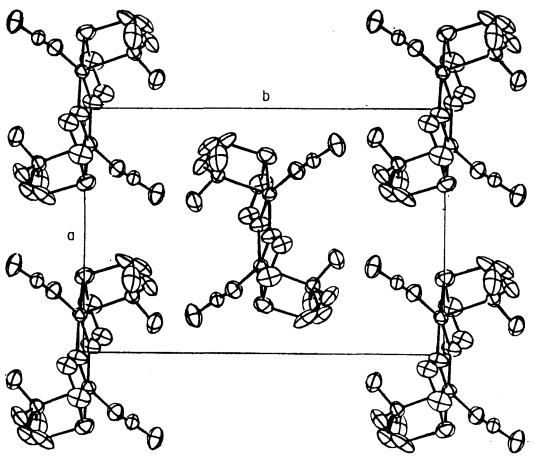

Fig. 1. Projection of the unit cell on the ab plane.

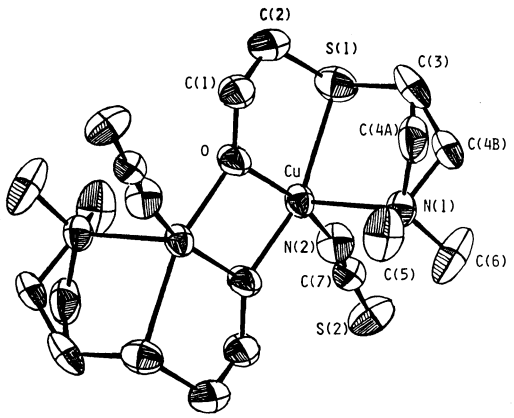

Fig. 2. Molecular structure of Cu(CH_3-nso)NCS. Thermal ellipsoids are drawn at 30% probability level.

alkoxo-bridged centrosymmetric binuclear units. The coordination geometry around each copper atom is best described as a distorted square pyramid with two alkoxo oxygen atoms, a thioether sulfur atom and an isothiocyanate nitrogen atom in the basal plane, and an amino nitrogen atom in the apical position. The copper atom deviates from the basal plane toward the apical N(1) atom by 0.233Å (Table 3). There is a tetrahedral distortion in the basal plane, because the deviations of the basal atoms from the least-squares plane are 0.088—0.129Å and the dihedral angle between the planes

TABLE 2. INTERATOMIC DISTANCES (l/Å) AND BOND ANGLES (ϕ/°) WITH THEIR ESTIMATED STANDARD DEVIATIONS IN PARENTHESES

(a) Copper coordination spheres			
Cu–Cu^i	3.009(2)	Cu–O^i	1.942(5)
Cu–S(1)	2.361(3)	Cu–N(1)	2.296(7)
Cu–O	1.902(7)	Cu–N(2)	1.940(9)
Cu–O–Cu^i	103.0(2)	O–Cu–N(2)	159.0(3)
S(1)–Cu–O	84.1(2)	O–Cu–O^i	77.0(2)
S(1)–Cu–O^i	160.8(2)	N(1)–Cu–N(2)	98.7(3)
S(1)–Cu–N(1)	84.4(2)	N(1)–Cu–O^i	102 5(2)
S(1)–Cu–N(2)	99.5(2)	N(2)–Cu–O^i	97.1(3)
O–Cu–N(1)	102.3(3)		
(b) CH_3 -nso moiety			
O–C(1)	1.386(9)	C(3)–C(4B)	1.422(26)
C(1)–C(2)	1.469(16)	N(1)–C(4A)	1.460(21)
S(1)–C(2)	1.788(14)	N(1)–C(4B)	1.432(20)
S(1)–C(3)	1.820(15)	N(1)–C(5)	1.448(15)
C(3)–C(4A)	1.489(25)	N(1)–C(6)	1.446(18)
Cu–O–C(1)	124.2(6)	C(3)–C(4B)–N(1)	113.4(18)
Cu^i–O–C(1)	132.0(6)	Cu–N(1)–C(4A)	107.3(10)
O–C(1)–C(2)	112.7(9)	Cu–N(1)–C(4B)	114.1(10)
C(1)–C(2)–S(1)	114.3(7)	Cu–N(1)–C(5)	109.4(7)
C(2)–S(1)–Cu	96.4(4)	Cu–N(1)–C(6)	111.9(6)
Cu–S(1)–C(3)	96.1(3)	C(4A)–N(1)–C(5)	88.0(11)
C(2)–S(1)–C(3)	103.4(7)	C(4B)–N(1)–C(5)	119.2(11)
S(1)–C(3)–C(4A)	119.0(12)	C(4A)–N(1)–C(6)	127.9(14)
S(1)–C(3)–C(4B)	124.0(12)	C(4B)–N(1)–C(6)	91.8(13)
C(3)–C(4A)–N(1)	107.9(15)	C(5)–N(1)–C(6)	109.1(9)
(c) Isothiocyanato group			
N(2)–C(7)	1.119(12)	C(7)–S(2)	1.605(9)
Cu–N(2)–C(7)	170.9(7)	N(2)–C(7)–S(2)	177.8(8)

i) $-x, -y, -z$.

Table 3. Deviation of the atoms from least-squares planes (l/Å) and dihedral angles between the planes (ϕ/°)

(I) Plane through Cu, O, Cu^{i}, O^{i}
$-0.0782X+0.9713Y+0.2380Z=0$[a)]
[Cu 0.000, O 0.000, Cu^{i} 0.000, O^{i} 0.000, S(1) 0.129, S(2) 1.721, N(1) −2.208, N(2) 0.675, C(1) −0.173, C(2) 0.306, C(3) −1.646, C(4A) −2.619, C(4B) −2.525, C(5) −3.045, C(6) −2.519, C(7) 1.113][b)]

(II) Plane through Cu, S(1), O
$-0.1195X+0.9747Y+0.2187Z=-0.0519$
[Cu 0.000, S(1) 0.000, O 0.000, N(1) −2.226, N(2) 0.683, C(1) −0.235, C(2) 0.176, C(3) −1.790, C(4A) −2.701, C(4B) −2.618, C(5) −3.018, C(6) −2.520]

(III) Plane through Cu, S(1), N(1)
$-0.6796X-0.4300Y+0.7946Z=-1.2163$
[Cu 0.000, S(1) 0.000, N(1) 0.000, O 1.843, N(2) −1.895, C(1) 2.540, C(2) 1.682, C(3) 0.142, C(4A) 0.732, C(4B) −0.241, C(5) 1.108, C(6) −1.234]

(IV) Plane through O, N(1), N(2)
$0.7333X+0.0973Y+0.3736Z=0.9207$
[O 0.000, N(1) 0.000, N(2) 0.000, Cu 0.022, S(1) 2.347, S(2) −0.354, O^{i} −1.841, C(1) 1.071, C(2) 2.368, C(3) 2.326 C(4A) 1.067, C(4B) 1.300, C(5) −0.951, C(6) −0.355, C(7) −0.165]

(V) Plane through O, O^{i}, N(2), S(1)
$-0.2113X+0.9128Y+0.4013Z=-0.0027$
[O 0.129, O^{i} −0.123, N(2) 0.088, S(1) −0.093, Cu −0.233, S(2) 0.659, N(1) −2.499,C(1) 0.091, C(2) 0.419, C(3) −1.887, C(4A) −2.774, C(4B) −2.867, C(5) −3.114, C(6) −3.062, C(7) 0.333]

(VI) Plane through Cu, S(1), N(2)
$-0.3706X+0.8335Y+0.5136Z=-0.4986$
[Cu 0.000, S(1) 0.000, N(2) 0.000, S(2) 0.157, O 0.675, O^{i} 0.322, N(1) −2.264, C(1) 0.692, C(2) 0.796, C(3) −1.768, C(4A) −2.478, C(4B) −2.751, C(5) −2.663, C(6) −3.014, C(7) 0.078]

Dihedral angles between the planes (ϕ/°)

(I) and (II)	3.1	(II) and (VI)	20.9
(I) and (III)	103.4	(III) and (IV)	98.1
(I) and (IV)	79.1	(III) and (V)	92.4
(I) and (V)	11.0	(III) and (VI)	82.1
(I) and (VI)	21.5	(IV) and (V)	80.3
(II) and (III)	103.0	(IV) and (VI)	85.1
(II) and (IV)	82.3	(V) and (VI)	10.8
(II) and (V)	11.2		

a) The equation of the plane is expressed as $LX+MY+NZ=D$, where X, Y, and Z are in Å units refered to the crystallographic axes. b) Deviations (l/Å) of atoms from the planes are listed in square brackets. Superscript (i) refers to the equivalent position $(-x, -y, -z)$.

Cu–O–O^{i} and Cu–S(1)–N(2) is 21.5°. This distortion is smaller than that in Cu(CH_3-nso)Br.[2)] The bond distances and angles with their estimated standard deviations are listed in Table 2. The Cu–Cu^{i} distance (3.009(2)Å) agrees well with the value found for Cu(CH_3-nso)Br (3.004(2) Å), while the Cu–O–Cu^{i} angle (103.0(2)°) is larger than that found for Cu(CH_3-nso)Br (102.2(2)°).[2)]

The Cu–O and Cu–N(1) distances of Cu(CH_3-nso)-NCS are 1.902(7) and 2.296(7)Å, respectively, which are slightly shorter than those of Cu(CH_3-nso)Br (Cu–O 1.930(5), Cu–N 2.334(6)Å). On the other hand, the Cu–S(1) bond length (2.361(3)Å) is longer than that (2.316(2)Å) of Cu(CH_3-nso)Br. The shortening of the Cu–O and Cu–N bonds should bring about a considerable strain in the fused chelate ring, although the elongated Cu–S bond may contribute to the releasing of the strain. In fact, the carbon atom of the chelate ring, C(4), is disordered. This is probably due to the strain of two adjacent five-membered chelate rings.[2)] It is noteworthy that all the atoms of the complex have considerably large temperature factors. This fact suggests that the conformation of the complex easily fluctuates.

The isothiocyanate group coordinates to the copper atom with the nitrogen atom. The infrared spectrum (ν_{CN}=2075 cm^{-1}; ν_{CS}=760 cm^{-1}) is consistent with this coordination mode.[13)] The Cu–N(2) distance (1.940(9) Å) is in the range of the normal in-plane coordination. The NCS group is nearly linear (the N(2)–C(7)–S(2) angle 177.8(8)°) and of nearly the same structure as found for other alkoxo-bridged copper(II) complexes containing an NCS group.[14–17)]

The electronic absorption spectrum in 1,2-dichloroethane solution resembles the diffuse reflectance spectrum, indicating that the molecular structure is essentially the same in the solution as in the solid state. The absorption spectrum shows a band centered at 13.9×10^3 cm^{-1} (ε=130) with a shoulder at *ca.* 11.1×10^3 cm^{-1}. These bands can be assigned to the d-d transitions of a five-coordinate copper(II) complex.[18)] A more intence band (ε=2350) occurs at 24.9×10^3 cm^{-1}. This is the band characteristic of alkoxo-bridged structure assigned to a charge transfer from a p_π orbital of the bridging oxygen atom to the unfilled d orbital of the copper ion.[2)]

The magnetic susceptibility was measured over the temperature range 90—300 K. The magnetic moment per copper atom is 0.90 BM at 299 K. The temperature dependence of the magnetic susceptibility is shown in Fig. 3. The susceptibility decreases gradually with lowering temperature from 300 to 240 K and then

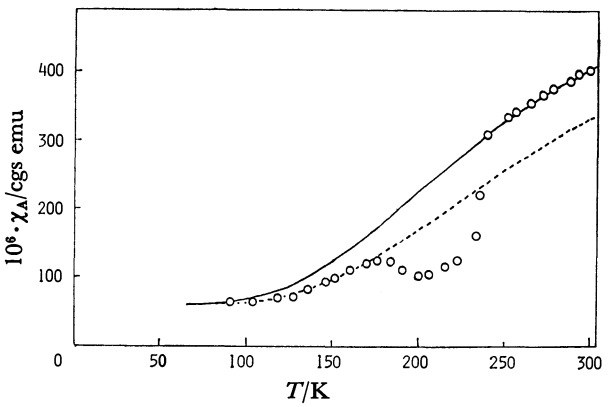

Fig. 3. Temperature dependence of magnetic susceptibility of Cu(CH_3-nso)NCS. The solid curve was calculated from Eq. 1 with g=2.10 and $-2J$=535 cm^{-1}; the bloken curve, from Eq. 1, using g=2.10 and $-2J$=595 cm^{-1}.

suddenly decreases in the range 240—230 K, reaching a minimum at 200 K. Below 200 K, the susceptibility increases to a maximum at about 180 K and finally decreases again. This fact suggests that a phase transition occurs in the temperature range 240—180 K. The susceptibility data were fitted to Eq. 1 (the Bleaney-Bowers equation[3]) separately in the two temperature ranges:

$$\chi_A = \frac{Ng^2\beta^2}{3kT}\left[1+\frac{1}{3}\exp(-2J/kT)\right]^{-1} + N\alpha, \qquad (1)$$

where $-2J$ is equal to the energy separation between the spin-singlet ground state and the lowest spin-triplet state and the other symbols have their usual meanings. Between 300 and 240 K, the experimental data fit Eq. 1 with $-2J=535$ cm^{-1} and $g=2.10$. Below 170 K, the susceptibility follows Eq. 1 with $-2J=595$ cm^{-1} and $g=2.10$. Although temperature dependence of J value was already noticed in some binuclear copper(II) complexes,[19-21] the present complex provides the most remarkable instance. Such a magnetic behavior may be attributed to the fact that the conformation of the chelate ring readily fluctuates with temperature variation. It is known that J values of binuclear copper(II) complexes depend sensitively on the Cu–O–Cu angle[22] or the tetrahedral distortion about the copper coordination.[23] Therefore, a slight variation in the conformation of the complex may lead to a marked change in the J value.

References

1) Part XL: M. Mikuriya, H. Okawa, and S. Kida, *Bull. Chem. Soc. Jpn.*, **54**, 2943 (1981).

2) M. Mikuriya, H. Okawa, and S. Kida, *Bull. Chem. Soc. Jpn.*, **54**, 2943 (1981).

3) B. Bleaney and K. D. Bowers, *Proc. R. Soc. London, Ser. A*, **214**, 451 (1952).

4) N. F. Curtis, *J. Chem. Soc.*, **1961**, 3147.

5) P. W. Selwood, "Magnetochemistry," Interscience Publishers, New York (1956).

6) B. N. Figgis and R. L. Martin, *J. Chem. Soc.*, **1959**, 1359.

7) D. W. J. Cruickshank, in "Computing Methods and the Phase Problem in X-Ray Analysis," ed by R. Pepinsky, J. M. Robertson, and J. C. Speakman, Pergamon Press, Oxford (1961), p. 45.

8) "International Tables for X-Ray Crystallography," Kynoch Press, Birmingham (1974), Vol. IV.

9) R. F. Stewart, E. R. Davison, and W. T. Simpson, *J. Chem. Phys.*, **22**, 3175 (1965).

10) S. Kawano, *Rep. Comp. Cent. Kyushu Univ.*, **13**, 39 (1980).

11) T. Sakurai, H. Iwasaki, Y. Watanabe, K. Kobayashi, Y. Bando, and Y. Nakamichi, *Rep. Inst. Phys. Chem. Res.*, **50**, 75 (1972).

12) C. K. Johnson, Report No. 3794, Oak Ridge National Laboratory, Oak Ridge, Tennessee (1965).

13) K. Nakamoto, "Infrared and Raman Spectra of Inorganic and Coordination Compounds," Wiley-Interscience, New York (1978), p. 270.

14) W. Haase, R. Mergehenn, and W. Krell, *Z. Naturforsch., Teil B*, **31**, 85 (1976).

15) A. Pajunen and K. Smolander, *Finn. Chem. Lett.*, **1974**, 99.

16) M. Mikuriya, Y. Nishida, S. Kida, T. Uechi, and I. Ueda, *Acta Crystallogr., Sect. B*, **33**, 538 (1977).

17) R. Mergehenn and W. Haase, *Acta Crystallogr., Sect. B*, **33**, 2734 (1977).

18) M. Ciampolini, *Struct. Bonding*, **6**, 52 (1969).

19) T. A. Kennedy, S. H. Choh, and G. Seidel, *Phys. Rev. B*, **2**, 3645 (1970).

20) D. M. Duggan and D. N. Hendrickson, *Inorg. Chem.*, **13**, 2929 (1974).

21) O. Kahn, I. Morgenstern-Badarau, J. P. Audiere, J. M. Lehn, and S. A. Sullivan, *J. Am. Chem. Soc.*, **102**, 5935 (1980).

22) D. J. Hodgson, *Prog. Inorg. Chem.*, **19**, 173 (1975); W. E. Hatfield, in "Theory and Applications of Molucular Paramagnetism," ed by E. A. Boudreaux and L. N. Mulay, Wiley-Interscience, New York (1976), p. 349.

23) E. Sinn, *J. Chem. Soc., Chem. Commun.*, **1975**, 665; R. J. Butcher and E. Sinn, *Inorg. Chem.*, **15**, 1604 (1976).

Tetrahedral Transition Metal Complexes of $[MW_{12}O_{40}]$-type ($M=Cu^{II}$, Fe^{III}, Co^{II}) with Dodecatungstate as Tetrahedral Ligand

Kenji Nomiya, Makoto Miwa,* Ryoichi Kobayashi, and Masahiro Aiso

Department of Industrial Chemistry, Faculty of Engineering, Seikei University, Musashino, Tokyo 180

(Received March 30, 1981)

Tetrabutylammonium salts of 12-heteropolytungstates with central transition metal ions in a tetrahedral oxygen environment, $MW_{12}O_{40}$ ($M=Cu^{II}$, Fe^{III}, Co^{II}), have been prepared and their spectroscopic data (infrared (IR), near-infrared, UV-vis, and magnetic circular dichroism (MCD)) presented.

12-Tungstometallate, $MW_{12}O_{40}$, is a typical 12-heteropolytungstate with the central transition metal in a tetrahedral oxygen environment. The compound is also considered as a transition metal complex with quadridentate dodecatungstate "ligand," $W_{12}O_{40}$, having tetrahedral cavity. Therefore, the formula can be rewritten as $MO_4W_{12}O_{36}$.

12-Tungstocuprate(II) anion, first reported by Brown and Mair,[1] is not easily prepared because of the extremely low yield and the difficulty of controling experimental conditions, pH and temperature, into the very narrow range allowed. Subsequently, except for the polarographic study by Wexell and Pope,[2] no precedent has been reported. On the contrary, 12-tungstocobaltate(II) and 12-tungstoferrate(III) anions, although purification takes time and yields are not so high, are not so difficult to prepare,[3-6] and many investigations have been reported.[7-14] Nevertheless, little spectroscopic data, especially IR data, of these heteropoly compounds have been reported.

Heteropoly compounds have contained different numbers of solvated water molecules (18 to 1), because the degree of hydration of K^+, Na^+, and Cs^+ salts of the anion varies according to the temperature of crystallization and the humidity at which the crystals are stored. Furthermore, most of the studies have been limited to aqueous systems. However, these compounds sometimes undergo hydrolytic decomposition in aqueous solution, the electronic spectra being influenced by the pH of the aqueous solvent because of the protonation of the dodecatungstate framework. We isolated these anions as tetrabutylammonium salts and measured the optical spectra in nonaqueous solution.

In this work, from a structural point of view, IR spectra of tetrabutylammonium salts of heteropolyanions with $M=Cu^{II}$ **1**, Fe^{III} **2**, and Co^{II} **3**, as heteroatom have been studied both in the solid and in the solution. On the basis of the results, the near-infrared and UV-vis spectra have been interpreted; MCD spectra have been measured to aid the resolution of the overlapping visible spectra.

Experimental

Near-infrared and UV-vis absorption spectra were measured on a Hitachi 340-spectrophotmeter with an attached computer key-board. MCD spectra were recorded by a JASCO J-40AS spectropolarimeter mounted with 10.0 kG electromagnet. The MCD intensity is expressed in terms of $\Delta\varepsilon=\varepsilon_l-\varepsilon_r$. Measurements were made at room temperature. IR spectra in acetonitrile were measured using a KBr cell with 0.1 mm optical path.

Preparation. $H_2[(C_4H_9)_4N]_4[CuW_{12}O_{40}]$, (*1*): Preparation of 12-tungstocuprate(II) is mainly performed according to the Brown-Mair's method.[1] Instead of using copper(II) nitrate solution, we modified as follows: the pH of sodium tungstate solution ($Na_2WO_4\cdot 2H_2O$ 56.2 g, 0.170 mol, in 300 cm^3 water) was adjusted within 4.5—5.0 by 1 mol dm^{-3} nitric acid and the temperature was maintained at 68—70°C. To this solution, the dropwise addition throughout 6 h of copper(II) sulfate solution ($CuSO_4\cdot 5H_2O$ 6.2 g, 2.48×10^{-2} mol, in 300 cm^3 water) was made with continuous stirring. During the process of purification, the metatungstate by-product should be removed. The product was dried on a steam bath followed by extraction with water; the separation of 12-tungstocuprate(II) and metatungstate was monitored by the near-infrared spectrum at *ca.* 1340 nm, until the spectra of its aqueous solution become unchanged.

The aqueous solution, acidified with nitric acid, of excess tetrabutylammonium bromide was added to the aqueous solution of purified 12-tungstocupric acid. The precipitate formed was filtered, washed thoroughly with water, dried *in vacuo* and recrystallized twice from acetonitrile (yield 1%, yellow). Found: C, 19.41; H, 3.83; N, 1.48%. Calcd for $H_2[(C_4H_9)_4N]_4[CuW_{12}O_{40}]$: C, 19.79; H, 3.76; N, 1.44%.

$H[(C_4H_9)N]_4[FeW_{12}O_{40}]$ (*2*): The 12-tungstoferrate(III) is prepared by a modification of the method reported by Pope and Varga,[4] and purified by Mair's method.[3] The compound structure is confirmed by the absorption spectrum of an aqueous solution as reported by Brown.[8] The aqueous solution, acidified with nitric acid, of excess tetrabutylammonium bromide was added into the aqueous solution of the purified 12-tungstoferric acid. The precipitate was washed thoroughly with water and recrystallized three times from acetonitrile (yield 1%, pale yellow). Found: C, 19.87; H, 3.95; N, 1.52%. Calcd for $H[(C_4H_9)_4N]_4[FeW_{12}O_{40}]$: C, 19.84; H, 3.74; N, 1.45%.

$K_2[(C_4H_9)_4N]_4[CoW_{12}O_{40}]\cdot CH_3CN$ (*3*): Potassium 12-tungstocobaltate(II) is prepared and purified by the method of Baker and McCutcheon.[5,6] The structure of the potassium compound is confirmed by the absorption spectrum of the aqueous solution as reported by Rollins.[11] This compound is converted to tetrabutylammonium salts (yield 1%, blue-green). Found: C, 19.58; H, 3.87; N, 1.49%. Calcd for $K_2[(C_4H_9)_4N]_4[CoW_{12}O_{40}]\cdot CH_3CN$: C, 19.83; H, 3.68; N, 1.75%.

$Na_2[(C_4H_9)_4N]_4[H_2W_{12}O_{40}]$ (*4*): Tungsten(VI) oxide monohydrate, $WO_3\cdot H_2O$ (yellow), obtained by acidic decomposition of $Na_2WO_4\cdot 2H_2O$, is converted to the sodium metatungstate (white) by Freedman's method.[15] This compound is converted to tetrabutylammonium salts as described above. Found: C, 20.18; H, 3.94; N, 1.46%. Calcd for $Na_2[(C_4H_9)_4N]_4[H_2W_{12}O_{40}]$: C, 20.12; H, 3.83; H, 1.47%. $[(C_4H_9)_4N]_4[SiW_{12}O_{40}]$ (**5**) and $[(C_4H_9)_4N]_3[PW_{12}O_{40}]$, (**6**) were prepared by the usual manner.[16]

Table 1. The IR data of tetrabutylammonium salts of $MW_{12}O_{40}$ anions in the solid[a)]

M						Assignment
Cu^{II}	Fe^{III}	Co^{II}	H_2	Si	P	
					1072 s	$\nu_3(F_2)$; ν(P–O)
1024 w	1025 w	1017 w		1010 m		
			956 s			ν(O–H, tetrahedral)
943 s	952 s	940 s	947 s	966 vs	969 s	ν(W–O, terminal)
				920 vs		$\nu_3(F_2)$; ν(Si–O)
875 vs	875 vs	870 vs	880 vs	882 m	887 s	ν(W–O–W, O_h edge-sharing)
			800 vs	805 vs	804 vs	ν(W–O–W, O_h corner-sharing)
765 vs	775 vs	760 vs				ν(W–O–W, O_h corner-sharing) and $\nu_3(F_2)$; ν(M–O)
					584 w	
				528 m		$\nu_4(F_2)$; δ(O–Si–O)
540—580 w	500—580 w	520—580 w	520—580 w			
					505 m	$\nu_4(F_2)$; δ(O–P–O)
				477 w	460 w	
437 m	440 m	441 m				$\nu_4(F_2)$; δ(O–M–O)
			410 s			ν(O–H, tetrahedral)

a) KBr disk, cm^{-1}.

Results and Discussion

IR Spectra. The IR spectra of heteropoly-compounds of M=Cu^{II}, Fe^{III}, and Co^{II} and metatungstate, recorded in KBr disks, in the metal-oxygen stretching region are shown in Fig. 1. The vibrational frequencies are presented in Table 1, together with the data of the M=Si and P compounds.

Fig. 1. IR spectra of tetrabutylammonium salts of $MW_{12}O_{40}$ heteropolyanions in 1000—400 cm^{-1} region measured in KBr disk; semi-dashed line (-·-·-) for M=Cu^{II}, dashed line (------) for M=Fe^{III}, full line (——) for M=Co^{II} and dotted line (·····) for metatungstate.

Three prominent bands in the tungstate spectra of **1**—**3** were assigned by comparison with the spectra of tetrabutylammonium salts of metatungstate $H_2W_{12}O_{40}^{6-}$ **4**, which is considered to be metal-free ligand, α-$SiW_{12}O_{40}^{4-}$ **5** and $PW_{12}O_{40}^{3-}$ **6**; ≈940 cm^{-1}, ν(W–O, terminal); ≈870 cm^{-1}, ν(W–O–W, octahedral edge-sharing); ≈770 cm^{-1}, ν(W–O–W, octahedral corner-sharing).[17] The characteristics of **1**—**3** compounds are as follows; (1) new bands appear at *ca.* 440 cm^{-1} and (2) the corner-sharing bands at *ca.* 770 cm^{-1} are more asymmetric and broader than that of **4**, and have some shoulder peaks.

In general, for an undistorted tetrahedron (T_d symmetry) of the MO_4^{n-} type ion there are four fundamental vibrational modes (A_1+E+2F_2), only triply degenerated F_2 modes of which are IR active; one of the F_2 is predominantly the M–O stretching motion, $\nu_3(F_2)$ and the other F_2 is the deformation by O–M–O angle bending motion, $\nu_4(F_2)$. The asymmetric stretch ν_3 is normally very strong in the IR and $\nu_3 > \nu_4$.[18] In the heteropolyanions **1**—**3**, by analogy with ν_3 and ν_4 of **4**, **5**, and **6** compounds, the new bands at *ca.* 440 cm^{-1} may be assigned to $\nu_4(F_2)$, and $\nu_3(F_2)$ band to be overlapped with the W–O–W octahedral corner-sharing band at *ca.* 770 cm^{-1}.

Table 2. Numerical data of the vibrational mode $\nu_4(F_2)$ of tetrabutylammonium salts of $MW_{12}O_{40}$ anions

M	In the solid (KBr disk) Max. cm^{-1}	In the solution (in CH_3CN)	
		Max. cm^{-1}	Half-width cm^{-1}
Cu^{II}	437[a)]	444[a)]	68±4
Fe^{III}	440	447	18±4
Co^{II}	441	450	39±4
Si	528[a)]	530[a)]	34±13
P	505	513[b)]	46±4

a) Asymmetric triplet. b) Center of doublet.

The expected splitting of ν_3 and ν_4 for different site symmetries has been described.[19] When the effects of crystal packing and/or environment upon ν_3 and ν_4 are eliminated, the spectral envelopes of both bands will show whether the central site symmetry is regularly tetrahedral or distorted. Accordingly, we have examined the variation in the frequencies and the widths of these vibrational modes, especially ν_4, in acetonitrile solution. The results are presented in Table 2. It was observed that the positions of the ν_4 band are essentially insensitive to the crystalline state and the apparent features of the envelopes are not significantly varied, except for the P compound.

The very symmetrical envelope and small width of the ν_4 for the Fe^{III} compound may be indicative of the regular tetrahedron of the FeO_4 moiety of this compound. The envelope for the Co^{II} compound is also very symmetrical, although the width is rather broad. This compound can be expected to retain excellent tetrahedral symmetry. On the contrary, the envelopes for the Cu^{II} and Si compounds are asymmetric; there are actually splittings into three bands and significant broadenings, indicating that the MO_4 moieties of these compounds possess far from perfect tetrahedral site symmetry. Since these bands are also asymmetric and broadened in the solid state (KBr disk), the features will not be caused by the effect of crystal packing, but mainly by the intrinsic structure of the tetrahedral complexes surrounded by dodecatungstate ligand. The significant distortion of the SiO_4 moiety in α-$Ba_2[SiW_{12}O_{40}]$ has been established by X-ray structural analysis.[20] The Cu^{II} compound is considered to have an intrinsic distortion on account of the Jahn-Teller effect of the d^9 configuration. It may be anticipated that the distortion reflects plausibly on the spectral envelope of ν_4 band. In the case of the P compound, the envelope of ν_4 band is very sharp and symmetric in the solid, whereas there is a splitting to two bands and the width is more broadened in the solution. If the above-mentioned hypothesis is true, the data indicate some departure from regular tetrahedral symmetry in the PO_4 moiety occurs.

Regarding the two W–O–W stretchings of **4**, there

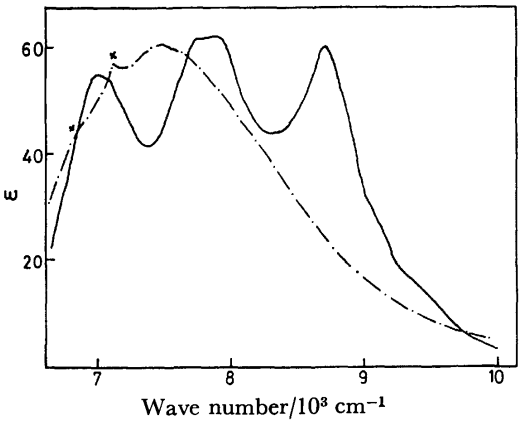

Fig. 2. Near-infrared spectra of tetrabutylammonium salts of $[Cu^{II}W_{12}O_{40}]^{6-}$ (-·-·-) and $[Co^{II}W_{12}O_{40}]^{6-}$ (——) in acetonitrile solution. The cross mark stands for the absorption of contaminated water.

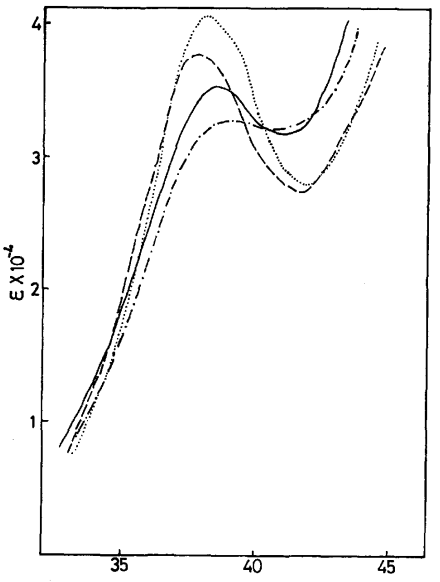

Fig. 3. UV spectra of tetrabutylammonium salts of $MW_{12}O_{40}$ heteropolyanions in acetonitrile solution; semidashed line (-·-·-) for $M=Cu^{II}$, dashed line (------) for $M=Fe^{III}$, full line (——) for $M=Co^{II}$ and dotted line (·····) for metatungstate.

are two cases as follows; where the heteroatom is a non-transition metal, those two bands are relatively unchanged or only slightly shifted to a higher frequency region, whereas if the heteroatom is a transition metal, the bands are shifted considerably to a low frequency region. Thus, the central transition metals may give rise to the strong electronic interaction with the dodecatungstate lattice.

Near-infrared, UV-vis, and MCD Spectra. The near-infrared and UV-vis spectra (Figs. 2 and 3) of an acetonitrile solution of 12-tungstocuprate(II) **1** shows a broad band at 7490 cm^{-1} (ε 60.1) and another at 39000 cm^{-1} (ε 32400). The former is slightly higher than that in water reported by Brown and Mair.[1] The former band is due to the d-d transition of Cu^{II} (d^9) displaced to this position in the tetrahedral oxygen lattice and is broadened by some components based on a Jahn-Teller effect in the ground state. Since the expected value should be around 4/9 of 12500 cm^{-1} (the value of 10 Dq for $Cu(H_2O)_6^{2+}$), *i.e.* around 5560 cm^{-1}, the ligand field strength by $W_{12}O_{40}$ "ligand" may be greater than the corresponding hypothetical four hydrate. A band at 39000 cm^{-1} is due to the charge transfer transition within the oxotungstate lattice and is observed in the spectra of other dodecatungstates of central nonmetals and transition metals.

The electronic and MCD spectra of 12-tungstoferrate(III) **2** in acetonitrile are shown in Figs. 3 and 4. This anion has perfect T_d symmetry; no distortion of the central FeO_4 tetrahedra would occur in solution. The three absorption bands observed at 20900 (ε 0.7), 24210 (ε 10.9) and 37590 cm^{-1} (ε 38400) are in good agreement with the results in aqueous solution, although the intensities of the visible absorptions are less than the halves of the previous data.[8] These have been assigned

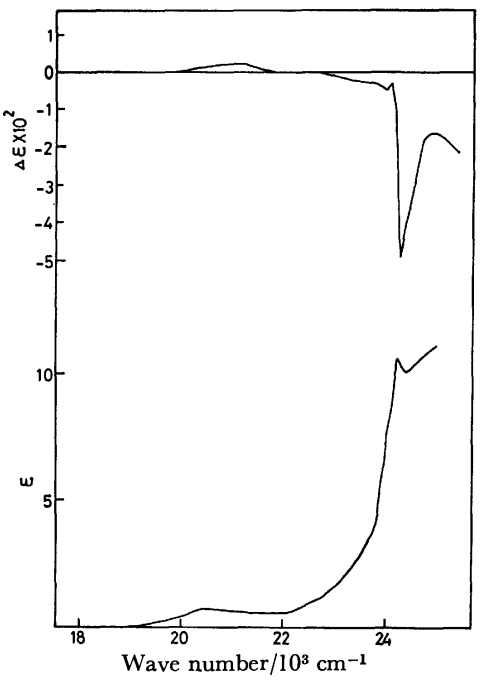

Fig. 4. Vis and MCD spectra of tetrabutylammonium salt of $[Fe^{III}W_{12}O_{40}]^{5-}$ in acetonitrile solution.

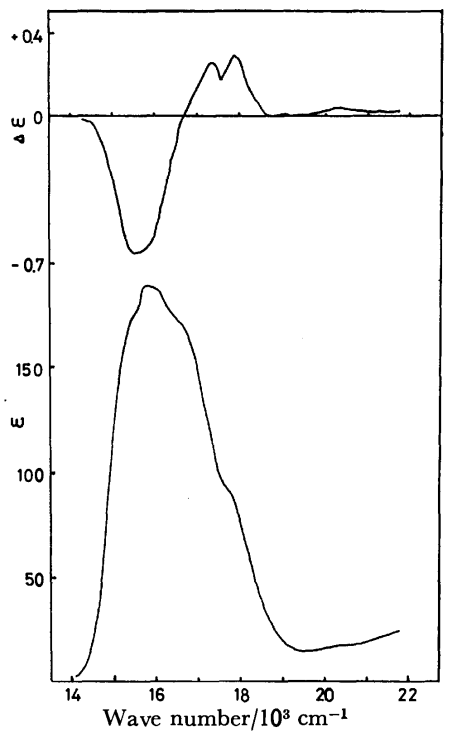

Fig. 5. Vis and MCD spectra of tetrabutylammonium salt of $[Co^{II}W_{12}O_{40}]^{6-}$ in acetonitrile solution.

to $^4T_1(G)\leftarrow{}^6A_1(S)$, $^4A_1(G)+{}^4E(G)\leftarrow{}^6A_1(S)$ and the charge transfer band, respectively. A very sharp band at 24210 cm^{-1} corresponds to a sharp band observed commonly in other high-spin d^5 ions such as $Mn(H_2O)_6^{2+}$ and $Fe(H_2O)_6^{3+}$, being on account of the independence of *Dq*. The negative MCD peak corresponding to this absorption is also very sharp. The very weak shoulder about 24×10^3 cm^{-1} which has been suggested as $^4T_2(G)\leftarrow{}^6A_1(S)$ from the spectral shape in the aqueous solution,[8] is obscure in this visible spectrum. However, the MCD spectrum shows such a band explicitly at 23950 cm^{-1}. The higher peaks due to d-d transitions of Fe(III) ion are swamped by the tail of the charge transfer band in both the electronic and the MCD spectra. These spectral data give us a 10 *Dq* value of 6200 cm^{-1} and a *B* value of 740 cm^{-1}, where the previously reported values are 6000 and 810 cm^{-1}, respectively. The 10 *Dq* value is in good agreement with the expected value, 4/9 of a 10 *Dq* value, 14200 cm^{-1}, for $Fe(H_2O)_6^{3+}$, *i.e.* about 6300 cm^{-1}.

The near-infrared, UV-vis absorption spectra, and the MCD spectrum in visible region of 12-tungstocobaltate(II) **3** are shown in Figs. 2, 3, and 5. The absorption spectrum shows the typical pattern of many common tetrahedral Co(II) complexes;[21] in the near-infrared region the spin-allowed transition to the excited quartet state, $^4T_1(F)\leftarrow{}^4A_2(F)$, at *ca.* 7.8×10^3 cm^{-1} and in the visible region $^4T_1(P)\leftarrow{}^4A_2(F)$ at *ca.* 16×10^3 cm^{-1}. In the UV region, there is a strong band at 38460 cm^{-1} (ε 35200) due to the charge transfer transition of the lattice. The near-infrared band exhibits much fine structure. Since many more peaks are observed than predicted by spin-orbit coupling, another causes must be sought; one may be a Jahn-Teller effect in the excited state.[21] The peak ($^4T_1(F)\leftarrow{}^4A_2$, 7.8×10^3 cm^{-1}) suggests a 10 *Dq* value of about 4100 cm^{-1}. This is estimated by using the energy level diagram for tetrahedrally coordinated Co(II), presented by Cotton and his coworkers.[21] The value is in good agreement with the expected values, 4/9 of 9200 cm^{-1} (the 10 *Dq* value of $Co(H_2O)_6^{2+}$), *i.e.* about 4090 cm^{-1} and the 10 *Dq* value of 4230 cm^{-1} for $Co(OH)_4^{2-}$.

The visible band is complicated because of a number of transitions to doublet excited states which occur in the same region, and these gain some of their intensity by means of spin-orbit coupling.[22] However, the corresponding MCD spectrum is much more resolved and suggests at least four different transitions; (1) intense and broad band with negative sign centered at *ca.* 15.6×10^3 cm^{-1}, (2) positive band at *ca.* 17.3×10^3 cm^{-1}, (3) positive band at *ca.* 17.9×10^3 cm^{-1}, and (4) weak and broad band with positive sign at *ca.* 20.4×10^3 cm^{-1}. There are further complications because each of (1), (2), and (3) includes some components. However, as suggested from the sign and the intensity of MCD, the band (1) will be mainly dominated by spin-allowed transition to a quartet excited state and the others (2)—(4) by transitions to doublet excited ones.

This type of heteropolyanions studied here is a real tetrahedral complex and stable even in dilute nonaqueous solution. These compounds lie in high-spin state, or paramagnetic state because of small 10 *Dq*. The crystal field theory and ligand field theory, which have been applied to the traditional octahedral coordination complexes, are acceptable to explain the spectral and magnetic properties.

References

1) D. H. Brown and J. A. Mair, *J. Chem. Soc.*, **1962**, 3946.
2) D. R. Wexell and M. T. Pope, *J. Chem. Soc., D*, **1971**,

886.
3) J. A. Mair, *J. Chem. Soc.*, **1950**, 2364.
4) M. T. Pope and G. M. Varga, *Inorg. Chem.*, **5**, 1249 (1966).
5) L. C. W. Baker and T. P. McCutcheon, *J. Am. Chem. Soc.*, **78**, 4503 (1956).
6) L. C. W. Baker and V. E. Simmons, *J. Am. Chem. Soc.*, **81**, 4744 (1959).
7) D. H. Brown and J. A. Mair, *J. Chem. Soc.*, **1962**, 1512.
8) D. H. Brown, *Spectrochim. Acta*, **16**, 1683 (1963).
9) H. So and M. T. Pope, *J. Chem. Phys.*, **55**, 2786 (1971).
10) L. C. W. Baker, V. E. S. Baker, S. H. Wasfi, G. A. Candela, and A. H. Cahn, *J. Chem. Phys.*, **56**, 4917 (1972).
11) O. W. Rollins, *Inorg. Chem.*, **11**, 3114 (1972).
12) P. G. Rasmussen and C. H. Brubaker, *Inorg. Chem.*, **3**, 977 (1964).
13) A. W. Chester, *J. Chem. Soc., D*, **1969**, 352; *J. Org. Chem.*, **35**, 1797 (1970).
14) G. M. Varga, E. Papaconstantionu, and M. T. Pope, *Inorg. Chem.*, **9**, 622 (1970).
15) M. L. Freedman, *J. Am. Chem. Soc.*, **81**, 3834 (1959).
16) E. O. North, "Inorganic Synthese," Vol. I, p. 129.
17) C. Rocchiccioli-Deltcheff, R. Thouvenot, and R. Franck, *Spectrochim. Acta, Part A*, **32**, 587 (1976).
18) F. Gonzalez-Vilchez and W. P. Griffith, *J. Chem. Soc., Dalton Trans.*, **1972**, 1416.
19) K. Nakamoto, "Infrared and Raman Spectra of Inorganic and Coordination Compounds," 3rd ed, John Wiley and Sons, New York (1978), p. 146.
20) A. Kobayashi and Y. Sasaki, *Bull. Chem. Soc. Jpn.*, **48**, 885 (1975).
21) F. A. Cotton, D. M. L. Goodgame, and M. Goodgame, *J. Am. Chem. Soc.*, **83**, 4690 (1961).
22) F. A. Cotton and G. Wilkinson, "Advanced Inorganic Chemistry," 4th ed, John Wiley and Sons, New York (1980), p. 770.

Optical Resolution of *rac*-5,5,7,12,12,14-Hexamethyl-1,4,8,11-tetraazacyclotetradecane (L), Circular Dichroism Spectra of Ni(II) Complexes with the Active Ligand, and the Absolute Configuration of $(-)_{589}$-[{Ni(*SS*-L)}$_2$(*d*-tart)(H$_2$O)](ClO$_4$)$_2$·2H$_2$O as Determined by the X-Ray Analysis

Haruko Ito,[†,††] Junnosuke Fujita,[†,††] Koshiro Toriumi,[†] and Tasuku Ito*[,†]

[†]*Division of Applied Molecular Science, Institute for Molecular Science, Okazaki 444*

[††]*Department of Chemistry, Faculty of Science, Nagoya University, Chikusa-ku, Nagoya 464*

(Received April 6, 1981)

The title ligand (L) has been resolved through its *d*-tartrato-nickel(II) complex. The X-ray analysis shows that the less-soluble $(-)_{589}$-diastereomer has a dimer structure with the folded macrocycles, [{NiL}$_2$(*d*-tart)(H$_2$O)]-(ClO$_4$)$_2$·2H$_2$O, and that the chiral carbon atoms have the absolute configuration of *S*. Axial methyl groups of geminal dimethyl pairs of each nickel(II) complex in the dimer provide stereoselective environment for the coordination site of the *d*-tartrate ion. Stereospecific hydrogen-bonds between a secondary amine group of the macrocyclic ligand or coordinated water and hydroxyl or carboxyl oxygens of the *d*-tartrate ion play also an important role in the optical resolution. Pairs of enantiomers of the free ligand and three isomers of the four-coordinate nickel(II) complex have been isolated. Circular dichroism spectra of various four- and six-coordinate complexes with the optically active ligand have been described.

Transition metal complexes of the tetraaza-fourteen membered macrocyclic ligand (L) **1** have been studied in depth.[1] However, the optically active form of the ligand has not been reported so far, although unsuccessful attempts of the optical resolution of its nickel(II) complex, [Ni(*rac*-L)]$^{2+}$, by column chromatography have been documented.[2] In this study, we aimed to resolve *rac*-L into the optically active form. The nickel(II) complex, [Ni(*rac*-L)]$^{2+}$, has been known to exist as three isomeric α-, β-, and γ-forms and their structures have been determined by X-ray analyses and ^{1}H NMR study as shown in structural formulae **2**—**4**.[3,4] The isomerism arises from a difference in conformations of six- and five-membered chelate rings associated with combination of chiralities of the four coordinated secondary amine nitrogens. Of these three isomers, only the α-isomer reacts readily with a bidentate ligand such as oxalate, acetylacetonate, acetate, or nitrate ion to form *cis*-type six-coordinate complexes with the macrocycle folded.[4-6] It was anticipated that optically active bidentate ligands such as (*R*)-1,2-propanediamine, (*S*)-amino acidate, and (*R*,*R*)-*d*-tartrate ions might react stereospecifically with the α-isomer to give sterically favored six-coordinate diastereomers and thereby the racemic ligand could be resolved into the enantiomers. The optical resolution of *rac*-L has been achieved successfully with *d*-tartrate ions. The absolute configurations of chiral centers have been determined by the X-ray crystallographic analysis of the less-soluble diastereomer. Preparations and circular dichroism spectra of various nickel(II) complexes with the optically active ligand are also described. Throughout this paper, abbreviations, *SS*-L and *RR*-L, are used for the ligand with the C(7)*S*,C(14)*S*- and C(7)*R*,C(14)*R*-configurations, respectively. The racemic mixture is designated as *rac*-L.

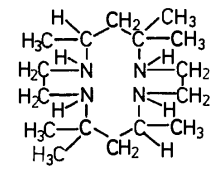

1

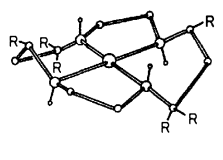

2(α)

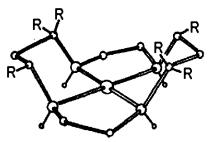

3(β)

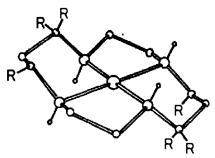

4(γ)

Experimental

Materials. The racemic complex, α-[Ni(*rac*-L)](ClO$_4$)$_2$, was prepared as reported previously.[4]

$(-)_{589}$-[{Ni(SS-L)}$_2$(d-tart)(H$_2$O)](ClO$_4$)·2H$_2$O. Addition of 7.2 g of tetrabutylammonium bromide to an acetonitrile solution of α-[Ni(*rac*-L)](ClO$_4$)$_2$ (4.0 g in 160 cm^3) gives green precipitate of the bromide salt (yield, 3.6 g). Found: C, 38.61; H, 7.43; N, 11.00%. Calcd for NiC$_{16}$H$_{36}$N$_4$Br$_2$: C, 38.20; H, 7.21; N, 11.14%. Four grams of the bromide (8.0 mmol) are dissolved in 160 cm^3 of water at room temperature and 0.50 g of sodium *d*-tartrate dihydrate (2.2 mmol) dissolved in a minimum amount of water are added portionwise. Color of the solution turns gradually greenish brown. After 30 min, 0.60 g of sodium perchlorate (4.0 mmol) dissolved in a minimum amount of water is added to this solution. Then the solution is chilled in an ice-bath for 1 h. The blue-violet precipitate is filtered and washed with chilled water, ethanol, and ether. Yield, 1.70 g. The filtrate (solution A) contains the other enantiomer and is used in the subsequent treatment (see below). The optical purity is checked by the *g*-value of the product in 1 mol dm^{-3} perchloric acid, where $g=|\Delta\varepsilon_{440}|/\varepsilon_{450}$ is 0.018 for the optically pure form. Judging from the *g*-value, the optical purity of the product at this stage is more than 90%. Recrystallization from acetonitrile gives blue-violet crystals. Found: C, 40.33; H, 7.71; N, 10.78%. Calcd for Ni$_2$C$_{36}$H$_{82}$N$_8$Cl$_2$O$_{17}$: C, 39.76; H, 7.60; N, 10.30%.

α-, β-, and γ-[Ni(SS-L)](ClO$_4$)$_2$. The optically active α-isomer is prepared by stirring 2.0 g of $(-)_{589}$-[{Ni(*SS*-L)}$_2$-(*d*-tart)(H$_2$O)](ClO$_4$)$_2$·2H$_2$O in 30 cm^3 of 70% perchloric acid at room temperature. Within a few min, the starting blue-violet complex decomposes to give a bright orange solution. A yellow product is obtained upon addition of cold water to the solution, and is recrystallized from 0.1 mol dm^{-3} perchloric acid. Found: C, 34.73; H, 6.73; N, 10.03%. Calcd for $NiC_{16}H_{36}N_4Cl_2O_8$: C, 35.45; H, 6.69; N, 10.34%. The β-derivative is prepared from the α-isomer following the reported procedure for the racemate[3] and recrystallized from 0.1 mol dm^{-3} perchloric acid. Found: C, 34.60; H, 6.53; N, 10.05%. Large red-orange crystals are obtained from a dilute solution of either α- or β-[Ni(*SS*-L)](ClO$_4$)$_2$ upon standing the solution for several days. These are identified with the ^{1}H NMR spectrum in CH$_3$CN-d_3 to be the γ-isomer. In contrast to the α- and β-isomers, the ^{1}H NMR spectrum of the γ-isomer shows that the six methyl groups are not pairwise equivalent.[3] Found: C, 34.88; H, 6.59; N, 10.32%.

(+)$_{589}$-[{Ni(RR-L)}$_2$ox](ClO$_4$)$_2$·H$_2$O. To the solution A (see above) is added 1.0 g of sodium oxalate and 1.0 g of sodium perchlorate. The solution is basified to pH ≈10 with aqueous sodium hydroxide to give a pale blue product. This is a well characterized racemic oxalate dimer, [{Ni(*rac*-L)}$_2$ox]-(ClO$_4$)$_2$,[1a,4] and is filtered off (*ca.* 1.3 g).[7] The pH of the blue filtrate is adjusted to ≈1 with dropwise addition of 60% perchloric acid in an ice-bath to yield a blue-violet product. This is almost optically pure $(+)_{589}$-[{Ni(*RR*-L)}$_2$ox](ClO$_4$)$_2$·H$_2$O (yield, 1.12 g) and is recrystallized from methanol. Found: C, 40.93; H, 7.54; N, 11.30%. Calcd for Ni_2C_{34}-$H_{74}N_8Cl_2O_{13}$: C, 41.12; H, 7.52; N, 11.30%. The structural formula is tentative. The addition of excess perchloric acid results in decomposition of the blue-violet product and formation of the yellow α-isomer.

α-, β-, and γ-[Ni(RR-L)](ClO$_4$)$_2$. α-, β-, and γ-Complexes of *RR*-L are obtained from $(+)_{589}$-[{Ni(*RR*-L)}$_2$ox]-(ClO$_4$)$_2$·H$_2$O in a manner similar to synthetic procedures for the *SS*-L complexes from $(-)_{589}$-[{Ni(*SS*-L)}$_2$(*d*-tart)(H$_2$O)]-(ClO$_4$)$_2$·2H$_2$O. Crude products are recrystallized from 0.1 mol dm^{-3} perchloric acid. Found for α: C, 34.65; H, 6.59; N, 10.09%. Found for β: C, 34.85; H, 6.60; N, 10.16%. Found for γ: C, 34.78; H, 6.63; N, 10.28%.

Optically Active Free Ligands. Following the reported procedures for the racemate,[8,9] the optically active free ligand is obtained from α-[Ni(*SS*- or *RR*-L)](ClO$_4$)$_2$ by sodium cyanide decomposition in strongly alkaline aqueous media (yield>90%). Found for *SS*-L: C, 66.03; H, 13.16; N, 19.18% (C/N=4.02). Found for *RR*-L: C, 66.14; H, 13.14; N, 19.43% (C/N=4.03). Calcd for $C_{16}H_{36}N_4$·0.5H$_2$O: C, 65.48; H, 12.70; N, 19.08% (C/N=4.00).

Measurements. The electronic absorption and circular dichroism spectra were recorded on a Hitachi 340 spectrophotometer and a JASCO J-40 spectropolarimeter, respectively. Optical rotations were measured with a JASCO DIP-4 polarimeter.

X-Ray Analysis. Blue-violet prismatic single crystals of the less-soluble diastereoisomer, $(-)_{589}$-[{Ni(*SS*-L)}$_2$(*d*-tart)-(H$_2$O)](ClO$_4$)$_2$·2H$_2$O, were obtained from an acetonitrile solution. A specimen with dimensions 0.28 mm × 0.32 mm × 0.36 mm was used for the X-ray study. Diffraction data were measured on a Rigaku AFC-5 diffractometer with graphite monochromatized Mo *Kα* radiation. Within the range $2\theta < 60°$, 5310 independent reflections with $|F_o| > 3\sigma(|F_o|)$ were obtained. Intensities were corrected for Lorentz and polarization factors but not for absorption.

Crystal data are: Monoclinic, P2$_1$, a=17.568 (3), b=11.482 (2), c=13.272 (2) Å, β=102.59 (1)°, U=2612.8 (6) Å^3, Z=2, D_m=1.39, D_x=1.39 g cm^{-3}, μ(Mo*Kα*)=8.95 cm^{-1}.

The structure was solved by the heavy atom method and refined by a block-diagonal least-squares method. The weighting scheme, $w=[\sigma_{count}{}^2+(0.015|F_o|)^2]^{-1}$, was employed. All hydrogen atoms except for those of water of crystallization and one of the methyl protons were located by the difference Fourier syntheses, and included in the final refinement with the isotropic temperature factors. The final R indicies were R=0.047 and R_w=0.057. Table 1 lists the final atomic coordinates.[10]

Table 1. Atomic coordinates (×10^5) and their standard deviations

Atom	x	y	z
NI(1)	22929(4)	46899(7)	5120(5)
N(1)	14435(30)	43099(45)	-8101(36)
N(4)	29849(29)	51602(45)	-5668(35)
N(8)	28850(32)	31323(47)	8746(39)
N(11)	15677(32)	40754(52)	15049(39)
C(2)	16762(38)	50050(80)	-16189(44)
C(3)	25082(39)	48219(74)	-15995(43)
C(5)	38319(37)	48193(65)	-3853(51)
C(6)	39191(39)	35212(65)	-824(57)
C(7)	37464(42)	31525(67)	9482(56)
C(9)	26961(49)	27670(71)	18625(56)
C(10)	18263(52)	28462(78)	17431(58)
C(12)	6908(42)	41677(73)	11990(56)
C(13)	4069(42)	37556(84)	884(59)
C(14)	6104(42)	44776(80)	-7743(54)
C(15)	41499(42)	49965(84)	-13688(59)
C(16)	42861(42)	56027(72)	4791(58)
C(17)	41212(65)	19516(93)	12419(87)
C(18)	2830(58)	34581(110)	19093(72)
C(19)	4787(46)	54388(90)	13195(75)
C(20)	598(59)	40334(195)	-17453(74)
NI(2)	27155(4)	100000(7)	53275(5)
N(1')	34506(27)	109031(40)	65493(33)
N(4')	18117(29)	111006(44)	56710(34)
N(8')	23286(28)	86615(45)	61711(34)
N(11')	36804(29)	88392(46)	52921(38)
C(2')	30096(41)	119391(55)	67336(48)
C(3')	21761(39)	116236(59)	66933(46)
C(5')	10034(39)	106290(65)	56060(48)
C(6')	10379(38)	95175(73)	62363(49)
C(7')	14599(39)	84574(62)	59521(46)
C(9')	27783(42)	76158(54)	59779(52)
C(10')	36093(39)	79254(58)	60450(54)
C(12')	44960(40)	92928(61)	53938(54)
C(13')	47127(35)	101024(67)	63421(51)
C(14')	42431(36)	112005(56)	63740(46)
C(15')	6505(41)	104245(77)	44512(53)
C(16')	4948(46)	115238(83)	60368(66)
C(17')	12525(46)	73939(76)	65269(63)
C(18')	45267(44)	99196(79)	43861(57)
C(19')	50927(47)	82937(80)	55467(70)
C(20')	46834(41)	120402(66)	71959(57)
C(21)	25793(36)	65048(56)	15315(46)
C(22)	27374(36)	75867(57)	22096(45)
C(23)	19873(35)	80733(52)	24096(41)
C(24)	21599(36)	91633(53)	30668(44)
O(1)	29411(25)	55796(40)	18505(31)
O(2)	20740(26)	65479(40)	6980(30)
O(3)	21508(25)	90698(35)	40120(29)
O(4)	23421(32)	100666(41)	26461(30)
O(5)	32666(28)	73141(47)	31679(37)
O(6)	15827(28)	72269(45)	28421(34)
OW(C)	29283(28)	113268(39)	42681(31)
CL(1)	65260(14)	37981(23)	9793(15)
OP(1)	63506(50)	38103(84)	-894(44)
OP(2)	58153(49)	35896(127)	13599(64)
OP(3)	70102(65)	28658(97)	13386(61)
OP(4)	68169(67)	47629(86)	13791(54)
CL(2)	20760(21)	-55488(21)	-52284(18)
OP(5)	16115(68)	-47162(68)	-57536(76)
OP(6)	19849(65)	-66050(76)	-56694(60)
OP(7)	21814(86)	-54949(82)	-42196(58)
OP(8A)	28025(156)	-54100(229)	-47074(206)
OP(8B)	27290(194)	-48853(256)	-57804(214)
OP(8C)	29587(215)	-59882(375)	-53608(210)
OW(1)	17872(47)	15638(79)	-8388(51)
OW(2A)	17027(81)	618(147)	4123(100)
OW(2B)	15627(131)	-15958(225)	-4642(155)

The calculations were carried out on the HITAC M-200H computer at the Computer Center of the Institute for Molecular Science with Universal Crystallographic Computation Program System UNICS III.[11]

Results and Discussion

Optical Resolution and Syntheses of the Nickel(II) Complexes with the Optically Active Ligand. The optical resolution of *rac*-L was performed by taking advantage of the characteristic nature of α-[Ni(*rac*-L)]$^{2+}$; this isomer readily forms *cis*-type six-coordinate complex with a bidentate chelate ligand. The use of *d*-tartrate has proved successful. But attempts by use of (*R*)-1,2-propanediamine and (*S*)-proline were ineffective, although they reacted with the α-complex to give six-coordinate complexes.

As has been well characterized, the α-isomer isomerizes in neutral or at much faster rate in basic media to the thermodynamically more stable β-isomer to give an equilibrium mixture.[4] Therefore, the perchlorate salt of the α-isomer was converted to the bromide salt so as to enhance the solubility and to dissolve quickly the racemic compound in the α-form in water. Reaction of α-[$NiBr_2$(*rac*-L)] with *d*-tartrate salt and subsequent addition of sodium perchlorate yielded the crystalline less-soluble diastereomer. Addition of excess sodium perchlorate gave less optically pure product. On account of the two facts mentioned above, the conversion of the perchlorate to the bromide is essential for the present synthetic procedures.

The less-soluble diastereomer was shown to be $(-)_{589}$-[{Ni(*SS*-L)}$_2$(*d*-tart)(H_2O)](ClO_4)$_2$·$2H_2O$ by the X-ray analysis (*vide infra*). The other enantiomer was isolated as the oxalate dimer, $(+)_{589}$-[{Ni(*RR*-L)}$_2$ox]-(ClO_4)$_2$·H_2O. When sodium oxalate is added to the filtrate obtained after the isolation of the less-soluble diastereomer, two kinds of oxalate dimers, optically active and racemic ones, are obtained. Since the perchlorate of the racemic compound is practically insoluble while the optically active one is fairly soluble in methanol, the separation of these two oxalate dimers are accomplished easily.

The optical purities of the diastereomer and the oxalate dimers were examined at each step of procedures by monitoring *g*-values ($\Delta\varepsilon_{440}/\varepsilon_{450}$) of the complexes dissolved in 1 mol dm^{-3} perchloric acid, where all the compounds are converted to four-coordinate complexes in the α-form.

The optically active four-coordinate complexes of α-, β-, and γ-[Ni(*SS*- or *RR*-L)](ClO_4)$_2$ were obtained from [{Ni(*SS*-L)}$_2$(*d*-tart)(H_2O)](ClO_4)$_2$·$2H_2O$ or [{Ni(*RR*-L)}$_2$ox](ClO_4)$_2$·H_2O in a way similar to the procedure for the isolation of the respective racemic complexes.

A pair of enantiomers of free ligand has been isolated successfully from the optically active nickel(II) complexes in a synthetic scale. Using these ligands, optically active complexes of other metal ions can be prepared.[12]

X-Ray Structure Analysis of $(-)_{589}$-[{*Ni*(SS-*L*)}$_2$(*d*-*tart*)(*H_2O*)](*ClO_4*)$_2$·*$2H_2O$*. The structure analysis revealed that the compound is a dimer of [Ni(*SS*-L)]$^{2+}$ with a bridged *d*-tartrate ion. A stereoscopic view of the dimer is shown in Fig. 1, in which only hydrogen atoms of NH groups and those bonded to chiral carbon atoms are depicted. Bond lengths and angles within the dimer are listed in Tables 2 and 3, respectively. Each Ni(II) in the dimer has a six-coordinate structure with

Table 2. Bond lengths (*l*/Å) within the complex cation and their estimated standard deviations

NI(1) -N(1)	2.087(4)	NI(2) -N(1')	2.112(4)
NI(1) -N(4)	2.140(5)	NI(2) -N(4')	2.154(5)
NI(1) -N(8)	2.072(5)	NI(2) -N(8')	2.100(5)
NI(1) -N(11)	2.142(6)	NI(2) -N(11')	2.165(5)
NI(1) -O(1)	2.148(4)	NI(2) -O(3)	2.102(4)
NI(1) -O(2)	2.191(5)	NI(2) -OW(C)	2.160(5)
N(1) -C(2)	1.465(9)	N(1') -C(2')	1.469(8)
N(1) -C(14)	1.487(9)	N(1') -C(14')	1.500(8)
N(4) -C(3)	1.493(7)	N(4') -C(3')	1.494(7)
N(4) -C(5)	1.506(8)	N(4') -C(5')	1.504(9)
N(8) -C(7)	1.495(9)	N(8') -C(7')	1.508(8)
N(8) -C(9)	1.482(10)	N(8') -C(9')	1.490(9)
N(11) -C(10)	1.495(11)	N(11')-C(10')	1.473(9)
N(11) -C(12)	1.509(9)	N(11')-C(12')	1.503(9)
C(2) -C(3)	1.471(10)	C(2') -C(3')	1.498(10)
C(5) -C(6)	1.543(11)	C(5') -C(6')	1.520(11)
C(6) -C(7)	1.524(11)	C(6') -C(7')	1.515(11)
C(5) -C(15)	1.541(11)	C(5') -C(15')	1.541(9)
C(5) -C(16)	1.537(10)	C(5') -C(16')	1.550(12)
C(7) -C(17)	1.541(13)	C(7') -C(17')	1.525(11)
C(9) -C(10)	1.504(13)	C(9') -C(10')	1.486(10)
C(12) -C(13)	1.525(10)	C(12')-C(13')	1.544(10)
C(13) -C(14)	1.518(12)	C(13')-C(14')	1.512(10)
C(12) -C(18)	1.536(14)	C(12')-C(18')	1.530(11)
C(12) -C(19)	1.523(13)	C(12')-C(19')	1.537(11)
C(14) -C(20)	1.521(13)	C(14')-C(20')	1.533(9)
C(21) -O(1)	1.263(8)	C(24) -O(3)	1.263(7)
C(21) -O(2)	1.259(7)	C(24) -O(4)	1.252(8)
C(22) -O(5)	1.437(7)	C(23) -O(6)	1.399(8)
C(21) -C(22)	1.524(9)	C(23) -C(24)	1.518(8)
C(22) -C(23)	1.507(9)		

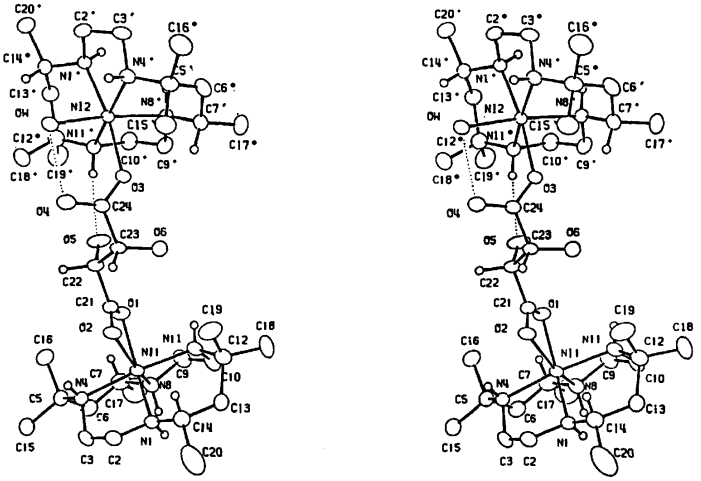

Fig. 1. Stereoview of the structure of $(-)_{589}$-[{Ni(*SS*-L)}$_2$-(*d*-tart)(H_2O)]$^{2+}$. Dotted lines indicate hydrogen-bonds.

TABLE 3. BOND ANGLES (ϕ/°) WITHIN THE COMPLEX CATION AND THEIR ESTIMATED STANDARD DEVIATIONS

N(1) -Ni(1) -N(4)	84,1(2)	N(1') -Ni(2) -N(4')	84,6(2)
N(1) -Ni(1) -N(8)	104,2(2)	N(1') -Ni(2) -N(8')	99,5(2)
N(1) -Ni(1) -N(11)	92,1(2)	N(1') -Ni(2) -N(11')	88,2(2)
N(1) -Ni(1) -O(1)	161,4(2)	N(1') -Ni(2) -O(3)	170,5(2)
N(1) -Ni(1) -O(2)	100,8(2)	N(1') -Ni(2) -Ow(C)	89,4(2)
N(4) -Ni(1) -N(8)	92,5(2)	N(4') -Ni(2) -N(8')	88,7(2)
N(4) -Ni(1) -N(11)	174,6(2)	N(4') -Ni(2) -N(11')	169,2(2)
N(4) -Ni(1) -O(1)	99,0(2)	N(4') -Ni(2) -O(3)	103,7(2)
N(4) -Ni(1) -O(2)	88,2(2)	N(4') -Ni(2) -Ow(C)	87,9(2)
N(8) -Ni(1) -N(11)	84,8(2)	N(8') -Ni(2) -N(11')	84,7(2)
N(8) -Ni(1) -O(1)	94,0(2)	N(8') -Ni(2) -O(3)	85,5(2)
N(8) -Ni(1) -O(2)	154,9(2)	N(8') -Ni(2) -Ow(C)	170,1(2)
N(11) -Ni(1) -O(1)	85,8(2)	N(11')-Ni(2) -O(3)	84,2(2)
N(11) -Ni(1) -O(2)	96,3(2)	N(11')-Ni(2) -Ow(C)	99,9(2)
O(1) -Ni(1) -O(2)	61,2(2)	O(3) -Ni(2) -Ow(C)	86,3(2)
Ni(1) -N(1) -C(2)	103,9(4)	Ni(2) -N(1') -C(2')	105,6(3)
Ni(1) -N(1) -C(14)	118,3(4)	Ni(2) -N(1') -C(14')	115,2(3)
Ni(1) -N(4) -C(3)	105,2(4)	Ni(2) -N(4') -C(3')	103,8(4)
Ni(1) -N(4) -C(5)	120,9(4)	Ni(2) -N(4') -C(5')	120,4(4)
Ni(1) -N(8) -C(7)	116,8(4)	Ni(2) -N(8') -C(7')	116,3(4)
Ni(1) -N(8) -C(9)	104,6(4)	Ni(2) -N(8') -C(9')	104,6(4)
Ni(1) -N(11) -C(10)	104,3(5)	Ni(2) -N(11')-C(10')	104,0(4)
Ni(1) -N(11) -C(12)	121,4(4)	Ni(2) -N(11')-C(12')	121,4(4)
C(2) -N(1) -C(14)	112,7(5)	C(2') -N(1') -C(14')	112,5(5)
C(3) -N(4) -C(5)	114,6(5)	C(3') -N(4') -C(5')	114,1(5)
C(7) -N(8) -C(9)	111,4(5)	C(7') -N(8') -C(9')	113,2(5)
C(10) -N(11) -C(12)	111,6(6)	C(10')-N(11')-C(12')	114,0(5)
N(1) -C(2) -C(3)	110,1(6)	N(1') -C(2') -C(3')	110,2(5)
N(1) -C(14) -C(13)	110,4(6)	N(1') -C(14')-C(13')	110,2(5)
N(4) -C(3) -C(2)	109,6(5)	N(4') -C(3') -C(2')	110,6(5)
N(4) -C(5) -C(6)	109,3(5)	N(4') -C(5') -C(6')	110,3(5)
N(8) -C(7) -C(6)	110,0(5)	N(8') -C(7') -C(6')	110,9(5)
N(8) -C(9) -C(10)	107,9(6)	N(8') -C(9') -C(10')	110,4(5)
N(11) -C(10) -C(9)	109,5(7)	N(11')-C(10')-C(9')	110,9(5)
N(11) -C(12) -C(13)	109,8(6)	N(11')-C(12')-C(13')	110,0(6)
N(1) -C(14) -C(20)	112,2(7)	N(1') -C(14')-C(20')	112,0(5)
N(4) -C(5) -C(15)	111,0(5)	N(4') -C(5') -C(15')	106,4(5)
N(4) -C(5) -C(16)	107,5(6)	N(4') -C(5') -C(16')	110,7(6)
N(8) -C(7) -C(17)	111,9(7)	N(8') -C(7') -C(17')	111,7(5)
N(11) -C(12) -C(18)	112,5(6)	N(11')-C(12')-C(18')	107,4(5)
N(11) -C(12) -C(19)	107,3(6)	N(11')-C(12')-C(19')	111,3(6)
C(5) -C(6) -C(7)	118,3(6)	C(5') -C(6') -C(7')	120,0(6)
C(12) -C(13) -C(14)	118,6(7)	C(12')-C(13')-C(14')	119,1(5)
C(6) -C(5) -C(15)	108,3(6)	C(6') -C(5') -C(15')	112,2(6)
C(6) -C(5) -C(16)	111,4(5)	C(6') -C(5') -C(16')	108,1(6)
C(15) -C(5) -C(16)	109,3(6)	C(15')-C(5') -C(16')	109,2(6)
C(6) -C(7) -C(17)	108,5(7)	C(6') -C(7') -C(17')	109,6(6)
C(13) -C(12) -C(18)	109,3(7)	C(13')-C(12')-C(18')	112,3(6)
C(13) -C(12) -C(19)	111,3(7)	C(13')-C(12')-C(19')	107,6(5)
C(18) -C(12) -C(19)	106,6(8)	C(18')-C(12')-C(19')	108,3(7)
C(13) -C(14) -C(20)	104,2(9)	C(13')-C(14')-C(20')	110,5(5)
Ni(1) -O(1) -C(21)	89,2(3)	Ni(2) -O(3) -C(24)	132,5(4)
Ni(1) -O(2) -C(21)	87,3(4)		
O(1) -C(21) -O(2)	122,3(6)	O(3) -C(24) -O(4)	125,0(5)
C(22) -C(21) -O(1)	118,3(5)	C(23) -C(24) -O(3)	117,2(5)
C(22) -C(21) -O(2)	119,3(5)	C(23) -C(24) -O(4)	117,7(5)
C(21) -C(22) -O(5)	110,2(5)	C(22) -C(23) -O(6)	110,9(5)
C(23) -C(22) -O(5)	110,3(5)	C(24) -C(23) -O(6)	113,1(5)
C(21) -C(22) -C(23)	110,6(5)	C(22) -C(23) -C(24)	109,5(5)

a folded macrocycle as anticipated. The bridged *d*-tartrate ion is coordinated to Ni(1) and Ni(2) unsymmetrically: one carboxyl group of the *d*-tartrate ion is coordinated to Ni(1) bidentately (O(1) and O(2)), while the other carboxyl group is coordinated to Ni(2) unidentately (O(3)). The sixth coordination site of Ni(2) is occupied by water (Ow(c)).

Each macrocycle (L) in the NiL dimer is folded about N(4)–Ni(1)–N(11) and N(4')–Ni(2)–N(11'). All these nitrogens are adjacent to the geminal dimethyl carbon atoms. A similar structural feature has been found in the crystal structure of [Ni(OAc)(*rac*-L)]$(ClO_4)_2$, where OAc is an acetate ion.[5] This is most likely owing to the following reason. When the macrocycle is folded from its coplanar nitrogen geometry, the nitrogen atom adjacent to the single methyl carbon is more easily lifted than that adjacent to the geminal dimethyl carbon atom is.[13] As a result, the more crowded side of the macrocycle, *i.e.*, that with the two geminal dimethyl groups, is directed toward the *d*-tartrate ion in each Ni(II) complex in the dimer. As a consequence, the axial methyl groups of the geminal dimethyl pairs in the folded macrocycle give stereoselective environments to the sites of *d*-tartrate coordination. Furthermore, stereospecific intramolecular hydrogen-bonds are observed between a secondary amine group of the macrocyclic ligand and hydroxyl oxygen of the *d*-tartrate ion and between a coordinated water molecule and the uncoordinated carboxyl oxygen : N(11')–H···O(5), 3.246(7) Å; Ow(c)···O(4), 2.605(6) Å (see Fig. 1). The preferred coordination of the *d*-tartrate ion to the *SS*-L complex over the *RR*-L complex is effected by the steric interactions with the axial methyl groups of the macrocyclic ligands and the stereospecific intramolecular hydrogen-bonds. In view of the fact that the use of (*S*)-prolinate ion or (*R*)-1,2-propanediamine as a resolving agent was not effective, the stereospecific hydrogen-bonds play more important roles in the optical resolution.

Each chelate ring adopts the most strain free conformation: all the six-membered rings take the chair form with the single methyl groups in equatorial positions; all the five-membered rings are in the gauche conformation. It should be noted that the macrocycle cannot adopt such a most strain free chelate ring conformation in the planar coordination.

The observed Ni–N and Ni–O distances are within the normal range for octahedral nickel(II) complexes. Chelation of the carboxyl group of the *d*-tartrate ion to Ni(1) results in a small angle of O(1)–Ni(1)–O(2) (61.0(2)°), giving a distorted octahedral geometry around the Ni(1) atom. The value is comparable to the corresponding angle of 62.4(3)° reported for [Ni(OAc)(*rac*-L)](ClO_4).[5]

Absolute configurations of the chiral centers were determined on the basis of that of the *d*-tartrate ion. All the chiral carbon atoms have the absolute configuration of *S* and all the chiral nitrogen atoms have *R*

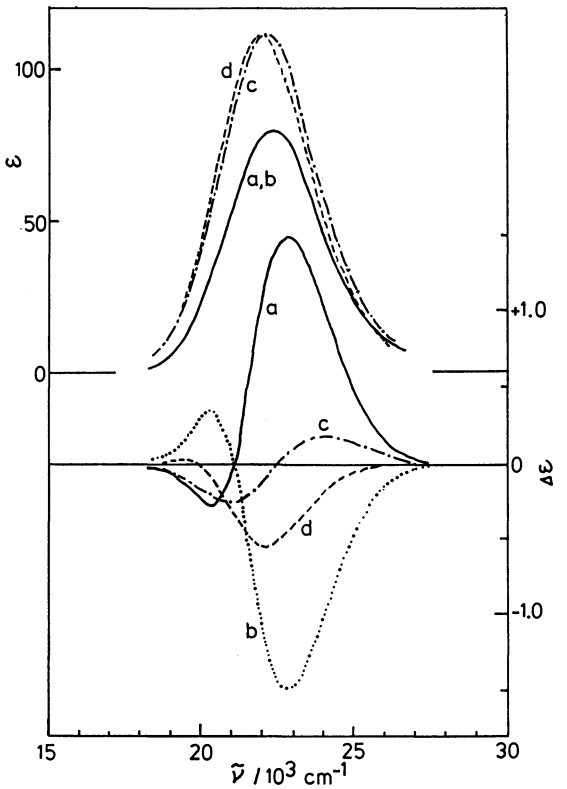

Fig. 2. AB (top) and CD (bottom) spectra of α-[Ni(*SS*-L)]$(ClO_4)_2$ (a) and α-[Ni(*RR*-L)]$(ClO_4)_2$ (b) in 60% $HClO_4$, and β-[Ni(*SS*-L)]$(ClO_4)_2$ (c) and γ-[Ni(*SS*-L)]$(ClO_4)_2$ (d) in 0.1 mol dm^{-3} $HClO_4$.

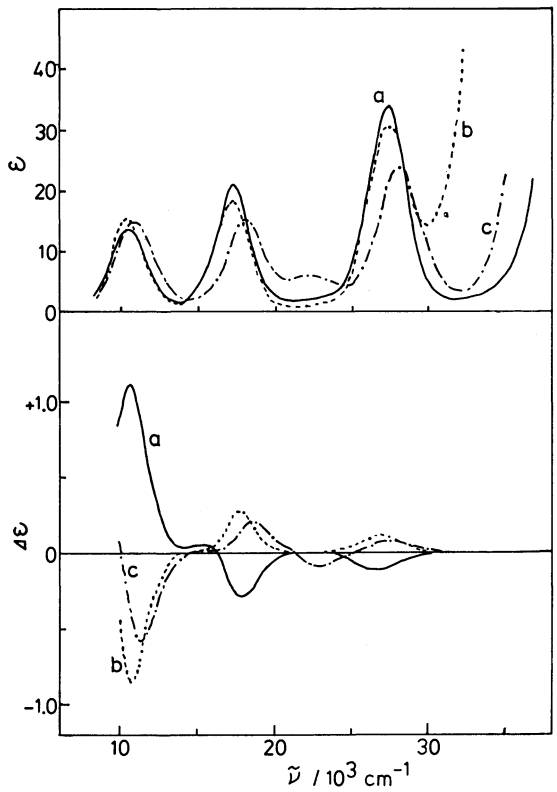

Fig. 3. AB (top) and CD (bottom) spectra of [{Ni(*SS*-L)}$_2$(*d*-tart) (H_2O)] (ClO_4)$_2$·2H_2O (a), [{Ni(*RR*-L)}$_2$-ox](ClO_4)$_2$}·H_2O (b), and α-[Ni(*SS*-L)](ClO_4)$_2$ (c) in CH_3CN at 20 °C.
Halves of the ε and Δε values are plotted for the dimers ((a) and (b)).

configuration.

Intermolecular hydrogen-bonds are observed among water of crystallization (Ow), secondary amine groups of the macrocyclic ligands, hydroxyl oxygen atom of the *d*-tartrate ion (O(6)), a coordinated water molecule, and perchlorate oxygen atoms (Op).[14] Other intermolecular contacts appear to be normal.

Absorption and Circular Dichroism Spectra. Absorption (AB) and circular dichroism (CD) spectra of some four- and six-coordinate complexes are presented in Figs. 2 and 3, respectively. The spectral data are summarized in Table 4. As reported for other tetraazamacrocyclic nickel(II) complexes,[1] AB spectra of the present complexes in the d-d region consists of single bands for four-coordinate complexes and three main bands for six-coordinate complexes.

As for the spectra of four-coodinate complexes, perchlorates of the three isomers in acidic aqueous solutions show similar AB spectra but their CD spectra are significantly different from each other (Fig. 2). The difference in the CD spectra provides some informations on subtle solution behaviors of the compounds, which had not been detected from absorption spectral studies.

It has been reported that α-[Ni(*rac*-L)](ClO_4)$_2$ gives blue, green, and violet solutions when dissolved in *N*,*N*-dimethylformamide, dimethylsulphoxide, and acetonitrile, respectively, in spite of the yellow-orange color in the solid state.[4] This has been interpreted as equilibria between four-coordinate species having singlet ground states and six-coordinate triplet species with two solvent molecules in the first coordination sphere:

α-[Ni(*rac*-L)]$^{2+}$+2 solvent⇌α-[Ni(*rac*-L)(solvent)$_2$]$^{2+}$.

Absorption spectra of these solutions show the charac-

Table 4. AB and CD spectral data in the d-d transition region[a]

Compound	Medium	AB $\tilde{\nu}/10^3$ cm^{-1} (ε)	CD $\tilde{\nu}/10^3$ cm^{-1} (Δε)	Assignment[b]
α-[Ni(*SS*-L)](ClO_4)$_2$	60% $HClO_4$	22.4(80)	20.3(−0.35), 22.8(+1.45)	s
	10^{-2} mol dm^{-3} $HClO_4$[c]	10.3(3.8)	10.4(+0.12)	t
		17.1(3.5)	17.4(−0.03)	t
		22.4(67)	20.4(−0.27), 23.0(+1.20)	s
	CH_3CN[c]	10.8(15)	11.2(+0.59)	t
		18.0(15)	18.5(−0.40)	t
		22.2(6)	22.7(+0.15)	s
		28.2(23)	27.8(−0.15)	t
α-[N(*RR*-L)](ClO_4)$_2$	60% $HClO_4$	22.4(80)	20.3(+0.35), 22.8(−1.47)	s
β-[Ni(*SS*-L)](ClO_4)$_2$	10^{-2} mol dm^{-3} $HClO_4$	22.1(111)	21.1(−0.27), 23.9(+0.15)	s
	CH_3CN	21.8(101)	20.7(−0.20), 23.6(+0.11)	s
γ-[Ni(*SS*-L)](ClO_4)$_2$	10^{-2} mol dm^{-3} $HClO_4$	21.8(111)	≈19.6(+0.01), 22.1(−0.55)	s
	CH_3CN	21.5(104)	≈19.0(+0.02), 21.9(−0.52)	s
α-, β-,or γ-[Ni(*SS*-L)](ClO_4)$_2$	10^{-3} mol dm^{-3} NaOH	22.2(104)	21.1(−0.24), 23.8(+0.15)	s
$(-)_{589}$-[{Ni(*SS*-L)}$_2$(*d*-tart)-(H_2O)](ClO_4)$_2$·2H_2O	CH_3CN	10.4(27)	10.6(+2.20)	t
		17.2(41)	17.8(−0.59)	t
		27.4(67)	26.5(−0.21)	t
$(+)_{589}$-[{Ni(*RR*-L)}$_2$ox]-(ClO_4)$_2$·H_2O	CH_3CN	10.3(31)	10.6(−1.68)	t
		17.2(36)	17.7(+0.55)	t
		27.4(61)	26.7(+0.22)	t

a) Data for the β- and γ-isomers of *RR*-L are not listed. They are enantiomeric to the data for the *SS*-L complexes. b) s: four-coordinate singlet species; t: six-coordinate triplet species. c) In this solvent, the compound exists as an equilibrium mixture. The apparent values for ε and Δε at 20 °C are given.

teristic absorptions both for four-coordinate singlet species and six-coordinate triplet species of nickel(II).[4] The AB and CD spectra in acetonitrile are shown in Fig. 3, the equilibrium being shifted toward the triplet form. In water, however, which should have strong coodinating ability, only an absorption band corresponding to the four-coordinate species has been reported.[4] This has been in contrast to the case with unsubstituted fully-saturated tetraaza-macrocyclic nickel(II) complexes, where such equilibria in water are clearly observed and the equilibrium constants and the thermodynamic parameters are studied in detail.[15-20] The CD spectrum of α-[Ni(*SS*-L)]$(ClO_4)_2$ in 0.01 mol dm^{-3} perchloric acid shows clearly a positive band ($\Delta\varepsilon=+0.12$) at 10400 cm^{-1} and a weak negative band ($\Delta\varepsilon=-0.03$) at 17400 cm^{-1} as well as strong bands due to the four-coordinate species. The exactly enantiomeric CD spectrum was observed with α-[Ni(*RR*-L)]$(ClO_4)_2$. These facts indicate an equilibrium between the four-coordinated and the diaquated six-coordinate species attains in water. It is difficult to detect the corresponding AB bands under usual experimental conditions because of the low solubility of the compound. But careful measurements revealed very weak AB bands at 10000 and 17100 cm^{-1} (see Table 4).

It is well known for analogous systems that the equilibria can be shifted toward the four-coordinate species by increasing the temperature and/or by increasing the concentration of perchlorate ions.[15-20] In 60% perchloric acid solution of the present α-complex, no AB and CD bands corresponding to the diaquated species were detected at 30 °C. From this spectrum, the molar extinction coefficient (ε) at the absorption maximum of the pure four-coordinate species was evaluated to be $\varepsilon_{447}=80$ dm^3 mol^{-1} cm^{-1}. Using this value, the equilibrium constant ($K=$[[α-Ni(*rac*-L)$(H_2O)_2$]$^{2+}$]/[α-[Ni(*rac*-L)]$^{2+}$]) in 0.01 mol dm^{-3} perchloric acid solution was determined to be 0.19 at 20 °C: the complexes in the solution consist of 16% six-coordinate and 84% four-coordinate species. The positions of the AB and CD bands due to the diaquated six-coordinate species are close to those observed for [{Ni(*SS*-L)}$_2$(*d*-tart)(H_2O)]$^{2+}$ and [{Ni(*RR*-L)}$_2$ox]$^{2+}$ (see Table 4). This indicates that the diaquated species of α-[Ni(*rac*-L)]$^{2+}$ has a *cis*-NiO_2N_4 structure. Compounds of the *trans*-NiO_2N_4 type show AB bands around 9000, 15000, and 29000—30000 cm^{-1}.[7,21,22]

The perchlorates of all the α-, β-, and γ-isomers give finally identical AB and CD spectra when dissolved in 10^{-3} mol dm^{-3} sodium hydroxide solution, where the compounds can isomerize to more stable forms. The resulting CD spectra are almost the same as that of the β-isomer in weakly acidic solution (Table 4). In the equilibrated solution, the predominant species is the β-form and the amounts of the α- and γ-forms are very small, if any. Nevertheless, the γ-isomer can easily be isolated as large crystals, because of the very low solubility, upon standing the equilibrated dilute solution for a long time.

As shown in Fig. 3, the AB spectra of $(-)_{589}$-[{Ni(*SS*-L)}$_2$(*d*-tart)(H_2O)]$^{2+}$ and $(+)_{589}$-[{Ni(*RR*-L)}$_2$-ox]$^{2+}$ are quite similar and their CD spectra are almost enantiomeric. This fact indicates that the CD patterns are determined by the chiralities associated with the coordinated macrocyclic ligand and that the effects of the *d*-tartrate ion on the CD pattern are small.

Figure 3 shows that the CD intensity of the α-isomer is stronger than those of the β- and γ-isomers. This is most likely because only the α-isomer has a skeletal chirality (see **2**—**4**). In view of the structure found in the crystal of the α-isomer of the racemic perchlorate **2**,[3] the optically active α-isomer containing *RR*-L would have six-membered rings in the λ twist conformation and five-membered rings in the δ gauche conformation.

References

1) For example, a) N. F. Curtis, *Coord. Chem. Rev.*, **3**, 3 (1967); b) D. H. Busch, *Helv. Chim. Acta, Fasciculus Extraordinarius Alfred Werner*, **1967**, 174; c) "Coordination Chemistry of Macrocyclic Compounds," ed by G. A. Nelson, Plenum, New York, N. Y. (1979).

2) L. G. Warner, Ph. D. Thesis, The Ohio State University, Colombus, Ohio, 1968.

3) a) N. F. Curtis, D. A. Swann, and T. N. Waters, *J. Chem. Soc., Dalton Trans.*, **1973**, 1963; b) The γ-perchlorate crystallizes with six-membered ring moieties randomly adopting the chair or twist conformation.[3a]

4) L. G. Warner and D. H. Busch, *J. Am. Chem. Soc.*, **91**, 4092 (1969).

5) P. O. Whimp, M. F. Bailey, and N. F. Curtis, *J. Chem. Soc., A*, **1970**, 1956.

6) N. F. Curtis, D. A. Swann, and T. N. Waters, *J. Chem. Soc., Dalton Trans.*, **1973**, 1408, and references cited therein.

7) The product contains a small amount of $(+)_{589}$-[{Ni(*RR*-L)}$_2$ox]$(ClO_4)_2$ in addition to the main component of [{Ni(*rac*-L}$_2$ox]$(ClO_4)_2$. These can be separated by methanol extraction (see text).

8) N. F. Curtis, *J. Chem. Soc.*, **1964**, 2644.

9) K. P. Wainwright, *J. Chem. Soc., Dalton Trans.*, **1980**, 2117.

10) The final atomic parameters and a list of the observed and calculated structure factors are kept in the Office of the Chemical Society of Japan (Document No. 8153). One of the two water molecules of crystallization (Ow(2)) is disordered and located at two positions, Ow(2a) and Ow(2b), with the populations of 0.7 and 0.3, respectively. The difference syntheses suggested large thermal oscillation, or static disorder, for the perchlorate oxygen atoms. One of the perchlorate oxygens, Op(8), was located at three positions Op(8a), O(8b), and Op(8c) with the population of 0.333.

11) T. Sakurai and K. Kobayashi, *Rikagaku Kenkyusho Hokoku(Rept. Inst. Phys. Chem.)*, **55**, 69 (1979).

12) Details will be reported elsewhere.

13) Yoshikawa *et al.* studied stereochemistry of *cis*-β type cobalt(III) complexes of methyl-substituted linear tetramines such as 3,7-diaza-1,9-nonanediamine and 4,7-diaza-1,10-decanediamine derivatives, which contain (2*R*,4*R*)-2,4-pentanediamine moiety, and proposed that a five-membered chelate ring orients so as to minimize the steric interaction with an axial methyl group on the adjacent six-membered ring, controlling thereby a total stereochemistry of the *cis*-β type complex: T. Ito, S. Yano, K. Toriumi, M. Ajioka, and S. Yoshikawa, Symposium on Stereochemistry and Optical Resolution of Coordination Compounds, Nagoya, January

1981, Abstr. pp. 65—68. The folding of the macrocyclic ligand in the present study can be explained in the same way.

14) Ow(1)···N(1), 3.251(11); Ow(1)···N(8), 3.250(9); N(4)···Op(3), 3.274(11); N(1′)···Op(4), 3.167(9); N(4′)···Op(7), 3.223(10); N(8′)···Op(3), 3.376(9); O(6)···Op(6), 2.917(10); Ow(c)···Op(7), 2.906(11) Å.

15) A. Anichini, L. Fabbrizzi, and P. Paoletti, *Inorg. Chim. Acta*, **24**, L21 (1977).

16) L. Fabbrizzi, *Inorg. Chem.*, **16**, 2667 (1977).

17) N. Herron and P. Moore, *Inorg. Chim. Acta*, **36**, 89 (1979).

18) L. Fabbrizzi, *J. Chem. Soc., Dalton Trans.*, **1979**, 1857.

19) L. Sabatini and L. Fabbrizzi, *Inorg. Chem.*, **18**, 438 (1979).

20) R. G. Swisher, J. P. Dayhuff, D. J. Stuehr, and E. L. Blinn, *Inorg. Chem.*, **19**, 1336 (1980).

21) N. F. Curtis, *J. Chem. Soc., A*, **1968** 1584.

22) M. Sugimoto, Ms. Dissertation, Nagoya University, Nagoya, 1981: 1,4,8,11-Tetraazacyclotetradecanenickel(II) perchlorate shows an absorption band at 9250 cm^{-1} in water.

  Bull. Chem. Soc. Jpn., 54, 2995—2999 (1981)

Crystal Structure and Absolute Configuration of *d*-Tartaric Acid-(+)$^{CD}_{500}$-Tris(2-aminoethanesulfenato)cobalt(III)-Water (1/1/1)

Masakazu KITA,* Kazuaki YAMANARI, Katsuki KITAHAMA,† and Yoichi SHIMURA

Department of Chemistry, Faculty of Science, Osaka University, Toyonaka, Osaka 560

†*The Institute of Scientific and Industrial Research, Osaka University, Yamadagaoka, Suita, Osaka 565*

(Received April 13, 1981)

The crystal structure and absolute configuration of diastereomeric molecular compound, *d*-$C_4H_6O_6\cdot(+)^{CD}_{500}$-$[Co\{S(O)CH_2CH_2NH_2\}_3]\cdot H_2O$, were determined by the X-ray diffraction method. The crystals are orthorhombic with space group $P2_12_12_1$, $Z=4$, and $a=13.034(4)$, $b=13.559(6)$, and $c=11.048(8)$ Å. The rifinement of 1724 reflections (Mo $K\alpha$ radiation) led to $R=0.068$. The complex molecule has the configuration *fac*(*S*)-*Λ*-(δ,δ,δ)-(*R*, *R*, *R*). All amino groups and the sulfenato oxygen atoms form hydrogen bonds with *d*-tartaric acid and/or water molecules three-dimensionally, which is responsible for the formation of the novel diastereomeric molecular compound.

Free sulfenic acids are recognized as important intermediates in reactions of many sulfur-containing organic compounds,[1,2] but a few ones have ever been isolated[1-3] because of the instability.[2,4,5] Some sulfenic acids which are S-coordinated to a cobalt(III) ion are stabler than their corresponding free acids,[6-11] their complexes providing a means for investigating the chemistry of sulfenic acids. Furthermore, sulfenato complexes are important for an understanding of redox reactions associated with metal-sulfur enzymes.[12]

The previous letter[11] reported the preparation and optical resolution for *fac*(*S*)-$[Co\{S(O)CH_2CH_2NH_2\}_n\{S(O)_2CH_2CH_2NH_2\}_{3-n}]$ type ($n=3$, 2, 1, and 0). In particular, one of the isomers of $[Co\{S(O)CH_2CH_2NH_2\}_3]$ was resolved by means of preferential crystallization of a diastereomeric molecular compound with *d*-tartaric acid, which is the first example of optical resolution by molecular compound formation in the field of metal complex chemistry. The crystal structure determination of this molecular compound, *d*-tartaric acid – (+)$^{CD}_{500}$-tris(2-aminoethanesulfenato)cobalt(III) – water (1/1/1), is especially of interest in connection with (1) the absolute stereochemistry of this complex (*i.e.*, the absolute configuration about the cobalt center (*Δ* or *Λ*) and those of the three asymmetric sulfur donor atoms (*R* or *S*)), (2) the intramolecular bond distances in comparison with those of monosulfenato complex $[Co\{S(O)CH_2CH_2NH_2\}(en)_2](SCN)_2$,[10] and (3) intermolecular interactions among the complex, *d*-tartaric acid, and water in the packing (en=ethylenediamine).

Experimental

Preparation of Compound. The diastereomeric molecular compound was prepared by the reported procedure.[11] Recrystallization of the compound from an ethanol-water (2 : 1) solution gave orange-red crystals in the form of rectangular prism. Found: C, 23.72; H, 5.22; N, 8.35%. Calcd for *d*-$C_4H_6O_6\cdot(+)^{D}_{500}$-$[Co\{S(O)CH_2CH_2NH_2\}_3]\cdot H_2O=C_{10}H_{26}N_3O_{10}S_3Co$: C, 23.86; H, 5.21; N, 8.35%.

Data Collection. Precession photographs exhibited systematic absences $h=$odd for $h00$, $k=$odd for $0k0$, and $l=$odd for $00l$, indicating the unique space group $P2_12_12_1$. An orange-red crystal, of approximate dimensions 0.18 mm × 0.20 mm × 0.30 mm, was mounted with its long dimension along the axis of a glass fiber to protect it from moisture. The diffraction intensities were measured using a Rigaku four-circle diffractometer, with a graphite monochromatized Mo $K\alpha$ radiation ($\lambda=0.71069$ Å). Accurate lattice parameters were obtained by least-squares refinement of ten high angle reflections. The crystal data are summarized in Table 1. Three standard reflections fluctuated within 4% in intensity over the time of data collection. Within the sphere $2\theta<50°$, 1968 unique reflections were obtained. Among them 1724 reflections were $|F_o|>3\sigma_{cs}$ (σ_{cs} is the standard deviation of F in counting statistics). Only these reflections were used for the structure determination and refinement. No absorption correction was applied.

Table 1. Crystal data

$C_{10}H_{26}N_3O_{10}S_3Co$	$F.W.=503.44$
Orthorhombic	Space group $P2_12_12_1$
$a=13.034(4)$ Å	
$b=13.559(6)$ Å	
$c=11.048(8)$ Å	
$U=1952.49$ Å^3	
$D_m=1.70(5)$ g cm^{-3} (by flotation)	
$D_c=1.72$ g cm^{-3}	$Z=4$
μ(Mo $K\alpha$)$=13.44$ cm^{-1}	

Structure Solution and Refinement. The structure was solved by the usual heavy-atom method; the positions of cobalt and sulfur atoms were picked up by means of the Patterson synthesis, and all the nonhydrogen atoms were located by the subsequent Fourier synthesis. Absolute configurations of the two asymmetric carbon atoms of *d*-tartaric acid were fitted to those reported previously.[13] Therefore, the absolute configuration of the metal complex molecule, $[Co\{S(O)CH_2CH_2NH_2\}_3]$, was determined definitely. The structure was refined by the block-diagonal least-squares method with the positional and isotropic thermal parameters for all nonhydrogen atoms. Further subsequent refinement was carried out using anisotropic thermal parameters for all nonhydrogen atoms. In the last cycles of least-squares refinement, 245 parameters were varied including an overall thermal parameter, a scale factor, positional and anisotropic thermal parameters for all nonhydrogen atoms. Convergence was achieved with $R=0.075$ ($R=\sum||F_o|-|F_c||/\sum|F_o|$). Although no hydrogen position was detected from the difference electron density map, hydrogen positions except those of carboxyl and hydroxyl groups of *d*-tartaric acid and those of water were tentatively calculated based on the following conditions; N-H=0.87 Å, C-H=0.97 Å, and tetrahedral geometry. Postulating $B=4.0$ Å^3 for each H atom, these twenty H atoms were added to the least-squares refinement, which gave the final R value of 0.068.

Atomic scattering factors from International Tables for

X-Ray Crystallography[14] were used for Co, S, O, N, C, and H atoms. Anomalous dispersion correction was made for Co and S atoms.[14] All computations were performed on an ACOS-S700 at Crystallographic Research Center, Institute for Protein Research, Osaka University. The computer programs used were RSSFR-5,[15] HBLS V,[16] DAPH,[17] and ORTEP.[18]

Final positional parameters, the corresponding isotropic thermal parameters which were calculated from respective anisotropic ones by Hamilton's method,[19] and their estimated standard deviations for nonhydrogen atoms are given in Table 2. The calculated positional parameters of hydrogen atoms, the anisotropic thermal parameters for all nonhydrogen atoms, and the complete list of the $|F_o|$ and $|F_c|$ values have been preserved by the Chemical Society of Japan (Document No. 8143).

TABLE 2. FRACTIONAL ATOMIC POSITIONAL AND ISOTROPIC THERMAL PARAMETERS FOR NONHYDROGEN ATOMS[a,b]

Atom	x	y	z	B[c] / Å^2
Co	0.1894(1)	−0.1105(1)	0.0817(1)	2.57(3)
S(1)	0.1471(2)	0.0473(2)	0.0988(3)	3.20(7)
S(2)	0.1071(2)	−0.1389(3)	0.2548(3)	3.79(8)
S(3)	0.3335(2)	−0.0819(2)	0.1843(3)	2.91(7)
O(1)	0.1998(7)	0.1060(7)	−0.0065(8)	3.9(3)
O(2)	−0.0072(7)	−0.1513(10)	0.2271(12)	6.4(4)
O(3)	0.3880(6)	−0.1823(7)	0.2046(9)	3.9(2)
O(4)	−0.3463(8)	0.0408(7)	0.2003(10)	5.1(3)
O(5)	−0.2511(10)	−0.0139(9)	0.0455(11)	6.3(3)
O(6)	−0.1983(7)	−0.1802(7)	0.1693(10)	4.7(3)
O(7)	−0.4144(6)	−0.1807(7)	0.1517(8)	3.2(2)
O(8)	−0.2913(8)	−0.2437(7)	0.4274(9)	4.6(3)
O(9)	−0.3532(7)	−0.3373(6)	0.2781(8)	4.0(2)
O(10)	0.4111(9)	−0.3021(8)	0.4179(13)	6.8(4)
N(1)	0.0608(7)	−0.1299(8)	−0.0135(10)	3.1(3)
N(2)	0.2210(8)	−0.2538(7)	0.0746(11)	3.6(3)
N(3)	0.2676(7)	−0.0860(8)	−0.0713(9)	3.2(2)
C(1)	0.0198(10)	0.0366(11)	0.0431(13)	4.0(4)
C(2)	0.0130(10)	−0.0381(11)	−0.0589(12)	4.1(4)
C(3)	0.1508(11)	−0.2637(10)	0.2737(13)	4.1(4)
C(4)	0.1538(11)	−0.3147(11)	0.1542(15)	4.5(4)
C(5)	0.4044(9)	−0.0306(9)	0.0590(13)	3.5(3)
C(6)	0.3783(9)	−0.0887(9)	−0.0530(12)	3.4(3)
C(7)	−0.2842(11)	−0.0223(11)	0.1452(14)	4.6(4)
C(8)	−0.2613(10)	−0.1111(11)	0.2270(12)	3.8(3)
C(9)	−0.3619(9)	−0.1639(9)	0.2598(12)	3.4(3)
C(10)	−0.3358(10)	−0.2550(10)	0.3228(12)	3.6(3)

a) The estimated error in the last digit is shown in parentheses. This form is used throughout. b) O(10) is for the water of hydration; the rest of numberings are as shown in Fig. 1. c) B is evaluated from the corresponding anisotropic thermal parameters according to Ref. 17. Isotropic thermal parameters are of the form $\exp\{-B(\sin^2\theta/\lambda^2)\}$.

Results and Discussion

Figure 1 shows the notation of the complex, *d*-tartaric acid, and the oxygen atom of water. Nonhydrogen atom bond distances and angles are given in Tables 3 and 4, respectively. Table 5 lists several selected plane equations, sets of deviations of atoms from the plane, and dihedral angles between the pair of planes.

Structure of $(+)^{CD}_{500}$-$[Co\{S(O)CH_2CH_2NH_2\}_3]$. The perspective view of the complex projected down its threefold axis is shown in Fig. 2. The cobalt(III) center is six-coordinate in approximately octahedral configuration (Table 5). The bidentate 2-aminoethanesulfenate coordinates to a cobalt(III) ion through sulfur and nitrogen atoms and the complex has *fac*(*S*) geometry. The average coordination angles of S–Co–S, N–Co–N, and S–Co–N (the S and N atoms are in trans) are 89.4°, 90.7°, and 177.7°, respectively (Table 4). The values indicate that the CoS_3 parasol constituted of three facial S atoms and a Co atom at the top is less blown

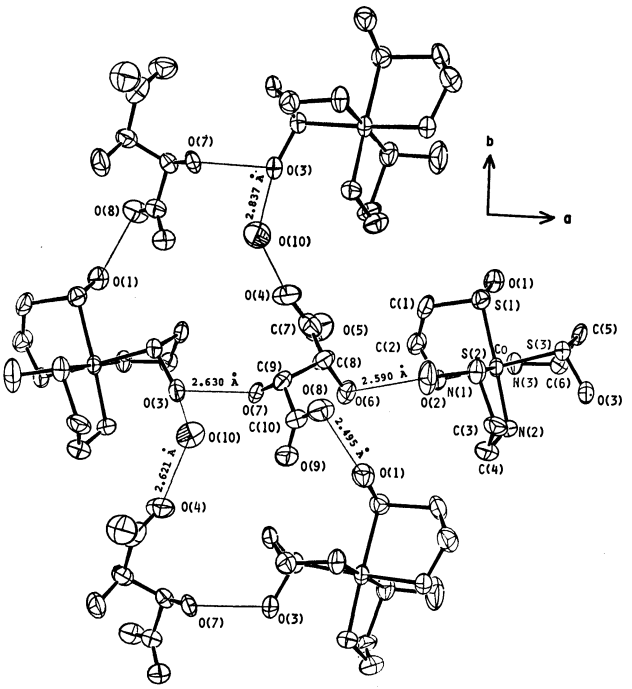

Fig. 1. A perspective view of a layer constituted by hydrogen bonds onto ab plane projected along c-axis, where line bonds denote hydrogen bonds within 3.10 Å. Thermal ellipsoids are drawn at the 50% probability level.

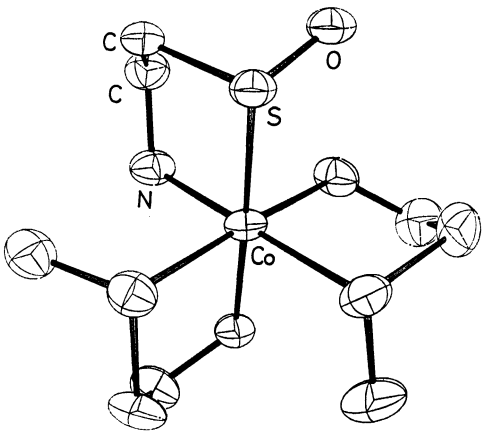

Fig. 2. A perspective drawing of the complex projected down the threefold axis of the complex (50% probability thermal ellipsoids).

Table 3. Intramolecular bond distances (l/Å)

For complex						Average
Co–S(1)	2.222(4)	Co–S(2)	2.228(4)	Co–S(3)	2.229(3)	2.226
Co–N(1)	2.015(11)	Co–N(2)	2.011(12)	Co–N(3)	2.012(11)	2.013
S(1)–O(1)	1.567(10)	S(2)–O(2)	1.531(13)	S(3)–O(3)	1.545(10)	1.548
S(1)–C(1)	1.793(15)	S(2)–C(3)	1.837(15)	S(3)–C(5)	1.823(14)	1.818
N(1)–C(2)	1.501(17)	N(2)–C(4)	1.479(20)	N(3)–C(6)	1.485(16)	1.488
C(1)–C(2)	1.535(20)	C(3)–C(4)	1.513(21)	C(5)–C(6)	1.516(19)	1.521
For *d*-tartaric acid						
O(4)–C(7)	1.333(19)	O(5)–C(7)	1.158(20)	O(6)–C(8)	1.390(17)	
O(8)–C(10)	1.303(17)	O(9)–C(10)	1.215(16)	O(7)–C(9)	1.394(16)	
C(7)–C(8)	1.569(21)	C(8)–C(9)	1.544(20)	C(9)–C(10)	1.494(19)	

Table 4. Intramolecular bond angles (ϕ/°)

For complex						Average
Metal coordination angles						
S(1)–Co–S(2)	88.4(1)	S(2)–Co–S(3)	89.9(1)	S(3)–Co–S(1)	89.9(1)	89.4
S(1)–Co–N(1)	88.4(3)	S(2)–Co–N(2)	88.5(4)	S(3)–Co–N(3)	88.8(3)	88.6
S(1)–Co–N(3)	91.9(3)	S(2)–Co–N(1)	91.5(3)	S(3)–Co–N(2)	90.8(4)	91.4
S(1)–Co–N(2)	176.8(4)	S(2)–Co–N(3)	178.6(3)	S(3)–Co–N(1)	177.8(3)	177.7
N(1)–Co–N(2)	91.0(5)	N(2)–Co–N(3)	91.2(5)	N(3)–Co–N(1)	89.8(4)	90.7
Intraligand angles						
Co–S(1)–O(1)	108.3(4)	Co–S(2)–O(2)	108.2(5)	Co–S(3)–O(3)	108.1(4)	108.2
Co–S(1)–C(1)	97.2(5)	Co–S(2)–C(3)	96.5(5)	Co–S(3)–C(5)	96.5(5)	96.7
O(1)–S(1)–C(1)	101.6(6)	O(2)–S(2)–C(3)	103.6(7)	O(3)–S(3)–C(5)	102.4(6)	102.5
S(1)–C(1)–C(2)	110.5(10)	S(2)–C(3)–C(4)	107.6(10)	S(3)–C(5)–C(6)	107.9(9)	108.7
C(1)–C(2)–N(1)	106.4(11)	C(3)–C(4)–N(2)	107.7(12)	C(5)–C(6)–N(3)	108.6(10)	107.6
Co–N(1)–C(2)	113.6(8)	Co–N(2)–C(4)	112.0(9)	Co–N(3)–C(6)	112.1(8)	112.5
For *d*-tartaric acid						
O(4)–C(7)–O(5)	126.5(15)	O(4)–C(7)–C(8)	110.6(12)	O(5)–C(7)–C(8)	122.9(14)	
O(6)–C(8)–C(7)	111.2(12)	O(6)–C(8)–C(9)	108.9(11)	C(7)–C(8)–C(9)	108.4(11)	
O(7)–C(9)–C(10)	112.1(11)	O(7)–C(9)–C(8)	107.5(11)	C(8)–C(9)–C(10)	106.1(11)	
O(8)–C(10)–O(9)	123.7(13)	O(8)–C(10)–C(9)	115.6(12)	O(9)–C(10)–C(9)	120.7(12)	

than the corresponding CoN_3 parasol. The three sulfenato sulfur atoms are three-coordinate (to the cobalt atom, the carbon atom of chelate ring, and the oxygen atom) in an approximately tetrahedral configuration counting the sulfur lone pair of electrons as occupying the fourth site. The oxygen atoms of sulfenato groups occupy the least repulsive positions on the *fac*(*S*) plane to one another. Therefore, the oxygen atoms are on the plane perpendicular to the threefold axis of the complex.

Since the sulfur atom of sulfenato group becomes chiral on coordination, the stereochemical possibilities for this *fac*(*S*) complex are as follows: (1) the wrapping of the chelate rings about the cobalt center may be either Δ or Λ, (2) the conformations of the three chelate rings generate four sets of isomers (δ,δ,δ), (δ,δ,λ), (δ,λ,λ), and (λ,λ,λ), and (3) four configurations (*R*,*R*,*R*), (*R*,*R*,*S*), (*R*,*S*,*S*), and (*S*,*S*,*S*) are possible from the combination of three chiral sulfur atoms. Therefore, 32 configurations in all, *i.e.*, 16 enantiomeric pairs of diastereoisomers are expected. However, the crystal contains only the configuration *fac*(*S*)-Λ-(δ,δ,δ)-(*R*,*R*,*R*). The result is consistent with the previous assignment based on the absorption, CD, and ^{13}C NMR spectra.[11]

Table 6 shows the selected bond distances and angles of the complex in comparison with those of Δ-{$\lambda'(S)$, λ,δ}[Co{S(O)$CH_2CH_2NH_2$}$(en)_2$]$^{2+}$.[10] There are no large differences between the two complexes in the bond distance and angle. In the monosulfenato complex ion, the Co–N distance (2.048 Å) *trans* to the sulfur donor atom is significantly larger than the average *cis* Co–N one (1.976 Å) which is consistent with the ordinary Co–N distance. Such a phenomenon is referred to as *structural trans effect* (*STE*).[10] The present *fac*(*S*) complex has exclusively the *trans* Co–N bond. The average Co–N distance is longer than the ordinary Co–N one but trivially shorter than the *trans* Co–N distance of the monosulfenato cobalt(III) complex ion. The Co–S bond distance (2.226 Å) is also somewhat shorter than that (2.253 Å) of the reference complex. The XPS data of both complexes show the existence of a significant amount of electron-transfer from the sulfenato sulfur donor atom to cobalt(III) ion in comparison with the tris(ethylenediamine)cobalt(III) complex.[20] The Co-$2p_{3/2}$, S-$2p_{3/2}$, and N-1s binding energies of the present complex (779.0, 163.8, and 398.9 eV, respectively) are lower than those of the monosulfenato complex (781.0, 164.9, and 400.1 eV, respectively). The results indicate that the saturation on the electron-transfer to cobalt(III) ion occurs

TABLE 5. DISPLACEMENTS OF ATOMS FROM LEAST-SQUARES PLANE AND DIHEDRAL ANGLES BETWEEN PLANES

For complex (coordination planes)

Plane1. [Co, S(1), S(2), N(2), and N(3)]

$-0.8403X-0.1657Y-0.5162Z+2.2964=0$

Co 0.0049, S(1) 0.0165, S(2) −0.0188, N(2) 0.0179, N(3) −0.0199, O(1) −0.0990

Plane 2. [Co, S(1), S(3), N(1), and N(2)]

$-0.5004X-0.1708Y+0.849Z+0.2069=0$

Co −0.0064, S(1) 0.0656, S(3) −0.0486, N(1) −0.0170, N(2) 0.0394, O(3) 0.0138

Plane 3. [Co, S(2), S(3), N(1), and N(3)]

$-0.2243X+0.9723Y+0.0658Z+1.9432=0$

Co −0.0100, S(2) −0.0149, S(3) 0.0201, N(1) 0.0226, N(3) −0.0171, O(2) 0.1446

Dihedral angles (ϕ/°)

between the planes 1 and 2	89.4
between the planes 1 and 3	90.4
between the planes 2 and 3	89.9
average	89.9

For *d*-tartaric acid

Plane 4. [C(7), C(8), C(9),and C(10)]

$0.0796X-0.5405Y-0.8376Z+1.5215=0$

C(7) 0.0531, C(8) −0.0319, C(9) −0.0670, C(10) 0.0523

Plane 5. [O(4), O(5), C(7), and C(8)]

$0.7944X+0.4826Y+0.3688Z+2.5013=0$

O(4) −0.0028, O(5) −0.0035, C(7) 0.0085, C(8) −0.0022

Plane 6. [O(8), O(9), C(9), and C(10)]

$0.8942X+0.0107Y-0.4476Z+5.5402=0$

O(8) 0.0023, O(9) 0.0026, C(9) 0.0020, C(10) −0.0068

Dihedral angles (ϕ/°)

between the planes 4 and 5	120.4
between the planes 4 and 6	63.9
between the planes 5 and 6	56.6

The *X*, *Y*, and *Z* coordinates in Å refer to the crystallographic axes.

according to the increase in number of sulfenato groups which lowers the S-$2p_{3/2}$ binding energy of the present complex. However, there is an apparent conflict between the XPS data and the Co–S bond distances: the present tris(sulfenato) complex with the more negative sulfur donor atoms has the shorter Co–S bond distance than the monosulfenato complex. This conflict may be interpreted as that the electron-transfer from sulfur to cobalt in sulfenato complex contains an antibonding character.

Structure of d-*Tartaric Acid.* The *d*-tartaric acid molecule has reasonable bond distances, angles, and dihedral angles as compared with other structure analyses[13] (Tables 3, 4, and 5). The carbon skelton C(7)–C(8)–C(9)–C(10) is planar, and the dihedral

TABLE 6. SELECTED BOND DISTANCES (l/Å) AND ANGLES (ϕ/°)

	Present complex[a]	Reference complex[b]
Bond	Average l	l
Co–S	2.226	2.253(1)
Co–N	2.013	2.048(3)[c]
		1.976[d]
S–O	1.548	1.552(3)
S–C	1.818	1.815(4)
N–C[e]	1.488	1.484(5)
C–C[e]	1.521	1.513(5)
Angle	Average ϕ	ϕ
Co–S–O	108.2	107.7(1)
Co–S–C	96.7	96.5(1)
O–S–C	102.5	102.3(2)

a) Data from Tables 2 and 3. b) Data from Ref. 10. c) *trans*-Position against S atom. d) Average for *cis*-positions against S atom. e) Associated with the sulfenato chelate ring.

TABLE 7. POSSIBLE HYDROGEN BONDING IN *d*-$C_4H_6O_6$·$[Co\{S(O)CH_2CH_2NH_2\}_3]$·$H_2O$[a]

B···(H–)A	B···A(l/Å)	X–B···A(ϕ/°)	B···A–Y(ϕ/°)
O(1)···O(8)^{I}	2.495(14)	111.3(5)	115.2(7)
O(2)···O(6)	2.590(17)	176.1(8)	110.5(8)
O(3)···O(7)^{II}	2.630(11)	114.3(5)	106.5(5)
O(3)···O(10)	2.837(16)	131.2(6)	92.1(8)[b]
O(10)···O(4)^{I}	2.621(17)	92.1(8)[b]	119.9(8)
A–H···B	A···B(l/Å)	H···B(l/Å)	A–H···B(ϕ/°)
N(1)–H(16)···O(7)^{III}	2.982(13)	2.205	148.5
N(2)–H(18)···O(6)^{III}	3.011(16)	2.262	144.2
N(3)–H(20)···O(9)^{III}	2.955(14)	2.204	144.4

a) Includes H bonding where A···B <3.1 Å. b) O(3)···O(10)···O(4) angle. I: Transformed to $-x,y+1/2,-z+1/2$. II: Transformed to $x+1,y,z$. III: Transformed to $x+1/2,-y-1/2,-z$.

angle between the planes [O(4), O(5), C(7), and C(8)] and [O(8), O(9), C(9), and C(10)] is 56.6°.Furthermore, a proof of no dissociation of its two carboxyl groups can be given by two kinds of bond distances C–O(–H) (1.333 Å, 1.303 Å) and C=O (1.158 Å, 1.215 Å), that is, the *d*-tartaric acid being not in resonance structure between

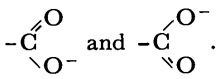

Crystal Packing. As for the intermolecular bond, possible hydrogen bond distances and angles are listed in Table 7. The perspective view of a layer constituted of hydrogen bonds onto ab plane projected along the c-axis is given in Fig. 1, where line bonds denote hydrogen bonds within 3.10 Å. This layer further interacts with the upper and lower layers by hydrogen bonds between the hydrogen atoms of amino groups of the complex and oxygen atoms of *d*-tartaric acid onto bc plane (Fig. 3). Thus, seven hydrogen bonds are possible

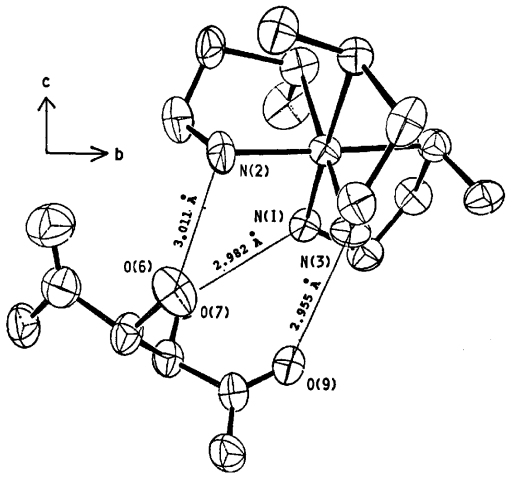

Fig. 3. The arrangement of the complex and *d*-tartaric acid molecule projected along a-axis (50% probability thermal ellipsoids). The line bonds represent possible hydrogen bonds (the distances within 3.10 Å).

per one *d*-tartaric acid molecule. The hydrogen bond distances between oxygen atoms of sulfenato groups and hydrogen atoms of carboxyl groups, hydroxyl groups, or water are considerably short (2.495—2.837 Å), that is, the sulfenato oxygens have a significantly basic character. The S–O bond distance (1.548 Å) is rather longer than that of the sulfinato group of $[Co\{S(O)_2\text{-}CH_2CH_2NH_2\}(en)_2]^{2+}$ (1.456 Å, 1.476 Å).[21] The facts indicate that the sulfur-oxygen bond of sulfenato complex has a large polarity (*right*) in analogy with

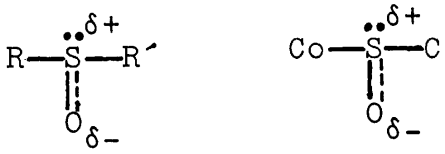

that of sulfoxide (*left*).[22] Such a basic property of oxygen atoms in sulfenato groups is confirmed for the first time. The hydrogen bonding mode in Fig. 3 is similar to the so-call *face-to-face close contact* between a triangular face of the octahedral complex cation and the hydrogen *d*-tartrate or the *d*-tartrate anion.[23] The hydrogen bond interaction between the neutral complex and the *d*-tartaric acid molecule seems to be a key for the successful optical resolution of this molecular complex.

We wish to thank Mr. Yoshihisa Baba of our University for his technical assistance. We are also grateful to Professor Shichio Kawai of our University for his support to this work. This work was partly supported by a Grant-in-Aid for Scientific Research No. 547041 from the Ministry of Education, Science and Culture.

References

1) J. R. Shelton and K. E. Davis, *J. Am. Chem. Soc.*, **89**, 718 (1967).
2) W. S. Allison, *Acc. Chem. Res.*, **9**, 293 (1976).
3) T. C. Bruice and J. Markiw, *J. Am. Chem. Soc.*, **79**, 3150 (1957).
4) E. Block and S. W. Weidman, *J. Am. Chem. Soc.*, **95**, 5046 (1973).
5) E. Block and J. O'Connor, *J. Am. Chem. Soc.*, **95**, 5048 (1973).
6) C. P. Sloan and J. H. Krueger, *Inorg. Chem.*, **14**, 1481 (1975).
7) W. G. Jackson, A. M. Sargeson, and P. O. Whimp, *J. Chem. Soc., Chem. Commun.*, **1976**, 934.
8) B. A. Lange, K. Libson, E. Deutsch, and R. C. Elder, *Inorg. Chem.*, **15**, 2985 (1976).
9) D. L. Herting, C. P. Sloan, A. W. Cabral, and J. H. Krueger, *Inorg. Chem.*, **17**, 1649 (1978).
10) I. K. Adzamli, K. Libson, J. D. Lydon, R. C. Elder, and E. Deutsch, *Inorg. Chem.*, **18**, 303 (1979).
11) M. Kita, K. Yamanari, and Y. Shimura, *Chem. Lett.*, **1980**, 275.
12) L. E. Bennett, *Prog. Inorg. Chem.*, **18**, 1 (1973).
13) F. Stern and C. A. Beevers, *Acta Crystallogr.*, **3**, 341 (1950).
14) "International Tables for X-Ray Crystallography," Kynoch Press, Birmingham (1974), Vol. IV.
15) T. Sakurai, "The Universal Crystallographic Computing System(I)," The Crystallographic Society of Japan (1967), p. 45.
16) T. Ashida, "HBLS V, The Universal Crystallographic Computing System-Osaka," The Computation Center, Osaka University (1979), p. 53.
17) T. Ashida, "DAPH, The Universal Crystallographic Computing System-Osaka," The Computation Center, Osaka University (1979), p. 61.
18) C. K. Johnson, "ORTEP-II : A FORTRAN Thermal-Ellipsoid Plot Program for Crystal Structure Illustrations, ORNL-5138, March 1976," Oak Ridge National Laboratory.
19) W. C. Hamilton, *Acta Crystallogr.*, **12**, 609 (1959).
20) M. Kita, K. Yamanari, K. Kishi, S. Ikeda, and Y. Shimura, *Chem. Lett.*, **1981**, 337.
21) R. C. Elder, L. R. Florian, R. E. Lake, and A. M. Yacynch, *Inorg. Chem.*, **12**, 2690 (1976).
22) D. Barnard, J. M. Fabian, and H. P. Koch, *J. Chem. Soc.*, **1949**, 2442; M. Tamers and S. Searles, Jr., *J. Am. Chem. Soc.*, **81**, 2100 (1959); R. H. Figueroa, E. Roig, and H. H. Szmant, *Spectrochim. Acta*, **22**, 1107 (1966); B. R. James and R. H. Morris, *J. Chem. Soc., Chem. Commun.*, **1980**, 31.
23) Y. Kushi, M. Kuramoto, and H. Yoneda, *Chem. Lett.*, **1976**, 135; M. Kuramoto, Y. Kushi, and H. Yoneda, *Bull. Chem. Soc. Jpn.*, **53**, 125 (1980) and the references cited therein.

Cobalt(III) Complexes with Tripodlike Quadridentate Ligands. I. Circular Dichroism Spectra of Quasi-enantiomeric Geometrical Isomers of [Co(tripod)(chiral bidentate)]-type Complexes

Keiji Akamatsu,* Takashi Komorita, and Yoichi Shimura

Department of Chemistry, Faculty of Science, Osaka University, Toyonaka, Osaka 560

(Received April 23, 1981)

Cobalt(III) complexes containing a tripodlike quadridentate ligand, tris(2-aminoethyl)amine or nitrilotriacetate, and a chiral bidentate, L-amino carboxylate or (*R*)-propylenediamine, are prepared and separated into their respective geometrical isomers. The two geometrical isomers have mutually quasi-enantiomeric configurations. Circular dichroism spectra in the d-d absorption band region are discussed in connection with this novel type of geometrical isomerism.

Two geometrical isomers, *trans*(*N*) and *cis*(*N*), of (L-amino carboxylato)(nitrilotriacetato)cobaltate(III) ion [Co(L-am)(ata)]$^-$ [1] which has been prepared by Koine *et al.*[2] show vicinal CD (circular dichroism) due to the coordinated chiral amino carboxylate ligand in the d-d absorption band region. But it has remained puzzling why the intensity of vicinal CD is much stronger than those of other simple (L-amino carboxylato)cobalt(III) complexes which have no tripodlike quadridentate ligand.

The present paper deals with CD spectra of several mixed cobalt(III) complexes of a tripodlike quadridentate ligand, ata^{3-} or tren[1] and a chiral bidentate one, α-amino carboxylate or 1,2-diamine. For each of these complexes two geometrical isomers are possible, which are denoted as in Fig. 1.

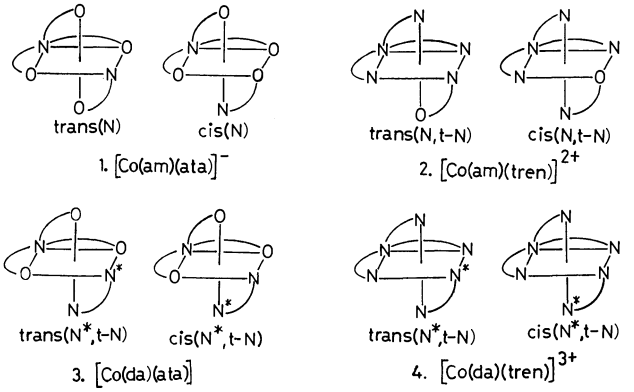

Fig. 1. Two geometrical isomers of [Co(tripod)(chiral bidentate)]type complex: tripod=ata^{3-} or tren, chiral bidentate=am$^-$ or da, and *N** and *t-N* mean the nitrogen atoms adjacent to the asymmetric carbon atom of the ligand and that of the tertiary amine of tripod ligand, respectively.

Experimental

Preparations. *(1) [Co(L-ala)(tren)]$^{2+}$ Salts*: To a solution of [$CoCl_2$(tren)]$ClO_4 \cdot 0.5H_2O$[3] (1 g) in 10 cm^3 of water was added an aqueous solution of L-alanine (0.3 g) neutralized with an equimolar amount of NaOH and the mixture was mechanically stirred for 2 h at 60 °C. The resulting red solution was poured into a cation-exchanger column (SP Sephadex C-25, Na^+ form) and the adsorbed band was eluted with a 0.07 M NaCl aqueous solution (1 M=1 mol dm^{-3}). The band split into three; orange, red, and purple one in the elution order. The third band turned out to be a trivalent complex cation, [Co(tren)$(H_2O)_2]^{3+}$, from the absorption spectrum and the column chromatographic behavior. The first and second eluates were evaporated almost to dryness on a rotary evaporator below 40 °C. A small amount of methanol was added to the residue to precipitate NaCl, which was filtered off. The repetition of this procedure enabled one to remove most of the sodium chloride. On addition of $NaClO_4$ to the solution the chloride perchlorate salt (orange isomer) or perchlorate (red isomer) deposited. They were recrystallized from warm water, washed with methanol and ether and dried in air. Found for the orange isomer: C, 24.98; H, 5.69; N, 16.50%. Calcd for [Co(L-ala)(tren)]Cl·ClO_4: C, 25.25; H, 5.66; N, 16.36%. Found for the red isomer: C, 21.71; H, 5.01; N, 14.37%. Calcd for [Co(L-ala)(tren)]$(ClO_4)_2$: C, 21.56; H, 5.04; N, 13.98%.

(2) Other tren Complexes with Amino Carboxylate: L-val, L-ser, L-phe, D-pgly, and L-cys complexes were prepared in the same way as that described in (1) using the corresponding amino carboxylate ligand instead of L-alaninate. Only orange isomer was isolated for these amino carboxylato complexes except for the L-cys one, for which only a brown isomer was isolated. Found for the L-val complex: C, 24.87; H, 5.50; N, 13.40%. Calcd for [Co(L-val)(tren)]$(ClO_4)_2$: C, 25.39; H, 5.44; N, 13.46%. Found for the L-ser complex: C, 20.67; H, 5.06; N, 13.34%. Calcd for [Co(L-ser)(tren)]$(ClO_4)_2$: C, 20.54; H, 4.99; N, 13.31%. Found for the L-phe complex: C, 31.80; H, 5.09; N, 12.51%. Calcd for [Co(L-phe)(tren)]$(ClO_4)_2$: C, 31.70; H, 4.98; N, 12.33%. Found for the D-pgly complex: C, 30.63; H, 4.67; N, 12.81%. Calcd for [Co(D-pgly)(tren)]$(ClO_4)_2$: C, 30.33; H, 4.74; N, 12.64%. Found for the L-cys complex: C, 25.04; H, 5.57; N, 16.10%. Calcd for [Co(L-cys)(tren)]ClO_4: C, 24.96; H, 5.60; N, 16.19%.

(3) [Co(ata)(en)] and [Co(ata)(R-pn)]: One gram of *cis*(*Cl*)-[$CoCl_2(NH_3)_2$(en)]Cl[4] was dissolved in 10 cm^3 of water and to this blue solution was added a solution (5 cm^3) containing nitrilotriacetic acid (1 g) and NaOH (0.46 g) with stirring. The mixture was stirred for 4 h at 70 °C until the evolution of gaseous ammonia ceased. The resulting red-violet solution was then poured into a cation-exchanger column (Dowex 50w-x8, Na^+ form) and after the adsorbed band had been eluted with water, the red-violet eluate obtained was evaporated on a rotary evaporator and to the residue was added methanol to precipitate the complex as a powder. It was recrystallized from water, washed with methanol and ether and air-dried. Found: C, 29.63; H, 4.92; N, 12.98%. Calcd for [Co(ata)(en)]·H_2O: C, 29.54; H, 4.97; N, 12.92%.

The corresponding *R*-pn complex was prepared using *cis*(*Cl*)-[$CoCl_2(NH_3)_2$(*R*-pn)]Cl[4] as a starting meterial. Found: C, 32.62; H, 5.18; N, 12.77%. Calcd for [Co(ata)-

(*R*-pn)]·0.5H_2O: C, 32.72; H, 5.20; N, 12.73%.

(4) [Co(en)(tren)]Br_3·0.5H_2O and [Co(R-pn)(tren)]Br_3: One gram of *cis(Cl)*-[$CoCl_2(NH_3)_2$(en)]Cl[4] was dissolved in 10 cm^3 of water and to the solution were added a small amount of activated charcoal and a solution (neutralized with NaOH) of tren·3HBr (1.4 g) in 10 cm^3 of water. The mixture was mechanically stirred for 3 h at 60 °C until the color of the solution turned orange. The resulting mixture was then diluted to 50 cm^3 with water and the activated charcoal was filtered off by suction. The filtrate was evaporated in a rotary evaporator almost to dryness. The residue was dissolved in 5 cm^3 of water and NaBr (0.5 g) was added to the solution. Yellow crystals deposited were filtered and recrystallized from warm water, washed with methanol and ether and dried in air. For the *R*-pn complex *cis(Cl)*-[$CoCl_2(NH_3)_2$-(*R*-pn)]Cl[4] was used as a starting material. Found for the en complex: C, 18.41; H, 5.05; N, 15.96%. Calcd for [Co(en)(tren)]Br_3·0.5H_2O: C, 18.69; H, 5.31; N, 16.35%. Found for the *R*-pn complex: C, 20.80; H, 5.50; N, 16.27%. Calcd for [Co(*R*-pn)(tren)]Br_3: C, 20.82; H, 5.45; N, 16.19%.

(5) Other Complexes: The [Co(L-ala)(ata)]$^-$ (*trans(N)* and *cis(N)*) and [Co(L-ala)$(NH_3)_4$]$^{2+}$ complexes were prepared in the same way as described in the literature.[2,5]

Measurements. The visible and ultraviolet absorption measurements were made by a Shimadzu UV-200 spectrophotometer in aqueous solutions. The CD spectra were recorded on a JASCO MOE-1 spectropolarimeter in aqueous solutions and the ^{1}H-NMR spectra were obtained in deuterium oxide on Varian XL-100-15 spectrometer using DSS (sodium 2,2-dimethyl-2-silapentane-5-sulfonate) as as internal standard.

Results and Discussion

(1) [Co(am)(ata)]$^-$ Complexes. The two isomers of [Co(L-ala)(ata)]$^-$, red-violet and blue-violet, have been assigned[2] to *trans(N)* and *cis(N)* structures, respectively, from the splitting pattern of the first d-d absorption band. A remarkable feature is observed in the CD curves of two isomers (Fig. 2); namely they are almost enantiomeric to each other in the d-d transition band region. This is probably related to the fact that the two geometrical isomers are mutually quasi-enantiomeric as is seen in Fig. 3. The CD curves in Fig. 2 are explained by the contributions from two kinds of chiralities, one being the (*S*) asymmetric carbon atom of the L-alaninate ligand and the other the quasi-enantiomeric orientation of substituent $-CH_3$ on the chelate ring.

On assumption that the CD contributions of both chiralities are additive, the following equations are obtained.

$$\text{CD[red-violet]} = \text{CD}[S] + \text{CD}[trans],$$

$$\text{CD[blue-violet]} = \text{CD}[S] + \text{CD}[cis],$$

and

$$\text{CD}[trans] = -\text{CD}[cis],$$

where CD[*S*] represents the contributions of (*S*) asymmetric carbon, and CD[*trans*] and CD[*cis*] those of the quasi-enantiomeric geometrical configuration. Two contributions, CD[*S*] and CD[*trans*] were calculated rom the equations,

$$\text{CD}[S] = 1/2\{\text{CD[red-violet]} + \text{CD[blue-violet]}\},$$

$$\text{CD}[trans] = -\text{CD}[cis]$$

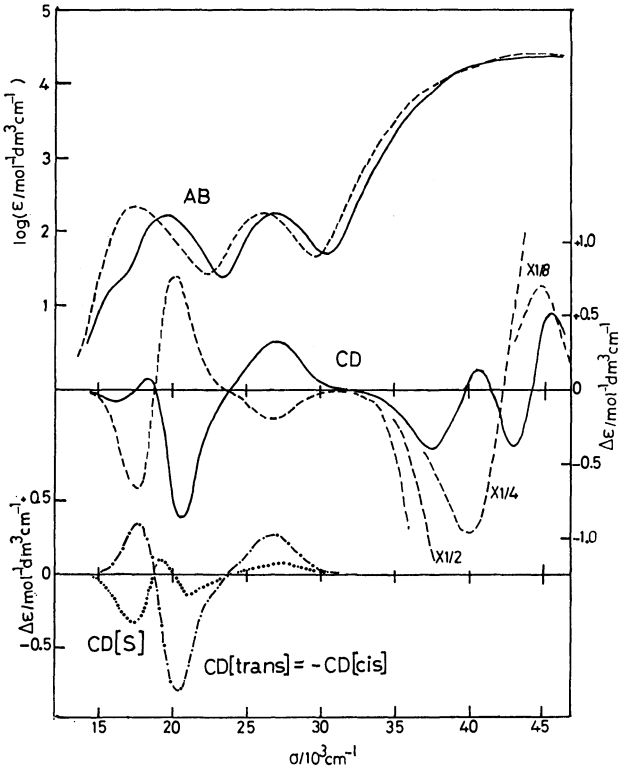

Fig. 2. Absorption (AB) and CD curves of *trans(N)* (——) and *cis(N)* (------) isomers of [Co(L-ala)(ata)]$^-$. Caclulated CD curves for asymmetric carbon (····) and quasi-enantiomeric (-···-) effects are also shown.

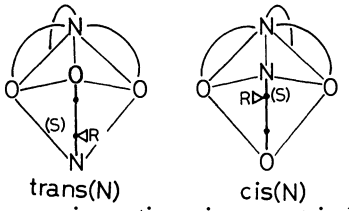

Fig. 3. Two quasi-enantiomeric geometrical isomers of [Co(am)(ata)]$^-$. (*S*) denotes absolute configuration of the asymmetric carbon.

$$= 1/2\{\text{CD[red-violet]} - \text{CD[blue-violet]}\}.$$

The obtained curves are also illustrated in Fig. 2. The CD[*S*] curve consists of three extrema (—, +, and —) from the longer wavelength side in the first d-d transition band region and the pattern and intensity are similar to the vicinal effect curve of the L-alaninate ligand in *trans(N)*-[Co(ox)(L-ala)$_2$]$^-$.[6] The CD[*trans*] curve shows two (+ and —) and one (+) component in the first and second d-d transition band region, respectively, and the contribution of CD[*trans*] or CD[*cis*] to the observed CD is larger than that of CD[*S*], the pattern of the observed CD being mainly determined by the quasi-enantiomeric effect.

(2) [Co(am)(tren)]$^{2+}$ Complexes. Kimura *et al.*[7] prepared tren complexes with amino carboxylate ligands and isolated two isomers, orange and red, of [Co(gly)(tren)]$^{2+}$. Recently it has been found from the X-ray crystal structure analyses that the orange isomer has *trans(N,t-N)* structure and the red one *cis(N,t-N)*.[8] Two isomers, orange and red, of the L-alaninato complex show absorption spectra analogous to those

TABLE 1. ABSORPTION DATA OF [Co(tripod)(bidentate)]-TYPE COMPLEXES
(Wave numbers and log ε values (in parentheses) are given in 10^3 cm^{-1} and mol^{-1} dm^3 cm^{-1}, respectively.)

Complex	d-d Tansition band		Ultraviolet band	
	1st	2nd		
trans(*N*)-[Co(L-ala)(ata)]$^-$	16 sh (1.3) 19.6 (2.22)	26.8 (2.24)	46.7 (4.35)	
cis(*N*)-[Co(L-ala)(ata)]$^-$	17.5 (2.34)	26.1 (2.24)	46.3 (4.37)	
trans(*N*,*t*-*N*)-[Co(gly)(tren)]$^{2+}$ [b]	21.2 (2.01)	29.2 (2.00)		
cis(*N*,*t*-*N*)-[Co(gly)(tren)]$^{2+}$ [b]	20.0 (1.96)	28.8 (1.88)		
trans(*N*,*t*-*N*)-[Co(L-ala)(tren)]$^{2+}$	21.2 (2.08)	28.9 (2.03)	44.4 (4.29)	
cis(*N*,*t*-*N*)-[Co(L-ala)(tren)]$^{2+}$	19.9 (2.06)	28.6 (2.01)	44.1 (4.27)	
trans(*N*,*t*-*N*)-[Co(L-val)(tren)]$^{2+}$	21.1 (2.09)	28.9 (2.04)	44.4 (4.28)	
trans(*N*,*t*-*N*)-[Co(L-ser)(tren)]$^{2+}$	21.1 (2.07)	28.9 (2 03)	44.6 (4.27)	
trans(*N*,*t*-*N*)-[Co(L-phe)(tren)]$^{2+}$	21.2 (2.09)	29.2 (2 05)	46.8 (4.35)	
trans(*N*,*t*-*N*)-[Co(D-pgly)(tren)]$^{2+}$	21.1 (2.16)	29 sh (2.1)	47.6 (4.34)	
trans(*N*,*t*-*N*)-[Co(L-cys)(tren)]$^{2+}$	16.5 sh (1.3) 20.7 (2.15)	26.5 sh (2.4)	34.7 (4.28)	47 (4.09)
[Co(en)(tren)]$^{3+}$	21.4 (2.04)	29.6 (1.98)	45.5 (4.27)	
[Co(*R*-pn)(tren)]$^{3+}$	21.3 (2.06)	29.6 (2.00)	45 sh (4.3)	49.5 (4.47)
[Co(ata)(en)]	17 sh 19.1 (2.19)	27.3 (2.25)	44.5 (4.33)	
[Co(ata)(*R*-pn)]	16.5 sh 19.2 (2.21)	27.4 (2.27)	44.7 (4.34)	

a) sh = Shoulder. b) Ref. 7.

TABLE 2. CD DATA OF [Co(tripod)(bidentate)]-TYPE COMPLEXES
(Wave numbers and $\Delta\varepsilon$ values (in parentheses) are given in 10^3 cm^{-1} and mol^{-1} dm^3 cm^{-1}, respectively.)

Complex	d-d Transition band		Ultraviolet band
	1st	2nd	
trans(*N*)-[Co(L-ala)(ata)]$^-$	16.1 (−0.083) 18.4 (+0.080) 20.6 (−0.863)	27.0 (+0.325)	37.6 (−0.40) 40.7 (+0.12) 42.9 (−0.40) 45.5 (+0.52)
cis(*N*)-[Co(L-ala)(ata)]$^-$	17.5 (−0.669) 20.3 (+0.763)	26.7 (−0.202)	40.0 (−3.76) 44.8 (+5.6)
trans(*N*,*t*-*N*)-[Co(L-ala)(tren)]$^{2+}$	19.5 (+0.194) 21.8 (−0.657)	29.0 (+0.118)	39.4 (−1.17) 46.3 (+0.57) 49.3 (−0.55)
cis(*N*,*t*-*N*)-[Co(L-ala)(tren)]$^{2+}$	18.8 (−0.160) 20.9 (+0.267)	26 (−0.05) 29.0 (−0.122)	39.4 (−0.66) 43.9 (+0.8) 48.2 (−1.11)
trans(*N*,*t*-*N*)-[Co(L-val)(tren)]$^{2+}$	19.4 (+0.215) 21.7 (−0.820)	29.0 (+0.149)	39.5 (−2.15)
trans(*N*,*t*-*N*)-[Co(L-ser)(tren)]$^{2+}$	18.7 (+0.020) 21.5 (−0.603)	29.0 (+0.077)	40.0 (−1.36)
trans(*N*,*t*-*N*)-[Co(L-phe)(tren)]$^{2+}$	19.5 (+0.062) 21.9 (−0.367)	29.3 (+0.055)	37.5 (−0.70)
trans(*N*,*t*-*N*)-[Co(D-pgly)(tren)]$^{2+}$	19.0 (−0.125) 21.7 (+1.685)	29.0 (−0.180)	39.1 (+3.44) 44.2 (−4.75)
trans(*N*,*t*-*N*)-[Co(L-cys)(tren)]$^+$	17.0 (+0.116) 18.7 (−0.016) 21.3 (+0.744)	25.6 (−0.787)	34.8 (−5.6) 39.5 (+1.5) 45 (+4.2) 48.5 (+6.3)
[Co(*R*-pn)(tren)]$^{3+}$	19.7 (−0.225) 22.1 (+0.397)	28.7 (−0.138)	44.8 (+4.1)
[Co(ata)(*R*-pn)]	17.4 (+0.059) 19.2 (−0.043) 21.4 (+0.228)	27.6 (−0.134)	46.1 (+4.2)

of the corresponding orange and red isomers of the glycinato complex, respectively (Table 1). Therefore, the orange isomer is *trans*(*N*,*t*-*N*) and the red *cis*(*N*,*t*-*N*). Though a pair of isomers, red-violet and blue-violet, were also isolated for each ata complex with the other amino carboxylates,[2] only orange isomer was obtained for each tren complex with L-val, L-ser, L-phe, and D-pgly. A series of hydrolysis studies[9] on $[CoCl_2(tren)]^+$ suggested that steric hindrance of hydrogen atoms on the aminoethyl chelate ring makes the chloro ligand *cis*

to the tertiary amine more labile, and X-ray crystal structure analyses of the two isomers of $[Co(gly)(tren)]^{2+}$ showed that unfavorable non-bonded interactions between the amino protons of the glycinate ring and the adjacent protons on the carbon and nitrogen atoms of tren make the *cis*(*N*,*t*-*N*) structure (red isomer) unstable[8] In fact, the formation ratio of the red isomer to the orange one was rather low for the tren complex with L-alaninate. Instability of the red isomer seems to increase with an increase in the bulkiness of a substituent on the amino carboxylate chelate ring. All orange isomers obtained have *trans*(*N*,*t*-*N*) structure from the same reason as that described for the L-alaninate complex. All these *trans*(*N*,*t*-*N*) isomers have similar CD patterns (+ and −) from the longer wavelength side in the first d-d transition band region, except for the D-pgly isomer, which shows the opposite sign pattern (− and +) (Table 2).

The two isomers of $[Co(L\text{-ala})(tren)]^{2+}$ show almost enantiomeric CD in the d-d transition band region (Fig. 4). On the basis of the same assumption as that for the ata complex, the CD contributions of (*S*) asymmetric carbon and the quasi-enantiomeric chirality were separated. The calculated CD contribution of the latter chirality is comparable in intensity to that of the former (Fig. 4). The pattern of the CD[*trans*(*N*,*t*-*N*)] is analogous to that of the CD[*trans*] for the ata complex; *i.e.*, two (+ and −) and one (+) components are

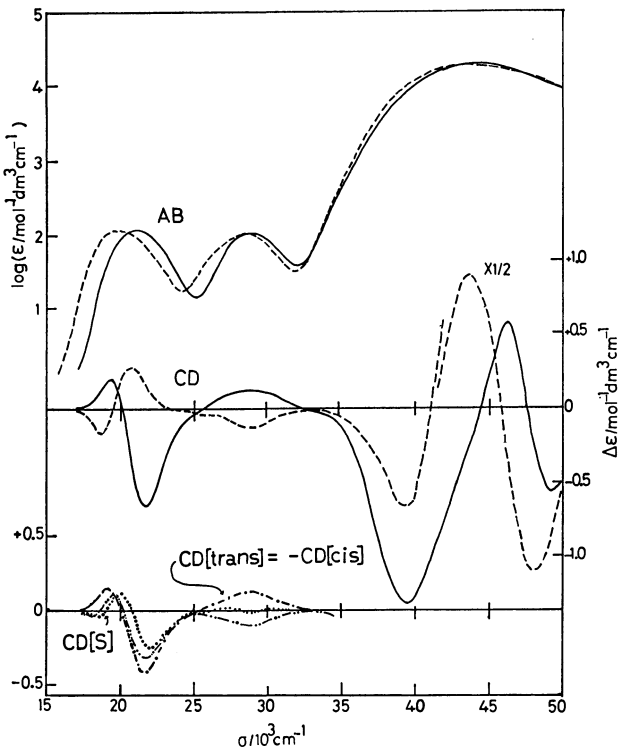

Fig. 4. Absorption (AB) and CD curves of *trans*(*N*,*t*-*N*) (——) and *cis*(*N*, *t*-*N*) (------) isomers of $[Co(L\text{-ala})(tren)]^{2+}$. Calculated CD curves for asymmetric carbon (····) and quasi-enantiomeric (-·-·-) effects are also shown. Another asymmetric carbon effect curve (-·-·-·-) is the observed one for $[Co(L\text{-ala})(NH_3)_4]^{2+}$ complex.

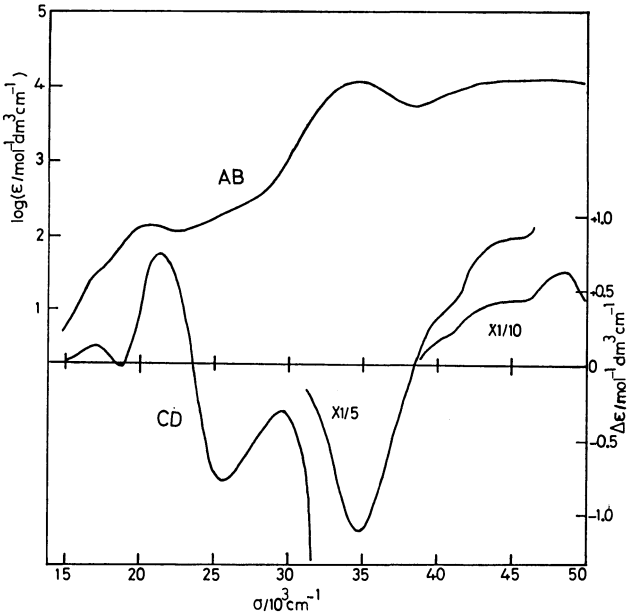

Fig. 5. Absorption (AB) and CD curves of *trans*(*N*, *t*-*N*)-$[Co(L\text{-cys})(tren)]^{+}$ complex.

present in the first and second d-d transition band region, respectively. The asymmetric carbon contribution CD[*S*] well coincides with the observed CD of the $[Co(L\text{-ala})(NH_3)_4]^{2+}$ in the first band region (Fig. 4).

The L-cysteinate complex is in a complicated situation. When L-cysteinate coordinates through the N and O donors, the α-substituent $-CH_2S^-$ is directed at the same side as in the other L-amino carboxylate complexes (Fig. 3), but when it does through N and S donors, the substituent $-CO_2^-$ is at the opposite side. Jackson *et al.*[10] first prepared two isomers, brown and ink-blue, of $[Co(L\text{-cys})(tren)]^{+}$ with N and S donors and assigned those to *trans*(*N*,*t*-*N*) and *cis*(*N*,*t*-*N*) structures, respectively, from their absorption, ^1H- and ^{13}C-nuclear magnetic resonance spectra. In the present work only the brown isomer, *trans*(*N*,*t*-*N*), was isolated, which showed a CD pattern enantiomeric to the L-alaninate complex of *trans*(*N*,*t*-*N*) structure in accordance with the *N*,*S*-coordination of L-cys ligand (Fig. 5).

(3) [Co(da)(ata)] Complexes. For en and *R*-pn, each only one complex of this type was prepared. The absorption spectrum of the *R*-pn complex was very similar to that of the en complex, having a broad first d-d band in agreement with the *mer*-CoN_3O_3 chromophore (Fig. 6 and Table 1). As the donor atoms at each end of *R*-pn have almost the same ligand-field strength, the discrimination of the two isomers, *trans*(*N**,*t*-*N*) and *cis*(*N**,*t*-*N*) in Fig. 1, is impossible only from the absorption spectra, in contrast to the case of amino carboxylate complex. In order to examine whether the isolated crystals contain only one isomer or both, the ^1H-NMR spectrum was measured.

It was found that the *R*-pn complex revealed two methyl doublets with about the same intensity (Fig. 7-a). Thus the complex is a 1 : 1 mixture of two isomers, *trans*(*N**,*t*-*N*) and *cis*(*N**,*t*-*N*), which are quasi-enantiomeric geometrical isomers (Fig. 8). If the same argument as that described for the L-ala complex is

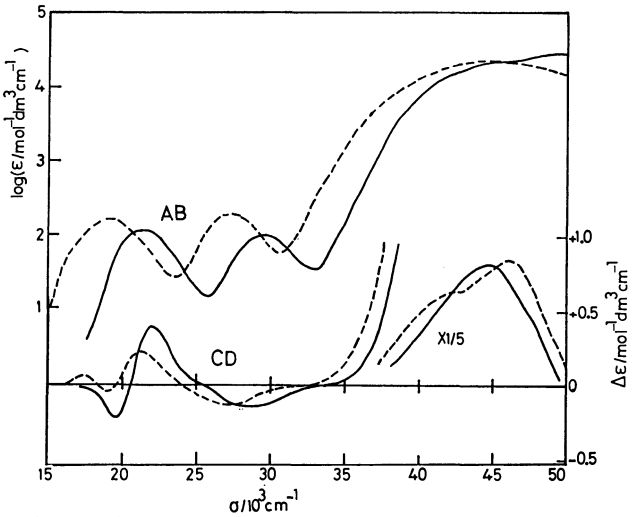

Fig. 6. Absorption (AB) and CD curves of [Co(ata)(*R*-pn)] (------) and [Co(*R*-pn)(tren)]$^{3+}$ (——).

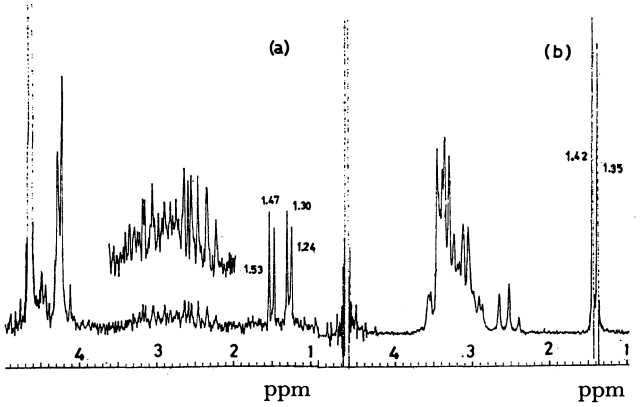

Fig. 7. ^{1}H-NMR spectra of (a) [Co(ata)(*R*-pn)] and (b) [Co(*R*-pn)(tren)]$^{3+}$.

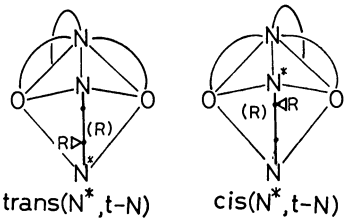

Fig. 8. Two quasi-enantiomeric geometrical isomers of [Co(ata)(*R*-pn)]. (*R*) denotes absolute configuration of the asymmetric carbon.

applicable to the *R*-pn complex, the observed CD curve (Fig. 6) should approximately correspond to a CD contribution CD[*R*], which contains two contributions, from (*R*) asymmetric carbon and λ-gauche conformation of the chelate ring.[11] In spite of a difference in the type of chromophore, the CD[*R*] contribution curve in Fig. 6 is roughly enantiomeric to the CD[*S*] curve of [Co(L-ala)(ata)]$^-$ (Fig. 2) or [Co(L-ala)(tren)]$^{2+}$ (Fig. 4) in the first and second d-d transition band region.

(4) [Co(da)(tren)]$^{3+}$ Complexes. Also in this case, only one complex was prepared for every 1,2-diamine (en or *R*-pn).

These complexes have a CoN_6 chromophore and their absorption spectra (Table 1) closely resembled that of [Co(en)$_3$]$^{3+}$ in regard to the position, intensity and half-width of the first d-d transition band. This indicates that the tripodlike ligand, tren, has about the same ligand-field strength as that of two en ligands. The ^{1}H-NMR spectrum of the [Co(*R*-pn)(tren)]$^{3+}$ complex showed only one methyl doublet (Fig. 7-b). Thus the complex consists of only one isomer, *trans(N*,t-N)* or *cis(N*,t-N)* in Fig. 1. Both isomers have unfavorable non-bonded interactions among the protons on the *R*-pn nitrogen atoms and on the carbon and nitrogen atoms of the tren. However, concerning the orientation of the substituent $-CH_3$, steric crowding in the *trans(N*,t-N)* structure is less unfavorable than that in *cis(N*,t-N)*; thus the only one isomer obtained is assigned to *trans-(N*,t-N)*. Therefore, its CD curve (Fig. 6) consists of two contributions, one from CD[*R*] and the other CD[*trans(N*,t-N)*]. Though the pattern of the observed CD for [Co(*R*-pn)(tren)]$^{3+}$ complex is similar to that for [Co(*R*-pn)$(NH_3)_4$]$^{3+}$, which has no quasi-enantiomeric effect and shows two (— and +) and one (—) component in the first and second d-d transition band region, respectively,[11] the intensity of the tren complex is much larger than that of the tetraammine complex. The subtraction of the CD curve for the tetraammine complex from that for the tren complex is expected to give an approximate CD[*trans(N*,t-N)*] contribution. The pattern of this CD contribution in the first and second d-d transition band region is analogous to that of CD[*R*] and the intensity for the CD[*trans(N*,t-N)*] is smaller than that for CD[*R*].

(5) Conclusion. The CD spectral data described above lead one to the following conclusion: 1. CD patterns of the [Co(L-am)(ata)]$^-$ or [Co(L-am)(tren)]$^{2+}$ complexes in the d-d band region are governed by the "vicinal effect" of amino carboxylate ligands, which consists of two contributions, the asymmetric carbon effect and the quasi-enantiomeric effect, the latter being dominant. 2. The *trans(N)* or *trans(N,t-N)* isomer shows two (+ and —) or three (—, + and —) CD components in the first d-d band region, and one (+) component in the second, while the *cis(N)* or *cis(N,t-N)* isomer shows two (— and +) and one (—) component in the first and second band region, respectively. 3. The CD patterns of this type of complex are not affected from the varieties of the first coordination spheres or chromophore (for example, the two isomers of the ata complex belong to *trans-* and *cis-*CoN_2O_4 chromophore and those of the tren complex CoN_5O). 4. For the corresponding *R*-pn complexes, the quasi-enantiomeric effect has a sign opposite to that for the L-ala complexes because the substituent $-CH_3$ is at the opposite side.

References

1) Abbreviations of ligands: L-ala=L-alaninate, am=amino carboxylate, ata=nitrilotriacetate, L-cys=L-cysteinate-(2-), da=1,2-diamine, en=ethylenediamine, gly=glycinate, L-phe=L-phenylalaninate, D-pgly=D-phenylglycinate, L-ser=L-serinate, *R*-pn=(*R*)-propylenediamine, tren=tris(2-aminoethyl)amine, and tripod=tripodlike quadridentate.

2) N. Koine, N. Sakota, J. Hidaka, and Y. Shimura, *Bull. Chem. Soc. Jpn.*, **42**, 1583 (1969).

3) K. Kuo and S. K. Madan, *Inorg. Chem.*, **8**, 1580 (1969).

4) C. J. Hawkins, J. A. Stark, and C. L. Wong, *Aust. J. Chem.*, **25**, 273 (1972).
5) T. Yasui, J. Hidaka, and Y. Shimura, *Bull. Chem. Soc. Jpn.*, **39**, 2417 (1966).
6) N. Matsuoka, J. Hidaka, and Y. Shimura, *Bull. Chem. Soc. Jpn.*, **48**, 458 (1975).
7) E. Kimura, S. Young, and J. P. Collman, *Inorg. Chem.*, **9**, 1183 (1970).
8) Y. Mitsui, J. Watanabe, Y. Harada, T. Sakamaki, Y. Iitaka, Y. Kushi, and E. Kimura, *J. Chem. Soc., Dalton Trans.*, **1976**, 2095.
9) S. Yuan, W. V. Miller, and S. K. Madan, *Inorg. Chim. Acta*, **7**, 134 (1973).
10) W. C. Jackson and A. M. Sargeson, *Inorg. Chem.*, **17**, 2165 (1978).
11) K. Ogino, K. Murano, and J. Fujita, *Inorg. Nucl. Chem. Lett.*, **4**, 351 (1968).

Synthesis and Structures of Steroidal Oxathiolanes

Shafiullah,* Hasrat Ali, Haruo Ogura,† and Hiroaki Takayanagi†

Steroid Research Laboratory, Department of Chemistry, Aligarh Muslim University, Aligarh-202001, India

†*School of Pharmaceutical Sciences, Kitasato University, Shirokane, Minato-ku, Tokyo 108*

(Received July 25, 1980)

Synthesis of isomeric oxathiolanes from 6-oxosteroids is described. Configurations at spirocyclic carbon in these compounds have been established on the basis of CD and NMR spectra with the use of shift reagent [Eu(dpm)$_3$].

As an extension of a previous study,[1] the synthesis and spectrochemical studies of steroidal oxathiolanes have been carried out.

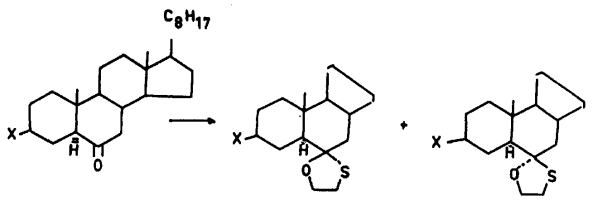

Results and Discussion

Reaction of ketone **1** with 2-mercaptoethanol in acetic acid ($BF_3 \cdot Et_2O$ as catalyst, room temperature) afforded a compound melting at 56 °C and a noncrystallizable oil. These compounds gave molecular ion peaks at *m/e* 446 ($C_{29}H_{50}OS$). The compound, mp 56 °C, showed characteristic bands at 1225 (–S–CH_2)[2] and 1065 cm^{-1} (monothioacetal group),[3] and the oil bands at 1220 (–S–CH_2) and 1070 cm^{-1} (monothioacetal group) in IR spectra. The NMR spectrum of the compound, mp 56°C, gave two distorted triplets at δ 4.32 and 3.92 (–O–CH_2) each integrating for 1 proton, and a double doublets at δ 2.78 (–S–CH_2; J=3.7 Hz) for 2 protons. The oil gave a distorted triplet for 2 protons at δ 4.03 (–O–CH_2) and a clean triplets for 2 protons at δ 2.93 (–S–CH_2).

The configuration of the –O–CH_2 and –S–CH_2 in the products could not be assigned with these spectral data, and [tris(dipivalomethanato) europium III] was employed as a shift reagent. Addition of the reagent to the compound, mp 56 °C, caused no significant change in the chemical shift of the signals in its NMR spectrum (Table 1), while its addition to the oily isomer showed a remarkable difference in the chemical shift of the NMR signals (Table 2). This confirmed that the –O–CH_2 group of monothioacetal ring attached to C(6) has an equatorial orientation in the oil, and an axial one in the compound, mp 56 °C.[4] Thus the compound is considered to be (6*S*)-6,6-oxyethylenethio-5α-cholestane **4** and the oil (6*R*)-6,6-oxyethylenethio-5α-cholestane **7**. CD data for compounds **4** (negative Cotton effect) and **7** (positive Cotton effect) (Fig. 1) further support configurational asignments for the monothioacetal ring in these compounds.[5]

By a similar treatment ketones **2** and **3** afforded oxathiolanes **5**, **8**, and **6**, **9** respectively. In NMR spectra, the splitting pattern of –O–CH_2 and –S–CH_2 protons of **5** and **6** was found identical with **4**, and oxathiolanes **8** and **9** provided similar NMR peaks for –O–CH_2 and –S–CH_2 protons as in **7**. On the basis of the NMR peak pattern the configurations at spirocyclic carbon in compounds **5**, **6**, and **8**, **9** were assigned similarly to **4** and **7**, respectively. This is supported by the negative Cotton effect (Figs. 2 and 3) for compounds **5** and **6** and positive Cotton effect (Figs. 2 and 3) for compounds **8** and **9**.

The parent ketones **1**—**3** were generated when monothioacetals **4**—**9** were treated with aqueous acetic acid.

Table 1. Induced chemical shifts (δ) of various protons of compound **4** with increasing amount of shift reagent Eu(dpm)$_3$

	–O–CH_2	–S–CH_2	C(10)–CH_3	C(13)–CH_3
Sample(20.29 mg) neat	4.05	2.85	0.98	0.66
Sample(20.29 mg)+Eu(dpm)$_3$ (5.79 mg)	4.00	2.83	0.96	0.66
Sample (20.29 mg)+Eu(dpm)$_3$ (11.54 mg)	4.06	2.78	1.00	0.67
Sample (20.29 mg)+Eu(dpm)$_3$ (12.30 mg)	4.15	2.80	0.94	0.61

Table 2. Induced chemical shifts (δ) of various protons of compound **7** with increasing amount of shift reagent Eu(dpm)$_3$

	–O–CH_2	–S–CH_2	C(10)–CH_3	C(13)–CH_3
Sample(22.00 mg) neat	4.03	2.93	0.98	0.67
Sample (22.00 mg)+Eu(dpm)$_3$ (6.0 mg)	4.20	3.00	0.98	0.67
Sample (22.00 mg)+Eu(dpm)$_3$ (11.16 mg)	4.63	3.03	1.03	0.70
Sample (22.00 mg)+Eu(dpm)$_3$ (15.81 mg)	4.91	3.34	1.14	0.72

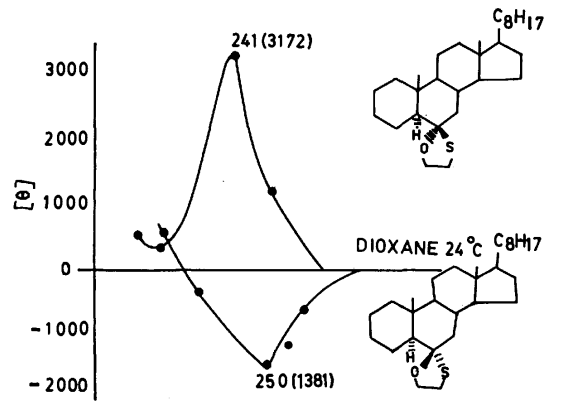

Fig. 1. CD curves of compounds **4** and **7** in dioxane at 24 °C.

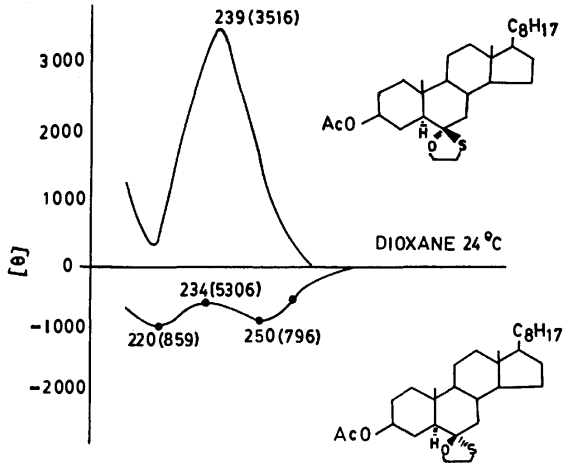

Fig. 2. CD curves of compounds **5** and **8** in dioxane at 24 °C.

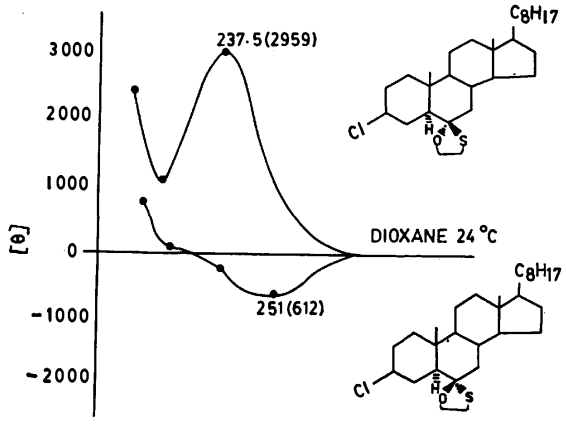

Fig. 3. CD curves of compounds **6** and **9** in dioxane at 24 °C.

Experimental

All melting points are uncorrected. IR spectra were recorded on a Perkin-Elmer 237 spectrophotometer, and ^{1}H-NMR spectra in $CDCl_3$ on a Varian A60 instrument (δ scale. TMS=0 ppm). CD curves were measured with a JASCO J-20 spectropolarimeter in dioxane. Mass spectra were measured on a Varian AJMS D100 mass spectrometer. TLC were performed with silica gel (BDH) and column chromatography with silica gel (BDH-60-120 mesh). NMR values in ppm (s=singlet; dd=double doublets; t=triplet; mc=multiplet centred at).

(6S)-6,6-Oxyethylenethio-5α-cholestane **4** *and (6R)-6,6-Oxyethylenethio-5α-cholestane* **7**. A solution of ketone **1**[6] (5.0 g) in AcOH (200 cm^3) was treated with 2-mercaptoethanol (10 cm^3) and $BF_3 \cdot Et_2O$ (2 cm^3) and left to stand at room temperature for 1 h. The solution was diluted with MeOH (25 cm^3), poured into water and extracted with ether. The ethereal layer was washed successively with water, $NaHCO_3$ solution (5%), water and dried (anhydrous Na_2SO_4). The oil (5.0 g) obtained after removal of ether under reduced pressure was chromatographed over silica gel (100 g). Elution with light petroleum ether afforded **4**; solidified on being left at room temperature (2.0 g); mp 56 °C; MS (70 eV) *m/e* 446 (30%) (M^+); Found: C, 78.03; H, 11.01%. Calcd for $C_{29}H_{50}OS$: C, 78.02; H, 11.20%; CD (dioxane) $[\theta]^{20}$(nm): −1380 (250). NMR ($CDCl_3$): δ 0.68, 0.82, 0.92, and 0.98 (C(10)−; C(13)− and side chain methyl protons).

Further elution with light petroleum ether afforded **7** (2.10 g) as an oil; MS (70 eV) *m/e* 446 (28.3%) (M^+); Found: C, 78.03; H, 11.01%. Calcd for $C_{29}H_{50}OS$: C, 78.02, H,11.20; CD (dioxane) $[\theta]^{20}$ (nm): +3170 (241). NMR ($CDCl_3$): δ 0.67, 0.70, 0.75, and 0.98 (C(10)−; C(13)− and side chain methyl protons).

3β-Acetoxy-(6S)-6,6-oxyethylenethio-5α-cholestane **5** *and 3β-Acetoxy(6R)-6,6-oxyethylenethio-5α-cholestane* **8**. The ketone **2**[7] (5.0 g) was treated with 2-mercaptoethanol (10 cm^3) and $BF_3 \cdot Et_2O$ (2 cm^3) in AcOH (200 cm^3) in the same way as for **1**. The oil obtained after removal of the solvent was chromatographed over silica gel (100 g). Elution with light petroleum ether–ether (22 : 1) afforded **5**, recrystallized from light petroleum ether (2.20 g); mp 142 °C, MS (70 eV) *m/e* 504 (12.5%) (M^+); Found: C, 73.81; H, 10.49%. Calcd for $C_{31}H_{52}O_3S$: C, 73.8; H, 10.51%; CD (dioxane) $[\theta]^{20}$ (nm): −860 (220) and −800 (250). IR (KBr): 1740 (CH_3–CO–O–), 1240 (C–O), and 1030 cm^{-1} (monothioacetal group); NMR ($CDCl_3$): δ 4.7 (mc, $W_{1/2}$=16 Hz, C(3)α-H), 4.28, 3.9 (distorted tripletes, –O–C$\underline{H}_2$–), 2.86 (dd, J=3.6 Hz, –S–C$\underline{H}_2$–), 2.03 (s, C(3)–O–CO–C$\underline{H}_3$), 0.70, 0.83, 0.93, and 1.0 (C(10)–, C(13)–, and side chain methyl protons).

Further elution with light petroleum ether-ether (20 : 1) yielded **8** recrystallized from light petroleum ether (2.0 g), mp 106°C; MS (70 eV) *m/e* 504 (11.4%) (M^+); Found: C, 73.80; H, 10.49%. Calcd for $C_{31}H_{52}O_3S$: C, 73.8; H, 10.51%; CD (dioxane) $[\theta]^{20}$ (nm): +3520 (239). IR (KBr): 1740 (CH_3–CO–O–), 1240 (C–O–), and 1030 cm^{-1} (monothioacetal group); NMR ($CDCl_3$): δ 4.73 (mc, $W1/2$=16 Hz, C(3)α-H), 4.03 (distorted triplet, –O–C$\underline{H}_2$–), 1.96 (t, –S–C$\underline{H}_2$–), 2.03 (s, C(3)β-O–CO–C$\underline{H}_3$), 0.70, 0.80, 0.90, and 0.98 (C(10)–(C(13)–, and side chain methyl protons).

3β-Chloro-(6S)-6,6-oxyethylenethio-5α-cholestane **6** *and 3β-Chloro-(6R)-6,6-oxyethylenethio-5α-cholestane* **9**. The ketone **3**[8] (5.0 g) was treated with 2-mercaptoethanol (10 cm^3) and $BF_3 \cdot Et_2O$ (2 cm^3) in AcOH (200 cm^3) in the same way as for **1** and **2**. Compounds **6** and **9** were separated. Compound **6** was recrystallized from light petroleum ether (1.8 g), mp 152 °C; MS (70 eV) *m/e* 480/482 (3 : 1) (26.0%) (M^+); Found C, 72.30; H, 10.10%. Calcd for $C_{29}H_{49}OSCl$: C, 72.5; H, 10.20%; CD (dioxane) $[\theta]^{20}$ (nm): −610 (251). IR (KBr): 1070 (monothioacetal group), and 760 cm^{-1}; NMR ($CDCl_3$): cm^{-1}; NMR ($CDCl_3$): δ 4.0 (mc, C(3)α-H, –O–C$\underline{H}_2$), 3.86 (dd, J=3.6 Hz, –S–C$\underline{H}_2$–), 0.68, 0.80, 0.92, and 1.0 (C(10)–, C(13)–, and side chain methyl protons).

Conpound **9** was recrystallized from petroleum ether (1.75 g); mp 115 °C; MS (70 eV) *m/e* 480/482 (3 : 1) (7.0%) (M^+); Found: C, 72.31; H, 10.12%. Calcd for $C_{29}H_{49}OSCl$: C,

72.5; H, 10.20%; CD (dioxane) $[\theta]^{20}$ (nm): +2960 (237.5). IR (KBr): 1070 (monothioacetal group), and 760 cm^{-1} (C–Cl); NMR ($CDCl_3$): δ 4.05 (mc, C(3)α-H, –O–C<u>H</u>$_2$–), 2.97 (t, –S–C<u>H</u>$_2$–), 0.68, 0.78, 0.92, 0.98 (C(10)–, C(13)–, and side chain methyl protons).

We are grateful to Prof. W. Rahman, Head, Department of Chemistry for providing necessary facilities and Prof. M. S. Ahmad for valuable discussions. Financial assistance from CSIR (New Delhi) is acknowledged.

References

1) Shafiullah and H. Ali, *J. Steroid. Biochem.*, **13**, 467 (1980).
2) I. F. Trotter and H. W. Thompson, *J. Chem. Soc.*, **1946**, 481.
3) C. Djerassi and M. Gorman, *J. Am. Chem. Soc.*, **75**, 3704 (1953).
4) J. E. Herz, V. M. Rodriguez, and P. J. Nathan, *Tetrahedron Lett.*, **1971**, 2949.
5) C. H. Robinson, L. Milewich, G. Snatzke, W. Klyne, and S. R. Wallis, *J. Chem. Soc., C*, **1968**, 1245.
6) D. N. Jones, J. R. Lewis, C. W. Shoppee, and G. H. R. Summers, *J. Chem. Soc.*, **1955**, 2876.
7) I. M. Heilbron, E. H. R. Jones, and F. S. Spring, *J. Chem. Soc.*, **1937**, 801.
8) C. W. Shoppee and G. H. R. Summers, *J. Chem. Soc.*, **1952**, 1786.

Aromatic Nucleophilic Substitution. XV.[1] Stopped-flow Kinetics of the Formation and Decomposition of 1,3- and 1,1-Disubstituted Meisenheimer Complexes in the Reactions of 1-Dialkylamino-2,4-dinitronaphthalenes with Potassium Methoxide in Dimethyl Sulfoxide–Methanol

Shizen SEKIGUCHI,* Toshio TAKEI, Kohji MATSUI, Noboru TONE, and Noboru TOMOTO†

Department of Synthetic Chemistry, Gunma University, Ten-jin-cho, Kiryu, Gunma 376

†*Faculty of Engineering, Miyazaki University, 1-1-1 Kirishima, Miyazaki 880*

(Received October 8, 1980)

The formation of 1,3-disubstituted anionic σ complexes, followed by 1,1-disubstituted ones was confirmed by means of absorption and NMR spectra in the reactions of 1-dialkylamino-2,4-dinitronaphthalenes with potassium methoxide in DMSO–CH_3OH. The rates and activation parameters were determined by kinetic studies with use of stopped-flow and conventional spectrophotometers. The rate constants for the formation of 1,3-disubstituted one decreased in the order 1-dimethylamino-$>$1-(*N*-methylbutyl)amino-$>$1-piperidino-$>$1-diethylamino-2,4-dinitronaphthalenes, those for its decomposition being comparable with each other. On the other hand, the rate constant for the formation of 1,1-disubstituted one decreased in the same order as above while that for its decomposition decreased in the order 1-dimethylamino-$>$1-(*N*-methylbutyl)amino-$>$1-diethylamino-$>$1-piperidino-2,4-dinitronaphthalenes. The mechanism was discussed from activation parameters.

Many Jackson-Meisenheimer complexes (anionic σ complex) have been prepared by nucleophilic attack on polynitroaromatic compounds[2] as shown by

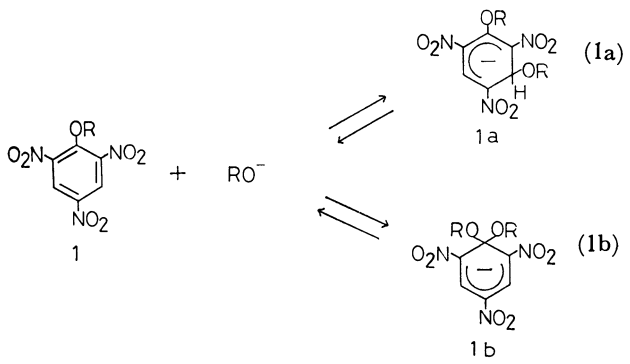

Especially in the reactions of 1-alkoxy- or 1-amino-substituted activated benzenes or heteroaromatics with alkoxides or amines, two anionic σ complexes, 1,3- and 1,1-disubstituted ones (**1a** and **1b**) are usually formed.[3–22] Upon addition of bases **1a** is formed at first, undergoing isomerization to **1b**; the former is said to be a kinetically controlled product and the latter an equilibrium-controlled one.[23,24]

However, with activated naphthalene derivatives 1,3-disubstituted complexes such as **1a** have hardly been found. As a few exceptional cases, Millot and Terrier testified the formation of **2a** by stopped-flow spectrophotometric technique,[14] although its evidence was considered to be somewhat uncertain. Fendler *et al.*[25] attempted the reaction of 1-methoxy-2,4-dinitronaphthalene (**2**) with alkoxide, but were unsuccessful in the identification of **2a**. Their failure is due to the insufficient stability of such complexes as **2a**, as compared with those formed from benzene derivatives.

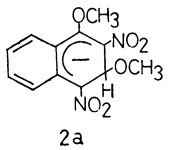

2a

Thus, if the stability of **2b** (naphthalene analog corresponding to **1b**) could be reduced, the energy barrier between **2a** and **2b** would become smaller, elongating the life of **2a** and making the identification easier. Such attempts were successful in the reactions of 1-amino-2,4-dinitronaphthalenes with alkoxides.[26,27] Replacement of amino for alkoxyl groups clearly deactivates the C-1 position of a naphthalene moiety, necessitating the slower isomerization of **2a** to **2b**.

As a result, it would be interesting to investigate the kinetic and thermodynamic parameters of the reactions of 1-dialkylamino-2,4-dinitronaphthalenes with alkoxides.[28]

This paper reports the stopped-flow kinetics of the formation and decomposition of the 1,3- and 1,1-disubstituted anionic σ complexes in the reactions of various 1-dialkylamino-2,4-dinitronaphthalenes (**3**—**6**) with potassium methoxide in DMSO–CH_3OH (90/10 v/v).

Results

General Features. The reaction of 1-dimethylamino-2,4-dinitronaphthalene (**4**) with potassium methoxide in DMSO–CH_3OH afforded **4a** at first and then **4b** in quantitative yields (Fig. 1). Spectrum (b) obtained by stopped-flow spectrophotometry just after addition of methoxide is due to **4a**, absorbance scale being arbitrary; Spectrum (c), attributable to **4b**, was obtained in 12 min after addition.[29,30] From the results, the reaction is expected to proceed in a mode similar to that of Eq. 1.

NMR technique is considered useful for elucidating the structures of anionic σ complexes.[23] Just after addition of methanolic potassium methoxide (1.40×10^{-4} mol) to a DMSO solution (0.5 ml) of **4** (1.40×10^{-4} mol) at room temperature, the solution turned red at once, suggesting the formation of a complex. Just after addition, H_3 sharp singlet (δ 8.63) of **4** shifted upfield

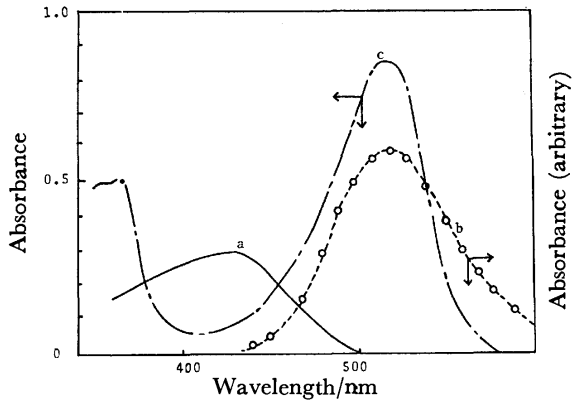

Fig. 1. Spectral changes relevant to the reaction of 1-dimethylamino-2,4-dinitronaphthalene (**4**) with CH_3OK in DMSO–CH_3OH (90 : 10, v/v); (a) **4** (3.25×10^{-5} M (1M=1 mol dm^{-3}) at room temperature; (b) obtained by means of a stopped-flow method (**4** 5.0×10^{-4} M and CH_3OK 4.5×10^{-3} M); (c) 12 min after addition of CH_3OK.

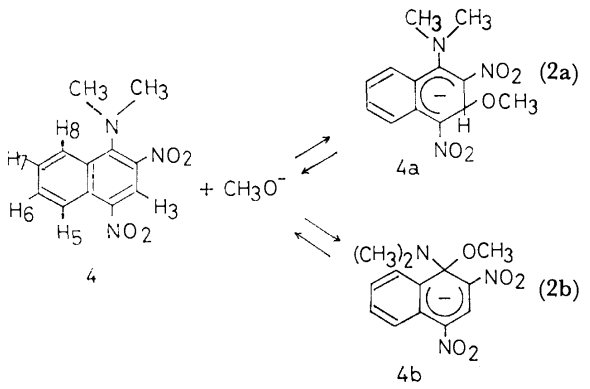

(δ 6.33, H_3 of **4a**). Fast sweep time (500 Hz/50 s) and fast procedure are indispensable for detecting spectral changes, 2.5 min after addition, a new singlet, due to H_3 of **4b** appeared at δ 9.31 at the expense of the singlet at δ 6.33 (measured at the normal sweep time, 250 Hz/50 s, in this case) which appeared faintly.

The results also support the reaction paths (Eq. 2). Similar results were obtained for **3**, **5**, and **6**.[31] It is thus expected that the discrete kinetics of formation and decomposition of **4a** and **4b** is possible.

Kinetic Runs. Let us rewrite Eq. 2 in a form convenient for quantitative discussion as Eq. 3. Stage I kinetics (**4**⇄**4a**, Eq. 3a) is much faster than Stage II

$$\mathbf{4} + {}^-OCH_3 \underset{k_{-1}}{\overset{k_1,\ K_1}{\rightleftharpoons}} \mathbf{4a} \quad (3a)$$

$$K_1 = \frac{k_1}{k_{-1}},\quad K_2 = \frac{k_2}{k_{-2}}$$

$$\mathbf{4a} \underset{k_{-2}}{\overset{k_2,\ K_2}{\rightleftharpoons}} \mathbf{4b} \quad (3b)$$

reaction (**4a**⇄**4b**, Eq. 3b). Thus, when Stage I kinetics is taken into account, Stage II reaction can be neglected, since the former reaction is completed in several thousandths seconds (Table 3), making the contamination by the latter negligible.

Stage I. The pseudo-first-order rate constant, k_ψ, for the attainment of an equilibrium is the sum of forward and reverse components. For the system (Eq. 3a) the following expression should hold:

$$k_\psi = k_1([CH_3O^-]+[4]) + k_{-1}. \quad (4)$$

Under the usual condition $[CH_3O^-]\gg[4]$, Eq. 4 is simplified to

$$k_\psi = k_1[CH_3O^-] + k_{-1}. \quad (5)$$

As a result, dependence of k_ψ on methoxide concentration would afford the linear relationship, and k_1 and k_{-1} are estimated from the slope and the intercept, respectively. The dependence of k_ψ on methoxide concentration is given in Table 1, involving estimated rate constants and equilibrium constants. The relationship between k_ψ and methoxide concentration at 15, 25, and 35 °C indicates that Eq. 5 holds fairly well (Fig. 2). The temperature dependence of K_1, k_1, and k_{-1} was determined at four temperatures. Kinetic and activation parameters obtained from the Arrhenius plot (not shown) are summarized in Table 3, which includes the results obtained for **3**, **5**, and **6**. The k_1 values decrease in the order **4**>**5**>**3**>**6** and the k_{-1} values in the order **3**>**6**>**4**>**5**. The enthalpy and entropy of activation for **3**, **4**, **5**, and **6** ($\Delta H_1^{\ddagger}$ and $\Delta S_1^{\ddagger}$) compensate with each other, and those ($\Delta H_{-1}^{\ddagger}$ and $\Delta S_{-1}^{\ddagger}$) also do the same except for **3**, in which the k_{-1} value depends upon $\Delta S_{-1}^{\ddagger}$ rather than $\Delta H_{-1}^{\ddagger}$.

Stage II. As shown in Fig. 1, the change from Spectrum a to Spectrum b (**4**⇄**4a**) obtained by stopped-flow spectrophotometry is instantaneous, whereas that from Spectrum b to Spectrum c (Stage II reaction) is relatively slow. As a result, Stage II reaction (**4a**⇄**4**⇄**4b**), in which Stage I process (**4**⇄**4a**) is involved as equilibrium, is much slower than Stage I reaction. Therefore, Stage I reaction can be treated as equilibrium, lying almost entirely on the right in the treatment of Stage II kinetics. Table 3 shows that Stage I reaction

Table 1. Rate and equilibrium for the formation and decomposition of 1,3-disubstituted anionic σ complex formed from 1-dimethylamino-2,4-dinitronaphthalene (**4**) and potassium methoxide in DMSO–CH_3OH (90: 10 v/v) at 25 °C[a]

10^3 [CH_3OK] / M	k_ψ[b] / s^{-1}	k_1 / $M^{-1}s^{-1}$	$10\,k_{-1}$ / s^{-1}	K_1 / M^{-1}
2.16	1.95			
2.26	2.11			
3.53	2.94			
4.24	3.19			
4.50	3.38			
4.94	3.63	596[c]	7.24[d]	820[e]
5.40	3.92			
5.65	4.04			
6.35	4.66			
7.20	5.08			
8.10	5.49			

a) $[4]_0$ 2.0×10^{-4} M; μ 0.05 M ($KClO_4$). b) Measured at 565 nm with a stopped-flow method. Estimated limit of error ±2.5%. c) Calculated from Eq. 5. Estimated limit of error ±7.3%. d) Calculated from Eq. 5. Estimated limit of error ±10.0%. e) Calculated from $K_1=k_1/k_{-1}$.

Table 2. Temperature dependence of k_1, k_{-1}, and K_1 for theformation and decomposition of 1,3-disubstituted anionic σ complex formed from 1-dimethylamino-2, 4-dinitronaphthalene (**4**) and potassium methoxide in DMSO–CH_3OH (90: 10 v/v)[a]

Temp °C	k_1[b] $M^{-1}s^{-1}$	$10\,k_{-1}$[c] s^{-1}	K_1[d] M^{-1}
15	325	2.83	1150
25	596	7.24	820
35	1150	14.8	780
40	1570	20.2	710

a) $[\mathbf{4}]_0$ 2.0×10^{-4} M; μ 0.05 M ($KClO_4$). b) Calculated from Eq. 5. Estimated limit of error ±7.3%. c) Calculate from Eq. 5. Estimated limit of error ±10.0%. d) Calculated from $K_1=k_1/k_{-1}$. Estimated limit of error ±17.3%.

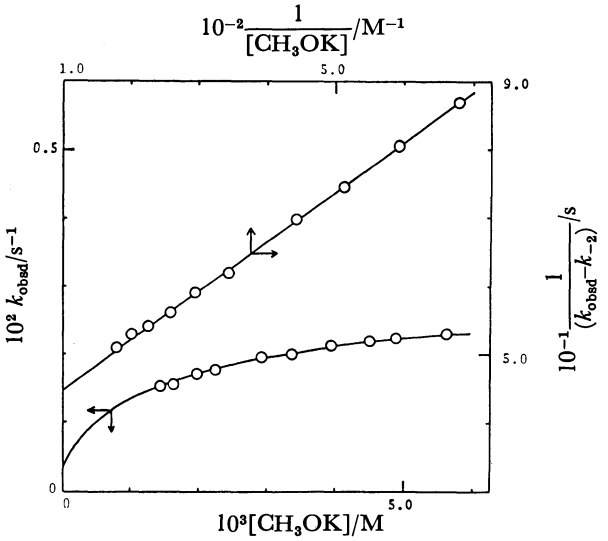

Fig. 2. Relationship between k_{obsd} and $[CH_3OK]$ and between $1/(k_{obsd}-k_{-2})$ and $1/[CH_3OK]$ in the reaction of 1-dimethylamino-2,4-dinitronaphthalene with CH_3OK in DMSO–CH_3OH (90 : 10, v/v) at 25 °C.

nearly completed in several thousandths of a second, very small in the time scale for Stage II reaction.

As to the rate of Stage II reaction, the general kinetic expression derivable from Eq. 3 should take account of the possibility that the substrate may be split between **4** and **4a**. Putting $[\mathbf{4}]_{st}=[\mathbf{4}]+[\mathbf{4a}]$, and K_1 the equilibrium constant for Stage I reaction, we obtain

$$k_{obsd}=k_{-2}+\frac{k_2[CH_3O^-]}{1+K_1[CH_3O^-]}, \quad (6)$$

where k_{obsd} is the pseudo-first-order rate coefficient for Stage II reaction, and k_2 and k_{-2} the rate coefficients for forward and reverse reactions. Consequently, dependence of k_{obsd} on methoxide concentration would afford a curvilinear relationship, in which the curve would not pass through the origin. If the k_{-2} value can be obtained by extrapolation from the relationship between k_{obsd} and methoxide concentration, we obtain the following equation by substituting the value into Eq. 6, and rearranging. Thus, k_2 and k_1 can be obtained from the slope and intercept in the plot of $1/(k_{obsd}-k_{-2})$ against $1/[CH_3O^-]$.

$$\frac{1}{k_{obsd}-k_{-2}}=\frac{1}{k_2[CH_3O^-]}+\frac{K_1}{k_2} \quad (7)$$

The dependence of k_{obsd} on methoxide concentration involves estimated rate and equilibrium constants (Table 4). Figure 2 shows the dependence of k_{obsd} on methoxide concentration and the inversion plot. Equation 6 and 7 are seen to hold. Objection might arise that the relation between k_{obsd} and methoxide concentration (Fig. 2) would afford a straight line within the range of methoxide concentration. This would be expected if $K_1[CH_3O^-]\ll1$ in Eq. 6. Although an increase in k_{obsd} with increasing methoxide concentration is much smaller at 25 °C, the plot of k_{obsd} against methoxide concentration were steeply convex upward at higher temperatures (*e.g.*, 35 and 40 °C), indicating that Eq. 6 holds. The k_{-2} value was so determined that the best linear relationship would be established in the inversion plot (Eq. 7). There might be some

Table 3. Kinetic and thermodynamic parameters for the formation and decomposition of 1,3-disubstituted anionic σ complexes in DMSO–CH_3OH (90: 10 v/v) at 25 °C

R, R'[a]	 **3**	CH_3, CH_3 **4**	CH_3, n-C_4H_9 **5**	C_2H_5, C_2H_5 **6**
$k_1/M^{-1}s^{-1}$	480±35	596±44	540±40	410±30
k_{-1}/s_{-1}	1.04±0.11	$7.24\pm0.08\times10^{-1}$	$7.20\pm0.08\times10^{-1}$	$7.56\pm0.08\times10^{-1}$
K_1/M^{-1}	460±80	820±150	750±140	540±90
$\Delta H_1^{\neq}$/kcal mol^{-1}	11.5±2.3	10.6±2.2	11.2±2.3	12.1±2.5
$\Delta S_1^{\neq}$/cal deg^{-1} mol^{-1}	−7.1±5.3	−10.0±7.6	−8.1±6.5	−5.7±4.3
$\Delta H_{-1}^{\neq}$/kcal mol^{-1}	13.5±3.6	13.4±3.6	13.7±3.6	14.1±3.7
$\Delta S_{-1}^{\neq}$/cal deg^{-1} mol^{-1}	−10.9±9.2	−14.1±12.0	−12.9±10.9	−11.4±9.7
$\Delta H_{1.3}^{\circ}$/kcal mol^{-1}[b]	−2.0±5.9	−2.8±5.8	−2.5±5.9	−2.0±6.2
$\Delta S_{1.3}^{\circ}$/cal deg^{-1} mol^{-1}[c]	3.8±14.5	4.1±19.6	4.8±17.4	5.7±14.0
$\Delta G_{1.3}^{\circ}$/kcal mol^{-1}[d]	−3.1±10.2	−4.0±11.6	−3.9±11.2	−3.7±10.3

a) Only the substituent at C-1 of 2,4-dinitronaphthalene is indicated. b) $\Delta H_{1.3}^{\circ}=\Delta H_1^{\neq}-H_{-1}^{\neq}$. c) $\Delta S_{1.3}^{\circ}=S_1^{\neq}-S_{-1}^{\neq}$. d) $\Delta G_{1.3}^{\circ}=\Delta H^{\circ}-T\Delta S^{\circ}$.

TABLE 4. RATE AND EQUILIBRIUM FOR THE FORMATION AND DECOMPOSITION OF 1,1-DISUBSTITUTED ANIONIC σ COMPLEX FORMED FROM 1-DIMETHYLAMINO-2,4-DINITRONAPHTHALENE (**4**) AND POTASSIUM METHOXIDE IN DMSO–CH_3OH(90: 10 v/v) AT 25 °C[a]

10^3 [CH_3OK]	$10^2 k_{obsd}$[b]	k_2	$10^3 k_{-2}$	K_1	K_2
M	s^{-1}	$M^{-1}s^{-1}$	s^{-1}	M^{-1}	M^{-1}
1.47	1.51				
1.69	1.60				
1.96	1.70				
2.25	1.76				
2.93	1.97	14.3[c]	3.6[d]	540[e]	3970[f]
3.37	2.05				
3.91	2.13				
4.49	2.20				
4.89	2.25				
5.62	2.31				

a) $[4]_0$ 3.20×10^{-5} M; μ 0.05 M ($KClO_4$). b) Measured at 520 nm. Estimated limit of error ±2.0%. c) Calculated from Eq. 7. Estimated limit of error ±13.5%. d) Calculated from Eq. 6. Estimated limit of error ±8.3%. e) Estimated limit of error ±16.5%. f) Calculated from $K_2=k_2/k_{-2}$. Estimated limit of error ±21.7%.

ambiguity in the k_{-2} values. The temperature dependence of K_1, K_2, k_2, and k_{-2} at four temperatures is given in Table 5. The Arrhenius plot affords kinetic and activation parameters (Table 6), together with the results obtained for **3**, **5**, and **6**. Although there is some difference between the K_1 values obtained from Stage I and II kinetics, the agreement could be considered to be fairly good. Formation of 1,3-disubstituted anionic σ complex is kinetically controlled and that of 1,1-disubstituted one equilibrium-controlled, which is reflected in the K_1 and K_2 values (Tables 3 and 6).

Discussion

1,3-Disubstituted Anionic σ Complex. The rates and activation parameters (Table 3) do not differ much, since

TABLE 5. TEMPERATURE DEPENDENCE OF K_1, K_2, k_2, AND k_{-2} FOR FORMATION AND DECOMPOSITION OF THE 1,1-DISUBSTITUTED ANIONIC σ COMPLEX FORMED FROM 1-DIMETHYLAMINO-2,4-DINITRONAPHTHALENE (**4**) AND POTASSIUM METHOXIDE IN DMSO–CH_3OH (90: 10 v/v) AT 25 C[a]

Temp	k_2[b]	$10^3 k_{-2}$[c]	K_1[d]	K_2[e]
°C	$M^{-1}s^{-1}$	s^{-1}	M^{-1}	M^{-1}
15	6.7	2.5	680	2680
25	14.3	3.6	540	3970
35	28.5	5.1	440	5580
40	41.8	5.8	400	7200

a) $[4]_0$ 3.20×10^{-5} M; μ 0.05 M ($KClO_4$). b) Estimated limit of error ±13.5%. c) Estimated limit of error ±8.3%. d) Estimated limit of error ±16.5%. e) Estimated limit of error 21.7%.

methoxide ion attacking at the C-3 position does not get the direct effect of a dialkylamino group at the C-1 position. Some comments are given in the following. (a) The entropy of activation for k_{-1} is negative, as compared with that for k_1 with each substrate. This indicates that the entropy refers to unimolecular reactions in line with the view that part of the negative charge delocalized in the anionic σ complex becomes concentrated on the incipient methoxide ion in the transition state of decomposition, increasing the solvation of activated complexes and giving rise to negative entropy of activation.[33] (b) The enthalpy and entropy of activation for k_1 ($\Delta H_1^{\ddagger}$ and $\Delta S_1^{\ddagger}$) compensate each other, in line with the view that the solvation of methanol to the dialkylamino group of a substrate, in which the F- and B-strains proposed by Brown *et al.*[34–36] occur,

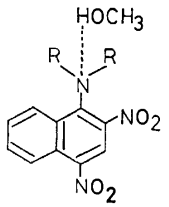

TABLE 6. KINETIC AND THERMODYNAMIC PARAMETERS FOR THE FORMATION AND DECOMPOSITION OF 1,1-DISUBSTITUTED ANIONIC σ COMPLEXES IN DMSO–CH_3OH (90: 10 v/v) AT 25 °C

R, R'[a]		CH_3, CH_3	CH_3, n-C_4H_9	C_2H_5, C_2H_5
	3	**4**	**5**	**6**
$k_2/M^{-1}s^{-1}$	2.53±0.29	14.3±1.9	3.88±0.38	1.09±0.14
k_{-2}/s^{-1}	$1.8\pm1.3\times10^{-4}$	$3.6\pm0.3\times10^{-4}$	$1.2\pm0.1\times10^{-4}$	$3.3\pm0.3\times10^{-4}$
K_1/M^{-1}	310±50	540±90	350±60	290±50
K_2/M^{-1}	14100±3050	3970±860	2400±520	2200±710
$\Delta H_2^{\ddagger}$/kcal mol^{-1}	12.2±2.5	12.1±2.5	13.1±2.7	14.4±3.0
$\Delta S_2^{\ddagger}$/cal deg^{-1} mol^{-1}	−15.4±10.2	−12.8±8.5	−12.3±8.1	−11.9±7.9
$\Delta H_{-2}^{\ddagger}$/kcal mol^{-1}	27.2±7.2	5.3±1.4	11.4±3.0	8.2±2.1
$\Delta S_{-2}^{\ddagger}$/cal deg^{-1} mol^{-1}	−15.8±1.5	−51.9±4.9	−33.3±3.1	−48.7±4.6
$\Delta H_{1.1}^{0}$/kcal mol^{-1}	−15.0±9.7	6.8±3.9	1.7±5.7	6.2±5.1
$\Delta S_{1.1}^{0}$/cal deg^{-1} mol^{-1}	0.4±11.7	39.1±13.4	21.0±11.2	36.8±12.5
$\Delta G_{1.1}^{0}$/kcal mol^{-1}	−15.1±12.2	−4.8±4.9	−4.6±9.0	−4.8±8.8

a) Only the substituent at C-1 of 2,4-dinitronaphthalene is indicated. b) $\Delta H_{1.1}^{0}=\Delta H_2^{\ddagger}-\Delta H_{-2}^{\ddagger}$. c) $\Delta H_{1.1}^{0}=\Delta H_2^{\ddagger}-\Delta H_{-2}^{\ddagger}$. d) $\Delta G_{1.1}^{0}=\Delta H_{1.1}^{0}-T\Delta S_{1.1}^{0}$.

would make amino nitrogen ammonium-nitrogen-like, which exerts the less electron-donating resonance contribution (due to the lone pair electrons of the amino nitrogen), giving rise to the reduced deactivation of the C-3 position indirectly. Naturally, the bulkier an amino group, the less it is solvated by methanol. Thus, the compensation would be evolved between the enthalpy and entropy of activation ($\Delta H_1^{\ddagger}$ and $\Delta S_1^{\ddagger}$). As regards the enthalpy and entropy of activation for k_{-1} ($\Delta H^{\ddagger}_{-1}$ and $\Delta S^{\ddagger}_{-1}$), those on **4**, **5**, and **6** linearly compensate each other except for **3**. With **3**, the compensation between $\Delta H^{\ddagger}_{-1}$ and $\Delta S^{\ddagger}_{-1}$ was found to deviate somewhat from the linear relationship. The conformation of **3** could be taken into account. In veiw of solvation ($-NR_2\cdots HOCH_3$), the 2,5-dinitro-1-naphthyl group should be put into an equatorial position at the nitrogen atom of piperidine. The same conformation could be held also in the anionic σ complex (**3a**). In the unimolecular decomposition of **3a**, the less solvation of methanol to the incipient methoxide ion at the C-3 position would be respon sible for the deviation to some extent, because 1-methoxy-2,6-dinitro-4,5-benzo-3-cyclohexadienylido group is very large.

It is of interest to compare our results with those of Millot and Terrier,[11] who carried out the kinetics of the reaction of **2** with potassium methoxide in DMSO–CH_3OH (90 : 10, v/v) at 20 °C, although their identification of the 1,3-disubstituted anionic σ complex was somewhat imcomplete (Eq. 8). Their values are as follows: k_1 7800 $M^{-1}\,s^{-1}$; k_{-1} 8.5 s^{-1}; K_1 916 M^{-1}.

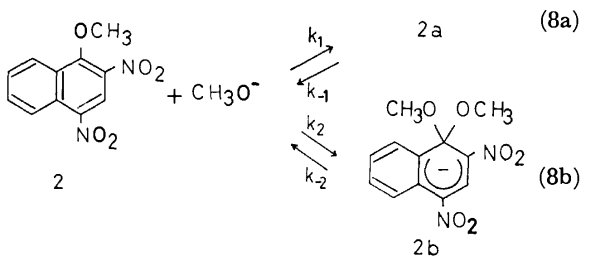

2 2a (8a) 2b (8b)

Their reaction temperature is a little lower than ours, but the k_1 and k_{-1} values are considerably larger; the difference in the K_1 values is not large. The stronger inductive (−I) and weaker resonance (+R) effects, that is, the more electron-attracting effect of methoxyl group than those of dialkylamino group, activate the C-3 position more strongly, making the attack of methoxide ion faster (k_1). The effects of methoxyl group activate the C-1 position also more strongly, making the 3→1 migration of methoxyl group easier (k_{-1}).

1,1-Disubstituted Anionic σ Complex. The k_2 and k_{-2} values are expected to vary with the steric and activating effects of a substituent at the C-1 position (Table 6). The k_2 value increases in the order **6**<**5**<**4**, depending on the enthalpy of activation ($\Delta H_2^{\ddagger}$) rather than on the entropy of activation ($\Delta S_2^{\ddagger}$), in which the same effect ($-NR_2\cdots HOCH_3$) might function. However, in the case of **3**, the decrease in the k_2 value, seems to depend on the negative and large entropy of activation, which might occur from the steric interference of piperidyl group with the bimolecular attack of methoxide ion at the C-1 position.

Non-linear compensation takes place among the enthalpy and entropy of activation for the decomposition of complex. Especially in the case of **3**, the k_{-2} value depends on the enthalpy of activation rather than on the entropy of activation. The steric strain at the C-1 position of **3**, due to the bulkiness of piperidyl group would be relieved during the formation of complex. This might make the complex more stable, making the k_{-2} value smaller.

Millot and Terrier[11] reported the following constants for the formation and decomposition of 1,1-disubstituted anionic σ complex (Eq. 8b): k_2 2100 $M^{-1}\,s^{-1}$; k_{-2} too small to be decided.

In the case of **2**, the k_{-2} value is very small, and the K_2 value might be very large. The conpicuous constrast is the difference in the k_2 values, which indicates the steric and inductive advantageousness of methoxyl group. The k_1/k_2 ratios are *ca.* 40—380 in our case, whereas it is *ca.* 4 in the case of Millot and Terrier, which also represents the advantageousness.

In the reaction course of 1-dialkylamino-2,4-dinitronaphthalenes with potassium methoxide in DMSO–CH_3OH, the existance of 1,1- and 1,3-disubstituted anionic σ complexes was confirmed, the life of the latter being much shorter.

Experimental

NMR spectra were recorded on a Varian A-60D spectrometer and UV-VIS absorption spectra on a Hitachi Model 200-10 spectrophotometer.

Materials. The compounds (**3**, **4**, **5**, and **6**) were prepared according to the method described previously.[38] A small amount of calcium hydride was added to commercial dimethyl sulfoxide, which was then distilled under reduced pressure. Methanol was refluxed with magnesium for 1 h and distilled. Commercial potassium perchlorate of special grade was used without further purification.

Rate Measurement. As regards the kinetics of formation and decomposition of 1,3-disubstituted anionic σ complex, the transmittance of complex was measured in order to estimate the apparent rate constants(k_ψ) with a thermostatted stopped-flow spectrophotometer (Union RA-1300 Stopped-Flow Analyser). The kinetic measurements for the formation and decomposition of 1,1-disubstituted ones (k_{obsd}) were made with a thermostatted Hitachi Model 200-10 Spectrophotometer.

This research was supported in part by Grant-in-Aid for Scientific Research No. 455330 from the Ministry Education, Science and Culture.

References

1) Part XIV: S. Sekiguchi, T. Aizawa, and M. Aoki, *J. Org. Chem.*, in press.

2) F. Pietra, *Q. Rev. Chem. Soc.*, **23**, 504 (1969); T. J. deBoer and I. P. Dirkx, "The Chemistry of the Nitro and Nitroso Groups," ed by H. Feuer, Interscience, New York (1968),Part I.; J.Miller,"Aromatic Nucleophilic Substitution," American Elsevier, New York (1968); E. Buncel, A. R. Norris, and K. E. Russell, *Q. Rev, Chem. Soc.*, **22**, 123 (1968); S. D. Ross, *Prog. Phys. Org. Chem.*, **1**, 31 (1963); J. F. Bunnett, *Q. Rev. Chem. Soc.*, **49**, 273 (1951); J. F. Bunnett and R. E. Zahler, *Chem. Rev.*, **49**, 273 (1951); C. F. Bernasconi, *Acc. Chem. Res.*, **11**, 147 (1978); C. F. Bernasconi, *MTP. Int. Rev. Soc.*: *Prg.*

Chem., Ser. One, **3**, 33 (1973).
3) F. Terrier, F. Millot, and R. Schaal, *J. Chem. Soc., Perkin Trans. 2*, **1972**, 1192.
4) F. Terrier, A.-P. Chatrousse, and R. Schaal, *J. Org. Chem.*, **37**, 3010 (1972).
5) A.-P. Chatrousse, F. Terrier, and R. Schaal, *J. Chem. Res. (M)*, **1977**, 2413.
6) F. Terrier, A.-P. Chatrousse, R. Schaal, C. Paulmier, and P. Patour, *Tetrahedron Lett.*, **1972**, 1961.
7) R. Schaal, F. Terrier, J.-C. Halle, and A.-P. Chatrousse, *Tetrahedron Lett.*, **1970**, 1393.
8) A.-P. Chatrousse and F. Terrier, *Bull. Soc. Chim. Fr.*, **1972**, 4549.
9) F. Millot and F. Terrier, *Bull. Soc. Chim. Fr.*, **1974**, 1823.
10) M. P. Simonnin, M. J. Lecourt, F. Terrier, and C. A. Dearing, *Can. J. Chem.*, **50**, 3558 (1972).
11) F. Millot and F. Terrier, *Bull. Soc. Chim. Fr.*, **1971**, 3897.
12) F. Terrier, F. Millot, and P. Letellier, *Bull. Soc. Chim. Fr.*, **1970**, 1743.
13) F. Terrier and J.-C. Halle, *Tetrahedron Lett.*, **1975**, 2987.
14) F. Millot and F. Terrier, *Bull. Soc. Chim. Fr.*, **1969**, 2692.
15) F. Terrier, F. Millot, and J. Morel, *J. Org. Chem.*, **41**, 3892 (1976).
16) F. Terrier, A.-P. Chatrousse, and C. Paulmier, *J. Org. Chem.*, **44**, 1634 (1970).
17) M. R. Crampton and V. Gold, *J. Chem. Soc., B*, **1966**, 893.
18) M. R. Crampton and V. Gold, *Chem. Commun.*, **1964**, 298.
19) M. R. Crampton and H. A. Khan, *J. Chem. Soc., Perkin Trans. 2*, **1973**, 710.
20) M. R. Crampton and M. J. Willison, *J. Chem. Soc., Perkin Trans. 2*, **1976**, 901.
21) B. Gibson and M. R. Crampton, *J. Chem. Soc., Perkin Trans. 2*, **1979**, 648.
22) M. R. Crampton, B. Gibson, and F. W. Gilmore, *J. Chem. Soc., Perkin Trans. 2*, **1979**, 91.
23) M. J. Strauss, *Chem. Rev.*, **70**, 667 (1970).
24) S. Sekiguchi, *Yuki Gosei Kagaku Kyokai Shi*, **36**, 633 (1978).
25) J. H. Fendler, E. J. Fendler, W. E. Byrne, and C. E. Griffin, *J. Org. Chem.*, **33**, 977 (1968).
26) S. Sekiguchi, K. Shinozaki, T. Hirose, K. Matsui, and T. Itagaki, *Tetrahedron Lett.*, **1974**, 1745.
27) S. Sekiguchi, S. Fujisawa, and Y. Ando, *Bull. Chem. Soc. Jpn.*, **49**, 1451 (1976).
28) S. Sekiguchi, T. Takei, T. Aizawa, and M. Okada, *Tetrahedron Lett.*, **1977**, 1209.
29) S. Sekiguchi, K. Tsutsumi, H. Shizuka, K. Matsui, and T. Itagaki, *Bull. Chem. Soc. Jpn.*, **49**, 1521 (1976).
30) S. Sekiguchi, T. Hirose, K. Tsutsumi, T. Aizawa, and H. Shizuka, *J. Org. Chem.*, **44**, 3921 (1979).
31) S. Sekiguchi, S. Fujisawa, and Y. Ando, *Bull. Chem. Soc. Jpn.*, **49**, 1451 (1976).
32) See, for example, J. J. Laidler, "Chemical Kinetics," McGraw-Hill, New York (1965), p. 19. Strictly speaking, $[\mathbf{4}]_e$ and $[CH_3O^-]_e$ (the suffix e represents the concentration at the attainment of equilibrium) should be substituted for [**4**] and $[CH_3O^-]$.
33) C. F. Bernasconi, *J. Am. Chem. Soc.*, **90**, 4982 (1968).
34) H. C. Brown and K. L. Nelson, *J. Am. Chem. Soc.*, **75**, 24 (1953).
35) H. C. Brown and M. Grayson, *J. Am. Chem. Soc.*, **75**, 20 (1953).
36) H. C. Brown and A. Cahn, *J. Am. Chem. Soc.*, **77**, 1715 (1955).
37) The solvent composition affects the k_1, k_{-1}, k_2, and k_{-2} values largely. The k_1 and k_2 values increase and the k_{-1} values decrease with increasing DMSO content.[11])
38) S. Sekiguchi, T. Hirose, K. Okada, K. Matsui, and T. Aizawa, *Research Report of the Asahi Glass Foundation for the Contribution to Industrial Technology*, **27**, 207, 221 (1975).

Amino Sugars. XXXII. Ammonolysis and Azidolysis of Benzyl 2,3-Anhydro-4-azido-4-deoxypentopyranosides

Hironobu HASHIMOTO,* Koichi ARAKI, and Juji YOSHIMURA

Laboratory of Chemistry for Natural Products, Faculty of Science, Tokyo Institute of Technology, Nagatsuta, Midori-ku, Yokohama 227

(Received December 23, 1980)

Ammonolysis and azidolysis of four benzyl 2,3-anhydro-4-azido-4-deoxypentopyranosides of α-D-*lyxo*, α-D-*ribo*, β-L-*lyxo*, and β-L-*ribo* configurations, were studied. Ratios of two ring-opening isomers and relative reaction rates were determined, factors controlling the direction of ring opening being discussed.

The ring-opening reaction of anhydro sugars with nucleophiles has been widely used not only for amino sugar synthesis by the reaction with ammonia or azide ion[1] but also for various kinds of carbohydrate derivatives.[2] In these reactions the formation of two kinds of *trans* α-hydroxy products is possible, depending on which carbon atom is attacked by the nucleophiles. Anhydropyranosides are well known to exist mainly in half-chair conformation.[3,4] When the conformation is fixed by a fused-ring such as in 4,6-*O*-benzylidene-2,3-anhydrohexopyranosides and 1,6 : 2,3-dianhydrohexopyranoses,[2] the predominant product is a *trans*-diaxial ring-opening product as postulated by the Fürst-Plattner rule.[5] On the other hand, the conformationally flexible anhydropyranoside like anhydropentopyranoside gives two ring-opening products in various ratios according to substituents on the pyranoside and to the character of nucleophiles. There is little systematic study on such ring-opening reaction, and the finding of the reversed ring-opening mode between ammonolysis and azidolysis of benzyl 2,3-anhydro-4-azido-4-deoxy-β-L-ribopyranoside (**4**)[6] prompted us to study the same reactions of all four stereochemical counterparts of benzyl 2,3-anhydro-4-azido-4-deoxypentopyranoside.

Results

All four stereochemical counterparts, namely, α-*lyxo* (**1**),[7] α-*ribo* (**2**),[7] β-*lyxo* (**3**),[8] and β-*ribo* (**4**)[6] isomers of benzyl 2,3-anhydro-4-azido-4-deoxypentopyranoside were prepared as reported previously. D-Enantiomer and L-enantiomer were used, for the α-anomers and β-anomers, respectively, because of availability of their starting materials.

Ammonolysis reactions of **1**,[6] **3**,[7] and **4**[8] in methanol at 90—95 °C gave 2-amino derivatives predominantly (40—70% yields of isolation). The ratios of two ring-opening isomers, 2-amino and 3-amino derivatives, were determined by means of densitometer (Method A) and optical rotational values (Method B). In method A the reaction mixture was developed on a silica gel TLC plate using benzene–pyridine as a solvent, the spots being detected by ninhydrin or sulfuric acid. In method B the ratio was calculated from the optical rotational value of the product mixture using that of each component. When the two isomers were well separated on TLC, the weights of products isolated by preparative TLC were also used for the estimation of the ratios of products (Method C). The results are summarized in Table 1. In each case the yield of the product mixture was over 90%. The ratios obtained by the different methods agreed with each other. In the case of **2**, closer mobility on TLC of two products may cause a slightly larger deviation of the ratios by method A. Thus, predominant formation of 2-amino derivatives could be ascertained for all four isomers.

Structures of newly obtained ammonolysis products of **2** were elucidated easily by NMR data, *viz.*, the

Table 1. Ratios of ammonolysis and azidolysis products

2,3-Anhydro sugars	Products[a]	Ratios of 2- and 3-substituted products/%							
		Ammonolysis				Azidolysis			
		NH_3/MeOH			NH_3/H_2O				
		A[b]	B[b]	C[b]	A	A	B	C	D[b]
1 (α-lyxo)	2-	64		60*	61	22[c]		15[c]*	16
	3-	36		40*	39	78[c]		85[c]*	84
2 (α-ribo)	2-	64	72*		55	44	52	51*	
	3-	36	28*		45	56	48	49*	
3 (β-lyxo)	2-	75	71*		73	57[c]		55[c]*	57
	3-	25	29*		27	43[c]		45[c]*	43
4 (β-ribo)	2-	60	66*		65	30	23	18*	
	3-	40	34*		35	70	77	82*	

a) 2- =2-Substituted product, 3-=3-substituted product. b) The following methods were used for estimation; A: densitometer, B: optical rotation, C: weight, D: NMR (see Experimental). c) Isolated as 3-acetates. *These values were used for the estimation of relative rates described in Discussion.

Table 2. NMR data of ammonolysis and azidolysis products (100 MHz, $CDCl_3$)

Compound	Chemical shifts δ							Coupling constants/Hz						Other signals
	H-1	H-2	H-3	H-4	H-5a	H-5e	$PhCH_2O$	$J_{1,2}$	$J_{2,3}$	$J_{3,4}$	$J_{4,5a}$	$J_{4,5e}$	$J_{5a,5e}$	
7a	4.17	2.99	3.75		3.56	4.04	4.55, 4.91	7.5	9.1	2.3	1.5	2.3	12.5	2.79(NH_2+OH)
8a	4.89	3.38	2.93	3.28	3.59	3.74	4.50, 4.78	3.5	10.1	9.0	9.0	6.2	10.5	2 25(NH_2+OH)
5c	5.01	3.15	5.48	3.60—3.82			4.58, 4.80	3.5	10.5	~9.5	—	—	—	2.20(OAc)
6c	4.43	5.15	3.74	3.82	3.57	4.02	4.53, 4.83	6.0	8.3	3.9	1.8	4.0	12.2	2.05(OAc)
7b	4.32	3.65		3.77	3.50	4.02	4.61, 4.90	6.8	—	3.0	2.0	3.0	12.9	2.82(OH)
8b	4.93	3.20—3.80					4.52, 4.78	2.0	—	—	—	—	—	2.36(OH)
8b[a]	4.70	2.52	3.06	3.60	3.82	4.19	4.72, 5.12	3.5	9.5	9.5	10.5	4.7	10.5	2.56(OH)
9c	4.36	3.44	4.89	3.62	3.20	4.06	4.66, 4.91	8.9	10.2	10.2	10.8	5.3	11.5	2.14(OAc)
10c	5.15	5.09		3.6—4.3			4.51, 4.74	3.9	9.3	—	—	—	—	2.11(OAc)
10c[b]	5.10	5.25	3.65	2.86	3.16	3.32	4.10, 4.38	3.6	10.5	3.9	1.7	1.5	12.3	1.67(OAc)
11b	5.03	3.52	4.26	3.93	3.76	3.95	4.58, 4.76	3.4	10.2	3.5	2.5	1.5	10.9	2.52(OH)

a) **8b**: $Pr(FOD)_3$ ≒6:1. b) In C_6D_6.

Table 3. Reaction rates of ammonolysis and azidolysis

	2,3-Anhydro sugars	Conversion ratios/%			Relative reaction rates[a]
		1h	3h	6h	
Ammonolysis[b]	1	63.6	100	100	3.5
	2	18.8	26.7	38.3	1.0
	3	19.3	28.2	35.3	1.0
	4	41.1	69.5	84.9	2.2
		30 min	70 min	130 min	
Azidolysis[c]	1	39.3	55.6	73.4	1.0
	2	76.1	94.0	95.8	1.9
	3	44.8	70.5	85.7	1.1
	4	58.3	80.3	95.1	1.5

a) Calculated from the conversion rates at 1 h for ammonolysis and 30 min for azidolysis. b) In methanol at 95°C (sealed tube). c) In 2-methoxyethanol at 110 °C.

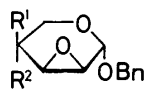

	R^1	R^2
1 (α-*lyxo*)	H	N_3
4 (β-*ribo*)	N_3	H

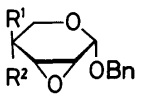

	R^1	R^2
2 (α-*ribo*)	H	N_3
3 (β-*lyxo*)	N_3	H

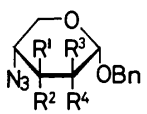

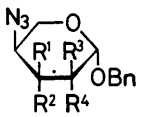

	R^1	R^2	R^3	R^4
5a	OH	H	H	NH_2
5b	OH	H	H	N_3
5c	OAc	H	H	N_3
6a	H	NH_2	OH	H
6b	H	N_3	OH	H
6c	H	N_3	OAc	H
7a	H	OH	NH_2	H
7b	H	OH	N_3	H
8a	NH_2	H	H	OH
8b	N_3	H	H	OH

	R^1	R^2	R^3	R^4
9a	H	OH	NH_2	H
9b	H	OH	N_3	H
9c	H	OAc	N_3	H
10a	NH_2	H	H	OH
10b	N_3	H	H	OH
10c	N_3	H	H	OAc
11a	OH	H	H	NH_2
11b	OH	H	H	N_3
12a	H	NH_2	OH	H
12b	H	N_3	OH	H

chemical shift of H_1 and the coupling constants of ring protons. H_1 signals of 2-amino (**7a**) and 3-amino (**8a**) derivatives appear at δ 4.17 ($J_{1,2}$=7.5 Hz) and δ 4.89 ($J_{1,2}$=3.5 Hz), indicating axial-axial and equatorial-axial orientations of H_1 and H_2, respectively. This and the coupling constants of other ring protons confirmed α-D-*arabino* (**7a**) and α-D-*xylo* (**8a**) configurations (Table 2).

Ammonolysis reaction in aqueous ammonia was also examined. In this reaction, the anhydro sugar did not dissolve at first, but went into solution with the progress of the reaction. Little difference was observed between the two solvents, methanol and water (third column, Table 1). The reason for the slightly different ratio for the products of **2** is not clear.

The 2,3-anhydro sugars was then treated with sodium azide in 2-methoxyethanol containing 5% water at 110 °C in the presence of ammonium chloride. The ratios of two ring-opening products, 2-azido and 3-azido derivatives, were determined by the same method as described above.

Estimation from NMR spectra was used as the fourth method (Method D) in the cases of azidolysis products of **2** and **3** because of poor separation on TLC. The reaction mixture could be separated on TLC after *O*-acetylation, the ratios being determined also by Methods A and C. As shown in Table 1 the results obtained from the various methods agree with each other. The error of these values was estimated to be about 5%, but the densitometric method may give a larger error since the difference of color development for each compound has

Table 4. Conformational equilibria of benzyl 2,3-anhydro-4-azido-4-deoxypentopyranosides

2,3-Anhydro sugars	Solvents	Coupling constants/Hz				Ratios of conformers $^0H_5$: $^5H_0$
		$J_{1,2}$	$J_{3,4}$	$J_{4,5a}$ [a]	$J_{4,5e}$ [a]	
1	$CDCl_3$ [7]	<0.5	<0.5	8.0 [b]	8.0 [b]	77 : 23 ($J_{4,5a}$)
	CD_3OD	<0.5	— [c]	7.7 [b]	7.7 [b]	74 : 26 ($J_{4,5a}$)
2	$CDCl_3$ [7]	2.7	—	—	—	82 : 18* ($J_{1,2}$)
	$CDCl_3$+Eu(FOD)$_3$	3.0	<0.5	9.3	4.2	95 : 5 ($J_{1,2}$) 93 : 7 ($J_{4,5a}$)
	$CDCl_3$+Pr(FOD)$_3$	3.0	<0.5	12.0	5.5	95 : 5 ($J_{1,2}$) 100 : 0 ($J_{4,5a}$)
	CD_3OD	2.9	—	—	—	91 : 9* ($J_{1,2}$)
3	$CDCl_3$	2.0	—	2.4	1.3	— [d]
	CD_3OD	1.3	—	2.8	2.0	— [e]
4	$CDCl_3$	<0.5	—	3.8	—	73 : 27 ($J_{4,5a}$)
	$CDCl_3$+Pr(FOD)$_3$	<0.5	3.8	4.5	3.0	57 : 43 ($J_{3,4}$) 64 : 36 ($J_{4,5a}$)
	CD_3OD	<0.5	—	4.5	—	64 : 36* ($J_{4,5a}$)

a) The suffixes 5a and 5e designate the axially and equatorially oriented protons on C-5, respectively, in the $^0H_5$ conformation. b) Analyzed as AB_2 and confirmed by simulation. c) Could not be obtained from the spectrum. d) The ratios estimated by $J_{1,2}$ and $J_{4,5a}$ are 50 : 50 and 89 : 11, respectively. e) The ratios estimated by $J_{1,2}$ and $J_{4,5a}$ are 18: 82 and 85 : 15, respectively. *These values were used for the estimation of relative rates (see Discussion).

not been considered.

Structures of these azidolysis products could be ascertained by their NMR data (Table 2). The products from **1** and **3** were characterized again as *O*-acetyl derivatives.

In order to elucidate the above result, *i.e.* the different regioselectivity in the ammonolysis and azidolysis reactions, the relative reaction rates and the conformations of these 2,3-anhydropentopyranosides were examined. The reactions were carried out in sealed tubes and followed by TLC. The conversion ratios determined densitometrically and the relative reaction rates estimated from the conversion ratios after the shortest reaction time examined are summarized in Table 3. The relative reaction rates are qualitative, but show a clear difference in the relative reactivities of the 2,3-anhydro sugars.

The pyranoside ring in 2,3-anhydropyranosides takes two half-chair forms, $^0H_5$ and $^5H_0$. The conformational equilibrium between these two forms was estimated by the coupling constants of vicinal ring protons, $J_{4,5}$ together with $J_{1,2}$ and $J_{3,4}$. The following standard values[4] were used for estimation: $J_{4a,5a}$ 9.9, $J_{4e,5e}$ 1.5; *cis*-$J_{1peq,2}$ 3.1, *cis*-$J_{1pax,2}$ 0.9; *cis*-$J_{3,4peq}$ 5.4, *cis*-$J_{3,4pax}$ 1.7 Hz.[9] Although the ratios estimated by $J_{4,5}$ should be more reliable considering the magnitude of difference in two conformers, those by $J_{1,2}$ and $J_{3,4}$ also indicate predominant conformers in the cases of the isomers having *cis*-relationship between H_1 and H_2, or H_3 and H_4. While the first-order analysis of H_4, H_5, and H_5, in **3**[8] and **4**[6] were possible, the NMR signals of the corresponding protons in **1** and **2** were not well separated. Coupling constants concerning these protons could be obtained in the aid of lanthanoid shift reagents or simulation (Table 4).

Predominance of $^0H_5$ conformation was confirmed in the cases of **1** and **2**, while **4** adopts $^0H_5$ conformation slightly preferentially than $^5H_0$ conformation (last column, Table 4). The use of lanthonoid shift reagents seems to cause no remarkable change of conformation[10] as supposed in the cases of **2** and **4**. In the case of **3** the ratios estimated by $J_{1,2}$ and $J_{4,5}$ are totally different, indicating a deviation from the half-chair conformation. The values of $J_{1,2}$, $J_{4,5a}$ and $J_{4,5e}$ are in line with the flattened half-chair conformation. The dihedral angles H-1–C-1/C-2–H-2, H-4–C-4/C-5–H-5a, and H-4–C-4/C-5–H-5e are 40°, 55°, and 65°, respectively. They were determined by assuming the Karplus-type dependence of coupling constants.[11,12] Thus, the predominant existence of $^0H_5$ conformation in **1**, **2**, and **4**, and also the flattened half-chair conformation of **3** confirm the importance of the anomeric effects on the conformational stability, observed in some 2,3-anhydropyranosides taking half-chair conformation.[13]

Discussion

In order to examine the factors affecting the regiospecificity of ring-opening reactions the results were analysed with the following assumptions.

1) The epoxides **1**, **2**, and **4** react with the nucleophiles in one of two half-chair conformations according to the Fürst-Plattner rule (Fig. 1).

2) The mutual conformational inversion is much faster than the reaction.

3) Epoxide **3** reacts in the flattened half-chair conformation, where the attack of nucleophiles can take place both at C-2 and C-3.

Although the deviation from the Fürst-Plattner rule, *i.e.*, *trans* diequatorial ring opening, was observed even in the conformationally rigid system especially when the favorable reaction site due to this rule is C-2, which is contrariwise the electronically unfavorable one[14] in the case of 2,3-anhydropyranosides such as 2,3-anhydro-4,6-*O*-benzylideneallopyranosides,[15] the contribution of such ring opening may be negligible as the first approximation. The expected relative small value of the free energy of conformational inversion in these epoxides also supports the assumption. The second assumption may be admitted for a reaction, whose activation energy is much higher than the free energy of conformational conversion. The reactions discussed here seem to

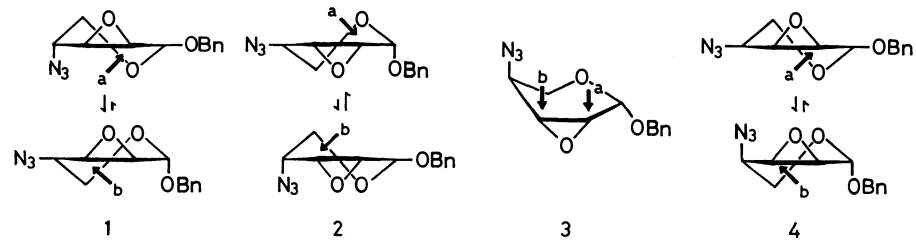

Fig. 1. Conformations and stereoelectronically preferred reaction sites of 2,3-anhydro-4-azido-4-deoxypentopyranosides.

correspond to this case, judging from those of substituted cyclohexene derivatives (25—30 kJ/mol),[16] which adopt a similar half-chair conformation to 2,3-anhydropentopyranoside.

The relative reaction rate of each conformer or site, K_a and K_b, were estimated by means of the equations,

$$K = N_a K_a + N_b K_b,$$

$$\frac{P_a}{P_b} = \frac{N_a K_a}{N_b K_b},$$

where N and P represent the mole fractions of two conformers (Table 4) and products (Table 1), respectively, and K is the relative reaction rate of each epoxide (Table 3). Suffixes a and b indicate the conformers or positions which give the 2- and 3-substituted products, respectively. The following relative reaction rates were obtained, where the standards are the same as in Table 3 and the comparison is significant only in the same reaction. In general the azidolysis reaction is faster than the ammonolysis. These results give useful informations for synthetic purpose.

	1a	**1b**	**2a**	**2b**	**3a**	**3b**	**4a**	**4b**
Ammonolysis	12	1.7	0.8	3.1	0.7	0.3	4.0	1.2
Azidolysis	0.8	1.0	1.1	10	0.6	0.5	0.75	1.9

(a) Among several possible interactions between the nucleophile and the reactant epoxide the dipole-dipole interaction between C_2---nucleophile and two C_1–O dipoles in the transition state may be the most effective factor as indicated in the cases of **1a** and **4a**. These conformers show higher reactivities than the other in ammonolysis, and lower reactivities in azidolysis. The differene ccould be explained by reverse direction of C_2---nucleophile diople as shown in Fig. 2.[17] A comparison of the reactivity between **2a** and **4a** shows the effect, which affects only **4a**. Thus the electronic character of the nucleophile controls the direction of ring opening.

(b) If the reactivity is not markedly increased or decreased by the dipole-dipole interaction, the attack of the nucleophile at the electronically favorable C-3 position predominates, as is well known in the reaction of 2,3-anhydro sugars.[1] In ammonolysis, **2b**, **1b**, and **4b** have higher reactivities except **1a** and **4a**, while in azidolysis **2b** and **4b** show the same tendency.

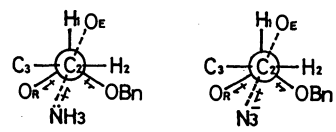

Fig. 2. Dipole-dipole interactions at the transition state of substitution on C-2 (O_E and O_R represent the oxygens in the epoxide and pyranoside rings, respectively.)

(c) The electronic or steric interactions between the nucleophile and the quasi-axial substituent (azido or benzyloxy group on the carbon adjacent to the epoxide) were also suggested by comparing **1a** with **4a** and **2b** with **4b**. There seems to be a little difference in the nature of the interactions between these groups and the nucleophiles. The axial azido group accerelates ammonolysis and retards azidolysis, while the axial benzyloxy group retards both reactions.

The evaluation of these interactions would be helpful for prediction of the ammonolysis and azidolysis products of 2,3-anhydropentopyranosides.

Experimental

General. Melting points were determined with a Beckmann Mel-temp melting point apparatus and are not corrected. Optical rotations were measured in methanol (M), unless otherwise stated, using a 0.5-dm tube with a Carl Zeiss LEP-Al or a JASCO DIP-4 polarimeter. IR spectra were recorded with a Hitachi EPI-G2 grating spectrometer, and NMR spectra with a JEOL JNM PS-100 spectrometer in chloroform-*d* containing tetramethylsilane as an internal reference. Chemical shifts and coupling constants are recorded in δ and Hz units, IR frequencies in cm^{-1}. All NMR data are summerized in Table 2. Evaporation was carried out in a rotary evaporator under reduced pressure. The products were recrystallized from ethanol unless otherwise stated. TLC was performed on silica gel (Merck Kieselgel H type 60) using the following developing solvent: A, benzene–pyridine (3 : 2); B, benzene–pyridine (7 : 3); C, benzene–methanol (200 : 1).

Benzyl 2,3-anhydro-4-azido-4-deoxypentopyranosides having α-D-*lyxo* (**1**), α-D-*ribo* (**2**), β-L-*lyxo* (**3**), and β-L-*ribo* (**4**) configurations were prepared according to published procedure.[6-8]

Ammonolysis of 2,3-Anhydropentopyranosides. A solution of 2,3-anhydro sugar (250 mg, 1 mmol) in methanol (20 ml) saturated with ammonia was heated in a sealed tube at 95 °C. After complete disappearance of the starting material the reaction solution was evaporated to give a crystalline mixture of products, which was separated on preparative TLC with the developing solvent A or B. Ammonolysis products of **1** (**5a** and **6a**),[6] **3** (**9a** and **10a**),[7] and **4** (**11a** and **12a**)[8] have been reported.

*Benzyl 2-Amino-4-azido-2,4-dideoxy-α-*D*-arabinopyranoside (**7a**) and Benzyl 3-Amino-4-azido-3,4-dideoxy-α-*D*-xylopyranoside (**8a**).* Ammonolysis of **2** was performed for 48 h, two isomeric products being separated as described above. **7a**: mp 119—121 °C, $[\alpha]_D$ +42.7° (*c* 1.1, M); IR (KBr): 3260 and 3330 (NH_2 and OH), 2100 (N_3), 700, and 730 (Phenyl). Found: C, 54.25; H, 5.97; N, 20.80%. Calcd for $C_{12}H_{16}N_4O_3$: C,

54.55; H, 6.10; N, 21.20%. **8a**: mp 122—124 °C, $[\alpha]_D$ +118° (*c* 0.75, M); IR(KBr): 3320 (NH_2 and OH), 2100 (N_3), 700 and 735 (Phenyl). Found: C, 54.41; H, 6.13; N, 20.95%. Calcd for $C_{12}H_{16}N_4O_3$: C, 54.55; H, 6.10; N, 21.20%. NMR data: see Table 2.

Azidolysis of 2,3-Anhydropentopyranosides. A suspension of 2,3-anhydro sugar (250 mg, 1 mmol), sodium azide (250 mg, 3.8 mmol), and ammonium chloride (100 mg, 1.9 mmol) in 2-methoxyethanol–water (14 : 1, 20 ml) was heated in a sealed tube at 110 °C. After the reaction had been completed, the insoluble material was filtered off, and the filtrate evaporated. The residue was extracted with methanol, the mixture of two isomeric products obtained by evaporation of the extract being separated by preparative TLC with multiple development using solvent C.

Benzyl 3-O-Acetyl-2,4-diazido-2,4-dideoxy-α-D-xylopyranoside (5c) and Benzyl 2-O-Acetyl-3,4-diazido-3,4-dideoxy-α-D-arabinopyranoside (6c). Azidolysis of **1** was performed for 4 h as described above. Since a mixture of two isomeric products (**5b** and **6b**) obtained could not be separated on TLC, it was acetylated with acetic anhydride in pyridine in the usual way to give **5c** and **6c**, which were separated by prepaprative TLC with developing solvent C. **5c**: sirup $[\alpha]_D$ +229° (*c* 0.6, M); IR(NaCl): 2100 (N_3), 1755 (OAc), 695, and 738 (Phenyl). Found: C, 50.66; H, 4.92; N, 24.89%. Calcd for $C_{14}H_{16}N_6O_4$: C, 50.60; H, 4.85; N, 25.29%. **6c**: sirup, $[\alpha]_D$ +49.9° (*c* 1.7, M); IR(NaCl): 2100 (N_3), 1745 (OAc), 695, and 740 (Phenyl). Found: C, 51.04; H. 4.86; N, 24.93%. Calcd for $C_{14}H_{16}N_6O_4$: C, 50.60; H, 4.85; N, 25.29%. NMR data: see Table 2.

Benzyl 2,4-Diazido-2,4-dideoxy-α-D-arabinopyranoside (7b) and Benzyl 3,4-Diazido-3,4-dideoxy-α-D-xylopyranoside (8b). Azidolysis of **2** as described for **1** gave **7b** and **8b**, which could be separated without acetylation. **7b**: sirup, $[\alpha]_D$ +26.5° (*c* 0.6, M); IR(NaCl): 3320 (OH), 2110 (N_3), 700, and 745 (Phenyl). Found: 49.30; H, 4.48; N, 28.68%. Calcd for $C_{12}H_{14}N_6O_3$: C, 49.65; H, 4.86; N, 28.95%. **8b**: sirup, $[\alpha]_D$ +259° (*c* 0.7, M); IR(NaCl): 3400 (OH), 2110 (N_3), 700, and 745 (Phenyl). Found: C, 49.27; H, 4.52; N, 28.67%. Calcd for $C_{12}H_{14}N_6O_3$: C, 49.65; H, 4.86; N, 28.95%. NMR data: see Table 2.

Benzyl 3-O-Acetyl-2,4-diazido-2,4-dideoxy-β-L-xylopyranoside (9c) and Benzyl 2-O-Acetyl-3,4-diazido-3,4-dideoxy-β-L-arabinopyranoside (10c). Azidolysis of **3** and separation of the isomeric products were carried out in the same way as described for **5c** and **6c**. **9c**: mp 107—110 °C, $[\alpha]_D$ +18.0° (*c* 0.6, M); IR(KBr): 2100 (N_3), 1755 (OAc), 715, and 750 (Phenyl). Found: C, 50.60; H, 4.64; N, 24.96%. Calcd for $C_{14}H_{16}N_6O_4$: C, 50.60; H, 4.85; N, 25.29%. **10c**: sirup, $[\alpha]_D$ +168° (*c* 0.9, M); IR(NaCl): 2105 (N_3), 1748 (OAc), 700, and 740 (Phenyl). Found: C, 50.24; H, 4.59; N, 24.91%. Calcd for $C_{14}H_{16}N_6O_4$: C, 50.60; H, 4.85; N, 25.29%. NMR data: see Table 2.

Benzyl 2,4-Diazido-2,4-dideoxy-β-L-arabinopyranoside (11b) and Benzyl 3,4-Diazido-3,4-dideoxy-β-L-xylopyranoside (12b). Azidolysis of **4** and separation of the isomeric products were carried out in the same way as described for **7a** and **8b**. **11b**: sirup, $[\alpha]_D$ +173° (*c* 0.7, M); IR(NaCl): 3380 (OH), 2100 (N_3), 700 and 740 (Phenyl). Found: C, 49.76; H, 4.60; N, 28.91%. Calcd for $C_{12}H_{14}N_6O_3$: C, 49.65; H, 4.86; N, 38.95. **12b**: reported.[8] NMR data: see Table 2.

Ratios of Ammonolysis and Azidolysis Products. Method A. In order to estimate the ratio with a densitometer, TLC was performed using Merck silica gel plate and self-made one, whose uniformity of thickness was checked densitometrically before use, with solvent A or B for the ammonolysis products and C for azidolysis ones. Each spot was detected by sulfuric acid and also by ninhydrin in the case of the ammonolysis products, and measured at 560 nm with an Atago Kemic densitometer. Each sample was developed, detected, and determined densitometrically three times separately, and the values were averaged. Method B. An analytically pure mixture of the products was obtained by preparative TLC with the same solvent system as described for Method A. Its rotational value compared with that of each component gave the desired ratio. Method C. In some cases, where the products could be well separated on TLC, the ratios were also obtained from the amount of isolated isomers by preparative TLC using the same solvents as described above. Method D. The ratio was estimated from the intensity of H_1 and H_{5a} signals in the NMR spectra of the analytically pure mixture of azidolysis products obtained by Method B.

This work was supported in part by a Grant-in-Aid for Scientific Research No. 554158 from the Ministry of Education, Science and Culture.

References

1) N. R. Williams, *Adv. Carbohydr. Chem. Biochem.*, **25**, 109 (1970).
2) D. Horton in "The Amino Sugars," ed by R. W. Jeanloz, Academic Press, New York (1969), Vol. 1A, p. 27.
3) S. A. S. Al Janabi, J. G. Buchanan, and A. R. Edgar, *Carbohydr. Res.*, **35**, 151 (1974).
4) D. Achmatowicz and B. Szechner, *Carbohydr. Res.*, **50**, 23 (1976).
5) A. Fürst and P. A. Plattner, *Abstr. Papers Int. Congr. Pure Appl. Chem.*, 12th, New York (1951), p. 409; J. A. Mills, cited by F. H. Newth, and R. F. Homer in *J. Chem. Soc.*, **1953**, 989.
6) The ratios of 2- and 3-substituted derivatives were 3 : 2 for ammonolysis and 1 : 3 for azidolysis, respectively. H. A. Khan, H. Hashimoto, and J. Yoshimura, *Bull. Chem. Soc. Jpn.*, **51**, 951 (1978).
7) H. Hashimoto, F. Chiba, K. Araki, and J. Yoshimura, *Carbohydr. Res.*, **72**, 261 (1979).
8) H. Hashimoto, T. Nishide, F. Chiba, and J. Yoshimura, *Carbohydr. Res.*, **60**, 75 (1978).
9) Abbreviations; a=axial, e=equatorial, peq=pseudo-equatorial, pax=pseudo-axial.
10) O. Hofer, "The Lanthanide Induced Shift Technique: "Applications in Conformational Analysis," in "Topics in Stereochemistry," ed by N. L. Allinger and E. L. Eliel, John Wiley and Sons, New York (1976), Vol. 9.
11) M. Karplus, *J. Chem. Phys.*, **30**, 11 (1959); S. Sternhell, *Quart. Rev. Chem. Soc.*, **23**, 236 (1969).
12) K. Tori, T. Komeno, and T. Nakagawa, *J. Org. Chem.*, **29**, 1136 (1964).
13) R. U. Lemieux, K. A. Watanabe, and A. A. Pavia, *Can. J. Chem.*, **47**, 4413 (1969).
14) In the case of 2,3-anhydropyranosides the attack of nucleophiles at C-2 is considered to be electronically favored due to the inductive effect of the anomeric carbon.[1]
15) R. D. Guthrie and D. Murphy, *J. Chem. Soc.*, **1963**, 5288; W. H. Myers and G. J. Robertson, *J. Am. Chem. Soc.*, **65**. 8 (1943); H. Hashimoto, A. Ando, and J. Yoshimura, unpublished results.
16) F. A. L. Anet and R. Anet, "Dynamic Nuclear Magnetic Resonance Spectroscopy," ed by L. M. Jackman, and F. A. Cotton, Academic Press, New York (1975), p. 543.
17) A. C. Richardson, *Carbohydr. Res.*, **10**, 395 (1969).

Reactions of 5,6-Dilithioacenaphthene-*N,N,N',N'*-Tetramethyl-1,2-ethanediamine Complex with α-Diketones. I. *cis*-Directing 1 : 1 Cyclic Additions with Acyclic and Cyclic α-Diketones and Related Compounds[1]

Norio TANAKA and Toshiyasu KASAI*

Department of Chemistry for Engineering, Tokyo Institute of Technology, O-okayama, Meguro-ku, Tokyo 152

(Received January 8, 1981)

The title complex (**3**) is readily generated from 5,6-dibromoacenaphthene with butyllithium and the diamine in ether at −10—0 °C. The reaction of **3** with biacetyl gave *cis*-1,2,5,6-tetrahydro-1,2-dimethylcyclopent[*fg*]-acenaphthylene-1,2-diol but no *trans*-isomer, whereas the reaction of pyracenequinone (PYQ) with methylmagnesium bromide gave both the *cis*- and *trans*-diols. The reactions of **3** with acenaphthenequinone and PYQ also gave *cis*-diols. On treatment with phenylboronic acid, these *cis*-diols quantitatively yielded the corresponding cyclic esters. The diols and their derivatives tend to form crystalline molecular compounds with solvent molecules. The stereoselectivity of the cyclic addition between **3** and the acyclic α-diketone can be best explained in terms of five-membered chelate-ring formation in a transition state.

5,6-Dilithioacenaphthene (**1**)[2,3] can be regarded as a nucleophile like 1,8-dilithionaphthalene (**2**)[4,5] which possesses two reaction sites at the peri positions of a naphthalene nucleus; thus, its synthetic conditions and reaction modes are of interest in connection with the peri interaction in naphthalene derivatives.[6] This paper describes an improved method for the generation of **1** as a *N,N,N',N'*-tetramethyl-1,2-ethanediamine (TMEDA) complex, and reports its *cis*-directing 1 : 1 cyclic additions with some α-diketones.

Results and Discussion

Generation of 5,6-Dilithioacenaphthene–TMEDA Complex (3).[7] The dihaloprecursor, 5,6-dibromoacenaphthene (**4**), can readily be prepared in a 15—20% yield from the reaction of acenaphthene (**5**) with *N*-bromosuccinimide by use of the procedure developed in our laboratory.[2]

An ethereal suspension of **4** was quantitatively converted into the solution of **3** by a 1 : 1 mixture of butyllithium (*n*-BuLi)[8] and TMEDA[9] at −10—0 °C within 15—30 min. Such mild conditions are preferable to those without TMEDA, in which case at least 1 h of refluxing is essential.[2] The substantially quantitative formations of 5,6-acenaphthenedicarboxylic anhydride (**6**) and 5,6-diiodoacenaphthene (**7**) confirm that the structure of **3** possesses two reaction sites at the peri positions (Eq. 1).[10]

cis-Directing 1 : 1 Cyclic Additions between 3 and α-Diketones. The reactions of **3** were investigated with three α-diketones: acenaphthenequinone (ACQ), pyracenequinone (5,6-dihydrocyclopent[*fg*]acenaphthylene-1,2-dione; PYQ), and biacetyl (Ac_2). Reaction conditions and results are summarized in Table 1.

The 1 : 1 cyclic additions of both ACQ and PYQ with **1** have been reported by Mitchell *et al.*[3] The reactions of the TMEDA complex (**3**) also gave the identical products (**8** and **9**) in almost the same yields

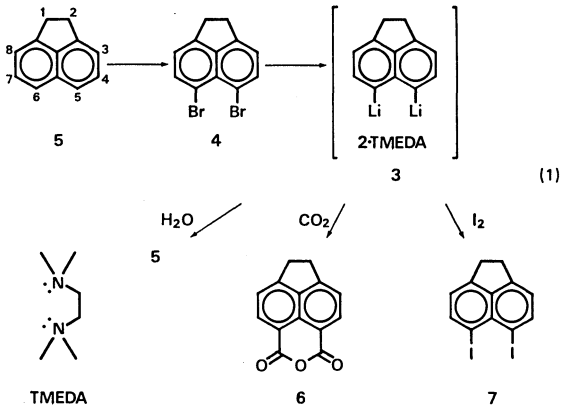

Table 1. Reactions of 5,6-dilithioacenaphthene–TMEDA complex (**3**) with α-diketones (in Et_2O)

α-Diketone	Mole ratio (diketone/**3**)	Reaction time/h[a] i	ii	iii	iv	Consumption of **3**/%[b]	Recovery of diketone/%	Product	Yield/%[c] A	B	Mp/°C[d]
ACQ	1.0	0.5	2	1	0	70	10	**8**[e]		22	320.0—322.0 (dec/Ar)
PYQ	0.5	0.5	4	1	0	60	16	**9**[f]		18	347.0—348.0 (dec/Ar)
	1.0	0.5	2	1	0	60	28	**9**		18	
	1.5	0.5	2	1	0	93	31	**9**	27		
	2.0	0.5	2	1	0	96	37	**9**	27		
Ac_2	1.1	0.5	1	1	1	85	—	**10**	40		134.0—135.0
	1.6	0.5	1	1	0	86	—	**10**	41		

a) Step i: Adding of diketone to **3** at −10—0 °C; Step ii: Stirring at −10—0 °C; Step iii: Warming to room temperature; Step iv: Refluxing. b) Based on GLC-peak-area of acenaphthene in hydrolyzed sample. c) A: Based on 5,6-dibromoacenaphthene; B: Based on α-diketone used. d) See Experimental. e) Lit,[3] mp 304—308 °C (dec), 10—20% yield. f) Lit,[3] mp 316—320 °C (dec), 13—26% yield.

as those reported. The use of TMEDA considerably shortened each reaction-time (see Table 1) in comparison with that in the literature[3] (14 h at room temperature or 6 h on refluxing in ether). The reactions of **8** and **9** with phenylboronic acid (dihydroxyphenylborane; $PhB(OH)_2$)[5] quantitatively yielded cyclic esters **8B** and **9B**, respectively (Eq. 2). These facts prove the *cis*-conformation of the 1,2-diols.

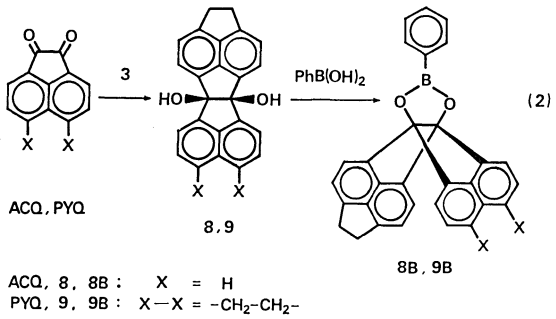

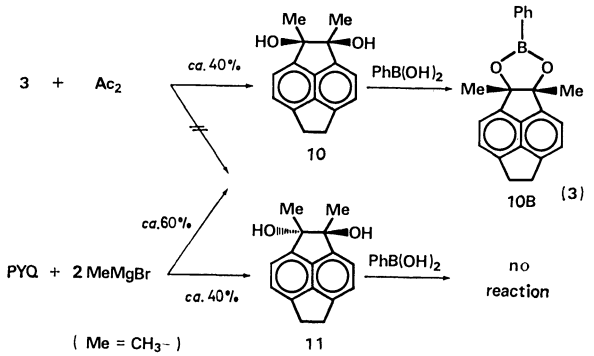

A 1 : 1 cyclic addition also took place between **3** and biacetyl and gave *cis*-diol **10** (mp 134—135 °C), which was quantitatively converted into cyclic ester **10B** with $PhB(OH)_2$. The *trans*-isomer (**11**; mp 171—172 °C) was separately synthesized from the reaction of PYQ with methylmagnesium bromide, and did not react with $PhB(OH)_2$. In this Grignard reaction, *cis*-diol **10** was also yielded in the *cis* : *trans* ratio of about 3 : 2 (Eq. 3). On the other hand, no **11** was detected in the reaction mixture of **3** with biacetyl. Hence, it is concluded that the cyclic addition of each of the three α-diketones to **3** proceeds in a completely *cis*-directing mode.

As Letsinger and Gilpin[5] have discussed in the case of **2** with ACQ, the five-membered *o*-quinone parts of ACQ and PYQ sterically require the *cis*-orientation of the addition product with **1** or **2**. But biacetyl itself, whose quasi-*trans*-conformation has been confirmed in the literature,[11] does not require the *cis*-directing cyclization. The possibility that biacetyl forms a chelate (**12**) and adopts a *cis*-conformation before the addition (Scheme, path B) has been disproved spectroscopically: The electron spectrum of biacetyl was uninfluenced by the presence of lithium cation.[12] The cyclic addition is, therefore, considered to be a two-step process that involves an α-oxide ketone intermediate (**13**) in which a five-membered chelate-ring permits only the *cis*-directing intramolecular cyclization (Scheme, path A). An analogous transition state has been proposed by Cram

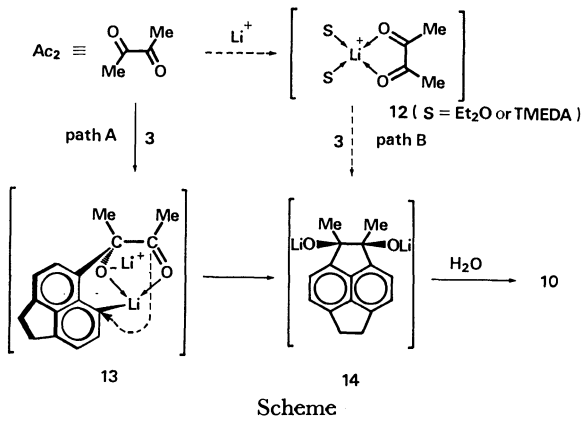

Scheme

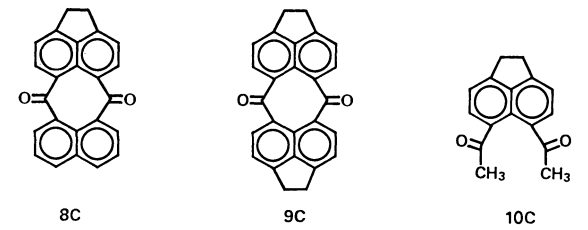

et al.[13] in order to explain the stereoselectivities in the reactions of α-hydroxy ketones and α-methoxy ketones with monofunctional organolithium compounds. In comparison with their results, the stereoselectivity of the present system is very high. This must be ascribed to the specific structure of **3** described before.

The reactions of *cis*-diols **8**, **9**, and **10** with lead(IV) acetate gave diketones **8C**, **9C**, and **10C** in 81, 84, and 92% yields, respectively, under the appropriate conditions described later. Because it has been confirmed that the reaction of **5** with acetyl chloride in the presence of aluminium chloride yields only 3,6-diacetylacenaphthene (mp 149 °C),[14] the cleavage of **10** is a new method for the synthesis of authentic 5,6-diacetylacenaphthene (**10C**; mp 156—157 °C).

It is worth noting that diols **8**, **9**, **10**, and **11**, cyclic esters **8B** and **9B**, and diketones **8C** and **9C** tend to form crystalline molecular compounds with some solvent molecules. Some of them are listed in Table 2. Notice that *cis*-diol **10** (mp 134—135 °C) formed a white molecular compound (mp 143—144 °C) with **5** (mp 94—95 °C). The solvent molecules in these crystals did not dissociate under an aspirator pressure at room temperature, whereas recrystallizations from suitable solvents separated their components, except in the case

Table 2. Crystalline molecular compounds

Component A	Component B	Composition (A : B)[a]	Mp/°C
10	Acenaphthene	2 : 1	143.0—144.0
10	Benzene	3 : 1	127.0—129.0
11	Cyclohexane	3 : 1	170.0—171.0
9B	Benzene	1 : 1	302.0—304.0[b]
9B	Cyclohexane	1 : 1	190[b]

a) Determined by elemental analysis and ^1H NMR spectrum. b) Dissociation in an argon-filled, sealed capillary.

of cyclohexane- or benzene-**9B** (see Experimental). "Solvated" crystals were also observed in the following systems: **8**/ethanol, **8**/acetone, **9**/benzene, **10**/cyclohexane, **11**/carbon tetrachloride, **8B**/cyclohexane, **8C**/acetic acid, and **9C**/acetic acid. By reference to analogous compounds known as "clathrate compounds,"[15] the three-dimensional bulkinesses of the diols and their derivatives seem to be related to the solvent inclusions.

The reactions of benzil and 9,10-phenanthrenequinone with **3** gave no 1 : 1 cyclic addition product, but rather gave unexpected, novel products. Their details will be reported separately.[16]

Experimental

General Procedures. All melting points except that over 360 °C are corrected; some of them were measured in argon-filled, sealed capillaries after degassing. Electron spectra were determined on a Shimadzu UV-200 double beam spectrophotometer. Fluorescence excitation- and emission-spectra were measured on a Shimadzu RF-501 recording spectrofluorophotometer. IR spectra were taken on a JASCO IRA-1 spectrophotometer, using KBr pressed discs. ^{1}H NMR spectra were recorded on a JEOL JNR-PS-100 (100 MHz) or a Hitachi R-40 (90 MHz) spectrometer. Chemical shifts are given in ppm relative to tetramethylsilane as an internal standard. In assignments, abbreviations PhH, NpH, ActH, and ArH mean benzene-, naphthalene-, and acenaphthene-ring protons and aromatic protons, respectively. Mass spectra were taken on a JEOL JMS-D-100 or a Hitachi RMU-7M mass spectrometer at an ion-source temperature of 200 °C and an ionizing voltage of 70 eV unless otherwise indicated. Analytical determinations by GLC were performed on a Shimadzu GC-3BT gas chromatograph operated at 220 °C with a 3 m×3 mm column of 10% SE-30 on Celite 545SK and with helium as carrier gas.

Pyracenequinone was prepared according to the reported method;[17] mp 304.0—306.0 °C (dec), (lit,[17a] mp 305—306 °C). All other chemicals were obtained commercially.[18] Acenaphthenequinone[18a] was recrystallized from toluene. Each of the quinones was ground down and degassed *in vacuo* before use. The biacetyl used was freshly distilled. Lithium perchlorate[18c] was dried at 200 °C/0.1 mmHg† for 2 h. Acetonitrile (Dotite Spectrosol)[18b] was dried with Molecular Sieves 5A. Under an argon atmosphere, "dry" solvents (diethyl ether and benzene) were distilled from sodium wire and then stored with Molecular Sieves 4A or 5A. TMEDA[18a] was refluxed with calcium hydride for 2—3 h and distilled.

All the reactions of **3** and of lead(IV) acetate were carried out under an argon atmosphere. All organic extracts were washed with aqueous concd sodium chloride and dried with anhydrous magnesium sulfate unless otherwise indicated. All evaporations were carried out under a reduced pressure on a rotary evaporator below *ca.* 50 °C.

5,6-Dibromoacenaphthene (4). This was prepared by the method of Yoshiwara[2] with modifications. To a *N,N*-dimethylformamide (DMF) suspension of acenaphthene (77.1 g, 0.50 mol in 250 cm^3), a DMF solution of *N*-bromosuccinimide (NBS)[18c] (89.0 g, 0.50 mol in 250 cm^3) was added dropwise over a period of 90 min at 30—40 °C. After the mixture had been stirred for 1 h at about 30 °C, additional NBS (133.5 g, 0.75 mol) was added in portions over a period of 90 min, the temperature being maintained at 30—40 °C. The dark mixture which formed was stirred for 2 h at about 30 °C and then allowed to stand overnight in a refrigerator. The pale yellow crystalline **4** which precipitated was filtered off, washed with a small amount of DMF and 100 cm^3 of methanol, and dried *in vacuo*. This crude product (mp 166.5—171.5 °C) was recrystallized from carbon tetrachloride,[19] giving 24—31 g (15—20%) of pure **4** as almost colorless needles: mp 174.0—176.0 °C, (lit,[3] mp 173—175 °C).

Generation of 3. All solutions of **3** were prepared just before use as follows. All glassware pieces were heated in a drying oven (*ca.* 100 °C) and then quickly assembled; **4** (1.560 g, 5.00 mmol) was introduced into a four-necked 500 cm^3-flask which was then equipped with a thermometer, a stopcock for sampling, a pressure-equalizing addition funnel joined with a stopcock, and a reflux condenser joined with a three-way stopcock for attachment to a vacuum-line and an argon-line. During a few repetitions of the pumping—argon-introducing cycle, the crystals of **4** were milled with a magnetic stirrer. Dry ether (300 cm^3 or 150 cm^3) was introduced into the flask with syringe-technique and then cooled on an ice–ethanol bath. During the period of cooling, *n*-BuLi (12.0 mmol in 5.5 cm^3 of hexane) was injected into the addition funnel and then mixed with TMEDA (2 cm^3, 13.3 mmol). After the yellow suspension which resulted had been allowed to stand for 15 min, it was added dropwise to the ethereal suspension over a period of 15 min with gentle stirring, and the pale red solution which formed was then stirred for 15 min. During these operations, the temperature was maintained at −10—0°C. A 0.5—1.0 cm^3 of sample of the solution was added to aqueous ammonium chloride and then analyzed gas-chromatographically. The relative peak-area of acenaphthene is usually≥99% within 5—12 min after the adding of *n*-BuLi–TMEDA. In case that a theoretical amount of *n*-BuLi was used, 5—10% of 5-bromoacenaphthene[20] was observed.

5,6-Acenaphthenedicarboxylic Anhydride (6). A solution of **3** (5.00 mmol in 150 cm^3 of ether) was cooled below −70 °C and poured onto crushed dry ice under an argon atmosphere. After the mixture had been allowed to come to room temperature, the white salt which formed was filtered off, washed with ether, and dried *in vacuo*. The quantitative yield of lithium salt (mp>340 °C) was extracted with 30 cm^3 of aqueous 5% sodium carbonate, and the extract was acidified with concd hydrochloric acid, giving 1.11 g (91.4%) of crude 5,6-acenaphthenedicarboxylic acid: mp 282.0—289.0 °C (dec/Ar); IR 3600—2400 (broad band) and 1670 cm^{-1} (C=O). Recrystallization from acetic acid gave anhydride **6**: mp 298.5—299.5 °C (under Ar), (lit,[21] mp 293—294 °C); $UV_{max}(C_2H_5OH)$ 213.5 (log ε 4.20), 237 (4.41), 247 (4.34), 332 (3.89), and 352 nm (3.88); IR 1790, 1765, and 1740 cm^{-1} (C=O).

(Found: C, 75.41; H, 3.26%).

5,6-Diiodoacenaphthene (7). To a solution of **3** (5.00 mmol in 300 cm^3 of ether), a solution of iodine (2.82 g, 11.1 mmol in 25 cm^3 of ether) was added dropwise over a period of 30 min at −10—0 °C. The dark mixture was stirred for 30 min with cooling and for 1 h without cooling. To the mixture 100 cm^3 of aqueous 5% sodium thiosulfate was added with vigorous stirring. The organic layer which separated was washed with aqueous sodium thiosulfate and then water, dried, and evaporated. The pale brown residue, 1.94 g (95.4%) of crude **7** (mp 144.0—148.5 °C), was recrystallized from hexane and then ethanol,[19] giving 1.26 g (62%) of pure **7**: mp 159.0—160.5 °C (dec), (lit,[22] mp 159—160 °C).

(Found: C, 35.44; H, 1.90; I, 62.24%).

cis-1,2-Dihydrocyclopenta[1,2-a: 3,4,5-f'g'] diacenaphthylene-4b,10b-diol (8). Acenaphthenequinone (0.900 g, 4.94 mmol)

† 1 mmHg≃133.3 Pa.

was added to a solution of **3** (5.13 mmol in 300 cm^3 of ether) with vigorous stirring over a period of 30 min at −10—0 °C. The deep violet suspension which resulted was stirred for 2 h with cooling and for 1 h without cooling. Aqueous ammonium chloride (30 g/100 cm^3) was added to the suspension with vigorous stirring. The dark yellow solid which precipitated was filtered off, washed with water and ether, and dried *in vacuo*; 87 mg (9.7%) of the quinone being recovered. The combined organic layer was washed, dried, and evaporated. The residue was washed with hot carbon tetrachloride and water and dried *in vacuo*, giving 326 mg (21.8%) of crude **8** (mp 280—283 °C (dec)). Recrystallization from benzene[19] gave 269 mg (16.2%) of pure **8** as white needles: mp 320.0—322.0 °C (dec/Ar), (lit,[3] mp 304—308 °C (dec)); UV_{max} (C_2H_5OH) 219 (log ε 4.89), 265 (3.54), 275 (3.75), 287 (3.88), 316 (4.13), and 330 nm (4.15); $Fluorescence_{max}$ (C_2H_5OH) 398 nm (excitation at 325 nm); IR 3500 and 3350 cm^{-1} (OH); MS (215 °C, 30 eV), *m/e* (rel intensity), 336 (100), 318 (34), 317 (21), and 290 (25).

(Found: C, 85.89; H, 4.58%).

cis-*1,2,7,8-Tetrahydropentaleno*[*1,2,3*-fg: *4,5,6*-f′g′]*diacenaphthylene-4b,10b-diol* (**9**). A solution of **3** (5.00 mmol in 300 cm^3 of ether) was treated with pyracenequinone (1.60 g, 7.67 mmol) as described above for **8**. After hydrolysis, the unreacted pyracenequinone was extracted with aqueous 10% sodium hydrogensulfite,[17] 499 mg (31.2%) of the quinone being recovered. Crude **9** (27.4%, mp 292—295 °C (dec)) was recrystallized from benzene[19] and then acetone, giving 386 mg (21.3%) of pure **9** as a white powder: mp 347.0—348.0 °C (dec/Ar), (lit,[3] mp 316—320 °C (dec)); UV_{max} (C_2H_5OH) 216 (log ε 4.80), 230 (4.87), 259 (3.28), 269 (3.51), 280 (3.78), 291 (3.96), 319 (4.19), and 333 nm (4.24); $Fluorescence_{max}$ (C_2H_5OH) 394 nm (excitation at 328 nm); IR 3435 and 3315 cm^{-1} (OH); MS, *m/e* (rel intensity), 362 (100), 361 (27), 360 (44), 359 (23), 345 (29), 344 (69), 343 (36), 334 (19), 333 (36), and 332 (16).

(Found: C, 86.22; H, 4.79%).

cis-*1,2,5,6-Tetrahydro-1,2-dimethylcyclopent*[fg]*acenaphthylene-1,2-diol* (**10**). To a solution of **3** (10.0 mmol in 300 cm^3 of ether), a solution of biacetyl (1.35 g, 15.6 mmol in 50 cm^3 of ether) was added over a period of 30 min at −10—0 °C. The pink suspension which resulted was stirred for 1 h with cooling and for 1 h without cooling, and then hydrolyzed with aqueous ammonium chloride (30 g/100 cm^3). The organic layer which separated was washed, dried, and evaporated. The dark residue was dissolved in 10 cm^3 of hot benzene and allowed to stand at room temperature for one day, giving 950 mg of a colorless crystal (mp 127.0—129.0 °C). This was spectrally identical with the molecular compound, benzene-**10**, prepared separately; the yield as $C_6H_6 \cdot 3C_{16}H_{16}O_2$ was 35.7%. The combined filtrate was evaporated and allowed to stand for four days, giving 162 mg of a pale brown crystal (mp 133.0—143.0 °C). This was spectrally identical with the molecular compound, acenaphthene-**10**, the yield as $C_{12}H_{10} \cdot 2C_{16}H_{16}O_2$ being 5.1%. Each of the molecular compounds was recrystallized from hexane,[19] giving a total of 914 mg (38.0%) of pure **10** as white needles: mp 134.0—135.0 °C; UV_{max} (*c*-C_6H_{12}) 226sh (log ε 4.71), 232 (4.87), 250 (2.83), 260sh (3.09), 273sh (3.58), 284 (3.84), 292sh (3.90), 296 (3.93), 305 (3.78), 311 (3.69), 319sh (3.12), and 325 nm (3.27); $Fluorescence_{max}$ (*c*-C_6H_{12}) 386 nm (excitation at 303 nm); IR 3350 (OH), 3035, 2975, 2930 sh, 2915, 2835, 1165, and 1090 cm^{-1}; NMR ($CDCl_3$) δ=7.33 (2H, d, *J*=7.0 Hz, *m*-CH_2-ActH), 7.26 (2H, broad d, *J*=7.0 Hz, *o*-CH_2-ActH), 3.42 (4H, s, $2CH_2$), 3.14 (2H, s, exch., 2OH), and 1.59 (6H, s, $2CH_3$); MS, *m/e* (rel intensity), 240 (14), 222 (12), 221 (16), 207 (48), 198 (17), 197 (100), and 179 (19).

Found: C, 79.95; H, 6.72%; M^+ 240.1121. Calcd for $C_{16}H_{16}O_2$: C, 79.97; H, 6.71%; M, 240.1150.

Molecular Compounds of **10**. *With Benzene*: A recrystallization of **10** from benzene gave benzene-**10** (1/3) as white needles; mp 127.0—129.0 °C. The IR spectrum and NMR spectrum were identical with those of pure **10**, except for the bands at 1485 and 680 cm^{-1} and δ 7.29 ppm, which are characteristic of benzene. The ratio of NMR peaks was ArH : CH_2 : OH : CH_3=6 : 4 : 2 : 6. The benzene molecule in the crystal did not dissociate at 20 °C/20 mmHg, but the crystal sublimed at 100 °C/0.1 mmHg, giving pure **10**.

Found: C, 81.18; H, 6.79%. Calcd for $C_6H_6 \cdot 3C_{16}H_{16}O_2$: C, 81.17; H, 6.81%.

With Acenaphthene: Acenaphthene (64 mg) and **10** (99 mg) were dissolved in 6 cm^3 of ether and allowed to stand for one day at −20 °C. A white precipitate formed (76 mg, mp 142—144 °C); this was filtered off and recrystallized once from ether, giving acenaphthene-**10** (1/2); mp 143.0—144.0 °C; UV_{max} (*c*-C_6H_{12}) 228 (log ε based on the assumption that the molecular weight is 317.40: 4.99), 250 sh (2.88), 286 (3.97), 292 (4.02), 296 (4.01), 305 (3.85), 310 (3.71), 320 (3.31), and 325 nm (3.26); IR 3350 and 3310 sh (OH), 3070, 3035, 2995, 2970, 2920, 2840, 1165, and 1090 cm^{-1}; NMR ($CDCl_3$) δ= 7.57—7.18 (7H, m, ArH), 3.42 (4H, s, CH_2 of **10**), 3.37 (2H, s, CH_2 of **5**), 3.00 (2H, s, exch., 2 OH), and 1.60 (6H, s, $2CH_3$).

Found: C, 82.87; H, 6.59%. Calcd for $C_{12}H_{10} \cdot 2C_{16}H_{16}O_2$: C, 83.25; H, 6.67%.

Reaction of Pyracenequinone with Methylmagnesium Bromide. Under an argon atmosphere, methylmagnesium bromide[18a] (16.8 mmol in 5.6 cm^3 of dibutyl ether) and 150 cm^3 of dry ether were introduced into a three-necked 300 cm^3-flask, and pyracenequinone (848 mg, 4.07 mmol) was added to the solution over a period of 30 min. After 2 h of refluxing, the mixture was cooled on an ice bath and hydrolyzed with aqueous ammonium chloride (15 g/50 cm^3). The organic layer which separated was washed, dried, and evaporated. The resulting dibutyl ether suspension was allowed to stand at −20 °C for 16 h. The pale yellow precipitate was then filtered off, washed with carbon tetrachloride, and dried *in vacuo*, giving 287 mg (29.3%) of crude *trans*-diol **11** (mp 168.5—170.0 °C). The combined filtrate was treated three times in a similar manner, giving 200 mg (20.4%) of crude *cis*-diol **10** (mp 130.0—132.5 °C) and 452 mg in total of a mixture of **10** and **11** (NMR spectral isomeric ratio *cis* : *trans*= 8 : 1—4 : 1). Averaged over repeated runs, the total yield of **10** and **11** was >95% and the total *cis* : *trans* ratio was approximately 3 : 2. The crude **10** and **11** on this run were individually recrystallized from hexane,[19] giving 123 mg (12.6%) of pure **10** and 237 mg (24.2%) of pure **11**: mp 171.0—172.0 °C; UV_{max} (*c*-C_6H_{12}) 224sh (log ε 4.63), 232 (4.89), 273sh (3.58), 284 (3.83), 295 (3.92), 305 (3.76), 310sh (3.65), 320sh (3.12), and 325 nm (3.18); $Fluorescence_{max}$ (*c*-C_6H_{12}) 387 nm (excitation at 304 nm); IR 3330 (OH), 3085, 3045, 2975, 2925, 2840, 1180, 1055, and 1025 cm^{-1}; NMR ($CDCl_3$) δ=7.34 (2H, d, *J*=7.5 Hz, *m*-CH_2-ActH), 7.28 (2H, broad d, *J*=7.5 Hz, *o*-CH_2-ActH), 3.44 (4H, s, $2CH_2$), 1.85 (2H, s, exch., 2OH), and 1.70 (6H, s, $2CH_3$); MS (150 °C, 75 eV), *m/e* (rel intensity), 240 (30), 222 (12), 221 (15), 207 (36), 198 (18), 197 (100), and 179 (11).

Found: C, 80.04; H, 6.70%; M^+ 240. Calcd for $C_{16}H_{16}O_2$: C, 79.97; H, 6.71%; M, 240.

Molecular Compound of **11** *with Cyclohexane*: A recrystallization of **11** from cyclohexane gave cyclohexane-**11** (1/3) as white hair-like crystals; mp 170.0—171.0 °C; IR 3340 (OH), 3085, 3040, 2980, 2925, 2840, 1180, 1055, and 1025 cm^{-1}.

The NMR spectrum was identical with a 1 : 3 mixture of cyclohexane and **11**. The cyclohexane molecule in the crystal did not dissociate at 20 °C/20 mmHg for 48 h, but did at 20 °C/0.1 mmHg, the weight-loss-ratio being 9.95% after 8 h (Calcd for: 10.45%).

Found: C, 80.07; H, 7.28%. Calcd for $C_6H_{12}\cdot 3C_{16}H_{16}O_2$: C, 80.56; H, 7.51%.

1,2-Dihydro-14-phenyl-4b,10b-(epoxyboroxy)cyclopenta[1,2-a : 3,4,5-f'g']diacenaphthylene (8B). A mixture of *cis*-diol **8** (168.25 mg, 0.5002 mmol) and phenylborenic acid[18a] (62.39 mg, 0.5116 mmol) in 50 cm³ of benzene was refluxed for 2 h. After a trace amount of suspended matter had been filtered off, the solution was evaporated to dryness, giving a quantitative yield of crude **8B** (mp 303—305 °C (under Ar)). Recrystallization from benzene gave 187.3 mg (88.7%) of pure **8B** as white needles: mp 307.0—308.0 °C (under Ar); UV_{max} (c-C_6H_{12}) 220sh (logε 4.79), 227 (4.81), 254 (3.50),264 (3.69), 274 (3.91), 280sh (3.75), 285 (4.01), 300sh (3.96), 313 (4.18), and 328 nm (4.22); $Fluorescence_{max}$ (c-C_6H_{12}) 390 nm (excitation at 322 nm); IR 3045, 2915, 2835, 1605, 1385, 1345 (-B-O-), and 1085 cm⁻¹; NMR ($CDCl_3$) δ=8.04—7.96 (2H, m, α-NpH), 7.89 (2H, d, J=7.1 Hz, m-CH_2-ActH), 7.89—7.78 (2H, m, o-B-PhH), 7.78—7,51 (4H, m, β-NpH), 7.43—7.17 (3H, m, m- and p-B-PhH), 7.27 (2H, d, J=7.1 Hz, o-CH_2-ActH), and 3.41 (4H, s, $2CH_2$); MS (220 °C, 75 eV), m/e (rel intensity), 422 (100), 421 (23), 318 (21), 300 (23), 288 (22), 262 (73), 186 (84), 149 (66), 104 (42), and 77 (30).

Found: C, 85.38; H, 4.44%; M⁺ 422 and 421. Calcd for $C_{30}H_{19}BO_2$: C, 85.33; H, 4.53%; M-^{11}B, 422 and M-^{10}B, 421.

1,2,7,8-Tetrahydro-14-phenyl-4b,10b-(epoxyboroxy)pentaleno[1,2,-3-fg : 4,5,6-f'g']diacenaphthylene (9B) and Its Molecular Compounds. *cis*-Diol **9** (181.44 mg, 0.5006 mmol) was treated with phenylboronic acid (62.41 mg, 0.5119 mmol) in 50 cm³ of benzene as described above for **8B**. The white crystalline residue was dried overnight under an aspirator pressure, giving 262.4 mg (99.6%) of crude benzene-**9B** (mp 299—302 °C (under Ar)). Recrystallization from benzene gave pure benzene-**9B** (1/1) as white needles: mp 302.0—304.0 °C (under Ar); MS (150 °C, 75 eV), m/e (rel intensity), 448 (100) and 78 (48). The λ_{max}'s of the UV spectrum in cyclohexane were identical with those of pure **9B** and the logε's, based on the assumption that the molecular weight is 526.44, were consistent with those of **9B** within ±0.03. The IR spectrum and NMR spectrum were identical with those of pure **9B**, except for the bands at 3090, 3075, 1485, and 680 cm⁻¹ and δ 7.33 (6H, s).

Found: C, 87.06; H, 5.00%. Calcd for $C_6H_6\cdot C_{32}H_{21}BO_2$: C, 86.70; H, 5.17%.

On recrystallization from cyclohexane, benzene-**9B** was converted into cyclohexane-**9B** (1/1). Under an argon atmosphere, these white needles melt at 190 °C with foaming and immediately solidify, and then re-melt at 300.0—301.0 °C. The UV spectrum, IR spectrum, NMR spectrum, and MS confirmed the composition to be the same as in the case of benzene-**9B**.

Found: C, 85.51; H, 5.87%. Calcd for $C_6H_{12}\cdot C_{32}H_{21}BO_2$: C, 85.71; H, 6.25%.

On heating at 100 °C/0.1 mmHg for 16 h and at 160 °C/0.1 mmHg for 8 h, 47.749 mg of cyclohexane-**9B** (1/1) gave 40.311 mg of pure **9B**: mp 306.0—307.0 °C; Weight loss, found: 15.58%, calcd: 15.81%; UV_{max} (c-C_6H_{12}) 224sh (logε 4.96), 230 (5.01), 258sh (3.01), 268 (3.56), 275sh (3.68), 278 (3.85), 286sh (3.81), 290 (4.04), 304sh (4.00), 315 (4.23), and 330 nm (4.30); $Fluorescence_{max}$ (c-C_6H_{12}) 390 nm (excitation at 326 nm); IR 3030, 2915, 2835, 1605, 1380, 1345 (-B-O-), 1115, and 1080 cm⁻¹; NMR ($CDCl_3$) δ=7.87 (4H, d, J=7.1 Hz, m-CH_2-ActH), 7.88—7.78 (2H, m, o-B-PhH), 7.36—7.22 (3H, m, m- and p-B-PhH), 7.27 (4H, d, J=7.1 Hz, o-CH_2-ActH), and 3.40 (8H, s, $4CH_2$); MS (150 °C, 75 eV), m/e (rel intensity), 448 (100), 447 (27), 420 (8), 344 (12), 343 (16), 326 (8), 316 (10), 315 (10), 313 (11), 262 (17), 186 (13), 149 (34), 104 (5), and 77 (25).

Found: C, 85.69; H, 4.65%; M⁺ 448 and 447. Calcd for $C_{32}H_{21}BO_2$: C, 85.73; H, 4.72%; M-^{11}B, 448 and M-^{10}B, 447.

1,2,4b,7a-Tetrahydro-4b,7a-dimethyl-6-phenylcyclopent[5,6]acenaphtho[1,2-d][1,3,2]dioxaborole (10B). *cis*-Diol **10** (240.76 mg, 1.002 mmol) was treated with phenylboronic acid (126.10 mg, 1.034 mmol) as described above for **8B**. A quantitative yield of crude **10B** (mp 164—168 °C) was recrystallized from hexane, giving 262.8 mg (80.4%) of pure **10B**: mp 169.5—171.0 °C; UV_{max} (c-C_6H_{12}) 227 (logε 4.83), 231 (4.93), 254 (3.21), 261sh (3.41), 269sh (3.62), 274 (3.72), 279sh (3.81), 283 (3.90), 291 (3.95), 295 (3.99), 304 (3.83), 310 (3.71), 319 (3.09), and 324 nm (3.13); $Fluorescence_{max}$ (c-C_6H_{12}) 387 nm (excitation at 303 nm); IR 3060, 2985, 2945, 2915, 1600, 1390, 1385, 1350 (-B-O-), and 1090 cm⁻¹; NMR ($CDCl_3$) δ=7.81—7.71 (2H, m, o-B-PhH), 7.49 (2H, d, J=7.1 Hz, m-CH_2-ActH), 7.43—7.14 (3H, m, m- and p-B-PhH), 7.29 (2H, broad d, J=7.1 Hz, o-CH_2-ActH), 3.43 (4H, s, $2CH_2$), and 1.86 (6H, s, $2CH_3$); MS (160 °C, 75 eV), m/e (rel intensity), 326 (100), 325 (24), 311 (4), 283 (66), 282 (17), 222 (22), 221 (19), 207 (15), 205 (12), 189 (10), 179 (18), 178 (13), 152 (12), 149 (8), 104 (16), and 77 (12).

Found: C, 81.24; H, 5.81%; M⁺ 326 and 325. Calcd for $C_{22}H_{19}BO_2$: C, 81.01; H, 5.87%; M-^{11}B, 326 and M-^{10}B, 325.

1,2-Dihydronaphtho[1',8': 5,6,7]cyclooct[1,2,3-fg]acenaphthylene-5,12-dione (8C). A mixture of diol **8** (132.5 mg, 0.3939 mmol) and lead(IV) acetate[18a] (291 mg, 1.50 molar ratio) in 30 cm³ of dry benzene was stirred at room temperature for 2 h, refluxed for 30 min, and allowed to come to room temperature. To the mixture 20 cm³ of dil hydrochloric acid was added dropwise. The pale yellow precipitate which formed was filtered off, washed with benzene, dil hydrochloric acid, and then water, and dried *in vacuo*, giving 106 mg (80.5%) of crude **8C**. Recrystallization from benzene gave pure **8C**: mp 343.0—345.0 °C (dec/Ar), (lit,[3] mp 330—334 °C (dec)); UV_{max} (C_6H_6) 320sh (logε 4.08) and 334 nm (4.13); $Fluorescence_{max}$ (C_6H_6) 401 nm (excitation at 333 nm); IR 1680 cm⁻¹ (C=O); MS, m/e (rel intensity), 334 (100), 333 (45), 306 (17), 278 (41), 277 (52), 276 (61), and 275 (12).

(Found: C, 85.84; H, 3.78%).

1,2,8,9-Tetrahydrocycloocta[1,2,3-fg : 5,6,7-f'g']diacenaphthylene-5,12-dione (9C). A mixture of diol **9** (135.0 mg, 0.3725 mmol) and lead(IV) acetate (300 mg, 1.63 molar ratio) in 20 cm³ of dry benzene was treated as described above for **8C**, giving 112.8 mg (84.0%) of almost pure **9C**. Recrystallization from benzene gave pure **9C** as pale yellow needles: mp 390—400 °C (uncorrected, dec/Ar), (lit,[3] mp >330 °C (dec)); UV_{max} (C_6H_6) 326sh (logε 4.04) and 341 nm (4.12); $Fluorescence_{max}$ (C_6H_6) 400 nm (excitation at 339 nm); IR 1680 cm⁻¹ (C=O); MS (240 °C, 35 eV), m/e (rel intensity), 360 (100), 359 (24), 332 (9), 331 (20), 304 (9), and 303 (13).

(Found: C, 86.63; H, 4.21%).

5,6-Diacetylacenaphthene (10C). A mixture of diol **10** (240.6 mg, 1.001 mmol) and lead(IV) acetate (600 mg, 1.22 molar ratio) in 25 cm³ of dry benzene was treated as described above for **8C**, except that the lead(II) acetate which precipitated was filtered off and the filtrate was chromatographed on a column of Wakogel C-200[18b] (40 g). After tarry matters (mainly silicone grease) had been extracted with benzene, the effluent with chloroform was collected and evaporated to dryness, giving 219 mg (91.8%) of crude **10C** (mp 153—155

°C). Recrystallization from cyclohexane gave 156 mg (65.4%) of pure **10C** as pale yellow plates: mp 156.0—157.0 °C; UV_{max} (c-C_6H_{12}) 230 (logε 4.60), 277sh (3.63), 310 (3.93), and 324sh nm (3.84); (Fluorescence was not detected.); IR 3045, 3015, 2940, 2910, 1670 (C=O), 1605, 1275, 1210, and 1115 cm^{-1}; NMR ($CDCl_3$) δ=7.80 (2H, d, J=7.1 Hz, o-CH_3CO-ActH), 7.35 (2H, broad d, J=7.1 Hz, o-CH_2-ActH), 3.44 (4H, s, $2CH_2$), and 2.70 (6H, s, $2CH_3CO$); MS (70 °C, 75 eV), m/e (rel intensity), 238 (29), 224 (19), 223 (100), 195 (14), 165 (22), 152 (21), 151 (10), 150 (5), and 149 (5).

Found: C, 80.53; H, 5.84%; M^+ 238. Calcd for $C_{16}H_{14}O_2$: C, 80.65; H, 5.92%; M, 238.

References

1) Presented partly at 37th National Meeting of the Chemical Society of Japan, Yokohama, April 1978, Abstr. No. 2D04.

2) T. Kasai and J. Yoshiwara, 34th National Meeting of the Chemical Society of Japan, Hiratsuka, April 1976, Abstr. No. 2G22.

3) R. H. Mitchell, T. Fyles, and L. M. Ralph, *Can. J. Chem.*, **55**, 1480 (1977).

4) R. L. Letsinger, J. A. Gilpin, and W. J. Vullo, *J. Org. Chem.*, **27**, 672 (1962); J. Meinwald, D. Dauplaise. F. Wudl, and J. J. Hauser, *J. Am. Chem. Soc.*, **99**, 255 (1977); J. F. Blount, F. Cozzi, J. R. Damewood, Jr., L. D. Iroff, U. Sjöstrand, and K. Mislow, *ibid.*, **102**, 99 (1980) and the references cited therein.

5) R. L. Letsinger and J. A. Gilpin, *J. Org. Chem.*, **29**, 243 (1964).

6) For an extensive review, see V. Balasubramaniyan, *Chem. Rev.*, **66**, 567 (1966).

7) See a) B. J. Wakefield, "The Chemistry of Organolithium Compounds," Pergamon Press, New York (1974); b) J. M. Mallan and R. L. Bebb, *Chem. Rev.*, **69**, 693 (1969).

8) Probably because of technical losses, a 10—20% excess of n-BuLi was required for the quantitative conversion of **4** into **3** (see Experimental).

9) Refs. 7a p. 8 and 7b p. 695.

10) Apparently the metal–bromine exchange exceeded the abstraction of the benzylic hydrogens[10a,b] in reaction rate: a) L. D. Kershner, J. M. Gaidis, and H. H. Freedman, *J. Am. Chem. Soc.*, **94**, 985 (1972); b) W. E. Rhine, J. H. Davis, and G. Stucky, *J. Organomet. Chem.*, **134**, 139 (1977).

11) P. H. Cureton, C. G. Le Fèvre, and R. J. W. Le Fèvre, *J. Chem. Soc.*, **1961**, 4447 and the references cited therein.

12) λ_{max}/nm (acetonitrile, [biacetyl]=0.02293 mol dm^{-3}) 270 (ε 16.8), 280sh (15.4), 416 (19.95), and 436sh (16.9); λ_{max}/nm (acetonitrile, [biacetyl]=0.02293 mol dm^{-3}, [$LiClO_4$] =0.024 mol dm^{-3}) 270 (ε 16.9), 280sh (15.7), 416 (19.9), and 436sh (16.8). Metal cation effects in UV spectra of some other diketones have been reported by K. Sasaki and A. Kitani, *J. Electroanal. Chem. Interfacial Electrochem.*, **94**, 201 (1978).

13) D. J. Cram and D. R. Wilson, *J. Am. Chem. Soc.*, **85**, 1245 (1963); *cf.* Ref. 7a p. 131.

14) H. J. Richter and F. B. Stocker, *J. Org. Chem.*, **24**, 214 (1959); L. A. Carpino and S. Göwecke, *ibid.*, **29**, 2824 (1964).

15) N. Kaneniwa, *Kagaku No Ryoiki*, **15**, 252, 345, 427 (1961); K. Takemoto, "Hosetsu-kagoubutsu No Kagaku," Tokyo Kagaku Dojin, Tokyo (1969).

16) N. Tanaka and T. Kasai, *Bull. Chem. Soc. Jpn.*, **54**, 3026 (1981).

17) a) B. M. Trost, *J. Am. Chem. Soc.*, **91**, 918 (1969); b) J. K. Stille, G. K. Noren, and L. Green, *J. Polym. Sci., Part A-1, Polym. Chem.*, **8**, 2245 (1970).

18) a) Tokyo Kasei Kogyo Co., Ltd.; b) Wako Pure Chemical Industries, Ltd.; c) Nakarai Chemicals, Ltd.

19) The hot solution was treated with decolorizing charcoal.

20) Authentic 5-bromoacenaphthene (mp 54.0—55.0 °C, lit,[3] mp 53.5—55.0 °C) was prepared according to the reported method: S. D. Ross, M. Finkelstein, and R. C. Petersen, *J. Am. Chem. Soc.*, **80**, 4327 (1958).

21) M. Freund and K. Fleischer, *Justus Liebigs Ann. Chem.*, **399**, 182 (1913).

22) R. L. Clough, P. Mison, and J. D. Roberts, *J. Org. Chem.*, **41**, 2252 (1976).

Reactions of 5,6-Dilithioacenaphthene-*N,N,N',N'*-Tetramethyl-1,2-ethanediamine Complex with α-Diketones. II.[1] Competitive Oxophilic and Carbophilic Additions and Redox Reactions

Norio TANAKA and Toshiyasu KASAI*

Department of Chemistry for Engineering, Tokyo Institute of Technology, O-okayama, Meguro-ku, Tokyo 152

(Received January 8, 1981)

The reaction of the title complex (**3**) with benzil did not give the 1 : 1 cyclic addition product expected, but gave 5,6-dibenzoylacenaphthene, 5-(1-hydroxy-2-oxo-1,2-diphenylethyl)-6-(2-oxo-1,2-diphenylethoxy)acenaphthene (**5**), 5-benzoyl-6-(1-hydroxy-2-oxo-1,2-diphenylethyl)acenaphthene, benzoin, and benzilic acid. Compound **5** suggests a new type of oxophilic addition accompanied by a carbophilic addition. The reaction of **3** with 9,10-phenanthrenequinone in a 1 : 1 molar ratio gave both the oxidative homo-coupling product of **3**, 1,2,7,8-tetrahydrodicyclopenta[*cd* : *lm*]perylene, and the hydroquinone dianion, which was converted into 9,10-diacetoxyphenanthrene on acetolysis. The differences in the reaction modes between **3** and α-diketones can basically be understood in terms of the redox potentials and the steric factors of the α-diketones.

5,6-Dilithioacenaphthene (**1**)[2,3] can be regarded as a nucleophile like 1,8-dilithionaphthalene (**2**)[4–8] which possesses two reaction sites at the peri positions of a naphthalene nucleus; thus, its synthetic conditions and reaction modes especially with bifunctional electrophiles are of interest in connection with the peri interaction in naphthalene derivatives.[9] A 1 : 1 cyclic condensation or addition is the most possible reaction path in the reaction systems of **1** and **2** with 1,2-dichlorodisilanes,[2,8] 1,3-dichlorodisiloxanes,[2] or acenaphthenequinone (ACQ),[3,5] **1** with pyracenequinone (5,6-dihydrocyclopent[*fg*]acenaphthylene-1,2-dione; PYQ),[3] and **2** with dialkyldichlorosilanes[6] or organotin dihalides.[7] No other reaction mode except a 2 : 2 cyclic condensation in the last case[7] has been reported.

In the course of studies on the synthetic conditions of **1**, the authors have found that the 5,6-dilithioacenaphthene-*N,N,N',N'*-tetramethyl-1,2-ethanediamine (TMEDA) complex (**3**)[1] reacts with some α-diketones in unexpected, novel modes which may illustrate new aspects of the peri interaction. This paper is chiefly concerned with the complicated reactions of **3** with benzil (Bz_2) and the redox reaction between **3** and 9,10-phenanthrenequinone (PQ). The factors that govern the reaction modes will also be discussed.

Results and Discussion

Competitive Complex Reactions of 3 with Benzil; Oxophilic Addition, Carbophilic Additions, and Reduction of Benzil. The *cis*-directing 1 : 1 cyclic additions of **3** with ACQ, PYQ, and biacetyl (Ac_2), reported separately,[1] prompted us to examine the reaction with benzil. The product expected, *cis*- or *trans*-1,2,5,6-tetrahydro-1,2-diphenylcyclopent[*fg*]acenaphthylene-1,2-diol (**4**), however, was not detected in the reaction mixture. Five products were isolated and identified as follows: 5-(1-hydroxy-2-oxo-1,2-diphenylethyl)-6-(2-oxo-1,2-diphenylethoxy)-acenaphthene (**5**), 5-benzoyl-6-(1-hydroxy-2-oxo-1,2-diphenylethyl)acenaphthene (**6**), 5,6-dibenzoylacenaphthene (**7**), benzoin (**8**), and benzilic acid (**9**). Typical yields are cited in Table 1. The structure of **5** was determined by means of a single-crystal X-ray analysis. The details of this analysis are reported elsewhere.[10] Figure 1 shows one of the two crystallographically independent molecules of **5**. Probably because of packing forces, their geometries are slightly different.[10]

The ^1H NMR spectrum of **5** shows some unusual features, one of which is that the signal assigned to the methine proton of the *O*-substituted benzoin moiety

Table 1. Reactions of 5,6-dilithioacenaphthene–TMEDA complex (**3**) with α-diketones (in Et_2O)

α-Diketone	Mole ratio (diketone/**3**)	Reaction time/h[a] i	ii	iii	iv	Consumption of **3**/%[b]	Recovery of diketone/%	Product	Yield/%[c] A	B	Mp/°C[d]
Bz_2	2.0	0.5	2	0.5	1	100	3.7	**5**	7.9		181.0—182.5
								6	4.1		201.0—204.0 (dec/Ar)
								7[e]	21		209.0—210.0
								8[f]		19	135.0—136.0
								9[f]		4.3	151.0—152.0
PQ	1.0	0.1	1	1	0	76	62	**10**	20		345.0—346.0 (dec/Ar)
	2.1	0.1	1	1	0	98	69	**10**	27		
	1.0	0.1	4	2+1[g]	0	87	0	**10**	27		
								11[h]		48	203.0—204.0

a) Step i: Adding of diketone to **3** at −10—0 °C; Step ii: Stirring at −10—0 °C; Step iii; Stirring without cooling; Step iv: Refluxing. b) Based on GLC-peak-area of acenaphthene in hydrolyzed sample. c) A: Based on 5,6-dibromoacenaphthene; B: Based on α-diketone used. d) Some melting points were measured in argon-filled, sealed capillaries. e) Lit,[11] mp 207—208 °C. f) An authentic sample was obtained commercially. g) Treatment with Ac_2O/pyridine. h) Lit,[12] mp 203—203.5 °C.

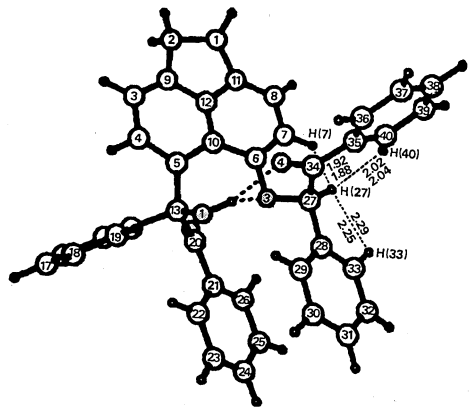

Fig. 1. Molecular structure of **5**. Some close H–H contacts (Å) are also shown, e.s.d.'s being 0.06—0.08 Å.

appears as a doublet (J=7.5 Hz) at δ 6.45 coupling with an aromatic proton, the signal of which appears as a multiplet at 7.00 (in $(CD_3)_2SO$).[13] This remarkably large long-range coupling-constant must ascribed to the specific conformation of **5** in which the methine H-atom, H(27), is in contact with three aromatic H-atoms: H(7), H(33), and H(40) (Fig. 1).[10,14]

The structure of **5** suggests a new type of oxophilic addition which cooperates with a normal carbophilic addition. This is the first example of the heterophilic addition of an organolithium compound with an α-diketone; in the case of Grignard reagent, not a few instances of this type of reactions have been reported.[15] These heterophilic additions have shown the radical character of some Grignard reactions with certain carbonyl compounds.[16] As discussed below, products **5** and **8** also suggest strongly that the radical processes that involve the benzil radical anion ($Bz_2^{-\cdot}$) take an important part in the reaction with **3**.

According to the reports published on the reduction of benzil,[17-21] $Bz_2^{-\cdot}$ generated *via* a single-electron-transfer (SET) in the presence of metal cation forms an ion pair, $Bz_2^{-\cdot}Li^+$ (≡**12a**⇌*cis*-**12b**⇌*trans*-**12b**), and disproportionates to benzil and dilithium stilbenediolate (**13**) which is converted into **8** on hydrolysis (Scheme 1, path A). The formation of **5** can most readily be accounted for when the redox reaction of benzil with a probable intermediate (**14**) is assumed: The SET between the two followed by the coupling of the resulting radicals, **15** and **12b**, will yield stilbene derivative **16**, which can be converted into **5** on hydrolysis[22] (Scheme 1, path B). The other coupling product (**17**), sterically unfavorable, was not detected in the reaction mixture.

Although **7** is the major product, no positive evidence that elucidates a mechanism for its formation has been obtained. However, a by-product expected for the oxidative fission of **17** (R=H), benzoic acid, was not detected in the reaction mixture. There is a possibility that 1 : 1 cyclic addition product **4** is formed but decomposes to yield **7**. This seems to be excluded because of the stabilities of *trans*-**4**,[11] *cis*-diaryl-1,2-acenaphthenediols,[23] and the methyl analogues, *cis*- and *trans*-1,2,5,6-tetrahydro-1,2-dimethylcyclopent[*fg*]-acenaphthylene-1,2-diols,[1] though the exact factor that prevents the formation of **4** is not yet clear.

An acidification of the aqueous layer after hydrolysis gave benzilic acid. On treatment of benzil in an ethereal solution with an aqueous lithium hydroxide in the presence of TMEDA, benzilic acid rearrangement[24] did not take place. Hence, the acid must be formed in the reaction system before hydrolysis.[25]

In order to evaluate the reducing potential of the butyllithium (*n*-BuLi)–TMEDA complex, it was allowed to react with benzil in a molar ratio of *n*-BuLi : Bz_2= 2 : 1 under the conditions similar to those in the case

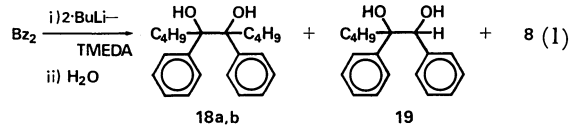

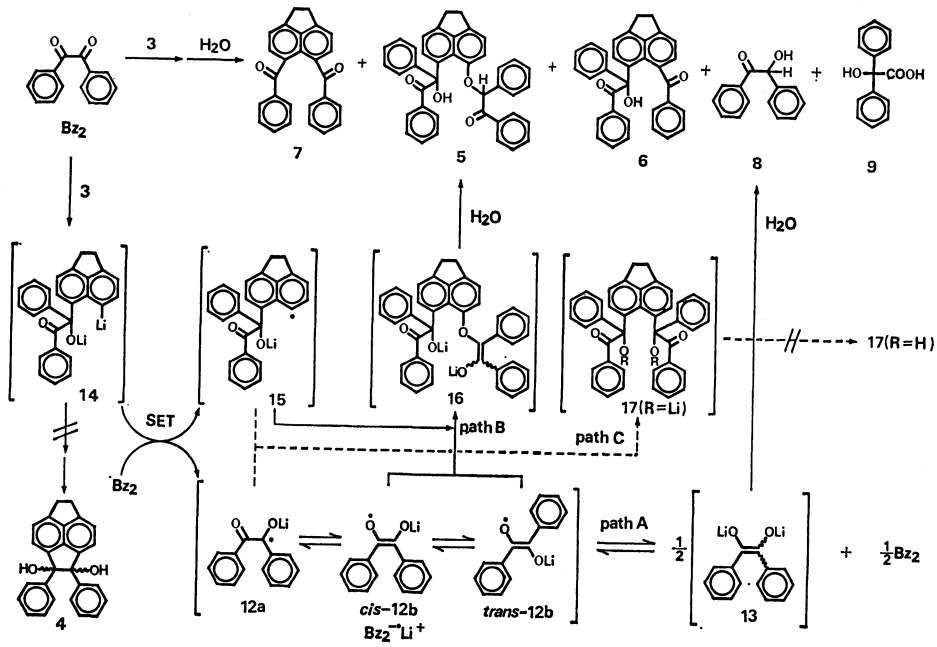

Scheme 1.

of **3** with Bz_2. From the reaction mixture, *erythro*- or *threo*-5,6-diphenyl-5,6-decanediol (46% of **18a** and 22% of 1 : 4 mixture of **18a** and **18b**),[26] 5% of 1,2-diphenyl-1,2-hexanediol (**19**), and 2% of benzoin were isolated (Eq. 1). Thus, the reducing effect of an excess *n*-BuLi which may remain in the solution of **3**[27] is negligible.

Oxidative Homo-coupling of 3. Although the reactions of *o*-quinones ACQ and PYQ with **3** yield 1 : 1 cyclic addition products,[1] another *o*-quinone, 9,10-phenanthrenequinone (PQ), has not yielded such a product (**20**). The reaction of **3** with PQ in a 1 : 1 molar ratio gave both the oxidative homo-coupling product of **3**, 1,2,7,8-tetrahydrodicyclopenta[*cd* : *lm*]-perylene (**10**; 27%), and the hydroquinone dianion (PQ^{2-}), which was converted into 9,10-diacetoxy-phenanthrene (**11**; 48%) on acetolysis, as described below in detail. Thus, the redox reaction between **3** and PQ took place preferentially. This is a novel instance of the behavior of a bifunctional organolithium compound in the system with quinones, although the homo-coupling of monofunctional Grignard reagent or organolithium compound is often induced by certain quinones.[28] In the case of PQ, however, many normal additions with such organometals[29] and some oxophilic additions with aryl and allyl Grignard reagents[15] have been reported, but homo-coupling products are described only in the cases of *p*-tolyl-[29c] and *p*-methyl-benzyl-[29d] magnesium bromides.

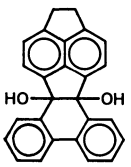

20

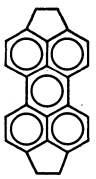

10

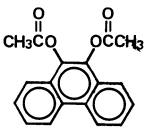

11

The molar ratio of PQ to **3** dramatically changed the appearance of the reaction. When an equivalent mol of PQ was added to a pale red solution of **3** over a period of 5 min, every portion of the yellow powder of PQ rapidly dissolved, the solution developed instantaneously a brilliant green color; just after the adding had been ended, the consumption-ratio of **3** was 50—60% and the reaction mixture became a dark green suspension involving a dark yellow powder of **10**. When the reaction was allowed to continue, the consumption-ratio increased and finaly reached to *ca.* 90%, and the suspension gradually changed to yellow. After a treatment with an aqueous iron(III) chloride, 60—70% of PQ was recovered, while a treatment with acetic anhydride gave a *ca.* 50% yield of 9,10-diacetoxy-phenanthrene and no PQ. When a 2 molar ratio of PQ was used, the consumption of **3** was approximately quantitative just after the adding and the dark green suspension which resulted did not change its color for at least 2 h. The maximum yield of **10** was 27% regardless of the molar ratio, but in the case of that of 1 : 1, the yield depended on the reaction-time (Table 1).

The reduction of PQ and the behavior of its radical anion ($PQ^{-\cdot}$) and dianion (PQ^{2-}) in the presence of metal cation have been well documented.[15a,30-32] On the bases of these reports, the observations described

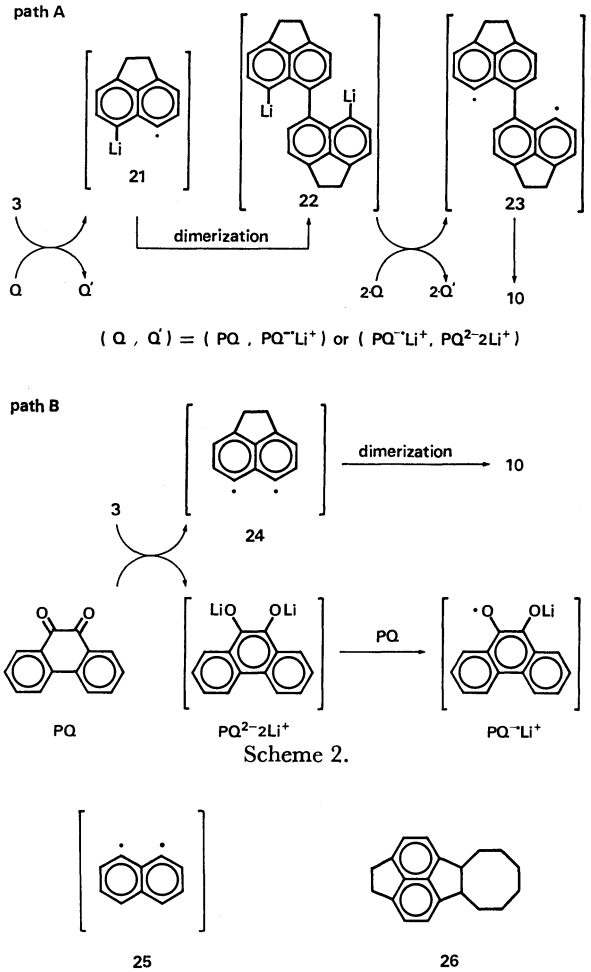

Scheme 2.

above strongly suggest that a SET between PQ or $PQ^{-\cdot}Li^+$ and **3** or **22** (Scheme 2, path A) is more operative than a single two-electron-transfer between PQ and **3**, followed both by the homo-coupling of the resulting biradical (**24**) and by the redox reaction between PQ^{2-} and PQ[31] (Scheme 2, path B). This idea was further examined.

By reference to the trapping experiments of 1,8-dehydronaphthalene (**25**),[33] the reaction of **3** with PQ was investigated in the presence of a 77 molar ratio of cyclooctene,[34] but the yield of **10** was not decreased (26%) and no cyclooctene adduct (**26**) was detected. This may disprove the presence of the *free* biradical (**24**).[35]

The oxidative homo-coupling reactions of aromatic dilithium compounds by transition metal halides have been reported in the cases of **2**,[33] *o*-dilithiobenzene,[36] and 2,2'-dilithiobiphenyl,[37] and no evidence for the corresponding biradicals has been obtained. For comparison, the reaction of **3** with a 2 molar ratio of cobalt(II) chloride was investigated: complex **3** was readily decomposed by $CoCl_2$ above −30 °C, the consumption-ratio reached to ≥95% within 2 h, and **10** was isolated in a 28% yield.

The similarities between the reactions with PQ and $CoCl_2$ in the reaction rate and the yield of **10** are quite in agreement with the idea that oxidative homo-coupling of **3** proceeds in a step-wise SET pathway regardless of the oxidizing agent. In fact, the reactions of **3** with

Table 2. Cyclic voltammetric data for reduction of α-diketones (in CH_3CN, [diketone]=1.3 mmol dm^{-3}, $[Et_4NClO_4]$=0.2 mol dm^{-3}, at 20 °C)

α-Diketone	Scan rate / V s^{-1}	1st wave			2nd wave		
		A/V	*B*/mV	*C*	*A*/V	*B*/mV	*C*
PQ	0.2	−1.13	60	1.0	−1.82	105	1.0
ACQ	0.14	−1.39	60	1.0	−2.15	80	1.0
PYQ	0.2	−1.52	140	1.0	−2.25	155	1.0
	0.01	−1.52	75	1.0	−2.25	85	1.0
Bz_2	0.2	−1.66	85	1.0	−2.31	155	0.7
	0.01	−1.66	50	1.0	−2.24	100	0.5
Ac_2	0.2	<−1.8	—	—	—	—	—

A: Half-wave potential *vs.* Ag/satu. $AgNO_3$. *B*: Peak-separation. *C*: Anodic-peak-current/cathodic-peak-current.

some *p*-quinones also yielded **10** (see Experimental). On the other hand, detailed examinations confirmed that other α-diketones (ACQ, PYQ, Bz_2, and Ac_2) did not induce the homo-coupling of **3**. This indicates that the redox potential of α-diketone may be an important control-factor of the reaction modes.

Redox Potentials of α-Diketones. As Table 2 shows, the one- and two-electron reductions of the α-diketones are easier in the order of

$$PQ > ACQ > PYQ > Bz_2 > Ac_2, \quad (2)$$

under the conditions where the ion-pairing effect[17c,32] is negligible. Then, the effects of lithium cation and TMEDA, which may prevent the ion-pairing,[38] were examined.

All the cyclic voltammograms measured in the presence of lithium perchlorate in an acetonitrile solutions[39] are complex and correspond to irreversible steps; thus, quantitative discussions are difficult. In the case of PQ, however, the clear, positive shifts of the cathodic peaks were observed. This can be explained in terms of the formation of an ion pair $PQ^{-\cdot}Li^+$, as in the literature.[32] As expected, these positive shifts were reduced by adding TMEDA, but its effect was relatively slight. In the cases of ACQ, PYQ, and Bz_2, the positive shifts were not so clear as in the case of PQ, and no distinct effect of TMEDA was observed at any scan rate (<0.27 V s^{-1}). These findings suggest that the order of the reduction potentials (Eq. 2) may be unchanged in the ethereal solution containing Li^+–TMEDA. Thus, PQ is the most reducible α-diketone in those investigated regardless of the presence of Li^+. The relatively low reducibility of benzil even under the influence of ion-pairing supports the idea that only the sterically hindered intermediate, **14**, is able to reduce benzil in the reaction system with **3**, as discussed before. On the other hand, the difference between PQ and ACQ in redox potential seems to be too small to contribute to the distinct disparity in their reaction modes toward **3**. In fact, the reactions of these *o*-quinones with monofunctional organometals proceed in almost the same modes involving normal[23,29] and unusual[40] carbophilic additions and redox reactions.[15a] It is clear that the specific structure of **3** has revealed an unknown difference between the two *o*-quinones, though its exact nature can not yet be explained.

Experimental

General Procedures. Melting points, electron spectra, fluorescence excitation- and emission-spectra, IR spectra, ^1H NMR spectra, and mass spectra were recorded according to the methods given in the previous paper.[1] The solution of **3** was prepared from 5,6-dibromoacenaphthene, *n*-BuLi, and TMEDA in dry ether at −10—0 °C just before use, as in the previous paper.[1] All other chemicals were obtained commercially.[41] Benzil[41a] and 9,10-phenanthrenequinone[41a] were recrystallized from ethanol and benzene, respectively, and ground down and degassed *in vacuo* before use. Tetraethylammonium perchlorate[41b] was dried *in vacuo* at room temperature. Lithium perchlorate[41c] was dried at 200 °C/0.1 mmHg† for 2 h. Acetonitrile (Dotite Spectrosol)[41b] was dried with Molecular Sieves 5A and degassed with argon-bubbling. All reactions were performed under an argon atmosphere. All evaporations were carried out under a reduced pressure on a rotary evaporator below *ca.* 40 °C. Chromatographic separations were carried out on the columns (2.2 cm × 60—90 cm) of Wakogel C-200.[41b] Analytical determinations by GLC were carried out according to the previous paper.[1]

Reactions of 3 with Benzil. To a solution of **3** (10.0 mmol in 300 cm^3 of ether), a solution of benzil[42] (4.280 g, 20.36 mmol in 50 cm^3 of ether) was added with stirring over a period of 30 min at −10—0 °C. The solution became at first dark brown, changed to dark green, and finally to a brown purple suspension. This was stirred for 2 h at −10—0 °C and for 0.5 h without cooling, and then refluxed for 1 h. After the suspension was allowed to stand for 30 min, aqueous ammonium chloride (30 g/100 cm^3) was added to it with vigorous stirring. The hydrolysate was then cooled on an ice bath for 2 h. The pale yellow precipitate which formed was filtered off, washed with water and ether, and dried *in vacuo*, giving a mixture of **5** and **7**. This was chromatographed on a silica-gel column (150 g) with benzene and chloroform as successive eluents, giving 286 mg of crude **5** (mp 177—180 °C) and then 461 mg of crude **7** (mp 199—205 °C). The combined filtrate was separated and the organic layer was washed with 3 × 100 cm^3 of aqueous concd sodium chloride. The combined aqueous layer was acidified with concd hydrochloric acid and allowed to stand for a few days, giving 160 mg of pure benzilic acid (**9**). The acidic solution was then extracted with ether and gave additional **9** (39 mg); the total yield was 4.3%: mp and mixed mp 151.0—152.0 °C. The organic mother layer was dried ($MgSO_4$), concentrated to about 50 cm^3, and then cooled for one day at −15 °C, giving 167 mg of crude **5** (mp 174—176 °C). The filtrate was then evaporated and the residue was triturated with ether, giving 432 mg of crude **8** (mp 122—133 °C). The filtrate of this trituration was evaporated to dryness and chromatographed on a silica-gel column (150 g) with benzene as eluent. The dark brown solution became dark green on this column. The first green eluent was collected and evaporated, and the brown residue was dissolved in carbon tetrachloride. The solution was then diluted with hexane, giving 108 mg of crude **6** as a pale brown crystal (mp 194—205 °C (dec)). The second yellowish green eluent was treated as described above for the first, giving 159 mg (3.7%) of benzil. The filtrate of this treatment was evaporated to dryness and the residue was recrystallized from ethanol, giving 83 mg of crude **6** (mp 180—182 °C). After the third deep green eluent (unknown), extraction with chloro-

† 1 mmHg ≃ 133.3 Pa.

from gave the fourth pale yellow eluent. This was evaporated to dryness, giving 390 mg of crude **8** (mp 128—132 °C). The fifth dark green eluent with chloroform was evaporated to dryness and then recrystallized from benzene, giving 306 mg of crude **7** (mp 206.5—208.5 °C). The total of 822 mg (19%, based on benzil used) of crude benzoin was decolorized in a short benzene-silica-gel column and then recrystallized from ethanol,[43] giving 547 mg (12.7%) of pure **8**; mp and mixed mp 135.0—136.0 °C.

*5-(1-Hydroxy-2-oxo-1,2-diphenylethyl)-6-(2-oxo-1,2-diphenylethoxy)acenaphthene (**5**)*: A total of 453 mg (7.9%) of crude product was recrystallized from benzene,[43] giving 331 mg (5.8%) of pure **5** as white plates: mp 181.0—182.5 °C; UV_{max} (C_2H_5OH) 214 (logε 4.65), 240 (4.69), 300 (3.99), 318sh (3.87), and 334sh nm (3.66); $Fluorescence_{max}$ (C_2H_5OH) 402 nm (excitation at 341 nm); IR 3425 (OH),3065, 3035, 2920, 1670 (C=O), 1600, 1450, 1265, 1225, 1140, 965, 855, 770, 750, 720, 705, and 695 cm^{-1}; NMR $\delta(CDCl_3)=7.83$—7.73 (4H, m, ArH), 7.68—6.80 (20H, m, ArH), 6.64 (1H, d, $J=7.5$ Hz, CH), and 3.30 (4H, s, $2CH_2$), $\delta((CD_3)_2SO)=7.98$—7.91 (2H, m, ArH), 7.70—6.80 (22H, m, ArH), 6.45 (1H, d, $J=$ 7.5 Hz, CH), and 3.29 ((4H), s, $2CH_2$); MS (270 °C, 75 eV), *m/e* (rel intensity), 574 (2.6), 572 (2.7), 558 (2.1), 556 (2.1), 540 (3.2), 469 (5.3), 452 (9.2), 451 (23), 450 (6.5), 435 (5.0), 364 (4.0), 363 (4.9), 362 (3.1), 361 (4.0), 347 (5.4), 346 (4.3), 345 (3.6), 285 (4.0), 269 (4.4), 257 (5.9), 241 (4.4), 240 (3.7), 239 (5.1), 167 (5.4), 152 (4.2), 105 (100), and 77 (70).

Found: C, 83.39; H, 5.01%; M^+ 574. Calcd for $C_{40}H_{30}O_4$: C, 83.60; H, 5.26%; M, 574.

*5-Benzoyl-6-(1-hydroxy-2-oxo-1,2-diphenylethyl)acenaphthene (**6**)*: A total of 191 mg (4.1%) of crude product was recrystallized from ethanol,[43] giving 144 mg (3.1%) of pure **6** as yellow rods: mp 201.0—204.0 °C (dec/Ar); UV_{max} (c-C_6H_{12}) 227 (logε 4.68), 253sh (4.17), 292sh (3.90), 304 (3.98), and 320 nm (3.85); (Fluorescence was not detected.); IR 3500 (OH), 3065, 3040, 2915, 2840, 1750 and 1675 (C=O), 1595, 1450, 1415, 1230, 1150, 1025, 840, 775, 730, 710, and 700 cm^{-1}; NMR ($CDCl_3$) $\delta=7.72$—7.56 (3H, m, ArH), 7.36—6.82 (13H, m, ArH), 6.69—6.53 (3H, m, ArH), 5.88 (1H, sharp s, exch., OH), and 3.38 (4H, broad s, $2CH_2$); MS (250 °C, 75 eV), *m/e* (rel intensity), 468 (38), 364 (33), 363 (100), 346 (12), 286 (10), 285 (21), 262 (23), 257 (30), 186 (23), 165 (24), 152 (15), 105 (90), and 77 (80).

Found: C, 84.64; H, 4.94%; M^+ 468. Calcd for $C_{33}H_{24}O_3$: C, 84.59; H, 5.16%; M, 468.

*5,6-Dibenzoylacenaphthene (**7**)*: A total of 767 mg (21.2%) of crude product was recrystallized from ethanol,[43] giving 612 mg (16.9%) of pure **7** as white needles: mp 209.0—210.0 °C, (lit,[11] mp 207—208 °C); UV_{max} (c-C_6H_{12}) 236 (logε 4.74), 248sh (4.53), and 316 nm (3.99); (Fluorescence was not detected.); IR 3080, 3040, 2905, 1655 and 1645 (C=O), 1600, 1270, 1230, 940, and 710 cm^{-1}; NMR ($CDCl_3$) $\delta=7.80$—7.70 (4H, m, o-CO-PhH), 7.58 (2H, d, $J=7.1$ Hz, o-CO-ActH), 7.52—7.20 (6H, m, m- and p-CO-PhH), 7.35 (2H, broad d, $J=7.1$ Hz, o-CH_2-ActH), and 3.49 (4H, s, $2CH_2$); MS (225 °C, 75 eV), *m/e* (rel intensity), 362 (46), 286 (16), 285 (62), 258 (25), 257 (92), 256 (10), 255 (14), 228 (16), 227 (23), 226 (32), 186 (16), 151 (10), 105 (62), and 77 (100).

(Found: C, 86.62; H, 4.81%).

Reaction of Benzil with n-*BuLi–TMEDA Complex*. Under an argon atmosphere, n-BuLi (25.3 mmol in 11 cm^3 of hexane) and TMEDA (4 cm^3, 26.6 mmol) were introduced into a four-necked 200 cm^3-flask, the mixture was stirred for 15 min, and then 35 cm^3 of dry ether was added to the mixture . To this solution a solution of benzil (2.150 g, 10.23 mmol in 50 cm^3 of ether) was added dropwise over a period of 30 min at −10—0 °C. The yellowish orange solution which resulted was stirred at −10—0 °C for 1 h and for 0.5 h without cooling, and then refluxed for 0.5 h. After the solution was allowed to stand for 30 min, it was hydrolyzed with aqueous ammonium chloride (15 g/50 cm^3). The organic layer was separated, washed with aqueous concd sodium chloride, dried ($MgSO_4$), and evaporated to dryness. The residue was recrystallized from 10 cm^3 of hexane, giving 1.401 g (42.0%) of crude **18a** (mp 118—120 °C). The filtrate was chromatographed on a silica-gel column (100 g) with hexane, benzene, and chloroform as successive eluents, giving 1.387 g of a mixture of **18a** and **18b** as a yellow oil, 44 mg (2.0%) of almost pure benzoin (mp 130—133 °C), and then 213 mg (7.7%) of crude **19** (mp 108—118 °C). The oily mixture was dissolved in 3 cm^3 of hexane and allowed to stand; it gave 145 mg (4.3%) of crude **18a** (mp 119—121 °C). The filtrate of this operation was chromatographed on a silica-gel column (120 g) with hexane–benzene as eluent, giving 743 mg (22.3%) of 1 : 4 mixture of **18a** and **18b** as a colorless solid: mp 76.0—84.0 °C (found: C, 80.98; H, 9.36%); UV_{max} (c-C_6H_{12}) 253 (logε 2.50), 259 (2.59), and 265 nm (2.41); IR 3535 (OH), 3095, 3060, 3035, 2960, 2865, 1445, and 1150 cm^{-1}; NMR ($CDCl_3$) $\delta=7.14$ (10H, broad s, PhH), 2.55 (1.6H, s, exch., OH of **18b**), 2.22 (0.4H, s, exch., OH of **18a**), 2.32—1.43 (4H, m), and 1.30—0.64 (14H, m).

(5R, 6R*)- or (5R*, 6S*)-5,6-Diphenyl-5,6-decanediol (**18a**)*: A total of 1.546 g (46.3%) of crude product was recrystallized from hexane, giving 1.341 g (40.2%) of pure **18a** as colorless prisms: mp 121.0—122.0 °C; UV_{max} (c-C_6H_{12}) 218sh (logε 4.13), 253sh (2.47), 259 (2.62), and 265 nm (2.50); IR 3600 (OH), 3055, 3035, 2955, 2930, 2865, 1445, and 1160 cm^{-1}; NMR ($CDCl_3$) $\delta=7.19$ (10H, s, PhH), 2.22 (2H, s, exch., 2OH), 2.47—2.15 (2H, m), 1.77—1.48 (2H, m), and 1.36—0.70 (14H, m); MS (150 °C, 20 eV), *m/e* (rel intensity), 326 (1.5), 309 (0.9), 292 (0.8), 164 (14), 163 (100), 162 (58), 120 (5), 107 (5), 105 (3), 85 (5), 71 (1.3), 57 (6), and 43 (1.4).

Found: C, 80.93; H, 9.53%; M^+ 326. Calcd for $C_{22}H_{30}O_2$: C, 80.94; H, 9.26%; M, 326.

*1,2-Diphenyl-1,2-hexanediol (**19**)*: The crude product was recrystallized from hexane, giving 131 mg (4.7%) of pure **19** as white hair-like needles: mp 123.0—124.0 °C; UV_{max} (c-C_6H_{12}) 253 (logε 2.51), 259 (2.59), and 264 nm (2.48); IR 3410 and 3355 (OH), 3065, 3035, 2940, 2865, 1450, and 1040 cm^{-1}; NMR ($CDCl_3$) $\delta=7.16$—6.80 (10H, m, PhH), 4.77 (1H, d, $J=3.9$ Hz, CH), 2.51 (1H, d, $J=3.9$ Hz, exch., OH), 2.49 (1H, s, exch., OH), 2.13—1.97 (2H, m), and 1.47—0.77 (7H, m); MS (135 °C, 23 eV), *m/e* (rel intensity), 270 (0.7), 252 (0.7), 213 (0.7), 195 (1.8), 164 (18), 163 (100), 145 (2), 120 (3), 108 (5), 107 (11), 105 (8), 103 (4), 85 (13), 79 (8), 77 (4), 71 (4), 57 (17), 43 (4), and 41 (3).

Found: C, 79.99; H, 8.12%; M^+ 270. Calcd for $C_{18}H_{22}O_2$: C, 79.96; H, 8.20%; M, 270.

*Oxidative Homo-coupling of **3**. 1,2,7,8-Tetrahydrodicyclopenta-[cd : lm]perylene (**10**). A) **3** : PQ (1/2)*: To a solution of **3** (5.00 mmol in 150 cm^3 of ether), 9,10-phenanthrenequinone (2.154 g, 10.3 mmol) was added with gentle stirring over a period of 5 min at −10—0 °C. The dark green suspension which resulted was stirred for 1 h at −10—0 °C and for 1 h without cooling. Aqueous iron(III) chloride (30 g/100 cm^3) was then added to the supension. After 0.5 h of stirring, the dark brown solid which had precipitated was filtered off with 10 g of Celite and washed with water and ether. The combined filtrate was separated and the organic layer was washed with aqueous concd sodium chloride, dried ($MgSO_4$), and evaporated. The residue was then chromatographed on a silica-gel column (150 g) with benzene as eluent, giving

472 mg of PQ. The residue containing Celite was exhaustively extracted with hot benzene. This extract was dried ($MgSO_4$), concentrated, and chromatographed on a silica-gel column (150 g) with benzene as eluent, giving 205 mg (26.9%) of crude **10** (mp 335—337 °C (dec/Ar)) and then 1.011 g of PQ. Total recovery of the quinone was 68.8%. The crude **10** was recrystallized from benzene, giving 180 mg (23.7%) of pure **10** as brilliant red rods: mp 345.0—346.0 °C (dec/Ar); UV_{max} (c-C_6H_{12}) 382 (logε 3.78), 402 (4.27), 426 (4.64), 443sh (4.41), 450sh (4.66), and 455 nm (4.82), (C_6H_6) 386 (3.70), 407 (4.18), 431 (4.56), and 460 nm (4.69); $Fluorescence_{max}$ (c-C_6H_{12}) 462 (rel intensity 100), 489 (87), 524 (20), and 565 nm (3) (excitation at 450 nm), (C_6H_6) 470 (100), 495 (100), and 530 nm (29) (excitation at 455 nm); IR 3065, 3030, 2905, 2830, 1620, 1585, 1395, 1375, 840, and 815 cm^{-1}; NMR (CS_2) δ= 7.76 (4H, d, J=7.5 Hz, m-CH_2-ArH), 7.09 (4H, broad d, J=7.5 Hz, o-CH_2-ArH), and 3.31 (8H, s, $4CH_2$); MS (200 °C, 70 eV), m/e (rel intensity), 304 (100), 303 (33), 302 (19), 301 (18), 300 (17), and 276 (6); $m/2e$, 152 (12), 151.5 (8), 151 (11), 150.5 (10), 150 (17), and 149.5 (3); $m/3e$, 101.7 (0.2), 101.3 (0.3), 101 (0.1), 100.7 (0.8), 100.3 (0.8), and 100 (1.8).

Found: C, 95.13; H, 5.15%; M^+ 304. Calcd for $C_{24}H_{16}$: C, 94.70; H, 5.30%; M, 304.

B) 3 : PQ (1/1): This was carried out exactly as described above for run *A*), except that 1.077 g (5.17 mmol) of PQ was used. The consumption-ratio of **3** changed as follows: 59% (5 min), 67% (50 min), and 76% (2 h). Column-chromatography gave 150 mg (19.7%) of **10** and 665 mg (61.7%) of PQ.

C) 3 : PQ (1/1) with Acetolysis: This was carried out exactly as described for run *A*), except that 1.070 g (5.14 mmol) of PQ was used and that the reaction mixture was treated with acetic anhydride (45 cm^3, 0.48 mol) and pyridine (5 cm^3), and then with 100 cm^3 of dil hydrochloric acid. After the addition of PQ, the consumption-ratio of **3** and the color of the reaction mixture changed as follows: 3—60 min, 65%, dark green; 2—4 h, 73—82%, dark green and partly dark yellow: 5—6 h, 86—87%, dark yellow. Column-chromatography gave 207 mg (27.2%) of **10** and then 703 mg (47.8%) of crude **11**. The latter was recrystallized from benzene, giving 619 mg (42.1%) of pure 9,10-diacetoxyphenanthrene (**11**); mp 203.0—204.0 °C, (lit,[12] mp 203—203.5 °C); IR 3075, 2930, and 1785 and 1770 cm^{-1} (C=O); NMR ($CDCl_3$) δ=8.75—8.56 (2H, m), 7.95—7.78 (2H, m), 7.78—7.50 (4H, m), and 2.46 (6H, s).

(Found: C, 73.20; H, 4.72%).

D) 3 : PQ (1/2) in the Presence of Cyclooctene: Freshly distilled cyclooctene (from sodium wire) (50 cm^3) was added to a solution of **3** (5.00 mmol in 150 cm^3 of ether) and the mixture was treated with PQ (2.195 g, 10.5 mmol) as described for run *A*). Column-chromatography gave 200 mg (26.3%) of **10** and 1.64 g (73.5%) of PQ.

E) 3 : $CoCl_2$ (1/2): Anhydrous cobalt(II) chloride[41b] (1.580 g, 12.2 mmol) was dried at 120 °C/0.1 mmHg for 4 h, and then added to a solution of **3** (5.00 mmol in 150 cm^3 of ether) over a period of 15 min at −78 °C . During 1 h of stirring, the solution became pale brown and *ca.* 10% of **3** was consumed. The reaction mixture was then allowed to come to room temperature gradually; after 2 h, ≥95% of **3** was consumed. The black suspension which resulted was treated as described for run *A*), giving 210 mg (27.6%) of **10**.

F) 3 : 2,3-Dibromo-1,4-naphthoquinone (1/1): This was carried out exactly as described for run *A*), except that 1.617 g (5.12 mmol) of the quinone[44] was used. The consumption-ratio of **3** and the color changed as follows: 3 min, 94%, brown purple; 20 min, 98%, blue green; 1—2 h, 98%, dark green. Column-chromatography gave 40 mg (5.2%) of **10**.

G) 3 : 2,3-Dichloro-5,6-dicyano-1,4-benzoqinone (1/1): This was carried out as described for run *A*), except that 1.160 g (5.11 mmol) of the quinone[41d] was used and that the reaction mixture was refluxed for additional 1 h. Finally, approximately 50% of **3** was consumed and 76 mg (10%) of **10** was obtained.

The authors wish to thank Professor S. Aoyagi (Tokyo Institute of Technology) for the measurements of the cyclic voltammograms. We also would like to thank Professor Y. Sasada and Dr. A. Takenaka (Tokyo Institute of Technology, Nagatsuta) for their helpful discussions.

References

1) N. Tanaka and T. Kasai, *Bull. Chem. Soc. Jpn.*, **54**, 3020 (1981).

2) T. Kasai and J. Yoshiwara, 34th National Meeting of the Chemical Society of Japan, Hiratsuka, April 1976, Abstr. No. 2G22.

3) R. H. Mitchell, T. Fyles, and L. M. Ralph, *Can. J. Chem.*, **55**, 1480 (1977).

4) R. L. Letsinger, J. A. Gilpin, and W. J. Vullo, *J. Org. Chem.*, **27**, 672 (1962).

5) R. L. Letsinger and J. A. Gilpin, *J. Org. Chem.*, **29**, 243 (1964).

6) L. S. Yang and H. Shechter, *J. Chem. Soc., Chem. Commun.*, **1976**, 775.

7) J. Meinwald, S. Knapp, T. Tatsuoka, J. Finer, and J. Clardy, *Tetrahedron Lett.*, **1977**, 2247.

8) J. S. Kiely and P. Boudjouk, *J. Organomet. Chem.*, **182**, 173 (1979).

9) For an extensive review, see V. Balasubramaniyan, *Chem. Rev.*, **66**, 567 (1966).

10) N. Tanaka, T. Kasai, A. Takenaka, and Y. Sasada, *Acta Crystallogr., Sect. B*, **37**, 715 (1981).

11) H. J. Richter and F. B. Stocker, *J. Org. Chem.*, **24**, 366 (1959); H. J. Richter and W. C. Feist, *ibid.*, **25**, 356 (1960).

12) H. Cho and R. G. Harvey, *J. Chem. Soc., Perkin Trans. 1*, **1976**, 836.

13) Other features are that the signal of the methylene protons at the ethano bridge appears as a sharp singlet in spite of the different substituents at their opposite peri positions (*cf.* the corresponding signal of **6**), and that the signal of the hydroxy proton can not clearly be discerned in the solvents used.

14) Analogous large J values are known in strained, saturated ring systems: N. F. Chamberlain, "The Practice of NMR Spectroscopy with Spectra-Structure Correlations for Hydrogen-1," Plenum Press, New York (1974), p. 99; R. M. Silverstein, G. C. Bassler, and T. C. Morrill, "Spectrometric Identification of Organic Compounds," 3rd ed, John Wiley and Sons, New York (1974), p. 191.

15) a) C. Blomberg, H. H. Grootveld, T. H. Gerner, and F. Bickelhaupt, *J. Organomet. Chem.*, **24**, 549 (1970); b) D. Wege, *Aust. J. Chem.*, **24**, 1531 (1971); c) P. Beak, J. Yamamoto, and C. J. Upton, *J. Org. Chem.*, **40**, 3052 (1975) and the references cited therein.

16) E. C. Ashby, J. D. Buhler, I. G. Lopp, T. L. Wiesemann, J. S. Bowers, Jr., and J. T. Laemmle, *J. Am. Chem. Soc.*, **98**, 6561 (1976); E. C. Ashby and J. S. Bowers, Jr., *ibid.*, **99**, 8504 (1977); E. C. Ashby and T. L. Wiesemann, *ibid.*, **100**, 189, 3101 (1978).

17) a) R. H. Philp, Jr., T. Layloff, and R. N. Adams, *J. Electrochem. Soc.*, **111**, 1189 (1964); b) J. Simonet and H. Lund, *Bull. Soc. Chim. Fr.*, **1975**, 2547; c) M. D. Ryan and D. H. Evans, *J. Electroanal. Chem. Interfacial Electrochem.*, **67**, 333 (1976).

18) M. Gomberg and W. E. Bachmann, *J. Am. Chem. Soc.*, **49**, 2584 (1927); W. E. Bachmann, *ibid.*, **53**, 2758 (1931); N. L. Bauld, *ibid.*, **87**, 4788 (1965).

19) A. G. Evans, J. C. Evans, and E. H. Godden , *Trans. Faraday Soc.*, **63**, 136 (1967).

20) D. R. Tallant and D. H. Evans, *Anal. Chem.*, **41**, 835 (1969); D. H. Eargle, Jr., *J. Org. Chem.*, **39**, 1295 (1974).

21) C. F. G. C. Geraldes, V. M. S. Gil, and D. H. Eargle, Jr., *J. Chem. Phys.*, **59**, 1171 (1973).

22) The stereochemistry of **5**[10] must result on this hydrolysis.

23) W. E. Bachmann and E. J.-H. Chu, *J. Am. Chem. Soc.*, **58**, 1118 (1936); *cf.* N. Campbell and R. S. Gow, *J. Chem. Soc.*, **1949**, 1555.

24) E. S. Gould, "Mechanism and Structure in Organic Chemistry," Henry Holt and Co., New York (1959), pp. 157 and 635; *cf.* F. G. Baddar, A. F. M. Fahmy, and N. F. Aly, *J. Indian Chem. Soc.*, **50**, 586 (1973).

25) An analogous benzilic acid rearrangement in an ethereal solution has been reported in the system of benzil with sodium acetylide: J. Cymerman-Craig, M. Moyle, P. Rowe-Smith, and P. C. Wailes, *Aust. J. Chem.*, **9**, 391 (1956).

26) Crawford *et al.* obtained a product (mp 184 °C) from the reaction of benzil with butylmagnesium bromide and described as **18**. However, analysis did not confirm the composition suggested: H. M. Crawford. M. E. Saeger, and F. E. Warneke, *J. Am. Chem. Soc.*, **64**, 2862 (1942); *cf.* R. D. Chambers and M. Clark, *J. Chem. Soc., Perkin Trans. 1*, **1972**, 2469.

27) A 10—20% excess of *n*-BuLi is needed for the quantitative conversion of 5,6-dibromoacenaphthene into **3**.[1]

28) H. M. Relles, *J. Org. Chem.*, **34**, 3687 (1969) and the references cited therein.

29) a) W. E. Bachmann and E. J.-H. Chu, *J. Am. Chem. Soc.*, **57**, 1095 (1935); b) R. Criegee, E. Höger, G. Huber, P. Kruck, F. Marktscheffel, and H. Schellenberger, *Justus Liebigs Ann. Chem.*, **599**, 81 (1956); c) E. J. Moriconi, F. T. Wallenberger, L. P. Kuhn, and W. F. O'connor, *J. Org. Chem.*, **22**, 1651 (1957); d) M. B. Rubin and P. Zwitkowits, *ibid.*, **29**, 2362 (1964); e) J.-C. Cognacq, R. Skowronski, W. Chodkiewicz, and P. Cadiot, *Bull. Soc. Chim. Fr.*, **1967**, 880.

30) K. Maruyama, *Bull. Chem. Soc. Jpn.*, **37**, 553 (1964).

31) T. L. Staples and M. Szwarc, *J. Am. Chem. Soc.*, **92**, 5022 (1970).

32) M. K. Kalinowski and B. Tenderende-Gumińska, *J. Electroanal. Chem. Interfacial Electrochem.*, **55**, 277 (1974).

33) C. W. Rees and R. C. Storr, *J. Chem. Soc., (C)*, **1969**, 756, 760, 765; *cf.* R. W. Hoffmann, G. Guhn, M. Preiss, and B. Dittrich, *ibid.*, **1969**, 769.

34) Another trapping agent, bromotrichloromethane,[33] did violently react with **3**.

35) There remains a possibility that the formation and subsequent coupling of **24** occurs within a solvent cage.[28]

36) G. Wittig and F. Bickelhaupt, *Chem. Ber.*, **91**, 883 (1958); H. J. S. Winkler and G. Wittig, *J. Org. Chem.*, **28**, 1733 (1963).

37) G. Wittig and G. Lehmann, *Chem. Ber.*, **90**, 875 (1957).

38) S. F. Nelsen, B. M. Trost, and D. H. Evans, *J. Am. Chem. Soc.*, **89**, 3034 (1967).

39) Unfortunately, supporting electrolytes dissolve very little in diethyl ether. For solvent effects, see Refs. 17c and 32.

40) H. M. Crawford, *J. Org. Chem.*, **28**, 3082 (1963); D. W. Cameron and M. Mingin, *Aust. J. Chem.*, **30**, 859 (1977).

41) a) Tokyo Kasei Kogyo Co., Ltd.; b) Wako Pure Chemical Industries, Ltd.; c) Nakarai Chemicals, Ltd.; d) Aldrich Chemical Co., Inc.

42) Adding as a powder gave the same results.

43) The hot solution was treated with decolorizing charcoal.

44) Mp 221.5—222.5 °C (lit, mp 216—218 °C: C. Liebermann and S. Schlossberg, *Ber.*, **32**, 2095 (1899)).

Diisobutylaluminum 2,6-Di-*t*-butyl-4-methylphenoxide. Novel Stereoselective Reducing Agent for Prostaglandin Synthesis[1)]

Sadahiko IGUCHI, Hisao NAKAI, Masaki HAYASHI,* Hisashi YAMAMOTO,† and Keiji MARUOKA†

Ono Pharmaceutical Co., Ltd., Research Institute, 3-1-1, Sakurai Shimamoto-cho, Osaka 618

†*Department of Chemistry, University of Hawaii, Honolulu, Hawaii 96822, U. S. A.*

(Received January 12, 1981)

In an effort to explore the selective reducing agents suitable for prostaglandin synthesis, diisobutylaluminum 2,6-di-*t*-butyl-4-methylphenoxide (**1**) is found to be among the best. Reduction of the C-15 ketone with **1** in toluene at −78 °C produced the desired 15*S*-alcohol in 95% yield with 92% stereoselectivity. The present procedure is suitable for the synthesis of prostaglandin derivatives and related polyfunctional natural products as shown in the conversion of PGE_2 methyl ester to $PGF_{2\alpha}$ methyl ester in 95% yield and 100% selectivity.

One major problem encountered in the synthesis of prostaglandins[2)] is stereoselective construction of the functional groups present in these molecules. Three of the four chiral centers of prostaglandin E_2, those at position 8, 11, and 12, are mutually *trans* and are relatively easily established. Stereochemical control of the fourth center at C-15, however, placed in a conformationally mobile side chain, and at a considerable distance from influence of the ring, poses a much more difficult problem. For example, introduction of the lower side-chain and establishment of the *trans*-C-13-ene unit are readily accomplished by simple Wadsworth-Emmons' reaction. The successive zinc borohydride or Meerwein-Ponndorf-Verley reduction of the resulting α,β-unsaturated ketone produced a 1 : 1 mixture of 15*S* and 15*R* allylic alcohols.

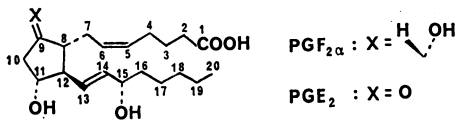

Fig. 1.

So far tremendous efforts have been devoted to solve this problem, and 15*S*/15*R* ratio of 92% was recorded in the reduction of the enone having a *p*-phenylphenylcarbamoyl protecting group at C-11 using a bulky trialkylhydroborate reagent at −130 °C.[3)] This result was explained on the basis that at low temperature the molecule is frozen into a conformation wherein the *p*-phenylphenylcarbamoyl group is lined up with the enone side-chain, effectively screening one side of the molecule. The hydride then attacks from the opposite side of the molecule, but can give rise to the desired 15*S* alcohol only if the enone is in a *S-cis* conformation.

Very recently an interesting asymmetric reduction of this enone with special binaphthol modified aluminum hydride reagent was reported.[4)] With this optically active reagent at −100 °C, 99.5% stereoisomeric purity was achieved.

Our interest has been focused on the stereoselective approach to the reduction of the C-9 and C-15 ketones in prostaglandins[5)] using the more practical reagent under mild reaction conditions. Diisobutylaluminum 2,6-di-*t*-butyl-4-methylphenoxide (**1**)[6)] has solved this problem practically, and has been found to be among the best selective reducing agent for the control of the stereochemistry at C-15.

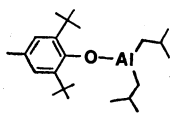

1

Fig. 2.

Results and Discussion

A solution of diisobutylaluminum 2,6-di-*t*-butyl-4-methylphenoxide (**1**) can be prepared from diisobutylaluminum hydride (DIBAH) in toluene and 2,6-di-*t*-butyl-4-methylphenol (molar ratio 1 : 1 to 1 : 2)[7)] in toluene at 0 °C for 1 h. Reduction of the C-11 hydroxy enone **2a** with the reagent **1** (10 equiv.) in toluene was

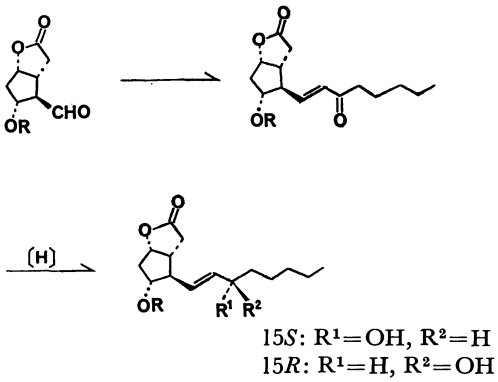

Scheme 1.

complete at −78 °C for 2 h, then at −40 °C for 1 h. The reaction mixture was then poured onto diluted hydrochloric acid and extracted with ethyl acetate. Short-path chromatographic separation to remove the recovered phenol gave allylic alcohol **3a** in 95% yield. The ratio of 15*S* to 15*R* isomers in several runs was 92/8 by high pressure liquid chromatographic analysis. When the aluminum reagent **1** was decreased to 3 equiv, the reaction proceeded slowly under the reaction conditions described above to give **3a** in 85% yield with the similar stereoselectivity (15*S*/15*R*=92/8).

The enone unit exists in both the *S-cis* and *S-trans* conformations, and the hydride attack can occur from either direction to give the 15*S* or 15*R* configuration. Therefore, reduction of the enone with sodium borohydride or zinc borohydride produced a 1 : 1 mixture

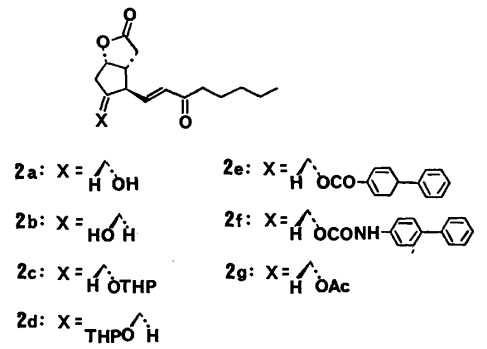

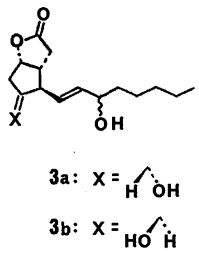

Fig. 3.

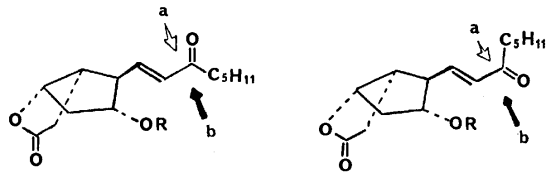

S-cis enone form *S-trans* enone form

Fig. 4.

of epimeric 15*S* and 15*R* alcohols. As previously reported, the examination of Corey-Pauling-Koltun models showed that van der Waals contact of the *p*-biphenylyl group in **2f** and the enone unit is indeed most favored when the enone is in the *S-cis* conformation. Clearly, the *p*-biphenylyl group must not only block approach from axis b but also stabilize the *S-cis* enone conformation in order to direct the formation of 15*S* alcohol. The present high stereoselectivity shown especially in **2a** can be attributed to the significant frontal steric bulk of the reagent **1** and at the same time to the substantial screening effect of *S-cis* enone chain to inhibit the α-approach of the reagent. Thus, the excess aluminum reagent, which is strongly coordinated at the C-11 hydroxyl function appears to play an important role as an exogeneous directing group to block the approach from axis b as well as to maintain *S-cis* enone conformation.

On the basis of this hypothesis, we examined the reduction of the THP ethers **2c** and **2d** using the reagent **1** under the standard conditions. It was thought that moderate selectivity for formation of 15*S* alcohol should be observed in these cases, since the aluminum reagent may be coordinated with ethers rather weakly.[6,8] The substrates and the observed 15*S*/15*R* ratios are shown in Table 1. In contrast to the high stereoselectivity in the

Table 1. Reduction of the enones containing the lactone function with diisobutylaluminum 2,6-di-*t*-butyl-4-methylphenoxide in toluene

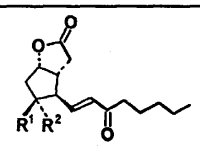

	15*S*/15*R*	%Total yield	Conditions
R^1=H, R^2=OH	92/8[a]	95	d) or e)
R^1=OH, R^1=H	85/15[a]	94	d)
R^1=H, R^2=OTHP	66/34[a]	98	d) or e)
R^1=OTHP, R^2=H	79/21[b]	92	d) or e)
R^1=H, R^2=OAc	50/50[a]	91	d) or e)
R^1=H, R^2=OCO-C_6H_4-C_6H_5-*p*	50/50[c]	90	e)

a) The ratio of 15*S* to 15*R* isomers was determined by high pressure liquid chromatography using a silica-gel column with a refractive index detector. b) After the removal of the THP group, the ratio was determined by high pressure liquid chromatography. c) The ratio was determined by high pressure liquid chromatography with UV (254 nm) index detector. d) The reaction conditions were −78 °C for 2 h, and then −40 °C for 1 h. e) The enone was added to the aluminum reagent at −78 °C and the temperature was raised gradually to −20 °C over 2 h.

Table 2. Reduction of the enones containing α-chain with diisobutylaluminum 2,6-di-*t*-butyl-4-methylphenoxide in toluene

Enones	15α-OH/ 15β-OH	%Total yield	Conditions
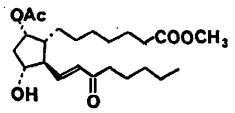	82/18[a]	95	c)
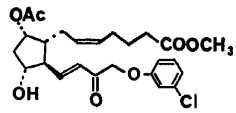	86/14[b]	83	c)
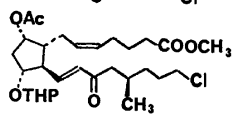	82/18[a]	95	c)
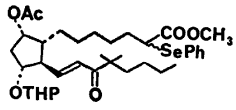	87/13[b]	92	d)

a) The ratio was determined by the isolation of each isomer using the usual silica-gel column chromatography. b) The ratio was determined by high pressure liquid chromatography. c) To a solution of the aluminum reagent in toluene cooled at −78 °C was added a solution of the enone in toluene and then the temperature was raised gradually to −20 °C over 2 h. d) The reaction conditions were −78 °C for 2 h, and then −40 °C for 1 h.

reduction of hydroxy ketones, the *p*-phenylbenzoyl ester **2e**[9] and the acetate **2g** afforded the corresponding alcohols without any stereoselectivity (15*S*/15*R*=1/1).

Although the reduction of the hydroxy enone **2a** with the lactone unit using the reagent **1** was complete within 2 h at −78 °C, the reduction of hydroxy enones

having α-chains proceeded considerably slowly at −78 °C to afford a trace of the product in 4 h. Therefore, the reaction mixture was warmed gradually to −20 °C over 2 h to produce 15α-allylic alcohols with moderate stereoselectivity as shown in Table 2. Presumably, in the reduction of the C-11 hydroxy enones with α-chains the *S-cis* enone conformation would be maintained at −78 °C by van der Waals contact of O-Al-OPh group and the enone moiety. However due to the steric hindrance of α-chains, the hydride attack along axis a would be unfavorable. At −20 °C, the stereoselectivity for formation of 15α-allylic alcohols is somewhat lost, since the *S-cis* enone conformation would not be stabilized at this temperature.

The stereoselectivity in the reduction of **7** was significantly influenced by the equivalent of the aluminum reagent **1**, as listed in Table 3. The best result was obtained using more than 10 equiv. of the aluminum reagent **1**. Surprisingly, with 2 equiv. of **1**, the 15*R* alcohol was produced predominantly. These results might be attributed to the relatively weak coordination of the reagent **1** to C-11 THP ether and then the direct attack of the coordinated aluminum reagent **1** to the substrate from the front side of the molecule (axis b). This is in sharp contrast with the reduction of **2a**, in which the stereoselectivity is essentially independent of the equivalent of **1** as described previously.

The substituent effect of the aryl group in the aluminum reagents upon the stereoselectivity of allylic alcohols was investigated using the enone **2c** and various diisobutylaluminum phenoxides in toluene. Under the similar reaction conditions, the use of 2,6-di-*t*-butylphenoxides gave higher stereoselectivity compared to other phenoxides in shorter reaction time (Table 5).

The significance of the frontal steric effect by the use of the aluminum reagent **1** was further demonstrated. Reduction of prostaglandin E with sodium borohydride or zinc borohydride proceeds in a nonstereoselective manner to give a mixture of C-9α and C-9β hydroxy compounds[10] with somewhat higher yield of the C-9β hydroxy isomer. Owing to the lack of the stereochemical control in this transformation, the design of chemical synthesis of these substances was extremely limited: the protected prostaglandin F_α derivative (*e.g.* **4**) may be prepared first, and oxidized to prostaglandin E derivative. Recently, some bulky trialkylhydroborate reagents[5] have been employed successfully for the reduction of prostaglandin E to prostaglandin F_α. Our aluminum reagent **1** can be also effective for the preparation of prostaglandin F_α with excellent stereoselectivity. Thus, reaction of prostaglandin E_2 methyl ester (**5a**) with **1** in toluene at −78 °C for 2 h produced prostaglandin

Table 3. Reduction of C_{11}-OTHP enone **7** with various equiv. of diisobutylaluminum 2,6-di-*t*-butyl-4-methylphenoxide (**1**)

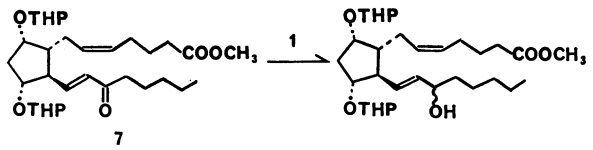

7

Equiv. of **1**	15*S*/15*R*[a]	%Total yield	Conditions
2	35/65	85	−78 °C→ 10 °C (2 h)
5	59/41	85	−78 °C→ 0 °C (2 h)
10	74/26	89	−78 °C→−20 °C (2 h)
20	68/32	85	−78 °C→−20 °C (2 h)

a) The ratio was determined by high pressure liquid chromatography.

Table 4. Reduction of C_{11}-hydroxy enone **2a** with diisobutylaluminum 2,6-di-*t*-butyl-4-methylphenoxide (**1**)

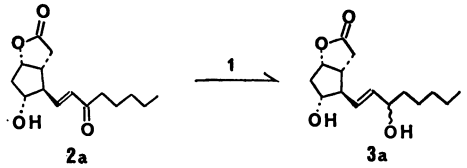

2a **3a**

Equiv. of **1**	15*S*/15*R*[a]	%Total yield	Coditions
3	92/8	85	−78 °C(2 h)→−40 °C(1 h)
10	92/8	95	−78 °C(2 h)→−40 °C(1 h)

a) The ratio was determined by high pressure liquid chromatography.

Table 5. Reduction of C_{11}-OTHP enone **2c** with various diisobutylaluminum phenoxides

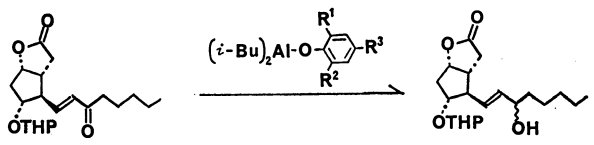

2c **11**

Phenoxide	15*S*/15*R*[a]	%Total yield	Conditions
$R^1=R^2=t$-Bu R^1=H or Me	66/34	(95)	−78 °C→−10 °C(3 h)
$R^1=R^2=R^3=t$-Bu	59/41	(95)	−78 °C→−40 °C(2 h)
$R^1=t$-Bu, R^2=H, R^3=H or Me	61/39	(94)	−78 °C→−10 °C(3 h)
$R^1=R^3=t$-Bu, R^2=H	54/46	(92)	−78 °C→−10 °C(3 h), 25 °C(1 h)
$R^1=R^2=i$-Bu, R^3=H	62/38	(90)	−78 °C→−40 °C(1 h), 25 °C(17 h)
$R^1=R^2$=Me, R^3=H	54/46	(95)	−78 °C (30 min), 0 °C (1 h)
$R^1=R^2=R^3$=H	63/37	(95)	−78 °C (30 min), 25 °C (12 h)

a) The ratio was determined by high pressure liquid chromatography.

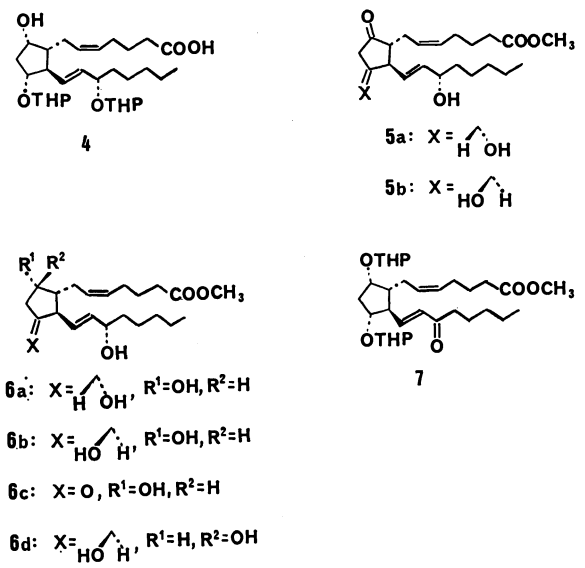

Fig. 5.

$F_{2\alpha}$ methyl ester (**6a**) cleanly in 95% yield with 100% selectivity. Furthermore, treatment of the C-11 epimeric prostaglandin E_2 methyl ester (**5b**) or prostaglandin D_2 methyl ester (**6c**) using **1** afforded the C-11 epimeric prostaglandin $F_{2\alpha}$ methyl ester (**6b**) with 76% or 98% selectivity.[11,12]

The generality of the new reagent **1** was examined using a simple hydroxy ketone and cyclic ketones with alkyl chains on the ring. Thus, treatment of 4-hydroxy-3-methyl-2-butanone with **1** at −78 °C gave a mixture of *erythro*- and *threo*-2-methyl-1,3-butanediols (ratio, 2 : 1) in 96% yield. Moreover, reduction of 4-*t*-butylcyclohexanone or 2-methylcyclohexanone with **1** at −78 °C furnished 4-*t*-butylcyclohexanol (84% yield; *cis*/*trans* ratio, 28 : 72) or 2-methylcyclohexanol (85% yield; *cis*/*trans* ratio, 75 : 25), respectively. The results of this investigation clearly reveal that unlike in the reduction of prostaglandin derivatives, the aluminum reagent **1** showed no remarkable stereoselectivity in the case of the simple unhindered hydroxy ketone. Therefore, the conformation of substrates also appears to be highly important to achieve the favorable frontal steric effect. It is also evident from the results that the reactivity of **1** is totally different from that of the usual bulky metal hydrides (*e.g.* Selectrides), which gave the less stable (*cis*) isomer predominantly in the reduction of cyclic ketones with an alkyl chain.[13]

A plausible mechanism for the reduction of ketones with **1** involves an initial coordination of the trivalent aluminum reagent to the carbonyl group, followed by an intramolecular hydride transfer from the β-carbon of the isobutyl group as shown in Scheme 2. Such a mechanism seems to be analogous to those in reductions

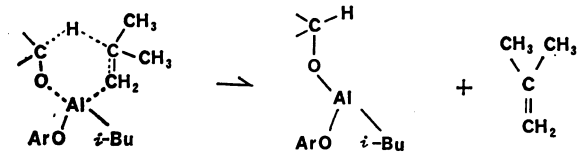

Scheme 2.

with Grignard reagents,[14,15] dialkylmagnesium compounds,[15] and triisobutylaluminum.[16] Therefore, in the reduction of α,β-unsaturated ketones only 1,2-reduction products can be obtained *via* the six-membered transition state. This is in sharp contrast with the reduction of enones using the bulky aluminum hydride reagents,[17] which afforded conjugate addition products predominantly.

Another mechanism may be considered for the

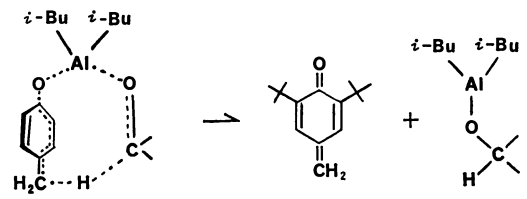

Scheme 3.

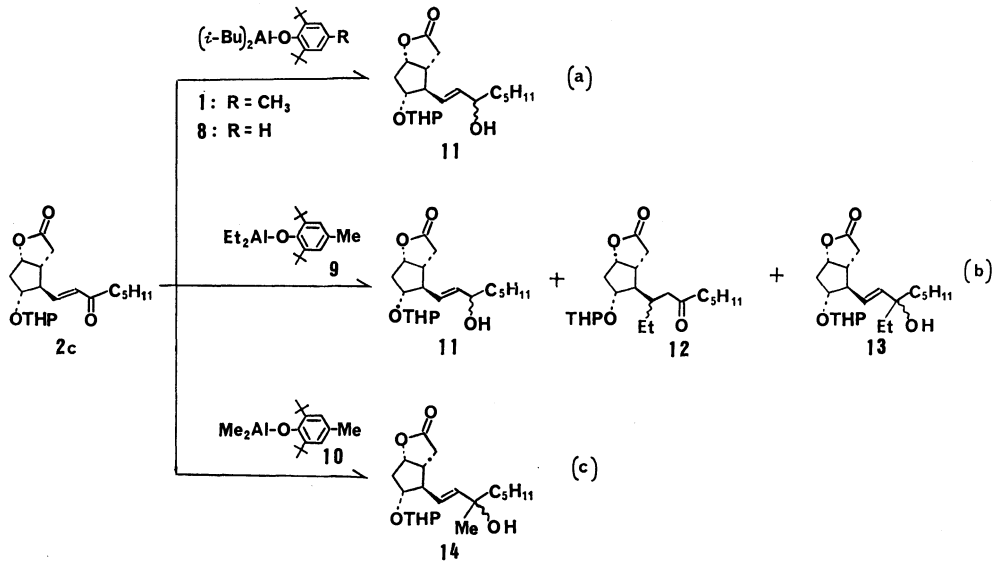

Scheme 4.

reduction with **1**, in which the actual hydride source of the reagent **1** is derived from the methyl group of phenoxide. This possibility was ruled out by the following experimental results. Scheme 4 represents the results obtained for the reduction of **2c** with several aluminum phenoxides. Since the reduction with diisobutylaluminum 2,6-di-*t*-butylphenoxide (**8**) afforded the same result as obtained with **1**, the methyl group of the reagent **1** is not necessary for reduction (Eq. a). The use of diethylaluminum 2,6-di-*t*-butyl-4-methylphenoxide (**9**) (Eq. b) produced three kinds of products: **11** (reduction product), **12** (Michael adduct to the enone **2c**), and **13** (ethylation product). In the reaction with dimethylaluminum 2,6-di-*t*-butyl-4-methylphenoxide (**10**), only the methylation product **14** was formed (Eq. c). It is evident from these results (Eqs. b and c) that at least a β-hydrogen of alkyl group of dialkylaluminum phenoxides is indispensable for reduction. Based on the above consideration we conclude that the mechanism shown in Scheme 2 is a most plausible one.

The reduction process which is described herein should be extremely useful for complex or polyfunctional molecules. The new aluminum reagent **1** for the reduction of ketone group of prostaglandins is characterized by the following features. (a) Yields are high and selectivities are unique. (b) No side reaction occurs. (c) Diisobutylaluminum hydride and 2,6-di-*t*-butyl-4-methylphenol are commercially available and inexpensive. (d) This reagent is stable and can be stocked. (e) There is no neccessity for protecting the C-11 hydroxy group with the special hindered function. (f) The process is operationally simple and can be done on a large scale.

Experimental

^{1}H NMR spectra were taken on a JEOL PMX-60 or a Varian XL-100 spectrometer in $CDCl_3$. Chemical shifts are reported as parts per million relative to TMS as the internal standard. The infrared spectra were recorded on a Hitachi EPI-G2 model. The mass spectra were obtained on a JMS-OlSG double focussing mass spectrometer. Molecular ion peaks of some compounds were too weak to be detected because of their low volatility, and in these cases the molecular weights were determined by their dehydration peaks.

For TLC analysis throughout this work, Merck TLC plates (Kieselgel 60 F_{254}, pre-coated, layer thickness 0.2 mm) were used. Column chromatography was carried out on silica gel (Merck, particle size 0.063—0.20 mm) or using Lobar Prepacked Column (Merck, silica gel). The isomeric ratio of the products was determined by high pressure liquid chromatography using a JASCO TRI ROTAR instrument equipped with a Waters μ-Porasil and a refractive index detector or a UV index detector.

Unless otherwise specified, all reactions were carried out under an atmosphere of argon.

*Preparation of Diisobutylaluminum 2,6-Di-*t*-butyl-4-methylphenoxide (**1**).* Diisobutylaluminum hydride in toluene (1.76 M (1 M=1 mol dm^{-3}), 21.7 ml, 38.2 mmol) was added slowly at 4 °C over 20 min to a solution of 2,6-di-*t*-butyl-4-methylphenol (16.81 g, 76.4 mmol) in toluene (180 ml) with the vigorous hydrogen gas evolution. During this operation, *ca.* 1 equiv. of hydrogen gas was collected. Strring was continued at 4 °C for 1 h. The reagent, thus prepared, was directly used for the following reduction, and is stable enough to be stored under argon at 0 °C for several weeks.

Reduction of Carbonyl Compounds. Method A: A solution of a carbonyl compound in toluene was added slowly below −60 °C to a solution of the aluminum reagent **1** (10 equiv.) in toluene. The mixture turned into orange. Further stirring was continued at −78 °C for 2 h, then at −40 °C for 1 h. The mixture was poured onto cold 1 M hydrochloric acid (*ca.* total volume of the reaction mixture), and extracted with ethyl acetate. The combined extracts were washed with aq sodium hydrogencarbonate, followed by brine, dried over magnesium sulfate, and concentrated by the evaporator. The residue was applied to column chromatography on silica gel with dichloromethane to separate 2,6-di-*t*-butyl-4-methylphenol, then with ethyl acetate to elute a mixture of 15*S* and 15*R* alcohols. The ratio of 15*S* and 15*R* isomers was determined Lobar Pre-packed Column (Merck) or high pressure liquid chromatographic analysis.

Method B: The reaction was carried out starting from −78 °C according to the method A. After addition of a carbonyl compound, the cooling bath was removed. The reaction mixture was allowed to warm to −10——20 °C over 2 h, stirred at this temperature for 30 min, and worked up as described above.

*Reduction of (1*S*, 5*R*, 6*R*, 7*R*)-7-Hydroxy-6-[(*E*)-3-oxo-1-octenyl]-2-oxabicyclo[3.3.0]octan-3-one (**2a**).* Reduction of **2a** (1.016 g, 3.82 mmol) with 2,6-di-*t*-butyl-4-methylphenol (16.81 g, 76.4 mmol) and DIBAH (25 g/100 ml in toluene; 21.7 ml, 38.2 mmol) was carried out using the method A to give a mixture of 15*S* and 15*R* isomers (0.964 g, 95% yield): TLC, R_f 0.229 for 15*S* isomer, 0.289 for 15*R* isomer (AcOEt–benzene, 2 : 1, 2 developments).[18] The ratio of 15*S* and 15*R* isomers was 92 : 8 by HPLC analysis (μ-Porasil, refractive index, AcOEt). Lobar Pre-packed Column chromatography on silica gel (Merck, size C, AcOEt–benzene, 4 : 1) separated the 15*S* isomer (833 mg) and the 15*R* isomer (72.3 mg): 15*S*: IR (film) 3400, 2950, 2850, 1770, 980 cm^{-1}; ^{1}H NMR δ 5.22—5.81 (2H, m, olefinic H), 4.55—5.02 (1H, m, C_1–H), 3.52—4.36 (2H, m, C<u>H</u>–OH), 0.87 (3H, t, CH_3); MS *m/e* 268 (M^+), 250 (M^+-H_2O), 232 (M^+-2H_2O); high resolution MS *m/e* 250.159 (dehydration peak, calcd for $C_{15}H_{22}O_3$, 250.157). The IR, ^{1}H NMR and MS spectra of the 15*R* isomer were identical with those of the 15*S* isomer: 15*R*: high resolution MS *m/e* 250.159 (dehydration peak, calcd for $C_{15}H_{22}O_3$, 250.157).

The reaction using the method B gave the similar results.

*Reduction of (1*S*, 5*R*, 6*R*, 7*S*)-7-Hydroxy-6-[(*E*)-3-oxo-1-octenyl]-2-oxabicyclo[3.3.0]octan-3-one (**2b**).* Reaction of the enone **2b** (50 mg, 0.188 mmol) and the aluminum reagent **1** in toluene (9 ml, 1.88 mmol) was carried out according to the method A to afford a mixture of 15*S* and 15*R* isomers (47 mg, 94% yield) after short column chromatography: IR (film) 3400, 2950, 2850, 1770, 980 cm^{-1}; ^{1}H NMR δ 5.66—5.89 (2H, m, olefinic H), 4.90—5.23 (1H, m, C_1–H), 4.20—4.42 (1H, m, $C_{3'}$–H), 3.91—4.20 (1H, m, C_7–H), 0.89 (3H, t, CH_3); high resolution MS *m/e* 268.165 (calcd for $C_{15}H_{24}O_4$, 268.168). HPLC analysis showed the ratio of 15*S* and 15*R* isomers to be 85 : 15 : TLC, R_f, 0.420 for the 15*S* isomer, 0.374 for the 15*R* isomer (ether–EtOH, 100 : 1, 3 developments). These R_f values were identical with those by the $NaBH_4$ reduction of **2b**. The configuration of two isomers was determined by comparison with the authentic samples, which were prepared as shown in Scheme A.

*Synthesis of (1*S*, 5*R*, 6*R*, 7*S*)-7-Hydroxy-6-[(1*E*, 3*S*)-3-hydroxy-1-ocetenyl]-2-oxabicyclo[3.3.0]octan-3-one (**19**).* A mix-

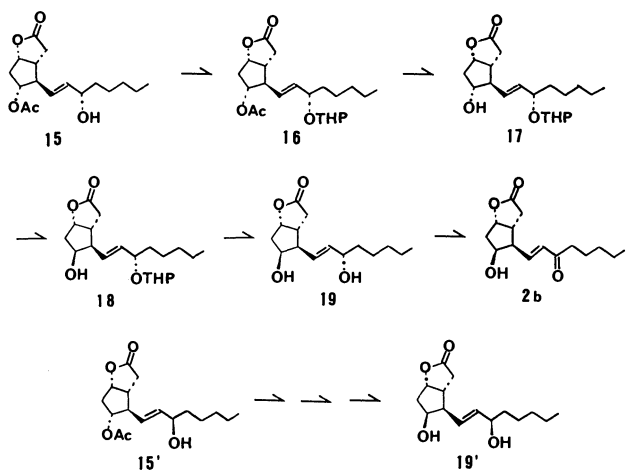

Scheme A.

ture of **15** (10 g, 32.3 mmol),[18] 2,3-dihydropyran (5.9 ml 64.5 mmol), and *p*-toluenesulfonic acid (60 mg) in dichloromethane (100 ml) was stirred in a water bath for 20 min. The reaction was terminated by the addition of pyridine (20 drops). Dilution with ethyl acetate (500 ml), washing with aq sodium hydrogencarbonate, followed by brine, being dried over magnesium sulfate, and concentration of the extracts left the residue, which was dissolved in methanol (120 ml) and stirred at 25 °C for 15 min after addition of anhydrous potassium carbonate (5.348 g). The solution was then acidified to pH 4 by the addition of acetic acid, diluted with ethyl acetate (500 ml), and washed with aq sodium hydrogencarbonate, then brine. Being dried over magnesium sulfate, and purification of the concentrated product by column chromatography (silica gel, 360 g; AcOEt–benzene, 1 : 1) gave **17** (10.846 g, 96% yield): TLC, R_f 0.273 (benzene–AcOEt, 2 : 1, 2 developments); IR (film) 3450, 2950, 2850, 1780, 980 cm^{-1}; ^1H NMR δ 5.25—5.65 (2H, m, olefinic H), 4.70—5.15 (1H, m, C_1–H), 4.61 (1H, br s, OCHO), 3.00—4.20 (4H, m, C_7, $C_{3'}$–H, OCH_2), 0.90 (3H, t, CH_3); MS *m/e* 352 (M^+), 334 (M^+-H_2O), 268 (M^+—DHP), 243 (M^+—OTHP—H_2O), 250 (M^+—HOTHP). The alcohol **17** (5.00 g, 14.2 mmol) in dry THF (70 ml) was treated with triphenylphosphine (7.443 g, 28.4 mmol) and benzoic acid (3.465 g, 28.4 mmol). Diethyl azodiformate (4.941 g, 28.4 mmol) in THF (10 ml) was then added slowly. The whole mixture was stirred at 25 °C for 30 min, and concentrated under reduced pressure. The residue, thus obtained, was dissolved in methanol (100 ml), treated with anhydrous potassium carbonate (3.919 g, 14.2 mmol) at 25 °C and stirred at 40—50 °C for 30 min. The mixture was cooled to 25 °C, acidified to pH 4 with acetic acid, diluted with ethyl acetate (500 ml), washed with aq sodium hydrogencarbonate followed by brine, dried over magnesium sulfate, and concentrated. Purification of the residue by column chromatography (silica gel, 150 g; cyclohexane–AcOEt, 2 : 1, then 1 : 1) gave **18** (4.689 g, 97% yield): TLC, R_f 0.357 (benzene–AcOEt, 2 : 1, 2 developments). The IR, ^1H NMR, and MS spectra of **18** were identical with those of **17**. The alcohol **18** (1.026 g) was dissolved in 65% acetic acid (30 ml) and THF (3 ml). The resulting mixture was stirred at 50 °C for 1 h, poured onto iced water (150 ml), and extracted with ethyl acetate. Concentration of the extracts left the residue, which was purified by column chromatography (silica gel, 30 g; AcOEt–cyclohexane, 2 : 1) to give **19** (664 mg, 85% yield): IR (film) 3600, 3450, 1760, 975 cm^{-1}; ^1H NMR δ 5.40—5.97 (2H, m, olefinic H), 4.98—5.25 (1H, m, C_1–H), 3.99—4.22 (2H, m, C_7, $C_{3'}$–H), 0.90 (3H, t, CH_3); MS *m/e* 268 (M^+), 250 (M^+-H_2O), 232 (M^+-2H_2O), high resolution MS *m/e* 268.165 (calcd for $C_{15}H_{24}O_4$, 268.167).

Synthesis of (1S, 5R, 6R, 7S)-7-Hydroxy-6-[(E)-3-oxo-1-octenyl]-2-oxabicyclo[3.3.0]octan-3-one (19'). The title compound (275 mg) was prepared starting from **15'** (633 mg)[17] according to the procedure described above. The IR, ^1H NMR, and MS spectra of **19'** were similar to those of **19**: high resolution MS *m/e* 268.165 (calcd for $C_{15}H_{24}O_4$, 268.167).

Reduction of (1S, 5R, 6R, 7R)-7-(Tetrahydro-2-pyranyloxy)-6-[(E)-3-oxo-1-octenyl]-2-oxabicyclo[3.3.0]octan-3-one (2c). Reduction of the enone **2c** (500 mg, 1.43 mmol) with the aluminum reagent **1** (14.3 mmol) in toluene (48 ml) using the method B gave a mixture of 15*S* and 15*R* isomers (490 mg, 98% yield): TLC, R_f 0.418 for the major product, 0.345 for the minor product (ether, 2 developments). The R_f values of these isomers were identical with those of the reduction product of **2c** with sodium borohydride. Column chromatography (silica gel, 40 g; ether–hexane–AcOEt, 2 : 1 : 1) separated the more polar isomer (92 mg), the less polar isomer (97 mg), and these mixture (199 mg). The two isomers gave the similar spectral data: IR (film) 3450, 1770, 975 cm^{-1}; ^1H NMR δ 5.10—5.17 (2H, m, olefinic H), 4.77—5.11 (1H, m, C_1–H), 4.64 (1H, br s, OCHO), 3.64—4.25 (4H, m, C_7, $C_{3'}$–H, OCH_2), 0.91 (3H, t, CH_3); MS *m/e* 352 (M^+), 334 (M^+-H_2O), 268 (M^+—DHP); high resolution MS *m/e* 334.215 (dehydration peak, calcd for $C_{20}H_{30}O_4$, 334.214). The two isomers were separately converted by the hydrolysis of the THP group (aq 65% AcOH, 40—45 °C, 2 h) into the corresponding diols, which were compared with the authentic samples[18] by TLC. The less polar isomer (major component) was the 15*S* alcohol. The ratio of 15*S* to 15*R* was 66 : 34 by HPLC analysis (μ-Porasil, refractive index, AcOEt–CH_2Cl_2, 1 : 1).

Reduction of (1S, 5R, 6R, 7S)-7-(Tetrahydro-2-pyranyloxy)-6-[(E)-3-oxo-1-octenyl]-2-oxabicyclo[3.3.0]octan-3-one (2d). Reduction of **2d** (101 mg, 0.289 mmol) with the aluminum reagent **1** (2.89 mmol) in toluene (20 ml) by the method B furnished a mixture of 15*S* and 15*R* isomers (90 mg, 90% yield). Hydrolysis of the THP group in these isomers gave the diols, which was characterized as described in the reduction of **2b**. IR, ^1H NMR, and MS spectra of the diols were identical with those of the reduction products of **2b**. HPLC analysis showed the ratio of 15*S* to 15*R* isomers to be 79 : 21.

Reduction of (1S, 5R, 6R, 7R)-7-(p-Phenylbenzoyloxy)-6-[(E)-3-oxo-1-octenyl]-2-oxabicyclo[3.3.0]octan-3-one (2e). Reduction of **2e** (89 mg, 0.201 mmol) with the aluminum reagent **1** (2.01 mmol) in toluene (15 ml) using the method B afforded a mixture of 15*S* and 15*R* isomers (82 mg, 93% yield): TLC, R_f 0.546, 0.452 (2-butanone–benzene, 15 : 85). Column chromatography of the mixture (42 mg) on silica gel (2-butanone–benzene, 10 : 90) separated the less polar isomer (13 mg), the more polar isomer (11 mg), and a mixture of these isomers (17 mg). The two isomers gave the similar ^1H NMR spectra: δ 7.23—8.09 (9H, m, Phenyl H), 5.23—5.42 (1H, m, C_7–H), 4.89—5.10 (1H, m, C_1–H), 5.35—5.65 (2H, m, olefinic H), 3.80—4.20 (1H, m, $C_{3'}$–H), 0.90 (3H, t, CH_3). The products by hydrolysis of the *p*-phenylbenzoyl group (1 equiv. of K_2CO_3 in MeOH, 25 °C for 2 h) was identical with the reduction products of **2a** by TLC. HPLC analysis (μ-Porasil, UV index 254 nm, hexane–AcOEt, 1 : 1) indicated the ratio of 15*S*/15*R* isomers to be 1 : 1.

Reduction of (1S, 5R, 6R, 7R)-7-Acetoxy-6-[(E)-3-oxo-1-octenyl]-2-oxabicyclo[3.3.0]octan-3-one (2g). Reduction of **2g** (195 mg, 0.635 mmol) with the aluminum reagent **1** (6.35 mmol) in toluene (30 ml) according to the method A produced

a mixture of 15*S* and 15*R* isomers (177 mg, 91% yield): TLC, R_f 0.523, 0.424 (ether, 2 developments). Comparison of the R_f values with those of the authentic sample[18] showed the less polar isomer to be the 15*S* alcohol. The mixture (100 mg), obtained above, was applied to column chromatography (silica gel, 20 g; ether–AcOEt–cyclohexane, 2 : 1 : 1) to furnish the less polar isomer (33 mg), the more polar isomer (23 mg), and their mixture (35 mg). Both isomers had the similar spectroscopic properties (IR, ^{1}H NMR, and MS), which were identical with those of the authentic sample: IR (film) 3450, 2950, 2850, 1780, 1760, 1250, 975 cm^{-1}; ^{1}H NMR δ 5.55—5.77 (2H, m, olefinic H), 4.86—5.23 (2H, m, C_{11}, C_7–H), 3.90—4.21 (1H, m, $C_{3'}$–H), 2.01 (3H, s, $CH_3C{=}O$), 0.90 (3H, t, CH_3); MS *m/e* 310 (M^+), 292 (M^+-H_2O), 250 (M^+-CH_3COOH); high resolution MS *m/e* 310.178 for the 15*S* isomer, 310.179 for the 15*R* isomer (calcd for $C_{17}H_{26}O_5$, 310.178). The ratio of 15*S*/15*R* isomers was 1 : 1 by HPLC analysis (μ-Porasil, refractive index, hexane–AcOEt, 1 : 1).

In the reduction products of enones with α-side chains using the aluminum reagent **1**, every less polar isomer correspond to the 15*R* alcohol. This was based on the transformation of both isomers into the end products, followed by the results of their biological activity. The 15*R* isomer had little activity.

Reduction of (5Z, 13E, 17R)-9α-Acetoxy-11α-(tetrahydro-2-pyranyloxy)-15-oxo-17-methyl-20-chloroprosta-5,13-dienoic Acid Methyl Ester. Reduction of the enone (1.8 g, 3.33 mmol) with the aluminum reagent **1** (33.3 mmol) in toluene (65 ml) using the method B produced a mixture of 15*R* and 15*S* isomers (1.71 g, 95% yield): TLC, R_f 0.42 for the 15*R* isomer, 0.31 for the 15*S* isomer (CH_2Cl_2–AcOEt, 4 : 1). Column chromatography (silica gel, 200 g; CH_2Cl_2–AcOEt, 5 : 1) separated the 15*R* isomer (295 mg) and the 15*S* isomer (1.346 g). Both isomers had the similar spectroscopic properties: IR (film) 3450, 2950, 2850, 1740, 980 cm^{-1}; ^{1}H NMR δ 4.80—5.93 (5H, m, olefinic H, and C_9–H), 4.52—4.55 (1H, m, OCHO), 3.63 (3H, s, $COOCH_3$), 3.50 (2H, t, CH_2Cl), 2.06 (3H, s, CH_3COO), 0.95 (3H, d, C_{17}–CH_3); MS *m/e* 524 (M^+-H_2O), 380 ($524-OCH_3-DHP$); high resolution MS *m/e* 524.290 for the 15*R* isomer, 524.291 for the 15*S* isomer (dehydration peak, calcd for $C_{29}H_{45}O_6Cl$, 524.290).

Reduction of (13E)-9α-Acetoxy-11α-hydroxy-15-oxoprost-13-enoic Acid Methyl Ester. Reduction of the enone (410 mg, 1.001 mmol) with the aluminum reagent **1** (10.01 mmol) in toluene (40 ml) using the method B afforded a mixture of 15*S* and 15*R* isomers (389 mg, 95% yield): TLC, R_f 0.46 for the 15*R* isomer, 0.26 for the 15*S* isomer (benzene–AcOEt, 1 : 2). Separation of the mixture (389 mg) by column chromatography (silica gel, 40 g; benzene–AcOEt, 1 : 1) gave the 15*R* isomer (299 mg) and the 15*S* isomer (65.8 mg). IR, ^{1}H NMR, and MS spectra of both isomers were identical: IR (film) 3450, 2950, 2850, 1740, 1250, 980 cm^{-1}; ^{1}H NMR δ 5.30—5.76 (2H, m, olefinic H), 4.92—5.30 (1H, m, C_9–H), 3.11 — 4.34(5H, m, C_{11}, C_{15}–H and $COOCH_3$), 2.31—2.82 [2H, br s, OH (disappearance in D_2O)], 2.05 (3H, s, CH_3COO), 0.90 (3H, t, C_{20}–H); MS *m/e* 394 (M^+-H_2O), 381 (M^+-OCH_3), 376 (M^+-2H_2O), 363 ($M^+-H_2O-OCH_3$), 334 (M^+-H_2O-AcOH); high resolution MS *m/e* 394.272 for both isomers (dehydration peak, calcd for $C_{23}H_{38}O_5$, 394.272). The 15*S* isomer was converted by treatment with potassium carbonate (1 equiv.) in MeOH at 45 °C for 2 h into the methyl ester of prostaglandin $F_{1\alpha}$ ($PGF_{1\alpha}$). The R_f value of this ester was in agreement with that of the authentic sample.

Reduction of (5Z, 13E)-9α-Acetoxy-11α-hydroxy-15-oxo-16-(3-chlorophenoxy)-17,18,19,20-tetranorprosta-5,13-dienoic Acid Methyl Ester. Reduction of the enone (388 mg, 0.812 mmol) with the aluminum reagent **1** (8.12 mmol) in toluene (20 ml) by the method B furnished a mixture of 15*R* and 15*S* isomers (329 mg): TLC, R_f 0.44 for the 15*R* isomer, 0.22 for the 15*S* isomer (benzene–AcOEt, 1 : 2). HPLC analysis (μ-Porasil, UV index 273 nm, CH_2Cl_2–AcOEt, 20 : 1) showed the ratio of 15*S*/15*R* to be 86 : 14. The mixture of 15*R* and 15*S* isomers: IR (film) 3450, 2950, 2850, 1740, 1600, 1450, 980, 780 cm^{-1}; ^{1}H NMR δ 6.70—7.22 (4H, m, phenyl H), 5.22—5.76 (4H, m, olefinic H), 5.05—5.23 (1H, m, C_9–H), 4.00—4.31 (1H, m, C_{15}–H), 3.55—4.00 (6H, m, C_{11}–H, CH_2OAr, and $COOCH_3$), 2.05 (3H, s, CH_3COO); MS *m/e* 462 (M^+-H_2O), 449 (M^+-OMe), 444 (M^+-2H_2O), 402 (M^+-H_2O-AcOH).

Reduction of (13E)-2-Phenylseleno-9α-acetoxy-11α-(tetrahydro-2-pyranyloxy)-15-oxo-16,16-dimethylprost-13-enoic Acid Methyl Ester. Reduction of the enone (448 mg, 0.644 mmol) with the aluminum reagent **1** (6.44 mmol) in toluene (20 ml) according to the method B afforded a mixture of 15*S* and 15*R* isomers (417 mg, 93% yield): TLC, homogeneous (CH_2Cl_2–AcOEt, 4 : 1). The ratio of 15*S*/15*R* was 87 : 13 by HPLC analysis (μ-Porasil, UV index 273 nm, CH_2Cl_2–AcOEt, 3 : 1). The mixture of 15*S* and 15*R* isomers: IR (film) 3400, 2950, 2850, 1740, 1580, 1440, 975, 790, 760 cm^{-1}; ^{1}H NMR δ 7.20—7.70 (5H, m, phenyl H), 5.50—5.72 (2H, m, olefinic H), 5.00—5.20 (1H, m, C_9–H), 4.50—4.70 (1H, m, OCHO), 3.62 (3H, s, $COOCH_3$), 2.05 (3H, s, CH_3COO), 0.80, 0.90, 0.91 (9H, s, s, t, CH_3); MS *m/e* 661 (M^+-H_2O), 648 (M^+-OMe), 619 (M^+-AcOH), 577 (M^+-H_2O-DHP).

Reduction of (5Z, 13E)-9α,11α-Bis(tetrahydro-2-pyranyloxy)-15-oxoprosta-5,13-dienoic Acid Methyl Ester (7). Reduction of the enone **7** (145 mg, 0.272 mmol) with aluminum reagent **1** (2.71 mmol) in toluene (5 ml) using the method B produced a mixture of 15*S* and 15*R* isomers (129 mg, 89% yield): TLC, R_f, 0.476 for the 15*R* isomer, 0.285 for the 15*S* isomer (benzene–AcOEt, 2 : 1). HPLC analysis (μ-Porasil, refractive index, CH_2Cl_2–AcOEt, 1 : 1) indicated the ratio of 15*R*/15*S* to be 74 : 26. Column chromatography (silica gel, 9 g; CH_2Cl_2–AcOEt, 7 : 1) separated the 15*S* isomer (96 mg) and 15*R* isomer (32 mg), which gave the similar spectral data: IR (film) 3450, 2950, 2850, 1740, 970 cm^{-1}; ^{1}H NMR δ 5.23—5.75 (4H, m, olefinic H), 4.50—4.83 (2H, m, OCHO), 3.30—4.20 (10H, m, s,$COOCH_3$, C_9 C_{11}, C_{15}–H, OCH_2), 0.90 (3H, t, CH_3); MS *m/e* 451 (M^+-THP), 434 ($M^+-HOTHP$), 332 ($M^+-2HOTHP$). Hydrolysis of the THP groups (65% aq AcOH, 40—45 °C for 2 h) in each isomer gave the corresponding triols. Their R_f values ($CHCl_3$–THF–AcOH, 10 : 2 : 1 or AcOEt) were identical with those of authentic samples ($PGF_{2\alpha}$ and its epimer).

Similarly, the enone **7** was reduced with 2, 5, and 20 equiv. of **1**, and their results are shown in Table 3.

Reduction of 2c with Various Diisobutylaluminum Phenoxides. The enone **2c** was reduced with various diisobutylaluminum phenoxides, which were prepared under the similar conditions as described for the synthesis of **1**. The reduction conditions are indicated in Table 5. The ratio of 15*S*/15*R* was determined by HPLC analysis (μ-Porasil, refractive index, CH_2Cl_2–AcOEt, 1 : 1).

Reduction of 2c with Diethylaluminum 2,6-Di-t-butyl-4-methylphenoxide (9). Triethylaluminum (2.71 mmol) in hexane was added dropwise at 0 °C to 2,6-di-*t*-butyl-4-methylphenol (715 mg, 3.25 mmol) in toluene (10 ml) under nitrogen. Stirring was continued at 0 °C for 30 min, then at 25 °C for 30 min. The solution was cooled to −78 °C, and the enone **2c** (210 mg, 0.600 mmol) in toluene (2 ml) was added dropwise at this temperature. Further stirring was carried out at −70 °C for 1 h, from −70 °C to 0 °C over 5 h, and at 25 °C for 1 h. The reaction was quenched by the addition of saturated

sodium hydrogentartarate. The crude product was extracted with ether, dried over $MgSO_4$, concentrated, and purified by column chromatography (silica gel, 5 g; CH_2Cl_2–cyclohexane, 1 : 1, then only AcOEt) to give a mixture of **11**, **12**, and **13**: TLC, R_f 0.727 for **2c**, 0.454 for **11**, and **13**, 0.808 for **12** (ether, 2 developments). Further purification by column chromatography (silica gel, 10 g; ether) afforded a mixture of **11** and **13** (105 mg), and **12** (32 mg): the mixture of **11** and **13**: IR (film) 3450, 1780, 1180, 980 cm^{-1}; ^1H NMR δ 5.30—5.55 (2H, m, olefinic H), 4.81—5.03 (1H, m, C_9–H), 4.61—4.70 (1H, m, OCHO), 3.02—4.05 (4H, m, C_{11},C_{15}–H, OCH_2), 0.90 (3H, t, CH_3); MS *m/e* 352 (M^+ of **11** $-H_2O$), 278 (M^+ of **13**—HOTHP), 250 (352—HOTHP): **12**: IR (film) 1780, 1720, 980 cm^{-1}; ^1H NMR δ 4.40—5.00 (2H,m, C_9–H, OCHO), 3.10—4.20 (3H, m, C_{11}–H, OCH_2), 0.90 (6H, t, CH_3); MS *m/e* 380 (M^+), 295 (M^+—THP).

Reduction of **2c** *with Dimethylaluminum 2,6-Di-t-butyl-4-methylphenoxide (***10***).* Trimethylaluminum (2.71 mmol) in hexane was added dropwise at 0 °C to a solution of 2,6-di-*t*-butyl-4-methylphenol (715 mg, 3.25 mmol) in toluene (10 ml) under nitrogen. Stirring was continued at 0 °C for 30 min, then at 25 °C for 30 min. The solution was cooled to −78 °C, and the enone **2c** (210 mg, 0.600 mmol) in toluene (2 ml) was added slowly over 5 min at this temperature. The whole mixture was stirred at −70 °C for 1 h, and warmed up to −5 °C over 2 h. The cooling bath was then removed and further stirring was carried out overnight. The reaction was terminated with saturated sodium hydrogentartarate. Extraction with ether, being dried over $MgSO_4$, concentration, and purification of the crude product by column chromatography (silica gel, 5 g; CH_2Cl_2–cyclohexane, 1 : 1, then only AcOEt) afforded the methylation product **14** with the recovery of **2c**: TLC, R_f 0.727 for **2c**, 0.461 for **14** (ether, 2 developments). Repurification by column chromatography (silica gel, 6 g; ether) furnished **2c** (50 mg) and **14** (100 mg): **14**: IR (film) 3450, 1770, 980 cm^{-1}; ^1H NMR δ 5.40—5.56 (2H, m, olefinic H), 4.75—5.00 (1H, m, C_9–H), 4.55—4.73 (1H, m, OCHO), 1.19 (3H, s, CH_3), 0.89 (3H, t, CH_3); MS *m/e* 366 (M^+), 348 (M^+ $-H_2O$), 264 (M^+ —HOTHP); high resolution MS *m/e* 366.242 (calcd for $C_{21}H_{34}O_5$, 366.241).

*Reduction of Prostaglandin E_2 Methyl Ester (***5a***).* A solution of the ester **5a** (104 mg, 0.284 mmol) in toluene (1 ml) was added slowly over 5 min to a solution of **1** (2.84 mmol) in toluene (15 ml) at −78 °C. The resulting mixture was stirred at −78 °C for 2 h, warmed up to −20 °C over 1 h, and again stirred at −20 °C for 30 min. The reaction mixture was poured onto cold 1 M hydrochloric acid (20 ml) and ethyl acetate (20 ml). The aqueous layer was extracted with ethyl acetate twice. The combined organic layers were washed successively with 1 M hydrochloric acid once, aq sodium hydrogencarbonate twice, then brine once, and dried over $MgSO_4$. Evaporation of the solvent, followed by purification of the residue by column chromatography (silica gel, 10 g; CH_2Cl_2, then AcOEt) gave $PGF_{2\alpha}$ methyl ester (**6a**) (99 mg, 95% yield): TLC, R_f 0.562 (homogeneous, AcOEt, 2 developments), which was in agreement with that of the authentic sample; boric acid impregnated TLC,[19] R_f 0.785 (homogeneous, AcOEt, 2 developments); IR (film) 3400, 2950, 2850, 1720, 1250, 975 cm^{-1}; ^1H NMR δ 5.22—5.65 (4H, m, olefinic H), 3.70—4.30 (3H, m, C_9, C_{11}, C_{15}–H), 3.66 (3H, s, $COOCH_3$), 0.90 (3H, t, CH_3); MS *m/e* 350 (M^+ $-H_2O$), 332 (M^+-2H_2O), 319 (M^+-H_2O-OMe), 314 (M^+-2H_2O), 301 (M^+ $-2H_2O-OMe$); high resolution MS *m/e* 350.244 (dehydration peak, calcd for $C_{21}H_{34}O_4$, 350.246). $PGF_{2\beta}$ methyl ester [TLC, R_f 0.424; boric acid impregnated TLC, R_f 0.462 (AcOEt, 2 developments)] was not detected in the reaction mixture.

*Synthesis of 11-Epiprostaglandin E_2 Methyl Ester (***5b***).* The ester **5b** was prepared starting from the diol **19** using the Corey method:[17] IR (film) 3400, 2950, 2850, 1740, 980 cm^{-1}; ^1H NMR δ 5.59—5.82 (2H, m, *trans* olefinic H), 5.26—5.45 (2H, m, *cis* olefinic H), 4.25—4.45 (1H, m, C_{11}–H), 3.92—4.15 (1H, m, C_{15}–H), 3.65 (3H, s, $COOCH_3$), 0.90 (3H, t, CH_3); MS *m/e* 348 (M^+-H_2O), 335 (M^+—OMe), 330 (M^+-2H_2O), 317 (M^+-H_2O-OMe); high resolution MS *m/e* 348.230 (dehydration peak, calcd for $C_{21}H_{32}O_4$, 348.230).

Reduction of **5b**. Reduction of the ester **5b** (200 mg, 0.546 mmol) with the aluminum reagent **1** (5.46 mmol) in toluene (30 ml) according to the method for reduction of **5a** afforded a mixture of 11-*epi*-$PGF_{2\alpha}$ methyl ester (**6b**) (major product) and 11-*epi*-$PGF_{2\beta}$ methyl ester (**6d**) (minor product) (188 mg, 94% yield): boric acid impregnated TLC, R_f 0.380 for **6b**, 0.565 for **6d** (AcOEt, 2 developments). These R_f values were in agreement with those of the reduction product from **5b** using $NaBH_4$.[20] Regular silica gel TLC plate showed a single spot with ethyl acetate (2 developments). The mixture of **6b** and **6d**: IR ($CHCl_3$) 3600, 3400, 1730, 980 cm^{-1}; ^1H NMR δ 5.48—5.72 (2H, m, *trans* olefinic H), 5.20—5.48 (2H, m, *cis* olefinic H), 3.82—4.43 (3H, m, C_9, C_{11}, C_{15}–H), 3.68 (3H, s, $COOCH_3$), 2.90—3.55 [3H, brs, OH disappearance in D_2O)], 0.89 (3H, t, CH_3): MS *m/e* 350 (M^+ $-H_2O$), 332 (M^+-2H_2O), 314 (M^+-3H_2O), 319 (M^+ $-H_2O-OMe$); high resolution MS *m/e* 350.243 (dehydration peak, calcd for $C_{21}H_{34}O_4$, 350.246). The ratio of **6b**/**6d** was determined by the conversion of **6b** and **6d** to the acids (2 M KOH–MeOH, 1 : 1, 25 °C for 2 h), then to the phenacyl esters (α,*p*-Dibromoacetophenone, Et_3N, CH_3CN, 25 °C for 3 min), followed by the HPLC analysis of these esters (μ-Porasil, UV index 264 nm, AcOEt–hexane, 4 : 1) to be 76 : 24.

*Reduction of Prostaglandin D_2 Methyl Ester (***6c***).* Reduction of **6c** (53 mg, 0.145 mmol) with the aluminum reagent **1** (1.61 mmol) in toluene (5 ml) using the method for the reduction of **5a** produced a mixture of 11-*epi*-$PGF_{2\alpha}$ methyl ester (**6b**) (major product) and $PGF_{2\beta}$ methyl ester (**6a**) (minor product) (49 mg, 92% yield): TLC, homogeneous; boric acid impregnated TLC, R_f 0.381 for **6b**, 0.501 for **6a** (AcOEt, 2 developments). The R_f values for **6b** and **6a** were completely identical with those for the reduction product of **5b**, and for the authentic $PGF_{2\alpha}$ methyl ester, respectively. The ratio of **6b**/**6a** (98/2) was determined, as described above, by the conversion of **6b** and **6a** into the corresponding phenacyl esters, followed by their HPLC analysis (μ-Porasil, UV index 264 nm, AcOEt–hexane, 4 : 1). The mixture of **6b** and **6a**: IR ($CHCl_3$) 3600, 3450, 1730, 980 cm^{-1}; ^1H NMR δ 5.50—5.69 (2H, m, *trans* olefinic H), 5.20—5.50 (2H, m, *cis* olefinic H), 3.96—4.46 (3H, C_9, C_{11}, C_{15}–H), 3.66 (3H, s, $COOCH_3$), 0.89 (3H, t, CH_3); MS *m/e* 350 (M^+-H_2O), 332 (M^+ $-2H_2O$), 319 (M^+-H_2O-OMe), 314 (M^+-3H_2O); high resolution MS *m/e* 350.246 (dehydration peak, calcd for $C_{21}H_{34}O_4$, 350.246).

Reduction of 4-Hydroxy-3-methyl-2-butanone. A solution of 4-hydroxy-3-methyl-2-butanone (500 mg, 4.90 mmol) in toluene (5 ml), which was cooled below −60 °C, was added dropwise to the aluminum reagent **1** (49 mmol) in toluene (100 ml) at −78 °C. The resulting mixture was stirred at −78 °C for 4 h, warmed up to −20 °C for 1 h, and again stirred at −20 °C for 30 min. The reaction mixture was poured onto 0.1 M hydrochloric acid (20 ml). Removal of the white solid by filtration, washing of the filtrate with brine, being dried over $MgSO_4$, and evaporation of the solvent left the crude oil, which was purified by column chromatography (silica gel, 150 g; CH_2Cl_2, then AcOEt) to furnish a

mixture of *erythro*- and *threo*-2-methyl-1,3-butanediol (480 mg, 96% yield): ^{1}H NMR (CD_3OD) δ 3.40—3.91 (3H, m, CH_2–O, CH–O), 1.41—1.70 (1H, m, CH_3–C<u>H</u>), 1.14, 1.16 (3H, two d, J=6.5 Hz, C_4–H), 0.87, 0.92 (3H, two d, J=7.0 Hz, C_2–CH_3); MS *m/e* 105 ($M^+ + 1$), 89 ($M^+ - CH_3$), 86 ($M^+ - H_2O$). The ratio of the peaks at δ 1.16 and 1.14 (or δ 0.92 and 0.87) was 2 : 1. The authentic *erythro* form[21] showed the peaks for 2 methyl groups at δ 1.16 (d, J=6.5 Hz) and 0.92 (d, J=7.0 Hz). Furthermore, the ^{1}H NMR analysis of the reduction product in the presence of the authentic *erythro* form showed the larger peaks at δ 1.16 and 0.92. Therefore, the ratio of *erythro* to *threo* form would be 2 : 1.

Reduction of 4-t-Butylcyclohexanone. A solution of 4-*t*-butylcyclohexanone (154 mg, 1 mmol) in toluene (2 ml) was added dropwise to the aluminum reagent **1** (10 mmol) in toluene (18 ml) at −78 °C. Stirring was continued at −78 °C for 4 h. Then the mixture was poured onto ice, and diluted with 1 M hydrochloric acid (75 ml). Extraction with ether, washing of the extracts with brine, being dried over $MgSO_4$, and concentration of the solvent left the crude oil, which was purified by column chromatography on silica gel (CH_2Cl_2, then CH_2Cl_2–AcOEt, 6 : 1) to afford the less polar isomer (37 mg, 24% yield) and the more polar isomer (94 mg, 60% yield) as white crystals: TLC, R_f 0.50 for the less polar isomer, 0.38 for the more polar isomer (AcOEt–CH_2Cl_2, 1 : 5). These R_f values were identical with those of the authentic samples (predominantly *cis*), which was prepared by the reduction of 4-*t*-butylcyclohexanone with L-Selectride in tetrahydrofuran at −78 °C.[22] The TLC analysis showed that the less polar isomer corresponded to the *cis* form, and therefore, the ratio of *cis*-/*trans*-4-*t*-butylcyclohexanol was 28 : 72. *cis*-4-*t*-Butyl-cyclohexanol: IR ($CHCl_3$) 3470, 1480, 1449, 1392, 1222, 1135, 1106, 949 cm^{-1}; ^{1}H NMR δ 3.93—4.18 (1H, m, CH–O), 1.14—2.04 (10H, m, aliphatic CH, OH), 0.87 (9H, s, *t*-Bu); MS *m/e* 156 (M^+), 141 ($M^+ - CH_3$), 138 ($M^+ - H_2O$), 123 ($M^+ - H_2O - CH_3$), 99 ($M^+ - t$-Bu); high resolution MS *m/e* 156.158 (calcd for $C_{10}H_{20}O$, 156.151). *trans*-4-*t*-Butylcyclohexanol: IR ($CHCl_3$) 3457, 1461, 1373, 1112, 1059, 978 cm^{-1}; ^{1}H NMR δ 3.29—3.80 (1H, m, CH–O), 0.80—2.23 (10H, m, aliphatic CH, OH), 0.83 (9H, s, *t*-Bu); MS *m/e* 138 ($M^+ - H_2O$), 123 ($M^+ - H_2O - CH_3$), 99 ($M^+ - t$-Bu), 81 ($M^+ - t$-Bu $- H_2O$).

Reduction of 2-Methylcyclohexanone. A solution of 2-methylcyclohexanone (112 mg, 1 mmol) in toluene (2 ml) was added dropwise to the aluminum reagent **1** (10 mmol) in toluene (18 ml) at −78 °C. Stirring was continued at −78 °C for 3.5 h, then at −20 °C for 3.5 h. The mixture was poured onto ice and diluted with 1 M hydrochloric acid (75 ml). Extraction with ether, washing of the extracts with brine, and purification of the concentrated crude product by column chromatography on silica gel (CH_2Cl_2, then ether) gave a mixture of *cis*- and *trans*-2-methylcyclohexanol (97 mg, 85% yield) as a colorless oil: IR ($CHCl_3$) 3490, 1452, 1378, 1220, 1123, 965 cm^{-1}; ^{1}H NMR δ 2.83—3.30, 3.63—3.97 (1H, m, CH–O), 1.10—2.12 (9H, m, aliphatic CH), 0.83—1.10 (3H, two d, CH_3); MS *m/e* 96 ($M^+ - H_2O$), 81 ($M^+ - H_2O - CH_3$). The ^{1}H NMR spectrum showed the ratio of the *cis* to *trans* isomers to be 75 : 25. This analysis was determined by an absorption due to the α-proton peak (C<u>H</u>–OH) of the hydroxyl group at δ 3.63—3.97 and 2.83—3.30.[23]

References

1) Preliminary communication: S. Iguchi, H. Nakai, M. Hayashi, and H. Yamamoto, *J. Org. Chem.*, **44**, 1363 (1979).

2) J. S. Bindra and R. Bindra ,"Prostaglandin Synthesis," Academic Press, New York (1977); A. Mitra, "The Synthesis of Prostaglandins," John Wiley and Sons, New York (1977); P. Crabbe, "Prostaglandin Research," Academic Press, New York (1977).

3) E. J. Corey, S. M. Albonico, U. Koelliker, T. K. Schaaf, and R. K. Varma, *J. Am. Chem. Soc.*, **93**, 1491 (1971); E. J. Corey, K. B. Becker, and R. K. Varma, *ibid.*, **93**, 8616 (1972).

4) R. Noyori, I. Tamino, and M. Nishizawa, *J. Am. Chem. Soc.*, **101**, 5843 (1979).

5) E. J. Corey and R. K. Varma, *J. Am. Chem. Soc.*, **93**, 7391 (1971); G. Stork and M. Isobe, *ibid.*, **97**, 4745 (1975).

6) H. Yamamoto and H. Nozaki, *Angew. Chem. Int. Ed. Engl.*, **7**, 169 (1978); A. Itoh, H. Nozaki, and H. Yamamoto, *Tetrahedron Lett.*, **1978**, 2903; K. B. Strarowieyski, S. Pasynkiewicz, and M. Skowronska-Ptasinska, *J. Organomet. Chem.*, **90**, C43 (1975).

7) Only one equiv. of phenol is involved in the reaction and *ca.* one equiv. of hydrogen gas evolution is observed during this operation.

8) General review of organoaluminum compounds, see T. Mole, and E. A. Jeffery, "Organoaluminum Compounds," Elsevier, Amsterdam (1972).

9) Using a bulky hydroborate in tetrahydrofuran–ether–pentane at −120 °C to −130 °C, it was possible to convert **2e** to a mixture of 15*S* and 15*R* alcohols in a ratio of 88 : 12, see Ref. 3).

10) S. Bergström, L. Kabisch, B. Samuelsson, and J. Sjövall, *Acta Chem. Scand.*, **16**, 969 (1962).

11) Reduction with zinc borohydride gives rise to C-9β isomer with 90% selectivity, see E. J. Corey, K. C. Nicolaou, Y. Machida, C. L. Malmsten, and B. Samuelsson, *Proc. Natl. Acad. Sci. U.S.A.*, **72**, 3355 (1975).

12) M. Hayashi and T. Tanouchi, *J. Org. Chem.*, **38**, 2115 (1973).

13) J. M. Fortunato and B. Ganem, *J. Org. Chem.*, **41**, 2194 (1976).

14) E. L. Eliel, "Stereochemistry of Carbon Compounds," McGraw-Hill Book Co., Inc., New York (1962), pp. 72—73.

15) E. S. Gould, "Mechanism and Structure in Organic Chemistry," H. Holt and Co., Inc., New York (1959), pp. 544—546.

16) H. Haubenstock and E. B. Davidson, *J. Org. Chem.*, **28**, 2772 (1963).

17) E. C. Ashby and J. J. Lin, *Tetrahedron Lett.*, **1976**,3685.

18) E. J. Corey, T. K. Schaaf, W. Huber, U. Koelliker, and N. M. Weischenker, *J. Am. Chem. Soc.*, **92**, 397 (1970).

19) Boric acid impregnated silica gel TLC plates were prepared by dipping the regulai TLC plates (30 s) in a solution of boric acid (4 g) in CH_3CN–EtOH (1 : 1, 200 ml), followed by dryness in the oven at 110 °C for 1 h. 1,3-*cis*-Diols should be less polar isomer on boric acid impregnated TLC. For references on the application of this TLC plate to the separation of prostaglandins, see a) E. L. Cooper and E. W. Yankee, *J. Am. Chem. Soc.*, **96**, 5881 (1974); b) F.H. Lincoln, W. P. Scheider, and J. E. Pike, *J. Org. Chem.*, **38**, 952 (1973).

20) Reduction of **5b** with $NaBH_4$ gave 11-*epi*-$PGF_{2\beta}$ methyl ester as the major product, which correspond to the less polar isomer on boric acid impregnated silica gel TLC plate. See Refs. 11 and 19b.

21) L. J. Dolby, F. A. Meneghini, and T. Koizumi, *J. Org. Chem.*, **33**, 3060 (1968).

22) H. C. Brown and S. Krishnamurthy, *J. Am. Chem. Soc.*, **94**, 7159 (1972).

23) Commercially available *trans*-2-methylcyclohexanol showed the α-proton peak (C<u>H</u>–OH) of the hydroxyl group at δ 2.75—3.40.

Photo-induced Radical Rearrangements of Hypoiodite of *N*-Acetyljervine and the Related *C*-nor-*D*-Homosteroid in the Presence of Mercury(II) Oxide and Iodine[1]

Hiroshi SUGINOME,*,** Kimitoshi KATO, and Tadashi MASAMUNE
Department of Chemistry, Faculty of Science, Hokkaido University, Sapporo 060

(Received February 3, 1981)

Irradiation of the hypoiodite of *N*-acetyljervine in benzene containing mercury(II) oxide and iodine gave a mixture of products. The major product was *N*-acetyl-11-oxojerva-5,12(13)-dien-3β-yl *N*-acetyl-*A*-homo-4-oxa-11-oxojerva-5,12(13)-dien-3α-yl ether (**4**) (25%). Four minor products, *N*-acetyl-2-iodo-11-oxo-*A*-nor-2,3-secojerva-5,12(13)-dien-3-yl formate, *N*-acetyl-3α,5-epoxy-6α-iodo-*A*-homo-4-oxa-5α-jerva-5,12(13)-dien-11-one, *N*-acetyl-4-oxajerva-5,12(13)-dien-11-one, and *N*-acetyl-4-oxa-*A*-homojerva-5,12(13)-diene-3,11-dione, were also isolated. Irradiation of the hypoiodite of 3β-hydroxy-17-ethyletiojerv-5-ene-11,20-dione also gave a dimer corresponding to **4**. The formation of **4** as the major product contrasts with the result of the corresponding reaction of cholesterol.

It has been shown that hypoiodites generated from a variety of steroidal alcohols undergo heat- or light-induced reaction to give products originating through alkoxy radical intermediates.[2,3] Mercuric oxide–iodine reagent has been shown to be an effective reagent for the formation of hypoiodites from steroidal alcohols.[4]

In previous papers,[5–7] we described the results of investigations of the photo- and thermally-induced rearrangements of hypoiodites of cholesterol and several related 5-cholesten-3-ols substituted with methyl groups on their C-3 and C-4 positions in the presence of mercury(II) oxide and iodine. It has been found that 3α,5-epoxy-*A*-homo-4-oxa-5α-cholestanes (type A) carrying α- or β-oriented iodine on their C-6 positions or 3α,5-epoxy-*A*-homo-4-oxa-5α-cholest-6-enes (type B) are usually formed when the reactions are induced by irradiation, although their yields varied widely; these products are usually accompanied by seco-iodide of type (C). It has also been found that methyl substituents on their C-3 or C-4 positions affect the relative yields of oxabicyclic compounds (type A) appreciably and that the presence of *gem* dimethyl group on the C-4 position results in the formation of 3-oxa-5-cholestenes (type D) with the loss of one carbon atom.[5,7] The products from thermally-induced reactions were almost parallel, but the thermally-induced reaction of cholesterol hypoiodite gave a novel dimeric product of type (E) as the major product.[5]

The pathways of the rearrangements which can explain the stereochemistry of these products have been advanced in the previous papers.[5–7] All the above products are formed from an allyl radical intermediate (F) derived from β-scission of the corresponding 3β-oxyl radicals.

In this paper, we report the results of the photo-induced reaction of hypoiodite of *C*-nor-*D*-homosteroid-5-en-3β-ols in which their C-ring is 5-membered instead of 6-membered as in normal steroids.

Results and Discussion

N-Acetyljervine (**1**)[8] and 3β-hydroxy-17α-ethyletiojerv-5-ene-11,20-dione (**11**)[9] were chosen as the substrates. The photo-induced reactions were conducted under the conditions reported previously;[5–7] irradiation of *N*-acetyljervine (**1**) in benzene containing mercury(II) oxide and iodine (*ca.* 3 mol equiv. each) with a 100-W high pressure mercury arc for 12 h under an atmosphere of nitrogen gave a mixture of products, from which five crystalline products (**8**) (5%), (**9**) (2%), (**6**) (1%), (**7**) (1%), and (**4**) (25%) in order of their mobility, were isolated by preparative TLC (Scheme 1). The noted yields of the products are those in pure crystalline states; thus the actual yield of each product is higher than those described above. The structures of all these products were deduced by the analysis of their spectra. The mass, IR, UV, and ^{1}H NMR spectra showed that the C, D, and heterocyclic rings in jervine were intact in all the five products.

The structure of the crystalline product (**8**) carrying iodine, which was the most mobile on the TLC plate, was proved to be *N*-acetyl-3-iodo-11-oxo-*A*-nor-2,3-secojerva-5,12(13)-dien-3-yl formate[10] by the following spectral evidence. Although the mass spectrum showed

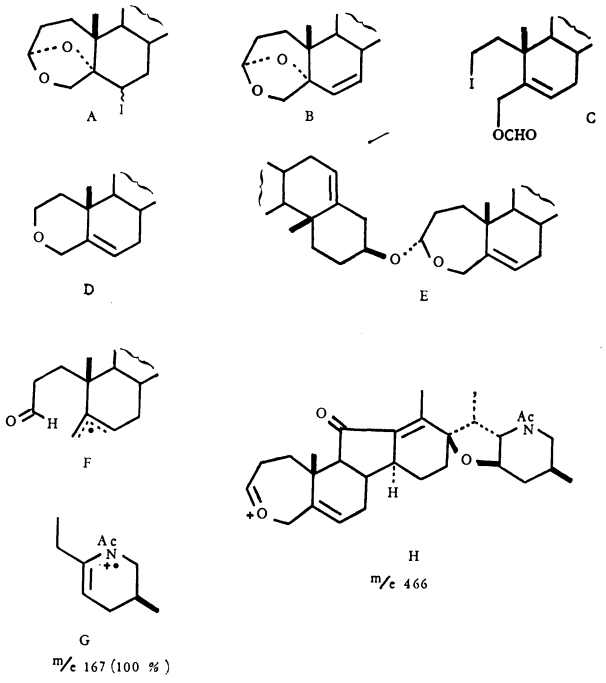

** Present address: Organic Chemistry Laboratory, Department of Chemical Process Engineering, Faculty of Engineering, Hokkaido University, Sapporo 060.

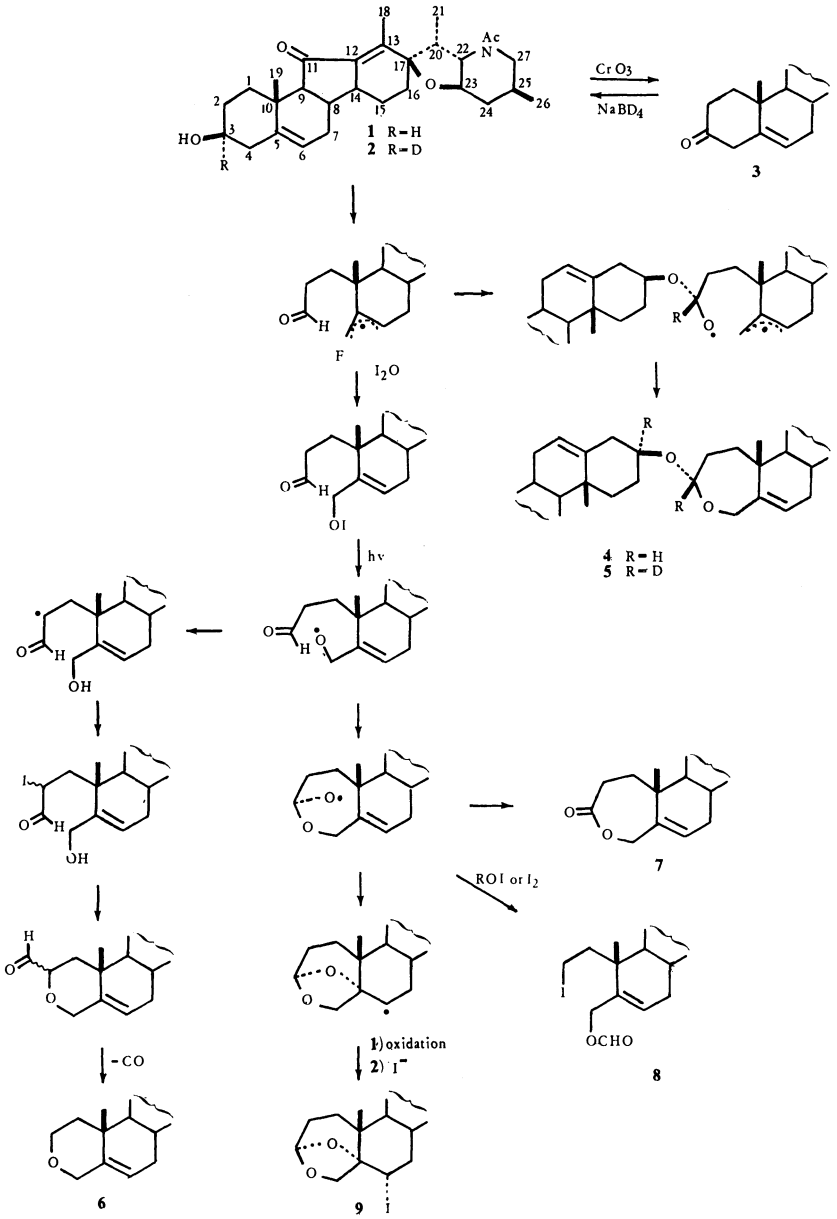

Scheme 1.

no molecular ion peak, the elemental analysis was in accord with the molecular formula $C_{29}H_{40}NO_5I$. A formate structure analogous to the formate[2] obtained from the hypoiodite of cholesterol was suggested by the presence of the 1H singlet at τ 1.91 in the ^1H NMR spectrum. The olefinic proton at the C-6 was present at τ 4.06 as a one-proton diffused doublet with J=4.5 Hz and the allylic C-3 methylene protons appeared as a broad singlet at τ 5.40 ($W_{1/2}$=5 Hz). The IR spectrum was also in agreement with the assigned structure. The pathway to this formate has already been discussed for the formation of an analogous formate from cholesterol in the previous paper.[5]

The crystalline product (**9**) carrying iodine was proved to be *N*-acetyl-3α,5-epoxy-6α-iodo-*A*-homo-4-oxa-5α-jerva-5,12(13)-dien-11-one[7] (**9**) from the following evidence: the molecular formula $C_{29}H_{40}NO_5I$ was determined by mass spectrometry (*m/e* 609, M^+) and elemental analysis. The ^1H NMR spectrum showed a broad one-proton singlet at τ 4.48, a one-proton double doublet at τ 5.55 with J=4.5 and 12.3 Hz, and an AB quartet at τ 5.84 and 6.24 with J=7.6 Hz. These signals were assigned to the 3β-H, the 6β-H, and the C-4a-methylene protons and were entirely analogous to those arising from the corresponding protons of 3α,5-epoxy-6β-iodo-*A*-homo-4-oxa-5α-cholestane[5] with respect to their chemical shifts and the coupling constants. The IR spectrum was also in accord with the assigned structure.

The molecular formula of the third TLC mobile crystalline product (**6**) was determined to be $C_{28}H_{39}NO_4$ by high resolution mass spectrometry. The structure was proved to be N-acetyl-4-oxajerva-5,12(13)-dien-11-one.[10] The ^1H NMR spectrum showed a one-proton doublet at τ 4.57 and a superimposed nine-proton multiplet (τ 5.81—7.20). The former is assigned to the olefinic 6-H and the latter is assigned to superimposed signals arising from the C-2-methylene protons, C-4-

methylene protons, 9α-H, 22β-H, 23α-H, and C-27-methylene protons. The shape of the multiplet signals is almost identical with that obtained by superimposing the signals due to 22-H, 23-H, C-27-methylene protons, and 9-H in the spectrum of *N*-acetyljervine and those due to C-2-methylene protons and C-4-methylene protons of 3-oxacholest-5-ene.[5] The IR spectrum was also in agreement with the assigned structure.

The molecular formula of the fourth TLC mobile crystalline product (**7**) was confirmed to be $C_{29}H_{39}NO_5$ by high resolution mass spectrometry. The results of the IR and NMR spectra were consistent with the structure, *N*-acetyl-4-oxa-*A*-homo-jerva-5,12(13)-diene-3,11-dione. In the IR spectrum, a new band arising from an unstrained lactone carbonyl band is present at 1737 cm^{-1}, together with the band due to the α,β-unsaturated carbonyl. In the ^1H NMR spectrum two doublets, at τ 5.36 and 5.84, and a one-proton doublet at τ 4.21 assigned to the C-4a methylene protons and the 6-H could be seen.

Finally, the structure of the most polar product (**4**), obtained in highest yield in this reaction, was deduced to be *N*-acetyl-11-oxojerv-5,12(13)-dien-3β-yl *N*-acetyl-*A*-homo-4-oxa-11-oxojerva-5-en-3α-yl ether, which was analogous to cholest-5-en-3β-yl *A*-homo-4-oxacholest-5-en-3α-yl ether obtained from thermal decomposition of cholesterol hypoiodite, on the basis of the spectroscopic, especially ^1H NMR spectral evidence. The molecular formula, $C_{58}H_{80}N_2O_8$, was deduced by the osmometric molecular weight determination[1] and the elemental analysis. The molecular weight was further confirmed by FD mass spectrometry, which showed the $M^+ + 1$ ion at *m/e* 933. The IR, UV, and ^1H NMR spectra proved that the C, D, and the heterocyclic ring portions of the starting jervine molecule were unchanged in this compound, as described earlier.

In the downfield region of the ^1H NMR spectrum, four signals (each one-proton) are present; these signals appeared at τ 4.45 (broad singlet), 4.69 (broad singlet), 5.12 (triplet, J=5.3 Hz) and 5.68 (doublet, J=13.5 Hz). These signals were assigned to those arising from 6-H of the *N*-acetyl-11-oxojerva-5,12(13)-dien-3β-yl portion, 6-H of the *A*-homo-4-oxa-11-oxojerva-5,12(13)-dien-3α-yl portion, and the 3β-H and 4a-H signals of *A*-homo-4-oxa-11-oxojerva-5,12(13)-dien-3α-yl portion on the basis of spin-decoupling experiments, deuterium labeling, acidic hydrolysis, and comparison of the spectrum with that of cholest-5-en-3β-yl *A*-homo-4-oxacholest-5-en-3α-yl ether.[5]

Decoupling experiments showed that the two signals at τ 4.45 and 4.69 collapsed into two clear singlets on irradiation at τ 7.5, while the triplet at τ 5.10 is only partially decoupled. The behavior of these two signals in the spin-decoupling is similar to those of C-6 olefinic proton of Δ^5-steroids. The diffused triplet at τ 5.10 was also partially decoupled to a broad singlet ($W_{1/2}$=7.0 Hz) on irradiation at τ 8.3. On the basis of an experiment which used 3α-deuterio-*N*-acetyljervine (**2**), this signal was confirmed to arise from C-3α-H of *N*-acetyljervine. 3α-Deuterio-*N*-acetyljervine (**2**) was prepared by reduction of *N*-acetyljerva-5,12(13)-diene-3,11-dione, which was prepared by the Jones oxidation of *N*-acetyljervine with $NaBD_4$. 3α-Deuterio-*N*-acetyljervine in benzene containing mercury(II) oxide and iodine was subjected to the photolysis to give a product (**5**) carrying deuterium. The ^1H NMR spectrum of **5** shows the absence of the triplet at τ 5.10 which was in the spectrum of product (**4**), proving that the triplet originated from 3α-H of the starting jervine.

The doublet at τ 5.68 in **4** was found to be a part of an AB quartet, and another doublet of the AB system superimposed with other signals was found at τ 6.48. On irradiation of the center of the doublet at τ 6.48, the doublet at τ 5.68 collapsed to a singlet. The irradiation at the center of the doublet at τ 5.68 caused a collapse of the doublet at τ 6.48 to a singlet without any change of the signal shapes at τ 4.45, 4.69 and 5.10. This AB quartet was thus assigned to an isolated C-4a methylene protons of *A*-homo-4-oxacholest-5-en-3α-yl portion.

The dimeric structure assigned to compound (**4**) was further confirmed by its acidic hydrolysis (Scheme 2).

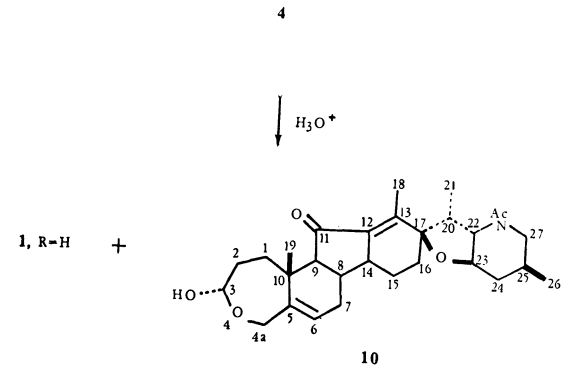

Scheme 2.

Hydrolysis of either **4** or **5** in THF containing dilute hydrochloric acid at room temperature gave only two products. As expected from the assigned structure, one of the products was found to be identical with *N*-acetyljervine (**1**) or 3α-deuterio-*N*-acetyljervine (**2**) by direct comparisons. All the spectra on the other product **10** were consistent with that of *N*-acetyl-*A*-homo-4-oxa-11-oxojerva-5,12(13)-dien-3α-ol or its 3β-deuterio compound. The MS spectrum showed the molecular ion at *m/e* 483. The IR spectrum shows the presence of a hydroxy and an α,β-unsaturated carbonyl. The ^1H NMR spectrum shows two one-proton signals at τ 4.41 and 4.86 and an AB quartet at τ 5.59 and 6.41, with J=13.3 Hz, together with a set of signals arising from the B, C and heterocyclic rings of jervine. The series of signals in the downfield region shows a remarkable similarity to the signals of compound **4** with respect to the chemical shifts and behavior in spin-decoupling. However, the spectrum shows the absence of a signal corresponding to the ones at τ 4.69 in the spectrum of compound **4**, proving that it originated from the *N*-acetyl-11-oxojerva-5,12(13)-dien-3β-yl portion.

All the foregoing results can be reconciled to the assigned structure **4**. It is noted that the signals arising from the *N*-acetyl, 18-H, 19-H, 21-H, and 26-H of the *N*-acetyl-11-oxojerva-5,12(13)-dien-3β-yl portion in the ^1H NMR spectrum were superimposed with those due

to the corresponding protons of the *N*-acetyl-*A*-homo-4-oxa-11-oxojerv-5-en-3α-yl portion.

The electron impact mass spectrum of compound **4** showed no peak above *m/e* 500 and showed weak peaks at *m/e* 465, 466, 467, and a base peak at *m/e* 167. The structures of the species of *m/e* 167 and 466 may be assigned to (G)[11] and (H). The ^{13}C FT NMR spectrum, with the aid of the off-resonance spectrum of **4**, fully supported the assigned formula. With the exceptions of the C-17 and the C-17′, the NAc and the N′Ac, and C-23 and C-23′, which appeared as the superimposed singlets at τ 172.97, 85.42, and 72.68 ppm, all the sp^2 carbon atoms and oxygen-bearing carbon atoms appeared as a pair of signals. Their assignments are as follows: C-11–CO and C-11′–CO (δ 206.65 ppm), C-5 and C-5′ (145.79 and 146.28), C-13 and C-13′ (142.46 and 144.22), C-6 and C-6′ (120.67 and 125.95), and C-3 of oxepane ring (99.08) and C-3′ (75.72).

To compare these results with those from a simpler *C*-nor-*D*-homosteroid, hypoiodite of 3β-hydroxy-17α-ethyletiojerv-5-ene-11,20-dione (**11**)[9] was subjected to the photolysis in the presence of mercury(II) oxide and iodine under the conditions described for *N*-acetyljervine hypoiodite. The results were found to be almost parallel to the case of *N*-acetyljervine (Scheme 3).

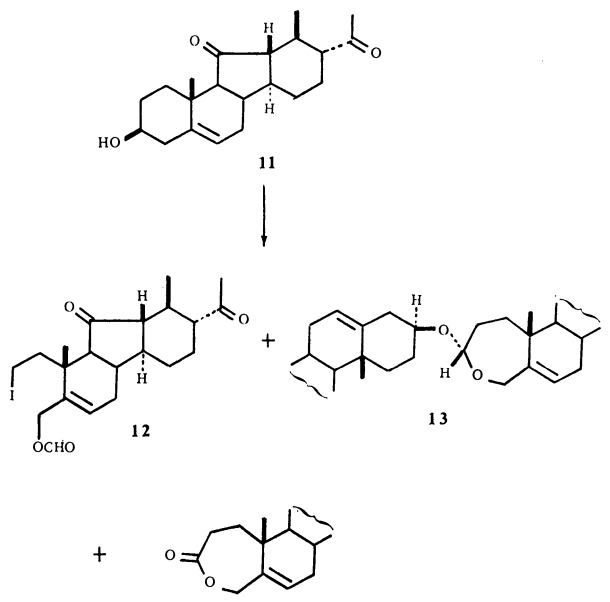

Scheme 3.

From a mixture of the products a formate (**12**), a dimer (**13**), and a lactone (**14**) were isolated in 32, 26, and 9% yields. The structures of these products were deduced by spectrometry in a manner analogous to the case of the products from *N*-acetyljervine. The results of the analysis of the spectra on each product are described in the experimental section, but the results of the electron impact mass spectrum of dimer **13** are only mentioned here. In contrast to the mass spectrum of dimer **4**, in which no molecular ion peak was present and the intensity of a fragment ion (H) was only 0.4%, that of dimer **13** showed the molecular ion peak at *m/e* 658 and the fragment ion of *m/e* 329 corresponding to the fragment (H) is the base peak. These results further supports the structure given to the product **4**. In this photolysis, two minor products (corresponding to **6** and **9**) were almost certainly present in the product mixture, but we failed to isolate these compounds in the pure forms. All the types of products, with the exceptions of lactone **7** and dimers **4** and **13**, obtained in this experiment were those already obtained in the photo-induced rearrangement of cholesterol[5] and the related 5-choleten-3-ols.[6,7] Changing the C-ring from 6-membered[5] to 5-membered, however, introduces appreciable variations in the products and their yields: dimeric acetal **4** was obtained as the major product, whereas no compound of this type was formed in the photo-induced reaction of cholesterol.[5] On the other hand, oxabicyclic compound **9** was formed in only a very minor amount although it is one of the major products in the corresponding reaction of cholesterol.[5] Unlike the cholesterol case,[5] we failed to isolate an oxabicyclic compound carrying β-oriented iodine.

The paths to dimeric acetal **4**, 4-oxa compound **6**, formate **8** and oxabicyclic compound **9** were already discussed in the previous papers.[5–7] All these products are derived from an allyl radical (F) formed by a β-scission of the 3β-oxyl radical. The Scheme 1 shows these pathways, including a path for the formation of lactone (**7**), the isolation of which in the present experiment strengthened the validity of our proposed pathways.[5] Although a further study is required for fuller understanding of origins of the variations in the products and their relative yields observed for *C*-nor-*D*-homosteroids and steroids,[5] one of the important factors would be slight changes in the geometries between groups or atoms introduced to the vicinity of the reaction center of the intermediary allyl radical. The change would affect the subtle balance between rates of intra- and intermolecular processes and would bring about appreciable differences in the products and their yields.

Experimental

For instruments used and general procedure see Ref. 2. Low resolution mass spectra of compounds, **2**, **3**, **7**—**9**, and **13** (70 eV), high resolution mass spectra of **2**, **3**, **7**, **9**, and FD mass spectra of **4**, and **5** were measured by Miss Yuko Chiba of the Faculty of Agriculture of this university. Low resolution mass spectra of compounds, **10**, **12**, and **14** (70 eV) were measured by the staff of Faculty of Pharmaceutical Sciences of this university. ^{13}C FT NMR spectra (25.1 MHz, solvent $CDCl_3$: TMS as internal reference) were determined by JEOL Ltd., Tokyo.

Irradiation of N-*Acetyljervine Hypoiodite in the Presence of Mercury(II) Oxide and Iodine.* *N*-Acetyljervine (**1**) (806 mg), mercury(II) oxide (763 mg), and iodine (1.346 g) in benzene (60 ml) in Pyrex vessel were irradiated for 12 h with a 100-W high pressure mercury arc under a nitrogen atmosphere. After the solution was filtered, the filtrate was evaporated to give a residue which was dissolved in chloroform. The chloroform solution was washed with 5% sodium thiosulfate solution and water (twice), and dried over anhydrous sodium sulfate. After the usual work-up, the residue was subjected to preparative TLC (SiO_2) with a chloroform–diethyl ether (10 : 1). Five products: **8**, **9**, **6**, **7**, and **4**, in order of their increasing mobility in TLC, were obtained. The product **8**, which was

the most mobile on the TLC plate, was recrystallized from ethanol to yield crystals (52 mg), mp 159—160.5 °C. The Beilstein test was positive. Found: C, 56.77; H, 6.64; N, 2.37%. Calcd for $C_{29}H_{40}NO_5I$: C, 57.12; H, 6.62; N, 2.30%. IR, 1719 and 1672 (α,β-unsaturated carbonyl), 1751 (formate carbonyl), 1627 (*N*-acetyl), 1176 (formate C=O), 895, and 840 cm^{-1}; NMR, τ 1.91 (1H, s, formate), 4.06 (1H, d, J=4.5 Hz, 6-H), 5.40 (2H, s, $W_{1/2}$=5 Hz, CH_2–OCHO), 7.75 (3H, s, 18-H), 7.90 (3H, s, N-Ac), 9.95 (3H, d, J=6, 21-H), 8.99 (3H, s, 19-H), and 9.13 (3H, d, J=7.5 Hz, 26-H); MS, *m/e* (rel intensity), 435 (1.9), 156 (100), and 114 (27.7).

Product **7** was recrystallized from acetone to yield crystals (21 mg), mp 218—220 °C. The Beilstein test gave a postive result. Found: C, 57.30; H, 6.69; N, 2.68%. Calcd for $C_{29}H_{40}NO_5I$: C, 57.12; H, 6.62; N, 2.30%. IR, 1710 and 1655 (α,β-unsaturated carbonyl), 1628 (*N*-acetyl), 1112 (C–O), 928, 910, and 890 cm^{-1}; NMR, τ 4.48 (1H, broad s, $W_{1/2}$= 3.9 Hz, 3-H), 5.55 (1H, dd, J=4.5 and 12.3 Hz, 6β-H), 5.84 and 6.25 (each 1H, AB quartet, J=7.6 Hz), 7.77 (3H, s, 18-H), 7.91 (3H, s, N-Ac), 8.96 (3H, d, J=6.3 Hz, 21-H), 9.08 (3H, s, 19-H), and 9.13 (3H, d, 26-H); MS, *m/e* (rel intensity), 609 (M^+ 0.4), 482 (M^+-I, 0.7), 167 (100), 152 (8.7), 74 (14.7), 59 (26.9), 45 (17.4), and 43 (8.4).

Product **6** was recrystallized from diethyl ether to yield crystals (8 mg), mp 165—167 °C. Found: C, 73.82; H, 8.73; N, 2.98%; M^+*m/e* 453.2842. Calcd for $C_{28}H_{39}NO_4$: C, 74.17; H, 8.67; N, 3.10%; M^+453.2877. IR, 1712 and 1671 (α,β-unsaturated carbonyl), 1624 (*N*-acetyl), 1262, 1100, and 904 cm^{-1}; NMR, τ 4.57 (1H, d, J=3.0 Hz, 6-H), 5.81—7.20 (9H, m, 2-H, 4-H, 9α-H, 22β-H, 23α-H, and 27-H), 7.77 (3H, s, 18-H), 7.92 (3H, s, N-Ac), 8.89 (3H, s, 19-H), 8.97 (3H, d, J=6.6 Hz, 21-H), and 9.14 (3H, d, J=7.5 Hz, 26-H); MS, *m/e* (rel intensity),453 (M^+, 0.5), 167 (100), and 152 (15.4).

Product **7** was recrystallized from diethyl ether to yield crystals (8 mg) mp 258—260 °C. Found: 481.2800. Calcd for $C_{29}H_{39}NO_5$: M, 481.2826. IR 1737 (7-membered lactone), 1712, and 1633, shoulder (α,β-unsaturated carbonyl), 1624 (*N*-acetyl), 1277, and 1028 cm^{-1}; NMR, τ 4.21 (1H, d, J= 3.0 Hz, 6-H), 5.36 and 5.84 (each 1H, AB quartet, J=13.5 Hz, 4a-H), 7.78 (3H, s, 18-H), 7.94 (3H, s, N-Ac), 8.94 (3H, s, 19-H), 8.97 (3H, d, J=6.6 Hz, 21-H), and 9.15 (3H, d, J= 6.9 Hz, 26-H); MS, *m/e* (rel intensity), 481 (M^+, 0.6), 167 (100), and 152 (14.7%).

Product **4** was recrystallized from acetone to yield crystals (201 mg), mp 216—218 °C. Found: C, 74.32; H, 8.80; N, 2.82. Calcd for $C_{58}H_{80}N_2O_8$: C, 74.64; H, 8.64; N, 3.00%. FD MS, (rel intensity), *m/e* 933 (M^++1, 100), 932 (43.4), 931 (26.9), 918 (M^+-CH_3, 21.0), and 777 (17.2); MS, (rel intensity), 467 (0.5), 466 (0.4), 465 (0.7), 330 (4.9), 167 (100), and 151 (10.6); IR, 1713 and 1633 (α,β-unsaturated carbonyl), 1659 (*N*-acetyl), 1094, 1074, 1032, and 762 cm^{-1}; NMR, τ 4.45 (1H, broad, s, 6-H of *N*-acetyl-11-oxojerva-5,12(13)-dien-3β-yl portion), 4.69 (1H, broad, s, 6-H of *A*-homo-4-oxa-11-oxojerva-5,12(13)-dien-3α-yl portion), 5.12 (1H, t, J=5.3 Hz, 3β-H of *A*-homo-4-oxa portion), 5.68 and 6.48 (each 1H, AB quartet, J=13.5 Hz, 4a-H of *A*-homo-4-oxa-11-oxojerva-5,12(13)-dien-3α-yl portion), 7.75 (6H, s, 18- and 18′-H), 7.92 (6H, s, *N*-acetyl and *N*′-acetyl), 8.97 (6H, d, J=6.6 Hz, 21-H and 21′-H), 9.00 (6-H, s, 19-H and 19′-H) and 9.14 (6H, d, J=7.5 Hz, 26-H and 26′-H).

Hydrolysis of N-*Acetyl-11-oxojerva-5,12(13)-dien-3β-yl* A-*Homo-4-oxa-11-oxojerva-5,12(13)-dien-3α-yl Ether with Aqueous Methanolic Hydrochloric Acid.* A suspension of the dimer (100 mg) in methanol (30 ml) containing concd hydrochloric acid (1 ml) was stirred at room temperature. The crystals gradually dissolved over a period of 1 h. The solution was stirred at room temperature for four more hours. After the addition of water, methanol was removed at room temperature and solution was extracted with chloroform. The chloroform solution was washed with aq sodium carbonate solution, washed with water, and dried over anhydrous sodium sulfate. The usual work-up of the solution left a residue which showed two spots on a TLC plate (SiO_2) (a 8:1 mixture of chloroform–acetone). The product was subjected to preparative TLC to give two products. The more TLC mobile product (39 mg) was recrystallized from acetone to yield a compound which was identical with *N*-acetyljervine. The less TLC mobile amorphous product (45 mg) could not be induced to crystallise. IR, 3380 (OH), 1706, and 1620, broad, (α,β-unsaturated carbonyl and *N*-acetyl), 1100, 1056, and 1025 cm^{-1}; NMR, τ 4.41 (1H, d, J=3.9 Hz), 4.86 (1H, t, J=6 Hz), 5.59 and 6.41 (each 1H, AB quartet, J=13.3 Hz, 4a-H), 7.76 (3H, s, 18-H), 7.91 (3H, s, N-Ac), 8.96 (3H, d, J=6.6 Hz, 21-H), 9.01 (3H, s, 19-H), and 9.14 (3H, d, J=7.2 Hz, 26-H); MS, *m/e* 483 (M^+).

Oxidation of N-*Acetyljervine with Jones Reagent.* To *N*-acetyljervine (652 mg) in acetone (40 ml) there was added Jones reagent dropwise until the solution turned brown. The solution was stirred for a few min. On addition of water (250 ml), crude 3-ketone crystallized out from the solution. The crystals were collected by filtration, washed with water and recrystallized from acetone to yield 255 mg of pure 3-ketone **3**, mp 172.5—174.5 °C. Found: *m/e* 465.2860. Calcd for $C_{29}H_{39}NO_4$: M, 465.2877. IR, 1714, 1640 (shoulder) and 1627 cm^{-1}(six-membered ring ketone, and α,β-unsaturated carbonyl), 1244, 1148, and 1096 cm^{-1}; NMR, τ 4.63 (1H, broad, s, 6-H), 7.73 (3H, s, 18-H), 7.91 (3H, s, NAc), 8.93 (3H, s, 19-H), 8.93 (3H, d, J=6.6 Hz, 21-H), and 9.12 (3H, d, J=7.2 Hz, 26-H); MS, *m/e* (rel intensity), 465 (M^+, 0.7), 167 (100), 152 (15.5), and 43 (14.4).

*Preparation of 3α-Deuterio-*N-*acetyljervine (2).* The 3-ketone (202 mg) in ethanol (40 ml) containing sodium borodeuteride (148 mg) was stirred for 50 min. After the addition of water, the solvent was evaporated and the residue was dissolved in chloroform. The chloroform solution was washed with water and dried over anhydrous sodium sulfate. The usual work-up of the solution gave a product which was recrystallized from acetone–diethyl ether to yield 3β-ol, **2**, mp 224.5—226.5 °C. Found: *m/e* 468.3086. Calcd for $C_{29}H_{40}DNO_4$: M, 468.3097. IR, 3407 (OH), 1712 and 1649 (α,β-unsaturated carbonyl), 1628 (NAc), and 960 cm^{-1}; NMR, τ 4.64 (1H, d, J=4.5 Hz, 6-H), 7.76 (3H, s, 18-H), 8.91 (3H, s, N-Ac), 8.96 (3H, d, J=6.6 Hz, 21-H), 9.00 (3H, s, 19-H), and 9.13 (3H, d, J=7.5 Hz); MS, *m/e* (rel intensity) 468 (M^+, 0.6), 167 (100), and 152 (8.7).

*The Irradiation of 3α-Deuterio-*N-*acetyljervine Hypoiodite in the Presence of Mercury(II) Oxide and Iodine.* 3α-Deuterio-*N*-acetyljervine (147 mg), mercury(II) oxide (157 mg), and iodine (243 mg) in benzene (30 ml) in a Pyrex vessel were irradiated for 26.5 h as in the case of *N*-acetyljervine. The usual work-up of the reaction product gave a product which was subjected to preparative TLC (SiO_2) with a 7 : 1 mixture of chloroform and acetone. The crude product (58 mg) was recrystallized from diethyl ether to yield a pure dimer incorporating deuterium. It had a mp of 220—222 °C. FD-MS, *m/e* (rel intensity), 936 (M^++D, 78.2), 935 [$(M+H)^+$, 100], 934 (M^+, 91.1), 878 (20.8), and 769 (16.5): IR, 1713 and 1633 (α,β-unsaturated carbonyl), 1659 (*N*-acetyl), 1104, 1065, and 1039 cm^{-1}; the NMR spectrum was identical with that of the corresponding dimer from *N*-acetyljervine, with the exception of the absence of a 1H triplet at τ 5.12.

*The Irradiation of 3β-Hydroxy-17α-ethyletiojerv-5-ene-11,20-dione (**11**) in Benzene Containing Mercury(II) Oxide and Iodine.* 3β-Hydroxy-17α-ethyletiojerv-5-ene-11,20-dione (**11**) (300 mg) in benzene (51 ml) containing mercury(II) oxide (581 mg) and iodine (695 mg) was irradiated for 5 h at room temperature under an argon atmosphere while stirring. The reaction mixture was worked up as usual. The product was a complex mixture and showed a pattern of spots on TLC similar to a mixture from *N*-acetyljervine. The product was subjected to preparative TLC (chloroform–acetone, 20 : 1) to give six fractions (A–F in the order of decreasing mobility). The most mobile product A (100 mg) was an amorphous formate **12**. IR ($CDCl_3$), 1724 (broad, formyl carbonyl, 11-carbonyl and 20-carbonyl) and 1162 cm^{-1} (formyl C–O); NMR, τ1.89 (1H, s, OCHO), 4.03 (1H, d, J=5.4 Hz, 6-H), 5.39 (2H, broad s, $W_{1/2}$=3.6 Hz, C-3 methylene), 6.93 (2H, m, C-2 methylene), 7.84 (3H, s, 17α-acetyl), 8.82 (3H, d, J=6.0 Hz, 18-H), and 8.94 (3H, s, 19-H). MS, *m/e* 469 (M^+). The fractions B (44 mg) and C (14 mg) were a mixture. The fraction D (57 mg) was crystals; they were identified to be a dimeric acetal **13**. After recrystallization from acetone it had a mp of 250—253 °C. Found: *m/e* 658.4229. Calcd for $C_{42}H_{58}O_6$: M, 658.4232. IR, 1727 (11-carbonyl), 1703 (20-carbonyl), and 1034 cm^{-1} (C–O); NMR, 4.39 (1H, d, J= 4.5,6- H of *A*-homo-17α-ethyletiojerv-5-ene-11,20-dion-3α-yl portion) 4.65 (1H, d, J=4.5, 6-H of 17α-ethyletiojerv-5-ene-11,20-dion-3β-yl portion, 5.14 (1H, t, J=6 Hz, 3β-H of *A*-homo-17α-ethyletiojerv-5-ene-11,20-dion-3α-yl portion), 5.75 and 6.50 (each 1H, d, J=12.8 Hz, 4a-methylene of *A*-homo-17α-ethyletiojerv-5-ene-11,20-dion-3α-yl portion), 7.85 (6H, s, two acetyls), 8.79 (3H, d, J=6.0 Hz, 18-H), 8.83 (3H, d, J=6.0 Hz, 18′-H), and 8.97 (6H, s, superimposed 19-H). MS (rel intensity), *m/e* 658 (M^+, 0.4), 347 (1.6), 346 (1.5), 329 (100), 312 (46.8), 311 (29.2), and 269 (31.2).

The fraction E (20 mg) was *A*-homo-4-oxa-17α-ethyletiojerv-5-ene-3,11,20-trione (**14**). IR ($CHCl_3$) 3440 (hydroxy), 1735 (11-carbonyl and lactone), and 1705 (20-carbonyl); NMR, τ 4.6 (1H, d, J=4.5 Hz, 6-H), 5.27 and 5.72 (each 1H, d, J= 13.5 Hz, 4a-H), 7.83 (3H, s, 21-H), 8.81 (3H, d, J=6.0 Hz, 18-H), and 8.87 (3H, s, 19-H). MS, *m/e* 342 (M^+).

The authors are grateful to Mrs. Satoko Araki and Mrs. Tomoko Okayama for the measurements of the ^1H NMR spectra and the spin decoupling experiments.

References

1) Photoinduced Transformations. Part 58: Preliminary Communications, H. Suginome, K. Kato, and T. Masamune, *Tetrahedron Lett.*, **1965**, 1161, 1165; Part 57: H. Suginome, S. Isayama, N. Maeda, A. Furusaki, and C. Katayama, *J. Chem. Soc., Perkin Trans. 1*, in press.

2) C. Meystre, K. Heusler, J. Kalvoda, P. Wieland, G. Anner, and A. Wettstein, *Helv. Chim. Acta*, **45**, 1317 (1962), and later papers.

3) For reviews of "the hypoiodite reaction" see K. Heusler and J. Kalvoda, *Angew. Chem.*, **76**, 518 (1964); J. Kalvoda and K. Heusler, *Synthesis*, **1971**, 501.

4) M. Akhtar and D. H. R. Barton, *J. Am. Chem. Soc.*, **86**, 1528 (1964). For mercury(II) oxide–iodine reagent, see also: A Goosen and H. A. H. Laue, *J. Chem. Soc., C*, **1969**, 383; *J. Chem. Soc., B*, **1969**, 995; C. P. Forbes, A. Goosen, and H. A. H. Laue, *J. Chem. Soc., Perkin Trans. 1*, **1974**, 2346.

5) H. Suginome, A. Furusaki, K. Kato, N. Maeda, and F. Yonebayashi, *J. Chem. Soc., Perkin Trans. 1*, **1981**, 236.

6) H. Suginome and N. Maeda, *Bull. Chem. Soc. Jpn.*, **53**, 2621 (1980).

7) H. Suginome and N. Maeda, *Bull. Chem. Soc. Jpn.*, **53**, 2626 (1980).

8) K. Saito, H. Suginome, and M. Takaoka, *Bull. Chem. Soc. Jpn.*, **11**, 172 (1936).

9) This compound was prepared from jervine *via* 8 steps. The details of the preparation will be published elsewhere. H. Suginome, H. Ono, and T. Masamune, unpublished results.

10) These compounds were erroneously formulated in our preliminary communications.[1] We now wish to retract the previous structures.

11) H. Budzikiewicz, C. Djerassi, and D. H. Williams, "Structure Elucidation of Natural Products by Mass Spectrometry," Holden-Day, Inc., San Francisco (1964), p. 21.

Studies of Reactions of Amines with Sulfur Trioxide. VI.[1] Thermal Reactions of Anilinium, Dimethylanilinium, and Trimethylanilinium Salts of Butylamidosulfuric Acid

Fujio KANETANI* and Hachiro YAMAGUCHI

Department of Applied Chemistry, Hiroshima University, Senda-machi, Naka-ku, Hiroshima 730

(Received March 20, 1981)

When the title compounds were heated in an evacuated reaction vessel, both transsulfonation and rearrangement occurred. At lower temperatures (80—120 °C) the corresponding phenylamidosulfates and sulfophenylamidosulfates (*transsulfonation products*) were the main products. Increasing temperature led to the formation of ring mono- and disulfonates (*rearrangement products*) at the expense of the transsulfonation products. The sulfonate group always migrated to the *ortho* and/or *para* position(s) to the amino group. In no case was any *meta*-product detected. There was no significant difference in the ease of transsulfonation among the anilinium salts studied except 2,6-dimethyl- and 2,4,6-trimethylanilinium salts. On the other hand, the ease of rearrangement and the orientation of ring sulfonation depended strongly on the structure of the substrate anilines. The thermal reactions of 2,4,6-trimethylanilinium butylamidosulfate produced (2,4,6-trimethylphenylimido)bis(sulfate) in addition to (2,4,6-trimethylphenylamido)sulfate. This is the first isolation of an arylimidobis(sulfate) from such reactions. Mechanisms of the transsulfonation and the rearrangement have been discussed.

Considerable attention has been paid to the chemistry of amidosulfuric acid and its *N*-substituted derivatives in recent years.[2] In particular, rearrangement of arylamidosulfuric acids ($ArNHSO_3H$) to the corresponding ring-sulfonated anilines is of great interest from both mechanistic and preparative viewpoints, because arylamidosulfuric acids have been postulated as intermediates in the sulfonation of aromatic amines with sulfuric acid[3] as well as in the "baking" process.[4-6]

Accordingly we studied the thermal reactions of amine salts of *N*-substituted amidosulfuric acids ($RNHSO_3^-R'NH_3^+$; R=*n*-Bu or *p*-$CH_3C_6H_4$, R'=*n*-Bu or *p*-$CH_3C_6H_4$) and showed[1] that: (1) at lower temperatures (80—120 °C) (4-methylphenylamido)sulfate and 4-methylaniline-*N*,2-disulfonate (transsulfonation products) are the main products; (2) at higher temperatures (120—180 °C) 4-methylaniline-2-sulfonate and 4-methylaniline-2,6-disulfonate (rearrangement products) predominate; and (3) the ease of both transsulfonation and rearrangement[7] depends on the basicity of both the parent amine (RNH_2) and the salt-forming amine ($R'NH_2$). On the basis of these results we proposed a tentative mechanism involving a preequilibrium thermal dissociation into the free acid ($RNHSO_3H$) and the salt-forming amine ($R'NH_2$) followed by a rate-determining nucleophilic attack by $R'NH_2$ on the tetracoordinate sulfur atom of the zwitterionic amidosulfuric acid ($RNH_2^+SO_3^-$) (Scheme 1).

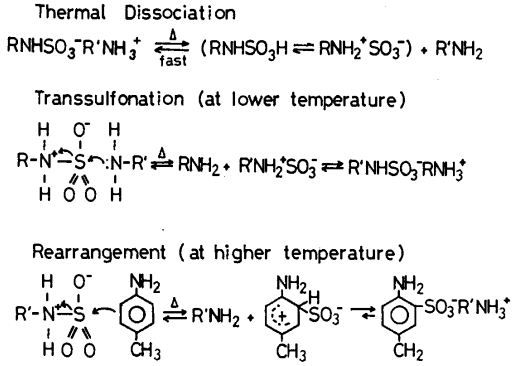

Scheme 1.

In order to obtain a better picture of the mechanism of thermal reaction, we studied the substituent effects both on the ease of transsulfonation and rearrangement and on the orientation of ring sulfonation in a series of methyl-substituted anilinium salts of butylamidosulfuric acid (*n*-$BuNHSO_3^-ArNH_3^+$).

Results and Discussion

Anilinium Butylamidosulfate (1). The thermal reaction of **1** at 100 °C for 8 h produced phenylamidosulfate (**2**) in an 85% yield. Aniline-*N*,4-disulfonate (**3**)[8] was also formed at the temperatures ranging 100—140 °C (Fig. 1). The structure of this new compound, **3**,[9] was unequivocally established by acid hydrolysis; namely, a sulfo-amidosulfate fraction from the reaction of **1** at 115 °C for 8 h gave aniline-4-sulfonic acid on acid hydrolysis. No isomeric aniline-*N*,2-disulfonate (which should give aniline-2-sulfonic

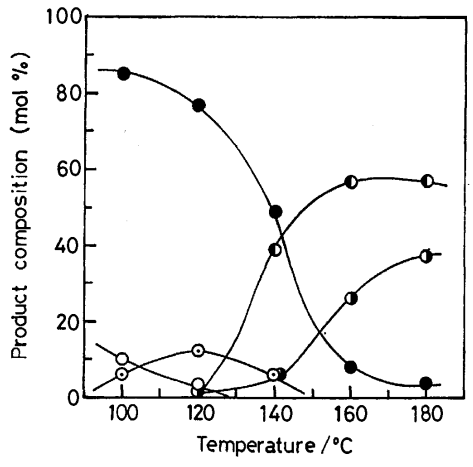

Fig. 1. Thermal reaction of anilinium butylamidosulfate. Reaction time 8 h.
○: *n*-$C_4H_9NHSO_3^-$, ●: $C_6H_5NHSO_3^-$, ◐: $NH_2C_6H_4SO_3^-$, ⊙: $C_6H_4(NHSO_3^-)(SO_3^-)$, ◑: $NH_2C_6H_3(SO_3^-)_2$.

acid on the hydrolysis) was detected on TLC.

The thermal reaction of **1** at 160 °C for 8 h gave a mixture of aniline-2- (**4**) and 4-sulfonate (**5**) (57%)[10] and aniline-2,4-disulfonate (+2,6-disulfonate) (26%);[11] neither **2** nor **3** was detected in the product.

In no run was any evidence obtained for the formation of aniline-3-sulfonic acid (*meta*-compound).

2,3-Dimethylanilinium Butylamidosulfate (6). Thermal reaction of **6** (120 °C, 8 h) gave (2,3-dimethylphenylamido)sulfate (**7**) in an 85% yield (Table 1). The amount of *N*,ring-disulfonate(s) (**8**) was negligibly small. The reaction at 140 °C for 8 h gave a mixture of **7** (13%), **8** (11%), 2,3-dimethylaniline-4-sulfonate (**9**) (27%), 2,3-dimethylaniline-6-sulfonate (**10**) (12%), and 2,3-dimethylaniline-4,6-disulfonate (**11**) (33%).[12]

Reaction of **6** at 160 °C for 8 h produced a mixture of **9** (5%), **10** (32%), and **11** (56%). The structure of **9** was established by direct comparison of its IR spectrum, R_f value (TLC), and melting point with those of an authentic sample prepared umambiguously (see Experimental section).

It is interesting to note here that increasing reaction temperature tends to increase the ratio of **10** : **9** (0.52 : 1 at 140 °C and 1.82 : 1 at 160 °C, respectively[13]).

2,4-Dimethylanilinium Butylamidosulfate (12). The reaction of **12** at 120 °C for 8 h gave (2,4-dimethylphenylamido)sulfate (**13**) in a 93% yield. 2,4-Dimethylaniline-6-sulfonate (**14**)[14] and 2,4-dimethylaniline-*N*,6-disulfonate (**15**) were also formed in small amounts. On the other hand, the thermal reaction of **12** at 160 °C for 8 h gave **14** in a 74% yield, together with **13** and **15**.

2,5-Dimethylanilinium Butylamidosulfate (16). The reaction of **16** at 100 °C for 8 h gave (2,5-dimethylphenylamido)sulfate (**17**) in a 91% yield. In contrast, the reaction at 120 °C for 8 h produced 2,5-dimethylaniline-4-sulfonate (**18**) (43.5%), and 2,5-dimethylaniline-*N*,4-disulfonate (**19**) (16%), together with **17** (32%). The reaction of **16** at 160 °C for 8 h yielded **18** predominantly; isomeric 2,5-dimethylaniline-6-sulfonate was formed in a small quantity (TLC). It should be noted that most of **19** remained unchanged and no trace of 2,5-dimethylaniline-4,6-disulfonate (**20**) was detected even at 160 °C. This fact indicates that the introduction of a sulfonate group into the 6 position of **18** is highly sterically hindered. This position is flanked by an amino and a methyl groups. Moreover, a buttressing effect of both 2-methyl and 4-sulfonate groups is operative (see also under the headings "3,5-dimethylanilinium butylamidosulfate" and "2,4,5-trimethylanilinium butylamidosulfate").

2,6-Dimethylanilinium Butylamidosulfate (21). In marked contrast with any other anilinium salt studied, **21** was thermally very unstable and showed a great tendency to dissociate into 2,6-dimethylaniline and butylamidosulfuric acid (even at room temperature).[15] Evidently this tendency is ascribable to B strain arising from the salt formation.[16]

It is to be expected that transsulfonation of **21** occurs much more readily than that of the other anilinium salts studied, because the transsulfonation of $RNHSO_3^-R'NH_3^+$ is believed to involve a preequilibrium thermal dissociation into the reacting species ($RNH_2^+SO_3^-$) and the substrate amine ($R'NH_2$) followed by a rate-determining transfer of a sulfonate group from $RNH_2^+SO_3^-$ to $R'NH_2$.[1] In fact, heating at 110 °C for as short as 30 min brought about *ca.* 90% transsulfonation.[17] The reaction for 2 h at the same temperature gave a mixture of (2,6-dimethylphenylamido)sulfate (**22**) (66%), 2,6-dimethylaniline-*N*,4-disulfonate (**23**) (21%), 2,6-dimethylaniline-4-sulfonate (**24**) (7%), and as little as 6% of the starting salt **21**. Heating at 110 °C for 8 h gave **24** in a 44% yield, in addition to **22** (38%) and **23** (15%).

When **21** was heated at 160 °C for 8 h, **24** was produced in a 90% yield. **22** disappeared almost completely (only a trace on TLC). No *meta*-isomer, 2,6-dimethylaniline-3-sulfonate, was detected.

Nitration of 2,6-dimethylaniline (**25**) and its *N*-acetyl derivative (**26**) with nitric acid or with mixed acid is known to occur exclusively at the *meta* position.[18] This anomalous behavior has been attributed to the steric inhibition of resonance.[19] The situation, however, is more complex, because bromination of **25** both in hydrobromic acid and in glacial acetic acid and chlorination of **25** in glacial acetic acid have been reported to give the 4-substituted compounds.[20] Bromination of **26** in hydrobromic acid leads to the formation of the 3-bromo derivative, whereas the bromination in glacial acetic acid gives a mixture of the 3- and the 4-isomers.[20]

These facts led us to examine the orientation of sulfonation of **25**. Our experiments showed that the "baking" of 2,6-dimethylanilinium hydrogensulfate in *o*-dichlorobenzene[21] yields **24** as the sole product, while the sulfonation with 25% oleum gave the *meta*-isomer (**27**) as the main product and, in addition, minor amounts of **24** and (a) disulfonic acid(s). **27** was also produced by reaction of **26** with $ClSO_3H$[22] and subsequent hydrolysis of the acetyl group.

The structure of **24** was established both by direct comparison with an authentic material prepared from 2-nitro-4,6-dimethylaniline and by chemical conversion of **24** to 3,5-dimethylbenzenesulfonic acid (see Experimental section).

Unlike the other *N*,ring-disulfonates, **23** failed to give the bis(tetraphenylphosphonium) salt; therefore, **23** was isolated and characterized as the dipotassium salt (Table 5). Its structure was proved by acid hydrolysis to **24**.

3,4-Dimethylanilinium Butylamidosulfate (28). Thermal reaction of **28** at 120 °C for 8 h gave (3,4-dimethylphenylamido)sulfate (**29**) in an 85% yield. Additionally, 3,4-dimethylaniline-*N*,6-disulfonate (**30**) (18%) was formed. No 3,4-dimethylaniline-6-sulfonate (**31**) was detected (TLC).

On the other hand, the reaction at 160 °C for 8 h produced **31** in a high yield. **29** and **30** were also formed in small amounts. No isomeric 3,4-dimethylaniline-2-sulfonate was found in the product.

3,5-Dimethylanilinium Butylamidosulfate (32). When heated at 110 °C for 8 h, anilinium salt **32** readily underwent transsulfonation to give (3,5-dimethylphenylamido)sulfate (**33**) in a 77% yield, but the subsequent rearrangement of **33** to 3,5-dimethylaniline-2-sulfonate (**34**) proceeded with difficulty and incom-

TABLE 1. THERMAL REACTIONS OF ANILINIUM SALTS OF BUTYLAMIDOSULFURIC ACID, n-$BuNHSO_3^-$-$ArNH_3^+$ [a)]

Ar	Temperature °C	Product composition (mol %)				
		n-$BuNHSO_3^-$	$ArNHSO_3^-$	$Ar(NHSO_3^-)$-(SO_3^-)	$Ar(NH_2)$-(SO_3^-)	$Ar(NH_2)$-$(SO_3^-)_2$
2,3-Dimethylphenyl	120	7.9	84.7	2.2	3.7	1.5
	160	0	1.1	trace	96.8[g)]	
2,4-Dimethylphenyl	120	2.9	92.7	2.2	2.2	0
	160	2.6	14.8	4.0	74.1	0
2,5-Dimethylphenyl	100	4.7	90.8	4.5	trace	0
	120	4.6	31.9	16.0	43.5	0
	160	1.2	trace	15.0	83.8	0
2,6-Dimethylphenyl	110[c)]	5.7	66.2	21.4	6.8	0
	110	3.1	37.8	14.8	44.3	0
	120	6.2	5.4	26.5	61.8	0
	160	1.9	trace	7.9	90.2	0
3,4-Dimethylphenyl	120	5.3	84.7	10.0	0	0
	160	1.7	3.0	7.9	87.3	0
2,4,5-Trimethylphenyl	130[b)]	0	98.3	1.7	0	0
	160	10.5	80.2	1.6	7.8	0
2,4,6-Trimethylphenyl	120[c)]	9.3	90.2	0.4[f)]	0	0
	120	2.6	74.3	23.1[f)]	0	0
	120[d)]	0	93.7	0	0	0
	160	5.2	70.3	19.4[f)]	0	0
	e)	9.5	69.7	6.1[f)]	0	0

a) Reaction time: 8 h. b) Reaction time: 4 h. c) Reaction time: 2 h. d) 2,4,6-Trimethylaniline was used as a reaction medium. e) The reaction was carried out in boiling 1,3,5-trimethylbenzene. f) (2,4,6-Trimethylphenylimido)bis(sulfate). g) A combined analytical yield of 2,3-dimethylaniline-4- and 6-sulfonate and 4,6-disulfonate.

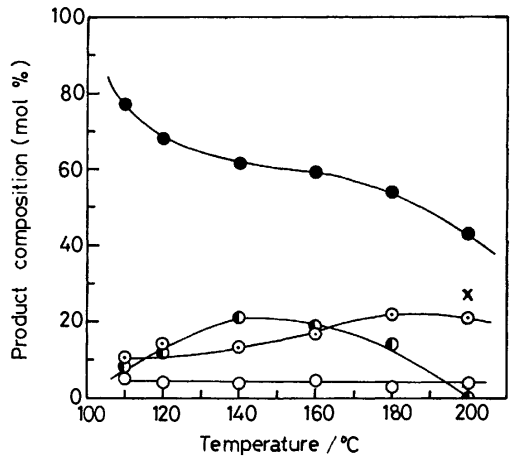

Fig. 2. Thermal reaction of 3,5-dimethylanilinium butylamidosulfate. Reaction time 8 h.
○: n-$C_4H_9NHSO_3^-$, ●: $Me_2C_6H_3NHSO_3^-$, ◐: $Me_2C_6H_2NH_2(SO_3^-)$, ⊙: $Me_2C_6H_2(NHSO_3^-)(SO_3^-)$ × : SO_4^{2-}.

pletely (see Fig. 2). Even after heating of **32** at 180 °C for 8 h, **33** was the main product (54%); 3,5-dimethylaniline-2-sulfonate (**34**) (14%), 3,5-dimethylaniline-*N*,2-disulfonate (**35**) (22%), and 3,5-dimethylaniline-2,6-(?)-disulfonate (a trace amount) were the minor products. The reaction at 200 °C gave rise to considerable decomposition.

It is particularly noteworthy that the sulfonation occurred almost exclusively at the *ortho* position, the *para*-isomer, 3,5-dimethylaniline-4-sulfonate (**36**) being formed in trace amounts.[23)]

These results show that the transfer of the sulfonate group to the aromatic ring is very subject to steric hindrance. Such preferential or exclusive sulfonation at a less hindered *ortho*- or *para*-position (as observed with **16**, **28**, **32**, and **37**) may be explained in terms of the steric requirements of the attacking species.[24)]

To determine the position of the sulfonate group in **34** we carried out the deamination of **34**; thus, diazotization followed by reduction with $NaBH_4$ in methanol gave *m*-xylene-4-sulfonic acid. The structure of **34** was proved additionally by direct comparison with a sample prepared *via* an unambiguous route outlined below:

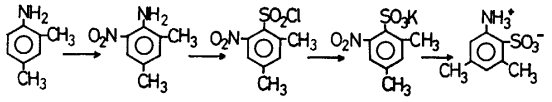

The structure of **35** was confirmed by acid hydrolysis to **34**.

A fourth component was isolated chromatographically in only a trace. This substance, which had the smallest R_f value on TLC, seemed to be 3,5-dimethylaniline-*N*,4-disulfonate, because this compound underwent hydrolysis on heating with dil HCl to give a spot corresponding to **36**.

2,4,5-Trimethylanilinium Butylamidosulfate (37). This salt, when heated at 130 °C for 4 h, yielded (2,4,5-trimethylphenylamido)sulfate (**38**) in an almost quantitative yield. 2,4,5-Trimethylaniline has one available position *ortho* to the amino group. This position, however, is highly sterically hindered by 1-amino and 5-methyl substituents. In addition there seems to be a "buttressing" effect of 2- and 4-methyl substituents.

In accord with this view, **38** rearranged to 2,4,5-trimethylaniline-6-sulfonate (**39**) with muth difficulty; thus, the thermal reaction of **37** at 160 °C for 8 h gave a mixture of the starting salt **37** (10.5%), **38** (80%), and **39** (9.4%).[25)] There was no evidence of the formation of either (2,4,5-trimethylphenylimido)bis(sulfate) or 2,4,5-trimethylaniline-*N*,6-disulfonate.

2,4,6-Trimethylanilinium Butylamidosulfate (40). This salt had some tendency to dissociate to 2,4,6-trimethylaniline (**41**) and butylamidosulfuric acid (**42**) at room temperature; consequently, **40** readily underwent transsulfonation to give (2,4,6-trimethylphenylamido)sulfate (**43**). Since **41** has no reactive site in the ring, any ring-sulfonated product cannot be formed. Deficiency of substrate amine **41** in the reaction mixture (caused by condensation of **41** on the cool wall of the reaction vessel) led to the formation of a new compound, (2,4,6-trimethylphenylimido)bis(sulfate) (**44**) in yields of 19—23% (Table 1). This is the first example of isolation of an arylimidobis(sulfate) from such reactions. **44** could also be obtained in an almost quantitative yield by fusion of an equimolar mixture of butylammonium (2,4,6-trimethylphenylamido)sulfate **43** and **42** (Scheme 2).[26]

$$n\text{-BuNHSO}_3^-\ 2,4,6\text{-Me}_3\text{C}_6\text{H}_2\text{NH}_3^+ \rightleftharpoons$$
40

$$(n\text{-BuNHSO}_3\text{H} \rightleftharpoons n\text{-BuNH}_2^+\text{SO}_3^-)$$
42

$$+\ 2,4,6\text{-Me}_3\text{C}_6\text{H}_2\text{NH}_2$$
41

$$\mathbf{41} + \mathbf{42} \rightleftharpoons 2,4,6\text{-Me}_3\text{C}_6\text{H}_2\text{NHSO}_3^-n\text{-BuNH}_3^+$$
43

$$\mathbf{42} + \mathbf{43} \rightleftharpoons 2,4,6\text{-Me}_3\text{C}_6\text{H}_2\text{N}(\text{SO}_3^-n\text{-BuNH}_3^+)_2$$
44

Scheme 2.

When the thermal reaction of **40** was carried out in **41** or 1,3,5-trimethylbenzene as reaction medium, the formation of **44** was suppressed.

Mechanistic Considerations. The thermal reactions of amine salts of amidosulfuric acids ($\text{RNHSO}_3^-\text{R'NH}_3^+$) are characterized by the initial thermal dissociation into the free acid (RNHSO_3H) and the salt-forming base (R'NH_2).[27] The degree of dissociation, of course, depends greatly on the basicity of R'NH_2; a decrease in the basicity of R'NH_2 favors the dissociation (Scheme 1).

Transsulfonation. There was no significant difference in the rate of transsulfonation among the anilinium salts examined except 2,6-dimethylanilinium and 2,4,6-trimethylanilinium butylamidosulfates. Evidently, in these two cases relief of B strain favors the dissociation.

It has been proved that free amidosulfuric acids exist as zwitterions ($\text{RNH}_2^+\text{SO}_3^-$) at least in the solid state;[2,28] the zwitterionic form is believed to be the reactive species.[1,2]

There are two possible mechanisms for the transfer of a sulfonate group from the zwitterionic amidosulfuric acid to the substrate amine. One involves rate-determining thermal cleavage of the N–S bond to give the parent amine and SO_3 (Eq. 1), followed by an electrophilic attack of SO_3 on the substrate (Eq. 2). The other involves a bimolecular nucleophilic substitution at the tetracoordinate sulfur atom (Eq. 3).

It should be noted that the transsulfonation occurs in the molten state (*viz.*, non-solvolytic conditions) at such low temperatures that the zwitterion, $n\text{-BuNH}_2^+\text{SO}_3^-$, is quite stable. As an example may be cited the fact that the transsulfonation of 2,6-dimethylanilinium butylamidosulfate (**21**) proceeds very rapidly at 110 °C (90% conversion of **21** occurred in 30 min at this temperature). The *gas-phase* reaction between sulfur trioxide and an amine such as trimethylamine is very exothermic.[29] These two facts suggest that, under "*non-solvolytic*" conditions, the dissociative process may be unlikely, whereas the latter process involving synchronous bond-forming and bond-breaking in the transition state is much more likely from the energetical point of view. It has been reported that *N*-substituted amidosulfate salts undergo acid-catalyzed hydrolysis mostly by an A-2 type mechanism (involving a bimolecular nucleophilic attack of water in the transition state) (Eq. 4).[2] It has also been suggested that the catalytic sulfation of 1-hexadecanol with amidosulfuric acid in the presence of DMF may involve the formation of a DMF–SO_3 complex by an S_N2 mechanism (Eq. 5).[30] Further, the rates of sulfation of eleven alcohols with $n\text{-Bu}_3\text{N}^+\text{–SO}_3^-$ have been measured and an S_N2-type mechanism has been proposed (Eq. 6).[31]

Unimolecular Transsulfonation. (S_N1-type dissociative mechanism)

$$n\text{-BuNH}_2^+\text{SO}_3^- \underset{\text{slow}}{\overset{\Delta}{\rightleftarrows}} n\text{-BuNH}_2 + \text{SO}_3 \quad (1)$$

$$\text{ArNH}_2 + \text{SO}_3 \underset{\text{fast}}{\rightleftharpoons} (\text{ArNH}_2^+\text{SO}_3^- \rightleftharpoons \text{ArNHSO}_3\text{H})$$

$$\xrightarrow[\text{fast}]{n\text{-BuNH}_2} \text{ArNHSO}_3^-n\text{-BuNH}_3^+ \quad (2)$$

Bimolecular Transsulfonation (S_N 2-type mechanism)

$$n\text{-BuNH}_2^+\text{SO}_3^- + \text{ArNH}_2 \rightleftharpoons$$

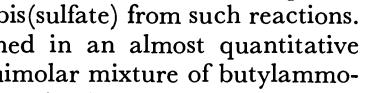

$$\rightleftharpoons$$

pentacoordinate transition state

$$n\text{-BuNH}_2 + \text{ArNH}_2^+\text{SO}_3^- \rightleftarrows \text{ArNHSO}_3^-n\text{-BuNH}_3^+ \quad (3)$$

$$\text{R}^1\text{R}^2\text{NSO}_3^- \overset{\text{H}^+}{\rightleftharpoons} \text{R}^1\text{R}^2\text{NH}^+\text{SO}_3^-$$

$$\xrightarrow[\text{slow}]{\text{H}_2\text{O}} \text{R}^1\text{R}^2\text{NH}_2^+\text{HSO}_4^- \quad (4)$$

$$\text{NH}_3^+\text{SO}_3^- + \text{DMF} \overset{\text{slow}}{\rightleftharpoons} \text{NH}_3 + \text{DMF}\cdot\text{SO}_3$$

$$\xrightarrow{\text{ROH}} \text{ROSO}_3^-\text{NH}_4^+ \quad (5)$$

$$n\text{-Bu}_3\text{N}^+\text{SO}_3^- + \text{RO}^- \xrightarrow{\text{slow}}$$

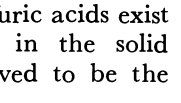

$$\longrightarrow \text{ROSO}_3^- + n\text{-Bu}_3\text{N} \quad (6)$$

Rearrangement. There are at least three possible mechanisms to be considered for the rearrangement.[32]

(a) Intramolecular Pathway: Any mechanism which does not involve the N–S bond cleavage before a ring-sulfonation, encounters geometrical difficulties; that is, direct transfer of the sulfonate group from the amino nitrogen to the *para*-position of the ring is improbable because of the large distance which would have to be

spanned in the transition state.[33]

In order to account for the intramolecularity of the nitramine rearrangement, Dewar has proposed a π-complex mechanism involving initial cleavage of the N-NO_2 bond, followed by a series of 1,2-shifts *via* π-complex intermediates.[34] The very ready rearrangement of butylammonium (2,6-dimethylphenylamido)-sulfate (**22**) to 2,6-dimethylaniline-4-sulfonate (**24**) could not be accounted for by this scheme, because the migration of the sulfonate group passing through the ring to the *para*-position should be highly sterically hindered (Fig. 3).

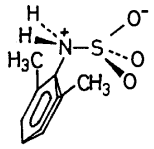

Fig. 3. (2,6-Dimethylphenylamido)sulfuric acid zwitterion.

Hughes and coworkers proposed the "cartwheel" mechanism in order to explain the intramolecular migration of the nitro group from the amino nitrogen to the *para*-position in the ring.[35] If a similar mechanism were to operate, the amidosulfuric acid rearrangement could be written as follows:

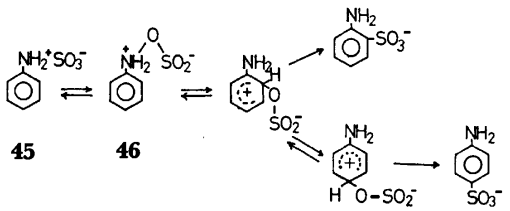

45 **46**

This mechanism seems unlikely from the following reasons. First, there is neither evidence nor analogy for such initial isomerization of **45** to *N*-phenylhydroxylamine-*O*-sulfite (sulfitoamine), **46**.[36] Secondly, **46**, a postulated intermediate in the reaction of *N*-phenylhydroxylamine with SO_2, has neither been isolated nor characterized.

It should be noted that the formation of disulfonated products does not eliminate the possibility of an intramolecular process, because a sulfonate group exchange between an arylamidosulfate and an aniline occurs very rapidly in the presence of the anilinium chloride (Eq. 7).[37]

$$ArNHSO_3^- + Ar'NH_2 \overset{H^+}{\rightleftharpoons} ArNH_2 + Ar'NHSO_3^- \quad (7)$$

(b) S_N2*-type Intermolecular Pathway*: A second possible mechanism is an S_N2-type intermolecular pathway involving a nucleophilic attack by a substrate amine at the tetracoordinate sulfur atom of the zwitterion (ligand-exchange) to form (a) σ-complex(es) leading to *ortho* and/or *para* sulfonates (Eq. 8).

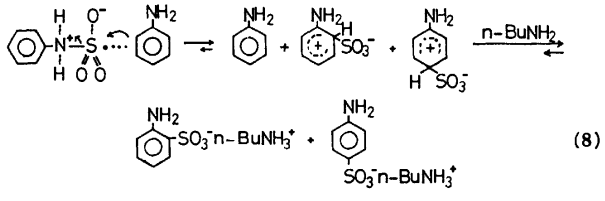

(8)

(c) S_N1*-type Intermolecular Pathways*: A third possible mechanism is an S_N1-type intermolecular process, which involves a unimolecular thermal cleavage of the zwitterion, $ArNH_2^+$–SO_3^-, to the substrate aromatic amine ($ArNH_2$) and SO_3 molecule. The latter species attacks at the *ortho*- and/or *para*-position(s) in the substrate (Eq. 9).

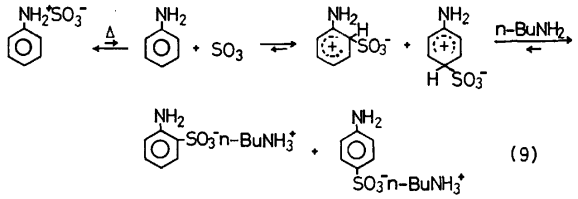

(9)

It is well known that, in marked contrast with amidosulfuric acid itself and its *N*-alkyl derivatives, arylamidosulfuric acids are very unstable and have a great tendency to undergo a hydrolytic and thermolytic N–S bond cleavage.[38] Further, it should be emphasized that (a) the composition of the product formed in the rearrangement of anilinium butylamidosulfate (160 °C, 8 h) closely resembled that of the product obtained by heating free phenylamidosulfuric acid, $C_6H_5NH_2^+SO_3^-$, in dioxane at 100 °C for 30 min (in the solid state)[28] and (b) in no case was any *meta*-sulfonated product detected.

These facts support the S_N1-type intermolecular mechanism (Eq.9). A mechanism whereby the sulfonate group is transferred directly from the amino nitrogen to the *ortho*- and/or *para*-position(s) of another molecule (Eq. 10) is excluded. If this mechanism were operative, one would expect *meta* substitution (positively charged nitrogen).[3]

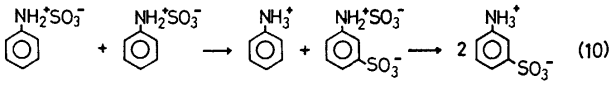

(10)

We suggested previously[1] that the transsulfonation and the rearrangement may occur concurrently. However, in the present study we have found that the former process proceeds much more rapidly than the latter; therefore, it seems more likely that both processes proceed consecutively.

Orientation of Ring Sulfonation. In marked contrast to the transsulfonation, the rearrangement was very subject to steric hindrance; *viz.*, both the ease and the orientation of the rearrangement were governed by steric factors. Relief of the steric strain around the amido-nitrogen markedly accelerated the rearrangement as observed with 2,6-dimethylanilinium butylamidosulfate. Two methyl substituents *ortho* to the reactive site hindered the introduction of a sulfonate group as observed typically with 3,5-dimethylanilinium butylamidosulfate. Moreover, a buttressing effect of 2- and 4-methyl substituents may operate. Thus, 2,4,5-trimethylanilinium butylamidosulfate underwent transsulfonation as rapidly as the other anilinium salts, but the subsequent rearrangement was very much retarded. The absence of 3,4-dimethylaniline-2-sulfonate in the

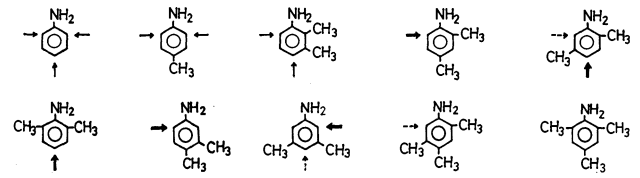

→ indicates the position where sulfonation occurs.
➡ indicates the position where sulfonation occurs (almost) exclusively.
⇢ indicates the position where sulfonation occurs to only a small extent.

Fig. 4. The orientation of ring sulfonation.

product of the rearrangement of 3,4-dimethylanilinium butylamidosulfate is also ascribable to this effect.

Formation of N, *Ring-disulfonates.* Deficiency of the substrate aniline caused by the partial condensation of the dissociated amine on the cool part of the reaction vessel gave rise to the formation of disulfonates compounds. Thus, the thermal reaction of **1** gave aniline-*N*,4- (**3**) and 2,4-disulfonates in addition to aniline-2- and 4-sulfonates and phenylamidosulfate (Fig. 1). No trace of the *N*,2-disulfonate was found in the product mixture. In contrast, the same reaction of **32** yielded 3,5-dimethylaniline-*N*,2-disulfonate (**35**), together with (3,5-dimethylphenylamido)sulfate and 3,5-dimethylaniline-2-sulfonate. 4-Sulfonate (**36**) and *N*,4-disulfonate (**47**) were formed in only traces.

There are three possible pathways to an *N*,ring-disulfonate: (1) *N*-sulfonation of a ring monosulfonate (route a); (2) ring sulfonation of an arylamidosulfate (route b); (3) rearrangement of an arylimidobis(sulfate) (route c) which could be formed by the *N*-sulfonation of the corresponding arylamidosulfate (Scheme 3).

The results described above can best be interpreted in terms of route a. The exclusive formation of **3** is accounted for by the preferential *N*-sulfonation of aniline-4-sulfonate. The *N*-sulfonation of aniline-2-sulfonate must be sterically unfavored. If route b were to be followed, **47** should be formed instead of **35**. Formation of **36** and **47** in only traces supports pathway b. Route c is unlikely, because this route is sterically unfavorable as compared with route a.

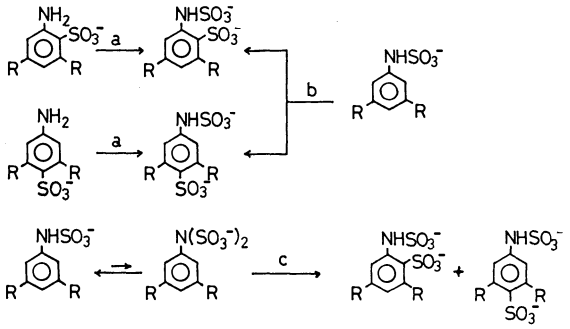

R = H, CH_3

Scheme 3.

Experimental

General experimental details have been described previously.[1]

Material. *Anilinium Salts of Butylamidosulfuric Acid (**42**)*: These compounds were prepared simply by neutralization of the free acid (**42**) with an appropriate aniline in methanol.[1]

2,6-Dimethylanilinium and 2,4,6-trimethylanilinium salts were prepared as follows and immediately used for the reactions: a large excess of the aniline was added to a methanol solution of **42**; the mixture was evaporated *in vacuo* to give a slurry of the salt. This was filtered, washed with benzene, and dried in a desiccator (Table 2).

Isolation and Identification of the Reaction Products. For details see Ref. 1. *Amidosulfates* were isolated by liquid chromatography (cellulose Whatman CF-11, dioxane-H_2O 4 : 1) or by extraction with EtOH of the product mixtures obtained (as the sodium salts) from the reactions at lower temperatures. The crude amidosulfates thus obtained were readily purified and characterized as the tetraphenylphosphonium salts (Table 3).

Table 2. Analytical and spectral data for anilinium salts of butylamidosulfuric acid *n*-$BuNHSO_3^-$ - $ArNH_3^+$

$ArNH_3^+$	Formula	N(%) (Calcd)	S(%) (Calcd)	IR spectra ($\tilde{\nu}$/cm^{-1}) νNH	$\nu_s SO_3^-$	$\nu_{as} SO_3^-$	Other prominent bands
Anilinium	$C_6H_{18}N_2O_3S$	11.46 (11.37)	13.15 (13.02)	3280	1048	1187 1229	748, 683
2,3-Dimethylanilinium	$C_8H_{22}N_2O_3S$	10.25 (10.21)	11.60 (11.68)	3210	1026	1147 1231	912, 880, 769, 705
2,4-Dimethylanilinium	$C_8H_{22}N_2O_3S$	10.20 (10.21)	11.65 (11.68)	3260	1026	1156 1235	916, 876, 807, 720
2,5-Dimethylanilinium	$C_8H_{22}N_2O_3S$	10.15 (10.21)	11.73 (11.68)	3268	1024	1156 1235	871, 828, 708
2,6-Dimethylanilinium	$C_8H_{22}N_2O_3S$	9.72 (10.21)	11.97 (11.68)	3260	1033	1161 1236	890, 777, 706
3,4-Dimethylanilinium	$C_8H_{22}N_2O_3S$	10.18 (10.21)	11.70 (11.68)	3240	1044	1170	807
3,5-Dimethylanilinium	$C_8H_{22}N_2O_3S$	9.98 (10.21)	11.68 (11.68)	3224	1038	1232	917, 855, 756—746, 684
2,4,5-Trimethylanilinium	$C_9H_{24}N_2O_3S$	9.68 (9.71)	11.14 (11.12)	3240	1027 1069	1160 1233	918, 876, 735
2,4,6-Trimethylanilinium	$C_9H_{24}N_2O_3S$	9.58 (9.71)	11.52 (11.12)	3260	1051	1186 1229	858

TABLE 3. ANALYTICAL AND SPECTRAL DATA FOR TETRAPHENYLPHOSPHONIUM AMIDOSULFATES,[a] $ArNHSO_3^-(C_6H_5)_4P^+$, ISOLATED FROM THE THERMAL REACTIONS OF n-$BuNHSO_3^-ArNH_3^+$

Ar	Formula	N(%) (Calcd)	S(%) (Calcd)	P(%) (Calcd)	IR spectra[b] ($\tilde{\nu}$/cm^{-1})			
					νNH	$\nu_s SO_3^-$	$\nu_{as} SO_3^-$	Other prominent bands
Phenyl	$C_{30}H_{26}NO_3PS$	2.72 (2.74)	6.50 (6.27)	5.97 (6.05)	3260	1039	1210 1227	885
2,3-Dimethylphenyl	$C_{32}H_{30}NO_3PS$	2.63 (2.60)	6.04 (5.94)	5.87 (5.74)	3308	1033	1210 1225	921, 834, 807, 778
2,4-Dimethylphenyl	$C_{32}H_{30}NO_3PS$	2.65 (2.60)	6.08 (5.94)	5.70 (5.74)	3280	1037	1206 1225	937, 864, 837
2,5-Dimethylphenyl	$C_{32}H_{30}NO_3PS$	2.62 (2.60)	6.03 (5.94)	5.82 (5.74)	3260	1035	1188 1231	950, 857, 813
2,6-Dimethylphenyl	$C_{32}H_{30}NO_3PS$	2.58 (2.60)	5.85 (5.94)	5.73 (5.74)	—	1036	1208 1228	875, 779, 745
3,4-Dimethylphenyl	$C_{32}H_{30}NO_3PS$	2.65 (2.60)	6.16 (5.94)	5.85 (5.74)	3236	1036	1205 1226	958, 868, 846, 816
3,5-Dimethylphenyl	$C_{32}H_{30}NO_3PS$	2.56 (2.60)	6.07 (5.94)	5.89 (5.74)	3216	1037	1203 1227	955, 844
2,4,5-Trimethylphenyl	$C_{33}H_{32}NO_3PS$	2.40 (2.53)	5.85 (5.79)	5.73 (5.59)	—	1029	1217	874
2,4,6-Trimethylphenyl	$C_{33}H_{32}NO_3PS$	2.38 (2.53)	6.04 (5.79)	5.61 (5.59)	3240	1033	1200 1218	864, 847, 819

a) Melting points of these phosphonium salts depended greatly on the rate of heating, probably because of the lability of the N-sulfonate group and hence the definite values could not be obtained. b) Absorbtions due to the tetraphenylphosphonium cation are omitted.

TABLE 4. ANALYTICAL AND SPECTRAL DATA FOR HEXYLAMMONIUM SALTS OF AMINOBENZENESULFONIC ACIDS (I) ISOLATED FROM THE THERMAL REACTIONS OF n-$BuNHSO_3^-ArNH_3^+$

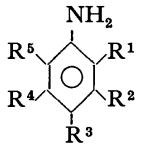

(I)

R^1	R^2	R^3	R^4	R^5	Mp/°C	Formula	N(%) (Calcd)	S(%) (Calcd)	IR spectra ($\tilde{\nu}$/cm^{-1})			
									νNH	$\nu_s SO_3^-$	$\nu_{as} SO_3^-$	Other prominent bands
SO_3H	H	H	H	H	190—190.5	$C_{12}H_{22}N_2O_3S$	10.13 (10.21)	11.66 (11.68)	3340 3408	1015 1110	1160 1200	748, 710
H	H	SO_3H	H	H	141—142	$C_{12}H_{22}N_2O_3S$	10.15 (10.21)	11.55 (11.68)		1037 1125	1162	822, 701
CH_3	CH_3	SO_3H	H	H	138.5—139.5	$C_{14}H_{26}N_2O_3S$	9.30 (9.26)	10.51 (10.60)	3352	1031	1175	650 971, 816, 711
CH_3	CH_3	H	H	SO_3H	172—173	$C_{14}H_{26}N_2O_3S$	9.15 (9.26)	10.53 (10.60)	3336 3428	1038 1079	1178 1221	800, 750, 700
CH_3	H	CH_3	H	SO_3H	153—154	$C_{14}H_{26}N_2O_3S$	9.22 (9.26)	10.48 (10.60)		1031	1172 1210	870, 797, 745
CH_3	H	SO_3H	CH_3	H	178.5—179.5	$C_{14}H_{26}N_2O_3S$	9.28 (9.26)	10.52 (10.60)	3340 3410	1065	1180	797, 728, 676 978, 912, 866
CH_3	H	SO_3H	H	CH_3	125—126.5	$C_{14}H_{26}N_2O_3S$	9.06 (9.26)	10.59 (10.60)	3360 3425	1034	1130 1220	888, 750, 737
H	CH_3	CH_3	H	SO_3H	214—216	$C_{14}H_{26}N_2O_3S$	9.31 (9.26)	10.51 (10.60)	3340 3420	1058	1165 1221	725, 663 985, 895, 868
SO_3H	CH_3	H	CH_3	H	138—139[a]	$C_{12}H_{22}N_2O_3S$[a]	10.25 (10.21)	11.64 (11.68)	3350 3430	1012 1075	1178	910, 830, 681
SO_3H	H	SO_3H	H	H	137—138	$C_{18}H_{37}N_3O_6S_2$	9.31 (9.22)	14.00 (14.07)	3365	1029 1090	1186 1215	817, 752, 691
CH_3	CH_3	SO_3H	H	SO_3H	178—179	$C_{20}H_{41}N_3OS_2$	8.60 (8.69)	13.40 (13.26)		1047	1182	750, 699 960, 878, 800
CH_3	H	CH_3	H	CH_3	—	$C_9H_{11}K_2NO_6S_2 \cdot H_2O$[b]	3.55 (3.61)	16.52 (16.50)	—	1028 1079	1223,1194 1284,1246	929, 730, 689

a) Butylammonium salt. b) Dipotassium (2,4,6-trimethylphenylimido)bis(sulfate) monohydrate.

TABLE 5. ANALYTICAL AND SPECTRAL DATA FOR BIS(TETRAPHENYLPHOSPHONIUM) AMIDOSULFATES (II)[a] ISOLATED FROM THE THERMAL REACTIONS OF *n*-$BuNHSO_3^-$-$ArNH_3^+$

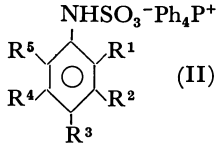

(II)

R^1	R^2	R^3	R^4	R^5	Formula	N(%) (Calcd)	S(%) (Calcd)	P(%) (Calcd)	IR spectra[c] ($\tilde{\nu}$/cm^{-1}) νNH	$\nu_s SO_3^-$	$\nu_{as} SO_3^-$	Other prominent bands
H	H	SO_3^- Ph_4P^+	H	H	$C_{54}H_{45}NO_6P_2S_2$	1.30 (1.51)	7.04 (6.90)	6.51 (6.66)	3250	1026	1206	890, 841
CH_3	H	SO_3^- Ph_4P^+	CH_3	H	$C_{56}H_{49}NO_6P_2S_2$	1.57 (1.46)	6.50 (6.69)	6.45 (6.47)	3245	1048 1076	1179 1220	870, 812, 797
CH_3	H	SO_3K	H	CH_3	$C_8H_9K_2NO_6S_2$[b]	3.90 (3.92)	17.85 (17.94)	—	3225	1041	1175 1218	920, 904, 806
H	CH_3	CH_3	H	SO_3^- Ph_4P^+	$C_{56}H_{49}NO_6P_2S_2$	1.75 (1.46)	6.75 (6.69)	6.39 (6.47)	3240	1035	1202	865, 814
SO_3^- Ph_4P^+	CH_3	H	CH^3	H	$C_{56}H_{49}NO_6P_2S_2$	1.42 (1.46)	6.85 (6.69)	6.55 (6.47)	3230	1032	1211	841

a) See footnote a) to Table 3. b) Dipotassium salt. c) Absorptions due to the tetraphenylphosphonium cation are omitted.

Amino-monosulfonic acids were easily isolated by treatment with hydrochloric acid of the sodium salt mixtures obtained from the reactions at higher temperature. These acids were characterized as the hexylammonium or butylammonium salts (Table 4).

Sulfo-amidosulfates (*N*, ring-disulfonates) were isolated by liquid chromatography or by fractional precipitation with $(C_6H_5)_4PCl$ from the disulfonate fractions (obtained as the insoluble residues of the foregoing ethanol extraction). The tetraphenylphosphonium amidosulfates were more soluble in acetone than the bis(tetraphenylphosphonium) *N*, ring-disulfonates; hence, the former salts can readily be removed by washing the precipitate with a small volume of acetone. Disodium 2,6-dimethylaniline-*N*,4-disulfonate could not be converted to the corresponding bis(phosphonium)salt by the double-decomposition method (Table 5).

(2,4,6-Trimethylphenylimido)bis(sulfate) was isolated by liquid chromatography. Isolation was also achieved as follows: the product from the reaction of **40** (2 mmol, 120 °C, 8 h) was dissolved in water and the solution was passed through a column of Dowex 50W (K^+ form). The eluate was evaporated to dryness and the residue was extracted three times with 99.5% ethanol. The residual solid [composed of potassium (2,4,6-trimethylphenylamido)sulfate and dipotassium (2,4,6-trimethylphenylimido)bis(sulfate)] was then dissolved in water (3 ml) containing a few drops of aqueous KOH; to this solution was added 60 ml of hot ethanol with vigorous stirring. The mixture was filtered immediately and the filtrate was left at room temperature overnight. The precipitate was collected by filtration; for further purification this was dissolved in hot water containing a few drops of aqueous KOH, and reprecipitated with hot ethanol, giving the pure *imidobis(sulfate)* as colorless needles (Table 4).

Confirmation of the Structures of the Products Isolated from the Thermal Reactions. Deamination of 2,6-Dimethylaniline-4-sulfonic Acid: The aminosulfonic acid [obtained from the thermal reaction (160 °C, 5 h) of **22**] was deaminated by diazotization followed by reduction with $NaBH_4$ in MeOH (5—10 °C, 5 h),[39] yielding *m*-xylene-5-sulfonic acid; this was converted to the sulfonamide, mp 133—134 °C (lit,[40] 133—134 °C), mixed mp 132—133.5 °C.[41]

Deamination of 3,5-Dimethylaniline-2-sulfonic Acid: The aminosulfonic acid isolated from the thermal reaction (180 °C, 8 h) of **33** was deaminated in the same way as described above. The product was identical with authentic *m*-xylene-4-sulfonic acid;[42] its anilinium salt melted at 203—204 °C (lit,[40] 197—199 °C); mixed mp 202.5—203.5 °C; IR: 1551, 1194 (SO_3^-), 1168, 1089 (SO_3^-), 1018, 833 (2H), 746 (5H), and 680 (5H) cm^{-1}.

Proof of the Constitutions of Aniline-N,4-disulfonate and 3,5-Dimethylaniline-N,2-disulfonate. Disodium aniline-*N*,ring-disulfonate [obtained from the thermal reaction of **2** (110 °C, 8 h)] was hydrolyzed by refluxing for 30 min with dil HCl. After cooling, the mixture was neutralized with $Ba(OH)_2$, filtered, and the filtrate was passed through a column of Amberlite IR-120B (H^+ form). The effluent was evaporated to dryness and the residual solid washed in a minimum quantity of ethanol. The product thus obtained gave a single spot on TLC. Its R_f value and IR spectrum were entirely in agreement with those of authentic aniline-4-sulfonic acid.

In the same manner, acid hydrolysis of disodium 3,5-dimethylaniline-*N*,ring-disulfonate gave 3,5-dimethylaniline-2-sulfonic acid, deamination of which yielded *m*-xylene-4-sulfonic acid.

Preparation of Authentic Compounds. (1) 2,3-Dimethylaniline-4-sulfonic Acid:[43] *Nitration of 2,3-Dimethylacetanilide*:[44,45] To a stirred solution of 2,3-dimethylacetanilide (mp 130—131 °C) (8.0 g) in concd H_2SO_4 (20 ml) was added HNO_3 (d 1.42; 3.3 ml) at 5—10 °C over a period of half an hour. The mixture was poured into ice water (250 ml) and the precipitate was filtered, washed, and dried.

2,3-Dimethyl-4-nitroaniline:[44] The foregoing nitroacetanilide was hydrolyzed by refluxing for 1 h with 60% sulfuric acid (100 ml). The product (6.91 g) was chromatographed on silica gel by use of CCl_4–acetone (15 : 1 v/v) as an eluent. The 4-nitro compound thus obtained was recrystallized from CCl_4; the pure product (2.48 g) melted at 114—115 °C (lit,[46] 115.5—116.5 °C).

2,3-Dimethyl-4-nitro-1-benzenesulfonic Acid: 2,3-Dimethyl-4-nitroaniline (2.2 g) was diazotized in the usual way and the excess of nitrous acid was destroyed with NH_2SO_3H. The mixture was poured in one portion into a cold, saturated solution of SO_2 (8.7 g) in CH_3COOH to which a solution of $CuCl_2$ (0.37 g) in water (0.80 ml) had been added. The

temperature was raised gradually to 40 °C. The mixture was stirred for 1 h at this temperature, then poured into water (150 ml), and neutralized carefully with a $NaHCO_3$ solution; the oily layer was extracted twice with benzene and the extract was washed with aqueous $NaHCO_3$, dried, and concentrated *in vacuo* to give the crude sulfonyl chloride. A mixture of the sulfonyl chloride, 50% aq MeOH (15 ml), and Na_2CO_3 (0.60 g) was boiled for 1 h. The reaction mixture was evaporated and the residual solid was dissolved in water (10 ml), filtered, and evaporated to dryness. The residue was again dissolved in methanol (35 ml). After filtration, the filtrate was concentrated to give the *sodium nitro-sulfonate*. IR: 1517 (NO_2), 1356 (NO_2), 1178 (SO_3^-) 1067 (SO_3^-), 1039, 828(2H), 802, and 663 (SO_3^-) cm^{-1}; *S*-(1-naphthylmethyl)isothiouronium salt, mp 222—222.5 °C.

2,3-Dimethylaniline-4-sulfonic Acid: The crude nitrosulfonate was reduced with activated iron powder (2.5 g). Work-up in the usual way gave the pure *sulfonic acid* as needles; IR: 1503, 1206 (SO_3), 1082, 1052 (SO_3), 818 (2H), and 695 cm^{-1}. Found: S, 14.58%. Calcd for $C_8H_{11}NO_3S \cdot H_2O$: S, 14.62%. The *hexylammonium salt* (from EtOH–AcOEt 1 : 2) melted at 138.5—139.5 °C. Found: S, 10.51%. Calcd for $C_{14}H_{26}N_2O_3S$: S, 10.60%.

(2) 2,5-Dimethylaniline-4-sulfonic Acid: Treatment of 2,5-dimethylacetanilide (mp 138—139 °C, 1.0 g) with $ClSO_3H$ (4.2 ml) (80 °C, 1 h)[47] and subsequent recrystallization from C_6H_6–AcOEt(1 : 1) gave N-*acetyl-2,5-dimethylaniline-4-sulfonyl chloride* (0.55 g); mp 159—160 °C (lit, [47]160 °C), IR: 1660 (CO), 1560 (NH_3^+), 1360 (SO_2), 1275, 1121 (SO_2), 895 (1H), and 829 cm^{-1}.

A mixture of the sulfonyl chloride (0.30 g), ethanol (1 ml), and concd HCl (5 ml) was refluxed for 1h. After cooling the *sulfonic acid* was collected and recrystallized from H_2O. IR: 1219, 1083, 1055, 900, and 873 cm^{-1}. Its *hexylammonium salt* melted at 178.5—179.5 °C. Found: S, 10.52%. Calcd for $C_{14}H_{26}O_3N_2S$: S, 10.60%. The sulfonic acid was converted to its sodium salt, which was then refluxed for 1 h with Ac_2O in pyridine to give the N-*acetyl derivative*. Its p-*toluidinium salt* melted at 232—233 °C. The same *N*-acetylated sulfonic acid was also prepared according to Junghahn's procedure.[48]

(3) 2,6-Dimethylaniline-3-sulfonic Acid: This acid was prepared by two methods.

(a) Sulfonation of 2,6-Dimethylaniline with Oleum: To 25% oleum (32 ml) was added, drop by drop, 2,6-dimethylaniline (5.1 ml) and the mixture was heated for 4 h at 80—90 °C. The reaction mixture was poured on cracked ice and neutralized with $BaCO_3$. After removal of $BaSO_4$ the filtrate was concentrated and treated with concd HCl (5 ml), giving the 3-sulfonic acid in a 30% yield. IR: 1607, 1185 (SO_3^-), 1044 (SO_3^-), 822 (2H), 741, and 694 cm^{-1}.

(b) Chlorosulfonylation of 2,6-Dimethylacetanilide.[49] To ice-cooled $ClSO_3H$ (18.69 g) was added the acetanilide (3.00 g) with stirring. The mixture was stirred at 5 °C for 15 min, then at 25 °C for 1 h, and finally at 40 °C for 10 min, and poured on cracked ice, yielding the *sulfonyl chloride*. IR: 3290 (NH), 1665 (CO), 1505, 1367 (SO_2), 1202, 1168 (SO_2), and 814 (2H) cm^{-1}. The sulfonyl chloride was treated with concd ammonia, giving N-*acetyl-2,6-dimethylbenzene-3-sulfonamide*. Recrystallization from water gave the pure sulfonamide; mp 263—264 °C. IR: 3345 (NH), 3235 (NH), 1638 (CO), 1327 (SO_2), 1120 (SO_2), and 810 (2H) cm^{-1}. The foregoing sulfonyl chloride was heated under reflux with concd HCl for 1 h to give the *3-sulfonic acid*.

(4) 2,6-Dimethylaniline-4-sulfonic Acid: This acid was prepared by "baking" 2,6-dimethylanilinium hydrogensulfate in *o*-dichlorobenzene (180 °C, 6 h).[21,51] No isomeric 3-sulfonic acid was detected. IR: 1618, 1529, 1438, 1222, 1190, 1154, 1111, 1045 (SO_3^-), 883 (1H), and 723 cm^{-1}.

(5) 3,4-Dimethylaniline-6-sulfonic Acid: This acid was prepared in a 76% yield by baking 3,4-dimethylanilinium hydrogensulfate in *o*-dichlorobenzene (171—175 °C, 3 h).[43,51,52] IR: 1603, 1553, 1502, 1258, 1167 (SO_3^-), 1048 (SO_3^-), 880 (1H), 787, 732, and 660 cm^{-1}.

(6) 3,5-Dimethylaniline-2-sulfonic Acid: This compound was prepared by three different methods.[43] *(a) Synthesis* via *2,4-Dimethyl-6-nitroaniline*: The procedure was almost the same as that for the synthesis of 2,3-dimethylaniline-4-sulfonic acid. 2,4-Dimethyl-6-nitroacetanilide, mp 171.5—172.8 °C (from H_2O) (lit,[53] 172 °C); 2,4-dimethyl-6-nitroaniline, mp 67—68 °C (from CCl_4) (lit,[54] 67—68 °C); potassium 4,6-dimethyl-2-nitrobenzene-1-sulfonate, IR; 1529 (NO_2), 1377 (NO_2), 1208 (SO_3^-), 1093, 1032 (SO_3^-), 852 (1H), and 773 cm^{-1}; 3,5-dimethylaniline-2-sulfonic acid (from H_2O), IR: 1200 (SO_3^-), 1162, 1123, 1087, 1015 (SO_3^-), 866 (1H), and 683 (SO_3^-) cm^{-1}; p-*toluidinium* N-*acetyl-3,5-dimethylaniline-2-sulfonate* melted at 180.5—181.5 °C (from H_2O), IR; 1662 (CO), 1580 (amide), 1322, 1184 (SO_3^-), 1082, 1017 (SO_3^-), 858 (1H), and 806 (2H). *(b) Sulfonation of 3,5-Dimethylaniline with 100% Sulfuric Acid*: Sulfonation of 3,5-dimethylaniline (2.5 g) with 100% H_2SO_4 (3.0 g) (170 °C, 1 h) gave almost exclusively the *2-sulfonic acid* (TLC, IR).[55] *(c) Sulfonation of 3,5-Dimethylaniline with Chlorosulfuric Acid*: Sulfonation of 3,5-dimethylaniline (2.0 g) with $ClSO_3H$ (3.25 g) in 1,1,2,2-tetrachloroethane (150 °C, 45 min)[56] also gave the *2-sulfonic acid* as the main product, together with the 4-sulfonic and 2,6-(?)-disulfonic acids.

(7) 3,5-Dimethylaniline-4-sulfonic Acid: This acid was prepared by chlorosulfonation of 3,5-dimethylacetanilide.[57] The sulfonyl chloride obtained was moderately soluble in water unlike the normal sulfonyl chlorides and considerably susceptible to hydrolysis. Accordingly, this chloride was immediately converted to the corresponding *sulfonamide*, which melted at 230—231 °C after repeated crystallization from dil alcohol. IR: 3245 (NH), 1660 (C=O), 1593 (NH), 1543, 1319 (SO_2), 1150 (SO_2), 872, 850, and 740 cm^{-1}.

The sulfonyl chloride was subjected to hydrolysis with aqueous K_2CO_3 (100 °C, 1 h), followed by acidification to give the *4-sulfonic acid*. IR: 1476, 1242 (SO_3^-), 1148, 1118, 1080, 1003 (SO_3^-), 860 (1H), and 680 (SO_3^-) cm^{-1}; the butylammonium salt melted at 168.5—170 °C.

*Formation of (2,4,6-Trimethylphenylimido)bis(sulfate) (**44**) by Reaction of (2,4,6-Trimethylphenylamido)sulfate (**43**) with Butylamidosulfuric Acid (**42**).* An intimate mixture of **43** (0.56 g) and **42** (0.30 g) was heated at 120 °C for 4 h in an evacuated tube; the product was dissolved in aqueous KOH. The solution was evaporated to dryness; the residual solid was dissolved in hot water (8 ml) containing two drops of aqueous KOH. This solution was added, with vigorous stirring, to boiling 99.5% ethanol (100 ml). The precipitated crystals were collected, and dried. Its IR spectrum was completely in accord with that of the material isolated from the thermal reaction of **40**.

References

1) Part V: F. Kanetani and H. Yamaguchi, *Bull. Chem. Soc. Jpn.*, **51**, 3039 (1978).

2) G. A. Benson and W. J. Spillane, *Chem. Rev.*, **80**, 151 (1980).

3) P. K. Maarsen and H. Cerfontain, *J. Chem. Soc., Perkin Trans. 2*, **1977**, 921, 929; 1008; and references cited therein.

4) A. Junghahn, *Chem. Ind. (Berlin)*, **26**, 57 (1903).

5) W. Huber, *Helv. Chim. Acta*, **15**, 1372 (1932).
6) Z. Vrba and Z. J. Allan, *Collect. Czech. Chem. Commun.*, **34**, 272 (1969).
7) In the present paper, the term "*transsulfonation*" refers to the transfer of a sulfonate group from one amino nitrogen to another and the term "*rearrangement*" refers to the migration of a sulfonate group from aromatic amino nitrogen to the ring.
8) This compound may be called (4-sulfophenylamido) sulfate or *N*-(4-sulfophenyl)sulfamate in accordance with IUPA Crules.
9) Aniline-*N*,2- and *N*,4-disulfonic acids have been postuated as intermediates in the sulfonation of aniline with sulfuric acid (Ref. 3).
10) The *ortho*: *para* ratios as calculated from the weights of the isolated products ranged from 0.66 : 1 to 0.82 : 1.
11) Product compositions are expressed in mol%.
12) In this paper, aminosulfonic acids are consistently named as the sulfonic acid derivative of the parent aniline in order to facilitate comparison; thus, the names of 2,3-dimethylaniline-4- and 6-sulfonate are used instead of 4-amino-2,3-dimethylbenzenesulfonic acid and 2-amino-3,4-dimethylbenzenesulfonic acid, respectively.
13) The ratios were calculated from the weights of the isolated products on the assumption that all of **8** was the *N*,4-disulfonate and that **11** comes equally both from **9** and from **10**.
14) See also A. Junghahn, *Ber.*, **35**, 3747 (1902).
15) 2,6-Dimethylaniline (pK_a 3.95) is weaker in basicity than aniline itself (pK_a 4.58) as well as 2,4-dimethylaniline (pK_a 4.91).
16) H. C. Brown and A. Cahn, *J. Am. Chem. Soc.*, **72**, 2939 (1950).
17) Immediately after the reaction had started, boiling of the reactant **21** and refluxing of 2,6-dimethylaniline occurred, but rapidly subsided in a few minutes. This observation is consistent with the ready transsulfonation of **21**.
18) E. Noelting and L. Stoeckling, *Ber.*, **24**, 564 (1891).
19) C. E. Ingham and G. C. Hampson, *J. Chem. Soc.*, **1939**, 981.
20) H. E. Dadswell and J. Kenner, *J. Chem. Soc.*, **1927**, 1102.
21) A. Burger and J. F. Siuda, *Arzneim. Forsch.*, **18**, 1220 (1968).
22) British Patent 1027060; *Chem. Abstr.*, **65**, 10905h (1966).
23) Sulfonation of 3,5-dimethylaniline with 100% H_2SO_4 and with $ClSO_3H$ also gave the 2-sulfonic acid almost exclusively (see Experimental section). A similar *ortho*-sulfonation of 3,5-dimethylphenol has been reported (F. Raschig, D. R. P. 283306; *Chem. Zentral.*, **1915 I**, 926).
24) Nitration of 3,5-dimethylaniline with mixed acid has been reported to give the 2- and 4-nitro compounds in yields of 55 and 24%, respectively [B. M. Wepster and P. E. Verkade, *Recl. Trav. Chim. Pays-Bas*, **68**, 88 (1949)]. Further, nitration of 3,5-dimethylanisole with nitric acid in $HClO_4$ has been reported to give *ca.* 1 : 1 mixtures of the 2- and 4-nitro isomers [R. B. Moodie, K. Schofield, and P. N. Thomas, *J. Chem. Soc., Perkin Trans. 2*, **1978**, 318]). In the present rearrangement the reacting species is probably SO_3, which is much larger than the species, NO_2^+, involved in nitration.
25) Paal and Hubalek have reported that (2,4,5-trimethylphenylamido)sulfuric acid as well as its ammonium salt did not rearrange to **39** at the temperatures up to 250 °C [C. Paal and M. Hubalek, *Ber.*, **50**, 1110 (1917).]. To the contrary a German patent claims that **39** is obtained by treatment of 2,4,5-trimethylaniline with an equimolar amount of $ClSO_3H$ in *o*-dichlorobenzene [I. G. Farbenindustrie A–G., DRP 541258; *Chem. Zentral.*, **1931 II**, 2057; *Chem. Abstr.*, **26**, 1942 (1932).]. It has been reported that *N*-bromo-2,4,5-trichloroacetanilide does not undergo the Orton rearrangement [M. J. S. Dewar and J. M. W. Scott, *J. Chem. Soc.*, **1957**, 1445.].
26) Diammonium imidobis (sulfate) is readily prepared by fusion of $NH_2SO_3NH_4$ or of an equimolar mixture of NH_3^+-SO_3^- and $NH_2SO_3NH_4$ [H.H. Sisler and L. F. Audrieth, *Inorg. Synth.*, Vol. II, 179 (1946)].
27) In the present experiment all of the anilinium salts melted in a few minutes at the reaction temperatures. Immediately after the reaction had started, the substrate amine ($ArNH_2$) was released and refluxed briskly. This refluxing subsided in 20—30 min.
28) F. Kanetani, *Chem. Lett.*, **1980**, 965.
29) Our unpublished data; see also H. Yamaguchi and F. Kanetani, *Yuki Gosei Kagaku Kyokai Shi*, **31**, 79 (1973) and references cited therein.
30) Yu. B. Kagan, L. I. Zvezdkina, A. Ya Rozovskii, G. M. Pakhomova, and A. N. Bashkirov, *Kinet. Katal.*, **15**, 368 (1974); Yu. B. Kagan, A. N. Bashkirov, E. B. Kozlovskaya, L. I. Zvezdkina, and A. Ya Rozovskii, *Neftekhimiya*, **15**, 433 (1975).
31) V. Parshikov, B. V. Passet, and N. Kopeina, *Org. React. (USSR)*, **13**, 310 (1976); B. V. Passet, and V. Parshikov, *ibid.*, **13**, 555 (1976).
32) See also W. Huber, *Helv. Chim. Acta*, **15**, 1372 (1932); E. D. Hughes and C. K. Ingold, *Quart. Rev.*, **6**, 51 (1952); Z. J. Allan and Z. Vrba, *Collect. Czech. Chem. Commun.*, **34**, 272 (1969).
33) In order to rationalize the alledged intramolecular rearrangement of phenylamidosulfuric acid in an excess of 97% sulfuric acid, Vrba and Allan postulated the deformation of the benzene ring so that the migrating SO_3H group was close to the *para*-position [Z. Vrba and Z. J. Allan, *Collect. Czech. Chem. Commun.*, **33**, 2502 (1968).]. However, this cannot be applied to our case.
34) M. J. S. Dewar, "Molecular Rearrangements," ed by P. de Mayo, Interscience Publishers, New York (1963), Part 1, Chap. 5, pp. 295—344. Dewar's π-complex theory has been criticized severely: D. V. Banthorpe, *Chem. Rev.*, **70**, 295 (1970).
35) D. V. Banthorpe, E. D. Hughes, and D. L. H. Williams, *J. Chem. Soc.*, **1964**, 5349.
36) On the contrary, the reverse isomerization, *viz.*, the rearrangement of certain sulfitoamines (obtained by reactions of tertiary amine oxides with SO_2) to the corresponding amidosulfuric acid zwitterions (tertiary amine–SO_3 complexes) has been reported: J. T. Edward and J. Whiting, *Can. J. Chem.*, **49**, 3502 (1971); see also H. Z. Lecher and W. B. Hardy, *J. Am. Chem. Soc.*, **70**, 1948 (1948).
37) Z. J. Allan and Z. Vrba, *Collect. Czech. Chem. Commun.*, **34**, 272 (1969); R. Lantz and P. Obellianne, *C. R. Acad. Sci.*, **238**, 2243 (1954).
38) First isolation and characterization of free phenylamidosulfuric acid and its ring-substituted derivatives has been reported by one of us very recently: see Ref. 28.
39) J. B. Hendrickson, *J. Am. Chem. Soc.*, **83**, 1251 (1961).
40) H. Asakura and Y. Muramoto, *Yuki Gosei Kagaku Kyokai Shi*, **35**, 828 (1977).
41) Authentic *m*-xylene-5-sulfonic acid was prepared by sulfonation of *m*-xylene with concd H_2SO_4 (200 °C, 3 h) (see Ref. 40). Its *sulfonamide* melted at 133.5—134 °C; IR: 3340 (NH), 3250 (NH), 1328 (SO_2), 1305, 1155 (SO_2), 894, and 860 (1H) cm^{-1}.
42) Authentic *m*-xylene-4-sulfonic acid was prepared by sulfonation of *m*-xylene with an equal volume of concd H_2SO_4 (80—90 °C, 2 h).
43) After the present work had been completed, we became aware of the publications on the syntheses of 2,3-dimethyl-

aniline-4-, 5-, and 6-sulfonic acids, 3,4-dimethylaniline-2-, 5-, and 6-sulfonic acids, and 3,5-dimethylaniline-2- and 4-sulfonic acids: A. Curtin and H.-R. von Tobel, *Helv. Chim. Acta*, **63**, 385 (1980); A. Curtin, *ibid.*, **60**, 1994 (1977).

44) H. von Euler and H. Hasselquist, *Arkiv Kemi.*, **12**, 259 (1958).

45) R. van Helden, P. E. Verkade, and B. M. Wepster, *Recl. Trav. Chim. Pays-Bas*, **73**, 39 (1954).

46) B. M. Wepster and P. E. Verkade, *Recl. Trav. Chim Pays-Bas*, **69**, 1393 (1950).

47) R. N. Johnson and S. Smiles, *J. Chem. Soc.*, **123**, 2384 (1923).

48) A. Junghahn, *Ber.*, **33**, 1364 (1900).

49) Parke, Davis & Co. British Patent 1027060 (1966); *Chem. Abstr.*, **65**, 10905 h (1966).

50) Casper and Petzold, P. B. Report 73911, FIAT Microfilm Reel N87, Frames 4648—4660 (1933).

51) J. Arient and J. Podstata, Czech. Patent, 157467 (1973); *Chem. Abstr.*, **83**, 96735f (1975).

52) Sulfonation of 3,4-dimethylaniline with concd H_2SO_4 (160—170 °C, 5 h) gave a mixture of 3,4-dimethylaniline-5- and 6-sulfonic acids. Both isomers were separated by fractional crystallization of their barium salts.

53) C. Willgerodt and F. Schmierer, *Ber*,. **38**, 1472 (1905).

54) K. Ibbotson and J. Kenner, *J. Chem. Soc.*, **123**, 1260 (1923).

55) The sulfonation with 25% oleum has been reported to give a 45 : 55 mixture of 3,5-dimethylaniline-2- and 4-sulfonic acids (Ref. 43).

56) British Dyestuffs Corp., British Patent 175019 (1922); *Chem. Zentral.*, **1922 IV**, 836.

57) J. Bolssens, J. A. C. T. Brouwers, J. H. Choufoers, A. Kats, P. E. Verkade, and B. M. Wepsters, *Recl. Trav. Chim. Pays-Bas*, **73**, 819 (1954).

X-Ray Crystallographic Studies on the Structure of Alnuserrudiolone Isolated from the Male Flowers of *Alnus serrulatoides*

Toshifumi HIRATA, Tadashi AOKI, and Takayuki SUGA*

Department of Chemistry, Faculty of Science, Hiroshima University, Higashisenda-machi, Naka-ku, Hiroshima 730

(Received March 23, 1981)

The structure of alnuserrudiolone was corroborated to be (12*R*,20*S*)-12,20-dihydroxy-24-methylenedammaran-3-one by the X-ray crystallography together with the ^{13}C NMR and the high resolution mass spectral measurements.

In connection with biochemical and physiological studies of pollination,[1] we investigated chemical constituents of the male flowers of *Alnus serrulatoides* CALL. (Japanese name: Kawara-hannoki) and reported the isolation and the structure elucidation of new C_{31} dammarane-type triterpenoids, alnuserol,[2] alnuseric acid,[3] and alnuselide.[3] In advance of these reports, the isolation of a new C_{31} dammarane-type triterpenoid, alnuserrudiolone, had been communicated, and structure (**1**) had been proposed to this triterpenoid on the basis of chemical and spectroscopic studies.[4] The structure has a feature of C_{31} dammarane-type triterpenoid having an acyclic side chain, in contrast to the above-described triterpenoids with the side chain including a tetrahydrofuran ring. It is, however, considered essential to establish the skeletal structure of **1**, because **1** has not been yet related to any compound having the well-defined structure. We, therefore, studied the structure of alnuserrudiolone by the X-ray crystallographic method together with the ^{13}C NMR and the high resolution mass spectral measurements.

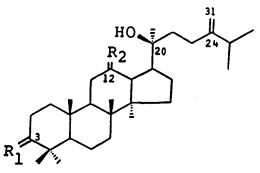

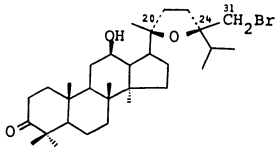

3

1: R_1=O, R_2= 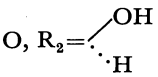

2: R_1=H_2, R_2=O

4: R_1=H_2, R_2= 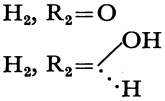

Results and Discussion

The male flowers of *Alnus serrulatoides* CALL. grown naturally on a river side were collected just before the flowering and immersed in acetone. An ether-soluble fraction of the acetone extract was subjected to chromatography using silica gel to give the sample of alnuserrudiolone (**1**), which showed completely the same physical (mp and optical rotation), spectral (IR, ^1H NMR, MS, and ORD) properties, and chemical behaviors as described previously.[4]

The acyclic side chain and functional groups characteristic of the previously-proposed structure (**1**) were first corroborated by measurement of ^{13}C NMR and high resolution mass spectra. Comparison of the ^{13}C NMR chemical shifts of **1** with those of the dammarane-type derivatives[2,5] indicated that **1** possesses a dammarane-type skeleton with a carbonyl group at the 3-position (δ_c 217.8), a secondary hydroxyl group on C-12 (δ_c 70.5), and a tertiary hydroxyl group on C-20 (δ_c 73.6). The last two signals showed that the chirality at C-12 and C-20 is *R* and *S*, respectively.[5] On the other hand, the signals at δ_c 156.5 and 106.2 indicated the presence of an acyclic side chain with a terminal methylene on C-24. This was further supported by the high resolution mass spectrum, which exhibited ions characteristic of such an acyclic side chain at *m/z* 141.1280 and 123.1279,[4,6,7] together with an ion derived from the 3-keto dammarane-type skeleton at *m/z* 205.1603.[6]

TABLE 1. FINAL ATOMIC COORDINATES ($\times 10^4$) OF **2**, WITH STANDARD DEVIATIONS IN PARENTHESES

Atoms	*x*	*y*	*z*	B_{eq}/Å^2 a)
O(1)	9963(19)	8721(13)	302(7)	6.6
O(2)	7328(16)	5223(11)	−1072(7)	5.8
C(1)	11293(34)	7677(23)	2902(16)	8.1
C(2)	11604(32)	7676(30)	3835(13)	7.3
C(3)	11780(37)	6285(25)	4512(14)	7.9
C(4)	9458(36)	6056(31)	4116(11)	7.1
C(5)	8521(34)	6498(28)	3317(14)	7.7
C(6)	6933(24)	5656(28)	3046(11)	7.6
C(7)	6066(26)	6145(25)	2316(12)	7.5
C(8)	7443(24)	6188(19)	1678(10)	4.9
C(9)	9070(26)	7057(18)	1921(10)	3.6
C(10)	9949(27)	6657(21)	2649(14)	7.9
C(11)	10433(22)	7208(18)	1293(9)	3.6
C(12)	9499(24)	7719(17)	590(10)	4.0
C(13)	7956(19)	6947(17)	319(9)	3.4
C(14)	6642(22)	6940(22)	964(10)	5.4
C(15)	5065(24)	6315(22)	559(12)	6.2
C(16)	5006(26)	6869(20)	−229(12)	8.3
C(17)	6978(25)	7311(19)	−406(12)	5.8
C(18)	7836(27)	4823(18)	1484(13)	6.4
C(19)	11035(35)	5326(25)	2630(13)	8.3
C(20)	7604(33)	6635(27)	−1116(10)	7.6
C(21)	9619(26)	6803(24)	−1226(11)	6.7
C(22)	6430(31)	7117(23)	−1807(11)	8.2
C(23)	6927(35)	6540(29)	−2528(12)	8.3
C(24)	5522(27)	6852(21)	−3155(12)	6.9
C(25)	3993(39)	5931(31)	−3083(17)	8.7
C(26)	4155(39)	4803(29)	−3749(18)	8.3
C(27)	2362(39)	6397(29)	−3131(26)	9.1
C(28)	8219(37)	6969(35)	4751(13)	7.9
C(29)	9167(43)	4671(20)	4275(13)	8.1
C(30)	6095(31)	8415(16)	1119(11)	8.3
C(31)	5756(41)	7694(28)	−3674(14)	8.5

a) $B_{eq}=8\pi^2(U_1+U_2+U_3)/3$, where U_1, U_2, and U_3 are the principal components of *U* matrix.

TABLE 2. INTERATOMIC DISTANCES (l/Å) OF **2**, WITH STANDARD DEVIATIONS IN PARENTHESES

C(1)–C(2)	1.67(3)	C(12)–C(13)	1.48(2)
C(1)–C(10)	1.56(3)	C(12)–O(1)	1.23(2)
C(2)–C(3)	1.60(4)	C(13)–C(14)	1.51(2)
C(3)–C(4)	1.60(4)	C(13)–C(17)	1.53(3)
C(4)–C(5)	1.61(3)	C(14)–C(15)	1.54(2)
C(4)–C(28)	1.60(4)	C(14)–C(30)	1.59(2)
C(4)–C(29)	1.49(3)	C(15)–C(16)	1.64(3)
C(5)–C(6)	1.52(3)	C(16)–C(17)	1.59(2)
C(5)–C(10)	1.61(3)	C(17)–C(20)	1.49(2)
C(6)–C(7)	1.56(3)	C(20)–C(21)	1.54(3)
C(7)–C(8)	1.54(3)	C(20)–C(22)	1.60(3)
C(8)–C(9)	1.55(2)	C(20)–O(2)	1.47(2)
C(8)–C(14)	1.61(2)	C(22)–C(23)	1.44(3)
C(8)–C(18)	1.47(2)	C(23)–C(24)	1.57(3)
C(9)–C(10)	1.57(2)	C(24)–C(25)	1.46(3)
C(9)–C(11)	1.48(2)	C(24)–C(31)	1.21(3)
C(10)–C(19)	1.54(3)	C(25)–C(26)	1.42(4)
C(11)–C(12)	1.52(2)	C(25)–C(27)	1.60(3)

TABLE 3. BOND ANGLES (ϕ/°) OF **2**, WITH STANDARD DEVIATIONS IN PARENTHESES

C(2)–C(1)–C(10)	111(2)	C(12)–C(13)–C(17)	121(2)
C(1)–C(2)–C(3)	129(2)	C(14)–C(13)–C(17)	100(1)
C(2)–C(3)–C(4)	102(2)	C(13)–C(14)–C(15)	109(1)
C(3)–C(4)–C(5)	131(2)	C(13)–C(14)–C(8)	110(1)
C(3)–C(4)–C(28)	100(2)	C(13)–C(14)–C(30)	108(1)
C(3)–C(4)–C(29)	101(2)	C(14)–C(15)–C(16)	106(2)
C(5)–C(4)–C(28)	103(2)	C(15)–C(16)–C(17)	96(2)
C(5)–C(4)–C(29)	113(2)	C(16)–C(17)–C(13)	111(2)
C(4)–C(5)–C(10)	109(2)	C(16)–C(17)–C(20)	111(1)
C(4)–C(5)–C(6)	116(2)	C(17)–C(20)–C(21)	113(1)
C(5)–C(6)–C(7)	114(2)	C(17)–C(20)–C(22)	109(1)
C(6)–C(7)–C(8)	109(2)	C(17)–C(20)–O(2)	110(1)
C(7)–C(8)–C(9)	111(1)	C(21)–C(20)–O(2)	105(1)
C(7)–C(8)–C(14)	108(1)	C(22)–C(20)–O(2)	104(1)
C(7)–C(8)–C(18)	107(1)	C(21)–C(20)–C(22)	116(1)
C(8)–C(9)–C(10)	116(1)	C(20)–C(22)–C(23)	115(2)
C(8)–C(9)–C(11)	115(2)	C(22)–C(23)–C(24)	112(2)
C(9)–C(10)–C(19)	115(1)	C(23)–C(24)–C(25)	111(2)
C(9)–C(11)–C(12)	112(1)	C(23)–C(24)–C(31)	124(2)
C(11)–C(12)–C(13)	115(1)	C(25)–C(24)–C(31)	125(2)
C(11)–C(12)–O(1)	120(1)	C(24)–C(25)–C(26)	125(2)
C(13)–C(12)–O(1)	125(1)	C(24)–C(25)–C(27)	127(2)
C(12)–C(13)–C(14)	116(2)	C(26)–C(25)–C(27)	108(2)

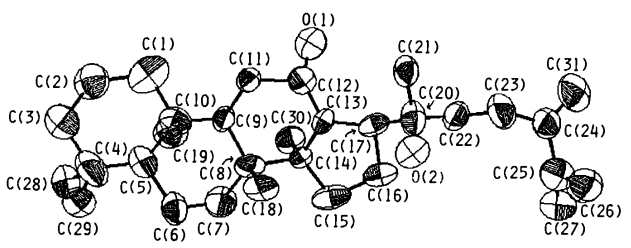

Fig. 1. Perspective view of **2**.

TABLE 4. FINAL ATOMIC COORDINATES ($\times 10^4$) OF **3**, WITH STANDARD DEVIATIONS IN PARENTHESES

Atoms	x	y	z	B_{eq}/Å^{2} a)
Br	1029(4)	2164(2)	2091(8)	6.9
O(1)	5727(23)	8986(12)	4576(5)	6.4
O(2)	−1003(18)	4085(11)	3435(4)	4.1
O(3)	−1492(16)	1846(10)	3245(4)	3.1
C(1)	3223(24)	7118(16)	3946(6)	3.6
C(2)	4326(31)	8189(18)	3982(8)	5.5
C(3)	5559(27)	8156(21)	4358(6)	5.1
C(4)	6536(28)	7044(19)	4437(6)	4.5
C(5)	5344(26)	5993(17)	4360(5)	3.4
C(6)	6258(27)	4828(18)	4396(6)	3.9
C(7)	4998(30)	3826(18)	4471(6)	4.4
C(8)	3717(25)	3756(16)	4095(5)	3.1
C(9)	2962(21)	4984(15)	4010(5)	2.2
C(10)	4267(21)	5970(14)	3949(5)	2.2
C(11)	1633(21)	4900(15)	3657(5)	2.2
C(12)	236(23)	4066(14)	3780(6)	2.8
C(13)	1074(23)	2859(15)	3842(5)	2.9
C(14)	2221(22)	2935(17)	4230(5)	2.5
C(15)	2650(27)	1630(18)	4280(7)	4.2
C(16)	994(31)	1091(19)	4274(7)	5.0
C(17)	−164(28)	1818(16)	3955(6)	3.9
C(18)	4734(26)	3270(16)	3702(6)	3.7
C(19)	5287(25)	5906(16)	3529(6)	3.3
C(20)	−778(32)	1095(16)	3572(6)	4.5
C(21)	−2209(31)	271(18)	3712(8)	5.2
C(22)	621(35)	454(16)	3316(7)	5.1
C(23)	−160(38)	372(17)	2867(9)	6.6
C(24)	−1026(31)	1533(15)	2825(7)	4.5
C(25)	−2604(31)	1573(26)	2520(7)	6.1
C(26)	−3485(32)	2718(18)	2488(7)	5.7
C(27)	−3973(42)	712(26)	2704(9)	8.5
C(28)	8064(26)	7055(21)	4140(6)	4.7
C(29)	7112(30)	7067(22)	4916(7)	5.5
C(30)	1406(28)	3308(20)	4643(5)	4.5
C(31)	258(29)	2441(14)	2684(6)	4.1

a) $B_{eq}=8\pi^2(U_1+U_2+U_3)/3$, where U_1, U_2, and U_3 are the principal components by U matrix.

The structure (**1**) for alnuserrudiolone was finally established by X-ray crystallography of a 3-deoxo-12-keto derivative (**2**) and a 31-bromo derivative (**3**) derived from **1**, because a good single crystal of **1** is not available. Huang-Minlon reduction of **1** gave a 3-deoxo compound (**4**), which could be converted to the 3-deoxo-12-keto derivative (**2**) by the Jones oxidation. The structure of **2** was determined by the direct method using MULTAN[8] and refined by full-matrix least-squares techniques to R=0.105 for 1876 reflections. Final atomic coordinates, bond lengths, and bond angles are given in Tables 1—3. A perspective view of the molecule of **2** is shown in Fig. 1. Since the ORD and the CD curves of **2** exhibited a negative Cotton effect similar to that of 3β-acetoxy-20-hydroxydammaran-12-one,[9,10] the absolute configuration is as given in **2**.

Bromination of **1** was carried out with pyridinium tribromide[11] with a view to preparing the bromo derivative of **1** for an X-ray crystallographic study. However, when **1** was treated with the above reagent,

Table 5. Interatomic distances (l/Å) of **3**, with standard deviations in parentheses

C(1)–C(2)	1.53(3)	C(12)–O(2)	1.49(2)
C(1)–C(10)	1.57(3)	C(13)–C(14)	1.55(2)
C(2)–C(3)	1.56(3)	C(13)–C(17)	1.60(3)
C(3)–C(4)	1.53(3)	C(14)–C(15)	1.56(3)
C(3)–O(1)	1.20(3)	C(14)–C(30)	1.54(3)
C(4)–C(5)	1.57(3)	C(15)–C(16)	1.46(3)
C(4)–C(28)	1.55(3)	C(16)–C(17)	1.62(3)
C(4)–C(29)	1.61(3)	C(17)–C(20)	1.57(3)
C(5)–C(6)	1.54(3)	C(20)–C(21)	1.56(3)
C(5)–C(10)	1.58(2)	C(20)–C(22)	1.58(3)
C(6)–C(7)	1.56(3)	C(20)–O(3)	1.48(2)
C(7)–C(8)	1.59(3)	C(22)–C(23)	1.58(3)
C(8)–C(9)	1.57(3)	C(23)–C(24)	1.52(3)
C(8)–C(14)	1.59(3)	C(24)–C(25)	1.60(3)
C(8)–C(18)	1.61(3)	C(24)–O(3)	1.45(2)
C(9)–C(10)	1.56(2)	C(24)–C(31)	1.54(3)
C(9)–C(11)	1.56(2)	C(25)–C(26)	1.51(4)
C(10)–C(19)	1.58(3)	C(25)–C(27)	1.60(4)
C(11)–C(12)	1.53(2)	C(31)–Br	2.03(2)
C(12)–C(13)	1.57(2)		

Table 6. Bond angles (ϕ/°) of **3**, with standard deviations in parentheses

C(10)–C(1)–C(2)	113(2)	C(13)–C(12)–O(2)	113(1)
C(1)–C(2)–C(3)	114(2)	C(12)–C(13)–C(14)	108(1)
C(2)–C(3)–C(4)	118(2)	C(8)–C(14)–C(13)	105(1)
C(2)–C(3)–O(1)	120(2)	C(8)–C(14)–C(30)	113(2)
C(4)–C(3)–O(1)	121(2)	C(13)–C(14)–C(15)	99(1)
C(3)–C(4)–C(5)	109(2)	C(14)–C(15)–C(16)	102(2)
C(3)–C(4)–C(28)	107(2)	C(15)–C(16)–C(17)	108(2)
C(5)–C(4)–C(29)	107(2)	C(13)–C(17)–C(16)	101(2)
C(4)–C(5)–C(6)	113(2)	C(13)–C(17)–C(20)	115(2)
C(4)–C(5)–C(10)	119(2)	C(16)–C(17)–C(20)	114(2)
C(6)–C(5)–C(10)	108(2)	C(17)–C(20)–C(21)	109(2)
C(5)–C(6)–C(7)	111(2)	C(17)–C(20)–C(22)	116(2)
C(6)–C(7)–C(8)	110(2)	C(21)–C(20)–C(22)	113(2)
C(7)–C(8)–C(9)	110(2)	C(22)–C(20)–O(3)	100(2)
C(7)–C(8)–C(18)	107(2)	C(20)–O(3)–C(24)	115(1)
C(7)–C(8)–C(14)	108(2)	C(20)–C(22)–C(23)	103(2)
C(8)–C(9)–C(10)	116(1)	C(22)–C(23)–C(24)	102(2)
C(8)–C(9)–C(11)	109(1)	C(23)–C(24)–O(3)	105(2)
C(9)–C(10)–C(1)	106(1)	C(23)–C(24)–C(31)	109(2)
C(9)–C(10)–C(19)	115(1)	C(25)–C(24)–O(3)	111(2)
C(5)–C(10)–C(1)	106(1)	C(24)–C(25)–C(26)	116(2)
C(5)–C(10)–C(9)	106(1)	C(24)–C(25)–C(27)	107(2)
C(9)–C(11)–C(12)	110(1)	C(26)–C(25)–C(27)	105(2)
C(11)–C(12)–C(13)	107(1)	C(24)–C(31)–Br	112(1)
C(11)–C(12)–O(2)	106(1)		

the bromination took place with the cyclization of the acyclic side chain of **1**. The presence of the brominated side chain including a tetrahydrofuran ring was evidenced by the high resolution mass spectrum, which exhibited ions at m/z 491.2332, 489.2344, and 139.1104. The ^{13}C NMR signals at δ_c 88.2, 87.5, and 32.9 also demonstrated the presence of the tetrahydrofuran ring[2,3] with a bromomethyl group on C-24. On the other hand, comparison of the high resolution mass and the ^{13}C NMR spectra of the bromo derivative (**3**) with those

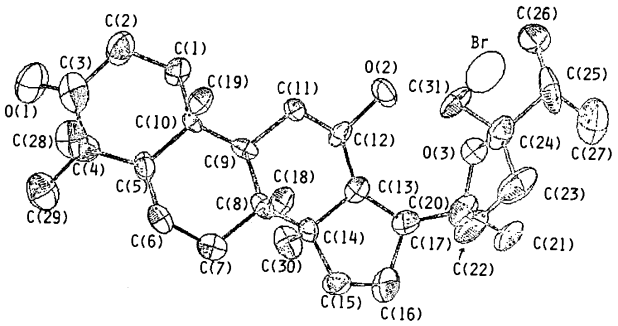

Fig. 2. Perspective view of **3**.

of **1** suggested that **3** possesses the same tetracyclic skeleton as **1**. Further, the bromo derivative (**3**) was confirmed to be convertible into **1** in a quantitative yield by treatment with zinc dust in acetic acid. The structural elucidation of **3** was carried out by X-ray crystallography using the heavy atom method. Refinement by least-squares calculation gave a final R value of 0.075 for 1707 reflections. Final atomic coordinates, bond lengths, and bond angles are shown in Tables 4—6. A perspective view of the molecule of **3** is shown in Fig. 2. The ORD and CD curves of **3** exhibited a positive Cotton effect, which indicated the absolute configuration to be as shown in **3**.

From the spectroscopic evidence of **1** and the X-ray crystallographic results of **2** and **3** derived from **1**, it has now been established that alnuserrudiolone is (12*R*,20*S*)-12,20-dihydroxy-24-methylenedammaran-3-one (**1**).

Experimental

The ^{1}H NMR spectra were taken on a Varian T-60 spectrometer using TMS as an internal standard. The ^{13}C NMR spectra were obtained on a JEOL JNM FX-60 (15.1 MHz) and a Hitachi R-42 FT NMR (22.6 MHz) spectrometers (δ_{TMS}=0). The ORD and the CD curves were taken on a JASCO ORD/UV-5 spectropolarimeter, equipped with a circular dichroism attachment, at 25 °C. The X-ray intensity data were collected on a syntex R3 and a Rigaku AFC-5 diffractometers using graphite-monochromated radiation.

Extraction and Isolation. The male flowers (10.3 kg) of *Alnus serrulatoides* Call. Grown naturally on a river side in the suburbs of Hiroshima city were collected just before the flowering in December, 1975. The flowers, after minced mechanically, were immersed in acetone (54 l) at room temp for 2 months. Removal of the solvent from the acetone solution gave a viscous sirup, which was extracted with ether (500 ml×5) to give a viscous oil (66.0 g). A part (7.0 g) of the viscous oil was subjected to centrifugal chromatography using silica gel (160 g) and a hexane–EtOAc mixture with EtOAc increasing 0 to 100% as a solvent, and then to preparative TLC (silica gel GF_{254}; 0.75 mm thick) with hexane–EtOAc (7 : 3 v/v) to give alnuserrudiolone (**1**) (1.27 g; R_f 0.20).

Alnuserrudiolone (1). Mp 174—175 °C; $[\alpha]_D^{25}$ +50.7° (c 0.61, $CHCl_3$); IR (0.005 M,† CCl_4) ν_{max} 3613 (free OH), 3432 (intramolecularly hydrogen-bonded OH), 1708 (C=O), 3082 and 1638 cm^{-1} (>C=CH$_2$); ^{1}H NMR ($CDCl_3$) δ=0.90—

† 1 M=1 mol dm^{-3}.

1.19 (Me×8), 3.60 (1H, br, >CH–OH), 4.71 and 4.73 (2H, br, >C=CH$_2$); ^{13}C NMR ($CDCl_3$) δ_c=217.8 (s, C-3), 156.5 (s, C-24), 106.2 (t, C-31), 73.6 (s, C-20), 70.5 (d, C-12), 26.7 (q, Me), 26.4 (q, Me), 21.9 (q, Me×2), 21.0 (q, Me), 16.8 (q, Me), 15.9 (q, Me), and 15.3 (q, Me); MS (70 eV) *m/z* 454.3869 (Calcd for $C_{31}H_{50}O_2$ (M−H_2O): 454.3808), 436.3731 ($C_{31}H_{48}O$ (M−2H_2O): 436.3705), 375.2911 ($C_{24}H_{39}O_3$: 375.2900), 205.1603 ($C_{14}H_{21}O$: 205.1592), 141.1280 ($C_9H_{17}O$: 141.1279), 123.1183 (C_9H_{15}: 123.1174); ORD (*c* 0.38, dioxane) $[\phi]_{600}$ +216°, $[\phi]_{589}$ +216°, $[\phi]_{315}$ +2095°, $[\phi]_{309}$ +2033°, $[\phi]_{305}$ +2077°, $[\phi]_{279}$ +73.9°; CD (*c* 0.56, dioxane) $[\theta]_{320}$ 0, $[\theta]_{293}$ +1170, $[\theta]_{243}$ 0.

Found: C, 79.00; H, 11.04%. Calcd for $C_{31}H_{52}O_3$: C, 78.76; H, 11.09%.

Huang-Minlon Reduction of 1. A mixture of **1** (200 mg), hydrazine hydrate (3 ml), and diethylene glycol (30 ml) was refluxed for 2 h to give a 3-deoxo compound (**4**) (157 mg): mp 167—168 °C; $[\alpha]_D^{25}$ +10.7° (*c* 0.56, $CHCl_3$); IR (0.0004 M, CCl_4) ν_{max} 3649, 3431 (OH), and 3081 cm^{-1} (>C=CH$_2$); ^{1}H NMR ($CDCl_3$) δ=3.64 (1H, br, >CH–OH), 4.73 (2H,br, >C=CH$_2$).

Found: C, 81.35; H, 12.16%. Calcd for $C_{31}H_{54}O_2$: C, 81.16; H, 11.87%.

Jones Oxidation of 4. The Jones reagent[12] (2 ml) was added to a solution of **4** (150 mg) in acetone (30 ml), followed by stirring for 1 h at 5 °C, to yield a 3-deoxo-12-keto derivative (**2**) (114 mg): mp 195—197 °C; $[\alpha]_D^{25}$ +44.3° (*c* 0.70, $CHCl_3$); IR (0.0002 M, CCl_4) ν_{max} 3652, 3452 (OH), 1702, 1689 (C=O), and 3083 cm^{-1} (>C=CH$_2$); ^{1}H NMR ($CDCl_3$) δ=4.73 (2H, br, >C=CH$_2$); MS (70 eV) *m/z* (rel. int.) 456 (M^+, 16), 438 (M−H_2O, 55), 359 (88), 315 (49), 191 (85), 141 (44), 124 (100), 123 (73); ORD (*c* 0.23, dioxane) $[\phi]_{600}$ +97°, $[\phi]_{589}$ +97°, $[\phi]_{309}$ −1069°, $[\phi]_{295}$ 0°, $[\phi]_{260}$ +3645°; CD (*c* 0.22, dioxane) $[\theta]_{318}$ 0, $[\theta]_{287}$ −1980, $[\theta]_{244}$ 0.

Found: C, 81.48; H, 11.30%. Calcd for $C_{31}H_{52}O_2$: C, 81.52; H, 11.48%.

Conversion of 1 to a Bromo Derivative (3). Pyridinium tribromide (264 mg)[11] was added to a warmed solution (55 °C) of **1** (300 mg) in EtOH (7.7 ml) and then the mixture was stirred for 1 min. After removal of the solvent, the reaction mixture was subjected to preparative TLC [silica gel GF_{254}; EtOAc–hexane (3 : 7 v/v); developed continuously for 3 h] to give a bromo derivative (**3**) (146 mg): mp 174—176 °C; $[\alpha]_D^{25}$ +33.5° (*c* 0.82, $CHCl_3$); IR (Nujol) ν_{max} 3329 (OH) and 1731 cm^{-1} (C=O); ^{1}H NMR ($CDCl_3$) δ=3.53 (2H, d, *J*=2.5 Hz, –CH_2Br); ^{13}C NMR ($CDCl_3$) δ_c=217.8 (d, C-3), 88.2 (s, C-24), 87.5 (s, C-20), 70.6 (s, C-12), 32.9 (t, C-31), 28.6 (q, Me), 26.7 (q, Me), 21.0 (q, Me), 18.0 (q, Me×2), 17.3 (q, Me), 16.2 (q, Me), 15.4 (q, Me); MS (70 eV) *m/z* 491.2332 (Calcd for $C_{28}H_{42}O_2Br$: 491.2347), 489.2344 ($C_{28}H_{42}O_2Br$: 489.2367), 205.1571 ($C_{14}H_{21}O$: 205.1591), 139.1104 ($C_9H_{15}O$: 139.1122), 43.0539 (C_3H_7: 43.0547); ORD (*c* 0.38, dioxane) $[\phi]_{600}$ +204°, $[\phi]_{589}$ +204°, $[\phi]_{317}$ +1750°, $[\phi]_{312}$ +1640°, $[\phi]_{308}$ +1714°, $[\phi]_{292}$ 0°, $[\phi]_{276}$ −985°, $[\phi]_{246}$ −79°; CD (*c* 0.38, dioxane) $[\theta]_{320}$ 0, $[\theta]_{292}$ +1224, $[\theta]_{264}$ 0.

Found: C, 67.24; H, 9.46%. Calcd for $C_{31}H_{51}O_3Br$: C, 67.60; H, 9.43%.

Conversion of 3 to 1. A suspension of **3** (8 mg) and Zn powder (5 mg) in ether (3 ml) and acetic acid (0.5 ml) was refluxed for 3 h at room temp. The reaction mixture was diluted with water and extracted with ether to give a crude product (6 mg), which was then purified by preparative TLC [silica gel GF_{254}; EtOAc–hexane (3 : 7 v/v)] to afford alnuserrudiolone (**1**) (mp 171—173 °C; direct comparison with mixed mp, ^{1}H NMR, and MS).

X-Ray Crystallographic Analyses. (i) 3-Deoxo-12-keto Derivative (2). The crystal used was about 0.7 mm×0.5 mm×0.05 mm in size. Cell dimensions were obtained by least-squares calculations from 2θ values of 15 well-centered, resolved Cu $K\alpha$ diffraction peaks. Crystal data: monoclinic, space group $P2_1$, two molecules per unit cell with dimensions a=7.629(5), b=10.438(5), c=17.714(6) Å, β=90.84(4)°; U=1410.4 Å^3; D_c=1.08 g cm^{-3}; D_m=1.12 g cm^{-3}; μ(Cu $K\alpha$)=4.30 cm^{-1}. A total of 2506 reflections were collected on an automatic four-circle diffractometer by the 2θ-ω scan method (θ_{max}=70°); 1876 reflections with intensities greater than 2.0 times the standard deviations were used in the structure determination. The phases of 456 strong reflections with $|E|>1.30$ were determined by the direct method, by the use of the program MULTAN.[8] The *E* map for the best solution yielded positions for all non-hydrogen atoms. The structure was refined by full-matrix least-squares methods. Anisotropic refinement for carbon and oxygen atoms reduced the *R* index to 0.105.

(ii) 3l-Bromo Derivative (3). The crystal used was about 0.2 mm×0.3 mm×0.6 mm in size. Cell dimensions were obtained by least-squares calculations from 2θ values of 14 well-centered, resolved Mo $K\alpha$ diffraction peaks. Crystal data: orthorhombic, space group $P2_12_12_1$, four molecules per unit cell with dimensions a=7.991(3), b=11.610(9), c=31.214(21) Å; U=2898.2 Å^3; D_c=1.26 g cm^{-3}; D_m=1.21 g cm^{-3}; μ(Mo $K\alpha$)=15.3 cm^{-1}. A total of 2702 reflections were collected by using the ω-scan technique (θ_{max}=60°); 1707 reflections with intensities greater than 1.96 times the standard deviations were used in the structure determination. The bromine atom position was obtained from a Patterson function, and then the positions of oxygen and carbon atoms were determined by difference-Fourier syntheses. A least-squares refinement using anisotropic temperature factors for bromine, carbon, and oxygen atoms and isotropic ones for hydrogen atoms reduced the *R* index to 0.075.

The complete F_o-F_c data and the tables of anisotropic thermal parameters for **2** and **3** are deposited as Document No. 8151, respectively, at the Office of the Editor of the Bulletin of the Chemical Society of Japan.

The authors thank Mr. Akio Wada of JASCO Instruments Co. Ltd. for useful advice for the X-ray crystallographic analyses and JEOL Co. Ltd. for obtaining the ^{13}C NMR spectra. The present work was partially supported by a Grant-in-Aid for Scientific Research No. 354189 (1978, to T.A.) from the Ministry of Education, Science and Culture and Matsunaga Science Foundation in 1977 (to T.H.).

References

1) J. Heslop-Harrison, "Pollen: Development and Physiology," London Butterworths Co. Ltd., London (1971).

2) T. Hirata and T. Suga, *J. Chem. Soc., Perkin Trans. 2*, **1978**, 347.

3) T. Suga and T. Hirata, *Bull. Chem. Soc. Jpn.*, **52**, 1153 (1979).

4) T. Suga, T. Hirata, and N. Iwata, *Chem. Lett.*, **1974**, 971.

5) P. M. Baker, E. J. L. Barreiro, and B. Gilbert, *Phytochemistry*, **15**, 785 (1976).

6) M. Tori, T. Tsuyuki, and T. Takahashi, *Bull. Chem. Soc. Jpn.*, **50**, 3349 (1977).

7) J. Asakawa, R. Kasai, K. Yamasaki, and O. Tanaka, *Tetrahedron*, **33**, 1935 (1977).

8) G. Germain, P. Main, and M. M. Woolfson, *Acta Crystallogr., Sect. A*, **27**, 368 (1971).
9) O. Tanaka, M. Nagai, and S. Shibata, *Chem. Pharm. Bull.*, **14**, 1150 (1966).
10) Y. Nagai, O. Tanaka, and S. Shibata, *Tetrahedron*, **27**, 881 (1971).
11) C. Djerassi and C. R. Scholy, *J. Am. Chem. Soc.*, **70**, 417 (1948).
12) K. Bowden, I. M. Heilbron, E. R. H. Jones, and B. C. L. Weedon, *J. Chem. Soc.*, **1946**, 36.

Intramolecular Interactions between a Group Bearing *n*-Electrons and a CH_2-X Where X is an Electronegative Group[1)]

Giichi Izumi, Gaku Yamamoto, and Michinori Ōki*

Department of Chemistry, Faculty of Science, The University of Tokyo, Bunkyo-ku, Tokyo 113

(Received April 17, 1981)

Conformational equilibrium of 9-(2-acyloxyethyl)-1,4-dimethoxytriptycenes in chloroform-*d* suggests that the stability of the $\pm sc$ conformation increases as the electronegativity of the acyl group increases. The results together with other pertinent data are discussed from the stand point that there is an attractive interaction between the acyloxymethyl and the methoxyl groups in proximity. Reflecting its high ionization potential, the chloro group in 1-position showed no stabilization of the $\pm sc$ conformation, although mass spectra and some chemical properties indicate that there is an interaction between the chloro group and highly electronegative CH_2X group. A possible correlation of these results with the incipient transition state for S_N2 reactions is suggested.

During the course of investigations on the reactivity-conformation correlations, we have encountered a striking difference in reactivities of 1,2,3,4-tetrachloro-9-(2-chloro-1,1-dimethylethyl)triptycene rotamers: the $\pm sc$ conformation reacted in the presence of titanium tetrachloride to afford Friedel-Crafts cyclization products, whereas the *ap* conformation remained intact under the conditions.[2)] The results suggest that there may be a kind of interaction between the CH_2–Cl group in the substituent at the bridgehead and the chloro group in the peri-position: the peri-chloro group stabilizes the transition state by delocalizing the partially developed positive charge on the carbon atom of the CH_2–Cl group. Although this phenomenon is concerned with the transition state of the reaction, the ground state of the molecule may be stabilized as well if we consider a charge-transfer interaction between the *n*-electrons of the chloro group and the σ^* orbital of the CH_2–Cl group.

Since we have succeeded in detecting the attractive interactions of *n*-electron-phenyl[3)] and *n*-electron-carbonyl[4)] in triptycene systems by looking at the population ratios of rotamers, we thought the same technique may be applied to the present case to diagnose the presence or absence of the interaction involving the CH_2–Cl group and a group carrying a lone pair of electrons. At the outset, it was thought that the attractive interaction could easily be observed if the group in 1-position of the triptycene system had a low ionization potential. Thus we first attempted to synthesize 9-(2-chloroethyl)-1,4-dimethoxytriptycene from the corresponding alcohol and thionyl chloride and observed that the treatment afforded only a cyclized product:[5)] it seemed that the interaction between a CH_2–Cl (or possibly the corresponding ion pairs) and a methoxyl group in this system was so strong that it caused a reaction. The results suggest that if we wish to find interactions instead of reactions, we should use a combination of a weaker electron acceptor than the CH_2–Cl group and a methoxyl group or that of CH_2–Cl group and a weaker electron donor than the methoxyl. Our choice was acyloxymethyl groups instead of the CH_2–Cl in combination with the methoxyl because the electronegativities and consequently the electron-accepting power of the former group can be easily modified by changing the acyl group. This paper reports the results of such investigations together with those of the interaction between a chloro group and a CH_2–X where X is either a chloro or a *p*-toluenesulfonyloxyl group.

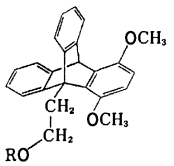

(**1**) R=H
(**2**) R=CH_3
(**3**) R=CH_3CO
(**4**) R=C_6H_5CO
(**5**) R=*p*-$CH_3OC_6H_4CO$
(**6**) R=*p*-$O_2NC_6H_4CO$
(**7**) R=$ClCH_2CO$
(**8**) R=Cl_2CHCO
(**9**) R=Cl_3CCO
(**10**) R=F_3CCO

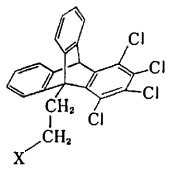

(**11**) X=OH
(**12**) X=CH_3COO
(**13**) X=Cl
(**14**) X=*p*-$CH_3C_6H_4SO_3$

Syntheses of the compounds were straightforward. 9-(Formylmethyl)-1,4-dimethoxytriptycene or 1,2,3,4-tetrachloro-9-(formylmethyl)triptycene was reduced to the corresponding alcohol (**1** and **11**). They were converted to esters by ordinary methods or to chloride by treatment with thionyl chloride.

Experimental

^1H NMR spectra were measured on a Hitachi R-20B spectrometer equipped with a temperature variation accessory. The temperature was read by the chemical shift differences of methanol protons. High resolution mass spectra were recorded on a JEOL JMS-D300 spectrometer.

*9-(2-Hydroxyethyl)-1,4-dimethoxytriptycene (**1**).* To a boiling solution of 1.3 g (3.7 mmol) of 9-(formylmethyl)-1,4-dimethoxytriptycene[4)] in 20 mL of dichloromethane and 20 mL of methanol, 0.5 g (13 mmol) of sodium tetrahydridoborate in 20 mL of methanol was added in 15 min. The mixture was heated for additional 30 min and evaporated. The residue was treated with dilute hydrochloric acid and extracted with dichloromethane. The alcohol, mp 220.8—221.5 °C, was obtained in 95% yield. Found: C, 80.30; H, 6.01%. Calcd for $C_{24}H_{22}O_3$: C, 80.42; H, 6.19%. ^1H NMR ($CDCl_3$, δ): 2.00 (1H, m), 3.50 (2H, t, J=7 Hz), 3.68 (3H, s), 3.77 (3H, s), 4.20 (2H, t, J=7 Hz), 5.88 (1H, s), 6.50 (2H, s), 6.80—7.70 (8H, m).

*1,2,3,4-Tetrachloro-9-(2-hydroxyethyl)triptycene (**11**),* mp 251—252 °C, was similarly prepared by sodium tetrahydridoborate

reduction of 1,2,3,4-tetrachloro-9-(formylmethyl)triptycene.[4] High resolution MS (M^+): 433.9798, 435.9763, 437.9694, and 439.9718. $C_{22}H_{14}OCl_4$ requires 433.9799, 435.9770, 437.9740, and 439.9708. The intensities of these observed M^+ peaks agreed well with those calculated from the natural abundance of ^{35}Cl and ^{37}Cl.

1,4-Dimethoxy-9-(2-methoxyethyl)triptycene (2). To a solution of 0.5 g (1.4 mmol) of 9-(2-hydroxyethyl)-1,4-dimethoxytriptycene (**1**) in 30 mL of tetrahydrofuran, was added 0.2 g (8 mmol) of sodium hydride which had been washed with hexane. The mixture was stirred for 1 h and then 0.5 mL (0.8 mmol) of methyl iodide was added to the mixture. Stirring was continued in a sealed system for 24 h and the solvent was evaporated. The residue was treated with dilute hydrochloric acid and extracted with dichloromethane. Evaporation of the solvent followed by recrystallization of the residue from benzene–hexane afforded the desired compound, mp 226—227 °C, in 92% yield. Found: C, 80.91; H, 6.66%. Calcd for $C_{25}H_{24}O_3$: C, 80.62; H, 6.49%. ^1H NMR ($CDCl_3$, δ): 3.45 (3H, s), 3.66 (3H, s), 3.74 (3H, s), *ca.* 3.5 (2H), 3.98 (2H, br t), 5.88 (1H, s), 6.46 (2H, s), 6.80—7.70 (8H, m).

Esters of 9-(2-Hydroxyethyl)-1,4-dimethoxytriptycene. A general procedure is given for acetylation. The other compounds were similarly prepared from the alcohol and acyl chloride except trifluoroacetate, in the preparation of which the acid anhydride was used.

A mixture of 0.6 g of the alcohol and 0.2 mL of acetyl chloride in 3 mL of pyridine was shaken for 5 min. To the mixture were added 30 mL of dichloromethane and dilute hydrochloric acid. The organic layer afforded, after chromatography on silica gel (benzene–hexane), the acetate (**3**), mp 167—168 °C, in 82% yield. Found: C, 77.77; H, 5.94%. Calcd for $C_{26}H_{24}O_4$: C, 77.98; H, 6.04%. ^1H NMR ($CDCl_3$, δ): 2.21 (3H, s), 3.56 (2H, br t, J=7 Hz), 3.70 (3H, s), 3.77 (3H, s), 4.78 (2H, t, J=7 Hz), 5.88 (1H, s), 6.50 (2H, s), 6.90—7.70 (8H, m).

Benzoate (4), mp 170.4—171.2 °C. Found: C, 80.56; H, 5.52%. Calcd for $C_{31}H_{26}O_4$: C, 80.50; H, 5.67%. ^1H NMR ($CDCl_3$, δ): 3.71 (3H, s), 3.79 (3H, s), 3.50—4.00 (2H), 5.07 (2H, t, J=7 Hz), 5.90 (1H, s), 6.51 (2H, s), 6.90—7.70 (11H, m), 8.10—8.30 (2H, m).

p-*Methoxybenzoate (5)*, mp 192.5—193.0 °C. Found: C, 77.86; H, 5.53%. Calcd for $C_{32}H_{28}O_5$: C, 78.03; H, 5.73%. ^1H NMR ($CDCl_3$, δ): 3.73 (3H, s), 3.80 (3H, s), 3.89 (3H, s), 3.50—4.00 (2H), 5.02 (2H, t, J=7 Hz), 5.90 (1H, s), 6.52 (2H, s), 6.90—7.70 (10H, m), 8.19 (2H, d, J=9 Hz).

p-*Nitrobenzoate (6)*, mp 254—255 °C. Found: C, 73.52; H, 4.71; N, 2.58%. Calcd for $C_{31}H_{25}NO_6$: C, 73.36; H, 4.97; N, 2.76%. This compound was so scarcely soluble in chloroform-*d* that the NMR measurement was not carried out.

Chloroacetate (7), mp 166—167 °C. Found: C, 71.80; H, 5.33; Cl, 8.15%. Calcd for $C_{26}H_{23}O_4Cl$: C, 71.69; H, 5.30; Cl, 8.10%. ^1H NMR ($CDCl_3$, δ): 3.56 (2H, br t, J=7 Hz), 3.71 (3H, s), 3.79 (3H, s), 4.20 (2H, s), 4.90 (2H, t, J=7 Hz), 5.88 (1H, s), 6.50 (2H, s), 6.90—7.60 (8H, m).

Dichloroacetate (8), mp 166.5—167.0 °C. Found: C, 66.39; H, 4.75; Cl, 14.97%. Calcd for $C_{26}H_{22}O_4Cl_2$: C, 66.53; H, 4.72; Cl, 15.11%. ^1H NMR ($CDCl_3$, δ): 3.60 (2H, br t), 3.72 (3H, s), 3.79 (3H, s), 5.00 (2H, t, J=6.5 Hz), 5.90 (1H, s), 6.62 (2H, s), 6.90—7.60 (8H, m).

Trichloroacetate (9), mp 178—179 °C. High resolution MS (M^+): 502.0485, 504.0471, 506.0357, and 508.0418. $C_{26}H_{21}O_4Cl_3$ requires 502.0507, 504.0477, 506.0448, and 508.0418. The observed intensities of the molecular ions agreed well with those calculated from the natural abundance of ^{35}Cl and ^{37}Cl. The base peak was 326.1292 to indicate that the loss of a trichloroacetoxyl and a methyl group occurred. ^1H NMR ($CDCl_3$, δ): 3.72 (3H, s), 3.80 (3H, s), *ca.* 3.75 (2H), 5.08 (2H, t, J=6.5 Hz), 5.90 (1H, s), 6.53 (2H, s), 6.90—7.60 (8H, m).

Trifluoroacetate (10), mp 170.0—170.3 °C. Found: C, 68.94; H, 4.86%. Calcd for $C_{26}H_{21}O_4F_3$: C, 68.72; H, 4.66%. ^1H NMR ($CDCl_3$, δ): 3.60 (2H, br t, J=6.5 Hz), 3.70 (3H, s), 3.79 (3H, s), 5.08 (2H, t, J=6.5 Hz), 5.85 (1H, s), 6.52 (2H, s), 6.90—7.60 (8H, m).

9-(2-Acetoxyethyl)-1,2,3,4-tetrachlorotriptycene (12), mp 192—193 °C, was similarly prepared from the corresponding alcohol (**11**). Found: C, 60.40; H, 3.58%. Calcd for $C_{24}H_{16}O_2Cl_4$: C, 60.28; H, 3.37%. ^1H NMR ($CDCl_3$, δ): 2.23 (3H, s), 3.86 (2H, t, J=7 Hz), 4.61 (2H, t, J=7 Hz), 6.01 (1H, s), 7.00—7.70 (8H, m).

1,2,3,4-Tetrachloro-9-(2-chloroethyl)triptycene (13). A solution of 0.1 g of the alcohol (**11**) in 30 mL of dichloromethane and 0.2 mL of thionyl chloride were stirred at 0 °C for 30 min and then refluxed for 30 min. The mixture was mixed with dilute aqueous sodium hydroxide and shaken. Evaporation of the organic layer followed by recrystallization of the residue from tetrahydrofuran–hexane afforded the desired material, mp 270—271 °C, in 93% yield. High resolution MS gave M^+ peaks at 451.9515, 453.9501, 455.9610, and 457.9221. Peaks corresponding to the loss of a hydrogen chloride and a chlorine were observed. The intensity ratios were in agreement with the calculated from the natural abundance of ^{35}Cl and ^{37}Cl. $C_{22}H_{13}Cl_5$ requires 451.9445, 453.9431, 455.9401, and 457.9372. ^1H NMR ($CDCl_3$, δ): 3.91 (2H, br t, J=6.5 Hz), 4.51 (2H, br t, J=6.5 Hz), 6.03 (1H, s), 6.90—7.70 (8H, m).

1,2,3,4-Tetrachloro-9-[2-(p-tolylsulfonyloxy)ethyl]triptycene (14). A mixture of 0.1 g of the alcohol (**11**), 10 mL of pyridine and 0.1 g of *p*-toluenesulfonyl chloride was stirred at room temperature for 24 h. The mixture was shaken with 40 mL of dichloromethane and dilute hydrochloric acid. The desired product was rather labile and hydrolyzed to the starting material on standing and on chromatography. ^1H NMR ($CDCl_3$, δ): 2.45 (3H, s), 3.88 (2H, t, J=7 Hz), 4.60 (2H, t, J=7 Hz), 5.99 (1H, s), 6.90—7.60 (10H, m), 7.88 (2H, d, J=8 Hz).

Deuterated Compounds. 9-Allyl-1,4-di(methoxy-d_3)triptycene was prepared as described elsewhere[5] from the Diels-Alder adduct between 9-allylanthracene and *p*-benzoquinone and di(methyl-d_3) sulfate. It was ozonized as reported to produce 9-(formylmethyl)-1,4-di(methoxy-d_3)triptycene which was reduced with sodium tetrahydridoborate. The alcohol (**1**-d_6) thus obtained was transformed into esters as described above.

The ^1H NMR spectrum of a chloroform-*d* solution of the acetate at −55 °C showed an AB quartet (δ 3.08 and 3.74, J=15 Hz) and a singlet (δ 3.74), whose relative intensities were 2.1±0.4, on irradiation at δ 4.76 corresponding to $AcOCH_2$ protons. Under the same conditions, the peak at δ 6.50 split into two peaks (δ 6.48 and 6.58). The intensity ratio (the low field peak over the high field peak) was 1.6±0.2.

The ^1H NMR spectrum of the trifluoroacetate at −50 °C gave the following data. 9-CH_2: quartet δ 3.28 and 3.82, J=15 Hz; singlet δ 3.74; intensity ratio (quartet/singlet) 2.9±0.8. Dimethoxybenzo protons: δ 6.51 and 6.42; intensity ratio (low/high) 3.1±0.3.

Results and Discussion

Determination of Conformations and Population Ratios.

Since the compounds studied here all carry a CH_2 group at the bridgehead of the triptycene skeleton, it should exhibit, in principle, a set of AB quartet if it is the $\pm sc$ conformation and a singlet if it is the *ap*. In practice, however, the determination of conformation poses difficult questions. Firstly, since the CH_2 (α) group at the bridgehead is connected to another CH_2 (β) group, it is necessary for seeing clearly a set of AB quartet and a singlet to irradiate the β-CH_2 protons for decoupling. Then, if the chemical shifts of these two methylene protons are very close, the α-CH_2 protons are partially saturated to make it difficult to obtain good data for the intensity. Secondly, the compounds carrying methoxyl groups give the methoxyl signals in the range of those due to α-CH_2 to cause heavy overlaps. And finally irradiation of β-CH_2 protons may not cause saturation completely because of its range.

These difficult situations were overcome by the following procedures. Since the overlap of the α-CH_2 signals can be avoided by deuterating the methoxyl groups, we first synthesized two triptycenes (acetate and trifluoroacetate) carrying the fully deuterated methoxyl groups in 1,4-positions. Their population ratios were observed by irradiating the β-CH_2 protons. We found that the population ratios obtained by integrating the AB quartet and the singlet due to $\pm sc$ and *ap* conformations, respectively, involve rather large errors but are in agreement with those obtained by integrating singlets which are formed by splitting of the signal at δ 6.5, if we assume that the signal at a higher magnetic field is due to the *ap* form and that at a lower field to the $\pm sc$ form. The protons which give a signal at δ 6.5 at room temperature are assigned to the aromatic protons of the dimethoxybenzeno bridge from the electronic density considerations. Since the splitting of the signal at δ 6.5 is definitely caused by freezing of the conformations, it is reasonable to assume that the intensities of these signals reflect conformational populations. Since the correspondence of the higher field signal to the population of the *ap* conformation and that of a lower field signal to the $\pm sc$ were unaltered in the cases examined, we may assume that the tendency is common in the series examined here, although the exact cause for the chemical shifts is unknown. As discussed later, this assumption afforded reasonable data about the conformational populations.

Conformational Equilibria. The population ratios of conformers of 1,4-dimethoxytriptycenes are listed in Table 1 together with pK_a values of the corresponding acids. Since the population ratio $\pm sc/ap$ of 9-ethyl-1,4-dimethoxytriptycene is known to be 1.0,[6] we cannot take the appearance of the $\pm sc$ conformer as evidence for the presence of attractive interactions as are the other cases.[4] Thus we take the 9-(2-methoxyethyl) compound (**2**) as a reference. This compound exhibits a low $\pm sc/ap$ value which is close to that of 9-ethyl-1,4-dimethoxytriptycene and can be taken that the attractive interaction between the methoxymethyl and the methoxyl groups is absent because of the low electron-accepting power of the former: thus this much of population ratio is expected in the absence of the attractive interaction.

Table 1. Populations ratios ($\pm sc/ap$) of 9-(2-acyloxy- or alkoxyethyl)-1,4-dimethoxytriptycene and pK_a's of the corresponding acids

Acyl (or Alkyl) group (R)	$\pm sc/ap$	Temp/°C	pK_a of ROH[7]
CH_3	0.7	−50	14.4
CH_3CO	1.5	−45	4.76
C_6H_5CO	1.7	−50	4.20
p-$CH_3OC_6H_4CO$	1.7	−50	4.47
$ClCH_2CO$	2.0	−45	2.86
Cl_2CHCO	2.5	−45	1.26
Cl_3CCO	3.0	−50	0.65
F_3CCO	3.0	−50	0.23

Inspection of the data in Table 1 reveals that all the compounds examined here exhibit larger $\pm sc/ap$ values than that of the 9-(2-methoxyethyl) compound (**2**). The results cannot be attributed to the electric effect although it was the case for some carbonyl-substituted triptycenes.[4] Although the conformation of the acyloxyl group is not well known, the important contribution for the interaction with the dipole of the peri-methoxyl group should be given by the CH_2–O group. Then the $\pm sc$ form is considered to be more polar since the two dipoles are arranged in a closer proximity: there cannot be an important compensation by solvent molecules. Therefore, if it is the electric nature which dominates as a factor in controlling the population, the $\pm sc$ form should be disfavored in nonpolar solvents such as chloroform. The difference between the methoxy (**2**) and acyloxy compounds cannot be accommodated by the steric repulsion either, because the steric sizes are, by and large, the same among the conformers examined.

The favoredness of the $\pm sc$ conformation relative to the *ap*, when an electronegative acyl group is introduced, should be attributed to the increased stability of the $\pm sc$ conformation, because no instability factor associated with the *ap* form is apparent. The results correspond to the fact that the acyloxyl group is more electronegative than the methoxyl and consequently the former group is more electron-accepting. pK_a values of carboxylic acids are associated with the electronegativities of the acyl group.[8] The fact that, among carboxylic esters, the larger is the pK_a of the corresponding acid, the smaller is the $\pm sc/ap$ value, although a minor change in pK_a does not seem to affect the $\pm sc/ap$ value to a significant extent, clearly shows that the attracting interaction is occurring between the acyloxymethyl group and the methoxyl group. The nature of the interaction is of the charge-transfer type, the acyloxymethyl group acting as an electron acceptor and the methoxyl group as an electron-donor.

Since the acyloxymethyl group should possess at least two low-lying vacant orbitals, it may be worthwhile to discuss the orbitals involved in the interaction here. Our choice is the σ^* orbital, which involves mainly the CH_2–O group, that is responsible to the interaction. It may be argued that the π^* orbital of the carbonyl group is responsible because of its electron-accepting ability. Indeed, the C–T interaction involving the carbonyl moiety is well documented.[4,9] However, we rule out

this possibility for the following reasons. The first is the fact that if the interaction between the carbonyl of the acyl group and the methoxyl had occurred, the ring formed there must be 8-membered. This kind of interaction is usually very unfavorable because of the decrease in entropy. It is especially so if we consider the weakness of the interaction discussed here. The second is indirect but is more convincing. Namely the attempt at synthesizing the tosylate of 9-(2-hydroxyethyl)-1,4-dimethoxytriptycene ended in the formation of a cyclic ether.[5] In this case, the result is best accommodated by assuming that the interaction between the SO_3–CH_2 and the methoxyl groups was so strong that it resulted in a reaction. Several phenomena related to this may be cited: that is the reactivities of 9-(2-chloroethyl) compound (**13**) which will be discussed later in this paper, where it becomes apparent that an interaction between a CH_2–Cl and a chloro group can take place. Finally the behavior of the trichloroacetate (**9**) may be taken into consideration. An attempted purification of the compound on a TLC plate which was inpregnated strongly activated silica gel ended in failure because a part of the compound reacted to give a cyclized compound, 6-methoxy-7,11b-*o*-benzeno-7,11b-dihydronaphtho[1,2,3-*de*]chromene.[5] The results together with the fact that the loss of a trichloroacetoxyl and a methyl groups was observed in the MS support the idea that it is the trichloroacetoxy-CH_2 group that is interacting with the methoxyl group in the peri-position. These considerations lead to a conclusion that σ^* orbital of the CH_2–O group is responsible to the interaction.

In contrast to the population ratios of the 1,4-dimethoxytriptycenes, 9-(2-acetoxyethyl)-1,2,3,4-tetrachlorotriptycene (**12**) showed the sole presence of the *ap* form at −50 °C. It was not possible to obtain a $\pm sc/ap$ ratio of 1,2,3,4-tetrachloro-9-(2-chloroethyl)-triptycene (**13**), since the NMR signals of α-CH_2 and β-CH_2 in this compound were too closely located to perform a decoupling experiment. 1,2,3,4-Tetrachloro-9-[2-(*p*-tolylsulfonyloxy)ethyl]triptycene (**14**) did show a sign of the presence of the $\pm sc$ form but the $\pm sc/ap$ value was practically zero. These results indicate that, being a weak electron-donor than a methoxyl group,[10] the chloro group is not a good enough electron-donor for the detectable interaction: that is best illustrated by the fact that compound **14** was prepared at room temperature in contrast to the facile cyclization of 1,4-dimethoxy-9-[2-(*p*-tolylsulfonyloxy)ethyl]triptycene.[5] The size of the chloro group is also responsible to the absence of the interaction.

Although the interaction between the CH_2–X and the chloro groups in compounds **12**, **13**, and **14** was not spectroscopically detectable, the chemical properties of the latter two compounds do indicate the presence of such an interaction. The CH_2–Cl compound (**13**) afforded 1,2,3,4-tetrachloro-9-(2-hydroxyethyl)triptycene (**11**) on chromatography on silica gel. Namely, the hydrolysis of the CH_2–Cl group in **13** is very easy. Probably the stabilization of a chloronium cation (**15**)[11] or the incipient transition state (**16**) for the formation of the chloronium cation is responsible to the phenomenon. A similar situation is found for the tosylate (**14**) as well: chromatography of this compound on silica gel or standing a solution of **14** in tetrahydrofuran–hexane in atmosphere caused hydrolysis to afford **11**. Fragmentation of **13** in mass spectroscopy is a further support to the above discussion: those corresponding to the chloronium ion (**15**) and to the loss of a hydrogen chloride molecule were observed as strong peaks, whereas the molecular ion peaks were rather weak in this compound.

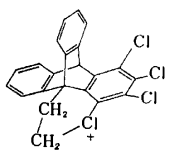

15

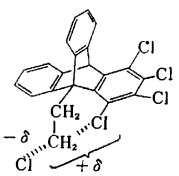

16

Establishing that there is an attractive interaction between the CH_2–Cl and the chloro group, we can now discuss the population ratios of 1,2,3,4-tetrachloro-9-(2-chloro-1,1-dimethylethyl)triptycene and 1,2,3,4-tetrachloro-9-(2-chloro-1-chloromethyl-1-methylethyl)triptycene.[12] As were discussed elsewhere,[13] the $\pm sc/ap$ ratio of 1,2,3,4-tetrachloro-9-(2-phenyl-1,1-dimethylethyl)triptycene is 0.48.[14] Being larger than a methyl, the chloromethyl group in 9-(2-chloro-1,1-dimethylethyl)- and 9-(2-chloro-1-chloromethyl-1-methylethyl)-1,2,3,4-tetrachlorotriptycenes should disfavor conformations in which the chloromethyl group is close to the peri-chloro group. In practice, however, the *ap* form of the latter which has two chloromethyl groups flanking the peri-chloro is unusually favored: $\pm sc/ap$ for the former is 0.96 and that for the latter is 1.80. We may attribute this anomaly to the attractive interaction between the CH_2–Cl and the chloro group.

Incipient Transition State for S_N2 *Reactions.* The above discussions reveal that the interaction as depicted by **16** is important. Then it implies that the molecules investigated here present models for the incipient transition state for S_N2 reactions. Here the peri-chloro or peri-methoxyl group acts as a nucleophile and the chloro or acyloxyl group in the 9-substituent as the leaving group in S_N2 reactions. This view is in conformity with the idea that pK_a values of acids corresponding to the leaving groups parallel with the leaving ability.[15] As we predicted before, the triptycene system has proved to be a good one in finding weak interactions which are otherwise not detectable. Dunitz *et al.* were able to show that the intramolecular nucleophile-carbonyl interaction could be taken as models for the nucleophilic addition to the carbonyl group.[16] We now add that the intramolecular interaction between a chloro or a methoxyl group and a CH_2–X group where X is an electronegative group can be considered as models for the incipient transition state of S_N2 reactions.

S_N2 reactions had originally been considered that it involves a single transition state.[17] However, data are accumulating for these days which suggest that S_N2 reactions may involve multisteps. Sneen *et al.* postulated that S_N2 reactions involve prior ionization from product distributions and rates of reaction studied as a function

of nucleophile concentration in competitive substitutions by solvent and nucleophile.[18] Ion cyclotron resonance study by Brauman and coworkers revealed that organic halides form complexes with nucleophiles before reaching the transition state for the S_N2 reactions.[19] Roberts *et al.*, using high-pressure mass spectrometry, have shown that various alkyl halides form complexes with nucleophiles.[20] Hayami and his coworkers have shown that a mixture of an organic halide and a nucleophile shows a definite shift in ^1H NMR spectroscopy and attributed this phenomenon to the formation of a hydrogen bond.[21] Since our system is a primary halide or a primary alkyl ester, the phenomenon may be attributed to the hydrogen bonding as well. However, we take the fact shown by Roberts *et al.* that even *t*-butyl bromide or carbon tetrachloride can form a complex significant. We prefer to state that, during the course of S_N2 reactions, there is a point which is stable due to interactions between *n*-electrons of a nucleophile and the σ^* orbital of a substrate.

We wish to acknowledge the receipt of a Grant-in-Aid for Scientific Research from the Ministry of Education, Science and Culture which made this work possible.

References

1) A preliminary note has been published: G. Izumi, G. Yamamoto, and M. Ōki, *Chem. Lett.*, **1980**, 969.

2) H. Kikuchi, T. Mitsuhashi, and M. Ōki, *Chem. Lett.*, **1980**, 209.

3) F. Suzuki and M. Ōki, *Tetrahedron Lett.*, **1974**, 2845; *Bull. Chem. Soc. Jpn.*, **48**, 596 (1975).

4) M. Ōki, G. Izumi, G. Yamamoto, and N. Nakamura, *Chem. Lett.*, **1980**, 213; *Bull. Chem. Soc. Jpn.*, in press.

5) G. Izumi, S. Hatakeyama, and M. Ōki, *Bull. Chem. Soc. Jpn.*, **54**, 258 (1981).

6) H. Nakanishi and O. Yamamoto, *Bull. Chem. Soc. Jpn.*, **51**, 1777 (1978).

7) "Constants of Organic Compounds," ed by M. Kotake, Asakura, Tokyo (1963).

8) H. C. Brown, D. H. McDaniel, and O. Häfliger, "Dissociation Constants," in "Determination of Organic Structures by Physical Methods," ed by E. A. Braude and F. C. Nachod, Academic Press, New York (1955), pp. 567—662.

9) N. J. Leonard, *Rec. Chem. Progr.*, **17**, 243 (1956).

10) Ionization potentials of 1,4-dimethoxybenzene and and 1,2,3,4-tetrachlorobenzene have been determined. M. Klessinger, P. Asmus, and U. Kraatz, *Tetrahedron*, **31**, 517 (1975); D. G. Streets and G. P. Ceasar, *Mol. Phys.*, **26**, 1037 (1973).

11) P. E. Peterson and E. V. P. Tao, *J. Am. Chem. Soc.*, **86**, 4503 (1964); G. A. Olah and P. E. Peterson, *ibid.*, **90**, 4675 (1968); N. S. Isaacs, "Reactive Intermediates in Organic Chemistry," John-Wiley, New York (1974), pp. 200—212.

12) S. Seki, T. Morinaga, H. Kikuchi, T. Mitsuhashi, G. Yamamoto, and M. Ōki, *Bull. Chem. Soc., Jpn.* **54**, 1465 (1981).

13) G. Yamamoto, M. Suzuki, and M. Ōki, *Angew. Chem.*, **93**, 580 (1981).

14) Since the population ratio is affected by the peri-substituent in this series, we may have to consider the solvation effect: if it is an isolated molecule, the phenyl in the 9-substituent should give little influence on the stability. However, to the first approximation, we may neglect the solvent molecules.

15) L. P. Hammett and H. L. Pfluger, *J. Am. Chem. Soc.*, **55**, 4079 (1933).

16) M. Kaftory and J. D. Dunitz, *Acta Crystallogr., Sect. B*, **30**, 1517 (1974); **31**, 2917 (1975).

17) C. K. Ingold, "Structure and Mechanism in Organic Chemistry," Cornell University Press, Ithaca (1953), pp. 306—418.

18) R. A. Sneen and H. M. Robbins, *J. Am. Chem. Soc.*, **94**, 7868 (1972) and earlier papers.

19) W. M. Olmstead and J. I. Brauman, *J. Am. Chem. Soc.*, **99**, 4219 (1977); M. J. Pellerite and J. I. Brauman, *ibid.*, **102**, 5993 (1980).

20) R. C. Doughety, J. Dalton, and J. D. Roberts, *Org. Mass Spectrom.*, **8**, 77 (1974); R. C. Dougherty, *ibid.*, **8**, 85 (1974).

21) J. Hayami, T. Koyanagi, N. Hihara, and A. Kaji, *Bull. Chem. Soc. Jpn.*, **51**, 891 (1978) and papers cited therein.

A New Method for Protein Sequence Analysis Using Edman-degradation, Field-desorption Mass Spectrometry and Computer Calculation. Sequence Determination of the *N*-Terminal BrCN Fragment of *Streptomyces erythraeus* Lysozyme

Yasutsugu SHIMONISHI,* Yeong-Man HONG, Itsuo KATAKUSE,† and Saburo HARA††

Institute for Protein Research, Osaka University, Suita, Osaka 565

†*Department of Physics, Faculty of Science, Osaka University, Toyonaka, Osaka 560*

††*Department of Chemistry, Faculty of Science, Osaka University, Toyonaka, Osaka 560*

(Received April 22, 1981)

A new method is described for protein sequence analysis. The principle is realized as follows: 1) determination by field-desorption mass spectrometry of the molecular weights of the constituents in peptide mixtures prepared from a polypeptide or protein by specific cleavage methods, 2) quantitation of the 3-phenyl-2-thiohydantoin derivatives of amino acids liberated successively from the constituent peptides in 1) by Edman-degradation, and 3) determination of amino acid sequences with a computer from the data obtained in 1) and 2). The method was applied to sequence determination of a polypeptide of unknown structure, the *N*-terminal BrCN fragment of *Streptomyces erythraeus* lysozyme.

The Edman method[1] is widely used for sequencing of polypeptides and proteins, making it possible to determine their partial or even almost complete sequences by cleavage and identification of the *N*-terminal amino acid residue in each degradation reaction. Recently, we[2-4] reported a new method for sequencing of peptide mixtures that cannot be achieved by Edman-degradation alone, by a combination of Edman-degradation and field-desorption mass spectrometry.[5] The principle of the method is based on the determination of the molecular weights of peptides and peptide fragments degraded by the Edman method in a mixture by the field-desorption ionization technique and calculation of possible mass differences before and after degradation. We also reported that when preparations of peptide mixtures are obtained from a polypeptide by two or more kinds of specific cleavage methods, the sequence of the polypeptide can be examined using the computer program "PROSEQ,"[6] the data for which consist of the molecular weights and partial amino acid sequences, determined by the method[2-4] described above, of constituent peptides in mixtures.

More recently, some of the authors and others[7,8] developed another method for sequencing of polypeptides and proteins. The procedure consists of the following steps: 1) determination by the field-desorption ionization technique of the molecular weights of peptides in mixtures, which are prepared from a polypeptide by two or more kinds of specific cleavage methods, and their peptide fragments obtained after one-cycle of degradation, 2) estimation of the 3-phenyl-2-thiohydantoin derivatives of amino acids released successively from peptides in mixtures, prepared in 1), by Edman-degradation, and 3) deduction of amino acid sequences from the data obtained in 1) and 2) using the computer program "PROSEQ2."[8] The program "PROSEQ2" uses the data on the 3-phenyl-2-thiohydantoin amino acids released from peptide mixtures in each cycle of Edman-degradation in place of those on partial amino acid sequences of constituent peptides used in "PROSEQ1." We named the procedure the "IPR-sequencing method." To appreciate the utility of the procedure, the sequence of a polypeptide of unknown structure was examined.

In this paper we report in detail the sequence determination of the *N*-terminal BrCN fragment of *Streptomyces erythraeus* lysozyme[9] (SE lysozyme) of unknown sequence, which consists of 55 amino acid residues with an Ala residue at the *N*-terminus,[10] by the procedure. The amino acid sequence of this polypeptide was determined from data on peptides prepared by tryptic and chymotryptic digestion.

Materials and Methods

The *N*-terminal BrCN fragment of SE lysozyme was isolated as described elsewhere.[10] Trypsin treated with L-(1-tosylamino-2-phenylethyl) chloromethyl ketone was purchased from Worthington Biochemical Corp. (USA) and chymotrypsin treated with L-(1-tosylamino-5-aminopentyl) chloromethyl ketone from Sigma Chemical Co. (USA). [Gly[1]]-ACTH-(1—18)-NH_2[11] was obtained from Shionogi Research Laboratory, Shionogi and Co., Ltd. (Osaka), by courtesy of Dr. K. Inouye. H-Val-Tyr-Ile-His-Pro-Phe-OH was synthesized by a conventional method in this laboratory. Reagents for Edman-degradation were obtained from Wako Pure Chemical Ind. Ltd. (Osaka). The solvents used were redistilled. All other reagents were reagent grade and were used without further purification.

BrCN Cleavage. A peptide was dissolved at a concentration of 1% (w/v) and in a ratio of its Met residue to BrCN of 50/1 (mol/mol) in 70% formic acid.[12] The solution was stood for 20 h at 25 °C, diluted with distilled water and lyophilized repeatedly.

Enzymic Digestion. The *N*-terminal BrCN fragment (0.7 mg (110 nmol) and 1.0 mg (160 nmol)) of SE lysozyme were digested with trypsin and chymotrypsin, respectively, at a substrate concentration of 1% (w/v) and in a ratio of substrate to enzyme at 50/1 (w/w) in 1% NH_4HCO_3 at pH 8.0 for 4 h at 37 °C, and the digests were lyophilized immediately after the reaction.

Field-desorption Mass Spectra. Field-desorption

mass spectra were measured with a second-order double focusing mass spectrometer[13] with a mono field-desorption ion source, equipped with a data processor (JEOL JMA-2000 mass data analysis system). Mass assignment was made using polypropylene glycol as a standard.[14] Silicon emitters[15] grown on a tungsten wire were used for measurements of field-desorption mass spectra. The lyophilized material of sample peptides was dissolved in a mixture of pyridine and water (1/1, v/v) and the solution (1—2 μl containing 1—2 μg of sample peptides) was loaded by the syringe technique[16] on the emitter. The conditions for measurement of field-desorption mass spectra were as described.[15]

Edman-degradation. Degradations were performed manually as described[1,4] using the following buffer solutions: a) a mixture of pyridine and water (1/1, v/v), pH 9.35; b) a mixture of pyridine and water (1/1, v/v), adjusted to pH 9.5 by adding *N*-methylmorpholine; c) a mixture of pyridine and water (1/1, v/v), adjusted to pH 9.5 by adding 30% aq trimethylamine and glacial acetic acid, and d) a mixture of pyridine and water (1/1, v/v), adjusted to pH 9.5 by adding *N,N*-dimethylallylamine and trifluoroacetic acid.[1] The resultant 3-phenyl-2-thiohydantoin derivatives of amino acids were subjected to high-performance liquid chromatography, and the remaining peptides in the water layer were subjected to field-desorption mass spectrometry.

High-performance Liquid Chromatography (HPLC). HPLC was performed on a Zorbax ODS column (4.6 mm × 25 cm) (Dupont) in a high-performance liquid chromatograph (Shimadzu HPLC LC-3A equipped with a data processor chromatopac C-R1A), for the quantitation of the 3-phenyl-2-thiohydantoin derivatives of amino acids released from sample peptides by Edman-degradation. Samples were dissolved in methanol and introduced into the sample holder. The solvent employed for chromatography was a mixture of CH_3CN and 0.01 M NaOAc (pH 4.5) (42/58, v/v).[17] Chromatography was performed at 62 °C at a flow rate of 1.0 ml/min for samples from the organic phase and at 2.0 ml/min for those from the aqueous phase.

Computer Calculation. The computer programs "PROSEQ1"[6] and "PROSEQ2"[8] were used for deducing the major portions of the sequences or the complete sequences of the polypeptide from the data on the peptides obtained by digestions of the polypeptide with trypsin and chymotrypsin. Calculations were carried out in the ACOS 700 computer of the Crystallographic Research Center (Institute for Protein Research, Osaka University).

Results and Discussion

Mass Spectra of Peptides Containing Homoserine Residues at the C-*Terminus.* The cleavage of a polypeptide or protein containing a Met residue(s) by BrCN[12] gives a peptide fragment(s) containing a homoserine residue at its (their) *C*-terminus and the *C*-terminal fragment of the original polypeptide or protein, as *N*-terminal BrCN fragments. Therefore, in this experiment,

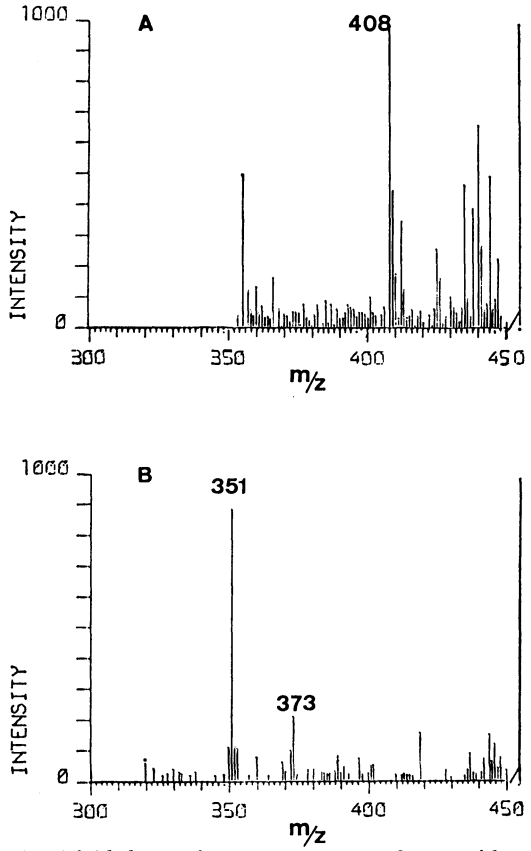

Fig. 1. Field-desorption mass spectra of a peptide mixture (A) prepared by cleavage of [Gly¹]-ACTH-(1—18)-NH_2 with BrCN and its one-step degraded peptide fragments (B). Spectra are shown in the range from 300 to 450 atomic mass units.

it was necessary to obtain information on whether peptides containing a homoserine residue at their *C*-termini give mass peaks with mass values of homoserine-peptides or those of homoserine-lactone peptides in mass spectra. As examples, we measured the field-desorption mass spectra of a peptide mixture obtained by cleavage with BrCN of [Gly¹]-ACTH-(1—18)-NH_2[11] containing a Met residue at the 5th position from the *N*-terminus and its peptide fragments prepared after one-cycle of Edman-degradation, as shown in Figs. 1A and 1B. The mass peaks of the peptide containing a homoserine residue in the mixture and its peptide fragment after Edman-degradation were observed at m/z=408 and 351, respectively, which corresponded to mass values of peptides containing homoserine lactones. However, when the peptides were measured after being kept for a long time, they gave mass values of homoserines opened at the *C*-terminal lactone rings. Generally, free "underivatized" peptides give mass peaks as quasi-molecular ions ($[M+H]^+$).[18,19] It is unknown whether peptides at their *C*-termini containing homoserine-lactones are observed as molecular ions $[M]^+$ or as quasi-molecular ions ($[M+H]^+$). The mass values (m/z=408 and 351) of the peptides containing homoserine residues observed above are responsible for the molecular ions. However, these mass values may be observed with a discrepancy of 1 atomic mass unit, because the mass peak at m/z=373 shown in Fig. 1B

is considered to be ($[M+Na]^+$) derived probably from 351 by addition of Na. This problem remains to be investigated further.

Edman-degradation and Field-desorption Mass Spectra. In our procedure of sequence determination, it was desirable to measure the mass spectra of peptides kept in the buffer solution for Edman-degradation. Therefore, we attempted to measure the mass spectra of several peptides in various buffer solutions. First we measured the mass spectra of peptides dissolved in a buffer solution containing *N,N*-dimethylallylamine as a base,[1] which is generally used in the coupling reaction of peptides with phenyl isothiocyanate in the Edman method. However, in this buffer the mass peaks could not be observed with high intensities in the spectra. The same phenomena were observed when some peptides were treated by the Edman method in the buffer solution and applied to the emitter. However, intense mass peaks could be obtained when the peptides were degraded in a mixture of pyridine and water without *N,N*-dimethylallylamine.[2,4]

Then we measured the mass spectra of a model peptide (H–Val–Tyr–Ile–His–Pro–Phe–OH) and its peptide fragments degraded successively under various conditions, as described in the Experimental section. Examples are illustrated in Figs. 2A and 2B. The model peptide and its peptide fragment gave mass peaks at $m/z=775$ and 676, respectively, with high intensities in all the buffer solutions examined except that containing *N,N*-dimethylallylamine. It was made not clear why the spectrum could not be obtained with high intensity in buffer solution with *N,N*-dimethylallylamine as base.

On the other hand, the 3-phenyl-2-thiohydantoin

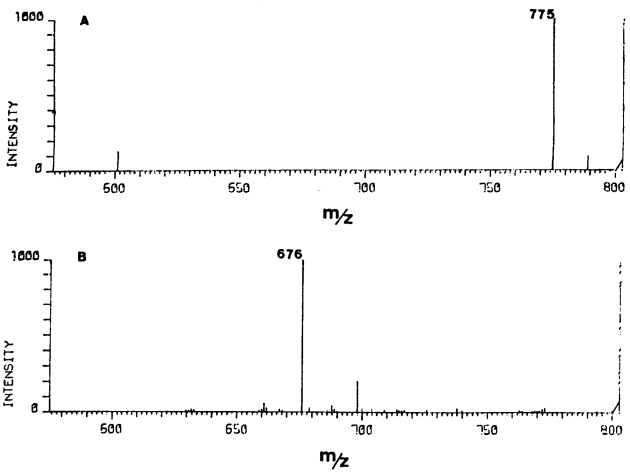

Fig. 2. Field-desorption mass spectra of H–Val–Tyr–Ile–His–Pro–Phe–OH (A) dissolved in a buffer solution containing *N*-methylmorpholine as a base (see text) and its peptide fragment (B) after one-cycle of degradation in the buffer solution.

derivatives of amino acids released from the model peptide in the degradation were quantitated by HPLC. The recoveries were similar in the all buffer solutions, but results seemed best in buffer solution containing *N*-methylmorpholine (data not shown), so, we used this buffer solution in Edman-degradation of the unknown polypeptide, as described below.

Mass Spectra of Tryptic and Chymotryptic Peptides of the N-Terminal BrCN Fragment of SE Lysozyme. We used trypsin and chymotrypsin, which specifically cleave different peptide bonds to each other, as methods for cleavage of the *N*-terminal BrCN fragment of SE

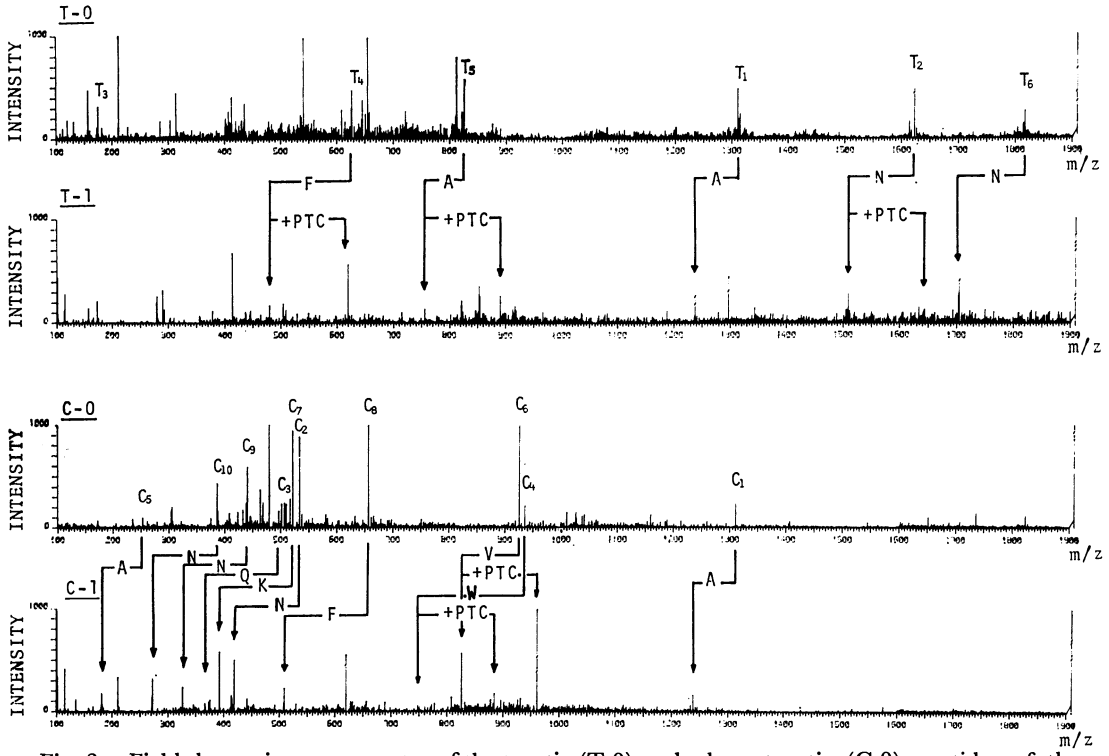

Fig. 3. Field-desorption mass spectra of the tryptic (T-0) and chymotryptic (C-0) peptides of the *N*-terminal BrCN fragment of SE lysozyme and their peptide fragments (T-1 and C-1) after one-step of degradation.

lysozyme. The tryptic and chymotryptic peptides and their peptide fragments obtained after the first-cycle of Edman-degradation gave the field-desorption mass spectra illustrated in Fig. 3. The spectra of the tryptic peptides and their degraded peptide fragments were simple, suggesting that the original polypeptide was specifically cleaved by this enzyme since it has only 3 Lys and 2 Arg residues. On the other hand, the spectra of the chymotryptic peptides and their degraded peptide fragments should be rather complicated, because the polypeptide contains many aromatic amino acid residues (6 Tyr, 3 Trp, and 2 Phe residues), which are susceptible to chymotryptic digestion. In fact, chymotryptic peptides and their degraded peptide fragments gave rather complicated spectra in the mass region up to 600 atomic mass units, as shown in Fig. 3. All the possible mass differences before and after the first-cycle of Edman-degradation of the tryptic and chymotryptic peptides were examined by the collation to the 3-phenyl-2-thiohydantoin derivatives of amino acids released in the degradation (Tables 1 and 2), as described previously.[2,4] In this case, the mass spectra were examined for mass peaks of $[M+Na]^+$, $[M+H-H_2O]^+$ and multiply charged ions $[M+2H]^{2+}$, *etc.*, which are occasionally observed with quasi-molecular ions $[M+H]^+$ in free "underivatized" peptides. Furthermore, the presence of peptides containing a Lys residue, giving mass peaks in the spectra with mass values that increased by addition of the phenylthiocarbamoyl group (135) after Edman-degradation,[4] was examined. The results revealed possible mass peaks of peptides obtained from the original polypeptide by enzymic digestion; namely, six tryptic peptides with R, F, A, and N[20] as *N*-termini and ten chymotryptic peptides with A, N, K, Q, F, W, and V as *N*-termini, as illustrated in Fig. 3. It was also found that the mass peaks at m/z=627, 826, and 1623 in tryptic peptides and at m/z=925 and 935 in chymotryptic peptides each contain a Lys residue. These findings are compatible with the presence of 3 Lys residues in the original polypeptide.

The molecular weight of the polypeptide was assumed to be within the range of 6280 and 6293 from the amino acid composition,[10] as described in Fig. 6, because Asp and Asn and Glu and Gln are quantitated together on amino acid analysis of acid hydrolysates of peptides and proteins. This molecular weight was compared with the sum of the molecular weights of the tryptic and chymotryptic peptides, which were obtained from the mass peaks in Fig. 3. The molecular weight of each peptide was obtained by subtracting one proton from the mass value of each peptide, because the mass peaks of free "underivatized" peptides are generally observed as quasi-molecular ions ($[M+H]^+$). Consequently, the tryptic peptides were assumed to be composed of peptides with mass values at m/z=175(R) : T_3, 627(F) : T_4, 826(A) : T_5, 1310(A) : T_1, 1623(N) : T_2 and 1818(N) : T_6 (amino acid residues in parentheses indicate the *N*-terminal amino acid residue of each peptide and T stands for tryptic peptide). Thus, the sum of the molecular weights of these six tryptic peptides was calculated as 6283. On the other hand, the chymotryptic peptides were suggested to be 253(A) : C_5, 386(N) : C_{10}, 440(N) : C_9, 496(Q) : C_3, 521(K) : C_7, 533(N) : C_2, 656(F) : C_8, 925(V) : C_6, 935(W) : C_4 and 1310(A) : C_1 (C stands for chymotryptic peptide). The peptide with a mass value of m/z=496 was assumed to have Q as the *N*-terminal residue, because the intense mass peaks at 479 and 501 were considered to be derived from a peptide with a mass value of m/z=496 by elimination of NH_3 during Edman-degradation or measurements of mass spectra and to correspond to $[M+H-NH_3]^+$ and $[M+Na-NH_3]^+$, respectively. Therefore, another peptide with the same mass difference (128) before and after the first-cycle of Edman-degradation as that of the peptide (m/z=496) and with a mass value at m/z=521 was expected to have *K* as the *N*-terminal residue, because one Lys residue, having the same residual weight (128) as that of Q, was observed in the 3-phenyl-2-thiohydantoin derivatives of amino acids released in the first-cycle of degradation, as shown in Table 2. The sum of the molecular weights of the chymotryptic peptides was calculated as 6283, and thus, completely coincided with that of the tryptic peptides and was definitely within the range (6280—6293) of the expected molecular weight of the polypeptide. Thus, the mass peaks of the tryptic and chymotryptic peptides

TABLE 1. RECOVERIES OF PHENYLTHIOHYDANTOIN DERIVATIVES RELEASED FROM TRYPTIC PEPTIDES OF THE *N*-TERMINAL BrCN FRAGMENT OF *Streptomyces erythraeus* LYSOZYME BY EDMAN-DEGRADATION

	Cycle of Edman-degradation										
	1	2	3	4	5	6	7	8	9	10	11
Asp	24	3	26	4	2	3	20	5	6	2	2
Asn	96	3*			2	2		—*	5	2	1
Glu			62	11	6	7	1	1	2	1	
Gln		—*	11*	8*	5	6	5	1*		t*	1
Ser		4*	—*	—*				—*	5	2*	3
Thr	1	80	8	1	12	3	1	1	2		2
Gly	6	12	3	25	28	16	7	3	5	14	6
Tyr			22*	—*	6	4	9	7	4	2	4
Ala	121	55	—*	32*	17	2					
Met											
Hse											
Val	3	58	29	8	3	1	1	14	6	1	3
Trp	2			2							
Pro		40	2						1	3	1
Lys	1	1			1			6	2		
Phe	44	2		9	1						1
Ile	1	4	1		1	20	4	1	1		1
Leu											
His											6
Arg	26	4									

Numerals are recoveries (nmol) from the *N*-terminal BrCN fragment (110 nmol). Ten % of the peptide fractions were removed for mass measurements before the 1st, 2nd and 3rd cycles of degradation. Thr was estimated in addition to *Δ*-Thr. The separations of Asn and Gln and Ser-derivatives and of Ala and Tyr-derivatives were not satisfactory in some cases. In these cases (*), recoveries were estimated as those of the main component. t means the presence of a trace of material.

Table 2. Recoveries of phenylthiohydantoin derivatives released from chymotryptic peptides of the *N*-terminal BrCN fragment of *Streptomyces erythraeus* lysozyme by Edman-degradation

	Cycle of Edman-degradation										
	1	2	3	4	5	6	7	8	9	10	11
Asp	62	30	46	8	4	3	33	8	3		1
Asn	277*	113*	11	2	1	1					
Glu	59	16*	75	37	45	9	12	4			
Gln	—*	11*	65*	31	5	1	1	2			2
Ser			—*				1		5	2	
Thr		64	13	25	7	7	10	3	3	1	1
Gly	28	51	33	39	43	34	10	19	8	19	6
Tyr		23	—*	25	17*	4	3	2	5	2	2
Ala	211	102	48*	64	22*	5	1	1			
Met											
Hse											
Val	67	47	75	15	3	2	2	24	5	1	1
Trp	69		—*	1							
Pro		2	50*	3							
Lys	113	71	5	29	2	1		1			
Phe	97	3	1				t				
Ile	3	15	2	1	1	39	5	1	1		
Leu											
His											10
Arg	8	8			3	5					

Numerals are recoveries (nmol) from the *N*-terminal BrCN fragment (160 nmol). Ten % of the peptide fractions were removed for mass measurements before the 1st, 2nd, and 3rd cycles of degradation. Thr was estimated in addition to *Δ*-Thr. The separations of Asn and Gln and Ser-derivatives and of Ala and Tyr-derivatives were not satisfactory in some cases. In these cases (*), recoveries were estimated as those of the main component. t means the presence of a trace of material.

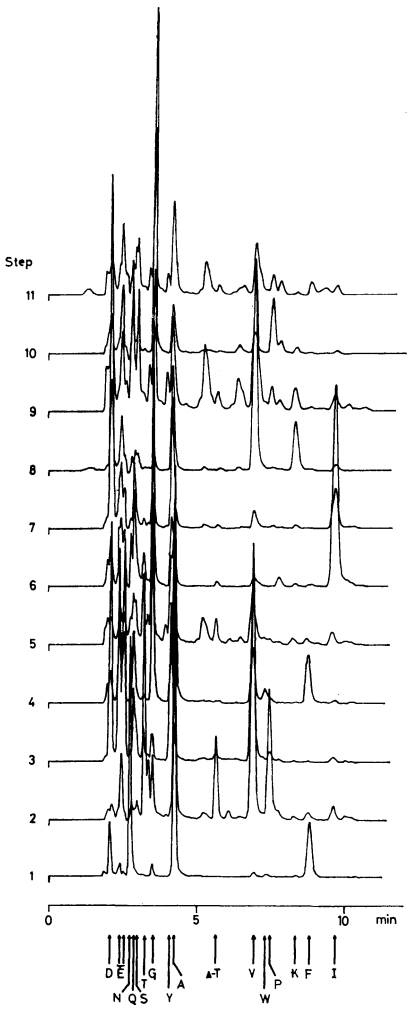

Fig. 4. High-performance liquid chromatograms of the 3-phenyl-2-thiohydantoin derivatives of amino acids released successively in the organic phase from the tryptic peptides of the *N*-terminal BrCN fragment of SE lysozyme. Numerals indicate the cycle of Edman-degradation. For conditions see text.

seemed to be selected correctly.

High-performance Liquid Chromatography of the 3-Phenyl-2-thiohydantoin Derivatives of Amino Acids Released from Tryptic and Chymotryptic Peptides. The 3-phenyl-2-thiohydantoin derivatives of amino acids released from peptide mixtures by Edman-degradation were quantitated using HPLC.[17] The chromatograms of the 3-phenyl-2-thiohydantoin derivatives of amino acids released from tryptic and chymotryptic peptides are illustrated in Figs. 4 and 5, respectively. The recoveries in each cycle of Edman-degradation are summarized in Tables 1 and 2. From these values, the kind and ratio of the 3-phenyl-2-thiohydantoin derivatives of amino acids released from the tryptic and chymotryptic peptides in each cycle of degradation were selected as interger values within the limits between possible maxima and minima, as described in Fig. 6, although the composition of the 3-phenyl-2-thiohydantoin derivatives of amino acids released were rather complicated. In these cases, the specificity of the enzymes used and the expected number of peptides in mixtures were considered. Furthermore, the fact that the recoveries of 3-phenyl-2-thiohydantoin derivatives of amino acids from larger peptides or Arg-containing peptides are generally better than those from smaller peptides was taken into consideration.

In this experiment, the 3-phenyl-2-thiohydantoin derivative of tryptophan was recovered with difficulty, because Edman-degradation was performed manually. Moreover, the 3-phenyl-2-thiohydantoin derivatives of homoserine and its lactone were not detected on the chromatograms.

Sequence Deduction with a Computer Program. The amino acid sequence of the *N*-terminal BrCN fragment of SE lysozyme was examined using the computer program "PROSEQ2,"[8] which was designed for deducing sequences of polypeptides or proteins from the molecular weights of the constituent peptides prepared from the polypeptides or proteins by two or more kinds of specific cleavage methods, the *N*-terminal amino acid residues or partial sequences of the constituent peptides and the 3-phenyl-2-thiohydantoin derivatives of amino acids released from the constituent peptides by successive degradation. The input data were as described in Fig. 6 and A and U (U denotes an Hse residue in this paper) as *N*- and *C*-terminal residues of the original

polypeptide,[10] respectively. There was only one output sequence, and it was complete as seen in Fig. 6. The results show that the procedure described above is applicable as a method for peptide or protein sequence analysis, and compares favorably with other methods,[1,21] although there may be no problem in sequencing a peptide as long as the *N*-terminal BrCN fragment tested with an automated sequencer.[22]

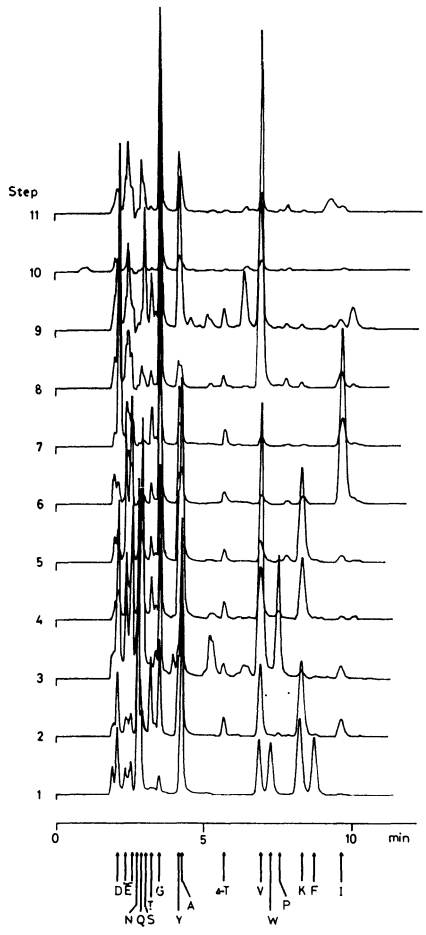

Fig. 5. High-performance liquid chromatograms of the 3-phenyl-2-thiohydantoin derivatives of amino acids released successively in the organic phase from the chymotryptic peptides of the *N*-terminal BrCN fragment of SE lysozyme. Numerals indicate the cycle of Edman-degradation. For conditions see text.

We express our sincere thanks to Professors Y. Izumi (Institute for Protein Research, Osaka University), H. Matsuda (College of General Education, Osaka University) and T. Ikenaka (Faculty of Science, Osaka University) for much helpful discussion and encouragement throughout this work.

References

1) P. Edman and A. Henschen, "Protein Sequence Determination," ed by S. B. Needleman, Springer-Verlag, Berlin-Heidelberg-New York (1975), p. 232.
2) Y. Shimonishi, Y.-M. Hong, T. Matsuo, I. Katakuse, and H. Matsuda, *Chem. Lett.*, **1979**, 1369.
3) T. Matsuo, I. Katakuse, H. Matsuda, Y. Shimonishi, Y.-M. Hong, and Y. Izumi, *Mass Spectroscopy (Japan)*, **28**, 169 (1980).
4) Y. Shimonishi, Y.-M. Hong, T. Kitagishi, T. Matsuo, H. Matsuda, and I. Katakuse, *Eur. J. Biochem.*, **112**, 251 (1980).
5) H. D. Beckey, *Int. J. Mass Spectrom. Ion Phys.*, **2**, 500 (1969).
6) T. Kitagishi, Y.-M. Hong, and Y. Shimonishi, *Int. J. Pept. Protein Res.*, **17**, 436 (1981).
7) Y. Shimonishi, Y.-M. Hong, T. Kitagishi, I. Katakuse, T. Matsuo, H. Matsuda, S. Hara, T. Ikenaka, and Y. Izumi, *Chem. Lett.*, **1981**, 499.
8) T. Kitagishi, Y.-M. Hong, and Y. Shimonishi, "Peptide Chemistry 1980," Proceedings of the 18th Symposium on Peptide Chemistry, ed by K. Okawa, Protein Research Foundation, Minoh, Osaka (1981), p. 135.
9) T. Morita, S. Hara, and Y. Matsushima, *J. Biochem. (Tokyo)*, **83**, 893 (1978).
10) S. Hara, M. Akira, E. Taketani, and T. Ikenaka, The 53rd Annual Meeting of the Biochemical Society of Japan (Tokyo), October 13—16 (1980).
11) H. Otsuka, M. Shin, Y. Kinomura, and K. Inouye,

INPUT DATA

AMINO ACID COMPOSITION

		N-TERM	C-TERM
G	7		
A	5	A	
U	1		U
S	2		
P	1		
V	4		
T	3		
L	0		
I	2		
N+D	7		
Q+E	6		
K	3		
M	0		
H	1		
C	0		
F	2		
R	2		
Y	6		
W	3		
TOTAL	55		

MOL WEIGHTS, N-TERMINAL SEQUENCES AND PTH-AMINO ACIDS IN EACH CYCLE

CHYMOTRYPTIC PEPTIDES

		2	3	4	5	6	7	8	9	10	11
252	A	G 1,0	1,0	1,0	1,0	1,0	0	1,0	0	1,0	0
385	N	A 2,0	1,0	2,0	1,0	0	0	0	0	0	0
439	N	U 1,0	1,0	1,0	1,0	1,0	1,0	1,0	1,0	1,0	1,0
495	Q	S 0	1,0	0	0	0	1,0	0	1,0	1,0	0
520	K	P 0	1,0	0	0	0	0	0	0	0	0
532	N	V 1,0	2,0	0	0	0	0	1,0	1,0	0	0
655	F	T 2,0	0	1,0	0	1,0	1,0	0	0	0	0
924	V	L 0	0	0	0	0	0	0	0	0	0
934	W	I 1,0	0	0	0	1,0	0	0	0	0	0
1309	A	N 2,0	0	0	0	0	0	0	0	0	0
		D 0	1,0	0	0	0	1,0	0	0	0	0
		Q 1,0	2,0	1,0	0	0	0	0	0	0	0
		K 1,0	0	1,0	1,0	0	0	0	0	0	0
		E 1,0	1,0	1,0	1,0	1,0	1,0	0	0	0	0
		M 0	0	0	0	0	0	0	0	0	0
		H 0	0	0	0	0	0	0	0	0	1,0
		C 0	0	0	0	0	0	0	0	0	0
		F 0	0	0	0	0	1,0	0	0	0	0
		R 0	0	0	1,0	1,0	0	0	0	0	0
		Y 2,0	1,0	2,0	2,0	0	1,0	1,0	1,0	1,0	1,0
		W 0	1,0	1,0	1,0	1,0	1,0	1,0	1,0	1,0	1,0

TRYPTIC PEPTIDES

		2	3	4	5	6	7	8	9	10	11
174	R	G 0	0	1,0	2,0	2,0	1,0	0	1,0	2,0	2,0
626	F	A 1,0	0	1,0	1,0	0	0	0	0	0	0
825	A	U 0	0	0	1,0	1,0	1,0	1,0	1,0	1,0	1,0
1309	A	S 1,0	0	0	0	0	0	0	2,0	1,0	2,0
1622	N	P 1,0	0	0	0	0	0	0	0	1,0	0
1817	N	V 1,0	1,0	1,0	0	0	0	1,0	1,0	0	1,0
		T 2,0	0	0	1,0	1,0	0	0	0	0	1,0
		L 0	0	0	0	0	0	0	0	0	0
		I 0	0	0	0	2,0	0	0	0	0	0
		N 0	0	0	0	0	0	0	2,0	1,0	1,0
		D 0	1,0	0	0	0	2,0	0	0	0	1,0
		Q 0	1,0	1,0	1,0	1,0	1,0	0	0	1,0	0
		K 0	0	0	1,0	0	0	1,0	1,0	0	0
		E 0	2,0	1,0	1,0	1,0	0	0	0	0	0
		M 0	0	0	0	0	0	0	0	0	0
		H 0	0	0	0	0	0	0	0	0	1,0
		C 0	0	0	0	0	0	0	0	0	0
		F 0	0	1,0	0	0	0	0	0	0	0
		R 0	0	0	0	0	0	0	0	0	0
		Y 0	2,0	0	1,0	1,0	1,0	1,0	1,0	1,0	1,0
		W 0	0	1,0	1,0	1,0	1,0	1,0	1,0	1,0	1,0

CANDIDATE SEQUENCE

1 ATVAGIDVSGHQRNVDWQYWWNQGKRFAYVKATEGTGYKNPYFAQQYNGSYNIGU

Fig. 6. Computer output sequence of the *N*-terminal BrCN fragment of SE lysozyme using "PROSEQ2."[8] U and W were put into as many data as possible, because the former derivative was not identified and the latter residue was possibly destroyed under our experimental conditions, as described in the text.

Bull. Chem. Soc. Jpn., **43**, 196 (1970).
12) E. Gross and B.Witkop, *J. Biol. Chem.*, **237**, 1856 (1962).
13) H. Matsuda, *Atomic Masses Fundam. Constants* **5**, 185 (1976).
14) T. Matsuo, H. Matsuda, and I. Katakuse, *Anal. Chem.*, **51**, 1329 (1979).
15) T. Matsuo, H. Matsuda, and I. Katakuse, *Anal. Chem.*, **51**, 69 (1979).
16) H. D. Beckey, A. Hendricks, and H. U. Winkler, *Int. J. Mass Spectrom. Ion Phys.*, **3**, app. 9 (1970).
17) C. L. Zimmerman, E. Appella, and J. J. Pisano, *Anal. Biochem.*, **77**, 569 (1977).
18) H. U. Winkler and H. D. Beckey, *Biochem. Biophys. Res. Commun.*, **46**, 391 (1972).
19) S. Asante-Poku, G. W. Wood, and D. E. Schmidt, Jr., *Biomed. Mass Spectrom.*, **2**, 121 (1975).
20) R. V. Eck and M. O. Dayhoff, "Atlas of Protein Sequence and Structure," ed by National Biomedical Research Foundation Publishers, Silver Spring, Md. (1966); A : Ala, D: Asp, E: Glu, F: Phe, G: Gly, H: His, I: Ile, K: Lys, L: Leu, M: Met, N: Asn, P: Pro, Q: Gln, R: Arg, S: Ser, T: Thr, V: Val, W: Trp, Y: Tyr.
21) J. A. Kelley, H. Nau, H.-J. Forster, and K. Biemann, *Biomed. Mass Spectrom.*, **2**, 315 (1975).
22) P. Edman and G. Begg, *Eur. J. Biochem.*, **1**, 80 (1967).

Synthesis and Properties of O^6-Substituted Guanosine Derivatives

Hristo Petrov DASKALOV, Mitsuo SEKINE, and Tsujiaki HATA*

Department of Life Chemistry, Tokyo Institute of Technology, Nagatsuta, Midori-ku, Yokohama 227

(Received April 27, 1981)

Reactions of 2′,3′,5′-tri-*O*-acetyl-N^2-protected or unprotected guanosine derivatives with phosphoryl, phosphinothioyl, arylsulfonyl, and silyl halides in dichloromethane gave the corresponding O^6-substituted guanosine derivatives in good yields. In these reactions, 4-(dimethylamino)pyridine (DMAP) was found to be very effective catalyst. The physical data of these products and their stabilities under acidic and basic conditions were described in detail. Selective detritylation of O^6-arylsulfonyl-N^2-tritylguanosine derivatives was accomplished by treatment with 80% acetic acid. It was found that O^6-dibutylphosphinothioyl derivatives were relatively stable under conditions where acetyl group was predominantly removed.

In recent years, introduction of new methodologies into nucleotide chemistry has facilitated dramatically the synthesis of oligonucleotides.[1] The modern phase of chemical synthesis of oligonucleotides rests mainly on the development of new types of condensing agents[2] and protecting groups[3] and the application of rapid purification and separation procedures.[4] For example, several (arylsulfonyl)azoles[2] have proved to be the most promising condensing agents since the reaction time for the condensation is being outstandingly shortened and the yields of oligomers are usually high. Narang[5] and Itakura[6] have recently showed rapid and practical methods for the synthesis of oligodeoxyribonucleotides demonstrating its successful application to the chemical synthesis of the fragments of the double stranded bioactive genes of lactose operator,[5a] human hormones,[6a,b] and insulin.[5b,c,6c,d] Ohtsuka and Ikehara[7] have also reported the utility of arenesulfonyl azoles in "unit-type" synthesis involving the total synthesis of $tRNA^{fMet}$. These new synthetic devices seem to be accepted satisfactorily. However, it appears that the preparation of guanosine-containing oligomers by the improved phosphotriester approach involves still synthetic problems, especially, on the aspect of the coupling yields. This problem is more severe in the case of the ribo-series. Several years ago, Reese[8-10] reported that guanosine derivatives were sulfonylated at the O^6-position of guanine moiety with arenesulfonyl chlorides in pyridine. It suggests strongly that during the elongation of oligonucleotide chains such unavoidable side reactions might occur at the O^6-position of guanosine. Indeed, we have met similar troubles owing to these side reactions in the synthesis of a guanosine monomer (as a unit nucleotide) and guanosine-rich oligomers. In connection with our project in oligoribonucleotide synthesis we have needed a highly lipophilic guanosine derivative capable for elaboration of a phosphate group at the 5′-ribose hydroxyl. Consequently, the coupling reaction between N^2-tritylguanosine and cyclohexylammonium *S,S*-bis(4-methoxyphenyl) phosphorodithioate (MPT) was performed by use of 2,4,6-triisopropylbenzenesulfonyl chloride (TPS) (TPS–MPT reaction) according to the established procedure.[11]

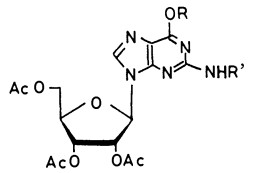

1: R = H, R′ = Tr
2: R = H, R′ = Bz
3: R = R′ = H

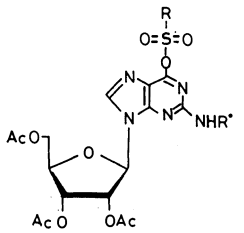

8a: R = 4-Me C_6H_4, R′ = Tr
b: R = 2,4,6-$(Me)_3C_6H_2$, R′ = Tr
c: R = 2,4,6-$(i\text{-}Pr)_3C_6H_2$, R′ = Tr
9: R = 2,4,6-$(i\text{-}Pr)_3C_6H_2$, R′ = Bz
10a: R = 4-MeC_6H_4, R′ = H
b: R = 2,4,6-$(Me)_3C_6H_2$, R′ = H
c: R = 2,4,6-$(i\text{-}Pr)_3C_6H_2$, R′ = H

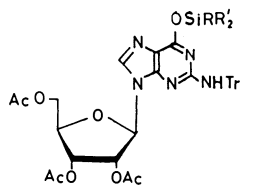

7a: R = R′ = Me
b: R = t-Bu, R′ = Me
c: R = t-Bu, R′ = C_6H_5

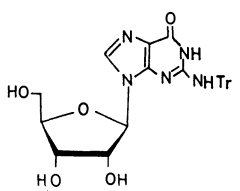

11

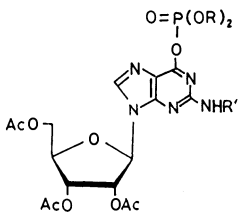

4a: R = Et, R′ = Tr
b: R = i-Pr, R′ = Tr
c: R = C_6H_5, R′ = Tr
d: R = 4-Cl-C_6H_4, R′ = Tr
5: R = C_6H_5, R′ = Bz

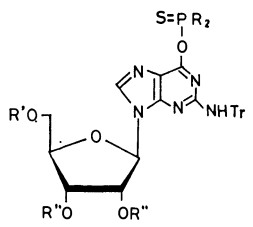

6a: R = Bu, R′ = R″ = Ac
b: R = Ph, R′ = R″ = Ac
12: R = Bu, R′ = R″ = H
13: R = Bu, R′ = Ac, R″ = H

However, the desired 5′-*O*-phosphorylated product was not obtained and some unidentified by-products were formed. Careful investigation of the TPS–MPT reaction on more simplified (*i.e.*, fully protected) guanosine derivatives such as 2′,3′,5′-tri-*O*-acetyl-N^2-trityl-guanosine (**1**) and 2′,3′,5′-tri-*O*-acetyl-N^2-benzoylguanosine (**2**) has revealed that O^6-substitution reactions of the above mentioned compounds occured easily under similar conditions. This led us to study extensively the protection of the O^6-position of guanosine residue, which would give some insight on the oligonucleotide synthesis.

In this paper, we wish to report the facile phosphorylation, sulfonylation, silylation of the O^6-position of guanosine derivatives and the properties of the O^6-substituted guanosine derivatives in detail.[12] During this work, we dealed mainly with N^2-tritylguanosine derivatives since the trityl group has proved to be useful and promising protecting group of the 2-amino group of guanine moiety because of its stability and great lipophilicity.

Results and Discussion

O^6-Substitution Reaction of Guanosine Derivatives. At first, pyridine was chosen as a solvent for the above mentioned O^6-substitution reaction, since it was the common solvent used for the TPS–MPT reaction. By use of pyridine, however, unsatisfactory results were obtained for O^6-sulfonylation and O^6-phosphorylation of N^2-substituted 2′,3′,5′-tri-*O*-acetylguanosines. Another disadvantage was difficult work-up procedure which allowed isolation of the O^6-substituted derivatives only in low yields. On the other hand, excellent results were obtained, when the reaction was carried out in the presence of a catalytic amount of 4-(dimethylamino)-pyridine (DMAP)[13,14] in dichloromethane. It can be

Table. 1 N^2-Substituted or unsubstituted 2′,3′,5′-tri-*O*-acetyl-O^6-(arylsulfonyl) guanosines

Compound	R^1	Sulfonylating agent[a]	Time h	Yield %	R_f value[b]	UV spectra, λ/nm $\lambda_{max}^{dioxane}$ ($\varepsilon \times 10^{-3}$)	UV spectra, λ/nm $\lambda_{min}^{dioxane}$
8a	Ph_3C	TsCl	3	75	0.58	303 (6.2) 258 (12.4)	278 248
8b	Ph_3C	MS	3	83	0.61	300 (6.2) 290 (6.2) 254 (12.3)	291 277 250
8c	Ph_3C	TPS	3	87	0.67	300 (7.7) 290 (7.7) 255 (14.9)	291 277 250
9	PhC(=O)	TPS	12	78	0.66	276 (7.3) 233 (12.0)	250 221
10a	H	TsCl	24	73	0.36	298 (8.1) 245 (12.4)	267 243
10b	H	MS	24	78	0.59	298 (6.2) 288 (6.2) 238 (12.4)	265 235
10c	H	TPS	24	80	0.43	299 (7.8) 289 (7.8) 240 (12.7)	265 238

a) TsCl=tosyl chloride. MS=mesitylenesulfonyl chloride. TPS=2,4,6-triisopropylbenzenesulfonyl chloride. b) Benzene–ethyl acetate (4 : 1, v/v).

Table 2. O^6-Phosphorylated 2′,3′,5′-tri-*O*-acetyl-N^2-tritylguanosines (**4—6**)

Compound	R	Phosphorylating agent	Yield %	R_f value[a]	UV spectra, λ/nm $\lambda_{max}^{dioxane}$ ($\varepsilon \times 10^{-3}$)	UV spectra, λ/nm $\lambda_{min}^{dioxane}$
4a	Ph_3C	$(EtO)_2P(O)Cl$	b)	0.23	b)	b)
4b	Ph_3C	$(i\text{-}PrO)_2P(O)Br$	35—40	0.31	291 (8.3) 257 (13.9)	277 244
4c	Ph_3C	$(PhO)_2P(O)Cl$	30—40	0.51	291 (7.5) 261 (13.3)	277 245
4d	Ph_3C	$(p\text{-}ClC_6H_4O)_2P(O)Cl$	30—40	0.65	292 (6.3) 257 (12.1)	286 250
5	PhC(=O)	$(PhO)_2P(O)Cl$	*ca.* 30	0.49	c)	c)
6a	Ph_3C	$Bu_2P(S)Br$	90—98	0.67	300 (9.25) 258 (12.9)	277 246
6b	Ph_3C	$Ph_2P(S)Cl$	50—60	0.66	299 (8.0) 256 (15.3)	279 247

a) Benzene–ethyl acetate (4 : 1, v/v). b) Compound **4a** was too unstable to be isolated in pure form. c) Compound **5** was not purified by chromatography because of partial decomposition.

TABLE 3. O^6-SILYLATED 2′,3′,5′-TRI-*O*-ACETYL-N^2-TRITYLGUANOSINES (**7**)

Compound	Silylating agent	R_f value[a)]	Yield %	UV spectra, λ/nm $\lambda_{max}^{dioxane}$ ($\varepsilon \times 10^{-3}$)	$\lambda_{min}^{dioxane}$
7a	Me_3SiCl	b)	b)	b)	b)
7b	*t*-$BuMe_2SiCl$	0.64[c)]	d)	c)	c)
7c	*t*-$BuPh_2SiCl$	0.66	98	290 (8.04) 271 (sh) 265 (sh) 261 (11.4) 254 (sh)	276 243

Other physical data (^{1}H NMR and elemental analysis) are given as follows: **7c**: ^{1}H NMR ($CDCl_3$): δ 1.18 (9H, s, $(CH_3)_3C$), 1.93 (3H, s, 5′-acetyl protons), 2.06 (6H, br. s, 2′- and 3′-acetyl protons), 5.06—5.53 (3H, m, ribose protons), 5.63 (3H, br. s, ribose protons), 7.10 (15 H, br. s, ArH), 7.17—7.83 (11H, Ph_2Si and H-8); Found: C, 69.07; H, 5.80; N, 7.47%. Calcd for $C_{51}H_{51}N_5O_8Si$: C, 68.82; H, 5.78; N, 7.87%. a) Benzene–ethyl acetate (4 : 1, v/v). b) Compound **7a** was too unstable to characterize its properties (see the text). c) It was not possible, according to the techniques developed in this report, to isolate **7b** in pure form. Therefore, no elemental analysis, precise, UV, ^{1}H NMR data are given here. R_f value for **7b** should be accepted with some reservation due to partial decomposition of **7b** during TLC. d) The yield of **7b** was *ca.* 90—95% (determined by the amount of triethylammonium hydrochloride and ^{1}H NMR appearance of the partially purified product; see General Procedure B.

emphasized that O^6-substitution reactions took place by use of appropriate sulfonyl and phosphoryl halides in the presence of DMAP and the reactions were very clean and the results were also satisfactory. The reaction conditions and the results are summarized in Tables 1—3.

Concerning the reaction rate of O^6-substitution reaction, it depended on the lipophilicity of the guanosine derivatives. For instance, compound **1** containing trityl group was more reactive than 2′,3′,5′-tri-*O*-acetylguanosine (**3**) having no trityl group, while **1** entered in O^6-substitutions a little faster than **2**. As one could easily see from Tables 1—3, electronic and steric effects in the O^6-substitution reactions have apparently a little influence on the reaction rates.

The successful isolation of this type of guanosine derivatives (**4** and **5**) is of great interest since O^6-phosphorylated species have been discussed as by-products in the synthesis of oligonucleotides involving guanosines but they have never been characterized.

On the other hand, two kinds of phosphinothioyl halides, *i.e.*, dibutylphosphinothioyl bromide and diphenylphosphinothioyl chloride, were employed in place of the phosphoryl halides in order to introduce phosphinothioyl groups into the O^6-position of guanosine derivatives. As a consequence, the corresponding O^6-phosphinothioylated guanosine derivatives (**6a** and **6b**) were successfully obtained in 98 and 60% yields, respectively.

Furthermore, this DMAP/Et_3N/CH_2Cl_2 system could be also extended to the O^6-silylation. We examined the DMAP-catalyzed silylation of **1** using trimethylsilyl chloride, *t*-butyldimethylsilyl chloride, and *t*-butyldiphenylsilyl chloride. The superiority of DMAP/Et_3N/CH_2Cl_2 system was also confirmed in this case by comparison with the conventional system (imidazole/*N*,*N*-dimethylformamide/silyl chloride[15)]). Thus, the *t*-butyldiphenylsilyl derivative (**7c**) was successfully isolated in an excellent yield of 98%. However, in the case of the trimethylsilylation, it was impossible to isolate the silylated product (**7a**) and even to detect it on the TLC plate. Very rapid decomposition of **7a**

TABLE 4. ELEMENTAL ANALYSIS AND ^{1}H NMR SPECTRA OF **4** AND **6**[a)]

Compound formula	Elemental analysis (%) Calcd / Found C	H	N	[S] or (Cl)	^{1}H NMR ($CDCl_3$), δ
4b	60.36	5.68	8.58	—	1.38 (6H, d, J=6 Hz, $(CH_3)_2C$), 1.96 (3H, s, 5′-acetyl), 2.08 (6H, s, 2′,3′-acetyls), 4.16 (3H, br. s, ribose protons), 4.92 (2H, m, $(CH_3)_2CH$), 5.20—5.63 (3H, m, ribose protons), 6.56 (1H, s, NHTr), 7.23 (15H, br. s, ArH), 7.70 (1H, s, H-8)
$C_{41}H_{46}N_5O_{11}P$	60.29	5.69	8.53	—	
4c	63.86	4.80	7.92		1.93 (3H, s, 5′-acetyl), 2.08 (6H, s, 2′,3′-acetyls), 4.13 (3H, br. s, ribose protons), 5.13—5.55 (3H, m, ribose protons), 6.08 (1H, br. s, NHTr), 7.18 (25H, br. s, ArH), 7.70 (1H, s, H-8)
$C_{47}H_{42}N_5O_{11}P$	64.06	4.78	7.61		
4d	55.02	3.90	6.83	(6.94)	1.97 (3H, s, 5′-acetyl), 2.10 (6H, s, 2′,3′-acetyls), 4.17 (3H, br. s, ribose protons), 5.17—5.63 (3H, m, ribose protons), 6.27 (1H, br. s, NHTr), 7.20 (1H, s, H-8)
$C_{47}H_{40}N_5Cl_2O_{11}P \cdot 4H_2O$	55.04	3.98	6.46	(6.48)	
6a	61.00	5.91	8.27	[3.78]	0.67—2.43 (18H, m, C_4H_9), 2.00 (3H, s, 5′-acetyl), 2.06 (6H, s, 2′,3′-acetyls), 4.23 (3H, br. s, ribose protons), 5.22—5.80 (3H, m, ribose protons), 6.43 (1H, br, s, NHTr), 7.23 (15H, br. s, ArH), 7.73 (1H, s, H-8)
$C_{43}H_{50}N_5O_8PS \cdot H_2O$	61.39	6.06	8.03	[3.62]	
6b	64.34	4.82	7.98	[3.65]	1.93 (3H, s, 5′-acetyl), 2.04 (6H, s, 2′,3′-acetyls), 4.13 (3H, br. s, ribose protons), 5.17—5.63 (3H, m, ribose protons), 6.13(1H, s, NHTr), 7.08—8.10 (26H, br. s, H-8 and ArH)
$C_{47}H_{42}N_5O_8PS \cdot 1/2H_2O$	64.42	4.90	7.75	[3.45]	

a) Compounds **4a** and **5** could not be purified because of their instability during work-up procedure. Therefore no elemental analysis and ^{1}H NMR spectral data are given here.

Table 5. Elemental analysis and ^{1}H NMR spectra of **8**—**10**

Compound formula	Elemental analysis (%) Calcd / Found C	H	N	S	^{1}H NMR ($CDCl_3$), δ
8a	62.60	4.88	8.69	3.98	1.95 (3H, s, 5′-acetyl), 2.06 (6H, s, 2′,3′-acetyls), 2.40 (3H, s, para-methyl), 4.15 (3H, br. s, ribose protons), 5.10—5.63 (3H, m, ribose protons), 6.42 (1H, br. s, NHTr), 7.18 (17H, s, ArH), 7.7 (1H, s, H-8), 7.78 (2H, d, J=8 Hz)
$C_{42}H_{39}N_5O_{10}S$	63.07	5.09	8.41	3.78	
8b	63.37	5.20	8.40	3.84	1.93 (3H, s, 5′-acetyl), 2.09 (6H, s, 2′,3′-acetyls), 2.26 (3H, s, p-CH_3), 2.7 (6H, s, o-CH_3), 4.15 (3H, br. s, ribose protons), 5.13—5.53 (3H, m, ribose protons), 6.17 (1H, br. s, NHTr), 6.83 (2H, s, m-ArH), 7.17 (15H, br. s, ArH), 7.70 (1H, s, H-8)
$C_{44}H_{43}N_5O_{10}S$	63.40	5.21	7.89	3.76	
8c	65.41	6.04	7.63	3.49	1.20 (18H, d, J=6 Hz, $(CH_3)_2C$), 1.86 (3H, s, 5′-acetyl), 2.03 (6H, s, 2′,3′-acetyls), 3.05 (1H, m, p-$(CH_3)_2CH$), 4.06 (3H, br. s, ribose protons), 4.10 (2H, m, o-$(CH_3)_2CH$), 5.00—5.46 (3H, m, ribose protons), 6.08 (1H, br. s, NHTr), 7.13 (15H, br. s, ArH), 7.62 (1H, s, H-8)
$C_{50}H_{55}N_5O_{10}S$	65.06	6.08	7.36	3.40	
9	58.53	5.82	8.98	4.11	1.26(12H, d, J=6 Hz, o-$(CH_3)_2C$), 1.23 (6H, d=6 Hz, p-$(CH_3)_2$-C), 2.00—2.23 (9H, br. d, acetyl), 2.92 (1H, m, p-$(CH_3)_2CH$), 4.20 (2H, m, o-$(CH_3)_2CH$), 4.50 (3H, m, ribose protons), 5.85—6.18 (3H, m, ribose protons), 7.1—8.00 (8H, m, ArH)
$C_{38}H_{45}N_5O_{11}S$	58.76	5.77	8.62	3.90	
10a	49.02	4.47	12.43	5.69	2.03—2.20 (9H, three singlets, acetyls), 2.42 (3H, s, p-CH_3), 4.33 (3H, br. s, ribose protons), 4.98 (2H, br. s, NH_2), 5.57—5.97 (3H, m, ribose protons), 7.23 (2H, d, J=8 Hz, ArH), 7.72 (1H, s, H-8) 7.92 (2H, d, J=8 Hz, ArH)
$C_{23}H_{25}N_5O_{10}S$	49.07	4.59	12.22	5.53	
10b	51.76	4.94	11.84	5.42	2.00—2.20 (9H, br. s, acetyls), 2.30 (3H, s, p-CH_3), 2.74 (6H, s, o-CH_3), 4.38 (3H, br. s, ribose protons), 5.08 (2H, br. s, NH_2), 5.60—6.00 (3H, m, ribose protons), 6.93 (2H, s, ArH), 7.80 (1H, s, H-8)
$C_{25}H_{29}N_5O_{10}S$	51.68	4.99	11.44	5.30	
10c	55.10	6.12	10.36	4.74	1.28 (18H, d, J=6 Hz, $(CH_3)_2C$), 2.00—2.13 (9H, three singlets, acetyls), 3.05 (1H, m, p-$(CH_3)_2CH$), 3.70—4.23 (2H, m, o-$(CH_3)_2CH$), 4.37 (3H, m, ribose protons), 4.97 (2H, br. s, NH_2), 5.60—6.00 (3H, m, ribose protons), 7.13 (2H, s, ArH), 7.68 (1H, s, H-8)
$C_{31}H_{41}N_5O_{10}S$	54.79	6.12	9.99	4.63	

to the starting material was observed. However, indirect evidence of the O^6-silylation was supported by the fact that a stoichiometric amount of triethylamine hydrochloride was obtained from the reaction mixture. When t-butyldimethylsilyl chloride was used for the silylation, it was possible to detect the corresponding silylated product (**7b**) by TLC and to separate it as a material which was contaminated with DMAP and traces of triethylammonium chloride (see Procedure B in Experimental Section).

Stability of the O^6*-Substituted Guanosine Derivatives.* Since it was quite important for our synthetic purpose, we undertook a careful examination of the stability of the above mentioned compounds (**4**—**10**) either during work-up procedure, in solid state, or in several acidic and basic mediums. Consequently, their stabilities have varied in a quite wide range. The summary of the results is given below (for further details see Table 6 and Experimental Section). In connection with their stability in solid state, we have found that N^2-unsubstituted guanosine derivatives were unstable and after two months at room temperature a significant decomposition has been observed.

It was proved also that an introduction of the bulky substituents near O^6-oxygen of the O^6-substituted guanosines increases their stability both during work-up and in the solid state. Thus, in the O^6-sulfonylated derivatives of **3** the order of stability in the solid state was **10a**>**10b**>**10c**. On the other hand, in O^6-phosphorylation of **1**, it was found that the O^6-diethylphosphoryl derivative (**4a**) was not stable enoguh to be isolated in pure form, while the O^6-diisopropylphosphoryl compound (**4b**) could be isolated, although the yield was relatively low (*ca.* 30%).

Because of the circumstances under which this study was undertaken we have been in keen interest for lability of the substituent on O^6-guanosine oxygen, especially, in different basic mediums. Our principal goal is to obtain O^6- and N^2-disubstituted guanosines so that we can call them "fully protected" selectively in the guanine part. As a consequence, we tried to check the stability of O^6-substituted 2′,3′,5′-tri-O-acetyl-N^2-tritylguanosines in more detail. It was found that most of substituents of O^6-guanosine oxygen were too unstable in several alkaline mediums to serve as protecting groups for O^6-position of the compounds involved. The O^6-sulfonylated derivatives (**8**—**10**) were particularly susceptible to nucleophilic substitution at C^6 carbon. A similar reaction of 2′,3′,5′-tri-O-acetyl-O^6-mesitylsulfonylguanosine (**10b**) has been described by Reese.[9] Unfortunately, it was not possible to find a suitable reagent which would attack preferably ribose acetoxyl groups, but not the C^6-carbon in the guanine moiety.

In order to gain information on the possibility of using O^6-substituents as protecting groups some data on their stability in acidic mediums were also required. We have found that, as a rule, they were quite labile under acidic conditions (see Table 6). It was, however, possible to find removal conditions of trityl group selectively from 2′,3′,5′-tri-O-acetyl-O^6-sulfonyl-N^2-tritylguanosine (**8a**—**c**) where the sulfonyl groups remained intact to afford **10a**—**c** in almost quantitative yields. On

TABLE 6. REMOVAL OF THE PROTECTING GROUPS OF SOME O^6-SULFONYLATED PHOSPHORYLATED, OR SILYLATED COMPOUNDS IN ACIDIC OR BASIC MEDIUMS

Compound	Acidic or basic medium[a)]	Time/h	Product
8a	80% acetic acid in dioxane–water (4 : 1, v/v)	1.0	**10a**
8b		1.0	**10b**
8c		1.0	**10c**
8a	60% formic acid	0.5	**3**
8b		0.5	**3**
8c		0.5	**3**
8a	14% methanolic ammonia[c)]	2.0	b)
7c		24	**11**
6a	*t*-butylamine in methanol–dichloromethane[d)]	6.0	**12** and **13**[e)]
6a	butylamine in dichloromethane	48	no reaction
6a	*t*-butylamine in methanol	0.25	**12** and **13**[f)]

a) All operations were carried out at room temperature, if not otherwise stated. b) The TLC ($CHCl_3$– MeOH, 9 : 1, v/v) of the reaction mixture after 2 h showed that at least 4 products were formed (no starting material remained). No attempts were made to identify these compounds, but at least for one of them it could be judged (from R_f value) that it was N^2-tritylguanosine. c) In 5% methanolic ammonia a similar reaction took place. d) This was one of the best solvent systems which have been tested for aminolysis of **6a**. The reaction was sufficiently slow for isolation of monoacetyl- and deacetylated products of **6a**. e) See Experimental section. f) See the text.

the other hand, simultaneous removal of both trityl and arylsulfonyl groups could be accomplished by employing 60% formic acid (see Table 6).

The O^6-phosphorylated guanosine derivatives (**4** and **5**) were also quite labile in basic mediums, and the O^6–P bond was cleaved easily in either aqueous or anhydrous solvents to give rise to N^2-tritylguanosine (**11**) as a principal reaction product.

For aminolysis of 2′,3′,5′-tri-*O*-acetyl-O^6-dibutylphosphinothioyl-N^2-tritylguanosine (**6a**), ammonia, *t*-butylamine, and butylamine in different solvent systems were tested. It was found that both ammonia (in methanol) and butylamine (in methanol–dichloromethane) had given unsatisfactory results. The aminolysis was too fast and O^6-dibutylphosphinothioyl group was cleaved considerably. On the contrary, *t*-butylamine [in methanol and especially in methanol–chloroform (or dichloromethane)] had given good results both in terms of aminolysis reaction and stability of the O^6-dibutylphosphinothioyl group. The aminolysis with *t*-butylamine appeared to be very sensitive to the solvent system. For instance, there was no reaction between **6a** and *t*-butylamine in solvents such as dichloromethane, 2-propanol, and chloroform, while the reaction was very fast in methanol (only 15 min was enough for disappearance of **6a**) and relatively slow in ethanol. Thus, it was shown that the dibutylphosphinothioyl group was relatively stable during the aminolysis of the corresponding guanosine derivatives with *t*-butylamine. On the other hand, an easy cleavage of the group was detected in acidic mediums (for example, 80% acetic acid) to give **3**. Therefore, it seems to us that the dibutylphosphinothioyl group (BPT) is useful for O^6-protection of guanosine derivatives, because it has the following useful features; 1) ribose acetyl groups undergo more rapid aminolysis by *t*-butylamine than the O^6-BPT group; 2) it is possible to cleave easily O^6-BPT groups in either acidic or appropriate basic mediums; 3) the corresponding O^6-phosphinothioyl compounds could be obtained conveniently in high yields; 4) compounds **6a**—**c** are stable in solid state at room temperature for a long period of time and in aqueous pyridine for one day and can survive TLC or other purification procedures; 5) O^6-dibutylphosphinothioyl derivatives of N^2-tritylguanosine can be detected easily on TLC plates because of their characteristic blue fluorescence at 254 nm; 6) compounds **6**, **12**, or **13** have very characteristic UV spectra (see the later section); 7) butyl groups are easily detectable by ^1H NMR and it might be useful in nucleotide synthesis, because no significant signals appeared in that region.

Diphenylphosphinothioyl group showed similar properties to the BPT group but the introduction of the former to the O^6-imidoyl group was performed only in moderate yields and it does not have blue fluorescence like BPT-containing compounds.

Thus, as a result of this investigation, it seems that the BPT group might be useful for protection of the O^6-oxygen of guanosine. It could be a valuable starting point for designing similar and even better groups. Further efforts toward this goal are now in progress in our laboratory.

Solubility of O^6*-Substituted Guanosine Derivatives.* It is well documented by Guschlbauer that guanosine forms rigidly stable hydrogen bonded complexes of cyclic structure.[16)] This greatly diminishes the solubility of the molecule in many organic solvents and makes it impossible to perform some interesting synthetic transformations. Generally, in the oligonucleotide synthesis, the longer the chain of an oligonucleotide is, the poorer its solubility is so that the R_f becomes low and the separation of the oligonucleotide from other polar by-products is difficult. Therefore, from the two points of the prevention of the side reactions at the O^6-position of guanine moiety and the enhance of the solubility of guanosine derivatives, introduction of a protecting group into the O^6-imidoyl group seems to be important. The solubility of the O^6-substituted guanosine derivatives obtained in the present works increases dramatically in several organic solvents. For example, the *t*-butyldiphenylsilylated derivative (**7c**) is freely soluble in ether and fairly even in hexane. The high solubility of the O^6-substituted guanosine derivatives is seen from the R_f values described in Tables 1—3 and 7.

UV and ^1H *NMR Spectra of* O^6*-Substituted Guanosine Derivatives.* All O^6-substituted guanosines have similar UV spectra which are quite different from the corresponding UV spectral data of O^6-unsubstituted derivatives. All O^6-substituted compounds have a

Table 7. Some physical data for O^6-dibutylphosphinothioyl-N^2-tritylguanosine (**12**) and 5′-O-acetyl-O^6-dibutylphosphinothioyl-N^2-tritylguanosine (**13**)

Compound	Elemental analysis (%) Formula		R_f value[a]	UV spectra λ/nm		^{1}H NMR ($CDCl_3$), δ
	Calcd	Found		$\lambda_{max}^{dioxane}$ ($\varepsilon \times 10^{-3}$)	$\lambda_{min}^{dioxane}$	
12	$C_{37}H_{44}N_5O_5PS$ C, 63.32 H, 6.32 N, 9.98	 63.42 6.30 9.82	0.14	300 (8.75) 258 (10.6)	276 246	0.73—2.57 (18H, m, C_4H_9), 1.92 (3H, s, 5′-acetyl), 3.02 (1H, br. s, OH), 3.77—4.20 (5H, m, 2′,3′,4′, 5′-ribose protons), 5.38 (1H, d, $J_{1'-2'}$=1.1 Hz,H-1′), 6.47 (1H, s, NHTr), 7.23 (15H, br. s, ArH), 7.57 (1H, s, H-8)
13	$C_{39}H_{46}N_5O_6PS$ C, 62.97 H, 6.23 N, 9.41	 62.85 6.30 9.03	0.30	299 (8.6) 260 (12.4)	277 298	0.67—2.33 (18H, m, C_4H_9), 3.33—4.57 (8H, m, 2′, 3′,4′,5′-ribose protons and three OH groups), 5.53 (1H, d, $J_{1'-2'}$=1.1 Hz, H-1′), 6.47 (1H, s, NHTr), 7.27 (15H, br. s, ArH), 7.68 (1H, s, H-8)

a) Benzene–ethyl acetate (4 : 1, v/v).

maximum at 290—305 nm (ε=6000—9000) which is not characteristic of guanosine-type derivatives. In the case of the O^6-sulfonylated compounds this maximum lies between 300—305 nm, while the corresponding O^6-silylated and phosphinothioylated derivatives have their higher wavelength maximum at 290 and 300 nm, respectively.

^{1}H NMR spectra of O^6-substituted guanosines also have some very characteristic features. For instance, all O^6-substituted N^2-tritylguanosines have a moderately broad singlet around δ 6.0—6.5 (due to N^2-proton)[9] which disappears after D_2O exchange. Also all O^6-substituted 2′,3′,5′-tri-O-acetyl-N^2-tritylguanosines have their ribose protons split in two three protons groups, one located as a characteristic multiplet around δ 5.0—5.6 and the other as a broad singlet around δ 4.2. Resonance positions of trityl, acetyl, and H-8 protons are also of great value, but usually their chemical shift on NMR scale does not depend so crucially on O^6-substitution pattern. In the case of O^6-substituted 2′,3′,5′-tri-O-acetyl-N^2-benzoyl (or unsubstituted) derivatives the same pattern of resonance for the ribose protons was observed.

In conclusion, preparative new findings on the O^6-substitution reactions of guanosine derivatives have been obtained by use of 4-(dimethylamino)pyridine as a catalyst. All O^6-substituted guanosine compounds are highly soluble in many nonpolar organic solvents. It might be due to the cleavage of hydrogen bond between N^1 and O^6 by the introduction of the O^6-substituent. The O^6-dibutylphosphinothioyl derivatives are promising synthetic intermediates of guanosine compounds in nucleotide chemistry, because of some useful characteristics of the BPT group.

From the synthetic point of view in oligonucleotide synthesis, it is highly likely that coupling agents such as arenesulfonyl chlorides or azoles and phosphorylating species activated by the coupling agents attack the O^6-imidoyl group of guanine residue during the desired internucleotidic bond formation. This seems to be the reason why yields of the coupling reactions of oligonucleotides containing guanosine residue are remarkable unsatisfactory.

Experimental

Proton nuclear magnetic resonance spectra (60 MHz) were taken on a Hitachi Model R-24 spectrometer and are reported in parts per million from internal tetramethylsilane on the δ scale (δ=0). Ultraviolet spectra were recorded on a Hitachi Model 124 spectrophotometer. Elemental analyses were performed by the Microanalytical Laboratory, Tokyo Institute of Technology, at Nagatsuta. All solvents were distilled prior to use. Dichloromethane and pyridine were dried over 3A molecular sieves and calcium hydride, respectively. t-Butyldiphenylsilyl chloride,[17] diphenylphosphinothioyl chloride,[18] and dibutylphosphinothioyl bromide[19] were prepared according to the literature procedures.

General Procedure for O^6-*Sulfonylation, Silylation, or Phosphorylation of* N^2-*Substituted*[a] *or Unsubstituted 2′,3′,5′-Tri*-O-*acetylguanosines (Procedure A).* Two mmol of N^2-substituted or unsubstituted 2′,3′,5′-tri-O-acetylguanosine and 0.12 mmol of DMAP were dissolved[b] in 20 ml of dichloromethane and then to this solution were added successively 3.3 ml of triethylamine and 2.94 mmol of the corresponding sulfonyl, silyl, or phosphoryl halide.[c] After stirring of the homogeneous solution[d] for several hours,[e] the solvent was evaporated at 30 °C. The crystalline residue was redissolved[f] in 4 ml of dichloromethane and purified by column chromatography on silica gel. Elution was performed with benzene–ethyl acetate. Yields of the products are listed in Tables 1—3.

a) N^2-Substituent refers to trityl, benzoyl, or hydrogen. For a specific compound details are given in Tables 1—3.

b) In the case of 2′,3′,5′-tri-O-acetylguanosine, it was not possible to dissolve completely the guanosine derivative before addition of the corresponding sulfonylating, phosphorylating, or silylating reagent.

c) The corresponding silyl chloride (2.4 mmol) was used in the case of O^6-silylation reaction.

d) In the case of 2′,3′,5′-tri-O-acetylguanosine the reaction mixture became homogeneous after 30 min.

e) The reaction times for each individual compound are listed in Tables 1—3.

f) In some cases it was not possible to dissolve completely the white solid residue in 4 ml of dichloromethane. This did not, however, hamper the purification because it was possible to apply this suspension to the silica-gel column.

General Procedure for Partial Purification (Removal of Triethylammonium Chloride) of O^6-*Substituted* N^2-*Substituted or Unsubstituted 2′,3′,5′-Tri*-O-*acetylguanosines (Procedure B).* The general procedure A was followed until the solid residue was obtained after evaporation of the solvent. Then the solid was suspended

in 20 ml of dry ether, stirred for 10 min. and the white precipitate of triethylamine hydrochloride was filtered. The O^6-substituted-N^2-substituted or unsubstituted 2′,3′,5′-tri-*O*-acetylguanosine was in the filtrate together with DMAP and the excess of the corresponding sulfonylating, silylating, or phosphorylating agent. This procedure is especially useful for a quick confirmation that the reaction between guanosine derivative and the corresponding O^6-substitution reagent takes place. It is supported by the formation of triethylamine hydrochloride.

General Procedure for Aminolysis of Compounds 4—8 (Procedure C). O^6-Sulfonylated, O^6-phosphorylated, or O^6-silylated N^2-substituted 2′,3′,5′-tri-*O*-acetylguanosine (0.26 mmol) was dissolved in 1 ml of the corresponding organic solvent (dichloromethane, chloroform, methanol, ethanol, 2-propanol, or mixtures of two of them) and 2.8 mmol of the amine (ammonia, *t*-butylamine, or butylamine) in 2 mL of the above mentioned solvent was added at once. The course of the reaction was monitored by TLC (chloroform–methanol, 9 : 1, v/v). In the case of 2′,3′,5′-tri-*O*-acetyl-O^6-dibutylphosphinothioyl-N^2-tritylguanosine (**6a**: 1.59 mmol), *t*-butylamine (16.4 mmol) in methanol (12 ml) were stirred for 15 min at room temperature. The organic solvent was evaporated at 25 °C and the solid residue was chromatographed on silica gel with benzene–ethyl acetate to give **12** and **13** as white foams in 50 and 10% yields, respectively. In Table 7 the data are given for compounds **12** and **13**.

General Procedure for Acid Hydrolysis of O^6*-Sulfonylated 2′,3′,5′-Tri-*O*-acetyl-*N^2*-tritylguanosines to* O^6*-Sulfonylated 2′,3′,5′-Tri-*O*-acetylguanosines (Procedure D).* 2′,3′,5′-Tri-*O*-acethyl-O^6-arylsulfonyl-N^2-tritylguanosine[g] (0.1 mmol) was dissolved in 1 ml of 80% acetic acid in dioxane–water (4 : 1, v/v).[h] After 1 h water (4 ml) was added to the homogeneous reaction mixture and the resulting suspension was extracted with dichloromethane (3 × 2 ml). The combined dichloromethane solutions were washed with water (2 × 2 ml), dried over anhydrous sodium sulfate and evaporated at 25 °C. The remaining residue was redissolved in a small amount of dichloromethane and purified by column chromatography on silica gel (2 g). Benzene was used as the first eluent for removal of triphenylmethanol (about 10 ml of the eluate were collected) and the desired O^6-sulfonylated 2′,3′,5′-tri-*O*-acetylguanosine was eluted by ethyl acetate. The yield was nearly quantitative. The results are summarized in Table 6. All obtained 2′,3′,5′-tri-*O*-acetyl-O^6-(arylsulfonyl)guanosines (see Table 6) were proved to be identified (^{1}H NMR, R_f values, and UV spectra) with the corresponding 2′,3′,5′-tri-*O*-acetyl-O^6-(arylsulfonyl)guanosine obtained from direct O^6-sulfonylation of 2′,3′,5′-tri-*O*-acetylguanosine (see Table 1).

[g] Compounds **8a**—**c** were subjected to this reaction.

[h] No reaction took place in the absence of water.

*General Procedure for Conversion of 2′,3′,5′-Tri-*O*-acetyl-*O^6*-arylsulfonyl-*N^2*-tritylguanosines to 2′,3′,5′-Tri-*O*-acetylguanosine (Procedure E).* 2′,3′,5′-Tri-*O*-acetyl-O^6-arylsulfonyl-N^2-tritylguanosine (0.1 mmol) was suspended in 70% aqueous formic acid (2 ml) and stirred at room temperature for 30 min. The white precipitate of tritylcarbinol was filtered off and the colorless filtrate was poured into 8 ml of water and extracted with chloroform (3 × 2 ml). After evaporation of the chloroform at 30 °C the remaining residue was chromatographed on silica gel (2 g) with chloroform–methanol to give the desired 2′,3′,5′-tri-*O*-acetylguanosine (**11**). The yield of **11** was nearly quantitative in each experiment.

*2′,3′,5′-Tri-*O*-acetyl-*N^2*-tritylguanosine (1)* 2′,3′,5′-Tri-*O*-acetyguanosine (26.35 g, 64 mmol) was suspended in 400 ml of dry pyridine and heated at 100 °C and 53.9 g (0.193 mmol) of trityl chloride was added. After stirring at 100 °C for 6 h, the reaction mixture was poured into 1.5 l of water and extracted with dichloromethane (3 × 400 ml). The organic solvent was then removed by evaporation and the remaining oily residue was subjected to coevaporation with benzene (2 × 150 ml) for removal of the traces of pyridine. After that the dark brown oil (sometime it could crystallize) was suspended and stirred in 500 ml of ether for 1 h at room temperature. The resulting yellow precipitate was filtered off. After drying at 40 °C *in vacuo*, the crude 2′,3′,5′-tri-*O*-acetyl-N^2-tritylguanosine was dissolved in 90 ml of dichloromethane–methanol (9 : 1, v/v) and was purified by column chromatography on silica gel (60 g) by using dichloromethane–methanol as eluent. After evaporation of the eluate, the resulting light yellow solid was dissolved in 1.6 l of boiling methanol. The hot solution was filtered and the filtrate was concentrated by evaporation until 800 ml of methanol remained. External cooling (10—15 °C) was applied and after stirring of the suspension for 3 h the purified 2′,3′,5′-tri-*O*-acetyl-N^2-tritylguanosine was filtered and washed with a small amount of methanol. The yield was usually 70—80%.

We express great thanks to Prof. Hisashi Takei Tokyo Institute of Technology, for his kind gift of DMAP.

References

1) R. I. Zhdanov and S. M. Zhenodarova, *Synthesis*, **1975** 222; H. Kossel and H. Seliger, Fortschr. *Chem. Org. Naturstoffe* **32**, 298 (1975); V. Amarnath and A. D. Broom, *Chem. Rev.*, **77**, 183 (1977); C. B. Reese, *Tetrahedron*, **34**, 3143 (1978); M, Ikehara, E. Ohtsuka, and A. F. Markham, *Adv. Carbohyd. Chem. and Biochem.*, **36**, 135 (1978).

2) N. Katagiri, K. Itakura, and S. A. Narang, *J. Chem. Soc., Chem. Commun.*, **1974**, 325; N. Katagiri, K. Itakura, and S. A. Narang, *J. Am. Chem. Soc.*, **97**, 7332 (1975); J. Stawinski, T. Hozumi, and S. A. Narang, *Can. J. Chem.*, **54**, 670 (1976); J. Stawinski, T. Hozumi, S. A. Narang, C. P. Bahl, and R. Wu, *Nucleic Acids Res.*, **4**, 353 (1977); J. H. van Boom, P. M. J. Burgers, G. van der Marel, C. H. M. Verdegaal, and G. Wille, *ibid.*, **4**, 1047 (1977); C. B. Reese, R. C. Titmas, and L. Yau, *Tetrahedron Lett.*, **1978**, 2727; J. F. M. de Rooij, G. Wille-Hazeleger, P. H. van Deursen, J. Serdijn, and J. H. van Boom, *Recl. Trav. Chim. Pays-Bas*, **98**, 537 (1979); M. J. Gait and S. G. Popov, *Tetrahedron Lett.*, **21**, 2841 (1980); K. K. Ogilvie and R. T. Pon, *Nucleic Acids Res.*, **8**, 2105 (1980).

3) C. B. Reese and L. Yau, *J. Chem. Soc., Chem. Commun.* **1978**, 1050; E. Ohtsuka, T. Tanaka, T. Wakabayashi, Y. Taniyama, and M. Ikehara, *ibid.*, **1978**, 824; S. S. Jones and C. B. Reese, *J. Chem. Soc.*, **1979**, 2762; R. Arentzen, C. A. A. van Boeckel, G. van der Marel, and J. H. van Boom, *Synthesis* **1979**, 137; W. T. Markiewicz, *J. Chem. Research (S)*, **1979**, 24; J. B. Chattopadhyaya, C. B. Reese, and A. H. Todd, *J. Chem. Soc., Chem. Commun.*, **1979**, 987; A. Kaszewski, J. Stawinski, and M. Wiewiorowski, *Nucleic Acids Res.*, **10**, 2301 (1980); Z. J. Lesnikowski, W. J. Stec, and W. S. Zielinski, *Synthesis*, **1980**, 397; E. Uhlmann and W. Pfleiderer, *Tetrahedron Lett.*, **21**, 1181 (1980); C. C. M. Verdegaal, P. L. Jansee, J. F. M. de Rooij, and J. H. van Boom, *ibid.*, **21**, 1571 (1980).

4) R. L. Letsinger and W. B. Lunsford, *J. Am. Chem. Soc.*, **98**, 3655 (1976); K. K. Ogilvie, N. Theriault, and K. L. Sadana, *ibid.*, **99**, 7741 (1977); K. L. Agarwal and F. Riftina, *Nucleic Acids Res.*, **5**, 2809 (1978); K. K. Ogilvie, S. L. Beaucage, A. L. Schifman, and N. Y. Theriault, K. L. Sadana, *Can. J. Chem.*, **56**, 2768 (1978); R. Crea, T. Hirose, and K. Itakura,

Tetrahedron Lett., **1979**, 395; K. K. Ogilvie and N. Y. Theriault, *ibid.*, **1979**, 2111; K. Miyoshi and K. Itakura, *ibid.*, **1979**, 3635; M. J. Gait and R. C. Sheppard, *Nucleic Acid Res.*, **6**, 1259 (1979); G. R. Gough, C. K. Singleton, H. L. Weith, and P. T. Gilham, *ibid.*, **6**, 1557 (1979); V. K. Potapov, V. P. Veiko, O.N. Koroleva, and Z. A. Shabarova, *ibid.*, **6**, 2041 (1979); K. K. Ogilvie and N. Y. Theriault, *Can. J. Chem.*, **57**, 3140 (1979); M. D. Matteucci and M. H. Caruthers, *Tetrahedron Lett.*, **21**, 719 (1980); M. J. Gait, M. Singh, R. C. Sheppard, M. D. Edge, A. R. Green, G. R. Heathcliffe, T. C. Atkinson, C. R. Newton, and A. F. Markham, *Nucleic Acids Res.*, **8**, 1081 (1980); K. Greskowiak, R. W. Adamiak, and M. Wiewiorowski, *ibid.*, **8**, 1097 (1980); K. K. Ogilvie and R. T. Pon, *ibid.*, **8**, 2105 (1980); R. Crea and T. Horn, *ibid.*, **8**, 2331 (1980).

5) a) C. P. Bahl, R. Wu, K. Itakura, N. Katagiri, and S. A. Narang, *Proc. Natl. Acad. Sci. U.S.A.*, **73**, 91 (1976); b) H. M. Hsiung, R. Brousseau, J. Michniewicz, and S. A. Narang, *Nucleic Acids Res.*, **6**, 1371 (1979); c) W. L. Sung, H. M. Hsiung, R. Brousseau, J. Michniewicz, R. Wu, and S. A. Narang, *ibid.*, **7**, 2199 (1979).

6) a) K. Itakura, T. Hirose, R. Crea, A. D. Riggs, H. L. Heyneker, F. Bolivar, and H. W. Boyer, *Science*, **198**, 1056 (1977); b) D. V. Goeddel, H. L. Heyneker, T. Hozumi, R. Arentzen, K. Itakura, D. G. Yansure, M. J. Ross, G. Miozzari, R. Crea, and P. H. Seeburg, *Nature*, **281**, 544 (1979); c) R. Crea, A. Kraszewski, T. Hirose, and K. Itakura, *Proc. Natl. Acad. Sci. U.S.A.*, **75**, 5765 (1978); d) D. V. Goddel, D. G. Kleid, F. Bolivar, H. L. Heyneker, D. G. Yansura, R. Crea, T. Hirose, A. Kraszewski, K. Itakura, and A. D. Riggs, *ibid.*, **76**, 106 (1979).

7) E. Ohtsuka, T. Tanaka, and M. Ikehara, *J. Am. Chem. Soc.*, **101**, 6409 (1979); E. Ohtsuka, T. Tanaka, and M. Ikehara, *Chem. Pharm. Bull.*, **28**, 120 (1980).

8) P. K. Bridson, W. T. Markiewicz, and C. B. Reese, *J. Chem. Soc., Chem. Commun.*, **1977**, 447.

9) P. K. Bridson, W. T. Markiewicz, and C. B. Reese, *ibid.*, **1977**, 791.

10) C. B. Reese and A. Ubasawa, *Tetrahedron Lett.*, **1980**, 2265.

11) M. Sekine, K. Hamaoki, and T. Hata, *J. Org. Chem.*, **44**, 2325 (1979).

12) A preliminaly report of this work has already appeared: H. P. Daskalov, M. Sekine, and T. Hata, *Tetrahedron Lett.*, **21**, 3899 (1980).

13) H. Vorbrüggen, *Angew. Chem. Intern. Ed.*, **17**, 569 (1978).

14) S. K. Chaudhary and O. Hernandez, *Tetrahedron Lett.*, **1979**, 95, 99.

15) K. K. Ogilvie and D. J. Manitoba, *Tetrahedron Lett.*, **1973**, 317.

16) W. Guschlbauer and J. F. Chantot, "Synthesis, Structure, and Chemistry of Transfer Ribonucleic Acids and Their Compounds," Polish Academy Science (1976), p. 96.

17) S. Hanessian and P. Lavallee, *Can. J. Chem.*, **53**, 2975 (1975).

18) L. Maier, *Helv. Chim. Acta*, **47**, 120 (1964).

19) K. Furusawa, M. Sekine, and T. Hata, *J. Chem. Soc., Perkin Trans. 1*, **1976**, 1711.

Reaction of Hexafluoropropene Dimers with Organomagnesium and -lithium Reagents

Nobuo Ishikawa,* Sigmund Butler, and Masamichi Maruta
Department of Chemical Technology, Tokyo Institute of Technology, Ookayama, Meguro-ku, Tokyo 152

(Received May 20, 1981)

Nucleophilic reactions of *F*-2-methyl-2-pentene (**1**) and (*E*)-*F*-4-methyl-2-pentene (**2**), the dimers of hexafluoropropene, with organomagnesium and -lithium reagents were investigated. The reaction of **1** proceeded readily, giving two alkyl- or aryl-substituted polyfluoroalkenes which resulted from α- and γ-fluorine elimination, respectively. Only phenyllithium reacted with **2**, giving also α- and γ-fluorine eliminated phenylpolyfluoroalkenes. The reaction mechanism of γ-elimination was postulated in relation to the electropositive property of the organo group and to Mg–F or Li–F bond formation.

In our continuing studies on the chemistry of hexafluoropropene oligomers,[1] we have reported a number of reactions of the oligomers with various nucleophiles except those with C-nucleophiles such as organomagnesium or organolithium reagents. Although some reactions between terminal perfluoroalkenes and organometallic reagents of this type have been investigated,[2] none of reports on those of non-cyclized inner perfluoroalkenes have appeared in the literature.

In this paper we wish to reveal an interesting behavior of the dimers of hexafluoropropene, a typical inner perfluoroalkene, towards organomagnesium and organolithium reagents.

Results and Discussion

It is well known that two kinds of perfluoroalkenes are obtained by the anionic dimerization of hexafluoropropene:[1] *F*-2-methyl-2-pentene (**1**) and (*E*)-*F*-4-methyl-2-pentene (**2**).

The perfluoroalkene **1** is thermodynamically more stable than the other isomer **2**, and, nevertheless, **1** is much more reactive to O-, N- and S-nucleophiles than **2**.[3] This is ascribed to the higher stability of the carbanion (**3**) formed from **1** and a nucleophile, compared with the carbanion (**4**) derived from **2**, owing to the two electron-withdrawing trifluoromethyl groups attached to the anionic carbon atom.[3]

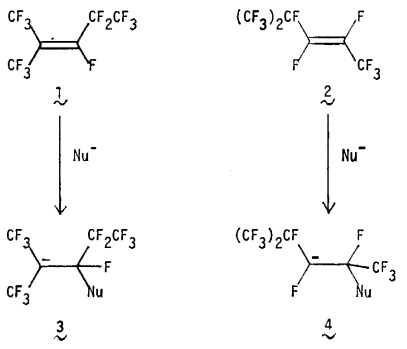

In a course of studies on the reactions of these dimers with organo-magnesium and -lithium reagents, we observed a similar tendency. The reaction of **1** was instantaneous and highly exothermic for all Grignard reagents except aryl one, while the less reactive isomer **2** with Grignard reagents, for example butylmagnesium bromide, did not produce any significant amount of products.

The products obtained by the reactions between **1** and alkylmagnesium halides were, however, always a mixture of two isomeric compounds which resulted from α- and γ-elimination of a fluoride ion from the intermediate carbanion **3** (Nu=R).

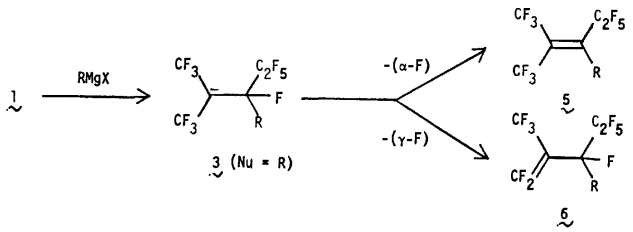

All the reactions were carried out in diethyl ether using about twice molar amounts of the Grignard reagents to ensure fast reaction. Although the two isomeric compounds in the products were not separable, the combined yield was over 70% (from ^{19}F NMR), and the structure of each isomer was readily established by careful checking of the ^{19}F NMR spectra. For example, the chemical shifts and coupling constants for the compound **5** and **6** (R=*n*-Bu) were as follows:†

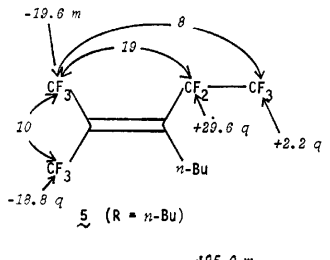

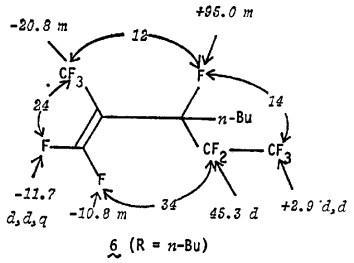

† All the ^{19}F chemical shifts throughout this article are shown in δ ppm upfield from external CF_3CO_2H. The coupling constants are given in Hz.

Table 1. Reaction of *F*-2-methyl-2-pentene (**1**) with Grignard reagents

$$(CF_3)_2C{=}CFCF_2CF_3 \xrightarrow[Et_2O]{RMgX} (CF_3)_2C{=}C(R)CF_2CF_3 + CF_2{=}C(CF_3)CF(R)CF_2CF_3$$

1 **5** **6**

Run	RX	RX/**1** mol/mol	Et_2O/RX ml/mmol	Temp °C[a]	Time min	Product, **5**+**6** Yield[b] %	Ratio **6**/**5**	Bp °C/mmHg[d]	Found (Calcd) (%) C	H
1	EtI	2.3	0.7	0	5	91	1.9	102—103/760	30.69 (30.98)	1.60 (1.63)
2	EtI	2.2	0.8	0	30	76	1.9			
3	EtBr	2.1	0.8	0	5	85	2.0			
4	EtBr	2.3	0.8	0	30	74	2.1			
5	*n*-PrI	2.4	0.7	0	5	87	1.3	54—55/72	33.51 (33.35)	2.24 (2.18)
6	*n*-PrBr	2.6	2.0	0	8	75	1.6			
7	*n*-PrBr	2.5	0.7	−45	8	75	1.0			
8	*n*-PrBr	2.4	0.7	0	60	78	1.4			
9	*n*-PrBr	2.2	0.8	+35	60	75	1.7			
10	*n*-BuBr	1.8	0.8	0	20	78	1.2	131—133/760	35.23 (35.50)	2.68 (2.68)
11	*n*-BuBr	1.2	2.5	+8	180	70[c]	1.4			
12	*n*-$C_8H_{17}Br$	2.0	0.6	0	30	87[c]	1.1	95—96/18	42.89 (42.60)	4.46 (4.35)
13	*c*-$C_6H_{11}CH_2Br$	2.7	0.8	0	7	88	1.0	83—85/22	41.58 (41.28)	3.54 (3.46)
14	$PhCH_2Br$	2.3	0.7	0	4	90	4.0	85—86/25	42.00 (41.95)	1.92 (1.90)
15	*i*-PrBr	2.4	0.7	0	4	77	7.4	42—43/40	33.09 (33.35)	2.18 (2.18)
16	PhBr	2.4	1.3	+23	60	46[c]	0.13	101—103/97	40.42 (40.24)	1.47 (1.41)
17	*p*-MeC_6H_4Br	2.4	0.8	+23	60	59	0.12	80—82/21	41.73 (41.95)	1.86 (1.90)

a) Deviation in the range of ±3 °C was allowed. b) Based on the ^{19}F NMR signal intensities unless otherwise noted.
c) Isolated yield. d) 1 mmHg≈133.322 Pa.

Although no evidence was found for isomerization of **6** into thermodynamically more stable **5** in the reaction system, and also in the post-treatment of the reaction mixture, the conversion was ascertained by the ^{19}F NMR to be realized readily by adding triethylamine in a polar solvent such as acetonitrile or *N*,*N*-dimethylformamide within 5 min, assisting confirmation of the structures.

The ratios of isomeric products in reaction mixtures, **6** *vs.* **5** or γ-elimination *vs.* α-elimination varied with the organo group of the reagents, reaction temperature, and other reaction conditions.

Thus, from Table 1, the order of percentage for γ-elimination forming **6** in ethereal solution was *i*-Pr> $PhCH_2$≫*n*-alkyl>aryl which is correlated to the relative reactivities of Grignard reagents, *i*-Pr>*s*-Bu>$PhCH_2$> *n*-alkyl.[4,5] Also the reactivity of Grignard reagents is correlated to the electropositivity of their identifying organo group[6] and, in fact, the order listed above shows a general, if imperfect, similarity to that of the electropositivities of organo groups, *i.e.* $PhCH_2$>*i*-Pr>*n*-alkyl>aryl.[7]

Regarding the mechanism of the reaction of **1** with Grignard reagents, α-elimination of a fluoride ion from the carbanion **3** resulting in a substituted product **5** is quite natural, and this type of reaction is frequently observed in the normal reactions of **1** with O- and N-nucleophiles.[1]

However, the formation of the rather unstable terminal alkene **6** resulted from γ-elimination is unusual. The elimination of a fluoride ion from the terminal trifluoromethyl group should be assisted by an electron donating group on one side and a fluoride ion-pulling group on another side. Thus we postulate that the magnesium behaves as a strong fluoride ion acceptor, as it can occupy a very close position to the fluorine atoms of CF_3, and as the Mg–F bond is thermodynamically very strong (462 kJ mol^{-1}).[8]

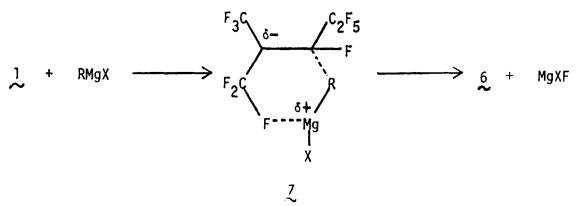

This kind of γ-elimination has been also observed in the reactions of **1** with thiols[9] and with ortho-difunctional benzenes.[10] The experimental fact mentioned above revealed that the more electropositive the organo group of the Grignard reagent is, the more γ-elimination becomes dominant. This is quite reasonable because an electropositive group will make the electron density more localized on a $^-C(CF_3)$ group, and will make magnesium more "metallic," and both effects will

render it easy to release a fluoride ion from the trifluoromethyl group. This assumption would be also supported by the difference in values **6**/**5** for RMgBr and RMgI. The more metallic organomagnesium bromide slightly prefers γ-elimination than organomagnesium iodide does. However, a fluoride ion elimination from a trifluoromethyl group is a process demanding higher energy because of a stronger carbon-fluorine bond in CF_3. So that it is natural that the reactions at higher temperatures enhanced the γ-elimination.

Similar reactions of another dimer, (*E*)-*F*-4-methyl-2-pentene, **2**, were sluggish and practically no products were formed with Grignard reagents. Phenyllithium, however, reacted with **2** and gave a significant amount of γ-elimination product (**9**) together with normal α-elimination product (**8**) in a ratio **9**/**8**=0.6.

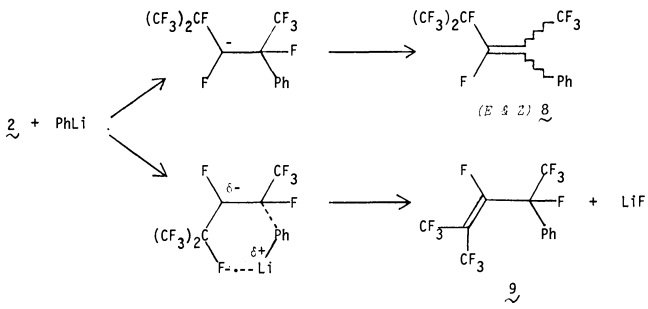

This value seems rather high because probability of γ-elimination for **2** should be one sixth of that for **1**. However, it should be understandable by considering that the Li–F bond is very strong (577 kJ mol^{-1})[8] and the tertiary fluorine atom would be released easily to give a stable perfluoro inner alkene. The structures of these isomers were also established by careful cheking of the ^{19}F NMR spectra for the mixture though it was unable to separate them from each other. The ratio of **8** to **9** was 5 : 3, of which **8** containing (*E*) and (*Z*) form (1 : 6.5). The chemical shifts and coupling constants were assigned to all fluorine atoms of the isomers as above:

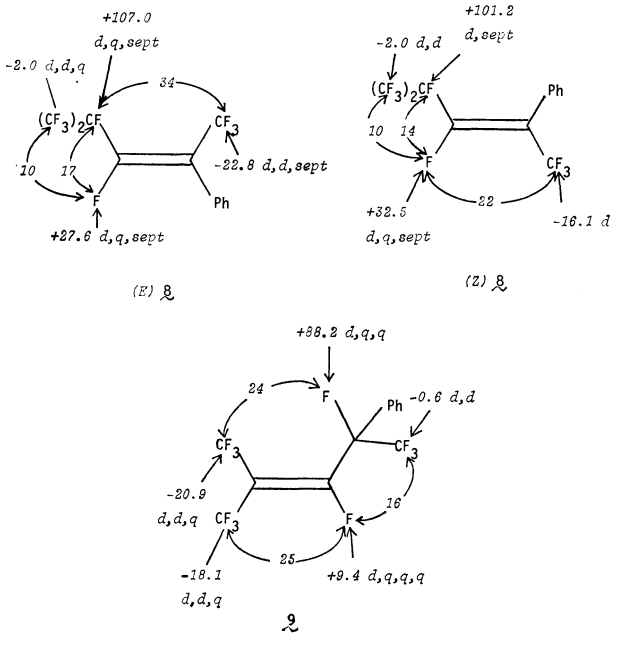

Experimental

Grignard Reactions of F-2-Methyl-2-pentene (1). Grignard reagents were prepared in a dried apparatus with air replaced by argon. Magnesium turnings and mild heating were used to initiate the reaction; in no case were chemical initiators necessary. The Grignard reagents in diethyl ether were very clear, almost colorless solution, except for aryl reagents which were dark brown. After formation of the Grignard reagent, the solution was brought to a specified temperature, and **1** was added with magnetic stirring. The addition was highly exothermic, and vigorous shaking of the bath was required to keep the temperature under control. Addition of the requisite amount of perfluoroalkene generally took about 5 min, after which the mixture was quenched by 2% HCl. Typical procedures are as follows.

Determination of Isomer Ratio. To the Grignard reagent prepared from magnesium turning (0.28 g, 11.5 mmol) and propyl bromide (1.51 g, 12.3 mmol) in dry diethyl ether (9 ml) was added **1** (purity over 95%, 1.62 g, 5.13 mmol) over 10 min at 0±3 °C. After stirring for 50 min at that temperature, the remaining Grignard reagent was quenched by the addition of dilute hydrochloric acid (2%, 2 ml). To the homogeneous ethereal solution, fluorobenzene (0.3784 g, 3.94 mmol) was added as internal standard. The ^{19}F NMR spectrum for this solution showed that the ratio of **6** to **5** (R=Pr) was 1.4, in a combined yield of 78%.

Isolation. To the Grignard reagent prepared from magnesium turning (2.65 g, 110 mmol) and octyl bromide (17.3 g, 90 mmol) in dry diethyl ether (55 ml) was added **1** (13 g, 41 mmol) at 0 °C. After 30 min the reaction was quenched by the addition of dilute hydrochloric acid (2%, 10 ml). The mixture was extracted with ether, washed with brine and dried over $MgSO_4$. After removing the solvent, distillation gave a mixture (15.2 g) of **5** and **6** (R=*n*-C_8H_{17}). The yield was 89%.

Isomerization of 6 to 5. To a mixture of **5** and **6** (R=alkyl) was added an approximately equal volume amount of acetonitrile in an NMR tube. It was ascertained by ^{19}F NMR that no isomerization occurred until a drop of triethylamine was added, upon which complete conversion of **6** to **5** occurred with 1 or 2 min. *N,N*-Dimethylformamide in the presence of triethylamine also effected the isomerization of **6** to **5** quantitatively.

Reaction with Phenyllithium. Into a solution of **1** (3.00 g, 10.0 mmol) in dry diethyl ether (20 ml), a solution of phenyllithium in diethyl ether (1.3 M (1 M=1 mol dm^{-3}), 10 ml) was dropped under nitrogen atmosphere at −60 °C, controlling the temperature with Dry Ice–acetone bath. The reaction mixture was stirred for 2 h allowing the temperature to rise up to room temperature. After additional stirring for 1 h at room temperature, the reaction was quenched by the addition of dilute hydrochloric acid and ethereal layer was washed with water and dried over $MgSO_4$. The solvent was removed and the residue was subjected to distillation *in vacuo* yielding a mixture of **5** and **6** (R=Ph) (2.25 g, 63%, **6**/**5**=0.16), bp 101—103 °C/97 mmHg. Found: C, 40.42; H, 1.47%. Calcd for $C_{12}H_5F_{11}$: C, 40.24; H, 1.41%.

In a similar manner, **2** (3.00 g, 10.0 mmol) and phenyllithium–diethyl ether solution (1.0 M, 20 ml) were allowed to react for 1 h at −70 °C. The reaction mixture was worked up as mentioned above and distillation under reduced pressure gave a mixture of **8** and **9** (2.80 g, 78%, **9**/**8**=0.6, (*Z*)**8**/(*E*)**8**=

6.5), bp 98—102 °C/115 mmHg. Found:C,40.04; H,1.48%. Calcd for $C_{12}H_5F_{11}$: C, 40.24; H, 1.41%.

References

1) Review: N. Ishikawa and M. Maruta, *Yuki Gosei Kagaku Kyokai Shi*, **39**, 51 (1981).
2) For example, L. A. Rozov, L. S. German, Yu. V. Zeifman, Ya. A. Cheburkov. and I. L. Knunyants, *Izv. Akad. Nauk SSSR, Ser. Khim.*, **1974**, 741; L. F. Rybakova, E. M. Panov, and K. A. Kocheshkov, *Zh. Org. Khim.*, **11**, 2576 (1975).
3) N. Ishikawa and A. Nagashima, *Bull. Chem. Soc. Jpn.*, **49**, 502 (1976).
4) T. Holm, *Acta Chem. Scand.*, **28** (Ser. B), 809 (1974).
5) W. A. Nugent, F. Bertini, and J. K. Kochi, *J. Am. Chem. Soc.*, **96**, 4945 (1974).
6) M. S. Kharasch and S. Weinhouse, *J. Org. Chem.*, **1**, 209 (1936).
7) H. O. Pritchard and H. A. Skinner, *Chem. Rev.*, **55**, 745 (1955).
8) CRC, "Handbook of Chemistry and Physics," 59th ed, (1978—1979), p. F 219.
9) M. Maruta and N. Ishikawa, *J. Fluorine Chem.*, **13**, 111 (1979).
10) M. Maruta, S. Kubota, N. Yoshimura, T. Kitazume, and N. Ishikawa, *J. Fluorine Chem.*, **16**, 75 (1980).

A Synthesis of Human Proinsulin C-Peptide[1)]

Ken'ichi IGANO, Yuriko MINOTANI, Nobuo YOSHIDA, Masao KONO, and Ken INOUYE*

Shionogi Research Laboratories, Shionogi and Co., Ltd., Fukushima-ku, Osaka 553

(Received December 6, 1980)

A peptide corresponding to the thirty-one amino acid sequence of human proinsulin C-peptide (positions 33—63 of proinsulin) was synthesized by the solid-phase method. The product was purified consecutively by gel filtration, DEAE-cellulose chromatography, and high-performance liquid chromatography (HPLC). The purified material behaved as a single component in reversed-phase HPLC, gave correct amino acid ratios, and was not distinguished from natural human C-peptide in terms of immunoreactivity and chromatographic behaviors. The $\alpha \rightarrow \beta$ transpeptidation at the Asp–Leu sequence, possible to occur associated with the HF cleavage, was studied using model peptides to demonstrate that the formation of β-peptide was 3—4% regardless of whether the β-carboxylic acid is free or protected as a benzyl ester.

Proinsulin synthesized in the β cells of the pancreas is transferred to the Golgi apparatus, where this precursor is degraded into insulin and C-peptide by certain proteolytic processes and both are released into the circulation.[2,3)]

The measurement of the concentration of C-peptide in peripheral venous plasma is of increasing importance for estimating the endogenous function of the pancreas, particularly in patients receiving insulin therapy. For this purpose Melani *et al.* first established a radioimmunoassay system using natural human C-peptide.[3)] However, the use of natural peptide is extremely limited and in addition human C-peptide can not be substituted by the animal peptides because C-peptides are highly species-specific in their primary structure. The chemical synthesis is thus the only means to meet the requirement for this peptide.

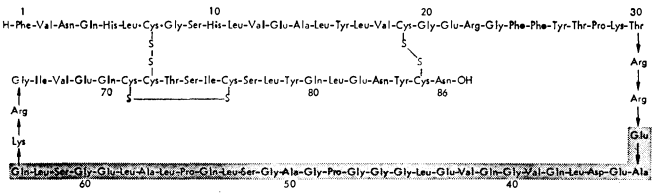

Fig. 1. Primary structure of human proinsulin.[4a)]
The shadowed portion indicates the region of C-peptide.

Human C-peptide (Fig. 1)[4)] is a thirty-one amino acid peptide corresponding to positions 33—63 of human proinsulin and contains none of aromatic amino acids, basic amino acids, and sulfur-containing amino acids. The synthesis by the conventional solution method has already been done by Naithani *et al.*,[5,6)] Geiger *et al.*,[7)] and Yanaihara *et al.*[8)] Yanaihara *et al.*[9)] also synthesized a derivative of human connecting peptide (Arg–Arg–C-peptide–Lys–Arg, positions 31—65 of proinsulin). These synthetic products were used in establishment of the radioimmunoassay system for C-peptide.[7,10,11)] The present paper describes our synthesis of human C-peptide by the solid-phase method.[12)] Synthesis of as large a peptide as C-peptide, particularly by the solid-phase technique, often presents considerable difficulty because it usually affords a highly heterogeneous product. Recently, however, HPLC has become a powerful tool for separation of closely related polypeptides[13,14)] including synthetic corticotropins and semisynthetic insulins.[14)] In the present synthesis of C-peptide also, reversed-phase HPLC played a major role in purification and characterization of the product.

Results and Discussion

The $\alpha \rightarrow \beta$ Rearrangement at the Aspartic Acid Residue. Human C-peptide contains a single Asp residue in position 36 (as numbered for proinsulin sequence) within the sequence Glu–Asp–Leu–Gln. It has been of special concern, particularly in the solid-phase synthesis, that Asp(OBzl)–Ser(Bzl)[15)] and Asp(OBzl)–Gly[16,17)] sequences are highly susceptible to cyclic imide formation when treated with HBr in TFA or with HF. The aspartimide formed is subject to nucleophilic attack at either carbonyl to give a mixture of α-Asp and β-Asp peptides. It is known, however, that Asp–Ser(Bzl) or Asp–Gly sequences containing a free β-COOH have little tendency to undergo this $\alpha \rightarrow \beta$ rearrangement.[15,18)] Thus, Yang and Merrifield[19)] proposed the use of the Pac group for temporary protection of the β-COOH. The Pac can be removed selectively after the completion of peptide synthesis but before the HF cleavage. This rearrangement is also known with other Asp peptides.[20)] Therefore, we tried to estimate the occurrence of the rearrangement in the present synthesis of C-peptide using Boc–Glu(OBzl)–Asp(OR)–Leu–Gly–OBzl (**1**: R=Bzl, **2**: R=H, **3**: R=Pac) as model compounds. The authentic samples of α-peptide, H–Glu–Asp(OH)–Leu–Gly–OH (**18**), and β-peptide, H–Glu–Asp(Leu–Gly–OH)–OH (**23**), were synthesized as illustrated in Fig. 2. They were well distinguished from each other and could, therefore, be determined easily on an amino acid analyzer.

The model compounds **1**—**3** were treated with HF–anisole in the usual manner and the product was

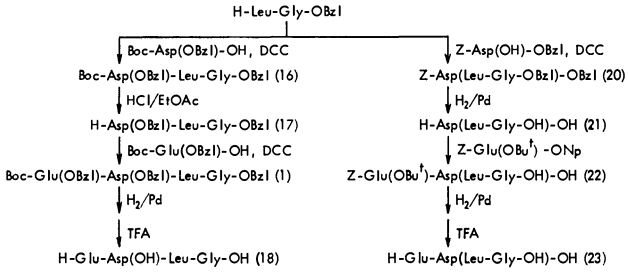

Fig. 2. Synthesis of model peptides.

Table 1. The $\alpha \rightarrow \beta$ rearrangement of aspartyl peptides, as examined with model compounds Boc–Glu(OBzl)–Asp(OR)–Leu–Gly–OBzl[a)]

R	Percent formation of	
	α-Peptide	β-Peptide
Bzl	96.9	3.1
H	95.9	4.1
Pac	49.4	50.6

a) For details see Experimental.

subjected to an amino acid analyzer before and after treatment with triethylamine. Before the base treatment β-peptide was not found in the product, but the chromatogram showed the presence of an unknown material. When treated with base, β-peptide became detectable, while the unknown peak had disappeared completely, indicating the latter to be an aspartimide, H–Glu–Asp> Leu–Gly–OH, the intermediate to β-peptide. The results are summarized in Table 1. The data show that compound **1** is not more susceptible to the α→β rearrangement than compound **2**, indicating that in compound **1** the rate of cyclization is much slower than the rate of cleavage of the benzyl ester, that is, the protecting group is removed first, then cyclization occurs very slowly as in compound **2**. Since the Asp(OBzl)–Leu sequence was thus found not to be more susceptible than the Asp–Leu sequence, which gave 4% of β-peptide under the conditions used, we decided to use the benzyl ester as a protecting group of Asp-36 in the present synthesis of C-peptide.

Compound **3** containing a β-Pac ester has a great tendency to undergo rearrangement as shown in Table 1. Therefore, the β-Pac ester has to be removed completely prior to the HF cleavage,[19)] or otherwise its incomplete removal will lead to ready formation of β-peptide.

Solid-phase Synthesis of Human C-Peptide. The synthesis was started with the introduction of Boc–Gln to the solid support using perhydrodibenzo-18-crown-6 as catalyst according to Roeske and Gesellchen.[22)] The resulting Boc–Gln-resin had a substitution of 0.35 mmol Gln/g. A 2.5-g portion (0.87 mmol) of the resin was placed in a peptide synthesizer and subjected to cycles of synthesis according to the procedure outlined in Table 2. The amino acid residues were introduced stepwise except for positions 50—51, 44—49, and 38—40, which were introduced by using Boc–Ala–Gly–OH (**4**), Boc–Leu–Gly–Gly–Gly–Pro–Gly–OH (**5**), and Boc–Gln–Val–Gly–OH (**6**), respectively.

The α-amino function was temporarily blocked by the Boc group and the side chain functional groups of Asp, Glu, and Ser were protected by the benzyl group. The Boc group was removed with TFA–CH_2Cl_2 (1 : 1 by vol).[23)] The coupling reactions were mediated by DCC throughout except for glutamines which were incorporated by the active ester method using Boc–Gln–ONp with DMF as solvent (steps 11—13 in Table 2).

The DCC couplings were performed with 3 equiv of reactants (reactons) (6 equiv in the case of Boc–Pro or Boc–Val) at room temperature for 2 h, while the active ester couplings were carried out for 16 h with 6 equiv of Boc–Gln–ONp. All the coupling reactions were performed twice by repeating steps 11—20 and the second coupling reaction was followed by acetylation with acetic anhydride to block any remaining amino function

Table 2. Schedule for solid-phase synthesis of peptide

Step	Operation and reagent[a)]	Number of operation	Mixing time (min)
1	50% TFA in CH_2Cl_2, 15 ml	1	3
2	50% TFA in CH_2Cl_2, 15 ml	1	20
3	CH_2Cl_2, 15ml	2	3
4	2-Propanol, 15 ml	2	3
5	CH_2Cl_2, 15 ml	3	3
6	5% DIEA in CH_2Cl_2, 15 ml	2	3
7	Repeat step 3		
8	Repeat step 4		
9	Repeat step 5		
10	Monitoring[b)]		
11	Boc–amino acid or Boc–peptide (3 equiv.)[c)] in CH_2Cl_2, 6 ml[d)]		
12	CH_2Cl_2 rinse, 6 ml		
13	DCC (3 equiv.) in CH_2Cl_2, 6 ml		120
11*	DMF, 15 ml	2	3
12*	Boc–Gln–ONp (6 equiv.) in DMF, 15 ml	1	960
13*	DMF, 15 ml	2	3
14—20	Repeat steps 3—9		
21	Monitoring[b)]		
22—31	Repeat steps 11—20		
32	Monitoring[b)]		
33	15% Ac_2O in CH_2Cl_2, 6 ml		
34	CH_2Cl_2 rinse, 6 ml		
35	15% DIEA in CH_2Cl_2, 6 ml		60
36—42	Repeat steps 3—9		
43	Monitoring[b)]		

a) For introduction of Boc–Gln follow steps 11*—13* in place of steps 11—13. b) See Table 3 for detailed prodcedure. Delete step 10 when it follows deprotection of a Boc–Gln derivative. c) Use 6 equiv. in case of Boc–Pro or Boc–Val. d) DMF–CH_2Cl_2 mixtures are used in cases of Boc–peptides which are of low solubility in CH_2Cl_2.

Table 3. Procedure for monitoring solid-phase synthesis by the picrate method

Step	Operation and reagent	Number of operation	Mixing time (min)
1	0.1 M Picric acid in CH_2Cl_2, 15 ml	1	3
2	CH_2Cl_2,15 ml	7	3
3	2-Propanol	2	3
4	CH_2Cl_2, 15 ml	3	3
5	5% DIEA in CH_2Cl_2, 15 ml	2	3
6	CH_2Cl_2, 15 ml	2	3
7	2-Propanol, 15 ml	2	3
8	CH_2Cl_2, 15 ml	3	3

a) The washings collected in steps 5—8 are combined and subjected, after appropriate dilution with 95% ethanol, to manual measurement of absorption at 358 nm. The procedure basically follows Gisin's.[24)]

completely (steps 33—42).

The progress of solid-phase synthesis was monitored by the picrate method,[24] which determines resin-bound free amino group by picric acid salt formation. The determination was carried out, according to the procedure shown in Table 3, after every reaction of the deprotection, couplings, and acetylation. Only when a Gln came to the N-terminal, the determination after deprotection was omitted to prevent the chain termination by possible formation of the pyrrolidone ring. The picric acid bound to the resin was displaced by DIEA and measured on a spectrophotometer based on the molar absorptivity of 16100 at 358 nm.[24] The results are shown in Fig. 3. The total free amino group, as determined after deprotection, decreased progressively from 0.87 mmol for Gln-63 to 0.32 mmol for Ala-34 at an average rate of 4.5% per cycle.

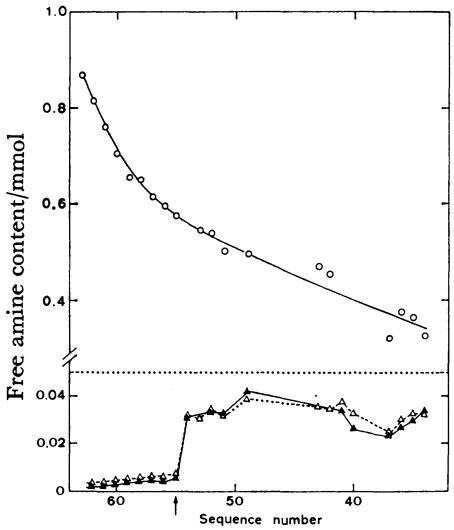

Fig. 3. Progress of solid-phase synthesis of human C-peptide as monitored by the picrate method.[24]
○—○: After deprotection (step 10 in Table 2), △---△: after 1st coupling (step 21 in Table 2), ▲—▲: after acetylation (step 43 in Table 2). Note that the scale is different between the upper part and the lower part of the ordinate. Sequence number (abscissa) represents position in the human proinsulin sequence. Positions 51—50, 49—44, and 40—38 were introduced as fragments. Glutamine residues occupy positions 54, 41, and 38, where the determination after deprotection (step 10 in Table 2) was eliminated. The arrow indicates the position of Pro-55. For details see text.

The free amino group was also determined after both first and second couplings. The values for the two determinations were nearly identical and were little affected by the subsequent acetylation, indicating that the reaction had been achieved satisfactorily by a single coupling operation. Therefore, the second coupling and acetylation might not be essential in the present synthesis. It is worthy of note that the picrate value showed a sudden rise by 0.02—0.03 mmol when Boc-Gln was introduced next to Pro-55. Schou *et al.*[25] suggested that an N-alkylation takes place between Pro and surplus chloromethyl group on the resin to form a tertiary amine. Such amine may be a cause for the apparent increase in free amino group which is seen in Fig. 3.

The protected peptide-resin obtained was found to contain 0.49 mmol of peptide, as calculated from the content of Leu. This value is significantly higher than the picrate value (0.32 mmol) obtained for Ala-34. The big difference might be a reflection of the accumulation of incomplete couplings not easily detectable by the picrate method.

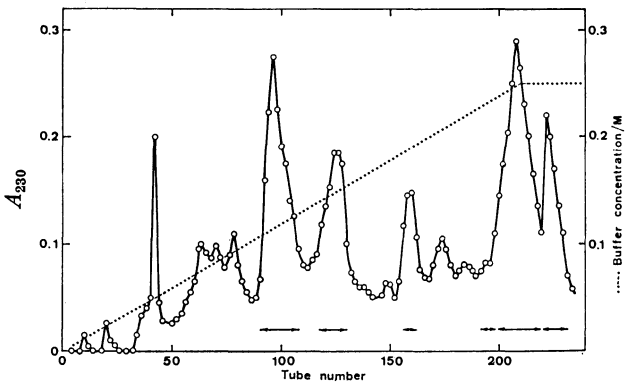

Fig. 4. Fractionation of crude human C-peptide preparation on DEAE-cellulose column.
Material: solid-phase synthetic product (gel-filtered through a Sephadex G-50 column), 237 mg; column: Whatman DE-52, 2.2×33 cm; eluent: 0—0.25 M NH_4HCO_3 (3000 ml) with a linear concentration gradient; fractionation: 14 ml/tube. Fractions, as indicated by the horizontal arrows, were collected.

The peptide-resin was deprotected with HF–anisole in the usual manner[21] and the resulting crude product was gel-filtered first and then subjected to DEAE-cellulose chromatography (Fig. 4). The fractions indicated by the horizontal arrows were collected and lyophilized. Tubes 199—220 and 221—234 had virtually the same and the simplest HPLC profile consisting of one major (**b**) and three minor components (**a**, **c**, and **d**) (Fig. 6A). These fractions were also shown to resemble human C-peptide more closely than any other fractions in the amino acid ratios. The combined amount of tubes 199—234 represented 25% of the crude product. Rechromatography of this preparation on a DEAE-cellulose column afforded a major peak (tubes 174—200, Fig. 5), from which a preparation containing components **a** and **b** but not **c** and **d** was obtained (Fig. 6B). For final purification, this was subjected to HPLC under conditions similar to those used for analytical HPLC. The eluate corresponding to component **b** was collected and desalted by gel filtration. The resulting preparation was shown to be fairly homogeneous by the criteria of HPLC (Fig. 6D) and TLC. The amino acid composition was consistent with that expected for human C-peptide and the optical rotation was identical with those reported in the literature.[5,6] Components **a**, **c**, and **d** have remained unidentified.

The synthetic peptide thus obtained was then compared with natural C-peptide preparations in order to establish their identity. For this purpose C-peptide was isolated from human urine and purified to a single

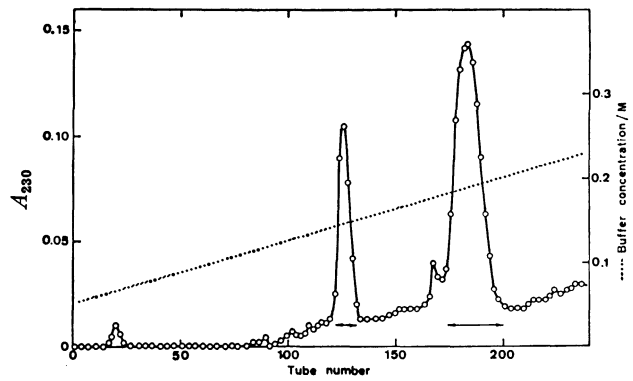

Fig. 5. Rechromatography of synthetic human C-peptide. Material: preparation from tubes 199—234 in Fig. 4, 21.3 mg; column: Whatman DE-52, 1.74×33 cm; eluent: 0.05—0.25 M NH_4HCO_3 (2000 ml) with a linear concentration gradient; fractionation: 6 ml/tube. Fractions, as indicated by the horizontal arrows, were collected.

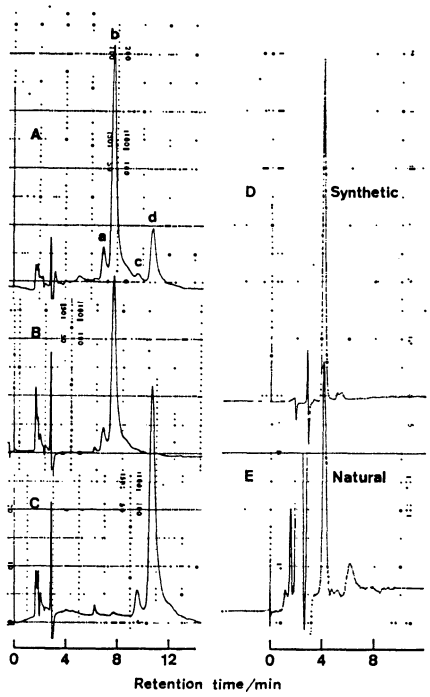

Fig. 6. HPLC of human C-peptide preparations.
A, tubes 199—220 in Fig. 4; B, tubes 174—200 in Fig. 5; C, tubes 122—132 in Fig. 5; D, synthetic C-peptide (component **b**, isolated by HPLC from tubes 174—200 in Fig. 5); E, natural C-peptide isolated from human urine. Peaks seen in E, but not in D, are those derived from a phosphate buffer used as solvent of natural C-peptide. HPLC conditions: column, Nucleosil $5C_{18}$, 0.4×25 cm; eluant, 0.1 M sodium phosphate (pH 7.0)–CH_3CN (79 : 21 by vol), 1 ml/min; detection, at 220 nm (0.04 AUFS).

component. This preparation contained all the constituent amino acids of human C-peptide in correct ratios. The isolation and purification of this urinary C-peptide will be described elsewhere. The identical HPLC profiles of the synthetic and natural preparations are shown in Fig. 6. Comparison between these two

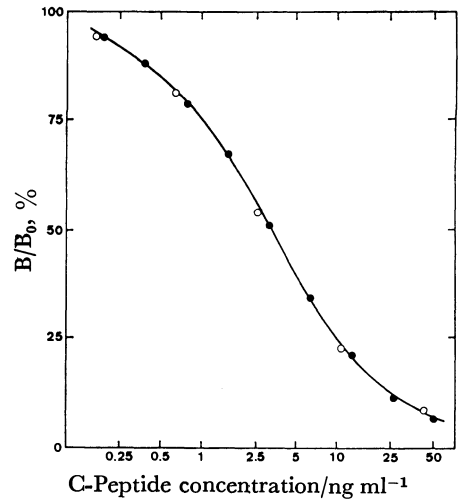

Fig. 7. Radioimmunoassay of human C-peptide preparations.
●—●: Synthetic C-peptide (component **b**), ○—○: natural C-peptide isolated from human urine. The assay was performed using a C-peptide assay system described elsewhere.[26]

preparations was also made in terms of the ability to displace [^{125}I]iodotyrosylated C-peptide specifically bound to the antibodies using a radioimmunoassay system developed by Kono *et al.*[26] As illustrated in Fig. 7, the displacement curves of the synthetic and natural preparations are perfectly superimposable. The identical results were also obtained in the radioimmunoassay performed with human pancreatic C-peptide as reference (data not shown).

These observations permit us to conclude that the synthetic peptide prepared in the present work is identical to human C-peptide.

Experimental

Protected amino acid derivatives, DCC, TFA, and chloromethylated copoly(styrene–2%-divinylbenzene) resin (200—400 mesh, 0.73 mmol Cl/g) were obtained from Protein Research Foundation, Osaka. DIEA (Aldrich) was distilled before use (bp 129—129.5 °C). Other reagents and solvents were of reagent grade and used without further purification. All melting points are uncorrected. TLC was performed on precoated silica gel plates (Kieselgel $60F_{254}$, Merck), unless otherwise specified, with the following solvent systems (ratios by vol): A, $CHCl_3$–MeOH (9 : 1); B, $CHCl_3$–MeOH (8 : 2); C, $CHCl_3$–MeOH–AcOH (90 : 10 : 3); D, $CHCl_3$–MeOH–AcOH (80 : 20 : 3); E, EtOAc–AcOH–H_2O (4 : 1 : 1); F, EtOAc–AcOH–H_2O (3 : 1 : 1). For detection the plate developed was sprayed with concd HCl, heated at 150 °C, and then sprayed with 0.2% ninhydrin in H_2O-saturated *n*-BuOH. Silica gel used for column chromatography was Kieselgel 60 (Merck). Amino acid analyses were performed on a Hitachi amino acid analyzer KLA-5 equipped with a Shimadzu data processor Chromatopac-ElA. Acid hydrolysis of peptide-resin samples was carried out in sealed evacuated tubes with concd HCl–propionic acid (1 : 1 by vol)[27] at 110 °C for 20 h. The hydrolysis of free peptides was carried out with 6 M HCl under similar conditions. Digestion with leucine aminopeptidase (Worthington) was performed as described by Hofmann *et al.*[28] in a substrate-enzyme ratio

of 10 (by wt). For HPLC a Waters Associates Model 6000A solvent delivery system, equipped with a Waters U6K injector, and a Japan Spectroscopic UVIDEC-100-II variable-wavelength UV detector were used throughout.

Peptide Synthesizer. A microcomputer-controlled semiautomated peptide synthesizer was designed and constructed in these Laboratories. The whole design basically followed that of Brunfeldt[29] except for the reaction vessel and its shaking device, which are rather similar to those of Merrifield's instrument.[30] The apparatus performed all the operations required for introduction of at least one amino acid residue or equivalent according to the schedule shown in Table 2. Although the apparatus is not equipped with any monitoring system, it performed transfer of reagents and solvents, for monitoring by the picrate method,[24] along the reservoir-reaction vessel-collecting bottle line. The spectrophotometric determination of the displaced picric acid was carried out manually.

Solid-phase Synthesis of Human C-Peptide. Neutralization of Boc–Gln–OH (2.1 g, 8.5 mmol) with KOH in 60% EtOH yielded Boc–Gln–OK, which was dried over P_2O_5 and then dissolved in DMF (100 ml). To this were added perhydrodibenzo-18-crown-6 (3.21 g, 8.6 mmol)[22] and chloromethylated copoly(styrene–2%-divinylbenzene) resin (10 g, 0.73 mmol Cl/g) and the mixture was gently stirred at 50 °C for 18 h. The Boc–Gln–resin thus obtained was filtered off, washed with DMF (30 ml×3), 75% DMF (30 ml×3), water (30 ml×2) and EtOH (30 ml×4) and dried over P_2O_5 *in vacuo* (11.2 g); Gln content: 0.35 mmol/g resin.

The Boc–Gln–resin (2.5 g, 0.87 mmol Gln) was placed in the peptide synthesizer and the synthesis was performed at room temperature according to the procedure shown in Table 2. On completion of the synthetic cycles the protected peptide-resin obtained was dried over P_2O_5 *in vacuo* (3.61 g).

A 1.08-g sample of the protected peptide-resin was treated with HF (7 ml) at −3—0 °C for 60 min in the presence of anisole (3 ml). After evaporation of the HF at the same temperature, the residue was triturated with EtOAc and the supernatant was discarded by decantation. The residue was washed with EtOAc two more times and then extracted with 0.05 M NH_4HCO_3. Lyophilization of the extract gave 320 mg of crude product.

The crude material (305 mg) was subjected to gel filtration on a column (3.3×91 cm) of Sephadex G-50 (superfine) with 0.05 M NH_4HCO_3 as eluent. Fractions (7.5 ml/tube) collected were monitored by absorbance at 230 nm and by TLC on a cellulose plate (Cellulose F_{254}, Merck) with *n*-BuOH–AcOH–pyridine–H_2O (30 : 6 : 20 : 24) as solvent. Tubes 40—83, which showed similar TLC patterns, were pooled and lyophilized (237 mg). This material was then fractionated on a DEAE-cellulose column (Whatman DE-52), as shown in Fig. 4, to give tubes 90—108 (40 mg), 118—130 (22 mg), 156—161 (11 mg), 191—198 (7 mg), 199—220 (60 mg), and 221—234 (17 mg). Amino acid ratios in acid hydrolysate of tubes 199—220: Asp 1.0 (1), Ser 1.8 (2), Glu 7.1 (8), Pro 2.5 (2), Gly 6.9 (7), Ala 3.0 (3), Val 1.9 (2), Leu 6.0 (6) (theoretical values for human C-peptide are given in parentheses).

Tubes 199—220 and 221—234 were combined and its small portion (21.3 mg) was rechromatographed on a DE-52 column (Fig. 5). The major peak at tubes 174—200 afforded 13.8 mg of peptide upon lyophilization. This was then subjected in ten separate portions (1.4 mg each) to HPLC on a column of Nucleosil $5C_{18}$ (1.0×30 cm) with a mixture of 0.01 M sodium phosphate buffer (pH 7.1) and CH_3CN (84.5 : 15.5 by vol) as eluent. The flow rate was 6 ml/min. The eluete corresponding to a major peak, as monitored by absorbance at 220 nm, was collected. Evaporation of the solvent gave a residue, which was desalted by gel filtration on a column (2.4×120 cm) of Sephadex G-25 (medium) with 5 mM NH_4HCO_3 as eluent. The peptide emerged was lyophilized and dried over P_2O_5; 7.6 mg (9% based on crude deprotection product), $[\alpha]_D^{26}$ −95.4±6.2° (*c* 0.2, 0.05 M NH_4HCO_3). Lit: $[\alpha]_D^{22}$ −95.4° (*c* 0.3, 0.05 M NH_4HCO_3),[5] $[\alpha]_D^{23}$ −96.2° (*c* 0.4, 0.05 M NH_4HCO_3),[6] $[\alpha]_D^{22}$ −92.3° (*c* 0.3, 0.1 M NH_3aq),[7] $[\alpha]_D^{20}$ −103.2° (*c* 1.00, 50% AcOH).[9] Amino acid ratios in acid hydrolysate: Asp 1.04 (1), Ser 1.88 (2), Glu 7.90 (8), Pro 2.24 (2), Gly 7.01 (7), Ala 3.09 (3), Val 1.95 (2), Leu 6.00 (6). TLC (cellulose): homogeneous in *n*-BuOH–AcOH–pyridine–H_2O (30 : 6 : 20 : 24). For HPLC see Fig. 6.

Synthesis of C-Peptide Fragments. *Boc–Ala–Gly–OBzl (**7**)*: Coupling of Boc–Ala–OH and H–Gly–OBzl (free base) with DCC in CH_2Cl_2 yielded compound **7**; 92%, mp 85—85.5 °C, $[\alpha]_D^{24.5}$ −28.1±0.7° (*c* 1.0, MeOH). Lit:[31] mp 83—84 °C, $[\alpha]_D^{20}$ −23.9° (*c* 1.0, $CHCl_3$). TLC: homogeneous in system C.

*Boc–Ala–Gly–OH (**4**)*: Catalytic hydrogenolysis of **7** gave **4** in 83% yield; mp 82—86 °C, $[\alpha]_D^{23.5}$ −25.1±0.6° (*c* 1.0, MeOH). Lit:[32] mp 78—80 °C, $[\alpha]_D$ −23° (MeOH). TLC: homogeneous in system C.

*Boc–Pro–Gly–OBzl (**8**)*: Coupling of Boc–Pro–OSu with H–Gly–OBzl (free base) in DMF yielded **8**; 88%, mp 71 °C, $[\alpha]_D^{25}$ −64.3±1° (*c* 1.0, MeOH). Lit:[33] mp 68—70 °C. TLC: homogeneous in system B.

*Boc–Gly–Pro–Gly–OBzl (**9**)*: Treatment of **8** with 1 M HCl in AcOH yielded H–Pro–Gly–OBzl·HCl, which was coupled with Boc–Gly–OSu in DMF in the presence of Et_3N to give **9**; 78%, mp 150—151 °C, $[\alpha]_D^{24}$ −81.3±1.6° (*c* 1.0, MeOH). Lit:[33] mp 145—147 °C. TLC: homogeneous in system B.

*Boc–Leu–Gly–Gly–OH (**10**)*: Coupling of Boc–Leu–OSu with H–Gly–Gly–OH (solubilized by Triton B) in DMF gave **10** as hygroscopic amorphous powder; 82%, $[\alpha]_D^{27}$ −8.1±0.5° (*c* 1.0, MeOH). TLC: homogeneous in system D. Found: C, 50.92; H, 7.74; N, 11.02%. Calcd for $C_{15}H_{27}N_3O_6\cdot 0.5H_2O$: C, 50.84; H, 7.96; N, 11.86%.

*Boc–Leu–Gly–Gly–NHNH$_2$ (**11**)*: Coupling of Boc–Leu–OSu with H–Gly–Gly–OBzl gave Boc–Leu–Gly–Gly–OBzl, from which compound **11** was derived by hydrazinolysis; 81%, $[\alpha]_D^{24}$ −8.3±0.5° (*c* 1.0, MeOH). TLC: homogeneous in system B. Found: C, 49.51; H, 7.83; N, 19.08%. Calcd for $C_{15}H_{29}N_5O_5\cdot 0.5H_2O$: C, 48.90; H, 8.21; N, 19.01%.

*Boc–Leu–Gly–Gly–Gly–Pro–Gly–OBzl (**12**)*: Treatment of **9** with 1 M HCl in EtOAc gave H–Gly–Pro–Gly–OBzl·HCl, which was coupled to **10** with DCC–HOSu[34] in DMF in the presence of Et_3N to yield **12** as amorphous solid; 87%, $[\alpha]_D^{24}$ −56.6±1.0° (*c* 1.0, MeOH). TLC: homogeneous in system B. Found: C, 56.61; H, 7.52; N, 12.56%. Calcd for $C_{31}H_{46}N_6O_9$: C, 56.78; H, 7.22; N, 12.81%.

Coupling of H–Gly–Pro–Gly–OBzl with the azide derived from **11** by the treatment with isopentyl nitrite[35] also produced **12** in 96% yield; $[\alpha]_D^{24.5}$ −57.0±0.9° (*c* 1.0, MeOH).

*Boc–Leu–Gly–Gly–Gly–Pro–Gly–OH (**5**)*: Catalytic hydrogenolysis of **12** in AcOH gave **5** as amorphous solid; 96%, $[\alpha]_D^{24.5}$ −55.9±1.0° (*c* 1.0, MeOH). TLC: homogeneous in system E. Found: C, 51.72; H. 7.18; N, 14.93%. Calcd for $C_{24}H_{40}N_6O_9$: C, 51.79; H, 7.24; N, 15.10%.

*Boc–Val–Gly–OBzl (**13**)*: Coupling of Boc–Val–OH and H–Gly–OBzl with DCC yielded **13**; 76%, mp 73—75 °C, $[\alpha]_D^{24}$ −27.1±0.7° (*c* 1.0, MeOH). Lit: mp 63—69 °C;[36] mp 74.5—76.5 °C, $[\alpha]_D^{20}$ −8.3° (*c* 2.0, DMF).[37] TLC: homogeneous in system A.

Boc-Gln-Val-Gly-OBzl (14): Treatment of **13** with TFA yielded H-Val-Gly-OBzl·TFA, which was coupled with Boc-Gln-ONp in DMF in the presence of DIEA to give **14**; 61%, mp 208—209 °C, $[\alpha]_D^{23}$ −47.9±1.3° (*c* 1.0, MeOH). TLC: homogeneous in system D. Found: C, 58.56; H, 7.10; N, 11.36%. Calcd for $C_{24}H_{36}N_4O_7$: C, 58.52; H, 7.34; N, 11.37%.

Boc-Gln-Val-Gly-OH (6): Catalytic hydrogenolysis of **14** in AcOH yielded **6** as amorphous solid; 76%, $[\alpha]_D^{26}$ −45.6 ±1.5° (*c* 0.5, MeOH). TLC: homogeneous in system F. Found: C, 50.47; H, 7.68; N, 13.76%. Calcd for $C_{17}H_{30}N_4O_7$: C, 50.47; H, 7.51; N, 13.92%.

Synthesis of Model Peptides. H-Leu-Gly-OBzl·HCOOH (15): Coupling of Boc-Leu-OH and H-Gly-OBzl with DCC followed by treatment with HCOOH for 5 h yielded **15**; 74%, mp 93—94 °C, $[\alpha]_D^{22.5}$ +7.4±0.5° (*c* 1.0, MeOH). Lit:[39] mp 92.5—93.5 °C, $[\alpha]_D^{20}$ +5.0° (*c* 1.0, MeOH). TLC: homogeneous in system E.

Boc-Asp(OBzl)-Leu-Gly-OBzl (16): Coupling of Boc-Asp-(OBzl)-OH and H-Leu-Gly-OBzl (free base derived from **15**) with DCC yielded **16**; 80%, mp 111—115 °C, $[\alpha]_D^{23}$ −38.6±0.8° (*c* 1.0, MeOH). TLC: homogeneous in system A. Found: C, 63.88; H, 7.19; N, 7.10%. Calcd for $C_{31}H_{41}N_3O_8$: C, 63.79; H, 7.08; N, 7.19%.

H-Asp(OBzl)-Leu-Gly-OBzl·HCl (17): Treatment of **16** with 1 M HCl in EtOAc produced **17**; 91%, mp 172—174 °C, $[\alpha]_D^{23}$ −19.7 ±0.6°, (*c* 1.0, MeOH). TLC: homogeneous in system B. Found: C, 59.83; H, 6.61; N, 8.10; Cl, 6.96%. Calcd for $C_{26}H_{33}N_3O_6$·HCl: C, 60.05; H, 6.59; N, 8.08; Cl, 6.82%.

Boc-Glu(OBzl)-Asp(OBzl)-Leu-Gly-OBzl (1): Boc-Glu-(OBzl)-OH and **17** were coupled with DCC in CH_2Cl_2 in the presence of DIEA to give compound **1** as amorphous solid after purification on a silica gel column with EtOAc–hexane (1 : 1) as solvent; 62%, $[\alpha]_D^{23}$ −30.1±0.7° (*c* 1.0, MeOH). TLC: homogeneous in system B. Found: C, 64.04; H, 6.80; N, 6.92%. Calcd for $C_{43}H_{54}N_4O_{11}$: C, 64.32; H, 6.78; N, 6.98%.

H-Glu-Asp-Leu-Gly-OH (18): Catalytic hydrogenolysis followed by treatment with TFA of compound **1** produced the TFA salt of **18**. This was treated with Amberlite CG-400 (acetate form) with 1 M AcOH as solvent. The resulting solution was lyophilized and the residue was subjected to chromatography on a column (1.2×29 cm) of DEAE-cellulose (Whatman DE-52) using an NH_4HCO_3 buffer (pH 7.8, 2000 ml) with a linear concentration gradient of 0—0.2 M. The fractions (10 ml/tube) were monitored by absorbance at 230 nm and those corresponding to a major peak were pooled and lyophilized. The resulting material was desalted by gel filtration on a Sephadex G-10 column with 0.1 M AcOH as eluent. A pure preparation of **18** was obtained as colorless powder upon lyophilization; 88%, $[\alpha]_D^{24}$ −36.2±1.4° (*c* 0.5, H_2O). TLC: homogeneous in system F. Found: C, 44.42; H, 6.82; N, 12.18%. Calcd for $C_{17}H_{28}N_4O_9\cdot 1.5H_2O$: C, 44.44; H, 6.80; N, 12.19%. Amino acid ratios in: acid hydrolysate: Asp 1.03 (1), Glu 1.03 (1), Gly 0.96 (1), Leu 1.00 (1); leucine aminopeptidase digest: Asp 0.97 (1), Glu 0.98 (1), Gly 0.97 (1), Leu 1.00 (1).

Z-Asp(OH)-OBzl (19): The Cs salt of Z-Asp(OBu^t)-OH was allowed to react with benzyl bromide at 25 °C for 3 d. The resulting Z-Asp(OBu^t)-OBzl was treated with 1 M HCl in EtOAc to give **19**; 39%, mp 83—84 °C, $[\alpha]_D^{25}$ −18.1±0.6° (*c* 1.0, MeOH). Lit:[40] mp 82—85 °C, $[\alpha]_D^{25}$ −15.3° (*c* 1.60, EtOH). TLC: homogeneous in system B.

Z-Asp(Leu-Gly-OBzl)-OBzl (20): Compound **19** and H-Leu-Gly-OBzl (free base derived from **15**) were coupled with DCC to yield **20**; 74%, mp 150 °C, $[\alpha]_D^{25}$ −35.2±0.8° (*c* 1.0, MeOH). TLC: homogeneous in system B. Found: C, 66.22; H, 6.53; N, 7.01%. Calcd for $C_{34}H_{39}N_3O_8$: C, 66.11; H, 6.63; N, 6.80%.

H-Asp(Leu-Gly-OH)-OH (21): Crystalline **21** was obtained from **20** by catalytic hydrogenolysis in AcOH; 93%, mp 236—237 °C dec, $[\alpha]_D^{26}$ −30.0±0.7° (*c* 1.0, H_2O). Found: C, 47.42; H, 7.09; N, 13.52%. Calcd for $C_{12}H_{21}N_3O_6$: C, 47.52; H, 6.98; N, 13.85%.

Z-Glu(OBu^t)-Asp(Leu-Gly-OH)-OH (22): Compound **21** was coupled with Z-Glu(OBu^t)-ONp in DMF in the presence of DIEA to give **22** as amorphous solid; 89%, $[\alpha]_D^{24}$ −24.9 ±0.6° (*c* 1.0, MeOH). TLC: homogeneous in system E. Found: C, 54.98; H, 6.88; N, 8.64%. Calcd for $C_{29}H_{42}N_4O_{11}\cdot 0.5H_2O$: C, 55.14; H, 6.86; N, 8.87%.

H-Glu-Asp(Leu-Gly-OH)-OH (23): Catalytic hydrogenolysis and subsequent treatment with TFA of **22** yielded **23**, which was purified in the same manner as described for **18**; 86%, $[\alpha]_D^{24.5}$ −8.0±0.5° (*c* 1.0, H_2O). TLC: homogeneous in system E. Found: C, 43.99; H, 6.71; N, 11.73%. Calcd for $C_{17}H_{28}N_4O_9\cdot 2H_2O$: C, 43.59; H, 6.89; N, 11.96%.

Boc-Asp(OPac)-Leu-Gly-OBzl (24): Boc-Asp(OPac)-OH derived from the dicyclohexylamine salt[19] and H-Leu-Gly-OBzl derived from **15** were coupled with DCC to give **24**; 84%, mp 233—233.5 °C, $[\alpha]_D^{22}$ −36.5±0.8° (*c* 1.0, MeOH). TLC: homogeneous in system B. Found: C, 62.89; H, 6.91; N, 6.78%. Calcd for $C_{32}H_{41}N_3O_9$: C, 62.83; H, 6.76; N, 6.78%.

H-Asp(OPac)-Leu-Gly-OBzl·HCl (25): Treatment of **24** with M HCl in EtOAc yielded **25**; 90%, mp 79—80 °C, $[\alpha]_D^{23}$ −7.4±0.5° (*c* 1.0, MeOH). TLC: homogeneous in system D. Found: C, 58.93; H, 6.17; N, 7.65; Cl, 6.55%. Calcd for $C_{27}H_{33}N_3O_7$·HCl: C, 59.17; H, 6.25; N, 7.67; Cl ,6.47%.

Boc-Glu(OBzl)-Asp(OPac)-Leu-Gly-OBzl (3): Coupling of Boc-Glu(OBzl)-OH and H-Asp(OPac)-Leu-Gly-OBzl (free base derived from **25**) with DCC yielded **3**, which was purified on a silica gel column with 20—30% EtOAc in CH_2Cl_2 as solvent; 68%, mp 142—143.5 °C, $[\alpha]_D^{23}$ −31.6 ±0.7° (*c* 1.0, MeOH). TLC: homogeneous in system B. Found: C, 63.33; H, 6.55; N, 6.91%. Calcd for $C_{44}H_{54}N_4O_{12}$: C, 63.60; H, 6.55; N, 6.74%.

Boc-Glu(OBzl)-Asp(OH)-Leu-Gly-OBzl (2): Compound **3** was treated with Zn in AcOH at 25 °C overnight to give the Zn salt of **2** as amorphous solid. TLC: almost homogeneous in system C. Found: C, 51.88; H, 6.25; N, 7.01%. Calcd for $C_{36}H_{47}N_4O_{11}Zn$: C, 50.95; H, 6.10; N, 7.21%.

The α→β Rearrangement of Aspartyl Peptides. The model compound (**1**, **2**, or **3**; 108 mg) was treated with HF (2 ml) in the presence of anisole (0.3 ml) at 0 °C for 60 min. The HF was evaporated at 0 °C *in vacuo* and the residue was dissolved in water. The solution was washed twice with Et_2O and then lyophilized (80 mg). A 30-mg portion of this product was dissolved in 1% Et_3N (5 ml) and the solution was kept at 37 °C for 16 h, after which the solvent was removed by lyophilization. The resulting material was subjected to determination on an amino acid analyzer. The contents of α-peptide [H-Glu-Asp(OH)-Leu-Gly-OH] and β-peptide [H-Glu-Asp(Leu-Gly-OH)-OH] were calculated with the authentic samples (**18** and **23**) as reference. The α-peptide and β-peptide had retention times of 103 and 91 min, respectively, and the ninhydrin color intensity of β-peptide was found to be 0.96 relative to that of α-peptide under the following conditions: column, Hitachi Custom No. 2613, 0.9× 55 cm; buffer, 0.2 M sodium citrate (pH 3.25), 30 ml/h; temp, 55 °C. The results are shown in Table 1.

The peptide synthesizer used in the present work was

constructed in these Laboratories in collaboration with Drs. Hiroshi Hakata and Tetsuo Takahashi and their groups including Nobuhiko Imamura, Masayoshi Shudou, Masamitsu Nakanishi, and Hiroyuki Miyamoto. Their valuable contributions are gratefully acknowledged. Thanks are also due to Dr. Tadashi Okabayashi, these Laboratories, for his advice and encouragement.

References

1) All the amino acid residues mentioned in this communication are of the L-configuration. Abbreviations used are those recommended by the IUPAC-IUB Commission on Biochemical Nomenclature [*Biochemistry*, **5**, 2585 (1966); **6**, 362 (1967); **11**, 1726 (1972)], and include: Boc, *t*-butoxycarbonyl; Z, benzyloxycarbonyl; Bu^t, *t*-butyl; Bzl, benzyl; Pac, phenacyl; ONp, *p*-nitrophenoxy; OSu, succinimidooxy; DCC, dicyclohexylcarbodiimide; DIEA, *N,N*-diisopropylethylamine; TFA, trifluoroacetic acid; DMF, *N,N*-dimethylformamide.

2) A. H. Rubenstein, J. L. Clark, F. Melani, and D. F. Steiner, *Nature*, **224**, 697 (1969); D. F. Steiner, J. L. Clark, C. Nolan, A. H. Rubenstein, E. Margoliash, B. Aten, and P. E. Oyer, *Recent Progr. Hormone Res.*, **25**, 207 (1969); W. Kemmler, J. D. Peterson, A. H. Rubenstein, and D. F. Steiner, *Diabetes*, **21**, 572 (1972); W. Kemmler, D. F. Steiner, and J. Borg, *J. Biol. Chem.*, **248**, 4544 (1973).

3) F. Melani, A. H. Rubenstein, P. E. Oyer, and D. F. Steiner, *Proc. Natl. Acad. Sci. U. S. A.*, **67**, 148 (1970).

4) a) P. E. Oyer, S. Cho, J. D. Peterson, and D. F. Steiner, *J. Biol. Chem.*, **246**, 1375 (1971); b) A. Ko, D. G. Smith, J. Markussen, and F. Sundby, *Eur. J. Biochem.*, **20**, 190 (1971).

5) V. K. Naithani, *Hoppe-Seyler's Z. Physiol. Chem.*, **354**, 659 (1973).

6) V. K. Naithani, M. Dechesne, J. Markussen, and L. C. Heding, *Hoppe-Seyler's Z. Physiol. Chem.*, **356**, 997 (1975).

7) R. Geiger, G. Jäger, and W. König, *Chem. Ber.*, **106**, 2347 (1973).

8) N. Yanaihara, C. Yanaihara, M. Sakagami, N. Sakura, T. Hashimoto, and T. Nishida, *Diabetes*, **27** (Suppl. 1), 149 (1978).

9) N. Yanaihara, T. Hashimoto, C. Yanaihara, M. Sakagami, D. F. Steiner, and A. H. Rubenstein, *Biochem. Biophys. Res. Commun.*, **59**, 1124 (1974).

10) T. Kaneko, H. Oka, M. Munemura, T. Oda, K. Yamashita, S. Suzuki, N. Yanaihara, T. Hashimoto, and C. Yanaihara, *Endocrinol. Jpn.*, **21**, 141 (1974).

11) O. K. Faber, J. Markussen, V. K. Naithani, and C. Binder, *Hoppe-Seyler's Z. Physiol. Chem.*, **357**, 751 (1976).

12) R. B. Merrifield, *J. Am. Chem. Soc.*, **85**, 2149 (1963); *Adv. Enzymol.*, **32**, 221 (1969); B. W. Erickson and R. B. Merrifield, "The Proteins," 3rd ed, ed by H. Neurath, R. L. Hill, and C.-L. Boeder, Academic Press, New York (1976), Vol. 2, pp. 255—527.

13) W. S. Hancock, C. A. Bishop, R. L. Prestidge, D. R. K. Harding, and M. T. W. Hearn, *Science*, **200**, 1168 (1978); J. Rivier, R. Kaiser, and R. Galyearn, *Biopolymers*, **17**, 1927 (1978); E. C. Nice and M. J. O'Hare, *J. Chromatogr.*, **162**, 401 (1979); M. J. O'Hare and E. C. Nice, *ibid.*, **171**, 209 (1979).

14) S. Terabe, R. Konaka, and K. Inouye, *J. Chromatogr.*, **172**, 163 (1979).

15) R. B. Merrifield, *Recent Progr. Hormone Res.*, **23**, 451 (1967).

16) M. A. Ondetti, A. Deer, J. T. Sheehan, J. Pluščec, and O. Kocy, *Biochemistry*, **7**, 4069 (1968).

17) G. W. Kenner and J. H. Seely, *J. Am. Chem. Soc.*, **94**, 3259 (1972).

18) S. S. Wang, C. C. Yang, I. D. Kulesha, M. Sonenberg, and R. B. Merrifield, *Int. J. Pept. Protein Res.*, **6**, 103 (1974).

19) C. C. Yang and R. B. Merrifield, *J. Org. Chem.*, **41**, 1032 (1976).

20) T. Baba, H. Sugiyama, and S. Seto, *Chem. Pharm. Bull.*, **21**, 207 (1976).

21) S. Sakakibara and Y. Shimonishi, *Bull. Chem. Soc. Jpn.*, **38**, 1412 (1965); S. Sakakibara, Y. Shimonishi, Y. Kishida, M. Okada, and H. Sugihara, *ibid.*, **40**, 2164 (1967).

22) R. W. Roeske and P. D. Gesellchen, *Tetrahedron Lett.*, **1976**, 3369.

23) B. Gutte and R. B. Merrifield, *J. Am. Chem. Soc.*, **91**, 501 (1969).

24) B. F. Gisin, *Anal. Chim. Acta*, **58**, 248 (1972). See also: R. S. Hodges and R. B. Merrifield, *Anal. Biochem.*, **65**, 241 (1975).

25) O. Schou, D. Bucher, and E. Nebelin, *Hoppe-Seyler's Z. Physiol. Chem.*, **357**, 103 (1976).

26) M. Kono, A. Yamauchi, S. Mori, Masa. Nakamura, A. Ueda, N. Yoshida, Masu. Nakamura, T. Shike, H. Tanaka, T. Kishida, K. Inouye, T. Okabayashi, and H. Kuzuya, *Saishin-Igaku*, **36**, 153 (1981).

27) J. Scotchler, R. Lozier, and A. B. Robinson, *J. Org. Chem.*, **35**, 3151 (1970).

28) K. Hofmann, H. Yajima, T.-Y. Liu, N. Yanaihara, C. Yanaihara, and J. L. Humes, *J. Am. Chem. Soc.*, **84**, 4481 (1962).

29) P. Villemoes, T. Christensen, and K. Brunfeldt, *Hoppe-Seyler's Z. Physiol. Chem.*, **357**, 713 (1976); K. Brunfeldt, J. Halstrøm, and P. Roepstorff, *Acta Chem. Scand.*, **23**, 2830 (1969).

30) R. B. Merrifield, J. M. Stewart, and N. Jernberg, *Anal. Chem.*, **38**, 1905 (1966).

31) R. D. Comell and J. H. Jones, *J. Chem. Soc., Perkin Trans. 1*, **1972**, 1809.

32) Y. Wolman, M. Schwarzberg, and M. Frankel, *Isr. J. Chem.*, **8**, 53 (1970).

33) C. M. Deber and E. R. Blout, *Isr. J. Chem.*, **12**, 636 (1974).

34) F. Weygand, D. Hoffmann, and E. Wünsch, *Z. Naturforsch., Teil B*, **21**, 426 (1966).

35) J. Honzl and J. Rudinger, *Collect. Czech. Chem. Commun.*, **26**, 2333 (1961).

36) D. Baron, L. G. Pease, and E. R. Blout, *J. Am. Chem. Soc.*, **99**, 8299 (1977).

37) H. Aiba and Y. Shimonishi, *Bull. Chem. Soc. Jpn.*, **53**, 201 (1980).

38) B. Halpern and D. E. Nitecki, *Tetrahedron Lett.*, **1967**, 3031.

39) V. P. Chernyshev, S. A. Riskal, G. A. Zhiglova, E. I. Filippovich, and R. P. Evstigneeva, *J. Gen. Chem. USSR*, **41**, 2596 (1971).

40) T. Hayakawa, K. Harada, and S. W. Fox, *Bull. Chem. Soc. Jpn.*, **39**, 391 (1966).

Preparations and Properties of Optically Active (Alkyl)bis(dimethylglyoximato)cobalt(III) Complexes

Yoshiaki Ohgo,* Seiji Takeuchi, Yukikazu Natori, Juji Yoshimura,†
Yuji Ohashi,† and Yoshio Sasada†

Niigata College of Pharmacy, 5829 Kamishin'ei-cho, Niigata 950-21

†*Laboratory of Chemistry for Natural Products, Tokyo Institute of Technology, Nagatsuta, Midori-ku Yokohama 227*

(Received January 29, 1981)

Optically active alkyl cobalt complexes, $CH_3CHXCo(Hdmg)_2$·Base [X=$COOCH_3$ or CN; Base=(*R*)- or (*S*)-1-phenylethylamine, H_2O, pyridine, or (1*R*,2*S*)-1,2-diphenyl-2-aminoethanol; Hdmg=dimethylglyoximate-(1-)], have been prepared, and their spectroscopic and chiroptical data are given. The rotational contribution of the chiral alkyl moiety was shown to be considerably greater than that of the chiral amine moiety. This suggests that the rotational sign (in the longer-wave length region of about 546 to 589 nm) may be useful for deducing the chirality of the alkyl moiety.

Transition-metal alkyl complexes are important intermediates in various catalytic reactions. The reactions with chiral alkyl transition metal complexes can provide a clearer description of the elementary process of catalytic reactions, especially catalytic asymmetric reactions. Studies on the mechanism of asymmetric hydrogenation catalyzed by the bis-(dimethylglyoximato)cobalt(II)–chiral amino alcohol system[1-5] prompted us to prepare optically pure (alkyl)bis(dimethylglyoximato)cobalt complexes which have chirality at the carbon coordinated directly to cobalt.

Two approaches are, in principle, possible in the preparation of such a complex. One is based on the stereospecific displacement of a labile group or atom of chiral-carbon compounds with metal complexes (1).[6] Another method is the resolution of diastereomeric complexes with a chiral ligand (L_1*) other than the alkyl group, followed by the displacement of the chiral ligand L_1* with an achiral ligand (L_2) (2). The optical purity gained by the former approach is completely dependent on the degree of stereospecificity of the reaction applied; also, there is no guarantee that the same stereospecificity will be afforded as in a model reaction. In fact, (−)-1-methylheptyl bromide ($[\alpha]_D$ −29°) reacts with bis(dimethylglyoximato)cobalt (I) anion to give bis(dimethylglyoximato)(1-methylheptyl)(pyridine)cobalt(III) of $[\alpha]_D$ +50°,[6a] while we could not detect the optical activity of the alkyl complex produced in a similar reaction with optically pure methyl 2-bromopropanoate. Therefore, the latter method (2) is considered to be favorable for obtaining optically pure alkyl complexes.

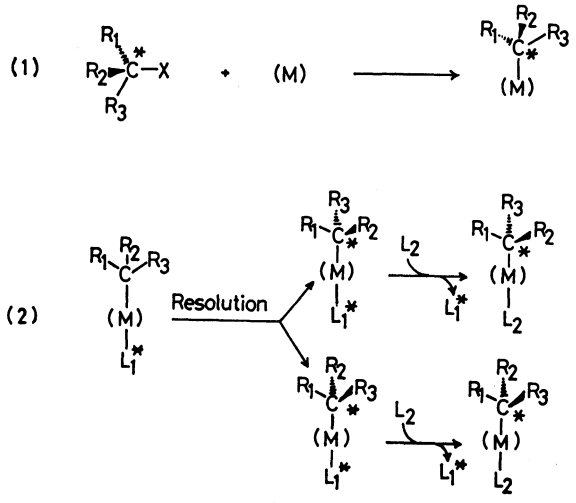

Fig. 1.

We wish here to report preparations and properties of some optically pure (alkyl)bis(dimethylglyoximato)-cobalt complexes.

Results and Discussion

Bis(dimethylglyoximato)cobalt(II) was allowed to react with methyl acrylate or acrylonitrile in methanol under weakly acidic conditions under a hydrogen atmos-

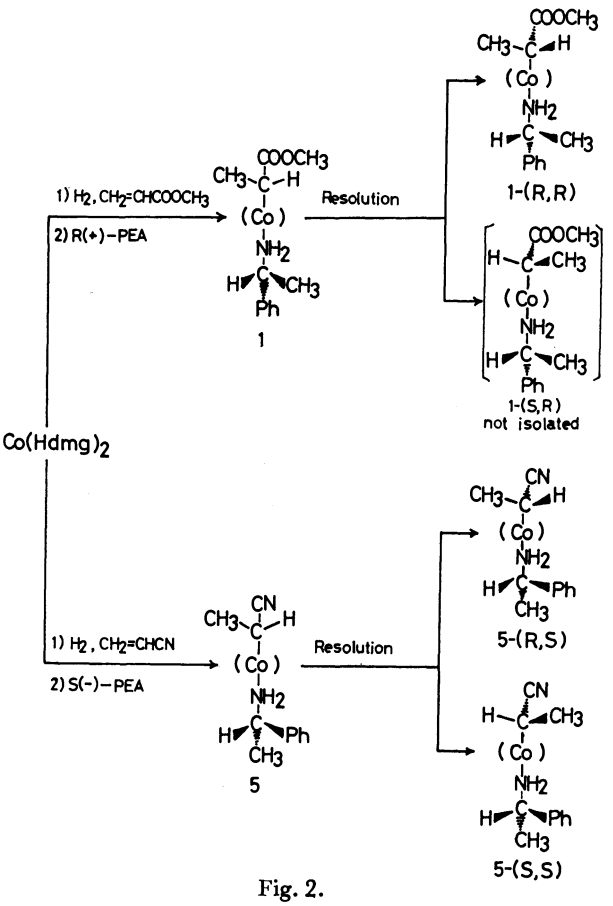

Fig. 2.

Table 1. ^{1}H NMR chemical shifts of diastereomeric pairs of 1-substituted ethyl-(1-phenylethylamine)cobaloximes, CH_3CHX–$Co(Hdmg)_2 \cdot NH_2CH(CH_3)Ph$

Substituent	Configuration		Chemical shift, δ							
	Alkyl	Amine	CH_3CHCo	CH_3CNH_2	$CHCo$	CH_3(Hdmg)	OCH_3	$CHNH_2$	NH_2	Ph
$COOCH_3$	*R*	*R*	0.32 (d, 3H)	1.22 (d, 3H)	1.96 (q, 1H)	2.20 and 2.24 (12H)	3.44 (s, 3H)	3.63 (q, 1H)	7.04 (m, 2H)	7.26 (m, 5H)
$COOCH_3$	*R*	*S*	0.32 (d, 3H)	1.22 (d, 3H)	1.94 (q, 1H)	2.20 and 2.24 (12H)	3.44 (s, 3H)	3.63 (q, 1H)	7.04 (m, 2H)	7.26 (m, 5H)
CN	*S*	*S*	0.48 (d, 3H)	1.25 (d, 3H)	1.98 (q, 1H)	2.25 (12H)		3.65 (q, 1H)	7.08 (m, 2H)	7.30 (m, 5H)
CN	*R*	*S*	0.48 (d, 3H)	1.25 (d, 3H)	1.96 (q, 1H)	2.25 and 2.27 (12H)		3.65 (q, 1H)	7.08 (m, 2H)	7.29 (m, 5H)

Table 2. Main IR absorpotion bands of diastereomeric pairs of 1-substituted ethyl(1-phenylethylamine)cobaloximes

Substituent	Configuration		Spectral bands, $\tilde{\nu}$/cm^{-1}				
	Alkyl	Amine	NH_2 *asym*	NH_2 *sym*	CN	$COOCH_3$	C=N
$COOCH_3$	*R*	*R*	3313	3266		1685	1555
$COOCH_3$	*R*	*S*	3305	3250		1686	1556
CN	*S*	*S*	3320	3232	2200		1559
CN	*R*	*S*	3304	3235	2199		1560

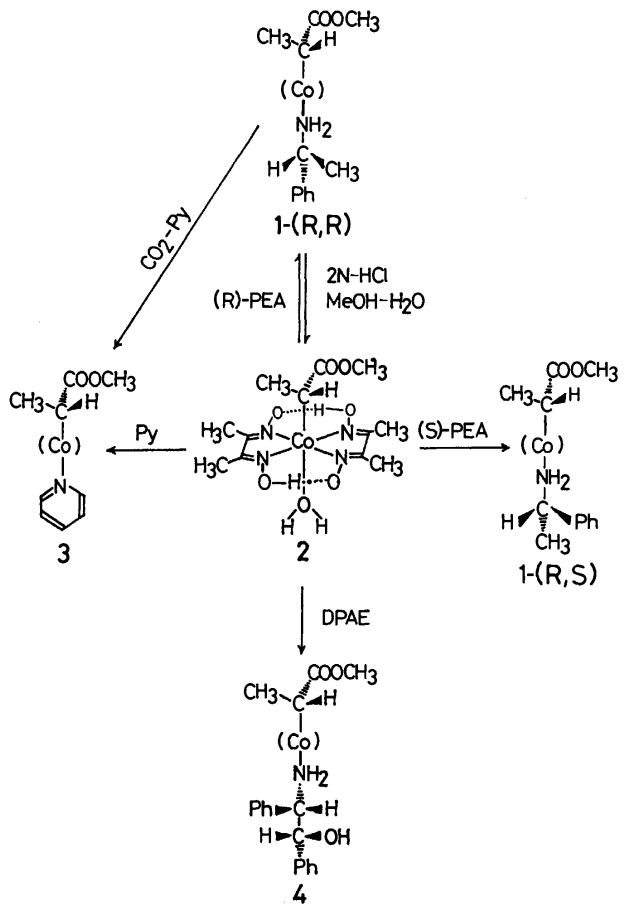

Fig. 3.

phere.[7] After neutralization, (*R*)- or (*S*)-1-phenylethylamine was added to give diastereomeric alkyl complexes with a chiral axial base (**1** or **5**; see Fig. 2). The repeated recrystallization of **1** from a mixture of methanol and water gave $(+)_{578}$-bis(dimethylglyoximato)[1-(methoxycarbonyl)ethyl]cobalt(III), **1**-(*R*,*R*), with $[\alpha]_{578}$ +211.3°. (*S*)-1-Phenylethylamine coordinated 1-cyanoethyl cobalt complexes were resolved into two diastereomers, **5**-(*R*,*S*) ($[\alpha]_{578}$ +55.85°) and **5**-(*S*,*S*) ($[\alpha]_{578}$ −60.13°). By the use of (*R*)-1-phenylethylamine, the enantiomer of the former, **5**-(*S*,*R*), was also obtained ($[\alpha]_{578}$ −55.6°).

The absolute configurations of cobalt-alkyl moieties of dextrorotating $(+)_{578}$-bis(dimethylglyoximato)-[1-(methoxycarbonyl)ethyl][(*R*)-1-phenylethylamine]-cobalt(III), dextrorotating $(+)_{578}$- and levorotating $(-)_{578}$-1-cyanoethylbis(dimethylglyoximato)[(*S*)-1-phenylethylamine]cobalt(III) were determined by the X-ray method to be (*R*), (*R*), and (*S*) respectively.[8–10]

The ^{1}H NMR spectra and main bands of the IR spectra of diastereomeric pairs of 1-(methoxycarbonyl)-ethyl and 1-cyanoethyl complexes are shown in Tables 1 and 2.

A diastereomeric difference appears in the ^{1}H NMR signals of the proton on the carbon attached to cobalt: the HC–Co proton signal of the *R*–*S* complex (**1**-(*R*,*S*), **5**-(*R*,*S*)) appears in a somewhat higher field (0.02 ppm) than that of the corresponding *R*–*R* or *S*–*S* complex (**1**-(*R*,*R*) or **5**-(*S*,*S*)). The absorption bands due to the asymmetric stretching vibration of $-NH_2$ of the *R*–*R* or *S*–*S* complex appear at a higher frequency than that of the diastereomer, the *R*–*S* complex, while the other absorption bands are almost identical.

Aquabis(dimethylglyoximato)[(*R*)-1-(methoxycarbonyl)ethyl] cobalt(III) was obtained in about a 60% yield by treating **1**-(*R*,*R*) with 2 mol dm^{-3} hydrochloric acid in aqueous methanol. The aqua ligand is so labile in this complex that the aqua complex is a useful intermediate in exchanging the axial ligand. Thus, the pyridine, (1*R*,2*S*)-1,2-diphenyl-2-aminoethanol, and (*S*)-1-phenylethylamine coordinated complexes were easily derived only by evaporating a methanol solution of an equimolar amount of the aqua complex and the axial base desired (Fig. 3). The pyridine complex (**3**) was also obtained in one step by treating **1**-(*R*,*R*) with CO_2

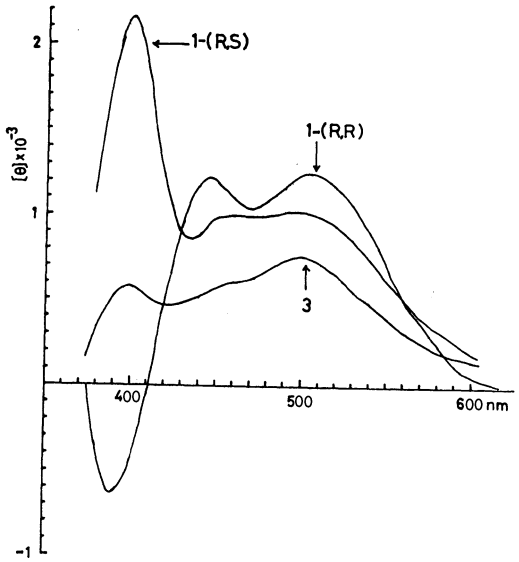

Fig. 4. CD spectra of 10^{-3} mol dm^{-3} dichloromethane solution of **1**-(*R*,*R*), **1**-(*R*,*S*), and **3**.

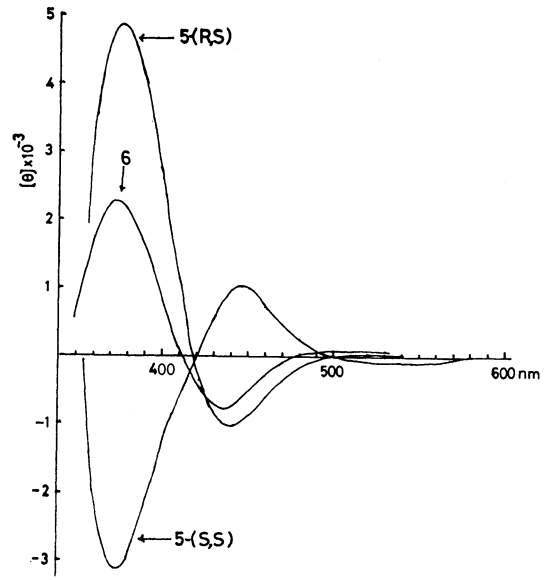

Fig. 5. CD spectra of 10^{-3} mol dm^{-3} dichloromethane solution of **5**-(*R*,*S*), **5**-(*S*,*S*), and **6**.

Table 3. Specific and molecular rotation of 1-substituted ethyl cobaloximes, CH_3CHX–$Co(Hdmg)_2$-base, and their configurations at α-carbon

	X	Axial base	Conf. at α-carbon	$[\alpha]_{578}^{RT}$	$[\phi]_{578}^{RT}$ [d]
1-(*RR*)	$COOCH_3$	(*R*)-1-PEA[a]	*R*[c]	+211($CHCl_3$)	+1051
1-(*RS*)	$COOCH_3$	(*S*)-1-PEA	*R*	+161($CHCl_3$)	+801
2	$COOCH_3$	H_2O	*R*	+160(MeOH)	+631
3	$COOCH_3$	Pyridine	*R*	+167($CHCl_3$)	+760
4	$COOCH_3$	(1*R*,2*S*)-DPAE[b]	*R*	+143($CHCl_3$)	+843
5-(*RS*)	CN	(*S*)-1-PEA	*R*[c]	+55.85($CHCl_3$)	+259
5-(*SR*)	CN	(*R*)-1-PEA	*S*[c]	−55.6($CHCl_3$)	−258
5-(*SS*)	CN	(*S*)-1-PEA	*S*[c]	−60.13($CHCl_3$)	−279
6	CN	Pyridine	*R*	+52.2($CHCl_3$)	+220

a) 1-PEA: 1-phenylethylamine. b) (1*R*,2*S*)-DPAE: (1*R*,2*S*)-1,2-diphenyl-2-aminoethanol. c) These configurations were determined by the X-ray method.[3-5] d) Molecular rotation.

Table 4. Estimation of partial contribution of alkyl and amine parts for molecular rotation of diastereomeric 1-substituted ethyl-(1-phenylethylamine)cobaloximes

Alkyl		Base	Parial contribution	
Substituent	Configuration		$[\phi_{alkyl}]_{578}$	$[\phi_{amine}]_{578}$
$COOCH_3$	*R*	(*R*)-1-PEA[a]	+925.9	+125.1
$COOCH_3$	*R*	(*S*)-1-PEA[a]	+925.9	−125.1
CN	*R*	(*S*)-1-PEA	+269.3	−9.9
CN	*S*	(*S*)-1-PEA	−269.3	−9.9

a) (*R*)-1-PEA: (*R*)-1-phenylethylamine.

and pyridine. 1-Cyanoethyl complex, **6**, was obtained by the same procedure. The structures of these complexes were characterized by IR, ^1H NMR, and/or elemental analyses.

No substantial racemization occurs during the ligand-exchange process: optical rotation did not decrease during 12 h under the conditions applied in ligand exchange, and the (*R*)-1-phenylethylamine complex, **1**-(*R*,*R*), regained through the aqua complex showed almost the same optical rotation ($[\alpha]_{578}$ +210°) as the original one.

The CD spectra of chiral 1-cyanoethyl and 1-(methoxycarbonyl)ethyl complexes are shown in Figs. 4 and 5 respectively. (*R*)-1-Cyanoethyl complexes (**5**-(*R*,*S*), **6**) have clear negative and positive Cotton effects at about 440 and 375 nm respectively; the (*S*)-1-cyanoethyl complex (**5**-(*S*,*S*)) also has clear but reverse Cotton effects at the corresponding wave lengths. However, the (*R*)-1-(methoxycarbonyl)ethyl complexes (**1**-(*R*,*R*), **1**-(*R*,*S*), **3**) give broad positive spectra, ranging from 600 to 400 nm, and the CD peak around 380 nm is greatly influenced by the chiral amine moiety rather than by the chiral alkyl. Thus, the configuration of the alkyl part can not simply be deduced from the sign of the Cotton effect.

The specific rotations and molecular rotations of the chiral alkyl-cobalt complexes prepared here are listed in Table 3. As may be seen from Table 3, the (*R*)-1-substituted alkyl complex and the (*S*)-1-substituted alkyl complex causes positive and negative rotation respectively. If the contribution from a chiral distortion of the inplane ligand is negligible, the molecular rotation of diastereomeric complex will be expressed by the sum of the partial contributions of the alkyl part ($[\phi_{alkyl}]$)

and the amine part ($[\Phi_{amine}]$):

$$[\Phi] = [\Phi_{alkyl}] + [\Phi_{amine}]. \quad (1)$$

The $[\Phi_{alkyl}]$ and $[\Phi_{amine}]$ values of the diastereomers are calculated (Table 4). From Table 4 it can be said that the partial contribution of the alkyl part is considerably greater than that of the amine part, and the calculated values of the partial contribution of the alkyl part, $[\Phi_{alkyl}]$, are comparatively near to the molecular rotations of the corresponding pyridine complex, **3** or **6**, which has no chirality on the axial base. Thus, the rotational sign (in the longer-wavelength region of about 546 to 589 nm) can be useful for deducing the configuration of the 1-substituted alkyl metal complexes. Further studies on this respect are now under way.

Experimental

The IR spectra were recorded on a JASCO A-3 spectrometer. The NMR spectra were obtained on a JEOL JNM-PS-100 spectrometer, using TMS as the internal standard. The optical rotations were measured on a Perkin-Elmer 241 polarimeter and a Carl Zeiss photoelectric precision polarimeter. The circular dichroism spectra were recorded on a JASCO J-40C spectrometer.

Bis(dimethylglyoximato) [(R)-*1-(methoxycarbonyl) ethyl*] [(R)-*1-phenylethylamine*]*cobalt(III)*, (**1**-(R,R)). To a methanol (100 cm³) solution of $Co(OCOCH_3)_2 \cdot 4H_2O$ (50 g) was added a hot solution of dimethylglyoxime (47 g) in methanol (400 cm³) under a nitrogen atomosphere with stirring. The solution was stirred for 5—10 min. The reaction vessel was then connected to a hydrogen-gas burret. 22.5 cm³ of methyl acrylate was added to the reaction vessel by means of a syringe. The reaction mixture was then stirred under a hydrogen atmosphere. After a theoretical amount of hydrogen had been absorbed, the reaction mixture was neutralized by an aqueous solution of sodium hydroxide (16 g) on cooling. To the resulting solution, 25.5 cm³ of *R*(+)-1-phenylethylamine ($[\alpha]_D^{23}$ +38°) was added. The products were extracted with dichloromethane (2 dm³) and washed several times with water. The dichloromethane solution was dried over anhydrous sodium sulfate and concentrated *in vacuo* to give a crystalline mass. The crude product was dissolved in methanol (370 cm³) at room temerature. The solution was filtered, and then, to the filtrate, water (445 cm³) was added gradually by means of a syringe on warming (30—35 °C). The solution was left standing overnight at room temperature. The dark red crystals thus deposited were collected by filtration; 25.4 g (1C-I). 1C-I (25.4 g) was recrystallized from methanol (240 cm³) and water (288 cm³) to give 15 g of crystals (1C-II), $[\alpha]_{578}$ +195.5° (*c* 0.404, chloroform). The recrystallization of 1C-II (14.9 g) from methanol (144 cm³) and water (156 cm³) gave 10.4 g of crystals (1C-III), $[\alpha]_{578}$ +211.3°, $[\alpha]_{546}$ +233,4° (*c* 0.407, chloroform). Found: C, 48.34; H, 6.33; N, 14.39%. Calcd for $C_{20}H_{32}N_5O_6Co$: C, 48.29; H, 6.48; N, 14.08%.

Aquabis(dimethylglyoximato) [(R)-*1-(methoxycarbonyl) ethyl*]*cobalt(III)*, (**2**). To a methanol (20 cm³) solution of 4.5 g of **1**-(*R*, *R*) was added 2 mol dm⁻³ hydrochloric acid (9 cm³), after which the solution was left standing for 2 h, and then 9 cm³ of 6 mol dm⁻³ hydrochloric acid was added. The resulting complexes were extracted with three 100-cm³ portions of dichloromethane. The extract was neutralized by adding an excess of solid potassium carbonate and 1 cm³ of water. After 10 min, the dichloromethane solution was concentrated under a reduced pressure to give a crystalline mass. The crude product was dissolved in acetone (10 cm³). In a few minutes crystals appeared which were collected by filtration; 1.7 g (48%). These are satisfactory enough for further syntheses. From the above filtrate another crop (0.9 g) of crystals was obtained by concentrating it, followed by treating the residue with acetone. The product was further purified by silica-gel column chromatography (Kiesel gel 60, Merck), using acetone–benzene as the eluent. Fractions giving a single spot on TLC [R_f 0.45, acetone (2)/benzene(1)] were collected and concentrated under reduced pressure to give a thick paste, which was then crystallized on addition of acetone. $[\alpha]_{578}$ +160° (*c* 0.206, methanol); IR(KBr): 3400 (OH), 1670 (ester), 1565 cm⁻¹ (C=N); ¹H NMR (D_2O): δ 0.05 (d, 3H, $\underline{CH_3}CHCo$), 2.28 and 2.29 (CH_3 of Hdmg), 3.38 (s, 3H, $-COOCH_3$), 4.75 (broad, HOD); Found: C, 37.05; H, 5.89; N, 14.50%. Calcd for $C_{12}H_{23}N_4O_7Co$: C, 36.56; H, 5.88; N, 14.21%.

Bis(dimethylglyoximato)[(R)-*1-(methoxycarbonyl)ethyl*]*(pyridine)-cobalt(III)*, (**3**). *Method (A)*: 2.7 g of bis(dimethylglyoximato)[(*R*)-1-(methoxycarbonyl)ethyl][(*R*)-1-phenylethylamine]cobalt(III) ($[\alpha]_{578}$ +209°) was dissolved in methanol (30 cm³), and pyridine (1.5 cm³) was then added. Carbon dioxide was bubbled through the solution for 20 min, and then 15 cm³ of water were added. The bubbling was continued for another 10 min. The reaction mixture was extracted with 200—250 cm³ of benzene and washed several times with water. The benzene layer was dried over anhydrous sodium sulfate and concentrated under reduced pressure to give a yellow crystalline powder; 2.14 g (87%). The crude product (1 g) was recrystallized from methanol (15 cm³) and water (25 cm³) to give leaflets (0.46 g), $[\alpha]_{578}$ +167°, $[\alpha]_{546}$ +198° (*c* 0.408, chloroform). The IR and ¹H NMR spectra were identical with those of the racemic compound.

Method (B): 8 g of bis(dimethylglyoximato)[(*R*)-1-(methoxycarbonyl)ethyl][(*R*)-1-phenylethylamine]cobalt(III) ($[\alpha]_{578}$ +196°) was dissolved in methanol (35 cm³), and then 12 cm³ of 2 mol dm⁻³ hydrochloric acid were added. After 1 h, pyridine (2.5 cm³) was added to the solution. The resulting solution was left standing for another 30 min, extracted with 200 cm³ of dichloromethane, and then washed with water. The dichloromethane layer was dried over anhydrous sodium sulfate and concentrated under reduced pressure to give a yellow crystalline powder; 7 g (96%). The IR and ¹H NMR spectra were identical with those of the racemic compound.

Mutarotation of Compound 3 in Methanol–Water: To a methanol (5 cm³) solution of the pyridine complex **3** (0.0303 g, 0.09 mmol) were added water (5 cm³) and pyridine (0.021 g, 0.27 mmol). The optical rotational change of the above solution was followed. The change was very slow (see below):

Time/h	α_{578}/°
0.0	+0.31
0.5	+0.31
12.0	+0.30
20.0	+0.28
111.0	+0.175

Bis(dimethylglyoximato) [(R)-*1-(methoxycarbonyl) ethyl*] [(S)-*1-phenylethylamine*]*cobalt(III)*, (**1**-(R,S)). 300 mg (0.76 mmol) of the *R*(+)-aqua complex (**2**) and 93 mg (0.76 mmol) of (*S*)-(−)-1-phenylethylamine were dissolved in methanol. The solution was concentrated *in vacuo* to dryness. The procedure was repeated three times. The IR and ¹H NMR spectra were shown in Tables 1 and 2. $[\alpha]_{578}^{21}$ +161°, $[\alpha]_{546}^{21}$

+186° (*c* 0.404, chloroform); Found: C, 47.97; H, 6.64; N, 13.93%. Calcd for $C_{20}H_{32}N_5O_6Co$: C, 48.29; H, 6.48; N, 14.08%.

Bis(dimethylglyoximato) [(R)-*1*-(*methoxycarbonyl*)*ethyl*] [(*1R*,-*2S*)-*1,2-diphenyl-2-aminoethanol*]*cobalt(III)*, (*4*). 250 mg (0.63 mmol) of the *R*(+)-aqua complex (**2**) and 135 mg (0.63 mmol) of (1*R*, 2*S*)-1,2-diphenyl-2-aminoethanol were dissolved in methanol. The solution was concentrated *in vacuo* to dryness. The procedure was repeated three times. ^{1}H NMR ($CDCl_3$): δ 0.25 (d, 3H, $C\underline{H}_3CHCOOCH_3$), 1.95 and 1.98 ($CH_3$(Hdmg) and $CH_3C\underline{H}Co$), 3.34 (s, 3H, $COOC\underline{H}_3$), 4.46 (d, 1H, $\underline{H}COH$), 6.84 (broad m, NH_2), 7.22 (m, 10H, Ph). $[\alpha]_{578}$ +143.3°, $[\alpha]_{546}$ +190° (*c* 0.30, chloroform).

[(R)-*1-Cyanoethyl*]*bis*(*dimethylglyoximato*) [(S)-*1*-*phenylethylamine*]*cobalt(III)*, (*5*-(R,S)), and [(S)-*1-Cyanoethyl*]*bis*(*dimethylglyoximato*)[(S)-*1-phenylethylamine*]*cobalt(III)*, (*5*-(S,S)). Acrylonitrile (8 cm^3) was added to a methanolic solution of bis(dimethylglyoximato)cobalt (II), prepared from Co $(OCOCH_3)_2 \cdot 4H_2O$ (25 g) and dimethylglyoxime (23.5 g) in methanol (250 cm^3). The reaction mixture was stirred under a hydrogen atmosphere at room temperature. After a theoretical amount of hydrogen had been absorbed, an aqueous solution of sodium hydroxide (8 g) and 13 cm^3 of (*S*)-1-phenylethylamine ($[\alpha]_D$ −39°) were successively added to the cooled reaction mixture. The resulting complexes were extracted with dichloromethane (1.5 dm^3) and washed several times with water. The dichloromethane solution was dried over anhydrous sodium sulfate and then concentrated under reduced pressure to give a crude product. It was dissolved in 150 cm^3 of methanol at room temperature. The solution was filtered, and 140 cm^3 of water were added by means of a syringe on warming (30—35 °C). The solution was then left standing overnight at room temperature. Dark red crystals deposited were collected by filtration; 26.7 g (5C-I), $[\alpha]_{578}$ +2°. 5C-I (25.3 g) was recrystallized from methanol (290 cm^3) and water (350 cm^3) to give 12.3 g of crystals (5C-II); $[\alpha]_{578}$ +32° (*c* 0.5, chloroform). 5C-II (11 g) was again recrystallized from methanol (140 cm^3) and water (200 cm^3) to give 6.68 g of crystals (5C-III); $[\alpha]_{578}$ +48.5°. 5C-III (6.68 g) was recrystallized from methanol (94 cm^3) and water (106 cm^3) to give 4.5 g of crystals (5C-IV); $[\alpha]_{578}$ +55.5° and $[\alpha]_{546}$ +60.5° (*c* 0.2, chloroform). Another experiment gave a constant rotation of $[\alpha]_{578}^{23}$ +55.85°, $[\alpha]_{546}^{23}$ +60.10°(*c* 0.188, chloroform). Found: C, 49.05; H, 6.45; N, 18.18%. Calcd for $C_{19}H_{29}N_6O_4Co$: C, 49.13; H, 6.29; N, 18.09%. From filtrates of 5C-I and 5C-II, 10 g of crystals (5F-I) ($[\alpha]_{578}$ −15.3°) and 2.5 g of crystals (5F-II) ($[\alpha]_{578}$ −47.7°) were obtained respectively. The repeated recrystallization of 5F-II (2 g) from methanol/water (1.2/1) gave 0.275 g of crystals with a constant rotation; $[\alpha]_{578}^{23.5}$ −60.13°, $[\alpha]_{546}^{23.5}$ −64.56° (*c* 0.158, chloroform). Found: C, 48.16; H, 6.34; N, 17.81%. Calcd for $C_{19}H_{29}N_6O_4Co$: C, 49.13; H, 6.29; N, 18.09%.

[(R)-*1-Cyanoethyl*]*bis*(*dimethylglyoximato*)(*pyridine*)*cobalt(III)*, (*6*). Pyridine (0.42 cm^3, 5.2 mmol) and water (6 cm^3) were added to a solution of [(*R*)-1-cyanoethyl]bis(dimethylglyoximato) [(*S*)-1-phenylethylamine]cobalt (III), **5**-(*R*,*S*), (0.8 g, 1.7 mmol) in methanol (12 cm^3). Carbon dioxide was bubbled through the solution for 20 min at room temperature. The reaction mixture was then extracted with benzene (200 cm^3) and washed several times with water. The benzene layer was dried over anhydrous sodium sulfate and concentrated *in vacuo* to give 0.65 g of a crude product (89%). The crude product (0.65 g) was recrystallized from methanol (19 cm^3) and water (35 cm^3) to give orange leaflets (0.08 g), $[\alpha]_{578}^{22}$ +52.2°, $[\alpha]_{546}^{22}$ +59.2° (*c* 0.157, chloroform). The IR and ^{1}H NMR spectra were identical with those of the racemic compound.

The authors wish to express their thanks to Mr. Hitoshi Matsumoto and Mr. Yuzuru Ishida for their NMR measurements.

References

1) Y. Ohgo, S. Takeuchi, and J. Yoshimura, *Bull. Chem. Soc. Jpn.*, **44**, 583 (1971).
2) S. Takeuchi, Y. Ohgo, and J. Yoshimura, *Chem. Lett.*, **1973**, 265.
3) Y. Ohgo, S. Takeuchi, Y. Natori, and J. Yoshimura, *Chem. Lett.*, **1974**, 33.
4) Y. Ohgo, Y. Natori, S. Takeuchi, and J. Yoshimura, *Chem. Lett.*, **1974**, 709.
5) Y. Ohgo, Y. Natori, S. Takeuchi, and J. Yoshimura, *Chem. Lett.*, **1974**, 1327.
6) a) D. Dodd and M. D. Johnson, *J. Chem. Soc., Chem. Commun.*, **1971**, 571; b) F. R. Jensen and R. C. Kiskis, *J. Am. Chem. Soc.*, **97**, 5825 (1975) and the references cited therein.
7) G. N. Schrauzer and R. J. Windgassen, *J. Am. Chem. Soc.*, **89** , 1999 (1967).
8) Y. Ohashi and Y. Sasada, *Bull. Chem. Soc. Jpn.*, **50**, 2863 (1977).
9) Y. Ohashi, Y. Sasada, S. Takeuchi, and Y. Ohgo, *Bull. Chem. Soc. Jpn.*, **53**, 627 (1980).
10) Y. Ohashi, Y. Sasada, S. Takeuchi, and Y. Ohgo, *Bull. Chem. Soc. Jpn.*, **53**, 1501 (1980).

One-step Oxidation of Olefins into α-Phenylseleno Carbonyl Compounds[1]

Makoto SHIMIZU and Isao KUWAJIMA*

Department of Chemistry, Tokyo Institute of Technology, Ookayama, Meguro-ku, Tokyo 152

(Received April 14, 1981)

Oxidation of olefins has been examined with the following three types of reagents; (i) $(C_6H_5Se)_2$–Br_2–$(Bu_3Sn)_2O$, (ii) $(C_6H_5Se)_2$–*t*-BuOOH, and (iii) $(C_6H_5Se)_2$–$(C_6H_5SeO)_2O$, and the corresponding α-phenylseleno carbonyl compounds have been obtained directly from the olefins.

Recent developments in organoselenium chemistry[2] have brought about a wide range of synthetic utilities of α-phenylseleno carbonyl compounds. They have been used for regioselective introduction of various functional groups, especially for that of unsaturation *via* well established *syn*-elimination process.[2] For their preparation, both electrophilic and uncleophilic organoselenium reagents are usually available as shown below:[3]

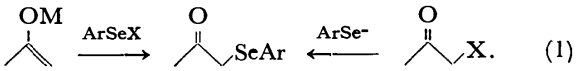

(1)

However, no simple and reliable route to α-phenylseleno carbonyl compounds from both internal and terminal olefins has been developed until now,[4] although olefinic compounds are in general readily accessible *via* a number of established synthetic procedures.

Electrophilic 1,2-addition of PhSeX species constitutes a potential methodology for the introduction of double functionalities into carbon-carbon double bonds.[2] It is expected that during this process if CH–X group is converted into a carbonyl simultaneously, α-phenylseleno carbonyl compounds may be produced directly from olefins (Eq. 2). In this paper, we describe an efficient approach for one-step oxoselenenylation reaction of olefins to afford α-phenylseleno carbonyl compounds.

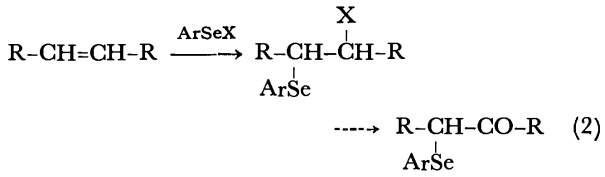

(2)

Oxidation of Olefins with $(C_6H_5Se)_2$–Br_2–$(Bu_3Sn_2)O$. Trialkylstannyl ethers are well known to be transformed into carbonyl compounds on treatment with bromine or *N*-chlorosuccinimide (NCS)[5] as shown in the following equation. In a related reaction, a formation of a

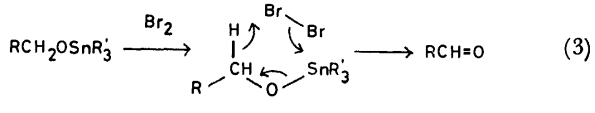

(3)

$$Bu_3SnOSnBu_3 \xrightarrow{Br_2} Bu_3SnOBr + Bu_3SnBr \quad (4)$$

hypohalite species, Bu_3SnOBr, is postulated through the reaction of hexabutyldistannoxane with bromine.[6] In a similar way, a formation of "$C_6H_5SeOSnBu_3$" **1** is expected on treatment of hexabutyldistannoxane with benzeneselenenyl bromide. Like other electrophilic species such as ArSeCl, ArSeBr, ArSeOAc, *etc.*,[2] **1** appears to behave as an electrophile to attack a C=C bond to form β-(phenylseleno)alkyl tributylstannyl ether **2** which may be converted to the corresponding α-phenylseleno carbonyl compounds **3** as usual with stannyl ethers. Treatment of styrene with diphenyl

$$Bu_3SnOSnBu_3 \xrightarrow{C_6H_5SeBr} \underset{\mathbf{1}}{Bu_3SnOSeC_6H_5} + Bu_3SnBr \quad (5)$$

$$RCH{=}CH_2 \xrightarrow{\mathbf{1}} \underset{\mathbf{2}}{RCH(OSnBu_3)-CH_2SeC_6H_5} \longrightarrow \underset{\mathbf{3}}{R\text{-}CO\text{-}CH_2SeC_6H_5} \quad (6)$$

diselenide (0.55 equiv.), bromine (0.50 equiv.), and hexabutyldistannoxane (1.0 equiv.) indeed afforded α-(phenylseleno)acetophenone in 38% yield. An optimum result was obtained when the reaction was performed with 2.2 equiv. of diphenyl diselenide, 2.1 equiv. of bromine, and 2.2 equiv. of hexabutyldistannoxane in refluxing chloroform for 2 h. Various olefins were also

$$C_6H_5CH{=}CH_2 \xrightarrow{(C_6H_5Se)_2,\ Br_2,\ (Bu_3Sn)_2O} C_6H_5CO\text{-}CH_2SeC_6H_5 \quad (7)$$

converted to the corresponding α-phenylseleno carbonyl compounds **3** in good yields by this procedure. The results are shown in Table 1.

Styrene gave a single regioisomer, whereas other terminal olefins usually afforded a mixture of α-phenylseleno ketones and α-phenylseleno aldehydes. Their ratios are dependent on the reaction conditions, especially on the solvent. Electron-deficient olefins such as vinyl bromide or α,β-unsaturated esters are almost inert to this oxidation reaction. The major drawbacks of this procedure are relatively troublesome work-up for removal of organotin moieties and lack of regioselectivity. To eliminate these disadvantages, other methods were investigated, especially for improvement of regioselectivity in the oxoselenenylation reactions.

Oxidation of Olefins with $(C_6H_5Se)_2$–t-BuOOH or $(C_6H_5Se)_2$–$(C_6H_5SeO)_2O$. It has been described that allylic alcohols are oxidized with benzeneselenenyl bromide and silver acetate to give α,β-unsaturated carbonyl compounds.[7] More recently, oxidation of aldehyde hydrazones with benzeneseleninic anhydride was reported,[8] which proceeded presumably *via* an intermediacy of selenenate esters. These examples indicate that alkyl selenenates appear to undergo fragmentation readily to afford carbonyl compounds and selenols.[9]

Benzeneselenenic anhydride "$C_6H_5SeOSeC_6H_5$" **4**, a rare class of compound, is expected to add to olefins to form alkyl selenenates **5** in a similar manner with other kinds of electrophilic organoselenium species,[2] and the resulting selenenate esters **5** may decompose to

Table 1. Oxidation of olefins with $(C_6H_5Se)_2$–Br_2–$(Bu_3Sn)_2O$[a]

Olefin	Solvent	Period/h	Product (ratio)	Yield/%[b]
1-Decene	CCl_4	7	$C_8H_{17}COCH_2SeC_6H_5$, $C_8H_{17}CH(SeC_6H_5)CH{=}O$ (68 : 32)	68
	CCl_4	10	(67 : 33)	54
	CCl_4	12	(72 : 28)	48
	THF	8.5	(58 : 42)	60
	C_6H_6	9	(80 : 20)	56
Ethyl 10-undecenoate	CCl_4	6.5	$C_2H_5O_2C(CH_2)_8COCH_2SeC_6H_5$, $C_2H_5O_2C(CH_2)_8CH(SeC_6H_5)CH{=}O$ (77 : 23)	60
Cyclooctene[c]	$C_6H_5CH_3$	7	2-Phenylselenocyclooctanone	72
Cyclododecene[c]	C_6H_6	8	2-Phenylselenocyclododecanone	52[d]
Cinnamyl acetate	$C_6H_5CH_3$	6.5	$C_6H_5COCH(SeC_6H_5)CH_2OAc$	73
α-Methylstyrene	CCl_4	2	$C_6H_5C(CH_3)(OH)CH_2SeC_6H_5$	62
β-Bromostyrene	CCl_4	12	No reaction	0
Ethyl cinnamate	CCl_4	6	No reaction	0

a) Reactions were performed on a 1 mmol scale with olefin : $(C_6H_5Se)_2$: Br_2 : $(Bu_3Sn)_2O$ = 1.0 : 2.0 : 2.0 : 2.0. b) Isolated yield. c) Olefin: $(C_6H_5Se)_2$: Br_2 : $(Bu_3Sn)_2O$ = 1.0 : 4.0 : 4.0 : 4.0. d) 2-Cyclododecenone was also formed in 20% yield.

give α-phenylseleno carbonyl compounds.

Woodbridge reported that the oxidation of diphenyl diselenide with ozone afforded benzeneseleninic anhydride,[10] presumably *via* an intermediate of benzeneselenenic anhydride **4**. We have examined the olefin oxidation under the expectation that the oxidation of diphenyl diselenide with *t*-butyl hydroperoxide may produce benzeneselenenic anhydride **4**.

$$(C_6H_5Se)_2 + t\text{-BuOOH} \longrightarrow \underset{\mathbf{4}}{\text{“}C_6H_5SeOSeC_6H_5\text{”}} + t\text{-BuOH} \quad (8)$$

Treatment of styrene with diphenyl diselenide (1.5 equiv.) and *t*-butyl hydroperoxide (2.0 equiv.) gave rise to α-(phenylseleno)acetophenone (48%) with 1-*t*-butoxy-1-phenyl-2-(phenylseleno)ethane (38%). The latter product was certainly produced *via* oxyselenenylation with $C_6H_5Se^+$ species and *t*-butyl alcohol formed from *t*-butyl hydroperoxide during the oxidation. The incorporation of *t*-butyl alcohol could be avoided by the removal of *t*-butyl alcohol after the oxidation of the diselenide with the peroxide followed by the addition of an olefin to the resulting solution. The optimum

$$C_6H_5CH{=}CH_2 \xrightarrow{\mathbf{4}} C_6H_5CO\text{–}CH_2SeC_6H_5 \quad (9)$$

conditions were examined about the reaction of styrene.

The results shown in Table 2 indicate that the use of *ca.* 2 equiv. of reagents leads to the optimum yield and a slightly higher reaction temperature is required for the completion of the reaction when compared with the previous system.

Displacement of *t*-butyl hydroperoxide to other oxidants did not lead to the satisfactory result. Oxidation of diphenyl diselenide with pyridinium chlorochromate (PCC), active manganese dioxide, or Jones reagent followed by the addition of styrene to the oxidation product gave only a trace amount of α-(phenylseleno)acetophenone.[11]

A remarkable result was obtained when styrene was treated with diphenyl diselenide (1.4 equiv.) and benzeneseleninic anhydride (0.7 equiv.) as oxidant in refluxing carbon tetrachloride. By this system, α-(phenylseleno)acetophenone was obtained in 77% yield. Generation of benzeneselenenic anhydride **4** may occur *via* disproportionation reaction of diphenyl diselenide and benzeneseleninic anhydride, and it seems to be this species which acts as an electrophile toward olefins to form selenenate ester intermediates.

$$2(C_6H_5Se)_2 + (C_6H_5SeO)_2O \longrightarrow 3\underset{\mathbf{4}}{\text{“}C_6H_5SeOSeC_6H_5\text{”}}$$

$$\xrightarrow{C_6H_5CH=CH_2} C_6H_5CO\text{–}CH_2SeC_6H_5 \quad (10)$$

Table 2. Oxidation of styrene with $(CH_5Se)_2$–*t*-BuOOH. comparison of reaction conditions[a]

t-BuOOH (equiv.)	$(C_6H_5Se)_2$ (equiv.)	Period/h	Yield % of α-(phenylseleno)-acetophenone
2.0	1.5	2	53
1.7	2.2	2	71
1.7	2.2	1	79
1.7	2.2	0.75	74
2.0	2.0	1	87[b]
2.1	2.1	1	80

a) Reactions were perormed in refluxing carbon tetrachloride. Yields were determined by NMR using a calibrated internal standard. b) Isolated yield.

Oxidation of Terminal Olefins. Oxidation of terminal olefins with $(C_6H_5Se)_2$–Br_2–$(Bu_3Sn)_2O$ system usually produces a mixture of α-phenylseleno ketones and aldehydes. The regioselectivity on the oxidation of terminal olefins with **4** was proved to be highly dependent on the reaction solvent. Predominant formation of α-phenylseleno ketones was observed in DMSO solvent, whereas the ratio of α-phenylseleno aldehydes increased in toluene, acetonitrile, sulfolane, and nitromethane. This tendency is explained in terms of the stabilization of the seleniranium intermediate which has often been involved in the addition process of ArSeX to olefins.[12]

Raucher has examined the addition of benzeneselenen-

Table 3. Oxidation of terminal olefins[a]

Olefin	Solvent	Temp/°C	Product (ratio)	Yield/%[b]
1-Decene	$C_6H_5CH_3$	110	$C_8H_{17}COCH_2SeC_6H_5$, $C_8H_{17}CH(SeC_6H_5)CH{=}O$ (66 : 34)	81
	CH_3CN	82	(55 : 45)	75
	$C_6H_5CH_3$[c]	110	(58 : 42)	85
	CH_3CN[c]	82	(54 : 46)	72
	CH_3NO_2[c]	80	(55 : 45)	66
	Sulfolane	110	(59 : 41)	79
	DMSO	110	(91 : 9)	70
(1 : 1)DMSO–$C_6H_5CH_3$[c]		110	(81 : 19)	86
Ethyl 10-undecenoate	DMSO[d]	110	$C_2H_5O_2C(CH_2)_8COCH_2SeC_6H_5$, $C_2H_5O_2C(CH_2)_8CH(SeC_6H_5)CH{=}O$ (94 : 6)	70
1-Dodecene	DMSO[d]	110	$C_{10}H_{21}COCH_2SeC_6H_5$, $C_{10}H_{21}CH(SeC_6H_5)CH{=}O$ (93 : 7)	71

a) Reactions were performed with olefin : $(C_6H_5Se)_2$: *t*-BuOOH = 1.0 : 2.0 : 2.0. b) Isolated yield. c) Olefin : $(C_6H_5Se)_2$: $(C_6H_5SeO)_2O$ = 1.0 : 1.4 : 0.7. d) Olefin : $(C_6H_5Se)_2$: *t*-BuOOH = 1.0 : 4.4 : 4.4.

Table 4. Oxidation of inetrnal olefins[a]

Olefin	Product	Yield/%
$C_6H_5CH{=}^{t}CHCH_2OAc$	$C_6H_5{-}CO{-}CH(SeC_6H_5)CH_2OAc$	83
$C_6H_5CH_2OCH_2CH{=}^{t}CHCH_2OCH_2C_6H_5$	$C_6H_5CH_2OCH_2{-}CO{-}CH(SeC_6H_5)CH_2OCH_2C_6H_5$	81
		67[b]
		56[c]

a) Reactions were performed in refluxing benzene with olefin: $(C_6H_5Se)_2$: *t*-BuOOH = 1.0 : 4.4 : 4.4 or olefin: $(C_6H_5Se)_2$: $(C_6H_5SeO)_2O$ = 1.0 : 2.8 : 1.4. b) Cyclododecenone was formed in 15% yield. c) Reported by Smith III, Nicolaou *et al.*, see Ref. 18.

yl bromide to terminal olefins and has observed the following regioselectivity: under thermodynamically controlled conditions, olefin-PhSeX adducts undergo equilibration to form Markownikoff type adducts predominantly, while under kinetically controlled conditions, the formation of *anti*-Markownikoff adducts are favored.[13] In this regard, in DMSO, oxygen atom on sulfoxide appears to associate with the seleniranium ion and stabilize it, which results in the equilibration of this intermediate to afford the Markownikoff adduct predominantly.

One disadvantage of this oxidation lies in the insolubility of olefins in this solvent, and for reproducible results the use of an excess reagent is required. DMSO–toluene solvent system has found a complemental use for insoluble olefins, although regioselectivity has been somewhat decreased.

We may exclude a possibility for the role of DMSO as oxidant by the following observations. It is well known that olefin–PhSeX adducts are very susceptible to solvolysis.[14] The reaction of these adducts with DMSO,

$$C_8H_{17}CH{=}CH_2 \xrightarrow[DMSO]{C_6H_5SeBr} C_8H_{17}{-}CO{-}CH_2SeC_6H_5 + C_8H_{17}CH(OH){-}CH_2SeC_6H_5 \quad (11)$$

Et_3N: 3% 6%

$AgBF_4$, EtN_3: 14% 80%

however, did not practically proceed. Even in the presence of silver tetrafluoroborate, a phenylseleno ketone was obtained in only low yield. These strongly suggest inefficiency of DMSO as an oxidant in the present system.

Displacement of diphenyl diselenide did not noticeably improve product distribution.

$$C_8H_{17}CH{=}CH_2 \xrightarrow[toluene]{\text{"ArSeOSeAr"}} C_8H_{17}CO{-}CH_2SeAr + C_8H_{17}CH(SeAr){-}CH{=}O \quad (12)$$

Ar: C_6H_5 58:42

$2,4,6\text{-}(CH_3)_3C_6H_2$ 69:31

Oxidation of Internal Olefins. By the procedures reported so far, oxidation of internal olefins to α-phenylseleno ketones appears to be quite difficult. For

example, treatment of (*E*)-3-hexene and (*E*)-6-dodecene with PhSeBr–$AgPF_6$–DMSO–Et_3N produced the corresponding β-hydroxy selenides in *ca.* 60% yield,[4b] whiles terminal olefins gave phenylselenomethyl ketones. The procedure developed by Tsuji *et al.*[4a] does not appear to be applicable to internal olefins due to a facile *syn*-elimination of the resulting selenoxides, although this point has not been tested. By the present method, internal olefins were smoothly oxidized to α-phenylseleno ketones in good yields. The results are listed in Table 4.

$$R\text{-}CH{=}CH\text{-}R \xrightarrow{\mathbf{4}} R\text{-}CO\text{-}\underset{\displaystyle SeC_6H_5}{\underset{|}{CH}}\text{-}R \qquad (13)$$

In general, however, internal olefins are less reactive than terminal ones even under the present oxidation conditions, and good conversion of the starting olefins calls for the use of *ca.* 4.4 equiv. of the reagent.

The difference of the reactivity of C=C bonds in a polyene has been studied by van Tamelen and Sharpless using addition reaction of a hypohalite.[15] More recently, Krief *et al.*[16] examined the reactivity of dienes bearing an internal and a terminal C=C bonds toward methane- and benzeneselenenyl bromide, and they observed selective addition to the terminal olefin. In the present oxidation, a terminal olefin was selectively oxidized to the corresponding α-phenylseleno ketone. For example, when an equimolar mixture of ethyl 10-undecenoate and cyclododecene was treated with diphenyl diselenide (2.8 equiv.) and benzeneseleninic anhydride (1.4 equiv.) in DMSO at 110 °C for 30 min, a mixture of ethyl 10-oxo-11-phenylselenoundecanoate and ethyl 11-oxo-10-phenylselenoundecanoate (92 : 8) was obtained in 64% yield with the recovered cyclododecene (90%). It is expected that the present system will find applications in selective oxidation of polyenes.

Reaction Mechanism. Sharpless and Reich have suggested a "Conproportionation" reaction between diphenyl diselenide and benzeneseleninic acid to yield benzeneselenenic acid as a reactive species to olefinic bonds.[17] Smith III and Nicolaou have also described

$$(C_6H_5Se)_2 + C_6H_5\overset{\displaystyle O}{\overset{\|}{S}}e\text{-}OH + H_2O \longrightarrow 3\text{“}C_6H_5SeOH\text{”} \qquad (14)$$

a cyclization reaction of dienes using this kind of species.[18]

We propose here a generation of benzeneselenenic anhydride **4** from both of the systems, which acts as a reactive species. However, it is not very clear whether the introduction of carbonyl proceeds *via* a selenenate ester or not. One possible alternative seems to be the involvement of the fragmentation of a seleninate ester

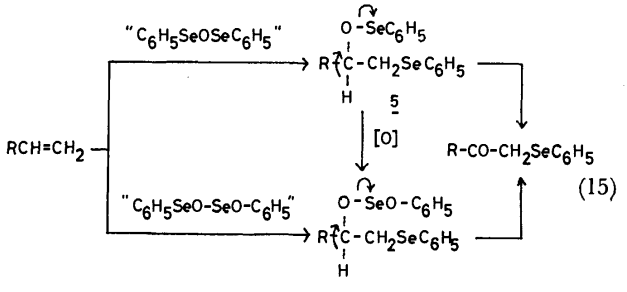

(15)

via addition of "$C_6H_5SeOSe(=O)C_6H_5$" species or oxidation of a selenenate ester intermediate. In regard to the reports dealing with fragmentation of seleninate esters proposed by Barton *et al.*,[19] we can not exclude the possibility of seleninates as the intermediates in this oxidation process.

Experimental

All reactions involving air- or moisture-sensitive compounds were performed under either argon or ultra-grade nitrogen atmosphere. NMR spectra were taken on a Hitachi R-24B spectrometer and chemical shifts are recorded in parts per million downfield from internal tetramethylsilane. IR spectra were taken on a Hitachi EPI- G3 or 260-10 spectrometer, and mass spectra on a Hitachi RMU-7M or RMU-6C spectrometer at 70 eV ionizing irradiation. Analytical gas liquid chromatography was performed on a Hitachi 063 or 163 instrument. Microanalyses were performed on a Perkin Elmer 240 instrument. Melting points which were taken in open capillaries and boiling points were uncorrected.

Diphenyl diselenide, bis(*p*-chlorophenyl) diselenide, and bis(2,4,6-trimethylphenyl) diselenide were prepared by the procedure reported by Sharpless and Reich.[3c,17] Benzeneseleninic anhydride was prepared according to the procedure of Woodbridge,[10] and was stored over P_2O_5.

Oxidation of Styrene with $(C_6H_5Se)_2$–Br_2–$(Bu_3Sn)_2O$. To a solution of diphenyl diselenide (686 mg, 2.2 mmol) and hexabutyldistannoxane (1.31 g, 2.2 mmol) in 3 ml of chloroform were added a carbon tetrachloride solution of bromine (1.55 ml of 1.35 M (1 M = 1 mol dm^{-3}) solution, 2.10 mmol) and then a solution of styrene (104 mg, 1.0 mmol) in 2 ml of chloroform. After stirring for 2 h under refluxing, the brown colored mixture was washed with 5% aq NaOH, and satd aq NaCl. The organic layer was dried over $MgSO_4$, concentrated, and purified by silica gel column chromatography followed by bulb-to-bulb distillation to afford α-(phenylseleno)acetophenone (204 mg,74%). Bp 150—160 °C/0.15 mmHg;[20] IR (neat): 1665 cm^{-1}; NMR ($CDCl_3$): δ 4.13 (s, 2H), 7.13—7.63 (m, 8H), 7.73—7.97 (m, 2H); MS:[21] *m/e* (%) 276 (M^+, 16), 105 (100), 77 (20), 52 (13); Found: C, 61.37; H, 4.62%. Calcd for $C_{14}H_{12}OSe$:C, 61.10; H, 4.40%.

Oxidation of 1-Decene with $(C_6H_5Se)_2$–Br_2–$(Bu_3Sn)_2O$. To a solution of diphenyl diselenide (686 mg, 2.2 mmol) and hexabutyldistannoxane (1.31 g, 2.2 mmol) in 5 ml of carbon tetrachloride in the presence of molecular sieves 3A (1 g) were added a carbon tetrachloride solution of bromine (1.3 ml of 1.64 M solution, 2.1 mmol) and then a solution of 1-decene (140 mg, 1.0 mmol) in 5 ml of carbon tetrachloride, and the mixture was heated to refluxing for 7 h. After a usual work-up, the crude oil was purified by silica gel column chromatography to give diphenyl diselenide (437 mg), 1-phenylseleno-2-decanone (143 mg, 46%), and 2-p henylselenodecanal(68 mg, 22%). *1-Phenylseleno-2-decanone*, Bp 168 °C/0.3 mmHg;[20] Mp 39—40 °C (hexane); IR (KBr): 1692 cm^{-1}; NMR (CCl_4): δ 0.60—1.90 (m, 15H), 2.50 (t, J=7.0 Hz, 2H), 3.47 (s, 2H), 6.70—7.60 (m, 5H); MS[21] *m/e* (%) 321 (M^+, 5), 155 (6), 141 (6), 77 (20), 57 (69), 43 (100); Found: C, 61.66; H, 7.68%. Calcd for $C_{16}H_{24}OSe$: C, 61.73; H, 7.77%. *2-Phenylselenodecanal*, Bp 142—143 °C/0.06 mmHg;[20] IR(neat): 1705 cm^{-1}; NMR (CCl_4): δ 0.70—2.20 (m, 17H), 3.20—3.90 (m, 1H), 7.10—7.70 (m, 5H), 9.40 (d, J=4.0 Hz, 1H); MS:[21] *m/e* (%) 312 (M^+, 18), 283 (18), 155 (19), 57 (75), 43 (100), 29 (59).

Ethyl 10-Oxo-11-phenylselenoundecanoate. Mp 37—38 °C (hexane); IR (KBr): 1730, 1695 cm^{-1}; NMR (CCl_4): δ 1.00—2.00 (m, 17H), 2.23 (t, J=8.0 Hz, 2H), 2.50 (t, J=7.0 Hz,

2H), 3.47 (s, 2H), 4.10 (q, J=5.0 Hz, 2H), 7.10—7.60 (m, 5H); MS: [21] *m/e* (%) 384 (M^+, 30), 339 (13), 213 (65), 171 (54), 157 (41), 97 (65), 83 (28), 77 (33), 69 (70), 46 (100); Found: C, 59.67; H, 7.42%. Calcd for $C_{19}H_{28}O_3Se$: C, 59.52; H, 7.36%.

Ethyl 11-Oxo-10-phenylselenoundecanoate. IR (neat): 1720, 1700 cm^{-1}; NMR (CCl_4): δ 0.85—1.90 (m, 19H), 2.13 (t, J=6.0 Hz, 2H), 3.20—3.60 (m, 1H), 3.97 (q, J=5.0 Hz, 2H), 7.00—7.50 (m, 5H), 11.5 (d, J=3.0 Hz, 1H); MS:[21] *m/e* (%) 384 (M^+, 5), 354 (2), 226 (5), 77 (8), 73 (92), 45 (12), 29 (100); Found: C, 59.34; H, 7.56%. Calcd for $C_{19}H_{28}O_3Se$: C, 59.52; H, 7.36%.

2-Phenylselenocyclododecanone. The reaction was carried out with cyclododecene (84 mg, 0.5 mmol) using diphenyl diselenide (2.2 equiv.), bromine (2.1 equiv.), and hexabutyldistannoxane (2.2 equiv.) in refluxing benzene for 8 h. Purification of the reaction mixture by silica gel column chromatography gave 2-cyclododecenone (18 mg, 20%) and the title compound (87 mg, 52%). Bp 148—152 °C/0.06 mmHg;[20] IR (neat): 1685 cm^{-1}; NMR (CCl_4): δ 0.70—2.35 (m, 18H), 2.53 (unresolved dd, J= 10.0 and 6.0 Hz, 2H), 3.90 (dd, J= 5.0 and 8.0 Hz, 1H), 7.10—7.60 (m, 5H); MS:[21] *m/e* (%) 338 (M^+, 2), 181 (6), 157 (28), 83 (61), 55 (100).

3-Oxo-3-phenyl-2-phenylselenopropyl Acetate. IR (neat): 1740, 1680 cm^{-1}; NMR (CCl_4): δ 1.90 (s, 3H), 4.40—4.90 (m, 3H), 7.10—7.55 (m, 8H), 7.75—8.00 (m, 2H); MS:[21] *m/e* (%) 348 (M^+, 8), 289 (90), 271 (7), 191 (40), 105 (100), 77 (45), 59 (88), 43 (40).

1-Phenylseleno-2-phenyl-2-propanol. Bp 127—130 °C/0.4 mmHg;[20] IR (neat): 3440 cm^{-1}; NMR (CCl_4): δ 1.57 (s, 3H), 2.80 (brs, 1H, disappeared on D_2O exchange), 3.38 (d, J= 6.0 Hz, 1H), 3.40 (d, J=6.0 Hz, 2H), 7.00—7.50 (m, 12H); MS:[21] *m/e* (%) 274 ($M^+ - 18$, 5), 172 (18), 117 (70), 115 (100), 77 (80).

Oxidation of Styrene with $(C_6H_5Se)_2$–t-BuOOH (General Procedure). To a solution of diphenyl diselenide (628 mg, 2 mmol) in 5 ml of carbon tetrachloride were added molecular sieves 3A (2 g) and a solution of 70% *t*-butyl hydroperoxide (256 mg, 2.0 mmol) in 5 ml of carbon tetrachloride, and the mixture was heated to refluxing for 1 h. Then all the solvent as well as *t*-butyl alcohol was removed *in vacuo*, and a solution of styrene (104 mg, 1.0 mmol) in 5 ml of carbon tetrachloride was added to the resulting pale yellow solid. After stirring for 1 h under refluxing, the reaction mixture was washed with satd aq NaCl and dried over $MgSO_4$. Removal of the solvent gave a brown oil, which was purified by silica gel column chromatography to give α-(phenylseleno)acetophenone (238 mg, 87%) and diphenyl diselenide (414 mg).

Oxidation with $(C_6H_5Se)_2$–$(C_6H_5SeO)_2O$ (General Procedure). To a solution of diphenyl diselenide (437 mg, 1.4 mmol) and benzeneseleninic anhydride (252 mg, 0.7 mmol) in 5 ml of the solvent were added an olefin (1 mmol) in 5 ml of solvent and molecular sieves 3A (2 g), and the mixture was stirred under refluxing until the starting olefin was all consumed. The resulting reaction mixture was worked up and purified as described above.

Oxidation of 1-Decene. 1-Decene (70 mg, 0.5 mmol) was oxidized with diphenyl diselenide (686 mg, 2.2 mmol) and *t*-butyl hydroperoxide (282 mg of 70% solution, 2.2 mmol) in DMSO at 110 °C for 1 h. A mixture (108 mg, 70%) of 2-phenylselenodecanal and 1-phenylseleno-2-decanone was obtained. The isomeric ratio was determined to be 9 : 91 by NMR analysis. Further purification gave both samples which exhibit similar spectroscopic properties to ones prepared previously.

Oxidation of Ethyl 10-Undecenoate. Ethyl 10-undecenoate (106 mg, 0.5 mmol) was oxidized with diphenyl diselenide (686 mg, 2.2 mmol) and 70% *t*-butyl hydroperoxide (282 mg, 2.2 mmol) in 10 ml of DMSO at 110 °C for 1.5 h. A mixture (134 mg, 70%) of ethyl 10-oxo-11-phenylselenoundecanoate and ethyl 11-oxo-10-phenylselenoundecanoate was obtained, and their ratio was determined to be 94 : 6 by NMR analysis. Separation of the mixture gave pure samples which exhibit similar spectroscopic properties to ones prepared previously.

Oxidation of 1-Dodecene. 1-Dodecene (84 mg, 0.5 mmol) was oxidized by the same procedure. A mixture of 1-phenylseleno-2-dodecanone and 2-phenylselenododecanal was obtained, and their ratio was determined to be 93 : 7 by NMR analysis. Separation of the mixture gave pure samples. *1-Phenylseleno-2-dodecanone*, IR (neat): 1705 cm^{-1}: NMR (CCl_4): δ 0.70—2.00 (m, 19H), 2.60 (t, J=7.0 Hz, 2H), 3.57 (s, 2H), 7.30—7.90 (m, 5H); MS:[21] *m/e* (%) 340 (M^+, 71), 172 (89), 15; (32), 133 (29), 109 (54), 95 (39), 91 (57), 85 (54), 77 (25), 71 (57), 57 (100). *2-Phenylselenododecanal*, IR (neat): 1705 cm^{-1}; NMR (CCl_4): δ 0.70—2.00 (m, 21H), 3.3—3.9 (m,1H), 7.40—7.90 (m, 5H), 9.50 (d, J=3.0 Hz, 1H).

3-Oxo-3-phenyl-2-phenylselenopropyl Acetate. Cinnamyl acetate (88 mg, 0.5 mmol) was oxidized by a similar procedure in benzene (5 ml) for 4 h, and the title compound (144 mg, 83%) was obtained as an oil. IR (neat): 1740, 1680 cm^{-1}; NMR (CCl_4): δ 1.90 (s, 3H), 4.40—4.90 (m, 3H), 7.10—7.55 (m, 8H), 7.75—8.00 (m, 2H); Found: C, 58.92; H, 4.78%. Calcd for $C_{17}H_{16}O_3Se$: C, 58.80; H, 4.64%.

2-Phenylselenocyclododecanone. Cyclododecene (91 mg, 0.5 mmol) was oxidized in a similar procedure in refluxing benzene for 3 h, and the title compound (118 mg, 67%) and 2-cyclododecenone (14 mg, 15%) were obtained.

1,4-Bis(benzyloxy)-3-phenylseleno-2-butanone. (*E*)-1,4-Bis-(benzyloxy)-2-butene (120 mg, 0.5 mmol) was oxidized in a similar procedure in refluxing benzene for 4.5 h, and the title compound (166 mg, 81%) was obtained. IR (neat): 3100, 1710, 1100, 750 cm^{-1}; NMR (CCl_4): δ 3.90—4.17 (m, 3H), 4.37 (d, J=5.0 Hz, 4H), 7.00—7.53 (m, 5H). Further deselenenylation with benzenethiol (0.15 ml) and triethylamine (1.0 ml) gave analytically pure deselenenylated product, 1,4-bis(benzyloxy)-2-butanone. IR (neat): 3100, 1705 cm^{-1}; NMR (CCl_4): δ 2.71 (t, J=7.0 Hz, 2H), 3.60 (t, J=7.0 Hz, 2H), 3.90 (s, 2H), 4.07 (s, 2H), 4.74 (s, 2H), 7.20 (s, 10H); Found: C, 76.19; H, 7.14%. Calcd for $C_{18}H_{20}O_3$: C, 76.037; H, 7.09%.

Oxidation of Ethyl 10-Undecenoate in the Presence of Cyclododecene. To a mixture of diphenyl diselenide (437 mg, 1.4 mmol) and benzeneseleninic anhydride (252 mg, 0.7 mmol) were added a solution of cyclododecene (83 mg, 0.5 mmol) and ethyl 10-undecenoate (106 mg, 0.5 mmol) in DMSO (10 ml) and then molecular sieves 3A (2 g). After stirring for 30 min at 110 °C, the reaction mixture was washed with satd aq NaCl and was extracted with ether. Cyclododecanone (91 mg) was added to the reaction mixture as an internal standard, and the resulting solution was examined by GLPC to give an indication that cyclododecene was recovered in 90%. Purification of the mixture by silica gel column chromatography afforded a mixture of ethyl 10-oxo-11-phenylselenoundecanoate and ethyl 11-oxo-10-phenylselenoundecanoate (123 mg, 64%). The ratio of the seleno ketone *vs.* the seleno aldehyde was determined to be 92 : 8 by NMR analysis.

References

1) Preliminary reports dealing with certain aspects of this work: I. Kuwajima and M. Shimizu, *Tetrahedron Lett.*, **1978**, 1277; M. Shimizu, R.Takeda, and I. Kuwajima, *ibid.*, **1979**,

419.

2) K. B. Sharpless, R. F. Lauer, D. W. Patrick, S. P. Singer, and M. W. Young, *Chem. Scr.*, **8A**, 9 (1975); D. L. J. Clive, *Tetrahedron*, **34**, 1049 (1978); *Aldrichim. Acta*, **11**, 43 (1978); H. J. Reich, *Acc. Chem. Res.*, **12**, 22 (1979).

3) a) D. L. J. Clive, *J. Chem. Soc., Chem. Commun.*, **1973**,695; b) K. B. Sharpless, R. F. Lauer, and A. Y. Teranishi, *J. Am. Chem. Soc.*, **95**, 6137 (1973); c) H. J. Reich, J. M. Renga, and I. L. Reich, *ibid.*, **97**, 5434 (1975); d) I. Ryu, I. Niwa, and N. Sonoda, *Synthesis*, **1977**, 874.

4) Recently two methods have been introduced for this purpose: a) T. Takahashi, H. Nagashima, and J. Tsuji, *Tetrahedron Lett.*, **1978**, 799; b) S. Raucher, *ibid.*, **1978**, 2261.

5) J. C. Pommier and D. Chevolleau, *J. Organomet. Chem.*, **74**, 405 (1974); K. Saigo, A. Morikawa, and T. Mukaiyama, *Bull. Chem. Soc. Jpn.*, **49**, 1656 (1976); T. Ogawa and M. Matsui, *J. Am. Chem. Soc.*, **98**, 1629 (1976).

6) Y. Ueno and M. Okawara, *Tetrahedron Lett.*, **1976**,4597.

7) K. B. Sharpless and R. F. Lauer, *J. Am. Chem. Soc.*, **94**, 7145 (1972).

8) D. H. R. Barton, D. J. Lester, and S. V. Ley, *J. Chem. Soc., Chem. Commun.*, **1977**, 445.

9) M. Shimizu and I. Kuwajima, *Tetrahedron Lett.*, **1979**, 2801.

10) G. Ayrey, D. Barnard, and D. T. Woodbridge, *J. Chem. Soc.*, **1962**, 2089.

11) Treatment of styrene with diphenyl diselenide (1.5 equiv.) and selenium dioxide (1.1 equiv.) in refluxing dioxane for 5 h afforded 1-phenyl-2-(phenylseleno)ethanol in 55% yield.

12) See, for example; G. H. Schmid and D. G. Garratt, *Tetrahedron Lett.*, **1975**, 3991.

13) S. Raucher, *J. Org. Chem.*, **42**, 2950 (1977); *Tetrahedron Lett.*, **1977**, 3909.

14) H. J. Reich, *J. Org. Chem.*, **39**, 428 (1974); K. B. Sharpless and R. F. Lauer, *ibid.*, **39**, 429 (1974).

15) E. E. van Tamelen and K. B. Sharpless, *Tetrahedron Lett.*, **1967**, 2655.

16) J. N. Denis, J. Vicens, and A. Krief, *Tetrahedron Lett.*, **1979**, 2697.

17) T. Hori and K. B. Sharpless, *J. Org. Chem.*, **43**, 1689 (1978); H. J. Reich, S. Wollowitz, J. F. Trend, F. Chow, and D. F. Wendelborn, *ibid.*, **43**, 1697 (1978).

18) R. M. Scarborough, Jr., A. B. Smith III, W.E. Barnette, and K. C. Nicolaou, *J. Org. Chem.*, **44**, 1742 (1979).

19) D. H. R. Barton, A. G. Brewster, R. A. H. F. Hui, D. J. Lester, and S. V. Ley, *J. Chem. Soc., Chem. Commun.*, **1978**, 952.

20) 1 mmHg=133.322 Pa.

21) Selenium-containing compounds exhibit the characteristic isotopic family in their mass spectra ^{74}Se (1), ^{76}Se (10), ^{77}Se (9), ^{78}Se (27), ^{80}Se (57), ^{82}Se (11), but only the peaks due to the most abundant isotope (^{80}Se) are described.

The Characterization of a Novel Metathesis Catalyst, β-Titanium Oxide-supported Molybdenum Oxide

Katsumi TANAKA, Koshiro MIYAHARA,* and Ken-ichi TANAKA**
Research Institute for Catalysis, Hokkaido University, Sapporo 060
***Faculty of Engineering, Hokkaido University, Sapporo 060*
(Received December 17, 1980)

The results of the X-ray photoelectron spectroscopy of a novel metathesis catalyst, MoO_x/β-TiO_2, are discussed with reference to its catalytic behavior. It is concluded that the active center for the metathesis reaction of olefin is the molybdenum ion with an oxidation higher than +4 on the average, and that the hydrogen scrambling of olefin during the metathesis is caused by the OH group on the TiO_2 surface. During the preparation of this catalyst, the decomposition of titanic acid to TiO_2 is found to be accelerated by MoO_3; a similar thing can be seen of the reduction of MoO_3 to zero-valent molybdenum by TiO_2.

Many active catalysts, homogeneous and heterogeneous, have been developed[1] for the olefin-metathesis reaction, and its mechanism has been investigated since 1964;[2] the simultaneous hydrogen scrambling of olefin has been an intricate problem. We ourselves have reported a novel solid catalyst, MoO_x/β-TiO_2 (x= 2.3—2.9), on which the metathesis reaction of olefin proceeds with a negligible extent of hydrogen scrambling of olefin.[3] When alumina and zirconia are used as catalyst supports, the hydrogen scrambling of olefin surpasses the metathesis.[4] In this paper, this novel catalyst was characterized, mainly by using X-ray photoelectron spectroscopy.

Experimental

The catalyst was prepared by impregnating a powder of β-titanic acid with an aqueous solution of ammonium molybdate and then dried at 120 °C. The sample (*ca.* 0.3 g) was oxidized with O_2 and evacuated at 500 °C in a conventional circulation apparatus with a volume of *ca.* 350 cm^3. Preceding the metathesis reaction, the following pretreatments of the catalyst were performed: it was reduced with hydrogen at 500 °C for 1 h and preconditioned by performing on it a reaction of N_2O (*ca.* 40 Pa) with H_2 (*ca.* 100 Pa) at 200 °C for 1 h.[4,5] By this pretreatment, the catalyst surface was controlled to give a characteristic activity for metathesis reaction; *i.e.*, it was active for metathesis, but had a negligible extent of hydrogen scrambling as well as of the isomerization of olefin.[4]

A mixture (1 : 1) of propene and [D_6]propene (CH_2=$CHCH_3$ and CD_2=$CDCD_3$) or *cis*-2-butene and [D_8]*cis*-2-butene was admitted at room temperature onto the catalyst at a total pressure of *ca.* 6×10^3 Pa, and its catalytic activities for the productive and degenerative metathesis, as well as for the hydrogen scrambling of olefin, were studied. The analysis of the products was carried out by GC, and the deuterated isomers separated by GC were analyzed by means of a mass spectrometer with low isonization voltages. The reagents used were of a chemically pure grade.

The X-ray photoelectron spectra of the catalyst were obtained by means of an ESCA-3 apparatus of the Vacuum Generator Co. The untreated samples prepared from ammonia molybdate and β-titanic acid were pressed on a sample hoder of the ESCA-3 apparatus and treated in a side chamber under conditions similar to those used in the catalyst pretreatments. The binding energies of Mo(3d) and Ti(2p) electrons were corrected using a reference of 530 eV for the ls electron from oxygen of oxide; this value is common for a variety of metal oxides.[6]

Results

The catalytic properties of 6.7 wt% MoO_3/TiO_2 change with the extent of reduction, as is shown in Fig. 1,[4] in which the extent of reduction (x in MoO_x) was estimated from the amount of hydrogen consumed in the reduction of an oxidized catalyst sample at 500 °C for 1 h. It was found that the molybdenum oxide supported on titanium oxide was finally reduced to the zero-valent state, although Ti^{3+} could not be detected by ESR during the reduction of the catalyst.[5]

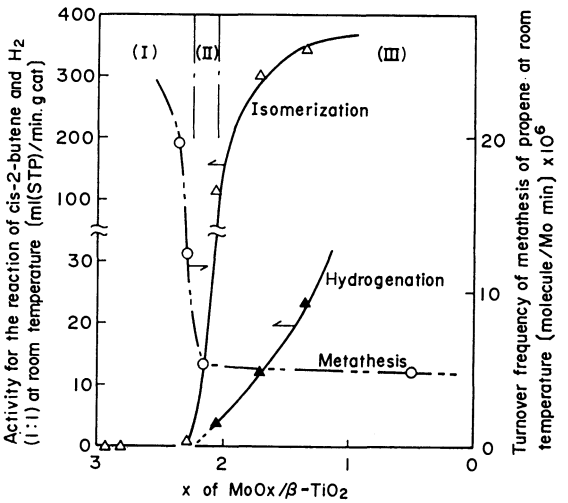

Fig. 1. Characteristic profile of the catalytic activity of MoO_x/β-TiO_2 for reactions of olefins at room temperature.

Only oxidation of olefin was caused by a catalyst, MoO_x/β-TiO_2, with an x value larger than 2.9. However, the catalyst of x=2.3—2.9, State I, gave preferentially olefin metathesis with little hydrogen scrambling of the olefins. As a result, a mixture of propene and [D_6]propene yielded mainly [D_2] and [D_4]propene by degenerative metathesis, and [D_0], [D_2], and [D_4]ethylene by productive metathesis, respectively. In contrast to the State I surface, the catalyst of x=2.0—2.3, State II, is active for the isomerization of olefin in the presence of hydrogen. The more reduced surface, described by State III, of a

catalyst with x value less than 2.0 can catalyze the isomerization in the absence of hydrogen. Such an isomerization caused by a process other than metathesis can be followed by interconversion between 1-butene and 2-butene.[7] The hydrogenation of olefin is also brought about over the catalyst surfaces of States II and III. A more reduced surface has a higher activity for hydrogenation. We found that a State I or II surface can be prepared from a reduced catalyst by carrying out on it the reaction of N_2O with H_2 at 200 °C or with CO at room temperature for 1 h.

Figure 2 shows the amount of hydrogen consumption in the reduction of oxidized catalyst samples at 500 °C for 1 h, in which the stoichiometric reduction of MoO_3 is brought about if the catalyst samples are loaded with less than *ca.* 10 wt% of MoO_3.

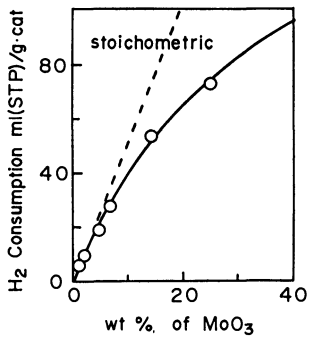

Fig. 2. Amounts of H_2 consumed in reduction of MoO_3/β-TiO_2 catalysts loaded with different amounts of MoO_3 at 500 °C for 1 h.

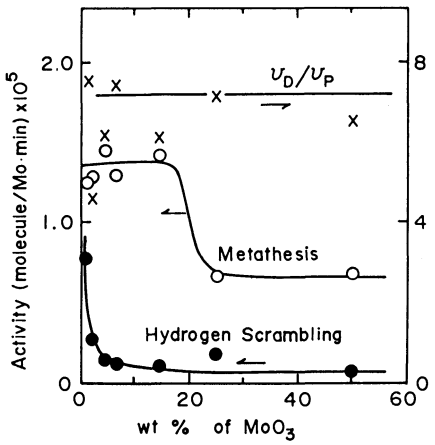

Fig. 3. Catalytic activity changes of MoO_x/β-TiO_2 (x= 2.3—2.9) depending on the amount of loaded MoO_3.

Figure 3 shows the specific activities for a metathesis reaction and for a simultaneous hydrogen scrambling of olefin over catalysts with various wt% MoO_3, where the catalysts were prepared by oxidation, and the reduction at 500 °C, followed by the reaction of N_2O with H_2 at 200 °C for 1 h and its evacuation at 500 °C. The ratio of a productive metathesis to a degenerative one is plotted in Fig. 3. The turnover frequency in this figure is evaluated by assuming that all the molybdenum loaded on TiO_2 is active for the reactions. Up to *ca.* 15 wt% MoO_3, the turnover frequency of metathesis is nearly constant,while that of hydrogen scrambling decreases steeply.

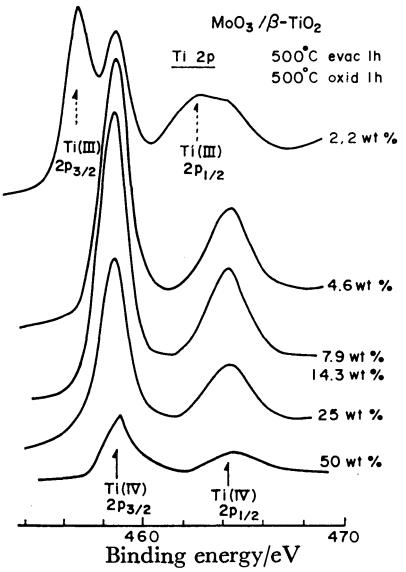

Fig. 4. XPS spectra of Ti(2p) electrons from surfaces of MoO_3/β-TiO_2 with different amounts of loaded MoO_3.

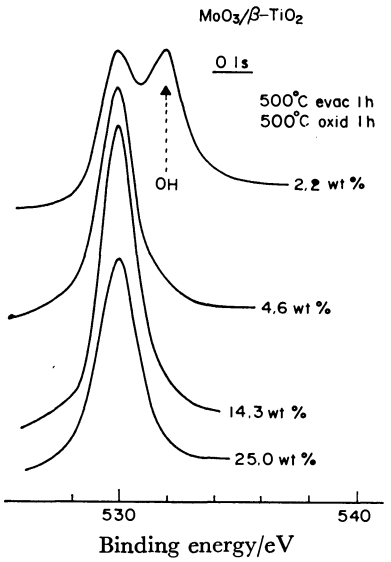

Fig. 5. XPS spectra of O(1s) electrons from surfaces of MoO_3/β-TiO_2 with different amounts of loaded MoO_3.

Figures 4 and 5 show the XPS spectra of Ti(2p) and O(1s) of oxidized samples with various wt% MoO_3. The XPS peak areas of Mo(3d), Ti(2p), and O(1s), observed as measures of the surface concentrations of these components, are plotted in Fig. 6 against the loaded amounts of MoO_3.

Discussion

The activity for metathesis reaction increases proportionally to the amount of loaded MoO_3 up to *ca.* 15 wt%, as can be seen from the constant turnover frequency for metathesis shown in Fig. 3. This result implies that molybdenum is dispersed rather homogeneously on the

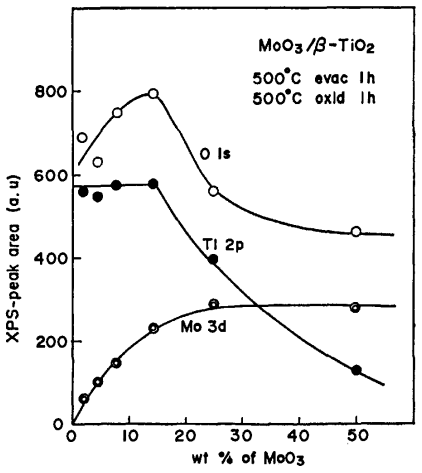

Fig. 6. Changes of XPS-peak areas of Mo(3d), Ti(2p), and O(1s) electrons from the surfaces of MoO_3/β-TiO_2 catalysts with different amounts of loaded MoO_3.

catalyst surface when the loaded MoO_3 is less than *ca.* 15 wt%. The valence state of the molybdenum ion is quite sensitive to a metathesis reaction, as is shown in Fig. 1, and a characteristic activity for metathesis reaction appears only in the range of $x=2.3$—2.9 of MoO_x/TiO_2. In contrast to the result of Iwasawa *et al.*,[8] the activity for metathesis reaction became higher when the average oxidation state was slightly higher than Mo^{4+}.

It was confirmed[7] that, in the hydrogen scrambing of olefin, the relative contribution of *n*- and *s*-alkyl species to the catalyst of State II is quite similar to that of the MoS_2 catalyst.[9] With the MoS_2 catalyst, the selectivity for isomerization and hydrogenation of olefin has been found to be sensitive to the degree of the coordinative unsaturation of the central Mo ion.[9]

The turnover frequency for a metathesis reaction decreases with an increase in the loaded amount of MoO_3 above *ca.* 20 wt%, as can be seen in Fig. 3, while the ratio of the degenerative metathesis to the productive one, v_D/v_P, is constant, irrespective of the loaded amount of MoO_3. These results imply that the active sites on MoO_x/TiO_2 are not influenced by the loaded amount of MoO_3. In contrast to this, the turnover frequency for the simultaneous hydrogen scrambling of olefin is quite sensitive to the amount of MoO_3 loaded on TiO_2. It was found that the O(1s) peak at 531.5 eV in the XPS spectra, which may be attributed to the OH group,[10] was observed in the present experiments only on a catalyst with 2.2 wt% MoO_3 (Fig. 5), and the hydrogen scrambling might be caused by this OH group on the TiO_2 surface.

As is shown in Fig. 6, the XPS peak area of Ti(2p) decreases steeply, while that of Mo(3d) increases to a plateau, with an increase in the loaded amount of MoO_3 above *ca.* 20 wt%. The samples subjected to XPS measurements were completely oxidized, so that this catalyst may be different from the catalyst used for the metathesis reaction. Titanium oxide is not influenced by the pretreatment of the catalysts, and the reproducible results shown in Fig. 2 were obtained. This fact may indicate that the distribution of the molybdenum ion on the catalyst surface is not changed by this pretreatment. The results given in Fig. 6 suggest that MoO_3 loaded with more than *ca.* 20 wt% causes its aggregation on the TiO_2 surface and is more difficult to be reduced by hydrogen, as is shown in Fig. 2. As a result, the specific activity for the metathesis reaction decreases with an increase in the loaded amount of MoO_3, as is shown in Fig. 3.

Figures 4 and 5 show the XPS spectra of a sample of 2.2 wt% MoO_3. It is interesting that the sample loaded with MoO_3 less than 4.6 wt% gives the exceptional peaks of the Ti^{3+} ion and the O(1s) peak of the OH group. This fact indicates that the decomposition of titanic acid to TiO_2 is accelerated by MoO_3 loaded more than 4.6 wt%. Furthermore, it has been reported[11] that the reduction of MoO_3/TiO_2 was far faster than those of MoO_3 supported on SiO_2, MgO, ThO_2, *etc.* It was found in this work that MoO_3 loaded on TiO_2 with *ca.* 10 wt% or less could be reduced to nearly the zero-valent state of molybdenum with hydrogen at 500 °C for 1 h, while MoO_3 loaded by an amount of more than 10 wt% was hard to be reduced to zero valence. This result is in contrast to the MoO_3 loaded on alumina, which is difficult to be reduced to a state lower than Mo^{4+}.[12] It may be concluded that a special interaction between molybdenum oxide and titanium oxide can keep the valence state of the molybdenum ion suitable for metatheses, while the coordinative unsaturation of oxygen on the molybdenum ion may be more important in hydrogenation and/or isomerization reactions, such as in the case of the MoS_2 catalyst.[7,9]

By referring to the results shown in Figs. 2, 3, and 6, we see that the catalyst of 6.7 wt% MoO_3, used by chance,[3,4,7] is one of the most effective catalysts for the selective metathesis of olefin, causing a negligible simultaneous hydrogen scrambling of olefin.

The present work was supported in part by a Grant-in-Aid for Scientific Research, No. 343001, from the Ministry of Education, Science and Culture and also by a grant from the Mitsubishi Foundation, 1979. We are much indebted to Professor Isamu Toyoshima ofthe Research Institute for Catalysis, Hokkaido University, for his valuable discussions of the XPS spectra.

References

1) G. C. Bailey, *Catal. Reg.*, **3**, 37 (1969); R. L. Banks, *Topic Curr. Chem.*, **25**, 39 (1972); J. C. Mole and J. A. Moulijin, *Adv. Catal.*, **24**, 131 (1975); J. J. Rooney and A. Stewart, *Catalysis (Spec. Period Rep.)*, **1**, 277 (1977).

2) R. L. Banks and G. C. Bailey, *Ind. Eng. Chem. (Product Res. Develop.)*, **3**, 170 (1964).

3) K. Tanaka, K. Tanaka, and K. Miyahara, *J. Chem. Soc., Chem. Commun.*, **1979**, 314; *Shokubai (Catalyst)*, **21**, 73 (1979).

4) K. Tanaka, K. Miyahara, and K. Tanaka, *Proceedings of The Internat. Congr. Catal., Tokyo*, **1981**, 1318.

5) T. Watanabe, K. Tanaka, K. Miyahara, and K. Tanabe, *Shokubai (Catalyst)*, **20**, 255 (1978).

6) T. J. Barr, *J. Phys. Chem.*, **82**, 1801 (1978).

7) K. Tanaka, *Doctoral Thesis, Hokkaido Univ.* (1980).

8) Y. Iwasawa, H. Kubo, M. Yamagishi, and S. Ogasawara, *Chem. Lett.*, **1980**, 1165.
9) K. Tanaka and T. Okuhara, *Catal. Rev.-Sci. Eng.*, **15**, 256 (1978).
10) H. Vinek, J. Latzel, and H. Noller, *J. Chem. Soc., Faraday Trans. 1*, **74**, 2092 (1978).
11) R. Nakamura, Y. Morita, M. Mori, and E. Echigoya, *Shokubai* (*Catalyst*), **13**, 130 (1971).
12) E. A. Lombardo, M. Hoialla, and W. K. Hall, *J. Catal.*, **51**, 256 (1978).

Magnetic Interaction in Solvent-free DPPH and DPPH-Solvent Complexes

Teruaki FUJITO†

Department of Chemistry, Faculty of Science, Kyoto University, Sakyo-ku, Kyoto 606

(Received December 19, 1980)

Magnetic interaction in solvent-free DPPH and DPPH–solvent complexes has been studied by means of measurements of the magnetic susceptibility, the proton magnetic resonance, and the low-field ESR at very low temperatures. The susceptibility of solvent-free DPPH shows a round maximum at 11 K, and then it decreases with a lowering of the temperature, no ordered state being observed. The DPPH–benzene (1 : 1) complex shows a round maximum of susceptibility at 0.65 K and antiferromagnetic ordering at about 0.40 K. The DPPH–CCl_4 (4 : 1) complex shows a curious temperature dependence of the susceptibility, which is interpreted in terms of a two-magnetic sublattice model; one sublattice is in the singlet spin state, while the other is in the paramagnetic state at low temperatures except below 0.45 K. Pair interaction is dominant both solvent-free DPPH and in solvent complexes of DPPH. A theoretical approach to the ordered state of DPPH–benzene is given by taking the inter-pair interaction into account.

Recently many studies have been made of the magnetic properties of some organic stable free radicals, such as 4-hydroxy-2,2,6,6-tetramethyl-1-piperidinoxyl (TANOL), diphenyl nitroxide (DPNO) and 1,3-bis-(biphenyl-2,2′-diyl)-2-phenylallyl (BDPA).[1,2] It has been found that the linear-chain interaction is dominant in these radicals. 2,2-Diphenyl-1-picrylhydrazyl (DPPH) is a well known, stable, organic free radicals, and its magnetic properties have been investigated by many workers using various techniques.[3-5] However, the results obtained by different workers have not been consistent with each other. For example, the results of NMR by Karimov and Schegolev[5] were different from those reported by Anderson, Pake, and Tuttle.[4] In 1965, Weil and Anderson[6] reported that there are three different crystal forms for the group of solvent-free DPPH and DPPH-solvent complexes (this group will be abbreviated as DPPHs hereafter). Subsequent X-ray investigations by Williams showed that there are indeed three types of crystal structures for DPPHs.[7] Hence, the complication of the magnetic properties of DPPHs is probably due to the differences in the crystal structures of the samples used by different workers. In order to understand the magnetism of DPPHs, it is, therefore, important to examine the relation between magnetism and crystal structure.

Previously, we measured the magnetic susceptibilities of several DPPHs samples obtained by recrystallization from different solvents.[8] The results showed that the magnetic susceptibilities are also classified into three types in accordance with the structure types reported by Williams. In this paper, the author will report the results of powder-magnetic-susceptibility, NMR, and ESR measurements of DPPH recrystallized from ether (hereafter abbreviated as free DPPH), DPPH–benzene (1 : 1) complex (DPPH–Bz), and DPPH–CCl_4 (4 : 1) complex (DPPH–1/4CCl_4), in addition to the single-crystal-susceptibility measurements of DPPH–Bz; he will also discuss the types of magnetic interactions existing in the different types of crystals.

Here let us review the crystal structure of DPPHs before we proceed to the analysis of the magnetic properties. In the free DPPH, DPPH molecules are more closely packed (d=1.485) than in any other crystals of DPPH–solvent complexes. The crystal parameters of the free DPPH have been reported, but their precise structure has not yet been established. The crystal structure of DPPH–Bz, on the other hand, was precisely determined.[7] In this case, DPPH molecules align face-to-face to form a chain along the a-axis (Fig. 1a). A DPPH molecule at site "A" is 0.776 nm from the adjacent DPPH molecule at the same site along the a-axis. The DPPH molecules at site "B" are in a similar situation. The DPPH molecules at site "A" and site "B" make an alternative array. The nearest distance between the centers of their N–N bonds is about 0.85 nm. Two phenyl rings, the α phenyl of A_0 and the β phenyl of B_0 in Fig. 1b, however, have the nearest carbon-carbon distance of 0.372 nm. Recently, the crystal structure of the DPPH-acetone (4 : 1) complex, considered to be very similar to that of DPPH–

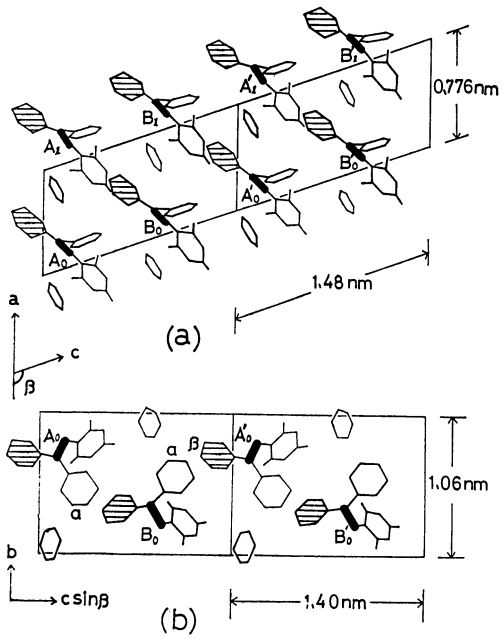

Fig. 1. The crystal structure of DPPH–Bz projected on the ac-plane(a) and on the bc-plane(b) from the Williams' work. N–N bonds are shown by rods. A and B mean DPPH molecules in site "A" and site "B", respectively. α represents α-phenyl rings and β does β-phenyl rings (shaded portion).

† Present address: JEOL Ltd., Akishima, Tokyo 196.

$1/4CCl_4$, was reported by Kiers *et al.*[9] This crystal has a hole with a diameter of at least 0.6 nm, which an acetone molecule possibly occupies, and four DPPH molecules in a unit cell ($z=4$). The four DPPH molecules are located in two different crystallographic sites. Two of the four DPPH molecules in the unit cell are related to each other by an inversion center and are close together, with a distance of only 0.595 nm between the centers of their N–N bonds. These molecules surround the hole mentioned above, so that the molecules have a relatively large freedom of motion. On the other hand, the other two molecules are separated by a distance of 0.692 nm between the centers of their N–N bonds. However, the nearest two phenyl rings of the latter lie parallel to each other at a carbon distance of 0.393 nm. Solvent–acetone molecules are randomly distributed in the holes which make channels along the c-axis. The number of the acetone molecules is about one-fourth that of the DPPH molecules.

These DPPHs show different magnetic properties. The susceptibility of DPPH–Bz and free DPPH were explained by a pair model of localized spins (localized model).[8,10,11] The DPPH–$1/4CCl_4$ complex shows a curious magnetic susceptibility which gives two Weiss constants, θ_{high} (above 30 K) and θ_{low} (below 4.2 K). The spin concentration in the low-temperature region (below 4.2 K) is half of that in the high-temperature region (above 30 K). In order to interpret this phenomenon, Duffy and Strandberg[3] proposed a "two-sublattice model," one featuring the coexistence of strong and weak pair interactions between the electron spins localized on the DPPH molecules in the crystal. On the other hand, Fedders and Kommandeur[12] applied a "narrow-band model" to explain the magnetic susceptibility of the DPPH complexes. They assumed a delocalization of unpaired electrons throughout the crystal, resulting in the formation of an energy band of the electrons.

In this paper, the present author tries to answer the following questions on the basis of the results of his magnetic measurements: (1) Which models are suitable to explain the magnetic behavior of the DPPHs crystals? (2) What types of magnetic interactions are dominant in these crystals? (3) How do the solvent molecules affect the magnetic properties of the DPPH–solvent complexes?

Experimental

The samples were prepared by the oxidation of 2,2-diphenyl-1-picryl-hydrazine($DPPH_2$) with PbO_2 in extra pure diethyl ether, benzene, carbon tetrachloride, carbon disulfide, or chloroform solutions; they were then recrystallized several times using the same solvents. It was confirmed by the elementary analyses and preliminary X-ray analyses that the free DPPH and DPPH–solvent complexes can be classified into three groups with the different, definite crystal structures (I, III, and DPPH–Bz) reported in Williams' paper.[7] Free DPPH has the same crystal structures as that of DPPH(I), while DPPH–Bz has the crystal structure identified by him. The crystal parameters of the complexes of DPPH with CS_2, CCl_4, and $CHCl_3$ are very close to those of DPPH(III) in Williams' paper[7] and those of DPPH(IIIa) in Kiers' paper.[9]

Magnetic-susceptibility(χ) measurements of polycrystalline samples were carried out with a magnetic torsion balance at temperatures between 1.2 K and 4.2 K and with a bridge method at the temperatures obtained by the adiabatic demagnetization described below. The measurement of the anisotropy of the magnetic susceptibility in DPPH–Bz was carried out in order to determine the phase-transition temperature (T_N) to an antiferromagnetic state using a single crystal of 1.34g in the adiabatic-demagnetization temperature region. Single crystals of free DPPH and DPPH–$1/4CCl_4$ were too small for us to measure the anisotropy of χ. The data obtained by the torsion balance above 1.7 K have been corrected for diamagnetism by the use of Pascal's constants. The data at the adiabatic-demagnetization temperatures were fitted to the data measured by the torsion balance at 4.22 K. The adiabatic demagnetization was carried out following the standard method. Samples were mixed with a high-vacuum diffusion oil and Apiezone-N-grease, and placed in contact with a coolant of chromium potassium alum (Cr–K–Alum) through 3000 Cu-formal wires. The temperatures were determined from the paramagnetic susceptibility of Cr–K–Alum to temperature measurement; this substance was thermally linked by copper wires to the samples. The temperature gradient between the sample and the coolant was calibrated by comparing the susceptibility of the coolant with that of Cr–K–Alum mixed with diamagnetic $DPPH_2$ at the same position. The temperatures, T^*, thus obtained were corrected to thermodynamic ones, T, by the use of T^*-*vs.*-T table.[13]

In order to study the paramagnetic shift, ^{1}H-NMR resonance (PMR) measurements were performed on powder samples (*ca.* 1 g), using Robinson and Pound-Knight-Watkins-type spectrometers operating at 12—40 MHz in the tempera-

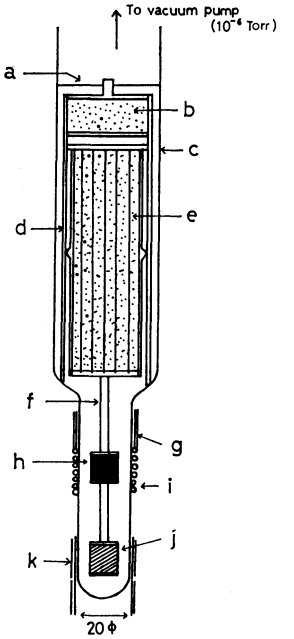

Fig. 2. Sample cell for low-field ESR in adiabatic demagnetization temperature region.
(a) Stainless steel spring, (b) heat guard; Mn-Tutton salt, (c) 40 mmϕ glass tube, (d) polycarbonate sample cell, (e) coolant; Cr–K–Alum, (f) Cu rod for heat link, (g) 3 mmϕ stainless steel tube for Lecher line, (h) sample, (i) RF coil (1.5 mmϕ, 6 turns), (j) Cr–K–Alum for thermometer, (k) coil for temperature measurement.

ture range of 1.3—77 K. Low-field ESR measurements were carried out with a Kushida-type spectrometer[14] with 80 Hz field modulation to confirm the presence of the antiferromagnetic state and T_N. The sample cell for low-field ESR in the adiabatic-demagnetization-temperature region is shown in Fig. 2. The field-modulation power and radio-frequency power were minimized to prevent sample heating.

Results

Magnetic Susceptibility. The data were analyzed with the isolated-pair model and also the interacting-pair model to be discussed later. The susceptibility in the isolated-pair model[15] is accurately given by:

$$\chi = \frac{N'g^2\beta^2S(S+1)}{3kT}\frac{1}{1+1/3\exp(\delta/kT)}, \quad (1)$$

where $\delta=2|J|$ and where N' is the number of spin pairs with $S=1$, which is half the Avogadro number. Here, δ means the singlet-triplet energy separation for the electron-spin pairs. The exponential function in Eq. 1 can be expanded in the series of δ/kT; the high-temperature approximation for Eq. 1 is given as follows:

$$\chi = \frac{N'g^2\beta^2S(S+1)}{4k(T+\delta/4k)} = \frac{C'}{T+\theta'}, \quad (2)$$

where $C'=N'g^2\beta^2S(S+1)/4k$ and $\theta'=\delta/4k$. Thus, the susceptibility in the pair model shows the same form as that of the Curie-Weiss law at high temperatures where $T\gg\delta/k$. Figure 3 shows the molar susceptibilities of DPPHs, with the theoretical curves calculated using Eq. 1.

Free DPPH: Free DPPH showed a magnetic behavior which can be well explained by the pair model with $\delta/k=17.6$ K at temperatures down to 5 K. In the temperature region between 1.8 and 2.5 K, on the other hand, a paramagnetic contribution to the susceptibility corresponding to a spin concentration of 2.5% was observed (see Fig. 3). From the comparison with

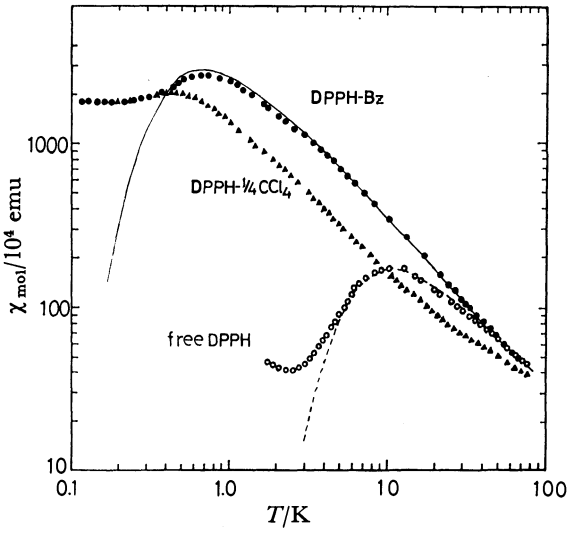

Fig. 3. Powder magnetic susceptibilities of free DPPH and DPPH solvent complexes, where 1 χ_{mol} (emu)= 4 $\pi\chi_{mol}$ (SI). Solid line : pair model curve with $\delta/k=$ 1.04 K. Dotted line : pair model curve with $\delta/k=$ 17.6 K.

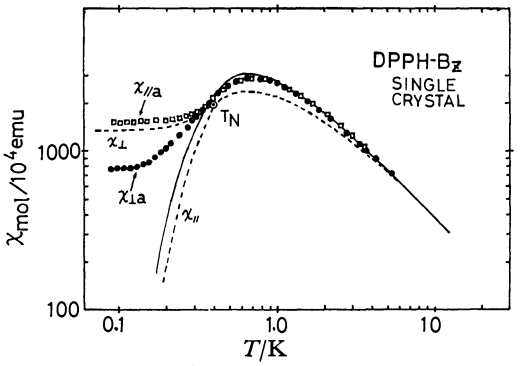

Fig. 4. Anisotropy of the magnetic susceptibility of DPPH–Bz single crystal. Solid line represents the pair model curve with $\delta/k=1.04$ K, and dotted line is the interacting-pair model for $\kappa=1.3$ (Ohya's model). $\chi_{//}$ and $\chi_{\perp}$ denote the susceptibilities parallel and perpendicular to the easy axis, respectively.

the paramagnetic shifts in the PMR spectra described below, it is concluded that the susceptibility increase below 2.5 K is due to an isolated paramagnetic "impurity."

DPPH–Bz: The susceptibility of DPPH–Bz reached a maximum χ_{max} at about 0.65 K and remained constant below 0.3 K. The data above 0.40 K are better fitted to the pair model with $\delta/k=1.04$ K than to other models, such as the linear-chain model. Figure 4 shows the anisotropy of the susceptibility in a DPPH–Bz single crystal. The squares (□) and filled circles (●) in the figure indicate the observed susceptibility along the a-axis ($\chi_{//a}$) and the directions perpendicular to the a-axis ($\chi_{\perp a}$) respectively; they show the anisotropy of the susceptibility below 0.40 K. These data suggest an antiferromagnetic ordering at about 0.40 K in the DPPH–Bz.

DPPH–1/4CCl_4: This sample is characterized by two Weiss constants, $\theta_{high}=-26$ K and $\theta_{low}=-0.3$ K, in the temperature ranges above 30 K and below 4.2 K respectively, which were obtained from a comparison of the experimental susceptibility and the Curie-Weiss law in Eq. 2. The spin concentration, C, in the low-temperature region (below 4.2 K) is about half the high-temperature one (above 30 K). In the intermediate region (4.2—30 K), θ and C gradually changed. The susceptibility increased with a lowering of the temperature from 1.7 K down to 0.45 K and remained constant below 0.45 K. The constant susceptibility, probably due to spin ordering below 0.45 K, had a value similar to that of the DPPH–Bz complex. In the high-temperature region (above 30 K), the best fit for the pair model is obtained by assuming δ/k(high)= 96 K. The remaining unpaired spins at temperatures between 4.2 and 0.45 K show an ordinary paramagnetic behavior, following the Curie-Weiss law with the Weiss constant $\theta=-0.3$ K.

A summary of the susceptibility data is given in Table 1, where C is the spin concentration obtained by comparing the observed and theoretical Curie constants.

Proton Magnetic Resonance. In the case of the powder samples, the PMR line-width (ΔH_i) is proportional to both the resonance field for the i-th proton, H_i,

TABLE 1. SUMMARY OF THE MAGNETIC SUSCEPTIBILITY DATA

Sample	T_{max} [a] / K	χ_{max} [b]	C	θ / K	δ / kK	$\lvert J\rvert$ / kK	T_N / K
Free DPPH	11.0	175	0.98	−10.0	17.6	8.8	Unknown
DPPH-Bz	0.65	2900	1.00	−0.5	1.04	0.52	0.40
DPPH-1/4CCl_4	60 0.45	15 2000	0.86[c] 0.44[d]	−26.0[c] −0.3[d]	96[c] —	48[c] —	Unknown

a) Temperature of χ_{max}. b) Maximum susceptibility in 10^{-4} emu/mol. c) Determined by measurements above 30 K. d) Determined by measurements below 4.2 K.

and the magnetic susceptibility, χ, because of the proton-electron dipolar interaction. The paramagnetic shift (δH_i) is also proportional to χ and H_i, as is given by:

$$\delta H_i = H_i - H_0 = -\frac{a_i \chi H_i}{g_N \beta_N}, \quad (3)$$

where H_0 is the resonance field for the free proton and where a_i is the hyperfine constant of the i-th proton. For $T \gg \delta/k$, this equation can be approximated as:

$$\delta H_i \cong \frac{-5.2 \nu_i a_i}{T+\theta} \quad (4)$$

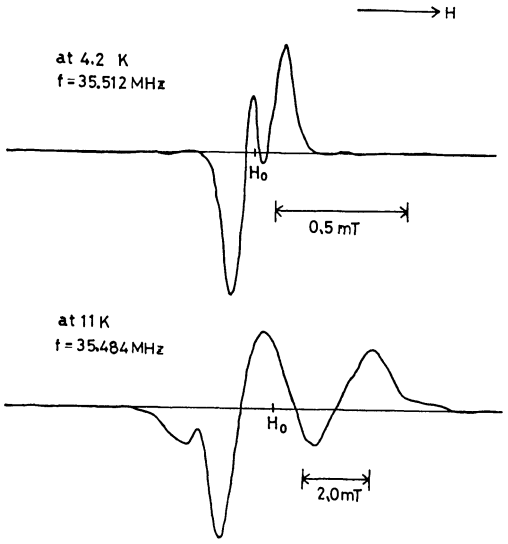

Fig. 5. PMR spectra of free DPPH at low temperatures.

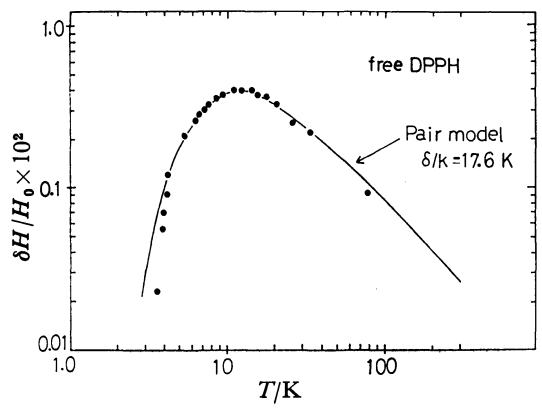

Fig. 6. Temperature dependence of the relative paramagnetic shift of free DPPH.

where ν_i is the observed resonance frequency in MHz and where $2\pi\nu_i = \gamma_N H_i$. Therefore, one can determine χ and the microscopic behavior of the compounds by measuring the temperature dependence of δH_i and ΔH_i.

Free DPPH: Figure 5 shows the PMR-derivative spectra of free DPPH at 4.2 and 11 K. At about 11 K, where the susceptibility shows χ_{max}, four lines were resolved, the ratio of the integrated line intensities being 2 : 4 : 3 : 3. It should be noted that the unshifted line does not appear at these temperatures. The distance between the inner two lines of the spectra, δH, has the same temperature dependence as that of the observed susceptibility, and agrees well with that predicted by the pair model with $\delta/k = 17.6$ K (Fig. 6). The pair-model curve in Fig. 6 was fitted to the experimental results so that its maximum value coincided with the experimental one at 11 K. In spite of an increase in the static magnetic susceptibility below 2.5 K, the spectra did not show any shifted lines down to 1.2 K, as in Verlinden's work.[16] It can be easily deduced from Eq. 3 that the disappearance of the shift leads to the decrease in χ. Therefore, the susceptibility increase below 2.5 K shown in Fig. 3 is due to isolated paramagnetic "impurity" spins, the concentration being about 2.5%.

DPPH-Bz: The PMR spectra of DPPH-Bz show five lines at 4.2 K, as given in a previous paper.[4] The intensity ratio of the five lines is about 2 : 4 : 6 : 3 : 3. This ratio is consistent with the number of protons at five different positions in DPPH-Bz: *i.e.*, two protons in metapicryl, four protons in metaphenyl, six protons in benzene, three protons at the ortho and para positions in α phenyl, and three protons at the ortho and para positions in β phenyl.[17] When the reciprocal of the paramagnetic shifts, δH_i, is plotted as a function of the temperature, the Weiss constant of $\theta = -0.5$ K is obtained by extrapolation to the absolute zero degree. This θ value is in good agreement with that obtained from the susceptibility measurements. As the temperature is lowered or frequency is increased, the shifted lines become broader and split further. The broadening of the lines is roughly proportional to χ. The central line due to benzene protons is easily saturated at 1.5 K, because the spin-lattice relaxation time, T_1, of the diamagnetic benzene protons is longer than those of the paramagnetic DPPH protons.

DPPH-1/4CCl_4: The PMR spectra of DPPH-1/4CCl_4 below 20 K showed a strong unshifted line which is easily saturated at 1.5 K, in addition to four weak, shifted lines (two high-field and two low-field shifted lines), as was shown in Karimov's paper.[5] Above 20 K,

four shifted lines coalesced into a broad central line. The intensity ratio of the unshifted central line to the sum of the four shifted lines at 18.082 MHz was determined to be 2.5 : 1 from the PMR absorption spectra at 4.2 K. The intensity of the central line increased as the frequency became higher. The unshifted line can be attributed not to the protons of the DPPH molecule in the paramagnetic state, but to the protons of DPPH in the singlet state.[16] The relative shift for this sample is somewhat larger than that for DPPH–Bz. The following results were obtained from the reciprocal plot of the paramagnetic shift *versus* the temperature. In the lower temperature region (below 4.2 K), the Weiss constant $\theta_{low}=-0.2$ K is in agreement with that obtained from the susceptibility measurement.

Low-field ESR. In order to confirm the long-range ordering observed by the anisotropy of χ for DPPH–Bz, low-field ESR measurements were carried out at 74.4 MHz in the range from 0.27 K to 4.2 K. The derivative spectra are shown in Fig. 7. The $g=2$ signal intensity decreased rapidly below 0.6 K. The line-width, ΔH_{pp}, increased with a lowering of the temperature and then diverged between 0.46 and 0.42 K. (Fig. 8) Below 0.42 K, the $g=2$ resonance became very small, and the $g=4$ resonance due to forbidden dipolar transition became dominant.[18] The rapid increase in the line-width observed in the paramagnetic region near 0.42 K is interpreted as follows: the critical fluctuation sets in the spin system and makes the exchange correlation time, τ_e, long[19] thus reducing the extent of exchange narrowing of the ESR line-width. Then, long-range ordering occurs at about 0.40 K. The transition temperature to the antiferromagnetic state (0.43 ± 0.03 K) is consistent with that determined from the magnetic-susceptibility measurements for a single-crystal sample.

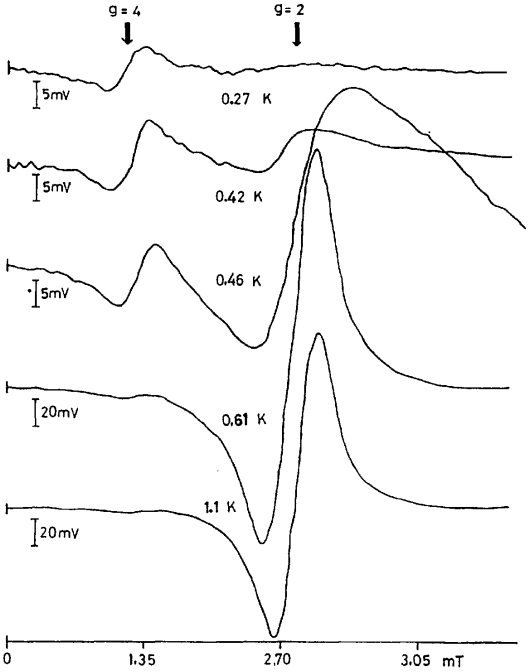

Fig. 7. Low-field ESR spectra of DPPH–Bz at 74.4 MHz.

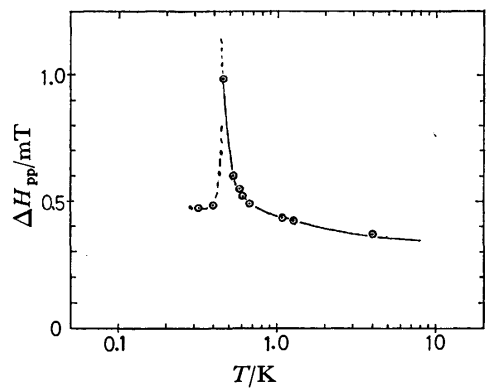

Fig. 8. Temperature dependence of low-field ESR ($g=2$) line-width of DPPH–Bz.

Discussion

Magnetic Interaction in the Paramagnetic State. From the results of the magnetic susceptibility shown in Fig. 3, it can easily be understood that, in the DPPH–solvent complexes, solvent molecules play an important part in constructing a spatial configuration of the magnetic moments. Different solvents form free DPPH and different solvent complexes with certain crystal structures. Therefore, the type and the intensity of magnetic interaction depend on the solvent used for preparing the crystal.

In the free DPPH, DPPH molecules are most closely packed in the crystal ($d=1.485$). The susceptibility results show that every two molecules make pairs with a strong antiferromagnetic exchange interaction ($J/k=-8.8$ K) and fall into a singlet ground state at low temperatures below about 3 K. The results of the paramagnetic shift in PMR spectra support this model. No fall in the PMR intensity was observed in the free DPPH below 3 K, at which point the paramagnetic shift lines are coalesced into an unshifted single line, while a sudden decrease in PMR intensity was observed in the BDPA and TANOL radicals in the vicinity of their antiferromagnetic transition.[20,21] In the low-field ESR measurements, a maximum of the line-width was observed in DPPH–Bz near the Néel temperature, while no such maximum was observed in the free DPPH. From these results, one can conclude that the magnetic properties of the free DPPH are characterized by the isolated-pair model.

In the case of DPPH–Bz, the powder magnetic susceptibility in Fig. 3 and that as well as the heat capacity measured by Duffy *et al.*[11] show that the pair interaction is rather dominant in this crystal. The pair interaction, however, does not lead to any long-range ordering. Therefore, some inter-pair exchange interaction must be taken into account in order to explain the antiferromagnetic ordering. Duffy *et al.* proposed the exchange paths for DPPH–Bz described below in order to explain the magnetic susceptibility in the paramagnetic region: DPPH molecules which are 0.776 nm apart from each other along the a-axis are considered to form a chain along this axis from the crystallographic point of view (Fig. 1a), suggesting the existence of linear-chain-type interaction along this axis.

In a DPPH molecule, the unpaired electron is not localized on a N–N bond, about 30% of it being distributed on the phenyl and picryl rings.[22] Therefore, the exchange interaction between the unpaired electron on Site "A" and on Site "B" will take place dominantly through the overlap of the $2p\pi$-orbitals on the adjacent α and β phenyl rings. (Fig. 1b) This interpretation is reasonable if we take the crystal structure into account. However, their heat capacity and susceptibility measurements were limited to the paramagnetic region, and there was no mention of the antiferromagnetic transition. Below we will discuss the phase transition using the interacting-pair model based on the interpretation of the exchange path mentioned above.

DPPH–1/4CCl_4 shows more complicated magnetic behavior. The magnetic susceptibility results have been explained by both the two-sublattice model and the narrow-band model. However, the PMR spectra can be analyzed in terms of the coexistence of weakly and strongly coupled spin pairs, supporting the two-sublattice model proposed by Duffy *et al.* This excludes the narrow-band model. The following exchange mechanism is suggested from the point of view of the two-sublattice model. DPPH–1/4CCl_4 has one CCl_4 molecule and four DPPH molecules in a unit cell. The two DPPH molecules are close together (0.595 nm) and are mutually coupled with a strong exchange interaction. They form singlet spin pairs at higher temperatures compared with free DPPH. On the other hand, the other two weakly coupled DPPH molecules (0.692 nm apart) interact with each other with some weak exchange interactions through both paths between nearest N–N bonds and between nearest phenyl rings, which may trigger an antiferromagnetic ordering of unpaired spins below 0.9 K.[23]

Phase Transition to Antiferromagnetic State. An antiferromagnetic ordering of DPPH–Bz was suggested by Prokhorov and Fedrov from the disappearance of the low-field ESR signal near 0.18 K.[24] In the present work, the low-field ESR signal disappeared at 0.43 ± 0.03 K, below which point the magnetic susceptibility of a powder sample approaches a finite constant value with a decrease in the temperature. In addition, the single crystal shows magnetic anisotropy below 0.40 K, as is shown in Fig. 4. All of these data support the appearance of an antiferromagnetic ordering about 0.40 K. The Néel temperature, T_N, is higher than that given by Prokhorov and Fedrov. As has been described already, the paramagnetic susceptibility of DPPH–Bz is rather well described by the isolated-pair model, although linear-chain interaction can be expected to be dominant from its crystallographic data. Duffy, Strandburg, and Deck reported the susceptibility and heat capacity of DPPH–Bz from 0.4 K up to room temperature, but neither the linear-chain model nor the quadratic-net Heisenberg model gives a satisfactory explanation of their data. The pair interaction, J, however, cannot cause a long-range ordering. Therefore, in order to explain the long-range ordering of a spin-pair system, inter-pair interaction must be considered. We try to explain the long-range ordering temperature and the magnetic behavior, in both paramagnetic and antiferromagnetic regions, by using the following model as a first-order approximation. This model is a modified version of Oguchi's "improved molecular field theory of the antiferromagnet,"[25] the details of which were recently described by Ohya-Nishiguchi.[26]

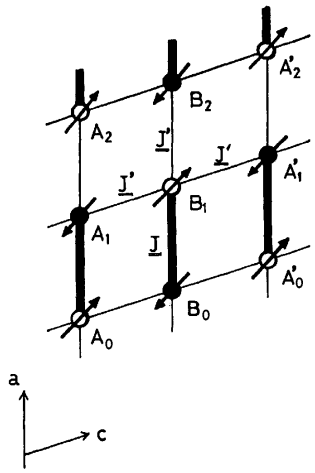

Fig. 9. Interacting-pair model for DPPH–Bz. The positions of DPPH molecules are projected in the ac-plane. J and J' represent intra-pair and averaged inter-pair interactions, respectively.

Assuming a spin pair i-j with intra-pair exchange interaction, J, having other exchange interactions with their neighboring spin pairs, averaged as $J'(|J'|<|J|)$, as is shown in Fig. 9. J' is treated as a kind of molecular field. For such a spin system, a two-body Hamiltonian is given by the following equation:

$$\begin{aligned} \mathcal{H} &= 2|J|(\boldsymbol{S}_i\cdot\boldsymbol{S}_j) + aS_i^z + bS_j^z \\ a &= 2|J'|Z'(-\langle S^z\rangle+\langle\delta S^z\rangle) - g\mu H^z \\ b &= 2|J'|Z'(\langle S^z\rangle+\langle\delta S^z\rangle) - g\mu H^z, \end{aligned} \tag{4}$$

where Z' is the number of the nearest interaction paths of i-spin with all neighboring spins except the j-spin and is equal to three in the case of Fig. 9. Calculation using Eq. 4 gives the following paramagnetic susceptibility, χ_{para}, and Néel temperature, T_N. The susceptibility of the antiferromagnetic region is discussed in Ohya-Nishiguchi's paper:[26]

$$\chi_{para} = \frac{N/2(g\mu)^2}{\kappa|J|+kT\left(1+\exp(|J|/kT)\times\dfrac{\cosh(|J|/kT)}{\cosh(g\mu H/kT)}\right)} \tag{5}$$

$$\exp(-|J|/kT_N)+\cosh(|J|/kT_N) = \kappa\times\sinh(|J|/kT_N), \tag{6}$$

where $\kappa=Z'\times|J'|/|J|$. In the case of $\kappa=0$, χ_{para} is equal to the pair-model susceptibility of Eq. 1. From Eq. 5, it can be seen that χ depends also on the external field, H. At 4.22 K, such a field effect is negligibly small, *i.e.*, $\chi(0)/\chi(0.829\text{ T})=0.98$. By taking the field effect into account, the susceptibility data obtained by the ballistic method in a zero external field were fitted to that obtained by means of a torsion balance in the field of 0.829 T at 4.22 K. A comparison of the theoretical values with the experimental ones shows that the $T_N/T(\chi_{max})$ ratio is best fitted to the experimental one, 0.6, which results in the value of $\kappa=1.3$. The theoretical susceptibility for the case of a single crystal obtained by Ohya-Nishiguchi's model is represented by a dotted

line in Fig. 4 in the case of $\kappa=1.3$; it is qualitatively well fitted to the experimental susceptibility. Using the value of $\kappa=1.3$, the inter-pair interaction $|J'|$ is estimated to be $0.43|J|$ for $Z'=3$ in the case of Fig. 9, while $|J'|=0.26|J|$ is obtained for the case of $Z'=5$ proposed by Duffy *et al.*, who take the other interaction paths into account, also.[11] In both cases, the inter-pair interaction is not so small compared with the intra-pair one.

In conclusion, a spin with antiferromagnetic interaction with a nearest-neighbor spin in free DPPH makes a singlet spin-pair as a ground state. However, in the case of DPPH–Bz spin-pairs interact with each other by means of second-exchange interaction, J', and an antiferromagnetic ordering takes place at a temperature of about 0.40 K. It is difficult, at present, to say definitely what kind of magnetic structure exists in DPPH–1/4CCl_4, but it is most likely that DPPH–1/4CCl_4 is the case of the coexistence of isolated pairs and mutually interacting pairs.

The author is greatly indebted to Professor Yasuo Deguchi for his continuous help and encouragement. Thanks are also due to Dr. Hiroaki Ohya-Nishiguchi, and Professor Noboru Hirota for their helpful advice and discussions, and to Dr. Toshiaki Enoki and Mr. Toshio Yoshioka for their collaboration. He also wishes to express his appreciation to Professor Ikuji Tsujikawa and Dr. Hanako Kobayashi for their courtesy in carring out the adiabatic demagnetization experiments and for their helpful discussions.

References

1) J. Yamauchi, *Bull. Chem. Soc. Jpn.*, **44**, 2301 (1971).
2) Yu. S. Karimov, *Soviet Phys. JETP*, **30**, 1062 (1970).
3) W. Duffy, Jr., and D. L. Strandburg, *J. Chem. Phys.*, **46**, 456 (1967).
4) M. E. Andereson, G. E. Pake, and T. R. Tuttle, Jr., *J. Chem. Phys.*, **33**, 1581 (1960).
5) Yu. S. Karimov and I. F. Schegolev, *Soviet Phys. JETP*, **13**, 1 (1961).
6) J. A. Weil and J. K. Anderson, *J. Chem. Soc.*, **1965**, 5567.
7) D. E. Williams, *J. Chem. Soc.*, **1965**, 7535; *J. Am. Chem. Soc.*, **89**, 4280 (1967).
8) T. Fujito, T. Enoki, H. Ohya-Nishiguchi, and Y. Deguchi, *Chem. Lett.*, **1972**, 557.
9) C. Th. Kiers, J. L. de Boer, R. Olthof, and A. L. Spek, *Acta Crystallogr., Sect. B*, **32**, 2297 (1976).
10) P. Grobet, L. Van Gerven, and A. Van den Bosch, *J. Chem. Phys.*, **68**, 5225 (1978).
11) W. Duffy, Jr., D. L. Strandburg, and J. F. Deck, *J Chem. Phys.*, **68**, 2097 (1978).
12) P. A. Fedders and J. Kommandeur, *J. Chem. Phys.*, **52**, 2014 (1970).
13) F. Din and A. H. Cockett, "Low-temperature Techniques," George Newnes, London (1960), p. 71.
14) G. B. Benedek and T. Kushida, *Phys. Rev.*, **118**, 46, (1960).
15) B. Bleaney and K. D. Bowers, *Proc. R. Soc. London, Ser. A*, **214**, 451 (1952).
16) R. Verlinden, P. Grobet, and L. Van Gerven, *Chem. Phys. Lett.*, **27**, 535 (1974).
17) T. Yoshioka, H. Ohya-Nishiguchi, and Y. Deguchi, *Bull. Chem. Soc. Jpn.*, **47**, 430 (1974).
18) R. S. Rhodes, J. H. Burgess, and A. S. Edelstein, *Phys. Rev. Lett.*, **6**, 462 (1961).
19) H. Mori, *Bussei*, **1968**, 399.
20) K. Uchino, J. Yamauchi, H. Ohya-Nishiguchi, and Y. Deguchi, *Bull. Chem. Soc. Jpn.*, **47**, 285 (1974).
21) S. Saito and T. Sato, *Phys. Lett. A*, **44**, 347 (1973).
22) R. W. Holmberg, R. Livingston, and W. T. Smith, Jr., *J. Chem. Phys.*, **33**, 541 (1960).
23) A. R. Kessel', B. M. Kozyrev, E. G. Kharakhash'yan, S. Ya. Khelebnikov, and Sh. Z. Shakirov, *JETP. Lett.*, **17**, 453 (1973).
24) A. M. Prokhorov and V. B. Fedrov., *Soviet Phys. JETP.*, **16**, 1489 (1963).
25) T. Oguchi, *Prog. Theor. Phys.*, **13**, 148 (1955).
26) H. Ohya-Nishiguchi, *Bull. Chem. Soc. Jpn.*, **52**, 3480 (1979).

  Bull. Chem. Soc. Jpn., 54, 3117—3121 (1981)

NMR Studies of Picolyl-type Carbanions. V.[1,2] ^{7}Li and ^{13}C Spectra of Picolyl-type Anions with Lithium as a Counter Ion

Kazuyori Konishi,* Akihiro Yoshino,† Morimatsu Katoh,† Kensuke Takahashi,†
Yuzo Kawada,†† Tadashi Sugawara,†† and Hiizu Iwamura††

The Industrial Technology Center of Mie Prefecture, Takajayakomori-cho, Tsu 514
†*Department of Industrial Chemistry, Nagoya Institute of Technology, Gokiso-cho, Showa-ku, Nagoya 466*
††*Division of Applied Molecular Science, Institute for Molecular Science, Myodaiji, Okazaki 444*

(Received December 24, 1980)

The ^{7}Li and ^{13}C NMR spectra have been observed for picolyl-type anions with lithium as a counter ion in polar solvents. With reference to the observed chemical shifts, it is concluded that these lithium salts are present in THF as tight ion pairs in which the anion-cation interaction takes place mainly at the ring nitrogen. Thus, the picolyl-type anions are characterized by their ion-pair structures.

In the previous reports on picolyl(pyridylmethyl)-type delocalized anions, the following points of interest were disclosed for I—IV (shown below) in polar solvents:[1,3] (1) The methylene carbon in I is virtually sp^2-hybridized; (2) for II, the observed ^{13}C chemical shifts are linearly related to the calculated π-electron densities; and (3) II—IV can be regarded as delocalized anions with the same significance as I. In order to delineate the nature of interaction between the picolyl-type anions under discussion and the lithium ion, the ^{7}Li, ^{13}C, and ^{1}H resonances of these ionic species have been investigated in polar solvents. The anions prepared are numbered as follows:

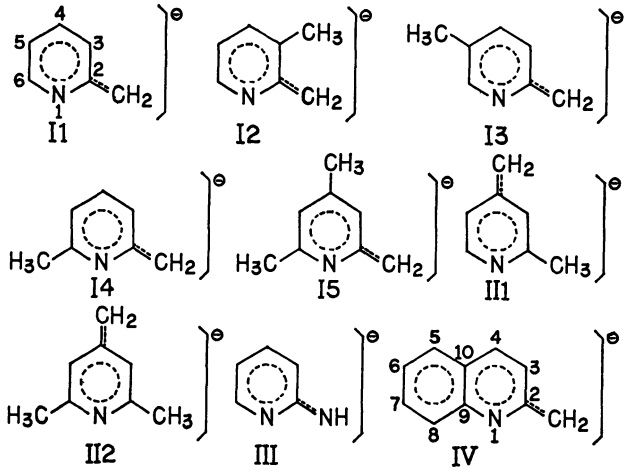

Experimental

The procedures used in this study are similar to those described in previous reports.[1,3] All the anions were produced by reacting methyl-substituted pyridines, 2-methylquinoline, and 2-aminopyridine with butyllithium.

The ^{7}Li and ^{13}C NMR spectra were measured on a Varian FT 80A spectrometer installed at the Institute for Molecular Science, operating in the FT mode at 30.913 and 20.000 MHz respectively. The measuring temperatures and sample concentrations were 36—37 °C and 0.8—1.3 mol dm^{-3}. The lithium chemical shifts were expressed relative to that for aqueous LiCl (0.5 mol dm^{-3}), used as an external reference. The carbon chemical shifts were evaluated with the solvent peaks used as an internal reference. The more shielded peaks of diethyl ether (DEE), tetrahydrofuran (THF), 1,2-dimethoxyethane (DME), the most shielded peak of tetraglyme (TG), and the peak of hexamethylphosphoric triamide (HMPA) were taken to be 17.1, 26.4, 58.8, 58.6, and 37.0 ppm from TMS respectively.

The PPP and CNDO/2 MO calculations for the 2- and 4-pyridylmethyl (picolyl) anions[4] were carried out using the Okitac-4300C and Hitac-8450 computer systems installed at The Industrial Technology Center of Mie Prefecture and at the Nagoya Institute of Technology respectively, using the same procedure as that described in the preceding paper.[1] The bond lengths between the methylene and 2-carbons and between the methylene and 4-carbons were set at 1.39 Å in the calculations.

Results and Discussion

Some typical spectra of the anions with lithium as a counter ion are shown in Figs. 1 and 2. The ^{7}Li and ^{13}C chemical-shift data are given in Tables 1 and 2 respectively.

Table 1. The lithium chemical shifts for the anions, in ppm[a]

Anion	Solvent	
I1	DEE	−0.52
	THF	−0.29
	DME	−0.62
	TG	−0.26
	HMPA	−0.05
I1′[b]	THF	−0.01
I1″[b]	THF	−0.26
I1‴[b]	THF	−0.40
I2	THF	−0.24
I3	THF	−0.34
I4	THF	−0.30
I5[c]	DEE	−0.10
II1	THF	−0.22
II2	THF	−0.03
	HMPA	−0.08
III	THF	1.08
	HMPA	0.78
IV	THF	−0.08
	HMPA	−0.10

a) Errors are estimated to be within ±0.05 ppm. b) In proportions of starting materials, 2-methylpyridine : butyllithium = 1.77 : 1, 1.31 : 1, and 0.58 : 1 for I1′, I1″, and I1‴ respectively. c) Contaminated with a small amount of II2.

Table 2. The carbon chemical shifts of the anions, in ppm[a)]

Anion	Solvent	Assignment										
		2-C	3-C	4-C	5-C	6-C	7-C	8-C	9-C	10-C	CH_2	CH_3
I1	DEE	165.5	118.8	134.7	102.0	149.8					57.5	
	THF	164.2	116.1	131.6	97.3	148.7					57.0	
	DME	163.5	115.7	131.3	96.2	148.8					58.0	
	TG	161.9	114.8	130.5	94.1	149.0					61.5	
	HMPA	161.3	113.6	129.8	92.2	149.8					62.6[b)]	
I2	THF	163.2	119.4	130.7	97.2	146.7					56.2	21.0
I3	THF	164.1	116.6	134.2	104.6	147.1					54.2	18.1
I4	THF	166.0	112.7	132.6	97.3	155.7					54.1	24.6
I5	DEE	169.1	114.2	144.7	104.7	156.8					52.9	22.6
												25.5
II1	THF	149.7	107.9	150.0	107.9	143.7					64.9	24.4
II2	THF	150.2	106.4	151.9	106.4	150.2					62.2	24.3
	HMPA	150.1	105.2	150.5	105.2	150.1					62.2	24.8
III	THF	174.2	113.3	136.3	104.7	148.1						
	HMPA	173.2	112.2	134.4	101.0	148.6						
IV	THF	159.0	126.0	128.6	126.3	111.8	128.2	117.7	155.8	122.7	70.2	
	HMPA	159.0	125.0	127.9	125.5	108.7	127.7	119.0	156.5	121.9	70.7	

a) Errors are estimated to be within ± 0.3 ppm. b) This value should be adopted, though it is somewhat different from the corresponding CH_2 value in Table 2 of Ref. 1.

NMR Spectra of the Anions with Lithium as a Counter Ion.[5)]
^{7}Li Spectra: A typical spectrum is shown in Fig. 1. With changes in the anion, the solvent, the concentration, and the temperature, the chemical shifts and/or linewidths varied. In the case of 2-pyridylmethyllithium (I1),[6)] the variation in the chemical shift was 0.24 ppm, and the linewidth increased about 6.5 times (*i.e.*, from about 14 to 90 Hz), with a change in solvent from THF to HMPA.

^{13}C Spectra: The signals were assigned by comparison with the ^{1}H spectra and by confirmation of a quarternary carbon by means of the off-resonance decoupling method. The 2- and 4-pyridylmethyl anions with lithium as a counter ion, produced from methyl-substituted pyridines by the action of butyllithium, were distinguishable by a difference in spectral pattern, as is shown in Fig. 2.

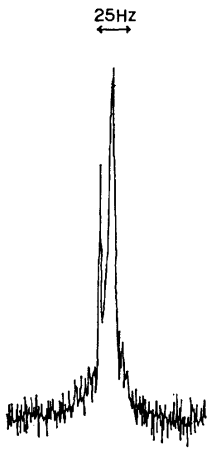

Fig. 1. ^{7}Li spectrum for I1 in THF. The less shielded peak is due to the signal of aqueous LiCl used as an external reference.

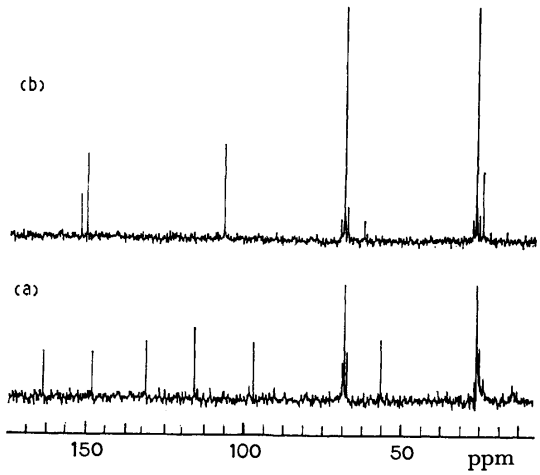

Fig. 2. ^{13}C spectra of pyridylmethyl anions in THF; (a) I1 and (b) II2.

Types and Structures of Ion Pairs Formed. In the ^{7}Li NMR spectra for I—IV, the signals appear at higher fields than those of typical alkyllithium compounds (*i.e.*, 1—2 ppm in ether, triethylamine, and cyclopentane)[7)] and at lower fields than those of typical aromatic lithium salts present in THF as primarily loose (or solvent-separated) ion pairs, such as fluorenyl-, 1,3-diphenylallyl-, triphenylmethyl-, and cyclononatetraenyllithium (*i.e.*, -1——-2 ppm in THF).[8)] These ^{7}Li spectra may indicate that the ionic natures of lithium salts of I—IV are different from those of the alkyllithiums and the loose ion pairs. As has already been reported,[9)] phenylmethyl-(benzyl-), 1-phenylallyl-, cyclopentadienyl-, and indenyllithium exist as tight (or contact) ion pairs in THF. The signals of phenylmethyl- (*i.e.*, -0.12 ppm in THF) and 1-phenylallyllithium (*i.e.*, -0.71) are found within a range (-1—1

ppm) similar to those for I—IV, but those of cyclopentadienyl-(*i.e.*, −8.37) and indenyllithium (*i.e.*, −6.12) show an upfield shift of more than 6 ppm from I—IV.[8,10] This large difference reflects the specific location of the counter ion in relation to the anion in a tight ion pair. Consequently, if I—IV form tight ion pairs with lithium cations, the cations are not situated so as to be strongly subject to the diamagnetic shielding of the induced ring current.[11]

The dependence of the lithium chemical shift with a solvent for the I1, II2, III, and IV given in Table 1 is relatively small. The lithium shift for I1 in DME is 0.33 ppm upfield from the THF value. This variation is similar to those for typical tight ion pairs, but is not large enough to indicate primarily loose ion pairs in THF and DME. An 1 ppm or greater difference between THF and DME should be observed for primarily loose ion pairs.[8]

The carbon chemical shifts of I1, II2, III, and IV in various solvents are given in Table 2. As can be seen from the table, the effect of a change in solvent is large on the carbon shifts of I1. The 5-carbon shift, being a well-defined index of electron delocalization,[1] appears in a higher field with the change to a more polar solvent in this order: DEE, THF, DME, TG, and HMPA; it is about 5 and 10 ppm upfield in HMPA from the THF and DEE values respectively. The same tendency is observed with the proton chemical shifts.[1,3,12] This upfield shift is induced by a change in the ion-pair equilibrium toward loose ion pairs or an increase in the external solvation of tight ion pairs.[13] Generally, the same overall trends for the carbon and proton shifts are observed on a lowering of the temperature as on an increase in the solvating ability of the solvent. The 5-proton shifts of I1 in THF and DME show a relatively large temperature dependence, but the magnitude of the upfield shift induced by changing the temperature from 40 °C to −30 °C in DME is slightly larger than that in THF.[1,3] The temperature dependence of the 5-proton shifts of I1 and I2 in DME is shown in Fig. 3. The shift of I1 at −60 °C is about 0.25 ppm upfield from the 40 °C value, but it is still about 0.2 ppm downfield from that at room temperature in HMPA, favoring loose ion pairs in comparison with DME. In addition, the two curves depicted in this figure cannot be claimed to be the remarkable sigmoid curves, which imply a change in the ion-pair equilibrium toward loose ion pairs in this temperature range.[13] Consequently, in THF and DEE, which favor tight ion pairs in comparison with DME at room temperature, the significant upfield shift induced by the change in solvent from DEE to THF can be accounted for by an increase in the external solvation of tight ion pairs. These results on the lithium and carbon shifts in various solvents and the proton shifts at various temperatures lead to the conclusion that I1 forms a tight ion pair with a lithium cation in THF, and that, therefore, so do I2—IV.

At concentrations in the range of 0.5—2.0 mol dm^{-3}, the variation in the lithium shifts for I1 in THF is negligibly small, but the linewidth at the half-peak height varies from 21 to 8 Hz. At 0.8—1.2 mol dm^{-3}, the variations for I1 in DME, and for I4 and III1 in THF are less than 0.05 ppm. Thus, no meaningful difference in lithium shift for I1 is observed on a change in the concentration in discrete solvents. Consequently, it is reasonable to assume that either the state of association does not change in this concentration range or that the effect of association is not important in determining the lithium shifts.[8]

The lithium shifts for I1′—I1‴ contaminated with an excess of the starting materials in THF are given in Table 1. With an increase in the proportion of 2-methylpyridine relative to butyllithium, the lithium signal is shifted to a lower field, and the linewidth becomes broader. In view of these shifts, the effect of contamination is negligibly small for the lithium salts prepared in this study. Further, when lowered to −76 °C, the peak for I1′ and I1″ is split into two, but not so for I1‴, as is shown in Fig. 4. The ratio of the two peak areas for I1′ is roughly 1.8 : 1, while that for I1″ is 0.22 : 1. One of the two peaks for I1′ and I1″ appears at about 1.35ppm, and the other, at −0.1—−0.2 ppm. It seems that the less and more shielded peaks with respect to inorganic lithium are attributable to

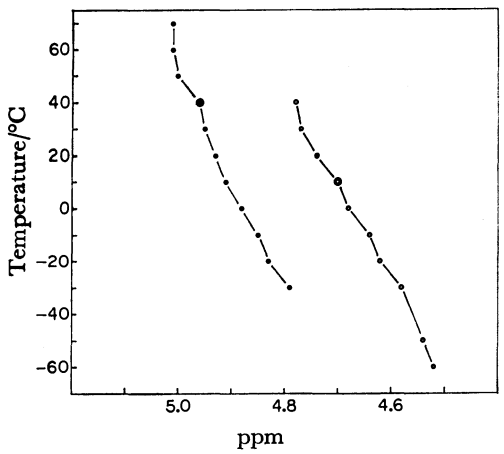

Fig. 3. Temperature dependence of the 5-proton chemical shifts of I1 and I2. ○: I1 in DME, ●: I2 in DME, and ◎: coalescence temperature of the two methylene proton peaks of I1, and ⊙: I2 in DME.

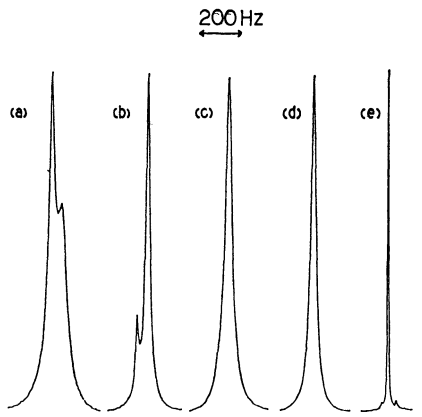

Fig. 4. ^{7}Li spectra; (a) I1′, (b) I1″,(c) I1, (d) I1‴, and (e) butyllithium in THF at −76°C.

the 2-pyridylmethyllithium–2-methylpyridine complex formed and to 2-pyridylmethyllithium respectively.

Turning now to the comparison of 2-pyridylmethyllithium (I1) with phenylmethyl alkali compounds, especially with phenylmethyllithium in THF, we note first that the preparation of I1 is indeed easy, and that I1 is thermodynamically very stable in THF and DME.[3] Secondly, it is apparent that phenylmethylpotassium is much more ionic than phenylmethyllithium in THF.[10,14,15] The ^{1}H and ^{13}C spectra of phenylmethylpotassium in THF are similar to those of I1 in DME, except for the positions bonded to the ring nitrogen, *i.e.*, the 2- and 6-positions. With the procedure reported for naphthylmethyl alkalis present as tight ion pairs in THF at room temperature,[16] the proton chemical shifts, calculated on the basis of the assumption that the cation radius for the phenylmethyl anion can be infinitely large (that is, that the phenylmethyl anion may form a loose ion pair or free ions with the cation), would be about 5.2, 5.7, and 4.2 ppm for the *o*-(3-), *m*-(4-), and *p*-(5-)protons respectively. These values are comparable to values of 5.16, 5.68, and 4.33 ppm for I1 in HMPA.[1] The π-electron densities, calculated using the PPP MO method, at the 3-, 4-, and 5-positions in the phenylmethyl anion are also comparable to those in I1. These suggest that I1 may be present as a loose ion pair in HMPA. Thirdly, we recall that the methylene carbon in I1 is virtually sp^2-hybridized.[3] Fourthly, an *o*-position in I1 is a nitrogen atom. The excess charge density, calculated using the PPP and CNDO/2 MO methods, at the *o*-nitrogen (ring nitrogen) is comparable to that at the methylene carbon. Thus, I1 has some different features as compared with phenylmethyllithium, apparently caused by the effect of *o*-nitrogen, but it seems to be monomeric in polar solvents, much like to phenylmethyl and naphthylmethyl alkalis.[16,17] Therefore, when I1 is present as a tight ion pair in THF, either the methylene carbon or the ring nitrogen can be regarded as the site where the anion-cation interaction mainly takes place.

A good correlation has been obtained between the carbon chemical shifts and the π-electron densities calculated using the PPP and CNDO/2 MO methods for the 2-pyridylmethyl anions I and 4-anions II. The relationship given in Fig. 5 shows that the π-electron densities at the carbons in both 2-anion I1 and 4-anion

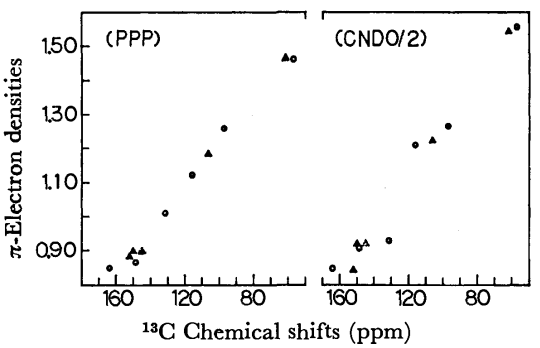

Fig. 5. π-Electron densities *vs.* ^{13}C chemical shifts.
○:I1, △: II2 in THF, and ⛬: 2- and 6-C corrected for effect of methyl group by reducing 5 ppm in II2.

II2 can be evaluated from the carbon chemical shifts using an identical scale. In addition, as is shown in Table 1, the lithium-shift difference between lithium salts of the 2-anions I and the 4-anions II is less than 0.31 ppm in THF; especially, that between I2 and III is negligibly small. These imply that both have essentially the same ion-pair structure in THF. However, it was previously reported that 2,4-dimethylpyridine and 2,4,6-trimethylpyridine underwent deprotonation to give 2-anions such as I, and that isomerization took place from the 2- to the thermodynamically more stable 4-anions II.[3] The lithium salts of the 4-anions II are indeed surprisingly stable, for about 30—40% of these lithium salts in TG could still be detected in the ^{1}H spectra after the samples had stood for 1 h at 100 °C, while the lithium salts of the 2-anions I completely changed to the corresponding methyl-substituted pyridines in TG. In view of these experimental facts, it is not reasonable to assume that the anion-cation interaction takes place mainly at the methylene carbon in lithium salts of the 2-anions I and the 4-anions II present as tight ion pairs in THF, for this assumption would predict a primarily loose ion-pair structure for both lithium salts I—II. Therefore, in both lithium salts I and II and, furthermore, in III—IV, the ring nitrogen can be regarded as the site where the anion-cation interaction mainly takes place.

It is concluded that I—IV are present in THF as tight ion pairs in which the anion-cation interaction takes place mainly at the ring nitrogen. Thus, the picolyl-type anions with lithium as a counter ion are characterized by their ion-pair structures.

This work was supported by the Joint Studies Program (1978—1979) of the Institute for Molecular Science.

References

1) Part IV in this series: K. Konishi and K. Takahashi, *Bull. Chem. Soc. Jpn.*, **50**, 2512 (1977).

2) K. Konishi, A. Yoshino, M. Katoh, K. Takahashi, Y. Kawada, T. Sugawara, and H. Iwamura, 18th Symposium on NMR Spectroscopy, Suita, November 1979, 13.

3) K. Konishi, K. Takahashi, and R. Asami, *Bull. Chem. Soc. Jpn.*, **44**, 2281 (1971); K. Takahashi, K. Konishi, M. Ushio, M. Takaki, and R. Asami, *J. Organomet. Chem.*, **50**,1 (1973); Kazuyori Konishi, A thesis submitted in partial fulfillment of the requirement for a Master's Degree, in the Department of Synthetic Chemistry, Nagoya Institute of Technology, March 1973; K. Konishi, Y. Onari, S. Goto, and K. Takahashi, *Chem. Lett.*, **1975**, 717.

4) On the basis of the assumption that lithium salts of these anions exist as completely free ions, the π-electron densities have been calculated using the PPP and CNDO/2 MO methods.

5) ^{14}N Spectra: The spectra of the starting materials could be easily observed, but it was difficult to observe those of the anions. At present, the signals can not be confirmed. ^{15}N Spectra: Further studies are now in progres.

6) The lithium salt of the I1 anion is expressed in the form of (I1).

7) T. L. Brown, *Acc. Chem. Res.*, **1**, 23 (1968).

8) R. H. Cox and H. W. Terry, Jr., *J. Magn. Reson.*, **14**, 317 (1974).

9) J. B. Grutzner, J. M. Lawlor, and L. M. Jackman, *J. Am. Chem. Soc.*, **94**, 2306 (1972); V. R. Sandel, S. V. McKinley, and H. H. Freedman, *ibid.*, **90**, 495 (1968).
10) R. Waack, M. A. Doran, E. B. Baker, and G. A. Olah, *J. Am. Chem. Soc.*, **88**, 1272 (1966).
11) C. F. Johnson, Jr., and F. A. Bovey, *J. Chem. Phys.*, **29**, 1012 (1958).
12) The values of the 5-proton chemical shift of I1 in DEE, THF, DME, TG, and HMPA are 5.14, 4.84, 4.77, 4.58, and 4.33 ppm respectively.
13) U. Edlund, *Org. Magn. Reson.*, **12**, 661 (1979); C. Gooijer and N. H. Velthorst, *ibid.*, **12**, 684 (1979).
14) V. R. Sandel and H. H. Freedman, *J. Am. Chem. Soc.*, **85**, 2328 (1963).
15) K. Takahashi, M. Takaki, and R. Asami, *Org. Magn. Reson.*, **3**, 539 (1971); K. Takahashi, Y. Kondo, R. Asami, and Y. Inoue, *ibid.*, **6**, 580 (1974).
16) F. J. Kronzer and V. R. Sandel, *J. Am. Chem. Soc.*, **94**, 5750 (1972).
17) P. West and R. Waack, *J. Am. Chem. Soc.*, **89**, 4395 (1967).

The Binding of Sodium Dodecyl Sulfate to Lysozyme in Aqueous Solutions

Kohsuke FUKUSHIMA,* Yoshio MURATA, Nagamune NISHIKIDO,
Gohsuke SUGIHARA, and Mitsuru TANAKA
Department of Chemistry, Faculty of Science, Fukuoka University, Fukuoka 814-01
(Received January 16, 1981)

The binding mode of sodium dodecyl sulfate to lysozyme and the accompanying structural change of lysozyme by binding have been investigated by means of the binding isotherm, the precipitation curve, and the CD spectra in pure water, NaCl, and borate buffer solutions. The precipitation phenomena could be explained in terms of the neutralization of the net charge of lysozyme due to dodecyl sulfate-ion binding. The analysis of the binding isotherms by the use of the BET equation gave the site number of the first layer corresponding to the positively charged residues at the pH studied. The conformational change from the β-structure to the α-helix has been observed in the second-layer binding. The environmental change of the side-chain residues has also been observed.

It has been well known that the denaturation of protein is caused or influenced by many factors, such as heat, the pH, and the addition of inorganic or organic substances.[1] Above all, it is interesting that most ionic surfactants behave uniquely as strong denaturants for proteins.[1-3] The addition of a surfactant to a protein solution causes a drastic change in the conformation of protein. Even in a very low surfactant concentration (far below the critical micelle concentration, CMC), the protein is denatured by surfactant molecules. For instance, the extent of the conformational change of serum albumin increases with the surfactant concentration, but it reaches a certain limit at a concentration close to 10^{-5} mol dm^{-3}.[4]

With respect to the hen egg-white lysozyme, an X-ray study revealed that the lysozyme is a rigid and stable enzyme.[5] In the range of physiological pH values, the lysozyme does not show any detectable change in its structure up to 77 °C, and at the physiological temperature no detectable change in the structure was observed with a pH change from 1.2 to 11.3. The stability of lysozyme has been attributed to the four disulfide bonds besides hydrogen bonds and hydrophobic interactions among the 129 amino-acid residues. Thus, it is supposed that the lysozyme molecule may be comparatively resistant to the addition of a surfactant.

The precipitation and the inactivation of the enzyme occurred when a surfactant mixture of sodium dodecyl sulfate (SDS) and sodium tetradecyl sulfate (STS) was added to the lysozyme. The mixing ratio of SDS to STS was 80 to 20.[6] In the past, these phenomena were interpreted in terms of the weight-mixing ratio of surfactant to protein. However, these experimental results should be interpreted with reference to binding isotherms.

In a study of the binding of SDS to various proteins including lysozyme, it was found that as much SDS bound to a protein as the weight of the protein itself,[7] and it was suggested, from the solubilizing ability of the SDS–protein complex for water-insoluble dye, that SDS formed a so-called hemimicelle containing a polypeptide as a core. We are interested in what type of hemimicelle is formed in the lysozyme–SDS system. Fortunately, the structure of lysozyme has been well defined, so that lysozyme may give some detailed information about the interaction.

In this work, the binding of SDS to lysozyme, and the precipitation and structural change upon binding are investigated as a function of the concentrations of SDS and the added NaCl, and the pH by means of circular dichroism (CD) measurement and potentiometry.

Experimental

Materials. Hen egg-white lysozyme (6 times recrystallized) was purchased from the Seikagaku Kogyo Co., Ltd., and was used without further purification. The SDS was synthesized from the purified 1-dodecanol according to the literature.[8] The product was purified by recrystallizing it three times from ethanol. The CMC of the SDS was determined by electric-conductivity measurements. The value of 8.28×10^{-3} mol dm^{-3} at 25 °C was consistent with that in the literature.[9] There was no minimum in the plot of the surface tension *vs.* the concentration. All the inorganic salts (Nakarai Chemical Co., Ltd.) were of a special grade and were used without further purification.

Precipitation Measurements. An aqueous solution of lysozyme and one of the SDS solution were mixed in a test tube, and then water was added to make a 25-ml solution. Throughout the series of experiments, the concentration of lysozyme in the test tube was kept constant. After the samples had been allowed to stand at 25 °C for over 20 h, the precipitates were separated through a membrane filter (pore size, 0.1 μm; Toyo Roshi, Co., Ltd.) The concentration of lysozyme in the filtrate was determined spectrophotometrically at 280 nm (Model 323 of Hitachi Mfg. Co.) using the molar extinction coefficient of 36500 for lysozyme.[10] The amount of protein precipitated was evaluated by comparing the absorbance of the filtrate with that of the reference solution without SDS.

Binding Isotherms. The binding isotherms of SDS to lysozyme were constructed by the determination of the equilibrium SDS concentration by means of potentiometry.[11] The electromotive force (emf) of the cell with a liquid membrane was measured by means of a digital multimeter(Takeda Riken TR 6856). The temperature of the solution in the cell was kept within 25 ± 1 °C using a thermostated water bath. The corresponding calibration curves of emf for SDS in pure water, NaCl, and buffer solutions showed a good linearity and gave a slope consistent with the Nernstian response (59.4 ± 0.5 mV per decade of change in SDS at 25 °C). After the mixed solutions of lysozyme and SDS had been allowed to stand for 1 d at 25 °C, the emf was measured. The concentration of lysozyme in the sample solution was constant (2×10^{-5} mol dm^{-3}) throughout the series of experiments. The coexistence of lysozyme in the solution has been reasonably assumed not to affect the response for the DS^- ion, and so the

change of emf should be ascribable specifically to the change in the free-DS^--ion concentration in solution.

The average number of SDS molecules ($\bar{\nu}$) bound to a lysozyme molecule can be given as:

$$\bar{\nu} = (C_t - C_e)/C_l, \quad (1)$$

where C_t is the total SDS concentration, C_e is the equilibrium SDS concentration, as determined from the curve of emf *vs.* the concentration, and C_l is the lysozyme concentration.

Circular Dichroism (CD). The CD spectra in the ranges of 240—200 nm and 320—270 nm were measured by the use of a spectropolarimeter (JASCO-A40) under nitrogen flush. Calibration was made with a D-10-camphorsulfonic acid solution. The path length of the cell used was 10 mm. The temperature was controlled at 25±0.1 °C by circulating thermostated water through the cell.

The CD spectra were obtained by accumulating 4 times for 240—200 nm and 8 times for 320—270 nm, with a microproccessor equipped with a spectropolarimeter, and their mean values were recorded. The data were expressed in terms of the mean residue ellipiticity.

All samples were equilibrated in a water bath at 25 °C for 1 d, and then the CD spectra were measured. The concentrations of lysozyme were 1.2×10^{-6} mol dm^{-3} and 2.7×10^{-5} mol dm^{-3} in the ranges of 240—200 nm and 320—270 nm respectively.

Results

Figure 1 shows the binding isotherm of SDS to lysozyme as well as the precipitation curve at two lysozyme concentration in pure water. The $\bar{\nu}$ was calculated according to Eq. 1. In the lower equilibrium concentration (4×10^{-5}—9×10^{-4} mol dm^{-3} SDS), the $\bar{\nu}$ is about 10, while in the range higher than 9×10^{-4} mol dm^{-3} the $\bar{\nu}$ gradually rises to about 20, and then it reaches a certain limit of measurement, *i.e.*, the upper limit of the linearity in the calibration curve of emf.

The shape of the precipitation curve of lysozyme depends on the lysozyme concentration when the total concentration of SDS, C_t, is taken as the abscissa. However, the data can be replotted against the equilibrium SDS concentration, C_e, which is calculated by using the binding isotherm. As is shown in Fig. 1, the precipitation curves at two different lysozyme concentrations coincide with each other when C_e at equilibrium is taken as the abscissa. It can be seen from Fig. 1 that the amount of the precipitate increases parallel with the binding, and thereafter it is kept constant (*i.e.*, the lysozyme is almost completely precipitated) when $\bar{\nu}$ is about 10. In the range of the binding number of 10, the lysozyme keeps being precipitated almost completely. With an increase in $\bar{\nu}$ from 10 to 20, the precipitation curve goes down to zero.

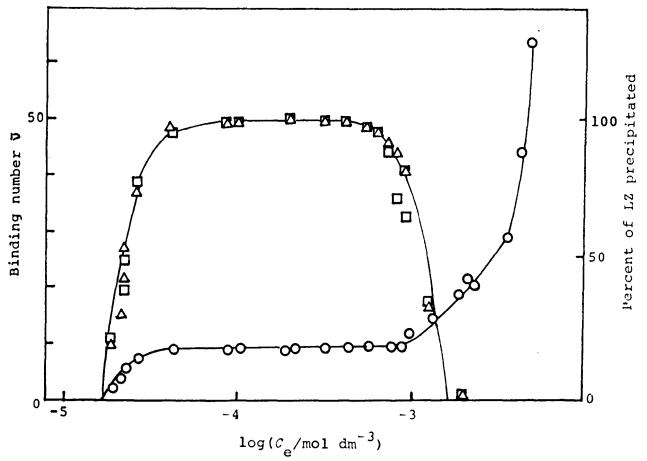

Fig. 1. The binding isotherm of SDS (○) and precipitation curve of lysozyme (LZ) in pure water (pH 5.8) at 25 °C. △: Lysozyme concentration 3.76×10^{-5} mol dm^{-3}, □: lysozyme concentration 2.19×10^{-5} mol dm^{-3}.

For the NaCl solution system whose ionic strength is 0.1, as may be seen in Fig. 2, the binding isotherm begins to rise at $C_e=1\times10^{-4}$ mol dm^{-3}. The region where the binding number is kept at 10 is very narrow as compared with Fig. 1. After reaching a $\bar{\nu}$ value of about 13, the binding isotherm is characterized by a sharp uprise. The precipitation (nearly 100%) is seen in the same manner as in a pure water system when $\bar{\nu}$ is also about 10. With an increase in $\bar{\nu}$ from 10 to 20, the amount of precipitate also goes down to zero. The region of the maximum precipitation is narrow, corresponding to the narrowness of the region where $\bar{\nu}=10$.

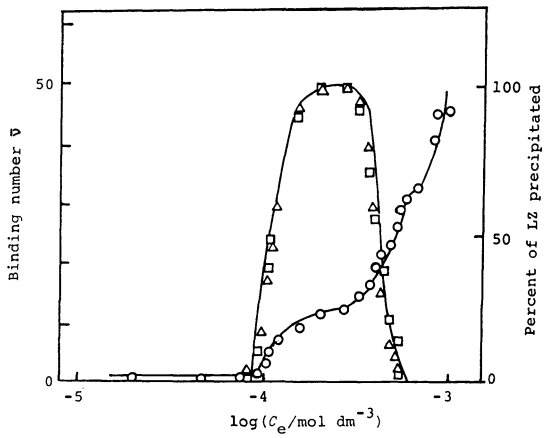

Fig. 2. The binding isotherm of SDS (○) and precipitation curve of lysozyme in NaCl solution (pH 5.8) at 25 °C. △: Lysozyme concentration 4.20×10^{-5} mol dm^{-3}, □: lysozyme concentration 2.56×10^{-5} mol dm^{-3}.

Figure 3 shows the binding isotherm and the precipitation curves in a borate buffer system, the pH and the ionic strength of which are 9.2 and 0.1 respectively. The binding isotherm shows a gradual rise in the range of 1×10^{-4}—1×10^{-3} mol dm^{-3} SDS up to the binding number of 35, and then it shows an abrupt increase up to 55, which seems to be followed by a levelling-off tendency near the CMC. Each precipitation curve has a maximum at $\bar{\nu}=9$. In this case, 100% precipitation does not occur, and the amount of the precipitate depends on the lysozyme concentration, unlike the case in Figs. 1 and 2.

The α-helix, β-structure, and random coil of proteins each have their own characteristic SDS spectra. The CD spectra of synthetic polypeptides are changed by various factors, such as the pH, the solvent, the temperature, and the addition of a surfactant, and have been used as the criteria of the α-helix, the β-structure, and the random coil.[12-15] However, the magnitudes of the CD spectra do vary among different helical, β-structured, and random-coiled polypeptides. In this work, we

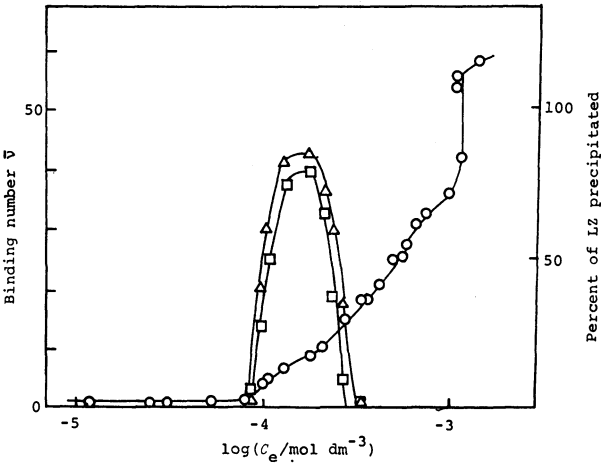

Fig. 3. The binding isotherm of SDS (○) and precipitation curves of lysozyme in borate-buffer solution (pH 9.2) at 25 °C. △: Lysozyme concentration 3.95×10^{-5} mol dm^{-3}, □: lysozyme concentration 2.70×10^{-5} mol dm^{-3}.

applied the criteria of the α-helix, the β-structure, and the random coil, which had been deduced from the CD spectra of 5 proteins (myoglobin, lysozyme, lactate dehydrogenase, papain, and ribonuclease) as analysed by means of X-rays.[16] The optical activity of the above three conformations is assumed to be additive and can be expressed as described below.

At any wavelength, λ,[16]

$$[\theta]_\lambda = f_H X_{H,\lambda} + f_B X_{B,\lambda} + f_R X_{R,\lambda}, \quad (2)$$

where $f_H+f_B+f_R=1$. $[\theta]$ is the mean residue ellipticity. The f is the fraction of each conformation in a protein molecule. The $X_{H,\lambda}$, $X_{B,\lambda}$, and $X_{R,\lambda}$ are the mean ellipticities for the helix (H), the β-structure (B), and the random coil (R) at a certain wavelength λ, respectively. The f_H, f_B, and f_R were determined by fitting the CD spectra of lysozyme to Eq. 2. The calculation by Eq. 2 was made by the least-squares method at 3 nm intervals from 240 to 200 nm. Figure 4a shows the typical CD spectra of lysozyme alone and those of lysozyme saturated with SDS in a pure-water system. The results calculated for lysozyme alone are consistent with those deduced from X-ray study.[5] In Fig. 5, we can see the correlation of the binding isotherm with the fraction of each conformation in the borate-buffer system. Below the concentration at which SDS binding begins to occur, none of the content of the conformations was affected by adding SDS. The dashed line shows the precipitation region where CD spectra can not be observed. The fractions of the α-helix and the β-structure change above the concentration where the redissolution of lysozyme takes place. With an increase in $\bar{\nu}$, the fraction of the α-helix increases, but that of the β-structure decreases. The fraction of the random coil is almost constant over the whole range of equilibrium concentrations of SDS. Similar results were also obtained in pure-water and NaCl-solution systems.

The typical near-ultraviolet CD spectra of lysozyme alone and that saturated with SDS in a pure-water system are shown in Fig. 4b. The change in the CD spectra in the near-ultraviolet region is more drastic than

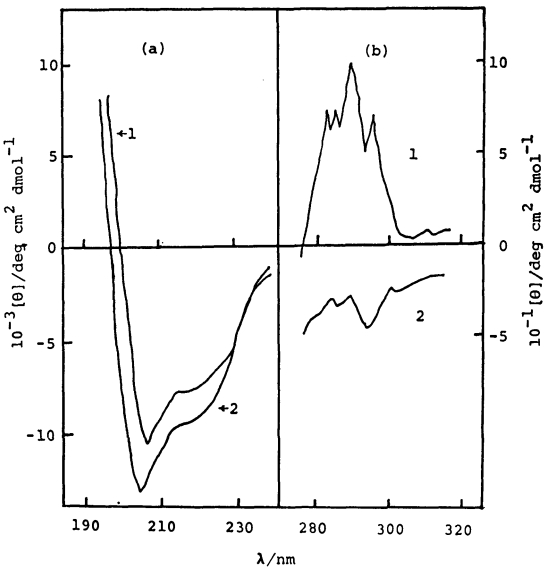

Fig. 4. The effect of the addition of SDS on CD spectrum of lysozyme (1) in pure water, (2) in SDS solution 1.03×10^{-2} mol dm^{-3}.

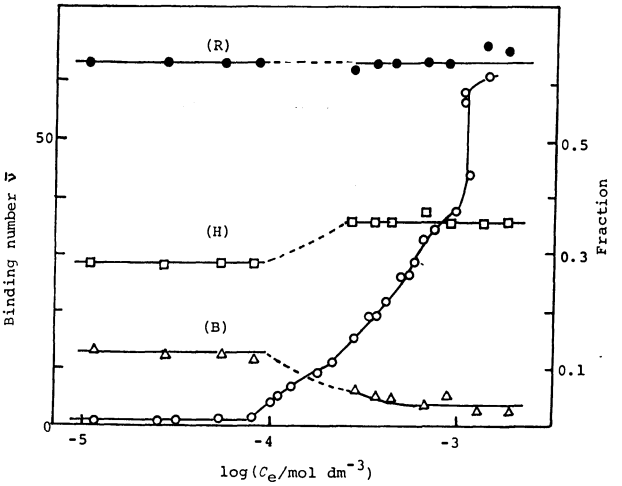

Fig. 5. The correlation of binding isotherm with the fraction of three conformations in borate-buffer solution. (H), (B), and (R) indicate the fractions of α-helix, β-structure, and random coil, respectively.

that in the far-ultraviolet region. Figure 6 shows the binding isotherm and the corresponding change in $[\theta]$ at 294 nm in a NaCl solution. The $[\theta]_{294}$ of the redissolved lysozyme solution is negative in contrast with that of a lysozyme solution without binding. In both pure-water and borate-buffer solutions, the corresponding plots showed the same tendency as that in a NaCl solution.

Discussion

The solubility of protein in an aqueous solution is on a critical balance between the net charge and the hydrophobicity. The net charge effect on the solubility of protein is typically demonstrated in the case of the precipitation at the isoelectric point. As is shown in Figs. 1—3, the binding number which gives the maximum

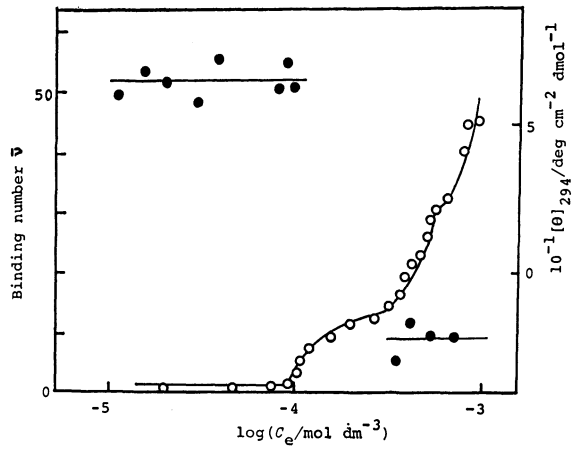

Fig. 6. The change of $[\theta]_{294}$ due to SDS binding in NaCl solution. (○): Binding isotherm, (●): $[\theta]_{294}$.

precipitation is about 10 in each case. If the change in the net charge of lysozyme caused by the binding of DS^- ion can be estimated, it must give a means of interpreting the precipitation.

The lysozyme molecule has ionizable residues (*i.e.*, 6 Lys's, 11 Arg's, and 1 His) as basic amino acid residues and 7 Asp's and 2 Glu's as acidic residues. At the pH's studied (pH 5.8 for pure water and a NaCl solution; pH 9.2 for a borate buffer solution), Lys and Arg are positively ionized, since their pK values on lysozyme are within the ranges of 10.3—10.6 and 12.7—13.3[17] respectively. This means that the lysozyme molecule has 17 positive charges. On the other hand, the negatively ionized residues are 7 Asp's and one Glu^7 in pure water and the NaCl solution system, since their pK values are within the ranges of 3.0—4.7 and 2.7—4.7[15] respectively. In the borate buffer solution of pH 9.2, Glu^{35}, whose pK is between 6 and 6.5,[17] is also ionized besides 7 Asp's and one Glu^7. Therefore, the value of the net charge of lysozyme is +9 in the solutions with and without NaCl (+17−8=+9) and +8 in the borate-buffer solution (+17−9=+8). The number of binding which gives the maximum precipitation seems to be consistent with the number of negative ions necessary to neutralize the net charge of lysozyme. Here, we have assumed that, in the competitive binding to lysozyme, the DS^- ion is much superior to its co-ion, Cl^-, because there exists a hydrophobic interaction between DS^- and lysozyme.

The binding of the DS^- ion introduces the hydrophobicity to the lysozyme (LZ) surface in addition to the neutralization of the positive charges, since DS^- consists of both ionic and hydrophobic parts. Once the DS^- ions have neutralized the net positive charge, the solubility of the LZ^+–DS^- complex will depend on the hydrophobicity of the complex itself. The number of DS^- neutralizing the net charge (+8) in a borate-buffer solution is smaller than those (+9) in pure water or a NaCl solution. Therefore, a number of DS^- ions necessary for the complete neutralization of lysozyme in the borate-buffer solution is one less than in pure water or the NaCl solution; *i.e.*, the surface of the LZ^+–DS^- complex with a zero net charge is less hydrophobic in the borate-buffer solution. This causes less precipitation than in pure water or the NaCl solution. On the other hand, Sophianopoulos and Van Holde have suggested that the lysozyme is in equilibrium with the dimer in alkaline pH.[18] If the dimerization was caused by the aggregation of the hydrophobic part of the lysozyme, the reduction of the hydrophobic area by dimerization would lead to the easy dissolution of lysozyme.

As is shown in Figs. 1—3, each isotherm has two or more steps. This means that there exist two or more kinds of mechanisms in the binding. It is well-known that the BET equation is applicable to the analysis of such a type of binding isotherm. According to Hill,[19] the statistical expression for the BET equation is given as:

$$\frac{\bar{N}}{M} = \frac{q_1\lambda}{(1-q_2\lambda+q_1\lambda)(1-q_2\lambda)}, \tag{3}$$

where $\bar{N}$ is the average number of molecules bound to protein; M, the number of sites; q_1, the partition function for the molecule in the first layer; q_2, the partition function for the molecule in the second and higher layers, and λ, the absolute activity of the free molecule in equilibrium with the bound molecule. Equation 3 is then rewritten as:

$$\frac{\bar{N}}{M} = \frac{KX}{(1-X+KX)(1-X)}, \tag{4}$$

where

$$K = q_1/q_2, \text{ and } X = q_2\lambda. \tag{5}$$

The chemical potential of SDS in solution, μ_{sol}, can be written, using the concentration, C, as:

$$\mu_{sol} = \mu^\ominus + kT\ln(C/\mathrm{CMC}), \tag{6}$$

where $\mu^\ominus$ is the chemical potential of SDS at CMC. From Eqs. 5 and 6, we obtain:

$$X = q_2 \exp(\mu^\ominus/kT) \times \frac{C}{\mathrm{CMC}}. \tag{7}$$

By analogy with the adsorption of vapor on an absorbent, we can consider that, as the SDS concentration increases, the amount of the binding species increases, especially on the hydrophobic surface of the lysozyme–DS complex, where the DS^- ion is concentrated. In a bulk solution, a subsequent increase in SDS causes micelle formation, and simultaneously the amount of DS^- per site, $\bar{N}/M$, rises abruptly. We assume that $\bar{N}/M \to \infty$ when $C \to$ CMC; thus, $\bar{N}/M \to \infty$ means that $X \to 1$, as is known from Eq. 4. Therefore, from Eqs. 6 and 7 we may obtain $q_2\exp(\mu^\ominus/kT)=1$, and then;

$$X = \frac{C}{\mathrm{CMC}}. \tag{8}$$

Using Eq. 8, Eq. 4 may be rewritten as follows:

$$\frac{C}{\bar{N}(\mathrm{CMC}-C)} = \frac{1}{MK} + \frac{K-1}{MK} \times \frac{C}{\mathrm{CMC}}. \tag{9}$$

Thus, if the BET equation reproduces the data, the plot of $C/\bar{N}(\mathrm{CMC}-C)$ against C/CMC will be linear, while M and K may be obtained from the slope and the intercept of the line. The plots of $C/\bar{N}(\mathrm{CMC}-C)$ against C/CMC for the pure-water, NaCl, and borate-buffer solution systems are given in Fig. 7. The slopes and the intercepts give values of $M=18$ and $K=10$

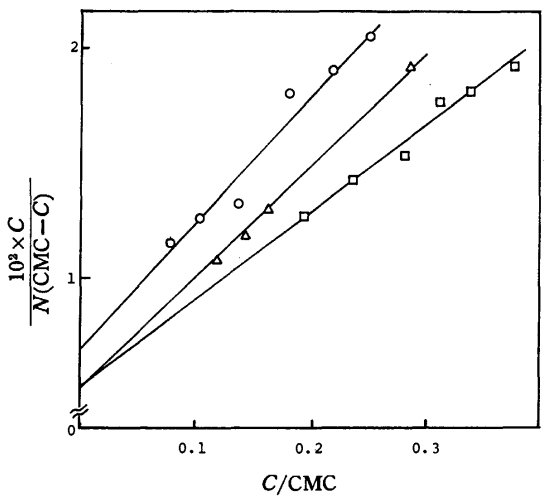

Fig. 7. BET plots for SDS binding on lysozyme in pure water (△), NaCl solution (○), and borate-buffer solution (□).

for the pure-water system, $M=16$ and $K=9$ for the NaCl-solution system, and $M=21$ and $K=11$ for the borate-buffer solution system. According to the BET theory, M is the number of sites, *i.e.*, the number of molecules forming the first layer. As has been mentioned above, the number of positively charged residues of lysozyme is 17 in the pH range studied. The values of M for both the pure-water and NaCl-solution systems are in fair agreement with the number of positively charged residues, but the value of $M=21$ for the borate-buffer system is somewhat large. This aspect of the borate-buffer system is attributable to the dimerization of lysozyme in an alkaline pH.[18]

Recalling that the precipitation is interpreted in terms of the neutralization of the net charge, and that the site number corresponds to the number of positively charged residues, the driving force for the binding of SDS to the first layer may be mainly attributed to the electrostatic interaction with the positively charged residues of lysozyme. The hydrocarbon tail of DS^- of the first layer can be expected to interact with the hydrophobic portion of the lysozyme surface, in addition to the ion-pairing of the head with the positively charged residue of lysozyme. Consideration by photo of the space-filling molecular models of lysozyme and SDS leads us to consider that the surface of lysozyme can be roughly covered with 17 DS^- ions, corresponding to the site number of the first layer, if they lay on lysozyme. This implies that mutual hydrophobic interaction between DS^-'s can be expected for the subsequent binding over the first layer. The subsequent binding is reflected in the sharp uprise of the binding isotherms. This mechanism is supported by the fact that the equilibrium SDS concentration at which the binding isotherms rise sharply is lower in NaCl and borate-buffer solution than in the pure-water solution, as in the case of the salt effect on the micelle formation.

The change in the secondary structure of lysozyme is caused by binding above an SDS concentration where the binding of SDS to the second layer begins to occur in each case. With an increase in the binding number, the helical content increases, but the β-structure decreases; later both reach constant values. An increase in the helical content of lysozyme in an aqueous solution containing more than 60% (v/v) of ethanol, methanol, and 2-propanol has been reported by Ikeda and Hamaguchi.[20] The increase in the helical content with the binding of SDS may be related to their finding that a development of the hydrophobic environment enhances the helical conformation. The tendency for the fraction of each conformation to reach a constant value indicates that the environment of lysozyme is no longer changed above a certain limit of the binding number of SDS, at which the surface of lysozyme is completely covered.

Taking into account the constant fraction of the random coil, it seems that the β-helix transition is induced partly by binding ($\bar{\nu}>10$). Hayakawa *et al.* have reported the β-helix transition of poly (L-lysine) upon the addition of sodium 1-octanesulfonate.[21] With respect to the surfactant-concentration dependence of the secondary structure, the renin substrate has been investigated by Yang and Wu.[22] At a low SDS concentration, the renin substrate shows the characteristic CD spectrum of β-structure, but at a high SDS concentration it shows the characteristic CD spectrum of the α-helix with double minima. These results surpport the idea that the β-structure of lysozyme changes to the α-helix above a certain SDS concentration.

The CD bands in the region between 275 and 300 nm originate in Trp and Tyr. The drastic change from the positive CD spectrum to the negative one upon binding, as is shown in Fig. 4b, means that the environment of these residues is largely altered.

Ikeda and Hamaguchi have demonstrated that the positive CD spectrum of lysozyme in the range from 275 to 300 nm is enhanced by the addition of alcohols (methanol, ethanol, and 2-propanol), but in a concentration of alcohols above 60% (v/v) it begins to decrease, finally becoming a negative CD spectrum. A similar decreasing tendency of the CD spectrum of lysozyme has been observed in the case of the oxidation of Trp's by *N*-bromosuccinimide.[20] These findings mean that Trp gives a clue to the CD spectrum in the range from 275 to 300 nm. The effect of the polarity of a solvent on the CD spectrum of amino-acid derivatives has been examined by Shiraki.[23] He showed that the positive CD spectrum of *N*-acetyltryptophan amide in water changed to a negative one in dioxane, and so he suggested that the sign of the CD spectrum of Trp residues in protein may be changed by the change in their surroundings. It seems reasonable that the reduction of the positive CD spectrum of lysozyme is attributable to the enhancement of the hydrophobic nature of surroundings of Trp on the binding SDS. Thus, the idea that lysozyme is covered with DS^- ions clustering like a micelle can explain the present CD spectrum obtained experimentally.

The present work has been performed within a research program sponsored by The Institute for Advanced Research, Fukuoka University. The authors are grateful to Professor Keishiro Shirahama, Saga

Univ., Professor Iwao Satake, Kagoshima Univ., and Professor Eiji Kimoto, Fukuoka Univ., for encouragement and help.

References

1) C. Tanford, "Advances in Protein Chemistry," Academic Press, New York (1968), Vol. 23, p. 121.
2) K. Aoki, *Hyomen*, **6**, 483 (1968).
3) K. Shirahama and T. Takagi, *Hyomen*, **11**, 383 (1973).
4) R. V. Decker and J. F. Foster, *Biochemistry*, **5**, 1242 (1966).
5) C. C. F. Blake, D. F. Koenig, G. A. Mair, A. C. T. North, D. C. Phillips, and V. R. Sarma, *Nature(London)*, **206**, 757 (1965).
6) H. N. Glassman and D. M. Molnar, *Arch. Biochem. Biophys.*, **32**, 170 (1951).
7) R. Pitt-Rivers and F. S. A. Impiombato, *Biochem. J.*, **109**, 825 (1968).
8) E. E. Dreger, G. I. Klein, and G. D. Miles, *Ind. Eng. Chem.*, **36**, 610 (1944).
9) P. Mukerjee and K. J. Mysels, "Critical Micelle Concentration of Aqueous Surfactant Systems," NSRDS-NBS-36, U. S. Government Printing Office, Washington D. C. (1971).
10) T. Imoto and J. A. Rupley, *J. Mol. Biol.*, **80**, 657 (1973).
11) B. J. Birch and D. E. Clarke, *Anal. Chim. Acta*, **61**, 159 (1972).
12) G. Holzwarth and P. Doty, *J. Am. Chem. Soc.*, **87**, 218 (1965).
13) R. Townend, T. F. Kumosinski, S. N. Timasheff, G. D. Fasman, and B. Davidson, *Biochem. Biophys. Res. Commun.*, **23**, 163 (1966).
14) F. Quadrifoglio and D. W. Urry, *J. Am. Chem. Soc.*, **90**, 2755 (1968).
15) P. K. Sarker and P. Doty, *Proc. Natl. Acad. Sci. U.S.A.*, **55**, 981 (1966).
16) Y. Chen, J. T. Yang, and K. H. Chau, *Biochemistry*, **13**, 3350 (1974).
17) T. Imoto, L. N. Johnson, A. C. T. North, D. C. Phillips, and J. A. Rupley, "Enzyme," 3rd ed, ed by P. D. Boyer, Academic Press, New York (1972), Vol. 7, p. 740.
18) A. J. Sophianopoulos and K. E. Van Holde, *J. Biol. Chem.*, **239**, 2516 (1964).
19) T. L. Hill, "An Introduction to Statistical Thermodynamics," Addison-Wesley, Reading, Mass. (1960), p. 134.
20) K. Ikeda and K. Hamaguchi, *J. Biochem. (Tokyo)*, **68**, 785 (1970).
21) K. Hayakawa, K. Ohara, and I. Satake, *Chem. Lett.*, **1980**, 647.
22) J. T. Yang and C. S. C. Wu, "Versatility of Protein," ed by C. H. Li, Academic Press, New York (1978), p. 99.
23) M. Shiraki, *Sci. Papers, College of Gen. Education, Univ. of Tokyo*, **19**, 151 (1969).

Dissociation of Micelles and Intermicellar Concentrations of Aqueous Solutions of Calcium and Sodium Decyl Sulfates

Masakatsu KOSHINUMA

Laboratory of Chemistry, Faculty of Education, Chiba University, Chiba 260

(Received January 26, 1981)

Activities of the surfactant ions and the counterions were calculated from the electromotive forces of concentration cell with ion-exchange membranes for the aqueous solutions of calcium ($Ca(DeS)_2$) and sodium (NaDeS) decyl sulfates. Moreover, the mean activities and the activity coefficients were obtained. From these activities, the valence effects of the counterions on the dissolved state of micellar solutions were studied. The following results were obtained: (1) The mean activities were not constant, but increased with the increase in the concentration of the two surfactants above the CMC; the slope of curve of the mean activity for $Ca(DeS)_2$ against its concentration was smaller than that for NaDeS. (2) The CMCs were 6.4 for $Ca(DeS)_2$ and 32.8 mmol dm^{-3} for NaDeS, respectively. (3) For the mechanism of micelle formation, the phase separation model was set up in both cases. (4) From this model, the degrees of dissociation of the micelles were calculated as 0.12 for $Ca(DeS)_2$ and 0.28 for NaDeS, respectively. (5) The intermicellar concentrations of the Ca^{2+}, the Na^+, and the decyl sulfate (DeS^-) ions were calculated; those of the counterions increased but those of the DeS^- ions decreased with the increase in their surfactant concentrations. Moreover, those of the DeS^- for $Ca(DeS)_2$ changed slowly while those for NaDeS changed steeply.

The dissolved state properties of surfactant solutions, *e.g.* the dissociation of micelles, a critical micellar concentration (CMC), effects of addition of electrolytes on the CMC and dissociation, theories and mechanisms of micelle formation, have been studied by many investigators in terms of surfactant concentrations but in disregard of the activity coefficients.[1] Taking surface energy of micelles into account, Hall and Pethica have proposed recently a detailed theory of micelle formation.[2] But on the other hand, from an experimental point of view, the activities of the surfactant ion and the counterion, being in equilibrium with the micelle, are necessary to investigate the dissolved state of micellar solution. This is because the micellar properties and validity of these theories can not be discussed without any assumption until the activities are obtained. Recently, correct measurements of activity for ionic surfactants by use of solid[3–6] or liquid[7–11] ion-exchange membranes have been reported. From these results for sodium alkyl sulfates, the following new knowledge has been obtained.[4–6] With an increase in the surfactant concentration, (1) the mean activity and the mean intermicellar concentration of the surfactant above the CMC increased; (2) the activity of the surfactant ion decreased, (3) while that of the counterion increased. (4) The activity of the surfactant ion above the CMC was approaching a constant when much more electrolyte was added into the surfactant solution.[10] (5) Depression of the surface tension above the CMC could be explained by the change of the mean activity.[4,5]

It has been well known that the bivalent-metal ions affected the dissolved state of a micellar solution. Some reports on the activities for monovalent-metal alkyl sulfates are available, but those for bivalent- and polyvalent-metal alkyl sulfates are few.[11] In the present paper, effects of valence in the counterions on the dissolved state are studied on the basis of the activities which are calculated from the membrane potentials developed across the ion-exchange membranes. Among these effects, we discuss the dissociation of micelles, the mechanism of micelle formation, and the intermicellar concentrations in the aqueous solutions of calcium ($Ca(DeS)_2$) and sodium (NaDeS) decyl sulfates.

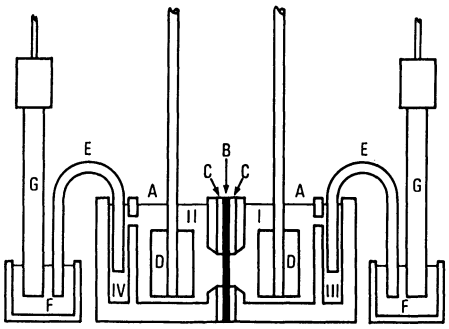

Fig. 1. Apparatus of surfactant concentration cell. A: Cell and solutions; (I) standard solution, (II), sample solution, and (III), (IV), compartments of bridge inserted. B: Anion or cation-exchange membrane. C: Silicon rubber washer. D: Stirrer. E: Agar bridge (2 M NH_4NO_3, 2% agar). F: Saturated KCl solution. G: Reference electrode.

Experimental

In order to obtain good stability and reproducibility in the measurement of electromotive force (EMF), the cell shown in Fig. 1 was used. The cell consisted of four compartments. A standard solution was poured into I and a sample solution into II. The compartments III and IV were connected to them through small holes to avoid any contamination of KCl by agar bridges into it, because EMF was greatly affected by such contamination. The solutions in I and II were gently stirred by means of stirrers, D, rotating at a constant velocity (130 rmp). The EMF developed across a solid ion-exchange membrane, B, was measured at 30 ± 1 °C by means of an electrometer (Keithley, model 610C) through agar bridges (2 M NH_4NO_3, 2%-agar), E, and reference electrodes (Orion, model 90-01), G, and was recorded with time. The EMF was determined as an extraporated value at the time zero since it changed during the first 5 min and then decreased very slowly with time after it had passed a flat region. The solutions of 5.0 and 1.0 mmol dm^{-3} for $Ca(DeS)_2$, and 10.0 and 2.0 mmol

dm^{-3} for NaDeS were used as the standard solutions. Other experimental conditions and procedures were the same as in a previous paper.[5]

Results and Discussion

Single Ionic Activities and Mean Activities. The EMFs developing in the concentration cell of surfactant solution were measured for the two surfactants. The experimental values of the Ca^{2+} ion, E_{Ca}, and of the decyl sulfate (DeS^-) ion, E_{DeS}, are plotted against the concentration of $Ca(DeS)_2$ in Fig. 2 and those of the Na^+ ion, E_{Na}, and of the DeS^- ion, E_{DeS}, against the concentration of NaDeS in Fig. 3. According to Nernst's equation, the single ionic activities are given by

$$\left.\begin{aligned} E_{Ca} &= -(2.303RT/2F)\log(a_{Ca}/a_{OCa}) \\ E_{Na} &= -(2.303RT/F)\log(a_{Na}/a_{ONa}) \\ E_{DeS} &= (2.303RT/F)\log(a_{DeS}/a_{ODeS}), \end{aligned}\right\} \quad (1)$$

where R, T, and F are the gas constant, the absolute temperature, and the Faraday constant, respectively. The activities of the Ca^{2+}, the Na^+, and the DeS^- ions in the sample solutions are represented as a_{Ca}, a_{Na}, and a_{DeS}; those of the corresponding ions in the standard solutions as a_{OCa}, a_{ONa}, and a_{ODeS}. Their values, which were determined in the same way as in the previous paper,[5,6] are listed in Table 1. The activities of the individual ions for $Ca(DeS)_2$, having been calculated by Eq. 1, are shown in Fig. 4 and for NaDeS in Fig. 5. All the activities increased linearly with the increase in the surfactant concentration up to the CMC; after that concentration, those of the DeS^- ions in the two surfactant solutions decreased, while those of the Ca^{2+} and the Na^+ ions increased monotonously. It is also notable that the changes of activity of the Ca^{2+} and the DeS^- ions with the concentration of $Ca(DeS)_2$ are smaller than those of the Na^+ and the DeS^- ions of NaDeS. This finding comes mainly from the difference in the valence between the counterions and will be discussed later in connection with the dissociation of micelle and the intermicellar concentration. The mean activities calculated from the single ionic activities according to the usual definition are shown in Fig. 6; the values of the CMC, which were determined from the breaking points in their curves, are listed in Table 2 and agreed with those reported in the literature.[11,12] Below the CMC, the slope of the curve (mean activity coefficient) for $Ca(DeS)_2$ was smaller than that of NaDeS. This result can be explained by the difference

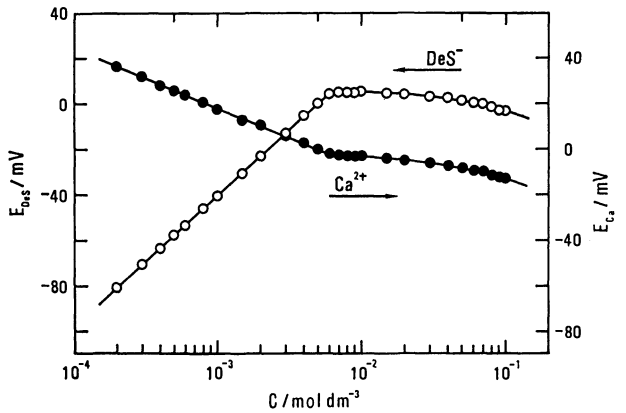

Fig. 2. Electromotive force of the Ca^{2+} and the DeS^- ions against concentration of Ca $(DeS)_2$.

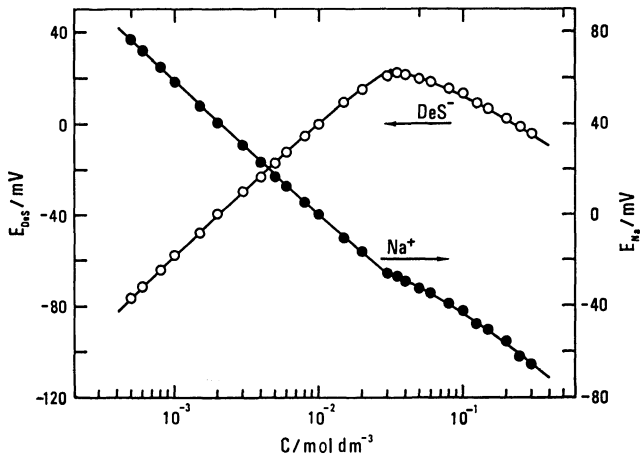

Fig. 3. Electromotive force of the Na^+ and the DeS^- ions against concentration of NaDeS.

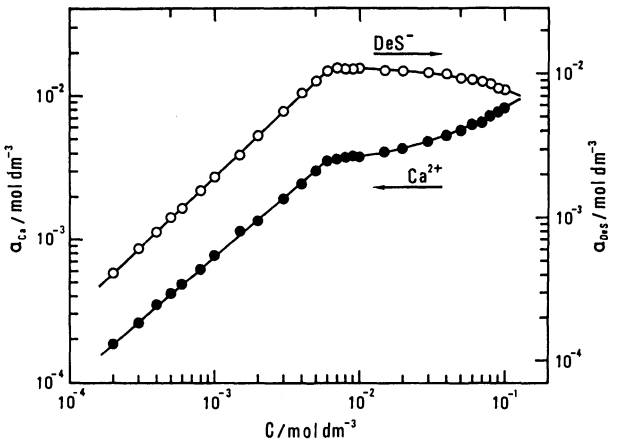

Fig. 4. Activities of the Ca^{2+} and the DeS^- ions against concentration of $Ca(DeS)_2$.

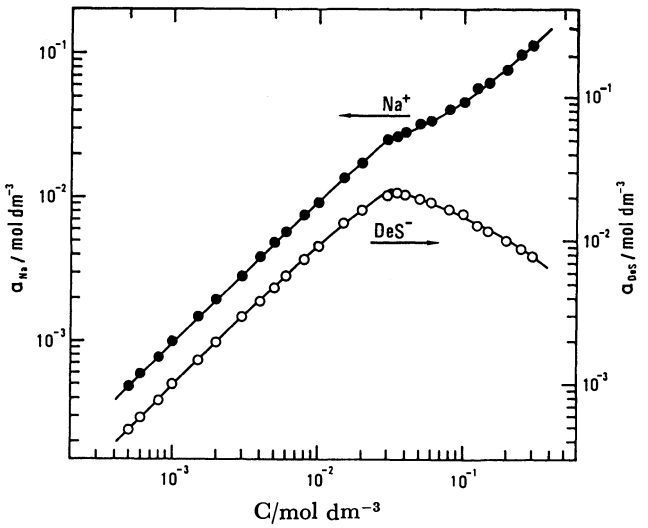

Fig. 5. Activities of the Na^+ and the DeS^- ions against concentration of NaDeS.

TABLE 1. ACTIVITIES OF THE STANDARD SOLUTIONS AND THE CONSTANTS OF K, L, AND M IN Eqs. 2 and 3

Surfactant	a_{ODeS} / mmol dm^{-3}	a_{OCa}, a_{ONa} / mmol dm^{-3}	$C\pm \leqq C_{CMC}$			$C\pm > C_{CMC}$	
			K	L	M	K	L
$Ca(DeS)_2$	8.85	3.01	0.078	0.274	—	0.984	2.087
NaDeS	9.16	9.16	0.022	0.073	97.0	0.898	1.477

TABLE 2. THEDEGREES OF COUNTERION ATTACHMENT (r) AND DISSOCIATION OF MICELLES, CONSTANT ($\log K_{CaD}$, $\log K_{NaD}$), AND THE CMC

Surfactant	r	Dissociation		$\log K$	CMC/mmol dm^{-3}	
		This exp.	Literature		This exp.	Literature
$Ca(DeS)_2$	0.44	0.12		−3.014	6.4	6.7(30 °C)[a]
			0.38[12]			
NaDeS	0.72	0.28	0.30[18]	−2.788	32.8	31.6(25 °C)[12] 33.0(25 °C)[10]
			0.23[10]			
$Co(DS)_2$[b]			0.10[11]			1.15(30 °C)[11]

a) The value was obtained as an extrapolated one by means of the reference(Y. Moroi, K. Motomura, and R. Matuura, *J. Colloid Interface Sci.*, **46**, 111 (1974).), when $K_g=0.95$ and $\sigma=8.64\times10^4$ were used. b) Cobalt dodecyl sulfate.

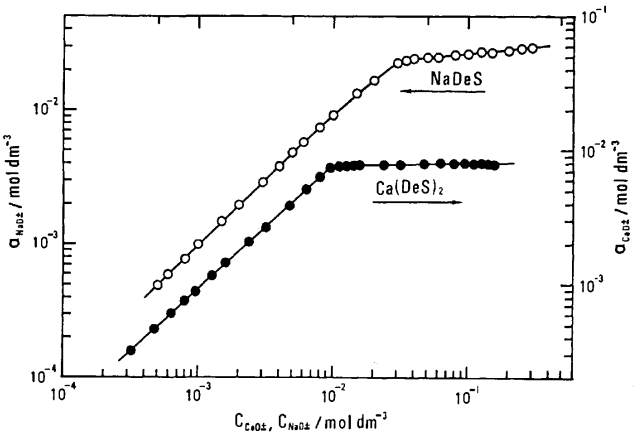

Fig. 6. Mean activities of $Ca(DeS)_2$ and NaDeS against their mean concentrations.

in the valence of the counterions, like that considered in simple electrolytes. In spite of the decrease in the activities of the DeS^- ion above the CMC (shown in Figs. 4 and 5), the mean activities of $Ca(DeS)_2$ and NaDeS did not remain constant, but increased gradually with the increase in their concentrations owing to a large increase in the activities of the corresponding counterions compensating completely for the decrease in the activities of the DeS^- ions. Figure 6 and K in Table 1, which will be defined by Eq. 2, show clearly that the mean activity of NaDeS above the CMC changes with the concentrations steeper than that of $Ca(DeS)_2$, but the activity of the DeS^- ion decreases slowly in comparison with that of NaDeS (Fig. 4). This is because the increase in the activity of the Na^+ ion was much larger than that in the activity of the Ca^{2+} ion. The mean activity coefficients of these surfactants within the concentration ranges illustrated are given by the following formula,[4-6] except for that of NaDeS below the CMC:

$$\log f_\pm = -(K\log C_\pm + L), \qquad (2)$$

where $f_\pm$ and $C_\pm$ denote the mean activity coefficient and the mean concentration of the surfactant, respectively. The constants of K and L are tabulated in Table 1. The activity coefficient of NaDeS solution below its CMC is expressed empirically and satisfactorily by

$$\log f_\pm = -(K\log C_\pm + L) - MC_\pm^2, \qquad (3)$$

where M is a constant and also shown in Table 1.

Formation and Dissociation of Micelles. Various mechanisms of micelle formation have been proposed, but little satisfactory experimental investigation has yet been reported. Recently the mechanism and the dissociation of micelles have been discussed by use of the activity only on 1-1 electrolytic surfactants, such as sodium dodecyl sulfate[4] or sodium tetradecyl sulfate.[5,6] But they should be also focussed on the micelles of 2-1 electrolytic surfactants such as $Ca(DeS)_2$ in connection with the valence effect of counterions. If a micelle of $Ca(DeS)_2$ is composed of $p$$DeS^-$ ions and $q$$Ca^{2+}$ ions which are always in equilibrium with the micelle, the micelle formation is expressed by

$$p\mathrm{DeS}^- + q\mathrm{Ca}^{2+} \rightleftarrows \mathrm{Ca}_q\mathrm{DeS}_p^{-(p-2q)}.$$

According to the mass action theory,[13-15]

$$a_M/(a_{DeS}{}^p\cdot a_{Ca}{}^q) = \text{const}$$

holds, where a_M denotes the activity of micelle. Then,

$$p\log a_{DeS} + q\log a_{Ca} \neq \text{const} \qquad (4)$$

is obtained. On the other hand, according to the phase separation theory,[15-17] in which a_M is assumed to be constant, the micelle formation is expressed by

$$a_{DeS}{}^p\cdot a_{Ca}{}^q = K_{CaD},$$

therefore, $$p\log a_{DeS} + q\log a_{Ca} = K_{CaD} \qquad (5)$$

holds, where K_{CaD} is a constant. We can test which mechanism of the two is applicable, by plotting $\log a_{DeS}$ against $\log a_{Ca}$. Figure 7 shows two linear relationships for $Ca(DeS)_2$ and NaDeS. Therefore, the phase separation theory is also a more probable mechanism for the micelle formation of $Ca(DeS)_2$, as in the cases of 1-1 electrolytic surfactants.[4-6] The degrees of counterion attachment, $r=-q/p$, for $Ca(DeS)_2$(r_{Ca}) and NaDeS (r_{Na}) were obtained from each slope of the straight lines, and the constants were also calculated independl-

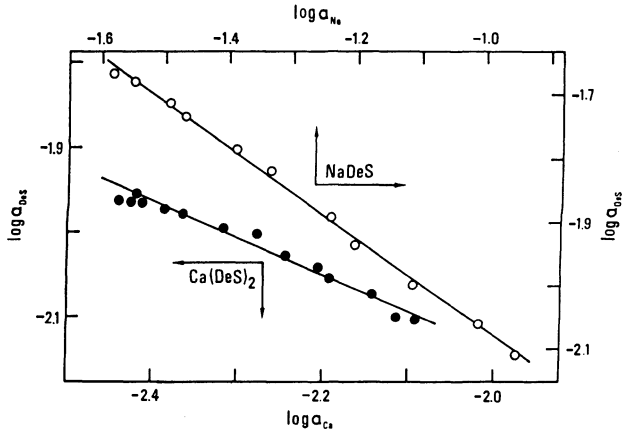

Fig. 7. Curves of log a_{Ca} and log a_{Na} against log a_{DeS} above their CMCs.

ently. The degrees of dissociation of micelles, therefore, are given as $1-2r_{Ca}$ and $1-r_{Na}$. Table 2 shows these values together with those reported.[10-12,18] It is found that the dissociation of $Ca(DeS)_2$ micelles was less than a half of that of NaDeS micelles. This finding can be explained by the idea that the Ca^{2+} ions remain rather near the surface of micelles because of the stronger coulombic interaction of the Ca^{2+} ion than that of the Na^+ ion; as the result of this, the micelle has a smaller dissociation. The observed degree of dissociation of $Ca(DeS)_2$ micelle can not be compared with ones reported in the literature, because there were few found. But the value, being slightly larger than that of bivalent-metal dodecyl sulfate as shown in Table 2, seems reasonable, because the shielding effect resulting from the high intermicellar concentration of $Ca(DeS)_2$ must lessen the counterion binding. The values for the NaDeS micelle in Table 2 scatter, but this discrepancy comes from the differences in the methods of measurement and in the assumptions made in the calculation. The value in the present study is reliable since it is almost free from assumption or approximations.

The smaller increase in the activity of the Ca^{2+} ion than in the Na^+ ion with the increasing concentrations of their surfactants above the CMCs observed already in Figs. 4 and 5 can be directly ascribed to the smaller degree of dissociation of the $Ca(DeS)_2$ micelle; in other words, the activity of Ca^{2+} ion varies with the increase in the intermicellar concentration of the Ca^{2+} ion which will be calculated later. Moreover, the mean activity of $Ca(DeS)_2$ is given by

$$a_{CaD\pm} = (a_{DeS}{}^2 \cdot a_{Ca})^{1/3} \tag{6}$$

according to the definition. If Eq. 5 is introduced into Eq. 6,

$$a_{CaD\pm} = (K_{CaD})^{2/3} \cdot a_{Ca}{}^{(1-2r_{Ca})/3} \tag{7}$$

is obtained. For NaDeS,

$$a_{NaD\pm} = (K_{NaD})^{1/2} \cdot a_{Na}{}^{(1-r_{Na})/2}, \tag{8}$$

where $a_{CaD\pm}$ and $a_{NaD\pm}$ denote the mean activities of $Ca(DeS)_2$ and NaDeS, respectively. The slope of the curves of mean activity are also given by

$$\left.\begin{aligned} \mathrm{d}\ln a_{CaD\pm}/\mathrm{d}\ln C_\pm &= [(1-2r_{Ca})/3]\cdot \mathrm{d}\ln a_{Ca}/\mathrm{d}\ln C_\pm, \\ \mathrm{d}\ln a_{NaD\pm}/\mathrm{d}\ln C_\pm &= [(1-r_{Na})/2]\cdot \mathrm{d}\ln a_{Na}/\mathrm{d}\ln C_\pm \end{aligned}\right\} \tag{9}$$

which are equal to the osmotic coefficients of their solutions.[4] As a_{Ca} and a_{Na} (shown in Figs. 4 and 5) increase, the gradual increases in their mean activities with the increasing concentration of their surfactants in Fig. 6 can be explained by Eqs. 7 and 8. Their increments are mainly restricted by the terms of $(1-2r_{Ca})/3$ and $(1-r_{Na})/2$ in Eq. 9. Therefore, the increment of $a_{CaD\pm}$ becomes smaller than that of $a_{NaD\pm}$. The osmotic coefficient of $Ca(DeS)_2$ was 0.03 and that of NaDeS was 0.10, which almost agreed with 0.07 of sodium dodecyl sulfate.[4]

Calculation of the Intermicellar Concentrations. From the definition, a_{Ca} and a_{DeS} above the CMC are expressed

$$a_{Ca} = f_{Ca} \cdot C_{Ca} \text{ and } a_{DeS} = f_{DeS} \cdot C_{DeS} \tag{10}$$

where f_{Ca}, f_{DeS}, C_{Ca}, and C_{DeS} are the activity coefficients and the intermicellar concentrations of Ca^{2+} and DeS^- ions, respectively. According to Eq. 6,

$$a_{CaD\pm} = f_{CaD\pm} \cdot C_{CaD\pm} \tag{11}$$

holds, where

$$f_{CaD\pm} = (f_{Ca} \cdot f_{DeS}{}^2)^{1/3} \tag{12}$$

and

$$C_{CaD\pm} = (C_{Ca} \cdot C_{DeS}{}^2)^{1/3} \tag{13}$$

are the mean activity coefficient and the mean intermicellar concentration, respectively. If micelles have no effect upon the relation between the mean activity and the mean intermicellar concentration, namely if the

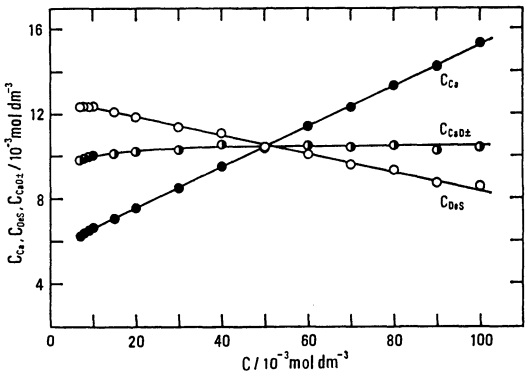

Fig. 8. Intermicellar concentrations of the Ca^{2+} and the DeS^- ions and intermicellar mean concentration against concentration of $Ca(DeS)_2$.

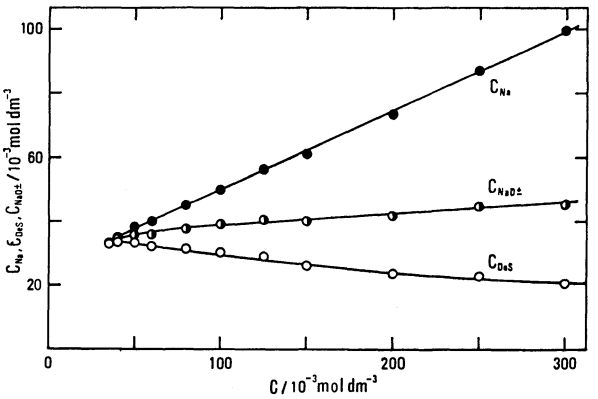

Fig. 9. Intermicellar concentrations of the Na^+ and the DeS^- ions and intermicellar mean concentration against concentration of NaDeS.

The values were calculated by use of $K=0.301$ and $L=0.591$ in Eq. 2 which was set up satisfactorily within the range of concentration from 10.0 to 30.0 mmol dm^{-3} in stead of Eq. 3.

mean activity coefficient shows the same behavior as just below the CMC, then Eq. 2 holds above the CMC. Moreover, the conditions of electrical neutrality hold

$$C_{Ca} = [(2C - C_{DeS})(1 - 2r_{Ca}) + C_{DeS}]/2, \quad (14)$$

where C is the concentration of $Ca(DeS)_2$. Substituting Eqs. 2, 6, 11, 12, and 13 into Eq. 14 yields

$$r_{Ca}C_{DeS}^3 + (1 - 2r_{Ca})C \cdot C_{DeS}^2 - 1000^{(L+\log a_{CaD_\pm})/(1-K)} = 0. \quad (15)$$

As a solution of Eq. 15, C_{DeS} is obtained, and then C_{Ca} is found by substituting C_{DeS} into Eq. 14. With respect to NaDeS, the intermicellar concentrations are given in a manner similar to that of $Ca(DeS)_2$.[4,6]

$$\left.\begin{aligned} C_{DeS} &= -(1 - r_{Na})(C/2r_{Na}) + (1/2r_{Na}) \\ &\quad \times [(1 - r_{Na})^2 \cdot C^2 + 4r_{Na}C_{NaD_\pm}^2]^{1/2} \\ C_{Na} &= -(1 - r_{Na})(C/2) - (1/2) \\ &\quad \times [(1 - r_{Na})^2 \cdot C^2 + 4r_{Na}C_{NaD_\pm}^2]^{1/2} \\ C_{NaD_\pm} &= 100^{(L+\log a_{NaD_\pm})/(1-K)} \end{aligned}\right\} \quad (16)$$

Figures 8 and 9 show the calculated results, which are essentially similar in the two surfactants: namely, the intermicellar mean concentrations and the intermicellar concentrations of counterions increase, while those of the DeS^- ion decrease monotonously. But the increment and the decrement of $Ca(DeS)_2$ with the increasing concentration are smaller than those of NaDeS.

References

1) K. Shinoda, T. Nakagawa, B. Tamamushi, and T. Isemura, "Colloidal Surfactants," Academic Press, New York (1966), Chaps. 1 and 2.

2) D. G. Hall and B. A. Pethica, "Nonionic Surfactants," ed by M. J. Shick, Marcel Dekker Inc., New York (1967), Chap. 16.

3) K. Kaibara, T. Nakahara, I. Satake, and R. Matuura, *Mem. Fac. Sci. Kyushu Univ., Ser. C*, **7**, 1 (1970).

4) T. Sasaki, M. Hattori, J. Sasaki, and K. Nukina, *Bull. Chem. Soc. Jpn.*, **48**, 1397 (1975).

5) M. Koshinuma and T. Sasaki, *Bull. Chem. Soc. Jpn.*, **48**, 2755 (1975).

6) M. Koshinuma, *Bull. Chem. Soc. Jpn.*, **52**, 1790 (1979).

7) C. Gavach and P. Seta, *Anal. Chem. Acta*, **50**, 407 (1970).

8) B. J. Birch and D. E. Clarke, *Anal. Chem. Acta*, **61**, 159 (1972).

9) S. G. Cutler, P. Meares, and D. G. Hall, *J. Chem. Soc., Faraday Trans. 1*, **74**, 1758 (1978).

10) A. Yamauchi, T. Kunisaki, T. Minematsu, Y. Tomokiyo, T. Yamaguchi, and H. Kimizuka, *Bull. Chem. Soc. Jpn.*, **51**, 2791 (1978).

11) A. Yamauchi, H. Tokunaga, S. Matsuno, and H. Kimizuka, *Nippon Kagaku Kaishi*, **1980**, 388 (1980).

12) I. Satake, I. Tahara, and R. Matuura, *Bull. Chem. Soc. Jpn.*, **42**, 319 (1969).

13) J. N. Phillips, *Trans. Faraday Soc.*, **51**, 561 (1955).

14) E. Matijevic and B. A. Pethica, *Trans. Faraday Soc.*, **54**, 587 (1958).

15) P. H. Elworthy and K. J. Mysels, *J. Colloid Interface Sci.*, **21**, 331 (1962).

16) K. Shinoda, *Bull. Chem. Soc. Jpn.*, **26**, 101 (1953); **28**, 340 (1955).

17) K. Shinoda and E. Hutchinson, *J. Phys. Chem.*, **66**, 577 (1962).

18) L. Shedlovsky, C. W. Jakob, and M. B. Epstein, *J. Phys. Chem.*, **63**, 650 (1959).

A Conductance Study of Alkali Metal Ion-18-Crown-6 Complexes in *N,N*-Dimethylformamide

Yasuyuki TAKEDA

Department of Chemistry, Faculty of Science, Chiba University, Yayoi-chō, Chiba 260

(Received February 5, 1981)

The formation constants, K_{ML}^+, for 1 : 1 complexes of 18-crown-6 (18C6) with alkali metal ions (Na^+, K^+, Rb^+, and Cs^+) and the limiting ionic molar conductivities, λ°, of the complexed cations in *N,N*-dimethylformamide have been determined conductometrically at 25 °C. The K_{ML}^+ sequences of the alkali metal ions with 18C6 are $K^+ > Rb^+ > Cs^+ > Na^+$. The stabilities and selectivities on complexation are governed by the solvent medium and the relative sizes of the cation and the 18C6 cavity. The λ° values of the 18C6 complexes with the alkali metal ions are all approximately equal except for Cs^+, suggesting that, in the cases of Na^+, K^+, and Rb^+, the charge of the alkali metal ion trapped in the 18C6 cavity is effectively screened by 18C6, while this is not true in the case of Cs^+. The ratio of the size of the alkali metal ion to that of the 18C6 cavity appears to be an important factor in determining the magnitude of λ° for alkali metal ion–18C6 complexes.

Complexation reactions of 18-crown-6 (18C6) with alkali metal ions in various solvents have been investigated from the thermodynamic point of view by several different methods, *e.g.* conductance,[1,2] calorimetry,[3,4] potentiometry,[5,6] and spectroscopy.[7,8] The stabilities and selectivities on complexation are governed by the solvent medium and the relative sizes of the cation and the 18C6 cavity.

In the present study, the formation constants for 1 : 1 complexes of 18C6 with alkali metal ions and the limiting ionic molar conductivities of the alkali metal ion–18C6 complexes in *N,N*-dimethylformamide (DMF) have been determined conductometrically at 25 °C; the complex-formation constants have been compared with those in other solvents in order to clarify the factors influencing the magnitude of the complex-formation constant; on the basis of the data for the limiting ionic molar conductivities of the alkali metal ion–18C6 complexes, the behavior of the complexes in DMF has been discussed.

Experimental

Materials. 18C6 (Nisso Co., Ltd.) was recrystallized from acetonitrile and, prior to use, dried at 70 °C in a vacuum oven. The rubidium and caesium perchlorates were prepared by adding an equimolar perchloric acid solution to aqueous solutions of rubidium and caesium chlorides respectively. The lithium, sodium, and potassium perchlorates were purchased commercially. All the perchlorates were recrystallized from water four times and, prior to use, dried at 150 °C in a vacuum oven. The DMF was distilled twice under nitrogen at approx. 12 mmHg.† The middle 70% of the distillate was used. The water content of the finally purified DMF, as determined by Karl Fischer titration, was less than 0.01%. The conductivity of the final product was less than 1×10^{-7} Ω^{-1} cm^{-1}.

Apparatus and Procedure. The conductance measurements were conducted on a Yanagimoto conductivity apparatus, model MY-7, in a water bath thermostated at 25.00± 0.01 °C. Three cells were used with cell constants of 0.05971, 0.09393, and 0.09776 cm^{-1}.

The experimental procedure to obtain the formation constants and the limiting ionic molar conductivities of 18C6 complexes with alkali metal ions was just the same as that described in a previous paper.[2]

† 1 mmHg≈133.322 Pa.

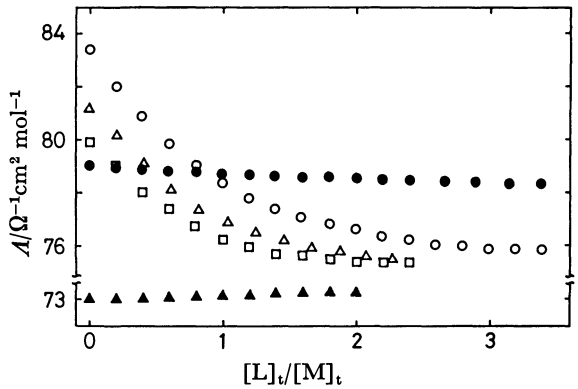

Fig. 1. Λ *vs.* $[L]_t/[M]_t$ curves for 18C6–alkali metal perchlorate systems in DMF at 25 °C.
▲: Li^+, ●: Na^+, □: K^+, △: Rb^+, ○: Cs^+, $[M]_t=5\times10^{-4}$ M.

Results

The molar conductivity, Λ, *vs.* $[L]_t/[M]_t$ plots in DMF at 25 °C are given in Fig. 1, where $[L]_t$ and $[M]_t$ are the total concentrations of 18C6 and the alkali metal ion respectively. The Λ *vs.* $[L]_t/[M]_t$ plots show a decrease in Λ with an increase in the 18C6 concentration, except for Li^+. In the case of Li^+, a very small increase in Λ is found with an increase in the 18C6 concentration. However, since the change in Λ is very small, the conductometric determination of the complex formation constant is impossible. It is assumed that the association between the cation and the perchlorate ion in DMF is negligible under these highly dilute experimental conditions and that, in this work, 18C6 forms the 1 : 1 complexes with the alkali metal ions in DMF. Since the 18C6 concentration was kept low ($<2.0\times10^{-3}$ M; 1 M=1 mol dm^{-3}) during these experiments, corrections for viscosity changes were neglected. The procedure for obtaining the complex-formation constant, K_{ML}^+, and the limiting ionic molar conductivity, λ°, of the alkali metal ion-18C6 complex was just the same as that described in a previous paper.[2] M^+ and L denote the alkali metal ion and 18C6 respectively. The log K_{ML}^+ and the λ° values of the alkali metal ion–18C6 complexes are listed in Tables 1 and 2, together

TABLE 1. log (K_{ML}^+/mol^{-1} dm^3) VALUES AT 25 °C AND CRYSTAL IONIC RADII OF ALKALI METALS (Å)

		Na^+	K^+	Rb^+	Cs^+
Crystal ionic radius[14]		0.95	1.33	1.48	1.69
AN	18C6	4.5_5[5]	5.7_0[5]		>4[7]
	DB18C6	4.8_5[5]	4.8_1[5]	3.7_0[15]	3.5_9[5]
		5.0_0[15]	4.7_0[15]		3.5_0[15]
		5.0[16]	4.8[16]		
PC	18C6	5.6_8[2]	6.2_4[2]	5.3_2[2]	4.4_8[2]
		5.2_5[5]	6.3_2[5]		4.5_2[5]
					4.2[7]
	DB18C6	5.2_0[5]	5.1_3[5]	3.9_1[5]	3.3_1[5]
H_2O	18C6	0.8_0[3]	2.0_3[3]	1.5_6[3]	1.0^3[3]
		0.8_2[17]	2.04_7[17]		0.9_8[17]
			2.0_6[6]		0.8[6]
	DB18C6	1.1_6[18]	1.6_7[18]	1.0_8[18]	0.8_3[18]
		1.1[5]	1.6[5]		
CH_3OH	18C6	4.3_2[6]	6.1[6]		4.6_2[6]
		4.3_6[4]	6.0_5[4]		
	DB18C6	4.3_6[6]	5.0_0[6]	4.2_3[5]	3.5_5[6]
		4.4[5]	5.0_5[5]		
		4.5[10]	5.1[10]		
			4.6_0[15]		
			4.6[16]		
DMF	18C6	2.4	4.3_1	3.9_8	3.6_7
					3.9[7]
	DB18C6	2.4[5]	2.8[5]	2.1[5]	1.5[7]
		2.8_0[19]			
DMSO	18C6	1.4_3[5]	3.2_1[5]		3.0[7]
	DB18C6	1.9_3[5]	2.4_6[5]	1.9[5]	1.3[7]
			2.5[20]		

with the literature values and the λ° values of the alkali metal and perchlorate ions in DMF at 25 °C respectively.

Discussion

As can be seen from Table 1, in the case of each crown ether-solvent system, except for Na^+, the more closely the alkali metal ion fits into the crown ether cavity (18C6 cavity radius: 1.3—1.6 Å[9]), the more stable is the alkali metal ion–crown ether complex. Of all the alkali metal ion–18C6 complexes in the same solvent, the log K_{ML}^+ value of the Na^+–18C6 complex is the second largest for acetonitrile (AN) and propylene carbonate (PC); however, it is the smallest for H_2O, CH_3OH, DMF, and DMSO. The log K_{ML}^+ value of the Na^+–dibenzo-18-crown-6 (DB18C6) complex is the largest for AN and PC, and the second largest for H_2O, CH_3OH, DMF, and DMSO. The difference in the log K_{ML}^+ values of Na^+ and K^+ with 18C6 about the same solvent is larger for H_2O, CH_3OH, DMF, and DMSO than for AN and PC. The difference in the log K_{ML}^+ values of Na^+ and Rb^+ with DB18C6 in relation to the same solvent is larger for AN and PC than for H_2O, CH_3OH, DMF, and DMSO; the same tendency is observed for the Na^+ and Cs^+ with the DB18C6 system. A possible interpretation for this is that, in every one of these solvents, Na^+ is the most strongly solvated of all the alkali metal ions (Na^+, K^+, Rb^+, and Cs^+), and that the differences in the free energies of the solvation of Na^+ and K^+, Na^+ and Rb^+, and Na^+ and Cs^+ are much smaller for AN and PC than for the others.[5]

The strength of the interaction of the alkali metal ion with the donor oxygen atoms of the crown ether is due to the basicity of the donor oxygen atoms. Since the aromatic ether oxygen atom is less basic than the aliphatic one, and since DB18C6 has four aromatic ether oxygen atoms, the stability of the DB18C6 complex with the same alkali metal ion may be lower than that of the 18C6 complex. For the same solvent, the log K_{ML}^+ value of the DB18C6 complex with the same alkali metal ion is smaller than that of the 18C6 complex except in the case of Na^+, which is consistent with this expectation; however, the log K_{ML}^+ value of the Na^+–DB18C6 complex is large for AN, H_2O, and DMSO, and nearly identical for PC, CH_3OH, and DMF, compared with 18C6 (Table 1). This result is unexpected. Because the charge density of Na^+ is the largest of all the alkali metal ions (Na^+, K^+, Rb^+, and Cs^+), Na^+ may attract the donor oxygen atoms of the crown ether much more strongly than the others. Thus, when a complexation reaction occurs between a flexible crown ether and the alkali metal ion, the greatest ligand-ring conformational change may be observed in the case of Na^+. Consequently, since 18C6 is more flexible than DB18C6, the 18C6 complex with Na^+ may be entropy destabilized much more than the DB18C6 complex, resulting in the small or nearly the same log K_{ML}^+ value of the Na^+–18C6 complex compared with DB18C6. This explanation may be supported by the following data. The values of the enthalpy (ΔH/kJ mol^{-1}) and entropy changes (ΔS/J K^{-1} mol^{-1}) in methanol are −35.0 and −34 for the Na^+–18C6 system,[4] −31.3 and −18.8 for the Na^+–DB18C6 system,[10] −56.13 and −72.4 for the K^+–18C6 system,[4] and −40.1 and −36.7 for the K^+–DB18C6 system[10] respectively. The reason why, in each case of Na^+ and K^+, the $-\Delta H$ value of DB18C6 is small and the $-\Delta S$ value of DB18C6 is very small compared with 18C6 may be largely due to the four aromatic ether oxygen atoms and the more rigid structure of DB18C6 respectively. Compared to DB18C6, the greater stability of the K^+–18C6 complex entirely depends on the much larger $-\Delta H$ value of the K^+–18C6 complex. However, in the case of Na^+, compared to DB18C6, the larger $-\Delta H$ value of 18C6 is greatly canceled by the much more unfavorable ΔS value of 18C6, resulting in the smaller log K_{ML}^+ value of 18C6. For H_2O, CH_3OH, DMF, and DMSO, the log K_{ML}^+ value of Na^+ with DB18C6 is the second largest; however, that with 18C6 is the smallest of all the alkali metal ions. Similarly, for AN and PC, that with DB18C6 is the largest; however, that with 18C6 is the second largest (Table 1). This may indicate that, from DB18C6 to 18C6, the Na^+ complex is much more entropy destabilized than the other alkali metal ion complexes because the structure of 18C6 is more flexible than that of DB18C6.

The solvation power sequences of the solvents for the same alkali metal ion are as follows:

Na^+: PC<AN<CH_3OH<H_2O<DMF<DMSO,

K^+: CH_3OH<PC<AN<H_2O<DMF<DMSO,

Rb^+: CH_3OH<PC<AN<H_2O<DMF<DMSO,

Cs^+: $CH_3OH < PC < AN < H_2O < DMF < DMSO$.[5]

The solvation power sequences of the aprotic solvents for the same alkali metal ion are PC<AN≪DMF<DMSO,[5] while, for both 18C6 and DB18C6, the log $K_{ML}{}^+$ value sequences of the aprotic solvents about the same alkali metal ion are completely the reverse except that, for the Cs^+–DB18C6 system, the log $K_{ML}{}^+$ value of AN is larger than that of PC (Table 1). For the aprotic solvents, between the group of PC and AN, and that of DMF and DMSO, there is a very great difference in the solvation power for the same alkali metal ion, and also a large difference in the log $K_{ML}{}^+$ value with regard to the same alkali metal ion in every system except for the Cs^+–18C6 system. These results indicate that, for the same alkali metal ion, the solvation power of the aprotic solvent is a very important factor in determining the $K_{ML}{}^+$-value sequences of the aprotic solvents for both 18C6 and DB18C6. For both 18C6 and DB18C6, the log $K_{ML}{}^+$ value of CH_3OH about the same alkali metal ion gains in ranking in these solvents with an increase in the size of the alkali metal ion. This may reflect the fact that, of all the solvents, the solvation power of CH_3OH for Na^+ is the third smallest, while those for K^+, Rb^+, and Cs^+ are the smallest. It is interesting that, although the solvation power of H_2O for the same alkali metal ion is the third largest of all the solvents, the log $K_{ML}{}^+$ value of H_2O is the smallest for every alkali metal ion–crown ether system (Table 1).

Table 2. ($\lambda^\circ/\Omega^{-1}\,cm^2\,mol^{-1}$) values of alkali metal ion–18C6 complexes, alkali metal ions, and a perchlorate ion in DMF at 25 °C

Ion	$\lambda^\circ/\Omega^{-1}\,cm^2\,mol^{-1}$	
		M^+–18C6
Na^+	29.7_9	24
K^+	30.6_7	$24._6$
Rb^+	32.4_3	$24._3$
Cs^+	34.7_2	$23._4$
$ClO_4{}^-$	52.8_3	

Table 2 shows that the λ° value of the alkali metal ion-18C6 complex is much smaller than that of the corresponding alkali metal ion, indicating that the alkali metal ion–18C6 complex is much bulkier than the corresponding alkali metal ion in DMF. The λ° values of the 18C6 complexes with the alkali metal ions are approximately equal except for Cs^+ (Table 2). From the data, it appears that, in the cases of Na^+, K^+, and Rb^+, the charge of the alkali metal ion trapped in the 18C6 cavity is effectively screened by the 18C6 and that the 18C6 complexes with the alkali metal ions are nearly equal to each other in size in DMF. Since Cs^+, whose size is larger than the cavity size of 18C6, cannot get into the plane of the oxygen atoms of 18C6, Cs^+ may protrude from the plane of 18C6. Thus, the exposed part of Cs^+ in the 18C6 complex may strongly interact with the DMF molecules. This may be the reason why the λ° value of the Cs^+–18C6 complex is smaller than those of the others. Judging from the above observations, the ratio of the size of the alkali metal ion to that of the 18C6 cavity appears to be an important factor in determining the magnitude of λ° for alkali metal ion–18C6 complexes.

Table 3. Stokes' radii, R_s, and crystal ionic radii, R_c, of alkali metal ion–18C6 complexes (Å)

Cation	R_c/Å	R_s/Å	
		DMF	PC[2]
Na^+	4.8	4.3	3.8_0
K^+	4.9	4.1_8	3.6_3
Rb^+	4.9	4.2_3	3.6_5
Cs^+	4.9	4.4_0	3.6_9

The crystal ionic radii, $R_C(ML^+)$, of the alkali metal ion–18C6 complexes may be approximately evaluated from the crystal ionic radii, $R_C(M^+)$, of the alkali metal ions held in the 18C6 cavity and from the 18C6 volume, V:

$$R_c(ML^+) = \{R_c(M^+)^3 + 3V/4\pi\}^{1/3}.$$

V may be approximated by summing the van der Waals volumes of the atoms or groups forming 18C6. The $R_c(ML^+)$ values are given in Table 3, together with the Stokes' radii, $R_s(ML^+)$, of the alkali metal ion–18C6 complexes calculated from this equation: $R_s(ML^+) = 0.819/\eta_0\lambda^\circ$, where η_0 is the viscosity of the pure solvent. For the same alkali metal ion–18C6 complex, the R_s value of DMF, whose dielectric constant (36.71 at 25 °C[11]) is smaller than PC (64.4 at 25 °C[11]), is larger than that of PC. The crystal ionic radii of the alkali metal ion–18C6 complexes are nearly equal to that of a tetrabutylammonium ion (4.94 Å[12]) (Table 3). The λ° values of the alkali metal ion–18C6 complexes are, however, smaller than that of the tetrabutylammonium ion (26.9[13]) (Table 2). This is the same tendency as that found in the alkali metal ion–18C6 complex–PC system.[2] Since, in the case of the tetrabutylammonium ion, four butyl groups effectively shield the surface charge of the central nitrogen atom, while, in the case of the alkali metal ion–18C6 complex, solvent contacts with the alkali metal ion trapped in the 18C6 cavity are still possible in the direction perpendicular to the plane of 18C6, the alkali metal ion–18C6 complex would much more strongly undergo specific solvation than the tetrabutylammonium ion. This may be the reason why the λ° value of the alkali metal ion–18C6 complex is smaller than that of the tetrabutylammonium ion for both DMF and PC.

References

1) H. P. Hopkins, Jr., and A. B. Norman, *J. Phys. Chem.*, **84**, 309 (1980).
2) Y. Takeda, H. Yano, M. Ishibashi, and H. Isozumi, *Bull. Chem. Soc. Jpn.*, **53**, 72 (1980).
3) R. M. Izatt, R. E. Terry, B. L. Haymore, L. D. Hansen, N. K. Dalley, A. G. Avondet, and J. J. Christensen, *J. Am. Chem. Soc.*, **98**, 7620 (1976).
4) J. Lamb, Ph. D. Thesis, Brigham Young University, Provo, Utah, 1978.
5) I. M. Kolthoff and M. K. Chantooni, Jr., *Anal. Chem.*, **52**, 1039 (1980).
6) H. K. Frensdorff, *J. Am. Chem. Soc.*, **93**, 600 (1971).
7) E. Mei, A. I. Popov, and J. L. Dye, *J. Phys. Chem.*, **81**, 1677 (1977).
8) A. J. Smetana and A. I. Popov, *J. Solution Chem.*, **9**,

183 (1980).
9) C. J. Pedersen, *J. Am. Chem. Soc.*, **92**, 386 (1970).
10) P. U. Früh and W. Simon, "Protides of the Biological Fluids-20th Colloquium," ed by H. Peeters, Pergamon Press, New York (1978).
11) G. J. Janz and R. P. T. Tomkins, "Nonaqueous Electrolytes Handbook," Academic Press, New York (1972), Vol. 1.
12) D. E. Arrington and E. Griswold, *J. Phys. Chem.*, **74**, 123 (1970).
13) N. Matsuura, K. Umemoto, and Y. Takeda, *Bull. Chem. Soc. Jpn.*, **48**, 2253 (1975).
14) L. Pauling, "The Nature of the Chemical Bond," 3rd ed, Cornell Univ. Press (1960).
15) A. Hofmanova, J. Koryta, M. Brezina, and M. Mittal, *Inorg. Chim. Acta*, **28**, 73 (1978).
16) D. F. Evans, S. L. Wellington, J. A. Nadis, and E. L. Cussler, *J. Solution Chem.*, **1**, 499 (1972).
17) H. Hφiland, J. A. Ringseth, and T. S. Brun, *J. Solution Chem.*, **8**, 779 (1979).
18) E. Shchori, N. Nae, and J. Jagur-Grodzinski, *J. Chem. Soc., Dalton Trans.*, **1975**, 2381.
19) E. Shchori, J. Jagur-Grodzinski, Z. Luz, and M. Schporer, *J. Am. Chem. Soc.*, **93**, 7133 (1971).
20) D. P. Nelson, Ph. D. Thesis, Brigham Young University, Provo, Utah, 1971.

  Bull. Chem. Soc. Jpn., 54, 3137—3142 (1981)

Liquid Crystal Formation in Binary Systems. IV.[1] Induction of Smectic Phases in Mixtures of *N*-(*p*-Nitrobenzylidene)-*p*-aminoazobenzene and Various Electron Donors of the Type *N*-(*p*-Substituted Benzylidene)-*p*-aminoazobenzene

Minoru FUKUI and Yoshio MATSUNAGA*

Department of Chemistry, Faculty of Science, Hokkaido University, Sapporo 060

(Received February 5, 1981)

A study of the phase diagrams of binary systems consisting of nematogenic *N*-(*p*-nitrobenzylidene)-*p*-aminoazobenzene and various electron donors of the type *N*-(*p*-*X*-benzylidene)-*p*-aminoazobenzene revealed the induction of a smectic A phase in the cases where X=MeO, EtO, *n*-PrO, Me_2N, and Et_2N and of a smectic B phase as well in the cases where X=EtO and *n*-PrO. The extent of thermal stability enhancement of the smectic A phase is larger with non-nematogenic dialkylamino derivatives than with nematogenic alkoxy derivatives; this supports our postulate that the smectic phases are stabilized by the intermolecular interaction of the electron donor-acceptor type. The induction of smectic A phases was shown also in all the combinations of the *p'*-ethoxy derivatives, including the cases where X=H, Me, and Ph.

We reported earlier that nematic and smectic liquid crystals can be induced by mixing the *p*-dimethylamino and *p*-nitro derivatives of *N*-benzylideneaniline, which are both potentially mesogenic.[2] The induction of the mesophases in these binary systems was attributed to the stabilization of the parallel molecular arrangement by the interaction of the electron donor-acceptor type. In order to seek further correlation between the donor-acceptor interaction and the formation of smectic liquid crystals, we have applied the phase diagram approach to mixtures of nematogenic *N*-(*p*-nitrobenzylidene)-*p*-aminoazobenzene and various electron donors of the type *N*-(*p*-*X*-benzylidene)-*p*-aminoazobenzene. The latter compounds themselves are nematogenic or non-nematogenic depending upon the substituent X. The following substituents were selected purely from the standpoint of the electron-donor strength: H, Me, MeO, EtO, *n*-PrO (hereafter abbreviated PrO), Me_2N, and Et_2N. As the nature of each of these terminal substituents is so different, the influence on the thermal stability of mesophases of the component compounds may be quite variable. In addition, we worked on mixtures of the *p'*-ethoxy derivatives.

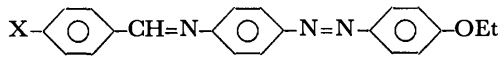

The appearance of a smectic phase has been noted by several research groups with a number of binary systems in which either one or both of the components are capable of giving nematic mesophases.[3-8] For instance, Schroeder and Schroeder have found the formation of a smectic phase in the system comprised of nematogenic 4,4'-bis(hexyloxy)azoxybenzene and non-nematogenic *N*-(*p*-methoxybenzylidene)-*p*-nitroaniline.[3] Engelen *et al.* have examined about thirty combinations and concluded that mixtures of terminal nonpolar and terminal polar nematogens usually induce a smectic phase of the type A.[5] While the nematogens with only alkyl and alkoxyl groups are considered to be nonpolar, the cyano and nitro derivatives are polar. A paper of Domon and Billard published a year later has referred to about ten systems which comprise two different nonpolar nematogens and yield smectic phases.[7] The donor-acceptor systems examined in our previous work consist of only polar components and markedly differ from theirs. Thus, it seems difficult to explain the role of terminal substituents and their dipole moments in the induction of smectic phases in binary mixtures. Recently, Sharma *et al.* have reported their work on the electron donor-acceptor complexes formed by two mesogenic component compounds and noted that the formation of smectic A phase is favored by such an interaction.[8] Their donor compounds are 4,4'-bis(alkylamino)biphenyls and the acceptors are various compounds carrying nitro, cyano, and/or carbonyl groups.

Experimental

Materials. The condensation reaction between *p*-X-substituted benzaldehyde and *p*-aminoazobenzene yields *N*-(*p*-X-benzylidene)-*p*-aminoazobenzene, as reported by Vorländer and Schuster.[9] The *p'*-ethoxy derivatives were similarly prepared. Hereafter, the component compounds are represented by their terminal substituents: that is, [X, H] in the first series and [X, EtO] in the second series. *p*-Amino-*p'*-ethoxyazobenzene needed for the latter series was prepared by the rearrangement of *p*-ethoxydiazoaminobenzene obtained by the coupling of benzenediazonium chloride with *p*-phenetidine.[10] Binary mixtures in known proportions were melted in small test tubes, shaken well to ensure homogeneity, and then rapidly cooled.

Measurements. The calorimetric curves were recorded on a Rigaku Denki differential scanning calorimeter, Model 8001 SL/C, during the processes of heating and cooling. The heating rate in the present work was 5 °C min^{-1}. The liquid crystals were identified by examining their texture with the aid of a polarizing microscope and/or by studying the continuous miscibility with a reference mesogen.

Results and Discussion

The [H, H] and [Me, H]–[NO_2, H] Systems. The acceptor compound [NO_2, H] has a nematic phase stable between 181 and 228 °C. The combination with non-mesogenic [H, H] yields no smectic phase (see Fig. 1a). A eutectic point is located at 122.5 °C and 14.5 mol% of [NO_2, H] and a peritectic point at 161 °C and 81 mol%.

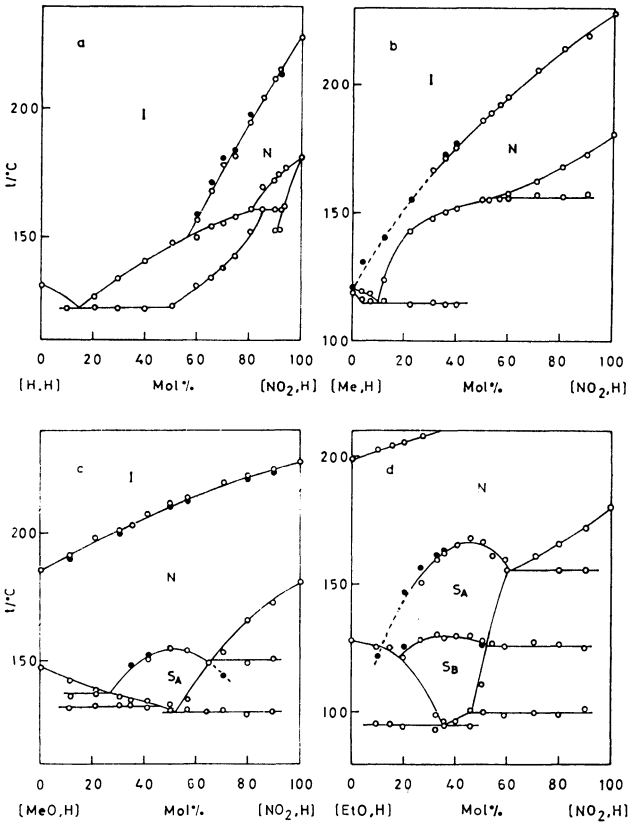

Fig. 1. Phase diagrams of (a) the *N*-benzylidene-*p*-aminoazobenzene–*N*-(*p*-nitrobenzylidene)-*p*-aminoazobenzene, (b) *N*-(*p*-methylbenzylidene)-*p*-aminoazobenzene–*N*-(*p*-nitrobenzylidene)-*p*-aminoazobenzene, (c) *N*-(*p*-methoxybenzylidene)-*p*-aminoazobenzene–*N*-(*p*-nitrobenzylidene)-*p*-aminoazobenzene, and (d) *N*-(*p*-ethoxybenzylidene)-*p*-aminoazobenzene–*N*-(*p*-nitrobenzylidene)-*p*-aminoazobenzene systems. The open and shaded circles are transitions observed in the processes of heating and cooling respectively.

The nematic liquid crystal-isotropic liquid (N-I) transition curve is met by the freezing point curve at 150 °C and 56.5 mol%. The extrapolation of the N-I transition curve, which is almost straight, to 0 mol% of the acceptor indicates that [H, H] has a latent N-I transition temperature around 50 °C. This temperature is far below its melting point, 131 °C.[9]

The compound [Me, H] exhibits a nematic phase stable between 118.5 and 120.5 °C. This temperature range is so narrow that the N-I transition is not detectable on the calorimetric curve recorded in the process of heating; however, the transition is well established in the process of cooling because of the delayed solidification. The N-I transition curve in the [Me, H]–[NO_2, H] system is slightly convex upwards (see Fig. 1b). A eutectic point is found at 114.5 °C and 10 mol% of [NO_2, H]. As the phase change at the former temperature is detected only below 50 mol%, the solid molecular compound melting incongruently at 156 °C may be of a 1 : 1 mole ratio. No smectic phase is induced in this system.

The [MeO, H], [EtO, H], and [PrO, H]–[NO_2, H] Systems. The donor [MeO, H] is nematogenic.[9] The liquid crystal is stable between 147.5 and 185.5 °C. The system [MeO, H]–[NO_2, H] gives a eutectic point located at 130 °C and 52 mol% of the acceptor. The N-I transition curve is convex upwards but only slightly. A smectic liquid crystal of the type A is induced and the maximum temperature of 154.5 °C is at 50 mol% (see Fig. 1c). The smectic liquid crystal-nematic liquid crystal (S-N) transition curve intersects the freezing point curve of the donor component at 137.5 °C and 27 mol% and that of the acceptor component at 150 °C and 65 mol%. The extrapolation of the S-N transition curve to 0 mol% gives a latent S_A-N transition temperature of donor at about 90 °C, while the extrapolation to 100 mol% yields a temperature of about 100 °C. Thus, the smectic phase is stabilized as much as 60 °C by the interaction between these two mesogens.

The nematic phase of [EtO, H] covers the temperature range from 128 to 199 °C. The system with [NO_2, H] shows a eutectic point at 95 °C and 36 mol% of [NO_2, H] and a peritectic point at 100 °C and 47 mol% (see Fig. 1d). There seems to be a solid molecular compound at 50 mol% with an incongruent melting point. Not only a smectic A phase but also a smectic B phase can be observed in this system. The maximum temperature of the former phase is about 167 °C and of the latter about 130 °C. The extrapolation of each transition curve to 0 mol% suggests that the donor has latent S_A-N and S_B-S_A transition temperatures at about 95 and 90 °C respectively. The existence of these two transitions has been confirmed by a study of the phase diagram of the system [EtO, H]–[NoO, H], *N*-(*p*-nonyloxybenzylidene)-*p*-aminoazobenzene. The reference compound gives a smectic B phase stable between 109.5 and 126 °C and a smectic A phase stable between 126 and 156 °C, in agreement with the data reported by Demus and Sackmann.[11] The freezing point curve of [EtO, H] is met by the S_A-N transition curve at 114 °C and 31 mol% of [NoO, H] and by the S_B-S_A transition curve at 105 °C and 44 mol% (see Fig. 2a). While the S_A-N transition curve above 31 mol% is convex upwards, the curve below this composition appears concave upwards. The extrapolation yields the latent transition temperatures of 95 and 89 °C which agree well with those suggested above. The latent S_B-S_A transition expected to be around 95 °C for [NO_2, H] is also supported by the phase diagram of the system with the same reference mesogen (see Fig. 2b). Here, the S_A-N transition curve is markedly convex upwards, as has been noted with the shorter alkoxy derivatives (see Figs. 1c and 1d). Passing the maximum at 177 °C and 60 mol% of [NoO, H], the transition curve is met by the freezing point curve of [NO_2, H] at 157.5 °C and 37 mol%. In contrast to the S_A-N transition curve, the curve separating the smectic A and B phases is slightly concave upwards. The intersection with the freezing point curve is found at 112 °C and 58 mol%. Consequently, the extents of stabilization of the smectic A and B phases in the [EtO, H]–[NO_2, H] system are estimated to be about 70 and 38 °C respectively.

With the [MeO, H]–[EtO, H] system, we have confirmed the ideal linear relationship of N-I transition

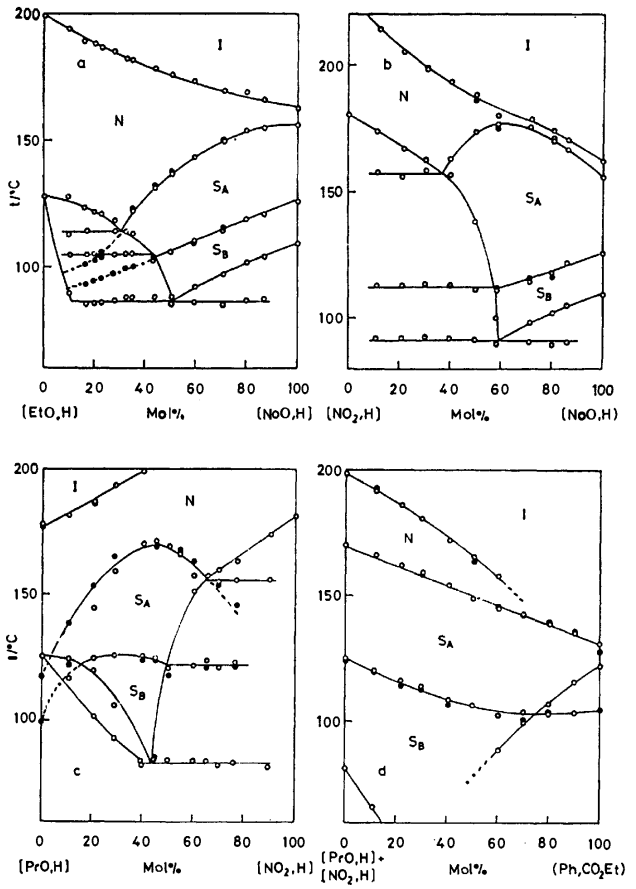

Fig. 2. Phase diagrams of (a) the *N*-(*p*-ethoxybenzylidene)-*p*-aminoazobenzene–*N*-(*p*-nonyloxybenzylidene)-*p*-aminoazobenzene, (b) *N*-(*p*-nitrobenzylidene)-*p*-aminoazobenzene–*N*-(*p*-nonyloxybenzylidene)-*p*-aminoazobenzene, and (c) *N*-(*p*-propoxybenzylidene)-*p*-aminoazobenzene–*N*-(*p*-nitrobenzylidene) -*p*-aminoazobenzene systems and (d) the system consisting of *N*-(*p*-phenylbenzylidene)-*p*-(ethoxycarbonyl)aniline and the 6 : 4 mixture of *N*-(*p*-propoxybenzylidene)-*p*-aminoazobenzene and *N*-(*p*-nitrobenzylidene)-*p*-aminoazobenzene. As to the open and shaded circles, see the caption of Fig. 1.

temperatures in the absence of a particular interaction. The single eutectic point is located at 115 °C and 56 mol% of [EtO, H]. It is rather surprising to see that solid [EtO, H] can dissolve [MeO, H] up to 30 mol%. On the other hand, the solubility of [EtO, H] into solid [MeO, H] is less than 10 mol%.

The nematic phase of [PrO, H] makes an appearance at 125 °C and is stable up to 178 °C. This donor has metastable smectic A and B phases: that is, the supercooled nematic phase is transformed into a smectic A phase at 117 °C and then into a smectic B phase at 99 °C. When mixed with [NO_2, H], a eutectic point appears at 83 °C and 44 mol% of the acceptor (see Fig. 2c). The smectic A phase has a region of existence from 4 to 65 mol% and the smectic B phase from 15 to 50 mol%. The upper temperature limit of the former mesophase is located at about 170 °C, which is higher by 62 °C than the straight line joining the S_A-N transition temperatures of the components. When the composition is lower than 30 mol%, the S_A-N transition temperatures recorded in the process of heating were found to deviate significantly from those recorded in the process of cooling. The curve was drawn on the basis of the latter points which are in conformity with the transition temperature of pure [PrO, H]. In contrast to the smectic A phase, the maximum deviation from the ideal linear relationship in the smectic B phase apparently occurs at a composition far from a 1 : 1 mole ratio. This phase at 30 mol% is stabilized by about 28 °C.

The induced smectic A and B phases could be identified by their characteristic fan-shaped texture. In addition, the classification has been confirmed by the selective miscibility with the smectic A phase of *N*-(*p*-phenylbenzylidene) -*p*- (ethoxycarbonyl) aniline (Ph,

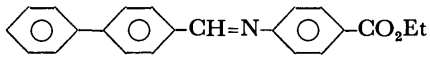

CO_2Et) which is stable between 121.6 and 131 °C.[12] Fig. 2d presents the diagram of the pseudo-binary system consisting of a mixture of [PrO, H] and [NO_2, H] at 40 mol% and the reference compound. The diagram is of the eutectic type. The N-I transition curve is slightly convex upwards and the nematic phase is not observable above 70 mol% of (Ph, CO_2Et). Doubtlessly the mesophases induced in the mixture at high temperatures form an uninterrupted series of mixed crystals with the smectic A phase of the reference compound. Another smectic phase appearing enantiotropically in the mixtures at lower temperatures is identical with the metastable smectic phase of (Ph, CO_2Et). The latter was classified into type B on the basis of its miscibility behavior with [NoO, H].

The smectic B phase could be found also in the system comprising a 1 : 1 mixture of [MeO, H] and [NO_2, H] and the reference mesogen. The phase is stable in the composition range from 5 to 68 mol% of (Ph, CO_2Et). The extrapolation of the transition curve to 0 mol% gives a temperature only a few degrees below the eutectic temperature of the [MeO, H]–[NO_2, H] system.

The [Me_2N, H] and [Et_2N, H]–[NO_2, H] Systems. The donor [Me_2N, H] is non-mesogenic. A eutectic point is located at 142 °C and 75.5 mol% of [NO_2, H]. A peritectic point appears at 146 °C and 59 mol% because of the formation of an incongruently-melting molecular compound, possibly of a 1 : 1 mole ratio. The mixtures give rise to a smectic A phase, as is shown in Fig. 3a. The induced S_A-N transition curve is met by the freezing point curve of the donor component at 152 °C and 48 mol% and by that of the acceptor component at 166 °C and 87 mol%. The maximum may be located around 190 °C in the composition range between 60 and 70 mol%. The steep slope on the donor-rich side suggests that the latent S_A-N transition temperature of [Me_2N, H] is very low. This may be the reason why the maximum of the transition curve is found at an acceptor-rich composition. As this temperature is higher by 90 °C than the estimated S_A-N transition temperature of [NO_2, H], the extent of the stabilization of the smectic phase certainly exceeds 100 °C.

Replacement of a dimethylamino group by a diethyl-

amino group in the donor compound seems to lower markedly the latent N-I transition temperature. As is shown in Fig. 3b, the N-I transitions lie on an approximately straight line in the diagram. The extrapolation to 0 mol% of [NO_2, H] yields −12 °C. The line intersects the induced S_A-N transition curve at 167 °C and 72 mol%. The maximum temperature of the smectic A phase is found at 168 °C near 75 mol%. The extent of induction is at least 90 °C, because the latent S_A-N transition of [Et_2N, H] is expected to be lower than the latent N-I transition. It must be noted that the smectic A phase induced over the range of composition below 72 mol% is thermally more stable than the nematic phase. At 83 mol% and 164.5 °C, the S_A-N transition curve is met by the freezing point curve of the acceptor.

In summary, the maximum temperature of the induced smectic A phase in the present series decreases in the following order: [Me_2N, H]>[PrO, H]>[EtO, H]≃[Et_2N, H]>[MeO, H]. Even though these results arise from the complex interplay of different molecular parameters determining the thermal stability of smectic phases, the extents of the stability enhancement with more electron-donating dialkylamino derivatives are clearly larger than those with less electron-donating alkoxy derivatives, 60—70 °C, supporting our postulate that the ordered arrangement of molecules characteristic of smectic phases can be achieved by the interaction of the electron donor-acceptor type. In the latter derivatives, the sequence of the extents is [EtO, H]>[PrO, H]≃[MeO, H]. It must be emphasized that the maximum deviation of the nematic phases from the ideal linear relationship is merely several degrees in the above-mentioned systems. Moreover, the induction of the smectic A phases is about twice as large as that of the smectic B phases when observable. As no smectic phase could be found in the [H, H] and [Me, H]–[NO_2, H] systems, we decided to take up the second series, mixtures of the *p'*-ethoxy derivatives. The unsubstituted compound [H, EtO] is an isomer of [EtO, H] and has been found to be nematogenic by the work of Vorländer.[10]

The [H, EtO] and [Me, EtO]–[NO_2, EtO] Systems. The compound [H, EtO] melts at 136 °C and has an enantiotropic nematic range up to 204 °C. The range is shifted upwards by several degrees compared with that of the isomeric [EtO, H]. When this donor is mixed with nematogenic [NO_2, EtO], a smectic A phase is produced in the composition range from 50 to 88 mol% of the acceptor (see Fig. 4a). At the latter composition, the induced S_A-N transition curve intersects the freezing point curve of the acceptor. The extrapolation of this transition curve to 100 mol% suggests that the acceptor has the latent transition temperature at about 155 °C. The smectic phase shows the maximum temperature of about 178 °C at 75 mol%. It must be added that the latent S_A-N transition temperature of pure [H, EtO] is apparently much lower than that of [EtO, H], which is located at 95 °C. This combination produces a congruently melting molecular compound, presumably at 33 mol%. Eutectic points are located at 118 °C and 22.5 mol% and at 127 °C and 47 mol%. The acceptor compound [NO_2, EtO] is transformed from a solid to a nematic liquid crystal at 177.5 °C.

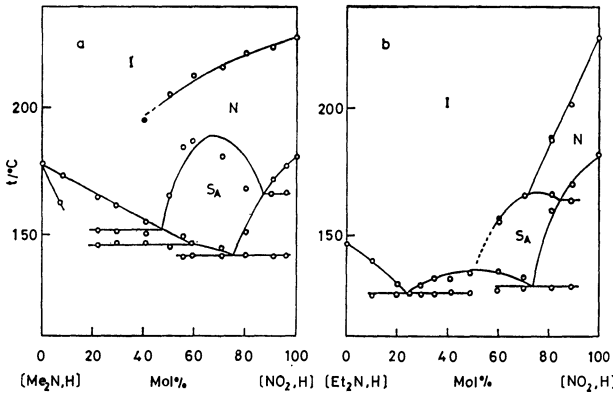

Fig. 3. Phase diagrams of (a) the *N*-[*p*-(dimethylamino)-benzylidene] - *p*-aminoazobenzene–*N* - (*p* - nitrobenzylidene)-*p*-aminoazobenzene and (b) *N*-[*p*-(diethylamino)benzylidene]-*p*-aminoazobenzene–*N*-(*p*-nitrobenzylidene)-*p*-aminoazobenzene systems. As to the open and shaded circles, see the caption of Fig. 1.

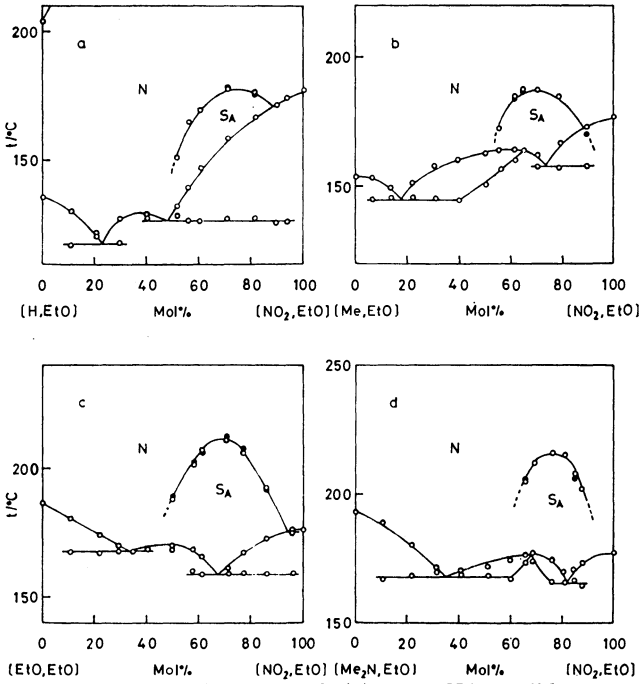

Fig. 4. Phase diagrams of (a) the *N*-benzylidene-*p*-amino-*p'*-ethoxyazobenzene–*N*- (*p*-nitrobenzylidene)-*p*-amino-*p'*-ethoxyazobenzene, (b) *N*-(*p*-methylbenzylidene)-*p*-amino-*p'*-ethoxyazobenzene–*N*-(*p*-nitrobenzylidene)-*p*-amino-*p'*-ethoxyazobenzene, (c) *N*-(*p*-ethoxybenzylidene)-*p*-amino-*p'*-ethoxyazobenzene–*N*-(*p*-nitrobenzylidene)-*p*-amino-*p'*-ethoxyazobenzene, and (d) *N*-[*p*-(dimethylamino)benzylidene]-*p*-amino-*p'*-ethoxyazobenzene–*N*-(*p*-nitrobenzylidene)-*p*-amino-*p'*-ethoxyazobenzene systems. As to the open and shaded circles, see the caption of Fig. 1.

The compound [Me, EtO] is nematogenic and melts at 154 °C. The mixtures with [NO_2, EtO] in the composition range from 55 to 90 mol% of [NO_2, EtO] yield a smectic A phase (see Fig. 4b). The maximum temperature of 188 °C is found at 70 mol%. The molecular compound formed in this system has a 1 : 2

mole ratio and melts congruently at 164 °C. Eutectic points are located at 145 °C and 18 mol% and at 158 °C and 74 mol%.

The [MeO, EtO], [EtO, EtO], and [PrO, EtO]–[NO_2, EtO] Systems. All the donor compounds are nematogenic. The donor [MeO, EtO] melts at 161 °C. When mixed with [NO_2, EtO], a smectic A phase is induced in the composition range from 55 to 88 mol%. The S_A-N transition curve has a maximum at 192 °C and 73 mol% and is met at 88 mol% by the freezing point curve of the acceptor. As the donor molecule has electron donating groups at the *p* and *p'* positions, the molecular complex formed in the smectic phase may be, at least, partly of a 1 : 2 mole ratio. A solid molecular compound is found at a 1 : 2 mole ratio and is stable up to its melting point, 164 °C. A eutectic point on the donor-rich side is located at 161 °C and about 48 mol%; therefore, the freezing point curve below this point is flat. Another eutectic point is found at 158 °C and 74 mol%.

The phase diagram of the [EtO, EtO]–[NO_2, EtO] system is presented in Fig. 4c. The donor compound has a nematic phase stable above 186 °C. The smectic mesophase appears in the range from 50 to 93 mol% of the acceptor. The upper temperature limit of the mixture's smectic range is found at 211.5 °C and 68 mol%. The equimolar solid molecular compound formed by the present combination melts at 170 °C. Eutectic points are located at 168 °C and 32 mol% and at 159 °C and 67 mol%.

The diagram of the [PrO, EtO]–[NO_2, EtO] system bears a similarity to the afore-mentioned one. The nematogenic [PrO, EtO] melts at 167 °C. The induced smectic A mesophase can be seen in the composition range from 45 to 90 mol%. The maximum in smectic phase stability occurs at 226 °C and 65 mol%. The intersection between the S_A-N transition curve and the freezing point curve on the acceptor-rich side may be at 176 °C and 93 mol%. The 1 : 1 molecular compound melts at 165°C. As this melting point and the eutectic temperature are not distinguishable from each other, the latter location could not be determined. Another eutectic point is at 150 °C and 67 mol%.

The [Me_2N, EtO], [Et_2N, EtO], and [Ph, EtO]–[NO_2, EtO] Systems. Contrary to [Me_2N, H], the donor [Me_2N, EtO] gives a stable nematic liquid crystal above 193 °C. As is shown in Fig. 4d, a smectic A phase is induced in the mixtures with [NO_2, EtO]. The maximum for the S_A-N transition is located at about 216 °C and 75 mol%. This combination yields a 1 : 2 molecular compound with a congruent melting point of 177.5 °C. Two eutectic points are at 168 °C and 35 mol% and at 165 °C and 82 mol%.

The compound [Et_2N, EtO] has a nematic range from 159.5 to 198.5 °C. The reduction of the enantiotropic N-I transition temperature by replacement of a dimethylamino group with a diethylamino group is in accordance with the trend suggested for the latent N-I transitions in [Me_2N, H] and [Et_2N, H]. The induced smectic A phase in the system with [NO_2, EtO] covers a wide composition range. One end of the S_A-N transition curve is the intersection with the freezing point curve of the donor located at 144 °C and 29 mol% and the other is the intersection with the freezing point curve of the acceptor, possibly around 98 mol%. The maximum temperature of 239 °C is found at about 77 mol%. The solid 1 : 2 molecular compound in this system is of lower stability and ceases to exist stably at 146 °C, producing a peritectic point at 64 mol%. The eutectic is at 138.5 °C and 34 mol%.

In addition to the above-mentioned systems, the phase diagram has been prepared for the combination of [Ph, EtO] and [NO_2, EtO]. The donor [Ph, EtO] is transformed from a solid to a nematic liquid crystal at 199 °C. The diagram has a eutectic point at 159 °C and 64 mol%. In this system too, only a smectic A phase is induced. The S_A-N transition curve recorded in the range from 30 to 90 mol% reaches its maximum at 234 °C and 54 mol%. The smooth extrapolation to 0 mol% suggests that the donor has the latent transition a little below 150 °C. The extent of induction may be about 90 °C.

As described above, the smectic A phases induced in the second series are found to exhibit maxima beyond 50 mol% of [NO_2, EtO]. Except for the last donor, the latent S_A-N transition temperatures are expected to be considerably lower than that of the acceptor. The large mole percentages at the upper temperature limits may be ascribed to the low latent transition temperatures of the donor compounds and also to the formation of 1 : 2 molecular complexes. The observed upper temperature limits of the induced mesophases give the following sequence of the donors:

[Et_2N, EtO]>[Ph, EtO]>[PrO, EtO]>[Me_2N, EtO]>
[EtO, EtO]>[MeO, EtO]>[Me, EtO]>[H, EtO].

The extent of induction may be concluded to be less only when both the temperature limit and the composition are lower. Judging by such a condition, the donors may be partially arranged in order of their decreasing ability of inducing a smectic A phase: namely,

[Me_2N, EtO]>[MeO, EtO]>[Me, EtO],
[Et_2N, EtO]>[PrO, EtO],
[Me_2N, EtO]>[EtO, EtO], and
[Me_2N, EtO]>[H, EtO].

A plausible explanation for these features is that the stabilization is provided by the intermolecular electron donor-acceptor interaction.

No smectic B phase could be observed in the second series. As the molecular compounds found in this series are more stable than those in the first series, the freezing point may be too high to allow the observation of the S_B-S_A transition. This assumption has been supported by a study on the system consisting of a 3 : 7 mixture of [Me, EtO] and [NO_2, EtO] and the reference compound [NoO, H]. The composition of the mixture has been chosen to correspond to the upper temperature limit of the induced smectic A phase (see Fig. 4b). The diagram shown in Fig. 5 strongly suggests that the mixture has a latent S_B-S_A transition located around 120 °C, which is not very different from the transitions exhibited by mixtures of [EtO, H] and [NO_2, H]. The

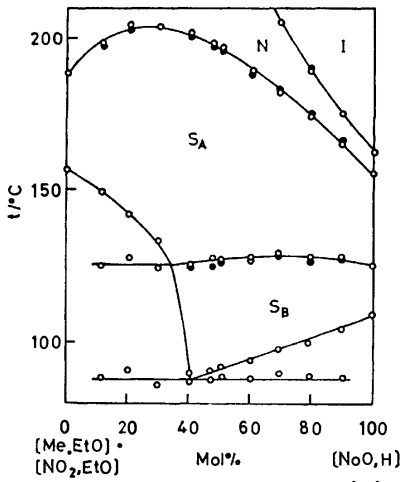

Fig. 5. Phase diagram of the system consisting of *N*-(*p*-nonyloxybenzylidene)-*p*-aminoazobenzene and the 3 : 7 mixture of *N*-(*p*-methylbenzylidene)-*p*-amino-*p'*-ethoxyazobenzene and *N*-(*p*-nitrobenzylidene)-*p*-amino-*p'*-ethoxyazobenzene. As to the open and shaded circles, see the caption of Fig. 1.

S_A-N transition curve is appreciably convex upwards and the maximum is located at about 25 mol% of [NoO, H]. These results imply that [NoO, H] is a better electron donor than [Me, EtO] is.

The present work was partly supported by a Grant-in-Aid for Scientific Research No. 543001 from the Ministry of Education, Science and Culture.

References

1) Part III: K. Araya and Y. Matsunaga, *Bull. Chem. Soc. Jpn.*, **54**, 2430 (1981).
2) K. Araya and Y. Matsunaga, *Bull. Chem. Soc. Jpn.*, **53**, 3079 (1980).
3) J. P. Schroeder and D. C. Schroeder, *J. Org. Chem.*, **33**, 591 (1968).
4) A. C. Griffin, R. F. Fisher, and S. J. Havens, *J. Am. Chem. Soc.*, **100**, 6329 (1978).
5) B. Engelen, G. Heppke, R. Hopf, and F. Schneider, *Ann. Phys. (Paris)*, **3**, 403 (1978).
6) L. J. Yu and M. M. Labes, *Mol. Cryst. Liq. Cryst.*, **54**, 1 (1979).
7) M. Domon and J. Billard, *J. Phys. (Paris), Colloq.*, **40**, C3-413 (1979).
8) N. K. Sharma, G. Pelzl, D. Demus, and W. Weissflog, *Z. Phys. Chem. (Leipzig)*, **261**, 579 (1980).
9) D. Vorländer and H. Schuster, *J. Prakt. Chem. (2)*, **140**, 193 (1934).
10) D. Vorländer, *Ber.*, **62**, 2824 (1929).
11) D. Demus and H. Sackmann, *Z. Phys. Chem. (Leipzig)*, **238**, 215 (1968).
12) D. Demus and H. Sackmann, *Z. Phys. Chem. (Leipzig)*, **222**, 127 (1963).

The Temperature Dependence of the Localization and Scavenging of Electrons in a Glassy 2-Methyltetrahydrofuran Matrix

Masato YOSHIZAKI, Masaaki OGASAWARA,* and Hiroshi YOSHIDA
Faculty of Engineering, Hokkaido University, Kita-ku, Sapporo 060
(Received February 21, 1981)

The nature and behavior of localized electrons in a γ-irradiated 2-methyltetrahydrofuran matrix were studied at 4 and 77 K by optical absorption measurements. Electrons localized in shallow traps generated at 4 K in a neat matrix showed one broad peak with ε_{max} of 1.2×10^4 mol^{-1} dm^3 cm^{-1} at 1490 nm. The yield was 1.9 (for 100 eV energy absorbed). This yield is less than the yield of electrons localized in deep traps at 77 K, 2.6. With an increasing concentration of biphenyl added to the matrix, the localized electrons were completely transformed into biphenyl anions. The scavenging efficiency was twice as high at 4 K as at 77 K. These results indicated that the electron scavenging took place by tunneling of the once localized electrons.

Glassy 2-methyltetrahydrofuran (MTHF) is a rigid organic matrix in which the nature and behavior of radiation-generated localized electrons at 77 K have been extensively studied by means of optical absorption and electron spin resonance (ESR) measurements.[1] The temperature dependence of an electron scavenging reaction in this glassy matrix was first studied by Higashimura and two of the present authors (M. O. and H. Y.). They used the 4 K γ-irradiation technique combined with the ESR method. From the observed temperature dependence it was inferred that the scavenging efficiency of biphenyl was higher by about a factor of four at 4 K than at 77 K. This was attributed to a temperature-dependent competition among localization, charge recombination, and scavenging of electrons.[2] In this early study, however, the ESR measurements were made after warming of the samples to 77 K, so that ambiguity caused by the effect of warming could not be avoided. Hase *et al.* have tried to study the relaxation of electrons localized in the MTHF matrix by a 4 K irradiation-optical absorption method, but the spectrum of localized electrons obtained prior to their relaxation was not clear enough, mainly because of the efficient electron-scavenging at 4 K by impurities contained in the sample.[3] Hager and Willard have studied the relaxation of localized electrons in this matrix by generating them photolytically in the temperature range 10—97 K.[4]

Owing to the recent progress in pulse radiolysis studies at low temperatures, electron tunneling from localized states to scavenger molecules has become the prevailing interpretation of the mechanism for electron scavenging reactions in rigid matrices.[5] In this respect, we thought it was necessary to re-examine the temperature dependence of the electron scavenging in the MTHF matrix in a more quantitative way and also to examine the absorption spectrum of the localized electrons before their relaxation.

Experimental

MTHF was washed with an aqueous NaOH solution, distilled over Na metal, and dried with a Na–K alloy. Solutions of zone-refined biphenyl in MTHF were degassed with freeze-pump-thaw cycles, sealed in Suprasil quartz cells (0.2 cm optical path) under a vacuum of 10^{-5} Torr,† frozen in liquid nitrogen into the glassy state, and transferred into a liquid helium cryostat. In order to avoid breakage of the cells in liquid helium, the glass in the cells was usually made moderately cracked by introducing a tiny piece of quartz.

The samples were irradiated with ^{60}Co γ-rays at a dose rate of 6.24×10^{18} eV g^{-1} h^{-1} at 77 K (in the cryostat filled with liquid nitrogen) or at 4 K, and subjected to optical absorption measurements at the irradiation temperatures with a Shimadzu MPS-5000 spectrophotometer. Post-irradiation annealing of the samples irradiated at 4 K was carried out by transferring them into liquid nitrogen, keeping them there for ten minutes, and transferring them back into the liquid helium cryostat again. All measurements and the handling of the samples were carried out in complete darkness. The absorption spectra were corrected for the background absorption recorded before the irradiation.

Results and Discussion

Spectra of Localized Electrons. The absorption spectrum due to localized electrons in neat MTHF irradiated at 4 K initially showed a broad single peak at 1490 nm and a long absorption tail to the high energy side as shown in Fig. 1. Annealing at 77 K changed the spectral shape; it became red-shifted and double-peaked at 1150 and 1300 nm. Such a spectral change has been observed previously and was attributed to the rearrangement of MTHF molecules around electron

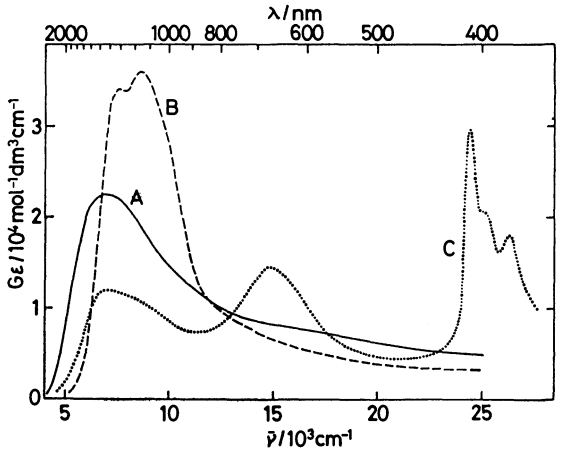

Fig. 1. Absorption spectra obtained from γ-irradiated MTHF at 4 K (A) in the absence and (C) presence of biphenyl. The spectrum B was obtained from γ-irradiated neat MTHF at 4 K after annealing the sample at 77 K for 10 min.

† 1 Torr≈133. 322 Pa.

traps.[3,4,6] The possibility that the spectral change is due to a redistribution of the electrons into deeper traps, as is the case for aqueous glasses[7] and (partly) for alcoholic glasses,[8] cannot yet be discarded however. Irrespective of the mechanism responsible for the spectral change, the localization of the electrons becomes deeper when the samples are annealed at 77 K. The spectral shape after the annealing is almost the same as that recorded from MTHF irradiated at 77 K.

The intensity increase at the absorption maximum during annealing seems to be complemented by a disappearance of the low-energy part of the absorption and an intensity decrease of the high-energy absorption tail. This kind of spectral change is theoretically expected from an effective deepening of electron traps on the basis of the cavity model.[9] Assuming no loss of electrons during annealing, the molar absorptivity at the absorption maximum, ε_{max}, of the electrons localized in shallow traps at 4 K is calculated to be 1.2×10^4 mol^{-1} dm^3 cm^{-1} at 1490 nm, based on the reported ε_{max} value, 1.9×10^4 mol^{-1} dm^3 cm^{-1} for the electrons localized in deep traps generated at 77 K.[10] It turns out that the yield (for 100 eV energy absorbed, *G*-value) of the localized electrons at 4 K is 1.9, which is significantly lower than the *G*-value at 77 K, 2.6.[11] This result is consistent with the previous finding[2] that the *G*-value at 4 K is 75% of that at 77 K in MTHF and is similar to the temperature-dependence of the *G*-values observed in glassy alkanes by steady-state measurements.[12] Klassen *et al.*,[13] however, have claimed, based on their pulse radiolysis study, that the apparent difference in the *G*-value is due to rapid decay of a fraction of localized electrons immediately after their formation. This is more significant at 4 K than at 77 K.

In the presence of a small amount of biphenyl in MTHF, the optical absorption signal recorded after the irradiation at 4 K is comprised of the spectrum due to localized electrons and that due to biphenyl molecular anions as is shown in Fig. 1C. Although the high-energy absorption tail of the electron spectrum could not be examined in detail because it was overlapped by the anion spectrum peaks at 395, 408, and 650 nm, the low-energy side of the electron spectrum is efficiently depleted. This depletion can probably be attributed to the selective scavenging by biphenyl of the localized electrons. In contrast, the electron spectrum at 77 K is depleted homogeneously by the addition of biphenyl. The heterogeneous depletion of electron spectra at 4 K has also been demonstrated for glassy ethanol.[14,15]

Electron Scavenging of Biphenyl. The yields of localized electrons and biphenyl anions were determined for 4 K and 77 K-irradiations as a function of the biphenyl concentration by graphically decomposing the recorded absorption curves into their component spectra. They are shown in Fig. 2. The electron yield at 77 K was determined from the absorption peak height at 1150 nm, while that at 4 K was estimated from the spectral intensity integrated down to 400 nm (below this wavelength, free radicals from MTHF contribute to the optical absorption[16]) to minimize the effect of the heterogeneous spectral depletion. The anion yield

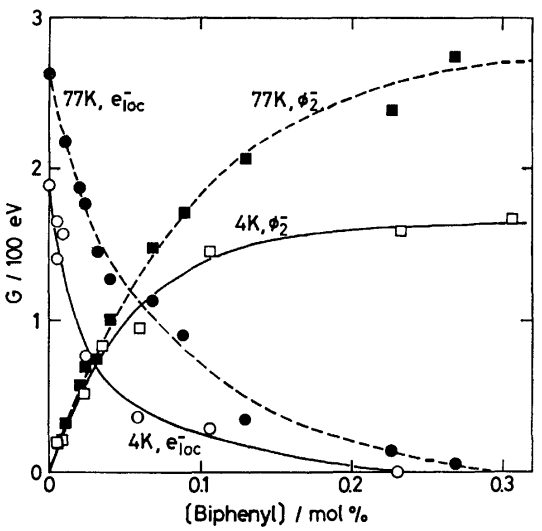

Fig. 2. Effect of biphenyl concentration on the yield of the localized electron, e^-_{loc}, and biphenyl anion, ϕ^-_2, in γ-irradiated MTHF at 4 and 77 K.

at 4 and 77 K was determined by using the ε_{max} at 408 nm measured at 77 K, 3.9×10^4 mol^{-1} dm^3 cm^{-1}, reported by Shida,[10] as the present study has shown ε_{max} to be independent of the temperature.

The plateau value of the anion yield at 77 K for high biphenyl concentrations agrees with the electron yield in the absence of the scavenger at the same temperature. The plateau value at 4 K is 1.7, which appears to be a little lower than the initial electron yield of 1.9. However, this small difference may be the result of the uncertainty in the ε_{max} value for the localized electrons at 4 K. If one assumes a partial disappearance of 10% of the localized electrons in the MTHF during annealing, then the ε_{max} value will be 1.1×10^4 mol^{-1} dm^3 cm^{-1} instead of 1.2×10^4 mol^{-1} dm^3 cm^{-1}, and agreement at 4 K will be attained between the yields of the localized electrons and the anions. Within the uncertainty of the present experiments, it can be concluded that the yield of scavengeable electrons is equal to the yield of stably localized electrons in the absence of the scavenger. The yield of such electrons is appreciably lower at 4 K than at 77 K.

Figure 2 also indicates the temperature dependence of the electron scavenging efficiency. The efficiency can be estimated from the reciprocal of that biphenyl concentration at which the electron yield is halved or from that where the anion yield is half of its plateau value. Biphenyl is about twice as efficient at 4 K as at 77 K in scavenging electrons. This temperature dependence is less significant but qualitatively consistent with the previous result obtained by ESR for the biphenyl–MTHF system.[2] When the concentration of added biphenyl exceeded 1 mol%, the *G*-value of the anion was found to decrease slowly at both 4 and 77 K. The reason for this is probably complicated.

Localization and Tunneling of Electrons. The temperature dependence of the electron yield combined with the complete conversion into biphenyl anions at a high enough biphenyl concentration naturally leads to the conclusion that at first the electrons are localized

in traps in the matrix; subsequently they are transferred to the scavenger molecules. If one assumes that the electrons are scavenged before localization, the observed temperature dependence of the electron yield can only be interpreted by the rather improbable hypothesis that the *G*-value of ionization is lower at 4 K than at 77 K, *i.e.*, that the *W*-value in the MTHF matrix is dependent on temperature. Otherwise, the plateau *G*-value of the anion should have been independent of temperature, as the electrons must be scavenged completely by biphenyl at sufficiently high concentrations.

The low *G*-value of localized electrons at 4 K is interpreted as a competition between electron localization and charge recombination. The former process will become less dominating at a lower temperature because of weaker interactions between the excess electron and the motions of the matrix molecules, so that the electron has a greater chance of encountering positive ions as its migration path is longer before being localized. An alternative interpretation is that a large fraction of the localized electrons have disappeared at low temperature before the steady-state measurements took place. This is the result of charge recombination by electron tunneling which competes with the slow relaxation of the localized electrons. This interpretation, however, seems unlikely as it predicts that the *G*-value of scavengeable electrons (the plateau *G*-value of the anions) is independent of temperature.

The transfer of the localized electrons to scavenger molecules has generally been explained by a tunneling mechanism.[5] The observed dependence of the electron and anion yields on the scavenger concentration is replotted in Fig. 3; this shows the survival probability of the localized electrons to decrease exponentially, consistent with the tunneling mechanism. The tunneling transfer of electrons in the MTHF matrix is also suggested by the previous observation that the rate of decay of the localized electrons by charge recombination deviates from an Arrhenius-type dependence in the low temperature region and is almost independent of temperature below 77 K.[17]

The slopes of the straight lines in Fig. 3 again indicate that the efficiency of scavenging of the localized electrons is about twice as high at 4 K as at 77 K. This

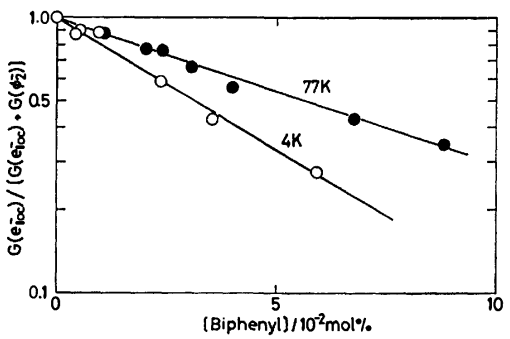

Fig. 3. Survival probability of the localized electron as a function of biphenyl concentration at 4 and 77 K.

temperature dependence can be understood qualitatively by taking into account that the height of the potential barrier to tunnel through is effectively lower for the electrons localized in shallow traps at 4 K than the ones in deep traps at 77 K. Unfortunately direct calculation of the tunneling probability is difficult or even impossible for the present case. The discrete electron energy pectrum of the chemical product of the scavenging reaction is unknown, so that the energy difference between electron-donating levels and electron-accepting levels can not be properly expressed in the calculation of the tunneling probability. Efficient scavenging of electrons localized in shallow traps has been reported also in glassy ethanol by using benzyl chloride[14] and toluene[15] as scavengers.

A part of this work was carried out in the Research Reactor Institute, Kyoto University. The authors wish to thanks Prof. Takenobu Higashimura for giving opportunity to use the experimental facilities.

References

1) See for examples: J. Paraszczak and J. E. Willard, *J. Chem. Phys.*, **70**, 5823 (1979); H. Yoshida and T. Higashimura, *Can. J. Chem.*, **48**, 504 (1970).

2) H. Yoshida, M. Ogasawara, T. Warashina, and T. Higashimura, *J. Chem. Phys.*, **56**, 4238 (1972).

3) H. Hase, M. Noda, and T. Higashimura, *J. Chem. Phys.*, **54**, 2975 (1971).

4) S. L. Hager and J. E. Willard, *J. Chem. Phys.*, **61**, 3244 (1974).

5) See for example: J. V. Beitz and J. R. Miller, *J. Chem. Phys.*, **71**, 4579 (1979).

6) L. Kevan, "Advances in Radiation Chemistry," ed by M. Burton and J. L. Magee, Wiley-Interscience, Publ., N. Y. (1974), Vol. 4, p. 181.

7) T. Q. Nguyen, D. C. Walker, and H. A. Gillis, *J. Chem. Phys.*, **69**, 1038 (1978); S. A. Dolivo and L. Kevan, *ibid.*, **68**, 4864 (1978).

8) M. Ogasawara, K. Shimizu, K. Yoshida, J. Kroh, and H. Yoshida, *Chem. Phys. Lett.*, **64**, 43 (1979); M. Ogasawara, K. Shimizu, and H. Yoshida, *Chem. Lett.*, **1980**, 1201; M. Ogasawara, K. Shimizu, and H. Yoshida, *Radiat. Phys. Chem.*, **17**, 331 (1981).

9) T. Ichikawa and H. Yoshida, *J. Chem. Phys.*, **73**, 1541 (1980).

10) T. Shida, *J. Phys. Chem.*, **73**, 4311 (1969).

11) D. R. Smith and J. J. Pieroni, *Can. J. Chem.*, **43**, 2141 (1965).

12) T. Kimura, N. Bremer, and J. E. Willard, *J. Chem. Phys.*, **66**, 1127 (1977).

13) N. V. Klassen and G. G. Teather, *J. Phys. Chem.*, **83**, 326 (1979).

14) T. Higashimura, A. Namiki, M. Noda, and H. Hase, *J. Phys. Chem.*, **76**, 3744 (1972).

15) S. Noda, K. Yoshida, M. Ogasawara, and H. Yoshida, *J. Phys. Chem.*, **84**, 57 (1980).

16) T. Ichikawa, H. Yoshida, and K. Hayashi, *J. Nucl. Sci. Tech.*, **9**, 34 (1972).

17) T. Ichikawa, H. Yoshida, and K. Hayashi, *Bull. Chem. Soc. Jpn.*, **46**, 812 (1973).

Adsorption Behavior of N-Containing Heterocycles at a Mercury/Water Interface

Osamu IKEDA,* Fumio GOTO, and Hideo TAMURA

Department of Applied Chemistry, Faculty of Engineering, Osaka University, Yamadaoka, Suita, Osaka 565

(Received March 11, 1981)

Adsorption behavior of 1-methylimidazole and 1-methylbenzimidazole at a mercury/water interface were investigated by electrocapillary measurement. These heterocycles showed a horizontal orientation at lower surface excesses, but at higher surface excesses a vertical one complicated by the presence of the horizontal one. In positive surface charge density, 1-methylbenzimidazole showed an anomalous behavior in which the potential drops across the inner layer, $\Delta_2^M\phi$ does not change with adsorption through the displacement of the water molecules on the electrode. The analysis of the electrosorption valency indicated the absence of a partial charge transfer between the electrode and the adsorbate. This anomalous behavior was interpreted by the compensation effect between the polarization of the water molecules due to the permanent dipoles and that of the 1-methylbenzimidazole molecules due to the dipoles induced in the electric field.

It has been observed that organic compounds with π-electron system show unique adsorption behavior, compared to the compounds lacking π-electron system. Gerovich *et al.*[1-4] studied adsorption of nonpolar organic compounds with π-electrons, such as benzene, anthracene, phenanthrene and chrysene, and found that the adsorbability of these compounds at positive surface charges increases with an increase in the number of benzene ring in the molecule and at the same time the potential of zero charge (p.z.c) shifts toward the negative potentials. They considered that these characteristics are due to a strong interaction between π-electrons and the positive charges. Similar consideration has also been given by Blomgren and Bockris,[5] and Conway and Barradas.[6,7] Damaskin *et al.* studied adsorption of aniline molecules[8] and anilinium cations[9] by the differential capacity measurement. They found that the capacity-potential curves at highly positive potentials measured in pure electrolyte solution and solution containing aniline or anilinium cation approximately coincide, and that the anode peak is caused by the reorientation process not the adsorption-desorption process. These results were explained as following: the aniline and the anilinium cations lie horizontally on the electrode surface with the positive charges and constitute a kind of extension of the metallic surface toward the solution; the double layer capacity changed very slightly.

Thereafter, the negative shift of the p.z.c due to adsorption of organic compounds with π-electron system has been attributed to the extension of the metallic surface[10] or the partial charge transfer.[11] However, the partial electron transfer from the adsorbed molecules to the electrode should increase the negative charge on the electrode, and as the result, the p.z.c seems to shift toward the positive direction. The possibility of this partial charge transfer was discussed in this study.

Furthermore, in the previous report[12] in which the adsorption behaviors of various N-containing heterocycles were studied, it was pointed out that imidazole adsorbed through aggregates due to intermolecular association,[13] because it did not take a vertical orientation owing to the large dipole moment.[14] It was also found that on positive surface charges the potential drop across the inner layer $\Delta_2^M\phi$ was not changed with adsorption of imidazole. This anomalous behavior was considered to result from an interaction between positive charges on the electrode and the aggregates at the outer layer without displacement of the water molecules adsorbed. In order to clarify the above two phenomena, namely the formation of aggregates and the anomalous adsorption behavior of a constant $\Delta_2^M\phi$, 1-methylimidazole (1-MI) without a possibility of intermolecular association,[15] and 1-methylbenzimidazole (1-MBI) with larger π-electron system were chosen, and their adsorption behavior at the mercury/water interface was studied. Besides the above two compounds which are classified into π-excessive heterocycles, quinoxaline, which is a π-deficient heterocycle, was also studied, but the adsorption equilibrium was not observed in the measurement of interfacial tension.

Experimental

All chemicals were analytical grade materials. 1-Methylimidazole (1-MI) was purified by distillation in a vacuum. 1-Methylbenzimidazole (1-MBI) was prepared by the methylation of benzimidazole,[16] and recrystallized twice from petroleum ether. Mercury was purified by treatment with dilute nitric acid, then triply distilled in vacuum. Nitrogen gas, after passing through a purification line, was used for deaeration of the solution. As the supporting electrolyte 0.099 M (1 M = 1 mol dm^{-3}) $NaClO_4$ containing 0.001 M NaOH was prepared from triply distilled water, and treated with purified active charcoal before use. The 0.001 M NaOH was used to depress the ionization of the adsorbates.

Adsorption behavior of 1-MI and 1-MBI was estimated from the analysis of the electrocapillary curves, which were measured by the maximum bubble pressure method.[17,18] The interfacial tension was measured at 50 mV intervals, except for positive and negative extrema where 25 mV intervals were chosen. The error of the measurement was ± 0.1 mN m^{-1} near the electrocapillary maximum, and ± 0.3 mN m^{-1} at positive and negative extrema. The measurement was carried out in a water bath thermostated at 25 ± 0.1 °C, and the potentials were measured against a normal calomel electrode (NCE).

Most of the parameters essential to adsorption were derived by analyzing the electrocapillary curves with a computer program. In the analysis, no corrections were made for the medium effect on the activity coefficient of the supporting electrolyte[19,20] and the activity coefficient of the adsorbate.[21]

Results and Discussion

Electrocapillary Curves. The electrocapillary data for 1-methylimidazole (1-MI) and 1-methylbenzimidazole (1-MBI) are summarized in Table 1. The interfacial tension, γ for 1-MBI dropped gradually with an increase in the concentration, C_{org}. However, such a change was not observed in quinoxaline (QX). Figure 1 shows the plot of γ at -0.5 V against log C_{org} with respect to 1-MBI and QX. The surface excess, Γ can be obtained by a differentiation of the above plot

$$(\partial\gamma/\partial \ln C_{org})_E = -RT\Gamma. \quad (1)$$

The interfacial tension for QX was nearly constant up to 1 mM, but fell abruptly beyond 2 mM, and then gradually at more than 5 mM. The surface excess obtained from the constant slope at higher concentrations is considered to be a saturated value of the surface excess, Γ_s. These values were 3.4×10^{-10} mol cm^{-2} for 1-MBI and 2.9×10^{-10} mol cm^{-1} for QX, which are in fair agreement with 2.9—3.0×10^{-10} mol cm^{-2} estimated from the projected areas assuming a horizontal orientation for both compounds, though somewhat large with 1-MBI.

Table 1. Electrocapillary data for 1-methylimidazole and 1-methylbenzimidazole

C_{org} / M	γ_{ecm} [a] / mN m^{-1}	$-E_{ecm}$ *vs.* NCE [b] / V
0(base soln) [c]	425.1	0.504
1-Methylimidazole		
0.005	423.7	0.505
0.007	423.2	0.504
0.010	422.7	0.507
0.015	421.8	0.510
0.020	421.2	0.511
0.030	419.8	0.510
0.040	418.8	0.510
0.050	417.9	0.512
0.070	416.3	0.505
0.100	414.4	0.502
0.150	412.2	0.501
0.200	410.2	0.499
0.300	307.2	0.491
1-Methylbenzimidazole		
0.00010	424.7	0.503
0.00015	424.2	0.506
0.00020	423.8	0.505
0.00030	422.9	0.505
0.00040	421.7	0.506
0.00050	420.6	0.508
0.00060	419.4	0.506
0.00070	418.4	0.515
0.00085	417.0	0.517
0.00100	415.7	0.528
0.00150	412.4	0.533
0.00200	409.9	0.540
0.00300	406.7	0.534

a) γ_{ecm} is the interfacial tension at the electrocapillary maximum. b) E_{ecm} is the potential of the electrocapillary maximum. c) Base solution consists of 0.099 M $NaClO_4$ and 0.001 M NaOH.

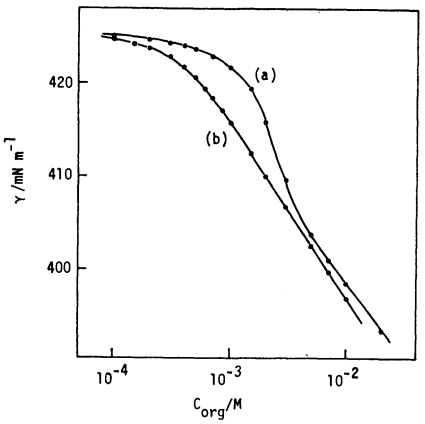

Fig. 1. Plot of γ at -0.5 V against log C_{org} for quinoxaline (a) and 1-methylbenzimidazole (b).

The relation for QX in Fig. 1 is similar to that in the presence of a diffusion limit, which was observed in the interfacial tension measurement due to drop time.[22] However, the concentration of 10^{-3} M where γ changes abruptly, is considered to be higher than that of 10^{-4} M observed for the diffusion limit. Probably, micelle formation[23] or polymeric aggregate formation due to an interaction with water molecules seems to be the cause.

Evaluation of Γ_s. The valuation of Γ_s is necessary to elucidate the adsorption state qualitatively. When adsorption can be described by a Langmuir isotherm, Γ_s is evaluated from the slope of the plot of x/Γ against x, where x is the molar fraction. If this is not the case, Γ_s can be evaluated simply from the extrapolation of the plot of $1/C_{org}$ against $1/\Gamma$ to $1/C_{org}=0$. From the nature of this plot, Γ_s obtained in this way reflects Γ_s at higher surface excesses. Therefore, the validity of the Γ_s at Γ_s should be confirmed by a fit to the isotherm molecular model.

The values of Γ_s evaluated by the above simple method are shown in Fig. 2 for 1-MI and 1-MBI. Various orientation parameters expected for 1-MI and 1-MBI were estimated using the CPK molecular model; these are shown in Fig. 3 for 1-MI and in Fig. 4 for

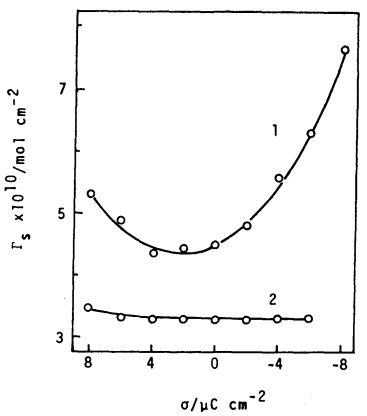

Fig. 2. Saturated value of surface excess as a function of surface charge density. (1) 1-Methylimidazole and (2) 1-methylbenzimidazole.

Table 2. Orientation parameters for 1-methylimidazole and 1-methylbenzimidazole

	1-Methylimidazole		1-Methylbenzimidazole	
	Horizontal	Vertical	Horizontal	Vertical
A_s/Å^2	35.7	21.5	54.6	29.7
Γ_s/mol cm^{-2}	4.7×10^{-10}	7.7×10^{-10}	3.0×10^{-10}	5.6×10^{-10}
d_1/Å	3.4	6.6	3.4	6.6

Here A_s and d_1 are the projected area and the molecular height from the electrode, respectively.

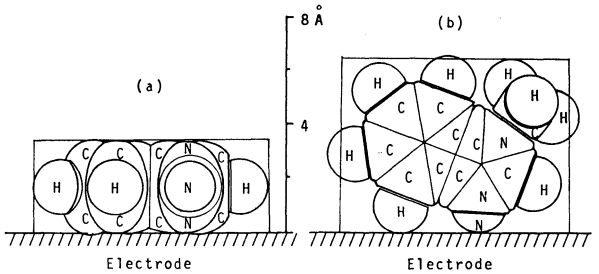

Fig. 3. Scale drawings of a 1-methylimidazole molecule adsorbed on the electrode through the horizontal orientation (a) and the vertical orientation (b). The area of rectangles enclosing the molecule in (a) and (b) correspond to the projected area of the vertical and the horizontal orientation, respectively.

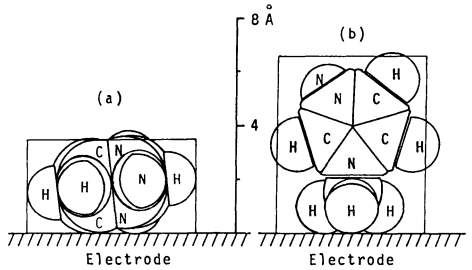

Fig. 4. Scale drawings of a 1-methylbenzimidazole molecule adsorbed on the electrode through the horizontal orientation (a) and the vertical orientation (b). The area of rectangles enclosing the molecule in (a) and (b) correspond to the projected area of the vertical and the horizontal orientation, respectively.

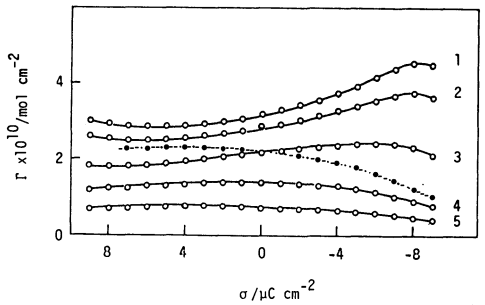

Fig. 5. Relations between surface excess and the surface charge density at various concentrations of 1-methylimidazole. The concentrations in M: (1) 0.3, (2) 0.2, (3) 0.1, (4) 0.03, and (5) 0.01. The broken line is for the 0.2 M imidazole.[12]

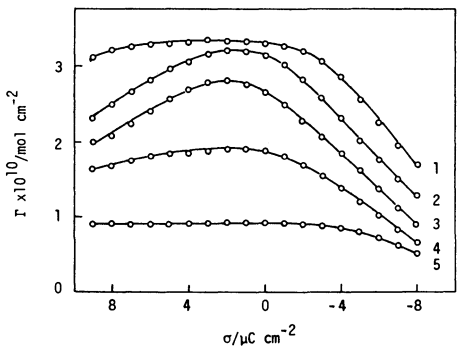

Fig. 6. Relations between surface excess and the surface charge density at various concentrations of 1-methylbenzimidazole. The concentrations in mM: (1) 3.0, (2) 1.0, (3) 0.6, (4) 0.4, and 0.2.

1-MBI. The paramenters obtained for a horizontal and a vertical orientation are summarized in Table 2.

Surface Excess. Figures 5 and 6 show the relations between Γ and surface change density σ with respect to 1-MI and 1-MBI, respectively. The broken line in Fig. 5 is the result for 0.2 M imidazole[12] obtained previously. Adsorption behavior of 1-MI is somewhat similar to that of imidazole at positive charges, but at negative charges it is quite different. From the results in Fig. 2 and Table 2, 1-MI is considered to take a horizontal orientation at lower surface excesses, but change to a vertical orientation at higher surface excesses, owing to the large dipole moment[24] and the absence of the intermolecular association.[15]

The difference in the adsorption behavior of imidazole and 1-MI supports the previous consideration[12] that imidazole adsorbs in an aggregate form. On the other hand, the adsorbability of 1-MBI is similar to that of imidazole, as can be seen from Fig. 6. This result also supports the formation of aggregate for imidazole, whose structure resembles that of 1-MBI with a large π-electron system and planarity.

Potential Drop across the Inner Layer, $\Delta_2^M\phi$. Figures 7 and 8 show the relations between $\Delta_2^M\phi$ at constant charge and Γ, with respect to 1-MI and 1-MBI, respectively. The values of $\Delta_2^M\phi$ were determined by the following equation

$$\Delta_2^M\phi = E - E_z - \phi_2, \qquad (2)$$

where E is the measured potential against NCE, E_z is the potential of zero charge obtained in the electrolyte without specific adsorption of ions (−0.472 V *vs.* NCE[25]), and ϕ_2 is the potential drop ascross the diffuse layer, which was determined using the Gouy-Chapman theory.[26]

The results in Fig. 7 also show that 1-MI changes its orientation from horizontal to vertical above a certain value of Γ. The change in the slope indicates that 1-MI at negative charges takes a vertical orientation with the positive pole of the dipole toward the electrode, but at positive charges it takes a vertical orientation with the

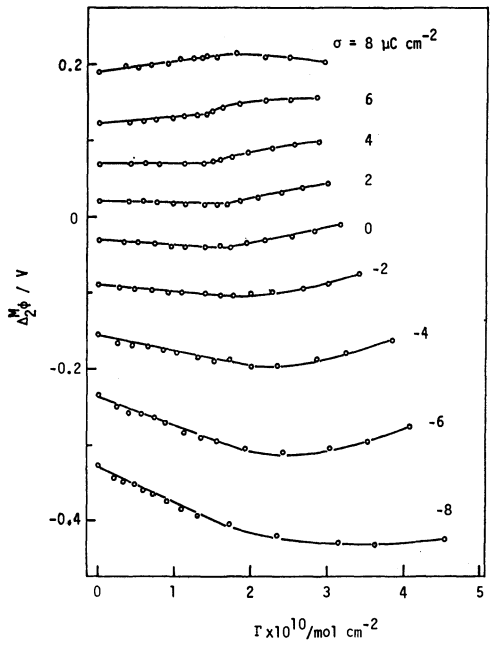

Fig. 7. Change in $\Delta_2^M\phi$ due to adsorption of 1-methylimidazole. Charge densities are indicated by each line.

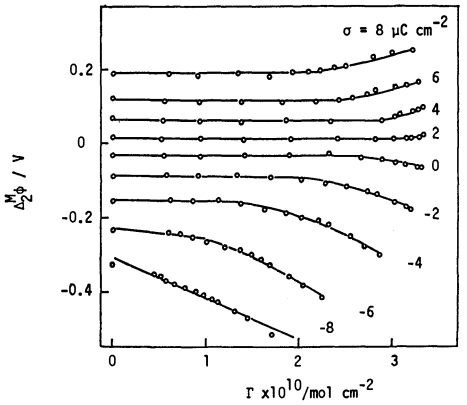

Fig. 8. Change in $\Delta_2^M\phi$ due to adsorption of 1-methylbenzimidazole. Charge densities are indicated by each line.

negative pole of the dipole towards the solution side.

The results in Fig. 8 show the presence of the region where $\Delta_2^M\phi$ does not change due to adsorption of 1-MBI, especially in $\sigma \geq -2\ \mu C\ cm^{-2}$. This is similar to the results obtained in imidazole.[12] In general, organic compounds without a net dipole moment, such as pyrazine, exhibit a constant $\Delta_2^M\phi$ around $\sigma = -4\ \mu C\ cm^{-2}$,[27] where the orientation of water molecules on the electrode becomes most disordered, they show linear lines with a positive or negative slope at more positive or negative charges than -2——$4\ \mu C\ cm^{-2}$, respectively. An example is shown in Fig. 9 for pyrazine. This was obtained in the previous experiment[12] and was nearly same as that reported by Conway *et al.*[28]

The anomalous adsorption behavior of 1-MBI appears to result from an adsorption without displacement of the adsorbed water molecules. However, such an adsorption seems to be unreasonable, because

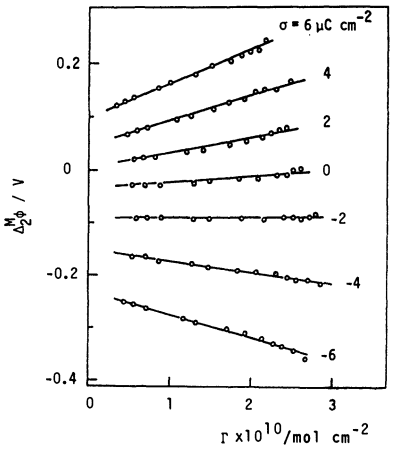

Fig. 9. Change in $\Delta_2^M\phi$ due to adsorption of pyrazine. Charge densities are indicated by each line.

adsorption due to the displacement of water actually occurs at fairly negative charges, as can be seen from Fig. 8; generally organic compounds without a net dipole moment adsorb strongly at low electric fields. This behavior of 1-MBI will be discussed precisely in the following sections.

The constancy of $\Delta_2^M\phi$ disappeared at higher surface excesses. The cause is not clear at the present time. However, note the following: (1) Γ_s of 1-MBI at the holizontal orientation was estimated from the projected area to be 3.0×10^{-10} mol cm^{-2}, which is somewhat smaller than that of 3.4×10^{-10} mol cm^{-2} determined from the experiment. A vertical orientation contributing to a change in $\Delta_2^M\phi$ through the dipole moment will be mixed with the horizontal orientation at higher surface excesses. (2) Specifically adsorbed perchlorate ions will be desorbed at higher surface excesses.

The Adsorption Isotherm and Free Energy of Adsorption. The determination of the adsorption isotherm and the free energy of adsorption at infinite dilution, $\Delta\bar{G}^\circ$, was carried out in the region where the change in the orientation was considered to be negligible, namely at lower surface excesses for 1-MI and that showed a constant $\Delta_2^M\phi$ for 1-MBI.

By examining a fit to various isotherms, 1-MI and 1-MBI were found to obey the Langmuir (Fig. 10) and the Frumkin isotherm (Fig. 11) with $\Gamma_s = 3.0\times10^{-10}$

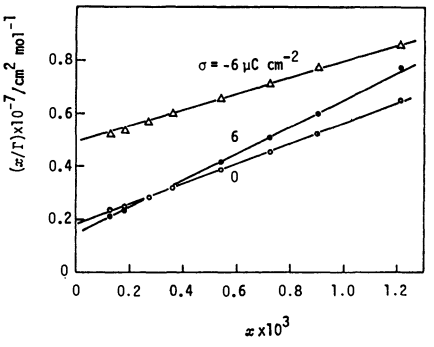

Fig. 10. Test of the Langmuir isotherm for adsorption of 1-methylimidazole at various charge densities. Charges are indicated by each line.

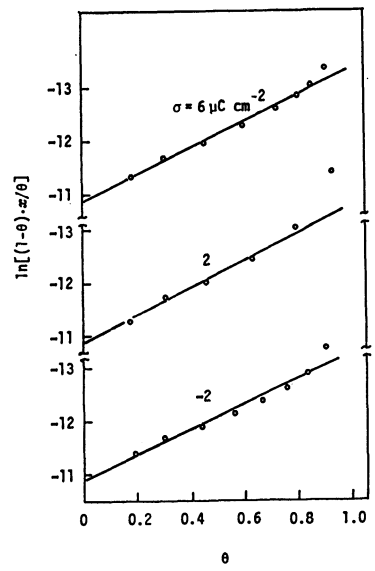

Fig. 11. Test of the Frumkin isotherm with $\Gamma_s=3.0\times10^{-10}$ mol cm^{-2} for adsorption of 1-methylbenzimidazole at various charge densities. Charges are indicated by each line.

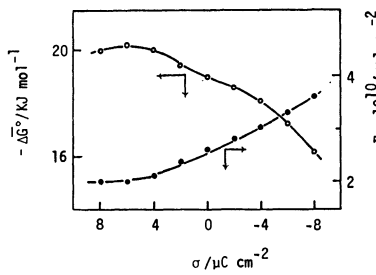

Fig. 12. Variation of $\Delta\bar{G}^\circ$ and Γ_s for 1-methylimidazole due to surface charge density.

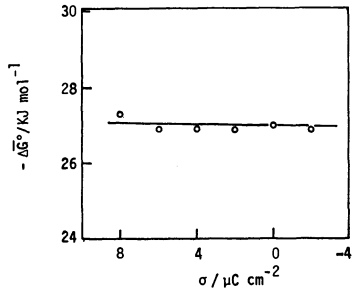

Fig. 13. Variation of $\Delta\bar{G}^\circ$ for 1-methylbenzimidazole due to surface charge density.

mol cm^{-2} and the interaction parameter $2a=2.5$, respectively.

Γ_s and $\Delta\bar{G}^\circ$ obtained for 1-MI are shown in Fig. 12. $-\Delta\bar{G}^\circ$ was increased with an increase in the surface charge, and the maximum was observed at highly positive charges. This behavior is typical to that of organic compounds with π-electrons. On the other hand, $\Delta\bar{G}^\circ$ for 1-MBI was charge independent, as shown in Fig. 13. If the isotherms are congruent to charge the slopes of linear lines in Fig. 8 are related to the change in $\Delta\bar{G}^\circ$ due to surface charge[29]

$$(\partial\Delta_2^M\phi/\partial\theta) = -RT\Gamma_s(\partial \ln\beta/\partial\sigma), \quad (3)$$

where $\beta=\exp(-\Delta\bar{G}^\circ/RT)$. Since both $(\partial\Delta_2^M\phi/\partial\theta)$ and $(\partial\ln\beta/\partial\sigma)$ are nearly zero, Eq. 3 is set up for adsorption of 1-MBI. This indicates that the experimental results are reliable and the final picture is consistent.

Quantitative Interpretation of Adsorption. From the fit to the adsorption isotherm, the horizontal orientation was approximately confirmed for both 1-MI and 1-MBI at lower surface excesses. Further to verify this, evaluation of the dipole moment at the adsorbed state was made at $\sigma=0$ μC cm^{-2}, to simplify the calculation.

In general, if the adsorption of an organic compound is charge congruent, the change in $\Delta_2^M\phi$ can be described by the following equation[30]

$$\Delta(\Delta_2^M\phi)/\theta = (\Gamma_sP_1/\varepsilon_1-\Gamma_snP_0/\varepsilon_0) + \sigma(1/C_1-1/C_0), \quad (4)$$

where P, ε, and C are the effective normal dipole moment, the permittivity of the inner layer and the inner layer capacity, respectively, n is the number of water molecules displaced by adsorption of one adsorbate molecule, and subscripts 1 and 0 denote the surface layer saturated with the adsorbate and water. The potential drop due to water dipoles, Δg^w_{dipole} can be represented by Eq. 5

$$\Delta g^w_{dipole} = -\Gamma_snP_0/\varepsilon_0. \quad (5)$$

The ε_1 can be obtained from C_1 using the relation, $C_1=\varepsilon_1/d_1$, where d_1 is the thickness of the adsorption layer. Further, the values of C_1 can be obtained by the extrapolation of the linear relation between $1/C^i$ and Γ at $\sigma=0$ μC cm^{-2}, as shown in Fig. 14, to the corresponding to Γ_s. They were 32.5 μF cm^{-2} for 1-MI and 40.0 μF cm^{-2} for 1-MBI.

One can obtain 30 mV as Δg^w_{dipole} at $\sigma=0$ μC cm^{-2} from Bockris and Habib's water adsorption model,[31] and 3.4 Å as d_1 from Table 2, and -20 mV for 1-MI and -13 mV for 1-MBI as $\Delta(\Delta_2^M\phi)/\theta$ from Figs. 7 and 8. By introducing the above values into Eq. 4, the effective normal dipole moment at $\sigma=0$ μC cm^{-2}, P_1 was found to be -1.1 Debye for 1-MI and -1.0 Debye for 1-MBI. The negative value of P_1 means an orientation with the negative pole of the dipole of the adsorbate toward the electrode. However, the above values seem to be too large, compared with the value

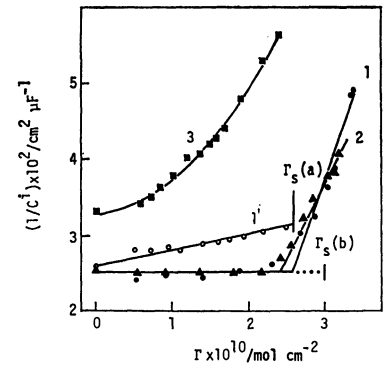

Fig. 14. Plot of $1/C^i$ against Γ at various charge densities. Open and closed symbols correspond to 1-methylimidazole and 1-methylbenzimidazole, respectively. Charge density in μC cm^{-2}: (1) and (1′) 0, (2) 6 and (3) -6. Γ_s (a) and Γ_s (b) represent Γ_s of 1-methylimidazole and 1-methylbenzimidazole at the horizontal orientation, respectively.

expected for the horizontal orientation, $P_1=0$ Debye, The cause of the large negative values is probably the presence of the specifically adsorbed perchlorate anions, which contribute to the negative dipole moment. Therefore, the effect of the specific adsorption of perchlorate anion was taken into consideration in the calculation of the true P_1. In this calculation, the data obtained by Payne[32] in the mixed solution of 0.1 M NH_4ClO_4 and 0.9 M NH_4F was used. The procedures are as follows: (i) If the specific adsorption of ClO_4^- is deducted, $\Delta_2^M\phi$ shifts towards a positive direction by 31 mV, which is the difference between $\Delta_2^M\phi$ at $\sigma=0$ μC cm^{-2} in the base solution of 0.099 M $NaClO_4$+ 0.001 M NaOH, -0.031 V and that in the 0.1 M NaF,[33] 0 V. (ii) In the absence of the specific adsorption of ClO_4^-, true surface charge density at -0.504 V. which is the p.z.c for the base solution, can be estimated to be -0.64 μC cm^{-2} from the result on 0.1 M NaF,[33] then Δg^{w}_{dipole} at that charge amounts to 24 mV.[31] (iii) True value of C_1, C_1^t is given by the following relation derived using the data of Payne[32]

$$1/C_1^t = 1/C_1^a + 4.73\times10^{-3}, \quad (6)$$

where C_1^a is the apparent value of C_1 in the presence of specifically adsorbed perchlorate ions. After the above treatment, the true P_1 was calculated to be -0.2 Debye for 1-MI and -0.1 Debye for 1-MBI. These values are reasonable for the horizontal orientation.

Electrosorption Valency.[11] It was discussed on the basis of the electrosorption valency whether the constancy of $\Delta_2^M\phi$ observed clearly in 1-MBI results from a partial charge transfer or not. Figure 15 shows a change in σ at constant $\Delta_2^M\phi$ due to adsorption of 1-MBI. The electrosorption valency, r is defined by Eq. 7

$$r = (1/F)(\partial\sigma/\partial\Gamma)_{\Delta_2^M\phi}, \quad (7)$$

where F is the Faraday constant. Further, r at $\Delta_2^M\phi=0$, r_N is represented by Eq. 8 with respect to neutral organic compounds

$$r_N = -\lambda(1-g) + K^{ad} - nK^w, \quad (8)$$

where λ is the partial charge transfer coefficient, g is the geometric factor defined as $(X_o-X_a)/X_0$, X_o, and X_a are the distance of the outer Helmholtz plane and the adsorption plane from the electrode, respectively, K_{ad} and K_w are the dipole terms of the adsorbate and water, and n is the same as used in Eq. 4. The value of r is plotted as a function of $\Delta_2^M\phi$ in Fig. 16, from which r_N was estimated to be 0.0035.

As can be seen from Fig. 14, and as Eq. 4 and the result in Fig. 8 predict, C_1 and C_0 for 1-MBI are nearly equal in the region where the constancy of $\Delta_2^M\phi$ is observed. This implies compensation between $(\Gamma_s P_1/\varepsilon_1)$ and $(-\Gamma_s n P_0/\varepsilon_0)$. Therefore, $(K_{ad}-nK_w)$ in Eq. 8 becomes also zero. If X_o and X_a can be represented by the sum of d_1 and the ionic radius of Na^+(0.96 Å), and the half of d_1, respectively, g is calculated to be 0.61. Finally one obtains λ near 0.01. However, this value is too small to be considered a partial charge transfer between the electrode and the adsorbed 1-MBI molecules.

What is the compensation between $(\Gamma_s P_1/\varepsilon_1)$ and $(-\Gamma_s n P_0/\varepsilon_0)$? If this effect results from a partial charge transfer, it corresponds to the increased negative dipole moment or charge in 1-MBI. That means the partial electron transfer from the electrode to the adsorbed 1-MBI molecules. Since the compensation is observed even at fairly positive charges, the above deduction is hard to accept. The most reasonable consideration will be an electronic polarization effect. Thus, the dipole moment of 1-MBI induced in the electric field compensates for the dipole moment of the water molecules displaced. Further, this effect is valid at positive charges and seems to disappear at highly negative electric field because of increased repulsion between π-electrons and the negative charges on the electrode surface.

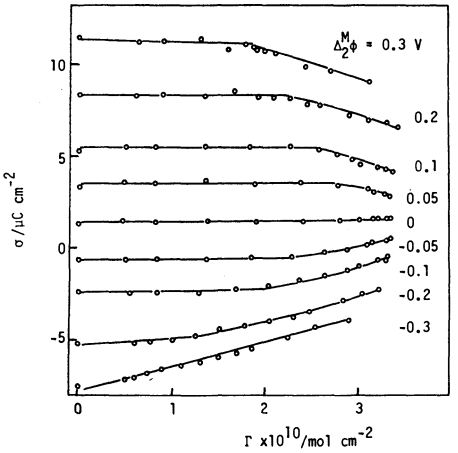

Fig. 15. Change in σ at constant $\Delta_2^M\phi$ due to adsorption of 1-methylbenzimidazole. The values of $\Delta_2^M\phi$ are indicated by each line.

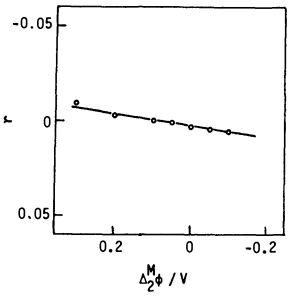

Fig. 16. Variation of electrosorption valency due to $\Delta_2^M\phi$.

The compensation effect observed in this study correlates with the constant adsorbability in positive charges. Such an adsorbability was clearly observed for heterocycles classified into π-excessive type, for example 1-MI and 1-MBI in this study, and imidazole and pyrazole,[12] but not so clearly observed for those classified into π-deficient type, for example pyrazine, pyrimidine and pyridazine.[12] These results are also considered to support the compensation effect observed in 1-MBI which has easily polarizable π-electrons. Recently, King *et al.*[34] explained the enormous intensity enhancement observed for Raman scattering from pyridine adsorbed on the electrode on the basis of a classical electrostatic theory, namely electronic polarization.

References

1) M. A. Gerovich and O. G. Ol'man, *Zh. Fiz. Khim.*, **28**, 19 (1954).
2) M. A. Gerovich, *Dokl. Akad. Nauk SSSR*, **96**, 543 (1954).
3) M. A. Gerovich, *Dokl. Akad. Nauk SSSR*, **105**, 1278 (1955).
4) M. A. Gerovich and G. F. Rybal'chenko, *Zh. Fiz. Khim.*, **32**, 109 (1958).
5) E. Blomgren and J. O'M Bockris, *J. Phys. Chem.*, **63**, 1475 (1959).
6) B. E. Conway and R. G. Barradas, *Electrochim. Acta*, **5**, 319 (1961).
7) B. E. Conway and R. G. Barradas, *Electrochim. Acta*, **5**, 349 (1961).
8) B. B. Damaskin, I. P. Mishutushkina, V. M. Gerovich, and R. I. Kaganovich, *Zh. Fiz. Khim.*, **38**, 1797 (1964).
9) S. L. Dyatkina and B. B. Damaskin, *Elektrokhimiya*, **2**, 1340 (1966).
10) Yu. M. Loshkarev, V. V. Trofimenko, and A. A. Kuznetsov, *Elektrokhimiya*, **11**, 1724 (1975).
11) J. W. Schultze and K. J. Vetter, *J. Electroanal. Chem.*, **44**, 63 (1973).
12) H. Tamura, O. Ikeda, and K. Kataoka, *Elektrokhimiya*, **14**, 699 (1978).
13) M. Mauret, J. P. Fayet, and M. Fabre, *Bull. Soc. Chim. Fr.*, **1975**, 1675.
14) W. Hückel, J. Datow, and E. Simmerbach, *Z. Phys. Chem.*, **186A**, 129 (1940).
15) L. Hunter and J. A. Mariott, *J. Chem. Soc.*, **1941**, 777.
16) A. F. Pozharskii and A. M. Simonov, *Zh. Obshch. Khim.*, **33**, 179 (1963).
17) D. J. Schiffrin, *J. Electroanal. Chem.*, **23**, 168 (1969).
18) O. Ikeda, Y. Matsuda, H. Yoneyama, and H. Tamura, *Electrochim. Acta*, **21**, 519 (1976).
19) A. De. Battisti and S. Trasatti, *J. Electroanal. Chem.*, **54**, 1 (1974).
20) D. M. Mohilner and H. Nakadomari, *J. Phys. Chem.*, **77**, 1594 (1973).
21) D. M. Mohilner, L. W. Browman, S. J. Freeland, and H. Nakadomari, *J. Electrochem. Soc.*, **120**, 1658 (1973).
22) R. Guidelli and M. R. Moncelli, *J. Electroanal. Chem.*, **89** , 261 (1978).
23) R. Tamamushi and T. Yamanaka, *Bull. Chem. Soc. Jpn.*, **28**, 673 (1955).
24) V. I. Minkin, O. A. Osipov, A. D. Garnovskii, and A. M. Simonov, *Zh. Fiz. Khim.*, **36**, 469 (1962).
25) P. Delahay, "Double Layer and Electrode Kinetics," Interscience, New York (1966), p. 23.
26) D. C. Grahame, *Chem. Rev.*, **41**, 441 (1947).
27) S. Trasatti, *J. Electroanal. Chem.*, **28**, 257 (1970).
28) B. E. Conway, H. P. Dhar, and S. Gottesfeld, *J. Colloid Interface Sci.*, **43**, 303 (1973).
29) R. Parsons, *Trans. Faraday Soc.*, **55**, 999 (1959).
30) R. Parsons, R. Peat, and R. M. Reeves, *J. Electroanal. Chem.*, **34**, 191 (1972).
31) J. O'M Bockris and M. A. Habib, *Electrochim. Acta*, **22**, 41 (1977).
32) R. Payne, *J. Phys. Chem.*, **70**, 204 (1966).
33) C. D. Russell, *J. Electroanal. Chem.*, **6**, 486 (1963).
34) F. W. King, R. P. Duyne, and G. G. Schatz, *J. Chem. Phys.*, **69**, 4472 (1978).

  Bull. Chem. Soc. Jpn., 54, 3153—3156 (1981)

"Macromolecular Ion Flotation" of MnO_4^- by Combined Use of Macromolecular Anion and Cationic Surfactant

Tsunetaka SASAKI,* Kiyoo MATSUBARA, and Ikuko MACHIDA

Department of Chemistry, Faculty of Science, Tokai University, 1117 Kitakaname, Hiratsuka 259-12

(Received March 26, 1981)

MnO_4^- ions in aqueous solution were subjected to macromolecular ion flotation, a process of flotation applied for an aqueous solution containing organic or inorganic ions to be floated, macromolecular ions including macroscopic or colloidal particles with an ion exchange capacity and polymer ions, and oppositely charged ionic surfactant. The macromolecular anions examined were basic aluminum chloride, polyaluminum chloride, carboxymethylcellulose, sodium polyacrylate, sodium alginate, potassium poly(vinyl sulfate), sodium hexametaphosphate, polyphosphoric acid, polyacrylic acid, bentonite, and sodium metasilicate. As a cationic surfactant, hexadecyltrimethylammonium chloride was used. All the above substances are effective for the MnO_4^- ion flotation, whereas low molecular substances such as Na_3PO_4 are ineffective, when used with the cationic surfactant. Molecular models of sublate formed during the macromolecular ion flotation are proposed.

In our prevous papers,[1-2] we have confirmed that combined use of macromolecular or polymer anions, such as bentonite and silicate ions, with a cationic surfactant is effective for the flotation of both organic and inorganic anions and cations. The purpose of the present investigation is to examine whether or not macromolecular anions, including both macroscopic or colloidal particles with cation exchange capacity and polymer anions, are in general effective for ion flotation when used in combination with a cationic surfactant.

MnO_4^- ions were adopted as the ions to be subjected to flotation. The macromolecular ions tested were aluminum chloride ($AlCl_3$) and polyaluminum chloride ($PAlCl_3$) in basic solution, carboxymethylcellulose (CMC), sodium polyacrylate (NaPA), sodium alginate (NaAlg), potassium poly(vinyl sulfate) (KPVS), sodium hexametaphosphate (NaHMP), polyphosphoric acid (PPA), polyacrylic acid (PAA), bentonite (Bt), and sodium metasilicate (NaMS); NaHMP and PPA, not high molecules, were adopted since they behave similarly to high polymer ions with respect to the flotation. The cationic surfactant tested was hexadecyltrimethylammonium chloride (HTAC) which had shown good floatability for both anions and cations.

Experimental

Materials. Commercial products of pure grade were used for $AlCl_3$ ($AlCl_3 \cdot 6H_2O$), $PAlCl_3$ ($AlCl_3 \cdot nAl_2O_3$, Al_2O_3 content 30 wt%), CMC (dp, 700—850), NaPA (dp, 22000—66000), NaAlg (relative viscosity, 15.67 at 30 °C), KPVS (dp, 1500), NaHMP ($[NaPO_3]_6$), PPA ($P_6O_4H_{13}$), PAA (dp, 8000—12000), Bt (montmorillonite), NaMS ($Na_2SiO_3 \cdot 9H_2O$), trisodium phosphate (TNaP), and potassium permanganate.

Measurement. The concentration of silicate ions was measured colorimetrically at the wavelength 450 nm[3] from the color developed by adding an aqueous solution of ammonium molybdate to a sample liquor. The concentration of permanganate ions was determined by the usual titrimetric method using a solution of sodium oxalate. The concentration of each of the remainder was determined by dissolving its known amount of dried substance in water; concentration of $PAlCl_3$ could not be determined accurately due to its Al_2O_3 content indicated 30 wt%, being qualitative.

The solution to be subjected to flotation processing was prepared to contain MnO_4^- ions at a constant concentration around 1.6×10^{-4} mol dm^{-3}, proper amounts of one or some macromolecular ions and HTAC, a small amount of NaPA if necessay, and HCl or NaOH for pH control when needed. A volume (12 cm^3 for the systems of Table 1 and 10 cm^3 for the other systems) of the solution thus prepared was put into a stoppered test tube, 1.6 cm in inner diameter and 19 cm in engths, equipped with a stop cock at its bottom. It was slowly mixed and kept standing for 1 min, then vigorously shaken by hand to float MnO_4^- ions. After 5 min of standing, the lower portion was taken out and its MnO_4^- concentration was measured by use of a Shimazu Model Spectronic-20 spectrophotometer at wavelength 525 nm; the specific absorbance had been confirmed to be independent of the pH range 1—11 at this wavelength. The floatability of MnO_4^- ions was calculated from the difference between concentrations before and after the flotation processing on MnO_4^- ions.

Results and Discussion

Table 1 shows results of preliminary measurements on the MnO_4^- ion flotation by the combined use of macromolecular ions and HTAC. In these measurements, the concentration of MnO_4^- ions was kept constant at 1.59×10^{-4} mol dm^{-3} in average. The concentrations of macromolecular ions and HTAC are not necessarily for the optimum flotation condition; Table 1 is compiled

Table 1. Macromolecular ion flotation of MnO_4^-

Macromolecule		HTAC	NaPA	pH	Floatability/%
Substance	Concn / ppm	Concn / ppm	Concn / ppm		
$AlCl_3$	996	55	1.67	9.8[a]	87
$PAlCl_3$	548	55	1.67	9.8[a]	88
CMC	666	833	—	6.3	100
NaPA	388	809	—	1.5[b]	98
NaAlg	1667	2447	—	6.8	98
KPVS	898	1691	—	1.1[b]	100
NaHMP	2196	3306	—	1.5[b]	100
PPA	10670	826	—	1.3	99
PAA	4514	1664	—	2.3	90
Bt	5839	662	—	8.8	100
NaMS	1314	500	—	11.2	98

a) NH_3 added. b) HCl added. $[MnO_4^-] = 1.59 \times 10^{-4}$ mol dm^{-3}. For the abbreviation of the substance names see text.

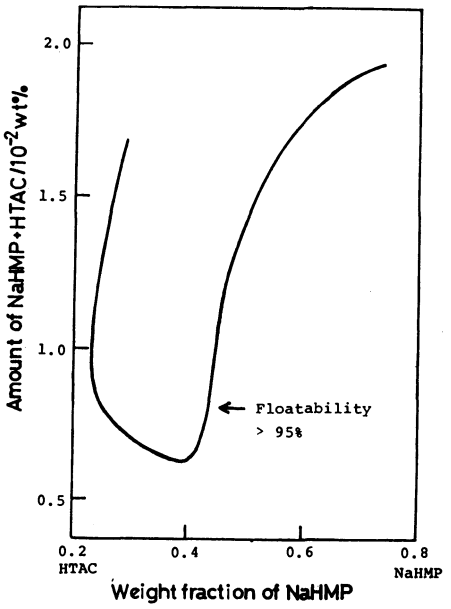

Fig. 1. Diagram of MnO_4^- ion flotation by NaHMP, HTAC, and HCl.
MnO_4^-: 1.49×10^{-4} mol dm^{-3}, pH: 1.4.

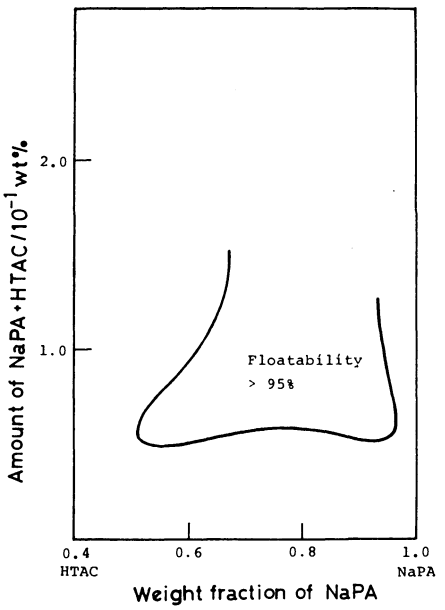

Fig. 3. Diagram of MnO_4^- ion flotation by NaPA, HTAC, and HCl.
MnO_4^-: 1.64×10^{-4} mol dm^{-3}, pH: 1.4.

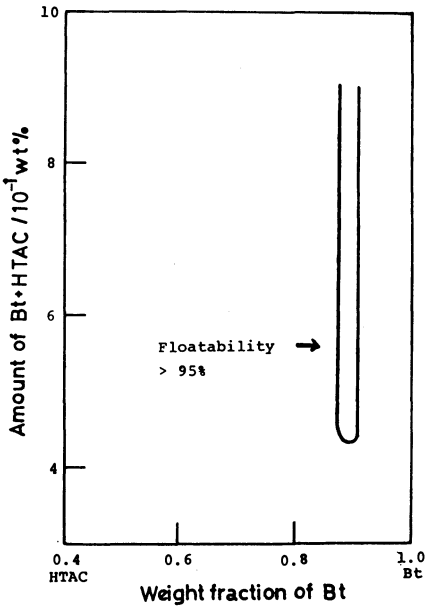

Fig. 2. Diagram of MnO_4^- ion flotation by Bt and HTAC.
MnO_4^-: 1.69×10^{-4} mol dm^{-3}, pH: 8.8.

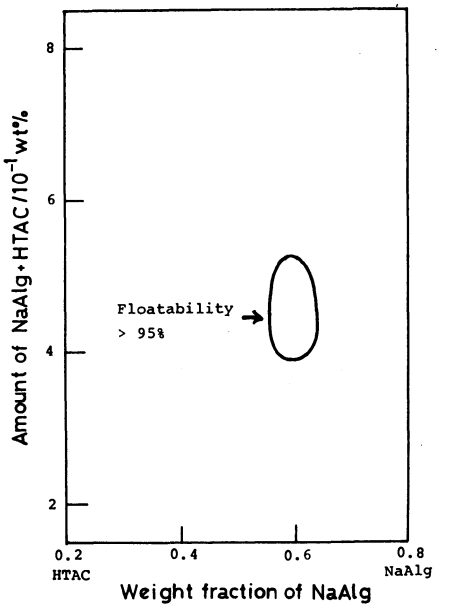

Fig. 4. Diagram of MnO_4^- ion flotation by NaAlg and HTAC.
MnO_4^-: 1.64×10^{-4} mol dm^{-3}, pH: 6.7.

merely to show a possibility of effective ion flotatition of MnO_4^- by combined use of macromolecular anions and cationic surfactant. As seen from Table 1, many macromolecular anions, when used with HTAC, are effective for the flotation of MnO_4^- ions, whereas low molecular electrolytes were found ineffective for that flotation, as exemplified by as low a floatability as 46% which TNaP showed at pH 1.1 (not indicated in Table 1). On the basis of this finding, the present authors propose the term "Macromolecular ion flotation" for such flotations as are effected by use of macromolecular or polymer ions and ionic surfactants both carrying charges opposite to each other; the present investigation has dealt with a case of combination of macromolecular anions with an cationic surfactant and the preceding paper[4] reported a case of effective use of poly(ethyleneimine) (cationic macromolecule) and sodium dodecyl sulfate (anionic surfactant).

For several systems in Table 1, flotation of MnO_4^- ions was studied in dedail by varying the ratio of macromolecular anions to HTAC and their total amount while the concentration of MnO_4^- ions was kept constant. The results obtained are shown in Figs. 1 to 5 for NaHMP+HTAC+HCl, Bt+HTAC, NaPA+HTAC+HCl, NaAlg+HTAC, and CMC+HTAC systems, respectively, each of which was treated similarly

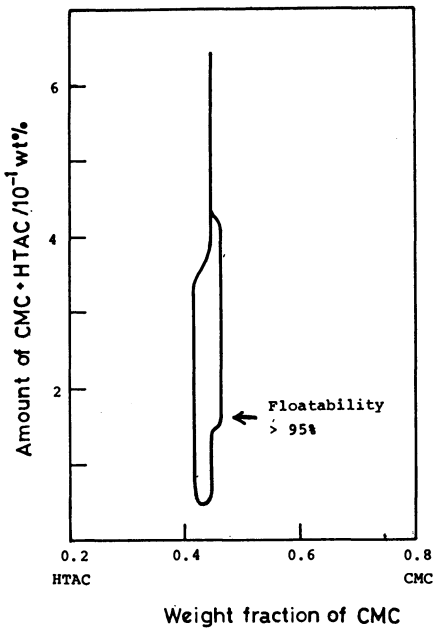

Fig. 5. Diagram of MnO_4^- ion flotation by CMC and HTAC.
MnO_4^-: 1.58×10^{-4} mol dm^{-3}, pH: 6.

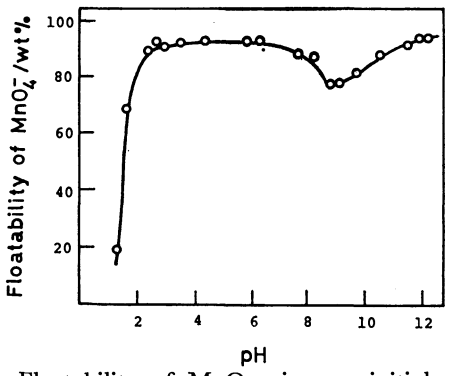

Fig. 6. Floatability of MnO_4^- ion *vs.* initial pH for NaMS+HTAC system.
MnO_4^-: 1.67×10^{-4} mol dm^{-3}, NaMS: 7570 ppm HTAC: 240.4 ppm.

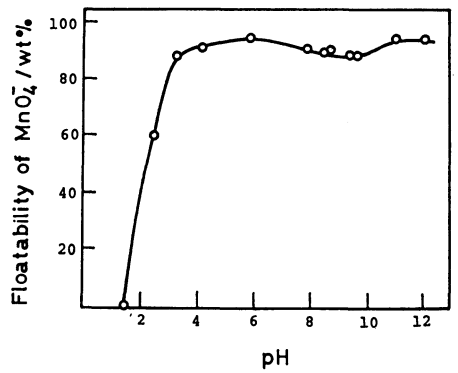

Fig. 7. Floatability of MnO_4^- ion *vs.* initial pH for NaAlg+HTAC system.
MnO_4^-: 1.67×10^{-4} mol dm^{-3}, NaAlg: 2000 ppm, HTAC: 2995 ppm.

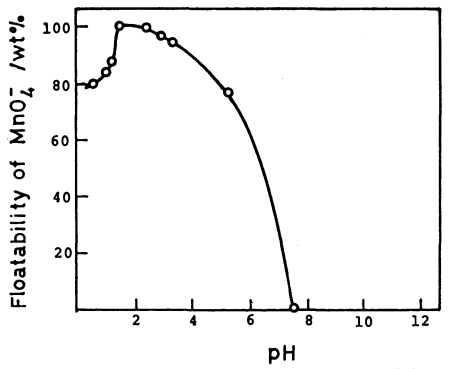

Fig. 8. Floatability of MnO_4^- ion *vs.* initial pH for NaPA+HTAC+HCL system.
MnO_4^-: 1.67×10^{-4} mol dm^{-3}, NaPA: 400.5 ppm, HTAC: 240.4 ppm.

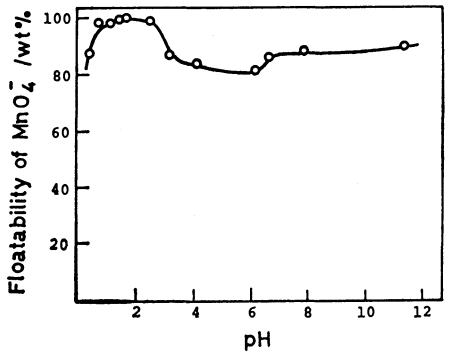

Fig. 9. Fostsbility of MnO_4^- ion *vs.* initial pH for NaHMP+HTAC system.
MnO_4^-: 1.67×10^{-4} mol dm^{-3}, NaHMP: 5365 ppm, HTAC: 5191 ppm.

to the NaMS+HTAC system already reported.[1] In each solution studied, the concentration of MnO_4^- ions and pH are given in the caption of each figure. In these diagrams, the floatability of the system is greater than 95% in the areas inside the curves. Thus we can confirm wide ranges of composition to be effective for ion flotation for the systems of Figs. 1 and 3, while we note narrow vertical ranges of the effective ion flotation, and only a small region for the system of Fig. 4. For the cases of Figs. 2 and 5, a nearly constant weight ratio of macromolecular ions to surfactant may be expected for the sublate composition, similarly to the case of NaMS+HTAC system already reported.[1]

To get the pH dependence of flotation efficiency of MnO_4^- ions, a study was made on the systems of NaMS+HTAC,** NaAlg+HTAC, NaPA+HTAC+HCl, and NaHMP+HTAC. The initial pH of solution was controlled by addition of HCl or NaOH. The results are shown in Figs. 6 to 9, where as a whole, floatabilities are seen to exceed 90% over a wide pH range, especially in acidic regions for the NaPA and NaHMP systems, attaining nearly 100%.

It is confirmed from the above results that the composition and total concentration of the set of macromolecular ions and surfactant as well as the pH of solution are important factors affecting the floatabiitly

** The corresponding composition diagram has been shown in the preceding paper.[1]

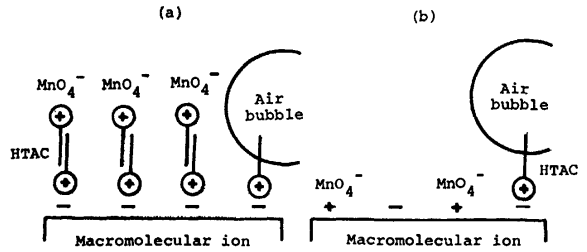

Fig. 10. Sublate structures of MnO_4^-+macromolecular ion+HTAC.
(a): The case of macromolecular anion, (b): the case of macromolecular ampholyte.

of MnO_4^- ions. In addition, it is noted that, although the NaPA+HTAC+HCl system is capable of effective MnO_4^- flotation in an acidic region, the system PAA with HTAC is not so effective at pH 2.3 as shown in Table 1. The reason is not clear at present, but it may be due to the different order of adding the flotation reagent, namely, in the former case, PAA is formed by the acidification after the reaction of NaPA with HTAC, while in the latter case, PAA is added without NaPA and this makes difficult the attachment of hexadecyltrimethylammonium ion to polyacrylate chain. These phenomena are similar to those observed in the case[1] of MnO_4^- ion flotation by NaMS and HTAC where the order of adding NaMS and HTAC sensitively affects the floatability.

A probable model of MnO_4^- sublate is given in Fig. 10a, which has already been proposed in the case of macromolecular anions.[1] On the other hand, for the case of ampholyte polymers like $AlCl_3$ and $PAlCl_3$ in alkaline solution, the model shown in Fig. 10b is applicable since it is in conformity with the observation, given in Table 1, that HTAC in less quantity than in the case of other macromolecular anions is capable of resulting in effective MnO_4^- flotation.

References

1) I. Takayanagi, K. Kobayashi, and T. Sasaki, *Bull. Chem. Soc. Jpn.*, **49**, 2419 (1976).
2) K. Kobayashi, K. Natori, M. Kamaya, and T. Sasaki, *Bull. Chem. Soc. Jpn.*, **51**, 439 (1978); T. Inakazu, K. Kobayashi, and T. Sasaki, *ibid.*, **48**, 3008 (1975); K. Kobayashi, H. Sato, K. Kachi, M. Nakamura, and T. Sasaki, *ibid.*, **48**, 3533 (1975); K. Kobayashi, N. Watabe, K. Hachisuka, and T. Sasaki, *ibid.*, **49**, 2701 (1976).
3) E. B. Sandell, "Colorimetric Determination of Traces of Metals," 3rd ed, Interscience Pub., New York (1956).
4) T. Sasaki, H. Kurosawa, K. Miyasaka, and M. Mizushima, *Bull. Chem. Soc. Jpn.*, **53**, 2506 (1980).

  Bull. Chem. Soc. Jpn., 54, 3157—3161 (1981)

Corrosion Inhibition and Adsorption Behavior of Some Thioamides on Mild Steel in Sulfuric Acid

Badr G. Ateya,*,† B. E. El-Anadouli, and F. M. A. El-Nizamy
Chemistry Department, Faculty of Science, Cairo University, Cairo, Egypt
(Received June 20, 1980)

The objective of this work was to evalulate the effect of changing functional and structural groups on the protection efficiency imparted by the various inhibitor molecules. It was found that the molecules which include a thiocarbonyl group *e.g.* thiourea (TU), thioacetamide (TA), and thiosemicarbazide (TSC) exhibited much higher protection efficiencies than the corresponding compounds which do not *e.g.* semicarbazide, guanidine, and aminoguanidine. Furthermore, it made only little difference whether the thiocarbonyl group was attached to two amino groups as in thiourea, an amino and a methyl group as in thioacetamide or an amino and a methyl group as in thioacetamide above certain concentrations both TU and TA lose their efficiency and eventually become corrosion promotors. The adsorption behavior of TU and TA was quist complicated whereas that of TSC points towards complete coverage at high concentrations. The differences in behaviour between TSC, TU, and TA have been explained on the basis of delocalization or resonance stabilization energy.

The use of organic compounds as inhibitors for the aqueous corrosion of metals dates back several hundred years. A large number of such compounds has been developed to suit various applications. The diversity of these compounds and their applications, as well as the sheer volume of the pertinent literature, are quite evident in a classical review in the corrosion handbook[1] which was published in 1947.

This area is still attracting considerable attention in efforts to obtain more efficient inhibitors and to further the understanding of the mechanisms involved in the corrosion and inhibition processes. The work published in the last thirty years is quite extensive and is directed more towards understanding the effect of inhibitors on the kinetics of the half-cell reactions. Some of this work has already been reviewed.[2-4]

The relationship between the structure of the inhibitor molecule and its efficiency has been the subject of several investigations.[5-16] On the other hand, much less attention has been paid to the dependence of the protection efficiency on the size and the electronic distribution in the inhibitor molecule. This is an important question especially for sulfur-containing compounds *e. g.* thioamides (–CS–NH_2), many of which have been found to be good inhibitors. In this connection, several questions may be asked, for example; what is the effect on the protection efficiency of replacing the amino group of thiourea by a methyl group ? or upon replacing the thiocarbamoyl group $\diagdown\!\!\!\!\diagup C{=}S$ by either a carbonyl or carbonimidoyl group $\diagdown\!\!\!\!\diagup C{=}NH$? What is the effect of the above changes on the degree of surface converage and the mechanism of adsorption? The objective of this work is to answer some of the above questions by experimental measurements.

Experimental

The system chosen for this study is the acid corrosion of mild steel. Several organic compounds have been chosen for the purpose of this work. Table 1 lists these compounds. The main criterion for their selection was to provide a number of variables *e. g.* effect of a $\diagdown\!\!\!\!\diagup C{=}S$ as against $\diagdown\!\!\!\!\diagup C{=}NH$ or $\diagdown\!\!\!\!\diagup C{=}O$ substitution of an $-NH_2$ by a $-CH_3$ group or by the hydra zino group $-NH\cdot NH_2$.

Table 1. Molecular structures and abbreviations of the inhibitors used

Compound	Abbreviation	Molecular formula
Thiourea	TU	$H_2N-\overset{\overset{S}{\|}}{C}-NH_2$
Thioacetamide	TA	$CH_3-\overset{\overset{S}{\|}}{C}-NH_2$
Thiosemiearbazide	TSC	$NH_2-NH-\overset{\overset{S}{\|}}{C}-NH_2$
Semicarbazide	SC	$NH_2-NH-\overset{\overset{O}{\|}}{C}-NH_2$
Urea	U	$H_2N-\overset{\overset{O}{\|}}{C}-NH_2$
Guanidine	G	$H_2N-\overset{\overset{NH}{\|}}{C}-NH_2$
Aminoguanidine	AG	$H_2N-NH-\overset{\overset{NH}{\|}}{C}-NH_2$

The experimental approach taken here was to evaluate the effect of the inhibitors on the overall corrosion rate, and on the rate of the hydrogen evolution reaction (h.e.r.) at different inhibitor concentrations. This was done using the steady state galvanostatic technique. From these results, the protection efficiency of the inhibitor and the degree of coverage of the metal surface was calculated. Details of the experimental procedure, cell design, electrode preparation, pre-electrolysis....*etc.* were given elsewhere.[17] The composition of the mild steel electrode was 0.08% C, 0.44% Mn, and trace amounts of both S and P. The temperature was adjusted to 30±0.1 °C using an air thermostat. The electrolyte was 1.0 mol dm^{-3} H_2SO_4. The compounds used as inhibitors were of the highest purity available.

Results and Discussion

Effect of Inhibitor Concentration. Figures 1a, 1b, and 1c show the effect of the concentrations of TSC,

† Present address: Faculty of Science, University of the United Arab Emirates, Al-Ain, Abu Dhabi, United Arab Emirates.

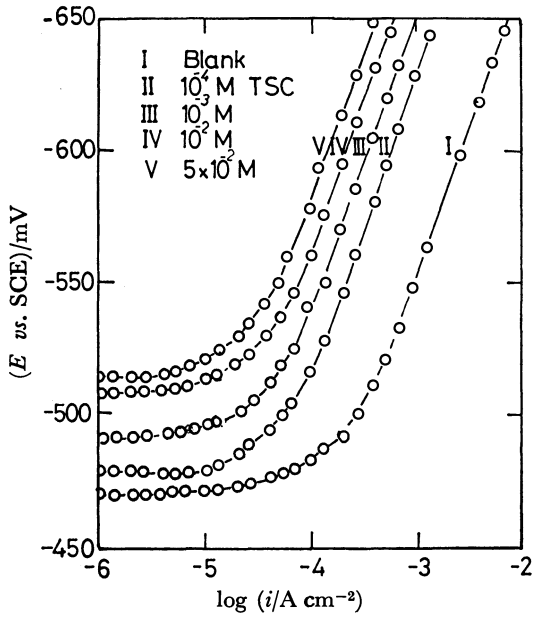

Fig. 1a. Effect of the concentration of thiosemicarbazide on the cathodic polarization curves of mild steel in 10 mol dm^{-3} H_2SO_4 at 30 °C.

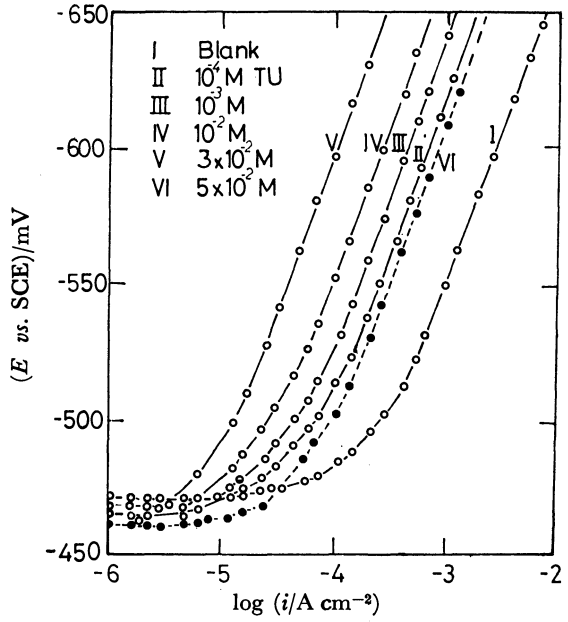

Fig. 1b. Effect of the concentration of thiourea on the cathodic polarization curves of mild steel in 1.0 mol dm^{-3} H_2SO_4 at 30 °C.

TU, and TA on the current-potential relations of hydrogen evolution on mild steel in 1.0 mol dm^{-3} H_2SO_4 at 30 °C. Clearly the concentrations of TSC, TU, and TA have a strong effect on the current-potential relations. Thus as their concentrations increase, it is seen that:

1) In case of TSC, the electrode potential at low current densities and the corrosion potential were shifted in the cathodic direction by about 10 to 40 mV, while in the cases of both TU and TA, the shifts were smaller in magnitude and in the anodic direction.

2) They caused large bodily shifts of the Tafel lines

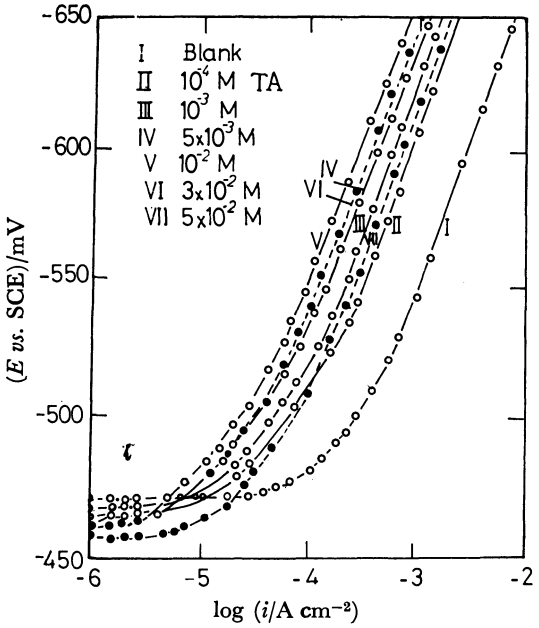

Fig. 1c. Effect of the concentration of thioacetamide on the cathodic polarization curves of mild steel in 1.0 mol dm^{-3} H_2SO_4 at 30 °C.

in the cathodic direction. In the case of TSC, the Tafel lines were shifted by 70 to 140 mV depending on the TSC concentration over the entire range. In the case of TU and TA, the magnitude of this shift also depended on their concentrations, only up to a critical value above which TU and TA became much less efficient (see below).

3) The Tafel slopes were approximately constant independent of inhibitor concentration.

The above two effects (2 and 3) indicate that TSC, TU, and TA have significant inhibiting effects on the hydrogen evolution reaction. From the Tafel slope, the transfer coefficient of the hydrogen evolution reaction is calculated to be $\beta=0.51$ which agrees with the generally accepted values.[18,19] The constancy of the cathodic transfer coefficient β in the presence and in the absence of the inhibitors indicates that their adsorption in the double layer does not change the mechanism of the hydrogen evolution reaction even though they significantly reduce its rate. This suggests that these inhibitors operate *via* a blocking adsorption mechanism.

It is recognized that the inhibitors which shift the entire current-potential curves in the cathodic direction are cathodic inhibitors, while those which shift them in the anodic direction are anodic inhibitors.[20] On the other hand, the inhibitors of the type of the mixed control shift the cathodic Tafel lines towards more cathodic potentials and the current-potential curves near the free corrosion potential towards less cathodic potentials. On the basis, TSC is characterized as a purely cathodic inhibitor while TU and TA exhibit dual inhibiting action, *i. e.* they inhibit both the cathodic and the anodic reactions, although to varying degrees.

Adsorption Behavior. The degree of surface coverage can be calculated from the currents obtained at constant potential in presence (i_2) and in absence (i_1) of inhibitor.[21,22] Thus

$$\theta = 1 - i_2/i_1. \quad (1)$$

Alternatively, the degree of coverage can be obtained at constant current.[23,24] Thus

$$\theta = 1 \exp(\beta\Delta\varepsilon/b), \quad (2)$$

where B is the transfer coefficient, $\Delta E = E_{inh} - E_{blank}$ is the difference between the electrode potential in the inhibited solution and that in the blank solution, and $b = RT/F$. Under the present conditions, Eqs. 1 and 2 gave virtually identical results.

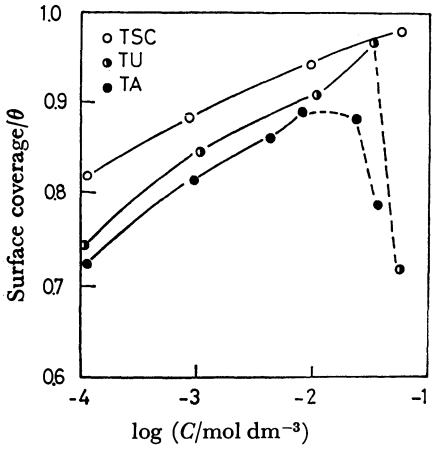

Fig. 2. Effect of inhibitor concentration on the surface coverage at 30 °C for mild steel in 1.0 mol dm^{-3} H_2SO_4.

Figure 2 shows the effect of inhibitor concentrations on coverage of the electrode surface. TSC is the only compound which displays a simple behavior over the tested concentration range. Its behavior points to the tendency to form a monolayer of adsorbed TSC. Both TU and TA undergo an apparent loss in the degree of surface coverage above certain concentrations. It is evident that at a certain inhibitor concentration, the tendency for adsorption is in the order TSC>TU>TA (see below).

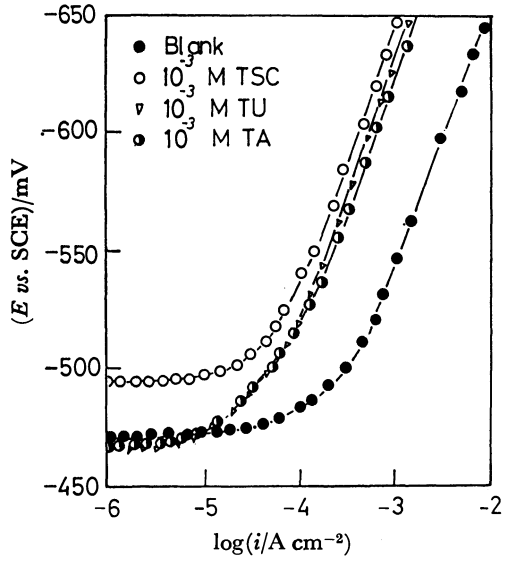

Fig. 3. Effect of the structure of molecules on the cathodic polarization curves of mild steel in 1.0 mol dm^{-3} H_2SO_4.

Effect of the Structure of the Inhibitor Molecule. Figure 3 shows a comparison of the cathodic polarization relations in the presence of TSC, TU, and TA at a concentration of 10^{-3} mol dm^{-3}. Clearly the differences among these compounds are not too large. The inhibiting effect of these compounds on the h.e.r. is in the order TSC>TU>TA as evident by the extent of the shift in Tafel lines in the cathodic direction. Alternatively, Fig. 4 shows the effect of the functional group on the current-potential relations for TSC, SC, and AG at a concentration of 10^{-2} mol dm^{-3}. Clearly aminoguanindine (AG) is a slightly better inhibitor than SC but TSC is far more efficient than both. The above evidence indicates that the inhibiting action of the compounds is mainly imparted by the thiocarbonyl group.

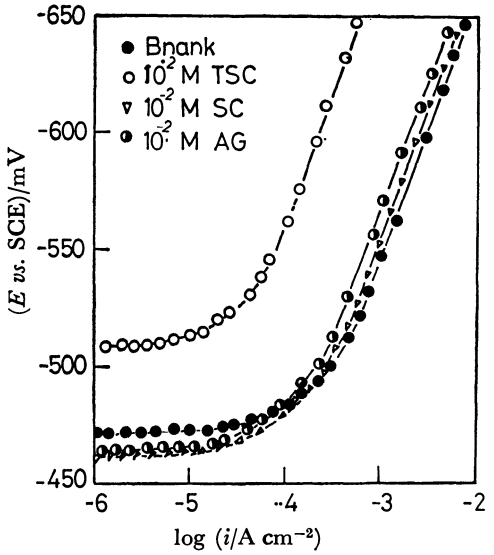

Fig. 4. Effect of TSC and AG molecules on the cathodic polarization curves of mild steel in 1.0 mol dm^{-3} H_2SO_4.

Table 2 shows the effect of TSC, TU, and TA concentrations on the exchange current density of hydrogen evolution i_0, corrosion current density i_{corr}, the protection efficiency, P, the degree of surface coverage θ and the polarization resistance R_p (see below). The protection efficiency is the parcent of relative decrease in the corrosion rate, given by

$$P(i_{corr}) = 100\left(1 - \frac{i_{corr}(\text{inhibited})}{i_{corr}(\text{blank})}\right). \quad (3)$$

The percent of relative decrease in the exchange current density is defined similarly.

The efficiency of a corrosion inhibitor may also be evaluated by measuring its effect on the polarization resistance which is defined by

$$R_p = \mathrm{d}(E - E_{corr})/\mathrm{d}i \quad \Omega\,cm^2, \quad (4)$$

where E and E_{corr} are in V and i in A cm^{-1}. Thus a plot of $(E - E_{corr})$ in the low polarization region, when $|E - E_{corr}| < 20$ mV, *vs.* current density i should give a straight line passing by the origin with a slope equal to the polarization resistance. Figure 5 shows such a

Table 2. Effect of the inhibitor concentration on: corrosion potential, tafel slope, exchange and corrosion current densities, and percentage decrease in each, degree of surface coverage, and polarization resistance for mild steel in 1.0 mol dm^{-3} H_2SO_4 at 30 °C

Inhibitor Concn 1	E_{corr} *vs.* SCE / mV	b / mV	i_0	$p(i_0)$	i_{corr} / $\mu A\ cm^{-2}$	$p(i_{corr})$	θ	$R_p/\Omega\ cm^2$
Thiosemicarbazide TSC								
0	−471	−116	5.2	—	220	—	—	83.0
10^{-4}	−480	−119	1.1	78.8	68	73.6	0.82	300.0
10^{-3}	−495	−118	0.93	82.1	48	78.2	0.89	366.7
10^{-2}	−510	−119	0.59	88.7	38	82.7	0.94	500.0
5×10^{-2}	−515	−118	0.4	92.3	32	85.4	0.96	666.7
Thiourea TU								
0	−472	−116	5.2	—	220	—	—	83
10^{-4}	−470	−117	2.0	61.5	71	67.8	0.72	530
10^{-3}	−467	−117	1.3	75.0	40	81.8	0.82	870
5×10^{-3}	−465	−117	0.98	81.2	32	85.5	0.87	1430
10^{-2}	−463	−117	0.8	84.6	24	89.1	0.90	2150
3×10^{-2}	−461	−117	0.89	82.9	22	90.0	0.79	909
5×10^{-2}	−451	−115	1.4	73.1	39	81.9	0.79	830
Thioacetamide TA								
0	−472	−116	5.2	—	22	—	—	83
10^{-4}	−469	−116	2.0	61.5	53	75.9	0.74	370
10^{-3}	−467	−116	1.0	80.8	28	87.3	0.85	630
10^{-2}	−465	−114	0.6	87.9	16	92.7	0.91	870
3×10^{-2}	−463	−114	0.1	96.3	60	97.3	0.97	2220
5×10^{-2}	−462	−116	1.9	63.5	56	79.1	0.72	350

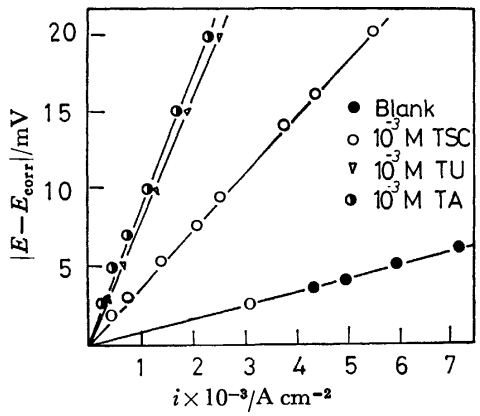

Fig. 5. The relationship between $|E-E_{corr}|$ and current density at low cathodoc polarization for mild steel in the presence of 10^3 mol dm^{-3} of each TSC, TU, and TA at 30 °C.

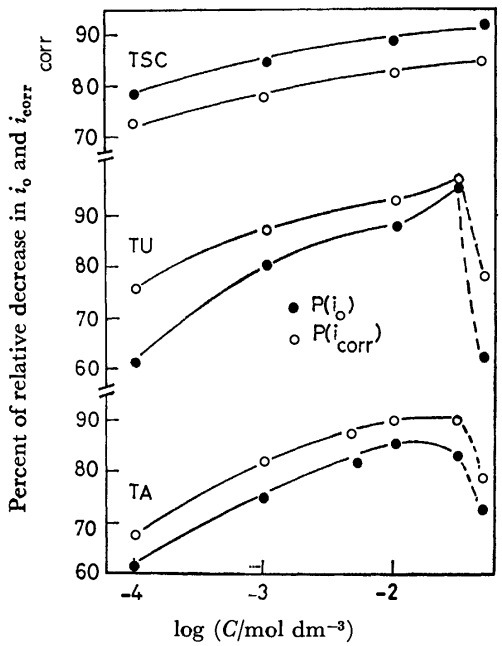

Fig. 6. Effect of inhibitor concentrations on the percent of relative decrease in i_o and i_{corr}.

plot for TSC, TU, and TA at a concentration of 10^{-3} mol dm^{-3} of each. Similar straight lines were obtained at various concentrations of each inhibitor (see Table 2).

Figure 6 shows a comparison between $P(i_{corr})$ and $P(i_0)$ for TSC, TU, and TA. It is seen that for TSC $p(i_0)>p(i_{corr})$ whereas for TU and TA $P(i_{corr})>P(i_0)$ over the entire concentration range. This indicates that for TU and TA the percentage decrease in corrosion rate is greater than the percentage decrease in the rate of the h.e.r. This can be true if the anodic reaction is also partially inhibited which supports the conclusions reached above, *viz.* that TU and TA are inhibitors of dual action.

From R_p calculations, as shown in Table 2, it is seen that for TSC the polarization resistance increases with inhibitor concentration over the indicated range. In the cases of TU and TA the polarization resistance increases with inhibitor or concentration up to a critical value above which TU and TA lose their inhibiting efficiency and eventually stimulate, rather than inhibit, corrosion. The value of this critical concentration at 30 °C is about 10^{-2} mol dm^{-3} in the case of TU and

about 3×10^{-2} mol dm^{-3} in the case of TA. Such a behaviour has not been observed with TSC up to a concentration of 5×10^{-2} mol dm^{-3}. Preliminary results suggest that this critical concentration is temperature dependent.

The reason for this behaviour of TU and TA is still in question. Thus whereas some workers[25,26] attribute it to the hydrolysis of TU to produce corrosion promoting species *e. g.* HS^- and S^{2-}, others[27,28] reported the disappearance of TU from the solution. The loss of TU in HNO_3 has been recently explained[2] by a scheme which involves its oxidation in solution followed by reduction at the metal surface. This scheme obviously cannot be applied in non-oxidizing acids *e. g.* HCl and H_2SO_4. On the other hand, the hydrolysis scheme cannot, as yet, be totally accepted since it is not clear why hydrolysis occurs to such an extent only in concentrated solutions and not in dilute ones. Determination of the equilibrium constant for such a reaction is required before a final judgement can be made with respect to this scheme.

Consideration of the Molecular Structure. The above results indicate that the order of the stability of the above thiocompounds in solution and the extent of their tendency to adsorb on, and hence protect, the iron surface are as follows: TSC>TU>TA$\gg$nonsulfur compounds. A qualitative explanation of this sequence may be found from a consideration of the electronic structure of these compounds (see Table 1). These are all similar on one side of the thiocarbonyl group and different on the other. The lone pairs of electrons on the nitrogen and sulfur atoms are delocalized and hence produce delocalization or resonance stabilization energy which stabilizes the compound.[29] There is reason to believe that the larger the number of delocalized electrons, the more stable is the structure and the more is the charge density on the "anchoring" atom (in this case S) and hence the larger is the extent of adsorption *i. e.* the larger is θ.

Therefore, where as the methyl group of TA has no delocalized electrons, the amino group of TU has one lone pair of such electrons and the hydrazine group of TSC has two such pairs. This explains the above sequence. In fact in 1.0 mol dm^{-3} H_2SO_4 medium, TA readily undergoes hydrolysis in presence of acid:

$$CH_3-\overset{\overset{S}{\|}}{C}-NH_2 + H_2O \rightleftharpoons CH_3-\overset{\overset{O}{\|}}{C}-NH_2 + H_2S. \quad (5)$$

The decomposition of TU does not go to the same extent. On the other hand, the results we obtained on TSC do not point towards measurable degree of decomposition or hydrolysis of the compound over the tested concentration range. The resulting H_2S or HS^- are known to be promotors of hydrogen discharge, hydrogen embrittlement and general acid corrosion.[30,31] Therefore, as the concentration of TA increases, the equilibrium of Eq. 5 shifts towards the right producing more H_2S which promotes the h.e.r. and hence the overall corrosion reaction. Similar considerations apply to the case of TU although obviously to a lesser extent.

References

1) G. G. Eldredge and J. C. Warner, "Corrosion Handbook," ed by H. H. Uhlig, Wiley, New York (1947), p. 905.
2) A. M. Shams El-Din, A. A. El-Hosary, R. M. Salah, and J. M. Abdel Kader, *Werkst. Korros.*, **28**, 26 (1977).
3) M. N. Desai, G. H. Thanki, and M. G. Ghandi, *Anticorrosion*, **1968**, 12; B. Bonnelly and Grzeskowiak, *Corros. Sci.*, **14**, 597 (1974).
4) G. Trabanelli and V. Carassatti, "Advances in Corrosion Science and Technology," ed by M. G. Fontana and R. W. Staehle, Plenum Press, N. Y. (1970), Vol. 1, p. 147.
5) N. Hackerman and A. C. Makrides, *Ind. Eng. Chem.*, **46**, 523 (1954).
6) N. Hackerman and R. M. Hurd, "1st Int. Congr. on Metallic Corr. London," Butterworths, London (1962), p. 166.
7) R. R. Annand, R. M. Hurd, and N. Hackerman, *J. Electrochem. Soc.*, **112**, 138, 144 (1965).
8) N. Hackerman, *Corrosion*, **18**, 322 (1962).
9) N. Hackerman, R. M. Hurd, and R. R. Annand, *Corrosion*, **18**, 37 (1962).
10) H. F. Finely and N. Hackerman, *J. Electrochem. Soc.*, **107**, 259 (1960).
11) H. Kaesche and N. Hackerman. *J. Electrochem. Soc.*, **105**, 191 (1958).
12) R. C. Ayers, Jr., and N. Hackerman, *J. Electrochem. Soc.*, **110**, 507 (1963).
13) F. M. Donahue and K. Nobe, *J. Electrochem. Soc.*, **112**, 886 (1965); **114**, 1012 (1967).
14) F. M. Donahue, A. Akiyama, and K. Nobe, *J. Electrochem. Soc.*, **114**, 1006 (1967).
15) Z. Szklarska-Smialowska and Kaminski, *Corros. Sci.*, **13**, 1 (1973).
16) B. Donnelly, T. C. Downie, R. Grazeskowiak, H. R. Hamburg, and D. Short, *Corros. Sci.*, **18**, 109 (1978).
17) B. G. Ateya, *J. Electroanal. Chem.*, **76**, 191 (1977).
18) B. E. Conway, "Electrochemical Data," Elsevier, N. Y. (1952), p. 347.
19) N. Tanaka and R. Tamamushi, *Electrochim. Acta*, **9**, 963 (1964).
20) I. A. Ammar and F. El-Khorafi, *Werkst. Korros.* **1973**, 702.
21) I. A. Ammar and S. A. Darwish, *Corros. Sci.*, **7**, 579 (1967).
22) H. Fischer, "Ann. Univ. Ferrarea," Sez. 5, Suppl. No. 3, 1 (1960), published (1961).
23) R. W. Hansen and B. H. Clampitt, *J. Phys. Chem.*, **58**, 808 (1954).
24) A. K. P. Chu and A. J. Sukava, *J. Electrochem. Soc.*, **116** 188, (1969); R. O. Loutfy and A. J. Sukava, *ibid.*, **116**, 1188 (1969); P. Seto and A. J. Sukava, *ibid.*, **119**, 852 (1972).
25) Z. A. Iofa "Ann. Univ. Ferrarea," Sez. 4, 93 (1966).
26) I. E. Titov and V. A. Guseva, *Zasch. Metal.*, **4**, 588 (1968).
27) T. F. Boyd and M. Galan, *Chem. Abstr.*, 568382 (1962).
28) A. F. Bogenschatz, C. Hemz, and J. L. Soctan, *Melalloberfl.*, **28**, 397 (1974).
29) A. Streitwieser, Jr., "Molecular Orbital Theory for Organic Chemists," Wiley, New York (1961), p. 43.
30) A. Kawashima, K. Hashimoto, and S. Shimodaira, *Corrosion*, **32**, 321 (1976).
31) Z. A. Iofa and F. L. Kam, *Zashch. Metall.*, **10**, 17 (1974).

Gas-Solid Chromatographic Studies of Organic Compounds on Zirconium Oxide Beads†

Nebojša M. Djordjević,†† Slobodan K. Milonjić, and Miroslav M. Kopečni*

Chemical Dynamics Laboratory, The Boris Kidric Institute of Nuclear Sciences, P.O. Box 522, 11001 Beograd, Yugoslavia

††*Chemical Industry "Petrohemija" LTCP, 26000 Pančevo, Yugoslavia*

(Received August 18, 1980)

Adsorption properties of synthetic zirconium oxide beads were investigated by the gas-solid chromatography (GSC) method. Retentions of numerous alkanes, alkenes, aromatics and chlorinated compounds were measured in a wide temperature region. It appears that the surface activity of an adsorbent can be easily changed by thermal treatment, and in connection with it, the role of crystallographic structure of the adsorbent is emphasized. Thermodynamic parameters obtained were used for explanation of the adsorbent-adsorbate interaction.

The role of GSC in chromatographic practice is twofold: its early application was mainly connected to the analytical problems, while recently there is an increasing interest in physicochemical applications of GSC, among them, special attention is devoted to the adsorption phenomena. GSC measurements offer numerous advantages, the most important are: speed, accuracy, wide temperature region, zero coverage of a surface and above all, this technique provides results in the dynamic conditions.

Apart from silica and alumina, which are extensively used both for practical and physicochemical purposes and therefore are well examined,[1-3] a very few data concerning other metal oxides are available in literature.[4-9] Analytical inapplicability of uncommon metal oxides, due to their surface inhomogeneity and polarity, makes that little attention is paid to those adsorbents. To overcome serious problems linked with surface inhomogeneity and polarity, modifications with various polymeric stationary phases are generally applied.

The first paper dealing with GSC properties of zirconium oxide,[4] thermally pretreated at 1173 K, appeared at the time when the present study was undertaken. Since zirconium oxide may appear in amorphous as well as in monoclinic and tetragonal crystal form, it is normally expected that each modification exhibits different adsorptive properties. There is no information on crystal form used by Lapteva and coworkers,[4] but thermal treatment applied strongly suggests the monoclinic structure. The authors[4] have used three alkanes, *n*-pentane to *n*-heptane, adsorption and thermodynamic data of which were evaluated for temperature region between 493 and 543 K.

Despite the lack of GSC data, zirconium oxide is widely used as an inorganic adsorbent both for anions and cations. It seems that this material deserves more detailed investigations as far as the organic molecule adsorption processes are concerned.

Experimental

The experiments were performed with zirconium oxide precipitated from aqueous zirconium dichloride oxide ($ZrOCl_2 \cdot 8H_2O$) solution with ammonia.[10]

The following procedure was adopted: 30 g of zirconium dichloride oxide was dissolved in 500 ml of 4 mol dm^{-3} of nitric acid, diluted by equal volume of deionized water, and precipitated by 1000 ml of 5% ammonia with vigorous stirring at room temperature. The resultant precipitates were filtrated, thoroughly washed with 1% ammonia solution till the negative reaction of chloride ion, then with deionized water till the neutral reaction. After that, the precipitants were dried in air at 383 K for the period of 10 d. This material was ground and sieved. The fraction of 45—60 mesh was splitted into three portions and each was thermally treated for 4,5 h in air, at 523, 873, and 1173 K, respectively. These materials were used then in GSC experiments as a column packing.

All the chemical used were of analytical grade.

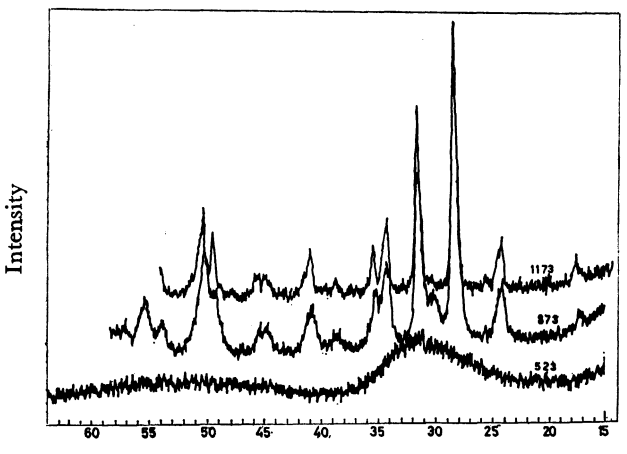

Fig. 1. X-Ray diffraction diagrams for zirconium oxide heated at various temperatures. The figures on the curves represent the heating temperatures, K.

The specific surface areas of the above materials were determined by a Ströhlein area meter using the single point nitrogen adsorption method. The values obtained were 220, 34, and 13 $m^2 g^{-1}$ for materials heated at 573, 873, and 1173 K, respectively. To determine the crystalinity of the packing used, X-ray diffraction patterns were recorded using a Siemens Kristalloflex 4 with a GM counter. The diffractograms obtained are shown in Fig. 1. Diffraction diagram for the material treated at 523 K shows a typical pattern of the amorphous species. The product heated at 873 K is mainly monoclinic with a metastable tetragonal phase indicated

† Presented at the 3rd World Chromatography Conference, July 3—4, 1980, Zürich, Switzerland.

with a small peak at 30 degrees of 2θ while that one at 1173 K shows the stable monoclinic phase only. These results are in agreement with the recent information published by Sato *et al.*[11]

All the organic compounds, obtained from various commercial sources, were of analytical reagent grade and used "as received."

A Perkin-Elmer model F 17 and 881 gas-chromatographs were used in the experiments. As a carrier, dry nitrogen was employed, and its flow, depending on the experimental conditions applied, varied in the range of 10 to 20 $cm^3\ min^{-1}$, as measured by a soap-bubble flowmeter. The adsorbates were injected as small vapour samples and the retention times were measured by a stop-watch. In all cases, stainless steel columns were used. Prior to the experiments, the packed column was conditioned overnight in a stream of nitrogen at 503 K.

The retention volumes for each adsorbate were measured at 413, 433, 453, 473, and 493 K, with the exception of adsorbates with retention times exceeding 90 min. An average retention from a multiple injection was for the following calculations, and the gas hold up time was assumed to be equal to the retention time of methane at the same temperature. No sample size and tailing effects were observed, except for aromatics at lower experimental temperatures, and such data were omitted from the calculations since they cannot be used for derivation of the thermodynamic data. Generally, sample size effect or tailing indicates inhomogeneity of the adsorbent surface, nonlinearity of the adsorption isotherm or multilayer adsorption.

The net retention volume, V_N, was calculated for each adsorbate from the usual relation,

$$V_N = j\, t'_R\, F_C, \qquad (1)$$

where t'_R is the adjusted retention time, F_C is the corrected carrier flow rate and j denotes the James-Martin pressure correction term. The net retention volumes were then converted into the adsorbate distribution coefficients, K_D, at a given temperature, deviding V_N by the total surface area of the adsorbent in the column. The values obtained correspond to the initial slope of the adsorption isotherm. The variation of K_D from one adsorbent to another for the same adsorbate was used then to quantify the changes in the properties of the adsorbents. The isosteric heat of adsorbtion, ΔH, was calculated by plotting $\ln (K_D/T)$ *vs.* $(1/T)$, where the linear least-square slopes of the plots were taken to be equal to $-\Delta H/R$ (assuming that ΔH is invariant over the temperature range examined here). The Gibbs free energies of adsorbtion, ΔG, were calculated from the relation $\Delta G = -RT \ln K_D$, where R is the gas constant. The corresponding entropies of adsorption, ΔS, were calculated from $\Delta S = (\Delta H - \Delta G/T)$.

Results and Discussion

As expected, the distribution coefficients of the adsorbates within the homologous series increase with the increasing chain length as well as with the increasing molecular weights or boiling points, the later dependence is shown in Fig. 2. The straight line connecting experimental points for benzene and its derivates is considerably above the paraffin line because of the specific interactions of adsorbent with the aromatic ring. If we assume that normal alkanes can interact with the surfacenons pecifically only, then the plots similar to Fig. 2 can be used to elucidate the nature of the specific adsorption process. Using this approach, the vertical

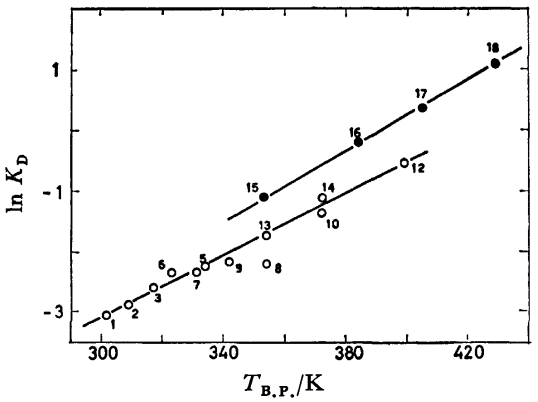

Fig. 2. Logarithm of distribution coefficient at 473 K *vs.* boiling point for zirconium oxide treated at 873 K. 1: 2-Methylbutane, 2: pentane, 3: cyclopentene, 5: 2-methylpentane, 6: 2,2-dimethylbutane, 7: 2,3-dimethylbutane, 8: cyclohexane, 9: hexane, 10: heptane, 12: Octane, 13: 2,4-dimethylpentane, 14: 2,2,4-trimethylpentane, 15: benzene, 16: toluene, 17: chlorobenzene, 18: bromobenzene.

distance between the normal alkane line (open circles) and any point on the plot for the aromatic line (filled circles) is related to the degree of specific interaction, shown by the compound representing that point.[12] The plots similar to those in Fig. 2 and conclusions that follow can be drawn for other thermal modifications of the zirconium oxide.

The role of a dominant element in GSC-geometrical factors, is evaluated by comparing the data for hexane and cyclohexane. Although cyclohexane boils 12 K higher than hexane, its retentions are shorter, regardless the thermal treatment of the column material. Due to the shorter retention, the point corresponding to cyclohexane (Fig. 2) lies considerably lower than the saturated hydrocarbon line. Explanation for such a behaviour can be easily found in geometric properties of the molecules under consideration. In the case of hexane, all the six carbon atoms can approach a plane, while for cyclohexane only three or four of them can interact with a surface at the same time, depending on the steric form that cyclohexane may take. Similarlly, the branched saturated hydrocarbons possess less carbon atoms available to contact and therefore to interact with the surface in comparison to the linear molecule with the same carbon atom number. Accordingly, all the branched hydrocarbons are eluted prior to the corresponding linear homologues.

Halogenated compounds interact with zirconium oxide to a great extent, due to their possibility to form stable zirconium dichloride oxide organic complexes.[13] We believe that this mechanism is responsible for permanent linking of chloroform, dichloromethane and carbon tetrachloride to the column material, even at higher experimental temperatures applied here. On the contrary, halogenated alkenes as well as 1,2-dichlorethane and halogenated benzene derivates are eluted from the column with quite reasonable retentions, in spite of the fact that some of these adsorbates have two possibilities to interact specifically with zirconium oxide, *e. g.* double bond and chlorine atom. Here, the

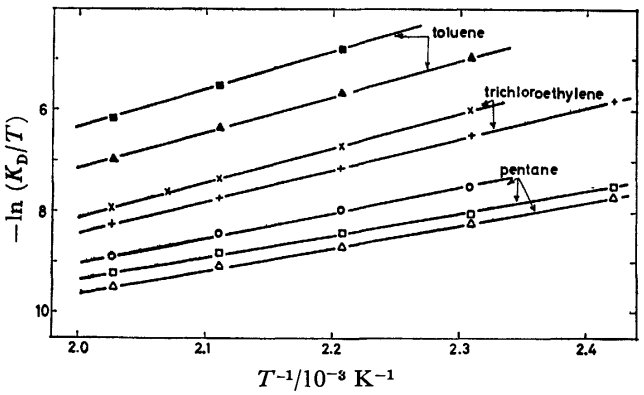

Fig. 3. Representive plots of $\ln(K_D/T)$ *vs.* $(1/T)$ for indicated adsorbates ○, ×, ● ZrO_2 heated at 523 K, △, +, ▲ heated at 873 K and □, ×, ■ heated at 1173 K.

geometric factor is obviously responsible for such a behaviour, a nature of which requires a more detailed examination.

Typical plots of the functionality, $\ln K_D = f(1/T)$ for pentane, trichlorethylene, and toluene are shown in Fig. 3. For other adsorbates studied, similar linear relationships were obtained. The ΔH values calculated from these plots and the corresponding entropies of adsorption are collected in Table 1.

The isosteric heat of adsorption for pentane, hexane and heptane reported by Lapteva and coworkers[4] are −28.9, −34.4, and −41.9 kJ mol^{-1}, respectively. These values are lower than those we found. The different temperature region used in determining the ΔH values can easily produce discrepancy between the values of the isosteric heats. In addition, the mode of preparation of the initial zirconium oxide material, may also contribute to the disagreement in ΔH values.

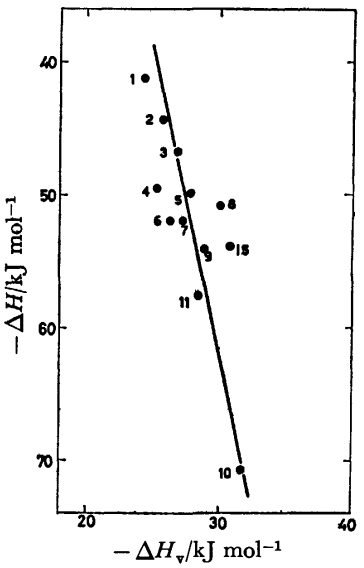

Fig. 4. Dependence of isosteric heat of adsorption on the corresponding heat of vaporization for ZrO_2 thermally treated at 523 K.
Symbols as in Fig. 2. 4: 1-Pentene, 11: 1-hexene.

Dependence of the isosteric heat of adsorption on the heat of vaporization, ΔH_v, are illustrated in Fig. 4, for zirconium oxide treated at 523 K. All the compounds lying on the common straight line represent the same interaction mechanism with the surface. The compounds falling out of the line, *e. g.* benzene, 1-pentene, and chlorinated compounds, are capable to interact, beside always acting nonspecific mode, with one or other specific mechanism.

The role of the specific part of the interaction can be evaluated considering the free energy of adsorption. The values of $\Delta(\Delta G)$ for a pair of adsorbates, benzene

Table 1. Isosteric heat of adsorption ($-\Delta H$/kJ mol^{-1}) and entropy of adsorption ($-\Delta S$/J mol^{-1} K^{-1}) values for named adsorbates on various thermally treated zirconium oxide

Absorbate	523 K		873 K		1173 K	
	$-\Delta H$	$-\Delta S$	$-\Delta H$	$-\Delta S$	$-\Delta H$	$-\Delta S$
Pentane	44.32	113	38.46	106	35.76	98
Hexane	54.07	125	45.74	115	44.70	111
Heptane	70.69	149	54.05	126	53.01	120
Octane	—	—	64.03	142	68.73	146
Cyclohexane	50.79	118	43.66	111	41.58	105
2-Methylbutane	41.12	107	38.05	106	35.34	98
2-Methylpentane	49.92	117	42.62	110	42.62	107
2,2-Dimethylbutane	51.80	122	42.62	111	39.92	103
2,3-Dimethylbutane	51.91	121	42.62	110	41.58	105
2,4-Dimethylpentane	—	—	48.86	118	49.90	117
2,2,4-Trimethylpentane	—	—	54.47	124	54.05	120
Cyclopentene	46.76	118	44.70	116	—	—
Benzene	53.95	119	54.47	124	—	—
Chlorobenzene	—	—	65.49	136	—	—
Bromobenzene	—	—	73.80	147	—	—
Toluene	—	—	60.29	129	63.20	128
1,2-Dichloroethane	40.73	115	45.32	121	—	—
Trichloroethylene	57.07	130	51.35	122	—	—
Tetrachloroethylene	62.21	135	55.72	128	—	—

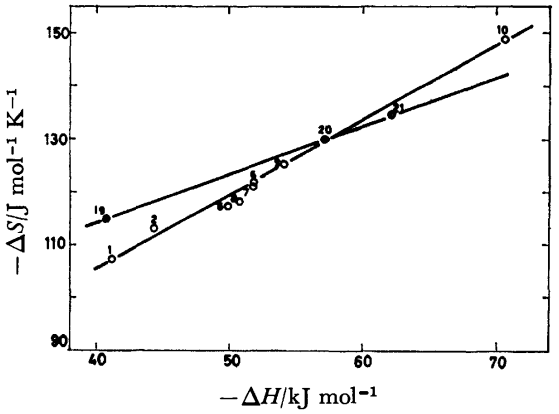

Fig. 5. Plots of ΔS *vs.* ΔH.
19: 1,2-Dichloroethane, 20: trichloroethylene, 21: tetrachloroethylene. Other symbols as in Fig. 2.

and hexane at 473 K, on the zirconia treated at 523, 873, and 1173 K are −2.82, −4.29, and −6.45 kJ mol^{-1}, respectively. These values represent the contribution of three double bonds from benzene ring. It is normal that $\Delta(\Delta G)$ increases with the increasing treatment temperature; such a treatment leads to dehydroxylation of the surface and therefore to the surface activation. The increased $\Delta(\Delta G)$ values are also connected to the thermal treatment which leads to the change of the crystalinity of zirconium oxide.

Empirical dependence of ΔS on ΔH, designated in literature as a compensation effect, is shown in Fig. 5 for the material preheated at 523 K. Nonspecific interacting adsorbates lie on the same straight line, although a separate line can be constructed for the chlorinated compounds. Two separate lines indicate two different types of interactions as pointed out above.

The values of the isosteric heats of adsorption of normal alkanes on zirconium oxide are similar to those obtained on silica.[14] On the other hand, the increment of ΔH for each CH_2 group is much higher when zirconia is used as adsorbent, implying the stronger nonspecific adsorption.

Many problems in the field of GSC thermodynamics remain without definite answers. A complete explanation of the nature of the interactions acting between adsorbate and metal oxides must await further experimentations.

We are indebted to Dr. S. Malčić, from the Boris Kidrič Institute of Nuclear Sciences, for crystallographic examinations, to Miss V. Roglić for careful corrections of English, and to M.Sc. M. Trtanj for zirconium oxide grant.

References

1) C. S. G. Phillips and C. G. Scott, "Progress in Gas Chromatography," ed by J. H. Purnell, Willey-Interscience, New York (1968), pp. 121—152.
2) A. V. Kiselev and Ya. I. Yashin, "Gazo-Adsorbtsionnaya Khromatografiya," Nauka, Moscow (1967).
3) K. K. Unger, "Porous Silica," Elsevier, Amsterdam (1979).
4) T. N. Lapteva, V. V. Moskovskikh, G. D. Kharlampovich, V. P. Timakov, and A. A. Pospelov, *Zh. Fiz. Khim.*, **53**, 980 (1979).
5) S. K. Milonjić and M. M. Kopečni, *J. Chromatogr.*, **172**, 357 (1979).
6) S. K. Milonjić, M. M. Kopečni, and Z. E. Ilić, *Bull. Soc. Chim. Beograd*, **44**, 541 (1979).
7) A. Betti, B. Lodi, C. Bighi, and F. Dondi, *J. Chromatogr.*, **106**, 291 (1975).
8) M. J. O'Brien and R. L. Grob, *J. Chromatogr.*, **155**, 129 (1978).
9) I. V. Kolosnitsyna and R. J. Petrova, *Kolloidn. Zh.*, **29**, 815 (1967).
10) G. H. Nancollans and R. Paterson, *J. Inorg. Nucl. Chem.*, **29**, 565 (1967).
11) T. Sato, F. Ozawa, T. Nakamura, H. Watanabe, and S. Ikoma, *Thermochimica Acta*, **34**, 211 (1979).
12) D. J. Brookman and D. T. Sawyer, *Anal. Chem.*, **40**, 106 (1968).
13) G. Guiochon and C. Pommier, "Gas Chromatography in Inorganics and Organometaillics," Ann Arbor Science, Ann Arbor (1973), pp. 209, 210, 223.
14) M. M. Kopečni, R. J. Laub, and S. K. Milonjić, *Anal. Chem.*, **52**, 1032 (1980).

Mössbauer Study of Solid State Photolysis of Alkali Tris(oxalato)ferrates(III)

Ajaib Singh BRAR* and Balwinder Singh RANDHAWA
Chemistry Department, Guru Nanak Dev University, Amritsar-143005, India
(Received August 25, 1980)

Solid state photolysis of alkali tris(oxalato)ferrates(III) (Li, Na, K, Cs, and NH_4) was studied with mercury radiation in the visible region by means of Mössbauer spectroscopy. The intermediate $K_6[Fe_2^{II}(ox)_5]$ is formed in the case of potassium tris(oxalato)ferrate(III) and $FeC_2O_4 \cdot 2H_2O$ in the case of other alkali tris(oxalato)ferrates-(III)[Li, Na, Cs, and NH_4].

Mössbauer spectroscopy is effective for detecting the change in oxidation state and structure.[1] By means of UV and visible spectroscopy and magnetic susceptibility measurements Wendlandt and Simmons[2] found that iron(II) oxalate is formed during the course of solid state photolysis of potassium tris(oxalato)ferrate(III). Bancroft *et al.*[3] reported the formation of $K_6[Fe_2^{II}(ox)_5]$ as an intermediate, the results contradicting the observation made by Wendlandt and Simmons.[2] Sato and Tominaga[4,5] investigated the photolysis of potassium bis- and tris(oxalato)ferrate(III) in solid state and frozen solutions using Mössbauer spectroscopy, their results supporting those obtained by Bancroft *et al.*[3] They also suggested the formation of metastable iron(II) species during the course of photolysis. In our earlier communication,[6] Mössbauer parameters of alkali tris-(oxalato)ferrates(III) have been reported. The effect of change of cation on the isomer shift values have been observed. In this communication, the effect of change of cation (Li, Na, K, Cs, and NH_4) on the intermediates formed during the course of solid state photolysis of these complexes is reported.

Experimental

Alkali Tris(oxalato)ferrates(III) $M_3[Fe(ox)_3]\cdot 3H_2O$ (M= Li, Na, K). These were prepared by mixing three volumes of 1.5 mol dm^{-3} alkali metal oxalate solution and one volume of 1.5 mol dm^{-3} iron (III) chloride solution with vigrous stirring. The precipitated green product, *i. e.* $M_3[Fe(ox)_3]\cdot 3H_2O$ (M=Li, Na, K), was recrystallized three times from warm water and dried in a current of warm air (45 °C) with a drier.[7] The solid product was stored in the dark in order to avoid chemical change.

Caesium Tris(oxalato)ferrate(III) Trihydrate $Cs_3[Fe(ox)_3]\cdot 3H_2O$. Caesium oxalate was prepared from caesium chloride and oxalic acid. Three volumes of 1.5 mol dm^{-3} caesium oxalate solution and one volume of 1.5 mol dm^{-3} iron (III) chloride solution were mixed with vigrous stirring. The reaction mixture was concentrated on a water bath until crystals of caesium tris (oxalato) ferrate (III) formed. The crystals were recrystallized from warm water and then stored and dried in the dark.

Ammonium Tris(oxalato)ferrate(III) Trihydrate $(NH_4)_3[Fe(ox)_3]\cdot 3H_2O$. This complex was prepared as reported.[8]

The percentage of iron in the alkali tris(oxalato)ferrates (III) was determined by electronic spectroscopy and found to agree with that of the expected value.[9] The percentage of sodium and potassium in sodium- and potassium tris(oxalato)ferrate-(III) trihydrate respectively was determined with a flame photometer.

For photo-irradiation, samples were exposed to medium pressure 125 watts mercury lamp radiations.

A Mössbauer spectrometer MBS-35 (ECIL, India) coupled with MCA-38B with constant acceleration drive was employed to record the spectrum. A 5-mi ^{57}Co (Rh) source was used. The values of isomer shift are reported with respect to naturaliron. All the spectra were recorded at temperature 25±2 °C. A sample containing approximately 10 mg/cm^2 of the natural iron was taken for each measurement. All the spectra have been fitted to Lorentzian line shape using program and fitting procedures[10] on microcomputer 2000 (DCM, India). The intensities of quadrupole doublets are almost equal, the Mössbauer spectra of the tris(oxalato)-ferrates(III) at room temperature being almost symmetrical. Slight deviations might be due to powdered random samples and due to spin lattice relaxation effect.[11]

Results and Discussion

The Mössbauer spectra of alkali tris(oxalato)ferrates-(III) at room temperature (25±2 °C) consist of a single broad absorption band due to an electronic spin relaxation effect.[11] The Mössbauer parameters of alkali tris-(oxalato)ferrates(III) are given in Table 1. The isomer shift value of 0.26 mm s^{-1} for potassium tris(oxalato)-ferrate(III) trihydrate agrees with the reported value.[1,3,4,12-14]

Table 1. Mössbauer parameters of alkali tris(oxalato)ferrates(III)

Name of complex	Isomer shift / mm s^{-1}	Width at half maximum / mm s^{-1}	Percentage absorption
$Li_3Fe(C_2O_4)_3\cdot 3H_2O$	0.03±0.02	1.39±0.02	6.09
$Na_3Fe(C_2O_4)_3\cdot 3H_2O$	0.15±0.02	1.37±0.02	2.35
$K_3Fe(C_2O_4)_3\cdot 3H_2O$	0.26±0.02	1.78±0.02	6.12
$Cs_3Fe(C_2O_4)_3\cdot 3H_2O$	0.39±0.02	0.85±0.02	3.81
$(NH_4)_3Fe(C_2O_4)_3\cdot 3H_2O$	0.21±0.02	1.16±0.02	2.07

The alkali tris(oxalato)ferrates(III) are high spin complexes having octahedral structure with oxidation state (+3) of iron. The sp^3d^2 hybridization is involued in bonding with the ligands (oxalates). The change in polarization of the alkali metal cation affects the 3s-electron density at the iron nucleus. The more electronegative cation will polarize the oxalato group causing a change in the electron density of the iron. The increase of electronegativity from caesium to lithium decreases the electron density in the 3d-orbital of iron

TABLE 2. MÖSSBAUER PARAMETERS OF THE PRODUCTS OF PHOTOLYSIS FROM ALKALI TRIS(OXALATO) FERRATES(III)

Product	Isomer shift / mm s^{-1}	Quadrupole splitting / mm s^{-1}	Tentative assignment
Product I	—	—	Parent compounds[a)]
Product II	1.16±0.04	3.89±0.04	$K_6[Fe_2^{II}(ox)_5]$
Product III	0.28±0.04	0.68±0.04	$M[Fe^{III}(ox)_2(H_2O)_2]$[b)]
Product IV	1.18±0.04	1.80±0.04	$FeC_2O_4\cdot 2H_2O$

a) The values of isomer shift and quadrupole splitting are given in Table 1. b) M=Na, K, Cs.

which affects the shielding of 3s-electron density at iron nucleus. Less electronegative cation would have less effect on the d orbital and the resulting s-electron density at the nucleus would decrease, giving higher isomer shift value. The effect of electronegativity of cation on the value of isomer shift is greater as compared with that in low spin octahedral complexes[15] [hexacyanoferrate(II) and hexacyanoferrate(III)] and high spin tetrahedral complexes[16] [alkalidithioferrate-(III)]. A linear relationship between cationic size and isomer shift has been observed in alkali tris(oxalato)-ferrates(III).[6]

The Mössbauer parameters of alkali tris(oxalato)-ferrates(III) products for the solid state photolysis are given in Table 2. The Mössbauer spectrum of potassium tris(oxalato)ferrate(III), irradiated for 30 h at room temperature (Fig. 1b) shows a broad band with isomer

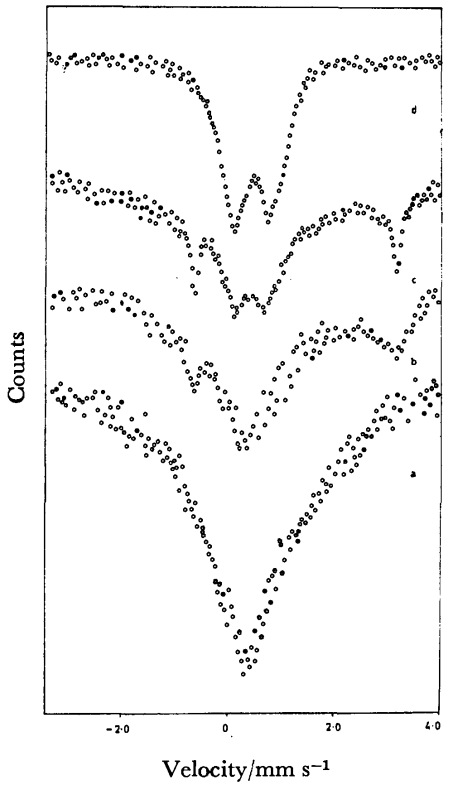

Fig. 1. Mössbauer spectra of potassium tris(oxalato)-ferrate(III) trihydrate at room temperature (25 °C). a: Unirradiated complex, b: irradiated for 30 h, c: irradiated for 60 h, d: irradiated for 200 h and on long standing in air.

shift 0.29 mm s^{-1}, indicating the presence of parent complex and a quadrupole doublet with isomer shift value 1.19 mm s^{-1} and quadrupole splitting value of 3.89 mm s^{-1} indicating the formation of $K_6[Fe_2^{II}(ox)_5]$. The Mössbauer spectrum of potassium tris(oxalato)-ferrate(III) irradiated for 60 h at room temperature (Fig. 1c) represents two sets of quadrupole doublets, one with isomer shift and quadrupole splitting value of 1.16 and 3.89 mm s^{-1}, respectively, indicating the formation of $K_6[Fe_2^{II}(ox)_5]$, and the other with isomer shift and quadrupole splitting values of 0.33 and 0.62 mm s^{-1}, respectively, indicating the formation of $K[Fe^{III}(ox)_2(H_2O)_2]$ species. Wendlandt and Simmons[2] observed the formation of FeC_2O_4 in the solid state photodecomposition of potassium tris-(oxalato)ferrate(III) by means of magnetic susceptibility measurements. However, no such results were obtained on the basis of Mössbauer studies. On further irradiation of the complex, oxidation of $K_6[Fe_2^{II}(ox)_5]$ to $K[Fe^{III}-(ox)_2(H_2O)_2]$ takes place. The isomer shift and quadrupole splitting values of this complex *i. e.* $K[Fe^{III}(ox)_2-(H_2O)_2]$ are 0.32 and 0.65 mm s^{-1}, respectively, showing that the complex has octahedral symmetry with oxidation state (+3). After irradiation with mercury radiations for a period of 200 h (Fig. 1d), the Mössbauer spectrum shows isomer shift and quadrupole splitting values of 0.32 and 0.62 mm s^{-1}, respectively, indicating complete photodecomposition to $K[Fe^{III}(ox)_2(H_2O)_2]$. No change in Mössbauer parameters has been observed on further irradiation. $K_6[Fe_2^{II}(ox)_5]$ is an unstable complex which, after being left to stand in the air for several days, gets oxidized to $K[Fe^{III}(ox)_2(H_2O)_2]$ (product III). It is possible that product III is formed by radiation and aerial oxidation. Sato and Tominaga[5] reported the formation of metastable iron(II) and $[Fe(ox)_2(H_2O)_2]^{2-}$ intermediate. The formation of these species was not observed in our experiments. This might be due to the difference in wavelength and experimental conditions. The mechanism of the solid state photodecomposition of potassium tris(oxalato)ferrate(III) is suggested as follows:

$$\underset{(I)}{K_3[Fe^{III}(ox)_3]} \xrightarrow{h\nu} \underset{(II)}{K_6[Fe_2^{II}(ox)_5]} \xrightarrow[\text{air}]{h\nu} \underset{(III)}{K[Fe^{III}(ox)_2(H_2O)_2]}.$$

The Mössbauer spectra of sodium and caesium tris(oxalato)ferrates(III) irradiated for a period of 60, 150, and 200 h are shown in Figs. 2 and 3, respectively. The Mössabauer spectra of these complexes irradiated for 60 h (Figs. 2b and 3b) show a doublet with isomer shift and quadrupole splitting values of 1.22 and 1.82

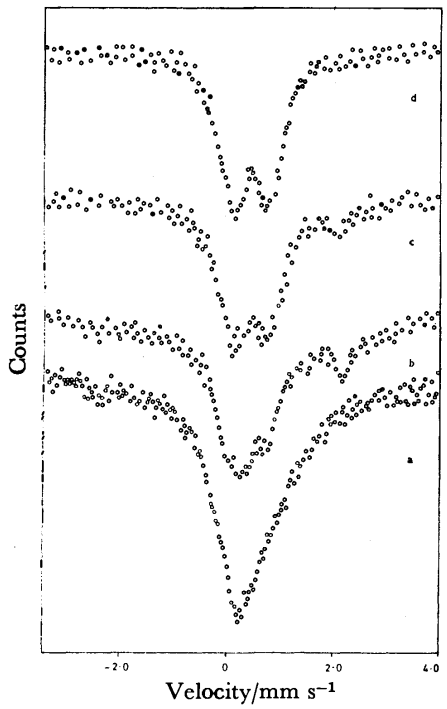

Fig. 2. Mössbauer spectra of sodium tris(oxalato)-ferrate(III) trihydrate at room temperature (25 °C).
a: Unirradiated complex, b: irradiated for 60 h, c: irradiated for 150 h, d: irradiated for 200 h.

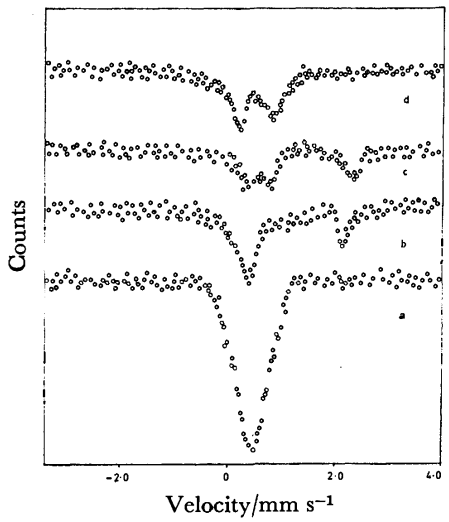

Fig. 3. Mössbauer spectra of caesium tris(oxalato)-ferrate(III) trihydrate at room temperature (25 °C).
a: Unirradiated complex, b: irradiated for 60 h, c: irradiated for 150 h, d: irradiated for 200 h.

mm s^{-1} in the case of sodium tris(oxalato)ferrate(III), and 1.18 and 1.77 mm s^{-1} in the case of caesium tris-(oxalato)ferrate(III). The values of isomer shift and quadrupole splitting are comparable to those reported for iron(II) oxalate dihydrate.[14] The same were observed in the Mössbauer spectrum of iron(II)oxalate-dihydrate (pure A.R.). On further irradiation, the Mössbauer spectrum shows a quadrupole doublet with isomer shift and quadrupole splitting values of 0.30 and 0.66 mm s^{-1} in sodium tris(oxalato)ferrate(III) (Fig. 2c) and 0.28 and 0.66 mm s^{-1} in the case of caesium tris(oxalato)ferrate(III) (Fig. 3c). These values indicate the formation of an octahedral complex with oxidation state(III). When these complexes (Na and Cs) were irradiated for 200 h and left to stand in the air for several hours, the Mössbauer spectrum represents a quadrupole doublet with isomer shift and quadrupole splitting values of 0.28 and 0.68 mm s^{-1} in sodium tris(oxalato)ferrate(III) (Fig. 2d) and 0.29 and 0.68 mm s^{-1} in the case of caesium tris(oxalato)ferrate(III) (Fig. 3d), indicating the formation of $M[Fe^{III}(ox)_2(H_2O)_2]$ complexes (M=Na, Cs). Further irradiation of these complexes shows on change in the Mössbauer spectra. The mechanism of photodecomposition of sodium- and caesium-tris(oxalato)ferrates(III) in solid state might be postulated as follows:

$$M_3[Fe^{III}(ox)_3] \xrightarrow{h\nu} \underset{(IV)}{Fe^{II}(ox)2H_2O} \xrightarrow[air]{h\nu} \underset{(M=Na,\ Cs)}{M[Fe^{III}(ox)_2(H_2O)_2]}.$$

These observations are similar to those for the products obtained by the photolysis of potassium tris(oxalato)-ferrate(III) in acidic solutions.[17] Potassium tris-(oxalato)ferrate(III) is used in actinometer. Photolysis of potassium tris(oxalato)ferrate(III) has extensively been investigated in solution as regards its use in actinometer. The formation of ferrous oxalate is observed in solutions.

In the case of lithium- and ammonium tris(oxalato)-ferrates(III) the Mössbauer spectra of these complexes irradiated for 100 h at room temperature indicate a quadrupole doublet with isomer shift and quadrupole splitting values of 1.20 and 1.77 mm s^{-1} in the case of lithium tris(oxalato)ferrate(III) (Fig. 4b) and 1.22 and 1.74 mm s^{-1} in the case of ammonium tris(oxalato)-

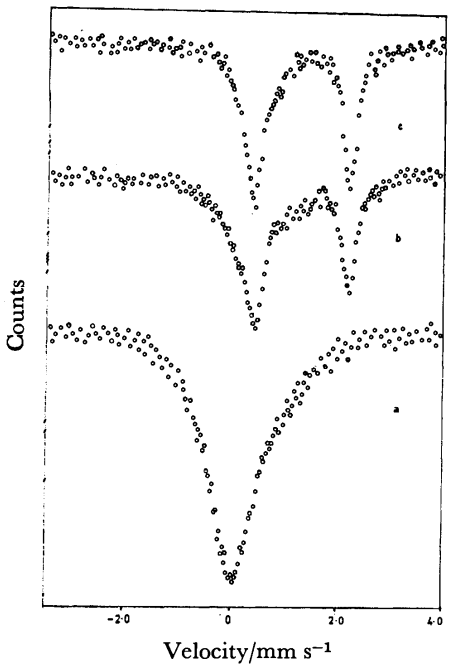

Fig. 4. Mössbauer spectra of lithium tris(oxalato)-ferrate(III) trihydrate at room temperature (25 °C).
a: Unirradiated complex, b: irradiated for 100 h, c: irradiated for 200 h.

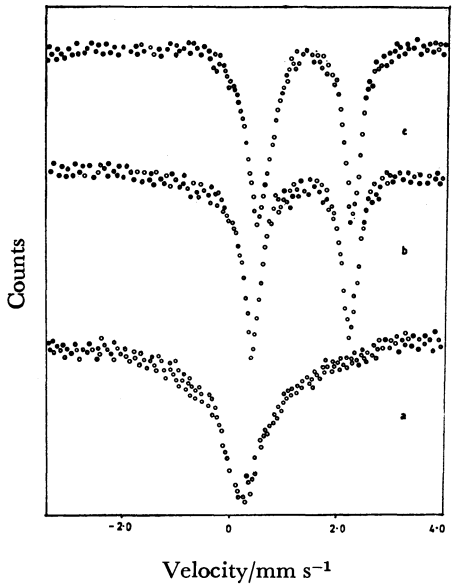

Fig. 5. Mössbauer spectra of Ammonium tris(oxalato)-ferrate(III) trihydrate at room temperature (25 °C).
a: Unirradiated complex, b: irradiated for 100 h, c: irradiated for 200 h.

ferrate(III) (Fig. 5b). On further irradiation upto 200 h (Figs. 4c and 5c) no change in the Mössbauer parameters was observed.

In the photolysis of potassium tris(oxalato)ferrate-(III), the $K_6[Fe^{II}_2(ox)_5]$ intermediate is formed and finally $K[Fe^{III}(ox)_2(H_2O)_2]$ is obtained. In sodium- and caesium tris(oxalato)ferrates(III), iron(II) oxalate has been observed as an intermediate. However, in the case of lithium- and ammonium tris(oxalato)ferrates-(III), iron(II) oxalate is formed upto 200 h of irradiation. It can be concluded that different intermediates are formed during the course of photolysis of alkali tris(oxalato)ferrates(III). The rate of photodecomposition is greater in the case of potassium- and ammonium tris(oxalato)ferrates(III). This might be the reason for the use of potassium tris(oxalato)ferrate(III) in an actinometer.

References

1) "Applications of Mössbauer Spectroscopy," ed by R. L. Cohen, Academic Press (1976).
2) W. W. Wendlandt and E. L. Simmons, *J. Inorg. Nucl. Chem.*, **28**, 2420 (1966).
3) G. M. Bancroft, K. G. Dharmawardena, and A. G, Maddock, *J. Chem. Soc., A*, **1969**, 2914.
4) H. Sato and T. Tominaga, *Radiochem. Radioanal. Lett.*, **30**, 165 (1977).
5) H. Sato and T. Tominags, *Bull. Chem. Soc. Jpn.*, **52**, 1402 (1979).
6) A. S. Brar and B. S. Randhawa, *Radiochem. Radional. Lett.*, **44**, 377 (1980).
7) J. G. Calvert and J. N. Pitts, "Photochemistry," John Wiley and Sons, Inc., New York (1967), p. 784.
8) T. Wada, Japan 8910 (57), Oct. 19; *Chem. Abstr.*, **52**, 13206 (1958).
9) C. G. Hatchard and C. A. Parker, *Proc. R. Soc. London, Ser. A*, 235, 518 (1956).
10) P. Gutlich, R. Link, and A. Trautwein, "Mössbauer Spectroscopy and Transition Metal Chemistry," Spring-Verlag Berlin Heidelberg (1978), p. 53.
11) M. Blume, *Phys. Rev. Lett.*, **14**, 96 (1965).
12) K. G. Dharamawardena and G. M. Bancroft. *J. Chem. Soc., A*, **1968**, 2655.
13) G. M. Bancroft, K. G. Dharamawardena, and A. G. Maddock, *Inorg. Chem.*, **9**, 223 (1970).
14) T. C. Gibb and N. N. Greenwood, "Mössbauer Spectroscopy," Chapman and Hall Ltd., London (1971), p. 158.
15) A. N. Garg and P. S. Goel, *J. Inorg. Nucl. Chem.*, **31**, 697 (1969); **32**, 1547 (1970).
16) D. Raj and S. P. Puri, *J. Chem. Phys.*, **50**, 3184 (1969).
17) V. Balzani and V. Carassiti, "Photochemistry of Cordination Compounds," Academic Press (1970), p. 167.

  Bull. Chem. Soc. Jpn., 54, 3170—3172 (1981) [Vol. 54, No. 10

The Design of Organic Metals. Dibenzotetrathiafulvalene-2,3-Dichloro-5,6-dicyano-*p*-benzoquinone (DBTTF-DDQ)

James J. MAYERLE* and Jerry B. TORRANCE*
IBM Research Laboratory, San Jose, California 95193, U. S. A.
(Received November 4, 1980)

The electrical and optical properties of the four charge-transfer salts formed between the two donors tetrathiafulvalene (TTF) and dibenzotetrathiafulvalene (DBTTF) and the two acceptors tetracyanoquinodimethan (TCNQ) and 2,3-dichloro-5,6-dicyano-*p*-benzoquinone (DDQ) are compared. The differences are rationalized on the basis of electrochemical considerations. DBTTF–TCNQ, the compound composed of the weakest donor and acceptor, is found to be a neutral complex. However, TTF–TCNQ and the new material DBTTF–DDQ are mixed valence and highly conducting. The latter material, which is the first highly conducting salt to contain the common acceptor DDQ, has a room temperature pellet electrical conductivity of 8 Ω^{-1} cm^{-1}. Finally, the combination of best donor and acceptor, TTF–DDQ, forms an insulating, completely ionic salt. The structure of this salt has been determined and found to crystallize with relatively isolated dimers of TTF and strongly distorted stacks of DDQ.

For the past few years we have been engaged in a program aimed at gaining a systematic understanding of the electronic and structural properties of organic charge-transfer complexes. As part of this work we have attempted to expand the range of materials that will form organic metals. We now report the electrical and optical properties of the new highly conducting salt DBTTF–DDQ,[1] the first[2] such material containing the common acceptor DDQ. In order to understand why DBTTF–DDQ is highly conducting, we will compare the electrical and optical properties of the four charge-transfer salts formed between the two donors DBTTF and TTF and the two acceptors DDQ and TCNQ.[1] This comparison will illustrate the dependence of the solid state electrical properties of organic charge-transfer complexes on the redox properties of the individual molecules and, consequently, will illustrate guidelines for how to make organic metals.

High conductivity requires that two conditions be fulfilled: first, the donor and acceptor must crystallize in separate (segregated) stacks and, second, the degree of charge transfer, ρ, from donor to acceptor must be fractional ($\rho<1$), *i.e.*, the resulting complex must be mixed valence. The criteria we use in selecting donors and acceptors that will meet these conditions have been discussed in detail elsewhere.[2–4] However, we will briefly mention under what conditions the criterion of incomplete charge-transfer is met[3] since it is of central importance to the results reported here.

The total binding energy of these materials per donor/acceptor pair, expressed as a function of ρ, the degree of charge-transfer, is given in Eq. 1,

$$E_B(\rho) = -\rho[\rho E_M - (I-A)], \quad (1)$$

where E_M is the Madelung (electrostatic binding) energy of the completely ionized lattice, I is the ionization potential of the donor, and A is the electron affinity of the acceptor. Since variations in E_M are smaller than variations in $(I-A)$ for the types of materials under discussion, differences in ρ between different materials should depend mainly on the quantity $(I-A)$. Since the values of I and A are generally not well known for organic molecules, however, we use the more readily obtained values of the electrochemical half-wave potentials ($E_{1/2}$) as a measure of relative donor/acceptor strength. Since ΔE_{REDOX}, the difference between the $E_{1/2}$ values of any donor/acceptor pair, can be related[5] to the quantity $(I-A)$ in Eq. 1, values of ΔE_{REDOX} can be used to predict the degree of charge-transfer in a given material. In particular, if ΔE_{REDOX} is large

TABLE 1. PROPERTIES OF DONOR/ACCEPTOR COMBINATIONS: ΔE_{REDOX}, VALENCE, AND ROOM TEMPERATURE PELLET ELECTRICAL CONDUCTIVITY

	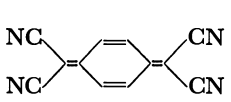 TCNQ ($E_{1/2}$=0.23 V)	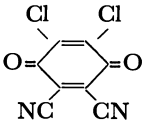 DDQ ($E_{1/2}$=0.56 V)
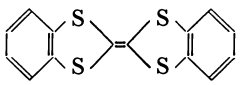 DBTTF ($E_{1/2}$=0.55 V)	+0.32 V Neutral 10^{-7} Ω^{-1} cm^{-1}	−0.01 V Mixed valence 8 Ω^{-1} cm^{-1}
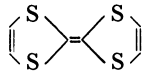 TTF ($E_{1/2}$=0.29 V)	+0.06 V Mixed valence 70 Ω^{-1} cm^{-1}	−0.27 V Ionic 10^{-8} Ω^{-1} cm^{-1}

and positive, a neutral charge-transfer complex results, *i.e.*, for a poor donor/acceptor combination, $\rho=0$. If ΔE_{REDOX} is large and negative, a fully ionic charge-transfer salt results, *i.e.*, for a good donor/acceptor combination, $\rho=1$. For intermediate values of ΔE_{REDOX}, estimated[3] as $-1/4\,V \lesssim \Delta E_{REDOX} \lesssim 1/4\,V$, there is incomplete charge-transfer and a mixed-valence, and therefore highly conducting, compound results.

Table 1 gives $E_{1/2}$ values[6] (in parentheses) for the two donors, TTF and DBTTF, and the two acceptors, TCNQ and DDQ, as well as the ΔE_{REDOX} values for the four donor/acceptor combinations. Since donor strength increases as $E_{1/2}$ decreases, it is apparent that TTF is a considerably stronger donor than DBTTF. On the other hand, since acceptor strength increases as $E_{1/2}$ increases, it can be seen that DDQ is a much stronger acceptor than TCNQ. Thus, for TTF–TCNQ, ΔE_{REDOX} is $+0.06$ V and the material is a mixed-valence, highly conducting salt. Because of its small value (-0.01 V) of ΔE_{REDOX}, one would predict that DBTTF–DDQ would also be a mixed-valence, highly conducting solid. This is what we have found. DBTTF–TCNQ, however, has a large, positive ($+0.32$ V) value of ΔE_{REDOX}. Hence, it is a neutral insulating ($\rho=0$) solid. The ΔE_{REDOX} value of -0.27 V for TTF–DDQ lies too near the ionic boundary ($\Delta E_{REDOX} \approx -1/4$ V) to allow one to predict whether TTF–DDQ would be mixed-valence or ionic. We have found it to be, in fact, completely ionic.

The reaction of DBTTF with DDQ in toluene results in a 1 : 1 compound[7] with the relatively high room temperature powder electrical conductivity of 8 Ω^{-1} cm^{-1}, compared to values in the range of 10^{-4}—10^{-10} Ω^{-1} cm^{-1} for any of the previously known compounds of DDQ, and compared to a value of 70 Ω^{-1} cm^{-1} for TTF–TCNQ. Although we have not been able to obtain single crystals of DBTTF–DDQ suitable for X-ray diffraction, the high electrical conductivity leaves no doubt that the material is composed of mixed-valence, segregated stacks of donors and acceptors. Convincing evidence for the mixed-valence nature of DBTTF–DDQ can also be obtained from its optical spectrum, Fig. 1. Like that of TTF–TCNQ, the spectrum consists of high energy bands largely characteristic of the individual ions. In addition, and most importantly, there is a low energy band at $\approx$0.4 eV which, in the case of TTF–TCNQ, has been shown to be a mixed-valence, intrastack charge-transfer transition.[8] This mixed-valence charge-transfer band is found in and is characteristic of all known organic metals.[8] Thus, DBTTF–DDQ is mixed-valence and is the first highly conducting material that contains DDQ. This compound is one of the rare examples[4] of a highly conducting organic charge-transfer salt that does not contain TCNQ or one of its derivatives as the acceptor molecule. This compound is also significant as one of the first highly conducting materials containing DBTTF, the oldest TTF-like molecule.[9] Metallic DBTTF compounds with BF_4^- and $TCNQCl_2$ have recently been reported.[10,11]

Slow diffusion of an acetonitrile solution of TTF into a DDQ solution of the same solvent yields small, dark red crystals of almost cubic habit. A projection of the structure (space group $P\bar{1}$ with $a=10.227(4)$, $b=12.195(5)$, $c=6.609(2)$ Å, $\alpha=77.51(2)$, $\beta=81.93(2)$, and $\gamma=87.30(4)°$, with 2 formula units per unit cell) onto the (001) plane is shown in Fig. 2(a). It consists of

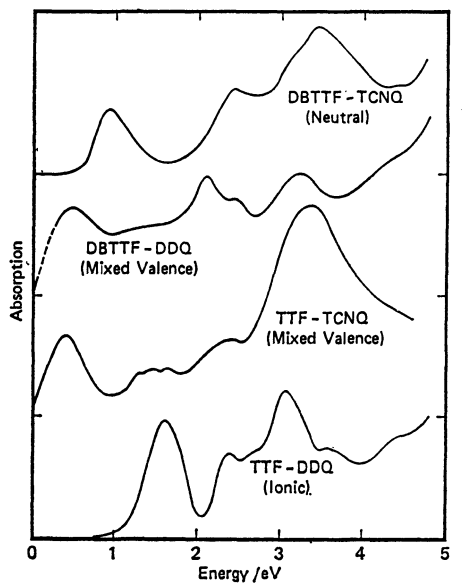

Fig. 1. Optical absorption spectra of the four complexes formed between the two donors TTF and DBTTF and the two acceptors DDQ and TCNQ.

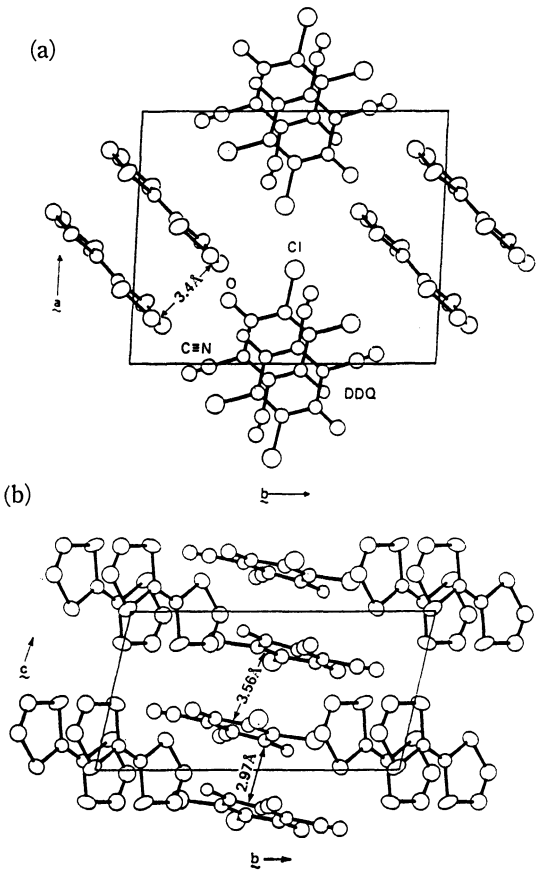

Fig. 2. Structure of TTF–DDQ projected onto the (a) (001) plane and (b) onto the (100) plane.

strongly distorted stacks of DDQ and isolated, eclipsed dimers of TTF. The interplanar spacing between the two TTF molecules comprising the dimer is ≈3.4 Å. There is virtually no overlap between adjacent dimers. The DDQ molecules also dimerize, but do so within the framework of infinite columns of DDQ stacked parallel to the c axis. The stacking of the DDQ molecules can be seen in the (100) projection of the structure, shown in Fig. 2(b). The interplanar spacing between molecules of the DDQ dimer is 3.0 Å. This is an extremely short distance. The interplanar spacing between molecules in adjacent dimers is 3.56 Å. This strong distortion of the DDQ stacks, as well as the existence of isolated dimers of TTF, accounts for the fact that there is no paramagnetic contribution to the magnetic susceptibility. The distortion of the acceptor stack is presumably caused by the same phenomenon[12] that causes the distortion in the low temperature phases of other fully ionic complexes, such as K–TCNQ.[13] The completion of the structural analysis (R=12%) has been complicated by the fact that the DDQ molecule is disordered, exhibiting partial interchange of -Cl and -C–N groups. Such disorder has previously been seen in the charge-transfer complex of DDQ with benzo[c]-phenanthrene.[14]

That ρ=1 in TTF–DDQ can be seen in its optical spectrum, shown in Fig. 1. The absence of a mixed valence charge transfer band near 0.4 eV indicates that this compound is not mixed valence. The optical spectrum is dominated by the stronger absorption of the TTF molecule and is nearly identical to that of $(TTF^+)_2$ dimers,[15] consistent with the dimers evident in the structure (Fig. 2). The optical absorption indicates that they are not neutral, but completely ionic (ρ=1) in agreement with the conclusions of Ikemoto and co-workers.[16]

The optical spectrum of DBTTF–TCNQ, also shown in Fig. 1, shows no evidence of any absorption[17] due to $TCNQ^-$ and hence must be a neutral (ρ=0) complex. (Absorption due to $DBTTF^+$, if it were present, would also appear near 2.0 eV, but would be considerably weaker than the $TCNQ^-$ absorption.) Recent ESR experiments[18] also indicate that DBTTF–TCNQ is a neutral complex. This is expected from the large positive value (+0.32 V) of ΔE_{REDOX} (Table 1). The energy of the charge transfer band at 0.91 eV is in agreement with a computed[19] value based on ΔE_{REDOX}. The second band near 2.4 eV is probably a second charge-transfer band.

In summary, it seems apparent that if the ΔE_{REDOX} value of the donor/acceptor pair in a 1 : 1 charge-transfer complex differs significantly from zero, the degree of charge-transfer in the complex will be either zero or one (ρ=0,1). If, however, ΔE_{REDOX}=0, the complex will probably be mixed-valence. As described above, we have used the ΔE_{REDOX} values in Table 1 to successfully predict that DBTTF–TCNQ would be neutral and that DBTTF–DDQ would be mixed-valence and, therefore, highly conducting. In so doing, we have convincingly demonstrated that by employing simple electrochemical considerations and readily obtainable data, one can reliably estimate the degree of charge-transfer which might be expected for a 1 : 1 compound. As a result, one can predict which combinations of donors and acceptors have a reasonable probability of giving rise to organic metals. This predictability has been used to obtain the first highly conducting salt of the common acceptor DDQ.

We wish to acknowledge the technical assistance of V. Y. Lee.

References

1) Abbreviations used are: DBTTF, dibenzotetrathiafulvalene; TTF, tetrathiafulvalene; DDQ, 2,3-dichloro-5,6-dicyano-*p*-benzoquinone; TCNQ, tetracyanoquinodimethan; $TCNQCl_2$, dichlorotetracyanoquinodimethan.

2) These results were first reported by us at the ACS/CSJ Chemical Congess, Honolulu, Hawaii, April 1—6, 1979.

3) J. B. Torrance, *Acc. Chem. Res.*, **12**, 79 (1979); J. J. Mayerle, in "Mixed-Valence Compounds," ed by D. B. Brown, D. Reidel Publishing Co., Dordrecht (1980), p. 451.

4) J. B. Torrance, J. J. Mayerle, K. Bechgaard, and V. Y. Lee, *J. Am. Chem. Soc.*, **101**, 4747 (1979).

5) V. D. Parker, *J. Am. Chem. Soc.*, **98**, 98 (1976); E. C. M. Chen and W. E. Wentworth, *J. Chem. Phys.*, **63**, 318 (1975).

6) $E_{1/2}$ values (*vs.* SCE) were measured in acetonitrile using a Pt electrode and a sweep rate of 100 mV/s.

7) The stoichiometry of DBTTF–DDQ was determined from both elemental analysis and solution optical data.

8) J. B. Torrance, B. A. Scott, and F. B. Kaufman, *Solid State Commun.*, **17**, 1369 (1975); J. Tanaka, M. Tanaka, T. Kawai, T. Takabe, and O. Maki, *Bull. Chem. Soc. Jpn.*, **49**, 2358 (1976).

9) W. R. H. Hurtlay and S. Smiles, *J. Chem. Soc.*, **1926**, 1821, 2263.

10) I. V. Krivoshei, V. A. Babiyczuk, I. M. Guella, I. F. Golovkina, N. V. Mansia, V. A. Starodub, and S. A. Cheva, *Phys. Status Solidi A*, **50**, K197 (1978).

11) C. S. Jacobsen, H. J. Pedersen, K. Mortensen, and K. Bechgaard, *J. Phys.*, **13**, 3411 (1980).

12) J. B. Torrance, *Ann. N. Y. Acad. Sci.*, **313**, 210 (1978); J. B. Torrance, J. J. Mayerle, and J. I. Crowley, *Bull. Am. Phys. Soc.*, **23**, 425 (1978).

13) M. Konno, T. Ishii, and Y. Saito, *Acta Crystallogr., Sect. B*, **33**, 763 (1977).

14) J. Bernstein, H. Reger, and F. H. Herbstein, *Acta Crystallogr., Sect. B*, **33**, 1716 (1977).

15) T. Sugano, K. Yakushi, and H. Kuroda, *Bull. Chem. Soc. Jpn.*, **51**, 1041 (1978); J. B. Torrance, B. A. Scott, B. Welber, F. B. Kaufman, and P. E. Seiden, *Phys. Rev. B*, **19**, 730 (1979).

16) I. Ikemoto, T. Sugano, and H. Kuroda, *Chem. Phys. Lett.*, **49**, 45 (1977).

17) Y. Iida, *Bull. Chem. Soc. Jpn.*, **42**, 71 (1969).

18) M. T. Jones, R. Kellerman, A. Troup, and D. J. Sandman, *Proc. Conf. Low-Dimensional Synthetic Metals, Chem. Scripta*, in press.

19) J. B. Torrance, J. Vazquez, J. J. Mayerle, and V. Y. Lee, *Phys. Rev. Letts.*, **44**, 253 (1981).

Studies in the Molten State. Viscosities of *trans*-Stilbene, *N*-Benzylideneaniline, and *N*-Benzylidene-*p*-toluidine Melts Near Their Melting Temperatures

Bimla KWATRA,† (the late)Venketachari RAMAKRISHNA, and Sushil Krishan SURI*
Chemistry Department, Indian Institute of Technology, Delhi, New Delhi-110016, India
(Received November 21, 1980)

The viscosities and densities of *trans*-stilbene, *N*-benzylideneaniline (BA) and *N*-benzylidene-*p*-toluidene (BT) melts at various temperatures near their respective melting temperatures have been determined. In all the cases, a precursor behaviour in crystal phase at temperatures below the melting temperature has been observed. The viscosity *vs.* temperature relationships have been discussed in two parts: one in the liquid state and the other in the supercooled region. The values of energy and entropy of viscous flow are indicative of molecular association in BA and BT. The enhanced viscosity in the supercooled region has been attributed to the cluster formation. The hinderance to molecular rotation, as a factor influencing viscosity can not be ruled out.

The measurement of viscosity (η) and its temperature dependence near transitions has yielded useful information regarding liquid structure both for normal and polymeric liquids and for those which are non-Newtonian.[1-5] Rotational and ordering characteristics of molecules, intermolecular complexing tendency including hydrogen bonding, precursor behaviours of melting in crystal phase at temperatures below the melting temperature (premelting phenomenon), cluster formation prior to freezing of the liquid phase (prefreezing phenomenon) and the molecular nature of the compounds have been confirmed from the log η *versus* reciprocal of temperature plots and from the thermodynamic parameters of viscous flow.[7,8] Though viscosity behaviour of many liquids like paraffins,[9] mono- and polysubstituted benzenes;[10-14] polycyclic hydrocarbons[7] *etc.* have been investigated, molecules having flexible aromatic rings as end groups attached to a rigid central group like $\diagdown\!\!\diagup C{=}C\diagdown\!\!\diagup$; $C{=}N-$, *etc.* have not received serious attention.[15,16] These type of molecules are of importance because a vast majority of compounds having such structure exhibit liquid crystallinity and constitute a potentially mesomorphic system. As a part of our investigations on such molecules,[17] we report in this paper the viscosities and densities of *trans*-stilbene, $C_6H_5CH{=}CHC_6H_5$; *N*-benzylideneaniline, $C_6H_5CH{=}NC_6H_5$ (BA); and, *N*-benzylidene-*p*-toluidine, $C_6H_5CH{=}NC_6H_4CH_3$(BT) melts at various temperatures near their respective melting region. These studies were aimed to investigate the behaviour of these compounds in molten liquid and supercooled region.

Experimental

Chemically pure sample of *trans*-stilbene (mp 124 °C) supplied by "Fluka AG" was used as such without any further purification. *N*-Benzylideneaniline (mp 51.5 °C) and *N*-benzylidene-*p*-toluidine (mp 34.2 °C) were prepared and purified following the standard established procedures.[18]

Densities of the melts were measured using a specifically designed pipette-like-pycnometer[12] of about 6 ml capacity. A fine orfice opening into the liquid prevented easy flow of the liquid after the pycnometer was filled thus reducing turbulence and crystallization in the supercooled region. The viscosities were determined with the help of an Ubbelohde suspended level viscometer. For measurements at <70 °C, a water thermostat with a temperature control of ±0.01 °C was used for maintaining constant temperature. Distilled, deionized and degassed water was used as a reference liquid in this temperature range and the literature values of the viscosities and densities[19,20] were used to calibrate the apparatus. For higher temperatures a glycerine bath was used with an accuracy in the maintenance of temperature up to ±0.03 °C. The calibration of pycnometer and viscometer was checked at different temperatures by measuring the density and viscosity of several known liquids in the desired temperature range. The maximum error in the density values was $\pm2\times10^{-5}$ g cm^{-3}. The viscosities at temperatures above the melting temperature was reproducible to within 1×10^{-6} N s cm^{-2} at temperature below 70 °C and to within 2×10^{-6} N s cm^{-2} at higher temperatures. The measurements in the supercooled region was particularly tedius and reproducibility was checked by repeating the measurements four or more times. Densities and viscosities in the supercooled region could not be reproduced to better than $\pm5\times10^{-5}$ g cm^{-3} and $\pm5\times10^{-6}$ N s m^{-2} respectively.

Results and Discussion

The densities and viscosities of the three compounds in the molten state at various temperature in the vicinity of their respective melting temperatures are recorded in Table 1.

The densities were found to vary linearly with the temperature, the deviations in most cases being within the experimental uncertainties of the data.

The results of viscosity measurements are plotted as log η *vs.* T^{-1} in Fig. 1. It is observed that the viscosities follow two different linear relationships, one above the melting point and the other in the supercooled region with a break at temperature T_t and some uncertain points around this temperature. This is an indication of premelting or prefreezing transitions taking place in these compounds. For BT the break in log η *vs.* T^{-1} plot below the melting point is not as sharp and curvature not as high as is normally expected for melts deviating from the Arrhenius equation. Nevertheless, we have satisfied ourselves that the deviations from the Arrhenius line below the melting point are significant being larger

† Present address: Chemistry Department, University College for Women, Miranda House, University of Delhi, Delhi-110007 india.

TABLE 1. DENSITIES AND VISCOSITIES OF COMPOUNDS IN THE MOLTEN STATE AT VARIOUS TEMPERATURES NEAR THE MELTING TEMPERATURE

Temperature K	Density g cm^{-3}	Viscosity × 10^4 N s m^{-2}	Temperature K	Density g cm^{-3}	Viscosity × 10^4 N s m^{-2}
	trans-Stilbene		329.15	1.0331	36.88
396.15	0.95932	10.595	331.15	1.0323	34.89
397.15	0.95861	10.398	333.15	1.0303	32.92
398.15	0.95789	10.296	335.15	1.0277	31.32
400.15	0.95635	10.096	337.15	1.0264	29.66
403.15	0.95421	9.756	339.15	1.0252	28.26
406.15	0.95168	9.357	341.15	1.0228	26.93
408.15	0.95029	9.112	343.15	1.0217	25.78
410.15	0.94875	8.866		*N*-Benzylidene-*p*-toluidine	
413.15	0.94652	8.545	293.15	1.0443	154.16
416.15	0.94433	8.376	296.15	1.0422	137.03
418.15	0.94282	8.245	298.15	1.0403	125.15
423.15	0.93908	7.915	300.15	1.0383	112.79
	N-Benzylideneaniline		302.15	1.0369	104.47
299.15	1.0580	106.30	304.15	1.0357	96.49
301.15	1.0563	96.53	306.15	1.0342	93.34
303.15	1.0546	87.30	308.15	1.0325	85.00
305.15	1.0530	80.55	310.15	1.0312	77.66
307.15	1.0513	73.65	313.15	1.0293	69.79
309.15	1.0496	68.12	315.15	1.0278	64.18
311.15	1.0479	63.28	317.15	1.0258	56.78
313.15	1.0462	58.84	319.15	1.0246	55.28
315.15	1.0447	54.59	321.15	1.0227	51.74
317.15	1.0431	51.46	323.15	1.0211	48.97
319.15	1.0411	47.87	325.15	1.0195	45.43
321.15	1.0391	45.22	327.15	1.0180	42.86
323.15	1.0378	42.87	329.15	1.0163	40.37
325.15	1.0371	41.72	331.15	1.0151	38.16
327.15	1.0352	39.13			

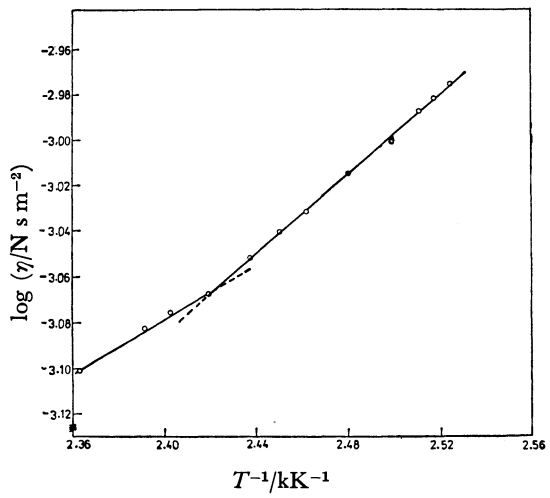

Fig. 1(a). The variation of viscosity (η) with temperature (T) for *trans*-stilbene.

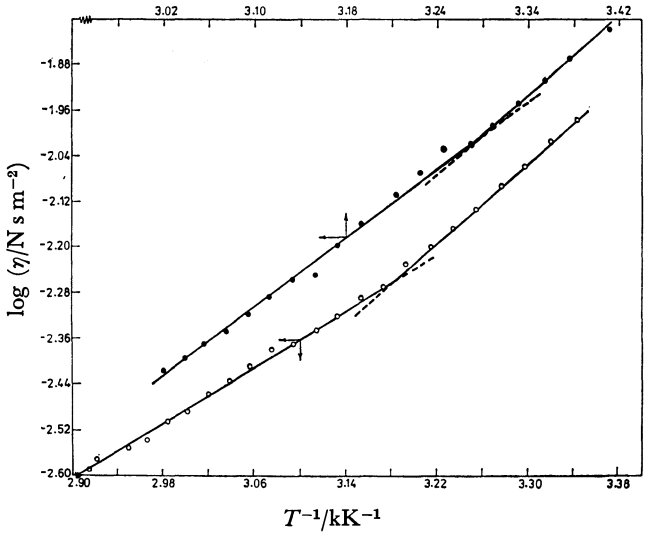

Fig. 1(b). The variation of viscosity (η) with temperature (T) for *N*-benzylideneaniline (○) and *N*-benzylidene-*p*-toluidine (●).

than the order of magnitude of the experimental error involved. It is observed that at any temperature, the liquid densities of the three compounds increases in the order *trans*-stilbene<BT<BA whereas the viscosities follow the order *trans*-stilbene<BA<BT. The viscosity of BT is higher than that of BA and reveals that the substitution of methyl group by hydrogen in BT facilitates its flow.

The Arrhenius parameters for the melts have been calculated for the two regions and recorded in Table 2.

TABLEE 2. ARRHENIUS PARAMETERS FOR THE MELTS

	Temperature range / K	Slope × 10^2	Intercept.	E_{vis} / kcal mol^{-1}	ΔG^* at T_t / kcal mol^{-1}	ΔS^* / cal K^{-1} mol^{-1}
trans-Stilbene	396.1—412.3	8.85	−5.209	4.05	4.92	−2.14
	412.3—423.1	5.85	−4.484	2.68		−5.46
N-Benzylidene aniline	299.1—314.2	17.17	−7.719	7.86	4.85	9.52
	314.2—343.1	12.58	−6.256	5.75		2.82
N-Benzylidene-*p*-toluidine	293.1—302.1	16.95	−7.592	7.76		8.78
	302.1—331.1	15.18	−7.008	6.95	5.12	6.11

According to Mclaughlin,[1] E_{vis} is made up of two terms namely the energy required to overcome the barrier for transport E_1; and the energy required for forming a hole, E_2. The former is related to the energy of vaporization, $E_{vap}(\simeq 3E_1)$. The magnitude of E_2 is normally small in comparison to E_{vap} for liquids at moderate temperatures. In fact, for most of the normal liquids, the ratio $E_{vaq} : E_{vis}$ is something between 3 and 4. At sufficiently low temperatures, and, for sufficiently bulky molecules, E_2 become predominant[2] and hence the ratio tend to a value lower than 3. Grumberg and Nissan[3] pointed out that the ratio for polar associated liquids would depend upon the extent of association both in the liquid and vapours state and the geometry of packing in the liquid state. The ratio of $E_{vap} : E_{vis}$ for *trans*-stilbene, BA and BT is ≈5.2, 1.9, and 1.2 respectively. Further, the ratio $E_{vap}/\Delta G^*$ for *trans*-stilbene is ≈2.8 in agreement with the reported ratio of 2.45. For BA and BT, the value is far less. These observations are clear indicative of intramolecular association in BA and BT. The entropy of activation values recorded in Table 2 support this surmise. Tyuzyo[4] reported a value of $\Delta S^* = -2.9$ cal deg^{-1} mol^{-1} for a large number of compounds including polar ones. For *trans*-stilbene, ΔS^* is more negative in the liquid region indicating less ordering in it. Higher values of ΔS^* for BA and BT suggest that the ordering in these compounds exists to a much larger extent especially in supercooled region as compared to many organic liquids. This is also confirmed by Batschinski's plot of the viscosity data.[5,6] According to Batschinski:

$$\frac{1}{\eta} = \frac{v}{c} - \frac{v_0}{c}, \qquad (1)$$

where, v=specific volume; v_0=limiting value of specific volume at infinite viscosity and c is a constant. The plots of η^{-1} *versus* v yielded straight line plots with break at T_t and uncertain region around this temperature. The value of v_0 for the three compounds obtained from these plots are recorded in Table 3. These values, though different from those reported for many other organic liquids,[5] are close to the one reported for Cresols[14] where strong hydrogen bonding and structuring exist in the liquid state.

Several functional relationships, emperical, semi-emperical and theoretical have been proposed[6] for the viscosity in the low temperature region. For many compounds the viscosity data in this region fit into the Doolittle equation.[21]

$$\log \eta = A' + B'/(T - T_0), \qquad (2)$$

where T_0 is evisaged as a second order transition temperature. The evidence of applicability of Doolittle equation for our systems was not conclusive because the region of supercooling is rather short. A rough numerical fit yielded T_0 values of <10 K for the three compounds. These values are unexpectedly low considering that normally T_0 is about 20—100 K less than the melting temperature.[22] We consider it reasonable therefore, to assume that even below the melting temperature, the supercooled liquid follow an Arrhenius equation with different values of the constants.

It is observed that the E_{vis} and ΔS^* values are more positive in the supercooled region as compared to the high temperature region indicating an increase in association between molecules and a non-cooperative mechanism of flow. Two approaches based on the hinderance to rotation at or below T_t and on the cluster formation may be proposed to explain the enhanced viscosity in the supercooled region. The most commonly used procedure to establish the existence of hinderance to rotation is to compare the volume swept by rotation of the molecule, V_r, about a suitable axis with the actual volume available to it on the basis of experimental density data. Following Ubbelohde's procedure,[7] V_r for the molecules around the longer axis have been calculated and compared with the molar volumes in Table 3. The V_r is far in excess of the available volume, indicating that the enhanced viscosity of melts may result from hinderance to rotation.

In the alternate approach in terms of cluster formation it is assumed that the increase in viscosity and hence E_{vis} is due to the formation of clusters, the volume fraction ϕ of clusters have been calculated from the

TABLE 3. SOME CALCULATED PARAMETERS OF THE COMPOUNDS

	v_0 at temperatures		V_r / cm^3 mol^{-1}	Molar volume range[a] / cm^3 mol^{-1}	E_{vap} / kcal mol^{-1}
	$<T_t$	$<T_t$			
trans-Stilbene	0.968	0.985	368	187—192	14.0
N-Benzylideneaniline	0.942	0.933	435	170.5—178	11.1[b]
N-Benzylidine-*p*-toluidine	0.952	0.947	500	185.5—191	8.0[b]

a) From liquid density data at temperatures around T_t. b) Extrapolated using Trouton's rule.

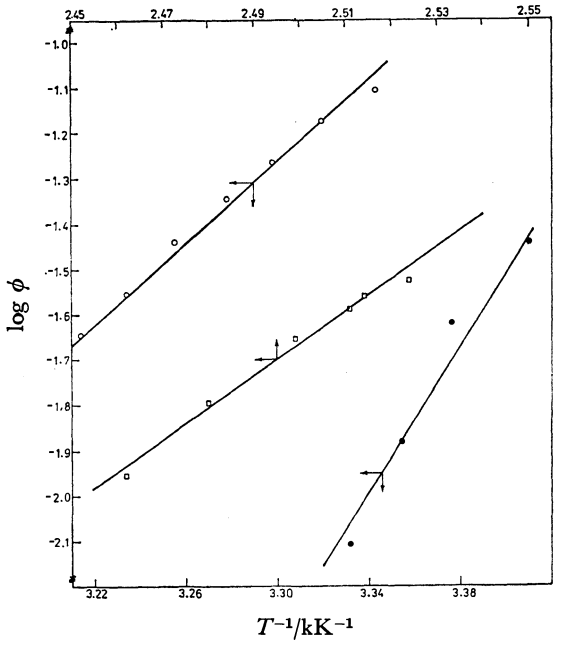

Fig. 2. The variation of Volumes fraction of Clusters (ϕ) with temperature (T) for *trans*-stilbene (□); *N*-benzylideneaniline (○); and *N*-benzylidene-*p*-toluidine (●).

Einstein equation.[23]

$$\eta/\eta_{ext.} = 1 + 2.5\phi + 7\phi^2, \quad (3)$$

where η_{ext} is the viscosity extrapolated from high temperature region and η is the actual viscosity. The plots of log ϕ *versus* T^{-1} are shown in Fig. 2. These are similar to the one obtained by Ubbelohde for dimeric, trimeric and even polymeric clusters of organic molecules. Following Ubbelohde,[23] the equilibrium constant K for the equilibrium

$$A_n \rightleftharpoons nA, \quad (4)$$

where n are the number of molecules in the cluster. We have calculated K at different temperatures for various values of n between 2 and 6, and also the heat of depolymerization of clusters, ΔH_d. It was found to be same for different values of n. The ΔH_d values have been compared with ΔH_f values for the compounds in Table 4. The ratio $\Delta H_d/\Delta H_f$, which is considered as the number of molecules in the cluster, n, is 2 for *trans*-stilbene, 3 for BA and 4 for BT. It is possible that these clusters also consitute the unit of flow thus raising the E_{vis} in the supercooled region. At the same time the volumetric effects due to the cluster formation seems to be too small to bring about any sharp change in density at T_t is passed.

References

1) E. Mclaughlin, *Trans. Faraday Soc.*, **55**, 28 (1959).
2) M. F. Mole, W. S. Homes, and J. C. Macoubrey, *J. Chem. Soc.*, **1964**, 5144.
3) L. Grunberg and A. H. Nissan., *Trans. Faraday Soc.*, **45**, 125 (1949).
4) K. Tyuzyo, *Bull. Chem. Soc., Jpn.*, **30**, 782 (1957).
5) A. A. K. Al-Mahdi and A. R. Ubbelohde, *Trans. Faraday Soc.*, **51**, 361 (1955).
6) S. G. Brush, *Chem. Revs.*, **62**, 513 (1962).
7) A. R. Ubbelohde, "Melting and Crystal Structure," Claredon Press, London (1965).
8) A. Bondi, "Physical Properties of Molecular Crystals," J. Wiley, N. Y. (1968).
9) R. J. Moore, P. Gibbs, and H. Eyring, *J. Phys. Chem.*, **57**, 172 (1953).
10) A. R. Dexter and A. J. Matheson, *Trans. Faraday Soc.*, **64**, 2632 (1968).
11) J. N. Andrews and A. R. Ubbelohde, *Proc. R. Soc. London, Ser. A*, **228**, 435 (1955).
12) U. S. Tewari, P. Vasudevan, and V. Ramakrishna, *J. Phys. Soc. Jpn.*, **30**, 843 (1971).
13) U. S. Tewari, P. Vasudevan, and V. Ramakrishna,

TABLE 4. VOLUME FRACTION OF CLUSTERS AND THEIR EQUILIBRIUM CONSTANT IN MELTS IN THE SUPERCOOLE D REGION

	Temp $(T^{-1}/kK^{-1}) \times 10^{-2}$	$\phi \times 10^3$	K	ΔH_f / kcal mol^{-1}	ΔH_d / kcal mol^{-1}
trans-Stilbene	252.4	29.7	64.3		
	251.8	27.5	69.8		
	251.2	25.5	75.5		
	249.9	22.0	87.7		
	248.0	16.0	122.1	7.1	15.0
	246.2	11.1	177.9		$n=2$
N-Benzylideneaniline	334.3	78.0	33.6		
	332.1	66.8	39.9		
	329.9	54.2	50.4		
	327.7	45.2	61.4		
	325.6	36.1	78.1		
	323.5	27.7	103.3	5.6	16.7
	321.4	22.5	128.1		$n=3$
N-Benzylidene-*p*-toluidine	341.1	36.0	104.2		
	337.7	23.9	160.4		
	335.4	13.1	298.4		
	333.2	7.8	505.8	6.7	25.8
					$n=4$

J. Phys. Soc. Jpn., **36**, 1418 (1974).
14) U. S. Tewari, P. Vasudevan, and V. Ramakrishna, *Indian J. Chem.*, **13**, 720 (1975).
15) G. W. Gray, "Molecular Structure and the Properties of liquid crystals," Academic Press, New York (1962).
16) R. S. Porter, E. M. Barrall, and J. F. Johnson, *J. Chem. Phys.*, **45**, 1452 (1966).
17) B. Kwatra and S. K. Suri, *Thermochim. Acta*, **44**, 373 (1981).
18) H. Gilman and A. H. Blatt, *Org. Synth.*, Coll. Vol. I, (1961).
19) G. S. Kell, *J. Chem. Eng. Data*, **15**, 119 (1970).
20) "Thermo Physical Properties of Matter,"ed by Y. S. Touloukian, S. C. Saxena, and P. Hestermans, Plenum, New York (1975), Vol. II.
21) M. H. Cohen and D. Turnbull, *J. Chem. Phys.*, **31**, 1164 (1959).
22) M. R. Carpenter, D. B. Davies, and A. J. Matheson, *J. Chem. Phys.*, **46**, 2451 (1967).
23) E. McLaughlin and A. R. Ubbelohde, *Trans. Faraday Soc.*, **56**, 988 (1960).

Spectrophotometric Determination of Copper, Cobalt, Nickel, and Tellurium after Extraction with Morpholine-4-carbodithioate into Molten Naphthalene

Mamta GAUTAM, R. K. BANSAL, and B. K. PURI*

Department of Chemistry, Indian Institute of Technology, Hauz Khas, New Delhi-110016, India

(Received March 25, 1980)

Potassium morpholine-4-carbodithioate has been examined as a reagent for the spectrophotometric determination of copper, cobalt, nickel and tellurium after extraction into molten naphthalene. The extracted mixture of metal complex and naphthalene was dissolved in chloroform and the trace amounts of these metals determined spectrophotometrically. Beer's law holds in the concentration range Cu: 5.0—70.0, Co: 5.0—81.0, Ni: 6.0—90.0, and Te: 5.7—125.0 μg per 10 ml of the final solution. The molar absorptivity and sensitivity are calculated to be Cu: 1.067×10^4 mol^{-1} cm^{-1}, 0.0059 μg/cm^2 (440 nm), Co: 1.350×10^4 mol^{-1} cm^{-1}, 0.0043 μg/cm^2 (360 nm), Ni: 7.920×10^3 mol^{-1} cm^{-1}, 0.0088 μg/cm^2 (390 nm), and Te: 1.075×10^4 mol^{-1} cm^{-1}, 0.0110 μg/cm^2 (415 nm). Aliquots containing 25.0 μg of copper, 27.0 μg of cobalt, 24.0 μg of nickel and 25.5 μg of tellurium gave a mean absorbance of 0.420, 0.620, 0.270, and 0.215 with a relative standard deviation of 0.0016, 0.0024, 0.0015, and 0.0013 respectively. The interference of various ions has been studied in detail. Only cobalt interfered in the determination of nickel which was eliminated by extraction first at low pH. Methods were developed for the determination of copper, cobalt and nickel in various alloys. A method was also developed for simultaneous determination of tellurium and selenium in the pure solution, based upon the thermal instability of seleniumelided carbodithioate complex.

Morpholine-4-carbodithioate has been suggested as a possible analytical reagent by Beyer and Ott[1] in the spectrophotometric[2,3] and volumetric[4] determination of some metals. Recently, it has been utilized in the gravimetric determination of tellurium, copper, bismuth, palladium and nickel.[5-8] The reagent was used in the thin layer[9] and paper[10] chromatographic separation of metal complexes. A preliminary study indicated that bismuth, copper, cobalt, nickel, and tellurium formed coloured, water insoluble and thermally stable metal complexes which may be extracted with molten naphthalene. The extraction-spectrophotometric determination of bismuth has been reported.[11] Conditions have been developed for the determination of copper, cobalt, nickel and tellurium and also for the analysis of alloys containing copper, cobalt and nickel. Based upon the thermal instability of selenium complex of this reagent, a method is suggested for the simultaneous determination of tellurium and selenium using this technique and liquid-liquid extraction at room temperature.

Experimental

Reagents. Potassium morpholine-4-carbodithioate was prepared by the method given by Macrotrigiano *et al.*,[12] 0.01 M aqueous solution being used when necessary. Solutions of copper sulfate, cobalt nitrate, nickel nitrate and potassium tellurite were prepared from samples (analytical grade) in distilled water and standardized.[13] Naphthalene and chloroform (analytical grade) were checked spectrophotometrically before use. 1% alkali salt and 0.1% metal salt solutions were used to study intereference. Dilute solutions of perchloric acid and ammonia were used to adjust pH.

Equipment. An Elico pH meter and a SP-700 spectrophotometer were used.

General Procedure. To an aliquot of each metal solution taken separately was added 1.0 ml of the reagent, the pH being adjusted (Fig. 2). After being transferred to round bottomed flasks with stopper and heated in a water-bath at *ca.* 60 °C, 2 g of naphthalene was added, heating being continued till naphthalene melted and formed a separate liquid-layer. This was stirred vigorously till the naphthalene separated out as a solid mass. The contents were again heated in the water-bath to remelt the naphthalene, shaken vigorously and allowed to stand. Naphthalene was separated from the aqueous phase by filteration, dried in folds of filter paper, dissolved in chloroform and made exactly 10 ml in each case. These solutions were dried by adding 2 g of anhydrous sodium sulfate, a portion being taken in a 1 cm cell and the absorbance measured against a reagent blank. This was referred to the calibration curve constructed under similar conditions in each case.

Results and Discussion

Absorption Spectra. The absorption spectra of potassium morpholine-4-carbodithioate and its copper, cobalt, nickel, and tellurium complexes were recorded in naphthalene-chloroform solution against water and reagent blank, respectively. Copper, cobalt, nickel, and tellurium morpholine-4-carbodithioates show absorptions at 440 nm, 360 nm, 385—390 nm, and 410—420 nm, respectively, the absorption of reagent being negligible at these wavelengths (Fig. 1).

Effect of pH. Extraction was carried out at different pH, other conditions being kept constant. The characteristics of all spectral curves were the same, indicating the presence of only one complex. The absorbances of the extracts were constant in the pH range of Cu: 4.5—8.0, Co: 3.5—9.5, Ni: 6.5—9.0 and Te: 4.0—6.5 respectively. The pH effect in each case is shown in Fig. 2.

Effect of Reagent. Extraction was carried out at optimum pH and varying amounts of reagent (Fig. 3). It was found to be quantitative in the volume range of Cu: 0.8—1.5 ml, Co: 1.0—2.0 ml, Ni: 1.0—2.5 ml and Te: 0.5—1.5 ml of 0.01 M reagent.

Effect of Naphthalene. Extraction was carried out by varying the amount of naphthalene from 0.25—4.5 g at optimum pH and under constant conditions. In all cases absorbance remained constant for 1.0—

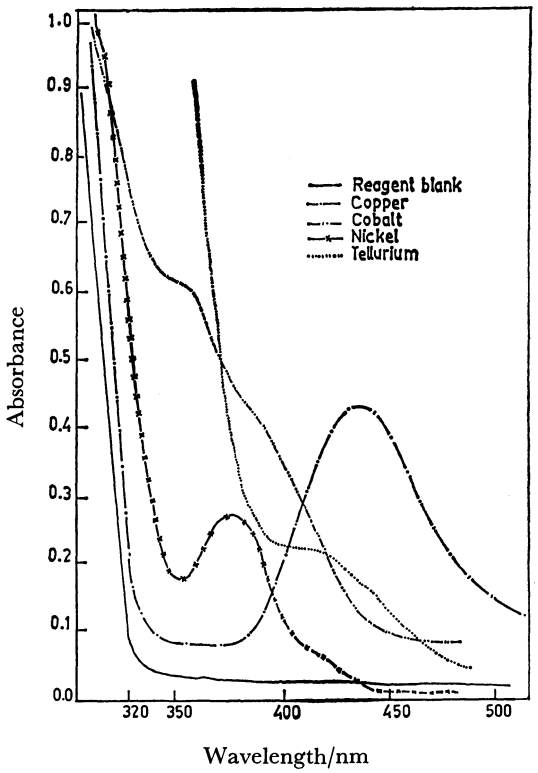

Fig. 1. Absorption spectra.
Reagent blank. Morpholine-4-carbodithioate (0.01 M): 1.5 ml, naphthalene: 2.0 g, reference: water. Cu: 25.0 μg, pH: 5.0; Co: 27.0 μg, pH: 6.5; Ni: 24.0 μg, pH: 7.5; Te: 25.5 μg, pH: 5.0; rest of the conditions were same as in reagent blank.
Reference: reagent blank.

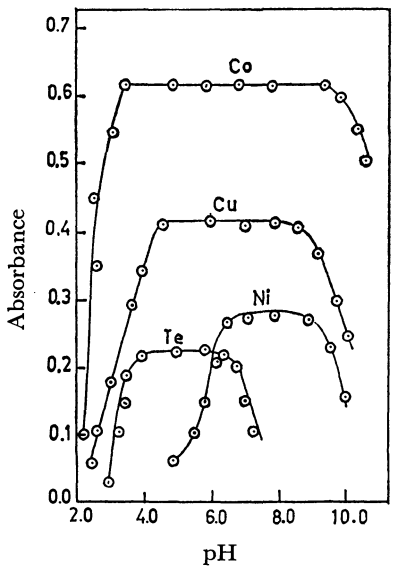

Fig. 2. Effect of pH.
Cu: 25.0 μg, wavelength: 440 nm; Co: 27.0 μg, wavelength: 360 nm; Ni: 24.0 μg, wavelength: 370 nm; Te: 25.5 μg, wavelength: 415 nm. Morpholine-4-carbodithioate (0.01 M): 1.5 ml, naphthalene: 2.0 g, reference: reagent blank.

3.5 g of naphthalene. Below 1.0 g the extraction was incomplete and above 3.5 g it was difficult to dissolve naphthalene in a limited amount of chloroform (Fig. 4).

Effect of Aqueous Phase. Since the amount of the organic phase is very small as compared to that of the aqueous phase the effect of the latter on extraction was studied. Extraction was quantitative

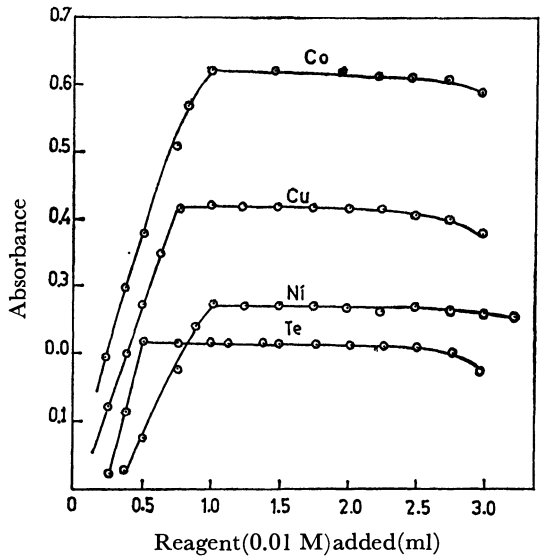

Fig. 3. Effect of reagent.
Conditions were same as in Fig. 2.

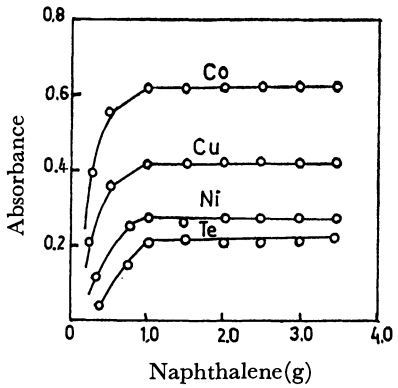

Fig. 4. Effect of naphthalene.
Conditions were same as in Fig. 2.

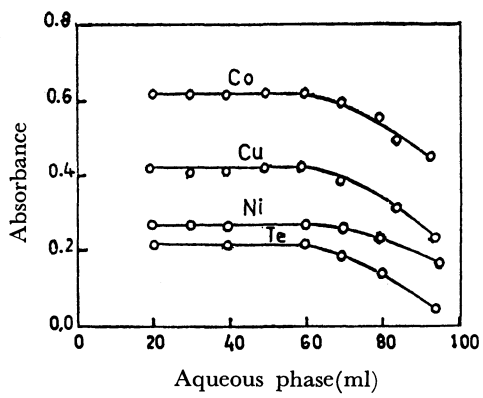

Fig. 5. Effect of the aqueous phase.
Conditions were same as in Fig. 2.

TABLE 1. EFFECT OF DIVERSE ANIONS
Cu: 25.0 μg, Co: 27.0 μg, Ni: 24.0 μg, Te: 25.5 μg.

Alkali salt added	Anion added (mg)	Absorbance at 440 nm	360 nm	390 nm	415 nm
—	—	0.420	0.620	0.270	0.215
Sodium acetate	40.00	0.420	0.615	0.270	0.220
Sodium oxalate	33.60	0.380	0.550	0.220	0.115
	25.20	0.420	0.620	0.270	0.215
Potassium, sodium tartrate	39.40	0.380	0.580	0.240	0.150
	29.50	0.415	0.620	0.272	0.215
Potassium bromide	33.60	0.420	0.620	0.270	0.210
Potassium chloride	23.80	0.420	0.620	0.270	0.215
Sodium citrate	31.45	0.370	0.590	0.245	0.140
	15.72	0.415	0.620	0.270	0.215
Potassium iodide	38.25	0.415	0.620	0.270	0.215
Sodium fluoride	22.60	0.380	0.580	0.245	0.150
	17.00	0.420	0.620	0.270	0.215
Sodium orthophosphate	25.00	0.420	0.615	0.270	0.220
Sodium thiosulfate	21.00	0.420	0.620	0.270	0.220
Potassium thiocyanate	29.85	0.420	0.620	0.270	0.215
Disodium EDTA	40.00	0.005	0.008	0.005	0.150
	20.00	0.008	0.008	0.005	0.210

TABLE 2. EEFECT OF DIVERSE CATIONS
Cu: 25.0 μg, Co: 27.0 μg, Ni: 24.0 μg, Te: 25.5 μg.

Metal salt added	Metal added (mg)	Absorbance at 440 nm	360 nm	390 nm	415 nm
—	—	0.420	0.620	0.270	0.215
Copper(II) chloride	0.431	—	0.550	0.240	0.110
	0.143	—	0.620	0.270	0.210
Manganese(II) acetate	0.480	0.420	0.620	0.270	0.210
Aluminium(III) nitrate	0.450	0.420	0.620	0.270	0.220
Lead(II) nitrate	0.616	0.415	0.620	0.270	0.210
Uranyl acetate	0.280	0.415	0.620	0.270	0.215
Zinc sulfate	0.596	0.415	0.615	0.270	0.215
Mercury(II) chloride	0.147	0.420	0.615	0.272	0.215
Zirconyl chloride	0.458	0.420	0.615	0.270	0.215
Thorium(IV) nitrate	0.160	0.420	0.620	0.270	0.210
Iron(III) chloride	0.200	0.350	0.550	0.220	0.180
	0.100	0.420	0.615	0.272	0.215
Nickel(II) chloride	0.450	0.420	0.620	—	0.215
Cobalt(II) sulfate	0.666	0.250	—	0.600	0.115
	0.111	0.415	—	0.800	0.215
Ammonium metavanadate	0.544	0.420	0.620	0.272	0.215
Sodium tungstate	0.577	0.420	0.620	0.270	0.215

when the aqueous phase did not exceed 60 ml but not quantitative, above 60 ml of the aqueous phase (Fig. 5).

Effect of Standing Time. Absorbance of the extract in naphthalene-chloroform was constant for at least 24 h for copper and cobalt, 40 h for nickel and 3 h for tellurium.

Effect of Electrolytes. Various electrolytes such as sodium chloride, sodium nitrate, and sodium acetate (0.01—0.08 M) caused no improvement in extraction, indicating that the extraction was complete.

Composition of the Complex. The composition of the copper, cobalt, nickel, and tellurium morpholine-4-carbodithioates was established by Job's method of continuous variation and the mole-ratio method. $Cu(C_4H_8ONCS_2)_2$, $Co(C_4H_8ONCS_2)_2$, $Ni(C_4H_8ONCS_2)_2$, and $Te(C_4H_8ONCS_2)_4$ have been extracted into molten naphthalene. It has been confirmed on the basis of gravimetric[5-8,14] volumetric[4,14] and conductometric[5] studies that the ligand acts as bidentate. The following tentative structures can be assigned to these metal complexes.

Table 3. Determination of copper in various alloys

Alloy	Certified % composition	Amount of Cu taken μg	Amount of Cu found μg	Average (μg)	Error %
Mallory No. 3	Cu: 99.2, Cr: 0.8	35.70	35.50 35.50 35.80 35.50 35.50	35.56	−0.39
Monel wire	Ni: 66.24, Cu: 31.18, Fe: 1.18, Mn: 1.08, Mg: 0.093, Al: 0.093, Si: 0.083, C: 0.083, S: 0.0037	46.80	46.50 46.50 46.50 47.00 46.50	46.60	−0.42
Monel 400	Ni: 63.0, C: 0.15, S: 0.0024, Mn: 0.01, Si: 0.5, Fe: 2.5, Cu: 31.0	35.65	35.50 35.50 35.60 35.50 35.50	35.52	−0.36
Brass No. 41.2	Cu: 58.18, Pb: 2.56, Zn: 38.99, Fe: 0.09, Sn: 0.12	30.55	30.50 30.60 30.60 30.60 30.10	30.66	+0.36

Table 4. Determination of cobalt in alloys

Alloy	Certified % composition	Amount of cobalt taken μg	Amount of cobalt found μg	Average (μg)	Error %
High speed steel	Co: 9.25, Mn: 0.40, Si: 0.35, S: 0.05, P: 0.05, Cr: 4.15, Mo: 5.5, W: 6—18.5	50.00	49.50 49.50 50.00 49.50 49.50	49.80	−0.40
Elgiloy (M-1712)	Co: 40.0, Cr: 20.0, Ni: 15.0, Mn: 2.0, Mo: 7.0, Fe: 15.0, Be: 0.05, C: 0.15	36.16	36.00 36.50 36.50 36.50 36.50	36.30	+0.39

Table 5. Determination of nickel in alloys

Alloy	Certified % composition	Amount of Ni taken μg	Amount of Ni found μg	Average (μg)	Error %
Monel wire	Ni: 66.24, Cu: 31.18, Fe: 1.18, Mn: 1.08, Mg: 0.093, Al: 0.093, Si: 0.083, C: 0.083, S: 0.0037	49.65	49.50 49.50 49.20 49.40 49.40	49.40	−0.54
Stainless steel No. 304	Ni: 9.68, Cr: 18.0, Fe: 70—71	35.50	35.80 36.50 35.50 35.40 35.80	35.80	−0.55
Inconel 600	Ni: 72.0, C: 0.15, Mn: 1.0, Fe: 8.0, S: 0.5, Cu: 0.50, Cr: 15.50, S: 0.015	30.60	30.50 30.30 30.60 35.80 35.80	30.46	−0.45

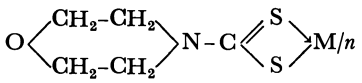

where $n=2$ for Cu, Co, and Ni, 4 for Te. Crystal structure study showed that in the case of the tellurium complex all four dithiocarbamate groups are bidentate and the eight sulphur atoms are bonded around the central tellurium atom in a slightly distorted dodecahedral manner;[15] in IR studies, the C···N and C···S stretching frequencies in Te(IV) complex were observed at 1000 cm^{-1} for the latter and 1480 cm^{-1} for the former. In the free ligand these modes were observed at 990 cm^{-1} and 1440 cm^{-1}, respectively.

Beer's Law and Sensitivity. Under optimum conditions described above, calibration curves were constructed at 440, 360, 385—390, and 410—420 nm against reagent blank, respectively. Beer's Law holds in the concentration range Cu: 5.0—70.0 μg, Co: 5.0—81.0 μg, Ni: 6.0—90.0 μg and Te: 5.7—125.0 μg per 10 ml of the final solution. The molar absorptivities and sensitivities in terms of Sandell's definition were calculated to be Cu: 1.067×10^4 mol^{-1} cm^{-1}, 0.0059 μg/cm^2 (440 nm); Co: 1.350×10^4 mol^{-1} cm^{-1}, 0.0043 μg/cm^2 (360 nm); Ni: 7.920×10^3 mol^{-1} cm^{-1}, 0.0088 μg/cm^2 (390 nm), and Te: 1.075×10^4 mol^{-1} cm^{-1}, 0.0110 μg/cm^2 (415 nm) respectively. Aliquots containing 25.0 μg of copper, 27.0 μg of cobalt, 24.0 μg of nickel and 25.5 μg of tellurium gave mean absorption of 0.42, 0.62, 0.27, and 0.215 with a relative standard deviation of 0.0016, 0.0024, 0.0015, and 0.0013, respectively.

Effect of Diverse Ions. 50 mg salt of the anions and 1.0 mg salt of the cations were added separately to aliquots containing 25.0 μg of copper, 27.0 μg of cobalt, 24.0 μg of nickel and 25.5 μg of tellurium, of the anions (Table 1) fluoride, citrate, tartrate, oxalate, and EDTA interfered in the determination of the metals, minor amounts of fluoride, citrate, tartrate and oxalate giving no serious effect. The extraction was almost nil in the presence of EDTA in the case of Cu, Co, and Ni probably due to higher stability of metal–EDTA complexes. A smaller amount of EDTA is allowable in the case of tellurium.

Of the cations (Table 2), Co (II) and Fe (III) interfered in the determination of copper, Cu (II) and Fe (III) in that of cobalt, and Cu (II) and Fe (III) and Co (II) in that of nickel. In all cases the relatively small amount can be tolerated except in the determination of nickel where Co(II) seriously interfered. Its interference can be eliminated by extraction first at low pH, then nickel being determined from the aqueous phase. In the determination of tellurium relatively small amounts of Cu (II), Co (II), and Fe (III) could be tolerated, nickel not interfering at all.

Determination of Copper, Cobalt, and Nickel in Various Alloys. 0.1 g of the alloy sample was taken in a beaker to which were added 10—15 ml of concentrated hydrochloric acid and a few ml of concentrated nitric acid. This was heated over a hot plate till the mixture dissolved completely and the solution was reduced to 5 ml. The solution was cooled, 10 ml of hydrochloric acid being added, then diluted and filtered. The final volume was made exactly 500 ml.

TABLE 6. SIMULTANEOUS DETERMINATION OF NICKEL AND COBALT IN AN ALLOY

Alloy	Amount of Ni/Co taken (μg)	Amount of Ni/Co found (μg)	Average (μg)	Error %
Elgiloy (M-1712)	Ni: 33.90	33.70 34.00 33.50 33.80 33.70	33.74	−0.74
	Co: 36.16	36.00 35.90 36.00 36.00 35.00	35.98	−0.55

An aliquot containing an appropriate amount of copper, cobalt or nickel was taken separately in a beaker, 1.0 ml of the reagent being added, the pH adjusted (Fig. 2), and determined by the general procedure. Results are given in Tables 3, 4, and 5 respectively.

Simultaneous Determination of Nickel and Cobalt in Alloys. Based upon the fact that the nickel complex is decomposed by ammonia to form a more stable complex whereas the cobalt morpholine-4-carbodithioate complex remains as such in chloroform, a method has been developed for the determination of nickel and cobalt present together.

An aliquot containing nickel and cobalt was taken, 2.0 ml of the reagent being added and the pH adjusted to 7.0. The solution was then extracted with molten naphthalene. Naphthalene containing nickel and cobalt morpholine-4-carbodithioate was dissolved in chloroform, the volume being made 10 ml. 5 ml of the solution was taken, dried with sodium sulfate, the absorbance being measured at 390 nm against a reagent blank. This corresponded to total absorbance due to cobalt and nickel complexes. To the other 5 ml of the solution was added 5 ml of 1:10 ammonia solution in a separating funnel. The organic phase was separated, dried by adding anhydrous sodium sulfate and the absorbance measured at 360 and 390 nm. The cobalt complex is not affected by shaking with ammonia, the absorbance at 360 nm corresponding to the amount of cobalt present. The absorbance was referred to the calibration curve for cobalt prepared under similar conditions. The amount of nickel was determined by the difference of total absorbance at 390 nm and that due to cobalt at 360 nm and referring it to the calibration curve for nickel at 390 nm. The results of the determination of nickel and cobalt in one alloy sample are given in Table 6.

Simultaneous determination may also be carried out by the control of pH. However, this is time consuming and less accurate since two steps are involved (the relative error $\approx1\%$).

Simultaneous Determination of Tellurium and Selenium. Preliminary investigations indicated that selenium is

Table 7. Simultaneous determination of tellurium and selenium

Tellurium	Selenium
Morpholine-4-carbodithioate (0.01 M): 1.0 ml.	Dithizone in CCl_4 (60 μmol/l): 5.0 ml.
Naphthalene: 2.0 g,	acidity: 6 M HCl,
Wavelength: 415 nm	Wavelength: 420 nm
pH: 5.5	

Amount present μg		Amount found μg		Average (μg)		Error %	
Tellurium	Selenium	Tellurium	Selenium	Tellurium	Selenium	Tellurium	Selenium
		51.0	10.5				
		50.5	10.5				
51.0	10.50	51.0	10.4	50.70	10.48	−0.58	−0.55
		50.5	10.5				
		50.5					
		50.5	7.8				
		51.0	7.7				
51.00	7.78	51.0	7.8	50.70	7.74	−0.58	−0.51
		50.5	7.7				
		50.5	7.7				
		25.4	7.7				
		25.4	7.7				
25.50	7.78	25.5	7.8	25.56	7.74	+0.55	−0.51
		25.5	7.8				
		25.0					
		25.5	10.5				
		25.4	10.5				
25.50	10.50	25.5	10.4	25.35	10.48	−0.58	−0.55
		25.2	10.5				
		25.15	10.5				

Table 8. The extraction-spectrophotometric behavior of metal morpholine-4-carbodithioates

Metal	λ_{max} / nm	Optimum pH	Morpholine-4-carbodithioate (0.01 M) (ml)	Extracted as	Concentration range from Beer's curve / μg(10 ml)$^{-1}$	Molar absorptivity / mol^{-1} cm^{-1}	Sandell's sensitivity S / μg cm^{-2}	Standard deviation
Copper	440	4.0—9.0	0.8—1.5	$Cu(C_4H_8ONCS_2)$	5.0—70.0	1.067×10^4	0.0059	0.0016
Cobalt	360	4.0—9.5	1.0—2.0	$Co(C_4H_8ONCS_2)_2$	5.0—81.0	1.350×10^4	0.0043	0.0024
Nickel	385—390	6.5—9.0	1.0—2.5	$Ni(C_4H_8ONCS_2)_2$	6.0—90.0	7.92×10^3	0.0088	0.0015
Tellurium	410—420	4.0—6.5	0.5—1.5	$Te(C_4H_8ONCS_2)_4$	5.7—125.0	1.075×10^4	0.0110	0.0013
Bismuth[a]	362—370	4.0—6.5	0.5—1.5	$Bi(C_4H_8ONCS_2)_3$	2.5—53.0	3.960×10^4	0.0052	0.0035

a) Ref.[11]

not extracted with molten naphthalene. A method has been developed for the simultaneous determination of tellurium and selenium.

An aliquot containing appropriate amounts of these two metals was taken, 1.0 ml of the reagent being added and the pH adjusted (Fig. 2). Tellurium was then determined. From the aqueous phase selenium was extracted in 6 M HCl as a dithizone complex in carbon tetrachloride.[16] The absorbance was measured at 420 nm against a reagent blank. The amount of selenium was determined by the calibration curve prepared under similar conditions (Table 7). Selenium can be extracted with a suitable organic solvent by liquid-liquid extraction as morpholine-4-carbodithioate, but not by spectrophotometry since the complex gives no absorption.

The extraction behavior of metal morpholine-4-carbodithioates is summarized in Table 8.

One of the authors (M.G.) is grateful to the Council of Scientific and Industrial Research, New Delhi, India, for the award of Senior Research Fellowship.

References

1) W. Beyer and R. D. Ott, *Mikrochim. Ichnoanal. Acta*, **1965**, 1130.
2) W. Beyer and W. Likussar, *Mikrochim. Acta*, **4**, 721 (1967).
3) W. Likussar, W. Beyer, and O. Wawshinek, *Mikrochim. Acta*, **4**, 735 (1968).
4) W. Beyer, R. D. Ott, and G. Pokorny, *Mikrochim. Acta*, **3**, 575 (1967).

5) N. Singh, R. Kumar, and R. C. Agarwal, *Curr. Sci.*, **46**, 851 (1977).
6) N. Singh, R. Kumar, and B. D. Kansal, *J. Indian Chem. Soc.*, **55**, 240 (1978).
7) N. Singh, R. C. Agarwal, V. K. Maheshwari, and R. Kumar, *J. Indian Chem. Soc.*, **55**, 961 (1978).
8) R. Kumar, N. Singh, and H. Singh, *J. Indian Chem. Soc.*, **56**, 838 (1979).
9) N. Singh, R. Kumar, and B. D. Kansal, *Chromatographia*, **11**, 408 (1978).
10) R. Kumar and N. Singh, *Curr. Sci.*, **47**, 422 (1978).
11) B. K. Puri and M. Gautam, *Zh. Anal. Khim.*, **35**, 1024 (1980).
12) G. Macrotrigiano, G. C. Pallacani, C. Preti, and G. Tosi, *Bull. Chem. Soc. Jpn.*, **48**, 1018 (1975).
13) A. I. Vogel, "A Textbook of Quantitative Inorganic Analysis," 3rd ed, Longman (1969).
14) A. B. Sakla, A. A. Helmy, W. Beyer, and F. E. Harhash, *Talanta*, **26**, 519 (1979).
15) S. Esperas and S. Hasebye, *Acta Chem. Scand.*, **29**, 185 (1975).
16) H. Mabuchi and M. Nakahara, *Bull. Chem. Soc. Jpn.*, **36**, 151 (1965).

  Bull. Chem. Soc. Jpn., 54, 3185—3190 (1981)

The Effects of the BF_2- and $B(C_2H_5)_2$-substitution for Bridging Hydrogen Atoms in the Cobalt(II), Nickel(II), and Copper(II) Complexes with Some Oximate Ligands

Yasuomi NONAKA* and Kohsuke HAMADA

Department of Chemistry, Faculty of Science, Kyushu University 33, Hakozaki, Higashi-ku, Fukuoka 812

(Received September 16, 1980)

Cobalt(II), nickel(II), and copper(II) complexes with dioximes substituted by BF_2- and $B(C_2H_5)_2$-groups for bridging hydrogen atoms were prepared. The BF_2-substitution caused a red-shift of d-d band and increase of $g_{//}$-value for copper(II) complexes and positive shift of polarographic half wave potential of nickel(II) complexes. In the case of the $B(C_2H_5)_2$-substituted complexes, such variations were not observed. The BF_2-substituted cobalt(II) complexes are stable under an open atmosphere at room temperature in a solid state and in a DMF solution. These were interpreted in terms of the electron-withdrawing ability of BF_2-group in the ligand.

In 1962, nickel(II) complexes with BF_2- or BR_2(R= CH_3, *n*-C_3H_7, *n*-C_4H_9, and *i*-C_4H_9)-linked dioximes were prepared and characterized by Schrauzer[1] (the structures and abbreviations of these complexes are shown in Fig. 1). In the electronic spectra of these complexes,

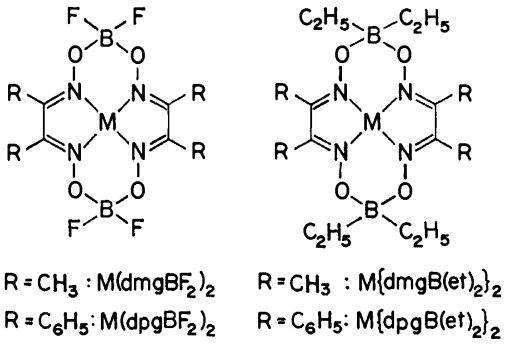

Fig. 1. Structures and abbreviations of the complexes used in this study.

little change due to the introduction of BF_2- or BR_2-group was observed. Therefore, it was concluded that these substituents exert no effect on the ligand field around the nickel ion. Recently, Gagnè[2] obtained the dark purple complex, $Cu(tnomBF_2)ClO_4$, from brown $Cu(tnomH)ClO_4$:

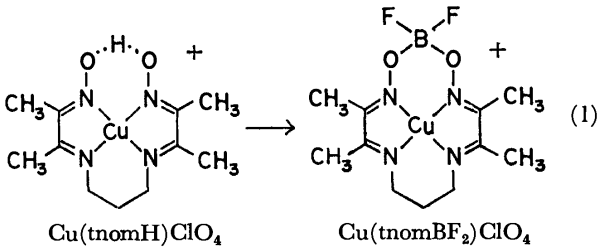

(1)

Drago and Gaul[3] found that $Co(dpgBF_2)_2(N\text{-meim})_2$ formed in a solution of $Co(dpgBF_2)_2 \cdot 2CH_3OH$ containing *N*-methylimidazole (*N*-meim) is stable under aerobic conditions. The discoloration by introduction of BF_2-group (Eq. 1) and the high stability of resulting $Co(dpgBF_2)_2(N\text{-meim})_2$ complex against molecular oxygen suggest that the electronic state of the complexes is affected by the introduction of BF_2-group. Then, the substitution of BF_2-group for the bridging hydrogen may bring about change in the ring size and/or the electron density on the nitrogen atoms.

In this study, we have systematically prepared cobalt(II), nickel(II), and copper(II) complexes with BF_2- or $B(C_2H_5)_2$-substituted macrocyclic ligands as shown in Fig. 1, in order to elucidate the effects of these substituents on the electronic state of the complexes, coordination geometry, the reactivity of cobalt(II) complexes with molecular oxygen, and the equilibrium of cobalt(II) complexes with some organic bases, such as pyridine, in DMF solution.

Experimental

Synthesis. Triethylborane was prepared by the procedure of Meerwein and Mitab.[4] This material ignites spontaneously in air and hence it was used for subsequent reactions as a diethyl ether solution (*ca.* 30%).

Cu(dmgBF$_2$)$_2$·2dioxane: To a suspension of $Cu(dmgH)_2$ (4.5 g) in dioxane (90 cm^3) was added dropwise a dioxane solution (50 cm^3) containing boron trifluoride etherate (10 cm^3) at 60 °C. Reaction mixture was stirred at 80 °C for 1 h. On standing overnight, fine dark purple crystals were separated. These were recrystalized from acetone–dioxane (1 : 1).

Found: C, 33.84; H, 4.97; N, 9.93%. Calcd for $C_{16}H_{28}N_4O_8B_2F_4Cu$: C, 33.98; H, 4.99; N, 9.91%.

Cu(dpgBF$_2$)$_2$·2dioxane: This was prepared in a procedure similar to that for $Cu(dmgBF_2)_2 \cdot 2$dioxane by using $Cu(dpgH)_2$ (5.5 g) instead of $Cu(dmgH)_2$.

Found: C, 53.24; H, 4.53; N, 6.88%. Calcd for $C_{36}H_{36}N_4O_8B_2F_4Cu$: C, 53.13; H, 4.46; N, 6.88%.

Cu{dmgB(et)$_2$}$_2$: To a suspension of $Cu(dmgH)_2$ (4.5 g) in dioxane (100 cm^3) was added dropwise at room temperature 40 cm^3 of a diethyl ether solution of triethylborane. Reaction mixture was stirred at 80 °C for 1 h and concentrated to *ca.* 70 cm^3. After being left to stand overnight, the product was collected and recrystallized from dichloromethane–benzene (1 : 1) to give brown fine crystals.

Found: C, 44.73; H, 7.51; N, 13.04%. Calcd for $C_{16}H_{32}N_4O_4B_2Cu$: C, 44.31; H, 7.41; N, 13.25%.

Cu{dpgB(et)$_2$}$_2$·dioxane·H$_2$O: This was obtained in a procedure similar to that for $Cu\{dmgB(et)_2\}_2$ by using $Cu(dpgH)_2$ (5.5 g) instead of $Cu(dmgH)_2$. Recrystallization was carried out from chloroform–dioxane (1 : 1).

Found: C, 60.78; H, 6.15; N, 6.94%. Calcd for $C_{40}H_{50}N_4O_7B_2Cu$: C, 61.28; H, 6.43; N, 7.14%.

Ni(dmgBF$_2$)$_2$ and Ni(dpgBF$_2$)$_2$: These were prepared by the procedure of Schrauzer.[1]

Ni{dmgB(et)$_2$}$_2$: To a suspension of $Ni(dmgH)_2$ (4.3 g) in

dichloromethane (80 cm^3) was added dropwise 40 cm^3 of a diethyl ether solution of triethylborane at 40 °C. The solid dissolved gradually forming a red solution. The solution was evaporated to *ca.* 60 cm^3 and left stand overnight to give reddish orange fine crystals. These were recrystallized from benzene–chloroform (1 : 1).

Found: C, 45.15; H, 7.62; N, 13.18%. Calcd for $C_{16}H_{32}N_4O_4B_2Ni$: C, 45.24; H, 7.59; N, 13.19%.

Ni{dpgB(et)$_2$}$_2$·1/2CH$_2$Cl$_2$: This was prepared in a procedure similar to that for Ni{dmgB(et)$_2$}$_2$ by using Ni(dpgH)$_2$ (5.5 g) instead of Ni(dmgH)$_2$. Recrystallization was carried out from dichloromethane–diethyl ether (2 : 1).

Found: C, 61.01; H, 6.08; N, 7.57%. Calcd for $C_{36.5}H_{41}N_4O_4B_2ClNi$: C, 61.27; H, 5.78; N, 7.83%.

Co(dmgBF$_2$)$_2$·2H$_2$O: This was prepared in a procedure similar to that for Cu(dmgBF$_2$)$_2$·2dioxane by using Co(dmgH)$_2$·2H$_2$O (4.2 g) instead of Cu(dmgH)$_2$. The operations were carried out under nitrogen atmosphere and then brown fine crystals were obtained. These were dried at 80 °C for several hours under a reduced pressure over P_2O_5.

Found: C, 23.05; H, 3.87; N, 12.98%. Calcd for $C_8H_{16}N_4O_6B_2F_4Co$: C, 22.84; H, 3.83; N, 13.31%.

Co(dpgBF$_2$)$_2$·2H$_2$O·dioxane: This was prepared in the procedure similar to that by Tovrog *et al.*[5] Recrystallization was carried out from acetone–dioxane (1 : 1) under nitrogen atmosphere to give marron fine crystals.

Found: C, 50.19; H, 4.35; N, 7.40%. Calcd for $C_{32}H_{32}N_4O_8B_2F_4Co$: C, 50.76; H, 4.26; N, 7.40%.

Physical Measurements. Electronic spectra were measured at 25.0±0.2 °C with a Shimadzu Multipurpose Spectrophotometer Model MPS-5000. ESR spectra were measured with a JES-ME-3X Spectrometer using an X-band at room and liquid nitrogen temperatures. DPPH and Mn/MgO were used as standard markers. Thermogravimetric analyses were carried out with a Rigaku-denki Thermogavimetric and Differential Thermal Analyzer Model 8075E-1. All polarographic measurements were made at 25.0±0.2 °C in *N,N*-dimethylformamide (DMF), which was dried over molecular sieves (4A—1/16 type) and was distilled under nitrogen atmosphere. Tetraethylammonium perchlorate (TEAP) was used as a supporting electrolyte (0.1 mol/dm^3). The concentration of complexes was maintained constant (5×10^{-4} mol/dm^3) except for Ni(dmgH)$_2$. In the case of Ni(dmgH)$_2$, the saturated solution was used. All solutions were deoxygenated by bubbling pure nitrogen gas. A Fuso Polarographic Analyzer Model 312 was used for sampled d. c. polarography.

A three-electrode system[6] consisting of the droping mercury, the platinum wire and the saturated calomel electrodes as a working, a counter and a reference electrodes, respectively, was adopted. The saturated calomel electrode was connected to the sample solution through a salt bridge.[7]

Determination of Adduct Formation Constant. Deoxygenated DMF solution (100 cm^3) of Co(dmgBF$_2$)$_2$·2H$_2$O, Co(dpgBF$_2$)$_2$·2H$_2$O·dioxane, or Co(dpgH)$_2$·2H$_2$O was placed into a three necked flask (200 cm^3, filled with dry nitrogen) fitted with a tube connected to the cell for spectral measurement, and another neck being fitted with a buret to drop DMF solution of an organic base. After an organic base had been added to as olution of the complex, the solution was stirred for 10 min with a magnetic stirrer. The reaction mixture was led to the cell for spectral measurements. Equilibrium constants were determined at 25.0±0.2 °C by the method of Marzilli *et al.*[8]

Results and Discussion

Results of the elemental analyses and the infrared spectra suggested that the molecules of dioxane and/or water are contained in crystals of some compounds obtained. These were confirmed by thermogravimetric analyses.

All attempts to isolate a BF_2-linked metal free ligand or its alkali metal salt were unsuccessful to obtain dimethylglyoxime.

Electronic Spectra of Copper(II) Complexes. The electronic spectra of Cu(dmgH)$_2$ in various solvents[9,10] seem to consist of a number of bands overlapping each other. The d-d band[9] observed at about 22.0×10^3 cm^{-1} as a shoulder is almost concealed by an intense CT band. A methanol solution of Cu(dmgBF$_2$)$_2$ exhibits a peak at 21.5×10^3 cm^{-1} with a shoulder at 20.0×10^3 cm^{-1}. These bands regarded as d-d bands

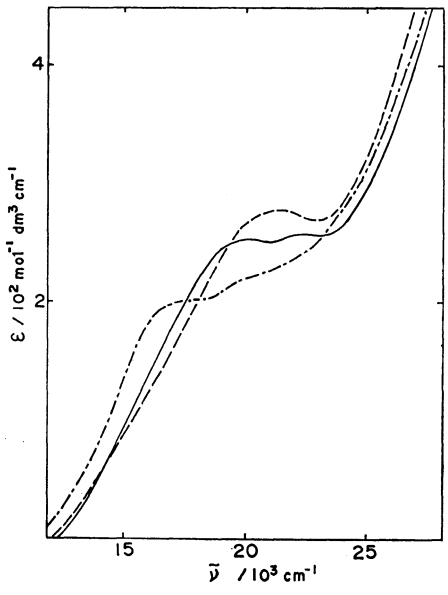

Fig. 2. Electronic spectra of Cu(dmgBF$_2$)$_2$ in methanol (----), acetone (——), and DMF (– – –).

Table 1. Electronic and ESR spectral data of copper(II) complexes

Compound	Solvent	$\tilde{\nu}$/10^3cm^{-1}	(ε/mol^{-1} dm^3 cm^{-1})	$g_{//}$	$A_{//}$/10^{-4} cm^{-1}
Cu(dmgH)$_2$	DMF	21.0*(1350)	29.0(5400)	2.148	197.8
Cu(dmgBF$_2$)$_2$	DMF	17.0*(200) 19.5(215)	32.0(2900)	2.170	196.2
Cu{dmgB(et)$_2$}$_2$	DMF	21.0*(660)	29.0(4100)	2.147	202.4
Cu(dpgH)$_2$	$CHCl_3$	21.0*(1220)	24.0*(1780)	2.146	188.8
Cu(dpgBF$_2$)$_2$	$CHCl_3$	19.0*(490) 20.8(540)	25.5*(950)	2.167	194.4
Cu{dpgB(et)$_2$}$_2$	$CHCl_3$	21.5*(1540)	25.5*(3280)	2.149	193.6

*: Shoulder.

were shifted to lower energy side in a DMF solution (Fig. 2). On the other hand, the spectrum of methanol solution of $Cu\{dmgB(et)_2\}_2$ is similar to that of $Cu(dmgH)_2$ (Table 1). Therefore, it can be concluded that no drastic change due to the substitution of BF_2- and $B(C_2H_5)_2$-groups for bridging hydrogen occurs in the geometric structure and that the equatorial ligand field around the copper ion is weakened on account of the electron-withdrawing effect of BF_2-group, bringing about the subsequent axial ligation of solvent molecules.

Then, the lowering of $\pi(2p)$-orbitals of nitrogen atoms should be larger than that of d_{xy}-orbital with an unpaired electron, *i.e.*, the energy separation between metal d_{xy}- and ligand $\pi(2p)$-orbitals is expected to increase. In fact, the charge transfer band at 28.5×10^3 cm^{-1} in $Cu(dmgH)_2$[9] is shifted by 2.5×10^3 cm^{-1} to higher energy side in $Cu(dmgBF_2)_2$.

ESR Spectra of Copper(II) Complexes. The ESR spectra of BF_2- or $B(C_2H_5)_2$-substituted copper(II) complexes were measured in DMF solution at room and liquid nitrogen temperatures. All these spectra are similar to those of $Cu(dmgH)_2$[11] at both temperatures and essentially axial. The characteristic feature is that the $g_{//}$-value of $Cu(dmgBF_2)_2$ is appreciably large compared with those of $Cu(dmgH)_2$ and $Cu\{dmgB(et)_2\}_2$ which are comparable to each other (Table 1). The $g_{//}$-value for copper(II) complexes with axial symmetry is approximated[12] by

$$g_{//} = 2.0 - \frac{8\lambda\alpha^2}{\Delta}, \qquad (2)$$

where λ is the spin-orbit coupling constant of the copper ion, α is the coefficient of d_{xy} in the molecular orbitals,[12,13] and Δ is the energy separation between d_{xy} and $d_{x^2-y^2}$. This shows that $g_{//}$-value increases with the decrease of energy separation Δ, because λ is negative. Therefore, the order of $g_{//}$-value is reasonable in view of that of the d-d band; $Cu(dmgH)_2 \approx Cu\{dmg(et)_2\}_2 > Cu(dmgBF_2)_2$. Such tendency is recognized in dpg-derivatives. These results support the conclusion mentioned above.

Polarography of Nickel(II) Complexes. The sampled d.c. polarograms of $Ni(dmgH)_2$, $Ni(dmgBF_2)_2$, and $Ni\{dmgB(et)_2\}_2$ were obtained in DMF solution containing TEAP (0.1 mol/dm^3). These complexes exhibited two reduction waves (Fig. 3). All these reduction waves are reversible one-electron reduction, judging from the results of coulometry. Olson and Vasilevskis[14] reported that a reduction wave corresponding to the electrode reaction, Ni(II)(14-diene)→Ni(I)(14-diene), was observed at −1.57 V *vs.* Ag–0.1 M $AgNO_3$ (1 M=1 mol/dm^3; −1.28 V *vs.* SCE) in the cyclic voltammetry of $Ni(14\text{-diene})(ClO_4)_2$ in acetonitrile. In view of this result, the first and the second waves should correspond to the following electrode processes,

$$Ni(II)L \xrightarrow{e^-} Ni(I)L$$
$$Ni(I)L \xrightarrow{e^-} Ni(O)L, \qquad (3)$$

where L denotes $(dmgH)_2$, $(dmgBF_2)_2$, and $\{dmgB(et)_2\}_2$.

The half-wave potential of $Ni(dmgBF_2)_2$ is more positive in both processes than those of $Ni(dmgH)_2$ and $Ni\{dmgB(et)_2\}_2$ which are approximatly comparable. The same tendency was found in dpg-derivatives. The BF_2-linked complexes are more facile to be reduced compared with corresponding hydrogen bridged or $B(C_2H_5)_2$-linked complexes, due to the electron-withdrawing effect of BF_2-group. Therefore, the electron-withdrawing effect of BF_2-group considerably exerts on the electronic states of the nikel(II) complexes, although Schrauzer[1] claimed that the BF_2-group little affects the ligand field around the nickel(II) ion.

The reduction potentials of $Ni(dpgX)_2$ (X denotes H, BF_2, and $B(et)_2$) are more positive than those of the corresponding $Ni(dmgX)_2$. This suggests that the electron density on nickel ion of $Ni(dpgX)_2$ decreases because of the rather weak electron-donating effect of phenyl group compared with that of methyl group.

Electronic Spectra of Nickel(II) Complexes. Schrauzer[1] reported that in the spectra of $Ni(dmgX)_2$ (X denotes H, BF_2, and BR_2) in chloroform the bands at 21.1 and 24.4×10^3 cm^{-1} of $Ni(dmgH)_2$ are little shifted by the substitution of BF_2- or BR_2-groups for bridging hydrogen atoms. We measured the spectra of these complexes in DMF and in pyridine (Fig. 4). These spectra suffer little solvent effect in these solvents except for increase of intensity, although some of these solvents are capable of coordinating to a metal ion. On the other hand, it was shown from our polarographic results that the electron density on nickel ion of $Ni(dmgBF_2)_2$ decreases considerably compared with $Ni(dmgH)_2$ and $Ni\{(dmgB(et)_2\}_2$. Consequently, the resemblance in the spectra of $Ni(dmgX)_2$ reported by Schrauzer is attributed to the fact that the axial coordination of solvents is not promoted by the substitution of BF_2-group for bridging hydrogen atom.

Formation Constants of $Co(dmgBF_2)_2(base)_n$ and $Co(dpgBF_2)_2(base)_n$ (n=1 or 2). A solution of $Co(dmgBF_2)_2$ in DMF exhibits an absorption band at 21.7×10^3 cm^{-1} (ε=2700) at 25 °C. When pyridine is added to this solution, the band diminished and a new band appeared at 23.5×10^3 cm^{-1} with an isosbestic point at 22.7×10^3 cm^{-1} (Fig. 5). The spectrum converged to one curve when pyridine concentration exceeded 0.1 mol/dm^3 (400 times of the complex

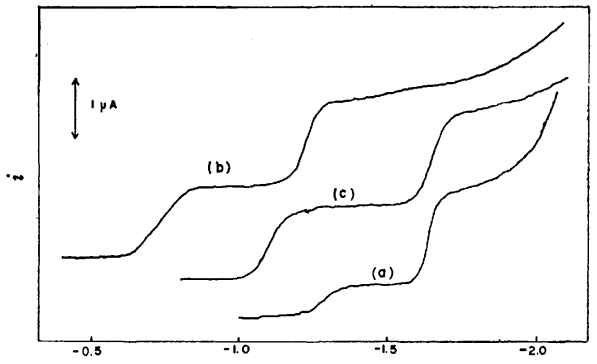

Fig. 3. Sampled d.c. polarograms of (a) $Ni(dmgH)_2$, (b) $Ni(dmgBF_2)_2$, and (c) $Ni\{dmgB(et)_2\}_2$ in DMF containing TEAP (0.1 mol/dm^3).

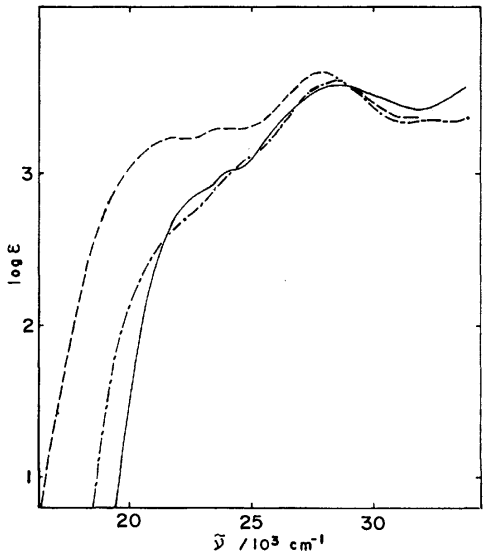

Fig. 4. Electronic spectra of $Ni(dmgBF_2)_2$ in chloroform (——), DMF (– – –), and pyridine (–·–·–).

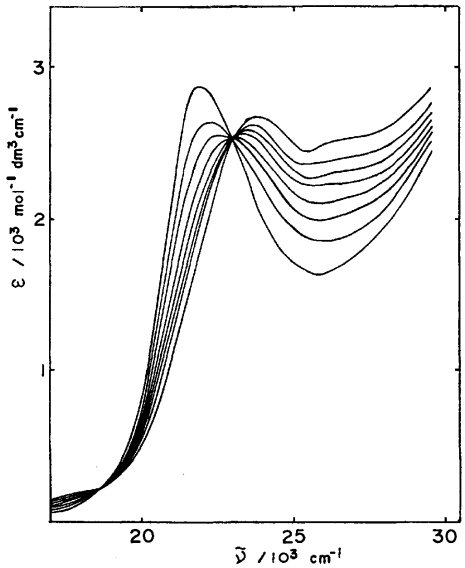

Fig. 5. Electronic spectra of $Co(dmgBF_2)_2$ in DMF with various contents of pyridine: 1), 0; 2), 1.4×10^{-3}; 3), 2.7×10^{-3}; 4), 5.9×10^{-3}; 5), 9.4×10^{-3}; 6), 1.5×10^{-2}; 7), 3.0×10^{-2}; 8), 1.0×10^{-1} mol/dm³. The concentration of $Co(dmgBF_2)_2$ is maintained constant (2.5×10^{-4} mol/dm³).

concentration). This spectral variation should correspond to the equilibrium,

$$Co(dmgBF_2)_2 + n\cdot py \rightleftharpoons Co(dmgBF_2)_2(py)_n (n=1 \text{ or } 2). \quad (4)$$

The equilibrium constant of this equation is given by the relation,

$$\beta = [Co(dmgBF_2)_2(py)_n]/[Co(dmgBF_2)_2][py]^n. \quad (5)$$

When A_0, A, and A_∞ denote the absorbances of $Co(dmgBF_2)_2$ at 21.7×10^3 cm^{-1} in the absence of pyridine, in the presence of pyridine and in the presence of large excess of pyridine, respectively, the equilibrium constant is given by

$$\log\beta = \log[(A_0-A)/(A-A_\infty)] - n\log[py]. \quad (6)$$

The free pyridine concentration [py] is corrected by

$$[py] = [py]_t - [(A_0-A)/(A_0-A_\infty)]\,[M], \quad (7)$$

where $[py]_t$ and [M] denote total concentrations of pyridine and the metal complex, respectively. Then, $\log[(A_0-A)/(A-A_\infty)]$ was plotted against log [py] which was calculated by Eq. 7 for both cases of $n=1$ and 2(Hill-plot). The plot for $n=1$ gives a straight line with a slope nearly equal to 1, and that for $n=2$ gives no straight line. Then, it became evident that one molecule of pyridine is bound to a cobalt ion. The equilibrium constant ($\log\beta$)was evaluated by extrapolating log [py] to zero. In the cases that the other organic base was used instead of pyridine, the equilibrium constants and n-values were evaluated in a similar manner as above (Table 2). For all the reactions between $Co(dmgBF_2)_2$ and organic bases, $n=1$ was

Table 2. Formation constants of $Co(dmgBF_2)_2(base)_n$, $Co(dpgBF_2)_2(base)_n$, and their related complexes

Compound	Base[c]	(pK_a)	n	log β (Temp/°C)	n*[d]	Solvent	Reference
$Co(dmgBF_2)_2$	im	(7.03)	1	4.04(25)	2	DMF	This work
$Co(dmgBF_2)_2$	py	(5.27)	1	2.25(25)	2	DMF	This work
$Co(dmgBF_2)_2$	2-etim	(7.99)	1	2.50(25)	1	DMF	This work
$Co(dmgBF_2)_2$	α-pic	(5.97)	1	0.16(25)	2	DMF	This work
$Co(dpgBF_2)_2$	im	(7.03)	2	7.19(25)	2	DMF	This work
$Co(dpgBF_2)_2$	γ-pic	(6.02)	2	4.46(25)	2	DMF	This work
$Co(dpgBF_2)_2$	py	(5.27)	2	4.20(25)	2	DMF	This work
$Co(dpgBF_2)_2$	2-etim	(7.99)	1	3.18(25)	1	DMF	This work
$Co(dpgBF_2)_2$	α-pic	(5.97)	2	0.97(25)	2	DMF	This work
$Co(dpgH)_2$	py	(5.27)	1	2.94(25)	2[e]	DMF	This work
$Co(dmgH)_2$	py	(5.27)	1	2.11(r.t.)	2[e]	CH_3OH	Ref. 15
Co(J-en)[a]	py	(5.27)	1	2.18(20)	2	DCE[f]	Ref. 16
Co(ppIXdme)[b]	py	(5.27)	1	3.27(20)	—	Toluene	Ref. 17
Co(ppIXdme)	py	(5.27)	1	3.78(23)	—	Toluene	Ref. 18

a) Jäger-type open-chain ligand. b) Protoporphyrin IX dimethyl ester. c) im: Imidazole, py: pyridine, 2-etim: 2-ethylimidazole, α-pic: α-picoline, γ-pic: γ-picoline. d) n* was evaluated from ^{14}N-superhyperfine splitting of the ESR spectrum. e) See Ref. 20. f) 1,2-Dichloroethane.

obtained. This shows that one molecule of the organic base links to the metal complex to form a five-coordinate complex $Co(dmgBF_2)_2(base)$.

The formation constants of $Co(dmgH)_2(py)$,[15] Co-(J-en)(py),[16] and Co(ppIXdme)(py)[17,18] at room temperature were reported (Table 2). In all cases, the mono-base adducts are predominant in the solution. Accordingly, it seems that square planer cobalt(II) complexes tend to form five-coordinate complexes with an organic base in solution. Thus, the present result that a five-coordinate complex, $Co(dmgBF_2)_2(base)$, is formed is consistent with this tendency.

On the other hand, two molecules of organic base coordinate to $Co(dmgBF_2)_2$ at apical sites at 77 K, judging from the five-lined ^{14}N-superhyperfine structure in ESR spectrum in DMF glass containing organic base (except for 2-ethylimidazole). Therefore, it was revealed that the coordination manner of the organic base to $Co(dmgBF_2)_2$ at room temperature is different from that at low temperature, as seen in Co(J-en)-pyridine system reported by Kubokura *et al.*[16]

The formation constants of $Co(dpgBF_2)_2(base)_n$ at 25 °C were evaluated by using the variation of absorbance at 20.0×10^3 cm^{-1} by a procedure similar to the case of $Co(dmgBF_2)_2(py)$. When pyridine, imidazole, α- and γ-picoline were used, $n=2$ was obtained from the slope of Hill-plots, and then, six-coordinate complexes $Co(dpgBF_2)_2(base)_2$ were shown to be formed, in contrast to the general tendency as mentioned above.

The electron-withdrawing effect of BF_2-group is more effectively exerted on $Co(dpgBF_2)_2$ than $Co(dmgBF_2)_2$, because the electron-donating ability of phenyl group is negligibly weak compared with that of methyl group. Consequently, the electron density on the cobalt(II) ion decreases and the axial coordination of ligands is facilitated.

When 2-ethylimidazole was used, the five-coordinate complex $Co(dpgBF_2)_2$(2-etim) was formed at 25 °C. This is explained in terms of the steric hindrance of ethyl group adjacent to the donating nitrogen atom.

Reaction of $Co(dmgBF_2)_2$ and $Co(dpgBF_2)_2$ with Molecular Oxygen. The electronic spectra of $Co(dmgBF_2)_2$ in DMF solution were measured under N_2-, O_2-, and an open atmospheres. The spectrum obtained under O_2-atmosphere is practically same as those under an open and N_2-atmospheres. This indicates that $Co(dmgBF_2)_2$ in the solution hardly reacts with molecular oxygen at room temperature.

The ESR spectrum of $Co(dpgBF_2)_2$ measured in acetonitrile frozen solution under an open atmosphere exhibited an axial pattern characteristic of low-spin, d^7-tetragonal complexes of cobalt(II) with $(d_{xy})^2(d_{z^2})^1$-ground state[19] (Fig. 6).

These results are noteworthy in contrast to the fact that the solutions of $Co(dmgH)_2$ and $Co(dpgH)_2$ are oxidized immediately on exposure to air. The d_{z^2}-orbital of $Co(dmgBF_2)_2$ and $Co(dpgBF_2)_2$ is lowlying relative to that of $Co(dmgH)_2$ and $Co(dpgH)_2$ because of the electron-withdrawing effect of BF_2-group. Accordingly, in the cases of BF_2-linked complexes the donation from metal-d_{z^2}-orbital to oxygen-π^*-orbital is

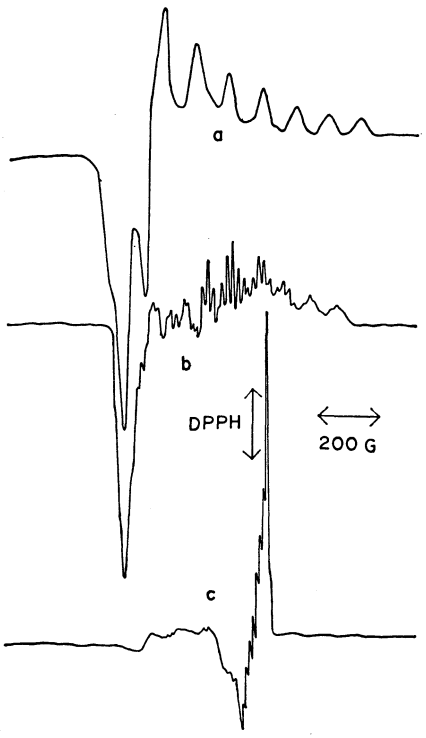

Fig. 6. ESR spectra of $Co(dpgBF_2)_2$ in (a) acetonitrile, (b) DMF–pyridine (19 : 1), and (c) DMF–2-etim (19 : 1) at liquid nitrogen temperature under aerobic conditions. ($1G=10^{-4}$ T).

diminished. Drago and Gaul[3] found that six-coordinate complex, $Co(dpgBF_2)_2(N\text{-meim})_2$, is prepared in the solution of $Co(dpgBF_2)_2$ containing *N*-methylimidazole (*N*-meim) and that no oxygenated complex is formed under aerobic conditions. The formation of the same type six-coordinate complexes is recognized in solutions of $Co(dpgBF_2)_2$ containing excess pyridine and γ-picoline under an open atmosphere (Fig. 6), although oxygenated complexes were found in a solution of $Co(dpgH)_2$ containing excess pyridine.[20] These facts suggest that decrease of the electron density on cobalt ion facilitates the formation of normal coordination bond between cobalt and organic base, and that the formation of such strong bond hinders the exchange an organic base for molecular oxygen.

ESR spectrum of the DMF frozen solution of $Co(dmgBF_2)_2$ containing excess pyridine under an open atmosphere exhibits a relatively weak, sharp signal at $g=ca.$ 2, in addition to main signal due to the di-base adduct, $Co(dmgBF_2)_2(py)_2$. This shows the slight formation of an oxygenated complex. The reason may be that the electron-withdrawing effect of BF_2-group is partially canceled by the electron-donating ability of methyl group.

The ESR spectra of $Co(dmgBF_2)_2$ and $Co(dpgBF_2)_2$ in DMF frozen solution containing excess 2-ethylimidazole under an open atmosphere (Fig. 6) are drastically different from those of the di-base adducts such as $Co(dmgBF_2)_2(py)_2$ and are characteristic of oxygenated complexes formally described as a superoxide-cobalt(III) complex.[21] As mentioned above, the five-coordinate complex is formed under an

unaerobic condition when 2-ethylimidazole was used. Thus, it becomes possible for a molecular oxygen to come close to a vacant sixth coordination site of cobalt ion.

The authors are deeply grateful to Professor Sigeo Kida, Kyushu University, for his helpful discussion. We also would like to thank Professor Makoto Aihara, Fukuoka Woman's University, for the polarographic measurements. The present work was partially supported by a Grant-in-Aid for Scientific Research from the Ministry of Education, Science and Culture.

References

1) G. N. Schrauzer, *Chem. Ber.*, **95**, 1438 (1962).
2) R. R. Gagnè, *J. Am. Chem. Soc.*, **98**, 6709 (1976).
3) R. S. Drago and J. H. Gaul, *Inorg. Chem.*, **18**, 2019 (1979).
4) H. Meerwein and Mitab, *J. Prakt. Chem.*, **147**, 226 (1936).
5) B. S. Tovrog, D. J. Kitko, and R. S. Drago, *J. Am. Chem. Soc.*, **98**, 5144 (1976).
6) S. Misumi, M. Aihara, and Y. Nonaka, *Bull. Chem. Soc. Jpn.*, **43**, 774 (1970).
7) K. Takaoka, *Rev. Polargo. (Kyoto)*, **14**, 63 (1966).
8) L. G. Marzilli, P. A. Marzilli, and J. Helpern, *J. Am. Chem. Soc.*, **93**, 1374 (1971).
9) R. Roose, *Acta Chem. Scand.*, **21**, 1855 (1967).
10) D. Dyrssen and D. Petkovič, *Acta Chem. Scand.*, **19**, 653 (1963).
11) K-E. Falk, E. Ivanova, R. Roose, and T. Vänngård, *Inorg. Chem.* **9**, 556 (1970); A. K. Wierema and J. J. Windle, *J. Phys. Chem.*, **68**, 2316 (1964).
12) A. H. Maki and B. R. McGavey, *J. Chem. Phys.*, **29**, 31, 35 (1958).
13) D. Kivelson and R. Nieman ,*J. Chem. Phys.*, **35**, 149 (1961).
14) D. C. Olson and Y. Vasilevskis, *Inorg. Chem.*, **8**, 1611 (1969).
15) A. Roekenbauer, É. B. Záhonyi, and L. I. Simándi, *J. Chem. Soc., Dalton Trans.*, **1975**, 1729.
16) K. Kubokura, H. Okawa, and S. Kida, *Bull. Chem. Soc. Jpn.*, **51**, 2036 (1978).
17) R. S. Drago, T. Beugelsdijk, J. A. Breese, and J. P. Cannady, *J. Am. Chem. Soc.*, **100**, 5374 (1978).
18) D. V. Stynes, H. C. Stynes, B. R. James, and J. A. Ibers, *J. Am. Chem. Soc.*, **95**, 1796 (1973).
19) Y. Nishida and S. Kida, *Coord. Chem. Rev.*, **27**, 275 (1979).
20) G. N. Schrauzer and L. P. Lee, *J. Am. Chem. Soc.*, **92**, 1551 (1970).
21) G. McLendon and A. E. Martell, *Coord. Chem. Rev.*, **19**, 1 (1976), and references therein.

  Bull. Chem. Soc. Jpn., 54, 3191—3196 (1981)

Preparation and Ligand Field Absorption Spectra of $[CrF_2(O\text{-}O)_2]^{3-}$ and $[CrF_2(O\text{-}O)(en)]^-$ Type Complexes

Sumio KAIZAKI,* Mieko AKAHO(nee ASADA), Yasuyo MORITA, and Kuniko UNO

Department of Chemistry, Faculty of Science, Nara Women's University, Nara 630

(Received December 15, 1980)

Two geometrical isomeric pairs of $[CrF_2(O\text{-}O)_2]^{3-}$ and either one of two possible geometrical isomers of $[CrF_2(O\text{-}O)(en)]^-$, where O–O denotes oxalate and malonate anions, were newly prepared and characterized by means of the spectral and chromatographic elution behaviors. It was found that $[CrF_2(ox)(en)]^-$ and $[CrF_2(mal)(en)]^-$ obtained take *cis* and *trans* forms, respectively. The ligand field absorption spectra of the present complexes were compared with one another, and with those of the corresponding aqua complexes of the same type. On the basis of the analyses of the absorption spectra in terms of the angular overlap model, the AOM parameters (e_σ and e_π) for the ligands concerned were estimated, and their transferability assumption and the anisotropic π interactions of Cr–O bonding with respect to the chelate plane of the dicarboxylate ligands were discussed.

There have been spectral as well as preparative studies on difluorochromium(III) complexes like *trans*-$[CrF_2(H_2O)_4]^+$ and *trans*-$[CrF_2(N)_4]^+$ type complexes.[1-4] Such complexes exhibit characteristic spectral pattern in the ligand field band region: significant splitting of the second band, which facilitates the application of the angular overlap model (AOM). These studies have been mainly concerned with linearly ligating ligands[5] such as saturated amines and halide ions, and with nonlinear ligators such as pyridine, but not with dicarboxylate chelates in which Cr–O bonding may be formed with different π-interactions vertical and parallel to the chelate planes besides with the σ-interactions.[5] The estimates of the AOM parameters for the dicarboxylate ligands provide a valuable clue to test the assumption of parameter transferability from one complex to another and to clarify the anisotropy of the Cr–O π-interactions with respect to the chelate planes. For this purpose, such high symmetry complexes as *trans*-$[CrF_2(O\text{-}O)_2]^{3-}$ and *trans*-$[CrF_2(O\text{-}O)(en)]^-$ with dicarboxylates are considered to be suitable as a simple model case, because their ligand field spectra are expected to give splitting patterns as observed for those of *trans*-difluoro chromium(III) complexes with aqua and/or ethylenediamine ligands. However, there has been known no such mixed difluorochromium(III) complex with dicarboxylates.

The present paper deals with the preparation and characterization of two geometrical isomers, *cis*- and *trans*-$[CrF_2(O\text{-}O)_2]^{3-}$, where O–O denotes oxalate and malonate ions, and those of *cis*-$[CrF_2(ox)(en)]^-$ and *trans*-$[CrF_2(mal)(en)]^-$. The spectral behavior in the ligand field band region of these complexes is explored in connection with that of the corresponding aqua complexes, $[CrF_2(H_2O)_4]^+$, $[CrF_2(en)(H_2O)_2]^+$, and $[Cr(ox)_2(H_2O)_2]^-$, and analyzed in terms of the AOM.

Experimental

Preparation of the Complexes. *(1)* cis- *and* trans-$[CrF_2(O\text{-}O)_2]^{3-}$: Five grams of *cis*-$K[Cr(ox)_2(H_2O)_2]\cdot 3H_2O$ and 0.86 g of potassium fluoride were dissolved in 300 cm^3 of water in a polyethylene beaker. After the solution was heated at 60 °C on a water bath for about 6 h, the color of the solution changed from red violet to dark green. By adding the resultant solution to a large amount of methanol, pale green precipitate was obtained. An aqueous solution of this precipitate was poured onto a column (4×60 cm) of anion exchanger (QAE-Sephadex A-25), and the column was swept with water. When the adsorbed band was eluted with a 0.1 mol dm^{-3} sodium chloride solution, the column gave five bands. Of these bands, the four faster eluted bands (B-I, B-II, B-III, and B-IV) were found to be the complexes containing fluoride, oxalate ion, and water as ligands by the qualitative analyses in terms of zirconium alizarin paper tests for fluoride and potassium permanganate tests for oxalate, and by the fact that their first d-d absorption bands are shifted to the lower frequency by increasing in pH (*ca.* 10) of the eluate with a 0.1 mol dm^{-3} sodium hydroxide solution. Taking into account of these facts and the position of the first absorption band as well as the chromatographic elution behavior, three faster eluted bands (B-I, B-II, and B-III) may be three possible geometrical isomers of $[CrF_2(ox)(H_2O)_2]^-$ and two later eluted bands (B-IV and B-V) two possible isomers of $[CrF_3(ox)(H_2O)]^{2-}$ or $[CrF(ox)_2(H_2O)]^{2-}$. But their characterization was not attempted. When the fifth band(B-V) was eluted with a sodium chloride solution (0.2 mol dm^{-3} in the early stage of elution, and then 0.25 and 0.3 mol dm^{-3} successively in the later stage), three bands (B-V′, B-VI, and B-VII) were separated. The slowest eluate (B-VII) was confirmed to be tris(oxalato)chromate(III) ion from the absorption measurement. The remaining two bands (B-V′ and B-VI) were found to be complex ions containing only fluoride and oxalate ions as ligands, because the first d-d absorption band of these eluates shows no shift with increase in pH and the qualitative analyses indicate the presence of fluoride and oxalate ions in the complexes. The yield of the B-VI band was much smaller than that of the B-V′ one. After dilution with water, each eluate was loaded again on each column of QAE-Sephadex A-25. Each adsorbed band was eluted with a 1 mol dm^{-3} sodium chloride solution. To each eluate was added a large excess of barium perchlorate. Then green fine powder was obtained. Each barium salt was converted to methylammonium salt by a batchwise method with a cation exchange resin of $CH_3NH_3^+$ form (Dowex 50w×8) in water. The resultant green solutions were separately condensed by a vacuum rotatory evaporator at about 30 °C. By adding acetone and ethanol to each condensed solution, green solid was crystallized. Each green powder was recrystallized from water and acetone. Found for the B-VI: C, 23.21; H, 5.02; N, 11.60%. Calcd for $(CH_3NH_3)_3[CrF_2(ox)_2]$: C, 22.84; H, 5.05; N, 11.24%. Found for the B-V′: C, 21.41; H, 4.33; N, 7.65%. Calcd for $(CH_3NH_3)_3[CrF_2(ox)_2]\cdot C_3H_6O\cdot 2.25NaCl$ (C_3H_6O= acetone): C, 21.71; H, 4.38; N, 7.62%.

(2) cis- *and* trans-$[CrF_2(mal)_2]^{3-}$ *Complexes*: After dissolving

3.8 g of *cis*-K[Cr(mal)$_2$(H_2O)$_2$]·3H_2O and 1.2 g of potassium fluoride in 100 cm^3 of water in a polyethlene beaker, the solution was heated at 60 °C on a water bath for about 4 h. The resulting green solution was added to a large amount of methanol. Then pale green precipitate was obtained. An aqueous solution of this precipitate was poured onto a column (4×60 cm) of QAE-Sephadex A-25. After washing the column with water, the adsorbed band was eluted with a sodium chloride solution (0.1 mol dm^{-3} in the early stage of elution, and then 0.2 and 0.3 mol dm^{-3} successively in the later stage). The column gave eleven bands. From the elution behavior and the absorption spectral change with increase in pH, the b-I—b-VIII bands were found to be univalent or bivalent complex anions containing H_2O, F^-, and mal^{2-} as ligands. The slowest eluted band (b-XI) was confirmed to be [Cr(mal)$_3$]$^{3-}$ from the absorption measurements. The two remaining eluates (b-IX and b-X) were found to be the complexes with only fluoride and malonate ions but not with water. After dilution of these eluates with water, they were reloaded on short columns of QAE-Sephadex A-25. After each column was washed well with a 0.01 mol dm^{-3} lithium chloride solution, each band was eluted with a 1.0 mol dm^{-3} lithium chloride solution. To the condensed solutions was added ethanol and acetone; then lithium salts being precipitated. Each green powder was recrystallized from water and acetone. Found for the b-IX: C, 19.41; H, 2.55%. Calcd for Li_3[CrF_2(mal)$_2$]·2.5H_2O: C, 20.02; H, 2.52%. Found for the b-X: C, 16.72; H, 2.20%. Calcd for Li_3[CrF_2(mal)$_2$]·3H_2O·1.5LiCl: C, 16.66; H, 2.33%.

The present oxalato and malonato complexes were also prepared from [CrF_2(H_2O)$_4$]NO_3, which was obtained by evaporating the reaction mixture of $Cr(NO_3)_3$·9H_2O with 40% hydrofluoric acid and formaldehyde.[2a]

(3) [CrF_2*(en)*(H_2O)$_2$]*Br*: This complex was used as a starting complex for the preparation of [CrF_2(O–O)(en)]$^-$ type complexes. The preparation of this complex was performed by the similar method to that of [CrF_2(pn)(H_2O)$_2$]Br[7] except that ethylenediamine(en) was used instead of 1,2-propanediamine(pn). Found: C, 9.14; H, 4.67; N, 10.46%. Calcd for [CrF_2(en)(H_2O)$_2$]Br: C, 9.03; H, 4.55; N, 10.53%.

(4) [CrF_2*(ox)(en)*]$^-$: A solution containing 1.0 g of [CrF_2(en)(H_2O)$_2$]Br and 0.7 g of potassium oxalate monohydrate was heated at 60 °C on a water bath for 2.5 h. After cooling the reaction mixture, the solution was added to a large amount of methanol to form violet precipitate. This solid was filtered and dissolved again in a small amount of water. The resultant solution was poured onto a column of anion exchange resin (Dowex 1×8, Cl^- form). The adsorbed band was washed with water and then eluted with a 0.05 mol dm^{-3} sodium chloride solution. The column gave three bands. The third eluate was confirmed to be [Cr(ox)$_2$(en)]$^-$ by the absorption measurement. The second band was proved to contain fluoride and oxalate ions but not water as ligands by means of the qualitative analyses for these ions and by the fact of no shift of the first band with increase in pH. This eluate was concentrated at about 25 °C by a vacuum rotatory evaporator. By adding methanol to the condensed solution, red violet crystals were obtained. Recrystallization was carried out from water and methanol several times. Found: C, 16.28; H, 3.48; N, 8.62%. Calcd for Na[CrF_2(ox)(en)]·0.75 H_2O·0.5 CH_3OH·0.6 NaCl: C, 16.60; H, 3.56; N, 8.60%.

(5) [CrF_2*(mal)(en)*]$^-$: This complex was prepared by the similar method to that of the corresponding oxalato complex as described in *(4)* except that potassium malonate was used in place of potassium oxalate. The sodium salt obtained was converted to lithium salt with a cation exchange resin (Dowex 50×8, Li^+ form) by a batchwise method. After concentrating the solution by a vacuum rotatory evapolator, red violet crystals were obtained by adding methanol and then cooling. Recrystallization was carried out from water and methanol. Found: C, 19.75; H, 4.97; N, 9.21%. Calcd for Li[CrF_2(mal)(en)]·2.5H_2O: C, 20.06; H, 5.00; N, 9.28%.

Measurements. Absorption spectra were obtained on a Shimadzu UV-200S spectrophotometer. Diffuse reflectance spectrum was measured by a Hitachi EPS-3T spectrophotometer with a reflectometer. CD curves were recorded on a JASCO MOE-1 spectropolarimeter, and infrared spectra on a JASCO DS-402G spectrophotometer.

Calculations. Computer programs for the calculations of the transition energies of the d-d bands and for the Gaussian analyses of the observed curves were based on the programs (AOM/2 and LGNCD) already obtained. The calculations were carried out by a FACOM 230-28 at the Nara Women's University.

Results and Discussion

Characterization. *1)* [CrF_2*(O–O)*$_2$]$^{3-}$ *Complexes*: In view of the chromatographic elution behavior and the absorption spectra as well as the elemental analyses for each pair of the oxalato (B-V′ and B-VI) and the malonato (b-IX and b-X) complexes, each of them corresponds to the geometrical isomeric pair with the same chemical composition. The first absorption bands of [CrF_2(O–O)$_2$]$^{3-}$ are observed near the positions predicted by the average of environment.[8] In such cases, it is empirically expected[9] that the first absorption band of *trans*-[CrF_2(O–O)$_2$]$^{3-}$ locates at the lower frequency side than that of *cis*-[CrF_2(O–O)$_2$]$^{3-}$, because the ligand fluoride lies below the ligands oxalate and malonate in the spectrochemical series.[8] Since the B-V′ isomer of the present oxalato complexes gives the first band at the lower frequency side than the B-VI one as shown in Fig. 1, the former and the latter isomers may be assigned to *trans* and *cis* forms, respectively. This assignment is confirmed by the fact that the elution order of the ion exchange chromatography agrees with that generally recognized for *cis* and *trans* geometrical

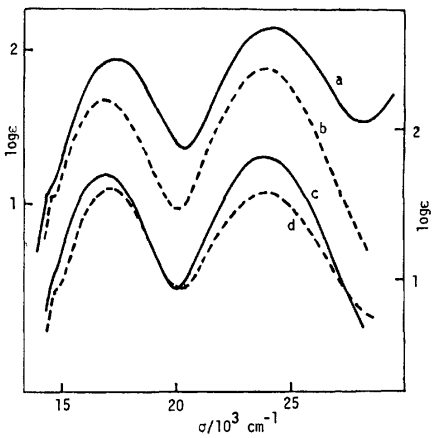

Fig. 1. Absorption curves of (a) *cis*-[CrF_2(ox)$_2$]$^{3-}$ (——), (b) *trans*-[CrF_2(ox)$_2$]$^{3-}$ (——) (left side ordinate), (c) *cis*-[CrF_2(mal)$_2$]$^{3-}$ (——), and (d) *trans*-[CrF_2(mal)$_2$]$^{3-}$ (——) (right side ordinate) in water.

isomers of $[MX_2L_4]$ type complexes,[10] and also supported by the fact that the B-VI (*cis*) isomer is found to have larger molar absorption coefficients of the d-d bands than the B-V′ (*trans*) one (Fig. 1) as noticed in the cases of $[Cr(CN)_2(en)_2]^+$[11] and $[Cr(NCS)_2(en)_2]^+$.[12] Further, the validity of this assignment is justified by the CD behavior in the first band region of these complexes in solutions containing chiral environmental substances as is applied to the structural assignments of $[SnCl_2(acac)_2]$ and the related complexes in *d*-malic acid systems.[13] That is, when the complexes at about 5×10^{-3} mol dm^{-3} in a mixture of water and acetone (1 : 1) containing *d*-cinchonine hydrochloride (15×10^{-3} mol dm^{-3}) were allowed to stand for about half an hour, the intensity of the CD extremum of the B-VI isomer in this region ($\Delta\varepsilon=+0.02$ mol^{-1} dm^{-3} cm^{-1} at 17750 cm^{-1}) is found to be much larger than that of the B-V′ isomer and to be as large as that of $[Cr(ox)_3]^{3-}$ in the analogous condition.[14] Since most bis(oxalato)-chromate(III) complexes are found to undergo rapid racemization,[15] the present complexes are expected to exhibit the CD associated with the enrichment of one enantiomer in terms of the so-called Pfeiffer effect. Thus, it appears that the B-VI isomer is a racemic mixture consisting of enantiomers with configurational chirality due to *cis* arrangement of two fluoride ions, and that the B-V′ isomer takes achiral configuration owing to *trans* coordination of two fluoride ions.

The corresponding malonato complexes show somewhat different spectral behavior from the oxalato complexes; the first absorption band of the faster eluted b-IX isomer was observed at a slightly higher frequency than that of the slower eluted b-X isomer. As shown in Fig. 1, the difference between the first band position of the b-IX isomer and that of the b-X one is too small to offer an any reliable clue for the assignment of the geometrical structures. The elution behavior on the column chromatography and the absorption intensities of the d-d bands seem to be more reliable for the structural assignments. As shown in Fig. 1, on the basis of these criterions, the b-IX and b-X isomers are to be assigned to *trans* and *cis* forms, respectively. This assignment is also supported by the CD behavior in a mixture of water and acetone containing *d*-cinchonine hydrochloride as in the case of the corresponding oxalato complexes. That is, the b-X (*cis*) isomer in such a solution gives a much stronger CD peak ($\Delta\varepsilon=+0.01$ mol^{-1} dm^3 cm^{-1} at 16880 cm^{-1}), probably due to the Pfeiffer effect, than the b-IX (*trans*) isomer. The infrared spectra of the malonato complexes may provide another clue for the assignment of the geometrical structure. Three infrared bands are observed at 1620, 1695, and 1720 cm^{-1} for the b-X isomer and only one at 1615 cm^{-1} for the b-IX isomer in the region of C=O asymmetric stretching as is observed for the corresponding diaquabis(malonato)chromate(III) complexes; *i.e.*, three components for the *cis*-isomer and one component for the *trans*-isomer. Such a difference in the number of the observed bands between the geometrical isomers of the malonato complexes may be mainly ascribed to the difference in symmetry of the complexes. Thus, these infrared spectral behavior of the malonato complexes confirms the assignment on the basis of the chromatographic elution orders, the molar absorption coefficients, and the Pfeiffer CD.

2) $[CrF_2(O-O)(en)]^-$ Complexes: For each of the oxalato and malonato complexes of this type, only one of two possible geometrical isomers could be isolated. The d-d absorption spectrum of the oxalato complex is symmetrical in shape and shows no splitting, whereas that of the malonato complex is of asymmetric shape and exhibits a shoulder at the higher frequency side for the first band and at the lower frequency side for the second band, as shown in Fig. 2. According to the

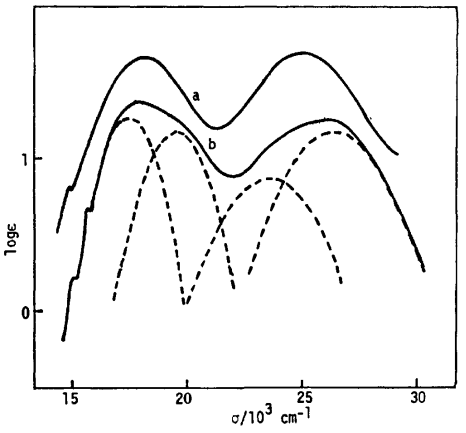

Fig. 2. Absorption curves of (a) *cis*-$[CrF_2(ox)(en)]^+$ and (b) *trans*-$[CrF_2(mal)(en)]^+$ in water, and the resolved curves of the latter complex (-----) using the Gaussian analysis.

Yamatera's rule,[16] it is suggested that the oxalato and malonato complexes take *cis* and *trans* forms, respectively. That is, it is predicted that the orbitally doubly degenerate and nondegenerate components of the $^4T_{2g}$ splitting states locate at 17390 and 19720 cm^{-1}, respectively, by using $10Dq(en)=21900$ cm^{-1}, $10Dq(F^-)=15050$ cm^{-1}, and $10Dq(mal^{2-})=17670$ cm^{-1}. These predicted transition energies lie close to the peaks and near the shoulder observed for $[CrF_2(mal)(en)]^-$. For the *cis* form, three splitting components are predicted to locate at 19100, 18100, and 17390 cm^{-1}. This splitting interval and the positions obtained may account for the observed symmetric pattern and the maximum of the first band for the oxalato complex (Fig. 2). In addition, this assignment may be confirmed by the solvent effect on the absorption spectra of these complexes. The second absorption band of *trans*-$[CrF_2(en)_2]^+$ in *N*-methylformamide (nmf) is more distinctly resolved into two components than that in water, and the corresponding *cis*-isomer gives almost unaltered behavior in these solvents. The present oxalato and malonato complexes exhibit the similar spectral behavior in water and nmf. The second band of the *trans*-difluoro malonato complex in nmf is more remarkably split than that in water, while that of the *cis*-difluoro oxalato complex remains unchanged.

Assuming that $[CrF_2(en)(H_2O)_2]^+$ takes *trans*(F) form as mentioned below, the formation of the malonato complex seems to take place with retention of configura-

tion, but the oxalato complex may be formed with conversion to *cis* configuration.

Ligand Field Absorption Bands. In spite of the fact that the ligand malonate lies at the higher position than the ligand fluoride in the spectrochemical series as in the case of the ligand oxalate,[8] the first absorption band of *trans*-$[CrF_2(mal)_2]^{3-}$ locates at the higher frequency side than that of the *cis* one; *i.e.*, contrary to the empirical prediction,[9] which is valid for the corresponding oxalato complexes as mentioned before. It is noted that the ligand field band of the malonato complexes behaves unlike that of the oxalato complexes to some significant degree. Such a difference in the ligand field band between the malonato and oxalato complexes is not observed for the absorption spectra of $[Cr(O-O)_n(en)_{3-n}]^{3-2n}$ type complexes; *e.g.*, the first band being observed at 20170 cm^{-1} for both $[Cr(ox)(en)_2]^+$ and $[Cr(mal)en)_2]^+$, at 18830 cm^{-1} for both $[Cr(ox)_2(en)]^-$ and $[Cr(mal)_2(en)]^-$, and at 17500 and 17670 cm^{-1} for $[Cr(ox)_3]^{3-}$ and $[Cr(mal)_3]^{3-}$, respectively. It is interesting to note that both the first and the second bands of the present dicarboxylato complexes are compared with those of the corresponding aqua complexes of the same types; *i.e.*, $[CrF_2(H_2O)_4]^+$, $[CrF_2(en)(H_2O)_2]^+$, and $[Cr(ox)_2(H_2O)_2]^-$. The absorption spectrum of *trans*-$[CrF_2(H_2O)_4]^+$ reported by Chia and King[1] shows a large splitting in the second absorption band region as in Fig. 3. *trans*-Diaquabis (oxalato)-

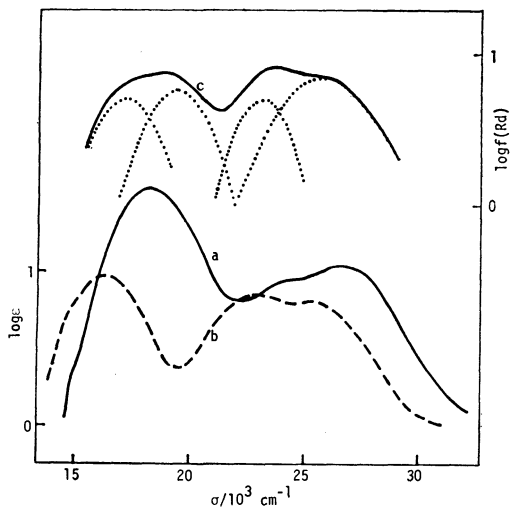

Fig. 3. Absorption curves of (a) *trans*(F)-$[CrF_2(en)(H_2O)_2]^+$ (——) and (b) *trans*-$[CrF_2(H_2O)_4]^+$ (----) (from Ref. 1) in water; diffuse reflectance spectrum of (c)*trans*-$K[Cr(ox)_2(H_2O)_2]\cdot 3H_2O$ (——) (right side ordinate) and its resolved curves using the Gaussian analysis (……).

chromate(III) complex also gives a splitting pattern for both the first and second bands, which is revealed with the aid of the Gaussian analysis of the diffuse reflectance spectrum (Fig. 3) as well as by the low-temperature single-crystal polarized spectral study.[17] Since the ligand field strength of the fluoride ligand is weaker than that of the aqua ligand,[8] it is anticipated that the splitting of the d-d absorption spectra for the present newly prepared *trans*-difluorobis(dicarboxylato) complexes is larger, at least in the first band region, than that for the diaqua complexes. Contrary to this expectation, however, both the present *trans*-difluoro complexes show the symmetrical shape and no splitting in their absorption spectra as in Fig. 1. The analogous situation is observed in the case of *trans*-$[CrF_2(O)_2(en)]$ type complexes. While the second absorption band of the malonato complex, *trans*-$[CrF_2(mal)(en)]^-$, is split similarly to that of *trans*(F)-$[CrF_2(en)(H_2O_2)]^+$, the first band exhibits a shoulder at the higher frequency side for the malonato complex, but not for the aqua complex as in Figs. 2—3.

In order to examine the different nature of Cr-ligand bonding, an attempt to estimate the angular overlap parameters is made by fitting the calculated transition energies to the observed positions of the d-d bands in terms of the angular overlap model on the assumption of orthoaxial ligation.[4] The theoretical calculations are carried out by diagonalizing full energy matrix incorporating all configurational interactions for the d^3 configuration.[18] The results are summarized in Tables 1 and 2 together with the AOM (e_σ and e_π) and Racah (B) parameter values as well as the assignments of the transition states. By using the AOM parameters for the fluoride and aqua ligands transferred from *trans*-$[CrF_2(N)_4]^+$ type and ammineaquachromium(III) complexes, $[Cr(NH_3)_n(H_2O)_{6-n}]^{3+}$,[3-4] the calculated positions of the ligand field bands for *trans*-$[CrF_2(H_2O)_4]^+$ and $[CrF_2(en)(H_2O)_2]^+$ (assumed *trans*(F) form) correspond fairly well to those of the observed ones, except that the rather large splitting of the first band is reproduced despite of the observed symmetrical envelope of this band (Fig. 1 and Table 1). Among several attempts to estimate the AOM parameters for *trans*-$[CrF_2(H_2O)_4]^+$,[19-20] the parameter values estimated by Keeton *et al.*[19] are close to the present values. Similar calculations are carried out for *trans*-$[Cr(ox)_2(H_2O)_2]^-$, *trans*-$[CrF_2(mal)(en)]^-$, and *trans*-$[CrF_2(O-O)_2]^{3-}$, assuming that the π orbitals vertical to

Table 1. Observed and calculated transition energies of *trans*-$[CrF_2(H_2O)_4]^+$ and *trans*-(F)-$[CrF_2(en)(H_2O)_2]^+$ complexes

trans-$[CrF_2(H_2O)_4]^+$		*trans*(F)-$[CrF_2(en)(H_2O)_2]^+$	
Obsd	Calcd (Assign)[b]	Obsd	Calcd(Assign)[b]
16.33[a]	16.09[a] (^4E)	18.42[a]	17.09[a] (^4E)
	17.20($^4B_2$)		19.10($^4B_2$)
22.70	22.68(^4E)	24.10	23.81(^4E)
25.50	25.47($^4A_2$)	26.81	26.92($^4A_2$)
37.00	35.98($^4A_2$)	38.30	37.78($^4A_2$)
	37.47(^4E)		39.92(^4E)
	e_σ(F)=7.43[a]		e_σ(F)=7.43[a]
	e_π(F)=1.78		e_π(F)=1.78
	$e_\sigma(H_2O)$=6.50		$e_\sigma(H_2O)$=6.50
	$e_\pi(H_2O)$=0.575		$e_\pi(H_2O)$=0.575
	B=0.73		e_σ(en)=7.00
			B=0.71

a) Wavenumbers are given in 1000 cm^{-1}. b) Assignments are made according to the results of the theoretical calculations.

Table 2. Observed and calculated transition energies of *trans*-$[CrF_2(mal)(en)]^-$ and *trans*-$[CrX_2(O-O)_2]^{-3}$ type complexes

trans-$K[Cr(ox)_2(H_2O)_2]\cdot 3H_2O$		*trans*-$[CrF_2(mal)(en)]^-$			*trans*$[CrF_2(O-O)_2]^{3-}$		
Obsd[a]	Calcd (Assign)[b]	Obsd[a]	Calcd I	II (Assign)[b]	Obsd(ox)	Obsd(mal)	Calcd(Assign)[b]
17.20[c]	17.12[c] (^4E)	17.46[c]	17.22[c]	17.05[c] (^4E)	16.80[c]	17.05[c]	16.33[c] (^4E)
19.44	19.05 ($^4B_2$)	19.50	19.50	19.20 ($^4A_2$)			17.40 ($^4B_2$)
23.13	23.81 (^4E)	23.60	23.42	22.95 (^4E)	23.90	23.90	23.09 (^4E)
25.85	25.75 ($^4A_2$)	26.40	26.53	27.07 ($^4A_2$)			24.83 ($^4A_2$)
	37.60 ($^4A_2$)	38.30	37.42	36.98 ($^4A_2$)	37.50	37.50	36.32 ($^4A_2$)
	39.32 (^4E)		39.81	39.69 (^4E)			37.48 (^4E)
	$e_\sigma(H_2O)=6.50$[c]		$e_\sigma(F)=7.00$[c]	7.43[c]			$e_\sigma(F)=6.20$[c]
	$e_\pi(H_2O)=0.575$		$e_\pi(F)=1.25$	1.78			$e_\pi(F)=0.825$
	$e_\sigma(O)$[d] $=6.35$		$e_\sigma(O)$[d] $=6.35$	5.80			$e_\sigma(O)$[d] $=5.80$
	$e_{\pi\perp}(O)$[d] $=0.50$		$e_{\pi\perp}(O)$[d] $=0.50$	0.00			$e_{\pi\perp}(O)$[d] $=0.00$
	$B=0.66$		$e_\sigma(en)=6.65$	7.00			$B=0.71$
			$B=0.63$	0.63			

a) The positions are obtained by the Gaussian analyses as shown in Figs. 2—3. b) Assignments are made according to the of the theoretical calculations. c) Wavenumbers are given in 1000 cm^{-1}. d) The parameter values for the dicarboxylate ligands; the same transition energies are obtained for the oxalato and malonato complexes owing to the assumption of orthoaxial ligation.

chelate planes participate predominately in the Cr–O π-interactions: $e_{\pi//} \gg e_{\pi\perp}$.[5],† Using the AOM parameter values for the aqua ligand from *trans*-$[CrF_2(H_2O)_4]^+$ and *trans*-(F)-$[CrF_2(en)(H_2O)_2]^+$, the reproduction of both the first and the second bands of *trans*-$[Cr(ox)_2(H_2O)_2]^-$ results in the estimation of the $e_\sigma(O)$ and $e_{\pi\perp}(O)$ values for the dicarboxylates as in Table 2. In addition, use of the transferred parameter values for the dicarboxylate ligand in calculating the transition energies for *trans*-$[CrF_2(mal)(en)]^-$ leads to the reproduction of four gaussian-analyzed band positions of this complex, though the values for the fluoride and ethylenediamine ligands used in this case are estimated to be smaller than those from the aqua complex, *trans*(F)-$[CrF_2(en)(H_2O)_2]^+$, as shown in Calcd I of Table 2. The parameter values obtained for the dicarboxylates agree fairly well with those estimated by the less sophisticated analyses for the ligand field bands of oxalato Cr(III) complexes.[21] On the other hand, use of the parameters for the fluoride and ethylenediamine ligands transferred from the aqua complex requires a significant decrease in the $e_\sigma(O)$ and $e_{\pi\perp}(O)$ values for the dicarboxylate ligand (Calcd II of Table 2), in order to account for the four observed bands of *trans*-$[CrF_2(mal)(en)]^-$. The similar situation may be also encountered for $[CrF_2(O-O)_2]^{3-}$ type complexes. That is, the reproduction of the small splitting expected from the symmetrical shape of the first and the second bands of *trans*-$[CrF_2(O-O)_2]^{3-}$ results in the unlikely decrease in the AOM parameters for the fluoride and dicarboxylate ligands as is tentatively estimated (Table 2). By comparing the present parameter values which are not always the best fit ones for the ligands of the complexes concerned, it is difficult to extract some quantitative information about the bonding nature of Cr and ligator. Within the framework of the AOM, however, it is concluded that the anisotropic Cr–O π-interactions in the dicarboxylato complexes play an important role in the splitting of the ligand field band for *trans*-$[Cr(ox)_2(H_2O)_2]^-$ and *trans*-$[CrF_2(mal)(en)]^-$, and that both the σ and π antibonding interactions between Cr and ligators in the fluoro complexes with the dicarboxylate ligands become weaker than those in the aqua complexes with the fluoride or dicarboxylate ligands.

† In this case, $\Delta(10Dq)$ equals to $3e_\sigma - 2e_{\pi\perp} - 2e_{\pi//} \simeq 3e_\sigma - 2e_{\pi\perp}$.

One of the authors (S.K.) wishes to express his thanks to Professor Yoichi Shimura of Osaka University for his kind guidance and valuable discussions throughout this work and also for making the circular dichroism and infrared spectra available for the present work. Grateful acknowledgement is made to Dr. Kiyoshi Isobe of Osaka City University for his aid in obtaining the elemental analyses of the fluoro complexes. The authors also wish to thank Dr. Takashi Komorita, Osaka University, for his generous offer of the LGNCD and AOM/2 computer programs.

References

1) T. Y. Chan and E. L. King, *Discuss. Faraday Soc.*, **29**, 109 (1966); E. L. King, private communication for the absorption data.

2) J. Glerup, J. Josephsen, K. Michelsen, E. Pedersen, and C. E. Schäffer, *Acta Chem. Scand.*, **24**, 247 (1970); b) J. Glerup and C. E. Schäffer, *Inorg. Chem.*, **15**, 1408 (1976).

3) T. J. Barton and R. C. Slade, *J. Chem. Soc., Dalton Trans.*, **1975**, 651.

4) J. Glerup, O. Mønsted, and C. E. Schäffer, *Inorg. Chem.*, **15**, 1399 (1976); **17**, 3153 (1978).

5) C. E. Schäffer, *Proc. R. Soc. London, Ser. A*, **297**, 96 (1967); C. K. Jørgensen, "Modern Aspects of Ligand Field Theory," North-Holland Publishing Company, Amsterdam (1971), Chap. 17.

6) C. E. Schäffer, *Pure Appl. Chem.*, **24**, 361 (1970).

7) J. W. Vaughn and J. Marzowski, *Inorg. Chem.*, **12**, 2346 (1973).

8) C. K. Jørgensen, "Absorption Spectra and Chemical Bonding in Complexes," Pergamon Press, Oxford (1962).

9) Y. Shimura, *Bull. Chem. Soc. Jpn.*, **25**, 49 (1952); R. G.

Wilkins and J. G. Williams, "Modern Coordination Chemistry," ed by J. Lewis and R. G. Wilkins, Interscience Publications, New York (1960), p. 190.
10) L. F. Druding, *Coord. Chem. Rev.*, **3**, 409 (1968).
11) S. Kaizaki, J. Hidaka, and Y. Shimura, *Bull. Chem. Soc. Jpn.*, **48**, 902 (1975).
12) W. A. Baker and M. G. Phillips, *Inorg. Chem.*, **5**, 1042 (1966).
13) V. Doron and W. Durham, *Inorg. Nucl. Chem. Lett.*, **6**, 285 (1970).
14) K. Miyoshi, Y. Kuroda, J. Takeda, H. Yoneda, and I. Takagi, *Inorg. Chem.*, **18**, 1425 (1979).
15) S. Kaizaki, J. Hidaka, and Y. Shimura, *Bull. Chem. Soc. Jpn.*, **42**, 988 (1969); G. L. Welch and R. E. Hamm, *Inorg. Chem.*, **2**, 295 (1963).
16) H. Yamatera, *Bull. Chem. Soc. Jpn.*, **31**, 95 (1958).
17) R. Dingle, *Acta Chem. Scand.*, **22**, 2219 (1968).
18) J. R. Perumareddi, *Coord. Chem. Rev.*, **4**, 73 (1969).
19) M. Keeton, B. Fa-Chun, and A. B. P. Lever, *Can. J. Chem.*, **49**, 192 (1971).
20) D. S. McClure, *Adv. Chem. Coord. Compounds*, **6**, 498 (1961); A. B. P. Lever, *Coord. Chem. Rev.*, **3**, 119 (1968); L. Dubicki and R. L. Martin, *Aust. J. Chem.*, **22**, 839 (1969); H. U. Rahman, *Physica*, **53**, 256 (1971).
21) S. Bunel, C. Ibarra, and L. Adan, *J. Inorg. Nucl. Chem.*, **31**, 3203 (1969).

  Bull. Chem. Soc. Jpn., 54, 3197—3199 (1981)

Unusual Transposition of the Carbonyl Group in the Reduction of 2-Amino-1-indanone

Jack C. Kim

Department of Chemistry, Busan National University, Busan, Korea

(Received May 15, 1980)

The catalytic reduction procedure of 2-amino-4,5-dimethoxy-1-indanone hydrochloride gave a major reduction product of 2-amino-4,5-dimethoxyindan hydrochloride, along with a small amount of a rearranged 4,5-dimethoxy-2-indanone. The isolated intermediate, 2-amino-4,5-dimethoxy-1-indanol hydrochloride yielded exclusively 4,5-dimethoxy-2-indanone under catalytic reaction conditions (acid treatment). The unusual transformation product was verified on the basis of IR, NMR and the result of elemental analysis. A plausible mechanism for the rearrangement is discussed.

Apomorphine (**1**) which has assumed considerable importance in efforts at understanding the role of dopamine (**2**) in the etiology and therapy of Parkinsonism,[1] has structural similarities (see the dotted line) to dopamine. It is currently believed that apomorphine is a dopaminergic agonist and presumably it is through this mechanism that this agonist is effective clinically. By the Dreiding model inspection of apomorphine and dopamine, the 2-amino-4,5-indandiol hydrochloride (**3**) suggests itself as a candidate for possession of dopaminergic activity. This relationship has been noted by Rekker *et al.*[2] as the rationale for the biologically active pharmacophore of the catechole ring and the amino group of dopamine.

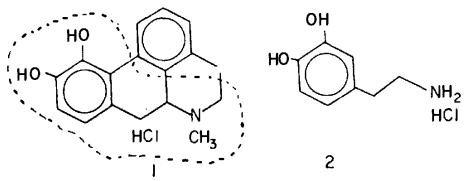

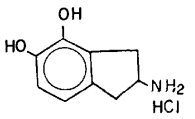

Our prior works have dealt with a synthesis[3] and dopamine-like effects[4] of 2-amino-4,5-indandiol series **3**. The objective of this investigation is to deal with the isolation and identification of an unusual rearranged product, 4,5-dimethoxy-2-indanone (**4**) from the catalytic reduction of 2-amino-4,5-dimethoxy-1-indanone (**5**).

Results and Discussion

Illustrating the previously published results[3] in brief (Scheme 1), the carbonyl group α to the benzene ring of the amino ketone **5** was removed by hydrogenolysis in the presence of palladium on charcoal; the intermediate amino alcohol, 2-amino-4,5-dimethoxy-1-indanol (**6**) was not isolated, but **6** was continuously hydrogenated in the presence of $HClO_4$ to bring about hydrogenolysis of the benzylic hydroxyl group directly to give 2-amino-4,5-dimethoxyindan (**7**). However, the catalytic reduction method of **5** gave exclusively a desired reduction product of **7**, along with a small amount of a white solid, having a higher mobility than that of **7** in thin layer chromatogram. Repeats of the catalytic hydrogenation reactions yielded consistently a small amount of a solid which has much lower melting point (89—90 °C) than those of the compounds **5** (193.5—194.5 °C) and **7** (205—206.5 °C).

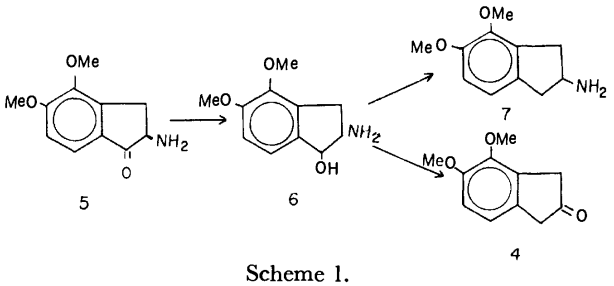

Scheme 1.

The IR spectrum (KBr) of the starting material **5** showed a benzylic carbonyl absorption peak at 1710 cm^{-1}. The unknown white solid showed a new absorption peak at 1740 cm^{-1} which is assumed to be a carbonyl stretching vibration of an isolated ketonic group. As the conjugation of the carbonyl group with the benzene ring results in delocalization of the π electrons from the carbonyl group, the C=O bond length as in **5** increases and the frequency of absorption decreases. An integration of nuclear magnetic resonance spectrum of the unknown compound demonstrated two methoxyl and two aromatic protons plus four aliphatic proton signals. The characteristic proton signal of the four aliphatic C-1 and C-3 protons gave two singlets (δ 2.51 and 2.53), quite different from those of the compounds, **5** and **7** which showed a multiplet.

The white compound is thus believed to be 4,5-dimethoxy-2-indanone **4**, in veiw of the spectral characteristics of the NMR and IR spectra, and the result of the elemental analysis.

In order to further test whether the unknown compound, 4,5-dimethoxy-2-indanone was derived from the intermediate **6**, we isolated the intermediate, 2-amino-4,5-dimethoxy-1-indanol **6**, before the $HClO_4$ treatment in the catalytic hydrogenation process (see Experimental), and treated **6** with a few drops of concentrated HCl. At this stage, a white solid **4** was exclusively obtained as a major product, and the mp and spectroscopic data of the compound was exactly identical with those of the compound obtained from the hydrogenolysis.

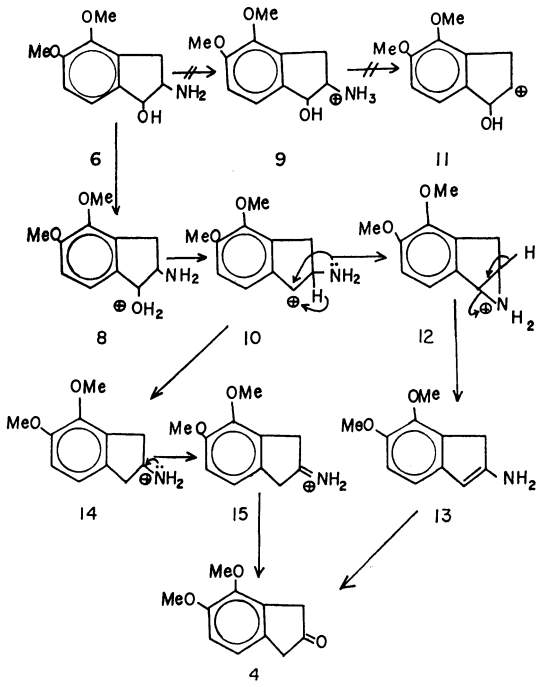

Scheme 2.

The following Scheme 2 shows a plausible mechanism for the rearranged product formation of **4** from **6**. A central problem in the fundamental understanding of a plausible mechanism at the amino alcohol intermediate stage, is the question of whether **6** involves either kinetically controlled protonation at the hydroxyl oxygen to form oxonium ion **8**, or thermodynamically controlled protonation at the basic nitrogen atom to form ammonium salt **9** under the acidic conditions of the catalytic hydrogenation step. Since the good leaving groups will be those that can best stabilize an extra pair of electrons, that is a week base,[6] the stronger base, NH_3 is hard to leave as a leaving group[7] as in **9**, and therefore the weaker base, OH_2 will become a better leaving group, thus making **8** the sole reactive intermediate. Secondly, the generated carbonium ion **10** has relatively good deal of influences on the speed of this ionization which partly depends on the stability of the carbonium ions formed. The much more stable, long-lived benzylic carbonium ion **10**, will predominantly favor the mechanistic routes in **8**→**10**→**12**, excluding a route **9**→**11**.

With these two controlling factors, the protonated oxonium ion **8** is preferentially formed and then converted to the enamine **13**,[8] which is hydrolyzed to give the rearranged product **4** eventually. However, the pinacol-pinacolone type rearrangement from the hydride shift of **10** to **14**, followed by the imminium salt **15**, has not been eliminated as a possibility. On the basis of the presently available data, the enamine-favored mechanistic path is more compatible, and it is reasonable to discard a route **9**→**11**.

Experimental

All melting points were determined using a Polytemp (Polyscience Corporation) or Fisher-Johns apparatus, and are uncorrected. The IR spectra were taken in KBr disks with a Shimadzu 400 spectrophotometer. The ^1H NMR spectra were obtained at 60 MHz using a Varian EM-60 spectrometer with TMS as an internal standard.

*2-Amino-4,5-dimethoxyindan Hydrochloride (**7**·**HCl**).* A mixture of 3 g (0.013 mol) of **5** and 0.6 g of 10% Pd/C in 100 ml of glacial AcOH was hydrogenated in a Parr apparatus at 38 °C under maximum pressure of 3.16 kg/cm². Uptake of 1 mol of H_2 was complete in 48 h. The reaction mixture was cooled and 3 ml of $HClO_4$ was added with rinsing with 3 ml of glacial AcOH, and hydrogenation was continued at 70 °C for 18 h employing a maximum pressure of 2.81 kg/cm². The catalyst was removed from the reaction mixture by filtration and the clear filtrate (yellow color) was treated with 6 g of KOAc; $KClO_4$ precipitated immediately and was removed by filtration. The filtrate was taken up to dryness under reduced pressure (steam bath) and 100 ml of aq 5% HCl was added to the residue and the small amounts of the insoluble solids were filtered. The aq solution was extracted with two 50 ml portions of Et_2O which were discarded. The aq phase was made strongly basic with 20% KOH, then was extracted with four 75 ml portions of Et_2O. The combined Et_2O extracts were washed with 75 ml of H_2O, 75 ml of 10% NaCl, and finally with 75 ml of H_2O and then dried ($MgSO_4$) and filtered. The filtrate was treated with ethereal HCl to form 2.13 g (71%) of a white solid. Recyrstallization from MeOH–Et_2O (charcoal) gave 1.92 g (66%) of white crystals, mp 205—206.5 °C. IR (KBr) showed a disappearance of a strong band at 1710 cm^{-1}. NMR (D_2O); δ 2.77—3.88 (m, 5H, Aliphatic H), 3.88 (s, 6H, –OMe), 7.07 (q, 2H, Aromatic H).

Found: C, 57.62; H, 7.13; N, 5.81%. Calcd for $C_{11}H_{16}ClNO_2$: C, 57.49; H, 7.02; N, 6.13%.

Evaporation of the filtrate under reduced pressure gave a yellow oil which was distilled through a "short path column" apparatus, as a clear colorless liquid, bp 115—119 °C (0.25 mmHg) to give the free base **7**.

*Isolation of the Intermediate, 2-Amino-4,5-dimethoxy-1-indanol Hydrochloride (**6**·**HCl**).* At the end of the complete uptake of 1 mol H_2, the catalyst was removed from the reaction mixture by filtration and the filtrate was evaporated under reduced pressure to obtain the oily residues. The residues were taken up into $CHCl_3$–Et_2O (1 : 6) and ethereal HCl was added to precipitate the salt. The amino-indan hydrochloride salt was very hygroscopic and was dried in a vaccum desicator. Recrystallization from EtOH–Et_2O gave a white solid, mp 163—165 °C. IR (KBr): 3327 (OH), 2892 (NH_3^+); NMR (D_2O): δ 3.18 and 3.98 (2s, 6H, OMe), 7.11 and 7.35 (dd, 2H, Aromatic H).

Found: C, 53.76; H, 6.56; N, 5.70; Cl, 14.14%. Calcd for $C_{11}H_{16}NClO_3$: C, 53.49; H, 6.51; N, 5.91%.

*Isolation of 4,5-Dimethoxy-2-indanone (**4**).* The insoluble solids and the "discarded" two 50 ml portions were combined, and evaporated under reduced pressure. The residue obtained, was crystallized from cyclohexane (charcoal) to yield a white solid, mp 89—90 °C. IR (KBr); 1740 cm^{-1}; NMR ($CDCl_3$): δ 2.51 and 2.53 (s, 4H, Aliphatic H), 3.81 and 3.87 (2s, 6H, OMe) and 7.19 (s, 2H, Aromatic H).

Found: C, 58.73; H, 6.29%. Calcd for $C_{11}H_{12}O_3$: C, 58.65; H, 6.21%.

*Reaction of **6**·**HCl** with Hydrochloric Acid (Preparation of 4,5-Dimethoxy-2-indanone).* The amino alcohol intermediate, **6**·**HCl** (1.11 g, 0.0022 mol) was dissolved in 100 ml of $CHCl_3$ and added 7 ml of concd HCl and the reaction mixture was refluxed for 18 h. At the end of the reaction, the reaction mixture was washed with three 30 ml portions of saturated $NaHCO_3$ solution, three 30 ml portions of NaCl solution,

three 30 ml portions of H_2O and the $CHCl_3$ layer was dried over $MgSO_4$. Fitration and evaporation *in vacuo* gave solid residue, which were crystallized from cyclohexane (charcoal) to give 0.39 g (55%) of white solids, mp 89—90 °C. The IR and NMR spectra were identical with that of the previously obtained compound.

References

1) G. C. Cotzias, P. S. Papavasilliou, C. Fehling, B. Kaufman, and I. Mena, *N. Engl. J. Med.*, **282**, 31 (1970).

2) R. F. Rekker, D. J. Engel, and G. G. Nye, *J. Pharm. Pharmacol.*, **24**, 589 (1972).

3) J. G. Cannon and J. C. Kim, *J. Med. Chem.*, **15**, 348 (1972).

4) J. P. Long, S. Heintz, J. G. Cannon, and J. C. Kim, *J. Pharmacol. Exp. Ther.*, **192**, 336 (1975).

5) H. O. House, "Modern Synthetic Reactions," 2nd ed, W. A. Benjamin, Calif. (1972), pp. 504, 573—575.

6) J. March, "Advanced Organic Chemistry," Reaction Mechanism and Structure, McGraw-Hill Co., New York (1968), pp. 296—295.

7) The strong base such as a NH_3 as a leaving group is seldom seen, except in the treatment of amino function with HNO_2.

8) T. H. Lowry and K. H. Richardson, "Mechanism and Theory in Organic Chemistry," Harper and Row Publishing (1976), pp. 223—226, 192—194.

Synthesis of Ethylene Glycol Acetates Catalyzed by Potassium Iodide and Metal Acetate[1)]

Kazuo SHIMIZU* and Juichi IMAMURA

National Chemical Laboratory for Industry, Yatabe-machi, Tsukuba-gun, Ibaraki 305

(Received February 9, 1981)

The catalytic activities of various kinds of binary systems consisting of KI and metal acetate were tested in liquid phase oxidation of ethylene in acetic acid at various pressures. KI–$Mn(OCOCH_3)_2$ was found to be the most reactive system and a new material, $CH_3COOCH_2CH_2OCOCH_2OCOCH_3$, was formed as a major by-product. It was also found that the main product at an early stage of the reaction was ethylene glycol monoacetate, from which other products were formed consecutively. It is considered that catalytic reaction does not proceed *via* ICH_2CH_2I, but *via* ICH_2CH_2OH which is formed by the oxidation of ethylene with HIO. On the basis of the rate equation and the results under various reaction conditions, a mechanism of the KI–$Mn(OCOCH_3)_2$-catalyzed reaction has been proposed.

At present, most of ethylene glycol is commercially manufactured by hydration of ethylene oxide. However, the total yield of ethylene glycol from ethylene is relatively low, because the selectivity of ethylene oxide production, in the vapor-phase oxidation of ethylene, is not so high.[2)] Therefore, other new methods of ethylene glycol synthesis, without ethylene oxide as an intermediate, have been proposed by several companies.[2)] Halcon International has developed a new process *via* ethylene glycol mono- and diacetates which are easily hydrolyzed to ethylene glycol and acetic acid.[3)] This process involved the acetoxylation of ethylene with KI-metal acetate catalyst. It recently attracted special interest because of the mild oxidizing conditions. Until now, however, the mechanism of this acetoxylation has not been published in detail. The authors have now studied the reaction mechanism and the results are published in this paper.

Experimental

Materials. The metal salts and acetic acid employed were all of a guaranteed grade and the ethylene and oxygen used were of a reagent grade; all were used without further purification.

Apparatus and Procedures. The reaction was performed in a closed system at higher pressure. A titanium-lined autoclave (300 ml) equipped with a magnetic stirrer and a thermocouple was used in conjunction with a pressure controller and a reservoir (469 ml) which was kept at 40 °C. The pressure inside the reservoir was measured by a strain gauge. The ethylene and oxygen gaseous mixture in a pressure ratio of 2 : 1 was preliminarily stored in this reservoir.

A mixture of the catalyst components and acetic acid was placed in the reaction vessel; the vapor phase was replaced with nitrogen, and the vessel was heated to the reaction temperature. At first, ethylene was introduced into the vessel until the desired pressure was obtained and then the mixture of ethylene and oxygen from the reservoir was introduced through the pressure controller until the pressure inside the vessel reached the reaction pressure. The gaseous mixture which decreased in pressure by dissolution and reaction was supplied continuously from the reservoir. Accordingly, the pressure inside the reaction vessel was held constant during the period of reaction.

The amount of mixed gas absorbed was measured by observing the pressure decrease inside the reservoir. The "reaction rate" means hereinafter the rate of pressure decrease during the initial stage of the reaction.

Identification and Analysis. Reaction products were identified by comparing their GC–MS(EI, CI) (JEOL, JMS-D300) and NMR (^1H, ^{13}C) (JEOL, JNM-FX100) spectra with those of authentic samples, and their amounts were determined by gas chromatography with a Shimadzu GC-4BT chromatograph (3m × 3 mm column packed with 20% Silicone DC-550 on Chromosorb WAW DMCS, from 60 to 170 °C, and 2 m × 3 mm column packed with Porapak Q, from 180 to 237 °C, He 40 ml/min). *o*-Dichlorobenzene was used as an internal standard.

Results and Discussion

Reaction Products. The major reaction products were ethylene glycol monoacetate (MA), ethylene glycol diacetate (DA), ethylene glycol (EG), $AcOCH_2CH_2OCOCH_2OH$ (**1**) (Ac means CH_3CO), $HOCH_2CH_2OCOCH_2OAc$ (**2**), $AcOCH_2CH_2OCOCH_2OAc$ (**3**), and $ICH_2CH_2OCOCH_2OAc$ (**4**)—the latter four will be designated the "higher boiling products." **3** was the new material with bp 219—220 °C; MS (70 eV), *m/e* (rel intensity), 174(13), 132(12), 131(12), 101(100), 87(18), and 73(16); MS (CI, NH_3) *m/e*=222, MS (CI,

Table 1. Product distibution for the oxidation of ethylene catalyzed by potassium iodide and different metal acetates

Catalyst Metal salts/mmol	Yield/g		
	DA	MA	EG
KI–$MnOA(c)_2 \cdot 4H_2O$	1.38	0.60	0
–$Ce(OAc)_3 \cdot H_2O$	1.26	0.65	0
–$Cr(OAc)_3 \cdot H_2O$	0.70	0.29	≈0
–$Co(OAc)_24H_2O$	0.46	0.12	0
–$Cu(OAc)_2H_2O$	0.69	0.22	0
–$Fe(OH)(OAc)_2$	0.48	0.17	0
–AgOAc	0.35	0.14	0
–$Ni(OAc)_2 \cdot 4H_2O$	0.38	0.14	0
–$Zn(OAc)_2 \cdot 2H_2O$	0.34	0.08	0

Reaction conditions; KI of 30 mmol, metal acetate of 5 mmol and acetic acid of 100 g (1.67 mol) were used, the ethylene pressure was 20 kg/cm², the oxygen pressure was 5 kg/cm², the reaction temperature was 140 °C and the reaction time was 60 min.

isobutane) m/e=205; ^{13}C-{^1H} NMR ($CDCl_3$) δ=171.2, 170.0, 168.2(3CO), 63.5, 62.3, 61.1($3CH_2$) and 21.2, 20.8($2CH_3$).

Minor products were ICH_2CH_2OH, ICH_2CH_2OAc, CH_2I_2, $AcOCH_2CH_2OCH_2CH_2OAc$, $AcOCH_2CH_2OCH_2CH_2I$, and $ICH_2CH_2OCH_2CH_2OH$. The seven major products were taken into account; ordinarily the yields of the others could be ignored.

Selection of Catalysts. The oxidation of ethylene at an applied pressure was carried out with different catalyst systems. The reaction conditions and results are shown in Table 1. The products which are not listed in the table are omitted because of their negligible yields under these reaction conditions. As Table 1 shows, KI–$Mn(OAc)_2$ is the most active catalyst for the oxidation; accordingly, the reaction with KI–$Mn(OAc)_2$ catalyst system was investigated in detail.

Change of Product Yield with Reaction Time. The yields of the reaction products were determined at selected time intervals. As Fig. 1 shows, MA was the main reaction product at 15 min, the yields of MA, **2** and **4** were maximum at 60 min and those of DA, EG, **3** and **1** increased with reaction time.

Effect of Oxygen Pressure. The reaction rate was of the first order in the oxygen pressure below 7.5 kg/cm and was independent of the pressure from 7.5 to 20 kg/cm^2 under the reaction conditions described in Fig. 2. The fact that the rate dependence on the oxygen pressure varied at 7.5 kg/cm^2 indicates that the reaction mechanism or the rate-determining step is different in the two regions. Figure 2 shows the effects of oxygen pressure on the product distributions after 90 min reaction. The yields of MA and **2** increased with an increase in the oxygen pressure, however, those of the other products were not affected greatly. The reaction was subsequently examined at an oxygen pressure of 7.5 kg/cm^2.

Effect of Ethylene Pressure. The reaction rate was of the first order in the ethylene pressure below 25 kg/cm^2, and independent of the pressure from 25 to 30 kg/cm^2 under the reaction conditions; KI=100 mmol, $Mn(OAc)_2\cdot4H_2O$=5 mmol, AcOH=100 g, the oxygen pressure of 7.5 kg/cm^2, the reaction temperature of 140 °C and the reaction time of 90 min. The reaction was subsequently investigated at an ethylene pressure of 20 kg/cm^2.

Effect of KI Concentration. The reaction rate was of the first order in the concentration of KI below 105 mmol/100 g AcOH under the reaction conditions destribed in Fig. 3; at concentrations above 120 mmol/100 g AcOH, a precipitate of KI was observed in the reaction mixture after the reaction. Figure 3 shows that the yields of DA and MA increased greatly with an increase in the KI concentration. On the basis of these results, the optimal concentration of KI for a fast reaction rate and selective formation of DA and MA is considered to be 120 mmol/100 g AcOH in the KI–$Mn(OAc)_2$-catalyzed reaction.

Effect of $Mn(OAc)_2$ Concentration. The reaction rate increased markedly with an increase in the $Mn(OAc)_2$ concentration between 0.1 and 1 mmol/100 g AcOH, and was independent of the concentration from

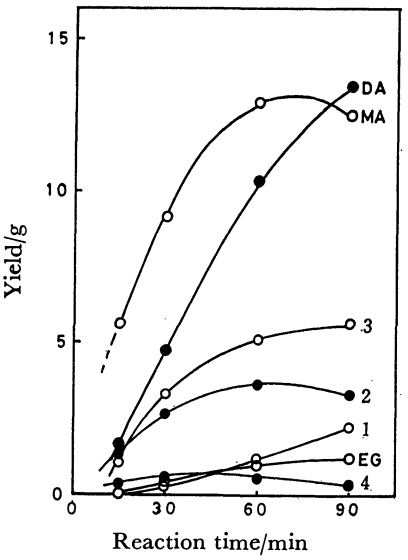

Fig. 1. Change of product yield with reaction time in the KI–$Mn(OAc)_2$-catalyzed reaction. Reaction conditions; KI=120 mmol, $Mn(OAc)_2\cdot4H_2O$=5 mmol, AcOH=100 g, the pressures of ethylene and oxygen were 20 and 5 kg/cm^2, respectively, and the reaction temperature was 140 °C.

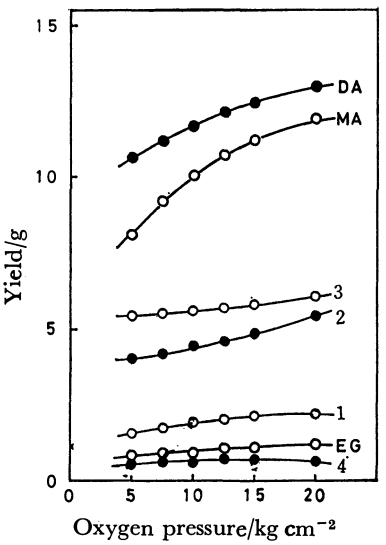

Fig. 2. Effect of the oxygen pressure on the product distributions. Reaction conditions; KI=120 mmol, $Mn(OAc)_2\cdot4H_2O$=1 mmol, AcOH=100 g, the ethylene pressure was 20 kg/cm^2, the reaction temperature was 140 °C and the reaction time was 90 min.

1 to 10 mmol/100 g AcOH under the conditions described in Fig. 4. Figure 4 shows that the $Mn(OAc)_2$ concentration hardly affected the product distributions. Therefore, the favorable region of concentration seems to be $1\leqq[Mn(OAc)_2]\leqq10$ mmol/100 g AcOH.

Mechanism of the Reaction. Y. Ogata and K. Aoki have proposed a mechanism for the reaction of propylene with a mixture of iodine and peracetic acid.[5] The mechanism of the KI–$Mn(OAc)_2$-catalyzed oxidation of ethylene is expressed as follows, by applying their mechanism to this reaction;

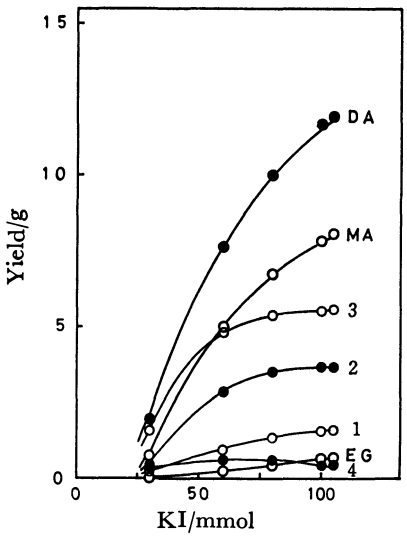

Fig. 3. Effect of the KI concentration on the product distributions. Reaction conditions; $Mn(OAc)_2 \cdot 4H_2O$ = 1 mmol, AcOH = 100 g, the pressures of ethylene and oxygen were 20 and 7.5 kg/cm², respectively, the reaction temperature was 140 °C and the reaction time was 90 min.

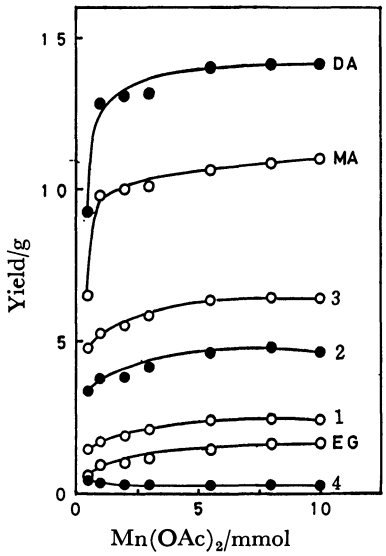

Fig. 4. Effect of the $Mn(OAc)_2$ concentration on the product distributions. Reaction conditions; KI = 120 mmol, AcOH = 100 g, the pressures of ethylene and oxygen were 20 and 7.5 kg/cm², respectively, the reaction temperature was 140 °C and the reaction time was 90 min.

Table 2. Reaction conditions and results

Run No.	Gas and pressure / kg/cm²	Catalyst/mmol and starting material/mmol[a]	Reaction time / min	Yield/g DA	MA	EG	1	2	3	4	Other product
1	C_2H_4(20) O_2(7.5)	$Mn(OAc)_2 \cdot 4H_2O$(10)	90	≈0	≈0	≈0	0	0	0	0	
2	C_2H_4(20) O_2(7.5)	KI(120)	90	3.56	1.84	≈0	0.14	0.41	0.99	0.19	
3	C_2H_4(20)	I_2(60)[b]	90	0.43	0	0	0	0	0	0	ICH_2CH_2I(5.0) ICH_2CH_2OAc(1.86)
4	C_2H_4(20) O_2(7.5)	I_2(60)[b]	15	1.68	0.05	0	0	0	0	0	ICH_2CH_2I(3.2) ICH_2CH_2OAc(1.86)
5	C_2H_4(20) O_2(7.5)	I_2(60)[b]	90	5.26	0.59	0	0	0	0	0	
6	O_2(7.5)	ICH_2CH_2I(20),KOAc(120)[b] $Mn(OAc)_2 \cdot 4H_2O$(5)	15	0.37	0.07	0	0	0	0	0	
7	C_2H_4(20)	I_2(60),KOAc(120)[b] $Mn(OAc)_2 \cdot 4H_2O$(5)	90	1.09	0.15	0	0	0	0	0	
8	O_2(7.5)	ICH_2CH_2OH(60),KI(60)[b] KOAc(60),$Mn(OAc) \cdot {}_2 4H_2O$(5)	15	3.25	2.02	≈0	0	0	0	0	ICH_2CH_2OAc(0.75) $ICH_2CH_2OCH_2CH_2OH$ trace
9	C_2H_4(20)	KIO(11),[c] AcOH(60 g)[b]	15	0.19	0.29	0	0	0	0	0	
10	C_2H_4(20)	KIO_3(60)[b]	15	3.56	2.54	0	0	0	0	0	
11	O_2(7.5)	KI(120),$Mn(OAc)_2 \cdot 4H_2O$(5) DA(20 g), AcOH(80 g)	15	20	≈0	0	0	0	0	0	
12	O_2(7.5)	KI(120),$Mn(OAc)_2 \cdot 4H_2O$(5)	15	0	0	0	0	0	0	0	$AcOCH_2COOH$(0)
13	O_2(7.5)	KI(120),$Mn(OAc)_2 \cdot 4H_2O$(5) A mixture of EG acetates (30 g),[d] AcOH(70 g)	15	23.3	9.97	0.43	0.16	1.53	1.68	0.03	ICH_2CH_2OH trace ICH_2CH_2OAc trace
14	O_2(7.5)	KI(120),$Mn(OAc)_2 \cdot 4H_2O$(5) A mixture of EG acetates (30 g),[d] AcOH(70 g)	30	22.3	8.28	0.67	0.56	1.63	3.28	0.02	
15	C_2H_4(20) O_2(7.5)	KI(120),$Mn(OAc)_2 \cdot 4H_2O$(5) H_2O(10 g), AcOH(90 g)	15	1.50	5.20	0.03	0	0	0	0	ICH_2CH_2OAc(0.29) ICH_2CH_2OH trace

Acetic acid (100 g) was used unless the amount is specified. The reaction temperature was 140 °C. a) All except the amount expressed in gram. b) A Teflon-lined autoclave was used. c) 5% aq solution of KIO(40 g) was used. d) A mixture of DA(12.33 g), MA(10.46 g), EG(2.14 g), and acetic acid(5.07 g).

$$CH_2{=}CH_2 + I_2 \rightleftharpoons CH_2 \overset{I_2}{\underset{\downarrow}{\mp}} CH_2 \xrightarrow{CH_3CO_2H} ICH_2CH_2OAc + HIO.$$

If the reaction proceeds by this mechanism, the main reaction product should be ICH_2CH_2OAc or DA which is formed from ICH_2CH_2OAc by the reaction with KOAc, because of the lack of water in the reaction mixture. However, Fig. 1 indicates that the initial reaction product is MA. Accordingly, this KI–Mn(OAc)$_2$-catalyzed reaction proceeds by a mechanism different from that proposed by them.

In order to study the mechanism of the KI–Mn(OAc)$_2$-catalyzed reaction, this reaction was investigated under various conditions. Table 2 shows the reaction conditions and the results obtained.

The catalytic reaction using Mn(OAc)$_2$ alone as a catalyst yielded practically no products (Run 1), however, the reaction using only KI yielded all of the products (Run 2). The reaction using I_2 alone in the absence of oxygen yielded ICH_2CH_2I and ICH_2CH_2OAc as the major products and DA as the minor one (Run 3). However, in the presence of oxygen the yields of the major two products decreased and those of DA and MA increased with reaction time (Runs 4, 5). The results of the I_2-catalyzed reactions indicate the following reaction pathway.

$$ICH_2CH_2I \longrightarrow ICH_2CH_2OAc \longrightarrow AcOCH_2CH_2OAc \longrightarrow AcOCH_2CH_2OH$$

Indeed, ICH_2CH_2I yielded much more DA than MA (Run 6).

However, as Fig. 1 shows, MA was the main product in the beginning of the reaction and DA and EG yielded consecutively. These results imply that the catalytic reaction does not proceed *via* ICH_2CH_2I.[2] Indeed, ICH_2CH_2I, in spite of its stability under the reaction conditions (Runs 3, 4), was not detected by means of lpc in the reaction mixture.

The reaction in the absence of oxygen yielded very small amounts of products (Run 7). This result implies that oxygen does not reoxidize the reduced catalyst, but takes part in the main reaction. That is to say, oxygen and iodine (or iodine-containing compound) may form a compound (for instance, HIO) which gives a precursor of MA (Run 8), and that compound then reacts with ethylene to form ICH_2CH_2OH. The catalytic reaction seems to proceed as described above, actually, KIO and KIO_3 gave MA and DA in the reaction conditions (Runs 9, 10).

The assumption that the first reaction product is ICH_2CH_2OH is supported by the fact that a much greater amount of $BrCH_2CH_2OH$ is formed in the KBr–Mn(OAc)$_2$-catalyzed reaction than that of ICH_2CH_2OH in the KI–Mn(OAc)$_2$-catalyzed reaction. This could be explained in terms of the difference of the reactivities with KOAc between these two.

Formation-path of Higher Boiling Products. The reactions with and without Mn(OAc)$_2$ as a catalyst component showed the same product distributions (Fig. 4, Run 2). This result indicates that the Mn salt does not take part in the formation of the higher boiling products. Furthermore, neither the higher boiling products formed form DA (Run 11), nor acetoxyacetate yielded from acetic acid (Run 12).

However, the higher boiling products are formed in high yields from a mixture of ethylene glycol acetates (Runs 13, 14). In addition, as Fig. 1 shows, **2** is formed first among the higher boiling products with **3** secondly and **1** only later. These results suggest that the hydrogen of the acetoxyl groups of MA is at first substituted by iodine which is replaced by acetoxyl groups to form **2**; then **3** is formed by the acetoxylation of **2**, followed by the hydrolysis of **3** to form **1**.

On addition of water to the reaction mixture, it was found that the yields of the higher boiling products decrease markedly and that of MA increases (Run 15). These facts support the idea that iodine was converted to HIO according to the equilibrium ($I_2+H_2O=HIO+HI$) in the presence of water, and that HIO promoted the formation of MA.

The reaction rate may be expressed as follows under the following conditions; oxygen pressure above 7.5 kg/cm^2, ethylene pressure below 25 kg/cm^2, KI concentration between 30 and 105 mol/100 g AcOH, Mn(OAc)$_2$ concentration between 1 and 10 mmol/100 g AcOH.

$$V = -dP/dt = k[KI][Mn(OAc)_2]^{\circ}P_{C_2H_4}P_{O_2}^{\circ}.$$

Furthermore, taking into account the above descriptions, the acidity of the reaction system and very little water in the reaction mixture in the beginning of the reaction, the catalytic reaction may be considered to proceed as follows;

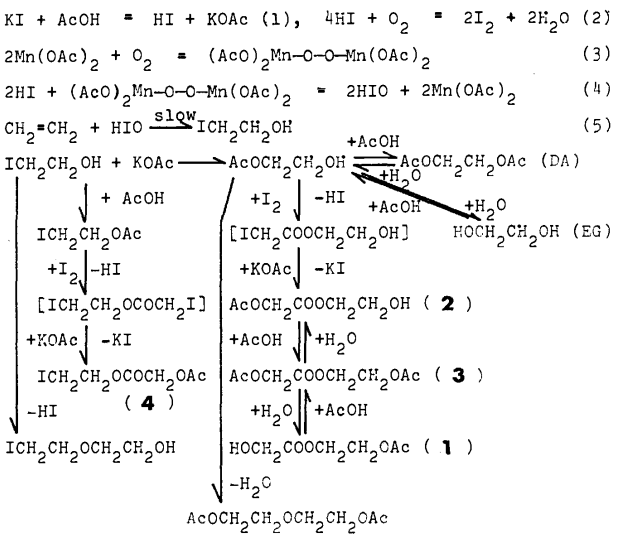

The main reaction rate should be determined at the beginning of the reaction, because by-products are formed from the product of the main reaction. The above rate equation can be derived from this mechanism, by assuming that Eq. 5 is the rate-determing step, Eqs. 1, 3, and 4 are in equilibrium, P_{O_2} and [AcOH] disappear seemingly because of their sufficient amounts in the reaction mixture, and equilibrium 1 lies to the left because of the liberation of acidic HI in acetic acid.

Mn^{3+} and HIO seem to be the chemical species that are easy to form by oxidation from the viewpoint of redox potential, because the redox potentials of (HIO+

$H^+ + e = 1/2\ I_2 + H_2O$) and ($Mn^{3+} + e = Mn^{2+}$) in aqueous solution at 25 °C are 1.45 and 1.51 V, respectively,[6] and the values are not so high, although application of the values in aqueous solution to the reaction system under different conditions is questionable. Of course, the actual participating structures in the reaction system are uncertain. However, some speculation concerning a likely mechanism can be made on the basis of the known data. J. A. Elvidge and A. B. P. Lever first reported the Mn–O–O–Mn complex with Mn phthalocyanine in pyridine.[7] It is not unreasonable to consider chemical species such as $(AcO)_2Mn–O–O–Mn(OAc)_2$ and HIO even in acetic acid at higher temperature. The addition of HIO to olefines is well known to occur.[8]

Y. Ogata and K. Aoki might have observed the results of acetoxylation of the first reaction product, halohydrin, during their classical analytical operations. These required a much longer time than more rapid analytical methods such as gas chromatography.[5] Indeed, MA and ICH_2CH_2OH give corresponding acetates after a long time standing in acetic acid at room temperature.

The authors wish to express their appreciation to Dr. K. Matsuura and Dr. K. Matsushita, of JEOL, for their cooperation in the mass spectrometry and NMR spectroscopy.

References

1) K. Shimizu and J. Imamura, 13th Oxidation Symposium, Kyoto, Japan, November 1979.
2) A. M. Brownstein, *Hydrocarbon Process*, **1974**, 129.
3) German Offen. 1 931 563 to Halcon International (1970).
4) N. Tamura, *Shokubai* (*Catalyst*), **21**, 168 (1979).
5) Y. Ogata and K. Aoki, *J. Org. Chem.*, **31**, 1625 (1966).
6) "Kagaku Binran, Kisohen II," ed by the Chemical Society of Japan, Maruzen, Tokyo (1966).
7) J. A. Elvidge and A. B. P. Lever, *Proc. Chem. Soc.*, **1959**, 195.
8) S. Oae, "Jikken Kagaku Koza," ed by the Chemical Society of Japan, Maruzen, Tokyo (1956), Vol. 20, p. 195; Y. Ogata, *Kagaku No Ryoiki*, **29** (5), 46 (1975).

The Splitting of the ESR Signal of Di-*t*-butyl Nitroxide Solubilized by Micellar Solutions

Shojun Isshiki and Yuhei Uzu*

Department of Chemistry, Faculty of Science, Shinshu University, Asahi, Matsumoto 390

(Received January 20, 1981)

Synopsis. In a hexadecyltrimethylammonium bromide solution containing the stable micelle, a solubilized di-*t*-butyl nitroxide facilitated the partial resolution of the high-field line of the ESR spectrum, which can be associated with the radical in aqueous and micellar phases. Further analysis of the lineshape was made as a function of the surfactant concentration or the temperature.

Stable nitroxide radicals have been widely used as molecular probes or labels in order to study the dynamic effects in a variety of micellar and related membrane-like systems.[1-4] In the present study, the investigation of the ESR lineshapes of di-*t*-butyl nitroxide was made for various types of ionic micellar solutions, with the purpose of further establishing the motional contribution to the ESR linewidths in micellar systems.

Sodium dodecyl sulfate (SDS), sodium tetradecyl sulfate (STS), hexadecyltrimethylammonium bromide (CTAB), and sodium 1,2-bis(2-ethylhexyloxycarbonyl)-ethanesulfonate (AOT) were chosen as the surfactants in this study. SDS and STS were synthesized according to the conventional method. Both CTAB and AOT were specially purified reagents. Surface-tension measurements for the surfactant solutions indicated no minima at 30 °C. The nitroxide probe, di-*t*-butyl nitroxide (DTBN), was synthesized by the method of Hoffman *et al.*[5,6] Prior to the ESR measurements, all the solutions were prepared by adding DTBN to the surfactant solutions and stirring them magnetically for several hours. The concentration of DTBN added was always 4.5×10^{-4} mol dm^{-3}. All the ESR spectra were recorded on a Japan Electron Optics Laboratory JES-ME-3X spectrometer operating at the X band.

Representative ESR spectra in various types of surfactants at 30 °C are presented in Fig. 1. As was observed from the earlier finding,[1] the spectrum of DTBN in an SDS aqueous solution at concentrations below the CMC was identical with that obtained in pure water (Figs. 1(a) and 1(b)). These normal three-line spectra of nearly equal width are characteristic of a variety of rapidly tumbling nitroxides, suggesting no significant variation that might indicate the formation of premicellar aggregates or DTBN-monomer interactions. On the other hand, the high-field hyperfine line of DTBN in a 33 mmol dm^{-3} SDS micellar solution above the CMC is markedly broadened as a consequence of its interaction with the micelles. The relative magnitude of the tumbling motion of the radical is predicted from the rotational correlation time (τ_c); this value was computed from the linewidth and height of the ESR signals by the method of Martinie *et al.*[7] The values obtained in water and SDS solutions with concentrations above the CMC, where the linewidth was essentially little dependent on the SDS concentrations, were approximately 10^{-11} s and 10^{-10} s respectively. It can

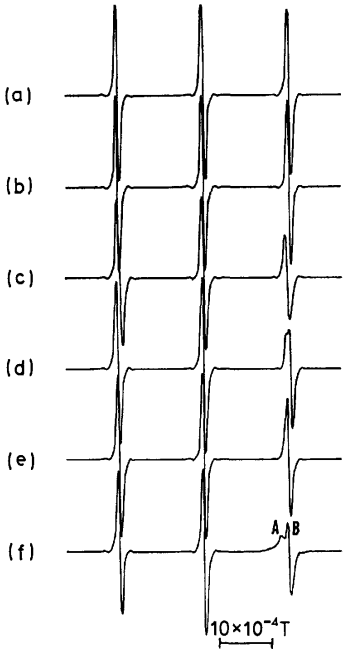

Fig. 1. Representative ESR spectra of 4.5×10^{-4} mol dm^{-3} DTBN at 30 °C.
(a): H_2O, (b): 5.5 mmol dm^{-3} SDS, (c): 33 mmol dm^{-3} SDS, (d): 14 mmol dm^{-3} STS, (e): 33 mmol dm^{-3} AOT, (f): 36 mmol dm^{-3} CTAB.

be seen that, although the experimental value for pure water agrees roughly with the one calculated (2.9×10^{-11} s) from the Stokes law (assuming the DTBN particle radius of 0.3 nm), the experimental values for the SDS solution are much smaller than that calculated for the radical rigidly adsorbed to a hypothetical rigid micelle (10^{-8} s). As has been stated in connection with other nitroxides,[1,3] the solubilized DTBN is considered to tumble too rapidly to be adsorbed on the micelles. Qualitatively, similar behavior was observed in solutions of the other surfactants studied, although there were some indications of the spectral distortion (or partial resolution) of the high-field line in both STS and CTAB micellar solutions (Figs. 1(d) and 1(f)). In the latter, most notably, the high-field line in a 36 mmol dm^{-3} CTAB micellar solution was replaced by two signals analogous to A and B. In this regard, the spectrum resembles that observed in the membrane-like system.[2] The explanation of the distortion is that signals from the radical molecule in two environments, *i.e.*, in the micelle and in the bulk aqueous solution, can be observed separately, indicating that the exchange of the radical between the two environments is very slow. On the contrary, the single signal of the high-field line observed in AOT and SDS suggests that the radical exchanges rapidly to produce a single symmetric signal, which is a weighted average of the spectra found in the two

environments. In these spectra, it seems to be unnecessary to consider the overlapping of two types of spectral lines due to the different environments of the probe. Especially, the very narrow line resulting for AOT suggests a motion which is very rapid compared with those of the other surfactants studied. In contrast with our result at 30 °C, Atherton *et al.*[5] found that the high-field line for SDS micellar solutions was barely resolved at 23 °C for DTBN in two environments. Accordingly, the rate of exchange of the radical probe for the SDS solution at 30 °C is presumed to be relatively slow compared to that of AOT; therefore, a motional behavior similar to that of STS may rather be expected. Therefore, the greater asymmetry of the lineshape, as well as the larger τ_c value, is observed with a longer length of the surfactant alkyl chain. From the ^{1}H NMR study of an SDS micellar solution containing a Tempo radical, Oakes *et al.*[4] showed that the radical-induced proton relaxation occurred preferentially at the α-methylene group of the SDS micelle. Based upon the chemical similarity of DTBN and Tempo, we find a strong indication for a solubilization mainly occurring in the outer region within the SDS micelles. With CTAB, the relative intensities of the A and B signals of the high-field line were strongly dependent upon the CTAB concentration (Fig. 2). As the concentration

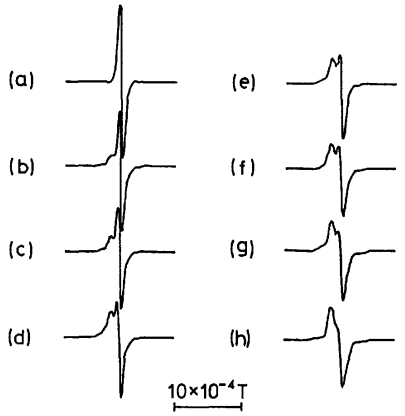

Fig. 2. Concentration dependence for the high-field line of ESR spectra in CTAB solutions at 30°C.
(a): 10, (b): 21, (c): 30, (d): 39, (e): 45, (f): 48, (g): 54, (h): 63 mmol dm^{-3} CTAB.

of CTAB is increased, an increase in Signal A and a concomitant decrease in Signal B are observed, until Signal B, due to the radical in the bulk aqueous phase, is no longer observable. This results from the relative population of the DTBN tumbling rapidly in each phase. Recently, the CTAB micelle has been described as being a more closely packed micelle or having a long-range order, giving it a somewhat solidlike character.[8] This suggestion is advantageous in explaining the above-mentioned incorporation of the DTBN in the CTAB micelle. That is, the small DTBN radical, which is nearly spherical, could rotate rapidly in a relatively rigid micelle; however, it would exhibit a slow chemical exchange of the radical between the micellar and the bulk aqueous phases. In solutions

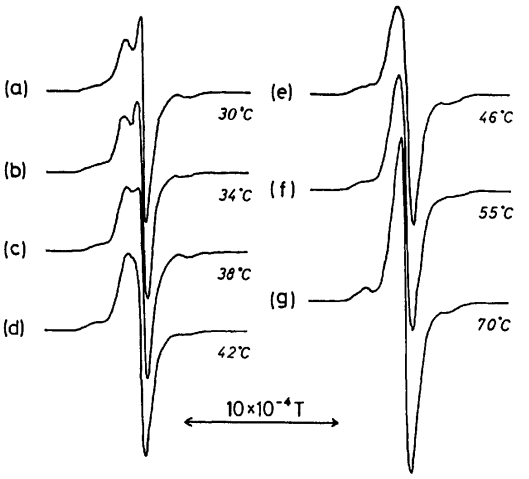

Fig. 3. Temperature dependence for the high-field line in 42 mmol dm^{-3} CTAB.

containing the more stable micelles, the DTBN radical can be expected to exhibit two distinct spectra of the high-field line.

The spectra for the 42 mmol dm^{-3} CTAB solution have also been studied over the temperature range of 30—86 °C. As the temperature is increased, the two signals of a high-field line progressively coalesce, until a single line is observed at *ca.* 46 °C (Fig. 3). The increase in the amount of solubilized radical in the micellar phase might be accounted for by the change in the micellar structure and in the solubilities of the radical in the aqueous phase. At higher temperatures above 46 °C, it is conceivable that the increase in the temperature could cause a linewidth decrease in the high-field line. This indicates that the narrowing due to the faster exchange rate between the two environments probably dominates in this temperature range. The most likely explanation is that the micelle would become less rigid as a result of the increased flexibility of the alkyl chains and that the above-mentioned packing restrictions would become less important, finally leading to a disruption of the micelles.

We are gratefully indebted to Professor Hiroshi Kato for his very generous hospitality and invaluable advice during the synthesis of di-*t*-butyl nitroxide.

References

1) A. S. Waggoner, O. H. Griffith, and C. R. Christensen, *Proc. Natl. Acad. Sci.*, **57**, 1198 (1967).
2) W. L. Hubbel and H. M. McConnell, *Proc. Natl. Acad. Sci.*, **61**, 12 (1968).
3) J. Oakes, *J. Chem. Soc., Faraday Trans. 2*, **68**, 1464 (1972).
4) N. M. Atherton and S. J. Strach, *J. Chem. Soc., Faraday Trans. 2*, **68**, 374 (1972).
5) N. Kornblum, R. J. Clutter, and W. J. Jones, *J. Am. Chem. Soc.*, **78**, 4003 (1956).
6) A. K. Hoffmann *et al.*, *J. Am. Chem. Soc.*, **86**, 639 (1964).
7) J. Martinie, J. Michon, and A. Rassat, *J. Am. Chem. Soc.*, **97**, 1818 (1975).
8) M. J. Povich, J. A. Mann, and A. Kawamoto, *J. Colloid Interface Sci.*, **41**, 145 (1972).

Electrochemical Behavior of Alkoxo-bridged Binuclear Copper(II) Complexes with *N,N*-Dialkyl-*N'*-(hydroxyalkyl)alkanediamine

Makoto AIHARA,* Yoshiko KUBO, Yuzo NISHIDA,† and Sigeo KIDA†

Faculty of Home Life Science, Fukuoka Women's University, Higashi-ku, Fukuoka 813

†*Faculty of Science, Kyushu University, Higashi-ku, Fukuoka 812*

(Received August 11, 1980)

Synopsis. The alkoxo-bridged binuclear copper(II) complexes with *N,N*-dialkyl-*N'*-(hydroxyalkyl)alkanediamine were investigated by electrochemical methods. The binuclear complexes exhibited two non-separable sequential, one-electron steps, the half-wave potentials of which were almost identical, in *N,N*-dimethylformamide. On the other hand, the complexes gave two distinctive one-electron reduction waves in acetonitrile.

Recently electrochemical investigations of binuclear copper(II) compounds have continued to increase. One of the interests in this field is the properties of the particular proteins in which a pair of copper(II) ions is strongly anti-ferromagnetically coupled.[1] The copper atoms bound in such proteins are referred to as type III coppers. Binuclear metal nuclei in proteins usually undergo two-electron reduction in one step. A tentative series of intermediates during the reduction has been proposed.[2] Synthetic binuclear copper(II) complexes exhibit either a one-electron reduction step[3–5] or a two-electron reduction step.[6–8]

The present report deals with the electrochemical behavior of the alkoxo-bridged binuclear copper(II) complexes with *N,N*-dialkyl-*N'*-(hydroxyalkyl)alkanediamine, $[Cu(R_2N(CH_2)_3NH(CH_2)_2O)]X$ (abbreviated hereafter as [Cu(R-3-2)]X, R=H, CH_3, C_2H_5 and $X=ClO_4^-$ or $B(C_6H_5)_4^-$) in non-aqueous solvents. A schematic structure of the complexes studied is illustrated in Fig. 1.

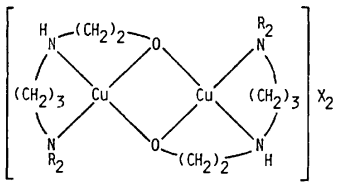

Fig. 1. Structure of the complexes of the [Cu(R-3-2)]X type.

Experimental

Synthesis of the Complexes: The complexes were prepared according to the method reported previously.[9]

Electrochemical Measurements: All measurements were carried out in an 0.1 M tetraethylammonium perchlorate (TEAP) solution of *N,N*-dimethylformamide (DMF) or acetonitrile (AN) at 25±0.1 °C. A Fuso model 312 polarograph and a DME (or HMDE) were employed for polarographic and cyclic voltammetric measurements. The reference electrode was SCE with a salt bridge.[10] Controlled-potential electrolysis was performed at a mercury pool under stirring. ESR controlled-potential electrolysis experiments were carried out under an atmosphere of nitrogen gas. The other apparatus was the same as described previously.[10]

Results and Discussion

The typical current-sampled dc polarogram for the binuclear copper(II) complex with the $[Cu(C_2H_5\text{-}3\text{-}2)]X$ formula in DMF is shown in Fig. 2. The second wave for the binuclear complex with the [Cu(H-3-2)]X type formula was observed at more negative regions (*ca.* −1.0 V *vs.* SCE) of potential, while the maxima were observed on the shoulder of the second waves for the binuclear complexes with $[Cu(C_2H_5\text{-}3\text{-}2)]X$ or $[Cu(CH_3\text{-}3\text{-}2)]X$ type formula. A detailed discussion of these waves, however, is omitted here.

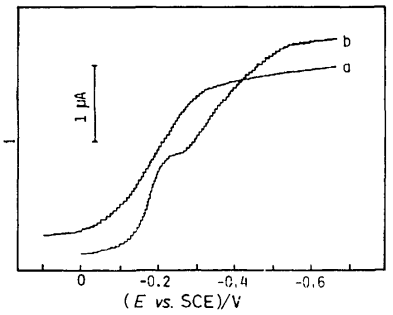

Fig. 2. Current-sampled d.c. polarograms of 0.5 mM $[Cu(C_2H_5\text{-}3\text{-}2)]X$ in DMF (curve a) and AN (curve b).

Table 1. Polarographic data for [Cu(R-3-2)]X in 0.1 M TEAP-solvent at 25 °C

	$E_{1/2}$ *vs.* SCE / V	I_d / μA	Slope / mV	$n^{a)}$
In DMF				
[Cu(H-3-2)]X	−0.498	1.20	62	2.0
$[Cu(CH_3\text{-}3\text{-}2)]X$	−0.327	1.70	79	2.0
$[Cu(C_2H_5\text{-}3\text{-}2)]X$	−0.212	1.50	110	1.9
In AN				
[Cu(H-3-2)]X	−0.560	2.04	116	2.1
$[Cu(CH_3\text{-}3\text{-}2\text{-})]X$	−0.237[b)]	0.73	*ca.* 50	
	−0.452[c)]	1.05	117	2.1
$[Cu(C_2H_5\text{-}3\text{-}2)]X$	−0.166[b)]	0.96	*ca.* 50	
	−0.364[c)]	1.23	116	2.0

a) These values for *n* were determined by controlledpotential electrolysis at −0.7 V *vs.* SCE. b) First wave. c) Second wave.

The limiting current of each of the first steps was found to be diffusion-controlled. Table 1 gives the results obtained.

The typical cyclic voltammogram for the binuclear complex with the $[Cu(C_2H_5\text{-}3\text{-}2)]X$ formula in DMF is shown in Fig. 3. The peak currents on the cathodic and anodic branches are nearly equal to each other, implying a reversible redox process, whereas the value of potential difference between the two redox peaks is larger than that (42 mV)[8] of the difference theoretically expected for the reversible two-electron redox step, suggesting a quasi-reversible one.

Constant potential electrolysis was performed at a fixed potential regions more negative than those of the first waves. The results of electrolysis showed the consumption of two electrons for each complex molecule, as summarized in Table 1, suggesting that this process is a two-electron reduction. On electrolytic reduction,

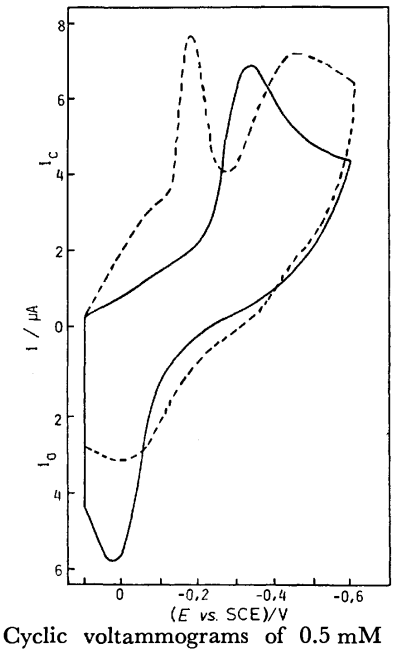

Fig. 3. Cyclic voltammograms of 0.5 mM [Cu(C_2H_5-3-2)]X in DMF (——) and AN (- - -) at HMDE, scan rate 200 mV.

the originally green solution became yellow. Exposure to air gradually restored the green color again, suggesting that chemical oxidation can take place reversibly.

The first waves observed in DMF for the binuclear complexes with the [Cu(CH_3-3-2)]X or [Cu(C_2H_5-3-2)]-X formula were found to split into two steps in AN as shown in Fig. 2. Differential pulse polarograms also showed two cathodic peak splittings.

The typical cyclic voltammogram of the binuclear complex with the [Cu(C_2H_5-3-2)]X formula in AN is shown in Fig. 3. The two peaks on the cathodic branch were clearly separated from each other, while those on the anodic one were not, suggesting an irreversible anodic process. Therefore, it was concluded that the chemical oxidation takes place reversibly, while the anodic oxidation cannot be followed due to the extremely rapid progress of the former even in a stream of nitrogen. The polarographic data are given in Table 1. Reduction of 1 mM [Cu(R-3-2)]X in AN solution at −0.7 V *vs.* SCE consumes two electrons per a complex molecule. The controlled-potential electrolysis at the potential region of the first wave in AN could not give any data available for the determination of number of electrons transferred because of a non-separable character of the first and the second waves, suggesting that no stable intermediate can exist. That is, the reduction product which had been prepared from the copper(II) complexes through the cathodic reduction did not show any anodic peak on the cyclic voltammogram. On the contrary, the reduced binuclear complexes with [Cu-(C_2H_5-3-2)]X formula in AN showed four-line ESR patterns as shown in Fig. 4. These four-line patterns obtained for the frozen solution suggest the location of odd electrons on a single copper nucleus on the ESR time scale.

Voltammetric results in DMF showed that the three complexes undergo two sequential, one-electron reduction steps in which the reduction potentials of both

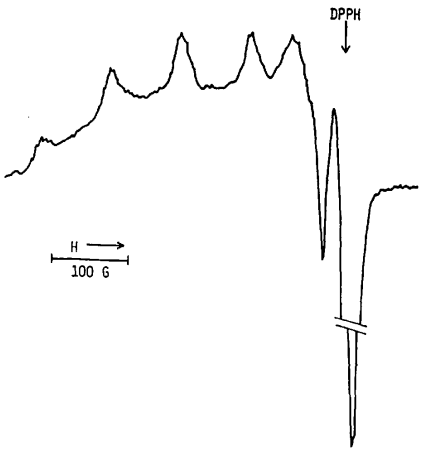

Fig. 4. ESR spectrum obtained for the frozen reduction product of the [Cu(C_2H_5-3-2)]X complex in AN, which was prepared by the controlled-potential electrolysis at −0.25 V *vs.* SCE.

steps are almost identical. The reduction process was quasi-reversible and the replacement of R by ethyl group caused a shift of the reduction potential of the first wave toward a more negative value.

On the other hand, voltammetric results in AN, coupled with those of ESR, showed two one-electron reduction steps occurring at different potentials as follows: Cu(II)-Cu(II)→Cu(II)-Cu(I)→Cu(I)-Cu(I). The solvation of AN may contribute to the formation of a "super complex" with a stable moiety of the Cu(II)-Cu(I) complex. The reduction potential of these complexes shift to a more positive direction of potential in order H-$<$ CH_3-$<$ C_2H_5-. The replacement of the *N*-substituent causes the sterical geometry of the complex to alter and simultaneously brings about the changes in properties of releasing electrons.

So far the effect of donor atoms on the standard redox potential of the coplanar Cu(II) complexes has been discussed and the order of positively-increasing redox potential of Cu(II)/Cu(I) couple was found to be $N_4$$<$$N_2O_2$$<$$N_2S_2$ donor sets.[7] The redox potential, E^0, of Cu(II)/Cu(I) couple for the binuclear complex with the [Cu(C_2H_5-3-2)]X formula in DMF was found to be −0.04 V *vs.* NHE, which was more positive than values of the Cu(II)/Cu(I) couple for the other synthetic complexes found in Ref. 7.

References

1) J. A. Fee, *Struct. Bonding (Berlin)*, **23**, 1 (1975).
2) R. Aasa, R. Branden, J. Deinum, B. G. Malmstrom, B. Beinhammer, and T. Vanngard, *Biochem. Biophys. Res. Commum.*, **70**, 1204 (1976).
3) P. J. M. W. L. Birker and H. C. Freeman, *J. Chem. Soc., Chem. Commun.*, **1976**, 1312.
4) R. R. Gagne, C. A. Koval, and T. J. Smith, *J. Am. Chem. Soc.*, **99**, 8367 (1977).
5) A. W. Addison, *Inorg. Nucl. Chem. Lett.*, **12**, 899 (1976).
6) J. T. Spence, *Inorg. Chem.*, **7**, 2545 (1968).
7) G. S. Patterson and R. H. Holm, *Bioinorg. Chem.*, **4**, 275 (1975).
8) D. E. Fenton and R. L. Lintvedt, *J. Am. Chem. Soc.*, **100**, 6370 (1978).
9) Y. Nishida, F. Numata, and S. Kida, *Inorg. Chim. Acta*, **11**, 189 (1974).
10) S. Misumi and M. Aihara, *Talanta*, **19**, 549 (1972).

Selective Separation of Cr(VI) from Cr(III) in Seawater by Cobalt-1-pyrrolidinecarboditioate Coprecipitation Method

Kitao FUJIWARA,* Shozo TODA,† and Keiichiro FUWA

Department of Chemistry Faculty of Science, The University of Tokyo, Hongo, Bunkyo-ku, Tokyo 113
†*Department of Agricultural Chemistry, Faculty of Agriculture, The University of Tokyo, Yayoi, Bunkyo-ku, Tokyo 113*

(Received November 28, 1980)

Synopsis. Specific coprecipitation of Cr(VI) in artificial seawater with Co(II)–APDC complex was investigated. The maximum recovery by coprecipitation was 60.6± 4.54% at pH 2 in which Cr(III) was completely separated from Cr(VI).

Historically, determination of Cr(VI)/Cr(III) ratio in seawater is one of the most important subjects, in chemical oceanography. From pure thermodynamic calculation, the amount of Cr(VI) is expected to be over 10^9 times more than that of Cr(III).[1,2] This means almost all chromium will exist in the Cr(VI) state. However, even under oxidative conditions, appreciable amount of Cr(III)[3,4] can be found in seawater. This discrepancy between the thermodynamic calculation and the actual finding of the Cr(VI)/Cr(III) ratio was sometimes explained in terms of the reduction of Cr(VI) by organic substances coexistent in the seawater or due to the catalytic participation of inorganic materials such as manganese nodules. On the other hand, the lack of an analytical method specific to Cr(VI) might also cause this discrepancy.

For Cr(III) ion, hydroxides of iron and zirconium have been successfully applied to seawater analysis.[4,5] Unfortunately, there is no specific method for Cr(VI) ion except solvent extraction.[5-8] However, solvent extraction might not be preferable for Cr(VI) stability because of the possibility that the use of large amount of organic solvent causes the reduction of Cr(VI), and also it is time-consuming when many samples have to be analysed.

In the present note, the coprecipitation with Co–APDC complex, which was first reported by Boyle *et al.*[9] was applied as a selective and specific method for separating Cr(VI) from seawater.

Experimental

As the chromium salts, $K_2Cr_2O_7$ and $Cr(NO_3)_3 \cdot 8H_2O$ were used. When coprecipitation was performed, the artificial seawater of 25—50 ml was taken, and 100 μl of *ammonium 1-pyrrolidinecarbodithioate* (APDC) solution (3%: ≈0.18 M) was added to the sample after adding 200 μl of cobalt solution (0.85 g $CoCl_2$-$6H_2O$/l: ≈0.3 mM). All the experiments in this paper were done with artificial seawater which was prepared according to Ref.10. Co-APDC suspension was left for about 1 h and centrifuged at 5000 $min^{-1} \times 20$ min. After drying the centrifuge tube, the precipitate was dissolved in 1 ml of 10% nitric acid solution, and chromium was determined by atomic absorption spectrometry with a carbon rod furnace (a Hitachi 170-50 atomic absorption spectrophotometer with a Jarrell-Ash FLA 100 atomizer).

Results and Discussion

The dependence of coprecipitation recovery of Cr(VI) and Cr(III) on pH of seawater is shown in Fig. 1. The values in the figure were the average of duplicate or triplicate measurements. Cr(VI) is well coprecipitated in the low pH region, being maximum at pH 1—3. When the solution was adjusted to pH 2, the recovery was 60.6±4.54% (standard deviation for nine independent coprecipitations). This value is almost constant against 0.2—10 ppb of Cr(VI) region. In the present experiment, the samples with Co–APDC suspension were left for 1 h before centrifuging. However, the recovery scarcely changed during the overnight standing of Co–APDC suspension.

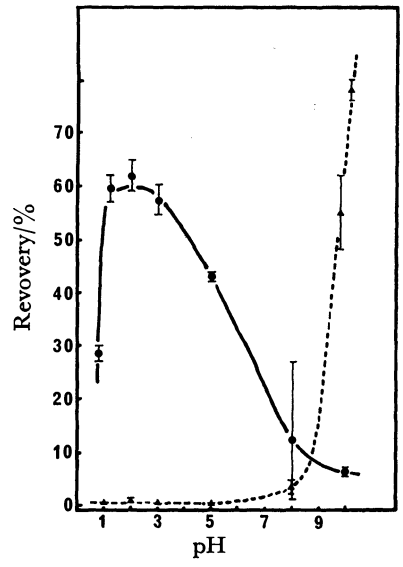

Fig. 1. Dependence of coprecipitation recovery on pH of seawater.
pH of seawater was adjusted by adding hydrochloric acid and sodium hydroxide solution. ●: Cr(VI), ▲: Cr(III).

On the other hand, the amounts of Cr(III) coprecipitated with Co–APDC are negligible at pH regions lower than 5. However, these values increase steeply above pH 9. The Cr(III) coprecipitation at low pH could be considered as contamination due to the incomplete separation of precipitate from the supernatant solution in the centrifugal process.

Figure 2 shows the effect of Cr(III) coexistence on the Cr(VI) coprecipitation. As can be seen in the figure, coexistence of Cr(III) up to 100 times more than Cr(VI) does not disturb the result of coprecipitation of Cr(VI) ion. Since oxidation of Cr(III) to Cr(VI) hardly proceeds in the present condition, the contamination of Cr(III) in the centrifugal separation might cause the increase of signal at the sample which contains 4000 ppm of Cr(III).

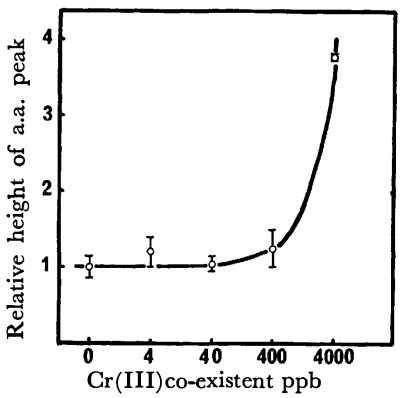

Fig. 2. The effect of Cr(III) coexistence on Cr(VI) coprecipitation.
All the solution contained 4 ppb of Cr(VI), and adjusted at pH 2.

From the present result, it has been confirmed that the cobalt 1-pyrrolidinecarbodithioate coprecipitation technique, which was first proposed for the analyses of Cu, Ni, and Cd in seawater,[9] is also effective for the selective and specific separation of Cr(VI) from seawater. Although the recovery of Co–APDC coprecipitation for Cr(VI) is only about 60%, this value is quantitative and reproducible. Therefore, the present method is a useful technique for the determination of Cr(VI) in seawater.

The authors would like to thank Prof. D. R. Kester, Univ. of Rhode Island for his suggestions concerning this work.

References

1) H. Elderfield, *Earth Planet. Sci. Lett.*, **9**, 10 (1970).
2) G. Arrhenius and E. Bonatti, "Progress in Oceanography," (1964), Vol. 3, p. 7.
3) R. Fukai, *Nature*, **213**, 901 (1967).
4) R. Cranston and J. Murray, *Anal. Chim. Acta*, **99**, 275 (1978).
5) A. Satō and N. Saitoh, *Bunseki Kagaku*, **25**, 663 (1976).
6) K. Kazuo, T. Owa, M. Takaoka, T. Tanaka, and A. Kuwahara, *Bunseki Kagaku*, **25**, 122 (1976).
7) S. Osaki, T. Osaki, S. Shibata, and Y. Takashima, *Bunseki Kagaku*, **25**, 358 (1976).
8) T. R. Gilbert and A. M. Clay, *Anal. Chim. Acta*, **67**, 289 (1973).
9) E. A. Boyle and J. M. Edmond, *Anal. Chim. Acta*, **91**, 189 (1977).
10) D. R. Kester, I. W. Duedall, D. N. Connors, and R. M. Pytkowicz, *Limnology and Oceanography*, **12**, 176 (1967).

Preparation of Sephadex Derivatives with Optically Active Groups and Column-chromatographic Application to the Resolution of Some Cobalt(III) Complexes

Miho FUJITA,* Masanobu SAKANO,† Yuzo YOSHIKAWA,† and Hideo YAMATERA†

Department of Chemistry, Nagoya City University, Mizuho-ku, Nagoya 467

†*Department of Chemistry, Faculty of Science, Nagoya University, Chikusa-ku, Nagoya 464*

(Received February 12, 1981)

Synopsis. Optically active cation-exchangers were newly prepared as Sephadex derivatives derived from L-alanine, L-valine, L-aspartic acid, and L-threonine. They were applied to the column-chromatographic resolution of some cobalt(III) complexes, partial resolution being attained.

The chromatographic method using an SP-Sephadex column has been successfully applied in the last decade to resolve optical isomers and to separate geometrical isomers of metal complexes. The method is useful for resolution, but it requires a considerable amount of optically active eluent. Direct column-chromatographic resolution without optically active eluents could be attained with use of an optically active stationary-phase. However, natural chiral substances such as quartz, starch, or lactose have been found to be unsuitable for a highly efficient resolution.

On the other hand, an ion-exchanger with optically active groups on itself could be applied to the column-chromatographic resolution of metal complexes. Two types of TA-Sephadex, TA(ET)- and TA(ES)-Sephadex, in which L-tartrate groups are linked to form ether and ester, respectively, were prepared and successfully applied to completely resolve $[Co(en)_3]^{3+}$ by column-chromatography.[1]

In the present study, a series of Sephadex derivatives with optically active cation-exchanging groups derived from L-amino acids were newly prepared and a couple of cationic and non-electrolyte complexes were chromatographed on their columns.

Experimental

Sephadex cation-exchanger with optically active groups was prepared by the following reactions:

$$\underset{\mathbf{1}}{\text{L-}H_2N\text{-}CH(R)\text{-}COOH} \xrightarrow[NaCl+NaNO_2]{1M\ HCl} Cl\text{-}CH(R)\text{-}COOH, \quad (1)$$

$$\underset{\mathbf{2}}{}$$

$$\underset{\mathbf{3}}{SD\text{-}OH} + Cl\text{-}CH(R)\text{-}COOH \xrightarrow[50\%\ NaOH]{benzene} SD\text{-}O\text{-}CH(R)\text{-}COONa, \quad (2)$$

$$\underset{\mathbf{4}}{}$$

where SD–OH (**3**) denotes Sephadex framework. The method of preparation for reaction (1) is similar to that for (*S*)(+)-2-chlorosuccinic acid from D-(−)-aspartic acid by Tosa *et al.*[2] For the reaction (2), Flodin's method of the preparation of CM-Sephadex was used with a slight modification.[3]

A typical procedure is as follows: Eighty-nine grams of L-alanine and 35 g of sodium chloride were dissolved in 900 ml of 1 M (1 M = 1 mol/dm^3) HCl by heating. To the cold solution (about 3 °C) was added 900 ml of a cold 4% $NaNO_2$ solution in small portions with stirring below 5 °C. The solution was then stirred for one day. Eight hundred milliliters of concd HCl was then added with stirring. The solution was filtered off from precipitated sodium chloride and extracted three times with ether. After concentrated extracts had been dried with anhydrous Na_2SO_4, 2-chloropropionic acid was obtained by distillation under reduced pressure: pale-yellow liquid (24 g), bp 105 °C/43 mmHg.

To the suspension of 60 g of dry Sephadex G-25 in 200 g of benzene, was added 90 g of 50% NaOH solution in small portions with stirring. Eighty-four grams of 2-chloropropionic acid was slowly poured into the mixture below 55 °C. The reaction mixture was kept standing at *ca.* 50 °C for 12 h, with constant stirring. This was filtered and washed throughly with water, methanol, and then water. This Sephadex derivative was converted into sodium form with sodium hydroxide.

The Sephadex derivative is denoted by PR-Sephadex (PR = propionate). By similar methods, three other types of Sephadex derivatives were prepared by using L-valine, L-aspartic acid, and L-threonine; they are denoted by IVA-, SU-, and HBU-Sephadex, respectively (IVA = isovalerianate, SU = succinate, and HBU = 3-hydroxybutyrate).

Five kinds of complexes were subjected to column-chromatography on each column of the Sephadex cation-exchangers prepared and CM-Sephadex (R = H, available from Pharmacia). A sodium sulfate solution was used as an eluent except for the case of *mer*-$[Co(gly)_3]$ which was eluted with water. Each 3 ml of effluent was collected and measured for the maximum absorbance of the first absorption band and for the maximum CD intensity in the corresponding region of the CD spectrum. From the results, the ratio of $\Delta\varepsilon/\varepsilon$, the apparent dissymmetric factor, was obtained for each fraction and used as a measure of resolution.

Results and Discussion

Configuration around an asymmetric carbon atom is inverted in reaction (1).[4] Thus, L-amino acids of *S*-chirality give chloro derivatives (**2**) of D-form with *R*-chirality.

Ion-exchange capacity for $[Co(en)_3]^{3+}$ of the Sephadex

Table 1. Ion-exchange capacity and column size

Sephadex derivatives	Capacity[a]	Column size
PR-Sephadex	0.91	1.8 cm × 130 cm
IVA-Sephadex	0.12	1.8 cm × 90 cm
SU-Sephadex	0.12	1.8 cm × 90 cm
HBU-Sephadex	0.53	1.8 cm × 150 cm
CM-Sephadex	1.23	1.8 cm × 130 cm

a) For $[Co(en)_3]^{3+}$ (in mmol/g).

Table 2. Apparent dissymmetric factors in the first and last fractions of elutions[a]

	PR-Sephadex	IVA-Sephadex	SU-Sephadex	HBU-Sephadex	CM-Sephadex
$[Co(en)_3]^{3+}$	—[b]	—[b]	—[b]	(+)5.8—(−)5.8 (26) (26)	(−)8.0—(+)9.2 (36) (41)
$[Co(gly)(en)_2]^{2+}$	(+)1.4—(−)2.5 (6.6) (12)	(+)0.8—(−)1.2 (3.8) (5.6)	(+)0.5—(−)0.5 (2.3) (2.3)	(+)6.0—(−)6.5 (28) (31)	(−)4.4—(+)5.5 (21) (26)
$[Co(ox)(en)_2]^{+}$	(+)2.3—(−)3.5 (9.6) (15)	(+)3.0—(−)2.9 (13) (12)	(+)2.0—(−)2.0 (8.4) (8.4)	(+)2.0—(−)3.5 (8.4) (15)	(+)11—(−)16 (46) (67)
c-$[Co(NO_2)_2(en)_2]^{+}$	—[b]	(+)2.0—(−)4.5 (11) (25)	(+)1.0—(−)1.0 (5.6) (5.6)	(+)0.8—(−)2.0 (4.5) (11)	(+)1.8—(−)2.4 (10) (14)
mer-$[Co(gly)_3]$	(−)1.6—(+)1.9	(−)3.2—(+)2.6	(−)2.2—(+)1.5	—[b]	(−)1.5—(+)1.7

a) Signs and figures denote $(\Delta\varepsilon/\varepsilon)\times 10^3$ values at the main CD peak. Figures in parentheses denote optical purity (%).
b) No significant resolution.

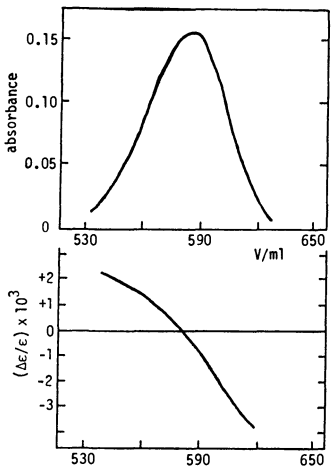

Fig. 1. The elution of $[Co(ox)(en)_2]^+$ on a PR-Sephadex column with a 0.07 M Na_2SO_4 solution.

derivatives prepared is given in Table 1 together with that of CM-Sephadex. Lower capacities of IVA- and SU-Sephadex might be attributed to lower yields of reaction (2).

The elution of $[Co(ox)(en)_2]^+$ from a PR-Sephadex column is shown as a representative example in Fig. 1. No clear-cut resolution is seen in the elution curve, but partial resolution is attained with a column of PR-Sephadex as well as other optically active Sephadex derivatives, as indicated by the change in dissymmetric factor from the top to the tail of the eluate.

The values of $\Delta\varepsilon/\varepsilon$ and optical purity in the first and the last fraction of each elution, together with the results on CM-Sephadex are summarized in Table 2. CM-Sephadex has no asymmetric centers on ion-exchange groups. Resolution with its column is, thus, due to the Sephadex skeleton which consists of dextran with a chirality similar to that of potato starch. With IVA- and SU-Sephadex, *mer*-$[Co(gly)_3]$ is resolved more efficiently than with CM-Sephadex, in spite of the fact that the ion-exchange capacities of the IVA- and SU-derivatives are only one-tenth of that of CM-Sephadex.

In the elution experiments of $[Co(gly)(en)_2]^{2+}$ with columns of Sephadex derivatives, the fast eluted enantiomer is the one with a negative CD peak. On the other hand, the enantiomer with a positive peak is eluted faster with a column of CM-Sephadex, as well as in the case of HBU-Sephadex for $[Co(en)_3]^{3+}$. Thus, optically active ion-exchanging groups on the Sephadex derivatives contribute to the resolution of the complexes. However, stereoselectivity for the complexes is opposite to that of Sephadex itself and the effect of optically active ion-exchanging groups for resolution is partially cancelled by the effect of the Sephadex skeleton.

References

1) M. Fujita, Y. Yoshikawa, and H. Yamatera, *Chem. Lett.*, **1974**, 1515; **1975**, 473; *J. Chem. Soc., Chem. Commun.*, **1975**, 941.

2) T. Tosa, T. Sato, R. Sano, K. Yamamoto, Y. Matuo, and I. Chibata, *Biochim. Biophys. Acta*, **334**, 1 (1970).

3) P. Flodin, "Dextran Gels and their Application in Gel Filteration," Pharmacia, Uppsala, Sweden (1962).

4) T. Kristiansen, M. Einarsson, L. Sundberg, and J. Porath, *FEBS Lett.*, **7**, 294 (1970).

Photochemical Nucleophilic Substitution Reactions of Methyl Substituted Derivatives of *p*- and *o*-Nitroanisole[1)]

Masaki SAWAURA and Toshio MUKAI*

Department of Chemistry, Faculty of Science, Tohoku University, Aoba, Aramaki, Sendai 980

(Received September 29, 1980)

Synopsis. Photosubstitution reactions of several methyl substituted derivatives of *p*- and *o*-nitroanisole with hydroxide ion were investigated. The methyl substituent seemed to show an uncertain (probably electronic) effect in addition to the steric effect for the replacement of both the methoxy and the nitro groups. Mainly, the replacement reaction of the nitro group is discussed.

It is well known that aromatic nucleophilic substitution reactions take place differently in the ground state and in the excited state.[2)] Theoretical calculations[3)] support the sharp contrast between them.[4)] In the photosubstitution reaction of *m*-nitroanisole with hydroxide ion, *m*-nitrophenol was produced as a single product as was expected from the orientation rule that the nitro group activates the replacement at the meta-position.[5)] However, with *o*- and *p*-nitroanisoles the meta-orientation rule is not useful for the prediction of the product. For instance, Letsinger[6)] and Havinga[7)] independently studied the photosubstitution reactions of *p*- and *o*-nitroanisoles (**1** and **5**) with hydroxide ion and obtained *p*- and *o*-methoxyphenols (**1b** and **5b**) in addition to *p*- and *o*-nitrophenols (**1a** and **5a**). The formation of **1b** and **5b** could be explained by the orientation rule that the methoxyl group activates at the *o*- and *p*-positions.[7)] However, it has not been rationalized why methoxyl group at para or ortho positions of the nitro group is replaced and why the product ratios (**1a**/**1b** and **5a**/**5b**) are inverted in the *o*- and *p*-isomers (see Table 1). Dudell's study on the flash photolysis of **1** and **5** showed that **1a** and **5a** were formed from the triplet states,[8)] but no clear explanation has been made on the reaction machanism. In order to gain an insight into the reaction mechanism, we studied the methyl substituent-effect on the replacement of the nitro- and the methoxyl group in the derivatives, **2**—**4** and **6**—**8**, with hydroxide ion. An expectation is that the ortho-substituted methyl group should supress more effectively the π-π^* excitation than the n-π^* excitation of the nitro group, thus resulting in decrease in the replacement of the methoxyl group.

Results and Discussion

The methyl substituent-effect on the photosubstitution reactions of **1**—**8** is discussed on the basis of the quantum yields shown in Table 1. The introduction of a methyl group at a position next to the nitro group, as in **2** and **6**, resulted in a great retardation of the replacement of both the methoxyl and the nitro groups. Neither **2b** nor **6b** were detected and **2a** and **6a** were formed only in poor yields. Decrease in the reactivity of **2** and **6** is clearly to be ascribed to the steric effect of the methyl group that inhibits the coplanarity of the nitro group and the phenyl moiety (see the UV spectra).[9)] The methyl group also prevents the attack of hydroxide ion to the nitro group. In addition to these effects, the photo-valence isomerization between the nitro-form (**9**) and the aci-form (**10**) should become a main decay process in the excited state of **2** and **6**. When **2** was irradiated in dioxane containing deuterium oxide, incorporation of deuterium was found to take place in the methyl group.

With **3** and **7**, the introduction of the neighboring methyl group led to the rapid formation of **3a** and **7a**.

Table 1. Quantum yields[a)] for the depletion of the reactants (**1**—**8**) and for the formation of the products (**1a**, **1b**—**8a**, **8b**)

REACTANT(-Φ)		PRODUCTS(Φ)			
1	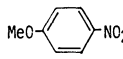 (0.111)	1a	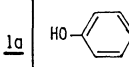 (0.020)	1b	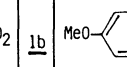 (0.091)
2	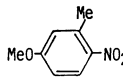 (0.005)	2a	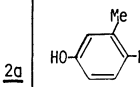 (0.005)	2b	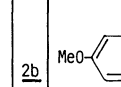 (0.000)
3	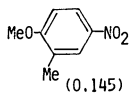 (0.145)	3a	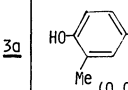 (0.056)	3b	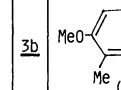 (0.089)
4	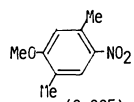 (0.005)	4a	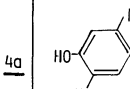 (0.003)	4b	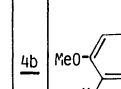 (0.002)
5	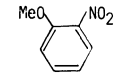 (0.028)	5a	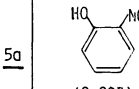 (0.022)	5b	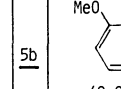 (0.006)
6	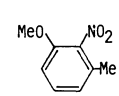 (0.003)	6a	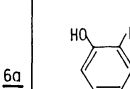 (0.003)	6b	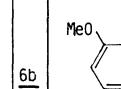 (0.000)
7	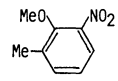 (0.044)	7a	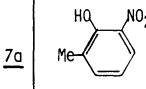 (0.044)	7b	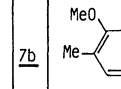 (0.000)
8	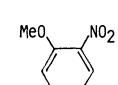 (0.008)	8a	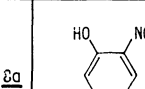 (0.004)	8b	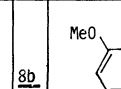 (0.004)

a) The quantum yields during the initial stage (less than 5 min) of the substitution reactionsare shown here. Side reactions appeared after prolonged irradiation.

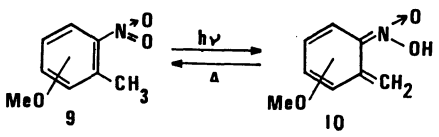

Compared with **1** and **5** the more sterically hindered methoxyl group was replaced more easily by hydroxide ion. This can be rationalized by the stabilization of the excited states, **3E** and **7E**, by the methyl substituent meta to the nitro group as shown in the following scheme.[11]

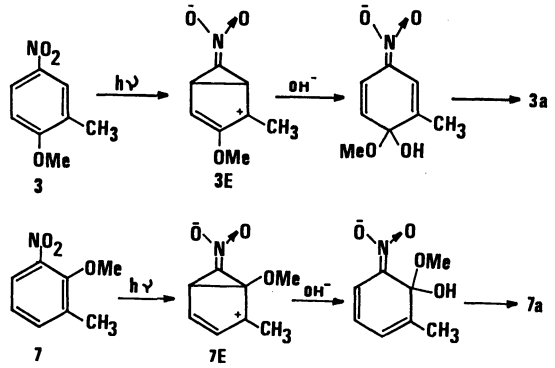

Contrary to this, the replacement of the nitro group in **3** and **7** seemed to be retarded very little by the methyl group located ortho to the methoxyl group.

The substitution reaction of 5-methyl-2-nitroanisole (**8**) was found to occur at a slow rate, even though the methyl group is not present at the positions next to the nitro and the methoxyl groups. The formation of **8b** was not affected by the methyl substituent, but that of **8b** was retarded compared to the formation of **5a**. However, this retardation could not be accounted for by the methyl substitution present.[12] Thus, it can be concluded that the methyl group enhances the replacement of the ortho-substituted methoxyl group in *m*-nitrotoluene derivatives such as **3** and **7**, but it retards the replacement of the para- or ortho-substituted methoxyl group in *o*- and *p*-nitrotoluene derivatives **2**, **6**, and **8**.

In the photosubstitution reaction of 2,5-dimethyl-4-nitroanisole (**4**), products **4a** and **4b** were obtained in poor yields. It is difficult to predict how methyl groups affect the substitution reaction of **4**, but the effect of the methyl group ortho to the nitro group seems to be stronger than that of the methyl group meta to the nitro group.

Experimental

Materials. Methyl derivatives of nitroanisole were prepared according to the literature[13–16] and identified by their mp and spectral data.

Measurements. A spectro-photofluoromenter Hitachi MPF-4 [xenon monochromatic light (UXL-150D)] was used as the light source for the irradiation. Absorption spectra were measured with a Hitachi 340 spectrophotometer. The quantum yields were obtained by using the potassium tris-oxalatoferrate(III) chemical actoinmeter.[17] A solution (1×10^{-4} mol/dm^3) of *p*-nitroanisole (**1**) in a mixture of *t*-butyl alcohol and water (1 : 3) containing 0.2 mol/dm^3 sodium hydroxide was irradiated with monochromatic light (at 313± 20 nm) in a quartz cell under nitrogen atomsphere. The absorption maximum of *p*-nitrophenol (at 420 nm, ε=20700) was used for the reference and the quantun yield of the formation of **1a** was measured spectroscopically based on the absorption coefficient at 420 nm. The UV spectrum of this reaction mixture corresponded well with a spectrum calculated for a mixture of 82% of *p*-methoxyphenol and 18% of *p*-nitrophenol (see report by Letsinger *et al.*[6]). On the other hand, the isolation of photoproducts, **1a** and **1b**, was carried out in preparative scale experiments. The photoreactions of other derivatives (**2**—**8**) were monitored in the same way as mentioned above and the quantum yields shown in Table 1 were thus obtained.

The authors wish to thank Dr. K. Okada for his helpful discussion.

References

1) Organic Photochemistry 50. Part 49: K. Okada and T. Mukai, *J. Chem. Soc., Chem. Commun.*, **1980**, 359.

2) E. Havinga, R. O. de Jongh, and W. Dorst, *Recl. Trav. Chim. Pays-Bas*, **75**, 378 (1956).

3) D. A. de Bie and E. Havinga, *Tetrahedron*, **21**, 2359 (1965).

4) E. Havinga, R. O. de Jongh, and M. E. Kronenburg, *Helv. Chim. Acta*, **50**, 2550 (1967).

5) E. Havinga and R. O. de Jongh, *Bull. Soc. Chim. Belg.*, **71**, 803 (1962).

6) R. L. Letsinger, O. B. Ramsay, and J. H. McCain, *J. Am. Chem. Soc.*, **87**, 2945 (1965).

7) J. Cornelisse and E. Havinga, *Chem. Rev.*, **75**, 353 (1975).

8) D. A. Dudell and J. T. Richards, "Lasers in Chemistry," London (1977), p. 349.

9) The absorption maximum and coefficient of **1**, **2**, **5**, and **6** are herein cited: **1**, λ_{max}=316 nm (ε=10000), **2**, λ_{max}= 313 nm (ε=8000), **5**, λ_{max}=333 nm (ε=3500), **6**, λ_{max}= 310—350 nm (ε=650—450, sh).

10) H. Morrison and B. H. Migdalof, *J. Org. Chem.*, **30**, 3996 (1965).

11) Such a stabilization effect at a cation site by the methyl group can be found in the photoreactions of santonine and its related compounds. See. K. Schaffner, *Adv. Photochem.*, **4**, 81 (1966).

12) The methyl substituent does not affect the stability of the excited state, **8E**. Compare **8E** with **3E** and **7E**.

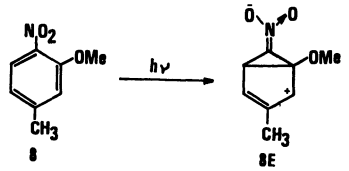

13) W. Staedel, *Ann.*, **217**. 153 (1884).

14) G. R. Allen, Jr., J. F. Poletto, and M. J. Weiss, *J. Org. Chem.*, **30**, 2897 (1965).

15) Y. Sugii and H. Shindo, *Yakugaku Zasshi*, **54**, 829 (1938).

16) K. G. Blakie and W. H. Perkin, Jr., *J. Chem. Soc.*, **1924**, 296.

17) C. G. Hatchard and C. A. Parker, *Proc. R. Soc. London, Ser. A*, **235**, 518 (1956).

Persistent Nitrogen-centered Free Radicals, *N*-(Arylthio)-3,5-di-*t*-butylphenylaminyls. Decomposition Reactions[1)]

Yozo Miura,* Akifumi Yamamoto, and Masayoshi Kinoshita

Department of Applied Chemistry, Faculty of Engineering, Osaka City University, Sumiyoshi-ku, Osaka 558

(Received November 27, 1980)

Synopsis. *N*-(4-Chlorophenylthio)-3,5-di-*t*-butylphenylaminyl was decomposed in oxygen-free benzene, and the products were examined. On the basis of the results, the decomposition mechanism of the radical is described.

In a previous report[1)] we described how *N*-(arylthio)-3,5-di-*t*-butylphenylaminyls are very persistent radicals and that they can be isolated as dimers which dissociate into the orginal radicals, even at room temperature ($K=[\text{radical}]^2[\text{dimer}]^{-1}=0.98\times10^{-4}$—$4.59\times10^{-4}$ mol l^{-1} in benzene at 27 °C). On standing in solution over a long period, however, the radicals gradually decompose. In order to elucidate the decomposition mechanism, *N*-(4-chlorophenylthio)-3,5-di-*t*-butylphenylaminyl (**1**), which is one of this family, was decomposed in oxygen-free benzene, and the products were examined. In this report the results will be described, and the decomposition mechanism of the radical will be presented.

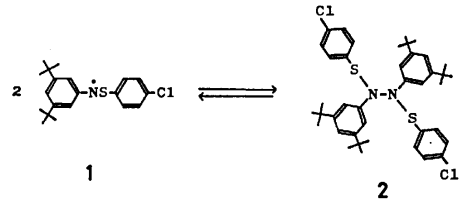

1 2

The dimer, **2**, was dissolved in 30 ml of benzene, and the resultant dark blue solution (λ_{max}: 602 nm), in which 0.498 mmol of **2** and 0.043 mmol of **1** were present,[2)] was allowed to stand under oxygen-free conditions (at ≈20 °C in the dark). After *ca.* three months, the solution turned orange, indicating the complete decomposition of **1** (and **2**). The orange solution was concentrated, and the residue was chromatographed on alumina. Elution with benzene–hexane (1 : 2) gave a mixture of five products, and the subsequent elution with benzene gave *N*-(4-chlorophenylthio)-3,5-di-*t*-butylaniline (**3**). The mixture was then run on a preparative TLC (silica gel; hexane) to give 1,3,5,7-tetra-*t*-butylphenazine (**4**), bis(4-chlorophenyl) disulfide (**5**), Product **6**, *N*,*N*-bis(4-chlorophenylthio)-3,5-di-*t*-butylaniline (**7**), and 3,3′,5,5′-tetra-*t*-butylazobenzene (**8**). The results are listed in Table 1 and the yields in the table are determined by weight. Since **3** and **5** are the known compounds, they were identified by means of the melting points and by a comparison of the IR and NMR spectra with those of authentic samples. The structures of the other products were determined by means of the IR, NMR, and mass spectra and the elemental analyses. Also, Product **7** was prepared independently by the reaction of 3,5-di-*t*-butylaniline with two equivs of 4-chlorobenzenesulfenyl chloride in the presence of triethylamine. Interestingly, the substance, on photolysis with a high-pressure mercury lamp, gave **1** effectively.

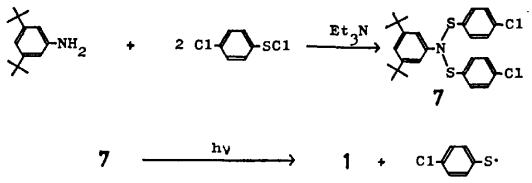

Table 1. Products of the decomposition of the dimer, **2**[a,b)]

Product	Yield mg (mmol)
3	68 (0.195)
4	34 (0.084)
5	9 (0.031)
6	18 (0.026)
7	150 (0.306)
8	49 (0.121)
Total	328

a) These data are compiled from three experiments. b) Dimer, 360 mg (0.519 mmol); benzene, 30 ml; ≈20 °C.

The major products of the decomposition are **3**,[3)] **4**, **7**, and **8**. In addition, small amounts of **5** and **6**[3)] were isolated. The sum of the products isolated is 328 mg, which corresponds to 91% of the starting material (360 mg). On the basis of the results shown in Table 1, we present a decomposition mechanism of **1** (and **2**) in Scheme 1. Product **3** is formed from **1** *via* hydrogen-atom abstractions, probably from **9** or an intermediate derived from **10** which finally gives the phenazine, **4**.

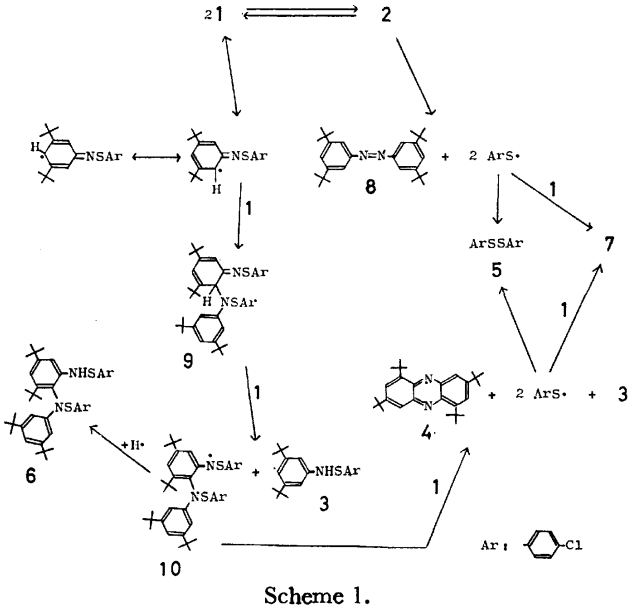

Scheme 1.

Product **7** is formed *via* the radical-coupling reaction between **1** and a thiyl radical. Also, **4** is derived from **10** with the loss of a hydrogen atom and two arylthiyl radicals, and **6** is formed from **10** *via* hydrogen-atom abstractions. On the other hand, the azo compound, **8**, is considered to be derived from the dimer, **2**, with the loss of two arylthiyl radicals. If this decomposition mechanism is reasonable, the mole quantity of **3** should be equal to twice that of **4** with respect to hydrogen atoms, and with arylthiyl radicals, the sum of the mole quantity of **5** and a half that of **7** should be equal to the sum of those of **4** and **8**. As can be seen in Table 1, these stoichiometric requirements are approximately satisfied.

Experimental

All the melting points were taken on a Yanaco Model melting-point apparatus and are uncorrected. The IR spectra were run on a JASCO Model IR-G spectrometer. The ^{1}H NMR spectra were recorded with a Hitachi Perkin Elmer R-20 spectrometer, with tetramethylsilane as the internal standard. The mass spectra were obtained on either a JEOL JMS-07 or a Hitachi M-60 mass spectrometer. The dimer, **2**[1] and 3,5-di-*t*-butylaniline[4] were obtained by the reported methods.

Decomposition of The Dimer. The dimer, **2** (360 mg, 0.519 mmol), and benzene (30 ml) were placed in a glass tube, and the solution was degassed by three freeze-pump-thaw cycles and sealed under a vacuum. On standing for three months at ≈20 °C in the dark, the dark blue solution turned orange. The solvent was evaporated under reduced pressure, and the resultant residue was subjected to column chromatograph (alumina; E. Merck Art 1097; column-size: 3×30 cm). Elution with benzene–hexane (1 : 2) gave a mixture of 1,3,5,7-tetra-*t*-butylphenazine (**4**), bis(4-chlorophenyl) disulfide (**5**), Compound **6**, *N*,*N*-bis(4-chlorophenylthio)-3,5-di-*t*-butylaniline (**7**), and 3,3′,5,5′-tetra-*t*-butylazobenzene (**8**), and elution with benzene gave *N*-(4-chlorophenylthio)-3,5-di-*t*-butylaniline (**3**) (68 mg). The mixture was then run on a preparative TLC (silica gel; E. Merek Art 7730; eluent: hexane) to give **4** (34 mg), **5** (9 mg), **6** (18 mg), **7** (150 mg), and **8** (49 mg). The products were purified by recrystallization from the appropriate solvents or sublimation.

Product **3** was identified by means of its melting point.

Product 4. Light yellow crystals; mp>305 °C (sublimation); ^{1}H NMR ($CDCl_3$): δ 1.48 (s, *t*-Bu, 18H), 1.74 (s, *t*-Bu, 18H), 7.64—7.82 (m, aromatic, 4H); MS (20 eV), *m/e* (rel intensity), 404 (5, M^+), 389 (21), 362 (19), 348 (29), 347 (94), 305 (20), 158 (40), 141 (20), 127 (26), 113 (33), 99 (42), 85 (94), 71 (100), 57 (90). Found: C, 82.63; H, 10.04; N, 6.80%. Calcd for $C_{28}H_{40}N_2$: C, 83.11; H, 9.97; N, 6.92%.

Product 6. Colorless plates; mp 167—168 °C (ethanol); IR (KBr): 3400 (NH), 2950—2850 cm^{-1} (CH); ^{1}H NMR ($CDCl_3$): δ 1.24, 1.27, and 1.30 (s, *t*-Bu, 36H), 4.97 (s, NH, 1H), 6.70—7.54 (m, aromatic, 13H); MS (30 eV), *m/e* (rel intensity), 694 (6, M^++2), 692 (6, M^+), 551 (27), 550 (25), 549 (27), 408 (16), 405 (19), 350 (59), 349 (100), 347 (42), 291 (19). Found: C, 69.11; H, 7.16; N, 4.31; Cl, 10.50; S, 9.21%. Calcd for $C_{40}H_{50}Cl_2N_2S_2$: C, 69.24; H, 7.26; N, 4.04; Cl, 10.22; S, 9.24%.

Product 7. Colorless plates; mp 119—121°C(methanol); ^{1}H NMR ($CDCl_3$): δ 1.24 (s, *t*-Bu, 18H), 6.93—7.33 (m, aromatic, 11H); MS (20 eV), *m/e* (rel intensity), 489 (5, M^+), 406 (13), 349 (21), 348 (19), 347 (63), 332 (15), 311 (27), 290 (16), 288 (75), 287 (15), 286 (100), 205 (17), 204 (15), 189 (38), 144 (38), 143 (41). Found: C, 63.33; H, 5.85; N, 2.81%. Calcd for $C_{26}H_{29}Cl_2NS_2$: C, 63.66; H, 5.96; N, 2.86%.

Product 8. Orange crystals; mp 210—212 °C (methanol); ^{1}H NMR ($CDCl_3$): δ 1.39 (s, *t*-Bu, 36H), 7.48—7.72 (m, aromatic, 6H); MS (75 eV), *m/e* (rel intensity), 406 (18, M^+), 363 (8), 190 (17), 189 (100), 147 (9), 133 (24), 91 (9), 57 (92). Found: C, 82.65; H, 10.88; N, 7.12%. Calcd for $C_{28}H_{42}N_2$: C, 82.70; H, 10.41; N, 6.89%.

Product **3** was identified by the melting point [148—150 °C (hexane), lit,[1] 150—151 °C] and its IR and NMR spectra, and Product **5**, by means of its IR spectrum.

Preparation of 7. 4-Chlorobenzenesulfenyl chloride, prepared by the treatment of 4-chlorobenzenethiol (1.72 g, 11.9 mmol) with chlorine in dry chloroform at 0—5 °C, was dissolved in 50 ml of dry ether, and the solution was added, drop by drop, to a stirred solution of 3,5-di-*t*-butylaniline (1.09 g, 5.32 mmol) and triethylamine (1.3 g, 13 mmol) in dry ether (200 ml) at 0—5 °C. After being stirred for 2 h at the same temperature, the reaction mixture was filtered, concentrated, and the residue was recrystallized from methanol to give colorless plates (119—120 °C) in a 17% yield (0.22 g).

References

1) Part 15 in the series: "ESR Studies of Nitrogen-Centered Free Radicals." For Part 14, see: Y. Miura, A, Yamamoto, Y. Katsura, and M. Kinoshita, *J. Org. Chem.*, **45**, 3875 (1980).

2) These values are derived from the equilibrium constant (K) at 20 °C (1.22×10^{-4} mol l^{-1}).

3) These products, like the other products, showed no detectable decomposition on standing in benzene at 20 °C for 2 months.

4) N. L. Allinger, H. M. Blatter, L. A. Freiberg, and F. M. Karkowski, *J. Am. Chem. Soc.*, **88**, 2999 (1966).

N-Sulfonylaminyls. The Isolation of Dimers and Their Properties[1)]

Yozo Miura,* Yuji Nakamura, and Masayoshi Kinoshita
Department of Applied Chemistry, Faculty of Engineering, Osaka City University, Sumiyoshi-ku, Osaka 558

(Received January 9, 1981)

Synopsis. From the reaction mixtures of sulfonamides [3,5-(t-Bu)$_2$C$_6$H$_3$NHSO$_2$C$_6$H$_4$CH$_3$-p and 3,5-(t-Bu)$_2$-C$_6$H$_3$NHSO$_2$CH$_3$] with di-t-butyl diperoxyoxalate, dimers of *N*-sulfonylaminyls were isolated as pure crystals which, in solution, dissociated into the corresponding *N*-sulfonylaminyls upon heating to 60 °C.

Since *N*-sulfonylaminyls (RṄSO$_3$R′) are important intermediates in organic and photochemical reactions,[2)] the radicals have been a subject of considerable interest and have been actively investigated by means of ESR spectroscopy.[3)] We have reported the ESR spectra of *N*-sulfonyl-(3,5-di-t-butylphenyl)aminyls (**2**), which are generated by the reaction of sulfonamides **1** with di-t-butyl diperoxyoxalate.[4)] Since *N*-sulfonylaminyls are transient species, it is quite difficult to isolate them in a pure form. However, the radicals may be isolated as dimers. If the dimers are isolated, we can confirm the assignments of their ESR spectra. Also, their chemical properties are of interest in connection with the structurally related dimers, **5** and **7**.[5,6)] For this purpose, we have carefully examined the products from the reaction of **1** with di-t-butyl diperoxyoxalate and have successfully isolated *N*-sulfonylaminyl dimers, **3**, in moderate yields. This is the first isolation of *N*-sulfonylaminyl dimers.[7)] In this report we will describe the isolation of **3** and their chemical properties.

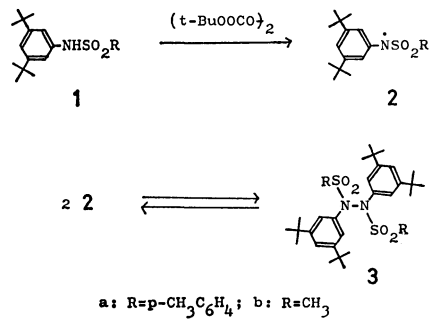

In the general procedure, an oxygen-free benzene solution of **1** and di-t-butyl diperoxyoxalate (excess) was allowed to stand for 3 d at room temperature, after which the reaction mixture was concentrated and chromatographed on silica gel, using benzene as the eluent. The second band was collected and the solvent was evaporated to give crude **3** in 17—23% yields; this was then recrystallized from hexane: colorless crystals; yield, 12—17%. In the IR spectra of the crystals, no N–H absorptions were found, and the NMR spectra and the elemental analyses were satisfactrily consistent with the structures of **3**. Also, in the mass spectra, the peaks corresponding to ions of M$^+$+1—SO$_2$C$_6$H$_4$CH$_3$ (for **3a**) and M$^+$—SO$_2$CH$_3$ (for **3b**) were found, though molecular-ion peaks could not be detected. Thus, we identified the crystals as **3** dimers.

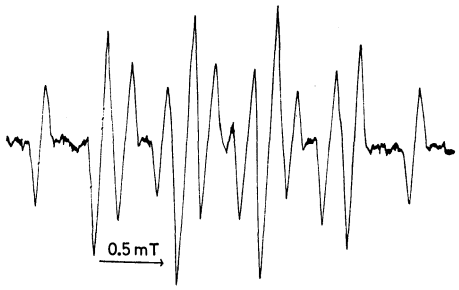

Fig. 1. ESR spectrum of **2b** detected from the solution of **3b** in benzene at 60 °C.

The dimers are highly soluble in most organic solvents, such as benzene, hexane, alcohols, and tetrahydrofuran, and the dimer solutions show no ESR signals. Thus, the dimers were found not to dissociate into **2** at room temperature. However, upon heating to 60 °C in benzene, the dimer solutions gave a relatively strong and clean ESR signal due to **2**, as is illustrated in Fig. 1; this finding clearly indicates that the dimer dissociate in part into **2** at this temperature. The assignments of the signals were based on their ESR parameters: a_N: 0.78; $a_{o\text{-}H}$: 0.56; $a_{p\text{-}H}$: 0.76 mT for **2a** and a_N: 0.77; $a_{o\text{-}H}$: 0.56; $a_{p\text{-}H}$: 0.77 mT for **2b**. These values are in good agreement with the previously reported values.[8)]

The equilibrium constants ([radical]^2[dimer]$^{-1}$) for the equilibria, however, are very small, even at 60 °C (probably$<10^{-9}$ mol l^{-1}). Also, upon heating at 60 °C in benzene for 2 h, trace amounts of the dimers were indicated by TLC analysis to decompose.

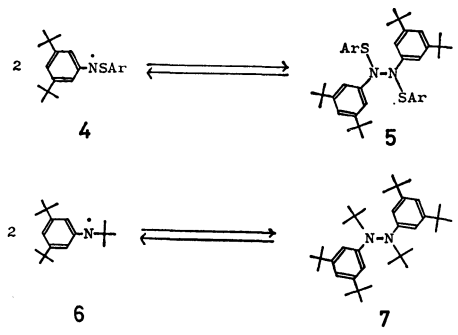

It is of interest to compare the equilibrium constants obtained for **3** with those reported for **5** and **7**. The reported values are 0.98×10^{-4}—4.59×10^{-4} mol l^{-1} for **5** (in benzene at 27 °C) and 6.00×10^{-6} mol l^{-1} for **7** (in methylcyclohexane at 44.7 °C). Thus, the magnitudes of the equilibrium constants of these dimers decrease in the following order: **5**>**7**>**3**. That is, when Y in **8** is an electron-donating group, –SR (dimers **5**). the equilibrium constants are remarkably increased, while when Y is an electron-withdrawing group,

$-SO_2R$ (dimers **3**), the equilibrium constants are, on the contrary, decreased. These changes in the magnitudes of the equilibrium constants may be reasonably interpreted as follows: in the case of **5**, the great electron-donating character of the –SR group enhances the dipolar repulsion between the nitrogen atoms, leading to a weakening of the nitrogen-nitrogen bond in **5**. In contrast, in the case of **3**, the electron-withdrawing character of the $-SO_2R$ group weakens the dipolar repulsion between the nitrogen atoms, leading to a strengthening of the nitrogen-nitrogen bond in **3**.

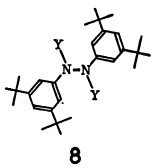

8

Experimental

All the melting points were taken on a Yanaco Model MP melting-point apparatus and are uncorrected, The IR spectra were run on a JASCO Model IR-G spectrometer, while the ^1H NMR spectra were recorded with a JEOL PS-100 spectrometer, with tetramethylsilane as the internal standard. The mass spectra were obtained on either a JEOL JMS-D-300 (for **3a**) or a Hitachi M-60 mass spectrometer (for **3b**). The ESR spectra were recorded with a JEOL JES-ME-3X spectrometer equipped with an X-band microwave unit and 100 kHz field modulation. The temperature was controlled with a JEOL JES-VT-3A temperature controller. The field sweep was calibrated by using a JEOL Mn^{2+} reference sample. *N*-(3,5-Di-*t*-butylphenyl)-*p*-toluenesulfonamide (**1a**) and *N*-(3,5-di-*t*-butylphenyl)methanesulfonamide (**1b**) were prepared by the previously reported method,[4] and di-*t*-butyl diperoxyoxalate was obtained according to Bartlett's method.[9]

N,N'-Bis(3,5-di-t-butylphenyl)-N,N'-bis(p-tolylsulfonyl)hydrazine (3a).[10] Sulfonamide **1a** (500 mg, 1.39 mmol), di-*t*-butyl diperoxyoxalate (500 mg, 2.13 mmol), and benzene (10 ml) were placed in a glass tube (1.5×40 cm), and the mixture was degassed by three freeze-pump-thaw cycles and then sealed under a vacuum. After the sealed tube had been allowed to stand for 3 d at room temperature (≈20 °C), the benzene solution was washed twice with a 10% $Na_2S_2O_3$ aqueous solution and twice with water, and then dried over anhydrous $MgSO_4$. After filtration, the solvent was evaporated under reduced pressure, and the residue was chromatographed on a silica-gel column (Mallinckrodt 100 mesh; column size: 3×50 cm), using benzene as the eluent. The second band was collected, and the solvent was evaporated to give 87 mg of crude **3a** (17%), which was afterward recrystallized from hexane to afford 61 mg of prisms (12%); mp 131—132 °C; (KBr): 2950—2850 (CH), 1160 cm^{-1} (SO_2); ^1H NMR (CCl_4) δ 1.20 (s, *t*-Bu, 36H), 2.42 (s, CH_3, 6H), 7.14—7.86 (m, aromatic, 14H); MS (70 eV), *m/e* (rel intensity), 562 ($M^+ + 1 - CH_3C_6H_4SO_2$, 6), 407 (10), 361 (20), 359 (100), 345 (24), 344 (98), 204 (42), 190 (20), 148 (20), 133 (44), 57 (37). Found: C, 70.71; H. 7.91; N, 3.74%. Calcd for $C_{42}H_{56}N_2O_4S_2$: C, 70.35; H, 7.87; N, 3.91%.

N,N'-Bis(3,5-di-t-butylphenyl)-N,N'-(methylsulfonyl)hydrazine (3b).[10] The hydrazine was prepared in a similar manner. Sulfonamide **1b** (400 mg, 1.41 mmol), di-*t*-butyl diperoxyxalate (500 mg, 2.13 mmol), and benzene (10 ml) were placed in a glass tube, degassed, and sealed as has been described above. After 3 d of standing at room temperature, the benzene solution was washed with a 10% $Na_2S_2O_3$ aqueous solution and then with water, and dried over anhydrous $MgSO_4$. After filtration, the solvent was evaporated, and the residue was chromatographed on silica gel as has been described above. The second band was collected, and the solvent was evaporated to give 90 mg of crude **3b** (23%), which was then recrystallized from hexane to afford 68 mg of needles (17%); mp 130.5—131.5 °C; IR (KBr): 2950—2850 (CH), 1160 cm^{-1} (SO_2); ^1H NMR (CCl_4) δ 1.32 (s, *t*-Bu, 36H), 3.14 (s, CH_3, 6H), 7.15—7.39 (m, aromatic, 6H); MS (30 eV), *m/e* (rel intensity), 486 ($M^+ + 1 - CH_3SO_2$, 22), 485 ($M^+ - CH_3SO_2$, 47), 408 (28), 407 (54), 341 (22), 284 (25), 269 (52), 190 (70), 133 (29), 57 (100). Found: C, 63.50; H, 8.46; N, 5.06%. Calcd for $C_{30}H_{48}N_2O_4S_2$: C, 63.79; H, 8.57; N, 4.96%.

Dissociation of 3. The dimer, **3** (20 mg), and benzene (0.2 ml) were placed in an ESR cell, and the solution was degassed as has been described above. The ESR spectra from the solution were recorded during heating at 60 °C.

References

1) Part 16 in the series: "ESR Studies of Nitrogen-centered Free Radicals." For Part 15, see: Y. Miura, A. Yamamoto, and M. Kinoshita, *Bull. Chem. Soc. Jpn.*, **54**, 3215 (1981).

2) For a review, see: R. S. Neale, *Synthesis*, **1971**, 1.

3) a) R. Istratoiu, I. Pascaru, and A. T. Balaban, *Z. Naturforsch., Teil B*, **28**, 543 (1973); b) G. Zomer and J. B. F. N. Engberts, *Tetrahedron Lett.*, **1977**, 3901; c) H. Teeninga and J. B. F. N. Engberts, *Recl. Trav. Chim. Pays-Bas*, **97**, 59 (1978); d) A. R. Forrester, E. M. Johansson, and R. H. Thomson, *J. Chem. Soc., Perkin Trans. I*, **1979**, 1112; e) H. Teeninga, B. Zomer, and J. B. F. N. Engberts, *J. Org. Chem.*, **44**, 4717 (1979); f) W. C. Danen and R. W. Gellert, *J. Am. Chem. Soc.*, **102**, 3264 (1980).

4) Y. Miura, Y. Nakamura, and M. Kinoshita, *Bull. Chem. Soc. Jpn.*, **51**, 947 (1978).

5) Y. Miura, A. Yamamoto, Y. Katsura, and M. Kinoshita, *J. Org. Chem.*, **45**, 3875 (1980).

6) S. F. Nelsen and R. T. Landis, *J. Am. Chem. Soc.*, **95**, 8707 (1973).

7) In Ref. 3d, the products derived from *N*-methoxy-*N*-sulfonylaminyl were carefully examined, but the radical dimer was not isolated.

8) For **2a**, a_N : 0.779; $a_{o\text{-}H}$: 0.564; $a_{p\text{-}H}$: 0.762 mT and for **2b**, a_N: 0.779; $a_{o\text{-}H}$: 0.559; $a_{p\text{-}H}$ 0.757 mT. See Ref. 4.

9) P. D. Bartlett, E. P. Benzing, and R. E. Pincock, *J. Am. Chem. Soc.*, **82**, 1762 (1960).

10) As has been pointed out in Ref. 9, it is advisable not to scrape the crystals of di-*t*-butyl diperoxyoxalate when treating them, especially when they are completely free of a solvent. Also, a large-scale experiment must be avoided in the preparation of the dimers, **3**.

Friedel-Crafts Acylation with 2-Methyl- or 2-Benzylbutanedioic Anhydride

Iwao HASHIMOTO

Department of Industrial Chemistry, Wakayama Technical College, Noshima, Nada-cho, Gobo 649-15

(Received January 8, 1981)

Synopsis. The $AlCl_3$-catalyzed acylation of benzene with 2-methylbutanedioic anhydride afforded a mixture of 3-benzoyl-2-methylpropanoic acid and 3-benzoylbutanoic acid. The intramolecular acylation of 2-benzylbutanedioic anhydride in the presence of $AlCl_3$ gave a mixture of 4-oxo-1,2,3,4-tetrahydro-2-naphthoic acid and 3-oxo-2-indanacetic acid. The results were discussed in terms of the solvent effect on the acylations.

We have previously reported[1,2] that the $AlCl_3$-catalyzed acylations of benzene with 2-phenyl-butanedioic or -pentanedioic anhydride proceeded by means of competitive inter- and intramolecular acylations, where an electron-attracting phenyl group in the anhydrides had a strong influence on the direction of each acylation. A more detailed mechanism of the acylation with unsymmetrical dibasic acid anhydrides may be get by introducing an electron-donating methyl group into the dibasic acid anhydride and by treating individually the inter- and intramolecular acylations. The present paper deals with the acylation of benzene with 2-methybutanedioic anhydride (**1**) in the presence of $AlCl_3$ as an example of the intermolecular acylation, and with the $AlCl_3$-catalyzed condensation of 2-benzylbutanedioic anhydride (**2**) as an intramolecular example.

TABLE 1. $AlCl_3$-CATALYZED ACYLATION WITH 2-METHYL- OR 2-BENZYLBUTANEDIOIC ANHYDRIDE AT 30 °C FOR 5 h

Anhydride	Solvent (20 cm)	$[AlCl_3]$ mmol	$[C_6H_6]$ mmol	Product yields[a] %	
1				**3**	**4**
	—	20	250[b]	62	39
	—	10	250[b]	28	14
	$(ClCH_2)_2$	20	10	61	34
	$(ClCH_2)_2$	10	10	14	6
	$C_6H_5NO_2$	30	10[c]	21	2
	$C_6H_5NO_2$	20	10[c]	12	1
2				**5**	**6**
	—	20	250[d]	37	63
	—	10	250[d]	28	37
	—	—[e]	250[d]	65	1
	—	—[f]	250[d]	34	66
	$(ClCH_2)_2$	20	10	34	59
	$(ClCH_2)_2$	10	10	26	35
	$(ClCH_2)_2$	20	0	32	60
	$C_6H_5NO_2$	30	10	81	5

a) Calculated on the basis of the amount of anhydride used. b) At 40 °C for 2 h. c) For 24 h. d) At 40 °C. e) Two hundred mmole of concd H_2SO_4 were used as the catalyst. f) Twenty mmol of $AlBr_3$ were used as the catalyst.

Several investigators[3,4] have isolated only 2-aroyl-2-methylpropanoic acid in the condensations of some aromatic compounds with **1** in the presence of $AlCl_3$. However, when 10 mmol of **1** was condensed in the presence of 20 mmol of $AlCl_3$ with benzene, which was used in a large excess as a reactant and as a solvent, a mixture of 3-benzoyl-2-methylpropanoic acid (**3**) and the isomeric 3-benzoylbutanoic acid (**4**) was obtained; the yield of **3** was about twice that of **4**. The predominant formation of **3** was also observed in the cases using a limited amount (10 mmol) of benzene in 1,2-dichloroethane or in nitrobenzene. The lower yield of the keto acids in nitrobenzene may be a complex formation between $AlCl_3$ and nitrobenzene. The small solvent effect on the acylation of benzene with **1** suggests that the actual acylating agent in this acylation is a type of oxonium compound (**3a** and **4a**); since they are less polarized than the acylium ions, the solvent effect on them appears smaller.

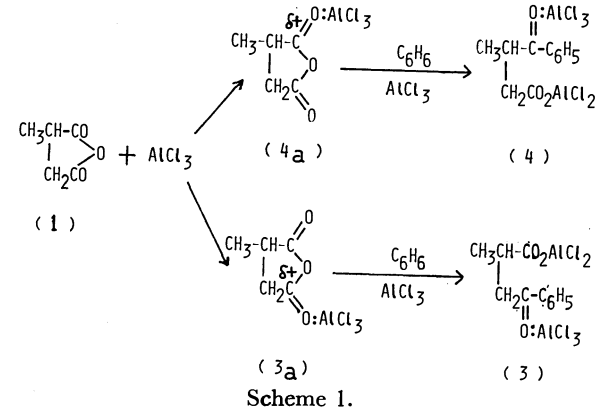

Scheme 1.

The electron-donating effect of a methyl group reduces the electrophilic reactivity of the $\overset{\delta+}{C}=O$ located closely to the methyl group; hence, the production of **3** is more favored than that of **4**.

The acylation with **2** in the presence of two equivalents of $AlCl_3$ in a large excess of benzene proceeded only intramolecularly to yield two isomeric keto acids, 4-oxo-1,2,3,4-tetrahydro-2-naphthoic acid (**5**) and 3-oxo-2-indanacetic acid (**6**), in a predominant yield, although early workers[5-8] in an analogous case succeeded in isolating only **5**. Similar results were also observed in 1,2-dichloroethane, whereas an overwhelming yield of **5** was obtained in nitrobenzene. Since the polarity of the solvent appears to affect markedly the relative yields between **5** and **6**, a reaction path including either the oxonium compounds (**5a** and **6a**) or the acylium ions (**5b** and **6b**) as the actual acylating agents may be formulated for the intramolecular acylation of **2** in the presence of $AlCl_3$.

The formation of **6a** is probably more favored than that of **5a** due to the electron-donating effect of a benzyl group,[9] although the electrophilic reactivity of $\overset{+}{C}-O$ of **5b** to a benzene nucleus may be greater than that of **6b**; a higher concentration of **6a** results in a predominant yield of **6**. On the other hand, in a polar

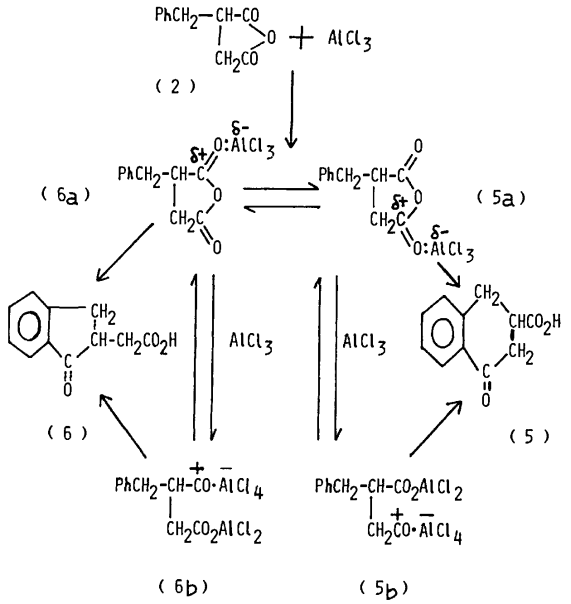

Scheme 2.

solvent such as nitrobenzene or in the presence of a large amount of concd H_2SO_4, the acylium ions bearing a more positive charge than the oxonium compounds may be greatly stabilized by solvation; therefore, a more reactive **5b** should give **5** in an overwhelming yield.

The product ratio obtained above dose not result from the thermodynamic equilibrium, since no isomerization between **5** and **6** was observed in the presence of two equivalents of $AlCl_3$ in 1,2-dichloroethane.

Experimental

Materials. 2-Methylbutanedioic anhydride: bp 238—240 °C. 2-Benzylbutanedioic anhydride was prepared by the method of Haworth *et al.*: mp 98.5 °C (lit,[7] mp 95—97 °C).

Acylation Procedures. The general procedure was as previously described.[1] A mixed solution of diethyl ether and methyl acetate was used to extract the keto acids.

Analyses of the Products. The acylation products of benzene with 2-methylbutanedioic anhydride, after being esterfied with an ethereal solution of diazomethane, were analyzed by GLC employing a Yanagimoto G-180 F model on a 1.5 m×3 mm column packed with Ucon Oil 50 LB 550 X (3 wt %) on Uniport KS of 60—80 mesh at 180 °C. GC analyses of the intramolecular acylation products of 2-benzylbutanedioic anhydride in the presence of $AlCl_3$ were made by using a column packed with Apiezon Grease L (3 wt %) at 170 °C or Ucon Oil 50 LB 550 X (3 wt %) at 171 °C. The compounds, **3**, **4** and **5**, were synthesized according to the method described in the literature: 3-benzoyl-2-methylpropanoic acid (**3**): mp 142 °C (lit,[10] mp 140.5 °C); 3-benzoylbutanoic acid (**4**): mp 55 °C (lit,[11] mp 59 °C); 4-oxo-1,2,3,4-tetrahydro-2-naphthoic acid (**5**): mp 149 °C (lit,[5] mp 149 °C).

3-Oxo-2-indanacetic Acid (**6**). A solution of 2-benzylbutanedioic anhydride (1.90 g) in benzene (12.1 cm^3) was treated with $AlBr_3$ (5.34 g) in benzene (10 cm^3) at 30 °C for 5 h. The reaction mixture was then work up in a usual manner. The crude keto acid was repeatedly recrystallyzed from acetic acid and then methyl acetate–petroleum ether: mp 150.5—151 °C; IR (KBr disk), 1750 (C=O), 1669, 1600 cm^{-1}; MS (methyl ester) *m/e* (%) 204 (M^+, 30), 173, 172 (M^+-OCH_3, 25), 145 ($M^+-COOCH_3$, 75), 131 ($M^+-CH_2COOCH_3$, 49), 116 (100); ^{1}H-NMR [$(CD_3)_2CO$] δ 7.4—7.7 (m, 4H, arom.), 3.5 (q, 1H, J=8), 3.0 (m, 2H), 2.7 (q, 2H, J=8); ^{13}C-NMR [$(CD_3)_2CO$] δ 209.0 (s, C=O), 175.5 (s, -COOH), 156.0 (s, C-9), 139.0 (s, C-4), 137.0, 129.5, 129.0 and 125.5 (d, C-arom.), 45.0 (d, C-2), 35.5 (t, $\underline{CH_2}$-COOH), 34.0 (t, C-3); Found: C, 69.43; H, 5.31%. Calcd for $C_{11}H_{10}O_3$: C, 69.46; H, 5.30%.

The author wishes to thank Professor Yoshiro Ogata, Nagoya University, for his valuable discussions.

References

1) I. Hashimoto and R. Takatsuka, *Bull. Chem. Soc. Jpn.*, **50**, 2495 (1977).
2) I. Hashimoto, *Bull. Chem. Soc. Jpn.*, **52**, 251 (1979).
3) W. Cocker, A. K. Fateen, and C. Lipman, *J. Chem. Soc.*, **1951**, 926.
4) W. Cocker and D. H. Hayes, *J. Chem. Soc.*, **1951**, 844.
5) A. J. Attwood, A. Stevenson, and J. F. Thorpe, *J. Chem. Soc.*, **123**, 1764 (1923).
6) E. L. Speight, A. Stevenson, and J. F. Thorpe, *J. Chem. Soc.*, **125**, 2185 (1924).
7) R. D. Haworth, B. Jones, and Y. M. Way, *J. Chem. Soc.*, **1943**, 10.
8) J. V. Braum, *Ber.*, **61**, 2602 (1927).
9) J. E. Leffler and E. Grunwald, "Rates and Equilibria of Organic Reactions," Wiley, New York (1963), p. 222.
10) E. R. Alexander and A. Mudrak, *J. Chem. Soc.*, **72**, 3195 (1950).
11) L. Higginbotham, A. Lapworth, and C. Simpson, *J. Chem. Soc.*, **125**, 2342 (1924).

Ring Monofluorinated Hydroxypyrazoles

Serry R. F. KAGARUKI, Tomoya KITAZUME, and Nobuo ISHIKAWA*

Department of Chemical Technology, Tokyo Institute of Technology, Ookayama, Meguro-ku, Tokyo 152

(Received January 16, 1981)

Synopsis. 3-Alkyl(or aryl)-4-fluoro-5-hydroxypyrazoles and their 1-methyl derivatives were prepared by the reaction of methyl α-fluoro-β-alkyl(or aryl)-β-keto esters with hydrazine hydrate or methylhydrazine in ethanol. The reaction of arylhydrazines with α-fluoro-β-keto esters gave only hydrazones which could not be cyclized to pyrazoles.

There has been the growing interest in utilization of some kind of monofluoro organic compounds because of their biological activities[1] and several practical methods for monofluorination of organic molecules have been developed in these days.[2] From this point of view, we have revealed that α-fluoro-β-keto esters (**1**), potent intermediates for monofluoroheterocycles, can be prepared easily from trifluoroethene or from hexafluoropropene.[3] As the first example of preparation of monofluoroheterocycles from α-fluoro-β-keto esters, we now wish to report the preparation of 3-alkyl(or aryl)-4-fluoro-5-hydroxypyrazoles by the reaction with hydrazine or with methylhydrazine. There has been no reports on pyrazole compounds carrying a fluorine atom directly attached to the ring.

β-Diketones are generally known to cyclize easily into pyrazoles by treating them with hydrazines.[4] The reactions between α-fluoro-β-keto esters with hydrazine or methylhydrazine proceeded smoothly in refluxing ethanol, and 3-alkyl(or aryl)-4-fluoro-5-hydroxypyrazoles (**2a**) were obtained as expected in good yields (Table 1).

TABLE 1. PREPARATION OF 3-ALKYL(OR ARYL)-4-FLUORO-5-HYDROXYPYRAZOLES **2a**[a]

R	R′	Yield %	Mp °C	^{19}F NMR[b] CF
Me	H	52	104—106	112
Pr	H	53	126—128	110
Ph	H	61	184—186	110
4-MeC$_6$H$_4$	H	98	205—206	110
4-ClC$_6$H$_4$	H	94	230—233	109
Me	Me	56	101—103	112.5
Pr	Me	58	123—125	111
Ph	Me	65	130—132	110
4-MeC$_6$H$_4$	Me	80	200—202	110
4-ClC$_6$H$_4$	Me	79	229—230	109
4-Me$_2$NC$_6$H$_4$	Me	58	250—252	110.5
3-MeC$_6$H$_4$	Me	52	220—221	110
4-FC$_6$H$_4$	Me	85	234—235	112

a) New compound: The structures were confirmed on the basis of their IR and NMR spectral data and the microanalysis was satisfactory agreement with the calculated value. b) Chemical shifts are given in δ ppm from ext. CF_3CO_2H in DMSO-d_6.

The structures of the fluoropyrazoles obtained was confirmed from their ^{19}F and ^{1}H NMR and mass

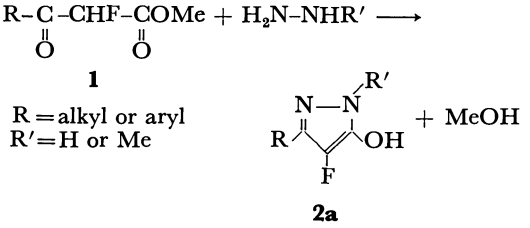

2a

spectra. The ^{19}F NMR spectra in DMSO-d_6 solution revealed only one singlet signal at about 110 ppm upfield from external CF_3CO_2H, while in the ^{1}H NMR spectra one broad signal due to the OH proton appeared at ≈δ 10 as well as the other signals due to alkyl or aryl protons. In addition, no absorption band due to a carbonyl group was observed in the spectra of these pyrazole compounds. These results suggest that these compounds prefer the hydroxypyrazole type structure to the pyrazolone type one. This may be ascribed to the hydrogen bonding formation between the oxygen atom and the fluorine atom, which stabilizes the enol form **2a** rather than the keto form **2b**.

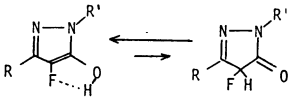

2a 2b

Arylhydrazines and tosylhydrazine, on the other hand, reacted with **1** to give only hydrazones **3** and none of cyclized compounds were obtained. This is in contrast to the case with non-fluorinated β-keto esters, which give readily pyrazolone compounds with arylhydrazines.

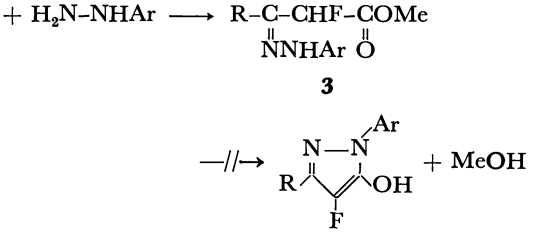

Experimental

Typical procedures are described below.

4-Fluoro-5-hydroxy-1-methyl-3-phenylpyrazole (2a) (R=Ph, R′=Me). A mixture of methyl α-fluorobenzoylacetate (1.96 g, 10 mmol), methylhydrazine (0.46 g, 10 mmol), and ethanol (5 ml) was refluxed for 3 h. On cooling the reaction mixture was filtered and the solid material was recrystallized from ethanol, affording a fluoropyrazole compound in 65% yield, mp 130—132 °C. ^{1}H NMR (DMSO-d_6) δ: 3.60 (CH_3), 7.50 (ArH), 9.87 (OH); ^{19}F NMR (DMSO-d_6) δ: 110 ppm from ext. CF_3CO_2H. Found: C, 62.86; H, 4.85; N, 14.61%. Calcd for $C_{10}H_9N_2OF$: C, 62.50; H, 4.72; N, 14.57%. M^+, 192.

2,4-Dinitrophenylhydrazone of Methyl α-Fluorobenzoylacetate. A mixture of methyl α-fluorobenzoylacetate (0.4 g, 2 mmol), 2,4-dinitrophenylhydrazine (0.42 g, 2 mmol), and concd sulfuric acid (2 ml) in ethanol (10 ml) was stirred for 24 h at room temperature. The solid material was collected by filtration and recrystallized from ethanol to give the hydrazone in 80% yield, mp 196—198 °C. IR (KBr): 3300 (NH), 1760 (C=O) cm^{-1}; ^1H NMR (DMSO-d_6) δ: 3.90 (CO_2CH_3), 6.77 (CHF, J_{H-F}=45 Hz), 7.52—9.07 (ArH), 11.87 (NH); ^{19}F NMR (DMSO-d_6) δ: 112 ppm from ext. CF_3CO_2H. Found: C, 49.29; H, 3.53; N, 15.25%. Calcd for $C_{15}H_{13}N_4O_6F$: C, 49.46; H, 3.60; N, 15.38%.

References

1) See reviews: R. Filler, "Organofluorine Chemicals and Their Industrial Applications," ed by R. E. Banks, Ellis Horwood, London (1979), p. 123; W. G. M. Jones, *ibid.*, p. 154; K. L. Kirk and L. A. Cohen, "Biochemistry Involving Carbon-Fluorine Bonds," ed by R. Filler, Am. Chem. Soc., Washington (1976), p. 23; R. W. Fuller and B. B. Molloy, *ibid.*, p. 77.

2) Review: C. M. Sharts and W. A. Sheppard, *Org, React.*, **21**, 125 (1974).

3) N. Ishikawa, A. Takaoka, H. Iwakiri, S. Kubota, and S. R. F. Kagaruki, *Chem. Lett.*, **1980**, 1107.

4) M. R. Grimmett, "Comprehensive Organic Chemistry," ed by P. G. Sammes, Pergamon Press (1979), Vol. 4, p. 400, and references cited therein.

A Product from the Photo-induced Reaction of Cholesterol in the Presence of Lead Tetraacetate and Iodine[1)]

Hiroshi SUGINOME*, ** and Kimitoshi KATO

Department of Chemistry, Faculty of Science, Hokkaido University, Sapporo 060

(Received February 3, 1981)

Synopsis. The irradiation of a benzene solution of cholesterol in the presence of lead tetraacetate and iodine gives cholest-5-en-3β-yl *A*-homo-4-oxacholest-5-en-3α-yl ether in a 23% yield.

Earlier parts of this series have described the results of the investigations of the photo- and thermally-induced rearrangements of hypoiodites of cholesterol[2)] and of the related 5-cholesten-3-ols[3)] and *C*-nor-*D*-homosteroid-5-en-3β-ols[1)] in the presence of mercury(II) oxide and iodine. Cholesterol (**1**) and epicholesterol hypoiodites in benzene have been found to give two oxabicyclic compounds, 3α,5-epoxy-6β-iodo-*A*-homo-4-oxa-5β-cholestane (**2**) and its 6α-isomer (**3**), accompanied by a moderate yield of 3-formyloxy-2-iodo-*A*-nor-2,3-seco-cholest-5-ene (**4**).[2)] The introduction of methyl groups on the C-3 or C-4 of 5-cholestene framework has been found to result in appreciable variations in the products and their yields.[3)] The pathways which explain the stereochemistry of the products and the effects of alkyl substitutions have been discussed in previous papers.[2,3)]

The reaction involved a new type of ring enlargement. The active species generated from mercury(II) oxide and iodine was believed to be iodine oxide, I_2O,[4)] which reacted with intermediary radical species to lead to the products. It is of interest to see, therefore, variations in the products caused by replacing mercury(II) oxide with other oxidizing reagents, *e.g.*, lead tetraacetate. The reaction of steroidal alcohols with lead tetraacetate and iodine reagent is also believed to proceed through hypoiodite or lead(IV) alkoxide.[5,6)]

In this paper we will report on a considerable variation in the products in this reaction when the mercury-(II) oxide and iodine reagents are replaced by lead tetraacetate and iodine.[5)]

The irradiation of cholesterol in dry benzene containing a freshly prepared lead tetraacetate and iodine through Pyrex with a 100-W high pressure mercury arc under an argon atmosphere for 5 h gave a mixture of products. The examination of the products by TLC proved the absence of any oxabicyclic compounds, **2** and **3**, and formate, **4**. It showed, however, the formation of an appreciable amount of cholest-5-en-3β-yl *A*-homo-4-oxacholest-5-en-3α-yl ether (**6**), obtained from the thermally-induced reaction of cholesterol hypoiodite in the presence of mercury(II) oxide and iodine.[2)] This ether, **6**, was isolated in a 23% yield as crystals by the aid of preparative TLC. A number of other unidentified products were also formed.

The variation in the products caused by lead tetraacetate is thus significant, but the role of the reagent which makes this difference is not certain, although the oxidation of intermediary radicals (*e.g.*, **5** in Scheme 1) to a cationic species with lead tetraacetate might play a part. A probable path *via* an allyl radical (**5**) has been suggested for the dimer **6**.[2)] Since cholesterol is the steroid most abundantly available, and since **5** is readily hydrolyzed to *A*-homo-4-oxacholest-5-en-3α-ol and cholesterol with acid,[2)] the reaction may be of use for the transformation of cholesterol into biologically useful compounds.

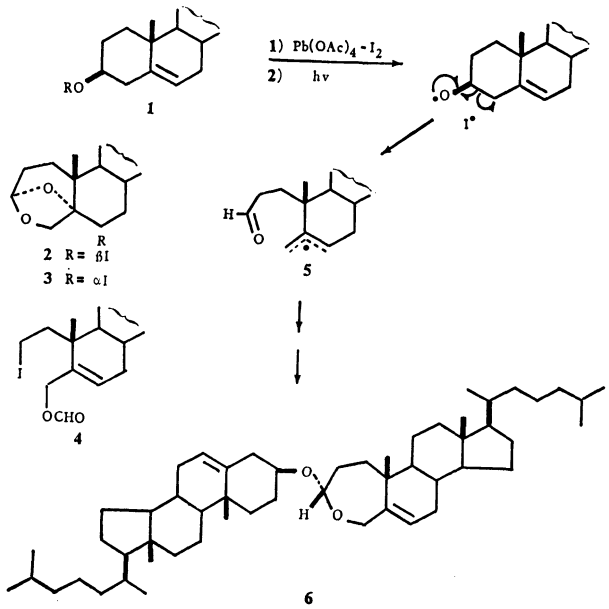

Scheme 1.

Experimental

For the instruments used and general procedures, see Ref. 2.

Irradiation of Cholesterol in Benzene Containing Lead Tetraacetate and Iodine. Cholesterol (300 mg) in benzene (44 ml) containing a freshly prepared lead tetraacetate (1.03 g) and iodine (600 mg) in a Pyrex vessel was irradiated with a 100-W high pressure mercury arc under an argon atmosphere for 5 h. The solution was then filtered, and the filtrate was washed with a sodium hydrogensulfite solution twice, a 10% sodium carbonate solution, and water successively and thereafter dried over anhydrous sodium sulfate. The evaporation of the solvent left a redidue which was subjected to preparative TLC with a mixture of 10 : 1 chloroform and acetone to give dimeric acetal, **6** (69 mg), together with a number of ill-defined products. The compound, **6**, was shown by a direct comparison to be identical with the specimen obtained from the thermal decomposition of cholesterol hypoiodite.[2)]

** Present address: Organic Chemistry Laboratory, Department of Chemical Process Engineering, Faculty of Engineering, Hokkaido University, Sapporo 060.

References

1) Photo-induced Transformations. Part 59. Previous paper in this series: H. Suginome, K. Kato, and T. Masamune, *Bull. Chem. Soc. Jpn.*, **54**, 3042 (1981).

2) H. Suginome, A. Furusaki, K. Kato, N. Maeda, and F.

Yonebayashi, *J. Chem. Soc., Perkin Trans. 1*, **1981**, 236.

3) H. Suginome and N. Maeda, *Bull. Chem. Soc. Jpn.*, **53**, 2621, 2626 (1980).

4) M. Akhtar and S. Marsh, *J. Chem. Soc., C*, **1966**, 937; C. P. Forbes, A. Goosen, and H. A. H. Laue, *J. S. African Chem. Inst.* **25**, 144 (1972); C. P. Forbes, A. Goosen, and H. A. H. Laue, *J. Chem. Soc., Perkin Trans. 1*, **1974**, 2346.

5) K. Heusler, J. Kalvoda, P. Wieland, G. Anner, and A. Wettstein, *Helv. Chim. Acta.*, **45**, 2575 (1962); J. Kalvoda, *J. Chem. Soc., Chem. Commun.*, **1970**, 1002.

6) For general reviews, see K. Heusler and J. Kalvoda, *Angew. Chem.*, **76**, 518 (1964); J. Kalvoda and K. Heusler, *Synthesis*, **1971**, 501.

The Synthesis of 2,5-Bis(*p*-methoxycinnamoyl)-1,3,4,6,7,8- and 4,5-Bis-(*p*-methoxycinnamoyl)-1,2,3,6,7,8-hexamethoxyxanthene[1)]

Heitaro OBARA,* Jun-ichi ONODERA, Takashi SAITO, Shingo SATO, Tsutomu SHIBATA, and Kimio SHIBAYAMA

Department of Applied Chemistry, Faculty of Engineering, Yamagata University, Yonezawa 992

(Received March 5, 1981)

Synopsis. In connection with studies of the structure of carthamin derivatives, 2,5-bis(*p*-methoxycinnamoyl)-1,3,4,6,7,8- and 4,5-bis(*p*-methoxycinnamoyl)-1,2,3,6,7,8-hexamethoxyxanthene were synthesized. The comparison of these two hexamethoxyxanthenes with carthamin derivatives is described.

Recently, we have obtained two hexamethoxyxanthene isomers, A-1 (mp 74—76 °C) and A-2 (mp 190—191 °C), which are presumed to be 2,5-bis(*p*-methoxycinnamoyl)-1,3,4,6,7,8-hexamethoxyxanthene (**1**) and 4,5-bis(*p*-methoxycinnamoyl)-1,2,3,6,7,8- or 2,7-bis(*p*-methoxycinnamoyl)-1,3,4,5,6,8-hexamethoxyxanthene (**2** or **3**) produced by the methylation of the hydrolysis products of carthamin, the red coloring matter of the flowers of safflower (*Carthamus tinctorius* L.).[1)]

In this paper, the synthesis of **1** and **2** and the comparison of the synthetic samples with carthamin derivatives will be described.

An equimolecular mixture of 2,3,4,6-tetrahydroxyacetophenone (**4**)[2)] and 3-formyl-2,4,5,6-tetrahydroxyacetophenone (**5**), obtained by the formylation of **4**, was refluxed in methanol containing a small amount of 50% sulfuric acid to afford the condensation product (**6**) as dark violet crystals. Compound **6** was hydrogenated in ethanol using 5% palladium charcoal as a catalyst. The reduction product was then methylated with dimethyl sulfate-potassium carbonate in acetone to give 2,5-diacetyl-1,3,4,6,7,8-hexamethoxyxanthene (**7**). The unsymmetrical structures of **6** and **7** were supported from the observation of the two separate signals of their acetyl groups in their ^{1}H-NMR spectra.

The condensation of **7** with *p*-methoxybenzaldehyde in methanol containing a 50% aqueous potassium hydroxide solution afforded **1** (mp 74—76 °C) in a 57% yield. The IR and ^{1}H-NMR spectra of **1** were completely identical with those of one of the natural derivatives, A-1.

Since the condensation of **4** with **5** did not give the other symmetrical compound, **2** was synthesized by the alternative method described below.

4,5-Diacetyl-1,2,3,6,7,8-hexamethoxyxanthene (**10**) was obtained by the methylation of 4,5-diacetyl-1,2,3,6,7,8-hexahydroxyxanthene (**9**), prepared by the C-acetylation of 1,2,3,6,7,8-hexahydroxyxanthene (**8**)[3)] with the boron trifluoride-acetic acid complex. 4,5-Bis(*p*-methoxycinnamoyl)-1,2,3,6,7,8-hexamethoxyxanthene (**2**) (mp 157—158 °C) was afforded by the condensation of **10** with *p*-methoxybenzaldehyde by a manner similar to that of **1**.

From the disagreement of this compound, **2**, with the natural derivative, A-2, it is assumed that the structure of another isomer, 2,7-bis(*p*-methoxycinnamoyl)-1,3,4,5,6,8-hexamethoxyxanthene (**3**), should be assigned for A-2.

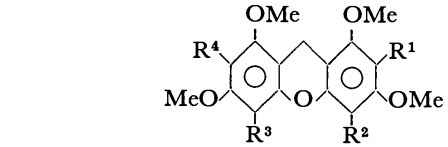

1 $R^1=R^3=COR$, $R^2=R^4=OMe$
2 $R^1=R^4=OMe$, $R^2=R^3=COR$
3 $R^1=R^4=COR$, $R^2=R^3=OMe$
$\left(R=-CH=CH-\langle\bigcirc\rangle-OMe\right)$

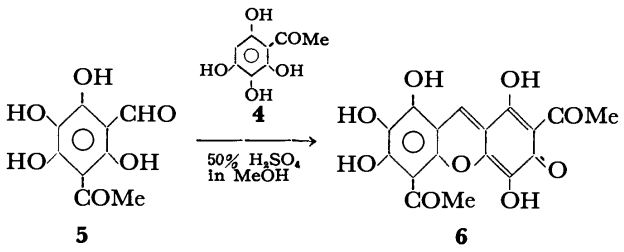

5 **6**

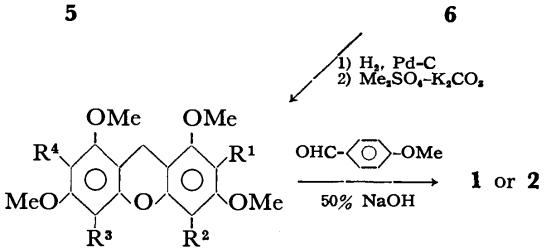

7 $R^1=R^3=COMe$, $R^2=R^4=OMe$
10 $R^1=R^4=OMe$, $R^2=R^3=COMe$

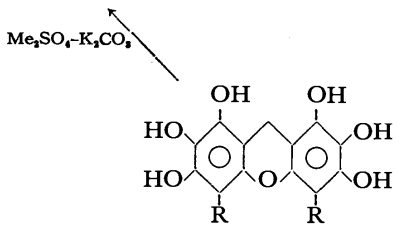

8 R=H
9 R=COMe

Experimental

All the melting points are uncorrected. The UV and IR spectra were recorded on a Hitachi 135 spectrophotometer, and a Hitachi EPI-S2 spectrophotometer respectively. The ^{1}H-NMR spectra were measured with a Hitachi R-22 spectrometer (90 MHz), using tetramethylsilane as the internal standard. The mass spectra were obtained on a Hitachi RMU-6M mass spectrometer.

3-Formyl-2,4,5,6-tetrahydroxyacetophenone (5). Into a solution of 2,3,4,6-tetrahydroxyacetophenone (**4**)[2)] (20 g), zinc cyanide (16 g), and anhydrous aluminium chlroride (18 g) in dry ether (300 ml), dry hydrogen chloride gas was stirred for

8 h under cooling with ice water. The reaction mixture was then allowed to stand overnight at 0 °C. After the solvent had been removed by decantation, the residue was refluxed with water (100 ml) for 3 h and then filtered. After cooling, **5** (9.2 g, 40%) was obtained from the filtrate. Mp 232—236 °C, ^{1}H-NMR (DMSO-d_6) δ 2.61 (3H, s, $-COCH_3$), 9.97 (1H, s, -CHO). Found: C, 50.67; H, 3.82%; M^+, 212. Calcd for $C_9H_8O_6$: C, 50.94; H, 3.77%; M, 212.

*Condensation Product of **4** with **5**.* A mixture of **4** (500 mg), **5** (570 mg), and 50% sulfuric acid (1 ml) in methanol (30 ml) was refluxed for 10 h. After cooling, the condensation product (**6**) was obtained as dark violet crystals (mp 280 °C) in a 19% yield. UV_{max} (EtOH) 352 and 540 nm, IR (KBr) 1700 and 1620 cm^{-1} (C=O), ^{1}H-NMR (DMSO-d_6) δ 2.67 and 2.82 (each 3H, s, $-COCH_3\times2$), 8.27 (1H, s, -CH=), MS *m/e* 360 (M^+). This compound was used without purification for the next reaction.

*2,5-Diacetyl-1,3,4,6,7,8-hexamethoxyxanthene (**7**).* Compound **6** (5.0 g) was hydrogenated in ethanol (300 ml), using 5% palladium charcoal (0.8 g) as the catalyst. The reaction mixture was filtered, and the filtrate was evaporated *in vacuo* to afford an unstable reduction product (4.8 g).

A mixture of the reduction product (300 mg), dimethyl sulfate (3 ml), and potassium carbonate (5 g) in dry acetone (70 ml) was refluxed for 3 h. The reaction mixture was then worked up in the usual manner, and the crude product was chromatographed on a column of silica gel with benzene–ethyl acetate (4 : 1) to give **7** in a 27% yield. Mp 119—120 °C (from methanol), IR (KBr) 1647 cm^{-1} (C=O), ^{1}H-NMR ($CDCl_3$) δ 2.49 and 2.61 (each 3H, s, $-COCH_3\times2$), 3.77 and 3.87 (each 3H, s, $-OMe\times2$), 3.84 and 3.90 (each 6H, s, $-OMe\times4$), 3.97 (2H, s, $-CH_2-$). Found: C, 61.79; H, 5.95%; M^+, 446. Calcd for $C_{23}H_{26}O_9$: C, 61.87; H, 5.87%; M, 446.

*2,5-Bis(p-methoxycinnamoyl)-1,3,4,6,7,8-hexamethoxyxanthene (**1**).* Into a mixture of **7** (500 mg) and *p*-methoxybenzaldehyde (1 ml) in methanol (10 ml), we added a 50% aqueous potassium hydroxide solution (2.0 g) ot room temperature. The reaction mixture was warmed to 50—60 °C for 1 h and then extracted with ether. The ether was evaporated *in vacuo*, and the residue was chromatographed on a column of silica gel with benzene–ethyl acetate (9 : 1) to afford crude **1**, which was further chromatographed on silica gel with chloroform–ethyl acetate (40 : 3). Compound **1** (380 mg, 50%), mp 74—76 °C, IR (KBr) 1632 cm^{-1} (C=O), ^{1}H-NMR ($CDCl_3$) δ 3.75 (2H, s, $-CH_2-$), 3.80—4.10 (24H, m, $-OMe\times8$), 6.95—7.60 (12H, m, *p*-substituted cinnamoyl$\times2$). Found: C, 68.63; H, 5.64%; M^+, 682. Calcd for $C_{39}H_{38}O_{11}$: C, 68.61; H, 5.61%; M, 682. This compounds was completely identical with the natural derivative A-1.

*1,2,3,6,7,8-Hexahydroxyxanthene (**8**).* This compound was prepared by the reduction of the condensation product of 1,2,3,5-benzenetetrol[4] with ethyl formate as has previously been reported.[3] Although this reduction product contained a small amount of an isomer, 1,3,4,6,7,8-hexahydroxyxanthene, it was used without purification for the next reaction.

*4,5-Diacetyl-1,2,3,6,7,8-hexamethoxyxanthene (**10**).* A mixture of 1,2,3,6,7,8-hexahydroxyxanthene (**8**) (2.5 g), containing a small amount of 1,3,4,6,7,8-hexahydroxyxanthene and the boron trifluoride–acetic acid complex (10 ml) was heated on a water bath for 2 h. The reaction mixture was then stirred into an aqueous potassium acetate solution, drop by drop. The resulting precipitate was filtered, and the filtrate was concentrated to dryness to afford 4,5-diacetyl-1,2,3,6,7,8-hexahydroxyxanthene (**9**) (mp$>$280 °C), containing a small amount of 2,5-diacetyl-1,3,4,6,7,8-hexahydroxyxanthene.

A mixed solution of the above crude **9** (1.0 g), dimethyl sulfate (3.2 ml), potassium carbonate (4.6 g), and dry acetone (50 ml) was refluxed for 6 h. The reaction mixture was worked up in the usual manner, and the crude product was chromatographed on a column of silica gel with benzene–ethyl acetate (8 : 1) to afford **10** (550 mg, 45%); mp 130—131 °C, IR (KBr) 1710 cm^{-1} (C=O). ^{1}H-NMR ($CDCl_3$) δ 2.44 (6H, s, $-COCH_3\times2$), 3.79 (2H, s, $-CH_2-$), 3.85, 3.87, and 3.96 (each 6H, s, $-OMe\times6$). Found: C, 61.58; H, 5.86%; M^+, 446. Calcd for $C_{23}H_{26}O_9$: C, 61.88; H, 5.87%; M, 446.

*4,5-Bis(p-methoxycinnamoyl)-1,2,3,6,7,8-hexamethoxyxanthene (**2**).* To a solution of **10** (50 mg) in methanol (0.3 ml), we added *p*-methoxybenzaldehyde (50 mg) and a 50% aqueous potassium hydroxide solution (0.2 g) at room temperature. The reaction mixture was then warmed to 50—60 °C for 1 h, and the resulting precipitate was recrystallized from methanol to give **2** as colorless needles (48 mg, 63%); mp 157—158 °C, IR (KBr) 1646 cm^{-1} (C=O), ^{1}H-NMR ($CDCl_3$) δ 3.80 (12H, s, $-OMe\times4$), 3.84 (2H, s, $-CH_2-$), 3.86 and 3.99 (each 6H, s, $-OMe\times4$), 6.68 and 7.22 (each 2H, d, J=16.0 Hz, -CH=CH-), 6.76 and 7.32 (each 4H, d, J=8.5 Hz, *p*-substituted phenyl$\times2$). Found: C, 68.42; H, 5.63%; M^+, 682. Calcd for $C_{39}H_{38}O_{11}$: C, 68.61; H, 5.61%; M, 682.

The authors wish to express their thanks to Mr. Kazuaki Sato for his microanalyses.

References

1) A part of this work was reported in a preliminary form: J. Onodera, T. Saito, and H. Obara, *Chem. Lett.*, **1979**, 1327.

2) H. Obara, J. Onodera, Y. Kurihara, and F. Yamamoto, *Bull. Chem. Soc. Jpn.*, **51**, 3629 (1978).

3) H. Obara, J. Onodera, T. Shibata, and K. Shibayama, *Bull. Chem. Soc. Jpn.*, **54**, 1261 (1981).

4) J. Onodera and H. Obara, *Nippon Kagaku Kaishi*, **1973**, 1808.

Low-temperature Reaction of *gem*-Dihalocyclopropanes with Activated Magnesium

Teiichi Ando,* Takeshi Muranaka, and Takashi Ishihara
Department of Industrial Chemistry, Faculty of Engineering, Kyoto University, Sakyo-ku, Kyoto 606
(Received March 23, 1981)

Synopsis. The reaction of 7-bromo-7-chlorobicyclo-[4.1.0]heptane and 7-bromo-7-fluorobicyclo[4.1.0]heptane with activated magnesium in THF at −50 to −40 °C gave 7-bromobicyclo[4.1.0]heptane, in addition to 7-chloro- and 7-fluorobicyclo[4.1.0]heptane, respectively.

Although much work has been done on the reaction of *gem*-dihalocyclopropanes with a variety of metals[1] or organometallic reagents,[2] there exists only scattered information on the reaction of *gem*-dihalocyclopropanes with metallic magnesium;[1c-e] the products reported are exclusively allenic compounds, derived from the intermediary cyclopropylmagnesium halides.

This paper describes the reaction of some *gem*-dihalocyclopropanes with activated magnesium, which resulted in reduction without ring opening.

Results and Discussion

The halogen compounds used in this study, 7,7-dibromo- (**1a**), 7-bromo-7-chloro- (**1b**), and 7-bromo-7-fluorobicyclo[4.1.0]heptane (**1c**), were prepared by the addition of the corresponding dihalocarbene to cyclohexene. The latter two compounds were obtained as a mixture of two geometrical isomers. The reaction was conducted by adding a solution of 7,7-dihalobicyclo-[4.1.0]heptane in THF to a suspension of finely powdered magnesium, prepared from anhydrous magnesium chloride and potassium metal in THF.[3] The products isolated in this reaction were bicyclo[4.1.0]heptane (**2**), 7-chloro- or 7-fluorobicyclo[4.1.0]heptane (**3**), 7-bromobicyclo[4.1.0]heptane (**4**), 7-(2-tetrahydrofuranyl)-bicyclo[4.1.0]heptane (**5**), and 7,7'-bi(bicyclo[4.1.0]-heptylidene) (**6**), whose structures were determined by comparison of their spectral data and other physical properties with those of authentic samples. The yields of the products were measured on GLC by use of an internal standard. Where only isomer distributions in the products (**3** and **4**) were desired, no internal standard was added. The results are summarized in Table 1.

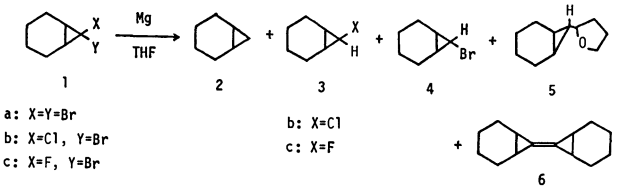

The reaction proceeded smoothly to give the reduction products (**2**, **3**, and **4**), together with a small amount of other products (**5** and **6**) derived from decomposition of 7-halobicyclo[4.1.0]hept-7-ylmagnesium compounds. Thus, **1a** gave an isomeric mixture of 7-bromobicyclo[4.1.0]heptane (**4**) in 80% yield. The reaction of **1b** and **1c** gave bromide (**4**), in addition to 7-chloro (**3b**) and 7-fluorobicyclo[4.1.0]heptane (**3c**), respectively. To be noted is that not only the bromine atom, which is usually much more susceptible to reduction, but also the chlorine or the fluorine atom is concurrently reduced. These findings suggest that the activated magnesium metal is in a highly reactive form and thus is relatively unselective toward halogen. The higher selectivity for chlorine than for bromine (see the reduction of **1b** to **3b** and **4**) or the concurrent reduction of bromine and fluorine (see the reduction of **1c** to **3c** and **4**) may be explained by strengthening of the C–Br bond or weakening of the C–Cl or the C–F bond caused by the presence of a geminal halogen atom. A support for this rationalization was afforded by the reaction of 7-halobicyclo[4.1.0]heptanes with activated magnesium: Under the same reaction conditions, 7-bromobicyclo[4.1.0]heptane (**4**) was readily reduced to give bicyclo[4.1.0]heptane in 65% yield whereas no

Table 1. Reaction of 7,7-dihalobicyclo[4.1.0]heptanes (**1**)

Halide (*endo*-X/*exo*-X)	Yield %	Composition of products/%				
		2	**3** (*endo*-X/*exo*-X)	**4** (*endo*-Br/*exo*-Br)	**5**	**6**
1a	95	4	—	84 (14/86)	11	1
1b (47/53)	70	3	42 (39/61)	43 (10/90)	12	0
1b (100/0)	56	1	30 (54/46)	59 (6/94)	10	0
1b (0/100)	76	3	34 (16/84)	41 (5/95)	22	0
1c (34/66)	61	4	51 (34/66)	39 (9/91)	6	0
1c (100/0)	71	4	59 (100/0)	33 (6/94)	4	0

reaction occurred with 7-chloro- (**3b**) or 7-fluorobicyclo-[4.1.0]heptane (**3c**), the starting halides being recovered quantitatively.

As shown in Table 1, the isomer ratios of 7-fluorobicyclo[4.1.0]heptane (**3c**) are identical with those of the initial halide (**1c**). This indicates that the reduction takes place with complete stereospecificity, *i.e.*, with complete retention of configuration. The reduction of 7-bromo-7-chlorobicyclo[4.1.0]heptane (**1b**) to 7-chlorobicyclo[4.1.0]heptane (**3b**) proceeds in a less stereospecific manner. These trends are entirely analogous to those found in the reduction of *gem*-dihalocyclopropanes with organotin(IV) hydride[2c] and in the Hunsdiecker reaction of α-halocyclopropanecarboxylic acids,[4] both of which are believed to proceed *via* α-halocyclopropyl radicals. From the stereochemical trends cited above, it is highly probable that the reduction with activated magnesium described herein proceeds by a radical mechanism rather than a carbanionic one. The latter mechanism, however, cannot be ruled out at the present time.[5]

Experimental

All boiling and melting points are uncorrected. Infrared spectra (IR) were recorded on a Shimadzu IR-400 infrared spectrometer. A Varian EM-360 spectrometer (60 MHz) was used to measure ^{1}H NMR spectra in solutions of CCl_4 with Me_4Si as an internal standard. Mass spectra (MS) were taken on a Hitachi RMS-4 spectrometer at an ionization potential of 70 eV. Gas chromatographic analyses (GLC) were performed with a Shimadzu GC-2C or GC-6A gas chromatograph.

7,7-Dihalobicyclo[4.1.0]heptanes (1a—c). 7,7-Dibromo- (**1a**), 7-bromo-7-chloro- (**1b**), and 7-bromo-7-fluorobicyclo-[4.1.0]heptane (**1c**) were prepared by the reaction of cyclohexene with dibromo-,[6] bromochloro-,[4] and bromofluorocarbene,[7] respectively, generated by basic decomposition of the corresponding trihalomethane: **1a**, 57% yield, bp 108—111 °C/16 mmHg; **1b**, 77% yield (*exo*-Br: *endo*-Br = 47 : 53), bp 69—72 °C/4 mmHg; **1c**, 63% yield (*exo*-Br: *endo*-Br = 34 : 66), bp 70—71 °C/22 mmHg. An isomeric mixture of **1b** or **1c** was treated with hot quinoline[8] to give pure 7-*exo*-bromo-7-*endo*-chlorobicyclo[4.1.0]heptane (bp 71—72 °C/6 mmHg) and 7-*exo*-bromo-7-*endo*-fluorobicyclo[4.1.0]heptane (bp 64—66 °C/13 mmHg). Isomerically pure 7-*endo*-bromo-7-*exo*-chlorobicyclo[4.1.0]heptane was obtained according to the method of Köbrich,[9] bp 76—77 °C/5 mmHg. 7-Halobicyclo[4.1.0]-heptanes (**3** and **4**) and bicyclo[4.1.0]heptane (**2**) were synthesized by the reduction of the corresponding 7,7-dihalo compound with organotin(IV) hydride[2c] and were used for determination of the yields and the structures of products.

Reaction of 7,7-Dihalobicyclo[4.1.0]heptanes with Activated Magnesium. To a suspension of activated magnesium, prepared from anhydrous $MgCl_2$ (12.6 mmol) and potassium metal (24.0 mg-atom) in THF (14 ml), was added under nitrogen a solution of a halide (10 mmol) in THF (2 ml) at such a rate that the temperature did not rise to −40 °C. After the addition, the mixture was stirred at −50 to −40 °C for 3—8 h. The reaction was quenched with a saturated solution of ammonium chloride and the resultant mixture was repeatedly extracted with ether. The combined extracts were dried over anhydrous Na_2SO_4, filtered, and concentrated under atmospheric pressure. The residual oil was analyzed on GLC by the internal standard method to measure the yields of products.

7-exo-(2-Tetrahydrofuranyl)bicyclo[4.1.0]heptane (5): Bp 86.5—87.5 °C/6 mmHg; n_D^{23} 1.4819 (lit,[9] n_D^{20} 1.4828); IR (film) 2932, 2860, 1452, 1371, 1355, 1342, 1175, 1128, 1062, 919, 770 cm^{-1}; ^{1}H NMR δ 0.2—2.2 (m, 15H), 3.2 (m, 1H), 3.7 (m, 2H).

cis-*7,7-Bi(bicyclo[4.1.0]heptylidene) (6)*: Bp 69—72 °C/2 mmHg; mp 80.5—81.5 °C (needles from methanol) (lit,[9] mp 77.5—78.5 °C); ^{1}H NMR δ 0.7—2.0 (m, 20H); IR (KBr) 2980, 2915, 2860, 1446, 1332, 1252, 1207, 1192, 1088, 991, 977, 949, 904, 840, 827, 782, 740 cm^{-1}; MS *m/e* (%) 188 (M^+, 11), 173 (21), 159 (30), 145 (68), 131 (64), 119 (31), 117 (49), 105 (55), 91 (100).

Found: C, 89.03; H, 10.92%.

trans-*7,7'-Bi(bicyclo[4.1.0]heptylidene) (6)*: Mp 124.0—125.0 °C (needles from methanol) (lit, mp 121.5—122.5 °C,[9] 124 °C[10]); IR (KBr) 2980, 2930, 2860, 1442, 1338, 1327, 1293, 1247, 1167, 1085, 988, 943, 840, 811, 787, 737 cm^{-1}; MS *m/e* (%) 188 (M^+, 12), 173 (21), 159 (30), 145 (68), 131 (63), 119 (30), 117 (49), 105 (54), 91 (100).

Found: C, 89.09; H, 10.93%. Calcd for $C_{14}H_{20}$: C, 89.29; H, 10.71%.

References

1) a) H. Yamanaka, R. Oshima, K. Teramura, and T. Ando, *J. Org. Chem.*, **37**, 1734 (1972); b) M. Schlosser and G. Heinz, *Angew. Chem.*, **79**, 617 (1967); c) P. D. Gardner and M. Narayama, *J. Org. Chem.*, **26**, 3518 (1961); d) T. J. Logan, *Tetrahedron Lett.*, **1961**, 173; e) W. E. Doering and P. M. LaFlamme, *Tetrahedron*, **2**, 75 (1958).

2) a) For organolithium compounds, K. G. Taylor, W. E. Hobbs, M. S. Clark, and J. Chaney, *J. Org. Chem.*, **37**, 2436 (1972); E. V. Dehmlow and G. C. Ezimora, *Tetrahedron Lett.*, **1971**, 563, and references cited therein; b) For Grignard reagents, D. Seyferth and B. Prokai, *J. Org. Chem.*, **31**, 1702 (1966); c) For organotin(IV) hydrides, D. Seyferth, H. Yamazaki, and D. L. Alleston, *ibid.*, **28**, 703 (1963); T. Ando, H. Yamanaka, F. Namigata, and W. Funasaka, *ibid.*, **35**, 33 (1970); J. Hatem and B. Waegell, *Tetrahedron Lett.*, **1973**, 2019, and references cited therein; d) For $LiAlH_4$, C. W. Jefford, U. Burger, M. H. Laffer, and N. Kabengele, *ibid.*, **1973**, 2483; J. Hatem and B. Waegell, *ibid.*, **1973**, 2023; H. Yamanaka, T. Yagi, K. Teramura, and T. Ando, *J. Chem. Soc., Chem. Commun.*, **1971**, 380, and references cited therein.

3) R. D. Rieke and P. M. Hudnell, *J. Am. Chem. Soc.*, **94**, 7178 (1972); R. D. Rieke and S. E. Bales, *ibid.*, **96**, 1775 (1974).

4) T. Ishihara, K. Hayashi, T. Ando, and H. Yamanaka, *J. Org. Chem.*, **40**, 3264 (1975).

5) The presence of the reduction products as such in the reaction mixture was confirmed by separate carbonation experiments; the amount of the carboxylic acids obtained was much less than that of the reduction products.

6) L. Skattebøl, G. A. Abskharoun, and T. Greibrokk, *Tetrahedron Lett.*, **1973**, 1367.

7) J. Hine and S. J. Ehrenson, *J. Am. Chem. Soc.*, **80**, 842 (1958); T. Ando, F. Namigata, H. Yamanaka, and W. Funasaka, *ibid.*, **89**, 5719 (1967).

8) T. Ando, H. Hosaka, H. Yamanaka, and W. Funasaka, *Bull. Chem. Soc. Jpn.*, **42**, 2013 (1969).

9) G. Köbrich and W. Goyert, *Tetrahedron*, **24**, 4327 (1968).

10) L. Skattebøl, *Tetrahedron Lett.*, **1961**, 167; *Acta Chem. Scand.*, **17**, 1683 (1963).

Use of 1,8-Diazabicyclo[5.4.0]undec-7-ene in Preparation of Trimethylsilyl Enol Ethers and Trimethylsilylacetylenes

Yoshiyuki TANIGUCHI, Junji INANAGA, and Masaru Yamaguchi*

Department of Chemistry, Kyushu University 33, Higashi-ku, Fukuoka 812

(Received March 23, 1981)

Synopsis. Trimethylsilyl enol ethers were prepared by using a combination of chlorotrimethylsilane and 1,8-diazabicyclo[5.4.0]undec-7-ene in good yields. Trimethylsilylation of acetylenes was also achieved with the same reagents in the presence of silver salt as catalyst.

Triethylamine is the most frequently used base for enol trimethylsilylation of carbonyl compounds[1] under equilibrating conditions. However, enol silylation with this base in combination with chlorotrimethylsilane requires rather vigorous conditions (refluxing in *N,N*-dimethylformamide for several hours),[2] and despite some modifications,[3] the yields have been less satisfactory than those with trimethylsilyl trifluoromethanesulfonate[4] or with trimethylsilyl nonafluorobutane-1-sulfonate formed *in situ*.[5,6]

Here, we wish to show that the use of 1,8-diazabicyclo-[5.4.0]undec-7-ene (DBU) as a base in combination with chlorotrimethylsilane, provides a rapid, mild, and efficient method of enol silylation of various carbonyl compounds.

$$RCH_2COR' \xrightarrow[CH_2Cl_2]{Me_3SiCl,\ DBU} RCH{=}CR' \quad (OSiMe_3)$$

The yields are summarized in Table 1 (entry 1—15). Ketones, aldehydes, and α,β-unsaturated ketones were smoothly enol silylated at the refluxing conditions in dichloromethane. An exceptionally low yield of 3,3-dimethyl-2-trimethylsiloxy-1-butene (entry 6 in Table 1) can be ascribed to the steric crowdness of the ether which is considered to be in equilibration with the starting ketone and chlorotrimethylsilane under the presence of chloride ion.[7] It is noteworthy that the addition of silver nitrate to the reaction mixture improved the yield to 92% (entry 8). In other cases examined, the addition of silver nitrate did not show much influence on the final yields.

The poor regioselectivity of the present method is demonstrated by the silylation of 2-methylcyclohexanone (entry 3 and 4 in Table 1 and notes therein). The ratio of the two isomers did not change after prolonged reaction time (50 h).[8]

$$RC{\equiv}CH \xrightarrow[CH_3Cl_3]{Me_3SiCl,\ AgCl(cat.),\ DBU} RC{\equiv}CSiMe_3$$

In trimethylsilylation of acetylenes, strong bases such as butyl lithium[9] or Grignard reagent[10] have usually been used for the generation of acetylide anions, except for one example where monosubstituted acetylenes were heated with trialkylchlorosilanes and triethylamine in the presence of catalytic amount (0.15 mol equiv.) of copper(I) chloride at 150 °C in an autoclave for 100—120 h.[11] When the present method with DBU was applied directly to trimethylsilylation of monosubstituted acetylenes, no silylation took place despite the modifications of the reaction conditions. However, the addition of a small amount of silver salt (0.1 mol equiv.) such as silver chloride or nitrate to the reaction mixture resulted in smooth silylation in refluxing dichloromethane in good yields. They are summarized in Table 1 (entry 16—23). Because of the mildness of the reaction conditions, the present method seems to have wide applicability. The use of triethylamine in place of DBU was ineffective. In experiments with phenylacetylene, copper(I) chloride gave a less satisfactory result than[silver chloride, and zinc chloride was almost useless.

Application of the method to the formation of ketene acetals from carboxylic esters was unsuccessful.

Experimental

Commercial DBU was distilled from calcium hydride. Commercial chlorotrimethylsilane was once distilled.

Silylation of Carbonyl Compounds. For the determination of the yield given in Table 1, chlorotrimethylsilane (0.55 mmol) was added to a stirred mixture of a ketone (0.50 mmol) and DBU (0.60 mmol) in dichloromethane (500 μl) at 40 °C. The progress of the reaction was followed by GLPC (SE-30) with the addition of an appropriate internal standard. The product was identified by comparing the retention time with that of the authentic specimen prepared by one of the reported procedures.[12]

In the experiment with silver nitrate as an additive, chlorotrimethylsilane (0.55 mmol) was added to a suspension of powdered silver nitrate (0.55 mmol) in dichloromethane and stirred for 15 min. The mixture was then warmed to 40 °C and a solution of a ketone (0.50 mmol) and DBU (0.60 mmol) in dichloromethane (300 μl) was added to this.

A typical example of the isolation experiment is as follow (entry 1, Table 1): A mixture of cyclopentanone (1.23 g, 14.7 mmol), chlorotrimethylsilane (1.76 g, 16.2 mmol), and DBU (2.68 g, 17.6 mmol) in dichloromethane (15 ml) was stirred at 40 °C for 1 h. The mixture was diluted with pentane (10 ml) and washed successively with dilute hydrochloric acid (1%) and aqueous sodium hydrogencarbonate, dried over magnesium sulfate, and distilled, giving 1-trimethylsiloxycyclopentene [1.83 g (80%), bp 85 °C (bath)/6670 Pa].

Silylation of Acetylenes. A typical example is given below (entry 23, Table 1). 1-Ethynylcyclohexyl acetate (1.054 g, 6.34 mmol) and DBU (1.16 g, 7.61 mmol) were successively added to a stirred suspension of silver chloride[13] (90.0 mg, 0.634 mmol) in dichloromethane (6.5 ml). The mixture was heated at 40 °C and chlorotrimethylsilane (0.827 g, 7.61 mmol) was added to this. After stirring for 25 h at the same temperature, the mixture was cooled, diluted with pentane (15 ml), washed successively with aqueous sodium hydrogencarbonate, hydrochloric acid (1%), and water, dried, and distilled. 1-(Trimethylsilylethynyl)cyclohexyl acetate: 1.36 g (90%), bp 149 °C (bath)/8000 Pa. NMR ($CDCl_3$) δ 0.17, [s, 9H, $-Si(CH_3)_3$], 1.4—1.8 (m, 10H, $-CH_2-$), and 2.03 (s, 3H, $-COCH_3$). Found: C, 65.40; H, 9.30%. Calcd for $C_{13}H_{22}O_2Si$: C, 65.50; H, 9.30%.

TABLE 1. SILYLATION OF CARBONYL COMPOUNDS AND MONOSUBSTITUTED ACETYLENES

Entry	Substrate	Additive (mole equiv.)	Time/h[a]	Product	Yield/%[b]
1		None	0.5		98 (80)
2		None	1		96 (84)
3		None	2	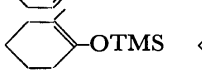 **a** **b**	92[d]
4		$AgNO_3$(1.1)	2		81[e]
5	$C_6H_5COCH_3$	None	0.25	$C_6H_5C(OTMS)=CH_2$	92 (82)
6	$(CH_3)_3CCOCH_3$	None	4	$(CH_3)_3CC(OTMS)=CH_2$	57
7		None	2.5[f]		73
8		$AgNO_3$(1.1)	4		92 (80)
9		$AgNO_3$(0.1)	2		75
10	$CH_3(CH_2)_5CHO$	None	0.25	$CH_3(CH_2)_4CH=CHOTMS$	97 (85)[g]
11		None	2[h]	$CH_3(CH_2)_4CH=CHOTBDMS$[i]	(81)[j]
12	$C_6H_5CH=CHCOCH_3$	None	0.5	$C_6H_5CH=CH-C(OTMS)=CH_2$	97
13		$AgNO_3$(1.1)	0.25		92
14	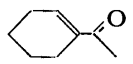	None	4	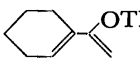	84
15		$AgNO_3$(1.1)	4		82
16	$C_6H_5C\equiv CH$	AgCl(0.1)	24	$C_6H_5C\equiv CTMS$	94
17		$AgNO_3$(0.1)	24		91 (83)
18		CuCl(0.1)	24		76
19		$ZnCl_2$(0.1)	24		6
20	$CH_3(CH_2)_5C\equiv CH$	AgCl(0.1)	21	$CH_3(CH_2)_5C\equiv CTMS$	84 (62)
21	$AcOCH_2C\equiv CH$[k]	AgCl(0.1)	24	$AcOCH_2C\equiv CTMS$[l]	(84)
22	$EtCH(OAc)CH_2C\equiv CH$[k]	AgCl(0.1)	24	$EtCH(OAc)CH_2C\equiv CTMS$[m]	(89)
23	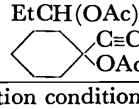	AgCl(0.1)	25	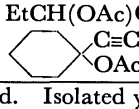	(90)

a) Other reaction conditions; see experimental section. b) GLPC yield. Isolated yield is given in parentheses. c) TMS = trimethylsilyl. d) **a** : **b** = 63 : 37 (GLPC). e) **a** : **b** = 57 : 43 (GLPC). f) HMPA was used as the solvent at 40 °C. g) E : Z = 30 : 70 (GLPC). h) ClSi(*t*-Bu)Me_2 (1.1 equiv.) and DBU (1.2 equiv.) were used. i) TBDMS = *t*-butyldimethylsilyl. Bp 104 °C (bath)/930 Pa. Found: C, 68.09; H, 12.37%. Calcd for $C_{13}H_{28}OSi$: C, 68 32; H, 12.35%. j) E: Z = 61 : 39. [NMR ($CDCl_3$): Olefinic proton β to oxygen appears at δ 4.98 (dt, J = 11.8 and J = 7.3 Hz) and 4.44 (dt, J = 5.9 and J = 7.1 Hz) for *E*-isomer and *Z*-isomer, respectively.]. k) The corresponding alcohol was acetylated with acetic anhydride and 4-dimethylaminopyridine. l) Bp 104 °C (bath)/9600 Pa. NMR ($CDCl_3$) δ 0.17 [s, Si $(CH_3)_3$]. Found: C, 56.30; H, 8.36%. Calcd for $C_8H_{14}O_2Si$: C, 56.43; H, 8.29%. m) Bp 136 °C (bath)/9870 Pa. NMR($CDCl_3$) δ 0.11 [s, $Si(CH_3)_3$]. Found: C, 62.03; H, 9.60%. Calcd for $C_{11}H_{20}O_2Si$: C, 62.21; H, 9.49%. n) Characterization: See experimental section.

This work was partially supported by a Grant-in-Aid for Scientific Research No. 443008 from the Ministry of Education, Science and Culture.

References

1) For recent reviews: J. K. Rasmussen, *Synthesis*, **1977**, 91; E. W. Colvin, *Chem. Soc. Rev.*, **7**, 15 (1978).

2) H. O. House, L. J. Czuba, M. Gall, and H. D. Olmstead, *J. Org. Chem.*, **34**, 2324 (1969).

3) S. Danishefsky and T. Kitahara, *J. Am. Chem. Soc.*, **96**, 7807 (1974); G. M. Rubottom and J. M. Gruber, *J. Org. Chem.*, **42**, 1051 (1977).

4) G. Simchen and W. Kober, *Synthesis*, **1976**, 259; H. Emde and G. Simchen, *Synthesis*, **1977**, 867.

5) H. Vorbruggen and K. Krolikiewicz, *Synthesis*, **1979**, 34.

6) Recently, a combination of iodotrimethylsilane and hexamethyldisilazane in pentane has been shown to provide a good silylating method: R. D. Miller and D. R. McKean, *Synthesis*, **1979**, 730.

7) Actually, when this enol ether was treated with 1 mole equivalent of DBU hydrochloride in dichloromethane at 40 °C, it gave an equilibrium mixture of a similar composition (trimethylsilyl enol ether: ketone = 60 : 40) in 5 min, and the ratio did not change by prolonged heating (1 h).

8) The ratio, **a** : **b** = 63 : 37, was different from the ratio, **a** : **b** = 78 : 22, reported by House et al. with triethylamine in refluxing DMF (Ref. 2). This seems to be due to the difference in reaction conditions.

9) C. Eaborn, A. R. Thompson, and D. R. M. Walton, *J. Chem. Soc., B*, **1969**, 859.

10) C. Eaborn, A. R. Thompson, and D. R. M. Walton, *J. Chem. Soc., C*, **1967**, 1364.

11) G. Deleris, J. Dunogues, and R. Calas, *J. Organomet. Chem.*, **80**, C45 (1974).

12) For silyl enol ethers: Ref. 2 (entry 2, 3, and 6); 3 (entry 14); 4 (entry 1, 2, and 5); R. D. Miller and D. R. McKean, *Synthesis*, **1979**, 730 (entry 12); and D. Ladjama and J. J. Riehl, *ibid.*, **1979**, 504 (entry 10). For silylacetylenes: Ref. 11 (entry 16) and K. Uchida, K. Utimoto, and H. Nozaki, *J. Org. Chem.*, **41**, 2215 (1976) (entry 20).

13) Silver chloride precipitated by mixing aqueous silver nitrate and aqueous sodium chloride at room temperature, was washed with water and dried at 100 °C/133 Pa for 3 h.

Reaction of Thiobenzophenone S-Oxide (Diphenylsulfine) with Carbon Nucleophiles

Atsuyoshi OHNO,* Misao UOHAMA, and Shinzaburo OKA
Institute for Chemical Research, Kyoto University, Uji, Kyoto 611
(Received March 26, 1981)

Synopsis. The reaction of diphenylsulfine with a Grignard reagent or alkyllithium gives a variety of products depending on the structure of the Grignard reagent or alkyllithium.

2,2,4,4-Tetramethyl-3-pentanethione *S*-oxide (di-*t*-butylsulfine) reacts with Grignard reagents affording a variety of products depending on the structure of the Grignard reagent.[1] The reactions were interpreted in terms of a delicate competition of thiophilic attack (one-electron transfer process) and proton-abstraction (acid-base reaction).

In this paper we wish to describe the reactions of thiobenzophenone *S*-oxide (diphenylsulfine) with various carbanionic reagents. The results will be compared with those from the corresponding reactions of di-*t*-butylsulfine.

Results and Discussion

The reactions were carried out, in general, by adding a solution of diphenylsulfine, **1a**, to a solution containing

$$R_2C{=}S{\rightarrow}O$$

1a: R=Ph
1b: R=*t*-Bu

a three-fold excess of Grignard reagent at room temperature. However, it was confirmed that inverse addition did not change the products. Reaction conditions and products are summarized in Table 1 together with data from the reactions with alkyllithiums.

Products obtained by the present reactions are quite different in type from those obtained from the reactions of di-*t*-butylsulfine, **1b**. Detailed analyses of product distribution have revealed that the differences can be accounted for by the difference in the structure of initially formed anions.

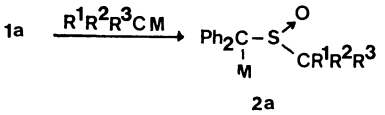

2a

(1)

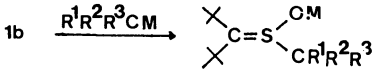

2b

The reaction course from **2a** seems to depend on the softness (polarizability, thiophilicity) and hardness (basicity) of the attacking reagent.

When a primary-alkyl reagent is employed in the reaction in DME, the hard base abstracts an acidic α-proton in **2a** resulting in the formation of a dianion, **3**, which is subsequently converted into an olefin through the corresponding thiocarbonyl ylide and thiirane. The electrocyclic ring-closure of a thiocarbonyl ylide has been reported.[2] Methyllithium in DME, on the other

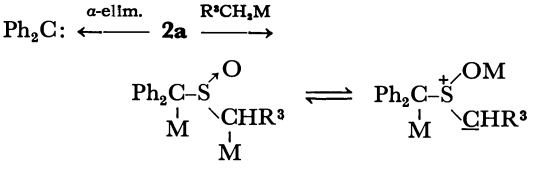

3a **3b** (2)

Table 1. Reaction of di phenylsulfine[a]

Reagent	Solvent	Product (Yield/%)[b]		Reagent	Solvent	Product (Yield/%)[b]	
CH_3MgI	Et_2O	$Ph_2C{=}CPh_2$	(77)	$PhCH_2MgCl$	Et_2O	Ph_2CSCH_2Ph | CH_2Ph	(86)
	DME	$Ph_2C{=}CH_2$	(69)				
CH_3Li	Et_2O	PHCHSCH$_3$ ↓ O	(87)		DME	$Ph_2C{=}CHPh$	(62)
				$Me_2CHMgCl$	Et_2O	$Ph_2CSCHMe_2$ | $CHMe_2$	(69)
	DME	$Ph_2C{=}CH_2$	(64)				
		Ph_2CHCH_3	(10)		DME	$Ph_2CHSCHMe_2$ ↓ O	(78)
C_2H_5MgBr	Et_2O	$Ph_2C{=}CHCH_3$	(52)				
	DME	$Ph_2C{=}CHCH_3$	(41)	$EtCHMgCl$ | Me	Et_2O	$Ph_2CSCH(Me)Et$ | $CH(Me)Et$	(78)
C_3H_7MgBr	Et_2O	$Ph_2C{=}CHEt$	(40)				
		Ph_2CSPr | Pr	(46)	Me_3CMgCl	Et_2O	$Ph_2CHSCMe_3$ ↓ O	(32)
C_3H_7Li[c]	Et_2O	Ph_2CHSPr ↓ O	(92)			$Ph_2C{=}CPh_2$	(6)
						Ph_2CH_2	(2)

a) At room temperature for 3 h. b) Isolated yield. c) At −20°C.

hand, is a very hard reagent, and the reaction with this reagent results in an α-elimination.[3-5] An extremely hard reagent, such as lithium compounds in ether, no further reaction takes place from **2a**. It is reported that both a sulfoxide and tetraarylethylene are formed by the reaction of a diarylsulfine with methyllithium in benzene.[6] Thus, the predominancy of a course (or courses) shown in Reaction 2 depends on the reaction conditions and reagents.

A secondary-alkyl reagent forms a sulfide by the reaction in ether. Since the secondary-carbanion is soft enough to attack the sulfur and a proton in **2a** is not acidic enough to be abstracted, the reaction scheme may be represented by Reaction 3. The process from **4**

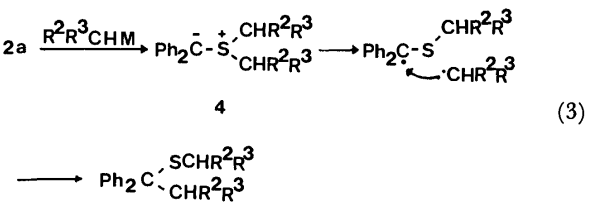

(3)

to the sulfide is well-known as the Stevens rearrangement.[7,8]

Benzylmagnesium chloride undergoes the secondary alkyl-type reaction in ether, whereas it behaves as a primary-alkyl reagent in DME. This is a marked difference between the reactions of **1a** and **1b**.[1] A further difference between the reactions of **1a** and **1b** with a secondary-alkyl reagent is that **1a** affords a sulfide which is composed of two parts of the alkyl reagent, whereas the sulfide from **1b** has only one part.[1]

t-Butylmagnesium chloride is a very soft reagent and may behave similarly to the secondary-alkyl reagent. However, the product from this reagent was the sulfoxide. Probably the steric effect of two *t*-butyl and a diphenylmethyl groups prevents this reagent from attack on sulfur.

Table 2. Reaction of diphenylmethyl alkyl(or aryl) sulfoxide[a]

R in $Ph_2CH-\overset{\uparrow}{\underset{O}{S}}-R$	Reagent	Product	Yield/%[b]
CH_3	CH_3MgI	$Ph_2C=CH_2$	34
		Ph_2CH_2	28
CH_3	CH_3Li	$Ph_2C=CH_2$	13
		Ph_2CHCH_3	53
CH_3	$PhCH_2MgCl$	$Ph_2C=CH_2$	25
		Ph_2CH_2	31
Me_2CH	CH_3MgI	$Ph_2C=CH_2$	64
Me_2CH	CH_3Li	No reaction[c]	—
Me_2CH	C_4H_9Li	No reaction[c]	—
$PhCH_2$	CH_3Li	$Ph_2C=CHPh$	58
$PhCH_2$	C_4H_9Li	$Ph_2C=CHPh$	64
$PhCH_2$	$PhCH_2MgCl$	$Ph_2C=CHPh$	55
Ph	CH_3MgI	No reaction	—
Ph	C_4H_9Li	No reaction	—

a) At room temperature in 1,2-dimethoxyethane (DME). b) Isolated yield. c) The formation of carbanion was recognized by color and H-D exchange.

In the above discussion we proposed that **2a** is an universal intermediate in the present reactions. To test the intermediacy of **2a**, we studied the reactions from diphenylmethyl alkyl (or aryl) sulfoxide by abstracting an α-proton and the results are summarized in Table 2.[9] The formation of 1,1-diphenylethylene from diphenylmethyl methyl sulfoxide is consistent with the proposed reaction scheme. However, it is recognized, by the isolation of diphenylmethane, that S_N2-type displacement on sulfur takes place in DME competitively with the proton-abstraction.[10]

Experimental

Materials. Thiobenzophenone[11] and thiobenzophenone *S*-oxide[12] were prepared according to literature procedures. Ether and 1,2-dimethoxyethane were dried over sodium weire and distilled prior to use. Sulfoxides were obtained by oxidation of the corresponding sulfides.

General Procedure. All reactions were carried out under a nitrogen atmosphere with stirring. Into 6 mmol of a Grignard reagent (or an alkyllithium) in 10 ml of ether was added 1 mmol of the sulfine in 10 ml of ether (or 1,2-dimethoxyethane) or *vice versa*. No difference was recognized in the result by the change of the addition order. When equivalent amounts ef a Grignard reagent and the sulfine were reacted, the reaction became slower but the product was the same as that obtained from the above reaction, though the yield was poor. After usual work-up, the products were subjected to column chromatography over silica gel with hexane–benzene (4 : 1 v/v) eluent. Analytically pure products were obtained by means of preparative VPC on a Varian Aerograph 920. The same procedure was employed for the reaction of sulfoxides.

The structure of products were confirmed by the identity of spectral data with those authentic samples.

References

1) A. Ohno, M. Uohama, K. Nakamura, and S. Oka, *J. Org. Chem.*, **44**, 2244 (1979).
2) T. B. Cameron and H. W. Pinniek, *J. Am. Chem. Soc.*, **101**, 4755 (1979).
3) J. Hine and J. J. Porter, *J. Am. Chem. Soc.*, **82**, 6178 (1960).
4) E. Schaumann and W. Walter, *Chem. Ber.*, **107**, 3562 (1974).
5) A. Ohno, K. Nakamura, Y. Shizume, and S. Oka, *Bull. Chem. Soc. Jpn.*, **50**, 1003 (1977).
6) A. G. Schultz and R. H. Schlessinger, *J. Chem. Soc., Chem. Commun.*, **1970**, 746, 748.
7) W. Ando, *Acc. Chem. Res.*, **10**, 179 (1977).
8) E. Block, "Reactions of Organosulfur Compounds," Academic Press, New York, N. Y. (1978), pp. 118—119 and 198—201.
9) Because of the solubility of sulfoxides, the reaction could not be carried out in ether.
10) T. Durst, M. J. LeBelle, R. Van den Elen, and K.-C. Tin, *Can. J. Chem.*, **52**, 761 (1974).
11) R. Ahmed and W. Lwowski, *Tetrahedron Lett.*, **1969**, 3611.
12) B. Zwanenburg and L. Thijs, *Recl. Trav. Chim. Pays-Bas*, **86**, 577 (1967).

The Effect of Hydration on the Thermal Stability of Ovalbumin as Measured by Means of Differential Scanning Calorimetry

Yukihisa FUJITA* and Yukinao NODA

Department of Chemistry, Hyogo College of Medicine, Mukogawa, Nishinomiya, Hyogo 663

(Received March 27, 1981)

Synopsis. The thermal denaturation of ovalbumin (egg albumin) was investigated by means of differential scanning calorimetry in the water-content range from 0.11 to 1.15 g of water per g of protein. At water contents above 0.76 g/g, the temperature, T_d, and the enthalpy, ΔH_d, of denaturation were scarcely dependent at all on the water content. At lower water contents, however, both T_d and ΔH_d showed a marked dependence on the water content. The degree of the hydration dependence of the T_d and ΔH_d suggested that the amount of water required to hydrate ovalbumin was 0.76 g/g and that at least two types of the hydration phase contributed to the thermal stability of the protein.

It is well known that water is an essential element in many biological processes. In spite of the importance of hydration in the maintaining of protein structure some important questions on protein hydration remain unresolved. As reviewed by Kuntz and Kauzmann,[1] approximately 0.3—0.5 g of water per g of protein is bound to globular protein; its properties are evidently different from those of pure water, *e.g.*, a lowered vapor pressure, a reduced mobility, and a much-reduced freezing point.

In previous papers,[2-4] the effect of hydration on the thermal stability of lysozyme and chymotrypsinogen A was investigated by means of differential scanning calorimetry (DSC). The essential hydration values for stabilizing the spatial structure of lysozyme and chymotrypsinogen A were considerably larger than those estimated by other techniques. It was also suggested that at least two types of the hydration phase contributed to the thermal stability of the proteins.

The present work was undertaken in order to investigate the effect of hydration on the thermal stability of ovalbumin and at the same time to confirm the above suggestions.

Experimental

Materials. The chicken ovalbumin (egg albumin) used in the present study was a salt-free, five-times-crystallized sample from Miles Laboratories, Inc. The molecular weight of ovalbumin was taken as 45000.[5]

Methods. The water content of the sample was adjusted by conditioning in a constant-humidity apparatus at the appropriate relative humidity for 7 d. Higher water contents were adjusted by placing the sample in saturated vapor at 293 K for an appropriate period. The water content was determined gravimetrically by drying at 378±5 K *in vacuo* for 24 h.

The calorimetric measurements were performed with a Rigaku Denki differential scanning calorimeter and a hermetic aluminum pan at a heating rate of 2.5 K/min.

Results and Discussion

The thermal denaturation of ovalbumin was measured by means of DSC in the water-content range from 0.11 to 1.15 g of water per g of protein. The DSC curves showed an endothermic peak, having a temperature width 10—15 K. The temperature, T_d, and the enthalpy, ΔH_d, of denaturation were estimated from the peak temperature and the peak area of the DSC curve here obtained respectively. The T_d and ΔH_d are plotted as functions of the water content in Fig. 1.

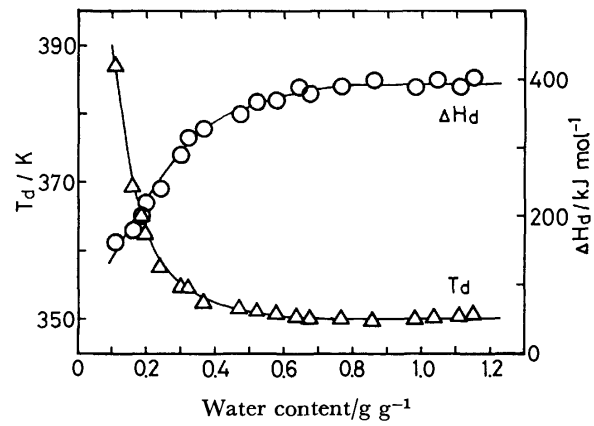

Fig. 1. The temperature, T_d, and the enthalpy, ΔH_d, of denaturation of ovalbumin as functions of the water content.

At water contents above 0.76 g/g, both T_d and ΔH_d were scarcely dependent at all on the water content. The mean values in this region were 350.5 K and 393 kJ/mol, values which were in rough agreement with those for ovalbumin in aqueous solutions.[6] Below the water content of 0.76 g/g, however, the T_d increased with a decrease in the water content. The increase became much more marked at water contents lower than about 0.35 g/g. On the other hand, the ΔH_d decreased gradually with a decrease in the water content in the same region, until the decrease became more pronounced at water contents below 0.34 g/g.

It is interesting that the T_d and ΔH_d values at water contents higher than 0.76 g/g hardly differ from those for the protein in an aqueous solution. From heat-capacity measurements on ovalbumin in the solid state with different amounts of water and in solution, Suurkuusk[7] has suggested that, between 0.1 g/g and a dilute solution, there can be no substantial change in the protein structure. It appears reasonable to assume that a conformational change similar to that which takes place in solution occurs in the solid state. In addition, it is suggested that the hydration for ovalbumin, an essential process for stabilizing its native structure, is completed at about 0.76 g/g. The hydration value is considerably higher than those determined by other techniques.[1]

According to Kauzmann,[8] the most important

contributor to the increase in heat capacity on protein denaturation is the interaction of nonpolar groups with water. At water contents below 0.76 g/g, the large decrease observed in ΔH_d may be substantially attributed to the reduction of the interactions between the exposed nonpolar groups with water, *i.e.*, the reduction of the hydrophobic hydration in the denatured state. In addition, it may be expected that, at a very low water content, the protein molecule does not completely unfold, because water is a competitor of the protein polar groups in creating "hydrogen bond." This causes a decrease in the enthalpy and entropy of protein denaturation.

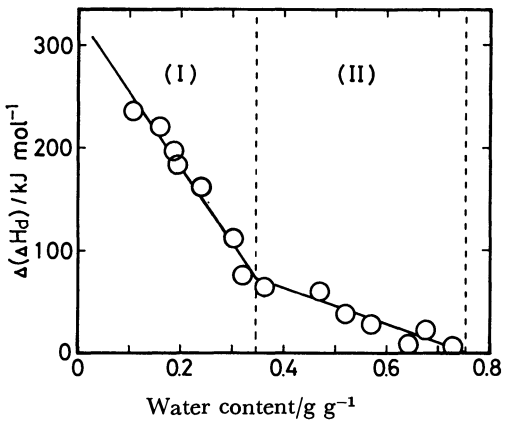

Fig. 2. The reduction in the denaturation enthalpy of ovalbumin by dehydration, $\Delta(\Delta H_d)$, as a function of the water content. The denaturation enthalpy at the full hydration is regarded as 393 kJ/mol.

Assuming that the denaturation enthalpy of ovalbumin at the full hydration is 393 kJ/mol, which is the mean at the water contents above 0.76 g/g, the reduction in the enthalpy of denaturation by dehydration, $\Delta(\Delta H_d)$, is expressed as follows:

$$\Delta(\Delta H_d) = 393 - \Delta H_d$$

where ΔH_d is the observed enthalpy of denaturation at the partial hydration. The $\Delta(\Delta H_d)$ is plotted as a function of the water content in Fig. 2. The relationship is represented by two segments of a straight line, with the break occurring at 0.34 g/g. This suggests that at least two types of phase exist in the hydration of the protein. The increase in T_d due to dehydration became much more marked at water contents below about 0.35 g/g. In an operational way, the hydration phase can be classified into two phases as follows: (I) the primary hydration phase, *i.e.*, the water contents below 0.34 g/g, and (II) the secondary hydration phase, *i.e.*, the water-content range of 0.34—0.76 g/g.

The primary hydration phase is completed at 0.34 g/g. This value is comparable to the amount of unfreezable water determined by NMR[9] and calorimetric studies,[10] which is barely sufficient to constitute a monolayer and which corresponds to 850 mol of water per mol of protein. These water molecules may be selectively arranged in the vicinity of the polar regions of a protein surface by hydrogen bonds and thus form part of a first hydration monolayer.

The secondary hydration phase is completed at 0.76 g/g. The real nature of the secondary hydration water is not yet clear, though it may be expected to play an important role in determining the structure and biological function of protein. In a recent calorimetric study of a frozen α-chymotrypsin solution, Luscher *et al.*[11] have suggested that the heat, entropy, and temperature of fusion of the secondary hydration water are lower in value than those of bulk water. This can be explained by hydrogen-bonding defects in the ice lattice. As has been pointed out by Kuntz and Kauzmann,[1] it is considered that the secondary hydration water has rotational properties only slightly different from those of bulk water and can not be readily differentiated by NMR and dielectric dispersion techniques, as there is little experimental evidence for the secondary hydration phase using either of the dispersion techniques.

References

1) I. D. Kuntz and W. Kauzmann, *Adv. Protein Chem.*, **28**, 239 (1974).
2) Y. Fujita and Y. Noda, *Bull. Chem. Soc. Jpn.*, **51**, 1567 (1978).
3) Y. Fujita and Y. Noda, *Bull. Chem. Soc. Jpn.*, **52**, 2349 (1979).
4) Y. Fujita and Y. Noda, *Int. J. Peptide Protein Res.*, **18**, 12 (1981).
5) H. Fevold, *Adv. Protein Chem.*, **6**, 187 (1951).
6) P. L. Privalov, *Biofizika*, **3**, 308 (1963).
7) J. Suurkuusk, *Acta Chem. Scand.*, **B 28**, 409 (1974).
8) W. Kauzmann, *Adv. Protein Chem.*, **14**, 1 (1959).
9) I. D. Kuntz, *J. Am. Chem. Soc.*, **93**, 514 (1971).
10) P. L. Privalov and G. M. Mrevlishvili, *Biofizika*, **12**, 22 (1967).
11) M. Luscher, P. Schindler, M. Ruegg, and M. Rottenberg, *Biopolymers*, **18**, 1775 (1979).

The Disproportionation of Dimethyldialkoxysilanes Catalyzed by Iodine Monobromide

Takeshi IBARAKI* and Katsuko ITO

Department of Natural Science, Osaka Women's University, Daisen-cho, Sakai, Osaka 590

(Received March 28, 1981)

Synopsis. Iodine monobromide is an extremely effective catalyst for the redistribution of alkoxyl groups on silicon atoms in dimethyldiakoxysilanes. The equilibrium constants of these reactions were determined at 40 °C by means of gas chromatography. Assuming that the reaction intermediate is the dative form of a dimethyldialkoxysilane–iodine monobromide complex, a mechanism of the reaction was proposed.

Although numerous examples of redistribution reactions in organosilicon compounds have been reported,[1–3] only a few studies concerning alkoxyl-alkoxyl exchange are found in the literature.[4–8] In these studies, the quantitative determination of the equilibria of the following reaction systems has been made by means of GLPC:

Tetramethoxysilane–Tetraethoxysilane[6,8]

Methyltrimethoxysilane–Methyltriethoxysilane[7]

Dimethyldimethoxysilane–Dimethyldiethoxysilane[7]

These reactions were carried out under rather severe conditions in the absence of a catalyst. Thus, to reach equilibrium the reaction mixtures were heated for 4 d at 150 °C,[6] 2 d at 120 °C,[8] or 7 d at 150 °C.[7] Consequently, the equilibrium data of such reactions at ordinary temperatures have not been available.

In the course of our studies of alkoxysilane–iodine complexing, we noticed that iodine or interhalogen compounds catalyzed alkoxyl-alkoxyl exchange, and that iodine monobromide was an especially favorable catalyst for the disproportionation of alkylalkoxysilanes. In the presence of iodine monobromide, the redistribution equilibrium was readily attained at the ambient temperature, and the equilibrium constants were determined by means of gas chromatography.

Results and Discussion

Redistribution Equilibria in Dimethyldialkoxysilanes. The following dimethyldialkoxysilane-systems were investigated at (40.0±0.1)°C:

$$Me_2Si(OEt)_2 + Me_2Si(OBu\text{-}n)_2 \rightleftharpoons 2Me_2Si(OEt)(OBu\text{-}n)$$

$$Me_2Si(OEt)_2 + Me_2Si(OBu\text{-}s)_2 \rightleftharpoons 2Me_2Si(OEt)(OBu\text{-}s)$$

$$Me_2Si(OEt)_2 + Me_2Si(OBu\text{-}i)_2 \rightleftharpoons 2Me_2Si(OEt)(OBu\text{-}i)$$

$$Me_2Si(OBu\text{-}n)_2 + Me_2Si(OBu\text{-}s)_2 \rightleftharpoons 2Me_2Si(OBu\text{-}n)(OBu\text{-}s)$$

$$Me_2Si(OBu\text{-}n)_2 + Me_2Si(OBu\text{-}i)_2 \rightleftharpoons 2Me_2Si(OBu\text{-}n)(OBu\text{-}i)$$

Both forward and reverse reactions proceeded in the presence of iodine monobromide. In most cases, the composition of the reaction mixture became constant within a few hours; the equilibrium constant was then evaluated from the composition. The values thus obtained for reactions from both sides agreed very well with each other; the results are summarized in Table 1.

Table 1. Equilibrium constants of the dispronportionatio of dimethyldialkoxysilanes catalyzed by iodine monobromide at (40.0±0.1) °C

$Me_2Si(OR)_2 + Me_2Si(OR')_2 \rightleftharpoons 2\ Me_2Si(OR)(OR')$

$K=[Me_2Si(OR)(OR')]^2/\{[Me_2Si(OR)_2][Me_2Si(OR')_2]\}$

Substituent OR	Substituent OR'	K (Forward reaction)	K (Reverse reaction)	K (Mean)
OEt	OBu-*n*	4.17±0.04	4.18±0.02	4.17±0.03
OEt	OBu-*s*	4.91±0.03	4.88±0.05	4.90±0.04
OEt	OBu-*i*	4.17±0.07	4.18±0.05	4.17±0.05
OBu-*n*	OBu-*s*	4.65±0.06	4.72±0.01	4.67±0.06
OBu-*n*	OBu-*i*	3.98±0.04	3.98±0.04	3.98±0.04

The K values of the reaction systems with ethoxy–butoxy, ethoxy–isobutoxy and butoxy–isobutoxy pairs are 4.17, 4.17, and 3.98, respectively, suggesting that these equilibria are close to the random distribution, where $K=4$. However, in the cases associated with the *s*-butoxyl group, $K=4.90$ and $K=4.67$, some deviation from random distribution is indicated.

Iodine monobromide was added to the reaction system as a piece of crystal, or solution in hexane, *o*- or *p*-xylene. The same equilibrium constant was obtained in each case; therefore, the influence of these solvents on the equilibrium state appeared to be negligible. The reaction was well-promoted in the presence of about 0.001 (mole fraction) of iodine monobromide.

It is noted that GLPC may be employed for the study of the disproportionation equilibria of alkylalkoxysilanes in which the rate of reaction is slow compared to the retention times of the reactants and products.[1] Hence, the following attempt was made to see if the GLPC technique could be employed for the study of the catalyzed reactions presented here.

The equilibrium mixture of the ethoxy–butoxy system was divided into two parts, one of which was treated with silver powder in order to allow it to react with iodine monobromide to remove the catalyst from the reaction system,[9] while the other was left untreated. The GLPC analysis of each sample gave virtually identical results, *i.e.*, $K=4.16$ was the mean value from the former case, and $K=4.15$, from the latter. (The mean value in the table is 4.17) This means that equilibrium does not shift during GLPC analysis even in the presence of iodine monobromide, and it was concluded that the composition of the equilibrium

mixture could be directly analyzed by GLPC.

Iodine Monobromide–Dimethyldialkoxysilane Complexes. The absorption spectra of iodine monobromide solutions in dimethyldialkoxysilanes were examined with a Shimadzu model UV-200 double-beam spectrophotometer, using stoppered silica cells with a path length of 10.0 mm. The visible and ultraviolet absorption peaks were observed at 428—436 nm and 218—234 nm respectively, indicating the formation of charge-transfer complexes,[10] similarly to the iodine–tetraethoxysilane system.[11]

A CT complex is usually represented as a resonance hybrid of a no-bond form and a dative form, and the dative form of a iodine monobromide–dimethyldialkoxysilane complex is regarded as $[(CH_3)_2Si(OR)_2\cdots I]^+Br^-$.

Proposed Reaction Mechanism. In the study of the disproportionation of ethyltrimethylsilane catalyzed by aluminum bromide, Russell postulated a reaction mechanism *via* a four-centered transition state.[12] An iodine monobromide–alkoxysilane complex is apparently of an ionic character, while an alkoxyl group also has considerable polarity. Consequently, in this case, a reaction intermediate with an ionic structure can be readily deduced, leading to the following mechanism, similar to that proposed by Russell:

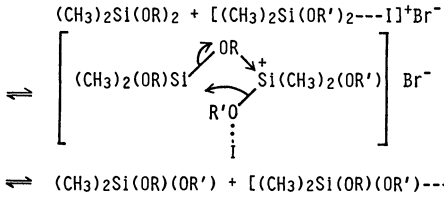

Experimental

General Procedure. In an about 10-cm³ reaction vessel with a sealing-cap, a certain amount of each alkoxysilane was placed; iodine monobromide was then added as a piece of crystal or a proper quantity of the solution in hexane, *o*- or *p*-xylene. Each reaction mixture thus prepared was divided into two or three parts and maintained in a thermostat setting of (40.0±0.1) °C. One of them was used to follow the time course of the reaction until the composition came to a constant, and then the others were used to determine the equillbrium composition.

Analysis. Analyses were performed by GLPC using a Shimadzu model GC-4B gas chromatograph with a thermal conductivity detector and equipped with a printing integrator.

In the case of the ethoxy–butoxy system, a 3 mm $\phi\times$5 m glass column with Neopak 1A (diatomaceous earth) supporting 25% PEG 4000 was employed at a column temp of 120 °C, the relative retention times being: $Me_2Si(OEt)_2$: 1, $Me_2(OEt)$-(OBu-*n*): 2.46, $Me_2Si(OBu\text{-}n)_2$: 5.85.

In the other cases, a 4 mm $\phi\times$6 m glass column with 5% Silicone OV-17 on Chromosorb W (diatomaceous earth) was used at a column temp of 110 °C. The relative retention times under these conditions were as follows: $Me_2Si(OEt)_2$: 1, $Me_2Si(OEt)(OBu\text{-}s)$: 2.30, $Me_2Si(OBu\text{-}s)_2$: 4.93, $Me_2Si(OEt)$-(OBu-*i*): 2.40, $Me_2Si(OBu\text{-}i)_2$: 4.95, $Me_2Si(OEt)(OBu\text{-}n)$: 3.30, $Me_2Si(OBu\text{-}n)(OBu\text{-}s)$: 6.67, $Me_2Si(OBu\text{-}n)(OBu\text{-}i)$: 6.68, $Me_2Si(OBu\text{-}n)_2$: 9.78.

Reagents. The dimethyldiethoxysilane was prepared by the reaction of octamethylcyclotetrasiloxane with tetraethoxysilane in the presence of potassium hydroxide.[13] The dimethyldibutoxysilanes and dimethylethoxybutoxysilanes were prepared by the iodine-catalyzed reaction of dimethyldiethoxysilane with butyl, *s*-butyl, or isobutyl alcohol. After the resulting ethanol and excess alcohol had been removed by distillation, each alkoxysilane was obtained by fractional distillation.

The dimethyldiethoxysilane was purified by repeated fractional distillation under ordinary pressure, while the dibutoxy-, di-*s*-butoxy-, and diisobutoxy-silanes were distilled under reduced pressure. The dialkoxysilanes with different alkoxyl groups were purified by means of GLPC fractional elution, employing a Shimadzu model GC-5A gas chromatograph, equipped with a model 4APP-5 autofraction collecteor. Stainless columns (8 mm $\phi\times$2.8—3.5 m) containing 25% Ucon oil on Chromosorb W or 35% PEG 6000 on Shimalite NAW were used at a column temp of 120—180 °C.

The iodine used in the alcoholysis of dimethyldiethoxysilane was purified by repeated sublimation with calcium oxide and potassium iodide. The iodine monobromide was prepared and purified by recrystallization as reported in the literature.[14]

References

1) K. Moedritzer, *Adv. Organomet. Chem.*, **6**, 171 (1968).
2) K. Moedritzer, *Organomet. Chem. Rev.*, **1**, 179 (1966).
3) J. C. Lockhart, *Chem. Rev.*, **65**, 131 (1965).
4) R. H. Krieble and C. A. Burkhard, *J. Am. Chem. Soc.*, **69**, 2689 (1947).
5) F. C. Boye and H. W. Post, *J. Org. Chem.*, **17**, 1389 (1952).
6) K. Moedritzer and J. R. Van Wazer, *Inorg. Chem.*, **3**, 268 (1964).
7) J. R. Van Wazer and K. Moedritzer, *J. Inorg. Nucl. Chem.*, **26**, 737 (1964).
8) D. N. Dolan and G. Nickless, *J. Chromatogr.*, **37**, 1 (1968).
9) W. T. Grubb and R. C. Osthoff, *J. Am. Chem. Soc.*, **77**, 1405 (1955).
10) L. J. Andrews and R. M. Keefer, *Adv. Inorg. Chem. Radiochem.*, **3**, 91 (1961).
11) K. Shinoda and J. H. Hildebrand, *J. Phys. Chem.*, **62**, 789 (1957).
12) G. A. Russell, *J. Am. Chem. Soc.*, **81**, 4815 (1959).
13) M. G. Voronkov, *J. Gen. Chem. USSR.*, **29**, 890 (1959).
14) A. I. Popov and N. E. Skelly, *J. Am. Chem. Soc.*, **77**, 3722 (1955).

The Reaction of 2-Ethoxy-1,3-oxathiolane with Carbonyl Compounds in the Presence of $ZnCl_2$ or $HgCl_2$

Shigeo TANIMOTO,* Shigeo JO,* Toyonari SUGIMOTO, and Masaya OKANO
Institute for Chemical Research, Kyoto University, Uji, Kyoto 611

(Received February 21, 1981)

Synopsis. In the reaction of 2-ethoxy-1,3-oxathiolane with carbonyl compounds in the presence of $ZnCl_2$ or $HgCl_2$, it has been found that only the breaking of the endocyclic bond (C–O or C–S bond) occurs, while the breaking of the exocyclic C–O bond to give the 1,3-oxathiolan-2-ium ion is unfavorable. This behavior is different from that of 2-ethoxy-1,3-dithiolane, in which the breaking of the endocyclic C–S bond occurs by means of $HgCl_2$ and the exocyclic C–O bond, by means of $ZnCl_2$.

It has already been shown[1] that the reaction of 2-ethoxy-1,3-dithiolane with acetone in the presence of $HgCl_2$ gives exclusively 2,2-dimethyl-1,3-dithiolane (**1**), whereas the employment of $ZnCl_2$, under otherwise identical conditions, yields 1-(1,3-dithiolan-2-yl)-2-propanone (**2**), along with **1**. The pathway leading to **1** involves the C–S bond fission of 2-ethoxy-1,3-dithiolane, and the breaking of the exocyclic C–O bond to give the 1,3-dithiolan-2-ium ion is necessary for the formation of **2**.

This report will describe the somewhat different behavior of 2-ethoxy-1,3-oxathiolane, in which these Lewis acids cause only the breaking of the endocyclic bond, with no evidence of the formation of the 1,3-oxathiolan-2-ium ion.

When 2-ethoxy-1,3-oxathiolane was allowed to react with aldehydes or ketones in dichloromethane at room temperature, in the presence of $ZnCl_2$, the corresponding 2-substituted or 2,2-disubstituted 1,3-oxathiolane (**3**) was produced as the main product in all cases.

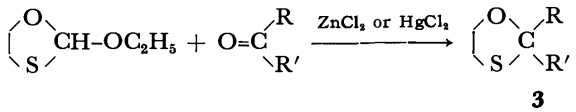

3

a: R=C_6H_5, R′=H **d**: R=R′=CH_3
b: R=$CH_3(CH_2)_2$, R′=H **e**: R=C_6H_5, R′=CH_3
c: R, R′=$-(CH_2)_5-$ **f**: R=C_6H_5CH=CH, R′=H

From the previously known data[1] it seems reasonable to propose that the coordination of the O atom in the ring with $ZnCl_2$ occurs preferentially, thus bringing about the formation of the resonance-stabilized thiocarbonium ion. The employment of $HgCl_2$ instead of $ZnCl_2$, under otherwise identical conditions, also yielded **3**. This may be also explained in terms of another path involving the intial coordination of the S atom with $HgCl_2$ and the subsequent formation of the resonance-stabilized oxycarbonium ion.

Ethyl acetoacetate, methyl acetoacetate, or acetylacetone was also used for the reaction with 2-ethoxy-1,3-oxathiolane in the presence of $ZnCl_2$ or $HgCl_2$. The reaction proceeded without a solvent at room temperature, and 1,3-oxathiolane derivatives of the **4** formula were isolated.

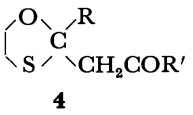

4

a: R=CH_3, R′=OC_2H_5
b: R=CH_3, R′=OCH_3
c: R=CH_3, R′=CH_3

The only product obtained was **4**; the remainder consisted of unchanged starting materials containing some resinous matter. Even in runs in which $ZnCl_2$

TABLE 1. REACTION OF 2-ETHOXY-1,3-OXATHIOLANE WITH ALDEHYDES OR KETONES

2-Ethoxy-1,3-oxathiolane, 20 mmol; Aldehyde or ketone, 20 mmol; $ZnCl_2$ or $HgCl_2$, 4 mmol; Dichloromethane, 35 ml. Reaction conditions: room temperature, 16 h.

Aldehyde or ketone R	R′	Catalyst	Product (yield/%)
C_6H_5	H	$ZnCl_2$	**3a**[a] (60), $C_6H_5CH(SCH_2CH_2OCHO)_2$[b] (14)
C_6H_5	H	$HgCl_2$	**3a**[a] (74), $C_6H_5CH(SCH_2CH_2OCHO)_2$[b] (4)
$CH_3(CH_2)_2$	H	$ZnCl_2$	**3b**[c] (53), $CH_3(CH_2)_2CH(SCH_2CH_2OCHO)_2$[d] (12)
$CH_3(CH_2)_2$	H	$HgCl_2$	**3b**[c] (72), $CH_3(CH_2)_2CH(SCH_2CH_2OCHO)_2$[d] (4)
$-(CH_2)_5-$		$ZnCl_2$	**3c**[e] (82), 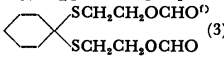 (3)
$-(CH_2)_5-$		$HgCl_2$	**3c**[e] (92)
CH_3	CH_3	$HgCl_2$	**3d**[g] (72)
C_6H_5	CH_3	$ZnCl_2$	**3e**[h] (43)
C_6H_5	CH_3	$HgCl_2$	**3e**[h] (42)
C_6H_5CH=CH	H	$HgCl_2$	**3f**[i] (39)

a) Bp 94.5—95 °C/2 Torr (lit,[2] 86—87 °C/5 Torr). NMR ($CDCl_3$): δ 7.5—7.1 (m, 5H), 5.97 (s, 1H), 4.6—4.3 (m,1H), 4.0—3.6 (m, 1H), 3.22—3.17 (m, 2H). b) Bp 170—171 °C/2 Torr. NMR ($CDCl_3$): δ 7.97 (s, 2H), 7.5—7.2 (m, 5H), 5.03 (s, 1H), 4.23 (t, 4H), 2.78 (d of t, 4H). c) Bp 83 °C/35 Torr (lit,[3] 84 °C/34 Torr). NMR ($CDCl_3$): δ 5.05 (t, 1H), 4.7—4.2 (m, 1H), 4.0—3.5 (m, 1H), 3.1—2.9 (m, 2H), 2.0—0.8 (m, 7H). d) Bp 119.5—120.5 °C/3 Torr. NMR ($CDCl_3$): δ 8.05 (s, 2H), 4.33 (t, 4H), 3.88 (t, 1H), 2.55 (d of t, 4H), 1.9—0.8 (m, 7H). e) Bp 59 °C/2.5 Torr (lit,[4] 47 °C/0.6 Torr). NMR ($CDCl_3$): δ 4.13 (t , 2H), 3.00 (t, 2H), 2.0—1.3 (m, 10H). f) Bp 153—154 °C/2 Torr. NMR ($CDCl_3$): δ 8.02 (s, 2H), 4.28 (t, 4H), 2.87 (t, 4H), 2.0—1.3 (m, 10H). g) Bp 44.5 °C/25 Torr (lit,[4] 70 °C/65 Torr). NMR ($CDCl_3$): δ 4.12 (t, 2H), 3.08 (t, 2H), 1.60 (s, 6H). h) Bp 78 °C/1.5 Torr (lit,[4] 96 °C/2 Torr). NMR ($CDCl_3$): δ 7.5—6.8 (m, 5H), 4.5—3.7 (m, 2H), 3.3—2.9 (m, 2H), 1.87 (s, 3H). i) Bp 98—101 °C/2.2 Torr. NMR ($CDCl_3$): δ 7.4—7.2 (m, 5H), 6.63 (d, 1H), 6.23 (d of d, 1H), 5.63 (d, 1H), 4.5—3.6 (m, 2H), 3.1—3.0 (m, 2H).

TABLE 2. REACTION OF 2-ETHOXY-1,3-OXATHIOLANE WITH SOME ACTIVE METHYLENE COMPOUNDS

2-Ethoxy-1,3-oxathiolane, 45 mmol; Active methylene compound, 30 mmol; Lewis acid catalyst: described in individual cases. Reaction conditions: room temperature, 24 h.

Active methylene compound R	R′	Catalyst (mmol)	Product (yield/%)
CH_3	OC_2H_5	$ZnCl_2$(7)	**4a**[a] (37)
CH_3	OC_2H_5	$HgCl_2$(11)	**4a**[a] (9)
CH_3	OC_2H_5	$FeCl_3$(6)	**4a**[a] (44)
CH_3	OCH_3	$ZnCl_2$(7)	**4b**[b] (66)
CH_3	CH_3	$ZnCl_2$(7)	**4c**[c] (28)

a) Bp 131—134 °C/25.5 Torr (lit,[4] 117 °C/20 Torr). NMR ($CDCl_3$): δ 4.17 (t, 2H), 4.13 (q, 2H), 3.06 (t, 2H), 2.87 (bs, 2H), 1.72 (s, 3H), 1.25 (t, 3H). b) Bp 82—83 °C/3 Torr. NMR (CCl_4): δ 3.98 (t, 2H), 3.53 (s, 3H), 2.92 (t, 2H), 2.70 (s, 2H), 1.62 (s, 3H). c) Bp 74—77 °C/2.5 Torr. NMR (CCl_4): δ 3.94 (t, 2H), 2.88 (t, 2H), 2.81 (s, 2H), 2.02 (s, 3H), 1.51 (s, 3H).

Table 3. Reaction of 2-ethoxy-1,3-dithiolane with some active methylene compounds using the $HgCl_2$ catalyst

2-Ethoxy-1,3-dithiolane, 33 mmol; Active methylene compound, 38 mmol; $HgCl_2$ (or $HgBr_2$) catalyst, 15 mmol. Reaction conditions: room temperature, 24 h.

Active methylene compound R	R	Catalyst	Product (yield/%)
CH_3	OC_2H_5	$HgCl_2$	**5a**[a] (35), 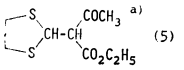 (5)
CH_3	OC_2H_5	$HgBr_2$	**5a**[a] (36), 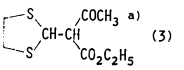 (3)
CH_3	OCH_3	$HgCl_2$	**5b**[a] (37), 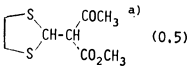 (0.5)
C_6H_5	OC_2H_5	$HgCl_2$	**5c**[b] (35), 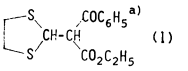 (1)
C_6H_3	CH_3	$HgCl_2$	**5d**[a] (30), 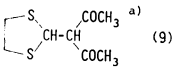 (9)
$-(CH_2)_3-$		$HgCl_2$[c]	**5e**[d] (7), 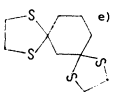 (5)
Diacetyl		$HgCl_2$	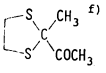 (28), 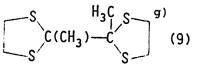 (9)

a) The data of these compounds can be seen in the literature.[5] b) Bp 163—165 °C/2 Torr. NMR ($CDCl_3$): δ 7.8—7.2 (m, 5H), 3.93 (q, 2H), 3.46 (s, 2H), 3.28 (s, 4H), 1.01 (t, 3H). c) Dichloromethane was used as the reaction solvent. d) Bp 134—136 °C/2 Torr (lit,[6] 130—136 °C/0.6 Torr). NMR ($CDCl_3$): δ 3.30 (s, 4H), 2.87 (bs, 2H), 2.5—1.9 (m, 6H). e) After the evaporation of **5e** from the crude product, the residue was column-chromatographied on silica gel, using 20% ether–hexane as the eluent, to afford this product. Mp 155—156 °C (ethanol) (lit,[7] 158—158.5 °C). NMR ($CDCl_3$): δ 3.28 (s, 8H), 2.71 (bs, 2H), 2.1—1.8 (m, 6H). f) Bp 82—84 °C/2 Torr. NMR ($CDCl_3$): δ 3.43 (bs, 4H), 2.39 (s, 3H), 1.81 (s, 3H). g) Mp 83—84 °C (ethanol) (lit,[8] 83 °C). NMR ($CDCl_3$): δ 3.5—3.3 (m, 8H), 2.03 (s, 6H).

was employed, none of the product which would arise from the intermediate 1,3-oxathiolan-2-ium ion was detected. On the other hand, in our previous work[5] on the reaction of 2-ethoxy-1,3-dithiolane with active methylene compounds in the presence of $ZnCl_2$, the exclusive formation of the intermediate 1,3-dithiolan-2-ium ion was observed. When $HgCl_2$ was used instead of $ZnCl_2$, the reaction with the dithiolane proceeded *via* a resonance-stabilized thiocarbonium ion. The formation of 1,3-dithiolane derivatives with the formula of **5** in this reaction suggests that the coordination of $HgCl_2$ with the S atom in the 1,3-dithiolane ring is favorable. The products obtained in the reaction are summarized in Table 3.

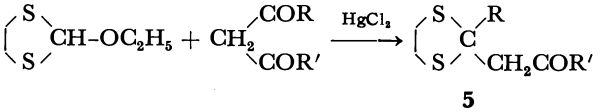

5

a: R=CH_3, R'=OC_2H_5 **d**: R=R'=CH_3
b: R=CH_3, R'=OCH_3 **e**: R, R'=$-(CH_2)_3-$
c: R=C_6H_5, R'=OC_2H_5

Experimental

Reaction of 2-Ethoxy-1,3-oxathiolane with Aldehydes or Ketones. To a mixture of 2-ethoxy-1,3-oxathiolane (20 mmol) and an aldehyde (or a ketone) (20 mmol) in dichloromethane (35 ml), we added $HgCl_2$ (or $ZnCl_2$) (4 mmol) at 0—5 °C. The mixture was stirred for 16 h at room temperature and then poured into a mixture of water and dichloromethane. The organic layer was separated, and then it was combined with a dichloromethane extract of the aqueous phase. The dichloromethane solution was washed with dilute aqueous $NaHCO_3$, and then with water, dried over $MgSO_4$, and distilled.

Reaction of 2-Ethoxy-1,3-oxathiolane with Active Methylene Compoundes. To a mixture of 2-ethoxy-1,3-oxathiolane (45 mmol) and an active methylene compound (30 mmol), we added a Lewis-acid catalyst (as is shown in Table 2) at 0—5 °C. The mixture was stirred for 24 h at room temperature and then worked up as above.

Reaction of 2-Ethoxy-1,3-dithiolane with Active Methylene Compounds in the Presence of $HgCl_2$. To a mixture of 2-ethoxy-1,3-dithiolane (33 mmol) and an active methylene compound (38 mmol), we added $HgCl_2$ (or $HgBr_2$) (15 mmol) at 0—5 °C. The mixture was stirred for 24 h at room temperature and then poured into a mixture of ice water and ether. The organic layer was separated and combined with an ethereal extract of the aqueous phase. The ethereal solution was washed with dilute aqueous $NaHCO_3$, and then with water, dried over $MgSO_4$, and distilled. The product was further purified by column chromatography on silica gel, if necessary (the eluent in most cases was 50% hexane–ether).

References

1) S. Jo, S. Tanimoto, T. Oida, and M. Okano, *Bull. Chem. Soc. Jpn.*, in press.
2) F. Kipnis and J. Ornfelt, *J. Am. Chem. Soc.*, **71**, 3555 (1949).
3) B. E. Leggetter and R. K. Brown, *Can. J. Chem.*, **41**, 2671 (1963).
4) C. Djerassi and M. Gorman, *J. Am. Chem. Soc.*, **75**, 3704 (1953).
5) S. Tanimoto, Y. Matsumura, T. Sugimoto, and M. Okano, *Bull. Chem. Soc. Jpn.*, **51**, 665 (1978).
6) M. P. Mertes, *J. Org. Chem.*, **26**, 5236 (1961).
7) E. E. Smissman and J. L. Diebold, *J. Org. Chem.*, **33**, 1466 (1968).
8) F. Chastrette, M. Hassambay, and M. Chastrette, *Bull. Soc. Chim. Fr.*, **1976**, 601.

Flavonoids of *Polygonum sieboldi* and *P. filiforme*

Takahiko Isobe,* Keiji Kanazawa, Makoto Fujimura, and Yukinao Noda
Department of Chemistry, Hyogo College of Medicine, Mukogawa-cho, Nishinomiya, Hyogo 663
(Received May 25, 1981)

Synopsis. Five flavonoids containing a new flavonol glycoside were isolated from *Polygonum sieboldi* and *P. filiforme*. The structure of the new compound was determined as quercetin 3-rhamnoside 2″-gallate by chemical and spectroscopic data.

Many flavonoids have been isolated from *Polygonum* species (*Polygonaceae*), and we previously reported the identification of five flavonoids from *P. nodosum* Pers.[1,2] Further investigation of this species has led to the isolation of several flavonoids containing a new compound. Two known compounds, quercetin (**1**) and quercetin 3-rhamnoside (**2**), were isolated from *P. sieboldi* Maxim. (Akino-unagitsukami in Japanese) and four known compounds, **1**, **2**, myricetin 3-rhamnoside (**3**), and quercetin 3-glucoside 2″-gallate (**4**), and a new flavonoid glycoside (**5**) were isolated from *P. filiforme* Thunb. (Mizuhiki in Japanese). The ^{13}C NMR spectrum of **5** and the ^{1}H NMR spectrum of the TMSi ether of **5** (**6**) were almost identical with that of **4** with the exception of the sugar part, which was assignable as L-rhamnose from these spectra.[3,4] The fragment ions of **5** by MS spectrum are assignable as quercetin (*m/z* 302), gallic acid (170), and galloyl group (153). The UV spectrum of **5** shows also the presence of a substituted hydroxyl group at C-3 of flavonol by bathochromic shifts in addition of both NaOAc and $AlCl_3$–HCl.[2,4] The compound obtained by the hydrolysis of **5** with aqueous ammonia was identical with **2** by TLC. From the ^{13}C shift values ($\Delta\delta$) of C-2, C-3, and C-4 of rhamnose of **5** having *ca.* −3.0, +1.0, and −2.0, respectively,[3] and the downfield shift of H-2 (δ 5.56) of rhamnose of **6** by ^{1}H NMR spectrum, the galloyl group may be attached to C-2 of rhamnose. Accordingly, compound **5** has the structure of quercetin 3-α-L-rhamnopyranoside 2″-gallate. The similar compound, myricetin 3-α-L-rhamnopyranoside 2″-gallate[5] had been isolated some years ago.

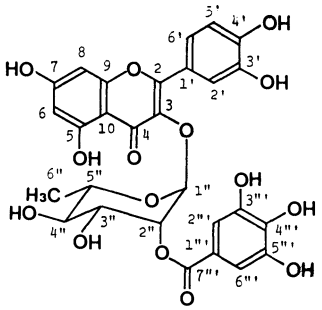

5

Experimental

Isolation of Flavonoids. By the previous reported procedure,[2] compounds **1** and **2** from *P. Sieboldi* Maxim., and compounds **1**, **2**, **3**, **4**, and **5** from *P. filiforme* Thunb. Compounds **1**, **2**, **3**, and **4** were identified as quercetin, quercetin 3-rhamnoside, myricetin 3-rhamnoside, and quercetin 3-glucoside 2″-gallate, respectively, by comparison with the TLC and the IR spectra of authentic samples and thier acetates.

Isolation of Quercetin 3-Rhamnoside 2″-Gallate (5). Compound **5**, yellowish plates from MeOH–H_2O, mp 207—208.5 °C; $[\alpha]_D^{25}$ −1.8 (*c*=0.9, MeOH); Found: C, 50.92; H, 3.94%. Calcd for $C_{28}H_{24}O_{15}\cdot 3H_2O$: C, 51.38; H, 4.62%; MS (20 eV) *m/z* 302, 170, and 153; UV (EtOH): λ_{max} 257 (sh), 267 (ε 27900), and 351 nm (ε 16400), (+$AlCl_3$): 276, 303 (sh), and 432 nm, (+$AlCl_3$+HCl): 271, 355, and 400 nm (sh), (+NaOAc): 273 and 359 nm; IR (Nujol): ν_{max} 3250, 1710, 1655, 1605, and 1205 cm^{-1}; ^{13}C NMR (25 MHz, DMSO-d_6): δ 17.7 (C-6″), 68.6 (C-3″), 70.8 (C-5″), 71.8 (C-2″ and 4″), 93.8 (C-8), 98.5 (C-1″), 98.9 (C-6), 104.1 (C-10), 109.0 (C-2‴ and 6‴), 115.7 (C-2′ and 5′), 119.3 (C-1‴), 120.6 (C-1′), 121.2 (C-6′), 133.4 (C-3), 138.6 (C-4‴), 145.3 (C-3′), 145.5 (C-3‴ and 5‴), 148.6 (C-4′), 156.5 (C-2), 157.3 (C-9), 161.3 (C-5), 164.3 (C-7‴), 165.0 (C-7), and 177.5 (C-4).

TMSi Ether of 5 (6). ^{1}H NMR (100 MHz, $CDCl_3$): δ 0.99 (3H, d, *J*=6 Hz, H-6″), 3.4 (1H, m, H-5″), 3.57 (1H, t, *J*=8 Hz, H-4″), 4.02 (1H, dd, *J*=8 and 2 Hz, H-3″), 5.56 (1H, t, *J*=2 Hz, H-2″), 5.66 (1H, d, *J*=2 Hz, H-1″), 6.26 (1H, d, *J*=2 Hz, H-6), 6.37 (1H, d, *J*=2 Hz, H-8), 6.97 (1H, d, 8 Hz, H-5′), 7.23 (2H, s, H-2‴ and 6‴), 7.37 (1H, d, *J*=2 Hz, H-2′), and 7.51 (1H, dd, *J*=8 and 2 Hz, H-6′).

Alkaline Hydrolysis of 5. To **5** (7 mg) were added 0.1 mol dm^{-3} aqueous ammonia (0.8 ml) and MeOH (1 ml) and the mixture allowed to stand for one day at room temperature. From the TLC of the reacting solution, the product was identified as quercetin 3-rhamnoside (**2**) [on silica gel plate; solvent, EtOAc–MeCOEt–HCO_2H–H_2O, 5 : 2 : 0.1 : 1].

We are grateful to Mr. Kozo Shibata, Osaka City University, for the measurement of ^{1}H and ^{13}C NMR.

References

1) T. Isobe, T. Fukushige, and Y. Noda, *Chem. Lett.*, **1979**, 27.
2) T. Isobe, N. Ito, and Y. Noda, *Phytochemistry*, **19**, 1877 (1980).
3) K. R. Markham, B. Ternai, R. Stanley, H. Geiger, and T. J. Mabry, *Tetrahedron*, **34**, 1389 (1978).
4) T. J. Mabry, K. R. Markham, and M. B. Thomas, "The Systematic Identification of the Flavonoids," Springer, New York (1970).
5) G. G. Zapesochnaya and G. P. Shnyakiana, *Khim. Prir. Soedin.*, **1975**, 720.

"Anomalous" Raman Polarization as Observed in Anthracene Anion

Etsuko FUJIMOTO, Toshio KAMISUKI, and Shiro MAEDA*

Research Laboratory of Resources Utilization, Tokyo Institute of Technology, Midori-ku, Yokohama 227

(Received December 27, 1980)

An example of "anomalous" Raman polarization is presented by measuring the polarization dispersion of a resonant depolarized line of anthracene anion near the first absorption band. The molecular origin of the asymmetric Raman tensor is discussed on the basis of a vibronic effect associated with the resonant electronic level.

Anomalous polarization refers to an unusual aspect of polarization in vibrational Raman scattering, in which the depolarization ratio exceeds the normal maximum value $\rho=3/4$ in isotropic media. This occurs when the scattering tensor becomes appreciably asymmetric under appropriate resonance conditions. Asymmetry of the scattering tensor is by no means unusual in the Raman transition between different electronic states.[1] In vibrational Raman transitions within the non-degenerate ground state, the tensor usually has a virtually symmetric form even when an asymmetry is claimed from the group theory, leading to the well-known rule $\rho \leqq 3/4$.

Deviation from the rule was first demonstrated by Spiro and Strekas for the extreme case of $\rho \simeq \infty$ (inverse polarization) in cytochrome C and hemoglobin.[2] This remarkable state of polarization arises from an entirely antisymmetric Raman tensor, which may really exist only in molecules with three-fold or higher symmetry axes. Namely, the orbital degeneracy of electronic excited states contributing to the scattering tensor plays an essential role in bringing about the antisymmetric tensor. Less striking cases of $3/4<\rho<\infty$ were subsequently found in various porphyrins and heme proteins,[3] but the tensor asymmetry in those systems could be understood in essentially the same vibronic scheme as in the original high symmetry case. Anomalous polarization of somewhat different origin was also found out in IrX_6^{2-},[4] where the degeneracy of the electronic ground state is responsible for the tensor asymmetry.

Now, confining our attention to the usual vibrational Raman spectrum in non-degenerate ground state, it may be noted that, from the group theoretical point of view, the scattering tensor is not always symmetric but is rather often asymmetric. Particularly, in lower symmetries without any three-fold or higher axes, which occur in a majority of organic molecules, the tensor of non-totally symmetric vibrations is always asymmetric, so that the depolarization ratio is greater than 3/4. Such an argument is of little significance in ordinary non-resonant Raman observations, where the antisymmetric part of the tensor almost dies out by the nature of wave-functions,[5] but may become more realistic if an appropriate resonance condition is found. An example substantiating this remark has been given in a previous study on dehydro annulenes of D_{2h} symmetry.[6] In some point groups, on the other hand, tensor asymmetry is also possible for totally symmetric vibrations: an example of such a type of anomaly was found out very recently in Fe(II)-bis[1-(2'-pyridylmethyleneamino)-2-aminoethane] ion of C_2 symmetry.[7]

In view of the particular significance of anomalous polarization in connection with the vibronic interaction, further experimental evidence should be sought. In this context, we take anthracene anion (An^-) as a promising candidate, because our previous resonance Raman study[8] of this system recorded a remarkably resonant depolarized line at 1466 cm^{-1}, which is supposed to be 'anomalous' intrinsically. In order to study the behavior of this line more definitely, the polarization dispersion has been carefully measured near the first absorption band.

Experimental

Anthracene anion was prepared by bringing anthracene into contact with metallic sodium in tetrahydrofuran (THF). The Raman spectra were obtained by $\approx 10^{-3}$ mol dm^{-3} THF solutions at room temperature. The intensity and depolarization ratio of 1466 cm^{-1} line were determined by the band area, using 914 cm^{-1} THF line as a standard. Since there exists a weak and broad depolarized band of THF extending over 1400—1550 cm^{-1}, due correction was made by subtracting the contribution from the measured area.

The MCD spectrum was recorded for a $\approx 10^{-6}$ mol dm^{-3} THF solution under the field strength of 10^4 G.

Results and Discussion

The whole span Raman spectrum recorded by 514.5 nm excitation is shown in Fig. 1 by the parallel and perpendicular scattered components. It is observed that the depolarization ratio of 1466 cm^{-1} line is slightly but certainly greater than 3/4 even in this

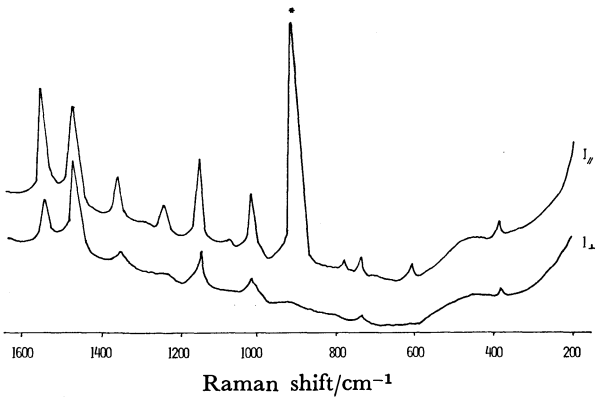

Fig. 1. Resonance Raman spectra of anthracene anion in THF solution by 514.5 nm excitation, obtained by parallel and perpendicular polarization conditions. Solvent line is marked by *.

moderately resonant condition. A partial spectral record of the interesting region is shown in Fig. 2 for some different exciting frequencies; here the dotted line indicates the baseline due to the solvent scattering as estimated in proportion to 914 cm^{-1} THF line. Uniform instrumental sensitivity for the two different analyzer settings has been confirmed by measuring well-defined depolarized lines of a known sample.

Since the deviation of ρ from the normal behavior was rather small in the observed region, the measurement was carefully made by repeated scanning with an alternating polarization sequence. The ρ values averaged for 6—7 records are plotted in Fig. 3 against the exciting laser frequency, together with the intensity plot and absorption curve. Scatter of the data was fairly small, and the composite error including the baseline uncertainty is estimated to be well within 10%. Although accurate measurement was impeded by increasing fluorescence in the more interesting region closer to the absorption maximum, the depolarization ratio has been verified to increase beyond the normal maximum of 3/4 along with the intensity, indicating the resonantly increasing tensor asymmetry.

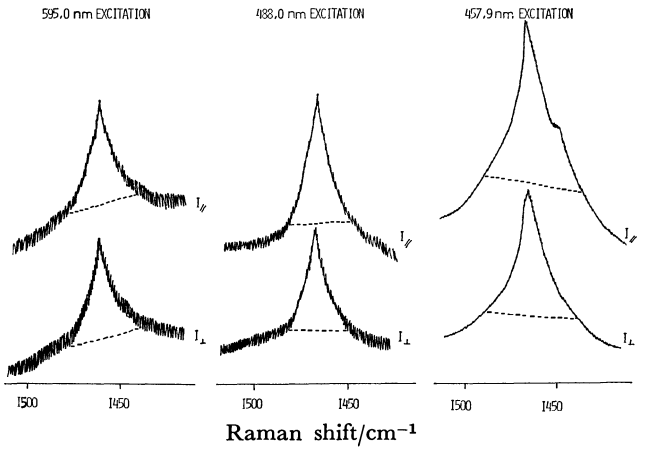

Fig. 2. Changes in polarization features of 1466 cm^{-1} line by different exciting light frequencies, where the dotted line indicates the baseline due to the solvent scattering.

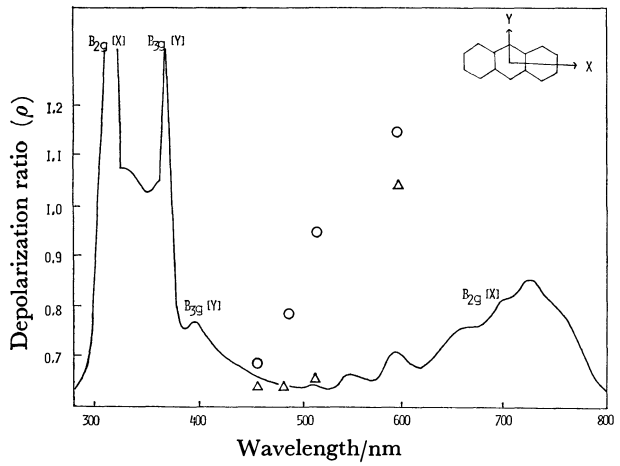

Fig. 3. Polarization dispersion (○) and excitation profile (△) of 1466 cm^{-1} line of anthracene anion in THF solution, with the electronic absorption spectrum.

The ρ value at 457.9 nm excitation is observed to be slightly lower than 3/4 in Fig. 3, in contradiction to the presumably non-totally symmetric nature of 1466 cm^{-1} mode. This is properly ascribed to the effect of a polarized line included in the measured area, because such a signal emerges at about 1450 cm^{-1} in the parallel component of 457.9 nm record as the result of much reduced resonance effect in 1466 cm^{-1} scattering. This polarized line may be reasonably assigned to an a_g mode corresponding to 1480 cm^{-1} of neutral anthracene.

The polarization dispersion as observed above is properly interpreted as due to the vibronic mixing that gives rise to a polarization change of the resonant electronic transition. In order to see the circumstances more precisely, the nature of the relevant electronic states has been investigated by a PPP-SCF-MO calculation and MCD measurement. The polarization of each transition predicted by the calculation is consistent with the sign of the observed ellipticity $[\theta]_M$, assuming B-term contributions in the MCD spectrum. The results are listed in Table 1 and the assignment of transitions is shown in Fig. 3. These results indicate that the first B_{2g} excited state with x-polarized transition moment has a good possibility to vibronically couple with the next B_{3g} states of y-polarization through b_{1g} in-plane vibrations. Then, the b_{1g} Raman tensor having the form $\begin{pmatrix} 0 & \alpha_{xy} & 0 \\ \alpha_{yx} & 0 & 0 \\ 0 & 0 & 0 \end{pmatrix}$ can be appreciably asymmetric for exciting laser frequencies sufficiently close to the first absorption band, because in such a resonant condition, the non-zero element is shown to be approximately represented[6] by the predominant term as

Table 1. Assignment of electronic absorption spectrum for anthracene anion

Observed transition			Calculated transion		
Abs. spectrum	MCD spectrum		PPP-SCF-CI		
Wavelength/nm	Wavelength/nm	$[\theta]_M$	Wavelength/nm	Symmetry type	Direction of polarization
726		+	822	$B_{2g}\leftarrow B_{1u}$	x
400	410	−	485	$B_{3g}\leftarrow B_{1u}$	y
366	365	−	344	$B_{3g}\leftarrow B_{1u}$	y
326	325	+	294	$B_{2g}\leftarrow B_{1u}$	x

$$\alpha_{xy} \propto \frac{\mu_x(\partial\mu_y/\partial Q)_0}{\nu_e+\nu_R-\nu+i\Gamma}, \quad \alpha_{yx} \propto \frac{\mu_x(\partial\mu_y/\partial Q)_0}{\nu_e-\nu+i\Gamma}. \tag{1}$$

Here μ, ν_e, and Γ are the moment, frequency, and damping factor of the resonant B_{1u} (ground)$\rightarrow B_{2g}$ transition, ν_R and Q are the frequency and normal coordinate of the b_{1g} Raman mode, and ν is the laser frequency. The depolarization ratio is thus given[6] by

$$\rho = \frac{3}{4}+\frac{5}{4}\left|\frac{\alpha_{xy}-\alpha_{yx}}{\alpha_{xy}+\alpha_{yx}}\right|^2 = \frac{3}{4}+\frac{5}{16}\frac{\nu_R^2}{(\nu_e+1/2\nu_R-\nu)^2+\Gamma^2}, \tag{2}$$

which is appreciably greater than 3/4 in the resonant region.

Further insight into the origin of the asymmetric tensor may be obtained by applying Warshel's model,[9] which approximately represents the transition moment derivative by an assembly of the products of transition monopoles q_i, allocated to individual atoms, and the corresponding components of normal mode vector $L^{i\sigma}$

$$\partial\mu_\sigma/\partial Q = \sum_i q_i L^{i\sigma}(m_i\nu_R)^{-1/2}. \quad m_i\text{: atomic mass} \tag{3}$$

The transition monopoles of the first absorption band as calculated by PPP-SCF-CI method are shown by the circles in Fig. 4.

Since available vibrational data of the anion have been quite insufficient for obtaining $L^{i\sigma}$ accurately, a normal mode calculation has been made for neutral anthracene using the library programs BGLZ and LSMB at the Computer Center, the University of Tokyo. The calculated Raman frequencies are shown in Table 2 together with those observed for neutral and anion species, the force constants being given in Table 3. The vibrational mode of 1466 cm^{-1} anion line may be properly related to ν_{16} and ν_{17} modes of the neutral molecule, which are shown in Fig. 4 by calculated atomic displacements. The MO calculation suggests that the anion mode is more closely allied to the neutral ν_{16} mode, because the change in bond order from neutral to anion predicts a down-shift of ν_{16} as large as 87 cm^{-1} in contrast with only 3 cm^{-1} up-shift of ν_{17}. Then, by putting the ν_{16} neu-

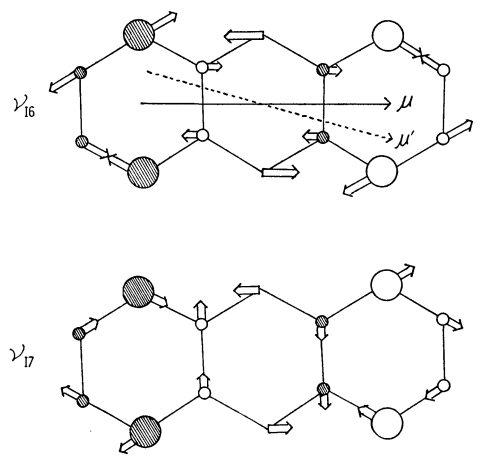

Fig. 4. Transition monopoles of the resonant An^- transition and the atomic displacements of b_{1g} modes of anthracene related with 1466 cm^{-1} An^- mode. Open and hatched circles designate positive and negative transition monopoles respectively. $\mu'-\mu$ gives the change of transition dipole.

Table 2. Assignment of Raman spectra for anthracene

		Calcd[a] $\tilde{\nu}$/cm^{-1}	Obsd $\tilde{\nu}$/cm^{-1}		
		Neutral	Neutral		Anion
			CCl_4 soln[10]	Crystal[11]	THF soln[8]
a_g	ν_1	3089			
	ν_2	3087			
	ν_3	3085			
	ν_4	1575	1561	1556 s	1545
	ν_5	1472	1479	1480 s	1450
	ν_6	1405	1406	1400 s	1363
	ν_7	1257	1260	1264 vs	1234
	ν_8	1145	1164	1164 vs	1153
	ν_9	1013	1006	1007 vs	1024
	ν_{10}	737		754 vs	738
	ν_{11}	665		625 w	
	ν_{12}	373	394	397 vs	390
b_{1g}	ν_{13}	3092			
	ν_{14}	3086			
	ν_{15}	1669	1634	1632 s	
	ν_{16}	1570		1574 w	1466
	ν_{17}	1346		1346 w	
	ν_{18}	1232		1273 w	
	ν_{19}	1173	1183	1187 vs	
	ν_{20}	1093		1102 w	
	ν_{21}	903		903 w	
	ν_{22}	544	523	521 vs	
	ν_{23}	405			

a) UBFF modified by taking into account the contribution of resonance of 4 Kekulé structures.

Table 3. Force constants for anthracene

Stretching	$K(C_1-C_2)$	5.0 mdyn $Å^{-1}$
	$K(C_2-C_3)$	4.3
	$K(C_3-C_4)$	6.1
	$K(C_4-C_5)$	4.4
	$K(C_2-C_7)$	4.4
	K(C-H)	4.8
Deformation	H(C-C-C)	0.30
	H(C-C-H)	0.20
Repulsion	$F(C_1\cdots C_3)$	0.70
	$F(C_2\cdots C_4)$	0.45
	$F(C_3\cdots C_5)$	0.45
	$F(C_1\cdots C_7)$	0.45
	$F(C_2\cdots C_{14})$	0.45
	F(C···H)	0.35
Kekulé constant		0.30

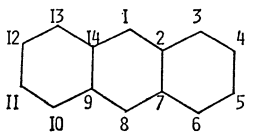

tral mode in place of the 1466 cm^{-1} anion mode, we can trace the ultimate source of the off-diagonal tensor elements, Eq. 1, to the wagging motion of $B_{1u} \rightarrow B_{2g}$ transition moment μ_x, which mostly comes from the rotational motion of the four equivalent carbon atoms at 3, 6, 10, and 13 positions which carry the predominant transition monopoles.

"Anomalous" polarization as reported above is by no means a unique occurrence theoretically, but should be observed quite generally as long as it is measured under well-resonant conditions. Nevertheless, it seems still worth investigating in view of its particular significance in studying the vibronic interaction in complex molecules.

The authors wish to thank Professor Makoto Miwa and Dr. Tomoko Komiyama of Seikei University for providing the facilities of MCD measurement.

References

1) A. Kiel and S. P. S. Porto, *J. Mol. Spectrosc.*, **32**, 458 (1969).
2) T. G. Spiro and T. C. Strekas, *Proc. Natl. Acad. Sci. U.S.A.*, **69**, 2622 (1972).
3) For example, D. W. Collins, D. B. Fitchen, and A. Lewis, *J. Chem. Phys.*, **59**, 5714 (1973); S. Sunder and H. J. Bernstein, *Can. J. Chem.*, **52**, 2851 (1974); A. L. Verma, R. Mendelsohn, and H. J. Bernstein, *J. Chem. Phys.*, **61**, 383 (1974).
4) H. Hamaguchi, I. Harada, and T. Shimanouchi, *Chem. Phys. Lett.*, **32**, 103 (1975); H. Hamaguchi and T. Shimanouchi, *ibid.*, **38**, 370 (1976).
5) A. C. Albrecht, *J. Chem. Phys.*, **34**, 1476 (1961).
6) E. Fujimoto, N. Yoshimizu, S. Maeda, M. Iyoda, and M. Nakagawa, *J. Raman Spectrosc.*, **9**, 14 (1980).
7) P. W. Jensen, *Chem. Phys. Lett.*, **77**, 267 (1981).
8) C. Takahashi and S. Maeda, *Chem. Phys. Lett.*, **22**, 364 (1973).
9) A. Warshel, *Chem. Phys. Lett.*, **43**, 273 (1976).
10) E. D. Schmid, H. Derner, and G. Berthold, *J. Raman Spectrosc.*, **4**, 329 (1976).
11) A. Bakke, B. N. Cyvin, J. C. Whitmen, S. J. Cyvin, J. E. Gustavsen, and P. Klaeboe, *Z. Naturforsch., Teil A*, **34**, 579 (1979).

1-Chloro-1,3-butadiene Copolymers. III. Reactivity of 1-Chloro-1,3-butadiene in Radical Copolymerizations

Shinzo KOHJIYA,* Hideo TAKEUCHI, Kohshi KAWAMOTO, and Shinzo YAMASHITA

Department of Chemistry, Kyoto Institute of Technology, Matsugasaki, Sakyo-ku, Kyoto 606

(Received November 14, 1980)

Radical copolymerizations of 1-chloro-1,3-butadiene (CB) were carried out with styrene (St), 1,3-butadiene (Bd), or chloroprene (Cp) in toluene at 70 °C by AIBN. The monomer reactivity ratios are found as follows: $r_{CB}=1.21\pm0.10$, $r_{St}=0.10\pm0.03$; $r_{CB}=0.27\pm0.02$, $r_{Bd}=0.56\pm0.03$. Copolymerization of CB and Cp showed CB was much less reactive than Cp. The Q and e values of CB were calculated to be 3.13 and +0.65, respectively. ^{1}H NMR and IR of poly(CB-co-St) showed 60% of CB units are of 1,4-configuration and the rest 3,4-configuration.

On the polymerization of 1-chloro-1,3-butadiene (CB), only a few papers[1-4] have been published up to now, while there have been so many works relevant to polychloroprene. This difference is probably due to their industrial significance. Carothers studied the polymerizations of 1,3-butadiene, chloroprene, and CB in the course of his research to synthesize a new synthetic rubber.[1] Klebanskii *et al.*[2] briefly reported the polymerizations of CB and 1-bromo-1,3-butadiene. Winston and Wichacheewa carried out the radiation-induced copolymerization of CB and styrene, and reported the monomer reactivity ratios.[3] They claimed all the CB units in the polymer are of 1,4-configuration.[3] However, in our previous studies on the polymer reactions and physical properties of CB–butadiene and CB–styrene copolymers,[4-7] it was pointed out that the CB units carried two different kinds of chlorine in their reactivity, suggesting the coexistence of two configurations of the CB unit, *i.e.*, 1,4- and 3,4-microstructures.[5-7]

In the present work, the reactivity of CB in radical polymerizations was determined relative to styrene, 1,3-butadiene or chloroprene, and the microstructure of CB units was analyzed by spectroscopic methods. This study will provide fundamental data of much importance in the syntheses and chemical modifications of CB copolymers.

Experimental

Materials. 1-Chloro-1,3-butadiene (CB) was prepared according to the method of Heasley and Lais.[8] The product was distilled twice just before use: bp 65—67 °C (lit,[8] 65—68.5 °C), yield 40%. Purity by GLPC was above 98%. Commercial 1,3-butadiene (Bd) was purified by the method previously reported.[9] Chloroprene (Cp) was distilled twice under a reduced pressure. Its purity by GLPC was 99.7%, and the trace amount of impurity (below 0.3%) was CB. Styrene (St), 2,2′-azobisisobutyronitrile (AIBN), toluene, and ethylbenzene were purified according to the usual procedures. As low mol-wt model compounds for CB units in the polymer, 1-chloro-2-butene (**1**, for the 1,4-microstructure) and 1-chloro-1-butene (**2**, for the 3,4-microstructure) were subjected to ^{1}H NMR measurements. The compound **2** was prepared by the method of Henne *et al.*,[10] and **1** was commercially available from Tokyo Kasei Kogyo Co., Ltd. Both were purified by repeated distillations.

Polymerization Procedures. Monomers, AIBN, and toluene were introduced into a glass ampoule. The ampoule was connected to a vacuum system, and was subjected to degassing, followed by the sealing *in vacuo*. When Bd was used as monomer, it was introduced into the ampoule by the vacuum distillation method. The ampoule was placed in a bath maintained at 70 °C and rotated at a speed of 24 min^{-1}. In the copolymerization of CB and Cp, the reaction was conducted under a nitrogen atmosphere and aliquots of the polymerization solution were withdrawn by a syringe at fixed time intervals. The aliquots then were mixed with acetone containing ethylbenzene as an internal standard for GLPC (carrier flow gas, hydrogen: column; LP 84, 65 °C).

Analyses of Polymers. IR and ^{1}H NMR spectra were measured on a Hitachi IR Spectrophotometer 215 and a Varian T-60A Spectrometer, respectively. Viscosity measurements were carried out in toluene using an Ubbelohde viscometer at 25.9 °C for the CB–Bd copolymer and at 30 °C for the CB–St copolymer. Copolymer compositions were determined by elemental analysis and/or ^{1}H NMR. Monomer reactivity ratios (MRRs) were calculated by the Fineman-Ross method.

Results and Discussion

Stability of CB Copolymers. The stability of poly(CB-co-Bd)s obtained by emulsion polymerization has been reported.[7] According to the results, the allylic chlorine in these CB–Bd copolymers was easily hydrolyzed to give a hydroxyl group because they were produced in an aqueous medium.[7] The CB copolymers obtained in toluene solution also contain allylic chlorines as will be described later in this paper. However, these polymers were produced under non-aqueous conditions, and could be kept unchanged for a few months. Table 1 shows the change of poly(CB-co-St) with standing time. Oxygen was detected from the CB copolymers obtained by emulsion polymeriza-

Table 1. Elemental analysis of poly(CB-co-St)[a]

Standing time[b] / d	C (%)	H (%)	Cl (%)	Total (%)
10	76.30	6.21	15.60	98.11
50	77.25	6.83	15.38	99.45
100	76.81	6.60	14.95	98.36
(Calcd)[c]	(77.59)	(6.51)	(15.90)	(100)

a) Polymer sample No. 3 in Table 2. b) Time in day after the polymerization. c) Calculated values for poly(CB-co-St) whose CB content is 43.9 mol%.

tion,[7] but it is not the case for the poly(CB-co-St) by solution polymerization as indicated in Table 1. While the found values of C, H, and Cl contents were in good agreement with the theoretical ones even after the storage for 100 d, these polymers began to color slightly and became darker with time in several months. Therefore, all the copolymer samples were treated in a few months after the polymerization.

Copolymerization of CB with St or Bd. Elemental analysis is applicable to the composition determination of many copolymers. The compositions of CB–St and CB–Bd copolymers were determined by the elemental analysis of chlorine. In case of CB–St copolymers, their ^{1}H NMR spectra also allow us to evaluate the compositions since the phenyl protons of St units in the copolymer appear separately from the others at a lower field as shown later in Fig. 3. Table 2 shows the results of composition determination of poly(CB-co-St) both by elemental analysis and by ^{1}H NMR. A very good agreement was found between the compositions obtained by two methods. Thus, ^{1}H NMR was equally employed to determine the composition of CB–St copolymers.

The copolymer composition curves, A for poly(CB-co-St), and B for poly(CB-co-Bd), are shown in Fig. 1. The times of polymerizations were adjusted to get the conversions below 10% so that Mayo-Lewis' equation could be used to evaluate the MRRs. From the experimental points in Fig. 1, MRRs were given as follows:

Copolymerization of CB (M_1) and St (M_2),

$$r_1 = 1.21\pm0.10,\ r_2 = 0.10\pm0.03;$$

Copolymerization of CB (M_1) and Bd (M_2),

$$r_1 = 0.27\pm0.02,\ r_2 = 0.56\pm0.03.$$

The solid lines in Fig. 1 are calculated ones from these values and fit well with the experimental points. Q and e values for CB were evaluated from the MRRs with St as follows:

$$Q = 3.13,\ e = +0.65.$$

The same values from the copolymerization with Bd were $Q=1.01$ and $e=+0.33$. These values are understandable because CB is a conjugated diene and has an electron-withdrawing chlorine. The composition curve, B, in Fig. 1 is of an inversed sigmoid shape, which suggests an alternating tendency for CB–Bd pair. Since Bd has a negative e value (-1.05[11]), the positive e value obtained for CB is in conformity with the observed alternating tendency.

Copolymerization of CB with Cp. Both CB and Cp are diene monomers of the same molecular formula. Consequently, it was difficult to determine the composition of the copolymer accurately by elemental analysis or ^{1}H NMR. Here, in order to compare the reactivity of the two monomers, the consumptions of monomers with the time of polymerization were determined by GLPC. Figure 2 shows the amount of residual monomers plotted against time of polymerization. Curves A and B indicate the decreases of CB and Cp in their homopolymerizations, respectively, and Cp was found to be polymerized faster than CB under the present conditions. Curves C and D show the decrease of CB and Cp in their copolymerization. Again Cp was consumed faster than CB, but the difference in their consumption rates is less enhanced in the copolymerization where both polymer

TABLE 2. COMPOSITION DETERMINATIONS OF poly(CB-co-St)[a]

No.	Monomer feed (mol%)		Conversion %	CB in copolymer (mol%)	
	CB	St		^{1}H NMR	Anal.[b]
1	100	0	17.8	100	
2	50	50	16.7	64.2	66.7
3	25	75	25.2	43.6	43.9
4	15	85	29.6	27.9	28.0
5	0	100	89.6	0	

a) [Monomer]=4.0 M, [AIBN]=0.02 M; temp, 70 °C; time, 86 h. (1 M=1 mol dm^{-3}) b) From elemental analysis of chlorine.

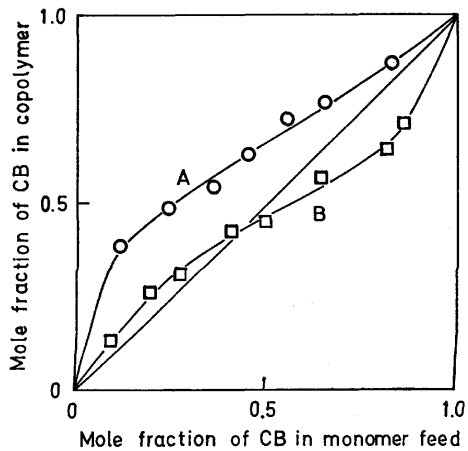

Fig. 1. Copolymer composition curves for CB–St(A) and CB–Bd(B). [Monomers]=4.0 M, [AIBN]=0.02 M; solvent, toluene; temp, 70 °C.

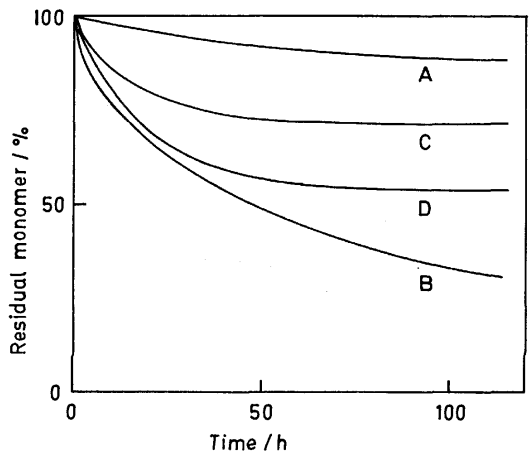

Fig. 2. Monomer consumption curves of CB(A, C) and Cp(B, D) in the homopolymerizations(A, B) and the copolymerization(C, D). Solution polymerizations in toluene at 70 °C: [AIBN]=0.04 M. Curve A; [CB]=5.4 M; curve B, [Cp]=5.4 M; curves C and D, [CB]=[Cp]=2.7 M.

radicals derived from CB and Cp are responsible for the propagation. Since the conversions from the weights of the resultant polymers agreed with those from monomer consumptions within the experimental error, it can be concluded that Cp is more reactive than CB in radical polymerization. This result is in accord with the reported difference in the reactivity between Cp and Bd ($r_{Cp}=3.41$ and $r_{Bd}=0.059$, or $r_{Cp}=2.86$ and $r_{Bd}=0.0$)[11] together with the comparable reactivity of CB with Bd described in the previous section.

Combining all the results of the polymerizations described above, we can propose the order of the monomer reactivity as follows:

$$Cp > CB \simeq Bd > St.$$

It has not been reported the successful synthesis of a new diene rubber containing chlorine by the copolymerization of Cp and Bd, probably because of the difference in their reactivities.[11] Now, CB is found to be a good candidate as a comonomer of Bd to synthesize a butadiene rubber containing chlorine. In fact, the emulsion copolymerization of CB and Bd was previously reported,[4] and the product is feasible for various chemical modifications due to allylic reactive chlorine.[6,7,12]

Intrinsic Viscosity of CB Copolymers. The three CB copolymers obtained in toluene were all soluble in toluene, and no insoluble fraction was found. In other words, the gelation did not occur in solution polymerizations, while it did occur and some insoluble parts were found in emulsion copolymerizations.[4] In Table 3 is shown the intrinsic viscosity of poly(CB-co-Bd)s prepared at various monomer feeds. The viscosities listed in Table 3 were much lower than those of the copolymers obtained by emulsion polymerization ($[\eta]=2.5$—5.5).[4] In addition, the viscosity of poly(CB-co-Bd) decreases with the increase of CB content in monomer feed. This tendency was also observed in poly(CB-co-St)s, the intrinsic viscosities of which were in the range of 0.15 to 0.30. CB monomer seems to be subject to monomer transfer reaction.

It is reasonable to get lower mol-wt copolymers by solution polymerization than by emulsion polymerization, because in the micelle the monomer can be regarded as being at the state of bulk and it is diluted in the solution. The produced polymer containing diene units is also more diluted in solution polymerization, and this fact could contribute to the absence of gelation.

Table 3. Intrinsic viscosity of poly(CB-co-Bd)[a]

No.	CB in monomer (mol%)	Conversion %	CB in copolymer (mol%)	$[\eta]$[b] of copolymer $dm^3\ g^{-1}$
1	0	21	0	0.163
2	20	15	25	0.111
3	40	17	42	0.109
4	65	16	57	0.081
5	85	16	70	0.069

a) Polymerization conditions: [monomer]=2.5 M, [AIBN]=1.25×10^{-2} M; solvent, toluene; temp, 70 °C; time, 40 h. b) Measured in toluene at 25.9 °C.

Microstructure of CB Unit. Four kinds of microstructures are possible for CB units in the polymer:

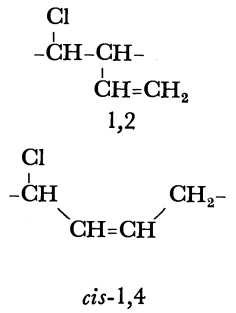

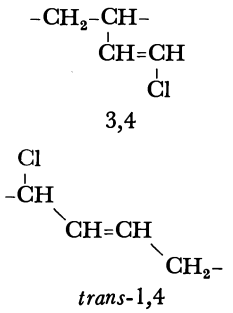

cis-1,4

trans-1,4

In the IR spectra of poly(CB-co-St), any peak ascribable to vinyl group (*ca.* 920 cm^{-1}) was not observed. In Fig. 3, ^1H NMR spectra of poly(St) (A), poly(CB) (B), and poly(CB-co-St) (C) are indicated. The peak due to olefinic methylene protons in the region of *ca.* 3.8 ppm is not observed. These two experimental findings suggest the absence of 1,2-microstructure in poly(CB-co-St), and its absence confirms the reluctance of 1,2-disubstituted olefins to polymerize,[13] because CB is involved in 1,2-propagation reaction as a 1,2-disubstituted olefin. Considering the spectra of model compounds *i.e.* **1** and **2**, an assignment of the peaks in ^1H NMR was made as listed in Table 4. It is noticeable that the protons of CB units are

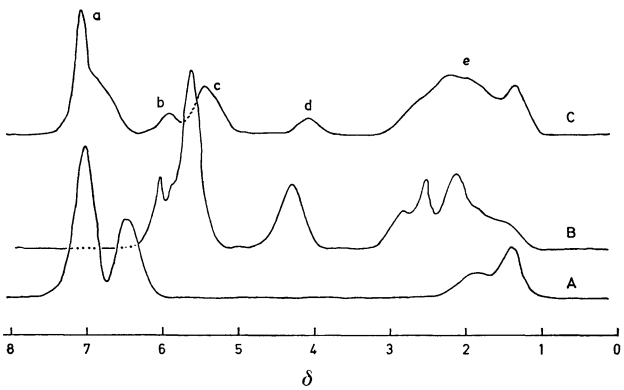

Fig. 3. ^1H NMR of polystyrene (A), poly(CB)(B), and poly(CB–co–St)(C) produced in toluene in the presence of AIBN.

Table 4. Assignment of ^1H NMR peaks in poly(CB-co-St)

Symbol	δ		Assignment
a	7.35	6.40	Phenyl proton (5H) in St
b	6.20	5.85	Olefinic proton (1H) geminal to chlorine in 3,4-CB
c	5.85	5.10	Olefinic proton in 1,4-CB (2H) and in 3,4-CB vicinal to chlorine (1H)
d	4.40	3.80	Methyne proton (1H) in 1,4-CB
e	3.20	1.10	Methyne proton in 3,4-CB (1H) and in St (1H), methylene proton in 1,4-CB (2H), in 3,4-CB (2H), and in St (2H)

subject to shielding to the higher field when CB units are incorporated in the copolymer with St. Similar shifts were observed in Bd–St and methyl methacrylate–St copolymers,[14] and this shielding effect has been interpreted in terms of the magnetic anisotropy of the phenyl group in St units. Therefore the observed shift may indicate that this poly(CB-co-St) is the true copolymer instead of the mixture of the homopolymers.

According to the assignment, the peak, a, is due to St units and the peaks, b, c, and d, are due to CB units, and the composition of poly(CB-co-St) was evaluated as shown in Table 2. Additionally, mol % of 1,4- and 3,4-microstructures could be evaluated from ^{1}H NMR, though *cis* and *trans* was not distinguishable. The results are shown in Table 5. We may conclude that in poly(CB-co-St) 60-mol% CB units are always of 1,4-configuration regardless of their contents, and the rests are of 3,4-configuration. This conclusion is in agreement with our previous estimation[5–7] from polymer reactions, while it is contrary to the result by Winston and Wichacheewa[3] who reported that all the CB units were of 1,4-configuration based on the results of the elimination reaction of hydrogen chloride from the poly(CB-co-St) obtained by the radiation-induced bulk copolymerization. Since both poly(CB-co-St)s were prepared by the radical polymerization, two copolymers have presumably almost the same microstructure. This discrepancy remains unsolved, but we suppose that their result is questionable due to the complex reactions following the hydrogen chloride elimination.

TABLE 5. MICROSTRUCTURE OF CB UNIT IN poly(CB-co-St)[a]

No.	CB in copolymer (mol%)	Microstructure[b]	
		1,4	3,4
1	100	66	34
2	87	55	45
3	77	57	43
4	73	60	40
5	64	57	43
6	54	66	34
7	52	59	41
8	39	70	30

a) Polymerization in toluene by AIBN at 70 °C. b) Mol% of CB unit in copolymer.

References

1) W. H. Carothers, *Ind. Eng. Chem.*, **26**, 30 (1934).
2) A. L. Klebanskii, P. M. Sorokina, and Z. Y. Khavin, *J. Gen. Chem. (USSR)*, **17**, 235 (1947); *Chem. Abstr.*, **42**, 514 h (1948).
3) A. Winston and P. Wichacheewa, *Macromolecules*, **6**, 200 (1973).
4) S. Yamashita, S. Atomori, S. Kohjiya, and T. Miyagawa, *J. Appl. Polym. Sci.*, **17**, 3049 (1973).
5) S. Kohjiya, Y. Imoto, H. Takeuchi, and S. Yamashita, *Polymer Preprints Japan*, **25**, 332, 639 (1976).
6) S. Yamashita, M. Tamura, J. Terada, and S. Kohjiya, *Rubber Chem. Technol.*, **50**, 364 (1977).
7) S. Yamashita, K. Sando, and S. Kohjiya, *J. Appl. Polym. Sci.*, **23**, 1951, 1963 (1979).
8) V. L. Heasley and B. R. Lais, *J. Org. Chem.*, **33**, 2571 (1968).
9) S. Yamashita, S. Kohjiya, A. Kita, and S. Shimizu, *J. Appl. Polym. Sci.*, **17**, 2935 (1973).
10) A. L. Henne, M. W. Renoll, and H. M. Leicester, *J. Am. Chem. Soc.*, **61**, 938 (1939); A. L. Henne and J. B. Hinkamp, *ibid.*, **67**, 1197 (1948).
11) G. E. Ham, "Copolymerization," Interscience, New York (1964), Appendices A and B.
12) S. Yamashita, S. Kohjiya, K. Sando, and M. Tamura, *Nippon Gomu Kyokai Shi*, **49**, 162 (1976).
13) T. Alfrey, Jr., J. J. Bohrer, and H. Mark, "Copolymerization," Interscience, N. Y. (1952), p. 49.
14) F. A. Bovey and G. V. D. Tiers, *Adv. Polym. Sci.*, **3**, 139 (1963); F. A. Bovey, "High Resolution NMR of Macromolecules," Academic Press, New York (1972), Chap. 10.

Kinetic Study of the Penetration of an Anthraquinoid Acidic Dye into Cationic Micelles

Yuuji MIYASHITA* and Shigeo HAYANO
Institute of Industrial Science, The University of Tokyo,
7-22-1 Roppongi, Minato-ku, Tokyo 106
(Received November 15, 1980)

The penetration of an anthraquinoid acidic dye into the micelle of a cationic surfactant, hexadecyltrimethylammonium bromide (HTAB), was studied kinetically by the stopped-flow method. The rate-determining step of this process was considered to be the dye reorientation from the micelle surface to its core. The apparent rate constants, k_{app}, of the dye penetration were determined by the first-order kinetics. The k_{app} values were a function of the surfactant micellar concentration. Above a certain micellar concentration (CMC) the k_{app} values become constant. The constant k_{app} was about 0.37—0.38 s^{-1} regardless of the total dye concentration. In the lower micellar concentration, there was a linear relationship between the k_{app} value and the number of the dye molecules which penetrated into a single micelle, n. This n was one of the factors which governed the dye penetration process.

Although the static properties of surfactant micelles, of their solubilization and of their interaction with organic compounds have been investigated extensively, only a few kinetic studies have been reported, probably due to the difficulty of measuring such rapid reactions. The development of modern techniques of analyzing fast reactions, such as the stopped-flow, the temperature-jump, the pressure-jump, and the ultrasonic relaxation methods, made it possible to discuss the kinetics of the micelle formation and dissociation.[1] Kinetic studies of the dye penetration into micelles have been reported recently.[2-4]

The micelles are in a dynamic equilibrium with themselves. The relaxation times obtained by the above techniques lead to the conclusion that there are at least two relaxation processes. The slower process is the micelle formation and dissociation, and its relaxation times are calculated to be about 10^{-2} s from the results of the temperature- and/or the pressure-jump experiments.[5] The faster one is the exchange of surfactant monomers between the aqueous and the micellar phases, and its relaxation times are estimated as 10^{-6} s by the ultrasonic relaxation method.[6] Since the micellization processes were faster than the dye penetration into micelles, these effects would be negligibly small in the kinetic study of the dye penetration.[2-4]

The kinetic studies of the dye penetration have been carried out by using ionic dyes with opposite charges to that of the surfactants, by the stopped-flow method.[2-4] In all cases, the apparent rate constants, which were calculated assuming a first-order reaction, increased with the increase in surfactant micellar concentration, and subsequently became constant. The mechanism at the lower micellar concentration was not discussed in detail, probably because of some complicated and unknown factors. In the region of constant k_{app} values, the mechanism was simplified, since these factors can be neglected. Thus, the discussions have been concentrated on this region.[7]

In the present paper, the rate constants of the penetration of an anthraquinoid acidic dye into cationic micelles were determined by measuring the change of dye absorbance, using the stopped-flow method. The main purpose is to develop a reasonable mechanism. The problem in the lower micellar concentration is discussed in detail, referring to the spectroscopic data[8] on the dye-surfactant system used in this study.

Experimental

Materials. Hexadecyltrimethylammonium bromide (HTAB), was obtained from Tokyo Kasei Industries Co. Ltd., and purified by recrystallizing from ethyl acetate containing 10 vol% ethanol and vacuum-drying at 80 °C. The CMC was determined to be 9.7×10^{-4} mol dm^{-3} by conductometry.

The dye, which was synthesized from the same process as used in a previous work,[4] has the structure shown in Fig. 1. The dye was paper-chromatographically pure, and the interaction among the dye molecules themselves was negligible spectrophotometrically in the concentration range used in this study.

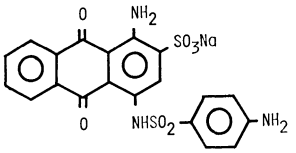

Fig. 1. Structure of an anthraquinoid acidic dye.

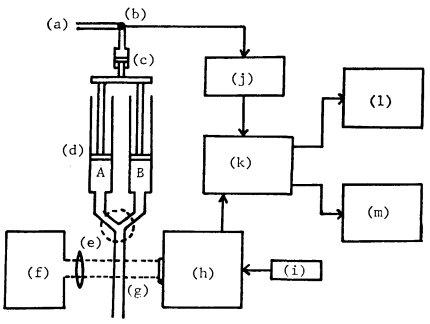

Fig. 2. Block diagram of RA-1100 and RA-108S systems.
(a): N_2 gas, (b): electromotive valve, (c): pushing syringe, (d): sample syringes, (e): mixing cell, (f): monochromator, (g): optical cell, (h): photomultiplier, (i): DC source, (j): trigger circuit, (k): digital memory RA-108S, (l): oscilloscope, (m): X-Y recorder.

Apparatus. The stopped-flow apparatus was a Fast Reaction Analyzer RA-1100 of Union Scientific Eng. Co. Ltd.. Its block diagram is shown in Fig. 2. The reagents were forced by a pressure of *ca.* 0.3 MPa into the optical cell, whose path was 10 mm, through a four-jet mixing cell. The mixing was established within 1 ms. The dye absorbance change at 547 nm against time was stored in the digital memory apparatus (RA-108S), and subsequently displayed on an oscilloscope or recorded on an X-Y recorder. During the experiment, the cell temperature was controlled by circulating water at 30±0.5 °C.

Methods. The sample syringes A and B were filled with a given concentration of dye solution and a certain concentration of the surfactant solution above CMC, respectively. The results were analyzed by first-order kinetics.

Results and Discussion

Some typical spectra of the dye in HTAB solution are shown in Fig. 3. The two characteristic bands at 510 and 547 nm are called α- and β-bands, respectively. The α-band appeared in absence of HTAB. In the presence of a sufficient amount of HTAB, the α-band changed to the β-band, indicating that dyes interacted with surfactants and/or micelles. The fact that the absorbance of both α- and β-bands increased in proportion to the dye concentration proved that there was no dye-dye interaction. The spectrum of the dye which had interacted with surfactants and/or micelles was similar to that the dye dissolved in methanol or acetone. These results lead to the inference that dyes are located in a methanol- or acetone-like atmosphere of the micelle core near the micellar surface. This is in agreement with the result of Sepulveda.[9]

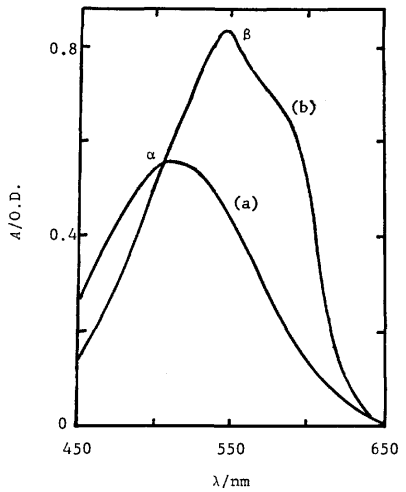

Fig. 3. Typical dye spectra.
(a) In absence of HTAB, (b) in presence of 10 mmol dm^{-3} of HTAB. The dye concentration is 0.1 mmol dm^{-3}.

Table 1. Mixing conditions and results

Run	A solution / mmol dm^{-3}	B solution / mmol dm^{-3}	Mixed solution / mmol dm^{-3}	Dynamic abs. change
1	Dye 0.2	Water	Dye 0.1	None
2	HTAB 20	Water	HTAB 10	None
3	Dye 0.2	HTAB 2	Dye 0.1 HTAB 1	Increase slightly
4	Dye 0.1 HTAB 1	HTAB 20	Dye 0.05 HTAB 10.5	Increase greatly
5	Dye 0.2	HTAB 20	Dye 0.1 HTAB 10	Increase greatly

After mixing solutions of dye and surfactant, the system was followed by the absorbance at 547 nm; the results are listed in Table 1. Then, the time scale for observation of absorbance change against time changed from 10 ms to 50 s in all the Runs. It was difficult to determine the rate constant in Run 3, since the absorbance change was very slight. On the contrary, appreciable changes were observed in Runs 4 and 5, and both the absorbance changes were nearly the same.

We have some data on the interaction between HTAB and the dye.[8] At first, the dye forms with HTAB an insoluble 1:1 salt (DS). The salt is resolved by further addition of HTAB below CMC, and the concentration of resolved salt is a linear function of that of HTAB. Thus, the authors assume that the dye forms a small complex with HTAB. The slope of the straight line shows that the complex consists of a single dye and three HTAB molecule. Moreover, the complex (DS_3) has similar spectroscopic characteristics, *i.e.* similar shape of the absorption curve and wavelength of maximum absorption (547 nm), to those of the dye which penetrated into micelles. Above CMC, the absorbance at 547 nm increases more intensively with the increase in the concentration of HTAB, and finally becomes constant. This absorbance is regarded to be caused by the dye penetration into the micelles. The magnitudes of the absorbances at 547 nm of both the complex below CMC and the dye which penetrated into micelles are proportional to the concentration of the dye, but the molar extinction coefficients are different, as shown in Table 2. The authors assume that the dye forms a complex with HTAB in the bulk of solution prior to the penetration in the mixing experiment. Consequently, the following sequence was proposed;

$$D + S \longrightarrow DS \longrightarrow DS_3 \longrightarrow D_m,$$

where D_m refers to the dye which penetrated into the micelles. Here, the process to forms DS_3 from DS would be very fast, because there exists a larger amount of DS_3 in Run 3 a short time after mixing. Accordingly, the process to form D_m from DS_3 will be the rate-determining step in the above sequence. If the dye penetration was established by the accu-

Table 2. Molar extinction coefficients of the dye

State of dye	ε at 547 nm[a] / dm^3 mol^{-1} cm^{-1}
Hydrated (D)	4470
Complex (DS_3)	7870
In micelle (D_m)	9620

a) Ref. 8.

mulation of HTAB molecules around DS_3 (refers to the induced micellization),[2] the rate would be comparable to the micellization from the HTAB monomers. But, the relaxation in this study is much slower (about 10 s) than the micellization. A more reasonable model is though to be the adhesion of DS_3 to the micelle surface. At first, DS_3 diffuses onto the micelle surface, then the dye reorients into the inner hydrophobic portion of the micelle. The diffusion coefficient of DS_3 would be larger than that of HTAB micelle; it was estimated to be about 10^{-6} cm^2 s^{-1} by the polarographic measurements.[10] Thus, as the diffusion process of DS_3 onto the micelle surface is also expected to be fast, it is not the rate-determining step. On the micelle surface, HTAB molecules in DS_3 may be replaced by that in the micelle and in the bulk in a short time.[11] Therefore, the dye would be in the state of DS_3 or a naked state in a dynamic equilibrium. As a result, the reorientation mentioned above is the most probable rate-determining step. The previous work[4] showed that the salt addition accelerated the reaction, probably due to the reduction of the surface potential of the micelle, and it supports the above assumption. During the dye penetration, the momentary fluctuation in the physical properties of the micelle, such as the aggregation number, can be neglected, because the micelle equilibrates much faster than the dye penetration.[11]

A reformed sequence for evaluating the apparent rate constants is proposed:

$$DS_3 \rightleftharpoons D_s \underset{k'}{\overset{k}{\rightleftharpoons}} D_m,$$

where D_s, k, and k' refer to the dye which exists on the micelle surface in the state of DS_3 and/or a naked state, and to the rate constants of the forward and backward reactions, repectively. The authors postulate similar extinction coefficients for DS_3 in the bulk and D_s, since the atomosphere of the dye chromophore of D_s is not so different from that of DS_3. The rate equation is expressed as

$$-\frac{d[D_s]}{dt} = k[D_s] - k'[D_m]. \quad (1)$$

In the adsorption process prior to the dye reorientation it is assumed that the dye exists predominantly on the micelle surface and that $[DS_3]$ in the bulk is negligible; thus the equilibrium constant is expected to be about 10^4 according to the previous paper.[2] Since $[D_m]=[D]_0-[D_s]$, and $k[D_s]_e=k'\times[D_m]_e$ at equilibrium, Eq. 1 is converted to Eq. 2:

$$-\frac{d[D_s]}{dt} = \frac{[D]_0}{[D]_0-[D_s]_e} k([D_s]-[D_s]_e). \quad (2)$$

An integration of Eq. 2 with respect to time yields

$$\ln\frac{[D_s]-[D_s]_e}{[D]_0-[D_s]_e} = -\frac{[D]_0}{[D]_0-[D_s]_e} kt = -k_{app}t, \quad (3)$$

where $[D_s]$ and $[D_m]$ are the concentrations of the adsorbed dye on the micelle surface and of the dye penetrated into the micelle, respectively, and $[D]_0$ stands for the total concentration of the dye, and the subscript e refers to equilibrium.

Figure 4 shows the typical reaction curve. Absorbance increased with elapsed time, and subsequently flattened out. The total absorbance change (ΔA_0) is in proportion to the amount of the dye which penetrated into the micelle at equilibrium ($[D_m]_e$), and ΔA refers to that during the relaxation process ($[D_m]$). The subtraction of $\Delta A/\Delta A_0$ from unity yields

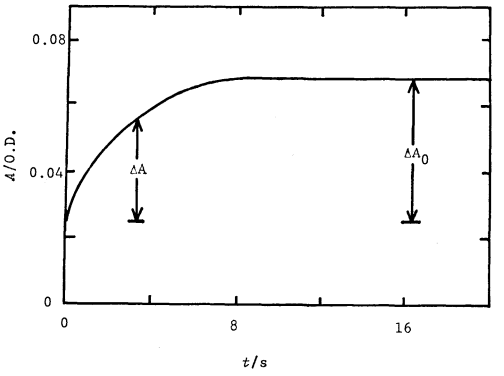

Fig. 4. Typical reaction curve.

$$1-\frac{\Delta A}{\Delta A_0} = 1-\frac{[D_m]}{[D_m]_e} = \frac{[D_s]-[D_s]_e}{[D]_0-[D_s]_e}. \quad (4)$$

Therefore, the logarithm of Eq. 4 is the same as the left-hand side of Eq. 3. The apparent rate constants, k_{app}, were calculated by Eqs. 3 and 4. The k_{app} values increased sharply with the increase in the surfactant concentration above CMC, and subsequently became constant, as shown in Fig. 5. The k_{app} had the same values regardless of the total dye concentration at high concentration of micellar surfactants.

At lower micellar concentration, some complicated factors may take part in the reaction. In papers by other workers,[2,3] there has been little explanation about the results obtained in this region. In our previous work, $[D_s]_e$ values were determined.[8] The k_{app} values were recalculated in consideration of $[D_s]_e$; these are connected by the dotted lines shown in Fig. 5. This treatment lowers k_{app} values to some extent, but no interesting result is obtained. Consequently, the $[D_s]_e$ values slightly affect k_{app} values.

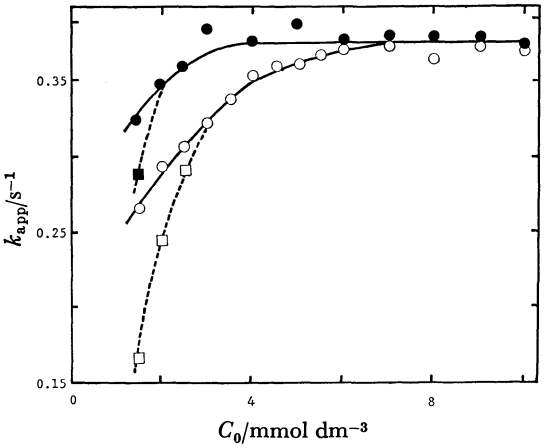

Fig. 5. Plots of k_{app} against HTAB concentration, $[C]_0$. ···●···: $[D]_0=0.05$ mmol dm^{-3}, ···○···: 0.1 mmol dm^{-3}. Recalculated k_{app} values in consideration of $[D_s]_e$ are connected by dotted line.

As one additional factor, the $[D_s]_e$ value induces the number of the dye molecules which penetrate into a single micelle, n. The n value shown in Fig. 6 was obtained use of the following equation:

$$n = \frac{N([D]_0 - [D_s]_e)}{[C]_0 - CMC}, \quad (5)$$

where N is the aggregation number of HTAB micelles,[1] and $[C]_0$ stands for the total HTAB concentration. The n decreased with the increase in the HTAB concentration until n attained unity. The n value is not actually less than unity even in the higher HTAB concentration, where there are micelles containing a single dye and those without dye. The

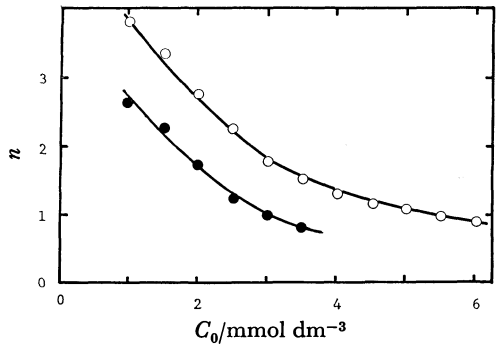

Fig. 6. Plots of the number of dye penetrated into a single micelle (n) *vs.* HTAB concentration, $[C]_0$. ···●···: $[D]_0$=0.05 mmol dm^{-3}, ···○···: 0.1 mmol dm^{-3}.

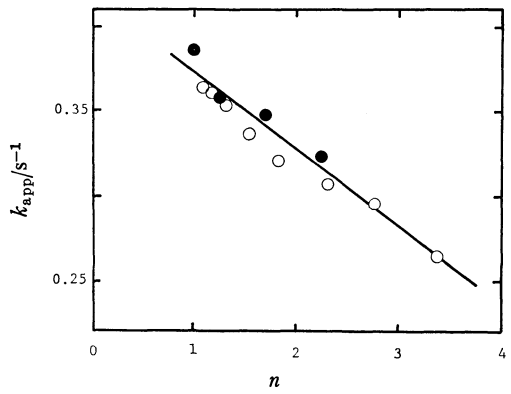

Fig. 7. Relation between k_{app} and n. ···●···: $[D]_0$=0.05 mmol dm^{-3}, ···○···: 0.1 mmol dm^{-3}.

k_{app} becomes constant at the same HTAB concentration for which n is unity. Moreover, in the lower HTAB concentration, there is a linear relationship between the k_{app} and the n value, as shown in Fig. 7. This suggests that the n value is one of the factors which govern the rate-determining step of the dye penetration. When n is unity, a single dye molecule reorients into a single micelle without any interaction with the other dyes. Then, the dye mortion seems to be dominated only by the dye structure and the properties of the micelle surface. When n values are more than unity, dyes on the surface of a single micelle reorient into its core slowly, since dyes are able to interact with each other directly and/or indirectly through the micellar surfactants. The increase in n value strengthens this interaction, and consequently the penetrating rates are further decelerated.

The dye penetration process consists of a number of elementary reactions. The inquiry into each reaction by other techniques will make it possible to gain more insight into the detailed mechanism.

We thank Dr. Noriko Shinozuka for her helpful discussions.

References

1) J. H. Fendler and E. J. Fendler, "Catalysis in Micellar and Macromolecular System," Academic Press, New York (1975), Chaps. 2 and 3.
2) B. H. Robinson, N. C. White, and C. Mateo, *Adv. Molecular Relaxation Processes*, **7**, 321 (1975).
3) K. Takeda, N. Tatsumoto, and T. Yasunaga, *J. Colloid Interface Sci.*, **47**, 128 (1974).
4) Y. Miyashita and S. Hayano, *Chem. Lett.*, **1978**, 987.
5) G. C. Kresheck, E. Hamori, G. Davenport, and H. A. Scheraga, *J. Am. Chem. Soc.*, **88**, 246 (1966).
6) T. Yasunaga, H. Oguri, and M. Miura, *J. Colloid Interface Sci.*, **23**, 352 (1967).
7) A. D. James, B. H. Robinson, and N. C. White, *J. Colloid Interface Sci.*, **59**, 328 (1977).
8) Y. Miyashita and S. Hayano, *Yukagaku*, **30**, 573 (1981).
9) L. Sepulveda, *J. Colloid Interface Sci.*, **46**, 372 (1974).
10) N. Shinozuka and S. Hayano, "Solution Chemistry of Surfactants," ed by K. Mittal, Plenum Press, New York, (1979), Vol. 2, p. 559.
11) J. Rassing, P. J. Sams, and E. Wyn-Jones, *J. Chem. Soc., Faraday Trans. 2*, **70**, 1247 (1974).

  Bull. Chem. Soc. Jpn., 54, 3253—3258 (1981)

Removal and Recovery of Organic Pollutants from the Aquatic Environment. VII. Adsorption of Phenol and Carboxylic Acids on Crosslinked Poly(4-vinylpyridine)

Nariyoshi KAWABATA,* Ichiro HIGUCHI, and Jun-ichi YOSHIDA

Laboratory of Environmental Chemistry, Department of Chemistry, Faculty of Polytechnic Science, Kyoto Institute of Technology, Matsugasaki, Sakyo-ku, Kyoto 606

(Received February 7, 1981)

Molecular adsorptions of phenols and carboxylic acids on crosslinked poly(4-vinylpyridine) were studied in comparison with those on various polymeric adsorbents. Enthalpies for the adsorption of phenol on various polymeric adsorbents were evaluated based upon the temperature dependence of the phenol adsorption isotherms. The enthalpy on crosslinked poly(4-vinylpyridine) was close to that on porous poly(styrene-divinylbenzene) resin with no ion exchange functional group, and was much smaller than that on commercial weak base anion exchange resin. The relative adsorption capacities of various polymeric adsorbents for carboxylic acids and substituted phenols indicated that the acid-base interaction as well as hydrophobic interaction between these organic acids and crosslinked poly(4-vinylpyridine) was an important factor in the adsorption.

In previous papers of this series, crosslinked poly(vinylpyridine) was reported to be an excellent polymeric adsorbent for removal and recovery of phenol[1] and carboxylic acids[2] from aqueous solution. The capacities of crosslinked poly(vinylpyridine) for the adsorption of these organic acids were scarcely affected by the presence of inorganic salts. On the contrary, the capacities of commercial strong base and weak base anion exchange resins for the adsorption of these organic acids were conspicuously reduced in the presence of inorganic salts. Elution of the adsorbed organic acids from crosslinked poly(vinylpyridine) was easily accomplished by a simple treatment with organic solvents such as acetone and methanol, which was notably easier than those from anion exchange resins, and crosslinked poly(vinylpyridine) was efficiently regenerated. These observations showed that an ion exchange mechanism could not explain the adsorption of these organic acids by crosslinked poly(vinylpyridine). On the other hand, the capacities of crosslinked poly(vinylpyridine) for the adsorption of these organic acids were remarkably higher than those observed with porous poly(styrene-divinylbenzene) resin with no ion exchange functional group, in spite of the fact that the crosslinked poly(vinylpyridine) in the pulverized form was used. Therefore, a simple physical interaction between these organic acids and crosslinked poly(vinylpyridine) could not wholly explain the ability of the polymer for the adsorption of these organic acids. In this work, we have investigated the mechanism of the adsorption of phenol and carboxylic acids on crosslinked poly(vinylpyridine).

Experimental

Materials. Crosslinked poly(4-vinylpyridine) containing 72 mol% 4-vinylpyridine was prepared by a copolymerization of 4-vinylpyridine with divinylbenzene followed by griding and sifting to 60—80 mesh as was described previously.[1] The mean particle diameter was 0.20 mm in the wet state. For comparison, three commercial resins supplied by Rohm and Haas Co., Philadelphia, Pa., U. S. A., were used in this work. Amberlite IRA-400 was used as a strong base anion exchange resin, which had a styrene-divinylbenzene matrix with quarternary ammonium group. The particle size of this resin in the chloride form was 0.38—0.45 mm. This resin was used in the hydroxide form. Amberlite IRA-45 was used as a weak base anion exchange resin, which had a styrene-divinylbenzene matrix with primary, secondary, and tertiary amino groups. This resin was used in the free base form. The particle size was 0.36—0.46 mm. Amberlite XAD-4 was used as a porous poly(styrene-divinylbenzene) resin with no ion exchange functional group, which had a styrene-divinylbenzene matrix. The supplier claimed that the surface area of the resin was 784 m^2/g. These resins were preconditioned as was described previously.[1] Commercial products of phenol, *p*-cresol, *p*-nitrophenol, carboxylic acids, and other chemicals were used without further purification. Deionized water was used throughout the experiments.

Procedure. Column studies were conducted using a 1.0-cm diameter glass column with a fritted glass filter connected with a dropping funnel in a down-flow fashion at room temperature as was described in a previous paper.[1] The adsorption capacity of resins was evaluated in two ways: (i) the breakthrough capacity, which was based upon the total amount of adsorbed organic acids until the effluent concentration reached 1 mg dm^{-3} (in the adsorption of substituted phenols), or until the effluent solution became acidic using Methyl Red as the indicator (in the adsorption of carboxylic acids); (ii) the total capacity, which was based upon the total amount of adsorbed organic acids until the effluent concentration reached the influent concentration. The concentrations of phenol, *p*-cresol, and *p*-nitrophenol were determined based upon the adsorptivities at 275, 279, and 318 nm, respectively, or with aid of 4-aminoantipyrine[3] using a Shimadzu UV-200S, UV-100-01 or UV-100-02 spectrophotometer. The concentrations of carboxylic acids were determined by titration with a standard 0.1 mol dm^{-3} sodium hydroxide solution using phenolphthalein as the indicator.

Equilibrium adsorption tests were conducted by placing weighed quantities of polymeric adsorbent and samples of aqueous solution of organic acids in a 300-cm^3 Erlenmeyer flask sealed by a rubber stopper with magnetic stirring at the prescribed temperature. After the mixture reached equilibrium, the concentration of organic acids was determined.

Results and Discussion

Enthalpies for Phenol Adsorption. The experimental isotherms of phenol adsorption on crosslinked poly(4-vinylpyridine), porous poly(styrene-divinylbenzene) resin with no ion exchange functional group (Amberlite XAD-4), and weak base anion exchange resin in the free base form (Amberlite IRA-45) are shown in Figs. 1, 2, and 3, respectively. The linear relationship of Figs. 1, 2, and 3 indicates that the adsorption isotherms of phenol on these polymeric adsorbents follow the Freundlich equation. The type of adsorption of phenol on crosslinked poly(4-vinylpyridine) appears to be not unusual but commonly observed in most of liquid-phase adsorptions. The temperature dependence of isotherms was large in the adsorption of phenol on weak base anion exchange resin in the free base form (Fig. 3), when compared with that on crosslinked poly(4-vinylpyridine) (Fig. 1) and that on porous poly(styrene-divinylbenzene) resin with no ion exchange functional group (Fig. 2).

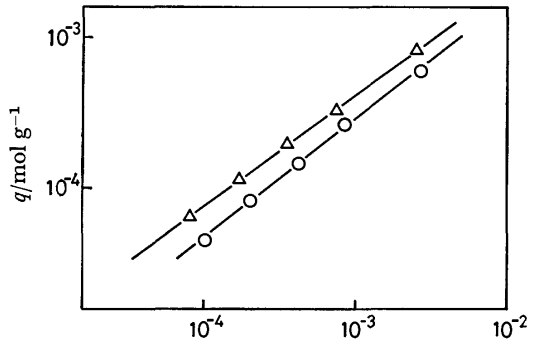

Fig. 1. Phenol adsorption isotherms on crosslinked poly(4-vinylpyridine).
△: 20 °C, ○: 50 °C.

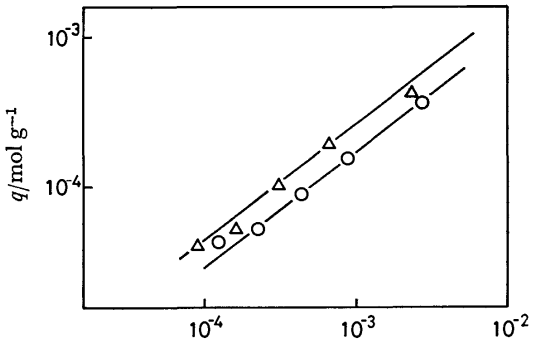

Fig. 2. Phenol adsorption isotherms on porous poly(styrene-divinylbenzene) resin with no ion exchange functional group (Amberlite XAD-4).
△: 20 °C, ○: 50 °C.

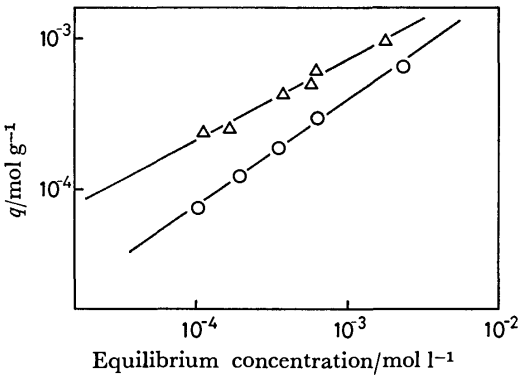

Fig. 3. Phenol adsorption isotherms on weak base anion exchange resin (Amberlite IRA-45) in the free base form.
△: 20 °C, ○: 50 °C.

In order to evaluate the temperature dependence of isotherms more quantitatively, we calculated the enthalpies for phenol adsorption on these three polymeric adsorbents. The enthalpy of adsorption on polymeric adsorbents is generally calculated from isotherms for adsorptions at two different temperatures by use of the following relationship:[4]

$$\Delta H^0 = \frac{2.303RT_1T_2}{T_2-T_1}(\log C_1 - \log C_2).$$

Here, ΔH^0 is the enthalpy of adsorption, R is the gas constant, C_1 and C_2 are the equilibrium concentrations of solute in moles per liter at the absolute temperatures T_1 and T_2, respectively. Enthalpies of phenol adsorption were calculated based upon the isotherms at 20 and 50 °C. The enthalpy of adsorption calculated by use of the above relationship depends upon the value of q, which is the number of moles of solute adsorbed per gram of dry adsorbent, and we calculated the enthalpy at four different values of q. Results are given in Table 1.

The enthalpy of phenol adsorption on weak base anion exchange resin (IRA-45) was large, and that on crosslinked poly(4-vinylpyridine) was close to that on porous poly(styrene-divinylbenzene) resin with no ion exchange functional group. These results show that the adsorption of phenol on crosslinked poly(4-

Table 1. Enthalpies for phenol adsorption

	q / mol g^{-1}	$-\Delta H^0$ / kcal mol^{-1}
Crosslinked poly(4-vinylpyridine)[a]	8.0×10^{-5}	3.8
	2.0×10^{-4}	3.4
	6.0×10^{-4}	2.7
	1.0×10^{-3}	1.9
Amberlite XAD-4[b]	8.0×10^{-5}	3.4
	2.0×10^{-4}	3.4
	6.0×10^{-4}	3.4
	1.0×10^{-3}	3.4
Amberlite IRA-45[c]	8.0×10^{-5}	11.0
	2.0×10^{-4}	8.6
	6.0×10^{-4}	5.0
	1.0×10^{-3}	4.4

a) Pulverized copolymer of 4-vinylpyridine with divinylbenzene containing 72 mol% 4-vinylpyrine. b) Porous poly(styrene-divinylbenzene) resin with no ion exchange functional group. Claimed to have a surface area of 784 m^2 g^{-1}. c) Weak base anion exchange resin in the free base form.

vinylpyridine) occurs through a different mechanism from that on anion exchange resin, and that the adsorption is rather close to physical adsorption.

Capacities for the Adsorption of Carboxylic Acids. Column studies were also performed in order to obtain detailed information concerning the nature and mechanism of the adsorption of phenol and carboxylic acids on crosslinked poly(4-vinylpyridine). Since the crosslinked poly(4-vinylpyridine) was developed as a polymeric adsorbent for removal and recovery of organic pollutants from waste water, the column studies were much more important and practical than the studies of adsorption equilibrium for this purpose. Relative adsorption capacities of these organic acids on the polymeric adsorbents were compared.

Effects of two factors, *i.e.*, hydrophobic interaction and acid-base or electrostatic interaction between the polymeric adsorbents and the organic acids, were evaluated on the basis of the relative adsorption capacites. The hydrophobic interaction between the polymeric adsorbents and the organic acids were evaluated in terms of the effect of the length of hydrocarbon chain. The acid-base or electrostatic interaction between the polymeric adsorbents and the organic acids were evaluated in terms of the effect of pK_a of the organic acids.

Breakthrough and total capacities of polymeric adsorbents for the adsorption of various carboxylic acids were determined by the continuous flow column method. In Table 2 are given the capacities of the porous poly(styrene-divinylbenzene) resin with no ion exchange functional group (Amberlite XAD-4). The adsorption capacity increased with the hydrocarbon chain length of the carboxylic acid, *i.e.*, in the order: formic < acetic < propionic < butyric < valeric acid. Similar tendency has been reported in the adsorption of carboxylic acids on a porous poly(styrene-divinylbenzene) resin,[5] although the results were obtained using the batch method.

The acidity of carboxylic acid did not affect significantly the adsorption capacity. For example, the adsorption capacities for valeric acid were 20—30 times larger than those for acetic acid, although pK_a values of these carboxylic acids are similar in magnitude. The adsorption capacities for formic and trifluoroacetic acid were much smaller than those for butyric and valeric acid, although the former carboxylic acids are more acidic.

In order to obtain a quantitative information about the effect of the structure of carboxylic acid on the adsorption capacity of the resin, the logarithm of the adsorption capacity was plotted against the number of carbon atoms in the carboxylic acid. The result is shown in Fig. 4. The straight line in Fig. 4 indicates that the logarithm of the adsorption capacity varies in proportion to the number of carbon atoms of the carboxylic acid.

It is widely held that the standard free energy change for transfer of hydrocarbon chains from aqueous solution to other phase varies in proportion to the num-

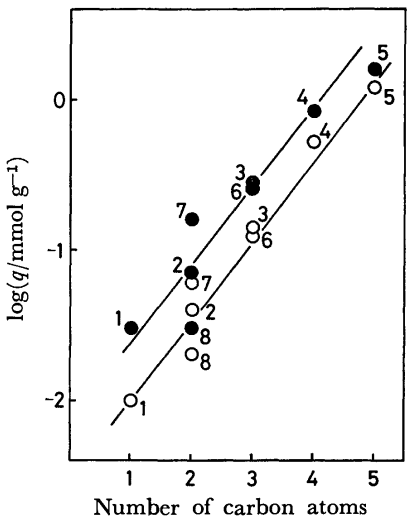

Fig. 4. Capacities of porous poly(styrene-divinylbenzene) resin with no ion exchange functional group (Amberlite XAD-4) for the adsorption of carboxylic acids as a function of the number of carbon atoms of the carboxylic acids.
●: Total adsorption capacity, ○: breakthrough capacity. 1: HCOOH, 2: CH_3COOH, 3: CH_3CH_2COOH, 4: $CH_3(CH_2)_2COOH$, 5: $CH_3(CH_2)_3COOH$, 6: CH_2=CHCOOH, 7: $ClCH_2COOH$, 8: CF_3COOH.

TABLE 2. CAPACITIES OF POROUS POLY(STYRENE-DIVINYLBENZENE) RESIN WITH NO ION EXCHANGE FUNCTIONAL GROUP FOR THE ADSORPTION OF CARBOXYLIC ACIDS FROM AQUEOUS SOLUTION[a]

Run	Carboxylic acid	pK_a	Breakthrough capacity[b] mmol g^{-1}	Total adsorption capacity[c] mmol g^{-1}
1	HCOOH	3.75 (25 °C)	0.01	0.03
2	CH_3COOH	4.76 (25 °C)	0.04	0.07
3	CH_3CH_2COOH	4.87 (25 °C)	0.14	0.28
4	$CH_3(CH_2)_2COOH$	4.82 (25 °C)	0.52	0.83
5	$CH_3(CH_2)_3COOH$	4.84 (25 °C)	1.20	1.55
6	CH_2=CHCOOH	4.26 (25 °C)	0.12	0.25
7	$ClCH_2COOH$	2.87 (25 °C)	0.06	0.16
8	CF_3COOH	0.25 (25 °C)	0.02	0.03

a) Determined by the continuous flow column method using 10 mmol dm^{-3} aqueous solution of carboxylic acids. Amberlite XAD-4 was used as the adsorbent. The flow rate was 3 bed volumes per hour. b) The total amount of adsorbed carboxylic acid until the effluent solution became acidic using Methyl Red as the indicator. c) The total amount of adsorbed carboxylic acid until the effluent concentration reached the influent concentration.

ber of carbon atoms.[6] For example, the standard free energy change for transfer of hydrocarbons from aqueous solution to pure liquid hydrocarbon was shown to be a linear function of the length of the hydrocarbon chain.[6,7] The free energy change for transfer of undissociated fatty acids from a dilute aqueous buffer solution to liquid heptane was also found to be proportional to the number of carbon atoms.[6,8] These relationships were explained in terms of hydrophobic interactions of the hydrocarbon chain.

The adsorption capacity obtained in column studies depends upon the diameter of the column, the flow rate, and other experimental factors. However, such factors were almost constant throughout the present study. Therefore, the relative adsorption capacity may closely relate to the thermodynamic adsorption equilibrium constant and its logarithm may correlate to the free energy change of transfer of a carboxylic acid from aqueous solution to the resin. The straight line in Fig. 4 suggests that such free energy change varies in proportion to the number of carbon atoms in the carboxylic acid.

On the basis of these arguments, it is reasonably considered that hydrophobic interactions between the hydrocarbon chain of the carboxylic acid and the resin matrix are responsible for the increase in adsorption capacity with the chain length of the carboxylic acid.

In Tables 3 and 4 are given the capacities of the weak base anion exchange resin (Amberlite IRA-45) in the free base form and those of strong base anion exchange resin (Amberlite IRA-400) in the hydroxide form for the adsorption of carboxylic acids. The adsorption capacities were not significantly affected by the chain length of the carboxylic acid. However, the adsorption capacities decreased with an increase in pK_a of the carboxylic acid. Thus, it was felt that the ion exchange or acid-base interaction between the carboxylic acid and the resin played an important role in the adsorption of carboxylic acid on these anion exchange resins.

In Table 5 are given the capacities of crosslinked poly(4-vinylpyridine) for the adsorption of carboxylic acids. The adsorption capacity for a series of saturated aliphatic carboxylic acids increased in the order: acetic<propionic<butyric<valeric acid. However, pK_a values indicate the similar acidity of these carboxylic acids. The relation between the logarithm of the adsorption capacity and the number of carbon atoms of the carboxylic acid is shown in Fig. 5. The figure shows a linear relationship for this series of saturated aliphatic carboxylic acids of similar pK_a. Therefore, hydrophobic interaction between the hydrocarbon chain of the carboxylic acid and the resin matrix seems to play an important role in the adsorption on the crosslinked poly(4-vinylpyridine).

TABLE 3. CAPACITIES OF WEAK BASE ANION EXCHANGE RESIN IN THE FREE BASE FORM FOR THE ADSORPTION OF CARBOXYLIC ACIDS FROM AQUEOUS SOLUTION[a]

Carboxylic acid	pK_a	Breakthrough capacity[b] mmol g^{-1}	Total adsorption capacity[c] mmol g^{-1}
HCOOH	3.75 (25 °C)	4.00	4.98
CH_3COOH	4.76 (25 °C)	3.13	4.08
CH_3CH_2COOH	4.87 (25 °C)	3.02	4.36
$CH_3(CH_2)_2COOH$	4.82 (25 °C)	3.25	4.91
$CH_3(CH_2)_3COOH$	4.84 (25 °C)	4.64	5.99
CH_2=CHCOOH	4.26 (25 °C)	3.44	5.15
$ClCH_2COOH$	2.87 (25 °C)	4.29	5.37
CF_3COOH	0.25 (25 °C)	4.29	5.45

a) Determined by the continuous flow column method using 100 mmol dm^{-3} aqueous solution of carboxylic acids. Amberlite IRA-45 was used as the adsorbent. The flow rate was 3 bed volumes per hour. b) See footnote (b) in Table 2. c) See footnote (c) in Table 2.

TABLE 4. CAPACITIES OF STRONG BASE ANION EXCHANGE RESIN IN THE HYDROXIDE FORM FOR THE ADSORPTION OF CARBOXYLIC ACIDS FROM AQUEOUS SOLUTION[a]

Carboxylic acid	pK_a	Breakthrough capacity[b] mmol g^{-1}	Total adsorption capacity[c] mmol g^{-1}
HCOOH	3.75 (25 °C)	3.15	3.87
CH_3COOH	4.76 (25 °C)	2.78	3.67
CH_3CH_2COOH	4.87 (25 °C)	2.75	3.74
$CH_3(CH_2)_2COOH$	4.82 (25 °C)	2.73	3.99
CH_2=CHCOOH	4.26 (25 °C)	2.95	3.88
$ClCH_2COOH$	2.87 (25 °C)	3.37	4.01
CF_3COOH	0.25 (25 °C)	3.01	3.35

a) Determined by the continuous flow column method using 100 mmol dm^{-3} aqueous solution of carboxylic acids. Amberlite IRA-400 was used as the adsorbent. The flow rate was 3 bed volumes per hour. b) See footnot (b) in Table 2. c) See footnote (c) in Table 2.

Table 5. Capacities of crosslinked poly(4-vinylpyridine) for the adsorption of carboxylic acids from aqueous solution[a]

Run	Carboxylic acid	pK_a	Breakthrough capacity[b] mmol g^{-1}	Total adsorption capacity[c] mmol g^{-1}
1	HCOOH	3.75 (25 °C)	2.61	3.03
2	CH_3COOH	4.76 (25 °C)	1.00	1.33
3	CH_3CH_2COOH	4.87 (25 °C)	1.75	2.02
4	$CH_3(CH_2)_2COOH$	4.82 (25 °C)	2.72	2.95
5	$CH_3(CH_2)_3COOH$	4.84 (25 °C)	4.21	4.70
6	CH_2=CHCOOH	4.26 (25 °C)	2.36	—
7	$ClCH_2COOH$	2.87 (25 °C)	2.45	4.78
8	CF_3COOH	0.25 (25 °C)	6.66	6.72

a) Determined by the continuous flow column method using 100 mmol dm^{-3} aqueous solution of carboxylic acids. The flow rate was 3 bed volumes per hour. Crosslinked poly(4-vinylpyridine) containing 72 mol% 4-vinylpyridine in the pulverized form was used as the adsorbent. b) See footnote (b) in Table 2. c) See footnote (c) in Table 2.

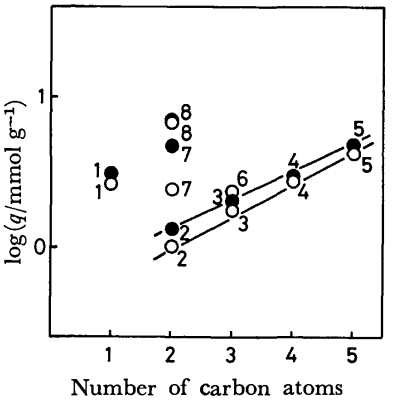

Fig. 5. Capacities of crosslinked poly(4-vinylpyridine) containing 72 mol% 4-vinylpyridine for the adsorption of carboxylic acids as a function of the number of carbon atoms of the carboxylic acids.
●: Total adsorption capacity, ○: breakthrough capacity. 1: HCOOH, 2: CH_3COOH, 3: CH_3CH_2COOH, 4: $CH_3(CH_2)_2COOH$, 5: $CH_3(CH_2)_3COOH$, 6: CH_2=CHCOOH, 7: $ClCH_2COOH$, 8: CF_3COOH.

However, marked deviations from the linear relationship of Fig. 5 were observed for formic acid (1), chloroacetic acid (7), and trifluoroacetic acid (8), in contrast to the relation shown in Fig. 4 for the adsorption on porous poly(styrene-divinylbenzene) resin with no ion exchange functional group. These carboxylic acids have much lower pK_a values than those of the saturated aliphatic carboxylic acids mentioned above. The effect of acidity on the capacity of crosslinked poly(4-vinylpyridine) for the adsorption of carboxylic acids is also demonstrated by a tendency that the adsorption capacity increased with the acidity in a series acetic<chloroacetic<trifluoroacetic acid. The larger capacity for the adsorption of acrylic acid than that for propionic acid can also be attributed to the difference in acidity of these carboxylic acids, since both of these carboxylic acids have a similar chain length. The larger adsorption capacity for formic acid than that for acetic acid cannot be explained in terms of the hydrophobic interaction, since such interaction seems to be smaller in the adsorption of formic acid as can be seen in Fig. 4. Higher acidity of formic acid may be responsible for the larger adsorption capacity. These observations clearly indicate the importance of acidity of the carboxylic acid in the adsorption on crosslinked poly(4-vinylpyridine). However, as was reported previously,[1,2] ion exchange mechanism does not appear to be suitable for the adsorption of phenol or carboxylic acids on crosslinked poly(4-vinylpyridine). Thus, the effect of acidity on the above adsorption capacity may be ascribable to the contribution of the acid-base interaction between the pyridyl group of the crosslinked poly(vinylpyridine) and the carboxyl group of the carboxylic acid. Because pyridine is an organic base, it is reasonable to consider the following interaction, where the pyridyl group of the resin uptakes a proton from the carboxylic acid to form a complex with the carboxylate anion as the associated counterion:

The formation of hydrogen bond may also contribute to the interaction between the pyridyl group and the carboxylic acid:

Such acid-base interactions may increase with acidity of carboxylic acid, and may be responsible for the remarkably higher capacity of the crosslinked poly(vinylpyridine) for the adsorption of carboxylic acid than that of the resin with no ion exchange functional group as Amberlite XAD-4.

Capacities for the Adsorption of Substituted Phenols. Breakthrough capacities of polymeric adsorbents for the adsorption of substituted phenols were also determined by the continuous flow column method. Results are given in Table 6.

Adsorption capacities of the porous poly(styrene-divinylbenzene) resin with no ion exchange functional group (XAD-4) for substituted phenols were in the order: *p*-nitrophenol ≈ phenol < *p*-cresol. The larger adsorption capacity for *p*-cresol than that for phenol may be attributed to the higher hydrophobicity

TABLE 6. BREAKTHROUGH CAPACITIES OF POLYMERIC ADSORBENTS FOR THE ADSORPTION OF SUBSTITUTED PHENOLS FROM AQUEOUS SOLUTION[a)]

Substituted phenol	pK_a	Breakthrough capacity mmol g^{-1} [b)]		
		XAD-4[c)]	IRA-45[d)]	PVP[e)]
p-Cresol	10.26 (25 °C)	2.41	2.38	3.88
Phenol	10.00 (20 °C)	1.59	2.89	2.93
p-Nitrophenol	7.15 (25 °C)	1.58	3.60	5.39

a) Determined by the continuous flow column method using 35 mmol dm^{-3} aqueous solution of substituted phenols. The flow rate was 3 bed volumes per hour. b) The total amount of adsorbed phenols before the effluent concentration reached 1 mg dm^{-3}. c) See footnote (b) in Table 1. d) See footnote (c) in Table 1. e) See footnote (a) in Table 1.

of *p*-cresol. The capacity for *p*-nitrophenol adsorption was close to that for phenol adsorption in spite of large difference in pK_a of the two phenols. This result implies that the acidity of phenolic hydroxyl group did not significantly affect the adsorption capacity. In contrast, the adsorption capacity of weak base anion exchange resin (IRA-45) in the free base form for substituted phenols was in the order: *p*-cresol < phenol < *p*-nitrophenol. Thus, the adsorption capacity increased with the acidity of adsorbate in this case. This result suggests the importance of the ion exchange or acid-base interaction between the substituted phenols and the resin.

In the adsorption on crosslinked poly(4-vinylpyridine), the capacity for *p*-cresol adsorption was higher than that for phenol adsorption. This fact may be explained in terms of higher hydrophobicity of the former adsorbate. Adsorption capacity for *p*-nitrophenol was also higher than that for phenol. Higher acidity of *p*-nitrophenol than that of phenol seems to be responsible for this result. These observations may suggest that both hydrophobic interaction and acid-base interaction played important roles in the adsorption of substituted phenols on crosslinked poly(4-vinylpyridine) as well as in the adsorption of carboxylic acids.

This work was supported in part by a Grant-in-Aid for Scientific Research No. 503042 from the Ministry of Education, Science and Culture.

References

1) N. Kawabata and K. Ohira, *Environ. Sci. Technol.*, **13**, 1396 (1979).
2) N. Kawabata, J. Yoshida, and Y. Tanigawa, *Ind. Eng. Chem., Prod. Res. Dev.*, **20**, 386 (1981).
3) S. Gottlieb and P. B. Marsh, *Ind. Eng. Chem., Anal. Ed.*, **18**, 16 (1946).
4) R. L. Gustafson, R. L. Albright, J. Heisler, J. A. Lirio, and O. T. Reid, *Ind. Eng. Chem., Prod. Res. Dev.*, **7**, 107 (1968).
5) H. Schneider, G. C. Kresheck, and H. A. Scheraga, *J. Phys. Chem.*, **69**, 1310 (1965).
6) C. Tanford, "The Hydrophobic Effect: Formation of Micelles and Biological Membranes," John Wiley & Sons, New York (1980), pp. 5—20.
7) C. McAuliffe, *J. Phys. Chem.*, **70**, 1267 (1966).
8) a) D. S. Goodman, *J. Am. Chem. Soc.*, **80**, 3887 (1958); b) R. Smith and C. Tanford, *Proc. Nat. Acad. Scid. U. S. A.*, **70**, 289 (1973).

  Bull. Chem. Soc. Jpn., 54, 3259—3264 (1981)

Nature of Acid Sites on TiO_2, and Their Reactions with OH and NH_2 Groups of 3-Amino-1-propanol, 1-Propanol, and 1-Propylamine

Toshinori KANTOH and Susumu OKAZAKI*

Department of Industrial Chemistry, Faculty of Engineering, Ibaraki University, Nakanarusawa, Hitachi 316

(Received February 19, 1981)

The IR spectra for pyridine adsorbed on the surfaces of TiO_2 (SA) (anatase type), prepared from titanium tetraisopropoxide, showed the existence of only Lewis acid sites which were not converted to the Brönsted type by the addition of water. However, TiO_2 (SB) (anatase type), prepared by the hydrolysis of titanium oxide sulfate, showed both Lewis and Brönsted acidities. The Lewis acidity of SB was converted to the Brönsted type by the introduction of water vapor. The 3-amino-1-propanol compound interacted with both Lewis and Brönsted acid sites on the TiO_2 surfaces in a manner similar to propylamine rather than to 1-propanol. However, in the case of SA, interactions between OH groups of the amino alcohol and surface OH groups seemed to take place to some extent. The mode of the surface reaction of TiO_2 differes markedly from that of SiO_2 which has no surface acidity. A linear relationship between the amount of surface OH groups on SB and the amount of the reaction of 3-amino-1-propanol at 235 °C in an autoclave was observed. The formation of oriented and closely packed layers of adsorbed molecules was observed for all the combination of SB and 3-amino-1-propanol, in which some condensation (mainly dimerization) seemed to be promoted by acid sites on SB.

Recently, the acid-base properties of the TiO_2 surfaces have become the object of practical attention because of their wide use for catalysts[1] and ion exchangers.[2] Accordingly, extensive studies of the reactivity of TiO_2 surfaces have been carried out to learn their specific properties.[3] It has been shown that hydroxyl groups and metal ions on the TiO_2 surfaces are active sites for chemisorption, and the interactions of these sites with alcohol[4,5] and amines[6] have been studied. However, the reactions of amino alcohols with the TiO_2 surfaces have not been investigated. It would be of great interest to know which of the groups, OH or NH_2, interact preferentially with active sites on the TiO_2 surfaces. Furtheremore, it is worthwhile to clarify the difference in mode of interaction between an amino alcohol with two functional groups and an alkylamines or alcohol, each of which has a single functional group.

In the present investigation, the interactions of OH and NH_2 groups in 3-amino-1-propanol with the surfaces of TiO_2 were studied by comparing the infrared spectra of the adsorbed molecules with those of 1-propanol and propylamine. The infrared spectra of pyridine adsorbed on TiO_2 were first examined in order to know the nature of acid sites which would interact with NH_2 or OH groups in organic reagents. For a further study of the reactivities of OH and NH_2 groups, the reactions of 3-amino-1-propanol, 1-propanol, and propylamine with TiO_2 surfaces were carried out in an autoclave. The reactions of other amino alcohols with various types of structures were also tested for comparative purposes.

Experimental

Materials. The TiO_2 samples were used to see the effect of the solid acidity on the surface reaction. The first of the samples was prepared by the hydrolysis of titanium tetraisopropoxide (Wako Pure Chemical Co.), followed by repeated washing with deionized water. The product contained no significant traces of sulfate or chloride ions. The sample was designated as SA. The other sample (SB) was prepared using an intermediate product from the sulfuric acid process, supplied by the Sakai Chemical Co. Even after repeated washing with deionized water, SB has a considerable amount of combined sulfate ions, possibly in the form of titanium oxide sulfate. Before use, both SA and SB were heat-treated at 500 °C for 3 h. The X-ray analysis showed that both crystalline forms of SA and SB are anatase after the heat-treatment.

The organic reagents used were of a special or reagent grade from the Wako Pure Chemical Co. The propylamine was dried over solid KOH, and the other reagents, over 4A molecular sieve. Immediately before adsorption, the reagents were purified by repeating a freeze-pump-thaw cycles. The water used was distilled from an aqueous solution of $KMnO_4$.

IR Absorption Experiment. The infrared spectra of the organic reagents adsorbed on TiO_2 were measured in an *in situ* cell equipped with NaCl windows. The TiO_2 samples were ground and fabricated into discs of 20 mm in diameter. The discs were heat-treated at 500 °C before insertion in the cell. Immediately before adsorption, the discs were further treated at 250 °C for 12 more hours under evacuation at pressure of 10^{-4} mmHg.† Oxygen treatment was done by introducing O_2 into the cell, followed by heat-treatment at 250 °C for 0.5 h to burn out any organic contaminants on the TiO_2 surface. Adsorption was carried out by bringing the saturated vapor of organic reagents into contact with the TiO_2 in the cell for 0.5 h at room temperature or at 250 °C. The infrared spectra were measured after evacuation at 120 °C for 0.5 h and then cooling to room temperature. IR transmission through SA was almost zero in the wavenumber range from 2800 to 4000 cm^{-1}, probably because of the reflection of the rays due to the large particle size of the TiO_2 sample. Therefore, the infrared spectra were measured in the range below 1750 cm^{-1}, since most of the essential bands for this study are in the lower-wavenumber region.

Reaction Procedure. SA or SB (5 g) was treated with a large excess of organic reagents (about 100 m mol) diluted with hexane (30 ml) in an autoclave having a volume of 100 ml. The reactions were carried out for 1 h at 235 °C (the critical temperature of hexane) with vigorous stirring. The products were washed with hexane and then with acetone, followed by drying under evacuation at about 100 °C.

Chemical Analysis, DTA, TG, and Measurements of Surface Area and Acid-Base Amount. The carbon and nitrogen

† 1 mmHg ≈ 133.322 Pa.

contents of the products were determined by the Pregl-Dumas method.[7] The specific surface areas were determined by the BET method using N_2 at −195 °C. The solid acidities were determined by titration with butylamine, using Methyl Red ($pK_a = +4.8$) as the indicator.[8] The amount of surface OH groups was determined by a modification of Boehm's method[9]. To ascertain the thermal-decomposition or decomposition temperature, DTA and TG were carried out using a Thermoflex (Rigaku Denki Co.) by heating the sample (20 mg) at a rate of 5 °C/min in an air flow.

Results and Discussion

Crystal Forms, SO_4^{2-} Content, and Surface Properties of Samples. As is shown in Table 1, the surface areas and amounts of the surface OH groups of SB were close to those of SA when both samples were treated at 500 °C. However, the acid amount on SB was more than ten times that on SA. The large acidity of SB is probably due to sulfate ions which diffused to the surface during the heat treatment.[10] The crystal forms of SA and SB were both anatase, and SB contained a considerable amount of sulfate ions.

IR Spectra of Pyridine Adsorbed on TiO_2. The infrared spectra of pyridine adsorbed on SA evacuated at room temperature showed adsorption bands at 1145, 1220, 1442, 1485, 1575, and 1603 cm^{-1} (Fig. 1b). Except for the band at 1142 cm^{-1} the bands almost coincide with those observed on rutile by Parfitt *et al.*[11] and are assignable to Lewis-acid sites. Unlike the other bands, the band at 1145 cm^{-1} became appreciably weaker under evacuation at 250 °C. Taking into account the fact that a weak shoulder at about 1140 cm^{-1} was assigned to weakly coordinated pyridine,[11] this band at 1142 cm^{-1} may also be attributable to weak Lewis acid sites. The band is clearly detectable in this study because the sample (anatase type) was heat-treated at a temperature not so high as the rutile. On exposure to water at room temperature, the bands attributed to Lewis acid sites became weaker, but the bands characteristic of Brönsted acid sites such as that at 1540 cm^{-1} [12] did not become apparent. These facts indicate that there is no conversion of Lewis acid to Börnsted acid with the addition of water to SA, much as with the result observed when water was added to the rutile sample.[11]

On the other hand, the spectra of pyridine adsorbed on SB showed an absorption band at 1537 cm^{-1} besides the bands attributed to Lewis-acid sites at 1445 and 1575 cm^{-1} (Fig. 2). The band at 1537 cm^{-1} may be taken as the principal band due to Brönsted acid sites.[13] Upon heating up to 250 °C, this band became considerably weaker in contrast to that of the band characteristic of Lewis acid sites at 1575 cm^{-1}, which became more distinct. With the addition of water vapor, the band due to Lewis acid sites almost disappeared, while the bands due to Brönsted acid sites became more prominent. Such a conversion of Lewis to Brönsted acid sites occasioned by the addition of water vapor has also been observed for other metal oxides[12] and for SiO_2–Al_2O_3,[13] but it was not observed in the case of SA, as has just been described. The band at 1375 cm^{-1} observed in the spectrum of SB is ascribed to –O–SO_2–O– groups, which should be found at 1330—1450 cm^{-1}.[14] The

Table 1. Surface properties of TiO_2 samples[a]

	SA[b]	SB[c]
Crystal form[d]	Anatase	Anatase
SO_4^{2-} content/wt%	Trace	4.7
Surface area/$m^2\ g^{-1}$	95	93
Amount of surface OH groups/mmol g^{-1}	0.55	0.58
Acid amount ($H_0 \leqq 4.8$)/mmol g^{-1}	0.02	0.35

a) Calcined at 500 °C. b) Prepared by the hydrolysis of titanium isopropoxide. c) Prepared by the sulfuric acid process. d) Incompletely crystallized.

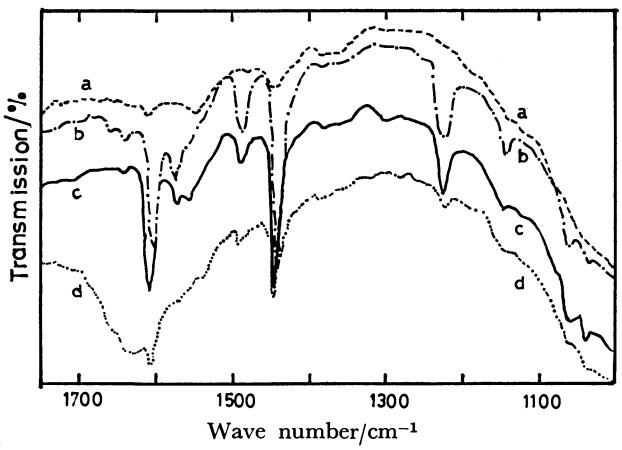

Fig. 1. IR spectra of pyridine adsorbed on SA.
(a) Initial surface, (b) exposed to pyridine at room temperature, evacuated at room temperature, (c) evacuated at 250 °C, (d) then, exposed to H_2O at room temperature, evacuated at room temperature.

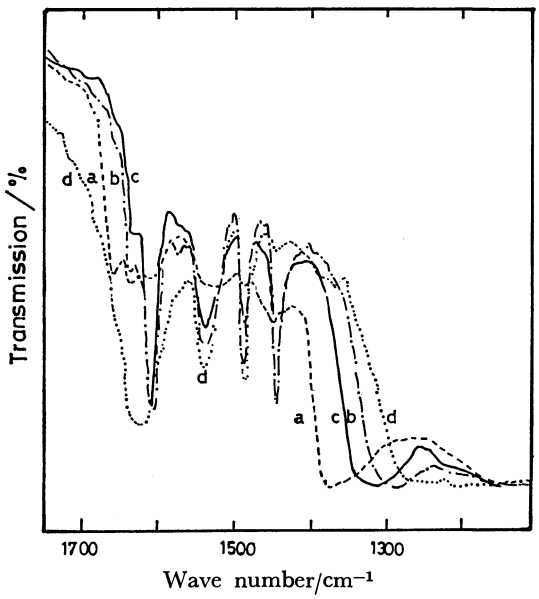

Fig. 2. IR spectra of pyridine adsorbed on SB.
(a), (b), (c), and (d) are the same as in Fig. 1.

groups may withdraw electrons from adjacent OH groups and make them Brönsted acids. Upon the addition of water vapor, the band at 1375 cm^{-1} was noticeably shifted to a lower-wave number region. Since the absorption bands due to $-SO_3H$ groups should be generally found at 1150—1260 cm^{-1},[14] the –O–S–O– bond on the surface might be broken by the attack of water, as is shown below;

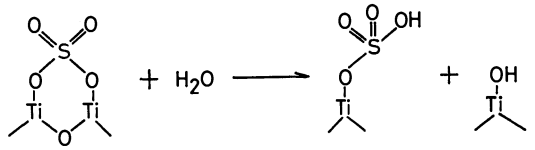

Also, this conversion, accompanied by the addition of water, should contribute to an increase in the Brönsted acidity.

IR Spectra of 3-Amino-1-propanol, 1-Propanol, and Propylamine Which Were Adsorbed on TiO_2. The spectra of 3-amino-1-propanol adsorbed on SA are given in Fig. 3. The spectra of 1-propanol and propylamine are given in Figs. 4 and 5 respectively for comparative purposes. The band at about 1600 cm^{-1} in the spectrum of liquid 3-amino-1-propanol (shown by Fig. 3, curve(d)) is shifted to near 1580 cm^{-1} (curves (b) and (c)) by the adsorption. Such a shift is also seen in the spectra of propylamine adsorbed on SA. Since a similar shift has been observed in the infrared spectrum of methylamine on alumina,[15] which is a typical Lewis acid, the band-shift observed here is considered to be due to the coordination of unshared electron pairs on the N atoms with Lewis acid sites or with exposed Ti ions on the surface. The shoulder at about 1650 cm^{-1} due to C=C bands in the spectra of 1-propanol adsorbed on SA (shown in Fig. 4, curves (b) and (c)) is not observed in the spectra of adsorbed 3-amino-1-propanol (Fig. 3). This fact indicates that the β-elimination of H_2O or NH_3 from the adsorbed molecules seems improbable for 3-amino-1-propanol.

Unlike the spectra of propylamine adsorbed on SA, three absorption bands, at about 1430, 1390, and 1245 cm^{-1}, are found in the spectra of the amino alcohol adsorbed on SA, and they become more marked on heating to 250 °C. The first band is also found in the spectrum of free amino alcohol (Fig. 3, curve (d)). The second band can be assigned to the C–O bond in titanium alkoxide by reference to the observation that a strong band has been found at 1385 cm^{-1} in the spectrum of aluminium ethoxide and in that of ethanol adsorbed on alumina.[16] The last band, at about 1245 cm^{-1}, was not found in the spectra of 1-propanol and propylamine, which were adsorbed on TiO_2 (SA and SB). The band is in the range of bands due to C–O stretching vibration (1000—1300 cm^{-1} [17]) and is especially assignable to the epoxy ring (strong absorption, near 1250 cm^{-1} [18]). The band in the C–N stretching vibration region (1120—1150 cm^{-1}) is broader and is shifted to a range lower than that found in the spectrum of propylamine adsorbed on SA at 250 °C. (Fig. 5(c)). Thus, it is

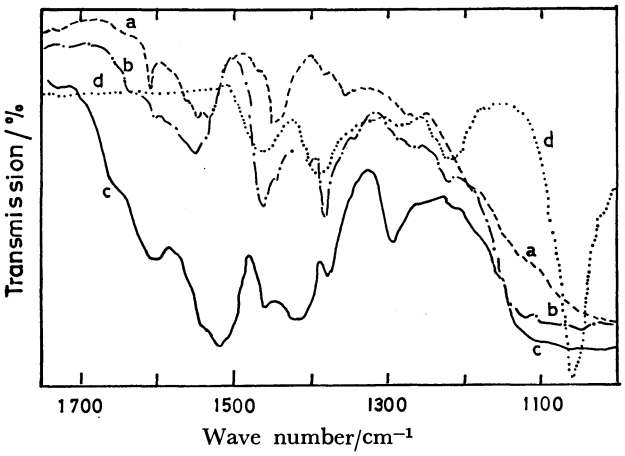

Fig. 4. IR spectra of 1-propanol adsorbed on SA.
(a) Initial surface, (b) exposed to 1-propanol at room temperature, evacuated at room temperature, (c) heated with 1-propanol vapor at 250 °C, evacuated at 120 °C, (d) 1-propanol (gas).

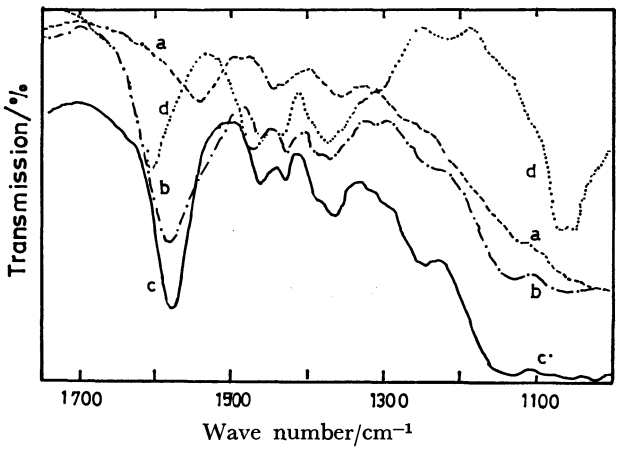

Fig. 3. IR spectra of 3-amino-1-propanol adsorbed on SA.
(a) Initial surface, (b) exposed to 3-amino-1-propanol at room temperature, (c) heated with 3-amino-1-propanol vapor at 250 °C, evacuated at 120 °C, (d) spectrum of 3-amino-1-propanol (liquid).

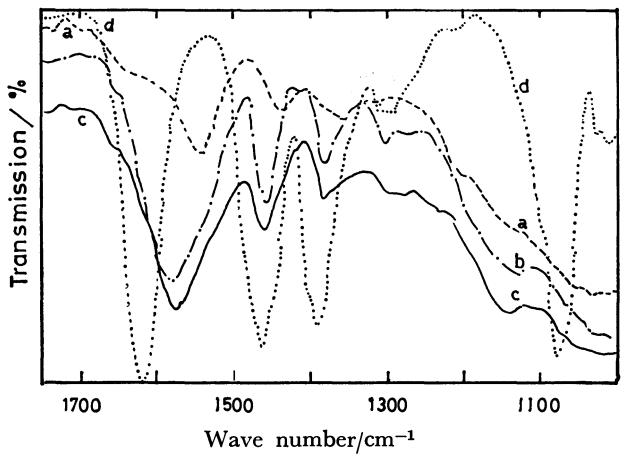

Fig. 5. IR spectra of 1-propylamine adsorbed on SA.
(a) Initial surface, (b) exposed to 1-propylamine at room temperature, evacuated at room temperature, (c) heated with 1-propylamine vapor at 250 °C, evacuated at 120 °C, (d) 1-propylamine (gas).

probable, although not certain, that, besides the N atom, the OH group of the amino alcohol may also participate in the surface reaction to some extent. Thus, the following reaction scheme is conceivable:

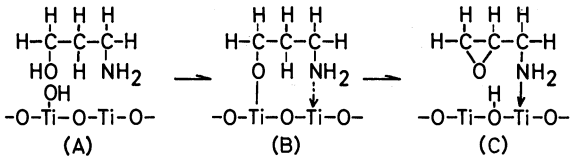

Here, the β-hydrogen atom in the (B) structure may become acidic as a result of the withdrawal of electrons by the surface Ti ion through the O atom, thus forming the OH group shown in (C) structure. The molecule formed on the TiO_2 surface may be adsorbed through the bond resulting from the coordination of the free electrons of the N atoms to the Ti ion, as is shown in the structure.

The infrared spectra of 3-amino-1-propanol, 1-propanol, and propylamine, which were all adsorbed on SB, are shown in Figs. 6, 7, and 8 respectively. As the 3-amino-1-propanol was adsorbed on SB, absorption bands at 1605 and 1510 cm^{-1} became observable. These are assigned to assymetric NH_3^+ (1560—1625 cm^{-1}) and symmetric NH_3^+ (1505—1550 cm^{-1} respectively.[19] The bands also show that Brönsted acid sites on TiO_2 probably take part in the surface reaction with the amino alcohol. The participation of Brönsted acid sites was observed in the interaction of propylamine with the SB surface at 250 °C (Fig. 8, curve(C)). However, when SB was heated up to 250 °C together with the amino alcohol, the bands due to NH_3^+ almost disappeared (Fig. 6(c)), while the band at about 1590 cm^{-1} related to the coordination bond between the Ti ion and the NH_2 groups became distinct with the heat-treatment. Such a change in the spectra indicates that the interaction of NH_2 groups with Lewis acid sites became predominant at higher temperature because of the decrease in the amount of OH groups, which may be Brönsted acid sites, as a result of dehydration. As is clear from the spectrum of the amino alcohol adsorbed on SA at 250 °C, there are no absorption bands which indicate the formation of C–O bonds. This suggests that the amino alcohol may interact with the SB surface mainly through the NH_2 groups.

Infrared spectroscopic studies of the reaction of 3-smino-1-propanol with SiO_2 surfaces have shown that free silanol reacted with alcoholic hydroxyl groups, while the NH_2 groups of the amino alcohol interacted only partially through hydrogen bonding.[20] The large difference in the mode of surface reaction between TiO_2 and SiO_2 may be due to the difference in the surface acidity. That is, the cation electronegativity

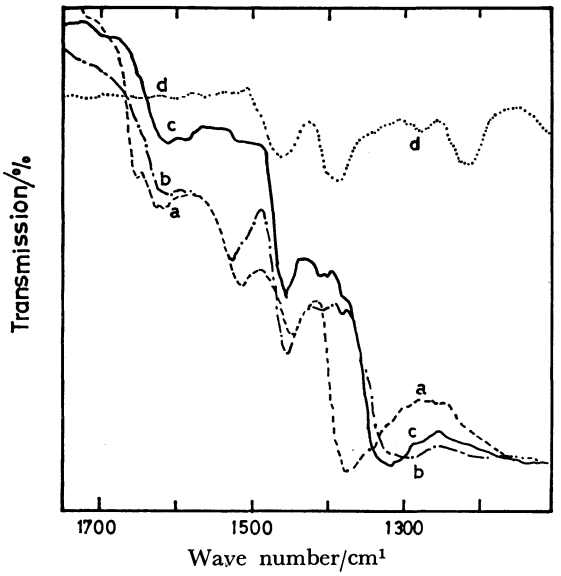

Fig. 7. IR spectra of 1-propanol adsorbed on SB.
(a), (b), (c), and (d) are the same as in Fig. 4.

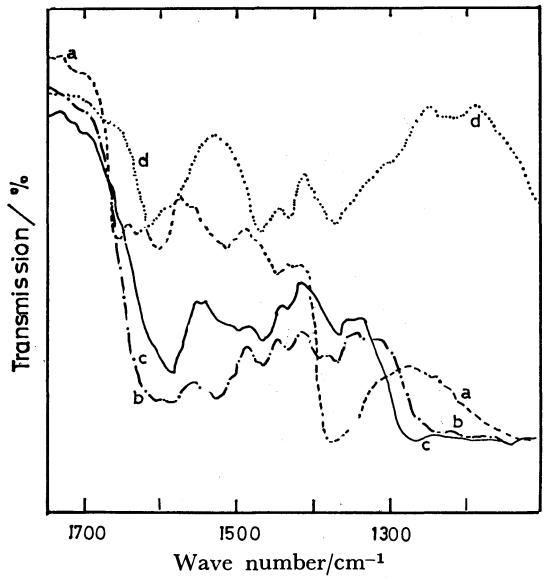

Fig. 6. IR spectra of 3-amino-1-propanol adsorbed on SB.
(a), (b), (c), and (d) are the same as in Fig. 3.

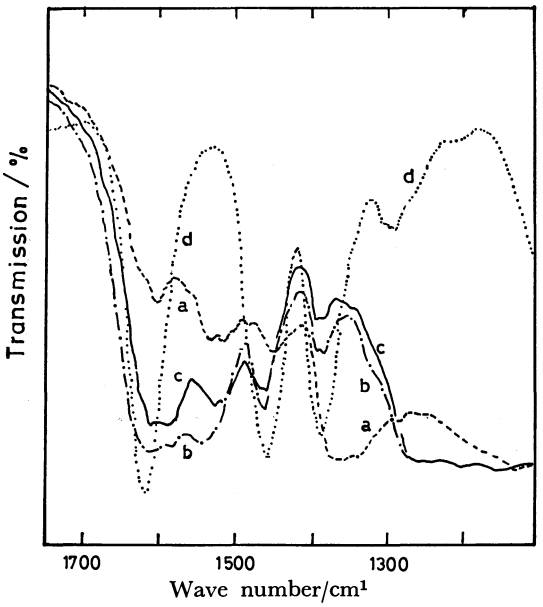

Fig. 8. IR spectra of 1-propylamine adsorbed on SB.
(a), (b), (c), and (d) are the same as in Fig. 5.

Table 2. Reactivity of TiO_2 to various reagents and decomposition temperatures of the products

Sample	Regent	Content in product wt% C	Content in product wt% N	Degree of reaction: Molecules per 100 Å² of surface calculated from content of C	Degree of reaction: Molecules per 100 Å² of surface calculated from content of N	Decomposition temperature °C: Beginning	Decomposition temperature °C: Active
SA	$CH_3(CH_2)_3OH$	2.67	0	4.9	—	140	240
	$CH_3(CH_2)_3NH_2$	2.20	0.94	4.0	4.4	160	240
	$HO(CH_2)_3NH_2$	2.67	0.99	5.0	4.7	150	230
SB	$CH_3(CH_2)_3OH$	2.54	0	4.8	—	190	260
	$CH_3(CH_2)_3NH_2$	2.45	1.12	4.6	5.4	210	255
	$HO(CH_2)_3NH_2$	3.86	1.52	7.5	7.7	180	260

of Ti^{4+} is much larger than that of Si^{4+};[21] the OH groups bound to Ti^{4+} are acidic in nature, unlike those bound to Si^{4+}, and so readily interact with NH_2 groups in the amino alcohol, resulting in the formation of NH_3^+ groups. In addition, Ti^{4+} also functions as a Lewis acid site, and the Lewis acidity should also make the reactivity of the TiO_2 surfaces higher than that of SiO_2. On the other hand, SiO_2 which has essentially no surface acidity,[22] forms only an ester due to the reaction of the silanol with the alcoholic OH groups of the amino alcohol.[20]

Comparison of the Reaction of 3-Amino-1-propanol with Those of 1-Propanol and Propylamine at Higher Temperatures in an Autoclave. Table 2 shows the results of the reactions for SA and SB. The degree of reaction was calculated on the assumption that there were no C–C bond scissions during the reaction. Except for the reaction between 3-amino-1-propanol and SB, the degree of the reaction was roughly the same for all the reactions; thus, the OH and NH_2 groups of the reagents appeared to have the same reactivity toward TiO_2 under the reaction conditions tried here. In addition, as is shown at the right end of Table 2, the temperatures at which the desorption or decomposition takes place actively were nearly the same for 3-amino-1-propanol, 1-propanol, and propylamine as long as they are adsorbed on the TiO_2 sample (SA or SB). Thus, the resistivity against heating of the adsorbed phase is considered not to differ much from reagent to reagent.

The degree of reaction per unit of surface area is calculated to be 4—5 molecules/100 Å² of the TiO_2 surface (Table 2). The areas occupied by one molecule of the reagents (20—25 Å²) nearly equal those occupied by normal alkylamine (20.5 Å²) and normal alkanols (21.6 Å²) in a unimolecular layer on water.[23] This fact suggests the formation of oriented and close-packed alkyl groups on TiO_2 surfaces. The exceptionally small value of the area occupied by 3-amino-1-propanol on SB (13 Å²) may be due to the condensation (mainly, dimerization) of the amino alcohol on the surface. The intermolecular reaction of the amino alcohol due to the OH and NH_2 groups is probably promoted by the acid sites on SB.

Effect of Surface OH Groups on the Reactivity of TiO_2 (SB). Figure 9 shows a plot of the amount of the reaction of 3-amino-1-propanol *vs.* the amount of surface OH groups on SB treated at various temperatures. Except for SB heat-treated at 300 °C, at which SB exists not as TiO_2 but as titanium hydroxide or hydrate of TiO_2,[24] a linear relationship is observed between the two amounts. From the slope of the straight line, the ratio of the amount of the reaction to that of the surface OH groups is determined to

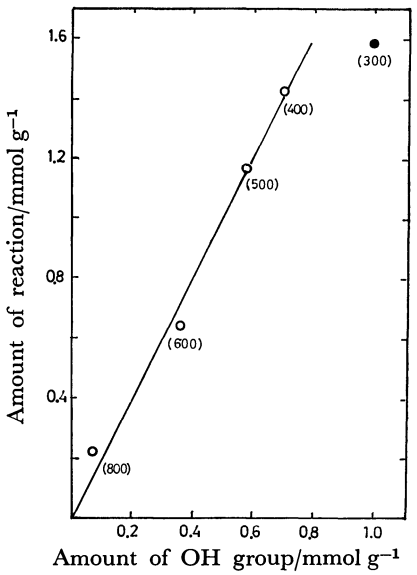

Fig. 9. Relationship between amount of reaction and that of surface OH groups on SB.
The numbers in parentheses show the heat-treatment temperature (centigrade) of the TiO_2 sample.

Table 3. Reactions of various aminoalcohols with TiO_2[a]

Sample	Aminoalcohol	Carbon content in products wt%	Density of organic groups: Number per 100Å² of surface
SA	$HO(CH_2)_2NH_2$	1.82	5.0
	$HO(CH_2)_2$ >NH $HO(CH_2)_2$	2.58	3.6
	$HO(CH_2)_2$ \ $HO(CH_2)_2$–N $HO(CH_2)_2$ /	3.29	3.1
SB	$HO(CH_2)_2NH_2$	3.98	12.0
	$HO(CH_2)_2$ >NH $HO(CH_2)_2$	6.59	10.4
	$HO(CH_2)_2$ \ $HO(CH_2)_2$–N $HO(CH_2)_2$ /	12.04	14.4

a) Preheated at 500 °C just before use.

be about 2. These facts show that NH_2 groups of the amino alcohol should react with surface OH groups on SB at a higher temperature under an autogeneous pressure, and that the amino alcohol may dimerize due to the NH_2 and/or OH groups of the molecules. The H_2O molecules generated by the dimerization or condensation may convert the Lewis acid sites on SB to Brönsted acid sites or acidic OH groups as was previously been observed in the IR study of pyridine adsorption.

Effect of Structure of Amino Alcohol on Reaction with TiO_2 Surfaces. The results of the surface reactions of various amino alcohols with SA and SB are shown in Table 3. For the reactions with SA, the amount of reaction per unit of surface area of TiO_2 decreased as the structure of amino alcohol became more complicated. For the reactions with SB, the amount of reaction per 100 Å^2 are $\geqq$10, markedly more than those for the reactions with SA. A maximum in the amount was obtained for the reaction of triethanolamine. The ratio of the amount of the reaction of the triethanolamine to that of the surface OH groups is above 4. Extensive condensations due to OH groups may be the main reason that the triethanolamine showed the highest value in the amount of the reaction in spite of its extremely bulky structure.

References

1) K. Tanabe, "Solid Acids and Bases," Kodansha, Tokyo (1970), p. 56.

2) C. H. Wirgiun and A. A. Yaron, *J. Appl. Chem.*, **15**, 445 (1965); *J. Inorg. Nucl. Chem.*, **28**, 2379 (1966); Y. Inoue and M. Tsuji, *Bull. Chem. Soc. Jpn.*, **49**, 111 (1976).

3) C. M. Hollabaugh and J. J. Chessick, *J. Phys. Chem.*, **65**, 1681 (1961); M. Primet, P. Pichat and M. V. Mathieu, *ibid.*, **75**, 1216, 1221 (1971); W. H. Wade and N. Hackerman, *ibid.*, **65**, 1681 (1961).

4) S. Okazaki and T. Kanno, *Nippon Kagaku Kaishi*, **1973**, 1285.

5) P. Jackson and G. D. Parfitt, *Trans. Faraday Soc.*, **68**, 1443 (1972).

6) Japanese Patents, Application No., 46-18858 (1971), 47-21686 (1972) (Titanium Geselshaft mit Farbenbriken Bayer).

7) For example, E. Kimura, "Yuki Biryo Teiryo Bunseki," ed by Yuki Biryo Bunseki Kenkyu Kondankai, Nankodo, Tokyo (1969), p. 330.

8) O. Johnson, *J. Phys. Chem.*, **59**, 287 (1955).

9) N. Yamagata, Y. Owada, S. Okazaki, and K. Tanabe, *J. Catal.*, **47**, 358 (1977).

10) T. Chinone and S. Okazaki, *Nippon Kagaku Kaishi*, **1978**, 1327.

11) G. D. Parfitt, J. Rambotham, and C. H. Rochester, *J. Chem. Soc., Trans. Faraday Soc.*, **67**, 1500 (1971).

12) M. Basila, T. R. Kanter, and K. H. Rhee, *J. Phys. Chem.*, **68**, 3197 (1964); M. R. Basila and T. R. Kanter, *ibid.*, **70**, 1681 (1966).

13) E. D. Parry, *J. Catal.*, **2**, 371 (1963).

14) S. Tanaka and Y. Iida, "Kikibunseki," Shokado, Tokyo (1977), p. 85.

15) K. Hirota, K. Fueki, and T. Sasaki, *Bull. Chem. Soc. Jpn.*, **35**, 545 (1962).

16) L. M. Roev and A. N. Terenin, *Dokl. Akad. Nauk SSSR*, **124**, 373 (1959); L. H. Little (translated by M. Hasegawa *et al.*), "Infrared Spectra of Adsorbed Species," Kagakudojin, Kyoto (1971), p. 181.

17) L. J. Bellamy, "The Infra-red Spectra of Complex Molecules," Chapman and Hall, London (1975), Vol. 2, p. 122.

18) Ref. 17, p. 131.

19) A. D. Cross and R. A. Jones (translated by N. Natori *et al.*), "An Introduction to Practical Infra-red Spectroscopy," Tokyo Kagaku Dojin, Tokyo (1977), p. 110.

20) R. G. Azrak and C. L. Angell, *J. Phys. Chem.*, **77**, 3048 (1973).

21) K. Tanaka and A. Ozaki, *J. Catal.*, **8**, 1 (1967).

22) S. Okazaki, "Kinzoku Sankabutsu To Fukugo Sankabutsu," ed by K. Tanabe, T. Seiyama, and K. Fueki, Kodansha Scientific, Tokyo (1978), p. 102.

23) "Kagakubinran (Kisohen)," ed by the Chemical Society of Japan, Maruzen, Tokyo (1966), p. 546.

24) J. Barksdale, "Titanium," The Ronald Press, New York (1966), p. 90.

Mechanisms of Light-initiated Redox Reactions of Copper(II)-Cyclic Polyamine Surfactant Assemblies

Yoshikiyo Moroi

Department of Chemistry, Faculty of Science, Kyushu University, Higashi-ku, Fukuoka 812

(Received March 2, 1981)

Photo-induced reduction of Cu^{2+} ion by organic electron donors was studied, main attention being paid to the decay kinetics of the cationized donor using two kinds of Cu^{2+} ions; one is free to move around the micellar surface of copper(II) dodecyl sulfate($Cu(DS)_2$), the other being fixed in a cyclic polyamine, Cu^{2+} complex of 2-tetradecyl-1,4,7,10-tetraazacyclododecane (CPA). Sodium 12-(10-phenothiazinyl)dodecanesulfonate (PTHDS) functions quite similarly to *N*-methylphenothiazine (MPTH) in an electron transfer reaction in $Cu(DS)_2$ micelles, and the reduced Cu^+ is ejected from the micelles.[1] In the MPTH–CPA system, $MPTH^+$ is completely ejected from the host micelle in the CPA micellar system. In consequence, the decay of the cationized donor obeys a second-order rate law, while the rate constant becomes much less. In PTHDS–CPA micellar system, on the other hand, the kinetics of the cationized donor is a superposition of two first-order decays of different rate constants, which suggests that the cationized donor can not escape into an intermicellar bulk phase due to the hydrophobic interaction between the long alkyl chain and its host micelle. A similar decay was also observed in the mixed micelles of the polyamine and hexadecyltrimethylammonium bromide.

Considerable effort has been expended on attempts to convert light energy to chemical energy,[2,3] and as a result mechanisms of photochemical reactions in micellar systems have become quite clear.[4–7]

Macrocyclic compounds with a long alkyl chain have been prepared for use as phase-transfer catalysts.[8] Micelle formation and surface activity of these compounds, as well as their cation transfer reaction[9] and complex formation with Cu^{2+} or Ag^+,[10] have been reported in recent publications. As described in our previous paper,[11] micellar aggregates of macrocyclic surfactant containing Cu^{2+} ion were found to exhibit a high efficiency in quenching the excited state of fluorophores such as cyanine dyes and pyrene. In the light of our previous discussion from the view point of the reaction mechanism concerning the light-induced reduction of Cu^{2+} ion by *N*-methylphenothiazine followed by the back electron transfer from the Cu^+ to the cationized *N*-methylphenothiazine in copper(II) dodecyl sulfate micelles,[12] it is worth carrying out an experimental investigation in pursuit for the effect of substitution of Cu^{2+} in the cyclic polyamine cage on the reaction sequence. Another interest is in the effect of the variation of electron donors, which would possibly cause some alteration of the decay mechanism.

The object of the present study is to make clear the mechanism of photo-redox reactions in the micellar system, *i.e.*, to derive kinetic equations capable of accounting for experimental results obtained from laser photolysis studies. Our first attention was concentrated on the difference in effects on reaction mechanism caused by two kinds of electron donors: one has a long hydrocarbon chain attached to the phenothiazine ring and the other has none. The former, even when positively charged, cannot escape into the intermicellar bulk phase due to hydrophobic interaction which is stronger than electrostatic repulsion with positively charged micelle. On the contrary, the latter, when positively charged, has the possibility of being ejected from the micelle. Our first interest was then shifted from the electron donors to electron acceptors, *i.e.*, two kinds of Cu^{2+} ions: one is free to move around the micellar surface and the other is fixed in the polyamine cage as a complex.

Experimental

Materials. The Cu^{2+} complex of 2-tetradecyl-1,4,7,10-tetraazacyclododecane (CPA) was kindly given us by Dr. P. Tundo of the Institute de Chimica Organica, University di Trino, and used as supplied. The *N*-methylphenothiazine (MPTH) and sodium 12-(10-phenothiazinyl)dodecanesulfonate (PTHDS) were synthesized by Dr. A. M. Braun in Dr. Grätzel's laboratory. The hexadecyltrimethylammonium bromide (HTAB) of certified grade was obtained from E. Merck, Darmstadt, and purified by repeated recrystallization from acetone–ethanol mixture. The copper(II) dodecyl sulfate($Cu(DS)_2$) was prepared by the method described previously.[13] The deionized water was distilled first from alkaline permanganate and then twice with a quartz still. All samples were deoxygenated by passage of nitrogen of high purity.

Apparatus. Time-resolved experiments were run by the laser photolysis technique; laser photolysis experiments employed a frequency doubled KJ-2000 ruby or neodymium laser with pulsewidth of 25 ns and energy output of *ca.* 20 mJ.

Analysis. In the cases where $PTHDS^+$ decay kinetics in PTHDS–cationic micellar systems can result from superposition of two kinds of first-order decays, the rate parameter (α_2) for slower decay was first determined from an oscilloscope trace of longer-time scale. The rate parameter(α_1) for faster decay was then evaluated from the difference between the total optical density and the extraporated optical density of the shorter-time scale which had been calculated from the optical density of longer-time scale with the aid of the rate parameter α_2.

Results and Discussion

The light-initiated redox reaction in question is represented as

$$A + D \underset{d}{\overset{h\nu}{\rightleftharpoons}} A^- + D^+, \quad (1)$$

where A and D stand for an electron acceptor and

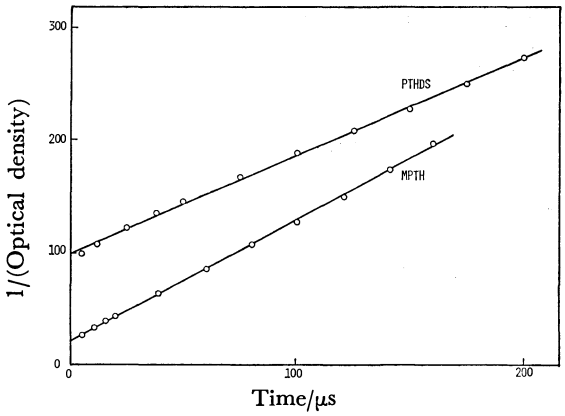

Fig. 1. Second-order plots of the 516 nm absorbance decay for MPTH (1.0×10^{-4} M†) and PTHDS (1.0×10^{-4} M) in $Cu(DS)_2$ (2.0×10^{-2} M) micellar systems.

donor, respectively, corresponding to Cu^{2+} ion and MPTH or PTHDS for the present experiment. The first requirement for analyzing the reaction mechanism is to pursue the decay rate of the cationized electron donor with absorption maximum at 516 nm on an oscilloscope screen. Quantum yields of the cationized and triplet states of the donors are given in our previous paper.[11] Figure 1 shows second-order plots of the 516 nm absorption decay for the MPTH– and PTHDS–$Cu(DS)_2$ micellar solutions. It can be seen that, down to 30 percent or less of the initial optical density, a good linear relation exists between the inverse of optical density and time, *i.e.*, that the cationized donor decays according to a second-order rate law. The slopes which are almost the same with each other give the following estimates:

$$k_{obsd} = 9.3\times10^{9}\ M^{-1}s^{-1} \text{ for MPTH},$$
$$k_{obsd} = 7.9\times10^{9}\ M^{-1}s^{-1} \text{ for PTHDS}.$$

This close equality indicates similar decay mechanism in operation. PTHDS plays the same role as MPTH in reduction of Cu^{2+} and subsequent reaction mechanism. That is to say, on the analogy of the MPTH case, the reduced electron acceptor Cu^{+} is detached from its host micelle not only by electrostatic substitution with Cu^{2+} but also *via* a hopping process before recombination with the oxidized donor.[12] With this view, attempt will be made to probe further into the effect of variation of electron acceptor on the decay mechanism of the cationized donor: one is free to move around the micellar surface and the other is fixed in the polyamine cage. For the latter acceptor, the hydrophobic electron donor, MPTH, is incorporated in the polyamine aggregate. The excited state of MPTH has such a propensity for strong reduction[1] as to be expected to react with Cu^{2+} in the complex as follows:

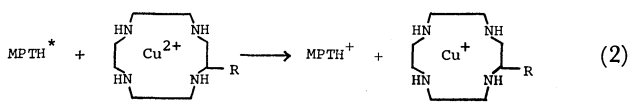

(2)

where R refers to $C_{14}H_{29}$ and MPTH* is the excited singlet state.[11] Figure 2 shows an oscilloscope trace illustrating a transient absorption at 516 nm for

† 1 M = 1 mol dm^{-3}.

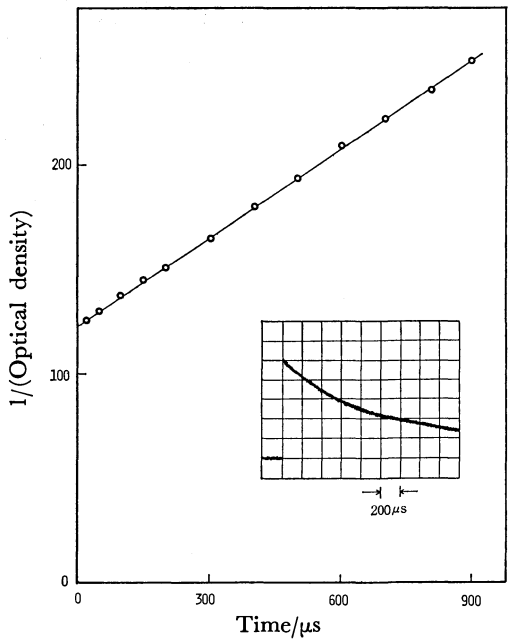

Fig. 2. Second-order plots of the 516 nm absorbance decay for MPTH (1.0×10^{-4} M) in Cu^{2+}-polyamine complex (5.0×10^{-3} M) micellar system. Insert: Oscilloscope traces showing the long-time $MPTH^{+}$ decay.

$MPTH^{+}$, together with plots of the inverse of optical density against time. The apparent decay process obeys the second-order kinetics in this case, too. The slope is, however, much less than those in the $Cu(DS)_2$ micellar assemblies.

$$k_{obsd} = 1.26\times10^{9}\ M^{-1}s^{-1}.$$

The discussion presented above leads to a possibility that either the oxidized $MPTH^{+}$ or the reduced Cu^{+} is ejected from its host micelle by electrostatic repulsion before the backward reaction occurs. If not, the decay should obey a first-order rate law because the cationized electron donor and the reduced electron acceptor ought to be paired in their host micelle. Another possibility is that both $MPTH^{+}$ and Cu^{+} leave the micelle. In this case, however, the k_{obsd} value should be larger than those for the MPTH– and PTHDS–$Cu(DS)_2$ systems because neither of the cations is trapped in the cationized micelle for a long time, resulting in a higher chance for them to come closer to each other for the backward electron transfer. In addition, not only Cu^{2+} but also Cu^{+} ions can form a stable complex with macrocyclic tetramine.[14–16] Hence, the chance that Cu^{+} leaves its mother micelle is very low.

In order to examine whether $MPTH^{+}$ is ejected, we succeeded in using PTHDS as an electron donor, since PTHDS, even when charged positively, cannot be detached from its host micelle. It will be discussed more in detail from an energy point of view. If MPTH is assumed to be twice as strong as benzene in hydrophobic interaction because of a presence of two benzene rings in the molecule, the free energy change of transfer of MPTH from aqueous bulk into micellar core is 6—7 kT.[17,18] A location of solubilized

aromatic molecules in the micellar phase is generally a palisade layer of micelle,[19] and the phenothiazine molecule is really solubilized in the palisade layer of alkyl sulfate micelles.[20] Accordingly, the free energy change for the present case is less than that value. On the other hand, the electrical surface potential is calculated[22] as 6.6 and 4.9 $e\Psi/kT$ for 1.0 and 0.2 of dissociation degree of the micelle, respectively, by using 50 A^2 for molecular surface area at the micellar surface, its CMC value for the counter-ion concentration, and 40 for the dielectric constant.[21] Suppose now that the free energy change of MPTH due to hydrophobic interaction is $6.5\,kT$. Then, a fraction of $MPTH^+$ ejected from the micelle is more than 50 and 16 percent for 1.0 and 0.2 of dissociation degree of the micelle, respectively. On the other hand, PTHDS has a longer alkyl chain of twelve carbon atoms and a free energy change of transfer per methylene group from aqueous bulk into micellar core is $1.1\,kT$.[22] Thus, the total free energy change due to hydrophobic interaction is about $22\,kT$, whereas the gross electrostatic repulsive energy due to micellar surface potential is zero even when the electron donor group is cationized, because the molecule has an SO_3^- group. Hence, just after the electron transfer reaction has taken place, some fraction of cationized donor groups is detached from its host micelle by electrostatic repulsion. However, the whole molecule cannot escape into the bulk phase, because the cationized group is anchored to the host micelle through the hydrophobic interaction between its alkyl chain and the hydrophobic micellar core.

The absorbance signal at 516 nm on the oscilloscope screen for the PTHDS–CPA system decays apparently in two steps, where the first component amounting to 55 percent of the total signal corresponds to the decay of the triplet of PTHDS. The kinetics obeys the first-order rate law with a time constant of $1.7\times10^7\ s^{-1}$.[11] The slow second component can be produced by neither the first nor the second-order kinetics but only by a superposition of two kinds of first-order decays (Fig. 3). Another difference in behavior between $MPTH^+$ and $PTHDS^+$ is that the latter decays much faster than the former as far as the apparent decay of the second component is concerned. This may be expected if the slow component is associated with the $MPTH^+$ which leaves the micellar aggregate and escapes into the intermicellar bulk phase. In contrast to $MPTH^+$ the detachment of $PTHDS^+$ will be incomplete, since the cation remains anchored to its mother micelle as mentioned above. Eventually, the charge recombination of $PTHDS^+$ and Cu^+ occurs giving rise to a faster decay process, and variation of laser intensity did not cause any change of this decay pattern, although two rate parameters, α_1 and α_2, altered in small amount (Table 1).

In the light of the above discussion, it will be inquired whether the schematic diagram for the decay processes assists us in explaining the decays of both $MPTH^+$ and $PTHDS^+$ in the Cu^{2+}–polyamine micellar systems. As was mentioned above, the forward electron transfer from the photoexcited MPTH or PTHDS (electron donor D) to Cu^{2+} in a complex form (electron acceptor A) occurs within the duration of the laser pulse. Hence, the $D^+\cdots A^-$ pairs produced at the end of the pulse are the starting state of the decay processes. The kinetic parameters in the present study are quite similar to those used in our previous paper.[12]

With the solution containing PTHDS in the micelle, $PTHDS^+$ cannot be ejected into the intermicellar phase for the above reasons. Therefore, the whole molecule of $PTHDS^+$ cannot be detached from its host micelle even during the completion of the cation decay; the relaxation time of the gross rate of micelle association reaction is more than a millisecond order.[23,24] This means that the decay of D^+ is associated with the electron transfer to D^+ either inside or outside the micelle. Thus, we have the decay processes depicted in the scheme of Fig. 4, where the rate parameter k_b^i refers to the electron back transfer of D^+ inside the micelle, k_b^o that of D^+ outside the micelle, k_e the reaction of D^+ escape from the micellar interior, and k_r the reaction of D^+ return into the micellar interior.

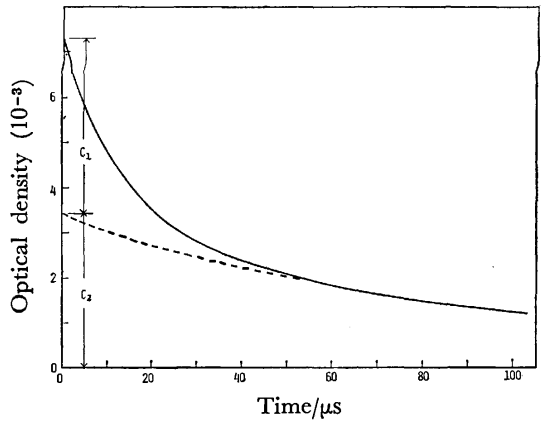

Fig. 3. The slower second-component decay of the absorbance at 516 nm for PTHDS (1.0×10^{-4} M) in Cu^{2+}–polyamine complex (5.0×10^{-3} M) micellar system.

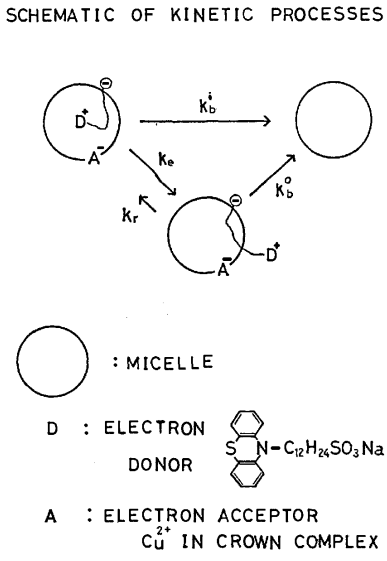

Fig. 4. Schematic illustration of the elementary processes for the decay kinetics of $PTHDS^+$ in Cu^{2+}–polyamine complex micellar system.

On the basis of the schematic diagram for the decay processes, we shall now develop kinetic equations to analyze the results. The following notations will be used for concentration terms: $C_{D^+_I}$ for micelles associated with D^+ inside the micelle; $C_{D^+_O}$ for micelles associated with D^+ outside the micelle.

$$\frac{dC_{D^+_I}}{dt} = -(k_b^I + k_e)C_{D^+_I} + k_r C_{D^+_O}, \quad (3)$$

$$\frac{dC_{D^+_O}}{dt} = -(k_b^O + k_r)C_{D^+_O} + k_e C_{D^+_I}. \quad (4)$$

From Eqs. 3 and 4, the decay rate of the total amount of the oxidized donor which is an experimentally observable quantity can be expressed as

$$\frac{d(C_{D^+_I} + C_{D^+_O})}{dt} = -k_b^I C_{D^+_I} - k_b^O C_{D^+_O}. \quad (5)$$

Introduction of Eqs. 3 and 4 into the time derivative equation of Eq. 3 gives

$$\frac{d^2C_{D^+_I}}{dt^2} + a\frac{dC_{D^+_I}}{dt} + bC_{D^+_I} = 0, \quad (6)$$

where

$$a = k_b^I + k_b^O + k_e + k_r \quad (7)$$

and

$$b = k_b^I k_b^O + k_b^I k_r + k_b^O k_e. \quad (8)$$

The solution of Eq. 6 becomes

$$C_{D^+_I} = A_1 e^{-\alpha_1 t} + A_2 e^{-\alpha_2 t}, \quad (9)$$

where $\alpha_1+\alpha_2=a$ and $\alpha_1\alpha_2=b$. Here, we assume $\alpha_1 > \alpha_2$. The boundary condition that the cation at time zero is totally $C_{D^+_I}$, reduces Eq. 9 to

$$A_1 + A_2 = C_0, \quad (10)$$

where C_0 is the total cationized donor concentration at time zero and A_1 and A_2 are integration constants. Introducing Eq. 9 into Eq. 3, $C_{D^+_O}$ can be obtained as

$$C_{D^+_O} = \frac{A_1(k_b^I + k_e - \alpha_1)}{k_r}e^{-\alpha_1 t} + \frac{A_2(k_b^I + k_e - \alpha_2)}{k_r}e^{-\alpha_2 t}. \quad (11)$$

As $C_{D^+_O}$ should be zero at time zero, we obtain for A_1 and A_2

$$A_1 = \frac{(k_b^I + k_e - \alpha_2)C_0}{\alpha_1 - \alpha_2}, \quad (12)$$

and

$$A_2 = \frac{(k_b^I + k_e - \alpha_1)C_0}{\alpha_1 - \alpha_2}. \quad (13)$$

Thus, the total decay of the cationized donor can be expressed as

$$C_{D^+_I} + C_{D^+_O} = C_1 e^{-\alpha_1 t} + C_2 e^{-\alpha_2 t}, \quad (14)$$

where

$$C_1 = \frac{A_1(k_b^I + k_e + k_r - \alpha_1)}{k_r}, \quad (15)$$

and

$$C_2 = \frac{A_2(k_b^I + k_e + k_r - \alpha_2)}{k_r}. \quad (16)$$

Hence, Eq. 14 indicates that the total decay is a superposition of the fast 1st-order decay on the slow 1st-order decay, which is the case with the present experiment. Now, we have to find a way to determine the rate parameters. Introducing Eqs. 9 and 11 into Eq. 5 and adopting the above two boundary conditions at time zero give k_b^I in the form,

$$k_b^I = \alpha_1\frac{C_1}{C_0} + \alpha_2\frac{C_2}{C_0}. \quad (17)$$

Using α_1, α_2, C_1, and C_2 which can be evaluated from the decay curves, k_b^I can be determined without any assumption and any mathematical approximation. Similarly, k_e value can also be determined by introducing Eqs. 9 and 11 into Eq. 4 and using the same boundary conditions in the following form,

$$k_e = \alpha_1\left(\frac{k_b^I + k_e - \alpha_2}{\alpha_1 - \alpha_2} - \frac{C_1}{C_0}\right) + \alpha_2\left(\frac{k_b^I + k_e - \alpha_1}{\alpha_2 - \alpha_1} - \frac{C_2}{C_0}\right). \quad (18)$$

As $k_b^I + k_e$ is nearly equal to α_1 (see Appendix), the third term cancels out and Eq. 18 can be rearranged using Eq. 17 into

$$k_e = \alpha_1 - k_b^I, \quad (19)$$

which means that Eq. 18 is consistent with the contents in the Appendix. Elimination of k_r term, using Eqs. 7 and 8, gives

$$k_b^O = \frac{k_b^{I2} + k_b^I k_e - (\alpha_1 + \alpha_2)k_b^I + \alpha_1\alpha_2}{k_e}. \quad (20)$$

Introducing k_b^I, k_b^O, and k_e thus obtained into Eq. 7, we obtain k_r value (Table 1). The k_r values for the systems are almost zero, if the experimental error is taken into account. Thus, the initial fast kinetics can be eventually represented by the equations in the Appendix. If the preceding reaction mechanisms are correct, the similar kinetic decay must be observed in the CPA–HTAB mixed micellar system. In fact, a superposition of two kinds of first-order decays took place in this system, too (Table 1), which assists the decay mechanism to be correct. A brief mention should be made of the difference in numerical values of the reaction parameters between the CPA and CPA–HTAB mixed micellar assemblies. Going back again to Table 1, we see that the k_b^I and k_e values in the mixed micellar system are much larger than those in the CPA micelle. It is highly likely, therefore, that the polyamine cage is much more mobile in the mixed micelle leading to higher k_b^I value and that the electrostatic surface potential is more positive in the mixed micelle, as reflected in the higher k_e value. The surface potential of HTAB is 9.4 $e\Psi/kT$ by a similar calculation, whereby a dissociation degree of the micelle is assumed to be 0.2, so that the value of 9.4 becomes less for the present mixed micellar system where a ratio of CPA to HTAB is 0.09. On the other hand, k_b^O is much less in the mixed system. This too is owing to higher surface potential which causes larger separation between Cu^+ and D^+ outside micelle.

Next, we proceed to the $MPTH^+$ cation decay in the Cu^{2+}–polyamine micellar system. As mentioned before, the decay kinetics obeys the 2nd-order law and $MPTH^+$, not Cu^+, escapes into an intermicellar phase due to an electrostatic repulsion between $MPTH^+$ and the positive micellar charge. This can be verified by 1) very large k_e value of the PTHDS–cationic

Table 1. Rate parameters for PTHDS (1.0×10^{-4} M) in Cu^{2+}-polyamine complex (5.0×10^{-3} M) and Cu^{2+}-polyamine complex/HTAB ($1.0\times10^{-3}/1.0\times10^{-2}$ M) mixed micellar systems

	α_1 / 10^4 s^{-1}	α_2 / 10^4 s^{-1}	k_b^i / 10^4 s^{-1}	k_b° / 10^4 s^{-1}	k_e / 10^4 s^{-1}	k_r / 10^4 s^{-1}
CPA	8.10 ± 0.36	1.04 ± 0.10	4.82	1.04	3.28	$\simeq0$
	$C_1/C_0=0.536$,	$C_2/C_0=0.464$				
CPA/HTAB	135 ± 10	0.261 ± 0.019	94.0	0.261	40.5	$\simeq0$
	$C_1/C_0=0.698$,	$C_2/C_0=0.302$				

The standard deviation for the numerical values of rate parameter is less than 10%.

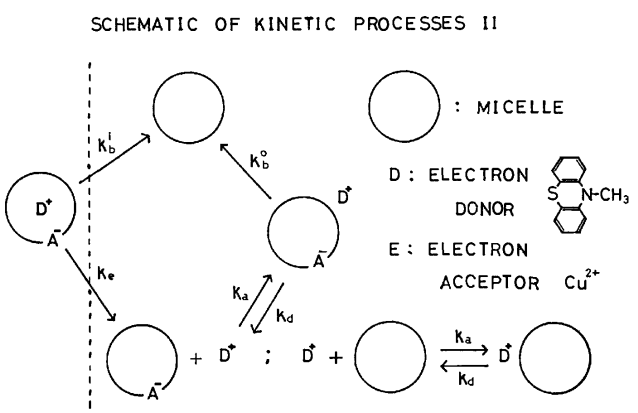

Fig. 5. Schematic illustration of the elementary processes for the decay kinetics of $MPTH^+$ in Cu^{2+}-polyamine complex micellar system.

micellar systems and 2) that the higher the surface potential of micelles, the larger the k_e value (see Table 1). In addition, as mentioned earlier, the k_r value was found to be almost zero. That is, the probability that the ejected cation donor goes back again into a micellar interior should be extremely small. Hence, the decay processes after the initial fast back electron transfer and after the cation ejection can be illustrated schematically in Fig. 5, where the reaction parameter k_a refers to the association reaction of D^+ with the micellar aggregate and k_d to the dissociation reaction of D^+ from the micellar aggregate. Now that the schematic diagram has been given, we can develop the kinetic equations for the decay processes. Following notations will be used for the concentration terms: $C_{D^+A^-}$ for micelles with simultaneous D^+ and A^- association (location of D^+ association is micellar surface); C_{D^+} for D^+ in the intermicellar bulk phase; C_{MD^+} for micelles with D^+ association; C_{MA^-} for micelles with A^- association; C_M for empty and D-containing micelles.

$$\frac{dC_{D^+A^-}}{dt} = k_a(k_b^\circ+k_d)C_{D^+A^-} + k_aC_{MA^-}C_{D^+}, \quad (21)$$

$$\frac{dC_{D^+}}{dt} = -k_aC_{D^+}(C_{MA^-}+C_M) + k_d(C_{D^+A^-}+C_{MD^+}), \quad (22)$$

$$\frac{dC_{MD^+}}{dt} = -k_dC_{MD^+} + k_aC_{D^+}C_M, \quad (23)$$

$$\frac{dC_{MA^-}}{dt} = -k_aC_{MD}C_{D^+} + k_dC_{D^+A^-}. \quad (24)$$

What we can observe experimentally is the sum of $C_{D^+A^-}+C_{D^+}+C_{MD^+}$. Hence, the decay rate of the total cationized donor is

$$\frac{d(C_{D^+A^-}+C_{D^+}+C_{MD^+})}{dt} = -k_b^\circ C_{D^+A^-}. \quad (25)$$

After the initial fast back electron transfer reaction, the concentration of D^+A^- becomes negligibly small and the system reaches a steady state for the concentration of $C_{D^+A^-}$ and for the partitioning of D^+ between the intermicellar phase and the micellar surface.[12]

$$\frac{dC_{D^+A^-}}{dt} = 0. \quad (26)$$

$$k_aC_{D^+}C_M = K_dC_{MD^+}. \quad (27)$$

An additional relationship is from the electroneutrality of the solution:

$$C_{MA^-} = C_{D^+} + C_{MD^+}. \quad (28)$$

Two equations which are derived by the introduction of Eq. 26 into Eqs. 21 and 25 give the total decay in the form,

$$\frac{d(C_{D^+}+C_{MD^+})}{dt} = -\frac{k_b^\circ k_aC_{MA^-}C_{D^+}}{k_b^\circ+k_d}. \quad (29)$$

Introducing Eqs. 27 and 28 into Eq. 29 gives

$$\frac{d(C_{D^+}+C_{MD^+})}{dt} = -k_{obsd}(C_{D^+}+C_{MD^+})^2, \quad (30)$$

where

$$k_{obsd} = \frac{k_b^\circ k_ak_d}{(k_b^\circ+k_d)(k_d+k_aC_M)}. \quad (31)$$

Thus, it has become clear that the cationized donor $MPTH^+$ is detached from the host micelle and that the decay rate of the total cation obeys the 2nd-order (Fig. 2). Namely, the mechanism depicted in Fig. 5 is consistent with the experimental results. Unfortunately, however, an evaluation of each rate parameter of this reaction system, unlike the system of MPTH in sodium dodecyl sulfate–europium decyl sulfate mixed micellar solution, can not be made only by increasing surfactant concentration,[12] because the micellar aggregation number of CPA increases with the surfactant concentration.[10] When the k_{obsd} value of $MPTH^+$ decay in the CPA micellar assembly is compared with that in the $Cu(DS)_2$ micellar assembly, we find that the former is as small as one-seventh of the latter. This is mainly attributable to the smaller k_a value for the former system which involves the repulsive force between $MPTH^+$ and the positive surface potential of CPA micelles, while, in the latter system, the

negative surface potential gives rise to an attractive force between Cu^+ and micellar surface.

The author is grateful to Professor M. Grätzel of École Polytechnique Fédérale de Lausanne in Switzerland for his helpful comments and generous permission to publish this work which was partly done during my stay there.

Appendix

In the schematic diagram of Fig. 4, the returning reaction of D^+ outside the micelle into micellar core must be very slow, because the probability that the cationized donor repelled from the micelle by an electrostatic repulsion goes back again into the micellar core must be very small. Therefore, especially when we are discussing the short-time decay just after the laser pulse, $k_r C_{D^+_o}$ term can be neglected in Eqs. 3 and 4. Hence they become

$$\frac{dC_{D^+_1}}{dt} = -(k_b^1 + k_e)C_{D^+_1}, \tag{32}$$

$$\frac{dC_{D^+_o}}{dt} = -k_b^o C_{D^+_o} + k_e C_{D^+_1}. \tag{33}$$

Integration of Eq. 32 yields

$$C_{D^+_1} = C_0 e^{-(k_b^1 + k_e)t}. \tag{34}$$

Introducing Eq. 34 into Eq. 33 and the subsequent integration give

$$C_{D^+_o} = \frac{k_e C_0}{k_b^o - (k_b^1 + k_e)}\{e^{-(k_b^1 + k_e)t} - e^{-k_b^o t}\}. \tag{35}$$

The total cation concentration then becomes

$$C_{D^+_1} + C_{D^+_o} = \frac{k_b^1 - k_b^o}{k_b^1 + k_e - k_b^o} C_0 e^{-(k_b^1 + k_e)t} \tag{36}$$

$$+ \frac{k_e}{k_b^1 + k_e - k_b^o} C_0 e^{-k_b^o t}. \tag{36}$$

Comparing Eq. 36 with Eq. 14 as respects the first part, we have the following equation concerning just the initial decay rate:

$$\alpha_1 = k_b^1 + k_e. \tag{37}$$

References

1) Y. Moroi, A. M. Braun, and M. Grätzel, *J. Am. Chem. Soc.*, **101**, 567 (1979).
2) a) S. A. Alkaitis, G. Beck, and M. Grätzel, *J. Am. Chem. Soc.*, **79**, 5723 (1975); b) S. A. Alkaitis and M. Grätzel, *ibid.*, **98**, 3549 (1976).
3) D. Meisil, M. S. Matheson, and J. Rabani, *J. Am. Chem. Soc.*, **100**, 1679 (1978).
4) P. P. Infelta, M. Grätzel, and J. K. Thomas, *J. Phys. Chem.*, **78**, 190 (1974).
5) F. H. Quina and V. G. Toscano, *J. Phys. Chem.*, **81**, 1750 (1977).
6) M. Maestri, P. P. Infelta, and M. Grätzel, *J. Chem. Phys.*, **69**, 1522 (1978).
7) a) M. Almgren, F. Grieser, and J. K. Thomas, *J. Am. Chem. Soc.*, **101**, 279 (1979); b) **101**, 2021 (1979).
8) a) C. M. Starks and R. M. Owens, *J. Am. Chem. Soc.*, **95**, 3613 (1973); b) M. Cinquini, F. Montanari, and P. Tundo, *Gazz. Chim. Ital.*, **107**, 11 (1977); c) D. Landini, A. Maia, F. Montanari, and P. Tundo, *J. Am. Chem. Soc.*, **101**, 2526 (1979).
9) J. L. Moigne, P. Gramain, and J. Simon, *J. Colloid Interface Sci.*, **60**, 565 (1977).
10) Y. Moroi, E. Pramauro, M. Grätzel, E. Pelizzetti, and P. Tundo, *J. Colloid Interface Sci.*, **69**, 341 (1979).
11) R. Humphry-Baker, Y. Moroi, M. Grätzel, E. Pelizzetti, and P. Tundo, *J. Am. Chem. Soc.*, **102**, 3689 (1980).
12) Y. Moroi, P. P. Infelta, and M. Grätzel, *J. Am. Chem. Soc.*, **101**, 573 (1979).
13) Y. Moroi, T. Oyama, and R. Matuura, *J. Colloid Interface Sci.*, **60**, 103 (1977).
14) J. M. Palmer, E. Papaconstantinou, and J. F. Endicott, *Inorg. Chem.*, **8**, 1516 (1969).
15) N. E. Tokel, V. Katovic, K. Farmery, L. B. Anderson, and D. H. Bush, *J. Am. Chem. Soc.*, **92**, 400 (1970).
16) D. C. Oslon and J. Vasilevskis, *Inorg. Chem.*, **10**, 463 (1971).
17) I. J. Lin, J. P. Friend, and Y. Zimmels, *J. Colloid Interface Sci.*, **45**, 378 (1973).
18) S. G. Dick, D. W. Fuerstenau, and T. W. Healy, *J. Colloid Interface Sci.*, **37**, 595 (1971).
19) P. Mukerjee, "Solution Chemistry of Surfactants," ed by K. L. Mittal, Plenum Publishing Corp., New York (1979), Vol. 1, p. 135.
20) Y. Moroi, M. Saito, and R. Matuura, *Nippon Kagaku Kaishi*, **13**, 483 (1980).
21) P. Mukerjee and J. R. Cardinal, *J. Phys. Chem.*, **82**, 1620 (1978).
22) Y. Moroi, K. Motomura, and R. Matuura, *J. Colloid Interface Sci.*, **46**, 111 (1974).
23) B. C. Bennion and E. M. Eyring, *J. Colloid Interface Sci.*, **32**, 286 (1970).
24) T. Yasunaga, K. Takeda, and S. Shirahama, *J. Colloid Interface Sci.*, **42**, 457 (1973).

  Bull. Chem. Soc. Jpn., 54, 3271—3273 (1981)

The Formation and Electronic Relaxation of Intermolecular Exciplex in the Vapor Phase

Yukio HANASHIMA and Michiya ITOH*

Faculty of Pharmaceutical Sciences, Kanazawa University, Takara-machi, Kanazawa 920

(Received March 2, 1981)

The intermolecular exciplex formation and electronic relaxation of 1,4-dicyanonaphthalene (DCN) with pentamethylbenzene (PMB) in the vapor phase have been studied by means of nanosecond fluorescence spectroscopy. The exciplex formation and decay-rate constants were independent of the excitation energy, while the decay-rate constants of DCN fluorescence was dependent on the excitation energy. The rate constants of the exciplex formation and decay kinetics were discussed in comparison with the collisional relaxation rate of the upper vibrational states.

The observation of the exciplex formation in the vapor phase provides valuable information concerning the electronic interaction between the electron donor and acceptor in the absence of solvent. It also provides information concerning vibrational effects on the radiative and nonradiative deactivation of the exciplex. Exciplex formation in the vapor phase has been reported on 9-cyanoanthracene and alkylamine systems.[1,2] Prochorow *et al.*[3] and Okajima and Lim[4] have reported on exciplex formation and electronic relaxation in the 1,2,4,5-tetracyanobenzene (TCNB) and *p*-xylene system in the vapor phase. Very recently, Itoh *et al.*[5,6] reported the intramolecular exciplex formation of 1-(9,10-dicyano-2-anthryl)-3-(1- or 2-naphthyl)propane (DCAN) in the vapor phase. In the collision-free vapor of DCAN, the excitation wavelength dependence in the $S_1 \leftarrow S_0$ spectral region of exciplex formation and the lifetimes was observed. A considerable blue shift of the exciplex fluorescence of the collision-free vapor on the excitation of the upper vibrational state was also observed in comparison with the excitation of the lower vibrational state. They suggested that the fluorescent relaxation from the upper vibrational state of the exciplex was significant.

This paper will describe the intermolecular exciplex formation and electronic relaxation of 1,4-dicaynonaphthalene (DCN) and also 1,4-dicyanonaphthalene-d_6 with pentamethylbenzene (PMB) in the vapor phase. The rate constants of the exciplex formation and decay kinetics were measured in the excitations at 337 and 293 nm. The lifetime of the exciplex fluorescence is independent of the excitation wavelength, while that of the DCN fluorescence is dependent. The reaction rates and the vibrational relaxation suggest that PMB may act not only as an electron donor, but also as a vibrational relaxer of the upper vibrational states of the S_1 state.

Experimental

The 1,4-dicyanonaphthalene was prepared and purified by known procedures.[7] 1,4-Dicyanonaphthalene-d_6 was prepared from naphthalene-d_8 (Merck, $C_{10}D_8$, 99%) by bromination in bromine vapor and by cyanogenation in a pyridine-d_5 (merck, C_5D_5N, 99%) solution, and was purified two times by means of silica-gel chromatography and recrystallization. Proton NMR gave an isotope purity of approximately 95%. The H-D exchange reaction was examined by the following method: after a mixture of DCN-d_6 and PMB (1:1) has been heated for 3 h at $\approx$523 K, the proton NMR signal shows that no H-D exchange reaction has occured between the two compounds. The spectral determinations in the vapor phase were made as follows: a rectangular quartz cell (1 cm) with graded seals containing solid DCN and PMB was degassed by means of a vacuum line and then sealed off. By using hexane as a buffer gas, a cell containing crystalline compounds and a trace of hexane corresponding to $\approx$500 Torr (1 Torr=133.32 Pa) at $\approx$503 K was degassed by the freeze-pump-thaw method. The absorption and fluorescence spectra and lifetimes were measured in a quartz Dewar vessel at a controlled temperature by means of a heated air flow. The absorption and fluorescence spectra were measured by means of Hitachi 220 and MPF-4 spectrophotometer, respectively. The fluorescence lifetimes were determined by excitation with a nitrogen laser and a dye laser (Molectron DL-14) with a frequency doubler (Rhamda Physik KDP unit). The fluorescence decays were measured by the use of a HTV R666 photomultiplier and by means of Tektronix 7904 (7A19 and 7B85) oscilloscope, and were analyzed by the deconvolution method.

Results and Discussion

The exciplex fluorescence at room temperature and also the excited-state complex fluorescence at low temperatures have been reported in a solution of 1,4-dicyanonaphthalene (DCN) and alkylbenzenes.[7] On the other hand, the fluorescence polarization of DCN in a rigid solution of 3-methylpentane at 77 K suggests that the absorption spectrum of DCN at 280—340 nm is attributable to the L_a ($S_1 \leftarrow S_0$) and L_b ($S_2 \leftarrow S_0$) bands. The absorption spectrum of DCN in the vapor phase shown in Fig. 1 may be ascribed to the L_a and L_b bands, though the spectral feature is quite different from that in solution. Figure 1 shows the fluorescence and excitation spectra of DCN and PMB vapor. The excitation spectra monitored at several wavelengths are identical with that of the DCN fluorescence determined in the vapor phase, which is attributable to the $S_1 \leftarrow S_0$ absorption band of DCN. The fluorescence spectrum exhibits the exciplex fluorescence ($\lambda_{max} \approx 395$ nm) in addition to the DCN fluorescence ($\lambda_{max} \approx 343$ nm). In the presence of a buffer gas (hexane, $\approx$500 Torr=6.65×10^4 Pa) which may act as a vibrational relaxer, both exciplex and DCN fluorescence increase in intensity in comparison with those in the absence of a buffer gas, as shown in Fig. 1. The fluorescence maximum of the vapor-phase exciplex exhibits a considerable blue shift from that

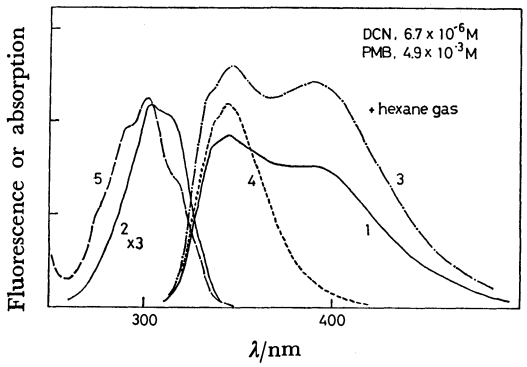

Fig. 1. (1) Fluorescence (excited at 300 nm) and (2) excitation (monitored at 450 nm) spectra of 1,4-dicyanonaphthalene and pentamenthylbenzene in the vapor phase at ≈503 K. (3) fluorescence spectrum determined in the identical condition with (1) except addition of hexane gas (≈500 Torr=6.6×10^4 Pa) as a vibrational relaxer (1 M=1 mol dm^{-3}). (4) Fluorescence (excited at 300 nm) and (5) absorption spectra of 1,4-dicyanonaphthalene vapor at ≈503 K.

in the nonpolar solution (λ_{max}≈416 nm in 3-methylpentane) at room temperature,[7] while that of the DCN fluorescence shows no significant spectral shift.

The well-known photochemical reaction scheme and decay kinetics of DCN and exciplex are as follows;[8]

$$\begin{array}{ccccc} & & A^* + D & \underset{k_4}{\overset{k_3}{\rightleftharpoons}} & (DA)^* \\ & \swarrow^{k_1} \quad \searrow^{k_2} & & & \swarrow^{k_5} \quad \searrow^{k_6} \\ A + h\nu & & A & & D + A + h\nu', \quad D + A \end{array}$$

$$[A^*] = c_1 \exp(-\lambda_1 t) + c_2 \exp(-\lambda_2 t)$$

$$[(DA)^*] = c_3 \exp(-\lambda_1 t) - c_3 \exp(-\lambda_2 t)$$

$$\lambda_1,\ \lambda_2 = \frac{1}{2}[k_1+k_2+k_3[D]+k_4+k_5+k_6 \mp (\{k_1+k_2+k_3[D]-(k_4+k_5+k_6)\}^2+4k_3k_4)^{1/2}],$$

where A and D are DCN and PMB, respectively. The time constants, λ_1 and λ_2 were determined in several concentrations of PMB in the excitation at 337 nm at ≈503 K. Figure 2 shows a plot of $\lambda_1+\lambda_2$ ($=k_1+k_2+k_3[D]+k_4+k_5+k_6$) *vs.* [D], the slope of which yields the rate constant of $k_3=1.2\times10^{11}$ dm^3 mol s^{-1}. Further, the fluorescence intensity ratio of DCN (excited at 337 nm) in the absence (I_0) and presence (I) of the electron donor (PMB) is expressed by the following equation:[8]

$$(I_0/I) - 1 = k_3[D](k_5+k_6)/(k_4+k_5+k_6)(k_1+k_2).$$

From k_3, the lifetimes of the exciplex and DCN, and the slope of the plot of I_0/I *vs.* [D], the dissociation rate constant (k_4) of the exciplex was determined to be 3.56×10^7 s^{-1}, as is summarized in Table 1.

The exciplex formation can be expressed by the following scheme:

$$\begin{array}{ccc} A^*(\nu_h) + D & \longrightarrow & (DA)^*(\nu_h) \\ \Big\downarrow + R & & \Big\downarrow + R \\ A^*(\nu_l) + D & \longrightarrow & (DA)^*(\nu_l), \end{array}$$

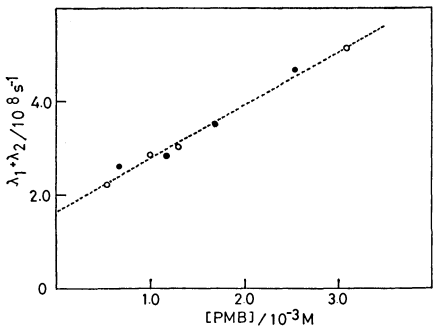

Fig. 2. Plots of $(\lambda_1+\lambda_2)$ *vs.* concentration of pentamethylbenzene in the vapor phase at 503 K; λ_1 and λ_2 were obtained from double exponential decay curves determined at 370 nm in the excitation at 337 nm.

TABLE 1. THE DECAY-RATE CONSTANTS AND THE FORMATION AND DISSOCIATION RATE CONSTANTS OF THE EXCIPLEX IN THE VAPOR PHASE AT 503 K IN THE EXCITATION AT 337 nm

Rate constant	DCN-PMB	DCN-d_6-PMB
(k_1+k_2)/s^{-1} a)	1.25×10^8	1.05×10^8
k_3/dm^3 mol^{-1} s^{-1}	1.2×10^{11}	1.2×10^{11}
$(k_4+k_5+k_6)$/s^{-1}	4.9×10^7 b)	5.2×10^7 c)
k_4/s^{-1}	3.56×10^7	4.1×10^7
k_q/dm^3 mol^{-1}	2.6×10^2	2.4×10^2

a) Determined in DCN and DCN-d_6 vapors. b) Determined in the DCN (6.7×10^{-6} mol dm^{-3}) and PMB (1.2×10^{-3} mol dm^{-3}) vapor. c) Determined in the DCN-d_6 (6.7×10^{-3} mol dm^{-3}) and PMB (1×10^{-3} mol dm^{-3}) vapor.

where ν_h and ν_l denote high and low levels of the vibrational state, respectively. R is a vibrational relaxer. In the excitation of the $S_1\leftarrow S_0$ absorption band at 337 nm, the fluorescence lifetimes of DCN vapor is 8.0 ns, while it is 3.6 ns for the $S_2\leftarrow S_0$ excitation at 292 nm. Since the energy level of the S_2 state may be very close to that of the S_1 state, and since the isoenergetic internal conversion from the S_2 state to the vibrationally hot S_1 state proceeds very rapidly, the short lifetime of DCN (3.6 ns) for the excitation of S_2 is attributable to decay from the upper vibrational state of S_1. However, the fluorescence lifetime of the exciplex in the DCN–PMB vapor does not exhibit any of the excitation-wavelength dependence mentioned above. Okajima and Lim[4] suggested that, in the vapor-phase exciplex of TCNB–*p*-xylene, the rate constant of the exciplex formation (7×10^{12} dm^3 mol^{-1} s^{-1}) between the vibrationally hot electron acceptor, A*(ν_h), *via* the S_2 excitation and the ground state of the electron donor is 10 times greater than that of the formation of (DA)*(ν_l), measured for excitation into S_1. Further, the rate constant of the intramolecular exciplex formation from the A*(ν_h) and D moieties in the collision-free vapor of DCAN was determined to be much greater than that from the A*(ν_l) and D moieties.[9] Therefore, if the rate constant of the (DA)*(ν_h) formation in the DCN–PMB vapor is assumed to be 5—10 times greater than the value of 1.2×10^{11} dm^3 mol^{-1} s^{-1} obtained in the (DA)*(ν_l) formation, the rate constant of the (DA)*(ν_h)

formation is estimated to be approximately 10^{12} dm^3 mol^{-1} s^{-1}. On the other hand, the concentration of PMB (10^{-2}—10^{-3} mol dm^{-3}) corresponds to the gas pressure of 50 Torr and to the collisional relaxation rate of 5×10^8 s^{-1} obtained by the use of a hard-sphere collision model.[4,10] Therefore, the rate of the (DA)*(ν_h) formation *via* S_2 excitation ($\approx10^{12}[D]$ s^{-1}) is greater than the decay of A*(ν_h) and the vibrational relaxation by ≈50 Torr of PMB. However, since the decay-rate constant of (DA)*(ν_h) is assumed to be approximately 3×10^7 s^{-1}, the vibrational relaxation of the upper vibrational state of (DA)*(ν_h) by PMB vapor may proceed at the rate of 5×10^8 s^{-1}, followed by the fluorescent decay from (DA)*(ν_l). These arguments are consistent with the absence of the excitation-wavelength dependence of the fluorescence lifetimes of the exciplex. The fluorescence-intensity ratio of the exciplex and DCN is not very much dependent on the absence or presence of the buffer gas, though the intensity ratio shows a slight increase in the latter, as shown in Fig. 1. This fact suggests that the exciplex formation and emission may take place according to the reaction scheme mentioned above. In the scheme, D and R are PMB as the electron donor and also as the vibrational relaxer.

The rate constants of the exciplex formation and decay kinetics were obtained in the DCN-d_6 and PMB system, as summarized in Table 1. Figure 3 compares the fluorescence spectrum of DCN-d_6 and PMB vapor with that of DCN–PMB vapor determined under identical conditions. The fluorescence-intensity ratio of the exciplex and DCN in DCN-d_6–PMB slightly increases in comparison with that of DCN–PMB. However, the rate constant of the exciplex formation (k_3) and the quenching constant (k_q) obtained from the plots shown in Figs. 2, show no significant difference between DCN-d_6 and DCN, as summarized in Table 1.[11] Okajima and Lim[4] reported that the Stern-Volmer quenching constant in the TCNB–*p*-xylene-d_{10} vapor is smaller by a factor of 1.4 than that for TCNB–*p*-xylene, and they suggested the occurence of important vibrational effects in the photoassociation. However, the lack of any significant effects of the deuterium substitution in DCN reported here suggests a slight contribution of C–D stretching to the high-frequency vibrational mode of a large molecule such as DCN in the exciplex formation and the radiationless deactivation.

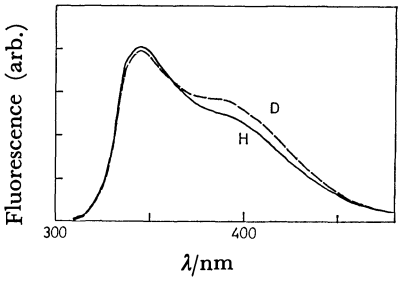

Fig. 3. (H) Fluorescence spectrum of 1,4-dicyanonaphthalene (6.7×10^{-6} mol dm^{-3}) and pentamethylbenzene (3.8×10^{-3} mol dm^{-3}) in the vapor phase at ≈503 K. (D) Fluorescence spectrum of 1,4-dicyanonaphthalene-d_6 (6.7×10^{-6} mol dm^{-3}) and pentamethylbenzene (3.8×10^{-3} mol dm^{-3}) determined in the identical condition with (H).

This work was partially supported by a Grant-in-Aid for Scientific Research from Ministry of Education, Science and Culture.

References

1) S. Hirayama, G. C. Abbott, and D. Phillips, *Chem. Phys. Lett.*, **56**, 497 (1978).
2) S. Hirayama, *Chem. Phys. Lett.*, **63**, 596 (1979).
3) J. Prochorow, S. Okajima, and E. C. Lim, *Chem. Phys. Lett.*, **66**, 590 (1979).
4) S. Okajima and E. C. Lim, *Chem. Phys. Lett.*, **70**, 283 (1980).
5) M. Itoh, T. Kotani, and Y. Hanashima, *Chem. Phys. Lett.*, **75**, 307 (1980).
6) M. Itoh, T. Kotani, and Y. Hanashima, *J. Am. Chem. Soc.*, **103**, 3271 (1981).
7) M. Itoh, S. Furuya, and T. Okamoto, *Bull. Chem. Soc. Jpn.*, **50**, 2509 (1977).
8) W. R. Ware, D. Watt, and D. Holmes, *J. Am. Chem. Soc.*, **96**, 7853 (1974).
9) M. Itoh and Y. Hanashima, *Chem. Phys. Lett.*, to be published.
10) H. Baba, "Laser and Chemical Reaction," ed by S. Tsuchiya, Gakkai Shuppan Center, Tokyo (1980), p. 62.
11) During the spectral determination in the vapor phase at a high temperature, it was confirmed that no H-D exchange reaction between DCN-d_6 and PMB occured, as mentioned in the Experimental section.

Magnetic Susceptibility and Crystal Structure of 1,5-Diphenyl-3-(4-chlorophenyl)verdazyl Radical[1)]

Nagao Azuma,*,** Kanji Tsutsui,† Yozo Miura,†† and Taiichi Higuchi*,†

Department of Chemistry, Faculty of Science, Kyoto University, Sakyo-ku, Kyoto 606
†*Department of Chemistry, Faculty of Science, Osaka City University, Sumiyoshi-ku, Osaka 558*
††*Department of Applied Chemistry, Faculty of Engineering, Osaka City University, Sumiyoshi-ku Osaka 558*

(Received March 4, 1981)

The magnetic susceptibility of 1,5-diphenyl-3-(4-chlorophenyl)verdazyl (Cl-TPV) has been measured on a powder sample in the temperature region between 1.8 and 80 K. It exhibited a round maximum at 21.0 K; this temperature is the highest among those observed for verdazyl monoradicals. The susceptibility can be well described by the Heisenberg linear chain model; the estimated exchange interaction parameter is $J/k=-16.4$ K. The crystal structure of Cl-TPV has been determined by means of X-ray diffraction. The crystal is orthorhombic, with the space group of Pbca and with $a=22.041(5)$, $b=7.166(4)$, $c=21.379(5)$ Å, and $Z=8$. The molecules are arranged in a column along the b axis. The exchange interaction has been discussed based on the crystal structure and the spin density distribution.

Electron spin-spin exchange interaction in a radical crystal is dependent on the crystal structure and the spin density distribution. In order to obtain the exchange interaction as a function of the interatomic distance and the spin density, 1,3,5-triphenylverdazyl (TPV) and its methyl derivatives, such as 1,3,5-triphenyl-6-methylverdazyl and 1,3-di-*p*-tolyl-5-phenylverdazyl (DTPV), have been studied to determine their magnetic susceptibilities, spin densities, and crystal structures.[2)] The C-phenyl ring in TPV lies in the nodal plane of the highest-occupied molecular orbital,[3)] so the replacement of the hydrogen atom in that ring scarcely perturbs the spin density distribution. Thus, a chlorine atom has been introduced into *para*-position and the molecular packing has been modified from that of TPV. The exchange interaction estimated from the magnetic susceptibility of this 1,5-diphenyl-3-(4-chlorophenyl)verdazyl (Cl-TPV) is the strongest among the verdazyl monoradicals examined. In order to understand the exchange interaction of Cl-TPV and to try the tractable function in Ref. 2, the crystal structure of this radical has been determined by means of X-ray diffraction.

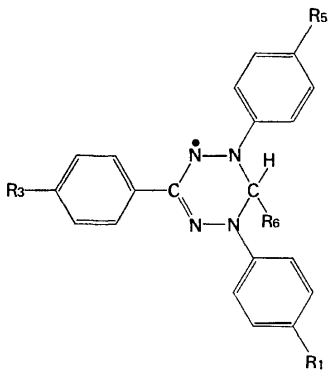

Fig. 1. Chemical structures of verdazyl radicals.

Radical	R_1	R_3	R_5	R_6
TPV	H	H	H	H
Cl-TPV	H	Cl	H	H
DTPV	CH_3	CH_3	H	H

Experimental

Cl-TPV was prepared from *p*-chlorobenzaldehyde, aniline and formaldehyde.[4)] The dark green crystals, elongated along the b axis, were purified several times through recrystallization from a mixed solution of acetone and methanol.

The magnetic susceptibility was measured on the powdered sample by means of a magnetic torsion balance.[5)] The temperature was determined using an AuCo–Cu thermocouple and a carbon resister. Manganese Tutton salt was used for the calibration of the thermometers and the field intensity.

ESR spectra of Cl-TPV and TPV in toluene were recorded on an X-band spectrometer at room temperature, in order to estimate the difference in the spin density distributions of these radicals.

The unit-cell parameters were obtained from the photographic data. The crystal data are summarized in Table 1. The Weissenberg intensity data ($h0l$—$h5l$, $0kl$—$1kl$) were collected with Cu $K\alpha$ radiation and corrected for Lorentz and polarization effects. There were 2326 independent reflections, of which 1741 were regarded as observed.

Table 1. Crystal data of Cl-TPV

Molecular formula	$C_{20}H_{16}N_4Cl$
Molecular weight	347.8
Melting point	144—145 °C
Crystal system	Orthorhombic
Space group	Pbca
Cell dimensions;	
a/Å	22.041(5)
b/Å	7.166(4)
c/Å	21.379(5)
V/Å^3	3376.5
Z	8
Density (calcd)/g cm^{-3}	1.368
Density (obsd)/g cm^{-3}	1.35

** Permanent address: Laboratory of Chemistry, Faculty of General Education, Ehime University, Matsuyama, Ehime 790.

Results of Magnetic Measurements

The susceptibility data were corrected for the diamagnetic contribution using Pascal's constants.[6] The paramagnetic molar susceptibility, χ_m, is shown in Fig. 2. The susceptibility follows the Curie-Weiss law with a negative Weiss constant, $\theta = -18.4$ K, in the high temperature region. However, the susceptibility deviates from the Curie-Weiss law at low temperatures, and it shows a round maximum with a value of $\chi_{max} = 6.70 \times 10^{-3}$ cgs emu mol^{-1} at $T_{max} = 21.0$ K.*** When the temperature is lowered further, the susceptibility decreases towards a finite value at 0 K. The radical concentration, as determined from the susceptibility data at high temperatures, is 100%, with an experimental error of 3%.

The ESR spectrum of TPV exhibited nine line splittings, with the hyperfine coupling constant of 0.59 mT due to the nearly equivalent four nitrogen nuclei; the splittings from protons were unresolved. On the other hand, the spectrum from Cl-TPV showed many incompletely resolved splittings due to the protons, as is shown in Fig. 3. However, the spacing of 0.59 mT of the nine line splittings was unchanged.

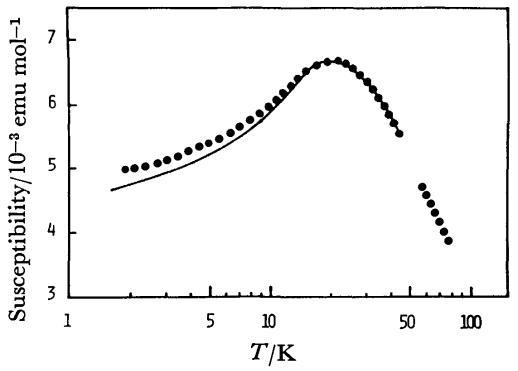

Fig. 2. Paramagnetic molar susceptibility of Cl-TPV powder. Solid circles show the experimental data and solid line is the susceptibility of the Heisenberg linear chain.

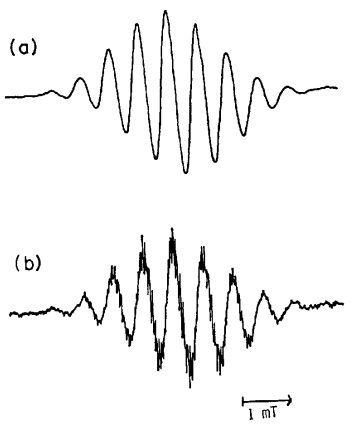

Fig. 3. ESR spectra of TPV (a) and Cl-TPV (b) in toluene.

***The value of the molar susceptibility in m^3 mol^{-1} (SI) can be obtained by multiplying the value in emu mol^{-1} (cgs) by $4\pi \times 10^{-6}$.

Structure Determination and Refinement

The crystal structure was solved by the direct method using a program written in our laboratory. The positions of all the 25 non-hydrogen atoms located on an E map were refined by the blockdiagonal least-squares procedure. The positions of all the 14 hydrogen atoms in the phenyl rings were deduced from a difference Fourier map, but both hydrogen atoms in the methylene group were located geometrically. The R value was reduced to 0.091 for 1741 observable reflections by blockdiagonal least-squares refinement with anisotropic thermal parameters for the non-hydrogen atoms and isotropic ones for the hydrogen atoms. The atomic coordinates are listed in Table 2. The atomic scattering factors for Cl, N, and C were those of the International Tables for X-Ray Crystallography.[7] For the hydrogen atom, the scattering factor was adopted from the table of Stewart *et al.*[8]

Description of the Structure

The molecular structure of Cl-TPV and the numbering system are illustrated in Fig. 4. The bond

Table 2. Fractional atomic coordinates of Cl-TPV[a]

Atom	$x \times 10^4$	$y \times 10^4$	$z \times 10^4$
C (1)	3709 (3)	95 (11)	2826 (3)
C (2)	2805 (3)	1300 (10)	2133 (3)
C (3)	4391 (3)	766 (10)	1901 (3)
C (4)	4875 (3)	−238 (11)	2168 (3)
C (5)	5441 (2)	−190 (10)	1878 (3)
C (6)	5533 (2)	827 (10)	1331 (3)
C (7)	5049 (3)	1822 (12)	1075 (3)
C (8)	4479 (3)	1790 (11)	1354 (3)
C (9)	3293 (2)	2100 (10)	3694 (2)
C (10)	2920 (3)	3507 (11)	3868 (3)
C (11)	2967 (3)	4291 (12)	4455 (3)
C (12)	3397 (3)	3633 (12)	4888 (3)
C (13)	3754 (3)	2208 (12)	4716 (3)
C (14)	3714 (3)	1328 (10)	4122 (3)
C (15)	2245 (3)	1398 (10)	1753 (3)
C (16)	2264 (3)	1832 (11)	1123 (3)
C (17)	1742 (3)	1929 (12)	773 (3)
C (18)	1193 (3)	1600 (11)	1060 (3)
C (19)	1156 (3)	1149 (11)	1678 (3)
C (20)	1686 (3)	1014 (11)	2027 (3)
N (1)	3815 (2)	767 (8)	2188 (2)
N (2)	3326 (2)	1038 (8)	1824 (2)
N (3)	2745 (2)	1684 (8)	2749 (2)
N (4)	3265 (2)	1379 (8)	3082 (2)
Cl	520 (1)	1814 (3)	631 (1)

a) The coordinates of hydrogen atoms, the anisotropic and isotropic thermal parameters, and the $F_o - F_c$ table are kept by the office of the Chemical Society of Japan (Document No. 8145).

lengths and the bond angles are listed in Table 3. The four nitrogen atoms are coplanar (N-plane) within ±0.001 Å and the *sym*-tetrazinyl ring has a deformed boat form; these have been observed in other verdazyls.[9-11] The atomic deviations from N-plane are as follows: C(1)=0.62, C(2)=0.14, C(3)=−0.34, C(9)=−0.42, and C(15)=0.30 Å. These values are close to those of DTPV and TPV except that C(9) (−0.22 Å in TPV). The dihedral angles between N-plane and each plane of N(1)-, N(4)- and C(2)-phenyl rings are 37.5, (−)35.7, and 25.5°, respectively. The twist angles around the inter-ring bonds, defined by the dihedral angle between the plane of each phenyl ring and the plane through α-, β-, γ-, and γ'-atoms, are 20.9, (−)15.6, and 25.2° for N(1)–C(3), N(4)–C(9), and C(2)–C(15) bonds, respectively. The last angle is much greater than those in the other verdazyls examined, this fact is attributed to the intermolecular packing forces, as can be seen from Fig. 5.

Table 3. Bond lengths (l/Å) and bond angles (ϕ/°)
The estimated standard deviations are less than 0.01 Å and 1°, respectively.

Bond	Length	Bond	Length
C (1)-N (1)	1.47	C (9)-N (4)	1.41
C (1)-N (4)	1.44	C (10)-C (11)	1.38
C (2)-C (15)	1.48	C (11)-C (12)	1.40
C (2)-N (2)	1.34	C (12)-C (13)	1.35
C (2)-N (3)	1.35	C (13)-C (14)	1.42
C (3)-C (4)	1.40	C (15)-C (16)	1.38
C (3)-C (8)	1.40	C (15)-C (20)	1.39
C (3)-N (1)	1.41	C (16)-C (17)	1.37
C (4)-C (5)	1.39	C (17)-C (18)	1.38
C (5)-C (6)	1.38	C (18)-C (19)	1.36
C (6)-C (7)	1.40	C (19)-C (20)	1.39
C (7)-C (8)	1.39	N (1)-N (2)	1.34
C (9)-C (10)	1.35	N (3)-N (4)	1.37
C (9)-C (14)	1.42	C (18)-Cl	1.75

Bond	Angle	Bond	Angle
N (1)-C (1)-N (4)	105	N (4)-C (9)-C (14)	119
C (1)-N (1)-N (2)	117	C (14)-C (9)-C (10)	121
N (1)-N (2)-C (2)	115	C (9)-C (10)-C (11)	121
N (2)-C (2)-N (3)	126	C (10)-C (11)-C (12)	121
C (2)-N (3)-N (4)	113	C (11)-C (12)-C (13)	118
N (3)-N (4)-C (1)	118	C (12)-C (13)-C (14)	123
C (1)-N (1)-C (3)	123	C (13)-C (14)-C (9)	117
N (2)-N (1)-C (3)	118	N (2)-C (2)-C (15)	117
N (1)-C (3)-C (4)	121	N (3)-C (2)-C (15)	116
N (1)-C (3)-C (8)	119	C (2)-C (15)-C (16)	122
C (8)-C (3)-C (4)	120	C (2)-C (15)-C (20)	120
C (3)-C (4)-C (5)	119	C (20)-C (15)-C (16)	119
C (4)-C (5)-C (6)	122	C (15)-C (16)-C (17)	121
C (5)-C (6)-C (7)	119	C (16)-C (17)-C (18)	119
C (6)-C (7)-C (8)	121	C (17)-C (18)-C (19)	122
C (7)-C (8)-C (3)	120	C (18)-C (19)-C (20)	119
C (1)-N (4)-C (9)	124	C (19)-C (20)-C (15)	120
N (3)-N (4)-C (9)	117	C (17)-C (18)-Cl	120
N (4)-C (9)-C (10)	120	C (19)-C (18)-Cl	119

Figure 5 shows how the Cl-TPV molecules are arranged in the unit cell. The molecules form columns along the b axis. The shortest intermolecular distance between the non-hydrogen atoms is 3.48 Å for the N(1)···C(19) contact in the column. This columnar structure seems very similar to that of DTPV, as can be seen from Fig. 6.[11] Within the column, the mean values of the intermolecular distances for the π-framework are actually 7.05 and 7.15 Å for Cl-TPV and DTPV, respectively, while they are 7.76—7.86 Å for the other verdazyls. However, there are some substantial differences between Cl-TPV and

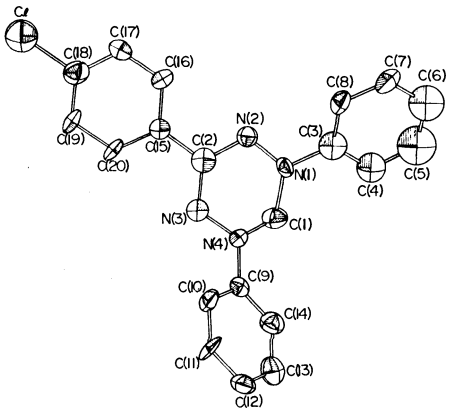

Fig. 4. Molecular structure of Cl-TPV and the numbering system.

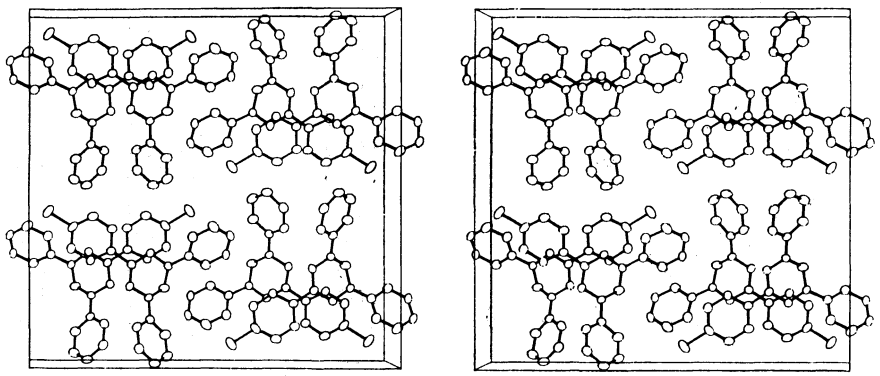

Fig. 5. Stereoscopic view of the crystal structure of Cl-TPV along the b axis. The a axis is horizontal, from left to right, and the c axis is downward vertical. The hydrogen atoms were omitted for clarity.

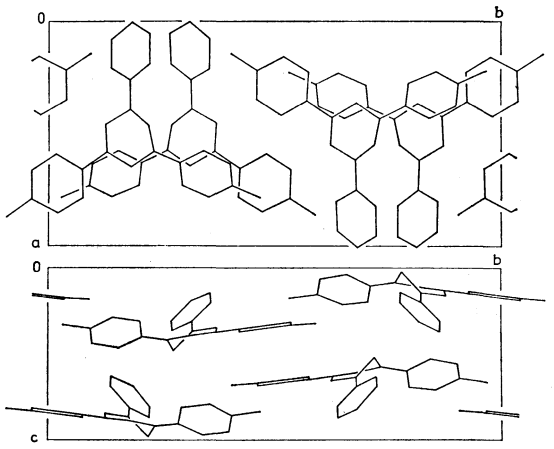

Fig. 6. Molecular packing of DTPV.[11]
The methyl carbon atom in C-tolyl group makes the outmost thorn of the column along the c axis.

DTPV, *e.g.* in the shortest N···N contact: 3.74 Å in the former, but 4.15 Å in the latter.

Discussion

The susceptibilities of a number of verdazyls have been described by the Heisenberg linear chain model.[2,12,13] The numerical study of the thermodynamic properties of the Heisenberg linear chain of $S=1/2$ spins has been made by Bonner and Fisher.[14] The theory predicts the following relation independent of the exchange parameter, J:

$$\chi_{max}T_{max} = 0.142. \quad (1)$$

The predicted susceptibility for antiferromagnetic coupling exhibits a round maximum at

$$T_{max} = 1.282|J|/k, \quad (2)$$

where k is the Boltzmann constant. The susceptibility of Cl-TPV gives 0.141 for Relation (1). Based on Eq. 2, the exchange parameter is estimated to be $J/k=-16.4$ K; this is the strongest antiferromagnetic exchange interaction among the verdazyl mono-radicals examined. The solid line in Fig. 2 is the susceptibility of the Heisenberg linear chain with this J value. The calculated susceptibility is very close to the observed one. The systematic disagreement in the lowest temperature region can be attributed to a small amount of impurities; it is hard to prepare and keep the radical completely pure. Therefore, an adequate model to describe the susceptibility of the Cl-TPV crystal is the Heisenberg linear chain model with $J/k=-16.4$ K.

Because the exchange interaction between the aromatic radicals is caused by the overlapping between the p_z π-orbitals, the Cl-TPV molecules in the column are coupled to one another by the exchange interaction. Therefore, a Cl-TPV crystal is a one-dimensional magnet in view of the molecular packing. This is consistent with the result derived from the susceptibility.

An approximated spin density Hamiltonian for the exchange interaction between the aromatic radicals A and B has been presented by McConnell:[15]

$$\mathscr{H}^{AB} = -\boldsymbol{S}^{A}\boldsymbol{S}^{B}\sum J_{ij}^{AB}\rho_i^A\rho_j^B, \quad (3)$$

where $\boldsymbol{S}^A$ and $\boldsymbol{S}^B$ are the total spin operators on molecules A and B, ρ_i^A and ρ_j^B are the π-spin densities on atoms i and j of A and B, respectively, and where J_{ij}^{AB} is the two-center exchange integral between i and j. The observed J corresponds to the summation in Eq. 3. Using this equation the ferromagnetic exchange interaction in a galvinoxyl radical crystal has been discussed.[16] The same procedure has been applied to TPV and its methyl derivatives.[2] According to that study, the order of the observed J's can be explained by means of the following tractable function for J_{ij}^{AB}:

$$J_{ij}^{AB} = -pC/r_{ij}^{AB}, \quad (4)$$

where C is a positive constant, r_{ij}^{AB} is the distance between atoms i and j, and where p is an angular correction. A possible angular correction is $p=\cos\theta_i^A\cos\theta_j^B$ where θ_i^A and θ_j^B are the angles between respective axes of the $p_z\pi$-orbitals of i and j atoms j and the vector distance $\boldsymbol{r}_{ij}^{AB}$.[17] However, the following rather crude correction factor was adopted:

$$p = \begin{cases} 1 & \text{when } r_{ij}^{AB} \leqq 6\text{ Å} \\ 0 & \text{when } r_{ij}^{AB} > 6\text{ Å}. \end{cases} \quad (5)$$

When the layered structure with the separation of 4 Å between the layers is assumed,

$$\left.\begin{array}{l} r_{ij}^{AB} \leqq 6\text{ Å corresponds to } \cos\theta_i^A\cos\theta_j^B \geqq 0.45 \\ \text{and} \\ r_{ij}^{AB} > 6\text{ Å corresponds to } \cos\theta_i^A\cos\theta_j^B < 0.45. \end{array}\right\} \quad (6)$$

When other functions for J_{ij}^{AB}, such as the overlap integral and exchange integral calculated by Dulčić and Herak,[18] were adopted, the order of the observed J's has been reversed.[2]

The spin densities on Cl-TPV are similar to those on TPV, in view of the same hyperfine coupling constant due to nitrogen nuclei. The same spin distribution as that of Cl-TPV can be reasonably assumed for DTPV. Therefore, the spin densities for Cl-TPV and DTPV used in the calculation are taken to be identical with those for TPV discussed elsewhere;[16] they are shown in Table 4.

Using Eqs. 4 and 5, the summation in Eq. 3 has been calculated for pairs of molecules along the three crystallographic axes. The results are summarized in Table 5, together with those for DTPV. The prominent negative value suggests the antiferromagnetic

Table 4. The π-spin density distribution in Cl-TPV

Atom	Spin density
N (1), N (4)	0.2040
N (2), N (3)	0.1944
C (2)	−0.0461
C (3), C (9)	−0.0345
C (4), C (8), C (10), C (14)	0.0473
C (5), C (7), C (11), C (13)	−0.0179
C (6), C (12)	0.0505
C (15)	0.0032
C (16), C (20)	−0.0179
C (17), C (19)	0.0067
C (18)	−0.0131

Table 5. Results of the calculation based on McConnell's spin density Hamiltonian

Direction in the crystal	Sum in Eq. 3[a]	
	Cl-TPV	DTPV[2]
Along the a axis	−3.41	
Along the b axis	−16.4	
along c axis		−21.3
Along the c axis	0.0369	
Observed J/k	−16.4 K	−11.1 K

a) The sums have been adjusted by using the factor obtained from the observed J for Cl-TPV and the calculated J along the b axis of the Cl-TPV crystal.

exchange coupling in the column along the b axis of the Cl-TPV crystal. The calculated exchange couplings between the columns are less than 1/5 of that within the column. These results are consistent with the fact derived from the susceptibility: an antiferromagnetic linear chain spin system. The ratio of the observed J of Cl-TPV to that of DTPV is 1.5. However, the calculated ratio is 0.8; this is not improved by adopting the squared cosine factor for ρ. The three other functions for J_{ij}^{AB} in Ref. 2 give the ratios of 0.7—0.004, where 0.7 is obtained with $J_{ij}^{AB}=-\rho C(r_{ij}^{AB})^{-3}$. In conclusion, Eq. 3 combined with Eqs. 4 and 5 has roughly explained the order of the observed J's of five verdazyl radicals. This tractable procedure would thus be practically more useful in correlating the exchange interaction with the crystal structure than complicated procedures, such as that adopted by Dulčić and Herak.[18]

The authors wish to thank Professors Yasuo Deguchi, Hiroaki Ohya-Nishiguchi, Noboru Hirota, and Masayoshi Kinoshita for their helpful discussions.

References

1) "The Magnetic Properties of Verdazyl Free Radicals," part XIII.
2) N. Azuma, in preparation.
3) P. H. H. Fischer, *Tetrahedron*, **23**, 1939 (1967).
4) C. Schiele, K. Halfar, and G. Arnold, *Z. Naturforsch.*, **226**, 105 (1967).
5) M. Mekata, *J. Phys. Soc. Jpn.*, **17**, 796 (1962).
6) P. W. Selwood, "Magnetochemistry," Interscience Publishers, New York (1956).
7) "International Tables for X-Ray Crystallography," Kynoch Press, Birmingham (1974), Vol. IV.
8) R. F. Stewart, E. R. Davidson, and W. T. Simpson, *J. Chem. Phys.*, **42**, 3175 (1965).
9) D. E. Williams, *Acta Crystallogr., Sect. B*, **29**, 96 (1973).
10) N. Azuma, Y. Deguchi, F. Marumo, and Y. Saito, *Bull. Chem. Soc. Jpn.*, **48**, 819, 825 (1975).
11) N. Azuma, *Bull. Chem. Soc. Jpn.*, **53**, 2671 (1980).
12) K. Mukai, K. Oishi, K. Ishizu, and N. Azuma, *Chem. Phys. Lett.*, **23**, 522 (1973).
13) N. Azuma, K. Ishizu, and K. Mukai, *J. Chem. Phys.*, **61**, 2294 (1974).
14) J. C. Bonner and M. E. Fisher, *Phys. Rev. A*, **135**, 640 (1964).
15) H. M. McConnell, *J. Chem. Phys.*, **39**, 1910 (1963).
16) N. Azuma, J. Yamauchi, K. Mukai. H. Ohya-Nishiguchi, and Y. Deguchi, *Bull. Chem. Soc. Jpn.*, **46**, 2728 (1973).
17) W. Duffy, Jr., D. L. Strandburg, and J. F. Deck, *J. Chem. Phys.*, **68**, 2097 (1978).
18) A. Dulčić and J. N. Herak, *Mol. Phys.*, **26**, 605 (1973).

Magnetic Circular Dichroism Studies of 4,4′-Disubstituted Biphenyls

Hiroyuki UCHIMURA, Akio TAJIRI, and Masahiro HATANO*

Chemical Research Institute of Non-aqueous Solutions, Tohoku University, Katahira, Sendai 980

(Received March 4, 1981)

The magnetic circular dichroism (MCD) and ultraviolet (UV) absorption spectra of 4,4′-disubstituted biphenyls were measured. The MCD spectra showed diverse spectral patterns reflecting the natures of the substituent groups. These observed MCD spectra were reproduced by the theoretical calculations based on the Pariser-Parr-Pople-SCF-CI method. The dihedral angles of 4,4′-disubstituted biphenyls were estimated to be about 20° by comparing the observed MCD spectra with the calculated ones. The assignments for the MCD bands of 4,4′-disubstituted biphenyls were given on the basis of these calculations. The substituent effects of biphenyls were interpreted by the use of the coefficients of the configuration interactions.

One of the most interesting aspects of the optical properties of biphenyl and its sterically hindered derivatives has been displayed by the appearance of an intense, structureless absorption band with its maximum at *ca.* 40000 cm^{-1}. The band is well known to be very sensitive to the variation in the torsional angle, θ, around the central carbon-carbon bond of biphenyl (see Fig. 1), giving rise to a change in both the location of the band and its intensity.[1] The conjugation between the two benzene rings becomes large with a decrease in the dihedral angle of biphenyl. Thus, if the dihedral angle decreases, this band shows a marked red-shift and an enhancement in its intensity; therefore, it is called the conjugation band. The stable conformation of biphenyl is, in principle, established on the basis of a balance between the two effects, electronic delocalization and electrostatic repulsion between non-bonded atoms.[2] Especially, however, repulsion among the hydrogen atoms at ortho positions (2, 6, 2′, and 6′ in Fig. 1) in the biphenyl skeleton is considered to be of primary importance. Accordingly, on substitution by bulky groups at the ortho positions, the dihedral angle of biphenyl increases due to the appreciable increase in steric repulsion, giving rise to a hypsochromic effect on the transition energy and a hypochromic effect on the intensity of the conjugation band. In fact, Beaven *et al.*[1] have reported that the conjugation band shifts toward a higher-energy region with a decrease in its intensity on successive substitution by methyl groups at the ortho positions of biphenyl.

On the other hand, the dihedral angle is considered to change only slightly or remain unchanged on substitution at the para positions (4 and 4′ in Fig. 1). Kurland[3] gave an equation in which the difference in chemical shift between the protons at the meta and ortho positions of biphenyl was expressed as a function of θ; using that equation, he then tried to estimate the dihedral angles, θ, of the 4,4′-disubstituted biphenyls, including 4,4′-dideuterated biphenyl. The experimental results were well reproduced by taking $\theta=45°$ in his equation. In addition, the dihedral angle is found to be independent of the substituent groups. On the other hand, Suzuki[4] tried to elucidate the UV spectra of biphenyl and estimated the dihedral angle, θ, by making use of the core-resonance integral for the central bond as a function of θ. He obtained 0°, 23°, and 43° for biphenyl in gas, solution, and a crystalline state respectively. According to his results, the dihedral angles of 4,4′-disubstituted biphenyls in solution may be expected to take a value of about 20°.

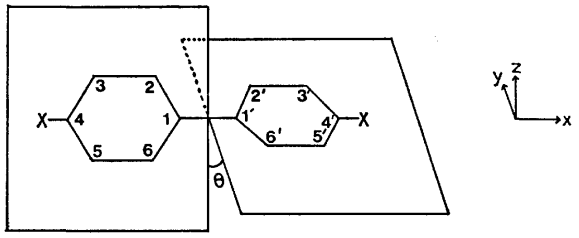

X = NH_2, OH, NO_2, CN, CH_3, Cl

Fig. 1. The nuclear skeleton and coordinate system of 4.4′-disubstituted biphenyl.

So far, MCD studies, which are very useful for the investigation of the electronic states of the compounds, have been carried out on biphenyl, para-substituted biphenyls with electron-donating groups and bridged biphenyls.[5,6] The 1st and 2nd MCD bands of the parent molecule, biphenyl, have positive and negative signs respectively, while those of the para-substituted derivatives have the opposite signs. Thus, the MCD spectra of biphenyls show an apparent substituent effect, suggesting that the MCD measurement is more sensitive with respect to the natures of the substituents than the UV measurement, and therefore useful in giving reasonable spectroscopic assignments.

The molecular orbital investigations of biphenyls were limited to those of biphenyl itself, using the Pariser-Parr-Pople method,[7,8] molecules in the molecule method,[9] and the CNDO/2 method.[10]

In this work, 4,4′-disubstituted biphenyls with various substituents are investigated by means of UV and MCD spectroscopies in order to examine the substituent effects in a systematic fashion. The calculations for the MCD spectra of these compounds were carried out on the basis of the PPP method so as to reproduce the observed MCD spectra and dihedral angles of 4,4′-disubstituted biphenyls in solutions. It seemed that it would be interesting to see to what extent the observed spectra for hindered biphenyls can be explained by theoretical calculations on the basis of a simple approximation.

Experimental

4,4′-Diaminobiphenyl, 4,4′-dihydroxybiphenyl, 4,4′-dinitrobiphenyl, 4,4′-dicyanobiphenyl, 4,4′-dichlorobiphenyl,

and 4,4'-dimethylbiphenyl obtained commercially were recrystallized several times from appropriate solvents.

All the measurements were carried out at room temperature, using ethanol, methanol, or cyclohexane as solvents for the derivatives with strong electron-donating groups, with electron-attracting groups, or with weak electron-donating groups respectively. The MCD and UV spectra were measured on a JASCO-J20A recording spectropolarimeter equipped with a 1.14 T electromagnet and on a Hitachi EPS-3T recording spectrophotometer respectively.

Theoretical

The electronic transition energies, oscillator strengths, and Faraday B values of 4,4'-disubstituted biphenyls were estimated on the basis of the PPP method,[11] including configuration interactions among singly excited configurations with transition energies below 10 eV. One-center-core and repulsion integrals were evaluated from the valence-state ionization potentials and electron affinities. Two-center-core integrals were calculated by the use of the Wolfsberg-Helmholtz equation.[12] Two-center repulsion integrals were evaluated by the use of the Nishimoto-Mataga equation.[13] The repulsion integral, γ_{pq}, within a benzene ring was evaluated according to the usual formula:

$$\gamma_{pq} = \frac{14.397}{R_{pq}+a_{pq}} \text{ (eV)}, \tag{1}$$

$$a_{pq} = \frac{28.794}{\gamma_{pp}+\gamma_{qq}}, \tag{2}$$

where R_{pq} is the distance between the p and q atoms and where γ_{pp} stands for the one-center repulsion integrals. The repulsion integral, γ_{pq}, in which the p and q atoms belong to different benzene rings was calculated using Eq. 1, while modifying a_{pq} as follows:

$$a_{pq} = \frac{28.794}{(\gamma_{pp}+\gamma_{qq})\cos^2\theta+(\gamma'_{pp}+\gamma'_{qq})\sin^2\theta}, \tag{3}$$

$$\gamma'_{pp} = \gamma_{pp} - 6F_2, \tag{4}$$

where θ is the dihedral angle and F_2 is the Slater-Condon parameter. The benzene rings in biphenyl were assumed to be regular hexagons. The coordinate system employed is represented in Fig. 1. The x axis lies along the long molecular axis, and the y axis bisects the dihedral angle, θ. Since the repulsions among orthoprotons in 4,4'-disubstituted biphenyls are considered to be equal to that in biphenyl, their dihedral angles have been assumed to be equal throughout the calculations.

The theoretical Faraday B term associated with an electronic transition, $j \leftarrow a$, is expressed as follows:

$$B(j\leftarrow a) = \mathrm{Im}\{\sum_{k\neq a}(\langle k|\vec{\mu}|a\rangle/(E_k-E_a))\cdot \langle a|\vec{M}|j\rangle \times \langle j|\vec{M}|k\rangle + \sum_{k\neq j}(\langle j|\vec{\mu}|k\rangle/(E_k-E_j))\cdot \langle a|\vec{M}|j\rangle \times \langle k|\vec{M}|a\rangle\}, \tag{5}$$

where $\vec{\mu}$ and $\vec{M}$ denote the magnetic and electronic dipole moment operators respectively. The quantities in the denominator, E_k *etc.*, are the energies of the k states. The electric-transition dipole moments were estimated on the basis of the dipole-velocity method. The atomic integrals of the electric and magnetic dipole moments were retained only for the nearest neighbor atoms, while those for the distant atoms were neglected because they were small and expected no decisive effect on the calculated results. The orthogonalized set of atomic orbitals obtained by the Löwdin procedure[14] was used for the calculations of these quantities. The calculations were carried out by using the ACOS-700 computer in the Computer Center of Tohoku University.

Results and Discussion

The UV and MCD spectra of 4,4'-dihydroxybiphenyl are represented in Fig. 2, where ε is the molar extinction coefficient in $dm^3\,mol^{-1}\,cm^{-1}$ and where $[\theta]_M$ is the molar ellipticity in degree $dm^3\,mol^{-1}\,cm^{-1}$

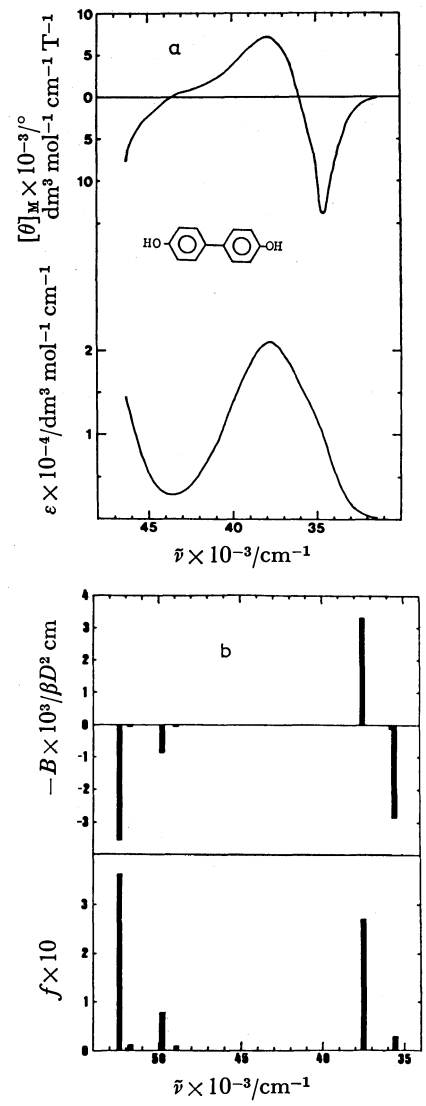

Fig. 2. The observed and calculated results of 4,4'-dihydroxybiphenyl.
(a) The MCD (top) and UV (bottom) spectra in ethanol measured at room temperature. (b) The calculated Faraday B value (top) and oscillator strength (bottom).

T^{-1}. The UV spectrum shows a single peak with its maximum at 37800 cm^{-1}, whereas the MCD spectrum exhibits a negative peak at 34600 cm^{-1} and a positive peak at 38000 cm^{-1}. 4,4′-Diaminobiphenyl shows a spectral profile (Fig. 3) similar to that of the dihydroxy derivative— a negative band at a lower frequency and a positive at a higher, but its MCD peaks shift toward a frequency region higher by about 2000 cm^{-1} in comparison with the dihydroxy derivative.

On the contrary, the MCD spectra of nitro and cyano derivatives show a positive band in the lower-frequency region and a negative in the higher, while the MCD extrema of the former are observed in a frequency region lower by about 3000 cm^{-1} than that of the latter (Figs. 4 and 5).

Furthermore, the signs of the MCD spectra of the methyl and chloro derivatives are all negative in the corresponding spectral region (Figs. 6 and 7). Thus, the UV spectrum of each compound is apparently observed as a single peak in the spectral region of 35000—40000 cm^{-1}, whereas the MCD spectra show various spectral patterns corresponding to the natures of the substituent groups.

The estimated Faraday B values (B) and oscillator strengths (f) are represented in Figs. 2—7. The longitudinal axis takes $-B$, since the Faraday parameter, B, appears as $-B$ in the expression of the molar ellipticity $[\theta]_M$. The estimated Faraday B values for the hydroxy and amino derivatives show positive signs in the lower-frequency region and negative signs in the higher, whereas those for the nitro and cyano derivatives are negative in the lower region and positive in the higher. The methyl derivatives are all predicted to have positive B values. The transition energies of hydroxy, amino, nitro, and methyl derivatives are in fairly good agreement with the experiments. However, in the cyano derivative the energy separation between the lst and 2nd MCD bands is too small in comparison with the observed

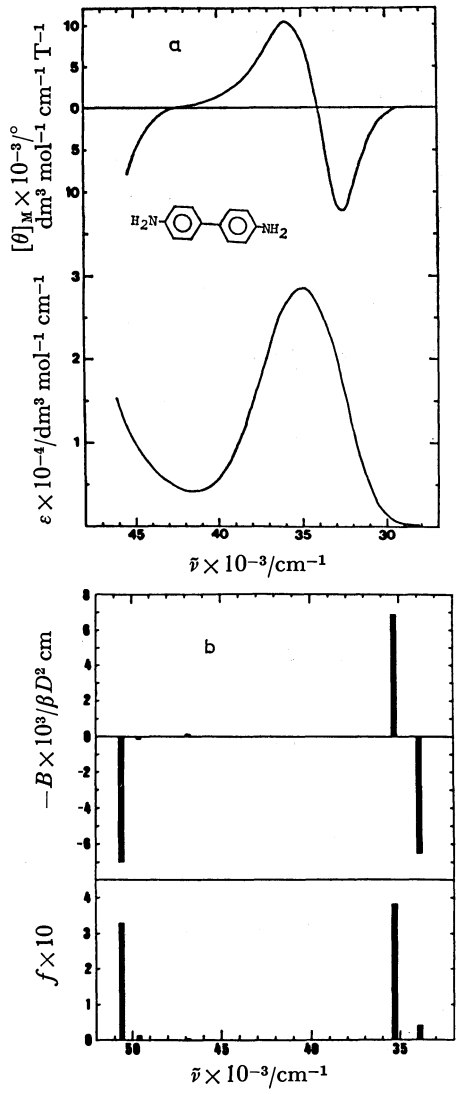

Fig. 3. The observed and calculated results of 4,4′-diaminobiphenyl.
(a) The MCD (top) and UV (bottom) spectra in ethanol measured at room temperature. (b) The calculated Faraday B value (top) and oscillator strength (bottom).

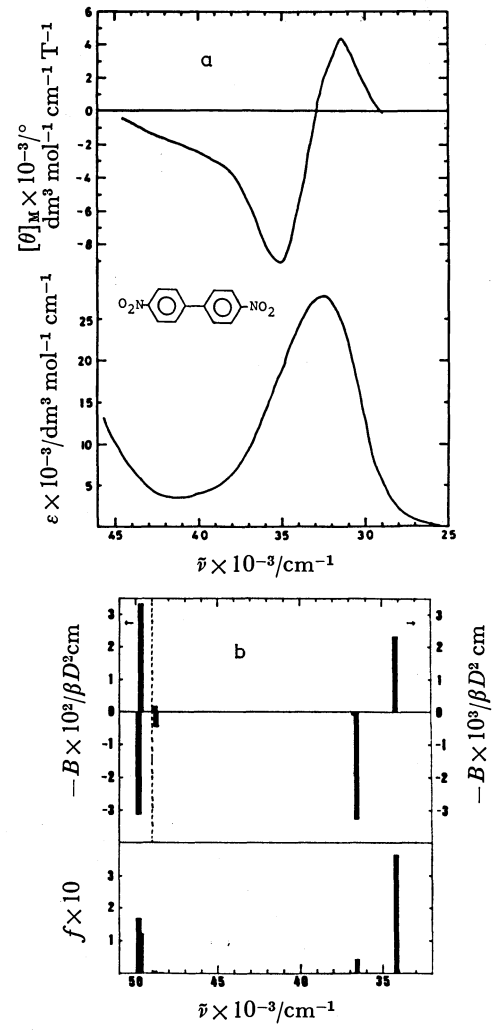

Fig. 4. The observed and calculated results of 4,4′-dinitrobiphenyl.
(a) The MCD (top) and UV (bottom) spectra in methanol measured at room temperature. (b) The calculated Faraday B value (top) and oscillator strength (bottom).

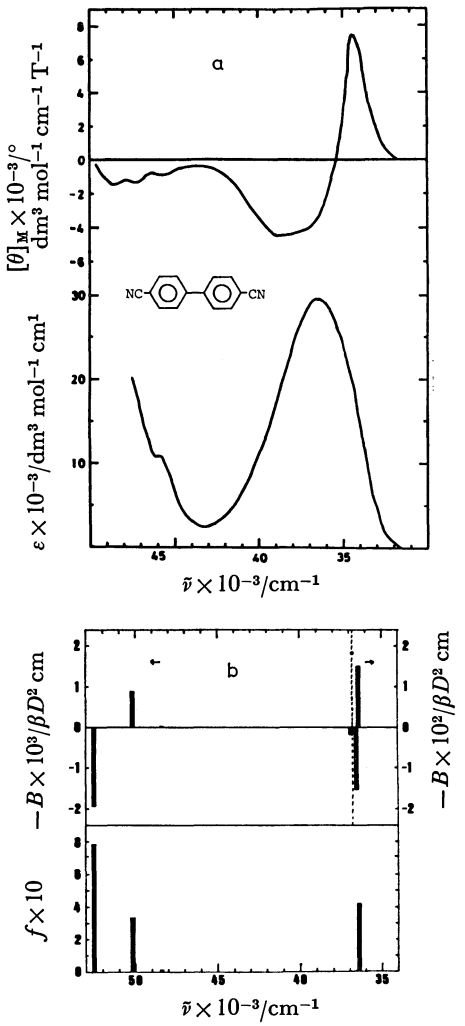

Fig. 5. The observed and calculated results of 4,4′-dicyanobiphenyl.
(a) The MCD (top) and UV (bottom) spectra in methanol measured at room temperature. (b) The calculated Faraday B value (top) and oscillator strength (bottom).

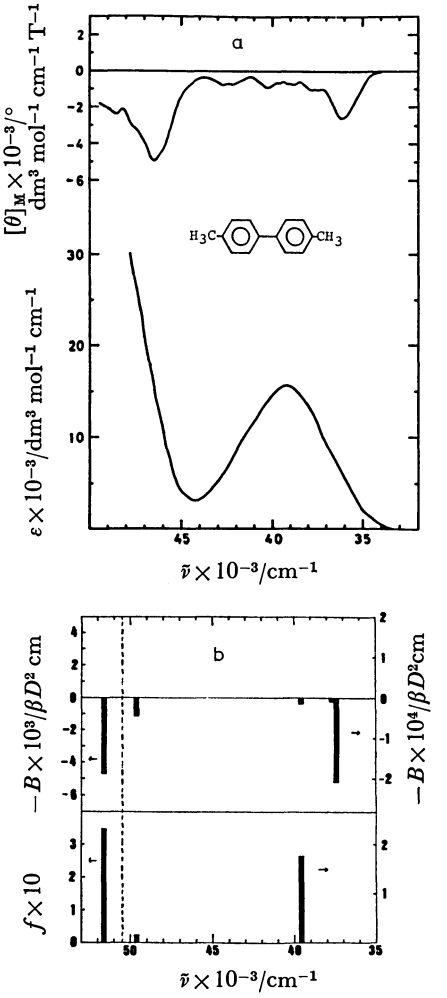

Fig. 6. The observed and calculated results of 4,4′-dimethylbiphenyl.
(a) The MCD (top) and UV (bottom) spectra in cyclohexane measured at room temperature. (b) The calculated Faraday B value (top) and oscillator strength (bottom).

one, and the experimental MCD signs of the chloro derivative are not reproduced. The disagreement between the calculations and experiments in cyano and chloro derivatives is mainly due to the parametrizations for atomic integrals in the present calculations.

The calculated results are summarized and listed in Table 1. The 4,4′-disubstituted biphenyls belong to the point group, D_2, as well as the parent molecule. The 1st, 2nd, and 3rd $\pi^* \leftarrow \pi$ transitions of the hydroxy, amino and methyl derivatives are calculated to be $^1B_2 \leftarrow {}^1A$, $^1B_1 \leftarrow {}^1A$, and $^1B_3 \leftarrow {}^1A$ respectively, whereas those in the nitro and cyano derivatives to be $^1B_3 \leftarrow {}^1A$, $^1B_2 \leftarrow {}^1A$, and $^1B_1 \leftarrow {}^1A$. Therefore, the 1st and 2nd MCD bands of the derivatives with electron-donating groups are assigned to the $^1B_2 \leftarrow {}^1A$ and $^1B_3 \leftarrow {}^1A$ transitions respectively, and those of derivatives with electron-attracting groups, to the $^1B_3 \leftarrow {}^1A$ and $^1B_2 \leftarrow {}^1A$ transitions. The $^1B_1 \leftarrow {}^1A$ transitions in the lower-frequency region of all the compounds are considered to be too weak to be distinctly observed.

In the above MCD calculations, the dihedral angles of all the compounds were assumed to be 20°. On the contrary, according to Kurland,[3] the dihedral angles of 4,4′-disubstituted biphenyls were supposed to be 45°; in that way the observed NMR spectra were well explained. The calculation of the transition energies and Faraday B parameters was carried out for the hydroxy, amino, and nitro derivatives, in which the dihedral angles were taken to be 45°. The results are summarized and listed in Table 2, along with the results with $\theta=20°$. The results calculated with $\theta=45°$ seemed to be in poor agreement, especially with respect both to the excitation energies and Faraday B values, with the experimental values. Accordingly, it is concluded that the dihedral angles of 4,4′-disubstituted biphenyls in solution are about 20°.

In Fig. 8 the molecular orbitals of biphenyl, 4,4′-diaminobiphenyl, and 4,4′-dinitrobiphenyl are schematically illustrated in order to show the interaction between biphenyl and the substituents. In the derivatives with electron-donating groups, the molecular orbitals of substituents interact, preferably with

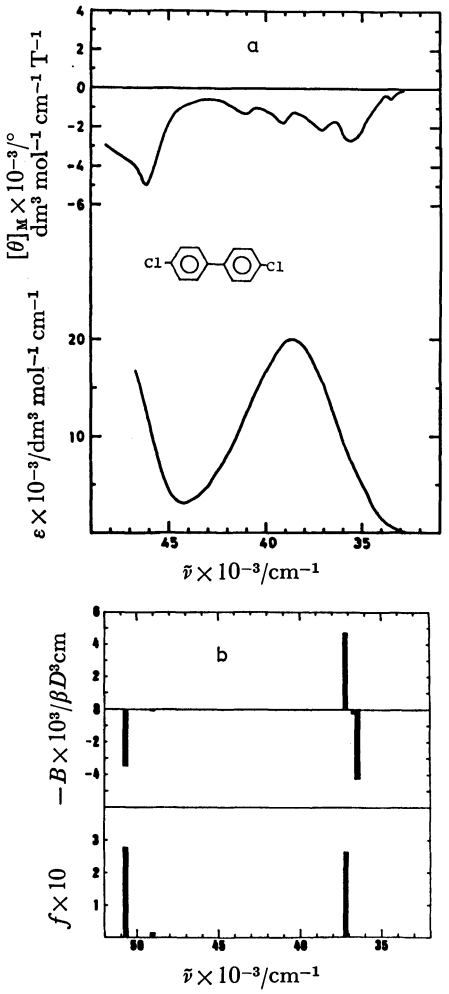

Fig. 7. The observed and calculated results of 4,4'-dichlorobiphenyl.
(a) The MCD (top) and UV (bottom) spectra in cyclohexane measured at room temperature. (b) The calculated Faraday B value (top) and oscillator strength (bottom).

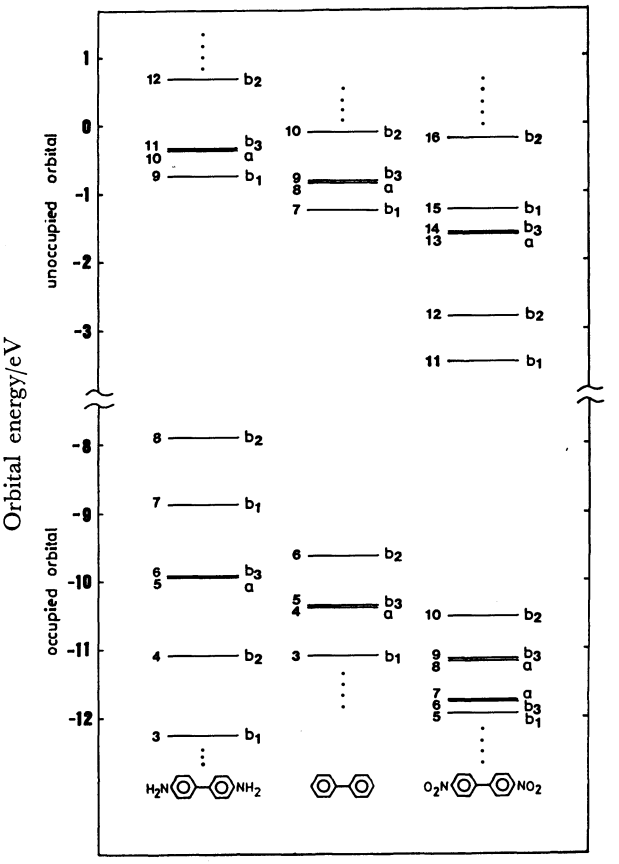

Fig. 8. The molecular orbitals of biphenyl, 4,4'-diaminobiphenyl, and 4,4'-dinitrobiphenyl.

the upper occupied orbitals of biphenyl, so that some of the occupied orbitals of biphenyl are destabilized. On the contrary, in the derivatives with electron-attracting groups, the molecular orbitals of substituents preferably interact with the lower unoccupied orbitals of biphenyl.

In Table 3 the wave functions which describe the three lowest excited states of biphenyl, 4,4'-diaminobiphenyl, and 4,4'-dinitrobiphenyl are shown, where $\psi_{k\to l}$ denotes a singly excited configuration from the k-th molecular orbital to the l-th. As is expected from Fig. 8, the lowest-energy excited state is considered to make a dominant contribution to the singly excited configuration arising from the LUMO← HOMO transition in each molecule. However, the lowest B_3 state is not able to be the lowest because of the weak configuration interaction with the higher B_3 states. On the contrary, the strong configuration interaction between $\psi_{5\to7}$ and $\psi_{6\to8}$ and that between $\psi_{4\to7}$ and $\psi_{6\to9}$ lower the B_2 and B_1 states below the B_3 state. This is also true for the amino derivative. In the nitro derivative, there exists a configuration with B_3 symmetry, $\psi_{5\to12}$, close to the $\psi_{10\to11}$ arising from the single excitation from the HOMO to the LUMO. The energy level of the B_3 state is lowered appreciably due to the configuration interaction, whereas the effect of the configuration interaction among the B_2 states, and also that among B_1 configurations, does not exceed the stabilization of the B_3 states. Consequently, the B_3 state is the lowest energy state in the nitro derivative.

The discrepancy of the MCD signs between the derivatives with the strong electron-donating groups and those with the attracting groups can then be explained. Here, only the strong MCD bands in the lower-frequency region in both derivatives are considered; they are assigned to the $^1B_2 \leftarrow {}^1A$ and $^1B_3 \leftarrow {}^1A$ transitions in the former and to $^1B_3 \leftarrow {}^1A$ and $^1B_2 \leftarrow {}^1A$ in the latter. As can clearly be seen from Eq. 5, the contribution of the 2nd term is considered to be of primary importance in the calculation of the Faraday B values because of its appreciable contribution to Eq. 5 thanks to the small energy difference in the denominator. Furthermore, the matrix element of the nearest neighboring state is of crucial importance; for example, the B_2 state mixes with B_3, and *vice versa*.

The excited electronic-wave functions of biphenyl derivatives are considered to be expressed for the lowest B_2 and B_3 states by a slight modification of the wave functions of biphenyl itself:

Table 1. Theoretical transition energies ($\tilde{\nu}$), oscillator strengths (f), and faraday B values (B) of 4,4′-disubstituted biphenyls

Compound	Symmetry	Theoretical			Experimental	
		$\tilde{\nu}\times10^{-3}$ / cm^{-1}	f	$-B\times10^{5}$ / βD^2/cm^{-1}	$\tilde{\nu}\times10^{-3}$ / cm^{-1}	$[\theta]_M^{max}\times10^{-3}$
4,4′-Dihydroxybiphenyl	$^1B_2\leftarrow{}^1A$	35.54	0.028	−286.3	34.60	−13.84
	$^1B_1\leftarrow{}^1A$	35.69	0.001	−11.7	—	—
	$^1B_3\leftarrow{}^1A$	37.54	0.270	331.9	37.88	7.10
4,4′-Diaminobiphenyl	$^1B_2\leftarrow{}^1A$	33.87	0.043	−652.8	32.68	−12.23
	$^1B_1\leftarrow{}^1A$	33.90	0.002	−24.2	—	—
	$^1B_3\leftarrow{}^1A$	35.31	0.381	689.1	36.10	10.37
4,4′-Dinitrobiphenyl	$^1B_3\leftarrow{}^1A$	34.20	1.346	233.6	31.45	4.36
	$^1B_2\leftarrow{}^1A$	36.64	0.139	−327.2	35.10	−9.01
	$^1B_1\leftarrow{}^1A$	36.72	0.005	−11.6	—	—
4,4′-Dicyanobiphenyl	$^1B_3\leftarrow{}^1A$	36.46	0.421	1512	34.36	7.44
	$^1B_2\leftarrow{}^1A$	36.61	0.003	−1546	38.50	−4.41
	$^1B_1\leftarrow{}^1A$	36.93	0.0002	−22.0	—	—
4,4′-Dimethylbiphenyl	$^1B_2\leftarrow{}^1A$	37.40	0.0003	−20.8	36.01	−2.51
	$^1B_1\leftarrow{}^1A$	37.71	0.000	−0.76	—	—
	$^1B_3\leftarrow{}^1A$	39.57	0.176	−1.50	39.30	−0.62
	$^1B_1\leftarrow{}^1A$	49.63	0.016	−4.59	46.51	−4.89
4,4′-Dichlorobiphenyl	$^1B_2\leftarrow{}^1A$	36.45	0.009	−425.6	35.52	−2.65
	$^1B_1\leftarrow{}^1A$	36.74	0.0004	−26.7	—	—
	$^1B_3\leftarrow{}^1A$	37.24	0.265	468.3	38.61	−2.16
	$^1A\leftarrow{}^1A$	46.83	forb.	—	—	—
	$^1B_1\leftarrow{}^1A$	49.04	0.014	−8.85	46.08	−4.95

Table 2. The calculated results of hydroxy, amino, and nitro derivatives with the dihedral angles of 20° and 45°

Compound	20°		45°		Experimental	
	$\tilde{\nu}\times10^{-3}$ / cm^{-1}	$B\times10^{5}$ / βD^2/cm^{-1}	$\tilde{\nu}\times10^{-3}$ / cm^{-1}	$B\times10^{5}$ / βD^2/cm^{-1}	$\tilde{\nu}\times10^{-3}$ / cm^{-1}	$B\times10^{5}$ / βD^2/cm^{-1}
4,4′-Dihydroxy-	35.54	286.3	36.16	171.9	34.60	338.0
	35.69	11.7	36.17	28.7	—	—
	37.54	−331.9	39.98	−197.4	37.88	−436.0
4,4′-Diamino-	33.87	652.8	34.45	257.8	32.68	456.0
	33.90	24.2	34.40	51.1	—	—
	35.31	−689.1	37.55	−346.5	36.10	−531.0
4,4′-Dinitro-	34.20	−233.6	36.17	−636.0	31.45	−161.0
	36.64	327.2	37.32	620.2	35.10	642.3
	36.72	11.6	37.30	116.8	—	—

Table 3. The wave functions of the $\pi^*\leftarrow\pi$ states of biphenyl and 4,4′-disubstituted biphenyls

Compound	State	Wave function
Biphenyl	$^1B_2$	$0.639\ (\psi_{5\to7}-\psi_{6\to8})+0.303\ (\psi_{4\to10}-\psi_{3\to9})$
	$^1B_1$	$0.634\ (\psi_{4\to7}+\psi_{6\to9})+0.312\ (\psi_{5\to10}+\psi_{3\to8})$
	$^1B_3$	$0.986\ \psi_{6\to7}+0.077\ (\psi_{6\to11}+\psi_{2\to7})+0.080\ \psi_{4\to9}+0.070\ \psi_{5\to8}$
4,4′-Diamino-	$^1B_2$	$0.813\ \psi_{8\to10}-0.376\ (\psi_{6\to9}+\psi_{7\to11})+0.222\ \psi_{5\to12}$
	$^1B_1$	$0.824\ \psi_{8\to11}-0.392\ \psi_{7\to10}+0.340\ \psi_{5\to9}-0.211\ \psi_{6\to12}$
	$^1B_3$	$0.981\ \psi_{8\to9}-0.152\ \psi_{7\to12}$
4,4′-Dinitro-	$^1B_3$	$0.969\ \psi_{10\to11}+0.233\ \psi_{5\to12}+0.040\ (\psi_{9\to13}+\psi_{8\to14})$
	$^1B_2$	$0.814\ \psi_{9\to11}+0.422\ \psi_{8\to12}-0.395\ \psi_{10\to13}$
	$^1B_1$	$0.824\ \psi_{8\to11}+0.441\ \psi_{9\to12}-0.352\ \psi_{10\to14}$

$$\Psi_{B_2} = C_1\psi_{5\to7} - C_2\psi_{6\to8} + C_3\psi_{4\to10} - C_4\psi_{3\to9}$$
$$\Psi_{B_3} = \psi_{6\to7}, \quad (6)$$

where the coefficients, C_1—C_4, are taken to be positive. In biphenyl, C_1 is equal to C_2, and C_3 to C_4.

The Faraday B terms of the B_2 and B_3 states are expressed as follows within this nearest-neighbor approximation:

$$B(B_2\leftarrow A) = -\mathrm{Im}\langle B_2|\mu_z|B_3\rangle\langle A|M_y|B_2\rangle \times\langle B_3|M_x|A\rangle/(E_{B_3}-E_{B_2})$$
$$B(B_3\leftarrow A) = \mathrm{Im}\langle B_3|\mu_z|B_2\rangle\langle A|M_x|B_3\rangle \times\langle B_2|M_y|A\rangle/(E_{B_2}-E_{B_3}). \quad (7)$$

As can clearly be seen from Eq. 7, $B(B_2\leftarrow A) = -B(B_3\leftarrow A)$. In amino derivatives the following equations hold for the energies and the off-diagonal matrix element of the μ_z operator:

$$E_{B_2} < E_{B_3} \quad (8)$$

$$\mathrm{Im}\langle B_2|\mu_z|B_3\rangle = \beta\{C_1\langle\phi_5|\vec{r}\times\vec{\nabla}|\phi_6\rangle_z - C_2\langle\phi_8|\vec{r}\times\vec{\nabla}|\phi_7\rangle_z\} \approx \beta\{0.7C_1+1.1C_2\} > 0, \quad (9)$$

where β is the Bohr magneton and where ϕ_k denotes the k-th molecular orbital of biphenyl.

The configurations, $\psi_{5\to7}$, $\psi_{6\to8}$, $\psi_{4\to10}$, and $\psi_{3\to9}$, in biphenyl correspond to $\psi_{6\to9}$, $\psi_{8\to10}$, $\psi_{5\to12}$, and $\psi_{7\to11}$ respectively in the amino derivative. If the para-positions of biphenyl are replaced by the electron-donating groups, such as $-NH_2$ or $-OH$, the energy levels of $\psi_{6\to8}$ and $\psi_{3\to9}$ are found to be lower than those of $\psi_{5\to7}$ and $\psi_{4\to10}$ respectively, as may be seen from Fig. 8 and Table 3. This means that $C_1 < C_2$ and $C_3 < C_4$. Then, the off-diagonal matrix element of M_y, $\langle A|M_y|B_2\rangle$, is expressed as:

$$\langle A|M_y|B_2\rangle = \sqrt{2}\{C_1\langle\phi_5|m_y|\phi_7\rangle - C_2\langle\phi_6|m_y|\phi_8\rangle + C_3\langle\phi_4|m_y|\phi_{10}\rangle - C_4\langle\phi_3|m_y|\phi_9\rangle\} \approx \sqrt{2}\{(C_1-C_2)m_1+(C_3-C_4)m_2\} < 0, \quad (10)$$

where;

$$\langle\phi_5|m_y|\phi_7\rangle \approx \langle\phi_6|m_y|\phi_8\rangle \equiv m_1 > 0,$$

and

$$\langle\phi_4|m_y|\phi_{10}\rangle \approx \langle\phi_3|m_y|\phi_9\rangle \equiv m_2 > 0.$$

In addition, the matrix element, $\langle B_3|M_x|A\rangle$, is calculated to be:

$$\langle B_3|M_x|A\rangle = \sqrt{2}\langle\phi_6|m_x|\phi_7\rangle > 0. \quad (11)$$

From Eqs. 7—11, the Faraday B values for the derivatives with strong electron-donating groups are found to be:

$$B(B_2\leftarrow A) = -B(B_3\leftarrow A) > 0. \quad (12)$$

On the contrary, in the nitro derivative,

$$E_{B_3} < E_{B_4}. \quad (13)$$

Equations 9 and 11 hold for the nitro derivative as well as the amino derivative, but with $C_1 > C_2$ and $C_3 > C_4$ the matrix element, $\langle A|M_y|B_2\rangle$, of the nitro derivative has the opposite sign of that of the amino derivative. Therefore, this leads to the following relationship:

$$\langle A|M_y|B_2\rangle > 0. \quad (14)$$

From Eqs. 9, 11, 13, and 14, the signs of the Faraday B values of the nitro derivative are shown to be the same as in Eq. 12; *i.e.*,

$$B(B_2\leftarrow A) = -B(B_3\leftarrow A) > 0.$$

Equation 12 implies that the MCD band which is assigned to the $^1B_2\leftarrow{}^1A$ transition must be negative and that the MCD band which is assigned to the $^1B_3\leftarrow{}^1A$ transition must be positive. In the hydroxy and amino derivatives, the electronic transitions are $^1B_2\leftarrow{}^1A$ and $^1B_3\leftarrow{}^1A$ in the increasing order of energy; therefore the MCD profile is negative for the 1st band and positive for the 2nd band. In the nitro and cyano derivatives, the situation is completely reversed; the MCD profile is positive for the 1st MCD band and negative for the 2nd band because of the inversion of the B_2 and B_3 excited states in these molecules.

The authors wish to thank Dr. Akira Kaito for his useful advice and stimulating discussions during the course of this work.

References

1) G. H. Beaven and G. W. Gray, "Steric Effects in Conjugated Systems," Butterworths Scientific Publications, London (1958), Chap. 3, p. 22.
2) I. Fisher-Hjalmars, *Tetrahedron*, **19**, 1805 (1963).
3) R. J. Kurland and W. B. Wise, *J. Am. Chem. Soc.*, **86**, 1877 (1964).
4) H. Suzuki, *Bull. Chem. Soc. Jpn.*, **32**, 1340, 1350, 1357 (1959).
5) H. Uchimura, A. Tajiri, and M. Hatano, *Chem. Phys. Lett.*, **34**, 34 (1975).
6) A. Tajiri, H. Uchimura, and M. Hatano, *Chem. Lett.*, **1975**, 1021.
7) R. Grinter, *Mol. Phys.*, **11**, 7 (1966).
8) Y. Gondo, *J. Chem. Phys.*, **41**, 3928 (1964).
9) A. Gamba, G. F. Tantardini, and M. Simonetta, *Spectrochim. Acta, Part A*, **28**, 1877 (1972).
10) A. Tajiri, S. Takagi, and M. Hatano, *Bull. Chem. Soc. Jpn.*, **46**, 1067 (1973).
11) R. Pariser and R. G. Parr, *J. Chem. Phys.*, **21**, 466, 767 (1953).
12) M. Wolfsberg and L. Helmholtz, *J. Chem. Phys.*, **20**, 837 (1952).
13) K. Nishimoto and N. Mataga, *Z. Phys. Chem. (N.F.)*, **12**, 335 (1957).
14) P. O. Löwdin, *J. Chem. Phys.*, **18**, 365 (1950).

Asymmetric Transformation of *N*-Acyl-DL-amino Acids

Chikara HONGO,* Shigeki YAMADA, and Ichiro CHIBATA
Research Laboratory of Applied Biochemistry, Tanabe Seiyaku Co., Ltd., 16-89, Kashima-3-chome, Yodogawa-ku, Osaka 532

(Received March 25, 1981)

The asymmetric transformation which converted *N*-acyl-DL-amino acids to the desired optically active isomers was studied. *N*-Acylamino acids such as *N*-butyrylproline, *N*-acetylleucine, and *N*-benzoylphenylglycine were easily racemized in the presence of a catalytic amount of acetic anhydride in melted states or in acetic acid or chloroform solutions. The racemic modification of these *N*-acylamino acids crystallized as a true racemic mixture suitable for optical resolution by a preferential crystallization procedure under the conditions of racemization. By combining preferential crystallization of the desired enantiomer by seeding from a supercooled melt or a supersaturated solution of a racemic modification and simultaneous racemization of the opposite isomer, *N*-acyl-DL-amino acid was partially converted to an optically active isomer and the whole reaction mixture became optically active (10—40% enantiomeric excess).

The optical resolution of DL-amino acids by a preferential crystallization procedure has been extensively investigated in our laboratory.[1-7] This procedure is considered to be one of the most useful methods for practical and industrial purposes since it enables the desired optical isomer to crystallize preferentially from a supersaturated solution of the racemic modification by simple inoculation of the same isomer.

Our previous report[6] showed that some *N*-acyl-DL-prolines were resolvable by the preferential crystallization procedure and that the undesired optically active isomer recovered from the mother liquor was completely racemized by heating at a temperature above its melting point in the presence of a catalytic amount of acetic anhydride and could be reused as the starting material. In the course of further studies, a large single crystal of almost optically pure *N*-butyryl-L-proline (*N*-Bu-L-Pro) was found to deposit in the reaction vessel when *N*-butyryl-D-proline (*N*-Bu-D-Pro) was completely racemized by heating with acetic anhydride and allowing the racemized melt to stand for 2 d at room temperature. This fact indicated that one of the optically active isomers preferentially crystallized from the super-cooled melt of *N*-butyryl-DL-proline (*N*-Bu-DL-Pro) by spontaneous crystallization of the isomer. If such optical resolution by preferential crystallization can be achieved at a high temperature, which enables the opposite isomer in the melt to racemize at a high rate, all of the racemic modification will be theoretically transformed to the optically active crystals. We were interested in the asymmetric transformation of *N*-Bu-DL-Pro by the combination of the preferential solidification from a melted racemic modification and simultaneous racemization of the opposite isomer in the melt. Besides *N*-Bu-DL-Pro, some *N*-acyl-DL-amino acids such as *N*-acetyl-DL-leucine[8] (*N*-Ac-DL-Leu) and *N*-benzoyl-DL-phenylglycine[9] (*N*-Bz-DL-PG) are known to form a true racemic mixture suitable for the optical resolution by a preferential crystallization procedure. These optically active isomers are expected to be readily racemized. Therefore, these substances were also chosen as test compounds; we sought the systems in which the asymmetric transformation took place by preferential crystallization under conditions of simultaneous racemization. The screening was carried out with combinations of the racemization process and two kinds of resolution procedures, *i.e.*, solidification from a melted racemic modification and the usual preferential crystallization from a supersaturated solution dissolving a racemic modification. In the former case, *N*-Bu-DL-Pro and *N*-Ac-DL-Leu were found to be partially converted to the respective optically active isomers and to become optically active as a whole. In the latter case, the asymmetric transformation was observed with *N*-Bu-DL-Pro, *N*-Ac-DL-Leu, and *N*-Bz-DL-PG. We wish to report here these results. A preliminary account of this work has been already published.[10]

Racemic and optically active *N*-Bu-Pro, *N*-Ac-Leu, and *N*-Bz-PG were prepared by the usual acylation of the respective amino acids. The physical properties are shown in Table 1; these indicate that these racemic modifications crystallize as a true racemic mixture suitable for the preferential crystallization procedure in the appropriate solvent. As shown in Table 2, these optically active isomers could be racemized at a very high rate by melting at a temperature near each one's melting point in the presence of a catalytic amount of acetic anhydride. Furthermore, as shown in Table 3, they could be easily racemized by heating at a relatively low temperature in acetic acid (for *N*-Ac-Leu and *N*-Bz-PG) or chloroform (for *N*-Bu-Pro) solution containing a small amount of acetic anhydride. In both cases, no racemization occurred without acetic anhydride, which was essential for the racemization process. Thus, the two important requirements for the intended asymmetric transformation were fulfilled.

The first approach for asymmetric transformation was carried out by preferential solidification from a super-cooled melt of a racemic modification. In the cases of *N*-Bu-Pro and *N*-Ac-Leu, the whole reaction mixtures became optically active (34% and 10% enantiomeric excess respectively). The second approach was carried out by preferential crystallization from a supersaturated solution of a racemic modification. In this case, two modes of operation were employed to maintain a supersaturation state during the asymmetric transformation, *i.e.*, continuous removal of solvent or addition of an inert solvent effective for reducing the solubility. In both operational modes, the asymmetric transformation of *N*-Bu-Pro, *N*-Ac-Leu, and *N*-Bz-PG was observed and the respective

Table 1. Properties of *N*-acylamino acids

N-Acylamino acid	Form	Mp/°C	$[\alpha]_D^{25}$/°	Solubility g/100 ml (Temp/°C)	Solvent	IR-Spectra[a]
N-Bu-Pro	DL	89— 90		152 (50) 194 (55)	$CHCl_3/Ac_2O$ (6/1)	Identical
				149 (50) 173 (55)	$CHCl_3$	
	L	114—116	−105.4 (*c* 1, H_2O)	—[b]	$CHCl_3/Ac_2O$ (6/1)	
				64 (50) 75 (55)	$CHCl_3$	
N-Ac-Leu	DL	159—160		65 (70) 88 (80)	AcOH/Ac_2O (10/1)	Identical
				55 (70) 75 (80)	AcOH	
	L	187—188	−24.9 (*c* 1, MeOH)	—[b]	AcOH/Ac_2O (10/1)	
				28 (70) 34 (80)	AcOH	
N-Bz-PG	DL	178—180		33 (70) 53 (80)	AcOH/Ac_2O (100/3)	Identical
				24 (70) 37 (80)	AcOH	
	L	195—196	+116.1 (*c* 1, MeOH)	—[b]	AcOH/Ac_2O (100/3)	
				8 (70) 12 (80)	AcOH	

a) The infrared spectra of L- and DL- forms which were crystallized from each solvent were compared. b) The solubility of L-isomer could not be determined because the dissolved L-isomer was readily racemized in the solvent system. L-Isomer was not dissolved in a saturated solution of DL-form.

Table 2. Racemization of *N*-acylamino acids by melting with acetic anhydride

N-Acylamino acid	Conditions: L-Isomer (g)	Ac_2O (ml)	Temp °C	Time h	Initial α_D^{25}/°	Final[a] α_D^{25}/°	Racemization[b] degree %
N-Bu-L-Pro	1.0	—	120	2	−1.713	−1.439	16
	1.0	0.05	97	0.5	−1.713	0.000	100
N-Ac-L-Leu	1.0	—	150[c]	0.5	−0.482	−0.482	0
	1.0	0.05	150	0.5	−0.482	0.000	100
N-Bz-L-PG	1.0	—	160[d]	1	+2.295	+2.295	0
	1.0	0.04	160	1	+2.295	+0.642[e]	72

a) After the reaction, the whole reaction mixture was dissolved in methanol (50 ml) and the optical rotation was measured. b) $\frac{\text{Initial optical rotation} - \text{final optical rotation}}{\text{Initial optical rotation}} \times 100$. c) *N*-Ac-L-Leu remained in solid state because the reaction temperature was lower than the melting point. At 190 °C for 30 min, the racemization was complete, but *N*-Ac-Leu partially decomposed. d) *N*-Bz-L-PG remained in solid state because the reaction temperature was lower than the melting point. At 200 °C for 30 min, the racemization was complete, but *N*-Bz-PG partially decomposed. e) The formation of by-products or decomposition was observed.

Table 3. Racemization of *N*-acylamino acids by heating in a solution containing acetic anhydride

N-Acylamino acid	Conditions: L-Isomer (g)	Ac_2O (ml)	Solvent (ml)	Temp °C	Time h	Initial α_D^{25}/°	Final[a] α_D^{25}/°	Racemization[b] degree %
N-Bu-L-Pro	1.0	—	$CHCl_3$, 1.2	50	4	−1.670	−1.670	0
	1.0	0.10	$CHCl_3$, 1.2	50	4	−1.670	−0.033	98
N-Ac-L-Leu	1.0	—	AcOH, 5	75	8	−0.453	−0.435	4
	1.0	0.11	AcOH, 5	75	2	−0.453	−0.009	98
N-Bz-L-PG	1.0	—	AcOH, 10	75	8	+1.955	+1.955	0
	1.0	0.07	AcOH, 10	75	8	+1.955	+0.059	97

a) After the reaction, the whole reaction mixture was diluted in methanol (50 ml) and the optical rotation was measured. b) $\frac{\text{Initial optical rotation} - \text{final optical rotation}}{\text{Initial optical rotation}} \times 100$.

optically active crystals were actually separated from the reaction mixture. From the mother liquor, the racemic modification was recovered. These results are shown in Table 4 and Table 5. In a typical experiment by addition of inert solvent, 4.70 g of *N*-Ac-L-Leu with an optical purity of 89.6% was obtained from 9.5 g of *N*-Ac-DL-Leu. From the mother liquor, 3.53 g of *N*-Ac-DL-Leu was recovered. In the usual optical resolution by the preferential crystallization procedure, the yield of the seeded isomer in one operating cycle is rather low, owing to the limitation of supersaturated state of the opposite isomer; it is usually 5 to 10% based on the original weight of racemic modification. On the other hand, the

Table 4. Asymmetric transformation by preferential crystallization procedure
(Crystallization by continuous removal of solvent)

N-Acyl-amino acid	Composition of solution			Seed crystals (g)	Reaction			Separated crystals		
	DL-Form (g)	Ac_2O (ml)	Solvent (ml)		Temp °C	Time h	Amount of removed solvent ml	Yield g	Optical purity %	Transformed[a] amount g
N-Bu-Pro	10.60	0.8	$CHCl_3$ 5.2	0.20	50	20	4.4	9.38 (—	41.3 —	3.67 —)[b,c]
N-Ac-Leu	10.00	1.1	AcOH 11.0	0.40	75	7	7.2	6.60 (0.40	50.2 0.0	2.91 0.00)[b]
N-Bz-PG	10.00	0.7	AcOH 25.0	0.60	75	7	14.0	7.12 (1.20	43.1 0.0	2.47 0.00)[b]

a) Weight of seed crystals was subtracted from the net weight of the active form obtained. b) The second crop was obtained by cooling the filtrate after the separation of the first crop; the data are shown in parentheses. c) Although a second crop could not be obtained, the filtrate did not show optical rotation.

Table 5. Asymmetric transformation by preferential crystallization procedure
(Crystallization by addition of inert solvent)

N-Acyl-amino acid	Composition of solution			Seed crystals (g)	Reaction			Separated crystals		
	DL-Form (g)	Ac_2O (ml)	Solvent (ml)		Temp °C	Time h	Added solvent (ml)	Yield g	Optical purity %	Transformed[a] amount g
N-Bu-Pro	10.60	0.8	$CHCl_3$ 5.2	0.60	50	7	*i*-Pr_2O 25	5.42 (2.00	60.6 0.0	2.68 0.00)[b]
N-Ac-Leu	9.50	1.0	AcOH 9.0	0.20	75	5	Toluene 50	4.70 (3.53	89.6 0.0	4.01 0.00)[b]
N-Bz-PG	9.00	1.0	AcOH 29.0	0.60	75	5	Xylene 50	3.30 (1.50	67.3 0.0	1.62 0.00)[b]

a) Weight of seed crystals was subtracted from the net weight of the active form obtained. b) The second crop was obtained by cooling the filtrate after the separation of the first crop; the data are shown in parentheses.

asymmetric transformation proposed here can give a high yield, since the concentration of the opposite isomer is decreased by the racemization and the total extent of supersaturation of the desired isomer can be increased by using the continuous operation methods described above.

The asymmetric transformation by a combination of optical resolution by selective precipitation of the less soluble diastereoisomeric salt and epimerization of the soluble diastereoisomeric salt is well known as an asymmetric transformation of second order.[11] However, the asymmetric transformation by a combination of preferential crystallization of a desired enantiomer by seeding from a supersaturated solution of a racemic modification and simultaneous racemization of the opposite isomer is unique and has not been reported except in the case of α-amino-ε-caprolactam–nickel chloride complex[12] and a few examples of somewhat analogous asymmetric transformations.[13–15] The proposed method is very promising for industrial application because of its operational simplicity. More detailed experiments on the mechanism of this asymmetric transformation and the best conditions for practical application will be described in a subsequent paper.

Experimental

Materials and Analyses. Analytical standard grade amino acids manufactured by our company, Tanabe Seiyaku Co., Ltd., were used. Other chemicals were obtained from Tokyo Kasei Kogyo Co., Ltd. All samples were dried overnight *in vacuo* at room temperature. Melting points were measured with a Yamato MP-21 melting point apparatus in an unsealed capillary tube and are uncorrected. Infrared spectra of samples were determined in nujol using a Shimadzu infrared spectrophotometer, Model IR-27G. Optical rotations were measured with a Perkin-Elmer 141 automatic polarimeter. Elemental analyses were performed with a Perkin-Elmer 240 elemental analyzer. Solubility was determined by approaching saturation equilibrium from the side of undersaturation. Solute concentration was measured with a Karl Zeiss immersion refractometer. Identification of *N*-acylamino acids was carried out by elemental analysis, IR-spectrum, specific rotation and thin-layer chromatography (solvent system: $CHCl_3$–MeOH–AcOH, 85:15:3, v/v/v) using the ascending technique on Merck's precoated Kieselgel 60 F_{254}. The chromatograms were sprayed with 40% hydrobromic acid, heated at 105 °C for about 5 min, and stained with ninhydrin at 105 °C for 5 min. The stained spots were compared with authentic samples.

Preparation of N-*Acylamino Acids.* *N*-Bu-L- and -DL-Pro were prepared from L- and DL-proline by acylation with *n*-butyryl chloride in chilled aqueous alkali, according to the usual manner described in our previous report.[6]

The racemic modifications and L-isomers of *N*-Ac-Leu and *N*-Bz-PG were similarly prepared from DL- and L-leucine and DL- and L-phenylglycine with acetyl chloride and benzoyl chloride, respectively (yield, 80—95%). The products were used for asymmetric transformation without further purification. The elemental analyses of these *N*-acylamino acids recrystallized from chloroform (for *N*-Bu-Pro) or acetic acid (for *N*-Ac-Leu and *N*-Bz-PG) corresponded to the respective theoretical values. The properties of these *N*-acylamino acids are shown in Table 1.

Racemization of N-*Acyl*-L-*amino Acids. *Racemization by Melting in the Presence of Small Amounts of Acetic Anhydride*: A mixture of *N*-Bu-L-Pro (1.0 g) and 0.1 molar equivalents of acetic anhydride (0.05 ml) was maintained at 97 °C in a sealed tube. The mixture was liquefied with the elapse of time. After 30 min, the liquefied sample was dissolved in methanol (50 ml) and the optical rotation was measured. The initial optical rotation before the reaction was α_D^{25} −1.713°. The reaction mixture did not show any optical rotation. Therefore *N*-Bu-L-Pro seemed to be completely racemized. In the absence of acetic anhydride, the optical rotation was α_D^{25} −1.439° even after heating at 120 °C for 2 h. In this case, the racemization degree was estimated to be 16%, based on α_D^{25} −1.713° of the initial optical rotation. In similar ways, *N*-Ac-L-Leu and *N*-Bz-L-PG were maintained at 150 °C for 30 min and at 160 °C for 1 h respectively in the presence of 0.1 molar equivalents of acetic anhydride. The racemization degrees were estimated as described above. The results were compared with those in the absence of acetic anhydride and are shown in Table 2. The racemization was also confirmed by separation of the reacted *N*-acylamino acids in the following way. After the complete racemization, the mixture was cooled to room temperature and the crystallized *N*-acylamino acid was suspended with a small amount of toluene (for *N*-Bu-Pro) or water/MeOH (2/1, v/v) (for *N*-Ac-Leu and *N*-Bz-PG). The suspended *N*-acylamino acid was collected and dried. The specific rotations, melting points, and IR spectra of these separated *N*-acylamino acids showed that the products were the respective racemic modifications and the true racemic mixtures. In the case of *N*-Bz-PG, however, a slight decomposition and some by-products formation were observed.

Racemization by Heating in a Solution Containing Small Amounts of Acetic Anhydride: *N*-Bu-L-Pro (1.0 g) was dissolved in chloroform (1.2 ml) containing 0.2 molar equivalents of acetic anhydride (0.10 ml). The mixture was maintained at 50 °C for 4 h. The whole reaction mixture was dissolved in methanol (50 ml) and the optical rotation was measured, α_D^{25} −0.033°. The racemization degree was estimated to be 98%, based on the initial optical rotation, α_D^{25} −1.670°. In the absence of acetic anhydride, the racemization did not occur. In similar ways, *N*-Ac-L-Leu and *N*-Bz-L-PG were racemized in acetic acid containing 0.2 molar equivalents of acetic anhydride and the racemization degrees were estimated as described above. The results were compared with those in the absence of acetic anhydride and are shown in Table 3.

The racemization was also confirmed by separation of respective *N*-acylamino acids from the reaction mixture. After the complete racemizations, the reaction mixtures were concentrated to a half volume, and the racemized *N*-acylamino acids were crystallized at room temperature. The precipitated crystals were collected and dried. The specific rotations, melting points, and IR spectra of these separated *N*-acylamino acids showed that the products were the racemic modifications and the true racemic mixtures.

Asymmetric Transformation by Preferential Solidification from Melted Racemic Modification. N-*Bu*-DL-*Pro*: A mixture of *N*-Bu-DL-Pro (10.00 g) and acetic anhydride (0.5 ml) was melted by heating at 100 °C. The complete melt was maintained at 70 °C, seeded with finely pulverized crystals of *N*-Bu-L-Pro (0.50 g), and gently stirred in a sealed flask for 7 h. During the reaction, the crystal growth of seeded L-isomer was observed. After 7 h, toluene (10 ml) was added into the reaction mixture at the same temperature and the precipitated crystals were quickly separated by filtration and dried to give *N*-Bu-L-Pro (6.30 g), $[\alpha]_D^{25}$ −64.7° (*c* 1, water), optical purity 61.4% (3.87 g of *N*-Bu-L-Pro plus 2.43 g of *N*-Bu-DL-Pro). After the separation of the first crop, the second crop was crystallized by cooling the filtrate and was separated by filtration to give *N*-Bu-DL-Pro (3.30 g), $[\alpha]_D^{25}$ 0.0° (*c* 1, water), mp 89—90 °C. The mother liquor did not show any optical rotation. Therefore, we subtract 0.5 g of seeded *N*-Bu-L-Pro from the net weight of *N*-Bu-L-Pro obtained, and find that 3.37 g of *N*-Bu-L-Pro was newly formed from *N*-Bu-DL-Pro. That is, 3.37 g of *N*-Bu-DL-Pro was transformed to *N*-Bu-L-Pro.

N-*Ac*-DL-*Leu*: A mixture of *N*-Ac-DL-Leu (10.00 g) and acetic anhydride (0.6 ml) was melted in a sealed flask by heating at 150 °C. The complete melt was cooled to 117 °C, seeded with finely pulverized crystals of *N*-Ac-L-Leu (0.05 g), and kept at the same temperature for 18 h in a sealed flask to allow the preferential solidification of L-isomer to proceed. Then, water/MeOH (2/1, v/v, 20 ml) was added into the reaction mixture at the same temperature and the precipitated crystals were quickly separated by filtration and dried to give *N*-Ac-L-Leu (1.21 g), $[\alpha]_D^{25}$ −21.4° (*c* 1, MeOH), optical purity 85.9% (1.04 g of *N*-Ac-L-Leu plus 0.17 g of *N*-Ac-DL-Leu). The second crop was crystallized from the filtrate by stirring at a room temperature and separated by filtration to give *N*-Ac-DL-Leu (4.20 g), $[\alpha]_D^{25}$ 0.0° (*c* 1, MeOH), mp 158—159 °C. The mother liquor did not show optical rotation. Therefore, we subtract 0.05 g of seeded *N*-Ac-L-Leu from the net weight of *N*-Ac-L-Leu obtained above, and find that 0.99 g of *N*-Ac-L-Leu was transformed from *N*-Ac-DL-Leu.

Asymmetric Transformation by Preferential Crystallization from Supersaturated Solution of Racemic Modification. Crystallization by Continuous Removal of Solvent: The supersaturation state was kept by continuous removal of solvent during the preferential crystallization of L-isomer and the simultaneous racemization of D-isomer. *N*-Bu-DL-Pro (10.60 g) was dissolved in chloroform (5.2 ml) at 70 °C and maintained at 50 °C. After acetic anhydride (0.8 ml) was added to the solution, the solution was seeded with finely pulverized crystals o *N*-Bu-L-Pro (0.20 g) and stirred for 20 h at the same temperature. Since the reaction was carried out in an open vessel without condenser, the solution was spontaneously concentrated. The amount of removed solvent was calculated to be 4.4 ml from the decrease in the weight of the reaction mixture. The precipitated crystals were quickly collected by filtration, washed with a small amount of cold chloroform, and dried to give *N*-Bu-L-Pro (9.38 g), $[\alpha]_D^{25}$ −43.5° (*c* 1, water), optical purity 41.3% (3.87 g of *N*-Bu-L-Pro plus 5.51 g of *N*-Bu-DL-Pro). Although the second crop was not obtained from the mother liquor, the mother liquor did not show optical rotation. Therefore, we subtract 0.20 g of seeded *N*-Bu-L-Pro from the net weight of *N*-Bu-L-Pro obtained above and find that 3.67 g of *N*-Bu-L-Pro was transformed from *N*-Bu-DL-Pro.

The reactions of *N*-Ac-DL-Leu and *N*-Bz-DL-PG were carried out at 75 °C for 7 h by using acetic acid as a solvent.

During the reaction, the solvent was removed at the rates of 1 ml/h for *N*-Ac-Leu and 2 ml/h for *N*-Bz-PG under a slightly reduced pressure. After 7 h, the precipitated crystals were quickly filtered, washed with a small amount of acetic acid, and dried. The second crops were obtained from the mother liquors which were stirred at room temperature. The results are shown in Table 4.

Crystallization by Addition of an Inert Solvent: During the preferential crystallization of L-isomer and the simultaneous racemization of D-isomer, the supersaturation state was maintained by addition of an inert solvent which was effective for reducing the solubility of racemic modification. *N*-Ac-DL-Leu (9.50 g) was dissolved in acetic acid (10.0 ml) containing acetic anhydride (1.0 ml) at 90 °C. The solution was maintained at 75 °C and seeded with finely pulverized crystals of *N*-Ac-L-Leu (0.20 g). Then toluene (50 ml) was added to the solution over a period of 5 h under stirring at the same temperature. The precipitated crystals were quickly collected by filtration and dried to give *N*-Ac-L-Leu (4.70 g), $[\alpha]_D^{25}$ −22.3° (*c* 1, MeOH), optical purity 89.6%, (4.21 g of *N*-Ac-L-Leu plus 0.49 g of *N*-Ac-DL-Leu). The second crop (3.53 g) was recovered from the mother liquor which was stirred at room temperature, $[\alpha]_D^{25}$ 0.0° (*c* 1, MeOH), mp 158—159 °C. Therefore, we subtract 0.20 g of seeded *N*-Ac-L-Leu from the net weight of *N*-Ac-L-Leu of the first crop and find that 4.01 g of *N*-Ac-L-Leu was transformed from *N*-Ac-DL-Leu. In similar ways, the reactions of *N*-Bu-Pro and *N*-Bz-PG were carried out at 50 °C for 7 h in chloroform solution and at 75 °C for 5 h in acetic acid solution, respectively. In these cases, diisopropyl ether (for *N*-Bu-Pro) or xylene (for *N*-Bz-PG) was added into the respective solutions to reduce the solubility of racemic modification. The results are shown in Table 5.

References

1) I. Chibata, S. Yamada, M. Yamamoto, and M. Wada, *Experientia*, **24**, 638 (1968).
2) S. Yamada, M. Yamamoto, and I. Chibata, *J. Agric. Food Chem.*, **21**, 889 (1973).
3) S. Yamada, M. Yamamoto, and I. Chibata, *J. Org. Chem.*, **38**, 4408 (1973).
4) S. Yamada, M. Yamamoto, C. Hongo, and I. Chibata, *J. Agric. Food Chem.*, **23**, 653 (1975).
5) S. Yamada, M. Yamamoto, and I. Chibata, *J. Org. Chem.*, **40**, 3360 (1975).
6) C. Hongo, M. Shibazaki, S. Yamada, and I. Chibata, *J. Agric. Food Chem.*, **24**, 903 (1976).
7) S. Yamada, C. Hongo, and I. Chibata, *Agric. Biol. Chem.*, **42**, 1521 (1978).
8) M. Shibazaki, Japan Patent, 1576 (1965); *Chem. Abstr.*, **62**, 13233 g (1965).
9) G. Bison, P. Janssen, and H. Schuebel, Ger. Offen. 2163033 (1973); *Chem. Abstr.*, **79**, 79175y (1973).
10) S. Yamada, C. Hongo, and I. Chibata, *Chem. Ind. (London)*, 539 (1980).
11) M. M. Harris, "Progress in Stereochemistry," ed by W. Klyne and P. B. D. Mare, Butterworths Scientific Publications, London (1958), Vol. 2, p. 157.
12) W. J. Boyle, Jr., S. Sifniades, and J. F. Van Peppen, *J. Org. Chem.*, **44**, 4841 (1979).
13) H. M. Powell, *Nature*, **170**, 155 (1952).
14) E. Havinga, *Biochim. Biophys. Acta*, **13**, 171 (1954).
15) R. E. Pincock and K. R. Wilson, *J. Am. Chem. Soc.*, **93**, 1291 (1971).

  Bull. Chem. Soc. Jpn., 54, 3291—3295 (1981)

Asymmetric Transformation of *N*-Acetyl-DL-leucine

Chikara HONGO,* Shigeki YAMADA, and Ichiro CHIBATA
Research Laboratory of Applied Biochemistry, Tanabe Seiyaku Co., Ltd., 16-89, Kashima-3-chome, Yodogawa-ku, Osaka 532
(Received March 25, 1981)

The asymmetric transformation of *N*-acetyl-DL-leucine by a combination of preferential crystallization of a desired isomer and simultaneous racemization of the opposite isomer was studied. The reaction was analyzed in detail and a practical method for the asymmetric transformation was established. A supersaturated solution of *N*-Ac-DL-Leu in acetic acid containing catalytic amounts of acetic anhydride was seeded with the crystals of *N*-Ac-L-Leu and cooled at a rate of 10 °C/h from 100 °C to 40 °C. As a result, almost optically pure *N*-Ac-L-Leu was obtained in a yield of 70%, based on the original weight of *N*-Ac-DL-Leu.

Our previous paper[1] reported some experimental facts demonstrating the asymmetric transformation of certain *N*-acylamino acids, including *N*-acetyl-DL-leucine (*N*-Ac-DL-Leu), *N*-butyryl-DL-proline, and *N*-benzoyl-DL-phenylglycine. The asymmetric transformation was achieved by a combination of an optical resolution process and racemization process. Among these experiments, a combination of the preferential crystallization of the seeded *N*-Ac-L-Leu from the acetic acid solution supersaturated with *N*-Ac-DL-Leu and racemization of the unseeded *N*-Ac-D-Leu remaining in the liquid phase was considered to be most promising for practical application. However, the details were not investigated and the yields were low. Subsequently to that work, the reaction was analyzed and a practical method for the asymmetric transformation of *N*-Ac-DL-Leu was established.

In the optical resolution process by preferential crystallization, the crystallization of the desired optical isomer (for example L-isomer) by seeding leads to an excess of the undesired opposite isomer (D-isomer) in the solution. This excess D-isomer also begins to crystallize spontaneously after a certain time, resulting in low enantiomeric purity of the product. Accordingly, the rate of racemization of the excess D-isomer in the optical resolution system is a very important factor in the asymmetric transformation by this type of optical resolution method. This is distinct from the common cases of a second order asymmetric transformation[2] which use the difference in solubility between the diastereoisomeric salts with a chiral resolving agent. Therefore, the factors accelerating the rate of racemization of *N*-Ac-D-Leu were investigated.

Since the presence of acetic anhydride was essential for accelerating the racemization of *N*-Ac-D-Leu, the effect of amounts of acetic anhydride was investigated at 75 °C using acetic acid as a solvent. If the racemization of *N*-Ac-D-Leu is complete in several hours, the rate of racemization is sufficient for practical asymmetric transformation. Although the rate of racemization was decreased with the decrease of the molar ratio of acetic anhydride, as can be seen in Fig. 1, a racemization rate sufficient for the asymmetric transformation was obtained even at 0.1 molar ratio of acetic anhydride. The effect of temperature on racemization was investigated under various conditions. The rate of racemization was greatly influenced by temperature and varied with the composition of the

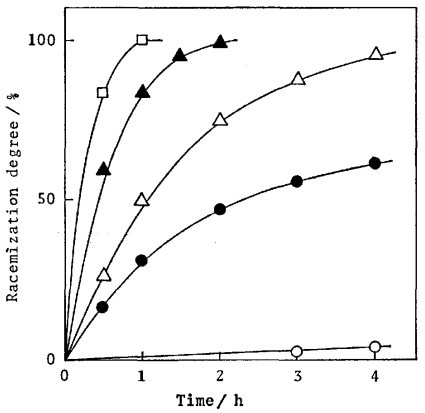

Fig. 1. Effect of acetic anhydride on racemization of *N*-Ac-D-Leu.
The solutions containing 6.0 g of *N*-Ac-D-Leu, 30 ml of AcOH and various amounts of Ac_2O were heated at 75 °C. Molar ratio of Ac_2O for *N*-Ac-D-Leu was varied from zero to 0.5: ○; zero, ●; 0.05, △; 0.1, ▲; 0.2, □; 0.5. Samples (0.5 ml) from the reaction mixture were diluted by methanol (10 ml) and optical rotations were measured. Racemization degree was calculated from the following equation:

$$\frac{\text{initial optical rotation} - \text{optical rotation after reaction}}{\text{initial optical rotation}} \times 100.$$

reaction mixture, as shown in Fig. 2. A temperature higher than 40 °C was necessary for practical racemization. The stability of crystalline optically active *N*-Ac-Leu was also investigated under the above conditions for racemization in a liquid phase. As a result, crystals of optically active *N*-Ac-Leu were found to be not racemized even at 90 °C. Thus the most essential requirement for this kind of asymmetric transformation was fulfilled.

Subsequently, optical resolution of *N*-Ac-DL-Leu by a preferential crystallization procedure was carried out at 80 °C under appropriate conditions to cause the rapid racemization of *N*-Ac-D-Leu in the liquid phase. After stirring for 1 h, all of the racemic modifications existing in excess as a supersaturation state, 12 g of *N*-Ac-DL-Leu per 100 ml of solvent, were converted to optically pure crystalline *N*-Ac-L-Leu and the filtrate was the saturated solution of *N*-Ac-DL-Leu. Figure 3 illustrates the above batch asymmetric transformation, compared with the ordinary optical resolu-

tion by a preferential crystallization procedure. In the asymmetric transformation, all of the racemic modifications existing in the supersaturation state are converted to crystalline optically active L-isomers and the supersaturation state is cancelled. On the other hand, in the ordinary optical resolution, some unseeded D-isomer remains in the liquid phase as an unstable supersaturation state. This is a marked difference between the two cases.

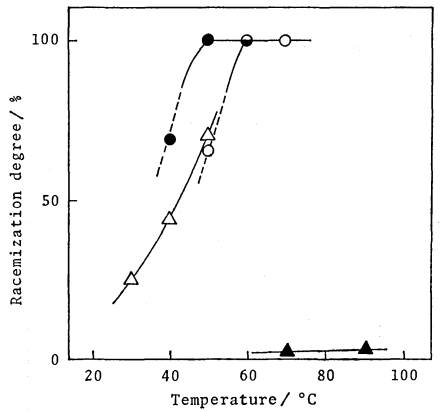

Fig. 2. Effect of temperature on racemization of *N*-Ac-D-Leu.
The mixture of the following composition was heated for 3 h. *N*-Ac-D-Leu/AcOH/Ac_2O (g/ml/ml): ○; 0.2/1.0/0.1, ●; 0.2/4.0/0.4, △; 0.2/8.0/0.8, ▲; 0.2/1.0/0.0. ----: The solid of *N*-Ac-D-Leu did not dissolve completely during the reaction. The whole reaction mixture was diluted with methanol (20 ml) and the optical rotation was measured. Racemization degree was calculated as shown in Fig. 1.

Since the driving force for the optical resolution by preferential crystallization procedure is provided only by the supersaturation degree of the racemic modification, the yield of the enantiomer produced by a simple batch experiment of this type of asymmetric transformation is dependent on the extent of the supersaturation state of the racemic modification dissolved in the reaction mixture. To obtain a higher yield of enantiomer, it is necessary to make up for the decrease of the supersaturation degree due to the preferential crystallization. This may be achieved by removal of solvent or addition of inert solvent effective for lowering the solubility of the racemic modification, as described in the previous report. In the present work, however, fresh racemic modification was added as a solid after completion of a batch asymmetric transformation and it was dissolved at an elevated temperature. In this case, fortunately, only *N*-Ac-DL-Leu in a solid mixture of newly added *N*-Ac-DL-Leu and previously crystallized *N*-Ac-L-Leu was dissolved and *N*-Ac-L-Leu was not dissolved because *N*-Ac-DL-Leu forms a true racemic mixture in the reaction system.[3] Thus a semicontinuous asymmetric transformation was able to be achieved by repeating the batch operation. The results are shown in Fig. 4, indicating that all of *N*-Ac-DL-Leu introduced successively into the reaction system was transformed to almost optically pure *N*-Ac-L-Leu. Using 2 g of seed crystals of *N*-Ac-L-Leu and 208 g of total *N*-Ac-DL-Leu on 100 ml scale, 130 g of *N*-Ac-L-Leu was obtained as 94% optically pure crystals. After the separation of *N*-Ac-L-Leu, 42 g of *N*-Ac-DL-Leu was recovered from the filtrate as the second crop.

From the practical view point, however, the above

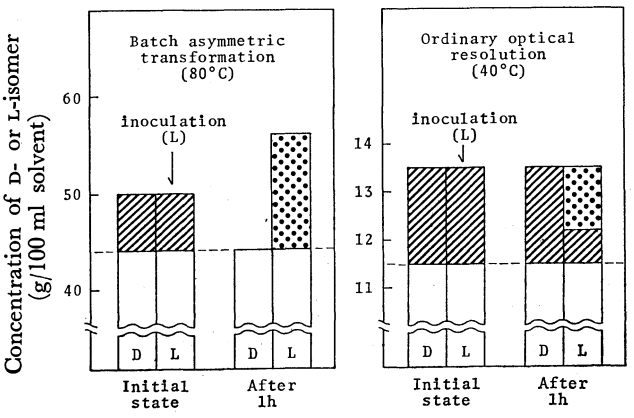

Fig. 3. Batch asymmetric transformation and ordinary optical resolution by preferential crystallization procedure of *N*-Ac-DL-Leu existing in excess as supersaturation state.
Batch asymmetric transformation was carried out under the conditions described in the text. Ordinary optical resolution was carried out at 40 °C using 0.1 g of seed crystals with the supersaturated solution of *N*-Ac-DL-Leu, 27 g/AcOH 100 ml. ----: Solubility of *N*-Ac-DL-Leu, 88 g/100 ml solvent at 80 °C and 23 g/100 ml AcOH at 40 °C, ▨: supersaturated part of *N*-Ac-Leu, ▩: crystals of *N*-Ac-L-Leu.

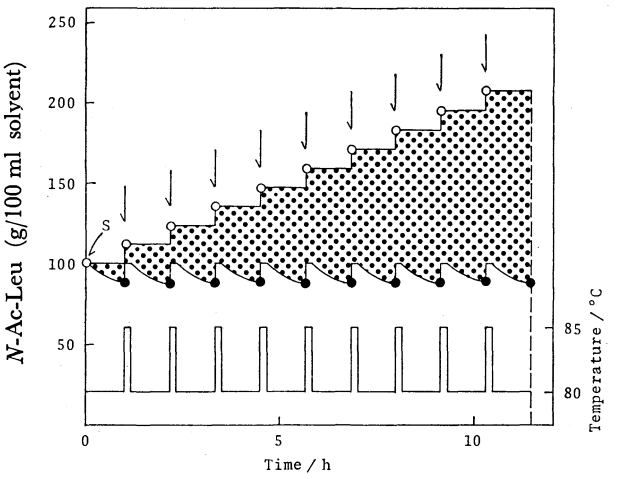

Fig. 4. Illustration of semicontinuous asymmetric transformation by repeating supply of DL-form in batch operation.
—○—: Total amount of *N*-Ac-Leu existing in the reaction mixture, —●—: concentration of *N*-Ac-Leu (almost DL-form) in the liquid phase, —: temperature, ▩: solid phase (almost L-form), ↓: addition of solid DL-form (12.0 g), S: seeding of *N*-Ac-L-Leu (2.0 g).

semicontinuous operation was considered to be complex and troublesome. The racemization experiments already demonstrated that the racemization proceeded at a rapid rate even at a relatively low temperature. Then, a continuous asymmetric transformation was carried out by a method in which the supersaturation state was continuously provided by cooling the solution from 100 °C to 40 °C. It is preferable that the rate of crystallization of the desired *N*-Ac-L-Leu is nearly equal to the rate of racemization of the undesired *N*-Ac-D-Leu in the solution. Therefore, the rate of cooling was controlled to meet those rates. When the temperature was decreased at a rate of 10 °C/h, which was selected as the optimum condition, the time course of the asymmetric transformation is shown in Fig. 5. In this experiment, acetic anhydride was supplemented after 2.5 h because its concentration had decreased at a relatively high rate, as can be seen in Fig. 5. Since the excess of the undesired *N*-Ac-D-Leu in solution was kept to a relatively low level (1±0.5 g/100 ml solvent) during the reaction,

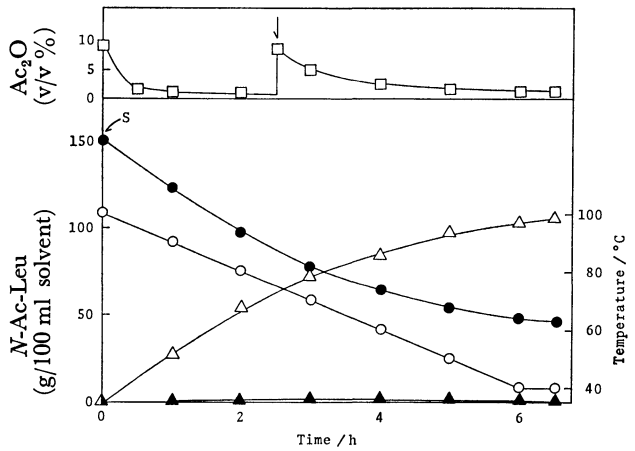

Fig. 5. Time course of continuous asymmetric transformation by gradient cooling from 100 °C to 40 °C. ○: Temperature, ●: concentration of *N*-Ac-Leu in the liquid phase, △: amount of precipitated crystals of *N*-Ac-L-Leu, which was calculated from decrease of the concentration of *N*-Ac-Leu in the liquid phase, ▲: concentration of *N*-Ac-D-Leu existing in excess in the liquid phase, □: concentration of Ac_2O, S: seeding of *N*-Ac-L-Leu (6.0 g), ↓: addition of Ac_2O (10.0 ml).

racemization seemed to proceed at a rapid rate to meet the preferential crystallization of *N*-Ac-L-Leu. The decrease in the concentration of acetic anhydride may be accounted for by the formation of a mixed anhydride or an azlactone of *N*-Ac-Leu, which are well known as racemizing intermediates.[4-6] After being cooled to 40 °C, the reaction mixture was allowed to stand for 30 min at the same temperature to complete racemization and crystallization. In this experiment, almost optically pure *N*-Ac-L-Leu was obtained in a high yield of 70%, based on the original weight of racemic modification (or 140% based on the enantiomer content of the racemic modification). The reproducibility of the reaction is demonstrated by the results of repeated runs given in Table 1.

The main disadvantage of the ordinary optical resolution by preferential crystallization is that crystallization of the desired isomer by seeding leads to an excess of the undesired isomer in the solution and the resolution system is racemic as a whole (Fig. 3). The resolution is not finished until the crystals of the desired isomer are separated from the mother liquor containing the undesired isomer. Furthermore, the yield is limited by the stability of the supersaturated state of the undesired isomer and is usually low because the supersaturation is relatively unstable. On the contrary, the asymmetric transformation now presented causes a substantial change of the composition of D- and L-isomers in the reaction system and almost optically pure crystals of the desired isomer is obtained in a high yield up to 140%, based on the enantiomer content of the racemic modification. The simplicity of the operation is also one of the advantages of the present asymmetric transformation. Therefore, application of the present method for the industrial production of L-leucine, an essential amino acid, is considered to be very promising if combined with a proper synthetic method for *N*-Ac-DL-Leu. The further applications of the asymmetric transformation combining optical resolution process and racemization process to other amino acids or their derivatives are under investigation.

Experimental

Materials and Analyses. *N*-Ac-DL-Leu, *N*-Ac-L-Leu, *N*-Ac-D-Leu, and other chemicals were the same as described

Table 1. Asymmetric transformation by cooling from 100 °C to 40 °C[a]

Exptl No.	First crop				Second crop[c]	
	Yield / g	$[\alpha]_D^{25}$/° (*c* 1, MeOH)	Optical purity / %	Transformed[b] amount / g	Yield / g	$[\alpha]_D^{25}$/° (*c* 1, MeOH)
1	112.6	−24.6	98.8	105.2	22.5	0.0
2	111.8	−24.4	98.0	103.6	25.4	0.0
3	113.5	−24.0	96.4	103.4	21.3	0.0
4	113.7	−24.3	97.6	105.0	18.5	0.0
5	110.2	−24.4	98.0	102.0	21.9	0.0

a) Reactions were carried out on a 100 ml-scale using 150 g of *N*-Ac-DL-Leu and 6.0 g of seed crystals of *N*-Ac-L-Leu. b) Amount of seed crystals was subtracted from the amount of net optically active form separated. c) The filtrate showed no optical rotation.

previously.[1] All samples for analyses were dried overnight *in vacuo* at 40 °C. Analytical and identification methods of *N*-acylamino acids were described in the previous paper.[1] The optical purity of separated crystals was determined by measuring the optical rotation with a Perkin-Elmer 141 automatic polarimeter. The total concentration of *N*-Ac-Leu in the reaction mixture was measured as total solute concentration with a Karl Zeiss immersion refractometer. The amount of *N*-Ac-D-Leu existing in excess in liquid phase was determined by refractometric and polarimetric measurements.[7] The amount of acetic anhydride remaining in a reaction mixture was determined by a Shimadzu gas chromatograph GC-3BT using a 3 m column of 20% Silicone DC-550 on Celite 545. Temperature control for reaction was carried out by using a Chino program setter NP-121-B and a Chino electronic recording controller ET-1561.

Racemization of N-*Ac-D-Leu. Effect of Amount of Acetic Anhydride*: *N*-Ac-D-Leu (6.0 g) was dissolved in AcOH (30 ml) at an elevated temperature and maintained at 75 °C. Various amounts (0.05, 0.1, 0.2, and 0.5 molar ratio) of acetic anhydride were added to the solution under stirring. The samples (0.5 ml) were taken out from the reaction mixture at intervals of 30 or 60 min, and were added into 10 ml of methanol. The optical rotation of the solution was measured and the racemization degree was evaluated on the basis of the initial optical rotation and its decrease. It was confirmed by thin-layer chromatography that significant degradation did not occur during the reaction. The data are shown in Fig. 1.

Effect of Temperature: Since the solubility of *N*-Ac-D-Leu varied largely with temperature, the reaction was carried out in three levels of the concentration of *N*-Ac-D-Leu corresponding to the reaction temperatures. A mixture of *N*-Ac-D-Leu (0.2 g) and various amounts of AcOH–Ac_2O (10:1,v/v) solution was heated at various temperatures in a sealed tube and shaken occasionally. After 3 h, the mixture was added into 20 ml of methanol and the optical rotation was measured. The racemization degree evaluated from the decrease of optical rotation is shown in Fig. 2.

Stability of Crystalline N-*Ac-L-Leu under Conditions of Racemization.* *N*-Ac-DL-Leu (12.5 g) was dissolved in 10 ml of AcOH–Ac_2O (10:1, v/v) solution at an elevated temperature to prepare the solution saturated with *N*-Ac-DL-Leu at 90 °C. To the saturated solution maintained at 90 °C, the crystals of *N*-Ac-L-Leu (10.0 g) were added. The heterogeneous reaction mixture was stirred for 5 h at the same temperature. The insoluble crystals were quickly separated by filtration, washed with a small amount of AcOH and then toluene, and dried. The insoluble crystals were proved to be optically pure *N*-Ac-L-Leu (8.5 g), $[\alpha]_D^{25}$ −24.9° (*c* 1, MeOH).

Asymmetric Transformation. Batch Transformation: *N*-Ac-DL-Leu (100.0 g) was dissolved in 100 ml of AcOH–Ac_2O (10:1, v/v) solution at 90 °C and maintained at 80 °C. In this case, 12.0 g of *N*-Ac-DL-Leu existed as a supersaturation state, because the solubility of *N*-Ac-DL-Leu at 80 °C was 88.0 g/100 ml solvent. The supersaturated solution was seeded with finely pulverized crystals of *N*-Ac-L-Leu (2.0 g) and stirred for one hour to achieve preferential crystallization of *N*-Ac-L-Leu and simultaneous racemization of *N*-Ac-D-Leu. The precipitated crystals were quickly collected by filtration, washed with a small amount of AcOH, and dried to give *N*-Ac-L-Leu (14.5 g), $[\alpha]_D^{25}$ −24.1° (*c* 1, MeOH), optical purity 96.8% (14.0 g of *N*-Ac-L-Leu and 0.5 g of *N*-Ac-DL-Leu). Subtracting 2.0 g of seeded *N*-Ac-L-Leu, 12.0 g of pure *N*-Ac-L-Leu was obtained. After the separation of *N*-Ac-L-Leu, the filtrate was stirred at 20 °C for 2 h and the precipitated crystals were collected by filtration to give *N*-Ac-DL-Leu (57.6 g), $[\alpha]_D^{25}$ 0.0° (*c* 1, MeOH). The filtrate showed no optical rotation. Consequently, all of *N*-Ac-DL-Leu (12.0 g) existing as supersaturation was completely transformed to *N*-Ac-L-Leu. The schematic comparison of the transformation with the ordinary optical resolution is shown in Fig. 3.

Semicontinuous Transformation by Repeating a Batch Run: *N*-Ac-DL-Leu (100.0 g) was dissolved in 100 ml of AcOH–Ac_2O (10:1, v/v) solution at 90 °C and cooled to 80 °C. The solution was seeded with the crystals of *N*-Ac-L-Leu (2.0 g, 65—100 meshes) and stirred for one hour at the same temperature for preferential crystallization of *N*-Ac-L-Leu and simultaneous racemization of *N*-Ac-D-Leu. Then, finely pulverized crystals of *N*-Ac-DL-Leu (12.0 g) were added into the heterogeneous system consisting of crystals of *N*-Ac-L-Leu and the solution saturated with *N*-Ac-DL-Leu. To dissolve the added *N*-Ac-DL-Leu, the mixture was heated at 85 °C for 10 min under stirring. All of the added *N*-Ac-DL-Leu was dissolved and most of the crystallized *N*-Ac-L-Leu remained in a solid state. The mixture was cooled again to 80 °C and stirred for one hour at the same temperature for the subsequent transformation. This operation was repeated nine times under heterogeneous conditions. After the last run, the precipitated crystals were quickly collected by filtration, washed with a small amount of toluene, and dried to give *N*-Ac-L-Leu (130.0 g), $[\alpha]_D^{25}$ −23.3° (*c* 1, MeOH), optical purity 93.6% (121.7 g of *N*-Ac-L-Leu and 8.3 g of *N*-Ac-DL-Leu). If we subtract 2.0 g of seeded *N*-Ac-L-Leu, we see that 119.7 g of *N*-Ac-L-Leu was obtained. After the separation of *N*-Ac-L-Leu, the filtrate was stirred for 2 h at 20 °C and the precipitated crystals were collected by filtration to give *N*-Ac-DL-Leu (41.8 g), $[\alpha]_D^{25}$ 0.0° (*c* 1, MeOH). The filtrate showed no optical rotation. Consequently, 119.7 g of the total *N*-Ac-DL-Leu (12.0 g × 10) used to make supersaturation state was transformed to *N*-Ac-L-Leu. The process of this experiment is illustrated in Fig. 4.

Continuous Transformation by Gradient Cooling of the Solution: *N*-Ac-DL-Leu (150.0 g) was dissolved in 100 ml of AcOH–Ac_2O (10:1, v/v) solution under reflux. The solution was cooled to 100 °C, seeded with finely pulverized crystals of *N*-Ac-L-Leu (6.0 g), and then the cooling was continued at the constant speed of 10 °C/h under stirring. After 2.5 h, Ac_2O (10.0 ml) was added into the reaction mixture at 75 °C. When the temperature reached 40 °C, the cooling was stopped and the reaction mixture was stirred for 30 min at the same temperature to complete racemization and crystallization. The precipitated crystals were quickly collected by filtration, washed with a small amount of AcOH, and dried to give *N*-Ac-L-Leu (112.6 g), $[\alpha]_D^{25}$ −24.6° (*c* 1, MeOH), optical purity 98.8% (111.2 g of *N*-Ac-L-Leu and 1.4 g of *N*-Ac-DL-Leu). If we subtract 6.0 g of seeded *N*-Ac-L-Leu, we see that 105.2 g of *N*-Ac-L-Leu was obtained. After the separation of *N*-Ac-L-Leu, the filtrate was concentrated *in vacuo* to about half the initial volume, and allowed to crystallize. The precipitated crystals were collected by filtration to give *N*-Ac-DL-Leu (22.5 g), $[\alpha]_D^{25}$ 0.0° (*c* 1, MeOH). The filtrate showed no optical rotation. Consequently, about 70% of the initially used *N*-Ac-DL-Leu was transformed to *N*-Ac-L-Leu. A typical time course of the transformation is shown in Fig. 5. The results of the five experiments carried out by the same procedure as described above are shown in Table 1.

References

1) C. Hongo, S. Yamada, and I. Chibata, *Bull. Chem. Soc. Jpn.*, **54**, 3286 (1981).
2) M. M. Harris, "Progress in Stereochemistry," ed by W. Klyne and P. B. D. Mare, Butterworths Scientific Publications, London (1958), Vol. 2, p. 157.
3) C. Hongo, M. Shibazaki, S. Yamada, and I. Chibata, *J. Agric. Food Chem.*, **24**, 903 (1976).
4) H. E. Carter and C. M. Stevens, *J. Biol. Chem.*, **133**, 117 (1940).
5) H. E. Carter and C. M. Stevens, *J. Biol. Chem.*, **138**, 627 (1941).
6) A. Neuberger, *Adv. Protein Chem.*, **4**, 297 (1948).
7) C. Hongo, S. Yamada, and I. Chibata, *Bull. Chem. Soc. Jpn.*, **54**, 1905 (1981).

Use of Propagators in the Hückel Model. IV. Chemical Reactivity in Radiation Field

Takayuki Ohmae, Kiyoshi Nishikawa, Kisaburo Deguchi, and Shigeyuki Aono*

Department of Chemistry, Faculty of Science, Kanazawa University, Marunouchi, Kanazawa 920

(Received April 7, 1981)

The propagator approach is applied to chemical reactivity in the presence of radiation field. The Woodward-Hoffmann's rule in photochemical reactions is generally derived. As an illustrative example, the ring closure or ring opening reactions are discussed.

In the previous work,[1] we have successfully applied the propagator theory to the problem of chemical reactivity and stability in the absence of radiation field. The treatment is fairly general, not restricted to the specified levels, *e.g.*, the highest occupied molecular orbital (HOMO) or the lowest unoccupied molecular orbital (LUMO) but whole electrons and levels are involved. The results have been shown analytically and, to some extent, quantitatively even though we are confined to the Hückel Hamiltonian.

In the present paper, we generalize the above theory to the chemical reactivity of photochemical reaction, and derive the Woodward-Hoffmann's rule in the presence of the radiation field.

General

As has been mentioned in early papers,[1,2] the total energy of the electronic system described by the Hamiltonian $\mathbf{H}$ is given as

$$E = \mathrm{Tr}\frac{1}{2\pi i}\int_c \mathrm{d}z\, z\mathbf{G}(z) = \mathrm{Tr}\frac{1}{2\pi i}\int_c \mathrm{d}z\, \mathbf{HG}(z), \tag{1}$$

where $\mathbf{G}(z)$ is the Green's function matrix with energy parameter z, and the integration contour, so called the Coulson contour, encloses only poles corresponding to the occupied levels. The second equality of Eq. 1. is obtained by adding and subtracting $\mathbf{H}$ to the right hand side of the first line and by noting that $(z-\mathbf{H})^{-1}=\mathbf{G}(z)$. It should be noticed that the expression of Eq. 1. is independent of the kind of representation.

Let us consider that the original system with Hamiltonian $\mathbf{h}$ is perturbed by a static interaction $\mathbf{v}$, under influence of the radiation field. The Hamiltonians to be considered are

$$\mathbf{H} = \mathbf{H}_0 + \mathbf{v}, \tag{2}$$

$$\mathbf{H}_0 = \mathbf{h} + \mathbf{F}, \tag{3}$$

where $\mathbf{F}$ denotes the radiation field and the interaction between radiation and electron. We now investigate the extra energy defined by

$$\Delta E = \mathrm{Tr}\frac{1}{2\pi i}\int_c \mathrm{d}z[\mathbf{HG}(z)-\mathbf{H}_0\mathbf{G}^0(z)]. \tag{4}$$

Substituting Eqs. 2. and 3 into Eq. 4, we obtain

$$\begin{aligned}\Delta E &= \mathrm{Tr}\frac{1}{2\pi i}\int_c \mathrm{d}z[(\mathbf{h}+\mathbf{F}+\mathbf{v})\mathbf{G}(z)-(\mathbf{h}+\mathbf{F})\mathbf{G}^0(z)] \\ &\cong \mathrm{Tr}\frac{1}{2\pi i}\int_c \mathrm{d}z[(\mathbf{h}+\mathbf{F}+\mathbf{v})(\mathbf{G}^0(z)+\mathbf{G}^0(z)\mathbf{v}\mathbf{G}^0(z)) \\ &\quad -(\mathbf{h}+\mathbf{F})\mathbf{G}^0(z)] \\ &\cong \mathrm{Tr}\frac{1}{2\pi i}\int_c \mathrm{d}z[\mathbf{v}\mathbf{G}^0(z)+(\mathbf{h}+\mathbf{F})\mathbf{G}^0(z)\mathbf{v}\mathbf{G}^0(z)].\end{aligned} \tag{5}$$

In this derivation, terms of first order with respect to $\mathbf{v}$ are retained. Further simplification shall be made: If we add and subtract z to the second term in Eq. 5, it yields that

$$\begin{aligned}&\frac{1}{2\pi i}\int_c \mathrm{d}z(\mathbf{h}+\mathbf{F})\mathbf{G}^0(z)\mathbf{v}\mathbf{G}^0(z) \\ &\quad = \frac{1}{2\pi i}\int_c \mathrm{d}z\, z\mathbf{G}^0(z)\mathbf{v}\mathbf{G}^0(z) \\ &\quad\quad -\frac{1}{2\pi i}\int_c \mathrm{d}z(z-\mathbf{h}-\mathbf{F})\mathbf{G}^0(z)\mathbf{v}\mathbf{G}^0(z).\end{aligned} \tag{6}$$

Noting that $\mathbf{G}^0(z)=(z-\mathbf{h}-\mathbf{F})^{-1}$, we can see that the second term of Eq. 6. cancel the first term by integration by part. Then we obtain

$$\Delta E \cong \mathrm{Tr}\frac{1}{2\pi i}\int_c \mathrm{d}z\, \mathbf{v}\mathbf{G}^0(z). \tag{7}$$

Certainly, Eq. 7. is exactly accordance with the first order term of our previous result (See Eq. 3. of Ref. 1.).

The Green's function, $\mathbf{G}^0(z)$ which describes the electronic structure of the system interacting with radiation, but without $\mathbf{v}$ is derived in the appendix as

$$\begin{aligned}\mathbf{G}^0(z) = [z-\mathbf{h}-&\sum_k \mathbf{f}^k n_k(z+\omega_k-\mathbf{h})^{-1}\mathbf{f}^k \\ &-\sum_k \mathbf{f}^k(1+n_k)(z-\omega_k-\mathbf{h})^{-1}\mathbf{f}^k]^{-1}.\end{aligned} \tag{8}$$

Here $\mathbf{f}^k$ is the interaction (matrix) between electron and radiation with the mode k, n_k, and ω_k are, respectively, number and angular frequency of photon with the mode k. The term with n_k is to do with absorption and the term with $(1+n_k)$ does emission.

First, if we confine ourselves, for simplicity, to the case of absorption with a single mode, it follows that

$$\mathbf{G}^0(z) = (z-\mathbf{h})^{-1} + (z-\mathbf{h})^{-1}\mathbf{f}n(z+\omega-\mathbf{h})^{-1}\mathbf{f}(z-\mathbf{h})^{-1}, \tag{9}$$

where we omitted the mode index k.

Substituting this into Eq. 7, and picking up the term relating with the radiation field, we obtain

$$\Delta E_f^a = n\,\mathrm{Tr}\frac{1}{2\pi i}\int_c \mathrm{d}z\, \mathbf{v}(z-\mathbf{h})^{-1}\mathbf{f}(z+\omega-\mathbf{h})^{-1}\mathbf{f}(z-\mathbf{h})^{-1}. \tag{10}$$

The Green's function, $(z-\mathbf{h})^{-1}$ has been precisely investigated in II[3] of this series for the case of the Hückel model.

Remembering that Eq. 10 has an expression independent of the kind of representation, we can manipulate this by the representation that the Green's functions are diagonal, namely by the MO representation. Thus

$$\Delta E_f^a = n \sum_{i,j,k} v_{ij} f_{jk} f_{ki} \frac{1}{2\pi i} \int_c dz \frac{1}{(z-\varepsilon_i)(z-\varepsilon_j)(z+\omega-\varepsilon_k)}, \tag{11}$$

where ε_i is the orbital energy or the eigenvalue of **h**. Now we impose an experimental condition usually met in the laboratory: suppose that the radiation field has a strong intensity at the frequency

$$\omega \cong \varepsilon_L - \varepsilon_H, \tag{12}$$

where ε_L and ε_H are orbital energies of LUMO and HOMO, respectively, and the electronic carries the oscillator strength only between LUMO and HOMO. Then Eq. 11 becomes

$$\Delta E_f^a = n v_{HH} |f_{HL}|^2 \frac{1}{2\pi i} \int_c dz \frac{1}{(z-\varepsilon_H)^2(z+\omega-\varepsilon_L)} + n v_{LL} |f_{LH}|^2 \frac{1}{2\pi i} \int_c dz \frac{1}{(z-\varepsilon_L)^2(z+\omega-\varepsilon_H)}. \tag{13}$$

The contour integration using the Coulson contour (Fig. 1) is easily carried out to yield

$$\Delta E_f^a = n|f_{HL}|^2 \left\{ \frac{v_{LL}}{(\varepsilon_H-\varepsilon_L-\omega)^2} - \frac{v_{HH}}{(\varepsilon_L-\varepsilon_H-\omega)^2} \right\} \cong -n|f_{HL}|^2 v_{HH}/(\varepsilon_L-\varepsilon_H-\omega)^2, \tag{14}$$

where the condition 12 is used to get the final result, neglecting the first term.

If we deal with the emission part of Eq. 8, the similar treatment gives rise to

$$\Delta E_f^e = (1+n)|f_{HL}|^2 \frac{v_{LL}}{(\varepsilon_L-\varepsilon_H-\omega)^2}. \tag{15}$$

Therefore, the net effect is

$$\Delta E_f = \Delta E_f^a + \Delta E_f^e = |f_{HL}|^2 \{-n v_{HH} + (1+n) v_{LL}\}/(\varepsilon_L-\varepsilon_H-\omega)^2, \tag{16}$$

the value of which should be negative for the photochemical reaction to take place. An analytical expression of the Woodward-Hoffmann's rule in the radiation field[4] is thus obtained.

Electrocyclic Reaction

As an illustrative example, we want to apply the general result 16 to the electrocyclic reaction. The ring closure and ring opening reactions are to be discussed, based on the same model that has been explained in III[2] of this seres. In Fig. 2 we display the model of the closure reaction of the conjugated chain molecule with N number of atoms; when the reaction path is con-rotatory the interaction between two ends, $v_{0,N-1}$ is positive, while when dis-rotatory, $v_{0,N-1}$ is negative.

In order to determine which of these two is likely to take place, it suffice to examine v_{HH} and v_{LL} in Eq. 16. As is shown in Fig. 2, the non-vanishing matrix elements of v are only $v_{0,N-1}$ and $v_{N-1,0}$, and then we can decompose these as follows

$$v_{AA} = \langle A|\mathbf{v}|A\rangle = \sum_{s,t}^{\text{sites}} \langle A|s\rangle\langle s|\mathbf{v}|t\rangle\langle t|A\rangle, \quad (A=L \text{ and } H)$$
$$= 2v_{0,N-1}\langle 0|A\rangle\langle A|N-1\rangle$$
$$= 2v_{0,N-1} \frac{1}{2\pi i} \int_A dz\, g(0, N-1; z). \tag{17}$$

The final expression is obtained by the use of the definition of the Green's function; $g(0,N-1;z)$ being the $(0,N-1)$ matrix element of the propagator. The contour A encloses only the pole at ε_A. In other words, the partial bond order between the 0-th and $(N-1)$-th atoms of the chain molecule is given by the pole strength of the corresponding propagator (except for the spin factor). The propagator $g(0, N-1; z)$ is given in II as

$$g(0, N-1; z) = \sin\theta/\sin(N+1)\theta, \quad z = 2\cos\theta. \tag{18}$$

Using these in Eq. 17, and noticing that

$$\theta_A = \pm\pi A/(n+1), \tag{19}$$

we obtain

$$v_{AA} = (-1)^{A+1} \frac{4v}{N+1} \sin^2 \pi A/(N-1), \tag{20}$$

when v is the abbreviation of $v_{0,N-1}$.

Here if we put $A=H$, and note that $L=H+1$, we obtain

$$\Delta E_f = (-1)^H v \frac{4}{N+1} \frac{|f_{HL}|^2}{(\varepsilon_L-\varepsilon_H-\omega)^2} \times \left\{ n \sin^2 \frac{\pi H}{N+1} + (1+n) \sin^2 \frac{\pi(H+1)}{N+1} \right\} \propto (-1)^H v. \tag{21}$$

This is the selection rule for the electrocyclic reaction in the presence of the radiation field. We shall examine in more detail conditions that the reaction takes place, or $\Delta E_f < 0$.

i) If H is even, the sign of v should be negative. In this case, the HOMO is designated to be the $2m$-th level (m is integer). If levels are doubly occupied up to the HOMO, namely concerned with $4m$ electrons system, the dis-rotatory reaction path is probable both for the ring closure and ring opening reaction.

ii) If H is odd, the sign of v should be positive. In this case, the HOMO is designated to be the $(2m+1)$-th level. If levels are doubly occupied up to the HOMO, namely concerned with $4m+2$ electrons system, the con-rotatory reaction path is probable both for the ring closure and the ring opening reaction. These selection rules are also tabulated in Table 1.

It should be mentioned that the above statements for the photochemical reaction give reverse prediction comparing with rules of the thermal electrocyclic reaction.[3]

Concluding Remarks

We have explained that even for the photochemical reaction the propagator approach works as well as for the ground state properties. In our theory the excited state are *virtually* taken into account, so that not only the absorption process but also the emission process are involved to photochemical reactivity. In

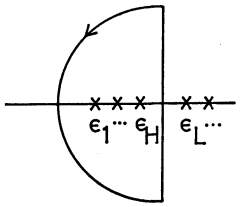

Fig. 1. Coulson contour and eigenvalues.

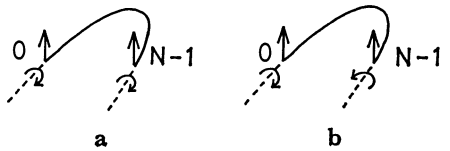

Fig. 2. Model for the ring closure reaction.
a: Con-rotatory, $v_{0,N-1}>0$, b: dis-rotatory, $v_{0,N-1}<0$.

Table 1. Selection rules of the electrocyclic reaction in the presence of radiation field

Number of electron	Condition	Path	Type of ring
$4m$	$v<0$	dis	Hückel ring
$4m+2$	$v>0$	con	Möbius ring

order to derive the Woodward-Hoffmann's rule as is written in a usual way, we have impose a special (laboratory) condition such as the relation (12) and the comments following it. However this restriction does not harm our general procedure, which ensures possibilities to analyze the more complicated phenomena and to get clear cut results.

Appendix

We derive $\mathbf{G}^0(z)$, the propagator of the electronic system in the radiation field, in a field theoretical way by means of the equation of motion method, combined by the decoupling procedure.[5,6] The Hamiltonian of the system under investigation is

$$H_0 = \sum_s \alpha_s a_s^\dagger a_s + \sum_{s,t} \beta_{st} a_s^\dagger a_t + \sum_{s,t,k} f_{st}^k a_s^\dagger a_t (c_k^\dagger + c_k) + \sum_k \omega_k c_k^\dagger c_k. \tag{A1}$$

Here matrix elements are written in the AO representation, indices s and t indicate atomic sites, and $a_s^\dagger$ (a_s) is the creation (annihilation) operator of electron at the site s, $c_k^\dagger$ (c_k) is the creation (annihilation) operator of photon with mode k, f_{st}^k, and ω_k being the electron-photon coupling constant and the photon frequency, respectively. The representation used above is only for convenience. The final result will be independent of the kind of representation.

We investigate the Green's function defined by

$$G_{rs}^0(t) = -i\langle T[a_r(t)a_s^\dagger(0)]\rangle, \tag{A2}$$

where $\langle\cdots\rangle$ denotes the ground state average, and T is the time ordering operator. The equation of motion of $G_{rs}^0(t)$ is Fourier transformed with respect to time as

$$zG_{rs}^0(z) = \delta_{rs} + \langle\langle[a_r, H_0]; a_s^\dagger\rangle\rangle_z \tag{A3}$$

where

$$G_{rs}^0(z) \equiv \langle\langle a_r; a_s^\dagger\rangle\rangle_z = \int_{-\infty}^{\infty} dt\, e^{izt}\langle\langle a_r(t); a_s^\dagger\rangle\rangle = \int_{-\infty}^{\infty} dt\, e^{izt} G_{rs}^0(z). \tag{A4}$$

The commutator in Eq. A3 is evaluated as

$$[a_r, H_0] = \alpha_r a_r + \sum_u \beta_{ru} a_u + \sum_{u,k} f_{ru}^k (c_k^\dagger + c_k) a_u. \tag{A5}$$

Using this in Eq. A3, we obtain

$$zG_{rs}^0(z) = \delta_{rs} + \alpha_r G_{rs}^0(z) + \sum_u \beta_{ru} G_{us}^0(z) + \sum_{u,k} f_{ru}^k \langle\langle c_k^\dagger a_u; a_s^\dagger\rangle\rangle_z + \sum_{u,k} f_{ru}^k \langle\langle c_k a_u; a_s^\dagger\rangle\rangle_z. \tag{A6}$$

If we want to evaluate $G_{rs}^0(z)$ utilizing this equation, we have to evaluate the higer order Green's functions:

$$M_{us}^{k+}(z) = \langle\langle c_k^\dagger a_u; a_s^\dagger\rangle\rangle_z,$$
$$M_{us}^{k}(z) = \langle\langle c_k a_u; a_s^\dagger\rangle\rangle_z. \tag{A7}$$

Again we set the equation of motions for these: this time the Kronecker delta does not appear, calculation being a little tedious, but straigtforward, and we obtain

$$zM_{us}^{k+}(z) = (a_u - \omega_k) M_{us}^{k+}(z) + \sum_v \beta_{uv} M_{vs}^{k+}(z) + \sum_{v,l} f_{uv}^l \langle\langle c_k^\dagger c_l^\dagger a_v; a_s^\dagger\rangle\rangle_z + \sum_{v,l} f_{uv}^l \langle\langle c_k^\dagger c_l a_v; a_s^\dagger\rangle\rangle_z - \sum_{v,t} f_{vt}^k \langle\langle a_v^\dagger a_t a_u; a_s^\dagger\rangle\rangle_z. \tag{A8}$$

At this stage we apply decoupling procedure as follows:

$$\langle\langle c_k^\dagger c_l a_v; a_s^\dagger\rangle\rangle_z = \langle c_k^\dagger c_l\rangle\langle\langle a_v; a_s^\dagger\rangle\rangle_z = \delta_{kl} n_k G_{vs}^0(z). \tag{A9}$$

Further we might assume that

$$\langle\langle c_k^\dagger c_l^\dagger a_v; a_s^\dagger\rangle\rangle_z = 0, \tag{A10}$$

since the two photon process described by this Green's function should be negligibly important, and we assume also

$$\langle\langle a_v^\dagger a_t a_u; a_s^\dagger\rangle\rangle_z = 0,$$

since this is a higher order correction to the electronic process. Accordingly Eq. A8 is approximately rewritten as

$$zM_{us}^{k+}(z) = (\alpha_u - \omega_k) M_{us}^{k+}(z) + \sum_v \beta_{uv} M_{vs}^{k+}(z) + n_k \sum_v f_{uv}^k G_{vs}^0(z), \tag{A11}$$

or in the matrix notation

$$z\mathbf{M}^{k+}(z) = (\mathbf{h} - \omega_k)\mathbf{M}^{k+}(z) + n_k \mathbf{f}^k \mathbf{G}^0(z),$$

or

$$\mathbf{M}^{k+}(z) = n_k (z - \mathbf{h} + \omega_k)^{-1} \mathbf{f}^k \mathbf{G}^0(z), \tag{A12}$$

where

$$\mathbf{h} = \boldsymbol{\alpha} + \boldsymbol{\beta}. \tag{A13}$$

In a similar way,

$$\mathbf{M}^{k}(z) = (1 + n_k)(z - \mathbf{h} - \omega_k)^{-1} \mathbf{f}^k \mathbf{G}^0(z). \tag{A14}$$

Substituting Eqs. A12 and A14 into Eq. A6, we obtain

$$z\mathbf{G}^0(z) = \mathbf{1} + \mathbf{h}\mathbf{G}^0(z) + \sum_k \mathbf{f}^k \mathbf{M}^{k+}(z) + \sum_k \mathbf{f}^k \mathbf{M}^{k}(z)$$
$$= \mathbf{1} + \mathbf{h}\mathbf{G}^0(z) + \sum_k \mathbf{f}^k n_k (z - \mathbf{h} + \omega_k)^{-1} \mathbf{f}^k \mathbf{G}^0(z) + \sum_k \mathbf{f}^k (1 + n_k)(z - \mathbf{h} - \omega_k)^{-1} \mathbf{f}^k \mathbf{G}^0(z),$$

or

$$\mathbf{G}^0(z) = [z - \mathbf{h} - \sum_k \mathbf{f}^k n_k (z - \mathbf{h} + \omega_k)^{-1} \mathbf{f}^k - \sum_k \mathbf{f}^k (1 + n_k)(z - \mathbf{h} - \omega_k)^{-1} \mathbf{f}^k]^{-1}. \tag{A15}$$

References

1) T. Ohmae, K. Nishikawa, K. Deguchi, and S. Aono, *Bull. Chem. Soc. Jpn.*, **54**, 2857 (1981).
2) S. Aono and K. Nishikawa, *Bull. Chem. Soc. Jpn.*, **53**, 3418 (1980).
3) S. Aono, T. Ohmae, and K. Nishikawa, *Bull. Chem. Soc. Jpn.*, **54**, 1645 (1981).
4) R. B. Woodward and R. Hoffmann, The Conservation of Orbital Symmetry, Academic Press, New York and London (1970).
5) D. N. Zubarev, *Soviet. Phys. Uspekhi.*, **3**, 320 (1960).
6) K. Nishikawa and S. Aono, *Prog. Theoret. Phys. (Kyoto)*, **50**, 830 (1973).

The Crystal Structure of *N*-Methylviologenium 2-Dicyanomethylene-1,1,3,3-tetracyanopropanediide, $[(CH_3 \cdot NC_5H_4 \cdot C_5H_4N \cdot CH_3)^{2+} \cdot (C_{10}N_6)^{2-}]$

Kenichi NAKAMURA,† Yasushi KAI, Noritake YASUOKA,†† and Nobutami KASAI*

Department of Applied Chemistry, Faculty of Engineering, Osaka University, Yamadaoka, Suita, Osaka 565

(Received April 13, 1981)

$[(CH_3 \cdot NC_5H_4 \cdot C_5H_4N \cdot CH_3)^{2+} \cdot (C_{10}N_6)^{2-}]$ crystallizes in the space group of $P2_1/c$, with four formula units. The unit-cell dimensions are; $a=14.625(2)$, $b=8.361(2)$, $c=17.332(3)$ Å, and $\beta=107.51(2)°$. The crystal structure was established by means of the symbolic addition method. For 2767 non-zero reflections, R is 0.074. In the crystal, divalent cations and divalent anions are stacked alternately to form infinite columns which are parallel to the b axis. Short atomic contacts are mostly involved between nitrogen atoms of the anion and carbon atoms of the cation. The $(C_{10}N_6)^{2-}$ anion takes a three-bladed propeller shape; however, it has no symmetry, unlike those in hexahydrated calcium and quinolinium salts. In the $[(CH_3 \cdot NC_5H_4 \cdot C_5H_4N \cdot CH_3)^{2+}]$ cation, two pyridine rings are twisted about the central C–C bond; the dihedral angle between the planes of two rings is 19.6(2)°.

In a series of structural studies of organic charge-transfer salts,[1-4] the crystal structure of *N*-methylviologenium 2-dicyanomethylene-1,1,3,3-tetracyanopropanediide, $[(CH_3 \cdot NC_5H_4 \cdot C_5H_4N \cdot CH_3)^{2+} \cdot (C_{10}N_6)^{2-}]$, has been determined by means of X-ray diffraction. This salt consists of a divalent cation and a divalent anion;

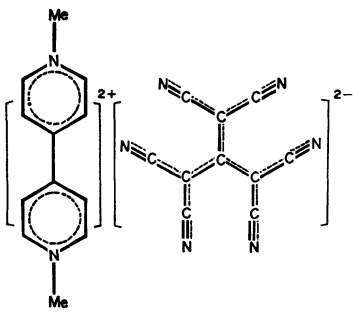

Interest in the structure of the anion in this crystal has also prompted the present study in relation to the structures of the anion in the quinolinium[3] and calcium salts.[5]

Experimental

Dark-red crystals of $[(CH_3 \cdot NC_5H_4 \cdot C_5H_4N \cdot CH_3)^{2+} \cdot (C_{10}N_6)^{2-}]$ were supplied by Professor H. Mikawa and his co-workers of this university. They were recrystallized from a saturated aqueous solution by slow evaporation at room temperature. Platelet crystals elongated along the b axis were usually obtained.

The unit-cell dimensions and the integrated intensities were measured on a Rigaku automated, four-circle diffractometer, using Ni-filtered Cu $K\alpha$ radiation. The crystal data are given in Table 1. A total of 2767 independent reflections was collected by means of the θ-2θ scan technique ($2\theta \leqq 115°$). The intensities were corrected for the usual Lorentz and polarization effects, but no absorption correction was made ($\mu/cm^{-1}=6.78$ for Cu $K\alpha$).

† Present address: Energy Conversion Research Laboratory, Matsushita Electric Industrial Co., Ltd., Kadoma, Osaka 571.

†† Present address: Institute for Protein Research, Osaka University, Yamadaoka, Suita, Osaka 565.

TABLE 1. CRYSTAL DATA OF $[(CH_3 \cdot NC_5H_4 \cdot C_5H_4N \cdot CH_3)^{2+} \cdot (C_{10}N_6)^{2-}]$

$C_{22}N_8H_{14}$, *F.W.* 390.41	
Monoclinic, Space group $P2_1/c$	
a/Å	14.625(2)
b/Å	8.361(2)
c/Å	17.332(3)
β/°	107.51(2)
V/Å^3	2021.9
D_m/g cm^{-3}	1.275 (by flotation in CCl_4–CH_3OH)
Z	4
D_c/g cm^{-3}	1.283

Solution of the Structure and Refinement

The structure was solved by the symbolic-addition procedure for the centrosymmetric space group.[6] The positional and thermal parameters were refined by the block-diagonal least-squares procedure. A difference Fourier synthesis was auxiliarily used to determine the location of hydrogen atoms. The neutral atomic-scattering factors used in the calculations were taken from those given by Hanson and his co-workers.[7]

The final positional and thermal parameters of the non-hydrogen atoms are listed in Table 2, while Table 3 gives those of hydrogen atoms.†††

Calculations of the symbolic addition procedure were done with the *SSGM* program revised by one of the present authors (N.Y.). The *HBLS* IV in the *UNICS*[8] and other programs in the *UNICS*-Osaka[9] were also used. Almost all the computations were done on a FACOM 230-60 computer at Kyoto University, with the rest being done on an ACOS Series 77 NEAC System 700 computer at Osaka University.

Results and Discussion

An *ORTEP* drawing[10] of the cation and anion is shown in Fig. 1.

††† Lists of the observed and calculated structure factors and anisotropic thermal parameters are kept at the Chemical Society of Japan; Document No. 8147.

Table 2. Fractional atomic coordinates and isotropic thermal parameters of non-hydrogen atoms, with e.s.d.'s in parentheses

Atom	x	y	z	B_{eq}/Å^2
C(1)	0.0814(4)	0.1936(7)	−0.0193(3)	5.2
C(2)	0.0660(3)	0.3663(6)	0.0904(3)	4.5
C(3)	0.2182(3)	0.3117(6)	0.0815(3)	3.9
C(4)	0.2589(3)	0.3931(6)	0.1512(3)	3.6
C(5)	0.1030(3)	0.4482(6)	0.1599(3)	4.3
C(6)	0.2023(3)	0.4639(5)	0.1934(3)	3.5
C(7)	0.2452(3)	0.5468(5)	0.2714(3)	3.3
C(8)	0.1936(3)	0.5716(6)	0.3262(3)	4.1
C(9)	0.3398(3)	0.5985(6)	0.2945(3)	4.2
C(10)	0.3782(3)	0.6693(6)	0.3675(3)	4.3
C(11)	0.2349(4)	0.6429(6)	0.3986(3)	4.2
C(12)	0.3710(4)	0.7729(7)	0.4975(3)	5.6
N(1)	0.1228(3)	0.2956(5)	0.0524(2)	3.8
N(2)	0.3267(3)	0.6924(5)	0.4188(3)	4.1
C(21)	0.2183(3)	−0.1223(6)	0.1331(3)	3.6
C(22)	0.3659(3)	0.0208(6)	0.1662(3)	4.2
C(23)	0.4453(3)	0.0489(6)	0.3358(3)	4.2
C(24)	0.3334(3)	0.1902(6)	0.3879(3)	3.7
C(25)	0.1628(3)	0.0065(6)	0.3500(3)	3.6
C(26)	0.0914(3)	0.0280(6)	0.2070(3)	3.8
C(27)	0.2848(3)	−0.0250(6)	0.1904(3)	3.4
C(28)	0.3482(3)	0.0877(5)	0.3278(3)	3.3
C(29)	0.1768(3)	0.0218(6)	0.2732(3)	3.4
C(30)	0.2705(3)	0.0283(5)	0.2632(3)	3.1
N(21)	0.1692(3)	−0.2016(6)	0.0844(3)	5.1
N(22)	0.4270(3)	0.0555(7)	0.1426(3)	6.7
N(23)	0.5238(3)	0.0161(7)	0.3459(3)	6.3
N(24)	0.3246(3)	0.2762(6)	0.4369(3)	5.3
N(25)	0.1475(3)	−0.0128(5)	0.4105(3)	4.5
N(26)	0.0213(3)	0.0381(6)	0.1561(3)	5.3

Table 3. Fractional atomic coordinates and isotropic thermal parameters of hydrogen atoms, with e.s.d.'s in parentheses

Atom	x	y	z	B/Å^2
H(1A)	0.084(4)	0.064(7)	0.000(4)	6.0(15)
H(1B)	0.115(4)	0.206(7)	−0.059(3)	5.3(14)
H(1C)	0.029(4)	0.202(8)	−0.035(4)	7.4(17)
H(2)	0.000(3)	0.359(5)	0.065(3)	2.4(10)
H(3)	0.252(4)	0.266(6)	0.050(3)	3.5(11)
H(4)	0.329(3)	0.390(5)	0.172(2)	0.5(7)
H(5)	0.055(3)	0.505(6)	0.182(3)	2.6(10)
H(8)	0.127(4)	0.533(6)	0.317(3)	4.2(12)
H(9)	0.378(3)	0.595(6)	0.261(3)	3.1(11)
H(10)	0.439(3)	0.708(5)	0.380(3)	1.3(8)
H(11)	0.202(3)	0.652(6)	0.444(3)	2.9(10)
H(12A)	0.396(5)	0.885(8)	0.489(4)	8.7(19)
H(12B)	0.407(4)	0.691(8)	0.530(4)	7.1(17)
H(12C)	0.329(4)	0.791(7)	0.523(4)	6.3(15)

Structure of the $[CH_3\cdot NC_5H_4\cdot C_5H_4N\cdot CH_3]^{2+}$ *Cation.* The skeleton of the cation, together with the bond lengths and bond angles, is illustrated in Fig. 2(a). Each pyridine ring is approximately planar (Table 4). These two rings are twisted about the C(6)–C(7) bond, the dihedral angle between the planes of two rings being 19.6(2)°. The methyl carbon, C(1), attached to the N(1) atom is considerably displaced (0.14 Å) from the (1) ring plane, whereas

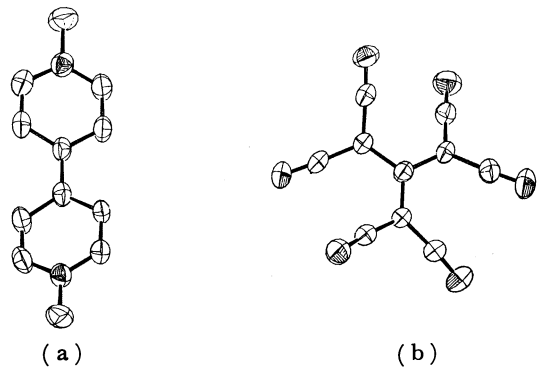

(a) (b)

Fig. 1. A perspective view of the cation(a) and anion (b). Non-hydrogen atoms are drawn by thermal ellipsoids with 50% probability level.

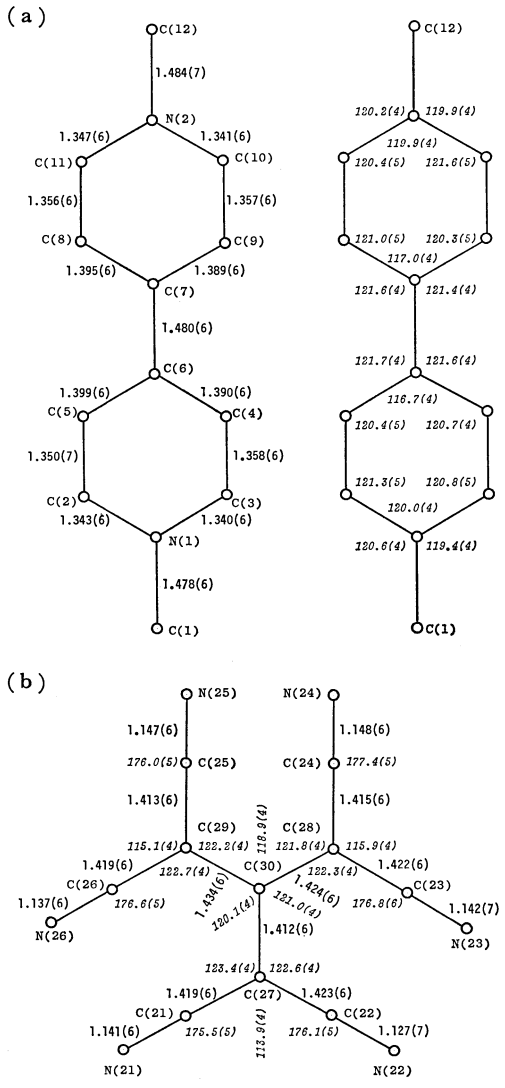

Fig. 2. Bond lengths (l/Å) and bond angles (ϕ/°) in the cation(a) and anion(b) with e.s.d.'s in parentheses.

TABLE 4. LEAST-SQUARES PLANES AND DIHEDRAL ANGLES

Least-squares planes	$AX+BY+CZ+D=0$, where $X=ax+cz\cdot\cos\beta$, $Y=by$, and $Z=cz\cdot\sin\beta$							
	A/Å	B/Å	C/Å	D/Å	Displacement of atoms from the plane (l/Å)			
$(CH_3\cdot NC_5H_4\cdot C_5H_4N\cdot CH_3)^{2+}$ ion:								
(1) Pyridine ring 1	−0.1340	−0.8389	0.5275	1.8375	N(1)	−0.010	C(4)	−0.002
					C(2)	−0.010	C(5)	0.009
					C(3)	−0.003	C(6)	0.017
(2) Pyridine ring 2	0.1812	−0.8925	0.4131	1.8331	N(2)	−0.004	C(9)	−0.000
					C(7)	−0.001	C(10)	0.003
					C(8)	−0.001	C(11)	0.003
$(C_{10}N_6)^{2-}$ ion:								
(3) Plane defined by C(27), C(28), C(29), and C(30)	−0.0762	0.9234	−0.3761	1.6176	C(27)	−0.001	C(29)	−0.001
					C(28)	−0.001	C(30)	0.003
(4) Plane defined by C(21), C(22), C(27), N(21), and N(22)	−0.3813	0.8153	−0.4359	2.7534	C(21)	0.008	N(21)	−0.005
					C(22)	−0.012	N(22)	0.007
					C(27)	0.001		
(5) Plane Defined by C(23), C(24), C(28), N(23), and N(24)	0.2540	0.7900	−0.5580	1.5843	C(23)	0.020	N(23)	−0.012
					C(24)	−0.013	N(24)	0.006
					C(28)	−0.001		
(6) Plane defined by C(25), C(26), C(29), N(25), and N(26)	0.0430	−0.9940	−0.1006	0.5878	C(25)	−0.025	N(25)	0.012
					C(26)	0.022	N(26)	−0.010
					C(29)	0.002		

Dihedral angles (ϕ/°) and angles between vectors and planes (ϕ/°)

Dihedral angles	between the (1) and (2) planes	19.6(2)
	between the (3) and (4) planes	18.9(2)
	between the (3) and (5) planes	23.1(2)
	between the (3) and (6) planes	27.9(2)
Angles between	N(1)-C(1) vector and the (1) plane	4.7
	N(2)-C(12) vector and the (2) plane	1.7

the deviation of C(12), attached to the N(2) atom, from the (2) plane is only 0.02 Å. This significant displacement of the methyl carbon, C(1), from the (1) ring plane probably depends upon the strong interaction between the cation and the anion. The structure of the same cation in the crystal of $[(CH_3\cdot NC_5H_4\cdot C_5H_4N\cdot CH_3)^{2+}\cdot(CuCl_4)^{2-}]$ has previously been reported;[11] in this structure two pyridine rings and two methyl carbons attached to the respective rings are all coplanar within the range of experimental error. However, in the present complex, the cations are considerably distorted, as has been mentioned above.

Structure of the $(C_{10}N_6)^{2-}$ Anion. The bond lengths and bond angles in the anion are also given in Fig. 2(b). The four central carbon atoms, C(27), C(28), C(29), and C(30), are coplanar (Table 4), while three dicyano-substituted carbon groups, $-C(CN)_2$, are tilted out of this plane; the tilt angle are 18.9(2), 23.1(2), and 27.9(2)° respectively (Table 4). The $(C_{10}N_6)^{2-}$ anion has a C_3-3 (or approximately D_3-32) symmetry in hexahydrated calcium salt[4] and a C_2-2 symmetry in quinolinium salt,[5] whereas in the present salt the anion has no symmetry. However, there is no considerable difference in the corresponding bond lengths and bond angles in these three salts.

Crystal Structure. The crystal structure as viewed along the b and a axes is shown in Figs. 3 and 4 respectively. The crystal consists of infinite columns parallel to the b axis. In the column the divalent cations and the divalent anions are stacked alternately. They lie roughly on the (022) plane. This

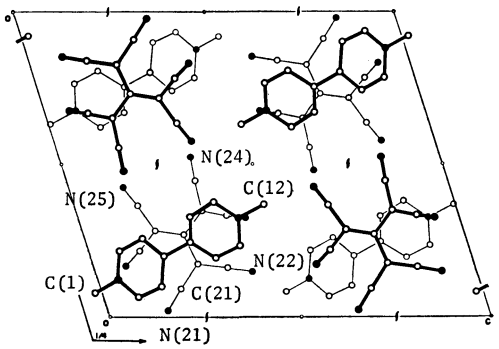

Fig. 3. Crystal structure projected along the b axis.

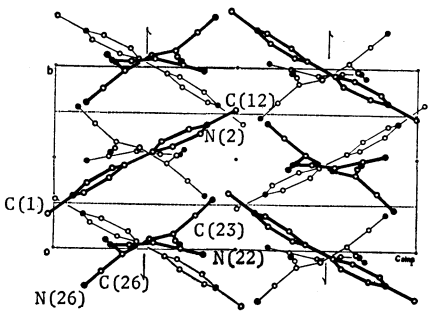

Fig. 4. Crystal structure projected along the a axis.

Table 5. Intermolecular atomic contacts (l/Å) less than 3.4 Å

1.	Cation(x, y, z) to anion(x, y, z)	
	C(2)···N(26)	3.115(7)
	C(3)···C(22)	3.290(7)
	C(3)···C(27)	3.367(6)
	C(8)···N(24)	3.353(6)
	C(11)···N(24)	3.322(6)
2.	Cation(x, y, z) to anion($x, 1+y, z$)	
	C(6)···N(21)	3.328(6)
	C(11)···C(25)	3.245(6)
	C(11)···N(25)	3.182(6)
3.	Cation(x, y, z) to anion($x, 0.5-y, -0.5+z$)	
	C(1)···N(25)	3.200(7)
	C(3)···N(25)	3.291(6)
4.	Cation(x, y, z) to anion($\bar{x}, \bar{y}, \bar{z}$)	
	C(1)···N(26)	3.080(7)
5.	Cation(x, y, z) to anion($1-x, 1-y, 1-z$)	
	C(12)···N(23)	3.214(7)
6.	Cation(x, y, z) to anion($\bar{x}, 0.5+y, 0.5-z$)	
	C(2)···N(25)	3.278(6)
	C(8)···N(26)	3.261(6)
7.	Cation(x, y, z) to anion($1-x, 0.5+y, 0.5-z$)	
	C(4)···N(23)	3.327(7)
	C(9)···N(22)	3.272(7)
	C(10)···N(22)	3.058(7)

structure well explains the particularly strong intensity of the 022 reflection. Short atomic contacts (less than 3.4 Å) between the cation and anion are listed in Table 5. Most of them are between electronegative nitrogen atoms of the anion and electropositive carbon atoms of the cation.

The authors wish to express their deep thanks to Professor Hiroshi Mikawa for the supply of crystals and for his helpful discussions. Thanks are also due to Mr. Takashi Mizuma for his help in the *ORTEP* drawings.

References

1) S. Sakanoue, Y. Kai, N. Yasuoka, N. Kasai, and M. Kakudo, *Bull. Chem. Soc. Jpn.*, **43**, 1306 (1970).
2) K. Nakamura, N. Yasuoka, N. Kasai, and M. Kakudo, *J. Chem. Soc., Chem. Commun.*, **1970**, 1135.
3) S. Sakanoue, N. Yasuoka, N. Kasai, and M. Kakudo, *Bull. Chem. Soc. Jpn.*, **44**, 1 (1971).
4) T. Tamamura, T. Yamane, N. Yasuoka, and N. Kasai, *Bull. Chem. Soc. Jpn.*, **47**, 832 (1974).
5) D. A. Bekoe, P. K. Gantzel, and N. K. Trueblood, *Acta Crystallogr.*, **22**, 657 (1967).
6) I. L. Karle, K. Britta, and P. Gum, *Acta Crystallogr.*, **17**, 496 (1964).
7) H. P. Hanson, F. Herman, J. D. Lea, and S. Skillman, *Acta Crystallogr.*, **17**, 1040 (1964).
8) "Universal Crystallographic Computing System," ed by T. Sakurai, The Crystallographic Society of Japan (1967).
9) "Universal Crystallographic Computing System-Osaka," The Computation Center, Osaka University (1973).
10) C. K. Johnson, *ORTEP* II, Oak Ridge National Laboratory, Tennessee (1974).
11) J. H. Russel and S. C. Wallwork, *Acta Crystallogr., Sect. B*, **25**, 1961 (1969).

Picosecond Laser Spectroscopy of Intramolecular Heteroexcimer Systems. Time-resolved Fluorescence Studies of p-$(CH_3)_2NC_6H_4$-$(CH_2)_n$-(9-Anthryl), p-$(CH_3)_2NC_6H_4$-$(CH_2)_n$-(1-Pyrenyl) Systems and 9,9′-Bianthryl

Masahito MIGITA, Tadashi OKADA, Noboru MATAGA,* Yoshiteru SAKATA,† Soichi MISUMI,† Nobuaki NAKASHIMA,†† and Keitaro YOSHIHARA††

Department of Chemistry, Faculty of Engineering Science, Osaka University, Toyonaka, Osaka 560

†*Institute of Scientific and Industrial Research, Osaka University, Suita, Osaka 565*

††*Institute for Molecular Science, Myodaiji, Okazaki 444*

(Received April 21, 1981)

In order to elucidate the details of elementary processes of photochemical charge transfer and heteroexcimer formation processes, and also in order to compare the obtained results with those of transient absorption spectral measurements, we have examined the following intramolecular heteroexcimer systems by means of ps time-resolved fluorescence measurements with a mode-locked Nd^{3+}: YAG laser and a streak camera: p-$(CH_3)_2NC_6H_4$-$(CH_2)_n$-(9-anthryl) (n=0, 1, 2, 3), p-$(CH_3)_2NC_6H_4$-$(CH_2)_n$-(1-pyrenyl) (n=1, 2, 3) and 9,9′-bianthryl. Effects of methylene chain length, solvent polarity and viscosity upon the intramolecular charge transfer processes have been clearly demonstrated. It is concluded that molecules with sandwich configuration in the ground state are not recognized in both n=3 compounds, and it takes a few ns for the heteroexcimer formation in hexane because of an extensive conformation change necessary to take sandwich configuration. Both conformation change and solvent reorientation are involved in the heteroexcimer formation processes in polar solvents, and heteroexcimer formation becomes faster with increase of solvent polarity and decrease of its viscosity. Moreover, two step conformation changes are observed in the case of the heteroexcimer formation of n=3 compounds in polar solvents, *i.e.* a heteroexcimer with loose structure is formed first, and then follows a structural change to the one of sandwich type. In acetonitrile, a strongly polar solvent, formation of heteroexcimer is very fast, occurring within the time-resolution of the picosecond apparatus.

The nature of CT (charge transfer) interactions in electronically excited states is a subject under lively investigation at present,[1] and the results appear to be important from the viewpoint of photochemical as well as photobiological reaction mechanisms.

In order to clarify the details of photo-induced CT and HE (heteroexcimer) formation processes, we have been examining intramolecular HE systems such as p-$(CH_3)_2NC_6H_4$-$(CH_2)_n$-(9-anthryl) (A_n, n=0, 1, 2, 3), p-$(CH_3)_2NC_6H_4$-$(CH_2)_n$-(1-pyrenyl) (P_n, n=1, 2, 3) and 9,9′-bianthryl (Bian), by means of ns time-resolved fluorescence and ns as well as ps time-resolved absorption spectral measurements.[2-10,12,14,16] It has been demonstrated that fluorescence spectra of A_1, A_2 and P_1 in nonpolar solvents can be ascribed to the anthracene or pyrene part (LE (locally excited state) fluorescence), and they show HE fluorescences only in polar solvents due to the solvent-induced change of electronic state during the excited state lifetime. Analogous results have been observed also for A_0. For A_3, P_3, and P_2 HE fluorescences can be observed not only in polar solvents but also in nonpolar solvents, due to a conformation change from an extended form to the sandwich or a similar structure during the excited state lifetime. Moreover, it has been demonstrated that the HE formation process is affected considerably by solvent polarity. By means of ps transient absorption measurements of P_3 in 2-propanol photoinduced CT has been found to produce at first a loose HE followed by a structural change to the more compact one.

In the present study, by means of ps time-resolved fluorescence measurements we have made direct observations of CT fluorescence rise curves as well as LE fluorescence decay curves of the above intramolecular exciplex systems in various solvents of different polarity, and have provided a systematic interpretation of photoinduced CT processes in solution.

Experimental

Apparatus and Measurements. The third harmonic (355 nm, 15 ps, 1 mJ) of a passively mode-locked Nd^{3+}:YAG laser was used as an exciting light source. The ps pulse repeated at 1 Hz. Fluorescence rise and decay curves were measured with a streak camera (HTV C979), the streak being digitized by a TV camera/microcomputer system (HTV C1000). Measurements in a few ns region were made also by a high speed tandem microchannel plate photomultiplier (HTV R1294X) connected to a transient digitizer (Tektronix R7912). All solutions for the measurements were de-aerated by freeze-pump-thaw cycles.

Materials. All solvents used were Merck spectrograde. Hexane, acetone and acetonitrile were used without further purification. 2-Propanol and butyronitrile were distilled before use. Bian was the same sample as used previously.[12] A_n (n=0, 1, 2, 3) and P_n (n=1, 2, 3) were synthesized and purified as described below.

All melting points are uncorrected. The NMR and MS spectra were recorded with a Hitachi Perkin-Elmer R-20 or a Varian XL-100 and a Hitachi RMU-7, respectively.

p-*(9-Anthryl)*-N,N-*dimethylaniline* (A_0). To a Grignard reagent prepared from p-bromo-*N,N*-dimethylaniline (20 g, 0.1 mol) and magnesium flake (2.4 g, 0.1 mol) in tetrahydrofuran, a solution of anthrone (5.82 g, 0.03 mol) in tetrahydrofuran was added with stirring over a period of 30 min at 0 °C under nitrogen atmosphere. After stirring for additional 1 h, the reaction mixture was worked up. The crude product was chromatographed on alumina and recrystallized from benzene.

A_0: yelloe granulars, 1.1 g (12.3%), mp 260—260.5 °C, NMR ($CDCl_3$) δ 3.11 (s, CH_3), 7.0—8.4 ppm (m, ArH).

Found: C, 88.94; H, 6.23; N, 4.72%; MS (*m/e*) 297 (M^+). Calcd for $C_{22}H_{19}N$: C, 88.85; H, 6.44; N, 4.71%; M, 297.38.

p-*Arylmethyl*-N,N-*dimethylaniline* (*A_1, P_1*). A mixture of *N,N*-dimethylaniline (2 ml) and 9-(bromomethyl)anthracene[19] (500 mg, 1.9 mmol) was stirred overnight at room temperature and at 40—50 °C for 30 min. After adding 10 ml of methanol to the reaction mixture, resulting precipitate was collected and washed with methanol. Recrystallization of the precipitate from acetone gave pale yellow plates of A_1 (180 mg, 30%), mp 133—134 °C. NMR ($CDCl_3$) δ 2.75 (s, CH_3), 4.82 (s, CH_2), 6.68 (m, ArH of phenyl), 7.0—8.3 ppm (m, ArH of Anthryl). Found: C, 88.45; H, 7.06; N, 4.50%, MS (*m/e*), 311 (M^+). Calcd for $C_{23}H_{21}N$: C, 88.70; H, 6.80; N, 4.50%; M, 311.41.

In a similar manner, P_1 was prepared. P_1: colorless needles from acetone, mp 103—105 °C. NMR ($CDCl_3$) δ 2.86 (s, CH_3), 4.62 (s, CH_2), 6.85 (m, ArH of phenyl), 7.7—8.4 ppm (m, ArH of pyrenyl). Found: C, 89.30; H, 6.23; N, 4.06%; MS (*m/e*), 335 (M^+). Calcd for $C_{25}H_{21}N$: C, 89.51; H, 6.31; N, 4.18%; M, 335.43.

p-*(2-Arylvinyl)*-N,N-*dimethylaniline* (*$I_{A,P}$*). To a stirred suspension of phosphonium salt (2.7 g, 5 mmol) in benzene, prepared from 9-(bromomethyl)anthracene[19] and triphenylphosphine, was added an ethereal solution of phenyllithium (1 mol dm^{-3}, 5 mmol) under nitrogen. To this mixture a solution of *p*-dimethylaminobenzaldehyde (0.75 g, 5 mmol) in benzene was added dropwise for 5 min. Stirring was continued overnight at room temperature. After working up in the usual manner the crude product was recrystallized from acetone to afford yellow needles of I_A (500 mg, 31%), mp 178—180 °C. Found: C, 88.89; H, 6.37; N, 4.26%. Calcd for $C_{24}H_{21}N$: C, 89.12; H, 6.55; N, 4.33%.

The synthesis of I_P was done in the same manner. I_P: yellow granulars from benzene–acetone, mp 193.5—195 °C. Found: C, 89.90; H, 6.08; N, 3.91%. Calcd for $C_{26}H_{21}N$: C, 89.87; H, 6.09; N, 4.03%.

p-*(2-Arylethyl)*-N,N-*dimethylaniline* (*A_2, P_2*). Catalytic hydrogenation of I_A (3.23 g, 10 mmol) in benzene was carried out by stirring with 5% Pd–C (200 mg) for 30 h. The reaction mixture was worked up and chromatographed on silica gel to afford yellow solid A_2 (1.97 g, 60.6%). A_2: yellow needles from acetone, mp 119.5—120.5 °C. NMR ($CDCl_3$) δ 2.92 (s, CH_3), 2.8—4.0 (m, CH_2), 6.9 (m, ArH of phenyl), 7.1—8.4 ppm (m, ArH of anthryl). Found: C, 88.50; H, 7.11; N, 4.26%; MS (*m/e*), 325 (M^+). Calcd for $C_{24}H_{23}N$: C, 88.57; H, 7.12; N, 4.30; M, 325.43.

The preparation of P_2 was accomplished in a similar manner. P_2: pale yellow granulars from acetone, mp 118—120 °C. NMR ($CDCl_3$) δ 2.92 (s, CH_3), 2.9—3.7 (m, CH_2), 6.94 (m, ArH of phenyl), 7.8—8.4 ppm (m, ArH of pyrenyl). Found: C, 89.41; H, 6.64; N, 3.99%, MS (*m/e*) 349 (M^+). Calcd for $C_{26}H_{23}N$: C, 89.36; H, 6.63; N, 4.01%; M, 439.45.

p-*(3-Aryl-3-oxo-1-propenyl)*-N,N-*dimethylaniline* (*$II_{A,P}$*). A mixture of 9-acetylanthracene (27.5 g, 125 mmol), *p*-dimethylaminobenzaldehyde (18.5 g, 125 mmol), and potassium cyanide (3 g, 45 mmol) in ethanol was heated under reflux for 4 h. The resulting precipitate was collected and recrystallized from toluene to yield ketone II_A (39 g, 90%), orange granulars, mp 188—189 °C. Found: C, 85.64; H, 5.76; N, 3.81%. Calcd for $C_{25}H_{21}NO$: C, 85.44; H, 6.02; N, 3.99%.

The preparation of II_P was done in the same manner. II_P: orange plates from acetone–benzene, mp 171.5—172.5 °C. Found: C, 86.12; H, 5.32; N, 3.63%. Calcd for $C_{27}H_{21}NO$: C, 86.37; H, 5.64; N, 3.73%.

p-*(3-Aryl-3-oxopropyl)*-N,N-*dimethylaniline* (*$III_{A,P}$*). The ketone II_A (20 g, 57 mmol) was reduced with lithium aluminium hydride (4 g, 110 mmol) in boiling diethyl ether for 20 h using an extractor of Soxhlet-type. After removal of the solvent, the residue was recrystallized from acetone to give pure III_A, yellow granulars, 17.4 g (87%), mp 103—103.5 °C. Found: C, 84.79; H, 6.41; N, 3.92%. Calcd for $C_{25}H_{23}NO$; C, 84.95; H, 6.56; N, 3.96%.

In the same manner III_P was prepared. III_P: yellow plates from acetone, mp 142—143 °C. Found: C, 86.09; H, 6.09;, N. 3.72%. Calcd for $C_{27}H_{23}NO$: C, 85.91; H, 6.14; N, 3.71%.

p-*(3-Arylpropyl)*-N,N-*dimethylaniline* (*A_3, P_3*). The dihydroketone III_A (2 g, 5.6 mmol) was added to a stirred suspension of lithium aluminium hydride (0.38 g, 9.8 mmol) and aluminium chloride (2.66 g, 19.6 mmol) in diethyl ether (50 ml). After stirring for 2 h under reflux, ethyl acetate, water, and 5% aq sodium hydroxide were successively added to the reaction mixture. It was extracted with diethyl ether, and the organic layer was worked up in the usual manner. The residual yellowish brown solid was chromatographed on silica gel to give A_3 (34 mg, 18%). A_3: colorless granulars from acetone, mp 105—106 °C. NMR ($CDCl_3$) δ 2.92 (s, CH_3), 1.9—3.8 (m, CH_2), 6.95 (m, ArH of phenyl), 7.3—8.3 ppm (m, ArH of anthryl). Found: C, 88.65; H, 7.29; N, 4.10% MS (*m/e*), 339 (M^+). Calcd for $C_{25}H_{25}N$: C, 88.45; H, 7.42; N, 4.13%; M, 339.46.

In the same manner P_3 was prepared. P_3: pale yellow powder, mp 97—97.5 °C. NMR ($CDCl_3$) δ 2.9 (s, CH_3), 2.0—3.5 (m, CH_2), 6.89 (m, ArH of phenyl), 7.1—8.2 ppm (m, ArH of pyrenyl). Found: C, 89.12; H, 6.95; N, 3.90%, MS (*m/e*), 363 (M^+). Calcd for $C_{27}H_{25}N$: C, 89.21; H, 6.93; N, 3.85%; M, 363.48.

Results

A_3 and P_3 in Hexane Solution. Fluorescence spectra of A_3 and P_3 in hexane are shown in Fig. 1. Decay times (τ_d) of LE fluorescence measured in the wavelength region of 390—420 nm and rise time (τ_r) of HE fluorescence observed through a filter transparent for the region longer than 550 nm are listed in Table 1. Both τ_d and τ_r values of each compound agree within experimental error.

It should be noted here that the rise curve of the HE fluorescence measured at 540 nm contains a considerable amount of the rapid component. However, the rapid component is negligible if the fluorescence is observed through a filter which is transparent above 550 nm (Fig. 2).

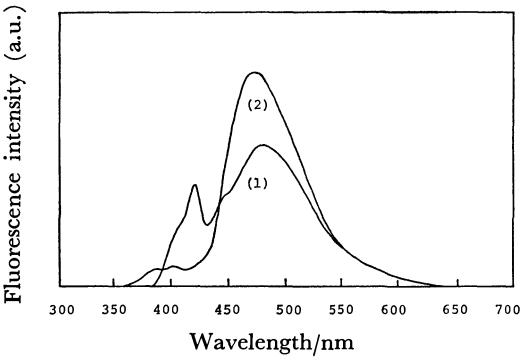

Fig. 1. Fluorescence spectra of A_3 and P_3 in hexane. (1): A_3, (2): P_3.

Table 1. Decay times of LE fluorescence and rise times of HE fluorescence of A_3 and P_3 in hexane

	τ_d/ns	τ_r/ns
A_3	2.3±0.1	2.6±0.4
P_3	4.6±1.0	3.9±0.6

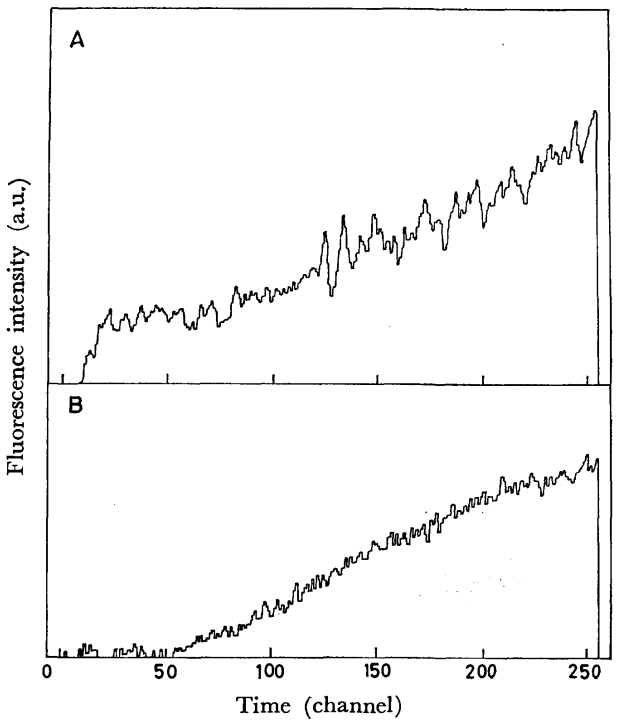

Fig. 2. Fluorescence rise curves of A_3 in hexane measured by means of ps streak camera.
A: Observed at 540 nm, B: observed through a filter which passes the wavelength region longer than 550 nm.

A_n and P_n in 2-Propanol Solution. Fluorescence spectra of A_n and P_n in 2-propanol solution are shown in Fig. 3. The HE band is shifted to considerably longer wavelength compared to that in hexane solution. Decay times of LE fluorescence observed in the region of 390—420 nm and rise times of HE fluorescence observed through a filter which is transparent above 520 nm are given in Table 2 for A_1, P_1, A_2, and P_2. The τ_d and τ_r values of each compound approximately agree, although there is a tendency that τ_r value is a little longer than that of τ_d for A_1 and P_1. As a typical example, the observed decay curve and also the rise curve of P_1 are shown in Fig. 4.

For A_3 and P_3, circumstances are somewhat complicated. By detailed observation of P_3 at 401 nm, we detected clearly a two-component decay of fluorescence as shown in Fig. 5A, from which decay times were estimated to be $\tau_d^1=340\pm20$ ps and $\tau_d^2=1.1\pm0.2$ ns.

We examined dynamic features of the HE fluorescence at several different wavelength regions. The measurement through a filter which is transparent above 680 nm indicated clearly rise and two-component decay curves (Fig. 5B). By analyzing this result, the

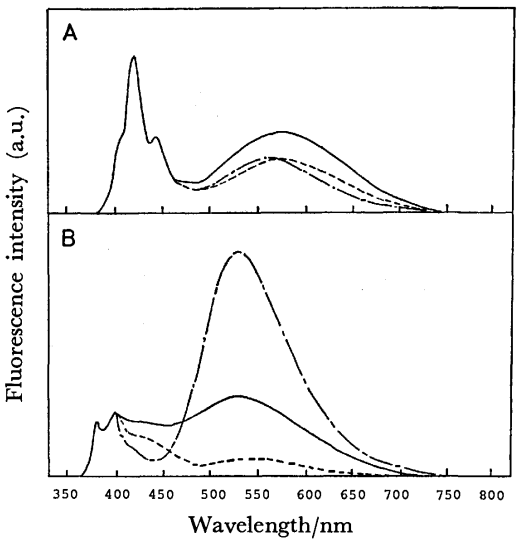

Fig. 3. Fluorescence spectra of A_n and P_n in 2-propanol.
A: A_n, B: P_n, (normalized at LE band maxima).
——: A_1, P_1, - - -: A_2, P_2, — - —: A_3, P_3.

Table 2. Decay times of LE fluorescence and rise times of HE fluorescence of A_1, P_1, A_2, and P_2 in 2-propanol solution

	τ_d/ps	τ_r/ps
A_1	40± 9	54± 9
A_2	98± 5	93±23
P_1	62± 6	93±20
P_2	170±39	192±39

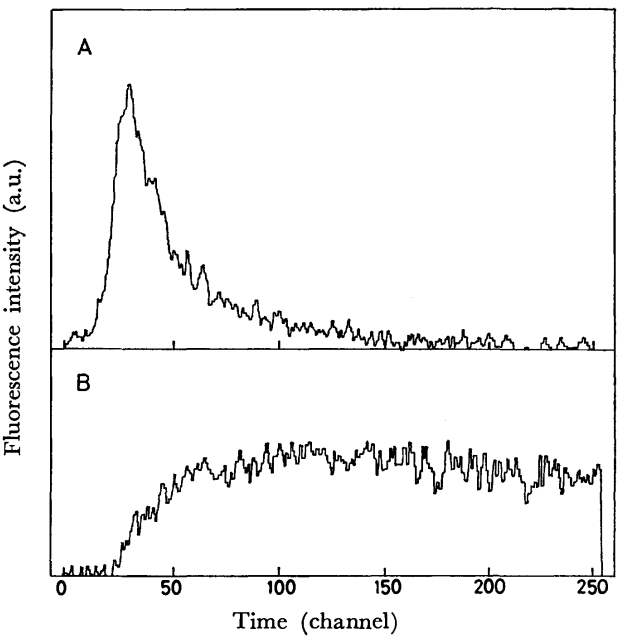

Fig. 4. Decay curve of LE fluorescence (A) and rise curve of HE fluorescence (B) of P_1 in 2-propanol.

fluorescence rise time and the decay time of the fast component of the two-component decay curve were estimated to be $\tau_r^{HE}=345\pm50$ ps and $\tau_d^{HE}=1.1\pm0.1$ ns, respectively. We can see a good agreement be-

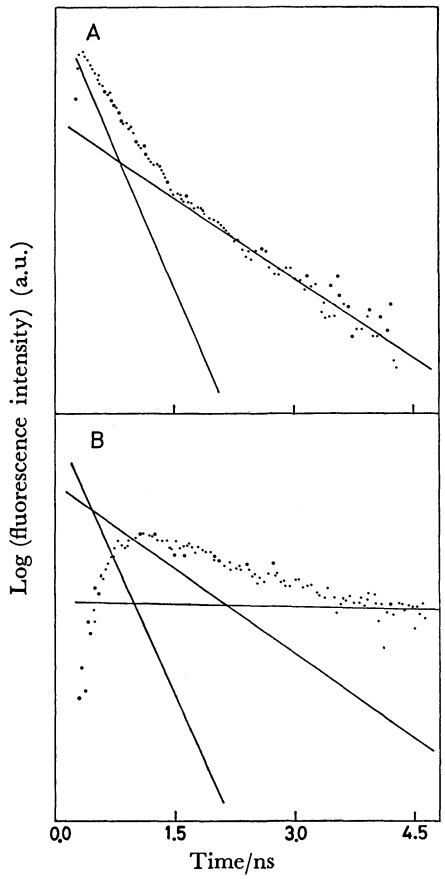

Fig. 5. Decay curve of LE fluorescence observed at 401 nm (A) and rise and decay curve of HE fluorescence observed through a filter which passes the wavelength region longer than 680 nm (B) in the case of 2-propanol solution of P_3. The observed results were calibrated for variations in the value of ps/channel in the following way. Conversion of n-th channel to the delay time $t(n)$ was made according to: $t(n)=\sum_{i=0}^{n}\Delta t(i)$, where $\Delta t(i)$ is the value of ps/channel of the i-th channel, and the observed intensity $I(i)$ at i-th channel was corrected according to: $I_{corr}(i)=I(i)/\Delta t(i)$.

tween τ_r^{HE} and τ_d^1 as well as between τ_d^{HE} and τ_d^2. Therefore, the results in Fig. 5 satisfy the ordinary kinetics of HE formation and decomposition. However, the measurement of HE fluorescence in the region including shorter wavelengths gave rather complicated results due to the contribution from the LE fluorescence.

Although we have not made such a detailed study for A_3 in 2-propanol, the circumstance seems to be analogous to P_3, since we have observed two component decay of the HE fluorescence by observing in the region longer than 650 nm and obtained the approximate τ_d^{HE} value of the fast component to be 1.5 ns.[16]

P_3 in an Acetone Solution. The results were similar to those in 2-propanol. However, the observed τ_d^1 value was much shorter (60 ps), while the τ_d^{HE} value was not so much different ($\approx$1 ns).

P_2 and P_3 in Acetonitrile Solutions. Both LE fluorescence decay and HE fluorescence rise times of P_2 in acetonitrile were shorter than 20 ps, the response time of the apparatus. The LE fluorescence decay time of P_3 was also shorter than 20 ps. Thus, the CT or HE formation becomes very fast in acetonitrile, a strongly polar and less viscous solvent. However, the ordinary kinetics for HE formation and decomposition as observed for P_3 in 2-propanol was not recognized clearly in this case.

A_0 and Bian in Polar Solvents. In the fluorescence spectra of these compounds in polar solvents, the LE and HE bands are not so distinct as those of A_n and P_n (n=1, 2, 3). One can recognize, however, that the vibrational structure of the LE band superposed upon the broad CT (HE) fluorescence band for Bian.[11,12] In accordance with this result, the decay curve of LE fluorescence in the region, 390—420 nm and the rise curve of CT fluorescence in the region above 520 nm for Bian were observed in 2-propanol (Fig. 6). In Fig. 6A, the fluorescence observed at longer delay times is due to the CT fluorescence band superposed upon the LE band. The decay time (τ_d) of the LE fluorescence and the rise time (τ_r) of the CT fluorescence of Bian in 2-propanol were estimated to be τ_d=80±17 ps and τ_r=80±20 ps. These values are in good agreement with each

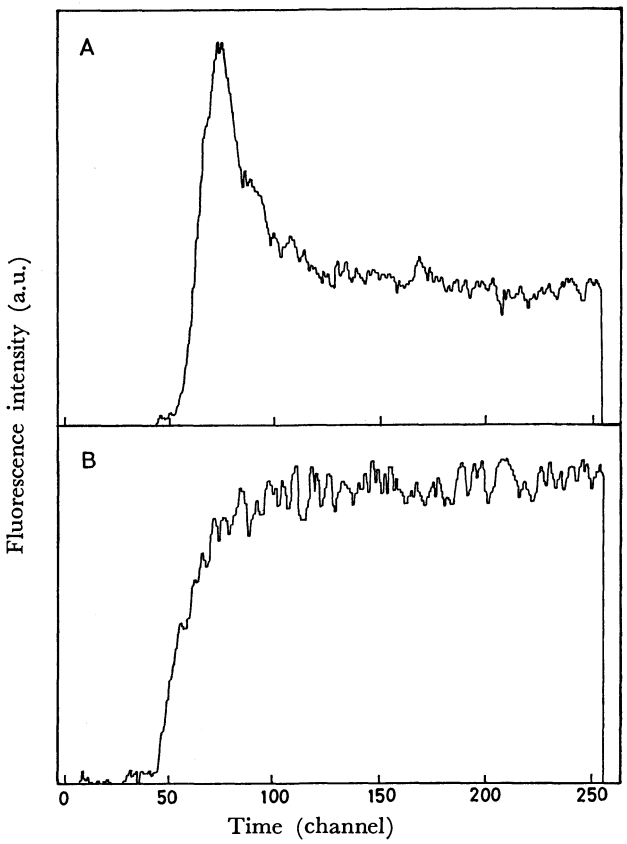

Fig. 6. Fluorescence decay and rise curves of Bian in 2-propanol.
A: Decay curve of LE fluorescence observed in the wavelength region of 320—420 nm. The long life tail is due to the CT fluorescence extending to this wavelength region, B: rise curve of CT fluorescence observed through a filter which passes the wavelength region above 520 nm.

other. Both the LE fluorescence decay and CT fluorescence rise times of Bian in acetone and acetonitrile were shorter than the response time of the apparatus (≈20 ps).

For A_0, the fluorescence spectra in polar solvents are more broad, and one cannot recognize clearly the LE fluorescence band.[2,6] In 2-propanol solution, we observed a decay curve in the region, 320—420 nm with the apparent decay time of approximately ≈70 ps, and a rise curve in the region longer than 520 nm with the apparent rise time of approximately ≈110 ps. Just as for Bian, both LE fluorescence decay and CT fluorescence rise times of A_0 in less viscous or more polar solvents like acetone, butyronitrile and acetonitrile were shorter than the response time of the apparatus (≈20 ps).

Discussion

HE Formation in Nonpolar Solvents. It is well established now that intramolecular HE formation is not possible for A_1, A_2, and P_1 in nonpolar solvents, while it is possible for A_3 and P_3 even in nonpolar solvents.[1-7] It has been confirmed already for P_3 in decalin solution that the rise time of the HE formation at room temperature is about 8 ns.[4,7] The fully slow formation process is ascribed to the internal rotations around CH_2–CH_2 bonds necessary for the conformation change and somewhat high viscosity of decalin. Both internal rotaions and solvent viscosity are affected by temperature, and the rise time becomes much longer by lowering temperature. For example, for P_3 in decalin, τ_r is 25 ns at −10 °C and 58 ns at −50 °C.[4,7]

Even if a less viscous solvent, hexane, is used, the rise of intramolecular HE fluorescence still takes a few ns for both A_3 and P_3, which indicates an important role of internal rotation for slowing down the HE formation process. Assuming the reaction mechanism of Eq. 1, where k_2 and k_3 are sum of radiative and non-radiative rate constants, the well-known Eq. 2 representing time dependence of each species is obtained.

$$\mathrm{S(A^*\ /\backslash/\backslash\ D)} \underset{k_{-1}}{\overset{k_1}{\rightleftharpoons}} \mathrm{HE_s}\left[\begin{array}{l}\text{sandwich}\\ \\ \text{heteroexcimer}\end{array}\right] \quad (1)$$

$$\downarrow k_2 \qquad\qquad \downarrow k_3$$

$$[\mathrm{S}] = C_1\exp(-\lambda_1 t) + (C_0 - C_1)\exp(-\lambda_2 t)$$
$$[\mathrm{HE_s}] = C_2[\exp(-\lambda_1 t) - \exp(-\lambda_2 t)]. \quad (2)$$

The values of λ_2^{-1} were determined as shown in Table 1, and these of λ_1^{-1} in hexane were given by the previous study as 130 ns and 87 ns for A_3 and P_3, respectively.[7]

The rapid component in the fluorescence rise curve observed at 540 nm (Fig. 2A) is indicative of the existence of ground state A_3 molecules in a sandwich configuration, which give HE fluorescence immediately after excitation as reported by Gnädig and Eisenthal.[13] However, this possibility is rejected, because no rapid component is found when the rise curve was observed only for the region longer than 550 nm (Fig. 2B).

Although the $S_n \leftarrow S_1$ spectrum of anthracene itself does not show any appreciable absorbance at 694 nm where Gnädig and Eisenthal monitored the transient absorbance of A_3 HE, we have confirmed by ps transient absorbance measurements on A_3 that the $S_n \leftarrow S_1$ spectra of anthracene are affected by alkyl substitution, and there arises some absorbance around 694 nm.[16] Thus, the rapid component observed in the ps transient absorption of A_3 can be ascribed to $S_n \leftarrow S_1$ spectra, and that shown in Fig. 2A must be ascribed to LE fluorescence.

Photo-induced CT and HE Formation of A_n and P_n (n=1, 2, 3) in Polar Solvents. In general, the wave equation and the Hamiltonian operator for the solute–solvent system may be given by

$$\mathscr{H}\Psi = E\Psi,\ \mathscr{H} = \mathscr{H}_0 + \mathscr{H}',\ \mathscr{H}' = -\vec{\mu}_{op}\cdot\vec{F}, \quad (3)$$
$$\vec{F} = \vec{\mu}\cdot f_\varepsilon/a^3,\ f_\varepsilon = 2(\varepsilon-1)/(2\varepsilon+1),\ \vec{\mu} = \langle\Psi|\vec{\mu}_{op}|\Psi\rangle,$$

where, $\mathscr{H}'$ represents the solute–solvent interaction, $\vec{\mu}_{op}$ is the dipole operator, $\vec{F}$ is the Onsager's reaction field and ε is the dielectric constant of solvent.

For an excited CT system, a simplified wavefunction may be given by

$$\Psi = C_1\Psi_{CT} + C_2\Psi_{LE}, \quad (4)$$

where Ψ_{CT} represents the CT structure A^-D^+, and Ψ_{LE} the LE structure A*D. By using Eqs. 3 and 4, the following matrix elements are defined:

$$\vec{\mu} = C_1^2\langle\Psi_{CT}|\vec{\mu}_{op}|\Psi_{CT}\rangle = C_1^2\cdot\vec{\mu}_0$$
$$\langle\Psi_{CT}|\mathscr{H}|\Psi_{CT}\rangle = \langle\Psi_{CT}|\mathscr{H}_0|\Psi_{CT}\rangle + \langle\Psi_{CT}|\mathscr{H}'|\Psi_{CT}\rangle$$
$$= E_c - \langle\Psi_{CT}|\vec{\mu}_{op}\cdot\vec{F}|\Psi_{CT}\rangle$$
$$= E_c - C_1^2(\mu_1^2/a^3)f_\varepsilon$$
$$\langle\Psi_{CT}|\mathscr{H}|\Psi_{LE}\rangle = \alpha,\ \langle\Psi_{LE}|\mathscr{H}|\Psi_{LE}\rangle = E_e. \quad (5)$$

With these matrix elements, the secular equations are written as

$$C_1(E_c - C_1^2(\mu_0^2/a^3)\cdot f_\varepsilon - E) + C_2\alpha = 0$$
$$C_1\alpha + C_2(E_e - E) = 0. \quad (6)$$

By solving these nonlinear equations and by adding the polarization energy of the solvent to the solution of Eq. 6, the energies of the states relevant to the fluorescence transition can be obtained.[1]

For A_1 and P_1, for example, α which is due to the electronic delocalization interaction between electron donor and acceptor groups may be negligibly small. Therefore, the energy of the CT state relaxed with respect to solvation may be given by,

$$E_{CT} = E_c - (1/2)(\mu_e^{eq2}/a^3)\cdot f_\varepsilon, \quad (7)$$

where $\vec{\mu}_e^{eq}$ is the dipole moment of the relaxed CT state. E_{CT} is higher than E_e in nonpolar solvents for A_1, P_1, and A_2. With increase of the solvent polarity, E_{CT} becomes lower than E_e. At the inversion point, there arises the orientational destabilization energy δE^{FC} in the Franck-Condon ground state of the fluorescence transition.

$$\delta E_g^{FC} = (1/2)\cdot(\mu_e^{eq2}/a^3)\cdot(f_\varepsilon - f_n)$$
$$f_n = 2(n^2-1)/(2n^2+1). \quad (8)$$

Therefore, in more polar solvents than that giving the inversion point, the frequency of the CT fluorescence is given by Eq. 9.

$$h\nu_e = \text{Const.} - (\mu_e^{eq2}/2a^3)(2f_\varepsilon - f_n). \quad (9)$$

We have actually observed, for A_1, P_1, and A_2, especially large red shifts of the HE fluorescence at the inversion point due to δE^{FC},[3-5] and have confirmed that Eq. 9 holds not only for the HE fluorescence of A_n and P_n (n=1, 2) but also for A_3 and P_3.[3-5]

In the present work, we are investigating the dynamic processes of appearance of the HE state. The simple picture described above seems to be especially suitable to the cases of A_1 and P_1. Thus, the time-resolved fluorescence measurements of these systems will reflect directly the solvation process in the CT state.

The results indicated in Table 2 and Fig. 4 for A_1 and P_1 in 2-propanol solution show that the relaxation processes of the decay of LE and appearance of the CT state take about 50—100 ps. These values, however, are considerably longer than the shorter reorientational relaxation time[15] (<30 ps) of 2-propanol liquid. This result seems to indicate two possibilities: (a) the relaxation process of the CT state formation involves not only the rapid reorientational relaxation of 2-propanol but also slower ones covering a wider region around the solute molecule and involving hydrogen bond breaking and formation; (b) the relaxation process involves not only the solvent reorientation and solvent-induced change in the electronic structure as outlined by Eqs. 3—7 but also the geometrical change *i.e.* internal rotations of the solute molecule around single bonds connecting the CH_2 group with two aromatic groups, and the relaxation time is inherent in this conformation change.

However, the fact the relaxation times for the CT state formation of Bian and A_0 in 2-propanol are likewise 50—100 ps indicates that this relaxation time is inherent in reorientation of 2-propanol molecules around the bichromophoric molecule in the excited CT state formation rather than its conformational change.

A little longer τ_r value than that of τ_d for A_1 and P_1 may be due to the time-dependent red shift of HE band during the rise of HE fluorescence.

The considerably longer relaxation times of A_2 and P_2 compared with those of A_1 and P_1 may be explained as due to more extensive conformational change necessary for the photo-induced CT and for taking the stable HE configuration.

The behavior of P_3 in 2-propanol is a good example of enhancement of photo-induced CT process in polar solvent, and also of the control or slowing down of the CT reaction by internal rotations which are necessary to bring A* and D to the mutual distance and orientation where the CT is possible. The latter effect of the internal rotations makes it possible to elucidate photo-induced CT processes in solution which are difficult to study in detail even by ps laser methods for free A* and D. This difficulty is caused by very rapid and mutually combined translational and rotational diffusions, and they make the result complicated.

The faster decay of LE fluorescence and the faster rise of HE fluorescence of P_3 in 2-propanol solution than in hexane solution despite the higher viscosity of 2-propanol suggest that the photo-induced CT in polar solvent is possible, even if A* and D are somewhat separated, because the energy of the CT state is lowered by the interaction with the polar solvent, and loose HE is formed. Moreover, our previous semi-quantitative studies of ps transient absorption spectra of P_3 in 2-propanol indicated a two step change of spectra which is probably due to loose HE formation followed by a conformational change into the one of sandwich-type.[8,10]

The double exponential decay of LE fluorescence observed at 401 nm and the rise as well as decay of HE fluorescence observed in the region longer than 680 nm can be well reproduced by assuming the reaction scheme of Eq. 10 and by Eq. 11 derived from it.

$$\begin{array}{ccccc} S(A^* \,/\backslash/\backslash\, D) & \underset{k_{-1}}{\overset{k_1}{\rightleftharpoons}} & HE_1 \left[\begin{array}{c}\text{loose}\\ \\ \text{heteroexcimer}\end{array}\right] & \xrightarrow{k_2} & HE_s \left[\begin{array}{c}\text{sandwich}\\ \\ \text{heteroexcimer}\end{array}\right], \\ \downarrow k_3 & & \downarrow k_4 & & \downarrow k_5 \end{array} \quad (10)$$

where k_3, k_4, and k_5 are sums of rate constants of radiative as well as radiationless deactivations, respectively.

$$\begin{aligned}[S] &= C_1' \exp(-\lambda_1' \cdot t) + (C_0' - C_1') \exp(-\lambda_2' \cdot t)\\ [HE_1] &= C_2'[\exp(-\lambda_1' \cdot t) - \exp(-\lambda_2' \cdot t)]\\ [HE_s] &= C_3[(\lambda_1' - k_5)\exp(-\lambda_2' \cdot t) - (\lambda_2' - k_5)\exp(-\lambda_1' \cdot t)\\ &\quad - (\lambda_2' - \lambda_1')\exp(-k_5 \cdot t)]. \end{aligned} \quad (11)$$

In view of the good correspondence between the τ values, the time-dependences of fluorescence observed at 401 nm and those observed in the region longer than 680 nm are assigned to S and HE_1, respectively, from which $\tau_d = \tau_r^{HE} = \tau'^{-1}_2 \approx 350$ ps and $\tau_d = \tau_d^{HE} = \tau'^{-1}_1 \approx 1.1$ ns were obtained. The assignment of the long wavelength band to the loose HE may be supported also by the fact that the ordinary (time-integrated) fluorescence spectra of P_1 and P_2 in 2-propanol are somewhat red-shifted compared to those of P_3 in the same solvent. The latter spectra can be attributed almost completely to HE_s because of its much longer lifetime ($\approx$100 ns) compared with HE_1. Moreover, our recent results of accurate ps time-resolved absorption measurements on the same system can be explained quantitatively assuming the same scheme (10), and they give the same λ' values.[16]

The results of similar measurements in acetone solution can be interpreted by the same scheme as Eq. 10, with $\lambda'^{-1}_2 \approx 60$ ps and $\lambda'^{-1}_1 \approx 1$ ns. Since the polarity of acetone is close to that of 2-propanol, it is necessary to have a similar conformation (HE_1) for

the photo-induced CT to occur. Therefore, the much shorter value of $\lambda'_2{}^{-1}$ might be due to the considerably lower viscosity of acetone compared to 2-propanol, resulting in faster conformation change. However, the reason why the value of $\lambda'_1{}^{-1}$ is not so much different from that in 2-propanol solution is not so clear at the present stage of investigation. Presumably, the HE_1 formation may occur by solvent reorientation and a small rotation of two chromophore groups with only a slight internal rotation around CH_2–CH_2 bonds, while the HE_s formation involves extensive internal rotations which seem to determine the velocity of the process irrespective of the solvent viscosity.

The photo-induced intramolecular CT process becomes much faster in acetonitrile, a strongly polar and less viscous solvent, since CT may be possible at longer mutual distance between A* and D due to the rapid and stronger solvation. In other words, the extent of the conformation change necessary for the photo-induced CT may be much smaller in acetonitrile than in 2-propanol.

Thus, both the LE fluorescence decay time and HE fluorescence rise time of P_2 are shorter than 20 ps, the response time of the apparatus. The LE fluorescence decay time of P_3 is also shorter than 20 ps, but the corresponding rise of the HE fluorescence was not observed. The fluorescence from the loose HE formed immediately after the rapid photo-induced CT may not be detectable in the case of P_3 because of the very small fluorescence yield due to strong solvation of the ion-pair state.

Behaviors of Bian and A_0 in Polar Solvents. Interestingly Bian shows in the excited state intramolecular CT from one anthracene nucleus to another, which is caused by the interaction with polar solvent molecules.[11] This is a solvent-induced "broken symmetry" phenomenon, *i.e.* the lowering of the symmetry of the solute molecule due to the interaction with polar solvent molecules, resulting in the CT state even if the molecule is composed of two identical chromophores.[12] Direct confirmation of the intramolecular CT was made by transient absorption spectral measurements in polar solvent.[12]

In the present work, we have directly demonstrated the CT state formation process and decay of the corresponding LE state in 2-propanol. Both the CT state rise and the LE state decay times are *ca.* 80 ps, which are considerably longer than the shorter reorientational relaxation time of 2-propanol liquid at room temperature. Just as in the cases of A_1 and P_1 in 2-propanol, two interpretations might be possible. One is the relaxation process which includes some contribution from slower processes involving solvent hydrogen bond breaking and formation. The other involves not only the solvent reorientation but also the geometrical structural change of Bian, *i.e.* the rotation around the 9–9′ bond which determines the observed relaxation time.

The two π-electronic systems of Bian are oriented perpendicular to each other because of a strong steric hindrance in the relaxed ground state as well as the Franck-Condon excited state. It was suggested that the stable conformation in the excited state may not be the perpendicular one but the oblique one.[11] Since the CT fluorescent state of excited Bian may be considered as a resonance hybrid of the CT configuration mixed with the LE configuration, its solvation by polar solvents will oppose the electronic delocalization between two chromophores, because the solvation energy increases with increasing charge separation in the CT system. When the conformation is the perpendicular one, the electronic delocalization will become very small. Therefore, the excited equilibrium conformation in polar solvents will be very close to that of the excited Franck-Condon state.

The above considerations lead to the conclusion that the rate of the photo-induced CT state formation of Bian will be determined by the solvent reorientation relaxation time and will become faster in a less viscous polar solvent. Actually, we have found that the LE fluorescence decay and the CT fluorescence rise times of Bian in acetone as well as in acetonitrile are much shorter (<20 ps) than those in 2-propanol.

Although the fluorescence spectra of A_0 are quite broad, we were able to observe the LE fluorescence decay in 2-propanol solution at the shorter wavelength edge of the fluorescence band, and the CT fluorescence rise process in the longer wavelength region. This result is somewhat analogous to those of A_1, P_1, and Bian. Although the CT character of S_1 state seems to be evident from the very large red shift of fluorescence with increase of solvent polarity, another evidence comes from the measurement of the effect of solvent polarity upon the $S_n \leftarrow S_1$ spectra.[6] It has been confirmed that the $S_n \leftarrow S_1$ spectra in moderately or strongly polar solvents are comparable to the superposition of those of anthracence anion and DMA cation.[6,17]

In this case too, the LE fluorescence decay time (≈ 70 ps) as well as the CT fluorescence rise time (≈ 110 ps) in 2-propanol are considerably longer than the shorter reorientation relaxation time of 2-propanol liquid at room temperature. A little larger value of the latter compared with the former can be explained as due to the time-dependent red shift of the CT fluorescence band occuring during the CT state rise process just as for A_1 and P_1. The fact that the CT fluorescence rise time agrees approximately with the LE fluorescence decay time for Bian in 2-propanol may be explained as due to the much smaller solvent-induced red shift of the CT fluorescence band of Bian compared with A_0. Namely, the wavenumber difference between the fluorescence band maxima of Bian in hexane and 2-propanol is *ca.* 1.4×10^3 cm^{-1}, smaller compared with the corresponding value of A_0, 5.3×10^3 cm^{-1}.

Thus, there arises a similar problem with A_1, P_1, and Bian concerning the mechanism of CT state formation in 2-propanol, *i.e.* the relaxation process includes some contribution from the slower process of solvent rearrangements involving hydrogen bond breaking and formation, or it involves structural changes of A_0. The possibility of an excited equilibrium structure of A_0 in polar solvents where molecular planes of two moieties are perpendicular to each other has been discussed already.[6,18] Moreover, we have also

confirmed that the LE fluorescence decay time as well as the CT fluorescence rise time of A_0 in less viscous and polar solvents, like acetone, butyronitrile and acetonitrile are much shorter than the response time (20 ps) of the apparatus. Analogously to the cases of A_1, P_1, and Bian, the rate of the CT state formation in polar solvents for A_0 seems to be determined by the solvent reorientations.

Summary

We have observed directly by means of ps time-resolved fluorescence measurements the intramolecular HE formation process and its solvent dependence for typical hydrocarbon–amine systems and have confirmed our prediction of the enhancement of intramolecular CT process with increase of solvent polarity. Existence of loose HE's as an intermediate during sandwich type HE formation in polar solvents has been demonstrated for three methylene-chain compounds and we have found that the loose HE emits at longer wavelength than sandwich type one. Moreover, it has been found that the loose HE in strongly polar solvents is non-fluorescent. These results demonstrate clearly the effect of solvent polarity upon the photo-induced CT and HE formation processes as well as upon the electronic and geometrical structures of the formed HE's.

The cost of the present investigation was partly defrayed by the grants given by Toray Science Foundation and Mitsubishi Foundation, and also by Grant-in-Aid for Special Project Research on Photobiology from the Japanese Ministry of Education, Science and Culture.

References

1) See for example: N. Mataga and M. Ottolenghi, "Molecular Association," ed by R. Foster, Academic Press, London (1979), Vol. 2.

2) T. Okada, T. Fujita, M. Kubota, S. Masaki, N. Mataga, R. Ide, Y. Sakata, and S. Misumi, *Chem. Phys. Lett.*, **14**, 563 (1972).

3) N. Mataga, "The Exciplex," ed by M. Gordon and W. R. Ware, Academic Press, New York (1975).

4) N. Mataga, T. Okada, H. Masuhara, N. Nakashima, Y. Sakata, and S. Misumi, *J. Luminescence*, **12/13**, 159 (1976).

5) S. Masaki, T. Okada, N. Mataga, Y. Sakata, and S. Misumi, *Bull. Chem. Soc. Jpn.*, **49**, 1277 (1976).

6) T. Okada, T. Fujita, and N. Mataga, *Z. Phys. Chem. N. F.*, **101**, 57 (1976).

7) T. Okada, T. Saito, N. Mataga, Y. Sakata, and S. Misumi, *Bull. Chem. Soc. Jpn.*, **50**, 331 (1977).

8) M. Migita, M. Kawai, N. Mataga, Y. Sakata, and S. Misumi, *Chem. Phys. Lett.*, **53**, 67 (1978).

9) J. Hinatu, H. Masuhara, N. Mataga, Y. Sakata, and S. Misumi, *Bull. Chem. Soc. Jpn.*, **51**, 1032 (1978).

10) N. Mataga, M. Migita, and T. Nishimura, *J. Mol. Struct.*, **47**, 199 (1978).

11) F. Schneider and E. Lippert, *Ber. Bunsenges. Phys. Chem.*, **72**, 1155 (1968).

12) N. Nakashima, M. Murakawa, and N. Mataga, *Bull. Chem. Soc. Jpn.*, **49**, 854 (1976).

13) K. Gnädig and K. B. Eisenthal, *Chem. Phys. Lett.*, **46**, 339 (1977).

14) M. Migita, T. Okada, N. Mataga, N. Nakashima, K. Yoshihara, Y. Sakata, and S. Misumi, *Chem. Phys. Lett.*, **72**, 229 (1980).

15) L. A. Hallidy and M. R. Topp, *Chem. Phys. Lett.*, **48**, 40 (1977).

16) T. Okada, M. Migita, N. Mataga, Y. Sakata, and S. Misumi, *J. Am. Chem. Soc.*, **103**, 4715 (1981).

17) T. Okada, M. Kawai, N. Mataga, Y. Sakata, S. Misumi, and S. Shionoya, unpublished.

18) A. Siemiarczuk, Z. R. Grabowski, A. Krowczynski, M. Asher, and M. Ottolenghi, *Chem. Phys. Lett.*, **51**, 315 (1977).

19) J. S. Meek, W. B. Evans, V. Godefroi, W. R. Benson, M. F. Wilcox, W. G. Clarks, and T. Tiedeman, *J. Org. Chem.*, **26**, 4281 (1961).

The Hartree-Fock and Electron-Hole Potential Methods from a Hypervirial Theorem Standpoint

Makoto Isihara

Department of General Education, Shotoku-Gakuen Women's Junior College, Gifu 500

(Received April 25, 1981)

The hypervirial theorem is introduced in the second quantized expanded form, and utilized for reviewing the Hartree-Fock and electron-hole potential methods. A possibility of going beyond the latter is suggested within the scope of handy methods. Brillouin's and the extended Brillouin's theorems are shown to be contained in the hypervirial theorem.

The hypervirial theorem (HVT)[1] is nothing other than the statement that the expectation value of any physically nonpathological operator does not depend on time in stationary states, and has vast range of application because of its great fundamentality. Essential explorations of the theorem in molecular quantum mechanics have been made already in 1960's from both variation-[2] and perturbation-theoretical[3] points of view, where the form of operators is either nonspecified or given as a function of coordinates and momenta. In this paper the HVT is introduced in the second quantized form, expanded under the exponential prescription,[4] and utilized for reviewing the Hartree-Fock (HF)[5] and electron-hole potential (EHP)[6,7] methods. We can immediately arrive at the HF method in the first order one-particle HVT for the ground state; that for the excited state leads us to the EHP method and further gives a possibility of a handy modification beyond the method. Brillouin's[8] and the extended Brillouin's[6] theorems are shown to be contained in the HVT. Supplementary remarks are added on what is implied in the first order two-particle HVT for the ground state and in connection with the perturbation-theoretical approach.

The Hypervirial Theorem

Let $|\psi\rangle$ be an eigenstate of a Hamiltonian H and W be an arbitrary operator, the restriction on W being only that $W|\psi\rangle$ should not jump outside the space considered. The HVT is simply written as

$$\langle\psi|[H, W]|\psi\rangle = 0. \tag{1}$$

Take a system of identical particles and denote the creation and annihilation operators for the one-particle quantum state j by $a_j^\dagger$ and a_j respectively. Then, any one-particle operator of the system is of the following form.

$$W = \sum_{jk} w_{jk} a_j^\dagger a_k.$$

The strong requirement that Eq. 1 must hold for any W leads to the one-particle HVT:

$$\langle\psi|[H, a_p^\dagger a_q]|\psi\rangle = 0 \quad \text{(any } p, q\text{)}. \tag{2}$$

Likewise we have the two-particle HVT,

$$\langle\psi|[H, a_p^\dagger a_r^\dagger a_s a_q]|\psi\rangle = 0 \quad \text{(any } p, q, r, s\text{)}, \tag{3}$$

and so on. For arbitrary products of the creation and/or annihilation operators we have

$$\langle\psi|[H, \prod_p a_p^\dagger \prod_q a_q]|\psi\rangle = 0. \tag{4}$$

However, unless the numbers of creation and annihilation operators are equal, the relation is trivial for the particle-conservative system.

Separating a Hamiltonian into the unperturbed Hamiltonian K and the perturbation λV with a real parameter λ,

$$H = K + \lambda V, \tag{5}$$

we can obtain a perturbation expansion of Eq. 1 on the assumption that an eigenstate $|\psi\rangle$ of H is attainable from the corresponding eigenstate $|\phi\rangle$ of K through a unitary transformation:

$$|\psi\rangle = \exp(S)|\phi\rangle, \tag{6}$$

where S is an antihermitian operator independent of the energy level index.[3,4] Noting that S has no zeroth order term, we put it in the power series of λ as

$$S = \lambda S_1 + \lambda^2 S_2 + \cdots \tag{7}$$

with antihermitian operators $\{S_i\}$. Substitution of Eq. 6 into Eq. 1 rewrites the HVT as a form of the unperturbed state expectation value:

$$\langle\phi|\exp(-S)[H, W]\exp(S)|\phi\rangle = 0,$$

which is expanded by means of Eqs. 5 and 7;

$$\lambda\langle\phi|([V, W] + [[K, W], S_1])|\phi\rangle + \lambda^2\langle\phi|([[V, W], S_1] + \frac{1}{2}[[[K, W], S_1], S_1] + [[K, W], S_2])|\phi\rangle + \cdots = 0. \tag{8}$$

Thus we have the first order HVT,

$$\langle\phi|([V, W] + [[K, W], S_1])|\phi\rangle = 0, \tag{9}$$

or, using the Jacobi-Lie identity,

$$\langle\phi|[V + [K, S_1], W]|\phi\rangle = 0. \tag{10}$$

To decompose S_i into the one-particle part $S_i^{(1)}$, the two-particle one $S_i^{(2)}$, and so on,

$$S_i = S_i^{(1)} + S_i^{(2)} + \cdots, \tag{11}$$

enables us to proceed a little further. Assuming that K is one-particle and that V consists of the one- and two-particle parts,

$$V = V^{(1)} + V^{(2)}, \tag{12}$$

we can write the first order HVT as

$$\sum_{n=1,2} \langle\phi|[Y^{(n)}, W]|\phi\rangle = 0 \tag{13}$$

with

$$Y^{(n)} = V^{(n)} + [K, S_i^{(n)}]. \tag{14}$$

The terms of $n=1$ and 2 in the left-hand side of Eq. 13 concern the one- and two-particle operators for

$W=a_p^\dagger a_q$ and two- and three-particle ones for $W=a_p^\dagger a_r^\dagger a_s a_q$ respectively. We can make all $S_1^{(n)}$'s vanish for n larger than 2.

The Hartree-Fock Method

The Hamiltonian of electrons in the fixed nuclear framework is given by

$$H=\sum_{\xi\eta\mu} h_{\xi\eta} a_{\xi\mu}^\dagger a_{\eta\mu} + \frac{1}{2}\sum_{\xi\eta\theta\tau\mu\nu} v_{\eta\tau}^{\xi\theta} a_{\xi\mu}^\dagger a_{\theta\nu}^\dagger a_{\tau\nu} a_{\eta\mu}, \tag{15}$$

where the second suffices, μ and ν, refer to the electron spin. It is assumed hereafter that the matrix elements, $\{h_{\xi\eta}\}$, $\{v_{\eta\tau}^{\xi\theta}\}$, and so on, are all spin-independent. Taking a relevant hermitian one-particle operator

$$X=\sum_{\xi\eta\mu} x_{\xi\eta} a_{\xi\mu}^\dagger a_{\eta\mu},$$

which is to be determined later, we rewrite the Hamiltonian in the molecular orbital representation as

$$H=\sum_{j\mu}\varepsilon_j a_{j\mu}^\dagger a_{j\mu} + \frac{1}{2}\sum_{jklm\mu\nu} v_{km}^{jl} a_{j\mu}^\dagger a_{l\nu}^\dagger a_{m\nu} a_{k\mu} - \sum_{jk\mu} x_{jk} a_{j\mu}^\dagger a_{k\mu}. \tag{16}$$

The molecular orbital coefficients $\{u_{\xi j}\}$ and their energies $\{\varepsilon_j\}$ are determined by the eigenvalue problem diagonalizing $\{h_{\xi\eta}+x_{\xi\eta}\}$:

$$\sum_\eta (h_{\xi\eta}+x_{\xi\eta})u_{\eta j} = u_{\xi j}\varepsilon_j. \tag{17}$$

Now let us take the unperturbed Hamiltonian in Eq. 16 as

$$K=\sum_{j\mu}\varepsilon_j a_{j\mu}^\dagger a_{j\mu} \tag{18}$$

and assume that its ground state $|F\rangle$ have a closed-shell form:

$$|F\rangle = a_{f\uparrow}^\dagger a_{f\downarrow}^\dagger \cdots a_{2\uparrow}^\dagger a_{2\downarrow}^\dagger a_{1\uparrow}^\dagger a_{1\downarrow}^\dagger |0\rangle,$$

where $\uparrow$ and $\downarrow$ stand for the up- and down-spin states, respectively, and $|0\rangle$ means the vacuum state. Denoting a set of the occupied orbitals $\{1,2,\cdots,f\}$ by F and that of the unoccupied by $\overline{F}$, we define the occupation indicator as

$$\mathrm{f}(j)=\begin{cases}1 & (j\in F)\\ 0 & (j\in\overline{F}).\end{cases} \tag{19}$$

Substituting

$$V^{(1)} = -\sum_{jk\mu} x_{jk} a_{j\mu}^\dagger a_{k\mu}, \tag{20}$$

$$V^{(2)} = \frac{1}{2}\sum_{jklm\mu\nu} v_{km}^{jl} a_{j\mu}^\dagger a_{l\nu}^\dagger a_{m\nu} a_{k\mu}, \tag{21}$$

$$S_1^{(1)} = \sum_{jk\mu} s_{jk} a_{j\mu}^\dagger a_{k\mu}, \tag{22}$$

$$S_1^{(2)} = \frac{1}{2}\sum_{jklm\mu\nu} s_{km}^{jl} a_{j\mu}^\dagger a_{l\nu}^\dagger a_{m\nu} a_{k\mu}, \tag{23}$$

and Eq. 18 into Eq. 13 through Eq. 14, we obtain the first order one-particle HVT putting $W=a_{p\sigma}^\dagger a_{q\sigma}$, since the present Hamiltonian includes no spin-changing term. For the ground state, putting $|\phi\rangle=|F\rangle$, we see the following condition result from the theorem.

$$(-x_{qp}+\tilde{v}_{qp}+(\varepsilon_q-\varepsilon_p)(s_{qp}+\tilde{s}_{qp}))(\mathrm{f}(q)-\mathrm{f}(p))=0, \tag{24}$$

the quantity with a tilde being defined as

$$\tilde{t}_{jk}=\sum_m (2t_{km}^{jm}-t_{mk}^{jm})\mathrm{f}(m).$$

Although for any $p\in F$ and $q\in\overline{F}$ the same equation is obtained as for any $p\in\overline{F}$ and $q\in F$, they are not independent of each other as far as X and V are kept hermitian and S antihermitian. If we use no S, that is, take an approximation that $|\phi\rangle=|\phi\rangle$, then Eq. 24 gives

$$x_{jk}=\tilde{v}_{jk} \quad (\text{any } j\in F, k\in\overline{F} \text{ and } \textit{vice versa}), \tag{25}$$

which is just the HF condition. Note that x_{jk}'s for $j,k\in F$ and $j,k\in\overline{F}$ are, as easily seen in Eq. 24, not conditioned here, the HF ambiguity being implied. Setting $x_{jk}=\tilde{v}_{jk}$ for all j and k, we have

$$x_{\xi\eta}=\sum_m (2v_{\eta m}^{\xi m}-v_{m\eta}^{\xi m})\mathrm{f}(m), \tag{26}$$

which gives the standard HF equation, substituted into Eq. 17. For general choices of X and S Eq. 24 should be read as a mutual restriction on them. Especially, under the HF choice of X, Eq. 25, the restriction is reduced to

$$s_{jk}+\tilde{s}_{jk}=0 \quad (\text{any } j\in F, k\in\overline{F} \text{ and } \textit{vice versa}). \tag{27}$$

Denoting the singlet and triplet excited states of K by

$$|vw\pm\rangle=\sum_\mu \mathrm{L}_\mu(\pm)a_{v\mu}^\dagger a_{w\mu}|F\rangle \quad (v\in\overline{F}, w\in F) \tag{28}$$

with

$$\mathrm{L}_\mu(\pm)=(\delta_{\mu\uparrow}\pm\delta_{\mu\downarrow})/\sqrt{2}, \tag{29}$$

where $+$ and $-$ stand for the singlet and triplet states respectively, we have

$$\langle F|H|vw\pm\rangle=\sum_\mu \mathrm{L}_\mu(\pm)\langle F|[H,a_{v\mu}^\dagger a_{w\mu}]|F\rangle, \tag{30}$$

since $\langle F|a_{v\mu}^\dagger$ vanishes. Thus Brillouin's theorem is contained in the HVT

$$\langle F|[H,a_{p\sigma}^\dagger a_{q\sigma}]|F\rangle=0 \quad (p\in\overline{F}, q\in F \text{ and } \textit{vice versa}) \tag{31}$$

or equivalently

$$\langle F|[H,a_{p\sigma}^\dagger a_{q\sigma}]|F\rangle=0 \quad (\text{any } p,q), \tag{32}$$

which characterizes the HF method.

The Electron-Hole Potential Method

The evaluation of excitation energies by the closed-shell HF method[9] is to be improved in the EHP method, as far as only one specific excitation is concerned.[6] A persuasive derivation of the EHP method consists of constructing the new occupied and unoccupied orbitals, respectively, from the occupied and unoccupied HF orbitals through the variational procedure for the excited state in question. Here, confining ourselves to the single configuration excitation case, we view the method from a HVT standpoint, which seems helpful in understanding a nature of the method.

The first order one-particle HVT for the singlet and triplet excited states are obtained by putting $|\phi\rangle=|vw\pm\rangle$ after substitution of Eqs. 18, 20, 21, 22, and 23 into Eq. 13 through Eq. 14:

$$(y_{qp}+\tilde{y}_{qp}+\dot{y}(v)_{qp}-\dot{y}(w)_{qp})(\mathrm{f}(q)-\mathrm{f}(p))$$
$$+\frac{1}{2}((y_{qp}+\tilde{y}_{qp})(\delta_{qv}-\delta_{qw}-\delta_{pv}+\delta_{pw})$$
$$-(y^{qv}_{pv}-y^{qv}_{vp})(\delta_{qw}-\delta_{pw})-(y^{qw}_{pw}-y^{qw}_{wp})(\delta_{qv}-\delta_{pv}))$$
$$\pm\frac{1}{2}(y^{qv}_{vp}(\delta_{qw}-\delta_{pw})+y^{qw}_{wp}(\delta_{qv}-\delta_{pv}))=0 \qquad (33)$$

with

$$y_{jk}=-x_{jk}+(\varepsilon_j-\varepsilon_k)s_{jk}$$

and

$$y^{jl}_{km}=v^{jl}_{km}+(\varepsilon_j+\varepsilon_l-\varepsilon_m-\varepsilon_k)s^{jl}_{km},$$

the quantity with a single dot being defined as

$$\dot{t}(m)_{jk}=t^{jm}_{km}-t^{jm}_{mk}/2.$$

Consider the single-determinant approximation, the case without S. Then, Eq. 33 is reduced to the condition that

$$-x_{vj}+\tilde{v}_{vj}-v^{vw}_{jw}+v^{vw}_{wj}\pm v^{vw}_{wj}=0 \qquad (j\epsilon\bar{F}'), \quad (34a)$$
$$-x_{jw}+\tilde{v}_{jw}+v^{jv}_{wv}-v^{jv}_{vw}\pm(-v^{jv}_{vw})=0 \qquad (j\epsilon F'), \quad (34b)$$
$$-x_{wj}+\tilde{v}_{wj}+v^{wv}_{jv}-v^{ww}_{jw}\pm v^{wv}_{vj}=0 \qquad (j\epsilon\bar{F}'), \quad (34c)$$
$$-x_{jv}+\tilde{v}_{jv}+v^{jv}_{vv}-v^{jw}_{vw}\pm(-v^{jw}_{wv})=0 \qquad (j\epsilon F'), \quad (34d)$$
$$-x_{jk}+\tilde{v}_{jk}+\dot{v}(v)_{jk}-\dot{v}(w)_{jk}=0 \qquad (j\epsilon F', k\epsilon\bar{F}'), \quad (34e)$$

and

$$v^{wv}_{vv}-v^{ww}_{vw}\pm(v^{wv}_{vv}-v^{ww}_{vw})=0, \qquad (34f)$$

where the primes on F and $\bar{F}$ mean the exclusion of w and v respectively. The complex conjugate equations are omitted for brevity. If we take the canonical and virtual HF orbitals, the first and second terms in each left-hand side of Eqs. 34a, b, c, d, and e cancel out. But the rest does not vanish in general, and we see the violation of the HVT by the standard HF method. Here it is worth while to note that the orbital symmetry tends to lessen the violation.

It enables us to make Eqs. 34a and b hold that the first order one-particle HVT for the ground state imposes no condition upon x_{jk}'s for $j,k\epsilon\bar{F}$ and $j,k\epsilon F$, Eq. 25 remaining satisfied. Determine the orbitals so as to satisfy

$$x_{jk}=\tilde{v}_{jk}-v^{jw}_{kw}+v^{jw}_{wk}\pm v^{jw}_{wk} \qquad (j,k\epsilon\bar{F}) \quad (35a)$$

and

$$x_{jk}=\tilde{v}_{jk}+v^{jv}_{kv}-v^{jv}_{vk}\pm(-v^{jv}_{vk}) \qquad (j,k\epsilon F). \quad (35b)$$

Then Eqs. 34a and b clearly hold and the violation occurs in the same form in Eqs. 34c, d, e, and f as the HF case. There the orbital symmetry still inclines to diminish the violation. If the HF orbitals $\{\underline{u}_{\underline{\xi}\underline{j}}\}$ and their energies $\{\underline{\varepsilon}_{\underline{j}}\}$ are already known, we have only to work out a set of eigenvalue problems that

$$\sum_{\underline{k}\epsilon\bar{F}}(\delta_{\underline{j}\underline{k}}\underline{\varepsilon}_{\underline{j}}+z(w\pm)_{\underline{j}\underline{k}})c_{\underline{k}m}=c_{\underline{j}m}\alpha_m \qquad (\underline{j}\epsilon\bar{F}) \quad (36a)$$

and

$$\sum_{\underline{k}\epsilon F}(\delta_{\underline{j}\underline{k}}\underline{\varepsilon}_{\underline{j}}-z(v\pm)_{\underline{j}\underline{k}})d_{\underline{k}m}=d_{\underline{j}m}\beta_m \qquad (\underline{j}\epsilon F) \quad (36b)$$

with

$$z(l\pm)_{\underline{j}\underline{k}}=-v^{\underline{j}l}_{\underline{k}i}+v^{\underline{j}l}_{i\underline{k}}\pm v^{\underline{j}l}_{i\underline{k}},$$

which is equivalent to the original form of the basic equations of the EHP method.

Noting that under Eqs. 35's the one-particle HVT for the excited states without S holds for a restricted region as

$$\langle vw\pm|[H,a^\dagger_{p\sigma}a_{q\sigma}]|vw\pm\rangle=0 \quad (p,q\epsilon F \text{ and } p,q\epsilon\bar{F}), \quad (37)$$

we can prove that the extended Brillouin's theorem in the EHP method,

$$\langle vw\pm|H|v'w\pm\rangle=0 \qquad (v\neq v') \quad (38a)$$

and

$$\langle vw\pm|H|vw'\pm\rangle=0 \qquad (w\neq w'), \quad (38b)$$

is contained in the HVT as follows. Arrange the left-hand side of Eq. 38a as

$$\langle vw\pm|H|v'w\pm\rangle$$
$$=\sum_{\mu\nu}\mathrm{L}_\mu(\pm)\langle vw\pm|Ha^\dagger_{v'\mu}\delta_{\mu\nu}a_{w\nu}|F\rangle$$
$$=\sum_{\mu\nu}\mathrm{L}_\mu(\pm)\langle vw\pm|Ha^\dagger_{v'\mu}(a_{v\mu}a^\dagger_{v\nu}+a^\dagger_{v\nu}a_{v\mu})a_{w\nu}|F\rangle$$
$$=\sum_\mu\langle vw\pm|Ha^\dagger_{v'\mu}a_{v\mu}|vw\pm\rangle$$
$$=\sum_\mu\langle vw\pm|[H,a^\dagger_{v'\mu}a_{v\mu}]|vw\pm\rangle, \quad (39)$$

where the terms under the summation of the last line are independent of μ. Hence the condition

$$\langle vw\pm|[H,a^\dagger_{v'\mu}a_{v\mu}]|vw\pm\rangle=0, \quad (40)$$

which is assured by Eq. 37, is equivalent to Eq. 38a. We have similar argument for Eq. 38b.

The EHP method is characterized by the HVT Eq. 37 besides Eq. 32, so it can be said that the EHP method satisfies the HVT better than the standard HF method. The hole potential method[10] may look characterized by the HVT defined in a smaller region of p and q than Eq. 37,

$$\langle vw\pm|[H,a^\dagger_{p\sigma}a_{q\sigma}]|vw\pm\rangle=0 \quad (p,q\epsilon\bar{F}), \quad (41)$$

besides Eq. 32. However, Eq. 41 is actually independent of v, and we have Eq. 41 for all of $v\epsilon\bar{F}$. Thus it is not necessarily appropriate to regard the hole potential method as an intermediate between the standard HF and EHP methods;[6] of course, when we confine ourselves to one specific excitation, it is correct that the EHP method satisfies the HVT better than the hole potential method.

Beyond the Electron-Hole Potential Method

Let us give a perturbation expansion to the excitation energy as preliminaries. Define the excitation energy $\Delta E(I\to J)$ from the state $|\phi_I\rangle$ to $|\phi_J\rangle$ as

$$\Delta E(I\to J)=\langle\phi_J|H|\phi_J\rangle-\langle\phi_I|H|\phi_I\rangle, \quad (42)$$

which is converted with Eqs. 5, 6, and 7 into

$$\Delta E(I\to J)=K_J-K_I$$
$$+\lambda(\langle\phi_J|V|\phi_J\rangle-\langle\phi_I|V|\phi_I\rangle)$$
$$+\lambda^2(\langle\phi_J|([V,S_1]+\frac{1}{2}[[K,S_1],S_1])|\phi_J\rangle$$
$$-\langle\phi_I|([V,S_1]+\frac{1}{2}[[K,S_1],S_1])|\phi_I\rangle)+\cdots, \quad (43)$$

where $|\phi_I\rangle$ and $|\phi_J\rangle$ are, respectively, the eigen-

states with the eigenvalues K_I and K_J of K. To first order the excitation energy is independent of S. Both the HF and EHP methods calculate Eq. 43 to first order with $|\phi_I\rangle=|F\rangle$ and $|\phi_J\rangle=|vw\pm\rangle$.

Now consider to satisfy the first order one-particle HVT for the excited state as well as the ground by including S as simple as possible. Under the EHP choice of X, Eqs. 35's together with Eq. 25, the following condition results from Eq. 33.

$$(\varepsilon_v-\varepsilon_j)(s_{vj}+\bar{s}_{vj}-s^{vw}_{jw}+s^{vw}_{wj}\pm s^{vw}_{wj})=0 \qquad (j\epsilon\bar{F}'), \tag{44a}$$

$$(\varepsilon_j-\varepsilon_w)(s_{jw}+\bar{s}_{jw}+s^{jv}_{wv}-s^{jv}_{vw}\pm(-s^{jv}_{vw}))=0 \quad (j\epsilon F'), \tag{44b}$$

$$y^{wv}_{jv}-y^{ww}_{jw}\pm y^{wv}_{vj}+(\varepsilon_w-\varepsilon_j)(s_{wj}+\bar{s}_{wj})=0 \quad (j\epsilon\bar{F}'), \tag{44c}$$

$$y^{jv}_{vv}-y^{jw}_{vw}\pm(-y^{jw}_{wv})+(\varepsilon_j-\varepsilon_v)(s_{jv}+\bar{s}_{jv})=0 \qquad (j\epsilon F'), \tag{44d}$$

$$\dot{y}(v)_{jk}-\dot{y}(w)_{jk}+(\varepsilon_j-\varepsilon_k)(s_{jk}+\bar{s}_{jk})=0 \qquad (j\epsilon F', k\epsilon\bar{F}'), \tag{44e}$$

and

$$y^{wv}_{vv}-y^{ww}_{vw}\pm(y^{wv}_{vv}-y^{ww}_{vw})=0. \tag{44f}$$

Here note that any term concerning $V^{(2)}$ has one of the following forms: y^{jv}_{kv}, y^{jv}_{vk}, y^{jw}_{kw}, and y^{jw}_{wk} ($j\epsilon F$, $k\epsilon\bar{F}$). This shows a way to attain the present purpose. Set the matrix elements of S as

$$s^{jl}_{ki}=s^{ij}_{ik}=-v^{jl}_{ki}/(\varepsilon_j-\varepsilon_k) \qquad \left(\begin{array}{c} j\epsilon F, k\epsilon\bar{F} \\ \text{and } \textit{vice versa}; \\ l=w,v \end{array}\right) \tag{45a}$$

$$s^{jl}_{ik}=s^{ij}_{ki}=-v^{jl}_{ik}/(\varepsilon_j-\varepsilon_k) \tag{45b}$$

$$s_{jk}=(2v^{jw}_{kw}-v^{jw}_{wk})/(\varepsilon_j-\varepsilon_k) \tag{45c}$$

and

$$s^{jl}_{km}=s_{jk}=0 \qquad \text{(otherwise)}, \tag{45d}$$

where the one-particle terms are prepared for the condition given by Eq. 27. Clearly this choice of S suffices for the satisfaction of Eq. 33 as well as Eq. 24, and gives the second order term in Eq. 43 for $|\phi_I\rangle=|F\rangle$ and $|\phi_J\rangle=|vw\pm\rangle$ as

$$\lambda^2\mathrm{Re}\left(\sum_{\substack{j\epsilon F\\ k\epsilon\bar{F}}}\frac{2A(vw\pm)_{jk}}{\varepsilon_k-\varepsilon_j}+\sum_{j\epsilon F}\frac{B(vw\pm)_j}{\varepsilon_v-\varepsilon_j}\sum_{j\epsilon\bar{F}}\frac{C(vw\pm)_j}{\varepsilon_j-\varepsilon_w}\right) \tag{46}$$

with

$$A(vw\pm)_{jk}=D(v)_{jk}(v^{kw}_{jw}-D(v)_{kj})+D(w)_{jk}(v^{kv}_{jv}-D(w)_{kj}) -v^{jw}_{wk}v^{kw}_{jw}-v^{jv}_{vk}v^{kv}_{jv}+(1\pm1)v^{jv}_{vk}v^{kw}_{wj}, \tag{47}$$

$$B(vw\pm)_j=|v^{vw}_{jw}|^2+|v^{vw}_{wj}|^2-2(1\pm1)v^{vw}_{wj}v^{vw}_{jw}, \tag{48}$$

and

$$C(vw\pm)_j=|v^{wv}_{jv}|^2+|v^{wv}_{vj}|^2-2(1\pm1)v^{wv}_{vj}v^{jv}_{wv}, \tag{49}$$

where

$$D(l)_{jk}=v^{jl}_{ki}-v^{jl}_{ik}.$$

In the first, second, and third summations in the above correction term 46, only j and k of the same symmetry, j of the same symmetry as v, and j of the same symmetry as w have only to be taken into account respectively.

In the EHP method the orbitals are determined under the influence of the scatterings of electrons inside F and $\bar{F}$ by the potentials due to the electron in v and the hole in w respectively. Roughly speaking, the adoption of the S of Eq. 45's means to take it into account the scatterings of electrons from F to $\bar{F}$ and from $\bar{F}$ to F by the electron and hole potentials. The first order correction to the excited state has one electron in $\bar{F}$ and one hole in F besides v and w in consequence:

$$(S^{(1)}_1+S^{(2)}_1)|vw\pm\rangle=\sum_{\substack{j\epsilon\bar{F}\\ k\epsilon F}}\sum G(vw\pm)^{\mu\nu}_{jk}a^\dagger_{j\nu}a_{k\nu}a^\dagger_{v\mu}a_{w\mu}|F\rangle \tag{50}$$

with

$$G(vw\pm)^{\mu\nu}_{jk}=\mathrm{L}_\mu(\pm)(v^{jw}_{kw}-v^{jv}_{kv}-\delta_{\mu\nu}(v^{jw}_{wk}-v^{jv}_{vk}))/(\varepsilon_j-\varepsilon_k). \tag{51}$$

The ground state is not affected, because it involves neither electron in v nor hole in w. As easily seen, we have

$$(S^{(1)}_1+S^{(2)}_1)|F\rangle=0. \tag{52}$$

Before we discuss the effect of the correction 46, a considerable amount of examinational numerical calculation is to be performed, and we would like to regard the recipe as a possibility at present.

Supplementary Remarks

The First Order Two-Particle HVT. To put $W=a^\dagger_{p\sigma}a^\dagger_{r\tau}a_{s\tau}a_{q\sigma}$ in Eq. 13 gives the first order two-particle HVT, which has the following expression for the ground state after substitution of Eqs. 18, 20, 21, 22, and 23 through Eq. 14.

$$(\delta_{qp}\hat{y}_{sr}+\delta_{sr}\hat{y}_{qp}-\delta_{\sigma\tau}(\delta_{qr}\hat{y}_{sp}+\delta_{sp}\hat{y}_{qr}))(\mathrm{f}(q)\mathrm{f}(s)-\mathrm{f}(r)\mathrm{f}(p)) -(y^{qs}_{pr}-\delta_{\sigma\tau}y^{qs}_{rp})(\mathrm{g}(qs:rp)-\mathrm{g}(pr:sq))=0 \tag{53}$$

with

$$\mathrm{g}(pr:sq)=\mathrm{f}(p)\mathrm{f}(r)(\mathrm{f}(s)+\mathrm{f}(q)-1), \tag{54}$$

and

$$\hat{y}_{jk}=y_{jk}+\bar{y}_{jk}.$$

Provided that the first order one-particle HVT for the ground state is satisfied, that is,

$$\hat{y}_{jk}=0 \qquad (j\epsilon F, k\epsilon\bar{F} \text{ and } \textit{vice versa}),$$

Eq. 53 results in

$$v^{qs}_{pr}-\delta_{\sigma\tau}v^{qs}_{rp}+(\varepsilon_q+\varepsilon_s-\varepsilon_r-\varepsilon_p)(s^{qs}_{pr}-\delta_{\sigma\tau}s^{qs}_{rp})=0 \qquad (q,s\epsilon\bar{F};\ p,r\epsilon F \text{ and } \textit{vice versa}), \tag{55}$$

which leads us to

$$s^{jl}_{km}=-v^{jl}_{km}/(\varepsilon_j+\varepsilon_l-\varepsilon_m-\varepsilon_k) \qquad \left(\begin{array}{c} j,l\epsilon\bar{F};\ k,m\epsilon F \\ \text{and } \textit{vice versa} \end{array}\right). \tag{56}$$

This shows that the electron correlation in the ground state can be taken into account first by including the contribution from the double excitation configurations for any choice of orbitals satisfying Eq. 24. In using the EHP orbitals, therefore, the first aid for the ground state $|F\rangle$ is to use the S in the form of Eq. 56 likewise in using the HF orbitals. Further adopting Eq. 56 together with Eqs. 45's, we can improve the ground state, the first order one-particle HVT for the excited state remaining alive, since s^{jl}_{km}'s for $j,l\epsilon\bar{F}$, $k,m\epsilon F$ and *vice versa* do not concern $\bar{s}_{jk}$'s.

The Perturbation-Theoretical Choice. It is never futile to add some remarks in connection with the perturbation-theoretical approach. Under the exponential prescription, Eq. 6, perturbation equations in the operator form are derived from[3,4,11]

$$[\exp(-S)H\exp(S), K] = 0. \quad (57)$$

Making use of Eqs. 5 and 7, we obtain the first order perturbation equation as

$$[V+[K, S_1], K] = 0, \quad (58)$$

which becomes the two separated equations corresponding to the one- and two-particle parts after calculation with Eqs. 18, 20, 21, 22, and 23:

$$\sum_{jk\mu} y_{jk}(\varepsilon_j-\varepsilon_k)a^\dagger_{j\mu}a_{k\mu} = 0 \quad (59a)$$

and

$$\sum_{jklm\mu\nu} y^{jl}_{km}(\varepsilon_j+\varepsilon_l-\varepsilon_m-\varepsilon_k)a^\dagger_{j\mu}a^\dagger_{l\nu}a_{m\nu}a_{k\mu} = 0, \quad (59b)$$

which lead us to

$$s_{jk} = x_{jk}/(\varepsilon_j-\varepsilon_k) \qquad (j, k \text{ such that } \varepsilon_j \neq \varepsilon_k) \quad (60a)$$

and

$$s^{jl}_{km} = -v^{jl}_{km}/(\varepsilon_j+\varepsilon_l-\varepsilon_m-\varepsilon_k) \quad \begin{pmatrix} j,k,l,m \text{ such that} \\ \varepsilon_j+\varepsilon_l-\varepsilon_m-\varepsilon_k \neq 0 \end{pmatrix}. \quad (60b)$$

The matrix elements of S other than these can be set to vanish by imposing such auxiliary restriction upon S as that S should be completely off-diagonal in the representation $\{|\phi\rangle\}$.[4] Clearly Eqs. 60's satisfy the first order one-particle HVT. This perturbation-theoretical choice requires nothing of orbitals but sufficient inclusion of configurations. Hence, unless we know the well-behaved orbitals suitable for purpose beforehand, the choice is not necessarily practical.

References

1) J. O. Hirschfelder, *J. Chem. Phys.*, **33**, 1462 (1960).
2) S. T. Epstein and J. O. Hirschfelder, *Phys. Rev.*, **123**, 1495 (1961); J. O. Hirschfelder and C. A. Coulson, *J. Chem. Phys.*, **36**, 941 (1962).
3) P. D. Robinson, *Proc. R. Soc. London, Ser. A*, **283**, 229 (1965); *J. Chem. Phys.*, **47**, 2319 (1967).
4) H. Primas, *Helv. Phys. Acta*, **34**, 331 (1961); *Rev. Mod. Phys.*, **35**, 710 (1963).
5) For example, A. C. Hurley, "Introduction to the Electron Theory of Small Molecules," Academic Press, London (1976), Chap. 7, Section 7.2.
6) K. Morokuma and S. Iwata, *Chem. Phys. Lett.*, **16**, 192 (1972); S. Iwata and K. Morokuma, *Theor. Chim. Acta*, **33**, 285 (1974).
7) E. R. Davidson, *J. Chem. Phys.*, **57**, 1999 (1972).
8) Ref. 5, p. 231.
9) C. C. J. Roothaan, *Rev. Mod. Phys.*, **23**, 69 (1951).
10) S. Huzinaga and C. Arnau, *Phys. Rev. A*, **1**, 1285 (1970); *J. Chem. Phys.*, **54**, 1948 (1971).
11) A. M. Arthurs and P. D. Robinson, *Proc. R. Soc. London, Ser. A*, **301**, 507 (1967).

  Bull. Chem. Soc. Jpn., 54, 3317—3321 (1981)

Transmission of Low-energy Electrons (0—15 eV) through Thin Films of Ethers, Ketones, Alcohols, and Ice. Determination of the Quasifree Electron State Energy

Kenzo HIRAOKA* and Masaji NARA

Faculty of Engineering, Yamanashi University, Takeda-4, Kofu 400

(Received May 6, 1981)

The transmission of low-energy electrons (0—15 eV) through 10—100 Å films of ethers, ketones, alcohols, and ice has been studied. Structures are indicated by electron current I_t transmitted through a thin film as a function of the incident electron energy V_1, displayed as dI_t/dV_1 *vs.* V_1. With increasing the film thickness, a decrease of the height of the first peak (due to injection of electrons in the film) and an appearance of a second peak are observed for ethers and alcohols. The energies of quasifree electron state V_0 are determined by measuring the energy of the second peak from the first peak for solid diethyl ether, tetrahydrofuran, 2-methyltetrahydrofuran, methanol, ethanol, 1-propanol, 2-propanol, 1-butanol, 1-pentanol, 1-hexanol, and 1-nonanol. For acetone, diethyl ketone, dimethyl sulfoxide, and ice, neither a decrease of the first peak nor an appearance of a second peak is observed, indicating that these compounds have negative V_0 values. From the energy of the onsets of broad negative peaks appeared at ≈14 eV for ethers and alcohols, the solid phase ionization energies I_s and the polarization energies of cations P^+ by the solid media are determined.

Condensed hydrocarbons are complex and electron interactions in them are the focus of much current interest. The energies of quasifree electron state V_0 have been reported for several liquid hydrocarbons.[1-5] However, attempts to measure V_0 directly in polar or nonpolar glassy matrices have failed.[5] The V_0 values in glassy matrices have been estimated by an indirect method using Eq. 1,[5-7]

$$I_1,\ I_s = I_g + P^+ + V_0 \qquad (1)$$

where I_1 and I_s are the ionization potential of an impurity molecule A in a liquid and solid solution, respectively, I_g the gas phase ionization potential of A, and P^+ the polarization energy of the medium by the positive ion A^+.

Recently, Hiraoka and Hamill[8] and Sanche[9] reported a simple method for measuring the electronic levels of molecules supported as ultrathin films on a metal surface at ≈80 K. The film was bombarded by a beam of low-energy electrons, and the current transmitted through the film (I_t) was measured as a function of the incident electron energy (V_1). The transmission spectra, displayed as dI_t/dV_1 *vs.* V_1, were found particularly useful for detecting optically forbidden electronic transitions.[8,9] In the previous work,[10] we reported direct measurements of V_0 for solid hexane and benzene by measuring the transmission spectra dI_t/dV_1 *vs.* V_1 for 10—100 Å films of these compounds deposited on the metal block at ≈80 K. In this work, the interactions of injected excess electrons with solid films are studied by measuring the transmission spectra for ethers, ketones, alcohols and ice. The main objective of this work is to relate the energy dependence of the transmission features to specific interactions occurring in solid films.

Experimental

The experimental procedure has been described.[8,10] The temperature of the stainless steel metal block was ≈80 K and the pressure was $\leq 10^{-7}$ Pa. The cathode was modulated by 0.3 V at 78 Hz by the reference signal of a lock-in amplifier. The cathode voltage was swept upward with $I_t \leq 2\times10^{-9}$ A transmitted through the thin film. The transmission spectra were displayed as dI_t/dV_1 *vs.* V_1, where eV_1 is the energy of the incident electron. Because no established sharp transitions are available as internal standards, the zero of the electron energy scale in the present work has been chosen arbitrarily as the onset of the first peak of the spectrum dI_t/dV_1 *vs.* V_1 (*i.e.* for electron injection). The film thickness was changed by changing the deposition time with the constant vapor pressure of a sample at 1.3×10^{-5} Pa.

Results and Discussion

In the previous work,[10] the transmission spectra dI_t/dV_1 *vs.* V_1 for benzene and hexane were examined in detail. It was found that there was almost no difference in shape (height and half-width) between the first peak for the metal block and those for 2 to 10 L† thick benzene films. On the contrary, the first peak of transmission spectra for hexane decreased drastically and a second peak appeared and grew as the film thickness was increased. From these experimental results, it was concluded that solid films of benzene and hexane have negative and positive V_0, respectively. The energy of quasifree electron state V_0 for hexane, 0.9 eV, was determined by measuring the energy of the second peak from the first peak of the spectrum for the metal block as a reference. In the following sections, the results for ethers, ketones, dimethyl sulfoxide (DMSO), alcohols, and ice are summarized, and a discussion is made for the determination of the energy of quasifree electron state V_0, the solid phase ionization energy I_s and the cation polarization energy P^+ by the solid media.

Ethers. The transmission spectra, dI_t/dV_1 *vs.* V_1, for diethyl ether, tetrahydrofuran (THF), and 2-methyltetrahydrofuran (2-MTHF) have been measured. The transmission spectra for diethyl ether and 2-MTHF are shown in Figs. 1 and 2. A drastic decrease of the first peak and an appearance of the

† The amount of the gas admitted in the vacuum chamber is expressed in Langmuir units (1 L = 1.33×10^{-4} Pa·s). When the sticking probability is unity, the surface will be covered by approximately one monolayer with 1 Langmuir gas admission.

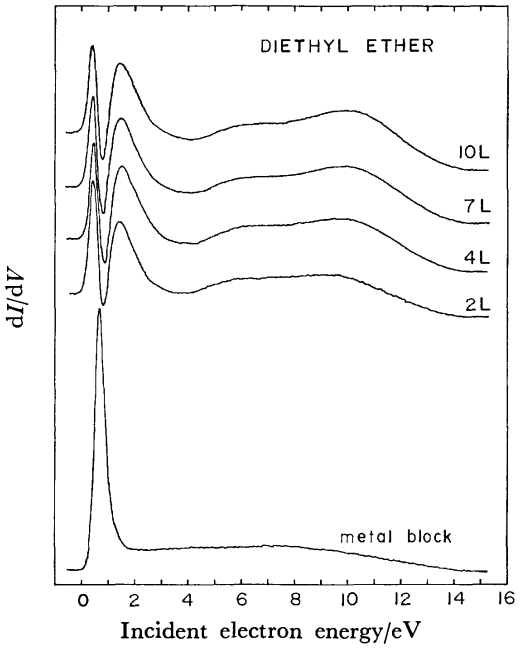

Fig. 1. The transmission spectra dI_t/dV_1 *vs.* V_1 for metal block and diethyl ether. The film thickness was changed from 2 to 10 L.

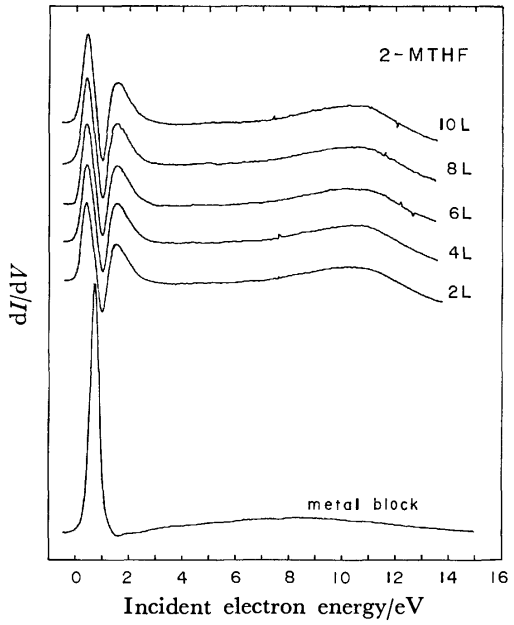

Fig. 2. The transmission spectra for metal block and 2-methyltetrahydrofuran (2-MTHF).

second peak and its strong growth are observed for all of these compounds, indicating that they have positive V_0.

Ketones and DMSO. The transmission spectra of acetone are shown in Fig. 3. The first peak of the transmission spectra for acetone and diethyl ketone shows only a slight decrease by the deposition of 2 L thick sample and the second peak does not show up for both of these compounds. These are characteristic features for solid films whose V_0 are negative. Thus the solid acetone and diethyl ketone are considered to have negative V_0s.

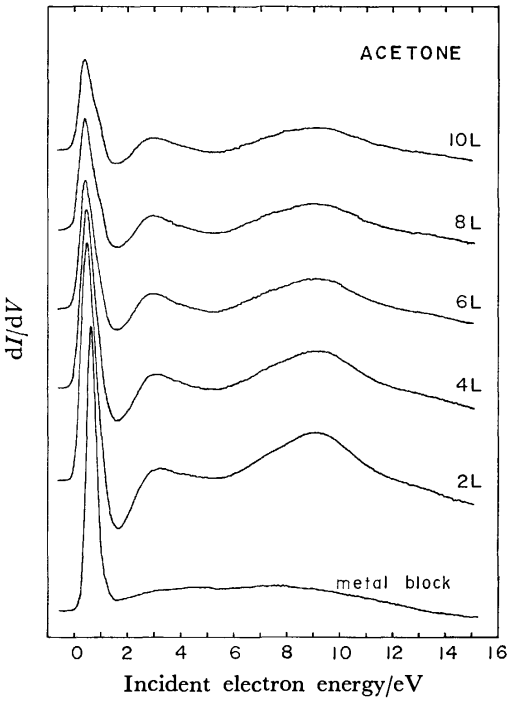

Fig. 3. The transmission spectra for metal block and acetone.

The continuous decrease of the first peak is observed for these compounds as the film thickness is increased from 2 to 10 L. This is due to the decrease of the electron emission efficiency of the cathode which is poisoned by the admission of ketone vapor in the vacuum system. The electron gun used in this experiment is a commercial TV gun (The Japan Lamp Industrial Co., Ltd) and has an indirectly heated oxide-coated cathode. This type of cathode was found to be easily poisoned by the admission of some kinds of organic vapors, especially ketones. Usually the 2 L thick film is prepared by the admission of 1.3×10^{-5} Pa vapor pressure of the sample for 20 s. In cases of acetone and diethyl ketone, 2 L thick sample was deposited by the admission of 3.3×10^{-6} Pa vapor pressure for 80 s in order to suppress the decrease of the electron emission efficiency of the cathode. This operation was successful only to some extent as shown in Fig. 3. After the samples were desorbed by increasing the temperature of the metal block, the transmission spectra were measured again. The height of the first peak for the bare metal block was found almost the same as those for 10 L thick samples at liq. N_2 temperature. If these compounds had positive V_0 values, the first peak should increase by the desorption of samples on the metal block.

In Fig. 4 are shown the transmission spectra of DMSO. The height of the first peak for 2 L thick film is even larger than that for the bare metal block and no second peak appears. There is no doubt that the solid DMSO film has a negative V_0 value.

Alcohols. The transmission spectra for methanol, ethanol, 1-propanol, 2-propanol, 1-butanol, 1-pentanol, 1-hexanol, and 1-nonanol have been measured. The transmission spectra for methanol and 1-

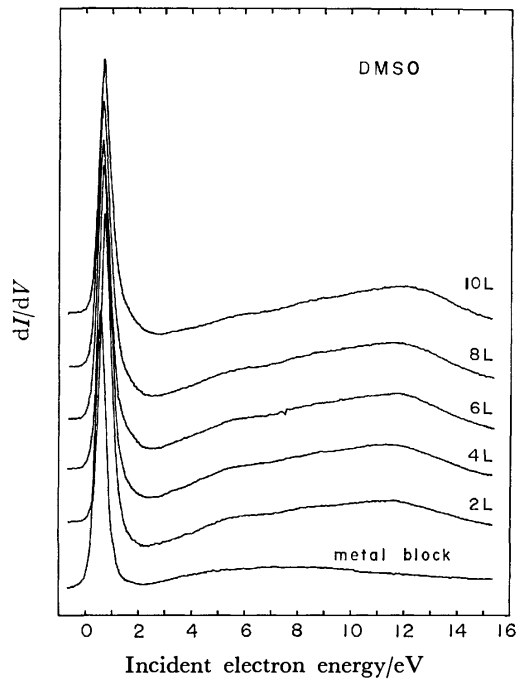

Fig. 4. The transmission spectra for metal block and dimethyl sulfoxide (DMSO).

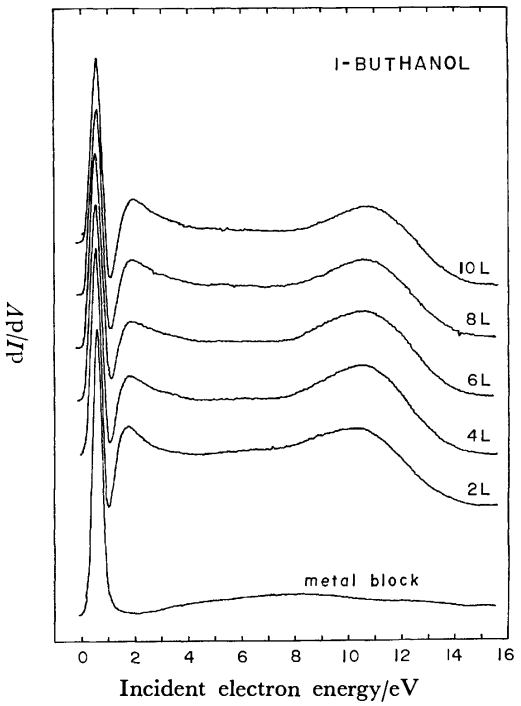

Fig. 6. The transmission spectra for metal block and 1-butanol.

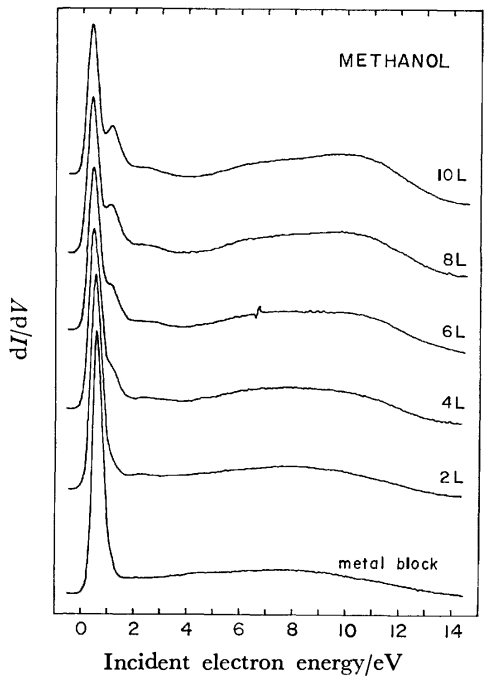

Fig. 5. The transmission spectra for metal block and methanol.

butanol are shown in Figs. 5 and 6.

A decrease of the first peak and a growth of the second peak are observed for methanol with an increase of the film thickness, indicating that the solid methanol has a positive V_0.

It was found that the film thickness dependence on the transmission spectra was very similar for ethanol and higher alcohols (see Fig. 6). For these compounds, a drastic decrease of the first peak and an appearance of a sharp second peak are observed by the deposition of 2 L thick film, indicating that these compounds have positive V_0. However, the decrease of the first peak and the increase of the second peak are only very gradual for further deposition of the sample. These results strongly suggest that electrons in solid alcohols with an energy lower than V_0 have a large contribution to the transmitted electron current to the anode.

Ice. The transmission spectra of ice are shown in Fig. 7. Contrary to the spectra of alcohols, the first peak neither decreases nor a growth of the second peak is observed with an increase of the film thickness, indicating that the energy of quasifree electron state V_0 in ice is negative.

Work Function Change of the Metal Block. It is worthy to note that in the spectra of ethers and some of alcohols, the first peak shows a negative shift when samples were deposited on the metal block. If the film was charged by the electron irradiation, the first peak should show a positive shift.[10] For all compounds measured in this experiment, the peaks of the spectra do not show any shifts under repeated electron irradiation under the present experimental conditions ($I_t \leq 2 \times 10^{-9}$ A), *i.e.*, the charging of the film is negligible. Therefore, the shift of the first peak must be due to the change of the current-voltage characteristic curve determined by the contact potential difference between the cathode and the metal block. After the samples were desorbed by increasing the temperature of the metal block, the first peak shifts back to the original energy value of the first peak for the metal block. This means that the shift of the first peak is due to the work function change of the metal block by the deposition of the sample

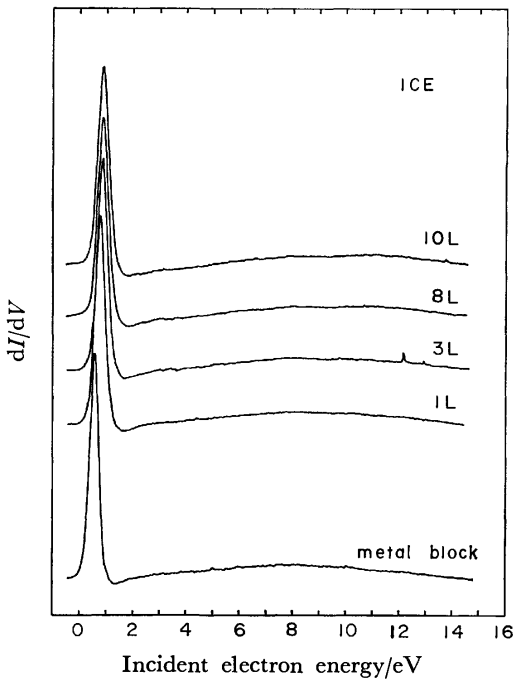

Fig. 7. The transmission spectra for metal block and ice.

on *it*.

Absorption is usually associated with a variation of the work function ϕ which provides a simple procedure for monitoring the state of a surface. Moreover, the sign of the work function change $\Delta\phi$ is connected with the direction of the electron transfer between the substrate and the adsorbate, *i.e.* with the dipole moment of the adsorbate complex. Although the surface of the stainless steel metal block used in this measurements is not characterized rigorously, it would be informative to discuss the work function changes observed by the deposition of several compounds.

The observed work function changes $\Delta\phi$ are summarized in Table 1 (column 6).†† The negative $\Delta\phi$s are observed for ethers and some of alcohols. For higher alcohols, $\Delta\phi$s are observed to become smaller. The positive $\Delta\phi$s are observed by the deposition of ice and DMSO. It has been observed that $\Delta\phi$s are nearly zero for alkanes and aromatic compounds at $\approx$80 K in the previous experiments.[10,11]

The sign and the amount of $\Delta\phi$ may give some information on the interaction of adsorbed molecules with the metal surface. The relatively large $\Delta\phi$s are observed for ethers. These compounds have large permanent dipole moments, but the positive charge is rather delocalized in molecules in comparison with the localized negative charge on oxygen atoms. Considering that the nonpolar compounds give very small $\Delta\phi$s, ethers are considered to be interacting with the metal surface directing the oxygen atoms toward the metal surface. Alcohols (protic solvents) have also negatively charged oxygen atoms but $\Delta\phi$s are generally smaller than those for ethers. This may be due to the fact that the molecules of the first monolayer on the metal surface form hydrogen bonds with molecules of the second monolayer and the dipole moments induced by the interaction between the substrate and the adsorbate are smaller than in cases for ethers. This may explain why $\Delta\phi$ becomes smaller for higher alcohols. The positive shifts for ice and DMSO are difficult to understand. It would only be suggested that the sign of the net dipole moments induced by the interactions between the substrate and these compounds are opposite to cases for ethers and alcohols.

It was found that $\Delta\phi$s are highly temperature-dependent and the sign of $\Delta\phi$s for some polar molecules changes as the temperature of the metal block is increased. A more detailed investigation on the work function changes in this respect is now in progress.

Table 1. V_0, I_s, I_g, P^+, and $\Delta\phi$

Compound	V_0/eV	I_s/eV	I_g/eV	P^+/eV	$\Delta\phi$/eV
Diethyl ether	1.0	8.4	9.5	−2.1	−0.2
THF	1.1	8.1	9.42	−2.4	−0.3
2-MTHF	1.1(1.15,[a] 0.98[b])	8.8			−0.3
Acetone	≤0				
Diethyl ketone	≤0				
DMSO	≤0				+0.1
Methanol	0.7(0.13,[a] −0.01[b])	9.2	10.84	−2.3(−1.99,[a] −1.84[b])	−0.1
Ethanol	1.1(0.34,[a] 0.24[b])	9.0	10.46	−2.5(−2.05,[a] −1.94[b])	−0.2
1-Propanol	1.1(0.38,[a] 0.36[b])	9.1	10.3	−2.3(−2.04,[a] −2.01[b])	−0.1
2-Propanol	1.0	8.9	10.12	−2.2	−0.1
1-Butanol	1.3(0.47[a])	8.8	10.04	−2.5(−2.08[a])	≈0
1-Pentanol	1.3	8.7			≈0
1-Hexanol	1.3	8.4			≈0
1-Nonanol	1.3	8.8			≈0
Ice	≤0(−0.36[b])				+0.2

a) Ref. 7. b) Ref. 5.

†† For acetone and diethyl ketone, $\Delta\phi$s are not given in Table 1 because the shifts of the first peak are partly due to the work function changes of the cathode.

The Energy of Quasifree Electron State V_0. In the previous work,[10] the V_0 values are determined by measuring the energy of the second peak from the first peak of the spectrum for the metal block as a reference. In the present study, the first peak of the spectrum for the metal block can not be chosen as a reference because the first peak shows positive or negative shifts by the deposition of the sample, as was mentioned in the previous section. In this work, V_0 is estimated by measuring the energy difference between the first and second peaks of a spectrum for each compound. Here, it is assumed implicitly that the first peak represents a crude profile of the electron energy distribution function. We think that this assumption is reasonable because the half-width of the first peak remains almost the same before and after the sample deposition. The estimated V_0s are listed in Table 1 (column 2). It is evident from our experimental results that V_0s for acetone, diethyl ketone, DMSO, and ice are negative, but the estimation of their values is difficult because of the lack of sharp structures in the transmission spectra for the calibration of the electron energy scale.

In Table 1, the values of V_0 in some solid alcohols and 2-MTHF measured by an indirect method[5,7] are also shown in parentheses of column 2. The agreement between these values and our directly measured values is good for 2-MTHF but poor for alcohols. The observed disagreement seems to be larger than the experimental errors in our measurements and it likely comes from the completely different experimental approaches for the determination of V_0. It is worthy to note that for almost all of solid alkanes,[5-7,10,11] a good agreement is observed between V_0 values determined by these two different methods. As shown in Table 1, V_0 values for alcohols obtained by an indirect method[5-7] are 0.6—0.8 eV lower than those obtained in this experiment. As is pointed out in the previous section, the contribution of electrons in solid alcohols with an energy lower than V_0 to the transmitted electron current is much larger than that in other solid samples whose V_0 are positive. This suggests the existence of dense trapping sites in solid alcohols for the efficient transport of nearly zero-energy electrons. In the indirect method, if the impurity molecules could be photoionized by ejecting electrons to the energy levels of pre-existing dense trapping sites, the onset of the recombination luminescence or of the appearance of the absorption of ionized impurity molecules would extend to lower photon energy and the rigorous determination of V_0 would be intrinsically difficult. This might explain the observed discrepancy. Although the Springett-Jortner-Cohen model[12] gives the rigorous theoretical definition for V_0, the experimentally determined V_0 represents the macroscopic "bulk" properties of the solid and the experimental V_0 could be highly dependent on each experimental method.

Cation Polarization Energy P^+ by the Medium. It has long been known that the ionization potential of a molecule in a condensed phase is lowered relative to the value measured in the gas phase. Lyons and his coworkers[13,14] emphasized the importance of the polarization of the medium P^+ around the cation and the ejected electron. Since I_g is known, the V_0 value may be derived by Eq. 1[5,7] if the cation polarization energy P^+ can be evaluated. So far, P^+ has been calculated by Eq. 2,

$$P^+ = -\frac{e^2}{2r_0}\left(1-\frac{1}{\varepsilon}\right) \quad (2)$$

where ε is the optical dielectric constant and r_0 the cation radius.

Since the V_0 values are directly measured in this experiment, P^+ may be derived by Eq. 1 if I_s can be measured experimentally. When a molecule in a solid film is ionized by an incident electron, the incident and ejected electrons in the film will have energies nearly equal to or larger than V_0 with respect to the vacuum. Because the produced hole (cation) in the film will be ultimately annihilated by a recombination or diffusion to the anode by tunneling or hopping mechanisms, the ionization of a molecule in a film by an incident electron must contribute to the "decrease" of the transmitted current. When the film has a positive V_0 value, the reflection coefficient for an electron at the film-vacuum interface is considered to be small enough that a discernable negative peak is expected to appear in the transmission spectrum. All transmission spectra for compounds whose V_0 are positive have broad negative peaks with onsets at around 9—10 eV. We think that these broad negative peaks observed at $\approx$14 eV are due to the ionization of molecules in a film.

For a film with a positive V_0, the threshold ionization energy I_s may be obtained by measuring the energy of the onset of a negative peak from the "second" peak as a reference. The measured I_s values are listed in Table 1 (column 3) with the reported I_g values (column 4). By knowing the values I_s, I_g, and V_0, the P^+ values can be derived by Eq. 1 which are shown in Table 1 (column 5), with the calculated P^+ by Eq. 2 in parentheses.[5,7] The error for values of I_s and thus P^+ which arises from the uncertainty for the determination of the onsets of the broad negative peaks may be estimated as $\pm$0.4 eV. The experimentally determined P^+ are a few tenths of an eV higher than the calculated P^+.

For a compound with $V_0<0$, the onset of a negative peak would not correspond to that for the ionization of a molecule in the film because the ejected electron with an energy $\approx V_0$ with respect to the vacuum can not escape to the vacuum due to the positive energy barrier ($-V_0$). Thus the I_s values for compounds with $V_0<0$ are difficult to estimate by the present method.

This work was partly supported by the Grant-in-Aid from the Ministry of Education, Science and Culture.

References

1) R. A. Holroyd and M. Allen, *J. Chem. Phys.*, **54**, 504 (1971).
2) R. A. Holroyd, *J. Chem. Phys.*, **57**, 3007 (1972).
3) R. A. Holroyd and R. L. Russell, *J. Phys. Chem.*,

78, 2128 (1974).
4) R. Schiller, Sz. Vass, and J. Mandics, *Int. J. Rad. Phys. Chem.*, **5**, 491 (1973).
5) S. Noda, L. Kevan, and K. Fueki, *J. Phys. Chem.*, **79**, 2866 (1975).
6) J. Bullot and M. Gauthier, *Can. J. Chem.*, **55**, 1821 (1977).
7) D. Grand and A. Bernas, *J. Phys. Chem.*, **81**, 1209 (1977).
8) K. Hiraoka and W. H. Hamill, *J. Chem. Phys.*, **56**, 3185 (1972); **57**, 3870, 3881, 4058 (1972); **58**, 3686 (1973); **59**, 5749 (1973).
9) L. Sanche, *Chem. Phys. Lett.*, **65**, 61 (1979); *J. Chem. Phys.*, **71**, 4860 (1979).
10) K. Hiraoka and M. Nara, *Bull. Chem. Soc. Jpn.*, **54**, 1589 (1981).
11) K. Hiraoka and M. Nara, *Proceedings of the 23rd Radiation Chemistry Conference*, Kyoto, October 1980; *J. Phys. Chem.*, (1981), in press.
12) B. E. Springett, J. Jortner, and M. H. Cohen, *J. Chem. Phys.*, **48**, 2720 (1968).
13) L. E. Lyons, *J. Chem. Soc.*, **1957**, 5001.
14) L. E. Lyons and J. C. Mackie, *Proc. Chem. Soc.*, **1962**, 71.

  Bull. Chem. Soc. Jpn., 54, 3323—3326 (1981)

Vibrational Spectra and Normal Coordinate Calculations for Trimethylgermane

Yoshika IMAI* and Koyo AIDA

Department of Engineering Science (Chemistry), Faculty of Engineering, Tohoku University, Sendai 980

(Received May 18, 1981)

Vibrational spectra of $(CH_3)_3GeH$, $(CH_3)_3GeD$, $(CD_3)_3GeH$, and $(CD_3)_3GeD$ were obtained. Assignments for all the fundamentals except internal torsions were made by assuming the C_{3v} molecular symmetry. Normal coordinate calculations were carried out to confirm the assignments.

In our previous paper,[1] we reported on a study of vibrational spectra and normal coordinate calculations for trimethylsilane. The study has now been extended to trimethylgermane. Although numerous vibrational studies on trimethylsilane have been reported,[2] only a limited number have been reported on trimethylgermane[3-6] and most of them relate to substituent effects on the GeH stretching mode. As far as we know, study on the assignment of all the active fundamentals has been made only by Van de Vondel and Van der Kelen.[6] They made also normal coordinate calculations with no data of isotopic compounds available by assuming the methyl group as a point mass. In the paper[1] on trimethylsilane, it was pointed out that the methyl rock, the SiH bend, and the asymmetric SiC_3 stretch are fairly strongly coupled with one another. Since it may highly be expected that a similar vibrational coupling will be operative also in the case of trimethylgermane, it seems inadequate to make the calculation by assuming that the methyl group is a point mass. In this paper, we will report vibrational spectra of trimethylgermane and its deuterated analogues and results of normal coordinate calculations on these compounds carried out without assuming the methyl group as a point mass.

Experimental

$(CH_3)_3GeH$ and $(CH_3)_3GeD$ were prepared by reduction of $(CH_3)_3GeI$ with $LiAlH_4$ and $LiAlD_4$, respectively. $(CH_3)_3GeI$ was prepared through a reaction of tetramethylgermane with I_2 in a sealed tube at 50 °C. The crude trimethylgermane was purified by vacuum distillation with a conventional vacuum line. $(CD_3)_3GeH$ and $(CD_3)_3GeD$ were prepared similarly to $(CH_3)_3GeH$ and $(CH_3)_3GeD$, respectively, by using $(CD_3)_4Ge$ instead of $(CH_3)_4Ge$. The purity of the compounds was checked by their infrared spectra in the gas phase.

Infrared spectra (4000—300 cm^{-1}) and far-infrared spectra (400—80 cm^{-1}) were recorded on a Hitachi 345 spectrophotometer and on a Hitachi FIS-III spectrophotometer, respectively, in the gas phase and with solid films at liquid nitrogen temperature.

Raman spectra were recorded with liquids in capillary tubes on a JEOL JRS-S1 Raman spectrophotometer equipped with a 50 mW NEC GLG 5800 He-Ne laser.

Results and Vibrational Assignments

If each methyl group in a molecule is staggered to both the Ge–H bond and the adjacent Ge–C bonds, the molecule will have a C_{3v} symmetry. On this assumption the 36 normal vibrations are made distributed as $8A_1+4A_2+12E$. The A_1 and E modes are active in infrared and Raman spectra but the A_2 modes inactive in both.

Symmetry coordinates have been classified, according to the description of the modes of methyl group and of the skeletons in the molecules, as given in Table 1, where the numbering of the symmetry coordinates is the same as that for the corresponding coordinates for trimethylsilane.[1] Figures 1 and 2 show the infrared spectra in the gas phase and the Raman spectra in the liquid phase, respectively. Tables 2—5 list the observed fundamental frequencies.

By taking into consideration the isotopic shift and polarization of Raman bands as well as data for related compounds,[7-9] assignments for the methyl stretches and the GeH and GeD stretches may easily be made.

There should be five methyl deformations. Asymmetric deformations bonded to a metal atom are usually relatively weak and broad, and their positions in spectra do not markedly shift with change in the nature of the metal atom, whereas symmetric methyl deformations usually give relatively strong and sharp bands and exhibit slight shifts with change in the nature of the metal atom.[10] For $(CH_3)_3GeH$ and $(CH_3)_3GeD$ the asymmetric deformations are observed at *ca.* 1410 cm^{-1}. Upon deuteration of the methyl groups, these shift to *ca.* 1040 cm^{-1}. The symmetric deformations are observed at *ca.* 1250 cm^{-1} for $(CH_3)_3GeH$ and $(CH_3)_3GeD$ and at *ca.* 970 cm^{-1} for $(CD_3)_3GeH$ and $(CD_3)_3GeD$.

Three methyl rocks, two GeC_3 stretches, and a GeH or GeD bend are expected to appear in the

Table 1. Description of the symmetry coordinates for trimethylgermane[a]

Vibrational mode	Coordinate		
	A_1	A_2	E
Stretching $(CH_3)_a$ or $(CD_3)_a$	S_1	S_9	S_{13}, S_{14}
Stretching $(CH_3)_s$ or $(CD_3)_s$	S_2		S_{15}
Stretching (GeH) or (GeD)	S_3		
Deformation $(CH_3)_a$ or $(CD_3)_a$	S_4	S_{10}	S_{16}, S_{17}
Deformation $(CH_3)_s$ or $(CD_3)_s$	S_5		S_{18}
Rocking (CH_3) or (CD_3)	S_6	S_{11}	S_{19}, S_{20}
Bending (GeH) or (GeD)			S_{21}
Stretching (GeC_3)	S_7		S_{22}
Deformation (GeC_3)	S_8		S_{23}
Torsion		S_{12}	S_{24}

a) Abbreviations used: a, asymmetric; s, symmetric.

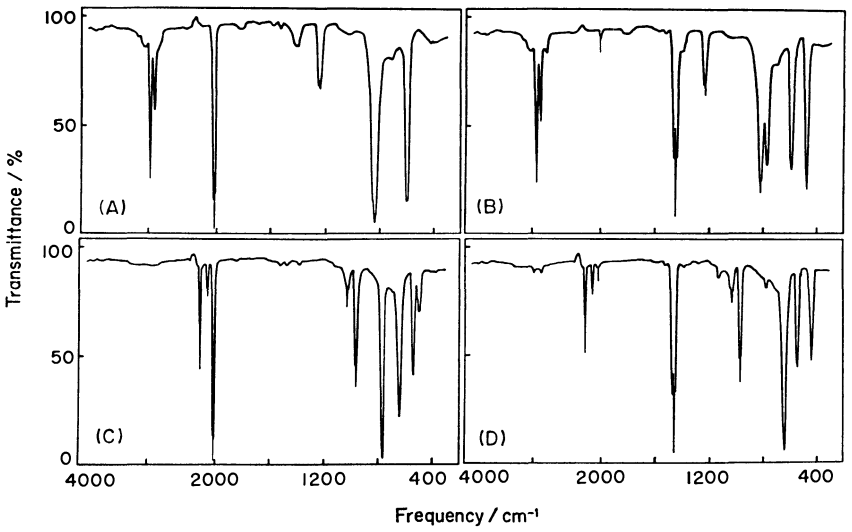

Fig. 1. Infrared spectra of $(CH_3)_3GeH$ (A), $(CH_3)_3GeD$ (B), $(CD_3)_3GeH$ (C), and $(CD_3)_3GeD$ (D) in the gas phase.

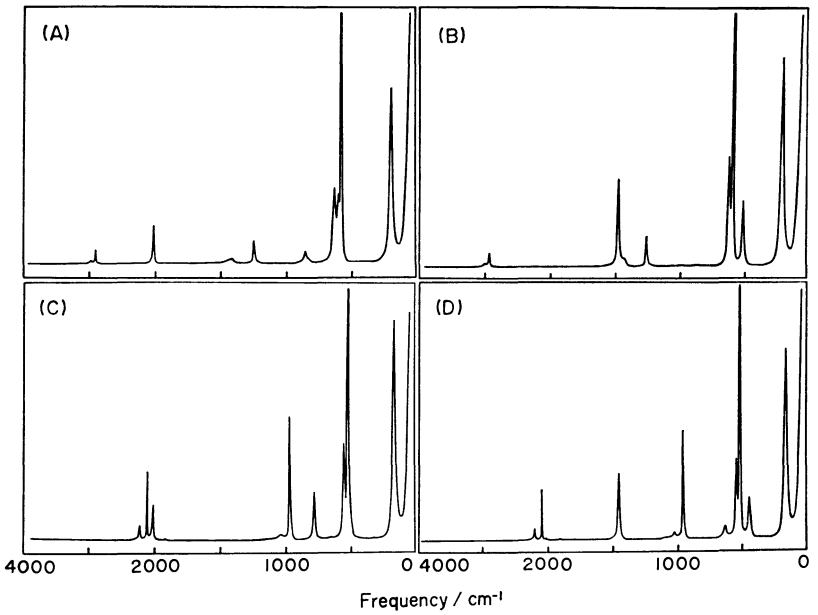

Fig. 2. Raman spectra of $(CH_3)_3GeH$ (A), $(CH_3)_3GeD$ (B), $(CD_3)_3GeH$ (C), and $(CD_3)_3GeD$ (D) in the liquid.

range 900—400 cm^{-1}. Of these vibrations the A_1 GeC_3 stretching mode should give an intense polarized Raman band. Therefore, the Raman bands at *ca.* 550 cm^{-1} for $(CH_3)_3GeH$ and $(CH_3)_3GeD$ may undoubtedly be assigned to this mode. Upon deuteration of methyl groups these shift to 520 cm^{-1}. A_1 methyl rocking frequencies are expected to be approximately identical with each other for $(CH_3)_3GeH$ and $(CH_3)_3GeD$ and for $(CD_3)_3GeH$ and $(CD_3)_3GeD$, since it is also the case with trimethylsilane (850 cm^{-1} for $(CH_3)_3SiH$ and 847 cm^{-1} for $(CH_3)_3SiD$; 704 cm^{-1} for $(CD_3)_3SiH$ and 705 cm^{-1} for $(CD_3)_3SiD$).[1] On this basis, to this mode we have assigned the Raman bands at 830 cm^{-1} for $(CH_3)_3GeH$ and $(CH_3)_3GeD$ and at *ca.* 650 cm^{-1} for $(CD_3)_3GeH$ and $(CD_3)_3GeD$. However, these Raman bands are only partly polarized. This suggests that there are some other vibrations in the E class coinciding on these bands. The most probable candidate is the E methyl rock, since the same accidental degeneracy is found in the A_1 and E methyl rocks in $(CH_3)_3GeCl$,[7] $(CH_3)_3GeCF_3$,[9] and $(CH_3)_3GeGeH_3$.[11]

The remaining bands observed in the range 900—400 cm^{-1} may be considered to be the vibrations due to the E modes but it is not easy to assign these bands. However, the 480 cm^{-1} band in $(CH_3)_3GeD$ and the 780 cm^{-1} one in $(CD_3)_3GeH$ are probably due to the GeD and GeH bends, respectively, since no corresponding Raman bands are observed for $(CH_3)_3GeH$ or $(CD_3)_3GeD$ in the same region. Assignment of the other bands is impossible without the aid of normal coordinate calculations.

The two GeC_3 deformation modes (A_1 and E) should be expected in the region below 300 cm^{-1},

Table 2. Observed and calculated frequencies (cm^{-1}) for $(CH_3)_3GeH$

No.	Infrared gas	Raman liquid	Calcd	PED
1	2982	2982	2986	$100S_1$
2	2922	2913	2914	$99S_2$
3	2040	2036	2041	$100S_3$
4	1426	1419	1425	$97S_4$
5	1246	1247	1250	$85S_5$, $10S_2$
6	833	830	830	$95S_6$
7	571*	573	578	$98S_7$
8	187	189	188	$77S_8$, $23S_6$
13	2982	2982	2987	$77S_{13}$, $23S_{14}$
14	2982	2982	2986	$77S_{14}$, $23S_{13}$
15	2922	2913	2914	$99S_{15}$
16	1426	1419	1425	$90S_{16}$
17	1426	1419	1425	$88S_{17}$
18	1246	1247	1251	$86S_{18}$, $10S_{15}$
19	624*	626	627	$44S_{19}$, $43S_{21}$, $12S_{22}$
20	833	830	834	$89S_{20}$
21	850*	850	852	$45S_{21}$, $43S_{19}$
22	592	597	604	$79S_{22}$, $12S_{21}$
23	187	189	188	$99S_{23}$

* The frequency is taken from the solid state spectrum.

Table 3. Observed and calculated frequencies (cm^{-1}) for $(CH_3)_3GeD$

No.	Infrared gas	Raman liquid	Calcd	PED
1	2982	2982	2986	$100S_1$
2	2920	2913	2914	$99S_2$
3	1470	1467	1454	$100S_3$
4	1410	1420	1425	$97S_4$
5	1248	1249	1250	$85S_5$, $10S_2$
6	833	830	829	$95S_6$
7	570*	574	578	$98S_7$
8	187	190	187	$77S_8$, $23S_6$
13	2982	2982	2987	$76S_{13}$, $24S_{14}$
14	2982	2982	2987	$76S_{14}$, $24S_{13}$
15	2920	2913	2914	$99S_{15}$
16	1410	1420	1424	$91S_{16}$
17	1410	1420	1425	$89S_{17}$
18	1248	1249	1251	$86S_{18}$, $10S_{15}$
19	787	785	783	$85S_{19}$, $10S_{21}$
20	833	830	836	$94S_{20}$
21	490	490	486	$78S_{21}$, $20S_{19}$
22	603	606	610	$94S_{22}$
23	187	190	188	$99S_{23}$

* See the footnote in Table 2.

Table 4. Observed and calculated frequencies (cm^{-1}) for $(CD_3)_3GeH$

No.	Infrared gas	Raman liquid	Calcd	PED
1	2236	2232	2227	$99S_1$
2	2129	2123	2121	$97S_2$
3	2041	2032	2041	$100S_3$
4	1043	1038	1030	$98S_4$
5	976	969	966	$75S_5$, $13S_2$, $12S_7$
6	654	650	649	$90S_6$
7	520*	520	515	$88S_7$
8	160	163	163	$73S_8$, $27S_6$
13	2236	2232	2225	$52S_{13}$, $47S_{14}$
14	2236	2232	2226	$52S_{14}$, $47S_{13}$
15	2129	2123	2121	$97S_{15}$
16	1043	1038	1031	$83S_{16}$, $15S_{17}$
17	1043	1038	1029	$82S_{17}$, $15S_{16}$
18	976	969	965	$75S_{18}$, $13S_{15}$
19	511	500	505	$76S_{19}$, $23S_{21}$
20	654	650	633	$90S_{20}$
21	787	780	780	$89S_{21}$, $10S_{19}$
22	552	553	548	$86S_{22}$
23	160	163	166	$97S_{23}$

* See the footnote in Table 2.

Table 5. Observed and calculated frequencies (cm^{-1}) for $(CD_3)_3GeD$

No.	Infrared gas	Raman liquid	Calcd	PED
1	2235	2232	2227	$99S_1$
2	2128	2122	2121	$97S_2$
3	1468	1463	1454	$100S_3$
4	1038	1037	1030	$98S_4$
5	976	969	966	$75S_5$, $13S_2$, $12S_7$
6	649	646	649	$90S_6$
7	520*	520	514	$88S_7$
8	161	163	163	$73S_8$, $27S_6$
13	2235	2232	2225	$56S_{13}$, $43S_{14}$
14	2235	2232	2226	$56S_{14}$, $43S_{13}$
15	2128	2122	2121	$97S_{15}$
16	1038	1037	1031	$82S_{16}$, $16S_{17}$
17	1038	1037	1029	$81S_{17}$, $16S_{16}$
18	976	969	965	$75S_{18}$, $13S_{15}$
19	649	646	646	$27S_{19}$, $34S_{20}$, $27S_{21}$
20	635*	646	626	$65S_{20}$, $20S_{21}$, $12S_{21}$
21	447	448	444	$55S_{21}$, $44S_{19}$
22	550	551	546	$81S_{22}$
23	161	163	166	$97S_{23}$

* See the footnote in Table 2.

However, only one band is observed in the infrared and Raman spectra for each isotopic compound below 300 cm^{-1}. It may be considered that these two vibrations coincide with each other in the present compounds, since in $(CH_3)_3GeCl$ the A_1 and E GeC_3 deformation modes are observed in the Raman spectra as two closely positioned bands at 193 and 185 cm^{-1}.[7]

Normal Coordinate Calculations and Discussion

Normal coordinate calculations were carried out by Wilson's GF-matrix method on an ACOS 77/900 computer at the Computer Center, Tohoku University, the iterative least-squares procedure being used in the usual way. The G matrix was calculated by

use of the molecular parameters determined from microwave study[12] (r(Ge–H)=0.1532 nm, r(Ge–C)=0.1947 nm, r(C–H)=0.1905 nm, ∠C–Ge–C=109.6°) and by assuming a tetrahedral angle around carbon atoms. In the calculations the observed frequencies were weighted by $(1/\lambda)$. The torsional mode was neglected in the E class.

A least-squares refinement was carried out in terms of symmetry force constants which had been fitted simultaneously to the observed frequencies for the four isotopic species. This refinement was carried out in the same manner as with the acetonitrile-borane adduct[13] and trimethylsilane.[1] The calculated frequencies have an average error of 0.39% for A_1 vibrations and 0.59% for E vibrations. The sum of the weighted squares of errors $\Sigma(\lambda_{obsd}-\lambda_{calcd})^2/\lambda_{obsd}$ was 1.7×10^{-3} for A_1 vibrations and 3.2×10^{-3} for E vibrations. The symmetry force constants, together with the uncertainty ranges from the last cycle in the least-squares refinement, are given in Table 6.

Table 6. Symmetry force constants for trimethylgermane[a]

	Constant	σ		Constant	σ
F_1	4.739	0.011	F_{13}	4.754	0.014
F_2	4.715	0.055	F_{14}	4.743	0.014
F_3	2.439	0.008	F_{15}	4.718	0.062
F_4	0.527	0.003	F_{16}	0.527	0.003
F_5	0.510	0.016	F_{17}	0.522	0.003
F_6	0.415	0.017	F_{18}	0.512	0.018
F_7	2.803	0.041	F_{19}	0.381	0.007
F_8	0.620	0.070	F_{20}	0.479	0.005
			F_{21}	0.482	0.007
$F_{2,5}$	−0.388	0.067	F_{22}	2.596	0.040
$F_{5,7}$	−0.145	0.032	F_{23}	0.457	0.018
$F_{6,8}$	−0.216	0.045			
			$F_{15,18}$	−0.388	0.076
			$F_{18,22}$	−0.144	0.033
			$F_{19,21}$	0.102	0.004
			$F_{21,22}$	0.016	0.026

a) The stretching force constants are given in 10^2 N m^{-1}, the deformation force constants in 10^{-18} N m rad^{-2}, and the stretching-deformation interaction constants in 10^{-8} N rad^{-1}. The subscript number i in F_i corresponds with that in S_i in Table 1.

Table 7. Comparison of force constants (10^2 N m^{-1}), bond distances (nm), and bond angles (°)

	f(Ge–CH_3)	r(Ge–CH_3)	(CH_3–Ge–CH_3)
$(CH_3)_3GeCN$	2.83[8]	0.1930±0.0006[15]	114.8±0.1[15]
$(CH_3)_3GeCl$	2.69[7]	0.1940±0.0003[16]	112.8±0.5[16]
$(CH_3)_3GeH$	2.67[a]	0.1947±0.0006[12]	109.6±0.2[12]
$(CH_3)_4Ge$	2.65[14]	0.1945±0.0003[17]	109.5[17]

a) Present work.

Potential energy distributions also are given in Tables 2—5. It is clear from these tables that the methyl rocks (S_{19} and S_{20}) and the GeH or GeD bend (S_{21}) are strongly coupled with each other.

The valence force constant of the Ge–CH_3 bond, derived from the symmetry force constants, is given in Table 7, together with those of the related compounds. The Ge–CH_3 bond distances and CH_3–Ge–CH_3 angles, determined by the microwave and electron diffraction study, are included for each compound in Table 7. The Ge–CH_3 force constant for the present compound is nearly equal to those for $(CH_3)_4Ge$ and $(CH_3)_3GeCl$ and slightly smaller than that for $(CH_3)_3GeCN$. This is in agreement with what might be expected from the Ge–CH_3 bond distances and CH_3–Ge–CH_3 bond angles.

This work was partly supported by a grant from the Asahi Glass Foundation for Industrial Technology to which our thanks are due. One of the authors (Y. I.) wishes to express his thanks to Prof. Fumio Watari, Iwate University, for the computer programs used in calculations.

References

1) Y. Imai and K. Aida, *Bull. Chem. Soc. Jpn.*, **54**, 925 (1981).
2) L. M. Sverdlov, M. A. Kovner, and E. P. Krainov, "Vibrational Spectra of Polyatomic Molecules," John Wiley & Sons, New York (1974), p. 562.
3) Y. P. Egorov, V. P. Morozov, and N. F. Kovalenko, *Ukr. Khim. Zh.*, **31**, 123 (1965); *Chem. Abstr.*, **63**, 3771b (1965).
4) R. Mathis, J. Satge, and F. Mathis, *Spectrochim. Acta*, **18**, 1463 (1962).
5) V. A. Ponomarenko, G. Y. Zueva, and N. S. Andreev, *Izv. Akad. Nauk SSSR, Otd. Khim. Nauk*, 1758 (1961); *Chem. Abstr.*, **58**, 3904e (1963).
6) D. F. Van de Vondel and G. P. Van der Kelen, *Bull. Soc. Chim. Belg.*, **74**, 467 (1965).
7) J. R. Durig, K. K. Lau, J. B. Turner, and J. Bragin, *J. Mol. Spectrosc.*, **31**, 419 (1969).
8) F. Watari, *J. Mol. Struct.*, **32**, 285 (1976).
9) R. Eujen and H. Bürger, *Spectrochim. Acta, Part A*, **35**, 1135 (1979).
10) J. Nakovich, Jr., S. D. Shook, and F. A. Miller, *Spectrochim. Acta, Part A*, **35**, 495 (1979).
11) R. D. George, K. M. Mackay, and S. R. Stobart, *J. Chem. Soc., A*, 3250 (1970).
12) J. R. Durig, M. M. Chen, Y. S. Li, and J. B. Turner, *J. Phys. Chem.*, **77**, 227 (1973).
13) F. Watari, *J. Phys. Chem.*, **84**, 448 (1980).
14) F. Watari, *Spectrochim. Acta, Part A*, **34**, 1239 (1978).
15) J. R. Durig, Y. S. Li, and J. B. Turner, *Inorg. Chem.*, **13**, 1495 (1974).
16) J. R. Durig and K. L. Hellams, *J. Mol. Struct.*, **29**, 349 (1975).
17) J. L. Hencher and F. J. Mustoe, *Can. J. Chem.*, **53**, 3542 (1975).

Mass-spectrometric Study of the Vaporization of Magnesium Oxide from Magnesium Aluminate Spinel

Tadashi SASAMOTO,*,† Hiroshi HARA,†† and Toshiyuki SATA

Research Laboratory of Engineering Materials, Tokyo Institute of Technology, 4259 Nagatsuta, Midori-ku, Yokohama 227

(Received Nobember 7, 1980)

The partial vapor pressures of Mg(g) over the spinel solid solution system, $MgO \cdot nAl_2O_3$(n=1.0, 2.0, and 2.8), have been measured by the mass-spectrometric Knudsen-cell method. In the temperature range from 1850 to 2300 K, the pressures are described by these equations:

$\log[P(\mathrm{Mg,g})\text{ over }1.0\text{-spinel/atm}] = 7.72 \pm 0.24 - (26900 \pm 490)/T$,

$\log[P(\mathrm{Mg,g})\text{ over }2.0\text{-spinel/atm}] = 7.72 \pm 0.32 - (27400 \pm 670)/T$,

$\log[P(\mathrm{Mg,g})\text{ over }2.8\text{-spinel/atm}] = 7.78 \pm 0.42 - (27900 \pm 1220)/T$.

These observed values were discussed in comparison with the calculated ones obtained by an approximate thermodynamic treatment of an ionic solid solution with composition-dependent vacancies.

In a previous paper[1] one of the present authors (T. Sata) reported that the vaporization of a magnesia component from spinels, $MgO \cdot 0.9Al_2O_3$ and $MgO \cdot 2.8Al_2O_3$, proceeds in two stages: the initial stage with a constant rate before the free surface is covered with the corundum precipitating during the preferential vaporization of the magnesia component, and the second stage controlled by the diffusion of O^{2-} ions through the corundum layer. It was concluded that the vaporization rate at the initial stage was controlled by the decomposition reaction, the activation energies of which were 587 and 327 kJ/mol for $MgO \cdot 0.9Al_2O_3$ and $MgO \cdot 2.8Al_2O_3$ respectively.

The aim of the present study is to measure the equilibrium vapor pressures and vaporization coefficients of Mg(g) and the activities of the magnesia component in the initial stage of the vaporization reaction in the spinel solid solution system, $MgAl_2O_4$–Al_2O_3, and to provide data for discussing the detailed mechanism of the vaporization of a defective spinel the vapor pressure of which is affected by vacancies induced by the dissolution of Al_2O_3, and to compare the observed vapor pressures with those calculated by the approximate treatment of thermodynamics, considering the electrical neutrality condition and the vacancy concentrations.

Experimental

Instrument. The instrument used for the measurement of the vapor pressure was a JMS-01BK-type double-focussing mass spectrometer equipped with a Knudsen-cell ion source, which had been described by Watanabe *et al.*[2,3] The main advantages of this mass spectrometer in the Knudsen measurement are: (1) high resolution, (2) the two ion-detecting systems of the electrical and photographic methods, and (3) the facility of sample exchange.

The Knudsen cell assembly, the ion source, and the slit system are shown in Fig. 1. The Knudsen cells, made of tungsten, sometimes has a ThO_2 liner; they were about 10 mm in both inner diameter and height. The knife-edge effusion orifice of the W or ThO_2 lid was 0.5 mm or 0.3 mm in diameter, so that the ratio of the effusion hole area to the sample surface area was less than about 1/400. The cell was set within the outer cell by means of the three legs and indirectly heated by the radiation from the outer cell, which was heated by electron bombardment. Although the temperature gradient in the cell was not checked, it must has been sufficiently small because the cell was set in an outer cell as a thermal block and the positions of the W-filaments for the electron bombardment were carefuly regulated. The cell temperature was measured both with the optical pyrometer, which was sighted into the orifice of the cell through a quartz window, and with a W-5%Re/W-26%Re thermocouple positioned under the bottom of the cell. The calibration for the thermocouple was carried out by comparison with the temperature of the cell with a graphite liner measured by the pyrometer calibrated against the standard lamp and by taking advantage of the plateau of the ion intensity on the basis of the constancy of the vapor pressure at the melting points of several high-purity metals. The estimated uncertainty of the determined temperature was less than ±1%.

The resolving power, $M/\Delta M$, measured using the peaks of two silver ions, $^{107}Ag^+$ and $^{109}Ag^+$, was about 2600 for

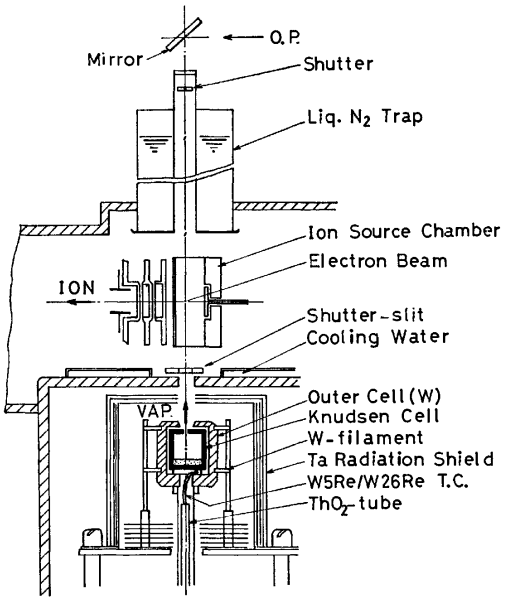

Fig. 1. Mass spectrometer with Knudsen-cell ion source.

† Present address: Tokyo National Technical College, 1220-2 Kunugida, Hachioji, Tokyo 193.

†† Present address: The Institute of Public Health, 4-6-1 Shirokanedai, Minato-ku, Tokyo 108.

the main slit width of 30 μm. It was enough for separating peaks of metal ions from the background peaks of hydrocarbon caused mainly by the decomposition of the diffusion oil. Since the shutter effect for permanent gases like oxygen was difficult to be obtained because of the imperfection of the slit mechanism and the insufficient evacuating ability, it was not possible for such a permanent gas to be distinguished from non-condensable residual gases in the source region of the mass spectrometer. The partial pressures of O_2 and O, therefore, could not be measured in this experiment.

The operational conditions of the ion source were as follows: ionization potential, 30 eV; ionization current, 500 μA; ion-accelerating voltage, 7.8 kV, and temperature of ionization chamber, 250 °C.

Procedure. About 350 mg of a sample (35—100 mesh grains) was placed in the cell with a weighed quantity of about 3 mg of the silver powder used as the reference material for vapor pressure. The Knudsen cell was then evacuated and heated by radiation from W-filaments up to 1400 K, followed by the electron bombardment. The vacuum was kept approximately in the 10^{-9} atm region at elevated temperatures.

When the temperature reached about 1300 K, the silver vapor beam effusing from the cell was ionized by electron impact with an energy of 30 eV, and the intensity of the $^{107}Ag^+$ ion beam was measured in order to determine the relation between the vapor pressure inside the cell and the intensity of the corresponding ion. After the silver had been completely vaporized, the temperature of the cell was rapidly raised up to a given temperature of from 1800 to 2300 K, and then we began to measure the Mg^+ ion intensity.

In the experiments using a photoplate as a detector, a few mg of copper were placed in the W-cell, together with a sample, as the reference material for both the vapor pressure and the calibration of the sensitivity of the photoplate(Ilford Q2). The conversion of the blackness of the spectrum on the plate into the relative ion intensity was carried out by means of Seidel's blackness *versus* relative ion-intensity curve, obtained by the two-line method using two isotope ions, $^{63}Cu^+$ and $^{65}Cu^+$. Sometimes, instead of copper, such stable background peaks as CO^+, N_2^+, O_2^+, and CO_2^+ were also successfully used.

The conversion of the ion intensities to the absolute pressures of Mg(g) was calculated by using the following equations:[4]

$$P(\mathrm{Mg}) = K_1 K_2 I(^{24}\mathrm{Mg}^+) T(\mathrm{Mg}), \quad (1)$$

$$K_1 = \frac{P(\mathrm{Ag}) r(^{107}\mathrm{Ag})}{I(^{107}\mathrm{Ag}^+) T(\mathrm{Ag})}, \quad (2)$$

$$K_2 = \frac{\sigma(\mathrm{Ag}) \Delta E(\mathrm{Ag}^+) \gamma(\mathrm{Ag}^+)}{\sigma(\mathrm{Mg}) \Delta E(\mathrm{Mg}^+) \gamma(^{24}\mathrm{Mg}^+)}, \quad (3)$$

where K_1 and K_2 were the proportionality constants and P was the vapor pressure; I, the ion current; T, the absolute cell temperature; σ, the first ionization cross section given by Mann;[5] r, the isotopic abundance ratio; γ, the electron multiplier efficiency for ions in the first stage of the dynode, and $\Delta E = E - E_{AP}$, where E_{AP} was the appearance potential, and E, the energy of the ionization electron in eV. K_1 is called the calibration factor or the sensitivity factor.

Samples. Three kinds of single-crystal spinels with molar ratios of MgO to Al_2O_3 of 1.0 to 1.0 (called 1.0-spinel for simplicity), 1.0 to 2.0 (2.0-spinel), and 1.0 to 2.8 (2.8-spinel), prepared by the flame-fusion method, were used. The molar ratios of MgO to Al_2O_3 were determined by measuring the X-ray lattice parameters on the basis of the data of Shirasuga *et al.*[6] The lattice parameters calculated from the (8.4.4), and (9.3.1) peaks were $a=8.079$ Å for the stoichiometric spinel, 1.0-spinel, $a=7.992$ Å for the 2.0-spinel, and $a=7.978$ Å for the 2.8-spinel.

Results

Vaporization of Spinel from Tungsten Cell. The intensities of ions formed from the gaseous species over the spinel/W-cell system were measured by the photographic detecting method. Figure 2 shows the time dependence of the ion intensities for the 2.8-spinel/W-cell system at 2180 K. Of these ions, the parent ones were determined from the appearance-potential data to be Mg^+, WO_2^+, WO_2^+, WO_3^+, Al^+, and AlO^+. This shows that the tungsten cell reacts with MgO to produce volatile W-oxides. The vapor pressure ratios, WO_2/WO_3 and AlO/Al, were about 2 and 27 respectively, these ratios agreed with those in the mass-spectrometric studies of the kinetics of the W–O_2 reaction by Berkowitz-Mattuck *et al.*[7] and Shissel *et al.*[8] and with those of the equilibrium vapor pressures in the W–Al_2O_3 system reported by Drowart *et al.*[9] Although the peak at $m/e=40$ corresponding to MgO(g) was observed, the existence of molecular species MgO(g) was ambiguous because of the superposition of the $^{40}(MgO)^+$ and $^{40}Ca^+$ peaks, as was pointed out by Drowart *et al.*[10] No other complex vapor, such as Al_2O, Al_2O_2, and $(WO_3)_n (n>4)$, was detected, since such vapors were present in quantities less than the detection limit of the instrument. The time dependences of the vapor-pressure ratios of Mg(g) to Al(g) at each temperature are shown in Fig. 3. These values lay approximately in the range from 10^2 to 10^3.

Figure 4 plots the partial vapor pressures of Mg(g),

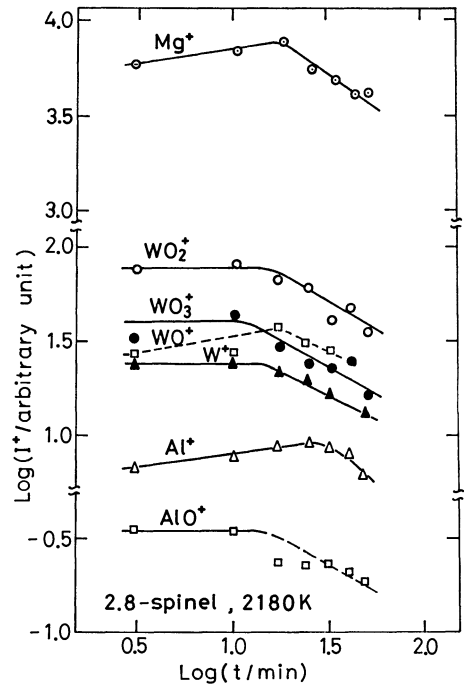

Fig. 2. Intensity of ions formed from gas species over the 2.8-spinel/W-cell system at 2180 K detected by a photographic plate.

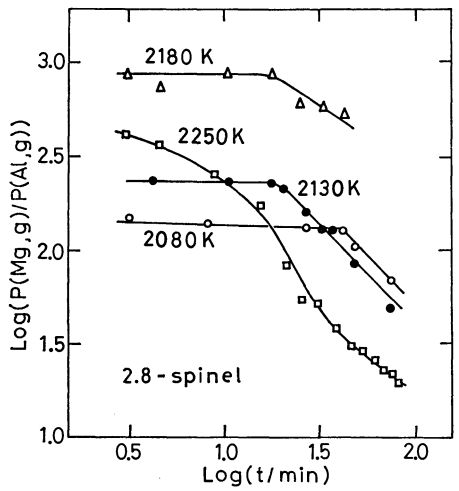

Fig. 3. Time-dependence of ratio of P(Mg,g) to P(Al, g) in the system 2.8-spinel/W-cell.

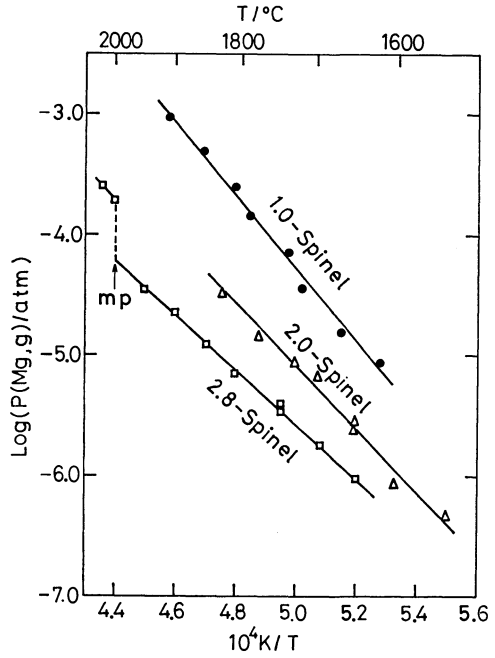

Fig. 4. Partial pressures of Mg(g) over the n-spinel/W-cell system as a function of reciprocal absolute temperature.

P(Mg), as a function of $1/T$. From the slopes of these lines, the heats of vaporization for Mg(g) over spinel were calculated to be 574, 494, and 436 kJ/mol for 1.0-, 2.0-, and 2.8-spinel respectively. The heat of vaporization for Mg(g) over pure MgO(s) was also determined to be 418 kJ/mol.

Vaporization of Spinels from W-Cell with a ThO_2 Liner. Figure 5 shows a typical time-dependence of the ion intensities of $^{24}Mg^+$ detected by means of a secondary electron multiplier (SEM) for 1.0- and 2.8-spinels. The appearance potential for Mg^+ obtained from the ionization efficiency measurement was 7.3 eV. This value means that the Mg^+ ion results from the simple ionization process. As can be seen in Fig. 5(A), a plateau of ion intensity was initially observed for the 1.0-spinel; a similar result was also obtained for the

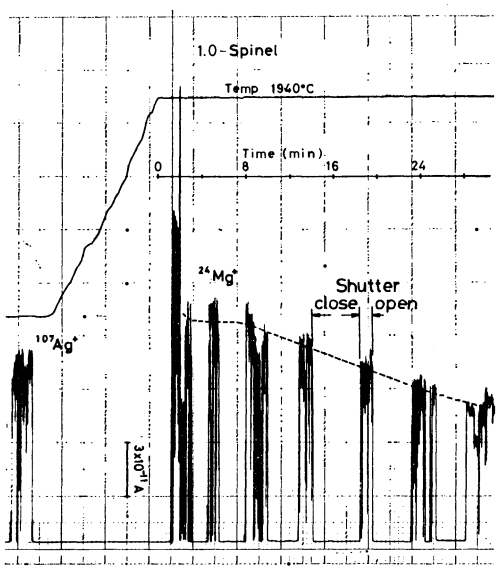

(A)

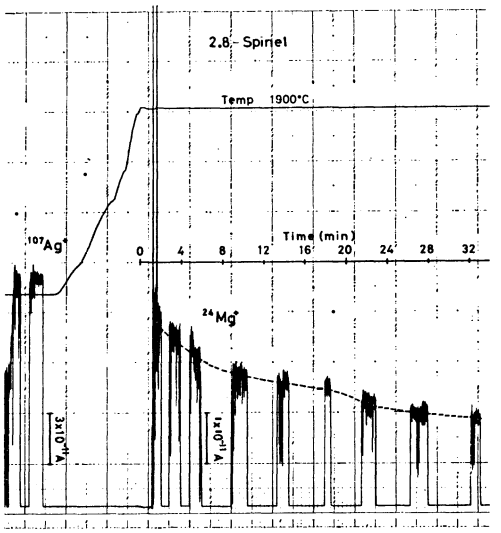

(B)

Fig. 5. Typical examples of the time-dependence of the ion intensities of $^{24}Mg^+$ on (A) 1.0-spinel and (B) 2.8-spinel.

2.0-spinel. In the case of the 2.8-spinel, however, no plateau appeared and the ion intensity decreased with time, as is shown in Fig. 5(B). This was because the vaporizing surface was gradually covered with the precipitated alumina. Therefore, the ion intensities extrapolated to the intercept of time=0 were employed in the calculation of the equilibrium vapor pressure.

Figure 6 shows the van't Hoff plots of magnesium vapor pressure over the 1.0-spinel, P(Mg, g), calculated from Eq. 1 using the values of the ion intensity obtained by the step-by-step measurement in which the temperature was raised, step by step, at intervals of from 5 to 10 min. The vapor pressures obtained by both the step-by-step and isothermal measurements were in good agreement with each other. The values of P(Mg) over the 1.0-spinel were about half of that over pure MgO and were formulated by the least-squares method in the temperature range from 1850

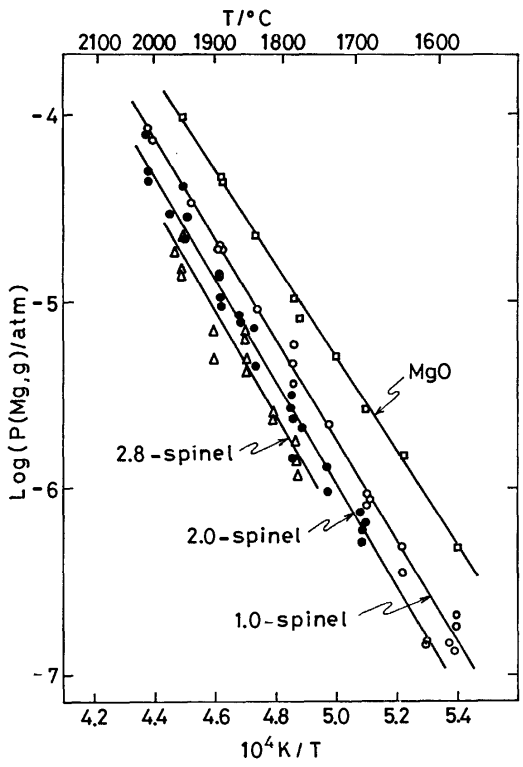

Fig. 6. Equilibrium vapor pressures of Mg(g) over the systems of *n*-spinel or magnesia/ThO_2-lined W-cell.

to 2300 K as follows:

$$\log[P(\mathrm{Mg,\ g})/\mathrm{atm}] = 7.72\pm0.24 - (26900\pm490)/T. \quad (4)$$

A similar temperature-dependence was obtained in the isothermal:

$$\log[P(\mathrm{Mg,\ g})/\mathrm{atm}] = 7.72\pm0.32 - (27400\pm670)/T. \quad (5)$$

For the 2.8-spinel, the initial values obtained in the isothermal experiment were plotted against $1/T$ for the reason described above, and the following equation was obtained:

$$\log[P(\mathrm{Mg,\ g})/\mathrm{atm}] = 7.78\pm0.42 - (27900\pm1220)/T. \quad (6)$$

The vapor pressures of P(Mg) over pure MgO(s) were given by this equation:

$$\log[P(\mathrm{Mg,\ g})/\mathrm{atm}] = 7.29\pm0.18 - (25200\pm310)/T. \quad (7)$$

Table 1 shows the activities of the magnesia component, a(MgO), as calculated by this equation:

$$a(\mathrm{MgO}) = \frac{P(\mathrm{Mg,\ g})\text{ over }n\text{-spinel(s)}}{P(\mathrm{Mg,\ g})\text{ over MgO(s)}}, \quad (8)$$

using P(Mg, g) over MgO and the *n*-spinel given by Eqs. 4 to 7.

Using the Langmuir vapor pressures given by Sata *et al.*,[1] the apparent vaporization coefficient of Mg(g) over the 1.0-spinel was given by this equation:

$$\log \alpha_v = \log[P_L(\mathrm{Mg,\ g})/P_K(\mathrm{Mg,\ g})], \quad (9)$$

$$= -0.833 - (1330/T) \quad (10)$$

where P_L is the vapor pressure in the Langmuir free vaporization, and P_K the Knudsen vapor pressure, the equilibrium vapor pressure. From this equation, α_v at the melting point, $\simeq$2100 °C, was found not to be equal to unity; this was also observed in the experiment on the 2.8-spinel/W-cell system, as is shown in Fig. 4. These results differed from those for α's for MgO[11] and $MgCr_2O_4$.[12]

Discussion

If we use the phase diagrams of the MgO–Al_2O_3 system[13,14] and the *JANAF Tables*[15] for the following reaction:

$$MgAl_2O_4(s) = Mg(g) + \frac{1}{2}O_2(g) + Al_2O_3(s), \quad (11)$$

and calculate the activities of the magnesium component, a(Mg), at 1800 °C in a spinel solution on the basis of Raoult's law, we could expect the relation between a(MgO) and Al_2O_3 composition shown in Fig. 7. The measured values plotted in the figure, however, greatly deviated from the expected ones. This might come from the application of Eq. 11 as the vaporization reaction for this case; the Al_2O_3 on the right-hand side in Eq. 11 should be replaced by the spinel solid solution ($n>1$), because $MgAl_2O_4$ and Al_2O_3 do not exist together, as can be seen from the phase diagram of Fig. 7. In fact, as is shown in Fig. 8, the P(Mg) values over $MgAl_2O_4$(s) calculated from the *JANAF Tables*[15] on the basis of $MgAl_2O_4(s) = Mg(g) + 1/2O_2(g) + Al_2O_3(s)$ were smaller than our values and those of the literature.[16,17] Altman[16] suggested that the alumina produced by the vaporization reaction immediately formed a spinel solid solution with $MgAl_2O_4$ and decreased the activity of MgO.

Considering the above discussion, the desired P-(Mg) over the single-phase of *n*-spinel, $P_{Mg/n\text{-spinel}}$, was determined by the following steps: first, P(Mg) over the two-phase region of the spinel-corundum, $P_{Mg/two\text{-}phase}$, was calculated using mainly the *JANAF*

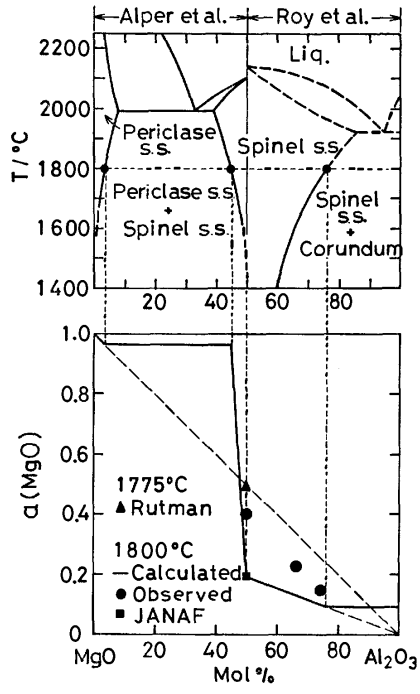

Fig. 7. Calculated relative vapor pressure of Mg(g) over the MgO–Al_2O_3 system assuming the Raoult's law.

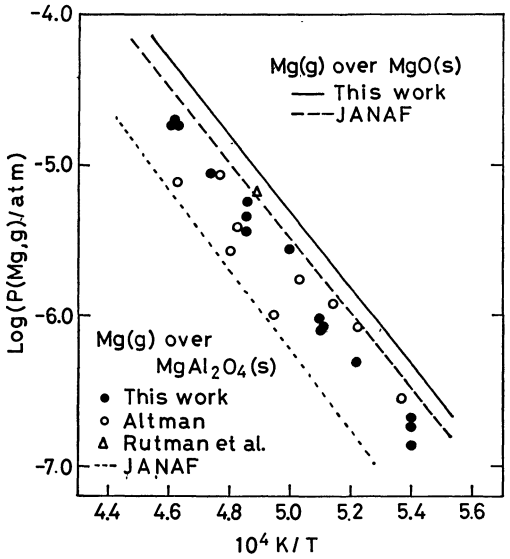

Fig. 8. Comparison of observed Knudsen vapor pressures of Mg(g) over 1.0-spinel with JANAF data.

Tables; next, the relative $P(\mathrm{Mg})$ over the single n-spinel on an arbitrary basis, $P'_{\mathrm{Mg}/n\text{-spinel}}$, was estimated as a function of the composition, n, by applying the method by Nakano[18] and Koumoto *et al.*;[19] and finally, $P'_{\mathrm{Mg}/n\text{-spinel}}$ was converted to $P_{\mathrm{Mg}/n\text{-spinel}}$ using an appropriate correction factor, which was obtained by comparing $P'_{\mathrm{Mg}/n\text{-spinel}}$ with $P_{\mathrm{Mg}/\mathrm{two\text{-}phase}}$ at the solubility limit of Al_2O_3 in the spinel.

The vaporization reaction in the two-phase region is as follows:

$$\mathrm{Mg}_{4/3n+1}\mathrm{Al}_{8n/3n+1}\mathrm{O}_4(\mathrm{s}) = \frac{4}{3n+1}\mathrm{Mg}(\mathrm{g}) + \frac{1}{3n+1}\mathrm{O}_2(\mathrm{g}) + \frac{4n}{3n+1}\mathrm{Al}_2\mathrm{O}_3(\mathrm{s},\alpha) + \Delta G_{\mathrm{v}}, \tag{12}$$

where α donates alpha-type alumina, *i.e.*, corundum. This reaction is decomposed into the following three reactions:

$$\frac{4}{3n+1}\mathrm{MgAl}_2\mathrm{O}_4(\mathrm{s}) + \frac{4(n-1)}{3n+1}\mathrm{Al}_2\mathrm{O}_3(\mathrm{s},\alpha) = \mathrm{Mg}_{4/3n+1}\mathrm{Al}_{8n/3n+1}\mathrm{O}_4(\mathrm{s}) + \Delta G_1, \tag{13}$$

$$\mathrm{MgO}(\mathrm{s}) + \mathrm{Al}_2\mathrm{O}_3(\mathrm{s},\alpha) = \mathrm{MgAl}_2\mathrm{O}_4(\mathrm{s}) + \Delta G_2, \tag{14}$$

$$\mathrm{MgO}(\mathrm{s}) = \mathrm{Mg}(\mathrm{g}) + \frac{1}{2}\mathrm{O}_2(\mathrm{g}) + \Delta G_3, \tag{15}$$

where ΔG denotes the Gibbs energy. By combining Eqs. 13, 14, and 15, the following equation was derived:

$$\frac{P_{\mathrm{Mg}/n\text{-spinel}}}{P_{\mathrm{Mg/MgO}}} = \exp\left[\frac{3n+1}{6}\left(\frac{\Delta G_1}{RT}\right)+\frac{2}{3}\left(\frac{\Delta G_2}{RT}\right)\right], \tag{16}$$

where $P_{\mathrm{Mg}/n\text{-spinel}}$ and $P_{\mathrm{Mg/MgO}}$ stand for the partial pressure of Mg(g) over the n-spinel(s) and MgO(s) respectively.

Here, ΔG_2 can be obtained from the *JANAF Tables*.[15] On the other hand, the ΔG_1 for the formation reaction of a solid solution in Eq. 13 is given as the sum of the following two Gibbs energies:

Table 1. Activities of magnesia component, $a(\mathrm{MgO})$, in the spinel solid-solution system $\mathrm{MgO}\cdot n\mathrm{Al}_2\mathrm{O}_3$

Specimen	a(MgO)			
	1700 °C	1800 °C	1900 °C	2000 °C
1.0-Spinel	0.376	0.408	0.444	0.481
2.0-Spinel	0.206	0.234	0.262	0.290
2.8-Spinel	—	0.154	0.177	0.200

$$\frac{4}{3n+1}\mathrm{MgAl}_2\mathrm{O}_4(\mathrm{s}) + \frac{3(n-1)}{3n+1}\mathrm{Al}_{8/3}\mathrm{O}_4(\mathrm{s},\gamma) = \mathrm{Mg}_{4/3n+1}\mathrm{Al}_{8n/3n+1}\mathrm{O}_4(\mathrm{s}) + \Delta G_1', \tag{17}$$

$$\frac{4(n-1)}{3n+1}\mathrm{Al}_2\mathrm{O}_3(\mathrm{s},\alpha = \frac{4(n-1)}{3n+1}\mathrm{Al}_2\mathrm{O}_3(\mathrm{s},\gamma) + \Delta G_1'', \tag{18}$$

$$\Delta G_1 = \Delta G_1' + \Delta G_1'', \tag{19}$$

where γ stands for γ-type alumina.

Shirasuka *et al.*[20,21] have recently reported, on the basis of the DTA experiment, that the exsolution of alumina from the spinel body with $n=1.5$—5.6 was exothermic. It is thought that this exothermic reaction resulted from the γ to α-transformation reaction, as is shown in Eq. 18.

The $\Delta G_1''$ in Eq. 18 can be obtained from the *JANAF Tables*. The $\Delta G_1'$ for Eq. 17 was obtained in the following manner. As the change in the volume of this reaction was very small (for examples, −0.16% for 3.0-spinel), the enthalpy change for the reaction was considered to be negligibly small. Therefore, $\Delta G_1'$ is reduced to:

$$\Delta G_1' \simeq -T\Delta S_{\mathrm{m}}, \tag{20}$$

where ΔS_{m} is the mixing entropy for Eq. 17. Here, ΔS_{m} is obtained by simple statistical thermodynamics on the assumption that the cations and cation vacancies are distributed randomly at tetrahedral and octahedral sites at a high temperature in the case of a spinel solid solution with the composition of $\mathrm{MgO}\cdot n\mathrm{Al}_2\mathrm{O}_3=(3n+1)/4\mathrm{Mg}_{4/(3n+1)}\mathrm{Al}_{8n/(3n+1)}\square_{(n-1)/(3n+1)}\mathrm{O}_4$. Let N_{t} be the total number of cation sites, and let N_{Mg}, N_{Al}, and N_{v} be the numbers of the Mg^{2+}, Al^{3+}, and cation vacancies respectively. Then, the following relationships hold:

$$\left.\begin{aligned} N_{\mathrm{t}} &= 3N_{\mathrm{A}},\\ N_{\mathrm{Mg}} &= \left(\frac{4}{3n+1}\right)\frac{N_{\mathrm{t}}}{3},\\ N_{\mathrm{Al}} &= \left(\frac{8n}{3n+1}\right)\frac{N_{\mathrm{t}}}{3},\\ N_{\mathrm{v}} &= N_{\mathrm{t}} - N_{\mathrm{Mg}} - N_{\mathrm{Al}} = \left(\frac{n-1}{3n+1}\right)\frac{N_{\mathrm{t}}}{3}, \end{aligned}\right\} \tag{21}$$

where N_{A} is Avogadro's constant. The number of distinguishable arrangements of cations and cation vacancies, W, is expressed as follows:

$$W = \frac{N_{\mathrm{t}}!}{N_{\mathrm{Mg}}!\,N_{\mathrm{Al}}!\,N_{\mathrm{v}}!}. \tag{22}$$

The contribution of mixing term to the entropy is expressed as:

$$S_{\mathrm{c}} = k\ln W, \tag{23}$$

Table 2. Gibbs energies relating to the vaporization reaction of spinels and the partial pressures of Mg(g) over various n-spinels

T/°C	n at T °C[a]	$\Delta G_1'$ for Eq. 17[b] kJ/mol	$\Delta G_1''$ for Eq. 18[c] kJ/mol	ΔG_2 for Eq. 14[c] kJ/mol	a(MgO) from Eq. 16	P(Mg) over n-spinel atm
1500	1.67	−6.116	8.588	−35.12	0.242	1.86×10^{-8}
1600	2.14	−7.428	7.775	−35.68	0.224	1.00×10^{-7}
1700	2.95	−8.077	6.950	−36.30	0.205	4.49×10^{-7}
1800	4.26	−7.951	6.129	−36.98	0.188	1.73×10^{-6}
1900	6.81	−6.941	5.291	−37.73	0.180	6.08×10^{-6}

a) n in $MgO\cdot nAl_2O_3$ on the solubility limit line at temperatures in the first column. b) Calculated from Eq. 25. c) From *JANAF Tables*.

where S_c denotes the configurational entropy. The substitution of Eqs. 21 and 22 into Eq. 23 yields the desired equation:

$$S_c(n) = -3R\left(\frac{N_{Mg}}{N_t}\ln\frac{N_{Mg}}{N_t}+\frac{N_{Al}}{N_t}\ln\frac{N_{Al}}{N_t}+\frac{N_v}{N_t}\ln\frac{N_v}{N_t}\right)$$
$$= \frac{-R}{3n+1}[4\ln4+8n\ln8n+(n-1)\ln(n-1)$$
$$-3(3n+1)\ln3(3n+1)], \quad (24)$$

and thus:

$$\Delta G_1' \simeq -T\Delta S_m$$
$$-\left[-T\left[S_c(n=n)-\frac{4}{3n+1}S_c(n=1)-\frac{3(n-1)}{3n+1}S_c(n=\infty)\right]\right]$$
$$= \frac{-RT}{3n+1}[8n\ln8n+(n-1)\ln(n-1)$$
$$-3(3n+1)\ln3(3n+1)+3.139n+10.045]. \quad (25)$$

The Gibbs energies of $\Delta G_1'$, $\Delta G_1''$, and ΔG_2 for the n-spinel on the solubility limit line at several temperatures between 1500 and 1900 °C are summarized in Table 2. From these Gibbs energies, and by applying Eq. 16, the ratios of P_{Mg} over the n-spinel(s) to P_{Mg} over MgO(s), *i.e.*, a(MgO), were calculated. The partial pressures of Mg(g) over the n-spinel, calculated using this a(MgO) and *JANAF* data for P(Mg) over pure MgO(s), are also shown in the last column in Table 2 and graphically in Fig. 9.

The partial pressures of Mg(g) over the spinel solid solution in the single-phase region are given by the following equation:[18,19]

$$\ln P(Mg,g)^{3/2} = \ln\frac{4}{3(3n+1)}\left[\frac{n-1}{3(3n+1)}\right]^{-1/4}+C$$
$$C = \frac{h_{MgO}-K_{Mg}-1/2K_{O_2}}{RT}, \quad (26)$$

where h_{MgO} is the enthalpy term and where K_{Mg} and K_{O_2} are constants independent of the composition. As it was assumed that a spinel solid solution is ideal; that $\Delta H_m\simeq0$, and that every vapor species behaves as a perfect gas, C should be constant. P(Mg) over n-spinel(s) in the single-solid solution region, therefore, can be obtained by shifting the P(Mg) calculated from Eq. 26 in the direction of the "pressure-axis" of the diagram for log$P$-*vs.*-n and joining it to the P(Mg) in the two-phase region. The results are shown in Fig. 9, along with the experimental values. The calculated values agreed with those obtained by mass spectrometry.

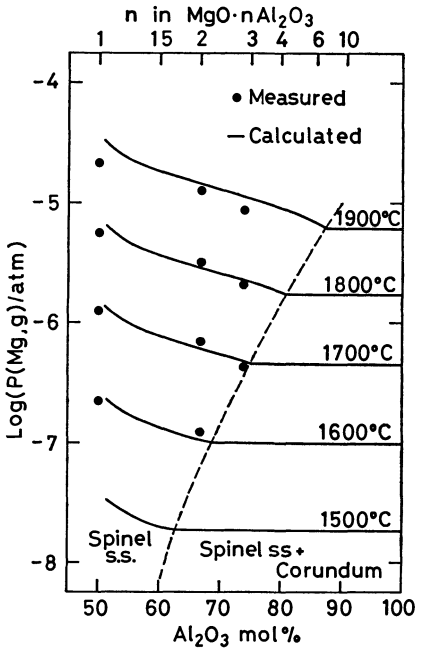

Fig. 9. Calculated and measured vapor pressures of Mg(g) over the system $MgAl_2O_4$–Al_2O_3.

We would like to thank Mr. Ryoichi Kondoh of the Tokyo Denki Kagaku Co., Ltd., for his assistance in obtaining the mass-spectrometric data.

References

1) T. Sata and T. Yokoyama, *Yogyo Kyokai Shi*, **81**, 501 (1973).
2) E. Watanabe and M. Naito, "Recent Developments in Mass Spectrometry," ed by K. Ogawa and T. Hayakawa, University of Tokyo Press (1970), p. 249.
3) E. Watanabe, M. Naitoh, and T. Aoyama, *Kogyo Kagaku Zasshi*, **67**, 1778 (1964).
4) R. T. Grimley, "The Characterization of High-Temperature Vapors," ed by J. L. Margrave, John Willey & Sons (1967), p. 222.
5) J. B. Mann, *J. Chem. Phys.*, **46**, 1646 (1967).
6) K. Shirasuka and G. Yamaguchi, *Yogyo Kyokai Shi*, **81**, 97 (1973); **82**, 650 (1974).
7) J. B. Berdowitz-Mattuck, A. Büchler, J. L. Engelke, and S. N. Goldstein, *J. Chem. Phys.*, **39**, 2722 (1963).
8) P. O. Scissel and O. C. Trulson, *J. Chem. Phys.*, **43**,

737 (1965).
9) J. Drowart, G. De Maria, R. P. Burns, and M. G. Inghram, *J. Chem. Phys.*, **32**, 1366 (1960).
10) J. Drowart, G. Exsten, and G. Verhaegen, *Trans. Faraday Soc.*, **60**, 1920 (1964).
11) T. Sasamoto, H.-L. Lee, and T. Sata, *Yogyo Kyokai Shi*, **82**, 603 (1974).
12) T. Sata and H.-L. Lee, *J. Am. Ceram. Soc.*, **61**, 326 (1978).
13) A. M. Alper, R. N. McNally, P. H. Ribble, and R. C. Doman, *J. Am. Ceram. Soc.*, **45**, 263 (1962).
14) D. M. Roy and E. F. Osborn, *J. Am. Cerm. Soc.*, **36**, 149 (1953).
15) JANAF Thermochemical Tables, 2nd ed.
16) R. L. Altman, *J. Chem. Phys.*, **67**, 366 (1963).
17) D. S. Rutman, I. L. Shchetnikova, E. I. Kelareva, and G. A. semenov, *Ogneupory*, No. 10, 40 (1968).
18) M. Nakano, *Yogyo Kyokai Shi*, **81**, 491 (1973).
19) K. Koumoto, S. Mizuta, and H. Yanagida, *Yogyo Kyokai Shi*, **88**, 217 (1980).
20) K. Shirasuka and G. Yamaguchi, *Yogyo Kyokai Shi*, **83**, 603 (1975).
21) K. Shirasuka, G. Yamaguchi, and M. Momoda, *Yogyo Kyokai Shi*, **84**, 523 (1976).

  Bull. Chem. Soc. Jpn., 54, 3334—3339 (1981) [Vol. 54, No. 11

The Formation Constants and Configurations of the Complexes of Cr(II), Mn(II), Fe(II), Co(II), Cu(II), and Zn(II) with 2,2′-Bipyridine and of Co(II) with 2,2′:6′,2″-Terpyridine in Hexamethylphosphoric Triamide

Yuriko Abe* and Goro Wada

Department of Chemistry, Nara Women's University, Nara 630

(Received December 13, 1980)

The absorption spectra and the first formation constants, K_1, of complexes $[M(bpy)]^{2+}$ (M(II)=Cr(II), Mn(II), Fe(II), Co(II), Cu(II), and Zn(II), bpy=2,2′-bipyridine) were determined spectrophotometrically in hexamethylphosphoric triamide(HMPA). The values of $\log K_1$ obtained were 4.61±0.02, 3.10±0.12, 4.82±0.04, 5.84±0.07, 7.33±0.02, and 1.77±0.07 for respective metal ions. The configurations of complexes $[M(bpy)]^{2+}$ were discussed on the basis of these data. The K_1 values of $[Cr(bpy)]^{2+}$, $[Mn(bpy)]^{2+}$, $[Fe(bpy)]^{2+}$, and $[Co(bpy)]^{2+}$ in HMPA are slightly larger than those in H_2O, indicating that their configurations are tetrahedral, whereas the value of $[Cu(bpy)]^{2+}$ in HMPA is slightly smaller than that in H_2O, indicating that its configuration in HMPA is either square planar or tetragonal. It seems that $[Zn(bpy)]^{2+}$ is octahedral in HMPA, because its K_1 value is smaller about three orders of magnitude than that in H_2O. In addition, the second formation constant, K_2, of complex $[Co(bpy)_2]^{2+}$, and the first and second formation constants of complexes $[Co(terpy)]^{2+}$ and $[Co(terpy)_2]^{2+}$ (terpy=2,2′:6′,2″-terpyridine) were also determined to be $\log K_2=3.59\pm0.03$ for the bpy complex, and $\log K_1=4.87\pm0.01$ and $\log K_2=3.35\pm0.01$ for the terpy complexes, respectively. These three complexes are concluded to be octahedral.

In a previous paper,[1] the configurations of solvated complex ions of the first transition metals (Mn(II), Fe(II), Co(II), Ni(II), Cu(II), and Zn(II)) in hexamethylphosphoric triamide (HMPA) were reported. It was found that the metal ions are tetrahedrally solvated in the cases of Mn(II), Fe(II), Co(II), and Cu(II), while equilibria are established among octahedral, square planar and tetrahedral solvated species in the case of Ni(II), and that Zn(II) forms probably an octahedrally solvated complex ion.

Now the problems on the complex-forming equilibria between the first transition metal ions and a ligand in HMPA are very interesting, since the configurations of the solvated ions in HMPA are widely different from those in water or in a number of other organic solvents, such as dimethyl sulfoxide, *N,N*-dimethylformamide, and methanol, in any of which the solvated ions are generally octahedral.

Up to date, however, no thermodynamic studies have been done yet except for the case of Co(II) complexes in HMPA.[2,3] In the present study, the absorption spectra and the values of the formation constants of the following complexes will be reported: the first formation constants, K_1, of complexes $[M(bpy)]^{2+}$ (M(II)=Cr(II), Mn(II), Fe(II), Co(II), Cu(II), or Zn(II), bpy=2,2′-bipyridine),† the second formation constant, K_2, of the complex $[Co(bpy)_2]^{2+}$, and the first and second formation constants of the complexes $[Co(terpy)]^{2+}$ and $[Co(terpy)_2]^{2+}$ (terpy=2,2′:6′,2″-terpyridine). The configurations of $[M(bpy)]^{2+}$ in HMPA will be discussed on the basis of these data.

Experimental

Materials and Procedure. HMPA of guaranteed reagent grade was purified as described elsewhere.[1] Bpy was recrystallized from hexane, and terpy was used without further purification. Anhydrous sodium perchlorate was prepared by heating monohydrous salt which had been recrystallized twice from water. Complexes of various metal ions $[M(hmpa)_4](ClO_4)_2$ (M(II)=Mn(II), Fe(II), Co(II), Cu(II), or Zn(II)) were synthesized according to the methods by Donoghue and Drago.[4,5] Stock solutions of these metal perchlorates were prepared, and portions of them were taken to analyze the metal ion concentrations by the spectrophotometric methods already published.[1] Complex solutions were prepared by mixing the aliquots of stock solutions of metal perchlorates with those of bpy or terpy solutions. The ionic strength was kept at $I=0.06$ mol dm^{-3} with sodium perchlorate.

Solution of chromium(II) perchlorate in HMPA was prepared under nitrogen atmosphere as follows. Metallic chromium was dissolved in aqueous solution of perchloric acid, and the hydrated perchlorate was crystallized from it. After the removal of water in vacuum at room temperature until the blue crystals turned white, the white crystals were treated with a slight excess of HMPA and an appropriate amount of ether and crystals of chromium perchlorate solvated by HMPA were obtained and dissolved in HMPA. The total chromium(II) ion concentration in solution was determined spectrophotometrically by diphenylcarbazide method[6] (molar absorptivity $\varepsilon=6.590\times10^4$ dm^3 mol^{-1} cm^{-1} at 540 nm).

Apparatus. The absorptivities of complex solutions were measured using a Hitachi Spectrophotometer Model 100-40 and a Hitachi Recording Spectrophotometer Model EPS-3T, with a thermostated cell compartment, respectively. The temperature was kept at 25.0±0.1 °C.

Results

The values of K_1 were obtained by a method by use of Job's curves (Method I),[7] the linear relationship method (Method II),[7] and the relative stability constant method (Method III).[8]

Determination of K_1 by Method I. The curves of Job's continuous variation method were obtained at two different total concentrations ($c=c_a$ and c_b) of M(II) (M(II)=Mn(II), Fe(II), Co(II), or Zn(II)) and bpy; an example is given in Fig. 1, essentially

† In this expression, HMPA molecules solvating the metal ions are omitted.

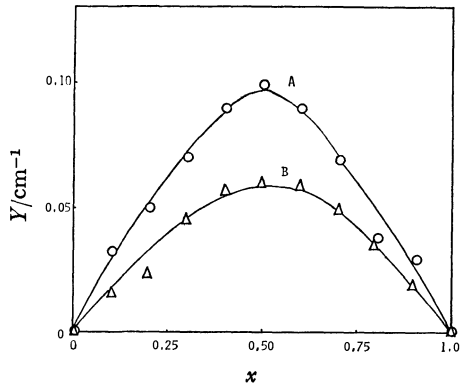

Fig. 1. Job's curves for Mn(II)+bpy system in HMPA at 317 nm.
Curve A: $c_a=1.00\times10^{-3}$ mol dm^{-3}, curve B: $c_b=7.00\times10^{-4}$ mol dm^{-3}.

similar data being obtained in other cases. Curves A and B indicate that the 1:1 complex $[M(bpy)]^{2+}$ is predominantly formed between M(II) and bpy, so that the following relations are established:

$$M^{2+} + bpy \overset{K_1}{\rightleftharpoons} [M(bpy)]^{2+}, \quad (1)$$

$$K_1 = \frac{[[M(bpy)]^{2+}]}{[M^{2+}][bpy]}. \quad (2)$$

In the Figure, the abscissa shows $x=[bpy]_0/c$, and the ordinate Y is defined as follows:

$$Y = (\varepsilon_1-\varepsilon_0-\varepsilon_b)[[M(bpy)]^{2+}] \quad (3)$$

in which ε_0, ε_1, and ε_b are the molar absorptivities of M^{2+}, $[M(bpy)]^{2+}$, and bpy, respectively. The values of K_1 and ε_1 are calculated by Eq. 3 and the following equations from curves A and B.[7]

$$[[M(bpy)]^{2+}] = \frac{x_a(1-x_a)c_a^2-x_b(1-x_b)c_b^2}{c_a-c_b}, \quad (4)$$

$$[M^{2+}] = x_a c_a - [[M(bpy)]^{2+}], \quad (5)$$

$$[bpy] = (1-x_a)c_a - [[M(bpy)]^{2+}], \quad (6)$$

where x_a and x_b are the x values having a common Y value on curves A and B. The results are summarized in Table 1.

Determination of K_1 and K_2 by Method II.[7] At concentrations of both M(II) and bpy low enough so that the amount of $[M(bpy)_2]^{2+}$ formed is negligibly small, the apparent molar absorptivity of M(II), ε, is expressed by a linear relationship, Eq. 7, with $(\varepsilon_0-\varepsilon)/[bpy]$.[7] When the molar absorptivity of M^{2+}, ε_0, is zero, Eq. 8 holds.

$$\varepsilon = \varepsilon_1 + \frac{1}{K_1}\frac{(\varepsilon_0-\varepsilon)}{[bpy]} \quad (7)$$

$$\frac{1}{\varepsilon} = \frac{1}{\varepsilon_1} + \frac{1}{K_1\varepsilon_1}\frac{1}{[bpy]} \quad (8)$$

Accordingly, plotting ε *vs.* $(\varepsilon_0-\varepsilon)/[bpy]$ or $1/\varepsilon$ *vs.* $1/[bpy]$ will give the values of K_1 and ε_1 from the slope and the intercept. Figure 2 shows the linear relationship of Co(II)+bpy system; similar relationships were obtained for Mn(II)+bpy and Fe(II)+bpy systems, respectively. The values of K_1 and ε_1 thus obtained are also summarized in Table 1. These values of K_1 are in good agreement with those obtained by Method I.

The second complex formation constant of $[Co(bpy)_2]^{2+}$, $K_2=[[Co(bpy)_2]^{2+}]/[[Co(bpy)]^{2+}][bpy]$, is obtained from Eq. 9 in the more concentrated regions for both Co(II) and bpy than in Fig. 2,

$$\varepsilon = \varepsilon_2 + \frac{1}{K_2}\frac{(\varepsilon_0-\varepsilon)+(\varepsilon_1-\varepsilon)K_1[bpy]}{K_1[bpy]^2}, \quad (9)$$

where ε_2 is the molar absorptivity of $[Co(bpy)_2]^{2+}$. The linearity is obvious between ε and $\{(\varepsilon_0-\varepsilon)+(\varepsilon_1-\varepsilon)K_1[bpy]\}/K_1[bpy]^2$ as shown in Fig. 3, giving the value of K_2 from the slope. The first and second formation constants of Co(II)-terpy complexes are also determined by the same method, the results being listed in Table 2.

Determination of K_1 by Method III.[8] When both M^{2+} and M_a^{2+} ions coexist in HMPA, equilibria (1)

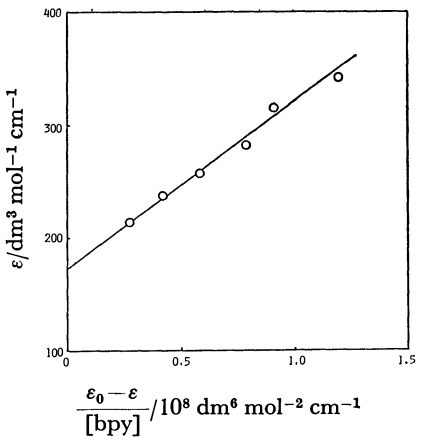

Fig. 2. Linear relation of ε against $(\varepsilon_0-\varepsilon)/[bpy]$ in HMPA at 630 nm.
$[Co(II)]=8.00\times10^{-4}$ mol dm^{-3}, $[bpy]_0=1.00\times10^{-4}$—$6.00\times10^{-4}$ mol dm^{-3}.

Table 1. First formation constants of the complexes of Mn(II), Fe(II), Co(II), or Zn(II) with bpy in HMPA by method I and method II

Method		Mn(II)	Fe(II)	Co(II)	Zn(II)
Method I	$\log K_1$	3.21±0.24	4.86±0.11	5.77±0.22	1.77±0.07
	$\log \varepsilon_1$	2.81±0.07[a]	3.88±0.02[b]	3.95±0.03[c]	3.10±0.06[d]
Method II	$\log K_1$	2.98±0.02	4.78±0.02	5.90±0.02	—
	$\log \varepsilon_1$	1.26±0.09[e]	2.42±0.04[f]	2.25±0.05[g]	—

The following values were adopted in Method I: a) $\log\varepsilon_0=0.60$, $\log\varepsilon_b=2.02$ at 317 nm, b) $\log\varepsilon_0=3.20$, $\log\varepsilon_b=2.90$ at 310 nm, c) $\varepsilon_0=0$, $\log\varepsilon_b=3.36$ at 305 nm, d) $\log\varepsilon_0=0.48$, $\log\varepsilon_b=2.02$ at 317 nm. The following wavelengths were used in Method II: e) 380 nm, f) 522 nm, g) 630 nm.

and (10) hold simultaneously among those ions and bpy,

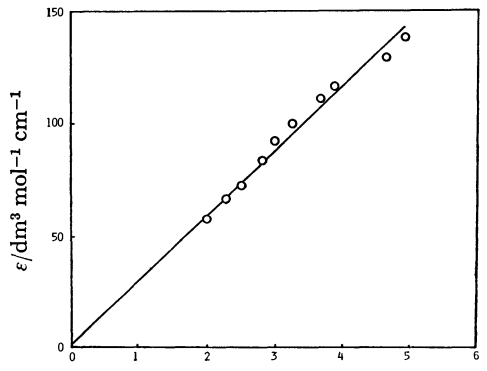

Fig. 3. Linear relation of ε against $((\varepsilon_0-\varepsilon)+(\varepsilon_1-\varepsilon)\times K_1[\mathrm{bpy}])/K_1[\mathrm{bpy}]^2$ in HMPA at 580 nm. $[\mathrm{Co(II)}]=3.20\times10^{-3}$ mol dm^{-3}, $[\mathrm{bpy}]_0=3.80\times10^{-3}$—$5.60\times10^{-3}$ mol dm^{-3}.

Table 2. Comparison of first and second formation constants of the complexes of Co(II) with bpy or terpy in HMPA and H_2O

Ligand	Solvent	$\log K_1$	$\log K_2$	$\log K_3$
bpy	HMPA	5.84±0.07	3.59±0.03	<1[a]
	H_2O[9]	5.65	5.60	4.80
terpy	HMPA	4.87±0.01	3.35±0.01	
	H_2O[9]	8.4	9.9	

a) This value was calculated on an assumption that ε of $[\mathrm{Co(bpy)_3}]^{2+}$ in HMPA is the same value as that in H_2O. $[\mathrm{Co(II)}]=1.00\times10^{-2}$ mol dm^{-3}, $[\mathrm{bpy}]_0=1.50\times10^{-1}$ mol dm^{-3}.

$$M_a^{2+} + \mathrm{bpy} \overset{K_a}{\rightleftharpoons} [M_a(\mathrm{bpy})]^{2+}, \quad (10)$$

where K_a is the formation constant of $[M_a(\mathrm{bpy})]^{2+}$. Therefore, an equilibrium (11) is also established with a formation constant K_r as expressed by Eq. 12.

$$M^{2+} + [M_a(\mathrm{bpy})]^{2+} \overset{K_r}{\rightleftharpoons} M_a^{2+} + [M(\mathrm{bpy})]^{2+}, \quad (11)$$

$$K_r = \frac{[M_a^{2+}][[M(\mathrm{bpy})]^{2+}]}{[M^{2+}][[M_a(\mathrm{bpy})]^{2+}]} = \frac{K_1}{K_a}. \quad (12)$$

The absorptivity of the solution, A, is defined by the following equation:

$$A = \varepsilon_0[M^{2+}] + \varepsilon_1[[M(\mathrm{bpy})]^{2+}] + \varepsilon_a[M_a^{2+}] + \varepsilon'_a[[M_a(\mathrm{bpy})]^{2+}], \quad (13)$$

where ε_a and ε_a' are the molar absorptivities of M_a^{2+} and $[M_a(\mathrm{bpy})]^{2+}$, respectively. When both the values of K_1 and K_a are considerably large, the concentration of free bpy will be negligibly small, and therefore, the total concentration of bpy, $[\mathrm{bpy}]_0$, will be equal to the sum of $[[M(\mathrm{bpy})]^{2+}]$ and $[[M_a(\mathrm{bpy})]^{2+}]$. Consequently, when the molar absorptivities of M^{2+}, $[M(\mathrm{bpy})]^{2+}$, M_a^{2+}, and $[M_a(\mathrm{bpy})]^{2+}$ are known, the value of K_r can be obtained because the total concentrations of M(II), M_a(II), and bpy and observed A are known. Therefore, the value of K_1 is given by virtue of the relationship $K_1=K_aK_r$ and the known K_a value. For the determination of the formation constants, K_1, of $[\mathrm{Cu(bpy)}]^{2+}$ and $[\mathrm{Cr(bpy)}]^{2+}$, Co(II) was used as M_a^{2+} ion in equilibrium (10). Since the molar absorptivity of $[M(\mathrm{bpy})]^{2+}$ can not be obtained directly, the absorptivity of the solution, A, was determined at the wavelength of the isosbestic point between M^{2+} and $[M(\mathrm{bpy})]^{2+}$ ($\varepsilon_0=\varepsilon_1$). The results are summarized in Tables 3 and 4.

Absorption Spectra of bpy- and terpy-Complexes. The absorption spectra of pure bpy- or terpy-complexes can be calculated from the apparent spectra of the

Table 3. First formation constant of the complex of Cu(II) with bpy in HMPA by method III[a]

[Cu(II)] / 10^{-4} mol dm^{-3}	[Co(II)] / 10^{-3} mol dm^{-3}	$[\mathrm{bpy}]_0$ / 10^{-4} mol dm^{-3}	$\log K_r$	$\log K_1$[b]
2.00	3.00	2.00	1.48	7.32
2.00	4.00	2.00	1.52	7.36
2.00	5.00	2.00	1.50	7.34
			mean	7.33±0.02

a) Measured at the isosbestic point 580 nm between Cu^{2+} and $[\mathrm{Cu(bpy)}]^{2+}$. $\log\varepsilon_0(Cu^{2+})=\log\varepsilon_1([\mathrm{Cu(bpy)}]^{2+})=0.88$, $\log\varepsilon_a(Co^{2+})=2.50$, $\log\varepsilon_a'([\mathrm{Co(bpy)}]^{2+})=2.12$. b) $\log K_a=5.84$ was used.

Table 4. First formation constant of the complex of Cr(II) with bpy in HMPA by method III[a]

[Cr(II)] / 10^{-2} mol dm^{-3}	[Co(II)] / 10^{-3} mol dm^{-3}	$[\mathrm{bpy}]_0$ / 10^{-3} mol dm^{-3}	$\log K_r$	$\log K_1$[b]
3.20	2.53	2.33	−1.21	4.63
2.85	2.12	2.40	−1.21	4.63
1.75	3.04	2.95	−1.25	4.59
1.50	2.92	2.65	−1.27	4.57
1.15	3.04	2.92	−1.27	4.57
0.91	2.63	2.60	−1.19	4.65
			mean	4.61±0.02

a) Measured at the isosbestic point 650 nm between Cr^{2+} and $[\mathrm{Cr(bpy)}]^{2+}$. $\log\varepsilon_0(Cr^{2+})=\log\varepsilon_1([\mathrm{Cr(bpy)}]^{2+})=1.11$, $\log\varepsilon_0(Co^{2+})=2.45$, $\log\varepsilon_a'([\mathrm{Co(bpy)}]^{2+})=2.00$. b) $\log K_a=5.84$ was used.

mixture of M^{2+} and bpy- or terpy-complexed M^{2+} ions by using the values of K_1 and K_2 listed in Tables 1—4. The observed absorption spectra of the solvated Mn^{2+}, Fe^{2+}, and Zn^{2+}, and the calculated ones of $[Mn(bpy)]^{2+}$, $[Fe(bpy)]^{2+}$, and $[Zn(bpy)]^{2+}$ are shown in Fig. 4, those of Co^{2+}, $[Co(bpy)]^{2+}$, $[Co(bpy)_2]^{2+}$, and $[Co(terpy)]^{2+}$ in Fig. 5, and those of Cu^{2+} and $[Cu(bpy)]^{2+}$ in Fig. 6, respectively.

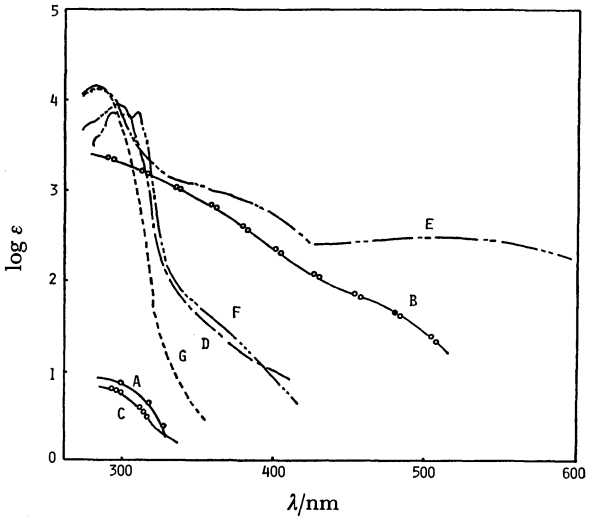

Fig. 4. Absorption spectra of solvated Mn^{2+} (A: —o—), Fe^{2+} (B: —oo—), Zn^{2+} (C: —ooo—), and those of $[Mn(bpy)]^{2+}$ (D: — - —), $[Fe(bpy)]^{2+}$ (E: ——), $[Zn(bpy)]^{2+}$ (F: ——), and bpy (G: ----) in HMPA.

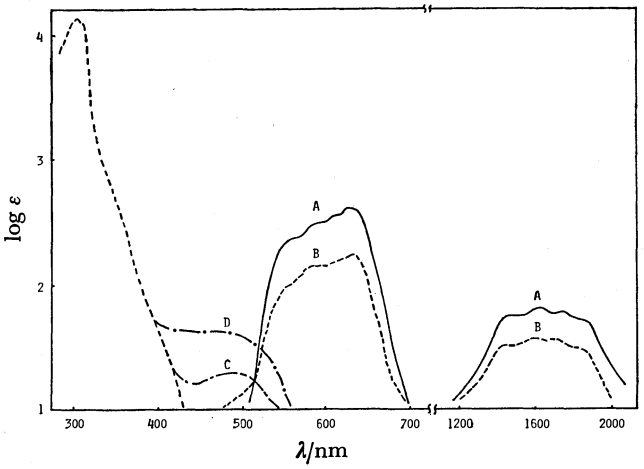

Fig. 5. Absorption spectra of solvated Co^{2+} (A:——), $[Co(bpy)]^{2+}$ (B:- - -), $[Co(bpy)_2]^{2+}$ (C:——), and $[Co(terpy)]^{2+}$ (D:—·—) in HMPA.

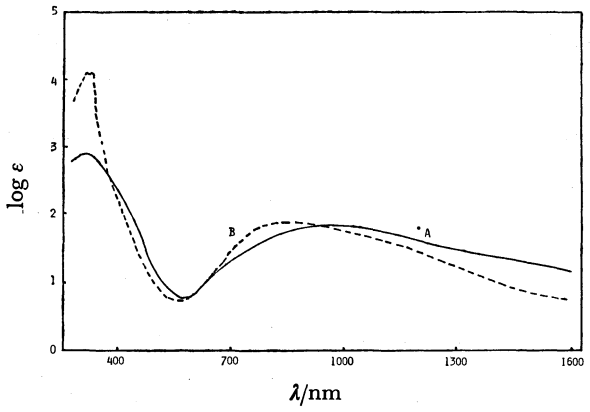

Fig. 6. Absorption spectra of solvated Cu^{2+} (A:——) and $[Cu(bpy)]^{2+}$ (B:----) in HMPA.

Discussion

Configurations of $[Cr(bpy)]^{2+}$, $[Mn(bpy)]^{2+}$, $[Fe(bpy)]^{2+}$, and $[Co(bpy)]^{2+}$ in HMPA. The K_1 values observed for bpy-complexes are in a sequence Cr(II)> Mn(II)<Fe(II)<Co(II)<Cu(II)>Zn(II) in HMPA. Figure 7 shows the comparison of the K_1 values in HMPA and in H_2O.[9] The factors which would make the values of the formation constants (K) in HMPA differ from those in H_2O or in other organic solvents might be the dielectric constants, basicities, and steric effects of the solvents. Since bpy and terpy ligands are electrically neutral, the K values might be little affected by the dielectric constant of the solvents. Since the competitive coordination to a metal ion occurs between bpy (or terpy) and the solvent molecules, the increase in basicity and in the degree of steric hindrance of the solvent would result in a decrease in K value.

It was reported[1] that the solvated Mn^{2+}, Fe^{2+}, Co^{2+}, and Cu^{2+} ions are tetrahedral in contrast with the octahedrally solvated Zn^{2+} ion in HMPA. Because an HMPA molecule is very bulky, solvated metal ions in HMPA will prefer the tetrahedral configurations to the octahedral ones.[1] If their bpy-complexes tend to form octahedral configurations in HMPA, K_1 values in HMPA would become smaller than those in H_2O or in DMSO because of a larger basicity and steric hindrance of HMPA molecules which would be more closely packed in the octahedral coordination sphere. However, since the observed K_1 values of Cr(II), Mn(II), Fe(II), and Co(II) in HMPA are slightly larger than those in H_2O as shown in Fig. 7, it is supposed that their bpy-complexes would not be octahedral. According to Gutmann *et al.*,[10] the donor strength of HMPA towards Co(II) is smaller

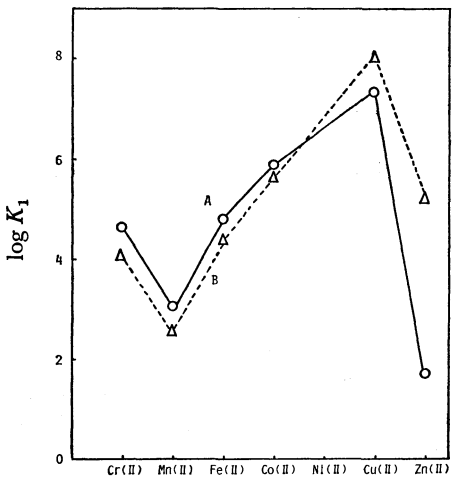

Fig. 7. Comparison of log K_1 in HMPA (A:—) and in H_2O (B:- - -).

than that expected from its donor number and the coordination center in $[Co(hmpa)_4]^{2+}$ is rattling within the tetrahedron formed by the bulky HMPA molecules. When their bpy-complexes in HMPA are also assumed to be tetrahedral, the K_1 values in HMPA would not be much smaller than those in H_2O because of the smaller steric hindrance and the decreased donor strength of HMPA molecules. Actually, the absorption spectrum of $[Co(bpy)]^{2+}$ in HMPA exhibits the spectral pattern characteristic of tetrahedral complexes as is seen in Fig. 5, having the absorption band due to $\nu_3(^4T_1(P)\leftarrow{}^4A_2)$, ($\varepsilon=100$—$2000$ dm^3 mol^{-1} cm^{-1}) in the visible region.[11] Although the configurations of bpy-complexes of Cr(II), Mn(II), and Fe(II) can not be judged from the observed absorption spectra, they would be also tetrahedral because their K_1 values in HMPA, as well as the K_1 value of tetrahedral $[Co(bpy)(hmpa)_2]^{2+}$, are similarly larger than those in H_2O. Then, the following equilibrium seems to be established in all these cases.

$$\underset{\text{tetrahedral}}{[M(hmpa)_4]^{2+}} + bpy \overset{K_1}{\rightleftharpoons} \underset{\text{tetrahedral}}{[M(bpy)(hmpa)_2]^{2+}} + 2hmpa \tag{14}$$

M(II) = Cr(II), Mn(II), Fe(II), or Co(II)

On the other hand, the absorption spectrum of bis(bpy)cobalt(II) complex in HMPA as is shown in Fig. 5 has a spectral pattern characteristic of the octahedral complexes, having the absorption band near 500 nm ($\varepsilon=5$—40 dm^3 mol^{-1} cm^{-1}).[11] Therefore, the following tetrahedral↔octahedral configurational equilibrium must be established;

$$\underset{\text{tetrahedral}}{[Co(bpy)(hmpa)_2]^{2+}} + bpy \overset{K_2}{\rightleftharpoons} \underset{\text{octahedral}}{[Co(bpy)_2(hmpa)_2]^{2+}}, \tag{15}$$

$$\underset{\text{octahedral}}{[Co(bpy)_2(hmpa)_2]^{2+}} + bpy \overset{K_3}{\rightleftharpoons} \underset{\text{octahedral}}{[Co(bpy)_3]^{2+}} + 2hmpa. \tag{16}$$

When terpy as a terdentate ligand coordinates to Co^{2+} ion, the 1:1 complex is octahedral as is shown from its absorption spectrum[11] in Fig. 5. Accordingly, this equilibrium is also a tetrahedral↔octahedral configurational change;

$$\underset{\text{tetrahedral}}{[Co(hmpa)_4]^{2+}} + terpy \overset{K_1}{\rightleftharpoons} \underset{\text{octahedral}}{[Co(terpy)(hmpa)_3]^{2+}} + hmpa, \tag{17}$$

$$\underset{\text{octahedral}}{[Co(terpy)(hmpa)_3]^{2+}} + terpy \overset{K_2}{\rightleftharpoons} \underset{\text{octahedral}}{[Co(terpy)_2]^{2+}} + 3hmpa. \tag{18}$$

As is evident from Table 2, the K_2 value of $[Co(bpy)_2]^{2+}$ and the K_1 value of $[Co(terpy)]^{2+}$ are remarkably smaller than those in H_2O, because the steric hindrance of HMPA molecules in octahedral $[Co(bpy)_2]^{2+}$ and octahedral $[Co(terpy)]^{2+}$ may be large. The reason why the K_3 value of $[Co(bpy)_3]^{2+}$ and the K_2 value of $[Co(terpy)_2]^{2+}$ in HMPA are extremely smaller than those in H_2O is probably the larger effect of the basicity of HMPA molecules than that due to their steric hindrance.

Configurations of $[Cu(bpy)]^{2+}$, and $[Zn(bpy)]^{2+}$ in HMPA. Since the steric hindrance caused by HMPA in the square planar complex or tetragonal complex is larger than that in the tetrahedral complex, but smaller than that in the octahedral one, it seems that K_1 value of the square planar or tetragonal complex in HMPA would be smaller than that in H_2O. According to both the K_1 value and the absorption spectrum observed for Cu(II)–bpy complex, it is safely said that its configuration is square planar or tetragonal.[11] Therefore, one of the following two equilibria may hold:

$$\left.\begin{aligned} &\underset{\text{tetrahedral}}{[Cu(hmpa)_4]^{2+}} + bpy \overset{K_1}{\rightleftharpoons} \underset{\text{square planar}}{[Cu(bpy)(hmpa)_2]^{2+}} + 2hmpa \\ &\text{or} \\ &\underset{\text{tetrahedral}}{[Cu(hmpa)_4]^{2+}} + bpy \overset{K_1}{\rightleftharpoons} \underset{\text{tetragonal}}{[Cu(bpy)(hmpa)_4]^{2+}}. \end{aligned}\right\} \tag{19}$$

We have reported that the solvated Zn^{2+} ion in HMPA may be octahedral, since its Stokes radius is larger than that expected if it were tetrahedral.[1] The fact that the K_1 value in HMPA is smaller about three orders of magnitude than that in H_2O is accounted for by a larger steric hindrance of HMPA molecules in octahedral $[Zn(bpy)(hmpa)_4]^{2+}$ and their larger basicity than those in the case of H_2O molecules. Accordingly, the following equilibrium seems to be established;

$$\underset{\text{octahedral}}{[Zn(hmpa)_6]^{2+}} + bpy \overset{K_1}{\rightleftharpoons} \underset{\text{octahedral}}{[Zn(bpy)(hmpa)_4]^{2+}} + 2hmpa. \tag{20}$$

General Conclusion. In HMPA, solvated Mn^{2+}, Fe^{2+}, Co^{2+}, and Cu^{2+} are tetrahedral, while solvated Zn^{2+} ion is octahedral.[1] Since an HMPA molecule is very bulky, it seems that solvated metal ions prefer the tetrahedral configurations to the octahedral ones. Gutmann and Weisz reported that mono-, di-, tri-, and tetrahalo complexes of cobalt(II) are tetrahedral in HMPA (halide ion=Cl^-, Br^-, or I^-).[2] When multidentate ligands such as bpy and terpy coordinate to metal ions in HMPA, the configurations of $[Cr(bpy)]^{2+}$, $[Mn(bpy)]^{2+}$, $[Fe(bpy)]^{2+}$, and $[Co(bpy)]^{2+}$ are also tetrahedral, while that of $[Cu(bpy)]^{2+}$ is either square planar or tetragonal. In the case of Zn(II), its configuration seems to be octahedral. The K_1 value and the absorption spectrum of Ni(II)-complex was not obtained, because the equilibria among the tetrahedral, square planar and octahedral solvated-species were too complicated to analyze them.[1] The configurations of both $[Co(bpy)_2]^{2+}$ and $[Co(terpy)]^{2+}$ are octahedral. In conclusion, it is likely that the complexes coordinated by more than three nitrogen atoms are mostly octahedral in HMPA.

References

1) Y. Abe and G. Wada, *Bull. Chem. Soc. Jpn.*, **53**, 3547 (1980).
2) V. Gutmann and A. Weisz, *Monatsh. Chem.*, **100**, 2104 (1969).
3) A. Weisz and V. Gutmann, *Monatsh. Chem.*, **101**, 19 (1970).
4) J. T. Donoghue and R. S. Drago, *Inorg. Chem.*, **1**, 866 (1962).
5) J. T. Donoghue and R. S. Drago, *Inorg. Chem.*, **2**, 1158 (1963).
6) "Japanese Industrial Standards; Testing Methods for Industrial Waste Water," ed by N. Tahara, Japanese Standards Association, Tokyo (1974), pp. 145—147.
7) G. Wada, *Bull. Chem. Soc. Jpn.*, **41**, 882 (1968).
8) V. L. Hughes and A. E. Martell, *J. Phys. Chem.*, **57**, 694 (1953).
9) L. G. Sillén and A. E. Martell, "Stability Constants Supplements No. 1 Special Publication 25," ed by The Chemical Society, Alden Press, Oxford (1971).
10) V. Gutmann, A. Weisz, and W. Kerber, *Monatsh. Chem.*, **100**, 2096 (1969).
11) A. B. P. Lever, "Inorganic Electronic Spectroscopy," Elsevier Publishing Company, Amsterdam (1968), Chap. 9.

The Kinetics and Mechanisms of the Racemization of Tris(*N,N'*-dimethylethanediimine)iron(II)

Satoshi TACHIYASHIKI*,† and Hideo YAMATERA
Department of Chemistry, Faculty of Science, Nagoya University, Chikusa-ku, Nagoya 464
(Received December 15, 1980)

Tris(*N,N'*-dimethylethanediimine)iron(II) (trivial name: tris(glyoxal-bis-*N*-methylimine)iron(II)[1]), $[Fe(gmi)_3]^{2+}$, has been resolved for the first time, and its racemization mechanism has been investigated in acid solutions. A mechanism similar to that for tris(2,2'-bipyridine)iron(II) was verified from the acid dependence of the racemization rate. At 69.4 °C, 30% of the racemization proceeded by means of an intramolecular bond-rupture mechanism and the remainder by means of an intramolecular twist mechanism. The activation enthalpy and the activation entropy for the twist path were 148($\Delta H^{\ddagger}$/kJ mol^{-1}) and 110($\Delta S^{\ddagger}$/J K^{-1} mol^{-1}) respectively. These values were compared with 127 and 114 for $[Fe(bpy)_3]^{2+}$ (bpy=2,2'-bipyridine) and with 119 and 91 for $[Fe(phen)_3]^{2+}$ (phen=1,10-phenanthroline). The racemization rate was larger in organic solvents, increasing in the order water<nitromethane<formamide<dimethyl sulfoxide, which is the same as the order for the bpy and phen complexes. The rate was less dependent on the solvent in the order $[Fe(phen)_3]^{2+}>[Fe(bpy)_3]^{2+}>[Fe(gmi)_3]^{2+}$. A salt effect on the racemization rates was also observed.

The intramolecular twist mechanism[2] is one of the basic mechanisms of the stereochemical rearrangement of metal chelates. The nature of the mechanism, however, does not seem to be fully understood.[3] Many investigations have been made concerning the intramolecular stereochemical rearrangement of stereochemically nonrigid complexes by means of dynamic nuclear magnetic resonance spectroscopy.[4] The mechanisms proposed in these studies have, however, been mainly based on indirect evidence. On the other hand, the studies of inert complexes based on rather classical kinetic methods have given more definitive evidence to show the reaction mechanisms.[5]

Tris(1,10-phenanthroline)iron(II)[6] is one of the few examples of such inert complexes which racemize by means of an intramolecular twist mechanism. Iron(II) forms very stable, strongly colored complexes not only with bpy and phen, but also with *N,N'*-dialkyl-1,2-diimines.[7] The racemization of the simple *N,N'*-dialkyl-1,2-diimine complex, $[Fe(gmi)_3]^{2+}$ (gmi=$CH_3N{=}CH{-}CH{=}NCH_3$), has been studied to disclose whether or not a twist mechanism also occurs in this case, and to gain a better understanding of the characteristics of the twist mechanism.

Experimental

Materials. Preparation and Resolution of the Complexes: Tris(*N,N'*-dimethylethanediimine)iron(II) iodide, $[Fe(gmi)_3]I_2\cdot 3H_2O$, was prepared by Krumholtz's method.[1] The complex was resolved for the first time by the fractional crystallization of its $(+)_{589}$-tartratoantimonate. Racemic iodide (2.0 g, 3.6×10^{-3} mol) was dissolved in water (10.5 cm^3), and, to the resulting solution, silver $(+)_{589}$-tartratoantimonate (2.8 g, 7.2×10^{-3} mol) was added with vigorous stirring. The stirring was continued for several minutes, during which double decomposition was completed to yield the solution of the $(+)_{589}$-tartratoantimonate of the racemic complex and the insoluble silver iodide. After the latter was filtered off, the solution was heated to 40 °C and ethanol was slowly added to it until the solution became slightly cloudy. The solution was then kept overnight at 0 °C to give a crystalline precipitate. Crystals of the $(+)_{589}$-tartratoantimonate of this complex, $(-)_{589}$-$[Fe(gmi)_3](Sbtart)_2$, were filtered off from the solution, and the crystals of $(+)_{589}$-$[Fe(gmi)_3](Sbtart)_2$ were precipitated by adding ethanol to the filtrate. By repeating the fractional crystallization five times, 0.15 g of $(+)_{589}$-diastereomer ($\Delta\varepsilon_{570}=+32$) and 0.32 g of $(-)_{589}$-diastereomer ($\Delta\varepsilon_{570}=-30$) were obtained. These diastereomers were converted into active bromide by the use of the anion-exchange resin, Dowex 2-X8, by the column method. The $[\alpha]_{589}$ values for $(+)_{589}$- and $(-)_{589}$-enantiomers were +950° and −900° respectively. Anal. $(+)_{589}$-$[Fe(gmi)_3]Br_2\cdot 3H_2O$: Found: C, 27.40; H, 5.49; N, 15.96; Calcd for $C_{12}H_{30}N_6O_3Br_2Fe$: C, 27.61; H, 5.75; N, 16.10.

Tris(1,10-phenanthroline)iron(II) perchlorate was resolved through precipitation as $(+)_{589}$-tartratoantimonate according to the method of Dwyer and Gyarfas;[8] $[\alpha]_{589}=+1460°$. The resolution of tris(2,2'-bipyridine)iron(II) perchlorate through precipitation as iodide $(+)_{589}$-tartratoantimonate was carried out in a manner similar to that previously described;[9] $[\alpha]_{589}=+4970°$.

Solvent: Nitromethane was refluxed with urea, dried with anhydrous sodium sulfate, and distilled. Dimethyl sulfoxide was distilled under reduced pressure, treated with alumina, and distilled again under reduced pressure. Formamide was dried with anhydrous sodium sulfate and distilled twice under reduced pressure.

Other Reagents: Guaranteed-grade potassium chloride and potassium iodide were recrystallized from water. Guaranteed-grade hydrochloric acid was purified by azeotropic distillation. Guaranteed-grade potassium thiocyanate was recrystallized from an aqueous ethanolic (1:1) solution. All the other chemicals were of a guaranteed grade and were used without purification.

Experimental Procedure. Racemization and Dissociation of $[Fe(gmi)_3]^{2+}$: The optically active bromide was dissolved in a given solvent ($(0.42-2.5)\times10^{-4}$ M††), containing other chemicals whenever necessary. Aliquots of the solution were sealed in eleven small test tubes. They were placed in a thermostat(±0.1 °C) and taken out, one by one, at proper intervals. They were then cooled in ice water, and their circular dichroism(CD) strength was measured at 570 nm and their absorbance, at 560 nm. The apparent racemization (rate constant: k_r^{app}) was studied by following the loss of optical activity for one to five half-lives. From the changes in the absorbance of the solution during the apparent racemization, the dissociation rate (rate constant: k_d) was calculated. Both the apparent racemization and the

† Present address: Kagawa Nutrition College, Sakado, Saitama 350-02.

†† 1 M=1 mol dm^{-3}.

dissociation were first-order with respect to the metal-complex concentration in the time range of the experiments. The net rate of racemization (rate constant: k_r^{net}) was obtained as $k_r^{net}=k_r^{app}-k_d$.

Racemization of $[Fe(bpy)_3]^{2+}$ *and* $[Fe(phen)_3]^{2+}$: The $(0.5-1.0)\times10^{-4}$ M solutions of optically active perchlorates were placed in a thermostatted (±0.1 °C) quartz cell, and the change in the optical rotation (at 510 nm for the phenanthroline complex, 525 nm for the bipyridine complex) was followed on a recorder. The temperature was measured during the reaction by putting a thermister directly in the solution. The reactions were followed for one to two half-lives.

Dissociation of $[Fe(bpy)_3]^{2+}$ *and* $[Fe(phen)_3]^{2+}$: The 0.5×10^{-4} M solutions of the complex were placed in a thermostatted (±0.1 °C) quartz cell, and the change in the absorbance (at 510 nm for the phen complex, 520 nm for the bpy complex) of the solution was followed on a recorder.

The racemization and dissociation rate constants were calculated by the usual method for first-order reactions. The racemization rate constant was defined as $k_r=[\ln(\alpha_0/\alpha_t)]/t$, where α_0 and α_t are the optical rotations or the CD strengths at time zero and t respectively.

Apparatus. A JASCO ORD/UV-5 with a CD attachment was used for measuring the CD strength and the optical rotation, and for recording the CD spectra. A Hitachi 323 Spectrometer was used for recording the absorption spectra, and Hitachi 101 and 124 Spectrophotometers, for measuring the absorbances.

Results and Discussion

CD Spectrum. Figure 1 shows the absorption and CD spectra of the resolved complex. The CD spectrum of the complex is very similar to those of the bpy and phen complexes;[10] the positive and negative CD peaks near 20×10^3 cm^{-1} are attributed to charge-transfer transitions by analogy with the corresponding bands in the bpy and phen complexes. The CD peak at 28.5×10^3 cm^{-1} is that of the d-d transition ($^1T_{2g}\leftarrow{}^1A_{1g}$ in octahedral approximation), in agreement with the assignment of the absorption band near 28.5×10^3 cm^{-1} by Ito *et al.*[11] On the other hand, the CD peaks at $(25-26)\times10^3$ cm^{-1} of $[Fe(phen)_3]^{2+}$ and $[Fe(bpy)_3]^{2+}$ were suggested to be

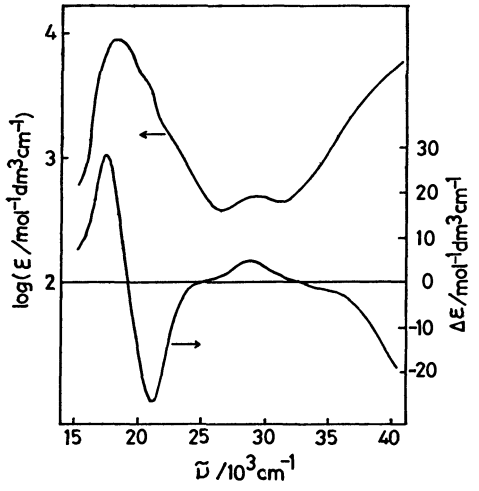

Fig. 1. Absorption (AB) and circular dichroism (CD) spectra of $(+)_{589}[Fe(gmi)_3]Br_2$ in aqueous solution.

of metal-to-ligand charge-transfer transitions.[10] In view of the d-d spectral parameters of $[Fe(phen)_3]^{2+}$ and $[Fe(bpy)_3]^{2+}$,[12] a d-d absorption band ($^1T_{2g}\leftarrow{}^1A_{1g}$ in O_h approximation) is suspected to exist around $(25-26)\times10^3$ cm^{-1}, though it is hidden by the strong CT-bands. Thus, the CD peaks of tris(1,2-diimine)-iron(II) at $(25-30)\times10^3$ cm^{-1} are probably of $^1T_{2g}\leftarrow{}^1A_{1g}$ d-d transition. The observed intensities of these CD peaks of magnetically forbidden d-d transitions may be attributed to a trigonal distortion of the complex and to mixing with charge-transfer transition.

Kinetics and Mechanism of Racemization. Racemization in a Neutral Solution: The apparent racemization, as measured by the change in optical activity, was first-order throughout approximately 90% of the reaction. The CD strength throughout the spectrum diminished monotonously to zero as the reaction proceeded. The decrease in absorbance (A) observed during this apparent racemization gave a straight line in the graph of log A *vs.* time. The decrease in absorbance was attributed to the dissociation of the complex, since the monotonous absorbance change occurred over the whole range of the absorption spectrum. The dissociation of the complex was an irreversible reaction, probably due to the immediate hydrolysis of the dissociated ligand. The formation of the bis complex from the tris complex was regarded as rate-determining;[13] *i.e.*, once one gmi ligand has been released from the tris complex, the complex will decompose irreversibly to yield an aqua-complex. Thus, the net racemization of this complex will take place exclusively by means of intramolecular mechanisms and not by intermolecular ligand-exchange processes. The net racemization rates were not affected by the presence of possible decomposition products of the complex (methylamine and/or glyoxal).

Racemization in an Acidic Solution: The decomposition of the complex is known to be acid-catalyzed,[14] and the rate expression is known to be similar to that for $[Fe(bpy)_3]^{2+}$,[6] which dissociates through an intermediate with one bond ruptured. In order to clarify the role of this process in the racemization, the racemization rate was measured at various acid concentrations. The results are depicted in Fig. 2. The observed acid dependence of the rates can be explained by the reaction scheme shown in Fig. 3. In the reaction scheme, k_r^t and $k_r^{b.r.}$ represent the rate constants of an intramolecular twist racemization process and that of an intramolecular bond-rupture racemization process respectively.

The rate constant for the apparent racemization, k_r^{app}, can be expressed as:

$$k_r^{app}=k_r^t+k_1\left(\frac{k_2+k_r^{b.r.}+k_3[H^+]}{k_{-1}+k_2+k_r^{b.r.}+k_3[H^+]}\right), \quad (1)$$

if the steady-state approximation is applied to the bond-rupture intermediate. The rate constant of acid dissociation, k_d, can be expressed as:

$$k_d=k_1\left(\frac{k_2+k_3[H^+]}{k_{-1}+k_2+k_3[H^+]}\right). \quad (2)$$

The net rate of racemization is given by: $k_r^{net}=k_r^{app}-k_d$.

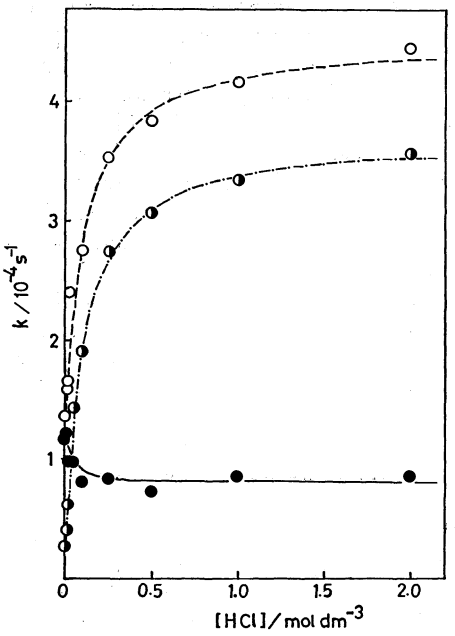

Fig. 2. Influence of acid concentration on the racemization and dissociation rate constants of $[Fe(gmi)_3]^{2+}$ at 69.4 °C and I=2.00 (HCl–KCl).
○: k_r^{app}, ◑: k_d, ●: k_r^{net}.

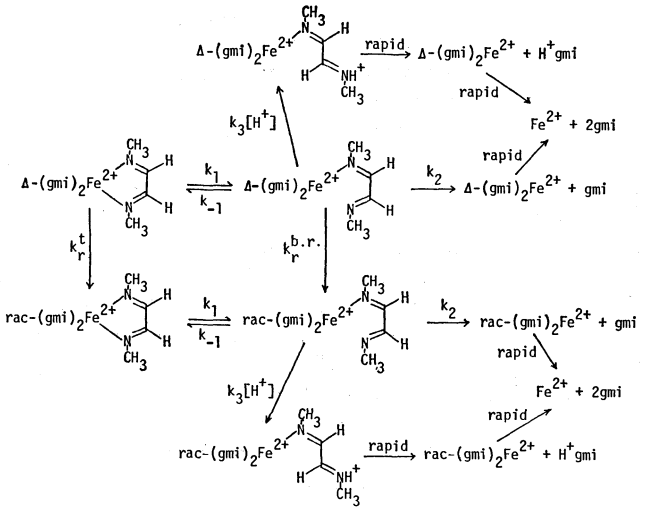

Fig. 3. The reaction scheme.

When [H⁺] is sufficiently low, the values of k_r^{app} and k_d will be approximately equal to the respective limiting values given by:

$$k_r^\circ = k_r^t + k_1\left(\frac{k_2+k_r^{b.r.}}{k_{-1}+k_2+k_r^{b.r.}}\right), \quad (3)$$

$$k_d^\circ = k_1\left(\frac{k_2}{k_{-1}+k_2}\right). \quad (4)$$

Then, Eqs. 1 and 2 can be transformed into:

$$k_r^{app} = (k_1+k_r^t) - \frac{k_{-1}+k_2+k_r^{b.r.}}{k_3}\frac{k_r^{app}-k_r^\circ}{[H^+]}, \quad (5)$$

$$k_d = k_1 + \frac{k_{-1}+k_2}{k_3}\frac{k_d-k_d^\circ}{[H^+]}. \quad (6)$$

In Fig. 4, the k_r^{app} and k_d values, observed in aqueous HCl–KCl solutions (I=2.00) at 69.4 °C, are plotted against $(k_r^{app}-k_r^\circ)/[H^+]$ and $(k_d-k_d^\circ)/[H^+]$ respectively. The values, $k_r^{app}=(1.39\pm0.02)\times10^{-4}$ s^{-1} and $k_d=(2.7\pm0.1)\times10^{-5}$ s^{-1}, observed in 2 M KCl were taken as the k_r° and k_d° values respectively. The intercepts and the slopes of the lines shown in Fig. 4 give $k_1=(3.70\pm0.10)\times10^{-4}$ s^{-1}, $(k_{-1}+k_2)/k_3=(0.102\pm0.005)$ mol dm^{-3}, $(k_1+k_r^t)=(4.52\pm0.12)\times10^{-4}$ s^{-1}, and $(k_{-1}+k_2+k_r^{b.r.})/k_3=(0.125\pm0.010)$ mol dm^{-3}. These values, together with $k_r^\circ=(1.39\pm0.02)\times10^{-4}$ s^{-1} and $k_d^\circ=(2.7\pm0.1)\times10^{-5}$ s^{-1}, lead to $k_{-1}/k_2=12.7\pm0.9$, $k_3/k_2=(129\pm13)$ mol^{-1} dm^3, and $k_r^{b.r.}/k_2=1.41\pm0.41$. The curves in Fig. 2 are the theoretical ones for k_r^{app}, k_d, and k_r^{net}, obtained on the basis of the above values.

Racemization Mechanism: The results discussed above indicate that, in a solution containing no hydrochloric acid at 69.4 °C, 70% of the racemization of $[Fe(gmi)_3]^{2+}$ occurred by way of an intramolecular twist mechanism, and the remainder, by means of an intramolecular bond-rupture mechanism. Thus, complexes with flexible ligands, such as bpy and gmi, racemize intramolecularly by means of a bond-rupture mechanism as well as by means of a twist mechanism. This is in contrast to $[Fe(phen)_3]^{2+}$, which is known to

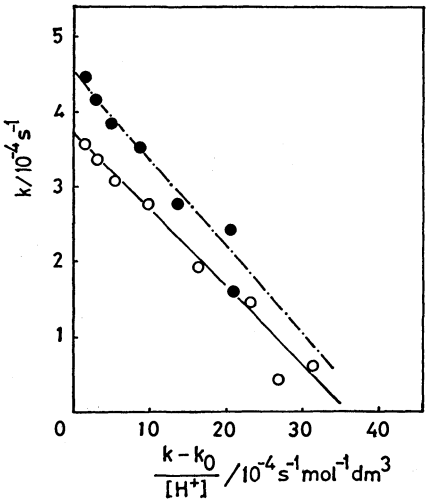

Fig. 4. Plots of k_r^{app} *vs.* $(k_r^{app}-k_r^\circ)/[H^+]$ for apparent racemization (●) and k_d *vs.* $(k_d-k_d^\circ)/[H^+]$ for dissociation (○) of $[Fe(gmi)_3]^{2+}$ at 69.4 °C and I=2.00 (HCl–KCl).

TABLE 1. THE RACEMIZATION AND DISSOCIATION RATE CONSTANTS OF $[Fe(gmi)_3]^{2+}$ IN VARIOUS MEDIA

t / °C	k_r^{app} / 10^{-5} s^{-1}	k_r^{net} / 10^{-5} s^{-1}	k_r^{app} / 10^{-5} s^{-1}	k_d / 10^{-5} s^{-1}
A. Water		C. 0.25 M HCl		
50.0	1.13±0.01	0.93±0.03	2.79±0.08	2.27±0.01
58.8	4.45±0.15	4.01±0.15	9.55±0.17	6.33±0.20
59.4	5.07±0.09	4.42±0.09	—	—
69.2	22.4±0.4	19.2±0.4	41.5±1.0	28.3±1.7
B. 2 M KCl		D. 2 M HCl		
50.0	0.62±0.01	0.50±0.01	2.41±0.02	2.15±0.01
58.9	2.66±0.17	2.35±0.17	9.54±0.17	7.49±0.16
69.2	13.9±0.2	11.6±0.2	38.7±2.7	32.3±1.0

Table 2. The rate constants of the racemization and dissociation of $[Fe(bpy)_3]^{2+}$ and $[Fe(phen)_3]^{2+}$ in 2 M HCl

$[Fe(bpy)_3]^{2+}$				$[Fe(phen)_3]^{2+}$			
t / °C	k_r / 10^{-3} s^{-1}	t / °C	k_d / 10^{-3} s^{-1}	t / °C	k_r / 10^{-3} s^{-1}	t / °C	k_d / 10^{-4} s^{-1}
15.0	0.219	15.0	0.159	20.0	0.214	20.5	0.283
20.0	0.543	19.9	0.400	22.6	0.339		0.287
22.4	0.705	22.4	0.588	25.0	0.493		
25.0	1.208	25.0	0.850	27.65	0.745	27.6	0.971
27.5	1.73	27.5	1.26	30.25	1.110		0.987
30.1	2.41	30.0	1.90	32.65	1.745		
	2.52			35.1	2.50	35.3	3.61
32.5	3.80	32.5	2.59				3.73
	3.94						

Table 3. The apparent racemization rate constants in ionic media[a)]

[KCl] / M	[HCl] / M	$[Fe(gmi)_3]^{2+}$ k / 10^{-4} s^{-1} [b)]	$[Fe(bpy)_3]^{2+}$ k / 10^{-3} s^{-1} [c)]	$[Fe(phen)_3]^{2+}$ k / 10^{-3} s^{-1} [c)]
0.00	0.00	2.24±0.04 (1.92±0.04)	2.17±0.14	1.92±0.02
0.25	0.00	1.87 (1.59)	—	—
1.00	0.00	1.67±0.01 (1.41±0.02)	1.88±0.10	1.76±0.02
2.00	0.00	1.39±0.02 (1.16±0.02)	1.68±0.01	1.70±0.03
2.00	0.00	1.43[d)] (1.17)	1.19±0.01[e)]	1.28±0.02[e)]
1.75	0.25	3.52[d)] (0.83)	1.96±0.05[e)]	—
1.50	0.50	3.83[d)] (0.73)	2.09±0.01[e)]	—
1.00	1.00	4.17[d)] (0.86)	2.43±0.03[e)]	1.14±0.01[e)]
0.00	2.00	4.45[d)] (0.86)	2.46±0.06[e)] (0.56±0.06)	1.12±0.02[e)] (0.97±0.02)

a) Data in parentheses are net racemization rates. b) Data at 69.2 °C. c) Data at 32.0 °C. d) Data at 69.4 °C. e) Data at 30.0 °C.

Table 4. The activation parameters for the reactions of $[Fe(1,2\text{-diimine})_3]^{2+}$ in various aqueous ionic media[a)]

Complex	Medium	k_r^{app} ΔH^* / kJ mol^{-1}	k_r^{app} ΔS^* / J K^{-1} mol^{-1}	k_d ΔH^* / kJ mol^{-1}	k_d ΔS^* / J K^{-1} mol^{-1}	k_r^{net} ΔH^* / kJ mol^{-1}	k_r^{net} ΔS^* / J K^{-1} mol^{-1}
$[Fe(gmi)_3]^{2+}$	Water	140±1	94±4	—	—	141±1	96±3
	2.0 M KCl	147±2	108±6	139±1	73±2	148±3	110±9
	0.25 M HCl	127±2	59±5	119±4	33±13	148±5	112±15
	2.0 M HCl	131±4	71±11	128±2	60±6	149±24	109±72
$[Fe(bpy)_3]^{2+}$	2.0 M HCl	117±0	93±0	114±0	78±1	127±1	114±3
	1.0 M HCl[b)]	—	—	112±2	71±4	106±8	50±29
$[Fe(phen)_3]^{2+}$	2.0 M HCl	120±0	93±0	128±0	104±0	119±1	91±2
	1.5 M HCl[b)]	—	—	132±2	117±8	119±8	88±29

a) Calculated by least-squares method. Errors are the standard deviations. b) Data from Ref. 6.

undergo intramolecular racemization only by means of a twist mechanism because of the rigidity of the ligand. It is not clear whether a twist process proceeds *via* a trigonal or a rhombic intermediate and whether the bond-rupture intermediate is a square pyramid or a trigonal bipyramid.

Activation Parameters: Table 1 shows the racemization and dissociation rate constants of $[Fe(gmi)_3]^{2+}$ at various temperatures. Those of $[Fe(bpy)_3]^{2+}$ and $[Fe(phen)_3]^{2+}$ are listed in Table 2 for the sake of comparison. The racemization rate constants in media of different salt and acid concentrations are given in Table 3. As has been described above for the case of $[Fe(gmi)_3]^{2+}$, the nearly identical values for the racemization rate constants at acid concentrations of 1 M and 2 M suggests that the net racemization rates of the complexes in 2 M HCl correspond to the rates of twist racemization. Table 4 shows the activation parameters of the three complexes for dissociation and twist racemization; the values obtained for $[Fe(phen)_3]^{2+}$ and $[Fe(bpy)_3]^{2+}$ are in good agreement with the literature values[6] (see Table 4) except that the low ΔH^* and ΔS^* values previously reported for the twist racemization of $[Fe(bpy)_3]^{2+}$ may be accompanied by greater errors than those accompanied by the present values, because the number of experimental data is smaller in the former case.

Although the complexes differ in hydrophobic properties, and thus in solvation, the entropies of activation for the twist racemization of the complexes are very similar. The large, positive activation entropies may be related to the formation of bond-expanded high-spin reaction intermediates[3] and/or to the rearrangement of the solvent sheath during the twist motion. These large, positive entropies of activation will lower the barrier for the operation of the twist mechanism by canceling a considerable part of the large activation enthalpies. The differences in activation enthalpies for the twist process between the complexes may come from differences in the ligand-field strength, which are shown by the CD spectra of the complexes. The ligand-field activation energies will become greater with the increase in the ligand-field strength if the reaction intermediates of racemization are similar for the three complexes. The observed activation parameters suggest that the ligand-field strength influences the ligand-field activation energy, but not so greatly as to change the mechanism.

The activation enthalpies of $[Fe(gmi)_3]^{2+}$ and $[Fe(bpy)_3]^{2+}$ for the dissociation *via* bond-rupture intermediates are lower than those for the twist racemization, while the enthalpy of activation for the dissociation of $[Fe(phen)_3]^{2+}$ is higher than that for the twist racemization. Unlike the flexible bpy and gmi, the rigid phenanthroline ligand hardly serves at all as a monodentate ligand to form a bond-rupture intermediate leading to dissociation. Thus, two bonds have to be broken simultaneously in order for the ligand to be liberated from the complex, and a greater activation enthalpy is required for the dissociation of $[Fe(phen)_3]^{2+}$.

Salt Effects: The racemization of $[Fe(phen)_3]^{2+}$ was found to be retarded by KCl and accelerated by KI and KSCN. These salt effects have been attributed to ion-pair formation.[15] The salt effects on the racemization of $[Fe(gmi)_3]^{2+}$ and $[Fe(bpy)_3]^{2+}$ have also been studied. The racemization rates of the complexes decreased with an increase in the KCl concentration, as is shown in Table 3. The racemization rates of $[Fe(gmi)_3]^{2+}$ increased in the presence of KSCN, but the addition of KI had no effect. The dissociation rates of $[Fe(gmi)_3]^{2+}$ increased in the presence of KSCN, but decreased slightly in the presence of KI. The results are shown in Fig. 5. Analyses of the data with due consideration of ion-pair formation[15] gave the racemization and dissociation rate constants of free and ion-paired complexes, and also the ion-association constants (Table 5). The curves in Fig. 5 were obtained by calculation on the basis of the values listed in Table 5.

The intramolecular racemization rates of the ion-pair increase in the order $I \approx Cl < SCN$, and the dissociation rates, $I < Cl < SCN$. The sequence is similar to that for $[Fe(phen)_3]^{2+}$; this gives support for the previously proposed mechanism of the nucleophilic

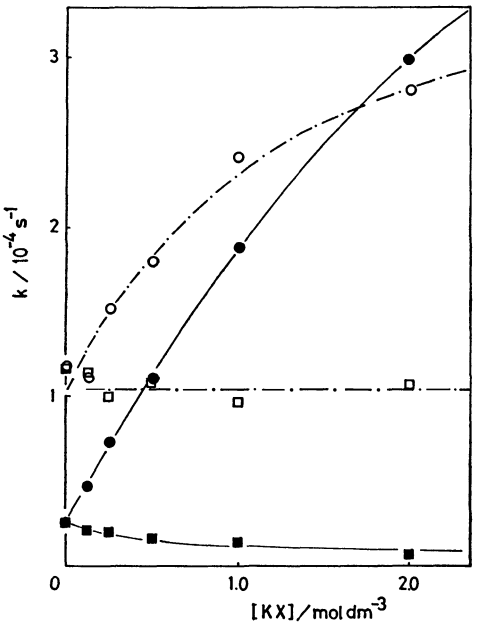

Fig. 5. Salt effects on the rates of racemization (open marks) and dissociation (full marks) at 69.1 °C and I=2.00 (KCl).
○,●: KSCN, □,■: KI.

TABLE 5. THE ION-ASSOCIATION CONSTANTS OF $[Fe(gmi)_3]^{2+}$ WITH AN ANION AND THE DISSOCIATION AND INTRAMOLECULAR RACEMIZATION RATE CONSTANTS OF $[Fe(gmi)_3]^{2+}$ IN AN ION-PAIR

Counter ion	$k^{IP}_{d(X)}$ / 10^{-4} s^{-1}	$k^{I,IP}_{r(X)}$ / 10^{-4} s^{-1}	$K^{IP}_{O(X)}$/mol dm^{-3}	
			Diss.	Racem.
H_2O[a]	0.32±0.02	1.86±0.14	—	—
Cl^-	0.22±0.02	1.08±0.11	4.0±3.5	3.7±2.4
SCN^-	3.21±0.41	2.74±0.15	5.6±3.4	6.1±3.0
I^-	0.06±0.02	0.90±0.07	6.4±3.4	—

a) The value for a free ion.

Table 6. Recemization rate constants in various solvents

Solvent	$[Fe(gmi)_3]^{2+}$ k / 10^{-5} s^{-1} a)	$[Fe(bpy)_3]^{2+}$ k / 10^{-4} s^{-1} b)	$Fe(phen)_3]^{2+}$ k / 10^{-4} s^{-1} b)
Water	4.12±0.11	2.86±0.14	2.80±0.14
Nitromethane	7.8±0.6	7.7±0.7	13.0±0.7
Formamide	21.5±0.4	15.9±0.3	32.8±0.2
DMSO	38.0±0.1	146±7	450±100

a) Data at 59 °C. Corrected for decomposition. b) Data at 20.1 °C.

interaction of the anions with complex cations.[15]

Solvent Effects: In spite of several investigations carried out thus far,[16] the nature of the solvent effects on the racemization rates of tris(1,2-diimine)iron(II) is not yet well understood. In order to compare the effects of solvents on the racemization rates of $[Fe(gmi)_3]^{2+}$, $[Fe(bpy)_3]^{2+}$, and $[Fe(phen)_3]^{2+}$, their racemization rates were observed in water, dimethyl sulfoxide (DMSO), nitromethane, and formamide. The results are summarized in Table 6. The net racemization rates were larger in organic solvents than in an aqueous solution. The dissociation rates of $[Fe(bpy)_3]^{2+}$ and $[Fe(phen)_3]^{2+}$ were reported to be not so large as the racemization rates in organic solvents.[16b,17] Thus, the increase in racemization rates in organic solvents can reasonably be considered to be due to the acceleration of the intramolecular process.

The abilities of the solvents accelerating the racemization were in the order DMSO>formamide>nitromethane>water for the three complexes. This order may be correlated with the polarizability of a solvent, by analogy with the fact that the effect of nucleophiles accelerating the intramolecular racemization of $[Fe(phen)_3]^{2+}$ in an aqueous solution is correlated with their polarizability.[15] The electronic polarization of a solvent is related to its refractive index on the Na D line, the values being 1.476, 1.446, 1.380, and 1.333 for DMSO, formamide, nitromethane, and water respectively; this order of decreasing refractive index is consistent with the decreasing order of the accelerating ability of a solvent shown above. However, this cannot be extended to other solvents. The order of the ability to accelerate the racemization of $[Fe(phen)_3]^{2+}$ was observed to be DMSO>acetone≈methanol > acetonitrile > formamide > nitrobenzene ≈ nitromethane>water,[18] whereas the order of the refractive index was nitrobenzene>DMSO>formamide >nitromethane>acetone > acetonitrile > water > methanol.

For the racemization of $[Ge(acac)_3]^{+}$ [19] and $[Ni(phen)_3]^{2+}$ [20] in organic solvents, the accelerating ability of the solvent was nicely correlated with Gutmann's donor number,[21] a parameter to express the electron-donating ability of a solvent molecule, although the mechanism for racemization differs from complex to complex. For the racemization of $[Fe(1,2\text{-diimine})_3]^{2+}$, the accelerating ability of a solvent may also be correlated with the donor number, the order of which is DMSO>methanol≳H_2O≳acetone>acetonitrile>nitrobenzene>nitromethane, in rough agreement with the trend in the acceleration of the racemization, if water is regarded as an exception. The correlation of the racemization rate of $[Fe(1,2\text{-diimine})_3]^{2+}$ in organic solvents with the polarizability and/or donor number of the solvents may indicate the assistance of solvent molecules in the twist racemization.

As is shown in Table 6, the extent to which the rate is affected by the solvent is decreased in the order $[Fe(phen)_3]^{2+}$>$[Fe(bpy)_3]^{2+}$>$[Fe(gmi)_3]^{2+}$. This order is consistent with the expectation that the most hydrophobic substance $[Fe(phen)_3]^{2+}$ would interact with an organic solvent most strongly, and the least hydrophobic substance $[Fe(gmi)_3]^{2+}$, least strongly. Thus, solvation plays some role in the racemization of tris(1,2-diimine)iron(II) complexes, as was suggested by Van Meter and Neumann.[16c]

References

1) P. Krumholtz, *J. Am. Chem. Soc.*, **75**, 2163 (1953).
2) P. Rây and N. K. Dutt, *J. Indian Chem. Soc.*, **20**, 81, (1943); J. C. Bailar, Jr., *J. Inorg. Nucl. Chem.*, **8**, 165, (1958); C. S. Springer, Jr., and R. E. Sievers, *Inorg. Chem.*, **6**, 852 (1967).
3) F. Basolo and R. C. Pearson, "Mechanisms of Inorganic Reactions," 2nd ed, Wiley, New York (1967), p. 314.
4) J. J. Fortman and R. E. Sievers, *Coord. Chem. Rev.*, **6**, 331 (1971); N. Serpone and D. G. Bickley, *Prog. Inorg. Chem.*, **17**, 391 (1972); R. H. Holm, "Dynamic Nuclear Magnetic Resonance Spectroscopy," ed by L. M. Jackman and F. A. Cotton, Academic Press, New York (1975), Chap. 9.
5) J. G. Gordon, Jr., and R. H. Holm, *J. Am. Chem. Soc.*, **92**, 5319 (1970); A. Y. Girgis and R. C. Fay, *ibid.*, **92**, 7061 (1970).
6) F. Basolo, J. C. Hayes, and H. M. Neumann, *J. Am. Chem. Soc.*, **76**, 3807 (1954).
7) P. Krumholtz, *Struct. Bonding*, **9**, 139 (1971).
8) F. P. Dwyer and E. C. Gyarfas, *J. Proc. R. Soc. N. S. Wales*, **83**, 263 (1950).
9) F. P. Dwyer and E. C. Gyarfas, *J. Proc. R. Soc. N. S. Wales*, **85**, 135 (1952).
10) J. Hidaka and B. E. Douglas, *Inorg. Chem.*, **3**, 1181 (1964).
11) T. Ito, N. Tanaka, I. Hanazaki, and S. Nagakura, *Bull. Chem. Soc. Jpn.*, **41**, 365 (1968).
12) E. König and K. Madeja, *Inorg. Chem.*, **6**, 48 (1967).
13) Gmi, one of the Shiff bases, is synthesized from glyoxal and methylamine by only a template reaction. It is not stable in a free form. Once the ligand has been released from the complex cation, it is immediately hydrolyzed to give the starting materials. This was supported by the fact that the addition of $CoCl_2$ or $NiCl_2$ (5×10^{-4}—0.5 M) as a masking agent of the released free ligand did not change the dissociation rates. The dissociation rate constant thus obtained was independent of the wavelength (in the visible range) where the measurements were made. The reaction was first-order in the complex from the very beginning. Thus, the formation of a bis complex from a tris one must be rate-determining, as was the case with $[Fe(bpy)_3]^{2+}$ and $[Fe(phen)_3]^{2+}$.
14) P. Krumholtz, *Proc. 7th Internat. Conf. Co-ordination Chem.*, Stockholm, p. 280 (1962).
15) S. Tachiyashiki and H. Yamatera, to be published; for the abstract, see the 28th Annual Meeting of Coordina-

tion Chemistry, Hamamatsu, Oct. 1979, Abstr. No 3C08.
16) a) N. R. Davis and F. P. Dwyer, *Trans. Faraday Soc.*, **50**, 1325 (1954); b) L. Seiden, F. Basolo, and H. M. Neumann, *J. Am. Chem. Soc.*, **81**, 3809 (1959); c) F. M. Van Meter and H. M. Neumann, *ibid.*, **98**, 1388 (1976).
17) D. J. Farrington, J. G. Jones, and M. V. Twigg, *J. Chem. Soc., Dalton Trans.*, **1979**, 221.
18) S. Tachiyashiki and H. Yamatera, unpublished results.
19) A. Nagasawa and K. Saito, *Bull. Chem. Soc. Jpn.*, **47**, 131 (1974).
20) T. Fujiwara and Y. Yamamoto, *Inorg. Nucl. Chem. Lett.*, **11**, 635 (1975).
21) K. Gutmann, "Coordination Chemistry in Non-aqueous Solutions," Springer, Wien (1968), p. 19.

  Bull. Chem. Soc. Jpn., 54, 3347—3350 (1981)

Study on the Regeneration of Mn_2O_3 Catalyst for Simultaneous Abatement of NO_x and SO_x

Toshio Sato, Akifumi Ueno,*,† Naoyuki Todo, Minoru Kurita, Hiroyuki Hagiwara, Akiko Nishijima, and Yoshimichi Kiyozumi

National Chemical Laboratory for Industry, Yatabe-cho, Tsukubagun, Ibaraki 305

(Received December 22, 1980)

A technique to regenerate catalysts used for the simultaneous abatement of NO_x and SO_x in flue gases was investigated. Formation of sulfate ions on the metal which is an active component of the catalyst was proved to be a poison for the catalysis. The most effective means to remove the sulfate ions on the catalyst is to heat the used catalyst at 300 °C in NH_3–water vapor.

It has been proposed to make use of coal for saving liquid fuels, although emission of NO_x and SO_x may be enhanced by the coal combustion. Hence, the development of catalysts to remove NO_x and SO_x simultaneously has been desired. The present authors have investigated catalysts for the removal of NO_x in flue gases using NH_3 as reducing reagent,[1] and have started to develop catalysts for the simultaneous removal of NO_x and SO_x on the basis of the results obtained so far. The principle of our techniques for the simultaneous abatement was reported in the previous paper.[2] It was also reported that Mn_2O_3 and Mn_2O_3/Co_3O_4 had the highest activities for the removal of NO_x and SO_x of all the transition metal oxides and their mixtures.[2] The activities, however, decreased with the reaction time, and became about 50% of the initial values. The purpose of the present work is to study the mechanism of the catalyst deactivation and to develop the techniques to regenerate the used catalysts.

Experimental

The catalyst employed in the present work is Mn_2O_3 which was prepared by the precipitation method using $Mn(NO_3)_2 \cdot 6H_2O$ and Na_2CO_3. The precipitates obtained were calcined in air at 550 °C for 3 h. The catalyst thus prepared was crushed to particles with ≈1 mm in diameter. The experiments were carried out using a conventional flow reactor with 5 ml of the catalyst at a space velocity of 10000 h^{-1}. The composition of the gas passed through the catalyst bed was as follows; ≈500 ppm of SO_2, ≈250 ppm of NO, ≈500 ppm of NH_3, ≈3% of oxygen, ≈10% of water vapor, and nitrogen as a balance gas. The activities were measured by the analyses of NO and SO_2 concentrations at the inlet and outlet of the reactor, which were made using an NO analyser of chemiluminescence type and an SO_2 analyser of NDIR type, respectively. The surface area of the catalyst was measured by the BET method using nitrogen at −196 °C. An infrared spectroscopy was used to identify the species formed on the catalyst during the reaction. Experiments for the catalyst regeneration were made in the same reactor employed for the activity measurements. The catalysts used were regenerated in the following gases: 1) ≈20% of water vapor in N_2, 2) ≈20% of water vapor in CO_2, and 3) ≈20% of water vapor and ≈5% of NH_3 in N_2 stream. The temperature employed in the regeneration experiment was in the range of 250—350 °C. To estimate the performance of the catalyst for practical use, a life test was performed for 200 h with the regeneration of the catalyst after every 20 h of the reaction. In this experiment a swing reactor[3] was employed, which consisted of two reactors with the same amount of catalyst peacked in each reactor. While one reactor was used for the reaction, the other was used for the regeneration.

† Present address: School of Materials Science, Toyohashi Univ. of Technology, 1-1 Hibariga-oka, Tempaku-cho, Toyohashi 440.

Results

The activity of Mn_2O_3 catalyst for SO_2 acceptance was measured at the temperatures between 150—400 °C (Fig. 1). The amount of SO_2 absorbed in the catalyst was estimated in a similar way shown in the previous paper.[2] Infrared spectra were measured for the catalysts used at various temperatures so as to identify the species formed by SO_2 absorption (Fig. 2). The regeneration of the catalyst which was used for the reaction at 200 °C for 40 h was done by heating it in various gases. The results obtained were summarized in Table 1. In Fig. 3 the surface area of the catalysts regenerated is shown. The result seems to indicate that the activities of the catalysts recovered were proportional to the surface areas of the catalysts regenerated. Accordingly, the life test of the catalyst was carried out with subsequent regeneration using ≈20% of water vapor and ≈5% of NH_3 in N_2 stream at 300 °C, under whose conditions the surface areas of the used catalysts were recovered almost completely. Infrared spectra of the catalysts regenerated were shown in Fig. 4. Figure 4-c shows an infrared spectrum of the catalyst regenerated by water vapor and NH_3 in N_2 stream at 300 °C for 2 h. Figure 4-d shows an infrared spectrum of the catalyst after 4 cycles of the reaction (20 h) and

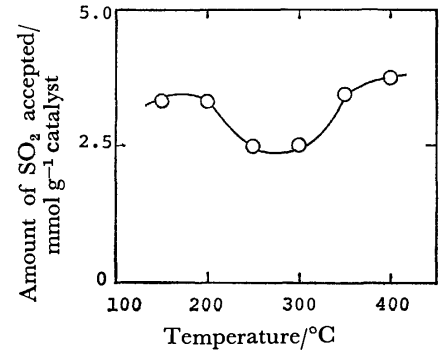

Fig. 1. Amount of SO_2 accepted in Mn_2O_3 at various temperatures.

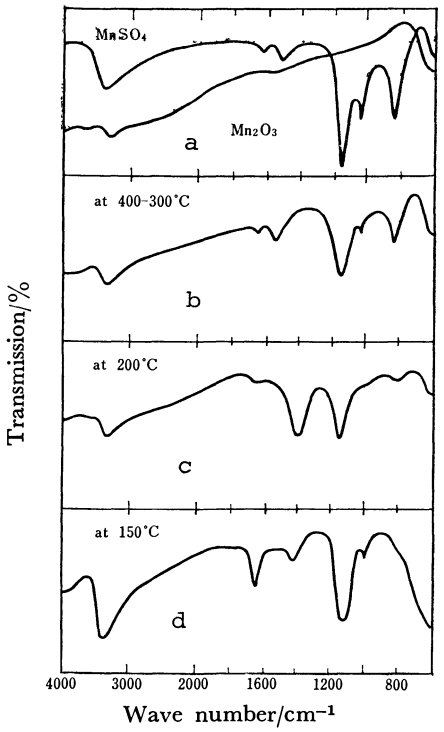

Fig. 2. Infrared spectra of the species formed on Mn_2O_3 by SO_2 adsorption at various temperatures. a): Infrared spectrum of Mn_2O_3, b): SO_2 adsorbed at 300—400 °C, c): SO_2 adsorbed at 200 °C, d): SO_2 adsorbed at 150 °C.

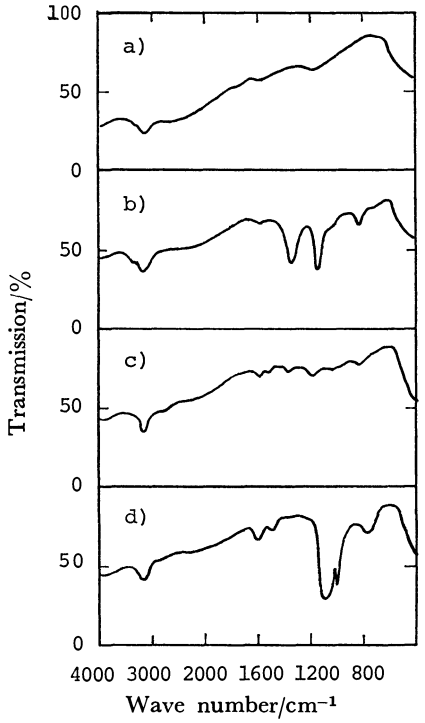

Fig. 4. Infrared spectra of the catalysts used and regenerated.
a): Fresh Mn_2O_3, b): used at 200 °C for 20 h, c): regenerated at 300 °C by water–NH_3, d): after 4th regeneration.

Table 1. Surface area and SO_2 acceptance of the catalyst regenerated by various regeneration methods
(The space velocity of the gases used for the regeneration was 5000 h^{-1} in each regeneration method.)

Regeneration methods	Surface area / $m^2\ g^{-1}$	SO_2 acceptance / mmol g^{-1}
(Fresh catalyst)	55.0	3.4
(Used at 200 °C for 30 h)	18.6	—
Water vapor/N_2 at 350 °C	35.1	2.1
CO_2-water vapor/N_2 at 350 °C	35.5	2.4
NH_3-water vapor/N_2 at 300 °C	42.5	3.1
N_2 at 850 °C	0.1	0

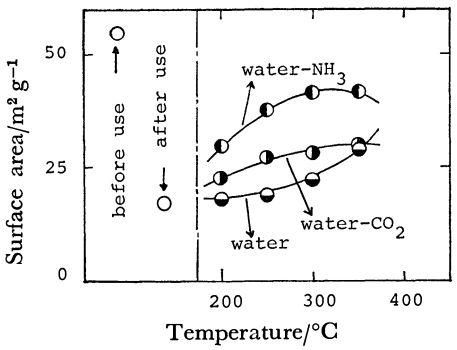

Fig. 3. Surface area of the catalyst regenerated.
◐: Regenerated by water–NH_3, ◑: regenerated by water–CO_2, ◒: regenerated by water.

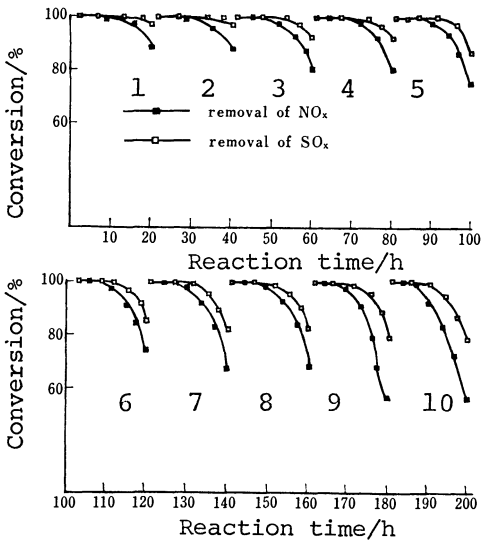

Fig. 5. Activity changes in the life test of the catalyst. (Odd run number for the catalyst in reactor A and even run number in reactor B. Reaction conditions: SV 5000 h^{-1}. Reaction temperature 200 °C. For gas composition see Experimental.)

the regeneration (2 h). These results mean that the sulfate ions accumulated in the catalyst during the cycle of the reaction and regeneration.

The change in the activity and the surface area during the life test were shown in Figs. 5 and 6, respectively. In this work a swing reactor was employed and the change in the activity in the reactor

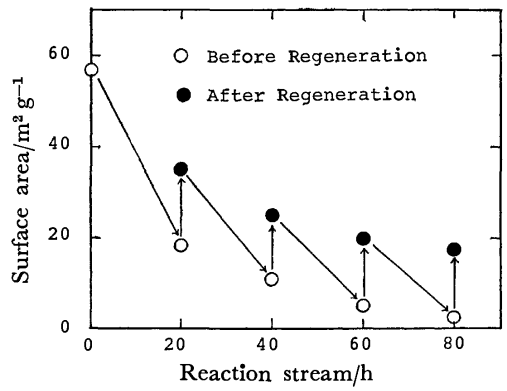

Fig. 6. Change in the surface area of the catalyst during the life test (Catalyst packed in reactor A). ○: Before regeneration, ●: after regeneration.

A was indicated by odd run numbers and those in the reactor B by even run numbers.

Discussion

The adsorption of SO_2 on metal oxides was studied by Galderbank *et al.*,[4] who reported that the adsorption isotherms at low temperatures were expressed in a different form from those at high temperatures. In the present work it was observed that the amount of SO_2 accepted in the catalyst decreased up to 250 °C, and then increased with the elevation of the temperature (Fig. 1). To understand this result, it is important to know the species formed on the catalyst when SO_2 was accepted at various temperatures. The catalyst used for the reaction was submitted to an infrared analysis. As is seen in Fig. 2, the species formed in the catalyst were different depending on the temperatures of the reaction. Manogue[5] and Lunsford[6] studied the adsorption of SO_2 on CuO and MgO, respectively, by means of infrared spectroscopy. They observed formation of sulfate and sulfite ions on both oxides. Furthermore, they revealed that sulfate ions in the bulk oxides showed infrared bands at the lower wave numbers (704 cm^{-1} for CuO and probably 860 cm^{-1} for MgO), while those on the surface of the oxides were not detected because of their structual symmetry. In the present study, an infrared band appeared at 820 cm^{-1} for the catalyst used at the temperatures higher than 300 °C (Fig. 2-b), while a trace or no absorption band was observed in the temperatures lower than 300 °C (Fig. 2-c). This means that the migration of the sulfate ions into the bulk of the catalyst will be enhanced at the temperatures higher than 300 °C, as was reported by Keppler[7] who observed the formation of bulk sulfate ions around 350 °C in metal oxides. When the catalyst was used at 200 °C, infrared bands were observed at 1410 cm^{-1} and 1175 cm^{-1}, and weakly around 3300 cm^{-1}. These bands mean that ammonium sulfates or sulfites were formed on the catalyst at this reaction temperature, since the band at 1410 cm^{-1} is characteristic of ammonium ions and that at 1175 cm^{-1} of both sulfates and sulfites. The weak band around 3300 cm^{-1} showed an existence of the species containing NH_x group. These bands were not observed at the higher temperatures due to the decomposition of the ammonium salts, their decomposition temperatures being about 250 °C. A band appeared at 1610 cm^{-1} when the reaction was carried out at 150 °C (Fig. 2-b). This band may be assigned to the water vapor condensed on the surface of the catalyst. As SO_2 and SO_3 on the catalyst may react with this water vapor to form H_2SO_3 and H_2SO_4, the band at 1175 cm^{-1} characteristic of sulfates and sulfites became strong (Fig. 2-d). The band at 1410 cm^{-1} shows that a small amount of ammonium salts were produced. From these observations it was concluded that the species formed on the catalyst were classified as follows depending on temperatures;

1) Temperatures around 150 °C: SO_2 was accepted in the forms of H_2SO_4 and H_2SO_3 as well as in the forms of ammonium salts.
2) Temperatures around 200 °C: Main species produced were ammonium salts.
3) Temperatures around 250 °C: The ammonium salts were decomposed to ammonia and SO_x adsorbed on the catalyst. A part of SO_x was released to gas phase and the others migrated into the bulk of the catalyst.
4) Temperatures higher than 300 °C: The migration of the sulfate ions was enhanced, and a large amount of the bulk sulfates was produced.

Thus, SO_2 was trapped and accumulated in the catalyst in the present experimental conditions. Hence, a regeneration technique was necessary to be developed for practical use of this catalyst. There have been several papers which proposed catalyst regenerations by heating at high temperatures. Kasaoka *et al.*[8] studied the sulfation of metal oxides and the thermal regeneration of the metal sulfates to the oxides at 700—750 °C in N_2 and air streams. After 30 min of sulfation, the catalysts were well regenerated. They did not mention, however, how well the catalysts were regenerated when the catalysts had been used for a prolonged time. In our experiments, it was observed that about 30% of Mn_2O_3 became $MnSO_4$ or $MnSO_3$ after 30 h reaction at 400 °C. It was also observed that the regeneration to Mn_2O_3 needed the temperature as high as 850 °C in N_2 and air streams. The surface area of the catalyst thus regenerated was less than 0.1 m^2/g, and no activity for the SO_2 acceptance was recovered (Table 1 and Fig. 3). Accordingly, we studied the regeneration at lower temperatures using a few kinds of gas mixtures to prevent reduction of the surface area of the catalyst.

Another point to be mentioned in our regeneration experiments was that the abatement reaction of both NO_x and SO_x was carried out at the temperatures as low as 200 °C, since the bulk sulfates formed at high temperatures were hard to be removed from the catalyst by our regeneration methods. The space velocity employed for the regeneration was 5000 h^{-1}. As the gas for regeneration CO_2 was employed, since $MnSO_4$ was expected to be regenerated to Mn_2O_3 through the formation of $MnCO_3$.[9] Ammonia was employed to let it react with SO_x adsorbed on the catalyst surface and form ammonium salts which are

then decomposed to NH_3 and SO_2 in the gas phase. This method seems to prevent the surface sulfate ions from migrating into the bulk of the catalyst. As is seen in Fig. 3 and Table 1, the most effective means to regenerate the surface area and the activity of the catalyst was to heat in the gas stream containing ≈20% water vapor and ≈5% of ammonia at 300 °C for 2 h. The infrared spectrum of the catalyst thus regenerated showed that a small amount of the sulfates remained unremoved (Fig. 4-c). Unfortunately, this bulk sulfates unremoved proved to accumulate in the catalyst in the every regeneration procedure, reducing the life of the catalyst. The most important point for the regeneration techniques seems to sweep out the sulfates completely from the catalyst. During the life test of the catalyst with the subsequent regeneration after 20 h of the reaction, a small part of the catalyst was submitted to the measurement of the surface area. The surface area of the catalyst regenerated decreased after every regeneration probably due to the accumulation of the sulfates. The rate of deactivation of the catalyst regenerated also became higher after every regeneration (Figs. 5 and 6). The infrared spectrum shown in Fig. 4-d corresponds to the catalyst observed after 4th regeneration procedure. This represents the accumulation of the sulfate ions in the catalyst.

References

1) A. Ueno, N. Todo, M. Kurita, H. Hagiwara, A. Nishijima, T. Sato, and Y. Kiyozumi, *Chem. Lett.*, **1979**, 557; N. Todo, and A. Ueno, *Shokubai (Catalyst)*, **20**, 333 (1978); A. Nishijima, T. Sato, Y. Kiyozumi, M. Kurita, H. Hagiwara, A. Ueno, and N. Todo, *Nippon Kagaku Kaishi*, **1978**, 512.

2) T. Sato, N. Todo, M. Kurita, H. Hagiwara, A. Ueno, A. Nishijima, and Y. Kiyozumi, *Chem. Lett.*, **1978**, 1073.

3) F. M. Dautzenberg, J. E. Naber, and A. J. J. Van Ginnekan, *Chem. Eng. Prog.*, **67**, 86, (1971).

4) P. H. Galderbank, *J. Appl. Chem.*, **2**, 484, (1952).

5) S. A. Kent, J. R. Katzer, and W. H. Manogue, *Ind. Eng. Chem., Fundam.*, **16**, 443, (1977).

6) R. A. Schoonheydt, and J. H. Lunsford, *J. Catal.*, **26**, 261, (1972).

7) G. Keppler, *Z. Angew. Chem.*, **21**, 579, (1908).

8) S. Kasaoka, Y. Sakata, M. Ito, and M. Ikeda, *Nippon Kagaku Kaishi*, **1975**, 2010.

9) R. W. Goodwin, *J. Air Pollution Control Assoc.*, **28**, 35, (1978); M. S. Mozes, *Environ. Sci. Technol.*, **12**, 163, (1978).

Metal Complexes Coordinating Pyridine Derivatives. II.[1] Circular Dichroism and Magnetic Circular Dichroism Spectra of Chromium(III) Complexes in the Region of Pyridine Ring Absorption Band

Yukihiro YAMAMOTO* and Yoichi SHIMURA

Department of Chemistry, Faculty of Science, Osaka University, Toyonaka 560

(Received December 22, 1980)

Dianionochromium(III) complexes coordinating (*S*)-*N*,*N*′-bis(2-pyridylmethyl)propylenediamine (abbrev. *S*-picpn) or (*S*)-1-(2-pyridyl)ethylamine (abbrev. *S*-pea) show CD spectra of a dispersion type in the region of pyridine ring absorption band. Utilizing the data of X-ray crystal structure analysis of *Δ-cis-α*-[$CrCl_2$(*S*-picpn)]Cl, the difluoro complex shows the correct exciton CD sign pattern expected from a simple theory but the dichloro and dibromo complexes the inverse sign pattern. The latter fact is explained in terms of overlapping of the pyridine ring absorption band with the halogeno-to-chromium charge transfer band, referring to MCD spectra. The absorption and MCD bands appeared in the region 30—35 × 10^3 cm^{-1} for all the chromium(III) complexes are assigned to the spin-forbidden $\pi\rightarrow\pi^*$ transition of the coordinated pyridine group.

When two or three ligands having a π electron system coordinate to take a chiral configuration around a metal ion, an exciton splitting of the CD (circular dichroism) band emerges in the region of the $\pi\rightarrow\pi^*$ transition,[2-4] 1,10-phenanthroline, 2,2′-bipyridine, acetylacetonato,[5,6] and tropolonato[7] ligands being typical examples. Several reports are available also for the exciton CD splitting of pyridine ring absorption band, but the treatment remained so far quite unsatisfactory. Bosnich pointed out firstly the occurence of exciton coupling in *cis-α*-[CoX_2(*S*-picpn)]$^{n+}$ and *cis*-[$CrCl_2$(*S*-picpn)]$^+$ complexes[8] (*S*-picpn=(*S*)-*N*,*N*′-bis-(2-pyridylmethyl))propylenediamine). Later Cragel and Brubaker discussed the case of the *cis-β*-cobalt(III) complexes,[9] but assigned incorrectly the *cis-β* structure for a violet $(+)^{C.D.}_{600}$-*cis-α*-[$CoCl_2$(*S*-picpn)]$^+$.[1] On the other hand, it has been claimed by Branca *et al.* that no exciton interaction occurs between the two pyridine rings in *trans* positions for iron(III) complexes coordinating *N*,*N*′-bis(2-pyridylmethyl)ethylenediamine (abbrev. picen) because of far distance of the two pyridine rings.[10]

In the present paper, we deal with the exciton splitting of chromium(III) and cobalt(III) complexes of *S*-picpn, picen, pma (=2-pyridylmethylamine), and *S*-pea (=(*S*)-1-(2-pyridyl)ethylamine), referring to the MCD (magnetic circular dichroism) spectra. Moreover, the assignment of a weak absorption band which emerges in the region of 30—35 × 10^3 cm^{-1} for the complexes having the coordinated pyridine group, is attempted.

Experimental

Ligands. *2-Pyridylmethylamine (pma)*: This ligand was purchased from Aldrich Co.

(S)-1-(2-Pyridyl)ethylamine (S-pea): The (*R*,*R*)-hydrogen tartrate diastereomer was prepared by the method in literature;[11] $[\alpha]_{589}$ +3.9° (c=1.00 × 10^{-2} g cm^{-1}, water) (lit,[11] $[\alpha]_{589}$ +4.3°). To an aqueous solution of the diastereomer was added an equimolar amount of barium chloride. After filtering off the precipitated barium (*R*,*R*)-tartrate, an excess amount of potassium hydroxide was added to the filtrate. An oily product separated was extracted with ether. The ether solution was dried on anhydrous sodium sulfate and ether was evaporated off to obtain the free amine. The free amine was distilled at atmospheric pressure; bp 189 °C, $[\alpha]^{14}_{589}$ −27.7° (c=0.01 g cm^{-3}, water).

(S)-N,N′-Bis(2-pyridylmethyl)propylenediamine (S-picpn) and N,N′-Bis(2-pyridylmethyl)ethylenediamine (picen): These were prepared from (*S*)-propylenediamine or ethylenediamine and 2-pyridinecarbaldehyde by the method of Goodwin and Lions.[12]

Cobalt(III) Complexes. *Δ-(−)*$_{589}$-[$CoCl_2$(*en*)$_2$]$Cl\cdot H_2O$: The racemic complex was resolved with ammonium $(+)_{589}$-(1*R*, 3*S*, 4*S*, 7*R*)-3-bromocamphor-9-sulfonate.[13]

trans(*py*)cis(*H_2O*)-[*Co*(H_2O)$_2$(*pma*)$_2$]$HSO_4\cdot SO_4$: The complex was prepared by the method of literature.[14]

cis-[*Co*(H_2O)$_2$(*en*)$_2$]Cl_3: This was prepared by the method of the literature.[15]

Δ-cis-α-[*$CoCl_2$*(S-*picpn*)]*Cl*: The complex was prepared previously.[1]

Chromium(III) Complexes. *Λ-(−)*$_{589}$-[*$CrCl_2$*(*en*)$_2$]$Cl\cdot H_2O$: The racemic complex was prepared as reported by Pedersen[16] and resolved by the method of Selbin and Bailar[17] with ammonium $(+)_{589}$-(1*R*,3*S*,4*S*,7*R*)-3-bromocamphor-9-sulfonate.

cis-[*CrF_2*(*en*)$_2$]*I*: This was prepared by the method of literature.[18]

trans-[*CrF_2*(*py*)$_4$]*Br*: This complex was prepared by the method of literature.[19]

Δ-trans(*py*)cis(*Cl*)-[*$CrCl_2$*(*pma*)$_2$]ClO_4, trans(*py*)cis(*F*)-[*CrF_2*(*pma*)$_2$]*Br*, trans(*py*)cis(*Cl*)-[*$CrCl_2$*(*pma*)$_2$]*Cl*, trans(*py*)-cis(*H_2O*)-[*Cr*(H_2O)$_2$(*pma*)$_2$](NO_3)$_3$, cis-α-[*$CrCl_2$*(*picen*)]*Cl*, *and* cis-*β*-[*$CrCl_2$*(*picen*)]NO_3: These were prepared by the methods of Michelsen.[20]

fac-[*$CrCl_3$*(*py*)$_3$]: This was prepared by the method in the literature.[21]

Λ-trans(*py*)cis(*Cl*)-[*$CrCl_2$*(S-*pea*)$_2$]*X*: The samples prepared by the following three methods showed the same CD spectra; that is, only one isomer was obtained.

(a) Chromium shot (0.5 g, 10 mmol) was crushed and dissolved in 6 mol dm^{-3} hydrochloric acid (15 cm^3) under a current of nitrogen. The blue solution was evaporated in a vacuum rotary evaporator and heated to dryness. To the residue was added *S*-pea (2.5 g, 20 mmol in 10 cm^3 pyridine). The mixture was heated and then a solution of iodine (1.2 g, 4.7 mmol in 4 cm^3 pyridine) was added. After refluxing for twenty minutes, the violet precipitate was filtered and washed with ethanol. The crude product was treated with silver chloride, the resulting iodide being filtered. The filtered solution was poured onto an SP-

Sephadex C-25 column ($\phi 35 \times 400$ mm) and eluted with 0.1 mol dm^{-3} sodium chloride aqueous solution acidified with hydrochloric acid (0.12 mol dm^{-3}). Only one band was eluted and collected in several fractions. The former 90% parts of the fractions showed the same CD spectrum; they were combined and concentrated in a vacuum rotary evaporator. The deposited sodium chloride was removed from the concentrated solution, to which was added sodium iodide. The desired violet complex precipitated. Found: C, 31.53; H, 4.43; N, 10.33%. Calcd for $[CrCl_2(S\text{-pea})_2]I \cdot 2H_2O = C_{14}H_{20}N_4Cl_2CrI \cdot 2H_2O$: C, 31.72; H, 4.56; N, 10.57%.

(*b*) The preparation was performed as in (*a*) using hydrobromic acid instead of hydrochloric acid. The obtained complex was adsorbed on an SP-Sephadex C-25 column and eluted with 0.5 mol dm^{-3} sodium chloride aqueous solution. The only one band was eluted and collected in several fractions, all of which showed the same CD spectrum. The product was a dinuclear complex. Found: C, 28.62; H, 4.12; N, 9.55%. Calcd for $[\{Cr(OH)(S\text{-pea})_2\}_2]I_4 \cdot 2.5H_2O = C_{28}H_{42}N_8O_2Cr_2I_4 \cdot 2.5H_2O$: C, 28.52; H, 4.02; N. 9.50%. The dinuclear complex was dissolved in water and sodium perchlorate was added. The obtained perchlorate salt of dinuclear complex was dissolved in concd hydrochloric acid. After 10 d, several drops of 70% perchloric acid was added. After ten more days, violet crystals of the desired mononuclear complex appeared. Found: C, 33.64; H, 4.74; N, 11.11%. Calcd for $[CrCl_2(S\text{-pea})_2]ClO_4 \cdot 2H_2O = C_{14}H_{20}N_4O_4Cl_3Cr \cdot 2H_2O$: C, 33.45; H, 4.81; N, 11.41%.

(*c*) Anhydrous chromium(III) chloride (3.9 g, 24.6 mmol) was suspended in dimethyl sulfoxide (12 cm^3). Six grams of *S*-pea (49.1 mmol) was added with stirring. After half an hour, ethanol (20 cm^3) was added to the reaction mixture, and the red-violet product was filtered. The product was extracted with an appropriate amount of hot water (70 °C). The extracted solution was poured onto an SP-Sephadex C-25 column ($\phi 40 \times 400$ mm) and eluted with 0.1 mol dm^{-3} sodium chloride aqueous solution acidified with hydrochloric acid (0.12 mol dm^{-3}). Five bands, a violet one (i), a red-violet one (ii), blue violet one (iii), and two violet ones (iv) and (v), were eluted in this order. Eluate (i) was condensed to a small volume in a vacuum rotary evaporator; violet crystals began to appear and whole was left in a refrigerator overnight. Violet crystals were filtered and washed with ethanol–water (1:1), ethanol and ether. Found: C, 37.75; H, 5.42; N, 12.51%. Calcd for $[CrCl_2(S\text{-pea})_2]Cl \cdot 2.5H_2O = C_{14}H_{20}N_4Cl_3Cr \cdot 2.5H_2O$: C, 37.56; H, 5.63; N, 12.51%. From eluates (ii), (iii), (iv), and (v), no pure crystals were obtained.

Λ-trans*(py)*cis*(F)*-[*CrF*$_2$(S-*pea*)$_2$]*Br*: To a solution of $[CrF_2(py)_4]Br$ (0.50 g) in 2-methoxyethanol was added *S*-pea (0.25 g) and the mixture was refluxed for twenty minutes, A saturated ethanol solution of LiBr was added to it and the precipitates obtained were recrystallized twice from water by adding a saturated ethanol solution of LiBr. Found: C, 30.37; H, 4.56; N, 10.09%. Calcd for $[CrF_2(S\text{-pea})_2]Br \cdot 2.5H_2O \cdot LiBr = C_{14}H_{20}N_4BrCrF_2 \cdot 2.5H_2O \cdot LiBr$: C, 31.05; H, 4.56; N, 10.34%. The complex was dissolved in concd HCl and saturated with HCl gas. After three days, the solution was concentrated and the precipitate was recrystallized from water. Found: C, 34.95; H, 5.02; N, 11.70%. Calcd for $[CrCl_2(S\text{-pea})_2]Br \cdot 2H_2O = C_{14}H_{20}N_4BrCl_2Cr \cdot 2H_2O$: C, 34.80; H, 5.01; N, 11.60%. The CD spectrum of this dichloro complex was the same as that of $[CrCl_2(S\text{-pea})_2]X$ prepared in the above section.

Δ-cis-α-[*CrCl*$_2$(S-*picpn*)]*Cl*, Λ-cis-α-[*CrCl*$_2$(S-*picpn*)]*Cl*, Δ-cis-α-[*CrBr*$_2$(S-*picpn*)]*I*, Λ-cis-α-[*CrBr*$_2$(S-*picpn*)]*Br*, *and* Λ-cis-α-[*CrF*$_2$(S-*picpn*)]*Br*: The preparations of these complexes was described in a previous paper.[1]

cis-α-[*CrF*$_2$*(picen)*]*Br*: To a solution of $[CrF_2(py)_4]Br$ in 2-methoxyethanol was added the stoichiometric amount of picen and the mixture was refluxed for thirty minutes. After cooling, a saturated ethanol solution of LiBr was added. The obtained precipitates were recrystallized from water. The product was eluted with 0.1 mol dm^{-3} NaCl aqueous solution on an SP-Sephadex C-25 column, only one band being observed. Found: C, 34.06; H, 4.85; N, 11.88%. Calcd for $[CrF_2(picen)]Br \cdot 2.5H_2O \cdot 0.3LiBr = C_{14}H_{18}N_4BrCrF_2 \cdot 2.5H_2O \cdot 0.3LiBr$: C, 34.58; H, 4.77; N, 11.52%. The complex was dissolved in concd HCl and saturated with HCl gas below −13 °C. The solution was left for three days and then concentrated with a rotary evaporator. The precipitated product was recrystallized from water and dried in a vacuum desiccator over $CaCl_2$. Found: C, 41.12; H, 4.43; N, 13.76%. Calcd for $[CrCl_2(picen)]Cl \cdot 0.5H_2O = C_{14}H_{18}N_4Cl_3Cr \cdot 0.5H_2O$: C, 41.05; H, 4.68; N, 13.68%. The absorption spectrum of this dichloro complex was the same as that of *cis*-α-$[CrCl_2(picen)]Cl$. Thus, the structure of the difluoro picen complex is determined to be *cis*-α.

Measurements. The visible and ultraviolet absorption spectra were measured with a Shimadzu UV-200 and a Hitachi 330 spectrophotometers. The CD and MCD spectra were measured on a JASCO MOE-1 spectropolarimeter. The specific rotation was measured with a JASCO DIP-4 polarimeter. All the measurements were performed at room temperature.

Results and Discussion

Structural Assignments of the Complexes. The structures of *S*-picpn complexes were assigned previously.[1] Only one isomer was prepared for the dinuclear *S*-pea complex, $[\{Cr(OH)(S\text{-pea})_2\}_2]^{4+}$, the structure of which has been determined as *Λ-trans*(py)*trans*(py),[22] the most probable one from the viewpoint of avoiding the steric hindrance between four pyridine rings. The $[CrCl_2(S\text{-pea})_2]^+$ complex derived from the dinuclear complex is assigned to the *trans*(py)*cis*(Cl) structure. The absolute configuration of this *S*-pea complex is assigned to *Λ* from the comparison of CD spectrum in the d-d transition region with that of *Λ*-$[CrCl_2(en)_2]^+$. No other isomer was obtained for the dichloro complex in any of the three different preparations. The stereospecificity may exist in the formation of $[CrCl_2(S\text{-pea})_2]^+$ complex to produce only the *Λ-trans*(py) isomer. The structures of $[CrF_2(S\text{-pea})_2]^+$ and $[CrF_2(picen)]^+$ are *Λ-trans*(py)*cis*(F), and *cis*-α, respectively (see Experimental).

Exciton Interaction between Pyridine Rings. When two identical chromophores (π system) exist in a chiral molecule, they couple to produce an exciton splitting in absorption and related CD bands, the splitting interval being expressed by exciton interaction energy $2V_{12}$ (Fig. 1).[23] The following explanation is restricted to the coupled chromophore having C_2 symmetry, being harmonized with all the present complexes, which have at least one C_2 or pseudo C_2 axis. In Fig. 1 is shown the exciton splitting for positive V_{12}; the splitting component due to the transition moment pair A symmetry is higher in energy than that of B. The rotatory strength R of A and B com-

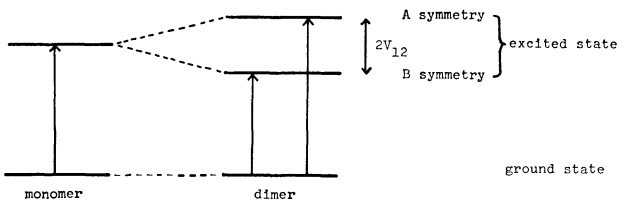

Fig. 1. The exciton splitting with positive V_{12}.

ponents are given by $(\pi\bar{\nu}/2)R'$ and $-(\pi\bar{\nu}/2)R'$, respectively, $\bar{\nu}$ being the wave number of the transition. The rotatory element, R', is written as follows:

$$\vec{R}' = \vec{\mu}_1 \times \vec{R}_{12} \times \vec{\mu}_2 \quad (1)$$

$$= \mu^2 d \sin\alpha \sin\beta \sin\theta, \quad (1)'$$

$$(0<\alpha<180°,\ 0<\beta<180°)$$

where $\vec{\mu}_k$ (k=1 or 2) are transition moments, $\vec{R}_{12}$ is vector from the center of gravity of $\vec{\mu}_2$ to that of $\vec{\mu}_1$, and μ is the magnitude of transition moment. The definition of parameters, d, α, β, and θ are shown in Fig. 2, where d is the distance between the two transition moments AB (chromophore 1) and A'B' (chromophore 2), and θ the dihedral angle between the two planes BCC' and B'C'C, its displayed orientation being taken as positive. Thus, R' is positive at $0<\theta<180°$; and negative at $0>\theta>-180°$.

The absorption spectrum of pma is shown in Fig. 3. In this study the lower energy band, ^1L_b, of pyridine ring at about 39800 cm^{-1} is treated. The transition moment direction of this absorption band is depicted with an arrow in Fig. 3, and supposed to be independent of the alkyl substitution (R) at 2 position of pyridine ring.

In Fig. 4 is shown the transition moments in the

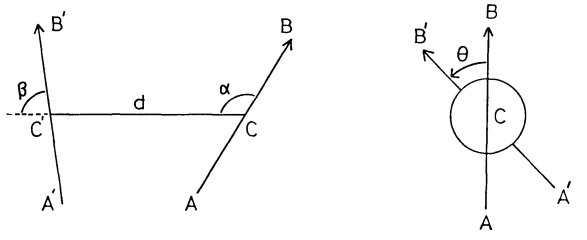

Fig. 2. The parameters, d, α, β, and θ defining the rotatory element R'.

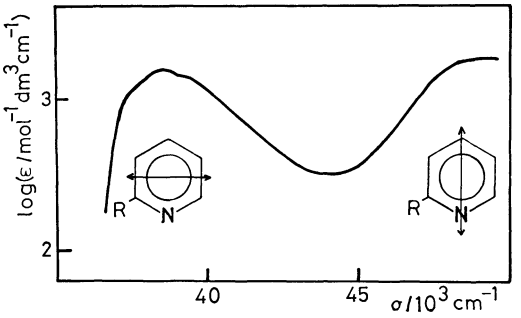

Fig. 3. Absorption Spectrum of pma ($R=CH_2NH_2$) in water, and the directions of transition moments for ^1L_b (lower energy) and ^1L_a (higher energy) bands.

case of Λ-*cis*-α-$[CrCl_2(picen)]^+$. The exciton interaction energy, V_{12}, is generally written,[23b]

$$V_{12} = \frac{1}{d^3}\{(\vec{\mu}_1\cdot\vec{\mu}_2) - 3(\vec{\mu}_1\cdot\vec{R}_{12})(\vec{\mu}_2\cdot\vec{R}_{12})/d^2\}. \quad (2)$$

The centers of gravity of transition moments being set on the x axis and the exciton interaction energy being approximated as coulomb interaction energy between point dipoles, V_{12} can be written as follows,[23b]

$$V_{12} = \frac{\mu^2}{d^3}(m_1m_2 + n_1n_2 - 2l_1l_2),$$

where l_k, m_k, and n_k (k=1 or 2) are the direction cosines for the transition moment k against the coordination axes x, y, and z, respectively (x, y, and z are taken as shown in Fig. 4).

It has been reported for Λ-*fac*-$[Co(S\text{-pea})_3]^{3+}$ [24] that the angles $<NCrN_{py}$ (N_{py} stands for pyridine nitrogen) in the chelate rings are not exactly 90°. Thus the angles ω_{x1} and ω_{x2}, which are the angles between the transition moments and the +x axis, are introduced as shown in Fig. 5, where $\omega_{x1}+\omega_{x2}=180°$. Consequently, the interaction energy V_{12} is approximately expressed as follows:

$$V_{12} = \frac{\mu^2}{d^3}(\cos\theta + 2\cos^2\omega_{x1}). \quad (2)'$$

The rotatory element R' and the exciton interaction energy V_{12} can be calculated approximately from the relative orientation of the transition moments on the two pyridine rings by Eqs. 1 and 2 (or Eqs. 1' and

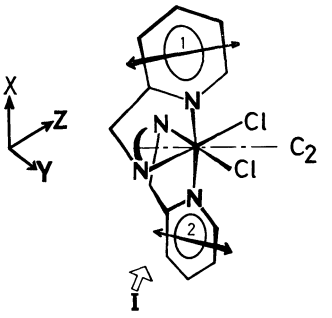

Fig. 4. The structure of Λ-*cis*-α-$[CrCl_2(picen)]^+$ and the directions of the transition moments for the ^1L_b band. The C_2 axis coincides with the bisector between y and z axis.

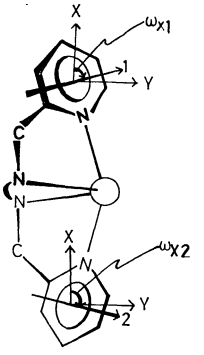

Fig. 5. The transition moment pair of A symmetry viewed from $-z$ direction (from the arrow I in Fig. 4).

2′) respectively. The expected CD patterns are given in Table 1 for the four combinations of R' and V_{12}; for example, when R' and V_{12} are positive, a negative and then a positive component from the lower energy side, (−,+), are expected.

CD and MCD Spectra of the Pyridine Ring Absorption Band (^1L_b Transition). The absorption and CD data of *cis*-α-$[CrX_2(S\text{-picpn})]^+$ (X=F, Cl, and Br) are exhibited in Table 2 (the band assignments are shown in the Table) and Figs. 6, 7, and 9. All the *S*-picpn complexes show (+,−) or (−,+) dispersion type CD pattern in the pyridine ring absorption band region (^1L_b transition). For the *Λ* difluoro complex, a typical (+,−) pattern is observed clearly (Fig. 6). The CD sign pattern is (−,+) from the lower energy side for the *Λ* complexes except for the difluoro complex, and that of the *Δ* complexes is (+,−) for the dichloro and the dibromo complexes (Table 2).

By using the atomic positions (Table 3) of pyridine ring carbon atoms determined in the X-ray structure analysis of *Λ*-*cis*-α-$[CrCl_2(S\text{-picpn})]Cl$,[25] the exciton CD pattern is estimated from Eqs. 1′ and 2. The numbering scheme of the carbon atoms is shown in Fig. 8. In the explanation of the component A symmetry, the directions of transition moments are taken from the midpoint of C(4) and C(5) to that of C(1) and C(2), and from the midpoint of C(10) and C(11) to that of C(13) and C(14). The evaluated values of R' and V_{12} from Eqs. 1′ and 2 are both negative. Thus the expected CD pattern is (−,+) from the lower energy side (Table 1), which is inverse to those observed for the dichloro and dibromo *Λ* complexes.

For the *Λ* complex, the expected exciton CD pattern is (+,−), since it is probable that the relative orientation of the two pyridine rings in the *Λ* complex is not so much different from the mirror image of that in the *Δ* complex. Only the difluoro *Λ* complex matches this calculated CD pattern.

The absorption and CD spectra of *cis*-$[CrX_2(en)_2]^+$ (X=F or Cl) are shown in Figs. 6 and 7. The ligand-to-metal charge-transfer (CT) band of the dichloro complex is located near the pyridine ^1L_b band, but

TABLE 1. EXPECTED CD PATTERN IN THE EXCITON REGION

R'	V_{12}	CD sign pattern from the lower energy side
+	+	(−, +)
+	−	(+, −)
−	+	(+, −)
−	−	(−, +)

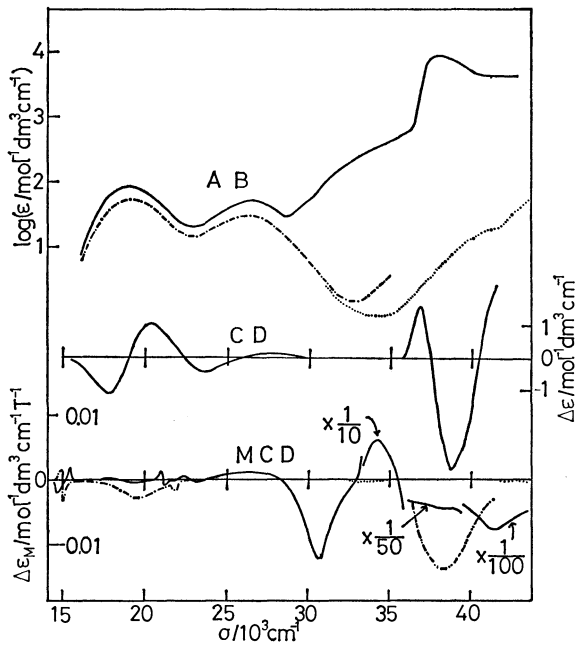

Fig. 6. Absorption (AB) and CD spectra of *Λ*-*cis*-α-$[CrF_2(S\text{-picpn})]Br$ in water (——). Absorption spectrum of *cis*-$[CrF_2(en)_2]I$ (-·-·-) and an eluted solution passed through Dowex 1-x8 (Cl^- form) (···). MCD spectra of *cis*-α-$[CrF_2(picen)]Br$ (——), *cis*-$[CrF_2(en)_2]I$ (-·-·-), the eluted solution (·····), and pma (-·-·-·-) in water.

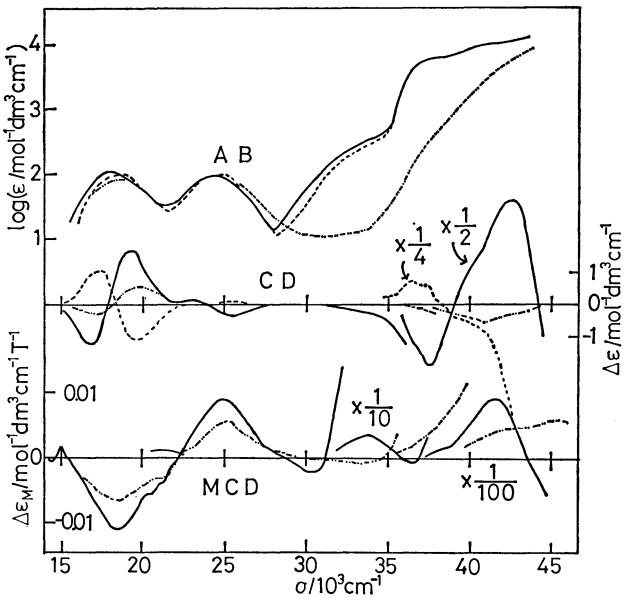

Fig. 7. Absorption (AB) and CD spectra of *Λ*-*cis*-α-$[CrCl_2(S\text{-picpn})]Cl$, (——), *Λ*-*cis*-α-$[CrCl_2(S\text{-picpn})]Cl$ (- - -), and *Λ*-*cis*-$[CrCl_2(en)_2]Cl$ (-·-·-·-) in 0.1 mol dm^{-3} HCl. MCD spectra of *cis*-α-$[CrCl_2(picen)]Cl$ in 0.1 mol dm^{-3} HCl (——) and *cis*-$[CrCl_2(en)_2]Cl$ (-·-·-·-) in methanol.

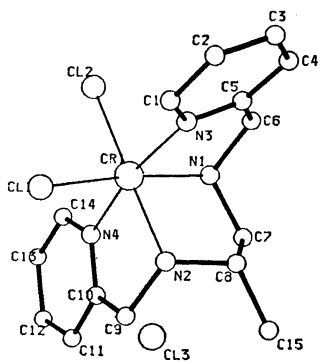

Fig. 8. The structure of *Λ*-*cis*-α-$[CrCl_2(S\text{-picpn})]Cl$ and the numbering scheme of the atoms.

Table 2. Absorption and CD data of Cr(III) and Co(III) complexes measured in 0.1 mol dm^{-3} HCl and in methanol (sh=shoulder)

Complex	Absorption (in HCl) σ_{max}/cm^{-1}	log ε[a]	CD (in HCl) σ_{ext}/cm^{-1}	$\Delta\varepsilon$[a]	Absorption (in methanol) σ_{max}/cm^{-1}	log ε[a]	CD (in methanol) σ_{ext}/cm^{-1}	$\Delta\varepsilon$[a]	Assignment
Λ-cis-α-[CrF_2(*S*-picpn)]Br[b,c]					18690	1.88	17180	−0.98	d-d
							19720	+0.79	
							23040	−0.69	
					26460	1.68	26740	+0.25	
	34000(sh)	2.4	29850	+0.06	33000(sh)	2.4	35000(sh)	+0.35	py(triplet)
			30960	+0.04					
			31750	+0.03					
	38020	3.89	36740	+1.69	37880	3.83	36630	+1.43	py(^1L_b)
			38760	−3.37					
			43670	+5.35			39060	−2.70	
Λ-trans(py)*cis*(F)-[CrF_2(*S*-pea)$_2$]Br[b]	19270	2.03	18350	−0.73	19010	1.88	18280	−0.60	d-d
			20580	+0.87			20450	+0.40	
	26810	1.77	25910	−0.28	27170	1.65	23810	−0.22	
							27550	−0.14	
	31000(sh)	2.2	28900	−0.07			33670	+0.15	py(triplet)
	34000(sh)	2.6	34250	+0.24					
	37740	3.90	37040	+6.79	38020	3.88	37040	+5.36	py(^1L_b)
			39840	−0.64			38760	−0.86	
			46080	+5.12			42370	+4.04	
cis-[CrF_2(en)$_2$]I[b]	19160	1.74							d-d
	26250	1.48							
cis-[CrF_2(en)$_2$]Cl[b]	40000(sh)	1.12							d-d
trans-[CrF_2(py)$_4$]Br[b]	19080	1.44			18760	1.42			d-d
	24450	1.04			24210	0.91			
	29410(sh)	1.49			29590(sh)	1.61			py(triplet)
	30300(sh)	1.74			30490(sh)	1.81			
	31750(sh)	2.11			31750(sh)	2.04			
	32790(sh)	2.33							
	37170(sh)	2.82			38460	3.99			py(^1L_b)
	38170	3.97							
	38610(sh)	3.95							
	45050	3.99			42190	4.01			
Λ-cis-α-[$CrCl_2$(*S*-picpn)]Cl[c]					18050	2.00	16860	+1.00	d-d
							19340	−1.03	
					24270	2.02	22730	+0.23	
			30300	+0.02	34000(sh)	2.6	34000(sh)	−0.27	py(triplet)
			31250	+0.05					
	34000(sh)	2.5	32260	+0.09					
	36500(sh)	3.6	36230	+3.13					py(^1L_b)
	37390	3.77	37040	+2.40	37000	3.8	36230	+1.59	
			39200(sh)	−1.7					
	48540	4.40	43860	−18.1			43290	−15.9	
Λ-cis-α-[$CrCl_2$(*S*-picpn)]Cl[c,e]					17700	2.03	16390	−1.09	d-d
							18800	+1.41	
					24100	2.10	21790	−0.24	
							23420	+0.07	
							25320	−0.27	
	34000(sh)	2.6	33500(sh)	−0.3	34000(sh)	2.6	34000(sh)	−0.25	py(triplet)
	36500	3.58	36360(sh)	−4.9	37000	3.8	37040	−5.08	py(^1L_b)
	37390	3.77	37310	−7.96			38760	+2.53	
			38170(sh)	−4.6					
			39600(sh)	+3.0					
			42370	+13.1			42020	+9.07	
			46950	−41.8					
Λ-trans(py)*cis*(Cl)-[$CrCl_2$(pma)$_2$]ClO_4	18520	1.97	17420	+0.63	18020	1.97	17180	+0.60	d-d
			19570	−0.85			19420	−0.58	

TABLE 2. (Continued)

Complex	Absorption (in HCl)		CD (in HCl)		Absorption (in methanol)		CD (in methanol)		Assignment
	σ_{max}/cm^{-1}	$\log \varepsilon$[a]	σ_{ext}/cm^{-1}	$\Delta\varepsilon$[a]	σ_{max}/cm^{-1}	$\log \varepsilon$[a]	σ_{ext}/cm^{-1}	$\Delta\varepsilon$[a]	
	24880	1.94	24570	+0.15	24630	1.97	23640	+0.17	
	34000(sh)	2.5	30670	−0.01	34000(sh)	2.5	29590	+0.02	py(triplet)
			31650	−0.02			30400	+0.02	
			33300	+0.15					
	37810	3.78	36830	−1.23	37000(sh)	3.7	35340	+0.34	py(^1L_b)
			38020	−1.14			37740	−3.31	
			38850	−1.10			39840	+0.84	
			44250	−14.6			43100	−9.94	
Δ-trans(py)*cis*(Cl)-[$CrCl_2$(*S*-pea)$_2$]Cl	18600	2.02	17480	−0.57	18180	2.02	17390	−0.48	d-d
			19570	+1.03			19490	+0.74	
	24060	1.99	24630	−0.21	24880	2.01	24000	−0.22	
	34000(sh)	2.4	28820	+0.02	33000(sh)	2.4	29070	+0.02	py(triplet)
			29940	+0.03			29760	+0.02	
			30770(sh)	+0.05					
			31550(sh)	+0.08					
	37000(sh)	3.7	36580	+3.85			35100	−0.25	py(^1L_b),CT
	37590	3.81	37790	(−)[d]			38760	+5.91	
			39900(sh)	+4.22					
			43980	+15.78			43500	+10.7	
Δ-cis-[$CrCl_2$(en)$_2$]Cl	19010	1.87	17240	−0.29					d-d
	19800		19800	+0.59					
	24810	1.83	24040	+0.23					
			40820	−1.70					CT
	47390	4.11	46080	+1.70					
Δ-cis-α-[$CoCl_2$(*S*-picpn)]Cl[c]	30000(sh)	3.1	30490	+2.34					CT
	34500(sh)	3.7	35590	−18.45					
	39530	4.30	39220	+36.60					py(^1L_b),CT
			43000(sh)	+16					
			46510	−21					
Δ-cis-[$CoCl_2$(en)$_2$]Cl	18690	1.98	16390	−0.55					d-d
			18870	−0.72					
	25640	1.95	24510	+0.22					
	32000(sh)	2.9	33670	−1.23					
	38500(sh)	4.1	37590	+7.97					CT
	42920	4.28	42370	−14.65					
Δ-cis-α-[$CrBr_2$(*S*-picpn)]I[c]					17180	2.07	16530	+0.78	d-d
							18940	−0.82	
					23420	2.18	24510	+0.07	
	33000	3.15	33000	+0.95	34000(sh)	3.5	31550	+0.81	CT
	37500(sh)	4.0	36560	−2.88			34960	−1.84	
			36830	(+)[d]	37600(sh)	4.0	36500	−1.23	py(^1L_b),CT
			39920	−9.60			39680	−8.61	
	44400	4.48	44250	+23.06					
Δ-cis-α-[$CrBr_2$(*S*-picpn)]Br[c]					17120	2.02	16130	−1.17	d-d
							18420	+1.53	
					23420	2.03	22320	+0.29	
							24390	−0.48	
	33000	3.3	32470	−1.68	34000(sh)	3.4	31250	−1.74	CT
			35090	+1.58			35090	+2.94	
			36300(sh)	+0.97					
	37500(sh)	4.0	37370	−2.59	37600(sh)	4.0	37170	−1.79	py(^1L_b),CT
			39630	+5.83			38910	+2.20	
			43860	−29.03			42640	−21.0	
2-Pyridylmethylamine	37500(sh)	3.04							py(^1L_b)
	38460	3.20							
	39500(sh)	3.13							

a) ε is defined in $mol^{-1}\,dm^3\,cm^{-1}$ unit. b) Measured in water. c) The data in the d-d transition region are reported in the previous paper.[1] d) The negative (positive) peak is in the positive (negative) area in fact because of the overlapping of intense positive (negative) band in close proximity. e) The perchlorate salt was measured in methanol.

Table 3. The positions of pyridine ring carbon atoms

	x	y	z
C (1)	2.25	2.56	3.86
C (2)	2.88	3.28	4.86
C (3)	3.02	2.78	6.13
C (4)	2.52	1.54	6.43
C (5)	1.96	0.78	5.41
C (10)	−1.38	−1.13	1.56
C (11)	−2.22	−1.98	0.83
C (12)	−1.72	−3.16	0.28
C (13)	−0.35	−3.45	0.48
C (14)	0.42	−2.59	1.26

that of the difluoro complex is far from the pyridine ^1L_b band (the absorption band at ca. 40000 cm^{-1} in *cis*-$[CrF_2(en)_2]^+$ is the third spin-allowed d-d transition band). Also in Figs. 6 and 7 are shown the MCD spectra of *cis*-α-$[CrX_2(picen)]^+$, *cis*-$[CrX_2(en)_2]^+$ (X=F or Cl), and pma. No MCD band was observed for the *cis*-$[CrF_2(en)_2]^+$ complex in the 35000—40000 cm^{-1} region, but a very strong tail of higher energy MCD band for the dichloro complex, *cis*-$[CrCl_2(en)_2]^+$, in that region. In *cis*-α-$[CrF_2(picen)]^+$ complex a broad MCD band of pyridine rings is observed, while in the *cis*-α-$[CrCl_2(picen)]^+$ complex, the rather complicated MCD spectra indicate an overlap of the bands due to pyridine ring and CT transitions.

It has been established that exciton coupling is not observed in MCD spectra of tris(phenanthroline) metal complexes.[26] Likewise, the present complexes having two pyridine rings show no exciton coupling in the MCD spectra. The exciton coupling CD pattern in the dichloro complexes is considered to suffer from the overlap of CT bands. The CD spectrum of the difluoro complex shows the unperturbed pattern and correct signs in this region. In the dibromo complexes, it is clear that the bromo-to-chromium CT bands overlap with the pyridine ring absorption band. The exciton treatment can not be made in the case of overlapping of charge transfer band to the pyridine ring absorption band and the overlapping of CT band can be distinguished more clearly by using MCD spectrum.

The absorption and CD spectra of *trans*(py)*cis*(F)-$[CrF_2(S\text{-pea})_2]^+$ are shown in Fig. 9 with the MCD spectrum of *trans*(py)*cis*(F)-$[CrF_2(pma)_2]^+$. The MCD spectra in the pyridine ring absorption band region shows a similarity to that of pma; that is, only the B term of pyridine ring is observed.[27] The exciton CD spectra of the difluoro complexes are expected to show the CD pattern estimated by the simple theory. Though the observed CD spectrum is somewhat shifted to the positive area, the CD pattern is (+,−) from the lower energy side. This case is explained by using the Eqs. 1′ and 2′ and Fig. 5. An X-ray analysis of *Δ-fac*-$[Co(S\text{-pea})_3](ClO_4)_3\cdot 2H_2O$ showed that the pyridine ring of each *S*-pea ligand is tilted against the plane determined by cobalt and two nitrogen atoms of the ligand.[24] The tilt angle is 13—17°. Since the central chelate ring in Fig. 5 is absent, the

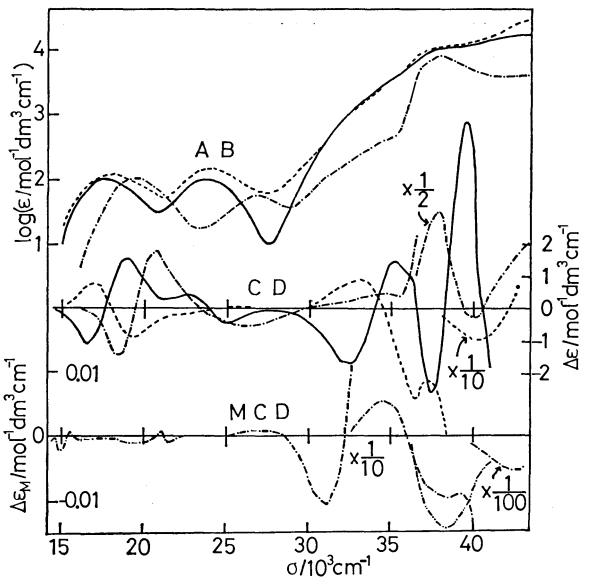

Fig. 9. Absorption (AB) and CD spectra of *Δ-cis*-α-$[CrBr_2(S\text{-picpn})]Br$ (- - -), *Λ-cis*-α-$[CrBr_2(S\text{-picpn})]I$ (——) in 0.1 mol dm^{-3} HCl, and *Λ-trans*(py)*cis*(F)-$[CrF_2(S\text{-pea})_2]Br$ in water (-·-·-). MCD spectra of *trans*(py)*cis*(F)-$[CrF_2(pma)_2]Br$ in water (-·-·-) and pma in water (-··-··-).

angle $|\theta|$ becomes larger than 90°, being estimated to be *ca.* 120°. From Eqs. 1′ and 2′ (ω_{x1}=*ca.* 84° was estimated from the X-ray analysis of *Δ-cis*-α-$[CrCl_2(S\text{-picpn})]Cl$[25]) the value of V_{12} becomes negative and R' is positive. Thus, a (+,−)CD pattern is expected from Table 1, which coincides with the observed pattern. It is established that the exciton CD between the two pyridine rings depends on the chelate ring conformations containing the pyridine rings.

In the case of *Λ-trans*(py)*cis*(Cl)-$[CrCl_2(S\text{-pea})_2]^+$ complex, (Fig. 10), the observed (+,−,+) CD pattern does not coincides with the expected exciton pattern. For the complex *Λ-trans*(py)*cis*(Cl)-$[CrCl_2(pma)_2]^+$, a vibrational pattern is observed in the CD spectrum. Moreover, the *S*-pea and pma complexes change the CD spectra by solvent change.

The observed CD pattern in the pyridine ring absorption band of *Δ-cis*-α-$[CoCl_2(S\text{-picpn})]^+$ (Fig. 10) coincides with the expected pattern. In the cobalt(III) complex, the chloro-to-cobalt CT band overlaps with the pyridine ring absorption band. Thus the coincidence between the observed and expected patterns might be accidental.

Solvent Effect. The absorption and CD spectra of all the chromium(III) complexes treated here were also measured in methanol and the spectral data are shown in Table 2. The absorption spectra in methanol are generally shifted to the lower energy side as compared with those measured in hydrochloric acid or water in the d-d transition region. But they show rather small change in the pyridine ring absorption band region. A solvent effect studies have been reported previously for the typical cobalt(III) and chromium(III) complexes,[28] which showed red shift by the solvent change from water to alcohols,

TABLE 4. MCD SPECTRAL DATA, MEASURED IN WATER OR 0.1 mol dm^{-3} HCl AND IN METHANOL (sh=shoulder)

Complex	σ_{ext}/cm^{-1} (in water or HCl)	$10^2\,\Delta\varepsilon_M$[a)]	σ_{ext}/cm^{-1} (in methanol)	$10^2\,\Delta\varepsilon_M$[a)]	Assignment
cis-α-[CrF_2(picen)]Br	14810	−0.39	14810	−0.21	d-d (doublet)
	15460	+0.21	15410	+0.17	
	17390	+0.05	20880	+0.15	d-d (quartet)
	20000	−0.10			
	20960	+0.31	21070	−0.21	d-d (doublet)
	21140	−0.31			
	21830	−0.05			
	22470	+0.09			
	23150	−0.07			d-d (quartet)
	26670	+0.17	26320	+0.4	
	30770	−2.1	30960	−1.6	py (triplet)
	34250	+9.9	34480	+11	
	36360	−34			py (^1L_b)
	37590	−33			
	41490	−132	41490	−82	
			46510	−100	
trans(py)*cis*(F)-[CrF_2($pma)_2$]Br	14930	−0.24	14840	−0.18	d-d (doublet)
	16390	−0.07	15420	+0.08	
	19610	−0.11	20900	+0.07	d-d (quartet)
	21050	+0.04	21280	−0.09	d-d (doublet)
	21510	−0.11			
	23150	−0.04			d-d (quartet)
	27030	+0.09	27030	+0.09	
	31060	−0.04	30960	−1.3	py (triplet)
	34480	+0.09	34480	+6.5	
	38460	−1.0	36360	−17	py (^1L_b)
	42550	−53	41670	−70	
cis-[CrF_2($en)_2$]I	14880	+0.15			d-d (doublet)
	15060	−0.36			
	19610	−0.31			d-d (quartet)
	21880	−0.19			d-d (doublet)
	23040	−0.06			d-d (quartet)
	26320	+0.13			
trans-[CrF_2($py)_4$]Br	14480	+0.03	14410	+0.01	d-d (doublet)
	14660	−0.04	14560	−0.01	
	14930	−0.03	14710	−0.01	
	15060	−0.03	14840	+0.04	
	15150	+0.01	15040	+0.06	
	15290	−0.05	15200	−0.02	
	15580	−0.01	15460	−0.08	
			15720	−0.07	
	23150	−0.03	18870	+0.02	d-d (quartet)
			22080	+0.02	
	29850	−0.08	30770	−0.51	py (triplet)
	34480	+3.92	34970	+6.42	
	39220	+52	39220	+63	py (^1L_b)
	41320	−18			
cis-α-[$CrCl_2$(picen)]Cl	14390	−0.11	14600	−0.12	d-d (doublet)
	14970	+0.16	14810	+0.06	
	18520	−1.1	17860	−0.97	d-d (quartet)
	20620	−0.56	20000	−0.42	d-d (doublet)
	21280(sh)	−0.39	20200	−0.46	
			20830	−0.27	
			21050(sh)	−0.23	
	25000	+0.89	25000	+0.87	d-d (quartet)
	30770	−0.22	30770	−0.73	py (triplet)

TABLE 4. (Continued)

Complex	σ_{ext}/cm^{-1} (in water or HCl)	$10^2\,\Delta\varepsilon_M$ [a]	σ_{ext}/cm^{-1} (in methanol)	$10^2\,\Delta\varepsilon_M$ [a]	Assignment
	33900	+3.5	33670	+5.3	
	36360	−10	35590	−0.60	py (^1L_b), CT
	41490	+94	40490	+68	
cis-β-$[CrCl_2(picen)]NO_3$	14900	+0.21			d-d (doublet)
	18180	−0.81	c)		d-d (quartet)
	19880	−0.51			d-d (doublet)
	20660	−0.50			
	24690	+0.73			d-d (quartet)
	30030	−0.54	29850	−1.1	py (triplet)
	33900	+4.2			
	39220	+62	37740	+39	py (^1L_b), CT
	42550	+44	42190	+57	
trans(py)*cis*(Cl)-$[CrCl_2(pma)_2]Cl$	14390	−0.36	14290	−0.19	d-d (doublet)
	15150	+0.13	15040	+0.34	
	18520	−0.85	17860	−1.4	d-d (quartet)
	20830	−0.430	20200	−0.52	d-d (doublet)
	21550(sh)	−0.33	20620	−0.67	
			21050	−0.45	
			21280(sh)	−0.46	
	25000	+0.76	25000	+1.4	d-d (quartet)
	303000	−0.26	30770	−1.3	py (triplet)
	33900	+3.0	33900	+7.5	
	37040	−4.0	35840	−2.8	py (^1L_b), CT
	41840	+75	39680	−120	
cis-$[CrCl_2(en)_2]Cl$ [b]			14490	−0.25	d-d (doublet)
			15150	+0.06	
			18520	−0.06	d-d (quartet)
			21510	−0.33	d-d (doublet)
			25000	+0.57	d-d (quartet)
			33330	−0.09	
			42000(sh)	+46	CT
			45450	+61	
2-Pyridylmethylamine	38460	−14			py (^1L_b)

a) $\Delta\varepsilon_M$ is given in $mol^{-1}\,dm^3\,cm^{-1}\,T^{-1}$. b) Measured in methanol, because of decomposition in water or in 0.1 mol dm^{-3} HCl. c) Data were not obtained because of low solubility. CT: Charge transfer band.

The same trend is observed in this study. The CD spectra of all the complexes show the red shift in the d-d transition region and large shift or change in the pyridine ring absorption band region. Especially, the dichloro complexes show remarkable changes in this region; that is, the (+,−) or (−,+) dispersion type CD pattern can more clearly be observed in methanol solution than in hydrochloric acid solution, large shift to the lower energy side being also observed.

The spectral change in the dibromo complexes is also distinctive in the pyridine ring absorption band region. The red shift in $30—35\times10^3\,cm^{-1}$ region is larger than that in the other regions.

Spin-forbidden Transition of the Coordinated Pyridine Groups. The MCD spectral data are shown in Table 4. In the pyridine ring absorption band region, the MCD change by the solvent change show a similar tendency to that observed in the CD spectra.

Some peculiar MCD spectra are observed in $30—35\times10^3\,cm^{-1}$ region. Only weak CD spectra are observed in this region for the difluoro and dichloro complexes, but a (−,+) MCD pattern from the lower energy side is observed in all the complexes with coordinated pyridine groups. In methanol solution the strength of the band is strengthened for all the complexes including *cis*-β-$[CrCl_2(picen)]^+$ (Fig. 11) and *trans*-$[CrF_2(py)_4]^+$ (Fig. 11). There are three possibilities for the assignment of this band.

(1) CT transition from pyridine to chromium ($\pi\rightarrow$ d),
(2) CT transition from chromium to pyridine (d$\rightarrow$ π^*),
(3) spin-forbidden transition of pyridine.

If it is the CT band (1), the position will change by changing the central metal, because the energy of the CT band is inversely proportional to the optical electronegativity of the metal (1.9 and 2.3 for Cr(III) and Co(III), respectively).[29] The absorption spectra of *cis*(H_2O)*trans*(py)-$[Cr(H_2O)_2(pma)_2]^{3+}$ and the cobalt(III) analog are shown in Fig. 11. The band for the chromium complex locates at lower energy than that for the cobalt complex. Moreover, from

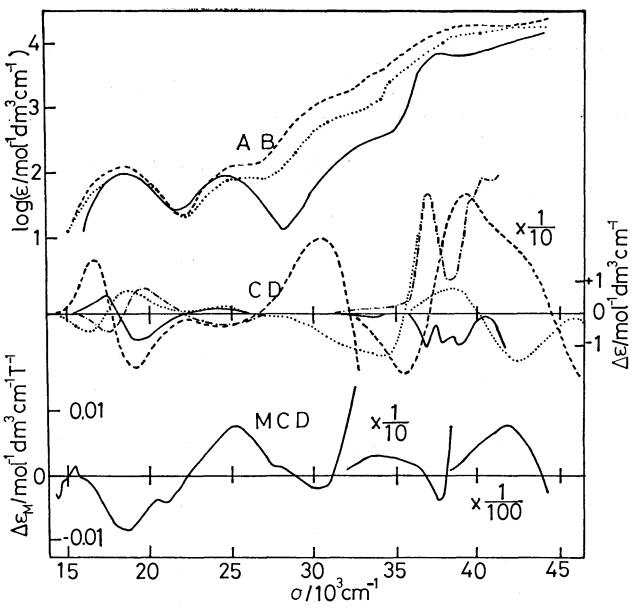

Fig. 10. Absorption (AB) and CD and MCD spectra of Δ- or *racemic-trans*(py)*cis*(Cl)-[$CrCl_2(pma)_2$]Cl in 0.1 mol dm^{-3} HCl (——). CD spectrum of Δ-*trans*-(py)*cis*(Cl)-[$CrCl_2$(*S*-pea)$_2$]Cl in 0.1 mol dm^{-3} HCl (-·-·-). Absorption (AB) and CD spectra of Δ-*cis*-α-[$CoCl_2$(*S*-picpn)]Cl (- - -), and Δ-*cis*-[$CoCl_2$-$(en)_2$]Cl (···) in 0.1 mol dm^{-3} HCl.

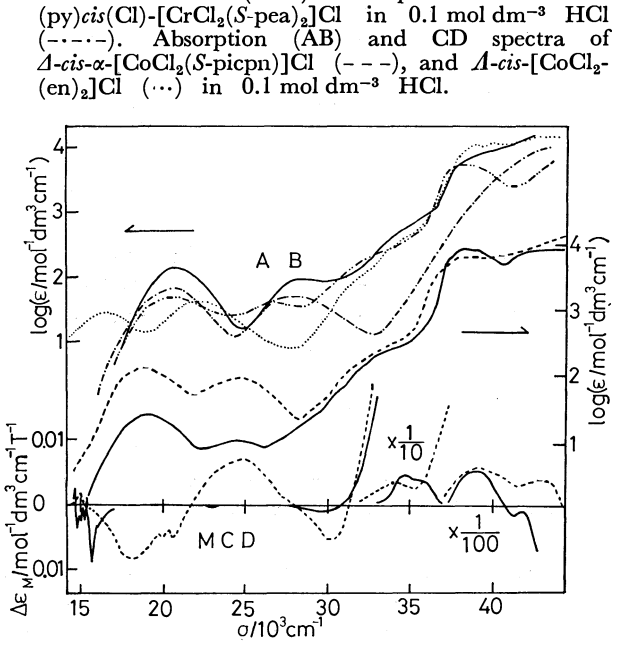

Fig. 11. Absorption (AB) (lower curves) and MCD spectra of *cis*-β-[$CrCl_2$(picen)]NO_3 in 0.1 mol dm^{-3} HCl (- - -) and *trans*-[$CrF_2(py)_4$]Br in water (——). Absorption (AB) (upper curves) spectra of *trans*(py)-*cis*(H_2O)-[$Co(H_2O)_2(pma)_2$]$HSO_4 \cdot SO_4$ (——), *cis*-[$Co(H_2O)_2(en)_2$]Cl_3 (-·-·-), *trans*(py)*cis*(H_2O)-[$Cr(H_2O)_2(pma)_2$]$(NO_3)_3$ (-···-···-) in 0.1 mol dm^{-3} HCl, and [$CrCl_3(py)_3$] in methanol (···).

the data of [$CrCl_3(py)_3$] and [$MoCl_3(py)_3$][30] this kind of bands are observed in almost the same position (the optical electronegativity value of Mo(III) is 1.7[29]). Accordingly, the possibility of (1) is diminished. Jørgensen observed such band for several iridium(III) complexes coordinating pyridine and named it "Ir-(III)-pyridine band,"[31] which changes the position by changing the number of the coordinated pyridine ligands or their relative positions in coordination octahedron. In our complexes treated here, the position does not change by the number of the coordinated pyridine groups. Furthermore, *cis*-α- and *cis*-β-[$CrCl_2$-(picen)]$^+$ complexes, which has *trans*(py) and *cis*(py) structure, respectively, show the MCD bands of the transition at about the same position (Table 4). Thus the assignment (2) is ruled out. The third assignment is most plausible because the position of this band in absorption or MCD spectra is not so much deviated from complex to complex. Evans found a fine structure of the spin-forbidden band of pyridine in this region under a high pressure of oxygen and assigned it $\pi \rightarrow \pi^*$ singlet-triplet transition.[32] A similar vibrational structure is observed for the *trans*-[$CrF_2(py)_4$]$^+$ complex in the absorption band (Fig. 11 and Table 2), and for some present complexes in the CD band (Table 2).

References

1) Part 1 of this series: Y. Yamamoto and Y. Shimura, *Bull. Chem. Soc. Jpn.*, **53**, 395 (1980).
2) S. F. Mason, *Inorg. Chim. Acta. Rev.*, **2**, 89 (1968).
3) B. Bosnich, *Acc. Chem. Res.*, **2**, 266 (1969).
4) C. J. Hawkins, "Absolute Configuration of Metal Complexes," Wiley-Interscience (1971), pp. 227—251.
5) E. Larsen, S. F. Mason, and G. H. Searle, *Acta Chem. Scand.*, **20**, 191 (1966).
6) I. Hanazaki and S. Nagakura, *Inorg. Chem.*, **8**, 654 (1969).
7) T. Ito, N. Tanaka, I. Hanazaki, and S. Nagakura, *Inorg. Nucl. Chem. Lett.*, **5**, 781 (1967).
8) B. Bosnich, *Proc. R. Soc. London, Ser. A*, **297**, 88 (1967).
9) J. Cragel, Jr., and G. R. Brubaker, *Inorg. Chem.*, **11**, 303 (1972).
10) M. Branca, P. Checconi, and B. Pispisa, *J. Chem. Soc., Dalton Trans.*, **1976**, 481.
11) K. Michelsen, *Acta Chem. Scand., A*, **28**, 428 (1974).
12) H. A. Goodwin and F. Lions, *J. Am. Chem. Soc.*, **82**, 5021 (1960).
13) J. C. Bailar, Jr., *Inorg. Synth.*, **2**, 222 (1946).
14) K. Michelsen, *Acta Chem. Scand.*, **26**, 769 (1972).
15) J. Springborg and C. E. Schäffer, *Inorg. Synth.*, **14**, 75 (1973).
16) E. Pedersen, *Acta Chem. Scand.*, **24**, 3362 (1970).
17) J. Selbin and J. C. Bailar, Jr., *J. Am. Chem. Soc.*, **79**, 4285 (1957).
18) K. R. A. Fehrmann and C. S. Garner, *J. Am. Chem. Soc.*, **82**, 6294 (1960).
19) J. Glerup, J. Josephsen, K. Michelsen, E. Pedersen, and C. E. Schäffer, *Acta Chem. Scand.*, **24**, 247 (1970).
20) K. Michelsen, *Acta Chem. Scand.*, **26**, 1517 (1972); **27** 1823 (1973); *A*, **31**, 429 (1977).
21) J. C. Taft and M. M. Jones, *Inorg. Synth.*, **7**, 132 (1963).
22) K. Michelsen, *Acta Chem. Scand., A*, **32**, 84 (1978).
23) a) J. A. Schellman, *Acc. Chem. Res.*, **1**, 144 (1968); b) K. Shingu, "Shin-jikken Kagaku Koza," ed by the Chemical Society of Japan, Maruzen, Tokyo (1977), Vol. 13, p. 850; c) P. M. Bayley, *Prog. Biophys. Mol. Biol.*, **27**, 1 (1973).
24) E. Bang, *Acta Chem. Scand., A*, **31**, 495 (1977).
25) Y. Hata, Y. Yamamoto, and Y. Shimura, *Bull. Chem. Soc. Jpn.*, **54**, 1255 (1981).
26) B. R. Hollebone, S. F. Mason, and A. J. Thomson, *Faraday Symp. Chem. Soc.*, **3**, 146 (1969).
27) A. Castellan and J. Michl, *J. Am. Chem. Soc.*, **100**, 6824 (1978).
28) K. Nakamoto, M. Kobayashi, and R. Tsuchida, *J. Chem. Phys.*, **22**, 957 (1963).
29) C. K. Jørgensen, "Orbitals in Atoms and Molecules," Academic Press, New York and London (1962), p. 95.
30) T. Komorita, S. Miki, and S. Yamada, *Bull. Chem. Soc. Jpn.*, **38**, 123 (1965).
31) C. K. Jørgensen, *Acta Chem. Scand.*, **11**, 166 (1957).
32) D. F. Evans, *J. Chem. Soc.*, **1957**, 3885.

  Bull. Chem. Soc. Jpn., 54, 3361—3365 (1981)

Kinetics of Monomerization or Polymerization Reaction for Bis(*N*-phenylsalicylideneaminato)nickel(II) and Bis(*N*-methylsalicylideneaminato)nickel(II) in Solid Phase

Kikuo Miyokawa,* Hidenori Hirashima, and Isao Masuda

Department of Chemistry, Faculty of Science, Fukuoka University, Nanakuma, Nishi-ku, Fukuoka 814-01

(Received January 12, 1981)

A kinetic investigation was carried out by means of a thermomagnetic analysis on two structural transformation reactions in solid phase: monomeric square planar-to-polymeric octahedral for Ni(*N*-Me-salam)$_2$ and polymeric octahedral-to-monomeric square planar for Ni(*N*-Ph-salam)$_2$. The polymerization process followed the Avrami-Erofeev equation ($n=2$) with $E_a=303$ kJ/mol and the monomerization followed the first order equation with $E_a=78$ kJ/mol. The thermal pyridine liberating reaction of Ni(*N*-Ph-salam)$_2$py$_2$, involving an octahedral-to-square planar transformation, has been investigated isothermally and found to follow the first order equation with $E_a=167$ kJ/mol.

Extensive investigations of the nickel(II) complexes having the formula Ni(*N*-R-X-salam)$_2$ (where *N*-R-X-salam represents an anion of the Schiff bases derived from the ring-substituted salicylaldehydes X-sal and amine R–NH$_2$) have revealed that the complexes exist in several structural forms with different coordination geometries: *i.e.*, square planar,[1] tetrahedral,[1-3] dimeric square bi-pyramidal,[4] and polymeric octahedral[5,6] structures. Isomerization reactions in solid phase have also been found to occur for some complexes of these structural forms.[3,6-9] However, the kinetics of the isomerization reaction has remained ambiguous.

In this work, the kinetics of the transformation reactions in solid phase, monomer-to-polymer of Ni(*N*-Me-salam)$_2$ and polymer-to-monomer of Ni(*N*-Ph-salam)$_2$, have been investigated by means of a thermomagnetic analysis measuring magnetic susceptibility changes of the sample under isothermal or dynamic conditions.

Experimental

Materials. Diamagnetic dark green complexes, Ni(*N*-Me-salam)$_2$ and Ni(*N*-Ph-salam)$_2$ (Form I), were prepared by the published procedure.[7,8,10,11] The paramagnetic light green modification (Form II) of Ni(*N*-Ph-salam)$_2$ was prepared in the following manner: the Form I complex was saturated into dichloromethane (50 ml) at *ca.* 35 °C, then to the solution was added ethanol (50 ml). The mixture was kept at room temperature under stirring until light green crystals separated.

The bis(pyridine) adduct Ni(*N*-Ph-salam)$_2$py$_2$ was precipitated from pyridine solution saturated with the Form I complex by addition of ethanol.

Found for Form II: C, 69.07; H, 4.51; N, 6.39; Ni, 13.19 %. Calcd for $C_{26}H_{20}N_2O_2Ni$: C, 69.22; H, 4.44; N, 6.21; Ni, 13.02%. Found for the pyridine adduct: Ni, 9.75%. Calcd for $C_{36}H_{30}N_4O_2Ni$: Ni, 9.64%.

Neodymium oxide was purified by repeating the following procedure: commercial reagent grade Nd_2O_3 was dissolved in aqueous HCl, and the solution was evaporated to dryness. The residue was dissolved in water, and to the resulting solution was added aqueous oxalic acid to precipitate neodymium oxalate. The oxalate thus obtained was collected on a filter, and then pyrolyzed at *ca.* 800 °C to give Nd_2O_3. The purity was ascertained by Nd-content analysis using the EDTA titration method.

Measurements. Thermogravimetric (TG) and differential scanning calorimetric (DSC) curves, and X-ray powder diffraction patterns were recorded as described in a previous paper.[12] Reflectance spectra were measured by means of an opal glass method[13] using a Shimadzu MPS 5000 spectrophotometer. The isothermal weight-loss measurements were made with a Sinku Riko micro DTA apparatus TGD-3000-RH, under a constant flow of nitrogen.

A thermomagnetic analysis[14] was carried out by using a thermomagnetic analysis instrument which was constructed by assembling a Faraday type magnetobalance and an infrared lamp furnace.[15] The sample was heated at a constant heating rate or kept at a desired temperature with a Sinku Riko temperature controller HPC-3000. On this instrument the following thermomagnetic curves were recorded: the isothermal thermomagnetic curve (hereafter abbreviated as ITM curve), obtained by plotting the magnetic susceptibility change of the sample against time while it was kept under isothermal conditions; the sample was usually heated to the desired temperature at a heating rate of 200 °C min^{-1}; and the dynamic thermomagnetic curve (DTM curve), obtained by plotting the magnetic susceptibility change of the sample under dynamic conditions against temperature; the sample was usually heated at a heating rate 1 °C min^{-1}. These measurements were carried out in a nitrogen atmosphere. The magnetobalance was calibrated by using $[Ni(en)_3]S_2O_3$ and Nd_2O_3, and the strenght of the applied magnetic field was regulated to an appropriate constant value around 0.85 T.

Results

The magnetic and electronic spectral data of the complexes in the solid state are given in Table 1. Whereas the dark green Form I isomer of Ni(*N*-Ph-salam)$_2$ is diamagnetic and is considered to have a square planar structure,[10] the light green Form II

Table 1. Magnetic and electronic spectral data

Complex	μ_{eff}[a] / μ_B	ν_{max}[b] / 10^3 cm^{-1}
Ni(*N*-Ph-salam)$_2$, Form I	dia[c]	16.3
Ni(*N*-Ph-salam)$_2$, Form II	3.28	10.1, 16.6
Ni(*N*-Ph-salam)$_2$py$_2$	3.09	9.9, 16.8
Ni(*N*-Me-salam)$_2$	dia	16.6
Ni(*N*-Me-salam)$_2$	3.30[d]	12.7, 18.0

a) Determined at room temperature, 22—25 °C. b) Powder reflectance. c) dia: Diamagnetic. d) See Refs. 7 and 8.

isomer prepared in the present work is paramagnetic with $\mu_{eff}=3.28\,\mu_B$. The electronic reflectance spectrum of the Form I isomer exhibits a peak with the maximum at $16.3\times10^3\,cm^{-1}$ ascribed to the square-planar crystal field band of Ni(II), $^1A_{1g}\rightarrow{}^1A_{2g}$ transition,[16] while the spectrum of the Form II isomer is composed of two peaks with the maxima at 10.1 and $16.6\times10^3\,cm^{-1}$; these may be ascribed respectively to the $^3A_{2g}\rightarrow{}^3T_{2g}$ and $^3A_{2g}\rightarrow{}^3T_{1g}(F)$ transitions of the octahedral crystal field bands.[16] The paramagnetism and the spectral data are indicative of an octahedral coordination and hence a polymeric structure for the Form II isomer.

The TG and DSC curves of the Form I and II isomers of Ni(*N*-Ph-salam)$_2$ are shown in Figs. 1-a and -b. No weight-loss is observed up to 320 °C in these TG curves. In the DSC curves of both isomers, however, an endothermic peak is observed at 280 °C due to the melting. An exothermic peak at 210 °C observed for the Form II isomer may be attributed to the transformation reaction into the Form I isomer. The X-ray diffraction pattern of the product obtained by heating the Form II isomer at 230 °C coincided with that of the Form I isomer.

As for diamagnetic Ni(*N*-Me-salam)$_2$, the TG curve shown in Fig. 1-c exhibits no weight-loss up to 290 °C; the DSC curve shows two endothermic peaks due to the melting at 215 and 302 °C. The former melting is found to be followed by the solidification of the melt; this does not disagree with the observation under microscope by Sacconi *et al.*[7] On heating diamagnetic Ni(*N*-Me-salam)$_2$ at 230 °C, a paramagnetic complex was obtained which showed quite different X-ray powder pattern from that of starting diamagnetic complex. Thus, the melting at 215 °C is thought to occur together with the transformation reaction of diamagnetic Ni(*N*-Me-salam)$_2$ into the paramagnetic complex; the latter melts at 302 °C with a partial decomposition.

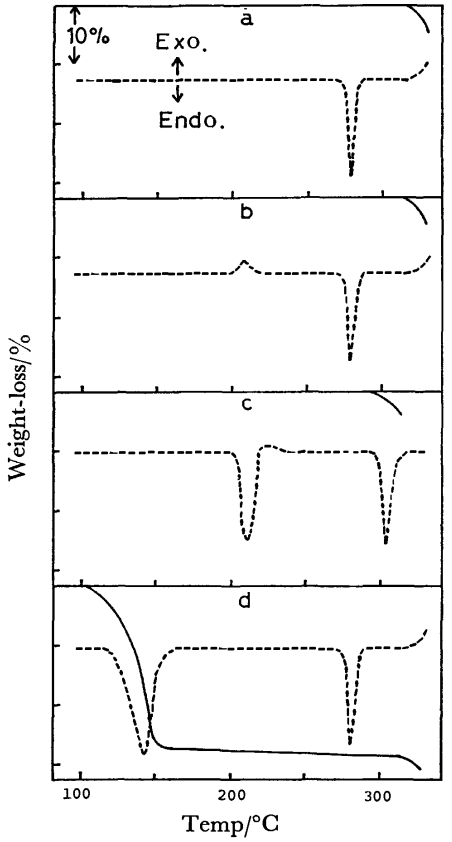

Fig. 1. TG(——) and DSC(- - -) curves; heating rate, 10 °C min^{-1}, in a static air atmosphere.
(a): Ni(*N*-Ph-salam)$_2$ (Form I), (b): Ni(*N*-Ph-salam)$_2$ (Form II), (c): diamagnetic Ni(*N*-Me-salam)$_2$, (d): Ni(*N*-Ph-salam)$_2$py$_2$.

The DTM curve of the paramagnetic Form II isomer of Ni(*N*-Ph-salam)$_2$ is presented in Fig. 2. When W mg of the sample is placed in the magnetic field, the response of the electrobalance, W' mg, is expressed by Eq. 1:

$$W' = W + W\cdot\chi_g^s\cdot H_c, \qquad (1)$$

where χ_g^s is the apparent gram magnetic susceptibility of the sample, and H_c a constant value which is determined by the apparatus and the strength of the applied magnetic field. The DTM curve shown by Fig. 2-a is obtained by plotting $(W'-W)/W$ value *vs.* temperature under dynamic conditions of a heating rate of 1 °C min^{-1}. In this curve a large decrease in the magnetic susceptibility of the Form II isomer is seen in the 170—230 °C region. This may correspond to the transformation reaction of the paramagnetic Form II to the diamagnetic Form I isomer, which is consistent with the results of the thermal analyses. On the basis of the DTM data, $\chi_{Ni(II)}$, the apparent susceptibility per mole of Ni(II), not corrected for the diamagnetism of all atoms, was calculated by Eq. 2:

$$\chi_{Ni(II)} = (W'-W)M/(H_cW), \qquad (2)$$

where M is relative molecular mass of the complex, 450.7. The H_c value has been determined by using

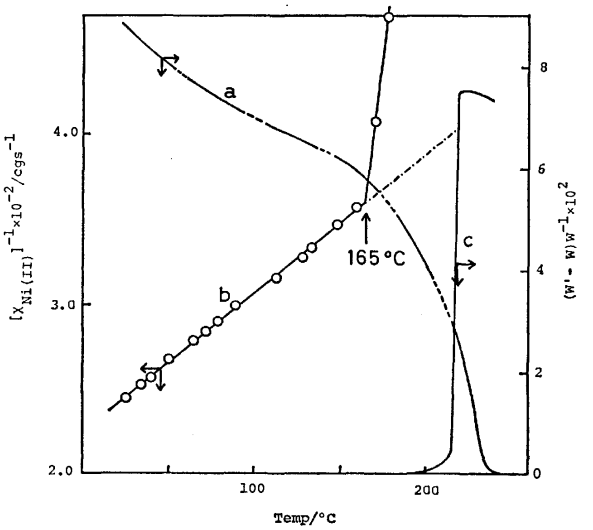

Fig. 2. DTM curve for Ni(*N*-Ph-salam)$_2$ (Form II), (a); plots of reciprocal $\chi_{Ni(II)}$ *vs.* temperature, for Form II, (b); sample, 18.40 mg. DTM curve for diamagnetic Ni(*N*-Me-salam)$_2$, (c); sample, 18.40 mg. Heating rate, 1 °C min^{-1}. On the dashed line in the curve (a) magnetic-field strength was attenuated to zero to check the base line.

Nd_2O_3 as a standard[17] to be 8.40×10^3 under the present experimental conditions; it is practically constant in the range 25—300 °C. And the plots of reciprocal $\chi_{Ni(II)}$ against temperature give a curve shown by Fig. 2-b. The curve indicates that a Curie-Weiss dependence of the magnetic susceptibility of the Form II isomer is broken at 165 °C; at this temperature the transformation reaction from the Form II to Form I isomer is thought to occur.

The ITM curves for the Form II isomer recorded under isothermal conditions at 175.6, 180.9, 186.1, and 191.3 °C are shown in Fig. 3. The apparent gram susceptibility of the sample, χ_g^s, can be expressed by Eq. 3, where χ_g^I, χ_g^{II}, and α are the gram susceptibilities of the Form I and II isomers, and the molar fraction of Form II transformed into Form I, respectively:

$$M\cdot\chi_g^s=[\chi_g^{II}(1-\alpha)+\chi_g^I\cdot\alpha]M. \quad (3)$$

Then, the α value is given as

$$\alpha=(\chi_g^s-\chi_g^{II})/(\chi_g^I-\chi_g^{II}). \quad (4)$$

The χ_g^I value was found to be practically zero and χ_g^{II} was evaluated from a Curie-Weiss dependence, *i.e.*, by extrapolating the linear part below 165 °C of the line in Fig. 2-b to each desired temperature. As shown in Fig. 4, the transformation reaction pursued at four different temperatures is found to be well described by the first order equation: $-\ln(1-\alpha)=kt$, where k and t are the rate constant and time. On the basis of these data, the activation energy E_a and pre-exponential factor A in the Arrhenius equation were determined to be 78 kJ/mol and 1×10^7.

In the case of diamagnetic Ni(N-Me-salam)$_2$, the DTM curve shown in Fig. 2-c indicates that the magnetic susceptibility begins to increase gradually at 190 °C, and rapidly increases at ⩾215 °C, which corresponds to the DSC peak temperature due to the melting. The ITM curves recorded at 186.7, 191.3, and 197.7 °C for the transformation to the paramagnetic form are shown in Fig. 5. In this case the χ_g^I and χ_g^{II} in Eq. 3 are the gram magnetic susceptibilities of the paramagnetic and diamagnetic Ni(N-Me-salam)$_2$, respectively. The χ_g^I values at these temperatures were determined after the reaction was completed, and χ_g^{II} was found to be practically zero. As shown

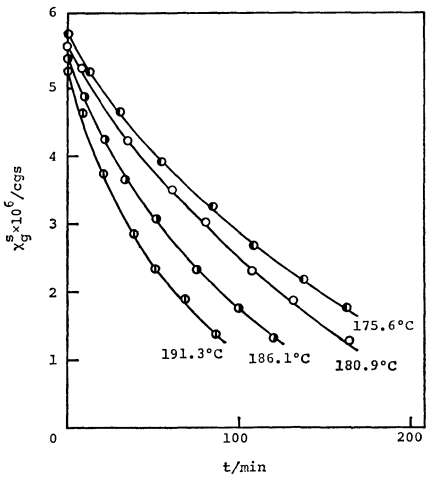

Fig. 3. ITM curves for Ni(N-Ph-salam)$_2$ (Form II); polymer-to-monomer transformation under isothermal conditions.

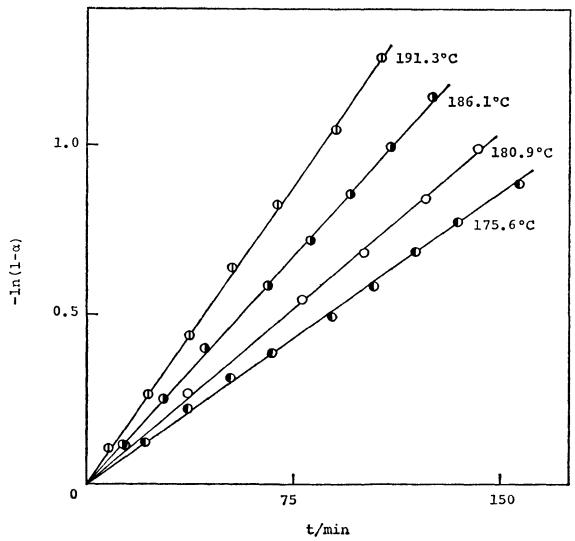

Fig. 4. First order rate plots for polymer-to-monomer transformation of Ni(N-Ph-salam)$_2$ (Form II).

Table 2. Kinetic data of transformation reactions in solid phase

Complex	Reaction Mode	Reaction Scheme	E_a / kJ mol^{-1}	log (A/min^{-1})	k / 10^{-2} min^{-1}	Temp / °C
Ni(N-Ph-salam)$_2$	a)	$-\ln(1-\alpha)=kt$	78± 5	7.0±0.6	0.723	175.6
					0.867	180.9
					1.13	186.1
					1.46	191.3
Ni(N-Me-salam)$_2$	b)	$-\ln(1-\alpha)=(kt)^2$	303±11	33±2	3.76	186.7
					7.81	191.3
					24.9	197.7
Ni(N-Ph-salam)$_2$py$_2$	c)	$-\ln(1-\alpha)=kt$	167±12	22±1	0.668	86.8
					0.937	88.8
					1.23	90.6
					1.73	93.0

a) Polymer-to-monomer. b) Monomer-to-polymer. c) Monomer(octahedral)-to-monomer(square-planar).

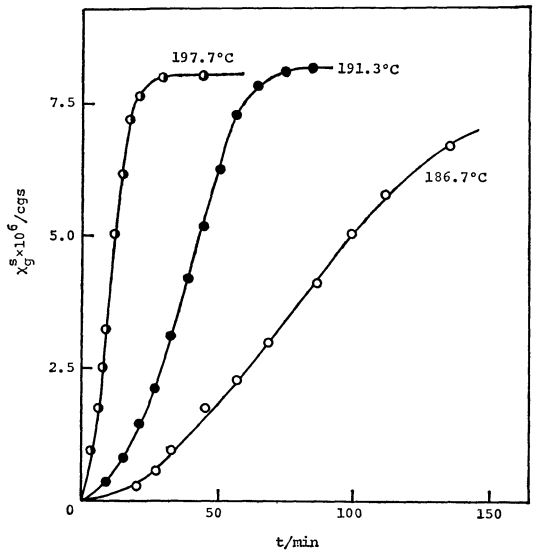

Fig. 5. ITM curves for diamagnetic Ni(*N*-Me-salam)$_2$; monomer-to-polymer transformation under isothermal conditions.

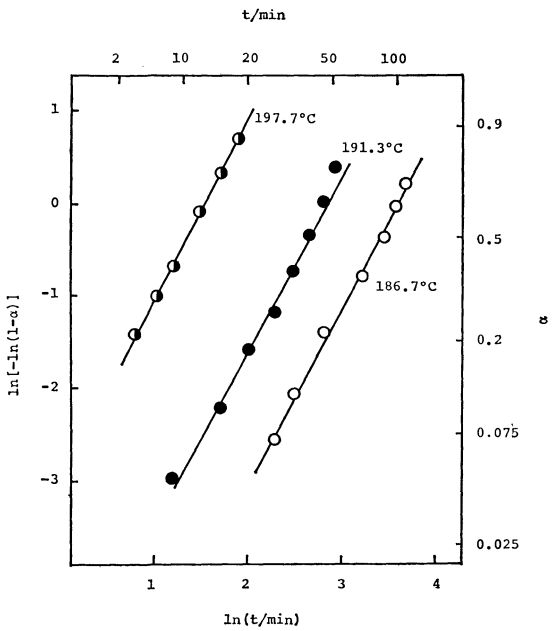

Fig. 6. Plots of ln[$-$ln(1$-\alpha$)] *vs.* ln(t) for monomer-to-polymer transformation of Ni(*N*-Me-salam)$_2$.

in Fig. 6, the transformation isotherms thus obtained are well fitted to the Avrami-Erofeev equation:[18]

$$-\ln[-\ln(1-\alpha)] = (kt)^n. \quad [n=1.94\text{—}2.02] \qquad (5)$$

The kinetic parameters, E_a and A, were calculated to be 303 kJ/mol and 1×10^{33}, respectively.

For the purpose of comparison, the thermal dissociation reaction of the axial pyridine molecules of Ni(*N*-Ph-salam)$_2$py$_2$ has been subjected to kinetic analysis. The DSC curve of the adduct shown in Fig. 1-d exhibits two endothermic peaks at 140 and 280 °C; the former peak is accompanied by 26.0% weight-loss in the range 100—150 °C, which corresponds to the elimination of 2 mol of pyridine per mol of the adduct, while the latter one is accompanied by no

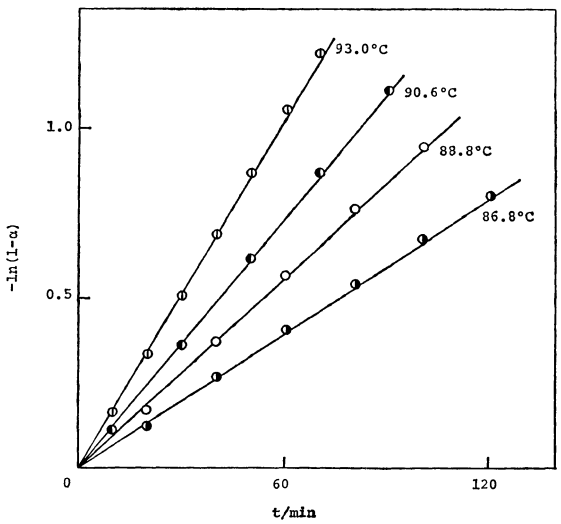

Fig. 7. First order rate plots for pyridine-liberating reaction of Ni(*N*-Ph-salam)$_2$py$_2$.

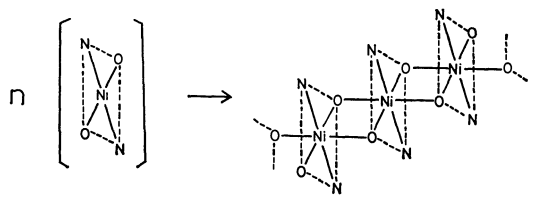

Fig. 8. Skeletal representation of monomer-to-polymer transformation.

weight-loss, and corresponds to the melting of the Form I isomer of Ni(*N*-Ph-salam)$_2$. The X-ray diffraction pattern of the sample obtained after heating at *ca.* 150 °C was identical to that of an authentic Form I isomer. The pyridine-liberating reaction of the adduct could easily be followed by the isothermal weight-loss measurements. The liberation isotherms obtained at 86.8, 88.8, 90.6, and 93.0 °C fit well to the first order equation, as shown in Fig. 7. The kinetic parameters, E_a and A, were calculated to be 167 kJ/mol and 1×10^{22}, respectively.

Discussion

The polymerization reaction of Ni(*N*-Me-salam)$_2$ including the alteration of the spin-state of central Ni(II), singlet(monomer)-to-triplet(polymer), has been considered to progress through the further coordination of the phenolato oxygen atoms in the complex molecule to a Ni(II) ion of adjacent molecules at the apical position, forming octahedral coordination geometry around the Ni(II) ion, as drawn above.[8] The polymerization kinetics is found to be depicted by the Avrami-Erofeev equation with n=2, suggesting that the reaction rate is determined either by two dimensional growth of nuclei[19] or by random nucleation and one dimensional growth of nuclei.[20] By taking into account the fact that the proposed polymeric structure includes a one-dimensionally extended monomer, the latter model seems to be preferable for the present polymerization. On the other hand, the monomerization reaction of Ni(*N*-Ph-salam)$_2$ includes the

spin-state alteration of Ni(II), triplet(polymer)-to-singlet(monomer); the monomerization kinetics fits the first order equation. The thermal pyridine liberating reaction of Ni(*N*-Ph-salam)$_2$py$_2$, which occurred with the accompanying triplet-to-singlet alteration of Ni(II) and the formation of monomeric Ni(*N*-Ph-salam)$_2$, is also depicted by the first order equation.

As shown in Table 2, the larger E_a and A values for the polymerization of Ni(*N*-Me-salam)$_2$ than those for the monomerization of Ni(*N*-Ph-salam)$_2$ could be understood by speculating that the progress of the polymerization requires more extensive movement of the molecules than that of the monomerization does.

We can compare the polymer complex and the pyridine adduct of Ni(*N*-Ph-salam)$_2$, both having octahedral and triplet Ni(II); the larger E_a value for the pyridine-liberating reaction than for the monomerization reaction seems to reflect a weaker association interaction than the adduct-formation interaction.

References

1) R. H. Holm and M. J. O'Connor, *Prog. Inorg. Chem.*, **14**, 241 (1971).

2) A. Takeuchi and S. Yamada, *Bull. Chem. Soc. Jpn.*, **44**, 1170 (1971).

3) A. Takeuchi and S. Yamada, *Inorg. Chim. Acta*, **8**, 225 (1974).

4) S. Yamada, K. Iwasaki, and A. Takeuchi, *Inorg. Chim. Acta*, **2**, 395 (1968).

5) R. H. Holm, *J. Am. Chem. Soc.*, **83**, 4683 (1961).

6) H. C. Clark and R. J. O'Brien, *Can. J. Chem.*, **39**, 1030 (1961).

7) L. Sacconi, P. Paoletti, and R. Cini, *J. Am. Chem. Soc.*, **80**, 3583 (1958).

8) C. M. Harris, S. L. Lenzer, and R. L. Martin, *Aust. J. Chem.*, **11**, 331 (1958).

9) N. Arai, M. Sorai, and S. Seki, *Bull. Chem. Soc. Jpn.*, **45**, 2398 (1972).

10) F. Basolo and W. R. Matoush, *J. Am. Chem. Soc.*, **75**, 5663 (1953).

11) W. Klem and K. H. Raddatz, *Z. Anorg. Allg. Chem.*, **250**, 207 (1942).

12) K. Miyokawa and I. Masuda, *J. Inorg. Nucl. Chem.*, **43**, 1495 (1981).

13) K. Shibata, "Methods of Biochemical Analysis," ed by D. Glick, Interscience, New York (1962), Vol. 4, p. 217.

14) W. W. Wendlandt, "Thermal Methods of Analysis," 2nd ed, John Wiley & Sons, New York (1974), p. 459.

15) K. Miyokawa and I. Masuda, *Fukuoka Univ. Science Reports*, **10**, 83 (1980).

16) A. B. P. Lever, "Inorganic Electronic Spectroscopy," Elsevier, Amsterdam (1968), p. 333.

17) "American Institute of Physics Handbook," 2nd ed, ed by D. E. Gray, McGraw-Hill, New York (1963), pp. 5—221.

18) M. Avrami, *J. Chem. Phys.*, **7**, 1103 (1939); **8**, 212 (1940); **9**, 177 (1941); B. V. Erofeev, *Dokl. Akad. Nauk SSSR*, **52**, 511 (1946).

19) O. Yamaguchi, M. Kamata, and K. Shimizu, *Bull. Chem. Soc. Jpn.*, **53**, 1973 (1980).

20) "Chemistry of Solid States," ed by W. E. Garner, Butterworth, London (1955), p. 184.

The Solvent Extraction of Np(III) by Means of Bis(2-ethyhexyl)-hydrogenphosphate in an Octane Solution and the Absorption Spectrum of the Organic Phase

Isamu KAWASUJI,* Akiko SATÔ, and Shin SUZUKI
The Research Institute for Iron, Steel and Other Metals, Tohoku University, Katahira, Sendai 980

(Received February 20, 1981)

Tervalent neptunium in an $HClO_4$ solution was extracted by means of bis(2-ethylhexyl)hydrogenphosphate, HDEHP, in an octane solution. The oxidation state of neptunium in the organic phase was determined by spectrophotometry. The intense peak in the absorption spectrum of tervalent neptunium was found at 348 nm, this peak was attributed to the $f \rightarrow d$ transition. The oxidation rate of the Np(III)–HDEHP complex in an oxygen-free octane solution was about 10%/h.

It has been well known that the tervalent neptunium ion in an acidic solution is fairly stable in an oxygen-free atmosphere. However, during a chemical operation like solvent extraction or ion exchange, it is difficult to maintain the neptunium ion in a tervalent state. Consequently, the study of the aqueous chemistry of Np(III) has been made mainly by means of the spectrophotometric technique. Shiloh and Marcus[1] found the characteristic absorption peaks of 384 nm and 387 nm in the chloride and bromide solution of Np(III) respectively. They determined the stability constants of the chloride and bromide complexes by measuring the increases in their characteristic peaks as the concentrations of the chloride and bromide ions increased.

Inoue *et al.*[2] recently investigated the effect of the neptunium concentration on the fraction of tervalent neptunium produced by hydrogen reduction. They concluded that neptunium was quantitatively reduced to the tervalent state at concentrations higher than 10^{-3} M (1 M=1 mol dm^{-3}), while the tracer concentrations of neptunium were quantitatively reduced to the tervalent state in the presence of more than 10^{-3} M Sn(II).

It has not been reported up to the present, however, that tervalent neptunium could be evidently extracted to the organic phase in the solvent extraction, which has been one of the most effective methods of investigating aqueous chemistry. In order to extract the tervalent neptunium, and in order to determine the oxidation state of the extracted neptunium by spectrophotometry, we made a specially designed reduction and extraction apparatus with reference to other authors'.[2,3] The apparatus was constituted of two parts: the spectrophotometric cell in which the extracted tervalent neptunium was introduced, and the reduction and extraction part.

HDEHP was used as the extractant, and octane, as the solvent, in this work.

Experimental

The ^{237}Np was obtained from the Radiochemical Centre, Amersham, and was purified by the method of Moore,[4] while the final stock solution was 10 M HNO_3. The concentration of ^{237}Np in the stock solution was determined by the α-counting method using a surface barrier Si-detector and the EDTA titration method. The results of the two methods agreed well within the limits of experimental error.

HDEHP was purified by the way of McDowell *et al.*[5] and was stocked as the copper salt. The desired quantities of the copper salt were weighed and then dissolved in octane. After the copper had been removed by shaking with an acid solution, the concentration of HDEHP in the octane solution was determined by the titration of the NaOH solution. The results of the titration method agreed well with the results of the gravimetry, within the limits of experimental error.

For the measurement of the absorption spectrum, a Hitachi 330 recording spectrophotometer was used.

The experimental apparatus used in this work is shown in Fig. 1. It was made of quartz, and at the top of it, a polyethylene plug was placed, through which Teflon tubes passed. At the end of the Teflon tubes, freshly prepared platinum-black-coils were fixed.

Three milliliters of the 2 M HDEHP/octane solution was placed in the spectrophotometric cell, while the same volume of a 0.3 M $HClO_4$ solution containing 20 mg of ^{237}Np (2.7×10^{-2} M) was placed in the other part.

The hydrogen gas, which had been deoxidized by passing through a pyrogallol–KOH solution, was bubbled into the Np/$HClO_4$ solution, and the neptunium was reduced to the tervalent state by the hydrogen gas catalyzed by the platinum-black-coil. A part of the deoxidized hydrogen gas was passed through the octane solution and then bubbled into the HDEHP/octane solution.

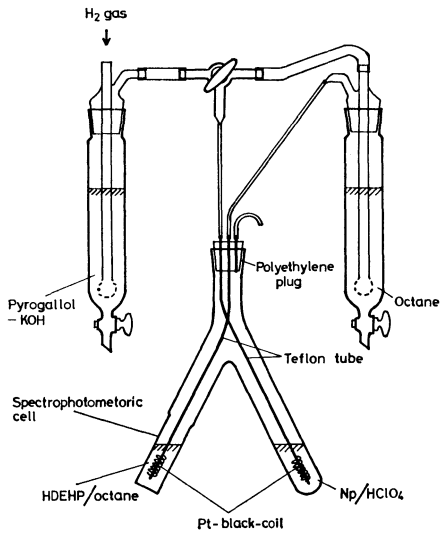

Fig. 1. Experimental apparatus.

The neptunium in the $HClO_4$ solution was completely reduced to the tervalent state about after three hours bubbling, as was recognized by the change in color. Then the apparatus was tilted and the HDEHP/octane solution in the spectrophotometric cell was introduced into the other part. The apparatus was shaken about ten minutes while the hydrogen gas was bubbling. After the two phases had separated, the organic phase was introduced to the spectrophotometric cell and the absorption spectrum was immediately measured. The Teflon tube and the platinum-black-coil were placed in the upper side so as not to disturb the measurement of the absorption spectra. The spectrophotometry of the organic phase was carried out every hour after the extraction in order to investigate the stability of the Np(III)–HDEHP complex in an octane solution. The absorption spectrum of the Np(IV)–HDEHP complex in an octane solution was measured after the oxidation had been completely concluded.

The absorption spectra of Np(III) and Np(IV) in 0.3 M $HClO_4$ solution were also measured.

An aliquot part of the organic phase was placed in the polyethylene test tube, and the concentration of the ^{237}Np was determined by γ-ray spectrometry. For the γ-ray spectrometry, a Tracor Northern TN-4000 pulse-height analyzer and a pure-Ge detector were used. The peak at 86.49 keV, the characteristic peak of ^{237}Np, was used to determine the concentration of neptunium. ^{233}Pa, the daughter of ^{237}Np, also has a weak peak at 86.59 keV. These two peaks could not be separated, so the contribution of the peak at 86.59 keV to the peak at 86.49 keV was eliminated by the γ-ray spectrometry of pure ^{233}Pa.

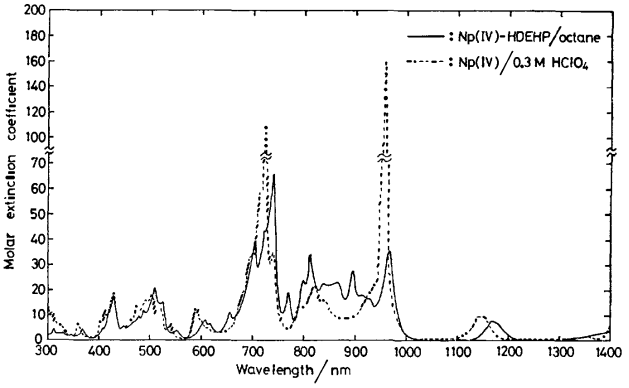

Fig. 2. Absorption spectra of Np(IV) in $HClO_4$ solution and Np(IV)–HDEHP complex in octane solution.

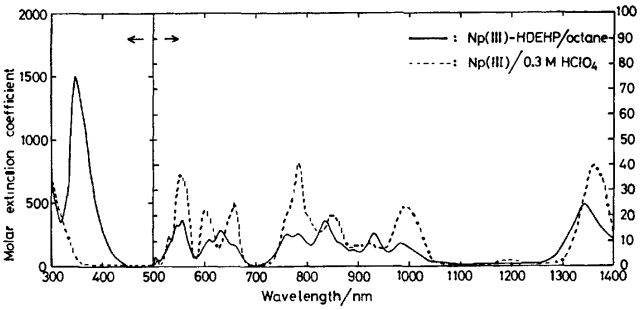

Fig. 3. Absorption spectra of Np(III) in $HClO_4$ solution and Np(III)–HDEHP complex in octane solution.

Results and Discussion

The absorption spectrum of the Np(IV)–HDEHP complex in an octane solution shown in Fig. 2 is very similar to the spectrum of Np(IV) in a 0.3 M $HClO_4$ solution except in the region of 900 nm. The characteristic peaks of the former are 427, 508, 735, 812, 896, 968, and 1167 nm, and the former shifts toward a lower energy compared with the latter. This shift may be caused by the nephelauxetic effect.[6]

On the other hand, the absorption spectrum of the Np(III)–HDEHP complex (shown in Fig. 3) is not so similar to the spectrum of Np(III) in the 0.3 M $HClO_4$ solution. This shows that the $f \rightarrow f$ transition was affected by the environment, *e.g.*, the ligand or the crystal field. The characteristic peaks of the former are 348, 557, 630, 760, 782, 835, 931, 987, and 1345 nm. Among these, the peak of 348 nm is clearly distinguished from the other peaks, which are attributed to the $f \rightarrow f$ transition in the visible and near-infrared regions. The molar extinction coefficient, ε_m, of this peak is about 1500, while the half-width toward the lower energy, $\sigma(-)$, is 1500 cm^{-1}. This peak is attributed to the $f \rightarrow d$ transition or the electron-transfer-from-ligand transition. Usually, the former band is relatively more intense and narrow than the latter.[7] However, it is difficult to discriminate between them. Poturaj-Gutniak and Taube[8] identified the absorption peak as the $f \rightarrow d$ transition by $\varepsilon_m > 3000$, and $\sigma(-) < 2000$ cm^{-1}, and as electron-transfer by $\varepsilon_m < 3000$, and $\sigma(-) > 2000$ cm^{-1}.

The characteristic peaks of Np(III) in concentrated LiCl and LiBr solution found by Shiloh and Marcus[1] are $\varepsilon_m = 1170$ and $\sigma(-) = 2400$ cm^{-1} at 384 nm (26000 cm^{-1}) in LiCl and $\varepsilon_m = 830$ and $\sigma(-) = 2400$ cm^{-1} at 387 nm (25800 cm^{-1}) in LiBr. These bands are attributed to the $f \rightarrow d$ transition.

The peak at 348 nm (28700 cm^{-1}) found in this work seemed to have the same cause as the peaks found by Shiloh and Marcus described above. The shifts of these peaks effected by the ligands are small. Generally, the shift of the $f \rightarrow d$ transition with a ligand is much less than that observed in the case of the electron-transfer band.[7] For example, the shift of the electron-transfer is 7000—9000 cm^{-1}; on the other hand, that of the $f \rightarrow d$ transfition is about 1000 cm^{-1} in tervalent actinoide hexahalides.[9] Therefore, the peak at 348 nm is ascribed to the $f \rightarrow d$ transition.

The Np(III)–HDEHP complex in an octane solution is unstable and is oxidized to the quadrivalent state, even in an oxygen-free atmosphere. The oxidation rate was found to be about 10%/h by the spectrophotometry that was carried out every hour after the extraction.

The color of the Np(III)–HDEHP complex in an octane solution is golden yellow, while that of the Np(IV)–HDEHP complex is slightly greenish yellow. It is difficult to distinguish between them by color, especially at a low concentration of neptunium.

References

1) M. Shiloh and Y. Marcus, *J. Inorg. Nucl. Chem.*, **28**, 2725 (1966).

2) Y. Inoue, O. Tochiyama, and N. Shinohara, *J. Inorg. Nucl. Chem.*, **42**, 757 (1980).
3) R. Sjoblom and J. C. Hindman, *J. Am. Chem. Soc.*, **73**, 1744 (1951).
4) F. L. Moore, *Anal. Chem.*, **29**, 941 (1957).
5) W. J. McDowell, P. T. Perdue, and G. N. Case, *J. Inorg. Nucl. Chem.*, **38**, 2127 (1976).
6) C. E. Schäffer and C. K. Jørgensen, *J. Inorg. Nucl. Chem.*, **8**, 143 (1958).
7) J. L. Ryan, "Absorption Spectra of Actinide Compounds," in "MTP International Review of Science," ed by H. J. Emeléus, Butterworth & Co., London (1972), Vol. 7, Chap. 9.
8) S. Poturaj-Gutniak and M. Taube, *J. Inorg. Nucl. Chem.*, **30**, 1005 (1968).
9) L. J. Nugent, R. D. Baybarz, and J. L. Burnett, *J. Phys. Chem.*, **77**, 1528 (1973).

High-performance Liquid Chromatographic Determination of Organic Substances by Metal Chelate Derivatization. I. Dithiocarbamate Chelates of Aliphatic Amines

Masataka Moriyasu,* Yohei Hashimoto, and Masaru Endo**

Kobe Women's College of Pharmacy, Motoyamakita-machi, Higashinada-ku, Kobe 658

***Kinki District Narcotic Control Office, Uchikyuhoji-machi, Higashi-ku, Osaka 540*

(Received March 2, 1981)

The use of the conversion of aliphatic primary and secondary amines into metal dithiocarbamate chelates was examined for high-performance liquid chromatographic determination of these amines. Characteristic chromatogram patterns based on the difference in the rate of ligand exchange were obtained for different central metal ions. When Hg(II) chelates were tested, trace determination of individual secondary amines was possible because only the peaks of binary complexes corresponding to each amine appeared on chromatograms. When Ni(II) and Pd(II) chelates were tested, peaks to ternary complexes as well as those of binary complexes appeared on chromatograms. This phenomenon was applied to the determination of optical purity of optically active amines. A description is given of applications to microdetermination of antiasthmatic ephedrine isomers, to determination of their optical purity in Chinese crude drugs, and to their preparation.

The metal chelate formation is widely applied to the colorimetric determination of metal ions. Since most chelating reagents are synthesized from organic substances, there have been made several attempts to determine organic substances after their conversion into metal chelates. Along with the recent progress of high-performance liquid chromatography(HPLC), a large number of UV-visible derivatization methods have been presented, but with little attention paid to utilization of the metal chelate formation for derivatization reactions of organic substances; this situation seems ascribable to the presumption that, as is often the case in gas chromatography, metal chelates usually undergo decomposition in course of chromatography. The purpose of the present series research is to clarify to what extent the metal chelate formation is useful for the UV-visible derivatization method in HPLC. The present report is concerned with conversion of aliphatic primary and secondary amines into dithiocarbamate chelates. We have described[1] an HPLC determination of various metal ions with the aid of their conversion into diethyldithiocarbamate chelates, and successively characterized[2,3] their chromatograms by means of ligand exchange. In experimental investigation on the application of the metal chelate formation to an analysis of organic substances, we should take into account the following two factors: (1) the organic substance needs to be converted into so stable a chelate as to undergo no decomposition in course of chromatography; (2) the ratio of central metal ion to ligand is of importance. If only 1:1 complexes are allowed to form, the determination of each organic substance may be performed easily. If 1:2 complexes are allowed to form, the ternary complex formation needs to be taken into consideration. When the ternary complex is very labile, it will undergo disproportionation into two binary complexes ($2MAB \rightarrow MA_2 + MB_2$) as soon as it gets separated; in this case, only the peaks for the binary complexes appear on the chromatogram, making the determination of individual organic substances possible. When the ternary complex is fairly inert, the peaks for ternary complex MAB will also appear on the chromatogram, complicating the chromatogram.

Experimental

Reagents. Sodium salts of various *N,N*-disubstituted and *N*-monosubstituted dithiocarbamic acids were prepared by mixing an aliphatic amine, carbon disulfide, and sodium hydroxide. The following aliphatic primary and secondary amines were used: dimethylamine, diethylamine, dipropylamine, dibutylamine, diisopropylamine, diisobutylamine, pyrrolidine, piperidine, perhydroazepine, morpholine, dibenzylamine, methylamine, ethylamine, propylamine, phenethylamine, and *l*-ephedrine. Each sodium salt was recrystallized from chloroform–methanol or chloroform–hexane. Standard solutions of each metal ion (0.1 M, 1 M=1 mol dm^{-3}) were prepared by dissolving each metal salt in water. The metal ions used are Mn(II), Fe(III), Co(II), Ni(II), Cu(II), Zn(II), Ag(I), Cd(II), Hg(II), Pb(II), Bi(III), and Pd(II).

Apparatus. The HPLC apparatus used was the same as the one used previously.[1-3] Absorption spectra of metal chelates were recorded on a Model-124 Hitachi double-beam spectrometer.

Results and Discussion

Relationship between Stability Constant and Chromatographic Behavior of Metal Chelates. Solutions of various dithiocarbamate chelates were prepared by mixing each of sodium dithiocarbamates and each metal ion at a suitable pH. The chelate formed was extracted with chloroform. Except Fe(III) and Mn(III), all the dithiocarbamate chelates derived from the secondary amines gave solutions stable at least for 2 d. Since dithiocarbamates derived from primary amines in general have a strong reducing property, the metal chelates for Ag(I), Hg(II), and Cu(II) decomposed readily, whereas those for Pd(II), Ni(II), and Co(III) were stable.

The HPLC of various metal diethyldithiocarbamate chelates has been described in several reports[4-8] and ours.[1] Chromatographic behaviors of various dithiocarbamate chelates were examined. Of the chelates tested, Hg(II), Pd(II), Cu(II), Ni(II), and Co(III) chelates gave good chromatograms without any occurrence of decomposition. All of these chelates, except chemically unstable Hg(II) and Cu-

(II) chelates derived from primary amines, gave linear calibration curves over the range from a few μg to a few ng. Chelates of other metals, Mn(III), Fe(III), Zn(II), Cd(II), Pb(II), and Bi(III), sometimes accompanied decomposition when sample amounts were small, giving nonlinear calibration curves. Ag(I) chelates were adsorbed on the silica-gel surface too strongly to be eluted out. The stability of metal dithiocarbamate chelates has been investigated by several workers.[9-13] For example, Bode and Tusche reported the following order of increasing stability: Mn(III) < Fe(III) < Zn(II) < Cd(II) < Co(III) < Pb(II) < Bi(III) < Ni(II) < Cu(II) < Ag(I) < Pd(II) < Hg(II). The present results suggest that no decomposition occurs when the metal chelate is very stable (Hg(II), Pd(II), Cu(II), and Ni(II)) or robust (Co(III)).

Formation of Dithiocarbamate Chelates and Exchange of Central Metal Ion. An examination was made in pursuit for the optimum conditions for the formation of metal dithiocarbamate chelates from aliphatic amines. Since, of various metal ions, Hg(II), Pd(II), Cu(II), Ni(II), and Co(III) had formed chelates stable enough for amine analysis, the examination was limited to these metal ions. The formation of dithiocarbamates and metal chelates is expressed by

$$R_1R_2NH + CS_2 + OH^- \rightleftharpoons R_1R_2NCSS^- + H_2O \quad (1)$$

and

$$nR_1R_2NCSS^- + M^{n+} \longrightarrow M(R_1R_2NCSS)_n. \quad (2)$$

Reaction 1 cannot go to completion in the forward direction because in acidic media the backward reaction is allowed to proceed. As the metal chelate formation proceeds and the chelate formed is caused to go into the the organic layer, free dithiocarbamate ion in aqueous solution gets removed from the aqueous layer, thereby leading the entire reaction to completion. Of various procedures tested, the following was capable of giving quantitative results: To 1 cm^3 of dilute amine solution were added 1 cm^3 of 0.1 M standard solution of each metal ion, 1 cm^3 of conc aqueous ammonia, and 5 cm^3 of chloroform containing 2% carbon disulfide. The mixed solution in a test tube equipped with a ground glass stopper was shaken vigorously for about 30 s to complete the reaction. The chloroform layer was washed with water three times. Pd(II), Ni(II) and Co(III) chelates allowed the reaction to proceed quantitatively (>98%) for both primary and secondary amines. Cu(II) gave quantitative results only for secondary amines since the Cu(II) chelates obtained from primary amines were chemically unstable. This procedure was inapplicable to Hg(II) chelates because Hg(II) salts are insoluble in conc aqueous ammonia. Hg(II) chelates of secondary amines were formed quantitatively by means of exchange of central metal ion as follows. To chloroform solution of corresponding Ni(II) dithiocarbamate chelates, which are brownish yellow, $HgCl_2$ aqueous solution was added and the mixture was shaken vigorously for a few seconds. Since stability constants of Hg(II) chelates are much larger than those of Ni(II) chelates, exchange of central metal ion occurred according to

$$[Ni(R_1R_2NCSS)_2]_{org} + [Hg(II)]_w \longrightarrow [Hg(R_1R_2NCSS)_2]_{org} + [Ni(II)]_w, \quad (3)$$

where org and w denote the organic and the aqueous phase, respectively. Hg(II) chelates allowing no absorption in the visible range, the brownish yellow color of chloroform layer was caused to disappear, indicating the completion of the exchange of central metal ion. Hg(II) chelates thus prepared gave good chromatograms without any occurrence of decomposition.

Chromatograms of Ni(II) and Pd(II) Complexes. Various dithiocarbamate chelates were prepared by the methods given above and their elution behaviors put into examination. When diethylamine was used, the following elution sequence for central metal ions was obtained in parallel with increase in retention time: Hg(II) < Cu(II) < Ni(II) < Pd(II) < Co(III). Similar results were obtained for diisopropylamine and piperidine. For Ni(II) chelates derived from various amines was obtained the increasing order of retention time as follows: dibutylamine < diisobutylamine < dipropylamine < dibenzylamine < diisopropylamine < perhydrazepine < diethylamine < piperidine < pyrrolidine < dimethylamine < propylamine < phenethylamine < morpholine < ethylamine < methylamine < *l*-ephedrine; the retention time was found to increase with increase in the carbon number of alkyl chains. This may be interpreted in terms of the solubility of metal chelates in eluents because the solubility increases with increase in the chain length of hydrophobic alkyl groups. The prolonged retention times of morpholine and *l*-ephedrine may be interpreted from the fact that oxygen atoms included in these amines will be adsorbed strongly on the silica-gel surface.

Chromatograms of mixtures of two different amines were examined, the results being exemplified in Fig. 1. Both Ni(II) (Fig. 1(a)) and Pd(II) (Fig. 1(b)) gave three peaks. This implies that a ternary complex is formed according to the following equation and that the ternary complex formed is inert enough to be eluted out without being subjected to disproportionation during the course of chromatographic run:[2,3]

$$MA_2 + MB_2 \rightleftharpoons 2MAB \quad (4)$$

with

$$K = [MAB]^2/[MA_2][MB_2]. \quad (5)$$

This phenomenon which results in complicate chromatogram patterns has led Liska *et al.*[14] to claim that it is difficult to determine amines by application of the conversion into dithiocarbamate chelates. However, as described previously,[15] the present authors think that this phenomenon has some analytical value for the determination of optical purity of optically active amines. When an racemic mixture of amines exists in solution, the following optically active chelates will be formed:

$$MD_2 + ML_2 \rightleftharpoons 2MDL, \quad (6)$$

where D and L represent derivatives derived from *d*- and *l*-isomers, respectively. Since MD_2 and ML_2 are enantiomers and their chemical properties except optical activity are identical, they cannot be separated

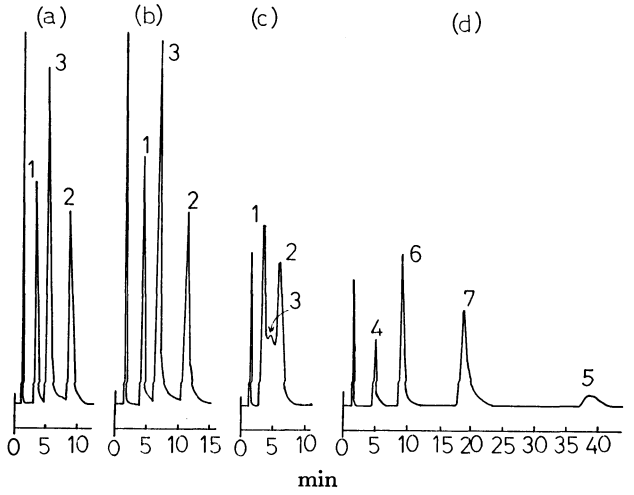

Fig. 1. Chromatogram patterns of dithiocarbamate chelates derived from the mixture of two amines.
Column: LiChrosorb SI 100 (4 mm×15 cm).
Eluent: hexane:ethyl acetate=100:3 (water saturated). Flow rate: 2.5 cm³/min. Detector: (a) 325 nm, (b) 308 nm, (c) 270 nm, (d) 268 nm. Sample: (a) Ni(II), (b) Pd(II), (c) Cu(II), (d) Co(III). Sample size: 50 μl (Concentrations of each amine were about 0.2 mM).
1: MA_2, 2: MB_2, 3: MAB, 4: MA_3, 5: MB_3, 6: MA_2B, 7: MAB_2. A=$(C_3H_7)_2NCSS^-$, B=$(CH_2)_5NCSS^-$.

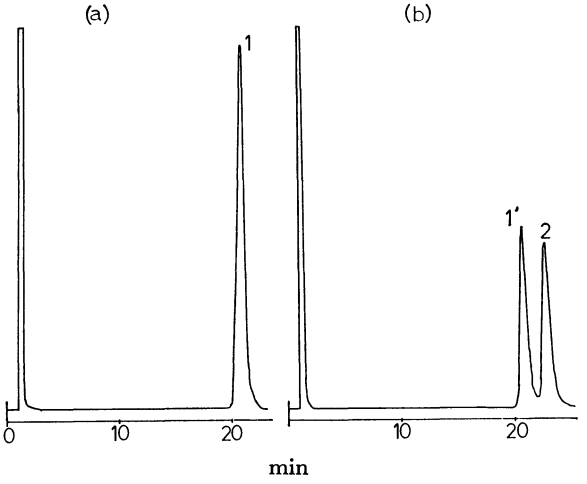

Fig. 2. Chromatograms of Ni(II) dithiocarbamate chelates derived from optically active and racemic ephedrines.
Column: LiChrosorb SI 100 (4 mm×25 cm).
Eluent: hexane:isopropyl acetate=100:11.5 (water saturated). Flow rate: 2.5 cm³/min. Detector: 325 nm. Sample: (a) 0.2 mM *l*-ephedrine(*d*-ephedrine gave similar chromatograms), (b) 0.2 mM *dl*-ephedrine Sample size: 50 μl.

from each other. On the other hand, MD_2 (or ML_2) and MDL are diastereomers, and can possibly be separated. Figures 2(a) and (b) show chromatograms of Ni(II) chelates derived from *l*- and *dl*-ephedrine, respectively. The *l*-isomer exists in nature and has widely been used as an antiasthmatic agent. On the contrary, *d*-isomer, not known to exist in nature, is ineffective as antiasthmatic agent. As shown in Fig. 2(b), the racemate gave two peaks, one being assigned to MD_2+ML_2 and the other to MDL. In Fig. 2(b), the peak area of the former (S_1) is equal to that of the latter (S_2), which suggests that the ternary complex formation according to Eq. 6 is controlled statistically ($K=[MDL]^2/([MD_2][ML_2])=4.0$). The optical purity of *dl*-mixture is determined as follows: When the initial concentrations of *d*- and *l*-isomers and d_0 and l_0, respectively, the equilibrium concentrations of MD_2 and ML_2 are $d_0-r/2$ and $l_0-r/2$, respectively, where r is the concentration of MDL. Since the ternary complex formation is controlled statistically, it is derived that $r=2d_0l_0/(d_0+l_0)$. The following relation will then hold between two peak areas S_1 and S_2:

$$\begin{aligned} S_2/(S_1+S_2) &= [MDL]/([MD_2]+[ML_2]+[MDL]) \\ &= r/(l_0+d_0) = 2d_0l_0/(d_0+l_0)^2 = 2p(1-p) \\ &= -2(p-1/2)^2+1/2, \end{aligned} \quad (7)$$

where $p=d_0/(d_0+l_0)$. Figure 3 shows parabolic plots for Eq. 7 with different ratios of *d*- to *l*-isomer. Both the calculated and observed results agreed well. The total ephedrine content was determined from the sum of the two peak areas S_1+S_2.

Pd(II) chelates gave similar results, with retention times slightly longer than those of corresponding Ni(II) complexes.

Chromatograms of Co(III) Complexes. It is well known that, when Co(II) ion reacts with dithiocarbamates to form metal chelates, Co(III) chelates are formed as a result of oxidation of Co(II) ion.[16] As shown in Fig. 1(d) four peaks, each assigned to MA_3, MA_2B, MAB_2, and MB_3, appeared on chromatograms when Co(II) solution was added. This result indicates that oxidation of the central metal ion occurs with formation of 1:3 complexes. No further investigation was made toward analytical application.

Chromatograms of Cu(II) Complexes. Figure 1(c) shows an example chromatogram for a mixture of two Cu(II) chelates. Since Cu(II) chelates are labile, their ternary complexes partially undergo disproportionation into two binary complexes during the course

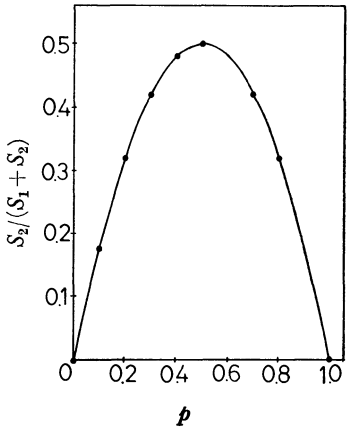

Fig. 3. Plot of Eq. 7 at various *d*- and *l*-isomer ratio chromatographic conditions were similar to those shown in Fig. 2.
——: Calculated value, ●: observed value.

of chromatographic run. The degree of the progress of disproportionation was sensitive to experimental conditions[3] such as the flow rate of pump and column temperature. The disproportionation within the column proceeded with increased proportions at higher column temperatures or at lower flow rates. Since the chromatogram pattern is very sensitive to experimental conditions, the analytical application seems unpromising.

Chromatograms of Hg(II) Complexes. Figure 4 shows chromatograms of Hg(II) chelates derived from mixtures of various aliphatic secondary amines. Unlike the other metal ions, only the peaks of the binary complexes corresponding to each amine appeared on chromatograms. The following aleternative explanations are plausible, the second being more likely: (1) no ternary complex formation occurs for Hg(II) chelates; (2) since Hg(II) complexes are very labile, the ternary complexes formed in the equilibrium state undergo disproportionation almost instantaneously after they are separated from the binary complexes. This seems a reasonable explanation because the rate of ligand exchange for Hg(II) complexes is known to be very high.

Figure 4 suggests that determination of individual amines will be possible when Hg(II) chelates are used. The mixture of samples shown in Fig. 4 was diluted to various concentrations and supplied for HPLC. The chromatograms were unsusceptible to experimental conditions and calibration curves were linear within a wide range of sample amounts. Thus, about 5 ng of each amine could be detected.

Application to Antiasthmatic Agents. Aliphatic amines usually show no or weak absorption in the UV or visible range. Since metal dithiocarbamate chelates show very strong absorption in th UV or visible range (log $\varepsilon > 4$), the present method will be useful for color-producing reactions. The present method was applied to the determination of ephedrines in crude drugs and Chinese crude drug preparations.

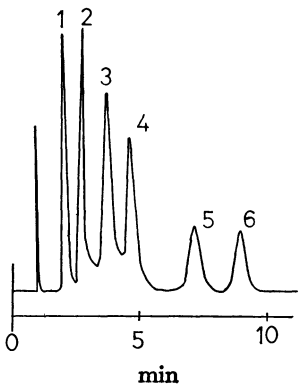

Fig. 4. Chromatograms of Hg(II) chelates derived from the mixture of various secondary amines.
Column: LiChrosorb SI 100 (4 mm × 15 cm).
Eluent: hexane:ethyl acetate=100:3 (water saturated). Flow rate: 2.5 cm³/min. Detector: 273 nm. Sample size: 50 μl (Concentrations of each amine were about 0.03 mM).
1: Dipropylamine, 2: dibenzylamine, 3: diethylamine, 4: piperidine, 5: pyrrolidine, 6: dimethylamine.

Four ephedrine isomers, *l*-, *d*-, *l*-pseudo, and *d*-pseudoephedrine exist. Ephedra herba, which is one of the most important Chinese crude drugs and has widely been used as an antiasthmatic agent or for cough remedy, contains two isomers, *l*- and *d*-pseudoephedrine, the former being more effective. The synthesized racemates *dl*- and *dl*-pseudoephedrine are less pharmacologically active because *d*- or *l*-pseudoephedrine is not effective. Thus, the determination of total content and optical purity of ephedrines is important. Sample treatment was made as follows: to 200 mg of powdered ephedra herba or Chinese crude drug preparations, 40 cm³ of 0.5 M H_2SO_4 was added. The extraction was carried out for 1 hr three times. Then, to the combined extract 100 cm³ of 0.05 M $NiCl_2$ in conc aqueous ammonia and 40 cm³ of chloroform containing 2% carbon disulfide were added, and the mixture was shaken vigorously for about 30 s. A brownish yellow color appeared in the chloroform layer. The chloroform layer was washed with water three times and the

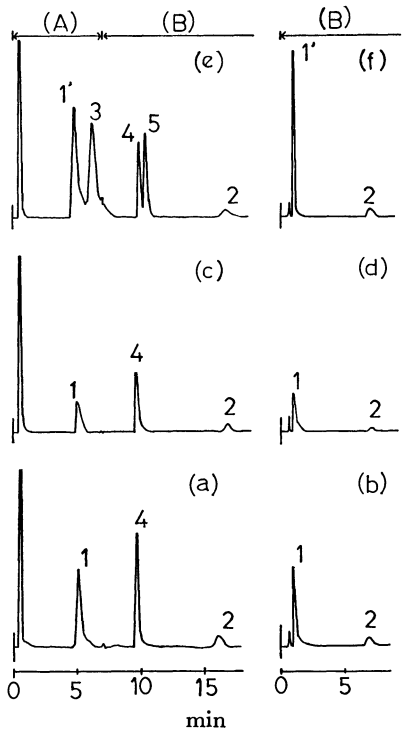

Fig. 5. Chromatograms of ephedrines in Ephedra herba and Chinese crude drug preparations.
Column: LiChrosorb SI 100 (4 mm × 15 cm).
Eluent: hexane:isopropyl acetate=(A) 100:12 (B) 100:25 (water saturated). Flow rate: 2.5 cm³/min. Detector: (a)(c), and (e) 325 nm, (b), (d), and (f) 273 nm. Sample size: 50 μl.
Sample: (a) and (b) ephedra herba, (c) and (d) chinese crude drug preparations (Kakkonto), (e) and (f) ephedra herba+*d*-ephedrine: (a),(c), and (e) Ni(II) chelates (b), (d), and (f) Hg(II) chelates. 1: M(*l*-EP)$_2$, 1′: M(*d*-EP)$_2$+M(*l*-EP)$_2$, 2: M(*d*-ϕ-EP)$_2$, 3: M(*l*-EP)(*d*-EP), 4: M(*l*-EP)(*d*-ϕ-EP), 5: M(*d*-EP)(*d*-ϕ-EP). *l*-EP, *d*-EP, and *d*-ϕ-EP denote dithiocarbamates derived from *l*-ephedrine, *d*-ephedrine, and *d*-ϕ-ephedrine, respectively.

extract was divided into two parts, one of which was supplied directly for HPLC (Ni(II) chelates). To the other part 1 mM $HgCl_2$ aqueous solution was added and the mixture was shaken for a few seconds. The brownish yellow color disappeared immediately as a result of the progress of the exchange of central metal ion according to Eq. 3. The solution was then supplied for HPLC (Hg(II) chelates). Figure 5 shows example chromatograms. Since *l*- and *d*-pseudoephedrine are diastereomers, two peaks corresponding to individual amines appeared on chromatograms when Hg(II) chelates were tested (Figs. 5(b) and (d)). Contrary to this, three peaks including the peak of ternary complex appeared on chromatograms when Ni(II) chelates were tested (Figs. 5(a) and (c)). Figures 5(a) and (c) show that no *d*-ephedrine is contained in these samples. Figure 5(e) shows chromatograms of Ni(II) chelates when a small amount of *d*-ephedrine was added. Two new peaks, assignable to ternary complexes M(*d*-EP)(*d*-ϕ-EP) and M(*d*-EP)(*l*-EP), appeared on chromatograms (Fig. 5(e)). The optical purity of *dl*-mixture of ephedrine in this sample can be determined by the following two methods: (1) equation 7 gives optical purity by comparing two peak areas of peaks 1′ ($M(l\text{-EP})_2+M(d\text{-EP})_2$) and 3 (M(*d*-EP)(*l*-EP)); (2) the ratio of two peak areas of peaks 4 (M(*l*-EP)(*d*-ϕ-EP)) and 5 (M(*d*-EP)(*d*-ϕ-EP)) directly indicates the ratio of *d*- and *l*-isomer. Contrary to the case with Ni(II) chelates, no chromatogram patterns of Hg(II) chelates were affected by addition of *d*-ephedrine (Fig. 5(f)). The peak height of the former was increased by addition of *d*-ephedrine while that of the latter unaffected. The area of the former peak 1 indicates the total content of *dl*-mixture of ephedrine. These results permit the calculation of individual contents of *l*-, *d*-, and *d*-pseudoephedrine.

References

1) M. Moriyasu and Y. Hashimoto, *Anal. Lett.*, **A11**, 593 (1978).
2) M. Moriyasu and Y. Hashimoto, *Chem. Lett.*, **1980**, 117.
3) M. Moriyasu and Y. Hashimoto, *Bull. Chem. Soc. Jpn.*, **53**, 3590 (1980).
4) P. Heizmann and K. Ballschmiter, *J. Chromatogr.*, **137**, 153 (1977).
5) P. C. Uden and I. E. Bigley, *Anal. Chim. Acta*, **94**, 29 (1977).
6) G. Schwedt, *Chromatographia*, **11**, 145 (1978).
7) J. W. O'Laughlin and T. P. O'Brien, *Anal. Lett.*, **A 11**, 829 (1978).
8) O. Liska, J. Lehotay, E. Brandstererova, G. Guichon, and H. Colin, *J. Chromatogr.*, **172**, 384 (1979).
9) L. Malatesta, *Chim. Ind. (Milan)*, **23**, 319 (1941).
10) V. Sedivec and V. Vasak, *Chem. Listy*, **43**, 269 (1949).
11) R. Wickbold, *Z. Anal. Chem.*, **152**, 259 (1956).
12) G. Echert, *Z. Anal. Chem.*, **155**, 23 (1957).
13) H. Bode and K. I. Tusche, *Z. Anal. Chem.*, **157**, 414 (1957).
14) O. Liska, G. Guichon, and H. Colin, *J. Chromatogr.*, **171**, 145 (1979).
15) M. Moriyasu, Y. Hashimoto, and M. Endo, *Chem. Lett.*, **1980**, 761.
16) A. Hulanicki, *Talanta*, **14**, 1371, (1967).

Kinetic Studies of Fast Equilibrium by Means of High-performance Liquid Chromatography. III. Ternary Complex Formation between Ni(II) Diethyldithiocarbamate and Other Unlike Ni(II) Chelates

Masataka Moriyasu* and Yohei Hashimoto

Kobe Women's College of Pharmacy, Motoyamakita-machi, Higashinada-ku, Kobe 658

(Received March 23, 1981)

The labile ternary complex formation ($MA_2+MB_2 \rightleftarrows 2MAB$ with $K=[MAB]^2/([MA_2][MB_2])$) between Ni(II) diethyldithiocarbamate(MA_2) and other several Ni(II) chelates(MB_2) was investigated by high-performance liquid chromatography; two solutions of MA_2 and MB_2 were mixed and equilibrated. The tendency to form a ternary complex is summarized as follows: (1) no ternary complex formation takes place (B=dimethylglyoxime and 1-(2-pyridylazo)-2-naphthol), for which high structural stability of binary complex MB_2 is responsible; (2) the ternary complex formation is controlled statistically ($K=4.0$), suggesting the absence of any factor to stabilize or unstabilize the ternary complex (B=*N*,*N*-disubstituted dithiocarbamates and *N*-monosubstituted dithiocarbamates); (3) the ternary complex formation is favored ($K>4.0$) (B=xanthates); and (4) all initial binary complexes are converted into a very stable species which is possibly a ternary complex (B=dithizone). Kinetic characteristics of these ternary complex formations are examined.

Ternary complex formation usually occurs as follows when two solutions of labile binary complexes are mixed:

$$MA_2 + MB_2 \underset{k_-}{\overset{k}{\rightleftharpoons}} 2MAB \qquad (1)$$

with

$$K = [MAB]^2/[MA_2][MB_2] = k/k_-. \qquad (2)$$

Study of the ternary complex formation has been carried out mainly by the spectroscopic method since many ternary complexes have characteristic absorption bands. However, this method cannot be applied if the ternary complex gives rise to no characteristic absorption. Our previous studies[1,2] made use of the high-performance liquid chromatography (HPLC) to investigate the ternary complex formation between two different *N*,*N*-disubstituted dithiocarbamate chelates of Ni(II) or Cu(II). In this method two solutions of MA_2 and MB_2 are mixed, kept standing to reach the equilibrium state for the ternary complex formation, and a portion of the mixture is subjected to the HPLC. The separation speed of HPLC is so high that labile ternary complexes are allowed to be eluted out without undergoing any disproportionation. Thus, considerably fast equilibria can be traced by the HPLC based on the conventional principle. Rate constants k and k_- can be determined as follows: when two very dilute solutions of MA_2 and MB_2 are mixed, the ternary complex will gradually be produced until the equilibrium shown in Eq. 1 is attained. During the progress of ternary complex formation, portions of the mixed solution are taken out to be subjected to HPLC. The progress of the reaction is caused to stop immediately after the solution is injected into the column. Thus, concentrations of each species can be determined as a function of time, allowing the determination of k and k_-.

It was confirmed in our previous report[2] that labile ternary complex formations between two different *N*,*N*-disubstituted dithiocarbamate chelates are controlled statistically with a factor of $K=4.0$ in the case of Ni(II) and Cu(II); different factors are expected in cases where two binary complexes whose coordinated ligands are different in property from each other are mixed, depending on the nature of the ligands. The purpose of the present study is to clarify to what extent the HPLC is applicable to the investigation of labile ternary complex formation. We selected Ni(II) chelates since they provide ternary complex formations of such a moderately high rate as to allow kinetic studies to be carried out easily.

Experimental

Reagents. The chelating reagents used are sodium diethyldithiocarbamate (NaDEDTC), sidum ethyldithiocarbamate (NaEDTC), sodium propyldithiocarbamate (NaPDTC), pottasium ethylxanthate (KEXAN), pottasium propylxanthate (KPXAN), 1-(2-pyridylazo)-2-naphthol (HPAN), dimethylglyoxime (HDMG), dithizone (H_2Dz), oxine, salicylaldehyde oxime, 1-nitroso-2-naphthol, and (*E*)-benzoin oxime. NaEDTC and NaPDTC were prepared by the usual procedure[3] from alkylamine, carbon disulfide, and sodium hydroxide. KPXAN was prepared from 1-propanol, carbon disulfide, and pottasium hydroxide.[4] These salts were recrystallized from chloroform–methanol. The other chelating reagents were obtained commercially and purified when necessary. NaDEDTC, NaEDTC, NaPDTC, KEXAN, and KPXAN were dissolved in water. H_2Dz was dissolved in chloroform and the content was determined by measuring the absorption at 606 nm ($\varepsilon=4.06\times10^4$).[5,6] The other chelating reagents which are sparingly soluble in water were dissolved in suitable organic solvents such as chloroform and methanol. The standard solution of Ni(II) was prepared by dissolving $NiCl_2\cdot6H_2O$ in water. The content of Ni(II) was determined by colorimetry on its diethyldithiocarbamate. Before use all solvents used for HPLC were saturated with water.

Apparatus. The HPLC apparatus used in this study is similar to the one described previously.[1,7] Absorption spectra of each metal chelate were measured by a Model-124 Hitachi double-beam spectrometer.

Procedure. The Ni(II) chelates of DEDTC, EDTC, PDTC, EXAN, and PXAN were prepared by mixing the Ni(II) standard solution and the corresponding chelating reagent in water. The metal chelates prepared were extracted with chloroform under the condition for complete extraction. In order to remove residual free ligands in chloroform, the extract was washed with water four times. The Ni(II) chelate of dithizone was prepared in the following

way: To the Ni(II) aqueous standard solution, a slight excess of dithizone in chloroform was added. Since in acidic media the rates of formation and extraction of Ni(II) dithizonate are slow,[8] a small amount of dilute aqueous ammonia (0.5 vol%) was added and the mixture was shaken vigorously for 30 min. Then, the chloroform layer was washed three times with 0.2 vol% aqueous ammonia to remove the residual free dithizone in chloroform. The solutions of the other Ni(II) chelates were prepared by mixing the Ni(II) standard solution and the corresponding chelating reagent in an organic solvent, and diluting the resulting solution with chloroform to a proper concentration.

Results and Discussion

HPLC of Various Ni(II) Chelates. Chromatographic behavior of various Ni(II) chelates was examined on silica gel packings. Among them, Ni(DEDTC)$_2$, Ni(EDTC)$_2$, Ni(PDTC)$_2$, Ni(EXAN)$_2$, Ni(PXAN)$_2$, Ni(DMG)$_2$, Ni(PAN)$_2$, and Ni(HDz)$_2$ gave good chromatograms. Calibration curves of these metal chelates are linear over a wide range of sample amounts. Contrary to this, the Ni(II) chelates of oxine, salicylaldehyde oxime, 1-nitroso-2-naphthol, and (*E*)-benzoin oxime gave no quantitative results because partial or complete decomposition takes place in the course of chromgatography. Silica gel seems too active for these chelates of relatively low stability and other less active packings are expected to give satisfactory results. In the present research these Ni(II) chelates which failed to give quantitative results on silica gel packings were left omitted from further examination.

Ni(DEDTC)$_2$–Ni(EDTC)$_2$. These two binary chelates were mixed at 25 °C and after kept standing long enough to attain the equilibrium, the mixture was supplied for HPLC. Three peaks corresponding to Ni(DEDTC)$_2$, Ni(EDTC)$_2$, and Ni(DEDTC)(EDTC) appeared on chromatograms (Fig. 1). The heights of each peak were independent of flow rate, suggesting that no disproportionation of the ternary complex occurs in course of chromatography. Similar to the system composed of two different Ni(II) *N,N*-disubstituted dithiocarbamate chelates,[1,2] the equilibrium constant K was 4.0. The system Ni(DEDTC)$_2$–Ni(PDTC)$_2$ gave similar results. From these results it can be concluded that the ternary complex formation according to the following equations is controlled statistically, *i.e.*, there exists no factor in operation which makes the ternary complex stable or unstable:

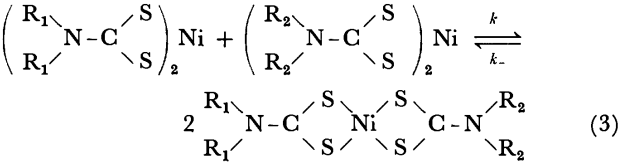

(3)

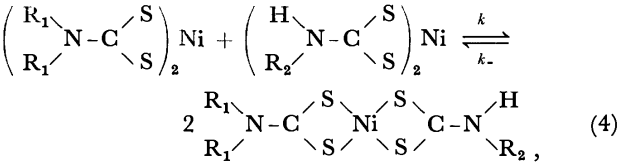

(4)

where R_1 and R_2 denote alkyl groups.

Rate constants k and k_- were determined by the following equation with a procedure similar to the one described in our previous report:[2]

$$k = -(1/a_0 t)\ln(1-y/a_0) \tag{5}$$

with

$$k_- = k/4, \tag{6}$$

where the initial concentrations of two binary complexes MA_2 and MB_2 are designed to be the same ($=a_0$) with each other and y is the concentration of ternary complex MAB at a reaction time t after mixing. Thus, rate constants k and k_- were determined to be $(1.6\pm0.25)\times10^2$ mol^{-1} dm^3 s^{-1} and $(4.0\pm0.6)\times10^1$ mol^{-1} dm^3 s^{-1}, respectively, for the system Ni(DEDTC)$_2$–Ni(EDTC)$_2$ (in chloroform: ethyl acetate: hexane=1:1:3) at 25 °C. These values are similar to those reported in our previous report[2] for corresponding complex formations between Ni(DEDTC)$_2$ and other various Ni(II) *N,N*-disubstituted dithiocarbamate chelates.

Ni(DEDTC)$_2$–Ni(EXAN)$_2$. Both dithiocarbamates and xanthates are *S,S*-coordinates chelating reagents and their chemical structures are similar to one another. When solutions of two binary complexes of Ni(II) dithiocarbamate and xanthate are mixed, the following ternary complex formation occurs:

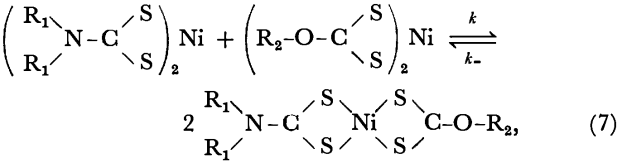

(7)

as evidenced by Fig. 2. Unlike the system composed

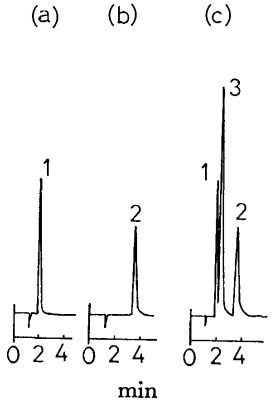

Fig. 1. Ternary complex formation between Ni(DEDTC)$_2$ and Ni(EDTC)$_2$.
Column: Shodex silipak (4 mm×15 cm). Eluent: (hexane:ethyl acetate=100:15 (water saturated). Flow rate: 3.2 cm^3/min. Detector: 325 nm. Sample size: 50 μl.
Sample: (a) 2.5×10^{-4} mol dm^{-3} Ni(DEDTC)$_2$, (b) 2.5×10^{-4} mol dm^{-3} Ni(EDTC)$_2$, (c) 2.5×10^{-4} mol dm^{-3} Ni(DEDTC)$_2$+2.5×10^{-4} mol dm^{-3} Ni(EDTC)$_2$. These samples are solutions in hexane:chloroform: ethyl acetate=3:1:1 at 25 °C.
1: Ni(DEDTC)$_2$, 2: Ni(EDTC)$_2$, 3: Ni(DEDTC)(EDTC).

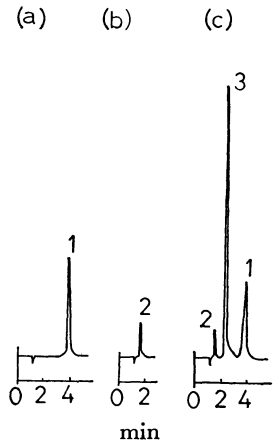

Fig. 2. Ternary complex formation between Ni(DEDTC)$_2$ and Ni(EXAN)$_2$
Column: Shodex silipak (4 mm × 15 cm). Eluent: hexane:ethyl acetate=100:8 (water saturated). Flow rate: 3.2 cm^3/min. Detector: 315 nm. Sample size: 50 μl.
Sample: (a) 2.5×10^{-4} mol dm^{-3} Ni(DEDTC)$_2$, (b) 2.5×10^{-4} mol dm^{-3} Ni(EXAN)$_2$, (c) 2.5×10^{-4} mol dm^{-3} Ni(DEDTC)$_2$+2.5×10^{-4} mol dm^{-3} Ni(EXAN)$_2$. These samples are solutions in hexane:chloroform:ethyl acetate=3:1:1 at 25 °C.
1: Ni(DEDTC)$_2$, 2: Ni(EXAN)$_2$, 3: Ni(DEDTC)-(EXAN).

of two Ni(II) dithiocarbamate chelates, this system gave an equilibrium constant K larger than 4.0 (8.3±1.2, in chloroform:ethyl acetate:hexane=1:1:3) at 25 °C, and about 60% of the initial binary complexes was converted into the ternary complex. This result suggests the presence of some factor to stabilize the ternary complex, even though there seem to exist none of apparent driving factors in favor of the ternary complex formation, such as steric factors, π-bond formation, hydrogen bond formation, and neutralization of the charge.[9]

When K is not equal to 4.0, rate constants k and k_- should be determined from the following rather complicated equation[10] derived on the assumption that a bimolecular collisional process is operating in the ternary complex formation:

$$k = (2/m_0t)\left[\ln\frac{\left(\frac{2a_0+m_0}{1-4/K}-y\right)}{\left(\frac{2a_0-m_0}{1-4/K}-y\right)}+\ln\left(\frac{2a_0-m_0}{2a_0+m_0}\right)\right], \quad (8)$$

where

$$m_0 = 4a_0\sqrt{1/K}. \quad (9)$$

Two solutions of MA_2 and MB_2 were mixed at 25 °C and after a measured time a portion of the mixed solution was supplied for HPLC. With the lapse of time the peak of the ternary complex rose while those of the binary complexes fell, the results being plotted in Fig. 3. The validity of the bimolecular collisional process was confirmed by changing the initial concentration a_0. Rate constants k and k_- were determined to be $(1.3\pm0.1)\times10^2$ mol^{-1} dm^3 s^{-1} and $(1.6\pm0.2)\times10^1$ mol^{-1} dm^3 s^{-1}, respectively, (in chloroform:

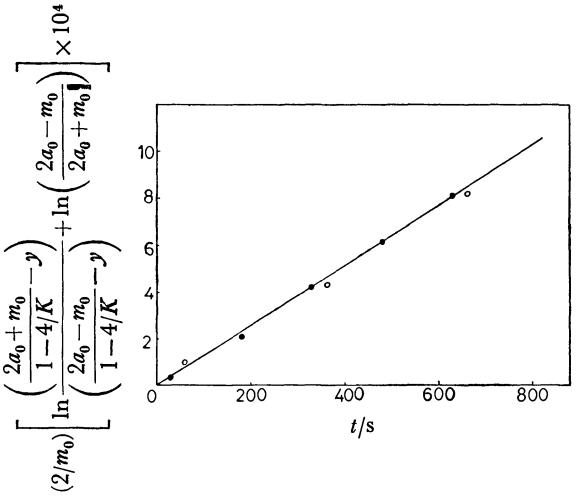

Fig. 3. Plot of Eq. 8.
Chromatographic conditions were similar to those shown in Fig. 2.

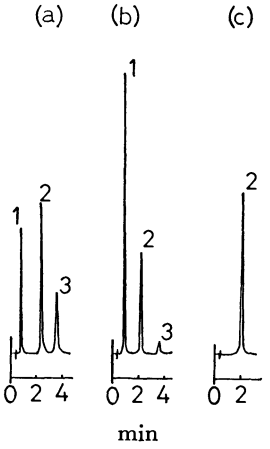

Fig. 4. Chromatograms of a mixture of Ni(DEDTC)$_2$, Ni(PAN)$_2$, and Ni(DMG)$_2$.
Column: Shodex silipak (4 mm × 15 cm). Eluent: hexane : ethyl acetate=100:25 (water saturated). Flow rate: 3.2 cm^3/min. Detector: (a) 254 nm, (b) 325 nm, (c) 530 nm. Sample sizes: 5 μl.
1: Ni(DEDTC)$_2$, 2: Ni(PAN)$_2$, 3: Ni(DMG)$_2$.

ethyl acetate:hexane=1:1:3) at 25 °C.

Similar results were obtained for the system Ni(DEDTC)$_2$–Ni(PXAN)$_2$. Equilibrium constant K and rate constants k and k_- for the ternary complex formation were also determined ($K=7.6\pm1.4$, $k=(1.0\pm0.1)\times10^2$ mol^{-1} dm^3 s^{-1}, and $k_-=(1.3\pm0.25)\times10^1$ mol^{-1} dm^3 s^{-1}, in chloroform:ethyl acetate:hexane=1:1:3) at 25 °C.

Ni(DEDTC)$_2$–Ni(PAN)$_2$–Ni(DMG)$_2$. When these two or three binary metal chelates were mixed, the peaks of the initial binary chelates alone appeared on chromatograms (Fig. 4). Then, an attempt was made to cause ternary complexes to be formed in the following way: Two or three free chelating reagents in methanol were mixed and then the Ni(II) aqueous solution was added to form metal chelates. The metal chelates were extracted with chloroform and then supplied for HPLC. The chromatogram

patterns were similar to those shown in Fig. 4, excluding the possibility of the formation of any stable ternary complexes. Thus, the following alternative explanations are plausible: (1) no ternary complex formation occurs because initial binary complexes have very stable structures; and (2) a very labile ternary complex is formed. In this case, the ternary complex formed should undergo disproportionation into two binary complexes almost instantaneously in the column, resulting in the appearance of only the peaks of binary complexes on chromatograms. The present authors regard the former explanation as the more plausible for the following reasons: as shown below, $Ni(DMG)_2$ has a very stable structure by dint of hydrogen bond formation[11] and $Ni(PAN)_2$ has a stable six-coordinated structure.[12] When a ternary complex

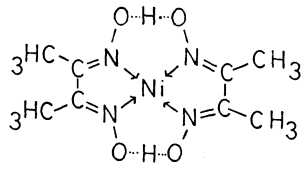

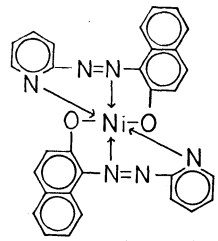

is to be formed, either the hydrogen bond should be broken or the five-coordinated ternary chelate formed. These ternary chelates will be rather unstable energetically. The chromatogram patterns shown in Fig. 4 were independent of experimental conditions such as flow rate, column temperature, and initial concentrations of binary complexes, which is in favor of the former explanation.[2] If the latter explanation is correct, the Ni(II) ternary complex formed should be extraordinarily labile in comparison with other various Ni(II) chelates.

$Ni(DEDTC)_2$–$Ni(HDz)_2$. When these two binary complexes were mixed, characteristic chromatograms different from those for the other systems were obtained. As ashown in Fig. 5, with the lapse of time, the peaks of binary complexes fell while a new peak appeared and grew gradually. The progress of the reaction was slow at room temperature. After 1-d standing, the peaks of the binary complexes disappeared completely when the initial concentrations of two binary complexes had been chosen the same ($=a_0$). There seems to remain some debatable points on what reaction occurred in the mixed solution. To the solution given in Fig. 5(g), in which the reaction had been completed, dilute aqueous ammonia (0.5 vol%) was added and the mixture was shaken vigorously for about 30 s. No free dithizone was extracted out into the aqueous layer, excluding the possibility of free dithizone being liberated in the reaction. It is reported[8] that Ni(II) dithizonate may exist in two forms, *i.e.*, as the keto-form complex $Ni(HDz)_2$ and enol-form complex NiDz. The Ni(II) chelates used in the present research was spectroscopically confirmed to be the keto-form complex. The absorption spectrum of the species produced, shown in Fig. 6(c), is different from those of such species as the initial binary complexes and free dithizone. It is different also from the one of the enol-form complex NiDz.[13] These results suggest that a new species was produced in the reaction. The absorption spectrum of the new species resembles the one of $Ni(HDz)_2$ in the visible range, with weaker absorption; in the UV range the absorption maximum ($=312$ nm) appeared between those of $Ni(DEDTC)_2$ ($=325$ nm) and $Ni(HDz)_2$ ($=280$ nm). These phenomena may be interpreted well in terms of the ternary complex formation. The possibility of the formation of higher-order complexes such as polynuclear com-

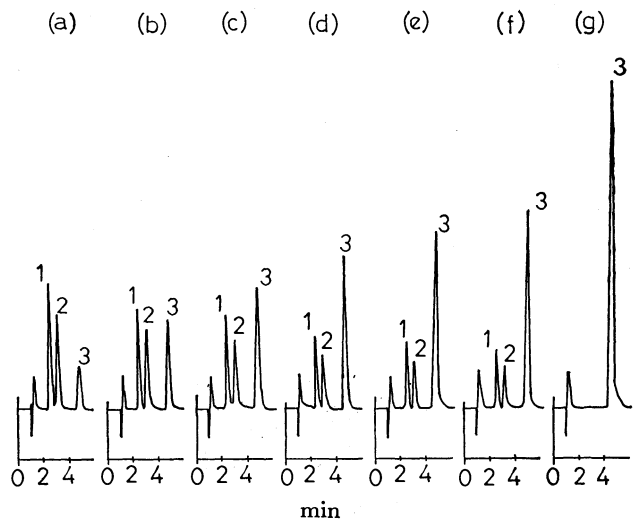

Fig. 5. Change of chromatogram patterns of the mixture of $Ni(DEDTC)_2$ and $Ni(HDz)_2$.
Column: LiChrosorb SI 100 (4 mm×25 cm). Eluent: hexane:ethyl acetate=100:10 (water saturated). Flow rate: 3.2 cm³/min. Detector: 312 nm. Sample size: 50 μl. Sample: 2.5×10^{-5} mol dm^{-3} $Ni(DEDTC)_2$+2.5×10^{-5} mol dm^{-3} $Ni(HDz)_2$ (a); after mixing 1 min, (b); 3.5 min (c); 6 min, (d); 8.5 min, (e); 11 min, (f); 13.5 min, (g); 1 d. These samples are solutions in chloroform:ethyl acetate: hexane=1:1:3 at 50 °C.
1: $Ni(DEDTC)_2$, 2: $Ni(HDz)_2$, 3: a new species (see text).

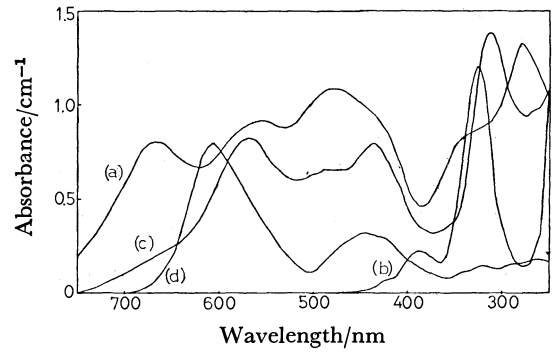

Fig. 6. Absorption spectra of various species in the system $Ni(DEDTC)_2$–$Ni(HDz)_2$.
(a): 4.0×10^{-5} mol dm^{-3} $Ni(HDz)_2$, (b): 4.0×10^{-5} mol $Ni(DEDTC)_2$, (c): the reaction product between 4.0×10^{-5} mol dm^{-3} $Ni(HDz)_2$ and 4.0×10^{-5} mol dm^{-3} $Ni(DEDTC)_2$, (d): 2.0×10^{-5} mol dm^{-3} H_2Dz. These samples are solutions in chloroform.

plex, however, cannot completely be ruled out for the following reason: It should be noted that Ni(HDz)$_2$ has the *N,N*-coordinated structure,[14] though most of other metal dithizonates have the *N,S*-coordinated structure. Some intramolecular structural rearrangement which stabilizes the ternary complex might occur during the course of ternary complex formation. The structure of the possible ternary complex will be as follows, provided that no structural rearrangement occurs.

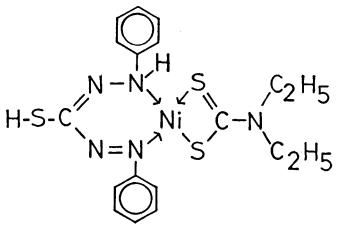

The following chemical equation will hold for the possible ternary complex formation since the reverse reaction can be neglected:

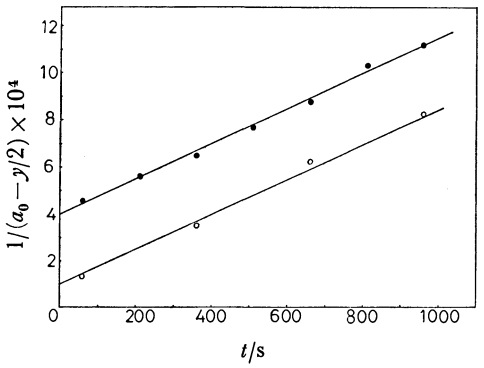

Fig. 7. Plot of Eq. 12.
Chromatographic conditions were similar to those shown in Fig. 5.
○: $a_0=1.0\times10^{-4}$ mol dm^{-3}, ●: $a_0=2.5\times10^{-5}$ mol dm^{-3}.
These samples are solutions in chloroform:ethyl acetate: hexane=1:1:3 at 50 °C.

$$\mathrm{Ni(DEDTC)_2} + \mathrm{Ni(HDz)_2} \xrightarrow{k} 2\mathrm{Ni(DEDTC)(HDz)}. \quad (10)$$

Rate constant k of this reaction will be obtained from the following equations based on the bimoelcular collisional process:

$$1/x = 1/a_0 + kt \quad (11)$$

$$1/(a_0-y/2) = 1/a_0 + kt, \quad (12)$$

where x and y are concentrations of Ni(DEDTC)$_2$ (=Ni(HDz)$_2$) and Ni(DEDTC)(HDz), respectively, at a reaction time t after mixing. Figure 7 shows plots for Eq. 12. The validity of the bimolecular process was confirmed by changing the initial concentration a_0. Rate constant k was thus determined to be $(1.8\pm0.2)\times10^1$ mol^{-1} dm^3 s^{-1} and $(7.4\pm0.4)\times10^1$ mol^{-1} dm^3 s^{-1} at 25 °C and 50 °C, recepectively (in chloroform: ethyl acetate:hexane=1:1:3).

References

1) M. Moriyasu and Y. Hashimoto, *Chem. Lett.*, **1980**, 117.
2) M. Moriyasu and Y. Hashimoto, *Bull. Chem. Soc. Jpn.*, **53**, 3590 (1980).
3) A. W. Hofmann, *Chem. Ber.*, **1**, 25 (1868).
4) C. C. Price and G. W. Stacy, *Org. Synth.*, **28**, 82 (1948).
5) S. S. Cooper and S. L. Sullivan, *Anal. Chem.*, **23**, 613 (1951).
6) A. S. Landry and S. F. Fedondo, *Anal. Chem.*, **26**, 732 (1954).
7) M. Moriyasu and Y. Hashimoto, *Anal. Lett.*, **A11**, 593 (1978).
8) T. Ashizawa, *Bunseki Kagaku*, **10**, 558 (1961).
9) H. Sioge, *Angew. Chem. Int. Ed. Engl.*, **14**, 397 (1975).
10) M. Bodenstein, *Z. Phys. Chem.*, **13**, 56 (1894); **22**, 1 (1897); **29**, 295 (1898).
11) L. E. Godycki and R. E. Rundle, *Acta Crystallogr.*, **6**, 487 (1953).
12) F. Umland, "Theorie und praktische Anwedung von Komplexbildenern," Akad. Verlagsges, Frankfurt/Main (1971), p. 471.
13) T. Ashizawa, *Bunseki Kagaku*, **10**, 350 (1961).
14) K. S. Math, Q. Fernando, and H. Freiser, *Anal. Chem.*, **36**, 1762 (1964).

Kinetics of the Oxidation of *N*-(2-Hydroxyethyl)ethylenediamine-*N*,*N*′,*N*′-triacetate Complex of Di-μ-oxo-bis[oxomolybdenum(V)] with Hexachloroiridate(IV) and μ-Hyperoxo-bis[pentaamminecobalt(III)] Ions in Aqueous Media

Yoichi SASAKI* and Reiko KAWAMURA

Department of Chemistry, Faculty of Science, Tohoku University, Aoba, Aramaki, Sendai 980

(Received March 5, 1981)

Kinctics of outer-sphere oxidations of $[Mo^{V}_{2}O_4(hedta)(H_2O)]^-$ (**1**) (H_3hedta=*N*-(2-hydroxyethyl)ethylenediamine-*N*,*N*′,*N*′-triacetic acid) with $[Ir^{IV}Cl_6]^{2-}$ ($[H^+]=10^{-5.8}$—0.10 M (1 M=1 mol dm^{-3}); ionic strength, I=0.1 M (adjusted with $LiClO_4$); 25—45 °C) and with $[(NH_3)_5Co^{III}(\mu\text{-}O_2^{(-)})Co^{III}(NH_3)_5]^{5+}$ ($[H^+]$=0.01—0.30 M; I=0.1 and 2.0 M; 10—30 °C), were studied under pseudo-first-order conditions (the reductant in large excess). The following reaction scheme is consistent with the observed rate laws:

$$\mathbf{1} \overset{K_a}{\rightleftharpoons} [Mo^{V}_{2}O_4(hedta)(OH)]^{2-} (\mathbf{2}) + H^+$$

$$\mathbf{1} + [Ir^{IV}Cl_6]^{2-} \xrightarrow{k_{(a)}} (Mo^{V}Mo^{VI}) + [Ir^{III}Cl_6]^{3-}$$

$$\mathbf{2} + [Ir^{IV}Cl_6]^{2-} \xrightarrow{k_{(b)}} (Mo^{V}Mo^{VI}) + [Ir^{III}Cl_6]^{3-}$$

$$\mathbf{1} + [\mu\text{-}O_2^{(-)}]^{5+} \overset{K_{IP(a)}}{\rightleftharpoons} IP(a) \text{ (ion-pair)}$$

$$\mathbf{2} + [\mu\text{-}O_2^{(-)}]^{5+} \overset{K_{IP(b)}}{\rightleftharpoons} IP(b) \text{ (ion-pair)}$$

$$IP(b) \xrightarrow{k_{e(b)}} (Mo^{V}Mo^{VI}) + [\mu\text{-}O_2^{(2-)}]^{4+}$$

$$(Mo^{V}Mo^{VI}) + \text{oxidant} \xrightarrow{\text{fast}} 2(Mo(VI)).$$

At 25 °C and I=0.1 M, K_a, $k_{(a)}$, $k_{(b)}$, $K_{IP(a)}$, $K_{IP(b)}$, and $k_{e(b)}$ are 7.9×10^{-4} M, 23 M^{-1} s^{-1}, 1.11×10^{4} M^{-1} s^{-1}, 40.5 M^{-1}, 1046 M^{-1}, and 2.56 s^{-1}, respectively. Activation parameters for the $k_{(b)}$ path are $\Delta H^{*}=38\pm8$ kJ mol^{-1} and $\Delta S^{*}=-25\pm29$ J K^{-1} mol^{-1}. The product $k_{e(b)}K_{IP(b)}K_a$ is 7.35×10^{-2} s^{-1} at 25 °C and I=2.0 M, and the corresponding activation parameters are $\Delta H^{*}=67\pm8$ kJ mol^{-1} and $\Delta S^{*}=-34\pm29$ J K^{-1} mol^{-1}. The oxidation of **2** is *ca.* 10^4 times as fast as that of **1**. The results are compared with the oxidation reactions of other $Mo^{V}_{2}O_4^{2+}$-complexes.

Redox reactions of molybdenum(V) complexes are attracting interest not only of coordination chemists but also of biochemists because of their importance in biochemical studies and biomimetic approach to complex catalysis.[1] We reported the kinetics of oxidations of two molybdenum(V) complexes containing di-μ-oxo-bis[oxomolybdenum(V)] ($Mo^{V}_{2}O_4^{2+}$) core, $[Mo^{V}_{2}O_4(edta)]^{2-}$ (H_4edta=ethylenediaminetetraacetic acid) and $[Mo^{V}_{2}O_4(H_2O)_n]^{2+}$, with $[(NH_3)_5Co^{III}(\mu\text{-}O_2^{(-)})Co^{III}(NH_3)_5]^{5+}$ in aqueous perchloric acid solution,[2] and of $[Mo^{V}_{2}O_4(pdta)]^{2-}$ (H_4pdta=propylenediaminetetraacetic acid) with $[(en)_2Co^{III}(\mu\text{-}NH_2,O_2^{(-)})Co^{III}(en)_2]^{4+}$ (en=ethylenediamine) in aqueous solution at pH 4.6.[3] Sykes and his co-workers studied the oxidation of edta and aqua complexes of the molybdenum(V) dimer with $[Fe^{III}(phen)_3]^{3+}$ (phen=1,10-phenanthroline) and with $[Ir^{IV}Cl_6]^{2-}$ in aqueous perchloric acid solution.[4,5] All these reactions proceeded via the outer-sphere mechanism. The rate of oxidation of $[Mo^{V}_{2}O_4(edta)]^{2-}$ with these one-electron oxidants is of first-order with respect to the concentration of $[Mo^{V}_{2}O_4(edta)]^{2-}$ and of the oxidant at 1.0 and 2.0 M (1 M=1 mol dm^{-3}) of ionic strength I, and is independent of $[H^+]$ (0.01—0.5 M).[2,4]

The rate of the predominant pathway for the oxidation of $[Mo^{V}_{2}O_4(H_2O)_n]^{2+}$ is, on the contrary, independent of the concentration of the oxidant and reciprocally dependent on $[H^+]$.[2,5] The proposed mechanism involves a rate-determining cleavage of one of the oxo bridges in $[Mo^{V}_{2}O_4(OH)(H_2O)_{n-1}]^{+}$ to give a single-bridged molybdenum(V) dimer prior to electron-transfer.[2,5]

The ligand environment including the presence of aqua ligands should play an important role in determining the pattern of oxidation mechanism. In order to clarify the factors controlling the oxidation mechanism, we have extended our study to the oxidation of $[Mo^{V}_{2}O_4(hedta)(H_2O)]^-$ (H_3hedta=*N*-(2-hydroxyethyl)ethylenediamine-*N*,*N*′,*N*′-triacetic acid),[6] which is structurally similar to $[Mo^{V}_{2}O_4(edta)]^{2-}$ but has no coordinated water molecule. Kinetics of the oxidation of the hedta complex with $[Ir^{IV}Cl_6]^{2-}$, $[(NH_3)_5Co^{III}(\mu\text{-}O_2^{(-)})Co^{III}(NH_3)_5]^{5+}$, and $[(en)_2Co^{III}(\mu\text{-}NH_2,O_2^{(-)})Co^{III}(en)_2]^{4+}$ are discussed in this paper.

Experimental

Materials. Sodium aqua-μ(*N*,*N*′)-*N*-(2-hydroxyethyl)-ethylenediamine-*N*,*N*′,*N*′-triacetato-di-μ-oxo-bis[oxomolybdate(V)] dihydrate, $Na[Mo^{V}_{2}O_4(hedta)(H_2O)]\cdot2H_2O$,[6] μ-hyperoxo-bis[pentaamminecobalt(III)] perchlorate dihydrate, $[(NH_3)_5Co^{III}(\mu\text{-}O_2^{(-)})Co^{III}(NH_3)_5](ClO_4)_5\cdot2H_2O$,[2] and μ-amido-μ-hyperoxo-bis[bis(ethylenediamine)cobalt(III)] chloride trihydrate, $[(en)_2Co^{III}(\mu\text{-}NH_2,O_2^{(-)})Co^{III}(en)_2]Cl_4\cdot3H_2O$,[7] were prepared by the known methods. Sodium hexachloroiridate(IV) hexahydrate, $Na_2[Ir^{IV}Cl_6]\cdot6H_2O$ (Johnson Matthey Chemical Limited), was used without further purification. Aqueous solution of lithium perchlorate was prepared as described previously.[2]

Kinetic Runs. All the kinetic runs were carried out under pseudo-first-order condition with the molybdenum(V)

complex in at least ten fold excess to the oxidant. The oxidation with $[Ir^{IV}Cl_6]^{2-}$ was studied by the stopped-flow method. The decrease in the concentration of $[Ir^{IV}Cl_6]^{2-}$ was followed by using its absorption peak at 487 nm (ε= 4070 M^{-1} cm^{-1}).[4] The rate of oxidation with $[(NH_3)_5Co^{III}(\mu\text{-}O_2^{(-)})Co^{III}(NH_3)_5]^{5+}$ was markedly affected by the ionic strength of aqueous solution. The conventional spectrophotometry and the stopped-flow method were used for reactions at I=2.0 and 0.1 M, respectively. The decrease in the concentration of $[(NH_3)_5Co^{III}(\mu\text{-}O_2^{(-)})Co^{III}(NH_3)_5]^{5+}$ was followed by using its absorption peak at 670 nm (ε= 832 M^{-1} cm^{-1}).[8] The rate of oxidation with $[(en)_2Co^{III}(\mu\text{-}NH_2,O_2^{(-)})Co^{III}(en)_2]^{4+}$ was followed by the stopped-flow method by using its absorption peak at 690 nm (ε= 485 M^{-1} cm^{-1}).[7] Errors for the activation parameters were determined by the least squares treatment with a confidence level 0.95.

Measurements. A Hitachi 124 spectrophotometer with a Hitachi recorder QPD-34 and a Union-Giken RA-401 stopped-flow spectrophotometer were used for kinetic measurement. The acid dissociation constant of $[Mo^{V}_2O_4(hedta)(H_2O)]^-$ was determined by the pH titration with a Model E300B pH meter of Metrohm Herisau, which was standardized against perchloric acid solutions in 2.0 and 0.1 M $LiClO_4$ to find the concentration rather than the activity of hydrogen ions.

Results

Preliminary Studies. The binuclear complex anion $[Mo^{V}_2O_4(hedta)(H_2O)]^-$ undergoes acid hydrolysis in aqueous perchloric acid solution ($[H^+]>0.5$ M).[6] The complex is oxidized with $[Ir^{IV}Cl_6]^{2-}$, $[(NH_3)_5Co^{III}(\mu\text{-}O_2^{(-)})Co^{III}(NH_3)_5]^{5+}$, and $[(en)_2Co^{III}(\mu\text{-}NH_2,O_2^{(-)})Co^{III}(en)_2]^{4+}$ in aqueous solution. The μ-hyperoxo complex $[(NH_3)_5Co^{III}(\mu\text{-}O_2^{(-)})Co^{III}(NH_3)_5]^{5+}$ decomposes slowly in aqueous solutions containing less than 0.01 M H^+.[2] The other two oxidants are stable over the pH range 1—5.8. Stoichiometries of the oxidation with $[Ir^{IV}Cl_6]^{2-}$ and with $[(NH_3)_5Co^{III}(\mu\text{-}O_2^{(-)})Co^{III}(NH_3)_5]^{5+}$ were determined in 0.01 M perchloric acid solution at 25 °C. Solutions were prepared to contain 2 to 10 fold excess (in molar ratio of the complex ions) of the oxidant to the molybdenum complex (*ca.* 5×10^{-4} M). The amount of unreacted oxidant was estimated as soon as the redox reaction was completed, so that the error caused by the slow decomposition of the oxidant was minimized. Two moles of both oxidants are consumed per one mole of the molybdenum complex. The overall reaction can be written similarly to that of the oxidation of $[Mo^{V}_2O_4(edta)]^{2-}$ with these oxidants.[2,4]

$$[Mo^{V}_2O_4(hedta)(H_2O)]^- + 2[Ir^{IV}Cl_6]^{2-} \longrightarrow 2\text{"Mo(VI)"} + \text{"HEDTA"} + 2[Ir^{III}Cl_6]^{3-} \quad (1)$$

$$[Mo^{V}_2O_4(hedta)(H_2O)]^- + 2[(NH_3)_5Co^{III}(\mu\text{-}O_2^{(-)})Co^{III}(NH_3)_5]^{5+} \longrightarrow 2\text{"Mo(VI)"} + \text{"HEDTA"} + 4\text{"Co(II)"} + 2O_2 + 20NH_4^+. \quad (2)$$

Here, "Mo(VI)" and "Co(II)" represent Mo(VI) and Co(II) species, respectively, present in the solution, whose structures are not specified. "HEDTA" represents variously protonated forms of the ligand which would possibly coordinate to Mo(VI) and/or Co(II) under the given conditions.

Kinetics of the Oxidation with $[Ir^{IV}Cl_6]^{2-}$. This was studied at I=0.1 M for most runs and at 25—45 °C. First-order plots $\log(OD_t-OD_\infty)$ *vs.* t gave excellent straight lines up to almost completion of the reaction, where OD_t stands for the absorbance at 487 nm at time t. The first-order rate constant, k_{obsd}, was not affected by the concentration of $[Ir^{IV}Cl_6]^{2-}$ (hereafter $[Ir^{IV}]$) (1.89×10^{-5}—9.90×10^{-5} M) at $[H^+]$=0.1 and $10^{-5.1}$ M. Values of k_{obsd} at a given $[H^+]$ are proportional to the concentration of $[Mo^{V}_2O_4(hedta)(H_2O)]^-$ (hereafter $[Mo_2]$) (5.22×10^{-4}—4.28×10^{-3} M), and expressed by Eq. 3. The

$$-d[Ir^{IV}]/dt = k_{obsd}[Ir^{IV}] = k_1[Mo_2][Ir^{IV}] \quad (3)$$

dependence of k_1 on $[H^+]^{-1}$ ($[H^+]$=0.01—0.10 M) is given in Fig. 1. The plot gives a straight line with a small intercept (Fig. 1(a)), as formulated by Eq. 4.

$$k_1 = k_2 + k_3[H^+]^{-1}. \quad (4)$$

Values of k_2 and k_3 are 45±17 M^{-1} s^{-1} and 16.5±0.4 s^{-1} at 25 °C, and 58±32 M^{-1} s^{-1} and 27.7±0.7 s^{-1} at 35 °C, respectively.

The k_1 value increases further in lower $[H^+]$ regions to reach a limiting value (k_4) at about $[H^+]=10^{-4.5}$ M (Fig. 1(b)). Values of k_4 at $[H^+]=10^{-5.1}$ M are 2.22×10^4, 2.95×10^4, 4.08×10^4, 4.83×10^4, and 6.86×10^4 M^{-1} s^{-1} at 25, 30, 35, 40, and 45 °C, respectively. Activation parameters are ΔH^*=38±8 kJ mol^{-1} and ΔS^*=−29±29 J K^{-1} mol^{-1}. The effect of ionic strength was briefly investigated; k_4 values at I=0.5 and 1.0 M at $[H^+]=10^{-5.1}$ M are 3.42×10^4 and 4.23×10^4 M^{-1} s^{-1}, respectively, at 25 °C.

Kinetics of the Oxidation with $[(NH_3)_5Co^{III}(\mu\text{-}O_2^{(-)})Co^{III}(NH_3)_5]^{5+}$ *at Ionic Strength 2.0 M.* This was studied at 10—30 °C and $[H^+]$=0.01—0.30 M. First-order plots, $\log(OD_t')$ *vs.* t, were linear to more than 90% of the course of reaction for most runs, where

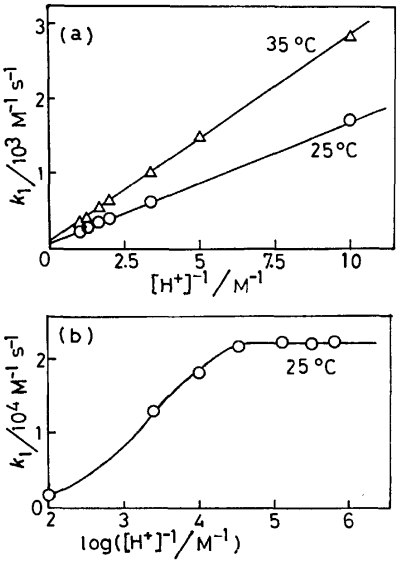

Fig. 1. The dependence of second-order rate constants, k_1, on $[H^+]^{-1}$ for the oxidation of $[Mo^{V}_2O_4(hedta)(H_2O)]^-$ with $[Ir^{IV}Cl_6]^{2-}$ at I=0.1 M ($LiClO_4$), (a) in aqueous perchloric acid solutions and (b) in acetate buffer solutions.

OD_t' stands for the absorbance at 670 nm at time t. The first-order rate constant, k_{obsd}, was not affected by the concentration of $[(NH_3)_5Co^{III}(\mu\text{-}O_2^{(-)})Co^{III}(NH_3)_5]^{5+}$ (hereafter $[\mu\text{-}O_2^{(-)}]$) ($(2.96-8.05)\times 10^{-4}$ M). First-order plot at $[H^+]=0.3$ M was not linear, probably due to acid hydrolysis of the oxidant,[6] and k_{obsd} was obtained from the initial part of the plot.

The k_{obsd} value depends linearly on $[Mo_2]$ at a given $[H^+]$ (Fig. 2), and is reciprocally dependent on $[H^+]$ at given concentrations of the reactants (Fig. 3). The rate law is expressed by Eq. 5. Values of

$$-d[\mu\text{-}O_2^{(-)}]/dt = k_{obsd}[\mu\text{-}O_2^{(-)}] = k_5[H^+]^{-1}[Mo_2][\mu\text{-}O_2^{(-)}] \quad (5)$$

k_5 are 3.17×10^{-2}, 6.39×10^{-2}, 0.100, 0.147, and 0.222 s^{-1} at 10.5, 16.0, 22.0, 25.5, and 30.0 °C, respectively. Activation parameters are $\Delta H^*=67\pm8$ kJ mol^{-1} and $\Delta S^*=-38\pm29$ J K^{-1} mol^{-1}.

Kinetics of the Oxidation with $[(NH_3)_5Co^{III}(\mu\text{-}O_2^{(-)})Co^{III}(NH_3)_5]^{5+}$ at Ionic Strength 0.1 M. This was studied at 25 and 30.6 °C and $[H^+]=0.02$—0.10 M. First-order plots deviated from straight lines for the initial part of the reaction for *ca.* 1 s regardless of reactant concentrations and of $[H^+]$. The first-order rate constant (k_{obsd}) was obtained from the linear part of the plot. The dependence of k_{obsd} on $[Mo_2]$ at a given $[H^+]$ was not linear (Fig. 4), but plot of k_{obsd}^{-1} *vs.* $[Mo_2]^{-1}$ gave a straight line with a positive intercept at each $[H^+]$. Therefore, k_{obsd} can be expressed by Eq. 6 at a given $[H^+]$. Values of x and

$$k_{obsd}^{-1} = x + y[Mo_2]^{-1} \quad (6)$$

y were obtained from 52 kinetic runs and their dependences on $[H^+]$ are shown in Figs. 5 and 6.

Kinetics of the Oxidation with $[(en)_2Co^{III}(\mu\text{-}NH_2,O_2^{(-)})Co^{III}(en)_2]^{4+}$. This was studied briefly at $[H^+]=10^{-5.1}$ and $10^{-5.8}$ M, $I=0.1$ M and at 25 °C. First-order plots gave good straight lines up to almost completion of the reaction. The k_{obsd} values for $[Mo_2]=1.04\times10^{-3}$ M at $[H^+]=10^{-5.1}$ and $10^{-5.8}$ M are 11.1 and 11.6 s^{-1}, respectively, suggesting that the dependence on $[H^+]$ is negligible in this $[H^+]$ range. The dependence of k_{obsd} on $[Mo_2]$ ($[Mo_2]=5.19\times10^{-4}$—3.11×10^{-3} M; [oxidant]$=9.24\times10^{-5}$ M) con-

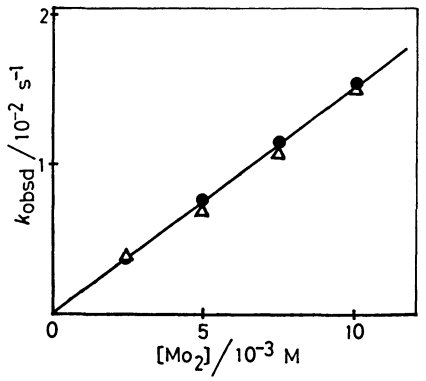

Fig. 2. The dependence of k_{obsd} on $[Mo_2^{V}O_4(hedta)(H_2O)^-]$ for the oxidation of $[Mo_2^{V}O_4(hedta)(H_2O)]^-$ with $[(NH_3)_5Co^{III}(\mu\text{-}O_2^{(-)})Co^{III}(NH_3)_5]^{5+}$ in 0.1 M $HClO_4$ solution at 25 °C and $I=2.0$ M. $[\mu\text{-}O_2^{(-)}]=5.21\times10^{-4}$ (●) and 2.96×10^{-4} M (△).

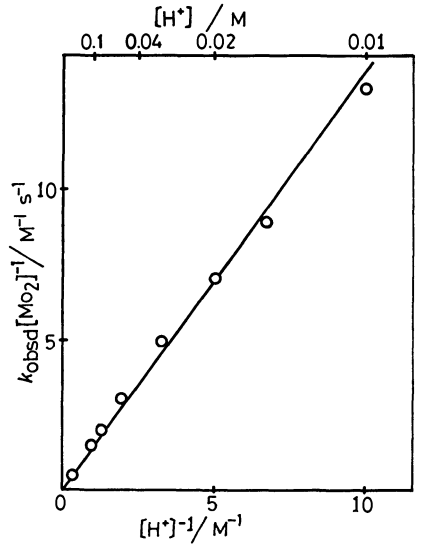

Fig. 3. The dependence of $k_{obsd}/[Mo_2]$ on $[H^+]^{-1}$ for the oxidation of $[Mo_2^{V}O_4(hedta)(H_2O)]^-$ with $[(NH_3)_5Co^{III}(\mu\text{-}O_2^{(-)})Co^{III}(NH_3)_5]^{5+}$ at 25 °C and $I=2.0$ M with $[Mo_2^{V}]$ in large excess.

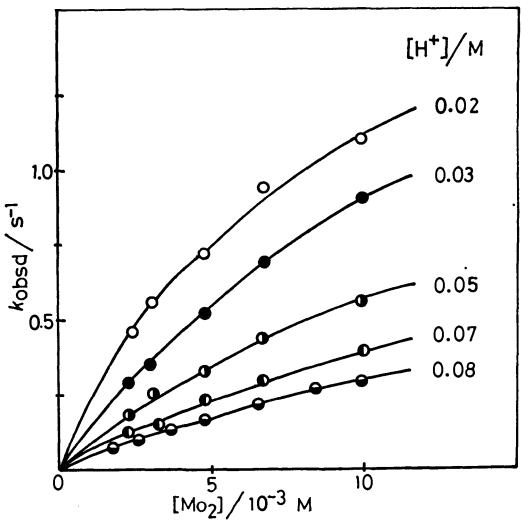

Fig. 4. The dependence of k_{obsd} on $[Mo_2^{V}O_4(hedta)(H_2O)^-]$ for the oxidation of $[Mo_2^{V}O_4(hedta)(H_2O)]^-$ with $[(NH_3)_5Co^{III}(\mu\text{-}O_2^{(-)})Co^{III}(NH_3)_5]^{5+}$ at $I=0.1$ M in aqueous perchlorate media ($HClO_4$–$LiClO_4$) at 25 °C and $[\mu\text{-}O_2^{(-)}]=3.0\times10^{-4}$ M.

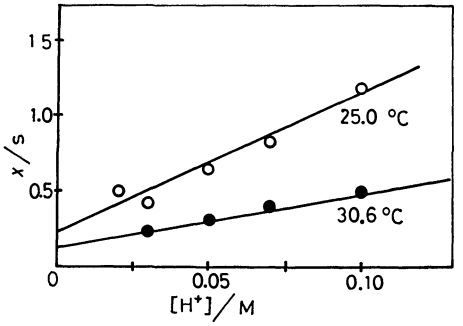

Fig. 5. The dependence of x on $[H^+]$ for the oxidation of $[Mo_2^{V}O_4(hedta)(H_2O)]^-$ with $[(NH_3)_5Co^{III}(\mu\text{-}O_2^{(-)})Co^{III}(NH_3)_5]^{5+}$ at $I=0.1$ M.

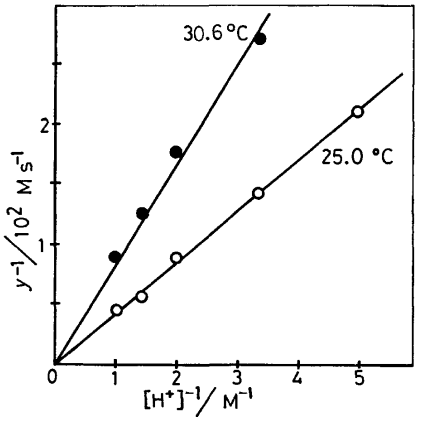

Fig. 6. The dependence of y^{-1} on $[H^+]^{-1}$ for the oxidation of $[Mo^{V}_2O_4(hedta)(H_2O)]^-$ with $[(NH_3)_5Co^{III}(\mu\text{-}O_2^{(-)})Co^{III}(NH_3)_5]^{5+}$ at I=0.1 M.

formed to the rate law (6). Values of x and y at $[H^+]=10^{-5.1}$ M are $(1.7\pm0.6)\times10^{-2}$ s and $(7.9\pm0.6)\times10^{-5}$ M^{-1} s, respectively.

Effect of Added Halide Ions. The effect of added chloride and bromide ions was studied with $[(NH_3)_5Co^{III}(\mu\text{-}O_2^{(-)})Co^{III}(NH_3)_5]^{5+}$ as oxidant at given concentrations of the reactants (Table 1). The pseudo-first-order rate constant becomes smaller on addition of halide ions. Various conditions shown in the footnote of Table 1 do not seem to change the degree of influence by the halide ions.

The pK_a Value of $[Mo^{V}_2O_4(hedta)(H_2O)]^-$. Values of p$K_a$ of this complex are 3.10 and 3.25 at 25 °C and I=0.1 and 2.0 M, respectively. The latter value was carefully determined, since it is clearly different from our previously determined value (3.02);[6] the value should therefore be revised to 3.25. At 35 °C pK_a is 3.18 (I=0.1 M).

Table 1. The effect of halide ions on the rate of oxidation of $[Mo^{V}_2O_4(hedta)(H_2O)]^-$ with $[(NH_3)_5Co^{III}(\mu\text{-}O_2^{(-)})Co^{III}(NH_3)_5]^{5+}$ at 25 °C[a]

Halide ion (X^-)	$[X^-]$/M	$k_{obsd}/10^3$ s^{-1}
Cl^-	0	6.70[b]
	0.1	6.35[b]
	0.5	4.37[b]
	0.5	4.00[c]
	0.5	4.02[d]
	0.5	4.02[e]
Br^-	0.5	4.46[b]

a) I=2.0 M ($LiClO_4$), $[H^+]$=0.10 M ($HClO_4$), $[Mo_2]=5\times10^{-3}$ M, $[\mu\text{-}O_2^{(-)}]=5\times10^{-4}$ M. b) The μ-hyperoxo complex solution containing lithium halide was mixed with the molybdenum solution to cause the electron transfer to start. c—e) The μ-hyperoxo complex solution was mixed with the molybdenum complex solution containing lithium chloride to cause the electron transfer reaction to start. Lithium chloride was added to the molybdenum complex solution c) 40 m, d) 220 m, and e) 345 m before the redox reagents were mixed.

Discussion

Interpretation of Kinetic Data. None of the three oxidants is likely to be protonated or deprotonated in the pH range employed. Therefore, the pH dependence of the oxidation rate should be interpreted by considering the protonation-deprotonation equilibrium of the reductant. A consideration similar to those for the oxidation[2,4] of $[Mo^{V}_2O_4(edta)]^{2-}$ suggests that the oxidation of the first molybdenum(V) ion in the dimer is the rate-determining step, which is followed by a rapid oxidation of the second molybdenum(V) ion.

The Oxidation with $[Ir^{IV}Cl_6]^{2-}$: Kinetic data were most reasonably interpreted in terms of the following mechanism.

$$[Mo^{V}_2O_4(hedta)(H_2O)]^- + [Ir^{IV}Cl_6]^{2-} \xrightarrow{k_{(a)}} \text{“}Mo^{V}Mo^{VI}\text{”} + [Ir^{III}Cl_6]^{3-}$$

$$K_a \downarrow\uparrow$$

$$[Mo^{V}_2O_4(hedta)(OH)]^{2-} + [Ir^{IV}Cl_6]^{2-} \xrightarrow{k_{(b)}} \text{“}Mo^{V}Mo^{VI}\text{”} + [Ir^{III}Cl_6]^{3-}$$

Rate law (7) is obtained for this mechanism. A

$$d[Ir^{IV}]/dt = \{2(k_{(a)}[H^+]+K_ak_{(b)})[Mo_2][Ir^{IV}]\}/(K_a+[H^+]) \quad (7)$$

comparison with the experimental rate law (4) indicates that $k_{(a)}$ and $K_ak_{(b)}$ correspond to $k_2/2$ and $k_3/2$, respectively, under the condition $K_{(a)}\ll[H^+]$. The term $k_{(b)}$ should correspond to $k_4/2$, since $k_{(a)}[H^+]$ is negligible as compared with $K_ak_{(b)}$ at $[H^+]\ll K_a$. The K_a values determined by the pH titration and the observed k_3 values give $k_{(b)}$ as 1.04×10^4 and 2.09×10^4 M^{-1} s^{-1} at 25 and 35 °C, respectively. These values are in excellent agreement with the experimentally obtained $k_4/2$ values at given temperatures. Also the pK_a values (3.13 and 3.17 at 25 and 35 °C, respectively) calculated from the observed values of k_3 and k_4 are in good agreement with those determined by the pH titration. These facts support the proposed mechanism. Activation parameters for $k_4/2$ must correspond to those for $k_{(b)}$ ($\Delta H^*=38\pm8$ kJ mol^{-1}, $\Delta S^*=-42\pm29$ J K^{-1} mol^{-1}). Those for $k_{(a)}$ were not obtained because of big uncertainty in k_2 values.

The Oxidation with $[(NH_3)_5Co^{III}(\mu\text{-}O_2^{(-)})Co^{III}(NH_3)_5]^{5+}$: The marked influence of ionic strength upon the rate suggests the importance of electrostatic interaction of the charged redox couple. The kinetics can be more precisely discussed at lower ionic strengths where such an interaction is expected to be stronger.

The observed rate law at I=0.1 M (Eq. 6) is consistent with a mechanism involving an ion-pair formation prior to electron transfer. Thus, the following mechanism is considered.[10] The terms $K_{IP(a)}$ and $K_{IP(b)}$ stand for the ion-pair formation constants for the original complex and its conjugate base, respec-

$$[Mo^{V}_{2}O_4L(H_2O)]^- + [\mu\text{-}O_2^{(-)}]^{5+} \overset{K_{IP(a)}}{\rightleftharpoons} [Mo_2O_4L(H_2O)\cdots\mu\text{-}O_2^{(-)}]^{4+} \xrightarrow{k_{e(a)}}$$
$$K_a \Big\downarrow\Big\uparrow \qquad\qquad K_a' \Big\downarrow\Big\uparrow \quad \text{(IP(a))}$$
$$[Mo^{V}_{2}O_4L(OH)]^{2-} + [\mu\text{-}O_2^{(-)}]^{5+} \overset{K_{IP(b)}}{\rightleftharpoons} [Mo_2O_4L(OH)\cdots\mu\text{-}O_2^{(-)}]^{3+} \xrightarrow{k_{e(b)}}$$
$$\text{(IP(b))}$$

tively, L^{3-} is $hedta^{3-}$, and $k_{e(a)}$ and $k_{e(b)}$ are the rate constants for the electron transfer within the ion-pairs, IP(a) and IP(b), respectively. The following rate law is derived for this mechanism. Thus, k_{obsd} is expressed by Eq. 9. The terms x and y in Eq. 6

$$-\frac{d[\mu\text{-}O_2^{(-)}]}{dt} = \frac{2\{k_{e(a)}K_{IP(a)}[H^+]+k_{e(b)}K_{IP(b)}K_a\}[Mo_2][\mu\text{-}O_2^{(-)}]}{K_a+[H^+]+\{K_{IP(a)}[H^+]+K_{IP(b)}K_a\}[Mo_2]} \quad (8)$$

$$k_{obsd} = \frac{2\{k_{e(a)}K_{IP(a)}[H^+]+k_{e(b)}K_{IP(b)}K_a\}[Mo_2]}{K_a+[H^+]+\{K_{IP(a)}[H^+]+K_{IP(b)}K_a\}[Mo_2]} \quad (9)$$

are expressed by Eqs. 10 and 11, respectively. Since $K_a \ll [H^+]$, Eq. 11 is rearranged to Eq. 12. A plot

$$x = \{K_{IP(a)}[H^+]+K_{IP(b)}K_a\}/2\{k_{e(a)}K_{IP(a)}[H^+] + k_{e(b)}K_{IP(b)}K_a\} \quad (10)$$

$$y = (K_a+[H^+])/2\{k_{e(a)}K_{IP(a)}[H^+]+k_{e(b)}K_{IP(b)}K_a\} \quad (11)$$

$$y^{-1} = 2\{k_{e(a)}K_{IP(a)}+k_{e(b)}K_{IP(b)}K_a[H^+]^{-1}\} \quad (12)$$

of experimental y^{-1} against $[H^+]^{-1}$ gives a straight line without intercept (Fig. 6). This fact suggests that $k_{e(a)}K_{IP(a)}$ is negligible as compared with $k_{e(b)} \times K_{IP(b)}K_a[H^+]^{-1}$ and x is rewritten to Eq. 13. A plot

$$x = \{K_{IP(a)}[H^+]/2k_{e(b)}K_{IP(b)}K_a\} + 1/(2k_{e(b)}) \quad (13)$$

of x against $[H^+]$ gives a straight line (Fig. 5). All the parameters are obtained as follows by use of the K_a value (7.9×10^{-4} M) at I=0.1 M and 25 °C: $K_{IP(a)}$= 40.5 M^{-1}, $K_{IP(b)}$=1046 M^{-1}, $k_{e(a)}$ not observed, and $k_{e(b)}$=2.56 s^{-1} at 25 °C; $K_{IP(a)}$=30 M^{-1}, $K_{IP(b)}$=1100 M^{-1}, $k_{e(a)}$ not observed, and $k_{e(b)}$=4.3 s^{-1} at 35 °C. These values are subject to nearly 50% uncertainty because of such a complicated analysis. No further trials for obtaining their temperature dependence were made. Nevertheless, the results provide additional example of first-order rate constant for the electron transfer within an ion-pair.[2,3,11,12]

For the reaction at I=2.0 M, the following assumptions are required to obtain a rate law which is of a form similar to the experimentally obtained rate law, Eq. 5: (i) the third term in the denominator of Eq. 9 is negligible (reasonable since the ion-pair formation at higher ionic strengths is expected to be less significant); (ii) $k_{e(a)}K_{IP(a)}$ is negligible as compared with $k_{e(b)}K_{IP(b)}K_a[H^+]^{-1}$ (this relation is experimentally derived at I=0.1 M (*vide supra*)); (iii) K_a is negligible as compared with $[H^+]$ (experimental condition). Under these assumptions Eq. 9 is simplified to Eq. 14.

$$k_{obsd} = 2k_{e(b)}K_{IP(b)}K_a[H^+]^{-1}[Mo_2] \quad (14)$$

The product $k_{e(b)}K_{IP(b)}K_a$ is 7.35×10^{-2} s^{-1} at 25.5 °C, thus $k_{e(b)}K_{IP(b)}$ is estimated to be 2.97×10^4 M^{-1} s^{-1} by use of the pK_a value (3.25).

The Oxidation with $[(en)_2Co^{III}(\mu\text{-}NH_2,O_2^{(-)})Co^{III}(en)_2]^{4+}$: The molybdenum(V) dimer is present almost entirely in the conjugate base form, $[Mo^{V}_{2}O_4(hedta)(OH)]^{2-}$, at $[H^+]=10^{-5.1}$ and $10^{-5.8}$ M. The following scheme is consistent with the kinetic behavior of the system (Eq. 6). The following rate law 15

$$[Mo^{V}_{2}O_4(hedta)(OH)]^{2-} + [\mu\text{-}NH_2,O_2^{(-)}]^{4+} \overset{K_{IP(c)}}{\rightleftharpoons} \text{IP(c)} \xrightarrow{k_{e(c)}} \text{products}$$

is derived for this mechanism. A comparison of Eq. 15 with Eq. 6 leads to the values $K_{IP(c)}=210\pm90$

$$k_{obsd} = 2k_{e(c)}K_{IP(c)}[Mo_2]/\{1+K_{IP(c)}[Mo_2]\} \quad (15)$$

M^{-1} and $k_{e(c)}=30\pm10$ s^{-1} at I=0.1 M and at 25 °C.

Ion-pair Formation Constants. The ion-pair formation constant between $[(NH_3)_5Co^{III}(\mu\text{-}O_2^{(-)})Co^{III}(NH_3)_5]^{5+}$ and $[Mo^{V}_{2}O_4(hedta)(OH)]^{2-}$ at I=0.1 M (1046 M^{-1} at 25 °C) is *ca.* 4 times bigger than that between the $\mu\text{-}O_2^{(-)}$ complex and $[Mo^{V}_{2}O_4(edta)]^{2-}$ (270 M^{-1} at 40 °C).[2] The electronic charge may be more localized in $[Mo^{V}_{2}O_4(hedta)(OH)]^{2-}$ than in the more symmetrical edta complex. Such a locarization would produce a more negatively charged site within the complex anion, at which the ion-pair formation would be more extensive.

Reaction Mechanism. Present reactions must proceed *via* the outer-sphere mechanism for the following reasons. The oxidation of $[Mo^{V}_{2}O_4(edta)]^{2-}$ with $[Ir^{IV}Cl_6]^{2-}$ and with $[(NH_3)_5Co^{III}(\mu\text{-}O_2^{(-)})Co^{III}(NH_3)_5]^{5+}$ are believed to occur by the outer-sphere mechanism, since these oxidants are unable to coordinate to the molybdenum(V) unless the edta ligand is partially displaced.[2,4,13] The present hedta complex has a coordinated water, for which the oxidant can substitute. The remarkable increase in the rate of oxidation on changing from $[Mo^{V}_{2}O_4(hedta)(H_2O)]^-$ to its conjugate base, $[Mo^{V}_{2}O_4(hedta)(OH)]^{2-}$, does not support the inner-sphere mechanism, however, since the OH^- ligand is more strongly coordinated than H_2O and should be less easily dissociated from the metal ion.[14] There seems to be no example that μ-hyperoxo-dicobalt(III) complexes behave as inner-sphere oxidants.[3,16]

The Marcus theory predicts that when a series of oxidants are reduced by two different reductants *via* the outer-sphere process, ratio of the two rate constants should be similar for all members of the series.[17,18] Such ratios are often used as a diagnostic criterion for assigning redox reactions involving chromium(II), vanadium(II), *etc.* as proceeding by an outer-sphere mechanism.[19] Ratios of the oxidation rate of $[Mo^{V}_{2}O_4(hedta)(OH)]^{2-}$ to that of $[Mo^{V}_{2}O_4(edta)]^{2-}$ ($k_{hedta(OH)}/k_{edta}$) are listed in Table 2. Ratios for the two oppositely charged oxidants are within one order of magnitude, and can be taken as an evidence for the outer-sphere mechanism for the present reactions.

Table 2. Ratios of the rate constant for the oxidation of $[Mo^{V}_{2}O_4(hedta)(OH)]^{2-}$ ($k_{hedta(OH)}$) to that of $[Mo^{V}_{2}O_4(edta)]^{2-}$ (k_{edta}) with the given oxidant at 25 °C

Oxidant	I/M	Order of the rate constant	$k_{hedta(OH)}/k_{edta}$
$[Ir^{IV}Cl_6]^{2-}$	1.0	second-order[b]	3.9×10^3
$[\mu\text{-}O_2^{(-)}]^{5+}$ [a]	0.1	first-order (k_e)[c]	9.8×10^3
	2.0	second-order (k_eK_{IP})[c]	29.7×10^3

a) $[\mu\text{-}O_2^{(-)}]^{5+}=[(NH_3)_5Co^{III}(\mu\text{-}O_2^{(-)})Co^{III}(NH_3)_5]^{5+}$. b) The $k_{hedta(OH)}$ value at $I=0.1$ M was estimated from those at $I=0.1$ and 2.0 M, to be 3.9×10^4 M^{-1} s^{-1}. c) The k_{edta} values at 25 °C were calculated from the activation parameters in Ref. 2, to be 2.60×10^{-4} s^{-1} and 8.81×10^{-3} M^{-1} s^{-1} at $I=0.1$ and 2.0 M, respectively.

Ratio of the first-order rate constants k_e for the oxidation with $[(NH_3)_5Co^{III}(\mu\text{-}O_2^{(-)})Co^{III}(NH_3)_5]^{5+}$ at $I=0.1$ M is *ca.* 3 times smaller than that of k_eK_{IP} at $I=2.0$ M, where k_e and K_{IP} values cannot be obtained separately. The difference in K_{IP} values should be responsible for such a difference in the ratios. This fact indicates that electrostatic interactions should significantly affect the ratio of the redox rates which are usually obtained as a product of k_e and K_{IP}.

Comparison with Other Reactions. Rate of the Reaction: The second-order rate constants of the oxidations of $Mo^{V}_{2}O_4^{2+}$-complexes with $[Ir^{IV}Cl_6]^{2-}$, $[Fe^{III}(phen)_3]^{3+}$, $[(NH_3)_5Co^{III}(\mu\text{-}O_2^{(-)})Co^{III}(NH_3)_5]^{5+}$, and $[(en)_2Co^{III}(\mu\text{-}NH_2,O_2^{(-)})Co^{III}(en)_2]^{4+}$ are summarized in Table 3. The following sequence is given for the decrease in oxidation rate. This sequence suggests

$[Mo^{V}_{2}O_4(hedta)(OH)]^{2-} > [Mo^{V}_{2}O_4(hedta)(H_2O)]^{-}$
$> [Mo^{V}_{2}O_4(edta)]^{2-} > [Mo^{V}_{2}O_4(H_2O)_n]^{2+}$

($[Mo^{V}_{2}O_4(OH)(H_2O)_{n-1}]^{+}$ must be more reactive than $[Mo^{V}_{2}O_4(hedta)(H_2O)]^{-}$)

that the total charge of the complex is not important in determining the rate. The two hydroxo complexes are significantly more reactive than thier conjugate acids. A possible interpretation may be that the stronger Lewis base, the hydroxide, makes the metal ion more negative and more electron donating. Outer-sphere oxidations of $[V^{III}(H_2O)_6]^{3+}$,[20] $[V^{IV}O(H_2O)_n]^{2+}$,[21] $[V^{IV}O(pmida)(H_2O)]$ ($H_2pmida=N$-(2-pyridylmethyl)-iminodiacetic acid),[22] $[V^{IV}O(nta)(H_2O)]^{-}$ (H_3nta =nitrilotriacetic acid),[22] and $[Ti^{III}(H_2O)_6]^{3+}$ [23,24] with various oxidants exhibit predominant rate-terms proportional to $[H^+]^{-1}$. The products in all of these reactions are mono- or dioxo metal ions; the number of oxo ligands increases and protons are reliesed on the oxidation. Such a structural requirement was claimed to be responsible for the higher reactivity of conjugate bases of these complexes.[24] A similar interpretation may be applied to the oxidation of $Mo^{V}_{2}O_4^{2+}$-complexes, although the rate-determining electron-transfer gives a mixed valence (V, VI) dimer as an immediate product, the structure of which is not known.

Activation Parameters: Table 4 shows that $\Delta H^{\neq}$ for $[Mo^{V}_{2}O_4(hedta)(OH)]^{2-}$ is significantly smaller than that for $[Mo^{V}_{2}O_4(edta)]^{2-}$ whenever a common oxidant is used. The big difference in oxidation rate between these two complexes seems to be due to the difference in $\Delta H^{\neq}$ rather than $\Delta S^{\neq}$.

The activation entropy for a given molybdenum(V) complex is more positive and the activation enthalpy is bigger for the oxidation with $[(NH_3)_5Co^{III}(\mu\text{-}O_2^{(-)})Co^{III}(NH_3)_5]^{5+}$ than those for the oxidation with $[Ir^{IV}Cl_6]^{2-}$. Such differences can be explained in terms of the change in solvation accompanied by the encounter complex formation from the separated reactants. Negative $\Delta S^{\neq}$ for redox reactions between reactants with charges of the same sign were claimed to be largely the result of the charge concentration on encounter complex formation, which causes substantial mutual ordering of the solvated water molecules.[25] On the other hand, the positive entropy brought about on the encounter complex (ion-pair) formation between oppositely charged reactants,[2,11] may be attributed to the weakening of solute-solvent interaction by the partial compensation of charges in the ion-pair. The change in $\Delta H^{\neq}$ with the charge of oxidant is more difficult to explain. The contributions of $\Delta H^{\neq}$ and $\Delta S^{\neq}$ to the rate constant seem

Table 3. A comparison of second-order rate constants/M^{-1} s^{-1} at 25 °C for the oxidations of some $Mo^{V}_{2}O_4^{2+}$-complexes with four oxidants

$Mo^{V}_{2}O_4^{2+}$-complexes	Oxidants				Ref.
	$[Ir^{IV}Cl_6]^{2-}$	$[Fe^{III}(phen)_3]^{3+}$	$[\mu\text{-}O_2^{(-)}]^{5+}$ [a]	$[\mu\text{-}NH_2,O_2^{(-)}]^{4+}$ [b]	
$[Mo^{V}_{2}O_4(edta)]^{2-}$	6.6[c]	1.9×10^3 [c]	8.8×10^{-3} [d,e]		2, 4
$[Mo^{V}_{2}O_4(pdta)]^{2-}$				1.87×10^{-1} [f]	3
$[Mo^{V}_{2}O_4(hedta)(OH)]^{2-}$	1.1×10^4 [g]		2.62×10^2 [e]	6.30×10^3 [g]	This work
$[Mo^{V}_{2}O_4(hedta)(H_2O)]^{-}$	2.3×10^1 [f]		5×10^{-2} [e]		This work
$[Mo^{V}_{2}O_4(OH)(H_2O)_{n-1}]^{+}$	$26<$[c,h,i]	$3000<$[c,h,i]	(Not observed)[j]		2, 5
$[Mo^{V}_{2}O_4(H_2O)_n]^{2+}$	5.7×10^{-2} [c]	1.6×10^1 [c]	(Not observed)[j]		2, 5

a) $[(NH_3)_5Co^{III}(\mu\text{-}O_2^{(-)})Co^{III}(NH_3)_5]^{5+}$. b) $[(en)_2Co^{III}(\mu\text{-}NH_2,O_2^{(-)})Co^{III}(en)_2]^{4+}$. c) $I=1.0$ M. d) Calculated from the activation parameters in Ref. 2. e) $I=2.0$ M. f) $I=0.2$ M. g) $I=0.1$ M. h) Estimated on the reasonable assumption that the acid-dissociation constant of $[Mo^{V}_{2}O_4(H_2O)_n]^{2+}$ is less than 10^{-3} M. i) For these reactions, significant part of the redox reaction proceeds *via* a pathway independent of the oxidant concentration.[5] j) The oxidation rate is independent of the concentration of the μ-hyperoxo complex.[2]

Table 4. Activation parameters for the oxidation of the complexes with $Mo^{V}_{2}O_4^{2+}$-core

Oxidant		I/M	$\Delta H^{\ddagger}$/kJ mol^{-1}	$\Delta S^{\ddagger}$/J K^{-1} mol^{-1}	Ref.
$[Ir^{IV}Cl_6]^{2-}$	$[Mo^{V}_{2}O_4(edta)]^{2-}$	1.0	56± 1	−42± 4	4
	$[Mo^{V}_{2}O_4(hedta)(OH)]^{2-}$	0.1	38± 8	−29±29	This work
$[\mu\text{-}O_2^{(-)}]^{5+}$ a)	$[Mo^{V}_{2}O_4(edta)]^{2-}$	0.1 b)	118±17	76±46	2
	$[Mo^{V}_{2}O_4(edta)]^{2-}$	2.0	111± 3	88±13	2
	$[Mo^{V}_{2}O_4(hedta)(OH)]^{2-}$	2.0	80±13	55±42	This work

a) $[(NH_3)_5Co^{III}(\mu\text{-}O_2^{(-)})Co^{III}(NH_3)_5]^{5+}$. b) For the first-order rate constant of the electron-transfer within the ion-pair. c) In evaluating $\Delta H^{\ddagger}$ and $\Delta S^{\ddagger}$, it is assumed that ΔH° and ΔS° for K_a are −8——15 kJ mol^{-1} and −80——100 J K^{-1} mol^{-1}, respectively, which were estimated from the K_a data at 25 and 35 °C as given in the text.

to compensate each other. Such a relationship is more clearly observed for the oxidations of $[V^{IV}O(pmida)(OH)]^{-}$ and $[V^{IV}O(nta)(OH)]^{2-}$ with $[Ir^{IV}Cl_6]^{2-}$ and $[(en)_2Co^{III}(\mu\text{-}NH_2,O_2^{(-)})Co^{III}(en)_2]^{4+}$ (isokinetic relationship is observed).[22] This fact suggests that the factors controlling $\Delta H^{\ddagger}$ must be closely related to those controlling $\Delta S^{\ddagger}$. Therefore, the solvation state of the encounter complex would be important in determining $\Delta H^{\ddagger}$. Activation enthalpy is smaller for redox reactions involving more solvated encounter complexes, and is larger for reactions between oppositely charged reactants which form less solvated encounter complexes.[22]

Reaction Pattern: Existence of a rate-term independent of the oxidant concentration is the characteristic feature of the oxidation of $[Mo^{V}_{2}O_4(OH)(H_2O)_{n-1}]^{+}$ with the three oxidants in Table 3.[2,5] The cleavage of one of the two oxo-bridges to give a single-bridged species was claimed to be the rate-determining step, the OH^{-} ligand being responsible for the bridge cleavage.[2] Chloride ions were found to catalyze markedly the oxidation of $[Mo^{V}_{2}O_4(H_2O)_n]^{2+}$ with $[(NH_3)_5Co^{III}(\mu\text{-}O_2^{(-)})Co^{III}(NH_3)_5]^{5+}$. The chloride ion was reckoned to substitute for the coordinated water and facilitate the bridge cleavage.[2] Such a mechanism is not plausible for the present reaction, since the rate formulae misses the term independent of the oxidant concentration and the positive catalytic effect by the halide ion was not observed. $[Mo^{V}_{2}O_4(H_2O)_n]^{2+}$ and $[Mo^{V}_{2}O_4(hedta)(H_2O)]^{-}$ are oxidized mainly *via* their conjugate bases, but mechanism is different. The present work stresses that the rate and mechanism of oxidations of the complexes with $Mo^{V}_{2}O_4^{2+}$-core depend significantly on the ligand environment.

This work is a part of the project supported by a Grant-in-Aid (511301) which is given to Professor Kazuo Saito from the Ministry of Education, Science and Culture. We are grateful to Professor K. Saito for his constant encouragement and valuable discussions throughout this work. We thank Mr. Susumu Kondo for the preparation of $[(en)_2Co^{III}(\mu\text{-}NH_2,O_2^{(-)})Co^{III}(en)_2]Cl_4\cdot 3H_2O$.

References

1) a) R. A. D. Wentworth, *Coord. Chem. Rev.*, **18**, 1 (1976); b) "Molybdenum Chemistry of Biological Significance", ed by W.E. Newton and S. Otsuka Plenum Press, New York (1980).

2) Y. Sasaki, *Bull. Chem. Soc. Jpn.*, **50**, 1939 (1977).

3) S. Kondo, Y. Sasaki, and K. Saito, *Inorg. Chem.*, **20**, 429 (1981).

4) R. K. Wharton, J. F. Ojo, and A. G. Sykes, *J. Chem. Soc., Dalton Trans.*, **1975**, 1526.

5) G. R. Cayley, R. S. Taylor, R. K. Wharton, and A. G. Sykes, *Inorg. Chem.*, **16**, 1377 (1977).

6) Y. Sasaki and T. S. Morita, *Bull. Chem. Soc. Jpn.*, **50**, 1637 (1977).

7) M. B. Stevenson and A. G. Sykes, *J. Chem. Soc., A*, **1969**, 2293.

8) Y. Sasaki, J. Fujita, and K. Saito, *Bull. Chem. Soc. Jpn.*, **42**, 146 (1969).

9) Transient absorption spectra during the course of the redox reaction measured by a rapid-scanning technique, did not show any evidence for intermediate formation. Since the deviation from the straight line for the first-order plot was small, we did not attempt to find the reason for the behavior further.

10) An alternative mechanism consistent with the rate law 6 is that the μ-hyperoxo complex formed an active intermediate which oxidized the molybdenum(V) dimer (a steady-state treatment for the active intermediate leads to the expected rate law). Although the kinetics of the oxidation with the μ-hyperoxo complexes were studied for various reductants, none of these reactions proceeded through such an active intermediate. Since the mechanism proposed in the text is reasonable, we exclude this alternative mechanism for the present reaction.

11) L. A. A. Oliveira, E. Giesbrecht, and H. E. Toma, *J. Chem. Soc., Dalton Trans.*, **1979**, 236.

12) P. L. Gaus and J. L. Villanueva, *J. Am. Chem. Soc.*, **102**, 4525 (1980), and references therein.

13) The dissociation of edta ligand from $[Mo^{V}_{2}O_4(edta)]^{2-}$ takes place in acid solution ($[H^{+}]>0.5$ M), the rate of which is accelerated as $[H^{+}]$ increases (Y. Sasaki and A. G. Sykes, *J. Chem. Soc., Dalton Trans.*, **1974**, 1468). The oxidation of $[Mo^{V}_{2}O_4(edta)]^{2-}$ is $[H^{+}]$ independent at $[H^{+}]=0.01$—0.10 M, which would not support the inner-sphere precursor complex formation accompanied by partial replacement of the edta ligand.

14) Partial dissociation of the hedta ligand, if occured, can be faster in the conjugate base complex, $[Mo^{V}_{2}O_4(hedta)(OH)]^{2-}$, than in $[Mo^{V}_{2}O_4(hedta)(H_2O)]^{-}$. We do not consider that the electron transfer mechanism involving an inner-sphere precursor formed by the rate-determining partial dissociation of the hedta ligand in $[Mo^{V}_{2}O_4(hedta)(OH)]^{2-}$, is likely, since the activation enthalpies for ligand substitution reactions *via* the conjugate base are usually bigger than 80 kJ mol^{-1},[15] while those for the present reactions are much smaller.

15) See for example, D. Seewald and N. Sutin, *Inorg. Chem.*, **2**, 643 (1963), and D. Thusius, *Inorg. Chem.*, **10**, 1106 (1971).

16) A. G. Sykes, *Chem. Britain*, **10**, 170 (1971).
17) R. A. Marcus, *J. Phys. Chem.*, **67**, 853 (1963).
18) Violation of such a prediction was discussed quantitatively (H.-M. Huck and K. Wieghardt, *Inorg. Chem.*, **19**, 3688 (1980)). The prediction would be valid for the present reactions, however, since the two oxidants have similar redox potentials.[2,5]
19) For example, a) T. D. Hand, M. R. Hyde, and A. G. Sykes, *Inorg. Chem.*, **14**, 1720 (1975); b) E. S. Gould, *Inorg. Chem.*, **18**, 900 (1979), and references therein.
20) R. N. F. Thorneley and A. G. Sykes, *J. Chem. Soc. A*, **1970**, 1307.
21) J. Birk, *Inorg. Chem.*, **16**, 1381 (1977), and references therein.
22) M. Nishizawa, Y. Sasaki, and K. Saito, unpublished results.
23) a) R. Marcec and M. Orhanovic, *Inorg. Chim. Acta*, **37**, 67 (1979); b) B. S. Brunschwig and N. Sutin, *Inorg. Chem.*, **18**, 1731 (1979); c) A. Adegite, J. E. Earley, and J. F. Ojo, *Inorg. Chem.*, **18**, 1535 (1979); d) M. Hery and K. Wieghardt, *Inorg. Chem.*, **17**, 1130 (1978), and references therein.
24) A. Bakac, R. Marcec, and M. Orhanovic, *Inorg. Chem.*, **16**, 3133 (1977), and references therein.
25) M. J. Weaver and E. L. Yee, *Inorg. Chem.*, **19**, 1936 (1980), and references therein.

Studies on Electronic Spectrum and Electron Spin Resonance of Vanadium(IV) Complexes with Organophosphorus Compounds and High Molecular Weight Amines

Taichi SATO* and Takato NAKAMURA

Department of Applied Chemistry, Faculty of Engineering, Shizuoka University, Johoku, Hamamatsu 432

(Received March 5, 1981)

In the extraction of vanadium(IV) from aqueous solutions containing hydrochloric acid and/or a mixture of hydrochloric acid and lithium chloride by bis(2-ethylhexyl) hydrogenphosphate (DEHPA; HX), trioctylmethylammonium chloride (Aliquat-336), trioctylamine (TOA), trioctylphosphine oxide (TOPO) and tributyl phosphate (TBP), the complexes formed in the organic phases have been examined by spectrophotometry and electron spin resonance spectroscopy. It is found that in the extraction by DEHPA, the vanadium in the organic phase exists as the monomeric species, $VO(X_2H)_2$, or the polymeric one, $(VOX_2)_n$, and that in the extractions by Aliquat-336, TOA, TOPO, and TBP, tetravalent vanadium complexes are stable in the organic phases extracted from a mixed solution of hydrochloric acid and lithium chloride, while complexes containing pentavalent vanadium and VOV^{4+} ions are formed in the organic phases extracted from hydrochloric acid solutions.

For the extraction of vanadium(IV) from hydrochloric acid solutions by trioctylmethylammonium chloride (Aliquat-336; $R_3R'NCl$), trioctylamine (TOA, R_3N), trioctylphosphine oxide (TOPO; R_3PO), and tributyl phosphate (TBP; $(RO)_3PO$), the spectral properties of the organic phases have been discussed in a previous paper.[1] The present paper extends the work to the extraction by bis(2-ethylhexyl) hydrogenphosphate (DEHPA; HX; $(RO)_2POOH$), and observations on the difference in the structure among the complexes formed in the organic phase with those acid, basic, and neutral extractants are reported on the basis of the results obtained by spectrophotometry and electron spin resonance (ESR) measurement.

Experimental

Chemicals. DEHPA (Daihachi Chemical Industry Co., Ltd.), Aliquat-336 (General Mills) and TBP (Daihachi Chemical Industry Co., Ltd.) were purified by the usual methods,[2-4] and diluted with hexane or benzene. TOA (Kao Soap Co., Ltd.) and TOPO (Hokko Chemical Industry Co., Ltd.) were used without purification. The vanadium(IV) chloride oxide solutions were prepared by dissolving vanadium(IV) chloride oxide, VCl_2O, in hydrochloric acid solutions of the required concentration. The chemicals used were of analytical reagent grade.

Extraction Procedures. Equal volumes (15 cm^3 each) of the aqueous and organic phases were shaken for 10 min in 50 cm^3 stoppered conical flasks in a thermostated water bath at 20 °C. The mixture was centrifuged and separated, and then the concentrations of vanadium in both phases were determined by edta titration as described already.[5] (In this case vanadium in the organic phase was stripped with 0.1 mol dm^{-3} hydrochloric acid). The complexes were isolated by drying the organic phases *in vacuo* at 50—60 °C.

Spectrophotometrical and ESR Measurements. The electronic spectra were obtained on a Shimadzu Model QV-50 spectrometer, using matched 1.00 cm fused silica cells. ESR spectra were recorded at 20 °C with a high sensitivity X-band spectrometer, designed in the Research Institute of Electronics, Shizuoka University, and at −30 °C with a JEOL JES-PE-3X X-band spectrometer, which operated at about 9.3 GHz using 100 kHz field modulation. Field calibration was checked by using DPPH and MnO doped in MgO. The calculation of ESR derivative line shape was made by using the computers of FACOM 230-45S and MELCOM COSMO 500.[6]

Results and Discussion

Electronic Spectra. The representative electronic spectra of organic phases for the extraction from aqueous hydrochloric acid solutions containing 0.036 mol dm^{-3} vanadium(IV) chloride oxide with 0.05 mol dm^{-3} DEHPA, 0.05 mol dm^{-3} Aliquat-336, 0.05 mol dm^{-3} TOA, 0.05 mol dm^{-3} TOPO, and 0.5 mol dm^{-3} TBP at 20 °C are shown in Fig. 1. The blue organic phase is obtained in the extraction by DEHPA. In the extractions by Aliquat-336, TOA, TOPO, and TBP,

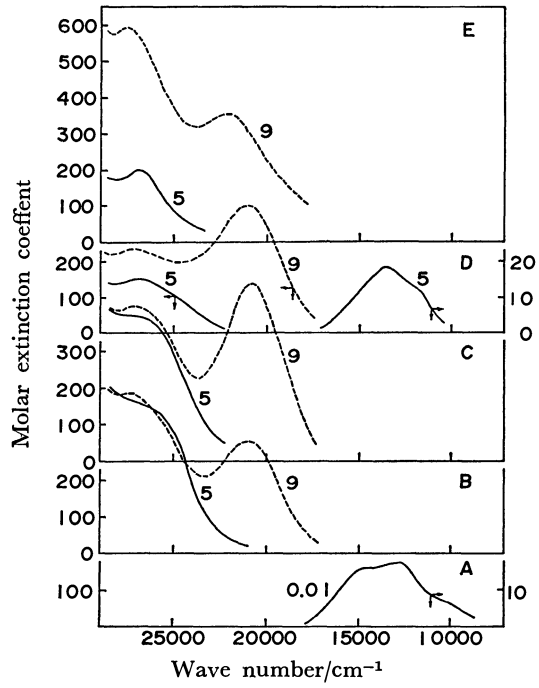

Fig. 1. Electronic spectra of organic phases from the extraction of aqueous solutions containing vanadium (IV) chloride oxide of 0.0036 mol dm^{-3} in hydrochloric acid with 0.05 mol dm^{-3} DEHPA (A), 0.05 mol dm^{-3} Aliquat-336 (B), 0.05 mol dm^{-3} TOA (C), 0.05 mol dm^{-3} TOPO (D), and 0.5 mol dm^{-3} TBP (E) (numerals on curves are hydrochloric acid concentrations in aqueous phase, mol dm^{-3}).

the organic phases depend on the kind of extractants in colour (yellow for Aliquat-336 and TOA, greenish yellow for TOPO, and pale yellow for TBP) at the aqueous hydrochloric acid concentration below 7 mol dm^{-3}, but at higher acidity above 8 mol dm^{-3} redish orange colour is developed in these organic extracts.

The spectra of the organic phases from the extraction by DEHPA, classified as acid extractant, show the d-d bands at 14700 and 12700 cm^{-1} accompanied by a shoulder around 9530 cm^{-1}. From the results obtained previously,[7] it is deduced that their bands rise from those of monomeric species VOX_4H_2 and/or polymeric one $(VOX_2)_n$. In both the complexes, the X^- group is bound to vanadium ion through the oxygen atoms which occupy the corner of a square, implying that the ligand field effect to vanadium ion resemble each other. Assuming that the extracted species is in a point group C_{4v} symmetry, the absorption bands at 14700 and 12700 cm^{-1} are assigned to the transitions $^2B_2 \rightarrow {}^2B_1$ and $^2B_2 \rightarrow {}^2E(I)$, respectively.

In the extractions by Aliquat-336 and TOA, classified as basic extractant, the spectra of yellow organic solutions exhibit no band due to the d-d transition of tetravalent vanadium ion but a band at 26000—27000 cm^{-1}. These organic solutions do not reveal a signal in the ESR experiment. In the extraction from 9 mol dm^{-3} hydrochloric acid solution, the absorption at about 21000 cm^{-1} appears in the spectra of redish orange organic solutions. This band probably arises from binuclear ion VOV^{4+}, which is an intermediate in the reaction between di- and tetravalent vanadium ions.[8] Accordingly it is considered that in the extractions by Aliquat-336 and TOA at the aqueous hydrochloric acid concentration below 7 mol dm^{-3}, the vanadium is oxidized during the extraction process, while the species formed in the extraction at higher acidity exists as a polymer containing ion such as VOV^{4+}.

In the extractions by neutral extractants, the spectra of organic phases for the extraction from 9 mol dm^{-3} hydrochloric acid solution are analogous to those with the basic extractants. In contrast, the spectrum of organic phase from 5 mol dm^{-3} hydrochloric acid solution with TOPO exhibits the absorption bands at 11600, 13500, and 26700 cm^{-1} due to $^2B_2 \rightarrow {}^2B_1$, $^2B_2 \rightarrow {}^2E(I)$, and $^2B_2 \rightarrow {}^2A_1$, respectively, indicating that the complex formed in the organic phase contains tetravalent vanadium ion. In addition the spectrum of the organic phase with TBP reveals a trace of band at about 14000 cm^{-1} similar to that with TOPO, although those absorption bands are hard to assign because of its low extractability.

On the other hand, the spectra of organic phase for the extraction from aqueous solution containing 0.036 mol dm^{-3} vanadium (IV) chloride oxide in a mixture of 0.06 mol dm^{-3} hydrochloric acid and 10 mol dm^{-3} lithium chloride by Aliquat-336, TOA, TOPO, and TBP exhibit the d-d bands in the range of 10000—14000 cm^{-1} (Fig. 2), which are characteristic bands of VO^{2+} ion. In the extraction by TOPO, the spectrum of the organic phase from mixed solution of hydrochloric acid and lithium chloride is similar to that from 5 mol dm^{-3} hydrochloric acid solution

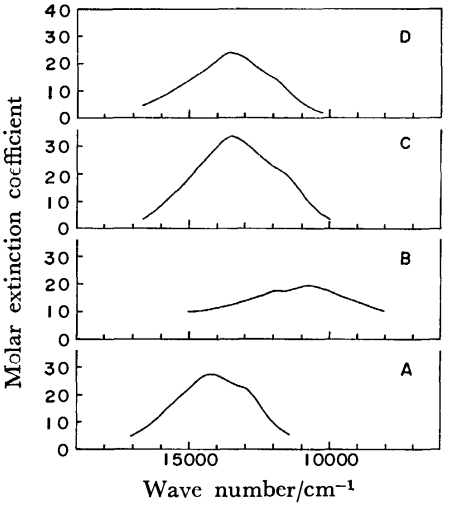

Fig. 2. Electronic spectra of organic phases from the extraction of aqueous solutions containing vanadium (IV) chloride oxide of 0.036 mol dm^{-3} in a mixture of 0.06 mol dm^{-3} hydrochloric acid and 10 mol dm^{-3} lithium chloride with 0.05 mol dm^{-3} Aliquat-336 (A), 0.05 mol dm^{-3} TOA (B), 0.05 mol dm^{-3} TOPO (C), and 0.5 mol dm^{-3} TBP (D) in benzene.

except that the former molar extinction coefficient of the band at 13500 cm^{-1} is larger than the latter one. This implies that the tetra- and pentavalent vanadium complexes coexist in the latter organic phase. In other spectra, the bands are assigned as follows: for Aliquat-336 26500, 14300, and 12800 cm^{-1} to $^2B_2 \rightarrow {}^2A_1$, $^2B_2 \rightarrow {}^2E(I)$, and $^2B_2 \rightarrow {}^2B_1$, respectively; for TOA 26700, 12300, and 10600 cm^{-1} to $^2B_2 \rightarrow {}^2A_1$, $^2B_2 \rightarrow {}^2B_1$, and $^2B_2 \rightarrow {}^2E(I)$, respectively; for TBP 27000, 13500, and 11800 cm^{-1} to $^2B_2 \rightarrow {}^2A_1$, $^2B_2 \rightarrow {}^2E(I)$, and $^2B_2 \rightarrow {}^2B_1$, respectively. As the complexes contained in these organic solutions could be formulated as $VOCl_2 \cdot R_3R'NCl \cdot xH_2O$, $VO(OH)Cl \cdot R_3NHCl$, $VO(OH)Cl \cdot 2R_3PO$, and $VO(OH)Cl \cdot 2(RO)_3PO$, respectively,[1] the following structures are presumed to satisfy an octahedral or square pyramidal coordination:

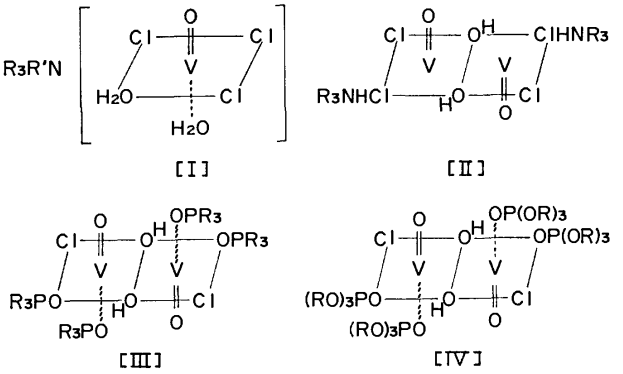

ESR Spectra. ESR spectra of organic phases from the extraction of aqueous solutions containing vanadium(IV) chloride oxide in 0.01 mol dm^{-3} hydrochloric acid with 0.05 mol dm^{-3} DEHPA in hexane at 20 °C are shown in Fig. 3. The well resolved hyperfine line with eight components is observed in the spectrum at the molar ratio of $[DEHPA]/[V]_{org} = 10.2$, which is assigned to that of the monomeric species

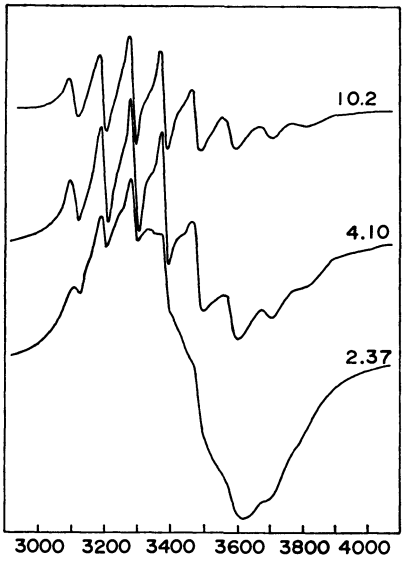

Fig. 3. ESR spectra of the organic phases from the extraction of vanadium(IV) by 0.05 mol dm^{-3} DEHPA in hexane (numerals on curves are the molar ratio of $[HX]/[V]_{org}$).

VOX_4H_2. On the one hand, the spectrum at the molar ratio of $[DEHPA]/[V]_{org}=4.10$ contains the broad line showing no hyperfine structure, and that at the molar ratio of $[DEHPA]/[V]_{org}=2.37$ is so broadened that the hyperfine structure is unresolved, although the spectra of aqueous solutions exhibit hyperfine structure, indicating that the vanadium ion concentration in the aqueous phases before extraction is magnetically diluted. This broadening is probably due to the exchange interaction among the unpaired electrons of vanadium ions, suggesting that the polymeric species is formed in the organic phase by substituting the hydrogen ions of the monomeric species VOX_4H_2 for VO^{2+} ion in the aqueous phase. It is thus considered that the anisotropy in ESR spectrum of the organic extract prepared by drying the organic phase for the extraction of 0.0072 mol dm^{-3} vanadium(IV) chloride oxide solution containing 0.01 mol dm^{-3} hydrochloric acid with 0.05 mol dm^{-3} DEHPA in hexane is due to that of the monomeric species

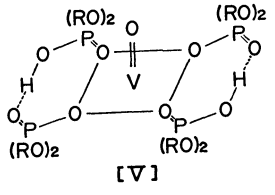

[V]

because of the molar ratio of $[DEHPA]/[V]_{org}=7.14>4$.

In the extraction of aqueous solution containing 0.036 mol dm^{-3} vanadium(IV) chloride oxide in a mixture of 0.06 mol dm^{-3} hydrochloric acid and 10 mol dm^{-3} lithium chloride with 0.05 mol dm^{-3} Aliquat-336, 0.05 mol dm^{-3} TOA, 0.05 mol dm^{-3} TOPO, and 0.5 mol dm^{-3} TBP in benzene, the ESR spectra of the frozen organic phases were measured at −30 °C in order to estimate ESR parameters (Fig. 4), because apparent change in the colour of organic phases was observed during the evaporation of benzene to isolate the complexes by drying. As the transition due to $S_1 \cdot S_2$ is not observed in the spectra of the organic solutions extracted with TOA, TOPO, and TBP, the exchange interaction between vanadium ion in the complexes [II], [III], and [IV] is presumed to be weak and/or less anisotropic. In addition the difference to be expected in the x, y components is not resolved in the spectra. Therefore those spectra can be described by the axially symmetric spin Hamiltonian including the terms of Zeeman and nuclear-electron hyperfine interactions:

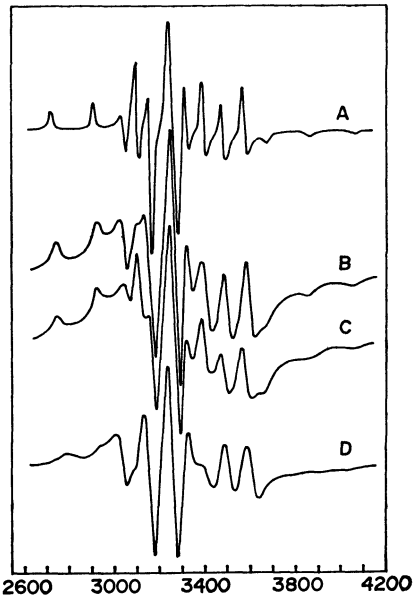

Fig. 4. ESR spectra of frozen organic phases from the extraction of aqueous solutions containing vanadium (IV) chloride oxide of 0.036 mol dm^{-3} in a mixture of 0.06 mol dm^{-3} hydrochloric acid and 10 mol dm^{-3} lithium chloride with 0.05 mol dm^{-3} Aliquat-336 (A), 0.05 mol dm^{-3} TOA (B), 0.05 mol dm^{-3} TOPO (C), and 0.5 mol dm^{-3} TBP (D) in benzene.

$$\boldsymbol{H} = \beta H(g_{//}S_z\cos\theta + 2g_{\perp}S_x\sin\theta) + A_zS_z + B(S_xI_x + S_yI_y) \quad (1)$$

where β is the Bohr magneton, H the applied magnetic field, $g_{//}$ and $g_{\perp}$ the g-tensor values parallel and perpendicular, respectively, to z-axis corresponding to the V=O bond direction, θ the angle between H and z-axis, $S_{x,y,z}$ and $I_{x,y,z}$ the components of the electron and nuclear spin vectors, respectively, and A and B the hyperfine splitting constants for vanadium nucleus. Computer simulation method described in an earlier paper[6] is used for determining the ESR parameters of VO^{2+} complexes with DEHPA, Aliquat-336, TOA, TOPO, and TBP. The resulting parameters are shown in Table 1.

The g-values and hyperfine splitting constants are related to the energy levels and bonding parameters. For the purpose of estimating approximate bonding parameters, it is assumed that the complexes are ap-

proximately in a point group C_{4v} symmetry, because the parameters indicating the difference in bonding between two perpendicular directions can not be obtained, and that the b_2 orbital is a non-bonding orbital. This leads to the following relationship:

$$\Delta g_{//} = 8\lambda_v\beta_1^{*2}/\Delta_{//}, \quad (2)$$

$$\Delta g_{\perp} = 2\lambda_v\varepsilon_\pi^{*2}/\Delta_{\perp}, \quad (3)$$

$$A = P[-(4/7+\kappa_v) - 8(\lambda_v\beta_1^{*2}/\Delta_{//}) - 6/7(\lambda_v\varepsilon_\pi^{*2}/\Delta_{\perp})], \quad (4)$$

and

$$B = P[2(2/7-\kappa_v) - 11/7(\lambda_v\varepsilon_\pi^{*2}/\Delta_{\perp})], \quad (5)$$

where $\Delta g_{//}=2.002-g_{//}$, $\Delta g_{\perp}=2.002-g_{\perp}$, β_1^{*2} and ε_π^{*2} are the fractional contributions of the orbitals $d_{x^2-y^2}$ and d_{xz} (and/or d_{yz}) in antibonding molecular orbitals $^2B_1$ and $^2E(I)$, respectively, λ the spin-orbital coupling constant for the free ion of vanadium, κ_v the Fermi contact term for the vanadium atom, $P=2.002g_N-\beta\beta_N\langle r^{-3}\rangle$ in which r is the distance from the central nucleus to the electron and β_N the nuclear magneton, $\Delta_{\perp}$ the energy in the transition $^2B_2\rightarrow{}^2E(I)$ and $\Delta_{//}$ the energy in the transition $^2B_2\rightarrow{}^2B_1$. The molecular parameters of the VO^{2+} complexes with DEHPA, Aliquat-336, TOA, TOPO, and TBP obtained from simultaneous solution of Eqs. 3—6 are given in Table 1. The values of β_1^{*2} for those complexes range from 0.50 to 0.59 except that of the complex with DEHPA being 0.78. This means that for the complexes with Aliquat-336, TOA, TOPO, and TBP the in-plane σ bonding is covalent so that the unpaired electron is delocalized, while somewhat covalent for that with DEHPA. This values of ε_π^{*2} range from 0.66 to 0.98, implying that the out-of-plane π bonding is almost completely ionic for the complexes with DEHPA, Aliquat-336, and TBP, somewhat covalent for that with TOPO and covalent for that with TOA.

Table 1. Estimated ESR parameters of the vanadium(IV) complexes with DEHPA, Aliquat-336, TOA, TOPO, and TBP

Parameter	Vanadium(IV) complex				
	DEHPA	Aliquat-336	TOA	TOPO	TBP
$g_{//}$	1.930	1.940	1.947	1.935	1.945
$g_{\perp}$	1.976	1.979	1.980	1.980	1.978
$\lvert A\rvert$/cm^{-1}	0.0147	0.0177	0.0170	0.0170	0.0155
$\lvert B\rvert$/cm^{-1}	0.0063	0.0067	0.0069	0.0069	0.0074

Conclusion

In the extraction by DEHPA, the monomeric species, $VO(X_2H)_2$, in which central vanadium ion possesses little π bonding of coordinated oxygen atoms of DEHPA, is formed when DEHPA is present in excess, and an increase in the organic vanadium concentration involves the formation of polymeric species arising from the substitution of the hydrogen ion of coordinated anion X_2H^- by vanadium ion in aqueous phase. In the extraction by Aliquat-336, the tetravalent vanadium species, $R_3R'NVOCl_3$, which is also deduced from the extractions of other metals, exists stably in the organic phase extracted from a mixed solution of hydrochloric acid and lithium chloride, and while the hydrolytic tetravalent vanadium species, $VO(OH)Cl\cdot nL$, are found in the extractions by TOA, TOPO, and TBP.

We wish to thank Dr. Kenzo Watanabe of the Research Institute of Electronics, Shizuoka University, and Prof. Takafumi Kanazawa, Dr. Hiroshi Kawazoe, and Mr. Hideo Hosono of the Department of Industrial Chemistry, Faculty of Technology, Tokyo Metropolitan University for the ESR spectral measurements, and also the Kao Soap Co., Ltd. for the sample of TOA, the Hokko Chemical Industry Co., Ltd. for the sample of TOPO, and the Daihachi Chemical Industry Co., Ltd. for the samples of DEHPA and TBP.

References

1) T. Sato, T. Nakamura, and S. Ikoma, *J. Inorg. Nucl. Chem.*, **41**, 223 (1979).
2) T. Sato, *J. Inorg. Nucl. Chem.*, **24**, 699 (1962); **27**, 1853 (1965).
3) T. Sato and H. Watanabe, *Anal. Chim. Acta*, **49**, 463 (1970).
4) K. Alcock, S. S. Grimly, T. V. Healy, J. Kennedy, and H. A. Mckay, *Trans. Faraday Soc.*, **52**, 39 (1956).
5) T. Sato and T. Takeda, *J. Inorg. Nucl. Chem.*, **32**, 3387 (1970).
6) T. Sato, T. Nakamura, and O. Terao, *J. Inorg. Nucl. Chem.*, **39**, 401 (1977).
7) T. Sato, T. Nakamura, and M. Kawamura, *J. Inorg. Nucl. Chem.*, **40**, 853 (1978).
8) T. W. Newton and F. B. Baker, *Inorg. Chem.*, **3**, 569 (1964).

Mass-spectrometric Measurement of Activities in Both Solid and Liquid Solutions of the KCl–NaCl System

Mitsuru ITOH,* Tadashi SASAMOTO,† and Toshiyuki SATA

Research Laboratory of Engineering Materials, Tokyo Institute of Technology, 4259 Nagatsuta, Midori-ku, Yokohama 227

(Received April 3, 1981)

The activities of the KCl–NaCl system were mass-spectrometrically determined by the ion-current-ratio method in the temperature range from 793 to 1083 K. As a result, the activities of KCl or NaCl in the solid solution showed greatly positive deviations from Raoult's law while the liquid solution at 1083 K gave slightly negative values. The heats of mixing in the solid solution were calculated from the temperature dependence of the modified ion-current ratios, $[(I_{Na_2Cl^+}/X^2_{NaCl})/(I_{K_2Cl^+}/X^2_{KCl})]$. The excess entropy of mixing in the solid solution was attributed to the change in the vibrational spectrum, and the vibrational contribution to the heat of mixing was evaluated.

The Knudsen-cell mass-spectrometric method developed by Belton and Fruehan[1] has been applied to the determination of the thermodynamic properties of metallic solutions at elevated temperatures and has proved to be very useful. However, there have been few reports concerning the application of this method in activity measurements in inorganic-solid-solution systems between compounds. In the case of the activity measurement of a solid-solution system, a difficult problem is a surface depletion caused by the preferential vaporization of certain components.

In this study, the applicability of the mass-spectrometric method has been checked for the measurement of activities in the KCl–NaCl system. This system is proper for a discussion of the adaptability of the mass spectrometry to the activity measurements in an inorganic-solid-solution system because of the relatively small difference in the vapor pressures of the components (the ratio of the vapor pressure of KCl to that of NaCl is about two) and the ease of thermodynamical analysis from the observed data.

Experimental

The instrument used was a doubly focused mass spectrometer (JEOL JMS-01/BK) with a Knudsen-cell source (*cf.* Fig. 1). The Knudsen cell(G), made of alumina, had dimensions of 8 mm I.D. by 8 mm in height and had a cylindrical orifice 0.2—0.7 mm in diameter bored in the center of a lid about 1 mm thick. The cell was heated by radiation from tungsten ribbon heaters(H). The temperature of the cell was measured with a W5%Re–W26%Re thermocouple attached at the inner bottom of the outer cell(F), which had been calibrated in advance from the difference in the temperatures between the inside and outside of the cell (containing a sample), the difference having been determined using a PR13 thermocouple (0.2 mm in diameter) inserted through the orifice. Samples in the KCl–NaCl solid solutions were prepared by the melting a mixture of exactly weighted KCl and NaCl powders dried in a vacuum for a day and by then quenching them to room temperature in a quartz tube. They were crushed to powder just before the measurement, and about 300 mg was used in the Knudsen cell for each run of an experiment.

The ion intensity for the derived species was measured by the usual mass-spectrometrical technique in the temperature range from 793 to 1083 K, changing the temperature in steps of 40 K intervals. The temperature was held for about 15 min at each temperature level in order to obtain the constant ion intensity indicating the chemical equilibrium. The total weight loss of the sample after each run was about 0.1 mg in the solid state and about 3 mg in the liquid state. If a perfect shutter effect could not be obtained because of the contamination by alkali halide vapors, the ion source was completely cleaned. The ionization potential of 25 eV was used.

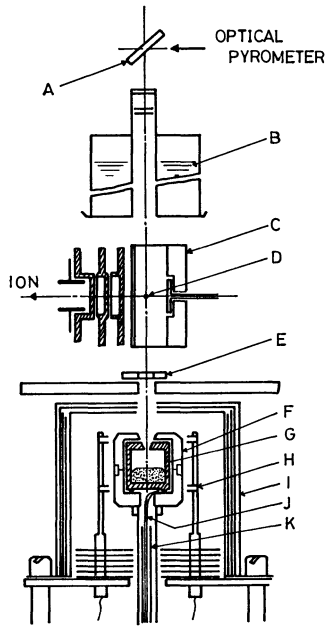

Fig. 1. Scheme of the mass spectrometer with Knudsen cell ion source.
A: Mirror, B: liquid N_2 trap, C: ion source chamber, D: electron beam, E: shutter slit, F: outer cell, G: Knudsen cell, H: filament, I: radiation shield, J: W5%Re–W26%Re thermocouple, K: ThO_2-tube.

Results and Discussion

The detected ion species were Na^+, K^+, $NaCl^+$, KCl^+, Na_2Cl^+, K_2Cl^+, $NaKCl^+$, and Cl^+. Their apperance potentials, referred to H_2O^+, were 10.3, 11.0, 10.0, 10.5, 10.0, 10.8, 10.5, and 15.5 eV respectively. The ion intensities of the $Na_3Cl_2^+$ and $K_3Cl_2^+$ trimers were under 1/100 for those of the Na_2Cl^+ and K_2Cl^+.

† Present address: Tokyo National Technical College, 1220-2, Kunugida, Hachioji, Tokyo 193.

Both by considering the temperature dependences of the ion currents and by using an analogy with other chlorides,[2,3] the formation processes of ions from the alkali-halide vapors were estimated to be as follows:

$$MCl + e^- = M^+ + Cl + 2e^-, \quad (1)$$

$$MCl + e^- = MCl^+ + 2e^-, \quad (2)$$

$$M_2Cl_2 + e^- = M_2Cl^+ + Cl + 2e^-, \quad (3)$$

$$MM'Cl + e^- = MM'Cl^+ + Cl + 2e^-, \quad (4)$$

$$Cl + e^- = Cl^+ + 2e^-, \quad (5)$$

where M and M′ stand for Na or K. That is to say, MCl^+, M_2Cl^+, and $MM'Cl^+$ were the molecular(or parent) ions formed by the simple ionization, while M^+ and Cl^+ were the fragment ions. Therefore, we considered that the sum of the ion currents of M^+ and MCl^+ was proportional to the vapor pressure of MCl(g).

In order to confirm the equilibrium in the cell, the dimer ion-current ratio, $I_{Na_2Cl^+}/I_{K_2Cl^+}$ was measured at 913 K as a function of the orifice diameter, as shown in Fig. 2. From the results, the equilibrium in the cell was confirmed.

Belton and Fruehan[1] have derived expressions relating to the activity of a solution which is favorable to mass spectrometry. The activity in the system was determined using the expression for the ion-current ratios of any two peaks for Na_2Cl^+, K_2Cl^+, or $NaKCl^+$. For example, the activity coefficient for the KCl component, γ_{KCl}, is given by:

$$\ln\gamma_{KCl} = -\int_{X_{KCl}=1}^{X_{KCl}} \frac{X_{NaCl}}{2} \times d\{\ln(I_{Na_2Cl^+}/I_{K_2Cl^+}) - \ln(X_{NaCl}/X_{KCl})^2\}, \quad (6)$$

where X_i is the mole fraction. This equation means that the activity can be determined from the ion-current ratio, $I_{Na_2Cl^+}/I_{K_2Cl^+}$, as a function of the composition. The experimental results are shown in Fig. 3 as plots of $\ln(I_{Na_2Cl^+}/I_{K_2Cl^+})$ *vs.* $1/T$. These plots for each composition fall on straight lines, the slopes of which are given in Table 1. The broken lines in Fig. 3, located on the gaps between the two straight lines in the lower and higher temperature sides, correspond to the regions where the solid and liquid coexist. The solidus and liquidus temperatures obtained from this figure agreed approximately with those in the phase diagram.[4] In order to graphically integrate Eq. 6, the term of $\{\ln(I_{Na_2Cl^+}/I_{K_2Cl^+}) - \ln(X_{NaCl}/X_{KCl})^2\}$ was plotted against the composition, X, as is illustrated in Fig. 4. Using this figure, the

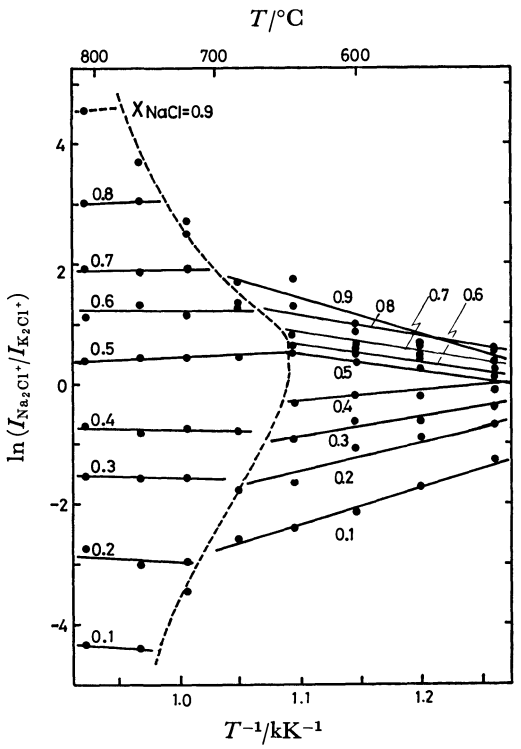

Fig. 3. The observed ion current ratio of dimer ions in the KCl–NaCl system.

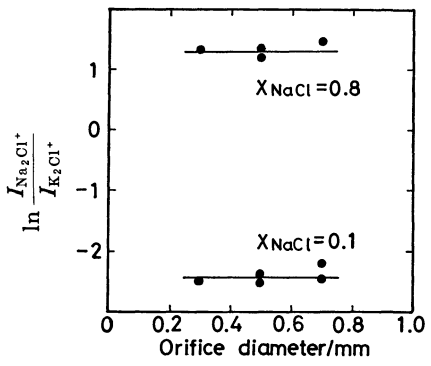

Fig. 2. Orifice diameter dependence of $\ln(I_{K_2Cl^+}/I_{Na_2Cl^+})$.

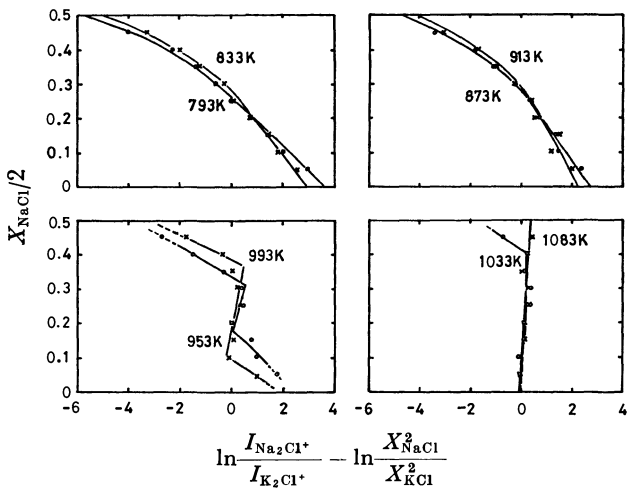

Fig. 4. Preliminary curves for the graphical integration in Eq. 6.

Table 1. Values of slopes for the lines drawn in Fig. 3

X_{NaCl}	0.1	0.2	0.3	0.4	0.5	0.6	0.7	0.8	0.9
$d\ln\left(\frac{I_{Na_2Cl^+}}{I_{K_2Cl^+}}\right)/d(1/T)$	6250	5030	3050	1240	−470	−990	−2970	−4310	−6830

activity coefficients for NaCl and KCl are calculated by the graphical integration on the basis of Eq. 6. The results are shown in Fig. 5.

The activity can be obtained also using a complex dimer, $NaKCl_2(g)$, in the following manner. The equilibrium reaction between the gas and the condenced phases containing the complex vapor:

$$Na_2Cl_2(g) + KCl(c) = NaKCl_2(g) + NaCl(c) \quad (7)$$

gives another expression for the activity coefficient corresponding to Eq. 6:

$$\ln\gamma_{KCl} = -\int_{X_{KCl}=1}^{X_{KCl}} X_{NaCl} \times d\{\ln(I_{NaKCl^+}/I_{K_2Cl^+}) - \ln(X_{NaCl}/X_{KCl})\}. \quad (8)$$

The obtained ion-current ratios *vs.* $1/T$ and the $\{\ln(I_{NaKCl^+}/I_{K_2Cl^+}) - \ln(X_{NaCl}/X_{KCl})\}$ *vs.* composition are shown in Figs. 6 and 7. The activities derived from Fig. 7 are shown in Fig. 8; they are in close agreement with those shown previously in Fig. 5. The closed circles in Fig. 8 indicate that the activities of NaCl at 1083 K were determined by the monomer-dimer method,[5] in which the following equation was used:

$$a_{NaCl} = (I_{Na_2Cl^+}/I_{NaCl^+})_{solution}/(I_{Na_2Cl^+}/I_{NaCl^+})_{pure}. \quad (9)$$

The plots were in good agreement with the values determined by the ion-current-ratio method. This fact supports the idea that the following fragmentation can be neglected:

$$Na_2Cl_2 + e^- \rightarrow Na^+ + NaCl + Cl + 2e^-, \quad (10)$$

$$Na_2Cl_2 + e^- \rightarrow NaCl^+ + NaCl + 2e^-. \quad (11)$$

Topor and Topor[6] have determined the activity of the KCl-NaCl system at 1153 K by means of the galvanic-cell method. The activity reported by them (Fig. 5) shows a great positive deviation from that for the ideal solution, while their values disagree with those extrapolated from our data up to 1153 K. When the excess partial entropy of mixing was evaluated using Topor and Topor's activity data and Hersh and Kleppa's calorimetric data,[7] the value of −0.72

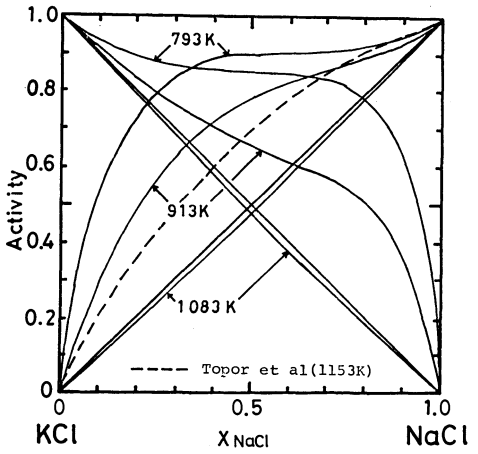

Fig. 5. Activities in the KCl-NaCl system.

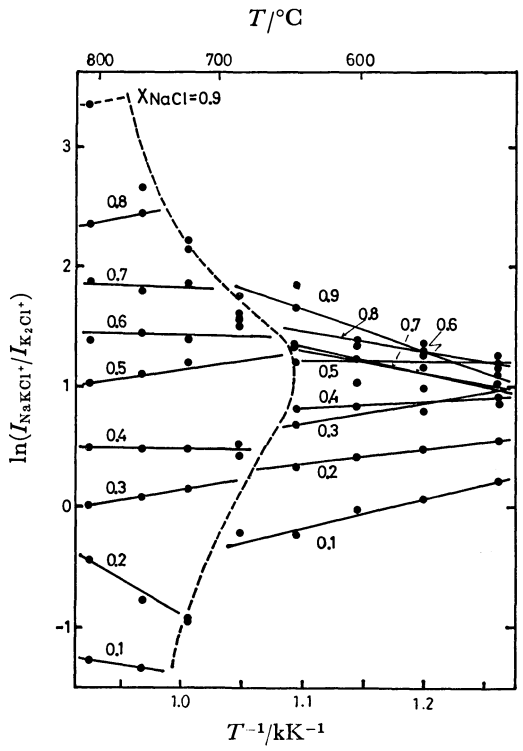

Fig. 6. The observed ion current ratio of dimer ions in the KCl-NaCl system.

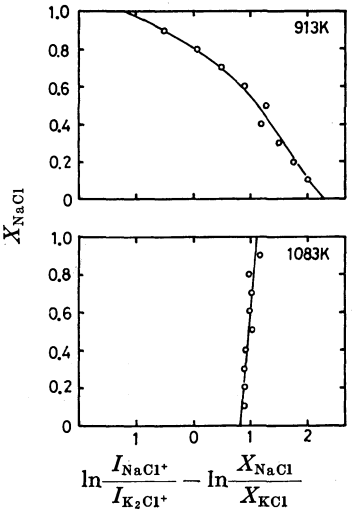

Fig. 7. Preliminary curves for the graphical integration in Eq. 8.

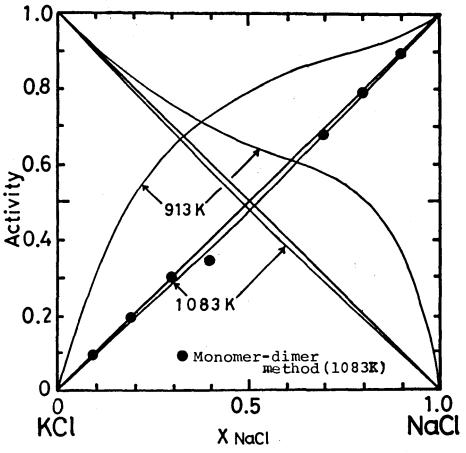

Fig. 8. Activities in the KCl-NaCl system.

e.u. was obtained for the composition of $X_{NaCl}=0.5$. This value, however, is considered to be too large for this simple system.

The heats of mixing, ΔH^M, for the solid solution were determined by a graphical integration of Eq. 12:[1]

$$\Delta\bar{H}_{KCl} = -R\int_{X_{KCl}=1}^{X_{KCl}} \frac{X_{NaCl}}{2} \times d\left[\frac{d\ln\{I_{Na_2Cl^+}\cdot X_{KCl}^3/I_{K_2Cl^+}\cdot X_{NaCl}^2\}}{d(1/T)}\right], \quad (12)$$

using the values of the slope given in Table 1. The integration along the curve in Fig. 9 yields Fig. 10. The large positive heat of mixing in the solid solution system probably arises from the difference in radius between the radii of Na^+ (0.96 Å) and K^+ (1.33 Å). As is shown in Fig. 10, $\Delta\bar{H}_{KCl}$ is larger than $\Delta\bar{H}_{NaCl}$. This is due to a requirement of a larger energy than that for the case of a small ion for the introduction of a large ion into a lattice. If the ionic radii in the state of solid solution and bulk moduli of the ions are known, the contribution of the strain energy to the heat of mixing can be estimated. In the KCl–NaCl system, the cations may take an arrangement with a short-range order in order to reduce the strain energy.

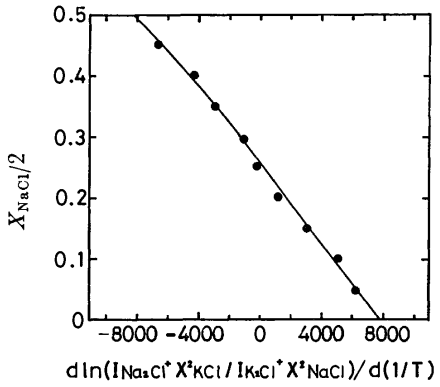

Fig. 9. Integration plot for the KCl–NaCl system.

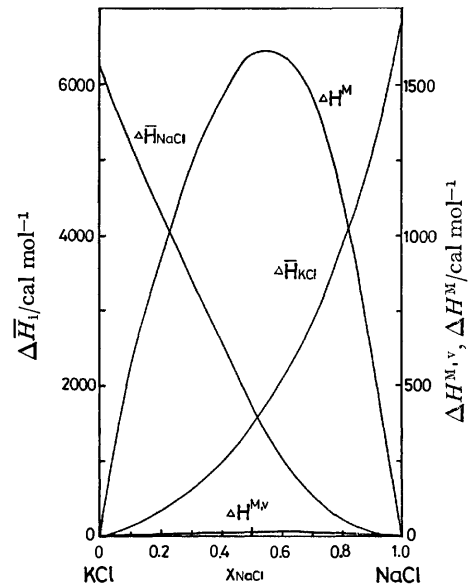

Fig. 10. Heats of mixing in the KCl–NaCl solid solution system.

The entropy of mixing, ΔS^M, in the solid solution was calculated from the well-known thermodynamic relation:

$$\Delta S^M = -(\Delta H^M - \Delta G^M)/T. \quad (13)$$

It is shown in Fig. 11. If the arrangement of the cations is close to the random state in the solid solution, the entropy is given by only the ideal configurational term, ΔS^M_{ideal}:

$$\Delta S^M_{ideal} = -R(X_{KCl}\ln X_{KCl} + X_{NaCl}\ln X_{NaCl}). \quad (14)$$

ΔS^M_{ideal} is also plotted in Fig. 11. Then the excess entropy, ΔS^M_{excess}, is given by:

$$\Delta S^M_{excess} = \Delta S^M - \Delta S^M_{ideal}. \quad (15)$$

The entropy of mixing in the liquid solution shown in Fig. 11 was calculated from the activities from Hersh and Kleppa's calorimetric data. The small excess entropy of mixing and the small heat of mixing suggest that the liquid solution is nearly an ideal solution. The large positive excess entropy of mixing in the solid solution is considered to arise from a change in the vibrational entropy associated with a change in the vibrational spectrum. The vibrational entropies(ΔS^M) of KCl and NaCl can be calculated from Debye's theory[8] using the Debye temperatures[9-11] of KCl (235 K) and NaCl (321 K). The vibrational entropy of solid solution(S^v) is the mean vibrational entropy, $S^v_{mean}(=X_{KCl}S^v_{KCl}+X_{NaCl}S^v_{NaCl})$, plus the excess entropy, ΔS^M_{excess}. The calculated S^v's are shown in Fig. 12. The Debye temperature of the solid solution was calculated from the S^v; it is shown in Fig. 13, along with the Debye temperature, θ_D, corresponding to the S^v_{mean}. It is also possible to calculate the heat capacity, C_v, for the KCl–NaCl solid solution. The change in the heat capacity to form the solid solution is:

$$\Delta C_v = C_{v,\text{solid solution}} - X_{KCl}C_{v,KCl} - X_{NaCl}C_{v,NaCl}. \quad (16)$$

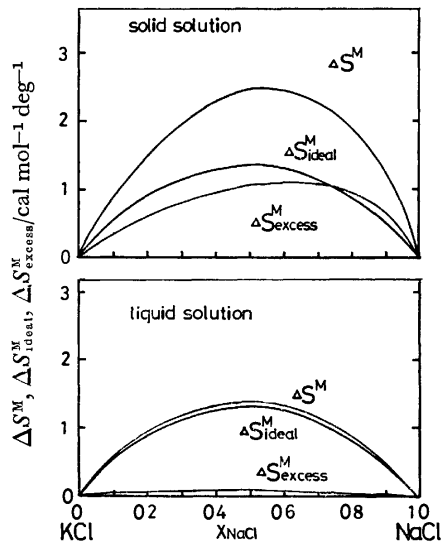

Fig. 11. Entropies of mixing in the KCl–NaCl solid solution and liquid solution systems.

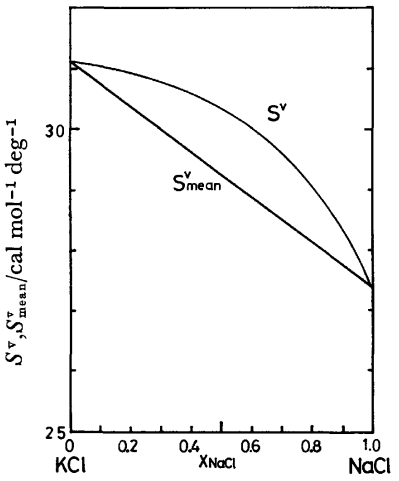

Fig. 12. Vibrational entropy and mean entropy of the KCl–NaCl solid solution system.

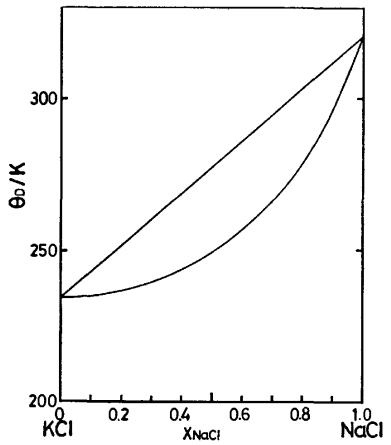

Fig. 13. Debye temperature for the KCl–NaCl solid solution system.

The change in the heat of mixing caused by the change in the vibrational spectrum is calculated using the following equation:

$$\Delta H^{M,v} = \int_0^T \Delta C_p dT. \quad (17)$$

The results are shown in Fig. 10. For the purposes of this study, it is possible to estimate that ΔC_p is close to ΔC_v. As is shown in Fig. 10, $\Delta H^{M,v}$ makes only a small contribution to ΔH^M.

Conclusion

(1) The activities of KCl and NaCl in the solid solution showed greatly positive deviations from Raoult's law, while the liquid solution gave slightly negative values.

(2) The large positive heat of mixing in the solid solution was attributed to the strain energy which arises from the difference in radius between the radii of Na^+ and K^+.

(3) The large positive excess entropy of mixing in the solid solution is considered to arise from a change in the vibrational spectrum.

References

1) G. R. Belton and R. J. Fruehan, *Metall. Trans.*, **2**, 291 (1971).
2) J. Berkowitz and W. A. Chupka, *J. Chem. Phys.*, **29**, 653 (1958).
3) T. A. Milne and H. M. Klein, *J. Phys. Chem.*, **64**, 1628 (1960).
4) R. G. Wolston and W. Kobes, *Mater. Res. Bull.*, **2**, 263 (1967).
5) J. Berkowitz and W. A. Chupka, *Ann. N. Y. Acad. Sci.*, **79**, 1073 (1960).
6) T. Topor and L. Topor, *J. Chim. Phys.*, **69**, 1465 (1972).
7) S. Hersh and O. J. Kleppa, *J. Chem. Phys.*, **42**, 247 (1965).
8) D. E. Gray, "American Institute of Physics Handbook," 3rd ed, McGraw-Hill (1972).
9) W. T. Bergand and J. A. Morrison, *Proc. R. Soc. London Ser. A*, **242**, 467 (1957).
10) P. H. Keeson and N. Pearman, *Phys. Rev.*, **91**, 1054 (1953).
11) F. J. Werb and J. Wilks, *Proc. R. Soc. London, Ser. A*, **230**, 549 (1955).

Reactions of Bis(β-diketonato)palladium(II) and -platinum(II) with Tertiary Phosphines††

Seichi OKEYA,* Yukio NAKAMURA,† and Shinichi KAWAGUCHI*,†

Faculty of Education, Wakayama University, Masago-cho, Wakayama 640

†*Faculty of Science, Osaka City University, Sumiyoshi-ku, Osaka 558*

(Received April 22, 1981)

Bis(β-diketonato)palladium(II) and -platinum(II) readily react with tertiary phosphines (L) to afford [M(β-dik)(β-dik-*O*)L], [M(β-dik)L_2](β-dik), [ML_4](β-dik)$_2$, [M(β-dik-*O*)$_2L_2$], and [M(β-dik)(β-dik-*C*)L] complexes, which were characterized mainly by infrared and ^{1}H and ^{13}C NMR spectroscopy. Factors influencing the relative stability of each bonding mode of β-diketonate anions were investigated.

Since bis(2,4-pentanedionato)palladium(II) was found to react readily with Lewis bases such as triphenylphosphine, pyridine, and diethylamine to convert one of the chelating ligands into the central-carbon-bonded state,[1] we have carried out comprehensive studies on the reactions of various bis(β-diketonato)palladium(II) and -platinum(II) complexes, [M(β-dik)$_2$], with a wide variety of nitrogen and phosphorus bases. In a previous paper[2a] the reactions of [Pd(β-dik)$_2$] with nitrogen bases were summarized in Scheme 1. Besides compounds **7** and **8** containing the carbon-bonded β-dik ligand, secondary and primary amines gave the cationic complexes **4** and **5**, respectively, which contain the β-dik anion as the counter ion in the outer sphere. In the platinum(II) case, compounds of the type **6** were also isolated as the linkage isomer of **4**.[2,3]

Since the kinetic study[4] revealed that compound **7** is produced *via* **4** and not directly from **1**, compound **4** seems to be formed *via* **3** which contains the oxygen-bonded β-dik as a unidentate ligand. However, no compounds of types **2** and **3** have been isolated in the reactions between [M(β-dik)$_2$] and nitrogen bases. Then the reactions with phosphorus bases have been examined, which proceed in a similar manner to those with nitrogen bases following Scheme 1, giving **2** and **3** as well as **4**, **5**, **6**, and **7**.

Several five-coordinate complexes [M(hfac)$_2$L] were prepared by the reactions of [M(hfac)$_2$] (M=Pd and Pt) with P(*o*-tolyl)$_3$, PCy_3, and PPh(*o*-tolyl)$_2$ as L. The square-pyramidal structure of these complexes was inferred by the ^{1}H, ^{13}C, and ^{19}F NMR studies, and confirmed by X-ray analysis in the case of [Pd(hfac)$_2$P(*o*-tolyl)$_3$] and [Pt(hfac)$_2$$PCy_3$].[5] Ito *et al.* also examined the reactions between [Pt(acac)$_2$] and phosphorus bases to obtain [Pt(acac-*O*)$_2$(PEt_3)$_2$][6] as well as [Pt(acac)(acac-*C*^{3})L] (L=PPh_3 and PCy_3),[7] which were characterized by the NMR spectroscopy. The present paper reports the other new compounds obtained by the reactions of [M(β-dik)$_2$] (M=Pd and Pt; β-dik=mainly acac, tfac, and hfac) as well as mixed-ligand chelates [M(acac)(tfac)] and [M(acac)(hfac)] with several kinds of tertiary phosphines.

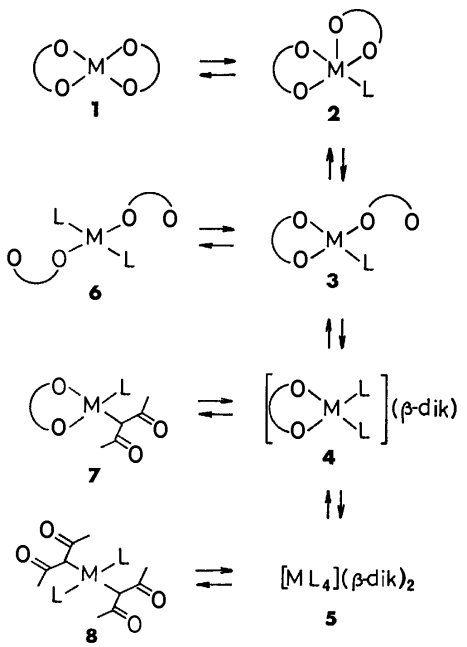

Scheme 1.

Experimental

Preparation of Complexes. The starting bis(β-diketonato)palladium(II) and -platinum(II) complexes were prepared by the methods reported recently.[8] Most of tertiary phosphines were purchased and used without further purification, but less stable triethylphosphine was distilled under reduced pressure before use and tri-*o*-tolylphosphine was purified by recrystallization from ethanol.

*1,1,1-Trifluoro-2,4-pentanedionato(1,1,1-trifluoro-2,4-pentanedionato-O)(tri-o-tolylphosphine)palladium(II), [Pd(tfac)(tfac-O){P(o-tolyl)$_3$}] (**3a**)*: Hexane (10 cm^3) was added to a red solution of [Pd(tfac)$_2$] (886 mg, 2.15 mmol) and P(*o*-tolyl)$_3$ (663 mg, 2.18 mmol) in hot benzene (15 cm^3) and the mixture was left to stand overnight at room temperature. Orange plates deposited were filtered, washed with diethyl ether (10 cm^3) and air-dried. The yield was 1.12 g (73%).

*[Pd(tfac)(tfac-O)(PCy_3)] (**3c**)*: [Pd(tfac)$_2$] (151 mg, 0.366 mmol) and tricyclohexylphosphine (PCy_3) (110 mg, 0.392 mmol) were dissolved in dichloromethane (2 cm^3) to result in a red solution. The solvent was allowed to evaporate spontaneously at room temperature to leave orange needles, which were recrystallized from hexane. The yield was 60 mg (24%).

†† In this paper the chelated, single oxygen bonded, and central carbon bonded anions of β-diketones such as 2,4-pentanedione (acacH), 1,1,1-trifluoro-2,4-pentanedione (tfacH), 1,1,1,5,5,5-hexafluoro-2,4-pentanedione (hfacH), 1-phenyl-1,3-butanedione (bzacH), and 1-(2-thienyl)-4,4,4-trifluoro-1,3-butanedione (ttaH) are represented by β-dik, β-dik-*O*, and β-dik-*C*, respectively, and β-dik in the outer sphere shows a counter ion. Other abbreviations: PCy_3, tricyclohexylphosphine; dpe, *cis*-1,2-bis(diphenylphosphino)-ethylene; dppe, 1,2-bis(diphenylphosphino)ethane.

*[Pd(acac)(tfac-O){P(o-tolyl)$_3$}] (**3d**)*: Hexane (2 cm^3) was added to a red solution of [Pd(acac)(tfac)] (108 mg, 0.301 mmol) and P(*o*-tolyl)$_3$ (94 mg, 0.31 mmol) in benzene (1.5 cm^3), and the mixture was left to stand at ambient temperature to deposit orange yellow columns. The product was filtered, washed with petroleum ether (bp$<$50 °C), and air-dried. The yield was 83 mg (42%).

*[Pt(acac)(acac-O){P(o-tolyl)$_3$}] (**3e**)*: A toluene solution (15 cm^3) containing [Pt(acac)$_2$] (327 mg, 0.831 mmol) and P(*o*-tolyl)$_3$ (1.024 mg, 3.36 mmol) was refluxed for 5.5 h. Hexane (20 cm^3) was added to the solution and the mixture was left to attain room temperature. Yellow needles formed were filtered, washed with hexane and dried *in vacuo*. The yield was 393 mg (68%).

*[Pt(tfac)(tfac-O){P(o-tolyl)$_3$}] (**3f**)*: A solution of *cis*-[Pt(tfac)$_2$] (300 mg, 0.599 mmol) and P(*o*-tolyl)$_3$ (203 mg, 0.667 mmol) in toluene (30 cm^3) was heated under reflux for 3 h. The solvent was then distilled away under reduced pressure to leave a yellow powder, which was washed with diethyl ether. The product was dissolved in dichloromethane and recrystallized by addition of hexane to afford yellow needles (271 mg) in a 56% yield. A similar reaction of *trans*-[Pt(tfac)$_2$] also gave **3f** in a 48% yield.

*[Pt(acac)(tfac-O){P(o-tolyl)$_3$}] (**3h**)*: The reaction of [Pt(acac)(tfac)] with three times molar amount of P(*o*-tolyl)$_3$ and work up in a similar manner as above gave tiny white needles of **3h** in a 46% yield.

*[Pt(acac)(tfac-O)(PPh$_3$)] (**3i**)*: [Pt(acac)(tfac)] (133 mg, 0.297 mmol) and triphenylphosphine (79 mg, 0.30 mmol) were dissolved in dichloromethane (1 cm^3) and the solvent was allowed to evaporate spontaneously at room temperature to leave yellow needles, which were gathered, washed with hexane, and dried *in vacuo*. The yield was 125 mg (59%).

*[Pt(acac)(tfac-O)(PEt$_3$)] (**3j**)*: A dichloromethane solution (2 cm^3) of triethylphosphine (25 mg, 0.21 mmol) was added dropwise to a solution of [Pt(acac)(tfac)] (73 mg, 0.163 mmol) in the same solvent with stirring. The solvent was then allowed to evaporate spontaneously at room temperature to deposit colorless cubes. Recrystallization from dichloromethane–hexane gave white plates (11 mg) in a 12% yield.

*Bis(tricyclohexylphosphine)(1,1,1-trifluoro-2,4-pentanedionato)-palladium(II) 1,1,1-Trifluoro-2,4-pentanedionate, [Pd(tfac)-(PCy$_3$)$_2$](tfac) (**4a**)*: [Pd(tfac)$_2$] (210 mg, 0.509 mmol) and PCy$_3$ (290 mg, 1.03 mmol) were dissolved in dichloromethane to afford an orange yellow solution. The solvent was allowed to evaporate spontaneously at room temperature to leave viscous red-orange oil, to which was added hexane (1 cm^3) to deposit a yellow precipitate. Recrystallization from dichloromethane–hexane gave a yellow crystalline solid (116 mg) in a 33% yield.

*[Pt(acac)(PPh$_3$)$_2$](tfac) (**4d**)*: A solution of [Pt(acac)-(tfac)] (145 mg, 0.324 mmol) and PPh$_3$ (176 mg, 0.671 mmol) in diethyl ether was kept in a refrigerator for two days to precipitate white plates, which were filtered and dried *in vacuo*. The yield was 232 mg (74%).

*Bis[cis-1,2-bis(diphenylphosphino)ethylene]palladium(II) 1,1,1-Trifluoro-2,4-pentanedionate, [Pd(dpe)$_2$](tfac)$_2$ (**5a**)*: To a suspension of [Pd(tfac)$_2$] (206 mg, 0.500 mmol) in dichloromethane (4 cm^3) was added dpe (396 mg, 1.00 mmol) to result in a clear yellow solution, which on standing for several minutes began to deposit pale yellow plates. After being left overnight, the precipitate was filtered, washed with dichloromethane, and dried *in vacuo*. The yield was 536 mg (89%).

*[Pd(PMe$_2$Ph)$_4$](hfac)$_2$ (**5b**)*: To a solution of [Pd(hfac)$_2$] (520 mg, 0.996 mmol) in diethyl ether (4 cm^3) was added a solution of about four times molar amount of dimethylphenylphosphine (PMe$_2$Ph) (0.7 cm^3) in the same solvent. Color of the solution changed immediately from red to orange yellow and yellow needles precipitated, which were filtered and washed five times with diethyl ether. Addition of hexane to a mixture of the filtrate and washings gave another crop of the product. The total yield of yellow crystals was 880 mg (82%).

*[Pd(dpe)$_2$](hfac)$_2$ (**5c**)*: When dpe (159 mg, 0.401 mmol) was added to a solution of [Pd(hfac)$_2$] (104 mg, 0.199 mmol) in dichloromethane (1 cm^3), the red color of the solution became light, precipitating white plates, which were filtered, washed with small portions of dichloromethane and diethyl ether, and dried *in vacuo*. The yield was 243 mg (92%).

*[Pt(PMe$_2$Ph)$_4$](tfac)$_2$ (**5d**)*: On addition of a solution of PMe$_2$Ph (100 mg, 0.725 mmol) in diethyl ether (1 cm^3) to a solution of *cis*-[Pt(tfac)$_2$] (106 mg, 0.212 mmol) in the same solvent, a creamy precipitate appeared immediately. After being washed three times with diethyl ether, the crude product (174 mg) was dissolved in hot dichloromethane (4 cm^3). A small amount of petroleum ether was added to the solution to deposit a white crystalline solid, which was filtered and washed with acetone. The yield was 82 mg (37%).

*[Pt(dppe)$_2$](tfac)$_2$ (**5e**)*: A white precipitate appeared immediately after addition of a solution of 1,2-bis(diphenylphosphino)ethane (dppe) (130 mg, 0.327 mmol) in dichloromethane (3 cm^3) to a solution of [Pt(tfac)$_2$] (80 mg, 0.16 mmol) in the same solvent (3 cm^3). Recrystallization from dichloromethane–hexane gave colorless columns (96 mg) in a 46% yield.

*[Pt(dppe)$_2$](hfac)$_2$ (**5h**) and [Pt(dppe)$_2$](acac)(tfac) (**5j**)*: Similar reactions of [Pt(hfac)$_2$] and [Pt(acac)(tfac)] with dppe in dichloromethane gave colorless plates of **5h** and pale yellow crystals of **5j** in 65 and 64% yields, respectively.

*[Pd(dpe)$_2$](tfac)$_2$·1/4CH$_2$Cl$_2$ (**5f**)*: To a solution of *cis*-[Pt(tfac)$_2$] (170 mg, 0.339 mmol) in dichloromethane (5 cm^3) was added dpe (278 mg, 0.702 mmol). After being left overnight, white plates produced were filtered, washed with dichloromethane, and dried *in vacuo*. The yield was 415 mg (93%).

*[Pt(dpe)$_2$](hfac)$_2$ (**5i**)*: White plates of **5i** were similarly prepared by the reaction between [Pt(hfac)$_2$] and dpe in dichloromethane. The yield was 96%.

*[Pt(PMe$_2$Ph)$_4$](hfac)$_2$ (**5g**)*: White columns of **5g** (109 mg) were obtained in a 38% yield by the reaction of [Pt(hfac)$_2$] (150 mg, 0.246 mmol) with PMe$_2$Ph (115 mg, 0.833 mmol) in diethyl ether (3 cm^3).

*Bis(1,1,1-trifluoro-2,4-pentanedionato-O)bis(triethylphosphine)-platinum(II), [Pt(tfac-O)$_2$(PEt$_3$)$_2$] (**6a**)*: To a solution of *cis*-[Pt(tfac)$_2$] (72 mg, 0.14 mmol) in dichloromethane (0.5 cm^3) was added PEt$_3$ (35 mg, 0.30 mmol) followed by a small amount of petroleum ether and the mixture was left overnight to allow spontaneous evaporation of the solvents. Colorless plates left were gathered, washed with a mixture of diethyl ether and ethanol (1:1 by volume) followed by neat ether, and air-dried. The yield was 67 mg (63%). *trans*-[Pt(tfac)$_2$] also gave the same product in *ca.* 50% yield.

*[Pt(tfac-O)$_2$(PCy$_3$)$_2$] (**6b**)*: The reaction of [Pt(tfac)$_2$] with PCy$_3$ in a similar manner as above afforded yellow plates of **6b** in an 87% yield. Recrystallization from dichloromethane–hexane gave rise to colorless transparent plates, which became opaque on drying *in vacuo*. The final yield was 112 mg (50%).

*[Pt(acac-O)(tfac-O)(PEt$_3$)$_2$] (**6c**)*: Addition of a dichloromethane solution (0.5 cm^3) of PEt$_3$ (57 mg, 0.48 mmol)

to a solution of [Pt(acac)(tfac)] (81 mg, 0.18 mmol) in the same solvent (1 cm^3) changed the solution colorless. Hexane (2 cm^3) was added to the solution and the mixture was left standing overnight at room temperature. The mixed solvent was then evaporated spontaneously to deposit colorless plates, which were washed repeatedly with ethanol until odor of the phosphine was lost and dried *in vacuo*. The yield was 89 mg (79%).

2,4-Pentanedionato(2,4-pentanedionato-C^3)(triethylphosphine)palladium(II), *[Pd(acac)(acac-C^3)(PEt_3)]* ***(7a)***: Triethylphosphine (43 mg, 0.36 mmol) was added dropwise to a solution of [$Pd(acac)_2$] (101 mg, 0.331 mmol) in chloroform (0.4 cm^3) with stirring. After addition of petroleum ether (0.5 cm^3) to the solution, the solvent mixture was vaporized spontaneously at ambient temperature to deposit yellow plates on the wall of vessel, which were filtered and washed with a mixture of ethanol and hexane (1:5 by volume). The yield was 31 mg (22%).

[Pd(acac)(acac-C^3)($PMePh_2$)] ***(7c)***: To a suspension of [$Pd(acac)_2$] (76 mg, 0.25 mmol) in benzene (2 cm^3) was added $PMePh_2$ (52 mg, 0.26 mmol) to result in a red solution. After addition of petroleum ether (2 cm^3) to the solution, the solvent mixture was allowed to evaporate spontaneously at room temperature to leave yellow plates on the wall, which were gathered and washed with diethyl ether. The crude product (74 mg, 59% yield) was dissolved in dichloromethane and recrystallized as yellow cubes on addition of petroleum ether. The final yield was 40 mg (32%).

1-Phenyl-1,3-butanedionato(1-phenyl-1,3-butanedionato-C^2)(triphenylphosphine)palladium(II), *[Pd(bzac)(bzac-C^2)(PPh_3)]* ***(7d)***: A mixture of [$Pd(bzac)_2$] (100 mg, 0.233 mmol) and PPh_3 (61 mg, 0.23 mmol) in diethyl ether (2 cm^3) was stirred for *ca.* 4 h at room temperature. A yellow precipitate formed was filtered and washed with diethyl ether. The yield was 57 mg (35%). Recrystallization was performed from dichloromethane–hexane.

1-(2-Thienyl)-4,4,4-trifluoro-1,3-butanedionato[1-(2-thienyl)-4,4,4-trifluoro-1,3-butanedionato-C^2](triphenylphosphine)palladium(II), *[Pd(tta)(tta-C^2)(PPh_3)]* ***(7e)***: The reaction of [$Pd(tta)_2$] with equimolar PPh_3 in diethyl ether in a similar manner as above gave a yellow powder of **7e** in a 60% yield.

Measurements. Infrared spectra were obtained in Nujol mull with Hitachi EPI-S and 295 infrared spectrophotometers. NMR spectra were recorded on JEOL-C60HL and JNM-MH100 (in the case of ^1H), FX60Q (for ^1H and ^{13}C), and FX90Q (for ^{19}F and ^{31}P) instruments. Molecular weight was determined in dichloromethane at 27 °C with a vapor pressure osmometer manufactured by Knauer, West Berlin, West Germany.

Results and Discussion

Tertiary phosphines react quite readily with [$M(\beta\text{-dik})_2$] (**1**) at room temperature. Table 1 lists the new compounds prepared by these reactions in appropriate organic solvents. In contrast to the case of nitrogen-base complexes, compounds **3** containing a tertiary phosphine as L and an O-unidentate β-dik ligand are sufficiently stable to be isolated and characterized. The π bonding between the d^8 metals and the phosphine ligands may strengthen not only the M–L bond but also the M–O(β-dik) bond by decreasing the electron density at the metal atom. Furthermore bulky phosphines are prone to prevent formation of the type **4** complexes.

In Table 2 are shown the infrared bands observed in the 1500—1800-cm^{-1} region for the representative complexes of each type. The frequencies of these bands assignable to the $\nu(C{=}O)+\nu(C{=}C)$ vibrations are helpful for diagnosing the bonding mode of β-dik anions. Ito *et al* pointed out that the $\nu(C{=}O)$ and $\nu(C{-}O)$ bands at 1650 and 1160 cm^{-1}, respectively, are characteristic of the unidentate acac ligand in [$Pt(acac\text{-}O)_2(PEt_3)_2$].[6] Each of compounds **3** and **6** also shows a band in the 1640—1660-cm^{-1} region ascribable to the $\nu(C{=}O)$ vibration of the O-bonded β-dik ligand. In addition, **3e** exhibits a strong $\nu(C{-}O)$ band at 1165 cm^{-1}. In the case of the tfac and hfac complexes, however, very strong $\nu(C{-}F)$ bands appear in the 1100—1200-cm^{-1} region, making the absorption due to the $\nu(C{-}O)$ vibration indiscernible.

Compared with **6**, compounds **3** show a few additional IR bands in the 1500—1625-cm^{-1} region caused by the chelated β-dik ligand. The tfac and hfac anions involved in the outer sphere of compounds **4** and **5** exhibit a single band in the 1604—1612-cm^{-1} and 1676—1680-cm^{-1} regions, respectively. The latter frequency coincides with that (1670—1680 cm^{-1}) recorded for the corresponding hfac compounds **4** and **5** containing nitrogen bases as L.[2] On the other hand, the former frequency for the tfac anions in **4** and **5** is *ca.* 30 cm^{-1} lower than that (1630—1640 cm^{-1}) observed for the corresponding nitrogen-base complexes.[2] The cause of this discrepancy is not rationalized at present. Compounds **7** show one or two bands in the 1650—1683-cm^{-1} region assignable to the $\nu(C{=}O)$ vibration of the C-bonded β-dik ligands.

^1H NMR Spectra. The ^1H NMR data for complexes **5** are listed in Table 3. A single set of the methyl and methine signals was observed for each complex, indicating that the two β-dik anions are environmentally equivalent. Much higher solubilities of **5** in methanol than in less polar solvents and absence of the Pt–H coupling in the proton signals from the β-dik anions in compounds **5d**—**5j** accord with the proposed salt-like structure. On the other hand, the methyl-proton signals from PMe_2Ph in **5d** and **5g** show coupling to platinum certifying that the phosphine is coordinated to the metal. The methine proton of the hfac anion in [$Pd(PMe_2Ph)_4$](hfac)$_2$ (**5b**) resonates at higher field (5.67 and 5.57 ppm in $CDCl_3$ and CD_3OD, respectively) than that in [$Pd(hfac)_2$] (6.42 and 6.50 ppm in respective solvents) because of the higher charge density on the noncoordinating anion. The methine signal from **5b** in C_6D_6 is shifted downfield by *ca.* 0.7 ppm, while the methyl signal from PMe_2Ph is shifted upfield by *ca.* 0.4 ppm as compared with the corresponding signals in $CDCl_3$. Similar phenomena were noted previously for analogous complexes containing nitrogen bases and attributed to the stereospecific interaction between the square planer complex and benzene molecules.[2]

In CD_3OD solution, the methine-proton signal from the tfac anion in **5** diminishes and instead a broad OH-proton signal becomes larger with time, attaining equilibrium in 2—3 h. Such a kind of H-D exchange is also observed in solutions of potassium β-diketonates

Table 1. Analytical data of the newly prepared complexes,[a] [M(β-dik)(β-dik-*O*)L] (**3**), [M(β-dik)L$_2$](β-dik) (**4**), [ML$_4$](β-dik)$_2$ (**5**), [Pt(β-dik-*O*)$_2$L$_2$] (**6**), and [Pd(β-dik)(β-dik-*C*)L] (**7**)

Compd	M	β-dik	L	Dec temp °C	Found(Calcd)(%) C	H
3a	Pd	tfac	P(*o*-tolyl)$_3$	164—166	51.72(51.93)	4.03(4.08)
3c	Pd	tfac	PCy$_3$	132—134	48.77(48.53)	6.02(5.96)
3d[b]	Pd	acac / tfac	P(*o*-tolyl)$_3$	160—165	56.11(56.16)	4.81(4.87)
3e	Pt	acac	P(*o*-tolyl)$_3$	190—192	53.02(53.37)	4.98(5.06)
3f	Pt	tfac	P(*o*-tolyl)$_3$	208—209	45.95(46.22)	3.57(3.63)
3h[b]	Pt	acac / tfac	P(*o*-tolyl)$_3$	220—226	49.43(49.53)	4.28(4.29)
3i[b]	Pt	acac / tfac	PPh$_3$	137—145	47.64(47.39)	3.68(3.69)
3j[b]	Pt	acac / tfac	PEt$_3$	135—138	34.02(33.98)	4.65(4.64)
4a	Pd	tfac	PCy$_3$	122—124	55.61(56.76)	7.67(7.66)
4d[b]	Pt	acac / tfac	PPh$_3$	131—134	56.79(56.85)	4.27(4.25)
5a	Pd	tfac	½dpe	150—155	61.30(61.76)	4.34(4.35)
5b	Pd	hfac	PMe$_2$Ph	114—116	47.36(47.01)	4.38(4.32)
5c	Pd	hfac	½dpe	204—209	56.09(56.70)	3.61(3.53)
5d	Pt	tfac	PMe$_2$Ph	136—138	48.05(47.85)	4.91(4.97)
5e	Pt	tfac	½dppe	226—227	57.42(57.36)	4.40(4.35)
5f[c]	Pt	tfac	½dpe	202—203	56.68(56.84)	4.10(4.02)
5g	Pt	hfac	PMe$_2$Ph	168—170	43.48(43.42)	4.02(3.99)
5h	Pt	hfac	½dppe	280—284	53.11(52.96)	3.58(3.58)
5i	Pt	hfac	½dpe	≈238	52.66(53.11)	3.41(3.31)
5j	Pt	acac / tfac	½dppe	208—213	58.75(59.85)	4.67(4.60)
6a	Pt	tfac	PEt$_3$	146—147	35.93(35.82)	5.25(5.19)
6b	Pt	tfac	PCy$_3$	196—199	52.32(52.02)	7.15(7.02)
6c	Pt	acac / tfac	PEt$_3$	145—146	39.03(38.65)	6.08(6.05)
7a	Pd	acac	PEt$_3$	131—132	45.34(45.45)	6.97(6.91)
7c	Pd	acac	PMePh$_2$	125—127	54.67(54.72)	5.42(5.39)
7d	Pd	bzac	PPh$_3$	154—156	65.72(66.05)	4.85(4.81)
7e	Pd	tta	PPh$_3$	115—125	49.81(50.35)	2.94(2.86)

a) The following compounds were not isolated, but characterized by IR and/or NMR spectroscopy in solution: [Pd(tfac)(tfac-*O*)(PPh$_3$)] (**3b**), [Pt(tfac)(tfac-*O*)(PPh$_3$)] (**3g**), [Pt(acac)(hfac-*O*)(PPh$_3$)] (**3k**), [Pd(tfac)(PPh$_3$)$_2$](tfac) (**4b**), [Pt(tfac)(PPh$_3$)$_2$](tfac) (**4c**), [Pt(acac)(PPh$_3$)$_2$](hfac) (**4e**), [Pd(acac)(acac-*C*^{3})(PMe$_2$Ph)] (**7b**), and [Pd(tfac)-(tfac-*C*^{3})(PPh$_3$)] (**7f**). b) The acac ligand is chelated. c) Including ¼CH_2Cl_2.

in D_2O and the rate decreases in the sequence of basicity: acac>tfac>hfac. The same trend is noted in the present complexes **5**–CD_3OD systems, the hfac anion reacting very slowly except that in **5g** which attains the exchange equilibrium in 24 h. Of the two methine proton signals from [Pt(dppe)$_2$](acac)(tfac) (**5j**), the one at δ 5.56 attains the exchange equilibrium in 3 min but the signal at δ 5.30 diminishes very slowly. Thus the former signal is assigned to the acac anion and the latter to tfac. Previously the analogous compounds **4** and **5** containing amines as L were found to exchange the amine protons and the methine proton of β-dik in the outer sphere with $CDCl_3$, the rate paralleling the basicity of β-dik.[2,9]

Compounds **4**, on the other hand, exhibit two sets of methyl and methine signals from tfac anions (Table 4). The signals assignable to acac in [Pt(acac)-(PPh$_3$)$_2$](tfac) (**4d**) are flanked by the ^{195}Pt satellites, while those from tfac are not, indicating that acac was retained in and tfac was repelled from the coordination sphere in the reaction of [Pt(acac)(tfac)] with PPh$_3$. When increasing amounts of PPh$_3$ was added to [Pt(acac)(hfac)] in $CDCl_3$, signals assignable to [Pt(acac)(hfac-*O*)(PPh$_3$)] (**3k**) grew at first (*vide infra*). After the amount of PPh$_3$ exceeded the equimolar level, signals attributable to [Pt(acac)-(PPh$_3$)$_2$](hfac) (**4e**) appeared and increased gradually at the expense of the **3k** signals, which disappeared almost completely when three times molar PPh$_3$ was added. Thus the difference in the coordinating ability of β-dik ligands in the mixed chelates is manifested by the reaction with PPh$_3$, the fluorinated β-dik ligands being displaced in preference to acac.

When twice molar PPh$_3$ reacted with *cis*-[Pt(tfac)$_2$] in $CDCl_3$, two sets of methyl and methine signals attributable to the tfac anions in [Pt(tfac)(PPh$_3$)$_2$]-

(tfac) (**4c**) were observed. Unfortunately, however, a spectrum distinct enough to allow the determination of exact coupling constants to ^{195}Pt could not be recorded, since the succeeding reactions gave rise to [Pt(tfac(2—)-*C,O*)(PPh_3)$_2$] containing a C,O-chelated 1,1,1-trifluoro-2,4-pentanedionate dianion.[10] On the contrary, the reaction mixture of [Pd(tfac)$_2$] and twice molar PPh_3 in CD_2Cl_2 at room temperature exhibited one set of broad methyl and methine signals, which became sharper with increasing temperature. At −45 °C, on the other hand, two sets of sharp signals were observed and assigned to the tfac anions in the inner and outer spheres of [Pt(tfac)(PPh_3)$_2$]-(tfac) (**4b**), and the temperature change of spectrum was reversible. The proposed structure is also supported by the ^{13}C NMR spectroscopy (*vide infra*). It is not certain at the present stage whether the rapid interchange of the tfac anions at room temperature occurs directly,

$$[Pd(tfac)(PPh_3)_2](tfac^*) \rightleftharpoons [Pd(tfac^*)(PPh_3)_2](tfac), \quad (1)$$

or is effected by the forward and reverse processes of

$$[Pd(tfac)(PPh_3)_2](tfac) \rightleftharpoons [Pd(tfac)_2] + 2PPh_3. \quad (2)$$

The fact that [Pd(tfac)(PCy_3)$_2$](tfac) (**4a**) shows no sign of the tfac exchange seems to suggest the associative nature of the ligand exchange, since the bulky PCy_3 ligands may prevent attack of tfac on palladium. Complex **4c** does not undergo the tfac exchange either, probably because of its substitution inertness as compared with the corresponding Pd(II) complex **4b**.

The methyl protons of the chelated β-dik ligands in complexes **4b**—**4e** resonate at δ 1.5—1.7. They are upfield shifted by 0.3—0.8 ppm compared with **4a** and complexes **4** containing nitrogen bases as L.[2] The phenyl rings of PPh_3 situated at the adjacent coordination sites seem to exert the anisotropic magnetic effect.[1a] Similar upfield shift of the methyl proton signals caused by the adjacent PPh_3 ligand is also noticed for complexes **3** and **7**.

Table 2. Characteristic IR bands in Nujol (cm^{-1})

Compd	ν(C=O)+ν(C=C)
3a	1649 m, 1614 vs, 1588 m, 1515 vs
3d	1650 s, 1565 vs, 1510 vs
3e	1647 s, 1561 vs, 1525 vs
3f	1651 m, 1612 vs, 1600 sh, 1520 vs
3h	1646 m, 1564 vs, 1517 vs
3j	1641 s, 1575 vs, 1515 vs
4a	1610 vs, 1560 vs, 1535 sh
4b[a]	1610 vs, 1550 vs, br
4d	1604 m, 1588 s, 1555 vs, 1526 vs
5b	1678 vs, 1547 vs, 1529 vs
5d	1612 s, 1545 vs, br
5g	1676 vs, 1548 vs, 1528 vs
6a	1660 vs, 1513 vs, br
6b	1670 sh, 1660 vs, 1540 vs, br
6c	1646 s, 1510 vs, br
7a	1683 vs, 1650 vs, 1568 vs, br, 1515 vs
7d	1653 vs, 1558 vs, 1517 vs
7f[b]	1715 vs, 1665 s, 1615 vs, br, 1523 vs

a) In $CDCl_3$. b) Orange red oil left after evaporation *in vacuo* of solvent from a solution of [Pd(tfac)(tfac-C^3)-(PPh_3)] (**7f**) of which formation by the reaction of [Pd(tfac)$_2$] with equimolar PPh_3 in $CDCl_3$ was confirmed by ^1H NMR spectroscopy.

Table 3. ^1H NMR data for complexes [ML_4](β-dik)$_2$ (**5**) and *trans*-[Pt(β-dik-*O*)$_2L_2$] (**6**)[a]

Compd	Solvent	β-dik		L		
		CH_3	CH	CH_3	CH_2	Ph
5a	CD_3OD	2.28	5.25[b]			7.4 br[e]
5b	$CDCl_3$		5.67	1.53		7.5 br
	C_6D_6		6.35	1.14		7.0—7.7 m
	CD_3OD		5.57	1.48		7.7 br
5c	CD_3OD		5.55			7.4 br[e]
5d	CD_3OD	2.11	5.23[b]	1.57 br{25}		7.7 br
5e	CD_3OD	2.27	5.22[b]		2.7$_3$ m, br	7.5 br
5f	CD_3OD	2.29	5.24[b]			7.4 br[e]
5g	CD_3OD		5.58[b]	1.58 br{25.$_4$}		7.7 br
5i	CD_3OD		5.56			7.4 br[e]
5j	CD_3OD	2.05 br[b]	5.56[b]		2.77 m, br	7.8 br
		2.32[c]	5.30[b,c]			
6a	$CDCl_3$	2.37{4.4}	6.41{12.7}	1.22[8] (8)[d]	1.66 m	
6b	$CDCl_3$	2.36{4.5}	6.58{11}		1.3 br, 1.9 br	
6c	$CDCl_3$	2.23{6}	6.31{14}	1.20[8] (8)[d]	1.53 m	
		2.06				
		2.35{3}[c]	6.49{12}[c]			

a) Chemical shifts in ppm from internal Me_4Si at 25 °C. Figures in braces, brackets, and parentheses are J(^{195}Pt-H), J(^{31}P-H), and ^3J(CH_2-CH_3) in Hz, respectively. m: multiplet, br: broad. b) The intensity decreases with time due to the H-D exchange reaction with the solvent. c) Signals from the tfac anion. d) Quintet due to the virtual coupling between the ^{31}P atoms located at the mutually trans positions. e) This large signal masks that from the vinyl protons of dpe.

Table 4. ^{1}H NMR data for complexes [M(β-dik)L$_2$](β-dik) (**4**)[a]

Compd	Solvent	β-dik(IS)		β-dik(OS)		L[c]
		CH_3	CH	CH_3	CH	Ph or Cy
4a	$CDCl_3$	2.47	6.08	2.27	5.34	1.9 br, 1.4 br
4b[d]	CD_2Cl_2[e]	2.01 br	5.47 br	2.01 br	5.47 br	7.36 br, 7.46 br
	CD_2Cl_2[f]	1.70	5.92	2.33	5.19	7.43 br
4c[d]	$CDCl_3$	1.47{≈5}	6.01	2.46	5.38	7.4 m, br
4d	$CDCl_3$	1.50{4}	5.51{6}	2.47	5.25	7.3 m, br
	CD_3OD	1.51{3}	5.65{6}	2.30[b]	5.23[b]	7.4 m, br
4e[d]	$CDCl_3$	1.48{3}	5.54{5}		5.61	7.4 m, br, 7.7 m, br

a), b) Same as footnotes for Table 3. IS and OS abbreviate the inner and outer spheres, respectively. c) L is PPh_3 except for **4a** which has PCy_3 as L. d) [M(tfac)(PPh$_3$)$_2$](tfac), where M=Pd (**4b**) and Pt (**4c**), were prepared in solution by the reactions of [M(tfac)$_2$] with twice molar PPh_3, and [Pt(acac)(PPh$_3$)$_2$](hfac) (**4e**) was formed by the reaction of [Pt(acac)(hfac)] with excess PPh_3. See text. e) The β-dik anions in IS and OS are interchanging with each other rapidly at 25 °C. f) At −45 °C.

The ^{1}H NMR data for complexes **6** are included in Table 3. They are quite similar to those for *trans*-[Pt(acac-*O*)$_2$(PEt$_3$)$_2$][6] and *trans*-[Pt(acac-*O*)$_2$(pip)$_2$],[3] where pip represents piperidine. Each of **6a** and **6b** exhibits single tfac-methyl signal flanked by the ^{195}Pt satellites, indicating that the acetyl oxygen is preferentially bonded to the metal. The characteristic quintet resonance (J=8 Hz) of the methyl protons of PEt_3 in **6a** and **6c** suggests the trans arrangement of the PEt_3 ligands.[11] Even when *cis*-[Pt(tfac)$_2$] reacted with the phosphine, the product was *trans*-[Pt-

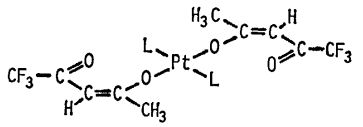

L=PEt_3 (**6a**) and PCy_3 (**6b**)

(tfac-*O*)$_2$L$_2$] exclusively. The trans configuration seems to be thermodynamically more stable and may have been realized by the geometrical isomerization catalyzed by the tertiary phosphine[12] contained in excess in the reaction mixture. The cis-trans isomerization may proceed by means of the intramolecular rearrangement of a five-coordinate intermediate. The dynamic behavior in solution of the five-coordinate complexes [M(hfac)$_2${P(*o*-tolyl)$_3$}] (M=Pd and Pt) was elucidated by the ^{13}C and ^{19}F NMR spectroscopy and interpreted based on a proposed mechanism.[5]

Complexes **3** are stable in solution. Molecular weights of **3a** and **3e** were determined in dichloromethane to be 716 and 659, which are near the calculated values, 717 and 698, respectively. The ^{1}H NMR data for **3** are listed in Table 5. Since the tfac anion is unsymmetric, the following two geometrical isomers are conceivable even though the unidentate tfac is bound to the metal preferentially *via* the more basic acetyl oxygen as was the case for com-

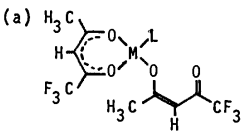

cis(Me,L)

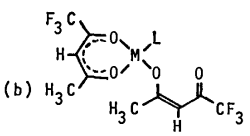

trans(Me,L)

plexes **6**. Thus four tfac-methyl signals are observed for **3f** at 1.63, 1.92, 1.97, and 2.11 ppm with the area ratio of 1:1:4:4, disclosing coexistence of the two isomers in the 1:4 ratio. The signal at the highest field is readily assigned to CH_3(a) of the chelating tfac in the *cis*(Me,L) isomer and in turn the signal at δ 1.92 to CH_3 of the O-unidentate tfac in the same isomer. The remaining signals at δ 1.97 and 2.11 are attributed to the *trans*(Me,L) isomer, but discrimination of them is not straightforward. The higher-field signal (δ 1.97) near the above one at δ 1.92 is tentatively assigned to CH_3 of the O-unidentate tfac and the one at δ 2.11 to CH_3(b) of the chelating tfac. The assignment is supported by the fact that the methyl protons of the chelating tfac in the *trans*(Me,L) isomer of [Pd(tfac)(tfac-*C*^{3})(PPh$_3$)] (**7f**) also resonate at 2.22 ppm. It is noteworthy that the CH_3(a) protons couple to ^{195}Pt (^4J=4 Hz) but CH_3(b) does not in accordance with the higher trans influence of the tertiary phosphine than that of the O-unidentate β-dik which is shown by the following ^{31}P NMR data.

Figure 1 displays the ^{19}F{^{1}H} NMR spectrum of **3f** in $CDCl_3$. Two overlapping triplets are observed at 72.81 and 72.96 ppm upfield from external $CFCl_3$,

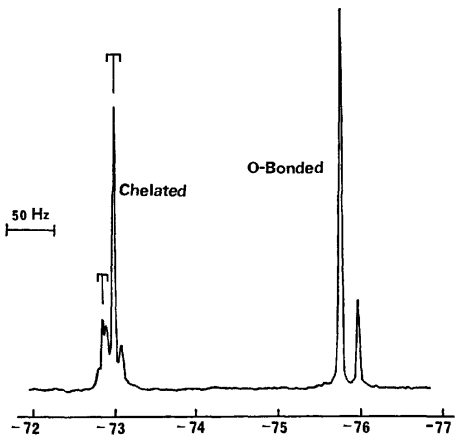

Fig. 1. ^{19}F{^{1}H} NMR spectrum at 84.31 MHz of [Pt(tfac)(tfac-*O*){P(*o*-tolyl)$_3$}] (**3f**) in $CDCl_3$.

TABLE 5. ^{1}H NMR DATA FOR COMPLEXES **3** AND **7** IN $CDCl_3$[a]

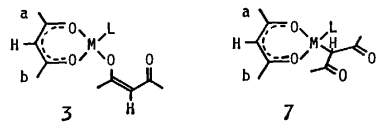

3 7

Compd	cis / trans	Isomer	Chelated β-dik			Unidentate β-dik		L	
			CH_3(a)	CH_3(b)	CH	CH_3	CH	CH_3	Ph[b]
3a	1/5	cis	1.74		c)	1.89	c)	2.29	7.87 dd[12](7), 1.9 br, 1.3 br
		trans		2.20	5.76	1.94	5.84		
3b		cis[c]							7.5 m, br
		trans		2.23	5.90	2.02	6.27		
3c	1/5	cis	2.13		5.70	2.17	5.94		Cy: 1.9 br, 1.3 br
		trans		2.52	5.94	2.20	6.30		
3d			1.56	2.05	5.44	1.93	5.91	2.33	7.88 dd[13](8), 7.2—7.6 m
3e			1.46{4}	1.98	5.43{6.5}	1.89, 1.82	5.72{7.5}	2.29	7.78 dd[13](7), 7.1—7.5 m
3f	1/4	cis	1.63{4}		c)	1.92	c)	2.27	7.84 dd[13](7), 7.2—7.6 m
		trans		2.11	5.85{6.5}	1.97{≈4}	5.94{7.5}		
3g	≈1/4	cis	1.72{4}		c)	c)	c)		7.4 m, br
		trans		2.11	5.92	1.97	6.33		
3h			1.48{5}	1.95	5.43{7.5}	1.95	5.88	2.28	7.82 dd[15](7), 7.0—7.4 m
3i			1.64{5}	2.00	5.52{7}	2.00{≈3}	6.39{8}		7.2—7.8 m
3i[d]			1.45{5}	1.81	5.23{7.5}	2.05{4}	6.44{9}		7.1—7.7 m
3j			c)	c)	5.48	c)	6.47		Et: c)
3k			1.54{5}	1.90	5.42{9}		5.59		7.3—7.9 m
7a			1.84	1.94	5.09	2.20	3.53[4]	1.26(6)	CH_2: 1.5—2.1 m
7b			1.92	1.99	5.37	2.06	3.55[5]	1.78[11]	7.2—7.8 m
7c			1.64	2.02	5.51	2.17	3.72[5]	2.11[11]	7.2—7.8 m
7d[e]	1/1	cis	1.55		5.94	2.60	4.38[5.4]		
		trans		2.16	5.98	2.58			
7e[f]	1/1				6.20		4.41[5]		Ph and thienyl: 7.2—7.8 m
					6.23		4.34[5]		
7f	1/3	cis	1.65		5.75	2.43	3.91[4]		7.3—7.8 m
		trans		2.22	5.76	2.41	3.98[4]		

a) Same as footnote(a) for Table 3. Cis and trans abbreviate *cis*(Me,L) and *trans*(Me,L), respectively. See text. b) dd: doublet of doublets. The coupling constants ^3J(P–H) and ^3J(C–H) are given in brackets and parentheses, respectively. c) Indiscernible because of overlapping with other signals. d) Determined in a mixture of $CDCl_3$ and C_6D_6 (2:1 by volume). e) Phenyl protons of the bzac and PPh_3 ligands resonate at 6.9—7.9 ppm. f) Two isomers coexist in approximately equal proportions but are indistinguishable.

^4J(Pt–F) being *ca.* 10 and 16 Hz, respectively. On the basis of their relative intensities, the more intense higher-field signal is assigned to CF_3 of the chelating tfac in the *trans*(Me,L) isomer and the lower-field one to that in the *cis*(Me,L) isomer. Two sharp singlets observed at 75.74 and 75.97 ppm upfield from external $CFCl_3$ with the area ratio of 4:1 are assigned to the CF_3 groups of unidentate tfac in the *trans*(Me,L) and *cis*(Me,L) isomers, respectively. It should be noted that the dangling CF_3CO group has no bonding interaction with the platinum atom, exhibiting a sharp ^{19}F singlet. The five coordinate complex [Pt(hfac)$_2$-{P(*o*-tolyl)$_3$}] containing the phosphine ligand in the basal plane of a square pyramid structure[5] exhibits an analogous ^{19}F NMR spectrum, but the higher-field singlet is broad, indicating coupling to platinum.

The ^{31}P{^{1}H} NMR spectrum of **3f** in $CDCl_3$ shows two signals at 4.5_1 and 5.2_5 ppm upfield from external H_3PO_4 flanked by the ^{195}Pt satellites with ^1J(Pt–P)= 4410 and 4380 Hz, respectively. Based on the relative intensities, they are assigned to the *cis*(Me,L) and *trans*(Me,L) isomers, respectively. The minor signal at 4.5_1 appears as a quartet with ^5J(F–P)=1.1 Hz, certifying that the CF_3 group occupies the trans position to the phosphine ligand in the *cis*(Me,L) isomer. The larger ^1J(Pt–P) value for the *cis*(Me,L) isomer than that for *trans*(Me,L) suggests that the poorer donor-ability of the CF_3CO moiety than that of CH_3CO decreases the charge density at platinum, suppressing the π-character and increasing the σ-character of the trans Pt–P bond.

Complex **3f** was produced by the reaction of P(*o*-tolyl)$_3$ with either of *cis*- and *trans*-[Pt(tfac)$_2$] and the ratio of *cis*(Me,L) and *trans*(Me,L) is almost constant. Geometrical isomerization catalyzed by the tertiary phosphine *via* a five-coordinate intermediate as mentioned above may have occurred to result in the equilibrium mixture of **3f**, since the bulkiness (cone angle 194°)[13] of P(*o*-tolyl)$_3$ seems to make the consecutive substitution mechanism (Eq. 3) *via* a bis(phosphine) complex less probable.

[Pt(acac)(acac-*O*){P(*o*-tolyl)$_3$}] (**3e**) exhibits four acetyl-methyl signals, which were assigned by reference to **3f** and [Pt(acac)(acac-*C*^{3})(PPh_3)].[7] Proton res-

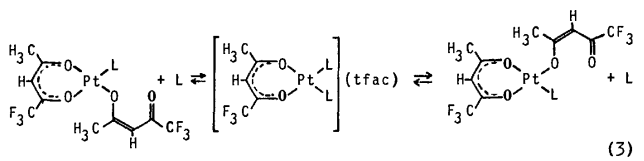

cis(Me,L) trans(Me,L) (3)

onances from other complexes **3** were assigned in a similar way and listed in Table 5. It should be noted that the CH_3(a) protons in [Pd(tfac)(tfac-*O*)(PCy$_3$)] (**3c**) resonate at much lower field as 2.13 ppm than those in other complexes containing the triarylphosphine as L.

[Pt(acac)(tfac-*O*){P(*o*-tolyl)$_3$}] (**3h**) exhibits two acetyl-methyl signals at 1.48 and 1.95 ppm in the area ratio of 1:2. The peak at δ 1.48 is assigned to CH_3(a) of the chelated acac and the other to CH_3(b) of acac and CH_3 of the O-unidentate tfac which resonate at the same field accidentally. If tfac were chelated alternatively to Pt and acac served as the unidentate ligand, more peaks (at most six) should appear, since two geometrical isomers are possible and the unidentate acac should exhibit two separate methyl signals. The corresponding palladium(II) complex **3d** shows three signals at 1.56, 2.05, and 1.93 ppm, of which the former two are assigned to the chelated acac and the last one to the unidentate tfac in a similar manner as above.

Thus the chelated tfac has stronger tendency than acac to transform into the O-unidentate state. In fact [Pd(acac)$_2$] did not react with three times molar P(*o*-tolyl)$_3$ even when kept in boiling toluene for 5 h, whereas [Pd(tfac)(tfac-*O*){P(*o*-tolyl)$_3$}] (**3a**) was formed in a good yield when equimolar amounts of [Pd(tfac)$_2$] and P(*o*-tolyl)$_3$ were mixed in hot benzene and the mixture was kept overnight at room temperature. However, compound **3d** is not so stable in $CDCl_3$, but about 30% of P(*o*-tolyl)$_3$ is liberated according to

$$[Pd(acac)(tfac\text{-}O)\{P(o\text{-tolyl})_3\}] \rightleftharpoons [Pd(acac)(tfac)] + P(o\text{-tolyl})_3. \quad (4)$$

On addition of excess phosphine, the equilibrium is shifted to left and proton signals from [Pd(acac)(tfac)] disappears. On the contrary, complex **3h** is quite stable in solution and shows no sign of dissociation. Thus the platinum(II) complexes of type **3** seem more stable than the corresponding palladium(II) complexes.

The proton signal pattern of [Pt(acac)(tfac-*O*)(PPh$_3$)] (**3i**) in $CDCl_3$ resembles quite well to that of **3h**. On addition of C_6D_6 to this solution, the overlapped methyl signal at 2.00 ppm was separated, giving rise to three equi-intensity methyl signals. It has been reported that as compared with the spectra in other solvents, C_6D_6 shifts the methyl and methine signlas from the chelated β-dik to the higher field and those from β-dik in the outer sphere to the lower field.[2,8b] The δ 1.45, 1.81, and 5.23 signals observed in the mixed solvent lie in the higher field than the corresponding ones in $CDCl_3$ and are assigned to CH_3(a), CH_3(b), and CH of the chelated acac, respectively. The remaining peaks at δ 2.05 and 6.44 are then ascribed to CH_3 and CH of the unidentate tfac, indicating that C_6D_6 shifts these resonances to the lower field in a similar way as it shifts the signals from β-dik in the outer sphere. Thus the two CH signals for **3i** were distinguished, the higher-field one being assigned to the chelated β-dik and the lower-field one to the O-unidentate β-dik. Similarly methine signals from each of compounds **3** were distinguished and listed in Table 5.

When PEt_3 was added in small portions to $CDCl_3$ solutions of [Pt(acac)$_2$] and [Pt(tfac)$_2$], proton signals attributable to [Pt(β-dik-*O*)$_2$(PEt$_3$)$_2$] (**6**) appeared, but those assignable to the intermediate complexes **3** could not be observed. On the other hand, addition of PEt_3 to a solution of [Pt(acac)(tfac)] in $CDCl_3$ gave rise to new signals at 5.48 and 6.47 ppm, which are assigned to methine protons of [Pt(acac)(tfac-*O*)(PEt$_3$)] (**3j**). Methyl resonances of **3j** were indiscernible because of overlapping with signals from **6c**, successor of **3j**. In a similar manner, addition of PPh_3 in limited amounts to a $CDCl_3$ solution of [Pt(acac)(hfac)] produced proton signals due to [Pt(acac)(hfac-*O*)(PPh$_3$)] (**3k**) as recorded in Table 5. Compound **3j** was isolated, while **3k** was not. However, characterization of these compounds in solution suggests that compounds [Pt(acac)(β-dik-*O*)L] containing chelated acac and unidentate β-dik other than acac are more stable than the corresponding compounds **3** containing one kind of β-dik.

As is noticed in Table 5, the *trans*(Me,L) isomers of compounds **3** containing tfac are invariably more stable than the *cis*(Me,L) isomers. The σ-donating ability of the CH_3CO moiety is higher than that of the CF_3CO moiety, strengthening the Pt–phosphine π-bonding. Although the σ-character of the Pt–P bond is decreased in this case as was evidenced by the lower ^1J(Pt–P) value for *trans*(Me,L)-**3f** than that for the cis isomer, the overall stability of the *trans*-(Me,L) isomer is higher, suggesting that the π-bonding of Pt–phosphine is more important than the σ-bonding in these complexes.

The ^{1}H NMR spectrum of the O-unidentate acac was first recorded for R_3Si(acac-*O*) by Pinnavaia and his collaborators.[14] It is composed of two sets of signals assignable to two geometrical isomers. The trans isomer, in which the acetyl and R_3SiO groups occupy the trans positions around the C=C bond, exhibits a methine multiplet and two acac methyl doublets as the result of the spin-spin coupling between the methine proton and both methyl groups. On the other hand, the cis isomer shows a methine singlet and a methyl singlet due to a rapid fluxional motion at room temperature interchanging intramolecularly the coordinating oxygen atom of the unidentate acac ligand. The unidentate acac in **3e** and **6c** exhibits one methine and two methyl resonances showing no coupling to each other. Similarly the unidentate tfac in each of other compounds **3** and **6** gives only one set of mutually uncoupled methine and methyl signals for the *cis*(Me,L) or *trans*(Me,L) isomer. These results indicate that the unidentate acac and tfac ligands always have the stereochemically rigid cis structure as depicted above. The O-unidentate β-dik originates from the O,O′-chelate and

cis configuration around the C=C bond was reserved during the reactions with phosphines under the mild conditions.

Table 5 includes the ^{1}H NMR data for complexes **7** inclusive of **7b** and **7f** which were not isolated. Proton signals from [Pd(acac)(acac-C^3)L] (L=PEt_3 (**7a**), PMe_2Ph (**7b**), and $PMePh_2$ (**7c**)) were assigned by reference to [Pd(acac)(acac-C^3)(PPh_3)].[18] There exist *cis*(Me,L) and *trans*(Me,L) isomers in the case of **7d**, **7e**, and **7f** containing unsymmetrical β-dik, and the signals were assigned by reference to the data for [Pt(etac)(etac-C^2)(PPh_3)],[15] of which etac represents the 1-ethoxy-1,3-butanedionate anion. Since [Pd(tta)(tta-C^2)(PPh_3)] (**7e**) lacks the methyl group, the geometrical isomers are indistinguishable though two sets of methine signals indicate their coexistence. When an equimolar amount of PPh_3 was added to a solution of [Pd(tfac)$_2$] in $CDCl_3$, proton signals ascribable to [Pd(tfac)(tfac-*O*)(PPh_3)] (**3b**) appeared first followed by those due to [Pd(tfac)(tfac-C^3)(PPh_3)] (**7f**), which is more stable and was the sole product after 1 h. [Pd(bzac)(bzac-C^2)(PPh_3)] (**7d**) is also stable in dichloromethane, giving a molecular-weight value of 640 near the calculated value (691).

^{13}C NMR Spectra. The ^{13}C NMR data for compounds **5** are listed in Table 6. None of the carbon signals from β-dik in **5** is flanked by ^{195}Pt satellites, indicating that the β-dik anions are not coordinated with the metal atom. The CH_3 and CF_3 carbon signals from β-dik in the outer sphere show downfield shift of 2—4 ppm, while the CH carbon upfield shift of 3—10 ppm as compared with the corresponding carbons in [M(β-dik)$_2$]. The ^1J(C-F) value for compounds **5** is more than 5 Hz larger and ^2J(C-F) is about 4 Hz smaller than those for the corresponding carbons in the bis-chelates. Similar trend was also noted for complexes of the type **5** containing nitrogen bases as L[2] and for [K(18-Crown-6)](β-dik).

Compound **4a** exhibits two sets of carbon signals from β-dik, which were easily assigned as is listed in Table 7 based on the above information. The CH_3 carbon of the chelated tfac appears as a doublet of doublets due to coupling to both ^{31}P atoms, ^4J(P-C) being 5 Hz to trans P and 2 Hz to cis P. The CF_3 carbon, on the other hand, couples only to trans P(^4J=9 Hz). The acetyl carbon, $CH_3\underline{C}O$, also couples only to trans P and the ^3J(P-C) is smaller (2.5 Hz) than that for CH_3 which is remote from P. Similar situation is observed for [Pt(β-dik)$_2$];[8] the ^3J(Pt-C) values for CH_3, CF_3, and CH are about twice

Table 6. ^{13}C NMR data for [ML_4](β-dik)$_2$ (**5**) in CD_3OD[a]

Compd	CH_3	CF_3	CH	$CH_3\underline{C}O$	$CF_3\underline{C}O$	L
5a	29.0	121.3	96.1	199.7	171.7	CH: 146.0 q((19)); Ph: P-C 125.0 m, *o*-C
	(127)	[290]	c)		[29]	134.0 q((3.4)), *m*-C 131.2 q((2.5)), *p*-C 134.6
5b[d]		118.1	85.5		173.7	CH_3: 14.5 br; Ph: 129—131
		[291]			[30]	complex
5c		119.3	85.8		175.2	CH: 146.1 q((19)); Ph: P-C 125.2 m, *o*-C
		[287]			[32]	134.2 q((3.4)), *m*-C 131.3 q((2.5)), *p*-C 134.7
5e	29.1	121.3	96.1	199.8	171.8	CH_2: 29.4 m; Ph: P-C 125.2 m, *o*-C 135.0
		[289]			[29]	br, *m*-C 130.8 q((2.5)), *p*-C 134.7
5f	29.0	b)	96.1	199.8	171.8	CH: 146.1 m, br; Ph: P-C 124.7 m, *o*-C
					[28]	134.2 q((3.4)), *m*-C 131.1 q((2.5)), *p*-C 134.6
5g		119.5	85.9		175.1	CH_3: 14.4 m; Ph: 130—134
		[290]			[31]	complex
5i		b)	85.9		b)	CH: 147.0 m; Ph: P-C 125.1 m, *o*-C 134.9
						q((3.4)), *m*-C 131.2 q((2.5)), *p*-C 134.8

a) Chemical shifts in ppm from internal Me_4Si. Figures in parentheses, double parentheses, brackets, and braces give ^1J(C-H), J(^{31}P-C), J(^{19}F-C), and J(^{195}Pt-C) in Hz, respectively. q: quintet, m: multiplet, br: broad. b) Indiscernible because of low intensity or overlapping with other signals. c) Indiscernible because of the fast H-D exchange with the solvent. d) In $CDCl_3$.

Table 7. ^{13}C NMR data for [Pd(tfac)L_2](tfac) (L=PCy_3 (**4a**) and L=PPh_3 (**4b**)) in $CDCl_3$[a]

Compd		CH_3	CF_3	CH	$CH_3\underline{C}O$	$CF_3\underline{C}O$	PCy_3[c] or PPh_3
4a	IS[d]	28.5	118.5	96.8 br	194.5	166.7	C^α 34.1 br((19)), 34.2 br((19));
		((5;2))	((9))		((2.5))	[34]	C^β 27.3 br((9)); C^γ 30.3 br;
			[284]				
	OS[d]	29.3	120.8	94.5	197.0	170.1	C^δ 25.8 br
			[292]			[28]	
4b[e]		28.4	b)	95.7	196.0	168	P-C 126.1 br((59)), *o*-C 134.1((11)), *m*-C
							129.0((11)), *p*-C 132.3

a, b) Same as footnotes for Table 6. c) 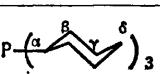 d) IS and OS refer to tfac in the inner and outer spheres.

e) Only one set of broad signals for tfac was observed due to the rapid exchange reaction between tfac anions in the inner and outer spheres.

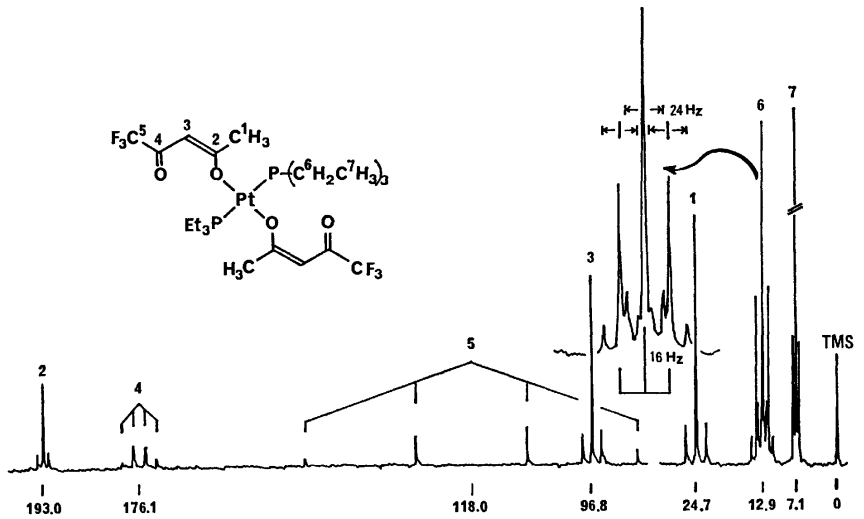

Fig. 2. $^{13}C\{^1H\}$ NMR spectrum at 15.04 MHz of [Pt(tfac-*O*)$_2$(PEt$_3$)$_2$] (**6a**) in $CDCl_3$. The J(Pt–C) values are 55, 28, and 55 Hz for CH_3, CO, and CH of tfac, respectively, and 24 and 15 Hz for CH_2 and CH_3 of PEt_3, respectively. ^1J(C–F)=292 Hz, ^2J(C–F)=31 Hz.

as large as the ^2J(Pt–C) values for $CH_3\underline{C}O$ and $CF_3\underline{C}O$.

Compound **4b** shows one set of carbon signals from β-dik, which are broad, sharpening at higher temperature, and their chemical shifts are rough average of those for tfac anions in the inner and outer spheres of **4a** except the CH_3 carbon. The exchange reaction between tfac anions in **4b** is occurring in $CDCl_3$ solution rapidly on the NMR time scale as was also evidenced by the ^1H NMR spectra (*vide supra*).

Figure 2 displays the $^{13}C\{^1H\}$ spectrum of [Pt(tfac-*O*)$_2$(PEt$_3$)$_2$] (**6a**) in $CDCl_3$. Each carbon of the CH_3COCH moiety couples to ^{195}Pt (J=55, 28, and 55 Hz, respectively), whereas CF_3 does not, implying that the tfac ligands coordinate to the metal *via* the acetyl oxygen without bonding interaction through CF_3CO. The CH_2 carbon of PEt_3 resonates at 12.9 ppm as a 1:2:1 triplet (J(P–C)=16 Hz) flanked by ^{195}Pt satellites. Although the $^{13}C\{^1H\}$ NMR spectra were first thought to provide a powerful tool for determining the stereochemistry of bis(phosphine) metal complexes,[16] later studies have questioned this proposal.[17] Nelson and his collaborators[18] showed that normally the ^{13}C resonances for the cis isomers of the square-planar $MX_2(PR_3)_2$ type complexes should appear as a quintet, a non 1:2:1 triplet, a doublet of doublets, or a doublet depending on the relative values of ^2J(P–P′) and $|^1J(P–C)^3-J(P'–C)|^2$, while those for the trans isomers with large ^2J(P–P′) always appear as 1:2:1 triplets. The 1:2:1 appearance of the CH_2 carbon of PEt_3 in **6a** seems to support the trans structure of **6a** in accordance with the ^1H NMR evidence (*vide supra*). The fact that the ^{13}C signals from the O-unidentate tfac ligands in **6a** show no coupling to ^{31}P is also in conformity with the trans structure.

The complex $^{13}C\{^1H\}$ NMR spectra of compounds **3** were analyzed based on the above-mentioned characteristics of the O-unidentate β-dik and also on the equilibrium ratio of the *cis*(Me,L) and *trans*(Me,L) isomers determined by the ^1H NMR spectroscopy. As is noticed in Table 8, the difference in the ^{13}C shielding between the two geometrical isomers is more remarkable for the chelated tfac than for the O-unidentate tfac. It seems to be caused by the larger difference in the trans influence between the tertiary phosphine and the O-unidentate tfac than that between the CH_3CO and CF_3CO moieties of the chelated tfac ligand.

The ^{13}C NMR data for [Pd(bzac)(bzac-*C*^{2})(PPh$_3$)] (**7d**) and [Pd(tfac)(tfac-*C*^{3})(PPh$_3$)] (**7f**), both having unsymmetric β-dik, are included in Table 8. Their spectra resemble those of [M(acac)(acac-*C*^{3})(PPh$_3$)] (M=Pd and Pt)[7] but are more complex due to coexistence of the geometrical isomers. The isomer ratio determined by the ^1H NMR spectroscopy was again helpful in assigning the ^{13}C signals. In a similar manner as the case of compounds **3**, the difference in the ^{13}C shielding between the *cis*(Me,L) and *trans*(Me,L) isomers is more remarkable for the chelated bzac and tfac ligands than for the central-carbon bonded ones. It is worth noting that the carbon-bonded tfac discriminates the geometry of the chelated tfac, whereas the carbon-bonded bzac is insensitive to the configuration of the chelated bzac. Thus the two signals assigned to C^8 of *cis*-**7f** and *trans*-**7f** are 0.5 ppm apart from each other, while C^8 of **7d** resonates as a single peak. The difference in trans influence between the CH_3CO and CF_3CO moieties in the chelated tfac seems to be larger than that between the CH_3CO and C_6H_5CO moieties in the chelated bzac.

The Sequence of Reactions between [M(β-dik)$_2$] and Tertiary Phosphines and Relative Stabilities of Various Products. Compounds **2**—**7** in Scheme 1 were obtained by the reactions of [M(β-dik)$_2$] with tertiary phosphines. When an equimolar amount of PPh_3 was added to a solution of [Pd(tfac)$_2$] in $CDCl_3$, the ^1H NMR signals attributable to **3b** appeared first prior to those assignable to **7f** which was the final product in this case. Employment of twice molar PPh_3 gave rise to **4b**, which was characterized in solution. Thus,

Table 8. ^{13}C NMR data for some complexes of types **3** and **7** in $CDCl_3$[a)]

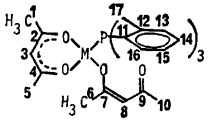

cis(Me, L)-3

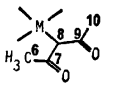

cis(Me, L)-7

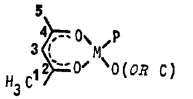

trans(Me, L)-3 and -7

Compd	Chelated β-dik					Unidentate β-dik					$P(o\text{-tolyl})_3$ or PPh_3						
	C^1	C^2	C^3	C^4	C^5	C^6	C^7	C^8	C^9	C^{10}	C^{11}	C^{12}	C^{13}	C^{14}	C^{15}	C^{16}	C^{17}
cis-**3a**	27.5 ((2)) (130)	195.7	95.7 (163)	169.5 [34]	b)	25.8 (128)	193.6	94.9 (154)	175.6 [30]	117.8 (292)	122.6 ((56))	142.9 ((8))	131.9 ((9))	131.8 ((3))	126.2 ((12)) (163)	135.2 ((12))	23.1 ((7)) (126)
trans-**3a**	28.1 ((7)) (130)	195.7 ((3))	97.1 (160)	166.2 [34]	b)						122.4 ((56))	143.0 ((8))	(161)	(161)	126.1 ((12)) (163)	(162)	22.9 ((7)) (126)
3e	b)	183.9 {24}	101.6 {69}	185.8 {16} ((3))	b)	b)	183.6 {30}	102.5 {22}	194.3	30.8	123.5 ((60)) {19}	142.8 ((9)) {18}	131.5 ((11))	131.3	125.6 ((12))	135.4 ((12)) {22}	22.8 ((6))
cis-**3f**	27.3	b)	97.7	b)	b)	24.8	b)	94.6	b)	118.0	122.4 ((65))	142.8	132.1	131.9	126.0 ((12))	135.2	22.9 ((≈6))
trans-**3f**	28.2 {b)} ((7))	193.2 {24} ((4))	98.9 {68}	165.0 [34]	b)	{55}	193.4 {27}	{23}	175.8 [31]	[292]	122.2 ((65)) {20}	((9)) {17}	((11))		125.8 ((12))	((13)) {19}	22.7 ((6))
cis-**7d**[c)]	27.5	186.9		177.8	b)				197.8								
			96.1 br	((3))		31.4	208.0	47.8		141.5							
trans-**7d**[c)]	29.2 ((7))	188.1 ((3))		178.8	b)			((5))	197.5								
cis-**7f**	28.2 br ((≈2))	193.6	95.7 br	167.9 [34]	b)	31.0	204.9	43.4 ((4))	186.4 [33]	b)	b)	134.1 ((11))	128.6	132.0 ((3))			
trans-**7f**	29.7 ((7))	194.5 ((3))		166.8 [33]	b)	31.1	204.3	43.9 ((4))	186.6 [32]	b)	126.8 ((49))	134.5 ((11))	((11))	131.5 ((3))			

a, b) Same as footnotes for Table 6. c) The phenyl-ring carbons of bzac and PPh_3 resonate in the 126.5—141.5 ppm region and are indiscernible because of overlapping except the quaternary carbon (C^{10}) of the C-bonded bzac resonating at 141.5 ppm and the ortho carbon of PPh_3 at 134.8 ppm with $^2J(P\text{-}C) = 11$ Hz.

compound **7** seems to be formed by a sequence of reactions **1**→(**2**)→**3**→**4**→**7** as was the case for [Pd(acac)(acac-C^3)Et$_2$NH].[4] The reaction **4**⇄**7** is reversible and controlled by relative concentrations of the reactants. The five-coordinate complex of the type **2** was not identified for this reaction system, but is presumed to be involved as an intermediate, since stable compound **2** was isolated in the reaction of [Pd(hfac)$_2$] with P(*o*-tolyl)$_3$.[5]

When *cis*-[Pt(tfac)$_2$] was allowed to react with an equimolar amount of PPh$_3$, the product was exclusively **3g**, which was converted to **4c** by the reaction with another equivalent of PPh$_3$. Similar NMR spectroscopic observation of the reaction sequence was also performed for [Pt(acac)(hfac)].

Relative stabilities of these ternary complexes are determined by the natures of the metal ion, β-dik, and L, and also by the combination of these components. The O-unidentate linkage of β-dik in complexes **3** and **6** seems to be more favorable for Pt(II) than for Pd(II) as suggested by Table 1. For instance, [Pt(acac)$_2$] reacts with P(*o*-tolyl)$_3$ to yield **3e**, while [Pd(acac)$_2$] does not. Both of [M(tfac)$_2$] (M= Pt and Pd) react with equimolar PCy$_3$ to produce compounds **3**, but the succeeding reactions with another mole of PCy$_3$ give rise to **6b** in the Pt(II) case, while to **4a** in the Pd(II) case. It is noteworthy that Pd(II) prefers [Pd(tfac)(PCy$_3$)$_2$](tfac) (**4a**) over the *trans*-[Pd(tfac-*O*)$_2$(PCy$_3$)$_2$] structure in spite of the mutual steric hindrance of the two PCy$_3$ ligands at the cis positions in **4a**.

The central carbon bonding in **7** is much more favorable for Pd(II) than for Pt(II). Thus the reaction of PEt$_3$ with [Pd(acac)$_2$] gives **7a** exclusively, whereas that with [Pt(acac)$_2$] results only in [Pt(acac-*O*)$_2$(PEt$_3$)$_2$].[6] In the reactions of [M(acac)$_2$] with secondary amines, Pd(II)[2a] gave complexes of types **4** and **7**, while Pt(II)[2b] **4** and **6**. On the other hand, [Pt(acac)$_2$] was reported to produce [Pt(acac-C^3)$_2$(py)$_2$] besides [Pt(acac)(acac-C^3)(py)],[19] but [Pd(acac)$_2$] gave only the latter type-**7** complex.[1a] Platinum looks to prefer carbon bonding with acac more strongly than palladium does in this [Pd(acac)$_2$]–py system, although reasonable rationalization is difficult.

As to the role of β-dik, the basicity is the most important factor. Thus the reactivity of [Pd(β-dik)$_2$] with nitrogen bases was in the sequence acac<tfac< hfac, half prefering most strongly to go out of the coordination sphere.[2] Similar trend is also observed for reactions with less bulky tertiary phosphines (Table 1). The type-**2** complexes were obtained only from [M(hfac)$_2$] whose acidity may be the highest among the [M(β-dik)$_2$] complexes due to the lowest basicity of hfac.

The unsymmetric tfac anion seems to stabilize the O-unidentate linkage as compared with acac, giving many kinds of compounds of the **3** and **6** types. On the other hand, [M(acac)$_2$] gave **7** by the reactions with phosphines[1a,7] except P(*o*-tolyl)$_3$ and PEt$_3$ which reacted with [Pt(acac)$_2$] to afford **3e** and the type-**6** complex,[6] respectively. The central carbon bonding is more favorable for acac than for tfac and hfac. Ito and Yamamoto[20] examined the reactions of [Pt(acac)(acac-C^3)(PPh$_3$)] with several β-dicarbonyl compounds (β-dikH) in refluxing toluene and found that the keto-favoring β-dikH could replace the carbon-bonded acac more easily.

The reactions of [M(acac)(β-dik)] with phosphines clearly distinguish the labilities of the β-dik ligands. The tfac or hfac chelate is preferentially cleaved firstly, the acac chelate being preserved intact. Complexes **3** and **4** derived from the mixed ligand chelates seem to be more stable than those from the binary chelates. The acac ligand preferring the chelated state and tfac which is suitable as the unidentate ligand or counter anion may cooperate to stabilize **3** and **4**.

The σ-basicity of tertiary phosphines was deduced from the frequency of the A_1 carbonyl mode of Ni(CO)$_3$L in CH$_2$Cl$_2$ to be in the sequence,[13] PCy$_3$> PEt$_3$ > PMe$_2$Ph > P(*o*-tolyl)$_3$ > PMePh$_2$ > PPh$_3$. The fact that the reaction of [Pt(acac)$_2$] with PPh$_3$ gives **7**,[7] whereas that with PEt$_3$ results solely in **6**[6] seems to reflect the electronic effect of phosphines on the choice of the bonding mode of β-dik ligands. In complexes **7**, less σ-basic and more π-acidic triarylphosphines will diminish the charge density on the metal atom, strengthening the bond with strong σ-donors such as the carbon-bonded β-dik. On the other hand, strongly σ-basic trialkylphosphines will prefer the O-unidentate β-dik which is a weak σ-donor to the carbon-bonded one, stabilizing complexes **6**.

The steric effect of tertiary phosphines is more remarkable. For example, P(*o*-tolyl)$_3$ can convert only one of the chelating ligands in [M(β-dik)$_2$] into the O-unidentate state to result in complexes **3**, but can not give succeeding products. Bulky P(*o*-tolyl)$_3$ (cone angle 194°)[13] in the coordination sphere might prevent attack of the second phosphine molecule on the central metal in both the kinetic and thermodynamic senses. On the other hand, PPh$_3$ (cone angle 145°)[13] can conduct reactions to give **3**→**4**→**7**. Less bulky PMe$_2$Ph (122°) and dppe (125°)[13] afford complexes **5** although the electronic factor might also be favorable.

We wish to thank Mr. Junichi Gohda for the elemental analysis and Mr. Tetsu Hinomoto of JEOL, Ltd. for the measurements of ^{19}F and ^{31}P NMR spectra. S. O. and S. K. are also grateful to the Ministry of Education, Science, and Culture for Grant-in-Aid for Scientific Research, Nos. 454196 and 243014, respectively.

References

1) a) S. Baba, T. Ogura, and S. Kawaguchi, *Bull. Chem. Soc. Jpn.*, **47**, 665 (1974); b) M. Horike, Y. Kai, N. Yasuoka, and N. Kasai, *J. Organomet. Chem.*, **72**, 441 (1974).

2) a) S. Okeya, H. Sazaki, M. Ogita, T. Takemoto, Y. Onuki, Y. Nakamura, B. K. Mohapatra, and S. Kawaguchi, *Bull. Chem. Soc. Jpn.*, in press; b) S. Okeya, Y. Nakamura, and S. Kawaguchi, to be published.

3) S. Okeya, F. Egawa, Y. Nakamura, and S. Kawaguchi, *Inorg. Chim. Acta*, **30**, L319 (1978).

4) S. Matsumoto and S. Kawaguchi, *Bull. Chem. Soc. Jpn.*, **53**, 1577 (1980).

5) S. Okeya, T. Miyamoto, S. Ooi, Y. Nakamura, and S. Kawaguchi, *Inorg. Chim. Acta*, **45**, L135 (1980).

6) T. Ito, T. Kiriyama, and A. Yamamoto, *Chem. Lett.*, **1976**, 835.
7) T. Ito, T. Kiriyama, and A. Yamamoto, *Bull. Chem. Soc. Jpn.*, **49**, 3250 (1976).
8) a) S. Okeya and S. Kawaguchi, *Inorg. Synth.*, **20**, 65 (1980); b) S. Okeya, S. Ooi, K. Matsumoto, Y. Nakamura, and S. Kawaguchi, *Bull. Chem. Soc. Jpn.*, in press.
9) S. Okeya, Y. Nakamura, and S. Kawaguchi, *J. Chem. Soc., Chem. Commun.*, **1977**, 914.
10) S. Okeya, N. Yanase, Y. Nakamura, and S. Kawaguchi, *Chem. Lett.*, **1978**, 699; S. Okeya, Y. Nakamura, S. Kawaguchi, and T. Hinomoto, *Inorg. Chem.*, in press.
11) G. W. Parshall, *J. Am. Chem. Soc.*, **88**, 704 (1966); W. J. Louw, *Inorg. Chem.*, **16**, 2147 (1977).
12) G. K. Anderson and R. J. Cross, *Chem. Soc. Rev.*, **9**, 185 (1980).
13) C. A. Tolman, *Chem. Rev.*, **77**, 313 (1977).
14) J. J. Howe and T. J. Pinnavaia, *J. Am. Chem. Soc.*, **91**, 5378 (1969); T. J. Pinnavaia, W. T. Collins, and J. J. Howe, *ibid.*, **92**, 4544 (1970).
15) S. Okeya and S. Kawaguchi, *Inorg. Chem.*, **16**, 1730 (1977).
16) B. E. Mann, B. L. Shaw, and R. E. Steinbank, *J. Chem. Soc., Chem. Commun.*, **1972**, 151.
17) *E. g.*, D. E. Axelson and C. E. Holloway, *J. Chem. Soc., Chem. Commun.*, **1973**, 455; M. Fild and W. Althoff, *ibid.*, **1973**, 933.
18) A. W. Verstuyft, J. H. Nelson, and L. W. Cary, *Inorg. Chem.*, **15**, 732 (1976); D. A. Redfield, L. W. Cary, and J. H. Nelson, *ibid.*, **14**, 50 (1975).
19) T. Ito, T. Kiriyama, Y. Nakamura, and A. Yamamoto, *Bull. Chem. Soc. Jpn.*, **49**, 3257 (1976).
20) T. Ito and A. Yamamoto, *J. Organomet. Chem.*, **174**, 237 (1979).

Synergistic Extraction of Vanadium(V, IV) with Dithizone

Hideo AKAIWA,* Hiroshi KAWAMOTO, and Etsuo HIYAMUTA
Department of Chemistry, Faculty of Technology, Gunma University, Kiryu, Gunma 376
(Received April 23, 1981)

By employing the synergistic extraction technique, vanadium(V,IV) has been found to form the primary dithizonate in the presence of a synergist. The extraction of the element proceeds according to the following equations.

$$VO_2^+ + H_2dz_{,org} + TBPO_{org} \rightleftharpoons VO_2(Hdz)(TBPO)_{org} + H^+,$$

and

$$VOOH^+ + H_2dz_{,org} + TOPO_{org} \rightleftharpoons VOOH(Hdz)(TOPO)_{org} + H^+,$$

where H_2dz, TBPO, and TOPO denote dithizone, tributylphosphine oxide and trioctylphosphine oxide, respectively, and the subscript org indicates the benzene phase. The resulting adduct $VO_2(Hdz)(TBPO)$ has an absorption maximum at 503 nm and is stable for at least 1 h. However, the red color of VOOH(Hdz)(TOPO) in benzene fades away during the standing time, probably due to the dimerization of the initially extracted monomeric species.

Since the introduction of dithizone(3-mercapto-1,5-diphenylformazan=H_2dz) into the field of analytical chemistry by H. Fischer,[1] extensive studies have been made with the reagent because of its excellent nature as a chelating agent.[2] However, the complexation of vanadium(V,IV) with dithizone has not been reported so far. In the work described below, sufficient evidence for the formation of dithizonatovanadium(V, IV) is given by employing the synergistic extraction technique.

Experimental

Reagent. A stock solution of vanadium(V) (100 μg cm^{-3}) was prepared by dissolving a weighed amount of ammonium metavanadate (NH_4VO_3, Wako Pure Chemicals) in water. Similarly, a stock solution of vanadium(IV) (100 μg cm^{-3}) was prepared by using vanadyl sulfate($VOSO_4$ $3H_2O$, Nakarai Chemicals). Trioctylphosphine oxide (TOPO), tributylphosphine oxide(TBPO), and dithizone were obtained from Wako Pure Chemicals and used without further purification. Benzene and all other reagents used in this work were of guaranteed grade.

Apparatus. The absorbance measurements were conducted with a Hitachi Model 200-10 type spectrophotometer and 1.00 cm glass cells. The pH of the aqueous phase was measured with a Hitachi-Horiba F-7_{ss} type pH meter, and the extraction was carried out by using a Iwaki KM type shaker.

Procedure. The aqueous phase containing 1.96×10^{-5} mol dm^{-3} vanadium(V) or vanadium(IV) was shaken vigorously for 10 min in a separatory funnel with an equal volume of the organic phase(benzene) containing dithizone and a synergist. After the phases were allowed to separate, the vanadium(V) or vanadium(IV) remaining in the aqueous phase was determined spectrophotometrically by using 4-(2-pyridylazo)resorcinol.[3] The pH of the aqueous phase, which was preliminarily adjusted with nitric acid or acetate buffer solution, was measured after the extraction. All experiments were conducted at room temperature.

Results and Discussion

No extraction of vanadium(V and IV) with dithizone(H_2dz) in benzene has been confirmed at any pH range, although vanadyl ion was reported to interfere with the spectrophotometric determination of lead(II).[4,5] In contrast, when the aqueous solution containing vanadium(V) or vanadium(IV) was shaken with a mixture of dithizone and trioctylphosphine oxide (TOPO), the organic phase was observed to change in its color from green to red though the color was not very stable. This phenomenon indicates the possible formation of dithizonatovanadium(V) and vanadium(IV) in the presence of a synergist.

Extraction of Vanadium(V). Although the mechanism was not clear, a stable reddish dithizonatovanadium(V) could be extracted into benzene by using tributylphosphine oxide(TBPO) as a synergist. In this extraction system, HVO_3 was reported to react with dithizone to form $VO_2(Hdz)(TBPO)$ by the present authors.[6] However, this conclusion has become dubious because the formation of $VO_2(Hdz)$-(TBPO) can also be explained by the reactive nature of VO_2^+ toward dithizone.

The effect of the TBPO concentration on the spectrum of the extract is given in Fig. 1. Below 2.0×10^{-3} mol dm^{-3} TBPO, each spectrum agrees with that of dithizone, indicating no formation of the colored

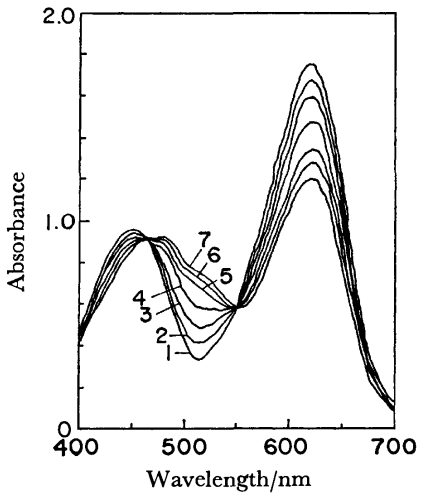

Fig. 1. Effect of TBPO concentration on the absorption spectrum of the organic phase.
H_2dz: 3.9×10^{-5} mol dm^{-3}, pH: 4.10, TBPO(mol dm^{-3}): 1; 2.0×10^{-3}, 2; 6.0×10^{-3}, 3; 1.0×10^{-2}, 4; 2.0×10^{-2}, 5; 4.0×10^{-2}, 6; 6.0×10^{-2}, 7; 1.0×10^{-1}.

vanadium(V) complex. On the other hand, in the higher concentration range of TBPO, the reddish dithizonatovanadium(V) is formed; this has an absorption maximum at 503 nm and is stable for at least 1 h (Fig. 2). The two isosbestic points seen in Fig. 1 suggest that only two kinds of colored species, dithizone and VO_2(Hdz)(TBPO), exist in the organic phase. The shape of the spectrum depends upon the pH of the aqueous phase, as can be seen in Fig. 3, and the existence of two isosbestic points here also supports the above assertion. Therefore, only VO_2(Hdz)(TBPO) is considered to be extracted at any pH region.

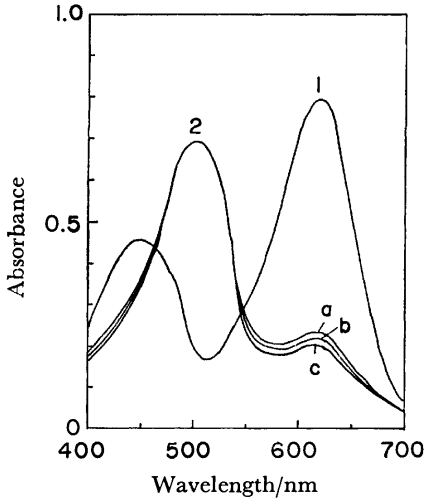

Fig. 2. Absorption spectra of the organic phase.
H_2dz: 1.95×10^{-5} mol dm^{-3}, TBPO: 1.0×10^{-1} mol dm^{-3}, vanadium(V): 1.96×10^{-4} mol dm^{-3}, pH: 4.0, 1: reagent balnk, 2: V(V)-H_2dz-TBPO complex, standing time after the extraction(min): a; 10, b; 30, c; 60.

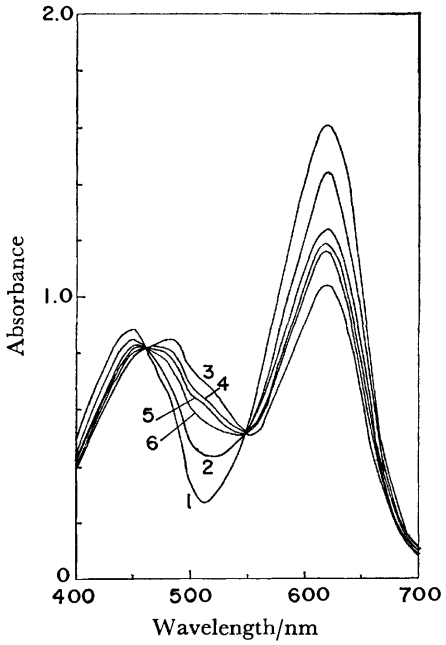

Fig. 3. Effect of pH on the absorption spectrum of the organic phase.
H_2dz: 3.9×10^{-5} mol dm^{-3}, TBPO: 1.0×10^{-1} mol dm^{-3}, pH: 1; 1.16, 2; 2.38, 3; 3.81, 4; 4.43, 5; 4.66, 6; 5.00.

Since the concentration of the polynuclear complex of vanadium(V), $H_1V_{10}O_{28}^{1-6}$ can be neglected compared with those of VO_2^+, HVO_3, and VO_3^-, according to the previous observation,[7] the reactions in the aqueous phase can be written by Eqs. 1 and 2 in all cases.

$$VO_2^+ + H_2O \rightleftharpoons HVO_3 + H^+ \quad (1)$$

and

$$HVO_3 \rightleftharpoons VO_3^- + H^+. \quad (2)$$

The equilibrium constants for the above reactions are defined by Eqs. 3 and 4.

$$K_1 = \frac{[HVO_3][H^+]}{[VO_2^+]} \quad (3)$$

and

$$K_2 = \frac{[VO_3^-][H^+]}{[HVO_3]}. \quad (4)$$

The extractions of vanadium(V) with 1-butanol (*n*-BuOH) and trialkylphosphine oxide(TAPO) were ascribed to the formations of $HVO_3(BuOH)_2$ and HVO_3-$(TAPO)_2$, respectively.[8,9] In both cases BuOH and TAPO can be considered to act as solvating agents, although the detailed scheme of solvation is still unknown. In our previous report, the extraction of vanadium(V) with a mixture of dithizone and TBPO was estimated to proceed according to the reaction: $HVO_3 + H_2dz_{,org} + TBPO_{org} \rightleftharpoons VO_2(Hdz)(TBPO)_{org} + H_2O$, where the subscript org denotes the organic phase.[6] And the pH of the maximal extraction of vanadium(V) in the dithizone-TBPO system agreed well with those obtained by alcohol extractions.[7,10] At that time, therefore, we concluded that HVO_3 might react with dithizone in this case. However, if we assume HVO_3 to be a reacting species, the extraction of vanadium(V) should be expressed as the OH^- releasing reaction: $VO_2(OH) + H_2dz \rightleftharpoons VO_2(Hdz) + H_2O$; here, HVO_3 seems to act as a base, in contradiction to Eq. 2. And the synergistic extraction of vanadium(V) with a chelating agent has generally been explained by the reactive nature of VO_2^+ instead of HVO_3.

Moreover, the extraction of 8-quinolinolatovanadium(V) in the presence of alcohol(ROH) was found to proceed according to the reaction: $VO_2^+ + 2HQ_{org} + ROH_{org} \rightleftharpoons VOQ_2(OR)_{org} + H^+ + H_2O$.[11] Similarly, vanadium(V)/2-thenoyltrifluoroacetone (TTA=Htta)/1-butanol or TOPO systems were explained by the reactions: $VO_2^+ + 2Htta_{,org} + BuOH_{org} \rightleftharpoons VO(tta)_2(BuO)_{org} + H^+ + H_2O$ and $VO_2^+ + Htta_{,org} + TOPO_{org} \rightleftharpoons VO_2(tta)(TOPO)_{org} + H^+$.[7] Consideration of these examples suggests that complexation of vanadium(V) with a chelating agent may start from VO_2^+ as a Lewis acid.

The extracted species was shown spectrophotometrically to be only one, *e.g.* VO_2(Hdz)(TBPO), which is formed by the reaction:

$$VO_2^+ + H_2dz_{,org} + TBPO_{org} \rightleftharpoons VO_2(Hdz)(TBPO)_{org} + H^+ \quad (5)$$

for which the extraction constant is defined as follows:

$$K_{ex} = \frac{[VO_2(Hdz)(TBPO)]_{org}[H^+]}{[VO_2^+][H_2dz]_{org}[TBPO]_{org}}. \quad (6)$$

The distribution ratio of vanadium(V) is written by Eq. 7:

$$D = \frac{[VO_2(Hdz)(TBPO)]_{org}}{[VO_2^+]+[HVO_3]+[VO_3^-]}. \quad (7)$$

Combining Eqs. 3, 4, 6, and 7, the following equation can be obtained:

$$\log D = \log \frac{K_{ex}}{K_1} + \log [H_2dz]_{org} + \log [TBPO]_{org} - \log\left(\frac{[H^+]}{K_1}+1+\frac{K_2}{[H^+]}\right), \quad (8)$$

where $[H_2dz]_{org}$=(total concentration of dithizone)−$[VO_2(Hdz)(TBPO)]_{org}$.

A logarithmic plot of D against $[H_2dz]_{org}$ is shown in Fig. 4; a straight line having a slope of unity is obtained. Similarly, the plot given in Fig. 5 shows a straight line with a slope of unity. The above results are in good agreement with those expected from Eq. 8. In addition, the pH dependence of log D also supports Eq. 8 (Fig. 6). By employing the curve-fitting method, K_1 and K_2 were estimated to be 1.9×10^{-4} and 1.3×10^{-4} respectively, K_{ex} being 3.0×10^2.

Extraction of Vanadium(IV). Vanadium(IV) was also found to react with dithizone in the presence of TOPO; the spectra of the resulting reddish complex, along with standing time in the organic phase, are given in Fig. 7. The vanadium(IV)–dithizone–TOPO complex is not very stable, but it is assumed that the complex may be stable during the extraction process and the changes in the spectrum may start after the phase separation. Assuming that the extraction of vanadium(IV) proceeds according to the following reaction:

$$VOOH^+ + H_2dz_{,org} + TOPO_{org} \rightleftharpoons VOOH(Hdz)(TOPO)_{org} + H^+, \quad (9)$$

the extraction constant may be defined by Eq. 10.

$$K^*_{ex} = \frac{[VOOH(Hdz)(TOPO)]_{org}[H^+]}{[VOOH^+][H_2dz]_{org}[TOPO]_{org}} \quad (10)$$

Neglecting $(VOOH)_2^{2+}$ compared with VO^{2+} and $VOOH^+$, the distribution ratio can be written as follows:

$$D = \frac{[VOOH(Hdz)(TOPO)]_{org}}{[VO^{2+}]+[VOOH^+]}. \quad (11)$$

Hydrolysis of VO^{2+} in the aqueous phase can be expressed by Eq. 12 and the equilibrium constant can be written by Eq. 13:

$$VO^{2+} + H_2O \rightleftharpoons VOOH^+ + H^+ \quad (12)$$

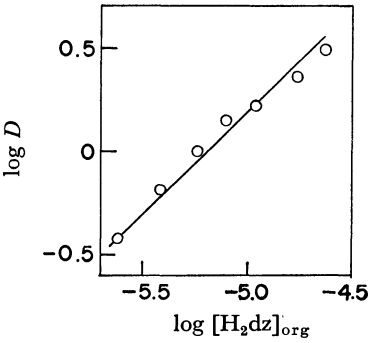

Fig. 4. Effect of dithizone concentration on the extraction of vanadium(V).
TBPO: 1.0×10^{-1} mol dm^{-3}, pH: 4.1.

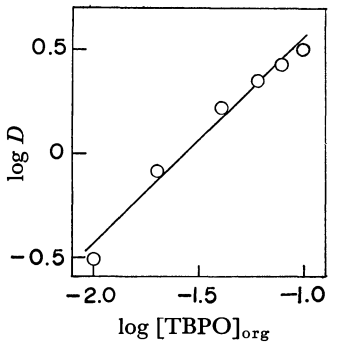

Fig. 5. Effect of TBPO concentration on the extraction of vanadium(V).
H_2dz: 3.9×10^{-5} mol dm^{-3}, pH: 4.1.

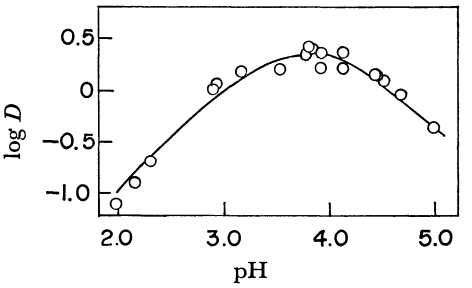

Fig. 6. Effect of pH on the extraction of vanadium(V).
H_2dz: 3.9×10^{-5} mol dm^{-3}, TBPO: 1.0×10^{-1} mol dm^{-3}, ○: experimental value, —: the best fitted normalized curve.

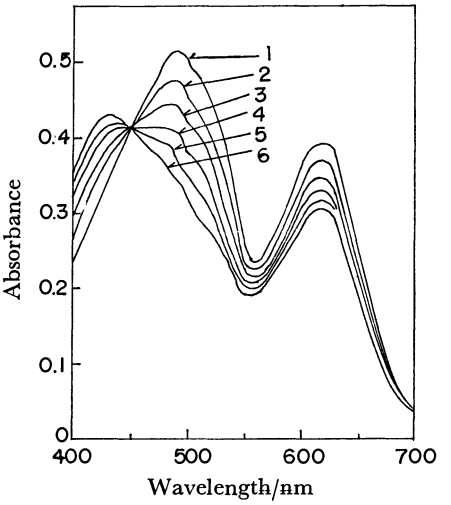

Fig. 7. Absorption spectra of the organic phase.
H_2dz: 3.9×10^{-5} mol dm^{-3}, TOPO: 1.0×10^{-1} mol dm^{-3}, vanadium(IV): 1.96×10^{-4} mol dm^{-3}, pH: 3.96, standing time after the extraction(min): 1; 10, 2; 20, 3; 30, 4; 40, 5; 50, 6; 60.

$$K_h = \frac{[VOOH^+][H^+]}{[VO^{2+}]}. \quad (13)$$

Combining Eqs. 10, 11, and 13, Eq. 14 can be obtained:

$$\log D = \log K^*_{ex} + \log [H_2dz]_{org} + \log [TOPO]_{org} + pH - \log\left(\frac{[H^+]}{K_h}+1\right). \quad (14)$$

As is seen in Fig. 8, a logarithmic plot of D against dithizone concentration shows a straight line having a slope of unity in the high concentration region of dithizone. Deviations from the straight line at low dithizone concentration may be due to extraction of vanadium(IV) with TOPO alone. A logarithmic plot of D against TOPO concentration given in Fig. 9 also shows a straight line having a slope of unity regardless of the presence of dithizone. But it should be mentioned that the D value obtained by TOPO alone is negligibly small compared with that given by a mixture of dithizone and TOPO. The above results coincide with those expected from Eq. 14. The pH dependency of log D given in Fig. 10 fits a curve obtained by calculation using $Y=pH-\log([H^+]/K_h+1)$, indicating that the extracted species may contain $VOOH^+$. This is also valid at low dithizone concentration region, in which the free concentration of dithizone can be calculated by using the equation: $[H_2dz]_{org}=$(total concentration of dithizone)$-[$vanadium(IV)$]_{org}$. A plot of $(\log D-\log [H_2dz]_{org})$ against pH also fits the above curve (Fig. 11). The deviations of some experimental values from the calculated ones above pH 4.6 may be due to the formation of unreactive $(VOOH)_2^{2+}$ in the aqueous phase. From the results given in Figs. 9 and 10, K_h was estimated to be $10^{3.6}$, K^*_{ex} being $10^{2.5\pm0.3}$. As a result, the synergistic extraction of vanadium(IV) with a mixture of dithizone and TOPO proceeds according to Eq. 9. For the composition of the extracted species, VOOH(Hdz)(TOPO), two types of structure can be assumed:

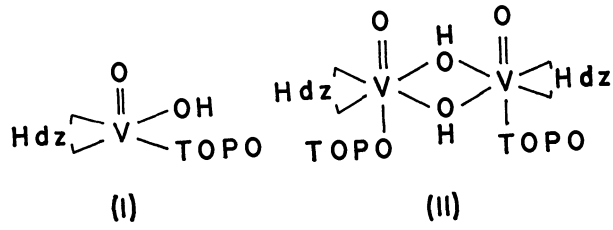

(I) (II)

where type I is a monomer and presumably extracted initially. The existence of an isosbestic point observed in Fig. 7 shows that VOOH(Hdz)(TOPO) in the organic phase may be converted to another stable complex, *e.g.* type II. That is to say, the instability

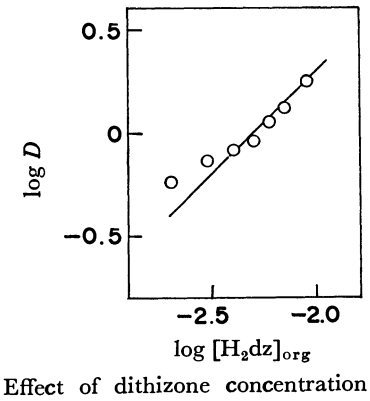

Fig. 8. Effect of dithizone concentration on the extraction of vanadium(IV).
TOPO: 1.0×10^{-2} mol dm^{-3}, pH: 4.0.

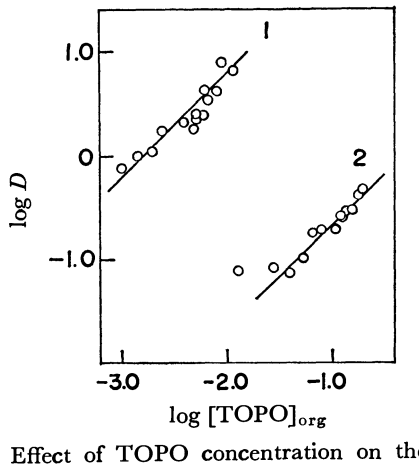

Fig. 9. Effect of TOPO concentration on the extraction of vanadium(IV).
H_2dz: 1; 3.9×10^{-4} mol dm^{-3}, 2; none.

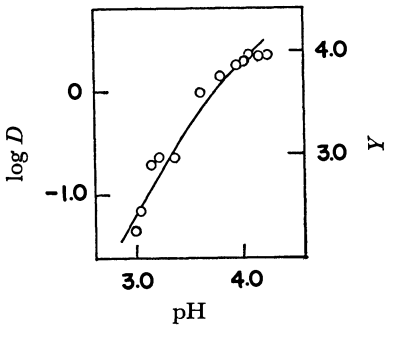

Fig. 10. Effect of pH on the extraction of vanadium (IV).
H_2dz: 1.56×10^{-4} mol dm^{-3}, TOPO: 1.0×10^{-2} mol dm^{-3}, O: log D *vs.* pH, —: Y *vs.* pH.

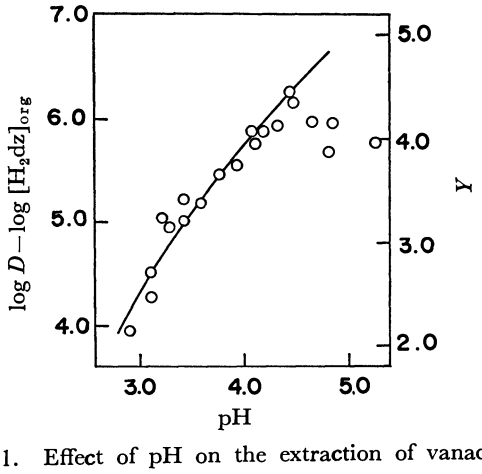

Fig. 11. Effect of pH on the extraction of vanadium (IV).
H_2dz: 3.9×10^{-5} mol dm^{-3}, TOPO: 1.0×10^{-1} mol dm^{-3}, O: log $D-$log $[H_2dz]_{org}$ *vs.* pH, —: Y *vs.* pH.

of VOOH(Hdz)(TOPO) can not simply be attributed to decomposition, as is observed in the cases of dithizonato complexes of manganese(II) and iron(II). It should be mentioned that stable dithizonatovanadium(IV) could be obtained by the extraction with a mixture of dithizone and TBPO. At present, we cannot explain the difference in the stability between TOPO and TBPO complexes.

References

1) H. Fischer, *Wiss. Veröffentlich. Siemes-Werken*, **4**, 158 (1925).
2) H. M. N. H. Irving, "Dithizone," ed by The Chemical Society, London (1977).
3) Y. Shijo and T. Takeuchi, *Bunseki Kagaku*, **14**, 115 (1965).
4) J. M. Bloch and J. Lazare, *Bull. Soc. Pharm.*, **35**, (1959).
5) J. M. Bloch and J. Lazare, *Bull. Soc. Chim. Fr.*, **1960**, 1148.
6) H. Akaiwa, H. Kawamoto, and E. Hiyamuta, *Chem. Lett.*, **1979**, 793.
7) H. Kawamoto and H. Akaiwa, *Nippon Kagaku Kaishi*, **1973**, 90.
8) H. Akaiwa, H. Kawamoto, and H. Kondo, *Bunseki Kagaku*, **23**, 402 (1974).
9) V. L. Bykhovtsov and G. N. Melikhova, *Zh. Prikl. Khim. (Leningrad)*, **43**, 954 (1970); *Chem. Abstr.*, **73**, 39238 (1970).
10) D. Dyrssen and T. Sekine, *J. Inorg. Nucl. Chem.*, **26**, 981 (1964).
11) M. Tanaka and I. Kojima, *J. Inorg. Nucl. Chem.*, **29**, 1769 (1967).

Synthesis and Magnetic Properties of Octaethylporphyrinatoiron(III) Perchlorate and Its Mono(amine) Adduct. Intermediate-spin State (S=3/2) Model for Ferricytochrome c′

Hisanobu Ogoshi,* Hiroshi Sugimoto,† Ei-ichi Watanabe,† Zen-ichi Yoshida,† Yutaka Maeda,†† and Hiroshi Sakai††

Department of Material Science, Technological University of Nagaoka, Nagaoka, Niigata 949-54
†*Department of Synthetic Chemistry, Kyoto University, Kyoto 606*
††*Research Reactor Institute, Kyoto University, Kumatori, Sennan, Osaka 590-40*

(Received December 26, 1980)

Octaethylporphyrinatoiron(III) perchlorate, its mono(pyridine) and mono(4-substituted pyridine) adducts and bis(tetrahydrofuran)octaethylporphyrinatoiron(III) perchlorate were prepared to mimic the ferricytochrome c′. Magnetic susceptibilities, Mössbauer spectra, and ESR spectra have been measured. Magnetic properties in the crystalline state revealed; (i) Octaethylporphyrinatoiron(III) perchlorate, $OEPFe^{III}ClO_4$ and bis(tetrahydrofuran)octaethylporphyrinatoiron(III) perchlorate, $OEPFe^{III}(THF)_2ClO_4$ are of intermediate-spin state(S=3/2). (ii) Magnetic susceptibilities and Mössbauer parameters of mono(pyridine) and mono(4-substituted pyridine)octaethylporphyrinatoiron(III) perchlorate, $OEPFe^{III}$(4-X-py)ClO_4 [X=CHO, X=CN, and X=H] are rather similar to those of the low-spin(S=1/2) states. Absorption spectra showed that octaethylporphyrinatoiron(III) perchlorate is of intermediate-spin state in dichloromethane solution, but of high spin state in acetone solution. Close spectral resemblance of these complexes to the ferricytochrome c′ at physiological pH suggests that the latter is in intermediate-spin state.

Ferrihemoproteins and ferriheme enzymes in general have been classified into two spin-states, that is, the five-coordinated high-spin (S=5/2) state and the six-coordinated low-spin (S=1/2) state. It is noted that the ferricytochrome c′ isolated from photosynthetic and denitrifying bacteria[1–4] have anomalous magnetic properties defined as intermediate-spin state (S=3/2). An unusual electronic spectrum is found in cytochrome c′. The oxidized form[5] in alkaline solution shows a hemichrome spectrum of the low-spin. Below pH 11 the spectrum reverts to a chracteristic of high-spin ferric hemes with split Soret bands. Further change of electronic spectrum is observed as pH decreases. The magnetic moment at physiological condition anomalously shows intermediate values between high-spin and low-spin.[6,7] Mössbauer spectra[8] show large quadrupole splittings which are comparable to those of methemoglobin with the opposite sign.

In order to aid understanding anomalous spin-state, there have been reported few simulations to intermediate-spin complexes by synthetic hemes. In previous communication,[9] we reported briefly syntheses and some magnetic properties of octaethylporphyrinatoiron(III) perchlorate and its mono(amine) adducts. We have described the unusual magnetic moments of these complexes at 288 K as an admixture of the high-spin and low-spin states as follows:

$$^6A_1 \rightleftharpoons {}^2T_2.$$

Since then, two groups have reinvestigated the physicochemical properties of the perchlorate salts of ferric porphyrins. Dolphin and his coworkers[10] reexamined magnetic moments and measured Mössbauer spectra of octaethylporphyrinatoiron(III) perchlorate and bis(ethanol)octaethylporphyrinatoiron(III) perchlorate. They have, however, suggested that these complexes possesses an intermediate-spin iron(III) atom, with the S=3/2 at the ground state possibly involving some high-spin character. Scheidt and his coworkers[11] have reported physicochemical properties of diaqua-$\alpha,\beta,\gamma,\delta$-tetraphenylporphyrinatoiron(III) perchlorate and perchlorate-$\alpha,\beta,\gamma,\delta$-tetraphenylporphyrinatoiron(III). We have studied crystal structure of the perchlorate complex[12] and its paramagnetic ^{1}H-NMR spectra in organic solvents.[13] In a previous communication,[9] we also reported the first syntheses of mono(amine) adducts and their magnetic moments at room temperature. We wish to report here elaborate measurements on magnetic susceptibilities, Mössbauer spectra, and ESR spectra of octaethylporphyrinatoiron(III) perchlorate, and three mono(amine) adducts in solid state.

Experimental

Preparation of Compounds. Ocatethylporphyrinatoiron(III) Perchlorate [$OEPFe^{III}ClO_4$] (1): To 500 mg of $OEPFe^{III}Cl$[14] in benzene (200 ml) was added 500 mg of anhydrous silver perchlorate and the solution was refluxed gently for 1 h. The hot solution was filtered and then allowed to stand overnight at room temperature. The resultant needle crystals (450 mg) were collected, washed with petroleum ether and dried under vacuum. Bis(tetrahydrofuran)octaethylporphyrinatoiron(III) perchlorate [$OEPFe^{III}(THF)_2ClO_4$] (**2**). To 100 mg of **1** in dichloromethane (20 ml) was added tetrahydrofuran (10 ml). The solution was warmed for 15 min and allowed to come to room temperature. The crystals were collected, washed with tetrahydrofuran, and dried under vacuum (95 mg).

(4-Formylpyridine)octaethylporphyrinatoiron(III) Perchlorate [$OEPFe^{III}$(4-CHO-py)ClO_4] (3): To 100 mg of **1** in dry benzene (100 ml) was added 0.5 ml of 4-formylpyridine. The solution was refluxed for 2 h, condensed to a small volume and allowed to stand overnight at room temperature. The resulting dark brown crystals were filtered, washed with petroleum ether and dried under vacuum (90 mg).

(4-Cyanopyridne)octaethylporphyrinatoiron(III) Perchlorate [$OEPFe^{III}$(4-CN-py)ClO_4] (4): The preparative method is identical with that described above. The dark brown crystals (95 mg) were obtained from 100 mg of **1**.

(Pyridine)octaethylporphyrinatoiron(III) Perchlorate [$OEPFe^{III}$(py)ClO_4] (5): To 100 mg of **1** in dry benzene (100 ml)

		C (%)		H (%)		N (%)	
		Calcd	Found	Calcd	Found	Calcd	Found
(1)	$C_{36}H_{44}N_4O_4ClFe$	62.84	62.94	6.45	6.48	8.14	8.04
(2)	$C_{44}H_{60}N_4O_6ClFe$	63.50	63.45	7.27	7.26	6.73	6.79
(3)	$C_{42}H_{49}N_5O_5ClFe$	63.44	63.36	6.21	6.28	8.81	8.89
(4)	$C_{42}H_{48}N_6O_4ClFe$	63.67	63.40	6.10	6.26	10.61	10.32
(5)	$C_{41}H_{49}N_5O_4ClFe$	64.19	64.33	6.44	6.34	9.13	8.95

was added 0.5 ml of pyridine and the solution was refluxed for 20 min. The deep red precipitates were collected, washed with benzene, and dried under vacuum (95 mg). The results of elemental analyses are tabulated above.

Magnetic and Spectral Measurements. *Magnetic Susceptibilities*: A Faraday magnetic balance was employed for measurements of magnetic susceptibilities from 77 K to 300 K. The magnetic susceptibilities of anhydrous hexaammine-chromium chloride powder was used as a "thermometer" which was calibrated at each run to an atmospheric liquid nitrogen temperature with corrections for the Hg-barometer and gravitational constant following the procedure of Linder.[15] The accuracy for the measurements was not less than 10%. The diamagnetic susceptibilities of porphyrin ligand and axial ligands were corrected by measurement of free base octaethylporphyrin and by Pascal's rule.

Mössbauer Spectra: Mössbauer spectra were obtained with a scanned velocity spectrometer operating in the time mode. The velocity scale was calibrated absolutely from an independent Mössbauer run using a thin metallic iron absorber and the center of symmetry of the spectrum was taken as zero velocity. The velocity was determined to an accuracy of ± 0.01 mm/s.

ESR Spectra: The ESR spectra of polycrystalline sample and in dichloromethane glass were measured at 77 K and at 293 K by using a JEOL X-band spectrometer.

Results

Figure 1 shows effective magnetic moments of **1**, **2**, **3**, **4**, and **5** at various temperatures from 77 K to 270 K. The effective magnetic moments of **1** and **2** are lower than those of typical high-spin state (5.9 BM) and higher than typical low-spin state (2.15—2.72 BM).[16] On the other hand, for mono(amine) adducts, **3**, **4**, and **5**, the effective magnetic moments vary greatly with the kinds of substituent at 4-position of pyridine. The effective magnetic moments of mono(pyridine) adduct **5** and mono(4-cyanopyridine) adduct **4** are closely similar to the six-coordinated low-spin complexes[16] at low temperature, but at high temperature these values become larger than those of low-spin complexes. It is noted that the magnetic moments of the 4-formyl pyridine adduct **3** are larger than those of mono(amine) adducts **4** and **5**, but smaller than those of the perchlorates **1** and **2**.

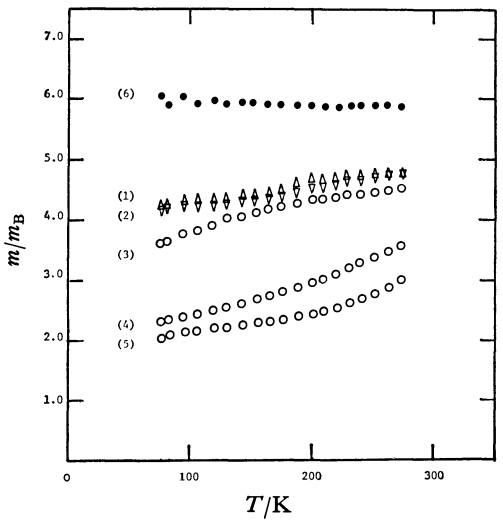

Fig. 1. Effective magnetic moments *versus* temperatures. (1): OEPFe(III)ClO_4, (2): OEPFe(III)$(THF)_2ClO_4$, (3): OEPFe(III)(4-CHO-py)ClO_4, (4): OEPFe(III)-(4-CN-py)ClO_4, (5): OEPFe(III)(py)ClO_4, (6): OEPFe(III)SCN.

Table 1 summarizes the Mössbauer parameters, isomer shifts δ (mm/s) and quadrupole splitting ΔE_Q (mm/s) of complexes at various temperatures. The isomer shifts of all these complexes are in the range of 0.2—0.4 mm/s, indicating typical iron(III) state. On the other hand, the quadrupole splittings of **1** and **2** show 3.14 and 3.08 mm/s at room temperature, respectively. These values are very large compared with those of usual iron(III) complexes and identical with those reported by Dolphin and his coworkers.[10] Mono(amine) adducts **3**, **4**, and **5** have smaller quadrupole splittings than the complexes **1** and **2**. In particular Mössbauer parameters of the mono(pyridine) adducts **3**—**5** are close to those of the six-coordinated low-spin complexes.[16] As shown in Figs. 2—6, high velocity lines of the complexes **4** and **5** are broadened at lower temperatures. Therefore, the sign of the quadrupole coupling can be determined to be positive. In the case of mono(4-formylpyridine) adduct **3**, the line broadening at high velocity due to the

Table 1. Mössbauer parameters

	Compound	T/K	ΔE_Q/mm s^{-1}	δ/mm s^{-1}
1	OEP·Fe(III)·ClO_4	RT	3.14	0.31
		77	3.57	0.39
		4.2	3.54	0.40
2	OEP·Fe(III)·	RT	3.04	0.31
	$(THF)_2$·ClO_4	77	3.34	0.42
3	OEP·Fe(III)·	RT	2.29	0.30
	(4-CHO-py)·ClO_4	77	2.35	0.38
		4.2	2.22	0.40
4	OEP·Fe(III)·	RT	2.34	0.27
	(4-CN-py)·ClO_4	77	2.05	0.25
		4.2	relax.	
5	OEP·Fe(III)·	RT	1.96	0.21
	(py)·ClO_4	77	1.95	0.27
		4.2	1.94	0.27

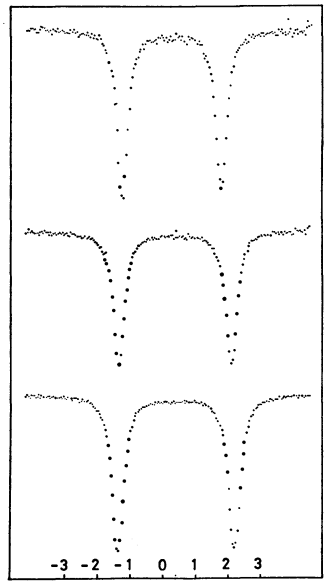

Fig. 2. Mössbauer spectra of OEPFe(III)ClO_4 at RT, 77 K, and 4.2 K.

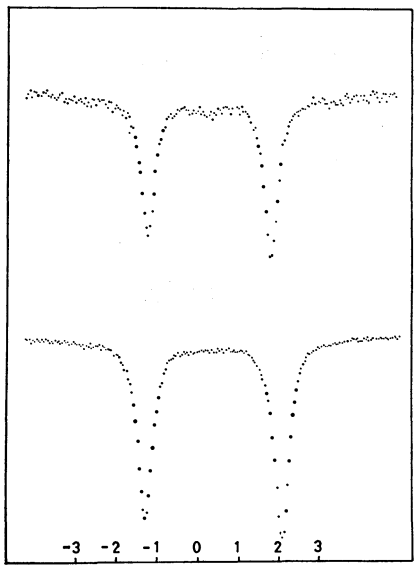

Fig. 3. Mössbauer spectra of OEPFe(III)$(THF)_2ClO_4$ at RT and 77 K.

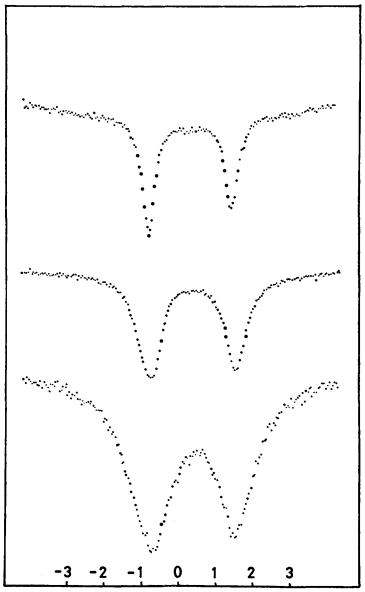

Fig. 4. Mössbauer spectra of OEPFe(III)(4-CHO-py)ClO_4 at RT, 77 K, and 4.2 K.

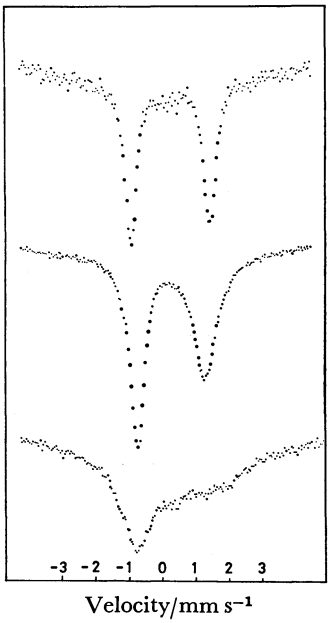

Fig. 5. Mössbauer spectra of OEPFe(III)(4-CN-py)-ClO_4 at RT, 77 K, and 4.2 K.

relaxating is much smaller than the other two mono-(amine) adducts even at 4.2 K.

ESR spectra of these complexes in solid state at 293 and 77 K are shown in Figs. 7 and 8, respectively, and observed g-values are summarized in Table 2. Complexes **1** and **2** show very broad signals at around $g=4$ at room temperature. On the other hand the mono(amine) adducts **3**, **4**, and **5** show also broad signals at $g=4.41$, 3.75, and 2.40 with very weak peaks around $g=2$, respectively. The line shapes and g-values of these complexes at room temperature are very much different from those of ordinary high-spin or low-spin iron(III) complexes hitherto reported. For mono(pyridine) adduct **5**, the signal at $g=2.06$ seems to be contaminated by organic radical species. The ESR spectra at 77 K were remarkably different from those at room temperature as shown in Fig. 8. The complex **2** shows still one broad signal at $g=4.61$ in solid state, but anisotropic g-values at $g=4.68$ and 2.00 in dichloromethane glass. The complex **1** shows a pair of anisotropic g-values at 5.83 and 1.48. On the other hand, three mono-(amine) adducts exhibit similar spectra with a pair of anisotropic g-values at low temperature, although the g-values are slightly different from each other. The g-values are markedly changed from 4.69 to 5.40 upon introduction of the formyl group at the 4-position of pyridine. The ESR spectra of **1** and **2** at 77 K show entirely different signals from those of

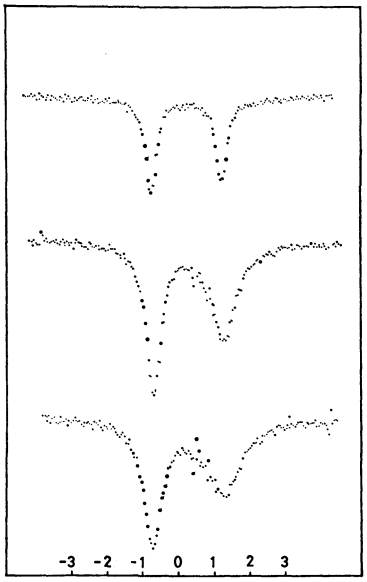

Velocity/mm s^{-1}

Fig. 6. Mössbauer spectra of OEPFe(III)(py)ClO_4 at RT, 77 K, and 4.2 K.

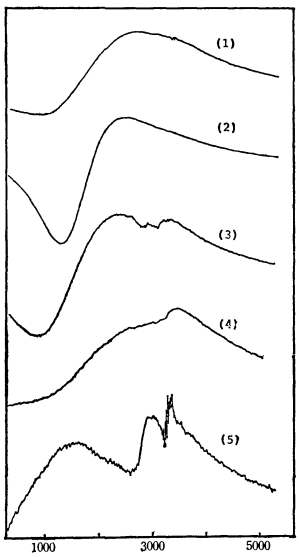

$G/10^{-4}$ T

Fig. 7. ESR spectra at RT.
(1): OEPFe(III)ClO_4, (2): OEPFe(III)$(THF)_2ClO_4$, (3): OEPFe(III)(4-CHO-py)ClO_4, (4): OEPFe(III)-(4-CN-py)ClO_4, (5): OEPFe(III)(py)ClO_4.

usual high-spin or low-spin complexes of ferric porphyrin. The ESR spectra of mono(amine) adducts **3**, **4**, and **5** exhibit the strong broad signals at high g-values(lower magnetic field) and the maximum absorption (zero derivative) is shifted towards lower g-values(higher magnetic field).

Absorption spectrum of the complex **1** changes remarkably with polarity of solvent as shown in Fig. 9. In acetone the complex **1** exhibits a spectral characteristic of the high-spin complexes, whereas in dichloromethane the Soret band is largely broadened and slightly splitted. The band at 630 nm assigned to a charge transfer band is shifted to longer wave length (636 nm) in dichloromethane than in acetone (628 nm).

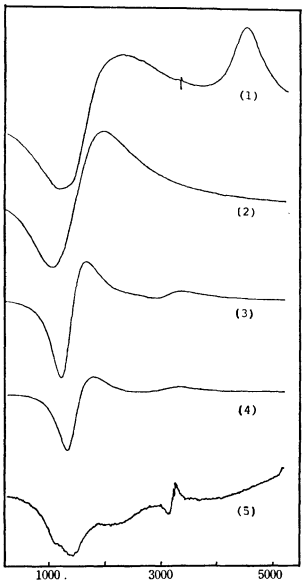

$G/10^{-4}$ T

Fig. 8. ESR spectra at 77 K.
(1): OEPFe(III)ClO_4, (2): OEPFe(III)$(THF)_2ClO_4$, (3): OEPFe(III)(4-CHO-py)ClO_4, (4): OEPFe(III)-(4-CN-py)ClO_4, (5): OEPFe(III)(py)ClO_4.

Table 2. ESR parameters

		RT		77 K	
		$g_{//}$	$g_\perp$	$g_{//}$	$g_\perp$
1	OEP·Fe(III)·ClO_4	3.9		1.5	5.8
2	OEP·Fe(III)·$(THF)_2$·ClO_4	3.9		4.6 2.0	 4.7[a]
3	OEP·Fe(III)·(4-CHO-py)·ClO_4	2.1	4.4	1.7	5.4
4	OEP·Fe(III)·(4-CN-py)·ClO_4	2.0	3.8	2.0	5.0
5	OEP·Fe(III)·(py)·ClO_4	2.1	2.4	2.5	4.7

	7 K	
	$g_{//}$	$g_\perp$
ESR spectral state A	1.99	4.77[20]
Protein state B_1	2.02	5.94[20]
Protein state A_1	1.99	4.75[20]
Protein state A_2	1.99	5.27[20]
Protein state B_2	2.00	5.68, 6.14[20]
Acid metmyoglobin	2.01	5.92[b]

a) Measured in dichloromethane glass. b) J. Peisah, W. E. Blumberg, S. Ogawa, E. A. Rachmilewitz, and R. Oltzik, *J. Biol. Chem.* **246**, 3342—3355 (1971).

Discussion

The complex **1** showed effective magnetic moments μ_{eff}=4.2 BM at 77 K and 4.7 BM at 275 K. Then these values are compared with calculated spin only values μ_{eff}=5.92, 3.87, and 1.73 BM for S=5/2, 3/2, and 1/2, respectively. The complexes **1** and **2** can be

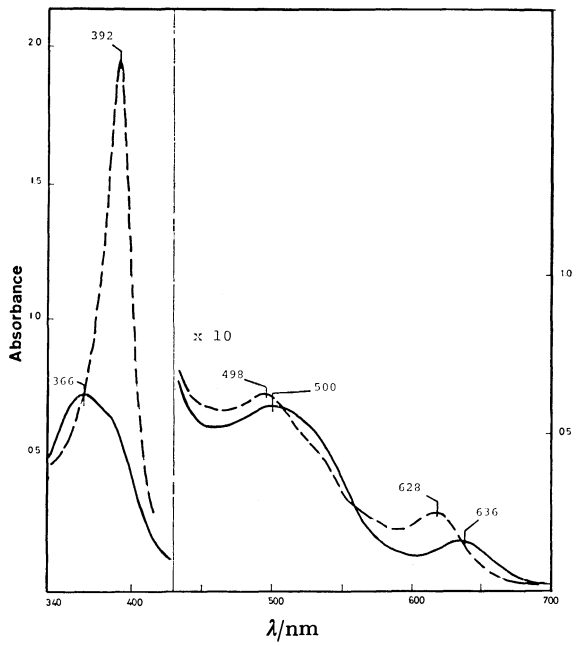

Fig. 9. Absorption spectra of OEPFe(III)ClO_4, (——) in CH_2Cl_2 and (----) in acetone.

regarded as intermediate-spin complexes. Harris has predicted a possible existence of pure quartet ground state ($S=3/2$) on theoretical consideration by using a strong crystal field model.[17] The ESR signals in the tetragonal symmetry might have only one transition between the exited state doublets with $g=2$ and 4. The intensity of this transition should be temperature dependent and also should vary with extent of spin-orbital coupling.[18] In fact the complexes **1** and **2** give a very broad signal at about $g=$ 3.9 as shown in Fig. 7, whose patterns are very similar to that of iron(III) bis(thiocarbamates) characterized as an intermediate-spin complex.[16] At low temperature, the complex **1** has some anisotropic character so that g-value at around 4 seems to split into the two values $g=5.83$ and 1.48, as shown in Fig. 8. On the other hand, the complex **2** in solid state has no anisotropic character even at 77 K, but in dichloromethane glass it gives anisotropic g-values at 4.68 and 2.00. The Mössbauer spectra of the complexes **1** and **2** did not show any relaxation broadning, as mentioned by Dolphin and his coworkers, suggesting fast spin relaxation between both $|\pm 1/2>$ and $|\pm 3/2>$ doublets. Comparison of the magnetic susceptibilities, the ESR spectra and the Mössbauer spectra leads us to conclude that the complexes **1** and **2** are of intermediate-spin state.

Mono(amine) adducts **3**, **4**, and **5** have effective magnetic moments between the low-spin and the intermediate-spin states. The ESR spectra of these compounds give anisotropic g-values at $g=5.47$—4.67 and $g=1.70$—2.05 at 77 K. In particular, the magnetic moments and Mössbauer parameters of the mono(pyridine) adduct **5** indicate that the spin state of **5** at low temperature is essentially low-spin state. However, the ESR spectrum of **5** is different from that of the hexa-coordinated low-spin complex. This fact suggests that mono(amine) adducts do not exist in pure low-spin state, but in a mixed spin state with low-spin($S=1/2$) and intermediate-spin($S=3/2$) states. Small differences in the magnetic properties among them may be attributed to the extent of admixture of two spin states. Weight of the quartet state in the mixed spin state increases in the following order, **3**>**4**>**5**. Magnetic properties of the 4-formylpyridine adduct **3** are very close to those of the complex **1**. Also magnetic properties of the mono(amine) adducts are consistent with the theoretical prediction for a quartet-doublet mixed spin iron(III) ion by Harris.[17] The effective magnetic moments of ferricytochrome c′ at pH 7[20] have been reported to be 5.15 BM at 293 K and 3.4 BM at 2.8 K. Ferricytochrome c′ shows anomalous feature in the ESR parameters and the shape of the Soret band in absorption spectrum. The ferricytochrome c′ at physiological pH exhibits a strong ESR absorption at high g-value $g=4.77$ and a weaker one at $g=1.99$.[20] The former absorption is much broadened and its maximum absorption (zero derivative) is shifted toward lower g-values than ferrimyoglobin and ferrileghemoglobin.[7] Maltempo has described unusual properties of ferricytochrome c′ by assuming that the electronic comfiguration of hemin at the ground state consists of substantial quantum mechanical admixture of intermediate-spin($S=3/2$) and high-spin($S=5/2$) states, coupled *via* the spin-orbit interaction. Therefore, intermediate spin complexes **1** and **2** seem to be good models for ferricytochrome c′ at physiological pH.

Present results lead us to postulate that a histidyl imidazole coordinates weakly to the iron(III) atom of ferricytochrome c′ even at physiological pH. Therefore, the mono(amine) adducts rather than complexes **1** and **2** are better model complexes for the ferricytochrome c′.

As is seen in Figs. 7 and 8, the mono(amine) adducts can duplicate unusual ESR specturm of ferricytochrome c′. The g-values of ferricytochrome c′ at the various conditions are referred in Table 2. Comparison of its g-values with model compounds suggests that the ground state of the ferricytochrome c′ at low temperature is similar to those of the mono(amine) adducts. Histidyl imidazole is considered to be most probable axial ligand to the heme in the enzyme. Analysis of amino acid sequence of apocytochrome c′ rationalizes possible ligation of the histidyl imidazole as fifth axial ligand.[21] There are, however, so many candidates of the sixth ligand such as water, aspartic acid, glutamic acid, and lysine.[22] On the basis of physicochemical properties of model complexes, it is proposed that relatively weak ligand coordinates to the hemin in cytochrome c′, and the bonding between iron atom and sixth ligand has more ionic character than that of the ferric hemoproteins. Positive charge seems to be localized on the iron(III) atom relative to the penta-coordinate ferric high-spin state. As is stated by Strekas and Spiro,[23] the differences of energy levels between d_π orbital and d_{z^2} or d_{z^2} and $d_{x^2-y^2}$ orbitals are very sensitive to the nature of axial ligands. Spin state of ferric porphyrin complex is markedly dependent on strength of axial ligation of the fifth and sixth ligands. Coordination of the histidyl

imidazole seems to be strongly influenced by changes in environment near proximity of the heme, which are induced by pH and temperature. Extensive investigations on the ferric porphyrin complex conclude that spin state is generally determined by coordination numbers of axial ligands. Namely it has been believed that the high-spin state and low-spin state constitute the five-coordinated complex of square pyramidal structure and the six-coordinated complexes of octahedral structure, respectively. We have found new iron(III) complexes having anomalous spin-state and coordination numbers, when a weak field ligand such ClO_4^- was employed.[13] Recently LaMar[24] and Scheidt's[11] groups have pointed out the existence of the six-coordinated high-spin species in the solution or in crystalline state.

Visible spectrum of ferricytochrome c′ shows absorptions at 400, 490, and 632 nm.[25] The absorption at 632 nm is explained as a charge transfer band. There is no essential difference between the electronic structure of d_π-orbital for intermediate spin($S=3/2$) and high spin($S=5/2$). Absorption spectra of **1** in CH_2Cl_2 and solid state can duplicate that of the oxidized form of cytochrome c′. Penta-coordinated iron(III) complex **1** shows remarkable solvent effect on electronic spectrum.[13] Axial ligation of polar solvent molecule results in formation of asymmetric hexa-coordinated (B) and symmetric hexa-coordinated iron(III) complex(C). The complex **2** is defined as the

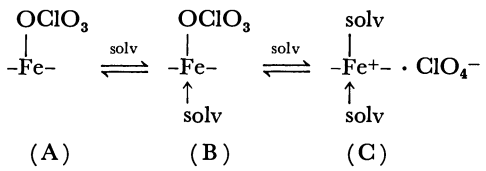

solv: solvent molecule

type (C). New hexa-coordinated complexes **3**—**5** constitute asymmetric coordinated complex at axial fifth and sixth sites. Addition of strong basic ligand such as imidazole to the hemin affords bis(imidazole) adduct. Consequently, spin state of the hemin is sensitive to coordination of axial ligand and delocalization of positive charge. These two factors are very important in biological systems. The spin state of the prosthetic heme in hemoproteins is determined by axial ligation of the residue of amino acid and polarity near proximity of the heme.

From present results, we are enforced to support that the ground state electronic configuration of the ferricytochrome c′ at physiological pH is of substantial quantum mechanical admixture of quartet and sextet states. Furthermore, a possibility of an admixture of quartet and doublet states is also proposed for the ferricytochrome c′ at low temperature.

This work was partially supported by a Grant-in-Aid for Special Project Research No. 511311 from Ministry of Education, Science and Culture.

References

1) H. Iwasaki and T. Mori, *J. Biochem.*, **42**, 375 (1955).
2) L. P. Vernon and M. D. Kamen, *J. Biol. Chem.*, **211**, 643 (1954).
3) K. Das, H. D. Klerk, R. G. Bartsch, T. Horio, and M. D. Kamen, *Proc. Natl. Acad. Sci. U.S.A.*, **57**, 367 (1967).
4) R. Lemberg and J. Barrett, "Cytochromes," Academic Press (1973).
5) T. Horio and M. D. Kamen, *Biochim. Biophys. Acta*, **48**, 266 (1961).
6) A. Ehrenberg and M. D. Kamen, *Biochim. Biophys. Acta*, **102**, 333 (1965).
7) A. Tasake, J. Otsuka, and M. Kotani, *Biochim. Biophys. Acta*, **140**, 284 (1967).
8) T. H. Moss, A. J. Bearden, R. G. Bartsch and M. A. Cusanovich, *Biochemistry*, **7**, 1583 (1968).
9) H. Ogoshi, E. Watanabe, and Z. Yoshida, *Chem. Lett.*, **1973**, 989.
10) D. H. Dolphin, J. R. Sams, and T. B. Tsin, *Inorg. Chem.*, **16**, 711 (1977).
11) M. E. Kastner, W. R. Scheidt, T. Mashiko, and C. A. Reed, *J. Am. Chem. Soc.*, **100**, 666 (1978); T. Mashiko, M. E. Kastner, K. Spartalian, W. R. Scheidt and C. A. Reed, *ibid.*, **100**, 6354 (1978); C. A. Reed, T. Mashiko, S. P. Benthy, M. E. Kastner, W. R. Scheidt, K. Spartalian, and G. Lang, *ibid.*, **101**, 2948 (1979).
12) H. Masuda, T. Taga, K. Osaki, H. Sugimoto, Z. Yoshida, and H. Ogoshi, *Inorg. Chem.*, **19**, 950 (1980).
13) H. Ogoshi, H. Sugimoto, and Z. Yoshida, *Biochim. Biophys. Acta*, **621**, 19 (1980).
14) H. W. Whitlock, Jr., R. Hanauer, M. Y. Oester, and B. K. Bower, *J. Am. Chem. Soc.*, **91**, 7486 (1969).
15) C. T. Linder, Research Report, R-94433-2-A (Westinghouse Research Laboratories).
16) L. M. Epstein, D. K. Straub, and C. Maricondi, *Inorg. Chem.*, **6**, 1720 (1967); L. Bullard, R. Panayappan, A. Thorpe, P. Hambright, and G. Ng., *Bioinorg. Chem.*, **3**, 41 (1973).
17) G. Harris, *Theor. Chim. Acta*, **10**, 119, 155 (1968).
18) M. M. Maltempo, *Chem. Phys. Lett.*, **60**, 441 (1979).
19) H. H. Wickman and F. R. Merritt, *Chem. Phys. Lett.*, **1**, 117 (1967); H. H. Wickman, A. H. Trozzolo, H. J. Williams, G. W. Hull, and F. R. Merritt,. *Phys. Rev.* **155**, 563 (1967); H. H. Wickman and A. H. Trozzolo, *Inorg. Chem.*, **7**, 63 (1968); G. E. Chapps, S. W. McCann, H. H. Wickman, and R. C. Sherwood, *J. Chem. Phys.*, **60**, 990 (1974).
20) M. M. Maltempo, T. H. Moss, and M. A. Cusanovich, *Biochim. Biophys. Acta*, **342** 289 (1974); M. M. Maltempo, *ibid.*, **379**, 95 (1975); M. M. Maltempo, *J. Chem. Phys.*, **61**, 2540 (1974); M. M. Maltempo, *Biochim. Biophys. Acta*, **434**, 513 (1976).
21) T. E. Meyer, R. P. Ambler, R. G. Bartsch, and M. D. Kamen, *J. Biol. Chem.*, **250**, 8416 (1975).
22) T. Kitagawa, Y. Ozaki, Y. Kyogoku, and T. Horio, *Biochim. Biophys. Acta*, **495**, 1 (1977).
23) T. C. Strekas and T. G. Spiro, *Biochim. Biophys. Acta*, **351**, 237 (1974).
24) M. Zobrist and G. N. Lamav, *J. Am. Chem. Soc.*, **100**, 1944 (1978).
25) S. Taniguchi and M. D. Kamen, *Biochim. Biophys. Acta*, **74**, 438 (1963).

A Reexamination of the Robinson Annelation of 2-Methylcyclohexanone with 3-Penten-2-one and 4-Phenyl-3-buten-2-one[1]

Mitsuko KIKUCHI* and Akira YOSHIKOSHI†

College of Engineering, Nihon University, Koriyama, Fukushima 963

† *Chemical Research Institute of Non-Aqueous Solutions, Tohoku University, Sendai 980*

(Received February 10, 1981)

The reported Robinson annelation of 2-methylcyclohexanone with 3-penten-2-one has been reexamined. In contrast to the previous result, it was found that the reaction product was not only obtained in a low yield, but also the solvent-depending stereoselectivity in the formation of *cis*-4,4a-dimethyl-4,4a,5,6,7,8-hexahydronaphthalen-2(3*H*)-one (**3a**) and its *trans* isomer (**3b**) was considerably lower than that reported. As expected, regioisomers, 4β,8α-dimethyl-4,4aβ,5,6,7,8-hexahydronaphthalen-2(3*H*)-one and 4β,8β-dimethyl-4,4aα,5,6,7,8-hexahydronaphthalen-2(3*H*)-one, were also formed in the annelation. A similar tendency was observed in the reaction with 4-phenyl-3-penten-2-one. The annelation products, **3a**, **3b**, *cis*-4-phenyl-4a-methyl-4,4a,5,6,7,8-hexahydronaphthalen-2(3*H*)-one, and *trans*-4-phenyl-4a-methyl-4,4a,5,6,7,8-hexahydronaphthalen-2(3*H*)-one, were also synthesized by an alternative route.

The Robinson annelation has most widely been employed as a useful method of synthesizing *cis*-1,8a-dimethyldecalins, the fundamental structures of eremophilanoids.

Scanio and Starrett[2] recently reported that *cis*-dimethyloctalone (**3a**) in an isomeric purity exceeding 95% was produced by the Robinson annelation of 2-methylcyclohexanone (**1**) with 3-penten-2-one (**2**) in dioxane, while change of the solvent to dimethyl sulfoxide dramatically altered the ratio of the diastereomers to give *trans*-dimethyloctalone (**3b**) in a high isomeric purity (over 95%) (Scheme 1). They also proposed a reaction mechanism (Scheme 2) for the predominant formation of the *trans*-isomer **3b** in dimethyl sulfoxide; the enolate, **4**, of 2-methylcyclohexanone (**1**) gives the 1,3-butadien-2-olate anion (**5**) by proton exchange, and the latter attacks the regenerated ketone, **1**, to yield olefinic alcohol, **6**. Under these reaction conditions, **6** is dehydrated to crossed dienone **7**, and its enol form, **8**, thermally cyclizes in a disrotatory manner to yield **9** predominantly.

To test their hypothesis concerning this unusual Robinson annelation in dimethyl sulfoxide, we reexamined their reaction of **1** and **2**, and also that of **1** and 4-phenyl-3-buten-2-one (**11**) for comparison.

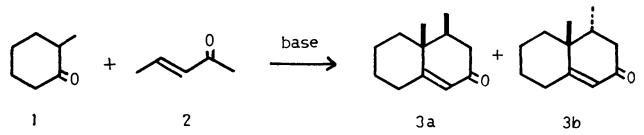

Scheme 1.

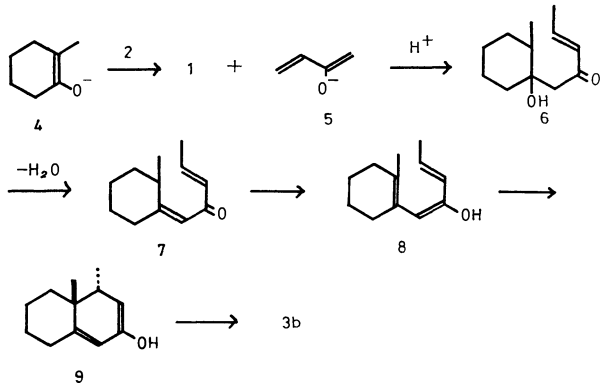

Scheme 2.

In order to obtain authentic samples for the GLC analysis of the annelation products, four octalones, **3a**, **3b**, **14a**, and **14b**, were synthesized by the alternative route shown in Scheme 3, because, contrary to the claim of Scanio and Starrett, these compounds were obtained only in poor yields under similar reaction conditions, as will be discussed later.

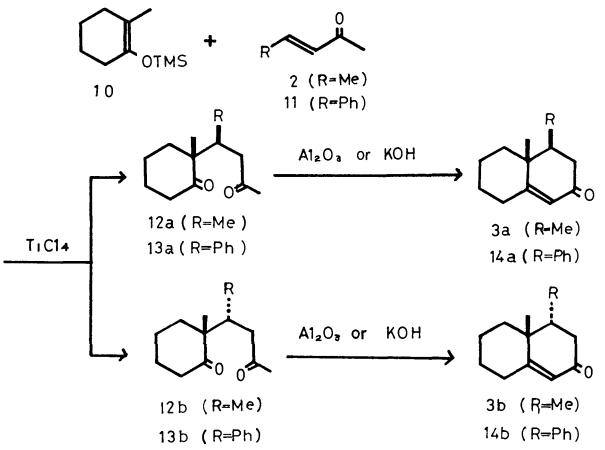

Scheme 3.

Silyl enol ether (**10**), prepared from 2-methylcyclohexanone (**1**), was treated with 3-penten-2-one (**2**) (or 4-phenyl-3-buten-2-one (**11**)) in dichloromethane in the presence of titanium tetrachloride,[3] thus giving a mixture of 1,5-diones **12a** and **12b** in a ratio of 25:75 (or **13a** and **13b** in a ratio of 71:29) and in a good yield. These diones were separated by chromatography and then submitted to aldol cyclization to give **3a** and **3b** (or **14a** and **14b**) respectively. The stereochemistry of the octalones thus obtained was assigned by means of ^{1}H NMR.[4] In the lanthanoid-shifted spectra of **3a** using Eu(dpm)$_3$, the signals of the protons on C(3) and C(4) were assigned by a concentration dependence of their chemical shifts on the shift reagent; coupling were confirmed by decoupling experiments, as is shown in Table 1 (cf. the conformational structure **15a**). The large coupling constant (J, 13 Hz) between H(1)- and H(3)-protons

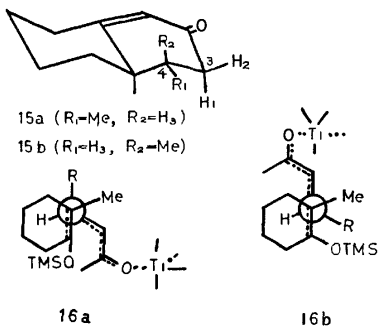

clearly demonstrated a *trans* diaxial disposition of these protons, leading to the *cis*-dimethyloctalone structure **3a**. On the other hand, the **3b** isomer showed a small coupling between these protons (J, 5 Hz), which indicated this compound to be a *trans*-dimethyloctalone, **3b** (*cf.* **15b**). Similar reasoning may also be applicable to **14a** and **14b**.

It is worth a short comment that, in the Lewis acid-promoted Michael addition of **10**, the erythro-threo ratio of the product was reversed, depending on the acceptor used. Considering two preferable conformations, **16a** and **16b**, in the transition states, the R substituent (methyl or phenyl) would control the population of these conformers. When R is methyl, **16b** is more favored than **16a** because the bulkier acetonyl would be disposed between the methyl and cyclohexane methylene groups, yielding the threo isomer, **12a**. Meanwhile, phenyl is bulkier than acetonyl, and the favored conformation in the transition state of the reaction with **11** must be **16a**, which leads to the erythro isomer, **13b**.

With the four authentic octalones, **3a**, **3b**, **14a**, and **14b**, in our hands, we set about the GLC analysis[5] of the Robinson annelation product of **1** with **2** or **11**. The results of the analysis are shown in Table 2.

Entry 1 indicates the analytical result of the enone fraction of the product obtained from **1** and **2** under the reaction conditions described by the original authors. The combined yield of enones was quite low, and the major products were, rather, the regioisomer, **17a** or **17b**, and the dienone, **18**. These by-products were separated by preparative GLC, and their structures were assigned spectroscopically; the enone showed a carbonyl absorption at 1668 cm^{-1} in the IR spectrum. Two pairs of methyl doublets in the ^1H NMR spectrum demonstrated this compound to be a regioisomer of **3a**; meanwhile, in the lanthanoid-shifted ^1H NMR, its C(3)-methylene protons exhibited a coupling pattern (J, 18 and 12 Hz for H(1) and 18 and 6 Hz for H(2)) which was very similar to that of **3a**. This result supported the idea that the C(4)-methyl in the regioisomeric enone must be equatorial. From these results, we concluded that the **17a** or **17b** stereostructure should be assigned to this compound because this compound was produced under equilibrating con-

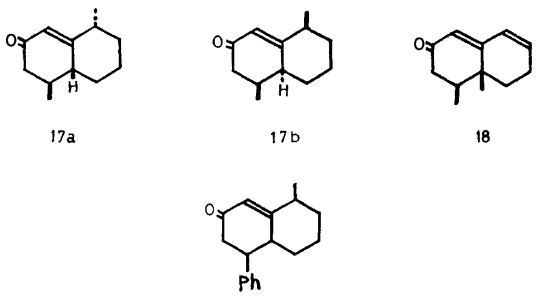

Table 1. Lanthanoid-shifted ^1H NMR of some protons of the octalones[a]

Octalone	Proton	Chemical shift, δ[b]	Coupling pattern and constants, Hz
3a	H_1	5.20	d.d, $J_{1,2}=18$, $J_{1,3}=12$
	H_2	5.44	d.d, $J_{1,2}=18$, $J_{2,3}=6$
	H_3	3.48	d.d, $J_{1,3}=12$, $J_{2,3}=6$
3b	H_1	5.82	d.d, $J_{1,2}=16$, $J_{1,3}=5$
	H_2	5.51	d.d, $J_{1,2}=16$, $J_{2,3}=8$
	H_3	3.36	d.d, $J_{1,3}=5$, $J_{2,3}=8$
14a	H_1	5.18	d.d, $J_{1,2}=18$, $J_{1,3}=16$
	H_2	4.70	d.d, $J_{1,2}=18$, $J_{2,3}=5$
	H_3	4.32	d.d, $J_{1,3}=16$, $J_{2,3}=5$
14b	H_1	4.55	d.d, $J_{1,2}=16$, $J_{1,3}=5$
	H_2	4.79	d.d, $J_{1,2}=16$, $J_{2,3}=9$
	H_3	4.00	d.d, $J_{1,3}=5$, $J_{2,3}=9$

a) $Eu(dpm)_3$ was added to a $CDCl_3$ solution of the substrate in a molar ratio of 1/3. b) Measured at 100 MHz.

Table 2. The robinson annelation of 2-methylcyclohexanone with 3-penten-2-one and 4-phenyl-3-buten-2-one

Entry	Enone	Reaction conditions			Combined yield/%	Ratio of products/%[b]		
		Solvent[a]	Temp/°C	Time/h		*cis*-Enone	*trans*-Enone	By-products identified
1	**2**	A	112—117	100	9	23	7	28(**17**), 40(**18**)
2	**2**	A	112—117	9	14	56	24	20(**17**)
3	**2**	B	75	6	22	25	75	
4	**2**	B	75	3	36	26	74	
5	**11**	A	112—117	6	29	53	15	32(**19a**)
6	**11**	A	112—117	3	36	54	16	30(**19a**)
7	**11**	B	75	6	26	37	34	10(**19a**), 19(**19b**)
8	**11**	B	75	3	26	37	36	8(**19a**), 12(**19b**)

a) A, dioxane; B, dimethyl sulfoxide. b) *Cf.* Ref. 5 for the analytical method,

ditions.

Another crystalline by-product showed a carbonyl absorption at 1659 cm^{-1} in the IR spectrum and a strong UV absorption at 239 nm, which indicated an $\alpha,\beta,\gamma,\delta$-unsaturated dienone chromophore. The dehydrogenation of **3a** with chloranil in *t*-butyl alcohol afforded the same dienone. Thus, this dienone is unambiguously shown by the formula **18**. This dienone was probably produced by the air oxidation of **3a** for a long period.

When the reaction time was shortened (Entry 2), the combined yield of the product was slightly raised and the only detectable by-product was the regioisomeric enone **17**.

In the reaction employing dimethyl sulfoxide as the solvent, the ratio of **3a** and **3b** was reversed (Entries 3 and 4), although the stereoselectivity of the reaction was not so high as Scanio and Starrett stated.[2] Unlike the reaction with 3-penten-2-one, no regioisomer was detectable in the reaction in dimethyl sulfoxide.

In the reaction of **1** and **11** employing dioxane as the solvent, the product was a mixture of *cis*- and *trans*-enone (**14a** and **14b**) and the regioisomer **19a**, in which the *cis*-enone **14a** was predominant (Entries 5 and 6). The structure of the regioisomer was supported by a carbonyl absorption at 1661 cm^{-1} in the IR spectrum and a three-proton doublet in the ^1H NMR spectrum. On the other hand, a comparable formation ratio of the *cis*- and *trans*-enones (**14a** and **14b**) was observed in the reaction using dimethyl sulfoxide as the solvent (Entries 7 and 8). Two regioisomers, **19a** and **19b**, were also isolated. The structures of the by-products were confirmed by the IR (1661 cm^{-1}) and ^1H NMR (a three-proton doublet) spectra, which demonstrated that these by-products must both be stereoisomers. However, we have obtained no evidence that allowed us to assign stereostructures to these regioisomers.

In conclusion, we could not observe such high stereoselectivity as was reported by Scanio and Starrett[2] in the Robinson annelation of 2-methylcyclohexanone and 3-penten-2-one, although a change in the formation ratio of the **3a** and **3b** stereoisomers was observed to some extent by replacing the reaction solvent. Accordingly, we are suspicious of the reaction mechanism (Scheme 2) they have proposed for the annelation in dimethyl sulfoxide, for if it will operate, the reaction would proceed much more stereoselectively.

Experimental

All the melting and boiling points are uncorrected. The IR spectra were taken on a Hitachi G-2 or 215 spectrophotometer. The ^1H NMR spectra were recorded on a Hitachi R-22 (90 MHz) or JEOL PS-100 (100 MHz) instrument, using TMS as the internal standard and $CDCl_3$ as the solvent. The recorded chemical shifts are on the δ (ppm) scale. The high resolution mass spectra were recorded on a JEOL JMS-OISC spectrometer. The GLC analysis was performed on a Shimadzu Model 5A instrument using the following columns: A (5% OV-17, 2 m×3 mm) and B (5% SE-30, 2 m×3 mm). The formation ratios of the reaction products were all determined by GLC.[5] The elemental analyses were performed in the microanalytical laboratory of the Chemical Research Institute of Non-Aqueous Solutions, Tohoku University.

2-Methylcyclohexanone (1). The ketone of a reagent grade (Tokyo Kasei Corp.) was distilled, and a fraction boiling at 163.2 °C was utilized.

3-Penten-2-one (2). This enone was prepared according to the method of Lawesson *et al.*[6] A fraction boiling at 52—54 °C/260 mmHg was immediately used.

1,5-Diketones 12a and 12b. These diketones were prepared according to the method of Mukaiyama *et al.*[3] A solution of $TiCl_4$ (570 mg, 3 mmol) in CH_2Cl_2 (12 ml) was cooled to −78 °C under N_2. Solutions of **2** (303 mg, 3.6 mmol) and **10**[8] (552 mg, 3 mmol) in the same solvent (5.4 and 4.5 ml respectively) were added successively to the above solution with stirring. After stirring for 30 min at −78 °C, the mixture was quenched with aqueous K_2CO_3 (1.05 g in 22 ml of water), and the resultant precipitates were filtered off. The filtrate was extracted with pentane, and the extract was washed with water and brine. After the removal of the solvent, the crude product (553 mg) was distilled in a vacuum to give the main fraction (374 mg; bp 102—126 °C (bath temperature)/1 mmHg††), which consisted of two isomers, **12a** and **12b** (25:75). Because the separation of these isomers by preparative TLC ($AgNO_3$-impregnated silica gel, hexane–AcOEt (5:1)) was incomplete, only one isomer, **12b** was separated in the pure state (21 mg, 13%). In order to separate the isomers completely, preparative GLC (Column B at 140 °C) was utilized. **12a**: R_t 6.7 min (Column B at 140 °C); IR ($CHCl_3$) 1700 cm^{-1}; ^1H NMR 0.86 (3H, d, J=7 Hz), 0.91 (3H, s), and 2.09 (3H, s). **12b**: R_t 7.8 min, IR ($CHCl_3$) 1700 and 1209 cm^{-1}; ^1H NMR 0.73 (3H, d, J=7 Hz), 0.94 (3H, s), and 2.17 (3H, s).

cis-4,4a-Dimethyl-4,4a,5,6,7,8-hexahydronaphthalen-2(3H)-one (3a). A mixture of **12a** (40 mg, 0.2 mmol), active alumina (activity II, 1.6 g), water (1.33 ml), and dioxane (4 ml) was heated at 105—109 °C under reflux for 3 h with stirring under N_2. Then the mixture was filtered, and the crude product (88 mg) was obtained from the filtrate on the removal of the solvent. Pure **3a** (21 mg, 58%) was obtained by preparative TLC repeated four times, using cyclohexane–AcOEt (10:1) as the solvent. IR ($CHCl_3$) 1660 and 1616 cm^{-1}; ^1H NMR 0.95 (3H, d, J=6 Hz), 1.09 (3H, s), and 5.98 (1H, d). The lanthanoid-shifted ^1H NMR spectra were taken as follows: an exact amount of $Eu(dpm)_3$ was added, portion by portion to a solution of **3a** (20 mg) in $CDCl_3$; the spectrum was recorded after each addition until the molar ratio of the substrate and the reagent reached 3:1. The experimental results obtained are shown in Table 1.

trans-4,4a-Dimethyl-4,4a,5,6,7,8-hexahydronaphthalen-2(3H)-one (3b). Pure **3b** (23 mg, 80%) was obtained from **12b** (32 mg, 0.16 mmol) in the same manner as has been described for **3a**. IR ($CHCl_3$) 1660 and 1618 cm^{-1}; ^1H NMR 0.98 (3H, d, J=6 Hz), 1.28 (3H, s), and 5.78 (1H, d). Found: C, 81.04; H, 10.34%. Calcd for $C_{12}H_{18}O$: C, 80.85; H, 10.18%.

1,5-Diketones 13a and 13b. A solution of freshly distilled $TiCl_4$ (380 mg, 2 mmol) in CH_2Cl_2 (8 ml) was cooled to −78 °C under N_2. A solution of **11**[7] (308 mg, 2.1 mmol) and **10** (450 mg, 2.4 mmol) in the same solvent (3 ml both) were added successively to the above solution with stirring. The mixture was then further stirred at −78 °C for 2.5 h. After quenching with aqueous K_2CO_3 (0.7 g in 15 ml of water), the resultant precipitates were

†† 1 mmHg≈133.322 Pa.

filtered off. The filtrate was extracted with CH_2Cl_2 and the extract was washed with water and brine. The subsequent removal of the solvent gave the crude product (598 mg). GLC (Column A at 180 °C) indicated two isomers (**13a** and **13b**, 71:29). Without distillation, the crude product was separated by preparative TLC, using hexane–AcOEt (5:1), to afford the respective isomers, **13a** (114 mg, 22%) and **13b** (211 mg, 41%). **13a**: R_t 9.4 min (Column A at 180 °C), IR ($CHCl_3$) 1702 and 1690 cm^{-1}; ^1H NMR 0.99 (3H, s) 1.98 (3H, s), 3.01 (H_1, dd, $J_{1,2}=16$, $J_{1,3}=10$ Hz), 2.48 (H_2, dd, $J_{1,2}=16$, $J_{2,3}=4$ Hz), 3.93 (H_3, dd, $J_{1,3}=10$, $J_{2,3}=4$ Hz) and 7.36 (5H, s). Found: C, 79.36; H, 8.91%. Calcd for $C_{17}H_{22}O_2$: C, 79.03; H, 8.58%. **13b**: R_t 10.1 min, IR ($CHCl_3$) 1701 and 1689 cm^{-1}; ^1H NMR 1.00 (3H, s). 2.03 (3H, s), 2.68 (H_1, dd, $J_{1,2}=16$, $J_{1,3}=4$ Hz), 3.03 (H_2, dd, $J_{1,2}=16$, $J_{2,3}=11$ Hz), 3.83 (H_3, dd, $J_{1,3}=4$, $J_{2,3}=11$ Hz), and 7.35 (5H, s). Found: C, 79.30; H, 8.83%. Calcd for $C_{17}H_{22}O_2$: C, 79.03; H, 8.58%.

cis-*4-Phenyl-4a-methyl-4,4a,5,6,7,8-hexahydronaphthalen-2(3H)-one (14a)*. Aqueous KOH (213 mg in 0.39 ml of water) was added to a mixture of **13a** (128 mg, 0.50 mmol) and ethanol (3 ml) with stirring under N_2. The whole mixture was heated at 90 °C under reflux for 4 h. The mixture was then cooled with ice, and 2% HCl was dropped into the mixture until the solution became pH 4. The resulting solution was extracted with CH_2Cl_2, and the extract washed with water and brine. The subsequent removal of the solvent gave the crude product (187 mg). Preparative TLC, using cyclohexane–AcOEt (4:1) as the solvent, gave the pure enone (90 mg, 76%), which solidified on distillation (bp 123—186 °C (bath temperature)/1 mmHg, mp 70.2—72 °C (recrystallized from pentane–benzene (5:1)); IR ($CHCl_3$) 1662 and 1616 cm^{-1}; ^1H NMR 1.10 (3H, s), 5.98 (1H, d), and 7.44 (5H, m). Found: C, 84.67; H, 8.29%. Calcd for $C_{17}H_{20}O$: C, 84.95; H, 8.39%.

trans-*4-Phenyl-4a-methyl-4,4a,5,6,7,8-hexahydronaphthalen-2-(3H)-one (14b)*. Pure **14b** (109 mg, 73%) was obtained from **13b** (161 mg, 0.63 mmol) in a similar manner. Distillation (bp 101—121 °C (bath temperature)/1 mmHg) of the enone gave a soft mass; mp 48.5—52 °C. No appropriate solvent was found for recrystallization. IR ($CHCl_3$) 1662 and 1614 cm^{-1}; ^1H NMR 1.35 (3H, s), 6.14 (1H, d), and 7.48 (5H, m). Found: C, 84.64; H, 8.29%. Calcd for $C_{17}H_{20}O$: C, 84.95; H, 8.39%.

The Annelation Reaction of 2-Methylcyclohexanone with 3-Penten-2-one. In Dioxane: NaH (178 mg, 3.6 mmol) was suspended in a solution of **1** (345 mg, 3.0 mmol) and dioxane (10 ml), and the mixture was stirred at 112—117 °C for 3 h under N_2. After cooling to room temperature, a solution of **2** (313 mg, 3.7 mmol) in dioxane (4 ml) was added, and the whole mixture was stirred for 9 h at room temperature. After the subsequent addition of a small amount of cold water, the mixture was extracted with pentane. The extract was washed with water and brine, and dried. After the removal of the solvent, the residue (512 mg) was distilled in a vacuum (bp 110—159 °C (bath temperature)/1 mmHg). The distillate (245 mg) was separated by preparative TLC, repeated four times, using cyclohexane–AcOEt (7:1) as the solvent; this gave two main fractions (R_f 4.8, 50 mg, 9% and R_f 5.3, 28 mg, 5%). The polar fraction was shown to be a mixture consisting of **3a** and **3b** (84:16), which was identified with authentic samples by GLC; however, the attempted separation of these isomers by GLC was fruitless. The by-product, **17a** (9 mg; mp 38.5—39 °C), in the less polar fraction was isolated by preparative GLC (Column A at 140 °C) and crystallized on standing, although no appropriate recrystallization solvent was found. IR ($CHCl_3$) 1668 and 1619 cm^{-1}; ^1H NMR 1.07 (3H, d, $J=6$ Hz), 1.16 (3H, d, $J=6$ Hz), and 5.86 (1H, s). Found: M^+ 178.1357. Calcd for $C_{12}H_{18}O$: M^+ 178.1357.

In a similar manner, **1** (337 mg, 3.0 mmol) and **2** (270 mg, 3.2 mmol) were allowed to react in dioxane for 100 h, after which the reaction mixture was worked up as above. A fraction (164 mg) obtained by short-path distillation was chromatographed on a silica-gel column, using hexane–AcOEt (7:1) as the solvent, thus giving an oil (46 mg, 9.0%). The GLC analysis (Column B at 140 °C) of the oil showed two peaks, **17a** (R_t 7.9 min) and **18** (R_t 11.2 min), along with those of **3a** and **3b**. Two by-products were separated by preparative GLC (Column B at 140 °C); **17a** (25 mg) and **18** (13 mg). The former by-product, **17a**, was identified by spectral comparison with the authentic compound. The latter one, **18**, solidified on standing; mp 39.8—42.5 °C; IR ($CHCl_3$) 1659 and 1622 cm^{-1}; ^1H NMR 0.98 (3H, d, $J=7$ Hz), 1.01 (3H, s), 5.72 (1H, s), and 6.21 (2H, br s); UV_{max} (95% EtOH) 239 nm (ε 12122); MS, *m/e* (rel intensity) 176 (M^+, 98), 134 (100), 119 (45), 105 (48), 91 (65).

This dienone was identified by spectral comparison with the authentic compound prepared by the dehydrogenation of **3a** (*vide post*).

In Dimethyl Sulfoxide (DMSO): A suspension of NaH (178 mg, 3.6 mmol) in DMSO (6 ml) was stirred at 75 °C for 30 min. After the addition of a solution of **1** (340 mg, 3 mmol) in DMSO (2 ml) and stirring for 3 h at room temperature, a solution of **2** (307 mg, 3 mmol) in the same solvent (3 ml) was added. The whole mixture was then stirred for 3 h at room temperature. After the subsequent addition of a small amount of ice water, the mixture was extracted with pentane. The extract was washed with water and brine, and dried. The evaporation of the solvent left an oil (373 mg), which was distilled in a vacuum (bp 114—158 °C (bath temperature)/1 mmHg) to give an oil (306 mg). The oil was purified by preparative TLC, repeated three times, using cyclohexane–AcOEt (7:1) as the solvent, to afford the main fraction (R_f 3.3, 193 mg, 36%). The GLC analysis of the fraction with a capillary column showed two peaks, **3a** and **3b** (29:71). Two other unidentified by-products were detected by the GLC (Column A at 140 °C, R_t 3.3 and 3.4 min) of the crude product.

Dehydrogenation of 3a with Chloranil. Authentic **18** was obtained by dehydrogenation according to the method of Agnello and Laubach.[10] A mixture of pure **3a** (36 mg, 0.2 mmol), chloranil (149 mg, 0.6 mmol), and *t*-butyl alcohol (5.5 ml) was heated at 80—90 °C for 3.5 h under N_2 with stirring. The reaction mixture was extracted with $CHCl_3$, and the extract was successively washed with water, 5% aqueous NaOH, water, and brine, and dried. After the removal of the solvent, the residue (30 mg) was purified directly by preparative TLC, using hexane–AcOEt (5:1) as the solvent, to give pure **18** (18 mg, 50%) as a soft mass (mp 39—42 °C).

The Annelation of 2-Methylcyclohexanone with 4-Phenyl-3-buten-2-one. In Dioxane: By a similar treatment, a crude product (952 mg) was obtained from **1** (336 mg, 3 mmol) and **11** (438 mg, 3 mmol) by allowing them to react at 112—117 °C for 3 h; subsequent distillation in a vacuum gave a fraction (bp 158—190 °C (bath temperature)/1 mmHg, 439 mg)) which was separated by preparative TLC, repeated twice, using hexane–AcOEt (15:1) as the solvent, to give two fractions (R_f 4.3 and 4.8). The two main compounds in the polar fraction (145 mg, 20%) were **14a** and **14b** (78:22), as identified with an authentic sample by GLC. The less polar fraction (113 mg, 16%) gave **19a** as the main

component upon preparative GLC (Column B at 180 °C, R_t 10.7 min, 9 mg); IR ($CHCl_3$) 1668 and 1619 cm^{-1}; ^1H NMR 1.19 (3H, d, J=7 Hz), 5.90 (1H, br s), and 7.24 (5H, m).

In DMSO: By a similar treatment, a crude product (990 mg) was obtained from **1** (449 mg, 4 mmol) and **11** (584 mg, 4 mmol) by a reaction at room temperature for 6 h. Vacuum distillation afforded a fraction (364 mg; bp 135—200 °C (bath temperature)/1 mmHg) which was subsequently separated by preparative TLC, using hexane–AcOEt (5:1) as the solvent, to give two fractions (R_f 3.5, 165 mg and R_f 4.0, 84 mg). Two enones, **14a** (10 mg) and **14b** (12 mg), were separated from the polar fraction by preparative GLC (Column A at 180 °C). **14a**, R_t 13.4 min; IR ($CHCl_3$) 1658 and 1616 cm^{-1}; ^1H NMR 1.09 (3H, s), 5.86 (1H, br s), and 7.31 (5H, m). **14b**, R_t 11.5 min; IR ($CHCl_3$) 1650 and 1618 cm^{-1}; ^1H NMR 1.33 (3H, s), 2.73 (1H, q, J=5 and 16 Hz), 3.0 and 3.12 (2H, in total), 5.96 (1H, br s), and 7.30 (5H, m). The two main components, **19a** (13 mg) and **19b** (24 mg), were separated from the less polar fraction by preparative GLC (Column A at 180 °C). **19a**, R_t 10.7 min; IR ($CHCl_3$) 1661 and 1601 cm^{-1}; ^1H NMR 1.19 (3H, d, J=7 Hz), 5.96 (1H, s), and 7.33 (5H, m). Found: M^+ 240.1520. Calcd for $C_{17}H_{20}O$: M^+ 240.1513. **19b**, R_t 12.3 min; IR ($CHCl_3$) 1661 and 1619 cm^{-1}; ^1H NMR 1.16 (3H, d, J=6 Hz), 5.79 (1H, s), and 7.36 (5H, m). Found: M^+ 240.1525. Calcd for $C_{17}H_{20}O$: M^+ 240.1513.

We wish to thank Professor Toshitaka Tamura, College of Science and Technology, Nihon University, for his measurements of the high-resolution mass spectra.

References

1) M. Kikuchi and A. Yoshikoshi, 22nd Symposium on the Chemistry of Terpenes, Essential Oils, and Aromatics, Yokohama, October 1978, Abstr., p. 258.
2) C. J. V. Scanio and R. M. Starrett, *J. Am. Chem. Soc.*, **93**, 1539 (1971).
3) K. Narasaka, K. Soai, and T. Mukaiyama, *Chem. Lett.*, **1974**, 1223.
4) T. J. Leitereg, *Tetrahedron Lett.*, **1972**, 2617.
5) An OV-17 capillary column (50 m) was used at 190 °C.
6) S. O. Lawesson, E. H. Larsen, G. Sundstrom, and H. J. Jakobsen, *Acta Chem. Scand.*, **17**, 2216 (1963).
7) N. L. Drake and P. Allen, Jr., *Org. Synth.*, Coll. Vol. I, 77 (1941).
8) H. O. House, L. J. Czuba, M. Gall, and H. D. Olmstead, *J. Org. Chem.*, **34**, 2324 (1969); G. Stork and P. F. Hudrlik, *J. Am. Chem. Soc.*, **90**, 4462 (1968).
9) Taken at 100 MHz.
10) E. J. Agnello and G. D. Laubach, *J. Am. Chem. Soc.*, **82**, 4293 (1960).

Preparation and Physicochemical Properties of Tervalent Cobalt Complexes of Porphyrins

Hiroshi SUGIMOTO,* Nobuhiro UEDA, and Masayasu MORI
Faculty of Science, Osaka City University, Sugimoto, Sumiyoshi-ku, Osaka 558

(Received March 9, 1981)

Tervalent cobalt complexes of octaethylporphyrin (OEP) and tetraphenylporphyrin (TPP), $[Co^{III}(OEP)(H_2O)_2]X$ (X=ClO_4, BF_4), $[Co^{III}(OEP)(THF)_2]ClO_4$, $[Co^{III}(TPP)(H_2O)_2]X$ (X=ClO_4, BF_4), and $[Co^{III}(TPP)(H_2O)Y]$ (Y=Cl, Br, SCN, N_3) were synthesized. Molecular weight measurements indicate that only $[Co^{III}(TPP)(H_2O)_2]BF_4$ and $[Co^{III}(TPP)(H_2O)_2]ClO_4$ aggregate at higher concentrations in chloroform. In polar solvents such as methanol, all are monomeric. In nonpolar solvents, all the complexes show Soret bands at shorter wavelengths and somewhat paramagnetic ^1H NMR spectra; these anomalies are absent in polar solvents. Tetrafluoroborates and perchlorates react with ethyl vinyl ether smoothly to form 2,2-diethoxyethylcobalt(III) complexes which are easily converted to formylmethylcobalt(III) complexes. ^1H NMR and absorption spectra of the amine adducts prepared in this study, $[Co^{III}(OEP)(L)_2]ClO_4$ (L=pyridine, 2-methylimidazole) and $[Co^{III}(TPP)(L')_2]ClO_4$ (L'=pyridine, 4-cyanopyridine, 4-methylpyridine), indicate that the two amine molecules coordinate to the central cobalt atom. As regards redox potentials for the Co(III)/Co(II) couple as measured by cyclic voltammetry, the cobalt(III) porphyrins are categorized into three groups: (i) BF_4 and ClO_4 salts with redox potentials at about 0.7 V; (ii) halides and pseudohalides with those at 0.2—0.3 V; and (iii) bis(amine) adducts with those at −0.3—+0.1 V. In polar solvents, however, the redox potentials of (i) and (ii) are very similar to one another.

It is well known that the active site of vitamin B_{12} is the cobalt complex of the corrin ligand and that its coenzyme form and related alkylcobalamin are the only organometallic compounds hitherto found in nature. Since the discovery of the cobalt σ-bond between cobalt(III) and 5'-carbon of an adenine moiety through crystallographic studies by Hodgkin,[1] a large number of model compounds have been synthesized to elucidate the basic chemistry of the cobalt-carbon bond in square planar macrocyclic systems.[2-8] Metal complexes of porphyrin are particularly suitable for model studies on the structure and reaction of coenzyme B_{12}, because both porphyrin and corrin[9] are of tetrapyrrole macrocycle. Since the rapture and recombination of the cobalt-carbon bond are key steps to achieve the enzymatic catalysis, main interes thas existed in the formation and cleavage of the cobalt-carbon bond by uni-, bi-, and tervalent metal complexes. The formation of the cobalt-carbon bond through nucleophilic reactions of Co(I) toward organic halides has been investigated in relation to the reaction of coenzyme B_{12}. Similar nucleophilic reactions of Co(I) species were found in porphyrin complexes of Rh(I)[10] and Ir.[11] On the other hand, another mode for the cobalt-carbon bond formation was recently found in an electrophilic reaction of coenzyme B_{12} having a tervalent cobalt atom[12] with alkyl vinyl ether. Ogoshi *et al.*[13] reported that a tervalent rhodium complex of porphyrin reacted with ethyl vinyl ether to give a rhodium-carbon bond. Silverman and Dolphin[12] also showed a cobalt-carbon bond formation by the electrophilic reaction of cobalt(III) oxime with vinyl ether. Dolphin suggested the intermediacy of an olefin π-complex of cobalt(III) in the reaction. However, there has hitherto been no report about the electrophilic reaction of cobalt(III) porphyrins toward electron rich olefins. This is probably because tervalent cobalt atoms of usual cobalt(III) porphyrin complexes have no sufficient cationic character to cause the reaction. Thus, usual cobalt(III) porphyrins are six-coordinated by inclusion of halogens and/or amines in the coordination sphere, such as $[Co^{III}(porphyrin)(amine)_2]X$ and $[Co^{III}(porphyrin)(amine)X]$, and the electrophilicity or cationic character of the central cobalt(III) ion is thereby reduced. In order that cobalt(III) porphyrins should have sufficient electrophilicity to react with various organic nucleophiles, therefore, the electron-donating ability of the counter anion should be sufficiently weak. In this sense it was thought of utmost importance to compare cobalt(III) complexes of porphyrins having various types of axial ligands: weak ligands such as BF_4 and ClO_4 ions; intermediate ligand such as halides and pseudohalides; and strong ligands such as amines. Although active investigations[14] have been made for bromides and chlorides and their amine adducts, for perchlorates only our research group[15,16] has recently reported of syntheses and X-ray crystallographic data. This paper is concerned with synthetic methods, electrophilic reactions toward electron rich olefins, and redox potentials for various tervalent cobalt complexes of octaethylporphyrin and tetraphenylporphyrin, and discusses the relation between mode of coordination of counter anions to the central cobalt atom and physicochemical properties such as absorption and ^1H NMR spectra, particularly redox potentials of the cobalt atom.**

Experimental

Synthesis. $[Co^{III}(OEP)(THF)_2]ClO_4$ (*1*): Octaethylporphyrinatocobalt(II) $Co^{II}(OEP)$, (100 mg) was dissolved in tetrahydrofuran (100 cm^3) containing 1 cm^3 of 70% perchloric acid. The reaction mixture was stirred for 24 h under an aerobic condition until black crystals

** Abbreviations used are: OEP, octaethylporphyrin; TPP, $\alpha,\beta,\gamma,\delta$-tetraphenylporphyrin; THF, tetrahydrofuran; py, pyridine; 2-MeIm, 2-methylimidazole; 4-CNpy, 4-cyanopyridine; 4-Mepy, 4-methylpyridine; TBAP, tetrabutylammonium perchlorate; TBAF, tetrabutylammonium fluoroborate; TBAB, tetrabutylammonium bromide; TBAC, tetra butylammonium chloride.

were precipitated. The crystals thus obtained were collected and washed with petroleum ether. Recrystallization from benzene–THF afforded reddish purple crystals (75 mg) in 53% yield. Found: C, 63.28; H, 7.43; N, 6.76%. Calcd for $C_{44}H_{60}N_4ClO_6Co$: C, 63.26; H, 7.24; N, 6.71%.

[Co^{III}(OEP)(H$_2$O)$_2$]ClO$_4$ (2): Recrystallization of **1** from benzene–dichloromethane saturated with water gave dark red, slightly hygroscopic crystals in a quantitative yield. Found: C, 59.00; H, 6.29; N, 6.99%. Calcd for $C_{36}H_{48}N_4ClO_6Co$: C, 59.46; H, 6.65; N, 7.70%.

[Co^{III}(OEP)(H$_2$O)$_2$]BF$_4$ (3): To a solution of Co^{II}(OEP) (100 mg) in methanol (100 cm^3) was added 10% tetrafluoroboric acid (2—3 cm^3) and the solution was stirred for several hours. Then the solvent was removed carefully under reduced pressure until fine purple crystals were precipitated. The crystals were collected, washed with water, and dried over P_2O_5 *in vacuo* to give **3** in 70% yield. Found: C, 61.62; H, 6.72; N, 7.87%. Calcd for $C_{36}H_{48}N_4BF_4O_2Co$: C, 60.51; H, 6.77; N, 7.84%.

[Co^{III}(OEP)(py)$_2$]ClO$_4$ (4): Recrystallization of **1** from benzene containing an excess amount of pyridine gave reddish purple crystals in almost a quantitative yield. Found: C, 64.56; H, 6.63; N, 9.69%. Calcd for $C_{46}H_{54}N_4ClO_4Co$: C, 65.05; H, 6.40; N, 9.89%.

[Co^{III}(OEP)(2-MeIm)$_2$]ClO$_4$ (5): Recrystallization of **1** from benzene–dichloromethane containing an excess amount of 2-methylimidazole afforded reddish purple crystals in a quantitative yield. Found: C, 61.94; H, 6.83; N, 12.90%. Calcd for $C_{44}H_{56}N_8ClO_4Co$: C, 61.78; H, 6.60; N, 13.10%.

[Co^{III}(OEP)CH$_2$CH(OCH$_2$CH$_3$)$_2$] (6): To an ethanol solution (100 cm^3) of **1** (100 mg) were added vinyl ethyl ether (100 mg) and triethylamine (0.5 cm^3). The reaction mixture was stirred at room temperature until a fine powder was precipitated. The powder thus obtained was collected and recrystallized from benzene–dichloromethane to afford reddish purple crystals (64 mg) in 75% yield. Found: C, 71.47; H, 7.55; N, 8.07%. Calcd for $C_{42}H_{57}N_4O_2Co$: C, 71.16; H, 8.10; N, 7.90%.

[Co^{III}(OEP)CH$_2$CHO] (7): A dichloromethane solution of **6** was treated with silica gel or allowed to stand for 1 d. The solvent was evaporated under reduced pressure. The residual solid was recrystallized from benzene to afford orange red crystals in almost a quantitative yield. Found: C, 71.14; H, 7.51; N, 8.46%. Calcd for $C_{38}H_{47}N_4OCo$: C, 71.90; H, 7.48; N, 8.84%.

[Co^{III}(TPP)(H$_2$O)$_2$]ClO$_4$ (8): To a suspension of Co^{II}(TPP) (100 mg) in methanol (100 cm^3) was added 10% perchloric acid (1—2 cm^3) and the solution was stirred for about 10 h to almost complete dissolution. The solvent was removed under reduced pressure. The residual solid was recrystallized from methanol–benzene to give reddish purple crystals in 75% yield. Found: C, 66.23; H, 3.77; N, 7.09%. Calcd for $C_{44}H_{40}N_4ClO_4Co$: C, 66.62; H, 4.32; N, 7.06%.

[Co^{III}(TPP)(H$_2$O)$_2$]BF$_4$ (9): To a solution of Co^{II}(TPP) (100 mg) in dioxane (100 cm^3) was added 10% tetrafluoroboric acid (2—5 cm^3) and the solution was stirred for about 1 h. Then the solvent was removed carefully under reduced pressure until fine crystals were precipitated. The crystals were collected, washed with water and dried over P_2O_5 *in vacuo* to give **9** in 65% yield. Found: C, 63.62; H, 4.42; N, 6.63%. Calcd for $C_{44}H_{36}N_4BF_4Co$: C, 63.63; H, 4.37; N, 6.75%.

[Co^{III}(TPP)(H$_2$O)I] (10): A dichloromethane solution of **8** was washed with an aqueous sodium iodide solution several times and then with water and dried over Na_2SO_4. The solvent was removed under reduced pressure. The residual solid was recrystallized from methanol to give reddish purple crystals in almost a quantitative yield. Found: C, 64.97; H, 4.08; N, 6.36%. Calcd for $C_{44}H_{30}N_4OICo$: C, 64.72; H, 3.70; N, 6.86%.

[Co^{III}(TPP)(H$_2$O)Br] (11): To a suspension of Co^{II}(TPP) in methanol was added 10% hydrobromic acid and the mixture was stirred for 20 h. Methanol was removed under reduced pressure. The residual solid was recrystallized from methanol to give reddish purple crystals in a quantitative yield. Found: C, 68.38; H, 3.96; N, 7.29%. Calcd for $C_{44}H_{30}N_4OBrCo$: C, 68.31; H, 4.17; N, 7.41%.

[Co^{III}(TPP)(H$_2$O)Cl] (12): This was synthesized by the method reported by Yamamoto *et al.*[14h,l]

[Co^{III}(TPP)(H$_2$O)SCN] (13): This was prepared by the same procedure as for **10** except that KI was replaced by KSCN. Found: C, 72.73; H, 3.86; N, 9.50%. Calcd for $C_{45}H_{30}N_5OSCo$: C, 72.28; H, 4.04; N, 9.37%.

[Co^{III}(TPP)(H$_2$O)N$_3$] (14): This complex also was prepared by the same procedure as for **10** but by using NaN_3 in place of KI. Found: C, 72.85; H, 4.12; N, 13.36%. Calcd for $C_{44}H_{30}N_7OCo$: C, 72.22; H, 4.13; N, 13.40%.

[Co^{III}(TPP)(py)$_2$]ClO$_4$ (15): Recrystallization of **8** from benzene–pyridine (10:1 vol/vol) gave reddish purple crystals in 80% yield. Found: C, 70.14; H, 4.33; N, 8.72%. Calcd for $C_{54}H_{38}N_6ClO_4Co$: C, 69.79; H, 4.12; N, 9.04%.

[Co^{III}(TPP)(4-CNpy)$_2$]ClO$_4$ (16): Recrystallization of **8** from benzene containing an excess amount of 4-cyanopyridine gave reddish purple crystals. Found: C, 68.37; H, 3.69; N, 11.39%. Calcd for $C_{56}H_{36}N_8ClO_4Co$: C, 68.68; H, 3.71; N, 11.44%.

[Co^{III}(TPP)(4-Mepy)$_2$]ClO$_4$ (17): Recrystallization of **8** from benzene containing an excess amount of 4-methylpyridine gave reddish purple crystals in a quantitative yield. Found: C, 70.78; H, 4.70; N, 9.19%. Calcd for $C_{56}H_{42}N_6ClO_4$: C, 70.25; H, 4.42; N, 8.78%.

[Co^{III}(TPP)(py)$_2$]Cl (18): Recrystallization of **12** from benzene–pyridine (1:1 vol/vol) gave reddish purple crystals. Found: C, 74.73; H, 4.87; N, 9.67%. Calcd for $C_{54}H_{46}N_6ClCo$: C, 74.60; H, 4.87; N, 9.67%.

[Co^{III}(TPP)(py)Cl] (19): This was prepared by the method previously reported,[14l] and also obtained from recrystallization of **18** from benzene–dichloromethane.

[Co^{III}(TPP)CH$_2$CH(OCH$_2$CH$_3$)$_2$] (20): The procedure for preparation was the same as that described for octaethylporphyrin complex **6**. Found: C, 75.73; H, 4.92; N, 7.32%. Calcd for $C_{51}H_{45}N_4O_2Co$: C, 76.10; H, 5.64; N, 6.96%.

[Co^{III}(TPP)CH$_2$CHO] (21): A dichloromethane solution of **20** was treated with silica gel as described for **7**. Found: C, 76.93; H, 4.42; N, 7.99%. Calcd for $C_{46}H_{35}N_4OCo$: C, 76.87; H, 4.91; N, 7.80%.

Molecular Weight. Molecular weights were measured by the vapour pressure osmometry at 31.5 °C in chloroform and methanol on a Knour vapour pressure osmometer.

Spectral Measurements. ^{1}H NMR spectra were obtained on Varian HA-100D and JEOL HM-100 spectrometers. Infrared spectra were measured on a Hitachi G-3 spectrometer and absorption spectra on a Hitachi model 200-10 spectrophotometer.

Cyclic Voltammetry. All solvents were dried and distilled before use. As a supporting electrolyte, tetrabutylammonium perchlorate (TBAP) was used after being subjected twice to crystallization from benzene. Cyclic voltammograms were obtained on a HA-104 potentiostat (Hokuto Denko) in combination with an HB-107A function generator. A three-electrode system was used which consisted of platinum working and counter electrodes and

a commercial saturated calomel electrode (SCE) separated from the bulk of solution by a bridge filled with solvent and supporting electrolyte. The bridge had its solution changed periodically to avoid aqueous contaminants from entering the cell *via* the SCE. All solutions were purged of oxygen by passing purified nitrogen through them for 10 min just before taking cyclic voltammograms. After the degassing a blanket of nitrogen was kept over the solution. The half-wave potential $E_{1/2}$ was taken as that potential lying midway between the oxidation and reduction peaks for a given couple. All experiments were carried out at room temperature (20 °C) and the potentials reported refer to the SCE.

Results and Discussion

Synthesis. All the tervalent cobalt complexes were prepared generally by air oxidation of their corresponding bivalent cobalt complexes in the presence of aqueous acid.[14] Perchlorate, tetrafluoroborate, bromide, and chloride salts of tetraphenylporphyrin complexes **8**, **9**, **11**, and **12** were obtained in methanol. Iodide and pseudohalide salts **10**, **13**, and **14** were obtained through anion exchange from the perchlorate salt. The bis(tetrahydrofuran) adduct of the perchlorate salt of cobalt(III) octaethylporphyrin **1** was obtained by using tetrahydrofuran as the solvent. This could easily be converted to bis(aqua) adduct **2** by recrystallization from benzene–dichloromethane saturated with water. The tetrafluoroborate salt of octaethylporphyrinatocobalt(III) was obtained by the same method as that for tetraphenylporphyrin derivative **9**. Bis(amine) adducts **4**, **5**, **15**, **16**, **17**, **18**, and **19** were prepared by recrystallization from benzene containing each amine in excess. The bis(pyridine) adduct of chloride salt **18** was easily converted into mono(pyridine) adduct **19** by recrystallization from benzene–chloroform. However, the bis(pyridine) adduct of perchlorate salt **15** could not be converted into mono(pyridine) adduct. These two types of pyridine adducts were confirmed by elemental analysis and ^{1}H NMR spectra.

Molecular Weights. For cobalt(III) complexes of porphyrin, no aggregation phenomena have been reported.[17] However, the molecular weight measurements in chloroform indicate that two of the complexes, **8** and **9**, tend to aggregate as the concentration is increased. For example, Fig. 1 shows the concentration dependence of molecular weight for **9** and **3**. At low concentrations around 0.01 mol dm^{-3}, both the complexes assume monomeric molecular weights. However, as the concentration is increased, the molecular weight of **9** is gradually increased. As high concentrations around 0.05 mol dm^{-3}, complex **9** is almost dimeric; in polar solvents such as methanol all of the tervalent complexes are monomeric at these high concentrations. As will be described below, ^{1}H NMR spectra of complexes **8** and **9** show no significant changes when the concentration is increased from 0.01 to 0.05 mol dm^{-3}. The observed molecular weights indicate that the complexes are not ionized in these solvents. When the anions are coordinated, the solute species are considered to be of nonelectrolyte; otherwise, they should be of ion pair or ion-pair aggregate.

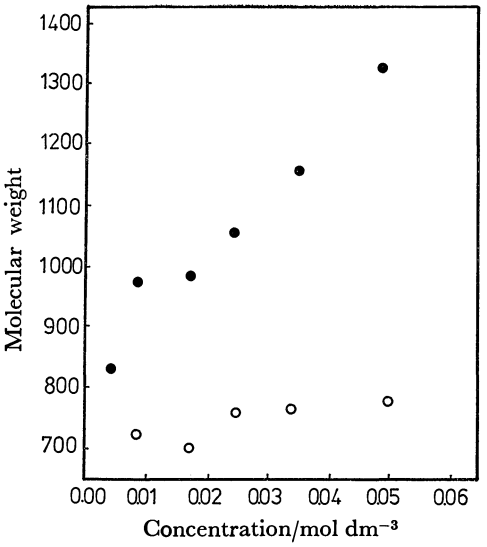

Fig. 1. Concentration dependency of the molecular weight in chloroform.
●: $[Co^{III}(TPP)(H_2O)_2]BF_4$, ○: $[Co^{III}(OEP)(H_2O)_2]BF_4$.

In the case of tetraphenylporphyrin derivatives **8** and **9** where higher molecular weights were observed, the aggregation mode of ion pair is not considered to be the stacking of porphyrin planes *via* a sort of the π-π interaction,[17] because such stacking is more difficult to be realized in the case of tetraphenylporphyrin derivatives because of the large steric hindrance of phenyl groups; this is contrary to the present situation. The most probable picture for the aggregation seems to be that in which the ion-pairs are bound through hydrogen bonding between the aqua ligands and the perchlorate (or tetrafluoroborate) anions as is realized in crystals.[16] Such hydrogen bonding seems to be more favorable in the case of tetraphenylporphyrin derivatives than in the case of octaethylporphyrin derivatives owing to the electron-withdrawing character of the former.

Absorption Spectra. Absorption spectral data are summarized in Table 1. Absorption spectra of the tervalent cobalt complexes except the amine complexes are highly dependent on properties of solvents.[15] Halides and pseudohalides **10**—**14** showed Soret bands at about 400—407 nm in nonpolar solvents such as dichloromethane. Addition of polar solvents such as methanol gave shifts toward longer wavelengths. In methanol the spectra of these complexes are very similar to one another. This can be explained in terms of the coordination of polar solvent molecules to form $[Co^{III}(TPP)(solvent)_2]^+$ species. On the other hand, BF_4 and ClO_4 salts **8** and **9** showed Soret bands at 426 nm in dichloromethane which are close to those in methanol (425 nm). This result indicates that, in dichloromethane, the cobalt atoms of BF_4 and ClO_4 salts are coordinated by water molecules as the fifth and sixth axial ligands.[16] In methanol these water molecules seem to be replaced with solvent molecules as suggested by the ^{1}H NMR and the cyclic voltammetry studies described below. The six-coordinated species $[Co^{III}(TPP)(H_2O)_2]^+$ or $[Co^{III}(TPP)(solvent)_2]^+$

Table 1. Absorption spectra of tervalent cobalt porphyrins

Compound	Solvent	λ_{max}/nm(log ε)		
1	CH_2Cl_2	378(4.82),	524(8.35),	557(3.86)
2	CH_2Cl_2	375(4.82),	524(3.85),	556(3.86)
	CH_3OH	409(4.98),	525(3.99),	559(3.99)
	py	418(5.09),	530(4.00),	562(3.98)
3	CH_2Cl_2	377(4.82),	524(3.35),	557(3.86)
4	CH_2Cl_2	418(5.09),	530(4.00),	562(3.98)
5	CH_2Cl_2	424(5.11),	536(4.01),	556(4.47)
6	CH_2Cl_2	393(5.30),	520(4.01),	556(4.47)
7	CH_2Cl_2	396(5.40),	522(4.03),	558(4.50)
8	CH_2Cl_2	426(4.98),	536(3.84)	
	CH_3OH	425(4.99),	539(3.88)	
9	CH_2Cl_2	426(4.99),	540(3.83)	
	CH_3OH	426(4.99),	539(3.89)	
10	CH_2Cl_2	407(5.01),	528(3.92)	
	CH_3OH	426(4.99),	540(3.88)	
11	CH_2Cl_2	405(4.99),	549(3.53)	
	CH_3OH	426(4.99),	542(3.90)	
12	CH_2Cl_2	404(5.00),	545(3.80)	
	CH_3OH	426(4.99),	543(3.99)	
13	CH_2Cl_2	400(5.00),	550(3.74)	
	CH_3OH	426(4.99),	542(3.98)	
14	CH_2Cl_2	403(4.99),	550(3.99)	
	CH_3OH	426(4.99),	550(3.89)	
15	CH_2Cl_2	434(5.01),	550(3.91),	584(3.41)
16	CH_2Cl_2	433(5.14),	545(3.99),	578(3.65)
17	CH_2Cl_2	434(5.13),	550(3.99),	585(3.66)
18	CH_2Cl_2	434(5.12),	550(3.99),	580(3.65)
19	CH_2Cl_2	437(5.00),	552(3.96),	588(3.60)
20	CH_2Cl_2	408(5.20),	526(4.00)	
21	CH_2Cl_2	407(5.21),	522(3.99)	

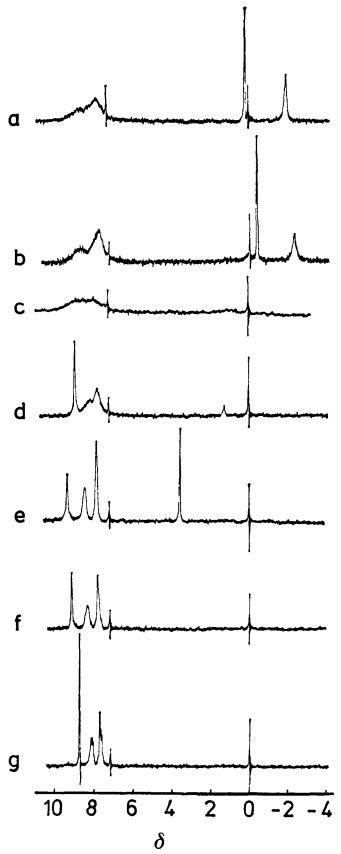

Fig. 2. ^{1}H NMR spectra in chloroform at 31.5 °C. (a): $[Co^{III}(TPP)(H_2O)_2]BF_4$, (b): $[Co^{III}(TPP)(H_2O)_2]ClO_4$, (c): $[Co^{III}(TPP)(H_2O)Cl]$, (d): $[Co^{III}(TPP)(H_2O)Br]$, (e): $[Co^{III}(TPP)(H_2O)I]$, (f): $[Co^{III}(TPP)(H_2O)N_3]$, (g): $[Co^{III}(TPP)(H_2O)SCN]$.

can be expected to have a cationic character, if the solvent molecule is allowed to dissociate easily due to weak solvation. Neither the bis(amine) adducts nor the mono(amine) adduct was much influenced by solvent polarity. This result indicates that there exists tight coordination of the amine molecules to the cobalt atom, which is consistent with results from ^{1}H NMR spectra.

^{1}H NMR Spectra. ^{1}H NMR data are summarized in Table 2. In nonpolar solvents such as dichloromethane and chloroform these tervalent cobalt complexes except the amine adducts and organocobalt complexes show very broad and shifted signals. Figure 2 illustrates the ^{1}H NMR spectra of **8**—**14** in chloroform at room temperature. The signals of the phenyl and β-pyrrole protons are significantly broad and shifted compared with those for usual diamagnetic spectrum. This phenomenon is qualitatively the same as that reported by Yamamoto *et al.* in the case of chloride salt **12**.[14k] It is noteworthy that the signals of the pyrrole β-protons for complexes **8** and **9** are very much shifted toward higher magnetic fields.[18] The magnetic moments of complexes **8** and **9** in chloroform at room temperature (31 °C) showed smaller paramagnetism (about 0.7 BM) than the one for a chloride salt (1.66 BM) previously reported.[14k] Such large upfield shifts of pyrrole β-protons and small paramagnetism, as compared with those of the chloride salt, suggest that the mechanisms of the spin delocalization on the porphyrin plane are somewhat different from each other. The difference in the mechanism of spin delocalization between the group of ClO_4 and BF_4 salts and the group of Cl, Br, I, and N_3 salts may result from the different coordination modes. Sakurai *et al.*[14h,i] reported that the cobalt atom in the chloride salt is coordinated by the chlorine atom as the fifth ligand. In perchlorate salt **8**, on the other hand, the cobalt atom is coordinated by two water molecules as described above.[16]

In polar solvents these complexes showed usual diamagnetic ^{1}H NMR spectra. The addition of amines such as pyridine gave also diamagnetic spectra which were very similar to those of bis(amine) adducts. For example, bis(tetrahydrofuran) adduct **1** showed only one broad signal at about 2 ppm in chloroform, but an addition of pyridine in twice the equivalent gave a spectrum indicating the existence of the bis(pyridine) adduct and free tetrahydrofuran.[15] The ^{1}H NMR spectra of amine adducts **4**, **5**, and **15**—**20** indicate a coordination of these amine molecules to the cobalt atom. In particular, it is noteworthy that both bis(pyridine) adduct **19** and mono(pyridine) adduct **20** can be isolated in the case of chloride salt,

TABLE 2. ^{1}H NMR DATA OF TERVALENT COBALT PORPHYRINS (δ VALUES)[a)]

	Solvent	*meso*	α-CH_2	β-CH_3	Others
1	CD_2Cl_2	Very broad signal at about 2			
	CD_2Cl_2+py	10.10(s, 4H),	4.04(q, 16H),	1.80(t, 24H)	3.56(m, 8H, THF), 1.68(m, 8H, THF) 5.66(t, 2H, γ-H of py), 4.50(t, 4H, β-H of py), 0.00(d, 4H, α-H of py)
2	CD_2Cl_2	Very broad signal at about 2			
	Acetone-d_6	9.10(s, 4H),	5.44(q, 16H),	1.81(t, 24H)	
	Methanol-d_4	10.78(s, 4H),	4.40(q, 16H),	2.04(t, 24H)	
	DMSO-d_6	10.41(s, 4H),	4.15(q, 16H),	1.77(t, 24H)	
3		Very broad signal at about 2			
4	CD_2Cl_2	10.06(s, 4H),	4.04(t, 16H),	1.80(t, 24H)	5.66(t, 2H, γ-H of py), 4.48(t, 4H, β-H of py), 0.00(d, 2H, α-H of py)
5	CD_2Cl_2	9.67(s, 4H),	5.88(q, 16H),	1.72(t, 24H)	3.88(m, 2H, 5-H of 2-MeIm), 1.26(m, 2H, NH), −1.04(t, 2H, 4-H of 2-MeIm), −2.76(s, 6H, 2-CH_3)
6	CD_2Cl_2	10.03(s, 4H),	4.13(q, 16H),	1.99(t, 24H)	1.09(m, 4H, $OC\underline{H}_2$-), 0.06(t, 6H, $OCH_2C\underline{H}_3$), −4.80(t, 1H, -$CH_2C\underline{H}$), −6.40(bd, 2H, -$C\underline{H}_2CH$)
7	CD_2Cl_2	10.34(s, 4H),	3.83(q, 16H),	1.88(t, 24H)	3.20(t, 1H, $C\underline{H}O$), −4.28(d, 2H, $C\underline{H}_2$)
		Pyrrole β	Phenyl		
8	$CDCl_3$	−2.2(br, 8H),	8(br, 20H)		
9	$CDCl_3$	−2.1(br, 8H),	8(br, 20H)		
	Acetone-d_6	9.18(s, 8H),	8.20(m, 8H),	7.80(m, 12H)	
10	$CDCl_3$	9.36(br, 8H),	8.44(br),	7.84(br)	
11	$CDCl_3$	10.0(br),	9.28(br),	8.76(br)	
12	$CDCl_3$	9.0(br),	8.8(br),	7.7(br)	
13	$CDCl_3$	8.8(br),	8.14(br),	7.72(br)	
14	$CDCl_3$	9.22(br),	8.38(br),	7.86(br)	
15	$CDCl_3$	9.13(s, 8H),	7.8(m, 20H)		6.21(t, 2H, γ-H of py) 5.06(t, 4H, β-H of py) 0.90(d, 4H, α-H of py)
16	$CDCl_3$	9.28(s, 8H),	7.9(m, 20H)		5.56(d, β-H of 4-CNpy) 1.20(d, 4H, α-H of 4-CNpy)
17	$CDCl_3$	9.02(s, 8H),	7.7(m, 20H)		4.84(d, 4H, β-H of 4-Mepy) 1.26(s, 6H, 4-CH_3) 0.66(d, 4H, α-H of 4-Mepy)
18	$CDCl_3$	9.13(s, 8H),	7.8(m, 20H)		6.21(t, 2H, γ-H of py) 5.06(t, 4H, β-H of py) 0.90(d, 4H, α-H of py)
19	$CDCl_3$	9.00(s, 8H),	8.8(m, 8H),	7.7(m, 12H)	5.82(t, 1H, γ-H of py) 4.84(t, 2H, β-H of py) 0.84(d, 2H, α-H of py)
20	$CDCl_3$	9.39(s, 8H),	8.04(m, 8H),	7.60(m, 12H)	1.44(m, 4H, -$OC\underline{H}_2$), 0.45(t, 6H, $OCH_2C\underline{H}_3$) −2.22(t, 1H, $CH_2C\underline{H}$) −4.06(d, 2H, $C\underline{H}_2CH$)
21	$CDCl_3$	8.82(s, 8H),	8.04(m, 8H),	7.60(m, 12H)	3.81(t, 1H, $C\underline{H}O$) −3.72(d, 2H, $C\underline{H}_2$)

a) Abbrebiations used: s, singlet; d, doublet; t, triplet; q, qualtet; m, multiplet; br, broad.

although mono(pyridine) adduct can not be isolated in the case of perchlorate salt. Moreover, the ^1H NMR spectrum of 2-methylimidazole adduct **5** showed tight coordination of such a sterically-hindered axial base.

Cyclic Voltammetry. The electrochemical behavior of cobalt porphyrin complexes has actively been investigated.[19,20] These studies usually dealt with cobalt(II) porphyrins and disclosed two distinct redox couples for the metal redox processes, Co(III)/Co(II) and Co(II)/Co(I). Addition of various types of amines to such systems was found to bring about shifts of the redox potentials for Co(III)/Co(II) to more negative values, the shift getting greater as the basicity of the amine is increased. The redox couple Co(II)/Co(I), on the other hand, was almost insensitive. However, there have been no reports on redox process of Co(III) porphyrins in which anions are present either as axial ligands or as counter ions. Study of such process seems to be of importance for estimation of the influence by such anions on the electrophilicity of cobalt atoms. There have been some reports on the effect of anions in the supporting electrolyte on the redox couple Co(III)/Co(II) associated with cobalt(II) porphyrins,[20a] but no study on such factors can give any direct information and we have no assurance that the anion is coordinated during the oxidation process.

Table 3 summarizes the half wave potentials ($E_{1/2}$) of tervalent cobalt porphyrins. One of the most outstanding features is that in dichloromethane these tervalent cobalt porphyrins have Co(III)/Co(II) redox couples varing in their combination significantly with counter anions or axial ligands and that accordingly, they can be categorized into three groups: Group (i) complexes have BF_4^- or ClO_4^- as the counter anion and have the most positive redox values similar to that of the bivalent complex $Co^{II}(TPP)$. Group (ii) includes salts of Cl^-, Br^-, SCN^-, and N_3^- and have less positive redox potentials by about 0.4 V which varies slightly with the kind of counter anions. These values reveal that there is no exchange of the axially coordinated anion with the perchlorate ion of the supporting electrolyte TBAP; otherwise, the redox values for these complexes would be close to that of the perchlorate salt. Group (iii) complexes have various amines as axial ligands and have the lowest redox potentials.

The difference between the redox potentials of Groups (i) and (ii) may be explained in terms of different modes of coordination. As previously discussed, two water molecules are coordinated axially in $[Co^{III}(TPP)(H_2O)_2]ClO_4$ and the same is expected to be true with the tetrafluoroborate salt and its corresponding OEP derivatives. The fact that the values for both Group (i) complexes and the bivalent complex are quite similar to one another, indicates that coordination of the axial water molecules is very weak and that it has little influence on the redox potentials in dichloromethane. On the other hand, the chloride anion, and probably other halide and pseudohalide anions, too, coordinate to the cobalt atom directly as the fifth ligand, and the increasing covalency of such axial ligands seems to lower the redox potential of the Co(III)/Co(II) couple.

It is interesting to compare the Co(III)/Co(II) potentials of Co(III) porphyrins with those of $Co^{II}(TPP)$ with various supporting electrolytes, reported by Truxillo and Davis.[20a] Thus, the redox values for $[Co^{III}(TPP)(H_2O)_2]X$ ($X=ClO_4$, BF_4) and $[Co^{III}(TPP)(H_2O)Y]$ ($Y=Br$, Cl) are +0.72, +0.72, +0.38, and +0.27, respectively. The redox values for the Co(III)/Co(II) couple of $Co^{II}(TPP)$ are reported to be +0.75, +0.94, +0.29, and +0.74 volt for electrolytes TBAP, TBAF, TBAB, and TBAC, respectively. Slightly lower values of the cobalt(III) porphyrin

Table 3. Half-wave potentials for bi- and tervalent cobalt porphyrins

Compound	Solvent	V *vs.* SCE	
		Co(III)/Co(II)	Co(II)/Co(I)
$Co^{II}(TPP)$	CH_2Cl_2	+0.71	−0.93
$[Co^{III}(TPP)(H_2O)_2]BF_4$		+0.72	−1.14
$[Co^{III}(TPP)(H_2O)_2]ClO_4$		+0.72	−1.05
$[Co^{III}(TPP)(H_2O)Br]$		+0.35	−1.03
$[Co^{III}(TPP)(H_2O)Cl]$		+0.27	−1.12
$[Co^{III}(TPP)(H_2O)SCN]$		+0.26	−0.94
$[Co^{III}(TPP)(H_2O)I]$		+0.23	−0.91
$[Co^{III}(TPP)(H_2O)N_3]$		+0.18	−0.89
$[Co^{III}(TPP)(4\text{-}CNpy)_2]ClO_4$		+0.15	−0.98
$[Co^{III}(TPP)(py)_2]ClO_4$		−0.05	−1.14
$[Co^{III}(TPP)(4\text{-}Mepy)_2]ClO_4$		−0.11	−1.04
$[Co^{III}(TPP)(imd)_2]ClO_4$		−0.31	−1.02
$[Co^{III}(TPP)(H_2O)_2]BF_4$	CH_2Cl_2-EtOH	+0.31	−0.85
$[Co^{III}(TPP)(H_2O)_2]ClO_4$		+0.32	−0.95
$[Co^{III}(TPP)(H_2O)Br]$		+0.27	−0.96
$[Co^{III}(TPP)(H_2O)Cl]$		+0.28	−0.99
$[Co^{III}(TPP)(H_2O)N_3]$		+0.29	−0.99

perchlorate and tetrafluoroborate than those of Co(II) porphyrin in TBAP and TBAF can reasonably be explained in terms of the presence of axially coordinated water molecules which have a weak electron-donating character. On the other hand, the much higher potential of the Co(II) porphyrin in the presence of TBAC than that of $[Co^{III}(TPP)(H_2O)Cl]$ indicates that the chloride ion in the supporting electrolyte coordinate neither to Co(II) porphyrin nor to Co(III) formed by the oxidation of Co(II) porphyrin during the time of voltage cyclings.

In dichloromethane–ethanol solution the tervalent cobalt complexes studies showed almost the same redox potentials with one another, referring presumably to $[Co^{III}(TPP)(EtOH)_2]^+$ (0.27—0.33 V), in conformity with the replacement of the axial anion by the solvent molecules as has just been concluded from the absorption spectra.

In the case of Group (iii) porphyrins, the redox potentials are still lower and dependent predominantly on the nature of axial ligands, which is consistent with the results in the case of bivalent cobalt porphyrins with various amines, reported by Walker *et al.*[20e] The ^1H NMR spectra of these complexes in chloroform indicate a tight coordination of two amine molecules. Large irreversibility for the bis(amine) adduct, compared with that for other tervalent complexes, suggests a considerable dissociation of the axial amines in the reduced state. In fact, it is well known that bivalent cobalt complexes prefer five-coordination to six-coordination.[22]

Reaction with Ethyl Vinyl Ether. We previously reported[15] that perchlorate salts **1** and **2**, and **8** react with ethyl vinyl ether to afford organocobalt(III) complexes **6** and **20**, respectively. Other halides and pseudohalides also gave similar reaction products in ethanol solution although their yields are low. This result indicates that the solvent-coordinated species (B) has sufficient electrophilicity toward ethyl vinyl ether to form organocobalt complex (D) probably *via* π-complex (C). The obtained 2,2-diethoxyethylcobalt(III) complexes **6** and **20** could easily be converted to formylmethylcobalt(III) complexes **7** and **21**, respectively. These organocobalt complexes have been well characterized by elemental analysis and spectroscopic measurements, in particular ^1H NMR spectra. Figure 3 shows the ^1H NMR spectra of **20** and **21**. The presence of 2,2-diethoxyethyl and

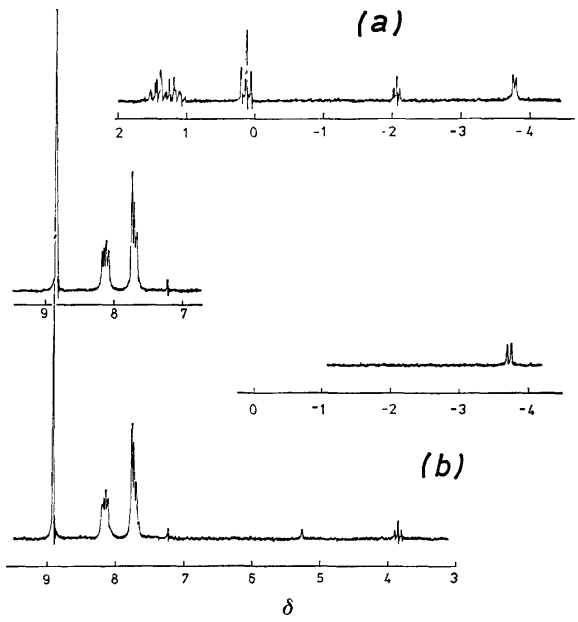

Fig. 3. ^1H NMR spectra of (a) $[Co^{III}(TPP)CH_2CH(OC_2H_5)_2]$ and (b) $[Co^{III}(TPP)CH_2CHO]$ in chloroform.

formylmethyl groups bonded to the central metal ion can reasonably be confirmed by the high field shift of the protons in the groups due to the large diamagnetic ring-current effect of porphyrin ring. Assignments of the protons are listed in Table 2.

This synthetic method for organocobalt(III) complexes of porphyrins is very convenient for the model study of vitamin B_{12}, because it is very simple and gives high yields, compared with the reaction of Co(I) species with organo halides.

On the other hand, bis(amine) adducts or mono(amine) adduct reacted with ethyl vinyl ether to give only reduced bivalent cobalt porphyrins. These results indicate that the strong electrophilic property of central cobalt(III) ion in the amine adducts is cancelled by the strong ligation of amine molecules and that only the electron transfer from ethyl vinyl ether to cobalt ion occurs.

The present work was partially supported by a Grant-in-Aid for Scientific Research from the Ministry of Education, Science and Culture.

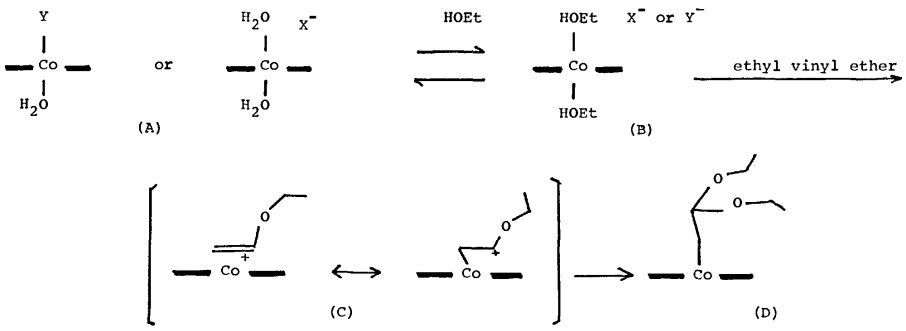

Scheme 1.

References

1) P. G. Lenhart and D. C. Hodgkin, *Nature (London)*, **192**, 937 (1961).

2) Reviews; G. N. Schrauzer, *Acc. Chem. Rec.*, **97** (1968); G. Costa, *Coord. Chem. Rev.*, **8**, 63 (1972); A. Biggetto, G. Costa, G. Mestroni, G. Pelliger, A. Puxeddu, E. Reisenhofer, L. Stefani, and G. Tauzher, *Inorg. Chim. Acta Rev.*, **4**, 41 (1970); D. Dodd and M. D. Johnson, *Organomet. Chem. Rev.*, **52**, 1 (1973); G. N. Schrauzer, *Angew. Chem.*, **88**, 465 (1976).

3) E. Ochiai, K. M. Long, C. R. Sperati, and D. H. Busch, *J. Am. Chem. Soc.*, **91**, 3201 (1969).

4) K. Farmery and D. H. Busch, *Inorg. Chem.*, **11**, 2901 (1972).

5) C. Y. Mok and J. E. Endicott, *J. Am. Chem. Soc.*, **99**, 1276 (1972); **100**, 123 (1978).

6) J. H. Esperson and A. H. Martin, *J. Am. Chem. Soc.*, **99**, 5953 (1977).

7) W. P. Schaefer, R. Walizman, and B. T. Huie, *J. Am. Chem. Soc.*, **100**, 5063 (1978).

8) H. Elroi and D. J. Meyerstein, *J. Am. Chem. Soc.*, **100**, 5540 (1978).

9) Y. Murakami and Y. Aoyama, *Bull. Chem. Soc. Jpn.*, **49**, 683 (1976); Y. Murakami, Y. Aoyama, and K. Tokunaga, *J. Am. Chem. Soc.*, **102**, 6736 (1980).

10) H. Ogoshi, J. Sestune, T. Omura, and Z. Yoshida, *J. Am. Chem. Soc.*, **97**, 6461 (1975); H. Ogoshi, J. Sestune, Z. Yoshida, *J. Chem. Soc., Chem. Commun.*, **1975**, 572.

11) H. Ogoshi, J. Sestune, and Z. Yoshida, *J. Organomet. Chem.*, **159**, 317 (1978).

12) R. B. Silverman and D. Dolphin, *J. Am. Chem. Soc.*, **95**, 1686 (1973); **96**, 7094 (1974); **98**, 4626 (1976).

13) H. Ogoshi, J. Sestune, Y. Nanbo, and Z. Yoshida, *J. Organomet. Chem.*, **159**, 329 (1978).

14) a) A. W. Johnson and I. K. Kay, *J. Chem. Soc.*, **1960**, 2979; b) J. W. Buchler, G. Eikelmann, L. Puppe, K. Rohbock, H. H. Schneege, and D. Weck, *Ann. Chem.*, **745**, 135 (1971); c) R. Bonnett and M. J. Dimsdale, *J. Chem. Soc., Perkin Trans. 1*, **1972**, 2540; d) N. Datta-Gupta and T. J. Bardos, *J. Pharm. Sci.*, **57**, 3000 (1968); e) W. R. Scheidt, J. A. Cunningham, and J. L. Hoard, *J. Am. Chem. Soc.*, **95**, 8289 (1978); f) D. A. Clarke, D. Dolphin, R. Grigg, A. W. Johnson, and H. A. Pinnock, *J. Chem. Soc., C*, **1968**, 881; g) J. A. Kaduk and W. R. Scheidt, *Inorg. Chem.*, **13**, 1875 (1974); h) T. Sakurai, K. Yamamoto, H. Naito, and N. Nakamoto, *Bull. Chem. Soc. Jpn.*, **49**, 3042 (1976); i) T. Sakurai, K. Yamamoto, N. Seino, and M. Katsuta, *Acta Crystallogr., Sect. B*, **31**, 2514 (1975); k) K. Yamamoto, J. Uzawa, and T. Chijimatsu, *Chem. Lett.*, **1979**, 89.

15) H. Sugimoto, M. Nagano, Z. Yoshida, and H. Ogoshi, *Chem. Lett.*, **1980**, 521.

16) H. Masuda, T. Taga, K. Osaki, H. Sugimoto, and M. Mori, *Bull. Chem. Soc. Jpn.*, in press.

17) "The Porphyrins," ed by D. Dolphin ,Vol. V, Chap. 7.

18) "The Porphyrins," ed by D. Dolphin, Vol. IV, Chap. 2.

19) "The Porphyrins," ed by D. Dolphin, Vol. V, Chap. 3.

20) a) L. A. Truxillo and D. G. Davis, *Anal. Chem.*, **47**, 2260 (1975); b) A. Giraudeau, H. J. Carrot, J. Jordan, I. Ezhar, and M. Gross, *J. Am. Chem. Soc.*, **101**, 3857 (1979); c) K. M. Kadish, L. A. Bottomley, and D. Beroiz, *Inorg. Chem.*, **17**, 1124 (1978); d) A. Wolbery and J. Manassen, *J. Am. Chem. Soc.*, **92**, 2982 (1970); e) F. A. Walker, D. Beroiz, and K. M. Kadish, *J. Am. Chem. Soc.*, **98**, 3484 (1976); f) M. J. Carter, D. P. Rillema, and F. Basolo, *J. Am. Chem. Soc.*, **96**, 392 (1974).

21) D. P. Rillema, J. F. Endicott, and E. Papaconstantniu, *Inorg. Chem.*, **10**, 1739 (1971); P. A. Rock, *ibid.*, **7**, 837 (1968).

22) F. A. Walker, *J. Am. Chem. Soc.*, **92**, 4235 (1970).

  Bull. Chem. Soc. Jpn., 54, 3433—3437 (1981)

Neighboring Effect of Mercapto Group in the Silver Ion-promoted Aminolysis of *S*-Monoacyldihydrolipoamide

Yoko NAMBU,* Takeshi ENDO, and Makoto OKAWARA

Research Laboratory of Resources Utilization, Tokyo Institute of Technology, Nagatsuta, Midori-ku, Yokohama 227

(Received December 10, 1980)

The aminolysis of *N*-benzyl-8-*S*-(*p*-nitrobenzoyl)dihydrolipoamide has been enhanced remarkably with excess silver perchlorate compared with that of *N*-benzyl-*S*,*S*′-bis(*p*-nitrobenzoyl)dihydrolipoamide. From the results of kinetics and complex formation followed by UV and IR spectra, the large enhancement in the reaction has been concluded to be derived from the activation of acyl group through the binding of two equivalents of silver ion to the neighboring mercapto group.

Whereas arenethiol ester is one of the activated esters which is able to be utilized for the activation of amino acids and peptide syntheses, less reactive alkanethiol esters are scarcely used for the activation of acyl group.

On the other hand, it is well known that 5-(1,2-dithiolan-3-yl)pentanoic acid (lipoic acid) plays an important role in transfer of acetyl group enzymatically from pyruvic acid-thiamine adduct to coenzyme A (CoASH), and the thiol ester (CoASAc) thus produced, in turn, is transferred into TCA cycle.

Further, the aminolysis of thiol esters has been shown to be catalyzed with various metal ions such as silver and mercuric ions.[1]

As part of the investigation on the synthesis and reaction of lipoic acid derivatives, we have already reported the silver ion-promoted acyl transfer on *S*,*S*′-diacyl-6,8-dimercaptooctanoic acid (*S*,*S*′-diacyldihydrolipoic acid) derivatives to nucleophiles such as amines and alcohols[2] and applied to the polymeric system to provide polymeric acylating agents.[3] In the previous report,[2] we mentioned briefly that aminolysis of 8-*S*-acetyldihydrolipoamide which had a neighboring mercapto group was enhanced remarkably with silver ion compared to that of *S*,*S*′-diacetyl derivatives. It is interesting to study the mechanism of the neighboring effect of mercapto group in this reaction, related to the similarity of the relative position between mercapto and acylthio groups in 8-*S*-acetyl derivative to the 6-*S*-acetyl isomer isolated from a natural enzymatic system, to the applicability of this system for polymeric acylating agents,[11] and to the activation of acyl group through complex formation in the metal-ion-promoted hydrolysis of 8-quinolyloxycarbonyl derivatives of amines.[4] We report here the mechanistic study on the aminolysis of *N*-benzyl-8-*S*-(*p*-nitrobenzoyl)dihydrolipoamide (**1**) with cyclohexylamine in the presence of silver perchlorate ($AgClO_4$) followed spectrophotometrically and the comparison of the result with that of the *S*,*S*′-diacyl derivative (**2**).

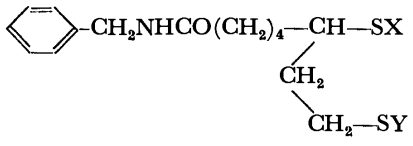

1: X=H, Y=-CO-R (R= 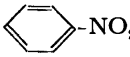)

2: X=Y=-CO-R (R= 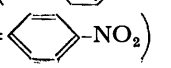)

Experimental

Materials. Silver perchlorate was purchased from Kojima Chemical Co., Ltd. *N*-Benzyl-*S*,*S*′-bis(*p*-nitrobenzoyl)dihydrolipoamide (**2**) was prepared by the method reported previously.[3] Solvents were purified by the usual procedure.

Preparation of N-*Benzyl-8-(*S-p-*nitrobenzoyl)dihydrolipoamide (**1**).* To a solution of *N*-benzyllipoamide[3] (295 mg, 1 mmol) in methanol (15 ml), sodium borohydride (95 mg, 2.5 mmol) was added portionwise at 0 °C and stirred for 2 h at room temperature under nitrogen. Reaction mixture was then acidified to pH 2 with 0.1 M† hydrochloric acid. The solution was extracted with dichloromethane (50 ml) and the organic layer was dried over $MgSO_4$. To the dichloromethane solution were added *p*-nitrobenzoyl chloride (196 mg, 1 mmol) and triethylamine (0.1 ml) under nitrogen, and the solution was stirred for 15 h at room temperature. The solvent was removed by evaporation and the obtained residue was dissolved in ether. The precipitated triethylamine hydrochloride was filtered off and the filtrate was evaporated to afford an oily residue, which was recrystallized from ether to give **1** (160 mg, 36%): mp 71—73 °C; NMR ($CDCl_3$) δ=1.41 (d, 1, J=7.5 Hz, SH), 1.5—2.0 (m, 8, CH_2), 2.2 (d, 2, J=6.0 Hz, $COCH_2$), 2.9 (m, 1, >CHS–), 3.3 (t, 2, J=6.0 Hz, CH_2SCO), 4.4 (d, 2, J=5.7 Hz, $C_6H_5CH_2$), 5.9 (s, 1, NHCO), 7.3 (s, 5, C_6H_5), and 8.2 ppm (q, 4, $C_6H_4NO_2$); IR (THF) 3550, 1670, 1525, and 1345 cm^{-1}; UV_{max}(THF)(log ε) 260 (4.15) and 290 nm (shoulder, 4.02); Found: C, 59.11; H, 6.00; N, 6.01%. Calcd for $C_{22}H_{26}N_2O_4S_2$: C, 59.18; H, 5.87; N, 6.28%.

Kinetic Measurements. To a tetrahydrofuran (THF) solution of acyl derivative **1** or **2** and cyclohexylamine, silver perchlorate was added at 35.5 °C under nitrogen. Final concentrations were [**1** or **2**]=2.5×10^{-4} M, [cyclohexylamine]=3—12×10^{-3} M, [$AgClO_4$]=1.5—10×10^{-3} M. A portion of the reaction mixture taken out with a pipet was centrifuged to remove the white thiolate. The supernatant was diluted with THF to obtain an appropriate absorbance in UV spectra. The absorbance at 290 nm was measured as a function of time. The measured data were treated as first-order kinetics by plotting $\ln|A_\infty - A_t|$ *versus* time. The slope of this line was taken as the pseudo-first-order rate constant k, k_0, or k'.

Reaction Products. A preparative scale experiment was carried out with mono(*S*-ester) **1**. The white precipitate formed was collected by centrifuging the reaction mixture. The precipitate was washed well with THF and dried to give the silver thiolate (**4**) which showed amide bands at 1540 and 1630 cm^{-1}, but showed no NO_2 band in IR spec-

† 1 M=1 mol dm^{-3}.

trum (Found: C, 24.73; H, 2.75; N, 2.14%. Calcd for $C_{15}H_{21}NO_5Ag_3Cl$: C, 25.17; H, 2.95; N, 1.95%). After evaporation of the supernatant, the resulting oily residue was dissolved in ethyl acetate and washed with aqueous hydrochloric acid. *N*-Cyclohexyl-*p*-nitrobenzamide (**3**) obtained from the organic layer was recognized by comparing the IR and UV spectra with those of the authentic sample, which was prepared from *p*-nitrobenzoyl chloride and cyclohexylamine (Found; C, 62.55; H, 6.48; N, 11.32%. Calcd for $C_{13}H_{16}N_2O_3$: C, 62.89; H, 6.50; N, 11.28%); IR (KBr) 3410, 1640, 1545, and 1345 cm^{-1}; UV_{max} (THF) (log ε) 266 nm (4.10).

Spectral Measurements. ^1H NMR spectra were measured with a varian EM 360 NMR spectrometer in chloroform-*d* with tetramethylsilane as the internal standard. IR spectra were recorded on a Hitachi EPI-S2 spectrophotometer. UV absorption spectra were recorded on a Hitachi 200-10 spectrophotometer.

Results and Discussion

Reaction of Mono(S-ester) 1 with Cyclohexylamine. Aminolysis of **1** with cyclohexylamine was carried out by mixing **1** and excess cyclohexylamine in THF at 35.5 °C. No appreciable reaction was observed in the absence of $AgClO_4$. A white precipitate (**4**), however, was produced gradually by adding $AgClO_4$. The change of absorption spectra at various time intervals for the supernatant liquid obtained by centrifuging the reaction mixture is shown in Fig. 1. The absorption spectrum (A) in Fig. 1 is ascribed to thiol ester **1** which was scarcely affected by adding excess cyclohexylamine, but changed to spectrum (B) immediately by adding $AgClO_4$. Spectrum (B) changed further to spectrum (C) in the rate depending on the concentration of $AgClO_4$. Spectrum (C) finally changed to spectrum (D) which corresponded to *N*-cyclohexyl-*p*-nitrobenzamide (**3**) in the slower rate than that of (B) to (C). The change in absorbance at 266 nm from (B) to (C) and from (C) to (D) followed first-order-kinetics, and the pseudo first-order rate constants k_0 for (B) to (C) and k for (C) to (D) were obtained.

As shown in the dependences of k_0 or k on the concentration of $AgClO_4$ (Fig. 2), only the change from (B) to (C) was observed at the lower concentration of $AgClO_4$. At the higher concentration of $AgClO_4$, however, faster change from (B) to (C) and slower change from (C) to (D) were observed. The both process were remarkably accelerated as the concentration of $AgClO_4$ increased, and k increased linearly at the concentration of $AgClO_4$ higher than that of cyclohexylamine.

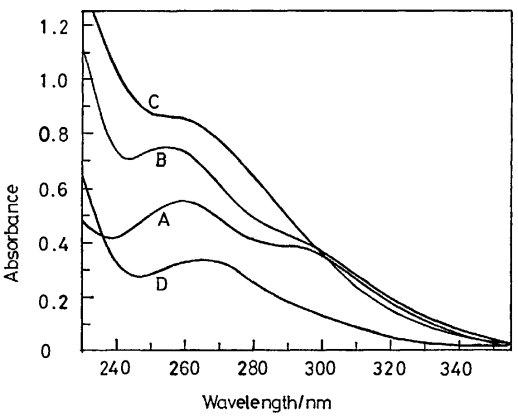

Fig. 1. Change of UV absorption in aminolysis of mono(*S*-ester) **1** with cyclohexylamine in the presence of $AgClO_4$, [**1**]$=2.5\times10^{-4}$ M, [$C_6H_{11}NH_2$]$=5.0\times10^{-3}$ M, [$AgClO_4$]$=4.8\times10^{-3}$ M, THF, 35.5 °C.
A: **1** and cyclohexylamine, B: 0 min, C: 60 min, D: 1 550 min.

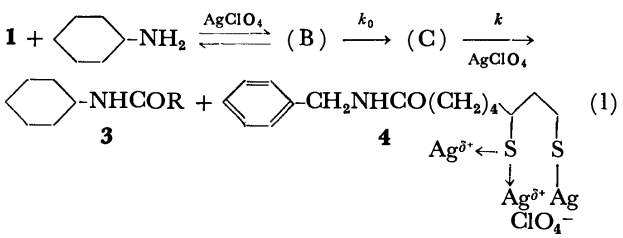

Figure 3 shows the dependence of k on the concentration of cyclohexylamine. Aminolysis was retarded considerably at the concentration of cyclohexylamine higher than that of $AgClO_4$.

Reaction of Di(S-ester) 2 with Cyclohexylamine. Aminolysis of **2** with cyclohexylamine was followed spectrophotometrically and the change of UV spectra

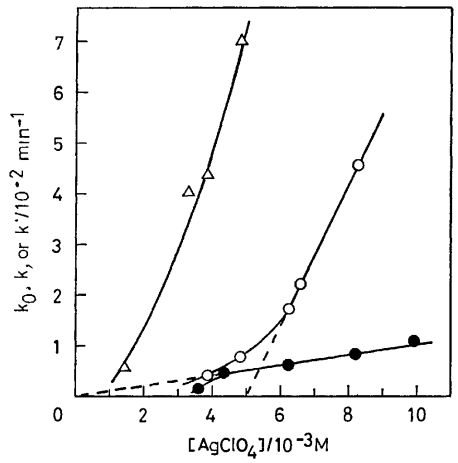

Fig. 2. Dependence of k_0, k, or k' on the concentration of $AgClO_4$ [**1** or **2**]$=2.5\times10^{-4}$ M (SCO unit), [$C_6H_{11}NH_2$]$=5.0\times10^{-3}$ M, THF, 35.5 °C.
△: k_0, ○: k, ●: k'.

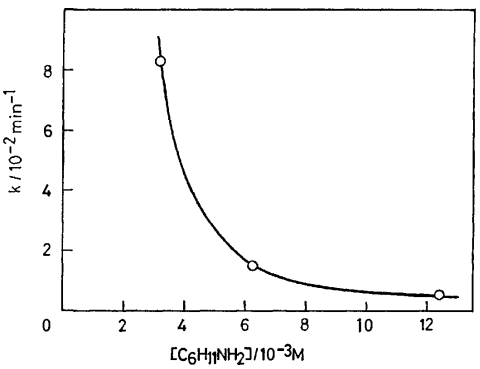

Fig. 3. Dependence of k on the concentration of $C_6H_{11}NH_2$, [**1**]$=2.5\times10^{-4}$ M, [$AgClO_4$]$=5.7\times10^{-3}$ M, THF, 35.5 °C.

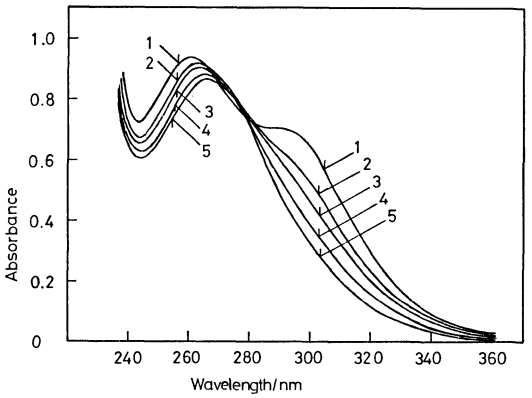

Fig. 4. Change of UV absorption in aminolysis of di(*S*-ester) **2** with cyclohexylamine in the presence of $AgClO_4$, $[\mathbf{2}]=1.2\times10^{-4}$ M, $[AgClO_4]=6.3\times10^{-3}$ M, $[C_6H_{11}NH_2]=5.0\times10^{-3}$ M, THF, 35.5 °C.
1: 0 min, 2: 80 min, 3: 125 min, 4: 240 min, 5: 410 min.

is shown in Fig. 4. Contrary to the case of mono(*S*-ester) **1**, di(*S*-ester) **2** showed no spectral change by adding $AgClO_4$. In the presence of excess $AgClO_4$ and cyclohexylamine, the spectrum of **2** changed gradually to that of amide **3**. Pseudo-first-order rate constant k' was obtained by following the decrease of absorbance at 300 nm. As shown additionally in Fig. 2, k' increased linearly by increasing the concentration of $AgClO_4$, but was not so much accelerated as in the case of **1**.

$$\mathbf{2} + \bigcirc\!\!-NH_2 \xrightarrow[AgClO_4]{k'} \mathbf{3} + \mathbf{4} \qquad (2)$$

Complex formation from Mono(S-ester) 1 and $AgClO_4$. The large enhancement of aminolysis of mono(*S*-ester) **1** at the higher concentration of $AgClO_4$ compared to that of di(*S*-ester) **2** is considered to be due to the formation of active complex from **1** and $AgClO_4$ as observed in the change of UV spectra of **1** (Figs. 1 (B) and (C)). This was further examined with molar ratio method,[5] by plotting the observed absorbances at 260 nm against the molar ratio of $AgClO_4$ to **1** with a fixed concentration of mono(*S*-ester) **1** in THF as shown in Fig. 5. The absorbance at 260 nm increased linearly by increasing the ratio of $AgClO_4$ to **1** up to 1, where the curve broke sharply. Further addition of $AgClO_4$ resulted in the minimum absorbance at a molar ratio of 2. These results suggested the formation of a tight 1:1 complex and a 1:2 complex respectively from **1** and $AgClO_4$. Further binding of $AgClO_4$ to the complex was presumed to be occurred from the increase of absorbance again by increasing the molar ratio. On the other hand, in the presence of excess cyclohexylamine, a different curve was obtained at a ratio of more than 1, as shown with the dotted line in Fig. 5. This result suggested that a different complex might be formed in the presence of amine.

Silver thiolates are well known to be formed from Ag^+ ion and thiols, therefore, the tight 1:1 complex deduced by the molar ratio method is presumed to be a thiolate (**5**) of mono(*S*-ester) **1**. Owing to the

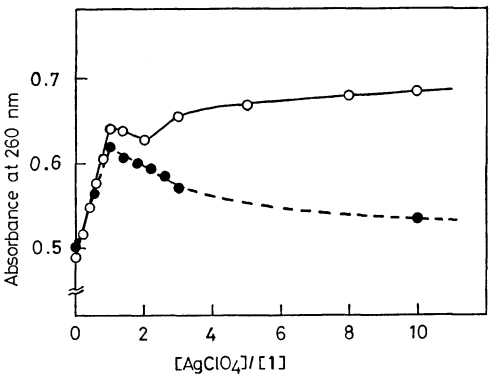

Fig. 5. Change of $A_{260\text{ nm}}$ in molar ratio method by complex formation from $AgClO_4$ and **1**, $[\mathbf{1}]=3.9\times10^{-5}$ M.
○: In the absence of amine, ●: in the presence of amine, $[C_6H_{11}NH_2]=9.9\times10^{-4}$ M.

strong affinity of silver ion to sulfur atom, further 1:2 complex (**6**) is considered to be formed through binding another Ag^+ ion to the sulfur atom of acylthio group.

In addition, silver thiolates are known to form further complexes with excess Ag^+ ion[6] (Eq. 3), which is suppressed in the presence of amine.[7]

$$RSAg + Ag^+ \longrightarrow (RSAg)Ag^+ \qquad (3)$$

In the present case, further binding of Ag^+ ion to the thiolate might be facilitated to form complex (**7**) in the presence of free Ag^+ ion. Thus complexes formed from **1** and $AgClO_4$ are formulated as follows.

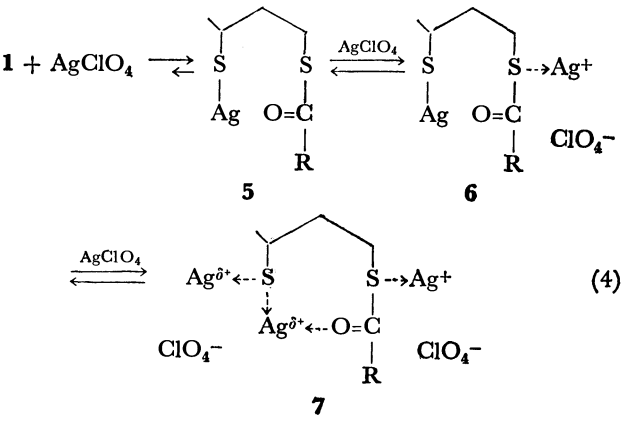

(4)

The IR spectrum of a THF solution of mono(*S*-ester) is shown in Fig. 6. In the presence of more than 3 equivalents of $AgClO_4$ to **1**, >C=O stretching band shifted from 1670 cm^{-1} to 1640 cm^{-1}, which might be attributed to the formation of the complex **7**.

Complex Formation from $AgClO_4$ and Cyclohexylamine. Ag^+ ion is known to form 1:1 and 1:2 complexes with amines in aqueous media.[8] Here the complex formation of $AgClO_4$ with cyclohexylamine in THF was examined by the molar ratio method in the presence of mono(*S*-ester) **1**. Figure 7 shows the change of absorbance at 260 nm against the molar ratio of cyclohexylamine to $AgClO_4$ with a fixed concentration of $AgClO_4$ (7.96×10^{-4} M) and **1** (3.92×10^{-4} M). The line bent gradually at a ratio of 1 and broke

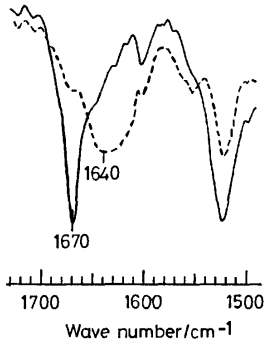

Fig. 6. IR spectra of **1** in THF.
—: **1**, ----: **1** and 3 eq. of $AgClO_4$.

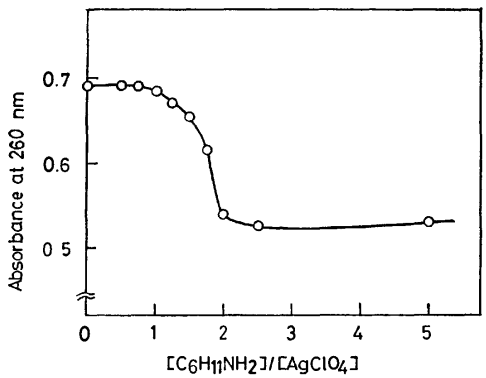

Fig. 7. Change of $A_{260\ nm}$ in molar ratio method by complex formation from $AgClO_4$ and cyclohexylamine in the presence of **1**, $[1]=3.9\times10^{-5}$ M, $[AgClO_4]=8.0\times10^{-4}$ M.

sharply at a ratio of 2. These results suggested that $AgClO_4$ might form a 1:1 complex (**8**) and a tight 1:2 complex (**9**) with cyclohexylamine (Eq. 5), and each complex formed further complex with mono(*S*-ester) **1** to cause the spectral change.

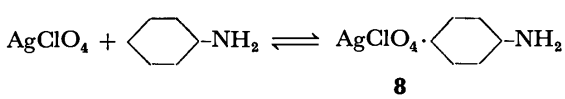

8

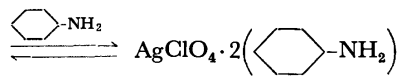

(5)

9

Mechanism of Acyl Activation by Silver Ion. From the results of kinetics and complex formation, Scheme 1 may be proposed for the silver ion-promoted aminolysis of mono(*S*-ester) **1** with cyclohexylamine.

At the lower concentration of $AgClO_4$, silver ion exists mainly in the form of complex **9** (Eq. 5), where silver ion has less affinity to sulfur atom, caused by the coordination of two basic ligands, therefore, the complex (**10**) losely formed from **1** and **9** showed no further change. Increasing the concentration of $AgClO_4$, complex **8** coexists with **9** following to Eq. 5 and complex **5** is formed immediately from **1** and **8**, corresponding to the spectral change from (A) to (B). Complex (**11**) is further formed from **5** and **8** which might be derived from the stronger affinity of one-coordinated silver ion to sulfur atom compared

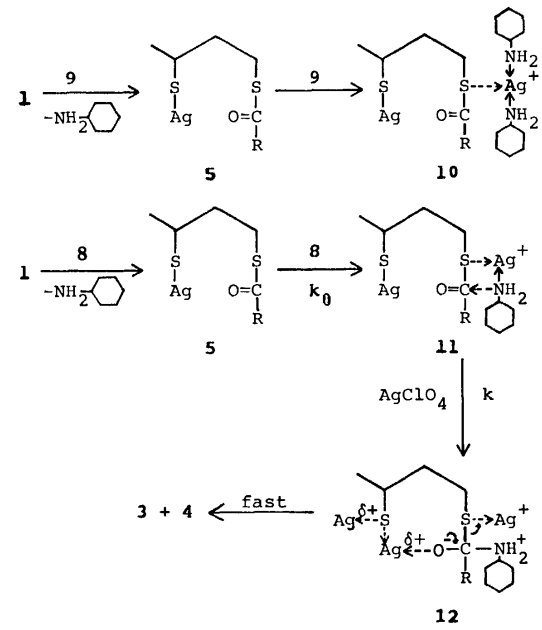

Scheme 1. Proposed mechanism.

to the two-coordinated one, corresponding to the spectral change from (B) to (C). The increase of the rate constant k_0 obtained from the spectral change of (B) to (C) by increasing the concentration of $AgClO_4$ might therefore correspond to the resulting increase of the concentration of **8**.

At the higher concentration of $AgClO_4$, active intermediate (**12**) would be formed from **11** in the presence of free silver ion to result in the activation of acyl group by interaction between Ag^+ ion binding to –SAg and >C=O group, which is well correlated to the lowering shift of >C=O band[9] in the IR spectrum of **1** in the presence of three equivalents of $AgClO_4$ (Fig. 6). Amide **3** and complex **4** are formed from **11** *via* activated intermediate **12**, corresponding to the spectral change from (C) to (D). Linear dependence of k on the concentration of $AgClO_4$ at this region is well correlated to Scheme 1.

In the presence of excess cyclohexylamine, the formation of **12** is suppressed by consumption of both free Ag^+ ion and complex **8** following to Eq. 5, which is also correlated to the rate-retardation at the higher concentration of amine as shown in Fig. 3.

Thus the acceleration effect of silver ion on the aminolysis of thiol ester having neighboring mercapto group is explained by the binding of 2 equivalents of silver ion to the mercapto group to lead to the activation of acyl group.

On the other hand, in the case of aminolysis of di(*S*-ester) **2**, the rate was accelerated linearly by increasing the concentration of $AgClO_4$ in the region that complex **8** was formed mainly. These results suggest that the rate-limiting step in this case is the binding of complex **8** to **2**, as reported in the case of aminolysis of *S*-ethyl thiobenzoate,[1b] where the acyl group was not so much activated as in the case of aminolysis of **1**. Therefore, the rate enhancement remained less than that in the aminolysis of **1** as shown in Fig. 1.

Takagi *et al.*[10] have reported the accelerated reaction of *S*-acyldihydrolipoic acid and alcohol with iodine. However, the probability of similar oxidative activation resulted in the formation of lipoic acid structure (S–S formation) with silver ion as formulated in Eq. 6 was ruled out in our case from the analysis of the reaction product **4**, as described in the experimental section.

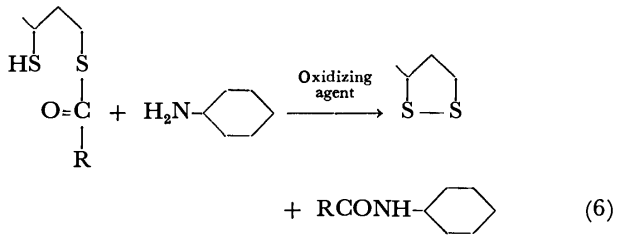

(6)

References

1) a) R. Schwyzer, *Helv. Chim. Acta*, **36**, 414 (1953); R. Schwyzer and C. Hürlimann, *ibid.*, **37**, 155 (1954); b) B. Boopsingh and D. P. N. Satchell, *J. Chem. Soc., Perkin Trans. 2*, **1972**, 1288.

2) M. Okawara, A. Fujimoto, and T. Endo, *Isr. J. Chem.*, **17**, 264 (1978).

3) Y. Nambu, T. Endo, and M. Okawara, *J. Polym. Sci., Polym. Chem. Ed.*, **18**, 2793 (1980).

4) E. J. Corey and R. T. Dawson, *J. Am. Chem. Soc.*, **84**, 4899 (1962).

5) J. H. Yoe and A. L. Jones, *Ind. Eng. Chem., Anal. Ed.*, **16**, 111 (1944).

6) K. Tunaboylu and G. Schwarzenbach, *Helv. Chim. Acta*, **54**, 235 (1971).

7) R. Cecil and J. R. McPhee, *Adv. Protein Chem.*, **14**, 255 (1959).

8) J. Bjerrum, *Chem. Rev.*, **46**, 381 (1950).

9) M. F. Lappert, *J. Chem. Soc.*, **1962**, 542.

10) M. Takagi, S. Goto, R. Ishihara, and T. Matsuda, *J. Chem. Soc., Chem. Commun.*, **1976**, 993.

11) Y. Nambu, T. Endo, and M. Okawara, *J. Polym. Sci., Polym. Chem. Ed.*, **19**, 1937 (1981).

Platinum Chloride–Diphosphine–Tin(II) Halide Systems as Active and Selective Hydroformylation Catalysts

Teruyuki HAYASHI,* Yasuziro KAWABATA, Toyoshiro ISOYAMA, and Ikuei OGATA
National Chemical Laboratory for Industry, Yatabe, Ibaraki 305
(Received January 8, 1981)

The hydroformylation of 1-alkenes was efficiently catalyzed by $PtCl_2$–diphosphine–SnX_2 systems whose diphosphines were 1,4-bis(diphenylphosphino)butane derivatives with rigid ring skeletons. The effects of the structure of diphosphines, the P/Pt atomic ratio, the sort of tin(II) halide or solvent, the reaction variables, and the structure of olefins on the relative rate and the product distribution were investigated. A higher reaction rate than when using $HRh(CO)(PPh_3)_3$, and a linearity of aldehydes up to 99%, were attained. The coordination structure of the effective diphosphines as well as the reasons for the rate enhancement and for the excellent selectivity were discussed.

Industrial hydroformylation processes have been carried out by the use of cobalt or rhodium-complexes as catalysts.[1] Of the two, the latter has been known to be 10^3 times more active than the former.[2] On the other hand, platinum-tin-complex catalysts were investigated by Orchin *et al.*[3] or by Knifton *et al.*[4] with triphenylphosphine as a ligand. They reported that the complex is more active than cobalt-complexes, but far less active than rhodium-complexes, and that, moreover, it gives aldehydes with a high molar ratio of a linear aldehyde to the total aldehydes from a 1-alkene without the addition of any excess of the phosphine. It has also been reported[4] that the activity of the complex was markedly reduced by the addition of 1,2-bis(diphenylphosphino)ethane which can make up a strong chelate ring.

The present authors have found, however, in the course of the study of asymmetric induction in the hydroformylation of butenes using the $PtCl_2$((−)-DIOP)–$SnCl_2$ system,[5] that (−)-DIOP, (4*R*,5*R*)-2,2-dimethyl-4,5-bis(diphenylphosphinomethyl)-1,3-dioxolane, strikingly raises the activity of the platinum-tin system, though it is one of the chelating phosphines. Through a study using $Ph_2P(CH_2)_nPPh_2$,[6] it was revealed that the diphosphine of $n=4$ is particularly effective, while (−)-DIOP is even more so. In this paper, the full details of the study will be described, along with those of further studies undertaken to elucidate the structure of the active catalyst species and the cause of the marked enhancement of the catalytic activity and the selectivity for linear aldehyde.

Experimental

1-Pentene was degassed before use. Thiophene-free benzene was dried over Na and distilled under N_2. The hydrogen was of a pure grade (99.99%), while the CO was of a research grade (99.95%).

The $PtCl_2(PhCN)_2$,[7] (1*R*,2*R*)-1,2-bis(diphenylphosphinomethyl)cyclohexane (II),[8] *trans*-1,2-bis(diphenylphosphinomethyl)cyclopentane (III),[9] (−)-DIOP,[10] (1*S*,2*S*)-1,2-bis(diphenylphosphinomethyl)cyclobutane (IV),[8] *trans*-1,2-bis(diphenylphosphinooxy)cyclopentane (VI),[11] and 1,4-bis(dicyclohexylphosphino)butane (VIII)[12] were prepared according to the literature. The $HRh(CO)(PPh_3)_3$ was purchased (Strem). The (+)-DIOP was presented by Dr. Iwao Ojima, Sagami Chemical Research Center. All the manipurations to prepare phosphines were carried out under N_2.

trans-2,3-Bis(diphenylphosphinomethyl)norbornane (V). To an ether (100 cm³) suspension of $LiAlH_4$ (7.8 g) was added an ether (800 cm³) solution of *trans*-5-norbornene-2,3-dicarboxylic acid[13] at a rate to maintain a gentle reflux. After a refluxing for further 40 min, water (7.8 cm³), 15% NaOH aq. solution (7.8 cm³) and three portions of water (7.8 cm³ × 3) were added to the cooled solution succesively. After the decomposition was complete, the solution was filtered to separate the precipitate and was dried over Na_2SO_4; this afforded 10.2 g (98%) of *trans*-5,6-bis(hydroxymethyl)-2-norbornene.

A methanol (100 cm³) solution of the diol was added to a methanol (10 cm³) suspension of PtO_2 (0.25 g), and the mixture was stirred under a H_2 atmosphere for 6 h at room temperature until the gas absorption ceased. The filtrate gave *trans*-2,3-bis(hydroxymethyl)norbornane (9.6 g, 93%). The diol was then dissolved in dry pyridine (50 cm³) and added to a pyridine (110 cm³) solution of tosyl chloride (35 g) at −20 °C. The solution was stirred for 4 h, while the temperature was allowed to rise to room temperature. The mixture was then poured into 250 cm³ of ice water, and the colorless precipitate thus formed was separated by filtration and dried *in vacuo*. Recrystallization from MeOH gave 25.8 g (90%) of the ditosylate; mp 101.8—102.8 °C.

The diphosphine was obtained from the ditosylate as a viscous oil according to the procedure in Ref. 8, bp 226—228 °C (bath temperature)/4×10^{-2} Pa, 16.6 g (78%). Found: C, 80.32; H, 7.06%. Calcd for $C_{33}H_{34}P_2$: C, 80.47; H, 6.96%.

2-endo-3-endo-2,3-Bis(diphenylphosphinomethyl)norbornane (XI). 2-*endo*-3-*endo*-2,3-Bis(hydroxymethyl)norbornane[14] (3.1 g) was ditosylated as above and recrystallized from MeOH; 4.6 g (51%). The diphosphine was again prepared according to Ref. 8 as a viscous oil; bp 245—248 °C (bath temperature)/5×10^{-2} Pa, 1.3 g (27%). Found: C, 79.84; H, 6.96%. Calcd for $C_{33}H_{34}P_2$: C, 80.47; H, 6.96%.

cis-1,2-Bis(diphenylphosphinomethyl)cyclohexane (X). X was prepared from the corresponding ditosylate as a viscous oil according to the procedure used for the *trans*-isomer II; bp 215—220 °C (bath temperature)/5×10^{-2} Pa. 65% Yield. Found: C, 79.88; H, 7.15%. Calcd for $C_{32}H_{34}P_2$: C, 79.98; H, 7.13%.

α,α′-Bis(diphenylphosphino)-o-xylene (VII). α,α′-Dibromo-*o*-xylene (Tokyo Kasei) (11 g) was added to a solution of $LiPPh_2$ (prepared from 21.8 g of PPh_3 and 2.6 g of Li in THF (140 cm³), followed by *t*-BuCl treatment) at 0 °C. After the addition, the mixture was stirred as the temperature rised and refluxed for 30 min. After the solution had cooled, the THF was removed and 40 cm³ of water was added. The diphosphine was extracted with benzene (100 cm³, 50 cm³ × 2) and recrystallized from EtOH–benzene twice; 13.4 g

(68%); mp 117.0—118.0 °C. Found: C, 81.58; H, 6.08%. Calcd for $C_{32}H_{28}P_2$: C, 81.00; H, 5.95%.

α,α'-Bis(diphenylphosphino)-p-xylene (IX). IX was prepared as above from α,α'-dibromo-*p*-xylene (6.1 g) and recrystallized from toluene; 5.5 g (50%); mp 177—179 °C. Found: C, 80.92; H, 6.03%. Calcd for $C_{32}H_{28}P_2$: C, 81.00; H, 5.95%.

Hydroformylation Procedure. A typical procedure was as follows: $PtCl_2(PhCN)_2$ 3.2×10^{-5} mol, (−)-DIOP 3.2×10^{-5} mol, and $SnCl_2\cdot2H_2O$ 1.6×10^{-4} mol were placed in a 50 cm³ Schlenk-tube type high-pressure reactor made of SUS-316, whose inside atmosphere was then replaced by N_2 (99.995%). Benzene (18 cm³) and 1-pentene (3 cm³) were added by the use of syringes. Carbon monoxide was pressurised up to 50 kg/cm² (at room temperature); then H_2 (up to 100 kg/cm²) was added into the reactor, and then heated in a 100 °C oil bath with magnetic stirring. The maximum slope of the pressure-*vs.*-time plot, recorded automatically, was adopted as the measure of the relative rate. The rate in the above reaction when $2PPh_3$ was used in place of (−)-DIOP was taken as the base (100). After the pressure drop had ceased, the reactor was cooled and the residual gas (which was usually about 65 kg/cm² at room temperature) was discharged. The reaction solution was then subjected to GLC analysis. Hydrocarbons were analyzed by gas chromatography on a Shimadzu GC-4B apparatus equipped with a column (2 mm i.d.×3 m) of VZ-7 at room temperature. The aldehydes were analyzed on a Shimadzu GC-4A apparatus with a Golay column of DDP-90 at 60 °C.

Results

Catalytic reactions were conducted with the amounts of platinum complexes of 3.2×10^{-5} mol in Figs. 1, 3, and 5, and Tables 2—4, or of 3.2×10^{-6} mol in Figs. 4, 7—13, and Table 1.

Effect of the Structure of Diphosphines. Several α,ω-bis(diphenylphosphino)alkanes, $Ph_2P(CH_2)_nPPh_2$ (n=1—6, 10), were used for activating the $PtCl_2$-$(PhCN)_2$–$SnCl_2\cdot2H_2O$ system as hydroformylation catalysts and compared with PPh_3. The results are presented in Fig. 1. Bis(diphenylphosphino)methane as well as 1,2-bis(diphenylphosphino)ethane were almost completely ineffective. The diphosphine of n=3 was equally as effective as PPh_3, and the rate enhancement effect attained maximum at n=4, where the reaction rate observed was several times higher than when PPh_3 was used. When n exceeded four, the effectiveness was reduced abruptly, and it gradually vanished. The linearity of the aldehydes formed, *i.e.*, the molar ratio of hexanal to the total aldehydes formed (hexanal, 2-methylpentanal, and 2-ethylbutanal) was 91—94%, and it did not greatly depend on the n of $Ph_2P(CH_2)_nPPh_2$ except in the case of n=3 in which the linearity was reduced to *ca.* 69%. This exceptional linearity at n=3 may be caused by the instability of the chelating coordination because of the steric repulsion of 1,3-diaxial phenyl groups of the six-membered chelate ring, which is made up by the coordination of the two phosphorus atoms to the platinum center. A similar exception to the regioselectivity of hydroformylation has been observed in the rhodium-diphosphine-catalyzed reaction of methyl methacrylate or methyl crotonate using $Ph_2P(CH_2)_3PPh_2$.[15]

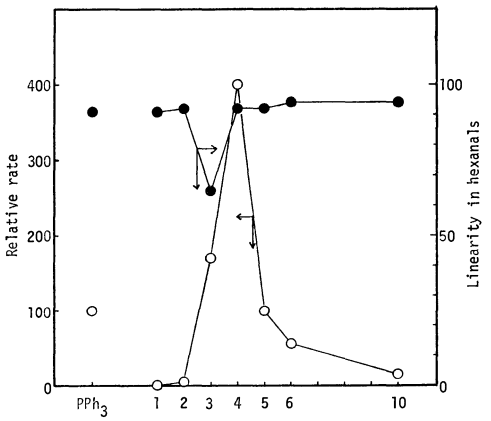

Fig. 1. Effect of methylene chain length of diphosphine ligands in $PtCl_2(PhCN)_2$–$SnCl_2\cdot2H_2O$-catalyzed hydroformylation of 1-pentene.
1-Pentene 3 cm³, benzene 18 cm³, $PtCl_2(PhCN)_2$ 3.2×10^{-5} mol, Pt/P/Sn=1/2/5 (atomic ratio), p(CO)=p(H_2)=50 kg/cm² initial at room temperature, reaction temperature 100 °C.

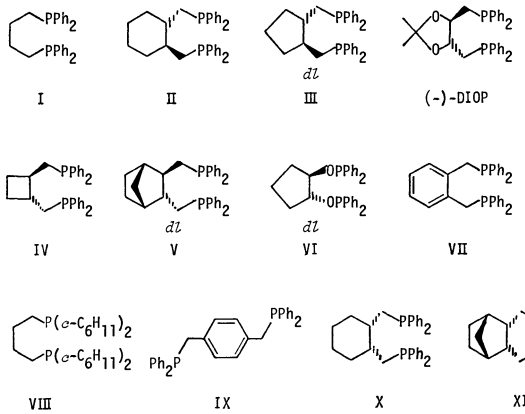

Fig. 2. Bidentate phosphorus ligands used with $PtCl_2$-$(PhCN)_2$–SnX_2 system.

In order to clarify the effect of the structure of the derivatives of 1,4-bis(diphenylphosphino)butane (I) and related compounds on the reaction rate and the product distribution, several diphosphines and phosphorus ligands capable of forming a seven-membered chelate ring like I were prepared and applied to the reactions (Fig. 2). The results are compared with that using the $HRh(CO)(PPh_3)_3$ catalyst. In these reactions, the catalyst concentration was reduced to one-tenth of that in Fig. 1 so that reaction rate could be compared exactly (Table 1).

Under these reaction conditions, the rate-enhancement effect of I (Run 2) was 7.5 times higher than that of PPh_3. It is noteworthy, however, that the reaction time required for complete conversion using I was incomparably shorter than that using PPh_3, because the dependence on the olefin concentration of a reaction rate using a diphosphine was smaller than that of one using PPh_3 as will be discussed later.

The effectiveness of I was further enhanced by bridging the 2- and 3-carbon to construct a rigid and

TABLE 1. EFFECT OF STRUCTURE OF BIDENTATE LIGAND IN THE HYDROFORMYLATION OF 1-PENTENE

Run	Ligand	Time / h	Relative rate[a]	Conversion / %	Product distribution/%[e]		
					Hexanals (Lin.)	Pentane	2-Pentenes
1	$2PPh_3$	24	10	4	79 (92)	8	13
2	I	10	75	100	71 (91)	14	15
3	II	18	60	100	76 (90)	13	10
4	III	4	170	100	73 (96)	9	18
5	(−)-DIOP	5	210	100	75 (96)	9	16
6	*dl*-DIOP	4	240	100	70 (96)	10	20
7	(+)-DIOP	4	240	99	71 (97)	10	19
8	(−)-DIOP[b]	4	210	99	89 (96)	3	8
9	IV	3	310	100	79 (99)	6	13
10	V	2	440	100	72 (99)	8	20
11	Rh[c]	4	240	100	100 (54)	0	0
12	VI	5	180	99	55 (94)	12	33
13	VII	10	80	95	68 (91)	10	22
14	IV[d]	2	400	100	89 (99)	3	8
15	Rh[c,d]	5	120	100	99 (70)	0	1

1-Pentene, 3 cm³; benzene, 18 cm³; $PtCl_2(PhCN)_2$, 3.2×10^{-6} mol; $SnCl_2\cdot2H_2O$, 1.6×10^{-5} mol; Pt/P = 1/2 (atomic ratio), $p(CO)=p(H_2)=50$ kg/cm² at room temperature; reaction temperature, 100 °C.
a) The maximum rate of the pressure drop in Run 1 was taken as the base (10). b) $p(CO)=150$ kg/cm². c) Rh: $HRh(CO)(PPh_3)_3$. d) Pt or Rh 3.2×10^{-5} mol, reaction temperature 70 °C. e) The molar ratio of each product. The deficiency was ascribed to some high-boiling product which might be formed through the condensation of aldehydes.

saturated ring skeleton. Both the reaction rate and the product linearity increased distinctly upon the use of *trans*-1,2-bis(diphenylphosphinomethyl)cyclopentane (III) (Run 4), and they increased further upon the use of (1*S*,2*S*)-1,2-bis(diphenylphosphinomethyl)cyclobutane (IV) with a saturated four-membered ring (Run 9). The effectiveness of (1*R*,2*R*)-1,2-bis(diphenylphosphinomethyl)cyclohexane (II) as a ligand (Run 3) was almost identical with that of I; that is, the attempt at the construction of a flexible six-membered ring skeleton was ineffective. The higher effectiveness of (−)-DIOP (Run 5) than that of III (Run 4) may be due to the somewhat smaller size of the dioxolane ring than that of the cyclopentane ring.

These diphosphines, however, accelerated not only the hydroformylation reaction, but also such side reactions as the hydrogenation[16] and isomerization of the olefin. Of course, the side reactions could be diminished by raising the carbon monoxide partial pressure, as is shown by the comparison of Runs 5 and 8. Even in this case, however, the reaction rate was not sacrificed because of the nearly zero-order rate dependence on the pressure, which will be discussed later. By the use of IV, which has a more rigid ring skeleton, the relative rate was increased 31 times in comparison with that when PPh_3 was used, and the product linearity was raised up to 99%. The reaction rate observed using IV was apparently higher than that in the reaction catalyzed by $HRh(CO)(PPh_3)_3$ in the absence of excess PPh_3 (Run 11). The superiority of the $PtCl_2$–IV–$SnCl_2\cdot2H_2O$ system to $HRh(CO)(PPh_3)_3$ was distinctly shown in the reactions with higher catalyst concentrations at the lower reaction temperature of 70 °C (Runs 14 and 15).

A bicyclic diphosphine, *trans*-2,3-bis(diphenylphosphinomethyl)norbornane (V) (Run 10), showed the highest effectiveness as a catalyst ligand; the observed relative rate was 44 times higher than that observed using PPh_3.

As has been shown by Knifton *et al.*[4] with various monodentate ligands, such as PPh_3 or $P(n\text{-}Bu)_3$, the electronic effect of phosphines did not influence the result in Pt-Sn catalyzed hydroformylation very much. This was fairly true for bidentate ligands; *trans*-1,2-bis(diphenylphosphinooxy)cyclopentane VI (Run 12) and III (Run 4), which are sterically similar but electronically different, gave similar results. Further, α,α′-bis(diphenylphosphino)-*o*-xylene VII (Run 13), which must be electronically different from II, caused an activity similar to that caused by II. Thus, the effectiveness of diphosphines as catalyst ligands is considered to be determined mainly by a steric factor. However, the difference in electron-donating ability between a diarylphosphino group and a dialkylphosphino one may be multiplied when they are in bidentate ligand. In fact, 1,4-bis(dicyclohexylphosphino)-butane (VIII) (Table 2) was far less effective than I, and also less effective than the monodentate ligand PPh_3, probably because its donating ability is too high.

In order to elucidate the further steric requirements, closely related isomers of diphosphines were prepared and their degrees of effectiveness were compared. The catalyst-system concentration was the same as in Fig. 1 (Table 2). α,α′-Bis(diphenylphosphino)-*p*-xylene (IX), which is unable to effect chelation, was distinctly less effective than the position isomer, VII, and also

TABLE 2. EFFECT OF STRUCTURE OF DIPHOSPHINE IN THE $PtCl_2(PhCN)_2$–DIPHOSPHINE–$SnCl_2 \cdot 2H_2O$-CATALYZED HYDROFORMYLATION OF 1-PENTENE

Diphosphine	Time / h	Relative rate	Conversion / %	Product distribution/%		
				Hexanals (Lin.)	Pentane	2-Pentenes
I	1.5	400	100	74(92)	12	14
VIII	17	50	76	63(91)	5	25
VII	2	370	100	64(87)	11	25
IX	6	80	94	62(85)	5	33
II	2	340	100	69(92)	11	14
X	2.5	180	100	71(90)	8	21
V	1	1880	100	53(97)	9	14
XI	1	720	100	42(92)	8	22
PPh_3	5	100	87	84(91)	5	11
PPh_3[a)]	3.5	180	100	58(86)	7	17
PPh_2Et	4	150	100	79(89)	7	15
PPh_2Et[a)]	4	120	100	62(86)	7	19

1-Pentene, 3 cm^3; benzene, 18 cm^3; Pt 3.2×10^{-5} mol; Pt/P/Sn=1/2/5 (atomic ratio); $p(CO)=p(H_2)=50$ kg/cm^2 at room temperature; reaction temperature, 100 °C.
a) Pt/P/Sn=1/1/5.

less effective than monophosphines. On the other hand, among the stereo isomers of 1,2-bis(diphenylphosphinomethyl)cyclohexanes (II and the *cis*-isomer X) and 2,3-bis(diphenylphosphinomethel)norbornane (V and the *endo*, *endo*-isomer XI), *cis*-isomers were half as effective as the corresponding *trans*-isomers. That is, a *trans*-configuration of the ring skeleton of the diphosphines was more favorable to rate enhancement than a *cis*-configuration, although the former seems to be fairly disadvantageous to chelating coordination.

Effect of P/Pt Atomic Ratio. It is well known that the amount of excess phosphine plays a significant role in the activity and selectivity of rhodium catalysts in hydroformylation.[17] However, in the $PtCl_2$–$SnCl_2$ catalyzed hydroformylation,[4] it was reported only that excess PPh_3 retarded the reaction, even at P/Pt=4. In contrast with this, the effect of the P/Pt ratio of diphosphines on the reaction rate was more serious than has been expected, as is shown in Fig. 3. That is, the optimum P/Pt ratio to attain the maximum reaction rate was between 1.0 and 2.0, but not so distinct when a monophosphine such as PPh_3 or PPh_2Et was used. In contrast, when diphosphine I was used, the optimum P/Pt value increased to 2.0 and became distinct. By the use of a more effective diphosphine, (−)-DIOP, this value became about 2.5—3.0. That is, the more effective the ligand, the higher the optimum P/Pt atomic ratio.

By the use of the most effective ligand, V, the effect of the P/Pt ratio was investigated with a catalyst amount one-tenth of that in Fig. 3. At this concentration, the optimum ratio of (−)-DIOP increased somewhat to about 3 as is shown in Fig. 4, while the reaction rate obtained by the use of V showed a plateau between 2.0—3.5 values of the P/Pt ratio.

Effect of Tin (II) Halide. It has been reported that the effectiveness of tin(II) halide as a cocatalyst for $PtCl_2(PPh_3)_2$ was in the order of $SnCl_2 \cdot 2H_2O$>

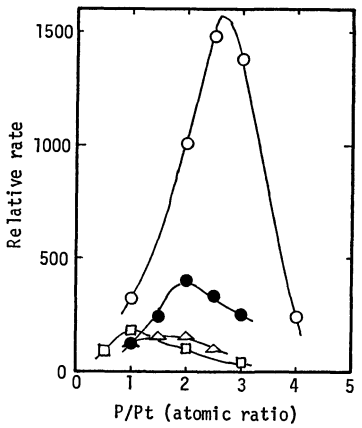

Fig. 3. Effect of phosphorus to platinum ratio in hydroformylation of 1-pentene catalyzed by $PtCl_2$-$(PhCN)_2$–phosphine–$SnCl_2 \cdot 2H_2O$ system.
Reaction conditions are the same as in Fig. 1 except phosphine amount. ○: (−)-DIOP, ●: I △: PPh_2Et, □: PPh_3.

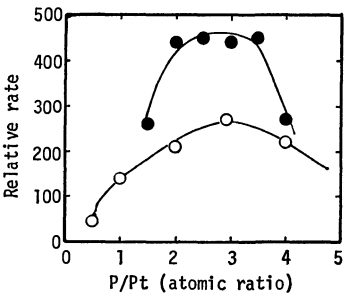

Fig. 4. Effect of phosphorus to platinum ratio in hydroformylation of 1-pentene catalyzed by $PtCl_2$-$(PhCN)_2$–diphosphine–$SnCl_2 \cdot 2H_2O$ system.
Reaction conditions are the same as in Table 1 except phosphine amount. ●: V, ○: (−)-DIOP.

TABLE 3. EFFECT OF THE SORT OF STANNOUS HALIDE IN THE $PtCl_2(PhCN)_2$–PHOSPHINE–SnX_2-CATALYZED HYDROFORMYLATION OF 1-PENTENE

Phosphine	SnX_2	Time / h	Relative rate	Conversion / %	Product distribution/%		
					Hexanals (Lin.)	Pentane	2-Pentenes
$2PPh_3$	SnF_2	24	25	61	87 (95)	5	8
	$SnCl_2 \cdot 2H_2O$	5	100	87	84 (91)	5	11
	$SnBr_2$	5	65	98	76 (92)	5	19
	SnI_2	24	5	26	85 (90)	4	11
(−)-DIOP	SnF_2	1.5	1180	100	75 (94)	9	15
	$SnCl_2 \cdot 2H_2O$	1	1010	100	75 (95)	10	15
	$SnCl_2$	0.5	1140	100	77 (96)	8	15
	$SnBr_2$	1	620	100	55 (96)	10	25
	SnI_2	8	45	100	64 (93)	8	28

The reaction conditions are the same as in Table 2.

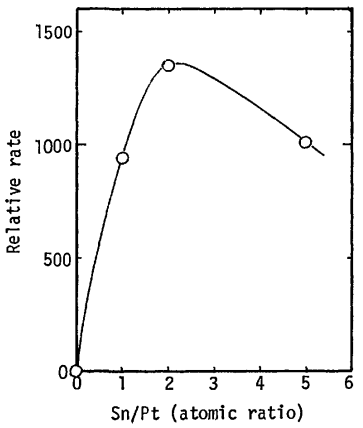

Fig. 5. Effect of tin to platinum ratio in $PtCl_2(PhCN)_2$–(−)-DIOP–$SnCl_2 \cdot 2H_2O$-catalyzed hydroformylation of 1-pentene.
Reaction conditions are the same as in Fig. 1 except $SnCl_2 \cdot 2H_2O$ amount.

$SnBr_2 > SnI_2$.[4] Tin(II) fluoride, which had not yet been used, was less effective than bromide (Table 3). However, the fluoride was more effective than $SnBr_2$, and as effective as $SnCl_2 \cdot 2H_2O$, when a diphosphine, (−)-DIOP, was used. Although it is uncertain how much SnX_2 operates as an anionic ligand, SnX_2Cl, as in the case of $SnCl_2$,[18] these results indicated that the effect of a cocatalyst was different depending on whether a phosphorus ligand was monodentate or bidentate.

The effect of the Sn/Pt atomic ratio was examined by the use of the most effective $SnCl_2 \cdot 2H_2O$ as a cocatalyst for $PtCl_2$–(−)-DIOP-system; the results are shown in Fig. 5. The system had no activity without tin(II) halide, and the significant activity appeared even at Sn/Pt=1, which suggests that one $SnCl_3$ group is necessary for, and also enough for the catalytically active species.

Choice of Solvent. The effect of the solvent on the reaction rate using the $PtCl_2$–diphosphine–$SnCl_2$ system was examined, the results are listed in Table 4. The relative rate was the highest when benzene or CH_2Cl_2 was used. In the latter, however, the linearity was low (89%), and, after the reaction, some metal deposit was observed. Acetone, which was one of the best solvents for the $PtCl_2(PPh_3)_2$–$SnCl_2$ system,[4] was not so suitable for the diphosphine system. Thus, it was best to carry out the reaction in benzene when diphosphines were used.

TABLE 4. RELATIVE RATE IN THE HYDROFORMYLATION OF 1-PENTENE CATALYZED BY $PtCl_2(PhCN)_2$–(−)-DIOP–$SnCl_2 \cdot 2H_2O$ IN VARIOUS SOLVENTS

Solvent	Relative rate
Benzene	1010
CH_2Cl_2	920
Acetone	350
THF	170
CH_3CN	130
Hexane	45
MeOH	5

The reaction conditions are the same as in Table 2 except for the solvent.

Effect of Reaction Variables. A diphosphine must coordinate to a platinum-metal center competing with olefin, hydrogen, and carbon monoxide. Therefore, the behavior of a diphosphine can be clarified if the effect of the catalyst or olefin concentration and the H_2 and CO partial pressure are examined. Thus, these variables were altered by the use of (−)-DIOP and benzene as diphosphine and solvent respectively, and the relative rate was measured.

The relative rate was plotted full-logarithmically against the charged amount of the catalyst system. The slope means that the order to the catalyst concentration was about 0.7 (Fig. 6)

On the other hand, the relation between the initial olefin concentration and relative rate (Fig. 7) showed the order of *ca.* 0.3, which was remarkably low for the dependence on the olefin concentration in hydroformylation. Hence, the reaction rate was nearly constant until almost all the olefin had been consumed, and the total reaction time required for a complete conversion was remarkably shorter than would be expected from the relative rate comparison between

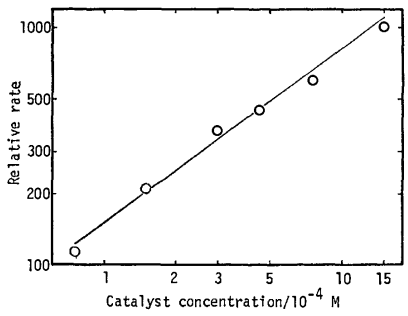

Fig. 6. Full-log plot of relative rate *vs.* catalyst system concentration in $PtCl_2(PhCN)_2$–(−)-DIOP–$SnCl_2 \cdot 2H_2O$-catalyzed hydroformylation of 1-pentene.
Reaction conditions are the same as in Table 1 except catalyst system concentration.

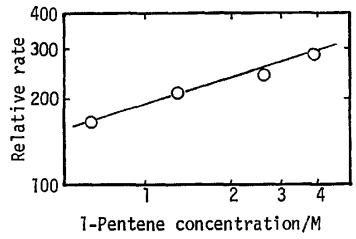

Fig. 7. Full-log plot of relative rate *vs.* 1-pentene concentration in $PtCl_2(PhCN)_2$–(−)-DIOP–$SnCl_2 \cdot 2H_2O$ catalyzed hydroformylation of 1-pentene.
Reaction conditions are the same as in Table 1 except 1-pentene concentration.

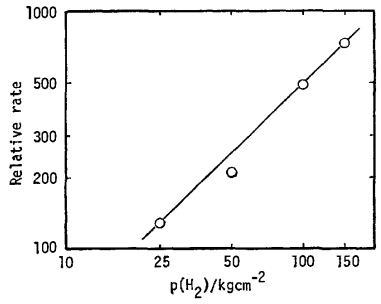

Fig. 8. Full-log plot of relative rate *vs.* $p(H_2)$ (initial at room temperature) in $PtCl_2(PhCN)_2$–(−)-DIOP–$SnCl_2 \cdot 2H_2O$-catalyzed hydroformylation of 1-pentene.
Reaction conditions are the same as in Table 1 except $p(H_2)$.

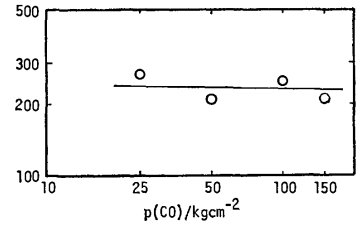

Fig. 9. Full-log plot of relative rate *vs.* p(CO) (initial at room temperature) in $PtCl_2(PhCN)_2$–(−)-DIOP–$SnCl_2 \cdot 2H_2O$-catalyzed hydroformylation of 1-pentene.
Reaction conditions are the same as in Table 1 except p(CO).

the case of (−)-DIOP and that of PPh_3.

The rate was proportional to the H_2 partial pressure, $p(H_2)$ (Fig. 8). The reaction order was almost 1.0 with respect to $p(H_2)$, as in other hydroformylation catalyst systems. On the other hand, the rate hardly depended on p(CO) at all, and Fig. 9 indicates an order of nearly zero.

The product distribution virtually did not depend at all on the reaction variables except on the partial pressures of CO and H_2. Isomerization was suppressed by increasing $p(H_2)$ or p(CO), while hydrogenation was suppressed by increasing p(CO) or decreasing $p(H_2)$.

Although the kinetic order described above was rather qualitative, the results can be represented by the following rate expression in the range of the above-mentioned reaction conditions:

$$\text{Rate} \propto [\text{Pt}]^{0.7}[\text{1-Pentene}]^{0.3}p(H_2)^{1.0}p(\text{CO})^{0.0}. \quad (1)$$

Effect of the Structure of Olefins. In the previous sections, 1-pentene has been used as the substrate because it is easy to handle and also easy to analyze the isomerization or hydrogenation products. The present catalyst system was further applied to propene or 1-butene hydroformylation, and the results were compared with that of 1-pentene. As is shown in Fig. 10, the shorter a 1-alkene was, the lower the product linearity. However, the effect of the rigid ring skeleton of a diphosphine on the linearity became distinct with shorter olefins.

Internal olefins reacted only sluggishly. For example, the rate of *cis*-2-pentene hydroformylation was one twentieth that of 1-pentene, and the product was composed of aldehydes (linearity 65%) 43%, *trans*-2-pentene 38%, *cis*-2-pentene 11%, and pentane 4%.

Effect of Temperature. The hydroformylation of propene was carried out at various temperatures between 80—140 °C by the use of the $PtCl_2$–IV–$5SnCl_2 \cdot 2H_2O$ catalyst system (Fig. 11). Lowering the reaction temperature improved the yield of aldehydes, which means the competitive hydrogenation or aldehyde loss was almost entirely suppressed. The linearity in aldehydes was also improved by lowering the temperature.

Effect of Total Pressure. It is important, from the industrial point of view to know to what degree

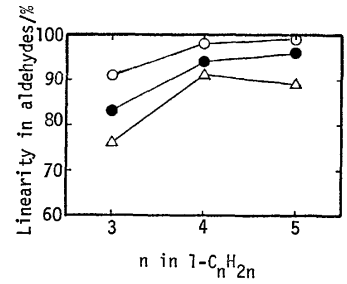

Fig. 10. Effect of the structure of diphosphines and the chain length of 1-alkene on the selectivity to the straight-chain aldehyde.
Other conditions are the same as in Table 1. ○: IV, ●: (−)-DIOP, △: II.

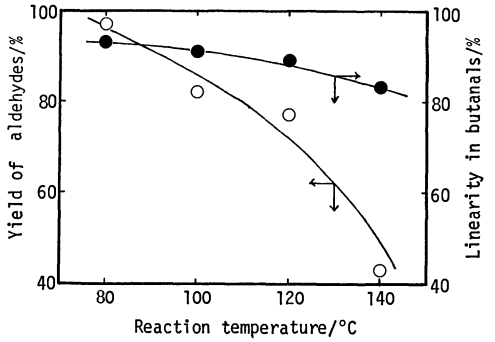

Fig. 11. Effect of reaction temperature in the hydroformylation of propene catalyzed by $PtCl_2(PhCN)_2$–IV–$SnCl_2 \cdot 2H_2O$-system.
Propene(l) 3 cm³, other conditions are the same as in Table 1 except reaction temperature.

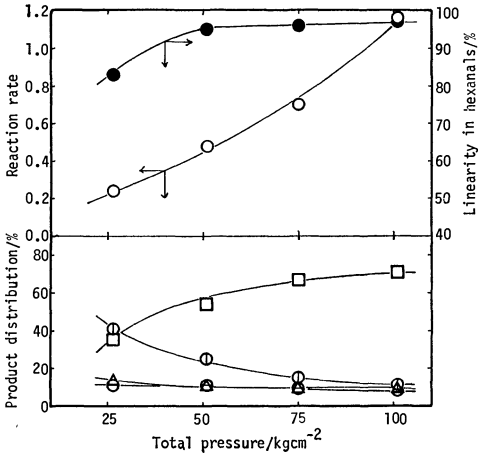

Fig. 12. Effect of total pressure ($CO/H_2=1$) on the product distribution, linearity in the aldehydes, and reaction rate in $PtCl_2(PhCN)_2$–(−)-DIOP–$SnCl_2 \cdot 2H_2O$-catalyzed hydroformylation of 1-pentene at constant pressure.
Reaction conditions are the same as in Table 1 except gas pressures. □: Hexanals, △: pentane, ⓘ: *trans*-2-pentene, ⊖: *cis*-2-pentene.

the total gas pressure can be lowered. Thus, 1-pentene was hydroformylated by the use of $PtCl_2(PhCN)_2$–[(−)-DIOP]–$SnCl_2 \cdot 2H_2O$ (Pt/P/Sn=1/2/5, atomic ratio) at a constant pressure (Fig. 12). Lowering the pressure decreased the relative rate, as was expected from the effect of partial pressures shown in Figs. 8 and 9. Aldehyde linearity was almost constant down to a pressure of 50 kg/cm², but it was lowered gradually below that pressure. The product distribution showed an interesting pattern; with a lowering of the total pressure, the yield of aldehydes was decreased until *ca.* 35% at 25 kg/cm², while those of *cis*-2-pentene and pentane remained almost constant, and only that of *trans*-2-pentene increased.

Also, in the reaction of propene carried out by the use of the most active catalyst system, $PtCl_2(PhCN)_2$–V–$SnCl_2 \cdot 2H_2O$, at the optimum atomic ratio of Pt/P/Sn (1/3/2.5) (Fig. 13), the relative rate decreased with a lowering of the pressure, as above. On the other hand, the yield of aldehydes and its

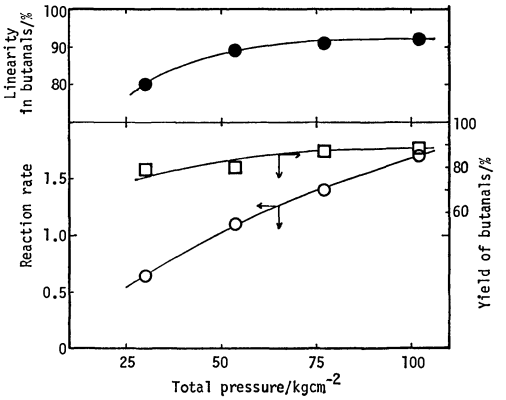

Fig. 13. Effect of total pressure ($CO/H_2=1$) on $PtCl_2(PhCN)_2$–V–$SnCl_2 \cdot 2H_2O$ catalyzed hydroformylation of propene at constant pressure.
Propene(l) 3 cm³, Pt/P/Sn=1/3/2.5, other conditions are the same as in Table 1 except gas pressures.

linearity was not so much lowered, because the isomerization of the olefin is excluded; *i.e.*, even at a total gas pressure of 25 kg/cm², both values were more than 80%.

Discussion

The rate-enhancement effect of diphosphines in hydroformylation has been observed in the rhodium-catalyzed reaction of 1-alkenes by the use of $Ph_2P(CH_2)_nPPh_2$ (n=2—4)[19] or IV.[20] However, the degree of the enhancement was low, *i.e.*, two times at the most. These effects can be interpreted as showing that a little excess of diphosphine plays the role of a large excess of monophosphine in keeping the rhodium complex catalytically active by coordination. The effect became more distinct in the rhodium-catalyzed hydroformylation of ethyl acrylate.[15] However, the operating mechanism of diphosphines in the rate enhancement seems to be qualitatively different from that of the platinum–diphosphine-catalyzed hydroformylation presented in this paper, because, in the rhodium-catalyzed reaction, $Ph_2P(CH_2)_nPPh_2$ are effective only for ethyl acrylate, and the diphosphines of n=2 and 3, which were ineffective in the platinum-catalyzed reaction, also accelerated this reaction.

Figure 14 shows the conceivable coordination types of diphosphines in square-planar platinum complexes. Among these, **A** was postulated for the $PtCl(SnCl_3)$-[(−)-DIOP] complex.[21] A complex of the **B** type was prepared with $(t\text{-Bu})_2P(CH_2)_nP(t\text{-Bu})_2$, $n \geqq 9$.[22] A di- or trinuclear complex of the **C** or **D** type was isolated by the use of $Ph_2P(CH_2)_nPPh_2$ of n=3 or 4 respectively.[23]

As has been reported in Ref. 4, 1,2-bis(diphenylphosphino)ethane, which is known to form a complex of the **A** type, inhibited the reaction almost completely. Moreover, $Ph_2PCH_2PPh_2$ was also completely ineffective (Fig. 1), and the recovered precipitate in the reaction solution showed a ^{31}P NMR spectrum which was ascribable to a chelating form rather than a bridged one.[24] However, many results in this paper support the idea that the active species has a form

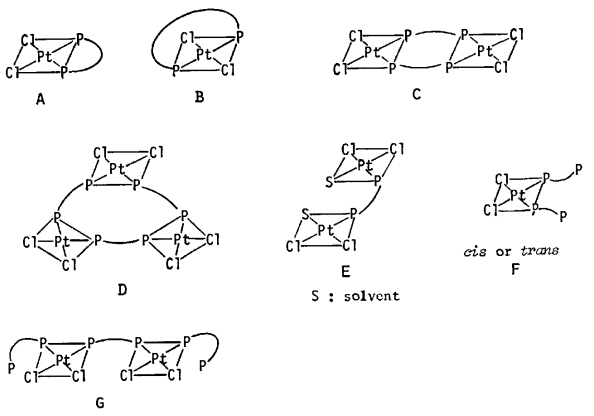

Fig. 14. Conceivable coordination types of diphosphines in square planar platinum complexes.

of the **A** type, where the chelating coordination is rather loose. In $Ph_2P(CH_2)_nPPh_2$ (n=1—10), only that of n=4 was prominent as a catalyst ligand (Fig. 1), and so the possibility of **B**-type coordination can be excluded. On the other hand, the possibility that a diphosphine bridges two platinum centers in the active species is negligible judging from the following considerations: 1) If the active species is a di- or trinuclear complex of the **C** or **D** type, with two or three bridging diphosphine molecules, the result of the reaction by the use of the *dl*-form of a diphosphine would be different from the result when only one antipode of the diphosphine is used, because the former might give a complex which has both antipodes. However, the result using *dl*-DIOP was almost the same as that when (−)-DIOP or (+)-one was used. 2) An α,α′-bis(diphenylphosphino)-*p*-xylene, IX, which is able to make only a bridging coordination, was much less effective than the *o*-isomer, VII, which is electronically similar to IX but which is able to form a *cis*-chelation complex of the **A** type. 3) The reaction rate depended on the charged-catalyst amount in the order of *ca.* 0.7 (Fig. 6), which may be due to the aggregation of the active species of the **A** type by the formation of inactive bridging complexes, such as **C** or **D**, with an increase in the catalyst concentration. Thus, the bridging-type coordination of **C** and **D** can be excluded.

As is shown in Fig. 3, the effectiveness of diphosphines I and (−)-DIOP was extremely low at the P/Pt atomic ratio of 1, in contrast with the inefficiency at P/Pt=2, and there was no significant difference either in rate enhancement or in product linearity between diphosphines and monophosphines so long as the P/Pt ratio in the reaction system was 1. This result suggests that, even if another bridging complex of the **E** type is formed at P/Pt=1, it operates as if it were a monophosphine complex of P/Pt=1. On the other hand, the presence of excess diphosphine retarded the reaction distinctly; the relative rate at P/Pt=4 was similar to that using PPh_2Et at P/Pt=2, probably because the diphosphines at a high P/Pt ratio behave as monodentate ligands, as in Type **F** or **G**.

Rather high optimum ratios of P/Pt of *ca.* 3 was observed for diphosphines with a rigid ring skeleton, as is shown in Figs. 3 and 4. This may be explained as follows. Because of the steric rigidity, it is difficult for these diphosphines to make a *cis*-chelating coordination. Therefore, not enough of the catalytically active species of Type **A** is formed at P/Pt up to 2, while some bridged complexes, such as **C** and **D**, may be formed. When excess diphosphine is added, it may displace one phosphorus end of bridging diphosphine in, for example, **C** to make up a bridging complex such as **G**, whose P/Pt ratio is 3. This dinuclear complex then dissociates to give the active species, **A**, and the inactive complex, **F**. Thus, some excess of diphosphine is necessary to maximize the concentration of the active species, **A**.

On the other hand, the ineffectiveness of 1,2-bis(diphenylphosphino)ethane and 1,4-bis(dicyclohexylphosphino)butane indicates the necessity of the dissociation of a chelating diphosphine during the catalytic cycle. The necessity of the loose *cis*-chelation of a diphosphine can be explained as follows. In contrast with a rhodium or cobalt system, $SnCl_3$ is necessary as a supplementary ligand, and it is considered to occupy one coordination site throughout the catalytic cycle; moreover, one phosphorus atom, probably trans to $SnCl_3$, has to dissociate to provide a vacant site for the activation of olefin, CO, and H_2. As Pt–P bonds are comparatively stable,[25] the dissociation can not easily occur without the aid of the instability of a seven-membered chelate ring, which is increased by the construction of a rigid ring skeleton.

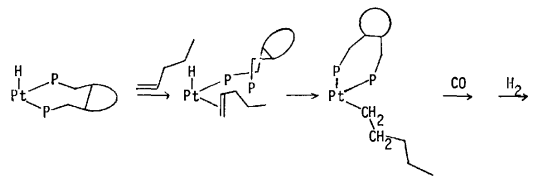

Scheme 1.

As is shown in Scheme 1, the reaction site for olefin is provided by the dissociation of one phosphorus end of the diphosphine, and the following *cis*-addition of H–Pt to the C=C bond of the olefin to give the σ-alkyl complex may be accelerated[26] by the recoordination of the dissociated phosphorus end, which is forced to be located near the reaction site by the steric bulkiness of the rigid ring skeleton of the diphosphine itself. This process may operate in successive steps of CO insertion and/or hydrogenolysis. In this manner, 1,4-bis(diphenylphosphino)butane derivatives can enhance the hydroformylation as well as competitive hydrogenation. On the other hand, the hydroformylation catalyzed by the $PtCl_2$–diphosphine–$SnCl_2\cdot 2H_2O$ system showed a low-order dependence of the rate on the CO partial pressure and on the olefin concentration in comparison with the reactions catalyzed by the $PtCl_2(PPh_3)_2$–$SnCl_2\cdot 2H_2O$ system,[4] $Co_2(CO)_8$,[27] and $Rh_4(CO)_{12}$[28] where the rate expressions were proportional to $[Pt]^{1.5}[Olefin]^{1.0}p(H_2)^{1.0}\cdot p(CO)^{-0.5}$, $p(H_2)/[p(H_2)+p(CO)]\times[Co][Olefin]$, and $[Rh][Olefin]p(H_2)/p(CO)$ respectively. The low dependence of the rate on [Olefin] suggests a spontaneous dissociation of one phosphorus end of the chelated

diphosphine, affording a vacant site. The low dependence on the CO partial pressure also suggests that the diphosphine keeps off the excess coordination of CO, which retards the reaction. However, the first-order dependence of the reaction rate on $p(H_2)$ is like that in a rhodium- or cobalt-catalyzed reaction, in which the rate-determining step is considered to be the hydrogenolysis of an acyl complex.

Not only the remarkable rate enhancement, but also the improvement of linearity in aldehydes produced was brought about by diphosphines bearing rigid ring skeletons. The linearity is originally as high as 92% (Table 1), even when the $PtCl_2(PPh_3)_2$–$SnCl_2 \cdot 2H_2O$ catalyst was used, much higher than when the $HRh(CO)(PPh_3)_3$ or cobalt catalyst was used, this difference may be ascribed to both the steric bulkiness of the $SnCl_3$ ligand and that of the two PPh_3 ones, which do not easily dissociate. The rigidity and bulkiness of the ring skeletons of diphosphines must cause a larger steric hindrance, not only when the diphosphine makes a *cis*-chelating coordination, but also when its one phosphorus end dissociates in order to receive substrate or reactant molecules.

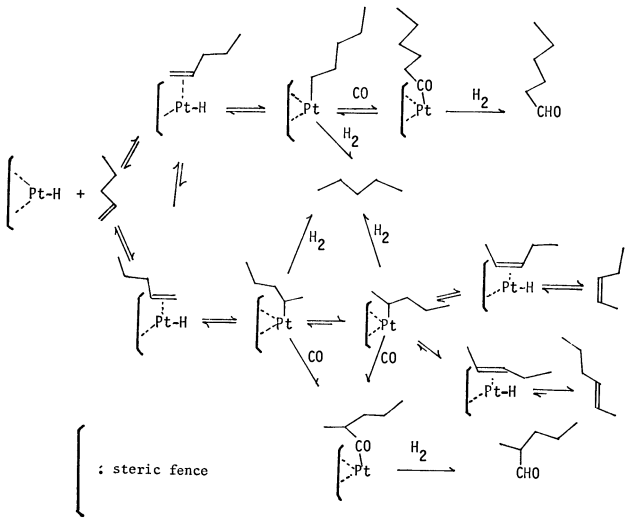

Scheme 2.

The process of how a terminal olefin gives linear aldehyde is shown schematically in Scheme 2. The increase in isomerized *trans*-2-pentene in comparison with *cis*-pentene with a prolonged reaction time can also be explained by the scheme. The steric hindrance is considered to prevent *trans*-2-pentene from taking part in the catalytic cycle again.

The authors wish to thank Mr. Kazuteru Ebata and Mr. Yukio Izawa for their experimental assistance.

References

1) K. Kuno, *Yuki Gosei Kagaku Kyokai Shi*, **35**, 683 (1977).
2) H. Wakamatsu, *Nippon Kagaku Zasshi*, **85**, 227 (1964).
3) C. -Y. Hsu and M. Orchin, *J. Am. Chem. Soc.*, **97**, 3553 (1975).
4) I. Schwager and J. K. Knifton, *J. Catal.*, **45**, 256 (1976).
5) Y. Kawabata, T. M. Suzuki, and I. Ogata, *Chem. Lett.*, **1978**, 361.
6) Y. Kawabata, T. Hayashi, and I. Ogata, *J. Chem. Soc., Chem. Commun.*, **1979**, 462.
7) F. R. Hartley, "The Chemistry of Platinum and Palladium," Applied Science, London (1973), p. 462.
8) T. Hayashi, M. Tanaka, Y. Ikeda, and I. Ogata, *Bull. Chem. Soc. Jpn.*, **52**, 2605 (1979).
9) T. P. Dang, J. -C. Poulin, and H. B. Kagan, *J. Organomet. Chem.*, **91**, 105 (1975).
10) H. B. Kagan and T. P. Dang, *J. Am. Chem. Soc.*, **94**, 6429 (1972).
11) T. Hayashi, M. Tanaka, and I. Ogata, *Tetrahedron Lett.*, **1977**, 295.
12) K. Issleib and D. -W. Müller, *Chem. Ber.*, **92**, 3175 (1959).
13) H. Koch, J. Kotlan, and H. Markut, *Monatsh. Chem.*, **96** 1646 (1965).
14) C. F. Culberson, J. H. Seward, and P. Wilder, Jr., *J. Am. Chem. Soc.*, **82**, 2541 (1960).
15) M. Tanaka, T. Hayashi, and I. Ogata, *Bull. Chem. Soc. Jpn.*, **50**, 2351 (1977).
16) J. -C. Poulin, T. -P. Dang, and H. B. Kagan, *J. Organomet. Chem.*, **84**, 87 (1975).
17) K. L. Olivier and F. B. Booth, *Hydrocarbon Process*, **49**, (4) 112 (1970).
18) J. C. Bailar, Jr., and H. Itatani, *Inorg. Chem.*, **4**, 1618 (1965).
19) A. R. Sanger, *J. Mol. Catal.*, **3**, 221 (1977/78).
20) Japan Kokai, 78-121711.
21) P. S. Pregosin and S. N. Sze, *Helv. Chim. Acta*, **61**, 1848 (1978).
22) A. Pryde, B. L. Shaw, and B. Weeks, *J. Chem. Soc., Dalton Trans.*, **1976**, 322.
23) A. R. Sanger, *J. Chem. Soc., Dalton Trans.*, **1977**, 1971.
24) M. P. Brown, R. J. Puddephatt, M. Rashidi, and K. R. Seddon, *J. Chem. Soc., Dalton Trans.*, **1977**, 951.
25) F. A. Cotton and G. Wilkinson, "Advanced Inorganic Chemistry, A Comprehensive Text," 2nd ed, 30·H John Wiley & Sons, New York (1966).
26) C. K. Brown and G. Wilkinson *J. Chem. Soc., A*, **1970**, 2753.
27) A. R. Martin, *Chem. Ind. (London)*, **1954**, 1536.
28) B. Heil and L. Markó, *Chem. Ber.*, **101**, 2209 (1968).

ortho-Disubstituted *F*-Benzenes. III. Preparation of (*F*-Benzo)heterocyclic Compounds from *F*-Benzoic Acid and *F*-Phenol, and the Reactions of Some Intermediary *F*-Benzoyl- and *F*-Phenoxy Compounds

Yoshinari INUKAI,† Yoshitsugu OONO, Takaaki SONODA, and Hiroshi KOBAYASHI*
Research Institute of Industrial Science, Kyushu University 86, Hakozaki, Higashi-ku, Fukuoka 812
(Received January 20, 1981)

With the intention of achieving the selective *ortho*-substitution of *F*-benzoic acid and *F*-phenol *via* intramolecular nucleophilic cyclization, preparation of some requisite precursory *F*-benzoyl- and *F*-phenoxy compounds and their nucleophilic cyclization reactions were examined. 1,2-(*F*-Benz)isoxazol-3(2*H*)-one, 2-(*p*-tolyl)-1,2-(*F*-benz)isoxazol-3(2*H*)-one, 1,3-dimethyl(*F*-benzo)pyrimidine-2,4(1*H*,3*H*)-dione, and 1,4-(*F*-Benz)oxazin-3(2*H*)-one were obtained from the respective precursory *F*-benzohydroxamic acid, *N*-(*p*-tolyl)-*N*-hydroxy-*F*-benzamide, *N*,*N*'-dimethyl-*N*-(*F*-benzoyl)urea, and 2-(*F*-phenoxy)acetohydrazide. Attempted cyclizations of 2-(*F*-phenoxy)acetohydroxamic acid and (*F*-phenoxy)acetic acid were accompanied by simultaneous ring-opening and resulted in the formation of the identical product: (2-hydroxy-*F*-phenoxy)acetic acid. Transamidation of ethyl *F*-benzoate with hydroxylamine failed to give *F*-benzohydroxamic acid, which was then obtained by the catalytic debenzylation of *N*-benzyloxy-*F*-benzamide.

In the continuation of studies on the preparation of (*F*-benzo)heterocyclic compounds[1] from simple and readily accessible monofunctional *F*-benzenes by intramolecular cyclization,[2,3] syntheses and cyclization of some precursory compounds were investigated by use of *F*-benzoic acid and *F*-phenol as the starting substances.

Results and Discussion

Preparation of the Requisite Precursors. From F-Benzoic Acid: The precursory *F*-benzoyl compounds were fabricated by *F*-benzoylation of the amino compound carrying a cyclizing agent by use of *F*-benzoyl chloride, as shown in Scheme 1.

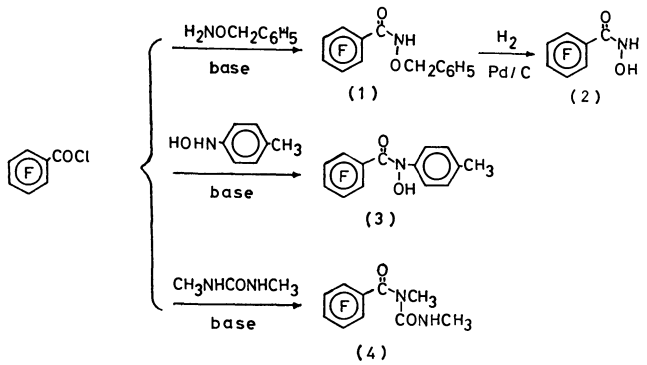

Scheme 1.

The oxygen in a *N*-hydroxycarbamoyl group is known to be one of the most effective nucleophiles, and is regarded as an effective cyclizing agent readily associable with an *F*-benzoyl group. Attempts to prepare *F*-benzohydroxamic acid (**2**)[4] from ethyl *F*-benzoate and hydroxylamine resulted in failure.[5] In the present case, *F*-benzohydroxamic acid (**2**) could be attained by the reductive debenzylation of *N*-benzyloxy-*F*-benzamide (**1**), which was derived from *F*-benzoyl chloride by the reaction with *O*-benzylhydroxylamine in the presence of base.

On the other hand, *N*-(*p*-tolyl)hydroxylamine reacted with *F*-benzoyl chloride to give *N*-(*p*-tolyl)-*N*-hydroxy-*F*-benzamide (**3**) in a usual manner.[6] Here, the *p*-tolyl group was introduced onto the amide nitrogen in such a way as to be favorable to the subsequent intramolecular cyclization due to its steric bulkiness.

The nitrogen of urea was also regarded as a nucleophile capable of replacing the fluorine atom on an *F*-phenyl nucleus. Then, we examined whether an *F*-benzoyl group could be combined with a urea molecule at the nitrogen only on one side. The reaction of *F*-benzoyl chloride with urea in the presence of pyridine, however, afforded none of the expected *N*-(*F*-benzoyl)urea (**5**). From the reaction mixture, di-(*F*-benzoyl)amine (**8**) was isolated and the mass spectrum of the crude product indicated the formation of a compound whose molecular weight corresponded to di(*F*-benzoyl)urea (**6**) as a minor by-product. Occurrence of the dibenzoylamine (**8**) indicates that, as shown in Scheme 2, the intermediary *F*-benzoyl derivatives, (**5**) and/or (**6**), cleaved in some way at the α–β bond relative to the *F*-benzoyl group prior to the intramolecular cyclization, to liberate di(*F*-benzoyl)amide anion (**7**) in the presence of pyridine.

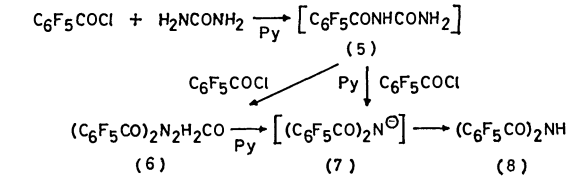

Scheme 2.

On the other hand, the reaction with *N*,*N*'-dimethylurea gave *N*,*N*'-dimethyl-*N*-(*F*-benzoyl)urea (**4**), in which no protic hydrogen was present at the α-amide nitrogen and the second *F*-benzoylation at the same site could not occur. Thus, the α–β bond cleavage seems to be suppressed. The electron-donation due to the methyl group on the nitrogen atom might also contribute to this stabilization.

† Present address: Government Industrial Research Institute in Kyushu, Shukumachi, Tosu, Saga 841.

From F-*Phenol*: For this purpose, we used ethyl (*F*-phenoxy)acetate (**9**), which was prepared by the reaction of potassium *F*-phenolate with ethyl chloroacetate.[7]

The carboxylic acid (**10**) from the ester (**9**), and its acyl derivatives, (**11**) and (**12**), were examined as the potential precursors for the subsequent intramolecular cyclization; they were prepared as shown in Scheme 3.

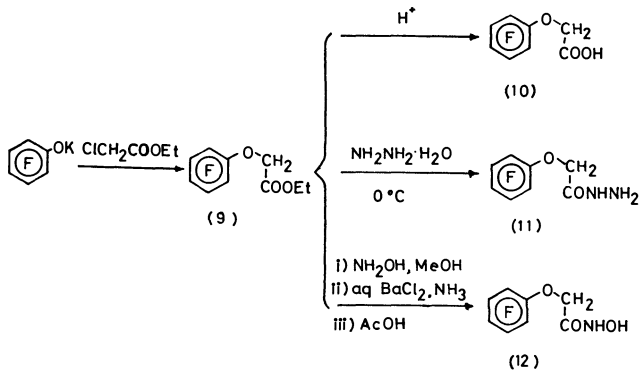

Scheme 3.

The ester function of the (*F*-phenoxy)acetate (**9**) was converted to a hydrazide to yield 2-(*F*-phenoxy)-acetohydrazide (**11**) by the reaction with hydrazine hydrate at 0 °C. Although the reactions were usually performed by heating under reflux,[8] the present ester (**9**) was treated under much milder conditions lest it should result in the formation of hydrazinium *F*-phenoxide.[9]

An oxygen nucleophile was fabricated at the terminal position of the side chain in the form of 2-(*F*-phenoxy)-acetohydroxamic acid (**12**), which was prepared in a usual manner.[5] Under a prolonged reaction time, the yield of the acetohydroxamic acid (**12**) decreased, while the more amount of *F*-phenol was generated as a by-product. The C–O bond fission to liberate *F*-phenol seems due to the higher stability of *F*-phenoxide, as often encountered in the reaction of *F*-phenoxy compounds in the presence of base.[10]

(*F*-Phenoxy)acetic acid (**10**) was regarded as another precursor carrying an oxygen nucleophile at the terminal position. The acetic acid (**10**) was obtained by the hydrolysis of the ester (**9**) in a good yield.[11]

Intramolecular Nucleophilic Cyclization. From F-*Benzoyl Compounds*: (*F*-Benzo)heterocyclic compounds were prepared by the base-catalyzed cyclization of the precursory *F*-benzoyl compounds (**2**, **3**, and **4**).

F-Benzohydroxamic acid (**2**) was refluxed with alkali in an aqueous solvent. The reaction proceeded to give 1,2-(*F*-benz)isoxazol-3(2*H*)-one (**13a**), *F*-aniline, and *F*-benzoic acid. The ^{1}H-NMR spectrum of the (*F*-benz)isoxazoline (**13**) indicated that it was a mixture of tautomers, (**13a**) and (**13b**). The ^{1}H-NMR signal in acetone-d_6 showed a broad peak centered at δ=6.2 at 35 °C, while at −58 °C the peak is separated into two peaks centered at δ=5.5 and 8.5, which correspond to the hydrogens of hydroxyl group in **13b** and amino group in **13a**. *F*-Aniline was the product which resulted from Lossen rearrangement[12]

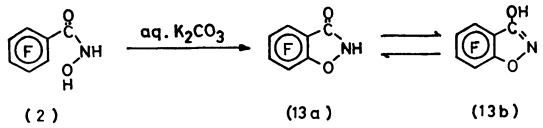

Scheme 4.

of *F*-benzohydroxamic acid (**2**), and *F*-benzoic acid could be generated by hydrolysis of the same compound (**2**). In order to prevent the hydrolysis, *F*-benzohydroxamic acid (**2**) was treated with base in anhydrous solvents such as DMF, DMSO, and pyridine. The reactions, however, were unsuccessful, resulting in a trace amount of the heterocyclic compound (**13**).

The reaction of *N*-(*p*-tolyl)-*N*-hydroxy-*F*-benzamide (**3**) showed somewhat peculiar behavior in basic media. In anhydrous pyridine, 2-(*p*-tolyl)-1,2-(*F*-benz)isoxazol-3(2*H*)-one (**14**) was isolated together with *N*-(*p*-tolyl)-*F*-benzamide (**15**) as a major product. When treated with base in an aqueous solvent of DMF, the sole product was the benzamide (**15**). The formation of the benzamide (**15**) suggested that the *N*-hydroxy-*F*-benzamide (**3**) favored the cleavage of N–O bond rather than the intramolecular cyclization in basic media. This N–O bond cleavage was presumably related with the electron-withdrawing effect of *F*-phenyl group. No further details of the mechanism were examined.

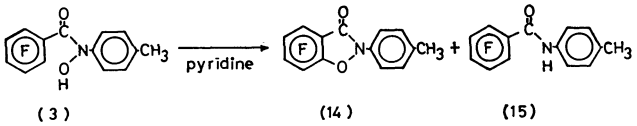

Scheme 5.

The *F*-benzoylurea (**4**) was intramolecularly cyclized to give 1,3-dimethyl-7-dimethylamino(*F*-benzo)pyrimidine-2,4(1*H*,3*H*)dione (**16**) in the presence of sodium hydride in anhydrous DMF. ^{19}F-NMR spectrum of the product shows three signals of equal intensity; their splitting patterns indicate that the product is of a 1,2,4-trisubstituted *F*-benzene structure. The assignment of the fluorine atom at 8-position of the product (**16**) is due to its multiplet peak, owing to the coupling between the adjacent *N*-methyl hydrogens and other fluorines.[13] The long-range coupling (J=9 Hz) of *N*-methyl hydrogens with the fluorine at the 8-position was also observed in the ^{1}H-NMR spectrum of the product (**16**). Such long-range coupling over five bonds between fluorine and hydrogen

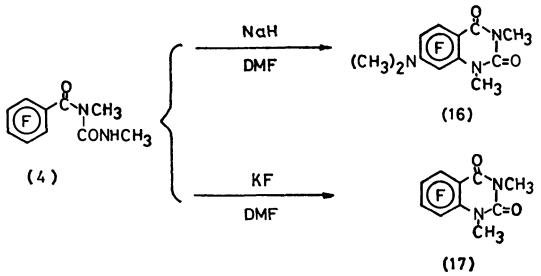

Scheme 6.

has been encountered sometimes in methylaminosubstituted *F*-benzenes.[14] On the other hand, the assignment of the fluorine atom at 5-position in the (*F*-benzo)pyrimidinedione (**16**) is based on its simple double-doublet peak due to the coupling with two unequivalent fluorines. The position of dimethylamino group is, therefore, assigned to 7-position of the product.

On the other hand, the *F*-benzoylurea (**4**) was cyclized into the expected 1,3-dimethyl(*F*-benzo)pyrimidine-2,4(1*H*,3*H*)-dione (**17**), in the presence of potassium fluoride in anhydrous DMF.[15] The ^{19}F-NMR spectrum of the product shows four signals of equal intensity, and their splitting patterns show that the product is of an *ortho*-disubstituted *F*-benzene structure. The long-range coupling (J_{8-H}=9 Hz) between the fluorine at the 8-position and *N*-methyl hydrogens was again observed in both ^{19}F- and ^{1}H-NMR spectra of the heterocyclic compound (**17**).[13]

The dimethylamino group present in the former product (**16**) is considered to come from DMF, where DMF plays the parts of both dimethylaminating agent and solvent in the nucleophilic cyclization reaction at the presence of sodium hydride.

From F-*Phenoxy Compounds*: The reaction of 2-(*F*-phenoxy)acetohydrazide (**11**) with potassium fluoride in DMF gave 1,4-(*F*-benz)oxazin-3(2*H*)-one (**18**), though in a poor yield. A great majority of the product was *F*-phenol, which resulted from the C–O bond cleavage during the reaction. The heterocyclic compound (**18**) was identical with that previously derived from *F*-aniline,[3] and would be formed by cyclization accompanied with the simultaneous cleavage of N–N bond of the terminal hydrazide functions. Under some other basic conditions, such as pyridine and potassium carbonate in DMF, no definite products were obtained except *F*-phenol.

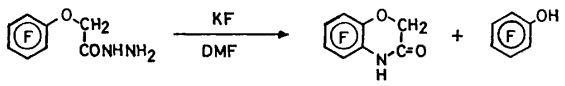

(11) (18)

Scheme 7.

We tried to cyclize the acetohydroxamic acid (**12**) by heating under reflux with potassium carbonate in DMF. The reaction proceeded to give (2-hydroxy-*F*-phenoxy)acetic acid (**21**), while the expected intermediary heterocyclic compound (**19**) could not be isolated. The ^{19}F-NMR spectrum of the product shows four signals of equal intensity; their splitting patterns indicate that the product is of an *ortho*-disubstituted *F*-benzene structure. The assignment of the fluorine atom at the 6-position in the product (**21**) is based upon its multiplet peak, due to the coupling with the adjacent *O*-methylene hydrogens and three other ring-fluorines. The assignment of the fluorine at the 3-position is based upon its doubled double-doublet peak, due to the coupling with three ring-fluorines.

We tried to cyclize the acetic acid (**10**) by refluxing it in the presence of potassium fluoride in DMF.[16,17] The reaction also proceeded to give (2-hydroxy-*F*-phenoxy)acetic acid (**21**); again the expected intermediary heterocyclic compound (**20**) could not be isolated.

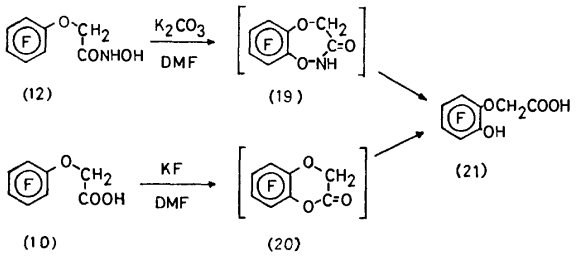

(12) (19) (21) (10) (20)

Scheme 8.

The reactions of the two different precursors, (**10**) and (**12**), resulted in the direct formation of the identical *ortho*-disubstituted *F*-benzene (**21**) under basic conditions.

Experimental

Melting points are uncorrected. The spectral data are those obtained on the following instruments and apparatus unless otherwise noted: IR spectra: JASCO DS-403G, A-1, and A-102. UV spectra: Hitachi 124 and 220. ^{1}H-NMR spectra: Varian A-60 and Hitachi R-24B against the internal TMS reference. ^{19}F-NMR spectra: JEOL PS-100 as the positive value downfield from the internal F-benzene reference. Mass spectra: JEOL JMS-07 and 01SG.

N-*Benzyloxy*-F-*benzamide (1)*. *F*-Benzoyl chloride (2.70 g, 12 mmol) was added dropwise to a stirred mixture of *O*-benzylhydroxylamine (31 mmol),[18] anhydrous pyridine (1.96 g, 25 mmol), and absolute ether (50 ml) over a 30-min period. The mixture was refluxed for an additional 1.5 h, cooled, and filtered. The filtrate was washed successively, with water, diluted hydrochloric acid, and water, and dried over magnesium sulfate. The residue obtained after evaporation *in vacuo* was recrystallized from benzene, to give *N*-benzyloxy-*F*-benzamide (**1**) (3.18 g, 85%) in colorless plates, mp 140.0—141.0 °C. IR(KBr): 3120 (NH) and 1670 cm^{-1} (C=O). ^{1}H-NMR (acetone-d_6) δ=5.50 (s, 2H, CH_2), 7.4 (s, 5H, arom.), and 10.7—11.1 (br. s, 1H, NH). Found: C, 52.95; H, 2.52; N, 4.32%. Calcd for $C_{14}H_8NF_5O_2$: C, 53.01; H, 2.54; N, 4.42%.

F-*Benzohydroxamic Acid (2)*. The *N*-(benzyloxy)amide (**1**) (1.73 g, 5.4 mmol) dissolved in methanol (50 ml) was hydrogenated in the presence of 5% palladium on charcoal (0.30 g) under atmospheric pressure at room temperature. The catalyst was filtered out, and the filtrate was evaporated to dryness *in vacuo*. Recrystallization from benzene gave *F*-benzohydroxamic acid (**2**) (1.00 g, 80%) in colorless needles, mp 140.0—141.0 °C. IR(KBr): 3230 (NH, OH) and 1650 cm^{-1} (C=O). ^{1}H-NMR (acetone-d_6) δ=7.35 (s, 1H, OH) and 9.4—10.1 (br. s, 1H, NH). Found: C, 37.04; H, 1.00; N, 6.60%. Calcd for $C_2H_2NF_5O_2$: C, 37.02; H, 0.89; N, 6.17%. The hydroxamic test using iron(III) chloride solution was positive.

N-(p-*Tolyl*)-N-*hydroxy*-F-*benzamide (3)*. *F*-Benzoyl chloride (3.30 g, 14 mmol) was added dropwise to a stirred mixture of ethereal *N*-(*p*-tolyl)hydroxylamine (2.10 g, 17 mmol in 80 ml of ether) and aqueous sodium hydrogencarbonate (2.60 g, 31 mmol in 15 ml of water) over a 1-h period at 0 °C. The mixture was stirred at 0 °C for an additional 2 h, and poured into ether. The ethereal solution was washed with water, dried over sodium sulfate, and evaporated to dryness *in vacuo*. The residue was recrystallized from aqueous methanol to give *N*-(*p*-tolyl)-*N*-hydroxy-*F*-

benzamide (**3**) (3.80 g, 84%) in colorless needles, mp 178—179 °C. IR(KBr): 3200 (OH) and 1650 cm^{-1} (C=O). Found: C, 53.05; H, 2.67; N, 4.40%. Calcd for $C_{14}H_8NF_5O_2$; C, 53.01; H, 2.54; N, 4.42%. The hydroxamic test using iron(III) chloride solution was positive.

Reaction of F-*Benzoyl Chloride with Urea.* *F*-Benzoyl chloride (1.00 g, 4.3 mmol) was added dropwise to a stirred mixture of urea (0.25 g, 4.2 mmol), anhydrous DMF (7 ml), and anhydrous pyridine (2 ml) over a 30-min period at room temperature and under a dry nitrogen atmosphere. The mixture was refluxed for an additional 30 min, cooled, and poured into ether. The ethereal solution was washed with water, dried over sodium sulfate, and evaporated to dryness *in vacuo*. The residue was recrystallized from aqueous methanol to give a white solid (315 mg). MS of the white solid; Found: *m/e*, 448. Calcd for $C_{15}H_2N_2F_{10}O_3$; 448. The solid was chromatographed on a silica-gel column. The fraction eluted with hexane–chloroform was sublimed to give di(*F*-benzoyl)amine (**8**) (27 mg, 3%) in colorless needles, mp 157—158 °C. IR(KBr): 3280, 3200 (NH), and 1750 cm^{-1} (C=O). Found: C, 41.54; H, 0.35; N, 3.56%; M^+, 405. Calcd for $C_{14}HNF_{10}O_2$: C, 41.50; H, 0.25; N, 3.46%; M, 405.

N,N′-*Dimethyl*-N-*(F-benzoyl)urea (4).* *F*-Benzoyl chloride (4.25 g, 18 mmol) was added dropwise to a stirred mixture of *N,N′*-dimethylurea (2.20 g, 25 mmol) and anhydrous pyridine (15 ml) over a 20-min period at room temperature. The mixture was refluxed for an additional 6 h, cooled, and poured into ether. The ethereal solution was washed with water, dried over sodium sulfate, and evaporated *in vacuo*. The residue was chromatographed on a silica-gel column. The fraction eluted with hexane–chloroform and that with chloroform–dichloromethane gave *N,N′*-dimethyl-*N*-(*F*-benzoyl)urea (**4**) (2.30 g, 44%). Recrystallization from cyclohexane afforded colorless needles, mp 62—63 °C. IR(KBr): 1720 cm^{-1} (C=O). ^{1}H-NMR ($CDCl_3$) δ=2.85 (d, J=4 Hz, 3H, NCH_3), 3.15 (s, 3H, CH_3), and 8.15—8.75 (br. s, 1H, NH). Found: C, 42.56; H, 2.50; N, 9.84%; M^+, 282. Calcd for $C_{10}H_7N_2F_5O_2$: C, 42.57; H, 2.50; N, 9.93%; M, 282.

2-(F-Phenoxy)acetohydrazide (11). A solution of ethyl (*F*-phenoxy)acetate (**9**) (8.10 g, 30 mmol) in ethanol (5 ml) was added dropwise to a stirred solution of 100% hydrazine hydrate (4.50 g, 90 mmol) in ethanol (5 ml) over a 10-min period at 0 °C. The mixture was stirred at 0 °C for an additional 20 min, and poured into saturated aqueous sodium chloride. The resulting solid was filtered, washed with water, and air-dried. Sublimation gave 2-(*F*-phenoxy)-acetohydrazide (**11**) (7.20 g, 94%) in colorless needles, mp 67—69 °C. IR(KBr): 3330 cm^{-1} (NH). Found: C, 37.52; H, 1.98; N, 10.94%. Calcd for $C_8H_5N_2F_5O_2$: C, 37.71; H, 2.14; N, 10.85%.

2-(F-Phenoxy)acetohydroxamic Acid (12). A solution of potassium hydroxide (2.40 g, 43 mmol) in methanol (7.5 ml) was added to a stirred solution of hydroxylamine hydrochloride (2.40 g, 35 mmol) in methanol (13.5 ml) at room temperature. Ethyl (*F*-phenoxy)acetate (**9**) (3.50 g, 13 mmol) was added to the stirred mixture, and then the mixture was filtered immediately. The filtrate was left standing overnight at room temperature, poured into water, and acidified with diluted hydrochloric acid. Barium chloride (3.50 g, 15 mmol) was dissolved in the acidified solution, and then the solution was basified with aqueous ammonia. The resulting precipitates were collected by filtration, washed with water, and air-dried. The solid (3.5 g) was warmed to dissolve in 10% aqueous acetic acid (20 ml) for a few minutes, and cooled to room temperature. The resulting precipitates were collected by filtration, washed with water, and air-dried. Recrystallization from petroleum ether–ethyl acetate gave 2-(*F*-phenoxy)acetohydroxamic acid (**12**) (2.10 g, 59%) in colorless plates, mp 106—108 °C. IR (KBr): 3220 (OH, NH) and 1650 cm^{-1} (C=O). Found: C, 37.37; H, 1.57; N, 5.45%. Calcd for $C_8H_4NF_5O_3$: C, 37.31; H, 1.62; N, 5.48%. The hydroxamic test using iron(III) chloride solution was positive.

1,2-(F-Benz)isoxazol-3(2H)-one (13a). A mixture of *F*-benzohydroxamic acid (**2**) (1.00 g, 4.4 mmol), potassium carbonate (1.00 g, 1.2 mmol), and water (20 ml) was refluxed for 10 h with stirring and cooled. *F*-Aniline (90 mg, 11%) deposited on the inside of a condencer, and was identified by comparison with an authentic specimen.[3] The reaction mixture was neutralized, and extracted with ether. The ethereal extract was dried over magnesium sulfate, and evaporated *in vacuo*. The residual solid was chromatographed on a silica-gel column by elution with benzene. An earlier fraction gave the starting material (**2**) (75 mg, 7.5%). A later fraction gave 1,2-(*F*-benz)isoxazol-3-(2*H*)-one (**13a**) (55 mg, 6%). Recrystallization from benzene afforded colorless prisms, mp 171.0—172.0 °C. IR (KBr): 3400 (OH), 3000 (NH), and 1665 cm^{-1} (C=N). ^{1}H-NMR (acetone-d_6) δ at 35 °C=6.2 (br. s); δ at −58 °C=5.5 (br. s) and 8.5 (br. s). Found; C, 40.44; H, 0.70; N, 6.25%; M^+, 207. Calcd for $C_7NHF_4O_2$; C, 40.60; H, 0.49; N, 6.77%; M, 207.

The neutral aqueous layer was acidified and then extracted with ether repeatedly. The combined extracts were treated in a similar manner to that described above. Upon elution chromatography with ethyl acetate–chloroform on a silica-gel column, an earlier fraction gave the heterocyclic compound (**13**) (85 mg, 9%). A later fraction gave *F*-benzoic acid (50 mg, 5%), which was identified by comparison with an authentic specimen.[20]

2-(p-Tolyl)-1,2-(F-benz)isoxazol-3(2H)-one (14). A solution of *N*-(*p*-tolyl)-*N*-hydroxy-*F*-benzamide (**3**) (427 mg, 1.3 mmol) in anhydrous pyridine (15 ml) was refluxed for 10 h with stirring, cooled, and poured into ether. The ethereal solution was washed with water and dried over sodium sulfate. Evaporation *in vacuo* gave a residual oil, which was chromatographed on a silica-gel column.

The fraction eluted with hexane gave 2-(*p*-tolyl)-1,2-(*F*-benz)isoxazol-3(2*H*)-one (**14**) (35 mg, 9%). Sublimation afforded colorless needles, mp 116.0—117.0 °C. IR (KBr): 1780 cm^{-1} (C=O). Found: C, 56.42; H, 2.35; N, 4.62; F, 25.50%; M^+, 297. Calcd for $C_{14}H_7NF_4O_2$: C, 56.58; H, 2.37; N, 4.71; F, 25.59%; M, 297.

The fraction eluted with hexane–chloroform and that with chloroform gave *N*-(*p*-tolyl)-*F*-benzamide (**15**) (80 mg, 20%). Recrystallization from cyclohexane–ethanol afforded colorless needles, mp 198.5—199.5 °C. IR (KBr); 3240 (NH) and 1670 cm^{-1} (C=O). Found: C, 55.89; H, 2.83; N, 4.59%. Calcd for $C_{14}H_8NOF_5$: C, 55.82; H, 2.68; N, 4.65%.

1,3-Dimethyl-7-dimethylamino(F-benzo)pyrimidine-2,4(1H,3H)-dione (16). A solution of *N,N′*-dimethyl-*N*-(*F*-benzoyl)urea (**4**) (595 mg, 2.1 mmol) in anhydrous DMF (10 ml) was added dropwise to a stirred suspension of sodium hydride (3.3 mmol) and anhydrous DMF (10 ml) over a 15-min period at room temperature. The mixture was refluxed for an additional 5 h, cooled, and poured into ether. The ethereal solution was washed with water, dried over sodium sulfate, and evaporated to dryness *in vacuo*. The residue was chromatographed on a silica-gel column. The fraction eluted with chloroform gave 1,3-dimethyl-7-dimethylamino(*F*-benzo)pyrimidine-2,4(1*H*,3*H*)-dione (**16**) (0.40 g,

66%). Recrystallization from benzene afforded colorless needles, mp 186—187.5 °C. IR (KBr): 1700 cm^{-1} (C=O). ^{1}H-NMR ($CDCl_3$) δ=3.05 (m, 6H, CH_3), 3.35 (s, 3H, CH_3) and 3.67 (d, J=9 Hz, 3H, CH_3). ^{19}F-NMR ($CHCl_3$) δ=9.5 (d.sep, 1F, F^6), 19.9 (dd, 1F, F^5), and 24.3 (m, 1F, F^8), (J_{5-8}=11.5, J_{5-6}=20.0, J_{H-6}=3.0 Hz). Found: C, 50.19; H, 4.23; N, 14.65; F, 19.6%; M^+, 287. Calcd for $C_{12}H_{12}N_3O_2F_3$: C, 50.18; H, 4.21; N, 14.63; F, 19.8%; M, 287.

1,3-Dimethyl(F-benzo)pyrimidine-2,4(1H,3H)-dione (17). A solution of *N,N'*-dimethyl-*N*-(*F*-benzoyl)urea (**4**) (2.44 g, 8.7 mmol) in anhydrous DMF (20 ml) was added dropwise to a stirred mixture of potassium fluoride (1.00 g, 18 mmol) and anhydrous DMF (30 ml) over a 30-min period at room temperature. The mixture was refluxed for an additional 7 h, cooled, and poured into ether. The ethereal solution was worked up in a similar manner to that described above. The chromatographic fraction eluted with hexane–chloroform gave 1,3-dimethyl(*F*-benzo)pyrimidine-2,4(1*H*,3*H*)-dione (**17**) (1.12 g, 49%). Recrystallization from cyclohexane afforded colorless needles, mp 102—104 °C. IR (KBr): 1720 cm^{-1} (C=O). ^{1}H-NMR ($CDCl_3$) δ=3.35 (s, 3H, CH_3) and 3.73 (d, J=9 Hz, 3H, CH_3). ^{19}F-NMR ($CHCl_3$) δ=0.05 (dd, 1F, F^6), 12.8 (ddq, 1F, F^8), 17.3 (ddd, 1F, F^7), and 24.2 (ddd, 1F, F^5), (J_{5-6}=J_{6-7}=23.0, J_{7-8}=21.0, J_{5-8}=13.0, J_{5-7}=11.5, J_{6-8}=1.0, and J_{8-H}=9 Hz). UV (EtOH); λ_{max} (log ε); 218 (4.49) and 313 nm (3.45). Found: C, 45.93; H, 2.34; N, 10.53; F, 29.1%; M^+, 262. Calcd for $C_{10}H_6N_2F_4O_2$: C, 45.82; H, 2.31; N, 10.69; F, 29.0%; M, 262.

Reaction of 2-(F-Phenoxy)acetohydrazide (11) with Potassium Fluoride in DMF. A mixture of 2-(*F*-phenoxy)acetohydrazide (**11**) (1.04 g, 4.0 mmol), potassium fluoride (0.57 g, 9.8 mmol), and anhydrous DMF (15 ml) was refluxed for 13.5 h with stirring and then, after being cooled, was poured into ether. The ethereal solution was washed with water, dried over sodium sulfate, and evaporated *in vacuo*. The residue was chromatographed on a silica-gel column. The fraction eluted with chloroform contained *F*-phenol, which was identified by spectral comparisons with an authentic specimen.[7] The residual solid from the fraction eluted with chloroform, was sublimed to give 1,4-(*F*-benz)-oxazin-3(2*H*)-one (**18**) (13 mg, 1.5%) in colorless needles, mp 190—191.5 °C measured in a sealed tube. The product was identified by comparison with an authentic specimen.[3] Found: M^+, 221.012. Calcd for $C_8H_3NF_4O_2$: M, 221.016.

Reaction of 2-(F-Phenoxy)acetohydroxamic Acid (12) with Base. A mixture of 2-(*F*-phenoxy)acetohydroxamic acid (**12**) (1.00 g, 3.9 mmol), potassium carbonate (0.60 g, 4.3 mmol), and anhydrous DMF (20 ml) was refluxed for 10 h, cooled, and poured into ether. The ethereal solution was washed with 3% hydrochloric acid and water, successively, and dried over magnesium sulfate. The residue from evaporation was sublimed to give (2-hydroxy-*F*-phenoxy)acetic acid (**21**) (95 mg, 11%). Recrystallization from cyclohexane–chloroform afforded colorless needles, mp 114—116 °C. IR (KBr): 3520 and 3460 (phenolic OH), and 1720 cm^{-1} (C=O). ^{19}F-NMR[21] (MeOH) δ=−2.2 (dm, 1F, F^6), 3.1 (ddd, 1F, F^3), 4.8 (ddd, 1F, F^4), and 11.8 (ddd, 1F, F^5), (J_{3-4}=J_{4-5}=J_{5-6}=22.5, J_{4-6}=3.0, J_{3-6}=5.5, and J_{3-5}=6.5 Hz). The phenol test using iron(III) chloride solution was positive.

Reaction of (F-Phenoxy)acetic Acid (10) with Potassium Fluoride. A mixture of (*F*-phenoxy)acetic acid (**10**)[22] (1.02 g, 4.2 mmol), potassium fluoride (0.57 g, 9.7 mmol), and anhydrous DMF (15 ml) was refluxed for 13.5 h with stirring, cooled, and poured into ether. The ethereal solution was washed with water, dried over sodium sulfate, and evaporated *in vacuo*. The residue was chromatographed on a silica-gel column. The fraction eluted with dichloromethane gave a solid product. Recrystallization from benzene followed by sublimation afforded (2-hydroxy-*F*-phenoxy)acetic acid (**21**) (56 mg, 6%) in colorless needles, mp 113—114 °C. The product was identified by comparison with an authentic specimen obatained by the above reaction.

We wish to express our sincere thanks to Professor Keihei Ueno of Kyushu University for his continuous encouragement throughout this study.

We also wish to thank Messrs. Akira Kito and Atsushi Iyoda of the Government Industrial Research Institute at Osaka for their measurements of the ^{19}F-NMR spectra. Financial support from the Ministry of Education, Science and Culture under a Grant-in-Aid for Developmental Scientific Research (2) (Project No. 585221) is gratefully acknowledged.

References

1) According to the revised nomenclature of highly fluorinated organic compounds by J. A. Young, *J. Chem. Document.*, **14**, 98 (1974); *J. Fluorine. Chem.*, **6**, 571 (1975).

2) Preceding Part II: Y. Inukai, T. Sonoda, and H. Kobayashi, *Bull. Chem. Soc. Jpn.*, **52**, 2657 (1979).

3) Y. Inukai, Y. Oono, T. Sonoda, and H. Kobayashi, *Bull. Chem. Soc. Jpn.*, **52**, 516 (1979).

4) The synthesis of *F*-benzohydroxamic acid from ethyl *F*-benzoate has been reported by A. Ostaszynski and H. Plenkiewicz, 6th International Symposium on Fluorine Chemistry, Durham, England (1971), Abstr. A-28; they gave no details of the experimental conditions.

5) W. B. Renfrow, Jr., and C. R. Hauser, *J. Am. Chem. Soc.*, **59** 2308 (1937).

6) Y. K. Agrawal and S. G. Tandan, *J. Indian Chem. Soc.*, **48**, 397 (1971).

7) J. M. Birchall and R. N. Haszeldine, *J. Chem. Soc.*, **1959**, 13.

8) R. B. Wagner and H. D. Zook, "Synthetic Organic Chemistry," John Wiley and Sons, New York (1953), p. 519.

9) E. J. Forbes, R. D. Richardson, M. Stacey, and J. C. Tatlow, *J. Chem. Soc.*, **1959**, 2019.

10) V. M. Vlasov and G. G. Yakobson, *Russ. Chem. Rev.*, **43**, 781 (1974).

11) G. M. Brooke and B. S. Furniss, *J. Chem. Soc.*, **1967**, 869.

12) H. L. Yale, *Chem. Rev.*, **33**, 242 (1943).

13) Two possible schemes of long-range coupling are conceivable between the *N*-methyl hydrogens and the ring-fluorine: one is the coupling with the fluorine atom at the 5-position and the other that at the 8-position. The magnitude of the observed J_{H-F} value, however, indicates the former scheme to be more likely.[14] Assignment of ^{19}F-NMR signals in the text is, therefore, tentative.

14) J. Burdon, *Tetrahedron*, **21**, 1101 (1965); J. G. Allen, J. Burdon, and J. C. Tatlow, *J. Chem. Soc.*, **1965**, 6329; J. Burdon, N. B. Hollyhead, and J. C. Tatlow, *ibid.*, **1965**, 6336.

15) For examples, R. Oda, *Kagaku*, **32**, 179 (1977); **33**, 75 (1978); **34**, 75 (1979); J. H. Clark and J. M. Miller, *J. Am. Chem. Soc.*, **99**, 498 (1977).

16) T. D. Petrova, V. P. Mamaev, G. G. Yakobson, and N. N. Vorozhtsov, Jr., *Khim. Geterotsikl. Soedin.*, **1968**, 771; *Chem. Abstr.*, **71**, 13104c (1969); V. P. Molosnova, V. A. Barkhash, and N. N. Vorozhtsov, *J. Gen. Chem., USSR,*

39, 1937 (1969); E. V. Aroskar, P. J. N. Brown, R. G. Plevey, and R. Stephens, *J. Chem. Soc.*, **1968**, 1569.

17) J. H. Clark, J. Emsley, and O. P. A. Heyte, *J. Chem. Soc., Perkin Trans. 1*, **1977**, 1091; J. H. Clark and J. M. Miller, *Tetrahedron Lett.*, **1977**, 599.

18) Benzyloxyamine was prepared by the neutralization of benzyloxyamine hydrochloride synthesized by A. Janny, *Chem. Ber.*, **16**, 170 (1883).

19) E. Bamberger, *Chem. Ber.*, **34**, 61 (1901).

20) J. M. Birchall and R. N. Haszeldine, *J. Chem. Soc.*, **1961**, 3719.

21) The chemical shifts were measured against the internal *F*-acetic acid reference. The values are given here after being converted against an *F*-benzene reference; the difference between the former reference and the latter one is taken to be 84.4 ppm.

22) (*F*-Phenoxy)acetic acid (**10**) was prepared from ethyl (*F*-phenoxy)acetate.[11]

  Bull. Chem. Soc. Jpn., 54, 3453—3455 (1981)

Photoreaction of *N,N'*-Dibromo-2,5-piperazinedione

Akira SERA,* Kuniaki ITOH, Hiroshi YAMADA, and Ryuichi AOKI

Department of Chemistry, Faculty of Science, Kobe University, Nada-ku, Kobe 657

(Received January 21, 1981)

The photolysis of *N,N'*-dibromo-2,5-piperazinedione in dichloromethane gave an unstable photoproduct. The alcoholysis of the photoproduct in the presence of a small amount of hydrogen bromide yielded 3,6-diethoxy-2,5-piperazinedione and its alcoholyzed products, ethyl diethoxyacetate, ethyl 2-(diethoxyacetylamino)-2-ethoxyacetate, *N*-(1-ethoxy-1-ethoxycarbonylmethyl)oxamide, and ethyl *N*-(diethoxyacetyl)glycinate. The reactions of the photoproduct with other nucleophiles also gave the corresponding substituted 2,5-piperazinediones. The structure of the primary photoproduct was deduced to be 3,6-dibromo-2,5-piperazinedione on the basis of these observations.

In recent years, attention has been focused on the chemical reactivity and selectivity of the succinimido radical produced from *N*-bromosuccinimide(NBS).[1-3] The preferential attack of the succinimido radical to a carbon-carbon double bond has been reported to proceed in competition with hydrogen abstraction reactions.[2,3] The presence of two states of the imido radical, a ground state π-radical and an exited state σ-radical was suggested to explain the reaction patterns observed under homogeneous conditions.

In the course of our investigation on the reactivity of *N,N'*-dibromo-2,5-piperazinedione (**1**, NBP), we reported a photo-induced alkoxybromination of some olefins with NBP in the presence of alcohols.[4] Because the structure of NBP is similar to that of NBS, photoreactions of NBP with olefins proceeded easily to give the corresponding addition products in aprotic media. A solvent incorporated product was also produced. However, no rearranged product was detected, such as was often found in the photoreactions of NBS. Thus, detailed examination of the photochemical behavior of NBP is desirable. This paper concerns the photoreaction of NBP in dichloromethane.

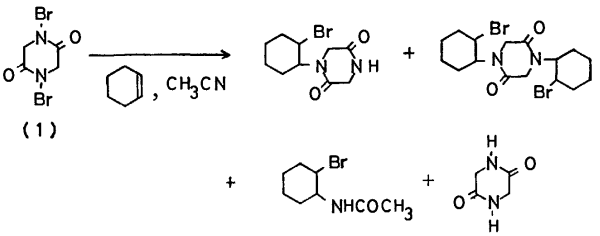

Results and Discussion

Photolysis of NBP in dichloromethane was carried out in a Pyrex apparatus. The concentration of NBP was usually around 0.4 mol dm^{-3}. Because of the low solubility of NBP in dichloromethane (and in most of organic solvents), the irradiation was carried out under heterogeneous conditions with agitation. In a few hours the reaction mixture turned red. After 8 h, the photolysate was filtered to give a pale yellow solid (**2**) which was found not to be NBP. The solid **2** was so unstable that we could not recrystallize it satisfactorily. However, the bromine analysis of a specimen of **2** (not completely pure)[5] revealed the presence of two bromine atoms in the molecule. The methine proton signal was observed at δ=5.0. A photo-enolization of the amide group of NBP and a subsequent 1,3-bromine shift might result in the unstable **2**.

Accordingly, immediately after filtration and quick rinsing with dichloromethane, **2** was allowed to react with ethanol to give 3,6-diethoxy-2,5-piperazinedione (**3a**, 3%), ethyl diethoxyacetate (**4**, 4%), ethyl 2-(diethoxyacetylamino)-2-ethoxyacetate (**5**, 25%), ethyl *N*-(diethoxyacetyl)glycinate (**6**, 16%), *N*-(1-ethoxy-1-ethoxycarbonylmethyl)oxamide (**7**, 2%), and ammonium bromide, respectively.

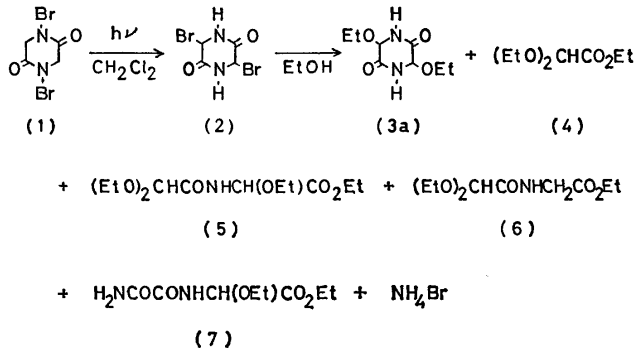

The structures of the above products were all determined taking into account their elemental analyses, and IR, NMR, and mass spectra. Compound **3a** had an infrared absorption pattern in its finger print region similar to that of 2,5-piperazinedione, except for the presence of C–O stretching bands in the former. The NMR spectrum of **3a** showed a distinct ring proton signal at δ=4.5 (dd, J=4 and 1 Hz), an NH proton signal (δ=8.9, d, J=4 Hz), and ethoxy proton signals. Elemental analysis and the MS fragment pattern[6] also confirmed the structure of **3a**. Compound **3a** was considered to be a primary alcoholysis product of **2** as described latter. The spectra of **4** were found to be identical with those of authentic ethyl diethoxyacetate prepared by the recorded method.[7] Compound **5** showed IR absorptions at 3400(ν_{NH}), 1760, 1710($\nu_{C=O}$)cm^{-1}, and its NMR spectra revealed the presence of two methine protons (δ=4.7, s and 5.3, d, J=9 Hz), one NH proton (δ=7.3, d, J=9 Hz), and four ethoxyl groups. Compound **6** also showed C=O (1760, 1690 cm^{-1}) and NH (3350 cm^{-1}) absorptions, and CH_2 (δ=3.9, d, J=6 Hz), CH (δ=4.7, s), NH (δ=7.0, t, J=6 Hz), and three ethoxyl proton signals. Both NMR spectra [δ=1.1 (CH_3), 3.5 (CH_2 of ethoxyl group), 4.1 (CH_2 of ethoxycarbonyl group),

5.2 (CH), 7.8 and 8.0 (NH_2), and 9.1 (NH)] and IR absorptions [3380 and 3270 (NH) and 1760 and 1680 (C=O) cm^{-1}] supported the structure of **7** to be that depicted above. The amide protons of **7** resonated at $\delta=7.8$ and 8.0 (DMSO-d_6) at ambient temperature. These two signals began to coalesce at around 100 °C, indicating the presence of restricted rotation around a formal single bond.[8]

Because the structure of **5** is composed of two glyoxalic acid units, **4** was thought to be produced from **5** in the course of the treatment of ethanol. Actually the ethanolysis of **5** in the presence of hydrochloric acid gave **4**. The same treatment of **6** also yielded **4** and ethyl glycinate hydrochloride. In addition, the treatment of **3a** with ethanol containing hydrogen bromide gave **4** and **5**. Thus **3a** was a key intermediate of the successive reactions of **2** giving **4** and **5**, where hydrogen bromide liberated from **2** played a catalytic role in the ethanolysis. The alcoholysis reactivity of **3a** seemed rather high, but one can anticipate that an addition of a hydrogen bromide scavenger can increase the yield of **3**. The yield of 3,6-dialkoxy derivative was found as follows. Reactions were carried out using methanol instead of ethanol: a 5% yield of 3,6-dimethoxy-2,5-piperazinedione (**3b**) was obtained by an irradiation of NBP in dichloromethane and a subsequent treatment of the remaining solid with methanol; 48% was obtained by the same irradiation followed by a treatment with methanol–pyridine. As expected, **2** reacted with other nucleophiles; water, acetic acid, and an azide ion.

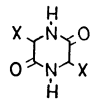

3b; X=OMe
3c; X=OH
3d; X=OAc
3e; $X=N_3$

The whole reaction scheme will be represented as follows: the photoisomerization of NBP gave the intermediate **2**, which on ethanolysis yielded **3a**. A nucleophilic attack of ethanol to the carbonyl group of **3a** and a subsequent ring opening followed by transacetalization gave **5**, which in turn yielded **4** by ethanolysis. A part of NBP was converted to *N*-bromo-2,5-piperazinedione by the protodebromination with hydrogen bromide.[9] A similar photoisomerization-ethanolysis of this *N*-bromo compound could give 3-ethoxy-2,5-piperazinedione and the corresponding ring opening product (**6**). The formation mechanism of **7** is not determined at present.

One of characteristic features of the photoreaction of NBP is the absence of the photo ring opening reaction, which has been often encountered in reactions of NBS giving 3-bromopropionyl isocyanate in a variety of conditions.[1,10] Massive evidence exists that the succinimido radical isomerizes to $\cdot CH_2CH_2CONCO$ by a photochemical α-cleavage-like reaction, and the latter radical abstracts a bromine atom of NBS to give 3-bromopropionyl isocyanate. However, in the case of NBP, this was not the case. This characteristic may arise from the structural feature of NBP, which is characterized as a bromide of cyclic diamide. Investigations are in progress to elucidate the dissimilarity of NBP to NBS in reactivity.

Experimental

Melting points were determined on a Yanagimoto hot stage and were uncorrected. NMR spectra were determined on a JEOL PMX-60 spectrometer using TMS as the internal standard. IR spectra were recorded on a JASCO IRA-1 spectrometer. Mass spectra were recorded on Hitachi RMU-6MG and JEOL JMS-01SG-2 spectrometers. All irradiations were carried out using Ushio UM 453B(450 w) and Halos EHB-WU(100 w) high pressure mercury arc lamps. Dichloromethane was washed with sulfuric acid to remove the contained ethanol, washed thoroughly with water, dried and distilled. *N,N'*-Dibromo-2,5-piperazinedione was prepared as described in the literature.[4]

Photoreaction of NBP. A suspension of NBP (**1**, 10 g) in 100 cm^3 of dichloromethane in a Pyrex vessel was irradiated by a high pressure Hg arc lamp for 8 h with stirring at ambient temperature. The mixture was filtered to give a pale yellow solid (**2**). In the filtrate, nothing was found but bromine. The solid **2** was quite unstable.[5] The color of **2** turned red, and meanwhile **2** decomposed spontaneously to a clear viscous liquid. Accordingly **2** was rinsed quickly with dichloromethane and was added into ethanol. The mixture was stirred overnight at room temperature, and was filtered to give white crystals. Recrystallization from ethanol gave 240 mg (3.3% based on NBP) of 3,6-diethoxy-2,5-piperazinedione (**3a**), mp 217 °C (dec). IR: 3230, 1680 cm^{-1}; NMR (DMSO-d_6): $\delta=1.1$ (6H, t, $J=7$ Hz), 3.5 (4H, q, $J=7$ Hz), 4.5 (2H, dd, $J=4$ and 1.2 Hz), 8.9 (2H, broad d, $J=4$ Hz); MS (*m/e*)[6]: 174 (M^+), 131, 115, 72, 60. Found: C, 47.83; H, 6.98; N, 13.97%. Calcd for $C_8H_{14}N_2O_4$: C, 47.52; H, 6.93; N, 13.86%.

The ethanolic filtrate was evaporated up to a syrup (11.5 g) which was separated on siliga-gel column to afford products in the following order. Yields are given on the basis of NBP employed.

Elution with benzene–ether (9:1) gave 530 mg (4.2%) of ethyl diethoxyacetate (**4**), a colorless liquid. IR: 1760 cm^{-1}; NMR (CCl_4): $\delta=1.1$ (9H, m), 3.5 (4H, q, $J=7$ Hz), 4.0 (2H, q, $J=7$ Hz), 4.6 (1H, s). Found: C, 53.88; H, 9.10%. Calcd for $C_8H_{16}O_4$: C, 54.55; H, 9.11%. The IR and NMR spectra of this compound were found to be identical to those of an authentic sample prepared by a recorded method.[7]

Further elution gave 2.48 g (24.8%) of ethyl 2-(diethoxyacetylamino)-2-ethoxyacetate (**5**) as a colorless liquid. IR: 3400, 1760, 1710 cm^{-1}; NMR (CCl_4): $\delta=1.2$ (12H, m), 3.5 (6H, q, $J=7$ Hz), 4.1 (2H, q, $J=7$ Hz), 4.7 (1H, s), 5.3 (1H, d, $J=9$ Hz), 7.3 (1H, broad d, $J=7$ Hz); MS (*m/e*): no M^+, 131, 130. Found: C, 51.25; H, 8.41; N, 4.79%. Calcd for $C_{12}H_{23}NO_6$: C, 51.95; H, 8.31; N, 5.05%.

Next the column was eluted with benzene–acetone (4:1) to give 128 mg (1.6%) of *N*-(1-ethoxy-1-ethoxycarbonylmethyl)oxamide (**7**) as white crystals, mp 163—165 °C. IR: 3380, 3270, 1760, 1690 cm^{-1}; NMR (DMSO-d_6): $\delta=1.1$ (6H, m), 3.5 (2H, q, $J=7$ Hz), 4.1 (2H, q, $J=7$ Hz), 5.2 (1H, d, $J=8$ Hz), 7.8 and 8.0 (2H, rotation restricted NH_2), 9.1 (1H, broad d, $J=8$ Hz); MS (*m/e*): 218 (M^+), 173, 145, 116. Found: C, 44.06; H, 6.60; N, 12.80%. Calcd for $C_8H_{14}N_2O_5$: C, 44.04; H, 6.42; N, 12.84%.

Elution with benzene–ethanol (9:1) afforded 1.11 g (13%) of ethyl *N*-(diethoxyacetyl)glycinate (**6**) as a yellow liquid.

IR: 3350, 1760, 1690 cm^{-1}; NMR (CCl_4): δ=1.2 (9H, m), 3.6 (4H, q, J=7 Hz), 3.9 (2H, d, J=6 Hz), 4.1 (2H, q, J=7 Hz), 4.7 (1H, s), 7.0 (1H, broad t, J=6 Hz); MS (*m/e*): no M^+, 174, 131, 130. Found: C, 51.38; H, 8.11; N, 5.77%. Calcd for $C_{10}H_{19}NO_5$: C, 51.50; H, 8.15; N, 6.01%.

Elution was continued using benzene–ethanol (4:1) and a compound was isolated. The structure of this compound has not been determined yet. Final elution with ethanol afforded ammonium bromide (2.3 g, 28%).

*Ethanolysis of 3,6-Diethoxy-2,5-piperazinedione (**3a**).* Compound **3a** (1 g) was refluxed in a 0.5 mol dm^{-3} ethanolic hydrogen bromide solution for 1.5 h. After the usual work-up and column chromatography, 270 mg (31%) of **4** and 230 mg (42%) of **5** were obtained.

*Ethanolysis of Ethyl 2-(Diethoxyacetylamino)-2-ethoxyacetate (**5**).* Compound **5** (1 g) was refluxed in an ethanol solution containing 0.5 mol dm^{-3} hydrochloric acid for 3 h. After the usual work-up and column chromatography, 570 mg (39%) of **4** and unchanged **5** (280 mg, 28%) were obtained.

*Ethanolysis of Ethyl N-(Diethoxyacetyl)glycinate (**6**).* A similar treatment of **6** (450 mg) gave **4** (138 mg, 38%), unchanged **6** (240 mg, 53%), and ethyl glycinate hydrochloride (100 mg, 35%): mp 133—135 °C; IR: 3400, 1750 cm^{-1}; NMR (DMSO-d_6): δ=1.1 (3H, t, J=7 Hz), 3.7 (2H, s), 4.1 (2H, q, J=7 Hz), 8.4 (2H, s).

*Reaction of the Primary Photoproduct (**2**) with Other Nucleophiles.* The reaction of **2** with methanol (or methanol–pyridine) for 6 h at room temperature gave 3,6-dimethoxy-2,5-piperazinedione (**3b**) in 5% (or 48%) yield; mp 226 °C (dec); IR: 3250, 3180, 1680 cm^{-1}; NMR (DMSO-d_6): δ=3.3 (6H, s), 4.5 (2H, dd, J=4 and 1.2 Hz), 8.9 (2H, broad d, J=4 Hz); Found: C, 41.38; H, 6.02; N, 16.30%. Calcd for $C_6H_{10}N_2O_4$: C, 41.38; H, 5.75; N, 16.09%.

Similar treatment of **2** with aqueous acetone, acetic acid–triethylamine, and sodium azide yielded 3,6-dihydroxy-, 3,6-diacetoxy-, and 3,6-diazido-2,5-piperazinediones, respectively. 3,6-Dihydroxy-2,5-piperazinedione (**3c**); 22% yield; mp 260 °C (dec); IR: 3380, 3200, 1690 cm^{-1}; NMR (DMSO-d_6): δ=4.6—4.8 (2H, dd, J=4 and 1.2 Hz and d, J=2 Hz), 5.9 (2H, broad s), 8.3 (1H, broad s), 8.4 (1H, broad d, J=4 Hz); Found: C, 32.73; H, 4.29; N, 19.19%. Calcd for $C_4H_6N_2O_4$: C, 32.88, H, 4.11; N, 19.18%. 3,6-Diacetoxy-2,5-piperazinedione (**3d**); 44% yield; mp 185 °C (dec); IR: 3200, 3120, 1760, 1720 cm^{-1}; NMR (DMSO-d_6): δ=2.1 (6H, s), 5.8 (2H, dd, J=5 and 1.2 Hz), 9.3 (2H, broad d, J=5 Hz), Found: C, 41.77; H, 4.63; N, 11.99%. Calcd for $C_8H_{10}N_2O_4$: C, 41.74; H, 4.35; N, 12.17%. 3,6-Diazido-2,5-piperazinedione (**3e**); 32% yield; mp 168 °C; IR: 3250, 2150, 1700 cm^{-1}; NMR (DMSO-d_6): δ=5.2—5.4 (2H, dd, J=4 and 1.2 Hz, and d, J=2 Hz), 9.1 (2H, broad s); Found: C, 24.57; H, 2.25; N, 57.08%. Calcd for $C_4H_4N_8O_2$: C, 24.49; H, 2.04; N, 57.14%.

References

1) P. S. Skell and J. C. Day, *Acc. Chem. Res.*, **11**, 381 (1978).
2) P. S. Skell and J. C. Day, *J. Am. Chem. Soc.*, **100**, 1951 (1978).
3) F-L. Lu, Y. M. A. Naguib, M. Kitadani, and Y. L. Chow, *Can. J. Chem.*, **57**, 1967 (1979).
4) A. Sera, H. Yamada, and K. Itoh, *Bull. Chem. Soc. Jpn.*, **53**, 219 (1980).
5) The bromine analysis of **2** (70% purity determined by NMR) showed the presence of two bromine atoms in one molecule of **2** (Found, Br, 50.3%; Calcd, Br, 49.5%). NMR (DMSO-d_6); δ=5.0 (2H, broad s), 8.8 (2H, broad s).
6) For MS analysis, 3,6-dimethoxy-2,5-piperazinedione (**3b**) was employed.
7) *Org. Synth.*, Coll. Vol. IV, 427 (1963).
8) J. A. Pople, W. G. Sneider, and H. J. Bernstein, "High Resolution Nuclear Magnetic Resonance," McGraw-Hill, New York (1959), p. 365.
9) J. S. Pizey, "Synthetic Reagents," (1974), Vol. II, p. 1.
10) J. C. Martin and P. D. Bartlett, *J. Am. Chem. Soc.*, **79**, 2533 (1957).

Electrochemical Conjugate Additions of the Allyl Groups in Substituted Allyl Halides to α,β-Unsaturated Esters

Shohei SATOH, Hiroshi SUGINOME, and Masao TOKUDA*

Department of Chemical Process Engineering, Faculty of Engineering, Hokkaido University, Sapporo 060

(Received January 30, 1981)

Electrolysis of allyl halides and diethyl fumarate (**2**) in *N,N*-dimethylformamide containing 0.2 M† tetraethylammonium tosylate gave a conjugate addition product, ethyl 3-(ethoxycarbonyl)-5-hexenoate, in a moderate yield. The electrochemical reaction of 1-chloro-3-methyl-2-butene (**4**) with **2**, that of allyl chloride **4** with methyl crotonate (**6**), and that of methyl 4-halo-2-butenoate with **2** likewise gave the corresponding conjugate addition products, ethyl 3-(ethoxycarbonyl)-6-methyl-5-heptenoate, methyl 3,4,4-trimethyl-5-hexenoate, and ethyl 3-(ethoxycarbonyl)-4-(methoxycarbonyl)-5-hexenoate, respectively. The addition reaction of **4** to **2** takes place at the α-carbon terminus of **4** exclusively, whereas the addition of **4** to **6** at the γ-carbon terminus of **4**. These regioselectivities of the additions and pathways of the reactions are discussed.

The electrochemical reduction of organic halides has been extensively studied, but most of these studies have been concerned with the elucidation of the mechanism of the cleavage of the carbon-halogen bond.[1] These studies have shown that the electrochemical reduction of carbon-halogen bonds generally gives radical or carbanion intermediates[2] which result in the formation of dimers or hydrocarbons.[1]

Although these species generated by ordinary chemical reaction are widely used in a variety of organic syntheses, only a limited number of investigations have been reported on the application of these species generated by the electrochemical reduction of organic halides to the formation of the carbon-carbon bond. These electrochemical investigations include ones on the cyclization of α,ω-dihalides,[3] cyclization of acetylenic halides,[4] alkylation of substrates containing an acidic hydrogen by alkyl halides,[5] acylation of benzyl halides,[6] and addition of alkyl halides to carbon-carbon[7] or to carbon-nitrogen double bonds.[8] The electrochemical addition of allyl bromide to acrylonitrile, ethyl acrylate, or diethyl maleate has also been reported to give a conjugate addition products.[7a]

In this paper we report a conjugate addition of the allyl group in allyl halides to α,β-unsaturated esters by the electrochemical reduction. The electrochemical conjugate additions of the allyl groups in substituted allyl halides to α,β-unsaturated esters were found to take place in a regioselective manner at either their α- or γ-carbon terminus.

Results and Discussion

The electrolysis of allyl chloride (**1a**), allyl bromide (**1b**), or allyl iodide (**1c**) together with diethyl fumarate (**2**) in *N,N*-dimethylformamide (DMF) containing 0.2 M tetraethylammonium tosylate as a supporting electrolyte gave a conjugate addition product, ethyl 3-(ethoxycarbonyl)-5-hexenoate (**3**), in the yields shown in Table 1. Electrolyses were carried out at a constant current in a normal undivided cell with two platinum plate electrodes. Electrolysis of **1b** in the presence of tenfold excess of **2** gave **3** in a 70% yield, although electrolysis of **1a** or **1c** under the same conditions gave a lower yield of **3**.

Table 1. Results of electrochemical additions of allyl groups in allyl halides (**1a**, **1b**, and **1c**) to diethyl fumarate (**2**)[a]

	1 (mmol)	2 (mmol)	F/mol	Conv./% of 1	Yield/%[b] of 3
1a	1.7	15	2	—	15
1b	1.5	1.5	4	100	36
	1.5	3	2	68	58
	1.5	3	4	75	61
	1.5	15	2	85	70
1c	1.5	15	2	90	39

a) Conducted at 5 mA/cm² in DMF containing 0.2 M Et_4NOTs. b) Yields are based on **1** consumed.

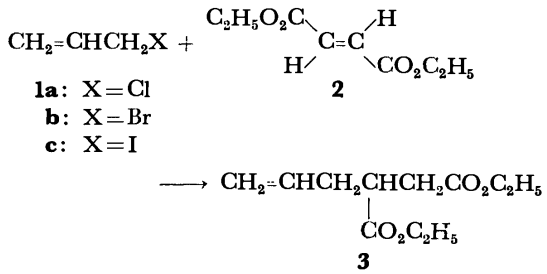

Scheme 1.

When substituted allyl halides are used in this electrolysis, the formation of a mixture of two isomers arising from the combination of the allyl halides at their α- and γ-carbon termini to α,β-unsaturated ester might be expected. The electrochemical reaction of a substituted allyl chloride, 1-chloro-3-methyl-2-butene (**4**), with a two-fold excess of diethyl fumarate (**2**) at 0 °C, however, gave exclusively ethyl 3-(ethoxycarbonyl)-6-methyl-5-heptenoate (**5**) in a 15% yield, in which a less heavily substituted carbon terminus of the allyl group was attached to the α,β-unsaturated ester. The electrolysis was conducted in DMF containing 0.2 M tetraethylammonium tosylate at a constant current of 25 mA/cm². Electricity passed was 2 Faraday per mole of **4**. On the other hand, the electrochemical reaction of **4** with methyl crotonate (**6**) gave methyl 3,4,4-trimethyl-5-hexenoate (**7**) as a single product, in which a more heavily substituted

† 1 M=1 mol dm⁻³.

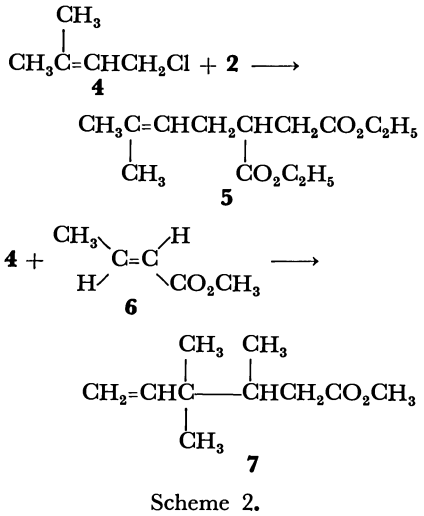

Scheme 2.

Table 2. Results of electrochemical additions of methyl 4-halo-2-butenoate (**8**) to diethyl fumarate (**2**)[a]

	8 (mmol)	**2** (mmol)	Curr. dens. mA cm^{-2}	F/mol	Yield/%[b] of **9**
8a	1.5	15	5[c]	2	16
	1.5	15	5	2	39
	1.5	15	5	4	18
	1.5	15	25	2	14
	1.5	5	5	2	20
	1.5	15	5[d]	2	27
	1.5	15	5[d]	4	31
8b	1.5	15	5	2	11
	1.5	15	5[d]	2	11

a) Conducted at −40 °C in DMF containing 0.2 M Et_4NOTs using a platinum cathode. b) Yields are based on **8** used. c) Conducted at 0 °C. d) Mercury pool was used as a cathode.

carbon of the allyl group was attached to the α,β-unsaturated ester, in a 22% yield. The structures of **5** and **7** were determined by elemental analyses and spectroscopies. The ^1H NMR spectrum of **7** gave well-resolved signals consistent with the assigned structure by an addition of 40 mol% of tris(dipivaloylmethanato)europium.

Electrolysis of methyl 4-bromo- (**8a**) or methyl 4-iodo-2-butenoate (**8b**) with ten-fold excess of **2** gave ethyl 3-(ethoxycarbonyl)-4-(methoxycarbonyl)-5-hexenoate (**9**) as the major product, in which the allyl group was again combined to the α,β-unsaturated ester with an allylic rearrangement. The structure of **9** was confirmed by the elemental analysis and spectroscopy. Traces of two isomeric products (**10** and **11**) were also obtained in this electrolysis. Table 2 shows the yields of **9** under various conditions. When electrolysis was conducted at −40 °C, **9** was obtained in a higher yield than at 0 °C. This is probably due to the decomposition or the condensation of the anion generated from **8** at room temperature. It is also seen that platinum is better than mercury as a cathode material.

The allyl groups were thus regioselectively com-

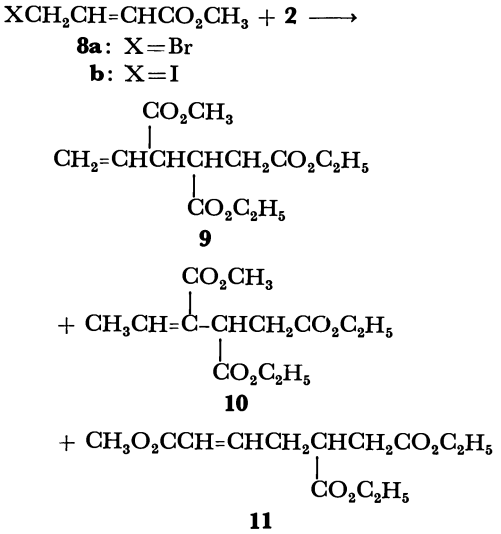

Scheme 3.

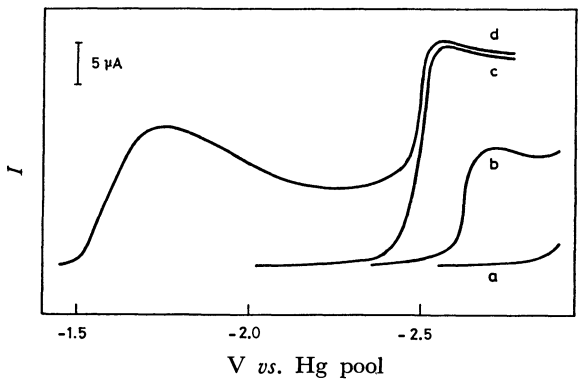

Fig. 1. Linear-sweep voltammograms of **4**, **2**, and **6** with a platinum disc electrode. Sweep rate, 0.023 V s^{-1}.
(a): 0.2 M Et_4NOTs in DMF, (b): 0.018 M **6** in 0.2 M Et_4NOTs–DMF, (c): 0.017 M **4** in 0.2 M Et_4NOTs–DMF, (d): 0.013 M **2** and 0.017 M **4** in 0.2 M Et_4NOTs–DMF.

bined to the two different α,β-unsaturated esters **2** and **6** at different sites. These regioselectivities can be interpreted by assuming the involvement of two different mechanisms. The reaction pathway of each electrochemical addition may be determined by whether a more readily reducible species in the electrolysis is α,β-unsaturated esters or allyl halides. Linear sweep voltammetry showed that allyl halides **4** and **8a** are reduced at about −2.5 and −1.1 V *vs.* Hg, while α,β-unsaturated esters **2** and **6** are reduced at −1.7 and −2.7 V *vs.* Hg, respectively (Fig. 1).

Therefore, in the electrochemical reaction of **4** with **2**, a preferential one-electron reduction of **2** generates an anion radical which reacts with the carbon atom of **4** carrying chlorine in an S_N2 fashion to give an intermediary radical species. A further reduction of the radical followed by a protonation of the resulting carbanion would give the observed addition product **5** [Scheme 4, (1)].

In the reaction of either **4** with **6** or **8** with **2**, however, a two-electron reduction of allyl halides **4** or

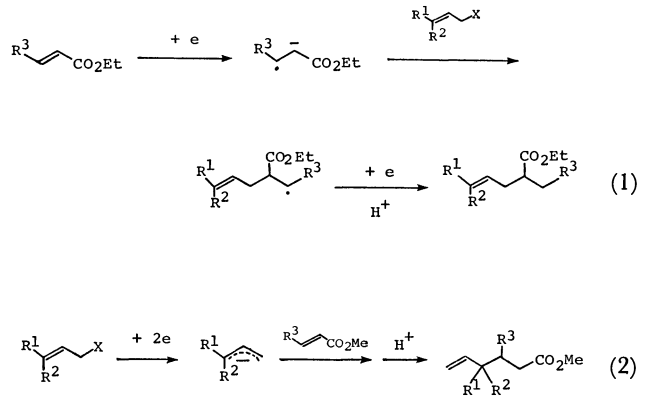

4: $R^1=R^2=CH_3$, X=Cl
8: $R^1=CO_2Me$, $R^2=H$, X=Br, I
2: $R^3=CO_2Et$
6: $R^3=CH_3$

Scheme 4.

8 may take place to generate allylic carbanions which then add to α,β-unsaturated esters to afford the observed addition products **7** or **9** [Scheme 4, (2)].

The aforementioned explanations are further supported by the results of ordinary chemical reactions. Several carbanions such as 2-substituted allyllithium,[9] dienolate anions derived from α,β-unsaturated acids,[10,11] or α-phenylsulfonyl carbanions[12] always undergo nucleophilic substitution on **4** at the less heavily substituted carbon terminus. On the other hand, the addition reactions of allylic carbanions derived from 3,3-dimethylallyl compounds to carbonyl group,[13] acyl halide,[14] acetal,[15] or α,β-unsaturated carbonyl compounds[16] take place at the more heavily substituted carbon terminus of **4** exclusively. Moreover, lithium dienolates derived from α,β-unsaturated esters undergo alkylation reactions at the α carbon of the ester almost exclusively.[10]

The formation of the addition product such as **5** having an allylic unit attached at a less heavily substituted carbon in the present electrochemical reaction is worth noting, since allylic organometallics always gave the addition products having the allyl groups at a more highly substituted carbon terminus.[16]

Experimental

All the products were isolated and purified by distillation and by preparative GLPC with a JEOL JGC-20K instrument. IR spectra were obtained with a Hitachi EPI-22 spectrometer, and NMR spectra in CCl_4 were measured with a Hitachi R-22 high-resolution spectrometer (90 MHz) using TMS as an internal reference. Mass spectra were obtained with a Hitachi RM-50GC mass spectrometer. Quantitative GLPC analyses were carried out with a Hitachi 063 instrument by an internal standard method.

Materials. *N,N*-Dimethylformamide (DMF) was shaken with phosphorus pentaoxide and then stirred overnight with potassium hydroxide. It was distilled under a reduced pressure of nitrogen atmosphere and then distilled over picric acid. The allyl halides used were washed with sodium thiosulfate solution, dried over calcium chloride, and then distilled.

1-Chloro-3-methyl-2-butene (**4**) was prepared from isoprene by the described procedure.[17] Dry hydrogen chloride (183 g) was added to isoprene (344 g) over a period of 2.5 h at −40 °C, and the resulting mixture was refluxed for 1 h. Distillation of the reaction mixture gave **4** (228 g, 43%): bp 107—109 °C; NMR δ 1.74 (3H), 1.78 (3H), 4.02 (2H), 5.44 (1H).

Methyl 4-bromo-2-butenoate (**8a**) was prepared from methyl crotonate by the described procedure.[18] To methyl crotonate (24 g) in carbon tetrachloride (100 ml) was added *N*-bromosuccinimide (25 g) and benzoyl peroxide (0.2 g) and the mixture was refluxed for 7 h. The usual work up and a distillation of the reaction mixture gave **8a**: bp 88—89° C/15 mmHg†† (lit,[18] 83—85 °C/13 mmHg); NMR δ 3.70 (3H, s), 3.98 (2H, m), 5.99 (1H, m), 6.96 (1H, m); MS *m/e* 180 (M^++2), 178 (M^+).

Methyl 4-iodo-2-butenoate (**8b**) was prepared from **8a** and sodium iodide by a literature procedure;[19] bp 108 °C/19 mmHg; MS *m/e* 266 (M^+).

General Procedure of Electrolysis. For most of the preparative electrolysis, a normal undivided cell (2.8 cm dia.) equipped with a magnetic stirrer, a reflux condenser, and a serum cap for introduction of nitrogen gas was used. Electrolysis was carried out under nitrogen atmosphere at a constant current using two platinum plate electrodes (2×2 cm^2). Amounts of the substrates in each electrolysis are shown in Tables 1 and 2. After electrolysis, the reaction mixture was dissolved in diethyl ether and the solution was washed with sodium thiosulfate solution and water, and dried over magnesium sulfate. The usual work up of the solution gave a product mixture which was subjected to distillation and preparative GLPC with a JEOL-20K instrument to give pure products.

Some physical properties of the products are recorded below.

*Ethyl 3-(Ethoxycarbonyl)-5-hexenoate (**3**)*: Bp 101—103 °C/18 mmHg; n_D^{24} 1.4330; IR (neat) 3090, 1735, 1645, and 925 cm^{-1}; NMR δ 1.24 (6H, t, $CO_2CH_2C\underline{H}_3$), 2.5 (5H, m, C-2H, C-3H, and C-4H), 4.10 (2H, q, $CO_2C\underline{H}_2CH_3$), 4.13 (2H, q, $CO_2C\underline{H}_2CH_3$), 5.05 (2H, m, C-6H), and 5.7 (1H, m, C-5H); MS *m/e* (rel intensity) 169 ($M^+-OC_2H_5$, 46), 140 (56), 123 (40), 95 (44), 67 (100), and 41 (42). Found: C, 61.29; H, 8.34%. Calcd for $C_{11}H_{18}O_4$: C, 61.66; H, 8.47%.

*Ethyl 3-(Ethoxycarbonyl)-6-methyl-5-heptenoate (**5**)*: Bp 118—119 °C/19 mmHg; n_D^{24} 1.4422; IR (neat) 3050, 1730, and 855 cm^{-1}; NMR δ 1.24 (6H, t, $CO_2CH_2C\underline{H}_3$), 1.61 (3H, s, $-C\underline{H}_3$), 1.70 (3H, s, $-C\underline{H}_3$), 2.5 (5H, m, C-2H, C-3H, and C-4H), 4.10 (2H, q, $CO_2C\underline{H}_2CH_3$), 4.12 (2H, q, $CO_2C\underline{H}_2CH_3$), and 5.07 (1H, m, C-5H); MS *m/e* (rel intensity) 242 (M^+, 12), 197 ($M^+-OC_2H_5$, 38), 168 (97), and 95 (78). Found: C, 64.13; H, 9.06%. Calcd for $C_{13}H_{22}O_4$: C, 64.44; H, 9.15%.

*Methyl 3,4,4-Trimethyl-5-hexenoate (**7**)*: Bp 117—120 °C/48 mmHg; IR (neat) 3090 and 1745 cm^{-1}; NMR δ 0.88 (3H, d, C-3-$C\underline{H}_3$), 0.97 and 0.99 (each 3H, s, $-C(C\underline{H}_3)_2$), 2.0 (3H, m, $-C\underline{H}C\underline{H}_2CO_2$), 3.62 (3H, s, $CO_2C\underline{H}_3$), 4.9 (2H, m, $C\underline{H}_2$=CH), and 5.80 (1H, m, =C$\underline{H}$); NMR (CCl_4, 40 mol% of Eu(DPM)$_3$ added) δ 1.79 and 1.84 (each 3H, s, $C(C\underline{H}_3)_2$), 3.41 (3H, d, C-3-$C\underline{H}_3$), 5.3—5.7 (2H, m, $C\underline{H}_2$=CH), 6.3—6.7 (1H, m, $-C\underline{H}$), 6.57—6.9 (1H, m, =C$\underline{H}$), 7.02 (1H, dd, J=10 Hz, J=15 Hz, $-C\underline{H}_2CO_2$), 7.54 (1H, dd, J=4 Hz, J=15 Hz, $-C\underline{H}_2CO_2$); MS *m/e* (rel intensity) 170 (M^+, 3), 96 (59), and 69 (100). Found: C, 70.33; H, 10.37%. Calcd for $C_{10}H_{18}O_2$: C, 70.55; H, 10.66%.

*Ethyl 3-(Ethoxycarbonyl)-4-(methoxycarbonyl)-5-hexenoate (**9**)*: Bp 67 °C/1 mmHg; n_D^{21} 1.4492; IR (neat) 3090, 1740,

†† 1 mmHg≈133.322 Pa.

1640, 935, and 860 cm^{-1}; NMR δ 1.26 (6H, t, $CO_2CH_2C\underline{H}_3$), 2.5 (2H, m, C-2H), 3.2 (2H, m, C-3H and C-4H), 3.70 (3H, s, $CO_2C\underline{H}_3$), 4.12 (4H, q, $CO_2C\underline{H}_2CH_3$), 5.2 (2H, m, C-6H), and 5.8 (1H, m, C-5H); MS *m/e* (rel intensity) 241 (M^+-OCH_3, 21), 240 (47), 227 ($M^+-OC_2H_5$, 82), 226 (44), 167 (56), 166 (53), 99 (68), 67 (65), and 29 (100). Found: C, 57.36; H, 7.37%. Calcd for $C_{13}H_{20}O_6$: C, 57.34; H, 7.40%.

*Ethyl 3-(Ethoxycarbonyl)-4-(methoxycarbonyl)-4-hexenoate (**10**)*: NMR δ 1.28 (6H, t, $CO_2CH_2C\underline{H}_3$), 1.97 (3H, d, J=7.5 Hz, C-6-$C\underline{H}_3$), 2.8 (3H, m, C-2H and C-3H), 3.78 (3H, s, $CO_2C\underline{H}_3$), 4.19 (4H, q, two $CO_2C\underline{H}_2CH_3$), and 7.07 (1H, q, J=7.5 Hz, C-5H). MS *m/e* 227 ($M^+-OC_2H_5$).

*Methyl Ethyl 5-(Ethoxycarbonyl)-2-heptene-1,7-dioate (**11**)*: NMR δ 1.24 and 1.26 (each 3H, s, $CO_2CH_2C\underline{H}_3$), 2.7 (5H, m, C-4H, C-5H, and C-6H), 3.71 (3H, s, $CO_2C\underline{H}_3$), 4.13 and 4.17 (each 2H, q, $CO_2C\underline{H}_2CH_3$), 5.85 (1H, d, J=16 Hz, C-2H), and 6.85 (1H, dt, J=16 Hz, J=8 Hz, C-3H). MS *m/e* 227 ($M^+-OC_2H_5$).

Voltammetry. Voltammetry was carried out with a Yanaco V8 potentionstat at a sweep rate of 0.023 V s^{-1} using a platinum disc electrode (1 mm dia.) in DMF containing 0.2 M Et_4NOTs. A potential was measured in V *vs.* Hg pool.

References

1) A. J. Fry, "Synthetic Organic Electrochemistry," Harper and Row Publishers, New York (1972), p. 170; M. R. Rifi, "Organic Electrochemistry," ed by M. M. Baizer, Marcel Dekker, Inc., New York (1973), p. 279; M. R. Rifi, F. H. Covitz, "Introduction to Organic Electrochemistry," Marcel Dekker, Inc., New York (1974), p. 194; M. R. Rifi, "Technique of Electroorganic Synthesis," ed by N. L. Weinberg, John Wiley and Sons, Inc., New York (1975), Part II, p. 170.

2) A. J. Bard and A. Merz., *J. Am. Chem. Soc.*, **101**, 2959 (1979).

3) M. R. Rifi, *J. Am. Chem. Soc.*, **89**, 4442 (1967); M. R. Rifi, *Collect. Czech. Chem. Commun.*, **36**, 932 (1971); R. Gerdil, *Helv. Chim. Acta*, **53**, 2100 (1970); A. J. Fry and W. E. Britton, *J. Org. Chem.*, **38**, 4016 (1973); S. Satoh, M. Itoh, and M. Tokuda, *J. Chem. Soc., Chem. Commun.*, **1978**, 481; S. Satoh, M. Itoh, H. Suginome, and M. Tokuda, *Bull. Fac. Eng. Hokkaido Univ.*, **102**, 33 (1981).

4) W. M. Moore, A. Salajegheh, and D. G. Peters, *J. Am. Chem. Soc.*, **97**, 4954 (1975).

5) M. Tokuda, T. Taguchi, O. Nishio, and M. Itoh, *J. Chem. Soc., Chem. Commun.*, **1976**, 606; M. Tokuda and O. Nishio, *ibid.*, **1980**, 188.

6) T. Shono, I. Nishiguchi, and H. Ohmizu, *Chem. Lett.*, **1977**, 1021.

7) M. M. Baizer and J. L. Chruma, *J. Org. Chem.*, **37**, 195 (1972); S. Satoh, T. Taguchi, M. Itoh, and M. Tokuda, *Bull. Chem. Soc. Jpn.*, **52**, 951 (1979).

8) T. Iwasaki and K. Harada, *J. Chem. Soc., Perkin Trans. 1*, **1977**, 1730.

9) G. Cardillo, M. Contento, and S. Sandri, *Tetrahedron Lett.*, **1974**, 2215.

10) J. A. Katzenellenbogen and A. L. Crumrine, *J. Am. Chem. Soc.*, **98**, 4925 (1976).

11) B. S. Pitzele, J. S. Baran, and D. H. Steinman, *J. Org. Chem.*, **40**, 269 (1975).

12) M. Julia and D. Arnold, *Bull. Soc. Chim. Fr.*, **1973**, 743.

13) V. Rautenstrauch, *Helv. Chim. Acta*, **57**, 496 (1974).

14) J. P. Pillot, J. Dunogues, and R. Calas, *Tetrahedron Lett.*, **1976**, 1871.

15) A. Hosomi, M. Endo, and H. Sakurai, *Chem. Lett.*, **1976** 941.

16) A. Hosomi and H. Sakurai, *J. Am. Chem. Soc.*, **99**, 1673 (1977).

17) W. J. Jones and H. W. T. Chorley, *J. Chem. Soc.*, **1946**, 832.

18) K. Ziegler, A. Späth, E. Schaaf, W. Shumann, and E. Winkelmann, *Ann.*, 80 (1942).

19) R. Fuson, R. Arnold, and H. Cooke, Jr., *J. Am. Chem. Soc.*, **60**, 2272 (1938).

The Rhodium Complex-catalyzed Synthesis of Quinolines from Aminoarenes and Aliphatic Aldehydes

Yoshihisa WATANABE,* Sang Chul SHIM,** and Take-aki MITSUDO
Department of Hydrocarbon Chemistry, Kyoto University, Sakyo-ku, Kyoto 606
(Received February 25, 1981)

A variety of aminoarenes react with aliphatic aldehydes in the presence of a catalytic amount of a rhodium complex and an excess amount of the corresponding nitroarenes at 180 °C to give 2-alkyl- and 2,3-dialkyl-substituted quinolines in excellent yields. Among the rhodium complexes examined, $[Rh(norbornadiene)Cl]_2$ exhibits the highest activity as a catalyst. Thus, 2-methyl-, 2-ethyl-3-methyl-, 2-propyl-3-ethyl-, and 2-butyl-3-propylquinoline derivatives are readily obtained from aminoarenes and ethanal, propanal, butanal, and pentanal respectively.

The Skraup and related syntheses are well known as methods for the preparation of quinolines from aminoarenes and carbonyl compounds.[1] These methods, however, have some disadvatages; the uncontrolled violence of the reaction and the use of a large amount of acid. Quinolines can be prepared from aminoarenes and olefins using transition-metal complexes as catalyst precursors.[2,3] Rhodium trichloride catalyzes the reaction between aniline and ethylene to give 2-methylquinoline in poor yields.[2] Octacarbonyldicobalt catalyzes the reaction between *N*-benzylideneaniline and ethyl vinyl ether in tetrahydrofuran under nitrogen to give 2-phenylquinoline in moderate yields.[3] More recently, we found that rhodium complexes such as μ,μ'-dichlorobis(norbornadiene)dirhodium(I) are active as catalysts for *N*-heterocyclization, the preparation of quinolines from aminoarenes and aliphatic aldehydes in a non-acidic medium.[4] This is a novel method for the preparation of 2-alkyl- and 2,3-dialkyl-substituted quinolines, applicable in a large-scale reaction. Here, a detailed study on the rhodium-catalyzed synthesis of quinolines will be described.

Results and Discussion

Aniline reacts with aliphatic aldehydes having two α-hydrogens in the presence of a catalytic amount of μ,μ'-dichlorobis(norbornadiene)dirhodium(I) and an excess amount of nitrobenzene as an oxidizing agent at 180 °C to give alkyl-substituted quinolines in moderate to excellent yields. The results are summarized in Table 1. This provides a convenient method for the synthesis of quinolines.

The combination of aniline with ethanal, propanal, butanal, and pentanal gives 2-methyl-, 2-ethyl-3-methyl-, 2-propyl-3-ethyl-, and 2-butyl-3-propylquinoline, respectively. 2-Methylquinoline was identified by comparing its IR and ^{1}H NMR spectra with those of the authentic sample. None of the ^{1}H NMR spectra (60 MHz in $CDCl_3$, with Me_4Si as the internal standard) of these products exhibited the peak at δ 8.8 ppm characteristic of the 2-H of the quinoline nucleus.[5] The ^{1}H NMR (60 MHz) spectrum of the product from aniline–propanal showed a typical pattern of the methyl and ethyl groups, while the ^{13}C NMR (25.05 MHz) spectrum showed three peaks, at 12.5(CH_3), 18.7(CH_3), and 29.1(CH_2) ppm, in the aliphatic carbon region, assignable to the 2-ethyl(12.5 and 29.1 ppm) and 3-methyl(18.7 ppm) groups. Accordingly, this is concluded to be 2-ethyl-3-methylquinoline.

Alkyl groups of 2,3-disubstituted quinolines produced from butanal and pentanal can be readily identified by means of the ^{1}H NMR (60 and 220 MHz) and ^{13}C NMR spectra. The products from aniline–butanal and –pentanal were assigned to 2-propyl(14.4, 22.5, and 37.5 ppm)-3-ethyl(14.4 and 25.0 ppm)quinoline and 2-butyl(14.0, 23.0, 31.7, and 35.4 ppm)-3-propyl-(14.0, 23.5, and 34.3 ppm)quinoline respectively.

The mass spectra of these products exhibited the corresponding molecular ions, and the elemental analysis gave satisfactory results.

The reaction of ethanal gave a considerable amount of a tarry material which appears to reduce the yield of 2-methylquinoline. An attempt of reduce the for-

Table 1. Rhodium-catalyzed synthesis of substituted quinolines from aniline and aldehydes

Exptl No.	Aldehyde	Product	Yield/%[a]
1	Ethanal	2-Methylquinoline	51 (30)[b]
2	Ethanal	2-Methylquinoline	14[c]
3	Ethanal	2-Methylquinoline	42[d]
4	Ethanal	2-Methylquinoline	40
5	Ethanal	2-Methylquinoline	23[e]
6	Ethanal	2-Methylquinoline	17[f]
7	2-Butenal	2-Methylquinoline	Trace
8	Paraldehyde $(CH_3CHO)_3$	No reaction	—
9	Metaldehyde $(CH_3CHO)_4$	No reaction	—
10	Propanal	2-Ethyl-3-methylquinoline	75 (59)
11	Butanal	2-Propyl-3-ethylquinoline	119 (82)
12	Pentanal	2-Butyl-3-propylquinoline	(45)

Under argon at 180 °C for 4 h. Molar ratio: Aniline (41 mmol)/aldehyde/nitrobenzene = 1.0/2.5/1.5. Rhodium complex: 0.03 mmol$[Rh(NBD)Cl]_2$. Solvent: Ethanol or benzene(20 ml).
a) Determined by GLC. Based on the amount of aniline used. The figures in parentheses show isolated yields. b) Benzene used as solvent. c) At 150 °C. d) Without solvent. e) Acetic acid(4.1 mmol) was added. f) Acetic acid (8.2 mmol) was added.

**Present address: Department of Industrial Chemistry, Kyung-park National University, Taegu, Korea.

mation of this tarry material was unsuccessful. The reaction at a low temperature (150 °C) or without a solvent gave 2-methylquinoline in poor yields. 2-Butenal gave only a trace of 2-methylquinoline, but a large amount of the tarry material. Paraldehyde [$(CH_3CHO)_3$] and metaldehyde [$(CH_3CHO)_4$] showed no reactivity for this reaction under the conditions used.

On the other hand, propanal, butanal, and pentanal give the corresponding 2,3-disubstituted quinolines in fairly good yields without the formation of any tarry material. The reaction between aniline and butanal was examined in some detail in order to determine the optimum conditions for the preparation of the quinoline; the results are summarized in Table 2. *N*-Butylaniline was formed as a by-product in 5—31% yields. The presence of excess amount of nitrobenzene reduced the formation of *N*-butylaniline. A hydrogen transfer should take place for the formation of the quinoline nucleus.

$$PhNH_2 + 2CH_3CH_2CH_2CHO \xrightarrow[PhNO_2]{[Rh]}$$

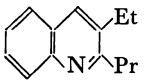

$$+ 2H_2O + 2H$$

The nitrobenzene appears to act as an oxidizing agent and to be partially reduced to aniline through the reaction. *N*-Butylaniline appears to be derived *via* *N*-butylideneaniline by hydrogenation. The reaction without nitrobenzene also gave a mixture of *N*-butylaniline and the quinoline, but in poor yields. When the aniline/butanal/nitrobenzene molar ratio is fixed at 1.0/2.2/0.33, the catalytic activity is highest with μ,μ'-dichlorobis(norbornadiene)dirhodium(I), followed by chlorotris(triphenylphosphine)rhodium(I) and hydridocarbonyltris(triphenylphosphine)rhodium(I).

The catalytic activity also depends on the amounts of the rhodium complex used. With μ,μ'-dichlorobis-(norbornadiene)dirhodium(I), the quinoline yield is highest (119%) when the rhodium catalyst of 0.03 mmol (20 mg) is used. The turn-over of the catalyst is calculated to amount to 1600, based on the yield (119%), and the product selectivity is estimated to be more than 95%, based on the butanal used. Higher (200 °C) or lower (160 °C) temperatures gave poorer yields of the quinoline.

Accordingly, the optimum conditions for the preparation of the quinoline are those of Exp. 3 in Table 2. This procedure is applicable for a variety of aniline derivatives combined with ethanal, propanal, and butanal. The reaction between aminoarenes and aldehydes was carried out in the presence of the corresponding nitroarenes as the oxidizing agent. The aminoarene/aldehyde/nitroarene molar ratio was fixed at 1.0/2.5/1.5 in the reaction. The results for *o*- and *p*-substituted anilines including methyl, methoxy, and chloro groups as substituents are summarized in Table 3.

p-Methyl-, *p*-methoxy-, and *p*-chloroaniline- reacted smoothly with ethanal, propanal, and butanal to give

Table 2. The rhodium-catalyzed synthesis of 2-propyl-3-ethylquinoline from aniline and butanal[a]

	Catalyst[b]	Molar ratio[c]	Product yield[d]/%	
			2-Propyl-3-ethyl-quinoline	*N*-Butyl-aniline
1	A	1.0/2.2/0.33	96	31
2	A	1.0/2.2/1.0	99	20
3	A	1.0/2.5/1.5	119	5
4	B	1.0/2.2/0.33	61	10
5	C	1.0/2.2/0.33	41	7
6	A	1.0/2.5/1.5	85[e]	
7	A	1.0/2.5/1.5	57[f]	

a) Under argon at 180 °C for 4 h in ethanol(20 ml). b) Rhodium complex, 0.03 mmol. A, $[Rh(NBD)Cl]_2$ (20 mg); B, $RhCl(PPh_3)_3$; C, $RhH(CO)(PPh_3)_3$. c) Molar ratio: Aniline (41 mmol)/butanal/nitrobenzene. d) Determined by GLC. Based on the amount of aniline used. e) $[Rh(NBD)Cl]_2$, 10 mg. f) $[Rh(NBD)Cl]_2$, 5 mg.

Table 3. Synthesis of quinoline derivatives from *o*- and *p*-substituted anilines and aldehydes[a]

Exptl No.	Aniline	Aldehyde	Product	Yield[b] %
13	*p*-MeO	Butanal	2-Propyl-3-ethyl-6-methoxyquinoline	65
14	*p*-MeO	Propanal	2-Ethyl-3-methyl-6-methoxyquinoline	70
15	*p*-MeO	Ethanal	6-Methoxy-2-methyl-quinoline	34
16	*p*-Me	Butanal	2-Propyl-3-ethyl-6-methylquinoline	60
17	*p*-Me	Propanal	2-Ethyl-3,6-dimethylquinoine	64
18	*p*-Me	Ethanal	2,6-Dimethylquino-line	30
19	*p*-Cl	Butanal	2-Propyl-3-ethyl-6-chloroquinoline	41
20	*p*-Cl	Propanal	2-Ethyl-3-methyl-6-chloroquinoline	48
21	*o*-MeO	Butanal	2-Propyl-3-ethyl-8-methoxyquinoline	39
22	*o*-MeO	Propanal	2-Ethyl-3-methyl-8-methoxyquinoline	25
23	*o*-MeO	Ethanal	8-Methoxy-2-methyl-quinoline	10
24	*o*-Me	Butanal	2-Propyl-3-ethyl-8-methylquinoline	59
25	*o*-Me	Propanal	2-Ethyl-3,8-dimethylquinoline	45
26	*o*-Me	Ethanal	2,8-Dimethyl-quinoline	24
27	*o*-Cl	Butanal	2-Propyl-3-ethyl-8-chloquinoline	25
28	*o*-Cl	Propanal	2-Ethyl-3-methyl-8-chloroquinoline	11
29	*o*-Cl	Ethanal	8-Chloro-2-methyl-quinoline	Trace

a) Under argon at 180 °C for 4 h. Solvent, ethanol (20 ml). $[Rh(NBD)Cl]_2$; 0.03 mmol(20 mg). Molar ratio: Aminoarene(41 mmol)/aldehyde/nitroarene = 1.0/2.5/1.5. b) Isolated yield based on the amount of aminoarene used.

2,6- or 2,3,6-substituted quinolines in fairly good yields. The reaction of ethanal has an inclination to give poorer yields because of the formation of the tarry material.

o-Methyl- and *o*-methoxyaniline also showed a moderate reactivity to give 2,3,8-substituted quinolines in good yields when combined with propanal and butanal. *o*-Chloroaniline, however, gave the product in poor yields, indicating that the chloro group located at the ortho position has an inhibitory effect on the reaction. The combination of *o*-chloroaniline with ethanal failed to give 8-chloro-2-methylquinoline almost entirely.

The results for *m*-methyl-, *m*-methoxy-, and *m*-chloroaniline are summarized in Table 4. These aminoarenes reacted with ethanal, propanal, and butanal to give 2,7-di-, 2,3,5-, and 2,3,7-trisusbtituted quinolines in fairly good yields. From *m*-substituted aminoarenes, two isomeric products are expected to be formed.

The products isolated from *m*-methoxyaniline–ethanal, –propanal, and –butanal were proved by GLC to be pure. Their ^{1}H and ^{13}C NMR spectra in the aliphatic region exhibited typical patterns of alkyl groups characteristic of 2-methyl, 2-ethyl-3-methyl, and 2-propyl-3-ethyl groups respectively. The ^{1}H NMR (220 MHz) spectra of the products from propanal and butanal in the aromatic region showed two singlets and two doublets, assignable to the isomeric 7-substituted quinoline, 2,3,7-substituted ones. The spectrum of the ring hydrogens of the 5-isomers, 2,3,5-substituted ones, should have a different pattern; one singlet, two doublets, and one doublet of doublet. Accordingly, the products from propanal and butanal are identified as 2-ethyl-3-methyl-7-methoxyquinoline and 2-propyl-3-ethyl-7-methoxyquinoline respectively. The ^{1}H NMR (220 MHz) spectrum of the product from ethanal exhibited one singlet and four doublets in the aromatic region, asssignable to the 7-isomer.

TABLE 4. SYNTHESIS OF QUINOLINE DERIVATIVES FROM *m*-SUBSTITUTED ANILINES AND ALDEHYDES[a]

Exptl No.	Aniline	Aldehyde	Yield[b] %	Distribution of products[c] 5-Isomer	7-Isomer
30	*m*-MeO	Butanal	44	0	100
31	*m*-MeO	Propanal	45	0	100
32	*m*-MeO	Ethanal	26	0	100
33	*m*-Me	Butanal	68	10	90
34	*m*-Me	Propanal	62	16	84
35	*m*-Me	Ethanal	38	15	85
36	*m*-Cl	Butanal	61	18	82
37	*m*-Cl	Propanal	55	17	83
38	*m*-Cl	Ethanal	20	18	82

a) Under argon at 180 °C for 4 h. Solvent, ethanol (20 ml). Rhodium complex; $[Rh(NBD)Cl]_2$, 0.03 mmol(20 mg). Molar ratio; *m*-Aminoarene(41 mmol)/aldehyde/*m*-nitroarene=1.0/2.5/1.5. b) Isolated yield based on the amount of *m*-aminoarene used. c) Determined by GLC. 5-Isomer, 2, 5- or 2, 3, 5-substituted quinolines; 7-isomer, 2, 7- or 2, 3, 7-substituted quinolines.

The 5-isomer from ethanal should have a different pattern; four doublets and one doublet of doublet. Thus, the product from ethanal is identified as 2-methyl-7-methoxyquinoline.

The reaction of *m*-toluidine and *m*-chloroaniline with ethanal, propanal, and butanal appeared to give mixtures of 5- and 7-isomers respectively. The distribution of the two isomers was determined by GLC analysis. The 7-isomers appear to predominate.

The ^{1}H and ^{13}C NMR spectra of the products from *m*-toluidine–butanal exhibited the typical pattern of the 7-isomer, assigned to 2-propyl-3-methyl-7-methylquinoline. The ^{13}C NMR spectrum clearly showed another pair of peaks with small intensities, assignable to the three alkyl groups (methyl, ethyl, and propyl) in the aliphatic carbon region and the quinoline ring in the aromatic region; nine peaks, five singlets and four doublets by off-resonance decoupling, were observed in the aromatic region. Therefore, the other product is believed to be the 5-isomer, 2-propyl-3-ethyl-5-methylquinoline.

The corresponding 5- and 7-isomers from *m*-toluidine and *m*-chloroaniline, combined with ethanal, propanal or butanal, were similarly analyzed by the spectroscopic method. The fact that the 7-isomers predominate in this procedure is consistent with the finding of the Skraup synthesis, the acid-catalyzed synthesis of quinoline.[6]

The results obtained here clearly demonstrate that the novel *N*-heterocyclization method catalyzed by rhodium complexes in a non-acidic medium is applicable to a veriety of combination of aminoarenes and aldehydes, giving 2-alkyl- and 2,3-dialkyl-substituted quinolines in good to excellent yields.

The Skraup synthesis is generally accepted to follow the following reaction sequence: the self-aldol condensation of aldehyde; the addition of an amine to the condensate, α,β-unsaturated aldehyde; ring closure by dehydration to form 1,2-dihydroquinoline, and the oxidation of the 1,2-dihydroquinoline. Acids such as concentrated sulfuric acid used as catalysts may participate in the ring-closure process of this sequence.

The mechanism of the rhodium-catalyzed synthesis

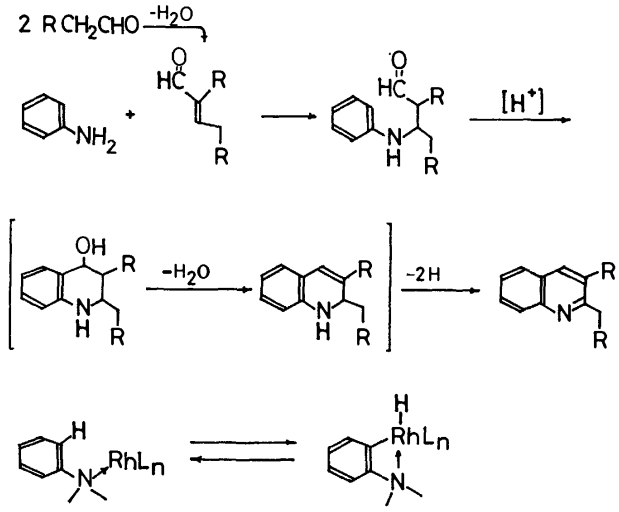

Scheme 1.

of quinolines is not yet clear, but the rhodium catalyst also seems to participate in the ring-closure process. Aminoarene reacts with the rhodium catalyst to form an *N*-coordinated complex in which the ortho hydrogen in a phenyl ring of aminoarene can be activated. The *N*-coordinated complex may be transformed into an ortho metallated complex by the intramolecular oxidative addition of the activated C–H bond, for it is the key intermediate for the ring-closure reaction. This consideration may be supported by the fact that triphenylphosphine complexes of iridium[7] and iron[8] give hydridometal complexes, ortho metallated complexes, by intramolecular oxidative addition and the fact that X-ray structures of triphenylphosphine complexes of ruthenium[9] and rhodium[10] reveal a short separation between metal and ortho hydrogen in a phenyl ring of the ligand. Aldehydes with two α-hydrogen atoms have a great tendency to aldol condensation under the conditions used, 180 °C in the presence of a base, suggesting that the formation of α,β-unsaturated aldehydes is also one of the key steps in the reaction. The nitroarenes used may be supposed to act as oxidizing agents in the final step, the oxidation of 1,2-dihydroquinolines.

Experimental

μ,μ′-Dichlorobis(norbornadiene)dirhodium(I), $[Rh(NBD)Cl]_2$, was prepared according to the method in the literature.[11] The ethanal, propanal, butanal, nitroarenes, aminoarenes, and other compounds employed in this study were all commercial products. The aldehydes, nitroarenes, and aminoarenes were distilled before use. The benzene and ethanol used were dried by the usual methods.

Analytical Procedure. The melting points and boiling points are uncorrected. The melting points were taken on a Yanagimoto capillary melting-point apparatus. The infrared spectra were measured on a Hitachi model 215 grating spectrophotometer. The ^1H NMR spectra were obtained at 60 MHz with a JEOL LNM-60 NMR or at 220 MHz with a Varian model HR-220 NMR spectrometer. The ^{13}C NMR spectra were determined at 25.05 MHz with a JEOL pulsed Fourier Transform spectrometer, model FX-100. Samples were dissolved in $CDCl_3$, and the chemical-shift values were expressed in δ ppm relative to Me_4Si as an internal standard. The mass spectra were recorded on a JMS O1SG mass spectrometer. The elemental analyses were performed at the Microanalytical Center of Kyoto University.

Reaction Procedure. A stainless steel autoclave (100 ml) equipped with a magnetic stirrer was used in the reaction. Ethanol (20 ml) and $[Rh(NBD)Cl]_2$ (20 mg, 0.03 mmol) were put into the autoclave. After the air in the autoclave had been replaced with argon, 88—100 mmol of aldehyde, 41 mmol of aminoarene, and 60 mmol of nitroarene were put into it, and then the remainder of the air was replaced with argon. The autoclave was kept at 180 °C by electrical heating for 4 h, and then the heating was turned off. The GLC analysis of the reaction products was made using a column (0.3 cmϕ × 3 m) packed with 10% Versamid on Neopak 60—80 mesh. After the solvents had been distilled off, the reaction products were subjected to fractional distillation. 2-Methylquinoline and 2-methyl-6-methoxyquinoline were identified by comparing their IR and ^1H NMR spectra with those of authentic samples (Aldrich). The other products were identified by means of the IR, ^1H NMR, ^{13}C NMR and MS spectra and by elemental analysis. Although the products could not be isolated in an analytically pure form in Exps. 13, 24, 32, 34, and 36, the corresponding quinoline derivatives were identified on the basis of their spectral data.

2-Ethyl-3-methylquinoline (Exptl 10): Yield, 59%; Yellow oil, bp 84—85 °C/0.35 Torr; ^1H NMR (60 MHz) ($CDCl_3$): δ (ppm) 1.32 (t, 3H, CH_3), 2.25 (s, 3H, CH_3), 2.86 (q, 2H, CH_2), 7.34—8.09 (m, 5H, Ar). ^{13}C NMR (25.05 MHz) ($CDCl_3$): δ (ppm) 12.5 (q, CH_3), 18.7 (q, CH_3), 29.1 (t, CH_2), 125.3 (d), 126.6 (d), 127.1 (s), 128.0 (d), 128.5 (d), 129.0(s), 135.2(d), 146.6(s), 162.5(s), MS (*m/e*): 171 (rel intensity 87, M^+), 170(100), 143(43), 115(44). Found: C, 84.28; H, 7.92; N, 8.13%. Calcd for $C_{12}H_{13}N$: C, 84.17; H, 7.65; N, 8.18%.

2-Propyl-3-ethylquinoline (Exptl 11): Yield, 82%; Yellow oil, 92 °C/0.3 Torr; ^1H NMR (220 MHz) ($CDCl_3$): δ (ppm) 1.05 (t, 3H, CH_3), 1.25 (t, 3H, CH_3), 1.82 (sex, 2H, CH_2), 2.73 (q, 2H, CH_2), 2.93 (t, 2H, CH_2), 7.36 (t, 1H), 7.57 (t, 1H), 7.66 (d, 1H), 7.77 (s, 1H), 8.07 (d, 1H). ^{13}C NMR ($CDCl_3$): δ (ppm) 14.2 (q, CH_3), 14.4 (q, CH_3), 22.5 (t, CH_2), 25.0 (t, CH_2), 37.5 (t, CH_2), 125.3 (d), 126.8 (d), 127.3 (d), 128.1 (s), 128.5 (s), 128.8 (s), 133.1 (s), 135.1 (s). Found: C, 83.78; H, 8.87; N, 6.86%. Calcd for $C_{14}H_{17}N$: C, 84.37; H, 8.60; N, 7.03%.

2-Butyl-3-propylquinoline (Exptl 12): Yield, 45%; Yellow oil, 115 °C/0.35 Torr; ^1H NMR (220 MHz) ($CDCl_3$): δ (ppm) 0.94 (t, 3H, CH_3), 0.95 (t, 3H, CH_3), 1.46 (sex, 2H, CH_2), 1.77 (qt, 2H, CH_2), 2.64 (t, 2H, CH_2), 2.95 (t, 2H, CH_2), 7.68 (s, 1H), 7.59 (d, 1H), 7.34 (t, 1H), 7.52 (t, 1H), 8.05 (d, 1H). ^{13}C NMR ($CDCl_3$): δ (ppm) 14.0 (q, $2CH_3$), 23.0 (t, CH_2), 23.5 (t, CH_2), 31.7 (t, CH_2), 34.3 (t, CH_2), 35.4 (t, CH_2), 125.5(d), 126.8(d), 127.2(s), 128.3(d, d), 133.7(s), 134.8(d), 146.3(s), 161.9(s). MS (*m/e*): 227 (rel intensity 13, M^+), 212 (23), 198 (27), 185 (69), 170 (85), 157 (100). Found: C, 84.55; H, 9.58; N, 5.99%. Calcd for $C_{16}H_{21}N$: C, 84.53; H, 9.31; N, 6.16%.

2-Propyl-3-ethyl-6-methoxyquinoline (Exptl 13): Yield, 65%; Yellow oil, bp 118 °C/0.3 Torr; ^1H NMR (220 MHz) ($CDCl_3$): δ (ppm) 1.02 (t, 3H, CH_3), 1.27 (t, 3H, CH_3), 1.77 (sex, 2H, CH_2), 2.73 (q, 2H, CH_2), 2.91 (t, 2H, CH_2), 3.66 (s, 3H, $-OCH_3$), 6.98 (s, 1H), 7.03 (d, 1H), 7.73 (s, 1H), 7.95 (d, 1H). ^{13}C NMR ($CDCl_3$): δ (ppm) 14.3 (q, $2CH_3$), 23.0 (t, CH_2), 25.0 (t, CH_2), 37.2 (t, CH_2), 55.4 (q, $-OCH_3$), 104.7(d), 113.9(s), 114.7(d), 121.0(d), 128.2 (s), 129.2(d), 133.3(d), 135.6(s), 157.2(s).

2-Ethyl-3-methyl-6-methoxyquinoline (Exptl 14): Yield, 70%; Yellow oil, bp 98 °C/0.3 Torr; ^1H NMR (60 MHz) ($CDCl_3$): δ(ppm) 1.33 (t, 3H, CH_3), 2.30 (s, 3H, CH_3), 2.87 (q, 2H, CH_2), 3.73 (s, 3H, $-OCH_3$), 6.80—8.00 (m, 4H, Ar). Found: C, 77.02; H, 7.88; N, 7.16%. Calcd for $C_{13}H_{15}NO$: C, 77.58; H, 7.51; N, 6.96%.

6-Methoxy-2-methylquinoline (Exptl 15): Yield, 34%; Yellow oil or yellow crystalline, bp 96 °C/0.4 Torr or mp 63—64 °C; ^1H NMR (60 MHz) ($CDCl_3$): δ(ppm) 2.67 (s, 3H, CH_3), 3.73 (s, 3H, $-OCH_3$), 6.67—7.93 (m, 5H, Ar). ^{13}C NMR ($CDCl_3$): δ(ppm) 24.8 (q, CH_3), 55.4 (q, $-OCH_3$), 105.1(d), 121.7(d), 122.0(d), 127.2(s), 129.8(d), 134.8(d), 143.7(s), 155.9(s), 156.9(s). MS (*m/e*): 173 (rel intensity 100, M^+), 158 (38), 130 (80), 103 (23), 77 (23). Found: C, 75.37; H, 6.48; N, 5.99%. Calcd for $C_{11}H_{10}NO$: C, 76.28; H, 6.40; N, 6.16%.

2-Propyl-3-ethyl-6-methylquinoline (Exptl 16): Yield, 60%; Yellow oil, bp 96—97 °C/0.2 Torr; ^1H NMR (220 MHz) ($CDCl_3$): δ(ppm) 1.02 (t, 3H, CH_3), 1.14 (t, 3H, CH_3), 1.84 (sex, 2H, CH_2), 2.30 (s, 3H, CH_3), 2.57 (q, 2H, CH_2),

2.84 (t, 2H, CH_2), 7.50 (s, 1H), 7.23 (s, 1H), 7.25 (s, 1H), 7.93 (d, 1H). ^{13}C NMR ($CDCl_3$): δ(ppm) 14.2 (q, CH_3), 14.4 (q, CH_3), 21.3 (t, CH_2), 22.5 (q, CH_3), 25.0 (t, CH_2), 37.5 (t, CH_2), 125.7 (d), 127.3(s), 128.4(s), 130.2(d), 132.7 (d), 134.7(s), 134.9(s), 145.2(s), 160.3(s). MS (*m/e*): 213 (rel int 26, M^+), 198 (39), 185 (100), 184 (62). Found: C, 84.44; H, 9.02; N, 6.51%. Calcd for $C_{15}H_{19}N$: C, 84.45; H, 8.98; N, 6.57%.

2-Ethyl-3-methyl-6-methylquinoline (Exptl 17): Yield, 64%; Yellow oil, bp 85—86 °C/0.17 Torr; ^1H NMR (220 MHz) ($CDCl_3$): δ(ppm) 1.32 (t, 3H, CH_3), 2.27 (s, 3H, CH_3), 2.30 (s, 3H, CH_3), 2.86 (q, 2H, CH_2), 7.25 (s, 1H), 7.30 (d, 1H), 7.48 (s, 1H), 7.89 (d, 1H). Found: C, 84.30; H, 8.46; N, 7.24%. Calcd for $C_{13}H_{15}N$: C, 84.28; H, 8.16; N, 7.56%.

2-Propyl-3-ethyl-6-chloroquinoline (Exptl 19): Yield, 40%; Yellow oil, bp 101—102 °C/0.2 Torr; ^1H NMR (220 MHz) ($CDCl_3$): δ(ppm) 1.02 (t, 3H, CH_3), 1.25 (t, 3H, CH_3), 1.82 (sex, 2H, CH_2), 2.73 (q, 2H, CH_2), 2.89 (t, 2H, CH_2), 7.44 (d, 1H), 7.52 (s, 1H), 7.57 (s, 1H), 7.89 (d, 1H). ^{13}C NMR ($CDCl_3$): δ(ppm) 14.1 (q, CH_3), 14.3 (q, CH_3), 22.5 (t, CH_2), 25.0 (t, CH_2), 37.4 (t, CH_2), 125.5 (d), 127.8(s), 129.0(d), 129.8(d), 131.1(s), 132.8(d), 136.3(s), 144.4(s), 162.1(s). Found: C, 71.74; H, 7.28; N, 5.90; Cl, 15.13%. Calcd for $C_{14}H_{16}NCl$: C, 71.94; H, 6.90; N, 5.99; Cl, 15.17%.

2-Ethyl-3-methyl-6-chloroquinoline (Exptl 20): Yield, 48%; Yellow oil, bp 101—102 °C/0.35 Torr; ^1H NMR (60 MHz) ($CDCl_3$): δ(ppm) 1.33(t, 3H, CH_3), 2.20(s, 3H, CH_3), 2.83 (q, 2H, CH_2), 7.20—8.00(m, 4H, Ar). Found: C, 70.04; H, 6.05; N, 6.74; Cl, 17.05%. Calcd for $C_{12}H_{12}NCl$: C, 70.07; H, 5.88; N, 6.81; Cl, 17.24%.

2-Propyl-3-ethyl-8-methoxyquinoline (Exptl 21): Yield, 39%; Yellow oil, bp 116—117 °C/0.2 Torr (mp 63.8—64 °C). ^1H NMR (220 MHz)($CDCl_3$): δ(ppm) 1.02(t, 3H, CH_3), 1.16 (t, 3H, CH_3), 1.84(sex, 2H, CH_2), 2.64(q, 2H, CH_2), 2.95 (t, 2H, CH_2), 3.86(s, 3H, $-OCH_3$), 6.75(d, 1H), 7.16(dt, 2H), 7.61(s, 1H). ^{13}C NMR($CDCl_3$): δ(ppm) 14.2(q, CH_3), 14.4(q, CH_3), 23.0(t, CH_2), 25.0(t, CH_2), 37.8(t, CH_2), 55.8(q, $-OCH_3$), 106.9(d), 118.9(d), 125.5(d), 128.5(s), 133.6(d), 135.6(s), 138.4(s), 155.1(s), 160.5(s). MS(*m/e*): 229(rel int 73, M^+), 228(59), 214(36), 201(100), 200(64). Found: C, 77.67; H, 8.31; N, 5.97; O, 7.26%. Calcd for $C_{15}H_{19}NO$: C, 78.56; H, 8.35; N, 6.11; O, 6.98%.

2-Ethyl-3-methyl-8-methoxyquinoline (Exptl 22): Yield, 25%; Yellow oil, bp 110 °C/0.8 Torr; ^1H NMR (60 MHz)($CDCl_3$): δ(ppm) 1.33(t, 3H, CH_3), 3.03(q, 2H, CH_2), 2.40(s, 3H, CH_3), 4.00(s, 3H, $-OCH_3$), 6.67—7.69(m, 4H, Ar). MS (*m/e*): 201(rel int 80, M^+), 200(100), 172(47), 171(41). Found: C, 77.51; H, 7.55; N, 7.15; O, 8.25%. Calcd for $C_{13}H_{15}NO$: C, 77.58; H, 7.51; N, 6.96; O, 7.95%.

8-Methoxy-2-methylquinoline (Exptl 23): Yield, 10%; Yellow oil, bp 108 °C/0.8 Torr; ^1H NMR (60 MHz)($CDCl_3$): δ(ppm) 2.77(s, 3H, CH_3), 4.03(s, 3H, $-OCH_3$), 6.86—8.00(m, 5H, Ar). Found: C, 76.15; H, 6.43; N, 8.19%. Calcd for $C_{11}H_{11}NO$: C, 76.28; H, 6.40; N, 8.09%.

2-Propyl-3-ethyl-8-methylquinoline (Exptl 24): Yield, 59%; Yellow oil, bp 90—92 °C/0.25 Torr; ^1H NMR(220 MHz) ($CDCl_3$): δ(ppm) 0.93(t, 3H, CH_3), 1.14(t, 3H, CH_3), 1.80 (sex, 2H, CH_2), 2.61(q, 2H, CH_2), 2.66(s, 3H, CH_3), 2.82 (t, 2H, CH_2), 7.13(t, 1H), 7.32(d, 1H), 7.43(d, 1H), 7.64 (s, 1H). ^{13}C NMR($CDCl_3$): δ(ppm) 14.2(q, $2CH_3$), 17.9 (q, CH_3), 21.7(t, CH_2), 25.0(t, CH_2), 37.3(t, CH_2), 124.8 (d), 125.1(d), 126.6(s), 127.1(s), 128.2(d), 133.5(d), 134.8 (s), 136.5(s), 159.9(s).

2-Ethyl-3,8-dimethylquinoline (Exptl 25): Yield, 45%; Yellow oil, bp 85 °C/0.25 Torr; ^1H NMR(60 MHz)($CDCl_3$): δ(ppm) 1.35(t, 3H, CH_3), 2.20(s, 3H, CH_3), 2.80(s, 3H, CH_3), 2.83(q, 2H, CH_2), 7.30—7.50(m, 4H, Ar). ^{13}C NMR ($CDCl_3$): δ(ppm) 11.7(q, CH_3), 17.8(q, CH_3), 18.4(q, CH_3), 28.9(t, CH_2), 124.6(d), 124.9(d), 126.9(s), 128.0(d), 128.7 (s), 134.9(d), 136.5(s), 145.5(s), 160.6(s). Found: C, 84.05; H, 8.32; N, 7.45%. Calcd for $C_{13}H_{15}N$: C, 84.28; H, 8.16; N, 7.56%.

2-Propyl-3-ethyl-8-chloroquinoline (Exptl 27): Yield, 25%; Yellow oil, bp 92 °C/0.35 Torr; ^1H NMR(220 MHz)($CDCl_3$): δ(ppm) 1.02(t, 3H, CH_3), 1.18(t, 3H, CH_3), 1.91(sex, 2H, CH_2), 2.61(q, 2H, CH_2), 2.86(t, 2H, CH_2), 7.16(t, 1H), 7.43(d, 1H), 7.55(d, 1H), 7.60(s, 1H). ^{13}C NMR($CDCl_3$): δ(ppm) 19.0(q, CH_3), 19.2(q, CH_3), 26.9(t, CH_2), 29.9 (t, CH_2), 42.3(t, CH_2), 130.1(d), 130.4(d), 130.9(s), 131.8 (d), 133.1(s), 132.2(d), 138.5(s), 150.5(s), 170.3(s). Found: C, 72.32; H, 7.19; N, 5.94; Cl, 14.19%. Calcd for $C_{14}H_{16}NCl$: C, 71.94; H, 6.89; N, 5.99; Cl, 15.19%. MS (*m/e*): 233(rel int 31, M^+), 235(11), 218(48), 205(100), 127(48).

2-Propyl-3-ethyl-7-methoxyquinoline (Exptl 30): Yield, 44%; Yellow oil, bp 122—123 °C/0.38 Torr; ^1H NMR (220 MHz) ($CDCl_3$): δ(ppm) 1.02(t, 3H, CH_3), 1.16(t, 3H, CH_3), 1.82 (sex, 2H, CH_2), 2.61(q, 2H, CH_2), 2.86(t, 2H, CH_2), 7.05 (d, 1H), 7.37(s, 1H), 7.45(d, 1H), 7.57(s, 1H). ^{13}C NMR ($CDCl_3$): δ(ppm) 14.2(q, CH_3), 14.4(q, CH_3), 22.9(t, CH_2), 24.9(t, CH_2), 37.6(t, CH_2), 55.1(q, $-OCH_3$), 106.5(d), 118.5 (d), 122.4(s), 127.8(d), 132.8(s), 133.6(d), 147.8(s), 159.9 (s), 161.7(s). MS(*m/e*): 229 (rel int 52, M^+), 214(40), 201 (100), 200(44), 190(62). Found: C, 78.35; H, 8.65; N, 6.22; O, 7.27%. Calcd for $C_{15}H_{19}NO$: C, 78.56; H, 8.35; N, 6.11; O, 6.98%.

2-Ethyl-3-methyl-7-methoxyquinoline (Exptl 31): Yield, 45%; Yellow oil, bp 99 °C/0.25 Torr; ^1H NMR (60 MHz)($CDCl_3$): δ(ppm) 1.27(t, 3H, CH_3), 2.23(s, 3H, CH_3), 2.87(q, 2H, CH_2), 3.73(s, 3H, $-OCH_3$), 6.00—8.00(m, 4H, Ar). Found: C, 77.62; H, 7.23; N, 7.06%. Calcd for $C_{13}H_{15}NO$: C, 77.58; H, 7.51; N, 6.96%.

7-Methoxy-2-methylquinoline (Exptl 32): Yield, 26%; Yellow oil, bp 90—92 °C/0.7 Torr; ^1H NMR (220 MHz)($CDCl_3$): δ(ppm) 2.67(s, 3H, CH_3), 3.83(s, 3H, $-OCH_3$), 6.91(d, 1H), 7.02(d, 1H), 7.32(s, 1H), 7.45(d, 1H), 7.73(d, 1H).

2-Propyl-3-ethyl-7-methylquinoline and 2-propyl-3-ethyl-5-methylquinoline (Exptl 33): Yield, 68%; Yellow oil, bp 100—102 °C/0.2 Torr; ^1H NMR (220 MHz)($CDCl_3$): δ(ppm) 1.00 (t, 3H, CH_3), 1.10(t, 3H, CH_3), 1.82(sex, 2H, CH_2), 2.30 (s, 3H, CH_3), 2.50(q, 2H, CH_2), 2.80(t, 2H, CH_2), 7.00 (d, 1H), 7.31(d, 1H), 7.43(s, 1H), 7.77(s, 1H). *7-Isomer*: ^{13}C NMR ($CDCl_3$): δ(ppm) 14.2(q, CH_3), 14.4(q, CH_3), 21.6(t, CH_2), 22.4(t, CH_2), 24.9(t, CH_2), 37.4(q, CH_3), 125.3(d), 126.5(d), 127.7(d), 133.0(s), 134.1(s), 137.8(s), 146.7(s), 161.1(s). *5-Isomer*; 18.3(q, CH_3), 18.7(q, CH_3), 21.2(t, CH_2), 25.2(t, CH_2), 29.2(t, CH_2), 36.8(q, CH_3), 114.0(d), 116.5(d), 117.2(d), 125.9(d), 127.0(s), 129.3(s), 135.6(s), 143.7(s). Found: C, 84.35; H, 9.02; N, 6.54%. Calcd for $C_{15}H_{19}N$: C, 84.45; H, 8.98; N, 6.56%.

2-Ethyl-3,7-dimethylquinoline and 2-ethyl-3,5-dimethylquinoline (Exptl 34): Yield, 62%; Yellow oil, bp 75 °C/0.35 Torr; ^1H NMR (220 MHz)($CDCl_3$): δ(ppm) 1.32(t, 3H, CH_3), 2.05(s, 3H, CH_3), 2.30(s, 3H, CH_3), 2.73 (q, 2H, CH_2), 7.00(d, 1H), 7.25(td, 2H), 7.77(s, 1H). ^{13}C NMR ($CDCl_3$): δ(ppm) 12.7(q, CH_3), 18.8(q, CH_3), 21.6(q, CH_3), 29.2(t, CH_2), 126.2(d), 127.5(d, d), 135.1(d), 128.1(s), 128.8(s), 137.9(s), 146.7(s), 162.6(s). *5-Isomer*; 18.3(q, CH_3), 21.1(q, CH_3), 26.7(q, CH_3), 30.1(t, CH_2), 117.4(d), 125.2(d).

2,7-Dimethylquinoline and 2,5-dimethylquinoline (Exptl 35): Yield, 38%; Yellow oil, bp 53—54 °C/0.25 Torr; ^1H NMR (220 MHz)($CDCl_3$): δ(ppm) 2.39(s, 3H, CH_3), 2.61(s, 3H,

CH_3), 7.00(d, 1H), 7.01(d, 1H), 7.45(d, 1H), 7.75(d, 1H), 7.77(s, 1H). *5-Isomer*; 2.45(s, 3H, CH_3), 2.62(s, 3H, CH_3), 7.00—8.00(m, 5H, Ar). Found: C, 83.80; H, 7.23; N, 8.48%. Calcd for $C_{11}H_{11}N$: C, 84.04; H, 7.05; N, 8.91%.

2-Propyl-3-ethyl-7-chloroquinoline (Exptl 36): Yield, 61%; Yellow oil, bp 119—120 °C/0.18 Torr; ^1H NMR (220 MHz) ($CDCl_3$): δ(ppm) 1.00(t, 3H, CH_3), 1.18(t, 3H, CH_3), 1.77 (sex, 2H, CH_2), 2.61(q, 2H, CH_2), 2.80(t, 2H, CH_2), 7.16 (d, 1H), 7.34(d, 1H), 7.52(s, 1H), 7.91(s, 1H). ^{13}C NMR ($CDCl_3$): δ(ppm) 14.0(q, CH_3) 14.3(q, CH_3), 22.4(t, CH_2), 25.0(t, CH_2), 37.5(t, CH_2), 125.4(d), 126.3(d), 127.3(d), 127.8(s), 128.0(d), 130.2(s), 133.3(s), 133.8(s), 162.8(s).

2-Ethyl-3-methyl-7-chloroquinoline (Exptl 37): Yield, 55%; Yellow oil or yellow crystalline, bp 95—96 °C/0.25 Torr (mp 54—56 °C). ^1H NMR (220 MHz)($CDCl_3$): δ(ppm) 1.34(t, 3H, CH_3), 2.43(s, 3H, CH_3), 3.00(q, 2H, CH_2), 7.39(d, 1H), 7.57(d, 1H), 7.80(s, 1H), 8.09(s, 1H). Found: C, 69.88; H, 5.84; N, 6.79; Cl, 17.20%. Calcd for $C_{12}H_{12}NCl$: C, 70.07; H, 5.88; N, 6.81; Cl, 17.24%.

7-Chloro-2-methylquinoline and 5-Chloro-2-methylquinoline (Exptl 38): Yield, 20%; Yellow oil, bp 70—71 °C/0.2 Torr; ^1H NMR (220 MHz)($CDCl_3$): δ(ppm) 2.63(s, 3H, CH_3), 7.09 (d, 1H), 7.25(d, 1H), 7.48(d, 1H), 7.80(d, 1H), 7.93(s, 1H). *5-Isomer*; 2.66(s, 3H, CH_3), 7.11(d, 1H), 7.24(d, 1H), 7.45(t, 1H), 7.84(d, 1H), 8.20(d, 1H). Found: C, 67.37; H, 4.57; N, 7.98; Cl, 19.72%. Calcd for $C_{10}H_8NCl$: C, 67.62; H, 4.54; N, 7.89; Cl, 19.95%.

The authors wish to express their thanks to Professor Yoshinobu Takegami for his helpful discussions.

References

1) H. Skraup, *Chem. Ber.*, **13**, 2086 (1880); R. H. F. Manske and M. Kulka, *Org. React.*, **7**, 59 (1953).
2) S. E. Diamond, A. Szalkiewicz, and F. Mares, *J. Am. Chem. Soc.*, **101**, 498 (1979).
3) T. Joh and N. Hagihara, *Tetrahedron Lett.*, **1967**, 4199.
4) Y. Watanabe, M. Yamamoto, S. C. Shim, T. Mitsudo, and Y. Takegami, *Chem. Lett.*, **1979**, 1025.
5) W. Seiffert, *Angew. Chem.*, **74**, 250 (1962).
6) M. H. Palmer, *J. Chem. Soc.*, **1962**, 3645.
7) M. A. Bennett and D. L. Milner, *J. Am. Chem. Soc.*, **91**, 6983 (1969).
8) G. Hata, H. Kondo, and A. Miyake, *J. Am. Chem. Soc.*, **90**, 2278 (1968).
9) S. J. LaPlaca and J. A. Ibers, *Inorg. Chem.*, **4**, 778 (1965); A. C. Skapski and P. G. H. Troughton, *J. Chem. Soc., Chem. Commun.*, **1968**, 123.
10) K. W. Muir and J. A. Ibers, *Inorg. Chem.*, **9**, 440 (1970).
11) J. Chatt and L. M. Venanzi, *J. Chem. Soc.*, **1957**, 4735.

Syntheses and Properties of α-Ethyl-substituted Bisdehydro-[13]annulenone and Its Benzo-annelated Derivatives

Jūro Ojima,* Yasushi Juni, Yoshiharu Yoneyama,
Kazuyo Wada, and Yoshiko Murosawa
Department of Chemistry, Faculty of Science, Toyama University, Gofuku, Toyama 930

(Received March 2, 1981)

2-Ethyl-5,10-dimethyl-, 13-ethyl-10-methyl-4,5-benzo-, 2-ethyl-10-methyl-4,5-benzo-, and 2-ethyl-4,5:10,11-dibenzo-6,8-bisdehydro[13]annulenone were synthesized. Influence of α-ethyl substitution upon the skeleton of the bisdehydro[13]annulenone ring system is discussed on the basis of ^{1}H NMR and UV spectra of these annulenones and their corresponding α-methyl-substituted derivatives.

In a previous paper[1] the synthesis of the paratropic 5,10-dimethyl- **1** and 2,5,10-trimethyl-6,8-bisdehydro-[13]annulenone **2** was reported and it was shown that α-methyl-unsubstituted annulenone **1** exists in the conformation indicated and, in contrast, the extra α-methyl group of trimethylbisdehydro[13]annulenone **2** causes a change of conformation due to rotation of the opposite double bond, **2** existing in the conformation of **2a** at −60 °C. The benzo-annelated derivatives of **1** and **2** were also prepared and it was shown that the extra α-methyl substituent and fused benzene ring(s) exert a considerable influence on the development of paratropic character and conformational mobility in the bisdehydro[13]annulenone system, as compared with that in the case of α-methyl-unsubstituted compounds.[2]

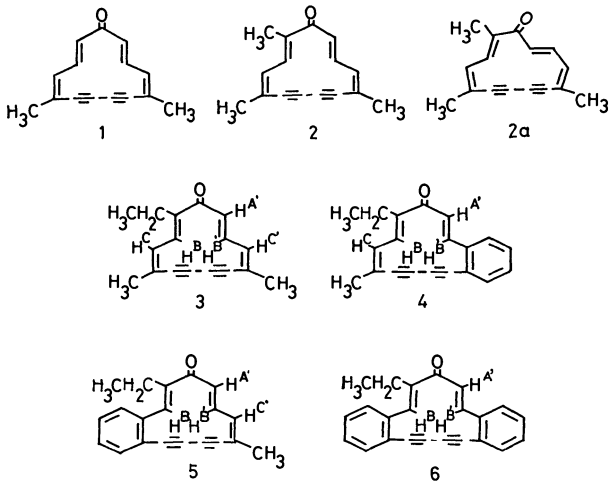

In view of these results, we investigated effects of different steric bulks of α-alkyl groups on the molecular skeleton of the bisdehydro[13]annulenone ring system. It required the preparation of 3-alkyl-2-alkanones of types **9** and **11** (R=alkyl, R′=H). In practice, we could obtain only 3-ethyl-2-alkanones **9b** and **11b** by acid-catalyzed aldol condensation from aldehydes **7** and **10** (Scheme 1). Thus we could prepare α-ethyl-substituted bisdehydro[13]annulenones **3**—**6**.

Results and Discussion

Synthesis. It is known that reaction of 2-butanone **8a**, an unsymmetrical aliphatic ketone, with aldehydes shows regioselectivity, depending on conditions used; base-catalyzed aldol condensation of 2-butanone **8a** favors C_1 of ketone as the position of attack, in contrast to C_3 favored by acid-catalyzed reaction.[3] In practice, reaction of 3-methyl-2-penten-4-ynal **7**[4] or *o*-ethynylbenzaldehyde **10**[5] with **8a** yielded **9a**[1] or **11a**[2] under acidic conditions but **9f**[1] or **11f** under basic conditions, respectively.

We examined aldol condensations of aldehydes **7** and **10** with 2-pentanone **8b** and its branched isomers **8c** and **8d**, as illustrated in Scheme 1. The results obtained demonstrate that only 2-pentanone **8b** shows regioselectivity for aldehydes **7** and **10**, as 2-butanone **8a** does. Under acidic conditions (acetic acid–sulfuric acid) **8b** yielded C_3-products, while both 4-methyl-**8c** and 4,4-dimethyl-2-pentanone **8d** yielded C_1-products. On the other hand, under basic conditions (sodium hydroxide in aqueous ethanol) all of **8b**—**d** gave C_1-products usually in higher yields than under

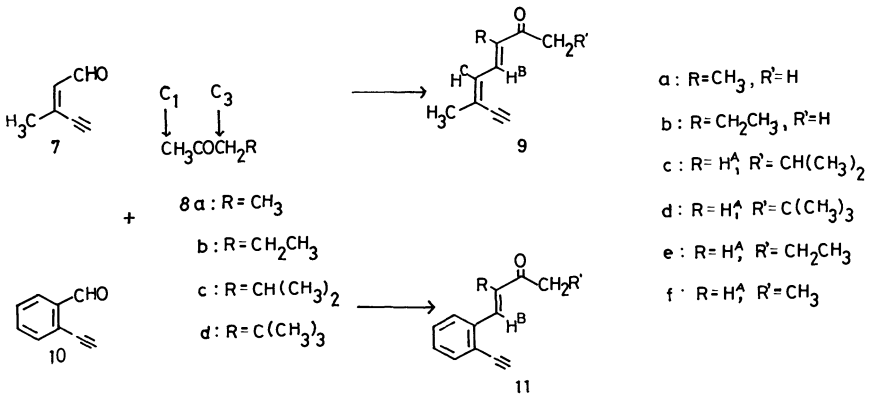

Scheme 1.

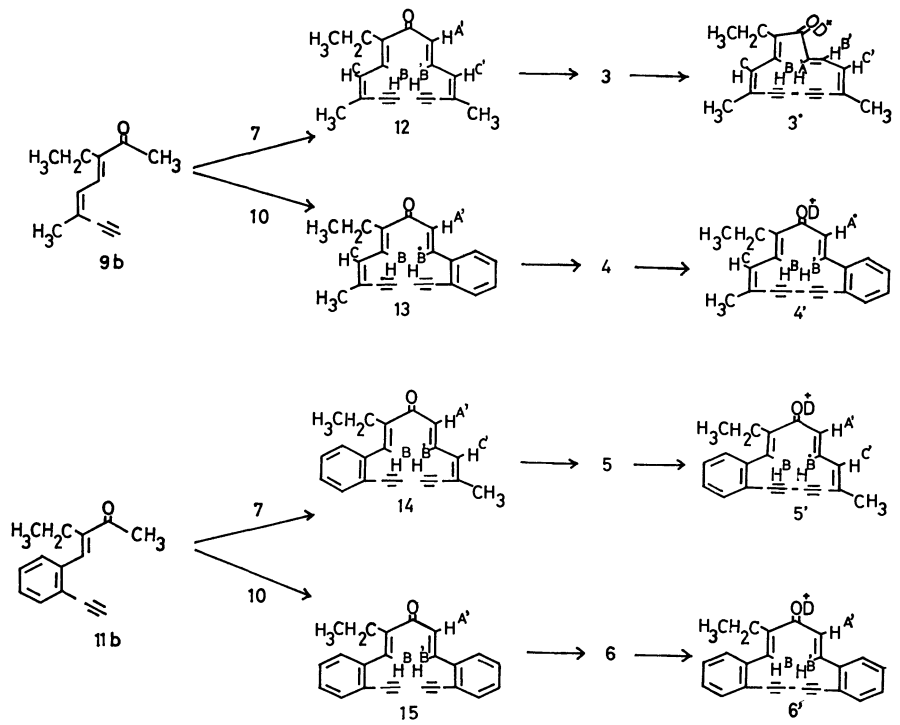

Scheme 2.

Table 1. Electronic absorption maxima of bisdehydro[13]annulenones in ether

λ_{max}/nm (ε_{max})

3		4		5		6	
210	(22900)	234 sh	(22700)	232 sh	(22800)	223	(36300)
250 sh	(15800)	276	(33900)	263	(25400)	268 sh	(23800)
263	(27100)	290 sh	(26400)	275	(30600)	281	(37600)
274	(28700)	388	(2980)	290 sh	(15700)	295	(39000)
390	(1000)			380	(3600)	352	(5510)

acidic conditions.

Thus, we could prepare only 3-ethyl-2-alkanones **9b** and **11b**. For ketones such as **9c—d** and **11c—d**, attempts were tried in vain to make them condense with aldehyde **7** or **10** to get their corresponding acyclic ketones. Starting with ketones **9b** and **11b**, syntheses of α-ethyl-substituted [13]annulenones **3—6** were carried out according to the previously reported procedure,[1,2] outlined in Scheme 2.

Ketone **9b** was condensed with (*Z*)-3-methyl-2-penten-4-ynal **7**[4] in the presence of ethanolic sodium ethoxide in ether to give the acyclic ketone **12** in 77% yield. Oxidative coupling of **12** with anhydrous copper(II) acetate in pyridine and ether at 50 °C[6] afforded annulenone **3** in 32% yield. Condensation of **9b** with *o*-ethynylbenzaldehyde **10**,[5] allowed to proceed similarly to that of **9b** with **7**, gave the acyclic ketone **13** in 47% yield. Oxidation of **13**, as with **12**, gave the monobenzannulenone **4** in 44% yield. Similarly, condensation of ketone **11b** with **7** gave ketone **14** in 28% yield, which was oxidized to give another monobenzannulenone **5** in 37% yield. Reaction of **11b** and **10** afforded ketone **15** in 47% yield. Oxidation of **15** gave dibenzannulenone **6** in 46% yield. The structures of these new compounds were established on the basis of their spectral properties and results of elemental analysis.

Treatment of annulenones **3—6** with trifluoroacetic acid or trifluoroacetic acid-*d* gave their corresponding protonated or deuteronated carbonyl species **3′—6′**, respectively; **3′—5′** were dark red and **6′** was yellow. Quenching of **3′—6′** with aqueous sodium hydrogencarbonate resulted in regeneration of **3—6**, respectively.

Properties. Electronic absorption maxima (in ether) of annulenones **3—6** are given in Table 1. As expected, the spectra are similar to one another, the medium bands exhibiting an appreciable bathochromic shift with increasing number of fused benzene rings, as observed for some benzo-annelated annulenes.[6] In contrast, the longest wavelength bands of these annulenones exhibit absorption shift toward longer wavelengths in the sequence of **3>4≃5>6**, demonstrating the sequence for the degree of extended conjugation of π-electron systems in the bisdehydro-[13]annulenone ring. Electronic absorption maxima of annulenones **3—6** in trifluoroacetic acid are given in Table 2, and it is evident that protonation with this acid causes a bathochromic shift of their main maxima.

Table 2. Electronic absorption maxima of bisdehydro-[13]annulenones in trifluoroacetic acid
λ_{max}/nm(Relative extinction coefficient)[a)]

3	4	5	6
250 sh (0.60)	277 sh (0.91)	273 sh (0.81)	285 sh (0.83)
268 sh (0.89)	292 (1.00)	287 (1.00)	299 (1.00)
281 (1.00)	354 sh (0.17)	342 sh (0.16)	352 sh (0.12)
345 sh (0.12)	420 sh (0.08)	415 (0.12)	413 sh (0.04)

a) All the spectra showed tailing to ≈700 nm.

^{1}H NMR chemical shifts of the protons of annulenones **3**—**6** and those of their corresponding acyclic ketones at 90 MHz are listed in Table 3, together with data for the deuteronated species **3′**—**6′**, obtained through dissolution in trifluoroacetic acid-*d*. Individual assignments were made on the basis of multiplicity, coupling constants (see Experimental), and data of closely related compounds.[1,2)] Variable-temperature ^{1}H NMR spectra of **3**—**6** were taken at 100 MHz over the range −60 to 60 °C, chemical shifts being summarized in Table 4. As indicated in Fig. 1, the spectra of ethyldimethyl-6,8-bisdehydro-[13]annulenone **3** are temperature-dependent. At 35 °C (and above), the $H^{A'}$, $H^{B'}$, and $H^{C'}$ bands of **3** are unresolved multiplets. On cooling, the bands become resolved, and the expected first-order pattern is observed at −30 °C. Further cooling results in increased separation of the $H^{A'}$ and the $H^{B'}$ bands. These observations are similar to those for the spectra of the corresponding α-methyl derivative **2**[1)] and indicate that the ethyldimethylbisdehydro[13]annulenone **3** exists as conformer **3a** and not **3b**. A marked

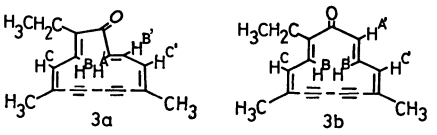

difference observed in variable-temperature ^{1}H NMR spectra between **2** and **3** is that a spectrum of complete first-order pattern for the structure of **3a** is attained at −30 °C, whereas for the structure of **2a** it is attained at −60 °C. This result reveals that the introduction of the extra ethyl group into **1** to give **3** is more effective than that of the extra methyl group into **1** to give **2**, causing a conformational change on the other *trans* double bond in this bisdehydro[13]-annulenone ring system. On the other hand, the spectra of annulenones **4**—**6** were found essentially temperature-independent (Table 4), revealing that the conformations indicated for **4**—**6** will remain unchanged over the range −60 to 60 °C; similar temperature independence has been obtained for their corresponding α-methyl derivatives.[2)]

If we judge the tropicity of these annulenones from differences in chemical shift among various protons for the cyclic ketone (annulenone) and its corresponding acyclic model (upfield shift for the outer protons and downfield shift for the inner) (Table 3), annulenone **3** is taken to be a paratropic molecule, while **4**—**6** to be atropic ones. It has been observed that the paratropicity of the α-unsubstituted bisdehydro-[13]annulenone series decreases with increasing number of fused benzene rings.[7)] However, an examination of the data shown in Table 3 reveals that α-ethyl-substituted series (**3**—**6**) does not show such a trend.

Table 3. ^{1}H NMR chemical shifts of **3**—**6**, **12**—**15** (in $CDCl_3$), and **3′**—**6′** (in CF_3COOD) at 90 MHz, determined at 35 °C (τ Value; Internal standard, Me_4Si)

Compd	$H^{A'}$	H^{B}	$H^{B'}$	H^{C}	$H^{C'}$	ArH	$-CH_2CH_3$	$-CH_2CH_3$	CH_3
12	3.13	2.52	2.23	3.27	3.49		7.49	8.98	7.92, 7.97
3[a)]	2.10	0.38	2.50	3.37	3.73		7.69	9.00	8.17
3′	b)	−0.37	b)	3.45	3.79		7.65	8.95	8.20
Δ(**3**−**12**)	−1.03	−2.14	+0.27	+0.10	+0.24		+0.20	+0.02	+0.20—+0.25
Δ(**3′**−**12**)		−2.89		+0.18	+0.30		+0.16	−0.03	+0.23—+0.28
13	(2.25———2.75)		1.88	3.23		2.25—2.75	7.43	8.92	7.93
4	2.50	0.95	2.12	3.24		2.6—2.8	7.57	8.94	8.10
4′	2.18	0.18	1.93	3.25		2.6—2.9	7.54	8.90	8.10
Δ(**4**−**13**)			+0.24	+0.01			+0.14	+0.02	+0.17
Δ(**4′**−**13**)			+0.05	+0.02			+0.11	−0.02	+0.17
14	3.13	2.30	2.17		3.45	2.4—2.8	7.42	8.92	7.93
5	2.87	2.17	1.98		3.40	2.5—2.8	7.52	9.02	8.10
5′	3.12	2.28	1.31		3.25	2.5—2.7	7.47	8.97	8.00
Δ(**5**−**14**)	−0.26	−0.13	−0.19		−0.05		+0.10	+0.10	+0.17
Δ(**5′**−**14**)	−0.01	−0.02	−0.86		−0.20		+0.05	+0.05	+0.07
15	(2.4—2.8)	2.18	1.78			2.4—2.8	7.38	8.87	
6	2.18	1.86	1.97			2.5—2.8	7.40	8.90	
6′	1.98	1.66	1.72			2.4—2.8	7.35	8.89	
Δ(**6**−**15**)		−0.32	+0.19				+0.02	+0.03	
Δ(**6′**−**15**)		−0.52	−0.06				−0.03	+0.02	

a) At −25 °C. b) The $H^{A'}$ and $H^{B'}$ chemical shifts of **3′** appeared as a multiplet at τ 1.67—2.13, due to conformational mobility.

Table 4. ^{1}H NMR data for compounds **3**—**6** (in $CDCl_3$) at 100 MHz (τ Value; Internal standard, Me_4Si)

Compd	T/°C	$H^{A'}$	H^B	$H^{B'}$	H^C	$H^{C'}$	ArH	$-CH_2CH_3$	CH_3	$-CH_2CH_3$
3	+60	2.32	0.65	2.52	3.48	3.82		7.69	8.22, 8.24	9.00
	+22	2.31	0.58	2.53	3.47	3.82		7.70	8.22	9.01
	−30	2.18	0.48	2.56	3.43	3.81		7.70	8.19	9.01
	−60	2.09	0.42	2.63	3.41	3.80		7.70	8.18	9.01
4	+60	2.55	1.05	2.18	3.29		2.7—2.9	7.59	8.15	8.96
	+22	2.54	1.01	2.16	3.28		2.7—2.8	7.60	8.14	8.97
	−30	2.53	0.93	2.14	3.27		2.7—2.8	7.61	8.12	8.97
	−60	2.52	0.90	2.14	3.25		2.7—2.8	7.61	8.11	8.97
5	+60	2.89	2.24	2.09		3.48	2.7—2.9	7.55	8.12	9.02
	+22	2.94	2.22	2.02		3.45	2.7—2.8	7.54	8.11	9.02
	−30	3.10	2.24	1.84		3.41	2.7—2.8	7.51	8.09	9.03
	−60	3.22	2.26	1.73		3.38	2.7—2.8	7.50	8.07	9.04
6	+60	2.07	1.98	2.23			2.5—2.8	7.43		8.93
	+22	2.04	1.93	2.21			2.5—2.8	7.42		8.93
	−30	2.03	1.88	2.19			2.5—2.8	7.40		8.92
	−60	2.03	1.87	2.18			2.5—2.7	7.38		8.91

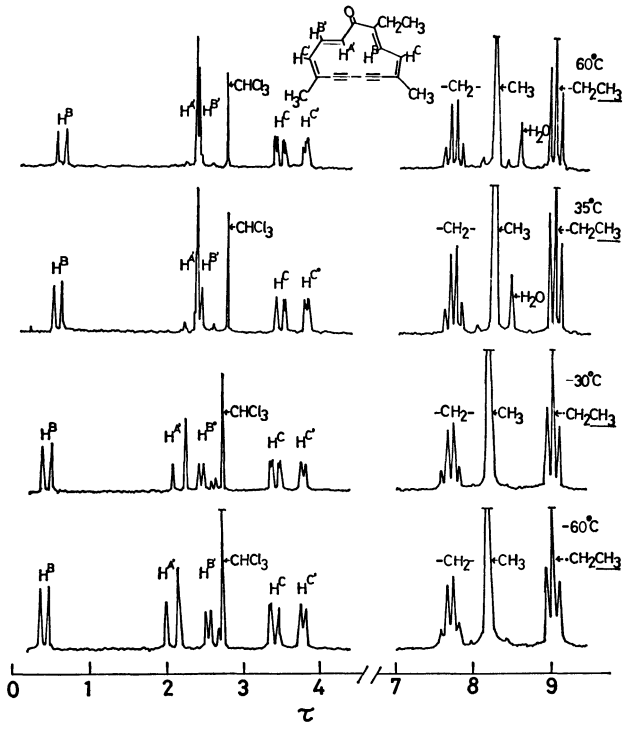

Fig. 1. The ^{1}H NMR FT spectra of **3** in $CDCl_3$ at 100 MHz (Internal standard, TMS).

Because it has been pointed out that annelation of an aromatic ring with an antiaromatic system exerts rather a minor effect on the paratropicity of the $4n\pi$ electron system,[8] and that the patatropicity of $4n$ moiety in the annelated [$4n$]annulene is quite sensitive to even a minor change in conformation,[9] the abovementioned trend observed in the series of α-ethyl-substituted bisdehydro[13]annulenone (**3**—**6**) should be ascribed to small change in the conformation of the [13]annulenone ring due to ethyl substitution at α-position and benzo-annelation, although the local anisotropic effect of the diacetylene unit can not be excluded.

In conclusion, the results obtained from this study indicate that the change of α-substituent from methyl to ethyl group causes both paratropic nature and conformational stability to decrease in the bisdehydro-[13]annulenone ring system.

Experimental

Deoxygenated ether was used to minimize oxidation of the compounds used for aldol condensation, and was freed from peroxide by passage through a short column of basic alumina (Woelm Act. I) followed by flushing with nitrogen immediately before use. Melting points were uncorrected. Mass spectra were recorded by the direct insertion technique with a JEOL JMS-200 spectrometer operating at 75 eV. IR spectra were taken on a Hitachi EPI-S2 spectrophotometer; only those absorptions characteristic of the carbonyl group are given in cm^{-1} for compounds **9** and **11**. UV spectra were measured on a Hitachi 124 instrument in ethanol solution, unless otherwise specified, and recorded in nm. ε-Values are given in parentheses, shoulders being denoted by sh. ^{1}H NMR spectra were recorded on a Varian EM-390 (90 MHz) or a JEOL FX-100 (100 MHz) spectrometer, and the data taken with a Varian EM-390 instrument are specified in this section by τ-value in $CDCl_3$ solution, TMS being used as an internal standard, unless otherwise stated. The coupling constants (J) are given in Hz. Alumina (Act. II—III) was used for column chromatography.

*3-Ethyl-6-methyl-3,5-octadien-7-yn-2-one (**9b**).* A solution of aldehyde **7**[4] (3.00 g, 32 mmol) in acetic acid (16 ml) was added dropwise during 2 h to a stirred solution of 2-pentanone **8b** (10.0 g, 16 mmol) and concentrated sulfuric acid (2.8 ml) in acetic acid (110 ml) at ambient temperature. The solution was stirred for a further 4.5 h, and then was cautiously poured into saturated aqueous potassium carbonate (200 ml). The mixture was diluted with water, and extracted with benzene. The extracts were washed with saturated aqueous sodium chloride solution, and dried over sodium sulfate. The residue obtained after removal of the solvent was chromatographed on alumina (80 g) with 5% ether in hexane. The early fractions gave ketone **9b** (2.08 g, 40%) as a light yellow oil; MS, *m/e*, 162 (M^+, 70%) and 119 (100); mol wt 162.2; IR (neat) 1660 cm^{-1}; UV_{max} 304 nm (51600); NMR τ=2.47 (d, 11, 1H, H^B), 3.27 (d, 11, 1H, H^C), 6.33 (s, 1H, $-C\equiv CH$), 7.57 (q, 8, 2H, $-C\underline{H}_2CH_3$), 7.60 (s, 3H, CH_3), 7.90 (s, 3H, CH_3), and 9.02 (t, 8, 3H, $-CH_2C\underline{H}_3$).

Found: C, 79.86; H, 8.40%. Calcd for $C_{11}H_{14}O$: C,

81.44; H, 8.70%. Attempts to improve the elemental analysis failed.

*2,8-Dimethyl-5,7-decadien-9-yn-4-one (**9c**)*: Yield 12% (acidic conditions) and 23% (basic conditions); light yellow oil; MS, *m/e*, 176 (M^+, 13%) and 119 (100); mol wt 176.2; IR (neat) 1680 and 1660 cm^{-1}; UV_{max} 305 nm (33500); NMR τ=2.40 (dd, 15.5, 11, 1H, H^B), 3.56 (d, 11, 1H, H^C), 3.80 (d, 15.5, 1H, H^A), 6.43 (s, 1H, $-C\equiv CH$), 7.53 (d, 7, 2H, $-C\underline{H}_2CH-$), 7.76 (m, 1H, $-CH_2C\underline{H}-$), 7.95 (s, 3H, CH_3), and 9.03 (d, 7, 6H, $-CH(C\underline{H}_3)_2$). Found: C, 81.94; H, 8.95%. Calcd for $C_{12}H_{16}O$: C, 81.77; H, 9.15%.

*2,2,8-Trimethyl-5,7-decadien-9-yn-4-one (**9d**)*: Yield 18% (acidic conditions) and 25% (basic conditions); light yellow oil; MS, *m/e*, 190 (M^+, 16%) and 134 (100); mol wt 190.2; IR (neat) 1675, 1660, and 1650 cm^{-1}; UV_{max} 304 nm (39700); NMR τ=2.42 (dd, 16, 12, 1H, H^B), 3.55 (d, 12, 1H, H^C), 3.80 (d, 16, 1H, H^A), 6.42 (s, 1H, $-C\equiv CH$), 7.52 (s, 2H, $-C\underline{H}_2-$), 7.95 (s, 3H, CH_3), and 8.95 (s, 9H, $-C(C\underline{H}_3)_3$). Found: C, 79.78; H, 9.15%. Calcd for $C_{13}H_{18}O$: C, 82.06; H, 9.54%. Attempts to improve the elemental analysis faield.

Ketones **9c** and **9d** were prepared by reaction of **8c** and **8d** with **7**, respectively, in a manner similar to that described above for the preparation of **9b**. Compounds **9c** and **9d** were also prepared by the reaction, under basic conditions, described below for the preparation of **9e**, and the yields under both acidic and basic conditions are given below.

*8-Methyl-5,7-decadien-9-yn-4-one (**9e**)*. A solution of 2.6% aqueous sodium hydroxide (7.0 ml) was added to an ice-cooled stirred solution of aldehyde **7** (1.0 g, 11 mmol) and **8b** (2.8 g, 33 mmol) in ethanol (6 ml). The solution was stirred for a further 2 h at 3 °C, and aqueous sulfuric acid (2 M, 10 ml) was then added. The solution was diluted with water and extracted with benzene. The extracts were washed with aqueous sodium hydrogencarbonate and sodium chloride solution, and dried over sodium sulfate. The residue obtained after removal of the solvent was chromatographed on alumina (70 g). The fractions eluted with 5% ether in hexane afforded ketone **9e** (425 mg, 35%) as a light yellow oil: MS, *m/e*, 162 (M^+, 17%) and 129 (100); mol wt 162.2; IR (neat) 1685 and 1660 cm^{-1}; UV_{max} 301 nm (27000); NMR τ=2.37 (dd, 16, 11, 1H, H^B), 3.54 (d, 11, 1H, H^C), 3.79 (d, 16, 1H, H^A), 6.37 (s, 1H, $-C\equiv CH$), 7.42 (t, 8, 2H, $-C\underline{H}_2CH_2-$), 7.97 (s, 3H, CH_3), 8.34 (m, 8, 2H, $-CH_2C\underline{H}_2-$), and 9.05 (t, 8, 3H, $-CH_2C\underline{H}_3$). Found: C, 81.24; H, 8.44%. Calcd for $C_{11}H_{14}O$: C, 81.44; H, 8.70%.

Reactions of **8b—d** with aldehyde **10**[5] were carried out similarly to those with aldehyde **7** under both acidic and basic conditions.

*3-Ethyl-4-(o-ethynylphenyl)-3-buten-2-one (**11b**)*. Yield 29%; yellow oil; MS, *m/e*, 198 (M^+, 23%) and 155 (100); mol wt 198.2; IR (neat) 1665 cm^{-1}; UV_{max} 227 sh (25100), 239 (31700), and 281 nm (19600); NMR τ=2.17 (s, 1H, H^B), 2.33—2.80 (m, 4H, ArH), 6.52 (s, 1H, $-C\equiv CH$), 7.52 (s, 3H, CH_3), 7.53 (q, 7, 2H, $-C\underline{H}_2CH_3$), and 8.90 (t, 7, 3H, $-CH_2C\underline{H}_3$). Found: C, 84.71; H, 7.15%. Calcd for $C_{14}H_{14}O$: C, 84.81; H, 7.12%.

*6-(o-Ethynylphenyl)-2-methyl-5-hexen-4-one (**11c**)*. Yield 17% (acidic conditions) and 67% (basic conditions); yellow oil MS, *m/e*, 212 (M^+, 15%) and 155 (100); mol wt 212.2; IR (neat) 1680, 1670, and 1660 cm^{-1}; UV_{max} 228 (31900), 242 (40900), 247 sh (39700), and 293 nm (37100): NMR τ= 1.92 (d, 16, 1H, H^B), 2.29—2.70 (m, 4H, ArH), 3.23 (d, 16, 1H, H^A), 6.45 (s, 1H, $-C\equiv CH$), 7.44 (d, 7, 2H, $-C\underline{H}_2-$), 7.52—7.99 (m, 1H, $-CH\langle$), and 9.02 (d, 7, 6H, $-CH-(C\underline{H}_3)_2$). Found: C, 84.68; H, 7.35%. Calcd for $C_{15}H_{16}O$: C, 84.87; H, 7.60%.

*2,2-Dimethyl-6-(o-ethynylphenyl)-5-hexen-4-one (**11d**)*. Yield 34% (acidic conditions) and 71% (basic conditions); yellow oil; MS, *m/e*, 226 (M^+, 6%) and 155 (100); mol wt 226.3; IR (neat) 1680 and 1650 cm^{-1}; UV_{max} 229 (22400), 243 (27900), 248 (27400), and 294 nm (26100); NMR τ=1.88 (d, 16, 1H, H^B), 2.23—2.68 (m, 4H, ArH), 3.18 (d, 16, 1H, H^A), 6.50 (s, 1H, $-C\equiv CH$), 7.40 (s, 2H, $-C\underline{H}_2-$), and 8.90 (d, 9H, $-C(C\underline{H}_3)_3$). Found: C, 84.84; H, 7.95%. Calcd for $C_{16}H_{18}O$: C, 84.91; H, 8.02%.

*6-(o-Ethynylphenyl)-5-hexen-4-one (**11e**)*. Yield 37%; light yellow cubes from hexane–benzene; mp 64—65.5 °C; MS, *m/e*, 198 (M^+, 14%) and 155 (100); mol wt 198.2; IR (KBr disk) 1675 cm^{-1}; UV_{max} 228 (14200), 242 (19800), 247 sh (19000), and 292 nm (18100); NMR τ=1.90 (d, 16, 1H, H^B), 2.35—2.80 (m, 4H, ArH), 3.22 (d, 16, 1H, H^A), 6.49 (s, 1H, $-C\equiv CH$), 7.33 (t, 7, 2H, $-C\underline{H}_2CH_2-$), 8.28 (m, 7, 2H, $-CH_2C\underline{H}_2-$), and 9.01 (t, 7, 3H, CH_3). Found: C, 84.99; H, 7.00%. Calcd for $C_{14}H_{14}O$: C, 84.81; H, 7.12%.

*5-(o-Ethynylphenyl)-4-penten-3-one (**11f**)*. Yield 38%; light yellow oil; MS, *m/e*, 184 (M^+, 14%) and 155 (100); mol wt 184.2; IR (neat) 1685 and 1665 cm^{-1}; UV_{max} 229 (16300), 243 (22400), 249 (21500), 261 (8340), and 290 nm (18500); NMR τ=1.89 (d, 16, 1H, H^B), 2.2—2.7 (m, 4H, ArH), 3.20 (d, 16, 1H, H^A), 6.43 (s, 1H, $-C\equiv CH$), 7.25 (q, 8, 2H, $-C\underline{H}_2-$), and 8.80 (t, 8, 3H, CH_3). Found: C, 83.60; H, 6.39%. Calcd for $C_{13}H_{12}O$: C, 84.75; H, 6.57%. Attempts to improve the elemental analysis failed.

*6-Ethyl-3,11-dimethyl-3,5,8,10-tridecatetraene-1,12-diyn-7-one **12***. To a mixture of aldehyde **7**[4] (1.30 g, 14 mmol) and ketone **9b** (562 mg, 3.4 mmol) in deoxygenated ether (20 ml) was added a 20% methanolic potassium hydroxide solution (1.7 ml) with stirring at 0 °C. The mixture was then stirred for 6 h at the same temperature. Neutralization with acetic acid (4.6 ml) followed by pouring into water (200 ml) and extraction with benzene gave an organic extract which was worked up as usual. The residue obtained by evaporation of the solvent was chromatographed on alumina (100 g). The initial fractions gave the unchanged ketone **9b** (164 mg). The following fractions eluted with hexane–ether (4:1) afforded ketone **12** (626 mg, 77%) as a solid. Recrystallization from hexane–benzene afforded yellow needles; mp 74.5—75 °C, MS, *m/e*, 238 (M^+, 10%) and 165 (100); mol wt 238.3; IR (KBr disk) 3250 ($-C\equiv CH$), 2100 ($-C\equiv C-$), 1645 (C=O), 1605, 1590, 1580 (C=C), and 980 cm^{-1} (*trans* C=C); UV_{max} (ether) 251 (19200), 256 (19300), 269 sh (17200), 293 (15300), 324 sh (27500), 336 (29800), and 354 nm sh (20900); NMR τ=2.23 (dd, 15, 11, 1H, $H^{B'}$), 2.52 (d, 11, 1H, H^B), 3.13 (d, 15, 1H, $H^{A'}$), 3.27 (d, 11, 1H, H^C or $H^{C'}$), 3.49 (d, 11, 1H, H^C or $H^{C'}$), 6.46 (s, 1H, $-C\equiv CH$), 6.52 (s, 1H, $-C\equiv CH$), 7.49 (q, 8, 2H, $-C\underline{H}_2CH_3$), 7.92 (s, 3H, CH_3), 7.97 (s, 3H, CH_3), and 8.98 (t, 8, 3H, $-CH_2C\underline{H}_3$). Found: C, 85.39; H, 7.63%. Calcd for $C_{17}H_{18}O$: C, 85.67; H, 7.61%.

*2-Ethyl-5,10-dimethyl-6,8-bisdehydro[13]annulenone (**3**)*. A solution of ketone **12** (825 mg, 3.5 mmol) in pyridine (48 ml) and dry ether (18 ml) was added dropwise during 3.5 h to a stirred solution of anhydrous copper(II) acetate (4.40 g) in pyridine (100 ml) and dry ether (35 ml) at 49—53 °C (bath). The solution was stirred at the same temperature for a further 1.5 h and then cooled. After addition of benzene (200 ml), the mixture was filtered through a Hyflo Super-Cel. The precipitates were washed with benzene (100 ml × 3) and the filtrate was poured into water. The organic layer was separated and the aqueous layer was extracted with benzene. The combined organic extracts were washed successively with 7% hydrochloric acid,

aqueous sodium hydrogencarbonate, and water, and dried over sodium sulfate. The dark red liquid obtained after removal of the solvent was chromatographed on alumina (80 g). The fractions eluted with hexane–ether (9:1) afforded annulenone **3** (257 mg, 32%), which formed red plates from hexane; mp 49—50 °C, MS, *m/e*, 236 (M^+, 28%) and 178 (100); mol wt 236.3; IR (KBr disk) 2150 (–C≡C–), 1650 (C=O), 1620 (C=C), and 985 cm^{-1} (*trans* C=C); UV, see Tables 1 and 2; NMR (−25 °C) τ=0.38 (d, 10, 1H, H^B), 2.10 (d, 16, 1H, $H^{A'}$), 2.50 (dd, 16, 6, 1H, $H^{B'}$), 3.37 (d, 10, 1H, H^C), 3.73 (d, 6, 1H, $H^{C'}$), 7.69 (q, 8, 2H, $-C\underline{H}_2CH_3$), 8.17 (s, 6H, CH_3), and 9.00 (t, 8, 3H, $-CH_2C\underline{H}_3$), and see Figure 1; NMR (CF_3COOD) τ=−0.37 (d, 10.5, 1H, H^B), 1.67—2.13 (m, 2H, $H^{A'}$ and $H^{B'}$), 3.45 (dd, 10.5, 1.5, H^C), 3.79 (dd, 6, 1.5, 1H, $H^{C'}$), 7.65 (q, 8, 2H, $-C\underline{H}_2CH_3$), 8.20 (broad s, 6H, CH_3), and 8.95 (t, 8, 3H, $-CH_2C\underline{H}_3$). Found: C, 86.30; H, 6.76%. Calcd for $C_{17}H_{16}O$: C, 86.40; H, 6.83%.

*4-Ethyl-1-(o-ethynylphenyl)-7-methyl-1,4,6-nonatrien-8-yn-3-one (**13**).* A solution of *o*-ethynylbenzaldehyde **10**[5] (1.40 g, 10.6 mmol) in deoxygenated ether (20 ml) was added dropwise during 30 min with ice-bath cooling to a stirred solution of ketone **9b** (1.20 g, 7.3 mmol) in deoxygenated ether (35 ml) containing ethanolic sodium ethoxide (2.1 ml) [from sodium (760 mg) and absolute ethanol (50 ml)]. After stirring for a further 6 h at the same temperature, the reaction was quenched by addition of aqueous oxalic acid. The mixture was poured into water (100 ml) and extracted with benzene. After working up as usual, the red liquid obtained was chromatographed on alumina (100 g). The early fractions gave the recovered aldehyde **10** (285 mg). The following fractions eluted with hexane–ether (17:3) gave ketone **13** (1.18 g, 47%) as a solid. Recrystallization from hexane–benzene afforded light yellow needles: mp 114—115 °C; MS, *m/e*, 274 (M^+, 15%) and 245 (100); mol wt 274.3; IR (KBr disk) 3250 (–C≡CH), 2150 (–C≡C–), 1645 (C=O), 1590 (C=C), 990, and 980 cm^{-1} (*trans* C=C); UV_{max} (ether) 230 (21600), 252 (22100), 259 sh (20600), 309 sh (17200), 327 (19700), and 352 nm sh (13600); NMR τ=1.88 (d, 16, 1H, $H^{B'}$), 2.25—2.75 (m, 6H, $H^{A'}$, H^B, and ArH), 3.23 (d, 11, 1H, H^C), 6.42 (s, 1H, –C≡CH), 6.51 (s, 1H, –C≡CH), 7.43 (q, 8, 2H, $-C\underline{H}_2CH_3$), 7.93 (s, 3H, CH_3), and 8.92 (t, 8, $-CH_2C\underline{H}_3$). Found: C, 87.38; H, 6.45%. Calcd for $C_{20}H_{18}O$: C, 87.56; H, 6.61%.

*13-Ethyl-10-methyl-4,5-benzo-6,8-bisdehydro[13]annulenone (**4**).* A solution of ketone **13** (1.1 g, 4 mmol) in pyridine–dry ether (3:1, 84 ml) was added dropwise during 3 h to a stirred solution of anhydrous copper(II) acetate (5.0 g) in pyridine–dry ether (3:1, 180 ml) at 45—50 °C (bath). The solution was stirred for a further 30 min at the same temperature and then cooled. After working up as in the preparation of **3**, the red liquid obtained was chromatographed on alumina (100 g). The fractions eluted with hexane–ether (17:3) gave monobenzannulenone **4** (481 mg, 44%). Recrystallization from hexane–benzene afforded yellow needles; mp 119—120 °C; MS, *m/e*, 272 (M^+, 20%) and 229 (100); mol wt 272.3; IR (KBr disk) 2150 (–C≡C–), 1650 (C=O), 1600 (C=C), and 980 cm^{-1} (*trans* C=C); UV, see Tables 1 and 2, NMR τ=0.95 (d, 11, 1H, H^B), 2.12 (d, 16.5 1H, $H^{B'}$), 2.50 (d, 16.5, 1H, $H^{A'}$), 2.6—2.8 (m, 4H, ArH), 3.24 (dd, 11, 1, 1H, H^C), 7.57 (q, 8, 2H, $-C\underline{H}_2CH_3$), 8.10 (d, 1, 3H, CH_3), and 8.94 (t, 8, 3H, $-CH_2C\underline{H}_3$); NMR (CF_3COOD) τ=0.18 (d, 11, 1H, H^B), 1.93 (d, 16.5, 1H, $H^{B'}$), 2.18 (d, 16.5, 1H, $H^{A'}$), 2.6—2.9 (m, 4H, ArH), 3.25 (d, 11, 1H, H^C), 7.54 (q, 8, 2H, $-C\underline{H}_2CH_3$), 8.10 (s, 3H, CH_3), and 8.90 (t, 8, 3H, $-CH_2C\underline{H}_3$). Found: C, 88.40; H, 5.67%. Calcd for $C_{20}H_{16}O$: C, 88.20; H, 5.92%.

*2-Ethyl-1-(o-ethynylphenyl)-7-methyl-1,4,6-nonatrien-8-yn-3-one (**14**).* Potassium hydroxide–ethanol (5.0 ml; 10% W/V) was added to a solution of ketone **11b** (2.40 g, 12.1 mmol) in dry tetrahydrofuran (35 ml), and a solution of aldehyde **7** (2.3 g, 24 mmol) in dry tetrahydrofuran (17 ml) was then added dropwise during 40 min with stirring at 9—10 °C. After stirring for a further 3 h at the same temperature, the reaction was quenched by addition of acetic acid (7 ml). The resulting solution was poured into water (150 ml) and extracted with benzene. The usual working up afforded a red liquid which was chromatographed on alumina (120 g). The early fractions gave the recovered ketone **11b** (586 mg). The following fractions, eluted with hexane–ether (9:1), gave ketone **14** (885 mg, 28%) as a partly crystallized liquid. Crystallization from hexane–benzene afforded yellow cubes: mp 90—92 °C; MS, *m/e*, 274 (M^+, 5%) and 217 (100); mol wt 274.3; IR (KBr disk) 3300, 3250 (–C≡CH), 2100 (–C≡C–), 1650 (C=O), 1595 (C=C), and 980 cm^{-1} (*trans* C=C); UV_{max} (ether) 226 (21000), 244 (18000), and 315 nm (22200); NMR τ=2.17 (dd, 15, 11, 1H, $H^{B'}$), 2.30 (s, 1H, H^B), *ca.* 2.4—2.8 (m, 4H, ArH), 3.13 (d, 15, 1H, $H^{A'}$), 3.45 (d, 11, 1H, $H^{C'}$) 6.50 (s, 1H, –C≡CH), 6.60 (s, 1H, –C≡CH), 7.42 (q, 8, 2H, $-C\underline{H}_2CH_3$), 7.93 (s, 3H, CH_3), and 8.92 (t, 8, 3H, $-CH_2C\underline{H}_3$). Found: C, 87.59; H, 6.40%. Calcd for $C_{20}H_{18}O$: 87.56; H, 6.61%.

*2-Ethyl-10-methyl-4,5-benzo-6,8-bisdehydro[13]annulenone (**5**).* A solution of ketone **14** (737 mg, 2.7 mmol) in pyridine–dry ether (3:1, 56 ml) was added dropwise during 2.5 h to a stirred solution of anhydrous copper(II) acetate (3.4 g) in pyridine–dry ether (3:1, 120 ml) at 45—50 °C (bath). The solution was stirred at the same temperature for a further 45 min and then cooled. After working up as in the preparation of **3**, the red liquid obtained was chromatographed on alumina (100 g). The fractions eluted with hexane–ether (9:1), gave benzannulenone **5** (269 mg, 37%). Recrystallization from hexane–benzene afforded yellow cubes: mp 101—102 °C; MS, *m/e*, 272 (M^+, 100%); mol wt 272.3; IR (KBr disk) 2150 (–C≡C–), 1625 (C=O), 1595 (C=C), and 970 cm^{-1} (*trans* C=C); UV, see Tables 1 and 2; NMR τ=1.98 (dd, 16, 9, 1H, $H^{B'}$), 2.17 (s, 1H, H^B), 2.5—2.8 (m, 4H, ArH), 2.87 (d, 16, 1H, $H^{A'}$), 3.40 (d, 9, 1H, $H^{C'}$), 7.52 (q, 8, 2H, $-C\underline{H}_2CH_3$), 8.10 (s, 3H, CH_3), 9.02 (t, 8, 3H, $-CH_2C\underline{H}_3$); NMR (CF_3COOD) τ=1.31 (dd, 16, 11, 1H, $H^{B'}$), 2.28 (s, 1H, H^B), 2.5—2.7 (m, 4H, ArH), 3.12 (d, 16, 1H, $H^{A'}$), 3.25 (d, 11, 1H, $H^{C'}$), 7.47 (q, 8, 2H, $-C\underline{H}_2CH_3$), 8.00 (s, 3H, CH_3), and 8.97 (t, 8, 3H, $-CH_2C\underline{H}_3$). Found: C, 88.44; H, 5.76%. Calcd for $C_{20}H_{16}O$: C, 88.20; H, 5.92%.

*2-Ethyl-1,5-bis(o-ethynylphenyl)-1,4-pentadien-3-one (**15**).* A solution of *o*-ethynylbenzaldehyde **10** (2.0 g, 15 mmol) in deoxygenated ether (17 ml) was added dropwise during 30 min with ice-bath cooling to a stirred solution of ketone **11b** (0.86 g, 4 mmol) in deoxygenated ether (43 ml) containing ethanolic sodium ethoxide (24 ml) [from sodium (0.38 g) and absolute ethanol (50 ml)]. After stirring for a further 8 h at the same temperature, the reaction was quenched by addition of aqueous oxalic acid. The mixture was poured into water (100 ml) and extracted with benzene. After usual working up, the semi-solid obtained was chromatographed on alumina (120 g). The early fractions gave the recovered aldehyde **10** (434 mg). The following fractions eluted with hexane–ether (4:1) gave ketone **15** (626 mg, 47%). Recrystallization from hexane–benzene afforded light yellow needles: mp 117—118 °C; MS, *m/e*, 310 (M^+, 13%) and 155 (100); mol wt 310.3; IR (KBr disk) 3250 (–C≡CH), 2150 (–C≡C–), 1655 (C=O), 1600 (C=C), and 980 cm^{-1} (*trans* C=C); UV_{max} (ether) 225

(28800), 245 (25200), 254 sh (20600), and 302 nm (16700); NMR τ=1.78 (d, 16, 1H, $H^{B'}$), 2.18 (s, 1H, H^{B}), *ca.* 2.4—2.8 (m, 9H, $H^{A'}$ and ArH), 6.54 (s, 1H, $-C\equiv CH$), 6.62 (s, 1H, $-C\equiv CH$), 7.38 (q, 8, 2H, $-C\underline{H}_2CH_3$), and 8.87 (t, 8, 3H, $-CH_2C\underline{H}_3$). Found: C, 89.18; H, 5.67%. Calcd for $C_{23}H_{18}O$: C, 89.00; H, 5.85%.

2-Ethyl-4,5:10,11-dibenzo-6,8-bisdehydro[13]annulenone (6). A solution of ketone **15** (0.52 g, 1.7 mmol) in pyridine–dry ether (3:1, 36 ml) was added dropwise during 3.5 h to a stirred solution of anhydrous copper(II) acetate (2.2 g) in pyridine–dry ether (3:1, 80 ml) at 45—50 °C. The solution was stirred for a further 30 min at the same temperature and then cooled. After working up as in the preparation of **3**, the brown solid obtained was chromatographed on alumina (90 g). The fractions eluted with hexane–ether (3:2) gave dibenzannulenone **6** (241 mg, 46%). Recrystallization from hexane–benzene afforded yellow needles: mp 154 °C (dec); MS, *m/e*, 308 (M^+, 100%); mol wt 308.3; IR (KBr disk) 2200 (–C≡C–), 1660 (C=O), 1610 (C=C), 995 and 985 cm^{-1} (*trans* C=C); UV, see Tables 1 and 2; NMR τ=1.86 (s, 1H, H^{B}), 1.97 (d, 16, 1H, $H^{B'}$), 2.18 (d, 16, 1H, $H^{A'}$), *ca.* 2.5—2.8 (m, 8H, ArH), 7.40 (q, 8, 2H, $-C\underline{H}_2CH_3$), and 8.90 (t, 8, 3H, $-CH_2C\underline{H}_3$); NMR (CF_3COOD) τ=1.66 (s, 1H, H^{B}), 1.72 (d, 16, 1H, $H^{B'}$), 1.98 (d, 16, 1H, $H^{A'}$), *ca.* 2.4—2.8 (m, 8H, ArH), 7.35 (q, 8, 2H, $-C\underline{H}_2CH_3$), and 8.89 (t, 8, $-CH_2C\underline{H}_3$). Found: C, 89.31; H, 5.00. Calcd for $C_{23}H_{16}O$: C, 89.58; H, 5.23%.

This work was financially supported in part by a Grant-in-Aid for Scientific Research No. 554141 from the Ministry of Education, Science and Culture, and from the Itô Science Foundation.

References

1) T. M. Cresp, J. Ojima, and F. Sondheimer, *J. Org. Chem.*, **42**, 2130 (1977).
2) J. Ojima and M. Fujiyoshi, *J. Chem. Soc., Perkin Trans. 1*, **1980**, 466.
3) H. O. House, "Modern Synthetic Reactions," 2nd ed, ed by W. A. Benjamin, Menlo Park, California (1972), Chap. 10, and the references cited therein.
4) J. Ojima, T. Katakami, G. Nakaminami, and M. Nakagawa, *Bull. Chem. Soc. Jpn.*, **49**, 292 (1976).
5) J. Ojima, T. Yokomachi, and A. Kimura, *Bull. Chem. Soc. Jpn.*, **49**, 2840 (1976).
6) N. Darby, T. M. Cresp, and F. Sondheimer, *J. Org. Chem.*, **42**, 1960 (1977).
7) J. Ojima, Y. Yokoyama, and M. Enkaku, *Bull. Chem. Soc. Jpn.*, **50**, 1522 (1977).
8) M. Nakagawa, *Angew. Chem.*, **91**, 215 (1979); *Angew. Chem. Int. Ed.*, **18**, 202 (1979).
9) Y. Aso, M. Iyoda, and M. Nakagawa, *Tetrahedron Lett.*, **1979**, 4217.

Syntheses and Properties of α-Ethyl-substituted Bisdehydro-[15]annulenones

Jūro Ojima* and Yoshiko Murosawa

Department of Chemistry, Faculty of Science, Toyama University, Gofuku, Toyama 930

(Received March 2, 1981)

2-Ethyl-5,10-dimethyl- and 15-ethyl-5,10-dimethyl-6,8-bisdehydro[15]annulenone were synthesized. Influence of α-ethyl substitution upon the skeleton of the bisdehydro[15]annulenone ring system is discussed on the basis of ^{1}H NMR and UV spectra of these annulenones and their α-methyl-substituted derivatives.

In a previous paper[1] we reported the synthesis of the diatropic bisdehydro[15]annulenones **1**—**3** and showed that the planarity, *i.e.*, the rigidity of molecular skeleton, of bisdehydro[15]annulenone ring system decreases in the sequence of **1**>**2**>**3**, reflecting the effect of perturbation caused by the introduction of α-methyl substituent. Since 3-ethyl-2-alkanones **6**[2] and **9** were made available, we examined the effect of α-ethyl group on the molecular skeleton of bisdehydro[15]annulenone ring system.

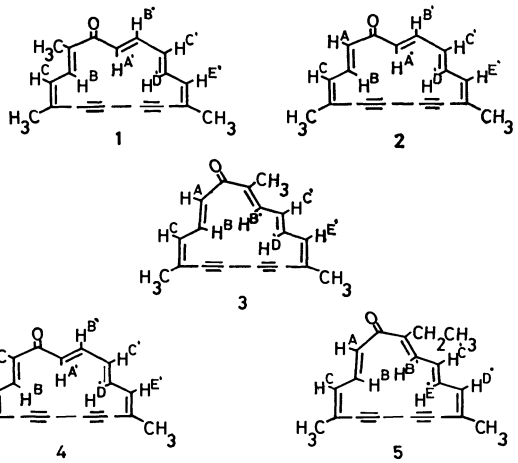

Results and Discussion

Synthesis. Annulenones **4** and **5** were synthesized by a reaction sequence similar to that used for their corresponding α-methyl derivatives.[1] Condensation of ketone **6**,[2] obtained from aldehyde **10**[3] and 2-pentanone, with (2*E*,4*Z*)-5-methyl-2,4-heptadien-6-ynal **7**[4] in the presence of ethanolic sodium ethoxide in ether gave the acyclic ketone **8** in 75% yield. Oxidative coupling of **8** with anhydrous copper(II) acetate in pyridine and dry ether at 50 °C[5] gave annulenone **4** in 38% yield. Acid-catalyzed aldol condensation of **7** with 2-pentanone yielded ketone **9** in 34% yield. Reaction of **9** and **10**, under the same conditions as for **6** and **7**, afforded ketone **11** in 36% yield. Oxidation of **11**, as with **8**, afforded another annulenone **5** in 34% yield. 2-Ethyl-5,10-dimethyl-**4** and 15-ethyl-5,10-dimethyl-6,8-bisdehydro[15]annulenone **5** formed yellow needles (mp 145—146 °C) and orange cubes (mp 97—98 °C), respectively; both **4** and **5** appear to be considerably stable. All the new compounds gave spectral data consistent with the assigned structures and satisfactory results of elemental analysis were obtained except for the unstable acyclic ketone **11**.

Treatment of annulenone **4** or **5** with trifluoroacetic acid or trifluoroacetic acid-*d* gave a red solution indicating formation of the protonated or deuteronated species **4'** or **5'**, respectively. Quenching of **4'** or **5'** with aqueous sodium hydrogencarbonate resulted in regeneration of **4** or **5**, respectively.

Properties. Electronic absorption maxima of these annulenones **4** and **5** as well as related derivatives **1**—**3**[1] are listed in Table 1. As expected, the spectra are similar to one another. However, the main and longest wavelength bands exhibit a small bathochromic shift in the sequence of **4**>**1**>**2** as the α-substituent at C_2-position passes from ethyl *via* methyl to hydrogen, whereas in the spectra of **3** and **5**, the positions of these maxima are in relatively short wavelengths and appear to be independent of alkyl substitution at C_{15}-position, reflecting that the molecular skeletons of **3** and **5** are less planar than those of **1**, **2**, and **4**. The absorption maxima of these annulenones **1**—**5** in tri-

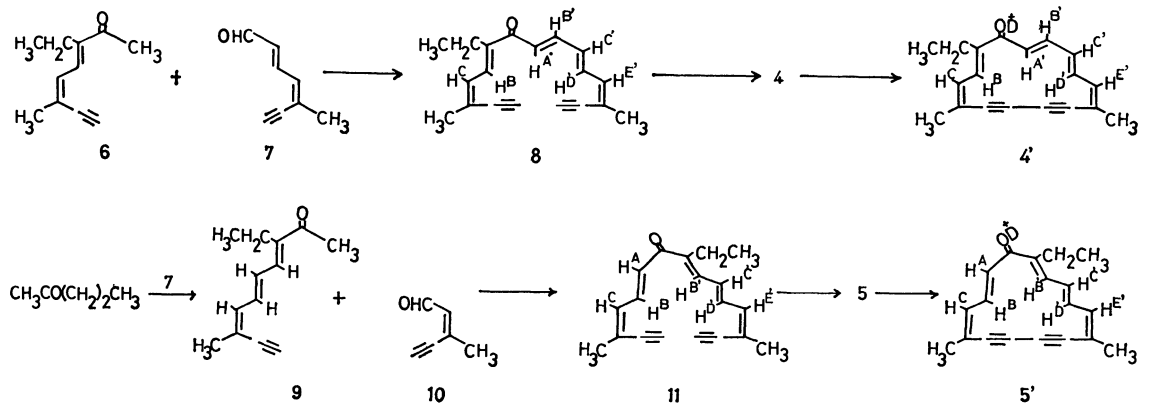

Table 1. Electronic absorption maxima of bisdehydro[15]annulenones in ether λ_{max}/nm (ε_{max})

1[a]		**2**[a]		**3**[a]		**4**		**5**	
232 sh	(13400)	247 sh	(13000)	247 sh	(12500)	221 sh	(17500)	247 sh	(12600)
246	(13800)	258	(14300)	257 sh	(14200)	247	(12200)	252 sh	(13300)
258	(14800)	301	(33200)	298	(40500)	258	(13700)	258 sh	(14700)
304	(42600)	382	(5700)	366	(6530)	308	(41200)	297	(37800)
310 sh	(41200)					387	(7350)	369	(6540)
384	(7880)								

a) See Ref. 1.

Table 2. Electronic absorption maxima of bisdehydro[15]annulenones in trifluoroacetic acid λ_{max}/nm (Relative extinction coefficient)

1[a]		**2**[a]		**3**[a]		**4**		**5**	
298 sh	(0.08)	292	(0.08)	350	(1.00)	356 sh	(0.72)	350	(1.00)
356 sh	(0.72)	352 sh	(0.68)	366 sh	(0.72)	371	(1.00)	366 sh	(0.74)
370	(1.00)	367	(1.00)	502	(0.35)	470 sh	(0.07)	502	(0.34)
470 sh	(0.11)	496 sh	(0.15)	536	(0.35)	500 sh	(0.16)	536	(0.33)
500 sh	(0.18)	513	(0.19)			524	(0.20)		
524	(0.23)	555	(0.34)			562	(0.25)		
562	(0.29)								

a) See Ref. 1.

Table 3. ^{1}H NMR chemical shifts of **1**—**5**, **8**, **11** (in $CDCl_3$), and **1′**—**5′** (in CF_3COOD) at 90 MHz, determined at 35 °C (τ Value; Internal standard, Me_4Si)

Compd	H^A	$H^{A'}$	H^B	$H^{B'}$	H^C	$H^{C'}$	$H^{D'}$	$H^{E'}$	CH_3	$-C\underline{H}_2CH_3$	$-CH_2C\underline{H}_3$
1[a]		4.50	4.48	2.37	2.57	3.15	4.71	2.75	7.71, 7.79		
1′[a]		10.57	10.60	0.17	0.60	1.20	10.69	0.80	6.68, 6.75, 6.80		
2[a]	3.35	4.37	4.17	2.44	2.75	3.19	4.53	2.75	7.76, 7.82		
2′[a]	1.31	10.10	9.92	0.29	0.89	1.28	10.15	0.89	6.73, 6.82		
3[a]	3.33		4.38	4.53	2.73	2.87	4.61	2.91	7.79, 7.90, 7.95		
3′[a]	1.60		8.52	8.05	1.30	1.25	8.95	1.33	6.89, 7.07, 7.12		
8		3.12	2.48	2.57	3.26	3.52	2.87	3.56	7.90, 7.98	7.47	8.97
4		4.47	4.50	2.36	2.56	3.14	4.69	2.73	7.70, 7.80	7.25	8.84
4′[b]		10.53	10.58	0.17	0.60	1.20	10.67	0.77	6.60, 6.73	6.18	8.30
Δ(**4**−**8**)		+1.35	+2.02	−0.21	−0.70	−0.38	+1.82	−0.83	−0.10—−0.28	−0.22	−0.13
Δ(**4′**−**8**)		+7.41	+8.10	−2.40	−2.66	−2.22	+7.80	−2.79	−1.17—−1.38	−1.29	−0.67
11	3.15		2.25	2.85	3.50	2.93	3.35	3.50	7.97	7.47	8.97
5	3.30		4.38	4.58	2.73	2.82	4.62	2.90	7.80, 7.92	7.42	9.00
5′[b]	1.60		8.46	8.02	1.30	1.23	8.83	1.30	6.93, 7.07	6.60	8.50
Δ(**5**−**11**)	+0.15		+2.13	+1.73	−0.77	−0.11	+1.27	−0.60	−0.05—−0.17	−0.05	+0.03
Δ(**5′**−**11**)	−1.55		+6.21	+5.17	−2.20	−1.70	+5.48	−2.20	−0.90—−1.04	−0.87	−0.47

a) See Ref. 1. b) Determined with CH_2Cl_2 as an internal standard.

Table 4. ^{1}H NMR chemical shifts of compounds **4** and **5** (in $CDCl_3$) at 100 MHz (τ Value; Internal standard, Me_4Si)

Compd	T/°C	H^A	$H^{A'}$	H^B	$H^{B'}$	H^C	$H^{C'}$	$H^{D'}$	$H^{E'}$	$-C\underline{H}_2CH_3$	CH_3	$-CH_2C\underline{H}_3$
4	+60		4.44	4.46	2.45	2.66	3.24	4.62	2.83	7.30	7.75, 7.84	8.88
	+22		4.51	4.54	2.42	2.64	3.20	4.73	2.80	7.30	7.73, 7.82	8.88
	−30		4.60	4.68	2.36	2.58	3.14	4.89	2.73	7.29	7.69, 7.79	8.88
	−60		4.63	4.74	2.32	2.54	3.09	4.95	2.68	7.28	7.65, 7.76	8.88
5	+60	3.40		4.33	4.59	2.86	2.94	4.58	3.01	7.46	7.84, 7.96	9.01
	+22	3.36		4.43	4.63	2.81	2.90	4.66	2.98	7.45	7.82, 7.92	9.02
	−30	3.30		4.60	4.74	2.76	2.80	4.78	2.92	7.44	7.77, 7.88	9.02
	−60	3.26		4.68	4.77	2.72	2.75	4.83	2.88	7.41	7.74, 7.83	9.02

fluoroacetic acid are given in Table 2, and it is evident that protonation of **4** and **5** with this acid causes shift of main maxima to longer wavelengths, similarly to the case of **1**—**3**. The main maxima of these annulenones in trifluoroacetic acid exhibit a bathochromic shift in the order of **4**≃**1**>**2**>**3**≃**5**, suggesting that the positions of main maxima do not depend on alkyl substitution, but on molecular planarity (*vide infra*). Also, the bathochromic shifts (53—63 nm) of the main maxima of **4** and **5** by protonation are much larger than that observed for their corresponding α-ethyl-substituted bisdehydro[13]annulenone (7 nm);[2] similar relations have been observed between [4*n*−2]- and [4*n*]annulenes and dehydroannulenes.[6]

^{1}H NMR chemical shifts of the protons of **4**, **5**, **8**, and **11**, together with those of **1**—**3** reported by us[1] are summarized in Table 3. The individual assignments, some of which are tentative, were made on the basis of multiplicity, coupling constants (Experimental), and data of closely related compounds.[1]

A comparison of the ^{1}H NMR chemical shifts of various protons of annulenones **4** and **5** with those of their corresponding acyclic ketones **8** and **11** indicates that both **4** and **5** are diatropic, as might be expected with 14π-electron systems. This follows from the fact that all the inner protons in **4** and **5** resonate at higher fields than their corresponding protons in **8** and **11**, respectively, whereas essentially all the outer protons (including allylic methylene and methyl protons) in **4** and **5** resonate at lower fields.

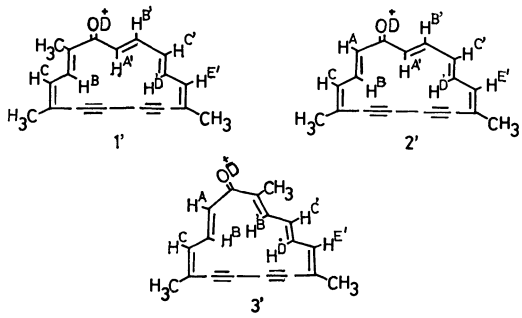

^{1}H NMR chemical shifts of the deuteronated species **1**′—**5**′, obtained through dissolution in trifluoroacetic acid-*d*, are also given in Table 3. It is evident that the conformations of **4** and **5** are unchanged. A comparison of the chemical shifts of various protons of **4**′ and **5**′ with those of their corresponding acyclic models **8** and **11**, as with **4** and **5** mentioned above, indicates that the diatropicities of the deuteronated species **4**′ and **5**′ are much more marked than those of annulenones **4** and **5**, respectively.

Variable-temperature ^{1}H NMR spectra of **4** and **5**, recorded over the range of −60 to 60 °C and summarized in Table 4, show that temperature has essentially no effect on spectra of **4** or **5**. Spectra of ethyldimethylbisdehydro[13]annulenone **5**, expected to be more mobile than **4**, are shown in Fig. 1. On cooling, the resonance of the inner (H^B, $H^{B'}$, $H^{D'}$) protons of **5** shifts to a slightly higher field, whereas that of the outer (H^A, H^C, $H^{C'}$, $H^{E'}$) protons (including allylic methylene and methyl protons) to a slightly

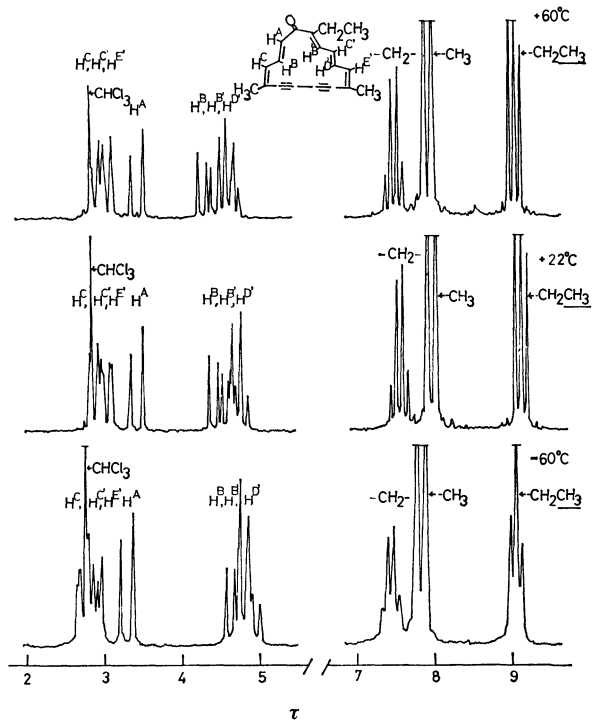

Fig. 1. The ^{1}H NMR FT spectra of **5** in $CDCl_3$ at 100 MHz (internal standard, TMS).

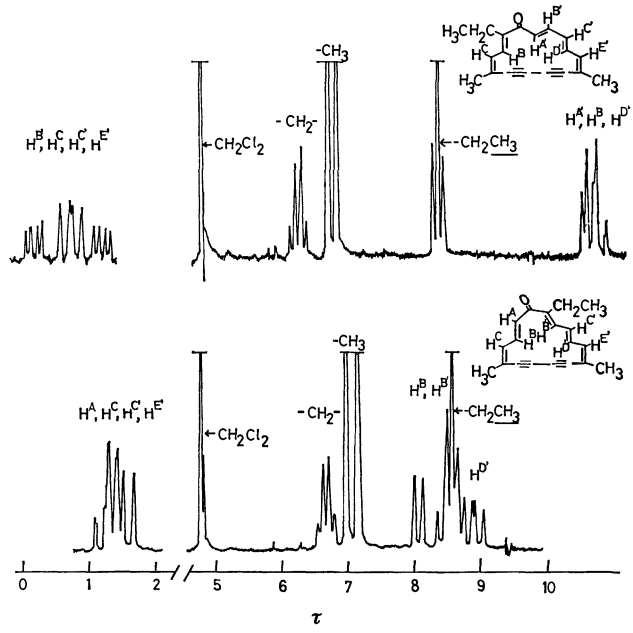

Fig. 2. The 90 MHz ^{1}H NMR spectra of **4** and **5** in CF_3COOD at 35 °C.

lower field. However, the $J_{B,C}$ value (11 Hz), indicating an s-*trans* relationship of the H^B and H^C bonds, does not vary in the range −60—60 °C, excluding any change in conformation due to rotation of the CH^A=CH^B double bond over this temperature range, in contrast to the case of α-ethyl-substituted bisdehydro[13]annulenones.[2] The signals of both the inner and outer protons of **4** exhibit less temperature dependence than those of **5** in the range −60—60 °C (Table 4), reflecting an enhanced rigidity in the mo-

lecular skeleton of **4**. This tendency is manifested very markedly in the spectra of **4** and **5** in trifluoroacetic acid-*d*, illustrated in Fig. 2. It is to be noted that the magnitudes of upfield shifts of the inner protons and of downfield shifts of the outer and methyl protons decrease in the order of **4**>**5**. Also, the chemical shifts of the olefinic and methyl protons of **4**′ are almost the same with those of their corresponding protons of **1**′. Similar relations in chemical shift are seen between **3**′ and **5**′ (Table 3). This fact suggests that the planarity, *i.e.*, the rigidity, of this bisdehydro[15]annulenone ring system decreases in the sequence of **4**≃**1**>**2**>**3**≃**5**. This interpretation, already presented on a different basis, is supported by the fact that their bathochromic shifts in main maxima as well as the longest wavelength bands are in the same sequence in both ether and trifluoroacetic acid (Tables 1 and 2).

Thus, the difference in behavior observed for the bisdehydro[15]annulenone ring system against the α-ethyl and α-methyl substitutions is not so large as that for the corresponding bisdehydro[13]annulenone system,[2] reflecting higher planarity of the molecular skeleton of the former system.

Experimental

Deoxygenated ether was prepared and used as reported.[1,2] Melting points were uncorrected. IR spectra were taken with a Hitachi EPI-S2 spectrophotometer. UV spectra were measured on a Hitachi 124 spectrophotometer and recorded in nm. ε-Values are given in parentheses, shoulders being denoted by sh. Mass spectra were recorded with a JEOL JMS-200 spectrometer operating at 75 eV. ^{1}H NMR spectra were recorded with a Varian EM-390 (90 MHz) or a JEOL FX-100 (100 MHz) spectrometer. Data taken with a Varian EM-390 instrument at 35 °C are specified by τ-value for $CDCl_3$ solution, TMS being used as an internal standard unless otherwise stated. Coupling constants (J) are given in Hz. Merck alumina (Act. II—III) was used for column chromatography. Sodium sulfate was used as drying agent, and solvents were evaporated at the water aspirator pressure.

6-Ethyl-3,13-dimethyl-3,5,8,10,12-pentadecapentaene-1,14-diyn-7-one (8). A solution of aldehyde **7**[4] (1.10 g, 9.3 mmol) in deoxygenated ether (17 ml) was added dropwise during 30 min to a stirred ice-cooled solution of ketone **6**[2] (1.0 g, 6.2 mmol) in deoxygenated ether (47 ml) containing ethanolic sodium ethoxide (6.7 ml) [from sodium (760 mg) and absolute ethanol (50 ml)]. After stirring for 5 h, portions of the ethanolic sodium ethoxide (each 2.0 ml) were added every 2 h. After stirring for a total 8 h, the reaction was quenched by addition of aqueous oxalic acid. The solution was poured into water and extracted with benzene. The benzene extracts were washed successively with aqueous sodium hydrogencarbonate and brine, and then dried. The semi-solid obtained after removal of the solvent was chromatographed on alumina (80 g). The early fractions gave the recovered ketone **6** (188 mg). The later fractions eluted with hexane–ether (4:1) gave ketone **8** (1.23 g, 75%) as a solid. Recrystallization from hexane–benzene afforded orange needles: mp 69—70 °C; MS, *m/e*, 264 (M^+, 74%) and 192 (100); mol wt 264.3; IR (KBr disk) 3300 (–C≡CH), 2100 (–C≡C–), 1640 (C=O), 1610, 1585 (C=C), and 1085 cm^{-1} (*trans* C=C); UV_{max} (ether) 225 sh (10300), 231 (10900), 253 sh (16100), 266 (20500), 277 (20800), 290 (21400), 304 (22800), 340 sh (32000), 356 (36100), and 373 nm sh (29600); NMR τ=2.48 (d, 11, 1H, H^B), 2.57 (dd, 15, 11, 1H, $H^{B'}$ or $H^{C'}$ or $H^{D'}$), 2.87 (dd, 15, 11, 1H, $H^{B'}$ or $H^{C'}$ or $H^{D'}$), 3.12 (d, 15, 1H, $H^{A'}$), 3.26 (d, 11, 1H, H^C or $H^{E'}$), 3.52 (dd, 15, 11, 1H, $H^{B'}$ or $H^{C'}$ or $H^{D'}$), 3.56 (d, 11, 1H, H^C or $H^{E'}$), 6.43 (s, 1H, –C≡CH), 6.53 (s, 1H, –C≡CH), 7.47 (q, 8, 2H, $-C\underline{H}_2CH_3$), 7.90 (s, 3H, CH_3), 7.98 (s, 3H, CH_3), and 8.97 (t, 8, 3H, $-CH_2C\underline{H}_3$). Found: C, 86.05; H, 7.43%. Calcd for $C_{19}H_{20}O$: C, 86.32; H, 7.63%.

2-Ethyl-5,10-dimethyl-6,8-bisdehydro[15]annulenone (4). A solution of ketone **8** (1.17 g, 4.4 mmol) in pyridine (79 ml) and dry ether (27 ml) was added dropwise to a stirred solution of anhydrous copper(II) acetate (5.3 g) in pyridine (159 ml) and dry ether (53 ml) during 6 h at 49—52 °C. The solution was stirred for a further 30 min at the same temperature, and then cooled. After addition of benzene (300 ml), the mixture was filtered through a Hyflo Super-Cel. The precipitates formed were washed with benzene (100 ml×3) and the filtrate was poured into water. The organic layer was separated and the aqueous layer was extracted with benzene. The combined organic extracts were washed successively with 7% hydrochloric acid, aqueous sodium hydrogencarbonate, and brine, and then dried. The semi-solid obtained after removal of the solvent was chromatographed on alumina (80 g). The fractions eluted with hexane–ether (7:3) gave annulenone **4** (434 mg, 38%). Recrystallization from hexane–benzene afforded yellow needles: mp 145—146 °C; MS, *m/e*, 262 (M^+, 27%) and 203 (100); mol wt 262.3; IR (KBr disk) 2170 (–C≡C–), 1635 (C=O), 1610 (C=C), and 975 cm^{-1} (*trans* C=C); UV, see Tables 1 and 2; NMR τ=2.36 (dd, 16, 5, 1H, $H^{B'}$ or $H^{C'}$), 2.56 (d, 11, 1H, H^C or $H^{E'}$), 2.73 (d, 11, 1H, H^C or $H^{E'}$), 3.14 (dd, 16, 5, 1H, $H^{B'}$ or $H^{C'}$), 4.47 (d, 16, 1H, $H^{A'}$), 4.50 (d, 11, 1H, H^B), 4.69 (dd, 16, 11, 1H, $H^{D'}$), 7.25 (q, 8, 2H, $-C\underline{H}_2CH_3$), 7.70 (s, 3H, CH_3), 7.80 (s, 3H, CH_3), and 8.84 (t, 8, 3H, $-CH_2C\underline{H}_3$); NMR (CF_3COOD, determined with CH_2Cl_2 as an internal standard) τ=0.17 (dd, 15, 7, 1H, $H^{B'}$ or $H^{C'}$), 0.60 (d, 12, 1H, H^C or $H^{E'}$), 0.77 (d, 12, 1H, H^C or $H^{E'}$), 1.20 (dd, 15, 7, 1H, $H^{B'}$ or $H^{C'}$), 6.18 (q, 8, 2H, $-C\underline{H}_2CH_3$), 6.60 (s, 3H, CH_3), 6.73 (s, 3H, CH_3), 8.30 (t, 8, 3H, $-CH_2C\underline{H}_3$), 10.53 (d, 15, 1H, $H^{A'}$), 10.58 (d, 12, 1H, H^B), and 10.67 (dd, 15, 11, 1H, $H^{D'}$), and see Fig. 2. Found: C, 87.15; H, 6.84%. Calcd for $C_{19}H_{18}O$: C, 86.98; H, 6.91%.

3-Ethyl-8-methyl-3,5,7-decatrien-9-yn-2-one (9). A solution of aldehyde **7**[4] (3.0 g, 25 mmol) in acetic acid (13 ml) was added dropwise during 20 min to a stirred solution of 2-pentanone (15.1 g, 0.175 mol) and concentrated sulfuric acid (4.7 ml) in acetic acid (95 ml) at 8—9 °C. The solution was stirred for a further 3 h, and then cautiously poured into saturated aqueous potassium carbonate (200 ml). The mixture was diluted with water, and extracted with benzene. The extracts were washed with saturated aqueous sodium chloride solution, and then dried. The dark red liquid obtained was chromatographed on alumina (80 g). The fractions eluted with hexane–ether (9:1—4:1) gave ketone **9** (1.59 g, 34%) as a yellow liquid: MS, *m/e*, 188 (M^+, 80%) and 159 (100); mol wt 188.2; IR (neat) 3250 (–C≡CH), 2100 (–C≡C–), 1655 (C=O), 1610, 1595 (C=C), and 980 cm^{-1} (*trans* C=C); UV_{max} (ether) 227 (5600), 236 (5710), 310 sh (23700), 331 (32800), and 341 nm sh (32500); NMR τ=2.89 (d, 11, 1H, H^B), 2.95 (dd, 15, 11, 1H, H^D), 3.38 (dd, 15, 11, 1H, H^C), 3.52 (d, 11, 1H, H^E), 6.55 (s, 1H, –C≡CH), 7.56 (q, 8, 2H, $-C\underline{H}_2CH_3$), 7.63 (s, 3H, CH_3), 7.98 (s, 3H, CH_3), and 8.01 (t, 8, 3H, $-CH_2C\underline{H}_3$). Found:

C, 82.68; H, 8.29%. Calcd for $C_{13}H_{16}O$: C, 82.93; H, 8.57%.

*8-Ethyl-3,13-dimethyl-3,5,8,10,12-pentadecapentaene-1,14-diyn-7-one (**11**).* A solution of ethanolic sodium ethoxide (2.4 ml) [from sodium (760 mg) and absolute ethanol (50 ml)] was added to a solution of ketone **9** (1.0 g, 5.3 mmol) in deoxygenated ether (47 ml), and a solution of aldehyde **10**[3] (1.0 g, 11 mmol) in deoxygenated ether (16 ml) was then added dropwise during 15 min with stirring and ice-bath cooling. After stirring for a further 14.5 h at room temperature, the reaction was quenched by addition of aqueous oxalic acid. The mixture was poured into water, and extracted with benzene. After working up as in the preparation of **8**, the semi-solid obtained after removal of the solvent was chromatographed on alumina (100 g). The early fractions gave the recovered ketone **9** (438 mg). The following fractions eluted with hexane–ether (4:1) gave ketone **11** (498 mg, 36%). Recrystallization from hexane–benzene afforded brown needles: mp 92—93 °C; MS, *m/e*, 264 (M^+, 100%); mol wt 264.3; IR (KBr disk) 3250 (–C≡CH), 2100 (–C≡C–), 1640 (C=O), 1580 (C=C), and 985 cm^{-1} (*trans* C=C); UV_{max} (ether) 233 sh (12600), 250 sh (18500), 260 sh (22400), 275 sh (26600), 287 (29900), 299 (29300), 342 sh (44900), 358 (50100), and 375 nm sh (43800); NMR τ=2.25 (dd, 15, 12, 1H, H^B), 2.85 (d, 12, 1H, $H^{B'}$), 2.93 (dd, 15, 12, 1H, $H^{C'}$), 3.15 (d, 15, 1H, H^A), 3.35 (dd, 15, 12, 1H, $H^{D'}$), 3.50 (d, 12, 2H, H^C and $H^{E'}$), 6.53 (s, 1H, –C≡CH), 6.60 (S, 1H, –C≡CH), 7.47 (q, 8, 2H, $-C\underline{H}_2CH_3$), 7.97 (s, 6H, CH_3), and 8.97 (t, 8, $-CH_2C\underline{H}_3$).

Crystals of **11** decomposed rapidly on exposure to diffused light and air at room temperature. Compound **11** gave unsatisfactory results of elemental analysis, which seems attributable to its instability. Found: C, 85.64; H, 7.35%. Calcd for $C_{19}H_{20}O$: C, 86.32; H, 7.63%.

*15-Ethyl-5,10-dimethyl-6,8-bisdehydro[15]annulenone (**5**).* A solution of ketone **11** (370 mg, 1.4 mmol) in pyridine–dry ether (3:1, 32 ml) was added dropwise during 2.5 h to a stirred solution of anhydrous copper(II) acetate (1.8 g) in pyridine–dry ether (3:1, 64 ml) at 48—50 °C. The solution was stirred at 49—51 °C for a further 30 min and then cooled. After working up as in the preparation of **4**, the semi-solid obtained after removal of the solvent was chromatographed on alumina (70 g). The fractions eluted with hexane–ether (3:1—2:3) gave annulenone **5** (124 mg, 34%) as a yellow liquid. Crystallization from hexane–benzene afforded orange cubes: mp 97—98 °C; MS, *m/e*, 262 (M^+, 25%) and 203 (100); mol wt 262.3; IR (KBr disk) 2150, 2100 (–C≡C–), 1620 (C=O), 1590 (C=C), 1000, and 970 cm^{-1} (*trans* C=C); UV, see Tables 1 and 2; NMR τ=2.73 (d, 11, 1H, H^C), 2.82 (dd, 16, 11, 1H, $H^{C'}$), 2.90 (d, 11, 1H, $H^{E'}$), 3.30 (d, 16, 1H, H^A), 4.38 (dd, 16, 11, 1H, H^B), 4.58 (d, 11, 1H, $H^{B'}$), 4.62 (dd, 16, 11, 1H, $H^{D'}$), 7.42 (q, 8, 2H, $-C\underline{H}_2CH_3$), 7.80 (s, 3H, CH_3), 7.92 (s, 3H, CH_3), and 9.00 (t, 8, 3H, $-CH_2C\underline{H}_3$), and see Fig. 1; NMR (CF_3COOD, determined with CH_2Cl_2 as an internal standard) τ=1.23 (dd, 15, 11, 1H, $H^{C'}$), 1.30 (d, 11, 2H, H^C and $H^{E'}$), 1.60 (d, 15, 1H, H^A), 6.60 (q, 8, 2H, $-C\underline{H}_2CH_3$), 6.93 (s, 3H, CH_3), 7.07 (s, 3H, CH_3), 8.02 (d, 11, 1H, $H^{B'}$), 8.46 (dd, 15, 11, 1H, H^B), 8.50 (t, 8, 3H, $-CH_2C\underline{H}_3$), and 8.83 (dd, 15, 11, 1H, $H^{D'}$), and see Fig. 2. Found: C, 87.18; H, 6.82%. Calcd for $C_{19}H_{18}O$: C, 86.98; H, 6.91%.

This work was financially supported in part by a Grant-in-Aid for Scientific Research (No. 554141) from the Ministry of Education, Science and Culture, and from the Itô Science Foundation.

References

1) J. Ojima, K. Wada, K. Kanazawa, and Y. Nakagawa, *J. Chem. Soc., Perkin Trans. 1*, **1981**, 947.

2) J. Ojima, Y. Juni, Y. Yoneyama, K. Wada, and Y. Murosawa, *Bull. Chem. Soc. Jpn.*, **54**, 3466 (1981).

3) J. Ojima, T. Katakami, G. Nakaminami, and M. Nakagawa, *Bull. Chem. Soc. Jpn.*, **49**, 292 (1976).

4) J. Ojima, M. Ishiyama, and A. Kimura, *Bull. Chem. Soc. Jpn.*, **50**, 1584 (1977).

5) N. Darby, T. M. Cresp, and F. Sondheimer, *J. Org. Chem.*, **42**, 1960 (1977).

6) a) P. J. Garratt and K. Grohmann, *Methoden Org. Chem. (Houben-Weyl)*, **5**, 533 (1972); b) J. Ojima, Y. Shiroishi, K. Wada, and F. Sondheimer, *J. Org. Chem.*, **45**, 3564 (1980).

Reduction by a Model of NAD(P)H. 32. Stereoselective Reduction of Camphoroquinone by a Chiral NAD(P)H Model

Atsuyoshi Ohno,* Takehiko Goto, Jun-ichi Nakai, and Shinzaburo Oka
Institute for Chemical Research, Kyoto University, Uji, Kyoto 611

(Received March 9, 1981)

(+)-, (−)-, and racemic camphoroquinones (CQ) were reduced by each of four NAD(P)H-models such as *N*-(α-methylbenzyl)-1-propyl-2,4-dimethyl-1,4-dihydronicotinamide (Me_2PNPH) in the presence of magnesium ion in acetonitrile with a view to elucidating the intermolecular arrangement in the transition state for asymmetric reduction. Partial rate factors for each attacking mode were calculated. Electronegative substituents in the substrate prefer to facing the carbamoyl group in Me_2PNPH, which is the most important factor determining the stereochemical course of the reduction. 1-Methyl group in CQ has a tendency to interfere with the dihydropyridine moiety in Me_2PNPH approaching the C_2-carbonyl group in CQ. This interference is more important for the selectivity than the intrinsic *exo*/*endo* reactivity difference.

Quite a few organic chemists have tried to design their reactions after the model of biochemical transformations which exhibit too high reactivity and stereospecificity. Dihydropyridine nucleotides, NADH and NADPH, are coenzymes of NAD(P)H-dependent dehydrogenases that reduce carbonyl and other unsaturated compounds stereospecifically in almost all organisms. Hence, for bioorganic chemists, reduction by models of NAD(P)H has been an interesting subject to study. In the course of our study on the biomimetic chemistry of NAD(P)H, we have found that bivalent metal ions such as Mg^{2+} and Zn^{2+} affect reduction of carbonyl compounds by models of NAD(P)H.[1-9] A series of investigations has revealed that the reduction is composed of a three-step electron-proton-electron transfer process and that the bivalent metal ion catalyzes the process of initial electron-transfer.[3,6,9,10]

The bivalent metal ions also control stereospecificity of the reduction.[1,2,11-15] For example, reduction of certain carbonyl compounds with *N*-(α-methyl benzyl)-1-propyl-2,4-dimethyl-1,4-dihydronicotinamide (Me_2PNPH) in the presence of magnesium ion results in an excellent asymmetric induction.[15] The configuration of predominant enantiomer of product alcohol is determined from the configuration of the C_4-position of Me_2PNPH. On an assumption that the carbonyl-oxygen in a substrate points toward the ring-nitrogen of Me_2PNPH, it has been proposed that an electronegative polar group in a substrate faces the electronegative carbamoyl group in Me_2PNPH in the transition state for reduction (**1**) and that the relative

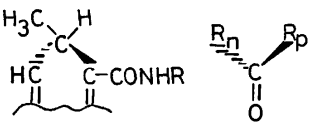

1

R_p: polar substituent
R_n: nonpolar substituent

bulkiness of substituents R_n and R_p plays no important role in determining the configuration of product alcohol.[15] The proposal that two electronegative groups face each other contradicts to a common idea of electronic effect. However, when it gets proved to be correct, it may suggest that the magnesium ion positions itself between the substrate and Me_2PNPH by coordinating two electronegative groups to freeze the intermolecular configuration in the transition state, as an origin of the stereospecificity of the magnesium ion-catalyzed reduction. Thus, it is important, for understanding the role of magnesium ion in the reduction, to get information about the intermolecular arrangement in the transition state for the reduction; for this reason we studied the reduction of 1,7,7-trimethylbicyclo[2.2.1]heptane-2,3-dione (camphoroquinone, CQ) with Me_2PNPH. CQ has two carbonyl groups constrained in a rigid framework, and the oxygen atom in the reacting carbonyl group will be caused to point toward the ring-nitrogen of Me_2PNPH in the transition state because of the large steric effect.

Results

(−)-CQ, (+)-CQ, and (±)-CQ were reduced by (4*R*)-N-[(*R*)-α-methylbenzyl]-1-propyl-2,4-dimethyl-1,4-dihydronicotinamide (*RR*-Me_2PNPH), *SS*-Me_2-PNPH, [(*R*)-α-methylbenzyl]-1-propyl-1,4-dihydronicotinamide (*R*-PNPH), 1-propyl-1,4-dihydronicotinamide (PNAH), or 1-benzyl-1,4-dihydronicotinamide (BNAH). All reactions were carried out in dry acetonitrile in the presence of magnesium ion in equivalent amount at room temperature under an argon atmosphere in the dark. The reduction did not proceed without magnesium ion. (−)-CQ afforded a mixture of diastereomeric isomers of four α-keto

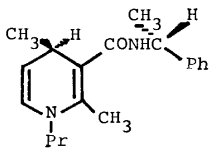

RR-Me_2PNPH

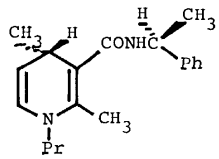

SS-Me_2PNPH

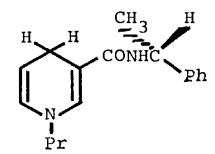

R-PNPH

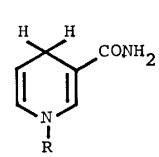

R = Pr : PNAH

R = $PhCH_2$: BNAH

alcohols: (2*S*)-2-*exo*-hydroxy-1,7,7-trimethylbicyclo-[2.2.1]heptan-3-one (2*S*-*exo*-hydroxyepicamphor, *X*-**2a**), (2*R*)-2-*endo*-hydroxy-1,7,7-trimethylbicyclo[2.2.1]-heptan-3-one (2*R*-*endo*-hydroxyepicamphor, *D*-**2a**), (3*R*)-3-*exo*-hydroxy-1,7,7-trimethylbicyclo[2.2.1]heptan-2-on (3*R*-*exo*-hydroxycamphor, *X*-**3a**), and (3*S*)-*endo*-hydroxy-1,7,7-trimethylbicyclo[2.2.1]heptan-2-one(3*S*-*endo*-hydroxycamphor, *D*-**3a**), whereas (+)-CQ afforded a mixture of their corresponding enantiomeric isomers *X*-**2b**, *D*-**2b**, *X*-**3b**, and *D*-**3b** (Scheme 1).

Structures and relative yields of products were determined on the basis of ^{1}H-NMR spectra.[16] Results for the reductions with BNAH, PNAH, and *R*-PNPH are summarized in Table 1 and those with Me_2PNPH in Table 2. It was confirmed that no isomerization took place between isomeric products.

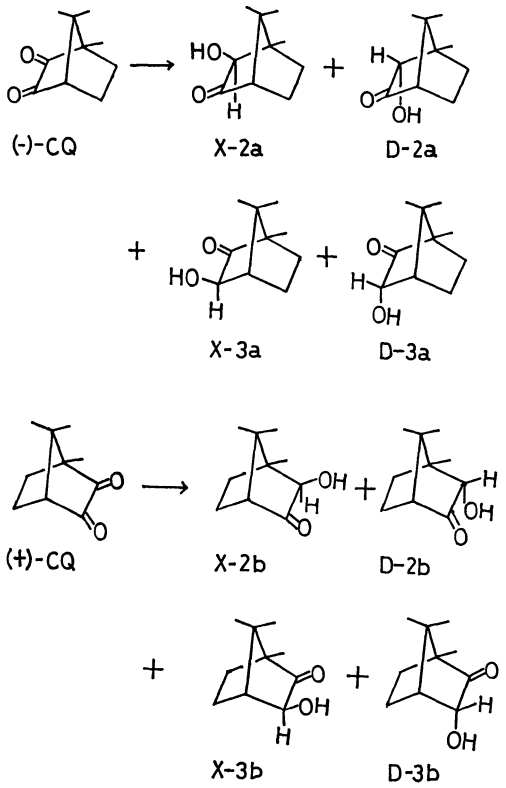

Scheme 1.

Discussion

CQ has two prochiral carbonyl groups and it is potentially possible that four isomers are to be formed as reduction products. Since these carbonyl groups are frozen to the *Z*-configuration on a rigid hydrocarbon framework which has diastereotopic faces, the ratio of the yields of these isomers reflects the configurational requirement for the carbonyl group in the transition state for the reduction. The results in Table 1 indicate that the *exo*-C_3-attack (see Scheme 2) is the most preferential process in the reduction with such models as have two available hydrogens on the C_4-position, whereas the other modes of attack

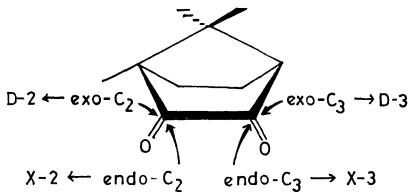

Scheme 2.

Table 1. Reduction of camphoroquinone with NAD(P)H-models

Substrate	Model	*T*/h[a]	CQ_{rec}(%)[b]	*Y*/%[c]	Product ratio[d]			
					X-**2a**	*D*-**2a**	*X*-**3a**	*D*-**3a**
(−)-CQ	BNAH	235	42.3	7.3	14	13	16	57
(−)-CQ	PNAH	48	65.6	4.3	13	11	24	52
(−)-CQ	*R*-PNPH	91	50.2	8.6	15	9	14	62
					X-**2b**	*D*-**2b**	*X*-**3b**	*D*-**3b**
(+)-CQ	*R*-PNPH	91	61.6	6.8	8	10	20	62

a) *T* is reaction time. b) CQ_{rec} is the recovered, isolated CQ. c) *Y* is the yield of product isolated. d) Relative intensities of ^{1}H-HMR signals.

Table 2. Reduction of camphoroquinone with *N*-(α-methylbenzyl)-1-propyl-2,4-dimethyl-1,4-dihydronicotinamide (Me_2PNPH)

Substrate	Config. of Me_2PNPH	*T*/h[a]	CQ_{rec}(%)[a]	*Y*/%[a]	Product ratio[a]			
					X-**2a**	*D*-**2a**	*X*-**3a**	*D*-**3a**
(−)-CQ	*RR*	52	57.7	40.6	8	19	68	5
(−)-CQ	*SS*	52	36.2	67.6	20	16	6	58
					X-**2b**	*D*-**2b**	*X*-**3b**	*D*-**3b**
(+)-CQ	*RR*	52	53.1	47.3	21	14	7	58
(+)-CQ	*SS*	52	50.9	58.7	7	21	62	10
					X-**2**[b]	*D*-**2**[b]	*X*-**3**[b]	*D*-**3**[b]
(±)-CQ[c]	*SS*	52	46.0	54.1	14	16	27	43

a) See footnotes in Table 1. b) Mixture of **a** and **b**. c) Racemic camphoroquinone.

appear to have no practical predominance. The chirality of the side chain of *R*-PNPH plays no important role in determining the stereochemistry of the product. The observation reveals that the stereochemistry of the reduction depends on the structural preference of substrate and that no enantiotopic difference for the dihydropyridine ring has any effect. It should be noted that it is the C_1-methyl group that makes the C_3-attack preferential to the C_2-attack. Although not yet given any reasonable explanations, this methyl group plays an important role in determining the intermolecular arrangement in the transition state for the reduction, for which mention will be made later.

Contrary to the above, the stereochemistry of the reduction with Me_2PNPH mainly reflects the configuration of this model compound, the intrinsic reactivity of each position in CQ having only a minor influence. Validity of the product ratios listed in Table 2 is supported by the fact that identical results have been obtained from the following two pairs of reactants essentially the same with each other in composition: (−)-CQ and *RR*-Me_2PNPH *vs.* (+)-CQ and *SS*-Me_2PNPH; and (−)-CQ and *SS*-Me_2PNPH *vs.* (+)-CQ and *RR*-Me_2PNPH. Since the plane of dihydropyridine-ring in Me_2PNPH is not enantiotopic but diastereotopic, these results can be interpreted only on the basis of such an idea that CQ and Me_2PNPH have a preference for the orientation of substituents in the transition state for the reduction.

Before discussing the orientation, it is helpful to evaluate partial rate factors with all the reaction modes for (−)- and (+)-CQ; this evaluation may be effected by solving linear simultaneous equations for eight variables (eight reaction modes) by using the data listed in Table 2. The result is shown in Table 3. First of all, the calculated values predict that the susceptibility of (−)-CQ toward reduction with *SS*-Me_2PNPH will be 66/34 times greater than that of (+)-CQ. This prediction was in excellent agreement with an experimental result that, after the reaction with racemic CQ, the recovered CQ was subjected to a measurement for optical rotation $[\alpha]_D$ and a ratio 61/39 of consumed CQ's was obtained.

The most preferable mode of attack is *exo*-C_3 for (−)-CQ. In this mode the carbamoyl moiety in *SS*-Me_2PNPH will face the electron-rich carbonyl group of the substrate. It is interesting that for (+)-CQ the second preferable mode is not *exo*-C_2 but *endo*-C_3. Although, as already mentioned, CQ has a higher intrinsic reactivity for the *exo*-attack than for the *endo*-attack, the presence of the C_1-methyl group prevents so much the reaction of (+)-CQ from preceding in this mode that even the less realizable *endo*-attack is chosen. Thus, the effect of the methyl group overwhelms the *exo*/*endo* reactivity difference. Alcohol *D*-**2b** is one of the least abundant products. A similar result has been obtained in our laboratory for reductions of a series of 2-pyridyl alkyl ketones.[17]

Table 3. Partial rate factors in the reduction of (−)- and (+)-camphoroquinone with (4*S*)-*N*-[(*S*)-α-methylbenzyl]-1-propyl-2,4-dimethyl-1,4-dihydronicotinamide (*SS*-Me_2PNPH)

Reaction mode	Product	Camphoroquinone (−)	Camphoroquinone (+)
endo-C_2	*X*-**2**	0.13	0.02
exo-C_2	*D*-**2**	0.10	0.07
endo-C_3	*X*-**3**	0.04	0.22
exo-C_3	*D*-**3**	0.39	0.03
Total		0.66	0.34
Obsd[a]		0.61	0.39

a) See text.

Two explanations are feasible for this phenomenon: it is established that magnesium ion will interact with non-reacting electron-rich substituents of substrates.[8] Since the methyl group is an electron-releasing group, the carbonyl-oxygen on C_2 becomes more electron-rich than the one on C_3. Consequently, the carbonyl-oxygen on C_2 becomes the coordinating site, with the carbonyl group on C_3 remaining as the reacting moiety. The other possibility is that the steric effect of 1-methyl group prevents the approach of the dihydropyridine moiety of Me_2PNPH. Although no investigations with CPK-molecular models have predicted such an effect, the orientation of methyl group seems quite important, if this is the case, because none of such effects have been recognized for the *endo*-attack.

For concluding the discussion, we would like to emphasize that the intermolecular arrangement in the transition state for the reduction has proved to be such as shown in **1**, with polar groups facing each other, possibly because the magnesium ion assists their approach by getting into coordination with these groups.

Experimental

Melting points were not corrected. ^{1}H-NMR spectra were recorded on a JNM-FX100 spectrometer. Optical rotation was observed on a Perkin-Elmer 241 polarimeter.

Materials. Racemic camphoroquinone purchased from Aldrich Chemical Co. was recrystallized from hexane: mp 199 °C.

Anhydrous magnesium perchlorate was dried at 80 °C overnight and used immediately. Acetonitrile was distilled three times over phosphorus pentaoxide before use.

(−)- and (+)-Camphoroquinone (CQ). The Evans' procedure[18] with modifications was employed as follows. A mixture of (+)-camphor (10 g, 0.07 mol) and selenium dioxide (15 g, 0.14 mol) in 10 cm^3 of acetic anhydride was heated at 150 °C overnight. After the mixture had been cooled to room temperature, selenium metal was removed from the mixture by filtration and the metal was washed with acetic acid. The combined orange-yellow filtrate was neutralized carefully with a 30% aqueous potassium hydroxide. Yellow crystals appeared, which were filtered and washed with water to yield 10 g (93% yield) of (−)-CQ. The crude (−)-CQ thus obtained was recrystallized several times from hexane: mp 199 °C (lit,[18] mp 199 °C); $[\alpha]_D^{27}$ −108° (c=1.93, benzene) (lit,[16] $[\alpha]_D^{23}$ −122±3° (c=1.825, benzene)).

(+)-CQ was prepared by the same method: mp 199 °C; $[\alpha]_D^{20}$ +105° (c=1.96, benzene).

Models of NAD(P)H. The methods of preparation adopted for BNAH,[19] PNAH,[19] *R*-PNPH,[12] and Me_2PNPH[15] have already been described in literature.

General Procedure. To a mixture of a substrate, a model compound, and magnesium perchlorate, each of 1 mmol, in a flask filled with argon and sealed, 20 cm^3 of dry acetonitrile was added through a syringe. The mixture was allowed to react at room temperature for an appropriate period with stirring in the dark. The reaction was quenched by addition of 10 cm^3 of water and the solution was concentrated *in vacuo* below 30 °C. The organic materials were extracted with chloroform several times and the solvent was evaporated slowly from the extract *in vacuo* below 30 °C. Ample caution was exercised so as not to cause the materials to sublime. The residue was chromatographed on a column of silica gel (Wakogel 200 M) with benzene–ether (4:1 v/v) as eluent, affording unchanged CQ and a mixture of reduction products. The mixture and the recovered CQ were weighed to obtain their yields. An analysis of ^{1}H-NMR spectra of the products in $CDCl_3$ led to the assignment of a mixture of four isomeric α-keto alcohols *X*-**2**, *D*-**2**, *X*-**3**, and *D*-**3**:[16] δ=3.55 s, 1H for *X*-**2**), 3.75 (s, 1H for *X*-**3**), 3.87 (s, 1H for *D*-**2**), and 4.22 (s, 1H for *D*-**3**). Relative yields of these four isomeric products were obtained from the peak areas for each.

Optical rotation observed for the recovered (±)-CQ was $[\alpha]_D^{20}$ +22.4 (c=1.935, benzene), indicating that the mixture was composed of 61% (−)-CQ and 39% (+)-CQ.

Conversion of Physical Unit. The unit used for temperature is correlated with the SI-unit by

$$t/°C = T/K - 273.15.$$

References

1) Y. Ohnishi, M. Kagami, and A. Ohno, *J. Am. Chem. Soc.*, **97**, 4766 (1975).

2) Y. Ohnishi, T. Numakunai, T. Kimura, and A. Ohno, *Tetrahedron Lett.*, **1976**, 2699.

3) A. Ohno, T. Kimura, H. Yamamoto, S. G. Kim, S. Oka, and Y. Ohnishi, *Bull. Chem. Soc. Jpn.*, **50**, 1535 (1977).

4) A. Ohno, H. Yamamoto, T. Okamoto, S. Oka, and Y. Ohnishi, *Bull. Chem. Soc. Jpn.*, **50**, 2385 (1977).

5) A. Ohno, S. Yasui, K. Nakamura, and S. Oka, *Bull. Chem. Soc. Jpn.*, **51**, 290 (1978).

6) A. Ohno, S. Yasui, H. Yamamoto, S. Oka, and Y. Ohnishi, *Bull. Chem. Soc. Jpn.*, **51**, 294 (1978).

7) A. Ohno, S. Yasui, R. A. Gase, S. Oka, and U. K. Pandit, *Bioorg. Chem.*, **9**, 199 (1980).

8) A. Ohno, S. Yasui, and S. Oka, *Bull. Chem. Soc. Jpn.*, **53**, 2651, 3244 (1980).

9) A. Ohno, H. Yamamoto, and S. Oka, *J. Am. Chem. Soc.*, **103**, 2041 (1981).

10) A. Ohno, T. Shio, H. Yamamoto, and S. Oka, *J. Am. Chem. Soc.*, **103**, 2045 (1981).

11) Y. Ohnishi, T. Numakunai, and A. Ohno, *Tetrahedron Lett.*, **1975**, 3813.

12) A. Ohno, T. Kimura, S. G. Kim, H. Yamamoto, S. Oka, and Y. Ohnishi, *Bioorg. Chem.*, **6**, 21 (1977).

13) A. Ohno, H. Yamamoto, T. Kimura, S. Oka, and Y. Ohnishi, *Tetrahedron Lett.*, **1977**, 4585.

14) A. Ohno, T. Kimura, S. Oka, and Y. Ohnishi, *Tetrahedron Lett.*, **1978**, 757.

15) A. Ohno, M. Ikeguchi, T. Kimura, and S. Oka, *J. Am. Chem. Soc.*, **101**, 7036 (1979).

16) B. Pfrunder and Ch. Tamm, *Helv. Chim. Acta*, **52**, 1630 (1969).

17) A. Ohno, J. Nakai, K. Nakamura, T. Goto, and S. Oka, *Bull. Chem. Soc. Jpn.*, **54**, 3486 (1981).

18) W. C. Evans, J. M. Ridgion, and J. L. Simonsen, *J. Chem. Soc.*, **1934**, 137.

19) D. Mauzerall and F. H. Westheimer, *J. Am. Chem. Soc.*, **77**, 2261 (1955).

Reduction by a Model of NAD(P)H. 33. Steric and Electronic Effects on Asymmetric Reduction of 2-Acylpyridines

Atsuyoshi Ohno,* Jun-ichi Nakai, Kaoru Nakamura,
Takehiko Goto, and Shinzaburo Oka
Institute for Chemical Research, Kyoto University, Uji, Kyoto 611

(Received March 26, 1981)

Series of alkyl and fluorinated alkyl 2-pyridinyl ketones have been reduced by a chiral NAD(P)H-model (Me_2PNPH) in the presence of magnesium ion in acetonitrile. Optical yield decreases in the order of substituent: $CH_3 > C_2H_5 > C(CH_3)_3 > CH(CH_3)_2$ and $CH_3 > CH_2F > CHF_2 > CF_3$. The results have been interpreted in terms of conformation of the substrates for alkyl 2-pyridinyl ketones and of electronic competitional effect between two substituents for fluorinated alkyl 2-pyridinyl ketones. Magnesium ion freezes intermolecular arrangement at the transition state of the reduction.

Chiral *N*-(α-methylbenzyl)-1-propyl-2,4-dimethyl-1,4-dihydronicotinamide (Me_2PNPH) reduces certain ketones in the presence of magnesium ion in acetonitrile resulting in excellent chemical and optical yields.[1] Conformation of the product from the reaction reveals that the carbonyl-oxygen in a substrate points toward the ring-nitrogen of Me_2PNPH and the polar (electronegative) substituent in the ketone faces against the (electronegative) carbamoyl group of Me_2PNPH.[2] Relative bulk of substituent on the carbonyl group in a substrate seems to have little influence on intermolecular arrangement at the transition state of the reduction. Namely, the pyridinyl moiety behaves as a polar substituent in the reduction of 2-acetylpyridine, whereas trifluoromethyl group is a polar substituent in the reduction of α,α,α-trifluoroacetophenone. The stereospecificity of the reduction is so excellent that it is interesting to obtain further insight into the factor(s) that is operating to determine the stereochemical course of the reduction. Evidence obtained from the study may provide an information on the mechanism of stereochemical transformation.

In this paper, we wish to report results from the reduction of series of 2-acylpyridines and α-fluorinated 2-acylpyridines.

Results

2-Acylpyridines (**1a—d**) and α-fluorinated 2-acylpyridines (**1e—g**) were reduced to the corresponding alcohol by *RR*-Me_2PNPH in the presence of equivalent amount of magnesium perchlorate in dry acetonitrile at room temperature in the dark. Chemical yields and conversion percentages are listed in Table 1. For the products **2a** and **2b**, enantiomer excess was calculated from their observed optical rotations, whereas those for the other products were calculated from their ^1H- and ^{19}F-NMR spectra by the aid of α-methoxy-α-trifluoromethylphenylacetic acid (MTPA).[3] Absolute configurations of the products were elucidated independently from their signs of optical rotations and CD spectra as well as chemical shifts in NMR spectra of the corresponding MTPA esters. Results are summarized in Table 2.

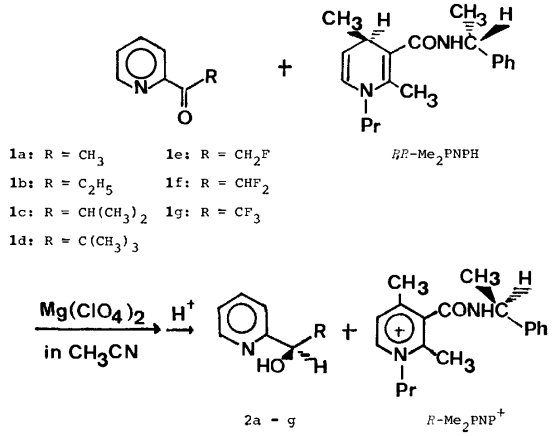

Complexation constants, *K*, for complexes of 2-acylpyridines and magnesium ion were measured spectrophotometrically,[4] and the results are listed in Table 3.

It has been confirmed that C_4-hydrogen in Me_2PNPH is transferred onto the carbonyl-carbon in a substrate without exchange and that the chirality on the carbamoyl-side chain exerts no influence on the stereochemical course of the reduction in the presence of

Table 1. Chemical yields and conversion percentages from the reduction

Substrate	R in **1**	Yield/%[a]	Conversion/%[b]
1a	CH_3	50.1	100
1b	C_2H_5	45.2	76
1c	$CH(CH_3)_2$	78.3	92
1d	$C(CH_3)_3$	40.3	47
1e	CH_2F	43.3	98
1f	CHF_2	39.4	100
1g	CF_3	35.7	100

a) Isolated yield. b) The amount of consumed substrate.

Table 2. Enantiomer excess and absolute configuration of excess enantiomer

Alcohol	R in **2**	e.e./%	Configuration
2a	CH_3	62.8	*R*
2b	C_2H_5	52.1	*R*
2c	$CH(CH_3)_2$	≈0	—
2d	$C(CH_3)_3$	43.4	*R*
2e	CH_2F	53.5	*S*
2f	CHF_2	30.3	*S*
2g	CF_3	16.5	*S*

Table 3. Complexation constant for complexes of 2-acylpyridines and magnesium ion[a)]

Acylpyridine	R in **1**	K/M^{-1}
1a	CH_3	283
1b	C_2H_5	279
1c	$CH(CH_3)_2$	124
1d	$C(CH_3)_3$	18.6
1e	CH_2F	—b)
1f	CHF_2	—b)
1g	CF_3	—b)

a) In acetonitrile at 25 °C. Estimated error is ±2%.
b) Too small to be observed accurately.

magnesium ion.[1)]

Discussion

α-Fluorinated 2-Acylpyridines. Configurations of alcohols **2a** and **2e—g** reveals that, regardless the number of fluorine atom, the pyridinyl moiety in the ketone faces against carbamoyl group in Me_2PNPH at the transition state of the reduction as depicted by **3**. However, the stereospecificity is largely affected

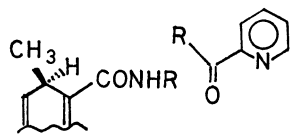

3

by the number of fluorine-substituent. The result can be accounted for by the difference in electronegativity of substituents on the carbonyl group: as the number of fluorine atom in the substituent R increases, the difference in electron-withdrawing ability between R and pyridinyl group becomes smaller and recognition of polarity-difference becomes difficult. Consequently, magnesium ion can coordinate onto both pyridinyl and fluorinated alkyl groups (See structures **4a—c**).

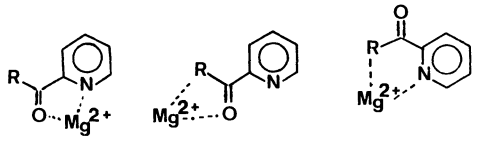

4a 4b 4c

Note that trifluoromethyl group is the coordination-site in the reduction of α,α,α-trifluoroacetophenone and that complexation constants for **1e**, **1f**, and **1g** are too small to be measured with a reasonable accuracy. The latter evidence indicates that the pyridinyl-nitrogen has no lone-electron pair available for the coordination at least at the ground state of these ketones.

2-Acylpyridines. According to the structure **3**, the substituent R faces against the open-side of Me_2PNPH. Nevertheless, the increase in bulk of R results in the decrease in the stereospecificity of the reduction. The substrate **1c** exerts an abnormal stereospecificity. It is obvious that relative bulk of the substituents cannot account for the result.

Previously we suggested that the change in complexation constant is due to the distortion of dihedral angle between the planes of pyridinyl and acyl groups.[4)] Free 2-acylpyridine in a solution exists with the conformation in which pyridinyl-nitrogen and carbonyl-oxygen sit themselves in the *E*-form.[5)] On the other hand, ^{13}C-NMR, IR, and other spectroscopic studies have revealed that some 2-acylpyridines serve as bidentate ligands that coordinate onto a bivalent metal ion with the nitrogen and oxygen being in the *Z*-form.[6-8)] 2-Acetyl- (**1a**) and 2-propionyl- (**1b**) pyridines are 2-acylpyridines of this kind (Fig. 1a). A large complexation constant suggests that the conformation of the complex is rigid. In these 2-acylpyridines, steric repulsion between the substituent R and pyridinyl-hydrogen on C_3 is negligibly small.

An inspection with a CPK-model, however, suggests that the *t*-butyl group in **1d** is so bulky that the dihedral angle in a stable conformation of complexed **1d** should be about 90° (Fig. 1b). The conformation shown in Fig. 1b′ has extremely high steric strain because of Mg^{2+}–Bu^t repulsion. Small complexation constant for this compound supports the idea that **1d** is no more a bidentate ligand to magnesium ion. Although magnesium ion cannot behave as a fixer

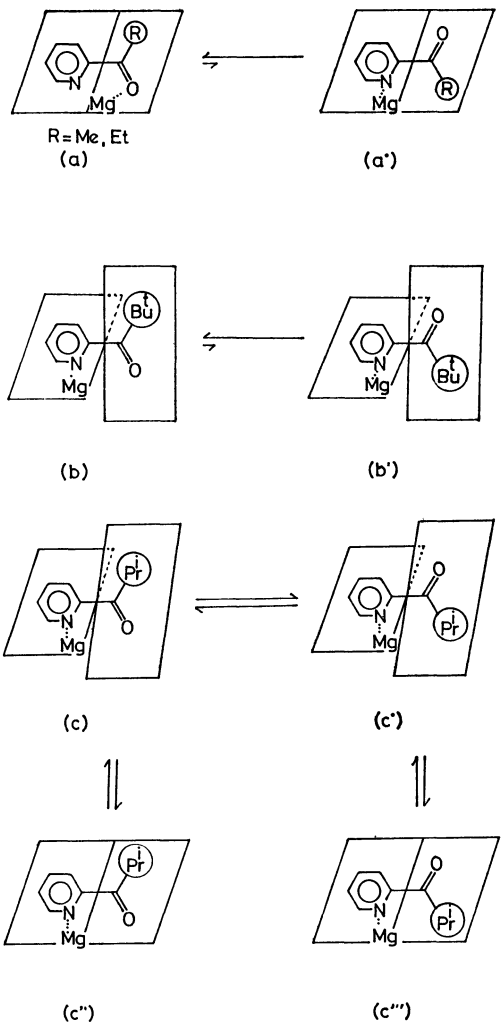

Fig. 1. Conformations of (a) 2-acetyl- and 2-propionylpyridines, (b) 2-pivaloylpyridine, and (c) 2-isobutyrylpyridine in the complex with magnesium ion.

of conformation of **1d**, the steric bulk of *t*-butyl group itself freezes the conformation intrinsically resulting in relatively satisfactory stereospecificity.

The situation is different in **1c**. The steric bulk of 2-propyl group is too large to set two planes coplanar, but it is not large enough to freeze the conformation. Stabilization energy by bidentate coordination onto magnesium ion is not so large as those for **1a** and **1b** but larger than that for **1d**, as seen in the magnitude of complexation constant. Therefore, all four possible rotomers (Fig. 1c) are available as a part of the transition-state complex of the reduction with **1c**, and net result appears non-stereospecific.

Role of Magnesium Ion. The substituent effect on the stereospecificity described above coincide with the idea proposed previously[1,2] that stereospecificity of the reduction is mainly defined by electronic effect. The steric effect has only secondary importance, if any, to define intermolecular arrangement at the transition state of the reduction. However, steric bulk of a substituent in a substrate exerts intrinsic effect on the conformation of the substrate.

Magnesium ion-catalysis for the stereospecificity has an origin in tetradentate sandwich-type coordination to freeze the configuration of transition-state complex (Fig. 2): dihydropyridinyl-nitrogen and carbamoyl-oxygen in Me_2PNPH on one side and pyridinyl-nitrogen or other electronegative substituent and carbonyl-oxygen in a substrate on the other side.[9]

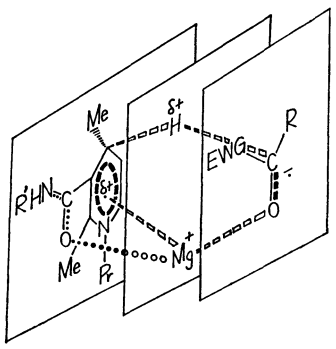

Fig. 2. Schematic illustration of the transition state of the reduction.

Experimental

Instruments. UV, IR, NMR, and mass spectra were recorded on Union Giken SM-401, Hitachi EPI-S2, JEOL JNMFX-100, and JEOL JMSO-1SG or Hewlett Packard 5992B GC/MS spectrometers, respectively. The optical activity was measured on a Perkin-Elmer 241 polarimeter. The CD spectra were obtained with a JASCO J-20 spectropolarimeter. A Yanaco G-1800F and Varian Aerograph Model 920 were used for VPC, and a Yanaco Model L-2000 was used for high-pressure liquid chromatography. Melting and boiling points were not corrected.

Materials. Acetonitrile was distilled three times over phosphorus pentaoxide and stored over 4A molecular sieves under an atmosphere of argon. Anhydrous magnesium perchlorate was dried at 100 °C and stored in a vacuum desiccator over phosphorus pentaoxide. 2-Acetylpyridine (**1a**) (bp 95 °C/34 mmHg) was purchased from Nakarai Chem. Co.

2-Propionylpyridine (**1b**) (bp 96.5—97.5 °C/20 mmHg),

Table 4. Optical rotations of product alcohols

Alcohol	$[\alpha]_D$	*c*	Temp/°C	Solvent
2a	+35.6	1.03	25	EtOH
	+26.8	1.95	25	CCl_4
2b	+38.0	1.68	25	EtOH
	+23.8	1.59	25	CCl_4
2c	+0.390	0.770	25	EtOH
	+0.232	0.818	25	CCl_4
2d	+27.0	0.215	20	EtOH
	+12.8	1.67	25	CCl_4
2e	+36.9	0.255	20	MeOH
	−3.04	1.19	20	CCl_4
2f	+6.21	0.145	20	MeOH
	−10.3	0.800	20	CCl_4
2g	+10.2	0.420	20	MeOH
	−0.821	0.875	20	CCl_4

Table 5. ^{1}H- and ^{19}F-NMR chemical shifts of (+)-MTPA esters of the product alcohols

Alcohol	Config. of alcohol	^{1}H Chemical shift[a]			^{19}F Chemical shift[b]	
		Acid-OMe	Alcohol-H	Alcohol-R	Acid-CF_3	Alcohol-R
2a	*R*	—	—	—	72.01	—
	S	—	—	—	72.01	—
2b	*R*	—	—	—	71.87	—
	S	—	—	—	71.87	—
2c	*R*	3.49	5.82	0.88	71.71	—
	S	3.55	5.82	0.88	71.79	—
2d	*R*	3.52	5.76	0.92	71.45	—
	S	3.52	5.71	0.97	71.56	—
2e	*R*	3.64	6.36	4.82	71.97	154.89
	S	3.53	6.36	4.82	72.29	156.31
2f	*R*	3.55	6.29	6.30	72.16	129.41
	S	3.55	6.25	6.30	72.48	129.16
2g	*R*	3.61	6.40	—	72.18	75.32
	S	3.50	6.43	—	72.36	75.47

a) δ from TMS in $CDCl_3$. b) δ from CCl_3F in $CDCl_3$.

2-isobutyrylpyridine (**1c**) (bp 99.0—100.0 °C/19 mmHg), and 2-pivaloylpyridine (**1d**) (bp 100.5—101.5 °C/20 mmHg) were prepared from the corresponding alkyl cyanides and 2-pyridinyllithium.[10] 2-(Fluoroacetyl)pyridine (**1e**) (mp 70.0—71.0 °C), 2-(difluoroacetyl)pyridine (**1f**) (purified on a silica-gel column), 2-(trifluoroacetyl)pyridine (**1g**) (mp 84.0—85.0 °C) were synthesized from the corresponding esters and 2-pyridinyllithium.[11] Elemental analyses and spectral data were satisfactory for all materials. Racemic alcohols as authentic samples of the products were obtained by reducing the corresponding ketones with sodium borohydride.[12]

General Procedure for the Reduction. One millimole each of *RR*-Me_2PNPH and magnesium perchlorate were dissolved in 25 ml of anhydrous acetonitrile in a sealed flask. One millimole of the substrate in 5 ml of anhydrous acetonitrile was added by injection by using a syringe, and the mixture was allowed to react at room temperature (about 25 °C) for an appropriate reaction time in the dark in an argon atmosphere. The reaction was stopped by the addition of water, and the product was extracted three times with dichloromethane. The combined dichloromethane solution was dried over sodium sulfate. After evaporation of the solvent at below 30 °C under reduced pressure, the residue was chromatographed on a column of silica gel. The product was further purified by preparative VPC or high-pressure liquid chromatography when neccesary. The purity of the product was confirmed by VPC and by elemental analyses. Columns used for VPC were mainly Silicone DC 200 5% (1 m) and DEGS 10% (1 m). Appropriate mixtures of benzene–ethyl acetate or benzene–ether were employed as the eluents for column chromatography. Thus obtained products were subjected for the measurement of optical rotations or converted into the corresponding MTPA esters for NMR spectroscopy. Optical rotations of the products and NMR chemical shifts of the corresponding esters are summarized in Tables 4 and 5, respectively.

Correlation of Physical Units. Physical units used in this report are correlated with SI-units by the following relationship.

1 M=1 mol dm^{-3}, $t/°C = T/K - 273.15$, p mmHg$=13.5951 \times 980.665 \times 10^{-2} p$ Pa.

References

1) A. Ohno, M. Ikeguchi, T. Kimura, and S. Oka, *J. Am. Chem. Soc.*, **101**, 7036 (1979).

2) A. Ohno, T. Goto, J. Nakai, and S. Oka, *Bull. Chem. Soc. Jpn.*, **54**, 3478 (1981).

3) J. A. Dale, D. L. Dull, and H. S. Mosher, *J. Org. Chem.*, **34**, 2543 (1969); J. A. Dale and H. S. Mosher, *J. Am. Chem. Soc.*, **95**, 512 (1973).

4) A. Ohno, S. Yasui, and S. Oka, *Bull. Chem. Soc. Jpn.*, **53**, 2651 (1980).

5) J. Barassin, G. Queguiner, and H. Lumbroso, *Bull. Soc. Chim. Fr.*, **1967**, 4707.

6) R. R. Osborne and W. R. McWhinnie, *J. Chem. Soc., A*, **1967**, 2075.

7) Y. Kidani, M. Noji, and H. Koike, *Bull. Chem. Soc. Jpn.*, **48**, 239 (1975).

8) R. A. Gase and U. K. Pandit, *J. Am. Chem. Soc.*, **101**, 7059 (1979).

9) *Cf.* also, A. Ohno, T. Kimura, H. Yamamoto, S. G. Kim, S. Oka, and Y. Ohnishi, *Bull. Chem. Soc. Jpn.*, **50**, 1535 (1977).

10) J. P. Wibaut, A. P. de Jonge, H. G. P. van der Voort, and P. Ph. H. L. Otto, *Recl. Trav. Chim. Pays-Bas*, **70**, 1054 (1951).

11) T. F. McGrath and R. Levine, *J. Am. Chem. Soc.*, **77**, 3656 (1955).

12) M. R. Johnson and B. Rickborn, *J. Org. Chem.*, **35**, 1041 (1970).

Reduction by a Model of NAD(P)H. 34. Substituent Effect on Asymmetric Reduction of Trifluoroacetophenones

Atsuyoshi Ohno,* Jun-ichi Nakai, Kaoru Nakamura,
Takehiko Goto, and Shinzaburo Oka
Institute for Chemical Research, Kyoto University, Uji, Kyoto 611

(Received March 26, 1981)

Substituted and unsubstituted α,α,α-trifluoroacetophenones were reduced by a chiral NAD(P)H-model (*RR*-Me_2PNPH). Both electron-releasing and -withdrawing substituents give better optical yields than unsubstitued compound. The result has been interpreted in terms of three-step mechanism which involves initial electron-transfer process.

Kinetics, isotope effects, and other evidence have proved that the reduction of certain ketones by 1,4-dihydronicotinamide derivatives proceeds through three-step electron-proton-electron transfer processes.[1] Magnesium ion catalyzes the reduction by assisting the initial electron-transfer process.

On the other hand, it has been demonstrated that the reduction proceeds with excellent stereospecificity when a chiral 1,4-dihydronicotinamide derivative is used as a reductant.[2] Stereospecificity is also catalyzed by magnesium ion. Namely, substituted and unsubstituted α,α,α-trifluoroacetophenones are reduced by a chiral *N*-(α-methylbenzyl)-1-propyl-2,4-dimethyl-1,4-dihydronicotinamide (Me_2PNPH) in more than 90% enantiomer excess in the presence of magnesium ion.[2] Magnesium ion plays a role to freeze the conformation of transition state complex,[3] and electronic substituent effect is more important than the steric effect to difine the stereochemical course.[3,4]

We have been interested in to study whether the reduction of a series of α,α,α-trifluoroacetophenones without magnesium ion results in variation of enantiomer excess due to electronic substituent effect and whether the stereochemical result can be explained by the proposed three-step mechanism without contradiction.

Results

α,α,α-Trifluoroacetophenone and its *p*-methoxy, *p*-methyl, *p*-chloro, *p*-bromo, and *m*-trifluoromethyl derivatives were reduced by *RR*-Me_2PNPH in dry acetonitrile at room temperature in the dark.

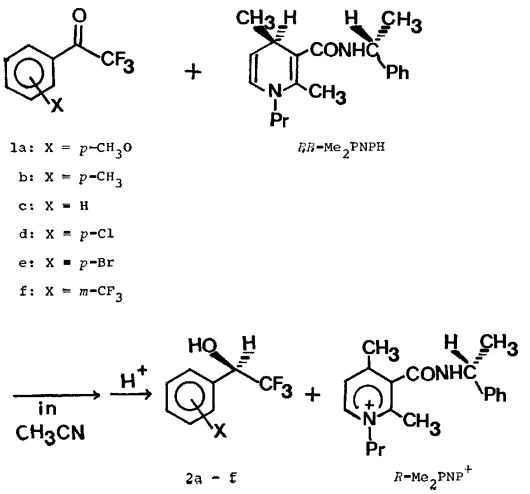

The enantiomer excess in the product alcohols (**2**) and their absolute configurations were determined on ^{1}H- and ^{19}F-NMR spectroscopies[5] as well as by VPC (15% BDS, 1 m) after the alcohols were converted into their corresponding α-methoxy-α-trifluoromethylphenylacetic acid (MTPA) esters. Chemical yield, conversion percentage, enantiomer excess, and the configuration of the product are summarized in Table 1. In Fig. 1 logarithms of the isomer ratios are plotted against Hammett σ-values for the substituent.

Discussion

Both electron-releasing and -withdrawing substituents increase the stereospecificity of the reduction. The

Table 1. Chiral reduction of substituted and unsubstituted α,α,α-trifluoroacetophenones

Product	Yield/%[a]	Conversion/%[b]	e.e./%	Configuration
2a	78.4	97	80.2	*R*
2b	33.6	95	76.4	*R*
2c	68.0	100	71.3	*R*
2d	55.3	99	82.5	*R*
2e	52.5	100	82.2	*R*
2f	58.0	99	85.9	*R*

a) Isolated yield. b) The amount of consumed substrate.

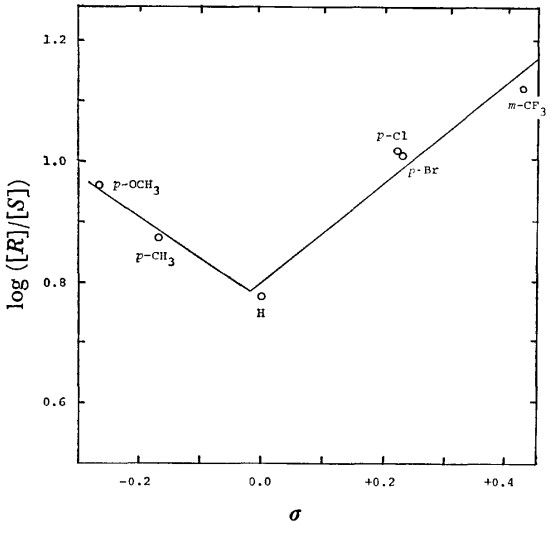

Fig. 1. A plot of log[*R*]/[*S*] against σ.

result cannot be accounted for by simple steric or electronic substituent effect in a unit reaction.

However, the multi-step mechanism with an initial electron-transfer process explains the variation of stereospecificity. An electron-releasing substituent reduces the electron-affinity of a substrate and the electron-transfer to a substrate of this sort requires high activation energy as shown in Fig. 2a. In this category, only a substrate which has proper intermolecular arrangement can form an electron-transfer complex with Me_2PNPH. Since the intermediate electron-transfer complex is an unstable species, the following proton-transfer step proceeds almost spontaneously. That is, the stereochemistry of the net reduction is defined kinetically in the process of initial electron-transfer.

The selectivity-reactivity relationship[6] predicts that the less the electron-releasing power of a substituent on the substrate, or the less the activation energy for the electron-transfer process, the less the difference in energy between preferred and other conformations (Fig. 2b). Consequently, the reduction becomes less stereospecific.

With a strongly electron-withdrawing substituent on a substrate, on the other hand, the electron-transfer takes place quite rapidly and the intermediate electron-transfer complex becomes more stable than the reactant system (Fig. 2c). The preferential course of reduction in this category is, therefore, controlled by thermodynamic stability of the intermediate. It is noteworthy that the reaction mixture with **1d**, **1e**, or **1f** turned dark green during the reaction and the color disappered at the end of the reaction. The color change suggests the formation of a stable long-living intermediate. Thus, stereochemical course of the reduction is determined by the complex-forming process. When the complex is unstable, stereochemistry is controlled kinetically, whereas when the complex is stable, thermodynamics controls the course. Since magnesium ion catalyzes the electron-transfer process, stereochemistry of the reduction in the presence of magnesium ion is controlled thermodynamically yielding quite high enantiomer excess.[2]

The energy diagrams shown in Fig. 2 are the same as those proposed previously. In conclusion, we would like to emphasize that not only kinetic bihavior but

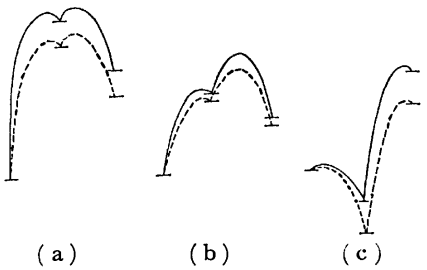

Fig. 2. Schematic representation of energy diagram for the reduction. Electron-withdrawing power increases in the order: (a)<(b)<(c).

Table 2. Optical rotation of product alcohol[a]

Alcohol	$[\alpha]_D$	c
2a	−35.9	1.35
2b	−24.0	0.825
2c	−9.32	1.18
2d	−19.0	1.05
2e	−21.5	1.04
2f	−17.1	1.58

a) In ethanol at 20 °C.

Table 3. VPC analysis of product alcohol and its (+)-MTPA ester[a]

Alcohol	Column temp/°C	Retention time/min		
		Alcohol	Ester of (*R*)-alcohol	Ester of (*S*)-alcohol
2a	170	7.9	24.5	30.7
2b	150	5.5	19.7	25.0
2c	150	4.0	14.0	17.6
2d	170	5.9	13.0	16.6
2e	170	10.0	21.4	27.9
2f	135	6.9	17.0	21.3

a) The analyses were done on a Yanaco G-1800F with a 1 m, 15% BDS column.

Table 4. ^1H- and ^{19}F-NMR spectra of (+)-MTPA esters of product alcohols

Alcohol	Config. of alcohol	^1H Chemical shift[a]		^{19}F Chemical shift[b]	
		Acid-OMe	Alcohol-H	Acid-CF_3	Alcohol-CF_3
2a	*R*	3.58	6.18	72.31	76.31
	S	3.46	6.26	72.31	76.49
2b	*R*	3.58	6.21	72.31	76.26
	S	3.47	6.29	72.31	76.47
2c	*R*	3.59	6.24	72.29	76.13
	S	3.46	6.31	72.29	76.39
2d	*R*	3.60	6.22	72.18	76.25
	S	3.47	6.29	72.18	76.47
2e	*R*	3.60	6.21	72.18	76.26
	S	3.47	6.28	72.18	76.48
2f	*R*	3.60	6.30	72.21	76.13
	S	3.46	6.37	72.21	76.42

a) δ from TMS in $CDCl_3$. b) δ from CCl_3F in $CDCl_3$.

also stereochemical result can be explained by the three-step reduction mechanism which proposes initial electron-transfer step as the driving force of the reduction.

Experimental

Instruments and general procedure for the reduction were described in a previous paper.[1,3] Melting and boiling points were not corrected.

Materials. Me_2PNPH,[2] acetonitrile,[1,3] and magnesium perchlorate[1,3] were prepared or purified as described before.

p-Methoxy- (**1a**) (bp 114—115 °C/20 mmHg),[7] *p*-methyl- (**1b**) (bp 77.5—78 °C/20 mmHg),[7] unsubstituted (**1c**) (150 °C/760 mmHg),[7] *p*-chloro- (**1d**) (81 °C/20 mmHg),[8] *p*-bromo- (**1e**) (95 °C/4 mmHg),[9] and *m*-trifluoromethyl-α,α,α-trifluoroacetophenone (**1f**) (77 °C/50 mmHg)[1] were synthesized according to the literature procedures.

Configurational Analyses of Products. Optical rotations of the product alcohols are listed in Table 2. Results of VPC-analyses and chemical shifts in ^1H- and ^{19}F-NMR spectra of MTPA esters of the alcohols are summarized in Tables 3 and 4, respectively.

Correlation of Physical Units. Physical units used in this report are correlated with SI-units by the following relationship.

1 M=1 mol dm^{-3}, $t/°C = T/K - 273.15$, p mmHg = $13.5951 \times 980.665 \times 10^{-2}$ p Pa.

References

1) A. Ohno, H. Yamamoto, and S. Oka, *J. Am. Chem. Soc.*, **103**, 2401 (1981); A. Ohno, T. Shio, H. Yamamoto, and S. Oka, *ibid.*, **103**, 2405 (1981).

2) A. Ohno, M. Ikeguchi, T. Kimura, and S. Oka, *J. Am. Chem. Soc.*, **101**, 7036 (1979).

3) A. Ohno, J. Nakai, K. Nakamura, T. Goto, and S. Oka, *Bull. Chem. Soc. Jpn.*, **54**, 3482 (1981).

4) A. Ohno, T. Goto, J. Nakai, and S. Oka, *Bull. Chem. Soc. Jpn.*, **54**, 3478 (1981).

5) J. A. Dale, D. L. Dull, and H. S. Mosher, *J. Org. Chem.*, **34**, 2543 (1969); J. A. Dale and H. S. Mosher, *J. Am. Chem. Soc.*, **95**, 512 (1973).

6) J. E. Leffler and E. Grunwald, "Rates and Equilibria of Organic Reactions," John Wiley and Sons, Inc., New York, N. Y. (1963), pp. 162—164.

7) R. Stewart and R. van der Linden, *Can. J. Chem.*, **38**, 399 (1960).

8) F. E. Herkes and D. J. Burton, *J. Org. Chem.*, **32**, 1311 (1967).

9) K. J. Klabunde and D. J. Burton, *J. Org. Chem.*, **35**, 1711 (1970).

Reduction by a Model of NAD(P)H. 35. Spectroscopic Detection of Charge-transfer Intermediate

Atsuyoshi Ohno,* Hiroyuki Yamamoto, and Shinzaburo Oka
Institute for Chemical Research, Kyoto University, Uji, Kyoto 611

(Received March 26, 1981)

4,4-Disubstituted 1,4-dihydropyridine derivatives are employed as models of NAD(P)H. Electronic and ESR spectroscopies have proved that these models form charge-transfer complexes with certain substrates, which supports a mechanism of the reduction with 1,4-dihydronicotinamide derivatives to be initiated by initial electron-transfer.

It has been proposed that the reduction of an unsaturated compound with an NAD(P)H-model involves at least one intermediate.[1-3] The nature of the intermediate has been discussed, but direct evidence has scarcely reported.[2,4,5]

Recently, we reported that results from the studies on kinetics and isotope effects for the reduction of a series of substituted and unsubstituted α,α,α-trifluoroacetophenone with 1-propyl-1,4-dihydronicotinamide revealed the importance of initial electron-transfer.[3] Stereochemistry of the reduction with a chiral model compound also supported the proposed mechanism.[6] However, since the intermediate undergoes further reaction spontaneously, it is not easy to detect it. Only when the intermediate becomes thermodynamically more stable than the reactant system, the detection has been succeeded.[2,4,5]

In order to obtain direct evidence for an unstable intermediate, we studied electronic and ESR spectroscopies by the aid of model compounds that have no C_4-hydrogen.

Results

1-Propyl-4,4-dimethyl-1,4-dihydropyridine (**1a**) and 1-phenyl-4,4-dimethyl-1,4-dihydropyridine (**1b**) were employed as reductants.

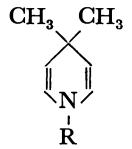

1a: R=C_3H_7
1b: R=C_6H_5

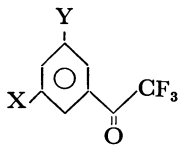

2a: X=H, Y=Br
2b: X=H, Y=CF_3
2c: X=H, Y=NO_2
2d: X=CF_3, Y=NO_2

Electronic Spectra. To test the formation of a stable charge-transfer (CT) complex with **1a** or **1b**, strongly electron-demanding substrates such as TCNQ, *N*-methylacridinium iodide, and 1,3,5-trinitrobenzene were used for the spectroscopy. Note that these substrates are known to form stable intermediates with an ordinary NAD(P)H-model which has a C_4-hydrogen.[2,3,7,8] When, TCNQ was mixed with **1a** in anhydrous acetonitrile at 50 °C, the solution turned green and exhibited a spectrum with absorption maxima at 746, 764, 825, and 846 nm as shown in Fig. 1. The complexation constant was measured to be 116 M^{-1}. The spectrum is identical to those reported previously.[9,10] 1,3,5-Trinitrobenzene (Fig. 2)[11] and *N*-methylacridinium iodide (Fig. 3)[2] also showed CT-bands when they were mixed with **1b** in acetonitrile.

m-Bromo- (**2a**), *m*-trifluoromethyl- (**2b**), *m*-nitro- (**2c**), and *m*-trifluoromethyl-*m'*-nitro- (**2d**) α,α,α-trifluoroacetophenones were, then, subjected to the spectroscopy. Kinetics and other evidence have predicted that the intermediates formed from these substrates are thermodynamically less stable than their corresponding reactant systems.[3] Yet, their mixtures with **1a** in acetonitrile clearly showed new absorptions with maxima at 367, 369, 371, and 374 nm for **2a**, **2b**, **2c**, and **2d**, respectively, as shown in Fig. 4. The

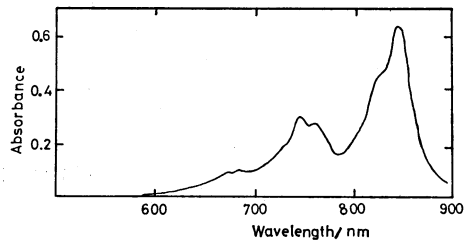

Fig. 1. Electronic spectrum of anion radical of TCNQ.

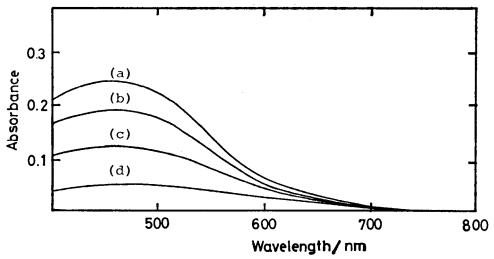

Fig. 2. CT spectra of 1,3,5-trinitrobenzene and 1-phenyl-4,4-dimethyl-1,4-dihydropyridine; (a) [TNB] $=3.56\times10^{-2}$ M, [**1b**] $=3.15\times10^{-2}$ M; (b) [TNB] $=3.67\times10^{-2}$ M, [**1b**] $=2.32\times10^{-2}$ M; (c) [TNB] $=3.79\times10^{-2}$ M, [**1b**] $=1.44\times10^{-2}$ M; (d) [TNB] $=3.91\times10^{-2}$ M, [**1b**] $=0.495\times10^{-2}$ M.

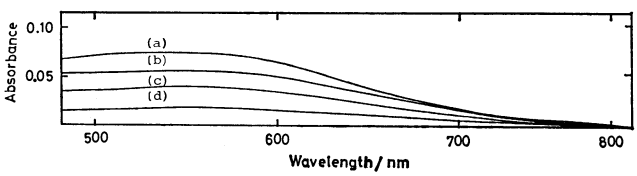

Fig. 3. CT spectra of *N*-methylacridinium iodide and 1-phenyl-4,4-dimethyl-1,4-dihydropyridine; (a) [AI] $=1.20\times10^{-2}$ M, [**1b**] $=6.35\times10^{-2}$ M; (b) [AI] $=1.30\times10^{-2}$ M, [**1b**] $=4.31\times10^{-2}$ M; (c) [AI] $=1.38\times10^{-2}$ M, [**1b**] $=2.74\times10^{-2}$ M; (d) [AI] $=1.47\times10^{-2}$ M, [**1b**] $=0.973\times10^{-2}$ M.

new absorptions satisfied well-known criteria for CT-complexation in solution.[12]

ESR Spectra. A mixture of TCNQ with **1a** in tetrahydrofuran at room temperature (about 25 °C) gave well-resolved ESR signals that were attributable to the signals from anion radical of TCNQ.[10,13] The spectrum is shown in Fig. 5. On the other hand, substrates **2a**—**d** did not give signals under the same condition. However, when magnesium perchlorate was added to the system, broad but distinct signals were recorded. A spectrum from **2d** is shown in Fig. 6 as a representative. The spectrum with $g=2.003$ is characterized by a large width of about 100 G, which indicates that the splitting due to fluorine atoms is involved in the spectrum. The recorded spectrum is identical to that observed from the system of **2d** and sodium metal (Fig. 6b). The signal width is identical to that reported for anion radical of α,α,α-trifluoroacetophenone.[14]

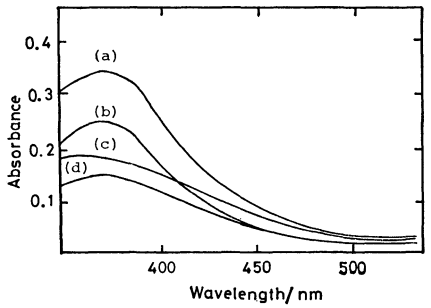

Fig. 4. CT spectra of substituted α,α,α-trifluoroacetophenones and 1-propyl-4,4-dimethyl-1,4-dihydropyridine; (a) [**2d**]$=1.39\times10^{-2}$ M, [**1a**]$=5.58\times10^{-2}$ M; (b) [**2c**]$=1.23\times10^{-2}$ M, [**1a**]$=1.98\times10^{-2}$ M; (c) [**2a**]$=4.57\times10^{-2}$ M, [**1a**]$=6.42\times10^{-2}$ M; (d) [**2b**]$=4.71\times10^{-2}$ M, [**1a**]$=3.84\times10^{-2}$ M.

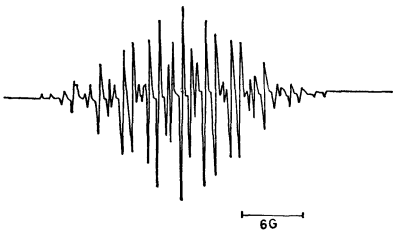

Fig. 5. ESR spectrum of anion radical of TCNQ.

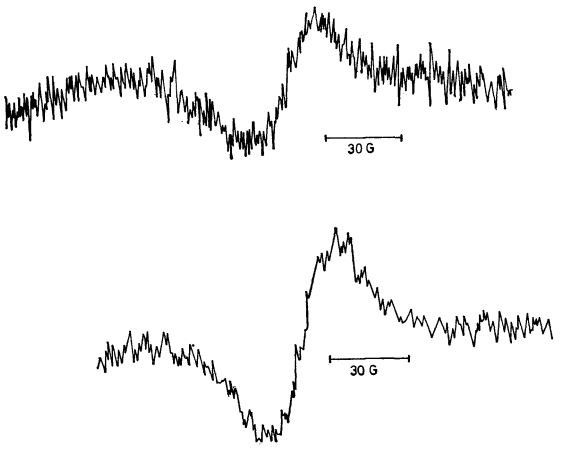

Fig. 6. ESR spectra from mixtures of *m*-trifluoromethyl-*m'*-nitro-α,α,α-trifluoroacetophenone and (a) 1-propyl-4,4-dimethyl-1,4-dihydropyridine and (b) sodium metal.

Discussion

Thus, both electronic and ESR spectroscopies have proved that 1,4-dihydropyridine can transfer an electron onto certain substrate forming a CT-complex. However, there still remains a question whether the detected intermediate is abortive or real. In this connection, it should be noted that the substrates **2a**—**c** are those the reduction of which is catalyzed by magnesium ion.[3] If magnesium ion increased the concentration of abortive CT-complex to exhibit an ESR signal, or if the concentration of reacting substrate were decreased by the addition of magnesium ion, the reduction in the presence of magnesium ion must be slower than that in its absence. The fact that the increase in reduction rate corresponds with the increase in concentration of CT-complex reveals that the CT-complex is not an abortive species but is a real intermediate of the reduction.

In conclusion, we have succeeded to prove that the initial step of the reduction with an NAD(P)H-model is an electron-transfer process.

Experimental

Materials. Acetonitrile was distilled three times on phosphorous pentoxide. Tetrahydrofuran was distilled and dried over sidium, then dried over alloy of potassium and sodium under reduced pressure. TCNQ and 1,3,5-trinitrobenzene were purchased from Nakarai Chem. Co. and purified by recrystallization. *N*-Methylacridinium iodide (mp 87 °C),[12] *m*-bromo-α,α,α-trifluoroacetophenone (bp 78 °C/15 mmHg) (**2a**),[15] *m*-trifluoromethyl-α,α,α-trifluoroacetophenone (bp 150 °C/760 mmHg) (**2b**),[3] *m*-nitro-α,α,α-trifluoroacetophenone (mp 54 °C) (**2c**),[15] and *m*-trifluoromethyl-*m'*-nitro-α,α,α-trifluoroacetophenone (bp 90 °C/8 mm Hg) (**2d**)[3] were prepared according to literature procedures. 1-Propyl-4,4-dimethyl-1,4-dihydropyridine (bp 72 °C/47 mmHg) (**1a**)[16] and 1-phenyl-4,4-dimethyl-1,4-dihydropyridine (mp 36 °C) (**1b**)[17] were also synthesized according to literature procedures. All materials gave satisfactory results from elemental analyses and spectroscopies.

Visible Spectra. Acetonitrile was flushed with dry argon prior to use. A solution of a substrate in acetonitrile was prepared and placed in a cell (1 cm) equipped with a silicone-rubber stopper, then the solution of a model compound in acetonitrile was injected into this solution. Visible spectra was obtained with Union Giken SM-401 spectrometer, the cell-compartment of which was filled with dry argon and kept at 50.0±0.1 °C.

The measurement of association (complexation) constant of TCNQ with **1a** was carried out by the procedure described below. The concentration of **1a** was kept at 2×10^{-4} M and the concentration of TCNQ was changed from 1.58×10^{-3} to 6.32×10^{-3} M. The change in the intensity at 746 nm was measured. The slope of the double reciprocal plot of the intensity and the concentration of TCNQ gave a linear line.

Spectra of the other substrates were obtained with the

Table 1. Concentrations of reagents for the observation of charge-transfer spectra

Substrate	Concn/10^{-2} M	Model	Concn/10^{-2} M
1,3,5-Trinitrobenzene	3.50—3.90	**1b**	0.5—3.2
N-Methyl acridinium iodie	1.25—1.50	**1b**	1.0—6.3
2a	4.40—5.50	**1a**	1.0—8.0
2b	4.40—4.90	**1a**	1.0—8.0
2c	1.21—1.25	**1a**	1.0—3.0
2d	1.39—1.48	**1a**	2.0—5.6

concentrations listed in Table 1.

ESR Spectra. Appropriate amounts of a substrate and **1** were placed in a sample tube and desired amount of the purified dry tetrahydrofuran was brought into the tube in a vacuum. The spectra were obtained on a JEOL-JMS-ME-3X spectrometer at room temperature or below.

Correlation of Physical Units. Physical units used in this report are correlated with SI-unit by the following relationship.

1 M=1 mol dm^{-3}, t/°C=T/K−273.15, p mmHg=13.5951 ×980.665×10^{-2} p Pa.

References

1) J. J. Steffens and D. M. Chipman, *J. Am. Chem. Soc.*, **93**, 6694 (1971).

2) J. Hajdu and D. S. Sigman, *J. Am. Chem. Soc.*, **98**, 6060 (1976).

3) A. Ohno, H. Yamamoto, and S. Oka, *J. Am. Chem. Soc.*, **103**, 2041 (1981); A. Ohno, T. Shio, H. Yamamoto, and S. Oka, *ibid.*, **103**, 2045 (1981).

4) A. Ohno and N. Kito, *Chem. Lett.*, **1972**, 369.

5) Y. Ohnishi and A. Ohno, *Chem. Lett.*, **1976**, 697.

6) A. Ohno, J. Nakai, K. Nakamura, T. Goto, and S. Oka, *Bull. Chem. Soc. Jpn.*, **54**, 3486 (1981).

7) A. Ohno, H. Yamamoto, and S. Oka, *Tetrahedron Lett.*, **1979**, 4061.

8) G. Sato and A. K. Colter, *Tetrahedron Lett.*, **1977**, 3325.

9) A. Rembaum, A. M. Hermann, F. E. Stewart, and F. Gutmann, *J. Phys. Chem.*, **73**, 513 (1969).

10) L. R. Melby, R. J. Harder, W. R. Hertler, W. Mahler, R. E. Benson, and W. E. Mochel, *J. Am. Chem. Soc.*, **84**, 3374 (1962).

11) C. N. R. Rao, "Spectroscopy of the Nitro Group," in "The Chemistry of the Nitro and Nitroso Groups," ed by H. Feuer, Interscience Publ., New York, N. Y. (1969), Part 1, pp. 116—120.

12) G. Mooser, H. Schulman, and D. S. Sigman, *Biochemistry*, **11**, 1595 (1972).

13) E. M. Kosower, *Prog. Phys. Org. Chem.*, **3**, 81 (1965).

14) C. P. Andrieux and J. M. Savéant, *Bull. Soc. Chim. Fr.*, **1973**, 2090.

15) R. Stewart and R. van der Linder, *Can. J. Chem.*, **38**, 399 (1960).

16) J. Foos, F. Steel, S. Q. A. Rizvi, and G. Fraenkel, *J. Org. Chem.*, **44**, 2522 (1979).

17) E. M. Kosower and T. S. Sorensen, *J. Org. Chem.*, **27**, 3764 (1962).

Intramolecular [2+2]Photocycloaddition of the 3-(3-Butenyloxy)-2-cyclohexenone System

Takashi UMEHARA, Yoshinobu INOUYE,* and Hiroshi KAKISAWA

Department of Chemistry, The University of Tsukuba, Sakura-mura, Niihari-gun, Ibaraki 305

(Received March 25, 1981)

The irradiation of 5,5-dimethyl-3-(4-methyl-3-pentenyloxy)-2-cyclohexenone gave regioselectively, 6,6,10,10-tetramethyl-2-oxatricyclo[5.4.0.0^{1,5}]undecan-8-one, while, that of 5,5-dimethyl-3-[(3-methylcyclohexenyl)methoxy]-2-cyclohexenone afforded, regio- and stereoselectively, 1,5,5-trimethyl-8-oxatetracyclo[8.3.1.0^{2,7}.0^{1,5}]tetradecan-3-one.

Since a successful synthesis of caryophyllene by Corey and his co-workers in 1963,[1] a number of [2+2]-photocycloaddition reactions have been reported as an important step[2] in the synthesis of natural products. Most of them were intermolecular reactions, for example, the addition of an α,β-unsaturated carbonyl moiety of one molecule to a double bond of a second one, but intramolecular approaches have limited to a few cases.[3-5] Nevertheless, the latter are very worthy of investigation because bond formation is expected to be prompted by the closer situation of reaction sites compared to the case of intermolecular reactions and becuase regio- and/or stereoselectivities will be enhanced by a specific and limited arrangement of reaction sites.

We will here report two intramolecular [2+2]-photocycloadditions of 3-(3-butenyloxy)-2-cyclohexenone derivatives, **7** and **10**. These cyclohexenones can be easily prepared from a β-diketone and a 3-butenyl alcohol derivative or a corresponding halide, as will be described below.

A simple system of 3-alkenyloxy-2-cyclohexenones had been investigated by Tamura and his co-workers.[6] In their work, 5,5-dimethyl-3-allyloxy-2-cyclohexenone-(**1**) changed into a tricyclic compound **2** upon irradiation with a Hg lamp, while 3-(3-butenyloxy)-2-cyclohexenone **3** was reversed in regioselectivity to give another tricyclic compound **4**. The reaction of the dimethyl compound **5** proceeded differently to afford a tetrahydrofuran derivative **6** as a result of a facile ene reaction. Therefore, we initially tried the photoreaction of 5,5-dimethyl-3-(4-methyl-3-pentenyloxy)-2-cyclohexenone(**7**), a dimethyl derivative of **3**, in order to clarify the influence of dimethyl groups on the reaction paths. The dimethyl compound **7** was prepared from dimedone and 5-chloro-2-methyl-2-pentene.[7]

The irradiation of a 1% hexane solution of **7** with an Ushio high-pressure mercury arc lamp gave a single photoadduct as a crystal in a 63% yield. The

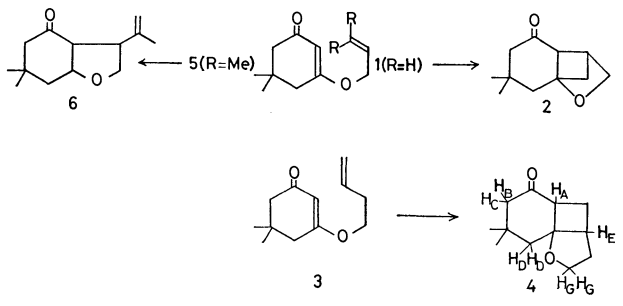

mass spectrum shows that the reaction was intramolecular, while the absorption at 1695 cm^{-1} in IR and the four methyl singlets at 0.94, 1.05, 1.05, and 1.08 ppm in NMR spectra clearly indicate that the reaction proceeded by means of [2+2]cycloaddition. Either structure, **8** or **8'**, is possible for the adduct; the NMR spectrum, a broad singlet at 2.35 (H_A), an AB center at 2.03 of J=18 Hz (H_B, H_C), a singlet at 1.90 ($2\times H_D$), and a complex multiplet between 3.60 and 4.20 ($-CH_2-O-$) are consistent with both structures, although, in **8'**, the coupling constant between H_A and H_E is nearly zero, as is to be anticipated from the dihedral angle (90°) of these two protons in the Dreiding models.

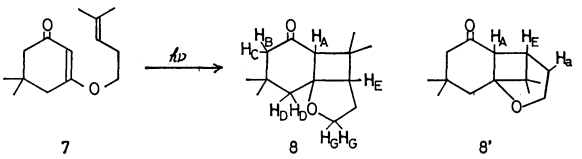

The pseudo-contact shift with Eu-FOD was measured; the results are shown in Fig. 1 and in Table 1. The three protons (H_A, H_B, and H_C) adjacent to the carbonyl group are most deshielded, and the magnitudes of the shifts are very close to each other. This shows that the shift reagent nearly comes in contact with the carbonyl oxygen and on the same side with H_A (see **9**). On the other hand, the H_E proton shifts

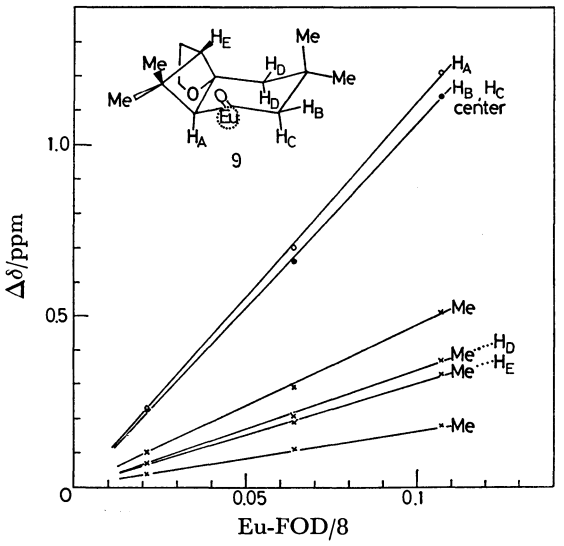

Fig. 1. Pseudocontact shifts of **8** with Eu-FOD in CCl_4.

Table 1. Pseudocontact shifts of **4**, **8**, and **16** with the addition of 0.1 mol equivalent of Eu-FOD in CCl_4

Proton	Δδ Values in ppm		
	4	**8**	**16**
H_A	1.18	1.12	1.18
H_B,H_C	1.08[a)]	1.05[a)]	1.14[a)]
H_D	0.40	0.34	0.34
H_E		0.30	0.26
H_G	0.2_5[b)]	0.3_7[b)]	0.28
	0.2_0[b)]	0.1_9[b)]	0.19
CH_3	0.36	0.47	0.49
	0.31	0.34	0.32
		0.30	0.17
		0.17	

a) Shifts at AB-type center. b) Less precise because of complex multiplets.

less than H_A and has a magnitude similar to that of H_D. These facts well accord with the structure **8**. In the alternate structure, **8'**, the H_E proton is situated closer to the carbonyl group than H_D; thus, it must have a larger Δδ value. Furthermore, H_E was found to be a double doublet with the coupling constants of 7 and 5 Hz upon the addition of the shift reagent. This is also inconsistent with the structure **8'**, in which the dihedral angle between H_E and the neighbouring axial proton (H_a) is very close to 90°.

Different from the case of **1** *vs.* **5**, the dimethyl group did not exert any influence on the reaction path and regioselectivity in the case of 3-(3-butenyloxy)-2-cyclohexenone **3** *vs.* **7**. This remarkable regioselectivity to give the bicyclo[3.*m*.0]-system has been observed in other cases.[3b,4,8)]

The successful conversion of **7** into **8** led us to investigate the photochemical reaction of 5,5-dimethyl-3-[(3-methyl-2-cyclohexenyl)methoxy]-2-cyclohexenone-(**10**), which has a less flexible olefinic side chain containing one asymmetric carbon atom.

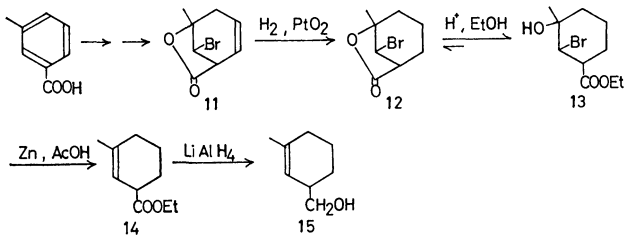

The bromo lactone **11**, prepared[9)] from *m*-toluic acid, was hydrogenated over the Adams catalyst to give a saturated lactone **12**. As the direct reduction of **12** with zinc in acetic acid gave a mixture of an olefinic acid and a debromo lactone, probably produced during the isolation procedure, **12** was initially changed into an ethyl ester **13** and then reduced with Zn–AcOH to afford an unsaturated ester **14**. The ester group in **14** was reduced with lithium aluminum hydride to give an alcohol **15**. The reaction of dimedone with **15** in the presence of *p*-toluenesulfonic acid afforded the enol ketone **10** as an oil.

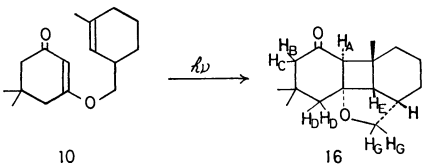

A similar irradiation of **10** gave a photoadduct in a 47% yield. Its spectroscopic properties well accord with the structure **16**: the carbonyl absorption at 1690 cm^{-1} in the IR spectrum and the three methyl singlets at 0.92, 1.00, and 1.01, the one broad proton singlet at 2.68, an AB-type quartet at 1.98 of J=18 Hz, a two proton singlet at 1.88, and the two triplets at 3.64 (J=9 Hz) and 3.94 (J=9 Hz) in the NMR spectrum. The *cis*-anti-*cis* stereochemical assignment was deduced from the fact that **16** was unchanged upon treatment with lithium diisopropylamide. The predominant formation of one diastereoisomer seems to be characteristic of the intramolecular reaction and is largely due to the steric requirement in the transition state.

Experimental

All the melting points are uncorrected. The IR spectra were taken on a Hitachi 215 grating spectrophotometer. The NMR spectra were obtained with Hitachi H-60 and JEOL MH-100 spectrophotometers, using TMS as the internal standard. The mass spectra were obtained with a Hitachi RMU-6MG mass analyzer. The flash chromatographies were performed using the Wakogel C-300 as the adsorbent.

Irradiation Procedure. A test solution of 170 mg of 5,5-dimethyl-3-(3-butenyloxy)-2-cyclohexenone (**3**) [$\nu(CHCl_3)$: 1640 and 1605 s cm^{-1}], prepared from dimedone and 4-bromo-1-butene in the presence of potassium methoxide, in 20 ml of hexane was irradiated in a Pyrex test tube with an Ushio 450 W high-pressure mercury arc lamp under nitrogen for 30 min. The solvent was then evaporated, and the residue was chromatographed with hexane–ethyl acetate (4:1) to give the known adduct, **4**[6a)] (120 mg, 72%). *m/e*: 194 (M^+) and 124 (base); $\nu(CCl_4)$: 1700, 1065, and 1040 cm^{-1}; δ (CCl_4, 100 MHz): 1.00 (s, 3H), 1.06 (s, 3H), 1.71 (AB center, 2H, J=15 Hz), 2.15 (AB center, 2H), 2.62 (dd, 1H, J=11 and 6 Hz), 1.5—2.0 (m, 2H), 2.0—2.4 (m, 4H), 2.5—2.8 (m, 1H), and 3.7—4.2 (m, 2H).

5,5-Dimethyl-3-(4-methyl-3-pentenyloxy)-2-cyclohexenone (7). A solution of dimedone (2.48 g) in 15 ml of dry HMPA was added, drop by drop, to a solution of potassium methoxide, prepared from 1.02 g of potassium, 5 ml of dry methanol, and 10 ml of HMPA. 5-Chloro-2-methyl-2-pentene[7)] (2.14 g) was added to the mixture, and the whole was heated at 100 °C overnight. Water was added, and the products were taken up in hexane. The solvent was evaporated, and the residue was chromatographed with hexane–ethyl acetate (9:2) to give **7** (741 mg, 19%) as an oil. An analytical sample was prepared by Kugelrohr distillation [bath temp: 70 °C/2 mmHg(1 mmHg=133.322 Pa)]. *m/e*: 222 (M^+) and 83 (base); ν (CCl_4): 1660, 1615, and 1220 cm^{-1}; δ (CCl_4): 1.08 (s, 6H), 1.65 (br. s, 3H), 1.73 (br. s, 3H), 2.08 (s, 2H), 2.23 (s, 2H), 2.37 (q, 2H, J=7 Hz), 3.78 (t, 2H, J=7 Hz), 5.1 (br. t, 1H, J=7 Hz), and 5.18 (s, 1H). Found: C, 75.35; H, 9.96%. Calcd for $C_{14}H_{22}O_2$: C, 75.63; H, 9.97%.

6,6,10,10-Tetramethyl-2-oxatricyclo[5.4.0.0^{1,5}]undecan-8-one (8).

A solution of 573 mg of **7** in 86 ml of hexane was divided into four Pyrex test tubes. The solution was then irradiated under nitrogen for 30 min. The solvent was evaporated, and the residual oil was chromatographed with hexane–ethyl acetate (5:1) to give colorless **8** (361 mg, 63%). Bath temp: 92 °C/2 mmHg; mp 48—49 °C (from pentane); *m/e*: 222 (M^+) and 83 (base); *v* (CCl_4): 1695, 1180, and 1050 cm^{-1}; *δ* (CCl_4, 100 MHz): 0.94 (s, 3H), 1.00 (s, 3H), 1.05 (s, 3H), 1.08 (s, 3H), 1.90 (s, 2H), 2.02 (AB center, 2H, *J*=18 Hz), 1.7—2.4 (m, 3H), 2.34 (s, 1H), and 3.6—4.2 (m, 2H); *δ* (CCl_4, 100 MHz, with the addition of a 0.11 equivalent of Eu-FOD): 1.20 (s, 3H), 1.27 (s, 3H), 1.45 (s, 3H), 1.56 (s, 3H), 1.9—2.2 (m, 2H), 2.27 (s, 2H), 2.48 (dd, 1H, *J*=7 and 5 Hz), 3.17 (AB center, 2H, *J*=18 Hz), 3.56 (s, 1H), and 3.9—4.4 (m, 2H). Found: C, 75.57; H 10.06%. Calcd for $C_{14}H_{22}O_2$: C, 75.63; H, 9.97%.

*8-Bromo-*cis*-5-methyl-6-oxabicyclo[3.2.1]octan-7-one (12).* The known bromo lactone **11**[9] (1.02 g) in 20 ml of ethyl acetate was hydrogenated over the Adams catalyst (109 mg) at a pressure of 1 atm for 80 min. The catalyst was then removed by filtration, and the filtrate was evaporated to give crystals. Recrystallization from pentane gave **12** (0.59 g, 93%); mp 59—60 °C. *v* (CCl_4): 1790s and 1105 cm^{-1}; *δ* (CCl_4): 1.45 (s, 3H), 1.0—2.5 (m, 6H), 2.75 (m, 1H), and 4.37 (d, 1H, *J*=6 Hz). Found: C, 43.97; H, 4.99%. Calcd for $C_8H_{11}O_2Br$: C, 43.86; H, 5.06%.

3-Methyl-2-cyclohexenylmethanol (15). A solution of **12** (13.4 g) in 60 ml of ethanol was refluxed in the presence of a catalytic amount of hydrochloric acid for 2 d. The mixture was passed through a sodium carbonate layer and then evaporated. The residue, after having been made free from a carboxylic acid produced, weighed 12.9 g. The IR spectrum of the residue showed that it was a mixture of **12** ($\nu_{C=O}$ 1790 cm^{-1}) and **14** ($\nu_{C=O}$ 1735 cm^{-1}) in the ratio of 1:3. The mixture was refluxed in 10 ml of acetic acid with 12.8 g of freshly activated (HCl) zinc powder. The solids were removed by filtration and washed with 20 ml of hexane. The filtrate and the washing were combined and then evaporated to give an oil (5.6 g). The oil was dispersed in a 5% sodium hydroxide solution and extracted with ethyl acetate. The extracts were washed with water, dried over Na_2SO_4, and then evaporated to give an ethyl ester **14** (4.4 g) as an oil; *v*(CCl_4): 1730 and 1175 cm^{-1}.

A solution of **14**, without further purification, in 50 ml of dry THF was added, drop by drop, to a cooled solution of lithium aluminum hydride (1.06 g) in 50 ml of dry THF. The mixture was stirred at room temperature for 30 min and then treated successively with 1 ml of water, 1 ml of a 15% sodium hydroxide solution, and 3 ml of water. The granular precipitates were removed by filtration and washed with THF. The filtrate and the washing were combined and then evaporated to give an alcohol **15** (2.5 g, 33% from **12**). Bp 55—63 °C/1 mmHg; *v* (CCl_4): 3400br, 1060, and 1030 cm^{-1}; *δ* (CCl_4): 1.65 (s, 3H), 1.1—2.4 (m, 8H), 2.83 (s, 1H, OH), 3.37 (d, 2H, *J*=6 Hz), and 5.30 (br.s, 1H).

Elemental analysis was performed on its *p*-nitrobenzoate derivative; mp 78—80 °C (from hexane); *v* (KBr): 1715, 1520, 1345, 1285, 1270, and 815 cm^{-1}. Found: C, 65.60; H, 6.14; N, 4.71%. Calcd for $C_{15}H_{17}NO_4$: C, 65.44; H, 6.22; N, 5.08%.

5,5-Dimethyl-3-[(3-methyl-2-cyclohexenyl)methoxy]-2-cyclohexenone (10). A mixture of 200 mg of dimedone, 179 mg of **15**, and 25 mg of *p*-toluenesulfonic acid was heated under refluxing with 40 ml of toluene for 43.5 h, while the water was being removed continuously by means of a water-separator. The mixture was then washed with a 15% sodium hydroxide solution and water until the washing was neutral. After having been dried, the solvent was evaporated to give an oil. The oil was chromatographed with hexane–ethyl acetate (4:1) to give **10** (204 mg, 58%). Bath temp: 60—65 °C/2 mmHg; *m/e*: 248 (M^+) and 108 (base); *v* (CCl_4): 1660, 1616, and 1220 cm^{-1}; *δ* (CCl_4): 1.08 (s, 6H), 1.66 (br.s, 3H), 2.08 (s, 2H), 2.25 (s, 2H), 1.0—2.8 (m, 10H), 3.65 (d, 2H, *J*=6.5 Hz), 5.22 (br.s, 1H), and 5.2—5.5 (m, 1H). Found: C, 77.08; H, 9.77%. Calcd for $C_{16}H_{24}O_2$: C, 77.37; 9.74%.

1,5,5-Trimethyl-8-oxatetracyclo[8.3.1.0^{2,7}.0^{1,5}]tetradecan-3-one (16). A solution of 200 mg of **10** in 22 ml of hexane was irradiated for 6 h. The solvent was then evaporated, and the residue was chromatographed with hexane–ethyl acetate (5:1) to give **16** (93 mg, 47%); mp 76—77 °C (from hexane); *m/e*: 248 (M^+) and 108 (base); *v* (CCl_4): 1690, 1050, and 1045 cm^{-1}; *δ* (CCl_4, 100 MHz); 0.92 (s, 3H), 1.00 (s, 3H), 1.01 (s, 3H), 1.88 (s, 2H), 1.98 (AB center, 2H, *J*=18 Hz), 1.98 (d, 1H, *J*=10 Hz), 2.68 (br.s, 1H), 3.64 (t, 1H, *J*=9 Hz), and 3.94 (t, 1H, *J*=9 Hz). Found: C, 77.28; H, 9.74%. Calcd for $C_{16}H_{24}O_2$: C, 77.37; H, 9.74%.

16 was unchanged even when it was treated with 5 equivalents of lithium diisopropylamide at room temperature overnight.

The present work was partially supported by a Grant-in-Aid for Scientific Reseach (No. 564174) from the Ministry of Education, Science and Culture.

References

1) E. J. Corey, R. B. Mitra, and H. Uda, *J. Am. Chem. Soc.*, **85**, 362 (1963); **86**, 485 (1964).

2) a) J. Kossanyi, *Pure Appl. Chem.*, **51**, 181 (1979); b) S. F. Martin, *Tetrahedron*, **36**, 419 (1980).

3) a) M. Mellor, D. A. Otieno, and G. Pattenden, *J. Chem. Soc., Chem. Commun.*, **1978**, 138; b) M. J. Begley, M. Mellor, and G. Pattenden, *ibid.*, **1979**, 235; c) A. M. Birch and G. Pattenden, *ibid.*, **1980**, 1195.

4) a) W. Oppolzer and S. C. Burford, *Helv. Chim. Acta*, **63**, 788 (1980); b) W. Oppolzer and R. D. Wylie, *ibid.*, **63**, 1198 (1980).

5) M. C. Pirrung, *J. Am. Chem. Soc.*, **101**, 7130 (1979).

6) a) Y. Tamura, H. Ishibashi, Y. Kita, and M. Ikeda, *J. Chem. Soc., Chem. Commun.*, **1973**, 101; b) Y. Tamura, H. Ishibashi, M. Hirai, Y. Kita, and M. Ikeda, *J. Org. Chem.*, **40**, 2702 (1975); c) Y. Tamura, H. Ishibashi, and M. Ikeda, *ibid.*, **41**, 1277 (1976).

7) T. A. Faworskaja and Sh. A. Fridman, *Zh. Obshch. Khim.*, **15**, 422 (1945).

8) S. Takahashi, T. Kusumi, Y. Sato, Y. Inouye, and H. Kakisawa, *Bull. Chem. Soc. Jpn.*, **54**, 1777 (1981).

9) W. E. Barnett and L. L. Needham, *J. Org. Chem.*, **40**, 2843 (1975).

Reactions of Group V Metal Compounds with Sulfur Trioxide

Fumio Ando, Jugo Koketsu,* and Yoshio Ishii
Department of Industrial Chemistry, Chubu Institute of Technology, Matsumoto-cho, Kasugai 487
(Received April 11, 1981)

Trialkylphosphines react with equimolar amounts of sulfur trioxide to form the 1:1 adducts $R_3P^{\oplus}$–$SO_3^{\ominus}$. Trialkylarsines and -stibines undergo sulfur trioxide insertion reactions across the metal-carbon bond to give the trisulfonates of the metal $M(OSO_2R)_3$ (M=As, Sb). The reactions of trialkyl phosphites, with sulfur trioxide yield trialkyl phosphates, trialkyl thiophosphates, dialkyl alkylphosphonates, dialkyl sulfates, and polymers which contain phosphorus atoms. The reactions of trialkoxyarsines and -stibines result in the insertion of sulfur trioxide across the metal-oxygen bond to form the alkoxymetal alkylsulfates $(RO)_{3-n}M(OSO_3R)_n$ (M=As, Sb; n=1, 2, 3) depending on the stoichiometric ratios of the reagents used. Pyrolysis of the metal sulfates gives dialkyl sulfates and undistillable residues containing the metals.

In a previous paper,[1] we reported that the reactions of trialkoxyarsines and -stibines with sulfur dioxide gave dialkyl sulfites and metal oxides, whereas trialkyl phosphites were oxidized to the phosphates and the thiophosphates. There are a few reports[2-4] concerning the reaction of sulfur trioxide with tervalent arsenic or antimony halides. Recently, Touzin and Mitacek[5] reported that arsenic(III) fluoride forms the mono-, di-, and tri-SO_3 insertion products $F_{3-n}As(OSO_2F)_n$ depending on the stoichiometric molar ratios. On the other hand, Schmidt and Bipp[6] reported that the 1:1 adducts of triphenyl-, diphenylchloro-, and phenyldichlorophosphines with sulfur trioxide were obtained by the reaction at −78 °C, but phosphine oxides and sulfur dioxide were formed by the reaction at room temperature. Becke-Gogehring and Thielemann[7] reported that triphenyl- and tricyclohexylphosphines, -arsines, and -stibines gave the sulfates $(C_6H_{11})_3AsSO_4$ and $(C_6H_5)_3SbSO_4$ in addition to the corresponding adducts $(C_6H_5)_3P^{\oplus}$–$SO_3^{\ominus}$, $(C_6H_{11})_3P^{\oplus}$–$SO_3^{\ominus}$, and $(C_6H_5)_3As^{\oplus}$–$SO_3^{\ominus}$. However, there has been no report about the insertion reaction of sulfur trioxide across the metal-carbon or metal-oxygen bond of the compounds containing the group V elements. We have investigated the reactions of trialkyl- and trialkoxyphosphines, -arsines, and -stibines with sulfur trioxide.

Results and Discussion

Trialkylphosphines. Trialkylphosphines reacted readily with sulfur trioxide in dichloromethane at −78 °C to give 1:1 adducts of the type $R_3P^{\oplus}$–$SO_3^{\ominus}$ in good yields. The adduct of trialkylphosphine (**1a**)

$$R_3P + SO_3 \longrightarrow R_3P^{\oplus}\text{-}SO_3^{\ominus} \quad (1)$$

is a colorless crystal (mp 35—39 °C); it disproportionated to triethylphosphine oxide and a small amount of triethylphosphine sulfide with evolution of sulfur dioxide on distillation under reduced pressure. The adduct of triisopropylphosphine (**1b**) is a stable crystal and has a very high melting point compared with the others. $Ph_2Bu^nP^{\oplus}$–$SO_3^{\ominus}$ (**1c**) was obtained in 70% yield by the equimolar reaction of butyldiphenylphosphine with sulfur trioxide. The IR spectrum of the adduct (**1c**) shows the symmetric and asymmetric stretching vibrations of the $SO_3^{\ominus}$ group[8] at 1270, 1120, and 1038 cm^{-1}. Assignments of the ^{13}C NMR spectra of the adducts were done according to the literature.[9] Both the large P–C coupling constants observed for the all adducts and the upfield shift of ipso-carbon of the phenyl group of the adduct (**1c**) are characteristic of the phosphonium compounds.[10-12] The 1:1 adduct of triethylphosphine with SO_3 (**1a**) reacted at room temperature with 3 molar excess of triethylphosphine to give 3 mol of triethylphosphine oxide and 1 mol of triethylphosphine sulfide. The

$$\mathbf{1a} + 3Et_3P \longrightarrow 3Et_3PO + Et_3PS \quad (2)$$

phosphonium ion structures of the adducts were also confirmed by their reactions with methyllithium, hydrogen chloride, and acetic acid. The structures of

$$\mathbf{1a} + MeLi \longrightarrow Et_3MePSO_3Li \quad (3)$$

$$\mathbf{1a} + HCl \longrightarrow Et_3ClPSO_3H \quad (4)$$

$$\mathbf{1a} + CH_3COOH \longrightarrow Et_3P(OCOCH_3)SO_3H \quad (5)$$

these reaction products were confirmed by their spectroscopic data and also by elemental analyses.

Trialkylarsines and -stibines. Arsenic or antimony tris(alkanesulfonate) were formed on treatments of trialkylarsines or -stibines with a 3 molar excess of sulfur trioxide. The yields and some spectroscopic data of

$$R_3M + 3SO_3 \longrightarrow M(OSO_2R)_3 \quad (6)$$
$$M=As, Sb$$

these insertion products are shown in Table 1. The reactivity order among the trialkyl derivatives was found to be $R_3Sb > R_3As$. Trialkylarsines and -stibines behave quite differently from triphenylarsine and -stibine[7] and also trialkylphosphines during the reactions with sulfur trioxide. This difference in the chemical behavior might be attributable to the fact that the metal-carbon bond of trialkylarsines and -stibines is weaker than the metal-phenyl or the phosphorus-alkyl bond.[13]

Trialkyl Phosphites. When sulfur trioxide was added to an equimolar amount of trimethyl phosphite at −78 °C, a violent reaction took place to give trimethyl phosphate, trimethyl thiophosphate, dimethyl methylphosphonate, dimethyl sulfate, and polymeric compounds containing phosphorus atoms. The reaction does not obey a simple stoichiometry. Table 2

$$(RO)_3P + nSO_3 \longrightarrow (RO)_3PO + (RO)_3PS + (RO)_2P(O)R + (RO)_2SO_2 + \text{"P-polymers"} \quad (7)$$

shows the effects of the alkyl group of trialkyl phosphite, the molar ratio of the reactants, and the reaction temperature on the distribution of reaction products,

Table 1. Sulfonation product of trialkylarsine and -stibine; $M(SO_3R)_3$

M	R	Yield %	IR $\nu(SO_2)/cm^{-1}$	^{13}C-NMR(δ) C_1	C_2	C_3	C_4	^1H-NMR(δ)
As	*i*-Pr	88	1185 1035	37.9	18.0			1.58(t, 3H) 3.68(m, 1H)
	n-Bu	92	1190 1045	34.0	24.9	24.9	13.2	1.00(t, 3H) 1.17—2.25(m, 4H) 3.07(t, 2H)
Sb	*i*-Pr	90	1195 1050	37.9	18.0			1.67(d, 6H) 3.56(m, 1H)
	n-Bu	84	1185 1040	34.3	26.5	25.0	13.3	0.97(*t*, 3H) 1.13—2.16(m, 4H) 2.80(t, 2H)

Table 2. Effect of alkyl group, molar ratio, and temperature on the reaction of trialkyl phosphite with SO_3

$P(OR)_3$	Molar ratio $P(OR)_3/SO_3$	Temp °C	Products distribution/% $(RO)_3PO$	$(RO)_3PS$	$(RO)_2SO_2$	$(RO)_2P(O)R$
R=Me	1/1	−50	7	0	93	0
Me	1/1	−78	22	4	55	19
Me	1/1	−95	100	0	0	0
Me	3/1	−50	56	0	18	26
Me	4/1	−50	55	1	12	32
Me	4/1	−78	48	16	3	9
Me	4/1	−95	25	4	0	71
Et	1/1	−50	55	0	17	28
Et	1/1	−78	64	0	14	22
Et	4/1	−50	64	21	3	11
Et	4/1	−78	70	23	2	5
Et	1/2	−78	30	0	65	5
Et	1/3	−78	2	0	97	1
i-Pr	1/1	−50	18	0	72	0
i-Pr	4/1	−50	67	25	8	0
n-Bu	1/1	−50	70	0	28	2
n-Bu	4/1	−50	64	22	2	12

The relative amounts of the products varied depending on the molar ratio of the reactants and the temperature. The selective oxidation of phosphite was observed at low temperature with formation of sulfur dioxide. The formation of sulfates is favored at high temperature and by increasing the amounts of sulfur trioxide. The formation of thiophosphates occured mainly under the reaction conditions where the excess amount of trialkyl phosphite was used. From these results of product distributions, we wish to propose a tentative reaction mechanism as follows:

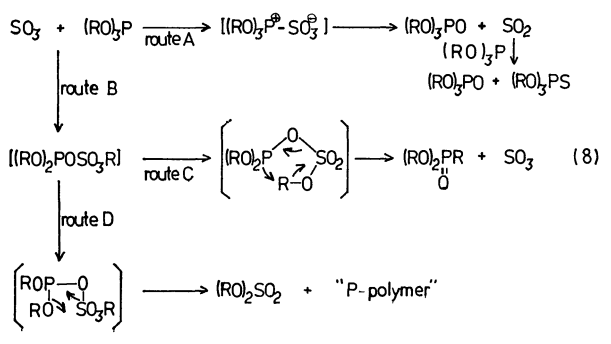

Trialkyl phosphite is an electron donor which forms a donor-acceptor complex with various electron acceptors. The sulfur atom of sulfur trioxide is the most electrophilic center in the molecule. Therefore, it is reasonable to assume that trialkyl phosphite reacts preferentially with the sulfur atom of sulfur trioxide to give alkoxyphosphonium intermediate (route A), which is not stable because of the electron-withdrawing alkoxyl group on the phosphorus atom. The phosphonium ion decomposed to trialkyl phosphate and sulfur dioxide, which, in turn, reacts with an additional trialkyl phosphite to give trialkyl phosphate and thiophosphate.[1] To explain the formation of dialkyl sulfate and dialkyl alkylphosphonate, we propose a mechanism involving the insertion of sulfur trioxide across the P–O bond of phosphite (route B). The formation of dialkyl alkylphosphonate can be explained by an intramolecular rearrangement of the insertion intermediate with elimination of sulfur trioxide (route C). An analogous mechanism has been reported by Lemper and Tieckman[14] for the rearrangement of diethyl 1-methylallyl phosphite to the phosphonate. Dialkyl sulfate and "P-polymers" might

be formed through the route D. Concerning the formation of dialkyl sulfate and "P-polymers," there might be another mechanism involving the reaction of trialkyl phosphate (formed through route A) with sulfur trioxide as reported by Du Plessis.[15] The reaction of trimethyl phosphate with sulfur trioxide gave dimethyl sulfate and methyl polyphosphates.[15] Trialkyl phosphates whose alkyl substituents were higher than the ethyl group, however, formed stable 1:1 adducts with sulfur trioxide and the corresponding dialkyl sulfates and "P-polymers" were not obtained from the adducts.[16] Therefore, the route D in the reaction mechanism proposed is much more probable than the latter route.

$$(MeO)_3PO + SO_3 \longrightarrow (MeO)_2SO_2 + \text{"P-polymers"} \quad (9)$$

Trialkoxyarsines and -stibines. When sulfur trioxide and trialkoxyarsines were allowed to react at −50 °C in 1:1, 1:2, and 1:3 molar ratios, the corresponding insertion products were obtained almost quantitatively. The insertion products are sensitive to moisture and oxygen, while they are stable at room temperature under an inert atmosphere. Attempts to distill the insertion products under reduced pressure (0.1 mmHg (1 mmHg≈133.322 Pa)) resulted in decomposition giving dialkyl sulfates and white or brown-black residues containing arsenic atoms.

$$As(OR)_3 + nSO_3 \longrightarrow (RO)_{3-n}As(OSO_3R)_n \quad (10)$$
$$n=1,\ 2,\ 3$$

Trialkoxystibines also gave the corresponding insertion products with cleavage of the Sb–O bond. The reactivity of trialkoxystibines toward sulfur trioxide is somewhat greater than that of trialkoxyarsines because of higher polarizability of the metal-oxygen bond of trialkoxystibines than that of trialkoxyarsines. The insertion products were viscous liquids and very sensitive to air and moisture. Attempts to purify these products by distillation or recrystallization were unsuccessful. Pyrolysis under reduced pressure gave dialkyl sulfates along with charred decomposition products containing antimony atoms. The IR, ^1H NMR, and ^{13}C NMR spectra of the arsenic or antimony mono-, bis-, and tris(alkyl sulfates) are given in Table 3 along with the parent metal alkoxide. The IR spectra exhibit symmetric and asymmetric stretching vibrations of SO_2 group at 1220 and 1390 cm^{-1}, respectively. In the ^{13}C NMR spectra, α-methylene carbons shift to low field by the shielding effect of SO_2 group.[17]

$$Sb(OR)_3 + nSO_3 \longrightarrow (RO)_{3-n}Sb(OSO_3R)_n \quad (11)$$
$$n=1,\ 2,\ 3$$

Experimental

All reactions were carried out under an atmosphere of argon or nitrogen. Infrared spectra were recorded on a Shimadzu IR 430 spectrometer. ^1H NMR spectra were recorded on a JEOL C 60 HL spectrometer and ^{13}C NMR spectra on a JEOL JNM-FX 60 FT NMR instrument. Analytical GLC was carried out on a Shimadzu GC 60A apparatus using a 3 m grass column packed with PEG 6000 (10%) with helium as a carrier gas. Dichloromethane was dried over calcium chloride and distilled through a fractionating column.

Reagent. Sulfur trioxide (bp 46 °C) was distilled from sulfuric anhydride (Yotsuhata Chem. Co.) into an ice-cooled flask containing dichloromethane. The concentration of sulfur trioxide was determined by a titration with a standard

Table 3. Spectroscopic data of the alkoxyarsenic or alkoxyantimony alkyl sulfates; $(ROSO_3)_nM(OR)_{3-n}$

M	R	n	^1H NMR(δ)		^{13}C NMR(δ)		IR
			$ROSO_3$	RO	$ROSO_3$	RO	$\nu(SO_3)/cm^{-1}$
As	CH_3	0	—	3.60 (s)	—	50.0	—
		1	4.01 (s, 1H)	3.90 (s, 2H)	58.0	52.5	1400 1218
		2	4.07 (s, 2H)	3.98 (s, 1H)	59.1	54.1	1390 1216
		3	4.11 (s)	—	59.4	—	1388 1218
As	C_2H_5	0	—	1.27 (t, 3H) 3.94 (q, 2H)	—	18.1 58.5	—
		1	1.42 (t, 3H) 4.34 (q, 2H)	1.33 (t, 6H) 4.17 (q, 4H)	14.7 68.4	17.6 61.3	1400 1218
		2	1.46 (t, 2H) 4.49 (q, 2H)	1.38 (t, 1H) —	14.5 71.1	17.2 65.2	1390 1216
		3	1.43 (t, 3H) 4.46 (q, 2H)	—	14.5 71.3	—	1388 1215
Sb	C_2H_5	0	—	1.37 (t, 3H) 4.01 (q, 2H)	—	19.8 58.9	—
		1	1.38 (t, 3H) 4.34 (t, 2H)	1.40 (t, 6H) 4.29 (q, 4H)	14.8 67.2	18.8 61.3	1392 1230
		2	1.41 (t, 6H) 4.40 (q, 4H)	1.45 (t, 3H) 4.36 (q, 2H)	14.7 68.7	17.1 63.7	1388 1210
		3	1.43 (t, 3H) 4.49 (q, 2H)	—	14.6 67.7	—	1389 1216

solution of sodium hydroxide. Trimethyl phosphite, triethyl phosphite and tributyl phosphite were of commercial material and distilled before use. Tripropyl phosphite (bp 84—87 °C/14 mmHg) and triisopropyl phosphite (bp 63—66 °C/12 mmHg) were prepared by the method described in the literature.[18] Trialkoxyarsines and -stibines[19] were prepared by the reaction of arsenic or antimony trichloride with an appropriate alcohol in the presence of ammonia; $As(OMe)_3$; bp 95—96 °C/35 mmHg, $As(OEt)_3$; bp 59—60 °C/14 mmHg, $Sb(OEt)_3$; bp 49—52 °C/14 mmHg.

Equimolar Reaction of Trialkylphosphine with Sulfur Trioxide. Sulfur trioxide (19.7 mmol in 5 cm³ of dichloromethane) was added to a solution of triethylphosphine (2.31 g, 19.6 mmol) in 10 cm³ of dichloromethane at −78 °C. The mixture was kept for 2 h at −78 °C and then warmed up gradually to room temperature. After removal of the solvent, the product was recrystallized from petroleum ether/chloroform (5/1) to give $Et_3P^{\oplus}-SO_3^{\ominus}$ (3.27 g, 84%), mp 35—39 °C. ^1H NMR ($CDCl_3$): $\delta=1.40$ (dt, 3H, $^3J_{PH}=19.2$ Hz) and 2.49 (dq, 2H, $^2J_{PH}=12.0$ Hz). ^{13}C NMR ($CHCl_3$): $\delta=5.2$ (d, $^2J_{PC}=4.9$ Hz) and 18.2 (d, $^1J_{PC}=64.7$ Hz). ^{31}P NMR ($CHCl_3$): $\delta=-79.5$. IR ($CHCl_3$): $\nu(SO_3^-)$ 1276, 1160, and 1040 cm⁻¹. Found: C, 36.9; H, 7.74; P, 15.0%. Calcd for $C_6H_{15}O_3PS$: C, 36.36; H, 7.63; P, 15.62%. An attempted distillation resulted in a decomposition which gave triethylphosphine oxide (78%) and triethylphosphine sulfide (5%). In a similar way, reaction of triisopropylphosphine (2.05 g, 12.8 mmol) with an equimolar amount of sulfur trioxide gave white crystals, $i\text{-}Pr_3P^{\oplus}-SO_3^{\ominus}$ (2.27 g, 74%), mp 201—203 °C (dec). ^1H NMR ($CDCl_3$): $\delta=1.59$ (dd, 6H, $^3J_{PC}=16.8$ Hz) and 2.87 (m, 1H). ^{13}C NMR ($CHCl_3$): $\delta=17.3$ (d, $^2J_{PC}=2.9$ Hz) and 24.8 (d, $^1J_{PC}=51.9$ Hz). IR (KBr): $\nu(SO_3^-)$ 1238, 1168, and 1020 cm⁻¹. Found: C, 45.3; H, 8.73; P, 13.1%. Calcd for $C_9H_{21}O_3PS$: C, 44.98; H, 8.81; P, 12.89%. Reaction of butyldiphenylphosphine (1.03 g, 4.25 mmol) with an equimolar amount of sulfur trioxide gave $Ph_2BuP^{\oplus}-SO_3^{\ominus}$ (0.96 g, 70%); ^{13}C NMR ($CHCl_3$): $\delta=28.2$ ($^1J_{PC}=70.8$ Hz), 23.2 ($^2J_{PC}=1.2$ Hz), 23.9 ($^3J_{PC}=12.2$ Hz), 13.4 ($^4J_{PC}\approx0$ Hz), 129.8 (ipso, $J_{PC}=100.1$ Hz), 130.92 (ortho, $J_{PC}=9.77$ Hz), 129.06 (meta, $J_{PC}=12.21$ Hz), and 132.7 (para, $J_{PC}=3.1$ Hz). IR (neat): $\nu(SO_3^-)$ 1270, 1120, and 1038 cm⁻¹.

Reactions of $Et_3P^{\oplus}-SO_3^{\ominus}$ with Various Reagent. Triethylphosphine (1.94 g, 16.4 mmol) was added to $Et_3P^{\oplus}-SO_3^{\ominus}$ (1.09 g, 5.47 mmol) in 5 cm³ of dichloromethane at −78 °C. The mixture was warmed up to room temperature and an exothermic reaction took place to give triethylphosphine oxide (1.61 g, 55%) and triethylphosphine sulfide (0.53 g, 16%). The structures of both compounds were confirmed by comparison of the physical properties and spectroscopic data with those of authentic samples.[20] An equimolar reaction of $Et_3P^{\oplus}-SO_3^{\ominus}$ (1.01 g, 5.12 mmol) and methyllithium in ether gave the lithium sulfonate Et_3PMeSO_3Li (0.93 g, 87%), a brown solid, mp>250 °C. ^{13}C NMR ($CHCl_3$): $\delta=6.2$ ($^2J_{PC}=4.6$ Hz, CH_3CH_2), 17.4 ($^1J_{PC}=35.6$ Hz, CH_2), and 19.3 ($J_{PC}=66.7$ Hz, CH_3P). Found: P, 14.1%. Calcd for $C_7H_{18}PSO_3Li$: P, 14.07%. Reaction of $Et_3P^{\oplus}-SO_3^{\ominus}$ (1.84 g, 9.29 mmol) with anhydrous hydrogen chloride in ether gave the sulfonic acid $Et_3P(Cl)SO_3H$ (2.09 g, 96%) as a viscous liquid. ^1H NMR ($CDCl_3$): $\delta=1.28$ (dt, 9H, $^1J_{PH}=19.1$ Hz), 2.23 (dq, 6H, $^2J_{PH}=12.4$ Hz), and 12.44 (s, 1H, SO_3H). ^{13}C NMR ($CHCl_3$): $\delta=5.1$ ($^2J_{PC}=5.5$ Hz) and 17.2 ($^1J_{PC}=62.9$ Hz); IR (neat): $\nu(OH)$ 2240, $\nu(SO_2)$ 1198, 1050, and $\nu(P-C)$ 560 cm⁻¹. Found: P, 13.5%. Calcd for $C_6H_{16}PSO_3Cl$; 13.20%. Reaction of $Et_3P^{\oplus}-SO_3^{\ominus}$ (0.58 g, 2.93 mmol) with acetic acid (0.20 g, 3.33 mmol) gave the corresponding acetate $Et_3P(OCOCH_3)-SO_3H$ (0.69 g, 92%) as a viscous liquid. ^1H NMR ($CDCl_3$): $\delta=1.26$ (dt, 9H, $^2J_{PH}=19.4$ Hz), 2.18 (dq, 6H, $^3J_{PH}=12.6$ Hz), 2.09 (s, 3H, CH_3CO), and 12.41 (s, 1H, SO_3H): ^{13}C NMR ($CHCl_3$): $\delta=5.0$ ($^2J_{PC}=5.1$ Hz), 16.6 ($^1J_{PC}=16.6$ Hz), 20.9 (CH_3CO), and 176.1 (CH_3Co). IR (neat): $\nu(C=O)$ 1724 cm⁻¹. Found: P, 11.6%. Calcd for $C_8H_{19}-O_5PS$: P, 11.99%.

Reaction of Trialkylarsines with Sulfur Trioxide. Sulfur trioxide (20.5 mmol in 10 cm³ of dichloromethane) was added to triisopropylarsine (1.40 g, 6.83 mmol) in 10 cm³ of dichloromethane at −50 °C. After removal of the solvent, arsenic tris(2-propanesulfonate) (2.67 g, 88%) was obtained as a viscous liquid. Found: C, 24.3; H, 4.83%. Calcd for $C_9H_{21}AsO_9S_3$: C, 24.32; H, 4.74%. Reaction of tributylarsine (1.78 g, 7.28 mmol) with 3 molar excess of sulfur trioxide gave arsenic tris(1-butanesulfonate) (3.26 g, 92%). Found: C, 28.9; H, 5.52%. Calcd for $C_{12}H_{27}-AsO_9S_3$: C, 29.63; H, 5.60%.

Reaction of Trialkylstibines with Sulfur Trioxide. Triisopropylstibine (2.06 g, 8.20 mmol) and sulfur trioxide (24.6 mmol) were treated in 20 cm³ of dichloromethane at −50 °C. Antimony tris(2-propanesulfonate) (3.62 g, 90%) was obtained as a viscous liquid. Found: C, 22.4; H, 4.56%. Calcd for $C_9H_{21}O_9S_3Sb$: C, 21.96; H, 4.30%. Tributylstibine (2.08 g, 7.11 mmol) and 3 molar excess of sulfur trioxide gave antimony tris(1-butanesulfonate) (3.18 g, 84%), a viscous liquid. Found: C, 27.4; H, 5.12%. Calcd for $C_{12}H_{27}O_9S_3Sb$: C, 27.03; H, 5.10%.

Reaction of Trialkyl Phosphite with Sulfur Trioxide. A typical reaction is described. When a solution of sulfur trioxide (19.2 mmol in 5 cm³ of dichloromethane) was added to trimethyl phosphite (2.38 g, 19.2 mmol) in 10 cm³ of dichloromethane at −78 °C, a violent reaction took place. After removal of the solvent, the mixture was distilled under reduced pressure to give a fraction (2.57 g) of the bp range of 60—86 °C/12 mmHg. The following substances were isolated from this fraction (1.50 g) by column chromatography on silica gel (changing eluent from cyclohexane to benzene and then to chloroform): trimethyl phosphate (0.33 g), trimethyl thiophosphate (0.06 g), dimethyl methylphosphonate (0.30 g), and dimethyl sulfate (0.82 g). All these compounds were identified by comparing the physical and spectroscopic (IR, ^1H, ^{13}C, and ^{31}P NMR) data with those of the authentic samples.[21] In a similar manner, the reactions of other trialkyl phosphites with sulfur trioxide were performed and the distribution of the reaction products were analyzed by analytical GLC.

Reaction of Triakoxyarsines with Sulfur Trioxide. A solution of sulfur trioxide (17.3 mmol in 5 cm³ of dichloromethane) was added slowly to trimethoxyarsine (2.93 g, 17.4 mmol) in 10 cm³ of dichloromethane at −50 °C. After the solvent was evaporated, dimethoxyarsenic methyl sulfate (3.90 g, 90%) was obtained as a colorless liquid. A distillation of the crude product (2.65 g) under reduced pressure gave pure dimethoxyarsenic methyl sulfate (1.01 g, 39%), bp 96—97 °C/0.22 mmHg; Found: C, 14.3; H, 3.63%. Calcd for $C_3H_9O_6SAs$: C, 14.52; H, 3.66%, along with dimethyl sulfate (0.35 g, 27%) and a residue (1.18 g) containing arsenic atoms. Reaction of trimethoxyarsine (1.65 g, 9.82 mmol) and sulfur trioxide (19.7 mmol) was carried out under similar conditions. The white crystals which formed were washed with hexane. Methoxyarsenic bis(methyl sulfate) (3.03 g, 94%) was obtained, mp 59—63 °C. The distillation of the crude methoxyarsenic bis(methyl sulfate) (1.93 g) gave methoxyarsenic bis(methyl sulfate) (0.54 g, 28%), bp 98—103 °C/0.2 mmHg; Found: C, 10.7;

H, 2.89%. Calcd for $C_3H_9O_9S_2As$: C, 10.98; H, 2.76%, dimethyl sulfate (0.52 g, 38%) and a grayish residue (0.60 g). Reaction of trimethoxyarsine (1.97 g, 11.7 mmol) with sulfur trioxide (35.2 mmol) gave crude arsenic tris(methyl sulfate) (4.49 g, 94%). Distillation of this crude product gave arsenic tris(methyl sulfate) (19%), bp 82—85 °C/0.08 mmHg, Found: C, 8.76; H, 2.28%. Calcd for $C_3H_9O_{12}S_3As$: C, 8.83; H, 2.20%, and dimethyl sulfate (21%). Equimolar reaction of triethoxyarsine (1.65 g, 7.86 mmol) and sulfur trioxide gave diethoxyarsenic ethyl sulfate (2.02 g, 88%). The distillation gave diethoxyarsenic ethyl sulfate (44%), bp 107—110 °C/0.1 mmHg and diethyl sulfate (36%), bp 94—96 °C/18 mmHg; IR (neat): $\nu(SO_2)$ 1385, and 1158 cm^{-1}; ^1H NMR (CCl_4): $\delta=1.43$ (t, 3H), and 4.30 (q, 2H); ^{13}C NMR ($CHCl_3$): $\delta=14.6$, and 69.8. When reaction of triethoxyarsine with sulfur trioxide was carried out in 1:2 and 1:3 molar ratios of the reagents, the corresponding oily insertion products were obtained in 97 and 92% yields, respectively. Attempted distillation of the adducts caused a complete decomposition which afforded diethyl sulfate (54 and 40%, respectively).

Reaction of Triethoxystibine with Sulfur Trioxide. A solution of sulfur trioxide (20.0 mmol in 10 cm^3 of dichloromethane) was added to triethoxystibine (5.12 g, 19.9 mmol) in 10 cm^3 of dichloromethane at −50 °C. In a few minutes, white crystals were formed. The mixture was warmed to room temperature and the crystals were collected by filtration. Recrystallization from benzene/chloroform (9/1) gave diethoxyantimony ethyl sulfate (5.9 g, 88%), mp 76—80 °C. Found: C, 20.5; H, 4.54%. Calcd for $C_6H_{15}O_6SSb$: C, 21.38; H, 4.49%. An attempted distillation of the diethoxyantimony ethyl sulfate (1.23 g, 3.64 mmol) caused the decomposition which gave diethyl sulfate (0.40 g, 2.58 mmol) and a residue (0.82 g). A solution of sulfur trioxide (19.7 mmol in 5 cm^3 of dichloromethane) was added to triethoxystibine (2.55 g, 9.92 mmol) in 10 cm^3 of dichloromethane at −50 °C. After removal of the solvent, the residue was dried under reduced pressure (5 h, at 15—20 °C/0.07 mmHg), leaving a brown viscous liquid (3.96 g) which was used without further purification for ^1H and ^{13}C NMR and IR spectra measurements. These spectra proved the product to be ethoxyantimony bis(ethyl sulfate) (96%). Found: C, 17.8; H, 3.42%. Calcd for $C_6H_{15}O_9S_2Sb$: C, 17.28; H, 3.62%. In a similar way, the reaction of triethoxystibine (3.37 g, 13.1 mmol) and sulfur trioxide (39.4 mmol) in 20 cm^3 of dichloromethane gave antimony tris(ethyl sulfate) (6.03 g, 93%), orange oil. Found: C, 14.5; H, 3.00%. Calcd for $C_6H_{15}O_{12}S_3Sb$: C, 14.49; H, 3.04%. Pyrolysis of the tris (sulfate) (2.00 g, 4.02 mmol) under reduced pressure gave diethyl sulfate (0.53 g, 3.42 mmol) and a charred residue (1.37 g).

References

1) F. Ando, J. Koketsu, and Y. Ishii, *Bull. Chem. Soc. Jpn.*, **52**, 807 (1979).
2) E. L. Muetterties and D. D. Coffman, *J. Am. Chem. Soc.*, **80**, 5914 (1958).
3) R. J. Gillespie and J. W. Oubridge, *Proc. Chem. Soc.*, **1960**, 308.
4) H. A. Lehmann and L. Riesel, *Z. Anorg. Allg. Chem.*, **371**, 281, 289 (1969).
5) J. Touzin and L. Mitacek, *Collect. Czech. Chem. Commun.*, **44**, 1521 (1979).
6) M. Schmidt and H. Bipp, *Sitzber, Ges. Befoerder. Ges. Naturw. Marburg.*, **83/84**, 523 (1961/1962).
7) M. Becke-Gogehring and H. Thielemann, *Z. Anorg. Allg. Chem.*, **308**, 33 (1962).
8) P. J. Butterfield, J. C. Tebby, and D. V. Griffiths, *J. Chem. Soc., Perkin Trans. 1*, **1979**, 1189.
9) J. Koketsu, *Nippon Kagaku Kaishi*, **1980**, 1835.
10) E. E. Schweizer and M. A. Calcagno, *J. Org. Chem.*, **42**, 2641 (1977).
11) F. J. Weigert and J. D. Roberts, *J. Am. Chem. Soc.*, **91**, 4940 (1969).
12) G. A. Gray and S. E. Cremer, *J. Org. Chem.*, **37**, 3470 (1972).
13) H. A. Skinner, *Adv. Organomet. Chem.*, **2**, 49 (1964).
14) A. L. Lemper and H. Tieckman, *Tetrahedron Lett.*, **1964**, 3054.
15) Du Plessis, *J. S. Afr. Chem. Inst.*, **26**, 30 (1973).
16) A. F. Turbak and J. R. Livingston, Jr., *I & EC Product Research and Development*, **2**, 229 (1963).
17) A. H. Fawcett, K. J. Ivin, and C. D. Stewart, *Org. Magn. Reson.*, **11**, 360 (1978).
18) A. H. Ford-Moore and B. J. Perry, *Org. Synth.*, Coll. Vol. 4, 955 (1963).
19) T. B. Brill and N. C. Cambell, *Inorg. Chem.*, **12**, 1884 (1973).
20) G. M. Kosolapoff and L. Maier, "Organic Phosphorus Compounds," Wiley-Interscience (1972), Vol. 3, Chap. 6 and Vol. 4, Chap. 7.
21) G. M. Kosolapoff and L. Maier, "Organic Phosphorus Compounds," Wiley-Interscience (1973), Vol. 6, Chap. 15 and (1976), Vol. 7, Chaps. 18 and 19.

Photochemistry of 9-[2-(*N*-Substituted Aminomethyl)-1-naphthyl]-phenanthrenes. Intramolecular Addition of Amines to Excited State of Phenanthrene in Conformationally Rigid System

Akira Sugimoto, Ryozo Sumida, Naoto Tamai, Hiroo Inoue, and Yoshio Otsuji*

Department of Applied Chemistry, College of Engineering, University of Osaka Prefecture, Mozu-Umemachi, Sakai, Osaka 591

(Received April 23, 1981)

Irradiation of benzene solutions of 9-[2-(*N*-substituted aminomethyl)-1-naphthyl]phenanthrenes (**3a—d**) gave pyrroline derivatives by the attack of the NH group on the C-9 carbon atom of the phenanthrene ring. The reactions were highly selective in regio- and stereochemical senses, and occurred through exciplexes formed by intramolecular interaction between the amino group and the excited phenanthrene moiety in **3a—d**. Mechanistic features of these photoreactions are discussed on the basis of chemical and photochemical properties of substrates and products.

The photochemical reactions of aromatic hydrocarbons with amines have been studied extensively in recent years. For example, primary and secondary amines undergo the photoaddition to aromatics such as benzene[1] and anthracene[2] mainly at their nitrogen atoms, and tertiary amines generally at their carbon atoms α to the amino groups. Similar photoaddition was observed for naphthalene[3] and stilbene.[4] Substituted aromatics sometimes undergo the photosubstitution by amines.[5] It has been reported that these reactions occur through exciplexes or solvated radical anion-radical cation pairs produced by an intermolecular interaction between the excited aromatics and the ground state of amines. However, since these reactions usually afford several products at the same time, the mechanistic interpretation of the reactions often becomes equivocal.

Intramolecular interactions between excited aromatic hydrocarbons and ground state of amines have also been studied in bichromophoric molecules containing both an aromatic moiety and a tertiary amino group.[6] These studies have mainly manifested photophysical processes such as intramolecular electron-transfer and exciplex formation, but the photochemical properties of these systems have not been much elucidated.

In this study, we synthesized 9-[2-(*N*-substituted aminomethyl)-1-naphthyl]phenanthrenes (**3a—f**) from 9-(2-methyl-1-naphthyl)phenanthrene (**1**), and studied their photochemical behavior. In these compounds (Scheme 1), phenanthrene ring (electron acceptor) and amino group (electron donor) are connected by naphthylmethyl group, whereby the spatial relationship between both groups is rendered relatively rigid for a steric reason: a molecular model shows that in these compounds, the two chromophoric groups can be situated in a neighboring position in their favorable conformations. Consequently, these compounds may serve as a good candidate for the elucidation of photochemical properties in a bichromophoric system.

In this paper we demonstrate that the RN group and hydrogen atom of the amino functions in **3a—d** add respectively to the C-9 and C-10 atoms of the phenanthrene ring in a *cis* mode to form a pyrroline ring system. This reaction is highly selective in regio- and stereochemical senses and occurs through exciplexes formed by intramolecular interaction between the amino groups and the excited phenanthrene moiety.

Results and Discussion

Preparations of the Compounds. The compounds **3a—f** were prepared by the route shown in Scheme 1. The structures of these compounds were secured from their elemental analyses and spectral data (see Experimental).

Preparative Photochemistry and Properties of Products. Irradiation of a degassed benzene solution of **3a** in Pyrex tube with a high-pressure mercury arc gave **4a** as a sole isolable product in high yield. Similar irradiation of **3b—d** gave the corresponding cyclized compounds, **4b—d**, also in high yields (Scheme 2). However, **3e** and **3f** were essentially unreactive under similar conditions, although prolonged irradiation of **3e** afforded a mixture containing at least four compounds. The results are summarized in Table 1. The structures of **4a—d** were established from their elemental analyses, spectral data, and chemical properties. The relevant ^{1}H NMR spectral data are listed in Table 2.

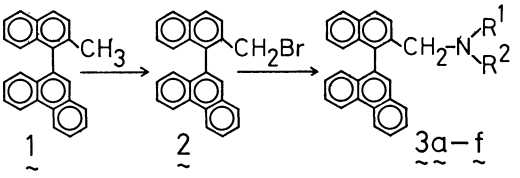

a: $R^1=C_6H_5$, $R^2=H$; **b**: $R^1=CH_3$, $R^2=H$; **c**: $R^1=C_6H_{11}$, $R^2=H$; **d**: $R^1=t\text{-}C_4H_9$, $R^2=H$; **e**: $R^1=C_6H_5$, $R^2=CH_3$; **f**: $R^1=R^2=CH_3$

Scheme 1.

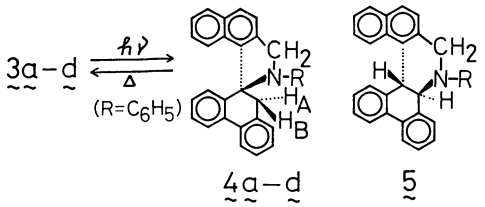

a: $R=C_6H_5$, **b**: $R=CH_3$, **c**: $R=C_6H_{11}$, **d**: $R=t\text{-}C_4H_9$

Scheme 2.

Table 1. Photoreaction of **3a—d**

Solvent	Compd	Concn / mol l^{-1}	Irradiation time/h	Product	Yield/%
Benzene	**3a**	0.016	1	**4a**	93
	3b	0.016	5	**4b**	30
	3c	0.016	3	**4c**	86
	3d	0.016	3	**4d**	84
Acetonitrile	**3a**	0.006	1	**4a**	82
	3b	0.018	5	**4b**	<2
	3c	0.016	3	**4c**	<2
	3d	0.016	3	**4d**	75
Methanol	**3a**	—	1	—	—
	3b	0.018	5	**4b**	<2
	3c	0.016	3	**4c**	10[a]
	3d	0.016	3	**4d**	45

a) Ethanol was used as solvent.

Table 2. ^{1}H NMR characteristic signals of **3a—f** and **4a—d**[a]

Compd	Aromatic-H[b]	CH_2	H_A	H_B	J_{AB}/Hz
3a	8.6—8.8	4.10	—	—	—
3b	8.4—8.8	3.50	—	—	—
3c	8.4—8.8	3.50	—	—	—
3d	8.5—8.8	3.50	—	—	—
3e	8.5—8.8	4.10, 4.30 (AB-q, J=17 Hz)	—	—	—
3f	8.4—8.7	3.15	—	—	—
4a	—	5.00	3.45	3.97	19
4b	—	4.20	3.14	3.58	17
4c	—	4.38	3.04	3.68	17
4d	—	4.50	3.37	3.61	18

a) δ Values. Solvent for **3c** and **3f** was CCl_4 and that for others was $CDCl_3$. b) Signals in the region of δ 8.4—8.9 ppm were shown.

The ^{1}H NMR spectrum of **3a** (Fig. 1a) remarkably changed after irradiation. A characteristic multiplet around δ 8.6—8.8 (2H, H-4 and H-5 of phenanthrene ring) shifted to higher field region (δ 6—8, usual aromatic region). A broad singlet at δ 3.80 (1H, NH) and a singlet at δ 4.10 (2H, CH_2NH) of **3a** disappeared and shifted, respectively. Instead, a singlet at δ 5.00 (2H) and an AB quartet (J_{AB}=19 Hz) centered at δ 3.45 (1H) and 3.97 (1H) appeared (Fig. 1b). The singlet at δ 5.00 was assigned to the methylene protons in the pyrroline ring of **4a**. The higher field signals in the AB quartet were assigned to the H_A proton in the cyclohexadiene ring in **4a** and the lower field ones to the H_B proton in the same ring. A downfield shift of H_B proton compared to the H_A proton may be due to a deshielding effect of lone-pair electrons on the adjacent nitrogen atom. Further support for the structure of **4a** was derived from the following observations.

Irradiation of **3a** in D_2O-saturated benzene led to the formation of a monodeuterated compound of **4a** (**4a**-D_B): it must be noticed here that the NH hydrogen in **3a** is replaced by deuterium through a rapid H-D exchange to form **3a**-ND before irradiation. The ^{1}H NMR spectrum of **4a**-D_B (Fig. 1c) showed a singlet at δ 3.45 (1H), which indicates that the H_B atom of **4a** is displaced by deuterium atom in the photoreaction of **3a**-ND (see Scheme 3).

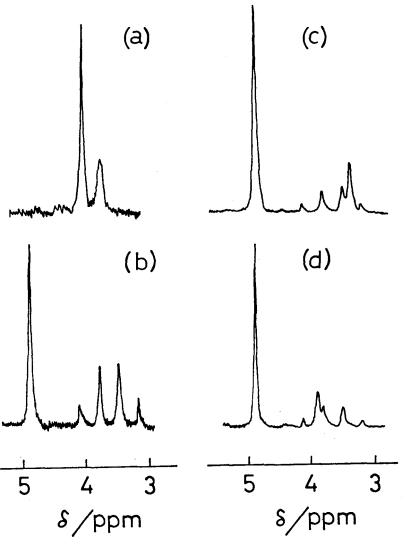

Fig. 1. ^{1}H NMR spectra of **3a** and **4a** in the region of 3—5 ppm.
(a): **3a**, (b): **4a**, (c): **4a**-D_B contaminated by **4a**, (d): **4a**-D_A contaminated by **4a**.

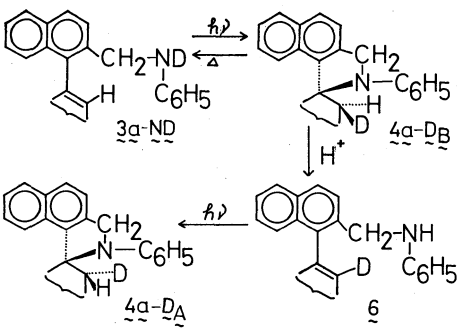

Scheme 3.

Compound **4a** was quantitatively converted back into **3a** by heating at its melting point or by treating with sulfuric acid. Compound **3a** thus obtained gave again **4a** in high yield upon irradiation in benzene. However, the compound obtained by heating **4a**-D_B, followed by irradiation in benzene showed the different ^{1}H NMR spectrum from that of the other compound which was obtained by treating **4a**-D_B with sulfuric acid, followed by irradiation in benzene. The ^{1}H NMR spectral examination revealed that the former compound is **4a**-D_B (Fig. 1c) contaminated by a small amount of **4a**. However, the ^{1}H NMR spectrum of the latter compound displayed a singlet at δ 3.93 (1H) (Fig. 1d), indicating that at this time the H_A atom of **4a** is replaced with deuterium atom to give **4a**-D_A.

All of the above observations can be explained in terms of the pathway illustrated in Scheme 3. Irradiation of **3a**-ND causes the addition of the ND function to the C-9 and C-10 carbons of the phenanthrene ring in a *cis*-mode to give **4a**-D_B. Thermolysis of

4a-D_B gives **3a**-ND by *cis*-elimination of the ND function. On the other hand, treatment of **4a**-D_B with acid affords the deuterium-incorporated compound **6** by *trans*-elimination of the N–H bond. Irradiation of **6** results in the formation of **4a**-D_A.

The ^1H NMR spectral data of **4b—d** shown in Table 2 strongly support that they also have the structures given in Scheme 2. The possibility of the structure of **5** for these compound can be neglected.

Spectral Studies. Fluorescence of aromatic hydrocarbons is often quenched by amines. It has been demonstrated that such quenching occurs through exciplexes produced by interaction between the excited aromatics and the ground state of amines, and that the exciplexes thus formed have a high polarity due to electron-transfer from the latter to the former.[7]

Compound **1**, which has no amino group in the molecule, emitted strongly fluorescence upon irradiation in benzene. Its spectral pattern was similar to that of phenanthrene. The fluorescence was efficiently quenched by adding triethylamine into the solution. It is therefore supposed that there exists intermolecular electron-transfer interaction between the amine and the excited phenanthrene moiety in **1**.

Figure 2 shows the fluorescence spectra of **3b**, **e**, **f** in benzene; the fluorescence of **3a** was too weak to be detected. The spectral pattern of these compounds was similar to that of phenanthrene and also of **1**. However, the intensities of the fluorescent lights were appreciably weaker than the intensity of fluorescent light of **1**, and decreased with decreasing ionization potentials of the amino moieties of these compounds.[8] In addition, the intensity of fluorescence of **3b** in benzene decreased by adding acetonitrile into the solution (Fig. 3), whereas that of **1** remained substantially unchanged by the addition of acetonitrile. Furthermore, new broad emissions were observed in benzene in 440 nm region for photochemically unreactive compounds, **3e** and **3f**. The maxima of these new emissions shifted to longer wavelength side by the addition of acetonitrile. Therefore, these emissions are attributable to the formation of exciplexes.

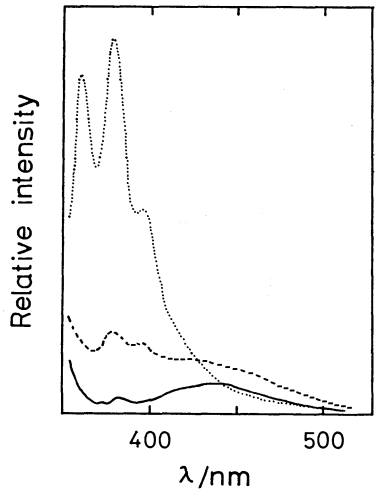

Fig. 2. Fluorescence spectra of **3b**, **3e**, and **3f** in benzene.
·····; **3b**, ——; **3e**, - - - -; **3f**.

These results suggest that intramolecular interaction between the amino groups and the excited phenanthrene ring occurs upon irradiation of **3a—d** and also **3e—f**, and that the interaction has a character of electron-transfer.

Mechanism and Solvent Effect on the Photochemical Reactivity. We now propose a mechanistic pathway shown in Scheme 4 for the photoreaction of **3a—d**.

In an initial stage, intramolecular exciplexes **7** are formed by interaction between the amino groups and the excited phenanthrene moiety. The exciplexes may dissociate to the cation radical-anion radical pairs **8** in polar solvents. The addition of the NH group to the C-9, C-10 bond of phenanthrene ring occurs from **7** or **8** only if the pairs exist in a solvent cage. This reaction takes place almost in a concerted fashion and selectively in a mode of *cis*-addition to form **4a—d**. When **7** have no hydrogen on the nitrogen as in the cases of **3e** and **3f**, the addition reaction does not occur. In these cases, the emissions from exciplexes can be observed.

This mechanistic pathway is consistent with the solvent effect on the photochemical reactivity. The results of Table 1 and Fig. 4 indicate that the yields of **4a—d** decrease with increasing solvent polarity, and the yield depression of **4b** in polar solvent is particularly remarkable.

If **7** and **8** are in a nonpolar solvent, their amino and phenanthryl groups exist in a neighboring position. In such a case, the addition of the amino groups to

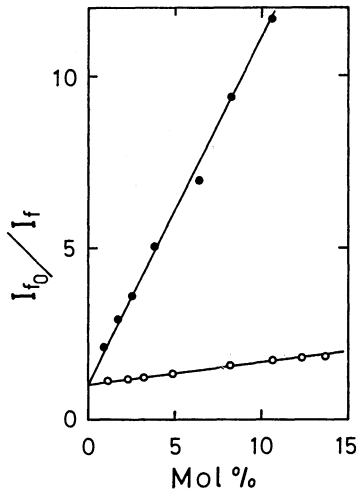

Fig. 3. Effect of addition of polar solvents on the intensity of fluorescent light of **3b** in benzene (ordinate: relative fluorescence intensities; abscissa: mol% of polar solvents in benzene).
—●—: Acetonitrile, —○—: methanol.

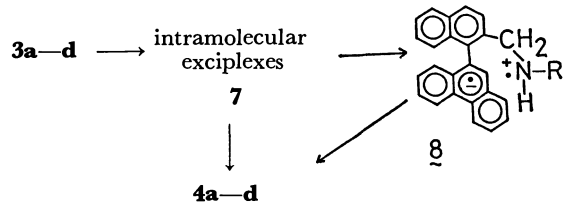

Scheme 4.

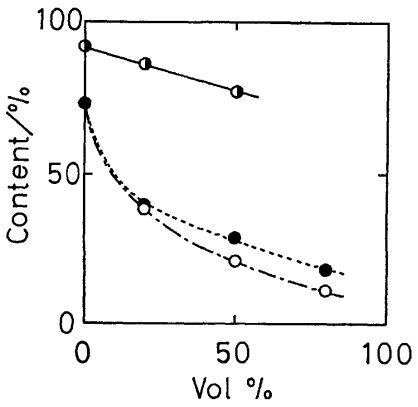

Fig. 4. Contents of the photoproducts **4a** or **4b** in the reaction mixtures obtained by the photoreactions of **3a** or **3b** in mixed solvents (abscissa: vol% of polar solvents in benzene).
—◑—: R=C_6H_5, C_6H_6–CH_3OH, irradiated for 1 h,
—●—: R=CH_3, C_6H_6–CH_3OH, irradiated for 4 h,
—○—: R=CH_3, C_6H_6–CH_3CN, irradiated for 4 h.

the phenanthrene moiety occurs efficiently. On the other hand, they may dissociate in polar solvents to form solvent separated ion pairs which will go back to the component neutral species by back electron-transfer. This assumption accounts for both the stereochemical course of the reaction and the solvent effect on the reactivity. A molecular model shows that in **3a—d**, particularly in **3a**, the amino and phenanthryl groups lie in close proximity in their prefered conformation. The preponderance of the conformation will be multiplied by the attachment of a bulky group on the amino nitrogen. As a result, **3a** reacts smoothly to give **4a** in any solvent.

Experimental

All melting points are uncorrected. IR spectra were obtained on a Hitachi 215 infrared spectrophotometer. ^1H NMR spectra were recorded on a Hitachi R-24A spectrometer (60 MHz) with tetramethylsilane as an internal standard. Ultraviolet and visiblelight absorption spectra were obtained on a Hitachi EPS-3T spectrometer. Fluorescence spectra were recorded on a Shimadzu RF-501 fluorophotometer.

Materials. *9-(2-Methyl-1-naphthyl)phenanthrene (**1**)*: Grignard reagent, prepared from 1-bromo-2-methylnaphthalene (6.8 g, 30 mmol), magnesium (0.75 g, 30 mmol), and a small amount of iodine in ether–benzene (1:1, v/v), was added over 30 min to a solution of 9-bromophenanthrene (5.5 g, 20 mmol) and dichlorobis(triphenylphosphine)nickel(II) (0.15 g) in anhydrous ether (50 ml). The mixture was refluxed for 5 h and acidified with dil hydrochloric acid. The organic layer was separated, dried ($MgSO_4$), and evaporated. The gummy residue was triturated with a small amount of hexane to give a white solid. The solid was filtered off and recrystallized from ethanol–benzene (2:1, v/v), giving **1** (4.8 g, 70% based on 9-bromophenanthrene): mp 148—150 °C; NMR (CCl_4) δ=2.12 (3H, s, CH_3) and 6.5—8.8 (15H, m, aromatic). Found: C, 94.32; H, 5.58%. Calcd for $C_{25}H_{18}$: C, 94.30; H, 5.70%.

*9-(2-Bromomethyl-1-naphthyl)phenanthrene (**2**)*: A mixture of **1** (3 g, 9.4 mmol), *N*-bromosuccinimide (1.7 g, 9.5 mmol) and benzoyl peroxide (3 mg) in CCl_4 (50 ml) was refluxed for 8 h. After cooling, the deposited solid was filtered off. Evaporation of the filtrate left a gummy substance which solidified upon treatment with a small amount of petroleum ether. The NMR spectrum showed that this solid contains **2** in 90—97% purity. Chromatography of the crude material on silica gel with hexane gave pure compound: mp 123—125 °C; NMR (CCl_4) δ=4.14 and 4.32 (2H, AB-type q, J=10 Hz, CH_2) and 6.8—8.8 (15H, m, aromatic). Found: C, 75.91; H, 4.14%. Calcd for $C_{25}H_{17}Br$: C, 75.57; H, 4.31%.

*9-(2-Anilinomethyl-1-naphthyl)phenanthrene (**3a**)*: A mixture of **2** (3.4 g, 8.5 mmol) and aniline (3.2 g, 34 mmol) in 1,2-dimethoxyethane (60 ml) was stirred for 24 h at room temperature, and the deposited solid was removed by filtration. The filtrate was concentrated under reduced pressure, and the oily residue crystallized immediately upon adding a small amount of methanol. The solid was recrystallized from benzene–hexane (1:1, v/v) to give **3a** (2.41 g, 64%): mp 169—170 °C; IR (KBr) 3400 (NH) and 1320 cm^{-1} (CN); NMR ($CDCl_3$) δ=3.80 (1H, broad s, NH), 4.10 (2H, s, CH_2), 6.2—8.0 (18H, m, aromatic) and 8.6—8.8 (2H, m, aromatic). Found: C, 90.84; H, 5.56; N, 3.47%. Calcd for $C_{31}H_{23}N$: C, 90.92; H, 5.66; N, 3.42%.

*9-(2-Methylaminomethyl-1-naphthyl)phenanthrene (**3b**)*: A solution of **2** (2.5 g, 6.3 mmol) in 1,2-dimethoxyethane (15 ml) was added to a mixture of methylamine hydrochloride (17 g, 0.25 mol) in methanol (80 ml). Solid potassium hydroxide (14 g, 0.25 mol) was then added in 3 g portions with stirring. After stirring for 12 h, the deposited solid was filtered off, and the filtrate was concentrated *in vacuo*. The residue was poured into water and extracted with ether. The extract was concentrated and chromatographed on silica gel with benzene–ether (1:1, v/v) to give **3b** (0.83 g, 38%): mp 65—67 °C; NMR ($CDCl_3$) δ=1.4 (1H, s, NH), 2.12 (3H, s, CH_3), 3.50 (2H, s, CH_2), 7.0—8.0 (13H, m, aromatic), and 8.4—8.8 (2H, m, aromatic). Found: C, 89.63; H, 6.11; N, 3.87%. Calcd for $C_{26}H_{21}N$: C, 89.88; H, 6.09; N, 4.03%.

*9-(2-Cyclohexylaminomethyl-1-naphthyl)phenanthrene (**3c**)*: A mixture of **2** (2.0 g, 5 mmol) and cyclohexylamine (5 ml) in 1,2-dimethoxyethane (20 ml) was stirred for 12 h at room temperature, and the deposited solid was removed by filtration. The filtrate was poured into 100 ml of water, and extracted with benzene. Evaporation of the solvent gave a white solid which was purified by chromatography on silica gel with benzene–ether (1:1, v/v), yielding **3c** (1.43 g, 73%): mp 160.5—161.5 °C; NMR (CCl_4) δ=0.3—2.4 (12H, m, cyclohexyl and NH), 3.50 (2H, s, CH_2), 6.7—8.3 (13H, m, aromatic), and 8.4—8.8 (2H, m, aromatic). Found: C, 89.44; H, 7.25; N, 3.44%. Calcd for $C_{31}H_{29}N$: C, 89.59; H, 7.03; N, 3.37%.

*9-(2-t-Butylaminomethyl-1-naphthyl)phenanthrene (**3d**)*: This compound was prepared by the method similar to that for **3c**. The product was purified by chromatography on silica gel with benzene. The yield of **3d** was 85%: mp 64—70 °C; NMR ($CDCl_3$) δ=0.65 (9H, s, CH_3), 1.0—1.2 (1H, broad s, NH), 3.50 (2H, s, CH_2), 7.0—8.0 (13H, m, aromatic) and 8.5—8.8 (2H, m, aromatic). Found: C, 89.39; H, 6.98; N, 3.55%. Calcd for $C_{29}H_{27}N$: C, 89.42; H, 6.99; N, 3.60%.

*9-[2-(N-Methylanilinomethyl)-1-naphthyl]phenanthrene (**3e**)*: This compound was prepared from **2** and *N*-methylaniline in 1,2-dimethoxyethane by the method applied for the preparation of **3a**: mp 167.5—168.5 °C; NMR ($CDCl_3$) δ= 2.80 (3H, s, CH_3), 4.10 and 4.30 (2H, AB-type q, J=17 Hz, CH_2) and 6.4—8.8 (20H, m, aromatic). Found: C, 90.53; H, 5.90; N, 3.38%. Calcd for $C_{32}H_{25}N$: C, 90.74;

H, 5.95; N, 3.30%.

9-(2-Dimethylaminomethyl-1-naphthyl)phenanthrene (3f): This compound was prepared from dimethylamine hydrochloride and **2** by the method applied for the preparation of **3b**: mp 115—117 °C; NMR (CCl_4) δ=1.97 (6H, s, CH_3), 3.15 (2H, broad s, CH_2), 6.8—7.9 (13H, m, aromatic), and 8.4—8.7 (2H, m, aromatic). Found: C, 89.97; H, 6.36; N, 3.89%. Calcd for $C_{27}H_{23}N$: C, 89.71; H, 6.41; N, 3.88%.

Photoreactions. A general procedure is shown in an example of the photoreaction of **3a**: a solution of **3a** (100 mg, 0.25 mmol) in benzene (10 ml) in a Pyrex tube was degassed by three freeze-pump-thaw cycles under argon and the tube was sealded under reduced pressure. Irradiation was carried out by using a merry-go-round apparatus (Eikosha PIH-300) with a 300 W high-pressure mercury lamp cooled with water. After irradiation, benzene was evaporated under reduced pressure. The residue was dissolved in $CDCl_3$ and its ^1H NMR spectrum was recorded. The yield of the photoproduct **4a** was estimated from the intensities of methylene signals.

Benzene-d_6 solutions of **3a**—**d** (8×10^{-2} M) sealded in NMR measureing tubes were irradiated in a manner similar to that employed for preparative photoreactions. The rates of the photoreactions were measured by following the changes in intensities of signals in the NMR spectra at appropriate time intervals. Yields were estimated on the basis of the relative intensities of methylene signals of each cyclic compound to that of tetramethylsilane used as an internal standard.

Photoproducts. The photoproducts were purified by chromatography on silica gel (**4a** and **4b**) or recrystallization from methanol (**4c** and **4d**). **4a**: mp 105—120 °C (dec); NMR ($CDCl_3$) δ=3.97 and 3.45 (2H, AB-type q, J=19 Hz, CH_2), 5.00 (2H, s, CH_2), and 6.2—8.1 (19H, m, aromatic). Found: C, 90.84; H, 5.65; N, 3.53%. Calcd for $C_{31}H_{23}N$: C, 90.92; H, 5.66; N, 3.42%. **4b**: mp 65—75 °C (dec); NMR ($CDCl_3$) δ=2.05 (3H, s, CH_3), 3.58 and 3.14 (2H, AB-type q, J=17 Hz, CH_2), 4.20 (2H, s, CH_2) and 6.8—8.0 (14H, m, aromatic). Found: C, 90.03; H, 6.40; N, 4.00%. Calcd for $C_{26}H_{21}N$: C, 89.88; H, 6.09; N, 4.03%. **4c**: mp 125—130 °C (dec); NMR ($CDCl_3$) δ=0.5—1.7 (m, cyclohexyl), 3.04 and 3.68 (AB-type q, J=17 Hz, CH_2), 4.38 (s, CH_2) and 6.8—8.0 (m, aromatic). Found: C, 88.97; H, 7.52; N, 3.49%. Calcd for $C_{31}H_{29}N$: C, 89.59; H, 7.03; N, 3.37%. **4d**: mp 100—110 °C (dec); NMR ($CDCl_3$) δ=0.92 (s, CH_3), 3.37 and 3.61 (AB-type q, J=18 Hz, CH_2), 4.50 (s, CH_2), and 6.9—8.0 (m, aromatic). Found: C, 90.06; H, 7.33; N, 3.58%. Calcd for $C_{29}H_{27}N$: C, 89.42; H, 6.99; N, 3.60%.

The present work was partially supported by a Grant-in-Aid for Scientific Research from the Ministry of Education, Science and Culture (No. 510206).

References

1) M. Bellas, D. Bryce-Smith, and A. Gilbert, *J. Chem. Soc., Chem. Commun.*, **1976**, 263, 862; M. Bellas, D. Bryce-Smith, M. T. Clarke, A. Gilbert, G. Klunkin, S. Krestonosich, C. Manning, and S. Wilson, *J. Chem. Soc., Perkin Trans. 1*, **1977**, 2571, and references cited therein.

2) R. S. Davidson, *J. Chem. Soc., Chem. Commun.*, **1969**, 1450; N. C. Yang and J. Libman, *J. Am. Chem. Soc.*, **95**, 5783 (1973); N. C. Yang, D. M. Shold, and B. Kim, *ibid.*, **98**, 6587 (1976).

3) J. A. Barltrop and R. J. Owers, *J. Chem. Soc., Chem. Commun.*, **1970**, 1492.

4) M. Kawanishi and K. Matsunaga, *J. Chem. Soc., Chem. Commun.*, **1972**, 313; T. Kubota and H. Sakurai, *Chem. Lett.*, **1972**, 923, 1249; A. Couture, A. Lablache-Combier, and H. Oftenberg, *Tetrahedron*, **21**, 2023 (1975); F. D. Lewis and T.-I. Ho, *J. Am. Chem. Soc.*, **99**, 7991 (1977).

5) M. Ohashi, K. Miyake, and K. Tsujimoto, *Bull. Chem. Soc. Jpn.*, **53**, 1683 (1980), and references cited therein.

6) R. Ide, Y. Sakata, S. Misumi, T. Okada, and N. Mataga, *J. Chem. Soc., Chem. Commun.*, **1972**, 1009; Rev., F. C. De Schryver, N. Boens, and J. Put, "Advances in Photochemistry," ed by J. N. Pitts, Jr., G. S. Hammond, and K. Gollnick, John Wiley & Sons. Inc., New York (1977), Vol. 10, p. 359.

7) H. Leonhardt and A. Weller, *Ber. Bunsenges. Phys. Chem.*, **67**, 791 (1963); N, Mataga, T. Okada, and H. Masuhara, Kagakusousetsu, No. 24, p. 101 (1979).

8) This conclusion was derived from the assumption that the ionization potentials of the amino moieties in these compounds can be estimated from those of the corresponding *N*-substituted methylamines: for example, 8.36 eV for $(CH_3)_2NH$, 8.12 eV for $(CH_3)_3N$, and 7.36 eV for $(CH_3)_2NC_6H_5$ were used as the ionization potentials of the amino moieties in **3b**, **3f**, and **3e**, respectively.

Branched-chain Sugars. XXIII. Stereoselectivities in the Addition of Nucleophiles to Several 4-Uloses[1]

Masafumi MATSUZAWA, Ken-ichi SATO, Toshio YASUMORI, and Juji YOSHIMURA*

Laboratory of Chemistry for Natural Products, Faculty of Science, Tokyo Institute of Technology, Nagatsuta, Midori-ku, Yokohama 227

(Received April 24, 1981)

The stereoselectivities in the 1,2-addition of nucleophiles such as methylmagnesium iodide, vinylmagnesium bromide, and 2-lithio-2-methyl-1,3-dithiane to seven kinds of 4-uloses were examined. The configurations of *C*-vinyl derivatives obtained were determined from the chemical shifts of α-carbons in ^{13}C-NMR spectra.

In the preceding paper of this series[1] benzyl 2,3-di-*O*-benzyl- (**1**) and 2,3-*O*-methylene-β-L-*threo*-pentopyranosid-4-uloses (**2**), benzyl 2,3-di-*O*-benzyl-6-deoxy- (**3**) and 6-deoxy-2,3-*O*-methylene-α-D-*xylo*-hexopyranosid-4-uloses (**4**), and methyl 6-deoxy-2,3-*O*-methylene-α-D-*ribo*-hexopyranosid-4-ulose (**5**) were synthesized as the starting materials for the synthesis of 2,3-*O*-methylene-4-*C*-substituted aldonolactones found in orthosomycins.[2] For this purpose, a two-carbon unit should be stereoselectively introduced into the carbonyl function of **2** and **4**. In this paper, stereoselectivities in the addition of nucleophiles to the above 4-uloses were examined, together with newly synthesized methyl 6-deoxy-2,3-*O*-methylene-α-D-*lyxo*-hexopyranosid-4-ulose (**6**) and known methyl 2,3-di-*O*-benzyl-6-deoxy-α-D-*xylo*-hexopyranosid-4-ulose (**7**).[3]

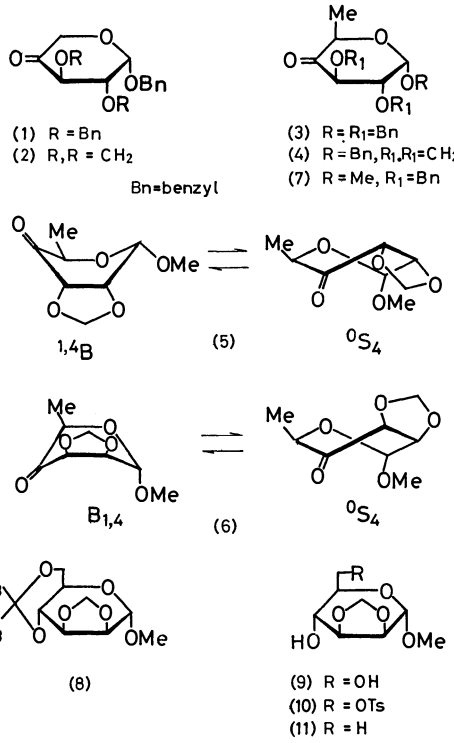

Results and Discussion

The new 4-ulose **6** was synthesized as follows. Reaction of methyl 4,6-*O*-isopropylidene-α-D-mannopyranoside[4] in *N*,*N*-dimethylformamide with sodium hydride and dibromomethane gave the corresponding 2,3-*O*-methylene derivative (**8**) in 61% yield. Partial hydrolysis of **8** in 70% acetic acid at room temperature for 16 h gave the corresponding *O*-deisopropylidenated product (**9**) in quantitative yield. Monotosylation of **9** gave the 6-*O*-tosylate (**10**) in 63% yield. Reduction of **10** in tetrahydrofuran with lithium aluminium hydride gave the 6-deoxy derivative (**11**) in 78% yield. Oxidation of **11** with dimethyl sulfoxide–trifluoroacetic anhydride[5] gave **6** in 93% yield.

The coupling constants of **5** ($J_{1,2}$=4.2, $J_{2,3}$=8.8, $J_{3,5}$=0.8 Hz) and **6** ($J_{1,2}$=0, $J_{2,3}$=6.4 Hz) indicate that these compounds exist in a boat or a skew-boat conformation, but not in the usual *C*1 conformation. Collins and Whitton[6] suggested the $^{\circ}S_4$ conformation to the 2,3-*O*-isopropylidene analogue ($J_{1,2}$=3.8, $J_{2,3}$=9.0, $J_{3,5}$=1.2 Hz) of **5**, however, the assingment of ^{1,4}B for **5** and the $^{\circ}S_4$ for **6** will be more probable from $J_{2,3}$ values.

As the nucleophiles for 1,2-addition to 4-uloses, methylmagnesium iodide, methyllithium, vinylmagnesium bromide, and 2-lithio-2-methyl-1,3-dithiane were used, and the results were summarized in Table 1.

The configuration of products in these reactions was mainly determined from the chemical shifts of the branching α-carbons in ^{13}C NMR spectra. Application of the fact that equatorially oriented *C*-methyl carbons are deshielded with respect to axially oriented methyl carbons for the configurational assignment of *C*-methylhexopyranosides[7] has been extended to the 1,3-dithian-2-yl,[8] hydroxymethyl,[9] nitromethyl,[10] and benzoylaminomethyl[10] derivatives. As shown in Table 2, this principle was successfully used for the determination of the configuration of 4-*C*-vinyl derivatives, by the comparison of the chemical shifts of methin carbons in the vinyl groups. However, this trend could not be observed in those of methylene carbons in vinyl groups. Miljkovic *et al.* depicted that there are *ca.* 6 ppm difference in the chemical shifts between axial and equatorial *C*-methyl carbons.[7] The smaller differences between **12** and **13**, and **14** and **15** indicate that the conformation of pentopyranosides having an axial substituent tends to deviate from *C*1.

The configurations of epimeric 4-*C*-(2-methyl-1,3-dithian-2-yl) derivatives (**16** and **17**) were determined from the fact that **16** exists in 1*C* ($J_{1,2}$=1.3, $J_{2,3}$=3.0 Hz), whereas **17** in *C*1 ($J_{1,2}$=4.0, $J_{2,3}$=9.2 Hz) conformation. It is known that this bulky group in axial orientation causes a similar inversion of the conformation to that of **16**.[11] The reliability of these assignments was proved by the actual derivation of **15**, **22**, and **28** into naturally occuring branched-chain sugars[12,13] and also by the establishment of a principle for the determination of the chirality of

TABLE 1. NUCLEOPHILIC REACTIONS OF 4-ULOSES

Run	4-Ulose	Nucleophile	Conditions		Ratio of products				Yield/%
			Solvent	Temp	Axial : equatorial attack				
1	**1**	MeMgI	Ether	−78 °C	(**12**)	1 : 2.6	(**13**)		98
2		MeMgI	Ether-THF	RT	(**12**)	2.5 : 1	(**13**)		84.5
3		MeLi	Ether	RT	(**12**)	1 : 0			32
4		CH_2=CHMgBr	THF	RT	(**14**)	2.5 : 1	(**15**)		48
5		DTNLi[a]	THF	−30 °C	(**16**)	2.5 : 1	(**17**)		35
6	**2**	MeMgI	Ether-THF	RT	(**18**)	1 : 2.8	(**19**)		72
7		CH_2=CHMgBr	THF	RT	(**20**)	1 : 4.6	(**21**)		59
8	**3**	CH_2=CHMgBr	THF	RT		0 : 1	(**22**)		44
9	**7**	MeMgI	Ether	RT	(**23**)	1 : 2.2	(**24**)		86
10	**4**	MeMgI	Ether-THF	RT		0 : 1	(**25**)		89
11		CH_2=CHMgBr	THF	RT	(**26**)	1 : 15	(**27**)		55
12		DTNLi[a]	THF	RT		0 : 1	(**28**)		35
13	**5**	MeMgI	Ether-THF	RT	(**29**)	1 : 0			95
14	**6**	MeMgI	Ether	RT		0 : 1	(**30**)		96

a) The abbreviation of 2-lithio-2-methyl-1,3-dithiane.

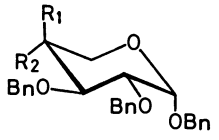

(12) R_1=Me, R_2=OH
(13) R_1=OH, R_2=Me
(14) R_1=-CH=CH_2, R_2=OH
(15) R_1=OH, R_2=-CH=CH_2
(16) R_1=DTN, R_2=OH
(17) R_1=OH, R_2=DTN

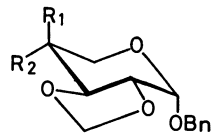

(18) R_1=Me, R_2=OH
(19) R_1=OH, R_2=Me
(20) R_1=-CH=CH_2, R_2=OH
(21) R_1=OH, R_2=-CH=CH_2

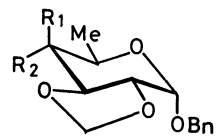

(25) R_1=OH, R_2=Me
(26) R_1=-CH=CH_2, R_2=OH
(27) R_1=OH, R_2=-CH=CH_2
(28) R_1=OH, R_2=DTN

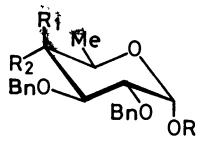

(22) R = Bn, R_1=OH, R_2=CH=CH_2
(23) R = Me, R_1=Me, R_2=OH
(24) R = Me, R_1=OH, R_2=Me

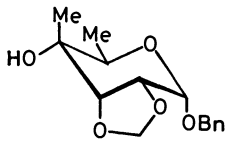

(29)

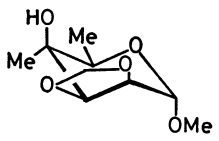

(30)

Bn=benzyl

TABLE 2. DETERMINATION OF THE CONFIGURATIONS OF 4-EPIMERS FROM THE CHEMICAL SHIFTS OF BRANCHING α-CARBONS IN ^{13}C-NMR SPECTRA

Chemical shifts (ppm) of α-carbons of 4-*C*-substituted epimers			
C-Methyl derivatives		*C*-Vinyl derivatives	
Axial	Equatorial	Axial	Equatorial
20.4(**12**)	22.8(**13**)	137.1(**14**)	138.5(**15**)
15.8(**18**)	22.0(**19**)	135.2(**20**)	137.2(**21**)
14.9(**23**)	22.3(**24**)		139.7(**22**)
	22.1(**25**)	132.7(**26**)	137.6(**27**)
18.4(**29**)			
	21.1(**30**)		

1-hydroxyethyl groups introduced *via* the corresponding vinyl and ethylidene derivatives.[14]

In the results of **1** (Runs 1—5) shown in Table 1, it is characteristic that the axial attack generally predominates over the equatorial attack, excepting the Grignard reaction in ether at −78 °C. The complementary stereoselectivity between the Grignard and methyllithium reactions at lower temperature was also observed in the cases of methyl 2,3-di-*O*-methyl- and 2,3-di-*O*-mesyl-6-*O*-trityl-α-D-*xylo*-hexopyranosid-4-uloses.[7] The reason for this remarkable fact should be pursued in more detail. The predominancy of the axial attack will be attributed again to changeable conformation of **1**, because the equatorial attacks are predominant in the case of **2** (Runs 6, 7) in which the 2,3-*O*-methylene ring prohibits the inversion of the *C*1 conformation. A similar trend is also observed in the reaction of **7** and **4** (Runs 9, 10) with methylmagnesium iodide, though the equatorial attack is predominant in these hexopyranosides. In the cases of **5** and **6**, the nucleophile exclusively approaches to the carbonyl function from the opposite side of the bulky 2,3-*O*-methylene ring. Similar stereoselec-

Table 3. ^{1}H NMR parameters of 4-*C*-methyl derivatives

4-*C*-Methyl derivative	Chemical shifts (δ) and coupling constants (Hz)						
	H-1 ($J_{1,2}$)	H-2 ($J_{2,3}$)	H-3	H-5e ($J_{5e,5a}$)	H-5a ($J_{5,6}$)	H-6	Other protons
12	4.76 d (2.8)	3.49 dd (7.2)	3.66 d	3.66 d (11.5)	3.41 d		7.4—7.1(Ph; m), 4.4—5.1(CH_2Ph; m), 2.50(OH), 1.20(CMe)
13	4.90 d (3.1)	3.85 dd (9.6)	3.68 d	3.64 d (12.0)	3.45 d		7.5—7.0(Ph; m), 4.4—5.1(CH_2Ph; m), 2.35(OH), 1.14(CMe)
18	5.26 d (3.8)	3.32 dd (9.8)	3.90 d	3.50 d (11.3)	3.34 d		7.4—7.2(Ph; m), 5.13 and 5.10 (OCH_2O; each s), 4.8—4.5(CH_2Ph; m), 2.16(OH), 1.39(CMe)
19	5.35 d (3.1)	3.84 dd (10.0)	3.72 d	3.50 s			7.5—7.3(Ph; m), 5.14 and 5.08 (OCH_2O; ABq, J=1.0), 4.7—4.4 (CH_2Ph; m), 2.40(OH), 1.39(CMe)
23	4.55 d (3.8)	3.44 dd (9.8)	3.74 d		3.74 q (6.0)	1.11 d	7.4—7.2(Ph; m), 4.4—5.1(2×CH_2Ph; 2×ABq, J=11.5, 11.8), 3.36(OMe), 1.99(OH), 1.13(CMe)
24	4.60 d (3.8)	3.86 dd (9.5)	3.58 d		3.71 q (6.5)	1.21 d	7.4—7.2(Ph; m), 4.5—5.0(2×CH_2Ph; 2×ABq, J=11.5, 10.8), 3.38(OMe), 2.27(OH), 1.12(CMe)
25	5.30 d (3.2)	3.78 dd (10.5)	3.77 d		3.58 q (6.4)	1.18 d	7.5—7.2(Ph; m), 5.10 and 5.15 (OCH_2O; ABq, J=1.0), 4.72 and 4.68 (CH_2Ph; ABq, J=12.0), 2.25(OH), 1.31(CMe)
29	4.68 d (5.2)	4.21 t (5.6)	3.86 d		3.93 q (6.7)	1.22 d	5.25 and 5.02(OCH_2O; ABq, J=2.0), 3.38(OMe), 2.35(OH), 1.21(CMe)
30	5.00 d (0.5)	3.88 dd (5.3)	3.76 d		3.70 q (6.6)	1.23 d	5.31 and 4.91(OCH_2O; ABq, J=1.4), 3.43(OMe), 2.40(OH), 1.14(CMe)

Table 4. ^{1}H NMR parameters of 4-*C*-vinyl derivatives

4-*C*-Vinyl	Chemical shifts (δ) and coupling constants (Hz)[a]								
	H-1 ($J_{1,2}$)	H-2 ($J_{2,3}$)	H-3	H-5e ($J_{5e,5a}$)	H-5a ($J_{5,6}$)	H-6	H-4α and H-4β ($J_{trans,cis,gem}$)	OH	OCH_2O (J_{ABq})
14	4.51 d (3.0)	3.83 dd (10.0)	3.92 d	3.72 dd (11.5)	3.35 d		5.80 dd, 5.50 dd, 5.27 dd (16.2, 9.8, 2.1)	2.71 d [b]	
15	4.82 d (2.9)	3.56 dd (9.1)	3.74 d	3.74 d (11.5)	3.63 d		6.09 dd, 5.49 dd, 5.26 dd (16.7, 10.0, 2.0)	3.22	
20	5.26 d (3.3)	3.37 dd (9.2)	4.01 d	3.62 d (10.8)	3.56 d		6.12 dd, 5.52 dd, 5.32 dd (17.6, 11.0, 1.8)	2.96	5.09 d, 5.03 d (1.0)
21	5.38 d (3.0)	3.90 dd (9.4)	3.97 d	3.54 d (11.0)	3.47 d		5.86 dd, 5.53 dd, 5.30 dd (16.7, 10.0, 2.0)	3.05	5.15 d, 5.07 d (1.0)
22	4.83 d (3.0)	3.80 dd (9.8)	3.88 d		3.93 q (6.5)	1.11 d	5.77 dd, 5.41 dd, 5.28 dd (17.0, 10.0, 2.0)	2.54	
26	5.28 d (3.5)	3.52 dd (10.0)	4.03 d		3.75 q (6.5)	1.05 d	5.99 dd, 5.55 dd, 5.46 dd (17.6, 11.0, 2.0)	2.47	5.12 d, 5.07 d (1.0)
27	5.35 d (3.0)	3.88 dd (9.5)	4.01 d		3.72 q (7.0)	1.12 d	5.84 dd, 5.48 dd, 5.32 dd (17.0, 10.4, 1.9)	2.14	5.18 d, 5.10 d (1.0)

a) Data of protons in benzyl groups were omitted. b) $J_{OH,5e}$=3.0 was observed.

tivities were also observed in the reduction of 2,3-*O*-isopropylidene analogue of **5**[6] and 2,3-*O*-isopropylidene analogue of **6**[15] and the Grignard reaction[16] of the enantiomer of the latter. It is obvious that bulkier nucleophiles such as vinylmagnesium bromide and 2-lithio-2-methyl-1,3-dithiane (Runs 7, 8, 11, 12) afford selectively the equatorial attack products, unless otherwise a special steric hindrance is present.

^{1}H NMR parameters of 4-*C*-methyl and 4-*C*-vinyl derivatives thus obtained were shown in Tables 3 and 4, respectively. Among *C*-methyl derivatives, coupling constants ($J_{1,2}$ and $J_{2,3}$) of **29** and **30** indicate that these compounds exist in the usual *allo* and *talo* configurations, respectively. The parameters shown in the both tables will be reasonable for the individual compounds.

Experimental

General Methods. Melting points were determined with a Mel-Temp melting point apparatus and not corrected. Optical rotations were measured at room tem-

perature in 0.5 dm tube with Carl Zeiss LEP-A1 or JASCO DIP-4 polarimeter, using chloroform as a solvent. ^{1}H-NMR spectra were recorded with a JEOL JNM PS-100 spectrometer in deuteriochloroform containing tetramethylsilane as the internal reference. ^{13}C-NMR data (Table 2) were obtained at 30 °C on a JEOL JNM FX-100 spectrometer in the pulse Fourier transform/proton noise decoupled mode at 25.15 MHz in deuteriochloroform. Each spectrum was obtained after 1000 transients with a frequency range of 5000 Hz. The pulse angle of 45° was used, with an acquisition time of 0.8 s and a pulse delay of 0.7 s. Chemical shifts and coupling constants were recorded in δ (ppm) and Hz units. Evaporations were conducted under diminished pressure.

Methyl 4,6-O-Isopropylidene-2,3-O-methylene-α-D-mannopyranoside (8). To a solution of methyl 4,6-*O*-isopropyridene-α-D-mannopyranoside (5.0 g, 21.3 mmol) and sodium hydride (1.5 g, 65 mmol) in *N,N*-dimethylformamide (10 ml, DMF) was added dibromomethane (11.5 g, 65 mmol) at 0 °C. After keeping the mixture at 0—5 °C for 2 h, the solution was poured into cold water, and extracted with ether. The extract was washed with water, dried, and evaporated to give a syrup which was purified on a silica-gel column (benzene–ethyl acetate 5:1) to give a colorless syrup **8** (3.2 g, 60.9%). $[\alpha]_D$ +2.0° (*c* 1.9); NMR: 5.19 and 4.94. (each s, 2H, OCH_2O), 4.97 (s, 1H, H-1), 4.25—3.50 (m, 6H, H-2,3,4,5,6,6'), 3.38 (s, 3H, OMe), 1.50 and 1.42 (each s, 6H, 2×CMe). Found: C, 53.54; H, 7.52%. Calcd for $C_{11}H_{18}O_6$: C, 53.65; H, 7.37%.

Methyl 2,3-O-Methylene-α-D-mannopyranoside (9). Partial hydrolysis of **8** (2.0 g, 8.1 mmol) in 70% acetic acid (20 ml) under reflux for 2 h gave the corresponding *O*-deisopropylidenated product **9** in quantitative yield (1.67 g). Mp 74—75 °C (ethyl acetate), $[\alpha]_D$ +29.6° (*c* 1.1); NMR: 5.17 and 4.98 (each s, 2H, OCH_2O), 4.96 (s, 1H, H-1), 4.21 (dd, 1H, $J_{2,3}$=5.8, $J_{3,4}$=7.0, H-3), 3.89 (d, 1H, H-2), 3.85 (d, 2H, $J_{5,6}$=3.4, H-6 and H-6'), 3.80—3.55 (m, 2H, H-4 and H-5), 3.40 (s, 3H, OMe). Found: C, 46.75; H, 6.90%. Calcd for $C_8H_{14}O_6$: C, 46.60; H, 6.84%.

Methyl 2,3-O-Methylene-6-O-p-tolylsulfonyl-α-D-mannopyranoside (10). To a solution of **9** (1.0 g, 4.85 mmol) in pyridine (10 ml) was added *p*-toluenesulfonyl chloride (1.4 g, 7.4 mmol) in dry benzene (15 ml) at 0 °C with stirring. After standing at 0 °C for 16 h, the solution was poured into ice–water and extracted with chloroform. The extract was processed as usual to give a syrup. The syrup was purified on a silica-gel column (benzene–acetone 8:1) to give a colorless **10** (1.1 g, 62.9%). $[\alpha]_D$ +6.5° (*c* 1.2); NMR: 7.78 and 7.30 (each d, 4H, *J*=8.0, Ph), 5.13 and 4.95 (each s, 2H, OCH_2O), 4.88 (s, 1H, H-1), 4.27 (d, 2H, $J_{5,6}$=3.6, H-6 and H-6'), 4.16 (q, 1H, $J_{2,3}$=5.8, $J_{3,4}$=7.0, H-3), 3.86 (d, 1H, H-2), 3.40—3.76 (m, 2H, H-4 and H-5), 3.55 (s, 3H, OMe), 2.44 (s, 3H, CMe). Found: C, 50.10; H, 5.75; S, 8.65%. Calcd for $C_{15}H_{20}O_8S$: C, 49.99; H, 5.59; S, 8.90%.

Methyl 6-Deoxy-2,3-O-methylene-α-D-mannopyranoside (11). To a solution of **10** (1.0 g, 2.8 mmol) in dimethyl sulfoxide (30 ml, DMSO) was added sodium borohydride (530 mg) and the mixture was kept at 80 °C for 4 h, poured into water (150 ml), and extracted with ether. The etheral extract was treated as usual to give syrupy **11** (410 mg, 77.7%) showing a single component on TLC and NMR. $[\alpha]_D$ +30.8° (*c* 0.9); NMR: 5.14 and 4.96 (each s, 2H, OCH_2O), 4.87 (s, 1H, H-1), 4.11 (dd, 1H, $J_{2,3}$=6.0, $J_{3,4}$=7.0, H-3), 3.87 (d, 1H, H-2), 3.65 (oct, 1H, $J_{4,5}$=9.2, $J_{5,6}$=6.0, H-5), 3.30 (dd, 1H, H-4), 1.29 (d, 3H, H-6), 3.37 (s, 3H, OMe), 2.80 (broad s, 1H, OH). Found: C, 50.47; H, 7.55%. Calcd for $C_8H_{14}O_5$: C, 50.52; H, 7.42%.

Methyl 6-Deoxy-2,3-O-methylene-α-D-lyxo-hexopyranosid-4-ulose (6). To a chilled solution (−78 °C) of DMSO (143 mg, 2 mmol) in dichloromethane (2 ml) was successively added a solution of trifluoroacetic anhydride (318 mg, 1.5 mmol) in dichloromethane (2 ml) with stirring, and after 10 min, a solution of **11** (135 mg, 0.7 mmol) in dichloromethane (4 ml) dropwise. After stirring for 1 h, the reaction mixture was carefully neutralized with triethylamine at −78 °C, and then poured into ice–water. The resulting solution was extracted with chloroform. The usual work-up of the extract gave **6** (125 mg, 93.6%) as a syrup, showing a single component on TLC and NMR. NMR: 5.17 (s, 1H, H-1), 4.98 and 4.88 (each s, 2H, OCH_2O), 4.33 (d, 1H, $J_{2,3}$=6.4, H-2), 4.37 (d, 1H, H-3), 4.24 (q, 1H, $J_{5,6}$=7.0, H-5), 3.47 (s, 3H, OMe), 1.37 (d, 3H, H-6).

This syrup was used for the next reaction, without further purification and measurement of the rotational value, because a small amount of impurities detectable in the NMR spectrum could not be removed.

Reaction of 4-Uloses with Methylmagnesium Iodide. Synthesis of 4-*C*-methyl derivatives is illustrated by the preparation of benzyl 2,3-di-*O*-benzyl-4-*C*-methyl-α-D-xylopyranoside (**12**) and -β-L-arabinopyranoside (**13**). To a chilled solution (−78 °C) of methylmagnesium iodide in ether (2 ml), prepared from magnesium turnings (0.12 g, 4.9 mmol) and methyl iodide (1 g, 7 mmol), was added dropwise a solution of **1** (0.3 g, 0.72 mmol) in ether (1 ml), and the mixture was stirred for 2 h at the same temperature, diluted with ether, and then poured into water. The ether layer was washed with water, dried, and then evaporated to give a syrup. Fractionation of the syrup on a silica-gel column (hexane–ethyl acetate 3:1) gave **12** and **13** as syrups in 27% (84 mg) and 70.6% (220 mg) yield, respectively.

When the reaction was carried out in ether–THF (1:1) at room temperature, **12** and **13** were obtained in 60.5 and 24% yield, respectively. **12**: $[\alpha]_D$ +90.1° (*c* 1.1); **13**: $[\alpha]_D$ +102° (*c* 5.0). Found for **12**: C, 74.23; H, 7.08, and for **13**: C, 74.13; H, 7.18%. Calcd for $C_{27}H_{30}O_5$: C, 74.63; H, 6.96%.

A similar reaction of **2** (0.2 g, 0.8 mmol) with methylmagnesium iodide in ether–THF at room temperature and separation of the epimeric products gave benzyl 4-*C*-methyl-2,3-*O*-methylene-α-D-xylopyranoside (**18**) and -β-L-arabinopyranoside (**19**) in 19% (40 mg) and 53% (112 mg) yield, respectively. Found for **18**: C, 62.86; H, 6.75%, and for **19**: C, 63.02; H, 6.63%. Calcd for $C_{14}H_{18}O_5$: C, 63.14; H, 6.81%.

In a similar way, methyl 2,3-di-*O*-benzyl-6-deoxy-4-*C*-methyl-α-D-glucopyranoside (**23**) and -α-D-galactopyranoside (**24**) were obtained from **7** as syrups in 27 and 59% yield, respectively. **23**: $[\alpha]_D$ +43.9° (*c* 1.1), **24**: $[\alpha]_D$ +81.6° (*c* 1.3). Found for **23**: C, 70.81; H, 7.35%, and for **24**: C, 70.65; H, 7.47%. Calcd for $C_{22}H_{28}O_5$: C, 70.94; H, 7.58%.

The reaction of **5** and **6** with methylmagnesium iodide as above gave selectively one epimer, methyl 6-deoxy-4-*C*-methyl-2,3-*O*-methylene-α-D-allopyranoside (**29**) and -α-D-talopyranoside (**30**), respectively. **29**: syrup, $[\alpha]_D$ +81.7° (*c* 0.8), **30**: mp 105—108 °C, $[\alpha]_D$ +13.3° (*c* 1.3). Found for **29**: C, 52.76; H, 7.95%, and for **30**: C, 52.87; H, 7.99%. Calcd for $C_9H_{16}O_5$: C, 52.93; H, 7.90%.

Reaction of 4-Uloses with Vinylmagnesium Bromide. Synthesis of 4-*C*-vinyl derivatives is typically presented by the preparation of benzyl 2,3-di-*O*-benzyl-4-*C*-vinyl-α-D-xylopyranoside (**14**) and -β-L-arabinopyranoside (**15**). To a solution of vinylmagnesium bromide, prepared from magnesium turnings (1.2 g, 49 mmol) and vinyl bromide (6 g, 56 mmol),

in THF (5 ml) was added with stirring a solution of **1** (3 g, 7.2 mmol) in THF (5 ml) at room temperature, and the mixture was stirred for 1 h, poured into a saturated aqueous ammonium chloride solution and then extracted with ether. The usual work-up of the extract and separation of the epimeric products on a silica-gel column (hexane–ethyl acetate 15:1) gave **14** and **15** as syrups in 34.4% (1.1 g) and 14% (0.45 g) yield, respectively. **14**: $[\alpha]_D$ +109° (*c* 0.8), **15**: $[\alpha]_D$ +152° (*c* 1.2). Found for **14**: C, 75.59; H, 6.58%, and for **15**: C, 75.31; H, 6.80%. Calcd for $C_{28}H_{30}O_5$: C, 75.31; H, 6.77%.

A similar reaction of **2** (1.1 g, 4.4 mmol) and vinylmagnesium bromide in THF (10 ml), prepared from magnesium turnings (0.8 g, 32.9 mmol) and vinyl bromide (4.0 g, 37.3 mmol), and separation of the epimeric products with a preparative TLC (developed four times with hexane–ethyl acetate 4:1) gave benzyl 2,3-*O*-methylene-4-*C*-vinyl-α-D-xylopyranoside (**20**) and -β-L-arabinopyranoside (**21**) as syrups in 10.5% (129 mg) and 47.8% (585 mg) yield, respectively. **20**: $[\alpha]_D$ +137° (*c* 3.0), **21**: $[\alpha]_D$ +170° (*c* 1.2). Found for **20**: C, 64.87; H, 6.49%, and for **21**: C, 64.24; H, 6.48%. Calcd for $C_{15}H_{18}O_5$: C, 64.73; H, 6.52%.

Reaction of **3** (664 mg, 1.5 mmol) as above gave one epimer, benzyl 2,3-di-*O*-benzyl-6-deoxy-4-*C*-vinyl-α-D-galactopyranoside (**22**) as a syrup in 43.8% (310 mg) yield. $[\alpha]_D$ +141° (*c* 6.0). Found: C, 74.83; H, 6.72%. Calcd for $C_{29}H_{32}O_5$: C, 75.63; H, 7.00%.

A similar reaction of **4** (4 g, 15.1 mmol) in THF with vinylmagnesium bromide and separation of the epimeric products with a lobar column (hexane–ethyl acetate 4:1) gave benzyl 6-deoxy-4-*C*-vinyl-2,3-*O*-methylene-α-D-glucopyranoside (**26**) and -α-D-galactopyranoside (**27**) as syrups in 3.4% (0.15 g) and 51.8% (2.29 g) yield, respectively. **26**: $[\alpha]_D$ +167° (*c* 2.3). **27**: $[\alpha]_D$ +141° (*c* 6.8). Found for **26**: C, 64.96; H, 6.61%, and for **27**: C, 65.98; H, 6.72%. Calcd for $C_{16}H_{20}O_5$: C, 65.74; H, 6.90%.

Reaction of 4-Uloses with 2-Lithio-2-methyl-1,3-dithiane. Synthesis of 4-*C*-[2-methyl-1,3-dithian-2-yl] derivatives is illustrated by the preparation of benzyl 2,3-di-*O*-benzyl-4-*C*-(2-methyl-1,3-dithian-2-yl)-α-D-xylopyranoside (**16**) and -β-L-arabinopyranoside (**17**). To a chilled solution of 2-methyl-1,3-dithiane (1 g, 7.5 mmol) in THF (5 ml) was added dropwise butyllithium (10%, 1.3 ml, 2 mmol) in hexane at −30 °C (Dry Ice–carbon tetrachloride) under argon atmosphere, and the mixture was stirred for 3 h. A solution of **1** (0.3 g, 0.72 mmol) in THF (2 ml) was further added to the mixture at −78 °C, and stirred for 1 h. The reaction mixture was poured into water and extracted with ether. The usual work-up of the extract and separation of the eprimeric products on a silica-gel column (benzene–acetone 16:1) gave **16** and **17** as syrups in 25.2% (0.1 g) and 10.1% (0.04 g) yield, respectively. **16**: $[\alpha]_D$ +82.4° (*c* 3.5), NMR: 7.6—7.3 (m, 15H, 3×Ph), 4.76 (d, 1H, $J_{1,2}$=1.3, H-1), 5.05—4.51 (m, 6H, 3×CH_2Ph), 4.30 (dd, 1H, $J_{2,3}$=3.0, $J_{3,5a}$=1.0, H-3), 4.30 and 3.96 (ABq, 2H, J=11.3 H-5e and H-5a), 3.60 (dd, 1H, H-2), 3.54—1.70 (m, 6H, $SCH_2CH_2CH_2S$), 1.57 (s, 3H, CMe). **17**: $[\alpha]_D$ +82.4° (*c* 3.5); NMR: 7.6—7.3 (m, 15H, 3×Ph), 5.04—4.37 (m, 6H, 3×CH_2Ph), 4.83 (d, 1H, $J_{1,2}$=4.0, H-1), 4.47 (dd, 1H, $J_{2,3}$=9.2, $J_{3,5e}$=1.0, H-3), 4.18 and 3.98 (ABq, 2H, J=12.8, H-5e and H-5a), 3.96 (dd, 1H, H-3), 3.20—1.50 (m, 6H, $SCH_2CH_2CH_2S$), 1.96 (s, 3H, CMe). Found for **16**: C, 67.29; H, 6.34; S, 11.25%, and for **17**: C, 67.41; H, 6.71; S, 11.32%. Calcd for $C_{31}H_{36}O_5S_2$: C, 67.36; H, 6.57; S, 11.60%.

In a similar manner, benzyl 6-deoxy-4-*C*-(2-methyl-1,3-dithian-2-yl)-2,3-*O*-methylene-α-D-galactopyranoside (**28**) was obtained from **4** as a syrup in 35% yield. $[\alpha]_D$ +116° (*c* 8.0), NMR: 7.6—7.3 (m, Ph), 5.77 and 5.67 (ABq, 2H, J=12.0, CH_2Ph), 5.26 (d, 1H, $J_{1,2}$=3.8, H-1), 5.16 and 5.09 (ABq, 2H, J=1.0, OCH_2O), 4.29 (d, 1H, $J_{2,3}$=9.7, H-3), 4.28 (q, 1H, $J_{5,6}$=6.2, H-5), 3.90 (dd, 1H, H-2), 3.22—1.72 (m, 6H, $SCH_2CH_2CH_2S$), 2.00 (s, 3H, CMe), 1.52 (d, 3H, H-6). Found: C, 57.28; H, 6.58; S, 15.88%. Calcd for $C_{19}H_{26}O_5S_2$: C, 57.26; H, 6.58; S, 16.09%.

Reaction of 1 with Methyllithium. To a solution of **1** (0.1 g, 0.24 mmol) in ether (10 ml), a 1 M (1 M=1 mol dm^{-3}) ethereal solution (1 ml) of methyllithium was added with stirring at room temperature. After the reaction mixture was stirred for 1 h, water was added, the ethereal layer was separated, and the aqueous layer was extracted two times with ether (10 ml). The usual work-up of the combined ethereal solution and purification of the product on a preparative TLC (hexane–ethyl acetate 3:1) gave syrupy **12** in 32% (34 mg) yield.

The present work was supported by a Grant-in-Aid for Scientific Research No. 347023 from the Ministry of Education, Science and Culture, Japan. The authors wish to thank Mr. Y. Nakamura for the measurements of the ^{13}C NMR spectra.

References

1) Part XXII. M. Matsuzasa, K. Kubo, H. Kodama, M. Funabashi, and J. Yoshimura, *Bull. Chem. Soc. Jpn.*, **54**, 2169 (1981).
2) W. D. Ollis, C. Smith, and D. E. Wright, *Tetrahedron*, **35**, 105 (1979) and literatures cited therein.
3) C. L. Stevens and S. H. Czerreki, *Carbohydr. Res.*, **63**, 307 (1978).
4) M. E. Evans and F. W. Parrish, *Carbohydr. Res.*, **54**, 105 (1977).
5) J. Yoshimura, K. Sato, and H. Hashimoto, *Chem. Lett.*, **1977**, 1327.
6) P. M. Collins and B. R. Whitton, *Carbohydr. Res.*, **33**, 25 (1974).
7) a) M. Miljkovic, M. Gligorijevic, T. Satoh, and D. Miljkovic, *J. Org. Chem.*, **39**, 1379 (1974); b) M. Miljkovic, M. Gligorijevic, T. Satoh, D. Glisin, and R. D. Pitcher, *ibid.*, **39**, 3847 (1974).
8) A. M. Sepulchre, B. Septe, G. Lukacs, and S. D. Gero, *Tetrahedron*, **30**, 905 (1974).
9) P. M. Collins and V. R. N. Munasinghe, *Carbohydr. Res.*, **62**, 19 (1978).
10) K. Sato, M. Matsuzawa, K. Ajisaka, and J. Yoshimura, *Bull. Chem. Soc. Jpn.*, **53**, 189 (1980).
11) H. Paulsen and V. Sinnwell, *Chem. Ber.*, **111**, 879 (1978).
12) M. Matsuzawa and J. Yoshimura, *Carbohydr. Res.*, **81**, C5 (1980).
13) J. Yoshimura and M. Matsuzawa, *Carbohydr. Res.*, **85**, C1 (1980).
14) J. Yoshimura, *Pure Appl. Chem.*, **53**, 113 (1981).
15) C. L. Stevens, R. P. Glinski, and K. G. Taylor, *J. Org. Chem.*, **33**, 1586 (1968).
16) B. M. Gough, W. Gunner, W. G. Overend, and N. R. Williams, *Carbohydr. Res.*, **14**, 173 (1970).

Oxidation of Olefins into α-Phenylseleno Carbonyl Compounds. Highly Regioselective *anti*-Markownikoff Type Oxidation of Allylic Alcohol Derivatives[1]

Makoto SHIMIZU, Ryo TAKEDA, and Isao KUWAJIMA*

Department of Chemistry, Tokyo Institute of Technology, Ookayama, Meguro-ku, Tokyo 152

(Received April 30, 1981)

By using $(C_6H_5Se)_2$–*t*-BuOOH or $(C_6H_5Se)_2$–$(C_6H_5SeO)_2O$ system, oxoselenenylation reactions of C=C bonds have been examined with allylic and homoallylic alcohol derivatives, and substituted cyclohexenes, and allyl *t*-butyldimethylsilyl ethers are found to undergo regioselective conversion into β-siloxy α-phenylseleno carbonyl compounds in high yields.

Regioselective introduction of various functional groups into the carbon atom adjacent to a carbonyl constitutes a major concern in synthetic organic chemistry. For this purpose, α-halo or α-phenylthio substituted carbonyl compounds offer one of the most promising methodologies to distinguish α from α′ carbons to a carbonyl group.

Recent developments in organoselenium chemistry[2] have realized that carbanions stabilized by arylseleno group are capable of attacking various electrophiles[3] and that arylseleno group is readily removed *via syn*-elimination reaction through selenoxides,[2] reduction with Raney nickel or trialkyltin hydride,[4] and so on.

Recently, several methods have been introduced by us[1,5] and others[6] for the direct preparation of α-phenylseleno carbonyl compounds from olefins. However, high regioselectivity in these oxidation reactions has only been achieved with terminal olefins to yield phenylselenomethyl ketones. We have examined steric and electronic effects of substituents for determining regiochemistry in the oxidation of olefins by using a system of diphenyl diselenide and *t*-butyl hydroperoxide, or diphenyl diselenide and benzeneseleninic anhydride.[1]

In this paper, we describe oxidation reactions of allylic and homoallylic alcohol derivatives, together with those of substituted cyclohexenes. Although a real reactive species in this reaction has not been confirmed yet,[7] it still appears to be reasonable for us to assume benzeneselenenic anhydride **1** as a plausible one as shown in the following equations.

$$\left.\begin{array}{l} (C_6H_5Se)_2 + t\text{-BuOOH} \longrightarrow \text{“}C_6H_5SeOSeC_6H_5\text{”} \\ \qquad\qquad\qquad\qquad\qquad\qquad\qquad\qquad \mathbf{1} \\ 2(C_6H_5Se)_2 + (C_6H_5SeO)_2O \\ \qquad\qquad \longrightarrow 3\text{“}C_6H_5SeOSeC_6H_5\text{”} \\ \qquad\qquad\qquad\qquad\qquad\qquad\qquad\qquad \mathbf{1} \\ \qquad\qquad\qquad\qquad\qquad\quad OSeC_6H_5 \\ \qquad\qquad\qquad\qquad\qquad\quad | \\ R^1CH{=}CHR^2 \xrightarrow{1} R^1CH\text{-}CHR \\ \qquad\qquad\qquad\qquad\qquad\quad | \\ \qquad\qquad\qquad\qquad\qquad\quad SeC_6H_5 \\ \qquad\qquad \longrightarrow R^1CH\text{-}CO\text{-}R^2 + C_6H_5SeH \\ \qquad\qquad\qquad\qquad\qquad\quad | \\ \qquad\qquad\qquad\qquad\qquad\quad ScC_6H_5 \end{array}\right\} \quad (1)$$

Oxidation of Allylic Alcohol Derivatives. Allylic alcohols are in general easily accessible *via* a number of standard procedures. Neighboring carbonyl group participation (Eq. 2) for allylic esters,[8] and steric

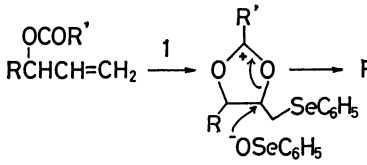

(2)

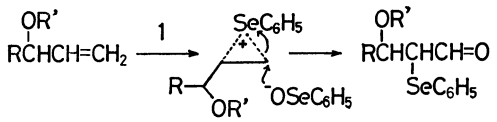

(3)

and electronic effects (Eq. 3) for allylic ethers are considered to play important roles which direct the site of introducing carbonyl functionality in the oxidation of carbon-carbon double bonds. Effects of substituents on oxygen atom were initially surveyed using 1-phenyl-4-hexen-3-ol derivatives. Thus, diphenyl diselenide was oxidized with an equimolar amount of *t*-butyl hydroperoxide in carbon tetrachloride, and *t*-butyl alcohol formed was removed together with the solvent *in vacuo*. The allylic alcohol derivatives were then treated with the resulting solid in refluxing benzene or toluene for an appropriate period and the corresponding oxoselenenylation products **2** and **3** were isolated. The results are listed in Table 1.

Comparison of these results implies that increasing steric conjestion around C=C bonds may enhance regioselectivity to introduce carbonyl functionality onto the remote carbon atoms of the double bonds. Trimethylsilyl ethers did not survive the reaction conditions to result in the formation of complex mixtures; a possible side-reaction may involve generation of the parent allylic alcohols which undergo oxidation under the present reaction conditions.[9] But, *t*-butyldimethylsilyl ether gave a remarkable result; only a single isomer was obtained in excellent yield. Satisfactory regioselectivity was also observed even with benzyl ether. In contrast, an effect based on neighboring group participation shown in Eq. 2 appeared to have little influence on the direction of this reaction.

Based on these results, similar oxidation was examined with a variety of allyl *t*-butyldimethylsilyl ethers. On treating with diphenyl diselenide and benzeneseleninic anhydride, they underwent regiospecific oxoselenenylation reaction to give the corresponding β-*t*-butyldimethylsiloxy α-phenylseleno carbonyl compounds **4**—**8** in excellent yields, without any contamination of their regio-isomers (see Table 2).

Table 1. Regioselectivity on the oxidation of 4-alkoxy-6-phenyl-2-hexene[a)]

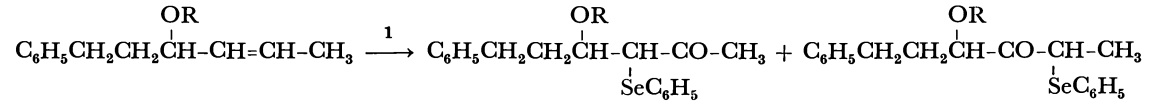

2a—d **3a—d**

R	Solvent	Period (h)	Ratio (**2**/**3**)	Yield/%
a) CH_3CO-	Toluene	3.0	67 : 33	71
b) $(CH_3)_3CCO$-	Toluene	10.0	75 : 25	60
c) $C_6H_5CH_2$-	Benzene	6.5	95 : 5	79
d) $(CH_3)_3CSi(CH_3)_2$-	Benzene	4.0	100 : 0	89

a) Reactions were carried out in a refluxing solvent with olefin: $(C_6H_5Se)_2$: *t*-BuOOH = 1.0 : 4.4 : 4.4.

Table 2. Oxidation of allyl *t*-butyldimethylsilyl ethers[a)]

Olefin	Product	Yield/%
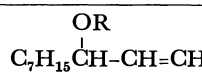	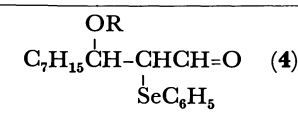 (**4**)	87
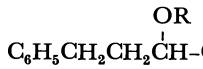	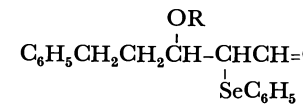 (**5**)	81
	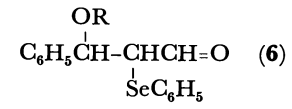 (**6**)	79
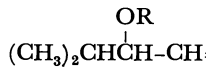	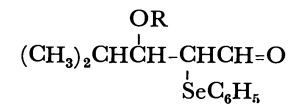 (**7**)	74
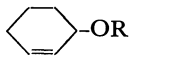	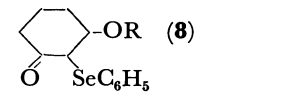 (**8**)	76
	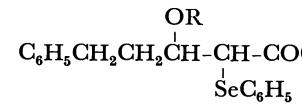 (**2d**)	89

a) Reactions were carried out in reflxing toluene with olefin: $(C_6H_5Se)_2$:$(C_6H_5SeO)_2O$ = 1.0:1.4:0.7 for terminal olefins and 1.0:2.8:1.4 for internal olefin. b) R = $(CH_3)_3CSi(CH_3)_2$-.

It should be remarkable that the ethers possessing a terminal olefin can be cleanly converted to the corresponding β-siloxy α-phenylseleno aldehydes exclusively, although such type of addition process appears to be disfavored electronically. β-Hydroxy or β-alkoxy aldehydes are usually quite unstable to undergo dehydration, but in these cases the products could be isolated without such kind of decomposition.

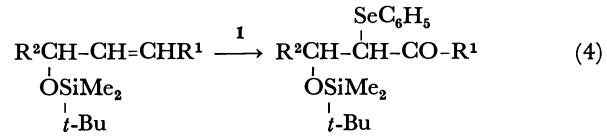

(4)

As the reaction solvent, benzene or toluene is preferable for this transformation. In other low-boiling solvents, a concomitant formation of β-hydroxy selenide was observed. The effect of *t*-butyldimethylsiloxy group was also prominent in the case with cyclohexene derivative, but the oxidation of 3-*t*-butyldimethylsiloxy-1-cyclopentene **9** afforded a mixture of 3-siloxy-2-phenylselenocyclopentanone **10**, 2-phenylseleno-2-cyclopentenone **11**, and 3-siloxy-2-phenylseleno-1-cyclopentanol **12**.

In addition to the bulky *t*-butyldimethylsiloxy group, substituents on the allylic position appear to have a marked influence on the regioselectivity; allyl *t*-butyldimethylsilyl ether derived from primary allylic alcohol did not show good regioselectivity to give a mixture of **13** and **14**.

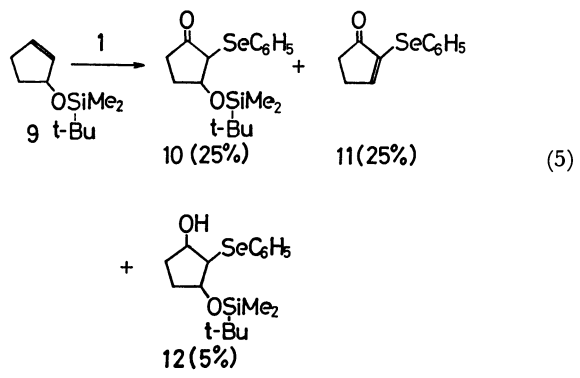

(5)

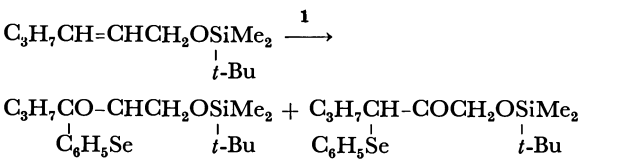

(6)

Addition of hypohalite to terminal olefins bearing tertiary carbon at their allylic position has been reported to proceed in a highly regioselective manner, and the *anti*-Markownikoff adducts were formed exclusively although the yields were low.[10] In a related system, *anti*-Markownikoff type oxidation was found to take place exclusively with methyl ethers of tertiary allylic alcohols in the present procedure. The results are shown in Table 3. However, in the case with a highly hindered olefin, the reaction did not proceed

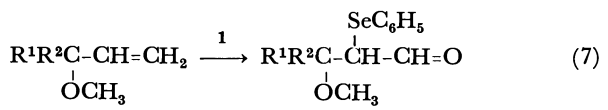

(7)

practically under the same conditions to recover the starting olefin.

The aldol type products obtained by the present procedure undergo a facile conversion to the corresponding α-phenylseleno enals on treatment with fluoride anion.[11] The use of other stronger bases such as lithium diisopropylamide (LDA), potassium *t*-butoxide, or tetrabutylammonium hydroxide led to formation of a mixture composed of several products. On the other hand, acidic treatment led to a mixture of α-phenylseleno enal and deselenenylated enal.[12] The products arising from the oxidation of allyl methyl ethers were more easily transformed into α-phenylseleno enals. They readily liberated methanol on treatment with silica gel.

Table 3. Oxidation of *t*-allyl methyl ethers[a]

Allyl methyl ether	Product		Yield/%
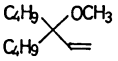	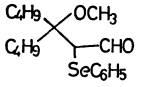	**15**	93
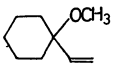	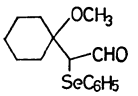	**16**	86
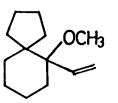	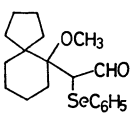		trace[b]

a) Reactions were carried out in refluxing toluene with olefin: $(C_6H_5Se)_2$: $(C_6H_5SeO)_2O$ = 1.0:1.4:0.7. b) Most of the starting material was recovered.

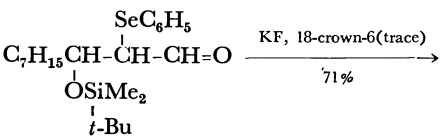

(8)

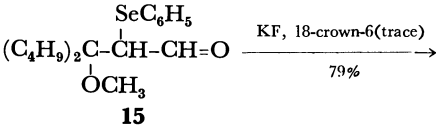

(9)

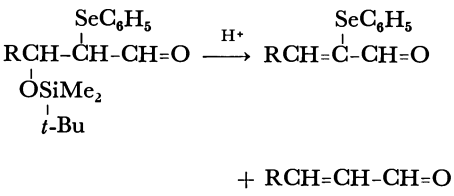

(10)

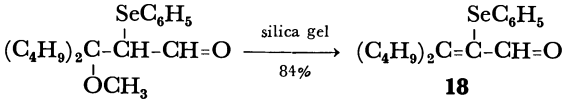

(11)

In addition, removal of phenylseleno group can also be readily performed. For example, treatment of 2-*t*-butyldimethylsiloxy-3-phenylselenocyclohexanone **8** with an excess amount of benzenethiolate anion in tetrahydrofuran afforded the deselenenylated ketone **19** in 88% yield.[13]

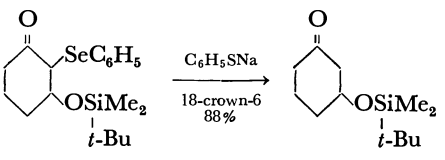

(12)

Considering that the starting materials are easily accessible, this procedure may be employed as a useful alternative for the synthesis of aldols or α,β-unsaturated carbonyl compounds.

Table 4. Oxidation of 6-phenyl-3-trialkylsiloxy-1-hexene

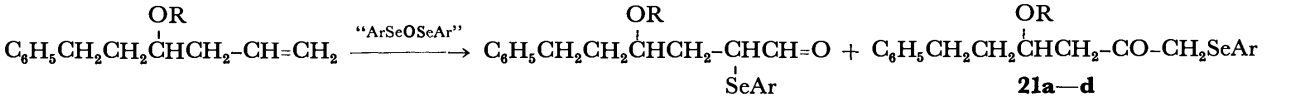

20a—d

	R	Ar	Ratio (**20**/**21**)	Yield/%
a)	$Si(CH_3)_2C(CH_3)_3$	C_6H_5	60 : 40	70[a]
b)	$Si(CH_3)_2C(CH_3)_3$	2,4,6-$(CH_3)_3C_6H_2$	75 : 25	74[b]
c)	$Si(C_6H_5)_3$	C_6H_5	73 : 27	72[a]
d)	$Si(C_6H_5)_3$	2,4,6-$(CH_3)_3C_6H_2$	77 : 23	71[b]

a) Reactions were carried out in refluxing benzene with olefin: $(C_6H_5Se)_2$:$(C_6H_5SeO)_2O$=1.0:1.4:0.7. b) Reactions were carried out in refluxing benzene with olefin: $(ArSe)_2$:*t*-BuOOH=1.0:2.0:2.0.

Table 5. Oxidation of 1-*t*-butyldimethylsiloxy-3-pentene[a]

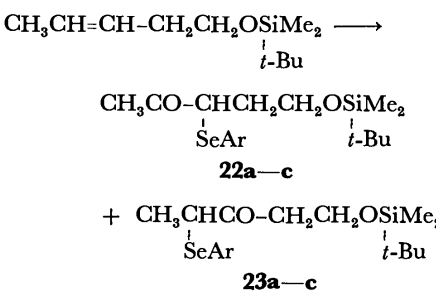

22a—c

23a—c

	Ar	Ratio (**22**/**23**)	Yield/%
a)	C_6H_5	75 : 25	78
b)	2,4,6-$(CH_3)_3C_6H_2$	66 : 34	88
c)	*p*-ClC_6H_4	80 : 20	72

a) Reactions were carried out in refluxing benzene with olefin: $(ArSe)_2$:$(ArSeO)_2O$=1.0:2.8:1.4.

Table 6. Oxidation of 5-alkoxy-5-propyl-2-octene[a]

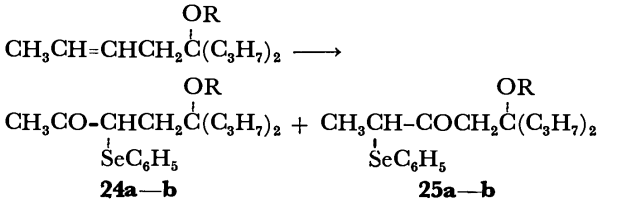

24a—b **25a—b**

	R	Ratio (**24**/**25**)	Yield/%
a)	CH_3	78 : 22	71
b)	$C_6H_5CH_2$	85 : 15	75

a) Reactions were carried out in refluxing benzene with olefin: $(C_6H_5Se)_2$:$(C_6H_5SeO)_2O$=1.0:2.8:1.4.

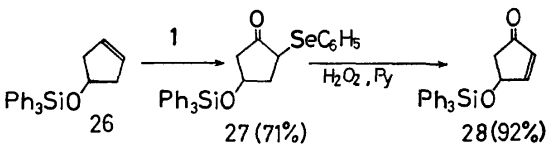

(13)

Oxidation of Homoallylic Alcohol Derivatives. As described above, the *t*-butyldimethylsilyl group has worked quite effectively on directing the site of introducing carbonyl functionality in the oxidation of allyl alcohol derivatives. Application of this procedure to homoallylic alcohol analogues has found relatively good regioselectivity.

As typical examples, we have examined the oxidation of 1-phenyl-5-hexen-3-ol, 3-penten-1-ol, and 4-propyl-6-octen-4-ol. The results are listed in Tables 4, 5, and 6.

The results shown in the tables reveal that the effects of homoallylic substituents are not so sufficient to distinguish the remote sp^2 carbon from the other as those of allylic ones. In these cases, the highest ratio of γ-alkoxy α-phenylseleno ketones to their regioisomers is approximately 4:1. From a synthetic point of view, the present method is not so useful for this kind of transformation.

On the other hand, this system offers a convenient route to 4-siloxy-2-cyclopentenone **28**, a useful precursor for the synthesis of prostaglandin derivatives.[14] Thus, oxidation of 4-triphenylsiloxycyclopentene **26** by the present procedure followed by treatment with hydrogen peroxide afforded the cyclopentenone **28** in 65% overall yield.

Oxidation of Cyclohexene Derivatives. In the addition process to cyclohexene derivatives, two major interactions which may direct the site of introduction of anionic species, *e.g.*, $C_6H_5SeO^-$, appear to be involved; one is 1,3-diaxial interaction and the other is 1,2-interaction based on tortional strain. In the case with 3,3-disubstituted cyclohexene, if 1,3-diaxial interaction severely prevents the introduction of $C_6H_5SeO^-$ species to C-1 carbon, oxidation at C-2 may predominate, whereas the attack at C-1 will be a subject of tortional strain. Table 7 lists the results.

The result of the oxidation of spiro compound **29** indicates that 1,2-interaction predominates over 1,3-interaction. Apparently, this interaction was not so prominent for 3-monosubstituted cyclohexene, and the selectivity was greatly decreased with the substrate **31**. Other cases, *e.g.*, 4,4-disubstituted derivatives did not show any preference for regioselectivity of 1,2-electrophilic addition, probably because the steric congestions are almost same for both olefinic carbons and because there is little difference of electronic

Table 7. Oxidation of substituted cyclohexenes[a)]

Substrate	Product (ratio)	Yield/%
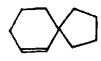 29	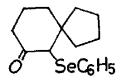	72
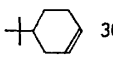 30	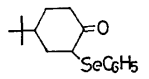 (55:45)	70
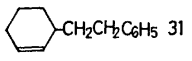 31	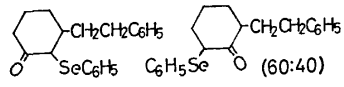 (60:40)	67
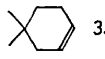 32	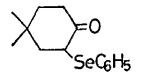 (57:43)	68

a) Reactions were carried out in refluxing benzene with olefin: $(C_6H_5Se)_2$:*t*-BuOOH = 1.0:4.4:4.4.

effects.

Experimental

All reactions were performed under either argon or ultra grade nitrogen atmosphere. NMR spectra were taken on a Hitachi R-24B spectrometer and chemical shifts are recorded in parts per million downfield from internal tetramethylsilane. IR spectra were taken on a Hitachi EPI G-3 or 260-10 spectrometer, and mass spectra on a Hitachi RMU-7M or RMU-6C spectrometer at 70 eV ionizing irradiation. Boiling points were uncorrected.

Diphenyl diselenide, bis(*p*-chlorophenyl) diselenide, and bis(2,4,6-trimethylphenyl) diselenide were prepared by the procedure reported by Sharpless[15)] or Reich.[16)] Benzeneseleninic anhydride was prepared according to the procedure of Woodbridge,[17)] and was stored over P_2O_5.

Oxidation of 4-Alkoxy-6-phenyl-2-hexene with $(C_6H_5Se)_2$-t-BuOOH. Examination of Regioselectivity (General Procedure). To a solution of diphenyl diselenide (1.382 g, 4.4 mmol) in 10 ml of carbon tetrachloride were added molecular sieves 3A (4 g) and a solution of 70% *t*-butyl hydroperoxide (563 mg, 4.4 mmol) in 10 ml of carbon tetrachloride, and the mixture was heated to refluxing for 1 h. Then, *t*-butyl alcohol formed as well as the solvent was removed *in vacuo*, and a solution of 4-alkoxy-6-phenyl-2-hexene (1 mmol) in 5 ml of benzene or toluene was added to the resulting solution. After heated to refluxing for the period indicated in Table 1 followed by usual work-up, the ratio of the regio-isomers was determined on the bases of chromatographycally pure samples.

*4-Acetoxy-6-phenyl-3-phenylseleno-2-hexanone (**2a**).* IR (neat): 1730, 1710 cm^{-1}; NMR (CCl_4): δ 1.80—2.41 (m, 2H), 2.21 (s, 3H), 2.30 (s, 3H), 2.42—3.00 (m, 2H), 3.43—4.00 (m, 1H), 5.01—5.32 (m, 1H), 7.00—7.52 (m, 10H); Found: C, 61.91; H, 5.50%. Calcd for $C_{20}H_{22}O_3Se$: C, 61.71; H, 5.69%.

*4-Acetoxy-6-phenyl-2-phenylseleno-3-hexanone (**3a**).* IR (neat): 1730, 1710 cm^{-1}; NMR (CCl_4): δ 1.83—2.10 (m, 2H), 1.91 (d, J=4.0 Hz, 3H), 2.20 (s, 3H), 2.51—3.00 (m, 2H), 3.35 (q, J=6.0 Hz, 1H), 5.06—5.32 (m, 1H), 7.00—7.52 (m, 10H); Found: C, 61.82; H, 5.63%. Calcd for $C_{20}H_{22}O_3Se$: C, 61.71; H, 5.69%.

*4-Pivaloyloxy-6-phenyl-3-phenylseleno-2-hexanone (**2b**).* IR (neat): 1725, 1710 cm^{-1}; NMR (CCl_4): δ 1.20 (s, 9H), 2.10—2.42 (m, 2H), 2.31 (s, 3H), 2.35—2.62 (m, 2H), 3.60—4.02 (m, 1H), 4.91—5.42 (m, 1H), 6.98—7.62 (m, 10H); Found: C, 64.23; H, 6.50%. Calcd for $C_{23}H_{28}O_3Se$: C, 64.04; H, 6.54%.

*4-Pivaloyloxy-6-phenyl-2-phenylseleno-3-hexanone (**3b**).* IR (neat): 1725, 1705 cm^{-1}; NMR (CCl_4): δ 1.10 (d, J=4.5 Hz, 2H), 1.21 (s, 9H), 1.93—2.42 (m, 2H), 2.43—3.01 (m, 2H), 4.00—4.20 (m, 1H), 4.92—5.45 (m, 1H), 6.88—7.71 (m, 10H); Found: C, 63.90; H, 6.41%. Calcd for $C_{23}H_{28}O_3Se$: C, 64.04; H, 6.54%.

*4-Benzyloxy-6-phenyl-3-phenylseleno-2-hexanone (**2c**).* IR (neat): 1705 cm^{-1}; NMR (CCl_4): δ 1.80—2.33 (m, 2H), 2.12 (s, 3H), 2.47—2.83 (m, 2H), 3.57—4.08 (m, 2H), 4.50 (s, 2H), 6.85—7.53 (m, 15H); Found: C, 68.35; H, 6.09%. Calcd for $C_{25}H_{26}O_2Se$: C, 68.64; H, 5.99%.

*3-Benzyloxy-6-phenyl-2-phenylseleno-3-hexanone (**3c**).* IR (neat): 1705 cm^{-1}; NMR (CCl_4): δ 1.30 (d, J=6.5 Hz, 3H), 1.76—2.30 (m, 2H), 2.37—2.80 (m, 2H), 4.00—4.37 (m, 2H), 4.50 (s, 2H), 6.90—7.50 (m, 15H). These spectra were identical with those of the authentic samples prepared in the following manner: addition of sodium benzeneselenolate to 4-benzyloxy-6-phenyl-2-hexene oxide followed by oxidation with benzeneseleninic anhydride and diphenyl diselenide.[9)]

*4-t-Butyldimethylsiloxy-6-phenyl-3-phenylseleno-2-hexanone (**2d**).* IR (neat): 1700 cm^{-1}; NMR (CCl_4): δ 0.11 (s, 6H), 0.92 (s, 9H), 2.00—2.60 (m, 2H), 2.30 (s, 3H), 2.70—3.00 (m, 2H), 4.00 (d, J=6.0 Hz, 1H), 4.10—4.42 (m, 1H), 7.00—7.81 (m, 10H); Found: C, 62.25; H, 7.39%. Calcd for $C_{24}H_{34}O_2SeSi$: C, 62.45; H, 7.42%.

Preparation of Allyl t-Butyldimethylsilyl Ethers. Silyl ethers were prepared by silylation of the corresponding alcohols.[18)] They exhibit the following spectroscopic properties.

3-t-Butyldimethylsiloxy-1-decene. IR (neat): 1640, 1460, 1255, 1080, 1010, 995, 925, 840, 780 cm^{-1}; NMR (CCl_4): δ 0.00 (s, 6H), 0.73—1.80 (m, 24H including singlet at 0.82 (9H, *t*-Bu)), 3.73—4.17 (m, 1H), 4.90 (dd, J=8.0 and 3.0 Hz, 1H), 5.00 (dd, J=16 and 3.0 Hz, 1H), 5.70 (ddd, J=16.0, 8.0, and 6.0 Hz, 1H).

3-t-Butyldimethylsiloxy-5-phenyl-1-pentene. IR (neat): 1640, 1600, 1460, 1255, 1090, 1010, 995, 925, 845, 780, 750, 700 cm^{-1}; NMR (CCl_4): δ 0.00 (s, 6H), 0.90 (s, 9H), 1.50—2.00 (m, 2H), 2.43—2.80 (m, 2H), 4.10 (dt, J=5.5 and 5.5 Hz, 1H), 5.00 (dd, J=8.5 and 2.0 Hz, 1H), 5.12 (dd, J=16.0 and 2.0 Hz, 1H), 5.80 (ddd, J=16.0, 8.5, and 5.5 Hz, 1H), 7.07 (s, 5H).

3-t-Butyldimethylsiloxy-3-phenyl-1-propene. IR (neat): 1640, 1600, 1460, 1255, 1130, 1090, 1070, 1010, 990, 940, 925, 870, 840, 780, 700 cm^{-1}; NMR (CCl_4): δ −0.03 (s, 3H), 0.67 (s, 3H), 0.90 (s, 9H), 4.90—5.40 (m, 3H), 5.90 (ddd, J=16.0, 10.0, and 4.0 Hz, 1H), 7.22 (s, 6H).

3-t-Butyldimethylsiloxy-4-methyl-1-pentene. IR (neat): 1690, 1470, 1255, 1080, 1010, 995, 925, 865, 845, 780 cm^{-1}; NMR (CCl_4): δ 0.00 (s, 6H), 0.80 (d, J=6.0 Hz, 6H), 0.83 (s, 9H), 1.65 (ses, J=6.0 Hz, 1H), 3.80 (dd, J=5.0 and 5.0 Hz, 1H), 5.00 (dd, J=8.0 and 2.0 Hz, 1H), 5.03 (dd, J=16.0 and 2.0 Hz, 1H), 5.73 (ddd, J=16.0, 8.0, and 5.0 Hz, 1H).

3-t-Butyldimethylsiloxy-1-cyclohexene. IR (neat): 1250, 1080 cm^{-1}; NMR (CCl_4): δ 0.11 (s, 6H), 0.98 (s, 9H), 1.64—2.21 (m, 6H), 4.08—4.36 (m, 1H), 6.15—6.80 (m, 2H).

4-t-Butyldimethylsiloxy-6-phenyl-2-hexene. IR (neat): 3010, 1250, 1100 cm^{-1}; NMR (CCl_4): δ 0.12 (s, 6H), 0.97 (s, 9H), 1.61—2.10 (m, 3H), 1.89 (d, J=5.0 Hz, 2H), 2.50—2.86 (m, 2H), 3.84—4.30 (m, 1H), 5.43—5.63 (m, 2H), 7.17 (s, 5H).

*3-t-Butyldimethylsiloxy-2-phenylselenodecanal (**4**) (General Pro-*

cedure for the Oxidation of Allyl t-Butyldimethylsiloxy Ethers). To a solution of diphenyl diselenide (874 mg, 2.8 mmol) and benzeneseleninic anhydride (504 mg, 1.4 mmol) in 5 ml of toluene was added a solution of 3-*t*-butyldimethylsiloxy-1-decene (540 mg, 2.0 mmol) in 15 ml of toluene. After stirring for 30 min under refluxing, the reaction mixture was washed with satd aq NaCl and the aqueous layer was extracted with ether. Drying and concentration of the combined extracts followed by purification by silica gel column chromatography afforded the title compound (764 mg, 87%) as an oil and diphenyl diselenide (1.03 g). IR (neat): 1710 cm^{-1}; NMR (CCl_4): δ 0.03 (s, 6H), 0.80—2.00 (m, 15H), 0.83 (s, 9H), 3.23—3.70 (m, 1H), 3.90—4.30 (m, 1H), 6.90—7.77 (m, 5H), 9.23 (d, J=6.0 Hz, C<u>H</u>=O), 9.43 (d, J=4.0 Hz, C<u>H</u>=O); Found: C, 60.11; H, 8.90%. Calcd for $C_{22}H_{38}O_2SeSi$: C, 59.84; H, 8.67%.

3-t-Butyldimethylsiloxy-5-phenyl-2-phenylselenopentanal (5). Bp 110 °C/0.25 mmHg;[19] IR (neat): 1710 cm^{-1}; NMR (CCl_4): δ 0.03 (s, 6H), 0.87 (s, 9H), 1.73—2.33 (m, 2H), 2.33—2.90 (m, 2H), 3.30—3.83 (m, 1H), 3.93—4.40 (m, 1H), 6.70—7.80 (m, 10H), 9.36 (d, J=5.0 Hz, C<u>H</u>=O), 9.43 (d, J=3.0 Hz, C<u>H</u>=O); MS:[20] *m/e* (%) 311 (M^+ −137, 2), 262 (2), 216 (7), 157 (4), 132 (22), 129 (17), 117 (9), 115 (9), 104 (9), 91 (78), 77 (57), 76 (100); Found: C, 62.17; H, 7.37%. Calcd for $C_{23}H_{32}O_2SeSi$: C, 61.73; H, 7.21%.

3-t-Butyldimethylsiloxy-3-phenyl-2-phenylselenopropanal (6). Bp 115—120 °C/0.02 mmHg;[19] IR (neat): 1710 cm^{-1}; NMR (CCl_4): δ −0.02, −0.015, and 0.08 (s, 6H), 0.90 (s, 9H), 3.56—3.83 (m, 1H), 5.07 (d, J=7.0 Hz, C<u>H</u>OSi), 5.22 (d, J=4.0 Hz, C<u>H</u>OSi), 7.00—7.50 (m, 10H), 9.43 (d, J=4.0 Hz, C<u>H</u>=O), 9.50 (d, J=8.0 Hz, C<u>H</u>=O); MS:[20] *m/e* (%) 283 (M^+ −137, 9), 264 (2), 258 (3), 218 (4), 205 (4), 177 (6), 176 (6), 157 (7), 137 (20), 131 (18), 117 (6), 115 (5), 105 (10), 103 (12), 77 (62), 76 (100); Found: C, 60.06; H, 6.57%. Calcd for $C_{21}H_{28}O_2SeSi$: C, 60.13; H, 6.73%.

3-t-Butyldimethylsiloxy-4-methyl-2-phenylselenopentanal (7). Bp 100—105 °C/0.025 mmHg;[19] IR (neat): 1705 cm^{-1}; NMR (CCl_4): δ 0.18 (s, 6H), 0.85—1.20 (m, 1H), 1.10 (d, J=2.0 Hz, 6H), 1.00 (s, 9H), 3.57—3.87 (m, 1H), 3.87—4.13 (m, 1H), 6.70—7.53 (m, 5H), 9.30 (d, J=4.0 Hz, C<u>H</u>=O), 9.33 (d, J=4.0 Hz, C<u>H</u>=O); MS:[20] *m/e* (%) 303 (M^+ −83, 8), 249 (M^+ −137, 33), 182 (23), 170 (27), 167 (47), 155 (40), 142 (20), 130 (18), 127 (33), 113 (7), 95 (33), 77 (17), 76 (70), 75 (100); Found: C, 56.39; H, 7.88%. Calcd for $C_{18}H_{30}O_2SeSi$: C, 56.09; H, 7.84%.

3-t-Butyldimethylsiloxy-2-phenylselenocyclohexanone (8). IR (neat): 1710 cm^{-1}; NMR (CCl_4): δ 0.11 (s, 6H), 0.92 (s, 9H), 1.22—2.90 (m, 6H), 3.31—4.50 (m, 2H), 6.98—7.61 (m, 5H); Found: C, 56.09; H, 7.42%. Calcd for $C_{18}H_{28}O_2SeSi$: C, 56.39; H, 7.36%.

Oxidation of 3-t-Butyldimethylsiloxy-1-cyclopentene (9). Diphenyl diselenide (312 mg, 1.0 mmol) was oxidized with 70% *t*-butyl hydroperoxide (141 mg, 1.0 mmol) in refluxing carbon tetrachloride (5 ml) for 1 h. Then all the solvent as well as *t*-butyl alcohol was removed from the reaction mixture, to which was added a solution of 3-*t*-butyldimethylsiloxy-1-cyclopentene (100 mg, 0.5 mmol) in 12 ml of benzene. After heating to refluxing for 2 h, the mixture was washed with satd aq NaCl and the aqueous layer was extracted with ethyl acetate. The combined extracts were dried and concentrated to give an oil, which was purified by preparative TLC to afford 3-*t*-butyldimethylsiloxy-2-phenylselenocyclopentanone **10** (46 mg, 25%), 2-phenylseleno-2-cyclopentenone **11** (30 mg, 25%), and 3-*t*-butyldimethylsiloxy-2-phenylseleno-1-cyclopentanol **12** (9 mg, 5%).

3-t-Butyldimethylsiloxy-2-phenylselenocyclopentanone (10). IR (neat): 1730 cm^{-1}; NMR (CCl_4): δ 0.12 (s, 6H), 0.91 (s, 9H), 1.67—2.30 (m, 4H), 3.42—3.65 (m, 1H), 3.71—4.05 (m, 1H), 7.10—7.71 (m, 5H).

2-Phenylseleno-2-cyclopentenone (11). IR (neat): 1690 cm^{-1}; NMR (CCl_4): δ 2.41—2.87 (m, 4H), 7.01 (t, J=3.0 Hz, 1H), 7.20—7.70 (m, 5H).

3-t-Butyldimethylsiloxy-2-phenylseleno-1-cyclopentanol (12). IR (neat): 3350 cm^{-1}; NMR (CCl_4): δ 0.12 (s, 6H), 0.92 (s, 9H), 2.12—2.70 (m, 5H), 3.10—3.40 (m, 1H), 3.43—3.76 (m, 2H), 7.12—7.62 (m, 5H).

1-t-Butyldimethylsiloxy-2-phenylseleno-3-hexanone (13). IR (neat): 1705 cm^{-1}; NMR (CCl_4): δ 0.11 (s, 6H), 0.92 (s, 9H), 1.05—1.82 (m, 5H), 2.34—2.72 (m, 2H), 3.54—4.05 (m, 3H), 7.01—7.52 (m, 5H); Found: C, 56.22; H, 8.01%. Calcd for $C_{18}H_{30}O_2SeSi$: C, 56.08; H, 7.84%.

1-t-Butyldimethylsiloxy-3-phenylseleno-2-hexanone (14). IR (neat): 1705 cm^{-1}; NMR (CCl_4): δ 0.19 (s, 6H), 0.93 (s, 9H), 1.05—1.81 (m, 7H), 3.66—3.90 (m, 1H), 4.20 (d, J=7.0 Hz, 2H), 7.00—7.51 (m, 5H); Found: C, 56.18; H, 7.96%. Calcd for $C_{18}H_{30}O_2SeSi$: C, 56.08; H, 7.84%.

3-Butyl-3-methoxy-2-phenylselenoheptanal (15) (General Procedure). To a solution of diphenyl diselenide (874 mg, 2.8 mmol) and benzeneseleninic anhydride (504 mg, 1.4 mmol) in 2 ml of toluene was added a solution of 3-butyl-3-methoxy-1-heptene (368 mg, 2 mmol) in 3 ml of toluene. After stirring for 30 min at refluxing temperature, the reaction mixture was washed with satd aq NaCl and the aqueous layer was extracted with ether. Drying and concentration of the combined extracts followed by purification by silica gel column chromatography (SiO_2 deactivated with 20% of water was used) afforded the title compound (649 mg, 91%) and diphenyl diselenide (960 mg). IR (neat): 1700 cm^{-1}; NMR (CCl_4): δ 0.67—2.00 (m, 18H), 3.20 (s, 3H), 3.50 (d, J=7.0 Hz, 1H), 7.00—7.60 (m, 5H), 9.77 (d, J=7.0 Hz, 1H); Found: C, 61.03; H, 7.98%. Calcd for $C_{18}H_{28}O_2Se$: C, 60.84; H, 7.94%.

2-(1-Methoxycyclohexyl)-2-phenylselenoacetaldehyde (16). Bp 110—115 °C/0.02 mmHg;[19] IR (neat): 1700 cm^{-1}; NMR (CCl_4): δ 1.00—2.20 (m, 10H), 3.17 (s, 3H), 3.62 (d, J=7.0 Hz, 1H), 7.00—7.67 (m, 5H), 9.42 (d, J=7.0 Hz, 1H); MS:[20] *m/e* (%) 312 (M^+, 13), 277 (7), 230 (7), 197 (8), 157 (40), 123 (73), 113 (60), 95 (60), 81 (60), 77 (100), 67 (60); Found: C, 57.87; H, 6.39%. Calcd for $C_{15}H_{20}O_2Se$: C, 57.88; H, 6.48%.

2-Phenylseleno-2-decenal (17). To a suspension of potassium fluoride (102 mg, 1.77 mmol) in 1 ml of benzene were added a solution of 3-*t*-butyldimethylsiloxy-2-phenylselenodecanal (78 mg, 0.177 mmol) in 2 ml of benzene and 18-crown-6 (4.7 mg, 0.018 mmol) in 1 ml of benzene. After stirring for 12 h at room temperature, the reaction mixture was washed with satd aq NaCl and the aqueous layer was extracted with ether. Drying and concentration of the combined extracts followed by purification by silica gel column chromatography (SiO_2 deactivated with 20% water) afforded the title compound (38 mg, 71%) as an oil. Bp 115—118 °C/0.37 mmHg;[19] IR (neat): 1685 cm^{-1}; NMR (CCl_4): δ 0.67—1.80 (m, 13H), 2.26—2.83 (m, 2H), 6.83—7.50 (m, 6H), 9.20 (s, 1H); MS:[20] 310 (M^+, 5), 187 (5), 157 (20), 115 (23), 91 (28), 81 (45), 78 (50), 77 (60), 67 (65), 55 (100).

3-Butyl-2-phenylseleno-2-heptenal (18). To a suspension of silica gel (2 g) in 10 ml of carbon tetrachloride was added a solution of 3-butyl-3-methoxy-2-phenylselenoheptanal (196 mg, 0.55 mmol) in 2 ml of carbon tetrachloride. After stirring for 2 h under refluxing, the reaction mixture was filtered. Concentration followed by purification by silica gel column chromatography (SiO_2 deactivated with 20%

water) gave the title compound (150 mg, 84%). Bp 95—100 °C/0.01 mmHg;[19] IR (neat): 1680 cm^{-1}; NMR (CCl_4): δ 0.50—1.90 (m, 14H), 2.30—2.90 (m, 4H), 7.00—7.33 (m, 5H), 9.53 (s, 1H); MS:[20] *m/e* (%) 324 (M^+, 4), 314 (8), 234 (4), 167 (10), 166 (10), 157 (19), 139 (17), 132 (56), 123 (13), 111 (40), 97 (25), 95 (77), 91 (13), 83 (33), 81 (40), 77 (40), 69 (33), 55 (100); Found: C, 60.56; H, 7.81%. Calcd for $C_{17}H_{24}OSe$: C, 60.84; H, 7.94%.

*3-t-Butyldimethylsiloxycyclohexanone (**19**).* To a solution of sodium hydride (55% in mineral oil, 18 mg, washed twice with hexane) in 1 ml of THF was added a solution of benzenethiol (90 mg, 0.8 mmol) in 1 ml of THF at room temperature, and the mixture was stirred for 5 min. Then a solution of 3-*t*-butyldimethylsiloxy-2-phenylselenocyclohexanone (76 mg, 0.2 mmol) and a trace amount of 18-crown-6 in 2 ml of THF was added to the resulting solution. After allowed to stand for 6 h at room temperature, the mixture was washed with satd aq NaCl, and the aqueous layer was extracted with ether. The combined extracts were dried and concentrated to give an oil, which was purified by silica gel column chromatography to afford the title compound **19** (41 mg, 88%). IR (neat): 1705 cm^{-1}; NMR (CCl_4): δ 0.11 (s, 6H), 0.92 (s, 9H), 1.22—2.41 (m, 8H), 3.91—4.20 (m, 1H); Found: C, 63.24; H, 10.37%. Calcd for $C_{12}H_{24}O_2Si$: C, 63.10; H, 10.59%.

1-Phenyl-5-hexen-3-ol was prepared by the reaction of 3-phenylpropanal with allylmagnesium bromide. 3-Penten-1-ol was prepared by treating 1-bromo-3-pentene with aq sodium acetate and then with aq sodium hydroxide. 4-Propyl-6-octen-4-ol was preapared by treating ethyl 3-pentenoate with 2.2 eq of propylmagnesium bromide in ether.

*4-t-Butyldimethylsiloxy-6-phenyl-2-phenylselenohexanal (**20a**).* IR (neat): 1700 cm^{-1}; NMR (CCl_4): δ 0.11 (s, 6H), 0.98 (s, 9H), 1.46—2.33 (m, 4H), 2.51—2.88 (m, 2H), 3.30—3.61 (m, 1H), 4.08—4.30 (m, 1H), 7.02—7.48 (m, 10H), 8.30 (d, J=2.0 Hz, C<u>H</u>=O), 8.80 (d, J=2.0 Hz, C<u>H</u>=O); Found: C, 62.71; H, 7.58%. Calcd for $C_{24}H_{34}O_2SeSi$: C, 62.45; H, 7.42%.

*4-t-Butyldimethylsiloxy-6-phenyl-1-phenylseleno-2-hexanone (**21a**).* IR (neat): 1700 cm^{-1}; NMR (CCl_4): δ 0.12 (s, 6H), 0.97 (s, 9H), 1.41—2.31 (m, 4H), 2.31—2.85 (m, 2H), 3.17 (s, 2H), 3.72—4.01 (m, 1H), 7.01—7.55 (m, 10H); Found: C, 62.57; H, 7.63%. Calcd for $C_{24}H_{34}O_2SeSi$: C, 62.45; H, 7.42%.

*4-t-Butyldimethylsiloxy-6-phenyl-2-mesitylselenohexanal (**20b**).* IR (neat): 1700 cm^{-1}; NMR (CCl_4): δ 0.12 (s, 6H), 0.92 (s, 9H), 1.44—1.78 (m, 4H), 2.00—2.75 (m, 2H), 2.28 (s, 3H), 2.45 (s, 6H), 3.31—3.52 (m, 1H), 4.05—4.31 (m, 1H), 6.86 (s, 2H), 7.00—7.40 (m, 5H), 8.31 (d, J=3.0 Hz, C<u>H</u>=O), 8.78 (d, J=3.0 Hz, C<u>H</u>=O); Found: C, 64.51; H, 8.19%. Calcd for $C_{27}H_{40}O_2SeSi$: C, 64.39; H, 8.01%.

*4-t-Butyldimethylsiloxy-6-phenyl-1-mesitylseleno-2-hexanone (**21b**).* IR (neat): 1700 cm^{-1}; NMR (CCl_4): δ 0.13 (s, 6H), 0.92 (s, 9H), 1.42—1.75 (m, 4H), 2.00—2.85 (m, 2H), 2.27 (s, 3H), 2.43 (s, 6H), 2.98 (s, 2H), 4.01—4.30 (m, 1H), 6.83 (s, 2H), 7.00—7.40 (m, 5H); Found: C, 64.60; H, 8.23%. Calcd for $C_{27}H_{40}O_2SeSi$: C, 64.39; H, 8.01%.

*6-Phenyl-4-triphenylsiloxy-2-phenylselenohexanal (**20c**).* IR (neat): 1705 cm^{-1}; NMR (CCl_4): δ 1.62—2.38 (m, 4H), 2.42—2.83 (m, 2H), 3.41—3.73 (m, 1H), 4.08—4.31 (m, 1H), 6.67—7.74 (m, 25H), 8.53 (d, J=3.0 Hz, C<u>H</u>=O), 8.80 (d, J=3.0 Hz, C<u>H</u>=O); Found: C, 71.52; H, 5.80%. Calcd for $C_{36}H_{34}O_2SeSi$: C, 71.38; H, 5.66%.

*6-Phenyl-4-triphenylsiloxy-1-phenylseleno-2-hexanone (**21c**).* IR (neat): 1710 cm^{-1}; NMR (CCl_4): δ 1.50—2.35 (m, 4H), 2.41—2.80 (m, 2H), 3.19 (s, 2H), 4.01—4.32 (m, 1H), 6.62—7.75 (m, 25H); Found: C, 71.59; H, 5.76%. Calcd for $C_{36}H_{34}O_2SeSi$: C, 71.38; H, 5.66%.

*2-Mesitylseleno-6-phenyl-4-triphenylsiloxyhexanal (**20d**).* IR (neat): 1700 cm^{-1}; NMR (CCl_4): δ 1.53—2.15 (m, 4H), 2.17—2.70 (m, 2H), 2.27 (s, 3H), 2.47 (s, 6H), 3.41—3.62 (m, 1H), 4.07—4.30 (m, 1H), 6.67—7.64 (m, 20H), 6.85 (s, 2H), 8.56 (d, J=3.0 Hz, C<u>H</u>=O), 8.83 (d. J=3.0 Hz, C<u>H</u>=O); Found: C, 72.53; H, 6.47%. Calcd for $C_{39}H_{40}O_2SeSi$: C, 72.31; H, 6.22%.

*1-Mesitylseleno-6-phenyl-4-triphenylsiloxy-2-hexanone (**21d**).* IR (neat): 1700 cm^{-1}; NMR (CCl_4): δ 1.57—2.16 (m, 4H), 2.21—2.72 (m, 2H), 2.28 (s, 3H), 2.48 (s, 6H), 3.05 (s, 2H), 4.06—4.32 (m, 1H), 6.68—7.64 (m, 20H), 6.86 (s, 2H); Found: C, 72.18; H, 6.09%. Calcd for $C_{39}H_{40}O_2SeSi$: C, 72.31; H, 6.22%.

*5-t-Butyldimethylsiloxy-3-phenylseleno-2-pentanone (**22a**).* IR (neat): 1700 cm^{-1}; NMR (CCl_4): δ 0.11 (s, 6H), 0.92 (s, 9H), 1.62—2.01 (m, 2H), 2.31 (s, 3H), 3.51—3.93 (m, 3H), 7.01—7.54 (m, 5H); Found: C, 54.91; H, 7.52%. Calcd for $C_{17}H_{28}O_2SeSi$: C, 54.97; H, 7.60%.

*5-t-Butyldimethylsiloxy-2-phenylseleno-3-pentanone (**23a**).* IR (neat): 1700 cm^{-1}; NMR (CCl_4): δ 0.11 (s, 6H), 0.92 (s, 9H), 1.45 (d, J=8.0 Hz, 3H), 2.62 (t, J=8.0 Hz, 1H), 2.67 (t, J=6.0 Hz, 2H), 3.40—3.90 (m, 2H), 7.00—7.50 (m, 5H); Found: C, 54.85; H, 7.54%. Calcd for $C_{17}H_{28}O_2SeSi$: C, 54.97; H, 7.60%.

*5-t-Butyldimethylsiloxy-3-mesitylseleno-2-pentanone (**22b**).* IR (neat): 1705 cm^{-1}; NMR (CCl_4): δ 0.11 (s, 6H), 0.92 (s, 9H), 1.05—1.35 (m, 2H), 2.01 (s, 3H), 2.32 (s, 3H), 2.71 (s, 6H), 3.10—3.90 (m, 3H), 6.85 (s, 2H); Found: C, 58.21; H, 8.12%. Calcd for $C_{20}H_{34}O_2SeSi$: C, 58.09; H, 8.29%.

*5-t-Butyldimethylsiloxy-2-mesitylseleno-3-pentanone (**23b**).* IR (neat): 1700 cm^{-1}; NMR (CCl_4): δ 0.11 (s, 6H), 0.92 (s, 9H), 1.38 (d, J=6.0 Hz, 3H), 2.21—2.41 (m, 2H), 2.25 (s, 3H), 2.50 (s, 6H), 3.42 (q, J=6.0 Hz, 1H), 3.51—3.87 (m, 2H), 6.85 (s, 2H); Found: C, 58.35; H, 8.08%. Calcd for $C_{20}H_{34}O_2SeSi$: C, 58.09; H, 8.08%.

*5-t-Butyldimethylsiloxy-3-(p-chlorophenylseleno)-2-pentanone (**22c**).* IR (neat): 1705 cm^{-1}; NMR (CCl_4): δ 0.11 (s, 6H), 0.92 (s, 9H), 1.74—2.03 (m, 2H), 2.28 (s, 3H), 3.52—4.03 (m, 3H), 7.01—7.45 (m, 4H); Found: C, 50.28; H, 6.79%. Calcd for $C_{17}H_{27}O_2ClSeSi$: C, 50.30; H, 6.70%.

*5-t-Butyldimethylsiloxy-2-(p-chlorophenylseleno)-3-pentanone (**23c**).* IR (neat): 1705 cm^{-1}; NMR (CCl_4): δ 0.11 (s, 6H), 0.92 (s, 9H), 1.31 (d, J=6.0 Hz, 3H), 2.72 (t, J=6.0 Hz, 2H), 3.53—4.05 (m, 3H), 7.00—7.30 (m, 4H); Found: C, 50.20; H, 6.69%. Calcd for $C_{17}H_{27}O_2ClSeSi$: C, 50.30; H, 6.70%.

*5-Methoxy-5-propyl-3-phenylseleno-2-octanone (**24a**).* IR (neat): 1700 cm^{-1}; NMR (CCl_4): δ 0.70—1.61 (m, 16H), 2.13 (s, 3H), 2.92 (s, 3H), 3.57—3.90 (m, 1H), 7.00—7.61 (m, 5H); Found: C, 61.02; H, 8.06%. Calcd for $C_{18}H_{28}O_2Se$: C, 60.84; H, 7.94%.

*5-Methoxy-5-propyl-2-phenylseleno-3-octanone (**25a**).* IR (neat): 1705 cm^{-1}; NMR (CCl_4): δ 0.75—1.65 (m, 17H), 1.92 (s, 2H), 2.95 (s, 3H), 3.82—4.10 (m, 1H), 7.02—7.61 (m, 5H); Found: C, 61.13; H, 8.11%. Calcd for $C_{18}H_{28}O_2Se$: C, 60.84; H, 7.94%.

*5-Benzyloxy-3-phenylseleno-5-propyl-2-octanone (**24b**).* IR (neat): 1705 cm^{-1}; NMR (CCl_4): δ 0.73—1.68 (m, 16H), 2.15 (s, 3H), 3.72—4.01 (m, 1H), 4.31 (s, 2H), 7.01—7.58 (m, 10H); Found: C, 67.02; H, 7.68%. Calcd for $C_{24}H_{32}O_2Se$: C, 66.81; H, 7.48%.

*5-Benzyloxy-2-phenylseleno-5-propyl-3-octanone (**25b**).* IR (neat): 1700 cm^{-1}; NMR (CCl_4): δ 0.78—1.72 (m, 17H), 1.85 (s, 2H), 3.72—3.95 (m, 1H), 4.34 (s, 2H), 7.01—7.55 (m, 10H); Found; C, 66.95; H, 7.56%. Calcd for C_{24}-

$H_{32}O_2Se$: C, 66.81; H, 7.48%.

2-Phenylseleno-4-triphenylsiloxycyclopentanone (27). IR (neat): 1740 cm^{-1}; NMR (CCl_4): δ 2.39—2.53 (m, 4H), 3.29—3.60 (m, 1H), 4.54 (t, J=5.0 Hz, 1H), 7.07—7.62 (m, 20H).

4-Triphenylsiloxy-2-cyclopentenone (28). To a solution of 2-phenylseleno-4-triphenylsiloxycyclopentanone (155 mg, 0.3 mmol) and pyridine (0.07 ml, 0.72 mmol) in 1 ml of dichloromethane were added 30% hydrogen peroxide (0.28 ml, 2.6 mmol) and water (0.28 ml) at 0 °C. After stirring at 0 °C for 30 min, the reaction mixture was washed with 7% $NaHCO_3$ and then with 4% HCl. Drying and concentration of the extracts followed by purification with preparative TLC gave the title compound (99 mg, 92%) as an oil. IR (neat): 1680 cm^{-1}; NMR (CCl_4): δ 2.21—2.40 (m, 2H), 3.74—4.00 (m, 1H), 4.83—5.11 (m, 1H), 5.80—6.00 (m, 1H), 7.00—7.66 (m, 15H); Found: C, 77.32; H, 5.40%. Calcd for $C_{23}H_{20}SiO_2$: C, 77.49; H, 5.65%.

Oxidation of Substituted Cyclohexenes. Oxidation of these compounds was performed in a similar manner with that of 4-alkoxy-6-phenyl-2-hexene in refluxing benzene for 3—5 h. The reaction mixtures were treated with benzenethiolate anion as described above, and the resulting deselenenylated products were identified by comparison with the authentic samples. Ratios of the regio-isomers were also determined with the deselenenylated products by GLPC analyses.

References

1) Preliminary reports dealing with certain aspects of this work: M. Shimizu, R. Takeda, and I. Kuwajima, *Tetrahedron Lett.*, **1979**, 419, 3461.

2) K. B. Sharpless, R. F. Lauer, D. W. Patrick, S. P. Singer, and M. W. Young, *Chem. Scr.*, **8A**, 9 (1975); D. L. J. Clive, *Tetrahedron*, **34**, 1049 (1978); D. L. J. Clive, *Aldrichim. Acta*, **11**, 43 (1978); H, J. Reich, *Acc. Chem. Res.*, **12**, 22 (1979).

3) D. Seebach and N. Peleties, *Angew. Chem.*, **81**, 465 (1969); D. Seebach and N. Peleties, *Chem. Ber.*, **105**, 511 (1972); D. Seebach and A. K. Beck, *Angew. Chem. Int. Ed. Engl.*, **13**, 806 (1974); D. Seebach, N. Meyer, and A. K. Beck, *Justus Liebigs Ann. Chem.*, **1977**, 846; B, T. Grobel and D. Seebach, *Chem. Ber.*, **110**, 867 (1977); W. Dumont, P. Bayet, and A. Krief, *Angew. Chem. Int. Ed. Engl.*, **13**, 804 (1974); D, Labar, W. Dumont, L. Hevesi, and A. Krief, *Tetrahedron Lett.*, **1978**, 1145; H. J. Reich, F. Chow, and S. K. Shah, *J. Am. Chem. Soc.*, **101**, 6638 (1979), and references cited therein.

4) K. C. Nicolaou and Z. Lysenko, *J. Am. Chem. Soc.*, **99**, 3185 (1977); D. L. J. Clive, G. Chittattu, and C. K. Wong, *J. Chem. Soc., Chem. Commun.*, **1978**, 41; K. C. Nicolaou, D. A. Claremon, W. E. Barnette, and S. P. Seitz, *J. Am. Chem. Soc.*, **101**, 3704 (1979); K. C. Nicolaou, S. P. Seitz, W. J. Sipio, and J. F. Blount, *ibid.*, **101**, 3884 (1979); D. L. J. Clive, G. J. Chittattu, V. Farina, W. A. Kiel, S. M. Menchen, C. G. Russel, A. Singh, C. K. Wong, and N. J. Curtis, *ibid.*, **102**, 4338 (1980).

5) I. Kuwajima and M. Shimizu, *Tetrahedron Lett.*, **1978**, 1277; M. Shimizu and I. Kuwajima, *Bull. Chem. Soc. Jpn.*, **54**, 3100 (1981).

6) T. Takahashi, H. Nagashima, and J. Tsuji, *Tetrahedron Lett.*, **1978**, 799; S. Raucher, *ibid.*, **1978**, 2261.

7) R. A. Gancarz and J. L. Kice, *Tetrahedron Lett.*, **22**, 1661 (1981).

8) S. Current and K. B. Sharpless, *Tetrahedron Lett.*, **1978**, 5075.

9) M. Shimizu and I. Kuwajima, *Tetrahedron Lett.*, **1979**, 2801.

10) See, for example, A. Hassner and F. W. Fowler, *J. Org. Chem.*, **33**, 2686 (1968); D. R. Dalton, V. P. Dutta, and D. C. Jones, *J. Am. Chem. Soc.*, **90**, 5498 (1968).

11) Fluoride anion has been proved to be a relatively weak base; I. Kuwajima, T. Murofushi, and E. Nakamura, *Synthesis*, **1976**, 602.

12) J. Remion, W. Dumont, and A. Krief, *Tetrahedron Lett.*, **1976**, 1385; J. Remion and A. Krief, *ibid.*, **1976**, 3743.

13) Deselenenylation of α-phenylseleno ketones was briefly described; H. J. Reich, J. M. Renga, and I. L. Reich, *J. Am. Chem. Soc.*, **97**, 5434 (1975).

14) A. Mitra, "The Synthesis of Prostaglandins," John Wiley and Sons, New York, N. Y. (1977), pp. 247—277.

15) T. Hori and K. B. Sharpless, *J. Org. Chem.*, **43**, 1689 (1978).

16) H. J. Reich, S. Wollowitz, J. F. Trend, F. Chow, and D. F. Wendelborn, *J. Org. Chem.*, **43**, 1697 (1978), and Ref. 13.

17) G. Ayrey, D. Barnard, and D. T. Woodbridge, *J. Chem. Soc.*, **1962**, 2089.

18) E. J. Corey and A. Venkateswarlu, *J. Am. Chem. Soc.*, **94**, 6190 (1972).

19) 1 mmHg=133.322 Pa.

20) Selenium-containing compounds exhibit the characteristic isotopic family in their mass spectra, ^{74}Se (1), ^{76}Se (10), ^{77}Se (9), ^{78}Se (27), ^{80}Se (57), ^{82}Se (11), but only the peaks due to the most abundant isotope (^{80}Se) are described.

  Bull. Chem. Soc. Jpn., 54, 3518—3521 (1981) [Vol. 54, No. 11

Synthesis and Kinetic Investigation of the Atropisomerization of *meso*-Tetra(2-cyanophenyl)porphine

Keiichiro HATANO,* Kazunori ANZAI, Tadashi KUBO, and Shoko TAMAI

Department of Pharmaceutical Sciences, Nagoya City University, Mizuho-ku, Nagoya 467

(Received May 7, 1981)

Tetra(2-cyanophenyl)porphine (ToCNPP) has been synthesized and isolated into the four respective atropisomers. The rotation of a cyanophenyl ring about the bond to the methine carbon of the porphyrin leads to interconversion reactions among the isomers. The isomerization reactions have been studied kinetically by the separation and quantitative measurement of each isomer on thin layer chromatography plates. The results show that the free energy of activation for the hindered rotation is an average of $\Delta G^* = 110$ kJ/mol at 50 °C. This is the highest barrier ever measured in similar porphyrin atropisomers. The apparent interaction between adjacent cyano groups is observed. The energy of interaction is estimated to be about 2.0 kJ per mole unit of interaction.

Rotational isomerism of some tetraarylporphyrins and their metal derivatives have been investigated by several groups of workers.[1-5] The principal features of the atropisomerism, *i.e.*, tautomerism and statistical distribution of isomers, have been known since the resolution and isomerization of tetra(2-hydroxyphenyl)porphine (ToOHPP) was communicated twelve years ago.[1] Many nuclear magnetic resonance (NMR) studies have also ratified the features.[2-4]

On the other hand, the isolation of a particular $\alpha,\alpha,\alpha,\alpha$ atropisomer of tetra(2-aminophenyl)porphine ($ToNH_2PP$) brought great advances in studies of synthetic models of the hemeproteins, such as the "picket fence" porphyrins.[6-8] We are interested in the steric control of ligand coordination and redox reactions of the central metal ions of metalloporphyrins[9] in connection with the catalytic selectivity and activity of various heme enzymes. Tetra(2-cyanophenyl)porphine (ToCNPP) is expected to be a good and new source for the synthetic models as well as $ToNH_2PP$.

In the course of our study to synthesize and isolate the desired isomer, $\alpha,\alpha,\alpha,\alpha$-isomer, of ToCNPP, we have found a new, but unfavorable for this isomer, effect of the cyano substituents on the atropisomerism. There is a steric repulsion between the CN groups through the space above the porphyrin plane, that disturbs the statistical distribution of isomers, especially, low yields of the $\alpha,\alpha,\alpha,\alpha$-isomer. This is the first report describing the kinetic analysis of the steric interaction as well as the synthesis and rotational isomerization of ToCNPP.

Experimental

Materials. A typical procedure to synthesize ToCNPP is as follows: 2-Cyanobenzaldehyde (10 g, 76 mmol) and pyrrole (5.3 ml, 76 mmol) in a mixture of acetic acid and pyridine (4:1 in volume, total 400 ml) were refluxed for 2 h. After the reaction mixture was cooled down to room temperature, twice the volume of methanol was added and the solution was allowed to stand for at least 2 d. Crystalline products precipitated in the solution were separated by filtration, washed with methanol, and dried in an oven at 50 to 70 °C. It was further purified by chloroform extraction using a Soxhlet extractor. The resulting purple crystals in the solution were collected by filtration (yield: *ca.* 0.4 g, 3%). Found: C, 80.22; H, 3.25; N, 15.11%. Calcd for $C_{48}H_{26}N_8$: C, 80.66; H, 3.67; N, 15.68%. IR (KBr) cm^{-1}: $\nu_{C\equiv N}$ 2230. UV ($CHCl_3$) λ_{max} nm ($\varepsilon \times 10^{-4}$): 419 (37.4), 512 (2.12), 544 (0.72), 587 (1.04), 644 (0.57). Mp >300 °C.

Since ToCNPP is a mixture of four atropisomers, each component was separated by column chromatography using silica gel 100 (70—230 mesh, Merck) and dry chloroform. The chloroform solution of each isomer was evaporated *in vacuo* immediately after elution from the column. Before kinetic experiments, the atropisomers were purified further by preparative thin layer chromatography (TLC) (silica gel 60, 0.5 mm thick, Merck).

All reagents and solvents of reagent grade were used without further purification except chloroform which was washed with water, dried over CaH_2, and distilled.

Measurement of the Isomerization Rates. A chloroform solution of each atropisomer (*ca.* 5 mg/20 ml) in a flask was placed in a water bath kept at 50 or 60 °C. A few microliters of the solution was sampled with a glass capillary at appropriate intervals, and spotted on a TLC plate (silica gel 60, 0.25 mm thick, Merck). The rotational isomerization reaction of an isomer to the additional three components was monitored by measurements of the quantity of respective isomers which were separated with 98:2 chloroform–acetone on a TLC plate. The quantity was measured by spectrometry after the extraction of each isomer from the TLC plate with chloroform. The mole fractions of minor components determined by this method have relatively larger errors than the fraction of major ones. Under the present reaction conditions, no product other than the isomers was detected by TLC even after the reaction for 3 d.

Processing of the Data. The digital integration of the differential rate equations,

$$d[A_i]/dt = \sum_j \sum_l k_j[A_l],$$

where k_j is the first-order rate constant for the j th reaction concerning the A_i species, was performed at small increments of time by a local Fortran program using the Runge-Kutta approximation.[10] An initial set of inputs, *i.e.*, rate constants and concentrations of isomers, was the experimental data obtained by the usual graphic method adapted to the initial stage of the reactions. The rate constants were refined by trial and error to fit the computed values to the experimental values of all isomers for the entire time course of the reaction.

The general structural parameters of the porphyrin skeleton[11] and atomic coordinates of cyano(*meso*-tetraphenylporphinato)manganese(III)[12] in the crystal were tentatively used for calculating the distances between atoms and for drawing.[13] The positions of the CN substituents were determined by assuming that the carbon and nitrogen atoms were on the linear extension from the center of phenyl ring to the ortho carbon with distances of C_{ortho}–C=1.5 Å and

C–N=1.15 Å. All calculations were carried out at the computing center of this university using a NEAC system 700S computer.

Results and Discussion

The Synthesis of ToCNPP. Two solvent systems have been proposed for the general syntheses of *meso*-tetraarylporphyrins in solution[14,15] besides Rothemund's original method and its applications.[16–18] Utilization of propionic acid, as proposed by Adler *et al.*,[14] to make ToCNPP has resulted in a large amount of tarry and black by-products which hamper the purification of the porphyrin in gram-quantities. On the other hand, Treib's procedure,[15] using 1:2 pyridine–acetic acid, for this porphyrin gave no precipitate even though the reaction mixture was allowed to stand for 2 d in a refrigerator.

The precipitation of crystalline products of reasonable purity and high yield from a simple reaction batch is considered to be the most important merit of the preparative procedure. We have determined the optimal conditions for preparing ToCNPP by varing the ratio of pyridine to acetic acid and by following the time course of the formation. The product yields obtained *in situ* by spectrometric methods increase from 4 to 8% by increasing the pyridine ratio from 10 to 33 v/v%. ToCNPP is found to be appreciably soluble in pyridine but much less soluble than the by-products, while ToCNPP is insoluble in acetic acid. Thus, the purest porphyrin products and highest isolated yield of a batch process have been obtained in 20% pyridine as described in Experimental. The total spectrometric yield reaches 7 to 8% level, but the complete isolation of the porphyrin is very difficult. The formation of ToCNPP in the boiling solution seems finished within 30 min and longer reaction time do not improve the yield.

The pyridine–acetic acid solvent system is also found to improve the isolation of crystalline tetra(2-nitrophenyl)- and tetra(2,6-dichlorophenyl)porphines from the single batch compared to the literature methods.[6,19]

Separation and Identification of the Atropisomers. The TLC of the reaction products show three distinct spots with R_f values of 0.47, 0.41, and 0.23 together with several minor spots at 0 to 0.2 when it is developed with 98:2 chloroform–acetone. The three materials extracted from the main spots display identical electronic absorption spectra with characteristic porphyrin maxima[19] and a common IR spectrum with a single C≡N stretching band. Each of the three compounds mutually interconverts in chloroform solution, and a new species at R_f=0.04 on TLC is generated in the interconversion. Thus the four spots on TLC correspond to the four atropisomers of ToCNPP. The distribution of the four isomers, equilibrated at 50 °C for 3 d, is 39 (±4), 24 (±3), 35 (±3), and 2 (±1)%, in the order of decreasing R_f values.

The compound with the smallest R_f value and mole fraction is easily assigned to α,α,α,α-isomer (iv) by consideration of the molecular polarity seen on TLC and the steric hindrance to assembling four cyano groups on the same side of the porphyrin plane. The kinetic studies mentioned below distinguish the α,α,α,β-isomer (iii) from the others as it is the only primary product of the isomerization of every isomer. We have tentatively identified the first and second eluents of chromatography to the α,β,α,β- (i) and α,α,β,β- (ii) isomers, respectively, based on the polarity on TLC. This assignment of the four atropisomers is consistent concerning the order of R_f values on TLC with that of $ToNH_2PP$ reported by Collman *et al.*[6] The crystal structure of ii may be analysed for a definitive assignment elsewhere.

The proton NMR spectra of the isomers have been poorly characterized owing to the complex multiplicity of the phenyl protons and low solubility in NMR solvents at room temperature.

The Kinetic Studies of the Isomerization. Rotation of any one of the four phenyl rings of ToCNPP about the bond to the porphyrin skeleton leads to the stereochemical isomerizations as shown in Fig. 1. Two or more rings can rotate simultaneously, but this can be ignored in the kinetic analysis as a secondary perturbation of small statistical probability. Intramolecular isomerization reactions are generally first-order reactions. The present case is also found to be first-order from the analysis. The designation of the rate constants for the six isomerization reactions is displayed in Fig. 1.

The equilibrium constants defined by $K_m=k_j/k_{j+1}$ are conveniently determined by the distribution of four isomers at 50 °C mentioned above, and the values obtained at 40 and 60 °C are invariant within experimental error. Each of the purified isomers were subjected to the rate determinations.

The refined rate constants are listed in Table 1 and the computer simulations of them are reasonable matches for all experiments at 50 and 60 °C. Two examples are displayed in Figs. 2a) and 2b). The solid lines in the figures are the computer simulations. The rate constants are also consistent with the equilibrium constants obtained experimentally.

The activation energies determined by the Arrhenius equation are found to spread over 84 to 94 kJ/mol for the six reactions, hence, they are averaged into an E_a which is reported in Table 2.

The Rotational and Steric Effects of the Cyano Substituent. The free energy of activation (ΔG^*) is considered to reflect the height of the rotational barrier principally generated by the friction between an ortho substituent and a pyrrole proton of the porphyrin. Our result, a weighted average value $\Delta G^*=110$ kJ/mol given by the Eyring equation at 50 °C, can be compared with the published kinetic data[1–4] for ortho substituted tetraphenylporphyrins. The comparison of ΔG^* should be done at the same temperature. However, since the entropy of activation or the substitute for it is unavailable, we must adapt our data to the extensions of temperatures by assuming that the activation energy (E_a) is employable over the temperature range of 23 to 180 °C. This assumption is plausible because of the intrinsic independence of E_a with temperature. The ΔG^* values of the present isomerization, calculated at appropriate temperatures, are summarized in Table 2, and compared with the bar-

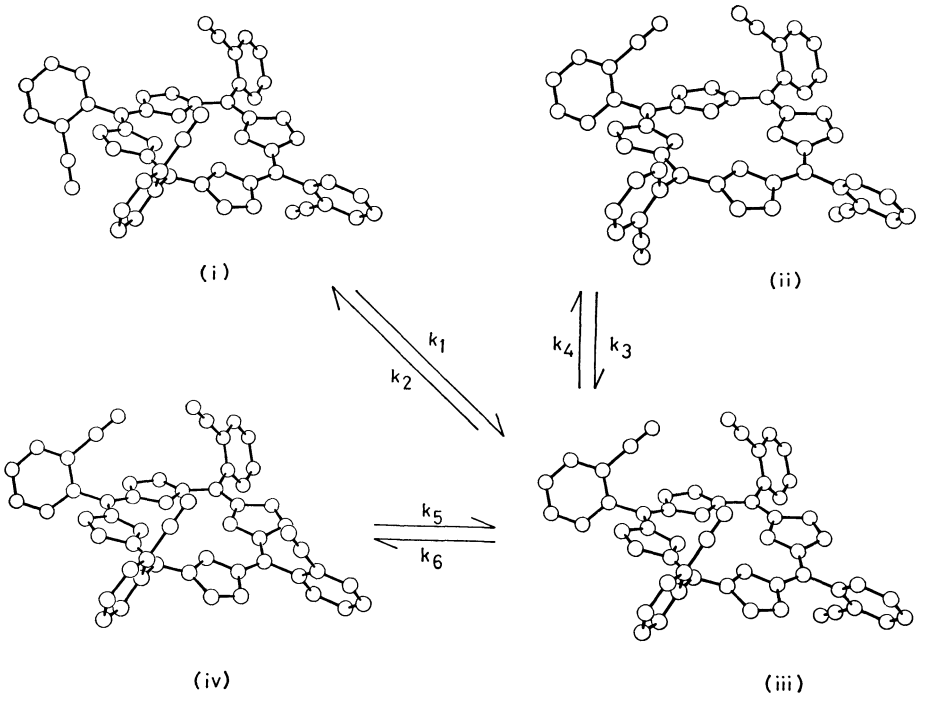

Fig. 1. Schematic representation of the rotational isomerizations of ToCNPP. The k_1 denote the first-order rate constant of the reaction.
(i) α,β,α,β-, (ii) α,α,β,β-, (iii) α,α,α,β-, (iv) α,α,α,α-, conformations.

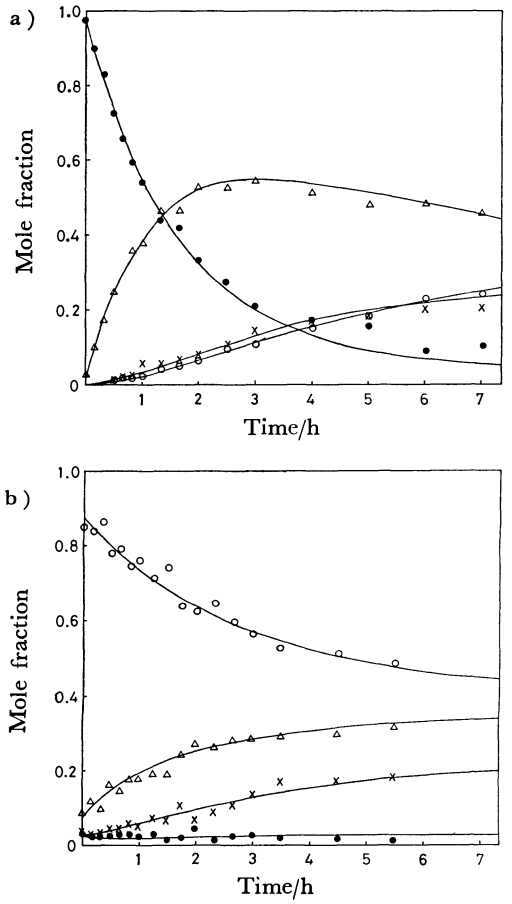

Fig. 2. Time course of isomerization reactions starting from (a) iv at 50 °C and (b) i at 60 °C.
(○) i; (×) ii; (△) iii; (●) iv. The solid lines represent the computer simulations.

TABLE 1. THE FIRST-ORDER RATE CONSTANTS FOR THE ROTATIONAL ISOMERIZATION OF ToCNPP

Temp °C	Rate constants/h^{-1}					
	k_1	k_2	k_3	k_4	k_5	k_6
50	0.089	0.100	0.220	0.135	0.609	0.052
60	0.228	0.256	0.583	0.361	1.730	0.148

riers reported in literature.[1-4]

The order $CN > CH_3 \approx CH_3O \approx OH$ is seen in the barriers. The cyano substituent on the ortho position of a phenyl ring has a higher rotational barrier, as expected by the bulk of the constituted atoms, than OH or CH_3. Moreover, since the CN group is erected linearly from the phenyl ring while CH_3O is bent at the oxygen atom, the awkwardness of CN passing through the porphyrin plane may contribute some kJ/mol to the activation state as compared with the flexible methoxide. The calculated rate constant for the rotation about one cyanophenyl-porphyrin bond at 23 °C is of the order of 10^{-6} s^{-1}. This value allows direct comparison with the only explicit parameter reported for ToOHPP.[1] That the rate in ToCNPP is about a tenth of that in ToOHPP indicates the reasonable substitution effect for CN.

The abundance ratio of the ToCNPP isomers deviates from the statistical expectation. This is the first reported example of the quantitative measurement for a nonstatistical distribution of porphyrin atropisomers. This can be interpreted as the non-bonded interactions of a CN substituent to CN substituent. The small mole fraction of iv indicates the interaction to be repulsive or maybe electrostatic. With consideration of the statistical ratios, the relative free

Table 2. Activation energy and free energy of activation for a phenyl ring rotation, and energy of steric interaction between neighboring substituent groups at ortho position of the phenyl ring in several porphyrins

Substituent group	E_a / kJ mol^{-1}	ΔG^*/kJ mol^{-1}			E_{int}[c] / kJ mol^{-1}	Ref.
		296 K	433 K	453 K		
CN	88.5[a]	108	118	120	2.0	This work
OH	—[b]	100	—	—	0	1
OCH_3	—[b]	—	108	—	0	4
CH_3[d]	—[b]	—	—	>109	0	2

a) Averaged value. b) The data were not shown. c) See text. d) Ni complex.

energy differences of any one of the isomers can be determined by the relationship $\Delta G^\circ = -RT \ln K$. The energy levels of ii, iii, and iv lie at 3.2, 4.0, and 7.9 kJ/mol above the level of i, respectively, based on the experimental data observed at 50 °C. The repulsive forces are thought to be due to the nitrogen atom of CN, because no such effect is reported for OH, NH_2, or CH_3 substituents. The intramolecular atomic distances of the nitrogen to the adjacent or diagonal nitrogen are interesting parameters to evaluate the long range and weak non-bonded interactions. Supposing that the dihedral angles between the porhyrin plane and all phenyl rings are 90° in molecule iv, the distances are estimated to be 6.1 Å between the adjacent nitrogens and 8.6 Å between the diagonal ones. The latter does not seem to be responsible for the interaction as it must be further than the distance between the adjacent nitrogens of NH_2 in α,α,α,α-ToNH$_2$PP. This static model leads to the conclusion that the energy of an interaction between two nitrogens of CN 6.1 Å apart is 2.0 kJ per mole unit of interaction, since iv has four interactions. This value is also consistent with the interactions in iii. The smaller value seen in ii is perhaps the result of lessened contacts between adjacent cyano phenyl rings resulting from tilting a bit more away from each other, but without making any new closer contacts. However, we do not necessarily predict that the dihedral angles between the porphyrin plane and phenyl planes in the crystal of ii are as small as the smallest angles found in metallotetraphenylporphyrins.[20] There are many examples of intermolecular contacts shorter than 6.1 Å, a result of crystal packing effects. We do, however, claim that the long range (6.1 Å) and appreciable (2.0 kJ/mol·interaction) interaction between the CN groups is observed in the atropisomers of ToCNPP. The unfavorable effect on the isolation of α,α,α,α-isomer may be overcome by the utilization of the intermolecular interaction, *e.g.*, adsorbance,[5] selective crystalization and so on.

We thank Prof. W. R. Scheidt for discussion and editorial assistance.

References

1) L. K. Gottwald and E. F. Ullman, *Tetrahedron Lett.*, **36**, 3071 (1969).
2) F. A. Walker and G. L. Avery, *Tetrahedron Lett.*, **52**, 4949 (1971).
3) S. S. Eaton and G. R. Eaton, *J. Am. Chem. Soc.*, **73**, 3660 (1975).
4) J. W. Dirks, G. Underwood, J. C. Matheson, and D. Gust, *J. Org. Chem.*, **44**, 2551 (1979).
5) C. M. Elliot, *Anal. Chem.*, **52**, 666 (1980); J. Lindsey, *J. Org. Chem.*, **45**, 5215 (1980).
6) J. P. Collman, R. R. Gagne, C. A. Reed, T. R. Halbert, G. Lang, and W. T. Robinson, *J. Am. Chem. Soc.*, **97**, 1427 (1975).
7) J. E. Baldwin and J. Huff, *J. Am. Chem. Soc.*, **95**, 5257 (1973); G. B. Jameson and J. A. Ibers, *ibid.*, **102**, 2823 (1980).
8) D. A. Buckingham, M. J. Gunter, and L. N. Mander, *J. Am. Chem. Soc.*, **100**, 2899 (1978); C. M. Elliot, *J. Chem. Soc., Chem. Commun.*, **1978**, 399.
9) K. Hatano, K. Usui, and Y. Ishida, *Bull. Chem. Soc. Jpn.*, **54**, 413 (1981).
10) H. Margenau and G. M. Murphy, "The Mathematics of Physics and Chemistry," D. Van Nostrand Company, Inc. (1943).
11) W. R. Scheidt, "The Porphyrins," ed by D. Dolphin, Academic Press, N. Y. (1978), Vol. III.
12) W. R. Scheidt, K. Anzai, and K. Hatano, unpublished.
13) A. local version of "ORTEP II" (C. K. Johnson) was employed.
14) A. D. Adler, F. R. Longo, J. D. Finarelli, J. Goldmacher, J. Assour, and L. Korsakoff, *J. Org. Chem.*, **32**, 476 (1967).
15) A. Treibs and N. Haberle, *Justus Liebigs Ann. Chem.*, **718**, 183 (1968).
16) P. Rothemund, *J. Am. Chem. Soc.*, **58**, 2010 (1935).
17) D. W. Thomas and A. E. Martell, *J. Am. Chem. Soc.*, **78**, 1335 (1956).
18) G. M. Badger, R. A. Jones, and R. L. Laslett, *Aust. J. Chem.*, **17**, 1028 (1964).
19) J. B. Kim, J. J. Leonard, and F. R. Longo, *J. Am. Chem. Soc.*, **94**, 3986 (1972).
20) W. R. Scheidt, D. A. Summerville, and I. A. Cohen, *J. Am. Chem. Soc.*, **98**, 6623 (1976) reported 54.0°.

Asymmetric Synthesis of Axially Dissymmetric 1,1′-Binaphthyls *via* an Intramolecular Ullmann Coupling Reaction of (*R*)- and (*S*)-2,2′-Bis(1-bromo-2-naphthylcarbonyloxy)-1,1′-binaphthyl[1,2]

Sotaro Miyano,* Masayuki Tobita, and Harukichi Hashimoto
Department of Applied Chemistry, Faculty of Engineering, Tohoku University, Aramaki-Aoba, Sendai 980

(Received May 7, 1981)

An Ullmann reaction of the chiral bifunctional substrate containing two 1-bromo-2-naphthyl moieties, (*S*)-2,2′-bis(1-bromo-2-naphthylcarbonyloxy)-1,1′-binaphthyl, gives an intramolecularly coupled 12-membered cyclic diester in a 36% isolated yield. The intramolecular coupling reaction proceeds with virtually complete diastereoselectivity to induce *S*-chirality into the newly formed bond between the two naphthyl units.

A number of 2,2′-disubstituted 1,1′-binaphthyls have been resolved into atropisomers, and proved to be highly resistant to thermal racemization.[3] The axially dissymmetric binaphthyl structure would be effective for chiral recognition because of its steric bulkiness and structural rigidity.[4,5] Having only the C_2 axis for the element of chirality, and thus minimizing the possibility of complex diastereomeric interactions, the biaryl moiety may also be useful for the elucidation of the mechanism of asymmetric induction. Thus, much attention has recently been centered on asymmetric reactions by the use of axially dissymmetric biaryl derivatives; in some cases a remarkable success has been accomplished.[6,7]

Although there are a number of methods currently available for the synthesis of biaryls,[8] direct routes to their atropisomers are limited:[7a,9] optical resolution of racemates has been adopted in conventional practices for the preparation of the prerequisite atropisomeric binaphthyl skeletons. In 1971, Jacques *et al.*[10] showed that the readily available 1,1′-binaphthyl-2,2′-diol (**1**) can be easily resolved into its antipodes *via* a phosphate ester. We have for some time been trying to utilize the axial dissymmetry of atropisomeric **1** for asymmetric synthesis of other biaryls, and here we wish to describe copper-promoted Ullmann biaryl coupling of 1-bromo-2-naphthoates of **1**.[1]

Results and Discussion

The synthesis of 1-bromo-2-naphthoates of **1** (**3** and **4**, and their atropisomers) is outlined in Scheme 1. 1-Bromo-2-naphthoyl chloride, prepared from 1-bromo-2-naphthoic acid[11] by reaction with thionyl chloride, was allowed to react with **1** in pyridine-benzene to give the corresponding monoester **2** and diester **3**. Each ester product was cleanly separated by column chromatography on alumina; benzene eluted the latter only, while ethanol–benzene could be used to liberate the former. The hydroxy ester (**2**) was in turn treated with 2-naphthoyl chloride to yield the mixed diester **4**. Optically active substrates were synthesized by use of (*S*)- and (*R*)-**1**.

Although the optical yield was poor, the Ullmann coupling reaction of the chiral substrates, (*R*)- and (*S*)-**4**, induced (*R*)- and (*S*)-chirality, respectively, into the newly formed 1,1′-binaphthyl bond, as evidenced as follows: In a typical reaction, (*R*)-**4** was treated with freshly activated copper powder in gently refluxing DMF under nitrogen. Debromination of the substrate ((*R*)-**4**) was completed within 5 h by heating under reflux to give a 15:85 mixture of the reduction ((*R*)-**6**) and the coupled product ((*RRR*)-**5**) in an almost quantitative yield (Scheme 2). Reductive cleavage of the ester linkage of the coupled product ((*RRR*)-**5**) with lithium aluminum hydride (LAH) in boiling ether gave a sample of (*R*)-2,2′-bis(hydroxymethyl)-1,1′-binaphthyl ((*R*)-**7**), which had $[\alpha]_{546}^{23}$ +3.5° (*c* 0.8, acetone). This value corresponds to the optical purity of 4% on the assumption that the enantiomerically pure (*R*)-**7** has the value of $[\alpha]_{546}^{23}$ +86° (*vide infra*). The diol was transformed into (*R*)-α-methoxy-α-trifluoromethylphenylacetic acid ester ((*R*)-MTPA ester);[12] an ^{1}H NMR spectral study of

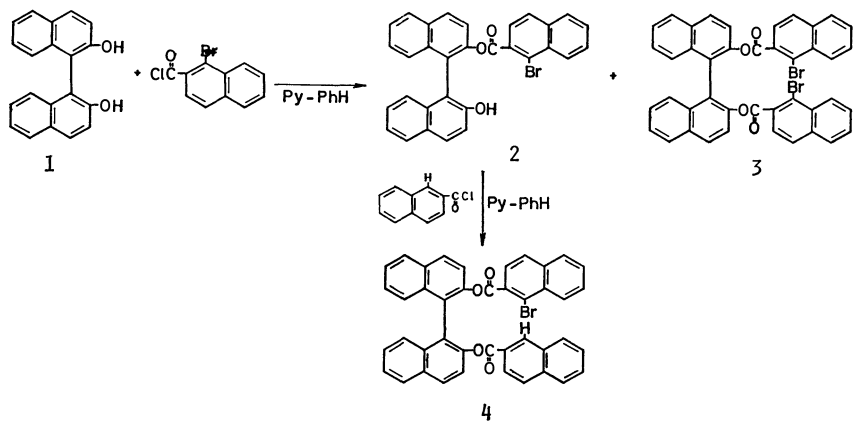

Scheme 1.

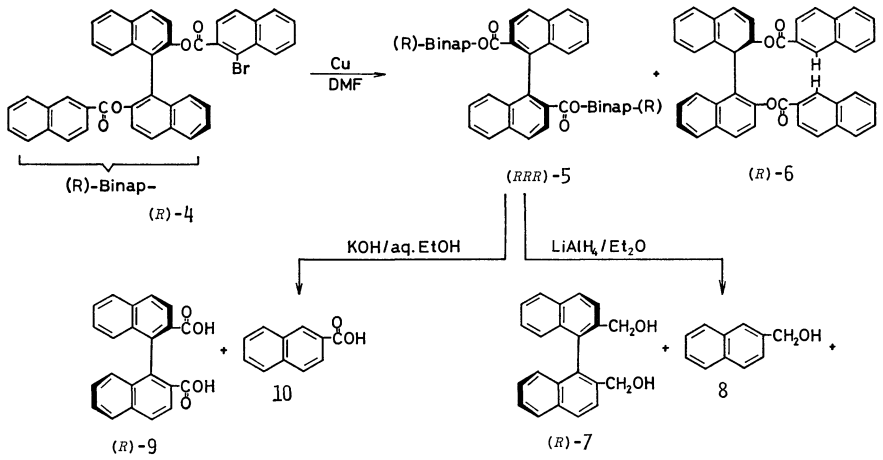

Scheme 2.

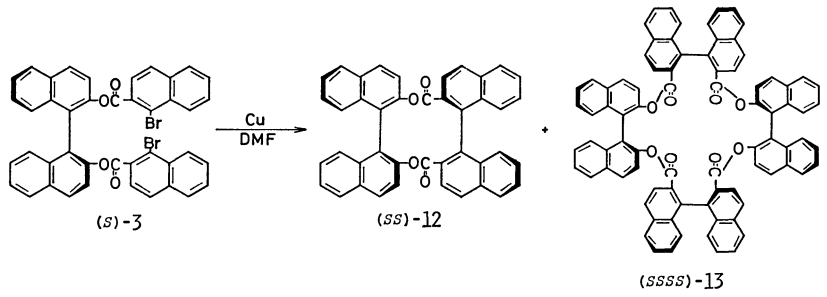

Scheme 3.

the ester in the presence of a chiral shift reagent, Eu(fod)$_3$, also showed the % e.e. of the sample to be 4—6%. Any significant racemization of the substrate ((*R*)-**4**) or products ((*RRR*)-**5** and (*R*)-**6**) under the reaction conditions was ruled out by considering the optical purity of the recovered (*R*)-**1**. Alternatively, (*R*)-1,1′-binaphthyl-2,2′-dicarboxylic acid (*R*)-**9** of 3% optical purity[13] was obtained *via* a hydrolytic treatment of a similar Ullmann product with KOH in boiling aq ethanol.

We have previously shown that an Ullmann coupling of *C*-chiral alcohol esters of 1-bromo-2-naphthoic acid induces axial dissymmetry into the 1,1′-binaphthyl bonds, but that the highest optical yield attained is only 13%.[9a] These and above results may imply that intermolecular Ullmann coupling of chiral substrates of type **11** is discouraging for asymmetric synthesis of binaphthyl atropisomers.

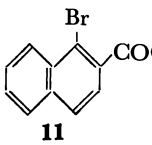

(R*: Chiral substituent)

11

On the other hand, we have found that copper-promoted reaction of bifunctional substrates, (*S*)- and (*R*)-**3**, is promising: Ullmann products from these diesters were hydrolyzed by heating under reflux with KOH in aq ethanol to give **9**'s in *ca.* 45% chemical yields. The apparent net optical yield for the joining of two binaphthyl units was estimated to be 30—45% on the basis of optical rotations of the recovered diacids. It seemed that these rather high asymmetric inductions should be attributed to *intramolecular* interactions of the substrates, as the *intermolecular* coupling of atropisomeric **4** scarcely induced axial dissymmetry.

Thus, we tried an attempt to enhance the unimolecular debromination of the diester, (*S*)-**3**. To a well stirred suspension of copper powder in gently refluxing DMF was slowly added a sample of (*S*)-**3** over 1 h period, and then heating was continued for another 5 h. As judged by TLC and HPLC, however, the intended intramolecular Ullmann coupling of (*S*)-**3** to **12** was accompanied by the formation of serious amounts of reduction product ((*S*)-**6**), dimeric ((*SSS*)-**5** and (*SSSS*)-**13**), and other higher oligomeric products (Scheme 3). It should be pointed out here that careful HPLC analysis, including variation of column and eluant, showed only one peak for the intramolecularly coupled product (**12**).[14] A chromatography of the Ullmann product on a silica-gel column using chloroform (1% ethanol) as the eluant gave a 36% isolated yield of the intramolecularly coupled cyclic diester ((*SS*)-**12**) as a white powder. The compound was characterized by elemental analysis, mass, IR, and other spectral studies as well as chemical transformation. Thus, treatment of the cyclic diester with LAH in ether–THF gave only two diols, (*S*)-**7** and (*S*)-**1**, the specific rotations being $[\alpha]_{546}^{23}$ −86.0° (*c* 1.4, acetone) and $[\alpha]_{D}^{24}$ −34.9°

(c 1.03, THF), respectively. These values compare well with literature ones claimed for enantiomerically pure samples; $[\alpha]_{546}^{23}$ −83.0° for (S)-**7**[11] and $[\alpha]_D^{25}$ −33.3° for (S)-**1**.[6,15] Furthermore, within the limits of the NMR detection at 60 MHz, the (R)-MTPA esters of these diols showed, in the presence of $Eu(fod)_3$, no indication of the presence of (R)-diols.

These observations unequivocally indicate that the two 1,1′-binaphthyl axes in the cyclic diester (**12**) have an *SS*-configuration of high enantiomeric purity. This leads to the conclusion that intramolecular Ullmann coupling of (S)-**3** proceeds, though under rather severe reaction conditions, with a virtually complete diastereoselectivity to give cyclic diester of *SS*-configuration ((*SS*)-**12**). An inspection of CPK models of the cyclic diester **12** suggests that two sets of Naph–COO–Naph moieties of (*SS*)-**12** arrange to a double helix-like structure to accommodate the 12-membered cyclic diester as schematically shown in Fig. 1, while those of (*SR*)-counterpart must be bent to a highly strained right angle in order to form the cycle (Fig. 2), thus strongly favoring the *SS*-configuration over *SR*-isomer. In conclusion, the origin of the remarkable diastereoselectivity in the intramolecular coupling may be attributed to the steric requirements of the product cyclic diester, while at present there is no basis for mechanistic conclusions with regard to the Ullmann reaction.

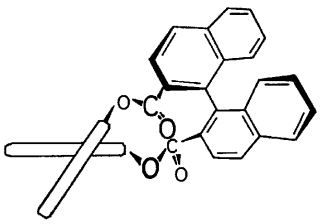

Fig. 1. (*SS*)-**12**.

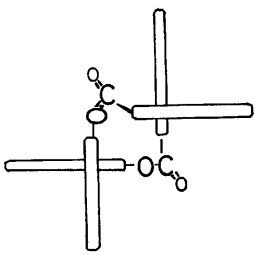

Fig. 2. (*SR*)-**12**.

It is interesting that both of the newly formed 1,1′-binaphthyl bonds in the cyclic dimer ((*SSSS*)-**13**) have also *SS*-chirality of rather high optical purity, though the paucity of the sample has been retarding the elucidation of their accurate structures. Further work along this line is in progress.

Experimental

Measurements. IR spectra were obtained on a Shimadzu IR 430 spectrophotometer. NMR spectra were determined on a Hitachi R-24A instrument using hexamethyldisiloxane as an internal standard in CCl_4 unless otherwise stated. Mass spectra were recorded on a JEOL JMS-D300 double focusing mass spectrometer with direct sample injection. Optical rotations were recorded on a Union PM-101 automatic digital polarimeter in a 1-cm cell at ambient temperature. High performance liquid chromatography (HPLC) was carried out on a JASCO TRIROTAR-III and/or JASCO FAMILIC-100 instrument using columns packed with JASCO SC-01 (ODS), HP-01 (styrene-divinylbenzene), and WC-03 (Carbowax 400) with conventional eluants. Molecular weight was determined in benzene solution with a Hitachi-Perkin-Elmer 115 vapor pressure osmometer. All melting points were corrected.

Materials. Analytical and preparative TLC were carried out on Merck Silica Gel 60H. Solvents for experiments requiring anhydrous conditions were distilled from CaH_2 and stored under nitrogen. 1-Bromo-2-naphthoic acid[11] (mp 188—190 °C), racemic **1**[17] (mp 217—218 °C), and 2-naphthoyl chloride[18] (bp 130—131 °C/400 Pa, mp 51.3—52.3 °C) were prepared according to the reported methods.

1-Bromo-2-naphthoyl Chloride: A mixture of 1-bromo-2-naphthoic acid (5.95 g, 23.7 mmol) and 10 ml† of thionyl chloride was refluxed for 3 h, and the resulting brown-red solution was evaporated to dryness. The residue was dissolved in hot cyclohexane, filtered hot from activated charcoal, and recrystallized to give pale yellow, feather-like crystals: yield, 5.40 g (84.5%); mp 82.5—83.5 °C; IR (KBr) 1780 cm^{-1} (>C=O). Found: C, 49.30; H, 2.10; halogen, 43.07%. Calcd for $C_{11}H_6BrClO$: C, 49.02; H, 2.24; halogen, 42.80%.

Resolution of **1**: The method of Jacques *et al.*[10] and Kyba *et al.*[6] was slightly modified. To a stirred solution of racemic **1** (50 g, 0.175 mol) in CH_2Cl_2 (200 ml) and pyridine (150 ml) was added dropwise 20 ml of $POCl_3$. The mixture was refluxed for 3 h, and then volatiles were evaporated under slightly reduced pressure. The residue was dissolved in a hot Na_2CO_3 (60 g) solution in water (2 l††). An amount of activated charcoal was added, and the mixture was filtered hot. The filtrate was made acidic by addition of 50 ml concd HCl, and the resulting white slurry was stirred overnight at room temperature. The white precipitate was collected and dried in a rotatory evaporator *in vacuo* to give 52.4 g (85.7% yield) of the acid phosphate of **1**. Resolution of the binaphthyl acid phosphate with cinchonine gave, after successive two runs of crystallization from MeOH–H_2O followed by HCl treatment, a 12.0 g sample of (+)-acid (46% yield): $[\alpha]_D^{23}$ +605° and $[\alpha]_{546}^{23}$ +717° (c 1.16, MeOH) (lit,[6] $[\alpha]_{546}^{25}$ +722° (c 0.9, MeOH). The levorotatory acid was recovered from the mother filtrate: 8.3 g (32% yield); $[\alpha]_D^{23}$ −608°; $[\alpha]_{546}^{23}$ −721° (c 0.824, MeOH) (lit,[6] $[\alpha]_{546}^{25}$ −734° (c 0.9, MeOH)). The (+)- and (−)-phosphoric acid were treated with LAH in THF[6] to give (S)-(−)- and (R)-(+)-**1**, respectively.

(S)-1: 8.69 g (88% yield based on the (+)-phosphoric acid); mp 209—210 °C (PhMe); $[\alpha]_D^{23}$ −35.0° (c 1.18, THF).

(R)-1: 5.72 g (84% yield); mp 208—210 °C (PhH); $[\alpha]_D^{23}$ +34.6° (c 0.892, THF).

2-Hydroxy-2′-(1-bromo-2-naphthylcarbonyloxy)-1,1′-binaphthyl (2): To a stirred, water-chilled solution of racemic **1** (1.0 g, 3.49 mmol) in PhH(20 ml)–pyridine(5 ml) was slowly added 0.945 g (3.51 mmol) of 1-bromo-2-naphthoyl chloride. The mixture was stirred overnight at ambient temperature and finally heated under reflux for 3 h. The reaction was quenched with 50 ml of 2 M (1 M=1 mol dm^{-3})

† 1 ml=1 cm^3.

†† 1 l=1 dm^3.

HCl, and extracted with portions of PhH. The combined extracts were washed successively with 2 M HCl, 1 M Na_2CO_3, and then H_2O, and dried over Na_2SO_4. The organic phase was concentrated to a *ca.* 5 ml volume, which was chromatographed on alumina column (Wako-Activated Alumina, 300 mesh). After a small amount of **3** (*vide infra*) was eluted with PhH, 1.32 g of **2** was recovered by use of PhH–EtOH (10:1) eluant (73% yield based on **1**): mp 202—203 °C (PhH); IR (KBr) 3450 (–OH) and 1735 cm^{-1} (>C=O). Found: C, 72.01; H, 3.88; Br, 15.60%. Calcd for $C_{31}H_{19}O_3Br$: C, 71.68; H, 3.69; Br, 15.38%.

Similar reactions of (*S*)- and (*R*)-**1** gave their corresponding atropisomeric **2**.

(S)-**2**: Mp 179—180 °C (PhH); $[\alpha]_D^{22}$ −32.0° (*c* 0.874, acetone); IR (KBr) 3450 (–OH) and 1730 cm^{-1} (>C=O). Found: C, 71.56; H, 3.69; Br, 15.72%.

(R)-**2**: Mp 177—178 °C (PhH); $[\alpha]_D^{23}$ +34.1° (*c* 1.38, acetone).

2,2′-Bis(1-bromo-2-naphthylcarbonyloxy)-1,1′-binaphthyl (**3**): Following the procedure used for the preparation of **2**, a 93% yield of **3** was obtained by the reaction of 2.2 g (8.16 mmol) of 1-bromo-2-naphthoyl chloride and **1** (1.10 g, 3.84 mmol) in PhH(20 ml)–pyridine(5 ml): yield, 2.69 g; mp 226.5—227 °C; IR (KBr) 1745 cm^{-1} (>C=O). Found: C, 67.04; H, 3.34; Br, 21.55%. Calcd for $C_{42}H_{24}O_4Br_2$: C, 67.04; H, 3.21; Br, 21.24%.

(S)-**3**: Mp 180—182 °C; $[\alpha]_D^{22}$ +34.7° (*c* 0.922, acetone); IR (KBr) 1750 cm^{-1} (>C=O). Found: C, 66.81; H, 3.16; Br, 20.84%.

(R)-**3**: Mp 177—180 °C; $[\alpha]_D^{24}$ −33.5° (*c* 1.08, acetone).

2,2′-Bis(2-naphthylcarbonyloxy)-1,1′-binaphthyl (**6**): Mp 211—213 °C; IR (KBr) 1730 cm^{-1} (>C=O). Found: C, 84.73; H, 4.46%. Calcd for $C_{42}H_{26}O_4$: C, 84.83; H, 4.40%.

2-(2-Naphthylcarbonyloxy)-2′-(1-bromo-2-naphthylcarbonyloxy)-1,1′-binaphthyl (**4**): A mixture of 3.71 g (7.14 mmol) of **2** and 1.41 g (7.40 mmol) of 2-naphthoyl chloride in PhH-(40 ml)–pyridine(5 ml) was stirred overnight at ambient temperature and then refluxed for 3 h. The reaction mixture was diluted with 50 ml of PhH, to which was added 100 ml of 2 M HCl. The solid was filtered off and recrystallized from $CHCl_3$ to give 3.86 g (5.73 mmol) of **4**: yield 80.3%; mp 248—249 °C; IR (KBr) 1725 and 1745 cm^{-1} (>C=O). Found: C, 74.66; H, 3.68; Br, 12.12%. Calcd for $C_{42}H_{25}O_4Br$: C, 74.89; H, 3.74; Br, 11.86%.

Optically active **4**'s were soluble in benzene and purified by alumina column chromatography.

(S)-**4**: Vitreous powder; $[\alpha]_D^{24}$ ≈0°; $[\alpha]_{436}^{24}$ +20.3° (*c* 1.03, acetone); IR (KBr) 1730 cm^{-1} (>C=O, broad).

(R)-**4**: Vitreous powder; $[\alpha]_{436}^{24}$ −18.9° (*c* 2.17, acetone).

Ullmann Reaction of (R)-**4**. Just prior to the reaction, 1.0 g of copper powder (200 mesh, Junsei Chemical Co.) was pretreated for activation according to a literature procedure,[19] except that all manipulations were carried out under nitrogen and that the acetone-moist powder was further washed with several portions of PhH. The copper powder and 0.524 g (0.778 mmol) of (*R*)-**4** were charged into a 30 ml round-bottomed flask equipped with a reflux condenser topped with nitrogen inlet. The whole system was evacuated and refilled with nitrogen, and then 10 ml of DMF was added to the flask. The mixture was magnetically stirred and heated to gentle reflux under nitrogen. After 5 h heating, the cooled mixture was diluted with 50 ml of PhH, and solids were filtered off. The filtrate was washed with 2 M HCl and then water, and dried over Na_2SO_4. Evaporation of the solvent *in vacuo* afforded a pale yellow residue, 0.458 g (0.770 mmol, calculated as **6**), which was comprised of a 15:85 mixture of (*R*)-**6** and (*RRR*)-**5**, as judged from the peak areas of UV absorption at 254 nm on HPLC (JASCO SC-01 column, MeCN/H_2O (98/2) eluant). A negative Beilstein test confirmed the absence of the unreacted ester. A preparative TLC of an aliquot of the Ullmann product (0.40 g) using PhH as eluant gave 21 mg of (*R*)-**6** and 0.302 g of (*RRR*)-**5**. The (*RRR*)-**5** melted gradually over a temperature range of 150—160 °C (dec); $[\alpha]_D^{23}$ +91.8° (*c* 1.0, acetone). Found: C, 84.85; H, 4.31%. Calcd for $C_{84}H_{50}O_8$: C, 84.98; H, 4.24%.

The (*RRR*)-**5** (0.25 g) was boiled with 0.2 g of LAH in ether for 3 h. The reaction was worked up as usual, and a preparative TLC with $CHCl_3$/AcOEt (4/1) enabled the recovery of (*R*)-**7** (36 mg, $[\alpha]_{546}^{23}$ +3.5° (*c* 0.8, acetone)), (*R*)-**1** (80 mg, $[\alpha]_D^{23}$ +35.2° (*c* 0.90, THF)), and **8** (26 mg). The diol ((*R*)-**7**) was completely acylated in CCl_4 with excess acid chloride of (*R*)-(+)-MTPA in the presence of excess 4-dimethylaminopyridine to give the diastereomeric pair of di-(*R*)-MTPA ester.[12b] NMR ($CDCl_3$): δ 3.33 (3H, $-OCH_3$), 2H at 4.76 ($-CH_2-$ for (*RR*)-isomer) and 4.82 ($-CH_2-$ for (*SR*)-isomer), 7.25 (10H, –Ph), and 6.7—8.1 (12H, Naphthyl). Addition of $Eu(fod)_3$ caused separation of the $-OCH_3$ signal, where the induced downfield shift for the (*SR*)-ester was larger than that for the (*RR*)-isomer.

Ullmann Reaction of (R)- *and* (S)-**3**. *Procedure A*: The following example is typical. As above, a mixture of (*R*)-**3** (1.00 g, 1.33 mmol) and activated copper powder (prepared from 1.2 g of Cu) in 10 ml of DMF was refluxed for 5 h with vigorous stirring under nitrogen. The organic residue obtained weighed 0.785 g, $[\alpha]_D^{24}$ +70.4° (*c* 0.83, PhH). This sample was refluxed with 2 g of KOH in 95% aq EtOH (20 ml) for 5 h. After the solvent was evaporated, the residue was dissolved in 30 ml of H_2O and made acidic with concd HCl to give a white precipitate. The mixture was extracted with portions of ether. Combined ether extracts were then extracted with 1 M Na_2CO_3; after usual work-up of the aq layer, 2-naphthoic acids ((*R*)-**9**+**10**) were recovered (0.42 g, 92% yield) while diol ((*R*)-**1**) was obtained from the ether layer (0.34 g, 89%, $[\alpha]_D^{24}$ +33.2° (*c* 1.00, THF)). After a TLC (EtOH/28% NH_4OH/H_2O= 16/3/1) of the acid mixture, 0.203 g of diacid ((*R*)-**9**, 44.6% yield based on (*R*)-**3**) and 0.140 g of monoacid (**10**) were obtained.

(R)-**9**: $[\alpha]_D^{24}$ +34.0° (*c* 0.78, 0.1 M NaOH); mp 255—265 °C (dec).

In another run, 0.302 g (0.401 mmol) of (*S*)-**3** was treated with Cu (1 g) in 10 ml of DMF at 120—130 °C for 10 h. The specific rotation of the diacid ((*S*)-**9**) was $[\alpha]_D^{24}$ −49.4° (*c* 0.85, 0.1 M NaOH); the yield was 60 mg.

Procedure B: To a well stirred, gently refluxing suspension of freshly activated copper powder (prepared from 3 g of Cu) in 50 ml of DMF was slowly added (*S*)-**3** (1.54 g, 2.05 mmol) over 1 h period under nitrogen, and heating was continued for another 5 h. The pale yellow organic residue (1.21 g, $[\alpha]_D^{24}$ −196.5° (*c* 1.11, PhH)) was analyzed by HPLC (JASCO SC-01 column, MeCN) to show the presence of, in the order of elution, (*SS*)-**12** (1.00), (*S*)-**6** (0.20), (*SSSS*)-**13** (0.21), (*SSS*)-**5** (0.19), and other higher oligomeric products (in parentheses are shown relative peak areas of UV absorption at 254 nm). A chromatography on a silica-gel column (Wako Gel C-200) using $CHCl_3$ (1% EtOH) as eluant gave 0.437 g of (*SS*)-**12** and 40 mg of (*SSSS*)-**13** as well as trace amounts of (*S*)-**6** and (*SSS*)-**5**.

(SS)-*Tetranaphtho*[*2,1*-b:*1,2*-d:*2,1*-h:*1,2*-j][*1,6*]*dioxacyclododeca-2,4,8,10-tetraene-7,12-dione* ((SS)-**12**): Mp >350 °C; $[\alpha]_D^{23}$ −457.6° (*c* 0.507, PhH); IR (KBr) 1752 cm^{-1} (>C=

O); MS (70 eV), *m/e* (%), 592 (M^+, 27.1), 280 (8.3), 268 (26.6), 252 (4.2), and 239 (4.2). Found: C, 85.41; H, 3.81%. Calcd for $C_{42}H_{24}O_4$: C, 85.12; H, 4.08%.

The cyclic diester ((*SS*)-**12**, 0.332 g, 0.56 mmol) was treated with 0.15 g of LAH in ether(30 ml)–THF(10 ml). After a TLC ($CHCl_3$/AcOEt=4/1), 0.149 g (0.474 mmol) of (*S*)-**7** ($[\alpha]_{546}^{23}$ −86.0° (*c* 1.43, acetone)) and 0.124 g (0.433 mmol) of (*S*)-**1** ($[\alpha]_D^{24}$ −34.9° (*c* 1.03, THF)) were recovered.

(SSSS)-***13***: Mp >400 °C; M.W. 1220 (calibrated with (*SS*)-**12** (M.W.=592)); $[\alpha]_D^{25} \approx 0°$ (*c* 0.304, PhH); $[\alpha]_{436}^{24}$ −291° (*c* 0.134, PhH); IR (KBr) 1745 cm^{-1} (>C=O). Found: C, 84.75; H, 3.63%. Calcd for $C_{84}H_{48}O_8$: C, 85.12; H, 4.08%.

LAH treatment of the cyclic dimer (*ca.* 30 mg) gave a *ca.* 8 mg sample of (*S*)-**7**, the specific rotation of which was estimated to be $[\alpha]_{546}^{23}$ −75—−85° (acetone).

(*S*)-***6***: MS (70 eV), *m/e* (%), 594 (M^+, 22.3), 440 (2.5), 268 (2.7), 156 (8.1), and 155 (56.3).

The (*SSS*)-**5** was inferred from its retention volume on HPLC and IR spectrum.

We are grateful to Professor Shozo Yamaguchi and Dr. Kuninobu Kabuto in our University for helpful suggestions and kind offering of reagents for the preparation of the (*R*)-MTPA esters. This work was partly supported by a Grant-in-Aid for Scientific Research No. 465280 from the Ministry of Education, Science and Culture.

References

1) Preliminary communication: S. Miyano, M. Tobita, M. Nawa, S. Sato, and H. Hashimoto, *J. Chem. Soc., Chem. Commun.*, **1980**, 1233.

2) This work was presented at the 43rd National Meeting of the Chemical Society of Japan, Tokyo, March—April 1981, Abstr. No. 3I18.

3) For example a) S. F. Mason, R. H. Seal, and D. R. Roberts, *Tetrahedron*, **30**, 1671 (1974); b) K. Mislow, M. A. W. Glass, R. E. O'Brien, P. Rutkin, D. H. Steinberg, J. Weiss, and C. Djerassi, *J. Am. Chem. Soc.*, **84**, 1455 (1962); c) H. Akimoto and S. Yamada, *Tetrahedron*, **27**, 5999 (1971); d) W. L. F. Armarego and E. E. Turner, *J. Chem. Soc.*, **1957**, 13, and references cited therein.

4) J. A. Berson and M. A. Greenbaum, *J. Am. Chem. Soc.*, **80**, 653 (1958).

5) D. J. Cram and J. M. Cram, *Acc. Chem. Res.*, **11**, 8 (1978).

6) E. P. Kyba, G. W. Gokel, F. de Jong, K. Koga, L. R. Sousa, M. G. Siegel, L. Kaplan, G. D. Y. Sogah, and D. J. Cram, *J. Org. Chem.*, **42**, 4173 (1977).

7) a) K. Tamao, H. Yamamoto, H. Matsumoto, N. Miyake, T. Hayashi, and M. Kumada, *Tetrahedron Lett.*, **1977**, 1389; b) S. Miyano, M. Nawa, and H. Hashimoto, *Chem. Lett.*, **1980**, 729; c) M. Nishizawa, M. Yamada, and R. Noyori, *Tetrahedron Lett.*, **22**, 247 (1981).

8) For example, a) K. Tamao, A. Minato, N. Miyake, T. Matsuda, Y. Kiso, and M. Kumada, *Chem. Lett.*, **1975**, 133; b) R. L. Clough, P. Mison, and J. D. Roberts, *J. Org. Chem.*, **41**, 2252 (1976); c) A. McKillop, A. G. Turrell, D. W. Young, and E. C. Taylor, *J. Am. Chem. Soc.*, **102**, 6504 (1980), and references cited therein.

9) a) S. Miyano, M. Tobita, S. Suzuki, Y. Nishikawa, and H. Hashimoto, *Chem. Lett.*, **1980**, 1027; b) J. M. Bobbitt, I. Noguchi, H. Yagi, and K. H. Weisgraber, *J. Org. Chem.*, **41**, 845 (1976); c) B. Feringa and H. Wynberg, *J. Am. Chem. Soc.*, **98**, 3372 (1976); d) B. Feringa and H. Wynberg, *Bioorg. Chem.*, **7**, 397 (1978).

10) J. Jacques, C. Fouquey, and R. Viterbo, *Tetrahedron Lett.*, **1971**, 4617.

11) D. M. Hall and E. E. Turner, *J. Chem. Soc.*, **1955**, 1242.

12) a) J. A. Dale and H. S. Mosher, *J. Am. Chem. Soc.*, **95**, 512 (1973); b) K. Kabuto, F. Yasuhara, and S. Yamaguchi, *Tetrahedron Lett.*, **21**, 307 (1980); **22**, 659 (1981).

13) (*S*)-**9**: $[\alpha]_D$max −110° (0.1 M NaOH); A. K. Colter and L. M. Clemens, *J. Am. Chem. Soc.*, **87**, 847 (1965).

14) In other words, it may be said that even if the coupled product (**12**) had been comprised of a diastereomeric mixture, chromatographic separation of these isomers apparently would not have occurred.

15) Literature values for (*R*)-**1** vary from $[\alpha]_D^{26}$ +43.0° (*c* 0.9, THF)[3c] to $[\alpha]_D^{25}$ +33° (*c* 0.103, THF).[16]

16) E. W. Hoffmann, W. Kuchen, W. Poll, and H. Wunderlich, *Angew. Chem. Int. Ed. Engl.*, **18**, 415 (1979).

17) R. Pummerer, E. Prell, and A. Rieche, *Ber. Dtsch. Chem. Ges.*, **59**, 2159 (1926).

18) E. B. Hershberg and J. Cason, *Org. Synth.*, Coll. Vol. III, p. 627 (1955).

19) R. C. Fuson and E. A. Cleveland, *Org. Synth.*, Coll. Vol. III, p. 339 (1955).

The Biotransformation of Foreign Substrates by Tissue Cultures. I. The Hydroxylation of Linalool and Its Related Compounds with the Suspension Cells of *Nicotiana tabacum*

Toshifumi HIRATA, Tadashi AOKI, Yoshio HIRANO, Takashi ITO, and Takayuki SUGA*

Department of Chemistry, Faculty of Science, Hiroshima University, Higashisenda-machi, Naka-ku, Hiroshima 730

(Received May 22, 1981)

It was found that the tissue cultures of *Nicotiana tabacum* "Bright Yellow" possess the ability to transform selectively the *trans*-methyl group in the 3-methyl-2-butenyl group of such foreign substrates as linalool and the related compounds into the hydroxymethyl group. Also, the cultures were found to have the ability to hydrolize the acetoxyl group of their acetates.

In connection with studies on the biosynthetic ability of plant callus tissues,[1] we are considerably interested in their ability to transform foreign substrates. Recently, it has been documented that some plant cell cultures have the ability to transform administered substrates, and such an ability may be used for the transformation of chemical substances.[2-9] However, there have been few systematic studies on their transformation ability and pattern. We, therefore, began investigating the transformation of acyclic monoterpenoid alcohols by the cultured cells of *Nicotiana tabacum* "Bright Yellow." As the acyclic monoterpenoid alcohols, linalool (**1**), linalyl acetate (**2**), dihydrolinalool (**3**), and dihydrolinalyl acetate (**4**) were used. The results have been partly outlined in the preliminary communication.[10] We will here report details of the results.

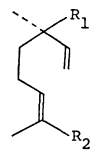

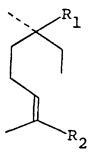

1: R_1=OH, R_2=CH_3
2: R_1=OAc, R_2=CH_3
5: R_1=OH, R_2=CH_2OH
7: R_1=OH, R_2=CHO
8: R_1=OAc, R_2=CH_2OH
10: R_1=OAc, R_2=CHO

3: R_1=OH, R_2=CH_3
4: R_1=OAc, R_2=CH_3
6: R_1=OH, R_2=CH_2OH
9: R_1=OAc, R_2=CH_2OH

Results and Discussion

Callus tissues induced from the stem of *Nicotiana tabacum* "Bright Yellow" were used in this work. The callus tissues were precultured for 3—4 weeks in Murashige and Skoog's medium[11] prior to the administration of the substrates. A sample of the monoterpenoids was administered to the suspension cells. The suspension cultures were incubated at 25 °C for 7 d under shaking in the dark. After incubation, transformation products were detected by comparing the ether-soluble constituents of both the cultured mass and the culture medium with those of the metabolites of *N. tabacum* suspension cells by means of GLC and TLC. The transformation products were separated by chromatographic methods.

In the biotransformation of linalool (**1**), compound **5** was a major product, as shown in Table 1. The compound (**5**) exhibited the ^{1}H NMR signal at δ 4.00 due to $-C\underline{H}_2OH$, instead of the 8- or 10-methyl signal of **1**. This suggested that the product is a C(8)- or a C(10)-hydroxylated derivative of **1**. The dihydroxy compound (**5**) was selectively hydrogenated with PtO_2 to give a dihydro derivative **6**, which showed a 17% NOE between the hydroxymethyl group (δ 3.94) and the C(6)–H (δ 5.42). The NOE[12] indicated that the hydroxymethyl group is *trans* to the C(1)–C(5) chain portion. This was further supported by the agreement of the observed chemical shift (δ 6.45) of the C(6)–H of the hydroxy aldehyde **7**, with the evaluated shift value (δ 6.40) calculated for the *trans* isomer by fitting Pascual's equation.[13,14] Thus, the product **5** was elucidated to be 8-hydroxylinalool.

When linalyl acetate (**2**) was fed to the tobacco suspension cells, two transformation products, 8-hydroxylinalool (**5**) and 8-hydroxylinalyl acetate (**8**), were found, as shown in Table 1. However, linalool (**1**) resulting from linalyl acetate (**2**) by hydrolysis was not found. Accordingly, the preferential formation of 8-hydroxylinalool (**5**) seems to indicate oc-

TABLE 1. BIOTRANSFORMATION OF LINALOOL (**1**) AND ITS DERIVATIVES (**2**, **3**, AND **4**) BY *Nicotiana tabacum* SUSPENSION CELLS

Substrates	Products	Yield/%[a]
Linalool (**1**)	8-Hydroxylinalool (**5**)	16.5
Linalyl acetate (**2**)	8-Hydroxylinalool (**5**)	14.8
	8-Hydroxylinalyl acetate (**8**)	1.9
Dihydrolinalool (**3**)	8-Hydroxydihydrolinalool (**6**)	14.9
Dihydrolinalyl acetate (**4**)	8-Hydeoxydihydrolinalool (**6**)	15.5
	8-Hydroxydihydrolinalyl acetate (**9**)	2.2

a) The weight percent of the products per the administered substrates.

currence of the hydrolysis of linalyl acetate (**2**) followed by the immediate hydroxylation at C(8) or occurrence of the immediate hydroxylation at C(8) of **2** followed by the hydrolysis of the acetoxyl group. The quite similar results were obtained in the administration of dihydrolinalool (**3**) and dihydrolinalyl acetate (**4**), as shown in Table 1.

We now have established that the suspension cells of *Nicotiana tabacum* "Bright Yellow" have the ability to hydroxylate selectively in the *trans*-methyl group in the 3-methyl-2-butenyl group of linalool (**1**) and its related compounds (**2**—**4**), but not in the *cis*-methyl group. Also, it was found that the cultured cells are capable of hydrolizing the acetoxyl group of the acetates.

Experimental

NOE experiments were carried out on a Hitachi R-22 spectrometer in the frequency-swept and internal-TMS-locked mode. The sample solution was prepared in concentration of 5% (w/v) in CCl_4 and carefully degassed just prior to measurements. GLC analyses were performed on a Shimadzu GC-6A equipped with a FID and a glass column (3 mm×2 m) packed with 2% OV-17 and 10% DEGS on Chromosorb AW-DMCS (80—100 mesh) at 120 °C and 150 °C, respectively, for each case. TLC analyses were carried out with silica gel (Kieselgel GF_{254}; 0.25 mm thick) by using two different solvent systems [(i) EtOAc–hexane (3:7, v/v) and (ii) MeOH–benzene (1:24, v/v)] for each case.

Sample Used. Linalool and its acetate donated from Takasago Perfumery Co. Inc. were purified by column chromatography (silica gel) with a hexane–EtOAc mixture with EtOAc increasing 0 to 15% to give (−)-linalool (**1**) [$[\alpha]_D^{25}$ −19.9° (neat); n_D^{25} 1.4600; d_4^{25} 0.8639; >99.5% pure on GLC] and (−)-linalyl acetate (**2**) [$[\alpha]_D^{25}$ −2.1° (neat); n_D^{25} 1.4550, d_4^{25} 0.8991; >99.5% pure on GLC]. (−)-Dihydrolinalool (**3**) [$[\alpha]_D^{25}$ −2.5° (*c* 1.8, MeOH); n_D^{25} 1.4558; d_4^{25} 0.8601; >99.5% pure on GLC] and (−)-dihydrolinalyl acetate (**4**) [$[\alpha]_D^{25}$ −1.8° (*c* 2.5, MeOH); n_D^{25} 1.4502; d_4^{25} 0.8983; >99.5% pure on GLC] were prepared from **1** and **2**, respectively, by selective hydrogenation with Adams' PtO_2.

Feeding of the Monoterpenoids to the Tobacco Suspension Cells. In this work, we used the callus tissues which were derived from the stem of *Nicotiana tabacum* "Bright Yellow" and then subcultured for about 5 years. Just before use for the transformation, the callus tissues were transplanted to freshly prepared Murashige and Skoog's medium[11] (100 ml per one flask) containing 2 ppm of 2,4-dichlorophenoxyacetic acid and 2% sucrose and then grown with continuous shaking for 3—4 weeks at 25 °C in the dark. To the suspension cells (40—60 g per one flask), the monoterpenoids (20 mg per one flask; total 200 mg) were administered, and then the suspension cultures were incubated at 25 °C for 7 d on a rotary shaker (70 min^{-1}) in the dark.

Isolation of the Products. After incubation as described above, the cells were filtered off and triturated with methanol. The methanol solution, after the removal of the solvent, was extracted with ether. The culture medium filtered from the cells was extracted with ether. These ether soluble fractions were compared by means of GLC and TLC with those of the metabolites of the suspension cells. Transformation products were isolated from the ether soluble fractions by chromatography on a 3% $AgNO_3$–silica-gel plate (1 mm thick) with EtOA–hexane (3:7, v/v) and/or preparative GLC with a glass column (5 mm×2 m) packed with 10% DEGS on Chromosorb AW-DMCS (80—100 mesh) at 150 °C. These products were identified as shown below. The identified products and their quantities are shown in Table 1.

*Identification of the Products. 8-Hydroxylinalool (**5**)*: $[\alpha]_D^{25}$ −12.8° (*c* 1.08, MeOH); IR (Liq.) 3380 (OH) and 1640 cm^{-1} (C=C); ^1H NMR ($CDCl_3$) δ=1.30 (3H, s, C(9)–H_3), 1.68 (3H, bs, C(10)–H_3), 4.00 (2H, s, –C$\underline{H}_2$–OH), and 5.0—6.2 (4H, olefinic H); MS (70 eV), *m/z* (rel intensity) 152 (5, M−H_2O), 137 (7), 119 (9), 71 (51), 67 (37), and 43 (100); direct comparison with a synthetic specimen (co-TLC, co-GLC, IR, ^1H NMR, and MS).

*Derivation of 8-Oxolinalool (**7**) from 8-Hydroxylinalool (**5**)*: A mixture of 8-hydroxylinalool (**5**) (50 mg) and active MnO_2 (40 mg) in CCl_4 (5 cm^3) was stirred at room temp for 12 h. Removal of the solvent from the reaction mixture, after filtration from the inorganic solid, gave an oily product (36 mg). This product was subjected to preparative TLC (silica gel; 1 mm thick) with hexane–EtOAc (4:1, v/v) to give 8-oxolinalool (**7**) (28 mg): IR (Liq.) 2720, 1685 (CHO), and 1640 cm^{-1} (C=C); ^1H NMR (CCl_4) δ=1.33 (3H, s, C(9)–H_3), 1.73 (3H, bs, C(10)–H_3); 6.45 (1H, bt, >C=CH–), and 9.43 (1H, s, CHO); MS (70 eV), *m/z* (rel intensity) 150 (21, M−H_2O), 135 (5), 83 (82), 71 (99), and 43 (100).

*8-Hydroxydihydrolinalool (**6**)*: *m/z* 154 (M−H_2O); IR (Liq.) 3350 (OH) and 1620 cm^{-1} (C=C); ^1H NMR (CCl_4) δ=0.90 (3H, t, *J* 7.5 Hz, C(1)–H_3), 1.19 (3H, s, C(9)–H_3), 1.70 (3H, bs, C(10)–H_3), 3.94 (2H, s, –C$\underline{H}_2$OH), and 5.42 (1H, bt, *J* 7.0 Hz, >C=CH–); direct comparison with a synthetic specimen (co-TLC, co-GLC, MS, IR, and ^1H NMR).

*8-Hydroxylinalyl Acetate (**8**)*: *m/z* 212 (M^+); IR (Liq.) 3500 (OH), 1735 (OAc), 1638 (C=C), and 1250 cm^{-1} (C–O); ^1H NMR ($CDCl_3$) δ=1.55 (3H, s, C(9)–H_3), 1.67 (3H, bs, C(10)–H_3), 2.01 (3H, s, OAc), 4.00 (2H, s, –C$\underline{H}_2$OH), 4.65 (1H, bt, *J* 6.5 Hz, >C=CH–), and 5.0—6.2 (3H, olefinic H). Hydrolysis of **8** with 5% methanolic NaOH gave 8-hydroxylinalool (**5**).

*8-Hydroxydihydrolinalyl Acetate (**9**)*: *m/z* 214 (M^+); IR (Liq.) 3450 (OH) and 1735 cm^{-1} (OAc); ^1H NMR ($CDCl_3$) δ=1.50 (3H, s, C(9)–H_3), 1.69 (3H, bs, C(10)–H_3), 1.95 (3H, s, OAc), 3.99 (2H, s, –C$\underline{H}_2$OH), and 5.0—6.2 (4H, olefinic H). Hydrolysis of **9** with 5% methanolic NaOH gave 8-hydroxydihydrolinalool (**6**).

*Preparation of the Authentic Samples. 8-Hydroxylinalool (**5**)*: Following the reported procedure,[15] linalyl acetate (**2**) (980 mg) was oxidized with SeO_2 (560 mg) in 95% dioxane (5 cm^3) at 70 °C for 30 min. The reaction mixture was subjected to preparative TLC (Si gel; 1 mm thick) with hexane–EtOAc (4:1, v/v) to give 8-oxolinalyl acetate (**10**) (227 mg): IR (Liq.) 2701 and 1686 (CHO), 1734, 1368, and 1246 cm^{-1} (OAc); ^1H NMR (CCl_4) δ=1.54 (3H, s, C(9)–H_3), 1.70 (3H, s, C(10)–H_3), 1.95 (3H, s, OAc), 6.37 (1H, bt, *J* 7.0 Hz, C(6)–H), 9.34 (1H, s, CHO); MS (70 eV), *m/z* (rel intensity) 150 (21, M−AcOH), 135 (14), 121 (18), 107 (17), 71 (45), and 43 (100). Reduction of this oxolinalyl acetate (110 mg) with $LiAlH_4$ (120 mg) in ether under reflux gave dihydroxy compound **5** (56 mg); IR (Liq.) 3400 (OH), 1642, and 922 cm^{-1} (C=C); ^1H NMR ($CDCl_3$) δ=1.29 (3H, s, C(9)–H_3), 1.67 (3H, bs, C(10)–H_3), 4.00 (2H, s, –C$\underline{H}_2$OH), and 5.0—6.2 (4H, olefinic H); MS (70 eV), *m/z* (rel intensity) 152 (3, M−H_2O), 137 (6), 119 (10), 71 (49), 67 (39), and 43 (100).

*8-Hydroxydihydrolinalool (**6**)*: Selective hydrogenation of 8-hydroxylinalool (**5**) (15 mg) on Adams' PtO_2 (5 mg)

in MeOH (3 cm^3) gave **6** (12 mg): IR (Liq) 3350 (OH) and 1620 cm^{-1} (C=C); ^1H NMR (CCl_4) δ=0.90 (3H, t, J 7.5 Hz, C(1)–H_3), 1.19 (3H, s, C(9)–H_3), 1.70 (3H, bs, C(10)–H_3), 3.94 (2H, s, –C$\underline{H}_2$–OH), and 5.42 (1H, bt, J 7.0 Hz, >C=C$\underline{H}$–); MS (70 eV), m/z (rel intensity) 154 (12, M–H_2O), 139 (12), 125 (27), 73 (44), and 43 (100).

The authors wish to express their thanks to Dr. Kunihiko Ojima of Faculty of Agriculture, Tohoku University, for a gift of *Nicotiana tabacum* callus and to the Takasago perfumery Co. Inc., for a gift of sample of linalool and linalyl acetate.

References

1) T. Suga, T. Hirata, and Y. Yamamoto, *Agric. Biol. Chem.*, **44**, 1817 (1980).
2) S. J. Stohs and H. Rosenberg, *Lloydia*, **38**, 181 (1975).
3) "Plant Tissue Culture and Its Bio-technological Application," ed by W. Barz, E. Peinhard, and M. H. Zenk, Springer-Verlag, Berlin (1977), pp. 126—150.
4) H. Itokawa, K. Takeya, and S. Mihashi, *Chem. Pharm. Bull. (Tokyo)*, **25**, 1941 (1977).
5) D. P. Carew and R. J. Krueger, *Phytochemistry*, **16**, 1461 (1977).
6) D. Aviv and E. Galun, *Planta Med.*, **33**, 70 (1978).
7) G. E. Gallili, B. Yagen, and R. I. Mateleo, *Phytochemistry*, **17**, 578 (1978).
8) T. Yoshikawa and T. Furuya, *Phytochemistry*, **17**, 239 (1978).
9) A. W. Alfermann and E. Reinhard, *Bull. Soc. Chim. Fr.*, **1980**, II-35.
10) T. Suga, T. Hirata, Y. Hirano, and T. Ito, *Chem. Lett.*, **1976**, 1246.
11) T. Murashige and F. Skoog, *Physiol. Plant*, **15**, 473 (1962).
12) J. H. Noggle and R. E. Schirmer, "The Nuclear Overhauser Effect. Chemical Application," Academic Press, New York (1971).
13) C. Pascual, J. Meier, and W. Simon, *Helv. Chim. Acta*, **49**, 164 (1966).
14) The chemical shift evaluated for the *cis* isomer is δ 6.67.
15) R. Naegeli and G. Weber, *Tetrahedron Lett.*, **1970**, 959.

Muramyl Dipeptide Derivatives with Multiprenylacetyl Group. Synthesis and Immunological Activities[1)]

Tsunehiko FUKUDA, Shigeru KOBAYASHI,* Hidefumi YUKIMASA, Shinji TERAO, Masahiko FUJINO, Tetsuo SHIBA,† Ikuo SAIKI,†† Ichiro AZUMA,†† and Yuichi YAMAMURA†††

Central Research Division, Takeda Chemical Industries, Ltd., Yodogawa-ku, Osaka 532

†*Department of Chemistry, Faculty of Science, Osaka University, Toyonaka, Osaka 560*

††*Institute of Immunological Science, Hokkaido University, Kita-ku, Sapporo 060*

†††*Osaka University, Suita, Osaka 565*

(Received May 28, 1981)

Several linear and branched all-*trans*-multiprenylacetic acids were synthesised, and introduced to the 6 position of the sugar moiety of muramyl dipeptide and its analog, *via* an amino acid as a linking unit. Compared with the saturated stearoyl derivative, all the compounds having a multiprenylacetyl group exhibited more potent adjuvant activity on the induction of delayed-type hypersensitivity to *N*-acetyl-3-(4-arsonophenylazo)-L-tyrosine. The derivatives with larger branched side chains tended to have increased activity.

Following the finding that *N*-acetylmuramyl-L-alanyl-D-isoglutamine (MDP) is the effective minimal component of bacterial cell walls eliciting the function of Freund's complete adjuvant,[2)] many studies on the synthesis and evalutation of the activity of MDP and its analogs have been carried out.[3)] During these investigations, several attempts to apply these chemically well-defined compounds to immunotherapy of cancer and infectious disease have been undertaken. Particularly some derivatives with a lipophilic substituent introduced to the 6 position of the carbohydrate moiety of MDP showed interesting results. For example, 6-*O*-mycoloyl-*N*-acetylmuramyl-L-alanyl-D-isoglutamine, in which the mycoloyl moiety was of either natural[4)] or synthetic origin,[5)] and 6-*O*-quinonyl-*N*-acetylmuramyl-L-valyl-D-isoglutamine methyl esters[6)] suppressed syngeneic tumor growth (Meth-A fibrosarcoma in BALB/c female mice). Furthermore, 6-*O*-stearoyl-*N*-acetylmuramyl-L-alanyl-D-isoglutamine protected the mice from infections.[7)] The potent adjuvant activity of MDP for the induction of delayed-type hypersensitivity to *N*-acetyl-3-(4-arsonophenylazo)-L-tyrosine (ABA–Tyr) in guinea pigs was also retained in these compounds. The results indicate that the lipophilicity of the residues introduced to the MDP molecule plays an important role in potentiating the immunological activity of MDP. The incorporated fatty acid may furnish an affinity for the membranes of macrophages and/or lymphocytes to the molecule: the precise role of the quinone nucleus moiety in the quinonyl MDP derivatives is left to be solved in future.

In order to investigate further the role of the lipophilicity, we tried to introduce a lipophilic unsaturated carboxylic acid to the 6 position of the muramyl moiety of MDP. Thus, nine multiprenylacetic acids (**7**) with different chain lengths were first synthesized. In view of lability of these carboxylic acids to the final hydrogenolytic deprotecting procedure, a coupling of them with amino group of 6-*O*-aminoacyl-*N*-acetylmuramyl dipeptides (**8**)[8)] was attempted under mild conditions to give the desired compounds. The versatility of these compounds (**8**) as intermediates for the synthesis of MDP derivatives has been demonstrated.[8,9)]

In this paper, we describe the synthesis and immunological evaluation of eight new polyprenylacetylamino-acylated MDP derivatives (**9**). The compounds synthesized are presented in Table 3.

Chemistry

Synthesis of Multiprenyl Alcohols (2). All-*trans*-1-benzyloxy-3,7,11,15-tetramethyl-9-(*p*-tolylsulfonyl)-2,6,10,14-hexadecatetraene (**1a**)[10)] served as material for the synthesis of multiprenyl alcohols containing more than four isoprenyl units (**2a**—**c**) as shown in Scheme 1. All-*trans*-3,7,11,15-tetramethyl-2,6,10,14-hexadecatetraen-1-ol (**2a**) was prepared by reductive elimination of the sulfonyl and benzyl group of **1a** with lithium in ethylamine at −60 °C in 95.6% yield.

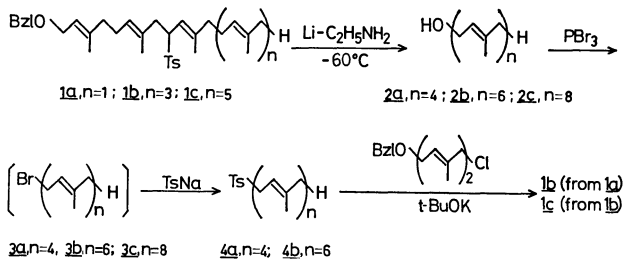

Scheme 1.

Compound **2a** was then converted to all-*trans*-1-bromo-3,7,11,15-tetramethyl-2,6,10,14-hexadecatetraene (**3a**) by treatment with PBr_3. Without further purification, the bromo compound (**3a**) was allowed to react with sodium *p*-toluenesulfinate dihydrate to give all-*trans*-3,7,11,15-tetramethyl-1-(*p*-tolylsulfonyl)-2,6,10,14-hexadecatetraene (**4a**) in an overall yield of 85%. Compound **4a** was coupled with *trans,trans*-1-benzyloxy-8-chloro-3,7-dimethyl-2,6-octadiene (**5**)[10)] in the presence of *t*-BuOK to give all-*trans*-1-benzyloxy-3,7,11,15,19,23-hexamethyl-9-(*p*-tolylsulfonyl)-2,6,10,14,18,22-tetracosahexaene (**1b**) (89%) which was subjected to reduction with lithium in ethylamine, giving all-*trans*-3,7,11,15,19,23-hexamethyl-2,6,10,14,18,22-tetracosahexaen-1-ol (**2b**) in 82% yield. The multiprenyl chain elongation of **2b** to all-*trans*-3,7,11,15,19,23,27,31-octamethyl-2,6,10,14,18,22,26,30-triacontaoctaen-1-ol (**2c**) was performed by repeating the above mentioned procedure (**2b**→**3b**→**4b**→**1c**→**2c**). Physicochemical properties of the multiprenyl alcohols (**2**) and their intermediates are listed in Table 1.

Table 1. Yields and data of elemental analysis of multiprenylalcohols (**2**) and their intermediates (**1** and **4**)

Compound	n	Yield %	Formula	Found (Calcd) (%) C	H	S
1a	1	91.0	$C_{34}H_{46}O_3S$	76.24 (76.36	8.89 8.67	6.19 6.00)
1b	3	88.9	$C_{44}H_{62}O_3S$	78.66 (78.75	9.46 9.31	4.69 4.78)
1c	5	86.4	$C_{54}H_{78}O_3S$	80.46 (80.34	9.79 9.74	3.98 3.97)
2a	4	95.6	$C_{20}H_{34}O$	82.95 (82.69	12.17) 11.80)	
2b	6	82.0	$C_{30}H_{50}O$	84.75 (84.44	12.19 11.81)	
2c[a)]	8	71.5	$C_{40}H_{66}O$	85.56 (85.34	12.13 11.82)	
4a	4	84.7	$C_{27}H_{40}O_2S$	75.78 (75.78	9.73 9.47	7.30 7.48)
4b	6	77.2	$C_{37}H_{56}O_2S$	78.75 (78.66	10.02 9.99	5.72 5.68)

a) Wax with low mp.

Table 2. Yields and data of elemental analysis of multiprenylacetic acids (**7**) and their intermediates (**6**)

Compound	n	R	Yield %	Formula	Found (Calcd) (%) C	H
6a	4	H	52.0	$C_{27}H_{44}O_4$	74.97 (75.02	10.35 10.26)
6a′	4		13.4	$C_{47}H_{76}O_4$	79.86 (80.12	10.89 10.79)
6b	6	H	38.0	$C_{37}H_{60}O_4$	78.48 (78.12	10.75 10.75)
6b′	6		44.0	$C_{67}H_{108}O_4$	82.27 (82.32	11.20 11.14)
6c[a)]	8	H	40.7	$C_{47}H_{76}O_4$	80.29 (80.06	11.05 10.87)
6c′[a)]	8		16.6	$C_{87}H_{140}O_4$	83.80 (83.59	11.37 11.29)
6d	2	H	54.2	$C_{17}H_{28}O_4$	69.17 (68.89	9.67 9.52)
6d′	2		27.1	$C_{27}H_{44}O_4$	75.23 (74.95	10.47 10.25)
7a	4	H	73.2	$C_{22}H_{36}O_2$	79.46 (79.46	11.20 10.91)
7a′	4		92.9	$C_{42}H_{68}O_2$	83.13 (83.38	11.52 11.32)
7b[a)]	6	H	100	$C_{32}H_{52}O_2$	81.74 (81.99	11.50 11.18)
7b′[a)]	6		74.6	$C_{62}H_{100}O_2$	85.12 (84.86	11.77 11.49)
7c[a)]	8	H	82.0	$C_{42}H_{68}O_2$	83.44 (83.38	11.47 11.32)
7c′[a)]	8		96.0	$C_{82}H_{132}O_2$	85.62 (85.65	11.79 11.57
7d	2	H	89.9	$C_{12}H_{20}O_2$	73.29 (73.42	10.57 10.27)
7d′	2		85.6	$C_{22}H_{36}O_2$	79.46 (79.46	11.02 10.91)
7e	3	H	—[11)]	$C_{17}H_{28}O_2$	77.55 (77.22	10.64 10.68)

a) Wax with low mp.

Synthesis of Mutiprenylacetic Acids (7). All-*trans*-5,9,13-trimethyl-4,8,12-tetracosatrienoic acid (**7d**) was synthesized according to the method reported by Fujita *et al.*[11] The eight other multiprenylacetic acids with different chain lengths were synthesized from multiprenyl alcohols (**2**, n=2—8) by the malonic ester method as shown in Scheme 2.

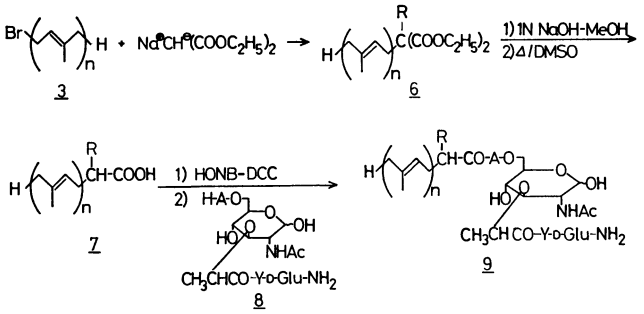

Scheme 2.

Multiprenyl alcohols (**2**) were converted to the corresponding bromides (**3**, n=2—8) by treatment with PBr_3. Using the resulting suitable multiprenyl bromides, diethyl malonate was alkylated in the presence of NaH to give the diethyl, mono- and disubstituted malonate (**6**). The molar ratio of the products of mono- (**6b**) and disubstituted (**6b'**) malonate was 2:1 when one equivalent of **3b**, for example, was allowed to react with diethyl malonate in the presence of one equivalent of NaH in DMF at room temperature for 2 h. The combined yield of **6b** and **6b'** was 82.1% based on **3b**. The reaction conditions that might affect the overall yield as well as the ratio of mono- and disubstituted compounds were not further exaimned since the result obtained was satisfactory for the present study. After the separation of the products by means of silica gel column chromatography with hexane–diisopropyl ether (15:1) as an eluent, each product was hydrolyzed in 1 M KOH (5 equivalent)–MeOH–THF (2:5:1) under reflux. The resulting dicarboxylic acids were subjected to decarboxylation in DMSO at 140—150 °C to give the straight and branched chain multiprenylacetic acids, *i.e.*, all-*trans*-5,9,13,17,21,-25-hexamethyl-4,8,12,16,20,24-hexacosahexaenoic acid (**7b**) and 2-(all-*trans*-3,7,11,15,19,23-hexamethyl-2,6,-10,14,18,22-tetracosahexaenyl)-all-*trans*-5,9,13,17,21,25-hexanethyl-4,8,12,16,22,24-hexacosahexaenoic acid (**7b'**). Physicochemical properties of the multiprenylacetic acids synthesized by this procedure are listed in Table 2 together with those of the intermediates (**6**).

Synthesis of 6-O-Multiprenylacylaminoacyl MDP Derivatives (9). The carboxylic acids prepared above were then converted to *N*-hydroxy-5-norbornene-2,3-

Table 3. Yields and physicochemical properties of MDP derivatives **9**, **10** and **11**

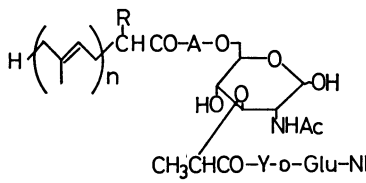

Compound	n	R	A	Y	Yield %	$[\alpha]_D$ (temp, c, solvent)	Formula	Found (Calcd) (%) C	H	N
9d	2	H	β-Ala	L-Ala	56.0	+28.2[b] (24, 0.5, H_2O)	$C_{34}H_{55}N_5O_{13}$ H_2O	53.71 (53.74	7.43 7.56	8.99 9.21)
9e	3	H	β-Ala	L-Ala	49.5	+38.4 (23, 0.5, DMF)	$C_{39}H_{63}N_5O_{13}$ H_2O	56.24 (56.57	7.96 7.91	8.43 8.45)
9a[a]	4	H	β-Ala	L-Ala	34.0	+25.8 (27, 0.4, EtOH)	$C_{44}H_{71}N_5O_{13}$ $2H_2O$	57.59 (57.81	7.95 8.27	7.62 7.66)
9b	6	H	L-Leu	Aib	17.9	+20.0 (25, 0.4, EtOH)	$C_{58}H_{95}N_5O_{13}$ H_2O	64.06 (64.00	8.96 8.98	6.32 6.44)
9c	8	H	L-Leu	Aib	14.1	+17.5 (23, 0.3, EtOH)	$C_{68}H_{111}N_5O_{13}$ H_2O	66.21 (66.68	9.38 9.30	5.73 5.72)
9d'	2		β-Ala	L-Ala	13.2	+24.7[b] (24, 0.3, H_2O)	$C_{45}H_{71}N_5O_{15}$ H_2O	57.07 (57.48	7.81 7.82	7.64 7.49)
9a'	4		β-Ala	L-Ala	28.0	+20.0 (27, 0.3, EtOH)	$C_{64}H_{103}N_5O_{13}$ $2H_2O$	64.58 (64.28	9.08 9.09	6.00 5.90)
9b'	6		L-Leu	Aib	13.5	+15.4 (25, 0.4, EtOH)	$C_{88}H_{143}N_5O_{13}$ H_2O	70.46 (70.60	9.79 9.76	4.59 4.68)
10	Stearoyl		β-Ala	L-Ala	66.3	+27.4[b] (27, 0.5, 70% EtOH)	$C_{40}H_{71}N_5O_{13}$ $2H_2O$	55.71 (55.47	8.88 8.73	8.12 8.09)
11[a]	Retinoyl		β-Ala	L-Ala	27.0	+23.9[b] (27, 0.5, H_2O)	$C_{42}H_{63}N_5O_{13}$ $5H_2O$	53.47 (53.85	7.19 7.86	7.43 7.48)

a) These compounds were reported previously.[8] b) Optical rotation was determined when mutarotation was completed (25 h).

dicaboximide (HONB)[12] active ester by dicyclohexylcarbodiimide (DCC) and coupled with 6-*O*-aminoacyl-*N*-acetylmuramyl dipeptide (**8**)[8] to give multiprenylacetyl derivatives of MDP with an amino acid as a linking unit (**9**) (Scheme 2). In this study, 6-*O*-β-alanyl-*N*-acetylmuramyl-L-alanyl-D-isoglutamine (**8a**) as an analog of a natural MDP type and 6-*O*-L-leucyl-*N*-acetylmuramyl-α-aminoisobutyryl-D-isoglutamine (**8b**) as an analog of an artificial MDP type with higher activity were used. In this acylation, the carboxylic acids with higher molecular weight gave the lower yields. Particularly the acylation with **7c'** could not be accomplished in spite of many trials. In addition to the steric effect, the large difference in the polarities of the two reactants (**7c'** and **8b**) may prevent access of each component to the reacting point. Stearoyl (**10**) and retinoyl (**11**) residues were introduced to **8a** in a similar manner for comparison of the biological activity. The resulting products were purified by column chromatography on silica gel with AcOEt–pyridine–AcOH–H_2O (80:10:3:5) as a solvent system. Rechromatography using Sephedex LH-20 with EtOH as an eluent gave the pure products listed in Table 3.

Biology

The adjuvant activity of these synthetic MDP analogs for the induction of delayed-typed hypersensitivity to *N*-acetyl-3-(4-arsonophenylazo)-L-tyrosine (ABA–Tyr) in guinea pigs was assayed by a method described earlier.[13] The reslults are shown in Table 4.

All the compounds reported in this paper showed more potent activity than the saturated stearoyl derivative (**10**). Among them, five compounds (**9b**, **9c**, **9b'**, **9d'**, **11**) revealed higher activity than MDP. The high activity of **9e**, in which the carbon number in the side chain is comparable to that of the stearoyl derivative (**10**), showed that the presence of the multiprenyl structure in the carbon chain is favorable for the activity. The activity of **9d'** is higher than **9a**, indicating that the branched structure of the chain is also favorable. The remarkable tendency for the compounds with larger side chains (**9b**, **9c**, and **9b'**) to possess increased activity is interesting although there was no clear-cut relation between the chain length and the activity. The high activity of retinoyl derivative (**11**), in spite of its small carbon number in the chain, suggested that there is some additional immunological function caused by retinoyl moiety as in the case of quinonyl derivatives[9] of MDP.

These results show that the introduction of lipophilic unsaturated carboxylic acids leads to the potentiation of the immunological activity of MDP, thus providing another approach to the development of a new family of immunologically active compounds.

Table 4. Adjuvant activity of MDP derivatives **9**, **10**, and **11** in delayed-type hypersensitivity to ABA-Tyr (100 μg) in guinea pigs

Compound[a]	Skin reaction (mm±s.e.)	
	24 h	48 h
9d	22.8±0.6	23.5±1.7
9e	25.0±1.3	26.3±1.6
9a	22.1±1.2	24.1±1.4
9b	24.3±0.7	28.9±1.3
9c	26.4±1.2	26.6±1.3
9d'	25.8±0.9	29.8±2.0
9a'	24.0±1.6	26.1±1.3
9b'	26.1±1.4	30.9±2.6
10	21.1±1.4	23.1±2.0
11	24.1±0.9	28.1±1.4
MDP	23.9±1.1	26.9±1.2
Control (ABA-Tyr+FIA)[b]	0	0

a) Dose: 100 μg. b) FIA: Freund's incomplete adjuvant.

Experimental

Optical rotations were determined with a Perkin-Elmer Model 141 polarimeter. NMR spectra were obtained on Varian EM-360 and EM-390 spectrometers. All chemicals and solvent were reagent grade and used without further purification. The reactions were monitored on TLC with Merck F_{254} silica-gel plates. Evaporation was carried out in a rotary evaporator under reduced pressure at temperatures below 45 °C.

All-trans-*3,7,11,15-tetramethyl-2,6,10,14-hexadecatetraen-1-ol (2a)*. Li (10.9 g, 2 g atom) was dissolved in $EtNH_2$ (300 ml) at −60 °C under N_2. After the solution became blue, a solution of all-*trans*-1-benzyloxy-3,7,11,15-tetramethyl-9-*p*-tolylsulfonyl-2,6,10,14-hexadecatetraene (**1a**) (21 g, 393 mmol) in anhydrous THF (40 ml) was added dropwise for 30 min. The mixture was stirred for 15 min at −60 °C, while blue color was kept. Isoprene (5 ml) and MeOH (100 ml) were carefully added to quench the excess Li. After the careful addition of water (500 ml), the organic solvents were evaporated. The residual aqueous solution was extracted with diisopropyl ether (150 ml×3). The organic layer combined was washed with water, and dried over Na_2SO_4. The solvent was evaporated and the resulting residue was purified by column chromatography (7×15 cm) on SiO_2 using hexane–diisopropyl ether (5:3, and then 1:2) as solvent: 10.9 g (95.6%) (Table 1). NMR ($CDCl_3$): 1.62 (9H, s), 1.70 (6H, s), 1.91—2.18 (12H, m), 4.15 (2H, d), 5.0—5.2 (3H, m), 5.43 (1H, t).

Other Multiprenyl Alcohols (*2b* and *2c*) were prepared from **1b** and **1c** in a similar manner.

All-trans-*3,7,11,15-tetramethyl-1-(*p*-tolylsulfonyl)-2,6,10,14-hexadecatetraene (4a)*. To a solution of **2a** (14.4 g, 49.6 mmol) in absolute THF (70 ml) was added a solution of PBr_3 (5.6 g, 20.7 mmol) in THF (70 ml) dropwise at −7—−10 °C. Then the mixture was stirred at the same temperature for 15 min. The solvent was evaporated and the residue was dissolved in hexane–diisopropyl ether (1:1, 200 ml). The solution was successively washed with 5% $NaHCO_3$ and water, and then dried over Na_2SO_4. The solvent was evaporated to give all-*trans*-1-bromo-3,7,11,15-tetramethyl-2,6,10,14-hexadecatetraene (**3a**). Without further purification, **3a** was dissolved in DMF (150 ml), and sodium *p*-toluenesulfinate tetrahydrate (24.8 g, 99.2 mmol) was added. After stirring for 1 h at room temperature, the mixture was diluted with hexane–diisopropyl ether (1:1, 400 ml), washed with water, and then dried over Na_2SO_4. After evaporation of the solvents, the resulting residue was purified by silica gel chromatography (6×25 cm) using hexane–diisopropyl ether (2:1) as solvent: 18.0 g (84.7%) (Table 1). NMR ($CDCl_3$): 1.36 (3H, d), 1.61 (9H), 1.68

(3H, s), 1.98—2.25 (12H, m), 2.44 (3H, s), 3.78 (2H, d), 5.10 (3H, m), 5.18 (1H, t), 7.31 and 7.74 (4H).

Compound ***4b*** was prepared from 2b in a similar manner.

*All-*trans*-1-benzyloxy-3,7,11,15,19,23-hexamethyl-9-(*p*-tolylsulfonyl)-2,6,10,14,18,22-tetracosahexaene (**1b**).* To a solution of **4a** (17.7 g, 41.3 mmol) and *trans,trans*-1-benzyloxy-8-chloro-3,7-dimethyl-2,6-octadiene (**5**) (13.1 g, 47 mmol) in absolute THF (100 ml)–DMF (12 ml) was added *t*-BuOK (6.96 g, 62 mmol) at −20 °C. After stirring for 20 min at the same temperature, the mixture was diluted with hexane–diisopropyl ether (1:1, 400 ml), and washed with 5% phosphoric acid (400 ml) and water, and then dried over Na_2SO_4. The solvent was evaporated, and the residue was chromatographed on a silica-gel column (5.5×20 cm) with hexane–diisopropyl ether (1:1) as an eluent: 24.6 g (88.9%) (Table 1). NMR ($CDCl_3$): 1.25 (3H, d), 1.55 (3H, s), 1.62 (12H, s), 1.70 (3H, s), 1.85—2.16 (16H, m), 2.44 (3H, s), 2.88 (2H, dd), 3.80 (1H, dd), 4.01 (2H, d), 4.50 (2H, s), 4.90 (1H, d), 4.95—5.24 (4H, m), 5.37 (1H, t), 7.30 and 7.71 (4H, m), 7.33 (5H, s).

Compound ***Ic*** was prepared from **4b** and **5** in a similar manner.

*Ethyl 2-Ethoxycarbonyl-all-*trans*-5,9,13,17,21,25-hexamethyl-4,8,12,16,20,24-hexacosahexaenate (**6b**)* and *Ethyl 2-(All-*trans*-3,7,11,15,19,23-hexamethyl-2,6,10,14,18,22-tetracosahexaenyl)-2-ethoxycarbonyl-all-*trans*-5,9,13,17,21,25-hexamethyl-4,8,12,16,20,24-hexacosahexaenate (**6b′**).* All-*trans*-3,7,11,15,19,23-hexamethyl-2,6,10,14,18,22-tetracosahexaen-1-ol (**2b**) (2.13 g, 5 mmol) was converted to the corresponding bromo-compound (**3b**) in a manner similar to that described in the synthesis of **4a**. To a solution of diethyl malonate (800 mg, 5 mmol) in absolute DMF (10 ml) NaH (240 mg, 5 mmol; 50% suspension in mineral oil) was added under N_2 with stirring. After stirring for 20 min at room temperature, the solution was cooled to −10 °C. A solution of **3b** in absolute THF (10 ml) was added dropwise at −10—−6 °C. After 30 min, the mixture was allowed to react at room temperature and stirring was continued for an additional 2 h. Water (100 ml) was carefully added and the solution was extracted with diisopropyl ether (100 ml). The organic layer was washed with water and dried over Na_2SO_4. The solvent was evaporated and the resulting residue was chromatographed on a silica-gel column (4.2×15 cm) with hexane–diisopropyl ether (15:1) to give pure **6b** and **6b′**: 1.09 g (38.0%) and 1.08 g (44.0%) (Table 2). NMR ($CDCl_3$) for 6b:1.27 (6H, t), 1.64 (21H, s), 1.88—2.19 (20H, m), 2.57 (4H, dd), 3.33 (1H, t), 4.17 (4H, q), 4.92—5.62 (6H, m).

*Other Esters (**6a**, **6a′**, **6c**, **6c′**, **6d**, and **6d′**)* were prepared from the appropriate alcohols and diethyl malonate in a similar manner. Geraniol for the preparation of **6d** and **6d′** was purchased from Wako Pure Chemical Industries, LTD, Osaka.

*2-(All-*trans*-3,7,11,15,19,23-hexamethyl-2,6,10,14,18,22-tetracosahexenyl)-all-*trans*-5,9,13,17,21,25-hexamethyl-4,8,12,16,20,24-hexacosahexaenoic Acid (**7b′**).* A solution of **6b′** (1.08 g, 1.1 mmol) in 1 M KOH–MeOH–THF (2:5:1, 22 ml) was heated under reflux for 100 h. After cooling to room temperature, 0.5 M HCl (50 ml) was added and the solution was extracted with AcOEt (40 ml). The organic layer was washed with water, dried over Na_2SO_4, and then evaporated. The residue (dicarboxylic acid) was dissolved in DMSO (5 ml) and the solution was heated at 150 °C for 20 min, during which time the evolution of CO_2 was completed. After cooling to room temperature, the mixture was diluted with H_2O (30 ml) and extracted with AcOEt–diisopropyl ether (1:1, 50 ml). The organic layer was washed with water, dried over Na_2SO_4, and evaporated. The resulting residue was chromatographed on a silica-gel column (3.8×6 cm) with hexane–diisopropyl ether (4:1): 720 mg (74.6%). (Table 2). NMR ($CDCl_3$): 1.61 (42H, s), 1.95—2.45 (45H, m), 4.95—5.21 (12H, m).

*Other Multiprenylacetic Acids (**7a**, **7a′**, **7b**, **7c**, **7c′**, **7d**, and **7d′**)* were prepared from the corresponding esters in a similar manner.

*N-Acetyl-6-O-[[2-(all-*trans*-3,7,11,15,19,23-hexamethyl-2,6,10,14,18,22-tetracosahexaenyl)-all-*trans*-5,9,13,17,21,25-hexamethyl-4,8,12,16,20,24-hexacosahexaenoyl]-L-leucyl]muramyl-α-aminoisobutyryl-D-isoglutamine (**9b′**).* To a solution of **7b′** (87.7 mg, 0.1 mmol) and HONB (21.6 mg, 0.12 mmol) in AcOEt–acetonitrile (1:1, 2 ml) was added DCC (24.7 mg, 0.12 mmol) at 0 °C. The mixture was stirred at 0 °C for 1 h and then at room temperature for 3 h. After filtration of precipitates, the solvent was evaporated. The resulting active ester, *N*-acetyl-6-*O*-(L-leucyl)muramyl-α-aminoisobutyryl-D-isoglutamine (**8**)[8] (62 mg, 0.1 mmol) and NEM (26 μl) were dissolved in DMF (1 ml), and the mixture was stirred at 60 °C for 70 h. After evaporation of the solvent, the residue was purified by chromatography on a column of silica gel (2×12 cm) with AcOEt–pyridine–AcOH–water (80:10:3:5), followed by rechromatography on a column of Sephadex LH-20 (1.5×90 cm) with EtOH as an eluent: 20 mg (13.5%) (Table 3).

*Other MDP Derivatives with Acylated Amino Acid (**9**)* listed in Table 3 were prepared from the appropriate carboxylic acids and MDP derivatives with an amino acid in a similar manner.

Biological Assays. Determination of the adjuvant activity on induction of delayed-type hypersensitivity was carried out according to the method described earlier.[13]

We wish to thank Dr. Masao Nishikawa of this division for discussion.

References

1) Part of this work was presented at the 7th Symposium on Progress in Organic Reactions and Syntheses, Gifu, November 1980, Abstr. P. 92. Abbreviations used are those recommended by IUPAC-IUB Commission on Biochemistry Nomenclature in July 1965 and 1966; *Biochemistry* **5**, 2435 (1966); **6**, 362 (1967). Other abbreviations: Aib=α-aminoisobutyric acid.

2) F. Ellouz, A. Adam, R. Ciorbaru, and E. Lederer, *Biochem. Biophys. Res. Commun.*, **59**, 1317 (1974); S. Kotani, Y. Watanabe, F. Kinoshita, T. Shimono, I. Morisaki, T. Shiba, S. Kusumoto, Y. Tarumi, and K. Ikenaka, *Biken J.*, **18**, 105 (1975).

3) Review: P. Dukor, L. Tarcsay, and G. Bascbang, "Annual Reports in Medicinal Chemistry," ed by H.-J. Hess, Academic Press, New York (1979), Vol. 14, p. 146; E. Lederer, *J. Med. Chem.*, **23**, 819 (1980).

4) Y. Yamamura, I. Azuma, K. Sugimura, M. Yamawaki, M. Uemiya, S. Kusumoto, S. Okada, and T. Shiba, *Proc. Jpn. Acad.*, **53**, 63 (1977); T. Shiba, S. Okada, S. Kusumoto, I. Azuma, and Y. Yamamura, *Bull. Chem. Soc. Jpn.*, **51**, 3307 (1978).

5) S. Kusumoto, M. Inage, T. Shiba, I. Azuma, and Y. Yamamura, *Tetrahedron Lett.*, **1978**, 4899.

6) S. Kobayashi, T. Fukuda, I. Imada, M. Fujino, I. Azuma, and Y. Yamamura, *Chem. Pharm. Bull.*, **27**, 3193 (1979).

7) W. A. Siddiqui, D. W. Taylor, S Ch. Kan, K. Kramer, S. M. Richmond-Crum, S. Kotani, T. Shiba, and S.

Kusumoto, *Science*, **201**, 1237 (1978); I. Azuma, M. Uemiya, I. Saiki, M. Yamawaki, Y. Tanio, S. Kusumoto, T. Shiba, T. Kusama, K. Tobe, H. Ogawa, and Y. Yamamura, "Immunobiology and Immunotherapy of Cancer," ed by W. D. Terry and Y. Yamamura, Elsevier North Holland Inc. (1979), p. 311.

8) S. Kobayashi, T. Fukuda, H. Yukimasa, I. Imada, M. Fujino, I. Azuma, and Y. Yamamura, *Bull. Chem. Soc. Jpn.*, **53**, 2917 (1980).

9) T. Fukuda, S. Kobayashi, H. Yukimasa, M. Fujino, I. Imada, I. Azuma, and Y. Yamamura, *Chem. Pharm. Bull.*, **29**, 2215 (1981).

10) S. Terao, K. Kato, M. Shiraishi, and H. Morimoto, *J. Chem. Soc. Perkin Trans. 1*, **1978**, 1101.

11) Y. Fujita, Y. Omura, T. Nishida, and K. Ito, Japan Patent, 76-29434 (1976).

12) M. Fujino, S. Kobayashi, M. Obayashi, T. Fukuda, S. Shinagawa, and O. Nishimura, *Chem. Pharm. Bull.*, **22**, 1857 (1974).

13) M. Uemiya, K. Sugimura, T. Kusama, I. Saiki, M. Yamawaki, I. Azuma, and Y. Yamamura, *Infect. Immun.*, **24**, 83 (1979).

Neighboring Group Participation in Solvolysis. XIII. Kinetic Isotope Effects in Solvolysis of 2-Arylethyl *p*-Nitrobenzenesulfonates[1,2]

Yasuhide YUKAWA, Takashi ANDO,* Katsuo TOKEN,† Mitsuru KAWADA, Kenichi MATSUDA, Seung-Geon KIM,†† and Hiroshi YAMATAKA

The Institute of Scientific and Industrial Research, Osaka University, Suita, Osaka 565

(Received May 29, 1981)

Carbon-14 kinetic isotope effects (k^{12}/k^{14}) were determined for the solvolysis of phenethyl (**1a**) and 2-(*p*-methoxyphenyl)ethyl (**1b**) *p*-nitrobenzenesulfonates in acetic, formic, and trifluoroacetic acids. Phenyl-1 carbon effects were all in the range of 1.02—1.04 except for the acetolysis of **1a** ($k^{12}/k^{14}=1.005$), which has been proved to proceed mainly *via* the aryl unassisted (k_s) pathway. In all other reactions, which proceed mainly *via* the aryl assisted (k_Δ) pathway, the phenyl-1 carbon apparently changes its bonding in the transition states. A large α-carbon effect (1.131) and a small β-carbon effect (1.013) as well as a medium phenyl-1 effect (1.022) were observed for the formolysis of **1b**, whose mechanism is thought to be exclusive k_Δ without troublesome ion-pair return. These observations, together with α- and β-deuterium effects reported already, enabled us to describe the qualitative nature of the bridged transition-state structure of the k_Δ pathway, *i.e.*, advanced C_α–O bond rupture, slight C_α–C_{Ph-1} bond formation, C_α–C_β double bond formation, slight C_β–C_{Ph-1} bond rupture, and breakdown of aromaticity at the phenyl-1 position. These characteristics are very similar to those of the phenonium ion.

After a long debate it has become a generally accepted idea that the solvolyses of all primary and most secondary 2-arylalkyl derivatives proceed through discrete aryl assisted (k_Δ) and/or aryl unassisted (k_s) pathways (Scheme 1).[3] A great deal of attention has been focused on the k_Δ pathway, since it can be regarded as a prototype of intramolecular catalysis, an important phenomenon in enzyme reactions, and also because it leads to the so-called phenonium ion intermediate whose structure has been a subject of discussion.[3] In 1969, we communicated the observation of normal carbon-14 kinetic isotope effects ($k^{12}/k^{14}>1.0$) of labeling at phenyl-1 in the solvolysis of 2-arylethyl *p*-nitrobenzenesulfonates (nosylates, **1**).[2] It was the first definitive evidence for the bonding change of the phenyl-1 carbon in the transition state of the reaction. Details of the study are described in the first half of this paper.

In order to obtain further detailed information concerning the structure of the transition state of the k_Δ pathway, it is desirable to observe kinetic isotope effects of labeling at several different atoms of 2-arylethyl esters. This type of approach is referred to as the successive labeling technique.[4] The first study along these lines has been carried out with 2-methyl-2-phenylpropyl (neophyl) esters (**2**).[5,6]

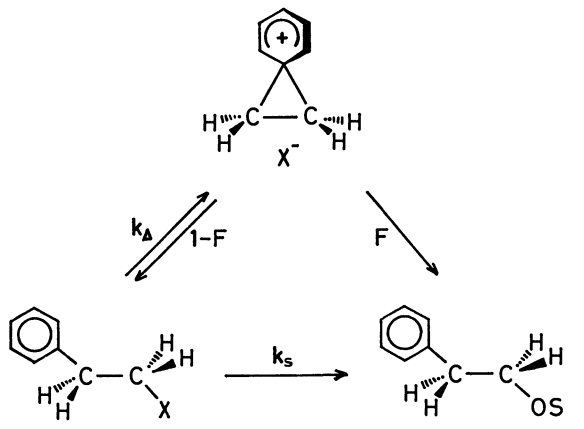

Scheme 1.

$ArCH_2CH_2OSO_2Ar'$

1a: $Ar=C_6H_5$, $Ar'=p\text{-}NO_2C_6H_4$

b: $Ar=p\text{-}CH_3OC_6H_4$, $Ar'=p\text{-}NO_2C_6H_4$

$ArC(CH_3)_2CH_2OSO_2Ar'$

2

Introduction of two methyl groups on the β-carbon of **1** not only causes the reaction to proceed *via* the k_Δ pathway almost exclusively but also inhibits scrambling of labels at α and β during the course of the reaction of **2**.[7,8] Thus, kinetic isotope effects have been successfully measured for α-^{14}C, α-D_2, β-^{14}C as well as phenyl-1-^{14}C in the solvolysis of **2**,[5,6] and the transition-state structure has been discussed both qualitatively and quantitatively using these data.[6]

In the present study, the successive labeling technique was extended to the parent 2-arylethyl system. The transition-state structure of the k_Δ pathway of 2-arylethyl esters is discussed with the kinetic isotope effects measured for the formolysis of 2-(*p*-methoxyphenyl)-ethyl nosylate (**1b**), and compared with that for the neophyl solvolysis.

Results

Labeling with carbon-14 at the specific carbons of phenethyl nosylate (**1a**) and 2-(*p*-methoxyphenyl)ethyl nosylate (**1b**) was performed by well-established procedures (see Experimental Section). The solvolyses of **1a** and **1b** in acetic, formic, and trifluoroacetic acids were followed by the gravimetric method, in which unreacted nosylates were recovered from the reaction solutions at various fractions of reaction, ranging from 0 to 70 or 80%. The recovery was quantitative for **1a** and almost so for **1b**; in the latter case the recovery factor was used in order to determine the fractions of reaction. The formolysis of **1b** was also followed by the spectrophotometric method. The rate con-

† Present address: Faculty of Science, Toyama University, Gofuku, Toyama 930.

†† Present address: Faculty of Science, Tokai University, Kitakaname, Hiratsuka, Kanagawa 259-12.

Table 1. Rate constants and carbon-14 kinetic isotope effects in solvolysis of phenethyl nosylate (**1a**) and 2-(*p*-methoxyphenyl)ethyl nosylate (**1b**)

Substrate	Label	Solvent	t/°C[a]	$k\times10^5$/s^{-1}	(r)[b]	k^{12}/k^{14}	n[c]	(r)[d]
1a	Phenyl-1[e]	CH_3CO_2H	100	4.65±0.04	(0.9997)	1.005±0.002	5	(0.76)
1a	Phenyl-1[e]	HCO_2H	60	6.67±0.07	(0.9997)	1.023±0.001	6	(0.994)
1a	Phenyl-1[e]	CF_3CO_2H	45	9.7±0.9	(0.97)	1.029±0.002	5	(0.991)
1a	Phenyl-1[e]	CF_3CO_2H[f]	30	5.96±0.12	(0.9992)	1.036±0.004	4	(0.991)
1b	Phenyl-1[g]	CH_3CO_2H	60	2.63±0.02	(0.9998)	1.028±0.002	5	(0.996)
1b	Phenyl-1[g]	HCO_2H	30	12.1±0.1	(0.9994)	1.022±0.002	5	(0.991)
1b	Phenyl-1[g]	CF_3CO_2H[f]	0[h]	3.24±0.04	(0.9996)	1.039±0.014	3	(0.94)
1b	α[i]	HCO_2H	30	12.2±0.1[j]	(0.998)	1.131±0.002	7	(0.998)
1b	β[i]	HCO_2H	30	12.2±0.1[j]	(0.998)	1.013±0.002	7	(0.96)

a) ±0.02 °C unless otherwise noted. b) Correlation coefficients of pseudo-first order rate plots. c) Number of radioassayed samples recovered at various fractions of reaction. See Ref. 10. d) Correlation coefficients for fit of radioactivities to Eq. 1. in the text. e) Substrate in 0.065 M (1M=1 mol dm^{-3}). f) Sodium trifluoroacetate (0.1 M) was added. g) Substrate in 0.059 M. h) ±0.1 °C. i) Substrate in 0.05 M. j) Determined spectrophotometrically.

stants obtained by these two methods agreed very well with each other. The linearity of the first-order rate plot for the trifluoroacetolysis of **1a** was rather poor in the absence of sodium trifluoroacetate, but it was much improved when the sodium salt was added to the reaction medium.

Carbon-14 kinetic isotope effects were determined according to the procedures described previously.[6] Calculation of isotope effects was carried out by the linear regression method using

$$\log A_x = \log A_0 - [1-(k^{14}/k^{12})]\log(1-x), \quad (1)$$

where x is the fraction of reaction, and A_0 and A_x are the molar radioactivities of the initial and recovered esters, respectively.[9,10] The results of kinetic isotope effects are summarized together with rate data in Table 1.

Discussion

Phenyl-1 carbon isotope effects were measured in seven cases for different substrates, solvents, and temperatures (Table 1). All the values were in the range of 1.02—1.04 except for the acetolysis of **1a**, for which a very small value close to unity (1.005) was obtained. Dissection of the rate constants (k_t) of the 2-arylalkyl solvolysis into the aryl assisted (Fk_Δ) and aryl unassisted (k_s) components has been carried out by a number of research groups.[3] They found that only the acetolysis of the phenethyl ester among all the systems studied here proceeds mainly *via* the k_s pathway,[11-14] although the dissection was usually studied not for nosylates but for tosylates or brosylates. The fraction of the k_Δ pathway (Fk_Δ/k_t) for the acetolysis of phenethyl tosylate was estimated to be 0.30—0.42 at 115 °C.[11-14] Because no bonding change for the phenyl-1 carbon is expected in the transition state of the k_s pathway, no isotope effect should be observed for this carbon. Thus, our observation of a small isotope effect in the acetolysis of **1a** is well in accord with the dissection studies by the tracer[11-13] or kinetic[14] method.

All the other values of the phenyl-1 carbon-14 isotope effects (1.02—1.04) definitely show that the bonding of the phenyl-1 carbon changes in the transition state of these reactions. Among these values, those for the trifluoroacetolysis (1.03—1.04) were slightly larger than those for the acetolysis or formolysis (1.02—1.03, Table 1). A similar phenomenon was also observed in the solvolysis of **2**; the phenyl-1 carbon-14 effect was 1.035 for the trifluoroacetolysis at 0 °C and 1.023 for the acetolysis at 75 °C.[5] Although the solvent effect on the isotope effects can not be completely neglected, since weaker solvation to the cationic moiety in a less nucleophilic solvent such as trifluoroacetic acid would result in decreased bonding and thus larger isotope effects, most of the difference in these isotope effects is likely to be attributable to the temperature dependence of the isotope effects. Trifluoroacetolysis was always carried out at a lower temperature than acetolysis and formolysis by 55—75 °C, and a definitive normal temperature dependence (a larger isotope effect at a lower temperature) was observed for this phenyl-1 carbon-14 effect in the acetolysis of **2**.[6] As a reported increase of the isotope effect was 0.003 for a decrease in temperature of 15 °C or 0.008 for 35 °C, the observed difference of 0.01 for **1** can be reasonably attributed to a difference in temperature of 55—75 °C.

In order to carry out the successive labeling study in the parent 2-arylethyl system, it is necessary to measure kinetic isotope effects in a solvolysis, in which the reaction not only proceeds exclusively *via* the k_Δ pathway, but is also free from an ion-pair return which is liable to cause scrambling of labels. The formolysis of **1b** is fitted for this purpose. According to the tracer study carried out with carbon-14 by Jenny and Winstein,[15] the formolysis of 2-(*p*-methoxyphenyl)ethyl tosylate proceeds exclusively *via* the k_Δ pathway ($Fk_\Delta/k_t=1.0$) without any ion-pair return ($F=1.00$). The strong ionizing power and the considerable nucleophilicity of formic acid as well as the fairly strong nucleophilicity of the neighboring *p*-methoxyphenyl group may be the reasons for this unique situation. Taking advantage of this, Saunders and Glaser have already studied secondary α- and β-deuterium isotope effects in this formolysis;[16] we

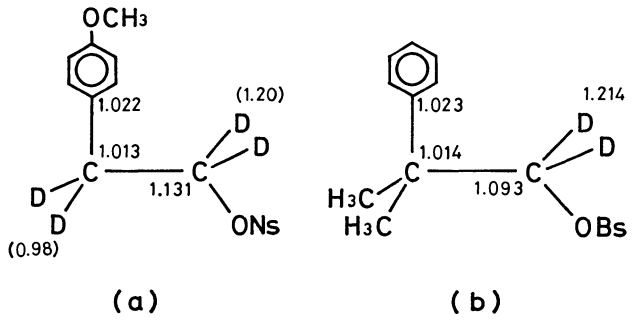

Fig. 1. Carbon-14 and deuterium isotope effects in the solvolysis of (a) 2-(*p*-methoxyphenyl)ethyl nosylate (**1b**) in formic acid at 30 °C, and (b) neophyl brosylate (**2**) in acetic acid at 75 °C. Deuterium effects in (a) are those reported by Saunders *et al.*[16] for the tosylate.

will use their results in our discussion.

Kinetic isotope effects observed in the formolysis of **1b** are summarized in Fig. 1, together with those reported for the acetolysis of **2** for comparison.[5]

It is obvious from Fig. 1 that the isotope effects for various atoms of **1b**, *i.e.*, a large α-^{14}C, medium α-D_2, small β-^{14}C, and medium phenyl-1-^{14}C effects, are almost the same as those for the corresponding atoms of **2**. These observations not only support the results of the dissection studies[7,8,15] that both the formolysis of **1b** and the acetolysis of **2** proceed *via* the k_Δ mechanism, but also indicate that the transition-state structures of both reactions are almost identical. This conclusion confirms the general assumption that neophyl solvolysis can be regarded as a model of the k_Δ process for phenethyl solvolysis.[13,17-19] Thus, the characteristics of the transition-state structure of **1b** can be discussed below in a similar manner to those of **2**[6] by use of the observed data of kinetic isotope effects.

The magnitude of the phenyl-1 carbon-14 effect, 1.022, is within the range (1.02—1.05) observed for the phenyl-1 carbon in a number of phenyl group rearrangements whose mechanisms have been proved to be concerted.[20-23] It is interesting that these medium carbon-14 effects show normal temperature dependence as mentioned above and as observed in the Beckmann rearrangement of acetophenone oxime.[23] When the bonding at the labeled position increases in the transition state, the isotope effect could be small normal, null, or even inverse, and the temperature dependence should be inverse. Thus, the total bonding of the phenyl-1 carbon should decrease, in spite of the hybridization change of this carbon from sp^2 to sp^3. In conclusion, the phenyl-1 carbon changes its bonding in the transition state of the k_Δ solvolysis as a result of C_{Ph-1}–C_α bond formation, breakdown of aromaticity in the benzene ring, and C_{Ph-1}–C_β bond rupture, among which the last two overwhelm the first one.

A large α-carbon-14 isotope effect comparable to those observed in S_N2[24] and a medium α-deuterium effect in contrast to large values for S_N1 and small ones for S_N2 are most characteristic of the k_Δ mechanism.[5,6,25] The importance of symmetry for a carbon isotope effect has been demonstrated in the S_N2 reaction,[26] in which the isotope effect of the central carbon atom becomes maximum when the two partial bonds are equal in strength. The magnitude of an α-deuterium effect is dependent on the vibrational frequencies of the bending motions including the C–H bond, and a larger effect is observed for a looser transition state.[27] Thus, the observed α-effects are compatible with a loose, pseudo-three-centered transition state composed of the phenyl-1 carbon, the α-carbon, and the oxygen of the leaving arenesulfonate.[5,6,25]

The difference between the α-carbon-14 effects for **1b** (1.131) and **2** (1.093), the only apparent difference in Fig. 1, is larger than that expected for the temperature dependence of this effect, since the reported increase in the effect is 0.004 for a decrease of 15 °C in the acetolysis temperature of **2**.[6] The difference in the solvent, formic acid *vs.* acetic acid, wolud not have much influence on the isotope effects. Therefore, the rest of the difference in the α-carbon-14 isotope effects may be attributed to the substituent effect of the phenyl group on the symmetry of the three-centered transition state.[6] The transition-state structure of **1b** may be more symmetric than that of **2** in terms of the breaking C_α–O bond and the forming C_α–C_{Ph-1} bond, resulting in a larger α-carbon isotope effect. Participation by the unsubstituted phenyl group in **2**, which is less nucleophilic than the *p*-methoxyphenyl group in **1b**, may lead to a later transition state with a stronger C_α–C_{Ph-1} bond and a weaker C_α–O bond, giving rise to a smaller isotope effect.[6,26]

A small β-carbon-14 isotope effect, 1.013, is consistent with small but distinct bonding changes at this carbon, which may include C_{Ph-1}–C_β bond rupture and C_α–C_β double bond formation.[28] It is interesting that this change has not been detected by the β-deuterium effect.[16] Quite recently, we observed negative CD_3 effects in the solvolysis of [γ-D_6]-**2** (0.959 per D_6 in acetic acid at 75 °C), which were attributed to the inductive effect by these nonmigrating methyl groups.[1] Nevertheless, the β-carbon-14 isotope effects of **1b** and **2** did not show any appreciable difference. The fact suggests that the inductive effect exerted on the β-carbon by the methyl groups may not greatly alter the structure of the transition state in this solvolytic rearrangement, although the rate of the reaction itself is enhanced to a great extent in the presence of these methyl groups.[29]

All of the above enable us to describe the qualitative nature of the transition-state structure of the k_Δ pathway in the phenethyl solvolysis as follows: (1) C_α–O bond rupture is well advanced, (2) the neighboring phenyl group behaves as an intramolecular nucleophile but C_α–C_{Ph-1} bond formation is not advanced, (3) the aromatic π-electron system of the phenyl group has broken down as a result of the participation, and (4) geometrical changes at C_β are small but may include partial C_β–C_{Ph-1} bond rupture and C_α–C_β double bond formation. Although a bridged ion intermediate does not necessarily follow this bridged transition state of the k_Δ solvolysis, as exemplified in the case of the

neophyl solvolysis, in which the rearranged tertiary cation is believed to be the first intermediate, it is important to point out that the phenonium ion, whose structure was estimated by molecular orbital calculations,[30,31] can be attained with the least structural changes from this transition state.

Experimental

Materials. [*phenyl*-1-^{14}C]Phenethyl alcohol was prepared from [*phenyl*-1-^{14}C]benzoic acid *via* benzoyl chloride, α-diazoacetophenone, and methyl phenylacetate; the last step made use of the Wolff rearrangement in methanol.[32] Esterification of the phenethyl alcohol with *p*-nitrobenzenesulfonyl chloride in pyridine gave [*phenyl*-1-^{14}C]-**1a**. The multistep synthesis of 2-(*p*-methoxy[*phenyl*-1-^{14}C]phenyl)ethyl nosylate ([*phenyl*-1-^{14}C]-**1b**) from [*phenyl*-1-^{14}C]toluene has already been reported.[33] 2-(*p*-Methoxyphenyl)ethyl nosylates labeled with carbon-14 at the α- and β-carbons ([α-^{14}C]- and [β-^{14}C]-**1b**, respectively) were prepared from *p*-methoxybenzyl cyanide (**3**) labeled at the cyanide- and benzyl-carbons, respectively, *via* acid hydrolysis, esterification with methanol, reduction with lithium aluminum hydride, and esterification with *p*-nitrobenzenesulfonyl chloride, successively. One of the precursors, [*cyanide*-^{14}C]-**3**, was synthesized from the reaction of *p*-methoxybenzyl chloride with sodium [^{14}C]cyanide.[34] The other, [*benzyl*-^{14}C]-**3**, was prepared by cyanation of *p*-methoxyphenyl bromide with copper(I) [^{14}C]cyanide[35,36] followed by hydrolysis, esterification, reduction, chlorination, and cyanation.[34] The chemical purity of the labeled compounds was verified by comparison of their physical constants and spectroscopic data with those for the unlabeled compounds. All ^{14}C labeled compounds had molar radioactivities of about 1.3—2.7 mCi/mol. The final arenesulfonates were carefully purified by repeated recrystallization until the molar activities remained constant. Phenethyl nosylate (**1a**): mp 102—103 °C (from hexane–carbon tetrachloride). 2-(*p*-Methoxyphenyl)ethyl nosylate (**1b**): mp 100.0—100.5 °C (from hexane–carbon tetrachloride or hexane–benzene).

Solvolysis Media. Acetic acid was refluxed over 2.0 wt% potassium permanganate, fractionally distilled, and the middle cut was refluxed with 1% pure acetic anhydride followed by fractional distillation (bp 119.1—119.3 °C).[37] Formic acid was purified according to the procedure described by Winstein and Marshall (bp 28.0—29.0 °C/6.60 kPa).[38] Trifluoroacetic acid was distilled through a 1 m, vacuum-jacketed column packed with glass helices. To the middle cut (bp 72.2—72.4 °C) was added 1 wt% freshly distilled trifluoroacetic anhydride.[39] Buffered medium (1.0 dm^3) was prepared by dissolving 0.1 mol of sodium trifluoroacetate in the above trifluoroacetic acid.

Quantitative Recovery of Nosylates ***1a*** *and* ***1b***. About 100 mg of **1a** or **1b** was weighed in a flask and dissolved in 11—30 cm^3 of solvolysis media. Cold distilled water (5 to 20 times the volume of the media used) was added to the solution, and the mixture was left overnight in a refrigerator. Precipitates of **1a** or **1b** were filtered with a weighed glass filtering crucible, washed thoroughly with cold distilled water, dried overnight in an oven at 70 °C (for **1a**) or in a vacuum desiccator over phosphorus pentaoxide (for **1b**), and weighed. The recovery of **1a** was 99.3±0.5% (acetic acid), 99.7±0.3% (formic acid), and 99.1±0.9% (trifluoroacetic acid), and that of **1b** was 97.6±0.1% (acetic acid), 98.4±0.1% (formic acid), and 95.9±1.4% (trifluoroacetic acid).

Kinetic Procedures. Samples of starting material large enough to yield about 100 mg unreacted esters after preselected fractions of reaction, ranging from 0 to 80% completion, were delivered to individual ampoules, dissolved in suitable volumes of the reaction media, and the ampoules were sealed. The reaction was started by placing the ampoules in a constant temperature bath, and quenched by cooling them in an ice bath or a Dry Ice–acetone mixture. After breaking the seal, the contents and the washings of the ampoules (5 cm^3 of the reaction media) were poured into cold water (5 to 20 times the combined volume of the reaction solution and the washing). After standing overnight in a refrigerator, the precipitates (unreacted esters) were filtered with a glass filtering crucible, and then treated as described above. The fractions of reaction were determined from the quantities of the samples used and recovered. For **1b** the recovery factors of 1.025 (acetic acid), 1.016 (formic acid), and 1.043 (trifluoroacetic acid) were used. Data points measured were usually seven.

The rate of formolysis of **1b** was also determined by a spectrophotometric method similar to that used for trifluoroacetolysis by Peterson,[40] in which the increase in the absorbance at 275 nm was followed. The rate constant determined by this method agreed very well with that determined by the gravimetric method (Table 1).

Radioactivity Measurement. The recovered precipitates of unreacted esters were recrystallized repeatedly, usually four times. The purified esters (5—10 mg) were oxidized in a modified Pregl micro combustion furnace,[41] and the ionization current of the radioactive carbon dioxide gas thus generated was measured in an ionization chamber (250 cm^3 capacity, Nuclear-Chicago) with a vibrating-reed electrometer (Nuclear-Chicago Model 6000 Dynacon electrometer system). The rate-of-charge method using a Model T4 interval timer was applied.[41] For the formolysis of [α-^{14}C]- and [β-^{14}C]-**1b**, the ionization current was measured with a Takeda Riken TR-84M vibrating-reed electrometer connected with a digital voltmeter and a computer.[6] It was confirmed that further recrystallization did not change the radioactivities beyond experimental errors.

References

1) For Part 12, see T. Ando, H. Yamataka, H. Morisaki, J. Yamawaki, and Y. Yukawa, *J. Am. Chem. Soc.*, **103**, 430 (1981).

2) Part of this work appeared in communication form: Y. Yukawa, T. Ando, K. Token, M. Kawada, and S.-G. Kim, *Tetrahedron Lett.*, **1969**, 2367; Y. Yukawa, T. Ando, M. Kawada, K. Token, and S.-G. Kim, *ibid.*, **1971**, 847.

3) For a review, see C. J. Lancelot, D. J. Cram, and P. v. R. Schleyer in "Carbonium Ions," ed by G. A. Olah and P. v. R. Schleyer, Interscience, New York (1972), Chap. 27.

4) A. Fry, *Pure Appl. Chem.*, **8**, 409 (1964).

5) Y. Yukawa, S.-G. Kim, and H. Yamataka, *Tetrahedron Lett.*, **1973**, 373; H. Yamataka, S.-G. Kim, T. Ando, and Y. Yukawa, *ibid.*, **1973**, 4767.

6) T. Ando, S.-G. Kim, K. Matsuda, H. Yamataka, Y. Yukawa, A. Fry, D. E. Lewis, L. B. Sims, and J. C. Wilson, *J. Am. Chem. Soc.*, **103**, 3505 (1981).

7) R. Heck and S. Winstein, *J. Am. Chem. Soc.*, **79**, 3432 (1957).

8) W. H. Saunders, Jr., and R. H. Paine, *J. Am. Chem. Soc.*, **83**, 882 (1961).

9) V. F. Raaen, G. A. Ropp, and H. P. Raaen, "Carbon-14," McGraw-Hill, New York (1968), Chap. 5.

10) Although the accuracy of radioactivity measurement

has been improved to a great extent in recent years, we still recommend measuring the activities of as many samples as possible, at least five or more, which are recovered from a wide range of the fractions of reaction in order to obtain accurate values of carbon-14 kinetic isotope effects. Unfortunately, it was impossible in some cases of the trifluoroacetolyses in the present study.

11) J. L. Coke, F. E. McFarlane, M. C. Mourning, and M. G. Jones, *J. Am. Chem. Soc.*, **91**, 1154 (1969).
12) M. G. Jones and J. L. Coke, *J. Am. Chem. Soc.*, **91**, 4284 (1969).
13) R. J. Jablonski and E. I. Snyder, *J. Am. Chem. Soc.*, **91**, 4445 (1969).
14) J. M. Harris, F. L. Schadt, P. v. R. Schleyer, and C. J. Lancelot, *J. Am. Chem. Soc.*, **91**, 7508 (1969).
15) E. F. Jenny and S. Winstein, *Helv. Chim. Acta*, **41**, 807 (1958).
16) W. H. Saunders, Jr., and R. Glaser, *J. Am. Chem. Soc.*, **82**, 3586 (1960).
17) A. Diaz, I. Lazdins, and S. Winstein, *J. Am. Chem. Soc.*, **90**, 6546 (1968).
18) F. L. Schadt, III, C. J. Lancelot, and P. v. R. Schleyer, *J. Am. Chem. Soc.*, **100**, 228 (1978).
19) S. Winstein and R. Heck, *J. Am. Chem. Soc.*, **78**, 4801 (1966).
20) T. Imamoto, S.-G. Kim, Y. Tsuno, and Y. Yukawa, *Bull. Chem. Soc. Jpn.*, **44**, 2776 (1971).
21) A. Fry "Isotope Effects in Chemical Reactions," ed by C. J. Collins and N. S. Bowman, Van Nostrand Reinhold, New York (1970), Chap. 6.
22) B. W. Palmer and A. Fry, *J. Am. Chem. Soc.*, **92**, 2580 (1970).
23) S.-G. Kim, T. Kawakami, T. Ando, and Y. Yukawa, *Bull. Chem. Soc. Jpn.*, **52**, 1115 (1979).
24) M. L. Bender and D. F. Hoeg, *J. Am. Chem. Soc.*, **79**, 5649 (1957); G. J. Buist and M. L. Bender, *ibid.*, **80**, 4308 (1958).
25) C. J. Collins, B. M. Benjamin, M. Hanack, and H. Stutz, *J. Am. Chem. Soc.*, **99**, 1669 (1977).
26) H. Yamataka and T. Ando, *Tetrahedron Lett.*, **1975**, 1059; *J. Am. Chem. Soc.*, **101**, 266 (1979); *J. Phys. Chem.*, **85**, 2281 (1981).
27) A. Streitwieser, Jr., R. H. Jagow, R. C. Fahey, and S. Suzuki, *J. Am. Chem. Soc.*, **80**, 2336 (1958).
28) Bonding changes at the β-carbon were fully discussed and quantitatively described for the neophyl ester **2**.[6]
29) S. Winstein, C. R. Lindegren, H. Marshall, and L. L. Ingraham, *J. Am. Chem. Soc.*, **75**, 147 (1953); A. H. Fainberg and S. Winstein, *ibid.*, **78**, 2763 (1956).
30) W. J. Hehre, *J. Am. Chem. Soc.*, **94**, 5919 (1972).
31) E. I. Snyder, *J. Am. Chem. Soc.*, **92**, 7529 (1970).
32) Y. Yukawa and T. Ibata, *Bull. Chem. Soc. Jpn.*, **42**, 802 (1969).
33) Y. Yukawa, K. Token, and T. Ando, *Radioisotopes*, **27**, 527 (1978).
34) L. Friedman and H. Shechter, *J. Org. Chem.*, **25**, 877 (1960).
35) W. R. Vaughan and D. I. McCane, *J. Am. Chem. Soc.*, **76**, 2504 (1954).
36) L. Friedman and H. Shechter, *J. Org. Chem.*, **26**, 2522 (1961).
37) S. Winstein, C. Hanson, and E. Grunwald, *J. Am. Chem. Soc.*, **70**, 812 (1948).
38) S. Winstein and H. Marshall, *J. Am. Chem. Soc.*, **74**, 1120 (1952).
39) J. E. Nordlander and W. G. Deadman, *J. Am. Chem. Soc.*, **90**, 1590 (1968).
40) P. E. Peterson, R. E. Kelly, Jr., R. Belloli, and K. A. Sipp, *J. Am. Chem. Soc.*, **87**, 5169 (1965).
41) V. F. Raaen, G. A. Ropp, and H. P. Raaen, "Carbon-14," McGraw-Hill, New York (1968), Chap. 11.

Reactions of Ketone Hydrazones and β-Keto Enamines with Disulfur Dichloride. New Synthesis of Thioketones and 5*H*-1,2,3-Dithiazoles

Renji Okazaki,* Kaoru Inoue, and Naoki Inamoto

Department of Chemistry, Faculty of Science, The University of Tokyo, Hongo, Bunkyo-ku, Tokyo 113

(Received June 19, 1981)

Ketone hydrazones react with disulfur dichloride in the presence of triethylamine to afford thioketones in good yields. The reaction mechanism involving *N*-thiosulfinylamine ($R_2C{=}N{-}N{=}S{=}S$) and *S*-thioxothioketone ($R_2C{=}S{=}S$) is proposed. The formation of di-*t*-butyl and di-1-adamantyl thioketones even at low temperatures has been interpreted as steric congestion alone being not enough to stabilize the corresponding *S*-thioxothioketones. The reaction of β-ketoenamines with disulfur dichloride gives 5*H*-1,2,3-dithiazoles *via* intramolecular cyclization of intermediary *N*-thiosulfinylamines.

We previously reported an interesting ring-chain tautomerism for *N*-thiosulfinylaniline **1a** which was prepared by reaction of disulfur dichloride with the corresponding aniline;[1] **1a** is in equilibrium with **1b** in solution, while only **1b** exists in the solid state.[2] The conversion of **1a** to **1b** can be regarded as intramolecular 1,3-dipolar cycloaddition of the *N*-thiosulfinyl group[3] or electrocyclization of 1,5-dipole.[4]

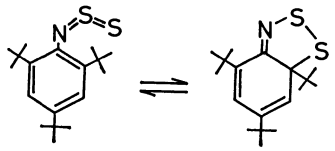

1a **1b**

Such a facile cyclization at the expense of loss of aromaticity observed for **1a** suggests that similar cyclizations are expected to occur also in other systems having X=Y–N=S=S structure.

We report in this paper that the reaction of ketone hydrazones and β-keto enamines with disulfur dichloride indeed proceeds *via* intramolecular cyclization of the *N*-thiosulfinyl group to form thioketones and 5*H*-1,2,3-dithiazoles, respectively.[5]

Results and Discussion

Reactions of Ketone Hydrazones with Disulfur Dichloride. Since a ketone hydrazone is considered to react with disulfur dichloride to give *N*-thiosulfinylamine **2**, which would undergo intramolecular cyclization in view of the tautomerism of **1**, we reasoned that this reaction would provide a route to a hitherto unknown *S*(IV)-thiocumulene, *S*-thioxothioketone **3**.[6]

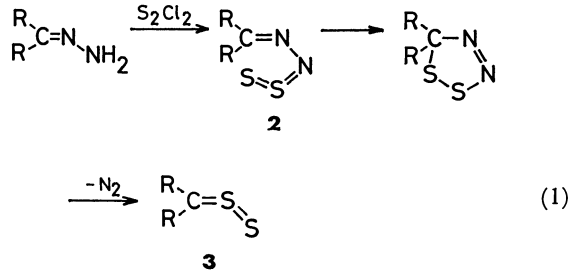

2

3 (1)

The reaction occurred, as expected, smoothly at a low temperature, but the product was not *S*-thioxothioketone but thioketone. For example, simultaneous addition of benzene solutions of di-*t*-butyl ketone hydrazone and disulfur dichloride to a benzene solution of triethylamine at 0 °C afforded di-*t*-butyl thioketone in 96% yield. The formation of di-*t*-butyl thioketone is most probably due to loss of a sulfur atom from the expected thioxothioketone which is unstable at the reaction temperature.

In the hope that the reaction at lower temperatures would enable the isolation of the thioxothioketone, the same reaction was carried out at −85 °C with toluene as solvent, but the product was again di-*t*-butyl thioketone (97%). The reaction using di-1-adamantyl ketone hydrazone in toluene at −90 °C also gave di-1-adamantyl thioketone (pink crystals, 71%). These reactions proceeded very fast, and the color due to the thioketones appeared during the addition of the reagents, suggesting that the thioxothioketone was too unstable to decompose into the thioketone even at such low temperatures.

Decomposition of *S*(IV)-thiocumulenes with loss of sulfur is generally believed[7] to proceed *via* cyclization into a three-membered ring as shown below and, therefore, such a change as from 3-coordinated to 4-coordinated carbon would be less favorable as R group becomes bulkier.

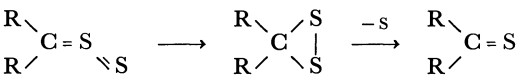

The failure of formation of thioxothioketone having such a bulky group as *t*-butyl or 1-adamantyl suggests that the steric congestion alone is not enough to stabilize the thioxothioketone.

It is known that as the electronegativity of X in thiocumulenes X=S=O or X=S=N–R increases, the S=O bond in the former or the S=N bond in the latter becomes stronger as suggested by shortening of the bond length.[8] If this is the case with the thioxothioketone, then the use of a hydrazone bearing strongly electron-withdrawing substituents is expected to lead to a more stable thiocumulene. To this end, hexafluoroacetone hydrazone (**4**)[9] was allowed to react with disulfur dichloride at −23 °C, but thioxothioketone **6** was not formed, the only characterizable

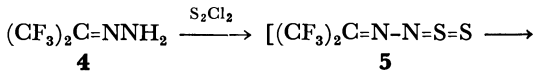

4 **5**

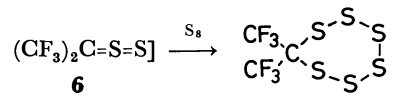

6 **7**

product being 7,7′-bis(trifluoromethyl)-1,2,3,4,5,6-hexathiacycloheptane (**7**) (3%) along with some sulfur.

A reaction closely related to the above has been reported;[10] *N*,*N*-bis(trimethylsilyl)sulfonamides **8** react with disulfur dichloride to give an eight-membered heterocycle **10**. Since the formation of **10** is explained by the reaction of thiosulfinylamine intermediate **9** with sulfur formed during the reaction,[10] a similar

$$\underset{\mathbf{8}}{R_2N\text{-}SO_2\text{-}N(SiMe_3)_2} \xrightarrow{S_2Cl_2} \underset{\mathbf{9}}{[R_2N\text{-}SO_2\text{-}N{=}S{=}S]} \xrightarrow{S_8} \underset{\mathbf{10}}{R_2NSO_2\text{-}N\langle S_5\rangle}$$

mechanism *via* **5** and **6** is thought to be operative in the formation of **7**.

An attempt to trap **6** by cycloaddition with dibenzoylacetylene was unsuccessful.[3]

Although the reaction of ketone hydrazones with disulfur dichloride did not give expected *S*-thioxothioketones, the formation of thioketones in good yields indicates that the present reaction provides a simple, new method for the synthesis of thioketones from hydrazones and the results using some hydrazones are listed in Table 1.

Table 1. Synthesis of thioketones from hydrazones ($R^1R^2C{=}NNH_2$)[a]

Hydrazones		Yield/% of thioketones	
R^1	R^2	UV	Isolated
t-Bu	*t*-Bu	Quant.	66
1-Ad[b]	1-Ad	71	59
$-Me_2CCH_2CH_2CMe_2-$[c]		Quant.	58
$C_{10}H_{16}$[d]		Quant.	54
$C_{10}H_{16}$[e]		63	
Ph	Ph	54	

a) The reactions were carried out in benzene at 5 °C except for di-1-adamantyl ketone hydrazone, where the reaction was done in toluene at −90 °C. b) 1-Ad denotes 1-adamantyl. c) 2,2,5,5-Tetramethylcyclopentanone hydrazone. d) Fenchone hydrazone. e) Camphor hydrazone.

The yields for sterically hindered thioketones are usually excellent although isolated yields are somewhat diminished. The simultaneous addition of the both substrates has to be done to get a good yield of thioketones. For example, the simultaneous addition method gave thiobenzophenone in 54% yield while the addition of a benzene solution of a hydrazone and triethylamine to disulfur dichloride in benzene formed the thioketone in 8%; the yield was 37% when the reverse addition was used.

The solvent effect of this reaction is remarkable. Although the reactions of di-*t*-butyl ketone hydrazone with disulfur dichloride in benzene and toluene gave di-*t*-butyl thioketone in 96 and 97% respectively as previously described, those in dichloromethane and ether resulted in the yields of 39 and 37% respectively. Thus, the aromatic hydrocarbon is a solvent of choice in the present reaction.

Another preparative method of thioketones from hydrazones, which uses the reaction of phosphoranes with sulfur, has recently been reported,[11] but we believe that the present method is simpler in manipulation and the reaction conditions are milder.

Although the pathway *via* thioxothioketone (Eq. 1) is considered to be a most likely mechanism for the formation of thioketones, other two mechanisms are also conceivable. One is oxidation of a hydrazone with disulfur dichloride to give a diazomethane, followed by the reaction with sulfur (Eq. 2)[12] and the other involves loss of the terminal sulfur from *N*-thiosulfinylamine intermediate to give thionitroso compound **11** followed by cyclization and loss of nitrogen molecule (Eq. 3).

$$R_2C{=}NNH_2 \xrightarrow{S_2Cl_2} R_2C{=}\overset{+}{N}{=}\overset{-}{N} \xrightarrow[-N_2]{S_8} R_2C{=}S \qquad (2)$$

$$R_2C{=}NNH_2 \xrightarrow{S_2Cl_2} \underset{\mathbf{11}}{R_2C{=}N\text{-}N{=}S{=}S} \xrightarrow{-S} R_2C{=}N\text{-}N{=}S$$

$$\longrightarrow \begin{array}{l} R_2C\text{—}N \\ \quad\| \quad\| \\ \quad S\text{—}N \end{array} \xrightarrow{-N_2} R_2C{=}S \qquad (3)$$

The possibility of Eq. 2 was eliminated by the fact that the reaction of diphenyldiazomethane with sulfur in the presence of triethylamine did not give thiobenzophenone under identical conditions. No di-*t*-butyl thioketone was formed by the reaction of di-*t*-butyl ketone hydrazone with sulfur dichloride (SCl_2) in the presence of triethylamine which is expected to yield **11** (R=*t*-Bu), thus ruling out the possibility of Eq. 3.

Reaction of β-Keto Enamines with Disulfur Dichloride. Since β-keto enamines **12** are known to exist as enamine form instead of imine form,[13] the reaction of β-ketoenamines with disulfur dichloride is expected to lead to *N*-thiosulfinylamine **13** or its cyclized form, 5*H*-1,2,3-dithiazole **14** (Eq. 4).

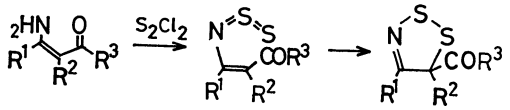

(4)

12 **13** **14**

a: $R^1R^2=(CH_2)_4$, $R^3=OEt$
b: $R^1R^2=(CH_2)_3$, $R^3=OEt$
c: $R^1=R^3=Me$, $R^2=H$
d: $R^1=Me$, $R^2=H$, $R^3=OEt$
e: $R^1=R^2=R^3=Me$
f: $R^1=Ph$, $R^2=R^3=Me$
g: $R^1=R^2=Me$, $R^3=OEt$

The reaction indeed proceeded as expected. 1-Amino-2-ethoxycarbonyl-1-cyclohexene (**12a**) was allowed to react with disulfur dichloride to give 6-ethoxycarbonyl-7,8-dithia-9-azabicyclo[4.3.0]non-1(9)-ene (**14a**) in 74% yield. The product was a stable yellow liquid and identified by spectral and analytical data. The electronic spectrum (λ_{max} 380 nm, ε 290) clearly inidicates that the product is not *N*-thiosulfinylamine **13** but 5*H*-1,2,3-dithiazole **14**; the *N*-thio-

sulfinylamine should have a strong absorption in the visible region (*e.g.*, 538 nm (ε 39000) for *p*-(dimethylamino)-*N*-thiosulfinylaniline[3] and 584 nm (ε 1280) for 2,4-di-*t*-butyl-6-methyl-*N*-thiosulfinylaniline).[1] The mass spectrum showing the fragment of M^+-CO_2Et as a strong base peak is also in keeping with the structure **14**, since cation **15** is a stable 6π-aromatic system and hence is easily formed. The strong peak of M^+-

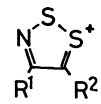

15

COR^3 (*i.e.* **15**) is characteristic of all the products **14 a,c′,d′,e,f** obtained in this study (see Experimental).

Contrary to the successful isolation of **14a**, the reaction of 1-amino-2-ethoxycarbonyl-1-cyclopentene **12b** with disulfur dichloride resulted in black polymeric products. In this case intermediary **13b** is unable to cyclize into **14b** probably because of strain due to two fused five-membered rings and polymerizes *via* intermolecular reaction. Since attempts to prepare 1-amino-2-ethoxycarbonyl-1-cycloheptene, 1-amino-2-ethoxycarbonyl-1-cyclooctene and 1-amino-2-ethoxycarbonyl-1-cyclododecene by the same procedure[13] as used for **12a** and **12b** were unsuccessful, the effect of a ring size on the stability of **14** ($R^1R^2=(CH_2)_n$) could not be studied.

The reaction of 4-amino-3-penten-2-one (**12c**) with disulfur dichloride in the presence of triethylamine at 0 °C in dichloromethane give a trace amount (0.75%) of 5-acetyl-5-methoxy-4-methyl-5*H*-1,2,3-dithiazole (**14c′**) instead of **14c** as a sole isolable product. Since the methoxyl group in **14c′** was thought to come from

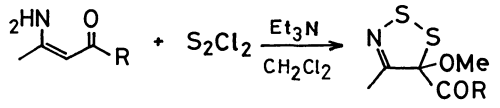

12c: R=Me
12d: R=OEt

14c′: R=Me
14d′: R=OEt

methanol present in dichloromethane as stabilizer, the reaction using an equimolar amount of methanol and two molar equivalents of disulfur dichloride and triethylamine was carried out to give 53% of **14c′**.

A similar reaction of ethyl 3-amino-2-butenoate (**12d**) with disulfur dichloride in the presence of triethylamine and methanol gave 35% of 5-ethoxycarbonyl-5-methoxy-4-methyl-5*H*-1,2,3-dithiazole (**14d′**) (R=OEt). The reaction without methanol under otherwise identical conditions gave no product other than sulfur.

The formation of **14c′,d′** can be explained in terms of oxidation of the hydrogen at 5-position in intermediary **14c,d** by disulfur dichloride followed by reaction of methanol with a resulting dithiazolium ion **15**. The relation of this reaction with the Herz reaction[14]

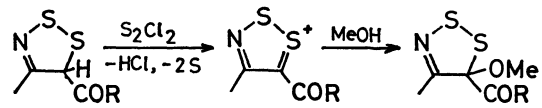

14c,d **15** **14c′,d′**

TABLE 2. SYNTHESIS OF 5*H*-1,2,3-DITHIAZOLES

Dithiazoles	Yield/%	Bp (°C, mmHg**)	Mp/°C
14a	73	115, 0.5	
14c′	53	136, 5	
14d′	35	100, 6	
14e	83	83, 6	
14f	6.4	110, 6	68—69

** 1 mmHg=133.322 Pa.

has already been discussed.[5b]

In support of the above mechanism, the reaction of 4-amino-3-methyl-3-penten-2-one (**12e**) where there is no hydrogen to be oxidized gave 5-acetyl-4,5-dimethyl-5*H*-1,2,3-dithiazole (**14e**) in 83% yield. A similar reaction also took place with 4-amino-3-methyl-4-phenyl-3-buten-2-one (**12f**) to afford 5-acetyl-5-methyl-4-phenyl-5*H*-1,2,3-dithiazole (**14f**) in 6.4% yield. Although 3-amino-2-methyl-2-butenoate (**12g**) was allowed to react under the same conditions, only polymeric products were obtained for reasons unclear to us yet.

The dithiazoles **14** are thought to be produced by the intramolecular cycloaddition of thiosulfinylamino group to the carbon-carbon double bond of **13**. This is the first synthesis of the compound with a 5*H*-1,2,3-dithiazole ring in the aliphatic system. The 5*H*-1,2,3-dithiazoles synthesized in the present study are summarized in Table 2.

The spectral data indicate that there is no equilibrium between **13** and **14** in the case of these dithiazoles in contrast to the system **1a**⇌**1b**. The visible spectra do not show any absorption due to *N*-thiosulfinyl group (–N=S=S) as mentioned previously. Any peak assignable to the open-chain structure **13** was not observed also in the NMR spectra. However, there still remains a possibility that **14** exists as an equilibrium mixture with **13** to such an extent that it cannot be detected spectroscopically. To check this possibility, the reactions of **14e** with some dipolarofiles (norbornadienes, *N*-phenylmaleimide, 4-phenyl-1,2,4-triazole-3,5-dione, dimethyl acetylenedicarboxylate) were carried out under various conditions,[3] but the cycloadducts were not obtained. These facts seem to suggest that **14** does not dissociate into **13** to an appreciable extent.

Experimental

NMR spectra were recorded at 60 MHz in deuteriochloroform on a Hitachi R-24B or a Hitachi R-24 spectrometer with tetramethylsilane as an internal standard. Mass spectra were measured on a Hitachi RMU-6L mass spectrometer. High resolution mass spectra were obtained with a JOEL D-300 mass spectrometer. Infrared spectra were recorded on a Hitachi EPI-G2 or a Hitachi 260-30 infrared spectrophotometer. Ultraviolet and visible spectra were taken on a Hitachi EPS-3 spectrophotometer or a Hitachi 340 recording spectrophotometer. All melting points were uncorrected. The reactions of hydrazones and enamines with disulfur dichloride were carried out under argon atmosphere.

Materials. Disulfur dichloride was distilled from sul-

fur and active carbon and stored in ampules in a refrigerator. Di-*t*-butyl ketone and di-1-adamantyl ketone hydrazones were prepared by the reported method.[15] The hydrazones of camphor, fenchone, 2,2,5,5-tetramethylcyclopentanone and benzophenone were prepared from the corresponding ketones by the method of Barton.[16] 2,2,5,5-Tetramethylcyclopentanone was prepared by the exaustive methylation of cyclopentanone.[17] Hexafluoroacetone hydrazone[9] was prepared from hexafluoroacetone. β-Ketoenamines were prepared from the corresponding β-diketones by the method of Kloek and Leshinsky,[13] and the new enamines **12 e,f,g** had following properties. **12e**: mp 118 °C; NMR ($CDCl_3$): δ=1.83 (3H, s), 1.95 (3H, s), 2.13 (3H, s), and 6.8—8.0 (2H, broad); IR (KBr): 3250, 3100, 1600, 1500—1420, 1280, 1220, 970, and 650 cm^{-1}; MS: *m/e* (rel intensity) 113 (M^+, 76), 98 (100), 70 (44), 55 (20), and 43 (38). Found: C, 63.54; H, 10.09; N, 12.25%. Calcd for $C_6H_{11}NO$: C, 63.69; H, 9.80; N, 12.38%. **12f**: mp 146.5—147.0 °C; NMR ($CDCl_3$): δ=1.66 (3H, s), 2.08 (3H, s), and 7.12 (s), 6.5—9.0 (broad) (7H in total); IR (KBr): 3250, 3100, 1600, 1500—1420, 1300, 1000, and 700 cm^{-1}; MS: *m/e* (rel intensity) 175 (M^+, 42), 174 (100), 160 (8), 105 (23), 98 (32), and 77 (31). Found: C, 75.28; H, 7.52; N, 7.72%. Calcd for $C_{11}H_{13}NO$: C, 75.40; H, 7.48; N, 7.99%. **12g**: mp 51.0—51.5 °C; NMR ($CDCl_3$): δ=1.23 (3H, t, J=7 Hz), 1.78 (3H, d, J=11 Hz), 4.03 (2H, q, J=7 Hz), and 5.5—7.0 (2H, broad); IR (KBr): 3370, 3120, 1600, 1500, 1270, 1220, 970, and 650 cm^{-1}. Found: C, 58.33; H, 9.16; N, 9.30%. Calcd for $C_7H_{13}NO_2$: C, 58.72; H, 9.15; N, 9.78%.

Reaction of Di-t-butyl Ketone Hydrazone with Disulfur Dichloride. a) In Benzene: To an ice-cold solution of triethylamine (1.06 g, 10.5 mmol) in benzene (20 cm^3) were added simultaneously benzene solutions (10 cm^3 each) of di-*t*-butyl ketone hydrazone (0.78 g, 5 mmol) and disulfur dichloride (0.71 g, 5.25 mmol) at about the same rate using two dropping funnels during 15 min. After stirring for 30 min at room temperature, the reaction mixture was washed with water and dried over anhydrous magnesium sulfate. The yield determined for the solution by the visible spectrum (λ_{max}(ethanol) 536 nm (ε 8.9))[18] was 96%. After removal of the solvent under reduced pressure, the residue was subjected to bulb to bulb distillation (bp 90—116 °C, 18 mmHg**) to give 521 mg (66%) of pure di-*t*-butyl thioketone as pink oil.[16]

b) In Other Solvents: Similar reactions in toluene (−85 °C), ether (−100 °C), dichloromethane (−90 °C) using 3 mmol of the hydrazone afforded the thione in 97, 37, and 39% (estimated by the visible spectra), respectively.

Reaction of Di-t-butyl Ketone Hydrazone with Sulfur Dichloride. To an ice-cold benzene solution (20 cm^3) of triethylamine (1.687 g, 16.7 mmol) were added simultaneously benzene solutions (15 cm^3 each) of di-*t*-butyl ketone hydrazone (1.241 g, 7.95 mmol) and sulfur dichloride (0.86 g, 8.35 mmol). After stirring for 1 h at room temperature, the deep red reaction mixture was washed with water and dried over anhydrous magnesium sulfate. The visible spectrum showed the absence of di-*t*-butyl thioketone. TLC of the reaction mixture also showed that di-*t*-butyl thioketone was not produced in this reaction. Removal of the solvent gave 1.267 g of red oil, 761 mg of which was subjected to bulb to bult distillation to give 251 mg (20%, based on the hydrazone) of di-*t*-butyl thioketone and 43 mg of unidentifiable yellow oil. This suggested that the thione was formed by the thermal decomposition of the reaction mixture.

Reaction of Di-1-adamantyl Ketone Hydrazone with Disulfur Dichloride. The reaction of the hydrazone (330 mg, 1.06 mmol) using the above simultaneous addition method was carried out at −85 °C, and the yield was determined for the reaction solution by the visible spectrum to be 71%. After removal of the solvent under reduced pressure, the residue was purified by TLC (silica gel, hexane) to give 195 mg (59%) of di-1-adamatyl thioketone as pink crystals: mp 184.5—185.0 °C; NMR ($CDCl_3$): δ=1.60—1.80 (18H, m) and 2.00—2.30 (12H, m); IR (KBr): 2950, 1730, 1610, 1440, 1290, 1220, 1140, 1100, 1020, and 720 cm^{-1}; MS *m/e* (rel intensity) 314 (M^+, 13), 179 (17), and 135 (100); UV: λ_{max} (benzene) 548 nm (ε 16.6), λ_{max} (hexane) 548 nm (ε 13.9); Found: C, 80.47; H, 9.35; S, 10.11%. Calcd for $C_{21}H_{30}S$: C, 80.19; H, 9.61; S, 10.19%.

Reaction of Other Hydrazones with Disulfur Dichloride. a) 2,2,5,5-Tetramethylcyclopentanone and Fenchone Hydrazones: The cyclopentanone (155 mg, 1.0 mmol) and fenchone hydrazones were allowed to react with disulfur dichloride in benzene at 5 °C by a method similar to that described for di-*t*-butyl ketone hydrazone (the simultaneous addition method). The yield was determined for the reaction mixture to be quantitative for both the thiones using the literature values of n-π^* absorption.[19,20] After removal of the solvent, the residue was subjected to bulb to bulb distillation to give pure thiones: the cyclopentane thione, 92 mg (58%), bp 116 °C (121 mmHg);[18] thiofenchone, 457 mg (54%), bp 120 °C (10 mmHg).[20]

b) Camphor and Benzophenone Hydrazones: The reactions of the two hydrazones were carried out by the simultaneous addition method in benzene at 5 °C. The reaction mixtures were analyzed for the corresponding thiones by the electronic spectra (n-π^* band), the yields of thiocamphor[19] and thiobenzophenone[20] being 63 and 54%, respectively. The addition of a solution of the benzophenone hydrazone and triethylamine to that of disulfur dichloride and the addition of a solution of disulfur dichloride to that of the hydrazone and triethylamine gave thiobenzophenone in 8 and 37% yields, respectively, as estimated by the electronic spectra.

Reaction of Hexafluoroacetone Hydrazone with Disulfur Dichloride. To a dichloromethane solution (30 cm^3) of triethylamine (5.34 g, 52.9 mmol) cooled with carbon tetrachloride–Dry Ice bath at −23 °C, were added simultaneously dichloromethane solutions (10 cm^3 each) of hexafluoroacetone hydrazone (5 g, 27.8 mmol) and disulfur dichloride (3.75 g, 26.5 mmol) during 1 h. After stirring for 30 min at room temperature, precipitated triethylamine hydrochloride was filtered off, the filtrate was passed through a short column of silica gel, and the solvent was removed under reduced pressure to give 4.12 g of a red-purple oil. Bulb to bult distillation (bp 110 °C, 0.5 mmHg) of the oil gave 1.15 g of a red oil, which was subjected to chromatographic separation (TLC, silica gel, carbon disulfide) to afford 254 mg (2.7%) of **7**: bp 110 °C (0.5 mmHg); IR (neat): 1280—1140, 925, 880, 840, 730, and 700 cm^{-1}; Found: *m/e* 341.8250. Calcd for $C_3F_6S_6$: M, 341.8228. MS: *m/e* (rel intensity) 342 (M^+, 34), 278 (100), 259 (9), 246 (3), 227 (2), 214 (60), and 182 (21).

*Reactions of β-Ketoenamines with Disulfur Dichloride. a) 1-Amino-2-ethoxycarbonyl-1-cyclohexene (**12a**)*: To a solution of **12a** (200 mg, 1.18 mmol) and triethylamine (2.51 mg, 2.49 mmol) in dichloromethane (20 cm^3) was added dropwise a solution of disulfur dichloride (168 mg, 1.24 mmol) in dichloromethane (10 cm^3) at room temperature during 30 min. After additional stirring at room temperature for 1 h, the reaction mixture was washed with water and dried over anhydrous magnesium sulfate. Removal of the solvent under reduced pressure left 271 mg of orange oil, which

**1 mmHg=133.322 Pa.

was purified by TLC (silica gel, dichloromethane) to give **14a** (203 mg, 74%) as yellow oil: bp 115 °C (0.5 mmHg); NMR ($CDCl_3$): δ=1.25 (t, J=7 Hz) and 1.0—3.1 (m) (11H in total), and 4.16 (2H, q, J=7 Hz); IR (neat): 2950, 1730, 1610, 1440, 1290, 1220, 1140, 1100, 1020, and 720 cm^{-1}; MS: *m/e* (rel intensity) 231 (M^+, 17) and 158 (100); UV: λ_{max} (hexane): 380 (ε 288), 278 (1890), and 234 nm (2010). Found: C, 46.48; H, 5.64; N, 5.92; S, 27.28%. Calcd for $C_9H_{13}O_2NS_2$: C, 46.73; H, 5.66; N, 6.05; S, 27.72%.

*b) 1-Amino-2-ethoxycarbonyl-1-cyclopentene (**12b**)*: To an ice-cold solution of **12b** (298 mg, 1.92 mmol) and triethylamine (427 mg, 4.23 mmol) in dichloromethane (20 cm^3) was added a solution of disulfur dichloride (286 mg, 2.11 mmol) in dichloromethane (10 cm^3) dropwise during 30 min. The color of the solution turned from yellow to black-brown at the end of the addition. Treatment of the reaction mixture gave no identifiable product.

*c) 4-Amino-3-penten-2-one (**12c**)*: The reaction of **12c** (1.043 g, 10.5 mmol) was carried out at 0 °C by the procedure described in *a)*. Chromatographic separation (DCC, silica gel, CCl_4) and Kugel Rohr distillation (bp 60 °C, 5 mmHg) gave 15 mg (0.75%) of **14c′** as yellow oil: NMR ($CDCl_3$): δ=2.05 (3H, s), 2.32 (3H, s), and 3.18 (3H, s); IR (neat): 3450, 3000—2900, 1720, 1430, 1360, 1080, 820 and 740 cm^{-1}; MS: *m/e* (rel intensity) 191 (M^+, 5), 160 (3), and 148 (100); UV: λ_{max}(hexane) 360 (ε 271), 282 (3210), and 244 nm (2710). Found: C, 37.42; H, 4.70; N, 7.49; S, 33.42%. Calcd for $C_6H_9NO_2S_2$: C, 37.68; H, 4.74; N, 7.32; S, 33.52%.

When a dichloromethane solution (10 cm^3) of disulfur dichloride (911 mg, 6.75 mmol) was added to an ice-cold dichloromethane solution (20 cm^3) of **12c** (318 mg, 3.21 mmol), triethylamine (1.36 g, 13.5 mmol), and methanol (0.1 g, 3.21 mmol), 326 mg (53%) of **14c′** was obtained after a similar work up to the above.

*d) Ethyl 3-Amino-2-butenecarboxylate (**12d**)*: A similar reaction with **12d** (372 mg, 2.89 mmol) to that in *c)* in the presence of methanol (92 mg, 2.89 mmol) gave a brown reaction mixture. After washing with water and removal of the solvent, it gave black-brown oil (555 mg), which was subjected to chromatographic separation (DCC, silica gel, dichloromethane–carbon tetrachloride 1:1) to give **14d′** (221 mg, 35%) as brown oil. It was purified by distillation (bp 110 °C, 3 mmHg) to give 194 mg of yellow oil: NMR ($CDCl_3$): δ=1.30 (3H, t, J=7 Hz), 2.15 (3H, s), 3.18 (3H, s), and 4.22 (2H, q, J=7 Hz); IR (neat): 3000—2900, 1740, 1440, 1260, 1100, and 740 cm^{-1}; MS: *m/e* (rel intensity) 221 (M^+, 9), 172 (31), 162 (38), 148 (100), 127 (64), and 126 (81); UV: λ_{max}(hexane) 352 (ε 273), 275 (2930), and 202 nm (3620). Found: C, 38.18; H, 4.85; N, 6.29; S, 29.65%. Calcd for $C_7H_{11}NO_3S_2$: C, 37.99; H, 5.01; N, 6.33; S, 28.98%.

*e) 4-Amino-3-methyl-3-penten-2-one (**12e**)*: The reaction of **12e** (3.56 g, 31.5 mmol) was carried out by the method described in *a)*. After usual work up, purification by Kugel Rohr distillation (bp 83 °C, 6 mmHg) afforded **14e** (4.59 g, 83%) as yellow oil: NMR ($CDCl_3$): δ=1.77 (3H, s), 2.05 (3H, s), and 2.41 (3H, s); IR (neat): 2980, 2930, 1710, 1600, 1430, 1360, 1190, 1090, 960, and 730 cm^{-1}; MS: *m/e* (rel intensity) 175 (M^+, 14), 132 (100), 91 (4), 74 (15), 59 (39), and 43 (68); UV: λ_{max}(hexane) 390 (ε 376), 352 (338), 280 (1530), and 236 nm (1980). Found: C, 41.39; H, 5.26; N, 8.11; S, 36.22%. Calcd for $C_6H_9NOS_2$: C, 41.12; H, 5.18; N, 7.99; S, 36.58%.

*f) 4-Amino-3-methyl-4-phenyl-3-buten-2-one (**12f**)*: The yellow reaction mixture obtained from the reaction of **12f** (300 mg, 1.71 mmol) by the procedure described in *a)* was, after usual work up, subjected to Kugel Rohr distillation to give **14f** (30 mg, 6.4%) as yellow oil which solidified upon standing: bp 110 °C (6 mmHg); mp 68—69 °C; NMR ($CDCl_3$): δ=1.82 (3H, s), 2.37 (3H, s), and 6.9—7.4 (5H, m); IR (KBr): 1705, 1370, 1350, 1200, and 690 cm^{-1}; MS: *m/e* (rel intensity) 237 (M^+, 9), 194 (100), 136 (13), 104 (15), 91 (46), 77 (17), 59 (26), and 43 (32): UV: λ_{max}(hexane) 408 (ε 2340), 348 (2450) 310 (3300), and 246 nm (9120). Found: C, 55.35; H, 4.46; N, 5.69%. Calcd for $C_{11}H_{11}NOS_2$: C, 55.67; H, 4.67; N, 5.70%.

*g) Ethyl 3-Amino-2-methyl-2-butenoate (**12g**)*: The reaction of **12g** (515 mg, 3.60 mmol) by the method described above gave a brown reaction mixture, the usual work up of which afforded no characterizable product.

The authors are grateful to Professor Nobuo Ishikawa of Tokyo Institute of Technology for a generous gift of hexafluoroacetone.

References

1) Y. Inagaki, R. Okazaki, and N. Inamoto, *Tetrahedron Lett.*, **1975**, 4575; *Bull. Chem. Soc. Jpn.*, **52**, 1988, 2008 (1979).
2) For X-ray analysis of **1b**, see F. Iwasaki, *Acta Crystallogr., Sect. B*, **36**, 1466 (1980).
3) Barton reported that the thiosulfinylamino group can act as 1,3-dipole towards some activated olefins. D. H. R. Barton and M. J. Robson, *J. Chem. Soc., Perkin Trans. 1*, **1974**, 1245.
4) We are grateful to Prof. Huisgen (München) for pointing out that this cyclization can be regarded as 1,5-electrocyclization. For 1,5-electrocyclization, see R. Huisgen, *Angew. Chem. Int. Ed. Engl.*, **19**, 947 (1980).
5) Preliminary reports: a) R. Okazaki, K. Inoue, and N. Inamoto, *Tetrahedron Lett.*, **1979**, 3673; b) R. Okazaki, K. Inoue, and N. Inamoto, *Heterocycles*, **15**, 803 (1981).
6) A. Senning, *Angew. Chem. Int. Ed. Engl.*, **18**, 941 (1979).
7) S. Tamagaki, K. Sakai, and S. Oae, *Bull. Chem. Soc. Jpn.*, **46**, 2608 (1971); L. Carlsen, N. Haait, and A. Holm, *J. Chem. Soc., Perkin Trans. 1*, **1976**, 1404.
8) Y. Inagaki and R. Okazaki, *Yuki Gosei Kagaku Kyokai Shi*, **36**, 1 (1978).
9) W. J. Middleton and C. G. Krespan, *J. Org. Chem.*, **30**, 1398 (1965).
10) R. Appel and M. Montenarh, *Chem. Ber.*, **111**, 759 (1978).
11) P. de Mayo, G. L. R. Petrasiunas, and A. C. Weedon, *Tetrahedron Lett.*, **1978**, 4621.
12) It is known that the reaction of a diazo compound with sulfur gives a thioketone. N. A. Korchevin, V. A. Usov, and M. G. Voronkov, *Zhur. Org. Chim.*, **12**, 2412 (1976).
13) J. A. Kloek and K. L. Leshinsky, *J. Org. Chem.*, **43**, 1460 (1978).
14) W. K. Warburton, *Chem. Rev.*, **57**, 1011 (1957).
15) J. H. Wieringa, H. Wynberg, and J. Strating, *Tetrahedron*, **30**, 3053 (1974).
16) D. H. R. Barton, F. S. Guziec, Jr., and I. Shahak, *J. Chem. Soc., Perkin Trans. 1*, **1974**, 1794.
17) M. J.-M. Conia, *Bull. Soc. Chim. Fr.*, **1950**, 537.
18) C.-P. Klages and J. Voss, *J. Chem. Res. (S)*, **1977**, 146.
19) J. Fabian and R. Mayer, *Spectrochim. Acta*, **20**, 299 (1964); D. C. Sen, *J. Indian Chem.*, **12**, 647 (1935); **14**, 214 (1937).
20) W. A. Lees and A. Burawoy, *Tetrahedron*, **20**, 1527 (1964).

Absolute Intensity Measurement of the ν_4 Band of Fluoroform by the Use of a Tunable Diode-laser Source

Susumu Sofue,† Kentarou Kawaguchi, Eizi Hirota, and Tsunetake Fujiyama*

Institute for Molecular Science, Myodaiji, Okazaki 444

†*Department of Chemistry, Faculty of Science, Tokyo Metropolitan University, Setagaya-ku Tokyo 158*

(Received May 6, 1981)

The absolute infrared absorption intensities have been measured for the $P_{35}(35)$ and $P_{36}(36)$ lines, which belong to the ν_4 fundamental of fluoroform, by the use of a tunable diode-laser source. The observed intensity, Γ, was 5360+220 $cm^2\ mol^{-1}$. This intensity value was compared with that observed by the conventional method.

The absorption intensities of the vibration spectra of gaseous molecules have been discussed as the intensities integrated over the whole absorption bands. This has been largely due to the fact that the limited resolution of a dispersion-type spectrometer is insufficient to observed individual vibration-rotation lines. Therefore, the experimental method based on the theory of Wilson and Wells[1] has conventionally been employed. In their method, the total pressure in the absorption cell is raised so that the rotational fine structures are completely smeared out, giving the band a smooth contour; this reduces the error resulting from the finite instrumental line-width. The disadvantage of this method is that the observed intensity value can be spoiled by some systematic errors. The two main origins of the systematic errors are:

1) the existence of hot bands originating from the combinations between the vibrational mode in question and the other modes,
and
2) the existence of the accidental coincidence of vibrational-energy levels.

Item 2) can further be divided into two categories: the anharmonic resonance (Fermi resonance) and the Coriolis interaction.

A high-resolution method has an advantage over the conventional method with respect to these problems. In the high-resolution method, it is enough to observe the intensities of several vibration-rotation lines in determining the intensity for the whole band. Since the instrumental line-width can be narrower than a Doppler width, two peaks whose frequency separation is larger than the Doppler width can be observed separately. Usually the molecular constants of the hot bands are slightly different from those of the fundamentals. Therefore, it is possible to detect this slight difference and to observe a spectrum corresponding to a single vibration-rotation transition. As for the problem of resonances, it should be remembered that it is the vibration-rotation levels that really interact with each other. Therefore, even if there are degeneracies with respect to the vibrational levels, only some vibration-rotation levels are considerably perturbed. The other vibration-rotation levels may be too far from their counter levels. Thus, it is possible to estimate the pure intensity for the vibration by observing the resonance-free transitions to these unperturbed vibration-rotation energy levels.

The purpose of this study is to examine the experimental possibility of intensity observation for a vibration spectrum by the use of a tunable diode-laser source spectrometer and to compare the intensity thus observed with that observed by the conventional method. Fluoroform was chosen because we have already determined its molecular constants on the ν_4 fumdamental.[2] The vibrational intensity for the ν_4 fundamental has also been reported as determined by the use of a conventional method.[3]

Experimental

Commercial fluoroform of a 99.95% purity was distilled several times just before the measurement. The sample cell was made of a Pylex tube (30 mm in diameter and 150 cm in length) with CaF_2 windows at its ends. The end planes of the Pylex tubes had been ground by means of a diamond grinder to make an angle of about 88° to the optical axis of the tube, thus avoiding interference. In order to produce the optimum transmittance under an appropriate pressure, it was often necessary to use several sample cells in a series. These cells were connected to a usual glass and grease manifold. The temperature of the sample was believed to be equal to the room temperature.

The measurement of the sample pressure is a critical problem in this kind of work. In the present experiment, a variable-inductance transducer (Tsukasa Sokken, model P90DL channeled to a special carrier amplifier) was connected to the vacuum system. By introducing air into the system, we calibrated the transducer against an MKS Baratron. We could not use the Baraton itself for our pressure measurements because the surface of the diaphragm is corroded by fluoride and so can be damaged by the sample fluoroform. The nonlinearity of the P90DL was estimated to be 4% up to 200 mTorr.†† This figure can serve to indicate the relative accuracy of the instrument as long as the Baratron is accurate. Although the transducer is rather sensitive to the temperature change, we did not use any thermostatting equipment in this work, for the room temperature was controlled well enough. It was recognized that the pressure of the system increased by 2—3% during the intensity measurement; this increase was ascertained to stem from the evaporation of the vacuum grease.

A laser diode, in a closed-cycle refrigerator operating at about 20 K, served as the source of monochromatic radiation. The emitted energy was focused on the entrace slit of a grating monochromator, which served both for the coarse frequency calibration and for the isolation of discrete laser modes. A mechanical vibrating chopper, operating at 400 Hz, was placed immediately before the entrance slit. The laser from the exit slit of the monochromator passed through the sample cells and was focused onto a HgCdTe or PbSnTe detector kept at 77 K. The chopped signal was amplified and fed to a lock-in amplifier, whose reference was obtained from the chopper. The DC signal

†† 1 Torr=133.322 Pa.

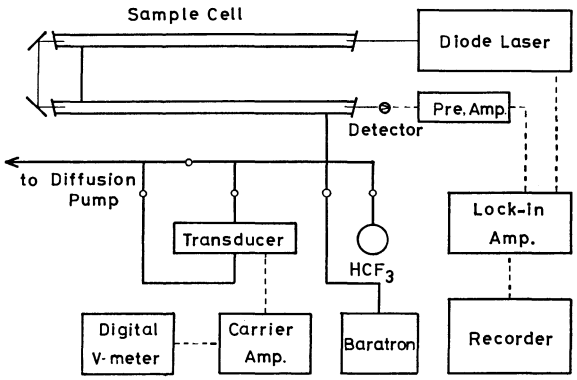

Fig. 1. The block diagram of the experimental arrangement for the intensity measurement.

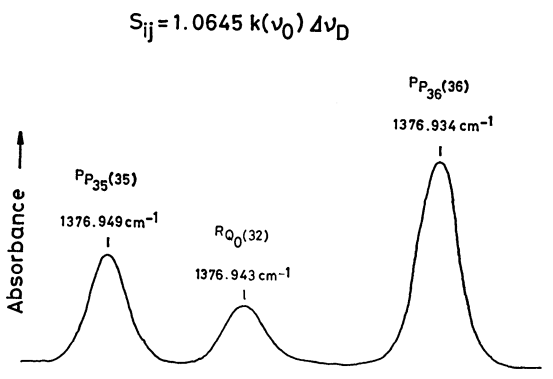

Fig. 2. The spectra for $P_{35}(35)$ and $P_{36}(36)$ of the ν_4 fundamental of fluoroform.

was channeled to an X-T recorder. The signal was strong enough for us to record lines with a high signal-to-noise ratio with a rather short time constant (300 ms) in comparison with the time needed to record an absorption line. Lines were identified in reference to the neighbouring lines. The FWMH (full-width at half maximum) was measured relative to the separation of three line peaks, with the middle one being measured. Figure 1 illustrates the experimental arrangement.

Results and Discussion

Observed Spectra. Figure 2 shows the spectra observed for the $^PP_{35}(35)$ and $^PP_{36}(36)$ lines of fluoroform. The length of the cell was 300 cm, and the pressure was 13.6 mTorr. The observation was made at 293 K. As the accurate frequencies had already been determined for these lines,[2] the FWHM's could be estimated for these two lines. They were 59.7 MHz for $^PP_{35}(35)$ and 63.3 MHz for $^PP_{36}(36)$. It is probable that these two line-shapes are governed by the Doppler broadening, for the calculated Doppler width is 60.5 MHz in this frequency region (HCF_3= 70, T=293 K). This postulation seems reasonable if the following three points are taken into account:

1) the line-width due to the collision broadening is of the order of 0.1 MHz (the pressure-broadening parameter for fluoroform is 18 MHz/Torr[4]),

2) the instrumental line-width can be narrower than 10^{-4} cm^{-1} (3 MHz),

and

3) the synthetic spectra calculated from the precise molecular constants[2] predict no overlapping from other lines with considerable intensities.

Determination of the Line Intensity. The absorption intensity associated with the transition from the energy level, i, to another energy level, j, is defined by this relation:

$$S_{ij} = \int_{-\infty}^{\infty} k(\nu)\mathrm{d}\nu, \tag{1}$$

where $k(\nu)$ is the absorption coefficient which appears in the Lambert-Beer law:

$$I(\nu) = I_0(\nu)\exp(-k(\nu)\chi). \tag{2}$$

In Eq. 2, I_0 and I correspond to the intensities for the incident and transmitted light respectively. χ is a measure of the number per unit of area of the absorbing molecules occurring along the direction of the propagation of the radiation in the sample gas. If the absorbing molecules are at a certain concentration, n, and are contained in a space with a certain length, l, in the direction in which the radiation travels

$$\chi = nl. \tag{3}$$

Knowledge about the dependence of the absorption coefficient on the frequency is needed to estimate S_{ij} from Eq. 1. That is, the explicit expression for the distribution function;

$$k(\nu) = S_{ij}f(\nu-\nu_0), \tag{4}$$

must be known. In the present study, f can be considered to have the form of a Doppler profile under appropriate conditions. Defining $\Delta\nu_D$ as a FWHM of the Doppler limited-absorption line, the following normalized distribution function is obtained:

$$f(\nu-\nu_0) = \frac{(\ln 2/\pi)^{1/2}}{(\Delta\nu_D/2)}\exp[-(\ln 2)\{(\nu-\nu_0)/(\Delta\nu_D/2)\}^2]. \tag{5}$$

By combining Eqs. 4 and 5, one can get this expression:

$$S_{ij} = 1.0645\, k(\nu_0)\Delta\nu_D, \tag{6}$$

which shows that only knowledge about the absorption coefficient at the peak frequency is required to evaluate the line intensity as long as the line shape is approximated by a Doppler profile.

The absolute line intensities estimated from Eq. 6 are summarized in Table 1. In the estimation, we used the theoretically estimated Doppler width, $\Delta\nu_D$= 60.5 MHz, instead of the experimentally observed linewidths, because the experimentally observed linewidths were not accurate enough for the quantitative work; this may be due to the irregularity in the scan rate of the electric current fed to the diode.

Determination of Transition Moment for the ν_4 Fundamental. The absolute line intensity defined by Eq. 1 can have another form in the quantum-mechanical expression. The time-dependent perturbation theory has shown that:

$$S_{ij} = \frac{8\pi}{3hc}(N_j-N_i)\nu_{ij}|\mu_{ij}|, \tag{7}$$

where h is Planck's constant; c, the velocity of light; N_s, the molecular density of the energy level, E_s ($E_j > E_i$); ν_{ij}, the transition frequency, and μ_{ij}, the transition dipole moment. Suppose that the molecules are

Table 1. Transition dipole moment deduced from absorption lines in ν_4 of HCF_3

Line	Pressure / mTorr	Intensity S / cm² atm	$\lvert\mu_{ij}\rvert$ / D	$\left(\frac{\partial\mu_x}{\partial Q_4}\right)\langle 0\lvert Q_4\rvert v_4=1\rangle\rvert$ / D
$^PP_{35}(35)$	13.6	0.153	0.110	0.111
	21.7	0.163	0.113	0.115
$^PP_{36}(36)$	13.6	0.310	0.112	0.114
	21.7	0.302	0.111	0.113

a) $D(\text{Debye}) = 10^{-18}\ g^{1/2}\ cm^{5/2}\ s^{-1}$.

in thermal equilibrium; that is, the molecules follow the Boltzmann distribution. Then, the density of molecules in the energy level, E_s, can be expressed as;

$$N_s = Ng_s\exp(-E_s/kT)/Z, \tag{8}$$

where N is the total molecular density and g_s, the degree of the degeneracy of the level, s. The estimation of g_s has been discussed in the previous paper.[2] Z is the total partition function, which can be evaluated by computor calculation. In this evaluation, we considered the rotational levels belonging not only to the vibrational ground state, but also to the $v_3=1$ and $v_6=1$ states. As the band origins are: $\nu_3=700$ cm^{-1} and $\nu_6=507$ cm^{-1}, the number of molecules in these energy levels at room temperature cannot be neglected. The vibrational-energy levels higher than 1000 cm^{-1} ($2\nu_6$, ν_2, ν_5, $\nu_3+\nu_6$, ν_4, $2\nu_3$, *etc.*) were neglected because the distribution density is very small. Then, Z can be expressed as the sum of the partition functions for three vibrational levels:

$$Z = Z_0 + Z_3 + Z_6. \tag{9}$$

For example, the explicit formula for Z_0 is:

$$Z_0 = \sum_{J=0}^{\infty}\sum_{J=-J}^{J}(2J+1)g_K g_I\exp(-E_{JK}/kT), \tag{10}$$

where E_{JK} is equal to the $E(J,K)$ of our previous paper,[2] and:

$$\left.\begin{aligned} &g_K = 1 \text{ for } K = 0,\\ &g_K = 2 \text{ for } K \neq 0,\\ &g_I = 2 \text{ for } K = 3n\ (n=1, 2, 3, \cdots), \text{ and}\\ &g_I = 1 \text{ for } K \neq 3n. \end{aligned}\right\} \tag{11}$$

The summation was executed until the term newly added became less than 10^{-10} of the sum theretofore. Z_3 and Z_6 were calculated in the same way, special attention being paid to the symmetry species of the vibration-rotation energy levels ($v_3=1$, A_1; $v_6=1$, E). The result was:

$$Z = 45836 + (3.21\times10^{-2}) \times 45991 + (8.26\times10^{-2})\times 91875 = 54904, \tag{12}$$

where (3.21×10^{-2}) and (8.26×10^{-2}) are the Boltzmann factors for $v_3=1$ and $v_6=1$ respectively. The transition dipole moments thus obtained are shown in Table 1.

On calculating the transition moment from the observed line intensities, we have to pay much attention to the mixing of the energy levels. In the case of the ν_4 fundamental of fluoroform, the possible perturbations are the x-y type Coriolis interaction with $2\nu_3$ and the l-type resonance. Fortunately, for the cases of $^PP_{35}(35)$ and $^PP_{36}(36)$ we do not have to consider the existence of the x-y type Coriolis interaction, because there are no counter levels in the $2\nu_3$ state.[5] The presence of the l-type resonance is not a critical problem for the determination of the transition moment. The degree of the mixing can be calculated exactly, for the eigenvectors can be calculated from the constant q_4.[6] However, there are no interacting pairs for these transitions.[7] In other words, $|0, 1: J, J, -1\rangle$ remains the eigenfunction of the overall Hamiltonian, and J, k, and l are good quantum numbers. The matrix elements of the direction cosine can then, readily be calculated.[8]

Now, the transition moment corresponding to the ν_4 fundamental can be derived. By expanding the components of the electric dipole moment with respect to the normal coordinates, we obtain:

$$\mu_x = (\mu_x)_0 + \sum_k\left(\frac{\partial\mu_x}{\partial Q_k}\right)_{Q_k=0}Q_k + \cdots \tag{13}$$

and by neglecting the terms higher than the quadratic, we can express the matrix element of μ_x by this relation:

$$\langle 0\lvert\mu_x\rvert v_4=1\rangle = \left(\frac{\partial\mu_x}{\partial Q_4}\right)\langle 0\lvert Q_4\rvert v_4=1\rangle. \tag{14}$$

The constant term of Eq. 13 vanishes so long as the anharmonicity is neglected. The numerically estimated values of Eq. 14 are summarized in Table 1.[8]

Comparison with the Results Obtained from the Conventional Method. The observed transition-moment values were converted into the absolute absorption-intensity values in order to compare the present results with the absorption intensities obtained by conventional method.[3] The relation between the absolute intensity, Γ, and the transition moment is:

$$\Gamma = \frac{8\pi^3}{3hc}(N_j - N_i)\left|\left(\frac{\partial\mu_x}{\partial Q_4}\right)\langle 0\lvert Q_4\rvert v_4=1\rangle\right|^2. \tag{15}$$

This equation has the same form as Eq. 7 when Γ is replaced by S_{ij}/ν_{ij}. $|\mu_{ij}|^2$ can be written for a vibrational transition as:

$$|\langle v''\lvert\mu_F\rvert v'\rangle|^2 = |\langle 0\lvert\mu_x\rvert v_4=1\rangle|^2 + |\langle 0\lvert\mu_y\rvert v=1\rangle^2 = 2|\langle 0\lvert\mu_x\rvert v_4=1\rangle|^2. \tag{16}$$

The coefficient of 2 corresponds to the degeneracy of the vibration, which is designated as k in Eq. 15. Again, the vibration-rotation partition functions were considered for the estimation of N_s. In Table 2, the Γ values calculated from Eq. 15 are compared with those obtained by the conventional method. The error for Γ was considered to arise mainly from the errors in the pressure measurement. The direct comparison of these intensity values is not possible because

Table 2. Absolute intensities I/cm^2 mol^{-1}

5360±220	Present result
6360±312	S. Saeki *et al.*[a]
4960±240	[b]

a) S. Saeki, M. Mizuno, and S. Kondo, *Spectrochim. Acta, Part A*, **32**, 403 (1976). b) The intensity for the ν_4 fundamentaal calculated from the value of a), assuming $T=293$ K.

the intensity values observed by the conventional method contain not only the absolute intensity for the ν_4 fundamental, but also the absolute intensities for such hot bands, like $\nu_6\rightarrow\nu_6+\nu_4$ and $\nu_3\rightarrow\nu_3+\nu_4$, or overtones like $2\nu_3$. For the subtraction of the contributions from these hot band, knowledge about the types of transitions and the intensities of these hot bands is necessary. As the symmetry species of ν_6 is E, the resultant level, $\nu_3+\nu_6$, has the symmetry of A_1+A_2+E. The direct product of the species of these two states:

$$E\times(A_1+A_2+E)=A_1+A_2+3E$$

shows the types of transition. The intensity of the A_1+A_2 type band is supposed to be quite weak, for it is governed by a higher-order derivative of the dipole moment. The $\nu_3\rightarrow\nu_3+\nu_4$ transition belongs to E. In order to discuss the overtone problem, it is necessary to know the magnitude of $|\langle 0|\mu_z|\nu_3=2\rangle|$. However, as we do not see any bands with considerable intensities in the 1400 cm^{-1} region of the survey spectra, $2\nu_3$ is supposed to be quite weak, and so its contribution to I might be negligible. Thus, we can estimate the relative intensities of these hot bands by calculating the Boltzmann factors.

Although Saeki *et al.* do not describe the temperature explicitly in their report,[3] we assumed that their intensity measurement had been carried out at 293 K. Then, the intensity value of Ref. 3 can be corrected for the hot-band effects. The intensity value of 6360 cm^2 mol^{-1} is reduced to:

$$6360\times\frac{1}{1+3\exp\left(-\frac{507}{293\,k}\right)+\exp\left(-\frac{700}{293\,k}\right)}=4960.$$

This intensity value agrees with our present result within the limits of experimental error. This, in turn, suggests that the present experimental procedure is effective enough to observe vibrational intensities with a high accuracy.

Effect of x-y Type Coriolis Interaction on Line Intensity. As the method is established for determining the line-intensities of individual rotation-vibration lines, it is of some interest to see the effects of an x-y type Coriolis interaction on line-intensities. For this purpose, we observed the line-intensities for the $^PP_{J-6}(J)$ series lines, because it has been established in our previous work[2] that the x-y type Coriolis interaction affects the energy levels of this line-series considerably.

A part of the observed results are summarized in Table 3. In can be seen from the table that the effective transition moment, $|\mu_{1j}|$, decreases in magnitude with the increase in J and K values for $v_4=1$. Using the spectral data for the $2\nu_3\leftarrow\nu_3$ band obtained by Graner *et al.*,[9] together with the molecular constants related to the ν_4 band,[2] we can ascertain that the energy level of the $|v_4=1, J, K=J-6>$ state is lower than the of $|v_3=2, J, K=J-5>$ for $J>36$, and *vice versa* for $J<36$. Therefore, the intensity behaviour of Table 3 may be explained by Coriolis coupling with the $2\nu_3$ band, whose intensity is rather weak in comparison with that of ν_4.

Table 3. Line intensites of $^PP_{J-6}(J)$

Line	S/cm^2 atm^{-1}	μ_{1j}/D
$^PP_{24}(30)$	0.277	0.121
$^PP_{27}(33)$	0.237	0.117
$^PP_{30}(36)$	0.191	0.111

D(Debye)$=10^{-18}$ g$^{1/2}$ cm$^{5/2}$ s^{-1}.

If we take a Coriolis interaction and a l-type resonance into account, the wave-function of an excited state may be expressed as:

$$\psi'=a\psi'_+(v_4=1, J, K+1)+b\psi'_0(v_3=2, J, K)+c\psi'_-(v_4=1, J, K-1), \quad (17)$$

where a, b, and c are constants. As the effect of the l-type resonance is negligible in the present case,[2] Eq. 17 can be simplified as:

$$\left.\begin{aligned}\psi'_1&=\cos\beta\psi'_0(v_3=2, J, K)+\sin\beta\psi'_-(v_4=1, J, K-1)\\ \psi'_2&=-\sin\beta\psi'_0(v_3=2, J, K)+\cos\beta\psi'_-(v_4=1, J, K-1)\end{aligned}\right\}, \quad (18)$$

where:

$$\cos2\beta=\frac{\Delta E}{2r},\ \text{and}\ \sin2\beta=\frac{-\xi_{334}}{r}[J(J+1)-K(K-1)]^{1/2}$$

with

$$r=\left[\left(\frac{\Delta E}{2}\right)^2+\xi_{334}^2\{J(J+1)-K(K-1)\}\right]^{1/2},$$

In the above relations, ΔE represents the energy difference between two unperturbed states, $|v_3=2, J, K>$ and $|v_4=1, J, K-1>$. The transition moment corresponding to the transition from the ground state, ψ'', is:

$$\begin{aligned}\langle\psi''|\mu|\psi'_2\rangle&=-\sin\beta\langle\psi''|\mu|\psi'_0\rangle+\cos\beta\langle\psi''|\mu|\psi'_-\rangle\\&=-\sin\beta\cdot M_r\cdot M_k{}^k+\cos\beta\cdot M_s\cdot M_k{}^{k-1}, \quad (19)\end{aligned}$$

where:

$$M_r=\left(\frac{\partial^2\mu_z}{\partial Q_3{}^2}\right)\langle 0|Q_3{}^2|v_3=2\rangle$$

and

$$M_s=\left(\frac{\partial\mu_x}{\partial Q_4}\right)\langle 0|Q_4|v_4=1\rangle$$

and $M_k{}^{k'}$ is a direction cosine matrix element. Thus, the rotation-vibration line-strength is shown to be proportional to this value:

$$\begin{aligned}|\langle\psi''|\mu|\psi'_2\rangle|^2&=\cos^2\beta(M_sM_k{}^{k-1})^2-\sin2\beta M_rM_sM_k{}^kM_k{}^{k-1}\\&\quad+\sin^2\beta(M_rM_k{}^k)^2\\&=(\cos^2\beta-\alpha\sin2\beta+\alpha^2\sin^2\beta)(M_sM_k{}^{k-1})^2, \quad (20)\end{aligned}$$

where:

$$\alpha=\frac{M_rM_k{}^k}{M_sM_k{}^{k-1}}.$$

According to the experimental results of Table 3, the line internsity of the ν_4 band decreases with the decrease in the energy difference between the levels interacting with each other through the Coriolis resonance. Therefore, the second term of Eq. 20 is positive; that is,

$$\alpha \sin 2\beta > 0$$

and, accordingly;[10]

$$\xi_{334} M_\tau M_s > 0. \tag{21}$$

The relation of Eq. 21 has been referred to as an "positive perturbation," following Mills, Smith, and Duncan.[11] As the $v_3=2$ state has not yet been studied with sufficient accuracy, though, the quantitative analysis of line intensities based upon Eq. 20 is left for the future. We can only conclude at this stage that the observed line-intensity values show that the perturbation is positive.

References

1) E. B. Wilson, Jr., and A. J. Wells, *J. Chem. Phys.*, **14**, 578 (1946).

2) S. Sofue, K. Kawaguchi, E. Hirota, and T. Fujiyama, *Bull. Chem. Soc. Jpn.*, **54**, 897 (1981).

3) S. Saeki, M. Mizuno, and S. Kondo, *Spectrochim. Acta, Part A*, **32**, 403 (1976).

4) C. H. Townes and A. H. Shawlow, "Microwave Spectroscopy," Dover Publications, New York (1955).

5) The matrix elements of the Hamiltonian for the Coriolis interaction between v_4 and $2v_3$ are expressed as:

$$\langle v_3=2,\ v_4=0;\ J, K, l=0\ |H_c|\ v_3=0,\ v_4=1;\ J, K\pm 1, l=\pm 1\rangle = \pm\xi_{334}[J(J+1)-K(K\pm 1)]^{1/2}.$$

Notice that $J>K$.

6) For the definition of q_4, see Ref. 2.

7) The perturbed energies can be obtained from the diagonalization of a 2×2 matrix of the form:

$$\begin{bmatrix} E(J,\ K-1,\ -1) & W \\ W & E(J,\ K+1,\ +1) \end{bmatrix}.$$

8) The following relations are used, where D_{fF} is a matrix element of a direction cosine matrix:

$$|\langle J,\ k|D_{xF}|J+1,\ k\pm 1\rangle|^2 = \frac{(J\pm k+1)(J\pm k+2)}{2(J+1)(2J+1)}$$

$$|\langle J,\ k|D_{xF}|J,\ k\pm 1\rangle|^2 = \frac{(J\mp k)(J\pm k+1)}{2J(J+1)}$$

$$|\langle J,\ k|D_{xF}|J-1,\ k\pm 1\rangle|^2 = \frac{(J\mp k)(J\mp k+1)}{2J(2J+1)}.$$

9) G. Graner, R. Anttila, and J. Kaouppinen, *Mol. Phys.*, **38**, 103 (1979).

10)

$$\sin 2\beta = \frac{M_r}{M_s}\frac{M_k{}^k}{M_k{}^{k-1}}(-\xi_{334})[J(J+1)-K(K-1)]^{1/2}/r$$

As M_K^K/M_K^{K-1} is negative, the product, $\xi_{334}M_\tau M_s$, is positive. Therefore, we obtain this relation:

$$\xi_{334}\left(\frac{\partial^2\mu_z}{\partial Q_3{}^2}\right)\left(\frac{\partial\mu_x}{\partial Q_4}\right) > 0.$$

11) I. M. Mills, W. L. Smith, and J. L. Duncan, *J. Mol. Spectrosc.*, **16**, 349 (1965); C. DiLauro and I. M. Mills, *ibid.*, **21**, 386 (1966).

  Bull. Chem. Soc. Jpn., 54, 3551—3555 (1981)

Kinetics and Mechanism of Oxidation of Dimethyl Sulfoxide by Peroxomonosulfate

Thanthoni PANDURENGAN and Pichai MARUTHAMUTHU*

Department of Chemistry, University of Madras, Autonomous post-Graduate Centre, Tiruchirapalli-620020, India

(Received January 23, 1981)

The kinetics of oxidation of dimethyl sulfoxide (DMSO) by peroxomonosulfate (PMS) was carried out in aqueous H_2SO_4 medium (0.1—0.5 M H^+†) and in buffered media, pH=4.6 and 7.0, at temperatures, 10 and 20 °C. The reaction obeys a total second order kinetics, first order each with respect to [PMS] and [DMSO]. The rate was found to be immeasurably fast at pH≥9 and T>20 °C. In strong acid medium, $[H_2SO_4]$=0.1—0.5 M, the reaction was found to follow an inverse first order dependence on $[H^+]$. The rate law for the disappearance of PMS is found to be

$$\text{Rate} = \{k_a + k_b[H^+]^{-1}\}[\text{PMS}][\text{DMSO}]$$

indicating both the acid-independent and inverse acid-dependent reactions occurring concurrently. Dimethyl sulfone was identified as the oxidation product and the reaction stoichiometry, [DMSO]:[PMS] was found to be 1:1. The kinetic and thermodynamic parameters evaluated strongly suggest the nucleophilic substitution mechanism characteristic of peroxides. A comparison is also made with the corresponding reactions of the similar peroxides, H_2O_2, $S_2O_8^{2-}$, $P_2O_8^{4-}$, and $H_2PO_5^-$.

There are many investigations on the oxidation of organic and inorganic compounds by the well-known oxidant, peroxodisulfate,[1,2] $S_2O_8^{2-}$, whereas the corresponding monoperoxo compound, namely peroxomonosulfate, HSO_5^- has received relatively little attention despite the fact that it is known to chemists nearly a century ago.[3] Peroxomonosulfate can be regarded as mono substituted hydrogen peroxide in which one of the hydrogens is replaced by a SO_3 group. Metal ion catalysed[4] and uncatalysed[5] thermal decomposition of peroxomonosulfate (PMS) and oxidation of chloride and halide[6] and nitrite[7] ions have already been carried out by Edwards and coworkers. Recently radiolytic chain decomposition[8] and oxidation of azide, azidopentamminechromiun(III)[9] and tris(2,2′-bipyridine)iron(II)[10] by peroxomonosulfate have been carried out. It has been observed that peroxomonosulfate is a better oxidant than peroxodisulfate in the reaction with halide ions.

It was the intention of the authors to utilize peroxomonosulfate in the oxidation reaction of various substrates to explore the possibility of its synthetic utility. As a part of this goal, dimethyl sulfoxide, which is emerging not only as a solvent but also as a versatile reagent, was chosen as the substrate for the present investigation to find out the ease with which an aprotic solvent is oxidized by peroxomonosulfate. In general, peroxoacids[11,12] are found to be effective oxidants in bringing about the oxidation of sulfides and sulfoxides. In the reactions of sulfides, it is inferred that the nucleophilic attack is made by the sulfur of sulfides on the peroxo oxygen of the oxidant and the reverse was found to be true in the case of sulfoxides. Peroxomonosulfate may resemble either peroxodisulfate (free radical mechanism) or organic peroxides (ionic mechanism) in its reactions. The present investigation focuses attention on (i) the kinetics of the reaction with the concurrent effect of pH and high acidity since the peroxides are prone to acid-catalysis (ii) mechanistic aspects with the kinetic and thermodynamic reasoning and (iii) the comparative behaviour of PMS with those of H_2O_2, $S_2O_8^{2-}$, $P_2O_8^{4-}$, and peroxomonophosphate, $H_2PO_5^-$, in effecting the oxidation of DMSO.

† 1 M=1 mol dm^{-3}.

Experimental

All the chemicals used were of analar grade. Potassium peroxomonosulfate was donated by Du Pont Chemical Co., U.S.A. under the trade name "oxone." It is a triple salt with the composition $2\,KHSO_5 \cdot KHSO_4 \cdot K_2SO_4$. The purity of this salt was estimated by cerimetry using ferroin indicator, as well as by iodometry and was found to be 96% pure. Tests with permanganate showed the absence of free hydrogen peroxide. No attempt was made to further purify this compound because all previous attempts have been reported unsuccessful.[8] From the methods of preparation of this compound, it is assumed that $KHSO_4$ or K_2SO_4 or both might account for the 4% difference between the formula and the analysis results[8]. Other chemicals such as dimethyl sulfoxide (Fluka), KI, $Na_2S_2O_3 \cdot 5H_2O$, NaH_2PO_4, Na_2HPO_4, CH_3COOH, and CH_3COONa (BDH) were all analytical grade samples. Perchloric acid (60%) was from E. Merck and all these chemicals were used as such.

Experiments were carried out in buffered media, pH 4.6 and 7, and in acidic medium provided by 0.1 to 0.5 M H_2SO_4. In buffered media, it was always necessary to use a high concentration of the buffer (0.1 M) since the product, HSO_4^-, is a stronger acid than the oxidant, HSO_5^-. Under the present experimental conditions, no spontaneous self-decomposition of peroxomonosulfate, even up to pH 12, was observed. The kinetics of the reaction was followed by estimating the amount of peroxomonosulfate disappeared by iodometry at different time intervals. The rate constants were obtained using integral method. The stoichiometry of the reaction was determined by taking a known excess concentration of peroxomonosulfate over dimethyl sulfoxide and allowing the reaction to completion at room temperature (30 °C). Different concentrations of DMSO (0.01—0.04 M) and PMS (0.02—0.08 M) were taken and after the reaction was over, the remaining PMS was estimated by iodometry. The stoichiometry of the reaction, [DMSO]:[PMS] in all the concentration range studied, was found to be 1:1. The only product of the reaction was identified to be dimethyl sulfone, a white solid, mp 109 °C;

IR: $\nu_{S=O}$ at 1310 and 1140 cm^{-1}, characteristic of sulfones. The error limits of the kinetic constants were calculated by the method of least squares. Duplicate experiments were carried out to check the reproducibility of the results and it was found that the results were reproducible within the error of ±5%.

Results and Discussion

All the experiments were carried out under pseudo-first-order conditions with [DMSO] at least ten times higher than that of PMS. The experiments could be done only at two different temperatures, 10 and 20 °C, and at higher temperatures, the reaction was found to be immeasurably fast. Plots of log $[PMS]_t$ *versus* time/min (Fig. 1) were found to be linear showing a first-order dependence on [PMS]. The pseudo-first-order rate constants, k'/s^{-1}, evaluated from the slopes of the above plots were found to be independent of the initial concentration of PMS (Fig. 1), further confirming the first-order dependence on [PMS]. The plots of log $[PMS]_t$ *vs.* time at different initial concentrations of DMSO and at a fixed concentration of PMS were found to be linear (Fig. 2) and the pseudo-first-order rate contants, k', evaluated from these plots were found to increase with increase in [DMSO]. Plots of k' *vs.* [DMSO] were found to be linear passing through origin (Fig. 3) showing a first-order dependence with respect to [DMSO] also. From the slopes of the above plots, the second-order rate constants, k_2 ($dm^3\ mol^{-1}\ s^{-1}$), were evaluated. In acid medium (H_2SO_4), the values of k_2 were found to decrease with increase in $[H^+]$ (0.1—0.5 M) and the plot of k_2 *vs.* $[H^+]$ was found to be linear with negative slope showing an inverse first-order dependence on $[H^+]$ and consequently the plot of k_2 $[H^+]$ *vs.* $[H^+]$ was linear with intercept on the ordinate (Fig. 4). The variation of pH from 4.6 to 7 was found to increase the rate (Table 1) and the reaction at pH≥9 was found

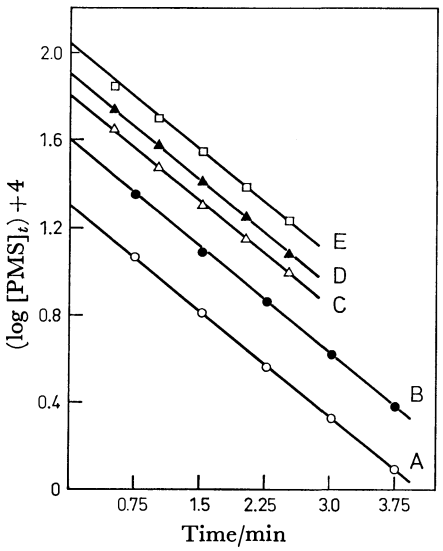

Fig. 1. First-order kinetics in [PMS]. pH=4.6; μ= 0.12 M, T=20 °C; [DMSO]=0.125 M; [PMS]= 2,4,6,8,10×10^{-3} M (A—E).

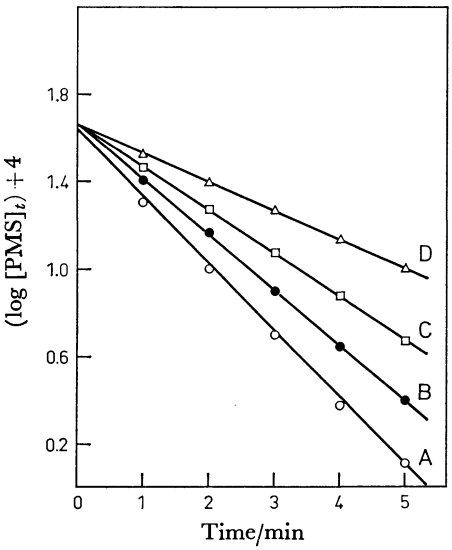

Fig. 2. Evaluation of pseudo-first-order rate constants at different [DMSO]. pH=4.6; μ=0.12 M; T=20 °C; [PMS]=4.3×10^{-3} M; [DMSO]=5,7.5,10, 12.5×10^{-2} M (A—D).

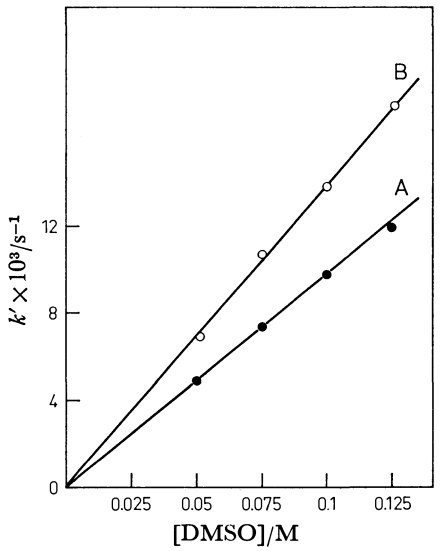

Fig. 3. First-order dependence on [DMSO]. plot A: pH 4.6; plot B: pH=7.0; μ=0.12 M; T=20 °C.

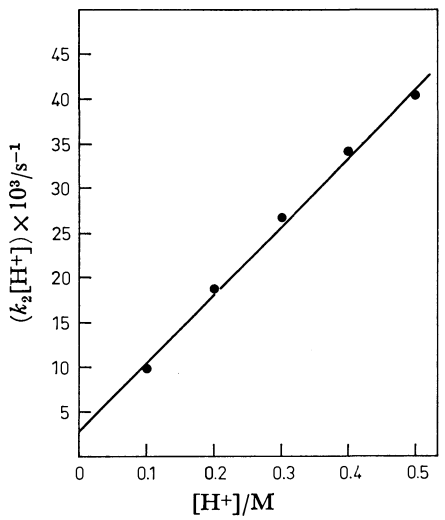

Fig. 4. Effect of $[H^+]$ on k_2. μ=0.6 M; T=20 °C.

Table 1. Kinetic and thermodynamic parameters

pH	T / °C	$k_2 \times 10^2$ / dm^3 mol^{-1} s^{-1}	E_a / kJ mol^{-1}	ΔH^* / kJ mol^{-1}	ΔS^* / J deg^{-1} mol^{-1}	ΔG^* / kJ mol^{-1}
4.6	10	4.80	50.2	47.7	−101.7	77.5
	20	9.90				
7.0	10	6.91	45.6	43.1	−114.7	77.5
	20	13.36				
0.3MH+	10	4.93	40.2	37.7	−146.1	80.8
	20	8.83				

to take place instantaneously and consequently no experiment was done at pH>7. The presence or absence of atmospheric oxygen was found to have no effect on the reaction rate. Added acrylonitrile monomer was found to polymerize in deaerated reaction systems containing (i) acrylonitrile and PMS and (ii) acrylonitrile, PMS, and DMSO when [DMSO]≤[PMS]. However, when the concentration of DMSO was increased to greater than ten times that of PMS, complete suppression of polymerization occurred and consequently no polymer formation was observed. This indicates that at low concentrations of DMSO and in the absence of it, the polymer formed was only due to the direct reaction between PMS and acrylonitrile and not due to the formation of any radical intermediate in the reaction between DMSO and PMS. The absence of any radical intermediate was also confirmed ESR by experiments.[13] DMSO and PMS were mixed in the ESR cavity in a flow system[14] and the ESR measurements were taken. No ESR signal corresponding to any radical species could be seen. Since peroxomonosulfate would give rise to $\cdot OH$ and $\dot{S}O_4^-$ by homolytic scission and $\dot{S}O_4^-$ and OH^- or $\dot{O}H$ and SO_4^{2-} with reducing agents,[10] such very reactive radical species, if they are formed, would have produced radicals such as $\dot{C}H_3$[15] from DMSO. Experiments were also conducted by mixing PMS solution and that of DMSO containing fumaric acid in the flow system and ESR signals were looked for. Since fumaric acid is an efficient spintrapping agent[16–18] for $\dot{O}H$, $\dot{S}O_4^-$, and organic radicals, absence of any ESR signal confirms positively the absence of radicals as the intermediate in the PMS–DMSO system.

Peroxomonosulfuric acid ($HO\text{–}OSO_3H$) has two ionisable protons. Strictly speaking, one is the sulfuric acid proton and the other is the hydrogen peroxide proton. The pK_a value of the sulfuric acid proton lies in a high acidity region and that of hydrogen peroxide proton[4] is 9.4. Since the rate was found to be increased enormously as the pH is increased and decreased as $[H^+]$ was increased and also from the nature of $k_2[H^+]$ *vs.* $[H^+]$ plot leaving intercept on the ordinate (Fig. 4), the following mechanism of oxidation involving acid-independent and inverse acid-dependent paths may be proposed.

$$HO\text{–}O\text{–}SO_3^- \overset{K}{\rightleftharpoons} {}^-O\text{–}O\text{–}SO_3^- + H^+ \quad (1)$$

$$(CH_3)_2SO + HO\text{–}OSO_3^- \xrightarrow{k_a} (CH_3)_2SO_2 + SO_4^{2-} + H^+ \quad (2)$$

$$(CH_3)_2SO + {}^-O\text{–}O\text{–}SO_3^- \xrightarrow{k_b} (CH_3)_2SO_2 + SO_4^{2-} \quad (3)$$

The rate equation for the disappearance of PMS is given as

$$\text{Rate} = \frac{-d[PMS]}{dt} = k_a[DMSO][HSO_5^-] + k_b[DMSO][SO_5^{2-}] \quad (4)$$

$$= k_a[DMSO][HSO_5^-] + \frac{k_bK[DMSO][HSO_5^-]}{[H^+]} \quad (5)$$

$$\frac{\text{Rate}}{[DMSO][PMS]} = k_2 = k_a + k_bK[H^+]^{-1}, \quad (6)$$

where k_2 is the overall second-order rate constant and k_a and k_b are acid-independent and inverse acid-dependent rate constants respectively. Equation 6 may be rearranged into a convenient form,

$$k_2[H^+] = k_a[H^+] + k_b[K]. \quad (7)$$

Using the rate constants at $[H^+]=0.1$—0.5 M, the plot of $k_2[H^+]$ *vs.* $[H^+]$ was drawn (Fig. 4). From the line of best fit, the value of $k_a=7.70\times10^{-2}$ M^{-1} was obtained as the intercept. From the slope of the above plot, k_bK, the value of $k_b=7.37\times10^6$ dm^3 mol^{-1} s^{-1} was obtained using the literature value[4] of $K=3.98\times10^{-10}$. It is seen that k_b is approximately eight orders of magnitude higher than k_a. So, it is not surprising that the reaction between DMSO and PMS is instantaneous at pH>9 where PMS exists as ${}^-O\text{–}O\text{–}SO_3^-$. This also points to the fact that the reaction occurs predominantly with SO_5^{2-} as the active species of PMS. In general, the reactions of peroxide are prone to acid-catalysis. The present investigation is interesting in that an inverse acidity dependence is observed. The higher reactivity of SO_5^{2-} than that of HSO_5^- may be considered to be in favour of a nucleophilic attack by the peroxide.

The foregoing kinetic results, second-order kinetics and inverse acidity dependence, may suggest a nucleophilic substitution mechanism on the sulfur atom in DMSO by PMS as shown below.

$$CH_3SOCH_3 + {}^-O\text{–}O\text{–}SO_3^- \longrightarrow \left[\begin{array}{l} CH_3 \\ \quad\ddot{S}\text{–}O\text{–}OSO_3^- \\ CH_3 \\ \quad O \end{array}\right] \longrightarrow (CH_3)_2SO_2 + SO_4^{2-}. \quad (8)$$

A similar mechanistic behavior involving the nucleophilic attack of peroxide oxygen on the sulfur atom of sulfoxide has been observed in the oxidation of diphenyl sulfoxide by perbenzoic acid.[12] There is also abundant evidence that peroxo anions are strongly

nucleophilic as pointed out in earlier work.[19] The kientic and thermodynamic parameters, for the present investigation, calculated by using standard equations are presented in Table 1. The thermodynamic parameters given are for the overall second-order rate constants, k_2, obtained only at two temperatures, 10 and 20 °C because the reaction was immeasurably fast above 20 °C. Nevertheless the values of activation parameters,

$\Delta H^* = 37.7$ to $47.7\,\mathrm{kJ\,mol^{-1}}$ and

$\Delta S^* = -101.7$ to $-146.1\,\mathrm{J\,deg^{-1}\,mol^{-1}}$

observed by us, are of the same order of magnitude as observed by Edwards[20] for typical nucleophilic second-order reactions,

$\Delta H^* = 37.7$ to $71.2\,\mathrm{kJ\,mol^{-1}}$ and

$\Delta S^* = -41.9$ to $-146.5\,\mathrm{J\,deg^{-1}\,mol^{-1}}$.

Comparison with the oxidation of sulfoxides by other inorganic peroxides:

Oxidations[12,20,21] of sulfides and sulfoxides by hydrogen peroxide and organic peroxoacids, are discussed in terms of nucleophilic reactions. In general, the reactions follow a second order rate law, first order each with respect to [peroxoacid] and [reductant]. In the case of sulfides, the nucleophilic attack on peroxo oxygen is made by sulfur of the sulfide and the reverse was found to be true in the case of sulfoxides.[12] The kinetic and thermodynamic parameters are found to be consistent with the mechanistic reasonings for an S_N2 mechanism.

Peroxodisulfate oxidation of DMSO has not been carried out so far. But from the available data[22,23] on the sulfoxides, such as diethyl and diphenyl sulfoxides, it can be understood that the oxidation rates at low concentrations of sulfoxides follow a total first order kinetics, first order with respect to $[S_2O_8^{2-}]$ and zero order with respect to [sulfoxide] and a total second order, first order each with respect to $[S_2O_8^{2-}]$ and [sulfoxide] at higher concentrations of sulfoxide. From the observation that oxygen does not affect the rate of the diethyl sulfoxide–$S_2O_8^{2-}$ reaction, Howard and Levitt[18,19] suggested that the reactions do not proceed by a free radical mechanism. But it is argued[2] that the increase in the rate of disappearance of peroxodisulfate ion in the presence of sulfoxide and the zero order dependence upon sulfoxide concentration would indicate that a chain reaction is operative.

The kinetics and mechanism of oxidation of dimethyl sulfoxide by peroxodiphosphate[24] was carried out recently. It was found that the reaction was strongly acid-catalysed. The reaction obeys a total first order, first order with respect to the [oxidant] and zero order with respect to [DMSO]. The kinetic data are rationalised by a free radical chain mechanism. Dimethyl sulfone was identified to be the sole product of oxidation, the stoichiometric reaction being

$$(CH_3)_2SO + H_3P_2O_8^- + H_2O \longrightarrow (CH_3)_2SO_2 + 2H_2PO_4^- + H^+. \quad (9)$$

The energy of activation for the reaction is 75.8 kJ mol^{-1} which is lower than the –O–O– bond energy of the peroxide. Comparison of the data on the oxidation of water by peroxodiphosphate indicated that the aprotic solvent, DMSO, was oxidised with more facility than the protic solvent, H_2O.

The kinetics of oxidation of dimethyl sulfoxide by peroxomonophosphate,[25] $H_2PO_5^-$, the phosphorus analog of peroxomonosulfate, was found to follow the similar rate law as in the present investigation except for the acid-dependence. The reaction is found to obey a second order kinetics, first order each with respect to [DMSO] and $[H_2PO_5^-]$. The reaction shows a direct first-order dependence on $[H^+]$ in strong acid (H_2SO_4) medium and the rate decreases with increase in pH in buffered media. This acid-dependence is in sharp contrast to that found in the present investigation wherein an inverse acidity dependence is observed. Comparison of rate constants under similar experimental conditions show that peroxomonosulfate is a more powerful oxidant than peroxomonophosphate and the former oxidant can be used as an analytical reagent to estimate dimethyl sulfoxide at room temperature, provided the estimation is done at alkaline pH.

References

1) D. A. House, *J. Chem. Soc.*, **62**, 185 (1962).
2) W. K. Wilmarth and A. Haim, "Peroxide Reaction Mechansims," ed by J. O. Edwards, Interscience, New York (1962), p. 175.
3) T. S. Price, *J. Chem. Soc.*, **89**, 54 (1906).
4) D. L. Ball and J. O. Edwards, *J. Am. Chem. Soc.*, **78**, 1125 (1956).
5) D. L. Ball and J. O. Edwards, *J. Am. Chem. Soc.*, **62**, 343 (1958).
6) R. W. Johnson and J. O. Edwards, *Inorg. Chem.*, **5**, 2073 (1966); D. H. Fortnum, C. J. Battaglia, S. R. Cohen, and J. O. Edwards, *J. Am. Chem. Soc.*, **82**, 718 (1960).
7) J. O. Edwards and J. J. Müller, *Inorg. Chem.*, **1**, 696 (1962).
8) P. Maruthamuthu and P. Neta, *J. Phys. Chem.*, **81**, 937 (1977).
9) R. C. Thompson, P. Wieland, and E. H. Appleman, *Inorg. Chem.*, **18**, 1974 (1979).
10) R. Somuthevan, R. Renganathan, and P. Maruthamuthu, *Inorg. Chim. Acta Lett.*, **45**, 165 (1980).
11) C. G. Overberger and R. W. Cummins, *J. Am. Chem. Soc.*, **75**, 4250 (1953).
12) H. H. Szmant, H. F. Harnsberger, and F. Krahe, *J. Am. Chem. Soc.*, **76**, 2185 (1954).
13) Experiments conducted by one of the authors (P.M.) at the Max-Planck-Institut für Strahlenchemie, Mülheim (Ruhr), West Germany.
14) B. C. Gilbert, R. O. C. Norman, and R. C. Sealy, *J. Chem. Soc., Perkin Trans. 2*, **1973**, 2174.
15) B. C. Gilbert, R. O. C. Norman, and R. C. Sealy, *J. Chem. Soc., Perkin Trans. 2*, **1975**, 303, 308.
16) P. Neta, *J. Phys. Chem.*, **75**, 2570 (1971).
17) Om P. Chawla and R. W. Fessenden, *J. Phys. Chem.*, **79**, 2693 (1975).
18) P. Maruthamuthu and H. Taniguchi, to be published: Fumaric acid was used successfully as an efficient spin-trapping agent to trap $\dot{O}H$ and $\dot{S}O_4^-$ in the photolysis

of aqueous solution of peroxomonosulfate.
19) C. A. Bunton, in Ref. 2, p. 11; W. P. Jencks and J. Carriuolo, *J. Am. Chem. Soc.*, **82**, 1778 (1960).
20) J. O. Edwards, in Ref. 2, p. 67.
21) S. D. Ross, *J. Am. Chem. Soc.*, **68**, 1484 (1946).
22) H. Howard, Jr., and L. S. Levitt, *J. Am. Chem. Soc.*, **75**, 6170 (1953).
23) R. L. Eager and C. A. Winkler, *Can. J. Res.*, **26** (B), 527 (1948).
24) P. Maruthamuthu and M. Santappa, *Ind. J. Chem.* **16A**, 43 (1978).
25) R. Viswamurthy and P. Maruthamuthu, *Oxidation Commun.*, in press.

Effects of Intermolecular Hydrogen-bonding on the Luminescence Properties of Acetophenone. Characterization of Emission States

Suniti Kumar GHOSHAL, Susil Kumar SARKAR, and Gouranga Sundar KASTHA*

Optics Department, Indian Association for the Cultivation of Science, Jadavpur, Calcutta 700032, India

(Received May 23, 1980)

The effects of intermolecular hydrogen-bond formation by protic solvents on the absorption and luminescence properties of acetophenone have been investigated. It has been concluded from analysis of the $T \leftarrow S_0$ absorption, phosphorescence excitation spectra and the emission characteristics that the lowest triplet state of acetophenone in its vapor phase and in nonpolar as well as in moderately polar solvents (*e.g.*, ethanol, EPA *etc.*) is of n-π^* character. In rigid polar media, acetophenone exhibits a very weak $^1\pi\text{-}\pi^* \rightarrow S_0$ fluorescence and a weak $^3\pi\text{-}\pi^* \rightarrow S_0$ phosphorescence superposed with the principal ^{3}n-$\pi^* \rightarrow S_0$ emission. A progressive enhancement of both of these emissions with increasing polarity of the solvent has been observed. It is shown that the fluorescence and the dual phosphorescence emissions from acetophenone in rigid polar media arise as a result of decreased efficiencies of the spin-orbit and vibronic coupling interactions due to intermolecular hydrogen-bond formation by the protic solvents.

In spite of extensive spectroscopic[1-18] and photophysical[19-21] studies ambiguity remains concerning the assignment of the lowest triplet state of acetophenone. The phosphorescent state of acetophenone in glassy nonpolar and moderately polar media (*e.g.*, ethanol, EPA) at 77 K has been shown to possess a n-π^* character by several investigators[1-6] and a π-π^* character by others.[7,8] More recently, Mathews and Lytle[9] characterized it as n-π^* and π-π^* type in polar (ethanol, methanol) and nonpolar media, respectively, at 77 K. In the case of pure acetophenone crystal, π-π^* assignment was made of its lowest triplet state on the basis of polarized phosphorescence-excitation spectra[11] and PMDR studies,[12] and n-π^* assignment on the basis of $T \leftarrow S_0$ absorption[10] and the polarization and Zeeman splitting measurement of the $T \leftarrow S_0$ absorption.[13]

As regards the origin of dual phosphorescence emissions in rigid polar media, the phenomenon has been interpreted on the basis of various assumptions.[14,17] Koyanagi *et al.*[6] proposed a model of highly distorted (triple minimum) potential surface in the lowest triplet state of acetophenone in order to explain its dual phosphorescence. A non-interacting density of states model has been postulated to account for the phenomenon. In each case a close proximity of the ^{3}n-π^* states has been assumed as an essential prerequisite for the occurrence of dual phosphorescence emission, but little information is given on the relative positions of the triplet levels in environments pertinent to the problem. The dual phosphorescence is observed in rigid polar media and H-bond acceptor properties of the aromatic ketones[5,22,23] but the possibility that this phenomenon could be associated with the solute–solvent intermolecular H-bonding interaction has not be considered.

Though the fluorescence activation of several aromatic aldehydes, ketones and other carbonyl compounds in protic media is well known[24] no investigation seems to have been made on the possibility of fluorescence activation in the case of acetophenone.

In view of the significance of luminescence properties of aromatic carbonyls in hydrogen bonding media and the conflicting assignment of the lowest triplet state of acetophenone, a detailed investigation on the absorption and emission characteristics of this aromatic ketone has been carried out. This study was carried out in order to obtain information on the relative positions of the n-π^* and π-π^* levels of acetophenone under various conditions, and to examine the effect of intermolecular H-bonding on the photophysical behavior of this phenyl alkyl ketone.

Experimental

Materials. Acetophenone (EGA-Chemie, West Germany) was purified by repeated fractional distillation till no impurity could be detected with a flame ionization detector column (Hewlett-Packard, Model 5730A). Spectrograde ethanol, ether, isopentane, and 3-methylpentane (3-MP) of E. Merck and hexane, pentane, and methylcyclohexane of BDH were further purified by fractional distillation. Freshly prepared and deoxygenated solutions of concentrations 10^{-4}—10^{-5} M were used for recording all the spectra except in the cases of $T \leftarrow S_0$ absorptions where more concentrated solutions (*ca.* 10^{-3} M) were used.

Apparatus: The room temperature (300 K) solution and vapor phase (*ca.* 10^{-2} Torr†) emission spectra and low temperature (77 K) emission, excitation and polarization spectra were recorded on a Perkin Elmer Model MPF 44A fluorescence spectrophotometer. The vapor phase absorption spectra with 10 cm quartz cell at 300 K and 760 Torr and the solution spectra at 300 K and 77 K with a 1 cm quartz cell were obtained with a Shimadzu 210A UV-VIS Absorption spectrophotometer. Photoselection technique was employed for the measurement of the degree of polarization, which was corrected following Azumi and McGlynn.[25] The phosphorescence lifetimes were determined by using Molectron UV-1000 N_2-Laser as the excitation source in conjunction with an EC storage Oscilloscope.

Results

Absorption Characteristics. Figure 1 shows the absorption spectrum of acetophenone in the vapor phase and in protic as well as aprotic solvents at room temperature (300 K). Appreciable solvatochromic effects, such as the hypso- and bathochromic shifts, respec-

† 1 Torr=133.322 Pa.

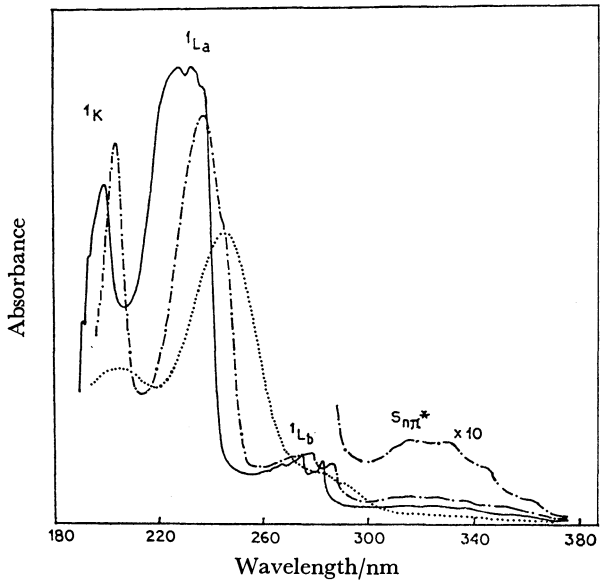

Fig. 1. Singlet-singlet absorption spectra of acetophenone in the vapor phase (——), 3-MP (—·—), and 1% HCl (·····) at 300 K.

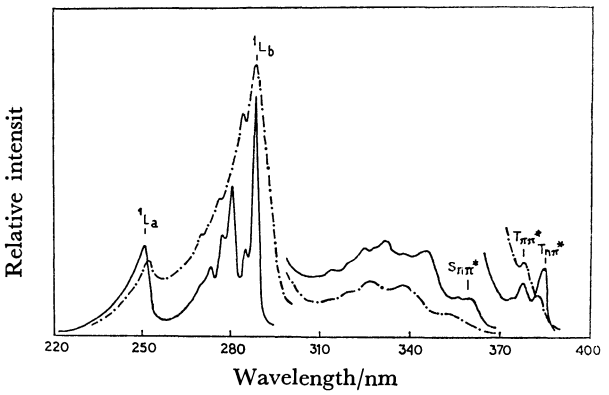

Fig. 2. Phosphorescence excitation spectra of acetophenone in 3-MP (——) and ethanol (—·—) at 77 K.

tively, of the n-π^* and π-π^* bands and noticeable hypochromic effect on both types of bands are evident from a comparison of the spectra. Although in moderately polar and H-bonding media (*e.g.*, ethanol) the higher energy π-π^* bands (^1L_a and ^1K) are relatively less affected, in highly polar and acidic media (*e.g.*, 1% HCl), the red-shifts and hypochromic effect on these bands are substantial but the n-π^* bands are completely obliterated. The results demonstrate the effects of intermolecular H-bonding on the various $\pi^*\leftarrow$n and $\pi^*\leftarrow\pi$ electronic transitions of acetophenone in protic media.

The phosphorescence excitation spectra of acetophenone (Fig. 2) in glassy polar ethanol and nonpolar 3-MP at 77 K provide further data attributable to the effect of solute-solvent H-bonding interaction (Table 1). An appreciable blue shift (*ca.* 464 cm^{-1}) and marked diminution and blurring out of vibrational structure of the ^{1}n-$\pi^*\leftarrow S_0$ bands in the excitation spectra are observed in going from 3-MP to ethanol. The ^{1}n-$\pi^*\leftarrow S_0$ excitation spectra show a significant

Table 1. Relative positions (cm^{-1}) of the n-π^* and π-π^* singlet and triplet states of acetophenone measured from the absorption spectra[a)]

Electronic energy levels	300 K			77 K	
	Vapor	3-MP	Ethanol	3-MP	Ethanol
^1L_a	42997	42092	41395	39875 (39892)	39740 (39749) (39358) b)
^1L_b	35387	34954	34712	34687 (34675)	34615 (34532) (34500) b)
^{1}n-π^*	27886	27692	31736	27769 (27776)	28003 (28240) (28481) b)
$^3\pi$-π^*	26946	26517	26510	26377 (26383)	26308 (26377) (26363) b)
^{3}n-π^*	25899	26000	—	25832 (25933)	25966 (26034) (26075) b)

a) Values in parentheses are obtained from the phosphorescence excitation spectra at 77 K. b) Data in ethanol-water mixture.

lowering (*ca.* 100 cm^{-1}) of the excited state carbonyl stretching frequency of the molecule in ethanol as compared to that in 3-MP glass (Table 2). With increase in the polarity of the medium (*e.g.*, from ethanol to predominantly ethanol–water mixture), further obliteration of the ^{1}n-$\pi^*\leftarrow S_0$ bands takes place. In highly polar and acidic media (1% HCl) these bands are no longer observable in the phosphorescence excitation spectra. The ^1L_a band also shows a similar solvent dependent intensity variation.

Both the vapor and solution phase $T\leftarrow S_0$ absorption spectra of acetophenone (Fig. 3) display two weak but distinct bands. The spectral positions of these bands under different environmental conditions are given in Table 1. From a consideration of the relative changes in absorbance and the solvatochromic shifts exhibited by the bands on passing from the vapor phase to hydrocarbon and to polar solvents, the respective assignments of these bands to $^3\pi$-$\pi^*\leftarrow S_0$ and ^{3}n-$\pi^*\leftarrow S_0$ transitions have been made (Fig. 3). The bands can be clearly discerned in the phosphorescence excitation spectra of acetophenone in polar as well as in nonpolar media at 77 K (Fig. 2). In glassy hydrocarbon (3-MP), the lower energy band (25933 cm^{-1}) has an eminent overlap with the phosphorescence band origin (25815 cm^{-1}), the higher energy one appearing at 26383 cm^{-1}, *i.e.* 450 cm^{-1} towards the higher frequency side of the former. The assignment of these bands to ^{3}n-$\pi^*\rightarrow S_0$ and $^3\pi$-$\pi^*\leftarrow S_0$, respectively on the basis of their characteristic solvatochromic shifts and hypochromic effects are analogous to and conform with those made in the case of absorption.

Emission Characteristics. *a) Phosphorescence Spectra*: Figure 4 shows the phosphorescence and the phosphorescence polarization (PP) spectra of acetophenone in glassy polar, EPA (ether, isopentane, and ethanol

TABLE 2. OBSERVED VALUES OF PHOSPHORESCENCE BAND ORIGIN, FUNDAMENTAL FREQUENCIES, MEAN PHOSPHORESCENCE LIFETIME (τ_p) AND QUANTUM YIELD RATIO (Φ_P/Φ_F) OF ACETOPHENONE

	300 K		77 K	
	Vapor	Isopentane	3-MP	Ethanol
Phosphorescence band origin/cm^{-1}	25670 25786[a]	25668	25815	26007
Fundamental frequency/cm^{-1}	1701	1709	45, 260, 1143, 1346*, 1710	95, 208, 1170, 1240*, 1666
τ_p/ms	2.2	2.4	2.5	5.0 1.2[b] × 10^3
Φ_P/Φ_F	—	—	—	500 400[c] 125[d]

a) Ref. 6. b) Lifetime in acidic media. c) Value in ethanol-water mixture. d) Value in 1% HCl. * C=O stretching frequencies obtained from ^{1}n-$\pi^*\leftarrow S_0$ phosphorescence excitation spectra at 77 K. Φ_P/Φ_F values are considered to be qualitative.

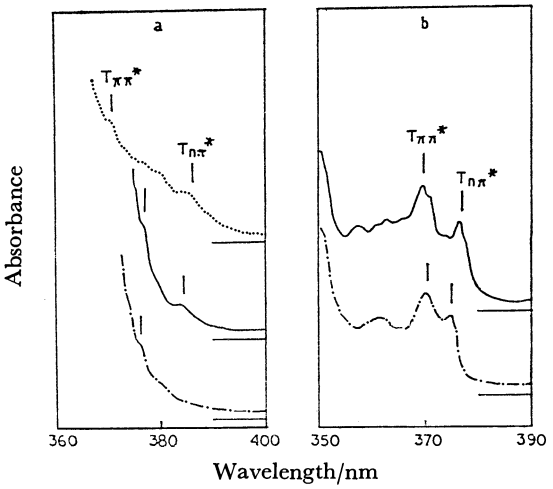

Fig. 3. Singlet-Triplet absorption spectra of acetophenone (a) in the vapor phase (·····), 3-MP (——) and ethanol (—·—) at 300 K. (b) In 3-MP (——) and ethanol (—·—) at 77 K.

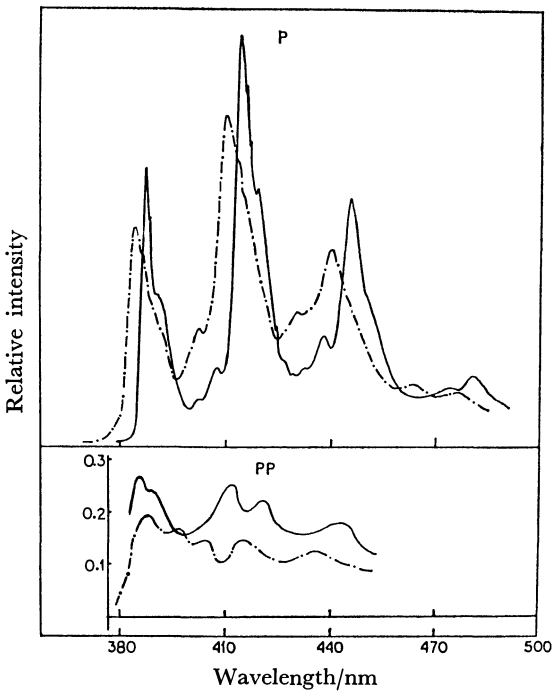

Fig. 4. Phosphorescence (P) and phosphorescence polarization (PP) spectra (with 250 nm excitation) of acetophenone in 3-MP (——) and EPA (—·—) at 77 K.

5:5:2) and nonpolar (3-MP) media under identical conditions. Despite the close resemblance of the two spectra, distinct changes in phosphorescence spectra brought about by the protic solvent are apparent:

(1) The sharp and structured phosphorescence spectrum observed in 3-MP at 77 K appears broadened in EPA glass.

(2) A substantial blue shift (*ca.* 190 cm^{-1}) of the phosphorescence band origin and lowering of carbonyl stretching frequency ($\nu_{C=O}$) occurs with the change of solvent from nonpolar to polar.

(3) A significant diminution in phosphorescence intensity of acetophenone takes place in polar media in comparison with that in glassy hydrocarbon matrices.

(4) Whereas the phosphorescence intensity on the smaller wavelength side of the 0-0 band in glassy hydrocarbon matrices falls steeply, in glassy polar media the band origin is accompanied by a short tail which extends to the higher frequency region beyond the band maximum (384.5 nm). In fact, the phosphorescence spectrum of acetophenone recorded with an expanded scale and higher resolution (Fig. 5) reveals a weak partially resolved blue shoulder at *ca.* 381 nm.

The phosphorescence polarization (PP) curves of acetophenone in glassy hydrocarbon (3-MP) and polar (EPA) media show that in both cases the phosphorescence is strongly positively polarized with respect to ^1L_a excitation, indicating a predominantly in-plane polarization of the phosphorescence emission (Fig. 4). The sharp fall in the value of the degree of polarization (P) in the 3-MP curve around the immediate vicinity of the phosphorescence band origin indicates the presence of some low frequency nontotally symmetric vibronic band in the phosphorescence spectrum. An important distinction between the PP curves in 3-MP

and EPA glass is that the P value is predominantly more positive in aprotic medium than in protic medium. The PP curve in EPA also shows markedly less positive value at 381 nm. A further decrement of the polarization is observed in more polar EWA (ether, water, and ethanol 5:1:4) glass at 77 K.

The phosphorescence decay curves for acetophenone show that while the nature of the decay is nearly exponential in the case of vapor and in hydrocarbon solutions, it is markedly nonexponential (in fact, biexponential) in rigid polar media like ethanol and water at 77 K (Fig. 6). The initial and final slopes of a first order plot from the decay curves of acetophenone in ethanol glass correspond to lifetimes (τ_p) of *ca.* 5 and 70 ms, respectively. The shorter lived component of the phosphorescence emission is, however, found to be contributing mostly (*ca.* 90% of the total intensity) to the phosphorescence intensity. In ethanol–water mixture at 77 K the τ_p values corresponding to the short and long lived components are 6 and 100 ms, respectively, in agreement with the earlier findings.[5]

As the polarity of the solvent is increased there occurs an enhancement in the intensity of the longer lived component of the dual phosphorescence emission until in strongly acidic media it overwhelms the shorter lived one. In this case the phosphorescence lifetime becomes of the order of seconds. This result is similar to that reported by Lamola.[3]

Thus, the predominantly in-plane polarization of the phosphorescence emission, the short lifetime, the solvent shifts and the vibronic structure of the phosphorescence emission provide the conclusive evidence for the n-π^* character of the lowest triplet state of acetophenone in its vapor phase and in nonpolar as well as moderately polar media (*e.g.*, EPA, ethanol) at 77 K. The $T \leftarrow S_0$ absorption spectra of the compound strongly confirm the n-π^* nature of its lowest triplet state in these media.

b) Fluorescence Spectra: In addition to its characteristic strong ^{3}n-$\pi^* \rightarrow S_0$ phosphorescence emission, acetophenone in rigid protic media at 77 K exhibits a very weak $^1\pi$-$\pi^* \rightarrow S_0$ fluorescence with ^1L_a and ^1L_b excitation (Fig. 7). Increase in the polarity or H-bond forming capacity (*e.g.*, ethanol+water, 1% HCl) of the media results in a progressive enhancement of such fluorescence but a gradual decrease in the phosphorescence intensity in the same order. The measured Φ_P/Φ_F values of acetophenone in these polar media are given in Table 2. The data when combined with the reported value of $\Phi_P(\approx 0.6)$ for acetophenone[4] yield an approximate Φ_F value of 1.2×10^{-3} for this molecule in ethanol. Under these conditions, no emission attributable to the ^{1}n-$\pi^* \rightarrow S_0$ fluorescence could be detected.

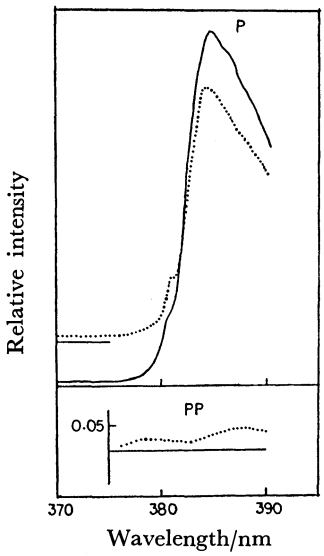

Fig. 5. Part of the phosphorescence (P) spectra (recorded on expanded scale) of acetophenone showing the phosphorescence band origins and the blue shoulder in ethanol (——), EWA (·····) glasses at 77 K and the corresponding phosphorescence polarization (PP) spectrum in EWA.

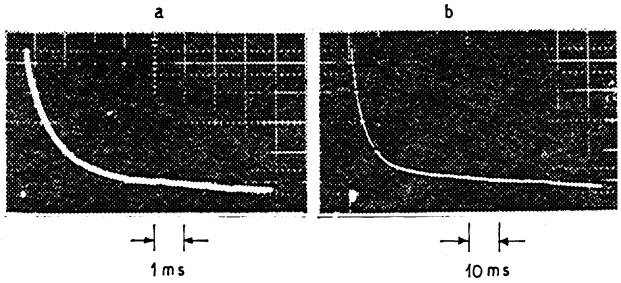

Fig. 6. Phosphorescence decay curves of acetophenone (a) in the vapor phase at 300 K (b) in ethanol at 77 K.

Discussion

Occurrence of the phenomena, *viz.*, blue-shifts of the n-π^* bands, hypochromic effect on the n-π^* and π-π^* (^1L_a) bands, significant lowering of ν_{CO}, fluorescence activation and dual phosphorescence emission from acetophenone in protic media and the progressive enhancement of each with increasing solvent H-bond

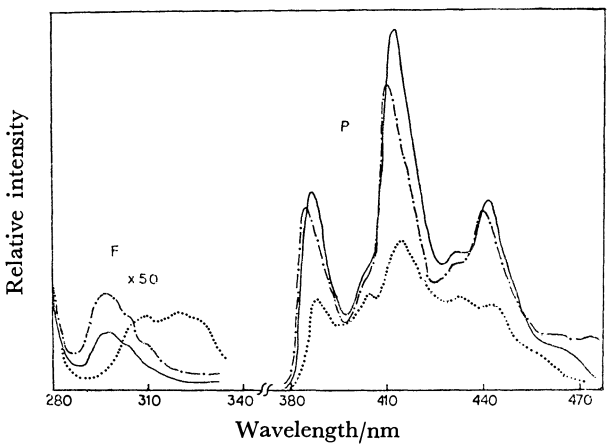

Fig. 7. Fluorescence (F) and phosphorescence (P) spectra of acetophenone in 3-MP (——), predominantly ethanol–water mixture (—·—), and in 1% HCl (·····) at 77 K (Note the broken wavelength scale.).

donor capacity, indicates a close interrelation with intermolecular H-bonding. It might be related to changes in the electronic configuration of the acetophenone molecules caused by solute-solvent interaction, in view of the importance of the electronic structure associated with the carbonyl group, particularly the nonbonding (n) orbital on the oxygen atom, in determining the photophysical behavior of the aromatic ketones and the possible involvement of the oxygen electrons in intermolecular H-bond formation.

The hypsochromic shift of $\pi^*\leftarrow$n transition bands of carbonyls in H-bonding media has now been established.[26,27] It is known by infrared and Raman studies[22,28,29] that the ν_{CO} of carbonyls decreases with increasing H-bonding. Our experimental results are in line with these findings.

Intermolecular H-bonding interaction between the proton acceptor carbonyls and the donor protic molecules affects the electronic configuration of the carbonyl group in several ways. It increases the polarity of the carbonyl group (in the direction C^+–O^-) by increasing the π electron charge on the carbonyl oxygen atom[28,30,31]. As a consequence, the C–O bond strength decreases leading to an increased C–O bond length and smaller ν_{CO}. Since the n electrons on the carbonyl are primarily involved in intermolecular H-bond formation, such solute-solvent interaction is expected to have a pronounced effect on the n orbital of the oxygen atom. The work of Hollas *et al.*[32] indicates that the s character of the n orbital and its extent of delocalization are important in determining the $\pi^*\leftarrow$n transition intensity in aromatic aldehydes and ketones. The marked diminution in the intensity of n-π^* bands of acetophenone observed in going from hydrocarbon to hydroxylic solvents suggests an appreciable decrease in the s character of the sp^2 hybridized[28,33,34] n orbital of the carbonyl oxygen atom.

In aromatic aldehydes and ketones, because of the presence of closely spaced n-π^* and π-π^* electronic states (the n-π^* states being the lower-lying one), the spin-orbit and vibronic interactions between n-π^* and π-π^* excited states are generally very strong. The radiationless deactivation processes, such as internal conversion (IC) and intersystem crossing (ISC) between the pertinent excited states, are very fast and efficient in these types of molecules. This largely accounts for their nonfluorescent nature. The occurrence of π-π^* fluorescence from acetophenone in protic media and the progressive enhancement of such emission with increasing H-bond donor capacity of the solvent thus imply a considerable decrease in the efficiency of ISC or IC, or of both in such media.

The rate or the efficiency of IC between the n-π^* and π-π^* states is dependent to a significant extent on the vibrational overlap integral between the states concerned. Since the magnitude of vibrational overlap integral between n-π^* and π-π^* states decreases as a result of decrease in the charge density of the nonbonding electrons following H-bond formation,[34,35] it is expected that the efficiency of IC between the $^1\pi$-π^* and ^{1}n-π^* states of acetophenone would decrease in protic media.

The magnitude of spin-orbit coupling between the $^1\pi$-π^* and ^{3}n-π^* states of aromatic aldehyde and ketone molecules is largely governed by factors such as the partial π electron density (C_ν^2) and Slater charge (Z_ν) on the carbonyl oxygen atom and the form (hybridization and extent of delocalization) of the n orbital on this atom.[36] It follows that while the π electron density on the carbonyl oxygen atom increases a little, the hybridization factor (γ) undergoes a significant decrement upon H-bond formation. The analysis of Del Bene[37] shows that the increase of π electron charge on the heteroatom due to H-bonding leads to the lowering of the effective nuclear charge (Z_ν) of the atom. Because of the dependence of the spin-orbit interaction matrix element, $|\beta|^2$ (Eq. 8, Ref. 36), on the higher power of Z and the fact that both γ and Z values decrease as a result of H-bonding, it seems that there is an overall decrease in the value of $|\beta|^2$, despite a small increment in the value of C_ν^2. Accordingly, the spin-orbit coupling between the $^1\pi$-π^* and ^{3}n-π^* states of acetophenone should decrease in H-bonding media, and so should the ISC rate between them. It is conceivable, therefore, that because of the decreased efficiencies or rates of $^1\pi$-π^* ⇝ ^{1}n-π^* IC and $^1\pi$-π^* ⇝ ^{3}n-π^* ISC, the $^1\pi$-$\pi^*\rightarrow S_0$ radiative process may become to some extent competitive with these radiationless processes such that some π-π^* fluorescence could be emitted from acetophenone molecules in protic media.

The ^1L_a state of aromatic aldehydes and ketones (*e.g.*, benzaldehyde and acetophenone) which provides the dipole allowed character and in-plane polarization to the lowest triplet state through spin-orbit coupling[1] is known[38] to possess considerable intramolecular charge transfer character. The marked diminution in the ^1L_a band intensity of acetophenone in protic media indicates that the intramolecular charge transfer character of the associated singlet-singlet $\pi^*\leftarrow\pi$ transition is perhaps inhibited as a result of solute-solvent H-bonding interaction. The significant lowering of the P values of phosphorescence emission from acetophenone molecules in H-bonding media, compared to those observed in nonhydrogen bonding media, could be related, at least partly, to the diminished spin-orbit coupling between $^1\pi$-π^* $(^1L)_a$ and ^{3}n-π^* state due to H-bonding. This may be interpreted as evidence in favor of the supposition that the spin-orbit coupling should decrease in H-bonding media.

The simultaneous emission of phosphorescence from both the triplet states (^{3}n-π^* and $^3\pi$-π^*) of acetophenone in protic media suggests that the solvent induced decrease in the efficiency of $^3\pi$-π^* ⇝ ^{3}n-π^* IC process could be at the basis of such phenomenon.

According to Avouris *et al.*,[39] the rate constant of the IC process between two states is given by

$$K_{if}^{ic} = 2\pi/\hbar V_{if}^2 \rho_f(E_i), \qquad (1)$$

where $\rho_f(E_i)$ is the density of closely spaced state 'f' (final) nearly degenerate with the initial state 'i' and V_{if} is the interaction matrix element for the IC process. V_{if} is dependent on the electronic factor β_{ei}^{ic} and vibrational overlap integral.

Intermolecular H-bonding can bring about a dimi-

nution in the overlap integral through the decrease of nonbonding charge density. It can be shown that the magnitude of V_{if} in the triplet manifold would also decrease as a result of intermolecular H-bond formation. We see from Eq. 1 that the density of states, $\rho_f(E_i)$ could also be an important factor contributing to the radiationless transition between the two triplet states. Because of the smaller energy gap between the T_2 (π-π^*)—T_1 (n-π^*) states of acetophenone in protic solvents, the level densities of T_1 near the T_2 origin are expected to be small. Consequently, internal conversion from the low-lying vibrational levels of T_2 to T_1 would be less efficient. As a result of the combined effect of a decrease in both these factors, it is possible that the $T_2 \rightsquigarrow T_1$ IC rate would become sufficiently slow so as to make the $^3\pi$-$\pi^* \rightarrow S_0$ radiative process to some extent competent with the IC process, leading to the observation of dual phosphorescence emission in the case of acetophenone. Several authors previously observed dual phosphorescence emission from other aromatic ketones, *e.g.*, *p*-benzoquinone,[40] indanone,[41] and related molecules in rigid polar media, and attributed the phenomenon to severely prohibited internal conversion from the $^3\pi$-π^* state to a lower lying ^{3}n-π^* state of these molecules.

Thus, the profound influence of the H-bonding solvents on the luminescence spectral properties of acetophenone is seen to arise primarily from the electronic effect of the intermolecular H-bonding interaction. When polarity or H-bond donor capacity of the solvent increases, the ISC and IC processes become progressively less efficient and a trend of progressive enhancement of the π-π^* fluorescence and $^3\pi$-$\pi^* \rightarrow S_0$ phosphorescence is observed. In strongly acidic media protonation of the carbonyl lone pair electrons occurs; the conjugation of the oxygen electrons across the carbonyl group and the intramolecular charge transfer character of the $^1L_a \leftarrow S_0$ transition are strongly affected. In this situation, as the n electrons on the carbonyl oxygen atom no longer remain nonbonding, the $\pi^* \leftarrow$n electronic transition loses its significance and the luminescence characteristics exhibited by the protonated species become more or less normal π-π^* type.

References

1) R. Shimada and L. Goodman, *J. Chem. Phys.*, **43**, 2027 (1965).
2) T. Takemura and H. Baba, *Bull. Chem. Soc. Jpn.*, **42**, 2756 (1969).
3) A. A. Lamola, *J. Chem. Phys.*, **47**, 4810 (1967).
4) T. F. Hunter, *Trans. Faraday Soc.*, **66**, 300 (1970).
5) M. B. Ledger and G. Porter, *J. Chem. Soc., Faraday Trans. 1*, **68**, 539 (1972).
6) M. Koyanagi, R. J. Zwarich, and L. Goodman, *J. Chem. Phys.*, **56**, 3044 (1972).
7) D. R. Kearns and W. A. Case, *J. Am. Chem. Soc.*, **88**, 5087 (1966).
8) Y. H. Li and E. C. Lim, *Chem. Phys. Lett.*, **7**, 15 (1970).
9) T. G. Mathews and F. E. Lytle, *J. Luminescence*, **21**, 93 (1979).
10) S. Dym and R. M. Hochstrasser, *J. Chem. Phys.*, **51**, 2458 (1969).
11) W. A. Case and D. R. Kearns, *J. Chem. Phys.*, **52**, 2175 (1970).
12) T. H. Cheng and N. Hirota, *Mol. Phys.*, **27**, 281 (1974).
13) Y. Tanimoto, T. Azumi, and S. Nagakura, *Bull. Chem. Soc. Jpn.*, **48**, 136 (1975).
14) N. C. Yang and S. L. Murov, *J. Chem. Phys.*, **45**, 4358 (1966).
15) P. Gacoin and Y. Mayer, *C. R. Acad Sci.*, **267**, 149 (1968).
16) R. N. Griffin, *Photochem. Photobiol.*, **7**, 159, 175 (1968).
17) P. J. Wagner, M. J. Mary, A. Haug, and D. R. Graber, *J. Am. Chem. Soc.*, **92**, 5269 (1970).
18) San-Yan Chu and L. Goodman, *Chem. Phys. Lett.*, **34**, 232 (1975).
19) G. Porter and P. Suppan, *Trans. Faraday Soc.*, **61**, 1664 (1965).
20) E. J. Baum, J. K. S. Wan, and J. N. Pitts, Jr., *J. Am. Chem. Soc.*, **88**, 2652 (1966).
21) N. C. Yang, D. S. McClure, S. L. Murov, J. J. Houser, and Ruth Dusenbery, *J. Am. Chem. Soc.*, **89**, 5466 (1967).
22) M. Ito, K. Inuzuka, and S. Imanishi, *J. Am. Chem. Soc.*, **82**, 1317 (1960).
23) E. Malwer and C. Marzzacco, *J. Mol. Spectrosc.*, **46**, 341 (1973); R. G. Lewis and J. J. Freeman, *ibid.*, **32**, 24 (1969).
24) K. Brederek, J. Forster, and H. G. Oesterlin, "Luminescence of Organic and Inorganic Materials," ed by H. P. Kallmann and G. M. Sprunch, Wiley, New York (1962), p. 161; J. F. Ireland and P. A. H. Wyatt, *J. Chem. Soc., Faraday Trans. 1*, **68**, 1053 (1972); H. Baba and M. Kitamura, *J. Mol. Spectrosc.*, **41**, 302 (1972); A. U. Acuna, A. Ceballos, and M. J. Molera, *J. Chem. Soc., Faraday Trans. 2*, **72**, 1469 (1976).
25) T. Azumi and S. P. McGlynn, *J. Chem. Phys.*, **37**, 2413 (1962).
26) N. Mataga and T. Kubota, "Molecular interactions and electronic spectra," Marcel Dekker, New York (1970), p. 293; George C. Pimentel and A. L. McClellan, *Ann. Rev. Phys. Chem.*, **22**, 347 (1971); C. N. R. Rao, S. Singh, and V. P. Senthilnathan, *Chem. Soc. Rev.*, **5**, 297 (1976).
27) S. N. Vinogradov and R. H. Linnel, "Hydrogen Bonding," Von Nostrand Reinhold Company, New York (1971).
28) L. J. Bellamy and R. J. Pace, *Spectrochim. Acta, Part A*, **27**, 705 (1971).
29) B. A. Zadorozhyyi and I. K. Ishchenko, *Opt. Spektrosk.*, **19**, 306 (1965).
30) L. Paoloni, A. Patti, and F. Manganu, *J. Mol. Struct.*, **27**, 123 (1975).
31) W. H. De Jeu, *Chem. Phys. Lett.*, **7**, 153 (1970).
32) J. M. Hollas, E. Gregorck, and L. Goodman, *J. Chem. Phys.*, **49**, 1745 (1968).
33) C. Dijkgraaf, *Spectrochim. Acta, Part A*, **23**, 365 (1967).
34) M. Kasha, "Light and Life," ed by W. D. McElroy and B. Glass, Baltimore, Johns Hopkins Press (1961), p. 31.
35) E. C. Lim, "Molecular Luminescence," ed by E. C. Lim, W. A. Benjamin, New York (1969), p. 475.
36) V. G. Plotnikov, *Opt. Spectrosc.*, **22**, 401 (1967).
37) J. E. Del Bene, *Chem. Phys.*, **50**, 1 (1980).
38) K. Kimura and S. Nagakura, *Theor. Chim. Acta*, **3**, 164 (1965).
39) P. Avouris, W. M. Gelbart, and M. A. El-Sayed, *Chem. Rev.*, **77**, 793 (1977).
40) M. E. Long, Y. H. Li, and E. C. Lim, *Mol. Photochem.*, **3**, 221 (1971).
41) M. E. Long and E. C. Lim, *Chem. Phys. Lett.*, **20**, 413 (1973).

Circular Dichroism of Chromium(III) Complexes. VII. Circular Dichroism in the Spin-forbidden Transitions of *cis*-$[Cr(N)_2(O)_4]$ Type Complexes with Ethylenediaminetetraacetate Analogues

Sumio KAIZAKI* and Hisako MORI

Department of Chemistry, Faculty of Science, Nara Women's University, Nara 630

(Received January 5, 1981)

Potassium (2*S*,4*S*)-2,4-pentanediaminetetraacetatochromate(III) monohydrate was newly prepared and was found to be formed stereospecifically with a $\Lambda(\Delta\Delta\Lambda)$ absolute configuration as has been revealed for the corresponding Co(III) complex. The circular dichroism spectra in the spin-forbidden transitions of this new complex along with the known analogues, $(-)_{589}$-ethylenediamine-*N*,*N'*-diacetato-*N*,*N'*-dipropionatochromate(III) and $(+)_{589}$-(*S*,*S*)-2,2'-(ethylenediimino)disuccinatochromate(III) complexes, were measured and discussed in comparison with those in the first spin-allowed transitions on the basis of the theoretical relations between the rotational strengths for the spin-forbidden and the spin-allowed transitions in trigonal and tetragonal fields.

In our previous papers of this series,[1-3] circular dichroism(CD) spectra in the spin-forbidden d-d transitions of trigonal and tetragonal Cr(III) complexes have been elucidated in comparison with those in the first spin-allowed d-d transitions by using the theoretical relations between the rotational strengths for the spin-forbidden and the spin-allowed transitions. No CD datum in the spin-forbidden transitions and few CD data in the spin-allowed transitions of chiral Cr(III) complexes with sexidentate ethylenediaminetetraacetate(edta) type ligands have been reported, whereas the CD spectra of several Co(III) complexes with edta analogues have been studied and discussed in relation with their absolute configurations and theories of optical activity.[5-7] The CD spectra in the first band region of such complexes have been dealt with the assumption of C_2 symmetry descending from trigonal(D_3) or tetragonal(D_4) symmetry.[4,5a-c,7a,8] To clarify these CD behavior, it is significant to reveal whether the CD in the spin-forbidden transitions of Cr(III) complexes with edta analogues will be elucidated in terms of the theoretical considerations for the rotational strengths in the d-d transitions on either the trigonal or tetragonal symmetry assumption. In this instance, it is desirable to examine the CD spectra in the spin-forbidden and the spin-allowed transitions of chiral Cr(III) complexes containing edta analogues with four glycinate rings as well as those of the known Cr(III) complexes,[4] $(-)_{589}$-*trans*(O_5)†-ethylenediamine-*N*,*N'*-diacetato-*N*,*N'*-dipropionatochromate(III), $(-)_{589}$-[Cr(eddda)]$^-$, and $(+)_{589}$-*trans*(O_5)†-(*S*,*S*)-2,2'-(ethylenediimino)disuccinatochromate(III), $(+)_{589}$-[Cr(*S*,*S*-edds)]$^-$, both of which have two five-membered and two six-membered N–O chelate rings. Apart from some racemic complexes of the former type,[9] no chiral Cr(III) complexes have yet been known.

This paper reports the preparation and stereospecific formation of a new chiral Cr(III) complex containing (2*S*,4*S*)-2,4-pentanediaminetetraacetate(*S*,*S*-ptnta^{4-}) as one of the closely similar sexidentate ligands to the edta ligand. The CD data in the spin-forbidden transitions as well as in the spin-allowed transitions of this complex are examined together with those in the spin-forbidden transitions of chiral *trans*(O_5) isomers of $(-)_{589}$-[Cr(eddda)]$^-$ and $(+)_{589}$-[Cr(*S*,*S*-edds)]$^-$, of which the CD spectra in the spin-allowed transitions have been previously reported by Radanovic and Douglas.[4] Their CD spectra in the whole region of the d-d transitions are compared with one another and discussed on the basis of both trigonal and tetragonal symmetry assumptions.

† Oxygens of five-membered chelate rings occupy transaxial coordination sites.

Experimental

Preparation of Ligands and Complexes. *1) (2S,4S)-2,4-pentanediaminetetraacetic Acid (S,S-ptntaH$_4$·1.5H$_2$O)*: This ligand was prepared from (2*S*,4*S*)-2,4-pentanediamine by the method for the racemic one.[6] Found: C, 43.27; H, 6.92; N, 7.63%. Calcd for *S*,*S*-ptntaH$_4$·1.5H$_2$O: C, 43.21; H, 6.97; N, 7.75%.

2) $(+)_{589}$-K[Cr(S,S-ptnta)]·H$_2$O: To a solution of 1.0 g of *S*,*S*-ptntaH$_4$·1.5H$_2$O in 15 cm^3 of water was added a solution containing 0.79 g of potassium hydroxide in 10 cm^3 of water. After dissolving 1.2 g of $Cr(NO_3)_3·9H_2O$ in this solution at 70 °C, the mixture was heated at 75—80 °C with stirring for about 16 h. The color of the solution changed gradually from violet to red violet. By adding ethanol to this chilled solution, red powder was obtained. Recrystallization was performed from warm water and ethanol. Found: C, 35.29; H, 4.61; N, 6.36%. Calcd for K[Cr(*S*,*S*-ptnta)]·H$_2$O: C, 35.53; H, 4.59; N, 6.38%.

3) $(-)_{589}$-[Cr(eddda)]$^-$ and $(+)_{589}$-[Cr(S,S-edds)]$^-$: The ligands, ethylenediamine-*N*,*N'*-diacetic-*N*,*N'*-dipropionic acid (edddaH$_4$)[5b] and (*S*,*S*)-2,2'-(ethylenediimino)disuccinic acid (*S*,*S*-eddsH$_4$),[7a] were prepared by the reported methods. $(-)_{589}$-[Cr(eddda)]$^-$ and $(+)_{589}$-[Cr(*S*,*S*-edds)]$^-$ were obtained by the method of Radanovic and Douglas.[4] The absorption and CD spectra along with the infrared spectra confirm that these complexes are *trans*(O_5) isomers which have been previously established.[4,10]

Measurements. Absorption spectra were recorded on a Shimadzu UV-200S spectrophotometer, and CD spectra on a JASCO MOE-1 spectropolarimeter. Infrared spectra were obtained by a JASCO DS-402S spectrophotometer.

Results and Discussion

Stereospecificity of [Cr(S,S-ptnta)]$^-$. The visible absorption spectrum of [Cr(*S*,*S*-ptnta)]$^-$ is quite similar in band position and intensities to that of the trimeth-

ylenediaminetetraacetatochromate(III) complex of the analogous type, [Cr(trdta)]$^-$, as shown in Fig. 1. This fact lends support to sexidentate coordination of an *S,S*-ptnta ligand as in the trdta complex. The CD intensities of the *S,S*-ptnta complex are found to be as large as those of $(-)_{589}$-[Cr(eddda)]$^-$ and $(+)_{589}$-[Cr(*S,S*-edds)]$^-$ as shown in Fig. 1 and Table 1. The CD pattern in the spin-allowed band region

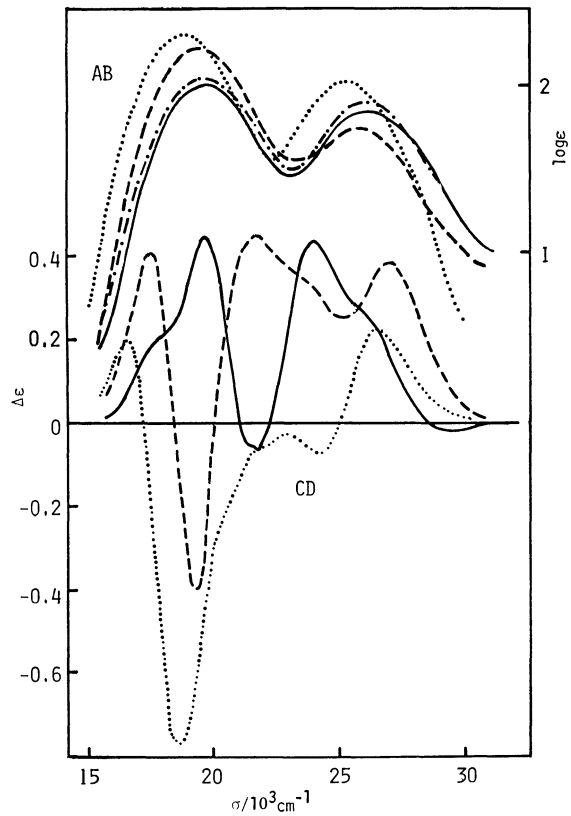

Fig. 1. Absorption and CD curves of $(+)_{589}$-[Cr(*S,S*-ptnta)]$^-$ (——), $(+)_{589}$-[Cr(*S,S*-edds)]$^-$ (– – –), and $(-)_{589}$-[Cr(eddda)]$^-$ (·····), and absorption curve of [Cr(trdta)]$^-$ (—·—) in water.

of the *S,S*-ptnta Cr(III) complex is much different from that of the corresponding Co(III) complex,[6] whereas the CD spectra of $(+)_{589}$-[Cr(*S,S*-edds)]$^-$ and $(-)_{589}$-[Cr(eddda)]$^-$ behave similarly to those of the corresponding chiral *trans*(O_5) isomers of the *S,S*-edds and eddda Co(III) complexes, respectively.[4,5b,7a] As has been revealed for [Co(*R,R*-ptnta)]$^-$,[6] the stereospecific formation of [Cr(*S,S*-ptnta)]$^-$ is expected to take place with a $\Lambda(\Lambda\Delta\Lambda)$ absolute configuration owing to the preference of the equatorial orientation of two methyl groups to the chelate rings.[6] It has been proposed for Co(III) complexes with edta type ligands[5,7] that the CD signs of the lowest frequency component in the first band region are correlated to the absolute configurations; the complexes giving a positive CD component at the lowest frequency side of the first band take a $\Lambda(\Lambda\Delta\Lambda)$ configuration, and *vice versa*. For the *S,S*-ptnta Cr(III) complex, the absolute configuration on the basis of the CD criterion is consistent with that determined in terms of stereospecificity arising from preferential coordination of sexidentate chiral ligands to Cr(III). That is, as in Fig. 1, [Cr(*S,S*-ptnta)]$^-$ with a $\Lambda(\Lambda\Delta\Lambda)$ configuration gives a positive CD component at the lowest frequency side of the first band as has been confirmed for $\Lambda(\Lambda\Delta\Lambda)$-$(-)_{589}$-[Cr(eddda)]$^-$ and $\Lambda(\Lambda\Delta\Lambda)$-$(+)_{589}$-[Cr(*S,S*-edds)]$^-$, of which the absolute configurations have been determined by the X-ray analysis[10] and the stereospecific formation,[4] respectively. Thus, the *S,S*-ptnta Cr(III) complex is formed stereospecifically with a $\Lambda(\Lambda\Delta\Lambda)$ configuration.

CD Spectra in the d-d Transitions. On the assumption of effective C_2 symmetry for the complexes of this type, the lowest-frequency CD component in the first band region is assigned to the $^4B(C_2)$ state, for which the CD signs are considered to be the same as those for the $^4B(C_2)$ state with $^4E(^4T_{2g})$ trigonal parentage or with $^4E(^4T_{2g})$ tetragonal parentage as in the case of the $^1T_{1g} \leftarrow {}^1A_{1g}$ transitions for Co(III) complexes.[4,5b,c,11]

Table 1. CD data of chromium(III) complexes with edta type ligands

$(+)_{589}$-[Cr(*S,S*-edds)]$^-$		$(-)_{589}$-[Cr(eddda)]$^-$		$(+)_{589}$-[Cr(*S,S*-ptnta)]$^-$		Assignment(D_4)
σ_{ext}[a]	$\Delta\varepsilon$[b]	σ_{ext}[a]	$\Delta\varepsilon$[b]	σ_{ext}[a]	$\Delta\varepsilon$[b]	
				13.92	(−0.0038)	$^2E(^2T_{1g})$
14.21	(+0.0348)	14.25	(+0.0352)	14.35	(+0.0055)	$^2A_1$ or $^2A_1+{}^2B_1(^2E_g)$
14.38	(−0.0024)			14.46	(+0.0058)	
14.53	(+0.0036)			14.62	(−0.0017)	
14.87	(−0.0120)	14.87	(−0.0092)	14.85	(+0.0014)	
				15.00	(−0.0021)	
15.44	(+0.0690)	15.26	(+0.0780)	15.31	(+0.0260)	$^2A_2(^2T_{1g})$
17.54	(+0.409)[c]	16.53	(+0.207)[c]	18.00	(*ca.* +0.2)[c]	$^4E(^4T_{2g})$
19.33	(−0.396)	18.62	(−0.765)	19.67	(+0.442)	
21.83	(+0.453)	20.33	(*ca.* −0.19)	21.67	(−0.064)	$^4B_2(^4T_{2g})$
23.33	(*ca.* +0.33)	22.17	(*ca.* −0.05)	24.00	(+0.435)	
27.03	(+0.386)	24.10	(−0.075)	25.25	(*ca.* +0.27)	
		26.53	(+0.23)	29.66	(−0.024)	

a) In units of 10^3 cm^{-1}. b) The $\Delta\varepsilon$ values are given in units of mol^{-1} dm^3 cm^{-1}. c) This band is assigned to the $^4B(C_2)$ state (see Text).

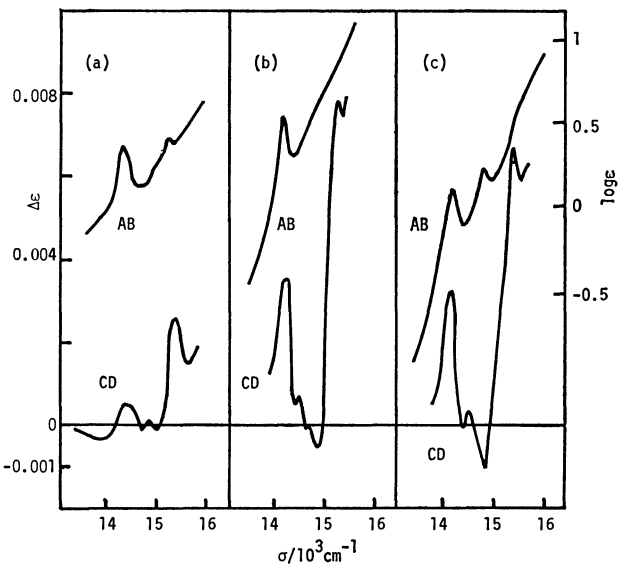

Fig. 2. Absorption (right side ordinate) and CD (left side ordinate) curves in the spin-forbidden transitions of (a) $(+)_{589}$-[Cr(*S*,*S*-ptnta)]$^-$, (b) $(-)_{589}$-[Cr(eddda)]$^-$, and (c) $(+)_{589}$-[Cr(*S*,*S*-edds)]$^-$ in water.

The CD spectra in the spin-forbidden transitions of the present complexes are shown together with the corresponding absorption spectra in Fig. 2. $(+)_{589}$-[Cr(*S*,*S*-edds)]$^-$ and $(-)_{589}$-[Cr(eddda)]$^-$ give a positive CD component near 15300 cm^{-1} and a positive CD one at 14300 cm^{-1} where the lowest-frequency absorption peak is observed. The positions of these two CD peaks coincide with those of the low-temperature absorption bands observed for bis(iminodiacetato)chromate(III) complex.[12] In the region between two strong CD peaks with a positive sign, a weak negative CD component is observed at 14870 cm^{-1} for both the *S*,*S*-edds and $(-)_{589}$-eddda complexes as shown in Fig. 2 and Table 1. Assuming pseudo D_3 symmetry for the complexes, the three CD peaks, (+) near 14300 cm^{-1}, (−) at 14870 cm^{-1}, and (+) near 15300 cm^{-1}, may be assigned to the $^2E(^2E_g)$, $^2A_2(^2T_{1g})$, and $^2E(^2T_{1g})$ states from the lower frequency side as in the case of $(+)_{546}$-[Cr(ox)$_2$(en)]$^-$.[1] The similar CD behavior is observed in the spin-forbidden transitions of the *S*,*S*-ptnta Cr(III) complex, except for the lowest-frequency CD component with a negative sign as shown in Fig. 2. That is, the positive CD peak at 14350 cm^{-1} corresponding to the lowest-frequency absorption peak of the *S*,*S*-ptnta complex and the positive highest-frequency CD peak may be due to the $^2E(^2E_g)$ and $^2E(^2T_{1g})$ states, respectively, as for the *S*,*S*-edds and $(-)_{589}$-eddda complexes. In the region corresponding to the $^2A_2 \leftarrow {}^4A_2$ transition, three weak CD peaks with alternate signs are observed for the *S*,*S*-ptnta complex. In view of these CD behavior, it appears that the correlation between the CD in the spin-forbidden transitions and the absolute configurations for tris-chelate complexes[1] holds also for the present complexes; the complexes giving two $^2E(D_3)$ CD components with a positive sign take a $\Lambda(\Lambda\Lambda\Lambda)$ configuration. From a theoretical point of view,[1] the rotatianal strengths for the $^2E(^2E_g) \leftarrow {}^4A_2$ transition and those for the $^2E(^2T_{1g}) \leftarrow {}^4A_2$ transition in trigonal field are predicted to have the same signs as the net rotational strengths for the $^4T_{2g} \leftarrow {}^4A_{2g}$ transitions and the rotational strengths for the $^4E(^4T_{2g}) \leftarrow {}^4A_2$ transition, respectively. In the case of the *S*,*S*-edds and *S*,*S*-ptnta complexes, such a theoretical relation for the rotational strengths in trigonal field is applicable to CD in the region of the $^2E(^2E_g)$ and $^2E(^2T_{1g}) \leftarrow {}^4A_2$ transitions, because the net CD signs in the first band region and the signs of the $^4B(C_2)$ CD component with ^4E trigonal parentage are positive. The CD of $(-)_{589}$-[Cr(eddda)]$^-$, however, does not follow this relation, since this complex gives a major negative CD band in the first band region, which is presumed to result in the sign inversion of the lowest-frequency CD in the spin-forbidden transitions. Assuming tetragonal symmetry for the complexes, the theoretical relation predicts[2] that the positive highest-frequency CD peak near 15300 cm^{-1} is due to the $^2A_2(^2T_{1g})$ state and the lower frequency one near 14300 cm^{-1} to the $^2A_1(^2E_g)$ or $[^2A_1+{}^2B_1](^2E_g)$ state; the rotational strengths for the $^2A_2$ and $^2A_1 \leftarrow {}^4B_1$ transitions being borrowed from those for the $^4E(^4T_{2g}) \leftarrow {}^4B_1$ transition, and the sum of the rotational strengths for the $^2A_1$ and $^2B_1 \leftarrow {}^4B_1$ transitions from the net one for the $^4T_{2g} \leftarrow {}^4A_{2g}$ transition. The remaining CD peaks may correspond to the $^2E(^2T_{1g})$ state. For $(-)_{589}$-[Cr(eddda)]$^-$, the assignment of the lowest-frequency CD peak to the $[^2A_1+{}^2B_1](^2E_g)$ state is questionable as in the case of the trigonal assumption as mentioned before, because the CD sign of this component is opposite to that of the major component in the first band region. Such a failure of the theoretical relations for the CD in the d-d transitions may be explained by the following approach.

The CD pattern in the spin-forbidden transitions of the *S*,*S*-edds complex is similar as a whole to that of the $(-)_{589}$-eddda complex despite the different CD patterns at the higher frequency side of the first band for these complexes as in Figs. 1 and 2. This fact suggests that the rotational strengths for the spin-forbidden transitions are little affected by those for the higher-frequency components of the $^4T_{2g} \leftarrow {}^4A_{2g}$ transitions but are dominantly borrowed from those for the lowest-frequency $^4B(C_2)^4T_{2g}(O_h) \leftarrow {}^4B(C_2)^4A_{2g}(O_h)$ transition. This intensity borrowing mechanism may be ascribed mainly to the difference in energy intervals between the doublet states and the quartet excited states as has been considered for the elucidation of CD in the spin-forbidden transitions of *trans*-[CrX$_2$(N)$_4$] type complexes.[2] This mechanism is supported by the fact that the CD intensities of the spin-forbidden bands for the present complexes increase in the order of increasing the lower-frequency shift of the lowest-frequency $^4B(C_2)$ CD component as shown in Figs. 1, 2, and Table 1. In such a situation, the contribution to the CD intensities of the spin-forbidden bands from the CD intensity of the negative major spin-allowed band of $(-)_{589}$-[Cr(eddda)]$^-$ is estimated to be only one-half that from the CD intensity of the positive lowest frequency band in the first band region. Therefore, it is probable that the relatively strong CD intensities of two

positive peaks near 14300 and 15300 cm^{-1} are accounted for by the dominant contribution from the CD intensity of the positive lowest frequency $^4B(C_2)$ component. And the minor contribution from the CD intensity of the negative higher-frequency band in the first band region may be responsible for the weakness of the CD peaks near 15000 cm^{-1}. However, the following consideration for the $^2E(^2T_{1g})$ state suggests that the assignment of the negative CD peaks near 15000 cm^{-1} to the electronic transitions is doubtful.

At the lowest frequency side in the spin-forbidden absorption band region for the *S,S*-ptnta complex, a negative CD peak is observed as in Fig. 2. The assignment for this CD component is attempted as follows. On the one hand, this CD peak is assumed to correspond to one of the splitting components of the ^2E_g state which arise from the interplay of the spin-orbit coupling and trigonal field,[13] as in the case of $(+)_{546}$-$[Cr(acac)_2(en)]^+$ and $(-)_{589}$-$[Cr(biguanide)_3]^{3+}$.[1] Then, provided that two positive lower-frequency CD components and a negative higher-frequency one are assigned to the $^4E(D_3)$ and $^4A_2(D_3)$ states, respectively, for the present complex, it may be predicted by the use of Eq. 6 and Table 2 of Ref. 1 that the CD components of the $^2E(^2E_g)$ splitting states, $\bar{E}$ and $2\bar{A}$, have positive and negative sings, respectively, and locate in this order from the lower frequency side. For the *S,S*-ptnta complex, however, this predicted CD pattern is reverse to the observed one. Thus, the lowest-frequency CD peak of this complex may not be assigned to one of the splitting components of the ^2E_g state.

On the other hand, the assumption of the holohedrized tetragonal symmetry for this complex makes alternative assignments possible. In this case, the positive lower-frequency and the negative higher-frequency CD components in the first band region are due to the ^4E and $^4B_2$ states, respectively. From the detailed analyses of the low temperature spin-forbidden absorption and luminescence spectra of $Na[Cr(ida)_2]\cdot 1.5H_2O$ (ida^{2-}=iminodiacetate),[12] it has been revealed that the $^2E(^2T_{1g})$ state is largely shifted to the lower frequency than the $^2A_1$ and $^2B_1(^2E_g)$ states. And this shift is considered to occur owing to the large configurational interaction between the $^2E(^2T_{1g})$ and $^2E(^2T_{2g})$ states as in the case of *trans*-$[CrF_2(en)_2]ClO_4$.[14] The present *S,S*-ptnta complex has the identical chromophore to the bis(iminodiacetato)chromate(III) complex except that two ida^{2-} ligands are joined by a 1,3-dimethyltrimethylene linkage. The doublet states for the *S,S*-ptnta complex are expected to behave similarly to the bis-ida complex as has been revealed from the magnetic circular dichroism measurements of several Cr(III) complexes with edta analogues.[15] Accordingly, the lowest-frequency CD component with a negative sign may be assigned to the $^2E(^2T_{1g})$ state in tetragonal field, though the position of this CD peak is shifted to the higher frequency than that of the absorption and phosphorescence bands.[12] The negative sign of this CD peak is elucidated by taking into account both the configurational interaction between the upper $^2E(^2T_{2g})$ and the lower $^2E(^2T_{1g})$ states and the strong spin-orbit coupling between the $^2E(^2T_{2g})$ state and the nearby $^4B_2(^4T_{2g})$ state, which may give rise to the splitting of the negative CD peaks near 22000 cm^{-1} as shown in Fig. 1. Then, the $^2E(^2T_{1g})\leftarrow{}^4B_1(^4A_{2g})$ transition attains the negative rotational strength by acquiring a piece of the negative rotational strength for the $^4B_2(^4T_{2g})\leftarrow{}^4B_1(^4A_{2g})$ transition to a larger extent than a piece of the positive rotational strength for the $^4E(^4T_{2g})\leftarrow{}^4B_1(^4A_{2g})$ transitions as has been found for the CD of *trans*-$[CrX_2(N)_4]$ type complexes with chiral diamines.[2] Thus, the assignments of these CD components to the electronic transitions suggest that the remaining weak CD peaks are due to the vibronic origin rather than the electronic one.

In conclusion, the CD behavior in the whole region of the spin-forbidden transitions for $(+)_{589}$-$[Cr(S,S\text{-ptnta})]^-$ and related complexes is elucidated on the tetragonal symmetry assumption more consistently than on the trigonal one as summarized in Table 1.

The authors wish to express their thanks to Prof. Yoichi Shimura, Osaka University, for his kind guidance and continuous encouragement throughout this work and also for making the circular dichroism and infrared spectra available for the present work.

References

1) S. Kaizaki, J. Hidaka, and Y. Shimura, *Inorg. Chem.*, **12**, 142 (1973).
2) S. Kaizaki and Y. Shimura, *Bull. Chem. Soc. Jpn.*, **48**, 3611 (1975).
3) S. Kaizaki and M. Ito, *Bull. Chem. Soc. Jpn.*, **54**, 2499 (1981).
4) D. J. Radanovic and B. E. Douglas, *J. Coord. Chem.*, **4**, 191 (1975).
5) a) C. W. Van Saun and B. E. Douglas, *Inorg. Chem.*, **8**, 1145 (1969); b) W. Byers and B. E. Douglas, *ibid.*, **11**, 1470 (1972); c) D. J. Radanovic and B. E. Douglas, *ibid.*, **14**, 6 (1975); d) G. G. Hawn, C. A. Chang, and B. E. Douglas, *ibid.*, **18**, 1266 (1979).
6) F. Mizukami, H. Ito, J. Fujita, and K. Saito, *Bull. Chem. Soc. Jpn.*, **43**, 3633 (1970).
7) a) J. A. Neal and N. J. Rose, *Inorg. Chem.*, **7**, 2405 (1968); b) J. I. Legg and J. A. Neal, *ibid.*, **12**, 1805 (1973); c) W. T. Jordan and J. I. Legg, *ibid.*, **13**, 2271 (1974).
8) C. J. Hawkins and E. Larsen, *Acta Chem. Scand.*, **19**, 1969 (1965).
9) J. A. Weyh and R. E. Hamm, *Inorg. Chem.*, **7**, 2431 (1968); H. Ogino, J. J. Chung, and N. Tanaka, *Inorg. Nucl. Chem. Lett.*, **7**, 125 (1971).
10) F. T. Helm, W. H. Watson, D. J. Radanovic, and B. E. Douglas, *Inorg. Chem.*, **16**, 2351 (1977).
11) A. J. McCaffery, S. F. Mason, and B. J. Norman, *J. Chem. Soc.*, **1965**, 5094.
12) C. D. Flint and A. P. Matthews, *J. Chem. Soc., Faraday Trans. 2*, **71**, 379 (1975).
13) S. Sugano and Y. Tanabe, *J. Phys. Soc. Jpn.*, **13**, 880 (1958).
14) C. D. Flint and A. P. Matthews, *J. Chem. Soc., Faraday Trans. 2*, **70**, 1307 (1974).
15) S. Kaizaki and H. Mori, *Chem. Lett.*, **1981**, 567.

Kinetics and Mechanism of Reduction of Hexacyanoferrate(III) by Sodium Tetrahydroborate

Mitra BHATTACHARJEE, Apurba K. BHATTACHARJEE, and Mahendra K. MAHANTI*

Department of Chemistry, North-Eastern Hill University, Shillong 793003 (Meghalaya), India

(Received January 20, 1981)

A kinetic investigation of the reduction of hexacyanoferrate(III) by sodium tetrahydroborate in buffered aqueous solution has been carried out. The rate of the reaction is proportional to the concentration of both, tetrahydroborate and hydrogen ions. The effect of the addition of some inorganic salts has been studied. The temperature has been varied, and the Arrhenius parameters have been evaluated. The rate of hydrolysis of tetrahydroborate has been separately studied. It has been observed that the activation energies for both the reactions—the reduction of hexacyanoferrate(III) and the hydrolysis of tetrahydroborate—are equal. A plausible mechanism for the reduction of hexacyanoferrate(III) has been proposed.

Sodium tetrahydroborate in water or methanol solution was found to be an effective reagent for the conversion of aldehydes and ketones to the corresponding alcohols.[1] The rate of reduction of ketones by sodium tetrahydroborate in isopropyl alcohol as solvent was found to follow second order kinetics.[2] It was though worthwhile to investigate the kinetics of reduction of hexacyanoferrate(III) ions by using this versatile reducing agent, $NaBH_4$, and to propose a mechanism consistent with the observed kinetic data. The decomposition of $NaBH_4$ as a function of time and temperature was separately studied with a view to support the mechanism proposed for this reaction.

Experimental

Materials. Sodium tetrahydroborate (Loba Chemical Co.) was kept under vacuum. The purity of $NaBH_4$ was checked by infrared analysis. Two sharp peaks were obtained at 2290 cm^{-1} and 1120 cm^{-1}, both being characteristic for $NaBH_4$. These have been assigned[3] as follows:

(i) 2290 cm^{-1}: $(B\text{-}H)_{asym}$ stretching

(ii) 1120 cm^{-1}: $B\begin{smallmatrix}/H\\ \backslash H\end{smallmatrix}$ deformation.

The $(B\text{-}H)_{asym}$ stretching mode was further split (2380 cm^{-1} and 2220 cm^{-1}). It has been suggested that the splitting was a consequence of the inability of the tetrahedral anion to rotate freely in the crystal lattice.[4]

All other substances used were of BDH(AR) grade.

Methods. Sodium tetrahydroborate was weighed out accurately and the solution was prepared in sodium hydroxide, whose strength had been determined. Potassium hexacyanoferrate(III) was weighed out accurately and the solution was prepared in sodium hydroxide. The pH of each solution was checked using a pH meter (Toshniwal, digital model). The two solutions were separately thermostated at 25 °C for 3 h. The solutions were then mixed in equal volumes, and the reaction was followed by observing the disappearance of hexacyanoferrate(III). Readings were taken at regular intervals of time, by noting the decrease in optical density at 420 nm,[5] using a spectrophotometer (Systronics, Mk II model). At this wave length, the absorption due to hexacyanoferrate(II) was negligible.[6] The pH of the reaction mixture was checked periodically, during the course of the reaction.

All infrared measurements were carried out using an IR 297 (Perkin-Elmer) spectrophotometer.

Product Analysis. Sodium tetrahydroborate (5×10^{-2} M†) in NaOH (1×10^{-2} M), and potassium hexacyanoferrate(III) (5×10^{-4} M) in NaOH (1×10^{-2} M), were mixed in equal volumes. The mixture was allowed to stand at room temperature for 48 h to ensure the completion of the reaction. The reaction mixture was slowly evaporated in a porcelain dish to near dryness; it was then digested with concentrated HCl and again evaporated to dryness to obtain the residue. The residue was recrystallized from hot water.

A small portion of the recrystallized product was taken in a porcelain dish, mixed with a small amount of concentrated H_2SO_4 to make a paste. About 3 ml of absolute methanol was added. The solution was heated and the vapours ignited. A green-edged flame was obtained, confirming the presence of the borate radical in the residue.

An infrared spectrum of the product sample was taken and compared with the infrared spectrum of a pure boric acid sample. Both the samples were found to be identical. This confirmed that the residue was boric acid.

Results and Discussion

Stoichiometry. The stoichiometry of the reaction was confirmed from colorimetric measurements in the following manner: reaction mixtures containing an excess of hexacyanoferrate(III) were allowed to go to completion, and then analyzed, spectrophotometrically, for the hexacyanoferrate(III) which was left. The results gave a 1:8 ratio according to

$$BH_4^- + 8Fe(CN)_6^{3-} + 2H_2O \longrightarrow BO_2^- + 8Fe(CN)_6^{4-} + 8H^+.$$

Kinetic Results. The rate of disappearance of hexacyanoferrate(III) was first order in each, the tetrahydroborate and hydrogen ions.

Effect of Tetrahydroborate. The rate of the reaction was found to be directly proportional to the concentration of BH_4^- ions. A plot of log k_1 *versus* the concentration of BH_4^- ions was linear, confirming the first order dependence of the reaction on the concentration of BH_4^- ions (Fig. 1).

Effect of Hydrogen Ions. The reaction was studied at varying pH. The rate of the reaction was found to vary as a function of the hydrogen ion concentration. The logarithm of the rate of disappearance of hexacyanoferrate(III) divided by BH_4^- ion concentration was plotted against pH. The plot was

† 1 M = 1 mol dm^{-3}.

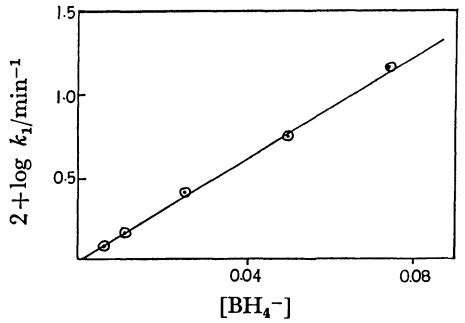

Fig. 1. Plot of logarithm of rate constant (k_1) *versus* the concentration of [BH_4^-].

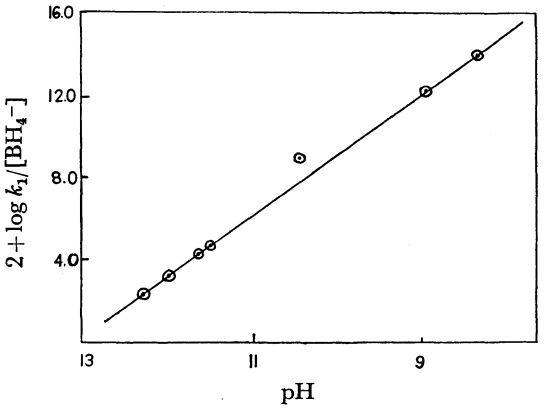

Fig. 2. Plot of logarithm of rate constant (k_1) divided by concentration of [BH_4^-] *versus* pH.

TABLE 1. EFFECT OF HEXACYANOFERRATE(III)

[Hexacyanoferrate(III)] / 10^4 M	$10^2 k_1$/min^{-1}
1.0	2.71
2.5	2.60
5.0	2.54
7.5	2.44
10.0	2.56
25.0	2.50
50.0	2.62

[BH_4^-] = 2.5×10^{-2} M; NaOH = 1×10^{-2} M; pH = 11.50; Temp = 25 °C.

linear, with a slope equal to unity (Fig. 2). This indicated a first order dependence of the reaction on the hydrogen ion concentration.

Effect of Hexacyanoferrate(III). The rate of the reaction was found to be independent of the concentration of hexacyanoferrate(III) ions in the range studied, from 1.0×10^{-4} M to 5.0×10^{-3} M (Table 1).

Effect of Hexacyanoferrate(II). The addition of hexacyanoferrate(II) ion to the reaction mixture resulted in a decrease in the rate of the reaction (Table 2). This decrease in the rate might suggest the possibility of an equilibrium being attained between the hexacyanoferrate(III) and the hexacyanoferrate(II). In the reaction of As(III) with hexacyanoferrate(III) in alkaline medium,[7] added hexacyanoferrate(II) was found to retard the rate of the reaction. In the reaction of mercaptoacetic acid with hexacyanoferrate(III)

TABLE 2. EFFECT OF HEXACYANOFERRATE(II)

[Hexacyanoferrate(II)] / 10^4 M	$10^3 k_1$/min^{-1}
0.0	9.50
1.0	4.86
2.5	2.29
4.0	0.84

Hexacyanoferrate(III) = 2.5×10^{-4} M; [BH_4^-] = 8×10^{-3} M; NaOH = 1×10^{-2} M; pH = 11.50; Temp = 25 °C.

TABLE 3. EFFECT OF COPPER(I) IONS

[Copper(I) ion] / 10^5 M	$10^3 k_1$/min^{-1}
0.0	9.50
2.5	7.50
5.0	4.36
7.5	3.05
10.0	1.84
12.5	1.07

Hexacyanoferrate(III) = 2.5×10^{-4} M; [BH_4^-] = 8×10^{-3} M; NaOH = 1×10^{-2} M; pH = 11.50; Temp = 25 °C.

in acid medium,[8] a similar retardation was also observed when hexacyanoferrate(II) was added to the reaction mixture.

Effect of Copper(I) Ions. The addition of copper(I) ions to the reaction mixture resulted in a decrease in the rate of the reaction (Table 3).

The choice of copper(I) ions was appropriate, since under the present experimental conditions, there was no possibility of further reduction of the copper(I) ions by the BH_4^- ion. The retardation in the rate of the reaction thus observed may be due to the formation of copper(I) tetrahydroborate ($CuBH_4$), which is stable at −12 °C, but undergoes decomposition at higher temperatures. At 25 °C, the $CuBH_4$ formed would be unstable and would undergo decomposition.

Effect of Added Salts. Potassium, rubidium, and caesium are known to form simple tetrahydroborates, $M(BH_4)_n$, which are stable or decompose only very slowly. The stability of these tetrahydroborates is in the order K<Rb<Cs, and can be related to two factors: (a) the electronegativities of the metal atom of the salts added (K, Rb, Cs), which are much lower than that of boron; and (b) the percentage ionic character. The greater the ionic character, the more stable will be the metal tetrahydroborate.

It is to be expected that the rates would follow the order of stability of these metal tetrahydroborates. This has been observed (Table 4).

Effect of Temperature. The reaction has been studied over the temperature range 25 °C to 55 °C. The rate of the reaction was found to be directly dependent on the temperature, the rate showing an increase with an increase in temperature (Table 5). The plot of log k_1 *versus* the reciprocal of temperature was linear, and the slope was used to calculate the activation energy. The Arrhenius parameters have been calculated and are shown in Table 6. The

Table 4. Effect of added salts

Concentration of salt 10^5 M	$10^3 k_1$/min^{-1} for K+	Rb+	Cs+
1.0	0.88	13.20	16.03
2.5	0.97	14.50	18.80
5.0	1.62	15.40	23.67
7.5	6.29	18.40	25.20

Hexacyanoferrate(III)$=2.5\times10^{-4}$ M; $[BH_4^-]=8\times10^{-3}$ M; NaOH$=1\times10^{-2}$ M; pH$=11.50$; Temp$=25$ °C.

Table 5. Effect of temperature

Temp/°C	$10^2 k_1$/min^{-1}
25	4.54
30	4.97
35	5.55
45	6.58
55	7.37

Hexacyanoferrate(III)$=2.5\times10^{-4}$ M; $[BH_4^-]=8\times10^{-3}$ M; NaOH$=1\times10^{-2}$ M; pH$=11.50$.

Table 6. Arrhenius parameters

Energy of activation (E_a)	$=19.14$ kJ mol^{-1}
Frequency factor (A)	$=1.59$ s^{-1}
Entropy of activation (ΔS)	$=-241.4$ J K^{-1} mol^{-1}
Enthalpy of activation (ΔH)	$=19.14$ kJ mol^{-1}

reaction has a large negative entropy of activation. Qualitatively, this would imply a lowering of the potential energy of the transition state. This would enable the facile formation of the transition state. Moreover, a large negative entropy of activation would correspond to a very low frequency factor; this has been observed for the reaction.

Decomposition of $NaBH_4$ as a Function of Time. It was thought appropriate to study the decomposition of $NaBH_4$, as a function of time. This would enable the determination of the rate of hydrolysis of $NaBH_4$ and would also throw some light on the probable mechanistic pathway of the hydrolytic reaction.

$NaBH_4$ (0.05 M) was prepared in water, and the solution was kept at 25 °C. At definite intervals of time, 5 ml aliquots of this solution were removed, and mixed with 5 ml of a solution of hexacyanoferrate(III) (5.0×10^{-4} M) in NaOH (2.0×10^{-2} M), also maintained at 25 °C. The reaction was followed by measuring the decrease in optical density at 420 nm. The rate constant (k_1) was determined, and the concentration of BH_4^- was calculated from the equation:

$$-\frac{d[Fe(CN)_6^{3-}]}{dt} = k_1[BH_4^-].$$

A plot of log C (concentration of BH_4^- ions) *versus* time was found to be linear, which indicated a first order dependence of the reaction on BH_4^- ion concentration.

The reaction was repeated at different temperatures, and the rate constant at each of these temperatures was calculated. The data are given in Table 7.

A plot of log k_1 *versus* the reciprocal of temperature was linear, and the slope was used to calculate the activation energy. The activation energy for the hydrolysis of $NaBH_4$ was found to be 19.14 kJ mol^{-1}. For the reaction involving the reduction of hexacyanoferrate(III) by $NaBH_4$, the value of the activation energy was also found to be 19.14 kJ mol^{-1} (Table 6).

Table 7. Decomposition of $NaBH_4$ as a function of time and temperature

Temperature °C	Time min	$10^2 k_1$/min^{-1}	$[BH_4^{-1}]$ $10^4\times$M
25	30	22.20	5.55
	60	14.60	3.65
	90	9.55	2.39
30	30	25.36	6.34
	60	16.60	4.15
	90	10.96	2.74
40	30	31.80	7.95
	60	20.70	5.17
	90	13.60	3.40

Hexacyanoferrate(III)$=2.5\times10^{-4}$ M; NaOH$=1\times10^{-2}$ M.

Mechanism

Since the rate of the reaction is proportional to the concentrations of both, tetrahydroborate and hydrogen ions, the chemical composition of the activated complex can be written as $H^+BH_4^-$.

The first step of the reaction is:

$$BH_4^- + H^+ \xrightarrow{k_1} H^+BH_4^-. \quad (1)$$

A kinetic scheme consisting of Eq. (1), followed by consecutive steps involving hexacyanoferrate(III) could be used as a basis to explain the experimental results. Each boron intermediate could react with either a hexacyanoferrate(III) ion or with a hydrogen producing species such as water.

The reaction could be represented by the following sequence of steps:

$$BH_4^- + H^+ \longrightarrow H^+BH_4^-,$$
$$H^+BH_4^- + 2Fe(CN)_6^{3-} + H_2O \longrightarrow BH_3OH^- + 2Fe(CN)_6^{4-} + 3H^+,$$
$$BH_3OH^- + 2Fe(CN)_6^{3-} \longrightarrow BH_2OH + 2Fe(CN)_6^{4-} + H^+,$$
$$BH_2OH + Fe(CN)_6^{3-} + H_2O \longrightarrow BH(OH)_2^- + Fe(CN)_6^{4-} + 2H^+,$$
$$BH(OH)_2^- + Fe(CN)_6^{3-} \longrightarrow BH(OH)_2 + Fe(CN)_6^{4-},$$
$$BH(OH)_2 + 2Fe(CN)_6^{3-} \longrightarrow BO_2^- + 2Fe(CN)_6^{4-} + 3H^+.$$

The overall stoichiometric reaction would then be:

$$BH_4^- + 8Fe(CN)_6^{3-} + 2H_2O \longrightarrow BO_2^- + 8Fe(CN)_6^{4-} + 8H^+.$$

The rate law could be expressed as

$$-\frac{d[Fe(CN)_6^{3-}]}{dt} = k_1[BH_4^-][H^+].$$

It has been found that for this reaction, k_1 has the frequency factor of 1.59 s^{-1}, and an activation energy of 19.14 kJ mol^{-1}.

The essential feature of this mechanism is that any given intermediate reacts only with a hydrogen producing species, or else with hexacyanoferrate(III). There is thus no competition for a given intermediate.

Further support of this mechanism is found from the rate measurements of the hydrolysis of BH_4^- ion, in the absence of hexacyanoferrate(III). The mechanism for the hydrolysis may be represented by:

$$BH_4^- + H^+ \longrightarrow H^+BH_4^-$$

followed by hydrogen yielding steps of the type:

(a) $BH_2OH + H_2O \longrightarrow BH(OH)_2 + H_2$,

(b) $2BH_2OH + 2H_2O \longrightarrow 2BH(OH)_2^- + 2H^+ + H_2$,

(c) $BH(OH)_2 + H_2O \longrightarrow H_3BO_3 + H_2$.

This mechanism would predict

$$-\frac{d[BH_4^-]}{dt} = k_1[BH_4^-][H^+].$$

The rate of hydrolysis of $NaBH_4$ was measured and it was found that the rate constant, k_1, corresponds to an activation energy of 19.14 kJ mol^{-1}. This was in agreement with the value determined from the kinetic studies, in the presence of hexacyanoferrate(III).

Intermediate Boron Compounds. The intermediate boron compounds, described in the reaction sequence, could not be isolated. However, there is evidence for the existence of such intermediates from the reaction of diborane with ice and with the "bound water" in silica gel.[9]

These intermediates differ in reducing capacity, and the formulas of the boron intermediates used are primarily intended to show the reducing capacity of the intermediate.

Consider the following steps:

(a) $BH_2OH + Fe(CN)_6^{3-} + H_2O \longrightarrow BH(OH)_2^- + Fe(CN)_6^{4-} + 2H^+$

and

(b) $2BH_2OH + 2H_2O \longrightarrow 2BH(OH)_2^- + 2H^+ + H_2$.

These steps describe a one-electron oxidation by hexacyanoferrate(III) and water respectively, to give the intermediate $BH(OH)_2^-$, which has three equivalents of reducing capacity.

Again, consider the following steps:

(a) $BH_2OH + 2Fe(CN)_6^{3-} + H_2O \longrightarrow BH(OH)_2 + 2Fe(CN)_6^{4-} + 2H^+$

and

(b) $BH_2OH + H_2O \longrightarrow BH(OH)_2 + H_2$.

These steps involve a two-electron oxidation to give $BH(OH)_2$, which has a two-electron reducing capacity

References

1) S. W. Chaikin and W. G. Brown, *J. Am. Chem. Soc.*, **71**, 122 (1949).
2) H. C. Brown, E. J. Mead, and B. C. Subba Rao, *J. Am. Chem. Soc.*, **77**, 6209 (1955).
3) W. C. Price, H. C. Longuet-Higgins, B. Rice, and T. F. Young, *J. Chem. Phys.*, **17**, 217 (1949).
4) T. C. Waddington, *J. Chem. Soc.*, **1958**, 4783.
5) I. M. Kolthoff, E. J. Meehan, M. S. Tsao, and Q. W. Choi, *J. Phys. Chem.*, **66**, 1233 (1962).
6) A. W. Adamson, *J. Phys. Chem.*, **56**, 859 (1952).
7) B. Krishna and H. S. Singh, *J. Inorg. Nucl. Chem.*, **31**, 2964 (1969).
8) R. C. Kapoor, O. P. Kachhwaha, and B. P. Sinha, *J. Phys. Chem.*, **73**, 1627 (1969).
9) I. Shapiro and H. G. Weiss, *J. Phys. Chem.*, **57**, 219. (1953).

The Synthesis of Antigenic Glycopeptides, 2-Acetamido-*N*-(β-L-aspartyl)-2-deoxy-4-*O*-β-(D-galactopyranosyl)-β-D-glucopyranosylamine. (*N*-Acetyllactosaminyl-L-asparagine)

Mohammed Abd El-Monem Shaban*,† and Roger W. Jeanloz††

Department of Chemistry, Faculty of Science, Alexandria University, Moharram Bey, Alexandria, Egypt

††*Laboratory for Carbohydrate Research, Department of Biological Chemistry and Medicine, Harvard Medical School and Massachusetts General Hospital, Boston, Massachusetts 02114, U.S.A.*

(Received January 5, 1981)

The title compound, serving as intermediate in the chemical and biochemical synthesis of glycopeptides and as a reference substance in the structure elucidation of glycoproteins, was synthesized. 2-Acetamido-4-*O*-allyl-3,6-di-*O*-benzyl-2-deoxy-β-D-glucopyranosyl azide was reduced to the corresponding β-D-glucosylamine and coupled with 1-benzyl *N*-benzyloxycarbonyl-L-aspartate to give 2-acetamido-4-*O*-allyl-3,6-di-*O*-benzyl-*N*-[(*S*)-3-benzyloxycarbonyl-3-benzyloxycarbonylamino)propionyl]-2-deoxy-β-D-glucopyranosylamine. Removal of the allyl group of the latter followed by condensation with 2,3,4,6-tetra-*O*-acetyl-α-D-galactopyranosyl bromide gave the fully protected *N*-acetyllactosaminyl-L-asparagine. De-blocking of the *O*-acetyl, benzyl, and benzyloxycarbonyl groups gave the title compound.

Carbohydrate chains attached to protein and to lipid moieties are known to be antigenic both at the surface of bacterial and mammalian cells. The role of carbohydrate in antigenic components at the surface of erythrocytes has been well established for the ABO and MN-antigen systems and suggested for I, P, and T-antigen systems.[1] Carbohydrate chains are also components of the cancer cells[2] and transplantation antigens.[3]

In view of these facts and the interest in (a) studying the inhibition of lectins in relation to the structure of receptor sites[4–6] and (b) structural indentification by gas-liquid chromatography combined with mass spectrometry,[7] a research program has been launched for the synthesis of antigenic oligosaccharides,[8] glycopeptides,[9] and isoprenoid sugar phosphates.[10]

The synthesis of *N*-acetyllactosaminyl-L-asparagine has been undertaken as a part of this program and because 2-amino-2-deoxy-4-*O*-β-D-galactopyranosyl-D-glucose (lactosamine) is the determinant group in the antigenic, Type XIV pneumococcus polysaccharide.[11] The synthesized glycopeptide may also be used as a starting material for the synthesis[9,12] and biosynthesis of larger glycopeptides.

Results and Discussion

In synthesizing *N*-acetyl-D-glucosamine-containing glycopeptides[12–17] it has been shown that derivatives of 2-acetamido-2-deoxy-β-D-glucopyranosyl azide[18] were the most convenient starting materials since they are stable, crystalline, and can be transformed, under mild conditions, into β-D-glucopyranosylamine derivatives ready for coupling with amino acids. In addition, β-D-glycosyl azides showed no sign of changing their anomerization throughout reduction and coupling.[17,19,20]

Taking these facts into consideration while designing a synthetic pathway for the title compound, one of three possible approaches may be adopted (a) starting with *N*-acetyllactosamine and going through the α-glycosyl halide, β-glycosyl azide, β-glycosylamine, and finally *N*-acetyllactosaminyl-L-asparagine; (b) Koenigs-Knorr condensation of α-D-galactosyl halide with a suitably protected 2-acetamido-2-deoxy-β-D-glucopyranosyl azide, followed by reduction of the azido group and coupling with aspartic acid; and (c) Koenigs-Knorr condensation of a suitably blocked 2-acetamido-2-deoxy-β-D-glucopyranosylamine-L-aspartic acid derivative with α-D-galactopyranosyl halide. The first approach suffers the disadvantages of the inavailability of *N*-acetyllactosamine, and the possible splitting of the glycosidic linkage during the preparation of the glycosyl halide.[16,17] Executing either of the two other alternatives requires the synthesis of a 2-acetamido-2-deoxy-β-D-glucopyranosyl azide blocked at positions 3 and 6 and having the 4-hydroxyl group available for Koenigs-Knorr condensation.

Previous work[21–23] has shown that the 4-hydroxyl group in 2-acetamido-2-deoxy-D-glucopyranosyl residues is not reactive in the Koenigs-Knorr reaction, and that, when both 4- and 6-hydroxyl groups are free, this reaction occurs exclusively at *O*-6.[22,23] Recourse to open chain intermediates[24] was necessary to prepare (1→4) linked *N*-D-glucosamine-containing oligosaccharides.[8,24–26] Although 2-acetamido-3,6-di-*O*-acetyl-2-deoxy-D-glucopyranosyl derivatives showed no reactivity at the 4-hydroxyl group, benzyl 2-acetamido-3,6-di-*O*-benzyl-2-deoxy-α- and β-D-glucopyranosides[8,27] were successfully condensed to give (1→4) linked oligosaccharides.[8,28] We decided, therefore, to prepare 2-acetamido-3,6-di-*O*-benzyl-2-deoxy-β-D-glucopyranosyl azide (**14**) as a suitable substrate for Koenigs-Knorr condensation with α-D-galactosyl halide to give β-*N*-acetyllactosaminyl azide.

2-Acetamido-4,6-*O*-benzylidene-2-deoxy-β-D-glucopyranosyl azide[13] (**2**) was prepared by a modified method in which 2-acetamido-2-deoxy-β-D-glucopyranosyl azide[18] (**1**) was treated with benzaldehyde and anhydrous formic acid as a dessicant instead of

† Present address: Department of Chemistry, Faculty of Science, King Abdul Aziz University, Jeddah, P.O. Box 9028, Saudi Arabia.

the usually used anhydrous zinc chloride. Benzylation of **2** with benzyl bromide in *N,N*-dimethylformamide and in the presence of a mixture of barium hydroxide and barium oxide, gave the 3-*O*-benzyl derivative **3**. Removal of the 4,6-*O*-benzylidene group was achieved by heating with 60% acetic acid to give **4**, which was tritylated to afford **5**. An attempt to prepare 2-acetamido-4-*O*-benzoyl-3-*O*-benzyl-2-deoxy-6-*O*-triphenylmethyl-β-D-glucopyranosyl azide (**7**) by benzoylating **5** with benzoyl chloride in the presence of pyridine at room temperature resulted in *N*- and *O*-benzoylation to give **6**. *O*-Benzylation, however, could be effected when the reaction was performed at −70 °C and in the presence of a limited amount of benzoyl chloride to give **7** in good yield (78%). Detritylation of **7** with hydrochloric acid in aqueous methanol for 4 h at room temperature gave **8**. Attempted conversion of 2-acetamido-4-*O*-benzoyl-3-*O*-benzyl-2-deoxy-β-D-glucopyranosyl azide (**8**) to 2-acetamido-4-*O*-benzoyl-3,6-di-*O*-benzyl-2-deoxy-β-D-glucopyranosyl azide (**9**) by benzylation with benzyl bromide and silver oxide, according to the method described by Sinaÿ[27] for a similar derivative, gave a mixture difficult to separate either by chromatography or fractional crystallization. This result, together with a previous similar one,[8] may be attributed to the partial migration of the 4-*O*-benzoyl group under the slightly alkaline conditions of the reaction.

Consequently, a new route for the synthesis of 2-acetamido-3,6-di-*O*-benzyl-β-D-glucopyranosyl azide (**14**) was contrived with intermediates containing the *O*-allyl protective group[29,30] instead of the benzoyl group. Allylation of **5** with allyl bromide and sodium hydroxide in benzene for 72 h gave 2-acetamido-4-*O*-allyl-3-*O*-benzyl-2-deoxy-6-*O*-triphenylmethyl-β-D-glucopyranosyl azide (**10**) in 77% yield. However, the reaction could be expedited (5 h) and the yield improved (89%) by carrying out the allylation in *N,N*-dimethylformamide. Detritylation of **10** with 60% acetic acid gave 2-acetamido-4-*O*-allyl-3-*O*-benzyl-2-deoxy-β-D-glucopyranosyl azide (**11**). Benzylation of the latter with benzyl bromide in *N,N*-dimethylformamide and in the presence of sodium hydroxide gave the expected *O*-benzylated product **12** in addition to the *O*- and *N*-benzylated product **13** in a 1 : 1.7 ratio. Attempted removal of the 4-*O*-allyl group of **12** by isomerization with tris(triphenylphosphine)-rhodium chloride in the presence of 1,4-diazabicyclo-[2.2.2]octane[8,31,32] followed by splitting of the resulting *O*-1-propenyl group with mercury(II) chloride,[8,33] failed giving a complex mixture of highly polar compounds devoid of the azido group. This may be attributed to the reaction of the azido group with the rhodium triphenylphosphine complex to give glycosylphosphinimines.[34,35] It was necessary, therefore, to reduce the azido group of **12**, and coupling the resulting glycosylamine with L-aspartic acid prior to the removal of the 4-*O*-allyl group.

The commonly used method[12–17] of reducing glycosyl azides by hydrogenation in the presence of Adam's catalyst, would be unsuitable for reducing compound **12** as it would lead to indiscriminate reduction of the azido and allyl groups. Saturation to *O*-propyl groups deprive the *O*-allyl groups their desirable selective removal in the presence of *O*-benzyl groups. Sodium borohydride was attempted as a selective reductant of the azido group without affecting the *O*-allyl function. In methanol, no such reduction took place and compound **12** was recovered unchanged. In *N,N*-dimethylformamide, however, the reduction took place smoothly at room temperatures to give the unstable glycosylamine **15** which showed a positive ninhydrin reaction.[36] The amine **15** was characterized by acetylation into the stable and crystalline 2-acetamido-*N*-acetyl-4-*O*-allyl-3,6-di-*O*-benzyl-2-deoxy-β-D-glucopyranosylamine (**16**).

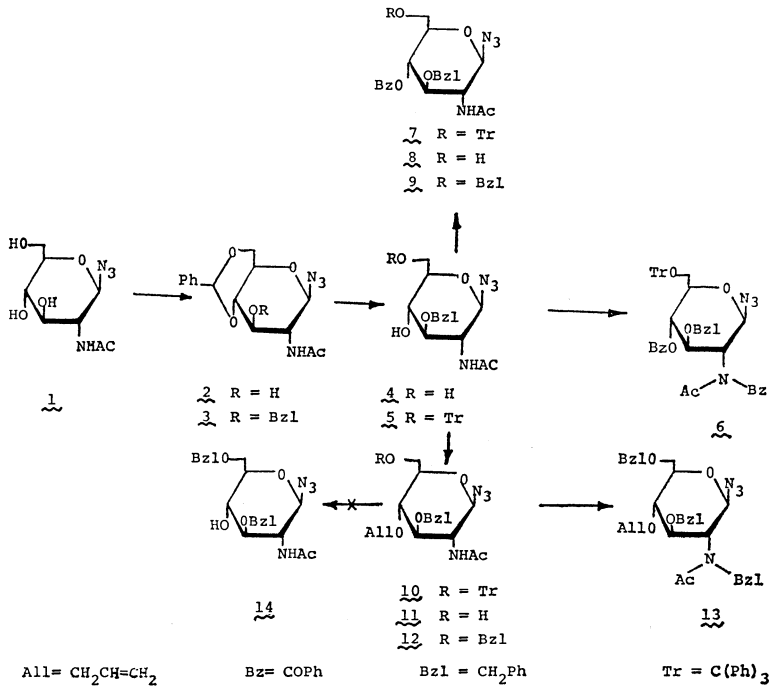

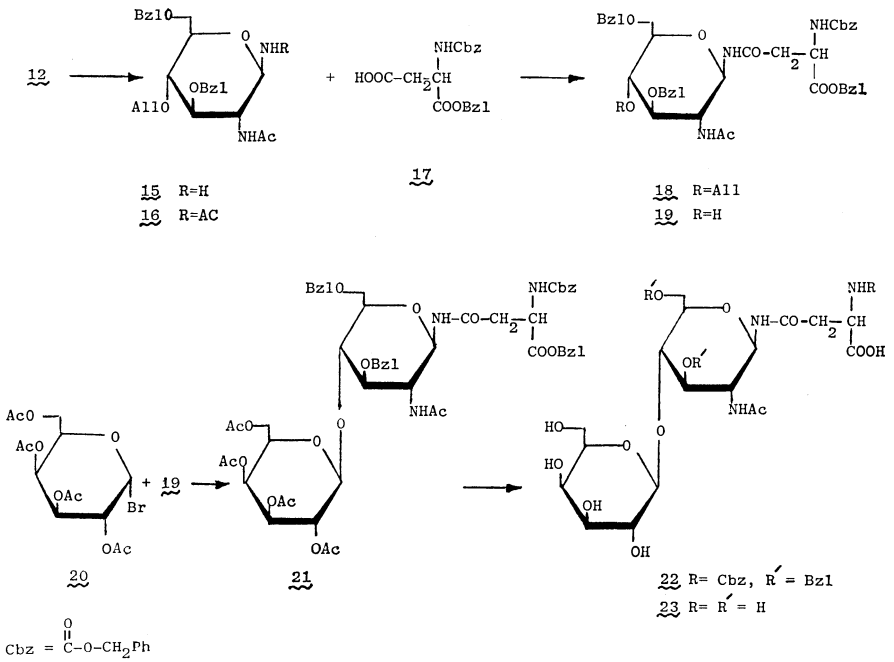

In order to prevent the formation of bis(glycosylamines),[17,19,37] the unstable amine **15** was used without further purification in the next step. Condensation of **15** with 1-benzyl-*N*-benzyloxycarbonyl-L-aspartate[38,39] (**17**) in the presence of dicyclohexylcarbodiimide gave crystalline 2-acetamido-4-*O*-allyl-3,6-di-*O*-benzyl-*N*-[(*S*)-3-benzyloxycarbonyl-3-(benzyloxycarbonylamino)propionyl]-2-deoxy-B-D-glucopyranosylamine (**18**) in 53% yield. Removal of the 4-*O*-allyl group of **18** using tris(triphenylphosphine)rhodium chloride and mercury(II)chloride gave crystalline **19**.

Koenigs-Knorr condensation of **19** with 2,3,4,6-tetra-*O*-acetyl-α-D-galactopyranosyl bromide[40] (**20**) in the presence of mercury(II) cyanide gave the fully protected *N*-acetyllactosaminyl-L-asparagine **21**. Assigning the β-D-configuration to the D-galactopyranosyl residue was based on the result of a previous synthesis.[16] Treatment of **21** with lithium hydroxide removed the protective *O*-acetyl groups of the D-galactopyranosyl moiety and the benzyl ester of L-aspartic acid giving **22**. Hydrogenolysis of the *N*-benzyloxycarbonyl and *O*-benzyl groups of **22** gave the title compound **23**.

Experimental

General. Melting points were determined with a Mettler FP2 hot stage equipped with a microscope, and correspond to "corrected" melting points. Optical rotations were determined for solutions in 1-dm, semimicro tubes with a Perkin-Elmer Model 141 polarimeter. Infrared spectra were recorded, for potassium bromide discs or for thin film, with a Perkin-Elmer Model 237 spectrophotometer. Chloroform used was analytical grade and contained about 0.75% ethanol. All solvent mixtures used were v/v. Solvents were dried over molecular sieve (type 5A, Grade 522, 8—12 mesh, Fisher Scientific Co., Fairlawn, N. J.). The cation-exchange resin used was in at least two-fold over the quantity necessary to effect complete ion exchange. Evaporations were performed in a rotary evaporator under diminished pressure, with an outside bath-temperature kept below 40 °C. Solutions (<5 ml) were evaporated under a stream of nitrogen. The microanalyses were performed by Dr. M. Manser, Zurich, Switzerland.

Chromatographic Methods. Column chromatography on silica gel was performed on Silica gel Merck (10—325 mesh, E. Merck A. G., Darmstadt, Germany) used without pretreatment. The ratio of the diameter of the column to its length was 1:8 to 1:12. The volume of the fractions eluted was 2 to 3 ml/g of substance to be chromatographed. The proportion of weight of substance to weight of silica gel was 1:60 to 1:100. Thin-layer chromatography (TLC) was performed on plates precoated with Silica gel G (layer thickness 0.25 mm. Merck), the plates supplied were cut to a length of 6 cm before use, but otherwise they were used without pretreatment. The distance of solvent-travel was 5 cm and the zones were detected by spraying the chromatograms with 1:1:18 *p*-anisaldehyde–sulfuric acid–ethanol[40] following by heating on a hot plate for a few minutes.

2-Acetamido-4,6-O-benzylidene-2-deoxy-β-D-glucopyranosyl Azide (2). A suspension of 2-acetamido-2-deoxy-β-D-glucopyranosyl azide[18] (**1**) (1.88 g) in freshly distilled benzaldehyde (15 ml) was stirred for 5 min at room temperature and then treated with 99% formic acid (20 ml). After stirring for a further 30 min, the reaction mixture was cooled in an ice-bath and gradually neutralized with a saturated aqueous solution of potassium carbonate. The heterogeneous mixture was distilled under reduced pressure and the excess benzaldehyde removed by repeated co-distillation with water. The residue, which remained, was triturated with water, filtered, washed with water, and dried. Crystallization from methanol gave 1.95 g (76%) of **2** as needles, mp and mixed mp[13] 214—216 °C (dec).

2-Acetamido-3-O-benzyl-4,6-O-benzylidene-2-deoxy-β-D-glucopyranosyl Azide (3). A solution of **2** (1.4 g) in dry *N,N*-dimethylformamide (30 ml) was treated with benzyl bromide (1.3 ml), barium oxide (5 g), and barium hydroxide octahydrate (1.3 g) and the mixture was stirred for 2 h at room temperature. Chloroform (50 ml) was added and the mixture was heated under reflux for 2 h while stirring

and then filtered while hot. The inorganic residue was washed with hot chloroform (3×50 ml) and the filtrate and washings were evaporated to dryness. Crystallization of the residue from chloroform–methanol gave 1.45 g (82%) of **3** as needles, mp 224—225 °C (dec); $[\alpha]_D^{30}$ −30° (*c* 2.1, pyridine); ν_{max}^{KBr} 3290 (NH), 2130 (N_3), 1655 (Amide I), 1555 (Amide II), 750, 725, and 690 cm^{-1} (Ph); TLC in 19:1 chloroform–ethanol R_f 0.32. Found: C, 62.18; H, 5.71; N, 13.16; O, 18.70%. Calcd for $C_{22}H_{24}N_4O_5$: C, 62.25; H, 5.70; N, 13.20; O, 18.85%.

2-Acetamido-3-O-benzyl-2-deoxy-β-D-glucopyranosyl Azide (4). A suspension of **3** (1.06 g) in 60% acetic acid (50 ml) was heated for 2 h at 90—95 °C. The clear solution was evaporated under diminished pressure and the residue was dried by several co-distillations with toluene. Chromatography of the residue on a column of silica gel with 19:1 chloroform–ethanol gave 655 mg (78%) of **4**, which crystallized from methanol–chloroform–ether; mp 173—174 °C (dec); $[\alpha]_D^{20}$ −29° (*c* 2.24, methanol); ν_{max}^{KBr} 3350 (OH), 3290 (NH), 2130 (N_3), 1645 (Amide I), 1550 (Amide II), 730, and 690 cm^{-1} (Ph); TLC in 4:1 chloroform–ethanol R_f 0.52. Found: C, 53.47; H, 5.99; N, 16.71; O, 23.58%. Calcd for $C_{15}H_{20}N_4O_5$: C, 53.57; H, 5.99; N, 16.66; O, 23.78%.

2-Acetamido-3-O-benzyl-2-deoxy-6-O-triphenylmethyl-β-D-glucopyranosyl Azide (5). A solution of **4** (700 mg) in dry pyridine (30 ml) was treated with chlorotriphenylmethane (1.4 g) for 30 h at room temperature. The mixture was poured onto a mixture of ice (200 g) and potassium carbonate (5 g), and then extracted with chloroform (4×50 ml). The extracts were washed with water (3×50 ml), dried (K_2CO_3) and evaporated. The last traces of pyridine was removed by several additions and evaporations of toluene. The residue was chromatographed on a column of silica gel with 19:1 chloroform–ethanol containing 0.1% of triethylamine, to give 1.16 g (84%) of **5**, which crystallized from dichloromethane–carbon tetrachloride as needles, mp 116—118 °C; $[\alpha]_D^{20}$ −22° (*c* 2.3, chloroform); ν_{max}^{KBr} 3500 (OH), 3280 (NH), 2120 (N_3), 1650 (Amide I), 1550 (Amide II), 740, and 690 cm^{-1} (ph); TLC in 19:1 chloroform–ethanol, R_f 0.32. Found: C, 63.79; H, 5.27; N, 8.62; O, 12.13%. Calcd for $C_{34}H_{34}N_4O_5 \cdot CH_2Cl_2$: C, 63.99; H, 5.37; N, 8.29; O, 11.84%.

2-(N-Acetylbenzamido)-4-O-benzoyl-3-O-benzyl-2-deoxy-6-O-triphenylmethyl-β-D-glucopyranosyl Azide (6). A solution of **5** (800 mg) in dry pyridine (30 ml) was treated with benzyl chloride (2 ml) for 2 h at room temperature. The mixture was poured into an ice-cold solution of sodium hydrogencarbonate and then extracted with chloroform (4×50 ml). The chloroform extracts were washed with water (3×50 ml), and dried (K_2CO_3). Evaporation of the solvent and removal of the residual pyridine by several co-distillations with toluene gave a residue which was chromatographed on a column of silica gel with chloroform. Fractions containing **6** were evaporated and the residue crystallized from dichloromethane–ether–pentane as needles (863 mg; 91%), mp 154—157 °C; $[\alpha]_D^{23}$ −33.4° (*c* 2.3, chloroform); ν_{max}^{KBr} 2120 (N_3), 1725 (O. COPh), 1700 (N. COPh), 1670 (N. $COCH_3$), 745, and 690 cm^{-1} (Ph); TLC in chloroform R_f 0.54. Found: C, 73.23; H, 5.42; N, 7.15; O, 14.20%. Calcd for $C_{48}H_{42}N_4O_7$: C, 73.27; H, 5.38; N, 7.12; O, 14.23%.

2-Acetamido-4-O-benzoyl-3-O-benzyl-2-deoxy-6-O-triphenylmethyl-β-D-glucopyranosyl Azide (7). A solution of **5** (664 mg) in dry pyridine (10 ml) was cooled to −70 °C and treated with a 14% (w/v) solution (1 ml) of benzoyl chloride in dry benzene. The mixture was kept at −20 °C for 16 h and then treated with a few drops of methanol, evaporated, and the residual pyridine removed by repeated addition and distillation of toluene. The syrupy residue which obtained could not be crystallized, and it was, therefore, chromatographed on a column of silica gel with 19:1 chloroform–ethanol to give 532 mg (78%) of **7**. It crystallized from dichloromethane–ether as needles, mp 169—170 °C; $[\alpha]_D^{20}$ +0.5° (*c* 2.8, chloroform); ν_{max}^{KBr} 3280 (NH), 2130 (N_3), 1730 (O. COPh), 1655 (Amide I), 1550 (Amide II), 740, and 680 cm^{-1} (Ph); TLC in 19:1 chloroform–ethanol R_f 0.38. Found: C, 72.10; H, 5.54; N, 8.12; O, 14.14%. Calcd for $C_{41}H_{38}N_4O_6$: C, 72.12; H, 5.61; N, 8.20; O, 14.06%.

2-Acetamido-4-O-benzoyl-3-O-benzyl-2-deoxy-β-D-glucopyranosyl Azide (8). A solution of **7** (1.9 g) in methanol (75 ml) was treated with 2 M hydrochloric acid until the mixture becomes just turbid (about 10 ml) and kept for 4 h at room temperature. The mixture was diluted with cold water (200 ml), extracted with chloroform (5×75 ml), and the extracts were washed with water (2×50 ml), saturated sodium hydrogencarbonate solution (2×50 ml), and water (3×50 ml), dried (Na_2SO_4), and evaporated. The residue was chromatographed on a column of silica gel with 9:1 chloroform–ethanol, to give 1.03 g (84%) of **8**, which crystallized from dichloromethane–ether; mp 178—190 °C (dec); $[\alpha]_D^{20}$ −28° (*c* 2.0, chloroform); ν_{max}^{KBr} 3480 (OH), 3280 (NH), 2130 (N_3), 1720 (O. COPh), 1655 (Amide I), 1550 (Amide II), 745, and 700 cm^{-1} (Ph); TLC in 19:1 chloroform–ethanol, R_f 0.20, and in 9:1 chloroform–ethanol, R_f 0.40. Found: C, 60.06; H, 5.49; N, 12.76; O, 21.98%. Calcd for $C_{22}H_{24}N_4O_6$: C, 59.99; H, 5.49; N, 12.72; O, 21.79%.

Attempted Synthesis of 2-Acetamido-4-O-benzoyl-3,6-di-O-benzyl-2-deoxy-β-D-glucopyranosyl Azide (9). Compound **8** (500 mg) in anhydrous benzene (30 ml) was treated with benzyl bromide (1.5 ml) and silver oxide (700 mg) and the mixture stirred for 24 h at 60—70 °C in the dark. After cooling to room temperature, the mixture was diluted with dichloromethane (30 ml) and filtered through a celite layer. To the filtrate pyridine (3 ml) was added and the mixture was evaporated and dried by several additions and distillations of toluene. The syrup obtained showed, on TLC, to contain more than four products. Attempted separation of these products by fractional crystallization or by repetitive column chromatography on silica gel using different solvent systems was unsuccessful.

Carrying the reaction at lower temperature (40—50 °C) and for a shorter duration (16 h) led to the same result.

2-Acetamido-4-O-allyl-3-O-benzyl-2-deoxy-6-O-triphenylmethyl-β-D-glucopyranosyl Azide (10). *Method A*: To a solution of **5** (500 mg) in dry benzene (20 ml) allyl bromide (110 mg) and powdered sodium hydroxide (1.25 g) were added and the mixture stirred for 72 h at room temperature. The mixture was filtered on a celite layer and the inorganic residue was washed with benzene (2×50 ml). The filtrate and washings were washed with water (3×50 ml), dried (Na_2SO_4), and evaporated. The residue which obtained was chromatographed on a column of silica gel with 19:1 chloroform–ethanol to give 360 mg (77%) of **10**, which crystallized from dichloromethanol–pentane as needles, mp 190—191 °C; $[\alpha]_D^{20}$ +1.4° (*c* 1.04, chloroform); ν_{max}^{KBr} 3300 (NH), 2130 (N_3), 1650 (Amide I), 1550 (Amide II), 740, and 680 cm^{-1} (Ph); TLC in 19:1 chloroform–ethanol R_f 0.44. Found: C, 71.72; H, 6.20; N, 9.05; O, 13.04%. Calcd for $C_{37}H_{38}N_4O_5$: C, 71.82; H, 6.19; N, 9.06; O, 12.93%.

Method B: A solution of **5** (500 mg) in *N*,*N*-dimethylformamide (20 ml) was treated with the same amounts of allyl bromide and sodium hydroxide as described in Method A. After completion of the reaction (5 h), the mixture

was diluted with chloroform (200 ml), washed with water (4×50 ml), and dried (Na_2SO_4). Evaporation of the solvents and chromotography of the residue gave 416 mg (89%) of **10** having the same properties as those just described.

*2-Acetamido-4-O-allyl-3-O-benzyl-2-deoxy-β-D-glucopyranosyl Azide (**11**).* A suspension of **10** (619 mg) in 60% acetic acid (50 ml) was heated for 2 h at 90 °C. The clear solution was evaporated and the residue, which obtained, was dried by several co-distillations with toluene and then chromatographed on a column of silica gel with 19:1 chloroform–ethanol to give 285 mg (79%) of **11**. It crystallized from dichloromethane–ether–pentane as needles, mp 188 °C; $[\alpha]_D^{20}$ −11° (*c* 2, chloroform); ν_{max}^{KBr} 3250 (OH), 3480 (NH), 2140 (N_3), 1650 (Amide I), 1550 (Amide II), 745, and 680 cm^{-1} (Ph); TLC in 19:1 chloroform–ethanol R_f 0.21 and in 9:1 chloroform–ethanol R_f 0.43. Found: C, 57.41; H, 6.45; N, 14.89; O, 21.89%. Calcd for $C_{18}H_{24}N_4O_5$: C, 57.44; H, 6.43; N, 14.88; O, 21.25%.

*2-Acetamido-4-O-allyl-3,6-di-O-benzyl-2-deoxy-β-D-glucopyranosyl azide (**12**) and 2-(N-Acetylbenzylamino)-4-O-allyl-3,6-di-O-benzyl-2-deoxy-β-D-glucopyranosyl Azide (**13**).* Benzyl bromide (1.2 ml) and powdered potassium hydroxide (3 g) were added to a solution of compound **11** (600 mg) in a mixture of anhydrous benzene (30 ml) and *N,N*-dimethylformamide (5 ml) and stirred for 3 h at room temperature. The mixture was cooled in an ice-bath, diluted with chloroform (200 ml), washed with ice–water (3×50 ml), 5% citric acid solution (2×50 ml), saturated sodium hydrogencarbonate solution (3×30 ml), and water (3×50 ml), and dried (Na_2SO_4). Evaporation of the solvents gave a syrup which on chromatography on a column of silica gel with 99:1 chloroform–ethanol gave 191 mg (33%) of **13** in the fast-moving fractions as a syrup which could not be crystallized, $[\alpha]_D^{20}$ +2.15° (*c* 1.6, chloroform), ν_{max}^{KBr} 2125 (N_3), 1650 (Amide I), 725, and 680 cm^{-1} (Ph); TLC in 29:1 chloroform–ethanol R_f 0.62. Found: C, 69.06; H, 6.46; N, 10.04; O, 14.60%. Calcd for $C_{32}H_{36}N_4O_5$: C, 69.05; H, 6.52; N, 10.06; O, 14.37%.

From the slow-moving fractions, 365 mg (56%) of **12** were obtained, which crystallized from methanol as needles, mp 159—160 °C; $[\alpha]_D^{20}$ +7.5° (*c* 2.7, chloroform), ν_{max}^{KBr} 3250 (NH), 2125 (N_3), 1645 (Amide I), 1550 (Amide II), 735, and 680 cm^{-1} (Ph); TLC in 29:1 chloroform–ethanol R_f 0.34. Found: C, 64.45; H, 6.52; N, 12.04; O, 17.25%. Calcd for $C_{25}H_{30}N_4O_5$: C, 64.36; H, 6.48; N, 12.01; O, 17.15%.

*Attempted Preparation of 2-Acetamido-3,6-di-O-benzyl-2-deoxy-β-D-glucopyranosyl Azide (**14**).* A solution of **12** (500 mg) and 1,4-diazabicyclo[2.2.2]octane (75 mg; Eastman Kodak Co., Rochester, N. Y. 14650) in 90% methanol (25 ml) was heated to boiling. Tris(triphenylphosphine)rhodium chloride (200 mg; Alpha Products, Ventron Corporation, Danvers, MA 01923) was added, and the mixture was boiled under reflux for 4 h, cooled to room temperature, filtered, and the filtrate, evaporated without being dried. A solution of the residue in chloroform (100 ml) was successively washed with 5% citric acid solution (2×25 ml) and water (2×25 ml), and evaporated without being dried. The residue was dissolved in 90% acetone (25 ml), and the solution was stirred with mercury(II) chloride (500 mg) and yellow mercury(II) oxide (500 mg) for 30 min at room temperature. The mixture was filtered on a celite layer, the inorganic residue was washed with acetone, and the filtrate and washings were evaporated to a syrupy residue (600 mg). TLC of this residue revealed the presence of a complex mixture of highly polar compounds and infrared showed the total loss of the characteristic azido group absorption.

*2-Acetamido-N-acetyl-4-O-allyl-3,4-O-benzyl-2-deoxy-β-D-glucopyranosylamine (**16**).* Attempted reduction of a solution of **12** (117 mg) in methanol (29 ml) with sodium borohydride (100 mg) for 16 h at room temperature or for 6 h at 80 °C was unsuccessful and gave the unchanged azido compound. Therefore, a solution of **12** (117 mg) in *N,N*-dimethylformamide (10 ml) was cooled to 0 °C and treated with sodium borohydride (100 mg) and then allowed to attain room temperature for 6 h. The mixture was treated with a few pieces of Dry Ice, diluted with chloroform (100 ml) and washed with water (5×25 ml), and dried (Na_2SO_4). Evaporation of the solvents gave a residue of 2-acetamido-4-*O*-allyl-3,6-di-*O*-benzyl-2-deoxy-β-D-glucopyranosylamine (**15**) which gave positive test with ninhydrin. The residue was dissolved in methanol (10 ml), treated with acetic anhydride (0.5 ml) for 2 h at room temperature, and evaporated. After several co-distillations with toluene, the substance was chromatographed on a column of silica gel with 19:1 chloroform–ethanol to give 95 mg (79%) of **16**, which crystallized from methanol, mp 214—216 °C; $[\alpha]_D^{20}$ +33° (*c* 1.12, methanol); ν_{max}^{KBr} 3280 (NH), 1650 (Amide I), 1550 (Amide II), 730, 680 cm^{-1} (Ph); TLC in 9:1 chloroform–ethanol R_f 0.53. Found: C, 67.11; H, 7.06; N, 5.69%. Calcd for $C_{27}H_{34}N_2O_6$: C, 67.20; H, 7.10; N, 5.80%.

*2-Acetamido-4-O-allyl-3,6-di-O-benzyl-N[(S)-3-benzyloxycarbonyl-3-(benzyloxycarbonylamino)propionyl]-2-deoxy-β-D-glucopyranosylamine(**18**).* A solution of compound **12** (1.1 g) in *N,N*-dimethylformamide (10 ml) was reduced with sodium borohydride (1 g), as described for the preparation of **15**. Carbon dioxide was bubbled into the solution while maintaining the temperature at 0 °C. The mixture was diluted with chloroform (300 ml), washed with water (6×50 ml), and the solvents were evaporated under reduced pressure with the bath temperature being kept below 30 °C. The residue, without further purification, was dissolved in dichloromethane (30 ml) and treated with 1-benzyl *N*-(benzyloxycarbonyl)-L-asparate[39] (**17**, 1 g) and dicyclohexylcarbondiimide (700 mg), and the mixture was stirred for 16 h at room temperature. The *N,N'*-dicyclohexylurea that had precipitated was filtered off, and the filtrate was evaporated. The residue was chromatographed on a column of silica gel which was first eluted with chloroform to remove the non-carbohydrate compounds, and then with 29:1 chloroform–ethanol to give 975 mg (53%) of **18**. It crystallized from dichloromethane–methanol as needles, mp 216—218 °C; $[\alpha]_D^{20}$ +43° (*c* 1.83, chloroform); ν_{max}^{KBr} 3300 (NH), 1740 (C=O ester), 1650 (Amide I), 1550 (Amide II), 725, and 680 cm^{-1} (Ph); TLC in 19:1 chloroform–ethanol R_f 0.33. Found: C, 67.73; H, 6.31; N, 5.34%. Calcd for $C_{44}H_{49}N_3O_{10}$: C, 67.76; H, 6.33; N, 5.39%.

*2-Acetamido-3,6-di-O-benzyl-N-[(S)-3-benzyloxycarbonyl-3-(benzyloxycarbonylamino)propionyl]-2-deoxy-β-D-glucopyranosylamine (**19**).* A boiling solution of **18** (780 mg) and 1,4-diazabicyclo[2.2.2]octane (80 mg) in 95% methanol (60 ml) was treated with tris(triphenylphosphine)rhodium chloride (250 mg) and the mixture was boiled under reflux for 5 h, and then processed as described for the attempted synthesis of **14**. The residue obtained was chromatographed on a column of silica gel with 19:1 chloroform–ethanol to give 503 mg (68%) of **19**, which crystallized from dichloromethane–ether; mp 163—165 °C, $[\alpha]_D^{20}$ +26° (*c* 2.4, chloroform), ν_{max}^{KBr} 3500 (OH), 3300 (NH), 1740 (C=O ester), 1650 (Amide I), 1545 (Amide II), 750, and 690 cm^{-1} (Ph); TLC in 19:1 chloroform–ethanol R_f 0.24. Found: C, 66.28; H, 6.27; N, 5.51%. Calcd for $C_{41}H_{45}N_3O_{10}$: C, 66.56; H, 6.13; N, 5.68%.

2-Acetamido-3,6-di-O-benzyl-N-[(S)-3-benzyloxycarbonyl-3-(benzyloxycarbonylamino)propionyl]-2-deoxy-4-O-(2,3,4,6-tetra-O-acetyl-β-D-galactopyranosyl)-β-D-glucopyranosylamine (21). A solution of **19** (740 mg) and mercury(II) cyanide (1.2 g) in 1:1 benzene–1,2-dichloroethane (250 ml) was distilled at atmospheric pressure until 100 ml of the solvents were distilled. The mixture was cooled to room temperature and treated with a solution of 2,3,4,6-tetra-*O*-acetyl-α-D-galactopyranosyl bromide[40] **20** (1.5 g) in dry 1,2-dichloroethane (50 ml) during 3 h, while being strirred. The mixture was stirred for a further 48 h, treated with additional amounts of mercury(II) cyanide (1 g) and **20** (1 g), and stirring was continued for a further 24 h. The mixture was diluted with chloroform (300 ml), filtered through a celite layer, and the filtrate was successively washed with water (3×50 ml), a saturated solution of sodium hydrogencarbonate (2×50 ml), a saturated solution of potassium iodide (3×25 ml), and water (3×50 ml), and dried (Na_2SO_4). Evaporation of the solvents gave a residue that was chromatographed on a column of silica gel with 19:1 chloroform–ethanol to give 480 mg (42%) of pure **21**. This could not be crystallized and was obtained as an amorphous powder by precipitation from an ethereal solution by addition of pentane; $[\alpha]_D^{20}$ +29° (*c* 1.1, methanol), ν_{max}^{KBr} 3300 (NH), 1740 (C=O ester), 1665 (Amide I), 1555 (Amide II), 750, and 690 cm^{-1} (Ph); TLC in 19:1 chloroform–ethanol R_f 0.29. Found: C, 57.84; H, 6.26; N, 3.63%. Calcd for $C_{55}H_{61}N_3O_{19}\cdot 4H_2O$: C, 57.79; H, 6.35; N, 3.68%.

2-Acetamido-3,6-di-O-benzyl-N-[N-(benzyloxycarbonyl)-β-L-aspartyl]-2-deoxy-4-O-β-D-galactopyranosyl-β-D-glucopyranosylamine (22). Compound **21** (570 mg) was stirred with a solution of lithium hydroxide (80 mg) in water (30 ml) for 2 h at room temperature. The solution was deionized by passage through Amberlite IRC-50 (H^+) ion-exchange resin, and then evaporated. The residue could not be induced to crystallize and **22** was obtained as an amorphous powder 351 mg (82%) from methanol–ether–pentane; $[\alpha]_D^{20}$ +13° (*c* 2.1, methanol), ν_{max}^{KBr} 3350 (broad, NH and OH), 1720, (COOH), 1650 (Amide I), 1550 (Amide II), 750, and 690 cm^{-1} (Ph); TLC in 8:2 chloroform–ethanol R_f 0.40. Found: C, 55.74; H, 5.80; N, 4.77%. Calcd for $C_{40}H_{49}N_3O_{15}\cdot 2.5\cdot H_2O$: C, 56.07; H, 6.35; N, 4.90%.

2-Acetamido-N-(β-L-aspartyl)-2-deoxy-4-O-β-D-galactopyranosyl-β-D-glucopyranosylamine (23). A solution of **22** (215 mg) in 50% methanol (100 ml) was hydrogenolyzed with hydrogen in the presence of 10% palladium-on-charcoal (100 mg) for 24 h at room temperature and 2 atm. The mixture was filtered on a celite layer and the filtrate was hydrogenolyzed for a second time as just described. Evaporation of the solvents gave a residue (108 mg, 81%) that showed a positive ninhydrin reaction.[36] This residue could not be crystallized and **23** was obtained as a hygroscopic amorphous powder from methanol–acetone–pentane; $[\alpha]_D^{20}$ +6° (*c* 1.1, methanol), ν_{max}^{KBr} 3400 (broad, NH_2 and OH), 1725 (COOH), 1650 (Amid I), and 1550 cm^{-1} (Amide II). Found: C, 40.51; H, 6.59; N, 7.72%. Calcd for $C_{18}H_{31}N_3O_{13}\cdot 2H_2O$: C, 40.53; H, 6.61; N, 7.88%.

References

1) G. F. Springer, "Amino Sugars," ed by E. A. Balazs and R. W. Jeanloz, Academic Press, New York (1966), Vol. IIB, p. 267.

2) See for example, H. C. Wu, E. Meezan, P. H. Black, and P. W. Robbins, *Biochemistry*, **8**, 2509 (1969); M. H. Burger and A. R. Goldberg. *Proc. Natl. Acad. Sci. U.S.A.*, **57**, 239 (1967).

3) K. Yamane and S. Mathenson, *Fed. Proc.*, **29**, 508 (1970).

4) M. Ingabr and L. Sachs, *Proc. Natl. Acad. Sci. U.S.A.* **63**, 1418, (1969); *Nature*, **223** 710 (1969).

5) M. M. Burger and Noonan, *Nature*, **228**, 512 (1971).

6) M. A. E. Shaban, D. K. Podolsky, and R. W. Jeanloz, *Carbohydr. Res.*, **52**, 129 (1967).

7) M. A. E. Shaban, V. N. Reinhold, and R. W. Jeanloz, *Carbohydr. Res.* **59**, 213 (1977).

8) M. A. E. Shaban and R. W. Jeanloz, *Carbohydr. Res.*, **52**, 115 (1976), and references cited therein.

9) M. A. E. Shaban and R. W. Jeanloz, *Carbohydr. Res.*, **43**, 281 (1975); H. G. Garg and R. W. Jeanloz, *ibid.*, **32**, 37 (1974), and references cited therein.

10) C. D. Warren, I. Y. Liu, A. Herscovics, and R. W. Jeanloz, *J. Biol. Chem.*, **250**, 8069 (1975), and references cited therein.

11) See Ref. 1, p. 316.

12) M. A. E. Shaban and R. W. Jeanloz, *Carbohydr. Res.*, **26**, 315 (1973).

13) M. A. E. Shaban and R. W. Jeanloz, *Carbohydr. Res.*, **21**, 347 (1972).

14) M. A. E. Shaban and R. W. Jeanloz, *Carbohydr. Res.*, **23**, 243 (1972).

15) M. Spinola and R. W. Jeanloz, *J. Biol. Chem.*, **245**, 158 (1970).

16) M. Spinola and R. W. Jeanloz, *Carbohydr. Res.*, **15**, 361 (1970).

17) E. Walker and R. W. Jeanloz, *Carbohydr. Res.*, **32**, 145 (1974).

18) F. Micheel and H. Wulff, *Chem. Ber.*, **89**, 1521 (1956).

19) C. H. Bolton, L. Hough, and M. Y. Khan, *Biochem. J.*, **101**, 184 (1966).

20) M. Kiyozumi, K. Kato, T. Komori, A. Yamamoto, T. Kawasaki, and H. Tsukamoto, *Carbohydr. Res.*, **14**, 355 (1970).

21) E. S. Rachaman and R. W. Jeanloz, *Carbohydr. Res.*, **10**, 435 (1969).

22) M. Shaban and R. W. Jeanloz, *Carbohydr. Res.*, **17**, 411 (1971).

23) M. Shaban and R. W. Jeanloz, *Carbohydr. Res.*, **19**, 311 (1971).

24) K. Heyns, K. Propp, R. Harrison, and H. Paulsen, *Chem. Ber.*, **100**, 2655 (1967).

25) M. Shaban and R. W. Jeanloz, *Carbohydr. Res.*, **20**, 17 (1971).

26) M. A. E. Shaban and R. W. Jeanloz, *Carbohydr. Res.*, **20**, 399 (1971).

27) J. C. Jacquinet, J. M. Petit, and P. Sinay, *Carbohydr. Res.*, **38**, 305 (1974).

28) J. C. Jacquinet and P. Sinaÿ, *Carbohydr. Res.*, **46**, 138 (1976).

29) P. A. Gent and R. Gigg, *J. Chem. Soc., Perkin Trans. 1*, 1446 (1974); 361 (1975).

30) A. Lubineau, A. Thiffery, and A. Veyrieres, *Carbohydr. Res.*, **46**, 143 (1976).

31) E. J. Corey and J. W. Suggs, *J. Org. Chem.*, **38**, 3224 (1973).

32) P. A. Gent and R. Gigg, *J. Chem. Soc., Chem. Commun.*, **1974**, 277.

33) R. Gigg and C. D. Warren, *J. Chem. Soc., C*, **1968**, 1903.

34) A. Messmer, I. Pinter, and F. Szego, *Angew. Chem.*, **76**, 227, (1964).

35) W. Mungall, G. L. Green, A. G. Heavner, and R. L. Lestinger, *J. Org. Chem.*, **40**, 1659 (1975).

36) S. Moore and W. H. Stein, *J. Biol. Chem.*, **176**, 367 (1948).
37) A. Y. Yamamoto, C. Miyashita, and H. Tsukamoto, *Chem. Pharm. Bull. (Tokyo)*, **13**, 1036 (1965).
38) M. Bergmann, L. Zervas, and L. Salzmann, *Ber.*, **66**, 1288 (1933).
39) Y. Yamamoto, *Biochem. Prep.*, **10**, 10 (1963).
40) H. Ohle, W. Marecek, and W. Bourjau, *Ber.*, **62**, 833 (1929).
41) P. J. Dunphy, J. D. Kerr, J. F. Pennock, K. J. Whittle, and J. Feeney, *Biochem. Biophys. Acta*, **136**, 136 (1967).

NOTES

Bull. Chem. Soc. Jpn., 54, 3577—3578 (1981)

Oxidation of Copper in Nitrogen Dioxide

Yoshio TAKASU,* Teruhide TOMO-OKA, and Yoshiharu MATSUDA
Department of Industrial Chemistry, Faculty of Engineering, Yamaguchi University, Tokiwadai, Ube 755

(Received January 8, 1981)

Synopsis. Thermal microgravimetry, mass spectrometry, and X-ray diffractometry were used to investigate the ability of NO_2 to oxidize copper. NO_2 oxidizes a copper plate with formation of oxide film consisting of Cu_2O (predominant) and CuO. The oxidation obeys a cubic law, and proceeds faster than in oxygen. An oxidation mechanism is presented on the basis of kinetic and structural data.

Although many studies have been made on high temperature oxidation of metals in oxygen, only a few have adopted NO_x as oxidizing agent.[1-3] We previously reported that copper could be oxidized in NO around 973 K but that the oxidation rate was much lower than that in oxygen.[4,5] The present investigation examined corrosive characteristics of nitrogen dioxide NO_2 for oxidation of copper by means of thermal microgravimetry, mass spectrometry, and X-ray diffractometry, mainly with a view elucidating the oxidation mechanism for this system.

Experimental

A poly-crystalline copper plate (99.99%Cu, 0.5 mm in thickness) was annealed *in vacuo* at 1073 K for 2 h, and then cut to the size 10×10 mm^2. After being abraded with an emery paper, the specimen was electropolished in an acid solution (H_2SO_4:H_3PO_4:H_2O=170:540:308 in volume), and rinsed in water and acetone. Highly pure NO_2, NO, and N_2O each in a glass cylinder (Takachiho Chemical Co., Ltd.) were used without further purification. The oxygen and argon were purified by bulb-to-bulb distillation with liquid nitrogen coolant. The oxidation process was followed by a Gulbransen-type microbalance contained in a conventional high-vacuum apparatus which could be evacuated to 2×10^{-5} Torr (1 Torr=133.3 N m^{-2}). Before use for the oxidation experiment, the test specimen was reduced in 20 Torr of hydrogen at 973 K for 1 h. Argon was used to determine the zero point of the microbalance. Oxide species were identified by an X-ray diffraction analysis (Cu $K\alpha$, 0.9 kW), in which the oxide film formed on each specimen was analyzed as it was. A mass spectrometer (JOEL, JMS-D-100) was used to determine the composition of the gas phase. Gas samplers for mass spectrometry were attached to the reaction tube of the microbalance equipment.

Results and Discussion

Figure 1 shows oxidation curves for copper plates placed at 673 K in 10 Torr of each of the corrosive gases NO_2, NO, N_2O, and O_2. Oxidation rate of copper in NO_2 was the highest and that in NO was the lowest. As indicated in Fig. 2, the oxidation of copper in NO_2 obeyed a cubic rate law $(\Delta W)^3=k_c\cdot t$, where ΔW signifies weight gain, k_c the cubic rate constant, and t oxidation time. According to

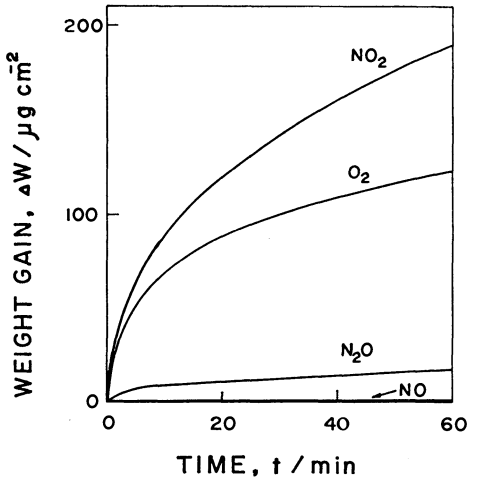

Fig. 1. Oxidation curves of copper plates in 10 Torr of NO_2, NO, N_2O, or O_2 at 673 K.

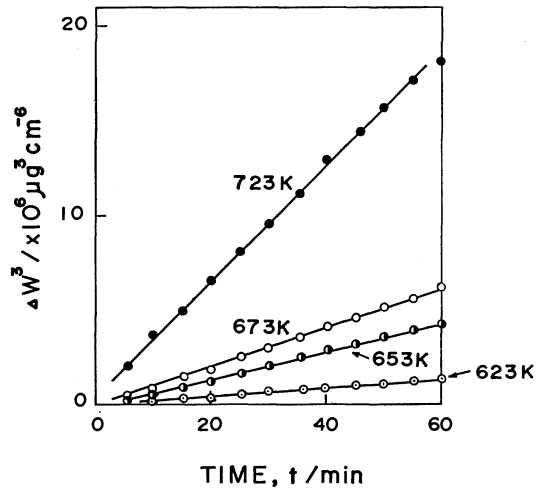

Fig. 2. Cubic plots of the oxidation curves of copper at various temperatures in 10 Torr of NO_2.

the mass spectrometry, the gas phase after a 1 h oxidation of copper at 673 K in 10 Torr of NO_2 consisted of about 97 per cent of NO_2 and a few per cent of NO and N_2O. Since the dissociation of nitrogen dioxide is not negrigible above 753 K, oxidation measurements were performed below 723 K. The oxide film formed in NO_2 was rather coarse and consisted of both Cu_2O (predominant) and CuO, while the one formed in O_2 was dense and consisted only of CuO. In Table 1, the oxidation law, rate constant, apparent activation energy, and kinds of the oxides formed were listed for comparison between oxidation behaviors of copper in NO_2 and O_2. According to

Table 1. Comparison between characteristics of NO_2 and O_2 for the oxidation of copper plates

Gas	Oxidation law	k_c[a] $\mu g^3\ cm^{-6}\ min^{-1}$	E_a[b] kJ mol^{-1}	Oxides
NO_2	Cubic	11×10^4	84	Cu_2O, CuO
O_2	Cubic	3.8×10^4	88	CuO

a) k_c is the rate constant at 673 K. b) E_a is apparent activation energy.

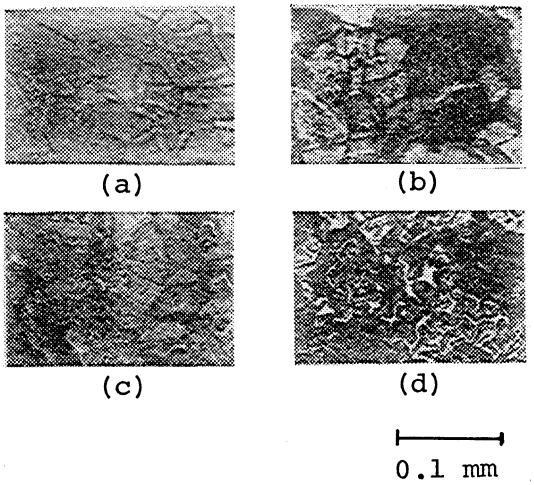

Fig. 3. Optical metallographs of the surfaces of Cu specimens oxidized in 10 Torr of O_2 or NO_2 at 673 K. (a): Non-oxidized(electropolished), (b): oxidized in 10 Torr of O_2 for 1 h, (c) and (d): oxidized in 10 Torr of NO_2 for 5 min and 1 h, respectively.

the Mott theory,[6-8] the rate determining process in the oxidation which obeys cubic rate law is the transfer of ions through the oxide layer under an electronic field formed between the adsorbed layer of gas and the oxide-metal interface. The reason for the higher rate of oxidation of copper in NO_2 than in O_2 is possibly in relation to the formation of a coarse oxide film as shown in Fig. 3. Such a coarse oxide film might result from formation of two different oxides Cu_2O and CuO. On the basis of the above results, the following oxidation mechanism is proposed in which only Cu_2O is considered as metal oxide species because it is predominant in the oxide layer.

Gas-oxide interface

$$NO_2 + e_x^- = NO_2^-, \quad (1)$$

$$2NO_2^- = Cu_2O + 2V^-_{Cu_x^+} + NO + NO_2, \quad (2)$$

$$6NO_2^- = 3Cu_2O + 6V^-_{C_x^+} + N_2O + 4NO_2, \quad (3)$$

In oxide

$$e_0^- \longrightarrow e_x^-, \quad (4)$$

$$V^-_{Cu_x^+} \rightleftarrows V^-_{Cu_0^+}. \quad (5)$$

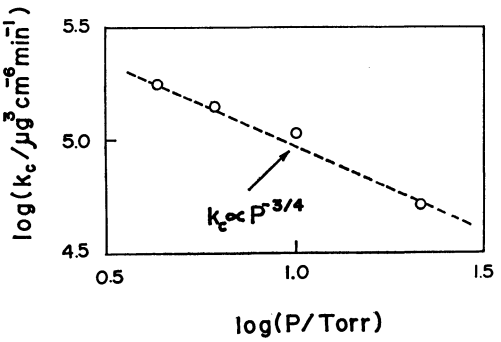

Fig. 4. The relation between the pressure of NO_2 and rate constant for the oxidation of copper at 673 K.

Oxide-metal interface

$$V^-_{Cu_0^+} + Cu = e_0^-, \quad (6)$$

where $V^-_{Cu_x^+}$, $V^-_{Cu_0^+}$, e_x^-, and e_0^- signify the cation vacancy at the gas-oxide interface, that at the oxide-metal interface, the electron at the gas-oxide interface, and the one at the oxide-metal interface, respectively. Considering the theory presented by Mott,[6-8] the cubic rate constant at a constant temperature can be given by $k_c \propto P^n_{NO_2}$, where $n=-1/2$ (in the case of Reaction 2) or $n=-3/2$ (in the case of Reaction 3).[9] The pressure dependence of oxidation constant obtained from this experiment is $-3/4$ as shown in Fig. 4. This value is within the region for the theoretical values given above, suggesting that both Reactions 2 and 3 are occurring in the oxidation process.

One of the authors (Y.T.) gratefully acknowledges the support of this research by a grant from the Itoh Kagaku Shinkokai.

References

1) M. Faber, A. J. Darnell, and D. M. Ehrenberg, *J. Electrochem. Soc.*, **102**, 446 (1955).
2) Y. Takasu, Y. Matsuda, S. Maru, and N. Hayashi, *Nature*, **255**, 544 (1975).
3) Y. Takasu, Y. Matsuda, S. Maru, N. Hayashi, H. Yoneyama, and H. Tamura, *J. Phys. Chem.*, **79**, 1480 (1975).
4) Y. Takasu, M. Takagi, and Y. Matsuda, *Chem. Lett.*, **1977**, 1403.
5) Y. Takasu and Y. Matsuda, *Bull. Chem. Soc. Jpn.*, **51**, 1225 (1978).
6) N. F. Mott, *Trans. Faraday Soc.*, **35**, 1175 (1939).
7) N. F. Mott, *Trans. Faraday Soc.*, **36**, 472 (1940).
8) N. F. Mott, *Nature*, **146**, 996 (1940).
9) M. Maeda, "Introduction to Surface Physics Engineering," (in Japanese), Asakura Shoten, Tokyo (1970), p. 176.

Partial Hydrogenation of Acetylenes on Modified Nickel Boride Catalysts

Yuriko NITTA, Toshinobu IMANAKA, and Shiichiro TERANISHI*

Department of Chemical Engineering, Faculty of Engineering Science, Osaka University, Toyonaka, Osaka 560

(Received January 12, 1981)

Synopsis. Ni–B catalysts modified with a small amount of copper(II) salt have a higher selectivity than palladium and modified Raney nickel catalysts for partial hydrogenation of phenylacetylene, 1-heptyne, 1-ethynylcyclohexene, and propargyl alcohol.

Our previous paper[1] reported that cobalt boride catalyst (Co–B), especially when modified with a small amount of metal salts, are much more effective than nickel boride catalyst (Ni–B) for selective hydrogenation of α,β-unsaturated aldehydes to α,β-unsaturated alcohols; however, for selective hydrogenation of acetylenes to olefins Ni–B is more selective than Co–B. This work investigated modifications of Ni–B by addition of a small amount of metal salts with a view to increasing the selectivity for the partial hydrogenation of acetylenes.

Although palladium has almost completely displaced nickel to be used as catalyst of choice for the partial hydrogenation of acetylenes, the lower price of nickel will make it more useful than palladium if equal or higher selectivity is to be obtained with it.[2] Thus it is worthwhile to study the partial hydrogenation on Ni–B which is very simple to prepare and to use and which is, in activity, equal to or, in some cases, superior to Raney nickel catalyst (R-Ni) for hydrogenation of many kinds of organic functions. With R-Ni, Elsner and Paul[3] reported that deactivation of the catalyst with copper(II) salt in ethanol might provide a selective catalyst for partial hydrogenation of octadecynes, without presenting any information on quantitative compositions of the products.

Experimental

Catalyst. Ni–B and R-Ni were prepared according to the method described previously.[4] Copper boride catalyst (Cu–B) and Co–B were prepared, respectively, with copper(II) chloride and cobalt acetate in a manner similar to that for Ni–B. The copper-modified nickel boride catalyst (Cu-modified Ni–B) was prepared by stirring Ni–B (0.2 g, by the P-1 method[4,5]) in a solution of copper(II) chloride (2—10 mol% of Ni) in 99% ethanol (10 ml) at 30 °C for 10 min. The copper-modified Raney nickel catalyst (Cu-modified R-Ni) was prepared in the same way by using R-Ni (0.2 g) activated at 70 °C. The coprecipitated nickel copper boride catalyst (Ni–Cu–B) was prepared by reducing a mixture of measured amounts of nickel acetate and copper(II) chloride with $NaBH_4$ in water.

Hydrogenation. Acetylenes (0.2 ml) were hydrogenated at 30 °C in ethanol or in cyclohexane (10 ml) under atmospheric pressure of hydrogen. The olefin selectivity of a catalyst was defined as the mol% of olefin in olefin plus paraffin determined by a GLC method at 30% conversion of acetylene. Selectivities of the catalysts were almost independent of the conversion of acetylenes up to 90%.

The other experimental details are the same as those described in our previous paper.[1]

Results and Discussion

Selectivities of boride catalysts in the partial hydrogenation of phenylacetylene fell in the order Cu–B> Ni–B>Co–B, which is considered to be reverse to the order of the strength of adsorption of the acetylene on the catalyst surface as based on the surface *d*-electron density.[1,8] 1-Phenyl-1-propyne, which is supposed to be adsorbed more weakly than phenylacetylene because of the steric hindrance of methyl group, was hydrogenated to the olefin more selectively than phenylacetylene on Ni–B. These facts support the idea, presented in our previous paper[1] concerning the selectivity of Co–B, that the stronger the adsorption bond between the C≡C bond and the metal, the lower the olefin selectivity.

The selectivity of Ni–B was enhanced by the modification with a small amount of copper(II) chloride even to such an extent as exceeds that of Cu–B or polymer-bound Pd complex catalyst (93%),[6] although the hydrogenation rate decreased considerably. In the case of R-Ni, it was necessary to add a larger amount of the copper(II) salt to obtain as high a selectivity as that of Cu–B, probably because of the larger surface area of R-Ni. The selectivity of a coprecipitated nickel copper boride catalyst was lower than those of Ni–B and Cu–B. This fact again shows

Table 1. The olefin selectivity(S) of various catalysts in the hydrogenation of acetylenes

Catalyst	Cu/Ni[a]	Reactant	S/%
Ni–B (P-1)[b]	—	Phenylacetylene	90.0
Ni–B (P-2)[b]	—	Phenylacetylene	91.3
R-Ni	—	Phenylacetylene	88.0
Cu–B	—	Phenylacetylene	92.0
Co–B	—	Phenylacetylene	79.0
Cu-modified Ni–B	0.02	Phenylacetylene	96.3
Cu-modified Ni–B	0.05	Phenylacetylene	97.7
Cu-modified Ni–B	0.10	Phenylacetylene	98.3
Cu-modified R-Ni	0.05	Phenylacetylene	84.1
Cu-modified R-Ni	0.10	Phenylacetylene	83.8
Cu-modified R-Ni	0.20	Phenylacetylene	93.2
Ni–Cu–B	0.10	Phenylacetylene	88.9
Ni–B (P-1)	—	1-Phenyl-1-propyne	92.3
Ni–B (P-1)	—	1-Heptyne	72.5
R-Ni	—	1-Heptyne	78.5
Cu-modified Ni–B	0.05	1-Heptyne	89.7
Cu-modified R-Ni	0.05	1-Heptyne	70.7
Cu-modified Ni–B	0.10	1-Ethynylcyclohexene	94±1
Ni–B (P-1)	—	Propargyl alcohol	68.0
Cu-modified Ni–B	0.10	Propargyl alcohol	80.3

a) Molar ratio of copper(II) salt to nickel salt. b) Prepared in water (P-1) or in 95% ethanol (P-2).

that the coprecipitation method for preparing binary boride catalysts is ineffective for increasing the catalytic selectivity, as already shown for the selective hydrogenation of α,β-unsaturated aldehydes in our previous paper.[1]

The addition of zinc or iron(II) salts instead of copper(II) salts to the Ni–B catalyst raised the selectivity only slightly.

The Cu-modified Ni–B was highly selective also for the partial hydrogenation of 1-heptyne, while Cu–B was almost inactive towards 1-heptyne. XPS studies on Cu-modified Ni–B and R-Ni indicated that the copper(II) ion was deposited as copper metal on the catalyst surface. From these facts, the high selectivity of Cu-modified Ni–B is supposed to be due to the synergetic effect between copper and nickel metals on the catalyst surface, where copper atoms adsorb acetylenes rather weakly but do not adsorb olefins in outer surface or at the top of rugged surface and where nickel atoms activate hydrogen in inner pores or at the bottom of rugged surface.

As an instance of partial hydrogenation of conjugated acetylenes, 1-ethynylcyclohexene was hydrogenated over the Cu-modified Ni–B in cyclohexane. After all reactant I had been exhausted, no further uptake of hydrogen was observed;

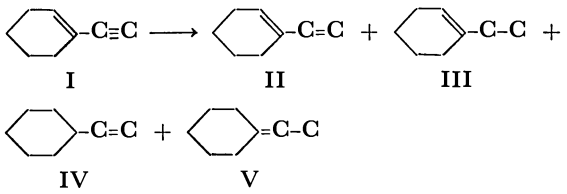

I II III

IV V

compositions of the products were as follows: II 94±1%, III+IV *ca.* 3%, and V and the others *ca.* 3%. Ethylcyclohexane was not detected. The yield of II was reported to be 86% at 94% conversion on the Lindler catalyst,[7] and to be 81% at 100% conversion on polymer-bound Pd complex catalyst.[6]

Propargyl alcohol was selectively hydrogenated to allyl alcohol on the Cu-modified Ni–B catalyst in ethanol without being accompanied by hydrogenolysis of the hydroxyl group.

These findings suggest that we can regard Cu-modified Ni–B as superior to the Lindler catalyst for the partial hydrogenation of acetylenes if we take into account both the ease of preparation and separation and the moderate price of nickel.

The authors wish to thank Dr. Yasuaki Okamoto for his valuable discussion and for his assistance in obtaining XPS data.

References

1) Y. Nitta, T. Imanaka, and S. Teranishi, *Bull. Chem. Soc. Jpn.*, **53**, 3154 (1980).
2) E. N. Marvell and T. Li, *Synthesis*, **1972**, 457.
3) B. B. Elsner and P. F. M. Paul, *J. Chem. Soc.*, **1953**, 3156.
4) Y. Nitta, T. Imanaka, and S. Teranishi, *Nippon Kagaku Kaishi*, **1976**, 1362.
5) C. A. Brown and H. C. Brown, *J. Am. Chem. Soc.*, **85**, 1003 (1963).
6) M. Terasawa, H. Yamamoto, K. Kaneda, T. Imanaka, and S. Teranishi, *J. Catal.*, **57**, 315 (1979).
7) E. N. Marvell and J. Tashiro, *J. Org. Chem.*, **30**, 3991 (1965).
8) G. C. Bond, "Catalysis by Metals," Academic Press, London and New York (1962), Chap. 5.

The Molecular Conformation of 6,14-Di-*O*-acetyl-3-*O*-(2-chlorobenzoyl)-grayanotoxin II as Revealed by X-Ray Methods

Akio FURUSAKI,* Nobuyuki HAMANAKA, and Takeshi MATSUMOTO
Department of Chemistry, Faculty of Science, Hokkaido University, Sapporo 060

(Received April 18, 1981)

Synopsis. An X-ray crystal analysis has revealed that the six-membered C-ring in the title compound takes a boat conformation, in contrast with that in grayanotoxin II itself.

A series of X-ray crystal analyses[1] revealed that the C-ring conformation of grayanotoxins[2] with the exocyclic double bond, C(10)=C(20), depends largely on the multiplicity of the C(15)–C(16) bond. When this is a single bond, the C-ring prefers a chair conformation. However, the enthalpy difference between the chair and boat conformations of the C-ring is supposed to be small, because the change of the B-ring conformation reduces that energy difference. In this paper, we wish to report an example of grayanoids in which, although the C(15)–C(16) and C(10)–C(20) bonds are single and double bonds respectively, the C-ring adopts a boat conformation.

Experimental

Colorless single crystals of 6,14-di-*O*-acetyl-3-*O*-(2-chlorobenzoyl)grayanotoxin II (**1**) were grown from an acetone-diisopropyl ether solution. The crystal data are as follows: $C_{31}H_{39}O_8Cl$, *M.W.*=575.1, orthorhombic, space group $P2_12_12_1$, a=12.51(1), b=22.12(2), c=10.39(1) Å, Z=4, D_m=1.33 g cm^{-3}, D_c=1.328 g cm^{-3}. The intensities were recorded on multiple Weissenberg photographs taken with Cu $K\alpha$ radiation for the 0th—10th layer around the a axis and for the 0th—8th layer around the c axis, and were measured visually with a calibrated intensity scale. The 2811 independent intensity data thus obtained were corrected for the Lorentz and polarization factors, but not for the absorption or the extinction effect.

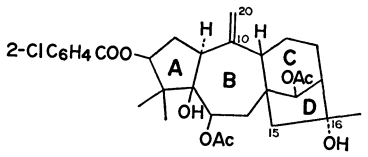

1

Structure Determination

Various attempts were made to solve the structure by the heavy-atom method or the symbolic-addition procedure,[3] but all such attempts were unsuccessful. Thus, the structure analysis was delayed more than 10 years. Since the Monte Carlo direct method was recently developed,[4] it was applied to the present phase determination. The 50 strongest reflections were chosen as the starting set. In order to extend the tentative-phase set derived from random numbers, 12 cycles of the tangent procedure were performed using 542 $|E|$ values above 1.30. Since the 24th phase set showed a low R_K value of 0.339 ($R_K=\Sigma||E_o|-|E_c||/\Sigma|E_o|$), 6 additional cycles of the tangent procedure were carried out using 658 $|E|$ values above 1.20; the R_K value was reduced to 0.249. An E-map based on 641 phases afforded all the 40 non-hydrogen atoms. The structure thus obtained was refined by the block-diagonal-matrix least-squares method with anisotropic temperature factors. The

Table 1. The final atomic parameters and estimated standard deviations

Atom	x(×10^4)	y(×10^4)	z(×10^4)	B_{eq}[a]/Å^2
Cl	11205(3)	2477(2)	1912(4)	5.74
O(1)	7972(5)	2183(3)	1716(7)	2.55
O(2)	6607(5)	2700(3)	4428(7)	2.27
O(3)	6954(5)	3892(3)	5049(7)	2.14
O(4)	4244(5)	4874(3)	4407(7)	2.21
O(5)	1930(6)	4763(3)	5323(7)	2.97
O(6)	9124(7)	2674(4)	411(8)	3.98
O(7)	6902(7)	4880(4)	4476(11)	4.82
O(8)	4276(8)	5509(4)	2688(9)	4.56
C(1)	5539(7)	2946(4)	2553(10)	1.98
C(2)	6114(8)	2432(5)	1837(11)	2.85
C(3)	7208(7)	2698(4)	1598(11)	2.36
C(4)	7410(8)	3203(5)	2601(10)	2.32
C(5)	6382(8)	3166(4)	3488(10)	2.20
C(6)	6080(7)	3748(4)	4178(9)	2.04
C(7)	5062(8)	3698(4)	5011(10)	2.20
C(8)	3992(7)	3793(4)	4320(9)	2.05
C(9)	3640(7)	3265(4)	3370(10)	2.02
C(10)	4479(7)	2770(4)	3138(9)	1.85
C(11)	3258(8)	3503(5)	2071(10)	2.37
C(12)	2422(8)	4011(4)	2171(10)	2.35
C(13)	2659(7)	4417(4)	3325(11)	2.06
C(14)	3877(8)	4387(4)	3555(10)	2.16
C(15)	3093(8)	3870(4)	5340(10)	2.26
C(16)	2193(7)	4217(4)	4639(10)	1.93
C(17)	1137(8)	3838(5)	4561(12)	3.04
C(18)	8468(9)	3120(6)	3376(13)	3.86
C(19)	7465(10)	3813(5)	1872(13)	3.60
C(20)	4202(9)	2189(5)	3385(14)	3.56
C(21)	8894(9)	2253(5)	1093(11)	2.84
C(22)	9590(8)	1709(5)	1279(11)	2.56
C(23)	10664(9)	1777(6)	1614(12)	3.38
C(24)	11375(10)	1276(7)	1681(14)	4.35
C(25)	10949(12)	722(7)	1497(15)	4.97
C(26)	9851(12)	625(6)	1225(17)	5.14
C(27)	9160(10)	1130(5)	1138(13)	3.66
C(28)	7315(9)	4472(5)	5106(12)	2.97
C(29)	8212(9)	4530(6)	6005(13)	3.57
C(30)	4476(9)	5408(5)	3800(12)	2.93
C(31)	4889(11)	5857(5)	4784(14)	4.25

a) $B_{eq}=8\pi^2(u_1^2+u_2^2+u_3^2)/3$, where u_i is the root-mean-square deviation in the ith principal axis of the thermal ellipsoid.

final R value was 0.123. The final atomic parameters are listed in Table 1. The table of the anisotropic temperature factors and the F_o-F_c table are kept at the Chemical Society of Japan (Document No. 8148).

All the calculations were performed on a HITAC M-200H computer at the Hokkaido University Computing Center, using our own programs. The atomic scattering factors were taken from the International Tables.[5]

Results and Discussion

The molecular framework of **1** and the torsion angles for the grayanane skeleton are shown in Figs. 1 and 2 respectively. The A-ring takes an envelope form; the C(2)–C(3)–C(4)–C(5) part is nearly planar. Since this conformation makes the O(1) atom and the C(18)H_3 group eclipse each other around the C(3)–C(4) bond, it is probably less stable than the envelope form with a planar C(5)–C(1)–C(2)–C(3) or C(1)–C(2)–C(3)–C(4) part. In fact, the present envelope form has not been observed in grayanotoxins I,[1a] II,[1b] XV,[6] XVI,[1c] and XIX.[1e] The B-ring has a chair form with an approximate mirror plane through the C(5) atom, while the C-ring adopts a deformed boat form. Force-field calculations indicate that, in grayanotoxins having the C(15)–C(16) single and C(10)–C(20) double bonds, the molecular conformation with the boat C-ring is less stable than that with the chair C-ring by about 4 kJ mol^{-1}.[7] If this is true, it follows that the occurrence of the present boat C-ring may be due to the molecular-packing effect. The D-ring takes a conformation intermediate between the envelope form with a mirror plane through the C(14) atom and the half-chair form with a two-fold rotation axis through the C(16) atom.

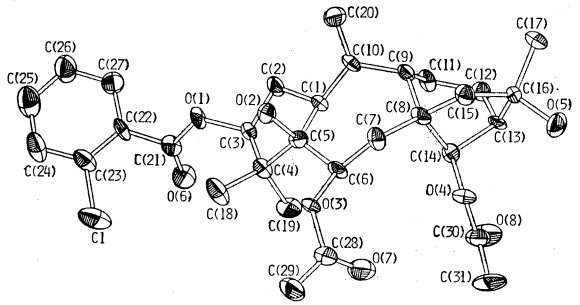

Fig. 1. A perspective view of the molecule of **1**.

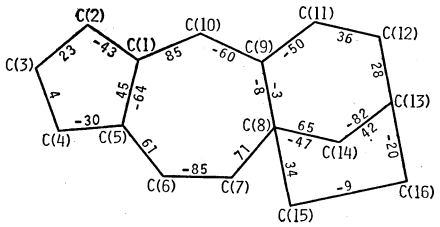

Fig. 2. The torsion angles (ϕ/°) for the grayanane skeleton.
Only the torsion angles relevant to atoms which form the same ring are given in the ring.

References

1) a) P. Narayanan, M. Rohl, K. Zechmeister, and W. Hoppe, *Tetrahedron Lett.*, **1970**, 3943; b) A. Furusaki, N. Hamanaka, and T. Matsumoto, *Bull. Chem. Soc. Jpn.*, **53**, 1956 (1980); c) A. Furusaki, S. Gasa, R. Ikeda, and T. Matsumoto, *ibid.*, **54**, 49 (1981); d) A. Furusaki, S. Gasa, R. Ikeda, T. Matsumoto, N. Yasuoka, and Y. Matsuura, *ibid.*, **54**, 657 (1981); e) **54**, 1622 (1981). We change the name of the new grayanoid in Ref. 1 d from grayanotoxin XVIII to grayanotoxin XX, since the names grayanotoxin XVIII and XIX have been already given to 14-deoxygrayanotoxin II (J. Sakakibara, N. Shirai, T. Kaiya, and H. Nakata, *Phytochemistry*, **18**, 135 (1979)) and to a new grayanoid (Ref. 1e) respectively.

2) S. Miyajima and S. Takei, *J. Agric. Chem. Jpn.*, **10**, 1093 (1934); H. Kakisawa, M. Kurono, S. Takahashi, and Y. Hirata, *ibid.*, **1961**, 59; J. Iwasa and Y. Nakamura, *Tetrahedron Lett.*, **1969**, 3937; H. Hikino, M. Ogura, T. Ohta, and T. Takemoto, *Chem. Pharm. Bull.*, **18**, 1072 (1970); T. Okuno, N. Hamanaka, H. Miyakoshi, and T. Matsumoto, *Tetrahedron*, **26**, 4765 (1970); N. Hamanaka, H. Miyakoshi, A. Furusaki, and T. Matsumoto, *Chem. Lett.*, **1972**, 779; S. Gasa, R. Ikeda, N. Hamanaka, and T. Matsumoto, *Bull. Chem. Soc. Jpn.*, **49**, 835 (1976).

3) J. Karle and I. L. Karle, *Acta Crystallogr.*, **21**, 849 (1966).

4) A. Furusaki, *Acta Crystallogr., Sect. A*, **35**, 220 (1979).

5) "International Tables for X-Ray Crystallography," The Kynoch Press, Birmingham (1974), Vol. IV.

6) The last paper but one in Ref. 2.

7) A. Furusaki and T. Matsumoto, unpublished.

Equilibrium Dissociation Pressure of Hydrogen in Molten LiCl–LiH Mixtures

Kazuhiko Ichikawa* and Kazutaka Kawamura†

Department of Chemistry, Faculty of Science, Hokkaido University, Sapporo 060

†*Research Laboratory of Nuclear Reactors, Tokyo Institute of Technology, Tokyo 152*

(Received April 23, 1981)

Synopsis. Pressure-composition-temperature data were collected for the LiCl–LiH system in the respective ranges 0.1—10 mmHg††, 4.5—22.3 mol% LiH, and 550—700 °C by measuring equilibrium hydrogen pressure in a Sieverts' apparatus. The square root of hydrogen pressure *vs.* composition isotherm follows Sieverts' relation for compositions below 10 mol% LiH.

The recent increased interest in physicochemical and thermodynamic properties of solutions containing lithium hydride as one component, such as those of hydrogen isotopes in liquid lithium,[1–4] has been motivated by their use for direct energy conversion devices. The simplest ionic crystal of LiH consisting of Li^+ and H^- has a NaCl-type structure, in which the ionic radius of H^- is as large as 0.2 nm. The molten LiH may be of simple ionic melt like molten lithium halide and may have a high decomposition-pressure of hydrogen at a temperature just above its melting point 686 °C under 1 atm of H_2(g). According to the study[5] on solid-liquid phase equilibrium the LiCl–LiH system has eutectic temperature 496 °C at 34.0 mol% LiH and no formation of solid solutions was observed. In this work we report variation of equilibrium dissociation pressure of hydrogen with concentration and temperature for molten LiCl–LiH binary mixtures.

Experimental

Experiments were carried out in a so-called Sieverts' apparatus[6] which consisted of four main sections designed, respectively, for (a) gas metering, (b) gas equilibration with LiCl–LiH melt, (c) gas pumping, and (d) gas supply. The gas metering section consisted of a mercury manometer (1—760 mmHg) and a McLeod gauge (10^{-4}—1 mmHg). The equilibration section was a fused-silica tube containing a molybdenum crucible filled with sample; the crucible was kept in a long sintered-Al_2O_3 tube because hydrogen is permeable through fused silica at higher temperatures. Before measuring the equilibrium hydrogen pressure, P_{H_2}, the apparatus, with no sample contained, was evacuated up to 10^{-5} mmHg at the high temperature of interest. P_{H_2} was measured as a function of temperature from 550 °C to 700 °C at each of the LiH concentrations, 4.5, 5.3, 7.5, 9.8, 12.3, 20.2, and 22.3 mol%.

Results and Discussion

Figure 1 shows variation of hydrogen pressure with temperature and Fig. 2 shows isothermal plots of the square root of hydrogen pressure *vs.* composition.

Since component LiH in a molten LiCl dissociates into a host of ions Li^+ and H^-, the binary solution has a common cation of Li^+ and the equilibrium

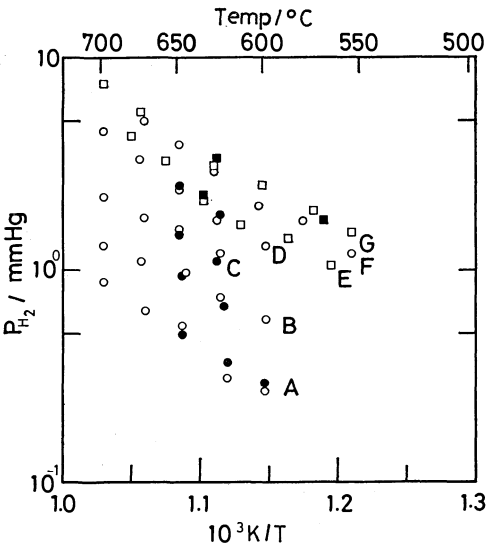

Fig. 1. Temperature dependence of hydrogen pressure for the LiCl–LiH system with each concentration of A: 4.5, B: 5.3, C: 7.5, D: 9.8, E: 12.3, F: 20.2, and G: 22.3 mol% LiH.
The measurements of P_{H_2} with increasing and decreasing temperatures correspond to the open circles or squares and the solid circles or squares, respectively.

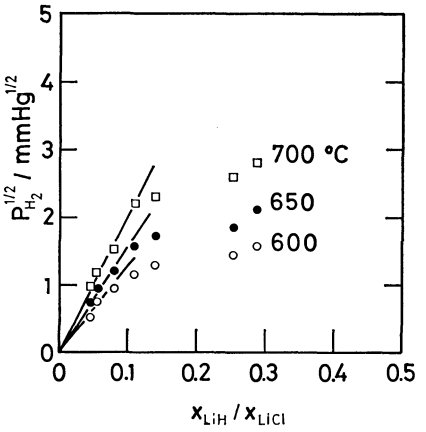

Fig. 2. Isothermal data on the square root of hydrogen pressure *vs.* mole fraction ratio, x_{LiH}/x_{LiCl}, for the LiCl–LiH system.

reaction between the gaseous and liquid phases may be written as

$$\frac{1}{2}H_2(g,\ T,\ P_{H_2}) + Cl^-(soln,\ T,\ P_{Cl_2}) \rightleftharpoons H^-(soln,\ T,\ P_{H_2}) + \frac{1}{2}Cl_2(g,\ T,\ P_{Cl_2}). \quad (1)$$

The equilibrium constant, $K(T)$, for this reaction is given by

†† 1 mmHg=133.322 Pa.

$$K(T) = a_{LiH}P_{Cl_2}^{1/2}/a_{LiCl}P_{H_2}^{1/2}, \quad (2)$$

where a is activity for each component and P is equilibrium pressure of H_2 or Cl_2. Activity coefficient of LiCl, γ_{LiCl}, has been calculated by use of the temperature-composition solid-liquid equilibrium diagram, with no formation of solid solutions, for the LiCl–LiH system.[5] It is equal to *ca.* unity up to 10 mol% LiH around 600 °C, whereas for component LiH at low concentrations γ_{LiH} may be interpreted as being equal to the constant $k(T)$ in Henry's law. The magnitude of $K(T)$, as evaluated with the aid of chemical potentials[7] of pure liquids LiH and LiCl and pure gases H_2 and Cl_2, indicates that the partial pressure of Cl_2 is very low as compared with that of H_2. If we assume that the square root of P_{Cl_2} is proportional to the concentration of chlorine anion or x_{LiCl}, the square root of P_{H_2} in Eq. 2 is given by

$$P_{H_2}^{1/2} = K_{app}(T)\frac{x_{LiH}}{x_{LiCl}}, \quad (3)$$

where $K_{app}(T)$ is apparent Sieverts' constant. The three straight lines shown in Fig. 2 correspond, respectively, to the values of $K_{app}(T)$, $K_{app}(700\,°C) = 20$, $K_{app}(650) = 16$, and $K_{app}(600) = 13$ $mmHg^{1/2}$/(mole fraction ratio, x_{LiH}/x_{LiCl}), though experimental values for the square root of P_{H_2} deviate from Sieverts' law toward the lower values for compositions above 10 mol% LiH. The experimentally determined $K_{app}(T)$ values are equal to *ca.* one third of those for the hydrogen isotope–lithium system.[4] The knowledge of the Sieverts' law constant is of importance to evaluate P_{H_2} for dilute solutions.

This work was supported in part by the Ministry of Education, Science and Culture of Japan.

References

1) E. Veleckis, E. H. Van Deventer, and M. Blander, *J. Phys. Chem.*, **78**, 1933 (1974).
2) H. Katsuta, T. Ishigai, and K. Furukawa, *Nucl. Technol.*, **32**, 297 (1977).
3) E. Veleckis, *J. Phys. Chem.*, **81**, 526 (1977).
4) J. Smith, J. D. Redman, R. A. Strehlow, and J. T. Bell, Proc. Symp. on Tritium Technol. related to Fusion Reactor Systems, Report ERDA-50, 41 (1975).
5) C. E. Johnson, S. E. Wood, and C. E. Crouthamel, *Inorg. Chem.*, **3**, 1487 (1964).
6) *E.g.*, K. Fujita, C. Kho, and M. Tada, *J. Jpn. Inst. Metals*, **43**, 601 and 611 (1979).
7) I. Barin and O. Knacke, "Thermodynamical Properties of Inorganic Substances," Verlag Stahleisen m.b.H., Düsseldorf (1973).

Pressure Effects on the Reaction of Hydroxide Ion with Sodium 2-Bromoethanesulfonate

Tsutomu ASANO* and Toshio OKADA

Department of Chemistry, Faculty of Engineering, Oita University, 700 Dannoharu, Oita 870-11

(Received May 21, 1981)

Synopsis. Kinetic effect of pressure on the reaction of hydroxide ion with 2-bromoethanesulfonate was studied. The reaction was moderately accelerated by pressure and the activation volumes suggest that the presence of the negative charge on the sulfonato group does not produce any measurable solvation increase during activation.

Although kinetic effects of pressure have been studied for a variety of organic reactions,[1] little work has been done for reactions between anions or cations. This is rather surprising because activation volume is known to be sensitive to solvational changes, and the approach of two ionic species with the same sign is expected to produce an increase in solvation. For example, when we compare the following two reactions, we would expect more negative activation volume for the latter because of the concentration of the negative charges.

$$A + B^- \longrightarrow [A\cdots B^-]^* \longrightarrow P \quad (1)$$

$$A^- + B^- \longrightarrow [A\cdots B^{2-}]^* \longrightarrow P \quad (2)$$

In fact, this effect of charge concentration on volume change has been observed in the ionization equilibria of some dicarboxylic acids. According to Høiland,[2] and Delben and Crescenzi,[3] the second ionization is accompanied by much larger volume contraction than the first ionization when the two carboxyl groups are located in close spatial proximity to each other (Table 1). Therefore, it is an interesting question whether a similar effect of charge concentration on volume can be observed in kinetic processes.

In this communication, the kinetic effects of pressure on the following elimination reaction[4] is discussed.

TABLE 1. VOLUME CHANGES FOR THE FIRST AND SECOND IONIZATIONS OF SOME DICARBOXYLIC ACID[a,b]

Compound	$\Delta\bar{V}_1^\circ$/mL mol^{-1}	$\Delta\bar{V}_2^\circ$/mL mol^{-1}
Oxalic acid	−6.72	−11.91
Malonic acid	−10.06	−18.55
Succinic acid	−12.86	−13.58
Glutaric acid	−13.17	−13.59
cis-1,2-Cyclohexane-dicarboxylic acid	−12.1	−22.9

a) From Refs. 2 and 3. b) At 25 °C in water.

$$BrCH_2CH_2SO_3^- + OH^- \longrightarrow CH_2{=}CHSO_3^- + Br^- + H_2O \quad (3)$$

The second-order rate constants of the reaction at various pressures are given in Table 2 and illustrated in Fig. 1. It is clearly seen in Fig. 1 that the application of pressure causes a moderate increase in the rate constant, and the plot of ln k against pressure is linear in the pressure range studied. The activation volumes of the reaction estimated from the slopes of the plots are given in the last column of Table 2. When we consider the volume change accompanying the approach of an ion toward a neutral substrate, two factors should be taken into account, *i.e.*, volume decrease caused by the partial bond formation between the two species, and volume increase caused by charge delocalization from the attacking ion to the substrate. These factors counterbalance each other, and as a result, moderately negative activation volumes are observed. A case in point is the base-catalyzed hydrolysis of alkyl acetates. The activation volumes for the reaction are in the range of −5.6—7.6 mL mol^{-1}.[5,6] On the other hand, if the substrate is electrically charged as in the present case, a stronger solute-solvent interaction in the transition state is con-

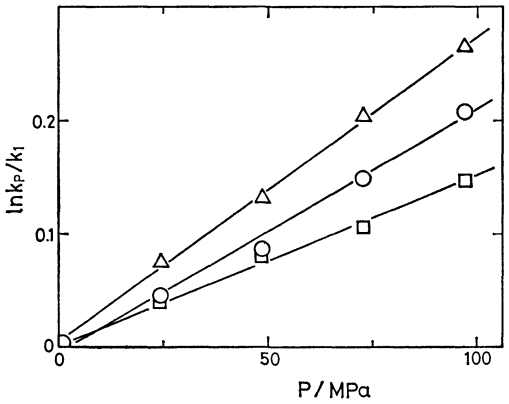

Fig. 1. Pressure dependence of the second-order rate constant for the reaction of hydroxide ion with 2-bromoethanesulfonate.
△: In H_2O at 10 °C, ○: in H_2O at 25 °C, □: in 60 wt% MeOH at 25 °C.

TABLE 2. SECOND-ORDER RATE CONSTANTS AND ACTIVATION VOLUMES FOR THE REACTION OF HYDROXIDE ION WITH 2-BROMOETHANESULFONATE ION

Solvent	T/°C	$k\times10^4$/M^{-1} s^{-1} at Pressure $\times10^{-5}$/Pa					ΔV^*/mL mol^{-1}
		1	245	490	736	981	
H_2O	10	2.22	2.39	2.53	2.72	2.89	−6.3
H_2O	25	11.3	11.8	12.3	13.1	13.9	−5.3
60 wt% MeOH	25	4.32	4.49	4.68	4.80	5.00	−3.6

ceivable and it might result in much larger negative activation volume. However, the activation volumes in water for the present reaction are in the same range as the saponifications, suggesting strongly the absence of solvation reinforcement by the presence of the negative charge on the sulfonato group. The results in aqueous methanol support this argument. If the solvation increase occurs in the activation step, more negative activation volume could be expected in less polar solvents. The experiment shows, however, it is not the case. The value is slightly less negative in aqueous methanol.

The comparison of the present results with the ionization of dicarboxylic acids reveals an interesting point. Since the hydroxide ion attacks a hydrogen atom on the α-carbon which bears the sulfonato group, the distance between the two charge centers in the transition state may be comparable to the one in malonate ion if the delocalization of the negative charge from the hydroxide ion to the substrate is not extensive. Such a transition state formation is expected to be accompanied by solvation increase as in the second ionization of malonic acid, but the activation volumes reported here are not in accordance with this expectation as discussed above. Therefore, it can be safely stated that the extensive negative charge delocalization is realized in the transition state and, probably, the hydration sheath around the sulfonato group remains intact while desolvation occurs around the hydroxide ion.

The present results also indicate that care must be taken when we use reaction volume values in the estimation of activation volumes.

Experimental

Sodium 2-bromoethanesulfonate was prepared as described.[7] The total consumption of hydroxide ion agreed with the theoretical value.

The reactions under pressure were performed by means of a high pressure vessel shown in Fig. 2. The reaction mixture, c, contained in a 50 mL glass syringe was withdrawn through the stainless steel capillary tubing, b, by opening the sampling valve, a, while the pressure of the system was kept constant by sending in pressurizing fluid, hexane. The decrease of the hydroxide ion was followed by titration after quenching the mixture by an excess amount of hydrochloric acid.

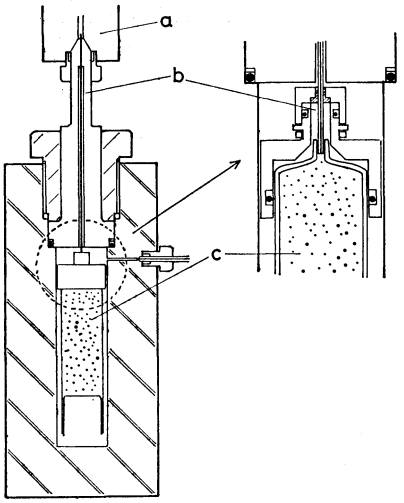

Fig. 2. High pressure reaction vessel with a sampling device.
a: Sampling valve, b: stainless steel capillary tubing, c: reaction mixture.

References

1) T. Asano and W. J. le Noble, *Chem. Rev.*, **78**, 407 (1978).
2) H. Høiland, *J. Chem. Soc., Faraday Trans. 1*, **71**, 797 (1975).
3) F. Delben and V. Crescenzi, *J. Solution Chem.*, **7**, 597 (1978).
4) E. F. Landau, W. F. Whitmore, and P. Doty, *J. Am. Chem. Soc.*, **68**, 816 (1946).
5) M. L. Tonnet and E. Whalley, *Can. J. Chem.*, **53**, 3414 (1975).
6) B. Andersen, F. Grønlund, and J. Olsen, *Acta Chem. Scand.*, **23**, 2458 (1969).
7) C. S. Marvel and M. S. Sparberg, *Org. Synth.*, Coll. Vol. II, 558 (1943).

Studies of Matrix Effects on ^{57}Co-Labelled Tris(β-diketonato)cobalt(III) by Means of Mössbauer Spectroscopy

Yoichi SAKAI, Kazutoyo ENDO,† and Hirotoshi SANO*,†

Department of Chemistry, Faculty of Science, The University of Tokyo, Hongo, Bunkyo-ku, Tokyo 113

† *Department of Chemistry, Faculty of Science, Tokyo Metropolitan University, Fukasawa, Setagaya-ku, Tokyo 158*

(Received September 26, 1980)

Synopsis. The emission Mössbauer spectra at 78 K of ^{57}Co-labelled $Co(dbm)_3$ (dbm=dibenzoylmethanato) dispersed in 2-methyltetrahydrofuran, or of ^{57}Co-labelled $Co(acac)_3$ (acac=acetylacetonato) dispersed in a mixed medium of oxalic acid and polystyrene, give no appreciable magnetic hyperfine structure (hfs), while those of ^{57}Co-labelled $Co(acac)_3$ dispersed in polystyrene and ^{57}Co-labelled crystalline $Co(dbm)_3$ give a magnetic hfs. The results indicate that the local radiolysis of EC-decay involves not only the labelled species itself, but also the neighbouring host matrix.

A number of emission Mössbauer spectroscopic studies of the ^{57}Co-labelled diamagnetic cobalt(III) compounds have shown practically no magnetic hyperfine structure (hfs), although the decayed ^{57}Fe(III)-paramagnetic species are considered to be magnetically diluted in a diamagnetic host.[1-5] The results are indicated in terms of an enhanced spin-spin interaction between the unpaired electrons of the ^{57}Fe and paramagnetic species produced through the EC-decay in the vicinity of ^{57}Fe. In our previous work,[6-7] however, a well-resolved paramagnetic hfs was found in the emission Mössbauer spectra of ^{57}Co-labelled tris(dibenzoylmethanato)cobalt(III), $Co(dbm)_3$, at 4.2 K. The results are explained from the viewpoint of the reduced formation of paramagnetic species (mainly organic radicals) in the vicinity of the decayed ^{57}Fe. It was also reported that the radical formation in the EC-Auger after-effects is small in such compounds that have ligands with a π-conjugated system and that the results are closely related to the radiolytic stability of the labelled compounds.[8]

In the present paper, we examined the emission Mössbauer spectra of the dispersion systems of ^{57}Co-labelled compound in order to get information about the matrix effects in the EC-decay. The dispersion systems of β-diketonates of cobalt(III) used are ^{57}Co-labelled $Co(acac)_3$ dispersed in a mixed medium of oxalic acid and polystyrene, and $Co(dbm)_3$ in 2-methyltetrahydrofuran.

Experimental

Preparation of Source Materials. ^{57}Co-labelled $Co(dbm)_3$ was prepared by following the method described previously.[7] The labelled complex was dissolved in 2-methyltetrahydrofuran, which is known to exist in vitreous structures when it is rapidly cooled. The solution was poured into a cell specially designed for the emission Mössbauer measurement. The cell was set in a cryostat and cooled by immersing it in liquid nitrogen as rapidly as possible.

A 100-mg portion of polystyrene and about 10 mg of $Co(acac)_3$ containing the ^{57}Co-labelled compound were dissolved into tetrahydrofuran, and then a 5-mg portion of oxalic acid was added to the mixture. Oxalic-acid crystals were dissolved on heating, after which the solution was allowed to stand in the air. The homogeneous dispersion of the sample prepared in the cold run was checked by X-ray diffractometry.

Measurement of Mössbauer Spectra. The emission Mössbauer spectra of the source materials at 78 K were measured against an ^{57}Fe-enriched stainless-steel absorber moving in a mode of constant acceleration. Velocity calibration was carried out by normalizing to iron metal.

Results and Discussion

The emission Mössbauer spectra at 78 K of ^{57}Co-labelled $Co(acac)_3$ dispersed in a mixed medium of oxalic acid and polystyrene give practically no magnetic hfs, as is shown in Fig. 1—a; they are similar to those found for pure crystalline ^{57}Co-labelled $Co(acac)_3$.[4] When the results are compared with the emission spectrum of ^{57}Co-labelled $Co(acac)_3$ dispersed in polystyrene,[7] they show that the oxalic acid plays a role in accelerating the rate of relaxation.

The emission Mössbauer spectrum at 78 K of ^{57}Co-labelled $Co(dbm)_3$ dispersed in 2-methyltetrahydrofuran is shown in Fig. 1—b. The magnetic hfs found in pure crystalline ^{57}Co-labelled $Co(dbm)_3$[6-7] decreased drastically in the present system.

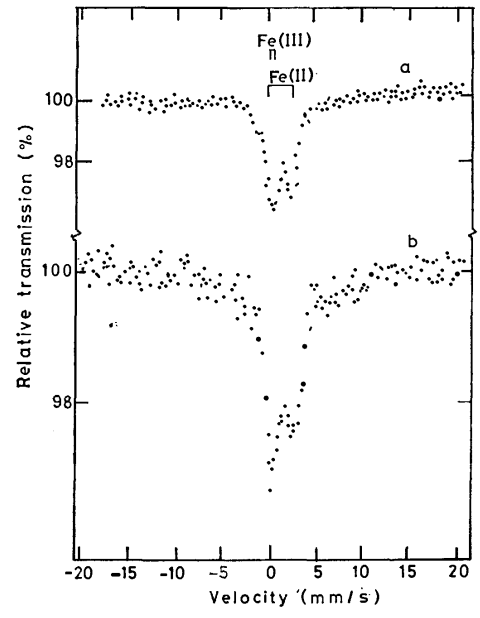

Fig. 1. Emission Mössbauer spectra at 78 K of ^{57}Co-labelled tris(acetylacetonato)cobalt(III) dispersed in a mixed medium of oxalic acid and polystyrene(a), and ^{57}Co-labelled tris(dibenzoylmethanato)cobalt(III) dispersed in 2-methyltetrahydrofuran(b).

We have explained that the appearance or disappearance of magnetic hfs in the emission Mössbauer spectrum of a cobalt(III) compound depends on the radiolytic stability of the source compounds; *i.e.* a compound which is stable against the local radiolysis of EC-decay gives a magnetic hfs.[8] The acceleration of the relaxation rate (or the disappearance of the magnetic hfs) in the present dispersion system can be explained by assuming an enhanced spin-spin interaction due to the increased radiolytic production of paramagnetic radicals in the vicinty of the decayed ^{57}Fe(III). Probably the radiolysis may occur in a dispersion medium as well as in a source compound, and it may be reasonable to conclude, from the results of the present experiment, that the radiation stability of a dispersion medium will contribute to change the rate of relaxation.

Although the relaxation rate is also enhanced by the spin-lattice interaction, this will make a minor contribution since the local heating due to the recoil energy of EC-decay should spread over the surrounding atoms by thermal diffusion in a much shorter time than the lifetime of the Mössbauer nuclear level.

References

1) H. Sano and M. Kanno, *Chem. Commun.*, **1969**, 601.
2) H. Sano, K. Sato, and H. Iwagami, *Bull. Chem. Soc. Jpn.*, **44**, 2570 (1971).
3) H. Sano and T. Ohnuma, *Chem. Lett.*, **1974**, 589; *Chem. Phys. Lett.*, **26**, 348 (1974); *Bull. Chem. Soc. Jpn.*, **48**, 266 (1975).
4) H. Sano, *J. Radioanal. Chem.*, **36**, 105 (1977).
5) H. Sano, M. Harada, and K. Endo, *Bull. Chem. Soc. Jpn.*, **51**, 2583 (1978).
6) K. Endo, M. Harada, Y. Sakai, and H. Sano, *J. Phys. (Paris), Colloq.* **40**, C2—420 (1979).
7) Y. Sakai, K. Endo, and H. Sano, *Bull. Chem. Soc. Jpn.*, **53**, 1317 (1980).
8) Y. Sakai, K. Endo, and H. Sano, *Int. J. Appl. Radiat. Isot.*, **32**, 435 (1981).

Some Aspects of the Solvent Extraction-spectrophotometric Determination of Copper Dithiocarbamate Complex in Strongly Acidic Media

Takeo TAKADA,* Yukio OKABE,** and Kunio NAKANO
Department of Chemistry, College of Science, Rikkyo (St. Paul's) University, Nishi-Ikebukuro, Toshima-ku, Tokyo 171
(Received December 1, 1980)

Synopsis. The time stability of the extracted complexes in isobutyl methyl ketone depends on the pH of the washing solution of the extract and on the stability of the metal complex. The extract is stable to concentrated acid when the organic extract is separated rapidly and washed with water. Copper(II) tetramethylenedithiocarbamate is quantitatively extracted from 1—6 and 1—2 mol dm^{-3} hydrochloric and nitric acid media respectively.

Sodium diethyldithiocarbamate(DDTC) and ammonium tetramethylenedithiocarbamate(Ammonium 1-pyrrolidinecarbodithioate, APCD) have been widely used as extraction and colorimetric reagents for many metal elements. There are a number of publications about the determination of copper(II) with those complexing agents.[1-8] The general principles are based on Sandell and others.[9-10] Many analytical procedures require precise adjustment of pH, usually in the range 2—4, and APCD is often preferred to DDTC when extractions are performed in acidic solution. However, some studies indicate that the pH-range for extraction with APCD is different for copper.[6-8] Moreover, these papers do not provide any information on the optimum range of strongly acidic concentration required for the extraction of copper(II). We have studied the time stability of copper(II)–DDTC and –PCD complexes in isobuthyl methyl ketone(IBMK) with the different acidities of the aqueous phase and the effect of pH of the washing solution on the extract, and we have applied this result to determine trace amounts of copper(II).

Experimental

Reagents. All solutions were prepared by dissolving analytical reagent grade chemicals in doubly distilled water. A 0.01 mol dm^{-3} copper(II) standard solution was prepared by dissolving recrystallized copper(II) sulfate pentahydrate in water, and diluted with water to give an adequate concentration before use. A 1% aqueous solution of DDTC and APCD were prepared. All other solvents were used without further purification.

Recommended General Procedure. The aqueous phase containing standard or sample should be acidified with hydrochloric or nitric acid; then adjust the acidity to the desired value. Add 10 cm^3 of the 1% DDTC or APCD solution, mix and allow to stand for 30 s. Extractions should be done in separatory funnels shaken for 7—10 min with 25 cm^3 of IBMK. After the aqueous phase is withdrawn, the organic phase should then be shaken with 50 cm^3 of water for about 5 min. After separating the two phases, the absorbance of the yellow copper complex in the IBMK phase can be measured at 435 nm against a reagent blank prepared in an identical manner.

** Present address: Denki Kagaku Keiki Co., Ltd. Kichijoji-kita, Musashino 180.

Results and Discussion

Effect of Washing Solution on the Stability of the Extracts. The extraction of metal complex into the organic phase depends upon the hydrogen-ion concentration of the aqueous phase. If the pH is less than some critical value, the amount of the metal ion extracted decreases steeply. Therefore, when the IBMK phase is not separated from the aqueous phase, the decomposition of the metal complex will be faster and will depend on the treatment of the extracts.

Figure 1 show that the time stability of the copper–PCD and –DDTC complexes in IBMK depends on the treatment of the extracts. In this experiment, the aqueous phase was adjusted to acidity 4 mol dm^{-3} with hydrochloric acid. It is seen that the absorbances of both extracts remain almost constant for at least 2 h after washing with water, whereas the use of 4 mol dm^{-3} hydrochloric acid as washing solution causes the very rapid change of the absorbance with time. It was thought that the copper–PCD and –DDTC complexes might be made stable in the IBMK if, after the extraction, the organic phase was washed with neutral water to prevent decomposition of extract by hydrogen ion attack.

Extraction Behavior in Hydrochloric Acid. The extractions of copper(II) with APCD and DDTC in

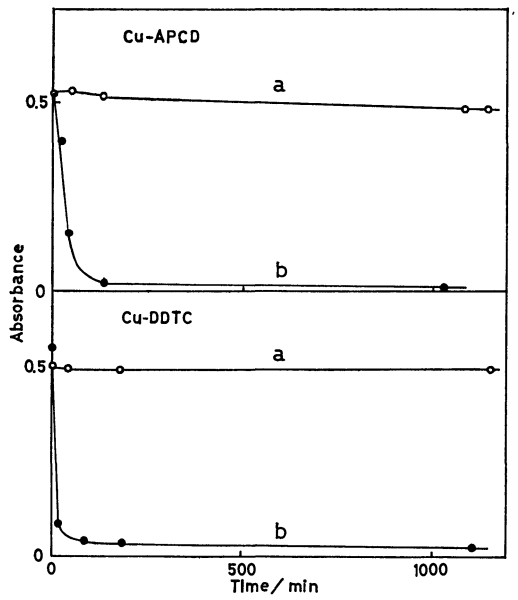

Fig. 1. Effect of acidity of washing solution on the absorbance of Cu–APCD and –DDTC complexes in IBMK.
a: Wash with 50 cm^3 of water, b: wash with 50 cm^3 of 4 M HCl, IBMK: 25 cm^3, Cu: 4×10^{-4} M.

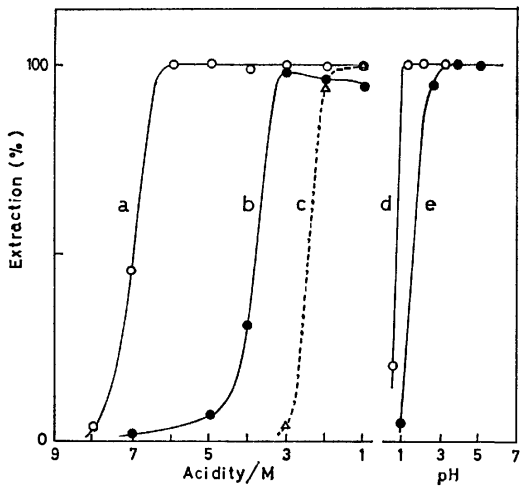

Fig. 2. Effect of acidity on the extraction of Cu(II) with APCD and DDTC in IBMK.
a: Cu–APCD–HCl system, b: Cu–DDTC–HCl system, c: Cu–APCD–HNO_3 system, d: Cu–APCD–HCl system, e: Cu–DDTC–HCl system. In the a, b, and c system, IBMK phase was washed with 50 cm^3 water, but in the d and e system, IBMK phase was not washed.
IBMK: 25 cm^3, Cu; 8×10^{-4} M.

IBMK were studied over the acidity range 1—8 mol dm^{-3}. The effects of acidity and the degree of extraction are shown in Fig. 2. With DDTC, the extraction is quantitative at acidity 1—3 mol dm^{-3}, but is incomplete at higher acid concentration. With APCD, copper(II) is completely extracted over the acidity range 1—6 mol dm^{-3}, but extraction is incomplete outside this acidity range. The decomposition of copper–PCD complex will be faster in the acidity range more than 6 mol dm^{-3} and will depend on the increase in the acidity of the aqueous phase.

Extraction Behavior in Nitric Acid. With APCD, copper(II) is extracted into IBMK at acidity less than 3 mol dm^{-3}, but the extraction of copper–DDTC complex is incomplete for acidity values. The oxidation decomposition of the dithiocarbamate complex with nitric acid is considered to occur in both the aqueous and organic phases. However, although the extraction range in nitric acid is very narrow compared to that in hydrochloric acid, it is noticeable that the stability of the copper–PCD complex in the organic phase is rather higher than that of the copper–DDTC complex.

Interferences. Synthetic mixtures were prepared with cations commonly found with copper in cadmium metal. No interference was observed in the determination of 5 μg of copper(II) with 1 mg of zinc(II), lead(II), iron(III), and thallium(II), and 10^6 times of cadmium(II).

Determination of Copper in Cadmium Metal. The method has been applied to the determination of a trace amount of copper in cadmium metals as follow: Dissolve 5 g of the sample into 100 cm^3 of 4 mol dm^{-3} nitric acid and rinse the beaker with 5 cm^3 of water. Transfer the solution to a 300 cm^3 separating funnel with 160 cm^3 of water. Add 10 cm^3 of 0.1% APCD solution. Shake the funnel for 8 min with 25 ml of IBMK. The two phases should be allowed to settle for 30 s; the aqueous phase was rapidly separated. The organic phase should then be shaken with 50 cm^3 of water for 5 min. The two phases thus separated. The yellow copper complex in the IBMK phase was measured photometrically at 435 nm against the reagent blank. Amounts of copper in various types of cadmium metals were determined and results were compared with those obtained by the atomic absorption method. The values were in good agreement. A study of the precision at 0.1 ppm level of copper showed the relative standard deviation of 1.3% for five replicates.

The procedure described in this paper is special additional step is unnecessary for stabilization of the extract; it is simple and permits the direct extraction of copper in various metals after decomposition of the metals with concentrated hydrochloric or nitric acid.

References

1) H. Bode, *Fresenius' Z. Anal. Chem.*, **144**, 165 (1965).
2) A. E. Martin, *Anal. Chem.*, **25**, 1260 (1953).
3) T. N. Tweeten and J. W. Knoeck, *Anal. Chem.*, **48**, 64 (1976).
4) E. Malissa, *Anal. Chim. Acta*, **27**, 402 (1962).
5) J. E. Allan, *Spectrochim. Acta*, **17**, 459 (1961).
6) E. Kovacs and H. Guyer, *Fresenius' Z. Anal. Chem.*, **186**, 267 (1962).
7) R. W. Looyenga and D. E. Boltz, *Talanta*, **19**, 82 (1972).
8) J. D. Kinrade and J. C. Van Loon, *Anal. Chem.*, **46**, 1894 (1974).
9) E. B. Sandell, "Colorimetric Determination of Traces of Metals," 3rd ed, Interscience, New York (1959), p. 444.
10) G. H. Morrison and H. Freiser, "Solvent Extraction in Analytical Chemistry," John Wiley & Sons, New York (1957), p. 181.

The Separation of Aluminium Trichloride and Iron Trichloride by Selective Hydrogen Reduction

Yuichi Shoji, Ryoko Matsuzaki, and Yuzo Saeki*

Research Laboratory of Resources Utilization, Tokyo Institute of Technology, 4259, Nagatsuta-cho, Midori-ku, Yokohama 227

(Received March 12, 1981)

Synopsis. When a gaseous mixture generated by heating a mixture of $AlCl_3$ and $FeCl_3$ (<19 wt%) was introduced, with a hydrogen stream, into a reaction zone held at various temperatures, the iron content in the sublimate decreased markedly above 300 °C; $AlCl_3$ containing less than 10 ppm of iron was obtained at 600 °C.

The production of aluminium *via* the electrolysis of aluminium trichloride($AlCl_3$) or the production of special-grade alumina from $AlCl_3$ requires pure $AlCl_3$. The $AlCl_3$ produced by the chlorination of aluminium-containing materials, however, contains impurities, such as iron, silicon, and titanium chlorides.

The separation of silicon tetrachloride or titanium tetrachloride from $AlCl_3$ presents no special problems because of the sufficient difference in relative volatility and the absence of vapor-phase complexes. The removal of iron trichloride($FeCl_3$) from $AlCl_3$ has been described as being considerably difficult despite the high volatility of pure $AlCl_3$ relative to the pure $FeCl_3$ phase,[1,2] because of the formation of a volatile complex, $AlFeCl_6$, on heating a mixture of $AlCl_3$ and $FeCl_3$.[1,3]

Considering the relative ease of the reduction of Fe(III) to Fe(II), the present authors examined the separation of $FeCl_3$ from $AlCl_3$ by means of selective hydrogen reduction.

Experimental

The $AlCl_3$ used was prepared by the reaction between aluminium (Al: 99.99%) and chlorine at 400 °C.[4] The $FeCl_3$ used was prepared by the reaction between iron (Fe: 99.98%) and chlorine at 500 °C.[5] The hydrogen used was purified up to a dew point below −70 °C by passing it through a membrane of palladium heated at 400 °C.

To examine the $FeCl_3$ content in the sublimate on heating a mixture of $AlCl_3$ and $FeCl_3$ in an argon stream, a mixture of $AlCl_3$ and $FeCl_3$ at a specified ratio in a quartz boat (width: 16 mm, length: 72 mm, depth: 9 mm) was placed in a straight, transparent quartz tube (inner diameter: 24 mm, length: 1000 mm) and heated at 150 °C for 1 h in the middle of a tubular electric furnace (heating length: 300 mm) in an argon stream at a flow-rate of 150 cm^3/min. The temperature of the sample part was controlled within ±2 °C.

For the experiments on the separation of $FeCl_3$ from $AlCl_3$ by means of selective hydrogen reduction, a gaseous mixture generated by heating a mixture of $AlCl_3$ and $FeCl_3$ at 150 °C was introduced, with a hydrogen stream at a flow-rate of 150 cm^3/min, into a reaction zone (inner diameter: 24 mm, length: 280 mm) held at a specified temperature for 1 h.

The total amount of aluminium and iron in the sublimate obtained outside the reaction zone was determined by chelatometric titration,[6] while the amount of iron was determined colorimetrically as 1, 10-phenanthroline complex[7] by using a Shimadzu double-beam spectrophotometer, Model UV-200S. The amount of aluminium was determined by subtracting the amount of iron from the above total amount of aluminium and iron. The chlorine content was determined gravimetrically as AgCl.

Throughout this work, chlorides of aluminium and iron were handled in an argon atmosphere to prevent any contamination by moisture in the air.

Results and Discussion

The $FeCl_3$ content in the sublimate obtained by heating 5.0 g of a mixture of $AlCl_3$ and $FeCl_3$ at a specified ratio in an argon stream was examined. Considering the vapor pressures of $AlCl_3$ and $FeCl_3$, the heating temperature was maintained at 150 °C ($P_{Al_2Cl_6}=11.53\times10^3$ Pa, $P_{Fe_2Cl_6}=1.4$ Pa).[8] The results are shown in Fig. 1.

Jorgensen and Moyle[9] have examined the equilibrium in the $AlCl_3$–$FeCl_3$–Cl_2 system and described that the vapor pressures of Al_2Cl_6, $AlFeCl_6$, and Fe_2Cl_6 at 160—180 °C are not changed by the initial $FeCl_3$ content in the range of 5—50 mol% (6—55 wt%). From the above description, we could well understood that the $FeCl_3$ content in the sublimate was constant on heating a mixture of $AlCl_3$ and $FeCl_3$ with an initial $FeCl_3$ content above 3 wt%. The results shown in Fig. 1 indicate that the clean separation of $FeCl_3$ from $AlCl_3$ is difficult by a repetition of the fractional sublimation.

Next, experiments for separating $FeCl_3$ from $AlCl_3$ by selective hydrogen reduction were carried out. The $FeCl_3$ content in the sublimate obtained by heating 5.0 g of a mixture of $AlCl_3$ and $FeCl_3$ at a specified ratio in a hydrogen stream at 150 °C was examined. The results obtained were the same as those obtained by the heating in an argon stream, shown in Fig. 1.

Then, the gaseous mixture generated by heating 5.0 g of a mixture of 95 wt% $AlCl_3$ and 5 wt% $FeCl_3$ at 150 °C (Fe content in the gaseous mixture: 1.4_6 wt% as $FeCl_3$ or 0.5_0 wt% as Fe) was introduced,

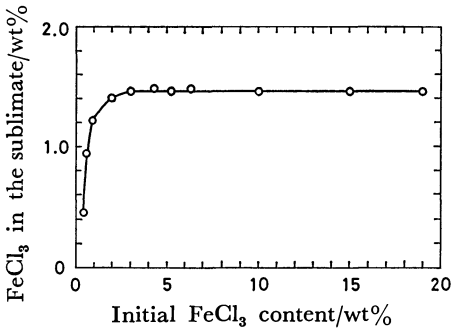

Fig. 1. $FeCl_3$ contents in the sublimates obtained by heating mixtures of $AlCl_3$ and $FeCl_3$ at various ratios in an argon stream.

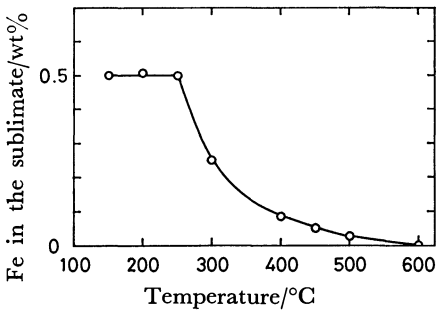

Fig. 2. Fe contents in the sublimates obtained by heating the gaseous mixture, generated by heating a mixture of $AlCl_3$ and $FeCl_3$, in a hydrogen stream at various temperatures.

with a hydrogen stream at a flow-rate of 150 cm^3/min, into a reaction zone held at various temperatures for 1 h. The iron content in the sublimate obtained outside the reaction zone was then examined. The results are shown in Fig. 2.

When the temperature of the reaction zone was below 250 °C, no change in the iron content was observed. Above 300 °C, the iron content decreased markedly, being reduced to 0.002 wt% at 600 °C. At 300—450 °C, it was observed that a colorless powder was deposited in the reaction zone. This colorless powder was identified as iron dichloride($FeCl_2$) by chemical analysis. Above 500 °C, the formation of iron in the form of thin film was observed in addition to $FeCl_2$.

The vapor pressure of $FeCl_2$ is negligible in the temperature range of this experiment.[8] However, it could also be considered that a part of the $FeCl_2$ formed was carried by the hydrogen stream and contaminated the sublimate. Therefore, the sublimate obtained above 400 °C was heated in an argon stream at 150 °C, and the iron content in the sublimate obtained outside the heating zone was examined. From the results, the iron contents were found to be 0.006 wt% at 400 °C, 0.004 wt% at 450 °C, 0.003 wt% at 500 °C, and <0.001 wt% at 600 °C.

From these experimental results, it is revealed that $AlCl_3$ containing less than 10 ppm of iron can be obtained by introducing a gaseous mixture, generated by heating a mixture of $AlCl_3$ and $FeCl_3$, with a hydrogen stream into a reaction zone held at 600 °C.

References

1) R. M. Fowler and S. S. Melford, *Inorg. Chem.*, **15**, 473 (1976).
2) B. D. Stepin, T. N. Naumova, I. G. Bykova, and T. A. Frolova, *Russ. J. Inorg. Chem.*, **18**, 1066 (1973).
3) K. N. Semenenko, T. N. Naumova, L. N. Gorokhov, and G. A. Semenova, *Dokl. Akad. Nauk SSSR*, **154**, 169 (1964).
4) Y. Shoji, K. Tatsumi, R. Matsuzaki, and Y. Saeki, *Bull. Chem. Soc. Jpn.*, **53**, 269 (1980).
5) Y. Saeki, R. Matsuzaki, and S. Fujiwara, *Bull. Chem. Soc. Jpn.*, **51**, 3527 (1978).
6) T. Dantsuka and K. Ueno, *Bunseki Kagaku*, **8**, 126 (1959).
7) F. D. Snell and C. T. Snell, "Colorimetric Methods of Analysis," 3rd ed, D. Van Nostrand (1957), Vol. 2, p. 316.
8) O. Kubaschewski, E. Ll. Evans, and C. B. Alcock, "Metallurgical Thermochemistry," 4th ed, Pergamon Press (1967).
9) F. R. A. Jorgensen and F. J. Moyle, *Proc. Australas Inst. Min. Metall.*, No. 269, 29 (1979).

The Preparation and Properties of Cobalt(III) Phosphine Complexes Containing Nitrite and Acetylacetonate Ions

Satoru HAYAKAWA, Hiroaki NISHIKAWA, Kazuo KASHIWABARA,** and Muraji SHIBATA*

Department of Chemistry, Faculty of Science, Kanazawa University, Kanazawa 920

(Received April 10, 1981)

Synopsis. Two complexes, $[Co(NO_2)(acac)_2(P)]$-(acac=acetylacetonate ion, P=PBu_3, PBu_2Ph, PMe_2Ph, and $PMePh_2$) and $[Co(NO_2)_2(acac)(PMe_2Ph)_2]$, were prepared by a reaction between $Na[Co(NO_2)_2(acac)_2]$ and phosphines. The geometrical structures were determined on the basis of the ^1H NMR, electronic, and IR spectra. A *cis*(NO_2, P) configuration was assigned to $[Co(NO_2)(acac)_2(P)]$, and a *trans*(P,P) configuration, to $[Co(NO_2)_2(acac)(P)_2]$.

There have been a few cobalt(III) phosphine complexes among the so-called Werner-type complexes.[1] The coordination of phosphine groups to a cobalt(III) ion may be affected by the kinds of other ligands coexisting in the complex. The unidentate phosphine complexes of cobalt(III) thus far prepared have been those with dimethylglyoximate,[2] acetylacetonate,[3] cyanide,[4,5] and halide[6] ions. Other types are, however, required to extend the study of the chemistry of cobalt-(III) phosphine complexes. This note will be concerned with the preparation and properties of cobalt-(III) phosphine complexes containing nitrite and acetylacetonate ions.

Experimental

The phosphines were prepared according to the procedures described previously,[7] and handled under a nitrogen atmosphere until they formed cobalt(III) complexes. The electronic spectra were measured with a Hitachi 139 spectrophotometer, the ^1H NMR spectra, with a JEOL C-60 H spectrometer in $CDCl_3$, using tetramethylsilane as the internal reference, and the IR spectra, with a JASCO DS-301 spectrometer.

Preparation. Nitrobis(acetylacetonato)tributylphosphinecobalt-(III): Tributylphosphine(PBu_3) (4 cm³, 12 mmol) was added to $Na[Co(NO_2)_2(acac)_2]$[8] (4 g, 10 mmol) in a mixture (200 cm³) of benzene and ethanol (4:1), after which the solution was stirred at 50 °C for 5 h. The resulting red-brown solution was evaporated under reduced pressure to dryness. The residue was extracted with a small amount of benzene, which was then chromatographed with a column (ϕ1.5×30 cm) of alumina, using a mixture of benzene and acetone (6:1) as the eluent. Red-brown crystals were obtained by concentrating the first main, red-brown eluate and by adding a proper amount of hexane. Found: C, 52.10; H, 8.54; N, 3.05%. Calcd for $[Co(NO_2)(acac)_2(PBu_3)]$: C, 52.31; H, 8.12; N, 2.77%. The materials remaining at the top of the column were not characterized.

Nitrobis(acetylacetonato)dibutylphenylphosphinecobalt(III): This complex was prepared by means of a reaction between $Na[Co(NO_2)_2(acac)_2]$ and dibutylphenylphosphine(PBu_2Ph) in a mixture of benzene and ethanol (4:1) by a method similar to that used for the PBu_3 complex. Found: C, 54.64; H, 7.15; N, 2.66%. Calcd for $[Co(NO_2)(acac)_2(PBu_2Ph)]$: C, 54.86; H, 7.10; N, 2.67%.

Nitrobis(acetylacetonato)dimethylphenylphosphinecobalt(III): A mixture of $Na[Co(NO_2)_2(acac)_2]$ (3 g, 9 mmol) and dimethylphenylphosphine(PMe_2Ph) (1 cm³, 9 mmol) in benzene (150 cm³) was stirred at room temperature for 48 h. The resulting solution was then subjected to procedures similar to those used for the PBu_3 complex except for the use of a mixture of benzene and acetone (15:1) as the eluent. Found: C, 48.37; H, 5.71; N, 2.96%. Calcd for $[Co(NO_2)(acac)_2(PMe_2Ph)]$: C, 48.99; H, 5.71; N, 3.17%.

Nitrobis(acetylacetonato)methyldiphenylphosphinecobalt(III): A mixture of $Na[Co(NO_2)_2(acac)_2]$ (3 g, 9 mmol) and methyldiphenylphosphine($PMePh_2$) (3 cm³, 15 mmol) in benzene (150 cm³) was stirred at room temperature for 48 h. The subsequent procedures were similar to those used for the PBu_3 complex. Found: C, 54.62; H, 5.57; N, 2.69%. Calcd for $[Co(NO_2)(acac)_2(PMePh_2)]$: C, 54.88; H, 5.41; N, 2.78%.

Dinitroacetylacetonatobis(dimethylphenylphosphine)cobalt(III): A mixture of $Na[Co(NO_2)_2(acac)_2]$ (3 g, 9 mmol) and PMe_2Ph (1.3 cm³, 12 mmol) in ethanol (100 cm³) was stirred at 50 °C for 2 h. The resulting red-brown solution was evaporated under reduced pressure to dryness. The residue was extracted with benzene, which was then chromatographed in a way similar to that used for the PBu_3 complex. The eluate was concentrated under reduced pressure to a small volume and then allowed to stand in a refrigerator to yield red-brown crystals. The presence of $[Co(NO_2)(acac)_2(PMe_2Ph)]$ in the solution was confirmed by the ^1H NMR spectrum. Found: C, 48.16; H, 5.64; N, 4.87%. Calcd for $[Co(NO_2)_2(acac)(PMe_2Ph)_2]$: C, 47.92; H, 5.55; N, 5.32%.

The yields for the above-mentioned complexes were 10—20%.

Results and Discussion

The facile substitution or solvolysis of a nitrite ion in $Na[Co(NO_2)_2(acac)_2]$ has been known and utilized for preparing other bis(acetylacetonato)cobalt(III) derivatives, such as $[Co(NO_2)(acac)_2L]$.[8,9] Tertiary monophosphines can also be expected to react with the dinitro complex in a similar manner. Trialkyl- or alkylarylphosphines react readily with the dinitro complex and yield complexes of the $[Co(NO_2)(acac)_2(P)]$ type, but triphenylphosphine does not yield the corresponding complex.

$[Co(NO_2)_2(acac)(PMe_2Ph)_2]$ was obtained from a reaction mixture of PMe_2Ph and $Na[Co(NO_2)_2(acac)_2]$ in ethanol, $[Co(NO_2)(acac)_2(PMe_2Ph)]$ also being involved in the solution. Free PMe_2Ph and the liberated NO_2^- might attack the $[Co(NO_2)(acac)_2(PMe_2Ph)]$ first formed, thus yielding $[Co(NO_2)_2(acac)(PMe_2Ph)_2]$.

A nitrite ion can coordinate to a metal ion through a nitrogen or oxygen atom. None of the complexes prepared in this study show the N–O stretching in the region of 1000—1100 cm⁻¹, indicating the coordination through the nitrogen atom.

There are two geometrical isomers for the [Co-

** Present address: Department of Chemistry, Faculty of Science, Nagoya University, Nagoya 464.

Table 1. Electronic (AB) and NMR spectral data

	AB $\tilde{\nu}/10^3$ cm^{-1}(log ε)	NMR, δ (J/Hz)[a]		
		-CH_3(acac)	-CH	P-CH_3
$[Co(NO_2)(acac)_2(PBu_2Ph)]$	19.8(2.54)	1.66 1.77 1.97 2.18	5.00 5.44	
$[Co(NO_2)(acac)_2(PBu_3)]$	20.6(2.50)	1.94[b] 2.02 2.25	5.40 5.52	
$[Co(NO_2)(acac)_2(PMePh_2)]$	19.2(2.56)	1.61 1.86 2.04 2.24	5.03 5.57	2.00(d, 13)
$[Co(NO_2)(acac)_2(PMe_2Ph)]$	19.7(2.50)	1.51 1.86 2.01 2.25	5.02 5.46	1.76(d, 13)
$[Co(NO_2)_2(acac)(PMe_2Ph)_2]$	20.8(3.34)	1.26	4.67	1.90(t, 8)
cis-$Na[Co(NO_2)_2(acac)_2]$[9]	19.2(2.25)	2.10 2.20	5.75	
trans-$Na[Co(NO_2)_2(acac)_2]$[8,9]	19.3(2.24)	2.18	5.79	

a) d; doublet, t; triplet, the J value refers to the interval of the two outer peaks. b) The peak intensity is twice that of the others because of accidental degeneracy.

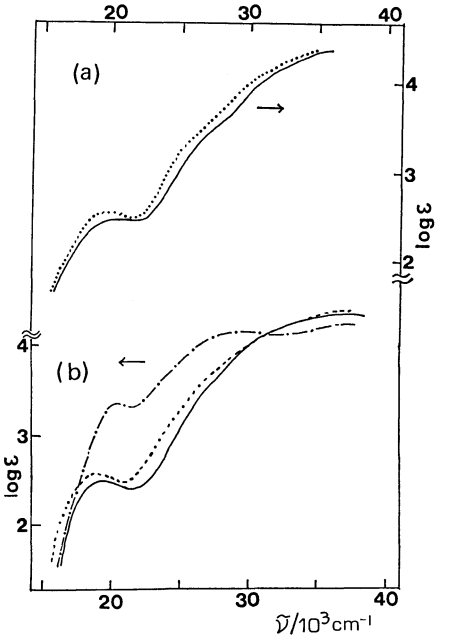

Fig. 1. Absorption spectra in dichloromethane. (a): $[Co(NO_2)(acac)_2(PBu_2Ph)]$ (----), $[Co(NO_2)(acac)_2(PBu_3)]$ (——), (b): $[Co(NO_2)(acac)_2(PMePh_2)]$ (——), $[Co(NO_2)(acac)_2(PMePh)]$ (----), $[Co(NO_2)_2(acac)(PMe_2Ph)_2]$ (—·—·—).

$(NO_2)(acac)_2(P)]$ complex. The ^{1}H NMR spectra can distinguish a *cis* or *trans* configuration. The spectral data are summarized in the table, together with those of the related compounds. All complexes of this type can be assigned to a *cis* configuration on the basis of the number of methyl and methine signals of the coordinated acetylacetonate. One of the methine peaks in each PBu_2Ph, PMe_2Ph, and $PMePh_2$ complex is shielded by a phenyl group on the phosphorus atom and is observed at high magnetic fields, 5.00—5.03 ppm.[10] The absorption spectra exhibit a broad first-absorption band around 20000 cm^{-1} (see Fig. 1). The replacement of the alkyl groups on a phosphorus atom by a phenyl group causes the red shift and increases the intensity of the first absorption band. The ligand-field strength of these phosphines is nearly identical with that of a nitro ligand, or slightly stronger.

There are three geometrical isomers for $[Co(NO_2)_2(acac)(PMe_2Ph)_2]$. The ^{1}H NMR spectrum shows one kind of methyl signal for the acetylacetonato ligand, indicating a *trans*(P,P) or *trans*(N,N) configuration. The remarkable high-field shift of the methine signal strongly suggests a *trans*(P,P) configuration where a phenyl group of the PMe_2Ph molecule is located over the acetylacetonate ring and shields the methine proton, causing it to resonate at a higher magnetic field.[10] The electronic and IR spectra also suggest a *trans*(P,P) configuration. The first absorption band shows a strong intensity (log ε=3.34), which is characteristic of the *trans*(P,P) arrangement of two phosphorus donor atoms.[11] The IR spectrum shows sharp peaks at 821 and 825 cm^{-1} attributable to the NO_2^- bending mode, the presence of two bands suggesting a *cis* configuration of two nitrite ions.[12]

References

1) "Transition Metal Complexes Containing Phosphorus, Arsenic and Antimony Ligands," ed by C. A. McAuliffe, Macmillan Press, London (1973); C. A. McAuliffe and W. Levason, "Phosphine, Arsine and Stibine Complexes of the Transition Elements," Elsevier, Amsterdam (1979).
2) G. N. Schrauzer and J. Kohnle, *Chem. Ber.*, **97**, 3056 (1964); W. C. Trogler and L. G. Marzilli, *Inorg. Chem.*, **14**, 2942 (1975); R. C. Stewart and L. G. Marzilli, *ibid.*, **16**, 424 (1977).
3) H. Nishikawa, K. Konya, and M. Shibata, *Bull. Chem. Soc. Jpn.*, **41**, 1492 (1968).
4) K. Watanabe, H. Nishikawa, and M. Shibata, *Bull. Chem. Soc. Jpn.*, **42**, 1150 (1969).
5) N. Maki and K. Ohshima, *Bull. Chem. Soc. Jpn.*, **43**, 3970 (1970).
6) K. A. Jensen, B. Nygaard, and C. Th. Pedersen, *Acta Chem. Scand.*, **17**, 1126 (1963); O. Stelzer, *Chem. Ber.*, **107**, 2329 (1974).
7) L. Maier, "Organic Phosphorus Compounds," ed by L. Maier and G. M. Kosolapott, Wiley, New York (1972), Vol. 1, p. 1.
8) L. J. Boucher and J. C. Bailar, Jr., *J. Inorg. Nucl. Chem.*, **27**, 1093 (1965).
9) B. P. Cotsoradis and R. D. Archer, *Inorg. Chem.*, **6**, 800 (1967).
10) K. Kashiwabara, I. Kinoshita, T. Ito, and J. Fujita, *Bull. Chem. Soc. Jpn.*, **54**, 725 (1981).
11) K. Kashiwabara, K. Katoh, J. Fujita, H. Nishikawa, and M. Shibata, *Chem. Lett.*, **1981**, 575.
12) B. M. Gatahouse, *J. Inorg. Nucl. Chem.*, **8**, 79 (1958); I. Nakagawa and T. Shimanouchi, *Spectrochim. Acta*, **23**, 2099 (1967).

Preparation and Circular Dichroism Spectrum of a (Triazacyclononane)-(tribenzo[*b,f,j*][1,5,9]triazacyclododecene)cobalt(III) Complex

Shuhei Fujinami,* Takao Hosokawa, and Muraji Shibata

Department of Chemistry, Faculty of Science, Kanazawa University, Kanazawa 920

(Received April 17, 1981)

Synopsis. A new $[Co(tacn)(tri)]^{3+}$ complex has been prepared and optically resolved (TACN represents 1,4,7-triazacyclononane, and TRI, tribenzo[*b,f,j*][1,5,9]triazacyclo dodecene). From the CD spectral similarity of $(+)^{CD}_{500}$-$[Co(tacn)(tri)]^{3+}$ with $(+)_{546}[Co(tri)_2]^{3+}$, it has been concluded that the metal-centered optical activity of the two tri complexes is derived from a chiral arrangement of (benzene ring)-C=N- moieties.

Cummings and Busch[1] have reported the formation of a macrocyclic terdentate ligand, tribenzo[*b,f,j*]-[1,5,9]triazacyclododecene (abb. as TRI), by the condensation of three molecules of *o*-aminobenzaldehyde in the presence of metal ions. There are two geometrical isomers in a bis(tri)cobalt(III) complex; one is chiral form and the other meso form. The former has been prepared and resolved by Cummings and Busch.[1] The absolute configuration of the $(+)_{546}[Co(tri)_2]^{3+}$ complex has been determined by Wing and Eiss[2] by means of X-ray analysis. The $(+)_{546}$ isomer exhibits a similar CD spectrum to that of the $(+)_{546}$-$[Co(en)_3]^{3+}$ complex in the first absorption band region; the arrangement of the donor atoms in the $(+)_{546}$-$[Co(tri)_2]^{3+}$ isomer also resembles that in the $(+)_{546}$-$[Co(en)_3]^{3+}$ complex to give a left-handed helix about the threefold symmetry axis. On these bases, Wing and Eiss regarded the bis(tri) complex as strong evidence for the metal-centered optical activity arising from the twisted crystal field. On the other hand, Mason and Seal[3] have explained the optical activity of the $[Co(en)_3]^{3+}$ complex in terms of a dynamic coupling model. Therefore, it is necessary to reinvestigate the source of the optical activity in the $[Co(tri)_2]^{3+}$ complex.

In this report, the preparation and optical resolution of a complex containing a symmetric cyclic-terdentate TACN ligand and a dissymmetric TRI ligand, $[Co(tacn)(tri)]^{3+}$, will be reported (TACN represents 1,4,7-triazacyclononane). The CD spectrum of the resolved complex will be compared with that of the $[Co(tri)_2]^{3+}$ complex in order to determine the sources of the metal-centered optical activity.

Experimental

Preparation and Optical Resolution of $[Co(tacn)(tri)]^{3+}$. The $[Co(NO_2)_3(tacn)]$ complex[4] (2.5 g, 7.7 mmol) was suspended in a mixture of ethanol (275 cm^3) and 64% $HClO_4$ (25 cm^3). The whole system was stirred at 60 °C for 3—4 h, whereupon the color of the solution turned from yellow to deep red-brown. After cooling of the resulting solution to room temperature and removal of some precipitated material by filtration, the filtrate was adjusted to pH 3 by a 2 mol/dm^3 ethanolic KOH solution, and then the precipitated $KClO_4$ was filtered off. To the filtrate was added freshly prepared *o*-aminobenzaldehyde[5] (5 g, 41 mmol), and the mixture was refluxed at 80 °C for 8—9 h. The resulting solution was cooled to room temperature, and the precipitated material was filtered and washed with small amounts of ethanol and acetone in turn. The product was dissolved in a large amount of water (*ca.* 2000 cm^3) which had been adjusted to pH 4 by diluted HCl (all adjustments of pH were carried out with diluted HCl, unless otherwise noted). The solution was charged on a column of SP-Sephadex C-25 (2.5×30 cm). The column was rinsed with water (pH 3), and then the adsorbed band was eluted with a 0.3 mol/dm^3 NaCl solution adjusted to pH 3. A yellow band of tervalent cation was collected in a fraction. The effluent was diluted with a large amount of water (*ca.* 2000 cm^3, pH 4), and then poured onto a column of SP-Sephadex C-25 (2×20 cm). The adsorbed band was eluted with a 0.3 mol/dm^3 $NaClO_4$ solution adjusted to pH 3 with diluted $HClO_4$, whereupon one species was eluted and the other remained. The former was identified to be the known $[Co(tacn)_2]^{3+}$ species.[6] The remaining band was then eluted with a 0.3 mol/dm^3 NaCl solution (pH 3). The effluent was concentrated by a rotary evaporator at *ca.* 35 °C, with simultaneous removal of the eluent. To the final filtrate was added small amounts of 64% $HClO_4$ and solid $NaClO_4$, and the whole was kept in a refrigerator for a few days. The yellow crystals which deposited were collected and washed with water (pH 3). The crystals were dried *in vacuo*. The yield was *ca.* 30 mg. Found: C, 40.75; H, 3.80; N, 10.56%. Calcd for $[Co(tacn)(tri)](ClO_4)_3$=$CoC_{27}H_{30}N_6O_{12}Cl_3$: C, 40.39; H, 3.75; N, 11.02%. The product is explosive on heating.

A partial optical resolution was attained by means of a column chromatography (SP-Sephadex C-25, 2 cm×110 cm) by use of a 0.3 mol/dm^3 $Na_2[Sb_2(d\text{-tart})_2]$ solution as eluent.[7] The earlier eluted species was $(+)^{CD}_{500}[Co(tacn)(tri)]^{3+}$ isomer.

Measurements. The absorption and CD spectra were measured with a Hitachi 323 spectrophotometer and a JASCO J-40CS automatic recording spectropolarimeter, respectively.

Results and Discussion

The absorption and CD spectra of the $(+)^{CD}_{500}[Co(tacn)(tri)]^{3+}$ complex are shown in Fig. 1, with those of the related $(+)_{546}[Co(tri)_2]^{3+}$ and $(+)_{546}[Ni(tri)(H_2O)_3]^{2+}$ complexes. The absorption spectrum of the $[Co(tacn)(tri)]^{3+}$ exhibits a shoulder at *ca.* 21000 cm^{-1} ($\log\varepsilon\simeq2.5$), which is assignable to the first absorption band. The band is observed at a frequency higher by 1000 cm^{-1} than the corresponding band for the $[Co(tri)_2]^{3+}$ complex, indicating that the ligand field strength of TRI is weaker than that of TACN. An absorption band observed at 34000 cm^{-1} is assigned intra-ligand transition.[2] Both $(+)^{CD}_{500}[Co(tacn)(tri)]^{3+}$ and $(+)_{546}[Co(tri)_2]^{3+}$ exhibit a positive CD peak at the lowest frequency in the d-d absorption band region, in contrast to $(+)_{546}[Ni(tri)(H_2O)_3]^{2+}$ which shows no apparent CD peak. In the region of 33000—37000 cm^{-1}, the three complexes exhibit one or two intense CD peaks with negative sign. These bands

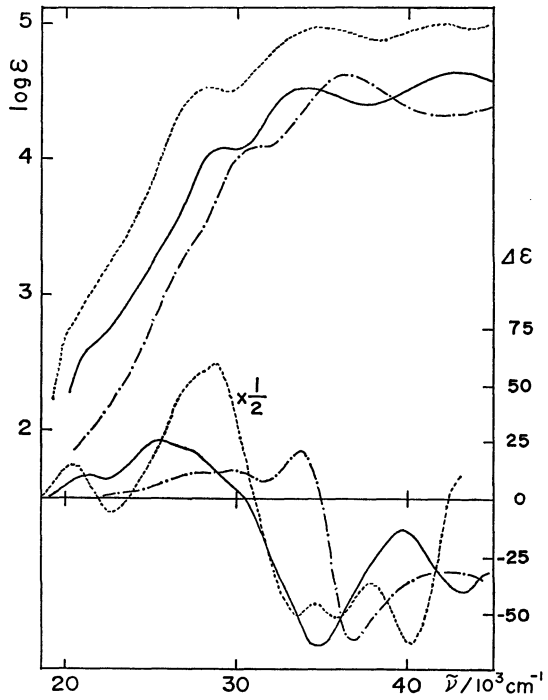

Fig. 1. Absorption and CD spectra.
——: $(+)^{CD}_{500}$[Co(tacn)(tri)]$^{3+}$, ----: $(+)_{546}$[Co(tri)$_2$]$^{3+}$,
—·—·—: $(+)_{546}$[Ni(tri)(H$_2$O)$_3$]$^{2+}$.

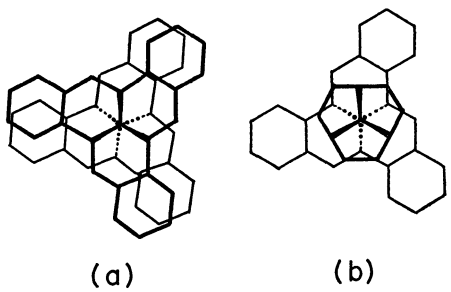

Fig. 2. Absolute configurations.
a): $(+)_{546}$[Co(tri)$_2$]$^{3+}$, b): $(+)^{CD}_{500}$[Co(tacn)(tri)]$^{3+}$.

are considered to be associated with a benzene ring inclining against a –C=N– bond, as is seen in a styrene chromophore.[8] Therefore, it is concluded that these complexes have the same absolute configuration with respect to the TRI ligand, namely, the pitch of the benzene rings has the sense of a left-handed screw.[2] The absolute configuration of $(+)^{CD}_{500}$[Co(tacn)(tri)]$^{3+}$ is predicted as shown in Fig. 2.

According to the X-ray analysis of $(+)_{546}$[Co(tri)$_2$]$^{3+}$,[2] there is a distortion around a threefold axis to give a twisted trigonal prism having the sense of a left-handed screw, due to a strong attractive interaction between two aromatic ligands. Wing and Eiss[2] have considered two sources of the metal-centered optical activity in the $(+)_{546}$[Co(tri)$_2$]$^{3+}$ complex; one is the arrangement of donor atoms distorted from octahedron, and another is structural features inherent in the TRI ligand such as a pitch of the benzene rings or a chiral arrangement of (benzene ring)–C=N– moieties. On the basis of the CD spectrum of $(+)_{546}$[Ni(tri)(H$_2$O)$_3$]$^{2+}$, they have concluded that one TRI ligand is ineffective in generating dissymmetric environment around a metal ion and that the former source is the principal one in $(+)_{546}$[Co(tri)$_2$]$^{3+}$.

On the other hand, the present [Co(tacn)(tri)]$^{3+}$ complex exhibits a clear CD peak in the d-d absorption band region, like $(+)_{546}$[Co(tri)$_2$]$^{3+}$ does. Furthermore, the distortion around the threefold symmetry axis seems to be small in $(+)^{CD}_{500}$[Co(tacn)(tri)]$^{3+}$, on account of a weak interaction between the TACN and TRI ligands, which is considered to be repulsive rather than attractive. Consequently, the crystal field distortion is not regarded as the principal source for the metal-centered optical activity in the $(+)^{CD}_{500}$[Co(tacn)(tri)]$^{3+}$ and $(+)_{546}$[Co(tri)$_2$]$^{3+}$ complexes. It is known[7] that the TACN chelate rings in [Co(tacn)$_2$]$^{3+}$ and [Co(gly)(NH$_3$)(tacn)]$^{2+}$ are flexible and the conformations are not fixed in an aqueous solution. Stereo models suggest that there is no preferential conformation of TACN in the [Co(tacn)(tri)]$^{3+}$ complex. Therefore, the optical activity due to conformations of TACN is considered to be small. It is reasonable to consider that the TRI complexes gain some activity from the chiral sequence of the (benzene ring)–C=N– moieties through the dynamic coupling mechanism.[3] A helical arrangement of the six benzene rings in $(+)_{546}$[Co(tri)$_2$]$^{3+}$ (in a sense of a left-handed helix, Λ) is also ineffective in raising the apparent metal-centered optical activity.

References

1) S. C. Cummings and D. H. Busch, *J. Am. Chem. Soc.*, **92**, 1924 (1970).
2) R. M. Wing and R. Eiss, *J. Am. Chem. Soc.*, **92**, 1929 (1970).
3) S. F. Mason and R. H. Seal, *Mol. Phys.*, **31**, 755 (1976).
4) M. S. Okamoto and E. K. Barefield, *Inorg. Chim. Acta*, **17**, 91 (1976).
5) L. I. Smith and J. W. Opie, *Org. Synth.*, **28**, 11 (1948).
6) H. Koyama and T. Yoshino, *Bull. Chem. Soc. Jpn.*, **45**, 481 (1972).
7) S. Shimba, S. Fujinami, and M. Shibata, *Bull. Chem. Soc. Jpn.*, **53**, 2523 (1980).
8) P. Crabbe, *Chem. Ind. (London)*, **1969**, 917.

Metal Complexes of Amino Acids. XIV.[1] Carbon-13 NMR of Cobalt(III) Complexes Containing *N*-Substituted Glycines

Tomoharu AMA,* Hiroshi KAWAGUCHI, and Takaji YASUI

Department of Chemistry, Faculty of Science, Kochi University, Akebono-cho, Kochi 780

(Received May 14, 1981)

Synopsis. The down-field shifts of α-carbons in *N*-alkylglycines, which were caused by the chelation to cobalt(III), were larger than those in *C*-alkylglycines. The down-field shifts of *N*-(carboxymethyl)glycine (ida) and *N*-(2-aminoethyl)glycine (enma) in fac complexes were also larger than those of ida and enma in mer complexes, respectively, and those of the *C*-alkylglycines.

In the previous paper,[2] we reported that the chelation of α-amino acids to cobalt(III) ion brigns about down-field changes in ^{13}C NMR chemical shifts of their carboxyl-carbons (C_{oxy}) and α-carbons (C_α). However, references were not made concerning the difference in ^{13}C NMR behavior between α-amino acids containing $-NH_2$ group and those containing –NH–R group. In the present paper, we will describe the difference in the NMR behavor. In addition, we will discuss about the relationship between the coordination forms of the tridentate ligand and the ^{13}C NMR chemical shifts, in connection with the chelation shifts of the α-amino acids containing the –NH–R group.

Experimental

The complexes examined were prepared by the procedures similar to those described in previous papers.[2-7]

^{13}C NMR spectra at 22.5 MHz were recorded on a JEOL FX-90Q spectrometer, in pulsed Fourier transform/proton noise decoupled mode. The field frequency ratio was stabilized by locking to internal D_2O. Peak positions were measured relative to internal dioxane (δ=67.40).

TABLE 1. ^{13}C CHEMICAL SHIFTS (ppm) OF SUBSTITUTED GLYCINES AND THEIR COBALT(III) COMPLEXES

Ligand (Structure and abbreviation (Acidic form))		δ (C_{oxy})[a]	δ_{ch} (C_{oxy})[b]	Δ_{ch} (C_{oxy})[c]	δ (C_α)[a]	δ_{ch} (C_α)[b]	Δ_{ch} (C_α)[c]
Glycine $NH_3^+CH_2COOH$, H_2gly)	$[Co(gly)(NH_3)_4]^{2+}$	170.14	186.15	+16.01	40.95	46.65	+5.07
L-Alanine ($NH_3^+CH(CH_3)COOH$, L-H_2ala)	$[Co(L\text{-}ala)(NH_3)_4]^{2+}$	173.02	186.97	+13.95	49.59	54.03	+4.44
α-Aminobutyric acid ($NH_3^+CH(C_2H_5)COOH$, α-H_2abu)	$[Co(\alpha\text{-}abu)(NH_3)_4]^{2+}$	172.38	186.44	+14.06	54.86	59.93	+5.07
Norvaline ($NH_3^+CH(C_3H_7)COOH$, H_2nva)	$[Co(nva)(NH_3)_4]^{2+}$	172.82	186.73	+13.91	53.44	58.13	+4.69
Sarcosine ($(CH_3)NH_2^+CH_2COOH$, H_2sar)	$[Co(sar)(NH_3)_4]^{2+}$	169.40	183.85	+14.45	49.59	57.88	+8.29
N-Ethylglycine ($(C_2H_5)NH_2^+CH_2COOH$, H_2etgly)	$[Co(etgly)(NH_3)_4]^{2+}$	169.60	184.43	+14.83	47.59	54.22	+6.63
N-Propylglycine ($(C_3H_7)NH_2^+CH_2COOH$, H_2prgly)	$[Co(prgly)(NH_3)_4]^{2+}$	169.31	184.39	+15.08	47.98	54.66	+6.68
L-Proline ($NH_2^+(CH_2)_3CHCOOH$, L-H_2pro)	$[Co(L\text{-}pro)(NH_3)_4]^{2+}$	172.24	186.97	+14.73	60.28	65.69	+5.42
L-Hydroxyproline ($NH_2^+CH_2CH(OH)CH_2CHCOOH$, L-$H_2hyp$)	$[Co(L\text{-}hyp)(NH_3)_4]^{2+}$	172.04	186.58	+14.54	58.96	64.47	+5.51
Iminodiacetic acid ($NH_2^+(CH_2COOH)_2$, H_3ida)	$[Co(ida)(NH_3)_3]^+$	169.16	184.68	+15.52	47.88	59.30	+11.42
	u-fac-$[Co(ida)_2]^-$		184.93	+15.77		59.59	+11.71
			184.19	+15.03		57.98	+10.10
	s-fac-$[Co(ida)_2]^-$		185.66	+16.50		58.32	+10.44
	mer-$[Co(ida)_2]^-$		184.53	+15.37		57.05	+9.17
			184.34	+15.18		56.91	+9.03
	$[Co(glygly)(ida)]^-$		184.19	+15.03		56.32	+8.44
Ethylenediamine-*N*-acetic acid ($NH_2^+(CH_2)_2NH_2^+CH_2COOH$, H_3enma)	$[Co(enma)(NH_3)_3]^{2+}$	169.11	185.17	+16.06	48.56	56.52	+7.96
	trans(O)-$[Co(enma)_2]^+$		185.32	+16.21		55.44	+6.88
	$[Co(glygly)(enma)]$		184.68	+15.57		53.83	+5.27

a) $\delta(C_\alpha)$ and $\alpha(C_{oxy})$: Chemical shifts of C_α and C_{oxy} in the free ligand (in acidic D_2O solution). b) $\delta_{ch}(C_\alpha)$ and $\delta_{ch}(C_{oxy})$: Chemical shifts of C_α and C_{oxy} in the chelated ligand. c) $\Delta_{ch}(C_\alpha)$ and $\Delta_{ch}(C_{oxy})$: $\Delta_{ch}(C_\alpha)=\delta_{ch}(C_\alpha)-\delta(C_\alpha)$ and $\Delta_{ch}(C_{oxy})=\delta_{ch}(C_{oxy})-\delta(C_{oxy})$.

Results and Discussion

The chemical shift changes arising from the chelation of amino acids are listed in Table 1, together with the structures and abbreviations of the ligands. The $\Delta_{ch}(C_\alpha)$ and $\Delta_{ch}(C_{oxy})$ values of *C*-alkylglycines ($NH_2CHRCOOH$) are smaller than those of glycine. This result is consistent with those described in the previous papers.[2,3] That is, the $\Delta_{ch}(C_\alpha)$ values of L-val, L-leu, L-ile, L-ser, L-thr, and L-phe were included in the range +3.8—+5.4 ppm, compared with +5.7 ppm of glycine.

On the other hand, the $\Delta_{ch}(C_\alpha)$ values of *N*-alkylglycines ($R-NHCH_2COOH$) are larger than that of glycine, though the $\Delta_{ch}(C_{oxy})$ values of the *N*-alkylglycines are smaller than that of glycine. The $\Delta_{ch}(C_\alpha)$ values of L-pro and L-hyp, which may belong to *N*-alkyl-*C*-alkylglycines, are intermediate between the $\Delta_{ch}(C_\alpha)$ value of the *N*-alkylglycine and that of the *C*-alkylglycine.

N-(Carboxymethyl)glycine (=iminodiacetic acid; ida) and *N*-(2-aminoethyl)glycine (=ethylenediamine-*N*-acetic acid; enma) containing –NH–R groups are able to coordinate to cobalt(III) in both of meridional (*mer*) and facial (*fac*) forms. It is known that the tridentate ida prefers the fac form to the mer form in both $[Co(ida)(NH_3)_3]^+$ and $[Co(ida)_2]^-$ complexes,[4–7] although recently the *mer*-$[Co(ida)_2]^-$ complex was isolated.[9,10] The $\Delta_{ch}(C_\alpha)$ values of the ida taking the fac form are larger than that of glycine. Similarly, the $\Delta_{ch}(C_\alpha)$ values of the enma, taking the fac form in $[Co(enma)(NH_3)_3]^{2+}$ and *trans*(*O*)-$[Co(enma)_2]^+$,[8] are larger than that of glycine. One of the important factors which are responsible for the large $\Delta_{ch}(C_\alpha)$ values will be the –NH–R groups of ida and enma, as is suggested by the present result that the $\Delta_{ch}(C_\alpha)$ values of *N*-alkylglycines are larger than that of glycine.

The chemical shifts of cobalt(III) complexes are affected by the anisotropic effect of cobalt(III) and by the trans influence of the coordinating atoms.[12–15] These effects in *mer*-$[Co(ida)_2]^-$ are equal to those in *s-fac*-$[Co(ida)_2]^-$. However, the $\Delta_{ch}(C_\alpha)$ value of *mer*-$[Co(ida)_2]^-$ is smaller than that of *s-fac*-$[Co(ida)_2]^-$. This difference may result from the difference of the geometrical structures of the ida. Similar result was obtained for the complexes containing diethylene-triamine (dien) by Ha *et al.*[16] They pointed out that the ^{13}C NMR spectral pattern of the *mer* forms of dien is distinguishable from the *fac* forms of dien. The carbons attaching to the central –NH– in the *mer* dien were resonated at lower field than those in the *fac* dien, that is, the Δ_{ch} values of the *mer* dien are smaller than those of the *fac* dien. The $\Delta_{ch}(C_\alpha)$ value of $[Co(glygly)(ida)]^-$, which includes a *mer* ida,[11] is also smaller than the $\Delta_{ch}(C_\alpha)$ values of the complexes including the *fac* ida. Similar result was obtained for the enma complexes. That is, the $\Delta_{ch}(C_\alpha)$ value of enma in *mer*-$[Co(glygly)(enma)]$,[11] is smaller than those of the *fac* enma in the other enma complexes (Table 1).

The differences of the $\Delta_{ch}(C_{oxy})$ values among the ligands examined were not so distinct as those of the $\Delta_{ch}(C_\alpha)$ values.

This work was partially supported by a Grant-in-Aid for Scientific Research No. 554189 from the Ministry of Education, Science and Culture.

References

1) Part XIII of this series: T. Ama, H. Kawaguchi, and T. Yasui, *Bull. Chem. Soc. Jpn.*, **54**, 448 (1981).
2) T. Ama and T. Yasui, *Bull. Chem. Soc. Jpn.*, **49**, 472 (1976).
3) Taken from the Ph. D. Thesis of T. Ama, Osaka University (1980).
4) J. Hidaka, Y. Shimura, and R. Tsuchida, *Bull. Chem. Soc. Jpn.*, **35**, 567 (1962).
5) A. Uehara, E. Kyuno, and R. Tsuchiya, *Bull. Chem. Soc. Jpn.*, **43**, 1394 (1970).
6) D. W. Cooke, *Inorg. Chem.*, **5**, 1141 (1966).
7) K. Okamoto, J. Hidaka, and Y. Shimura, *Bull. Chem. Soc. Jpn.*, **44**, 1601 (1971).
8) Y. Fujii, E. Kyuno, and R. Tsuchiya, *Bull. Chem. Soc. Jpn.*, **43**, 786 (1970).
9) N. Koine, T. Tanigaki, J. Hidaka, and Y. Shimura, presented at the 28th Symposium on the Coordination Chemistry, Matsuyama, Japan, October 1978, Abstract p. 309.
10) T. Ama, H. Kawaguchi, and T. Yasui, *Chem. Lett.*, **1981**, 323.
11) H. Kawaguchi, K. Maeda, T. Ama, and T. Yasui, *Chem. Lett.*, **1979**, 1105.
12) R. C. Stewart and L. G. Marzilli, *Inorg. Chem.*, **16**, 424 (1977).
13) N. Juranic, M. B. Celap, D. Vucelic, M. J. Malinar, and P. N. Radivojsa, *Inorg. Chim. Acta*, **25**, 229 (1977).
14) N. Juranic, M. B. Celap, D. Vucelic, M. B. Malinar, and P. N. Radivojsa, *Inorg. Chem.*, **19**, 802 (1980).
15) H. Yoneda, U. Sakaguchi, and Y. Nakashima, *Bull. Chem. Soc. Jpn.*, **48**, 209 (1975).
16) F. C. Ha, D. A. House, and J. W. Blunt, *Inorg. Chim. Acta*, **33**, 269 (1979).

The Reductive Coupling of Organic Halide Using Hydrazine and a Palladium Catalyst. II.[1] Homocoupling of 1-Iodoalkanes

Riichiro NAKAJIMA,* Kazuhiro MORITA, and Tadashi HARA
Department of Chemical Engineering, Faculty of Engineering, Doshisha University, Karasuma, Imadegawa Kamikyo-ku, Kyoto 602
(Received February 5, 1981)

Synopsis. The hydrogenolysis and dimerization of iodoalkanes were catalyzed by Pd in the presence of an appropriate reducing agent. Hydrazine was found to be effective for the coupling of 1-iodoeicosane to give tetracontane, $C_{40}H_{82}$, in a 74% yield. The yield of the coupling product decreased with the decrease of the number of the carbon atoms in the 1-iodoalkanes. Both alkylhydrazines and alkenes were shown not to take part in the reaction as a reaction intermediate.

We reported[1,2] that iodoarenes were converted to the corresponding biaryls in high yields by the use of a catalytic amount of palladium amalgam. No report has been published on the coupling of haloalkanes by the use of a catalytic amount of metal. Stille and Lau[3] reported that the reactive haloalkanes such as 9-bromofluorene were coupled with a stoichiometric amount of a palladium(0) complex. The present study has, therefore, been carried out in order to examine the homocoupling of the inert haloalkanes by the use of a catalytic amount of palladium metal or its salts. The higher iodoalkanes gave the corresponding bialkyls in high yield.

Results and Discussion

As shown in Table 1, 1-iodoalkanes reacted with hydrazine in the presence of catalytic amounts of palladium salt to produce coupling products. The highest yield was obtained in the case of 1-iodoeicosane. Palladium chloride was reduced in the initial stage of the reaction to give the metal, and the palladium metal formed was quantitatively recovered after the reaction. The coupling of iodoalkanes was examined with a catalytic amount of palladium metal in place of its salt to give the corresponding dimers in low yield (Eqs. 1 and 2).

$$2RI + Pd \longrightarrow RR + PdI_2 \quad (1)$$

$$PdI_2 + NH_2NH_2 \longrightarrow Pd + 2HI + N_2 + H_2 \quad (2)$$

To determine the products and the effect of hydrazine on the present reaction, the reaction involving 1-iodotetradecane(**1**) was examined, as shown in Table 2. The reaction products consisted of 1-methoxytetradecane(**2**), 1-tetradecene(**3**), tetradecane(**4**), and octacosane(**5**). The distribution of these products was strongly affected by the presence or absence of palladium and/or hydrazine. The highest yield of the dimer was obtained in the reaction with 85% hydrazine hydrate. In the absence of the catalyst, the methanolysis of iodoalkane occurred, and the hydrogenolysis and dimerization did not. No hydrazine was necessary for the coupling of iodoalkanes, in contrast with that of iodoarenes.[1]

The facts that an alkylhydrazine($RNHNH_2$) was prepared with anhydrous hydrazine and haloalkane[4] and that its decomposition produced the corresponding alkanes (RH and RR)[5] indicate that the reaction *via* alkylhydrazine derivative might be involved in the present system. Several results which exclude this are as follows: (1) The yield of **5** with tetradecylhydrazine (Run 4) was lower than that with hydrazine hydrate (Run 2)[6] and (2) No reaction of hydrazine hydrate with **1** occurred.

Since the reaction with methylhydrazine (Run 3) gave **3** in 46.4% yield, the dimerization of **3** was examined. Its intermediate may be denied from the following results: (1) No octacosene was detected (Run 2), and (2) No reductive coupling of **3** occurred under the experimental conditions in Run 2 except **1**, because **3** was quantitatively recovered.

It is consequently concluded that the coupling of

Table 1. Reductive homocoupling of 1-iodoalkanes using hydrazine and palladium catalyst[a]

Iodoalkane	Coupling product	Yield/%[b]
1-Iodohexane	Dodecane	0.7
1-Iodooctane	Hexadecane	5.4
1-Iododecane	Eicosane	7.9
1-Iodododecane	Tetracosane	14.8
1-Iodotetradecane	Octacosane	33.9
1-Iodotetradecane	Octacosane	44.5[c]
1-Iodohexadecane	Dotriacontane	40.3[d]
1-Iodooctadecane	Hexatriacontane	47.2[d]
1-Iodoeicosane	Tetracontane	55.3[d]
1-Iodoeicosane	Tetracontane	74.2[c,d]

a) A reaction mixture of iodoalkane(25.0 mmol), NaOH (125 mmol), and $PdCl_2$(2.5 mmol) in 16 ml of MeOH containing of 85% $NH_2NH_2 \cdot H_2O$(15 mmol) was refluxed for 6 h. b) Yield determined by GLPC. c) The 1.5-fold amounts of NaOH and 85% $NH_2NH_2 \cdot H_2O$ were used. d) Yield of the crude product.

Table 2. Effect of reducing agent on the reductive homocoupling of 1-iodotetradecane by the use of palladium chloride as catalyst[a]

Run	Reducing agent	Products/%[b]			
		2	**3**	**4**	**5**
1	None	11.0	15.1	59.8	13.3
2	85% $NH_2NH_2 \cdot H_2O$	12.2	19.5	36.4	33.9
3	CH_3NHNH_2	0.0	46.4	48.9	3.3
4	n-$C_{14}H_{29}NHNH_2$	5.1	44.1	99.5	8.0
5	$C_6H_5NHNH_2$	36.3	13.4	50.8	Trace

a) A mixture of **1**(25.0 mmol), $PdCl_2$(2.5 mmol), and NaOH(125 mmol) in 16 ml of MeOH containing the reducing agent(15 mmol) was refluxed for 6 h with stirring. b) Based on the iodoalkane.

1-iodoalkanes with hydrazine may not proceed through the hydrazine derivative and the alkene. Presumably, the hydrogenolysis and dimerization of 1-iodoalkanes proceed *via* an alkylpalladium complex, and the hydrazine used is consumed for reducing the palladium iodide formed.

Experimental

Materials. The reagents used were of commercial grade except of 1-iodooctane,[7] 1-iododecane,[7] 1-iodododecane,[7] 1-iodotetradecane(**1**),[7] 1-iodohexadecane,[7] 1-iodooctadecane[7] (mp 34.2—35.0 °C, lit,[8] 33.7—34.1 °C), 1-iodoeicosane[7] (mp 39.5—40.0 °C, lit,[8] 41.3—41.6 °C). Anhydrous hydrazine[9] was prepared by the methods given in the literature. The purity of all iodoalkanes determined by GLPC was over 98%.

Preparation of Tetradecylhydrazine(a New Compound): A mixture of anhydrous hydrazine (13 g, 0.38 mol), 1-bromotetradecane (21 g, 0.072 mol), and ethanol (15 ml) was refluxed with a magnetic stirrer for 35 h in a flask equipped a reflux condenser with a drying tube. The mixture was cooled until room temperature and then poured into water (50 ml) of 7 g of sodium hydroxide. The solid products and the ether-extractable materials were combined, and distilled under reduced pressure in a nitrogen atmosphere, giving 8.65 g (52%) of the hydrazine: bp 185—188 °C/1.5 kPa; white crystals, mp 40.5—42.0 °C. This melting point agreed closely with the value interpolated from the results of Westphal[4] for dodecylhydrazine (31 °C) and hexadecylhydrazine (57—58 °C). This new hydrazine was identified with maleic acid derivative. The *cis*-2-butenedioic dihydrazide showed: mp 116.5—117.3 °C; Found: C, 69.87; H, 10.60; N, 9.11%. Calcd for $C_{18}H_{32}N_2O_2$: C, 70.09; H, 10.46; N, 9.08%. Since the free hydrazine slowly decomposed in air, it was prepared before every use.

Reductive Coupling of 1-Iodoalkane Using Hydrazine and Palladium Catalyst. A mixture of 1-iodoalkane (25.0 mmol), NaOH (125 or 188 mmol), and $PdCl_2$ (2.5 mmol) in 16 ml of MeOH containing 85% $NH_2NH_2 \cdot H_2O$ (15 or 22.5 mmol) was refluxed for 6 h with stirring. The resulting mixture was filtered, and the residual metal was washed with hexane, and subsequently water. The organic layer was separated from the aqueous layer and evaporated. The yield of dimer was determined by GLPC. The dimers having more than twenty-eight carbon atoms were separated as a residue in the vacuum distillation using the Büchi Kugelrohrofen GRK-50, weighed, and recrystallized from hexane–methanol. Dotriacontane: mp 66.7—67.5 °C (lit,[10] 69.5—70.6 °C); Found: C, 85.38; H, 14.81%. Calcd for $C_{32}H_{66}$: C, 85.24; H, 14.76%. Hexatriacontane: mp 72.5—73.3 °C (lit,[10] 75.2—76.1 °C); Found: C, 85.20; H, 14.91%. Calcd. for $C_{36}H_{74}$: C, 85.29; H, 14.71%. Tetracontane: mp 78.8—79.5 °C (lit,[8] 81.2—81.4 °C); Found: C, 85.20; H, 14.82%. Calcd. for $C_{40}H_{82}$: C, 85.32; H, 14.68%.

Reductive Coupling of 1-Iodotetradecane with Various Reducing Agents. A mixture of **1** (25.0 mmol), $PdCl_2$ (2.5 mmol), and NaOH (125 mmol) in 16 ml of MeOH containing the reducing agent (15 mmol) was stirred for 6 h under reflux. The resulting mixture was filtered, and the residual metal was washed with hexane and then with water. After the organic layer was separated from the aqueous layer, the reaction products were obtained by the evaporation of the solvent, and analyzed by GLPC and GC-MS. Since both **3** and **4** gave an overlapped peak on the column used (SE-30), the peak of **3** was separated from that of **4** by brominating **4** with a bromine–tetrachloromethane solution, followed by the estimation of **4**. Octadecane and eicosane were used as the internal standards.

The present work was partially supported by a Science and Engineering Research Grant-in-Aid from the Science and Engineering Research Institute of Doshisha University.

References

1) Part I: R. Nakajima, Y. Shintani, and T. Hara, *Nippon Kagaku Kaishi*, **1981**, 249.

2) R. Nakajima, Y. Shintani, and T. Hara, *Bull. Chem. Soc. Jpn.*, **53**, 1767 (1980).

3) J. K. Stille and K. S. Y. Lau, *J. Am. Chem. Soc.*, **98**, 5841 (1976).

4) O. Westphal, *Ber.*, **74**, 759 (1941).

5) L. P. Kuhn, *J. Am. Chem. Soc.*, **73**, 1510 (1951).

6) In order to correct the amounts of the decomposition products of tetradecylhydrazine, an experiment was done under the same conditions as in Run 4 (Table 2) except for the absence of **1**; the decomposition products were different from those in Run 4: **3**(12.6%), **4**(62.4%), **5**(3.5%), and tetradecylamine (19.5%). This means that no correction is possible for the decomposition products of tetradecylhydrazine.

7) H. Stone and H. Shechter, *Org. Synth.*, Coll. Vol. IV, 323 (1963).

8) H. J. Becker and J. Strating, *Rec. Trav. Chem.*, **59**, 933 (1940).

9) L. I. Smith and K. L. Howard, *Org. Synth.*, **24**, 53 (1944).

10) Y. Abe, Y. Nakamura, A. Iwasaki, and N. Ono, *Yukagaku*, **20**, 224 (1971).

The Synthesis of New Electron Acceptors, 9,10-Bis[cyano-(ethoxycarbonyl)methylene]-9,10-dihydroanthracene and 10-[Cyano(ethoxycarbonyl)methylene]-9-anthrone

Takashi NOGAMI,* Yasuhiro KANDA, Hidekazu TANAKA, and Hiroshi MIKAWA

Department of Applied Chemistry, Faculty of Engineering, Osaka University, Yamadaoka, Suita, Osaka 565

(Received February 6, 1981)

Synopsis. We synthesized two new electron acceptor molecules. Their electron affinities were estimated by measuring the charge-transfer absorption spectra with three donor molecules in a 2-methyltetrahydrofuran solution. The former molecule was estimated to have an electron affinity comparable to 1,3,5-trinitrobenzene, and the latter, to *m*-dinitrobenzene.

3,6-Bis(dicyanomethylene)-1,4-cyclohexadiene (**1**), often called TCNQ, is known to form highly conductive organic complexes with various donor molecules.[1] The acceptor molecule, 9,10-bis(dicyanomethylene)-9,10-dihydroanthracene (**2**) is also expected to form highly conductive complexes, but it has not yet been synthesized. Although the attempt to prepare

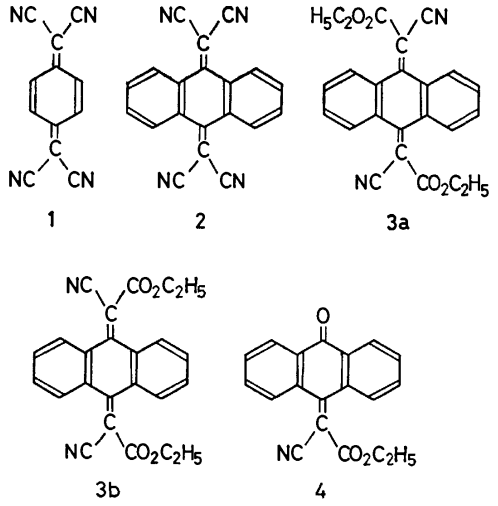

2 was unsuccessful, we could obtain the precursor of **2**, 9,10-bis[cyano(ethoxycarbonyl)methylene]-9,10-dihydroanthracene (**3**), and a by-product, 10-[cyano-(ethoxycarbonyl)methylene]-9-anthrone (**4**). Their electron affinities were estimated by measuring the charge-transfer (CT) absorption bands of the 2-methyltetrahydrofuran (MTHF) solution of these new acceptors and of three donor molecules.

Results and Discussion

Synthesis of the New Acceptors. The synthetic route is illustrated below. 9,10-Bis(cyanomethyl)anthracene (**5**) was synthesized by the procedures described in the literature.[2] The treatment of **5** with sodium ethoxide and diethyl carbonate, followed by hydrolysis, gave 9,10-bis[cyano(ethoxycarbonyl)methyl]anthracene (**6**). The dehydrogenation of **6** with *N*-iodosuccinimide (NIS) gave new electron acceptors, **3a**, **3b**, and **4**. The acceptors, **3a** and **3b**, were also obtained by the reaction of **5** with sodium ethoxide and diethyl carbonate, followed by the reaction with cyanogen chloride or cyanogen bromide.[3]

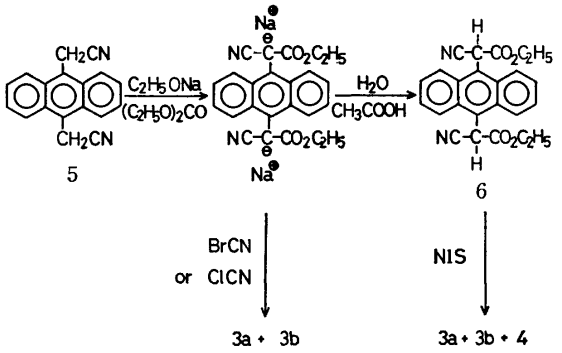

Measurements of the Charge-transfer Absorption Spectra. The CT-absorption spectra of the new acceptors were measured in a 2-methyltetrahydrofuran (MTHF) solution of **3** and **4** with three donor molecules at room temperature or at 77 K. *N,N,N',N'*-tetramethyl-*p*-phenylenediamine (TMPD), *N,N*-dimethyl-*p*-phenylenediamine (DMPD), and *N,N*-dimethylaniline (DMA) were used as the donors. Figure 1 shows the electronic-absorption spectra of these donor molecules with **3**. All these solutions showed a purple color at 77 K, although the color was not seen at room temperature even with the concentrated solution. New absorption bands were observed at the region of wavelengths longer than 400 nm.[4] The plot of the new

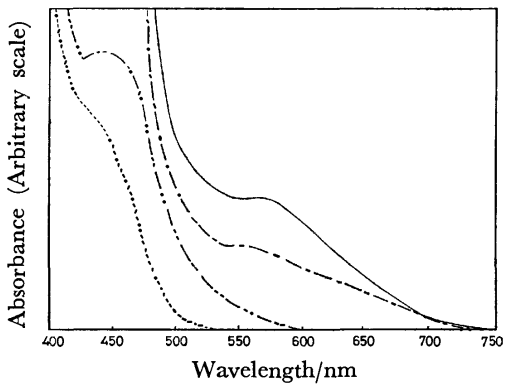

Fig. 1. Charge-transfer absorption spectra of **3** with TMPD, DMPD, and DMA in 2-methyltetrahydrofuran at 77 K.
[**3**] = 1.37×10^{-2} mol/l, [TMPD] = 1.45×10^{-2} mol/l, [DMPD] = 1.38×10^{-2} mol/l, [DMA] = 2.0 mol/l.
——: TMPD–**3**, – – –: DMPD–**3**, ———: DMA–**3**, ——: **3** only.

absorption peak positions ($h\nu_{CT}$) against the ionization potentials (I_p) of the donor molecules[5] gave the linear relation approximated as $h\nu_{CT}=1.1\ I_p-5.3$ in eV units, which is almost identical with that obtained by the use of 1,3,5-trinitrobenzene with various donor molecules.[5] Similarly the electronic-absorption measurements of **4** with the same donor molecules at room temperature gave the linear relation of $h\nu_{CT}=0.9\ I_p-3.3$, almost identical with that obtained by the use of *m*-dinitrobenzene with various donors.[5] Thus, the new absorptions are ascribed to the CT-transition. The electron affinities of **3** and **4** are roughly equal to those of 1,3,5-trinitrobenzene and *m*-dinitrobenzene.[6]

Experimental

Preparations of 9,10-Bis[cyano(ethoxycarbonyl)methylene]-9,10-dihydroanthracene (3) and 10-[Cyano(ethoxycarbonyl)methylene]-9-anthrone (4). 9,10-Bis[cyano(ethoxycarbonyl)methyl]anthracene (6): Sodium metal (0.5 g) was added to ethanol (20 ml), and the unreacted ethanol was distilled out. To the residual sodium ethoxide we then added a mixture of diethyl carbonate (10 g), toluene (3 ml), and **5** (1.5 g). The solution became yellow green. The resultant reaction mixture was stirred under reflux. Since the solvent was distilled out during the reaction, toluene was added from a dropping funnel in order to maintain a roughly constant volume of the reaction medium. After 1.5 h, the reaction mixture was cooled to room temperature and then hydrolysed by adding water (40 ml). Acetic acid (2 ml) was added, the mixtures was extracted three times with dichloromethane (50 ml), and the extract was shaken three times with 50 ml of water. The organic layer was separated and dried overnight over anhydrous magnesium sulfate. After the filtration of the magnesium sulfate, the dichloromethane was completely distilled out, hexane was added, we thus obtained 1.6 g of a brown solid (68%). After treatment with active charcoal, the raw material was recrystallized from diethyl ether to give a yellow powder of **6**: mp 198—205 °C; Found: C, 72.03; H, 5.01; N, 6.81%. Calcd for $C_{24}H_{20}N_2O_4$: C, 71.98; H, 5.03; N, 7.00%; MS: *m/e* 400 (M^+); IR (KBr): 2250 (C≡N), 1730 cm^{-1} (C=O); NMR ($CDCl_3$) $\delta=1.15$ (6H, m, CH_3), 4.20 (4H, m, CH_2), 6.20 (2H, s, tert H), 7.70 (4H, m, ring H), 8.30 (4H, m, ring H).

9,10-Bis[cyano(ethoxycarbonyl)methylene]9,10-dihydroanthracene (3a, 3b) and 10-[Cyano(ethoxycarbonyl)methylene]-9-anthrone (4) Method A: After **5** has been reacted with sodium ethoxide and diethyl carbonate by the procedures described above, BrCN (3.75 g) was stirred in, the mixture was heated gradually up to 55—60 °C for 2 h, and kept overnight at room temperature, and the toluene was distilled out. The addition of cold water, followed by the filtration of the precipitate, gave a raw product (**3**). An additional precipitate was obtained after keeping the filtrate for several days. Purification by means of a liquid chromatograph (Japan Analytical Industry, LC 07), using chloroform as the eluent, gave 1.58 g of **3** (66%) as a pale yellow powder. In the above procedure, ClCN can also be used instead of BrCN. Compound **3**: mp 145—152, 176—182 °C, arising from *cis*- and *trans*-isomers. Found: C, 72.70; H, 4.52; N, 6.96%. Calcd for $C_{24}H_{18}N_2O_4$: C, 72.35; H, 4.55; N, 7.03%. MS: *m/e* 398 (M^+); IR (KBr) 2210 (C≡N), 1720 (C=O), 1580 cm^{-1} (C=C); NMR ($CDCl_3$) $\delta=1.25$ (6H, m, CH_3), 4.30 (4H, m, CH_2), 7.50 (4H, m, ring H), 8.15 (4H, m, ring H).

Method B: The reaction vessel was covered with aluminum foil. Into the acetonitrile (12 ml) solution of *N*-iodosuccinimide (0.6 g) we stirred, drop by drop, an acetonitrile (60 ml) solution of **6** (0.5 g) under a nitrogen atmosphere. The solution was stirred for 3 h at room temperature under the nitrogen atmosphere, 400 ml of chloroform was added, and the solution was shaken four times with 200 ml of an aqueous solution of sodium thiosulfate and potassium hydroxide (both 5%) in the separatory funnel. The organic layer was washed with water until the aqueous layer became neutral. The solution was then dried overnight over calcium chloride, and the solvent was distilled out, we thus obtained a reddish-brown oil. The addition of hexane gave a yellow powder (0.32 g). The raw material was purified by liquid chromatograph, using chloroform as the eluent, to give **3** (0.2 g, 40%) and **4** (0.1 g, 43%). The recrystallization of **4** from a benzene–hexane mixed solvent gave yellow, needle-like crystals. Compound **4**: mp 146—147 °C. Found: C, 75.00; H, 4.06; N, 4.47%. Calcd for $C_{19}H_{13}NO_3$: C, 75.24; H, 4.32; N, 4.62%. MS: *m/e* 303 (M^+). IR (KBr) 2210 (C≡N), 1720, 1690 (C=O), 1580 cm^{-1} (C=C). NMR ($CDCl_3$) $\delta=1.20$ (3H, m, CH_3), 4.20 (2H, m, CH_2), 7.65 (4H, m, ring H), 8.24 (4H, m, ring H).

Electronic-absorption Measurements. The electronic-absorption spectra were measured by means of a Hitachi 340 recording spectrophotometer.

References

1) For example, "Molecular Metals," ed by W. E. Hatfield, Nato Conference Series, VI, Plenum Press, New York and London (1979).

2) M. W. Miller, R. W. Amidon, and P. O. Tawney, *J. Am. Chem. Soc.*, **77**, 2845 (1954); J. H. Golden, *J. Chem. Soc.*, **1961**, 3741; D. D. Reynolds and K. R. Dunham, U. S. Patent 2798971 (1957).

3) Attempts of the separation of **3a** from **3b** by repeated liquid chromatography, using chloroform as the eluent, were unsuccessful. The attempt to convert **3** or **4** to the corresponding acid amide by the reaction of **3** or **4** with aqueous ammonia or liquid ammonia was also unsuccessful.

4) The CT-absorption peak positions of **3** and **4** with three donor molecules (nm): **3**–TMPD 570; **3**–DMPD 550; **3**–DMA 475; **4**–TMPD 490; **4**–DMPD 465; **4**–DMA 430.

5) R. Foster, "Organic Charge-transfer Complexes," Academic Press, London and New York (1969), pp 40—69.

6) The electron affinities of 1,3,5-trinitrobenzene and *m*-dinitrobenzene are 0.7 eV and 0.3 eV respectively (see Ref. 5, p. 387). An irreversible chemical reaction occurred during the measurements of the cyclic voltammetry of **3** and **4**. Thus, we could not obtain their half-wave reduction potentials.

A Convenient Synthesis of 3-(Diethoxymethyl)alkanals

Kazuhiko SAIGO,* Shuji OKAGAWA, and Hiroyuki NOHIRA

Department of Applied Chemistry, Faculty of Engineering, Saitama University, Shimo-ohkubo, Urawa 338

(Received December 12, 1980)

Synopsis. 3-(Diethoxymethyl)alkanals were obtained in moderate yields by the diisobutylaluminium hydride reduction of ethyl 3-(diethoxymethyl)alkanoates, which were simply synthesized in one pot by the copper(II)-catalyzed reaction of ethyl diazoacetate with 1-trimethylsiloxy-1-alkenes, followed by the ring cleavage of the resulting cyclopropanes with concentrated sulfuric acid in the presence of triethyl orthoformate.

1,4-Dicarbonyl compounds are attractive intermediates, and their synthesis is of interest because they can be converted into cyclopentenones, furans, and lactones. Among the many synthetic methods for 1,4-dicarbonyl compounds, the method *via* the cyclopropanation of enol acetates,[1-3] enol ethers,[3-6] or silyl enol ethers[3,7-9] with carbenes generated from 2-diazo carbonyl compounds is the elegant one.

The cyclopropanation was applied to the one pot preparation of ethyl 3-(diethoxymethyl)alkanoates (**3**) based on the consideration that the ring cleavage of the cyclopropanes derived from 1-trimethylsiloxy-1-alkenes and ethyl diazoacetate with an acid in the presence of triethyl orthoformate would result in the one pot synthesis of **3**. When 1-trimethylsiloxy-1-hexene (**1a**) was allowed to react with ethyl diazoacetate (4 equimolar amounts) in cyclohexane in the presence of a catalytic amount of copper(II) sulfate under reflux, distillation under reduced pressure yielded a colorless oil, ethyl 2-butyl-3-(trimethylsiloxy)cyclopropanecarboxylate (**2a**), in 92% yield. Treatment of **2a** in ethanol with concentrated sulfuric acid in the presence of triethyl orthoformate for 24 h at room temperature gave ethyl 3-(diethoxymethyl)heptanoate (**3a**) in 91% yield (83% total yield from **1a**). On the other hand, when the ring cleavage was carried out without isolation of **2a** after the cyclopropanation, similar yield was achieved (78% total yield from **1a**). The reduction of **3a** with diisobutylaluminium hydride (1.5 equimolar amount) in a mixture of cyclohexane and ether (2:3) at −70 °C for 3 h, followed by thin layer chromatographic purification, gave 3-(diethoxymethyl)heptanal (**4a**) in 74% yield.

These results mean that the precursors for 3-substituted furan synthesis, 3-(diethoxymethyl)alkanals (**4**), could be conveniently obtained by the diisobutylaluminium hydride reduction of ethyl 3-(diethoxymethyl)alkanoates (**3**), which were simply synthesized in one pot through two reaction steps; step 1) the cyclopropanation of 1-trimethylsiloxy-1-alkenes (**1**) with ethyl diazoacetate, step 2) the ring cleavage of the resulting cyclopropanes (**2**) with concentrated sulfuric acid in the presence of triethyl orthoformate, as shown in Scheme 1.

Several runs were carried out giving similar ethyl 3-(diethoxymethyl)alkanoates (**3**) or 3-(diethoxymethyl)alkanals (**4**) (Table).

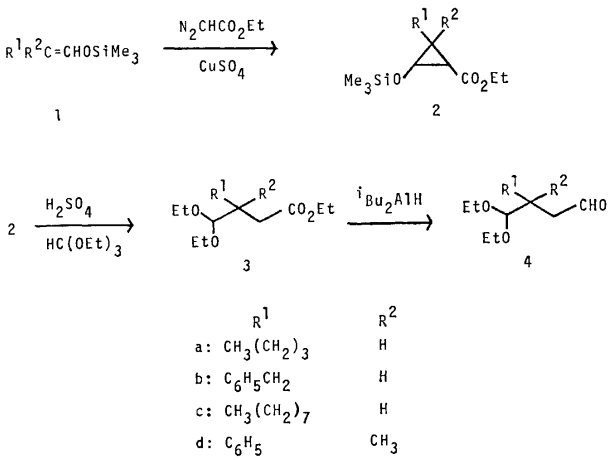

Scheme 1.

TABLE 1. SYNTHESES OF ETHYL 3-(DIETHOXYMETHYL)-ALKANOATES AND 3-(DIETHOXYMETHYL)ALKANALS

Starting Materials	Product	Yield/%	Bp/°C	(mmHg)[a]
1a	**2a**	92	64—67	(0.7)
2a	**3a**	91	93—94	(3)
1a	**3a**	78	90—91	(2)
1b	**3b**	84	118—120	(0.1)
1c	**3c**	86	110—113	(0.3)
1d	**3d**	71	121—124	(0.08)
3a	**4a**	72	[100[b]]	(12)][c]
3b	**4b**	67	[130[b]]	(0.9)][c]
3d	**4d**	76	[138[b]]	(0.8)][c]

a) 1 mmHg≈133.3 Pa. b) Bath temperature. c) The products were separated by TLC, and the boiling points were determined by bulb to bulb distillation.

Experimental

Boiling points are uncorrected. The ^{1}H-NMR spectra were recorded in CCl_4 solution at 60 MHz on a Varian A-60 Spectrometer using TMS as an internal standard. The IR spectra were determined on a JASCO IR-2A Spectrometer.

Materials. All silyl enol ethers were synthesized by the similar method described in the literature[10] giving mixtures of (*E*)- and (*Z*)-isomers, and they were used without separation. Ethyl diazoacetate and diisobutylaluminium hydride were prepared by the methods reported, respectively.[11,12]

Synthesis of Ethyl 3-(Diethoxymethyl)alkanoate (3). To a refluxing suspension of 1-trimethylsiloxy-1-alkene (**1**) (10 mmol) and anhydrous $CuSO_4$ (185 mg, 1.2 mmol) in dry cyclohexane (4 ml) was added ethyl diazoacetate (4.57 g, 40 mmol) in dry cyclohexane (19 ml) under argon atmosphere with vigorous stirring in a period of 2.5 h. After refluxing for additional 9.5 h, the reaction mixture was

cooled, and insoluble materials were filtered off and washed with cyclohexane (15 ml×3). The filtrate and the washings were combined and concentrated under reduced pressure. The oily product was dissolved in dry ethanol (5 ml). To the solution were added ethyl orthoformate (1.48 g, 10 mmol) and two drops of concentrated H_2SO_4. After standing for 24 h, H_2SO_4 was neutralized by addition of sodium ethoxide in dry ethanol. The insoluble mass appeared was filtered off and washed with ether (15 ml×3). The filtrate and the washing were combined and concentrated using a rotary evaporator. Distillation of the oil remained gave ethyl 3-(diethoxymethyl)alkanoate (**3**).

3a: IR (neat) 1740, 1180, 1130, and 1075 cm^{-1}; NMR (CCl_4) δ=0.90 (t, 3H, J=5 Hz), 1.03 (t, 3H, J=7 Hz), 1.14 (t, 3H, J=7 Hz), 1.22 (t, 3H, J=7 Hz), 1.1—1.6 (m, 6H), 1.9—2.7 (m, 3H), 3.49 (q, 2H, J=7 Hz), 3.50 (q, 2H, J=7 Hz), 4.06 (q, 2H, J=7 Hz), and 4.26 (d, 1H, J=4 Hz).

Found: C, 64.35; H, 10.56%. Calcd for $C_{14}H_{28}O_4$: C, 64.58; H, 10.84%.

3b: IR (neat) 1740, 1140, 1080, 1040, 760, and 710 cm^{-1}; NMR (CCl_4) δ=1.12 (t, 3H, J=7 Hz), 1.15 (t, 3H, J=7 Hz), 1.17 (t, 3H, J=7 Hz), 2.0—3.0 (m, 5H), 3.44 (q, 2H, J=7 Hz), 3.46 (q, 2H, J=7 Hz), 3.99 (q, 2H, J=7 Hz), 4.28 (d, 1H, J=4 Hz), and 7.16 (s, 5H).

Found: C, 69.23; H, 9.16%. Calcd for $C_{17}H_{26}O_4$: C, 69.36; H, 8.90%.

3c: IR (neat) 1730, 1160, 1115, and 1060 cm^{-1}; NMR (CCl_4) δ=0.89 (t, 3H, J=5 Hz), 1.17 (t, 3H, J=7 Hz), 1.24 (t, 3H, J=7 Hz), 1.25 (t, 3H, J=7 Hz), 1.2—1.5 (m, 14H), 1.9—2.5 (m, 3H) 3.50 (q, 2H, J=7 Hz), 3.54 (q, 2H, J=7 Hz), 4.09 (q, 2H, J=7 Hz), and 4.30 (d, 1H, J=4 Hz).

Found: C, 68.30; H, 11.46%. Calcd for $C_{18}H_{36}O_4$: C, 68.31; H, 11.47%.

3d: IR (neat) 1740, 1170, 1130, 1080, 750, and 700 cm^{-1}; NMR (CCl_4) δ=1.00 (t, 6H, J=7 Hz), 1.07 (t, 3H, J=7 Hz), 1.51 (s, 3H), 2.72 (s, 1H), 2.83 (s, 1H), 2.9—4.1 (m, 6H), 4.36 (s, 1H), and 7.0—7.5 (m, 5H).

Found: C, 69.17; H, 8.94%. Calcd for $C_{17}H_{26}O_4$: C, 69.36; H, 8.90%.

*Reduction of **3** to 3-(Diethoxymethyl)alkanal (**4**).* To a solution of ethyl 3-(diethoxymethyl)alkanoate (**3**) (1.0 mmol) in a mixture of cyclohexane (10 ml) and ether (15 ml) was added a solution of diisobutylaluminium hydride (1.5 mmol) in cyclohexane (1.5 ml) at −70 °C under argon atmosphere in a period of 10 min. After stirring for additional 3 h at −70 °C, water (0.5 ml) was added to remove excess diisobutylaluminium hydride, and the mixture was warmed to room temperature. To the resulting mixture was added water (10 ml), and the insoluble materials appeared were filtered off. The organic layer was separated, dried with sodium sulfate, and concentrated under reduced pressure. Silica gel thin layer chromatographic purification gave 3-(diethoxymethyl)alkanal (**4**).

4a: IR (neat) 1730, 1115, and 995 cm^{-1}; NMR (CCl_4) δ=0.90 (t, 3H, J=5 Hz), 1.14 (t, 6H, J=7 Hz), 1.2—1.7 (m, 6H), 2.0—2.5 (m, 3H), 3.48 (q, 2H, J=7 Hz), 3.52 (q, 2H, J=7 Hz), 4.23 (d, 1H, J=4 Hz), and 9.43 (t, 1H, J=1 Hz).

Found: C, 66.59; H, 11.34%. Calcd for $C_{12}H_{24}O_3$: C, 66.63; H, 11.18%.

4b: IR (neat) 1730, 1120, 990, 750, and 700 cm^{-1}; NMR (CCl_4) δ=1.13 (t, 3H, J=7 Hz), 1.15 (t, 3H, J=7 Hz), 2.2—2.9 (m, 5H), 3.45 (q, 2H, J=7 Hz), 3.49 (q, 2H, J=7 Hz), 4.22 (d, 1H, J=4 Hz), 7.23 (s, 5H), and 9.56 (t, 1H, J=1 Hz).

Found: C, 72.25; H, 8.71%. Calcd for $C_{15}H_{22}O_3$: C, 71.97; H, 8.86%.

4d: IR (neat) 1730, 1120, 1005, 750, and 700 cm^{-1}; NMR (CCl_4) δ=1.14 (t, 3H, J=7 Hz), 1.20 (t, 3H, J=7 Hz), 1.48 (s, 3H), 2.46 (d, 2H, J=1 Hz), 3.52 (q, 2H, J=7 Hz), 3.65 (q, 2H, J=7 Hz), 4.21 (s, 1H), 7.0—7.5 (m, 5H), and 9.50 (t, 1H, J=1 Hz).

Found: C, 71.83; H, 9.14%. Calcd for $C_{15}H_{22}O_3$: C, 71.79; H, 8.86%.

References

1) H. O. House and C. J. Blankley, *J. Org. Chem.*, **33**, 47 (1968).
2) J. E. McMurry and T. E. Glass, *Tetrahedron Lett.*, **1971**, 2575.
3) E. Wenkert, B. L. Buckwalter, A. A. Craveiro, E. L. Sanchez, and S. S. Sathe, *J. Am. Chem. Soc.*, **100**, 1267 (1978).
4) E. Wenkert, R. A. Mueller, E. J. Reardon, Jr., S. S. Sathe, D. J. Scharf, and G. Tosi, *J. Am. Chem. Soc.*, **92**, 7428 (1970).
5) E. Wenkert, C. A. McPerson, E. L. Sanchez, and R. A. Webb, *Synth. Commun.*, **3**, 255 (1973).
6) E. Wenkert, M. E. Alonso, B. L. Buckwalter, and K. J. Chou, *J. Am. Chem. Soc.*, **99**, 4778 (1977).
7) R. Le Goaller and J.-L. Pierre, *C. R. Acad. Sci., Ser. C*, **276**, 193 (1973).
8) R. M. Coates, L. O. Sandefur, and R. D. Smillie, *J. Am. Chem. Soc.*, **97**, 1619 (1975).
9) E. Wenkert, T. E. Goodwin, and B. C. Ranu, *J. Org. Chem.*, **42**, 2137 (1977).
10) H. O. House, L. J. Czuba, M. Gall, and H. D. Olmstead, *J. Org. Chem.*, **34**, 2324 (1969).
11) N. E. Searle, *Org. Synth.*, Coll. Vol. IV, 424 (1963).
12) J. S. McConaghy and J. J. Bloomfield, *J. Org. Chem.*, **33**, 3425 (1968).

Preparation of DL-Alanine by the Reaction of (±)-2-Chloropropionic Acid with Aqueous Ammonia under Pressure[1)]

Yoshiro OGATA* and Morio INAISHI

Department of Applied Chemistry, Faculty of Engineering, Nagoya University, Chikusa-ku, Nagoya 464

(Received January 23, 1981)

Synopsis. The effects of experimental conditions (molar ratio of reactants, concentration, temperature, and pressure) on the yield of DL-alanine produced by the reaction of (±)-2-chloropropionic acid with aqueous ammonia have been studied. Molar ratio of NH_3: $CH_3CHClCO_2H$ (*ca.* 10:1) much lower than that reported in the literature (68:1) can give a comparable yield (*ca.* 78%) by the reaction under pressure at 70 °C for 5 h, a much shorter time than that reported in the literature (over 96 h). Addition of ammonium carbonate does not increase the yield against the literature.[16)]

There are a number of methods for the chemical synthesis of 2-amino acids, *e.g.*, Strecker reaction with aldehyde–HCN–NH_3,[2-4)] Bücherer method[5)] using hydantoin with the components analogous to the Strecker's, and also ammonolysis of 2-halo acids with aqueous ammonia.[6-16)] The ammonolysis of 2-halo acids uses a large excess of ammonia (*e. g.*, NH_3: halo acid=60:1) at room temperature to avoid by-products, 2,2′-iminodipropionic and 2,2′,2″-nitrilotripropionic acid.

$$CH_3CHClCO_2H + NH_3 \longrightarrow \underset{\text{alanine}}{CH_3CH(NH_2)CO_2H}$$

$$+ \underset{\substack{\text{2,2′-iminodipropionic acid}\\(\text{Im})}}{[CH_3\dot{C}H(CO_2H)]_2NH} + \underset{\text{2,2′,2″-nitrilotripropionic acid}}{[CH_3\dot{C}H(CO_2H)]_3N}$$

However, this large excess of ammonia and a very long reaction time, *e. g.*, 4 d, are inconvenient, whereas the reaction at higher temperature in an open vessel gave a very poor yield because of the volatilization of ammonia. Hence we wished to shorten the reaction time and lower the molar ratio of (NH_3) : (halo acid), and we examined the effects of the molar ratio, reaction time, pressure, and temperature on the yield of DL-alanine produced by the reaction of (±)-2-chloropropionic acid with NH_3.

A few reports[6-16)] are available on this type of synthesis of 2-amino acid, but the reports discussing the effects of reaction conditions in detail are rare [10,16)] The present report is the summary of our data on the effect of several reaction parameters, especially pressure, on the yield of DL-alanine formed by the reaction of (±)-2-chloropropionic acid with aqueous saturated ammonia.

Results and Discussion

Effect of Temperature. A mixture of (±)-2-chloropropionic acid and 14.5 M (1 M=1 mol dm^{-3}) ammonia in a molar ratio of 10:1 was allowed to react in a sealed tube at various temperatures of 0—130 °C for 5 h, and the yield was measured by NMR. The results are shown in Fig. 1.

The optimum temperature was in a range of 50—70 °C; hence the increase of yield with progress of the reaction was recorded at 50, 60, and 70 °C. The results are shown in Fig. 2, which indicates that the optimum temperature is 70 °C, where a 78% yield based on (±)-2-chloropropionic acid is attained in 5 h reaction.

Effect of the Molar Ratio of Reactants. The ammonolysis was conducted with various ratios of $[NH_3]_0/[CH_3CHClCO_2H]_0$: 5/1, 10/1, 20/1, and 30/1.

The reaction with the molar ratio of 5:1 gave an appreciable amount of 2,2′-iminodipropionic acid (Im), while virtually no Im was found in the reaction with the ratio of 10:1. Consequently, we employed the ratio of 10:1 for most of the ammonolysis study. The higher ratio such as 68:1, which had been recommended in the literature[10,11)] gave really somewhat better yields, but the isolation of the product became troublesome due to dilution.

Effect of Initial Concentration of Ammonia. In order

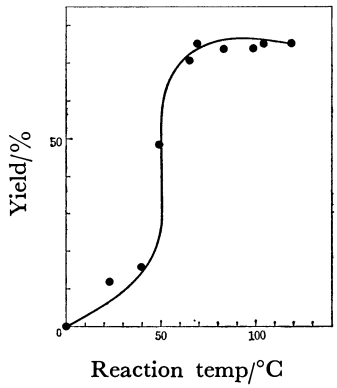

Fig. 1. Effect of the reaction temperature on the yield of DL-alanine formed by the reaction of (±)-2-chloropropionic acid with aqueous ammonia at 0—120 °C for 5 h with $[NH_3]_0$: $[ClCH(CH_3)CO_2H]_0$ =10:1.

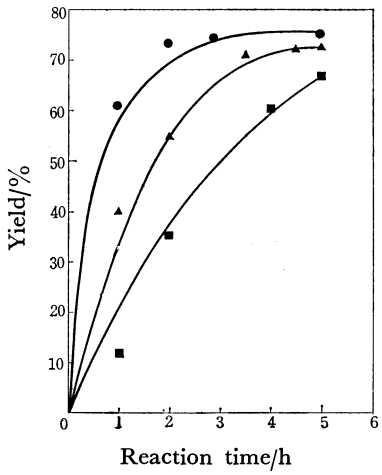

Fig. 2. Conversion curves for the formation of DL-alanine at various temperatures with $[NH_3]_0$:$[CH_3CHClCO_2H]_0$=10:1.
■: 50 °C, ▲: 60 °C, ●: 70 °C.

Table 1. Effect of initial concentration of NH_3 on the yield (%) of DL-alanine at various initial ratios of $[NH_3]_0/[CH_3CHClCO_2H]_0$

$\frac{[NH_3]_0}{[CH_3CHClCO_2H]_0}$	5	10	20	30
$[NH_3]_0=14.5$ M, yield/%	60.5	75.7	84.4	89.7
$[NH_3]_0=22.2$ M, yield/%	66.2	75.1	84.0	89.6

to find the effect of increasing concentration of ammonia, 22.8 M aqueous ammonia was prepared by passing gaseous NH_3 into the ice-cooled aqueous 14.5 M ammonia.

The effect of an increase in initial concentration of ammonia on the yield of DL-alanine at various initial molar ratios of reactants is shown in Table 1. The data in Table 1 show that the supersaturated solution of NH_3 cannot give a higher yield.

Effect of Agitation, Pressure and Addition of Ammonium Carbonate. Since there was no appreciable difference between the reaction in an autoclave and that in a sealed tube, the effect of agitation seems to be small. When the reaction was conducted at over 100 °C in an autoclave (*e. g.*, 130—140 °C at 17—19 atm), the yields of the by-products, Im, and DL-lactic acid, tended to increase.

Addition of ammonium carbonate was reported to give a better yield of DL-alanine,[16] but in our hands its addition reduced the yield to 37% accompanied by a rather high yield of DL-lactic acid.

Isolation of DL-Alanine. The NMR analysis of DL-alanine was checked by its isolation. The isolation was done by evaporation, addition of methanol and filtration. The decrease of alanine yield in the isolation and purification processes was *ca.* 32% in comparison with the yield based on the NMR analysis, whereas the yield of purified alanine which contained *ca.* 0.8 wt% NH_4Cl and no iminodipropionic acid, was 46%. The large loss of alanine in the purification process is due to a high solubility of alanine similar to that of NH_4Cl in aqueous solution. The analogous yield (43—46%) was reported in the reaction of 68 fold excess ammonia with chloropropionic acid carried out at room temperature for 96 h.[10,11] Although a better isolation yield may be obtained for bromopropionic acid due to small solubility of NH_4Br in methanol,[10] we did not attempt to use it because of its high cost.

Experimental

General. NMR spectra were measured on a 60 MHz Hitachi R-24B NMR spectrometer at 25 °C using dimethyl sulfoxide as an internal standard. Melting points were measured by a Yanagimoto micro melting point apparatus and uncorrected.

Materials. (±)-2-Chloropropionic acid (bp: 182.0—182.5 °C) was of guaranteed grade and used without further purification. Aqueous ammonia of 28% (14.5 M) was titrated by standard 0.1 M HCl. DL-Lactic acid with bp 130.0—134.0 °C (25 Torr), and DMSO with bp 81.0—83.5 °C (23 Torr) were of first-grade commercial products. 2,2′-Iminodipropionic acid was prepared according to the literature.[17] D_2O used was 99.8% pure.

Apparatus. Two sorts of apparatus were used for ammonolysis; one is a 1.5 mm thick sealed tube of 150 ml (38 mm × 200 mm) capacity dipped in a polyethylene glycol (PEG) thermostat; the other is a stainless steel autoclave made by Taiatsu Glass Ind. Co., TEM-D 300 type, of 250 ml capacity with a mechanical stirrer, which is dipped in a PEG thermostat.

Typical Procedure. A mixture of (±)-2-chloropropionic acid (0.07 mol, 3.4 g) and 14.5 M aqueous ammonia (50 ml, 0.73 mol) was placed in a sealed tube or an autoclave and heated in a PEG bath. The internal temperature was maintained in a range of ±3 °C.

Thus far, the yield of alanine was measured by isolating it by addition of methanol after completion of the reaction,[8-11] and evaporation of water, but poor solubility of accompanying NH_4Cl in methanol rendered the estimation of the yield rather inaccurate; hence the NMR measurement of the formed DL-alanine solution was employed for estimation of the yield as described below.

Identification and Estimation of Products. Aliquots (each 1 ml) of the reaction mixture were pipetted out, and each sample was added with DMSO as an internal standard, diluted with D_2O, and the NMR peak assigned to methyl proton of DL-alanine (δ: 1.43 d) was measured. The working curve was prepared with an aqueous 14.5 M ammonia solutions of given concentrations of DL-alanine at pH 10—11 containing NH_4Cl (2.0 g). Contaminated DL-lactic acid, (±)-2-chloropropionic acid, and 2,2′-iminodipropionic acid were also characterized and estimated analogously by using their characteristic NMR peaks, δ 1.40, 1.65, and 1.54 d, respectively.

Besides estimation of the yield by NMR analysis DL-alanine was isolated from the reaction mixture. The reaction of (±)-2-chloropropionic acid (0.07 mol) with 14.5 M aqueous ammonia (50 ml, 0.73 mol) was conducted at 70 °C for 5 h in an autoclave. Then the solution was concentrated under a reduced pressure to 10 ml, added with methanol (100 ml), and the product was filtered. The filtered mass weighing 4.6 g (60%) contained 18% NH_4Cl, and it was purified by reprecipitation from water (20 ml) with methanol (100 ml) and then standing the mixture overnight in a refrigerator. The filtered pure DL-alanine (2.9 g) contained 0.8 wt% NH_4Cl, and the yield was 46%.

References

1) Contribution No. 277.
2) A. Strecker, *Justus Liebigs Ann. Chem.*, **75**, 27 (1850).
3) D. T. Mowry, *Chem. Rev.*, **42**, 236 (1948).
4) Y. Ogata and A. Kawasaki, *J. Chem. Soc., B*, **1971**, 325.
5) H. T. Bücherer and W. Steiner, *J. Prakt. Chem.*, **140**, 291 (1934).
6) K. Kraut, *Ber.*, **23**, 2577 (1890).
7) G. R. Robertson, *J. Am. Chem. Soc.*, **49**, 2889 (1927).
8) J. M. Orten and R. M. Hill, *J. Am. Chem. Soc.*, **53**, 2797 (1931).
9) J. M. Orten and R. M. Hill, *Org. Synth.*, Coll. Vol. I, 300 (1941).
10) W. C. Tobie and G. B. Ayres, *J. Am. Chem. Soc.*, **59**, 950 (1937).
11) W. C. Tobie and G. B. Ayres, *Org. Synth.*, Coll. Vol. I, 23 (1941).
12) C. S. Marvel, *Org. Synth.*, Coll. Vol. III, 495 (1955).
13) C. S. Marvel, *Org. Synth.*, Coll. Vol. III, 523 (1955).
14) H. E. Carter and H. D. West, *Org. Synth.*, Coll. Vol. III, 774 (1955).
15) C. S. Marvel, *Org. Synth.*, Coll. Vol. III, 848 (1955).
16) N. D. Cheronis and H. Spitzmueller, *J. Org. Chem.*, **6**, 349 (1941).
17) G. Studnikoff, *Ber.*, **40**, 1014 (1907).

The Aromatization Observed on the Reaction of Terpinolene with Tetrahydrogeraniol in the Presence of Boron Trifluoride Etherate

Kimiko NAGAI* and Mitsuru NAKAYAMA†

Yasuda Women's University, Yasufuruichi-cho, Asaminami-ku, Hiroshima 731-01

Department of Chemistry, Faculty of Science, Hiroshima University, Higashisenda-machi, Naka-ku, Hiroshima 730

(Received February 16, 1981)

Synopsis. The reaction of terpinolene with tetrahydrogeraniol in the presence of boron trifluoride etherate gave an aromatic ether in addition to the corresponding aliphatic ether, along with *p*-cymene, *p*-cymen-8-ol, and the monoterpene hydrocarbons formed by double-bond migration. The aromatic ether was proved to form upon the treatment of the aliphatic ether with boron trifluoride etherate.

In connection with previous papers on the formation of ethers from monoterpene[1-6] and aliphatic[7,8] alcohols with boron trifluoride etherate, the effect of the same reagent on the addition reaction of tetrahydrogeraniol (**2**) to terpinolene (**1**) was examined.

In a typical experiment, equal portions (1.0 g) of terpinolene and tetrahydrogeraniol were mixed with boron trifluoride etherate (0.05 ml), after which the mixture was allowed to stand at room temperature for 5 days. The reaction mixture was then subjected to elution chromatography on silica gel, followed by preparative-GLC in Carbowax 6000, to give Compounds **3**, **4**, and **5** and also *p*-cymene. The structures of **3**, **4**, and **5** were characterized as 1-methyl-4-[1-(3,7-dimethyloctyloxy)-1-methylethyl]benzene, 1-methyl-4-[1-(3,7-dimethyloctyloxy)-1-methylethyl]-1-cyclohexene, and 1-methyl-4-(1-hydroxy-1-methylethyl)benzene (*p*-cymen-8-ol) respectively on the basis of their spectral data and chemical behavior.

Under mild conditions (Exp. No. 1, Table 1), the aromatic alcohol, **5**, *p*-cymene, and two ethers, **3** and **4**, were obtained as the major products. On the other hand, under vigorous conditions (Exp. No. 2), *p*-cymene was produced as the major product, together with small amounts of **3**, **4**, and **5** and three monoterpene hydrocarbons. Under these conditions, aromatic compounds were obtained as the main components. Furthermore, all the compounds were confirmed by GC/MS analysis. The aromatic ether, **3**, was also prepared albeit in a low yield, by treating the **4** ether with boron trifluoride etherate, as is shown in Table 2 and Scheme 1.

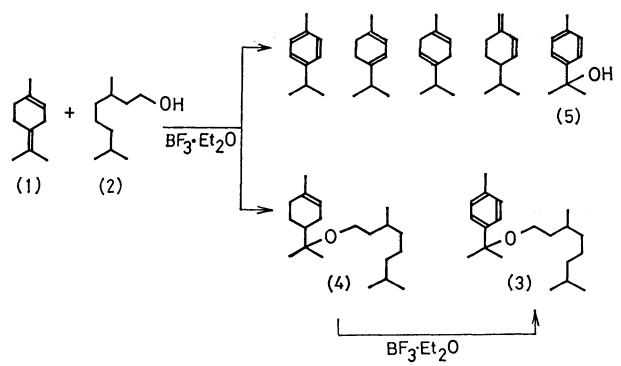

Scheme 1.

The results obtained in this paper are essentially comparable with those of previous works.[1,4-6] However, the formation of the aromatic compounds in considerable amounts is remarkable; this can be interpreted in terms of the participation of oxygen rather than disproportionation. In this connection, the obtaining of *p*-cymen-8-ol (**5**) is interesting; the mechanism of its formation is now under investigation.

Experimental

Apparatus. The IR spectra were taken in a CCl_4 solution, while the ^{1}H-NMR spectra were obtained in a CCl_4 solution, using TMS as the internal reference on a 60 MHz spectrometer. The mass spectra were measured by means of a Hitachi RMS-4 spectrometer under the following operating conditions: 80 eV, ionization-chamber voltage; 80 uA, total emission; 1800 eV, ion-accelerating voltage, and 200 °C, ionization-chamber temperature. The GLC was carried out on an FID-type apparatus in connection with a glass column (3 mm×2 m) packed with OV-1 (2%) on Diasolid L (60—80 mesh) and DEGS (3%) on Shimalite W (60—80 mesh) under a 20 ml/min flow rate of a N_2 carrier.

Materials. Commercial **1** and **2** were used after repeated fractional distillations. Each of them showed a single peak in GLC with OV-1 and DEGS-packed columns, and the IR and ^{1}H-NMR spectra of these materials were coincident with those of authentic ones.

A chemical-grade reagent of $BF_3 \cdot Et_2O$ (BF_3 47%) was used without any purification.

Reaction of 1 with 2 in the Presence of $BF_3 \cdot Et_2O$. To a mixture of **1** (1.0 g) and **2** (1.0 g), 0.05 ml or 0.15 ml of $BF_3 \cdot Et_2O$ was added, drop by drop. The mixture was then allowed to react at room temperature for 5 or 7 d respectively. The reaction mixture was shaken with a saturated aqueous solution of sodium carbonate to neutralize the remaining $BF_3 \cdot Et_2O$, washed with water, dried over anhydrous sodium sulfate, and separated through column chromatography on silica gel with a hexane–ethyl acetate mixture and through preparative-GLC with Carbowax 6000 (*cf.* Table 1).

Characterization of 3. A colorless oil was obtained in a 10% yield. λ_{max}^{EtOH}: 272 nm (220), 264 (260), 256 (250), 251 (280), 217_{sh} (5320), 212 (5580); IR (CCl_4, cm^{-1}): 1511 (aromatic ring), 1385, 1379, 1360 (CH_3–$\underset{|}{C}H$–CH_3, CH_3–$\underset{|}{C}$–CH_3, CH_3–$\underset{|}{C}H$–), 1162, 1075 (C–O–C); ^{1}H-NMR (CCl_4): δ 0.88 (9H, d, J=7 Hz, $C\underline{H}_3$–$\underset{|}{C}H$–$C\underline{H}_3$, $C\underline{H}_3$–$\underset{|}{C}H$–), 1.23 (8H, bs, –$C\underline{H}_2$–×4), 1.53 (6H, s, $(C\underline{H}_3)_2$–$\underset{|}{C}$–O–), 1.66 (2H, bs, –$\underset{|}{C}\underline{H}$–×2), 2.38 (3H, s, $C\underline{H}_3$–Ar), 3.20 (2H, t, J=7 Hz, –O–$C\underline{H}_2$–CH_2–), 7.25 (4H, bs, aromatic proton); Mass (*m/e*): 290 (4%, M^+, $C_{20}H_{34}O$), 135 (15), 133 (58), 112 (30), 110 (22), 105 (21), 91 (21), 81 (19), 71 (49), 70 (35), 69 (50), 57 (67), 43 (base).

Table 1. Reaction conditions and reaction products

Reaction conditions	Experiment No.	1	2
	Terpinolene (g)	1.0	1.0
	Tetrahydrogeraniol (g)	1.0	1.0
	$BF_3 \cdot Et_2O$ (ml)	0.05	0.15
	React. period/d	5	7
	React. temp/°C	20	23
Reaction products (yield/%)[a]	α-Terpinene	7.7	2.0
	β-Phellandrene	3.0	2.8
	γ-Terpinene	1.2	5.6
	p-Cymene	21.8	76.4
	p-Cymen-8-ol (**5**)	37.6	0.6
	Aromatic ether **3**	10.1	8.6
	Aliphatic ether **4**	14.2	1.4
	Others	4.4	2.6

a) The ratios of the components were calculated by means of GLC from their relative peak areas.

Characterization of **4**. A colorless oil was obtained in a 14% yield. IR (CCl_4, cm^{-1}): 1680, 895 (-CH=C-), 1390, 1369 (CH_3-CH-CH_3, CH_3-C-CH_3), 1165, 1142, 1121, 1082 (C-O-C); ^{1}H-NMR ($CDCl_3$): δ 0.85 (9H, d, J=6 Hz, $C\underline{H}_3$-CH-, $C\underline{H}_3$-CH-$C\underline{H}_3$), 1.10 (6H, s, $(C\underline{H}_3)_2$-C-O-), 1.67 (3H, s, $C\underline{H}_3$-C=CH-), 1.93 (4H, bs, -$C\underline{H}_2$-C=C-×2), 3.36 (2H, t, J=7 Hz, -O-$C\underline{H}_2$-CH_2-), 5.46 (1H, bs, $w/2$= 8 Hz, -$C\underline{H}$=C-); Mass (*m/e*): 294 (2%, M^+, $C_{20}H_{38}O$), 199 (8), 141 (5, $C_{10}H_{21}$), 136 (15), 121 (5), 95 (9), 93 (10), 81 (12), 59 (8), 55 (21), 43 (base), 41 (55), 39 (14).

Catalytic Hydrogenation of **4**. Compound **4** (300 mg) was hydrogenated over platinum oxide (30 mg) in acetic acid (7 ml) to take up 1 mol-equivalent of hydrogen, thus giving the dihydro derivative of **4** as a colorless oil in a yield of 80%. IR (CCl_4, cm^{-1}): 1383, 1368 (CH_3-CH-CH_3. CH_3-C-CH_3), 1173, 1151, 1121, 1071 (C-O-C); ^{1}H-NMR ($CDCl_3$): δ 0.85 (12H, d, J=6 Hz, $C\underline{H}_3$-CH-$C\underline{H}_3$, $C\underline{H}_3$-CH-×2), 1.10 (6H, s, $(C\underline{H}_3)_2$-C-O-), 3.34 (2H, t, J=7 Hz, -O-$C\underline{H}_2$-CH_2-).

Preparation of Dihydro **4**. Tetrahydrogeranyl bromide (1.0 g) and sodium dihydro-α-terpineolate (1.0 g) were treated according to the Williamson procedure to give the dihydro derivative of **4** as a colorless oil in a yield of 15%.

Conversion of **4** *into* **3** *by* $BF_3 \cdot Et_2O$. The ether **4** (20 mg), was dissolved in dried ether (1 ml) and mixed with 0.04 ml of $BF_3 \cdot Et_2O$. After the mixture had then been allowed to stand at room temperature for 9 d, a small amount of water was added to the reaction mixture to decompose the excess reagent. The reaction mixture thus reacted was then analyzed by means of gas chromatography on the DEGS separation column to determine the compositions (*cf.* Table 2). Each compound was identified by comparing the retention times with those of authentic samples.

Characterization of **5**. Compound **5** was isolated as a colorless oil in a yield of 38%. λ_{max}^{EtOH}: 272 nm (330), 263 (390), 257 (310), 251 (210), 221_{sh} (6920), 216 (8080), 213 (8020); IR (CCl_4, cm^{-1}): 3599 (-OH), 1511 (aromatic ring), 1380, 1364 (CH_3-C-CH_3), 1168, 1112 (C-O-C); ^{1}H-NMR (CCl_4): δ 1.56 (6H, s, $(C\underline{H}_3)_2$-C-O-), 1.76 (1H, bs, -O$\underline{H}$, disappeared with D_2O), 2.36 (3H, s, $C\underline{H}_3$-Ar), 7.21 7.40 (each 2H, d, J=8 Hz, aromatic proton); Mass (*m/e*): 150 (20%, M^+, $C_{10}H_{14}O$), 135 (base), 133 (16), 91 (24), 43 (21). The spectra were in good agreement with those of 1-methyl-4-(1-hydroxy-1-methylethyl)benzene, the synthesis of which will be described in the following section.

Preparation of **5**. Methyl *p*-methylbenzoate (500 mg) in ether (20 ml) was refluxed with 5% methyllithium in ether (7 ml) for 6 h. The mixture was then treated according to the usual procedure to give 1-methyl-4-(1-hydroxy-1-methylethyl)benzene in a 70% yield.

GC/MS of Reaction Products. GC/MS analyses of reaction products were carried out using a glass column (3 mm× 2 m) packed with 3% OV-1 on Gas Chrom. Q under a 7 °C/min temperature program from 80 to 230 °C; 70 eV, ionization voltage; 3500 eV, ion-accelerating voltage; 290 °C, the ion-source temperature, and 270 °C, the separator temperature. Each compound was gas-chromatographically identical with the respective authentic sample.

Table 2. Conversion of aliphatic ether **4** by $BF_3 \cdot Et_2O$ (%)

Unreacted ether	66.7
α-Terpinene	1.6
γ-Terpinene	1.4
p-Cymene	3.2
Tetrahydrogeraniol	14.5
Aromatic ether **3**	3.0
Others	9.6

The ratios of the components were calculated by means of GLC from their relative peak areas.

We wish to thank Professor Akira Hayashi, Kinki University, Faculty of Science and Technology, for the determination of the GC/MS.

References

1) K. Nagai, *Chem. Pharm. Bull.*, **18**, 2123 (1970).
2) K. Nagai, M. Nakayama, and S. Hayashi, *Chem. Lett.*, **1973**, 665.
3) K. Nagai, M. Nakayama, A. Matsuo, S. Eguchi, and S. Hayashi, *Bull. Chem. Soc. Jpn.*, **47**, 1193 (1974).
4) K. Nagai, *J. Sci. Hiroshima Univ., Ser. A*, **38**, 141 (1974).
5) K. Nagai, *Bull. Chem. Soc. Jpn.*, **48**, 2317 (1975).
6) K. Nagai, *Bull. Chem. Soc. Jpn.*, **49**, 265 (1976).
7) K. Nagai, M. Nakayama, and S. Hayashi, *Bull. Chem. Soc. Jpn.*, **51**, 3273 (1978).
8) K. Suga and S. Watanabe, *Nippon Kagaku Zasshi*, **81**, 1139 (1960).

Synthetic Photochemistry. XXIII.[1] The Photoreduction of Dioxetanes to *cis*-1,2-Glycols: ^{18}O-Labelling Experiments

Hitoshi TAKESHITA* and Toshihide HATSUI
Research Institute of Industrial Science, 86, Kyushu University, Hakozaki, Higashi-ku, Fukuoka 812
(Received March 25, 1981)

Synopsis. The Rose Bengal-sensitized photooxidation of some dioxetane-forming olefins, the Diels-Alder dimer of spiroheptadiene, indene, acenaphthylene, and thujopsene, under an $^{18}O_2$-atmosphere yielded the labelled analogs of the previously characterized *cis*-1,2-glycols. According to the mass-spectral analysis, both oxygens of the glycols were derived from the oxygen molecule.

Recently, we have shown the formation of *cis*-1,2-glycols in the Rose Bengal (RB)-sensitized photooxygenation of certain dioxetane-forming olefins.[2-4] It was deduced that the intermediate dioxetanes were involved in this reductive step. Should this be the case, both the oxygen atoms must come from the molecular oxygen. However, an accompanying formation of a *seco*-cyclopropane glycol (**A**), even in low yields, in the reaction of dispiro[cyclopropane-1,3′-tricyclo[5.2.1.$0^{2,6}$]deca-4′,8′-diene-10′,1″-cyclopropane] (**1**) arises the question that an epoxide (**B**) may be a precursor of both **A** and the *cis*-1,2-glycol (**2**). Consequently, to provide independent evidence, we have carried out ^{18}O-labelling experiments with **1**, indene (**3**),[4,5] a frequently studied dioxetane-forming olefin, and acenaphthylene (**4**),[4] as well as with thujopsene (**5**), a sesquiterpenoid cyclopropane derivative.[3]

Following the previous method,[2] the irradiation of **1** was performed by means of a tungsten lamp with a relatively large amount of RB, *ca.* 1.4 mmol/cm^3, in a mixed solution of methanol and pyridine under a 99%-enriched $^{18}O_2$-atmosphere[6] for 51 h by cooling with running water; the product mixture was then fractionated by silica-gel column chromatography to give the solvolyzed methoxy alcohol (**6**), 3%, and the glycol (**2**), 10%. The mass-spectral determination of **2** revealed an incorporation of two ^{18}O-atoms in the molecule with a more than 62% isotopic purity. Because of the weakness of the intensities of the molecular ions (less than 1% of the total ions), the peaks at *m/e*: 220 ($C_{14}H_{18}O^{18}O$) and 218 ($C_{14}H_{18}O_2$) were obscured under the noise level, and so the given figures (see Experimental) for the intensities of these weak peaks might be higher than the actual isotopic contents. At this stage, it can merely be pointed out that the solvolytic formation from **B** must be a minor path.

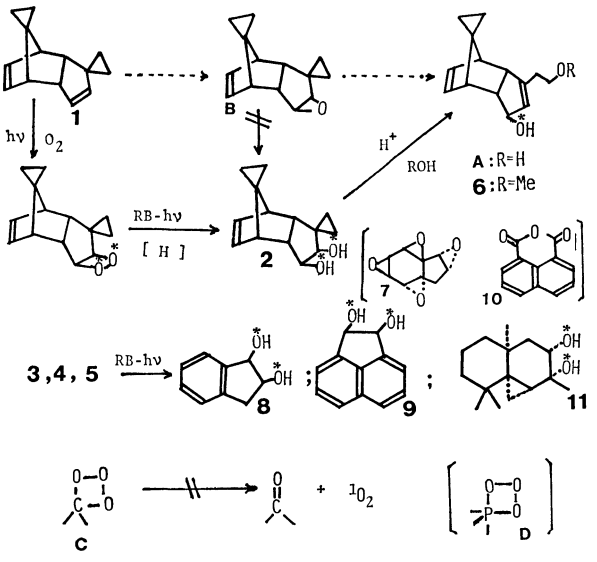

Scheme 1.

Next, a similar $^{18}O_2$-photooxygenation was carried out with indene (**3**); when the oxygenation was carried out at −40 °C in methanol, the major product was identified as the tetraepoxide (**7**), which was previously reported to be formed in the oxidation in aprotic solvents.[7] However, when the oxygenation was carried out at *ca.* 15—25 °C, after a work up by silica-gel column chromatography of the reaction mixture,[2,4] the desired *cis*-1,2-indandiol (**8**) was obtained in an 18% yield, together with other, previously identified products.[4,5] The mass-spectral analysis of **8** again confirmed the incorporation of two ^{18}O-atoms, with the relative intensity of *m/e*: 150, 152, and 154 being 2.3:1.7:96.

Although the relative rate of the oxygenation of acenaphthylene (**4**) is known to be very small, we have also carried out an $^{18}O_2$-experiment. The results were entirely the same as those of **8**; the *cis*-1,2-diol (**9**), obtained in a 24% yield, was shown to be $C_{12}H_8$-$^{18}O_2$, the relative intensity of the peaks at *m/e*: 186:188:190 being 8:6:86. The major product in this case was 1,8-naphthalic anhydride (**10**) (58%), whose mass spectrum indicated the incorporation of three ^{18}O-atoms.

As has previously been described, the solvolysis of the epoxy derivatives is known to give not only *trans*-1,2-diols, but, also the *cis*-glycols, **8** and **9**;[4] the present experiments can be employed to evaluate such solvolytic formation of *cis*-1,2-glycols by analyzing the mono-^{18}O-labelled products. The results show that this process is merely a side path; in the cases of **8** and **9**, a mass spectrometry gave estimates of *ca.* 2% and 6%. Consequently, the possible involvement of the epoxides in the sensitized photooxygenative formation of **8** and **9** has been unambiguously eliminated, and in turn, the intermediacy of the dioxetanes for the *cis*-glycol formation has been established.

Finally, the RB-sensitized photooxygenation of **5** was carried out in methanol under a recovered $^{18}O_2$-atmosphere, contaminated with $^{16}O_2$; after a usual work-up using silica gel column chromatography afforded the *cis*-glycol (**11**)[3] in a 15% yield, together with other products characterized previously. The mass-

spectral determination of **11** clarified the incorporation of two ^{18}O-atoms in the molecule; the relative intensity of the molecular ions for 238:240:242 was 54:4:42, where the peak due to the mono-^{18}O-labelled **11** was very weak compared to the peaks of the other isomers, providing firm evidence for eliminating a trioxetane precursor (**C**).[8] Should this be the case, these three peaks should have a ratio of *ca.* 7:4:5 on the basis of the observed ^{16}O:^{18}O ratio of 5:4. At the same time, it may be difficult for any mechanism involving two oxygen molecules to explain these isotope distributions.

Experimental

*RB-Sensitized Photooxidation of **1** with $^{18}O_2$. Isolation of **2** and **6**:* A mixed solution of methanol (20 cm^3) and pyridine (5 cm^3) containing **1** (735 mg) and RB (115 mg) was repeatedly degassed and flushed with nitrogen under reduced pressure at −70 °C, after which 99%-$^{18}O_2$ gas (100 cm^3) was introduced into the reaction vessel by means of a gas buret. The irradiation was performed by means of a 500-W tungsten lamp for 51 h at 15—20 °C with vigorous stirring of the solution by the use of a magnetic bar. The reaction was checked occasionally by the volumetric analysis of O_2-consumption. The mixture was then warmed *in vacuo* to remove the solvent, and the residue was chromatographed on a silica-gel column; together with the recovered **1** (265 mg), the vinyloxirane and the dialdehyde,[9] the glycol **2** (colorless needles, mp 56—57 °C (57 mg, 10%) [Found: *m/e*, 218(4.3), 219(3.7), 220(2.8), 221(1.6), 222(11.6)]), and methoxy alcohol (6)(a colorless oil (18 mg, 3%) [Found: *m/e*, 232(27.8, 233(8.2), 234(100), 235(26.5), 236(7.5)]), were isolated.

*RB-Sensitized Photooxidation of **3**. Formation of **7**:* A methanol solution (20 cm^3) of **3** (735 mg) was similarly irradiated with RB (135 mg) at −40 °C for 10.5 h. The only product consisted of colorless crystals (mp 175—176 °C (lit,[7] 178.5—180.5 °C)), whose NMR spectrum was identical with that of **7** [Found: *m/e*, 188.0567 (10.4, M$^+$, Calcd for $C_9H_8{}^{18}O_4$: 188.0592), 183(4.4), 185(1.7), 186(1.1), 187.0522 (100, M$^+$−1, Calcd for $C_9H_7{}^{18}O_4$: 187.0514, and $C_9H_9O^{18}O_3$ requires 187.0628)].

*RB-Sensitized Oxidation of **3** with $^{18}O_2$. Isolation of **8**:* A methanol solution (20 cm^3) of **3** (500 mg) was irradiated at 15—25 °C by means of a 500-W tungsten lamp in the presence of RB (100 mg) under an $^{18}O_2$-atmosphere for 8.5 h. The reaction mixture was then evaporated *in vacuo* to remove the solvent, and the residue was chromatographed on a silica-gel column; fractions eluted from hexane–ethyl acetate (8:2) contained two methoxy hydroperoxides, homophthalaldehyde and its cyclic acetal,[4] but no further characterization was attempted. From hexane-ethyl acetate (6:4), **8** (colorless crystals, mp 102.5—103 °C, 90 mg (18%) [Found: *m/e*, 154.0766 (M$^+$, Calcd for $C_9H_{10}{}^{18}O_2$: 154.0766)]) was isolated.

*RB-Sensitized Photooxidation of **4** with $^{18}O_2$. Isolation of **9** and **10**:* A methanol solution (12 cm^3) of **4** (430 mg) was irradiated at 15—25 °C by means of a 500-W tungsten lamp in the presence of RB (70 mg) under an $^{18}O_2$ atmosphere for 55 h. The reaction mixture was then evaporated *in vacuo* to remove the solvent, and the residue was chromatographed on a silica-gel column to give, after the elution of the recovered **4** (200 mg), colorless needles (mp 213—214 °C, **9**, 70 mg (24%) [Found: *m/e*, 190.0767 (M$^+$, Calcd for $C_{12}H_{10}{}^{18}O_2$: 190.0766)). The relative intensity of *m/e*: 186: 188:190=8:6:86], and 1,8-naphthalenedicarboxylic anhydride (**10**), mp 268—270 °C, 178 mg (58%) [Found: *m/e*, 204 ($C_{12}H_6{}^{18}O_3$)].

*RB-Sensitized Photooxygenation of **5**. Formation of **11**:* A mixed solution of methanol (8 cm^3) and acetone (6 cm^3) containing **5** (535 mg) and RB (75 mg) was irradiated by means of a 500-W tungsten lamp under an $^{18}O_2$-atmosphere (45%) for 35 h at 20—25 °C. The mixture was then chromatographed on a silica-gel column to give, after the elution of the recovered **5** (238 mg), colorless needles (mp 63—65 °C, **11** (53 mg, 15%) [Found: *m/e*, 242.2009 (M$^+$, Calcd for $C_{15}H_{26}{}^{18}O_2$: 242.2015)). The relative intensities of *m/e*: 240:241:242=54:4:42; *m/e*: 220:222=45:55].

References

1) Part XXII: H. Takeshita, I. Shimooda, and T. Hatsui, *Kyushu Daigaku Seisan Kagaku Kenkyusho Hokoku*, **72**, 15 (1980).

2) H. Takeshita and T. Hatsui, *J. Org. Chem.*, **43**, 3080 (1978).

3) H. Takeshita, T. Hatsui, and I. Shimooda, *Tetrahedron Lett.*, **1978**, 2889.

4) T. Hatsui and H. Takeshita, *Bull. Chem. Soc. Jpn.*, **53**, 2655 (1980).

5) a) P. A. Burns and C. S. Foote, *J. Org. Chem.*, **41**, 899 (1976); b) W. Fenical, D. R. Kearns, and P. Radlick, *J. Am. Chem. Soc.*, **91**, 7771 (1969); c) A. Frimer, *Chem. Rev.*, **79**, 359 (1979).

6) The 99%-enriched O_2 gas was purchased from the Prochem Co., Ltd.

7) C. S. Foote, S. Mazur, P. A. Burns, and D. Lerdal, *J. Am. Chem. Soc.*, **95**, 586 (1973).

8) A phosphorus analog (**D**) of **C** is known to generate singlet oxygen. See H. H. Wasserman, J. R. Scheffer, and W. A. Yager, *J. Am. Chem. Soc.*, **90**, 4160 (1968).

9) a) H. Takeshita, T. Hatsui, and H. Kanamori, *Tetrahedron Lett.*, **1973**, 1697; b) H. Takeshita, T. Hatsui, and H. Mametsuka, *Heterocycles*, **11**, 323 (1978).

Stereochemistry of Friedel-Crafts Alkylation of Benzene with Optically Active 2-Chlorobutane

Sohei SUGA,* Masahito SEGI, Kiyoyuki KITANO, Shinji MASUDA,** and Tadashi NAKAJIMA

Department of Industrial Chemistry, Faculty of Technology, Kanazawa University, Kodatsuno, Kanazawa 920

***Ashikaga Institute of Technology, Omae-cho, Ashikaga 326*

(Received April 2, 1981)

Synopsis. The alkylation of benzene with (+)-2-chlorobutane (**1**) by Lewis acid catalyst gave stereospecifically (−)-2-phenylbutane (**2**) with inversion of configuration at low temperature for short reaction times. A lowering of the stereospecificity of the reaction was found to be partly due to the racemization of (+)-**1** and (−)-**2**.

Friedel-Crafts alkylation has long been pointed out to proceed with almost complete racemization when an optically active alkylating reagent was used. For example, Price, Burwell, and Streitwieser reported that the alkylation of benzene with optically active 2-butanol and propan-1,1,1-d_3-2-ol gave almost racemic 2-phenylbutane and 2-phenylpropane-1,1,1-d_3, respectively, and concluded that these alkylations proceeded *via* a free carbonium ion intermediate.[1-3] However, some examples of the highly stereospecific reactions have been reported; the high degree of stereospecificity of the reactions was explained on the basis of the cyclic nature of the alkylating reagents or the formation of the cyclic intermediates.[6]

Recently, Rosenberg reported that the Friedel-Crafts alkylation of benzene with (+)-2-butanol by $AlBr_3$ catalyst gave (−)-2-phenylbutane with 27% inversion of configuration.[4] This is the only example of stereospecific Friedel-Crafts alkylation with such a simple alkylating reagent. On the other hand, Eliel reported that an optically active 2-phenylbutane was readily racemized under the influence of $AlCl_3$ at 0 °C.[5] These results prompted us to investigate the reaction with a simple acyclic reagent, optically active 2-chlorobutane (**1**).

Results and Discussion

Optically pure (*S*)-(+)-**1** was easily prepared from (+)-propylene oxide *via* (−)-2-butanol. The alkylation of benzene with (+)-**1** was carried out using a variety of Lewis acids as the catalyst. These reactions gave 2-phenylbutane (**2**) mainly and few by-products (<1%). The **2** produced was separated and its optical rotation was determined. The results are summarized in Table 1. The alkylations by $AlCl_3$, $FeCl_3$, and $AlCl_3$–CH_3NO_2 catalysts proceeded with inversion of configuration to give (*R*)-(−)-**2**. In the case of $AlBr_3$ catalyst the product was an almost racemic **2**.

In the case of the alkylation by $AlCl_3$ catalyst at −30 °C, the optical yield of the reaction decreased from 24%(50 s) to 14%(100 s) or 12%(120 s) with increasing reaction time. The product given at −10 °C for 20 min was completely racemic. The decrease of the optical yield appears to be due to a great extent to the racemization of (−)-**2** produced, because the alkylation proceeds to completion within 30 s even at −30 °C.

In the presence of $FeCl_3$ the racemization of (−)-**2** scarcely occurred for 60 min at 0 °C (Table 2). On the other hand, the starting (+)-**1** was racemized from $[\alpha]_D$ +27.0° to +6.1° by $FeCl_3$ catalyst in 1,2-dichloroethane for 4 min at 0 °C.

In the preceding paper,[6] we attempted to evaluate the net stereospecificity in the alkylation from the extent of alkylation and the remaining optical activity of the starting material by considering a kinetic model.[7] In the alkylation with (+)-**1** at 0 °C (4 min), **2** was obtained in 70% yield and in 24% optical yield, and the optical activity of the starting chloride was depressed to 22% of the initial value. The rate of alkylation and racemization of the chloride were calculated to be 5.0×10^{-3} s^{-1} and 6.3×10^{-3} s^{-1}, respectively. Therefore, the net stereospecificity in the

Table 1. Alkylation of benzene with (*S*)-2-chlorobutane (**1**) in the presence of lewis acids[a]

Lewis acid	Temp °C	Time min	Conv.[b] %	(*R*)-2-Phenylbutane (**2**) $[\alpha]_D$ (*c* 5, $CHCl_3$)	(*R*)-2-Phenylbutane (**2**) O.Y.[c] %
$AlCl_3$[d]	−30	0.8	100	−4.7°	24
$AlCl_3$[d]	−30	1.6	100	−2.8°	14
$AlCl_3$[d]	−30	2.0	100	−2.4°	12
$AlCl_3$[d]	−10	20	100	0.0°	0
$FeCl_3$[e]	0	4.0	70	−4.6°	24
$AlCl_3$–CH_3NO_2 (1:15)	30	15	30	−2.5°	13
$AlBr_3$[d]	−30	1.0	100	0.0°	0

a) Mole ratio is (*S*)-1: Lewis acid:benzene=1:0.15:30. The optical rotation of (*S*)-1 used was $[\alpha]_D$ +28.0° (neat). b) Determined by GLC. c) Calculated from the reported rotations of (*S*)-1 (+34.8°)[8] and (*R*)-2 (−23.6°).[9] d) A small amount of carbon disulfide was added. e) A small amount of 1,2-dichloroethane was added.

Table 2. Reaction of (*R*)-2-phenylbutane (**2**) in the presence of iron(III) chloride at 0 °C[a)]

Time / min	Recovered (*R*)-**2**	
	$[\alpha]_D$	O.P./%[d)]
0	−2.8° [b)]	12
5	−2.5° [b)]	10
60	−2.6° [c)]	11

a) Mole ratio is (*R*)-2: $FeCl_3$: benzene = 1:0.15:30. A small amount of carbon disulfide was added. b) Measured in benzene (*c* 5.0). c) Measured in benzene (*c* 3.0). d) Calculated from the reported rotation $[\alpha]_D$ −23.6° (neat).[9)]

alkylation step was calculated to be 40%.

Friedel-Crafts reactions of primary halides are thought to proceed in part by a displacement process.[10,11)] Such views are consistent with our stereochemical results about the reaction of 2-chlorobutane. However, the possibility of a carbonium ion character in the alkylating intermediate is not excluded. In addition, the lesser stereospecificity in the alkylations reported in the literature[1–3)] may be attributed in part to the successive racemization of the product and the simultaneous racemization of the starting material, which are caused by raising the reaction temperature and prolonging the reaction time.

Experimental

GLC analysis was carried out on a 2 m column of 10% Carbowax 20 M on Diasolid L with a Shimadzu GC-3BT instrument. Optical rotations were taken with a JASCO DIP-SL polarimeter using 1 or 0.5 cm tubes.

Benzene was washed with concentrated sulfuric acid and water, and distilled after drying on sodium ribbon. Other solvents were dried[12)] and distilled before use. Aluminium chloride was purified by sublimation under nitrogen. Other Lewis acids of commercial GR grade were used without further purification.

*(+)-2-Chlorobutane (**1**).* (+)-Propylene oxide[6)] (20 g, 0.35 mol) was added to an ethereal solution (400 ml) of methyllithium (1.0 mol) at 0 °C. After the addition, the reaction mixture was refluxed for 12 h, decomposed with water (50 ml), and extracted three times with 100 ml of ether. The extracts were fractionally distilled to give 19 g of (−)-2-butanol, $[\alpha]_D$ −11.8°(neat). Dichlorophenylphosphine (12.2 g, 0.0682 mol) and (−)-2-butanol (10 g, 0.137 mol) were mixed at 0 °C, stirred for 1 h, then distilled on a cooled trap *in vacuo*. The distillate was fractionated by a column to yield 4 g of (+)-**1**, bp 68 °C, $[\alpha]_D$ +28.0°(neat), [Lit,[8)] $[\alpha]_D$ +34.8°(neat)].

Alkylation. To a stirred mixture of benzene (13 g, 160 mmol), Lewis acid (0.81 mmol), and carbon disulfide (4 ml), (+)-**1** (500 mg, 5.4 mmol) was added at the prescribed temperature. The resulting mixture was allowed to stand at the above temperature for the prescribed period with stirring, then quenched with ice water (5 ml). The organic layer was separated, washed with water, and dried over anhydrous sodium sulfate. After the removal of solvent, the residue was distilled by fractionating column to give (−)-**2**, bp 68—70 °C/20 mmHg.

*Racemization of (+)-**1** or (−)-**2**.* A stirred mixture of (+)-**1** (500 mg, 5.4 mmol), iron (III) chloride (130 mg, 5.4 mmol), and 1,2-dichloroethane (14 ml) was treated at 0 °C for 4 min. After the usual work-up, the optical rotation of the recovered **1** was measured. Racemization of (−)-**2** was also carried out in a similar manner.

References

1) C. C. Price and M. Lund, *J. Am. Chem. Soc.*, **60**, 2499 (1938); **62**, 3105 (1940).

2) R. L. Burwell, Jr., and S. Archer, *J. Am. Chem. Soc.*, **64**, 1032 (1942).

3) A. Steitwieser, Jr., and P. J. Stang, *J. Am. Chem. Soc.*, **87**, 4953 (1965).

4) P. A. Spanninger and J. L. von Rosenberg, *J. Am. Chem. Soc.*, **94**, 1973 (1972).

5) E. L. Eliel, P. H. Wilken, and F. T. Fang, *J. Org. Chem.*, **22**, 231 (1957).

6) T. Nakajima, S. Suga, T. Sugita, and K. Ichikawa, *Bull. Chem. Soc. Jpn.*, **40**, 2980 (1967); *Tetrahedron*, **25**, 1807 (1969); S. Suga, T. Nakajima, Y. Nakamoto, and K. Matsumoto, *Tetrahedron Lett.*, **1969**, 3283; T. Nakajima, S. Masuda, S. Nakashima, T. Kondo, Y. Nakamoto, and S. Suga, *Bull. Chem. Soc. Jpn.*, **52**, 2377 (1979); J. I. Brauman and A. J. Pandel, *J. Am. Chem. Soc.*, **89**, 5421 (1967); J. I. Brauman and A. Solladié-Cavallo, *Chem. Commun.*, **1968**, 1124.

7) The effect of the difference between the solvents, benzene and 1,2-dichloroethane, was neglected in present calculation.

8) D. G. Goodwith and H. R. Hudson, *J. Chem. Soc., B*, **1968**, 1333.

9) D. J. Cram and W. D. Nielsen, *J. Am. Chem. Soc.*, **83**, 2174 (1961).

10) H. Jungk, C. R. Smoot, and H. C. Brown, *J. Am. Chem. Soc.*, **78**, 2185 (1956).

11) S. H. Sharman, *J. Am. Chem. Soc.*, **84**, 2945 (1962).

12) J. A. Riddick and E. E. Toops, Jr., "Organic Solvents," 2nd ed, Interscience Publishers, Inc., New York (1955).

MINDO/3 Calculations of Kinetic Isotope Effects in Heterolysis of Neopentyl Alcohol

Takashi Ando,* Hiroshi Yamataka, Satoshi Yabushita,†
Kizashi Yamaguchi,† and Takayuki Fueno*,†

The Institute of Scientific and Industrial Research, Osaka University, Suita, Osaka 565
† *Department of Chemistry, Faculty of Engineering Science, Osaka University, Toyonaka, Osaka 560*

(Received April 17, 1981)

Synopsis. Geometrical optimization of the protonated neopentyl alcohol and the transition state of its heterolysis was carried out using the MINDO/3 SCF-MO method. A cyclic structure was predicted for the transition state. Agreement between the calculated and experimental values for the carbon-14 kinetic isotope effects was excellent.

Neopentyl derivatives **1**, having a fully substituted carbon atom next to the reaction center, usually give rise to substitution and elimination products to be derived from the rearranged *t*-pentyl cation **2** under solvolytic conditions (Eq. 1). The timing of this rearrangement, concerted or stepwise, has long been a subject of controversy. Pieces of evidence for and against methyl participation have been accumulated from kinetic and stereochemical researches.[1,2]

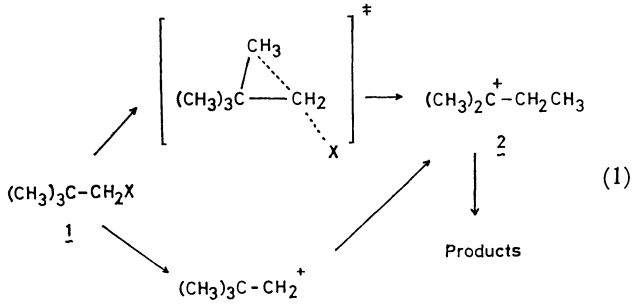

(1)

Recent studies using kinetic isotope effect (KIE) revealed that the three methyl groups are not equivalent in the role in governing the reaction rate, only the migrating methyl group showing a large isotope effect.[3,4] This fact, as well as the KIE data for α and β carbons, tends to support the concerted mechanism.[3,4]

However, methyl participation or bridging is not the only possible explanation for the observed inequality in the KIE for the methyl carbons. Hyperconjugation is also strongly angular-dependent, and the idea that hyperconjugation and bridging may merge has been presented.[5]

In order to gain an additional insight to the mechanism of neopentyl solvolysis, semiempirical SCF-MO calculations were carried out on the heterolysis process of neopentyl alcohol. Kinetic isotope effects were calculated from the molecular vibration frequencies of both the reactant and the transition state, and compared with the experimentally observed values.

Results and Discussion

Calculations were carried out by the MINDO/3 method.[6,7] The local minimum of the protonated neopentyl alcohol $(CH_3)_3CCH_2OH_2^+$ as reactant was determined by the geometrical optimization procedure based on the gradient method.[8] The results are shown in Fig. 1.

In order to determine the transition state geometry, the entire system at given C–O bond lengths was energetically optimized[9] with respect to the remaining degrees of freedom. As the C–O bond was elongated, the methyl group at the *s-trans* position was caused to draw nearer to the α-carbon to form a distorted triangle. The transition state was reached when the C–C distance in question was 1.819 Å, as shown in Fig. 2.

Force constants and molecular vibration frequencies were calculated for the reactant and the transition state. The former has 51 normal frequencies, while the latter has one imaginary ($430i$ cm^{-1}) and 50 normal

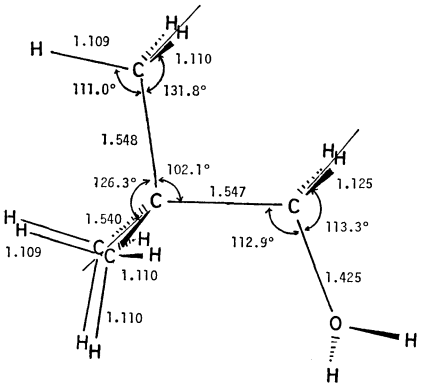

Fig. 1. Optimized structure of protonated neopentyl alcohol. Bond lengths appended are in units of Å.

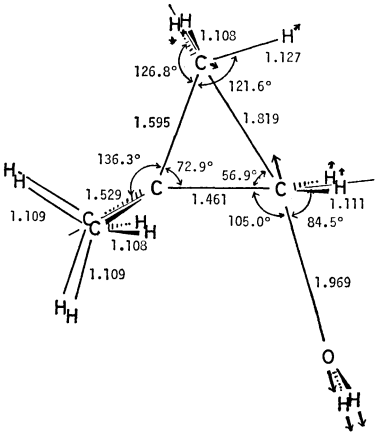

Fig. 2. Optimized structure of the transition state. Bond lengths in Å and reaction-coordinate motion are included.

Table 1. Calculated and experimental kinetic isotope effects in the heterolysis of neopentyl alcohol at 100 °C

Position[a)]	Calculated	Observed[b)]
α-^{14}C	1.084	1.073
α-D_2	0.982	1.187; 1.190
β-^{14}C	1.011	1.019
γ-^{14}C	1.022	1.037
γ-D_3	1.224	1.123
γ'-^{14}C	1.003	(1.00)[c)]
γ'-D_3	1.007	(0.95)[c)]

a) γ corresponds to the migrating methyl group while γ' to the nonmigrating groups. b) Combined data for the acetolyses of neopentyl *p*-nitrobenzenesulfonate and 2-methyl-2-adamantylmethyl brosylate (Ref. 3). c) Estimated from the data for the above-mentioned two compounds.

frequencies. The reaction-coordinate motion, *i.e.*, the mode of vibration with the imaginary frequency at the transition state, is also shown in Fig. 2. Kinetic isotope effects were calculated from the vibrational frequencies obtained.[10,11] The results are summarized in Table 1 together with the corresponding experimental data.

As can be seen from Table 1, the carbon-14 isotope effects calculated for the various carbon atoms involved agree reasonably well with the experimental data. The results lend strong support to the concept of the concerted mechanism for the neopentyl solvolysis. As for the deuterium isotope effects, however, the agreement between calculated and observed values is found to be rather poor. These contrasting results could best be reconciled by the view that the solvation effect, not considered in the present calculations, would perhaps be more important to those hydrogen atoms which embroider the skeleton carbon atoms and hence are exposed to the solvent environment to a higher extent.

In conclusion, the present calculations support the concerted mechanism for the neopentyl solvolysis, even though there is still some question with respect to the accuracy of MINDO/3 calculations on transition states for ionic reactions.

References

1) J. E. Nordlander, S. P. Jindal, P. v. R. Schleyer, R. C. Fort, Jr., J. J. Harper, and R. D. Nicholas, *J. Am. Chem. Soc.*, **88**, 4475 (1966); W. G. Dauben and J. L. Chitwood, *ibid.*, **90**, 6876 (1968), **92**, 1624 (1970); S. H. Liggero, R. Sustmann, and P. v. R. Schleyer, *ibid.*, **91**, 4571 (1969); I. L. Reich, A. Diaz, and S. Winstein, *ibid.*, **91**, 5635 (1969); P. C. Myhre and E. Evans, *ibid.*, **91**, 5641 (1969); G. Solladie, M. Muskatirovic, and H. S. Mosher, *J. Chem. Soc., Chem. Commun.*, **1968**, 809.

2) M. J. Blandamer and R. E. Robertson, *Can. J. Chem.*, **42**, 2137 (1964); W. M. Schubert and W. L. Henson, *J. Am. Chem. Soc.*, **93**, 6299 (1971); D. J. Raber, J. M. Harris, and P. v. R. Schleyer, "Ions and Ion Pairs in Organic Reactions," ed by M. Szwarc, Wiley, New York (1974), Vol. 2, p. 247.

3) T. Ando, H. Yamataka, J. Kuramochi, J. Yamawaki, and Y. Yukawa, *Tetrahedron Lett.*, **1976**, 1879; T. Ando, J. Yamawaki, and H. Morisaki, *ibid.*, **1979**, 117; T. Ando, H. Yamataka, H. Morisaki, J. Yamawaki, J. Kuramochi, and Y. Yukawa, *J. Am. Chem. Soc.*, **103**, 430 (1981).

4) V. J. Shiner, Jr., and J. J. Tai, *Tetrahedron Lett.*, **1979**, 127, *J. Am. Chem. Soc.*, **103**, 436 (1981).

5) For a recent review of the topic see: B. Capon and S. P. McManus, "Neighboring Group Participation," Plenum Press, New York (1976), Vol. 1, pp. 31—43.

6) R. C. Bingham, M. J. S. Dewar, and D. H. Lo, *J. Am. Chem. Soc.*, **97**, 1285 (1975).

7) The calculations were carried out using ACOS 900 computer at the Computation Center of Osaka University.

8) J. W. McIver, Jr., and A. Komornicki, *Chem. Phys. Lett.*, **10**, 303 (1971).

9) J. W. McIver, Jr., and A. Komornicki, *J. Am. Chem. Soc.*, **94**, 2625 (1972).

10) J. Bigeleisen and M. G. Mayer, *J. Chem. Phys.*, **15**, 261 (1947); J. Bigeleisen, *ibid.*, **17**, 675 (1949).

11) M. J. S. Dewar and G. P. Ford, *J. Am. Chem. Soc.*, **99**, 8343 (1977); S. B. Brown, M. J. S. Dewar, G. P. Ford, D. J. Nelson, and H. S. Rzepa, *ibid.*, **100**, 7382 (1978).

Preparation of (*R*)-*N*,*N*-Dimethyl-1-[2-(diphenylphosphino)ferrocenyl]-2-propanamines and Asymmetric Grignard Cross-coupling Catalyzed by Nickel Complexes with the Phosphine Ligands

Tamio HAYASHI, Mitsuo KONISHI, Takeshi HIOKI, Makoto KUMADA,*
Aleksander RATAJCZAK,† and Halina NIEDBAŁA†

Department of Synthetic Chemistry, Faculty of Engineering, Kyoto University, Yoshida, Sakyo-ku, Kyoto 606

† *Laboratory of Organic Chemistry, Institute of Chemistry, Silesian University, 40-006 Katowice, Poland*

(Received May 25, 1981)

Synopsis. A pair of diastereoisomeric phosphines, (*R*)-*N*,*N*-dimethyl-1-[2-(diphenylphosphino)ferrocenyl]-2-propanamines, have been prepared and used as ligands for nickel-catalyzed asymmetric cross-coupling of 1-phenylethylmagnesium chloride with vinyl bromide to give 3-phenyl-1-butene of 14—15% enantiomeric excess.

We have recently prepared various kinds of chiral ferrocenylphosphines, *e.g.*, (*S*)-*N*,*N*-dimethyl-1-[(*R*)-2-(diphenylphosphino)ferrocenyl]ethylamine [(*S*)-(*R*)-PPFA], starting with *N*,*N*-dimethyl-1-ferrocenylethylamine.[1] Some of them have been found to be effective ligands for several transition metal complex catalyzed asymmetric reactions giving rise to high optical yields.[2] Here we report the preparation of new chiral ferrocenylphosphines from *N*,*N*-dimethyl-1-ferrocenyl-2-propanamine and their use as ligands for nickel-catalyzed asymmetric Grignard cross-coupling.

Results and Discussion

(*R*)-*N*,*N*-Dimethyl-1-ferrocenyl-2-propanamine[3] (**1**) (80% ee) was lithiated with an excess of butyllithium in ether, and the lithiated ferrocene was then treated with chlorodiphenylphosphine. (*R*)-*N*,*N*-Dimethyl-1-[2-(diphenylphosphino)ferrocenyl]-2-propanamines (**2**), which consisted of two diastereomeric isomers in a 1:1 ratio, were obtained in 35% yield (Eq. 1). The

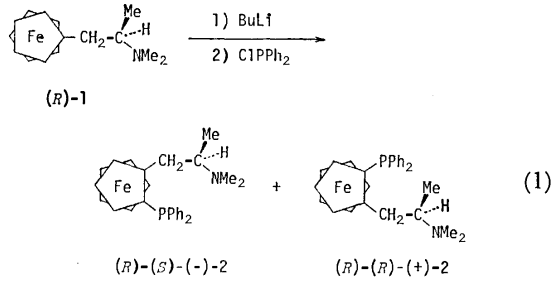

(1)

two isomers were isolated by alumina preparative TLC; the specific rotation of one isomer was $[\alpha]_D^{25}$ +187° and that of the other was $[\alpha]_D^{25}$ −219°. The configurations of ferrocene planar chirality of (+)- and (−)-**2** were estimated empirically[1] to be *R* and *S*, respectively. It should be noted that the lithiation of **1** is not stereoselective while the lithiation of *N*,*N*-dimethyl-1-ferrocenylethylamine has been reported to proceed with high stereoselectivity.[4]

The asymmetry inducing ability of (*R*)-(*R*)- and (*R*)-(*S*)-**2** as chiral ligands was examined in the nickel catalyzed cross-coupling of 1-phenylethylmagnesium chloride (**3**) with vinyl bromide (**4**) (Eq. 2). The

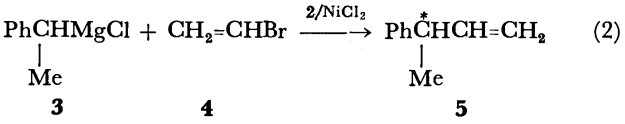

(2)

results are summarized in Table 1, which also contains the results obtained with (*S*)-(*R*)-PPFA ligand.[2a] The catalysts were prepared in situ by mixing nickel chloride and a chiral ligand. The ratio of nickel to ligand did not influence the stereoselectivity, and the catalytically active species is thought to consist of nickel and **2** or PPFA in a one-to-one ratio, not in a one-to-two ratio, regardless of the initial ratio of nickel chloride to the ligand.[2i] The Table contains three significant features. (1) The optical purity of the coupling product, 3-phenyl-1-butene (**5**), obtained here with **2** (14—15% ee) is much lower than that obtained with the PPFA ligand (61% ee). (2) The ferrocene planar chirality in **2** plays a more important role than the carbon central chirality, the diastereomeric isomers (*R*)-(*R*)- and (*R*)-(*S*)-**2** giving **5** with almost the same optical purity and different configurations. (3) The phosphine ligands (*R*)-(*R*)-**2** and (*S*)-(*R*)-PPFA, both of which have the same planar chirality *R*, exhibited opposite stereoselectivity.

The important role of the ferrocene planar chirality causing asymmetric induction is what has been always observed in asymmetric synthesis catalyzed by chiral ferrocenylphosphine-transition metal complexes.[2] The dimethylamino group on the ferrocene side chain has been thought to enhance the stereoselectivity by coordinating to the magnesium atom of the Grignard reagent.[2a] In ferrocenylphosphine **2** the dimethyl-

TABLE 1. ASYMMETRIC CROSS-COUPLING OF **3** WITH **4**[a]

Chiral ligand	Yield of **5**[b] %	$[\alpha]_D^{22}$ (neat)	Optical purity (%)[c] (configuration)	
(*R*)-(*R*)-**2**[d]	88	+0.86°	15(18)[e]	(*S*)
(*R*)-(*S*)-**2**[d]	77	−0.80°	14(17)[e]	(*R*)
(*S*)-(*R*)-PPFA[f]	95	−3.59°	61	(*R*)

a) The coupling reaction was carried out at 0 °C for 40 h. **3**:**4**:catalyst=400:200:1. b) Yields based on **4** used were determined by GLC. c) Optically pure (*R*)-(−)-3-phenyl-1-butene (**5**) has $[\alpha]_D^{22}$ −5.91±0.04° (neat): T. Hayashi, M. Fukushima, M. Konishi, and M. Kumada, *Tetrahedron Lett.*, **21**, 79 (1980). d) **2**:$NiCl_2$=0.8:1.0. e) Corrected for the optical purity of the phosphine ligand (80% ee). f) PPFA:$NiCl_2$=2.0:1.0.

amino group is one methylene farther away from the ferrocene nucleus than in PPFA. This greater distance between the amino group and the chiral ferrocene moiety in **2** must make the stereocontrol by coordination less effective.

Experimental

Optical rotations were measured with a Yanagimoto OR-50 polarimeter. ^{1}H NMR were measured with a JEOL MH-100 spectrometer in chloroform-*d* using tetramethylsilane as an internal standard.

(*R*)-*N*,*N*-Dimethyl-1-ferrocenyl-2-propanamine (**1**) ($[\alpha]_{546}^{20}$ −24.2° (*c* 1.075, ethanol)) was prepared from (*R*)-1-ferrocenyl-2-propanamine ($[\alpha]_{546}^{20}$ −3.29° (*c* 5, ethanol), 80% ee) according to the procedure previously reported,[3] which was obtained by optical resolution of the racemic amine via its tartaric acid salt.[3]

*(*R*)-*N*,*N*-Dimethyl-1-[(*R*)-2-(diphenylphosphino)ferrocenyl]-2-propanamine [(*R*)-(*R*)-**2**] and (*R*)-*N*,*N*-Dimethyl-1-[(*S*)-2-(diphenylphosphino)ferrocenyl]-2-propanamine [(*R*)-(*S*)-**2**].* To a stirred solution of 255 mg (1.1 mmol) of (*R*)-**1** (80% ee) in 2.5 ml of ether was added 3.4 ml of 1.6 M butyllithium (5.4 mmol) in hexane at room temperature under nitrogen. After 5 h stirring at room temperature, 1.3 ml (7.0 mmol) of chlorodiphenylphosphine was added at 0 °C. The reaction mixture was refluxed for 2 h, and then hydrolyzed with saturated aqueous sodium hydrogencarbonate. The resulting organic layer and benzene extracts from the aqueous layer were combined and extracted with 10% phosphoric acid. The aqueous layer was made alkaline with 10% sodium hydroxide, and extracted with ether. The ether solution was dried over anhydrous sodium sulfate, and evaporated under reduced pressure. The residue was purified by preparative TLC on silica gel (R_f 0.3—0.7 with 9:1 ethyl acetate–methanol) to give 160 mg (35% yield) of the product **2** as an orange-red oil. ^{1}H NMR spectrum showed that the product obtained consists of two diastereomeric isomers in one to one ratio. The two isomers were isolated by preparative TLC on alumina (3:5 chloroform–benzene). (*R*)-(*R*)-**2** (42 mg, 9%); R_f 0.7, $[\alpha]_D^{25}$ +187° (*c* 0.82, chloroform), NMR: δ 0.65 (d, 3H, J=7 Hz, CHC$\underline{H}_3$), 2.11 (s, 6H, NC$\underline{H}_3$), 2.33—2.62 (m, 1H, C$\underline{H}$CH$_3$), 2.63—2.82 (m, 2H, C$\underline{H}_2$), 3.75—4.52 (m, 3H, FeC$_5\underline{H}_3$), 3.92 (s, 5H, FeC$_5\underline{H}_5$), 7.13—7.75 (m, 10H, C$_6\underline{H}_5$). (*R*)-(*S*)-**2** (contaminated with 10% of (*R*)-(*R*)-**2**) (40 mg, 9%); R_f 0.6, $[\alpha]_D^{25}$ −219° (*c* 0.78, chloroform), NMR: δ 0.78 (d, 3H, J=7 Hz, CHC$\underline{H}_3$), 2.02 (s, 6H, NC$\underline{H}_3$), 1.94—2.30 (m, 2H, C$\underline{H}_2$), 2.93—3.21 (m, 1H, C$\underline{H}$CH$_3$), 3.65—4.43 (m, 3H, FeC$_5\underline{H}_3$), 3.95 (s, 5H, FeC$_5\underline{H}_5$), 7.08—7.70 (m, 10H, C$_6\underline{H}_5$). Found: C, 71.33; H, 6.58; N, 3.04%. Calcd for $C_{27}H_{31}NPFe$: C, 71.21; H, 6.64; N, 3.08%.

Asymmetric Grignard Cross-coupling. To a 100-ml pressure glass tube containing 13 mg (0.10 mmol) of anhydrous nickel chloride and 36 mg (0.08 mmol) of **2** was added at −78 °C 2.14 g (20 mmol) of vinyl bromide and 27 ml (40 mmol) of 1.5 M 1-phenylethylmagnesium chloride in ether. The glass tube was stoppered and allowed to warm up to 0 °C. The mixture was kept standing at 0 °C for 40 h, and hydrolyzed with 10% hydrochloric acid. After usual work-up, distillation through a short Vigreux column under reduced pressure followed by purification with preparative GLC (Silicone DC-550) gave 3-phenyl-1-butene. The yields and optical rotation data are shown in Table 1.

The present work was partly supported by a Grant-in-Aid for Scientific Research Nos. 510209 and 547080 from the Ministry of Education, Science and Culture.

References

1) T. Hayashi, T. Mise, M. Fukushima, M. Kagotani, N. Nagashima, Y. Hamada, A. Matsumoto, S. Kawakami, M. Konishi, K. Yamamoto, and M. Kumada, *Bull. Chem. Soc. Jpn.*, **53**, 1138 (1980).

2) a) T. Hayashi, M. Tajika, K. Tamao, and M. Kumada, *J. Am. Chem. Soc.*, **98**, 3718 (1976); b) T. Hayashi, K. Yamamoto, and M. Kumada, *Tetrahedron Lett.*, **1974**, 4405; c) T. Hayashi, T. Mise, S. Mitachi, K. Yamamoto, and M. Kumada, *ibid.*, **1976**, 1133; d) T. Hayashi, T. Mise, and M. Kumada, *ibid.*, **1976**, 4351; e) M. Zembayashi, K. Tamao, T. Hayashi, T. Mise, and M. Kumada, *ibid.*, **1977**, 1799; f) T. Hayashi, A. Katsumura, M. Konishi, and M. Kumada, *ibid.*, **1979**, 425; g) K. Tamao, T. Hayashi, H. Matsumoto, H. Yamamoto, and M. Kumada, *ibid.*, **1979**, 2155; h) T. Hayashi, K. Tamao, Y. Katsuro, I. Nakae, and M. Kumada, *ibid.*, **21**, 1871 (1980); i) T. Hayashi, M. Konishi, M. Fukushima, T. Mise, M. Kagotani, M. Tajika, and M. Kumada, *J. Am. Chem. Soc.*, in press.

3) a) A. Ratajczak and H. Zmuda, *Roczniki Chemii*, **49**, 215 (1975); b) A. Ratajczak and H. Zmuda, *Bull. Acad. Polon. Sci., Ser. Sci. Chim.*, **22**, 261 (1974).

4) D. Marquarding, H. Klusacek, G. Gokel, P. Hoffmann, and I. Ugi, *J. Am. Chem. Soc.*, **92**, 5389 (1970).

Fused Heterocycles. IV.[1] Synthesis of 7-(*o*-Hydroxyphenyl)-3,5-dimethyl-7,8-dihydro-6*H*-isoxazolo[4,5-*b*]azepines

Kooturu Malla Reddi, Citineni Janakirama Rao, and Ananthula Krishna Murthy*

Department of Chemistry, University College, Kakatiya University, Warangal 506009, India

(Received December 12, 1980)

Synopsis. Michael addition of acetylacetone to 3-methyl-4-nitro-5-(*o*-hydroxystyryl)isoxazoles gives 4-(*o*-acetoxyphenyl)-5-(3-methyl-4-nitro-5-isoxazolyl)-2-pentanones (**4**). Reductive cyclization of **4** with tin(II) chloride and concentrated hydrochloric acid leads to 7-(*o*-hydroxyphenyl)-3,5-dimethyl-7,8-dihydro-6*H*-isoxazolo[4,5-*b*]azepines. The formation of **4** has been rationalized through ortho effect. NMR and mass spectra of products have been discussed.

Though the formation of isoxazoles fused to a variety of heterocycles[2] has been extensively investigated, the isoxazoloazepines[3] have received very little attention. Furthermore, there is no general method of synthesis of isoxazoloazepines to date. Hence we recently reported the formation of hitherto unknown 3-methyl-5,7-diarylisoxazolo[4,5-*b*]azepines[4] by a facile reductive cyclization of ε-nitro ketones. In continuation of our interest, the report describes the preparation of title compounds.

Condensation of 3,5-dimethyl-4-nitroisoxazole (**1**) with various salicylaldehydes in boiling ethanol in the presence of piperidine gave the regioselective products namely, 3-methyl-4-nitro-5-(*o*-hydroxystyryl)isoxazoles (**2**).[5,6] Michael addition of acetylacetone to **2** has been carried out in boiling triethylamine for 4 h. The products which were insoluble in aq dil. sodium hydroxide and gave no colouration with iron(III) chloride have been identified as 4-(*o*-acetoxyphenyl)-5-(3-methyl-4-nitro-5-isoxazolyl)-2-pentanones (**4**) on the basis of IR (transparent in the hydroxyl region, 1775 cm^{-1} for ester >CO and 1725 cm^{-1} for ketonic >C=O) and NMR spectra (δ 2.35, s, 3H-$OCOCH_3$ and two doublets one each for 2H at 3.50 and 2.85 from two CH_2 groups). The 2-pentanone (**4**) might come through the intermediacy of **3** *via* **3A** and **3B** *i.e.*, due to ortho effect. The mechanism put forth is amply supported by the fact that 3-methyl-4-nitro-5-styrylisoxazoles (with no *o*-hydroxyl in the styryl moiety) and acetylacetone under identical conditions gave the β-diketones (**5**).[7]

The Michael products (**4**) on heating with tin(II) chloride and concd hydrochloric acid for 1.5—3.5 h underwent reductive cyclisation to 7-(*o*-hydroxyphenyl)-3,5-dimethyl-7,8-dihydro-6*H*-isoxazolo[4,5-*b*]azepines (**6**) through the intermediacy of the transient amino ketone. Five isoxazoloazepines thus prepared have been included in the table along with the characterization data. Chemical as well as spectroscopic evidence has been adduced for the occurrence of deacetylation during reduction. The cyclized product is not only soluble in dil. sodium hydroxide but also gives fairly intense colouration with iron(III) chloride. The IR spectrum shows no carbonyl absorption but a hydroxyl function (3300 cm^{-1}). Mass spectrum supports the same as it shows molecular ion at *m/e* 256. NMR spectrum shows only two methyls (δ 2.2, s, 3-CH_3; 1.8, s, 5-CH_3) and a hydroxylic proton at δ 3.8 which was neatly exchanged with D_2O. The four protons of the two methylenes and one methine proton of the azepine ring are not displayed distinctly and show complex splitting pattern in the region δ 2.4—3.5. Probably the chemical shift differences of these three types of protons are very little. The NMR

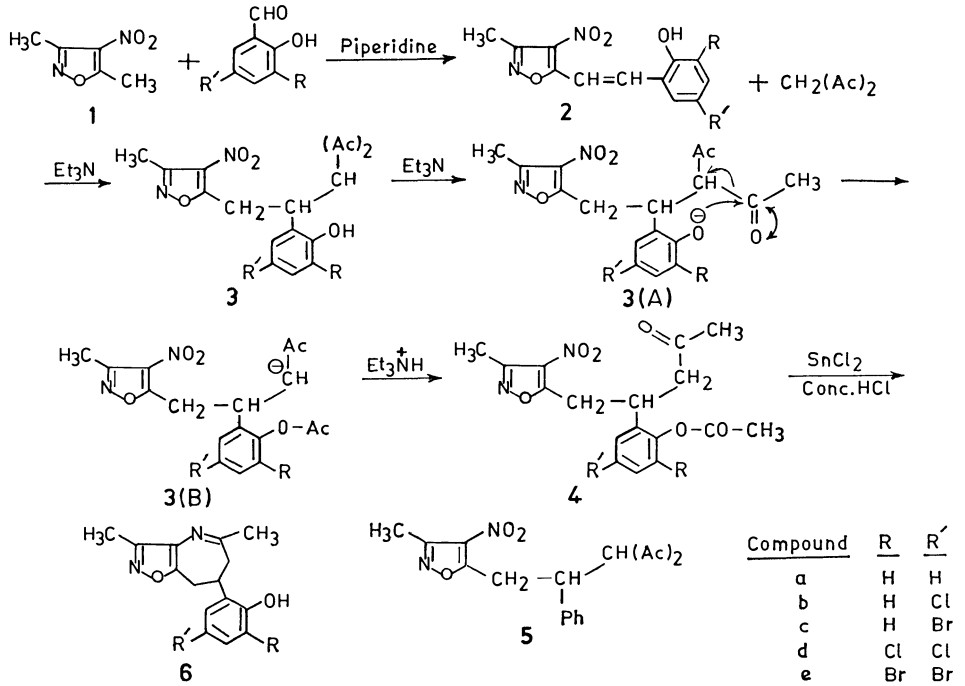

Fig. 1.

Table 1. The physical properties and elemental analysis of the products

Compound	Mp °C	Reaction time h	Yield %	Formula	Found (%) C	Found (%) H	Found (%) N	Calcd (%) C	Calcd (%) H	Calcd (%) N
2a	230	1.5	85	$C_{12}H_{10}N_2O_4$	58.40	3.99	11.10	58.53	4.06	11.30
2b	195	2.0	85	$C_{12}H_9N_2O_4Cl$	51.15	3.10	9.85	51.42	3.21	10.00
2c	250	2.0	80	$C_{12}H_9N_2O_4Br$	44.00	2.58	8.56	44.30	2.76	8.61
2d	203	2.5	82	$C_{12}H_8N_2O_4Cl_2$	45.52	2.37	8.78	45.71	2.53	8.88
2e	200	2.5	80	$C_{12}H_8N_2O_4Br_2$	35.27	1.75	6.80	35.64	1.98	6.93
4a	80	3.0	60	$C_{17}H_{18}N_2O_6$	58.65	5.10	8.00	58.95	5.20	8.09
4b	152	4.0	55	$C_{17}H_{17}N_2O_6Cl$	53.90	4.27	7.25	53.68	4.47	7.36
4c	95	4.5	50	$C_{17}H_{17}N_2O_6Br$	48.50	3.95	6.38	48.00	4.00	6.58
4d	155	4.5	40	$C_{17}H_{16}N_2O_6Cl_2$	49.10	4.00	6.59	49.15	3.85	6.74
4e	140	5.0	35	$C_{17}H_{16}N_2O_6Br_2$	40.25	3.25	5.43	40.47	3.17	5.55
6a	180	2.0	45	$C_{15}H_{16}N_2O_2$	70.25	6.00	10.82	70.31	6.25	10.93
6b	176	2.0	40	$C_{15}H_{15}N_2O_2Cl$	61.90	5.25	9.54	62.06	5.17	9.65
6c	166	2.0	45	$C_{15}H_{15}N_2O_2Br$	53.50	4.15	8.27	53.73	4.47	8.35
6d	178	2.5	30	$C_{15}H_{14}N_2O_2Cl_2$	55.17	4.52	8.50	55.38	4.30	8.61
6e	175	2.5	25	$C_{15}H_{14}N_2O_2Br_2$	43.60	3.28	6.67	43.47	3.38	6.76

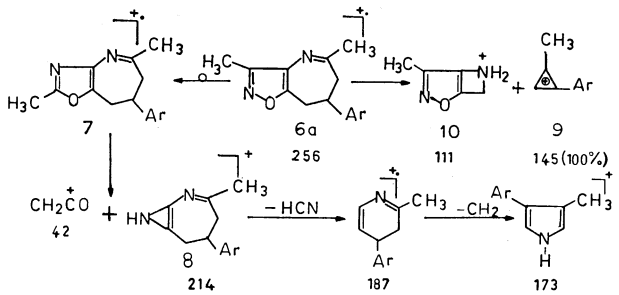

Fig. 2. Mass fragmentation of **6a**. Ar=*o*-OH-C_6H_4-

behaviour of these protons is in keeping with our eariler observation.[4]

In the mass spectrum of **6a**, the signal at *m/e* 214 is due to the ion **8** formed along with ketene by the fragmentation of **7** which comes from the molecular ion. This decomposition of the molecular ion is initiated by the cleavage of the N–O bond, the weakest linkage,[8] followed by ring transformation.[9] The base peak at *m/e* 145 is due to the resonance stabilised cation (**9**) formed together with **10** from the molecular ion.

Experimental

All the melting points are uncorrected. The purity of the compounds was checked by TLC. The IR spectra were recorded on Perkin-Elmer 283 model as KBr discs. ^{1}H NMR spectra were run on 90 MHz Varian EM-390 and 100 MHz JEOL spectrometers using TMS as internal reference and the mass spectra on Varian MAT CH-7 instrument at 70 eV. All the compounds prepared have been included in the table along with the characterization data.

3-Methyl-4-nitro-5-(o-hydroxystyryl)isoxazoles (2). 3,5-Dimethyl-4-nitroisoxazole (2.8 g, 0.02 mol) and salicylaldehydes (2 ml, 0.02 mol) were refluxed in ethanol (30 ml) in presence of traces of piperidine for 1.5 h. The reaction mixture was cooled and the products crystallized from ethanol–acetone.

4-(o-Acetoxyphenyl)-5-(3-methyl-4-nitro-5-isoxazolyl)-2-pentanones (4). 3-Methyl-4-nitro-5-(*o*-hydroxystyryl)isoxazoles (2.4 g, 0.01 mol), acetylacetone (3 ml, 0.03 mol), and triethylamine (35 ml) were refluxed for 3 h. Triethylamine was allowed to evaporate at room temperature. The residue was triturated with pet.ether and finally decomposed in methanol and filtered; colourless crystals from methanol. ^{1}H NMR ($CDCl_3$) of **4a**: δ 7.0—7.4 (m, 4H, Ar–H); 4.05 (m, 1H, >C–H); 3.5 (d, 2H, isoxazole–CH_2); 2.85 (d, 2H, –$COCH_2$–); 2.5 (s, 3H, isoxazole–CH_3); 2.35 (s, 3H, –$OCOCH_3$) and 2.05 (s, 3H, –$COCH_3$).

7-(o-Hydroxyphenyl)-3,5-dimethyl-7,8-dihydro-6H-isoxazolo-[4,5-b]azepines (6). Compound **4** (1.7 g, 0.005 mol), tin(II) chloride (12 g), and concd hydrochloric acid (15 ml) were heated together on water bath. Within a few minutes the reaction mixture became clear solution. After 0.5 h yellow crystalline compound began to separate. The heating is continued for further 2 h, cooled, filtered and washed with water. Recrystallization was effected from methanol. ^{1}H-NMR ($CDCl_3$) of **6a**: δ 6.9—7.2 (m, 4H, Ar–H); 3.8 (s, 1H, Ar–OH); 2.4—3.5 (5H, 6-CH_2–, 8-CH_2–, and >CH); 2.2 (s, 3H, 3-CH_3) and 1.8 (s, 3H, 5-CH_3).

The authors thank Prof. E. V. Sundaram, Head, Department of Chemistry, Kakatiya University for the facilities and Prof. P. Grunanger, University of Pavia, Italy, for helpful discussions. One of the authors (K. M. R) is grateful to the Director of Higher Education, Government of Andhra Pradesh, India, for the permission to carry out research.

References

1) Part III: C. J. Rao, K. M. Reddi, and A. K. Murthy, *Indian J. Chem.*, **20B**, 282 (1981).

2) E. C. Taylor and E. E. Garila, *J. Org. Chem.*, **29**, 2116 (1964); W. N. Speckamp, U. K. Pandit, and H. O. Huisman, *Recl. Trav. Chim. Pays-Bas Belg.*, **82**, 39 (1963); D. Govanni and G. Minoli, *Tetrahedron*, **26**, 1393 (1970).

3) P. K. Larsen, H. Hjeds, S. B. Christensen, and L. Brehm, *Acta Chem. Scand.*, **27**, 3251 (1973); M. Elliott, N. F. Janes, and K. A. Jeffs, *Chem. Ind. (London)*, **27**, 1175 (1967).

4) C. J. Rao and A. K. Murthy, *Indian J. Chem.*, **16B**, 636 (1978).

5) A. Quilico and C. Musante, *Gazz. Chim. Ital.*, **72**, 399 (1942).

6) A. K. Murthy, K. S. R. K. M. Rao, and N. V. S. Rao, *Indian J. Chem.*, **11**, 1074 (1973).

7) K. M. Reddi, C. J. Rao, and A. K. Murthy, *Indian J. Chem.*, **20B**, 607 (1981); Synthesis of Some Isoxazoles and Their Physiological Evaluation by C. J. Rao, Doctor thesis, Kakatiya University, 1980.

8) M. Ohashi, H. Kamachi, H. Kakisawa, A. Tatematsu, H. Yoshizumi, and H. Nakata, *Tetrahedron Lett.*, **3**, 379 (1968).

9) C. J. Rao and A. K. Murthy, *Indian J. Chem.*, **20B**, 335 (1981).

Theory of Molecular Deformation Due to the Vibronic Interaction between Two Closely-spaced Electronic Levels. I

Minoru KIMURA,† Kiyoshi NISHIKAWA, and Shigeyuki AONO*

†*Department of Physics, Faculty of Science, Kanazawa University, Marunouchi, Kanazawa, 920*

Department of Chemistry, Faculty of Science, Kanazawa University, Marunouchi, Kanazawa, 920

(Received July 3, 1980)

An theoretical investigation was made of the vibronic interaction between two electronic levels which are degenerate or nearly degenerate. Within the mean field approximation we derive a simplified effective Hamiltonian to analyze the problem of bond distortion of a molecule; the effective Hamiltonian is diagonalized by a linear canonical transformation of electronic operators. Thermodynamic arguments predict a possibility for appearance of a distorted phase below a characteristic temperature. The distorted phase is realized under a sufficiently strong coupling condition in a non-degenerate case, but under an arbitrarily small coupling condition in a degenerate case. The shift of electronic spectrum, the stabilization energy of the distortion, and thermodynamic quantities are expressed in terms of the parameters associated with the Hamiltonian. Change in electromagnetic properties due to the distortion is discussed. Magnitudes of the bond distortion and energy stabilization in the ground state are numerically estimated for cyclobutadiene, with results in good agreement with literature values.

Let us consider an electronic system with two discrete levels which are degenerate or nearly degenerate and coupled with each other through a vibronic interaction. Such a system can be taken as a prototype model for the variety of molecular distortion phenomena such as the Jahn-Teller or the pseudo Jahn-Teller effect and the bond alternation in conjugated molecules so-called the Peierls transition.[1)]

One attractive point with the present model is that it gives us a simple physical picture for the mechanism of molecular distortion; one can derive analogues with other similar problems in physics, *e.g.*, lattice distortions caused by electron-phonon interactions. It should be noted that there is a marked difference between the two problems, the lattice distortion and the present distortion; the former treats macroscopically large systems whereas the latter considers a single molecule or, at least, an aggregate of independent molecules. In our problem, therefore, we cannot expect any clear-cut transition at a finite temperature but can only anticipate a possible tendency with a large fluctuation towards transition to a new distorted ground state as temperature is lowered. Our finite temperature treatment, presented below, shows that phenomena are characterized by a temperature T_c below which this distortive character is expected to become noticeable. Within our present approximation this characteristic temperature is given by the apparent non-analyticity in free energy and electronic spectrum.

If temperature is much lower than T_c the molecule exists at its ground state where the distorted phase is well defined and stable as compared with the normal undistorted phase, provided the vibronic interaction is sufficiently strong.

To orient ourselves we will recapitulate the theory of bond alternation presented by Longuet-Higgins and Salem[2)] for conjugated molecules of linear polyenes and also present the iterative procedure developed by Nakajima *et al.*[3)] As the first step we tentatively adopt a structure with equal bond lengths and use the Hükel theory. We can thus specify molecular orbitals and orbital energies. From the former we find a set of bond orders, P_{rs}, between the rth and sth atomic sites. Next, we assume the relation of bond order, bond length, R_{rs}, and of bond length, resonance integral, β_{rs}, as

$$R_{rs} = R^0_{rs} + aP_{rs}, \tag{1}$$

$$\beta_{rs} = \beta^0_{rs} \exp(-bR_{rs}), \tag{2}$$

where R^0_{rs} and β^0_{rs} refer to the standarad geometry. Constant a in Eq. 1 is related to the force constant of lattice vibration which is assumed to be harmonic.[2)] Applying the P_{rs} obtained in the first step to Eq. 1, we can get a new set of bond lengths which enables us to estimate new resonance integrals by Eq. 2. We can then proceed to the next step on the eigenvalue problem. Such iterative treatments are repeated until a stable structure has been found. In the present theory, however, we can estimate stabilization energy and stable bond lengths in a single step.

Hamiltonian

The system in question is assumed to be well described by the Hamiltonian in the second quantized representation:

$$H = \sum_i \varepsilon_i a_i^+ a_i + \sum_q \omega_q b_q^+ b_q + \sum_{ijq} g_{ij:q} \phi_q a_i^+ a_j, \tag{3}$$

where a_i^+ and a_i are the creation and annihilation operators for the electron at the ith level, ε_i its energy, ω_q the phonon energy for mode q, $g_{ij:g}$ vibronic interaction constant, and ϕ_q is the phonon operator defined by

$$\phi_q = b_q^+ + b_q. \tag{4}$$

Throughout this article, we will use the unit of $\hbar = k_B = 1$ (k_B is the Boltzmann constant).

As mentioned above, we are considering only two electronic levels and, in order to avoid unnecessary complexity, the relevant phonon mode is also assumed to be single. It is convenient to use the following notations:

$$\varepsilon_1 = -\varepsilon, \ \varepsilon_2 = \varepsilon (\varepsilon > 0), \tag{5}$$

$$C = \begin{pmatrix} a_1 \\ a_2 \end{pmatrix}, \ C^+ = (a_1^+, a_2^+), \tag{6}$$

$$\hat{g} = \begin{pmatrix} 0 & g \\ g & 0 \end{pmatrix} = g\sigma_1. \tag{7}$$

Vibronic interaction constant g can be taken as real and we arrive at the model Hamiltonian:

$$H = C^+(-\varepsilon\sigma_3+q\sigma_1\phi)C + \omega b^+b, \tag{8}$$

where the Pauli matrices

$$\sigma_0=\begin{pmatrix}1&0\\0&1\end{pmatrix},\ \sigma_1=\begin{pmatrix}0&1\\1&0\end{pmatrix},\ \sigma_2=\begin{pmatrix}0&-i\\i&0\end{pmatrix},\ \sigma_3=\begin{pmatrix}1&0\\0&-1\end{pmatrix} \tag{9}$$

are used.

We further introduce the effective Hamiltonian, a good approximation to that of Eq. 8:

$$H^{eff} = -\varepsilon C^+\sigma_3 C + g\langle\phi\rangle C^+\sigma_1 C + \omega|\langle b\rangle|^2. \tag{10}$$

This form is based on an expectation that the so-called coherent state impling $\langle\phi\rangle\neq 0$ would be arranged by vibronic interaction.

Canonical Transformation

To diagonalize H^{eff} we will carry out a canonical transformation as follows:

$$\gamma = UC,\ \gamma^+ = C^+U^+, \tag{11}$$

where

$$U=\begin{pmatrix}u&-v\\v&u\end{pmatrix},\ U^+=\begin{pmatrix}u&v\\-v&u\end{pmatrix}, \tag{12}$$

$$u^2 + v^2 = 1. \tag{13}$$

For these equations u and v are real and we have $u>0$. It is obvious that U is unitary ($U^+=U^{-1}$), so we have

$$\begin{aligned} U &= u\sigma_0 - iv\sigma_2, \\ U^+ &= u\sigma_0 + iv\sigma_2. \end{aligned} \tag{14}$$

If we use the inverse transform of Eq. 11, Eq. 10 becomes

$$H^{eff} = \gamma^+(-\varepsilon U\sigma_3U^+ + g\langle\phi\rangle U\sigma_1U^+)\gamma + \omega|\langle b\rangle|^2. \tag{15}$$

Equation 14 readily gives

$$\begin{aligned} U\sigma_3U^+ &= u^2\sigma_3 + 2uv\sigma_1 - v^2\sigma_3, \\ U\sigma_1U^+ &= u^2\sigma_1 - 2uv\sigma_3 - v^2\sigma_1, \end{aligned} \tag{16}$$

so we have

$$H^{eff} = H^d + H^{od}, \tag{17}$$

where H^d and H^{od} are the diagonal and off-diagonal terms, respectively, as defined by

$$\begin{aligned} H^d &= -\gamma^+\{(u^2-v^2)\varepsilon + 2uvg\langle\phi\rangle\}\sigma_3\gamma + \omega|\langle b\rangle|^2, \\ H^{od} &= \gamma^+\{-2uv\varepsilon + (u^2-v^2)g\langle\phi\rangle\}\sigma_1\gamma. \end{aligned} \tag{18}$$

We determine u and v so as to make the off-diagonal term H^{od} vanish:

$$2uv\varepsilon = (u^2-v^2)g\langle\phi\rangle. \tag{19}$$

Combining this with Eq. 13, we get

$$\begin{aligned} u^2 &= \frac{1}{2}(1+\varepsilon/\sqrt{\varepsilon^2+\Delta^2}), \\ v^2 &= \frac{1}{2}(1-\varepsilon/\sqrt{\varepsilon^2+\Delta^2}), \end{aligned} \tag{20}$$

or alternatively,

$$\begin{aligned} u^2-v^2 &= \varepsilon/\sqrt{\varepsilon^2+\Delta^2}, \\ 2uv &= \Delta/\sqrt{\varepsilon^2+\Delta^2}, \end{aligned} \tag{21}$$

where

$$\Delta = g\langle\phi\rangle \quad (>0). \tag{22}$$

As will be explained in a later section, the molecular deformation arises from $\langle\phi\rangle\neq 0$. The positive sign adopted in Eq. 22 corresponds to specifying that we set the coordinate direction so as to make the molecular deformation have positive sign.

Under the condition of Eq. 20 H^d becomes

$$H^d = -\gamma^+\tilde{\varepsilon}\sigma_3\gamma + \omega|\langle b\rangle|^2, \tag{23}$$

where

$$\begin{aligned} \tilde{\varepsilon} &= (u^2-v^2)\varepsilon + 2uvg\langle\phi\rangle \\ &= \sqrt{\varepsilon^2+\Delta^2}. \end{aligned} \tag{24}$$

At this stage, we will look for the solution for a static deformation of molecule which satisfies

$$\langle\dot{\phi}\rangle = 0. \tag{25}$$

To make this explicit, we examine the equation of motion for operators b and b^+. For b we have

$$i\dot{b} = [b, H] = gC^+\sigma_1 C + \omega b. \tag{26}$$

The static condition of Eq. 25 leads to

$$\langle b\rangle = -\langle C^+\sigma_1 C\rangle\omega/g. \tag{27}$$

Since we can obtain entirely the same result for $\langle b^+\rangle$, we conclude that $\langle b\rangle$ and $\langle b^+\rangle$ are real and given by

$$\langle b\rangle = \langle b^+\rangle = \frac{1}{2}\langle\phi\rangle. \tag{28}$$

Therefore, combining this with Eq. 23, we arrive at the result:

$$H^d = -\gamma^+\tilde{\varepsilon}\sigma_3\gamma + \frac{\omega}{4g^2}\Delta. \tag{29}$$

Parameter Δ should be determined self-consistently.

Thermodynamics

Let us study thermodynamic properties of an assembly of molecules on the basis of the approximate Hamiltonian of Eq. 29. The partition function (per molecule) defined by

$$Z \equiv \mathrm{Tr}\exp(-H^d/T) \tag{30}$$

is easily calculated by use of Eq. 29. Using the relation

$$\gamma^+\sigma_3\gamma = \gamma_1^+\gamma_1 - \gamma_2^+\gamma_2, \tag{31}$$

we obtain

$$\begin{aligned} Z &= \exp(-\omega\Delta^2/4g^2T)\mathrm{Tr}\exp(-\tilde{\varepsilon}\gamma_1^+\gamma_1/T) \\ &\quad\times\mathrm{Tr}\exp(\tilde{\varepsilon}\gamma_2^+\gamma_2/T) \\ &= \exp(-\omega\Delta^2/4g^2T)\{\exp(-\tilde{\varepsilon}/2T)+\exp(\tilde{\varepsilon}/2T)\}^2, \end{aligned} \tag{32}$$

for which we have used the fact that the eigenvalue of $\gamma_i^+\gamma_i$ is 0 or 1.

The free energy of this system is given by

$$\begin{aligned} F &\equiv -T\ln Z \\ &= \omega\Delta^2/4g^2 - 2T\ln\{2\cosh(\tilde{\varepsilon}/2T)\}. \end{aligned} \tag{33}$$

Now we minize the free energy with respect to Δ:

$$\frac{\partial F}{\partial\Delta} = \frac{\omega\Delta}{2g^2} - \tanh(\tilde{\varepsilon}/2T)\frac{\partial\tilde{\varepsilon}}{\partial\Delta} = 0. \tag{34}$$

On application of Eq. 24 we get

$$\Delta\left\{\frac{\omega}{2g^2} - \frac{1}{\tilde{\varepsilon}}\tanh(\tilde{\varepsilon}/2T)\right\} = 0. \tag{35}$$

The nontrivial solution for Δ is determined from the relation:

$$\omega\tilde{\varepsilon}/2g^2 = \tanh(\tilde{\varepsilon}/2T). \quad (36)$$

This is the gap equation for Δ and has a solution ($\Delta \neq 0$) if

$$\omega\tilde{\varepsilon}/2g^2 < 1. \quad (37)$$

This is an important relation among the parameters included in the original Hamiltonian. If the two levels are degenerate, the above condition is always satisfied. In the case of non-degenerate levels sufficiently strong vibronic interactions can satisfy Eq. 37.

Characteristic temperature T_c at which Δ vanishes is obtained from Eq. 36 as

$$\omega\varepsilon/2g^2 = \tanh(\varepsilon/2T_c). \quad (38)$$

Now, we will tentatively examine other thermodynamic quantities. The entropy S of this system is estimated as follows:

$$S \equiv -\frac{\partial F}{\partial T} = -\left(\frac{\partial F}{\partial \Delta}\right)_T \frac{\partial \Delta}{\partial T} - \left(\frac{\partial F}{\partial T}\right)_\Delta$$

$$= 2\ln\{2\cosh(\tilde{\varepsilon}/2T)\} - \frac{\tilde{\varepsilon}}{T}\tanh(\tilde{\varepsilon}/2T). \quad (39)$$

In the above derivation, we have made use of Eq. 34. Using the gap equation (36), we get

$$S = 2\ln\{2\cosh(\tilde{\varepsilon}/2T)\} - \omega\tilde{\varepsilon}^2/2g^2T. \quad (40)$$

At the characteristic temperature,

$$S(T_c) = 2\ln\{2\cosh(\varepsilon/2T_c)\} - \frac{\varepsilon}{T_c}\tanh(\varepsilon/2T_c). \quad (41)$$

Since the entropy of the normal phase is given by

$$S_n(T) = 2\ln\{2\cosh(\varepsilon/2T)\} - \frac{\varepsilon}{T}\tanh(\varepsilon/2T), \quad (42)$$

the value of entropy changes continuously from the coherent phase ($\Delta \neq 0$) to the normal phase ($\Delta = 0$), *i.e.*,

$$S(T_c - 0) = S(T_c + 0). \quad (43)$$

On the other hand, heat capacity at constant volume

$$C \equiv T\frac{\partial S}{\partial T} \quad (44)$$

behaves in a different manner, as will be seen in what follows. From Eqs. 36 and 40 we get

$$\frac{\partial S}{\partial T} = -(\omega\tilde{\varepsilon}/2g^2T)\frac{\partial\tilde{\varepsilon}}{\partial T}. \quad (45)$$

We differenciate the gap equation (36) with respect to T and apply some algebraic treatments to have

$$\frac{\partial\tilde{\varepsilon}}{\partial T} = \tilde{\varepsilon}\{1-(\omega\tilde{\varepsilon}/2g^2)^2\}/T\{(\omega T/g^2)+(\omega\tilde{\varepsilon}/2g^2)^2-1\}, \quad (46)$$

which, in conjunction with Eqs. 44 and 45, leads to the formulation of heat capacity:

$$C = (\omega\tilde{\varepsilon}^2/2g^2T)\{1-(\omega\tilde{\varepsilon}/2g^2)^2\}/\{(\omega T/g^2)+(\omega\tilde{\varepsilon}/2g^2)^2-1\}$$

$$= \frac{\tilde{\varepsilon}}{T}\tanh(\tilde{\varepsilon}/2T)\,\mathrm{sech}^2(\tilde{\varepsilon}/2T)/\{(\omega T/g^2)-\mathrm{sech}^2(\tilde{\varepsilon}/2T)\}. \quad (47)$$

The heat capacity of the normal phase is obtained from Eq. 42 as

$$C_n = (\varepsilon^2/2T^2)\,\mathrm{sech}^2(\varepsilon/2T). \quad (48)$$

At the characteristic temperature, the heat capacities of the coherent and normal phases are given by

$$C = (\varepsilon^2/2T_c^2)\{1-(\omega\varepsilon/2g^2)^2\}/\{1+(g^2/\omega T_c)[(\omega\varepsilon/2g^2)^2-1]\}$$

$$C_n = (\varepsilon^2/2T_c^2)\{1-(\omega\varepsilon/2g^2)^2\}, \quad (49)$$

hence

$$\frac{C}{C_n} = 1/\{1+(g^2/\omega T_c)[(\omega\varepsilon/2g^2)^2-1]\} > 1. \quad (50)$$

We want to point out that, as T goes to 0, the heat capacities of these phases behave in accord with

$$C = (\tilde{\varepsilon}^2/2T^2)\exp(-\tilde{\varepsilon}/T),$$

$$C_n = (\varepsilon^2/2T^2)\exp(-\varepsilon/T). \quad (51)$$

It is seen that the former decreases faster than the latter because $\tilde{\varepsilon} > \varepsilon$.

Ground State Properties

At the limit of $T=0$, the gap equation (36) becomes

$$\tilde{\varepsilon} = \sqrt{\varepsilon^2+\Delta^2} = 2g^2/\omega, \quad (52)$$

which gives

$$\Delta^2 = (\varepsilon/s)^2(1-s^2), \quad (53)$$

where s is a dimensionless quantity defined by

$$s = \omega\varepsilon/2g^2 \quad (<1). \quad (54)$$

The ground state energy of the coherent phase is given as a sum of electronic and lattice parts:

$$\tilde{E} = -\tilde{\varepsilon} + \omega\Delta^2/4g^2$$

$$= -\varepsilon(1-s)^2/2s - \varepsilon. \quad (55)$$

Since the energy of the normal phase is $E=-\varepsilon$, the stabilization energy is thus obtained as

$$\delta E \equiv E - \tilde{E} = \varepsilon(1-s)^2/2s$$

$$= 2g^2/\omega\{1-(\omega\varepsilon/2g^2)\}^2. \quad (56)$$

It is seen that, if the inequality (37) holds, we have an energy depression.

The deformation of lattice is expressed as

$$\delta R_\alpha = \sum_q \sqrt{\frac{\hbar}{2M\omega_q}} L_{\alpha q}\langle\phi_q\rangle, \quad (57)$$

where α refers to the site and coordinate indicies and $L_{\alpha q}$ is the transformation matrix from the normal mode q to the real displacement. $L_{\alpha q}$ is calculated by the standard method for actual systems. If we restrict ourselves to treatment of a single mode as we have done so far, we can simplify Eq. 57 to

$$\delta R_\alpha = \sqrt{\frac{\hbar}{2M\omega}} L_{\alpha q}(2g/\omega)\{1-(\omega\varepsilon/2g^2)^2\}^{1/2}, \quad (58)$$

for which Eqs. 23 and 53 are used. The results obtained in this section will be applied to cyclobutadiene later.

Electromagnetic Properties

If the system has an induced dipole moment between levels 1 and 2, the interaction between the radiation field and the electron in our system is described as

$$H_{int} = -\mathbf{E}\cdot\mathbf{d}C^+\sigma_1 C$$

$$= -\mathbf{E}\cdot\mathbf{d}\gamma^+ U\sigma_1 U^+\gamma, \quad (59)$$

where $\mathbf{E}$ is the electric field associated with the applied radiation field and $\mathbf{d}$ is the induced dipole moment in the electronic system. Using Eq. 16, we can rewrite Eq. 59 as

$$H_{\text{int}} = -\mathbf{E}\cdot\mathbf{d}\gamma^{+}\{(u^2-v^2)\sigma_1-2uv\sigma_3\}\gamma, \tag{60}$$

hence we have for the radiative transition probability W_{21}

$$\begin{aligned} W_{21} &\propto (\mathbf{E}\cdot\mathbf{d})^2|\langle\tilde{2}|\gamma^{+}(u^2-v^2)\sigma_1\gamma|\tilde{1}\rangle|^2 \\ &= (\mathbf{E}\cdot\mathbf{d})^2(u^2-v^2)^2 \\ &= (\mathbf{E}\cdot\mathbf{d})^2\frac{\varepsilon^2}{\varepsilon^2+\Delta^2}. \end{aligned} \tag{61}$$

We have an additional information that, even if there is no permanent dipole in the normal phase, there will appear a permanent dipole in the coherent phase, as embodied by

$$\begin{aligned} \mathbf{P} &= -2uv\mathbf{d}\langle\gamma^{+}\sigma_3\gamma\rangle \\ &= -\frac{\mathbf{d}\Delta}{\sqrt{\varepsilon^3+\Delta^2}}\{\exp(2\tilde{\varepsilon}/T)+1\}^{-1}. \end{aligned} \tag{62}$$

It should be pointed out that increasing Δ causes the radiative transition probability to decrease but the permanent dipole to increase.

Illustrative Example. Cyclobutadiene

Cyclobutadiene is a fictious molecule, but has frequently been a subject for theoretical considerations. We will begin with an investigation on the assumption that cyclobutadiene is, in a crude approximation, a square molecule with bonds of equal length, 1.42 Å. This structure has two π electronic levels which are degenerate. The vibrational modes which connect these two levels have symmetries b_{1g} and b_{2g} as shown

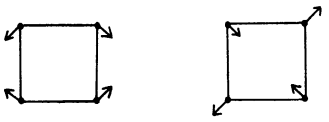

Fig. 1. Normal modes of molecular vibrations.
a: b_{1g} mode, b: b_{2g} mode.

in Fig. 1. Those vibronic coupling constants referring to those modes are designated g_1 and g_2, respectively. These constants are evaluated by the method of Murrel and Pople[4] as

$$\begin{aligned} g_1 &= 0.432/\sqrt{\nu_1}\ \text{eV}, \\ g_2 &= 0.112/\sqrt{\nu_2}\ \text{eV}, \end{aligned} \tag{63}$$

where ν_i is the wave number of the vibration in question in units of 1000 cm^{-1}; we adopt $\nu_i=1.5$, as is usually the case with hydrocarbons having several carbon atoms.

Wave function for the degenerate π levels are written as

$$\begin{aligned} \psi_1 &= \frac{1}{2}(\chi_1+\chi_2-\chi_3-\chi_4), \\ \psi_2 &= \frac{1}{2}(\chi_1-\chi_2-\chi_3+\chi_4), \end{aligned} \tag{64}$$

or alternatively,

$$\begin{aligned} \psi_1 &= \frac{1}{\sqrt{2}}(\chi_1-\chi_3), \\ \psi_2 &= \frac{1}{\sqrt{2}}(\chi_2-\chi_4), \end{aligned} \tag{65}$$

where χ_i is the $2p\pi$ atomic orbital at site i. Equation 64 is suitable for considering the b_{1g} vibrational mode, whereas Eq. 65 is applicable to the b_{2g} mode, so that the coupling matrix $\hat{g}$ is written as Eq. 7.

We can calculate stabilization energies using Eq. 56 with $\varepsilon=0$ (degenerate case) as

$$\begin{aligned} \delta E(b_{1g}) &= 0.831\ \text{eV (rectangle)}, \\ \delta E(b_{2g}) &= 0.107\ \text{eV (diamond)}. \end{aligned} \tag{66}$$

Apparently the former is much higher than the latter, in agreement with the most stable structure of this molecule being a rectangle. The stabilization energy, 0.831 eV, obtained here is very close to that obtained by Liehr, 0.907 eV.[5]

We turn to evaluation of δR_α ($\alpha=l,x$), with our interest restricted in the b_{1g} type distortion. Since $L_{\alpha q}$ has been estimated to be 0.0109 by the standard method,[6] we have from Eq. 58

$$\delta R_\alpha = 0.0325\ \text{Å}, \tag{67}$$

hence the longer and shorter bond distances are evaluated as

$$D_l = 1.485\ \text{Å}, \quad D_s = 1.355\ \text{Å}. \tag{68}$$

For reference, the following values have been obtained by Liehr[5] and by Salem:[7]

$$\begin{aligned} &D_l = 1.54\ \text{Å}, \quad D_s = 1.33\ \text{Å (Liehr)}, \\ &D_l = 1.463\ \text{Å}, \quad D_s = 1.388\ \text{Å (Salem)}. \end{aligned} \tag{69}$$

Similar arguments may be applicable to conjugated chain molecules. In these case, the b_{1g} vibrational mode is expected also to contribute dominantly to the stabilization; however, ε is finite in these case, though we can expect the inequality (37), to be applicable; both the stabilization energy and bond distortion would be smaller than those in the degenerate case discussed in this paper.

Discussion

We have presented the mean field theory for such an electronic system as is composed of two closely-spaced levels and strongly coupled with a phonon mode. Even though we have adopted quite a simple Hamiltonian given by Eq. 8, we have successfully derived some physically interesting results; the appearance of coherent phase and the condition for this phase to be more stable than the normal phase. Expressions for the stabilization energy and associated bond distortion have been derived and their numerical values estimated for cyclobutadiene, with results in good agreement with those obtained by conventional methods.

It should be pointed out that, for usual finite molecules, the characteristic temperature at which the coherent phase appears is so high (over 10000 °C as estimated by Eq. 38) that common molecules should be in the well-established coherent phase with respect to the phonon modes even at room temperature.

As to long chain molecules, there is a leading opinion that the stabilization is caused mostly by electron correlation.[8] We agree to this but want to stress that the electron correlation term, if included in our Hamiltonian, would rise a new problem to us.

Finally, we shoud note that the appearance of non-analyticity of free energy at the finite temperature T_c is to be taken as a shortcoming of our simplest approximation. Nevertheless, we can regard it as an important step of theoretical development, though fluctuating, on the distortion. The thermodynamic properties derived above also must be considered as indicating characteristic features below T_c for the transition towards the distorted ground state. At any rate, a more satisfactory theory is expected which gose over the present framework of approximation.

The problem treated here can also be manipulated by means of Green's function, which will be discussed in the following paper.

References

1) R. E. Peierls, "Quantum Theory of Solids," Clarendon Press, Oxford (1955), p. 108.

2) H. L. Longuet-Higgins and L. Salem, *Proc. R. Soc. London, Ser. A*, **251**, 172 (1959).

3) H. Yamaguchi, T. Nakajima and, T. L. Kunii, *Theor, Chim. Acta*, **12**, 349 (1968).

4) J. N. Murrel and J. A. Pople, *Proc. R. Soc. London, Ser. A*, **69**, 245 (1956).

5) A. D. Liehr, *Z. Phys. Chem.*, **9**, 338 (1956).

6) G. Herzberg, "Molecular Spectra and Molecular Structure. II, IR and Raman Spectra of Polyatomic Molecules," D. Van Nostrand Company, Inc., New York (1945), Chap. 2.

7) L. Salem, "Molecular Orbital Theory of Conjugated, System," W. A. Benjamin, Inc., New York (1966), Chap. 8.

8) A. A. Ovchinickov, I. I. Ukraiskii, and G. V. Kventsel, *Soviet Phys., Uspekhi*, **15**, 575 (1973). Other references are therein.

Theory of Molecular Deformation Due to the Vibronic Interaction between Two Closely-spaced Electronic Levels. II. Green's Function Treatment

Kiyoshi NISHIKAWA, Minoru KIMURA,† and Shigeyuki AONO*

Department of Chemistry, Faculty of Science, Kanazawa University, Marunouchi, Kanazawa, 920
†Department of Physics, Faculty of Science, Kanazawa University, Marunouchi, Kanazawa, 920

(Received July 3, 1980)

Vibronic interaction between two closely-spaced electronic levels was investigated by use of the temperature Green's function. A Green's function version for the mean field approximation was derived which is capable of reproducing results obtained in the preceding work. The spectrum of phonon in the normal phase was then calculated and the critical (strictly speaking, characteristic, since we are dealing with a finite system) temperature T_c was obtained where the phonon becomes completely soft causing lattice distortion. The fluctuation effect was investigated and the mean field theory was examined for its applicability. When the level spacing is comparable to or larger than the value of the electron-phonon coupling constant, the mean field theory is satisfactory, but when the two levels are nearly degenerate, it is not so good because the problem in question is in the regime involving extremely strong coupling.

In the preceding work (referred to as I hereinafter) we have developed the mean field theory for the title subject. The model considered there is outlined as follows. Let a_i^+ (a_i) be the creation (annihilation) operator of the electron at level i, and $b^+(b)$ the creation (annihilation) operator of phonon. To simplify formulations we introduce the notations

$$C^+ = (a_1^+ \; a_2^+), \; C = \begin{pmatrix} a_1 \\ a_2 \end{pmatrix}, \tag{1}$$

$$\phi = b^+ + b. \tag{2}$$

Thus, the Hamiltonian is given by

$$H = -\varepsilon C^+\sigma_3 C + g\phi C^+\sigma_1 C + \omega b^+ b, \tag{3}$$

where

$$\sigma_0 = \begin{pmatrix} 1 & 0 \\ 0 & 1 \end{pmatrix}, \; \sigma_1 = \begin{pmatrix} 0 & 1 \\ 1 & 0 \end{pmatrix}, \; \sigma_2 = \begin{pmatrix} 0 & -i \\ i & 0 \end{pmatrix}, \; \sigma_3 = \begin{pmatrix} 1 & 0 \\ 0 & -1 \end{pmatrix}, \tag{4}$$

are used. Later we will use the following marix for electron-phonon (vibronic) interaction:

$$\hat{g}\tilde{\varepsilon} = \begin{pmatrix} 0 & g \\ g & 0 \end{pmatrix} = g\sigma_1. \tag{5}$$

Within the mean field approximation, operators b^+ and b in Eq. 3 are replaced by their averages. This approximation reduces the Hamiltonian given by Eq. 3 to

$$H^{eff} = -\varepsilon C^+\sigma_3 C + g\langle\phi\rangle C^+\sigma_1 C + \omega|\langle b\rangle|^2. \tag{6}$$

This form is based on an expectation that the so-called coherent state impling $\langle\phi\rangle \neq 0$ will be arranged by the electron-phonon interaction. In I H^{eff} was diagonalized by a linear canonical transformation. The value of $\langle\phi\rangle$ has been determined on the condition that the free energy of our system is optimized with respect to $\langle\phi\rangle$. As a numerical example, the bond distortion and stabilization energy were calculated for cyclobutadiene, in good agreement with those obtained by a current theory.

In this paper, we will present the Green's function theory for the problem. In the first section, we will show that the result obtained in I is derivable on the basis of the simplest approximation on Green's function. In the remaining section, we will investigate the fluctuation effect to examine the validity of the mean field theory.

Phonon Softening

It is known well in the physics of one-dimensional (1-D) conductors[4,5] that the phonon softening induced by electron-phonon interaction causes lattice deformation in these systems. To show that an analogous mechanism is operative in the present problem, we will begin with investigating behaviors of the phonon propagator in the normal state; we will work with the simplest approximation for the polarization part of the phonon propagator as shown in Fig. 1. Analytically it is expressed by

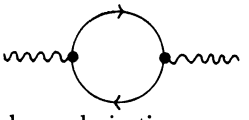

Fig. 1. First order polarization part of the phonon Green's function.

$$\Pi(i\nu_n) = T\sum_{i\omega_n} \mathrm{Tr}\,\hat{g}G^0(i\omega_n)\hat{g}G^0(i\nu_n - i\omega_n), \tag{7}$$

where $G^0(i\omega_n)$ is the Matsubara (temperature) Green's function[2] for a free electron and its expression can be obtained from the first term of Eq. 3 as

$$\begin{aligned} G^0(i\omega_n) &= (i\omega_n\sigma_0 + \varepsilon C^+\sigma_3 C)^{-1} \\ &= \begin{pmatrix} \dfrac{1}{i\omega_n + \varepsilon} & 0 \\ 0 & \dfrac{1}{i\omega_n - \varepsilon} \end{pmatrix} \\ &= \sum_k G_k^0(i\omega_n)\,\sigma_k \end{aligned} \tag{8}$$

with

$$\begin{aligned} G_0^0(i\omega_n) &= \frac{1}{2}\left(\frac{1}{i\omega_n + \varepsilon}\right) + \left(\frac{1}{i\omega_n - \varepsilon}\right) \\ G_3^0(i\omega_n) &= \frac{1}{2}\left(\frac{1}{i\omega_n + \varepsilon} - \frac{1}{i\omega_n - \varepsilon}\right). \end{aligned} \tag{9}$$

If we use Eqs. 5 and 8, Eq. 7 is rewritten as

$$\Pi(i\nu_n) = 2g^2\, T\sum_{i\omega n}\{G_0^0(i\omega_n)\, G_0^0(i\nu_n - i\omega_n) - G_3^0(i\omega_n)G_3^0(i\nu_n - i\omega_n)\}. \quad (10)$$

The frequency sum[3] in Eq. 10 leads to

$$\Pi(i\nu_n) = -g^2\frac{4\varepsilon}{\nu_n^2+4\varepsilon^2}\tanh(\varepsilon/2T). \quad (11)$$

The interacting phonon Green's function is obtained from the Dyson equation

$$D(i\nu_n) = D^0(i\nu_n)/\{1 - D^0(i\nu_n)\Pi(i\nu_n)\}, \quad (12)$$

where the free phonon propagator $D^0(i\nu_n)$ is given by

$$D^0(i\nu_n) = \frac{-2\omega}{\nu_n^2+\omega^2}. \quad (13)$$

Combining Eqs. 11, 13, and 12, we obtain

$$D(i\nu_n) = \frac{-2\omega(\nu_n^2+4\varepsilon^2)}{(\nu_n^2+\omega^2)(\nu_n^2+4\varepsilon^2)-8g^2\,\varepsilon\omega\tanh(\varepsilon/2T)}. \quad (14)$$

In this equation $i\nu_n$ is analytically continued to ν and thus the poles of Eq. 14 are found at

$$(\nu^2)_\pm = \frac{1}{2}(\omega^2+4\varepsilon^2) \pm \left\{\left(\frac{\omega^2+4\varepsilon^2}{2}\right)^2 + 8g^2\varepsilon\omega\tanh(\varepsilon/2T) - 4\varepsilon^2\omega^2\right\}^{1/2}. \quad (15)$$

First, we note that, if coupling constant g is extremely small, Eq. 15 reduces to

$$(\nu^2)_\pm \simeq \begin{cases}\omega^2 & \text{for } \omega > \varepsilon,\\ 4\varepsilon^2\end{cases} \quad (16a)$$

and

$$(\nu^2)_\pm \simeq \begin{cases}4\varepsilon^2 & \text{for } \omega < \varepsilon.\\ \omega^2\end{cases} \quad (16b)$$

They are spectra of independent electron and phonon. Aside from this simplest case, spectrum ν_- in general depends on temperature in a very specific way. In paticular, the behavior of ν_- is quite specific. If g is strong enough, it becomes soft as temperature is lowered. Complete softening of ν_- occurs at the temperature T_c in accordance with

$$\tanh(\varepsilon/2T_c) = (\varepsilon\omega/2g^2). \quad (17)$$

A unique solution is obtainable for T_c if g is so strong as to satisfy the inequality

$$g^2 > \varepsilon\omega/2. \quad (17a)$$

At the temperature T_c we get the spectrum

$$(\nu^2)_\pm = \begin{cases}\omega^2+4\varepsilon^2\\ 0\end{cases} \quad (18)$$

Equation 17 is equal to the relation defining the characteristic temperature for the distortive transition (given by Eq. 38 in I).

The above-demonstrated similarity to the case of 1-D conductor is of significance; however, it is worth while to take notice of the strong coupling condition (17a) applicable to our case, in contrast to the case of 1-D Peierls transition where any weak coupling can lead to the softening.

Electron Propagator

The description in the preceding section is inapplicable to the temperature range below the characteristic temperature T_c. To see how the system behaves at $T \lesssim T_c$, we consider the solution with deformation on the basis of the effective Hamiltonian (6). The propagator for a "free" electron suitable for this case is given by

$$G(i\omega_n) = (i\omega_n\sigma_0 + \varepsilon\sigma_3 - \Delta\sigma_1)^{-1}, \quad (19)$$

where

$$\Delta = g\langle\phi\rangle. \quad (20)$$

A straightforward calculation leads to an alternative form for Eq. 19

$$G(i\omega_n) = \sum_k G_k(i\omega_n)\sigma_k \quad (21)$$

$$G_k(i\omega_n) = \frac{1}{(i\omega_n-\tilde\varepsilon)(i\omega_n+\tilde\varepsilon)} \times \begin{cases} i\omega_n\\ \Delta\\ 0\\ -\varepsilon\end{cases} \text{ for } k = \begin{cases}0\\1\\2\\3\end{cases}, \quad (21a)$$

where

$$\tilde\varepsilon = \sqrt{\varepsilon^2+\Delta^2}. \quad (22)$$

To estimate $\langle\phi\rangle$, we now look for the solution of the static distortion as has been done in I, namely,

$$-\left\langle\frac{\partial}{\partial\tau}b\right\rangle = \langle[b,H]\rangle = 0, \quad (23)$$

which is the average of the Heisenberg equation of motion with respect to the imaginary time τ. Using Eq. 3 to make a calculation on Eq. 23, we obtain

$$\langle b\rangle = -\frac{g}{\omega}\langle C^+\sigma_1 C\rangle. \quad (24)$$

Obviously, for $\langle b^+\rangle$ we are led to entirely the same expression and it follows that

$$\Delta = g\langle\phi\rangle = -\frac{2g^2}{\omega}\langle C^+\sigma_1 C\rangle = \frac{g^2}{\omega}G_1(0^-), \quad (25)$$

where 0^- is negative infinitesimal and

$$G_1(0^-) = T\sum_{i\omega n} G_1(i\omega_n)\exp(i\omega_n 0^-) = T\sum_{i\omega_n}\frac{\Delta}{(i\omega_n-\tilde\varepsilon)(i\omega_n+\tilde\varepsilon)}\exp(i\omega_n 0^-) = (\Delta/2\tilde\varepsilon)\tanh(\tilde\varepsilon/2T). \quad (26)$$

Combining Eqs. 25 and 26, we arrive at the "gap" equation

$$(\tilde\varepsilon\omega/2g^2) = \tanh(\tilde\varepsilon/2T), \quad (27)$$

which is identical with Eq. 36 in I.

Thermodynamics

According to Ref. 6 the difference in free energy between the coherent and normal phases

$$\delta F = F - F_n \quad (28)$$

is given by

$$\delta F = \int_0^g dg\,\langle\phi C^+\sigma_1 C\rangle. \quad (29)$$

In the integrand in Eq. 29 the average $\langle\phi C^+\sigma_1 C\rangle$ is approximated to $\langle\phi\rangle\langle C^+\sigma_1 C\rangle$, which permits Eq. 29 with the aid of Eqs. 25, 26, and 27 to give

$$\delta F = -\int_0^g dg\, 2\langle\phi\rangle\frac{\Delta}{2\tilde\varepsilon}\tanh(\tilde\varepsilon/2T) = -\int_0^g dg\,(\omega\Delta^2/2g^3). \quad (29a)$$

The integration for Eq. 29a can be performed as follows:

$$\begin{aligned}\delta F &= \int_0^{g\omega\Delta^2/2} \mathrm{d}\left(\frac{1}{2g^2}\right) \\ &= \frac{\omega}{2}\int_{\varepsilon}^{\tilde{\varepsilon}} \Delta^2 \frac{\mathrm{d}}{\mathrm{d}\tilde{\varepsilon}}\left(\frac{1}{2g^2}\right)\mathrm{d}\tilde{\varepsilon} \\ &= \frac{\omega}{2}\int_{\varepsilon}^{\tilde{\varepsilon}} \Delta^2 \frac{\mathrm{d}}{\mathrm{d}\tilde{\varepsilon}}\left[\frac{1}{\tilde{\varepsilon}\omega}\tanh\left(\tilde{\varepsilon}/2T\right)\right]\mathrm{d}\tilde{\varepsilon} \\ &= \frac{1}{2}\int_{\varepsilon}^{\tilde{\varepsilon}} (\tilde{\varepsilon}^2-\varepsilon^2)\frac{\mathrm{d}}{\mathrm{d}\tilde{\varepsilon}}\left[\frac{1}{\tilde{\varepsilon}}\tanh\left(\tilde{\varepsilon}/2T\right)\right]\mathrm{d}\tilde{\varepsilon}, \end{aligned} \tag{30}$$

where for the second line the gap equation (27) has been used and for the third line the definition of $\tilde{\varepsilon}$ by Eq. 22 used. Finally, the integration by parts for Eq. 30 gives the free energy difference as

$$\begin{aligned}\delta F = &\frac{1}{2}\left[\frac{\tilde{\varepsilon}^2-\varepsilon^2}{\tilde{\varepsilon}}\tanh\left(\tilde{\varepsilon}/2T\right)\right] \\ &-2T\{\ln[2\cosh\left(\tilde{\varepsilon}/2T\right)] - \ln[2\cosh\left(\varepsilon/2T\right)]\}. \end{aligned} \tag{31}$$

For comparison we evaluate the free energy for the normal state; the partition function for this state is given by

$$\begin{aligned} Z_n &= \mathrm{Tr}\exp(-\varepsilon C^+\sigma_1 C/T) \\ &= \mathrm{Tr}\exp\left(-\varepsilon a_1^+ a_1/T\right)\times \mathrm{Tr}\exp(\varepsilon a_2^+ a_2/T) \\ &= [\exp\left(\varepsilon/2T\right) + \exp(-\varepsilon/2T)]^2 \end{aligned} \tag{32}$$

for which we have made use of the fact that the eigenvalue of $a_i^+ a_i$ is 0 or 1. Therefore, the free energy of the normal state is given by

$$F_n = -T\ln Z_n = -2T\ln[2\cosh\left(\varepsilon/2T\right)], \tag{33}$$

which, combined with Eq. 31, leads to

$$F = (\Delta^2\omega/4g^2) - 2T\ln[2\cosh(\tilde{\varepsilon}/2T)]. \tag{34}$$

Thus, we have obtained the free energy of the distorted state, which is identical with Eq. 33 in I; as far as the above treatment is concerted, the two methods have been shown to be identical.

Fluctuation Effect

Let us examine to what extent the above results are valid by estimating the correction due to fluctuation. To describe the deviation from the mean field quantities, new operator β, β^+, and ψ are defined by

$$b = \langle b\rangle + \beta,\ b^+ = \langle b\rangle + \beta^+, \tag{35}$$

$$\psi = \beta + \beta^+. \tag{36}$$

These definitions allow the Hamiltonian to be rewritten as

$$H = H_0 + H_{\mathrm{int}} + \omega\langle b\rangle\psi + \omega\beta^+\beta + \omega|\langle b\rangle|^2, \tag{37}$$

with

$$H_0 = C^+(-\varepsilon\sigma_3 + \Delta\sigma_1)C, \tag{38}$$

$$H_{\mathrm{int}} = C^+ g\psi\sigma_1 C. \tag{39}$$

In what follows, we attempt to estimate the fluctuation effect on electronic spectra within the lowest order of g by considering the self-energy contribution shown in Fig. 2.

Mean field electron propagator G (displayed in solid line in Fig. 2) is obtained from H_0 in Eq. 37. It has already been given by Eq. 21 with Δ to be determined by Eq. 27. Phonon propagator D^0 (displayed in wavy line in Fig. 2) is easily calculated from the third and fourth terms of Eq. 37 and is shown to be identical with Eq. 13.

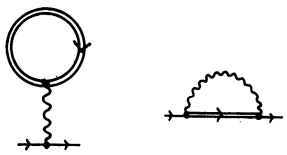

a b

Fig. 2. First order self-energy terms of the electron propagator.
a: Direct term, b: exchange term.

Using these expressions for propagators, we can express the self-energy parts in Fig. 2 analytically as

$$\Sigma = \Sigma_H + \Sigma_E, \tag{40}$$

where

$$\Sigma_H(\mathrm{i}\omega_n) = Tg^2\sigma_1 D^0(0)\sum_{\mathrm{i}\nu_n}\mathrm{Tr}\sigma_1 G(\mathrm{i}\nu_n) \tag{40a}$$

$$\Sigma_E(\mathrm{i}\omega_n) = -Tg^2\sum_{\mathrm{i}\nu_n}\sigma_1 G(\mathrm{i}\nu_n)D^0(\mathrm{i}\omega_n - \mathrm{i}\nu_n)\sigma_1. \tag{40b}$$

Σ_H is the contribution of Fig. 2a and Σ_E that of Fig. 2b. Following the usual procedure, we evaluate Σ_H as

$$\begin{aligned}\Sigma_H(\mathrm{i}\omega_n) &= (-4g^2/\omega)T\sum_{\mathrm{i}\nu_n}\sigma_1 G_1(\mathrm{i}\nu_n) \\ &= \sigma_1(4g^2/\omega)(\Delta/2\tilde{\varepsilon})\tanh\left(\tilde{\varepsilon}/2T\right) \\ &= \sigma_1\Delta. \end{aligned} \tag{41}$$

In the last step in Eq. 41 we have used the gap equation (27).

The calculation of Σ_E is tedious: First, the algebra of the Pauli matrices yields

$$\Sigma_E = \sigma_0\Sigma_0 + \sigma_1\Sigma_1 - \sigma_3\Sigma_3, \tag{42}$$

where

$$\Sigma_k(\mathrm{i}\omega_n) = -g^2T\sum_{\mathrm{i}\nu_n}G_k(\mathrm{i}\nu_n)D^0(\mathrm{i}\omega_n - \mathrm{i}\nu_n),\quad k = 0, 1, 3. \tag{42a}$$

Each term of this equation will be evaluated separately. The frequency summation of Σ_0 is performed to give

$$\Sigma_0(\mathrm{i}\omega_n) = g^2\left[\frac{\mathrm{i}\omega_n N_1}{(\mathrm{i}\omega_n)^2-(\tilde{\varepsilon}+\omega)^2} + \frac{\mathrm{i}\omega_n N_0}{(\mathrm{i}\omega_n)^2-(\tilde{\varepsilon}-\omega)^2}\right], \tag{43}$$

where

$$\begin{aligned} N_1 &= n(-\tilde{\varepsilon}) + n_b(\omega) \\ N_0 &= 1 - n(-\tilde{\varepsilon}) + n_b(\omega) \end{aligned} \tag{44}$$

and $n(-\tilde{\varepsilon})$ and $n_b(\omega)$ are, respectively, the Fermi and Bose function with corresponding arguments.

We have an approximation

$$(\mathrm{i}\omega_n)^2 - (\tilde{\varepsilon}+\omega)^2 \simeq \tilde{\varepsilon}^2 - (\tilde{\varepsilon}+\omega)^2 \simeq -2\tilde{\varepsilon}\omega \tag{45}$$

considering that $\tilde{\varepsilon}\gg\omega$; this approximation is possibly applicable to the example case discussed in I. Equation 43 can then be reduced to

$$\Sigma_0(\mathrm{i}\omega_n) \simeq \Sigma_0(\pm\tilde{\varepsilon}) = \mp\tilde{\varepsilon}/4. \tag{46}$$

The remaining two terms in Eq. 42 are evaluated in a similar manner as

$$\begin{aligned}\Sigma_1(\mathrm{i}\omega_n) &= -\Delta/4 \\ \Sigma_3(\mathrm{i}\omega_n) &= \varepsilon/4. \end{aligned} \tag{47}$$

Combining Eqs. 41, 46, and 47, we obtain

$$\Sigma(\mathrm{i}\omega_n) \simeq \Sigma(\pm\tilde{\varepsilon}) = \frac{1}{4}\begin{pmatrix}\mp\tilde{\varepsilon}-\varepsilon & 3\Delta \\ 3\Delta & \mp\tilde{\varepsilon}+\varepsilon\end{pmatrix}. \tag{48}$$

Finally, the full electron propagator

$$G(i\omega_n) = [G_0^{-1}(i\omega_n) - \sum(i\omega_n)]^{-1}$$

is given in the form

$$G(i\omega_n) \simeq \begin{pmatrix} i\omega_n \pm \frac{\tilde{\varepsilon}}{4} + \frac{5\varepsilon}{4} & -\frac{7\Delta}{4} \\ -\frac{7\Delta}{4} & i\omega_n \pm \frac{\tilde{\varepsilon}}{4} - \frac{5\varepsilon}{4} \end{pmatrix}^{-1}. \quad (49)$$

The electronic spectrum which involves the contribution from the fluctuation effect is determined from Eq. 49 as

$$\nu = \pm\tilde{\varepsilon}\left(1 + \frac{24}{25}\frac{\Delta^2}{\tilde{\varepsilon}^2}\right)^{1/2}. \quad (50)$$

According to this equation the electronic spectrum is to be corrected by a factor

$$\lambda = \left(1 + \frac{24}{25}\frac{\Delta^2}{\tilde{\varepsilon}^2}\right)^{1/2} - 1. \quad (51)$$

In the case where the two electronic levels are nearly degenerate, *i.e.*, $\varepsilon \simeq 0$, the factor (51) is considerably large since $\lambda \lesssim \sqrt{2} - 1$, whereas if ε is so large that $\tilde{\varepsilon} \gg \Delta$ the correction is small since $\lambda \simeq 0$. The latter inequality implies

$$\varepsilon \simeq 2g^2/\omega, \quad (52)$$

i.e., relatively weak coupling cases. Such cases as involve nearly degenerate levels belong to the extremely strong coupling regime.

Conclusion

We have made use of Green's functions to reproduce the results from the mean field theory presented in I and examined effects of fluctuation on electronic spectra. We are led to conclude that, as seen from Eq. 50, the mean field theory is not necessarily good; if the level spacing is fairly large, *i.e.*, $\varepsilon \simeq g$ or $\varepsilon \simeq \Delta$, the mean field theory is a pretty good approximation, but if the two levels are nearly degenerate, a substantial deviation is inevitable to the mean field theory. For this reason, the numerical estimate for cyclobutadiene (where $\varepsilon \simeq 0$) given in I, though in good agreement with results of other works, must be considered to be only qualitatively reliable.

In order to improve this situation and to reach better understanding of this problem, the perturbation scheme can be hardly suitable because we have no smaller parameters available for the series expansion. In paticular, the vertex renormalization which we have ignored can be expected to be superior to any other corrections. For metals we have the well-known Migdal theorem[7] which has demonstrated that the vertex correction is as small as the order of the small parameter m/M (electron-nucleus mass ratio). We do not think that the theorem is actually applicable to the case of finite systems such as molecules.

References

1) M. Kimura, K. Nishikawa, and S. Aono, *Bull. Chem. Soc. Jpn.*, **54**, 3619 (1981).
2) T. Matsubara, *Prog. Theor. Phys.*, **14**, 351 (1955).
3) A. L. Fetter and J. D. Walecka, "Quantum Theory of Many-Particle System," McGraw-Hill (1971), Chap. 7.
4) W. Kohn, *Phys. Rev. Lett.* **2**, 393 (1959).
5) A. M. Afanac'ev and Yu. Kagan, *Sov. Phys. JETP*, **16**, 1030 (1963).
6) A. L. Fetter and J. D. Walecka, *Loc. Cit.*, p. 449.
7) A. B. Migdal, *Sov. Phys. JETP*, **7**, 996 (1958).

Thermal Decomposition Studies of Ammonium Heptamolybdate(6-) Tetrahydrate by Means of High-temperature Oscillating X-Ray Diffraction with a Rotating Anode Type Large Capacity Generator

Kimio Isa* and (the late) Hajime Ishimura

Department of Chemistry, Faculty of Education, Fukui University, Bunkyo 3-9-1, Fukui 910

(Received October 28, 1980)

Ammonium heptamolybdate(6—) tetrahydrate (AHM) was studied by means of high temperature oscillating X-ray diffraction with a large capacity generator of 12 kW. Experimental conditions were determined precisely. It was possible to settle the maximum value of diffracted patterns, and the inherited error was about 1.5%. Thermal decomposition of AHM was studied by means of TG-DTA, but the first decrease of TG could not be explained as a single process of decomposition. Moreover it could also not be explained by means of high-temperature oscillating X-ray diffraction with a standard generator. However, with a large capacity generator, the first decrease of TG could be explained to be a convolution of three steps of decomposition. Moreover, the second and third steps could be explained by observing the microscopic structural change. In a high-temperature oscillating XRD, (heating rate 2 °C/min), a peak temperature of 96 °C was recognized, which had not been reported before. Also from 110 °C to 226 °C, a row of the small peak has been found. Finally, the first stage of decomposition which was thought to be a single step in the experiment of TG-DTA, could be seperated into three steps. Moreover, the onset and offset temperatures of changes of characteristic diffraction intensity are determined. It was proved that high-temperature oscillating X-ray diffraction is a powerful analysing method in thermal analysis.

Thermogravimetry (TG) is defined to be a single step process as illustrated in Fig. 1.[1] We have been studying thermal decomposition of ammonium heptamolybdate-(6—) tetrahydrate ($(NH_4)_6Mo_7O_{24}\cdot 4H_2O$, AHM) in the range of room temperature to 500 °C during several years. We first measured the thermal decomposition of AHM by means of TG under an atmosphere of static air. One of the typical results is shown in Fig. 2.[2] The intermediates (a), (l), and (n) are considered to be plateaus, but the intermediates (j), (k), and (m) are not. The steps (j) and (k) on a TG curve show gentle slopes. We must consider the gentle slopes owing either to some thermal decomposition or to an instrumental effect. From the definition of TG, the stages (j) and (k) contain multistep processes. However, this could be explained partly by DTA (differential thermal analysis). We hope to define elementary processes of this decomposition more precisely by studying the microscopic structure. The experimental methods used were mainly a simultaneous TG-DTA under various atmospheres, and a high-temperature oscillating XRD analysis (XRD: X-ray diffraction). The experimental results of the former have been already published partly.[2] The results of the latter will be discussed in this report.

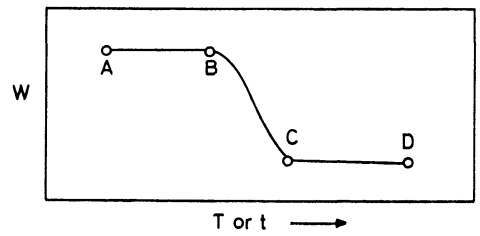

Fig. 1. TG curve of a single step process.
W, *T*, and *t* are weight change, temperature and time, respectively. AB and CD are plateaus.

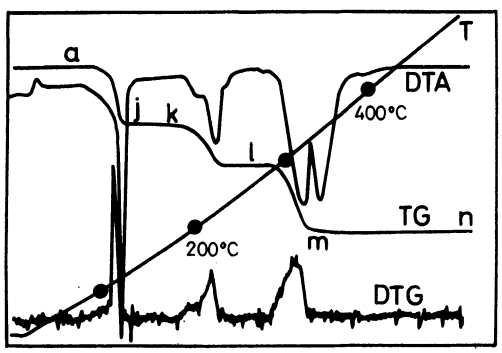

Fig. 2. One of the typical results of TG-DTG-DTA under a static air atmosphere.
Heating rate: 3 °C/min; TG full scale range: 10 mg; DTA full scale range: ±100 μV.

The decomposition of AHM has received considerable attention as it is an isopoly anion reaction. Numerous investigators have studied thermal decompositions of AHM by means of TG, TG-DTA, powder XRD, Ω-tron mass spectrometry, and infrared absorption spectrometry, *etc.* Moreover thermal decomposition of AHM was studied by simultaneous TG-DTG-DTA-HRMS (DTG: differential thermogravimetry, HRMS: high resolution mass spectrometry) under various atmospheres (static, dry air flow, wet air flow, and (NH_3+N_2) mixture gas flow).[2,3] Recently thermal decomposition of AHM was measured by means of DSC (DSC: differential scanning calorimetry) by the authors.[4] Furthermore, by using microscopic structural analysis, we observed a phase transition occurring at 175 °C in addition to those at 110 °C, 210 °C, and 297 °C by means of high-temperature oscillating XRD with a standard X-ray generator. The conditions were: heating rate 2.5 °C/min, ranges of scanning angle, 2θ: 10.5°—13.5°, and voltage and current of the standard X-ray generator 30 kV and 30 mA, respectively. Since the intensity of the X-ray is about 800 cps and the signal-to-noise ratio at a maximum value of diffracted patterns (2θ) is about 10,

the statistical error is about 9.7%. The result of this experiment did not elucidate a gradual decrease of the TG curve. Because of a large statistical error, we could estimate neither the order of the reaction, nor the Arrhenius parameter. Then, using a rotating anode type large capacity generator thermal decomposition of AHM was measured by means of high-temperature oscillating XRD (the maximum voltage and the current are 60 kV and 200 mA, respectively). An X-ray intensity with a brilliance over 6 times as bright as a conventional hermetically-sealed X-ray tube was obtained. As the current can be varied from 10 mA to 200 mA in steps of 5 mA, the maximum peak intensity of the diffracted X-ray can be kept constant, independent of grain size, thickness of the sample, or flatness of the sample surface. In the present experiment it is possible to settle the maximum value of the diffracted pattern at 7200 cps and the inherited error is about 2%. As the maximum value of the diffracted pattern is fixed to be 7200 cps, it will be possible to determine the reaction rate of the thermal decomposition in the case of constant heating.[5]

First we considered the optimum experimental conditions of high temperature oscillating XRD. This is discussed below.

Experimental

Details of the experimental conditions are described below.

X-Ray Tube Output. Patterns of XRD are obtained by JEOL ROTEX JRX-12 using Cu $K\alpha$ radiation. Precise performances are itemized in Table 1.

Table 1. Performances of JEOL ROTEX JRX-12

X-Ray output	12 kW (Cu anode type)
	$\lambda_{\alpha 1}=1.54050$ Å
Maximum tube current	200 mA
Maximum tube voltage	60 kV
Focus size	0.5×10 mm^2
X-Ray tube window	10 mmϕ (Beryllium)
Tube voltage stability	0.05%
(input power$\pm$10% fluctuation)	
Tube current stability	0.05%
(input power$\pm$10% fluctuation)	
Diameter of the rotating anode type generator	
	100 mmϕ
Anode type species	Cu $K\alpha$

High-temperature Sample Holder. The standard sample holder of the goniometer was replaced by a high-temperature sample holder, DX-GOH-V_2(JEOL) in Fig. 3. This is made of a Pt–20%Rh alloy, and the area of the sample setting is 18×12 mm^2, the setting depth being 0.15 mm. It has a low resistance and is heated directly by a large current. Improved temperature measurements have been made using a thin thermocouple wire, Pt–Pt13%Rh, welded to the ribbon sample heater of a high temperature oscillating XRD attachement. The output signal of the thermocouple was read by a digital voltmeter (Takeda Riken Co., TR-6855) *via* a cold junction compensator. Temperature control of the hot stage is done by a controller, ULVAC-RICO PLUG-IN MODULE type THERMAL PROGRAM CONTROLLER, Model HPC-5000 Series. In Fig. 4, a 1 : 13 wounded transformer is connected between the sample holder and the controller. Intensity of diffracted X-ray signal, angle marker signals of oscillating ranges and output reading of the thermocouple are recorded by a Desk Top Recorder D-2R-1S (Ohkura Denki Co.).†

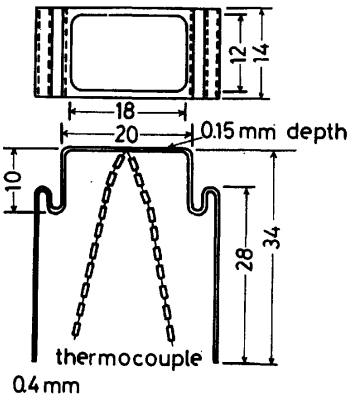

Fig. 3. A high temperature sample holder made of Pt–20%Rh alloy.

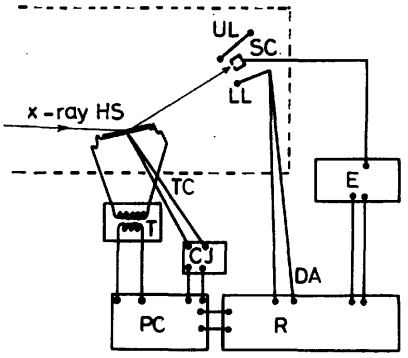

Fig. 4. An apparatus for high-temperature oscillating XRD.
HS: Hot stage; UL: upper limit switch; LL: lower limit switch; SC: scintillation counter; TC: thermocouple of Pt–Pt13%Rh; CJ: cold junction compensation; PC: thermal program controller; DA: diffraction angle; R: recorder; E: electric circuit.

Profiles of the Diffracted X-Ray Signal. Profiles of the diffracted X-ray signal are determined under the conditions described in Table 2. If more precise angular resolution that is described below is needed, the conditions shown in paren-

Table 2. Profiles of diffracted X-Ray signal

Glancing angle of X-Ray beam	4.5°
Soller slit, full opening angle	4.8°
Divergence slit	1° (1/2°)[a]
Scattering slit	1° (1/2°)[a]
Receiving slit	0.2 mm (0.05 mm)[a]
Filter species	Ni
Goniometer radius and angular accuracy	
	250 mm and $\pm$1/100°.

a) If more precise angular resolution of oscillating XRD is needed, the conditions shown in parentheses are used.

† In order to calibrate the linearity of the recorder, programmable DC voltage/current generator, TR-6141 (Takeda Riken K.K.), is used and its total accuracy is ± 5 μV.

theses in Table 2 are used.

Ranges of Oscillating Angles of Goniometer. The intensity of the diffracted angle, ranging between $2\theta_{low}$ and $2\theta_{high}$, is measured by high temperature oscillating XRD analysis, using limiting switches. At first usual powder XRD patterns are measured from $2\theta=5°$ to $2\theta=50°$. The angle of a maximum value of the diffracted X-ray signal is included in the range between $2\theta_{low}$ and $2\theta_{high}$. Moreover, on heating the sample in steps of 20 °C up to 500 °C, powder patterns of XRD are recorded. The angle of the highest dynamically changing value of the diffracted pattern is included in the range between $2\theta_{low}$ and $2\theta_{high}$ too. In the present case of the thermal decomposition of AHM, an angle of maximum intensity of the diffracted pattern, ($2\theta=9.7°$), is included in the range of the angle. Together with the angle of maximum intensity, more angles of strong intensity are included in the ranges of $2\theta_{low}=9.2°$ and $2\theta_{high}=13.2°$. Consequently the oscillating range of the goniometer is about 4°.

Selection of a Time Constant, τ, of the Electric Circuit. A time constant, τ, of a counting system is chosen below, *i.e.* "τ is smaller than half of the oscillation time of the slit."[6] Concerning the opening angle of the receiving slit, the goniometer scanning rate, its radius and the oscillation of the slit (described below), τ is chosen to be 0.172 s. Opening angle of the receiving slit, goniometer radius, and time width of the slit are found to be 0.0458°, 250 mm, and 0.344 s, respectively.

Conditions of the Experimental Room. In order to get rid of intensity variation due to scattering caused by the air in the path of the X-ray beam, measurements are done under the conditions of constant temperature and moisture. The present experiment is done at the constant temperature of 25 (±0.2) °C.

Heating Rate. The temperature difference, ΔT, between the temperature at an angle $2\theta_{low}$ and that at an angle $2\theta_{high}$ in the course of programmed heating, is defined by

$$\Delta T = \frac{\Delta 2\theta \cdot \mathrm{d}T/\mathrm{d}t}{S}, \qquad (1)$$

where S=scanning speed, $\mathrm{d}T/\mathrm{d}t$=heating or cooling rate, and $\Delta 2\theta=2\theta_{high}-2\theta_{low}$. In a typical experimental condition, ΔT is chosen to be 1 °C, under the conditions, $\Delta 2\theta=4°$, $\mathrm{d}T/\mathrm{d}t=$ 2 °C/min, and $S=8$ °/min.

Response of the Pen Recorder. The response of the pen recorder is 0.6 s for full scale. The half width of a peak is 5 mm and it takes 5 s to describe it. As the response time is shorter than this time, the use of this recorded for high temperature oscillating XRD is satisfactory.

Results and Discussion

Experimental Conditions. Time Constant, τ: As seen from Fig. 5 the best choice of the time constant τ is 0.1 s.

Stability of the Diffracted X-Ray Intensity: In order to examine the stability of the X-ray generator during a measurement, the intensity of the diffracted X-ray signal from the Pt-20%Rh ribbon heater versus experimental time was measured under the same conditions of the actual experiment described below, *i.e.* oscillation angle range from $2\theta_{low}=36.92°$ to $2\theta_{high}=41.17°$ and constant room temperature, during about 250 min. The peak intensity was measured versus experimental time and was averaged for during 250 min. During the first 24 min we observed a small increase of the signal of $2\theta=40.20°$ ($d=2.244$ Å), probably because the current of X-ray tube had not yet reached its stationary value. As the fluctuations of the X-ray intensity were below 1.5%, we may consider the stability of the X-ray source as fairly good.

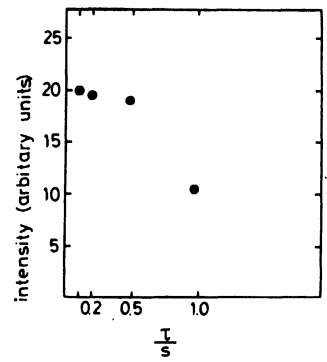

Fig. 5. Plot of intensity of XRD *versus* some time constant (τ).

High-temperature Oscillating XRD of AHM. AHM of Nakarai Co. (GR quality) was used in the form of a powder for the measurements. It was ground and sieved through standard sieves to seperate the fractions of 115—150 mesh, of 150—170 mesh and of 270—325 mesh. Moreover, for reference, a sample of Johnson-Matthey Co. of high purity (specpure chemical batch No. S84208**) was used for the measurements. In particular, in order to compare the experimental results, we mainly used samples of 150—170 mesh.

The intensity ratios of the peaks in the diffracted pattern are changed by the flatness and the thickness of the sample setting. So it is important how a sample is placed on the sample holder by a spatula, and was smoothed by a spoon. The intensity of the diffracted X-ray is about 90% of the full scale intensity (full scale is 2×10^4 cps in one case) of the recorder.

The intensity I of the characteristic X-ray is given by Eq. 2, C, A, V, and V_i are a constant, tube current, tube

$$I = C \cdot A \cdot (V-V_i)^{1.5} \qquad (2)$$

voltage, and exciting voltage, respectively. The intensity of the diffracted X-ray (I) of the diffraction angle, $2\theta=9.7°$ and the tube current are examined under the same experimental conditions as before. With A ranging from 10 mA to 150 mA, the relation (2) was examined experimentally. Considering I as a linear function of A : $I=aA+b$, we found by least squares method $a=0.34$ cps per Ampere and $b=1.85$ cps. Thinking b is small, it is satisfactory to use this X-ray generator for the present experiment under the conditions, mentioned above.

In the present experiment, high temperature oscillating XRD is measured at various heating rates, 0.5, 1, 2, 3, 4, 30, and 50 °C/min, *etc.* ΔT at the various heaintg rates is presented in Table 3. For the comparison with the results of TG-DTA and DSC, the heating in the high-temperature oscillating XRD is chosen to be 2 °C/min.

A result of a high temperature oscillating XRD of

** Specification: Cu below 7 ppm, Si below 2 ppm, Ca, Fe, and Mg below 1 ppm, respectively.

Table 3. ΔT (difference of the temperature between at $2\theta_{low}$ and $2\theta_{high}$ at the various heating rates

dT/dt (heating rate) °C/min	ΔT °C	dT/dt (heating rate) °C/min	ΔT °C
0.5	0.25	4	2
1.0	0.5	30	15
2.0	1.0	50	25
3.0	1.5		

S=8°/min, $\Delta 2\theta$=4°.

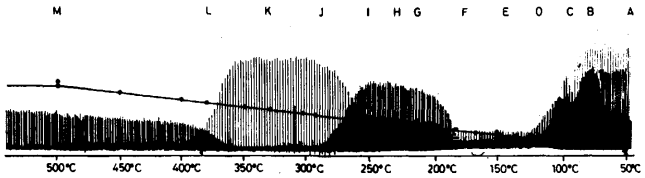

Fig. 6. One of the typical results of high-temperature oscillating XRD of AHM (115—150 mesh).
Experimental conditions: heating rate: 2 °C/min; chart spped: 5 mm/min; $2\theta_{low}$=9.37°; $2\theta_{high}$=13.43°; full scale of diffracted XRD: 1×10^4 cps; scanning speed: 8°/min; time constant: 0.1 s; divergency: 1°; receiving slit: 0.1 mm.

Table 4. Powder XRD patterns of various molybdates and molybdenum oxides in the ASTM X-Ray diffraction data files

ASTM index	Molecular formula	Crystal structure system
11-71	$(NH_4)_6Mo_7O_{24}\cdot 4H_2O$	Monoclinic
18-117	$(NH_4)_4Mo_8O_{26}$	Triclinic
21-0567	MoO_3	Hexagonal
5-0508	MoO_3	Orthorhombic

AHM (150—170 mesh) at the heating rate, 2 °C/min is shown in Fig. 6. Powder XRD patterns have been collected in the ASTM X-ray diffraction data files for the compounds given in Table 4. The XRD intensities for every plane index as a function of temperature are examined precisely. In the following I_0 stand for the maximum peak intensity.

ASTM Index 11-71, $(NH_4)_6Mo_7O_{24}\cdot 4H_2O$. The starting material was confirmed to be AHM by means of the standard powder XRD.

d = 9.08 Å, I/I_0 = 100, plane index (040), 2θ = 9.7°.

At about 65 °C this intensity shows a small increase and scattering becomes bigger. At about 84 °C the intensity begins to decrease drastically until about 95 °C and from that temperature it is gradually decreasing and finally at about 157 °C the peak disappears completely.

d = 7.56 Å, I/I_0 = 9, plane index (110), 2θ = 11.7°

This intensity begins to decrease from about 84 °C and disappears at about 100 °C.

d = 7.42 Å, I/I_0 = 9, plane index (110), 2θ = 11.9°

This intensity also begins to decrease from about 84 °C and disappears at about 100 °C.

d = 7.17 Å, I/I_0 = 20, plane index ($1\bar{2}1$), 2θ = 12.3°

This intensity also begins to decrease from about 77 °C and this decrease stops at about 90 °C and then it increases at about 97 °C from that temperature it begins to decrease again and at about 130 °C disappears completely.

The peak intensity of the d value, not described above, corresponding with the diffraction angle 2θ=9.7° begins to appear at about 118 °C. Moreover the peak at the diffraction angle, 2θ=13.4° begins to appear at about 110 °C and it is stable from about 124 °C to about 180 °C. From about 180 °C it begins to decrease and it disappears completely at about 226 °C.

ASTM Index 18-117, $(NH_4)_4Mo_8O_{26}$, Ammonium Octamolybdate(4−).

d = 7.21 Å, I/I_0 = 100, plane index undefined, 2θ = 12.2°.

This intensity begins to appear at about 176 °C and becomes stable at about 233 °C; it begins to decrease at about 266 °C and disappears completely at about 290 °C.

d = 9.21 Å, I/I_0 = 35, plane index undefined 2θ = 9.6°.

This intensity begins to appear at about 175 °C and becomes stable at about 200 °C. Moreover it becomes larger at about 250 °C.

ASTM Index 21-569, Hexagonal MoO_3.

d = 9.12 Å, I/I_0 = 80, plane index (100), 2θ = 9.7°.

The stable state of this peak produced from ammonium octamolybdate(4−) (AOM) is considered to be completed at about 175 °C, but at about 254 °C the peak becomes larger and becomes stable again at about 295 °C. In these temperature ranges, the intensity at the diffraction angle, 2θ=9.7°, of hexagonal MoO_3 is three times larger than that of AOM. It begins to decrease at about 355 °C and it disappears at about 405 °C.

ASTM Index 5-0508, Orthorhombic MoO_3.

d = 6.93 Å, I/I_0 = 34, plane index (020), 2θ = 12.7°.

This peak appears at about 358 °C, and becomes constant at about 426 °C. Its intensity is gradually increasing.

Meanwhile, in order to confirm an appearance temperature of maximum intensity at about 98 °C, we measured some high-temperature oscillating XRD's under the conditions described below. These conditions and the result are shown in Fig. 7.

Next, particular temperature stages of thermal decomposition are analysed by means of standard high

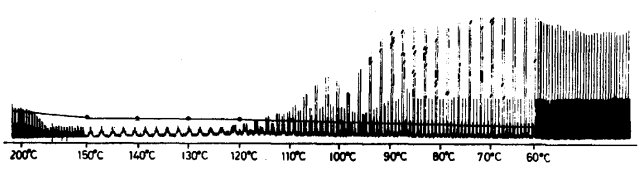

Fig. 7. One of the typical results of high-temperature oscillating XRD of AHM (115—150 mesh). Experimental conditions: heating rate: 2 °C/min; chart speed: 20 mm/min; $2\theta_{low}$=9.19°; $2\theta_{high}$=13.41°; full scale of diffracted XRD: 2×10^4 cps; scanning sped: 8°/min; time constant: 0.1 s; divergency: 1°; receiving slit: 0.1 mm.

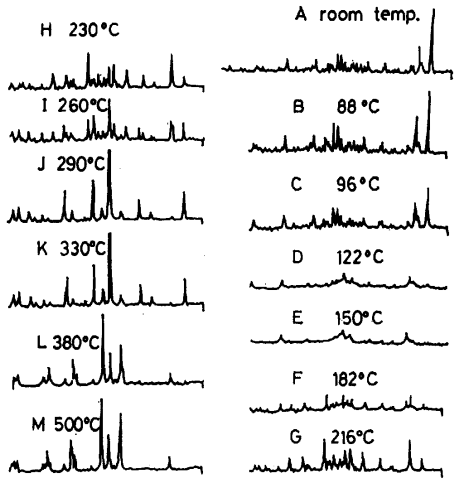

Fig. 8. The standard XRD at several temperatures.
(A) Room temperature; (B) 88 °C; (C) 96 °C; (D) 122°C; (E) 150 °C; (F) 182 °C; (G) 216 °C; (H) 230 °C; (I) 260 °C; (J) 290 °C; (K) 330 °C; (m) 380 °C; (M) 500 °C.

temperature XRD. At the desired temperature, the heating was stopped and after three minutes, the sample was cooled to room temperature, the standard powder XRD's are measured. The results are shown in Fig. 8, A)—M). The patterns of A), H), K), and M) are considered to be AHM, AOM, hexagonal MoO_3 and orthorhombic MoO_3, respectively.

Correspondence with the Results of TG-DTA and High-temperature Oscillating XRD. Thermal decomposition of AHM has been studied by E. Ma[7] and three clear steps were found to be:

$$(NH_4)_6Mo_7O_{24}\cdot 4H_2O \xrightarrow{130^\circ C} (NH_4)_4Mo_5O_{17},$$

$$(NH_4)_4Mo_5O_{17} \xrightarrow{240^\circ C} (NH_4)_4Mo_8O_{26},$$

$$(NH_4)_4Mo_8O_{26} \xrightarrow{360^\circ C} MoO_3.$$

We had already studied thermal decomposition of AHM by means of TG-DTG-DTA and DSC,[2,3],†† but the upper decomposition schemes are not consistent precisely with the present experimental results. The discrepancy can be explained partly by high-temperature oscillating XRD. Before explaining the experimental results, we summarize and XRD measurement method at high temperature step by step.

I. After confirming each reaction stage by means of TG-DTA, the sample of the intermediate product is taken out from a thermobalance and measured by means of standard powder XRD.

II. At constant high temperature stage, high temperature XRD's are measured.[8] In our experiment, using a strong X-ray generator, we are enabled to take only 5 min to measure a standard XRD. It is possible to find an intermediate more easily than in case I. The reaction proceeds further, because the temperature is kept constant during 5 min, so some intermediate may happen to be missed.

III. High temperature oscillating XRD is the best analysis in order not to miss an intermediate of thermal decomposition. This method allows to find the best setting angle ranges of oscillation. Using a large capacity generator, however, the signal-to-noise ratio improve and gains better accuracy than using a standard X-ray generator. At a desired temperature during high-temperature oscillating XRD, a standard XRD is easily measured in a short time. By this improved technique, the structural changes of the precise reaction stages are observed.

Next, in comparison with a high-temperature oscillating XRD, in Fig. 2 we show a typical TG-DTG-DTA result under a static air atmosphere. The temperature of onsets and offsets of TG decrease are shown in Table 5. Also initial, final, and peak top temperatures of DTA and DSC are shown in Table 6.

Table 5. The temperatures of onsets and offsets of TG decrease

Decomposition stage	Onsets temperatures of each stage	Offsets temperatures of each stage
I	92 °C	135 °C
II	185 °C	234 °C
III	277 °C	362 °C

Table 6. The initial, peak top, and final temperatures of DTA and DSC

Decomposition stage	Initial temperature	Peak top temperature	Final temperature
I	92 °C	103 °C, 112 °C[a)]	130 °C
II	165 °C	192 °C, 217 °C[a)] (223 °C, 239 °C)[a)]	236 °C
III	256 °C	263 °C, 305 °C (329 °C)	346 °C

a) indicates the bigger peak when two peaks appear. Temperatures in the parentheses are obtained by DSC.

The results of TG showed a sharp decrease of the first stage at about 92 °C and this decrease ends at about 132°C. From this temperature TG begins to decrease gradually. At about 185 °C the second step of TG begins and at about 277 °C the third step. High-temperature oscillating XRD experiments, however, show a decrease in intensity of the (040)-plane from about 84 °C to 95 °C. This intensity finally disappears completely at about 157 °C. These two tendencies of the intensity curve (rapid and gradual) decreases of high-temperature oscillating XRD are consistent with the decreasing tendency of the first stage of TG.

Concerning the plane $(1\bar{2}1)$, two tendencies, a decreasing intensity at about 77 °C and a peak at about 97 °C, are convolved. We tried to seperate them, but did not succeed until now.

Moreover, we considered the intensity of d=7.21 Å of AHM, the intensity of d=9.21 Å of AOM and the intensity of d=9.12 Å of hexagonal MoO_3 from 176 °C to 258 °C. As the difference of the interplanar spacing,

†† TG-DTG-DTA was measured by means of Rigaku Co. Thermoflex, model 8002 and DSC by means of Daini Seiko Co. DSC, model SSC/560S.

d of the last two cases (*i.e.*, d=9.21 Å and d=9.12 Å) is very small, we could not seperate these two interplanar spacings. There are two possible explanations: one is a co-existance of AOM and hexagonal MoO_3, and the other one is that we simply could not seperate the peaks. In order to consider the possibility of co-existence of AOM and hexagonal MoO_3, we compare with the standard high-temperature XRD's, H) and K), at 230 °C and 310 °C, respectively in Fig. 8. Though the difference of d=9.21 Å in AOM and of d=9.12 Å in hexagonal MoO_3 is recognized slightly, we could not seperate them in a high temperature oscillating XRD. This experiment shows two stable peaks of AOM, d= 7.21 Å and 9.21 Å. At the phase transition of AOM to hexagonal MoO_3, two peaks disappear partly and a new peak, d=9.12 Å of hexagonal MoO_3 appears. In order to confirm these results, we improved the angle resolution of high-temperature oscillating XRD. Under the conditions of D=0.5°, S=0.5°, R=0.05 mm, and $d2\theta/dt$=4°/min, we could not succeed in seperating both peaks. The results also show stable temperature ranges of hexagonal MoO_3 and orthorhombic MoO_3.

The results of TG and DTA may explain the production of MoO_3 only, but whether it is hexagonal or orthorhombic MoO_3 cannot be explained by TG-DTG-DTA alone.

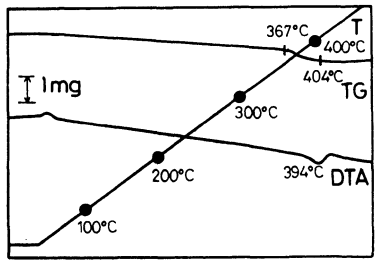

Fig. 9. Results of TG-DTA of a sample removed from the X-ray hot stage at about 330 °C, sample weight: 25.40 mg; TG full scale range: 10 mg; DTA full scale range: ±25 μV; chart speed: 20 cm/h; heating rate: 5 °C/min.

A sample of hexagonal MoO_3 was removed from the hot stage, and was analyzed by means of TG-DTA. The results are shown in Fig. 9 and two different decreasing types of TG are found. In one type the gradual weight loss of TG is about 2.4% from the room temperature to 300 °C. The other type is the rapid weight decrease of about 1.6% from 367 °C to 404 °C. Also the peak temperature of DTA is about 394 °C. The sample may not be simply MoO_3, but may be thought to be either $n\cdot(NH_4)_2O\cdot m\cdot MoO_3$ or $k\cdot H_2O\cdot MoO_3$ (n, m, k are positive integers). For the identification of this substance, a gas analysis is planned by means of simultaneous TG-MS. The weight loss of 2.4% may be due to desorption of water adsorbed by the sample after its removal from the hot stage. We conclude that the intermediate of (K) has hexagonal MoO_3 structure merely.

In X-ray spectroscopy there is always some background signal, and to decide whether or not this can be ignored is an important problem. Moreover, we must consider the accuracy of intensity measurements in high-temperature oscillating XRD. The statistical error depends on the peak intensity. If we define the number of signal intensity and of back ground as N_p and Nb, respectively, the statistical error $\sigma(\%)$ is given by the equation,[9]

$$\sigma(\%) = \frac{1}{\sqrt{Np}} \cdot \frac{\sqrt{1+Nb/Np}}{(1-Nb/Np)} \cdot 100. \qquad (3)$$

In the present experiment, Np and Nb are found to be 7040 cps and 440 cps, respectively, with σ=1.35%. For a standard X-ray tube (30 kV and 30 mA), Np and Nb were 650 cps and 70 cps, respectively, with now σ= 4.62%. Obviously the present experiment has a better accuracy, which enables to analyze a reaction rate and to determine Arrhenius parameters.

Table 7. The results of oscillating high temperature XRD

Decomposition stage	Temperature range of intensity plateaus	Cross point temperature
5 mm/min chart speed		
I_1	room temp—84 °C	89 °C
I_2	96 —100 °C	126 °C
I_3	128 —177 °C	183 °C, 187 °C
II	232 —251 °C	265 °C
III	295 —345 °C	384 °C
20 mm/min chart speed		
I_1	room temp—77 °C	99 °C
I_2	102 —104 °C	126 °C
I_3	129 —174 °C	183 °C, 187 °C

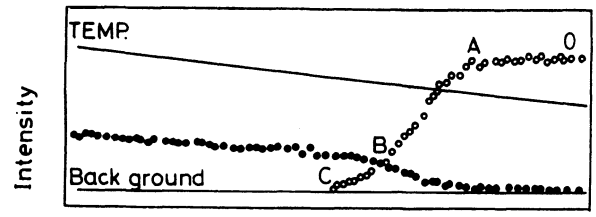

Fig. 10. Model of the result of high-temperature oscillating XRD. In the range OA one structural substance is present. In the range AC a mixture of more structural substances is present.

An appearance, disappearance, and cross point temperatures of the intensity of the diffraction patterns, are shown in Fig. 10. Moreover OA in Fig. 10 is considered to be a range of spacing versus sample temperature under programmed heating. From these measurements we may conclude that in the temperature range OA in Fig. 10, there is only one structural substance, but in the range AC, there is a mixture of structural substances. Finally we could measure points A and C more sharply by this experimental method. Consequently high-temperature oscillating XRD will become one of the most important methods of thermal analysis.

Some other inorganic salts (salts of isopoly acid) will be analyzed by high-temperature oscillation XRD method in future.

Summary

Thermal decomposition of AHM was measures by means of high-temperature oscillating XRD with a rotating anode type large capacity generator. This method enables us to measure microscopical structural changes in the field of thermal analysis. Especially, with improved S/N ratio, it is easy to determine the temperature of a phase transition and a reaction rate constant.

In a high-temperature oscillating XRD of AHM with the heating rate 2 °C/min, a peak temperature of 96 °C was found, which has not been reported before. Also from 110 °C to 226 °C, a series of small peaks was found. Finally, one stage of decomposition which was obtained in TG-DTA experiments, was seperated into three steps. The stability ranges of AOM, hexagonal MoO_3, and orthorhombic MoO_3 were clarified.

The X-ray generator is situated in the Research Institute for Material Science and Engineering, Fukui University. The author wishes to thank Professor Tohgoro Matsuo and Mr. Shigeru Hashiya for convenience of using their X-ray generator. The assistance of Miss Masayo Yoshimen during the early experiments is also acknowledged. The author would like to thank Dr. A. J. H. Boerboom and Dr. G. Harkvoort for critical reading of the manuscript. This work was partly supported by the Grant-in-Aid for Scientific Research from the Ministry of Education, Science and Culture.

References

1) G. Lombardi, "For Better Thermal Analysis," International Confederation for Thermal Analysis (1977).
2) K. Isa, Y. Hirai, and H. Ishimura, *Proc. of the 5th Int. Conf. on Thermal Analysis* (*Kyoto*), 348 (1977).
3) H. Ishimura and K. Isa, *Proc. of the 5th Int. Conf. on Thermal Analysis* (*Kyoto*), 488 (1977).
4) Unpublished.
5) Unpublished.
6) H. P. Klug and L. E. Alexander, "X-Ray Diffraction Procedures," John Wiley and Sons (1954).
7) E. Ma, *Bull. Chem. Soc. Jpn.*, **37**, 649 (1964).
8) P. F. Konovalov, A. I. Efremov, and B. V. Volkonskii, "Ionization X-Ray Equipment for Research on Crystalline Materials at Various Temperatures," (1958).
9) "Practical X-Ray Spectroscopy," ed by R. Jenkins and J. L. de Vries, Philips Technical Library, Macmillan (1972), Chap. 5, p. 90,

The Phosphorescence Spectra of Methyl-substituted 9,10-Anthraquinones in Solutions at 77 K

Akira KUBOYAMA* and Sanae Y. MATSUZAKI

National Chemical Laboratory for Industry, Tsukuba Research Center, Yatabe, Ibaraki 305

(Received February 6, 1981)

The phosphorescence spectra and their lifetimes of 9,10-anthraquinone and its 2-methyl and 2,3-dimethyl derivatives in various kinds of glassy solutions at 77 K have been obtained. In the non-hydrocarbon solutions, 2-methylanthraquinone shows, in most cases, a dual phosphorescence, consisting of a $n\pi^*$ phosphorescence and a $\pi\pi^*$ phosphorescence with different lifetimes, while 2,3-dimethylanthraquinone shows a very broad $\pi\pi^*$ phosphorescence spectrum. The quinone-solvent interactions and the relative positions of the close-lying $^3n\pi^*$ and $^3\pi\pi^*$ levels of these quinones are discussed on the basis of the experimental results.

Previously, we have studied the phosphorescence spectra of 9,10-anthraquinone[1,2] (AQ) in various solutions at 77 K. All the phosphorescence spectra observed have been of the $n\pi^*$ type, having a distinct progression of the C–O stretching vibration and a short lifetime around 3 ms. Recently, we have observed the $\pi\pi^*$ phosphorescence spectra of alkylsubstituted 1,4-naphthoquinones[3] in glassy solutions at 77 K, while in 1,4-naphthoquinone only the $n\pi^*$ phosphorescence spectra have been observed in all the solutions. This is thought to be due to the rise of the phosphorescent $n\pi^*$ level and the fall of the low-lying $^3\pi\pi^*$ level of 1,4-naphthoquinone in the alkyl derivatives, resulting from the alkyl-group substitutions and the specific (hydrogen-bond and charge-transfer) and dispersion-force[4] interactions between the quinones and solvents. In this work, the phosphorescence spectra of the methyl-substituted anthraquinones, 2-methyl- and 2,3-dimethyl-AQ's, in various kinds of glassy solutions at 77 K have been studied from this point of view. The phosphorescence spectra of AQ in those solutions have also been studied for the purpose of comparison.

Experimental

Measurements. The phosphorescence spectra and their lifetimes in solutions at 77 K were measured using a phosphoroscope in the manner described in previous papers.[1-3] The solvents used were methylcyclohexane, toluene, ethanol, methanol, and 1-chloro- and 1-bromobutanes. All the solutions were glassy at 77 K. In the toluene solutions, the crystalline state was also formed by slow-cooling.[2] The concentrations of the solutions used always less than 10^{-3} mol dm^{-3}.

Materials. The AQ and the methyl-substituted anthraquinones used were commercially available. The AQ and 2-methyl-AQ were zone-refined (mp 286.6—287.2 °C and 176.6—177.5 °C). The 2,3-dimethyl-AQ was twice recrystallized, from a toluene–cyclohexane (1 : 2) mixture and from acetic acid (mp 207.5—208.8 °C). Spectrograde methylcyclohexane, methanol, and toluene of the Dozin Yakukagaku Co., analytical-grade ethanol of Wako Pure Chemical Industries, and G.R.-grade 1-choro- and 1-bromobutanes of the Tokyo Kasei Kogyo Co. were used.

Results. The phosphorescence spectra obtained are shown in Figs. 1—6, while their observed lifetimes are shown in Table 1.[5] In the methyl-substituted anthraquinones, the phosphorescence spectra depend on the turning-rate of the sector and the excitation-wavelength in some cases, but show no concentration dependence. In AQ, the phosphorescence spectra show none of these dependences. In the captions of Figs. 3—5, the words in parentheses, "slow" and "fast", denote that the turning-rates of the sector are slow and fast respectively. In the captions of Figs. 5 and 6, the wavelengths in parentheses denote the excitation-wavelengths. When the phosphorescence spectra showed sector-turning-rate dependences, two kinds of lifetimes were obtained, the shorter ones of which were obtained with the sector turning relatively fast, and the longer ones of which, with the sector turning as slow as possible.

Discussion

AQ shows only the $n\pi^*$ phosphorescence spectra in the solvents used in this work at 77 K; they show a distinct progression of the C–O stretching vibration and short lifetimes (Figs. 1 and 2 and Table 1).[6] Therefore, AQ may have the T_1 $n\pi^*$ state in these cases.[7] The phosphorescence spectrum of AQ in a toluene crystal is at wavelengths longer by *ca.* 250 cm^{-1} than that in toluene glass, and is situated very close to that in methylcyclohexane. Therefore, the charge-transfer interaction between AQ and toluene in a toluene crystal may be very small. Similar phenomena are also observed in the cases of the methyl-substituted anthraquinones, as will be mentioned later.

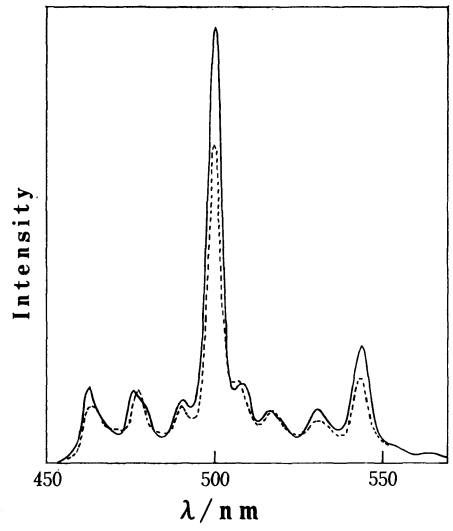

Fig. 1. Phosphorescence spectra of AQ and 2,3-dimethyl-AQ in methylcyclohexane at 77 K.
——: AQ, ------: 2,3-dimethyl-AQ.

TABLE 1. OBSERVED LIFETIMES, τ, OF THE PHOSPHORESCENCE SPECTRA

	τ/ms					
Solvent	Methylcyclohexane	Toluene	Ethanol	Methanol	1-Chlorobutane	1-Bromobutane
AQ	3.3	3.6 (3.4)[a]	3.3	3		3.1
2-Methyl-AQ	4.6	17 86 (4.7)	5	13 47	7 64	7 29
2,3-Dimethyl-AQ	5.1	100 (7.6)	92	150	73	19

a) The values in parentheses are the ones in toluene crystals.

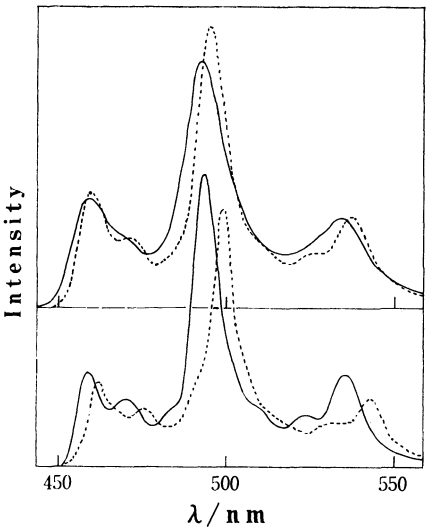

Fig. 2. Phosphorescence spectra of AQ in solutions at 77 K.
(1) Lower curves, ——: toluene glass, ------: toluene crystals, (2) Upper curves, ——: methanol, ------: 1-bromobutane.

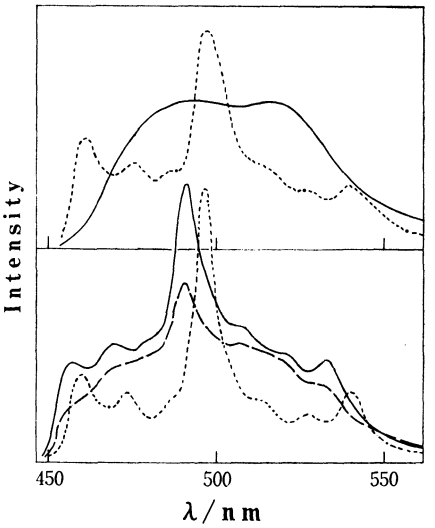

Fig. 3. Phosphorescence spectra of 2-methyl- and 2,3-dimethyl-AQ's in toluene at 77 K.
(1) Lower curves, 2-methyl-AQ, ——: glass (fast), — —: glass (slow),------: crystals, (2) upper curves, 2,3-dimethyl-AQ, ——: glass, ------: crystals.

The phosphorescence bands of the methyl-substituted anthraquinones in methylcyclohexane (Fig. 1)[13] may reasonably be assigned to the $n\pi^*$ spectrum because of their similarity to that of AQ and their short lifetimes (Table 1). Since the positions of the phosphorescence spectra of the methylsubstituted anthraquinones are very close to that of AQ, the rise in the T_1 $n\pi^*$ levels of the methyl-substituted anthraquinones relative to that of AQ may be very small. As may be seen in Table 1, the lifetime of 2-methyl-AQ is a little longer and a little shorter respectively than those of AQ and 2,3-dimethyl-AQ. This may be due to increases in the mixing[14–16] of the close-lying $^3\pi\pi^*$ state into the T_1 $n\pi^*$ state in these methyl-substituted anthraquinones, accompanied by decreases in the energy separation between these two states resulting from the methyl-group substitutions.

The phosphorescence spectrum of 2-methyl-AQ in toluene glass, obtained with the sector turning fast (Fig. 3), is considerably broader than that of AQ in toluene glass, while the one obtained with the sector turning slow is still broader. In this case, two considerably different lifetimes (17 and 86 ms) are obtained (Table 1). In these spectra, two kinds of phosphorescence spectra, the relatively sharp $n\pi^*$ spectrum and the broad $\pi\pi^*$ spectrum, seem to overlap. The above facts may be explained as follows. As the shorter lifetime (17 ms) is too long as that of the $n\pi^*$ spectrum, it is thought that 2-methyl-AQ in toluene glass has the T_1 $\pi\pi^*$ state and that the energy separation between the T_1 $\pi\pi^*$ state and the close-lying T_2 $n\pi^*$ state is distributed according to the degree of solvation of the quinone molecules.[17] Consequently, the degree of mixing of the T_2 $n\pi^*$ state into the T_1 $\pi\pi^*$ state and the rate of thermal population to the T_2 $n\pi^*$ state in the excited states[18] may take various values. Hence, dual phosphorescences, consisting of the $n\pi^*$ and $\pi\pi^*$ spectra, appear with various figures and lifetimes.

In the toluene glassy solution of 2,3-dimethyl-AQ, the very broad phosphorescence spectrum may be assigned to the $\pi\pi^*$ spectrum because of the absence of the C–O stretching vibrational structure and its long lifetime (100 ms). Previously, in the toluene glassy solution of 2-methyl-1,4-naphthoquinone, a similar, very broad phosphorescence spectrum with a short lifetime (2.0 ms) was observed. The difference in the lifetime between these two quinones is remarkable. Since the intensity of the latter phosphorescence spectrum is considerably weaker than that of the former, the short lifetime of the latter may be mainly due to the existence of some efficient non-radiative dissipative route from the

phosphorescence state.

The above differences in the phosphorescence spectra of 2-methyl- and 2,3-dimethyl-AQ's between the methylcyclohexane and toluene glass solutions may be partly due to the rise in the $^3n\pi^*$ levels resulting from the π-π type charge-transfer interaction between the quinones and toluene, and partly due to the fall in the $^3\pi\pi^*$ levels resulting from the relatively strong dispersion-force interaction between the quinones and toluene.[19] The phosphorescence spectra of the methylsubstituted anthraquinones in toluene crystal may be assigned to the $n\pi^*$ spectra because of their similarity to that of AQ and their short lifetimes, close to those in the methylcyclohexane solution.

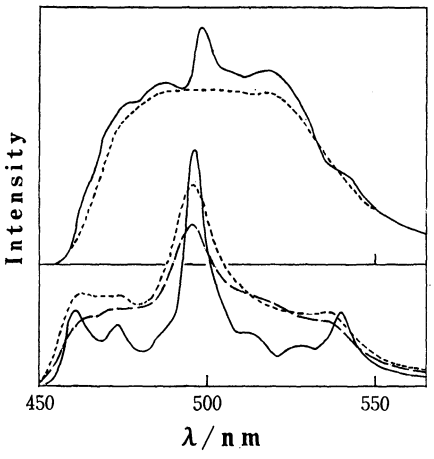

Fig. 4. Phosphorescence spectra of 2-methyl- and 2,3-dimethyl-AQ's in alcohols at 77 K.
(1) Lower curves, 2-methyl-AQ, ——: ethanol, ------: methanol (fast), — —: methanol (slow), (2) Upper curves, 2,3-dimethyl-AQ, ——: ethanol, ------: methanol.

In the methanol solution of 2-methyl-AQ (Fig. 4), a dual phosphorescence similar to that in the toluene solution is observed. As the shorter lifetime (13 ms) is close to that in the toluene solution, the T_1 state of 2-methyl-AQ in methanol is thought to be the $\pi\pi^*$ state, as in the toluene solution. On the other hand, in the ethanol solution of 2-methyl-AQ, the T_1 state may be the $n\pi^*$ state, as its phosphorescence spectrum show a distinct C–O stretching vibrational structure and its lifetime is short.

2,3-Dimethyl-AQ in methanol may have the T_1 $\pi\pi^*$ state because of the similarities of the phosphorescence spectrum and its lifetime to those in the toluene glassy solution. In the phosphorescence spectrum of 2,3-dimethyl-AQ in ethanol, the sharp $n\pi^*$ and broad $\pi\pi^*$ spectra seem to overlap, but the relative weight of the former seems to be far smaller than that of the latter. In view of the above relative weights of the two spectra and the sector-turning-rate independence of the phosphorescence spectrum, it is thought that the $^3\pi\pi^*$ level is lower than the $^3n\pi^*$ level, and that the $n\pi^*$ spectrum appears weakly because of the thermal population in the excited states. The above results indicate that the hydrogen-bond between ethanol and the quinones is,

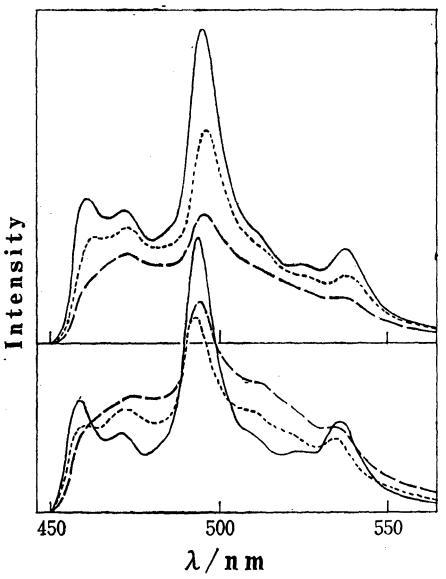

Fig. 5. Phosphorescence spectra of 2-methyl-AQ in 1-chloro and 1-bromobutanes at 77 K.
(1) Lower curves, 1-chlorobutane, ——: (fast, 313 nm), ------: (fast, 365 nm), — —: (slow, 313 nm), (2) upper curves, 1-bromobutane, ——: (fast, 313 nm), ------: (fast, 365 nm), — —: (slow 313 nm).

to some extent, weaker than that between methanol and the quinones.

In the 1-chloro- and 1-bromobutanes solutions of 2-methyl-AQ, dual phosphorescences similar to those in the toluene and methanol solutions are observed (Fig. 5). In these 1-halogenobutane solutions, however, as the shorter lifetimes (7 ms in both solutions) are considerably shorter than those in the toluene and methanol solutions, and are rather close to those in the methylcyclohexane and ethanol solutions, it is thought that differently solvated species which have either the T_1 $n\pi^*$ or the T_1 $\pi\pi^*$ state coexist and that the shorter

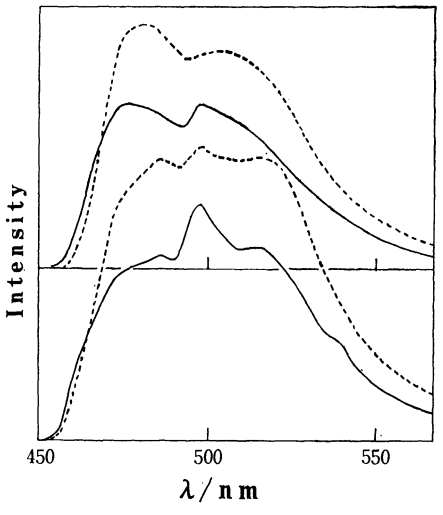

Fig. 6. Phosphorescence spectra of 2,3-dimethyl-AQ in 1-chloro and 1-bromobutanes at 77 K.
(1) Lower curves, 1-chlorobutane, ——: (313 nm), ------: (365 nm), (2) upper curves, 1-bromobutane, ——: (313 nm), ------: (365 nm).

TABLE 2. ASSIGNED T_1 STATES OF THE QUINONES[a)]

Solvent	Methylcyclohexane	Toluene	Ethanol	Methanol	1-Chlorobutane	1-Bromobutane
AQ	$n\pi^*$	$n\pi^*$ ($n\pi^*$)	$n\pi^*$	$n\pi^*$	$n\pi^*$	$n\pi^*$
2-Methyl-AQ	$n\pi^*$	$\pi\pi^*$ ($n\pi^*$)	$n\pi^*$	$\pi\pi^*$	$n\pi^*$, $\pi\pi^*$	$n\pi^*$, $\pi\pi^*$
2,3-Dimethyl-AQ	$n\pi^*$	$\pi\pi^*$ ($n\pi^*$)	$\pi\pi^*$	$\pi\pi^*$	$\pi\pi^*$	$\pi\pi^*$

a) The states in parentheses are the ones in toluene crystals.

lifetimes are due to the species which have the T_1 $n\pi^*$ state. In the 1-halogenobutane solutions of 2,3-dimethyl-AQ, in view of their phosphorescence spectra (Fig. 6), it is thought that the $^3\pi\pi^*$ level is lower than the $^3n\pi^*$ level, and that the weak appearances of the sharp $n\pi^*$ spectrum are due to the thermal population in the excited states, as in the ethanol solution.

As may be seen in Fig. 5, with the same turning-rate of the sector the weights of the sharp $n\pi^*$ spectrum relative to the broad $\pi\pi^*$ spectrum are considerably larger in the 313 nm excitation than in the 365 nm excitation. Similar excitation-wavelength dependences are seen in the case of 2,3-dimethyl-AQ in Fig. 6. In a previous work,[3)] a similar phenomenon was also observed in the phosphorescence spectrum of 2-methyl-1,4-naphthoquinone in ethanol at 77 K, where the weight of the sharp $n\pi^*$ spectrum relative to the broad $\pi\pi^*$ spectrum was larger in the 365 nm excitation than in the 313 nm excitation. No definitive explanation of these facts can be obtained at this stage.

In Table 1, the lifetimes corresponding to those of the $\pi\pi^*$ phosphorescence spectra of the methyl-substituted anthraquinones in 1-bromobutane are quite short in comparison with those in the 1-chlorobutane solutions. This may be due to the intermolecular heavy-atom effect[20)] brought about by the bromine atom in 1-bromobutane.

The T_1 states of these quinones in the solutions assigned in this work are shown in Table 2. When the quinone molecules with the T_1 $n\pi^*$ and $\pi\pi^*$ states are thought to coexist, both of the two states are described in Table 2. The results obtained in this work may be useful in studying the photochemistry of these quinones.

References

1) A. Kuboyama and S. Matsuzaki, *Bull. Chem. Soc. Jpn.*, **40**, 2475 (1967); *Rep. Gov. Chem. Ind. Res. Inst., Tokyo*, **64**, 105 (1969).

2) A. Kuboyama, *Bull. Chem. Soc. Jpn.*, **43**, 3373 (1970); *Rep. Gov. Chem. Ind. Res. Inst., Tokyo*, **66**, 176 (1971).

3) A. Kuboyama, *Bull. Chem. Soc. Jpn.*, **51**, 2771 (1978); *Rep. Gov. Chem. Ind. Res. Ins. Inst., Tokyo*, **75**, 1 (1980).

4) In general, the dispersion-force interaction between solutes and solvents brings about far larger red-shifts for $\pi\pi^*$ spectra than for $n\pi^*$ spectra, and so under this interaction the $\pi\pi^*$ levels become much lower than the $n\pi^*$ levels.

5) In a previous paper,[1)] the observed lifetime of the phosphorescence spectrum of AQ in a methylcyclohexane–toluene (4 : 1) mixture at 77 K (6.3 ms) is erroneous; the correct value is 3.8 ms.

6) The phosphorescence spectra of AQ in ethanol and 1-chlorobutane are similar to those of 2-methyl-AQ in ethanol (Fig. 4) and of AQ in 1-bromobutane (Fig. 2) respectively.

7) AQ is thought to have two low-energy triplet levels, $n\pi_+^*$ and $n\pi_-^*$, like *p*-benzoquinone.[8,9)] In the text, the $n\pi^*$ triplet level corresponds to the lower one of them, while the higher one is neglected in order to simplify the discussion. According to the CNDO/S-Cl[10)] calculations,[11)] in *p*-quinones the triplet $n\pi_-^*$ level (the $^3B_{1g}$ level in AQ) is lower than the $n\pi_+^*$ level (the ^3A_u level in AQ).[12)]

8) H. P. Trommsdorf, *J. Chem. Phys.*, **50**, 5358 (1972); Veenvliet and D. A. Wiersma, *Chem. Phys.*, **8**, 432 (1975); Y. Miyagi, M. Koyanagi, and Y. Kanda, *Chem. Phys. Lett.*, **40**, 98 (1976).

9) A. Kuboyama, *Bull. Chem. Soc. Jpn.*, **35**, 295 (1962); *Rep. Gov. Chem. Ind. Res. Inst., Tokyo*, **50**, 347 (1964).

10) J. DelBene and H. H. Jaffe, *J. Chem. Phys.*, **48**, 1807 (1968); R. L. Ellis, G. Kuehnlenz, and H. H. Jaffe, *Theor. Chim. Acta*, **26**, 131 (1972).

11) A. Kuboyama, Y. Kojima, and S. Matsuzaki, 43rd National Meeting of the Chemical Society of Japan, Tokyo, April 1981, Abstr. No. I, p. 517.

12) J. R. Swenson and R. Hoffmann, *Helv. Chim. Acta*, **53**, 2331 (1970); W. Hug, J. Kuhn, K. J. Seibold, H. Labhart, and G. Wagniere, *ibid.*, **54**, 1451 (1971).

13) The phosphorescence spectrum of 2-methyl-AQ in methylcyclohexane is similar to that of 2,3-dimethyl-AQ in Fig. 1.

14) Y. H. Li and E. C. Lim, *Chem. Phys. Lett.*, **7**, 15 (1970).

15) H. Hayashi and S. Nagakura, *Mol. Phys.*, **24**, 801 (1972).

16) T. H. Cheng and N. Hirota, *Mol. Phys.*, **27**, 281 (1974); **31**, 681 (1976).

17) A. A. Lamola, *J. Chem. Phys.*, **47**, 4810 (1967); H. J. Pownall and J. R. Huber, *J. Am. Chem. Soc.*, **93**, 6429 (1971).

18) E. Migirdicyan, *Chem. Phys. Lett.*, **12**, 473 (1972); S. W. Mao and N. Hirota, *Mol. Phys.*, **27**, 327 (1974); H. Hayashi and S. Nagakura, *ibid.*, **27**, 969 (1974).

19) The refractive index of toluene ($n_D^{20}=1.497$) is considerably larger than that of methylcyclohexane ($n_D^{20}=1.423$). Therefore, the dispersion-force interaction between quinones and toluene is thought to be considerably larger than that between quinones and methylcyclohexane.

20) S. P. McGlynn, T. Azumi, and M. Kinoshita, "Molecular Spectroscopy of the Triplet State," Prentice-Hall, New Jersey (1969), p. 307.

The Molecular Structures of Thiomethoxymethylbis(triphenylphosphine)-palladium Hexafluorophosphate and Perchlorate at −160 °C

Kunio MIKI,* Yasushi KAI, Noritake YASUOKA,** and Nobutami KASAI*

Department of Applied Chemistry, Faculty of Engineering, Osaka University, Yamadaoka, Suita, Osaka 565

(Received February 12, 1981)

The molecular structures of $[Pd(CH_2SCH_3)(PPh_3)_2]PF_6$(**3a**) and $[Pd(CH_2SCH_3)(PPh_3)_2]ClO_4$(**3b**) at −160°C were determined by means of X-ray diffraction. Crystals of both complexes belong to the monoclinic system: **3a**, $a=11.535(2)$, $b=17.990(4)$, $c=17.754(2)$ Å and $\beta=101.07(1)°$, space group $P2_1/c$ with $Z=4$; **3b**·CH_2Cl_2 solvate, $a=11.496(5)$, $b=20.872(9)$, $c=15.056(6)$ Å and $\beta=94.77(4)°$, space group $P2_1/n$ with $Z=4$. Both structures were solved by the heavy atom method and refined by the least-squares procedure to $R=0.141$ for 3906 reflections and $R=0.102$ for 4595 reflections for **3a** and **3b** respectively. The geometry around the Pd atom in each complex is essentially planar. However, the coordination behavior of the CH_2SCH_3 group in **3a** and in **3b** seems to be different. In **3a**, the CH_2SCH_3 group is bonded to the Pd atom through the Pd–C σ-bond and the donation of the sulfur to the metal atom, forming a Pd–C–S three-membered ring [Pd–CH_2=2.06(4), Pd–S=2.367(8), CH_2–S=1.77(4) and S–CH_3=1.78(4) Å]. On the other hand, the CH_2SCH_3 group in **3b** is coordinated to the metal atom as a methylenemethylsulfonium ion, containing a C=S double bond[Pd–CH_2=2.208(13), Pd–S=2.303(6), CH_2–S=1.678(14) and S–CH_3=1.86(4) Å].

We have hitherto studied the structural chemistry of a series of palladium complexes containing the CH_2SR(R=CH_3, C_6H_5) groups in order to elucidate their coordination behavior, especially that of the sulfur to the metal atom.[1-3] It is interesting that the CH_2SR group is coordinated to the transition metal not only as a monodentate ligand but also as a bidentate one.[4,5] Three types of coordination modes are possible for the thiomethoxymethyl(CH_2SCH_3) group, as shown below:

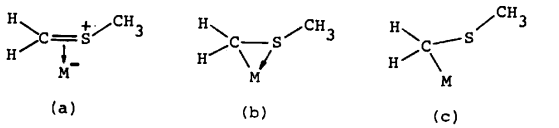

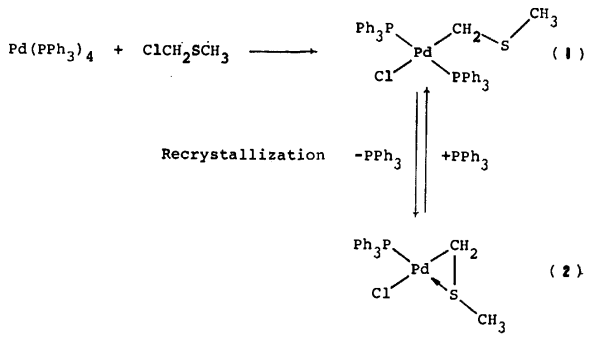

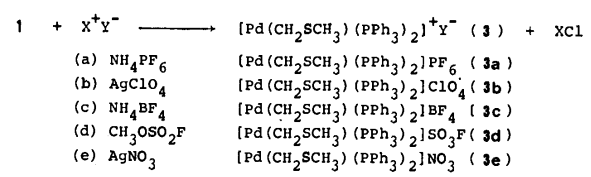

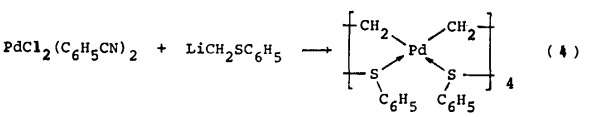

Scheme 1.

The CH_2SCH_3 group behaves as a π-bonded two-electron ligand in (a), as a bidentate ligand in (b), or as a σ-bonded monodentate ligand in (c).

Recently, a series of novel palladium complexes containing these CH_2SR groups have been prepared by Okawara, Yoshida, and their co-workers.[3,6-8] The outline of the reactions is summarized in Scheme 1.

We have previously carried out structure analyses of Complexes **1**,[1] **2**,[2] and **4**.[3] In Complex **1**,[1] the CH_2SCH_3 group is bound to the Pd atom through the Pd–C σ-bond (type c). On the other hand, in Complex **2**,[2] the CH_2SCH_3 group is coordinated with the type b mode to form a Pd–C–S three-membered ring. The thiophenoxymethyl ($CH_2SC_6H_5$) groups bridge four Pd atoms in Complex **4**,[3] which can be considered as an internuclear modification of type b. These differences in bonding modes may be due to the slight difference of the nucleophilicity of S atom in these complexes.

As a part of this study, we will report here the molecular structures of Complexes **3a** and **3b**, determined by means of X-ray diffraction at −160 °C, in order to reveal the coordination of the CH_2SCH_3 group in these cationic complexes.

Experimental

Several efforts were made for five kinds of complexes, **3a**—**e**, to obtain good single crystals from CH_2Cl_2 solutions. Crystals of $[Pd(CH_2SCH_3)(PPh_3)_2]SO_3F$(**3d**)[7] were too small to use for intensity data collection, and Complex **3e**, $[Pd(CH_2SCH_3)(PPh_3)_2]NO_3$, did not crystallize.[7] Crystals of $[Pd(CH_2SCH_3)(PPh_3)_2]BF_4$(**3c**)[7] were comparatively large, large enough to collect intensities. However, preliminary oscillation and Weissenberg photographs showed many diffuse spots near the normal Bragg reflections, suggesting a disordered structure. If all these diffuse spots can be disregarded, the **3c** crystals can be said to have a *C*-centered monoclinic unit cell with dimensions of $a=18.0$, $b=18.4$, $c=12.3$ Å, and $\beta=107°$.

The crystals of **3a** and **3b** are colorless needles and plates

** Present address: Crystallographic Research Center, Institute for Protein Research, Osaka University, Yamadaoka, Suita, Osaka 565.

Table 1. Crystal data

	$[Pd(CH_2SCH_3)(PPh_3)_2]PF_6$ (**3a**)		$[Pd(CH_2SCH_3)(PPh_3)_2]ClO_4\cdot 0.25CH_2Cl_2$ (**3b**)	
Formula	$C_{38}H_{35}P_2PdS\cdot PF_6$		$C_{38}H_{35}P_2PdS\cdot ClO_4\cdot 0.25CH_2Cl_2$	
Formula weight	837.1		812.8	
$F(000)$	1696		1658	
Crystal system	Monoclinic		Monoclinic	
Space group	$P2_1/c$		$P2_1/n$	
Z	4		4	
	[−160 °C]	[20 °C]	[−160 °C]	[20 °C]
a/Å	11.535(2)	11.650(2)	11.496(5)	11.526(4)
b/Å	17.990(4)	18.198(5)	20.872(9)	21.110(8)
c/Å	17.754(2)	17.956(3)	15.056(6)	15.328(5)
β/°	101.07(1)	101.24(2)	94.77(4)	94.42(4)
U/Å^3	3615.5(11)	3733.7(15)	3600(3)	3718(3)
D_c/g cm^{-3}	1.538	1.489	1.499	1.452
D_m/g cm^{-3} a)		1.49		1.44
μ (Mo $K\alpha$)/cm^{-1}	7.55	7.31	8.03	7.78

a) By flotation in carbon tetrachloride/hexane at 25 °C.

respectively. X-Ray structure analyses of these crystals have been performed, although they seemed not too suitable for X-ray diffraction study judging from their size, shape, and/or habits. Preliminary oscillation and Weissenberg photographs taken at room temperature with Cu $K\alpha$ raditaion determined their crystal system and space group. Accurate unit-cell dimensions at −160 and 20 °C were determined by a least-squares fit of the 2θ value of 25 strong reflections measured on a Rigaku diffractometer. The crystal data are summarized in Table 1.

Measurements of the integrated intensities were made at −160 °C on the Rigaku automated, four-circle, single-crystal diffractometer. The crystals used had approximate dimensions of 0.1 mm × 0.1 mm × 0.25 mm and 0.25 mm × 0.3 mm × 0.35 mm for **3a** and **3b** respectively. The low temperature was attained by the gas flow method using liquid nitrogen. The intensity data were collected by the θ-2θ scan technique, using graphite-monochromatized (for **3a**) and Zr-filtered (for **3b**) Mo $K\alpha$ radiation (λ=0.71069 Å). The scan speed was 4° min^{-1}, and the scan width was $\Delta 2\theta=(2.5+0.7\tan\theta)°$. The background intensities were measured for 5 s at both ends of a scan. Totals of 7899 and 7907 reflections with 2θ less than 54° were collected for **3a** and **3b** respectively, 3906 and 4595 reflections of which were considered as observed ($|F_o|>3\sigma(|F_o|)$). The standard reflections (600, 019, and 219 for **3a** and 800, 555, 008 and 0, 10, 0 for **3b**) monitored at regular intervals were constant throughout the data collection. Corrections for Lorentz and polarization factors were carried out in the usual manner, while neither absorption nor extinction correction was made.

Structure Solution and Refinement

Both structures were solved by the heavy atom method. The structures were refined by the block-diagonal least-squares procedure (*HBLS*-V[9]), the function minimized being $\sum w(|F_o|-|F_c|)^2$. The unit weights were employed throughout the refinement. The atomic scattering factors were taken from International Tables for X-Ray Crystallography[10] for non-hydrogen atoms and from those of Stewart *et al.*[11] for hydrogen atoms. The final atomic positional parameters are presented in Table 2.†

*$[Pd(CH_2SCH_3)(PPh_3)_2]PF_6$ (**3a**).* All the non-hydrogen atoms were reasonably located by the Patterson and Fourier syntheses. Several cycles of isotropic refinement reduced the R value ($R=\sum||F_o|-|F_c||/\sum|F_o|$) to 0.17. The temperature factors of the F atoms in the PF_6 anion showed relatively large values (maximum B=11.2 Å^2). Further anisotropic refinement in the usual manner did not go on straightforwardly, some abnormal temperature factors being observed. Therefore, the subsequent refinement was carried out step-by-step using small damping factors for the shifts of the parameters. On a Fourier map, a relatively high peaks, the peak height of which was about 80% of that of the C(1) atom, appeared 1.12 and 2.37 Å distant from the S and Pd atoms respectively. If this peak is identified as a disordered fragment of the S atom, the geometry around the Pd atom is far from the square-planar coordination. Therefore, this peak was ignored and not included in the subsequent refinement. The final R value is 0.141 for 3906 reflections.

*$[Pd(CH_2SCH_3)(PPh_3)_2]ClO_4\cdot 0.25CH_2Cl_2$ (**3b**).* The Fourier synthesis based on the coordinates of the Pd atom, determined from a three-dimensional Patterson map, revealed the locations of all the non-hydrogen atoms in the cation. A few cycles of isotropic refinement reduced the R value to 0.14. A difference Fourier map revealed the location of only the Cl atom of the ClO_4 anion, and its electron density was relatively low and very broad. Subsequent difference Fourier maps could locate only one of the four O atoms in the ClO_4 anion. These Cl and O atoms indicated abnormally large temperature factors in the further refinement. In addition, three other peaks were found on a Fourier map. They were interpreted as those of the solvent CH_2Cl_2 molecule. The calculated density for the formula weight, assuming that one molecule of CH_2Cl_2 is included in an asymmetric unit [1.566 g cm^{-3}], is

† Tables of the complete F_o—F_c data and of the final anisotropic temperature factors are deposited at the Chemical Society of Japan as Document No. 8150.

TABLE 2. FINAL ATOMIC PARAMETERS

Estimated standard deviations are given in parentheses. B_{eq} values are equivalent isotropic temperature factors calculated from anisotropic thermal parameters.[12]

(a) $[Pd(CH_2SCH_3)(PPh_3)_2]PF_6$ (**3a**)

Atom	x	y	z	B_{eq}/Å^2
Pd	0.67007(14)	0.02532(11)	0.22058(9)	2.0
S	0.4737(6)	0.0431(5)	0.1540(4)	3.5
P(1)	0.8027(5)	0.0113(3)	0.1363(3)	1.4
P(2)	0.7904(5)	0.0270(4)	0.3379(3)	1.6
C(1)	0.509(3)	0.0299(19)	0.2547(16)	4.0
C(2)	0.422(3)	−0.0465(16)	0.1216(17)	4.0
C(11)	0.9603(18)	0.0021(13)	0.1724(12)	2.0
C(12)	1.034(3)	0.0647(15)	0.1936(15)	3.1
C(13)	1.153(3)	0.057(3)	0.2267(16)	5.1
C(14)	1.201(2)	−0.0149(18)	0.2377(14)	3.5
C(15)	1.133(3)	−0.0780(18)	0.2190(14)	3.5
C(16)	1.0122(17)	−0.0656(14)	0.1866(11)	2.0
C(21)	0.7993(17)	0.0861(11)	0.0662(10)	1.2
C(22)	0.890(3)	0.0965(14)	0.0257(14)	2.7
C(23)	0.880(3)	0.1543(16)	−0.0267(14)	3.8
C(24)	0.782(4)	0.203(3)	−0.038(2)	5.6
C(25)	0.698(3)	0.2005(15)	0.0086(16)	3.2
C(26)	0.707(2)	0.1384(16)	0.0649(17)	3.6
C(31)	0.762(2)	−0.0702(14)	0.0806(13)	2.3
C(32)	0.791(3)	−0.0808(16)	0.0060(14)	3.2
C(33)	0.753(3)	−0.1461(16)	−0.0366(15)	4.1
C(34)	0.690(3)	−0.2019(14)	−0.0044(15)	3.3
C(35)	0.659(3)	−0.1909(18)	0.067(2)	4.9
C(36)	0.698(3)	−0.1252(16)	0.1053(16)	3.5
C(41)	0.7210(15)	0.0348(10)	0.4227(10)	1.1
C(42)	0.6496(19)	0.0966(12)	0.4276(12)	2.0
C(43)	0.599(3)	0.1029(15)	0.4932(16)	3.5
C(44)	0.621(3)	0.0489(16)	0.5508(13)	3.2
C(45)	0.687(2)	−0.0107(14)	0.5444(13)	2.7
C(46)	0.7395(19)	−0.0183(13)	0.4816(12)	2.1
C(51)	0.889(3)	0.1070(12)	0.3525(13)	2.2
C(52)	0.9790(19)	0.1157(13)	0.4191(13)	2.2
C(53)	1.055(2)	0.1755(13)	0.4251(13)	2.2
C(54)	1.042(3)	0.2272(13)	0.3686(15)	3.0
C(55)	0.954(3)	0.2195(13)	0.3025(12)	2.4
C(56)	0.877(3)	0.1587(14)	0.2950(12)	2.4
C(61)	0.8805(19)	−0.0566(12)	0.3545(11)	1.7
C(62)	1.000(3)	−0.0585(12)	0.3761(12)	2.3
C(63)	1.063(3)	−0.1269(14)	0.3881(12)	2.4
C(64)	0.999(3)	−0.1986(13)	0.3739(12)	2.1
C(65)	0.877(3)	−0.1935(14)	0.3518(13)	2.8
C(66)	0.817(3)	−0.1225(17)	0.3369(14)	3.3
P(3)	0.5228(7)	0.2723(4)	0.2220(4)	3.2
F(1)	0.4013(16)	0.2265(11)	0.2079(12)	5.8
F(2)	0.454(3)	0.336(2)	0.246(2)	15.2
F(3)	0.639(2)	0.3163(13)	0.2365(15)	8.1
F(4)	0.583(3)	0.2017(15)	0.207(3)	12.6
F(5)	0.493(3)	0.293(3)	0.1375(13)	13.0
F(6)	0.549(3)	0.249(3)	0.3079(13)	11.5

much larger than the observed value of 1.44 g cm^{-3}. These facts suggest a low occupancy of CH_2Cl_2. The occupancy factor for CH_2Cl_2 was then estimated as 0.25, which gives the calculated density of 1.452 g cm^{-3}. The coordinates of the C atom of CH_2Cl_2 were fixed in the further refinement. Several more cycles of refinement were carried out anisotropically for the Pd, S, P, and C atoms in the cation and isotropically for Cl, O, and C in the ClO_4 anion and the CH_2Cl_2 molecule. The final R factor is 0.102 for 4595 reflections.

(b) $[Pd(CH_2SCH_3)(PPh_3)_2]ClO_4 \cdot 0.25CH_2Cl_2$ (**3b**)

Atom	x	y	z	B_{eq} or B*/Å^2
Pd	0.04915(9)	0.13720(5)	0.17868(7)	2.4
S	0.0116(6)	0.1166(3)	0.0287(4)	5.7
P(1)	0.0635(3)	0.24730(16)	0.1976(3)	1.9
P(2)	0.0470(3)	0.09187(15)	0.3175(3)	1.8
C(1)	0.0133(12)	0.0517(6)	0.0945(9)	2.3
C(2)	−0.145(3)	0.1380(16)	0.0090(16)	8.6
C(11)	−0.0487(11)	0.2778(7)	0.2647(9)	2.6
C(12)	−0.1645(12)	0.2541(8)	0.2405(11)	3.4
C(13)	−0.2558(13)	0.2746(10)	0.2911(13)	5.2
C(14)	−0.2320(15)	0.3146(11)	0.3623(12)	5.3
C(15)	−0.1190(16)	0.3373(10)	0.3864(12)	5.1
C(16)	−0.0253(14)	0.3176(9)	0.3382(11)	4.0
C(21)	0.2024(10)	0.2823(6)	0.2391(8)	1.9
C(22)	0.2981(11)	0.2424(7)	0.2590(9)	2.3
C(23)	0.4068(12)	0.2683(8)	0.2850(10)	2.9
C(24)	0.4196(13)	0.3344(8)	0.2908(10)	3.5
C(25)	0.3255(12)	0.3745(7)	0.2717(10)	3.0
C(26)	0.2145(12)	0.3485(7)	0.2455(9)	2.7
C(31)	0.0371(10)	0.2898(6)	0.0913(9)	2.1
C(32)	0.1283(12)	0.2868(7)	0.0336(9)	2.6
C(33)	0.1167(12)	0.3197(7)	−0.0484(9)	2.5
C(34)	0.0152(12)	0.3532(6)	−0.0742(9)	2.3
C(35)	−0.0743(11)	0.3556(7)	−0.0179(9)	2.6
C(36)	−0.0650(11)	0.3247(6)	0.0660(9)	2.1
C(41)	0.1782(10)	0.0470(6)	0.3522(9)	1.9
C(42)	0.2668(11)	0.0424(6)	0.2909(9)	2.1
C(43)	0.3702(11)	0.0079(7)	0.3183(9)	2.5
C(44)	0.3847(12)	−0.0205(7)	0.4013(10)	2.7
C(45)	0.2974(11)	−0.0162(6)	0.4608(9)	2.3
C(46)	0.1956(11)	0.0176(7)	0.4342(9)	2.3
C(51)	0.0327(11)	0.1422(6)	0.4149(9)	2.2
C(52)	0.1176(11)	0.1876(7)	0.4365(9)	2.4
C(53)	0.1115(14)	0.2267(7)	0.5105(9)	3.1
C(54)	0.0178(13)	0.2190(7)	0.5655(9)	3.0
C(55)	−0.0669(12)	0.1728(7)	0.5452(9)	2.8
C(56)	−0.0621(11)	0.1329(7)	0.4688(9)	2.5
C(61)	−0.0753(11)	0.0359(6)	0.3152(8)	2.1
C(62)	−0.1868(12)	0.0603(8)	0.2881(11)	3.2
C(63)	−0.2836(12)	0.0197(8)	0.2816(11)	3.4
C(64)	−0.2677(12)	−0.0464(7)	0.2998(10)	2.9
C(65)	−0.1563(12)	−0.0696(7)	0.3275(10)	2.9
C(66)	−0.0603(12)	−0.0293(6)	0.3350(9)	2.2
Cl(1)	0.5065(15)	0.1197(9)	0.1529(11)	20.7(6)*
O(1)	0.579(3)	0.1116(14)	0.0822(19)	18.5(10)*
Cl(1S)	0.240(3)	0.0348(16)	−0.025(3)	9.1(8)*
Cl(2S)	0.378(3)	−0.0351(15)	0.092(2)	8.5(7)*
C(S)	0.380	0.013	0.003	8.9(28)*

Results and Discussion

Bond lengths and bond angles in the two complexes are listed in Tables 3 and 4 respectively.

In spite of the low temperature measurements, the precision of neither structure is high enough to make a detailed discussion. This is considered mainly due to the poor quality of the **3a** and **3b** crystals. In both **3a** and **3b** crystals, the PF_6 and ClO_4 anions have rather disordered structures, which may also be connected with the precision of the present structures.

Structures of PF_6 and ClO_4 Anions. In **3a**, six F atoms of the PF_6 anion, especially four out of those, show abnormally low peak heights and a broadening in the electron density distribution. As an example, an electron density map on the plane formed by the P and four F atoms is given in Fig. 1. The ^{19}F NMR studies of **3a** suggested that the PF_6 anions are rapidly reorienting about the octahedral axes[13] at random, or nearly so, even at liquid nitrogen temperature.[14]

The locations of three oxygen atoms in the ClO_4 anion

TABLE 3. BOND LENGTHS, WITH THEIR ESTIMATED STANDARD DEVIATIONS IN PARENTHESES

Length (l/Å)	**3a**	**3b**	Length (l/Å)	**3a**	**3b**
$[Pd(CH_2SCH_3)(PPh_3)_2]$ cation					
Pd–P(1)	2.350(5)	2.320(3)	Pd–P(2)	2.271(6)	2.297(3)
Pd–S	2.367(8)	2.303(6)	Pd–C(1)	2.06(4)	2.208(13)
S–C(1)	1.77(4)	1.678(14)	S–C(2)	1.78(4)	1.86(4)
P(1)–C(11)	1.82(3)	1.818(14)	P(2)–C(41)	1.84(2)	1.814(13)
P(1)–C(21)	1.83(2)	1.819(12)	P(2)–C(51)	1.82(3)	1.822(13)
P(1)–C(31)	1.78(3)	1.834(13)	P(2)–C(61)	1.82(3)	1.826(13)
C(11)–C(12)	1.42(4)	1.44(3)	C(41)–C(42)	1.40(3)	1.43(2)
C(12)–C(13)	1.39(5)	1.41(3)	C(42)–C(43)	1.40(4)	1.42(2)
C(13)–C(14)	1.41(5)	1.37(3)	C(43)–C(44)	1.40(4)	1.38(2)
C(14)–C(15)	1.38(5)	1.40(3)	C(44)–C(45)	1.33(4)	1.40(2)
C(15)–C(16)	1.42(4)	1.41(3)	C(45)–C(46)	1.37(4)	1.40(2)
C(16)–C(11)	1.36(4)	1.39(3)	C(46)–C(41)	1.40(3)	1.38(2)
C(21)–C(22)	1.39(4)	1.39(2)	C(51)–C(52)	1.43(4)	1.38(2)
C(22)–C(23)	1.39(4)	1.39(2)	C(52)–C(53)	1.38(4)	1.39(2)
C(23)–C(24)	1.41(5)	1.39(3)	C(53)–C(54)	1.36(4)	1.42(3)
C(24)–C(25)	1.39(5)	1.38(3)	C(54)–C(55)	1.40(4)	1.39(3)
C(25)–C(26)	1.49(4)	1.41(2)	C(55)–C(56)	1.40(4)	1.43(2)
C(26)–C(21)	1.42(4)	1.39(2)	C(56)–C(51)	1.37(4)	1.43(2)
C(31)–C(32)	1.44(4)	1.42(2)	C(61)–C(62)	1.36(4)	1.41(2)
C(32)–C(33)	1.42(5)	1.41(2)	C(62)–C(63)	1.43(4)	1.40(3)
C(33)–C(34)	1.42(5)	1.39(2)	C(63)–C(64)	1.48(4)	1.42(3)
C(34)–C(35)	1.39(5)	1.39(2)	C(64)–C(65)	1.39(4)	1.40(2)
C(35)–C(36)	1.40(5)	1.41(2)	C(65)–C(66)	1.45(4)	1.39(2)
C(36)–C(31)	1.36(4)	1.41(2)	C(66)–C(61)	1.40(4)	1.40(2)
PF_6 and ClO_4 anions					
P(3)–F(1)	1.60(3)		P(3)–F(2)	1.50(4)	
P(3)–F(3)	1.53(3)		P(3)–F(4)	1.50(4)	
P(3)–F(5)	1.52(4)		P(3)–F(6)	1.56(4)	
Cl(1)–O(1)[a]		1.42(4)			
CH_2Cl_2, crystalline solvent					
Cl(1S)–C(S)		1.69[b]	Cl(2S)–C(S)		1.68[b]

a) The other O atoms in the ClO_4 anion could not be located. b) The coordinates of the C(S) atom were not refined.

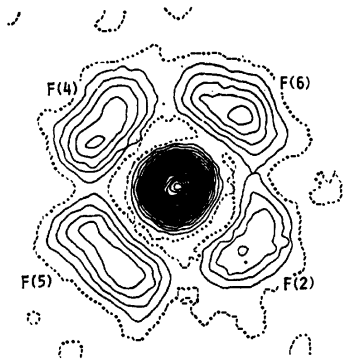

Fig. 1. Electron density distribution on the plane formed by the P(3), F(2), F(4), F(5), and F(6) atoms of the PF_6 anion in $[Pd(CH_2SCH_3)(PPh_3)_2]PF_6$ (**3a**). The contours are drawn at the interval of 1.0 e/Å^3. Zero contours are shown as broken lines while negative contours are omitted.

could not be determined in **3b**, because the electron densities around the central Cl atom are very broad and relatively low except for the O(1) atom. Disordered structures and large thermal motions of the ClO_4 anion have been reported in some complexes.[15]

Structures of $[Pd(CH_2SCH_3)(PPh_3)_2]$ *Cations.* Figure 2 shows *ORTEP* drawings[16] of the cations in these complexes. In Fig. 3, the coordination geometries around the Pd atom in **3a** and **3b** are compared with that of **2**.[2] The geometry around the Pd atom in each complex is essentially square-planar. The equations of the least-squares planes and the deviation of atoms from the planes are presented in Table 5. The planarity of the coordination plane in each complex is not so high, the maximum deviations from the plane being 0.17 and 0.10 Å for **3a** and **3b** respectively, while that in **2** is only 0.04 Å.[2]

Two PPh_3 groups are bonded to the Pd atom in *cis*-coordination. In both complexes, the Pd–P(1) bond lengths are slightly longer than those of the Pd–P(2). This is partly due to the difference in the *trans*-influences of the C and S atoms in the CH_2SCH_3 groups.

In the CH_2SCH_3 group in **3a**, the S–C(1) and S–C(2) bond lengths are close to the S–C single bond length [1.82 Å].[17] The Pd–C(1) bond length is considered to be a normal value for the Pd(II)–C(sp^3) σ-bond. Since these bond lengths, as well as the Pd–S, are comparable to the corresponding ones in **2**,[2] the coordination mode

Table 4. Bond angles, with their estimated standard deviations in parentheses

Angle (ϕ/°)	**3a**	**3b**	Angle (ϕ/°)	**3a**	**3b**
$[Pd(CH_2SCH_3)(PPh_3)_2]$ cation			C(35)–C(36)–C(31)	126.9(28)	118.5(12)
P(1)–Pd–P(2)	103.2(3)	107.58(12)	P(2)–C(41)–C(42)	117.8(15)	117.8(10)
P(1)–Pd–S	112.0(3)	108.10(17)	P(2)–C(41)–C(46)	122.0(15)	122.9(10)
P(2)–Pd–C(1)	99.0(10)	100.0(4)	C(46)–C(41)–C(42)	120.1(18)	119.3(12)
C(1)–Pd–S	46.5(10)	43.6(4)	C(41)–C(42)–C(43)	117.4(21)	118.0(12)
Pd–S–C(1)	57.7(11)	65.2(5)	C(42)–C(43)–C(44)	120.6(25)	121.0(13)
Pd–S–C(2)	105.7(11)	102.3(11)	C(43)–C(44)–C(45)	121.4(26)	120.8(13)
C(1)–S–C(2)	101.7(15)	104.6(12)	C(44)–C(45)–C(46)	119.9(24)	118.5(13)
Pd–C(1)–S	75.8(13)	71.2(6)	C(45)–C(46)–C(41)	120.7(21)	122.5(12)
Pd–P(1)–C(11)	121.0(8)	111.6(5)	P(2)–C(51)–C(52)	122.7(18)	118.4(10)
Pd–P(1)–C(21)	115.0(7)	119.5(4)	P(2)–C(51)–C(56)	117.5(18)	120.2(10)
Pd–P(1)–C(31)	107.7(8)	111.6(5)	C(56)–C(51)–C(52)	119.7(22)	121.3(12)
C(11)–P(1)–C(21)	101.3(10)	108.2(6)	C(51)–C(52)–C(53)	120.1(21)	120.8(13)
C(11)–P(1)–C(31)	105.3(11)	104.0(7)	C(52)–C(53)–C(54)	120.2(22)	119.4(14)
C(21)–P(1)–C(31)	105.1(10)	100.5(6)	C(53)–C(54)–C(55)	120.6(24)	120.3(14)
Pd–P(2)–P(41)	117.7(7)	113.8(5)	C(54)–C(55)–C(56)	120.1(23)	120.7(14)
Pd–P(2)–P(51)	113.3(8)	120.2(5)	C(55)–C(56)–C(51)	119.3(22)	117.5(13)
Pd–P(2)–P(61)	111.5(8)	108.2(5)	P(2)–C(61)–C(62)	125.7(18)	117.0(10)
C(41)–P(2)–C(51)	100.4(10)	101.2(6)	P(2)–C(61)–C(66)	114.2(18)	122.4(10)
C(41)–P(2)–C(61)	104.8(10)	107.2(6)	C(66)–C(61)–C(62)	119.9(22)	120.5(12)
C(51)–P(2)–C(61)	108.1(11)	105.3(6)	C(61)–C(62)–C(63)	121.7(23)	120.1(14)
P(1)–C(11)–C(12)	122.0(18)	115.1(11)	C(62)–C(63)–C(64)	120.2(22)	119.3(14)
P(1)–C(11)–C(16)	121.5(18)	123.5(12)	C(63)–C(64)–C(65)	115.7(22)	119.7(14)
C(16)–C(11)–C(12)	116.3(22)	121.3(14)	C(64)–C(65)–C(66)	121.9(24)	121.2(13)
C(11)–C(12)–C(13)	121.8(27)	118.2(15)	C(65)–C(66)–C(61)	120.0(25)	119.3(12)
C(12)–C(13)–C(14)	118.5(32)	119.8(18)	PF_6 anion		
C(13)–C(14)–C(15)	122.4(31)	122.0(20)	F(1)–P(3)–F(3)	179.3(14)	
C(14)–C(15)–C(16)	115.7(27)	119.9(19)	F(2)–P(3)–F(4)	171.3(21)	
C(15)–C(16)–C(11)	125.3(24)	118.6(16)	F(5)–P(3)–F(6)	178.0(21)	
P(1)–C(21)–C(22)	122.1(17)	119.2(10)	F(1)–P(3)–F(2)	87.0(16)	
P(1)–C(21)–C(26)	114.8(17)	120.2(10)	F(1)–P(3)–F(4)	87.7(17)	
C(26)–C(21)–C(22)	122.5(21)	120.5(12)	F(1)–P(3)–F(5)	87.2(17)	
C(21)–C(22)–C(23)	118.2(24)	120.3(13)	F(1)–P(3)–F(6)	90.8(16)	
C(22)–C(23)–C(24)	121.4(30)	119.5(14)	F(2)–P(3)–F(3)	92.7(17)	
C(23)–C(24)–C(25)	122.0(32)	120.9(15)	F(2)–P(3)–F(5)	93.2(20)	
C(24)–C(25)–C(26)	117.0(27)	120.0(14)	F(2)–P(3)–F(6)	87.0(20)	
C(25)–C(26)–C(21)	117.8(24)	118.9(13)	F(3)–P(3)–F(4)	92.5(18)	
P(1)–C(31)–C(32)	122.3(19)	115.9(10)	F(3)–P(3)–F(5)	93.4(18)	
P(1)–C(31)–C(36)	121.7(20)	124.1(10)	F(3)–P(3)–F(6)	88.6(17)	
C(36)–C(31)–C(32)	116.0(23)	120.0(12)	F(4)–P(3)–F(5)	93.4(21)	
C(31)–C(32)–C(33)	119.5(25)	119.6(12)	F(4)–P(3)–F(6)	86.3(20)	
C(32)–C(33)–C(34)	120.1(28)	120.5(13)	CH_2Cl_2, crystalline solvent		
C(33)–C(34)–C(35)	120.3(28)	119.7(12)	Cl(1S)–C(S)–Cl(2S)		106.6[a]
C(34)–C(35)–C(36)	117.0(30)	121.7(13)			

a) The coordinates of the C(S) atom were not refined.

of the CH_2SCH_3 group to the Pd atom in **3a** is considered to be virtually the same as in **2**. The CH_2SCH_3 group is bonded to the Pd atom by the Pd–C σ-bond, and also by the donation from the S to the Pd atom (the b-type mentioned above).

On the other hand, the coordination mode of the CH_2SCH_3 group to the Pd atom in **3b** is different from those in **2** and **3a**. In **3b**, the S–C(1) bond length is significantly shorter than those in **2** and **3a**, and it is close to the S=C double bond length [1.61 Å][17] rather than the S–C single bond length [1.82 Å].[17] The S–C(2) bond length is considered to be equal to the S–C single bond length. The Pd–C(1) distance is obviously longer than those in **2** and **3a**, and rather near to the Pd–C(olefin) lengths [2.174 and 2.233 Å] in $[Pd(\eta^5\text{-}C_5H_5)(PEt_3)(styrene)]BF_4$.[18] The Pd–S distance, somewhat shorter than those found in **2** and **3a**, is in good agreement with that in $[Pd(CS)_2(PPh_3)_2]$[2.31 Å].[19] These facts imply that the a-type coordination mode, where the CH_2SCH_3 group functions as a methylene-methylsulfonium ion, makes a great contribution to the bonding of the CH_2SCH_3 group.

Perspective views of the coordination mode are shown in Fig. 4. The C(1)–S–C(2) plane is almost perpendicular to the P(1)–Pd–P(2) plane in **3b**. The dihedral angles between these planes are 91.3° in **3b**, whereas

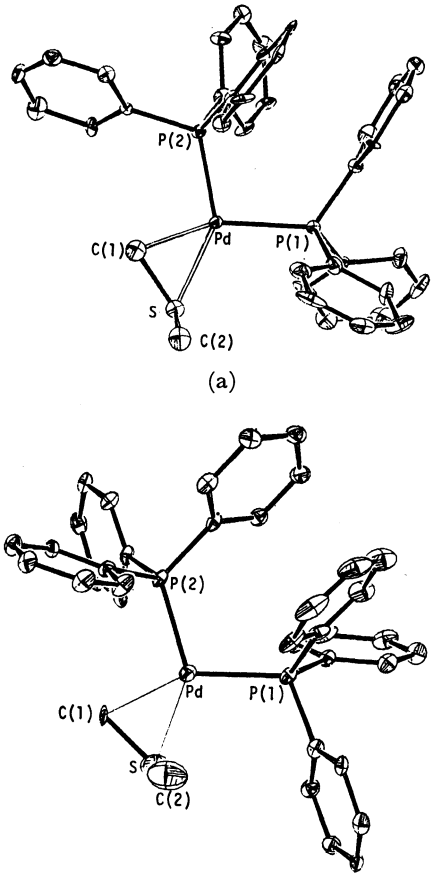

Fig. 2. An *ORTEP* drawing[16] of the $[Pd(CH_2SCH_3)(PPh_3)_2]$ cation. The thermal ellipsoids correspond to 30% probability levels. The atomic numberings for the phenyl groups of the triphenylphosphine groups are omitted. Six carbon atoms of the phenyl group are numbered as C(*n*1)—C(*n*6), where $n=1$—6. The C(11), C(21), and C(31) atoms are attached to the P(1) atom while C(41), C(51) and C(61) to P(2).
(a): $[Pd(CH_2SCH_3)(PPh_3)_2]PF_6$(**3a**), (b): $[Pd(CH_2SCH_3)(PPh_3)_2]ClO_4$(**3b**).

Table 5. Least-squares planes and atomic deviations from the planes

The equation of the plane is of the form: $AX+BY+CZ+D=0$, where X, Y, and Z are measured in Å units; $X=ax+cz\cos\beta$, $Y=by$, and $Z=cz\sin\beta$.

(a) Coordination plane of Pd through Pd, P(1), P(2), C(1), and S

(**3a**) $-0.119X-0.993Y+0.005Z+1.278=0$

(**3b**) $0.993X-0.117Y-0.029Z+0.174=0$

(b) Plane defined by Pd, P(1) and P(2)

(**3a**) $-0.091X-0.994Y+0.059Z+0.861=0$

(**3b**) $-0.996X+0.069Y-0.063Z+0.312=0$

Deviations of atoms from the plane (l/Å)

	Plane (a)		Plane (b)	
	(**3a**)	(**3b**)	(**3a**)	(**3b**)
Pd	+0.014	−0.101	0	0
P(1)	+0.042	+0.036	0	0
P(2)	−0.124	+0.045	0	0
C(1)	+0.171	−0.042	+0.133[a)]	+0.263[a)]
S	−0.066	+0.026	−0.200[a)]	+0.356[a)]
C(2)	+1.590[a)]	+1.836[a)]	+1.413[a)]	+2.176[a)]

a) Not included in the calculation of the plane.

they are 100.0° in **3a** and 100.9° in **2**. As presented in Table 5, the C(1) and S atoms in **3a** are located on the opposite sides of the P(1)–Pd–P(2) plane, 0.13 and −0.20 Å away from it respectively, while in **3b** these two atoms deviate by 0.26 and 0.36 Å on the same side of the P(1)–Pd–P(2) plane.

The resonance structures (d) and (e) presented below are suggested for the bonding of the CH_2SCH_3 group to the Pd atom,[8] which is connected with the stabilization of these complexes, although the main representation of the structure is probably (e). The contribution from (d) in the cationic complexes **3** may play a greater part than in a neutral complex such as **2**. However, the contributions from (d) in **3a** and **3b** seem to differ from each other, which may be due to the counter anions.

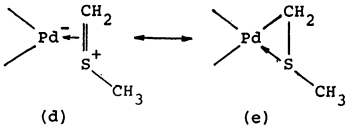

Table 6 shows the contacts between the $[Pd(CH_2SCH_3)(PPh_3)_2]$ cation and the PF_6 or ClO_4 anion in **3a** and **3b**. Both anions are considered to have the

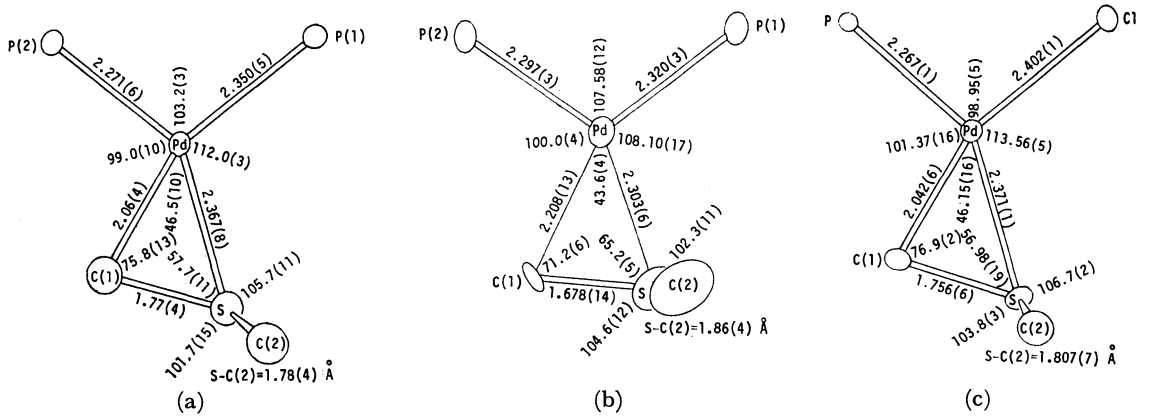

Fig. 3. The coordination geometry around the Pd atom along with selected bond lengths and bond angles.
(a): **3a**, (b): **3b**, (c): **2**.[2)]

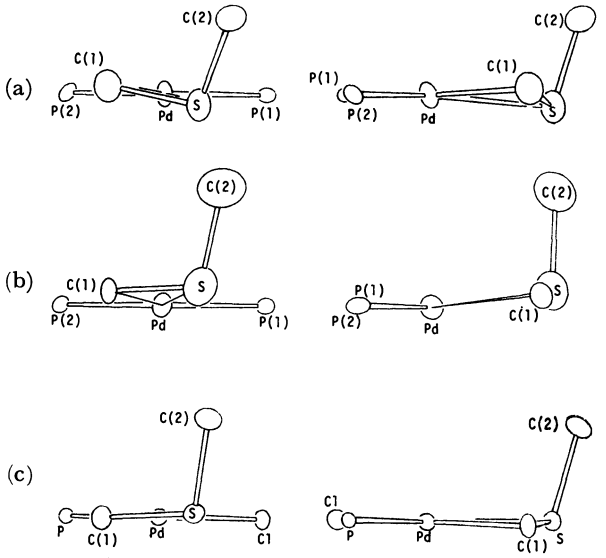

Fig. 4. Perspective views of the coordination geometry of the CH_2SCH_3 group to the Pd atom.
(a): **3a**, (b): **3b**, (c): **2**.[2)]

Table 6. Contacts between the $[Pd(CH_2SCH_3)(PPh_3)_2]$ cation and the PF_6 or ClO_4 anion

Distances between the Pd atom (the center of the cation) and the P (for PF_6 in **3a**) or Cl (for ClO_4 in **3b**) atom (the center of the anion) are shown.

Distance (l/Å)	(**3a**)	(**3b**)
	Pd(x,y,z)···P(3)	Pd(x,y,z)···Cl(1)
Nearest	4.759(8)(x,y,z)	5.317(17) (x,y,z)
Second	5 .252(8)($1-x$, $-1/2+y,1/2-z$)	6.288(17) ($-1+x,y,z$)

As shown in Fig. 5, only the above two contacts may exemplify significant interaction between the cation and the anion.

spherical symmetry. The distances between the Pd atom and the central atom of the anions (the P and Cl atoms) are compared with each other in Table 6. The radius of the PF_6 anion (P–F=1.54 Å) is larger than that of the ClO_4 anion (Cl–O=1.42 Å). Nevertheless, the Pd···P(3) distances in **3a** are sigificantly shorter than those of the Pd–Cl(1) in **3b**. These facts imply that **3a** may behave as a stronger ion-pair than **3b**, which is probably connected with the difference in the coordination modes between **3a** and **3b**.

Crystal Structure. The crystal structures of **3a** and **3b**, both projected along the a* axis, are given in Fig. 5. All the intermolecular atomic contacts in **3a** are considered as usual van der Waals distances, the shortest atomic contact being 3.22(4) Å [C(15)(x,y,z)··· F(3)($2-x,-1/2+y,1/2-z$)]. In **3b**, an abnormal short contact [2.82 Å] can be calculated for C(S)(x,y,z)··· C(S)($1-x,-y,-z$) distance. However, we can not discuss it further because of the low occupancy (0.25) of the CH_2Cl_2 molecule.

All the computations were carried out on NEAC 2200-700 and ACOS 800 computers at Computation Center, Osaka University, and on an ACOS 700 computer at Crystallographic Research Center, Institute for Protein Research, Osaka University.

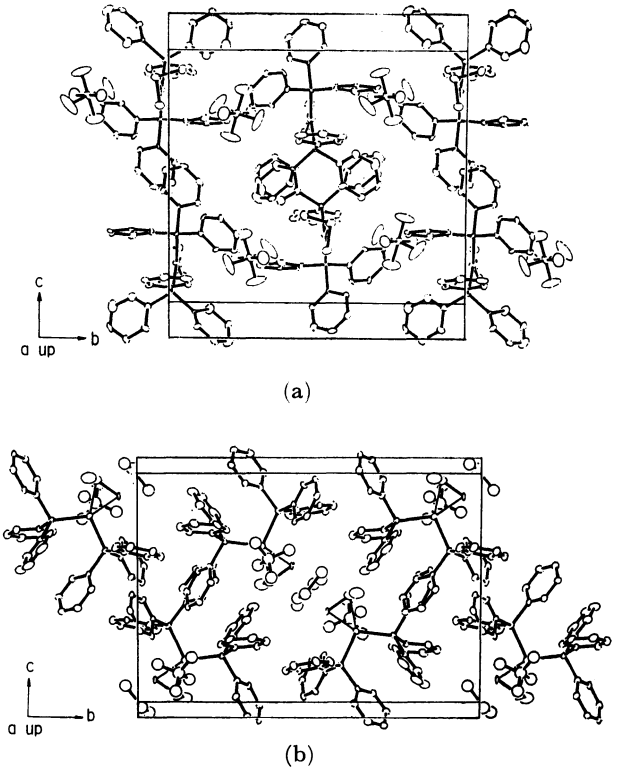

Fig. 5. The crystal structure projected along the a* axis.
(a) $[Pd(CH_2SCH_3)(PPh_3)_2]PF_6$ (**3a**).
Atoms are represented by thermal ellipsoids at 30% probability levels.
(b) $[Pd(CH_2SCH_3)(PPh_3)_2]ClO_4 \cdot 0.25CH_2Cl_2$ (**3b**).
Atoms of $[Pd(CH_2SCH_3)(PPh_3)_2]$ cation are represented by thermal ellipsoids at 30% probability levels, while those of the ClO_4 anion and the solvated CH_2Cl_2 molecule are drawn by circles with $B=7.0$ Å^2. The locations of three oxygen atoms in the ClO_4 anion are estimated from stereochemical consideration.

The authors wish to express their deep thanks to Professor Emeritus Rokuro Okawara, Dr. Hideo Kurosawa, and Dr. Gohei Yoshida of Osaka University for their kindness in supplying samples and their valuable discussions. Thanks are also due to Professor Hideko Kiriyama of Kobe University and Dr. Yoshihiro Furukawa of Nagoya University for their NMR studies of Complex **3a** and for their useful suggestions.

References

1) K. Miki, Y. Kai, N. Yasuoka, and N. Kasai, *J. Organomet. Chem.*, **165**, 79 (1979).
2) K. Miki, Y. Kai, N. Yasuoka, and N. Kasai, *J. Organomet. Chem.*, **135**, 53 (1977).
3) K. Miki, G. Yoshida, Y. Kai, N. Yasuoka, and N. Kasai, *J. Organomet. Chem.*, **149**, 195 (1978).
4) R. B. King and M. B. Bisnette, *Inorg. Chem.*, **4**, 486 (1965).
5) E. Rodulfo de Gil and L. F. Dahl, *J. Am. Chem. Soc.*, **91**, 3751 (1969).
6) G. Yoshida, Y. Matsumura, and R. Okawara, *J. Organomet. Chem.*, **92**, C53 (1975); G. Yoshida, H. Kurosawa, and R. Okawara, *ibid.* **113**, 85 (1976).
7) G. Yoshida, unpublished data.

8) G. Yoshida, H. Kurosawa, and R. Okawara, *J. Organomet. Chem.*, **131**, 309 (1977).
9) T. Ashida, "The Universal Crystallographic Computing System-Osaka," The Computation Center, Osaka University (1979), p. 53.
10) "International Tables for X-Ray Crystallography," Kynoch Press, Birmingham (1974), Vol. IV, p, 71.
11) R. F. Stewart, E. R. Davidson, and W. T. Simpson, *J. Chem. Phys.*, **42**, 3175 (1965).
12) W. C. Hamilton, *Acta Crystallogr.*, **12**, 609 (1959).
13) G. R. Miller and H. S. Gutowtky, *J. Chem. Phys.*, **39**, 1983 (1963).
14) The observed second moment is only 2.3 G^2 between 77 and 300 K, which is ascribable to interionic magnetic interactions; H. Kiriyama and Y. Furukawa, private communication (1978).
15) See, for example in case of the Pd complex containing the ClO_4 anion, A. J. Deeming , I. P. Rothwell, M. B. Hursthouse, and L. New, *J. Chem. Soc., Dalton Trans.*, **1978**, 1490.
16) C. K. Johnson, *ORTEP*-II, Report ORNL-5138, Oak Ridge National Laboratory, Tennessee (1976).
17) S. C. Abrahams, *Quart. Rev.* (London), **10**, 407 (1956).
18) K. Miki, O. Shiotani, M. Yama, Y. Kai, N. Tanaka, N. Kasai, and H. Kurosawa, 43rd National Meeting of the Chemical Society of Japan, Tokyo, April 1981, Abstr. I, p. 151 (4D17).
19) T. Kashiwagi, N. Yasuoka, T. Ueki, N. Kasai, and M. Kakudo, *Bull. Chem. Soc. Jpn.*, **40**, 1998 (1967).

Ultrasonic Absorption in Solutions of Sodium Iodide in Isopropyl Alcohol and Isopropyl Alcohol-Water Mixtures

Tsunemichi Okuwa* and Kozo Ohno†

Institute of Scientific and Industrial Research, Osaka University, Yamadakami, Suita, Osaka 565

†*Osaka Electro-communication University, Hatumachi, Neyagawa, Osaka 572*

(Received February 13, 1981)

Ultrasonic relaxational absorption was observed in solutions of NaI in *i*-PrOH. Assuming the excess ultrasonic absorption to be caused by the relaxation of the dissociation equilibrium of NaI in the solutions, the dissociation and recombination rates of NaI, the Arrhenius activation energy, and the enthalpy and volume changes due to dissociation were calculated; these were compared with the values estimated from other methods. An increase of the dissociation constant of NaI was observed with an increase in the concentration of H_2O in *i*-PrOH–H_2O mixtures.

Strong 1-1 electrolytes such as sodium iodide dissociate completely in aqueous solution. Ultrasonic absorptions due to chemical relaxation are not found in such solution. But in isopropyl alcohol, which has a lower dielectric constant than water, NaI would dissociate incompletely and a dissociation equilibrium would exist between the Na^+ ions, the I^- ions, and the undissociated NaI molecules. Then the excess ultrasonic absorption observed in *i*-PrOH would be caused by the relaxation of the reaction.

Experimental

The ultrasonic absorption spectra of NaI solutions in *i*-PrOH–H_2O mixtures were measured by the ultrasonic pulse method from 10 to 90 MHz at 20 °C. The concentrations of NaI were 0.1—0.3 molality (mol/1000 g solvent) and weight percentages of *i*-PrOH in *i*-PrOH–H_2O mixtures were 50, 60, 70, 80, 90, and 100%. The ultrasonic velocity was measured by the interference of the pulse wave and a continuous wave at 5 MHz.

Results and Discussion

The ultrasonic absorption α/f^2 in solutions of NaI in *i*-PrOH is shown in Fig. 1, where α is the absorption coefficient of amplitude and f the frequency. A single relaxation represented by the next equation fits the curves over the frequency range measured:

$$\frac{\alpha}{f^2} = \frac{A}{1+(f/f_{max})^2} + B,$$

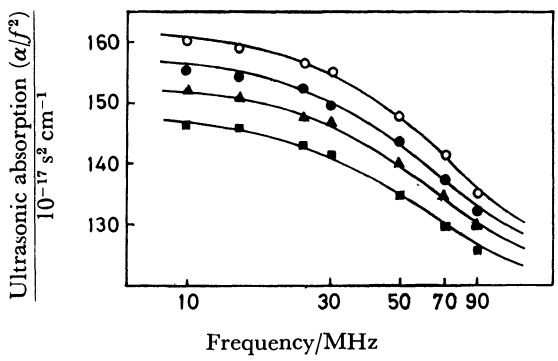

Fig. 1. Ultrasonic absorption in solutions of NaI in Molality of NaI, ■: 0.15, ▲: 0.20, ●: 0.25, ○: 0.30.

where f_{max} is the relaxational frequency, A the relaxational absorption, and B the non-relaxing absorptions due to viscosity, thermal conduction, *etc.* The relaxation parameters are listed in Table 1.

Table 1. The relaxation parameters in solutions of NaI in *i*-PrOH

Temp °C	Concn of NaI (molality)	A 10^{-17} s² cm⁻¹	B 10^{-17} s² cm⁻¹	f_{max} MHz
20	0.15	28.6	118	58.0
	0.20	33.3	120	61.3
	0.25	37.0	120	64.0
	0.30	40.0	122	66.8
25	0.15	27.0	110	64.1
	0.20	31.3	110	67.6
	0.25	34.5	110	70.7
	0.30	38.5	112	73.6
30	0.15	26.3	100	69.8
	0.20	30.3	100	73.0
	0.25	33.3	102	76.0
	0.30	37.0	102	78.4
35	0.15	25.6	90	75.8
	0.20	29.4	90	79.3
	0.25	32.3	92	82.1
	0.30	35.7	92	85.8

Here we assume the relaxation to be caused by the following equilibrium:

$$NaI \underset{k_b}{\overset{k_f}{\rightleftarrows}} Na^+ + I^-.$$

For such an equilibrium the relaxation frequency f_{max} is given by[1]

$$2\pi f_{max} = k_f + k_b \sigma \gamma_\pm^2 C\left(2+\frac{\partial \ln \gamma_\pm^2}{\partial \ln \sigma}\right), \quad (1)$$

where σ is the degree of dissociation, $\gamma_\pm$ means the ionic activity coefficient, k_f and k_b are the rate constants, and C is concentration. The dissociation constant K can be described by[2]

$$K = \frac{k_f}{k_b} = \frac{\sigma^2 C \gamma_\pm^2}{1-\sigma}, \quad (2)$$

$$K^{-1} = \frac{4\pi N}{1000}\left(\frac{e^2}{DkT}\right)Q(b), \quad (3)$$

$$b = \frac{e^2}{a_B DkT},$$

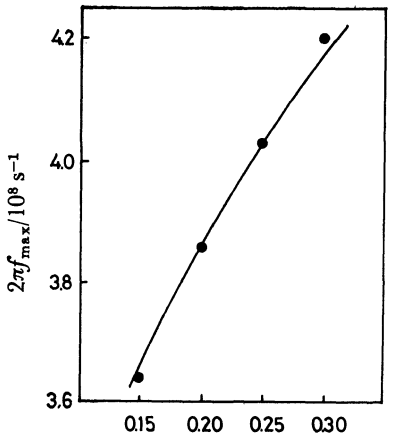

Fig. 2. Relation between f_{max} and concentration of NaI in *i*-PrOH at 20 °C.
●: Experimental value.

TABLE 2. THE KINETIC VALUES OF NaI in *i*-PrOH

Temp °C	K $10^{-3}M$[a]	k_b $10^{10}\ M^{-1}\ s^{-1}$	k $10^8\ s^{-1}$	a_B 10^{-8} cm
20	7.1±1.8	2.4±0.6	1.7±0.1	5.8±1.0
25	6.4±1.8	3.0±0.8	1.9±0.1	5.9±1.0
30	5.9±1.7	3.4±0.9	2.0±0.1	5.9±1.0
35	5.4±1.5	3.9±1.0	2.1±0.1	5.9±1.0

a) 1 M=1 mol dm^{-3}.

where a_B is the distance between the centers of the two ions forming the ion pair at their closest distance of approach, k is Boltzmann's constant, D dielectric constant, N Avogadro's constant, T absolute temperature, e the electronic charge, and $Q(b)$ is a function of b. By the method of successive approximation,[3] k_f, k_b, K, and a_B were calculated using Eqs. 1, 2, and 3. In Table 2, the kinetic values derived by this process are listed. The experimental and the calculated values of f_{max} are shown in Fig. 2. As may be seen in Table 2, the apparent Bjerrum distance $a_B \simeq 5.9$ Å is larger than the sum of the ion radii 3 Å and is independent of temperature. This result suggest that a solvated ion pair state exists and that the number of solvation would be invariable over the temperature range measured.

The rate constant k_b is given by Arrhenius as follows:

$$k_b = Pe^{-\Delta E/RT},$$

where P is a constant and ΔE is the activation energy.

When $\log k_b$ values are plotted against $1/T$, the activation energy is obtained from the slope. Using k_b values in Table 2, one obtains $\Delta E \simeq 5.4$ kcal mol^{-1}. This value is of the order of magnitude to be expected for a diffusion controlled process.[1] The rate constant k_b, as due to a diffusion controlled process, is given by[4]

$$k_b = \frac{8NkT}{3000\eta}\left(\frac{-b}{e^{-b}-1}\right) \quad (mol^{-1}\ s^{-1}),$$

where η is solvent viscosity. By substitution of the numerical values[5] at 25 °C, one gets $k_b \simeq 1.7\times10^{10}$ $mol^{-1}\ s^{-1}$. The agreement between the calculated and experimental values is fairly good.

The variation of the dissociation constant with temperature is given by

$$\left(\frac{\partial \ln K}{\partial T}\right) = \frac{\Delta H}{RT^2},$$

where ΔH is the enthalpy change. Taking the K values in Table 2, one gets $\Delta H \simeq -3.1$ kcal mol^{-1}. The energy diagram of NaI in the solution is shown in Fig. 3. The maximum excess ultrasonic absorption per wavelength at the relaxation frequency, μ_{max}, is given by[1,6]

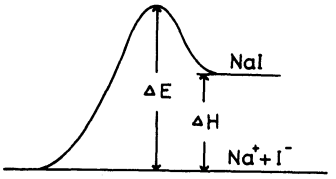

Fig. 3. Energy diagram of NaI in *i*-PrOH.
$\Delta E \simeq 5.4$ kcal mol^{-1}, $\Delta H \simeq 3.1$ kcal mol^{-1}.

$$\mu_{max} = \frac{\beta}{2\beta RTV}\left(\Delta V - \frac{l}{dC_p}\Delta H\right)^2 \frac{1}{\chi}, \quad (4)$$

$$\chi = \left(\frac{1}{n_{Na^+}} + \frac{1}{n_{I^-}} + \frac{1}{n_{NaI}}\right),$$

where ΔV is the volume change for the reaction, l the coefficient of thermal expansion, C_p the heat capacity at constant pressure, d density, V the volume, β the adiabatic compressibility, and n_{Na^+}, n_{I^-}, and n_{NaI}, are the numbers of the moles of the sodium ion, the iodide ion, and the undissociated sodium iodide. The adiabatic compressibility is obtained from the measured values of ultrasonic velocity. The number of the moles of species n_{Na^+}, n_{I^-}, and n_{NaI} are estimated from the degree of dissociation. Solvent parameters are given in Table 3. By substituting these values in Eq. 4, we find $\Delta V \simeq -15$ cm^3/mol. This value is of the same order as the volume change of NaI in *i*-BuOH:[10]

TABLE 3. THE SOLVENT PARAMETERS AT 20 °C

d g cm^{-3}	l 10^{-3} deg^{-1}	V m s^{-1}	C_p J g^{-1} deg^{-1}	D (c.g.s.e.s.u.)
0.7854[7]	1.03	1167.6	2.5524[8]	18.6[9]

The ultrasonic absorptions α/f^2 in solutions of NaI in *i*-PrOH–H_2O mixtures are shown in Figs. 4, 5, and 6. As may be seen in these figures, the addition of NaI in *i*-PrOH–H_2O mixture causes an increase in the magnitude of the relaxational absorption. This increase is attributed to the relaxation of dissociation equilibrium of NaI in the solution, assuming that the relaxational absorption of *i*-PrOH–H_2O mixture[11-13] is independent of the concentration of NaI. Therefore we assume the relaxational absorption due to dissociation of NaI to be

$$\left(\frac{\alpha}{f^2}\right)_{solution} - \left(\frac{\alpha}{f^2}\right)_{solvent} = \frac{A}{1+(f/f_{max})^2} + B,$$

where $(\alpha/f^2)_{solution}$ is the absorption of the NaI solution in the *i*-PrOH–H_2O mixture and $(\alpha/f^2)_{solvent}$ is the absorption of the *i*-PrOH–H_2O mixture. The relaxation parameters and the kinetic values are listed in Tables 4 and 5. As is seen in Table 5, the dissociation constants

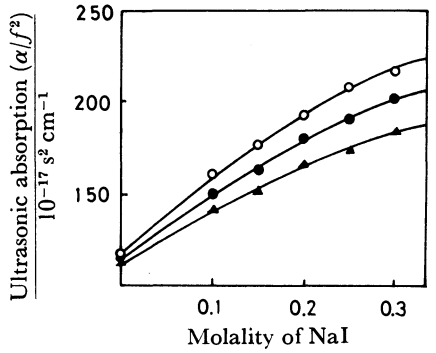

Fig. 4. Ultrasonic absorption in solutions of NaI in 90 wt% *i*-PrOH–10 wt% H_2O mixture at 20 °C.
○: 10 MHz, ●: 30 MHz, ▲: 50 MHz.

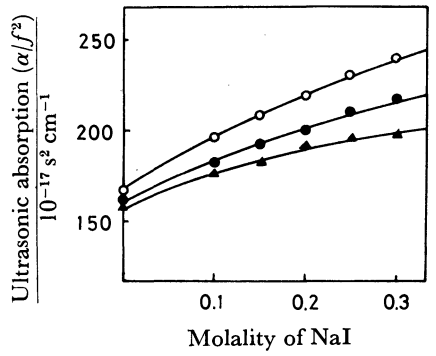

Fig. 5. Ultrasonic absorption in solutions of NaI in 80 wt% *i*-PrOH–20 wt% H_2O mixture at 20°C.
○: 10 MHz, ●: 30 MHz, ▲: 50 MHz.

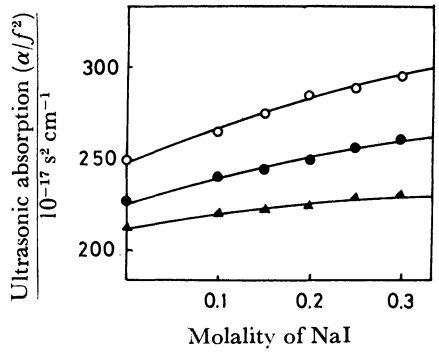

Fig. 6. Ultrasonic absorption in solutions of NaI in 70 wt% *i*-PrOH–30 wt% H_2O mixture at 20 °C.
○: 10 MHz, ●: 30 MHz, ▲: 50 MHz.

of NaI increase with decreasing the concentration of *i*-PrOH in mixtures. This increase is caused by an increase of dielectric constant in the solution. However, no relaxational absorption due to NaI was observed when the weight percent of *i*-PrOH in *i*-PrOH–H_2O mixtures were lower than 60. Perhaps NaI dissociates completely in such solutions.

Table 4. The relaxation parameters in solutions of NaI in *i*-PrOH–H_2O mixture at 20 °C

Concn of *i*-PrOH (wt%)	Concn of NaI (molality)	A / 10^{-17} s^2 cm^{-1}	B / 10^{-17} s^2 cm^{-1}	f_{max} / MHz
90	0.1	27.8	16	53.1
	0.15	41.7	18	57.0
	0.2	55.6	20	60.3
	0.25	66.7	22	63.5
	0.3	74.6	24	66.2
80	0.1	22.2	8	47.2
	0.15	32.3	9	50.7
	0.2	41.0	10	53.8
	0.25	48.8	11	55.0
	0.3	55.6	12	57.3

Table 5. The kinetic values of NaI in *i*-PrOH–H_2O mixture at 20 °C

Concn of *i*-PrOH (wt%)	K / 10^{-2} M	k_b / 10^{10} M^{-1} s^{-1}	k_f / 10^8 s^{-1}	a_B / 10^{-8} cm
90	1.0±0.3	1.7±0.5	1.7±0.1	6.0±1.2
80	2.0±1.0	0.8±0.3	1.6±0.1	6.1±2.2

Referencse

1) M. Eigen and L. De Maeyer, "Relaxation Methods," in "Technique of Organic Chemistry," John Wiley and Sons, N. Y. (1963).
2) N. Bjerrum, *Kgl. Danske Vidensk. Selskab*, **9**, 7 (1926).
3) S. Petrucci and G. Atkinson, *J. Phys. Chem.*, **70**, 2550 (1966).
4) E. F. Caldin, "Fast Reactions in Solution," John Wiley and Sons, N. Y. (1964).
5) International Critical Tables, **7**, 215 (1928).
6) G. G. Hammes and W. Knoche, *J. Chem. Phys.*, **45**, 4041 (1962).
7) International Critical Tables, **3**, 121 (1928).
8) "Landolt-Bornstein," Springer-Verlag, Berlin (1961), II Band, 4 Teil, p. 308.
9) G. Akerlof, *J. Am. Chem. Soc.*, **54**, 4125 (1932).
10) T. Okuwa, *Acustica*, **44**, 71 (1980).
11) M. J. Blandamer and D. Waddington, *Adv. Mol. Relaxation Process*, **2**, 1 (1970).
12) S. Nishikawa, M. Mashima, and T. Yasunaga, *Bull. Chem. Soc. Jpn.*, **49**, 1413 (1976).
13) R. E. Verall and H. Nomura, *J. Solution Chem.*, **6**, 1 (1977).

  Bull. Chem. Soc. Jpn., 54, 3651—3658 (1981)

Studies on the Electronic Structures of Hydrocarbon Diradicals by the Unrestricted Hartree-Fock Theory

Katsufumi HASHIMOTO* and Hideo FUKUTOME

Department of Physics, Kyoto University, Sakyo-ku, Kyoto 606

(Received February 16, 1981)

Electronic structures of low-lying states of cyclobutadiene, trimethylenemethane (**2**), and tetramethyleneethane (**3**) are studied by the unrestricted Hartree-Fock (UHF) theory. Characteristics of electronic correlations, called dynamical spin polarization effect, in these molecules are well described by corresponding orbitals and spin density structures of low-lying UHF solutions. The spin polarization of σ electrons is found to be relatively small but not negligible for quantitative discussion. The two low-lying singlet states of **2** are described by two UHF solutions with different spin density structures. The fact that the singlet UHF state of **3** lies a little below the triplet UHF state is explained by the difference in the spin polarization of the bonding π electrons between the singlet and triplet states. Two rules are given which predict the spin structure of low-lying UHF states and the spin multiplicity of ground states of hydrocarbon diradicals. These rules are applied to 1,1,2,3,3-pentamethylenepropane and 1,3-dimethylenecyclobutadiene, which confirms their validity.

Recent theoretical studies on cyclobutadiene (**1**) and trimethylenemethane (**2**) have revealed the importance

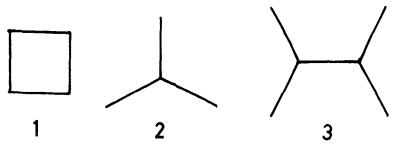

of correlation effects in determining the spin multiplicity of ground states and the stable geometry of low-lying states of hydrocarbon diradicals. Borden[1] showed that a strong correlation effect in **1** causes a violation of Hunt's rule and makes the ground state singlet. This effect was also shown to make the equilibrium geometry close to a square. These results are in agreement with experiments.[2] As for **2**, Yarcony and Schaefer III[3a] and Borden[3b] pointed out that the correlation of the two nonbonding (NB) electrons much reduces the energy difference in the singlet state between the planar geometry and the geometry with a methylene group orthogonal to the remaining allyl group.

These results indicate that in order to understand electronic properties of hydrocarbon diradicals, it is necessary to clarify correlation effects involved. As pointed out by Borden[1] and Kollmar and Staemmler,[4] the most important correlation effect in diradicals is similar to the spin polarization effect in free radicals. They called it the dynamical spin polarization effect. Therefore, the unrestricted Hartree-Fock (UHF) theory is powerful in analyzing the correlation effect. In this paper, we apply the UHF theory to three diradicals **1**, **2**, and tetramethyleneethane (**3**). We show that the corresponding orbitals and the spin density structure in the UHF theory well describe the dynamical spin polarization effect in low-lying states of the molecules. Concerning **3**, the singlet state is predicted to lie a little below the triplet state. From results for **1**, **2**, and **3**, we derive simple rules to predict the spin multiplicity of ground states and the spin structure of low-lying UHF solutions of hydrocarbon diradicals.

UHF calculations were made with the INDO approximation[5] using the computer program written by Takahashi and Igawa which uses the direct optimization method developed by Igawa and Fukutome[6] and is capable of calculating UHF solutions and their instabilities of any types. We use the notation proposed by Fukutome[7] for the types of UHF solutions and their instabilities.

Analysis of a Simplified Model of Diradicals with Two Electrons in Two NB MOs

Before performing all-valence-electron UHF analyses, we examine in this section UHF solutions for a simple model with two degenerate NB MOs ϕ_A and ϕ_B of different symmetries in a spatial symmetry group. In the model, there are one triplet state (Ψ_T) and three singlet states (Ψ_{S1}, Ψ_{S2}, and Ψ_{S3}) which are represented as

$$\Psi_T = (\phi_A\phi_B - \phi_B\phi_A)/\sqrt{2}\,\Theta_T,$$
$$\Psi_{S1} = (\phi_A\phi_A - \phi_B\phi_B)/\sqrt{2}\,\Theta_S,$$
$$\Psi_{S2} = (\phi_A\phi_A + \phi_B\phi_B)/\sqrt{2}\,\Theta_S,$$
$$\Psi_S{}^3 = (\phi_A\phi_B + \phi_B\phi_A)/\sqrt{2}\,\Theta_S,$$
$$\Theta_T = (\alpha\beta+\beta\alpha)/\sqrt{2},\ \Theta_S = (\alpha\beta-\beta\alpha)/\sqrt{2}.$$

Their energies are given by

$$E_T = 2K + \langle AA|BB\rangle - \langle AB|BA\rangle,$$
$$E_{S1} = 2K + \gamma - \langle AB|BA\rangle,$$
$$E_{S2} = 2K + \gamma + \langle AB|BA\rangle,$$
$$E_{S3} = 2K + \langle AA|BB\rangle + \langle AB|BA\rangle,$$

where

$$\langle AB|A'B'\rangle = e^2\int d1d2\phi_A(1)\phi_B(1)\phi_{A'}(2)\phi_{B'}(2)/r_{12},$$

and we assume that the single particle energies of ϕ_A and ϕ_B are equal to K and that $\langle AA|AA\rangle = \langle BB|BB\rangle = \gamma$. By the relation

$$\gamma > \langle AA|BB\rangle > \langle AB|BA\rangle > 0$$

the energetic order of the states except Ψ_{S3} is determined as

$$E_{S2} > E_{RHF} > E_{S1} > E_T,$$

where RHF means the restricted HF state $|\phi_A\alpha,\phi_A\beta|$ with the energy $E_{RHF} = 2K+\gamma$. The energetic position of Ψ_{S3} depends on the extent of the differential overlap

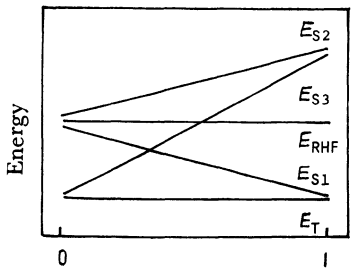

Fig. 1. The correlation diagram of low-lying states of diradicals against the extent of the differential overlap between the two NB MOs.

between ϕ_A and ϕ_B. Let's consider two extreme cases. When the overlap is nearly complete, $\langle AA|BB\rangle$ is nearly equal to γ, so that Ψ_{S3} is higher than the RHF and nearly degenerate with Ψ_{S2}. Ψ_{S1} and Ψ_T also are nearly degenerate. When ϕ_A and ϕ_B are disjoint, $\langle AA|BB\rangle$ is much smaller than γ, so that Ψ_{S3} is lower than the RHF and nearly degenerate with Ψ_T. Ψ_{S1}, Ψ_{S2}, and the RHF are also nearly degenerate. By connecting these extreme cases we obtain dependence of the energetic order of the four states on the overlap of ϕ_A and ϕ_B as shown in Fig. 1. It is found that in the two-electron model the ground state is always the triplet state. In the two extreme cases, however, the singlet state lies close to the triplet state, so that the enegetic order is possible to change in the all-valence-electron model. Figure 1 shows that in the case of the intermediate overlap the two singlet states Ψ_{S1} and Ψ_{S3} may lie below the RHF. In the following, we examine how the two singlet states are described by the UHF theory.

First we obtain the UHF solution emerging from the instability of the RHF. The four instability matrices ($^1ST_\pm$, $^3ST_\pm$)[7] of the RHF are 1×1 dimensional in the model and are given by

$$^1ST_+ = 2(a-b),\quad ^1ST_- = {}^3ST_+ = -2b,$$
$$^3ST_- = -2(a+b),$$
$$a = \langle AB|BA\rangle,\quad b = (\gamma-\langle AA|BB\rangle)/2,\quad a, b > 0.$$

Because the $^3ST_-$ instability matrix has the lowest negative eigenvalue, we consider this instability. The $^3ST_-$ instability of the RHS indicates that there is an axial spin density wave (ASDW) UHF solution (ASDW1) lower in energy than the RHF. The orbitals of ASDW1, which is a real DODS solution, are a spin polarized mixture of ϕ_A and ϕ_B

$$\text{ASDW1} = |\psi_{1+}\alpha, \psi_{1-}\beta|,\ \psi_{1\pm} = \cos\theta\phi_A \pm \sin\theta\phi_B,$$

and the energy is given by

$$E_{ASDW1} = E_{RHF} - (a+b)\sin^2 2\theta.$$

E_{ASDW1} has a minimum at $\theta=45°$, so that we obtain

$$\psi_{1\pm} = (\phi_A \pm \phi_B)/\sqrt{2},$$
$$E_{ASDW1} = 2K + (\gamma+\langle AA|BB\rangle)/2 - \langle AB|BA\rangle.$$

The wave function of ASDW1 is expanded as

$$(\Psi_{S1}-\Psi_T)/\sqrt{2},$$

showing that the singlet component of ASDW1 is Ψ_{S1}.

Next we examine the stability of ASDW1. The four instability matrices ($A_\pm M_\pm$)[7] of ASDW1 are 2×2 dimensional in the model and are given by

$$A_+M_+ = \begin{pmatrix} 2a, & 2b \\ 2b, & 2a \end{pmatrix},\quad A_+M_- = \begin{pmatrix} 2a, & 0 \\ 0, & 2a \end{pmatrix},$$
$$A_-M_\pm = \begin{pmatrix} -b, & -b \\ -b, & -b \end{pmatrix}.$$

The lowest eigenvalue of the A_+M_+ instability matrix is $2(a-b)$ with the eigenvector $\begin{pmatrix} 1 \\ -1 \end{pmatrix}$. Therefore, if $a-b<0$ which is the same condition as $E_{S3}<E_{S1}$, ASDW1 is A_+M_+ unstable, that is, ASDW1 is unstable for a spin unflip excitation and there is another ASDW solution (ASDW2) lower in energy than ASDW1. ASDW2's orbitals are determined by the eigenvector $\begin{pmatrix} 1 \\ -1 \end{pmatrix}$ of the A_+M_+ instability in the following form

$$\text{ASDW2} = |\psi'_{1+}\alpha, \psi'_{1-}\beta|,\ \psi'_{1\pm} = \cos\theta\psi_{1\pm} \pm \sin\theta\psi_{2\pm},$$
$$\psi_{2+} = \psi_{1-} = (\phi_A-\phi_B)/\sqrt{2},$$
$$\psi_{2-} = \psi_{1+} = (\phi_A+\phi_B)/\sqrt{2},$$

and the energy is given by

$$E_{ASDW2} = E_{ASDW1} + (a-b)\sin^2 2\theta.$$

E_{ASDW2} has a minimum at $\theta=45°$, so that we obtain

$$\psi'_{1+} = \phi_A,\ \psi'_{1-} = -\phi_B,\ E_{ASDW2} = 2K + \langle AA|BB\rangle.$$

Cleraly the singlet component of ASDW2 is Ψ_{S3}.

Last we examine the stability of ASDW2. The instability matrices of ASDW2 are

$$A_+M_+ = \begin{pmatrix} 2b, & 2a \\ 2a, & 2b \end{pmatrix},\quad A_+M_- = \begin{pmatrix} 2b, & 0 \\ 0, & 2b \end{pmatrix},$$
$$A_-M_\pm = \begin{pmatrix} -a, & -a \\ -a, & -a \end{pmatrix}.$$

Therefore, if $b-a<0$ which is the same condition as $E_{S1}<E_{S3}$, ASDW2 is A_+M_+ unstable. We can show similarly that the UHF solution arising from this instability is ASDW1.

The above results show that ASDW1 and ASDW2 well describe the two low-lying singlet states (Ψ_{S1} and Ψ_{S3}) which involve strong electronic correlations. The stability relations among the three HF solutions, the RHF, ASDW1, and ASDW2, are summerized in Table 1. We note that in the two-electron model, if $E_{S1}>(<)$ E_{S3}, ASDW1 (ASDW2) is always unstable, but that this is not necessarily the case with all-valence-electron calculations. This situation is also shown by the second scheme in Table 1.

Table 1. Possible instability relations among the three HF solutions of diradicals

$E_{RHF}>E_{S1}>E_{S3}$, RHF $\xrightarrow{^3ST_-}$ ASDW1 $\xrightarrow{A_+M_+}$ ASDW2	
($E_{RHF}>E_{S1}\approx E_{S3}$, RHF $\xrightarrow{^3ST_-}$ ASDW1.	ASDW2)
$E_{RHF}>E_{S3}>E_{S1}$, RHF $\xrightarrow{^3ST_-}$ ASDW1 $\xleftarrow{A_+M_+}$ ASDW2	
$E_{S3}>E_{RHF}>E_{S1}$, RHF $\xrightarrow{^3ST_-}$ ASDW1	

UHF Calculation on Cyclobutadiene

We performed an all-valence-electron UHF calculation on **1** by varying the C–C bond length (R) from

1.61 Å to 1.31 Å. The other geometrical parameters are fixed as shown in Fig. 2a. In the geometries the RHF π orbitals are a bonding (B) π MO (ϕ_1), two nearly degenerate NB π MOs (ϕ_2, ϕ_3), and an antibonding (AB) π MO (ϕ_4):

$$\phi_1 = (\chi_1+\chi_2+\chi_3+\chi_4)/2,\quad \phi_2 = (\chi_1+\chi_2-\chi_3-\chi_4)/2,$$
$$\phi_3 = (\chi_1-\chi_2+\chi_3-\chi_4)/2,\quad \phi_4 = (\chi_1-\chi_2-\chi_3+\chi_4)/2,$$

where χ_i is the π atomic orbital (AO) of the i-th carbon atom in Fig. 2a. The MOs ϕ_1—ϕ_4 are of b_{1u}, b_{2g}, b_{3g}, and a_u symmetries in the D_{2h} point group, respectively. As R is varied, the MOs ϕ_2 and ϕ_3 cross at square geometries, so that there are two RHF ground states with different occupancies of the π MOs: RHF1 = $(\phi_1)^2(\phi_2)^2$ and RHF2 = $(\phi_1)^2(\phi_3)^2$. RHF1 and RHF2 are the RHF ground states in the regions $R>R'$ and $R<R'$, respectively. Near the square geometry they become ^{3}ST- unstable. Because the differential overlap between the two NB MOs is complete, this case corresponds to the last scheme of Table 1 and an ASDW solution, ASDW1, emerges from the instability. ASDW1 connects smoothly RHF1 and RHF2. The correlation diagram of the π MOs and the adiabatic potentials of the RHFs and the UHF solutions are shown in Fig. 3. This shows that ASDW1 is the HF ground state near the square geometry and that the triplet ASDW solution is higher in energy than ASDW1 in contrast to the two-electron model. The equilibrium geometry of the singlet ground state obtained from ASDW1's potential becomes very close to the square one in contrast to the rectangular equilibrium geometries of the RHF's potentials. These features stem from the correlation effect which becomes important as the square geometry is neared.

In order to analyze the electronic correlation in

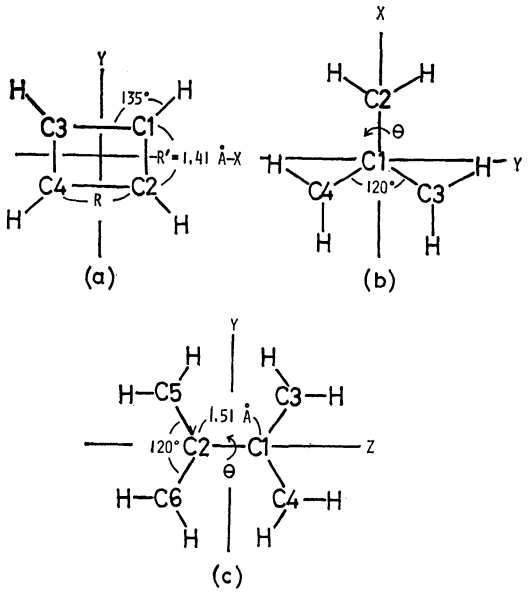

Fig. 2. Geometries used in the calculations for **1**, **2**, and **3**. All the C–H bond lengths are fixed to 1.1 Å, the C–C bond lengths, whose values are not indicated, to 1.41 Å, and all the H–C–H angles to 120°. **1** has the D_{2h} and D_{4h} symmetries at $R\neq R'$ and $R=R'$. respectively. **2** has the D_{3h}, C_{2v}, and C_2 symmetries at $\theta=0°$, 90°, and $\theta\neq 0°$ and 90°, respectively, and **3** has the D_{2h}, D_{2d}, and D_2 symmetries at $\theta=0°$, 90°, and $\theta\neq 0°$ and 90°, respectively.

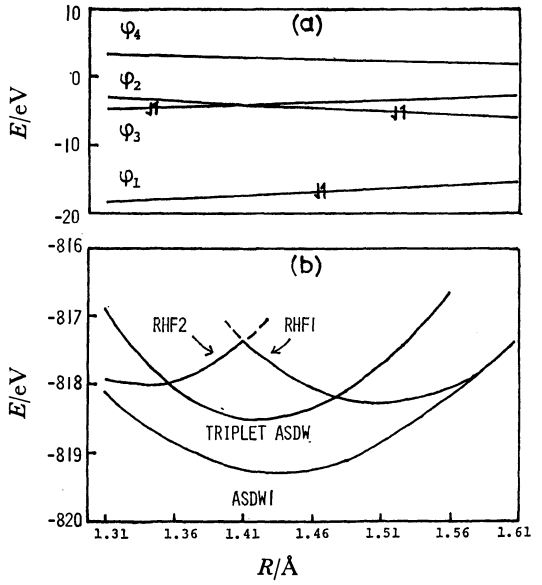

Fig. 3. The correlation diagram of the Hückel type π MOs (a), and the adiabatic potentials of the RHFs, ASDW1 and the triplet ASDW (b) of cyclobutadiene.

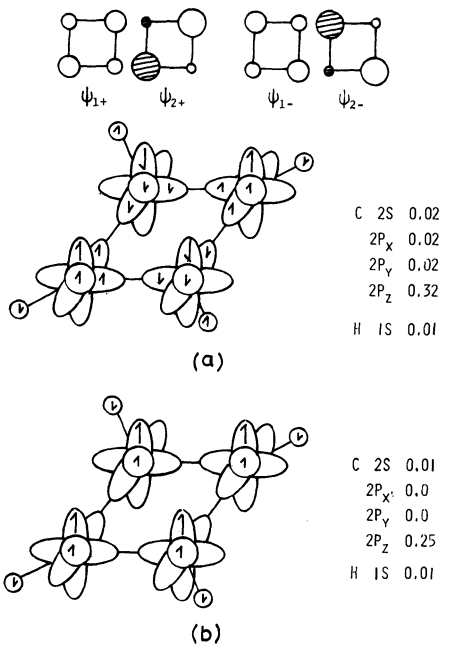

Fig. 4. The π corresponding orbitals and the spin density structure of ASDW1 (a) and the spin density structure of the triplet ASDW (b) of cyclobutadiene. The carbon π AOs with positive MO coefficients are represented by white circles and those with negative MO coefficients by shaded ones. The radii of the circles are proportional to the magnitudes of the MO coefficients. The spin densities with positive and negative z components are represented by up- and downward arrows, respectively. The magnitudes of the spin densities on carbon and hydrogen AOs are the same for all the C–H units except their signs.

ASDW1, we show in Fig. 4 the π corresponding orbitals and the spin density structure of ASDW1 at the equilibrium geometry. The spin density structure of the triplet ASDW is also shown for comparison. The excitations contributing to the $^3ST_-$ instability which produces ASDW1 from the RHF have the B_{1g} symmetry. Therefore, the π excitations $\phi_2 \rightarrow \phi_3$ (or $\phi_3 \rightarrow \phi_2$) and $\phi_1 \rightarrow \phi_4$ contribute to the instability. Consequently, not only the NB π orbitals but also the B π orbitals are spin polarized as follows:

$$\psi_{1\pm} = \cos\theta_1\phi_1 \pm \sin\theta_1\phi_4, \quad \psi_{2\pm} = \cos\theta_2\phi_2 \pm \sin\theta_2\phi_3.$$

The σ orbitals are also spin polarized, but to a smaller extent than the π orbitals, due to the σ excitation with the B_{1g} symmetry.

The triplet ASDW is obtained with the trial wave function

$$\Psi_T^0 = |\text{core}, \phi_1\alpha, \phi_1\beta, \phi_2\alpha, \phi_3\alpha|,$$

where core represents the doubly occupied RHF σ MOs. After the SCF procedure, the π orbitals remain unchanged but the core part is spin polarized with the corresponding orbitals retaining the same symmetries as the original RHF σ orbitals.

The spin polarization of the B π orbital ϕ_1 appears only in the singlet state. Its physical significance is as follows.[1] The splitting of the B π orbital occurs in such a way that $\psi_{1\pm}$ overlaps $\psi_{2\pm}$ more than $\psi_{2\mp}$ as shown in Fig. 4. Such coherent splittings of $\psi_{1\pm}$ and $\psi_{2\pm}$ reduce the Coulomb repulsion between the electrons of opposite spins because they are localized to different regions. The electrons of the same spin localize to the same region but this does not enhance the Coulomb repulsion between them because the Pauli principle prevents their close encounter. In contrast to the singlet state, the spin polarization of the B π electrons is not induced in the triplet state because the spin density of the NB π electrons is uniform in the triplet state. The spin polarization of the B π electrons which operates only in the singlet state makes the singlet ASDW lower in energy than the triplet ASDW.

Next we discuss on the spin polarization of the σ electrons shown in Fig. 4. The spin polarization of the σ electrons is induced in such a way that the σ spin densities on a carbon atom and that on adjacent hydrogen atom are arranged in the same and opposite directions, respectively, compared to that of the π spin density on the carbon atom. This enhances the exchange interaction between the σ electrons and the π electrons on each carbon atom and reduces the Coulomb repulsion between σ electrons. The magnitude of the σ spin polarization is relatively small. However, its effects are not so small as can be neglected in quantitative discussion.

UHF Calculation on Trimethylenemethane

We preformed a UHF calculation on **2** by rotating a methylene group out of the plane of the remaining allyl group. The other geometrical parameters are fixed as shown in Fig. 2b. At the planar geometry, the RHF π MOs are a B π MO (ϕ_1), two degenerate NB π MOs (ϕ_2, ϕ_3), and an AB π MO (ϕ_4):

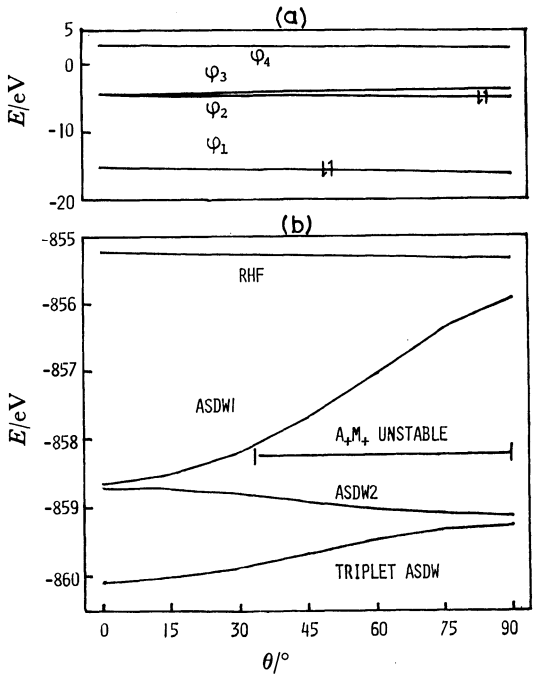

Fig. 5. The correlation diagram of the Hückel type MOs (a) and the adiabatic potentials of the RHF, ASDWs, and the triplet ASDW (b) of trimethylenemethane. The A_+M_+ instability domain of ASDW1 is also indicated. The region out of the domain corresponds to the second scheme in Table 1.

$$\phi_1 = a\chi_1 + b(\chi_2+\chi_3+\chi_4)/\sqrt{3}, \quad \phi_2 = (\chi_3-\chi_4)/\sqrt{2},$$
$$\phi_3 = (2\chi_2-\chi_3-\chi_4)/\sqrt{6},$$
$$\phi_4 = -b\chi_1 + a(\chi_2+\chi_3+\chi_4)/\sqrt{3}, \quad a \approx b \approx 0.7.$$

The MOs ϕ_1 and ϕ_4 belong to the a_2'' (b) symmetry and ϕ_2 and ϕ_3 to the e'' (a and b) symmetry at the planar D_{3h} geometry (nonplanar C_2 geometry). In the process of the internal rotation, the two NB MOs remain nearly degenerate (ϕ_2 lies a little below ϕ_3) as shown in Fig. 5a. The LCAO expression of ϕ_2 is unchanged while the main AO component of ϕ_3 turns out to be the p robe perpendicular to the twisted methylene group. Therefore, in the rotation the differential overlap between the two NB MOs varies from medium to nearly zero. This situation corresponds to the left half side of Fig. 1 and the first and second schemes of Table 1. Therefore, two singlet UHF states exist below the RHF. The UHF adiabatic potentials are shown in Fig. 5b. This calculation shows that the ground state is triplet and that its equilibrium geometry is planar. On the other hand, the lowest singlet UHF state (ASDW2) has the orthogonal equilibrium geometry. These results are in agreement with other calculations[3] and experiments.[8] It should be noted that at the planar geometry the two singlet states which are approximated by ASDW1 and ASDW2 are degenerate and belong to the E' representation of the D_{3h} point group. The calculated energies of ASDW1 and ASDW2 at the planar geometry are not exactly the same. However, the gap is very small and much reduced compared to the value in the RHF calculation of the two state.[3c]

In order to analyze the electronic correlation among

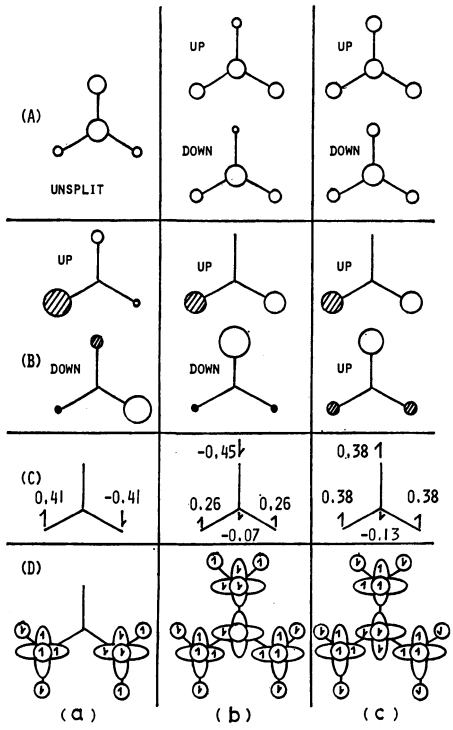

Fig. 6. The corresponding orbitals for the B π electrons (A) and for the NB π electrons (B), and the spin density structure on the π AOs (C) and on the σ AOs (D) of ASDW1 (a), ASDW2 (b), and the triplet ASDW (c) of planar trimethylenemethane. The numerals in (C) are the magnitudes of the spin densities. Those on the σ AOs are either ± 0.01 or ± 0.02.

the three UHF states, we show in Fig. 6 the π corresponding orbitals and the spin density structures of the UHF states at the planar geometry. The $^3ST_-$ instability which connects the RHF with ASDW1 has the B symmetry in the C_2 group. We adopted the C_2 symmetry because the RHF with the occupancy $(\phi_1)^2(\phi_2)^2$ of the π MOs is of symmetry adapted only to the C_2 group. The excitations $\phi_2 \rightarrow \phi_3$ and $\phi_2 \rightarrow \phi_4$ with the B symmetry contribute to the instability. Consequently, the NB orbitals in ASDW1 are spin polarized in the following manner:

$$\psi_{2\pm} = \cos\theta_1\phi_2 \pm \sin\theta_1(\cos\theta_2\phi_3 - \sin\theta_2\phi_4).$$

After the SCF procedure, ϕ_1 also is mixed into $\psi_{2\pm}$ because it has the same symmetry as ϕ_3 and ϕ_4 in the C_2 group.

ASDW2's orbitals are adapted to the C_2 symmetry and not to the D_{3h} one because its trial wave function

$$|\text{core}, \phi_1\alpha, \phi_1\beta, \phi_2\alpha, \phi_3\beta|$$

has the C_2 symmetry and not the D_{3h} one. Therefore, ϕ_1, ϕ_3, and ϕ_4 with the same b symmetry are mixed in ASDW2 after the SCF procedure, but ϕ_2 is unchanged:

$$\psi'_{3-} = \cos\theta_3\phi_3 + \sin\theta_3(\cos\theta_4\phi_4 + \sin\theta_4\phi_1),$$
$$\psi'_{1-} = \cos\theta_{5-}\phi_1 - \sin\theta_{5-}(\cos\theta_{6-}\phi_4 - \sin\theta_{6-}\phi_3),$$
$$\psi'_{1+} = \cos\theta_{5+}\phi_1 - \sin\theta_{5+}(\cos\theta_{6+}\phi_3 - \sin\theta_{6+}\phi_4).$$

The ASDW2's orbitals ψ'_{1-} and ψ'_{3-} have large MO weights on χ_1 and χ_2 AOs and ψ'_{+} does on χ_3 and χ_4 AOs so that electrons with different spins are caused to localize in different regions.

The triplet ASDW's orbitals are adapted to the D_{3h} symmetry because of the D_{3h} adaptation for the trial wave function

$$|\text{core}, \phi_1\alpha, \phi_1\beta, \phi_2\alpha, \phi_3\alpha|.$$

Therefore, only ϕ_1 and ϕ_4 with the same a_2'' symmetry are mixed in the triplet ASDW

$$\psi^t_{1\pm} = \cos\theta_{7\pm}\phi_1 \pm \sin\theta_{7\pm}\phi_4.$$

By the spin polarization of $\psi^t_{1\pm}$ a negative spin density appears on the central carbon atom.

We note that the spin structures of ASDW2 and the triplet ASDW are similar to those of the singlet and triplet GVB wave functions obtained by Davis and Goddard III.[3d] The forms of the orbitals of ASDW1 and ASDW2 are retained in the process of the rotation because the system has the C_2 symmetry throughout the process. The change in the spin polarization effect in the triplet ASDW also is small.

Next, we clarify the difference between ASDW1 and ASDW2. As mentioned above, ASDW2 is adapted to the C_2 symmetry, so that its spin structure is also invariant to the C_2 spatial rotation. The spin structure of ASDW1 is invariant not to the C_2 rotation but to the joint C_2 rotation of space and spin. This difference between the symmetries of the spin structures means that the singlet components of ASDW1 and ASDW2 belong to different C_2 symmetries as shown by Ozaki.[9] In fact, the singlet component of ASDW1 has the A symmetry but that of ASDW2 the B symmetry.

UHF Calculation on Tetramethyleneethane

We performed a UHF calculation on **3** by rotating the two allyl groups around the central C–C bond. The other geometrical parameters are fixed as shown in Fig. 2c. At the planar geometry the RHF π MOs are two B π MOs (ϕ_1, ϕ_2), two nearly degenerate NB π MOs (ϕ_3, ϕ_4), and two AB π MOs (ϕ_5, ϕ_6):

$$\phi_1 = a(\chi_1+\chi_2)/\sqrt{2} + b(\chi_3+\chi_4+\chi_5+\chi_6)/2,$$
$$\phi_2 = a'(\chi_1-\chi_2)/\sqrt{2} + b'(\chi_3+\chi_4-\chi_5-\chi_6)/2,$$
$$\phi_3 = (\chi_3-\chi_4+\chi_5-\chi_6)/2, \quad \phi_4 = (\chi_3-\chi_4-\chi_5+\chi_6)/2,$$
$$\phi_5 = -b(\chi_1+\chi_2)/\sqrt{2} + a(\chi_3+\chi_4+\chi_5+\chi_6)/2,$$
$$\phi_6 = -b'(\chi_1-\chi_2)/\sqrt{2} + a'(\chi_3+\chi_4-\chi_5-\chi_6)/2,$$
$$a \approx b' \approx 0.8, \quad b \approx a' \approx 0.6.$$

The MOs ϕ_1—ϕ_6 are of b_{3u}, b_{2g}, b_{1g}, a_u, b_{3u}, and b_{2g} symmetry in the D_{2h} group, respectively. In the process of the rotation, the two NB MOs remain nearly degenerate and cross at about $\theta = 40°$ as shown in Fig. 7a. The crossing occurs due to the spiroconjugation effect.[10] Therefore, there are two RHF ground states with the occupancies RHF1 $= (\phi_1)^2(\phi_2)^2(\phi_3)^2$ and RHF2 $= (\phi_1)^2(\phi_2)^2(\phi_4)^2$. RHF1 and RHF2 are the RHF ground states in the regions $\theta < 40°$ and $\theta > 40°$, respectively. The differential overlap between the two NB MOs is nearly complete throughout the rotation process, so that this case belongs to the last scheme of Table 1 and there is only a singlet ASDW state (ASDW1) below the RHF. The adiabatic potentials of the RHF and

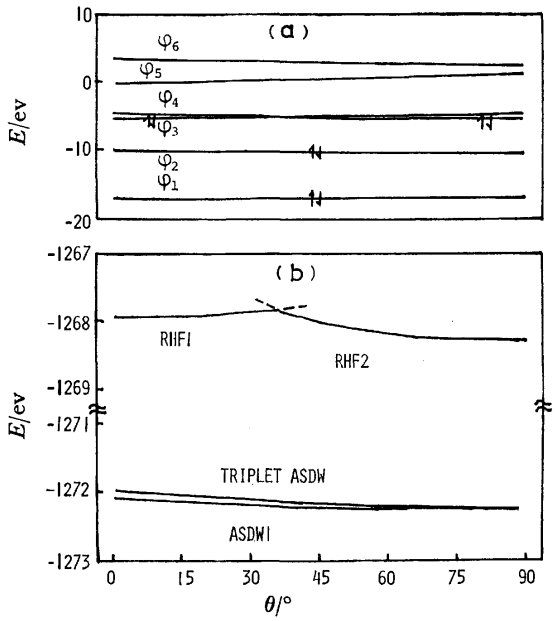

Fig. 7. The correlation diagram of the Hückel type MOs (a) and the adiabatic potentials of the RHFs, ASDW1 and the triplet ASDW (b) of tetramethyleneethane.

UHF states are shown in Fig. 7b. Our calculation, like a previous one,[10] shows a rather small energy change in the rotation. The singlet ASDW1 is found to lie a little below the triplet ASDW everywhere and has a very shallow potential minimum at about $\theta=50°$.

Next we examine the electronic correlation between the singlet and triplet ASDW states at the planar geometry. The $^3ST_-$ instability which connects the RHF and ASDW1 has the B_{1u} symmetry. Therefore, the excitations $\phi_3\rightarrow\phi_4$, $\phi_2\rightarrow\phi_5$, and $\phi_1\rightarrow\phi_6$ with the B_{1u} symmetry contribute to the instability. Consequently, all the orbital pairs are spin polarized as

$$\psi^s_{1\pm}=\cos\theta_1\phi_1\pm\sin\theta_1\phi_6,\quad \psi^s_{2\pm}=\cos\theta_2\phi_2\pm\sin\theta_2\phi_5,$$
$$\psi^s_{3\pm}=\cos\theta_3\phi_3\pm\sin\theta_3\phi_4.$$

The triplet ASDW's orbitals are adapted to the D_{2h} symmetry because its trial wave function

$$|\text{core},\ \phi_1\alpha,\ \phi_1\beta,\ \phi_2\alpha,\ \phi_2\beta,\ \phi_3\alpha,\ \phi_4\alpha|$$

has the B_{1u} symmetry in the D_{2h} group. After the SCF procedure, ϕ_2 and ϕ_6 with the b_{2g} symmetry and ϕ_1 and ϕ_5 with the b_{3u} one are mixed in the triplet ASDW to yield

$$\psi^t_{1\pm}=\cos\theta_{4\pm}\phi_1\pm\sin\theta_{4\pm}\phi_5,\quad \psi^t_{2\pm}=\cos\theta_{5\pm}\phi_2\pm\sin\theta_{5\pm}\phi_6.$$

The difference in the spin polarization of the B π MOs between the singlet and triplet ASDW states is that in the singlet ASDW it is produced by the mixing of the second π LUMO to the second π HOMO and of the third π LUMO to the third π HOMO, while in the triplet ASDW by the mixing of the third π LUMO to the second π HOMO and of the second π LUMO to the third π HOMO as shown in Fig. 8. As a result, the spin polarization of the second π HOMO is larger in the singlet ASDW, while that of the third π HOMO is larger in the triplet ASDW. Because the second π HOMO is spin polarized more easily than the third one, the spin polarization effect in the singlet ASDW

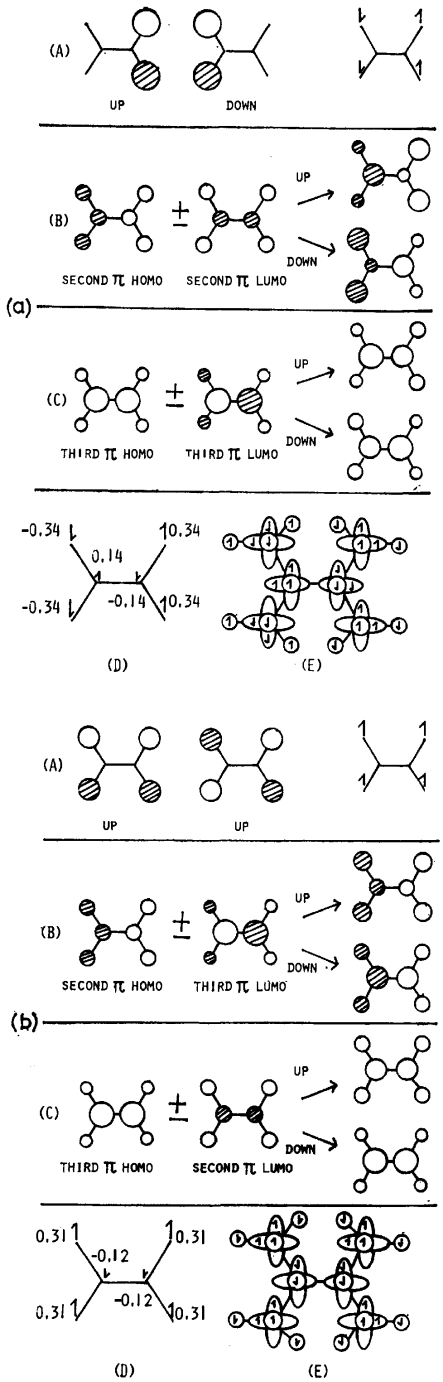

Fig. 8. The corresponding orbitals of the NB π MO (A), second π HOMO (B) and third π HOMO (C) of ASDW1 (a) and the triplet ASDW (b) of tetramethyleneethane. The spin density structures on the π AOs and σ AOs are also shown in (D) and (E), respectively. The numerals in (D) are the magnitudes of the spin densities. Those on the σ AOs are either ±0.01 or ±0.02.

is a little larger than that in the triplet ASDW. This explains why the singlet ASDW lies a little below the triplet ASDW.

The above UHF analysis indicates that the ground state of **3** is singlet and that a triplet state lies close to it. The result is in accord with the *ab initio* CI calcula-

tion by Borden and Davidson.[11] This suggests that the ESR signal of **3** which was observed at the boiling point of nitrogen[12] may be attributed to a thermally accessible triplet state. This prediction can be checked by measurement of the temperature dependence of the ESR signal. However, no such experiments have been carried out and the correctness of our prediction is left to be tested.

Simple Rules to Predict the Spin Multiplicity of the Ground State and the Spin Structure of Low-lying UHF States of Hydrocarbon Diradicals

The above results for **1**, **2**, and **3** show that the UHF theory gives the ground state of correct spin multiplicity. It should be stressed that all the ground states of **1**, **2**, and **3** have alternating spin structures. The results also show that the spin structure of the all-valence-electron UHF calculation is different from that of the two-electron model in such a manner that the weak spin density on an atom adjacent to the atom with large spin density is always antiparallel to the adjacent largest spin density. The preference of the antiparallel spin coupling manifested in the UHF results is consistent with the valence bond picture and seems to have a general validity. By generalizing these results, we can predict the spin multiplicity of the ground state and the spin structure of low-lying UHF states of hydrocarbon diradicals as follows.

Put spins on carbon atoms in alternating directions and if the number of the up and down spins in the alternating spin structure are the same with each other, the ground state is predicted to be singlet, whereas if their difference is two, the ground state is predicted to be triplet. This rule is much simpler than, but as effective as, the one proposed by Borden and Davidson.[11] The main aspect of the spin structure of low-lying UHF states is determined by the two-electron model. The all-valence-electron spin structures are obtained by modifying the directions of the weak atomic spin densities so as to make them antiparallel to the adjacent large spin densities.

To demonstrate the general validity of these rules, we apply them to 1,1,2,3,3-pentamethylenepropane (**4**) and 1,3-dimethylenecyclobutadiene (**5**). First we consider **4**. The two NB MOs (ϕ_A and ϕ_B) obtained with the Hückel Hamiltonian are shown in Fig. 9a. The figure shows that the differential overlap between them is nearly complete, so that there are a singlet ASDW (ASDW1) and a triplet ASDW below the RHF. The spin structures of the NB electrons of the two states are shown in Figs. 9b and 9c. Modifying the weak spin densities so that they are made antiparallel to the adjacent large ones, we obtain Figs. 9b and 9c′. There appear no spin densities on the two central carbons (4 and 5) in Fig. 9b because of the symmetry of the spin structure. The weak spin density on carbon 4 in Fig. 9c′ is made negative so as to be antiparallel to the adjacent one. The alternating spin structure corresponds to the triplet state of Fig. 9c′, so that the ground state is predicted to be triplet. We show in Fig. 9d the UHF results, which confirm our rules.

Next we consider **5**. The overlap between the two NB MOs (ϕ_A and ϕ_B) shown in Fig. 10a is medium, so that there are two singlet ASDWs (ASDW1 and ASDW2) and one triplet ASDW below the RHF. The spin structures of the two NB electrons in the three states are shown in Figs. 10b, 10c, and 10d. Modifying the weak spin densities so that they are made antiparallel

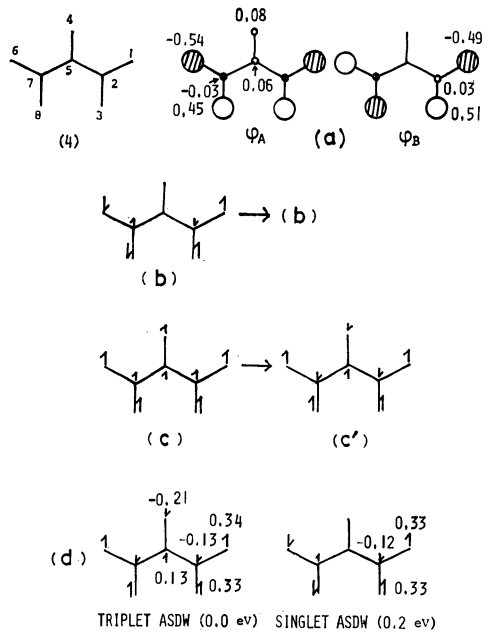

Fig. 9. Two NB MOs (a), the predicted spin structures of ASDW1 (b) and the triplet ASDW (c′), and the result of the all-valence-electron UHF calculation (d) of 1,1,2,3,3-pentamethylenepropane.

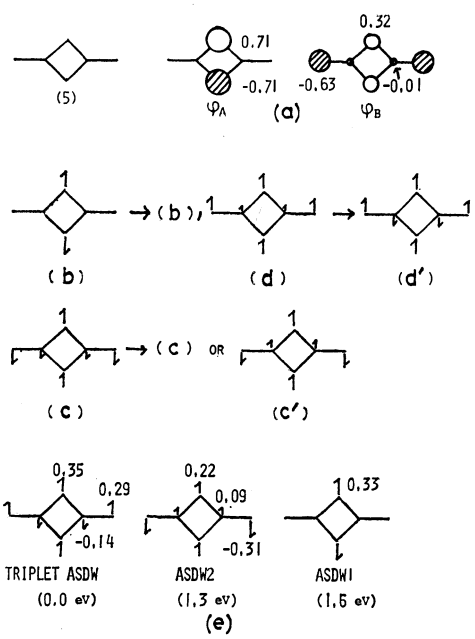

Fig. 10. Two NB MOs (a), the predicted spin structures of ASDW1 (b), ASDW2 (c′) and the triplet ASDW (d′), and the result of the all-valence-electron UHF calculation (e) of 1,3-dimethylenecyclobutadiene.

to the adjacent large ones, we obtain the spin structures shown in the right side of Figs. 10b, 10c, and 10d. The spin structure of Fig. 10b is unchanged because of its symmetry. The spin structure of Fig. 10c is possible to be modified in two different ways, but Fig. 10c' shows the feasible one because the terminal carbon atoms have the largest spin densities. The alternating spin structure corresponds to the triplet state in Fig. 10d', so that the ground state is predicted to be triplet. We show in Fig. 10e the UHF results, which also confirm our rules.

References

1) W. T. Borden, *J. Am. Chem. Soc.*, **97**, 5968 (1975).
2) G. Maier, *Angew. Chem. Int. Ed. Engl.*, **13**, 425 (1974); A. Krantz, C. Y. Lin, and M. D. Newton, *J. Am. Chem. Soc.*, **95**, 2744 (1973); O. L. Chapman, C. L. MacIntosh, and J. Pacansky, *ibid.*, **95**, 614 (1973); O. L. Chapman, D. De La Cruz, R. Roth, and J. Pacansky, *ibid.*, **95**, 1337 (1973).
3) a) D. R. Yarkony and H. F. Schaefer, III, *J. Am. Chem. Soc.*, **96**, 3754 (1974); b) W. T. Borden, *ibid.*, **97**, 2906 (1975), **98**, 2695 (1976); c) M. J. S. Dewar and J. S. Wasson, *ibid.*, **93**, 3081 (1971); d) J. H. Davis and W. A. Goddard, III, *ibid.*, **99**, 4242 (1977).
4) H. Kollmar and V. Staemmler, *J. Am. Chem. Soc.*, **99**, 3583 (1977).
5) J. A. Pople, D. L. Beveridge, and P. A. Dobosh, *J. Chem. Phys.*, **47**, 2026 (1967).
6) A. Igawa and H. Fukutome, *Prog. Theor. Phys.*, **54**, 1266 (1975).
7) H. Fukutome, *Prog. Theor. Phys.*, **52**, 115 (1974); **52**, 1766 (1974).
8) P. Dowd, *Acc. Chem. Res.*, **5**, 242 (1972).
9) M. Ozaki, *Prog. Theor. Phys.*, **63**, 84 (1980).
10) B. G. Odell, R. Hoffmann, and A. Imamura, *J. Chem. Soc., B*, **1970**, 1675.
11) W. T. Borden and E. R. Davidson, *J. Am. Chem. Soc.*, **99**, 4587 (1977).
12) P. Dowd, *J. Am. Chem. Soc.*, **92**, 1066 (1970).

Kinetics and Mechanism of Acylhydrazine Hydrolysis in Sulfuric Acid-Water Mixtures

Mitsuo MASHIMA,* Fujiko IKEDA, Takako DOI, and Sadakatsu NISHIKAWA

Department of Chemistry, Faculty of Science and Engineering, Saga University, Saga 840

(Received March 23, 1981)

The rates of acid-catalyzed hydrolysis of formylhydrazine, acetylhydrazine, chloroacetylhydrazine, propionylhydrazine, butyrylhydrazine, and octanoylhydrazine in sulfuric acid–water mixtures have been investigated over a wide range of acidities (about 1—18 M H_2SO_4) by means of spectrophotometric methods. First-order kinetics were obtained in all cases, and the pseudo-first-order rate constants showed one of two types of acidity dependences: (i) a rate maximum at intermediate acidities, followed by slow hydrolysis in highly concentrated acids; (ii) a rate maximum at intermediate acidities, followed by a sharp increase in rate at high acidities. This result was treated as a function of the Hammett acidity function, the water activity, and the total concentration of hydrogen ion to yield reaction parameters which are explicable in terms of a change in mechanism at a high acidity from A-2 to A-1. The mechanism change also was deduced from a criterion based on the values of activation entropies.

The rates of acid-catalyzed hydrolysis of amides have been studied systematically, but only a few results[1,2] have been obtained for those of acylhydrazines. Hydrazidinum ion $RCONHNH_3^+$, which is expected to exist in acid solutions,[1,3,4] would have a planar skeleton of O–C–N–N having two π-electrons and two lone-pair electrons. It is of interest to test how this electron system affects the kinetics.

Mechanisms of reaction in strong acid solutions have been recently reviewed in detail by Rochester[5] and Liler.[6] Empirical criteria of acid-catalyzed hydrolysis have been developed in terms of the acidity function, the water activity, the total concentration of hydrogen ions of acid media, and further in terms of the change of hydration number between reactants and transition states. For the hydrolysis containing pre-equilibrium, the value of the dissociation constant of the conjugate acid may also control the rate-determining step. Sulfuric acid-water mixtures are an exceptionally suitable medium to examine the factors affecting the kinetics of acid-catalyzed hydrolysis over a wide range of acid concentrations.

Experimental

Materials and Apparatus. The acylhydrazines were synthesized with methyl or ethyl esters of the corresponding acids and hydrazine hydrates, and purified by recrystallization from ether–ethanol mixtures. Purity was assured by melting point. Sulfuric acid–water mixtures were made by dilution of reagent grade acid with distilled water. The acid solutions were standardized by titration against a standard sodium hydroxide solution, exccpt for highly concentrated acids of which concentrations were determined by measurements of density. Molarities were calculated by calibration on the basis of the literature data of densities.[7]

The ultraviolet solution spectra were measured with a Hitachi EPS-3T Recording Spectrophotometer equipped with a thermostated cell compartment. The temperature in this compartment was controlled within ± 0.1 °C.

Rate Measurements. Reactions were followed by recording the change in absorbance A with time at the absorption maximum. Pseudo-first-order rate constants k were calculated graphically from plots of log $(A-A_\infty)$ *vs.* time (min) or by means of a computer program which gives, by adjustment of A_∞, the first-order rate constant which best fits the observed data. In view of the highly diluted reaction solutions, about 10^{-3} M (1 M = 1 mol dm^{-3}), used for spectrophotometric examination, no attempt was made to isolate reaction products from the reaction solutions. In order to check the A_∞, the absorption spectra of the prepared mock solutions were examined and compared with those of reaction solutions.

Results

Rate Profiles. The rate-acidity dependences of hydrolysis of the acylhydrazines were found to fit into one of two categories. The dependence of formylhydrazine and chloroacetylhydrazine is characterized by an initial rate increase with the acid concentration, passing through a maximum, followed by a rate decrease with further increasing acid concentration. Other acylhydrazines resemble this, except that the final increase occurs steeply at higher acid concentrations. It has been confirmed that the acylhydrazine hydrolysis also shows a rate maximum as amide[8] and ester[9] hydrolysis do, but at relatively high acidities: about 12 M H_2SO_4 for formylhydrazine, in contrast to about 5 M H_2SO_4 for formamide.[8a] The values of rate constants and acid concentrations at the maximum rate have been estimated graphically and collected in Table 2.

An important difference in reaction activities is found between the first two members of the aliphatic series $RCONHNH_2$, and an anomaly is found among the first three members, as pointed out for aliphatic acid amide homologues;[10] acetylhydrazine is less active than propionylhydrazine, but the difference is not very large. It also should be noted that the chlorine-substitution in the acyl group changes the reactivity in the low acidity region very little but does affect the reactivity at the very high acidity region.

Treatment of Rate Data. The pseudo-first-order rate constants, k, of hydrolysis of formylhydrazine and acetylhydrazine at 25 °C have been used in order to test several treatments which are useful for obtaining mechanistic conclusions in terms of the values of acidity function H_0,[11] activity of water a_w,[12] total concentration of hydrogen ion $[H^+]$,[13] and pK_{SH^+} of conjugate acid.[1,3]

One criterion of the reaction mechanism has been presented by Bunnett and Olsen,[14] who have found a

TABLE 1. PSEUDO-FIRST-ORDER RATE CONSTANTS OF HYDROLYSIS OF ACETYLHYDRAZINES $RCONHNH_2$ IN SULFURIC ACID–WATER MIXTURES

T °C	$[H_2SO_4]$ M	$10^2 k$ min^{-1}	T °C	$[H_2SO_4]$ M	$10^2 k$ min^{-1}	T °C	$[H_2SO_4]$ M	$10_2 k$ min^{-1}	T °C	$[H_2SO_4]$ M	$10^2 k$ min^{-1}
	R=H			R=CH_3			R=CH_2Cl			R=CH_3CH_2	
25.0	1.04	1.73	25.0	1.66	0.122	55.0	0.947	0.865	55.0	1.66	1.23
	1.66	2.64		2.67	0.180		1.40	1.32		2.72	2.14
	2.67	4.53		3.67	0.239		1.99	1.88		3.28	2.74
	3.67	6.23		4.18	0.269		2.72	2.72		4.39	3.40
	3.99	6.69		4.79	0.306		3.70	3.41		5.01	4.47
	4.18	7.24		5.70	0.352		4.64	4.23		6.19	5.66
	4.79	8.51		7.33	0.465		6.19	5.53		7.33	6.53
	5.70	10.9		8.15	0.517		7.80	6.09		8.58	7.25
	6.32	12.4		8.83	0.527		8.92	6.41		9.77	7.18
	7.74	16.0		9.40	0.499		10.3	6.57		10.6	6.85
	8.15	16.8		9.90	0.483		11.9	6.36		11.4	6.33
	8.40	17.4		11.1	0.356		13.3	5.64		12.3	5.51
	9.25	19.8		12.3	0.251		14.8	4.14		13.1	5.34
	10.2	22.1		13.7	0.144		15.8	3.11		14.0	6.95
	10.9	24.1		14.7	0.189		16.2	2.48		14.9	14.9
	11.2	24.7		15.6	0.572		17.0	1.60		15.9	30.3
	11.7	26.0		16.2	0.950		17.6	1.03		16.5	47.7
	12.4	24.5		16.5	1.41					17.3	94.8
	13.4	17.8		16.7	1.78						
	13.7	16.4		17.5	6.10		R=$CH_3(CH_2)_2$			R=$CH_3(CH_2)_6$	
	14.9	9.94		17.7	7.03	55.0	0.974	0.967	55.0	1.99	0.661
	15.5	6.35		17.9	8.70		1.40	1.03		2.90	0.994
	16.3	2.90	55.0	0.780	0.554		1.99	1.44		4.45	1.73
	16.5	2.03		1.38	0.992		2.90	2.23		5.10	1.93
	17.1	1.36		1.94	1.46		3.70	2.84		6.19	2.43
55.0	0.368	5.54		2.72	1.87		5.10	3.84		7.46	3.28
	0.510	7.64		3.67	2.73		6.19	4.45		7.95	3.44
	0.770	11.3		4.22	3.20		7.46	5.09		8.92	3.59
	1.04	15.3		5.10	4.03		8.92	4.86		9.77	3.56
	1.38	21.0		6.32	4.96		9.77	4.34		10.8	3.22
	1.54	23.7		7.80	6.42		10.8	3.85		11.7	3.01
	1.94	29.8		8.83	6.75		11.7	3.18		12.3	3.21
	2.85	43.9		9.63	6.80		12.3	2.90		13.1	4.21
	3.16	49.5		10.6	6.24		13.1	2.70		14.0	9.23
	3.67	55.9		11.1	5.98		14.0	5.33		14.8	17.7
	4.79	75.6		11.9	5.49		15.0	14.6		15.5	34.2
	5.70	92.1		12.6	4.78		15.5	21.1		15.9	46.8
	7.34	119		13.3	4.06		16.2	32.4		16.5	81.9
	8.92	142		14.0	4.14		16.5	42.2		17.3	143
	9.77	156		14.8	9.79		16.7	59.3			
	11.2	181		15.9	20.7		17.1	84.5			
	12.4	186		16.1	23.9		17.6	121			
	13.2	162		16.7	39.6						
	14.0	137		17.6	74.1						
	14.8	105		17.9	98.2						
	15.6	74.4									
	16.5	46.1									
	17.5	24.7									

linear correlation of $\log k+H_o$ *vs.* $H_o+\log[H^+]$ and proposed the values of the proportionality slope parameter ϕ as useful to characterize the medium dependence of rate constants. Typical ϕ plots are illustrated in Fig. 1, which shows the following: for formylhydrazine the points below 12 M H_2SO_4 give a good straight line ($\phi=0.95\pm0.01$), and above 13 M H_2SO_4 another straight line ($\phi=1.37\pm0.01$) can be drawn through the remaining points; for acetylhydrazine the similar linearities are obtained below about 10 M H_2SO_4 ($\phi=1.00\pm0.01$) and in the middle region of about 11—14 M H_2SO_4 ($\phi=1.29\pm0.00$), and one more linearity ($\phi=0.09\pm0.00$) is found above about 14 M H_2SO_4. It has been deduced[14,15] that for substrates

Table 2. Values of rate constant and acid concentration at maximum rate of hydrolysis of acetylhydrazines in sulfuric acid–water mixtures

R	$10^2 k$ / min^{-1}	$[H_2SO_4]$ / M	T / °C
H	26	12	25
	187	12	55
CH_3	0.53	9.1	25
	6.9	9.4	55
CH_2Cl	6.5	10	55
CH_3CH_2	7.3	9.0	55
$CH_3(CH_2)_2$	5.2	8.0	55
$CH_3(CH_2)_6$	3.6	9.2	55

protonated on N or O atom the ranges of ϕ values for different modes of water involvement in the rate-determining step are: $-0.34<\phi<0$ for water not involved, $0.18<\phi<0.47$ for water acting as a nucleophile, and $\phi>0.47$ for water acting as a proton transfer agent. Applying this criterion, the ϕ values obtained imply that the hydrolysis of formylhydrazine proceeds by the mechanism (A-2) involving water as a proton transfer agent over all the range of acid concentration studied; acetylhydrazine is hydrolyzed by the same mechanism up to about 14 M H_2SO_4, and above the acid concentration the hydrolysis mechanism changes into the one involving no water (A-1). A mechanistic conclusion similar to that for formylhydrazine is obtained for chloroacetylhydrazine, and a conclusion similar to that for acetylhydrazine is obtained for propionylhydrazine butyrylhydrazine and caprylylhydrazine (refer to the ϕ values in Table 3).

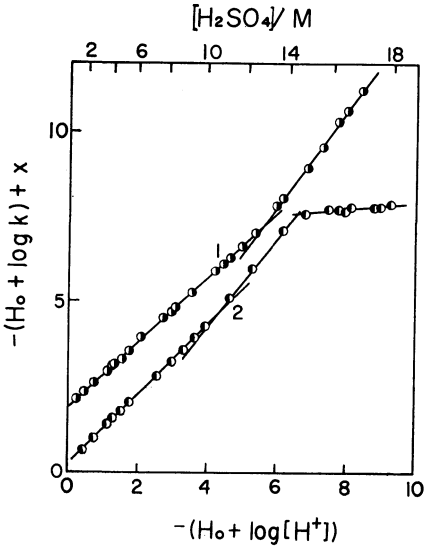

Fig. 1. Plots of $H_o+\log k_{obsd}$ *vs.* $H_o+\log [H^+]$ for hydrolysis in sulfuric acid at 25 °C; vertical displacement values $x=0$ for formylhydrazine (1) and $x=-3$ for acetylhydrazine (2).

Bunnett[16] noted that $\log k+H_o$ was correlated

Table 3. Values of ϕ, w, and w^* parameters[a] for the hydrolysis of acetylhydrazines $RCONHNH_2$ in sulfuric acid–water mixtures

R	T	ϕ	w	w^*
H	25	0.95±0.01 (1.04—11.7)	8.85±0.03 (1.04—2.67)	
		1.37±0.01 (13.4—17.1)	3.37±0.03 (3.99—8.15)	Not linear
			1.81±0.03 (10.23—17.1)	
	55	0.98±0.00 (0.510—9.77)	8.75±0.02 (0.150—3.16)	
		1.15±0.01 (11.2—17.5)	3.58±0.03 (3.67—8.92)	Not linear
			1.50±0.03 (12.4—17.5)	
CH_3	25	1.00±0.01 (1.66—9.90)	8.35±0.01 (1.66—3.67)	Not linear
		1.29±0.00 (11.1—13.7)	3.61±0.02 (4.18—8.83)	
		0.09±0.00 (14.7—17.9)	2.33±0.04 (9.90—13.7)	−1.96±0.02 (13.7—17.9)
			0.10±0.01 (14.7—17.9)	
	55	0.97±0.01 (0.780—7.80)	9.24±0.01 (0.780—1.94)	Not linear
		1.13±0.01 (8.83—13.3)	3.56±0.03 (4.22—8.83)	
		0.35±0.01 (14.0—17.9)	2.21±0.01 (10.6—13.3)	−1.78±0.04 (13.3—17.9)
			0.44±0.01 (14.0—17.9)	
CH_2Cl	55	1.02±0.01 (0.97—8.92)	8.74±0.01 (0.974—2.72)	
		1.11±0.00 (11.9—17.6)	3.62±0.01 (4.64—8.92)	Not linear
			1.47±0.05 (11.9—17.6)	
CH_3CH_2	55	0.95±0.01 (1.66—7.33)	8.48±0.01 (0.974—2.72)	
		1.10±0.00 (8.58—13.1)	3.53±0.00 (4.39—7.33)	Not linear
		0.37±0.00 (14.0—17.3)	2.41±0.08 (8.58—13.1)	
			0.64±0.01 (14.0—17.3)	−1.87±0.03 (14.0—17.3)
$CH_3(CH_2)_2$	55	1.00±0.01 (0.974—7.46)	9.67±0.00 (0.974—2.78)	
		1.15±0.00 (8.92—13.1)	3.65±0.01 (5.10—8.92)	Not linear
		0.33±0.00 (14.0—17.6)	2.35±0.05 (9.77—13.1)	
			0.40±0.01 (14.0—17.6)	−1.77±0.01 (15.0—17.6)
$CH_3(CH_2)_6$	55	0.94±0.01 (1.99—6.19)	6.02±0.03 (1.99—4.45)	
		1.07±0.00 (7.46—12.3)	3.04±0.01 (6.19—7.95)	Not linear
		0.33±0.00 (13.1—17.3)	2.41±0.04 (8.92—12.3)	
			0.41±0.01 (13.1—17.3)	−1.90±0.03 (14.0—17.3)

a) The values of H_o, $[H^+]$ and a_w at 25 °C are used for the kinetic data at 55 °C. b) The acid concentration range in which the parameters are calculated is inserted in the parentheses.

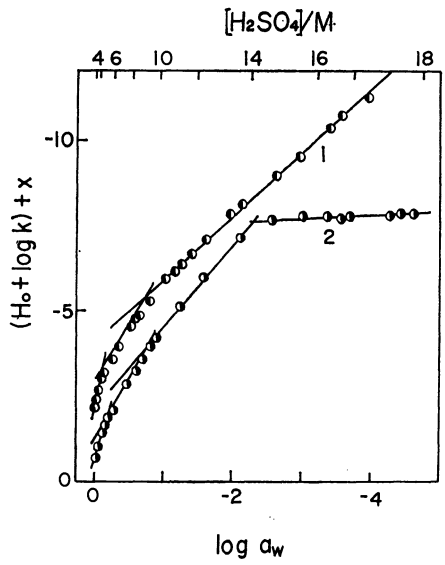

Fig. 2. Plots of $H_o+\log k_{obsd}$ *vs.* $\log a_w$ for the hydrolysis in sulfuric acid at 25 °C; vertical displacement values $x=0$ for formylhydrazine (1) and $x=-2$ for acetylhydrazine (2).

linearly with $\log a_w$ and that the values of the correlation slope parameter w were useful as the criterion of the reaction mechanism. Typical w plots are shown in Fig. 2. The plots should be divided into three (for formylhydrazine) or four (for acetylhydrazine) linear portions. The w values estimated for each portion are collected in Table 3, along with the acid concentration ranges in which the w values are calculated. A complementary parameter w^* was defined by Bunnett[16] as a useful index of the response of the reaction to the catalysis by concentrated acid, *e.g.* sulfuric acids above 4 M. The w^* plots, $\log k-H_o-\log[H^+]$ *vs.* $\log a_w$, are shown in Fig. 3. This clearly indicates that for acetylhydrazine the mechanism change expected from the magnitude of ϕ values takes place, *i.e.* for this compound a curved

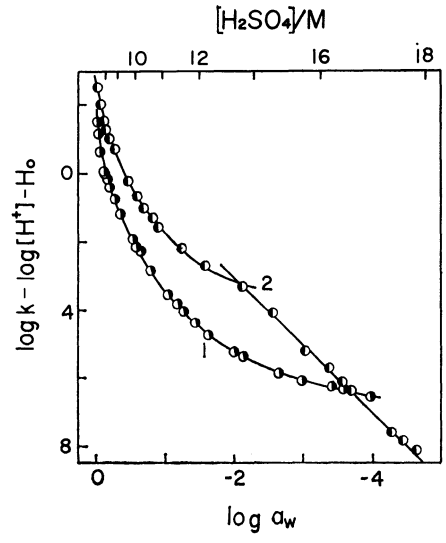

Fig. 3. Plots of $\log k_{obsd}-\log[H^+]-H_o$ *vs.* $\log a_w$ for the hydrolysis of formylhydrazine (1) and acetylhydrazine (2) at 25 °C.

line similar to that for formylhydrazine can be drawn through the points up to about 14 M H_2SO_4, while a good linearity is found beyond 14 M H_2SO_4.

The applicability of the Zucker-Hammett hypothesis[17] was also examined. However, the plot of $\log k$ *vs.* H_o showed no linearity over the range of acid concentration, except for a narrow range of very high acidity, and the plot of $\log k$ *vs.* $\log[H^+]$ also gave a linear portion in a narrow range at low acidities only.

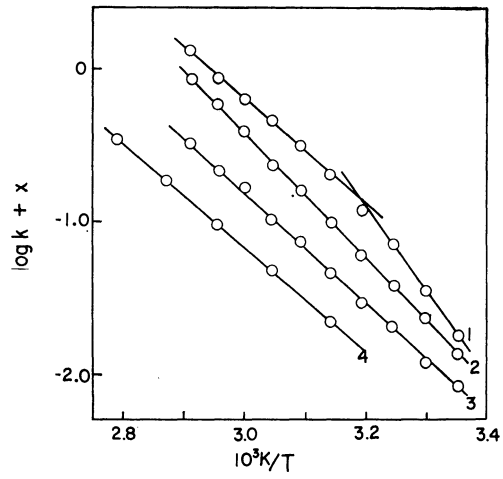

Fig. 4. Arrhenius plots for the hydrolysis of acetylhydrazine; vertical displacement value $x=0$ at 16.7 M H_2SO_4 (1), $x=0.6$ at 11.1 M (2), $x=0.2$ at 8.83 M (3), $x=0.4$ at 2.72 M (4).

Activation Parameters. The rate-temperature dependence was examined at several acid concentrations representative of linear portions in the plots mentioned in the foregoing section. Typical Arrhenius plots, $\log k$ *vs.* $1/T$, are shown in Fig. 4 for the hydrolysis of acetylhydrazine at 2.72, 8.83, 11.1, and 16.7 M H_2SO_4. The plots at high acid concentration for each substrate, except chloroacetylhydrazine, were divided into two linear portions. In these cases the rate constant-temperature dependence can be reasonably treated under the assumption that the activation heat capacities ΔC_p^* vary with temperature.[18] However, our present data do not seem to cover a sufficiently wide temperature range to do the treatment. Therefore, the values of activation parameters were calculated for each linear portion and are collected in Table 4.

After studying the acid-catalyzed hydrolysis of esters, Schaleger and Long[19] have suggested that the typical values of activation entropies are 0 to 42 J K^{-1} mol^{-1} for the A-1 mechanism and -63 to -126 J K^{-1} mol^{-1} for A-2. In fact, for the ethyl acetate hydrolysis[9] the ΔS^* value changed from a negative value (-64.0 J K^{-1} mol^{-1} at 40.2% H_2SO_4) typical of A-2 reactions to a small positive value ($+9.6$ J K^{-1} mol^{-1} at 98.4% H_2SO_4) typical of A-1 reactions; for the amide hydrolysis, which proceeds probably through the A-2 mechanism, the ΔS^* value[20] is -69.5 J K^{-1} mol^{-1} for formamide, -86.6 J K^{-1} mol^{-1} for acetamide, and 88.3 J K^{-1} mol^{-1} for propionamide in 1.00 M HCl.

The mechanistic change of acylhydrazine hydrolysis

Table 4. Activation parameters for hydrolysis of acetylhydrazines $RCONHNH_2$

R	$[H_2SO_4]$ / M	$\Delta E^{a)}$ / kJ mol^{-1}	ΔS^* / J K^{-1} mol^{-1}	$T^{b)}$ / °C
H	1.04	59.0 (25—65)	−121	25
	5.07	60.0 (10—40)	−92	25
	11.2	63.6	−88	25
	16.5	84.1 (25—45)	−38	25
		59.0 (55—75)	−113	55
CH_3	2.72	65.7 (45—85)	−121	55
	8.83	70.3 (25—70)	−96	25
	11.1	77.8	−71	25
	16.7	107 (25—35)	+38	25
		64.4 (57—70)	−100	55
CH_2Cl	1.99	72.0 (25—70)	−100	25
	7.80	73.2 (25—70)	−88	25
	15.8	74.5 (25—70)	−88	25
CH_3CH_2	3.28	63.2 (45—85)	−126	55
	11.4	72.0 (45—85)	−92	55
	17.3	89.1 (25—45)	−17	25
		35.1 (55—75)	−180	55
$CH_3(CH_2)_2$	5.10	64.4 (35—75)	−138	55
	11.7	74.9	−109	55
	15.5	108 (25—65)	+21	25
		26.4 (75—85)	−209	75
$CH_3(CH_2)_6$	4.45	68.2 (45—85)	−113	55
	12.3	77.4 (45—85)	−79	55
	15.5	105 (25—45)	+29	25
		54.8 (55—85)	−130	55

a) The linear Arrhenius plots were obtained in the temperature range which is indicated in the parentheses. b) The temperature at which ΔS^* was calculated.

from A-2 to A-1, at a very high acid concentration, was deduced again from the above-mentioned criterion in terms of the ΔS^* values. For each acylhydrazine the larger negative entropies were obtained in the acidity region in which the hydrolysis was expected to go through the A-2 mechanism, and in highly concentrated acids the ΔS^* values were positive or slightly negative, except for chloroacetylhydrazine. Although the ΔS^* values are based on pseudo-first-order rate constants which are dependent on acidity, the observed medium dependence of ΔS^* (see Table 4) would not be expected to lead to such a drastic change, unless a mechanism change was involved. However, for formylhydrazine no indication of the mechanism change from A-2 to A-1 was obtained from the criterion based on the reaction parameters ϕ, w, and w^*, while a relatively small negative value of ΔS^*, probably suitable to the A-1 mechanism, was obtained at a low temperature in 16.5 M H_2SO_4. This inconsistency may be due to the fact that the hydrolysis of formylhydrazine at high acidity is unimolecular (A-1), but is retarded by high activation energies. Even if this is the case, the Arrhenius plots involving two linear portions still need to be interpreted. For all the acylhydrazines with the exception of chloroacetylhydrazine, the values of activation energies and entropies, estimated from the linear portion of Arrhenius plot in higher temperature region and at high acidity, are identical with those obtained at lower acidities. This seems to indicate that change of hydrolysis mechanism occurs; in other words, there are two competing reactions, probably A-1 and A-2, which are predominant at low and high temperature, respectively.

Discussion

In the acidity region in which the hydrolysis proceeds through the A-2 mechanism, formylhydrazine has been observed to undergo hydrolysis about thirty times faster than acetylhydrazine (see Table 1). Acetylhydrazine is hydrolyzed as slow as chloroacetylhydrazine, with a k value of 4.12×10^{-1} min^{-1} at 25 °C in 7.8 M H_2SO_4 (not shown in the table). In spite of such a large rate difference, these three acylhydrazines give nearly equal values of activation energies and of entropies. Therefore, it may be said that the hydrolysis in the low acidity region is not entropy-controlled, nor is it an energy-controlled reaction. The greater stability of acetylhydrazine can not be ascribed to the electron-donating property of methyl group compared with the formyl hydrogen atom, because chloroacetylhydrazine, whose chloromethyl group has no electron-donation power, is as stable as acetylhydrazine. Thus the stability would come from the steric hindrance of the bulky acyl group which prevents it from attacking the water molecule. At high acidity, chloroacetylhydrazine shows no mechanism change from A-2 to A-1; this has been deduced from the criterion based on the reaction parameters and also from that based on activation entropies. The effect of substitution on acylhydrazine hydrolysis ought to be studied more widely. The regions of hydrolysis by the A-1 and A-2 mechanisms are usually separated by a minimum in the rate constant-acid concentration profile curves;[21] this is the case for the hydrolysis of acetylhydrazine, propionylhydrazine, butyrylhydrazine, and caprylylhydrazine.

The magnitude of the parameter used as the criterion of reaction mechanism depends upon how broad a range of acid concentration is covered by the kinetic experiments;[14] our present data, covering a sufficiently wide acidity range for the acylhydrazine hydrolysis, clearly reflect a medium change. The plots based on the linear free relationship[14] give a good linearity which covers all the examined range of acid concentration. However, the plots are divided into two or three linear portions (see Fig. 1 and Table 3). For the first one or two portions, the ϕ values are suitable to the A-2 mechanism, but the value for the higher acidity region is slightly larger than that for the lower acidity region. No acceptable interpretation of the small difference in ϕ values may be deduced from the ϕ plots only.

A striking behavior of the w^* plots, $\log k-H_o-\log[H^+]$ *vs.* $\log a_w$, is worth noting (see Fig. 3): the plot of acetylhydrazine gives a curved line up to an acid concentration which begins to give a linear portion, and so the mechanism change from A-2 to A-1 is expected to be involved; otherwise such a sudden change in curvature is not expected. Moreover, we should pay attention to the curved line portion, because the apparently continuous change of $\log k-H_o-\log[H^+]$

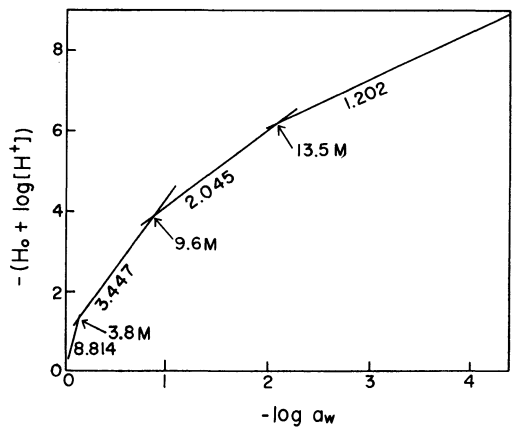

Fig. 5. The plots of $-(H_0+\log[H^+])$ *vs.* $-\log a_w$ for sulfuric acid-water mixtures.

which changing log a_w is considered to come from some affecting factors, which are continuously changed with acid concentration, on the hydrolysis rate. The relation between Hammett's acidity function and water activity has been discussed by several authors.[14,16,22,23] For sulfuric acid-water mixtures in the concentration range examined, the "excess acidity,"[23] $-(H_0+\log[H^+])$, is plotted against $-\log a_w$ by the use of data[11-13] available in Fig. 5. The plot is divided into four linear portions: the initial three portions in slope value and also in the acidity region correspond to the initial three linear portions of the w plots, *i.e.* the local linearlities of the plot of the excess acidity against the water activity are directly reflected on the w plot (compare the slope values and the range of acid concentration inserted in Fig. 5 with those presented in Table 3). Since the correspondence was found for all the acylhydrazines examined, it is not considered to be accidental. This means that the plot of log $k+H_0$ *vs.* $H_0+\log[H^+]$ (the Bunnett-Olsen ϕ plot[14]) gives a straight line with the ϕ value of unity; this is equivalent to the fact that the acidity dependence of rate constants comes from the change of total concentration of hydrogen ions, that is, the linear plot of log k *vs.* log $[H^+]$ with the slope value of unity (the Zucker-Hammett hypothesis[17]) is obtainable. In fact, the ϕ values nearly equal to unity were obtained over the acid concentration range in which the acylhydrazines were hydrolyzed through the A-2 mechanism. However, the ϕ values at lower acidity regions are slightly smaller than those at higher acidity regions; this was found for all the acylhydrazines which gave ϕ values which differed slightly from each other. This seems to imply that the hydration change which occurs with protonation and/or transition of substrate molecules also affects the rate constant-acidity dependence. Finally, we can say that the w^* parameter is greatly sensitive to small deviations from the Zucker-Hammett criteria and that the ϕ parameter will provide a more reliable criterion for the interpretation of the dependences of rate constants and also of reaction mechanisms on changes in acid concentration.

References

1) M. Mashima and F. Ikeda, *Bull. Chem. Soc. Jpn.*, **46**, 1366 (1973).
2) J. T. Edward, H. P. Hutchison, and S. C. R. Meacock, *J. Chem. Soc.*, 2520 (1955).
3) C. R. Lindergren and C. Niemann, *J. Am. Chem. Soc.*, **71**, 1504 (1949).
4) M. Mashima and F. Ikeda, *Chem. Lett.*, **1972**, 209.
5) C. H. Rochester, "Acidity Functions," Acad. Press, London (1970).
6) M. Liler, "Reaction Mechanisms in Sulphuric Acid," Acad. Press, London (1971).
7) N. A. Lange, "Handbook of Chemistry," 2nd ed Handbook Publications, Inc., Sandusky, Ohio (1937).
8) a) V. K. Krieble and K. A. Holst, *J. Am. Chem. Soc.*, **60**, 2976 (1938); b) B. S. Rabinovitch and C. A. Winkler, *Can. J. Res.*, **20**, 73 (1942).
9) See, for example, K. Yates, *Acc. Chem. Res.*, **4**, 136 (1971).
10) M. Willems and A. Bruylants, *Bull. Soc. Chim. Belg.*, **60**, 191 (1951).
11) P. Tickle, A. G. Briggs, and J. M. Wilson, *J. Chem. Soc., B*, **1970**, 65.
12) W. F. Giauque, E. W. Hornung, J. E. Kungler, and T. R. Rubin, *J. Am. Chem. Soc.*, **82**, 62 (1960).
13) E. B. Robertson and H. B. Dunford, *J. Am. Chem. Soc.*, **86**, 5080 (1964).
14) J. F. Bunnett and F. P. Olsen, *Chem. Commun.*, **1965**, 601; *Can. J. Chem.*, **44**, 1899, 1917 (1966).
15) Ref. 5, p. 125.
16) J. F. Bunnett, *J. Am. Chem. Soc.*, **83**, 4956, 4968, 4973, 4978 (1961).
17) L. Zucker and L. P. Hammett, *J. Am. Chem. Soc.*, **61**, 2791 (1939); F. A. Long and M. A. Paul, *Chem. Rev.*, **57**, 935 (1957).
18) For example, see G. Kohnstam, "Advances in Physical Organic Chemistry," ed by V. Gold, Acad. Press, London, (1967), Vol. 5, pp. 121—172.
19) L. L. Schaleger and F. A. Long, "Advances in Physical Organic Chemistry," ed by V. Gold, Acad. Press, London, (1963), Vol. 1, p. 24.
20) The values were calculated from the values of the Arrhenius parameter in Ref. 7 (b).
21) Ref. 6, pp. 195—196.
22) K. N. Bascombe and R. P. Bell, *Discuss. Faraday Soc.*, **24**, 158 (1957).
23) C. Perrin, *J. Am. Chem. Soc.*, **86**, 256 (1964).

An NMR Study on the Association Stabilities of Thiaheterohelicenes against 7,7,8,8-Tetracyanoquinodimethan. Effect of the Staggered Configuration of Helicene

Hisao TANAKA, Hiroko NAKAGAWA, Koh-ichi YAMADA, and Hiroshi KAWAZURA*
Faculty of Pharmaceutical Sciences, Josai University, Sakado, Saitama 350-02
(Received March 28, 1981)

In order to evaluate the influence of the staggered configuration of helicene on complex formation, a ^{1}H NMR technique was applied to the complexing equilibria of thiaheterohelicene homologs with 7,7,8,8-tetracyanoquinodimethan (TCNQ). Formation constants of the complexes showed irregular changes in the case of [5] and [7]-thiaheterohelicenes in which the staggerings occur. This irregularity could be interpreted on the basis of the observed abnormal decrease of the bonding entropy. The reduced bonding entropy was understood in terms of the incomplete quenching of internal freedom, which was expected from the peculiar orientation of the staggered thiaheterohelicene towards planar TCNQ in the charge-transfer complex.

To understand the molecular staggering due to the helical shape of helicenes, it will be useful to examine the thermodynamic stability of their charge-transfer (CT) complexes with an appropriate π-acceptor. In a series of studies[1-3] on thiaheterohelicenes with alternating thiophene and benzene rings, we have reported[1] that the thiaheterohelicene molecules act as π-donors to give the 1 : 1 CT complexes with a strong π-acceptor, 7,7,8,8-tetracyanoquinodimethan (TCNQ). Formation constants of the complexes, determined preliminarily by a Benesi-Hildebrand (B-H) treatment[4] on the CT-band intensities, were in the order of benzo[1,2-*b* : 4,3-*b'*]dithiophene (**3**)<[7]thiaheterohelicene (**5**)<[5]-thiaheterohelicene (**4**). This order was different from the ordinary trend in which formation constants in the complexes of cata-condensed aromatic donors increase with the number of aromatic rings. The reduced stability in the complex of [7]thiaheterohelicene has been considered to reflect its helical configuration, where two terminal thiophene rings are annularly overlapped.[5] However, it was difficult to inquire further into the thermal stabilities of the complexes, because of a lower degree of the accuracy of the formation constants which were determined by the B-H method on the weak CT absorptions.

A Hanna-Ashbaugh (H-A) treatment[6] on the ^{1}H NMR chemical shifts of interacting molecules was appropriate for the more exact determination of the formation constants and allowed us to estimate the enthalpy and entropy changes on complexation. This paper aims to clarify the steric effect caused by the staggering of helicene. The examination of thermodynamic parameters in the TCNQ complexes of thiaheterohelicene homologs: benzene (**1**), benzo[b]-thiophene (**2**), **3**, **4**, and **5** has led us to appreciate the importance of the entropy factor.

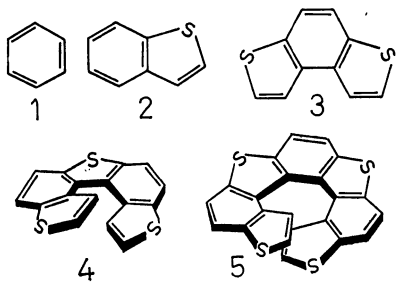

Experimental

Materials. Benzo[1,2-*b*: 4,3-*b'*]dithiophene(**3**), [5]-thiaheterohelicene(**4**), and [7]thiaheterohelicene(**5**) were synthesized[3,7] by photocyclization of the corresponding precursor olefins. Benzene-d_6 (**1**) and benzo[b]thiophene (**2**) were purchased from Merck Co. These compounds were purified as follows. **2** and **3** were column-chromatographed over alumina with hexane as an eluent, then sublimated under vacuum. **4** and **5** were also column-chromatographed over alumina with benzene, followed by recrystallization from benzene.

7,7,8,8-tetracyanoquinodimethan was purchased from Merck Co. and was purified by recrystallization three times from pure acetonitrile. 1,1,2,2-Tetrachloroethane-1,2-d_2 ($C_2D_2Cl_4$) used as an NMR solvent was of the spectroscopic grade (Merck; *Uvasol*).

Preparation and Measurement of NMR Samples. 1.77 mg of TCNQ crystals was dissolved in 3500 mm^3 of $C_2D_2Cl_4$ including a trace of tetramethylsilane (TMS). A 500 mm^3 portion of the solution was taken out with a micropipette (Gilson, Pipetman model P, $\pm$0.5% in error), and was put into each of the six 2000 mm^3-sample tubes containing various amounts (3—40 mg) of thiaheterohelicene which were weighed to a precision of 10^{-3} mg by a microbalance. After complete dissolution, a 400 mm^3 portion from each solution was transfered into a 5 mm-diameter NMR tube.

The ^{1}H NMR spectra of six samples thus prepared and of one sample containing only the TCNQ solution originally prepared were successively measured at a fixed temperature, then similarly measured at other temperatures. The measurements were done in the Fourier transform mode on a JEOL PFT-100 spectrometer operating at 100 MHz with an internal deuterium lock. 4096 or 8192 data points were taken over a 1 kHz spectral width at a tilt angle of 45°, repeated at 2.2 or 4.5 s intervals. The accumulation and data reduction of the NMR spectrum were performed on an EC-100 computer attached to the spectrometer. The error in reading the peak position of TCNQ protons was judged to be $\pm$0.3 Hz. The temperature of a given sample was regulated by a VT-3C variable temperature unit and was read from an Ohkura AM-1001 microvoltmeter connected to a copper–constantan thermocouple whose terminal was set in an NMR tube inside the probe. The temperature was constant within *ca.* 1 °C during each series of measurements.

Results

In the samples prepared, TCNQ was held at the low concentration of 2.5×10^{-3} mol/dm^3 to make sure that the amount of the thiaheterohelicene was in a large excess (10 to 100-fold excess to the amount of TCNQ),[8] which was requisite for an application of the H-A method. The ^{1}H NMR signal of TCNQ protons which was not hidden by the intense signals of thiaheterohelicene protons could be detected by 100—200 times of pattern accumulation. The observed signal moved noticeably to the up-field with an increase of the thiaheterohelicene concentration, as exemplified in the spectra of benzodithiophene (**3**)–TCNQ systems (Fig. 1). The net up-field shift $\Delta(=\delta_0-\delta)$, where δ and δ_0 are the chemical shifts of TCNQ protons in the complexing medium and in the uncomplexed state, respectively, was in close relation to the thiaheterohelicene concentration $[D]$, as shown by the fairly linear plots of Δ^{-1} *vs.* $[D]^{-1}$. This is seen in Figs. 2-A, B, and C for benzodithiophene (**3**)–TCNQ, [5]thiaheterohelicene (**4**)–TCNQ, and [7]thiaheterohelicene (**5**)–TCNQ systems, respectively. It is also seen from the figures that the intercepts of the plots at different temperatures show an excellent focussing.

Thus, the plots in Fig. 2 were analyzed by a least-squares method, using the H-A relation:[6]

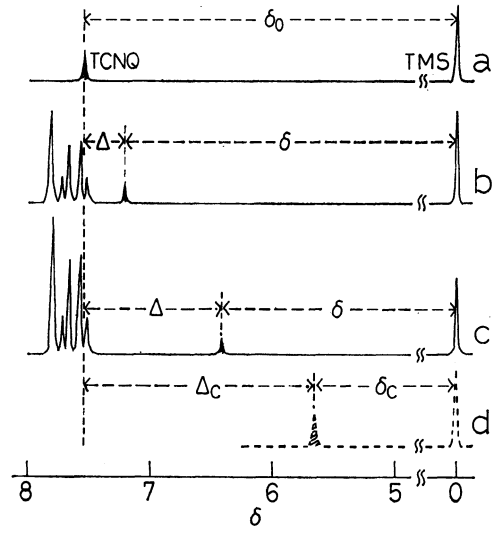

Fig. 1. ^{1}H NMR spectra of the complexing media of benzodithiophene(**3**)–TCNQ at 237 K and the definition of shifts, δ, δ_0, δ_c, Δ, and Δ_c. For $[A]=2.5\times10^{-3}$ mol/dm^3, a): $[D]=0$, b): $[D]=3.92\times10^{-2}$, c): $[D]=2.63\times10^{-1}$ mol/dm^3, d): extrapolated to $[D]=\infty$.

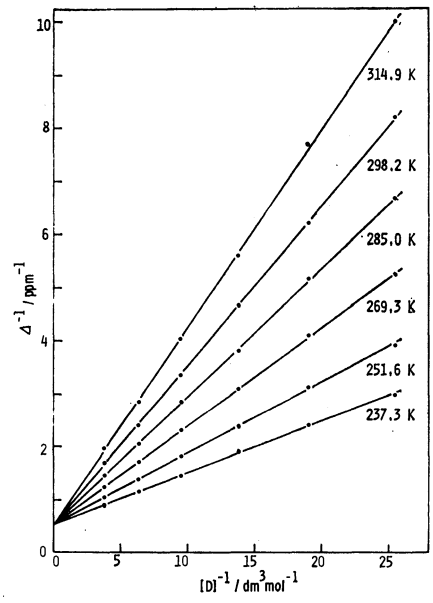

Fig. 2-A. Δ^{-1} *vs.* $[D]^{-1}$ plots for benzodithiophene(**3**)–TCNQ system; $[A]=2.5\times10^{-3}$ mol/dm^3 and $[D]=3.919\times10^{-2}$, 5.252×10^{-2}, 7.228×10^{-2}, 1.055×10^{-1}, 1.576×10^{-1}, and 2.627×10^{-1} mol/dm^3.

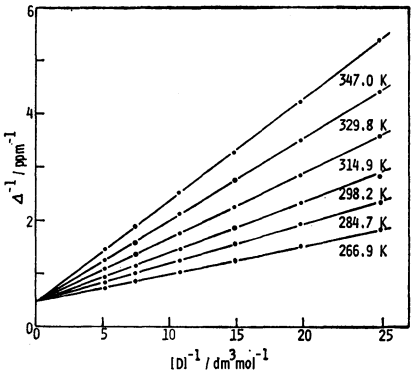

Fig. 2-B. Δ^{-1} *vs.* $[D]^{-1}$ plots for [5] thiaheterohelicene-(**4**)–TCNQ system; $[A]=2.5\times10^{-3}$ mol/dm^3 and $[D]=3.872\times10^{-2}$, 5.046×10^{-2}, 6.742×10^{-2}, 9.309×10^{-2}, 1.384×10^{-1}, and 1.945×10^{-1} mol/dm^3.

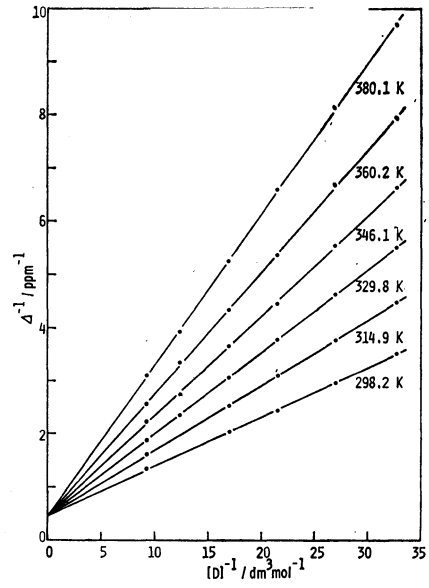

Fig. 2-C. Δ^{-1} *vs.* $[D]^{-1}$ plots for [7]thiaheterohelicene-(**5**)–TCNQ system; $[A]=2.5\times10^{-3}$ mol/dm^3 and $[D]=3.056\times10^{-2}$, 3.720×10^{-2}, 4.644×10^{-2}, 5.909×10^{-2}, 8.076×10^{-2}, and 1.085×10^{-1} mol/dm^3. The ^{1}H NMR signals of TCNQ for $[D]=8.076\times10^{-2}$ mol/dm^3 at 298.2 and 314.9 K were not observed because of overlapping with the donor signals.

Table 1. Shifts (Δ_c) and association constants (K) for the complexes at various temperatures(T)

Complex	T/K	Δ_c[a]/ppm	K[b]/dm^3 mol^{-1}	SD($\times 10^2$)
1–TCNQ	224.5	1.71	0.177	3.2
	244.9	1.78	0.157	7.4
	264.8	1.62	0.150	10.3
2–TCNQ	227.7	1.77	0.831	3.0
	239.3	1.84	0.725	3.8
	249.7	1.79	0.637	2.9
	264.2	1.75	0.548	4.1
3–TCNQ	237.3	1.84	5.63	3.2
	251.6	1.88	3.96	3.1
	269.3	1.86	2.90	2.4
	285.0	1.86	2.23	4.2
	298.2	1.93	1.73	3.1
	314.9	1.97	1.36	6.5
4–TCNQ	266.9	2.21	8.48	0.6
	284.7	2.16	6.37	1.7
	298.2	2.07	5.28	3.1
	314.9	1.98	4.34	1.9
	329.8	2.07	3.18	1.7
	347.0	2.13	2.48	1.2
5–TCNQ	298.2	2.21	4.85	2.3
	314.9	2.19	3.72	2.0
	329.8	2.34	2.75	2.0
	346.1	2.31	2.29	4.4
	360.2	2.17	2.01	4.5
	380.1	2.27	1.55	4.0

a) The averaged probable error; 3.8% of Δ_c. b) 4.5% of K.

$$\Delta^{-1} = (K\cdot\Delta_C)^{-1}\cdot[D]^{-1} + \Delta_C^{-1} \quad (1)$$
$$K = [AD]/[A]\cdot[D] \quad (A+D=AD).$$

Here K is the formation constant for the molecular complex and $\Delta_c(=\delta_0-\delta_c)$ the Δ in the pure complex (Fig. 1). Table 1 lists the K and Δ_c values, together with the standard deviations (SD) of the least-squares calculations, for the TCNQ complexes of **1**—**5** at various temperatures. Those values for benzene-d_6 (**1**)–TCNQ and benzothiophene (**2**)–TCNQ systems were determined only at lower temperatures owing to the smaller up-field shifts of TCNQ protons.

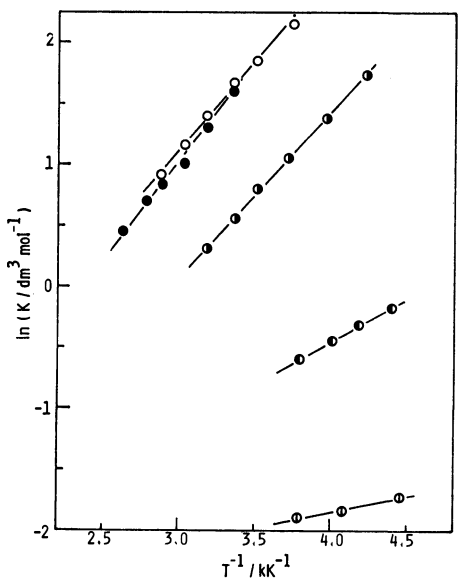

Fig. 3. Plots of ln K *vs.* T^{-1}. ◫): **1**–TCNQ, ◐): **2**–TCNQ, ◑): **3**–TCNQ, ○): **4**–TCNQ, ●): **5**–TCNQ.

Table 2. The enthalpy(ΔH) and entropy change(ΔS) in the complex formation

Complex	ΔH/kJ mol^{-1}	ΔS/J K^{-1} mol^{-1}
1–TCNQ	−2.0±0.8	−23.5±3.2
2–TCNQ	−5.7±0.5	−26.7±2.0
3–TCNQ	−11.2±0.2	−33.1±0.6
4–TCNQ	−11.7±0.5	−25.7±1.6
5–TCNQ	−13.0±0.4	−30.5±1.0

Figure 3 shows the plots of ln K to T^{-1}. The enthalpy (ΔH) and entropy changes (ΔS) collected in Table 2 were determined from the least-squares fitting of the plots to the van't Hoff equation:

$$\ln K = -(\Delta H/R)\cdot T^{-1} + \Delta S/R. \quad (2)$$

Discussion

Δ_c and K for the 1 : 1 Complex. The nice fit of the plots of Δ^{-1} *vs.* $[D]^{-1}$ to the H-A Eq. 1, which is judged from the small SD's in Table 1, allows us to assume[6,9] that only the 1 : 1 molecular complex is formed in the donor-acceptor equilibrium in the concentration range used for the present study. Table 1 also indicates that the intrinsic shifts Δ_c's for the 1 : 1 complex scatter independently of temperature and fall into a small range and that the averages are ordered as follows: 1.70 (**1**–TCNQ)< 1.79 (**2**–TCNQ) < 1.89 (**3**–TCNQ) < 2.12(**4**–TCNQ)<2.25 ppm(**5**–TCNQ). This ordering may be understood on the basis of the idea[10] that the shift Δ_c of TCNQ molecule facing the donor molecule is induced by the long range shielding due to the ring current which is accumulated with an increase of the number of rings of the donor. Thus, the parameter Δ_c exhibits a natural profile of the cata-condensed aromatic donors; however, it does not give a direct indication of the staggered configuration characteristic of helicenes.

On the other hand, an anomaly is observed for the association constants in the complex series: K's in $C_2D_2Cl_4$ at 25 °C are in the order of 0.13(**1**–TCNQ)< 0.41 (**2**–TCNQ) < 1.73 (**3**–TCNQ) < 4.85 (**5**–TCNQ) < 5.28 dm^3/mol(**4**–TCNQ), where the values for **1**–TCNQ[11] and **2**–TCNQ are obtained by extrapolating the van't Hoff plots in Fig. 3 to 298.2 K. We can note again a reduction of the K in **5**–TCNQ like that preliminarily found[1] from the B-H treatment of the CH_2Cl_2 solution. Interestingly, a similar result was also obtained[12] from a high performance liquid chromatography (HPLC) with a column of silica gel bonded with a strong π-acceptor, 2-(2,4,5,7-tetranitro-9-fluorenylideneaminooxy)propionic acid (TAPA). The elution order of the donors was **1**, **2**, **3**, **5**, and **4** giving the inversion of **4** to **5**, contrary to the absence of inversion in the case which used a column of silica gel only. Evidently, the CT interaction between donor molecule

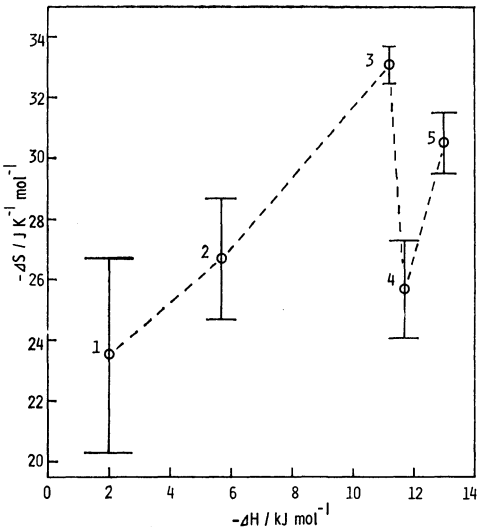

Fig. 4. Plots of $-\Delta S$ *vs.* $-\Delta H$. 1): **1**-TCNQ, 2): **2**-TCNQ, 3): **3**-TCNQ, 4): **4**-TCNQ, 5): **5**-TCNQ.

and fluorenylidene moiety of TAPA may produce this inversion. The inverse order is independent of solvent, detection method, or aromatic acceptor used, and so must be related to the inherently helical configuration of the donor.

ΔH and ΔS in the Complexation. Figure 4 shows the plots of $-\Delta H$ and $-\Delta S$ in the complex series. The enthalpy changes $-\Delta H$'s, *i.e.* bonding energies, tend to increase in the order of **1**, **2**, **3**, **4**, and **5**, although the increments among **3**, **4**, and **5** are smaller than those among **1**, **2**, and **3**. The above order may be interpreted in terms of the electron-donative abilities of the donors, which increase with ring accumulation. In fact, their ionization potentials[1] decrease in the same order as the above. As a result, the enthalpy changes suggest the effect of the staggering of **4** and **5**, but fail to explain the inversion in the K values.

The behavior of the entropy changes $-\Delta S$'s, *i.e.* degrees of bonding restriction, as seen in Fig. 4, is extraordinary: the $-\Delta S$ value reduces abruptly in the complex of **4** and still does not recover, in the complex of **5**, to the value in the complex of **3**. The inversion in the K values corresponds to the abnormal decrease of the $-\Delta S$.

It is known[13] that an increase of bonding energy causes an increase of bonding entropy in consequence of the stronger restriction between complexing species. This correlation may be valid in the case of absence of sterical hindrance, as demonstrated[13] in the iodine–alkylbenzene series. Indeed, the relation of the $-\Delta H$ and $-\Delta S$ among the complexes of planar molecules **1**, **2**, and **3** seems to follow the above general criterion. The abnormal decrease of the bonding entropy $-\Delta S$ in the complex of **4** should be a most direct proof for the existence of the sterical hindrance within the complex and certainly corresponds to the appearance of the staggered configuration in **4**, as revealed[2] by our X-ray structural analysis on the **4**-TCNQ complex. The change from **4** to **5** in Fig. 4 can be explained by the same criterion as in the case of **1**—**3**. This line of reasoning leads us to infer that a contribution of the staggering effect to the $-\Delta S$ approaches a limit against the ring accumulation, in so far as helicene and TCNQ molecules face each other.

Finally, we wish to comment on the decrease of bonding entropy, *i.e.* the gain of additional freedom, brought about by the staggering: the present complexes may be divided into two types with respect to the orientation manner of the donors towards planar TCNQ. In the complexes of planar **1**—**3**, the aromatic planes of donor and TCNQ molecules orient nearly parallel. But in the complexes of staggered **4** and **5**, both planes are much inclined[2] to each other. Hence the intensity distribution in the bonding interaction between aromatic planes is far from uniform. Thus, in the latter case, a possible displacement at the weakly interacting locus where both planes are widely separated may not change so steeply the total stabilization energy. This is a possible explanation for the existence of the additional freedom in the complexes of **4** and **5**, though the details must await an energy calculation of the complex system.

Here it should be noted that the staggering effect was visualized by looking not at the helicenes themselves, but at their molecular complexes. The influence of the staggering on the intramolecular properties; ionization potentials, transition energies,[14] and even spin densities of the radical anions[15] is not so easy to detect.

References

1) K. Yamada, T. Yamada, and H. Kawazura, *Chem. Lett.*, **1978**, 933.

2) M. Konno, Y. Saito, K. Yamada, and H. Kawazura, *Acta Crystallogr., Sect. B*, **36**, 1680 (1980).

3) K. Yamada, S. Ogashiwa, H. Tanaka, H. Nakagawa, and H. Kawazura, *Chem. Lett.*, **1981**, 433.

4) H. A. Benesi and J. H. Hildebrand, *J. Am. Chem. Soc.*, **71**, 2703 (1948).

5) M. Konno, Y. Saito, K. Yamada, and H. Kawazura, submitted for publication to *Acta Crystallogr.*

6) M. W. Hanna and A. L. Ashbaugh, *J. Phys. Chem.*, **68**, 811 (1964).

7) M. B. Groen, H. Schadenberg, and H. Wynberg, *J. Org. Chem.*, **36**, 2797 (1971).

8) Only in **1**-TCNQ and **2**-TCNQ systems, TCNQ was held at 5.0×10^{-3} mol/dm^3 and the donor was in 40 to 350-fold excess to the amount of TCNQ.

9) B. Dodson, R. Foster, A. A. S. Bright, M. I. Foreman, and J. Gorton, *J. Chem. Soc., B*, **1971**, 1283.

10) R. Foster, "Organic Charge-transfer Complexes," Academic Press, London and New York (1969), pp. 115—118. ^{1}H NMR signals of the donor also shifted to the up-field. This means that the partial charges induced by a CT interaction do not significantly contribute to the Δ_c.

11) The K for the benzene–TCNQ complex has been reported as 0.06 dm^3/mol in dioxane at 310 K (Ref. 6).

12) The HPLC experiments were performed according to the procedure of Mikes; see F. Mikes and G. Boshart, *J. Chromatogr.*, **149**, 455 (1978).

13) R. Keefer and L. J. Andrews, *J. Am. Chem. Soc.*, **77**, 2165 (1955).

14) S. Obenland and W. Schmidt, *J. Am. Chem. Soc.*, **97**, 6633 (1975).

15) H. Tanaka, S. Ogashiwa, and H. Kawazura, *Chem. Lett.*, **1981**, 585.

Redetermination of the Crystal Structure and the Electrical Resistivity of Rb-TCNQ-II

Hayao KOBAYASHI

Department of Chemistry, Faculty of Science, Toho University, Funabashi Chiba 274

(Received March 31, 1981)

The crystal structure of Rb-TCNQ-II was redetermined. The interplanar distance between the neighbouring TCNQ's is 3.25 Å, which is almost equal to those of highly conducting TCNQ salts. The electrical resistivity and the structure of the TCNQ columns suggest that the complete charge transfer in Rb-TCNQ-II makes this crystal low-conducting. The activation energy of the electrical conduction indicates that the dimerization gap appears below the monomer-dimer transition temperature. The temperature dependence of the electrical resistivities of Rb_2TCNQ_3 is also described.

Among the quasi-one-dimensional molecular crystals known at present, alkali metal salts of 7,7,8,8-tetracyanoquinodimethane (TCNQ) are of particular interest because of the simplicity of their crystal and electronic structures.[1] The crystal of Rb-TCNQ shows polymorphism. The crystal structure of Rb-TCNQ-II was reported eight years ago.[2] However, the recent studies of the crystal structures and the physical properties of alkali-TCNQ suggest that the reported interplanar distance of the TCNQ's of 3.43 Å in Rb-TCNQ-II is too long. Since the intensity data used in the previous work was not considered to be accurate enough,[3] the structure was redetermined on the basis of the newly collected intensity data.

Experimental

The crystals were prepared by a diffusion process of RbI and TCNQ in acetonitrile. All the crystals examined were twinned. The lattice constants were determined by means of a Rigaku automated four-circle diffractometer. The crystal data are:[4] $Rb^+(C_{12}H_4N_4)^-$, F.W.=289.6, triclinic, a=9.907(2), b=7.180(2), c=3.886(1) Å, α=88.55(2). β=86.86(2), γ=94.41(2)°, U=273.6(1) Å^3, d_c=1.757 g cm^{-3}, Z=1, space group $P\bar{1}$, $F(000)$=141, μ(Mo $K\alpha$)=45.5 cm^{-1}. The intensity data were collected with monochromated Mo $K\alpha$ radiation up to 2θ=60°. The crystal used had approximate dimensions of 0.3×0.23×0.07 mm^3. Of the 1718 accessible reflections, 1240 significant reflections were obtained ($|F_o| > 3\sigma(|F_o|)$).

Starting with the positional parameters previously obtained,[2] the structure was refined by the block-diagonal least-squares method. Since the twin ratio was not known, the scale factors of $|F(hkl)|$ were determined as: $S(l)\sum_{kh}|F_o(hkl)| = \sum_{kh}|F_c(hkl)|$, where $S(l)$ is the scale factor of the l-th layer (l=0, 1, 2, 3, 4, 5) and where $|F_o|$ and $|F_c|$ are the observed and calculated structure amplitudes respectively. The full-matrix least-squares refinement gave the following scale factors: $S(0)=0.846/\sqrt{2}$, $S(l)$=0.998—1.002 (l=1, 2, 3, 4, 5). The final R value was 0.059. The weighting scheme was: $w=1/[a+b|F_o|+c|F_c|^2]$ for $|F_o| \geqq 5.6$ (absolute scale), a=11.20, b=1.00, c=0.033; w=0.1 otherwise. The atomic coordinates are listed in Table 1.†

† List of the observed and calculated structure factors and tables of anisotropic thermal parameters for non-hydrogen atoms and atomic parameters for hydrogen atoms are kept at the Chemical Society of Japan as Document No. 8152.

TABLE 1. THE FINAL ATOMIC COORDINATES

The values for fractional coordinates are multipied by 10^4.

Atom	x	y	z	B_{eq}/Å^2 a)
Rb	0000	0000	0000	2.08
N(1)	9073(8)	6878(8)	5413(16)	3.43
N(2)	7633(7)	885(8)	5622(17)	3.80
C(1)	6137(6)	4621(7)	1871(14)	2.13
C(2)	5967(6)	6484(7)	838(15)	2.26
C(3)	5106(6)	3153(7)	977(15)	2.26
C(4)	7248(6)	4226(7)	3808(15)	2.34
C(5)	8265(6)	5693(8)	4675(15)	2.34
C(6)	7442(6)	2390(8)	4817(17)	2.48

a) Equivalent isotropic temperature factor as defined by H. C. Hamilton (*Acta Crystallogr.*, **12**, 609(1959)).

Results and Discussion

Figure 1 shows the crystal structure. The TCNQ's stack along the c axis to form monadic columns. There

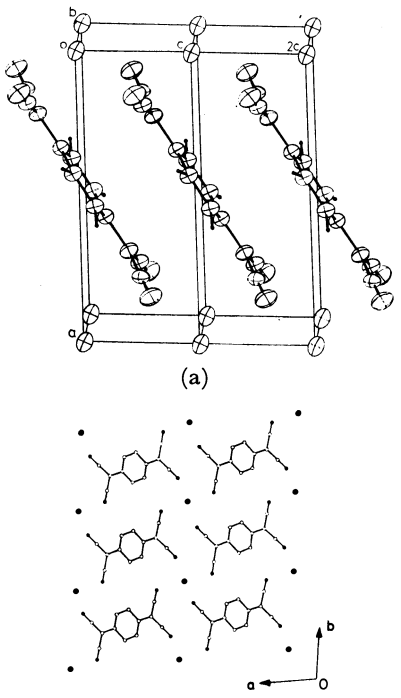

Fig. 1. (a) The crystal structure of Rb-TCNQ-II. (b) The molecular arrangement.

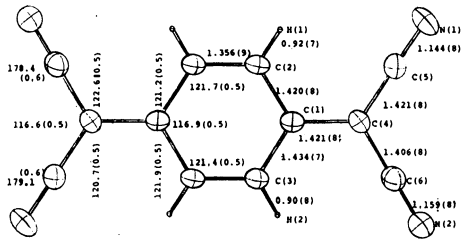

Fig. 2. The bond lengths and the bond angles of TCNQ with the standard deviations in parentheses.

are eight short contacts between Rb and the surrounding nitrogen atoms (≦3.27 Å). The shortest Rb···N distance is 3.052 Å. The bond lengths and the bond angles are shown in Fig. 2. The bond lengths agree well with those of the TCNQ anion[5] but significantly differ from those of neutral TCNQ:[6] the length of the C(1)-C(4) bond is 0.047 Å longer than the corresponding bond length of the neutral TCNQ molecule. The least-squares plane through TCNQ is: $-0.4973(X-0.5a)+0.1828(Y-0.5b)+0.8340Z=0.0$, where X, Y, and Z(Å) are the coordinates referred to the crystal axes a, b, and c respectively. The interplanar distance between adjacent TCNQ's of 3.248 Å is the shortest in alkali-TCNQ salts and almost equal to those of highly conducting salts: Na-TCNQ, 3.39 (80 °C);[7] K-TCNQ, 3.48 (120 °C);[8] NH_4-TCNQ, 3.31;[9] *N*-methylphenazinium-TCNQ (NMP-TCNQ), 3.25;[10] hexamethylenetetrathiafulvalene (2-(5,6-dihydro-4*H*-cyclopenta-1,3-dithiole-2-ylidene)-5,6-dihydro-4*H*-cyclopenta-1,3-dithiole)-TCNQ (HMTTF-TCNQ), 3.25;[11] quinolinium-TCNQ, 3.22;[12] acridinium-TCNQ, 3.26 Å.[13] As described in Ref. 2, the mode of overlap of TCNQ is of the "ring-external bond type" (see Fig. 3), which is found in every highly conductive TCNQ salts.[14]

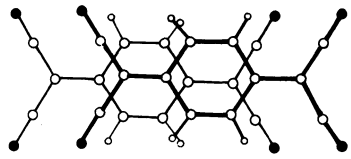

Fig. 3. The ring-external bond type overlapping in Rb-TCNQ-II.

Electrical Resistivities. The d.c. electrical resistivities of Rb-TCNQ-II were measured along the c-axis by the four-probe method (see Fig. 4). The room-temperature resistivity of 50 Ωcm is much smaller than those of the other alkali-TCNQ's,[14] which is consistent with the small intermolecular distance of Rb-TCNQ-II.

Although the structure of the TCNQ columns of Rb-TCNQ-II closely resembles those of NMP-TCNQ and HMTTF-TCNQ, the conductivities of NMP-TCNQ and HMTTF-TCNQ are four orderes of magnitude larger than that of Rb-TCNQ-II. This clearly shows the importance of the intramolecular Coulomb repulsion. Since the ρ of Rb-TCNQ-II is considered to be 1, Rb-TCNQ-II has a Coulomb gap at the Fermi wave number, k_F, where the ρ values of of NMP-TCNQ and HMTTF-TCNQ are 2/3[15] and

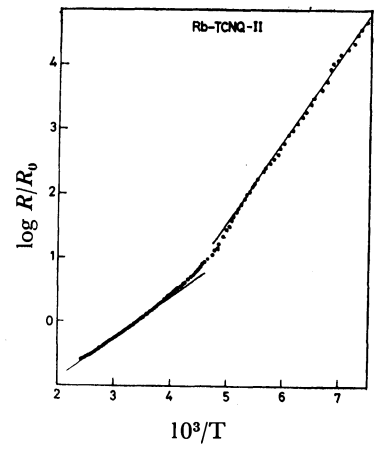

Fig. 4. The temperature dependence of the d.c. electrical resistivity of Rb-TCNQ-II.
The room-temperature resistivity R_0 is 50 Ω cm.

0.72[16] respectively. The importance of the Coulomb gap has been elucidated in a recent paper by Torrance *et al.*;[17] they thoroughly examined the physical properties of two isostructural HMTTF compounds, one metallic and the other insulating.

A change in the slope of the log R/R_0 *vs.* $1/T$ curve suggests a phase transition, which has been established by magnetic measurements (T_c=220 K).[18] X-Ray oscillation photographs taken around the needle axis showed the doubling of the lattice along the c axis below T_c. Therefore, the transition is a monomer-dimer (M-D) transition. It is well-known that the TCNQ columns in TTF-TCNQ and HMTTF-TCNQ exhibit $2k_F$ instability.[19,20] Although no long-range 3-D ordering is observed down to 20 K, a similar lattice modulation has been observed in NMP-TCNQ.[15] The $2k_F$-distortion in the crystals of organic metals arises from Peierls instability. On the other hand, the dimerization in alkali-TCNQ has been considered to be associated with the instability of the spin-Peierls type.[21] The transition temperatures (T_c) of some simple salts of TCNQ are plotted against the interplanar distances(d) in Fig. 5. Since the dimer structure of alkali-TCNQ

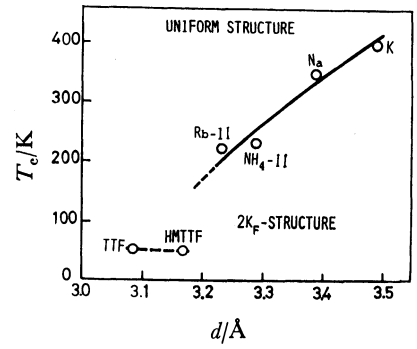

Fig. 5. The relationship between the interplanar distance of TCNQ's (d) and the phase transition temperature (T_c).
The thermal expansion of d was estimated by reference to the temperature dependence of the crystal structure of TTF-TCNQ (A. J. Schultz, C. D. Stuky, R. H. Blessing, and P. Coppens, *J. Am. Chem. Soc.*, **98**, 3197 (1976).

can be regarded as the $2k_F$-structure, the transitions presented in Fig. 5 are "uniform-$2k_F$ transitions." The M-D transition temperatures are almost linearly related to d. The nature of column instability appears to change around d=3.20 Å. Despite the close resemblance of the room-temperature structures of the TCNQ columns, the transition temperatures of Rb–TCNQ-II and HMTTF–TCNQ are quite different from each other.

The activation energies of the conductivities are 0.26 eV below T_c and 0.12 eV above T_c. The increase in the activation energy below T_c indicates the appearance of the dimerization gap. If the energy gap, E_g, is twice as large as the activation energy ($E_g=2E_a$), E_g is 0.24 eV. Since the Coulomb gap U ($\approx$1 eV[22]) is considered to be much larger than 0.24 eV, the conduction cannot be intrinsic.

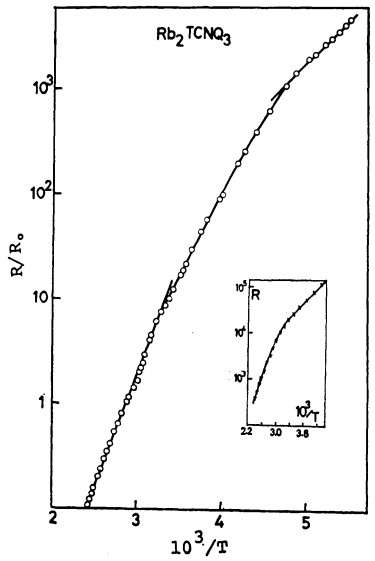

Fig. 6. The electrical resistivity of Rb_2TCNQ_3.
The diagram inserted is the resistivity by Lakhani and Hota (Ref. 23).

Recently, Lakhani and Hota have measured the electrical resistivity of Rb–TCNQ-II (see Fig. 6).[23] Their results are: (1) The room-temperature resistivity is 2×10^4 Ω cm. (2) Below room temperature, the conductivity is extrinsic and is due to the donor levels located 0.18 eV below the conduction band.[24] (3) Above 360 K, the intrinsic hole conduction becomes dominant where the activation energy is 0.44 eV. (4) The conductivity increases with the concentration of the impurity.

Since the room-temperature resistivity and the activation energies are quite different from those obtained by this work, and since their crystals have the form of a truncated pyramid while those used in this work were needle-shaped, the crystals used by Lakhani and Hota appear to be different from Rb–TCNQ-II. Figure 6 shows the resistivities of Rb_2TCNQ_3 measured along the most developed axis of the prismatic crystal ($//\boldsymbol{a}$), which is perpendicular to the TCNQ columns. The room-temperature resistivity is 10^5 Ω cm. E_a is 0.17 eV below 215 K and 0.43 eV above 310 K. Because

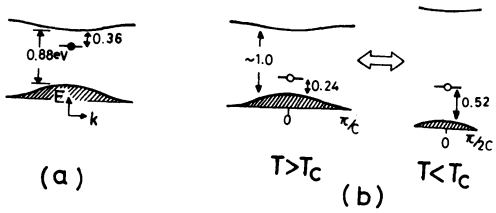

Fig. 7. Schematic representation of the energy-level diagram of Rb–TCNQ.
The intrinsic levels are presented as one-dimensional bands so as to indicate the doubling of the lattice constant at T_c. The band width and the dimerization gaps are assumed to be much smaller than 1 eV.
(a) The energy-level diagram of Rb_2TCNQ_3 based on the two carrier model by Lakhani and Hota (Ref. 23).
(b) The energy-level diagram of Rb–TCNQ-II.

these values agree well with those of Lakhani and Hota, their crystals are considered to be Rb_2TCNQ_3.

Based on the electrical resistivities and thermoelectric powers, Lakhani and Hota have proposed the two-carrier conduction model of Rb–TCNQ which is presented diagramatically in Fig. 7: donor levels are located 0.36 eV below the conduction band, and the band gap is 0.88 eV. Unlike as in the cases of Cs_2TCNQ_3[27] and Rb_2TCNQ_3, the thermoelectric powers of simple salts of alkali–TCNQ are positive ($T<$450 K), which indicates the hole conduction.[28] The activation energy of 0.12 eV ($T>T_c$) suggests that the impurity acceptor levels are located 0.24 eV above the filled band. Below T_c, the dimerization gap appears, which leads a slightly modified model of the energy diagram (see Fig. 7b). The magnitudes of the Coulomb gap and the band-width have been considered to be of the orders of 1 eV and 0.1 eV respectively. However, their precise evaluation will be required for the better understanding of the electrical properties of alkali–TCNQ.

References

1) "The Physics and Chemistry of Low Dimensional Solids," in "NATO Advanced Study Institute Series," ed by L. Alcacer, D. Reider Publishing Company, Dordrecht, Boston, and London (1980).

2) I. Shirotani and H. Kobayashi, *Bull. Chem. Soc. Jpn.*, **46**, 2595 (1973).

3) In a previous work, the reflections were collected by means of Weissenberg photographs and the intensities were estimated visually by comparison with a standard film strip. The crystal used was twinned. The twin ratio of 1 was tentatively assumed in order to compare $I(hkl)$ and $I(\bar{h}\bar{k}l)$.

4) There are errors in the lattice constants reported in Ref. 2: c and α should be corrected to: $c=3.903\pm0.02$ Å, and $\alpha=92.07\pm0.10$ °. The relationships between the old lattice vectors ($\mathbf{a}'$, $\mathbf{b}'$, $\mathbf{c}'$) and the new ones ($\mathbf{a}$, $\mathbf{b}$, $\mathbf{c}$) are: $\mathbf{a}=\mathbf{a}'$, $\mathbf{b}=\mathbf{b}'$, and $\mathbf{c}=-\mathbf{c}'$.

5) A. Hoekstra, T. Spoelder, and A. Vos, *Acta Crystallogr.*, **28**, 14 (1972); H. Kobayashi, T. Danno, and Y. Saito, *Acta Crystallogr., Sect. B*, **29**, 2693 (1973).

6) R. E. Long, R. A. Sparks, and K. N. Trueblood, *Acta Crystallogr.*, **18**, 932 (1965).

7) M. Konno and Y. Saito, *Acta Crystallogr., Sect. B*, **31**, 2007 (1975).

8) M. Konno, T. Ishii, and Y. Saito, *Acta Crystallogr., Sect. B*, **33**, 763 (1977).
9) H. Kobayashi, *Acta Crystallogr., Sect. B*, **34**, 2818 (1978).
10) C. J. Fritchie, *Acta Crystallogr.*, **20**, 892 (1966).
11) R. L. Greene, J. J. Mayerle, R. R. Schumaker, G. Castro, P. M. Chaikin, S. Etemad, and S. J. La Placa, *Solid State Commun.*, **20**, 943 (1976).
12) H. Kobayashi, F. Marumo, and Y. Saito, *Acta Crystallogr., Sect. B*, **37**, 373 (1971).
13) H. Kobayashi, *Bull. Chem. Soc. Jpn.*, **47**, 1346 (1974).
14) J. J. Andre and A. Bieber, *Ann. Phys., t. I.* **1976**, 145.
15) J. Pouget, S. Megtert, R. Comès, and A. J. Epstein, *Phys. Rev. B*, **21**, 486 (1980).
16) J. P. Pouget, S. Megtert, and R. Comès, "Quasi One-Dimensional Conductors I—Lecture Notes in Physics," ed by S. Barisic, A. Bjelis, J. R. Cooper, and B. Leontic, Springer-Verlag, Berlin, Heidelberg, and New York (1979).
17) J. B. Torrance, J. J. Mayerle, K. Bechgaard, B. D. Silverman, and Y. Tomkiewicz, *Phy. Rev. B*, **22**, 4960 (1980)
18) J. G. Vegter and J. Kommandeur, *Mol. Cryst. Liq. Cryst.*, **30**, 11 (1975).
19) V. J. Emery, "Chemistry and Physics of One-Dimensional Metals," ed by H. Keller, Plenum Press, New York and London (1977); S. Huizinga, J. Kommandeur, G. A. Sawatzky, B. T. Thole, K. Kopinga, W. J. M. de Jounge, and J. Roos, *Phys. Rev. B*, **19**, 4723 (1979).
20) R. Comès, "Chemistry and Physics of One-Dimensional Metals," ed by H. Keller, Plenum Press, New York and London (1977); R. Comes and G. Shirane, "Highly Conducting One-Dimensional Solids," ed by J. T. Devreese, R. P. Evrard, and V. E. van Doren, New York and London (1979).
21) J. B. Torrance, "Synthesis and Properties of Low-Dimensional Materials," in Annals of The New York Academy of Science," ed by J. S. Miller and A. J. Epstein, The New York Academy of Science, New York (1978), Vol. 313; Y. Lepine, A. Caille, and V. Larochelle, *Phys. Rev. B*, **18**, 3585 (1978).
22) J. F. Torrance, "Chemistry and Physics of One-Dimensional Materials," ed by H. Keller, Plenum Press, New York and London (1977).
23) A. A. Lakhani and N. K. Hota, *Solid State Commun.*, **33**, 233 (1980).
24) Since $E_a = W/2$ (W: ionization potential of donor), the donor levels are located 0.36 eV below the conduction band. The value of 0.18 eV in Ref. 23 must be revised.
25) B. van Bodegom, J. L. deBoer, and A. Vos, *Acta Crystallogr., Sect. B*, **33**, 602 (1977).
26) J. van der Wal and B. van Bodegom, *Acta Crystallogr., Sect. B*, **35**, 2003 (1979).
27) I. F. Shchegolev, *Phys. Status Solidi A*, **12**, 9 (1972).
28) N. Sakai, I. Shirotani, and S. Minomura, *Bull. Chem. Soc. Jpn.*, **45**, 3314 (1972).

A Study of the Electronic States of Iridium(III) Complexes Containing 1,10-Phenanthroline Ligands. The Contribution of a dd Excited State to the Lowest Triplet State

Yukako OHASHI*

The Institute of Physical and Chemical Research, Hirosawa, Wako 351

(Received April 17, 1981)

To investigate the solvent dependence of the dd contribution to the lowest excited state of *cis*-$[IrCl_2L_2]Cl$ (L=1,10-phenanthroline (phen) and 5,6-dimethyl-1,10-phenanthroline (5,6-Mephen)), the triplet-triplet absorption spectra (15000—25000 cm^{-1}) were measured in *N,N*-dimethylformamide (DMF)–water mixed solvents. From a smaller solvent-dependence of the absorption intensity for $[IrCl_2(5,6\text{-Mephen})_2]Cl$ than for $[IrCl_2(phen)_2]Cl$, the lowest triplet state of the former is considered to have a $\pi\pi^*$ character in 95% v/v DMF–water and 45% v/v DMF–water. However, in pure water a considerable decrease in the triplet-triplet absorbance was observed. Because the molar extinction coefficient of the triplet-triplet absorption of the dd-dd type is 10^{-2} times smaller than that of the $\pi\pi^*$-$\pi\pi^*$ type, the observed decrease in the absorbance is elucidated by the increase in the contribution of the dd state to the lowest triplet state. Using ethanol–methanol (4 : 1, v/v) as a solvent, it was confirmed that the triplet-triplet absorption spectrum shows no change when the solutions are degassed and the temperature is lowered (77 K).

Recently, several studies have been reported on the electronic character of the emitting state of *cis*-$[IrCl_2(phen)_2]Cl$, which is sensitive to the solvents, the temperature, and the methyl substitution of a ligand molecule.[1–5] This characteristic has been interpreted in terms of a change in the character of the lowest triplet state. In this complex, the lowest triplet state of the $d\pi^*$ (metal-to-ligand charge transfer) character and the lowest triplet state of the $\pi\pi^*$ (locally excitation of a ligand) character lie very close to each other. From the studies of the solvent effects on the energies and the lifetimes of the emission in alcoholic solvents at 77 K, Crosby *et al.* concluded that the emittive state is a state of a mixed character of $d\pi^*$ and $\pi\pi^*$, and that the contribution to the lowest triplet state of the two characters is affected by the environment.[1–3] On the other hand, Ballardini *et al.* studied the quantum yield of the photosubstitution reaction of a chloride ion for $[IrCl_2(phen)_2]Cl$ and $[IrCl_2(5,6\text{-Mephen})_2]Cl$ by using mixed solvents of DMF and water at room temperature.[6] They reported that the photochemical quantum yields depend on the solvents and the temperature in a very similar way for both complexes. Generally, the ligand substitution takes place through a dd excited state. Therefore, the observed change in the quantum yield reveals the close-lying dd excited state near the lowest triplet state. Recently, Watts *et al.* measured the weak emission of $[IrCl_2(phen)_2]Cl$ and $[IrCl_2(5,6\text{-Mephen})_2]Cl$ at room temperature and reported the emission from a dd excited state, besides the emission from the $d\pi^*$-$\pi\pi^*$ mixed state previously reported.[5]

We previously measured the triplet-triplet absorption spectra of $[IrCl_2(phen)_2]Cl$ and the related complexes in DMF–water mixed solvents.[7] For these complexes, the relevant solvent effect on the triplet-triplet absorption spectrum was observed, and the changes were interpreted in terms of the decrease in the $d\pi^*$ component in the lowest triplet state with the increase in the solvent polarity. The excited-state absorption spectrum sharply reflects the character of the lowest excited state. Therefore, in the present work we investigated the dd contribution to the lowest triplet state of $[IrCl_2(phen)_2]Cl$ and $[IrCl_2(5,6\text{-Mephen})_2]Cl$ using excited-state spectroscopy.

Experimental

Materials. *cis*-Dichlorobis(1,10-phenanthroline)iridium(III) chloride trihydrate, $[IrCl_2(phen)_2]Cl\cdot 3H_2O$, and *cis*-dichlorobis(5,6-dimethyl-1,10-phenanthroline)iridium(III) chloride trihydrate, $[IrCl_2(5,6\text{-Mephen})_2]Cl\cdot 3H_2O$, were prepared by following the procedure of Broomhead and Grumley.[8] After the yellow band has been eluted with 0.1 M HCl† from a cellulose cation-exchange column, the emission spectra of the eluted fractions were measured in ethanol–methanol (4 : 1, v/v) at 77 K. The fraction is considered to be pure when the emission decay is exponential and when the lifetimes monitored at 480 nm and 500 nm have the same value, because the by-product has its strong emission at a longer wavelength than that of pure $[IrCl_2(phen)_2]Cl$. Moreover, the emission in 95% v/v DMF–water was measured at 77 K and at room temperature and confirmed to give the same spectrum as a sample B, reported by Ballardini *et al.*[9] The *N,N*-dimethylformamide was of a spectroscopic grade, while the water was distilled four times.

Apparatus. The triplet-triplet absorption spectra were measured at room temperature and at 77 K using a nitrogen laser (Molectron UV24) as an exciting-light source and a pulsed xenon flash as a monitoring-light source.

Results and Discussion

Environmental Effect on the Triplet-Triplet Absorption Spectra. Figures 1 and 2 show the triplet-triplet absorption spectra of $[IrCl_2(phen)_2]Cl$ and $[IrCl_2(5,6\text{-Mephen})_2]Cl$ at room temperature in the solvents of 95% v/v DMF–water (**1**), 45% v/v DMF–water (**2**), and water (**3**). The concentrations of the six complex solutions were adjusted to take the same optical density for the ground-state absorption at the wavelength of the exciting-light source (337 nm). The concentrations of the complex solutions used are $\approx 10^{-3}$ M. Since

* Present address: Bunkyo University, Minamiogishima, Koshigaya 343.

† 1M=1 mol dm^{-3}.

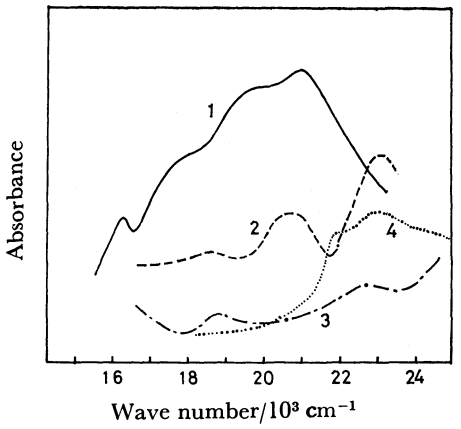

Fig. 1. Triplet-triplet absorption spectra at room temperature of $[IrCl_2(phen)_2]Cl$ in 95% v/v DMF–water (curve 1), in 45% v/v DMF–water (curve 2), in water (curve 3), and of phenathroline molecule in ethanol–methanol (4 : 1, v/v) (curve 4).

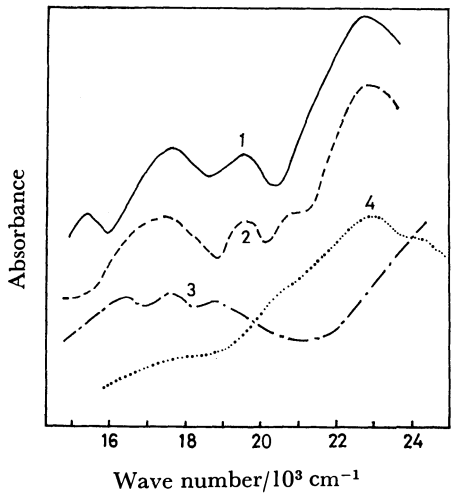

Fig. 2. Triplet-triplet absorption spectra at room temperature of $[IrCl_2(5,6\text{-Mephen})_2]Cl$ in 95% v/v DMF–water (curve 1), in 45% v/v DMF–water (curve 2), in water (curve 3), and of 5,6-dimethyl-1,10-phenanthroline molecule in ethanol–methanol(4 : 1, v/v) (curve4).

the two complexes show no fluorescence and contain a heavy atom (Ir^{3+}), the quantum yields of the intersystem crossing may safely be assumed to be very close to unity. Therefore, the concentrations of the singlet excited molecules populated by the laser radiation are assumed to be equal to that of the lowest triplet state. The absorbances of the six spectra (Curves 1—3 in Figs. 1 and 2) were measured under the same laser condition, so the changes in the absorbances correspond to the changes in the molar extinction coefficient of the triplet state. The absorbances of the free ligands in ethanol–methanol (4 : 1, v/v) are also shown in Figs. 1 and 2. The integrated absorbance of 5,6-Mephen is obtained to be larger by 1.5 times than that of phen.

At room temperature, the decay of the triplet-triplet absorption both of $[IrCl_2(phen)_2]Cl$ and $[IrCl_2(5,6\text{-Mephen})_2]Cl$ is exponential in 95% v/v DMF–water and in ethanol–methanol (4 : 1, v/v). In 45% v/v DMF–water, it deviates slightly from exponential behavior, but no time-dependence of the triplet-triplet absorption spectrum was observed. In water, the decay is very rapid (τ=25 ns for the non-degassed solutions of both complexes), so that the deviation from the exponential decay is not clear. Since the dearation is not carried out for the DMF–water mixed solvents, the observed lifetimes at room temperature are shorter by 0.6—0.7 times than those of the degassed solutions obtained from the emission measurements.[6] The lifetime of a degassed ethanol–methanol (4 : 1, v/v) of $[IrCl_2(phen)_2]Cl$ is determined from the absorption decay to be 59 ns. After a long radiation of 337 nm light, a dark violet material was produced, even at 77 K, in all the solvents examined. However, the emission and the triplet-triplet absorption spectra of the photoproducts were not found.

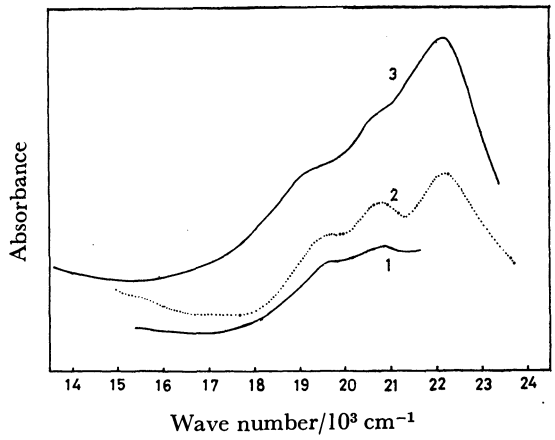

Fig. 3. Triplet-triplet absorption spectra of $[IrCl_2(phen)_2]Cl$ in ethanol–methanol(4 : 1, v/v) at room temperature (curve 1) and at 77 K (curve 2) in a degassed condition. Curve 3 is in a non-degassed ethanol–methanol(4 : 1, v/v) at room temperature. The sample concentrations of curves 1 and 2 are same but the correction of the volume contraction ($\times$0.80) was made for curve 2. The curve 3 is observed in a different concentration.

In order to examine the temperature effect on the triplet-triplet absorption spectrum, the measurements were carried out by using a degassed ethanol–methanol (4 : 1, v/v) solution of $[IrCl_2(phen)_2]Cl$ at 77 K and at room temperature (Fig. 3). The change in the absorption intensity and the spectrum is concluded to be insignificant between 77 K and room temperature after the correction for the volume contraction of the solvent. Over the range of 19500—21500 cm^{-1}, the emission is strong at 77 K, so that the correction was made for the emission contamination; the emission intensity is 1/4 of the decrease in the monitoring light by the absorption at the emission peak. From the comparison of the spectra of the non-degassed solution with that of the degassed solution (Fig. 3), no effect of the dearation on the spectra is observed at room temperature, but the triplet lifetime becomes longer upon dearation: 59 ns and 35 ns for the degassed and

the non-degassed solutions respectively. Therefore, the absorption spectra observed without dearation at room temperature can be assigned to the triplet-triplet transitions.

The Character of the Lowest Triplet State. With respect to $[IrCl_2(phen)_2]Cl$ and $[IrCl_2(5,6\text{-Mephen})_2]Cl$, recently two models were proposed for the electronic structure of the low-lying states. Model A assumes the close-lying dd state and the $d\pi^*$ (or $\pi\pi^*$) state to be thermally equilibrated at room temperature, while at a low temperature a barrier is assumed to exist between the two potential minima by virtue of a rigid matrix perturbation; the dd state lies 500 cm^{-1} below the lowest $d\pi^*$ state for $[IrCl_2(phen)_2]Cl$ and 100 cm^{-1} above the lowest $\pi\pi^*$ state for $[IrCl_2(5,6\text{-Mephen})_2]Cl$ in DMF.[5] The dd contribution to the emission is also determined by the use of the excitation and emission polarization spectra.[10] On the other hand, Model B gives a common interpretation for both $[IrCl_2(phen)_2]Cl$ and $[IrCl_2(5,6\text{-MePhen})_2]Cl$. It is proposed that a dd state lies close above the emitting state and that the energy separation between the two states decreases with the increase in the solvent polarity.[6,9]

In order to discuss the relation between the above two models and the present environmental effects of the triplet-triplet absorption spectra shown in Figs. 1—3, knowledge of the values of the molar-extinction coefficients of the triplet-triplet transitions (ε_{T-T}) is necessary. With respect to the $\pi\pi^*$-$\pi\pi^*$ transitions in the region of our experiments, the values of ε_{T-T} are evaluated to be in the order of 10^5 l/(mol cm) from the oscillator strengths calculated for free-lignad molecules: 0.2 for 1,10-phenanthroline and 0.4 for 2,2′-bipyridine.[7] The observed ε_{T-T} values for the ligands have not been reported, but the values for molecules with similar electronic structures have been reported:[11] for phenanthrene, ε_{T-T}=21000 l/(mol cm) at 20730 cm^{-1} and 41500 l/(mol cm) at 20410 cm^{-1}, and for biphenyl, ε_{T-T}=35400 l/(mol cm) at 27700 cm^{-1}. From these values, ε_{T-T} of the $\pi\pi^*$-$\pi\pi^*$ transitions are estimated to be of the order of 10^4—10^5 l/(mol cm), assuming the perturbation by the complex formation to be not very large. On the other hand, because the dd-dd transitions are generally weak due to a symmetry-forbidden property, ε_{T-T} is estimated to be of the order of 10—10^2 l/(mol cm), like the ε_G of the ground-to-dd transition, which is 10^2 l/(mol cm) for $[RhCl_2(phen)_2]Cl$[12] and 50 l/(mol cm) for $[IrCl_2(en)_2]Cl$ (en=ethylenediamine).[12] The intensity for the $d\pi^*$-$d\pi^*$ transitions becomes large only when the d orbital for the initial and the final states is common. Since the $d\pi^*$-$d\pi^*$ transition energy can be estimated roughly from the difference in the π^* orbital energies (e_j; j=8—14), the transition energies and the oscillator strengths shown in Table 1 are obtained from the SCF calculation of a free 1,10-phenanthroline. The $d\pi^*$ transition from a d orbital to the antibonding π^* orbital j is described as (d-j). The lowest $d\pi^*$ state, (d-8), degenerates almost to the (d-9) state. Therefore, we assigned the lowest $d\pi^*$ state to $1/\sqrt{2}\{(d\text{-}8)+(d\text{-}9)\}$. Then, the oscillator strengths of the $d\pi^*$-$d\pi^*$ transitions are calculated by means of the following equations:

$$f_j = 1.085 \times 10^{11}\,\sigma_j\,Q_j^2 \quad (\sigma_j \text{ in } cm^{-1} \text{ and } Q_j \text{ in cm})$$

$$Q_j = \int 1/\sqrt{2}\{(d\text{-}8)+(d\text{-}9)\}\,r(d\text{-}j)\,dv$$

$$\sigma_j = e_j - 1/2(e_8 + e_9).$$

From the calculated results, the transitions to be observed in the present measurement are the transitions to (d-11) or (d-12). Therefore, their oscillator strengths are of the same order as those of the $\pi\pi^*$-$\pi\pi^*$ transitions. Judging from the above-mentioned estimation, the ε_{T-T} of the dd-dd transition seems to be smaller by 10^2—10^4 than those of the $d\pi^*$-$d\pi^*$ and the $\pi\pi^*$-$\pi\pi^*$ transitions, so that the increase in the dd component in the lowest tripiet state causes a distinct intensity decrease in the triplet-triplet absorbances.

By the use of Model A, for $[IrCl_2(phen)_2]Cl$ the population ratio of $d\pi^*$ to dd states is estimated as 1/9 at 300 K, based on the reported dd-$d\pi^*$ separation (500 cm^{-1}). However, at 77 K a selective internal conversion is assumed to occur to the lowest $d\pi^*$ state after the excitation to the higher $\pi\pi^*$ state, so that a large increase in the population ratio results.[5] According to this scheme, the triplet-triplet absorbance should show a distinct increase with the temperature decrease. However, as may be seen in Fig. 3, the triplet-triplet absorption spectra at 77 K and at room temperature show no significant change in either the intensity or the peak position in ethanol–methanol (4 : 1, v/v). As far as the triplet-triplet absorption is concerned, the effect of the dd population was not observed at room temperature in this solvent, so that the lowest triplet state can be assigned to a $d\pi^*$ state, as was previously assigned.[2] Since the **1** solvent has a dielectric constant (39) similar to that (26) of the above solvent, and since we observed that the absorption spectra and intensities of the triplet-triplet transitions of the two solvents resembles each other, it is reasonable to make the same assignment for the complex in the **1** solvent.

Mechanism of Solvent Effect for $[IrCl_2(5,6\text{-Mephen})_2]Cl$. In a previous work, the present author suggested that the $\pi\pi^*$ character in the lowest triplet state increases considerably in water for $[IrCl_2(phen)_2]Cl$.[7] As may be seen in Fig. 1, this assignment is confirmed by the resemblance of the triplet-triplet absorption spectra of the complex in water and those of a free 1,10-phenanthroline.

The 5,6-dimethyl substitution of a 1,10-phenanthroline lowers the energy of the lowest $\pi\pi^*$ transition by 1500 cm^{-1} in ethanol–methanol (4 : 1, v/v) at 77 K.

Table 1. Transition energy and oscillator strength of the $d\pi^*$-$d\pi^*$ transition of $[IrCl_2(phen)_2]Cl$

Excited state	Transition energy σ_j/cm^{-1}	Oscillator strength
(d-8)	0	
(d-9)	81	
(d-10)	10500	0.05
(d-11)	13600	0.1
(d-12)	20200	0.1
(d-13)	30200	0.02
(d-14)	40300	0.007

Moreover, the emission energy does not show a solvent dependence, so that the lowest triplet state of $[IrCl_2(5,6\text{-Mephen})_2]Cl$ was assigned to a $\pi\pi^*$ state in alcoholic solvents at 77 K, independent of the solvent polarity.[2] Figure 2 shows that the intensity change of the triplet-triplet transition is small with respect to the spectra for **1** and **2** solvents, in contrast to the spectra of $[IrCl_2(phen)_2]Cl$. Consistent with the expectation from the assignment, the spectra for the two solvents resemble that of a free ligand (Fig. 2). The small intensity difference between the two solvents may be attributed to the change in the $d\pi^*$ component in the lowest triplet state. For this complex also, it has been reported that the lifetime changes from 66.3 μs to 236.1 μs at 77 K, but the emission energy does not change with the increase in the solvent dielectric constant (25—61).[2] Since the extent of the change in the lifetimes is comparable with that of $[IrCl_2(phen)_2]Cl$ (6.95—20.1 μs under the same conditions), the contribution of the $d\pi^*$ state to the emitting state can not be overlooked. Therefore, it is proposed that the lowest triplet state can be assigned to a $\pi\pi^*$ state with a small $d\pi^*$ component.

Considering the solvent dependence of the triplet-triplet absorption spectra,[7] the ground-state absorption spectra,[6] and the low-temperature emission energies[2] of $[IrCl_2(phen)_2]Cl$ and $[IrCl_2(5,6\text{-Mephen})_2]Cl$, the energy of the $d\pi^*$ transition is confirmed to shift to the higher energy side with the increase in the solvent polarity. Therefore, the character of the lowest triplet state should be mainly of the $\pi\pi^*$ character in water, so far as the contribution of the $d\pi^*$ and $\pi\pi^*$ states is concerned. However, as may be seen in Fig. 2, the absorbance in water shows a considerable decrease. This contradiction can be interpreted by means of Model B, which assumes the dd state to lie close above the emitting state and the energy separation to change with the solvent polarity. In the **1** and **2** solvents, the dd-$\pi\pi^*$ energy separation is large, but in water it becomes so small that the thermal distribution to the dd state causes a decrease in the triplet-triplet absorbance. With respect to $[IrCl_2(phen)_2]Cl$, it may be considered that the intensity decrease in water is attributed partially to the increase in the dd component in the lowest triplet state, besides to the increase in the $\pi\pi^*$ component. Since the emission energy of $[IrCl_2(5,6\text{-Mephen})_2]Cl$ is almost independent of the solvent polarity,[2] it may be suggested that the solvent shift of the dd state plays an important role and may be almost comparable to the small energy separation. This conclusion is reasonable because the dd transitions are generally sensitive to the environment, and the energy separation is suggested to be smaller for $[IrCl_2(5,6\text{-Mephen})_2]Cl$ than for $[IrCl_2(phen)_2]Cl$, judging from the work on photosubstitution.[6] For $[IrCl_2(5,6\text{-Mephen})_2]Cl$, Model A does not involve a knowledge of the solvent dependence of the dd-$\pi\pi^*$ energy separation, so the relation to the observed solvent dependence can not be discussed. From the above-mentioned discussion, it may be concluded that, in the polar solvents, the contribution of the dd state to the lowest triplet state can not be disregarded. The relevant evidence showing that the dd state is the lowest at room temperature for $[IrCl_2(phen)_2]Cl$ was not obtained using the technique of the triplet-triplet absorption measurements. However, the fact that the emissions in several solvents deviate from the exponential behavior shows some complicated interaction with the environment.

The formation of a photoproduct is inevitable in the photophysical experiment of the metal complexes. When the lowest excited state is of the $d\pi^*$ or $\pi\pi^*$ character in the complex molecule and of the dd character in the photoproduct, the triplet-triplet absorption measurement is a very adequate method to study the excited states of the complex, for it is not disturbed by the photoproduct.

The author is grateful to Professor Saburo Nagakura of The Institute for Solid State Physics and the Institute of Physical and Chemical Research for his support and valuable suggestions.

References

1) J. N. Demas and G. A. Crosby, *J. Am. Chem. Soc.*, **93**, 2841 (1971).
2) R. J. Watts, G. A. Crosby, and J. L. Sansregret, *Inorg. Chem.*, **11**, 1474 (1972).
3) R. J. Watts and G. A. Crosby, *Chem. Phys. Lett.*, **13**, 619 (1972).
4) R. J. Watts, T. P. White, and B. G. Griffith, *J. Am. Chem. Soc.*, **97**, 6914 (1975).
5) R. J. Watts and D. Missimer, *J. Am. Chem. Soc.*, **100**, 5350 (1978).
6) R. Ballardini, G. Varani, L. Moggi, V. Balzani, K. R. Olson, F. Scandola, and M. Z. Hoffman, *J. Am. Chem. Soc.*, **97**, 728 (1975).
7) Y. Ohashi and T. Kobayashi, *Bull. Chem. Soc. Jpn.*, **52**, 2214 (1979).
8) J. A. Broomhead and W. Grumley, *Inorg. Chem.*, **10**, 2002 (1971).
9) R. Ballardini, G. Varani, L. Moggi, and V. Balzani, *J. Am. Chem. Soc.*, **99**, 6881 (1977).
10) M. K. DeArmond, W. L. Huang, and C. M. Carlin, *Inorg. Chem.*, **18**, 3388 (1979).
11) J. B. Birks, "Photophysics of Aromatic Molecule," Wiley Interscience, London (1970), p. 280.
12) M. K. DeArmond and J. E. Hillis, *J. Chem. Phys.*, **54**, 2247 (1971).

The Cadmium-photosensitized Reaction of Saturated Tertiary Amines

Shunzo YAMAMOTO,* Masae YASUNOBU, and Norio NISHIMURA

Department of Chemivtry, Faculty of Science, Okayama University, Tsushima, Okayama 700

(Received April 18, 1981)

Rate constants for the quenching of the cadmium resonance line at 326.1 nm by triethylamine (TEA), *N*-ethylpiperidine (NEP), and 1-azabicyclo[2.2.2]octane (ABCO) were obtained. Relative rate constants for the formation of an exciplex between an excited cadmium atom and these amines and quantum yields for the emission from the exciplex were also obtained. Contrary to the case of primary amines, in which the electron-donating ability of the nitrogen atom is operative, the exciplex formation in the present case is mainly governed by the magnitude of the steric effect of ethyl groups on the interaction between the nitrogen atom and an excited cadmium atom. Gaseous products were hydrogen, methane, ethane (and/or ethylene), and butane. The quantum yields of these products indicate that the primary photochemical products are methyl and ethyl radicals for TEA and NEP. The amount of products for ABCO was considerably smaller than those for other amines.

In the cadmium-photosensitized reaction of saturated amines, the quenching of the resonance line at 326.1nm and the exciplex emission have been discussed in previous papers in terms of the following reactions:[1)]

$$Cd + h\nu(326.1) \longrightarrow Cd(^3P_1), \quad (1)$$

$$Cd(^3P_1) \longrightarrow Cd + h\nu(326.1), \quad (2)$$

$$Cd(^3P_1) + M \rightleftharpoons Cd(^3P_0) + M, \quad (3), (-3)$$

$$Cd^* + A \longrightarrow \text{quenching}, \quad (4)$$

$$Cd^* + A \longrightarrow CdA^*, \quad (5)$$

$$CdA^* \longrightarrow Cd + A + h\nu_e, \quad (6)$$

$$CdA^* + M \longrightarrow Cd + A + M. \quad (7)$$

Here, Cd* represents $Cd(^3P_1)$ and $Cd(^3P_0)$, and CdA* is an exciplex between Cd* and amines. A represents the amine and M stands for a third body. In general, the rate constant for Reaction 5 increases with a decrease in the ionization potential of amines, and for primary amines there is a good correlation between the rate constant and the ionization potential.[2)] The rate constants for secondary and tertiary amines are, however, somewhat smaller than the values predicted from the correlation mentioned above. It has been pointed out that the reactivity of amines is mainly governed by the electron-donating ability of the nitrogen atom, but partly by some other factor which supresses the formation of the exciplex in the cases of secondary and tertiary amines. This additional factor was attributed to the steric effect of the alkyl groups.[3)] It seems to be necessary to examine decomposition processes which compete with the exciplex formation. In the cadmium-photosensitized reaction of amines, however, products have not been yet reported.

In this study, in order to examine the influence of structural properties on the cadmium-photosensitized reaction of amine, we measured the quenching efficiency and the quantum yields for the exciplex emission and for the products of three saturated tertiary amines (TEA, NEP, and ABCO) which are considered to have different steric hindrances around the nitrogen atom.

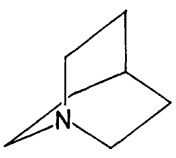

ABCO

Experimental

The apparatus and the procedure for measuring the emissions (resonance line at 326.1 nm and exciplex emission) were the same as those described previously.[4)] The measurements were done at 220±1 °C.

A Pyrex reaction cell used for measuring the product yields was 20.0 cm long and 2.2 cm in diameter, with a total volume, including access tubing, of about 86 cm^3. It was inserted in an electric furnace kept at 250±1 °C. A hand-made cadmium discharge lamp (filled with *ca.* 2 Torr argon, 1 Torr =133.32 Pa) made of Pyrex was also placed in the same furnace.

Reaction products were analyzed by means of a gas chromatograph using a column of 5 m VZ-7 (Gasukuro Kogyo Co., Ltd.) at 0 °C. In this column, we could not separate ethane from ethylene. The amounts of gases which are noncondensable at 77 K were determined volumetrically by a Toepler pump. The light intensity absorbed by cadmium atoms was estimated by using the *cis-trans* isomerization of *cis*-2-butene as an actinometer.

Cadmium metal used was high-purity grade (99.9999%) manufactured by the Osaka Asahi Metal Co. Ethylamine (EA), Diethylamine (DEA), TEA, piperidine (P), and NEP (G.R. grade) were used after drying over calcium hydride and repeated trap-to-trap distillation. ABCO·HCl was purchased from Pfaltz and Bauer, Inc. The free base was liberated by combining very concentrated ABCO·HCl and NaOH aqueous solutions. This solid amine was filtered and sublimed *in vacuo* through a layer of anhydrous BaO.

Results

In Fig. 1, the emission bands obtained for the cadmium-photosensitized reaction of TEA, NEP, and ABCO are shown. The band for ammonia is also shown for comparison. The quantum yields of the emission for TEA, NEP, and ABCO were determined by comparing the integrated intensities of the emission band with that for ammonia (whose emission quantum yield is known) under the same conditions. The values of quantum yields were found to be almost independent of amine pressure (0.1—1.2 Torr for TEA and NEP, and 0.1—2.0 Torr for ABCO) and argon pressure (50—200 Torr). The average values are listed in Table 1, together with the wavelengths at the peak of the emission bands.

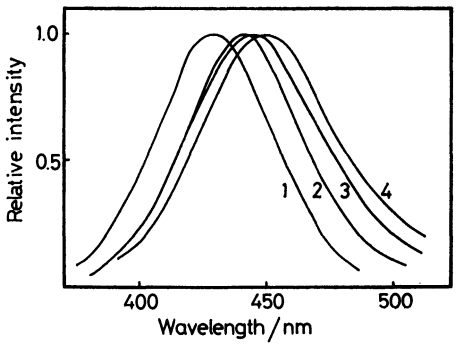

Fig. 1. Emission band contours for NEP (1), TEA (2), and ABCO (3). The curve for NH_3 (4) is derived from Ref. 5.

TABLE 1. WAVELENGTH AT THE PEAK OF THE EMISSION BAND AND QUANTUM YIELD OF THE EMISSION

Compound	$\frac{\lambda_{max}}{nm}$	ϕ_e
TEA	444	0.12±0.01
NEP	448	0.17±0.01
ABCO	442	0.87±0.02

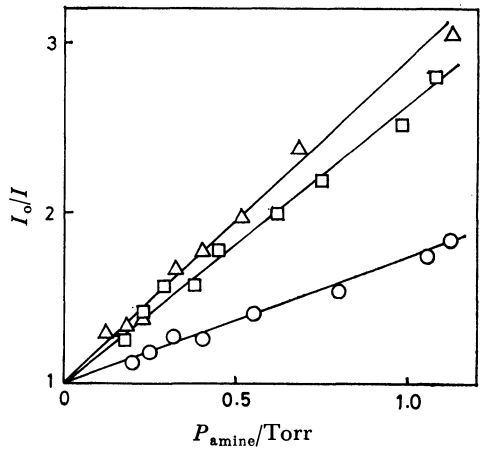

Fig. 2. Stern-Volmer plots for the quenching of the resonance line at 326.1 nm by TEA (□), NEP (△), and ABCO (○).

In order to estimate the efficiency of the quenching of the 326.1 nm resonance line, its emission intensity was measured as a function of the pressure of substrates. The Stern-Volmer plots are shown in Fig. 2, where I_0 and I are the intensities of the resonance line in the absence and in the presence of the substrates, respectively. Half-quenching pressures obtained from the slopes of the straight lines in Fig. 2 are listed in Table 2.

TABLE 2. HALF-QUENCHING PRESSURE FOR THE QUENCHING OF 326.1 nm RESONANCE LINE

Compound	Torr
TEA	0.61±0.02
NEP	0.52±0.02
ABCO	1.33±0.03

TABLE 3. QUANTUM YIELDS OF PRODUCTS IN CADMIUM-PHOTOSENSITIZED REACTION OF SATURATED AMINES[a,b]

Compound	H_2+CH_4	H_2	CH_4	C_2H_6 (C_2H_4)	C_4H_{10}	ϕ_d[c]
EA	0.071	0.001	0.070	0.073	0.013	0.169
DEA	0.162	0.001	0.161	0.143	0.022	0.348
P	0.027	0.001	0.026	0.023	0.033	0.115
TEA	0.147	0.002	0.145	0.289	0.044	0.522
NEP	0.049	0.002	0.047	0.050	0.022	0.141
ABCO	0.013	0.004	0.009	0.021	0	0.030

a) Uncertainties in quantum yields, except for hydrogen, are within 5%. b) Pressure of amines was 30 Torr. c) $\phi_d=\phi_{CH_4}+\phi_{C_2H_6}+2\phi_{C_2H_4}$.

The pressure dependence of the intensity at the peak of the emission band (which was expressed on the basis of that at 430 nm for Cd*-NH_3 system) is shown in Fig. 3. The emission intensities were independent of argon pressure.

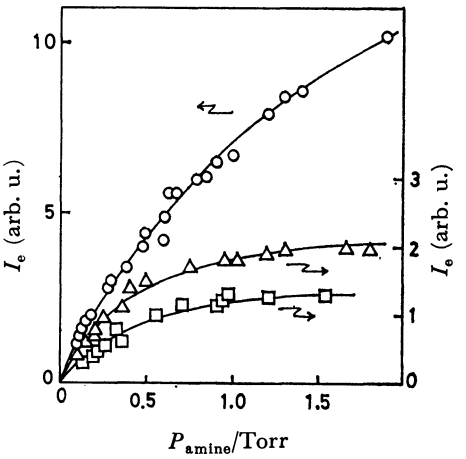

Fig. 3. The intensity at the peak of the emission band from the exciplex as a function of the pressures of TEA (□), NEP (△), and ABCO (○).

Quantum yields of products in the cadmium-photosensitized reaction of saturated amines are summarized in Table 3. In order to check the thermal reaction and the direct photolysis, 30 Torr of the amine was kept in the cell at 250 °C for a few hours in the absence of cadmium under irradiation of the 326.1 nm cadmium resonance line. No decomposition was detected for any amine. The light intensity absorbed by cadmium atoms was estimated to be 0.26×10^{-6} Einstein min^{-1}.

Discussion

In previous papers,[1] the quenching of the resonance line and the exciplex emission were explained according to Reactions 1—7. Because the equilibrium between $Cd(^3P_0)$ and $Cd(^3P_1)$ is easily established under the present experimental conditions,[6] we cannot discriminate the reactions of these two states.

A steady-state treatment leads to the following equation:

$$I_0/I = 1 + k_q[A]/k_2. \quad (8)$$

Here, I_0 and I represent the intensities of the resonance line (defined as $k_2[Cd(^3P_1)]$) in the absence and in the presence of amines respectively; k_q is the composite quenching rate constant: $k_q=k_4+(k_3/k_{-3})k_4'+k_5+(k_3/k_{-3})k_5'$ (k_4 and k_5 are rate constants for Reaction 4 and 5 in the case of $Cd^*=Cd(^3P_1)$ and k_4' and k_5' are those in the case of $Cd^*=Cd(^3P_0)$); $(k_3/k_{-3}=1.68$ at 220 °C). The Stern-Volmer plots in Fig. 1 are expressed by this equation. As was mentioned in previous papers,[1,6] the effective lifetime is almost independent of the pressure of foreign gases in the range we were studying. Therefore, k_2 may be set equal to $1/\tau_0$ (τ_0 is the natural lifetime of $Cd(^3P_1)$ and has been reported to be 2.39×10^{-6} s[7]). From the half-quenching pressure, the values of k_q can be estimated; they are listed in Table 4, together with those for some primary and secondary amines. As is shown in Table 4, the values of k_q for tertiary amines are smaller than those for primary and secondary amines. This tendency has been explained in terms of the steric hindrance of the alkyl groups.[4]

Table 4. The rate constants for the quenching of the resonance line and for the exciplex formation

Compound	$k_q\times10^{11}$ / cm^3 molecule^{-1} s^{-1}	$k_5/k_5^{NH_3}$	I_p[b] / kJ mol^{-1}
EA[a]	6.1±0.1	15.3	913.8
DEA[a]	17.0	43.1	832.6
P[a]	7.0±0.18	14.0	835.5
TEA	3.6±0.1	4.40	779.4
NEP	4.2±0.2	6.89	812.5[c]
ABCO	1.6±0.1	13.8	776.6

a) Ref. 4. b) Ref. 8. c) Value for *N*-methylpiperidine.

The steady-state treatment leads to the following equation for the intensity of the exciplex emission:

$$I[A]/I_e = \alpha(k_2/k_5)(1 + k_7[M]/k_6), \quad (9)$$

where I_e is the emission intensity at the peak of the band and I is the intensity of the resonance line at the same pressure of amines; α is the proportional factor between I_e and the total emission intensity. From the pressure dependence of the intensity at the peak of the emission band, relative values of k_5 have been estimated by the method described previously,[3,4] and are listed in Table 4.

In general, the rate constant for the exciplex formation increases with a decrease in I_p values of amines.[2] In the present case, the values of k_5 increase in the order: TEA<NEP<ABCO. This order is not in agreement with the order of the decrease in I_p. TEA is "flexible" in the sense that its ethyl groups hinder the access of the excited cadmium atom to the nitrogen atom. Meanwhile, ABCO is a rigid, bicyclic amine having bridgehead nitrogen atom and is little sterically hindered. Among these amines, if the steric effects overwhelm other factors affecting k_5, the smallest value of k_5 for TEA and the largest value for ABCO could be ascribed to the steric effects.

As mentioned above, the quantum yields of the emission for three tertiary amines are almost independent of amine and argon pressures, indicating that the exciplexes are little quenched by amine and argon. As ABCO has the largest quantum yield of the emission, we assumed that $\phi_e=k_5/k_q$ for ABCO. This indicates that the quantum yield of the emission is determined by the ratio of the rate constant (k_5) for the exciplex formation to the overall quenching rate constant (k_q). We obtained the value of k_5 (1.40×10^{-11} cm^3 molecule^{-1} s^{-1}) for ABCO by the observed values of ϕ_e and k_q. Further, we obtained the values of k_5 for other amines by using the relative values of k_5 shown in Table 4; these values are shown in Table 5. In Table 5, the values of k_5/k_q are also shown. These values are in fair agreement with the experimental values of ϕ_e. This indicates that the above assumption is valid for all these amines. Practically all of the exciplexes formed decay out through the emission process, that is, neither unimolecular decomposition nor a bimolecular quenching of the exciplex occurs.

Table 5. The values of k_5, k_5/k_q, and ϕ_r

Compound	$k_5\times10^{11}$ / cm^3 molecule^{-1} s^{-1}	k_5/k_q	ϕ_e	ϕ_r
EA	1.55	0.25	0.26[a]	0.57
DEA	4.37	0.26	—	0.39
P	1.42	0.20	0.20[a]	0.68
TEA	0.45	0.13	0.12	0.36
NEP	0.70	0.17	0.17	0.69
ABCO	1.40	0.87	0.87	0.10

a) Ref. 4.

As is shown in Table 3, gaseous products in the cadmium-photosensitized reaction of the saturated amines studied are hydrogen, methane, ethane (and/or ethylene), and butane. It has been reported that in the direct photolysis of TEA,[9] the primary products were hydrogen molecule and methyl and ethyl radicals produced from an excited TEA molecule and that from these radicals methane, ethane, ethylene, propane, and butane were formed. It is reasonable that, in the cadmium-photosensitized reaction of TEA, methyl and ethyl radicals are also precursors of products: methane, ethane, ethylene, and butane are produced *via* processes of hydrogen atom abstraction from amines, disproportionation, and recombination.

In the case of quenching of $Cd(^3P_{0,1})$ by alkane hydrocarbons, it has been pointed out that direct abstraction of a hydrogen atom to form CdH is a major quenching pathway. The quenching cross sections have been explained by assuming an additive cross section for each C–H bond of 1×10^{-5} nm^2, irrespective of type of C–H bond.[10] From the quenching cross section (4×10^{-3} nm^2) and the quantum yield of hydrogen (0.014) in the cadmium-photosensitized reaction of ammonia, the cross section corresponding to an abstraction of hydrogen atom for each N–H bond is similarly calculated to be about 1×10^{-5} nm^2. The quenching cross sections for the abstraction of hydrogen atom from saturated amines can be calculated by using these values. For example, the values for TEA, NEP, and ABCO are about 1.5×10^{-4}, 1.5×10^{-4}, and 1.3×10^{-4}

nm^2, since TEA, NEP, and ABCO have 15, 15, and 13 C–H bonds respectively. From these values and the overall quenching rate constants, the quantum yields of hydrogen (ϕ_{H_2}) for TEA, NEP, and ABCO are estimated to be 0.002, 0.002, and 0.004 respectively. These values are listed in Table 3, together with the values for other amines. The values of ϕ_{H_2} estimated for all amines investigated here are very small. The quantum yield of methane (ϕ_{CH_4}) are calculated by subtracting ϕ_{H_2} from $\phi_{H_2+CH_4}$. For P and ABCO, ϕ_{CH_4} is very small, as expected from molecular structure.

In the cadmium-photosensitized reaction of amines, the primary processes are expressed by the following reactions;

$$Cd^* + A \longrightarrow CdA^*, \quad (5)$$
$$\longrightarrow CdH + R, \quad (10)$$
$$\longrightarrow Cd + CH_3 + A', \quad (11)$$
$$\longrightarrow Cd + C_2H_5 + A'', \quad (12)$$
$$\longrightarrow Cd + \text{biradical}, \quad (13)$$
$$\longrightarrow Cd + A. \quad (14)$$

Reaction 10 indicates a hydrogen atom abstraction by excited cadmium atom from C–H or N–H bond of amines and Reaction 14 indicates a physical quenching process. A′ and A″ in Reactions 11 and 12 indicate the moieties of methyl and ethyl radicals respectively. In the cases of cyclic amines, the formation of biradical must be taken into account (Reaction 13). Reactions 10—14 are included in Reaction 4. In the cases of P and ABCO, Reactions 11 and 12 rarely occur.

The relative values of ϕ_d (defined as $\phi_d=\phi_{CH_4}+\phi_{C_2H_4,C_2H_6}+2\phi_{C_4H_{10}}$; it can be regarded as equal to the sum of initial quantum yields of methyl and ethyl radicals) are 1.00, 2.06, 3.09, and 0.83 for EA, DEA, TEA, and NEP. This ratio is almost the same that of the number of ethyl groups. This suggests that the reasoning that methane, ethane (and/or ethylene) and butane are primarily produced from methyl and ethyl radicals is valid. The values of ϕ_d for tertiary amines decrease in the order; TEA>NEP>ABCO. This decreasing order is in agreement with the increasing order of the emission quantum yield. It is difficult to explain the way by which methyl and ethyl radicals are produced for P and ABCO. In these cases the origin of products remains an open question.

The ratio of recombination to disproportionation of ethyl radicals has been reported to be about 7.4.[11] As is shown in Table 3, however, the ratios of the yields of butane to those of ethane (ethylene) are about 0.15—0.18 for EA, DEA, and TEA. This indicates that ethane is formed exclusively by the abstraction of a hydrogen atom from amines.

The contribution (ϕ_r) of Reactions 14 and/or 13 to the overall quenching processes is estimated by $\phi_r=1-(\phi_e+\phi_d+\phi_{H_2})$. The values of ϕ_r are listed in Table 5. For TEA, as Reaction 13 does not occur, the value of ϕ_r indicates the contribution of the physical quenching process; it is about one-third of the total quenching. On the other hand, in the case of NEP, both Reactions 13 and 14 contribute to the overall quenching processes. If the physical quenching process is almost the same for NEP and TEA, the difference in ϕ_r between NEP and TEA indicates the quantum yield for Reaction 13; it is 0.33. This value is about twice as much as ϕ_d for NEP; the difference is attributed to the number of bonds to be broken. Reaction 13 seems to be responsible for the large difference in ϕ_d between TEA and NEP. The same thing seems to hold between DEA and P. For ABCO, however, the quantum yields for processes other than the exciplex formation are very small. On the other hand, it has a large quantum yield for the emission (the largest value of those reported to date). That is, the quenching by ABCO can be concluded to occur overwhelmingly through the exciplex formation.

References

1) S. Yamamoto and S. Sato, *Bull. Chem. Soc. Jpn.*, **48**, 1382 (1975); S. Tsunashima, K. Morita, and S. Sato, *ibid.*, **50**, 2283 (1977); S. Yamamoto, M. Yasunobu, N. Nishimura, and S. Hasegawa, *Mol. Photochem.*, **9**, 277 (1979).

2) S. Yamamoto and S. Sato, *Bull. Chem. Soc. Jpn.*, **48**, 1381 (1975).

3) S. Yamamoto, K. Tanaka, and S. Sato, *Bull. Chem. Soc. Jpn.*, **48**, 2172 (1975).

4) S. Yamamoto, M. Yasunobu, N. Nishimura, and S. Hasegawa, *Mol. Photochem.*, **9**, 277 (1979).

5) S. Tsunashima, T. Toyono, and S. Sato, *Bull. Chem. Soc. Jpn.*, **46**, 2654 (1973).

6) S. Yamamoto, M. Takaoka, S. Tsunashima, and S. Sato, *Bull. Chem. Soc. Jpn.*, **48**, 130 (1975).

7) F. W. Byron, Jr., M. N. McDermott, and R. Novick, *Phys. Rev. A*, **134**, 615 (1964).

8) D. H. Aue, H. M. Webb, and M. T. Bowers, *J. Am. Chem. Soc.*, **98**, 311 (1976).

9) P. J. Kozak and H. Gesser, *J. Chem. Soc.*, **1960**, 448.

10) W. H. Breckenridge and A. M. Renlund, *J. Phys. Chem.*, **83**, 303 (1979).

11) J. A. Kerr and A. F. Trotman-Dickenson, "Progress in Reaction Kinetics," ed by G. Porteir, Pergamon Press, Oxford (1961), Vol. 1, p. 105.

Kinetics and Mechanism of 1,4-Cycloaddition between Tetracyanoethylene and Styrenes. II.[1] Effect of Para Substituents

Yasuhiro UOSAKI, Masaru NAKAHARA,* and Jiro OSUGI

Department of Chemistry, Faculty of Science, Kyoto University, Oiwake-cho, Kitashirakawa, Sakyo-ku, Kyoto 606

(Received April 24, 1981)

The 1,4-cycloaddition of TCNE to *p*-methyl-, *p*-chloro-, and *p*-bromostyrenes by way of the EDA complex has been studied in chloroform at 25 °C by the spectrophotometric method. The Hammett correlation obtained from the kinetic data provides -5.5 ± 0.2 as the reaction constant ρ. The negative value is large in magnitude relative to other common 1,4-cycloadditions, suggesting some large partial charges in the rate-determining transition state. A linear correlation between the logarithmic forms of the reaction rate and the EDA-complex formation constant is in favor of the reaction scheme where the complex is on the pathway of the cycloaddition.

The 1,4-cycloadduct of tetracyanoethylene (TCNE) with styrene and its derivatives has been discovered in solution by the low-temperature ^{13}C NMR technique combined with a high-pressure quenching method.[2] The effect of α-substituents on the 1,4-cycloaddition has been discussed in detail in a previous paper; a polar transition state is suggested based on the α-substituent effect.[1] The electronic effect of α-substituents is coupled to some extent with the steric hindrance because of the small distance from the reaction sites. For this reason, para substitution is more desirable to see exclusively the electronic effect of substituents on the 1,4-cycloaddition. For this purpose *p*-methyl-, *p*-chloro-, and *p*-bromostyrenes are employed in the present work.

The 1,4-cycloaddition (so-called Diels-Alder reaction) is a typical cycloaddition reaction and of great interest from theoretical and synthetic points of view. A large number of kinetic studies have been done to get insight into the mechanism of this simple and useful reaction, as recently well reviewed.[3] Most of the kinetic data are in favor of the concerted mechanism ((a) in Fig. 1). In the 1,4-cycloaddition studied here, styrenes serve as a diene instead of a dienophile; one unsaturated bond comes from the vinyl group and the other from the phenyl group, and as a result, the aromaticity is lost in the product. The aim of the present investigation is to elucidate the reaction mechanism of this unique 1,4-cycloaddition from the point of view of kinetics.

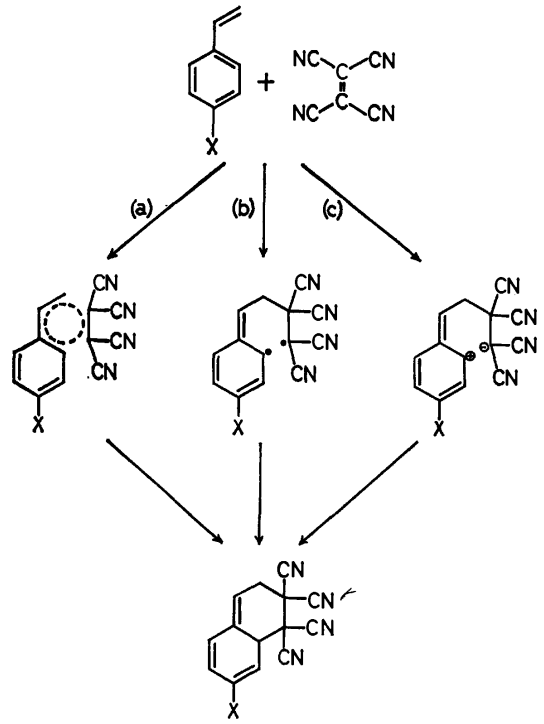

Fig. 1. Conceivable reaction mechanisms for 1,4-cycloaddition of TCNE to para-substituted styrenes (X= CH_3, H, Cl, and Br).

Experimental

p-Methyl-, *p*-chloro-, and *p*-bromostryenes were prepared by dehydrating the corresponding secondary alcohols with $KHSO_4$. The alcohols were synthesized by reducing the para-substituted acetophenones in ethanol with $NaBH_4$. All styrenes were repeatedly distilled at reduced pressure, stored in a refrigerator, and distilled again over CaH_2 before use. TCNE and chloroform were purified by repeated sublimation and distillation, respectively.

The apparatus and experimental procedures in the present work are the same as those described in detail in the previous paper.[1] Temperature was kept constant to ±0.1° C. The concentration of the donor was always much higher than that of the acceptor so as to simplify several equations utilized in the present analysis.

Results

Formation Constant of EDA Complex. When TCNE is mixed with each of the donors in chloroform, the electron-donor-acceptor (EDA) complex is formed instantaneously as a result of the diffusion-controlled reaction and exhibits two absorption maxima due to the first and second charge-transfer transitions in the visible region. All styrenes treated in this work and

Table 1. Spectroscopic parameters of EDA complexes in $CHCl_3$ at 25°C and some relevant properties of donors

X[a]	λ_{max} / nm	ε_{max} / mol^{-1} dm^3 cm^{-1}	K_c / mol^{-1} dm^3	I_P / eV	σ_p^+[e]
CH_3	531	1330±20	1.46 ±0.03	8.38[d]	−0.311
H	486[b]	1960±30[b]	0.467±0.010[b]	8.50[c]	0
Cl	493	1970±60	0.201±0.007	8.48[d]	+0.114
Br	497	2390±80	0.172±0.006	8.47[d]	+0.150

a) X denotes the substituent at the para site of styrene (see Fig. 1). b) From Ref. 1. c) From Ref. 5. d) From Eq. 2. e) From Ref. 6.

TCNE have no absorption in this region. Spectroscopic parameters of the complexes are summarized in Table 1 together with some relevant properties of the donors.

The complex formation constant (K_c) and molar absorption coefficient (ε_{max}) of the first charge-transfer band, listed in Table 1, are determined from the Scott equation 1,[4]

$$\frac{[D]_0[A]_0 l}{A_0} = \frac{1}{K_c \varepsilon_{max}} + \frac{[D]_0}{\varepsilon_{max}}, \quad (1)$$

where $[D]_0$ and $[A]_0$ are the initial concentrations of the donor and the acceptor, respectively, l the path length (1 cm) and A_0 the absorbance of the complex before the 1,4-cycloadduct is formed. Figure 2 shows plots of the left-hand side of Eq. 1 against $[D]_0$, the slopes and intercepts of which provide K_c and ε_{max} simultaneously.

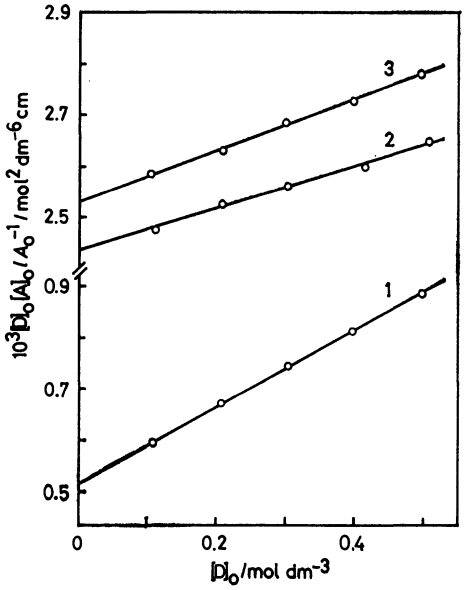

Fig. 2. Plots of $[D]_0[A]_0 l/A_0$ *vs.* $[D]_0$.
1: *p*-Methylstyrene, 2: *p*-bromostyrene, 3: *p*-chlorostyrene.

Since there is no photoelectron spectroscopic investigation on the para-substituted styrenes treated here, the ionization potentials (I_p) of these molecules in Table 1 are estimated by using the relation.

$$h\nu_{CT}/\text{eV} = 0.873(I_p/\text{eV}) - 4.89, \quad (2)$$

which is obtained on the basis of reported ionization potentials of some other styrene derivatives[5] and first charge-transfer transition energies ($h\nu_{CT}$) of their EDA complexes with TCNE.[1]

Reaction Rate of 1,4-Cycloaddition. Since the EDA-complex formation and 1,4-cycloaddition are reversible reactions, the following reaction scheme is assumed:

$$D + A \underset{}{\overset{K_c}{\rightleftharpoons}} \text{EDA Complex} \underset{k_{-1}}{\overset{k_1}{\rightleftharpoons}} P, \quad (3)$$

where k_1 and k_{-1} are the rate constants of the forward and backward reactions, respectively and P denotes the cycloaddition product. The rate equation for the reaction 3 is easily solved and affords the expression

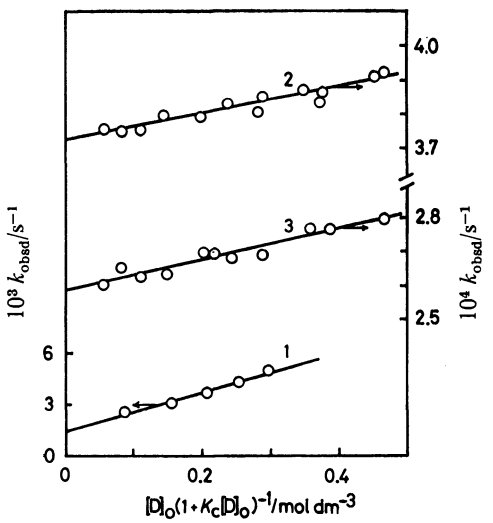

Fig. 3. Plots of k_{obsd} *vs.* $[D]_0/(1+K_c[D])$.
1: *p*-Methylstyrene, 2: *p*-chlorostyrene, 3: *p*-bromostyrene.

for [P] as a function of time (t):[1]

$$[P] = \frac{k_1[EDA]_0\{1-\exp(-k_{obsd}t)\}}{k_{obsd}}, \quad (4)$$

where

$$k_{obsd} = \frac{k_1 K_c [D]_0}{1+K_c[D]_0} + k_{-1}. \quad (5)$$

The pseudo-first-order rate constant, k_{obsd} was determined by the Guggenheim plot. As shown in Fig. 3, plots of k_{obsd} *vs.* $[D]_0/(1+K_c[D]_0)$ are linear, and from these slopes and intercepts we can get the values of k_1K_c and k_{-1}. The overall formation constant for the 1,4-cycloadduct K_p expressed as

$$K_P = \frac{[P]}{[D][A]} \quad (6)$$

$$= \frac{[EDA][P]}{[D][A][EDA]} \quad (7)$$

$$= K_c K_1 \quad (8)$$

$$= K_c k_1/k_{-1} \quad (9)$$

$$= k_f/k_{-1} \quad (10)$$

is given in Table 2 together with $k_f(=K_ck_1)$ and k_{-1}.

Table 2. Kinetic and thermodynamic parameters of 1,4-cycloadducts in $CHCl_3$ at 25°C

X[a]	$10^4 k_f$ / mol^{-1} dm^3 s^{-1}	$10^4 k_{-1}$ / s^{-1}	K_P / mol^{-1} dm^3
CH_3	115±4	14.5 ±0.09	7.93 ±0.33
H	1.77 ±0.05[b]	2.50±0.01[b]	0.708±0.023[b]
Cl	0.400±0.040	3.72±0.01	0.108±0.011
Br	0.454±0.049	2.59±0.01	0.175±0.020

a) X denotes the substituent at the para site of styrene.
b) From Ref. 1.

Discussion

The Hammett Correlation. The electronic effect of the para substitution (X in Table 1) on the formation of the 1,4-cycloadduct is expressed in terms of the

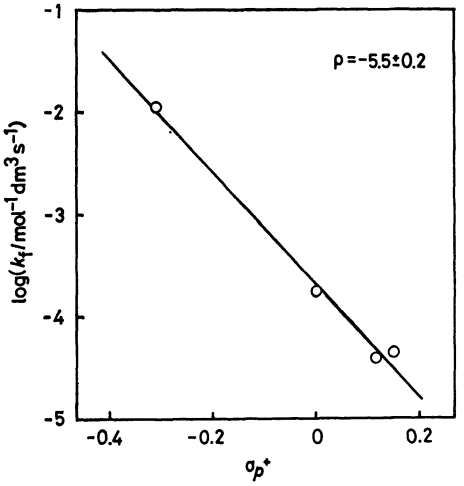

Fig. 4. A Hammett plot of log k_f *vs.* σ_p^+.

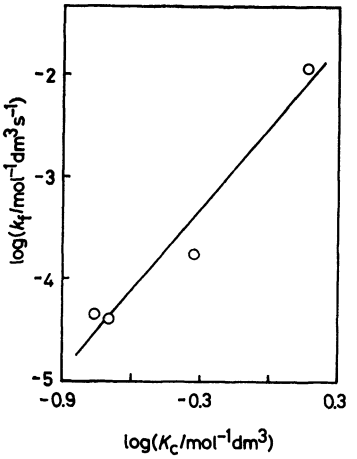

Fig. 5. A Plot of log k_f *vs.* log K_c.

reaction constant ρ, which is determined as -5.5 ± 0.2 from the Hammett plot of log k_f (in Table 2) *vs.* σ_p^+[6] (in Table 1) in Fig. 4. The ρ value obtained here is negative and considerably large in magnitude. Actually, ρ values are in the range of -1.8 to $+2.6$ for many other 1,4-cycloaddition reactions where CC-, NN-, and NO-double and CC-triplet bonds act as dienophiles.[3] The small ρ values found so far are considered to support the concerted mechanism (a) in Fig. 1. A large negative ρ value of -7.1 ± 0.5 has been reported for the 1,2-cycloaddition of TCNE to styrene derivatives having a strong electron-releasing substituent at the para site according to the Yukawa-Tsuno equation.[7] The large negative value for this 1,2-cycloaddition is regarded as an indication of a zwitterionic intermediate which is recognized in a similar 1,2-cycloaddition by various methods.[8] The large negative value found for the present reaction suggests some large partial charges in the rate-determining transition state. The following paper clarifies that the transition state has a dipole moment which is considerable but not so large as in a zwitterion existing in the 1,2-cycloaddition reaction.[9] Thus, the zwitterionic structure (c) in Fig. 1 contributes to the transition state of the 1,4-cycloaddition studied here to some extent. At the present time, however, we can not argue whether this 1,4-cycloaddition proceeds by one step or by two steps, because our attempt to trap any probable polar intermediate by using ice-cold methanol was unsuccessful.[10]

There is a frontier molecular orbital approach to the interpretation of the Hammett correlation.[11] It is not useful, however, in the present reaction because the ionization potential of the donor used as a measure of the HOMO energy (E_{HOMO}) does not correlate with the obtained k_f (see Table 1). In other words, the substituent constants σ_p^+ are not linearly correlated with ($E_{HOMO}-E_{LUMO}$) in the present series of the donors.

A Correlation of the Rate Constant k_f with the Complex Formation Constant K_c. In Fig. 5, the values of log k_f in Table 2 are plotted against log K_c. There exists a linear correlation, the correlation coefficient of which is 0.976. The linear correlation between log k_f and log K_c somehow supports the assumed reaction scheme shown by Eq. 3 because the free energy of the transition state of the 1,4-cycloaddition and the free energy of the complex are not necessarily expected to be linearly correlated in a reaction system where the complex formation is merely a side reaction. Similar correlations are reported in the 1,4-cycloaddition of TCNE to anthracenes[12] and some other kind of reactions.[13] In the former case, a negative activation enthalpy has been found, which is considered to support the scheme shown by Eq. 3 where the complex is on the pathway of the 1,4-cycloaddition reaction.[14] These linear correlations are often taken as evidence for the intermediacy of the EDA complex. The linear correlation found here between log k_f and log K_c suggests that the charge-transfer interaction between the donor and the acceptor is somehow important among interactions in the transition state.

References

1) The previous paper is designated as Part I of the present series: Y. Uosaki, M. Nakahara, and J. Osugi, *Bull. Chem. Soc. Jpn.*, **54**, 2569 (1981).
2) M. Nakahara, Y. Uosaki, M. Sasaki, and J. Osugi, *Bull. Chem. Soc. Jpn.*, **53**, 3395 (1980).
3) J. Sauer and R. Sustmann, *Angew. Chem. Int. Ed. Engl.*, **10**, 779 (1980).
4) R. L. Scott, *Recl. Trav. Chim. Pays-Bas*, **75**, 787 (1956).
5) J. P. Maier and D. W. Turner, *J. Chem. Soc., Faraday Trans. 2*, **69**, 196 (1975).
6) H. C. Brown and Y. Okamoto, *J. Am. Chem. Soc.*, **80**, 4979 (1958).
7) P. D. Bartlett, *Quart. Rev.*, **24**, 473 (1970).
8) R. Huisgen, *Acc. Chem. Res.*, **10**, 117 (1977).
9) Part III of the present series: Y. Uosaki, M. Nakahara, and J. Osugi, *Bull. Chem. Soc. Jpn.*, **55**, No.1 (1982), in press.
10) R. Huisgen and G. Steiner, *Angew. Chem. Int. Ed. Engl.*, **13**, 80 (1974).
11) O. Henri-Rousseau and F. Texier, *J. Chem. Educ.*, **55**, 437 (1978).
12) M. Lotfi and R. M. G. Roberts, *Tetrahedron*, **35**, 2131 (1979).
13) S. Fukuzumi and J. K. Kochi, *J. Phys. Chem.*, **84**, 2246 (1980).
14) V. D. Kiselev and J. G. Miller, *J. Am. Chem. Soc.*, **97**, 4036 (1975).

A Theoretical Approach to the Dielectric Relaxation of Alcohol Solutions. II.[1] The Effect of Dilution with Inert Solvents on the Principal Relaxation Times of Primary Alcohols

Ryuichi MINAMI, Koichi ITOH,* Hiroaki TAKAHASHI, and Keniti HIGASI

Department of Chemistry, School of Science and Engineering, Waseda University, Okubo, Shinjuku-ku, Tokyo 160

(Received May 8, 1981)

The concentration dependence of the principal relaxation times, τ_P, of primary alcohol/inert solvent solutions are analyzed based on the equation,

$$\tau_p = 2(1+Kx_A)\tau_H,$$

where x_A is the alcohol mole fraction, K the equilibrium constant corresponding to the formation of hydrogen bonded multimers, and τ_H the time constant characterizing the rotational activation process of the terminal OH groups of the multimers. By applying Eyring's absolute rate theory to the activation process, we calculated τ_P as a function of temperature and alcohol concentration. The results reproduce quite well the τ_P values observed for the ethanol/cyclohexane, 1-hexanol/cyclohexane, and 1-propanol/benzene solutions.

In the preceding papers[1,2] we studied the dielectric relaxation processes of pure alcohols and alcohol solutions by assuming the association equilibrium between hydrogen bonded chain multimers. The dipole inversion arising from the cooperative rotation of the OH groups of the multimers was considered to be the main mechanism of the dipole relaxation. To the dipole inversion process we applied the stochastic model of one-dimensional random walk with two absorption walls[3] and found that the relaxation time of an n-mer is given by

$$\tau_n = (1+n)\tau_H. \quad (1)$$

Here τ_H is the reciprocal of the rate constant in which the terminal hydroxyl groups of the n-mer are activated rotationally. The dielectric relaxation observed for liquid alcohols and alcohol solutions was considered to be the sum of the contributions from the dipole relaxation of each n-mer. Using Eq. 1 together with the stoichiometric relationships for the association equilibrium,[4,5] we obtained analytical equations for the dielectric dispersions of pure alcohols and alcohol solutions. It is well known that in a low-frequency region most of alcohols and alcohol solutions show a dielectric dispersion which conforms very well to the simple relaxation pattern of Debye.[6,7] Assuming that the above-mentioned analytical formula under the low frequency limit ($\omega \to 0$) can express the relaxation time corresponding to this dispersion (This has often been called as the principal relaxation time. In this paper we abbreviate it as τ_P.), we obtained τ_P as a function of K, K_b, and x_A, where K is the equilibrium constant of the formation of chain multimers, K_b the constant of the association between the chain-multimers and a solvent with a hydrogen-bonding capacity, and x_A is the mole fraction of alcohols.[1] From the result we successfully estimated the change in the principal relaxation times of primary alcohols due to dilution with solvents having a hydrogen-bond acceptor as well as with inert solvents.[8,9] In the case of alcohol/inert solvent systems we can put $K_b=0$, which leads to the following equation:

$$\tau_p = \frac{\tau_1}{(1+Kx_A)^2} + 2\left\{1 + Kx_A - \frac{1}{(1+Kx_A)^2}\right\}\tau_H, \quad (2)$$

where τ_1 is the dipole relaxation time of alcohol monomers. Under the condition of $Kx_A \gg 1$, the equation can be approximated by

$$\tau_p = 2(1 + Kx_A)\tau_H. \quad (3)$$

In the previous paper[1] we reported that the formula well represents the τ_P *vs.* x_A curves observed for 1-propanol/benzene and 1-butanol/benzene solutions.[8,10] For the cyclohexane solutions of primary alcohols, however, Sagal[11] and Komooka[12] observed a maximum in the τ_P *vs.* x_A curves. As stated previously, in order to explain these results it is necessary to consider the dependence of τ_H in Eq. 3 upon the atmosphere surrounding alcohol molecules or, rather, surrounding the end OH groups of the molecule. In this paper, we studied thermodynamics of the dilution effect of τ_H and discussed the variation of τ_P with x_A in further detail.

Thermodynamic Treatment on τ_P

The mechanism in which the hydroxyl group of one of the two terminal segments of multimers is brought into a rotational transition state can be regarded as a single relaxation process. Therefore, we can apply Eyring's absolute rate theory[13] to this process and get the equation,

$$\tau_H = \frac{h}{k_B T}\exp\left(-\frac{\Delta S^*}{R} + \frac{\Delta H^*}{RT}\right), \quad (4)$$

where h and k_B are the Planck and Boltzmann constants, respectively. ΔS^* the activation entropy, and ΔH^* the activation enthalpy.

As we are interested in the systems where the mole fraction of alcohols, x_A, is larger than 0.5, we can make a further approximation to Eq. 3 as follows:

$$\tau_p = 2Kx_A\tau_H = 2K(1-x_B)\cdot\tau_H(x_B), \quad (5)$$

where x_B ($=1-x_A$) is the mole fraction of an inert solvent B. In the last equation, τ_H is represented as a function of x_B to take the dilution effect on τ_H into consideration. This means that ΔH^* and ΔS^* in Eq. 4 are also a function of x_B. Substitution of Eq. 4 into Eq. 5 yields the following formula for τ_P:

$$\tau_P = \frac{2h(1-x_B)}{k_B T} \times \exp\left\{-\frac{-\Delta S^\circ + \Delta S^*(x_B)}{R} + \frac{-\Delta H^\circ + \Delta H^*(x_B)}{RT}\right\}. \quad (6)$$

In this expression we used the fact that the equilibrium constant K can be expressed as

$$K = \exp\left(\frac{\Delta S^\circ}{R} - \frac{\Delta H^\circ}{RT}\right), \quad (7)$$

where ΔS° and ΔH° are the entropy and enthalpy changes, respectively, due to the hydrogen-bond formation between multimers and a monomer. Equation 6 can be simplified to the equation,

$$\tau_p = \frac{A(x_B)}{T} \exp\left\{\frac{E_a(x_B)}{RT}\right\}, \quad (8)$$

by defining $E_a(x_B)$ and $A(x_B)$ as follows,

$$E_a(x_B) \equiv -\Delta H^\circ + \Delta H^*(x_B), \quad (9)$$

$$A(x_B) \equiv \frac{2h(1-x_B)}{k_B} \exp\left\{\frac{\Delta S^\circ - \Delta S^*(x_B)}{R}\right\}. \quad (10)$$

According to Eq. 8, the plot of $\ln(T\cdot\tau_P)$ against $1/T$ is represented as a straight line with the slope of $E_a(x_B)/R$ and the point of intersection with the vertical axis at $\ln\{A(x_B)\}$.[14,15] On the basis of these results we obtained the values of $E_a(x_B)$ and $A(x_B)$ as functions of x_B for ethanol/cyclohexane,[11] 1-hexanol/cyclohexane,[12] 1-octanol/cyclohexane,[12] and 1-propanol/benzene[16] solutions. Figures 1 and 2 were obtained by plotting $E_a(x_B)$ and $\ln\{A(x_B)/(1-x_B)\}$ against x_B, respectively. Each set of the plots conforms very well to a straight line especially in the region where $x_B<0.5$, indicating that $E_a(x_B)$ and $\ln\{A(x_B)/(1-x_B)\}$ can be approximated by the linear equations,

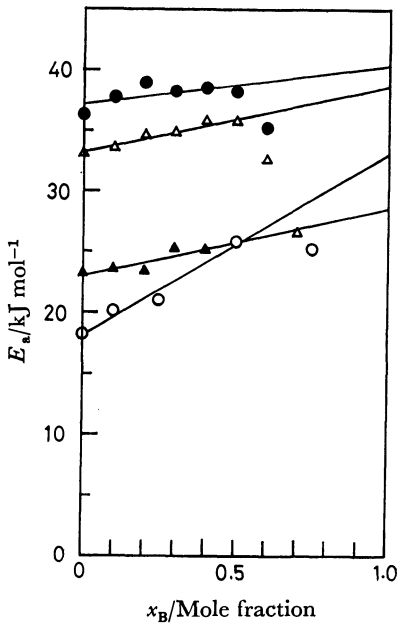

Fig. 1. Variation of E_a with the concentration of inert solvent, x_B, for the ethanol/cyclohexane (○), 1-hexanol/cyclohexane (△), 1-octanol/cyclohexane (●), and 1-propanol/benzene (▲) solutions. The straight lines are drawn to obtain the best fit with the data in the region of $x_B<0.5$ (see text.).

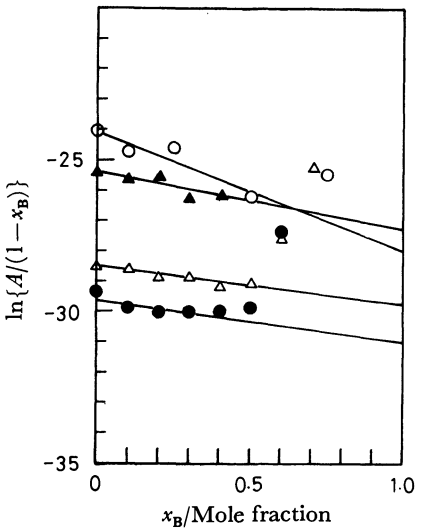

Fig. 2. $\ln\{A/(1-x_B)\}$ *vs.* x_B. The symbols have the same meaning as those in Fig. 1.

$$E_a(x_B) = E_a(0) + \alpha x_B, \quad (11)$$

$$\ln\{A(x_B)/(1-x_B)\} = \ln\{A(0)\} - \beta x_B/R, \quad (12)$$

where α and β are the constants characteristic of the solution in question. Equations 9 and 10 give the followings for pure alcohols ($x_B=0$),

$$E_a(0) = -\Delta H^\circ + \Delta H^*(0), \quad (13)$$

$$A(0) = \frac{2h}{k_B} \exp\left\{\frac{\Delta S^\circ - \Delta S^*(0)}{R}\right\}. \quad (14)$$

Using the above together with Eqs. 11 and 12, we can rewrite Eq. 6 to the following equation, which expresses τ_P explicitly as a function of x_B and T.

$$\tau_p = \frac{(1-x_B)A(0)}{T} \exp\left\{\frac{E_a(0)}{RT} - \left(\frac{\beta}{R} - \frac{\alpha}{RT}\right)x_B\right\} \quad (15)$$

Results and Discussion

Using the least-squares method we determined $E_a(0)$, α, $A(0)$, and β from Figs. 1 and 2. The results are given in Table 1. Inserting the $E_a(0)$, α, $A(0)$ and β values into Eq. 15, we calculated τ_P as a function of x_B and T for each set of the alcohol solutions listed in Table 1. The results are depicted by solid curves in Figs. 3, 4, and 5, where the observed values of τ_P are also included.

Figures 3, 4, and 5 show that the result of calculation for the region of $x_B<0.5$ well reproduces each set of the τ_P *vs.* x_B plots observed at various temperatures. In the region where x_B is larger than 0.5, however, the

Table 1. Estimated values for the parameters $E_a(0)$, α, $A(0)$, and β in Eqs. 11 and 12

Alcohol/Solvent	$E_a(0)$ kJ mol^{-1}	α kJ mol^{-1}	$A(0)$ ps K	β J K^{-1}mol^{-1}
Ethanol/Cyclohexane[11]	18.0	15.1	36.4	33.1
1-Hexanol/Cyclohexane[12]	33.1	5.9	0.41	10.5
1-Octanol/Cyclohexane[12]	36.8	5.0	0.13	11.7
1-Propanol/Benzene[16]	23.0	5.9	9.0	15.5

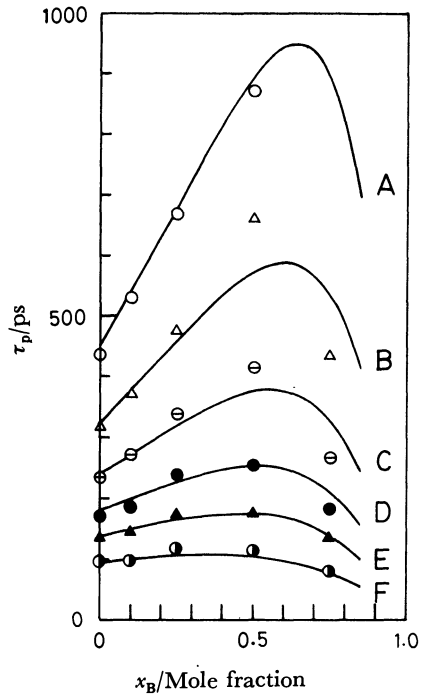

Fig. 3. Variation of τ_p with x_B for the ethanol/cyclohexane solutions. The solid lines show τ_p *vs.* x_B calculated by the use of Eq. 15 with the parameter values given in Table 1. Each set of points show the τ_p values observed at the following temperature.[11]
(A, ○): 268 K, (B, △): 278 K, (C, ⊖): 288 K, (D, ●): 298 K, (E, ▲): 308 K, (F, ◑): 323 K.

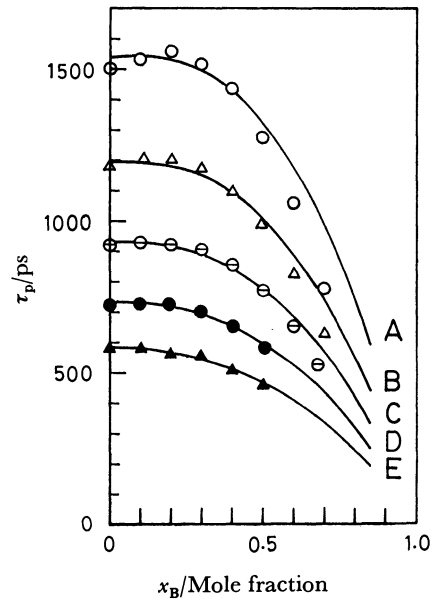

Fig. 4. τ_p *vs.* x_B for the 1-hexanol/cyclohexane solutions. The solid lines show τ_p *vs.* x_B calculated by the use of Eq. 15 with the parameter values given in Table 1. Each set of points show the τ_p values observed at the following temperature.[12]
(A, ○): 288 K, (B, △): 293 K, (C, ⊖): 298 K, (D, ●): 303 K, (E, ▲): 308 K.

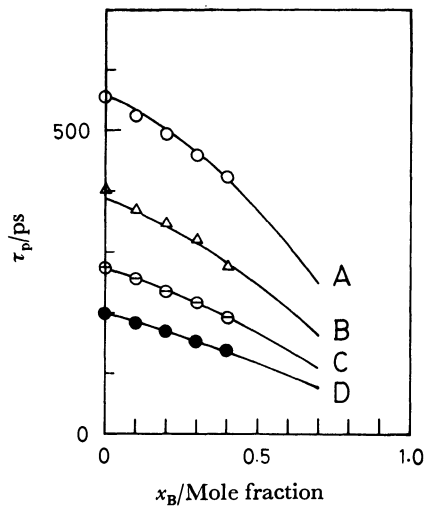

Fig. 5. τ_p *vs.* x_B for the 1-propanol/benzene solutions. The solid lines show τ_p *vs.* x_B calculated by the use of Eq. 15 with the parameter values given in Table 1. Each set of points show the τ_p values observed at the following temperature.[16]
(A, ○): 283 K, (B, △): 293 K, (C, ⊖): 303 K, (D, ●): 313 K.

results of calculation especially for the ethanol/cyclohexane (Fig. 3), 1-hexanol/cyclohexane (Fig. 4), and 1-octanol/cyclohexane solutions are not in good agreements with the data already reported.[11,12] In this region the approximate equations, (5), (11), and (12), cannot be applied to the systems in question. This is one of the main reasons for the deviation of the theoretical curves from the experimental data. In spite of such a deviation, the theoretical curves in Figs. 3 and 4 clearly predict the observations that the principal dielectric relaxation times of ethanol and 1-hexanol increase on the initial addition of cyclohexane, reach a maximum and then decrease. This result demonstrates the validity of our model proposed to the dielectric relaxation process of alcohol solutions.

From Eq. 3 it can be concluded that the principal relaxation times of alcohol solutions are determined by two factors. The first one is $(1+Kx_A)$, which depends on the distribution of chain lengths of hydrogen-bonded multimers,[17] and the other is τ_H. In the previous paper[1] we assumed that τ_H is constant. Using the thermodynamics of τ_H, which was explained in the preceding section, we can now discuss the dilution and temperature effects of τ_P in further detail.

Equation 9 indicates that the activation energy $E_a(x_B)$ is the sum of ΔH^* (the rotational activation energy of the terminal OH groups of hydrogen-bonded chain multimers) and $-\Delta H^\circ$ (the enthalpy change in the hydrogen-bond formation between chain-multimers and monomers). As the $-\Delta H^\circ$ values are in the region from 16 to 25 kJ/mol,[18] it is clear, from the $E_a(0)$ values listed in Table 1, that $\Delta H^*(0)$ of 1-hexanol and 1-octanol are larger than those of ethanol and 1-propanol; *i.e.*, the larger the hydrocarbon skelton of a primary alcohol is, the larger $\Delta H^*(0)$ becomes. The explanation for this can be given by a mechanism in which a third

alcohol molecule approaches with its oxygen atom oriented favorably to activate the OH group of the terminal molecule hydrogen-bonded to the neighboring one. With the increase in the size of the alcohol molecules the proximate presence of the hydrogen-acceptor atom to the terminal OH group becomes more and more scarce, causing the increase in the value of $\Delta H^*(0)$. In a similar manner we can explain the positive α values for the primary alcohols listed in Table 1. The addition of solvents such as cyclohexane and benzene to primary alcohols is considered to decrease the probability of the approach of an alcohol molecule near the terminal OH group, making it rotational activation more difficult. This will cause the increase in ΔH^* for the primary alcohol solutions.

Based on the activation energies observed for the ethanol/cyclohexane solutions and various pure alcohols, Sagal[11] proposed a mechanism to the dielectric relaxation process of alcohols. In his model the main mechanism of the relaxation is a switching process of hydrogen bonds. The reasoning for the explanation of the dependence of activation energy on the molecular size and shape of alcohols is similar to that given in this paper. Sagal, however, neither gave any explicit model to the structure of liquid alcohols and alcohol solutions, nor specify the OH group to any particular part of the structure. Therefore, although Sagal also noted that the energy necessary to reorient an OH group ($E_a(x_B)$) should be greater than that required to break a hydrogen bond ($-\Delta H^\circ$), he discussed the relationship between these two energies rather ambiguously.

References

1) Part I: R. Minami, K. Itoh, H. Sato, H. Takahashi, and K. Higasi, *Bull. Chem. Soc. Jpn.*, **54**, 1320 (1981).

2) R. Minami, K. Itoh, H. Takahashi, and K. Higasi, *J. Chem. Phys.*, **73**, 3396 (1980).

3) W. Feller, "An Introduction to Probability Theory and Its Applications," Wiley, New York (1957), Vol. 1.

4) I. Prigogine and R. Defay, "Chemical Thermodynamics," Longmans Green, London (1954), Chap. 26.

5) W. Dannhauser and L. W. Bahe, *J. Chem. Phys.*, **40**, 3058 (1964); W. Dannhauser, *ibid.*, **48**, 1911 (1968). See also Ref. 6, pp. 274—276.

6) N. E. Hill, W. E. Vaughan, A. H. Price, and M. Davies, "Dielectric Properties and Molecular Behaviour," Van Nostrand, London (1969), Chap. 5, p. 352.

7) J. Crossley, *Adv. Mol. Relax. Processes*, **2**, 69 (1970).

8) T. Koshii, E. Arie, M. Nakamura, H. Takahashi, and K. Higasi, *Bull. Chem. Soc. Jpn.*, **47**, 618, 623 (1974).

9) H. Sato, H. Takahashi, and K. Higasi, *Chem. Lett.*, **1976**, 623.

10) E. Arie, M. Nakamura, H. Takahashi, and K. Higasi, *Chem. Lett.*, **1973**, 533.

11) M. W. Sagal, *J. Chem. Phys.*, **36**, 2437 (1962).

12) H. Komooka, *Bull. Chem. Soc. Jpn.*, **45**, 1696 (1972).

13) S. Glasstone, K. J. Laidler, and H. Eyring, "The Theory of Rate Processes," McGraw-Hill, New York (1941), Chap. 9, pp. 547—551.

14) J. Middelhoek and C. J. F. Böttcher, "Molecular Relaxation Processes," *Chem. Soc. Spec. Publ.*, **20**, 69 (1966).

15) P. Bordewijk, F. Gransch, and C. J. F. Böttcher, *J. Phys. Chem.*, **73**, 3255 (1969).

16) T. Koshii, H. Takahashi, and K. Higasi, *Bull. Chem. Soc. Jpn.*, **48**, 993 (1975).

17) R. Minami, Doctor Thesis, Waseda University, Tokyo, Japan, 1981.

18) G. C. Pimentel and A. L. McClellan, "The Hydrogen Bond," W. H. Freeman & Company, San Francisco, California (1960), Chap. 7 and Appendices.

Reactions of Aromatic Radical Anions with Benzhydryl Chloride Studied by Pulse Radiolysis

Setsuo TAKAMUKU,* Hitoshi KIGAWA, Susumu TOKI, Kunihiko TSUMORI, and Hiroshi SAKURAI
The Institute of Scientific and Industrial Research, Osaka University, Suita, Osaka 565
(Received May 8, 1981)

Reactions of the aromatic radical anions with benzhydryl chloride have been investigated by pulse radiolysis. The second-order rate constants were determined for the reactions of benzhydryl chloride with various aromatic radical anions. On the basis of the linear relationship between the free energy and the activation energy, an irreversible electron transfer with an early transition state was elucidated.

Electron transfer reactions (ET) to generate radical-ion intermediates have been of wide-spread interest, especially in the photochemistry connected with solar energy storage. Of particular importance is a system where an endergonic and irreversible ET step is followed by a rapid chemical reaction. In such a system, chemical reactions *via* the radical ions of a substrate can be initiated by a mediator (radical ion) which possesses a lower redox potential than that of the substrate. The system is, thus, of great value for organic synthesis.[1] The interpretation of the kinetics for the system has been carried out by Schuster,[2] based upon the model proposed by Rehm and Weller.[3]

We report herein the measurement of the absolute rate constants for the reactions of aromatic radical anions with benzhydryl chloride and the mechanism of the irreversible ET by a pulse radiolysis technique. The reactions of aromatic radical anions with alkyl and aromatic halides have been investigated by using electrochemical reactions,[4] organometallic compounds,[5] and also pulse radiolysis technique.[6] The currently accepted reaction mechanism includes an initial ET, producing an alkyl radical, and immediately following competitive reactions of the alkyl radical, such as reduction to carbanions, addition to aromatic radical anions, and radical-radical reacaions.[7]

However, we have observed that in the case of intramolecular reactions of biphenyl radical anions with a terminal alkyl chloride which is linked to biphenyl moiety by a methylene chain, an intramolecular S_N2 reaction occurs.[8] Therefore, it seems essential to investigate the initial step of each respective reaction system, to determine whether it is an ET or S_N2 reaction.

Experimental

Materials. Benzhydryl chloride (Tokyo Kasei) was recrystallized twice from the ethanol solution and dried under high vacuum. The white crystal was stored in a refrigerator with silica gel as a drying agent (mp 16 °C). Biphenyl, phenanthrene, *trans*-stilbene, pyrene, and anthracene were purified by recrystallization or sublimation in the usual method. 2-Methyltetrahydrofuran (Wako Pure Chemicals) was distilled over $LiAlH_4$ three times.

Pulse Radiolysis. The L-band linear accelerator at Osaka University was used as the source of electron pulses.[9] The energy was 28 MeV and a 10 ns pulse width was selected for the present experiments. A detector (1P28 photomultiplier) and analyzing light produced by a 450W-Xenon pulse lamp (OPG-450, Osram) were used, and signals were monitored by a storage oscilloscope (Tektronix 7843) and a programmable digitizer (Tektronix 7912AD).

Fresh MTHF solutions were prepared just before irradiation and degassed under high vacuum. The following absorption bands were used in order to monitor the decay rate of the various aromatic radical anions: biphenyl (410 nm), phenanthrene (450 nm), *trans*-stilbene (500 nm), pyrene (495 nm), and anthracene (670 nm).

Results and Discussion

2-Methyltetrahydrofuran (MTHF) solutions of biphenyl containing benzhydryl chloride (BC) were irradiated with a 10 ns electron pulse of a 35 MeV L-band linear accelerator at room temperature. The transient absorption spectra were recorded at various times after the pulse; these are presented in Fig. 1.

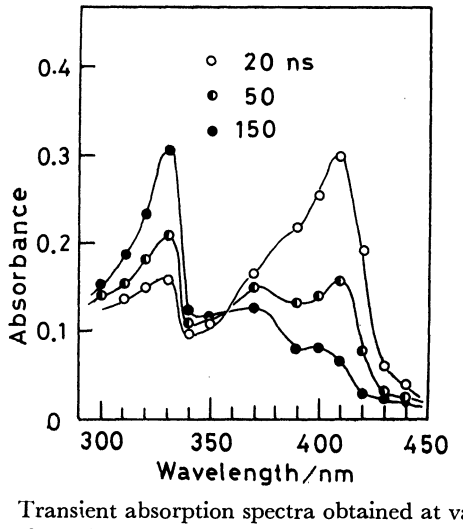

Fig. 1. Transient absorption spectra obtained at various times after a 10 ns pulse irradiation of a MTHF solution of biphenyl (50 mM) and BC (11 mM) mixture. Absorbed dose: 8.8 krad per pulse.

The spectrum observed immediately after the pulse has an absorption maximum at 410 nm, which is assigned to the biphenyl radical anions.[10] The 410-nm band decays according to the pseudo-first-order kinetics with the simultaneous formation of a 330-nm band. This latter band is assigned to a benzhydryl radical, by comparison with the spectrum obtained by the pulse radiolysis of a MTHF solution of BC.[11] The rate of formation of the 330-nm band is fully consistent with

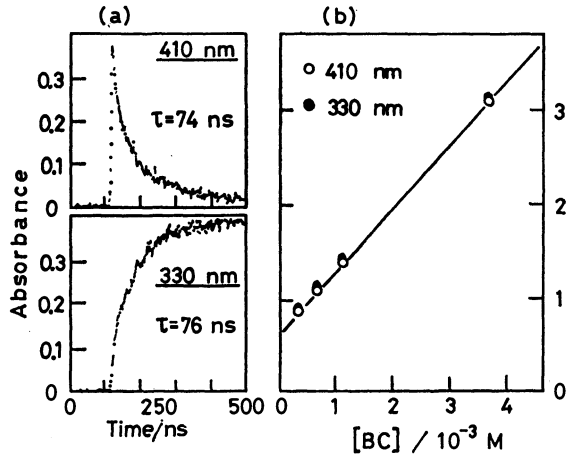

Fig. 2. Kinetic behavior of each band in Fig. 1 (a) The time dependency of transient absorption at 410- and 330-nm bands in Fig. 1. (b) The plot of the pseudo-first-order rate constant obtained from the 330-nm band formation and from the 410-nm band decay *vs.* BC concentration.

the decay rate of the 410-nm band, as shown in Fig. 2a. The plot of the pseudo-first-order rate constant *vs.* the BC concentration is linear; its slope results in the second-order rate constant: $k_S=7.0\times10^9$ M^{-1} s^{-1} (1 M=1 mol dm^{-3}). The two slopes obtained from the 330-nm band formation and the 410-nm band decay are in fair agreement within experimental error (Fig. 2b). Thus, the following equation is supported [M: biphenyl, BC: benzhydryl chloride]:

$$M^{\cdot-} + BC \xrightarrow{k_s} M + Ph_2CH\cdot + Cl^-.$$

In order to clarify the reaction mechanism, the second-order rate constants for the reaction of BC with aromatic radical anions of varying reduction potentials have been determined by a similar method to that described above. The plot of ln k_S as a function of the electrochemical half-wave potentials of the aromatic hydrocarbon (M)[12] yields a linear correlation, except for biphenyl, where the rate constant reaches the diffusion-controlled region, as shown in Fig. 3. The slope of the straight line is −9.45 in the units used here,† which corresponds to $-0.25/RT$.

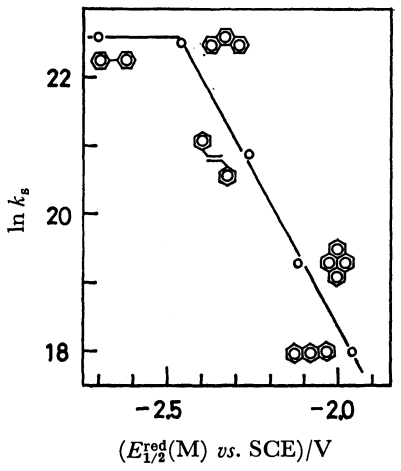

Fig. 3. Dependence of k_s on the reduction potential of various aromatic hydrocarbons.

According to Rehm and Weller,[3] the electron transfer mechanism can be described by the following reaction scheme.

$$M^{\cdot-} + BC \underset{k_{21}}{\overset{k_{12}}{\rightleftharpoons}} (M^{\cdot-}\cdots BC) \underset{k_{32}}{\overset{k_{23}}{\rightleftharpoons}} (M\cdots BC^{\cdot-}) \xrightarrow{k_{30}} M + Ph_2CH\cdot + Cl^-$$

In the present system, it is presumed that the ET step (k_{23}) is endergonic and that, even so, the $BC^{\cdot-}$ radical anion formed undergoes an irreversible bond cleavage at a rate faster than the back ET: thus, $k_{23}\ll k_{21}$ and $k_{32}\ll k_{30}$. Under such a circumstance, the following equation for the rate constant is obtained, applying a steady-state approximation:[2]

$$\ln k_s = \ln K_{12}k_i + \frac{\alpha E^{red}_{1/2}(BC)}{RT} - \frac{\alpha E^{red}_{1/2}(M)}{RT}, \quad (1)$$

where $K'_{12}=k_{12}/k_{21}$ and k_i is the rate constant for the reaction where $\Delta G_{23}=0$ and the activation barrier is $\Delta G_0^{\ddagger}$. $E^{red}_{1/2}$ is the electrochemical half-wave reduction potential of BC and M. The transfer coefficient α is defined as $\Delta G^{\ddagger}=\Delta G_0^{\ddagger}+\alpha\Delta G_{23}$ (see Ref. 2). The present observation appears to be in accord with the relationship expressed in Eq. 1, provided $\alpha=0.25$. If we presume the reversible ET step, the slope of the straight line should be $-1/RT$; this is incompatible with the present results.

Although a simple linear correlation between reactivities and the ionization potentials or the redox potentials of the substrates has been observed in many chemical reactions,[13] there is surprisingly little quantitative information and few discussions on the transfer coefficient. It is, however, worthwhile to mention that a reversible ET system affords a straight line with a slope of $-1/RT$, but a net α value is not obtained in such a system. The idea of the parameter α has been originally proposed by Horiuchi-Polanyi.[14] It is reasonable to accept that α reflects the position of the transition state, along with the reaction coordinate.[15]

Bank and Juckett reported a similar low α value (0.22) for the reaction of aromatic radical anions with alkyl bromides,[5] while $\alpha=0.72$ is calculated from the data presented for the reaction with chlorobenzene by Lund and coworkers.[4] On the basis of these observations, it seems that, when the C–X bond cleavage proceeds very rapidly, α becomes low. Such a low α value indicates an early transition state in which electrons localize mainly upon the aromatic hydrocarbon (M). Thus, it becomes questionable whether a full electron transfer from $M^{\cdot-}$ to BC goes to completion prior to the successive C–Cl bond cleavage in such a labile halide.

A simple estimation suggests that if α is less than one-half, ΔG should be negative.[15] Therefore, our interpretation is that in such a system where α is very low, an irreversible ET proceeds with an early transition state and this, therefore, closely correlates with a rapid C–Cl

† The slope is −9.45 when $E^{red}_{1/2}$ is expressed in V.

bond cleavage; a distinct discrimination between ET (k_{23}) and the successive bond cleavage (k_{30}) steps is difficult. The value of α would be considered as a parameter reflecting the extent of the ET in such a system.

The present work was supported in part by a Grant-in-Aid for Scientific Research No. 55334 from the Ministry of Education, Science and Culture.

References

1) M. M. Baizer, "Organic Electrochemistry," Marcel Dekker, New York (1973), Section G, p. 805; T. Shono, Y. Matsumura, J. Hayashi, and M. Mizoguchi, *Tetrahedron Lett.*, **1980**, 1867.

2) G. B. Schuster, *J. Am. Chem. Soc.*, **101**, 5851 (1979).

3) D. Rehm and A. Weller, *Israel J. Chem.*, **8**, 259 (1970).

4) H. Lund, M-A. Michel, and J. Simonet, *Acta Chem. Scand.*, **B 28**, 900 (1974).

5) S. Bank and D. A. Juekett, *J. Am. Chem. Soc.*, **97**, 567 (1975).

6) B. Bockrath and L. M. Dorfman, *J. Phys. Chem.*, **77**, 2618 (1973).

7) J. F. Garst, *Acc. Chem. Res.*, **4**, 400 (1971); J. F. Garst, R. D. Roberts, and B. N. Abels, *J. Am. Chem. Soc.*, **97**, 4925. (1975); J. F. Garst, R. D. Roberts, and J. A. Pacifici, *ibid.*, **99**, 3528 (1977).

8) H. Kigawa, S. Takamuru, S. Toki, N. Kimura, S. Takeda, K. Tsumori, and H. Sakurai, *J. Am. Chem. Soc.*, **103**, 5176 (1981).

9) H. Sakurai, M. Kawanishi, K. Hayashi, K. Tsumori, and S. Takeda, *Memoirs of the Inst. Sci. Ind. Res., Osaka Univ.*, **38**, 51 (1981).

10) N. Christodouleas and W. H. Hamill, *J. Am. Chem. Soc.*, **86**, 5413 (1964).

11) H. J. T. Chilton and G. Porter, *J. Phys. Chem.*, **63**, 904 (1959).

12) J. A. Dean, "Lange's Handbook of Chemistry," 11th ed, McGraw-Hill, New York (1973), p. 6.

13) S. Fukuzumi and J. K. Kochi, *J. Am. Chem. Soc.*, **102**, 7290 (1980).

14) S. Glasstone, K. J. Laidler, and H. Eyring, "The Theory of Rate Processes," McGraw-Hill, New York (1941), p. 145.

15) J. E. Leffler and E. Grunwald, "Rates and Equilibria of Organic Reactions," Wiley, New York (1963), p. 128.

The Application of Polarization Coherent Anti-Stokes Raman Spectroscopy to the Line-shape Analysis of Liquid Sample.

Ryosaku IGARASHI,* Fumisato IIDA,† Chiaki HIROSE,†† and Tsunetake FUJIYAMA

Institute for Molecular Science, Myodaiji, Okazaki 444

†*Department of Chemistry, Faculty of Science, Tokyo Metropolitan University, Setagaya-ku, Tokyo 158*

††*Research Laboratory of Resources Utilization, Tokyo Institute of Technology, Midori-ku, Yokohama 227*

(Received May 22, 1981)

The polarization CARS spectra were observed for a few typical Raman lines at various experimental settings. Based upon the observed and calculated spectra, the usefulness and the validity of the polarization CARS method for the study of the overlapped Raman lines observed for a condensed system have been emphasized.

The coherent anti-Stokes Raman scattering (CARS) experiment is a new method of Raman spectroscopy which utilizes the nonlinear optical phenomena induced by the macroscopic third-order nonlinear polarization, $\vec{P}^{(3)}$. This type of spectroscopy has been extensively applied in a wide range of laboratories utilizing the feature of the nonlinear phenomena.[1-5] The polarization CARS is one application of the CARS method, one in which the direction of the polarization of the incident and the scattered light are properly chosen.[6-8]

One of the most important and difficult problems in the field of application spectroscopy lies in the analyses of the spectral lines which are composed of two or more different lines whose resonance frequencies are very close to each other in comparison with their linewidths. For the analyses of the condensed-phase spectra, it is often necessary to resolve an observed line into a number of lines by assuming symmetric lineshape functions, like a Lorentzian or a Gaussian. This method is indeed useful for practical purposes. In many cases, however, the assumption of the lineshape functions is arbitrary in nature and falls short of experimental proof. We started the present work with the belief that we could perform this line-separation into multi-components on a purely experimental basis if we used the polarization CARS method.

In this study, we observe a few typical overlapped Raman lines by the polarization CARS method and ascertain the usefulness and validity of the application of the polarization CARS method for the study of the overlapped Raman lines observed for condensed systems.

Theoretical

Third-order Susceptibility in Liquid. CARS arises from a third-order nonlinear polarization which is induced in the medium at the frequency when $\omega_3 = 2\omega_1 - \omega_2$ by the incident lights, ω_1 and ω_2. This third-order nonlinear polarization at the ω_3 frequency can be expressed as:

$$\vec{P}^{(3)}(\omega_3) = \chi^{(3)}(\omega_3)\vec{E}(\omega_1)\vec{E}(\omega_1)\vec{E}^*(\omega_2), \quad (1)$$

where $\vec{E}(\omega_1)$ and $\vec{E}(\omega_2)$ are the amplitudes of the incident lights and where $\vec{P}^{(3)}(\omega_3)$ is the third-order susceptibility. As the CARS intensity is proportional to $|\vec{P}^{(3)}(\omega_3)|^2$, the CARS spectra are characterized by $\chi^{(3)}(\omega_3)$, which is a fourth-rank tensor. In general, $\chi^{(3)}(\omega_3)$ can be expressed as the sum of two terms:

$$\chi^{(3)}(\omega_3) = \chi^{NR} + \chi^{R}, \quad (2)$$

where χ^{NR} is an electronic or background susceptibility, and χ^{R}, a Raman susceptibility.

It has been established, for a spontaneous Raman scattering, that a totally symmetric Raman line is composed of two parts: an isotropic component and an anisotropic component. The linewidth of an anisotropic component is much broader than that of an isotropic one, because the isotropic linewidth is governed mainly by the reorientational relaxation process.[9] Therefore, it is preferable to write the χ^{R} of Eq. 2 in this form:

$$\chi^{R} = \sum_{r}\left(\frac{\chi^{rI}}{\delta_{rI} - i\Gamma_{rI}} + \frac{\chi^{rA}}{\delta_{rA} - i\Gamma_{rA}}\right), \quad (3)$$

where Γ_{rI} and Γ_{rA} are the linewidths of the isotropic and anisotropic components respectively; $\delta_r = \omega_r - (\omega_1 - \omega_2)$; ω_r is the Raman frequency of the r-th vibrational mode. In the derivation of Eq. 3, we assumed that $\omega_{rI} = \omega_{rA}$.[10]

In an isotropic medium, there are only two independent tensor components, $\chi^{(3)}_{1111}(-\omega_3 : \omega_1, \omega_1, -\omega_2)$ and $\chi^{(3)}_{1221}(-\omega_3 : \omega_1, \omega_1, -\omega_2)$, where 1 and 2 denote two distinguishable Cartesian axes. These tensor components are given by an orientational average of the susceptibilities of individual molecules. According to to Yuratich and Hanna,[11] χ^{rI} and χ^{rA} of Eq. 3 for an electronic non-resonant condition are given by these relations:

$$\chi^{rI}_{1111} = \frac{NL\alpha^2}{12\hbar}, \quad (4)$$

$$\chi^{rI}_{1221} = 0, \quad (5)$$

$$\chi^{rA}_{1221} = \frac{3}{4}\chi^{rA}_{1111} = \frac{NL}{12\hbar}\frac{\gamma_s^2}{15}, \quad (6)$$

where α^2 is the mean value and γ_s^2 is the symmetric part of the anisotropy of an usual Raman tensor. In this discussion we assumed that the antisymmetric part of the anisotropy is negligible. N is the number density of the Raman-active molecules, and L is the local-field correction factor.[1] It is important to add that the following relation holds approximately between the tensor components of χ^{NR}: it is known by the name of the Kleiman relation:

$$\chi^{NR}_{1111} = 3\chi^{NR}_{1221}. \quad (7)$$

Polarization CARS. From the above discussion

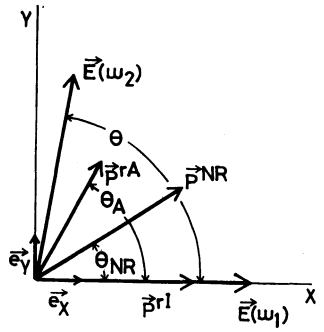

Fig. 1. Polarization directions for polarization CARS experiment.

it can be understood that the polarization, $\vec{P}^{(3)}(\omega_3)$, can be expressed as;

$$\vec{P}^{(3)}(\omega_3) = \vec{P}^{NR} + \sum_r (\vec{P}^{rI} + \vec{P}^{rA}), \tag{8}$$

where the superscripts correspond to those of Eqs. 2 and 3.

We set the experimental conditions as is shown in Fig. 1. One incident light, $\vec{E}(\omega_1)$, is linearly polarized to the X-direction, while the other incident light, $E(\omega_2)$, is polarized on the XY-plane at an angle; θ, with the X-direction. At this experimental setting, the terms of Eq. 8 are expressed by these relations:

$$\vec{P}^{NR} = 3\chi^{NR}_{1111} E_x^2(\omega_1)\{E_X(\omega_2)\vec{e}_X + \frac{1}{3}E_Y(\omega_2)\vec{e}_Y\}, \tag{9}$$

$$\vec{P}^{rI} = \frac{NL\alpha^2 E_x^2(\omega_1)E_X(\omega_2)}{4\hbar(\delta_{rI} - i\Gamma_{rI})}\vec{e}_X, \tag{10}$$

$$\vec{P}^{rA} = \frac{NL\gamma_S^2 E_x^2(\omega_1)}{60\hbar(\delta_{rA} - i\Gamma_{rA})}\left(\frac{4}{3}E_X(\omega_2)\vec{e}_X + E_X(\omega_2)\vec{e}_Y\right), \tag{11}$$

where $\vec{e}_X$ and $\vec{e}_Y$ are unit vectors in the directions of X and Y respectively. If we designate the angles between the X-axis and the vectors, $\vec{P}^{NR}$, $\vec{P}^{rI}$, and $\vec{P}^{rA}$, as θ_{NR}, θ_I, and θ_A respectively (see also Fig. 1), Eqs, 9, 10, and 11 lead to these relations:

$$\tan\theta_{NR} = \frac{E_Y(\omega_2)}{3E_X(\omega_2)} = \frac{1}{3}\tan\theta, \tag{12}$$

$$\tan\theta_I = 0, \tag{13}$$

and

$$\tan\theta_A = \frac{3E_Y(\omega_2)}{4E_X(\omega_2)} = \frac{3}{4}\tan\theta. \tag{14}$$

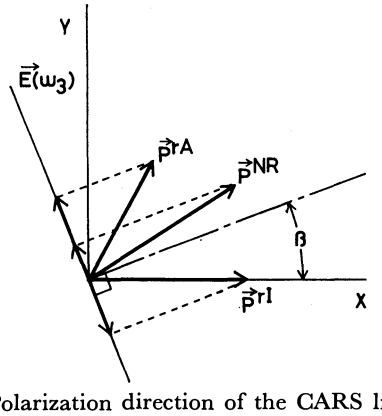

Fig. 2. Polarization direction of the CARS light which passed through the polarization analyzer.

The amplitude of the CARS light, $\vec{E}(\omega_3)$, is proportional to the polarization, $\vec{P}^{(3)}(\omega_3)$, so the observed amplitude, $\vec{E}(\omega_3)$, can have only one polarization state, which is defined by the vector-sum of $\vec{P}^{NR}$, $\vec{P}^{rI}$, and $\vec{P}^{rA}$. In this respect, the CARS light is obviously different from that of the spontaneous Raman scattering. As can be seen from Fig. 2, we can obtain various spectra by setting the polarization direction of the CARS light by putting a polarization analyzer in the path of the CARS light. If we cut off that light whose polarization direction makes an angle; β, with the X-axis, the amplitude, $E(\omega_3)$, which penetrates through the analyzer may be given by this relation:

$$E(\omega_3) \propto \{|\vec{P}^{NR}|\sin(\theta_{NR} - \beta) + \sum_r [|\vec{P}^{rI}|\sin(-\beta) + |\vec{P}^{rA}|\sin(\theta_A - \beta)]\}. \tag{15}$$

Especially, we can obtain "background-free" spectra if we set the experimental condition at $\beta = \theta_{NR}$.

Experimental

Apparatus for Polarization CARS Measurement. A schematic diagram of the polarization CARS spectrometer is shown in Fig. 3. A N_2 laser is oscillated at 337.1 nm with a peak output of 300 kW. The time-width of the N_2 laser is 7 ns, and the repetition rate is 4 Hz. This N_2 laser output is used to pump two dye lasers, 1 and 2, simultaneously. The frequency, ω_1, of the dye laser 1 is fixed at 19200 cm^{-1} (HWHM=0.4 cm^{-1}), while the frequency, ω_2, of the dye laser 2 (HWHM=0.6 cm^{-1}) is tunable. The directions of the polarization of ω_1 and ω_2 are adjusted by the use of two Glan-Laser prism polarizers, GP_1 and GP_2. The two light-beams, ω_1 and ω_2, are adjusted to be parallel with each other before a lens, L_1 (f= 10 cm), and then focused into a sample cell. The phasematching angle is adjusted by sliding a mirror, M_1. The scattered light is selected out by the use of an appropriate aperture. The polarization direction of the CARS light is selected out by means of a Glan-Laser prism polarizer, GP_3. After being passed through a depolarizer, DP, the CARS light is focused into a monochromator (JEOL, Model UI double-monochromator). Finally, the monochromated CARS light is detected by means of a photomultiplier (RCA-1P21) and averaged by the use of a laser photometer (Molectron, LP-20).

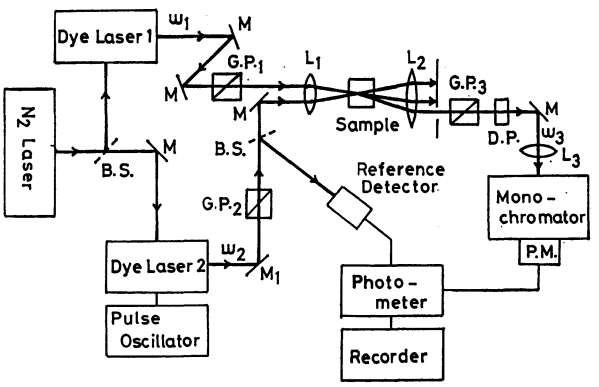

Fig. 3. Schematic representation of the experimental set-up.
BS: Beam splitter, M: mirror, GP: Glan prism, DP: depolarizer, PM: photomultiplier.

A part of the ω_2 is taken out by the use of a beamsplitter, BS, and used for the purpose of the normalization of the CARS light and for the triggering of the photometer. The depolarizer, DP, is used for the cancellation of the polarization characteristics of the monochromator.

Measurement of Ordinary Raman Spectra. The ordinary Raman spectra were recorded by a JEOL, JRS-400T Raman spectrophotometer equipped with an Ar^+-ion laser source (Spectra Physics, Model 164, 488.0 nm). A PL filter (Kenko) was used as a polarizer after being corrected for the polarization characteristics.

Sample. All the chemicals used in the present work were commercially available in a guaranteed grade and were used without further purification. The Raman spectra were observed for pure liquid toluene and chlorobenzene for a binary mixture (1 : 1 in volume) of them. The Raman spectra were also observed for pure liquid styrene.

Results and Discussion

For the purpose of dealing with the CARS lineshapes of Raman modes in liquid, we write the electric field of a CARS light being observed in this form:

$$E(\omega_3)=B\sin(\theta_{NR}-\beta)+\sum_r\left[\frac{R_{rI}\sin(-\beta)}{\delta_r-i\Gamma_{rI}}+\frac{R_{rA}\sin(\theta_A-\beta)}{\delta_r-i\Gamma_{rA}}\right], \quad (16)$$

where:

$$B\propto|\vec{P}^{NR}|=\sqrt{9+\tan^2\theta}\,\chi^{NR}_{1111}E_x^2(\omega_1)E_x(\omega_2), \quad (17)$$

$$R_{rI}\propto\frac{|\vec{P}^{rI}|}{\delta_r-i\Gamma_{rI}}=\frac{NL\alpha^2}{4\hbar}E_x^2(\omega_1)E_x(\omega_2), \quad (18)$$

and

$$R_{rA}\propto\frac{|\vec{P}^{rA}|}{\delta_r-i\Gamma_{rA}}=\sqrt{16+9\tan^2\theta}\times\frac{NL\gamma_s^2}{180\hbar}E_x^2(\omega_1)E_x(\omega_2). \quad (19)$$

Depolarized Raman Lines. A depolarized Raman line has only γ_s^2 in the Raman tensor. Therefore, the polarization CARS spectra expected for this case are represented by this relation:

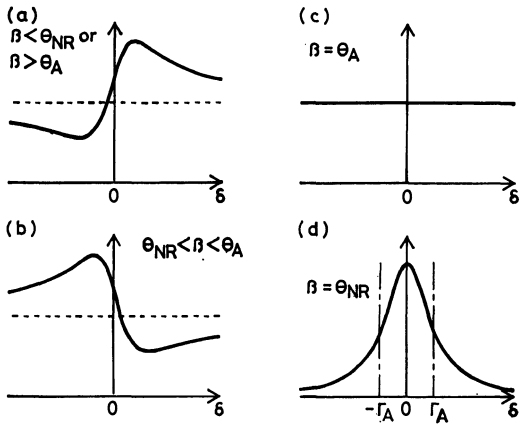

Fig. 4. Typical polarization CARS spectra for an isolated single Raman line.
Remark that (d) corresponds to a "background-free" spectrum.

$$|E(\omega_3)|^2=\left|B\sin(\theta_{NR}-\beta)+\frac{R_A\sin(\theta_A-\beta)}{\delta-i\Gamma_A}\right|^2. \quad (20)$$

The typical spectra expected for this case are illustrated in Fig. 4. It can be seen from the figure that the spectral features change dramatically with the change in β. It must be emphasized that this is the only case in which the Raman line is composed of only one component.

Totally Symmetric Raman Lines. A totally symmetric Raman line is characterized by γ_s^2 and α^2. Therefore, the polarization CARS spectra can be represented by this relation:

$$|E(\omega_3)|^2=\left|B\sin(\theta_{NR}-\beta)+\frac{R_I\sin(-\beta)}{\delta-i\Gamma_I}+\frac{R_A\sin(\theta_A-\beta)}{\delta-i\Gamma_A}\right|^2. \quad (21)$$

It must be emphasized that a totally symmetric Raman line is composed of two components, isotropic and anisotropic, although it seems to be a single line. Thus, Eq. 21 has two Raman-resonant terms, in good contrast to Eq. 20.

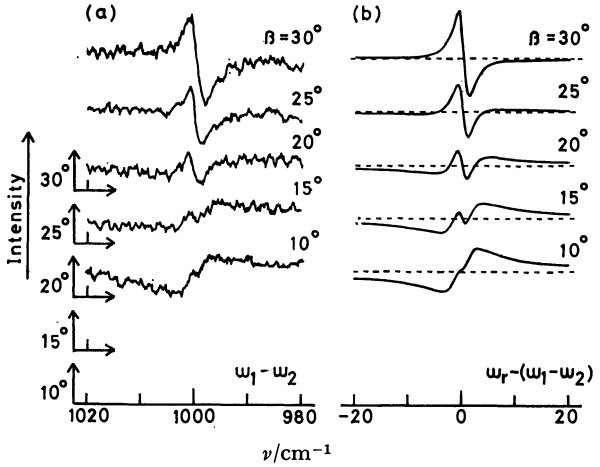

Fig. 5. Polarization CARS spectra for the 1000 cm^{-1} line of pure liquid styrene.
(a): Observed β-dependence, (b): Calculated β-dependence. The dotted lines indicate the background height; $B^2\sin^2(\theta_{NR}-\beta)$.

As an example, we observed the polarization CARS spectra of the 1000 cm^{-1} Raman line of pure liquid styrene for various β-values. Figure 5(a) shows the results for the experimental settings of $\theta=85°$ and $\beta=$ 10, 15, 20, 25, and 30°. The spontaneous Raman spectra of this line, on the other hand, are characterized by these spectral parameters: the polarization degree is 0.05, and the lineshapes are Lorentzian, with $\Gamma_I=$ 1.4 cm^{-1} for the isotropic line and with $\Gamma_A=2.5$ cm^{-1} for the anisotropic line. Using these spectral parameters, the polarization CARS spectra were calculated for this Raman line: the results are illustrated in Fig. 5(b).[12] The good agreement between the observed and the calculated spectra indicates that the physical meaning of the damping factors, Γ_I and Γ_A, which appear in the CARS formulation is essentially the same as that of the half-widths in the spontaneous Raman

scattering formulation.

It can be seen from Fig. 4 that we can clearly identify the existence of the two Raman components, the polarized and depolarized ones, by observing the polarized CARS spectra for various β-values. It is essential that, in the case of a totally symmetric Raman line, a Raman line should be considered to be overlapped lines whose frequencies are equal, but whose linewidths are different from each other.

Two Closely Located Totally Symmetric Raman Lines. In a case where two Raman lines are located very close to each other, we must consider the overlapping of four Raman lines: two isotropic components and two anisotropic components. As a model system, the binary mixture of toluene and chlorobenzene was chosen, because liquid toluene shows a Raman line at $\omega_r=1004$ cm^{-1}, with a depolarization degree of $\rho=0.018$ and with half-widths of $2\Gamma_I=2.1$ cm^{-1} and $2\Gamma_A=4.2$ cm^{-1}, while liquid chlorobenzene shows a Raman line at $\omega_r=1002.8$ cm^{-1}, with a depolarization degree of $\rho=0.025$ and with half-widths of $2\Gamma_I=1.5$ cm^{-1} and $2\Gamma_A=3.8$ cm^{-1}. These two Raman lines are assigned to the C–C stretching vibrations of the benzene rings and have almost equal intensities.

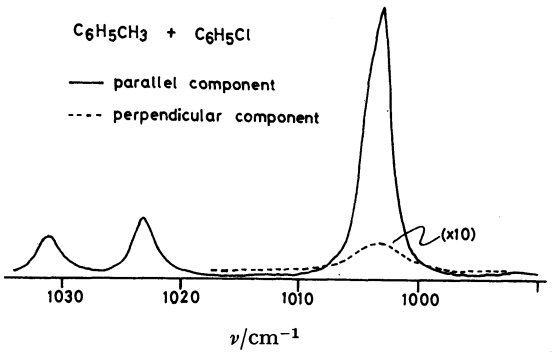

Fig. 6. Observed spontaneous Raman spectra for the binary mixture of toluene and chlorobenzene, (1 : 1 mixture in volume).

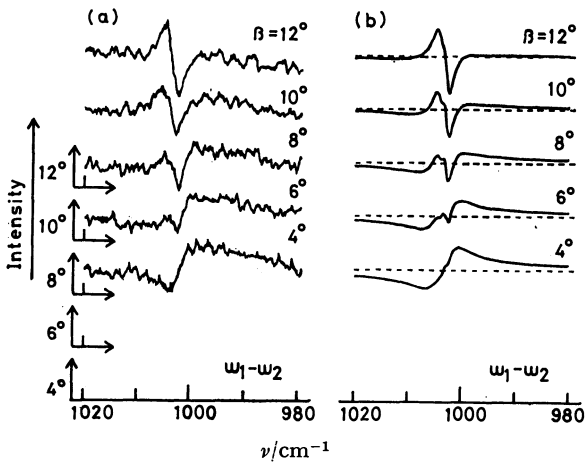

Fig. 7. Polarization CARS spectra for the binary mixture of toluene and chlorobenzene, (1 : 1 mixture in volume).
(a): Observed β-dependence, (b): Calculated β-dependence. The dotted lines indicate the background height, $B^2\sin^2(\theta_{NR}-\beta)$.

Figure 6 shows the Raman spectra observed for the binary solution of toluene and chlorobenzene. In this figure, two Raman lines are overlapped with each other at about 1000 cm^{-1}. It can be seen from the figure that it is almost impossible to separate this line into two Raman lines without knowing accurate spectral information about these individual lines. Figure 7(a) shows the observed polarization CARS spectra for $\theta=85°$ and for $\beta=4$, 6, 8, 10, and 12°. Figure 7(b) shows the results of the simulative calculation of the corresponding spectra on the basis of the above spontaneous Raman data. It can be seen from this figure that the overlapping of two Raman lines can easily be surmised by means of the asymmetric feature of the polarization CARS spectra. That is, the positive and negative peaks are quite different from each other both in shape and area, in good contrast with the spectra given in Fig. 5.[13]

Concluding Discussion. In the preceding paragraphs, the polarization CARS spectra have been discussed for three different cases: (1) a spectrum is composed of only one Raman line and only one component; that is to say, the line corresponds to one vibrational mode and one component: (2) a spectrum is composed of one Raman line which can be assigned to one vibrational mode, but is made from two components, namely, isotropic and anisotropic components, and (3) a spectrum corresponds to two overlapped Raman lines, each of which is made from isotropic and anisotropic components. From the results obtained, we can draw a few important conclusions with respect to the application of the polarization CARS method to the analysis of the overlapped Raman lines.

First, it has been shown that polarization CARS spectra should be analyzed by considering both isotropic and anisotropic scattering processes. It is essential to consider the difference between the isotropic and anisotropic linewidths. Therefore, the separation of the overlapped Raman lines into the individual vibrational lines is not so simple as has been described by Koroteev *et al.*[8] The apparent splittings in the CARS spectra cannot directly be related to the band-overlapping in ordinary Raman spectra.

Secondly, a polarization CARS method can be a useful technique to compare the isotropic and anisotropic components which are related to the same vibrational mode, because we can observe isotropic and anisotropic components separately by using a proper experimental setting. If we set $\beta=\theta_A$ or $\beta=\theta_I$, we can obtain a purely isotropic spectrum or a purely anisotropic spectrum respectively. For other angles, the spectra exhibit rather complicated features, namely, mixtures of isotropic and anisotropic spectra. As we can change the ratio of R_I and R_A properly by changing the θ, this method is extremely useful for the analysis of a Raman line whose depolarization degree is very small.

Thirdly, it has been shown that the polarization CARS spectra are quite sensitive to the change in the spectral parameters of component lines. Although the analyses of polarization CARS spectra themselves are rather complicated and difficult when several Raman modes are overlapped, the simultaneous use of spontaneous Raman and polarization CARS spectra is a very

promising method for the separation of the overlapped Raman lines into their component lines. We can ascertain the validity of the line-separation of overlapped ordinary Raman lines by simulating polarization CARS spectra using the spectral parameters obtained from the line-separation of ordinary Raman spectra. It must be emphasized, however, that this process is purely experimental.

References

1) M. D. Levenson and N. Bloembergen, *Phys. Rev. B*, **10**, 4447 (1974).

2) H. Lotem, R. T. Lynch, Jr., and N. Bloembergen, *Phys. Rev. A*, **14**, 1748 (1976).

3) J. W. Nibler and G. V. Knighten, "Coherent Anti-Stokes Raman Spectroscopy," in "Raman Spectroscopy of Gasses and Liquids," Topics in Current Physics, ed by A. Meber, Springer-Verlag (1979) Vol. II.

4) R. Igarashi, Y. Adachi, and S. Maeda, *J. Chem. Phys.*, **72**, 4308 (1980).

5) M. Shimizu, R. Igarashi, Y. Adachi, and S. Maeda, *J. Chem. Phys.*, **73**, 612 (1980).

6) S. A. Akhmanov and N. I. Koroteev, *Sov. Phys. JETP*, **40**, 650 (1975).

7) S. A. Akhmanov, A. F. Bunkin, S. G. Ivanov, and N. I. Koroteev, *Sov. Phys. JETP*, **47**, 667 (1978).

8) N. I. Koroteev, M. Endemann, and R. L. Byer, *Phys. Rev. Lett.*, **43**, 398 (1979).

9) F. J. Bartoli and T. A. Litovitz, *J. Chem. Phys.*, **56**, 404 (1972).

10) C. H. Wang and J. Mchale, *J. Chem. Phys.*, **72**, 4039 (1980).

11) M. A. Yuratich and D. C. Hanna, *Mol. Phys.*, **33**, 671 (1977).

12) The relative magnitude of R_I or R_A to B was determined from the simulation. The final parameters used for the simulation were: $\Gamma_I = 1.4\ cm^{-1}$, $\Gamma_A = 2.5\ cm^{-1}$, $R_I = 1.07B$, $R_A = 0.65B$, and $\omega_r = 1000.0\ cm^{-1}$.

13) The relative magnitudes of R_I and R_A to B were determined from the simulation. The final parameters were: $R_I = 1.03B$ and $R_A = 0.21B$ for toluene, and $R_I = 1.00B$ and $R_A = 0.30B$ for chlorobenzene.

Partition of Carboxylic Acids between Benzene and Aqueous Solution as Considered from the Regular Solution Theory

Yukio Fujii,† and Motoharu Tanaka*

†*Faculty of Engineering, Gifu University, Kagamihara, Gifu 504*

Laboratory of Analytical Chemistry, Faculty of Science, Nagoya University, Chikusa-ku, Nagoya 464

(Received July 10, 1981)

The partition of carboxylic acids between benzene and 0.1 mol dm^{-3}(H,Na)ClO_4 aqueous solution has been studied at 25 °C. Carboxylic acids used include acetic, propanoic, butanoic, pentanoic, hexanoic, and decanoic acids. The hydration of monomeric acids in benzene being taken into account, the hydration-corrected partition constant has been calculated. The effect of the chain length on the partition is accounted for with the aid of the newly estimated solubility parameters and empirical binary coefficients. Applicability of the empirical solubility parameter of water (35.89 $J^{1/2}$ $cm^{-3/2}$) has also been discussed.

The distribution behaviors of various organic compounds between two immiscible solvents have been extensively reviewed.[1-3] Milicevic[4] and Koshimura[5] have tried a systematic consideration on the solubility leading to a quantitative prediction of the partition of some organic compounds and metal chelates, respectively.

Of many attempts to introduce basic concepts into a general treatment of partition equilibria, the most successful one is the approach based on the theory of regular solution,[6] although its application to liquid-liquid partition is limited in some cases.[7]

The regular solution theory has been used to interpret the solvent effects on the extraction of organic compounds,[8,9] metal chelates,[10-12] halide complexes,[13,14] and ion pairs.[12,15] The same theory has been found useful in discussing the substituent effects on the partition of pyridine bases.[16]

In the previous papers,[17,18] we have presented the results of the partition of carboxylic acids between benzene and the aqueous solution. In this paper we attempt to interpret the effect of the chain length on the partition of carboxylic acids.

Theoretical

According to Hildebrand and Scatchard's theory of regular solution,[6] the activity of a solute HA, a_{HA}, is given by:

$$RT \ln a_{HA} = RT \ln x_{HA} + V_{HA}\phi_S^2(\delta_S - \delta_{HA})^2, \quad (1)$$

where x_{HA}, V_{HA}, and δ_{HA} denote the mole fraction, molar volume and solibility parameter, respectively, of the solute HA, and ϕ_S and δ_S the volume fraction and solubility parameter of the solvent S, respectively. The pure liquid was chosen as a standard state. The entropy of mixing molecules of the different size being taken into account, the following equation is relevant:

$$RT \ln a_{HA} = RT[\ln \phi_{HA} + \phi_S(1 - V_{HA}V_S^{-1})] + V_{HA}\phi_S^2(\delta_S - \delta_{HA})^2, \quad (2)$$

where the volume fraction of HA, ϕ_{HA}, is related with the molar concentration of HA, $[HA]_S$, as:

$$[HA]_S = 1000\,\phi_{HA}/V_{HA}. \quad (3)$$

Instead of using *the rigid geometric mean assumption* involved in the usual regular solution theory, we include an empirical binary coefficient,[19] $l_{HA,S}$, in Eq. 2. Then, we obtain:

$$RT \ln a_{HA} = RT(\ln [HA]_S - \ln 1000V_{HA}^{-1} + \phi_S(1 - V_{HA}V_S^{-1})) + V_{HA}\phi_S^2[(\delta_S - \delta_{HA})^2 + 2l_{HA,S}\delta_{HA}\delta_S]. \quad (4)$$

When the solute is partitioned between the aqueous and organic phases, *i.e.*, $a_{HA,w}=a_{HA,o}$, and that the concentration of HA is sufficiently low in both phases, *i.e.*, $\phi_w=1$ and $\phi_o=1$, we obtain from Eq. 4 the following expression for the partition constant of HA, $K_{D,HA}$:

$$\log K_{D,HA} = V_{HA}[(\delta_w-\delta_{HA})^2-(\delta_o - \delta_{HA})^2 + 2l_{HA,w}\delta_{HA}\delta_w - 2l_{HA,o}\delta_{HA}\delta_o + RT(V_o^{-1}-V_w^{-1})]/2.303RT, \quad (5)$$

where subscripts w and o denote the aqueous and organic phases, respectively. In Eq. 5 the aqueous solution is considered as a hypothetical regular solution.

Results and Discussion

Hydration and Partition Constants. At low pH, where anionic species may be neglected in the aqueous phase, the conditional partition constant of a monomeric carboxylic acid between the aqueous and organic phases, $K'_{D,HA}$, is written as:

$$HA_w \overset{\beta_{11}}{\rightleftharpoons} HA'_o, \quad K'_{D,HA} = [HA']_o/[HA]_w. \quad (6)$$

Measurement of water solubility[17,18] revealed that the monomeric acids are more or less hydrated in benzene contacted with water:

$$HA_o + H_2O_o \overset{\beta_{11}}{\rightleftharpoons} HA\cdot H_2O_o$$
$$\beta_{11} = [HA\cdot H_2O]_o/[HA]_o[H_2O]_o, \quad (7)$$

where β_{11} denotes the hydration constant. The conditional partition constant, $K'_{D,HA}$, determined from partition data is related with $K'_{D,HA}$, which is corrected for the hydration, as follows:

$$K_{D,HA} = K'_{D,HA}(1 + \beta_{11}[H_2O]_o)^{-1}, \quad (8)$$

where the monomer concentration of water in benzene at 25 °C is taken to be 0.0345 mol dm^{-3}.[18] The values for some aliphatic carboxylic acids are summarized in Table 1.

Evaluation of Solubility Parameters. If the heat of vaporization, ΔH^v/J mol^{-1}, is determined at a certain temperature, say 25 °C, the solubility parameter is given by:

$$\delta_{HA} = (\Delta H^v_{298} - RT)^{1/2}V_{HA}^{-1/2} \quad (9)$$

Table 1. Partition constant and hydration constant of carboxylic acids at 25 °C

Acid	$\log K'_{D,HA}$	$\log \beta_{11}$	$\log K_{D,HA}$ (obsd)	$\log K_{D,HA}$ (calcd)[g]
Acetic acid	−2.08	1.13	−2.25[a]	(−2.25)[f]
Propanoic acid	−1.34	0.99	−1.43[b]	−1.50
Butanoic acid	−0.97	0.98	−1.04[c]	−1.08
Pentanoic acid	−0.27	0.95	−0.39[c]	−0.43
Hexanoic acid	0.28	0.90	0.17[c]	0.16
Heptanoic acid	—	—	—	0.78
Octanoic acid	1.67[d]	—	—	1.35
Nonanoic acid	—	—	—	1.99
Decanoic acid	2.70[e]	—	2.62[a]	2.60

a) Y. Fujii, Y. Kawachi, and M. Tanaka, *J. Chem. Soc., Faraday Trans. 1*, **77**, 63 (1981). b) This work. c) Y. Fujii and M. Tanaka, *J. Chem. Soc., Faraday Trans. 1*, **73**, 788 (1977). d) G. K. Schweitzer and D. K. Morris, *Anal. Chim. Acta*, **45**, 65 (1969). e) M. Tanaka, N. Nakasuka, and S. Sasane, *J. Inorg. Nucl. Chem.*, **31**, 2591 (1969). f) Observed value used for calculation. g) Eq. 5.

where V_{HA}/cm^3 mol^{-1} is the molar volume of the pure liquid acid.

The lower monocarboxylic acids are known to dimerize in gas phase[20] even at pressure as low as 1 mmHg, and hence the heat of vaporization calculated from vapor pressure data only leads to erroneous results. The heat of vaporization from the vapor pressure data should be corrected for the heat of dimerization in the gas phase.[21] The heat of fusion should also be taken into account for the solid acids.[22] The corrected values of vaporization enthalpy in kJ mol^{-1} unit for fatty acids are given in Table 2. It has been shown by a number of workers[22-24] that there is a linear relationship between ΔH^v_{298} of the pure acids of a homologous series and its chain length. For a fatty acids, $CH_3(CH_2)_nCOOH$, we obtain the following best-fitting relation for the heat of vaporization ΔH^v_{298}/kJ mol^{-1} in Table 2:

Table 2. Heat of vaporization, molar volume, and solubility parameter of carboxylic acids at 25 °C

Acid	ΔH^v_{298} / kJ mol^{-1}	V_{HA}[d] / cm^3 mol^{-1}	δ_{HA}[e] / J$^{1/2}$ cm$^{-3/2}$
Acetic acid	51.5±1.7[a]	61.0	28.0
Propanoic acid	55.2±2.1[a]	77.5	26.1
Butanoic acid	58.6±4.2[a]	92.5	24.7
Pentanoic acid	62.3±2.9[b]	110.5	23.8
Hexanoic acid	73.2±2.1[b]	127.0	23.0
Heptanoic acid	72.0±1.7[b]	143.5	22.4
Octanoic acid	82.8±0.8[b]	160.0	21.9
Nonanoic acid	82.4±0.4[c]	176.5	21.5
Decanoic acid	89.5±2.1[c]	193.0	21.2

a) T. Konicek and I. Wadsö, *Acta Chem. Scand.*, **24**, 2612 (1970). b) C. G. Kruif and H. A. J. Oonk, *J. Chem. Thermodyn.*, **11**, 287 (1979). c) D. P. Baccanari, J. A. Novinski, Y. Pan, M. M. Yevitz, and H. A. Swain, *Trans. Faraday Soc.*, **64**, 1201 (1968). d) Calculated according to Eq. 11. e) Calculated according to Eq. 9 by employing calcul ated values of ΔH^v_{298} (Eq. 10) and V_{HA} (Eq. 11).

$$\Delta H^v_{298} = 50.3 + 4.9\,n, \tag{10}$$

where n denotes the number of CH_2 group. The increment in the heat of vaporization per CH_2, 4.9 kJ mol^{-1}, is in good agreement with that of (4.9±0.1) kJ mol^{-1} for normal alkanes, 1-alkenes, 1-alkanols, 1-alkanethiols, 1-chloro-, and 1-bromoalkanes and alkanoates.[23]

For the fatty acids, the molar volumes are proportional to chain length.[24-26] According to Rheineck and Lin,[26] the group contribution to the molar volume in cm^3 mol^{-1} unit is 34.0, 16.5 and 27.0 for methyl, methylene and carboxyl groups, respectively. Then the molar volume V_{HA}/cm^3 mol^{-1} for the fatty acids at 25°C is given by:

$$V_H = 61.0 + 16.5\,n, \tag{11}$$

where 61.0 cm^3 mol^{-1} for acetic acid was used as a standard for convenience.

With values of ΔH^v_{298} and V_{HA} in hand we calculate δ_{HA} of fatty acid by Eq. 9. Calculated δ_{HA} values are tabulated in Table 2.

As solubility parameter of the aqueous solution we used 47.9 J$^{1/2}$ cm$^{-3/2}$ calculated from the heat of vaporization of pure water.[27]

Determination of Binary Coefficients. We assume the additive property of excess enthalpy of mixing, ΔH^E, for functional groups in an organic compound X-$(CH_2)_n$-Y (abbreviated as X-n-Y), X, Y, and CH_2:

$$\Delta H^E_{X\text{-}n\text{-}Y} = \Delta H^E_X + n\Delta H^E_{CH_2} + \Delta H^E_Y. \tag{12}$$

The excess enthalpies of mixing of this compound and X, Y, and CH_2 are given by:

$$\Delta H^E_{X\text{-}n\text{-}Y} = V_{X\text{-}n\text{-}Y}[(\delta_s - \delta_{X\text{-}n\text{-}Y})^2 + 2l_{X\text{-}n\text{-}Y,s}\delta_{X\text{-}n\text{-}Y}\delta_s], \tag{13}$$

$$\Delta H^E_X = V_X[(\delta_s - \delta_X)^2 + 2l_{X,s}\delta_X\delta_s], \tag{14}$$

$$\Delta H^E_Y = V_Y[(\delta_s - \delta_Y)^2 + 2l_{Y,s}\delta_Y\delta_s], \tag{15}$$

$$\Delta H^E_{CH_2} = V_{CH_2}[(\delta_s - \delta_{CH_2})^2 + 2l_{CH_2,s}\,\delta_{CH_2}\delta_s], \tag{16}$$

where the subscript s denotes a solvent with which X-n-Y is mixed.

Substituting Eqs. 13—16 into Eq. 12 and assuming the additivity for the molar volume and the cohesive energy,[26] we obtain

$$\begin{aligned}(l_{X\text{-}n\text{-}Y,s} - 1)\delta_{X\text{-}n\text{-}Y}V_{X\text{-}n\text{-}Y} &= (l_{X,s} - 1)\delta_X V_X + n(l_{CH_2,s} - 1)\delta_{CH_2}V_{CH_2} \\ &\quad + (l_{Y,s} - 1)\delta_Y V_Y \qquad (17)\\ &= (l_{X\text{-}Y,s} - 1)\delta_{X\text{-}Y}V_{X\text{-}Y} + n(l_{CH_2,s} - 1)\delta_{CH_2}V_{CH_2}. \qquad (18)\end{aligned}$$

For an aliphatic carboxylic acid HA, X=CH_3 and Y=COOH. Then we may rewrite Eq. 18 as follows:

$$(l_{HA,s} - 1)\delta_{HA}V_{HA} = (l_{HA^\circ,s} - 1)\delta_{HA^\circ}V_{HA^\circ} + n(l_{CH_2,s} - 1)\delta_{CH_2}V_{CH_2}, \tag{19}$$

where HA° denotes acetic acid. Then the plot of the left hand side of Eq. 19 against n should give rise to a straight line with the intercept of $(l_{HA^\circ,s}-1)\delta_{HA^\circ}V_{HA^\circ}$ and the slope of $(l_{CH_2,s}-1)\delta_{CH_2}V_{CH_2}$.

The binary coefficient $l_{HA,W}$ of hexanoic to nonanoic acids was determined according to the following equation derived from Eq. 4:

$$\log[HA]_w = 3 - \log V_{HA} - 0.434\phi_w(1 - V_{HA}V_w^{-1}) - 0.434V_{HA}\phi_w^2[(\delta_w - \delta_{HA})^2 + 2l_{HA,w}\delta_{HA}\delta_w]/RT, \tag{20}$$

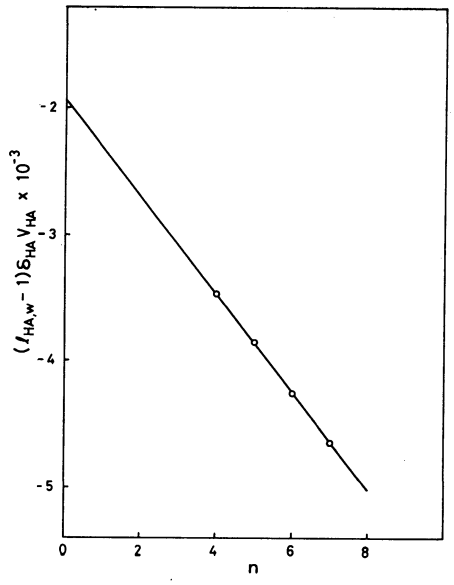

Fig. 1. Correlation between $(l_{HA,w}-1)\delta_{HA}V_{HA}$ and chain length. The line was drawn using the values $l_{CH_2,w}=-0.350$ and $l_{HA\circ,w}=-0.136$.

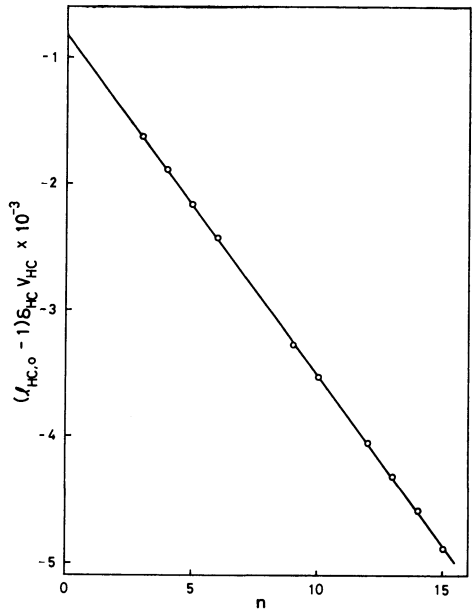

Fig. 2. Correlation between $(l_{HC,o}-1)\delta_{HC}V_{HA}$ and chain length. The line was drawn using the values $l_{CH_2,o}=0.055$ and $(l_{CH_3,o}-1)\delta_{CH_3}V_{CH_3}=-409$.

where $[HA]_w$ is the solubility of monomeric acid in water, corrected for the ionic dissociation. We utilized the solubility of carboxylic acids given by Ralston and Hoerr[28] interpolated to 25 °C.

As predicted from Eq. 19, $(l_{HA,w}-1)\delta_{HA}V_{HA}$ is linearly related with the number of methylene groups in carboxylic acids, n (see Fig. 1). By means of the method of least squares according to Eq. 19, we obtain

$$(l_{HA,w}-1)\delta_{HA}V_{HA}=-1940-386\,n. \quad (21)$$

That is $(l_{HA\circ w}-1)\,\delta_{HA\circ}V_{HA\circ}=-1940$ and $(l_{CH_2,w}-1)\times\delta_{CH_2}V_{CH_2}=-386$ in $J^{1/2}\,cm^{3/2}$ unit. From these equations together with values of $\delta_{HA\circ}V_{HA\circ}$ (Table 2) and $\delta_{CH_2}V_{CH_2}=286$ given by Rheineck and Lin,[26] the following binary coefficients are determined: $l_{HA\circ,w}=-0.136$ and $l_{CH_2,w}=-0.350$.

For hydrocarbons (abbreviated as HC), X=Y=CH_3 in Eq. 17. Then we obtain Eq. 22 for the subscript s=o

$$(l_{HC,o}-1)\delta_{HC}V_{HC}=2(l_{CH_3,o}-1)\delta_{CH_3}V_{CH_3}+n(l_{CH_2,o}-1)\delta_{CH_2}V_{CH_2}. \quad (22)$$

Table 3. Excess enthalpy of equimolar mixture at 298.15 K and derived binary coefficient

System	ΔH^E_{HC}/J mol^{-1}	$l_{HC,o}$
Pentane+Benzene	857[a]	0.028
Hexane+Benzene	898[b]	0.034
Heptane+Benzene	933[c]	0.037
Octane+Benzene	969[a]	0.039
Undecane+Benzene	1060[a]	0.045
Dodecane+Benzene	1101[a]	0.046
Tetradecane+Benzene	1183[a]	0.048
Pentadecane+Benzene	1207[a]	0.049
Hexadecane+Benzene	1256[a]	0.050
Heptadecane+Benzene	1289[a]	0.052

a) C. Menduina and M.Diaz-Pena, *Int. DATA Ser., Selec. Data Mixture, Ser. A*, p. 53, 55, 57—62 (1976). b) M. I. Paz-Andrade, *ibid.*, p. 100 (1973). c) J. P. E. Grolier, *ibid.*, p. 223 (1974).

Values of $l_{HC,o}$ for benzene was evaluated from the excess enthalpy of the system $C_6H_6+CH_3(CH_2)_nCH_3$ by means of Eq. 13. The results are tabulated in Table 3. Then the plot of the left hand side of Eq. 22 against n (Fig. 2) gives us the value $(l_{CH_3,o}-1)\,\delta_{CH_3}V_{CH_3}$ from the slope. By means of the method of least squares we obtain $(-270.3\pm1.0)J^{1/2}\,cm^{3/2}$ as $(l_{CH_3,o}-1)\,\delta_{CH_3}V_{CH_3}$ for benzene. $\delta_{CH_3}V_{CH_3}=286$ ($J^{1/2}\,cm^{3/2}$),[26] then we obtain $l_{CH_3,o}=0.055$.

Now according to Eq. 5 together with the known value of the partition constant of acetic acid (Table 1), we can determine the value of $l_{HA\circ,o}=0.034$ for benzene.

With these values of binary coefficients for benzene, we can rewrite Eq. 19 as follows:

$$(l_{HA,o}-1)\delta_{HA}V_{HA}=-1650-270\,n. \quad (23)$$

Values of $l_{HA,w}$ and $l_{HA,o}$ calculated by Eqs. 21 and 23, respectively, are summarized in Table 4.

Partition Constant of Aliphatic Carboxylic Acids. With thus determined values of $l_{HA,w}$ and $l_{HA,o}$ in hand, Eq. 5 enable us to predict the partition constant of aliphatic carboxylic acids. We utilized $\delta_w=47.9\,J^{1/2}$

Table 4. Binary coefficients of carboxylic acids

Acid	$l_{HA,w}\times10$		$l_{HA,o}\times10^2$
	Eq. 21	Solubility[a]	Eq. 23
Acetic acid	−1.36	—	3.4
Propanoic acid	−1.50	—	4.7
Butanoic acid	−1.68	—	5.4
Pentanoic acid	−1.78	—	6.2
Hexanoic acid	−1.93	−1.90	6.3
Heptanoic acid	−2.04	−2.05	6.5
Octanoic acid	−2.15	−2.14	6.5
Nonanoic acid	−2.23	−2.24	6.6
Decanoic acid	−2.29	—	6.7

a) Calculated from the data in Ref. 28.

$cm^{-3/2}$ and $\delta_o = 18.7\ J^{1/2}\,cm^{-3/2}$. Calculated values of the partition constant are listed in Table 1. It is evident that the values calculated by Eq. 5 compare very favorably with the experimental.

It is known that, in a homologous series, the partition constant $\log K_D$ is a linear function of the number of carbon atoms involved. According to Eq. 5, the increment of $\log K_D$ for an added methylene group may be written as:

$$\Delta \log K_D/CH_2 = V_{CH_2}[(\delta_w - \delta_{CH_2})^2 - (\delta_o - \delta_{CH_2})^2 + 2l_{CH_2,w}\delta_{CH_2}\delta_w - 2l_{CH_2,o}\delta_{CH_2}\delta_o + RT(V_o^{-1} - V_w^{-1})]/2.303RT. \quad (24)$$

Here we assume the additivity of molar volume and cohesive energy of functional groups. Now with $V_{CH_2} = 16.5$, $\delta_{CH_2} = 17.44$(Ref. 26), $l_{CH_2,w} = -0.350$ and $l_{CH_2,o} = 0.055$ for benzene, we obtain $\Delta \log K_D/CH_2 = 0.59$ for this solvent from Eq. 24. This value is consistent with the previous findings, *i.e.*, $\Delta \log K_D/CH_2 = 0.56$—$0.64$ for partition of alkanoic acids[3,29] and 1-alkanols[3] between benzene and water. It is worth noting from Eq. 24 that $\Delta \log K_D/CH_2$ depends on the organic solvent used, while it is independent of a polar group of alkyl compounds attached to the terminal. In Table 5 are listed values of $\Delta \log K_D/CH_2$ for several water-organic solvent systems together with $l_{CH_2,o}$, δ_o, and V_o. Interestingly values of $l_{CH_2,o}$ are very near to zero for all solvents as compared to $l_{CH_2,w} = -0.350$.

Table 5. $\Delta \log K_D/CH_2$ values for several organic solvent–water systems

Organic solvent	δ_o [e]	V_o [e]	$l_{CH_2,o} \times 10^2$ [f]	$\Delta \log K_D/CH_2$
Hexane	14.91	131.6	2.1	0.59
Cyclohexane	16.73	108.7	4.5	0.60
Carbon tetrachloride	17.48	97.1	3.9	0.59, 0.60[a]
Benzene	18.73	89.4	5.5	0.57, 0.60[b]
Nitrobenzene	20.45	102.7	4.0	0.56, 0.60[b]
1,2-Dichloroethane	20.16	79.6	2.2	0.60, 0.58[b]
Diisopropyl ether	14.48	142.3	2.3	0.57, 0.56[b]
1-Octanol	21.06	158.5	1.5	0.56, 0.54[c] 0.50[d]

a) S. S. Davis, T. Higuchi, and J. H. Rytting, *J. Pharm. Pharmacol.*, **24**, 30P (1972). b) I. Kojima, M. Yoshida, and M. Tanaka, *J. Inorg. Nucl. Chem.*, **32**, 987 (1970). c) A. Leo, C. Hansch, and D. Elkins, *Chem. Rev.*, **71**, 525 (1971). d) R. Collander, *Acta Chem. Scand.*, **5**, 774 (1951). e) Solubility parameter ($J^{1/2}\,cm^{-3/2}$) and molar volume ($cm^3\,mol^{-1}$) obtained from Refs. 24 or 27. f) Calculated according to Eq. 19.

Wakahayashi *et al.*[9] have used the following relationship for the partition constant $K_{B,o}$ of β-diketones and β-diketonates

$$\log K_{D,B} = V_B[(\delta'_w - \delta_B)^2 - (\delta_o - \delta_B)^2 + RT(V_o^{-1} - V_w^{-1})]/2.303RT, \quad (25)$$

where the subscript B denotes a solute partitioned between the aqueous and organic phases. Eq. 25 was successfully used for these systems with the empirical solubility parameter of water $\delta_w' = 35.89\ J^{1/2}\,cm^{-3/2}$.

Table 6. Empirical solubility parameter of water for different solute and solvent

System(solute–solvent)	$\delta'_w/J^{1/2}\,cm^{-3/2}$
Hexanoic acid–Benzene	34.6[a]
Decanoic acid–Benzene	35.1[a]
Aniline–Hexane	33.5[b]
Aniline–Carbon tetrachloride	33.8[c]
Aniline–Benzene	33.5[c]
Aniline–1-Octanol	34.5[d]
Nitropropane–Cyclohexane	34.4[e]
Nitropropane–Carbon tetrachloride	34.5[f]
Nitropropane–Toluene	36.0[e]
Nitropropane–Chloroform	36.4[e]
1-Pentanol–Hexane	35.4[g]
1-Pentanol–Benzene	35.3[g]
1-Pentanol–1-Octanol	37.1[h]
Phenol–Hexane	34.9[i]
Phenol–Benzene	35.5[i]
Phenol–1,2-Dichloroethane	35.1[j]
Phenol–1-Octanol	38.1[k]

Data source: a) This work. b) T. Sekine, Y. Suzuki, and N. Ihara, *Bull. Chem. Soc. Jpn.*, **46**, 995 (1973). c) W. Kemula, H. Buchowski, and W. Pawlowski, *Rocz. Chem.*, **43**, 1555 (1969). d) T. Fujita, J. Iwasa, and C. Hansch, *J. Am. Chem. Soc.*, **86**, 5175 (1964). e) W. Kemula, H. Buchowski, and J. Teperek, *Bull. Acad. Pol. Sci., Ser. Sci. Chem.*, **12**, 343 (1964). f) E. Kuznetsova, *Zh. Fiz. Khim.*, **48**, 2865 (1974). g) I. M. Korenman and Z. G. Chernorukova, *Zh. Prikl. Khim.*, **47**, 2523 (1974). h) A. Leo, C. Hansch, and D. Elkins, *Chem. Rev.*, **71**, 525 (1971). i) D. S. Abrams and J. M. Prausnitz, *J. Chem. Thermodyn.*, **7**, 61 (1975). j) W. Herz and W. Rathmann, *Z. Electrochem.*, **19**, 552 (1913). k) Ya. I. Korenman and V. Yu. Udalova, *Zh. Fiz. Chem.*, **48**, 1223 (1923).

δ_w' is considerably lower than the value obtained from the heat of vaporization $\delta_w = 47.9\ J^{1/2}\,cm^{-3/2}$. Comparison of Eq. 5 with Eq. 25 leads to the following:

$$(\delta'_w - \delta_B)^2 = (\delta_w - \delta_B)^2 + 2l_{B,w}\delta_B\delta_w - 2l_{B,o}\delta_B\delta_o, \quad (26)$$

in which δ'_w is correlated with the binary coefficients $l_{B,w}$ and $l_{B,o}$. From Eq. 26 it is obvious that δ'_w differs from solvent to solvent and from solute to solute. In Table 6 are listed values of δ'_w calculated for different solvents and solutes. If the values of δ'_w are compared for the same solute, they are close to each other for organic solvents of low polarity and limited tendency of hydrogen bonding. From this table may be seen the limit of the use of the empirical δ'_w values in the study of solvent effect on the extraction.

References

1) R. Collander, *Acta Chem. Scand.*, **3**, 717 (1949); **4**, 1085 (1950); **5**, 744 (1951).
2) A. Leo, C. Hansch, and D. Elkins, *Chem. Rev.*, **71**, 525 (1971).
3) S. S. Davis, *Sep. Sci.*, **10**, 1 (1975).
4) B. Milicevic, *Helv. Chim. Acta*, **46**, 1466 (1963).
5) H. Koshimura, *J. Inorg. Nucl. Chem.*, **38**, 1705 (1976); **39**, 148 (1977).
6) J. H. Hildebrand and R. L. Scott, "Solubility of

Nonelectrolytes," 3rd ed, Dover, New York (1957).
7) H. M. N. H. Irving, "Ion Exchange and Solvent Extraction," ed by J. A. Marinsky and Y. Marcus, Marcel Dekker, New York (1973), Vol. 6, p. 139.
8) W. Kemula, H. Buchowski, R. Lewandowski, W. Pawlowski, and J. Teperek, *Bull. Acad. Pol. Sci., Ser. Sci. Chim.*, **14**, 395 (1966).
9) T. Wakahayashi, S. Oki, T. Omori, and N. Suzuki, *J. Inorg. Nucl. Chem.*, **26**, 2255 (1964).
10) N. Suzuki, K. Akiba, and T. Kanno, *Anal. Chim. Acta*, **43**, 311 (1968).
11) H. A. Mottola and H. Freiser, *Talanta*, **13**, 55 (1966).
12) M. Tanaka, "Proc. Intern. Solvent Extraction Conference," ISEC 71, Soc. Chem. Industory, London (1971), Paper 66, Vol. 1, p. 18.
13) H. Irving and D. C. Lewis, *Proc. Chem. Soc.*, **1960**, 222.
14) S. Siekierski and R. Olszer, *J. Inorg. Nucl. Chem.*, **25**, 1351 (1963).
15) H. Freiser, *Anal. Chem.*, **41**, 1354 (1964).
16) K. Hirose and M. Tanaka, *J. Inorg. Nucl. Chem.*, **38**, 2285 (1976).
17) Y. Fujii and M. Tanaka, *J. Chem. Soc., Faraday Trans. 1*, **73**, 788 (1977).
18) Y. Fujii, Y. Kawachi, and M. Tanaka, *J. Chem. Soc., Faraday Trans. 1*, **77**, 63 (1981).
19) J. H. Hildebrand, J. M. Prausnitz, and R. L. Scott, "Regular and Related Solutions," Van Nostrand, New York (1970).
20) G. C. Pimentel and A. L. McClellan, "The Hydrogen Bond," W. H. Freeman, San Fransisco (1960).
21) T. Konicek and I. Wadsö, *Acta Chem. Scand*, **24**, 2612 (1970).
22) D. P. Baccanari, J. A. Novinski, Y. Pan, M. M. Yevitz, and H. A. Swain, *Trans. Faraday Soc.*, **64**, 1201 (1968).
23) M. Mansson, P. Sellers, G. Stridh, and S. Sunner, *J. Chem. Thermodyn.*, **9**, 91 (1977).
24) K. L. Hoy, "Tables of Solubility Parameters," Union Carbide Corp. (1961).
25) A. Dorinson, M. R. McCorkle, and A. W. Ralston, *J. Am. Chem. Soc.*, **64**, 2739 (1942).
26) A. E. Rheineck and K. F. Lin, *J. Paint Thechnol.*, **40**, 611 (1968).
27) A. F. M. Barton, *Chem. Rev.*, **75**, 731 (1975).
28) A. W. Ralston and C. W Hoer, *J. Org. Chem.*, **7**, 546 (1942).
29) I. Kojima, M. Yoshida, and M. Tanaka, *J. Inorg. Nucl. Chem.*, **32**, 987 (1970).

The Crystal and Molecular Structure of *trans*-2,2-Diphenyl-3,4-dichlorothietane

Shigekazu KUMAKURA

Department of Chemistry, Saitama University, 255 Shimo-okubo, Urawa 338

(Received December 8, 1980)

The crystal structure of the title compound has been determined by means of X-ray diffraction. The space group is $P\bar{1}$ with $a=11.665(4)$, $b=8.775(4)$, $c=7.092(2)$ Å, $\alpha=95.73(3)$, $\beta=84.36(3)$, $\gamma=104.90(2)°$, and $Z=2$. The structure was refined to $R=0.048$ for 1770 reflections collected on a four-circle diffractometer. The thietane ring is puckered with dihedral angles, C(2)SC(4)/C(2)C(3)C(4) and SC(2)C(3)/SC(4)C(3), of 150.1° and 149.9° respectively. The conformation of the C–Cl bonds with respect to the thietane skeleton is (3e4e), consistent with that in solution derived from the dipole moments. The average distance of the two C–Cl bonds is 1.781 Å. The C(2)–S, C(4)–S, and C(2)–C(3) bond distances are 1.872(4), 1.811(5), and 1.545(6) Å respectively; agreeing well with the corresponding bond distances observed in the *cis* isomer of the compound; however, the C(3)–C(4) of 1.506(6) Å is much shorter. The bisector of the bond angle formed by the ring substituents at each of the ring atoms is tilted out of the corresponding CCC or CCS planes within the thietane ring so as to increase the staggering of the neighboring substituents. The angle of tilt at C_β is larger than those at the C_α's. The intermolecular S···S contact of 4.080(5) Å is normal in view of the usual van der Waals radii.

Thietane is an example of four-membered ring molecules including a hetero-atom and differs from cyclobutane in the factors governing the geometry of four-membered ring systems. Recently theoretical and experimental investigations[1] on cyclobutane have indicated that the bisector of the methylene group is tilted out of the CCC plane of which the CH_2 group forms an apex and that the tilt of the CH_2 group appears to be an essential feature of bonding in the four-membered ring. Hence, detailed molecular geometries of thietane and its derivatives are required for comparative studies of the four-membered ring systems. The geometry of thietane itself was reported by Karakida and Kuchitsu;[2] however, the angles of tilts exhibited by the methylene groups are still unknown. Thus far, the only paper describing the tilting angle of the methylene group in thietane derivatives explicitly has been a microwave study of thietane 1-oxide by Bevan, Legon, and Millen;[3] the complete data of the molecular structure have not yet been presented. The present paper will describe a crystal-structure analysis of *trans*-2,2-diphenyl-3,4-dichlorothietane (abbreviated hereafter as *trans*-DCTE). The influence of the orientation of the ring substituents on the ring geometry is examined by comparing the molecular structure with that of *cis*-DCTE previously reported,[4] while the tilts of the ring substituents and the deformation of the thietane skeletons will be discussed in terms of the CNDO/2 method.

Experimental

The title compound was synthesised by a cycloaddition of thiobenzophenone to *trans*-dichloroethylene.[5] The crystals grown from a hexane solution are colorless plates. The lattice constants and intensity data were measured on a Philips PW 1100 automatic diffractometer, using Cu $K\alpha$ radiation monochromated by a graphite plate. The ω-2θ scan technique was employed with a scan speed of 4° min^{-1} in ω. The scan-width used was $(1.0+0.35\tan\theta)°$. A total of 1806 non-zero reflections were measured up to $\theta=78°$. 1770 reflections with $|F_o|\geq 3\sigma(|F_o|)$ were used for the analysis. Three standard reflections, monitored every two hours, showed a steady decline in intensity; at the end of data collection, the maximum reduction reached to 29%. The intensity data were put on a common scale by reference to the standard reflections. Lorentz and polarization corrections were applied, but no absorption correction was made ($\mu r\leq 0.5$). The crystal data are listed in Table 1.

Table 1. Crystal data

$C_{15}H_{12}Cl_2S$, F.W.=295.13
Triclinic, Space group: $P\bar{1}$
$a=11.665(4)$ Å
$b=8.775(4)$ Å
$c=7.092(2)$ Å
$\alpha=95.73(3)°$
$\beta=84.36(2)°$
$\gamma=104.90(2)°$
$V=696.02$ Å
$D_x=1.408$ Mg/m^3
$Z=2$
μ(Cu $K\alpha$)=5.345 mm^{-1}

Structure Analysis

The Cl and S positions were obtained from a sharpened Patterson map ($B=3.0$ Å^2). The positions of the remaining non-hydrogen atoms were determined by the heavy-atom method. A difference electron-density map computed at the stage of the R value of 0.07 revealed all the H atoms in plausible positions. Subsequent block-diagonal least-squares refinements including isotropic hydrogen atoms gave the final R value of 0.048. The weighting scheme of $w=1$ if $|F_o|\geq 10.0$ and $w=0.3$ otherwise was employed. The atomic scattering factors were taken from *International Tables for X-Ray Crystallography*.[6] The final atomic parameters are listed in Table 2. The atomic parameters for H atoms, the temperature factors for non-hydrogen atoms, and the list of observed and calculated structure factors are kept as Document No. 8149 at the Chemical Society of Japan.

The calculations were carried out on a HITAC 8700/8800 computer at the Computer Center of the

TABLE 2. FRACTIONAL ATOMIC COORDINATES ($\times 10^4$) AND EQUIVALENT THERMAL PARAMETERS (B_{eq}) FOR THE NON-HYDROGEN ATOMS, WITH e.s.d.'s IN PARENTHESES

	x	y	z	B_{eq}/Å^2
S	3295(1)	3658(1)	4876(2)	4.85
Cl(1)	3428(1)	2040(1)	−617(2)	4.68
Cl(2)	4945(1)	1504(2)	3726(2)	5.91
C(2)	2368(3)	3256(4)	2787(5)	3.70
C(3)	3146(4)	2148(5)	1896(6)	3.92
C(4)	4213(4)	2880(5)	3011(6)	4.44
C(11)	2458(3)	4729(5)	1721(6)	3.83
C(12)	3314(4)	6135(5)	2033(7)	4.89
C(13)	3352(4)	7432(5)	1011(8)	5.77
C(14)	2546(4)	7354(6)	−286(7)	5.66
C(15)	1701(4)	5949(6)	−629(7)	5.66
C(16)	1648(4)	4641(5)	376(6)	4.92
C(21)	1067(4)	2454(5)	3335(5)	3.88
C(22)	495(4)	1040(5)	2415(6)	4.53
C(23)	−714(4)	361(6)	2925(7)	5.18
C(24)	−1317(4)	1087(6)	4319(7)	5.74
C(25)	−756(5)	2507(6)	5278(7)	6.26
C(26)	459(4)	3178(5)	4768(7)	5.17

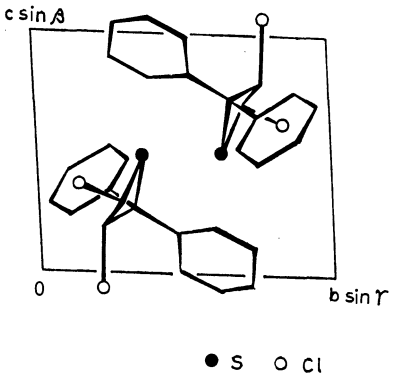

Fig. 1. A projection of the crystal structure along the a axis.

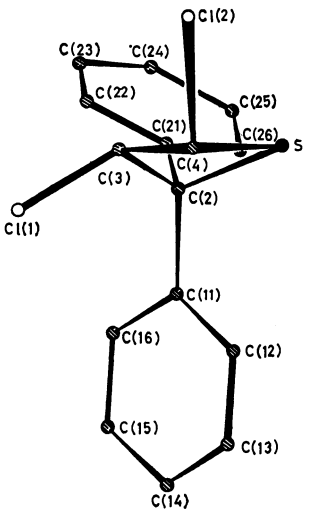

Fig. 2. The molecular conformation and the atomic numbering scheme.

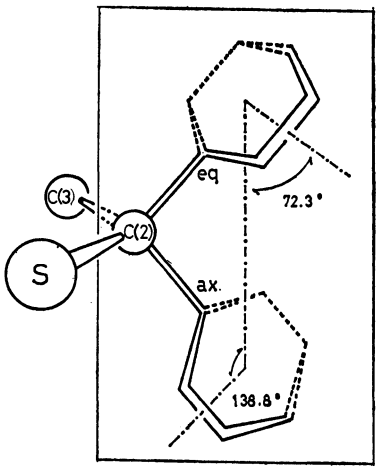

Fig. 3. Orientations of the equatorial and axial phenyl groups.

University of Tokyo and on a HITAC 8250 computer at Saitama University.

Description and Discussion of the Structure

The molecule is disymmetric, and both enantiomorphs exist in the crystal. A projection of the crystal structure viewed along the a axis is shown in Fig. 1. All the intermolecular contacts observed are normal in view of the usual van der Waals radii. The observed dipole moment of *trans*-DCTE (2.02 D) is close to that of *cis*-DCTE (2.16 D),[7] although their directions in the molecules are different from each other. The closest intermolecular contact of S···S=4.080(5) Å seems to be normal in contrast to the case of *cis*-DCTE (3.32 Å).

The molecular conformation and the atomic-numbering scheme employed are shown in Fig. 2. The conformation observed can be described as (3e4e), based upon the orientations of the Cl substituents with respect to the thietane skeleton; this agrees with that deduced from the dipole-moment study.[7] The two phenyl groups are planar; their orientations are illustrated in Fig. 3.

The bond lengths and angles are listed in Table 3, while the relevant non-bonded distances within the molecule are given in Table 4.

Ring Geometry. The thietane ring is puckered with the (C(2)SC(4)/C(2)C(3)C(4)) puckering angle of 29.9°(θ1) and the (SC(2)C(3)/SC(4)C(3)) puckering angle of 30.1°(θ2). All the inner angles within the thietane ring are much smaller than the values normally exhibited by the sp^3 carbon and the divalent sulfur respectively. The non-bonded S···C(3) and C(2)···C(4) distances are much smaller than the usual van der Waals contacts. The C(2)–S bond length of 1.872(4) Å is significantly longer than the C(4)–S bond length of 1.811(5) Å. The C(3)–C(4) of 1.506(6) Å is much shorter than the C(2)–C(3) (1.545(6) Å). The geometry of the thietane skeleton of *trans*-DCTE is compared with those of *cis*-DCTE, 3-cyano-3,5,7-trimethyl-6-oxo-1-thia-

TABLE 3. BOND LENGTHS (l) AND BOND ANGLES (ϕ)[a)]

Bond	l/Å	Bond	l/Å
S–C(2)	1.872(4)	C(13)–C(14)	1.364(7)
S–C(4)	1.811(5)	C(14)–C(15)	1.383(7)
C(2)–C(3)	1.545(6)	C(15)–C(16)	1.395(7)
C(3)–C(4)	1.506(6)	C(16)–C(11)	1.391(6)
C(2)–C(11)	1.536(6)	C(21)–C(22)	1.381(6)
C(2)–C(21)	1.529(6)	C(22)–C(23)	1.410(7)
C(3)–Cl(1)	1.778(4)	C(23)–C(24)	1.358(7)
C(4)–Cl(2)	1.784(5)	C(24)–C(25)	1.394(7)
C(11)–C(12)	1.387(6)	C(25)–C(26)	1.413(7)
C(12)–C(13)	1.398(7)	C(26)–C(21)	1.379(6)
Angle	**ϕ/°**	**Angle**	**ϕ/°**
C(2)SC(4)	76.6(2)	C(11)C(12)C(13)	120.2(4)
SC(2)C(3)	87.6(2)	C(12)C(13)C(14)	121.1(5)
C(2)C(3)C(4)	96.9(3)	C(13)C(14)C(15)	119.1(5)
C(3)C(4)S	91.0(3)	C(14)C(15)C(16)	120.7(5)
C(11)C(2)C(21)	110.6(3)	C(15)C(16)C(11)	120.2(4)
C(11)C(2)S	113.6(3)	C(16)C(11)C(12)	118.6(4)
C(11)C(2)C(3)	115.6(3)	C(21)C(22)C(23)	119.7(4)
C(21)C(2)S	111.9(3)	C(22)C(23)C(24)	120.3(5)
C(21)C(2)C(3)	115.9(3)	C(23)C(24)C(25)	121.0(5)
Cl(1)C(3)C(2)	117.4(3)	C(24)C(25)C(26)	118.4(5)
Cl(1)C(3)C(4)	115.5(3)	C(25)C(26)C(21)	120.6(5)
Cl(2)C(4)S	115.1(2)	C(26)C(21)C(22)	119.9(4)
Cl(2)C(4)C(3)	114.7(3)		

a) The C–H bond lengths are in the range of 0.98—1.14 Å.

TABLE 4. RELEVANT INTRAMOLECULAR NON-BONDED CONTACTS (l)

	l/Å		l/Å
S···C(3)	2.376(4)	Cl(1)···C(16)	3.442(5)
C(2)···C(4)	2.283(6)	Cl(1)···C(2)	2.841(4)
S···C(11)	2.857(4)	Cl(1)···C(4)	2.782(5)
S···C(12)	3.104(5)	Cl(1)···Cl(2)	3.824(2)
S···C(21)	2.825(4)	Cl(2)···C(3)	2.775(4)
S···C(26)	3.233(5)	Cl(2)···S	3.033(2)
Cl(1)···C(11)	3.134(4)		

5,7-diazaspiro[3.5]nonane (CTMTN),[8] 2-(2,6-dimethylphenylimino)-3,3-dimethyl-4,4-diphenylthietane (DDDTE),[9] and thietane itself[2] in Table 5. The puckering angles of *trans*-DCTE are slightly larger than those of *cis*-DCTE. The values of both compounds are larger than the others listed in the table. Significant deviations between the ring geometries of *trans*- and *cis*-DCTE's are found only for the C(3)–C(4) bond distances, the C(2)–S–C(4) angles, and the non-bonded C(2)···C(4) distances. The shortening of the C(3)–C(4) bond (0.074 Å in *trans*-DCTE) brings about a decrease in the C(2)–S–C(4) angle by 2.7° and a contraction of the C(2)···C(4) distance (0.077 Å); it also increases

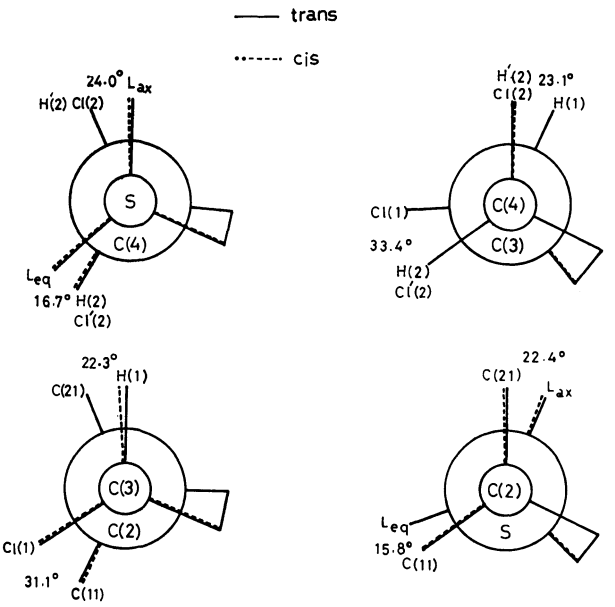

Fig. 4. Newman projections of *trans*- and *cis*-DCTE's along their ring bonds. L_{eq} and L_{ax} represent the directions of lone pairs on sulfur assumed to be in the tetrahedral disposition. H′ and Cl′ mean the atoms in the *cis* isomer.

TABLE 5. A COMPARISON OF RING-GEOMETRIES IN *cis*- AND *trans*-DCTE's, CTMTN, DDDTE, AND THIETANE

	cis-DCTE	*trans*-DCTE	CTMTN[a)]	DDDTE[b)]	Thietane
Bond length l/Å					
S–C(2)	1.89(1)	1.872(4)	1.844(3)	1.868(5)	1.846(2)
S–C(4)	1.81(1)	1.811(5)	1.817(3)	1.777(5)	1.846(2)
C(2)–C(3)	1.55(2)	1.545(6)	1.597(4)	1.591(7)	1.548(3)
C(3)–C(4)	1.58(2)	1.506(6)	1.541(4)	1.524(7)	1.548(3)
Non-bonded distance l/Å					
S···C(3)	2.38(1)	2.376(4)	2.432	2.455	2.421(3)
C(2)···C(4)	2.36(2)	2.283(6)	2.331	2.270	2.294(6)
Bond angle ϕ/°					
C(2)SC(4)	79.3(5)	76.6(2)	79.0(1)	77.0(2)	76.8(3)
SC(2)C(3)	86.7(7)	87.6(2)	89.6(2)	90.1(3)	90.6(3)
C(2)C(3)C(4)	98.1(9)	96.9(3)	95.8(2)	93.5(4)	95.6(4)
SC(4)C(3)	88.8(7)	91.0(3)	92.6(2)	95.8(3)	90.6(3)
Puckering angle ϕ/°					
$\theta 1$	28.9	29.9	18.3	20.0	26
$\theta 2$	28.1	30.1	18.7	21.2	

a) The C(2) is defined as the C_α linked to the spiro substituent. b) The C(2) is defined as the C_α linked to two phenyl groups.

TABLE 6. TILTING (γ), BENDING (δ), AND TWISTING (χ) ANGLES OF RING-SUBSTITUENTS IN *cis*- AND *trans*-DCTE'S AND CTMTN

	cis-DCTE			*trans*-DCTE			CTMTN		
	C(2)	C(3)	C(4)	C(2)	C(3)	C(4)	C(2)	C(3)	C(4)
γ/°	1.2	5.0	0.5	0.5	4.4	1.4	0.5	4.8	1.1
δ/°	4.7	0.5	2.0	3.5	4.1	0.9	2.9	0.7	3.1
χ/°	0.7	1.4	0.6	0.8	2.1	1.7	2.6	0.0	1.1

the puckering angle, $\theta 2$. Newman projections of the ring substituents in *trans*-DCTE are shown in Fig. 4, where those of *cis*-DCTE are superimposed. There are no significant deviations between them, although the *trans* arrangement of the substituted Cl atoms with the Cl(1)···Cl(2) contact of 3.824 Å seems to be stereochemically more favorable than that of the *cis* (3.25 Å). These observations indicate that the shortening of the C(3)–C(4) bond in *trans*-DCTE is a consequence of releasing a steric interaction between the Cl substituents on going from *cis* to *trans*. Furthermore, this C(3)–C(4) bond length is significantly shorter than the usual value for C(sp^3)–C(sp^3). This provides an interesting contrast to the longer bond observed for most cases of the four-membered ring systems, for example, thietane (C–C=1.548(3) Å)[2] and cyclobutane (C–C=1.548(3) Å).[10] A CNDO/2 calculation of the model molecules for *cis*- and *trans*-DCTE's[11] shows that the observed contraction of the C(3)–C(4) bond in the *trans* isomer may be attributed not only to the alleviation of steric hindrance between the Cl substituents, but also to an increased contribution of the 2s AO on C(4) to the C(3)–C(4) bonding. The C(2)–C(3) bond length in *trans*-DCTE is in good agreement with those in *cis*-DCTE, thietane, and CTMTN. The S–C(2) bond lengths in *cis*- and *trans*-DCTE's may be compared with the value in DDDTE, but they are longer than that in thietane. The carbon atoms at the ends of the longer C–S bonds are linked to two phenyl groups. These longer bonds may be a consequence of the lengthening effect due to the two phenyl groups at C_α. The C(4)–S bond length in *trans*-DCTE is in good agreement with those in *cis*-DCTE and CTMTN, but significantly shorter than that in thietane.

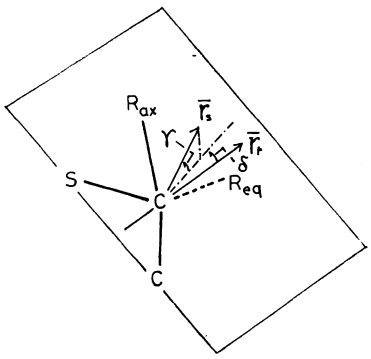

Fig. 5. A definition of the tilting, bending, and twisting angles (γ,δ,χ) exhibited by the ring substitutens. R_{ax} and R_{eq} represent the axial and equatorial substituents, respectively. The vectors, $\bar{r}_s$ and $\bar{r}_r$, are the bisectors of R_{ax}–C–R_{eq} and S–C_α–C_β angles, respectively. The angle, χ, stands for the angle of anticlockwise rotation of the $R_{ax}CR_{eq}$ plane around the vector $\bar{r}_s$.

Orientation of the Ring Substituents. The tilting, bending, and twisting angles (γ,δ,χ) exhibited by the ring substituents are defined as in Fig. 5. Table 6 lists these angles in *cis*- and *trans*-DCTE's and in CTMTN. Their e.s.d.'s are in the range of 0.3°—2°. It is commonly observed for all the compounds that the γ values are positive and that the γ at the C_β is larger than those at the C_α's. Although the puckering angles of *cis*- and *trans*-DCTE's are much larger than those of CTMTN, the γ values at the C_β's in the compounds are approximately equal to each other and agree well with the value of 4° predicted by Pasternak *et al.*[1c] based upon a geometrical model of cyclobutane composed of sp^3 carbons at the puckering angle of 30°. The γ's at the C_α's with the substituents are, however, much smaller than the predicted value. The CNDO/2 energies (E_t) for thietane and the model molecules assumed for *cis*- and *trans*-DCTE's[12] were calculated by varying the tilting angles, γ_1 and γ_2, at C_α and C_β in the range of 0°—6°. The values of γ_1 and γ_2 giving a minimum E_t value for thietane were found to be 1.5° and 3° respectively, while those for the model molecule of *cis*-DCTE were 1° and 5° respectively. The calculated values of these angles approximately agree with those observed for *cis*-DCTE and CTMTN. The tilting of the ring substituents is mainly caused by the resonance energy[13] in the electronic energy calculated; hence, it may be due to the nature of bonding in the thietane ring. On the other hand, the calculated values of γ_1 and γ_2 for the *trans* isomer were about 2°. Both these angles are positive, in accordance with those observed for *trans*-DCTE; however, this relative magnitude does not agree with that observed.

The author is grateful to Professor Yoshihiko Saito, Keiohgijuku University, and Professor Takashi Shimozawa for thier keen interest and valuable discussions. Thanks are also due to Professor Yoichi Iitaka, the University of Tokyo, for the use of the Philips PW 1100 diffractometer.

References

1) a) J. S. Wright and L. Salem, *Chem. Commun.*, **1969**, 1370; b) L. S. Bartell and B. Andersen, *J. Chem. Soc., Chem. Commun.*, **1973**, 786; c) R. Pasternak and A. Y. Meyer, *J. Mol. Struct.*, **20**, 351 (1974).

2) K. Karakida and K. Kuchitsu, *Bull. Chem. Soc. Jpn.*, **48**, 1691 (1975).

3) J. W. Bevan, A. C. Legon, and D. J. Millen, *J. Chem. Soc., Chem. Commun.*, **1974**, 659.

4) S. Kumakura and T. Kodama, *Bull. Chem. Soc. Jpn.*, **48**, 2339 (1975).

5) A. Ohno, Y. Ohnishi, and G. Tsuchihashi, *J. Am. Chem. Soc.*, **91**, 5038 (1969).

6) "International Tables for X-Ray Crystallography," The Kynoch Press, Birmingham (1968), Vol. III.

7) S. Kumakura, T. Shimozawa, Y. Ohnishi, and A. Ohno, *Tetrahedron*, **27**, 767 (1971).

8) J. Guilhem, *Cryst. Struct. Commun.*, **6**, 93 (1977).

9) V. Bertolasi and G. Gilli, *Acta Crystallogr., Sect. B*, **34**, 3403 (1978).

10) A. Almenningen, O. Bastiansen, and P. N. Skancke, *Acta Chem. Scand.*, **15**, 711 (1961).

11) In order to save computer time, the phenyl groups in *cis*- and *trans*-DCTE's were ignored. Calculations were made for the model molecules, *cis*- and *trans*-2,3-dichlorothietanes, the skeletal dimensions of which are assumed to be equal to those of *cis*- and *trans*-DCTE's. The dipole moments calculated by employing the (*sp*) basis sets are 2.19 D and 1.83 D, which are in good agreement with the observed values of the corresponding DCTE's.

12) The skeletal geometry of thietane observed was employed in the CNDO/2 calculations of thietane itself and of *cis*- and *trans*-2,3-dichlorothietanes. The tilting angles of the methylene groups calculated for thietane agree well those obtained by an *ab initio* calculation (P. N. Skancke, G. Fogarasi, and J. E. Boggs, *J. Mol. Struct.*, **52**, 259 (1980)).

13) The energy analysis was made by employing the method postulated by Pople (J. A. Pople and G. A. Segal, *J. Chem. Phys.*, **44**, 3289 (1966).

Spectrophotometric Determination of Formation Constants and Estimation of Molar Absorption Spectra of Individual Components in Chemical Equilibria. Infrared Study of Intermolecular Hydrogen Bonding of 2-Aminopyridine

Hiromu SUGETA

Institute for Protein Research, Osaka University, Suita, Osaka 565

(Received March 27, 1981)

A general method is developed for evaluating formation constants and molar absorption coefficients of constituent species from spectrophotometric data for a multicomponent equilibrium system. The method is applied to analyzing infrared spectra for the intermolecular hydrogen bond system of 2-aminopyridine in carbon tetrachloride solution. 2-Aminopyridine assumes a cyclic dimer structure by dint of an intermolecular hydrogen bonding and the formation constant for the dimerization is 1.4 ± 0.1 mol^{-1} dm^3 at 30 °C.

Spectroscopic methods have widely been used for studying equilibria in solutions. In very complex systems in which numerous equilibria exist, absorption curves of constituent species will overlap each other to give rise to complex envelopes of bands. For such complex systems methods for evaluating equilibrium constants from spectrophotometric data with the nonlinear least-squares method have been discussed by many investigators.[1-5] In their treatments the solution of mass balance equations and Jacobian matrix in the least-squares method were evaluated by numerical computations without resorting to analytical equations.

In this paper a general method for least-squares determination of formation constants and molar absorption coefficients of constituent species from spectrophotometric data is worked out in terms of matrix formulation and programed for electronic computers; a general method for solving mass balance equations for a multicomponent equilibrium system is derived; derivatives of equilibrium concentrations of constituent species with respect to formation constant are given in an analytical form; and a method for recasting the problem of least-squares determination in a simplified form is treated by using methods[6,7] for eliminating linear parameters in nonlinear least-squares adjustment. The method derived is applied to analyzing the intermolecular hydrogen bond system of 2-aminopyridine in carbon tetrachloride solution. Infrared spectra of 2-aminopyridine have been measured by Ramiah and Puranik[8] and Spinner,[9] and a normal coordinate treatment has been carried out by Berezin and Elkin,[10] but no quantitative analyses on intermolecular hydrogen bonding have yet been worked out. Therefore, the present infrared study on the intermolecular hydrogen bond of 2-aminopyridine was undertaken to investigate the molecular structure and formation constant of the hydrogen bond.

Method

Chemical Equilibrium of Multicomponent System. Let us consider the chemical equilibrium of a multicomponent system which consist of reactants X_i $(i=1,\cdots,m)$ and products Y_p $(p=1,\cdots,f)$. Let reaction equation for the system be given by

$$\sum_{i=1}^{m} n_{pi}X_i \rightleftharpoons Y_p \quad (p=1,\cdots,f), \tag{1}$$

where n_{pi} is the stoichiometric coefficient. Denoting the equilibrium concentrations of reactants X_i and products Y_p as $\tilde{\boldsymbol{x}}=[x_1\cdots x_m]$ and $\tilde{\boldsymbol{y}}=[y_1\cdots y_f]$, respectively, the total concentration of reactant X_i as $\tilde{\boldsymbol{x}}^t=[x_1^t\cdots x_m^t]$, and the formation constant of products Y_p as $\tilde{\boldsymbol{K}}=[K_1\cdots K_f]$ where $\sim$ represents the transpose of matrix, we have following equations for ideal solutions:

$$y_p = K_p \prod_{i=1}^{m} x_i^{n_{pi}}, \tag{2a}$$

$$\ln \boldsymbol{y} = \ln \boldsymbol{K} + \boldsymbol{N} \ln \boldsymbol{x}, \tag{2b}$$

$$x_i^t = x_i + \sum_{p=1}^{f} n_{pi} y_p, \tag{3a}$$

$$\boldsymbol{x}_i^t = \boldsymbol{x} + \tilde{\boldsymbol{N}}\boldsymbol{Y}, \tag{3b}$$

where $\ln \boldsymbol{x}$ represents the vector given by

$$\ln \tilde{\boldsymbol{x}} = [\ln x_1 \cdots \ln x_m], \tag{4}$$

and $\boldsymbol{N}$ is the stoichiometric coefficient matrix whose elements are n_{pi}. For a given set of stoichiometry $\boldsymbol{N}$, we can derive the following relations among infinitesimal changes in variables x_i, y_p, K_p, and x_i^t by differentiation of Eqs. 2a—3b:

$$[\boldsymbol{Y}]^{-1}\Delta\boldsymbol{y} = [\boldsymbol{K}]^{-1}\Delta\boldsymbol{K} + \boldsymbol{N}[\boldsymbol{X}]^{-1}\Delta\boldsymbol{x}, \tag{5a}$$

$$\Delta \ln \boldsymbol{y} = \Delta \ln \boldsymbol{K} + \boldsymbol{N}\Delta \ln \boldsymbol{x}, \tag{5b}$$

$$\begin{aligned}\Delta\boldsymbol{x}^t &= \Delta\boldsymbol{x} + \tilde{\boldsymbol{N}}\Delta\boldsymbol{y} \\ &= \tilde{\boldsymbol{N}}[\boldsymbol{Y}][\boldsymbol{K}]^{-1}\Delta\boldsymbol{K} + \{[\boldsymbol{X}] + \tilde{\boldsymbol{N}}[\boldsymbol{Y}]\boldsymbol{N}\}[\boldsymbol{X}]^{-1}\Delta\boldsymbol{x} \\ &= \tilde{\boldsymbol{N}}[\boldsymbol{Y}][\boldsymbol{K}]^{-1}\Delta\boldsymbol{K} + \boldsymbol{H}[\boldsymbol{X}]^{-1}\Delta\boldsymbol{x} \qquad (6a) \\ &= \tilde{\boldsymbol{N}}[\boldsymbol{Y}]\Delta \ln \boldsymbol{K} + \boldsymbol{H}\Delta \ln \boldsymbol{x}, \qquad (6b)\end{aligned}$$

where

$$\boldsymbol{H} = [\boldsymbol{X}] + \tilde{\boldsymbol{N}}[\boldsymbol{Y}]\boldsymbol{N}, \tag{7}$$

and $[\boldsymbol{X}]$, $[\boldsymbol{Y}]$, and $[\boldsymbol{K}]$ are the diagonal matrices whose elements are x_i, y_p, and K_p, respectively, and $\Delta\ln\boldsymbol{x}$ represents the vector given by

$$\Delta \ln \boldsymbol{x} = \begin{bmatrix} \Delta \ln x_1 \\ \Delta \ln x_2 \\ \vdots \\ \Delta \ln x_m \end{bmatrix} = \begin{bmatrix} \Delta x_1/x_1 \\ \Delta x_2/x_2 \\ \vdots \\ \Delta x_m/x_m \end{bmatrix} = [\boldsymbol{X}]^{-1}\Delta\boldsymbol{x}. \tag{8}$$

For a given set of formation constants $(\boldsymbol{K})$ and experimental formal concentrations of reactants $(\boldsymbol{x}^t)$, equilibrium concentrations of reactants $(\boldsymbol{x})$ can be calculated according to the method of Newton-Raphson iteration by making use of the following partial derivatives of total concentration $\boldsymbol{x}^t$ with respect to equilibrium

concentration $\boldsymbol{x}$ which can be derived from Eqs. 6a and 6b under the condition of $\Delta\boldsymbol{K}=0$:

$$(\partial \boldsymbol{x}^t/\partial \boldsymbol{x})_{\Delta \boldsymbol{K}=0} = \boldsymbol{H}[\boldsymbol{X}]^{-1}, \tag{9}$$

$$(\partial \boldsymbol{x}^t/\partial \ln \boldsymbol{x})_{\Delta \boldsymbol{K}=0} = \boldsymbol{H}, \tag{10}$$

where $(\partial \boldsymbol{x}^t/\partial \boldsymbol{x})$ represents the matrix whose i,j elements are $(\partial x_i^t/\partial x_j)$. Partial derivatives of equilibrium concentrations with respect to formation constant for a given set of experimental formal concentrations of the reactants are required for the least-squares determination of formation constants from spectrophotometric data. These derivatives can be derived from Eqs. 5a—6b under the condition of $\Delta \boldsymbol{x}^t=0$ as

$$(\partial \boldsymbol{x}/\partial \boldsymbol{K})_{\Delta \boldsymbol{x}^t=0} = -[\boldsymbol{X}]\boldsymbol{H}^{-1}\tilde{\boldsymbol{N}}[\boldsymbol{Y}][\boldsymbol{K}]^{-1}, \tag{11}$$

$$(\partial \ln \boldsymbol{x}/\partial \ln \boldsymbol{K})_{\Delta \boldsymbol{x}^t=0} = -\boldsymbol{H}^{-1}\tilde{\boldsymbol{N}}[\boldsymbol{Y}], \tag{12}$$

$$(\partial \boldsymbol{y}/\partial \boldsymbol{K})_{\Delta \boldsymbol{x}^t=0} = [\boldsymbol{Y}]\{\boldsymbol{E} - \boldsymbol{N}\boldsymbol{H}^{-1}\tilde{\boldsymbol{N}}[\boldsymbol{Y}]\}[\boldsymbol{K}]^{-1}, \tag{13}$$

$$(\partial \ln \boldsymbol{y}/\partial \ln \boldsymbol{K})_{\Delta \boldsymbol{x}^t=0} = \boldsymbol{E} - \boldsymbol{N}\boldsymbol{H}^{-1}\tilde{\boldsymbol{N}}[\boldsymbol{Y}], \tag{14}$$

where $\boldsymbol{E}$ represents unit matrix.

Least-squares Treatment of Spectrophotometric Data. Suppose a set of absorbance data at λ points in a given wavenumber region for s solutions of different concentrations containing n absorbing components in a chemical equilibrium system. The absorbance per unit path length, $D_{\nu r}$, at wavenumber ν in the rth solution, is expressed by the sum of absorptions of the n components in the system on the assumption of Beer's law:

$$D_{\nu r} = \sum_{i=1}^{n} A_{\nu i}C_{ir}(\boldsymbol{K}) \quad (\nu=1, \cdots, \lambda; r=1, \cdots, s), \tag{15}$$

where $A_{\nu i}$ is the molar absorption coefficient of the ith species at wavenumber ν, and C_{ir} is the concentration of the ith species in the rth solution which is a function of formation constants $\boldsymbol{K}$ and can be calculated by the method as described above. Equation 15 may be written in the matix notation as

$$\boldsymbol{D} = \boldsymbol{A}\boldsymbol{C}(\boldsymbol{K}), \tag{16}$$

where $\boldsymbol{D}$ is a $\lambda \times s$ absorbance matrix, $\boldsymbol{A}$ is a $\lambda \times n$ matrix of molar absorption coefficients, and $\boldsymbol{C}$ is an $n \times s$ concentration matrix. Introducing absorbance vector $\boldsymbol{d}$ and vector $\boldsymbol{a}$ of molar absorption coefficients as defined by

$$\tilde{\boldsymbol{d}} = [\tilde{\boldsymbol{D}}_1\tilde{\boldsymbol{D}}_2 \cdots \tilde{\boldsymbol{D}}_\lambda], \tag{17}$$

$$\tilde{\boldsymbol{a}} = [\tilde{\boldsymbol{A}}_1\tilde{\boldsymbol{A}}_2 \cdots \tilde{\boldsymbol{A}}_\lambda], \tag{18}$$

where $\tilde{\boldsymbol{D}}_\nu$ and $\tilde{\boldsymbol{A}}_\nu$ are row vectors of absorbance and molar absorption coefficients which are the νth rows of matrices $\boldsymbol{D}$ and $\boldsymbol{A}$, respectively,

$$\boldsymbol{D} = \begin{bmatrix} \tilde{\boldsymbol{D}}_1 \\ \vdots \\ \tilde{\boldsymbol{D}}_\lambda \end{bmatrix}, \tag{19}$$

$$\boldsymbol{A} = \begin{bmatrix} \tilde{\boldsymbol{A}}_1 \\ \vdots \\ \tilde{\boldsymbol{A}}_\lambda \end{bmatrix}, \tag{20}$$

Eq. 16 may be written as

$$\tilde{\boldsymbol{D}}_\nu = \tilde{\boldsymbol{A}}_\nu\boldsymbol{C}(\boldsymbol{K}) \quad (\nu = 1, \cdots, \lambda). \tag{21}$$

Now let us consider the problem of determining f formation constants $\boldsymbol{K}$ and $\lambda \times n$ molar absorption coefficients $\boldsymbol{A}$ from $\lambda \times s$ observed absorbances $\boldsymbol{D}^{\text{obsd}}$ by the least-squares method. In Eqs. 16 or 21 absorbances $D_{\nu r}$ are of linear function of molar absorption coefficients $A_{\nu i}$ but of nonlinear function of formation constants K_p. In such cases we can simplify the least-squares treatment into a reduced model by elimination of linear parameters as described in Appendix. For a given set of formation constants $\boldsymbol{K}$, the best least-squares estimate of molar absorption coefficients, $\boldsymbol{A}'(\boldsymbol{K})$, can be given in an explicit form as described in Appendix [Eq. A.6]:

$$\tilde{\boldsymbol{A}}'_\nu = \tilde{\boldsymbol{D}}_\nu^{\text{obsd}}\tilde{\boldsymbol{C}}(\boldsymbol{C}\tilde{\boldsymbol{C}})^{-1}, \tag{22}$$

$$\boldsymbol{A}' = \boldsymbol{D}^{\text{obsd}}\tilde{\boldsymbol{C}}(\boldsymbol{C}\tilde{\boldsymbol{C}})^{-1}. \tag{23}$$

Substitution of Eqs. 22 and 23 for Eqs. 21 and 16 gives the observation equations for the reduced model:

$$\tilde{\boldsymbol{D}}'_\nu = \tilde{\boldsymbol{A}}'_\nu\boldsymbol{C} = \tilde{\boldsymbol{D}}_\nu^{\text{obsd}}\tilde{\boldsymbol{C}}(\boldsymbol{C}\tilde{\boldsymbol{C}})^{-1}\boldsymbol{C}, \tag{24}$$

$$\boldsymbol{D}' = \boldsymbol{A}'\boldsymbol{C} = \boldsymbol{D}^{\text{obsd}}\tilde{\boldsymbol{C}}(\boldsymbol{C}\tilde{\boldsymbol{C}})^{-1}\boldsymbol{C}, \tag{25}$$

where the prime represents quantities for the reduced model which are functions of $\boldsymbol{K}$ only.

Small changes in absorbance, $\Delta\boldsymbol{D}$, caused by small increments in formation constants, $\Delta\boldsymbol{K}$, are expressed in terms of Jacobian matrix $\boldsymbol{J}'$ for reduced model:

$$\Delta \boldsymbol{D}'_\nu = \boldsymbol{J}'_\nu \Delta \boldsymbol{K}, \tag{26}$$

$$\Delta \boldsymbol{d}' = \boldsymbol{J}' \Delta \boldsymbol{K}, \tag{27}$$

$$\boldsymbol{J}' = \begin{bmatrix} \boldsymbol{J}'_1 \\ \vdots \\ \boldsymbol{J}'_\lambda \end{bmatrix}, \tag{28}$$

$$\boldsymbol{J}'_\nu = [(\partial \boldsymbol{D}'_\nu/\partial K_1) \cdots (\partial \boldsymbol{D}'_\nu/\partial K_f)]. \tag{29}$$

Elements $\partial D'_{\nu r}/\partial K_p$ of Jacobian matrix $\boldsymbol{J}'$ are given according to Eqs. A. 10—A. 12 derived in Appendix:

$$\begin{aligned} \partial \boldsymbol{D}'_\nu/\partial K_p &= (\partial \tilde{\boldsymbol{C}}/\partial K_p)\boldsymbol{A}'_\nu + \tilde{\boldsymbol{C}}(\partial \boldsymbol{A}'_\nu/\partial K_p) \\ &= [\boldsymbol{E} - \tilde{\boldsymbol{C}}(\boldsymbol{C}\tilde{\boldsymbol{C}})^{-1}\boldsymbol{C}](\partial \tilde{\boldsymbol{C}}/K_p)\boldsymbol{A}'_\nu \\ &\quad + \tilde{\boldsymbol{C}}(\boldsymbol{C}\tilde{\boldsymbol{C}})^{-1}(\partial \boldsymbol{C}/\partial K_p)(\boldsymbol{D}_\nu^{\text{obsd}} - \boldsymbol{D}'_\nu), \end{aligned} \tag{30}$$

$$\begin{aligned} \partial \boldsymbol{A}'_\nu/\partial K_p &= -(\boldsymbol{C}\tilde{\boldsymbol{C}})^{-1}\boldsymbol{C}(\partial \tilde{\boldsymbol{C}}/\partial K_p)\boldsymbol{A}'_\nu \\ &\quad + (\boldsymbol{C}\tilde{\boldsymbol{C}})^{-1}(\partial \boldsymbol{C}/\partial K_p)(\boldsymbol{D}_\nu^{\text{obsd}} - \boldsymbol{D}'_\nu). \end{aligned} \tag{31}$$

Derivatives $(\partial C_{ir}/\partial K_p)$ can be calculated by the method established in the preceding section (Eqs. 11 and 13). Equations 30 and 31 may be written with reference to Eqs. 19 and 20 as follows:

$$\begin{aligned} \partial \boldsymbol{D}'/\partial K_p &= \boldsymbol{A}'(\partial \boldsymbol{C}/\partial K_p) + (\partial \boldsymbol{A}'/\partial K_p)\boldsymbol{C} \\ &= \boldsymbol{A}'(\partial \boldsymbol{C}/K_p)[\boldsymbol{E} - \tilde{\boldsymbol{C}}(\boldsymbol{C}\tilde{\boldsymbol{C}})^{-1}\boldsymbol{C}] \\ &\quad + (\boldsymbol{D}^{\text{obsd}} - \boldsymbol{D}')(\partial \tilde{\boldsymbol{C}}/\partial K_p)(\boldsymbol{C}\tilde{\boldsymbol{C}})^{-1}\boldsymbol{C}, \end{aligned} \tag{32}$$

$$\begin{aligned} \partial \boldsymbol{A}'/\partial K_p &= -\boldsymbol{A}'(\partial \boldsymbol{C}/\partial K_p)\tilde{\boldsymbol{C}}(\boldsymbol{C}\tilde{\boldsymbol{C}})^{-1} \\ &\quad + (\boldsymbol{D}^{\text{obsd}} - \boldsymbol{D}')(\partial \tilde{\boldsymbol{C}}/\partial K_p)(\boldsymbol{C}\tilde{\boldsymbol{C}})^{-1}. \end{aligned} \tag{33}$$

Thus, formation constants $\boldsymbol{K}$ can be determined according to the usual procedure based on nonlinear least-squares with reference to observed data $\boldsymbol{D}^{\text{obsd}}$. The normal equations for the reduced model which give correction $\Delta\boldsymbol{K}$ in iteration cycles are given by

$$(\tilde{\boldsymbol{J}}'\boldsymbol{J}')\Delta \boldsymbol{K} = \tilde{\boldsymbol{J}}'(\boldsymbol{d}^{\text{obsd}} - \boldsymbol{d}') \tag{34}$$

$$\tilde{\boldsymbol{J}}'\boldsymbol{J}' = \sum_{\nu=1}^{\lambda} \tilde{\boldsymbol{J}}'_\nu \boldsymbol{J}'_\nu \tag{35}$$

$$\tilde{\boldsymbol{J}}'(\boldsymbol{d}^{\text{obsd}} - \boldsymbol{d}') = \sum_{\nu=1}^{\lambda} \tilde{\boldsymbol{J}}'_\nu (\boldsymbol{D}_\nu^{\text{obsd}} - \boldsymbol{D}'_\nu). \tag{36}$$

Experimental

2-Aminopyridine was recrystallized from carbon tetrachloride and dried. Spectroscopic grade carbon tetrachloride

dried over molecular sieves 3A was used as the solvent. Solutions were prepared in the concentration range of 0.5—0.005 M (1 M = 1 mol dm^{-3}). Infrared spectra were measured with a JASCO A-3 infrared spectrophotometer at 30°C. Absorbances were digitized with an AD converter over the range from 3600 to 3000 cm^{-1}. Absorbance data at 10 cm^{-1} intervals from 3550 to 3360 cm^{-1} and at 20 cm^{-1} intervals from 3360 to 3120 cm^{-1} were used for data analysis.

Results and Discussion

The observed spectra in the NH_2 stretching region of three solutions of 2-aminopyridine in CCl_4 are shown in Fig. 1. In the dilute solution the symmetric (ν_sNH_2)

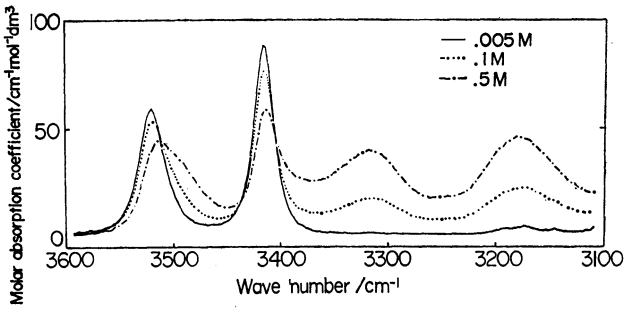

Fig. 1. Infrared spectra of 2-aminopyridine in CCl_4 solution.

and antisymmetric (ν_aNH_2) stretching vibrations of NH_2 group in free species are observed at 3415 and 3520 cm^{-1}, respectively. As the concentration increases both the peaks at 3520 and 3415 cm^{-1} decrease while the broad bands at 3315 and 3170 cm^{-1} grow up and the absorbances at about 3500 and 3390 cm^{-1} increase. These observations suggest that bands due to intermolecular association exist at those wavenumbers.

The concentration dependence of the observed absorbances was analyzed on the basis of the monomer-dimer equilibrium model by the least-squares method as described above. The formation constant for dimerization (K=[dimer]/[monomer]^2) was calculated to be 1.4±0.1 M^{-1} at 30 °C. The calculated molar absorption coefficients for monomer and dimer species are shown in Fig. 2, in which those for dimer species are

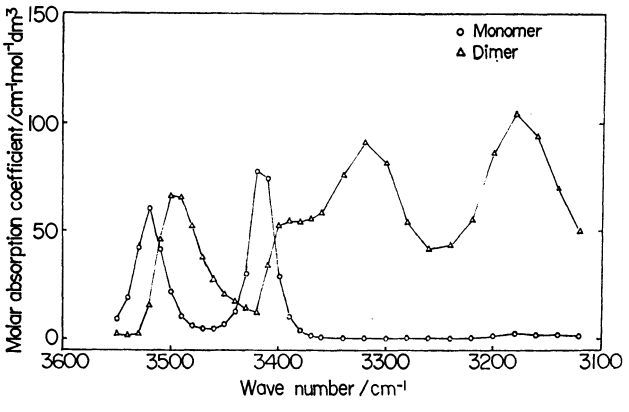

Fig. 2. Molar absorption coefficients for monomer and dimer of 2-aminopyridine.

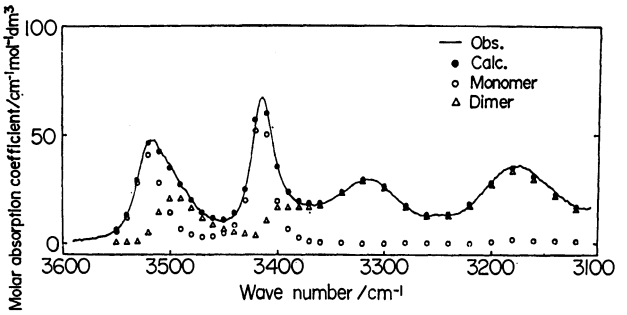

Fig. 3. Observed and calculated spectra for 0.25 M solution.

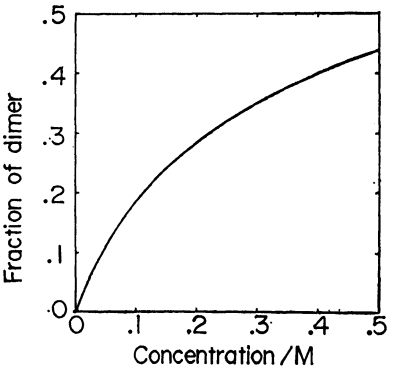

Fig. 4. Concentration dependence of the degree of dimer formation.

given in values per monomer unit. The observed spectra could be reproduced with a root-mean-squares deviation of 0.57 (in the unit of molar absorption). An example of comparison between observed and calculated spectra is shown in Fig. 3, together with contribution from monomer and dimer species for the 0.5 M solution. The concentration dependence of the degree of dimer formation is shown in Fig. 4. It turns out that the fraction of dimer changes from 1.4% at the lowest concentration of 0.005 M to 44% at the highest concentration of 0.5 M. The monomer-trimer model also was applied but the agreement between observed and calculated spectra was poor as compared with the monomer-dimer model. The least-squares treatment on the monomer-dimer-trimer model could give no convergence. Therefore, it can be concluded that dimerization is the predominant association in the concentration range employed.

The calculated molar absorption coefficients in Fig. 2 show that the monomer species has bands at 3520 and 3415 cm^{-1} which are assigned to vibrations ν_aNH_2 and ν_sNH_2, respectively, in the non-hydrogen-bonded species. The calculated dimer spectrum has peaks at 3495, 3320, and 3180 cm^{-1} and a shoulder at about 3390 cm^{-1}. The band at 3495 cm^{-1} can be assigned to the free N–H stretching vibration in the $\overset{\overset{H}{|}}{N}$–H···N hydrogen bond system. The two broad bands at 3320 and 3180 cm^{-1} can be assigned to the Fermi doublet caused by the resonance between the hydrogen-bonded N–H stretching vibration and the overtone of the NH_2

bending vibration at 1630 cm^{-1} in the $\overset{H}{\underset{|}{N}}$–H···N hydrogen bond system, similar resonance beeing observed in the hydrogen bond system of aniline by Wolf and Mathias.[11] The unperturbed hydrogen-bonded N–H stretching fundamental of dimer is estimated to be about 3240 cm^{-1}. The shoulder at 3390 cm^{-1} may be ascribed to the band caused by a Fermi resonance between the hydrogen-bonded N–H stretching fundamental and the overtone of the pyridine ring vibration at 1610 cm^{-1} or the combination tone of the NH_2 bending and ring vibrations.

From the fact that the calculated dimer spectrum has only one non-hydrogen-bonded N–H stretching band it turns out that one proton of NH_2 group is involved in the hydrogen bond while the other proton is free of the hydrogen bonding. It is consequently concluded that 2-aminopyridine in CCl_4 assumes a cyclic dimer structure by dint of an intermolecular hydrogen bond as shown in Fig. 5; it has been observed that 2-aminopyridine assumes the same cyclic dimer structure in the crystalline state.[12]

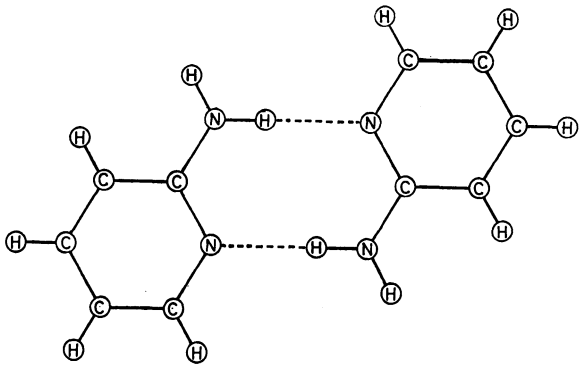

Fig. 5. Intermolecular hydrogen bonding of 2-aminopyridine.

Appendix: Elimination of Linear Parameters in Nonlinear Least-squares Treatment

Consider the problem of a least-squares estimation of the $m+n$ parameters of m nonlinear parameters $\tilde{\boldsymbol{\alpha}}=[\alpha_1\cdots\alpha_m]$ and n linear parameters $\tilde{\boldsymbol{\beta}}=[\beta_1\cdots\beta_n]$ with reference to the t observed values $\tilde{\boldsymbol{Z}}^{obsd}$ associated with the observation equations $\tilde{\boldsymbol{Z}}(\boldsymbol{\alpha},\boldsymbol{\beta})=[Z_1\cdots Z_t]$. Functions Z_q linear in β_k but nonlinear in α_i are generally written as

$$Z_q(\boldsymbol{\alpha},\boldsymbol{\beta}) = \sum_{k=1}^{n} F_{qk}(\boldsymbol{\alpha})\beta_k \quad (q = 1, \cdots, t), \tag{A. 1}$$

where F_{qk} is the nonlinear function of α_i. Eq. A.1 may be written in the matrix notation as

$$\boldsymbol{Z}(\boldsymbol{\alpha},\boldsymbol{\beta}) = \boldsymbol{F}(\boldsymbol{\alpha})\boldsymbol{\beta}. \tag{A. 2}$$

Residual vector $\boldsymbol{\varepsilon}$ and the sum of squared residuals S are given by

$$\boldsymbol{\varepsilon} = \boldsymbol{Z}^{obsd} - \boldsymbol{Z} = \boldsymbol{Z}^{obsd} - \boldsymbol{F}\boldsymbol{\beta}, \tag{A. 3}$$

$$S = \tilde{\boldsymbol{\varepsilon}}\boldsymbol{\varepsilon} = \tilde{\boldsymbol{\beta}}\tilde{\boldsymbol{F}}\boldsymbol{F}\boldsymbol{\beta} - 2\tilde{\boldsymbol{\beta}}\tilde{\boldsymbol{F}}\boldsymbol{Z}^{obsd} + \tilde{\boldsymbol{Z}}^{obsd}\boldsymbol{Z}^{obsd}, \tag{A. 4}$$

where $\sim$ represents the transpose of matrix.

Lawton and Sylvester[6] have pointed out that the $m+n$ dimensional problem with m nonlinear and n linear parameters in a least-squares adjustment could be reduced to an m dimensional problem by elimination of linear parameters. Golub and Pereyra[7] have treated the mathematics and algorism associated with that problem in detail but their derivation requires a familiarity with a somewhat advanced mathematics and is not familiar to chemists. Thus, a rather simple derivation using the elementary algebra will be given in a form appropriate to the present study.

The best least-squares estimate $\boldsymbol{\beta}'(\boldsymbol{\alpha})$ of linear parameters $\boldsymbol{\beta}$ associated with a given set of nonlinear parameters $\boldsymbol{\alpha}$ can be derived from the minimum condition for the sum of squared residuals S:

$$\begin{aligned}(1/2)\partial S/\partial\boldsymbol{\beta} &= (1/2)\partial(\tilde{\boldsymbol{\varepsilon}}\boldsymbol{\varepsilon})\partial/\boldsymbol{\beta} = -\tilde{\boldsymbol{F}}\boldsymbol{\varepsilon}\\ &= \tilde{\boldsymbol{F}}\boldsymbol{F}\boldsymbol{\beta} - \tilde{\boldsymbol{F}}\boldsymbol{Z}^{obsd} = 0,\end{aligned} \tag{A. 5}$$

$$\boldsymbol{\beta} = \boldsymbol{\beta}'(\boldsymbol{\alpha}) = (\tilde{\boldsymbol{F}}\boldsymbol{F})^{-1}\tilde{\boldsymbol{F}}\boldsymbol{Z}^{obsd}. \tag{A. 6}$$

Substitution of Eq. A.6 for Eq. A.2 gives reduced observation equations for the reduced model as

$$\boldsymbol{Z}'(\boldsymbol{\alpha}) = \boldsymbol{F}\boldsymbol{\beta}'(\boldsymbol{\alpha}) = \boldsymbol{F}(\tilde{\boldsymbol{F}}\boldsymbol{F})^{-1}\tilde{\boldsymbol{F}}\boldsymbol{Z}^{obsd}, \tag{A. 7}$$

where $\boldsymbol{Z}'$ is a function of only nonlinear parameters $\boldsymbol{\alpha}$ and the prime is used for representing quantities for the reduced model. Jacobian matrix $\boldsymbol{J}'$ for the reduced model is defined as

$$J'_{qi} = \partial Z'_q/\partial\alpha_i = \sum_{k=1}^{n}[(\partial F_{qk}/\partial\alpha_i)\beta'_k + F_{qk}(\partial\beta'_k/\partial\alpha_i)], \tag{A. 8}$$

$$\boldsymbol{J}' = \partial\boldsymbol{Z}'/\partial\boldsymbol{\alpha} = [\partial\boldsymbol{Z}'/\partial\alpha_1 \cdots \partial\boldsymbol{Z}'/\partial\alpha_m], \tag{A. 9}$$

$$\partial\boldsymbol{Z}'/\partial\alpha_i = (\partial\boldsymbol{F}/\partial\alpha_i)\boldsymbol{\beta}' + \boldsymbol{F}(\partial\boldsymbol{\beta}'/\partial\alpha_i), \tag{A. 10}$$

where $\partial\boldsymbol{\beta}'/\partial\boldsymbol{\alpha}$ can be derived through differentiation of Eq. A.6:

$$\begin{aligned}\partial\boldsymbol{\beta}'/\partial\alpha_i = &-(\tilde{\boldsymbol{F}}\boldsymbol{F})^{-1}[(\partial\tilde{\boldsymbol{F}}/\partial\alpha_i)\boldsymbol{F}\\ &+\tilde{\boldsymbol{F}}(\partial\boldsymbol{F}/\partial\alpha_i)](\tilde{\boldsymbol{F}}\boldsymbol{F})^{-1}\tilde{\boldsymbol{F}}\boldsymbol{Z}^{obsd}\\ &+(\tilde{\boldsymbol{F}}\boldsymbol{F})^{-1}(\partial\tilde{\boldsymbol{F}}/\partial\alpha_i)\boldsymbol{Z}^{obsd}\\ =&-(\tilde{\boldsymbol{F}}\boldsymbol{F})^{-1}\tilde{\boldsymbol{F}}(\partial\boldsymbol{F}/\partial\alpha_i)\boldsymbol{\beta}'\\ &+(\tilde{\boldsymbol{F}}\boldsymbol{F})^{-1}(\partial\tilde{\boldsymbol{F}}/\partial\alpha_i)\boldsymbol{\varepsilon}.\end{aligned} \tag{A. 11}$$

Substitution of Eq. A.11 for Eq. A. 10 gives

$$\begin{aligned}\partial\boldsymbol{Z}'/\partial\alpha_i = &[\boldsymbol{E} - \boldsymbol{F}(\tilde{\boldsymbol{F}}\boldsymbol{F})^{-1}\tilde{\boldsymbol{F}}](\partial\boldsymbol{F}/\partial\alpha_i)\boldsymbol{\beta}'\\ &+\boldsymbol{F}(\tilde{\boldsymbol{F}}\boldsymbol{F})^{-1}(\partial\tilde{\boldsymbol{F}}/\partial\alpha_i)\boldsymbol{\varepsilon}.\end{aligned} \tag{A. 12}$$

In terms of Jacobian matrix $\boldsymbol{J}'$ given by Eqs. A.9 and A.12 the normal equations for the reduced model are given by

$$(\tilde{\boldsymbol{J}}'\boldsymbol{J}')\Delta\boldsymbol{\alpha} = \tilde{\boldsymbol{J}}'\boldsymbol{\varepsilon}, \tag{A. 13}$$

and

$$\Delta\boldsymbol{\alpha} = (\tilde{\boldsymbol{J}}'\boldsymbol{J}')^{-1}\tilde{\boldsymbol{J}}'\boldsymbol{\varepsilon}. \tag{A. 14}$$

The improved nonlinear parameters $\boldsymbol{\alpha}+\Delta\boldsymbol{\alpha}$ for the next iteration are calculated from Eq. A.14 and the best companion linear parameters $\boldsymbol{\beta}$ are given by Eq. A.6. The method of least-squares with the reudced observation equations given by Eq. A.7 is evidently superior to the one with the original model given by Eq. A.2: The dimension of problem could be reduced to as low as m in the reduced model from $m+n$ in the original model by the elimination of n linear parameters. This reduced dimension could result in a faster convergence, a stabilization of convergence, and a reduction of memories. The initial guess requires only m nonlinear parameters rather than $m+n$ parameters in the original model.

References

1) For example, Refs. 2—5 and references therein.
2) K. Nagano and D. E. Metzler, *J. Am. Chem. Soc.*, **89**, 2891 (1967).
3) J. J. Kankare, *Anal. Chem.*, **42**, 1322 (1970).

4) E. A. Sylvestre, W. H. Lawton, and M. S. Maggio, *Technometrics*, **16**, 353 (1974).
5) D. J. Legget and W. A. E. McBryde, *Anal. Chem.*, **47**, 1065 (1975).
6) W. L. Lawton and E. A. Sylvestre, *Technometrics*, **13**, 461 (1971).
7) G. H. Golub and V. Pereyra, *SIAM J. Numer. Anal.*, **10**, 413 (1973).
8) K. V. Ramiah and P. G. Puranik, *J. Mol. Spectrosc.*, **7**, 89 (1961).
9) E. Spinner, *J. Chem. Soc.*, **1962**, 3119.
10) V. I. Berezin and M. D. Elkin, *Opt. Spectrosc.*, **36**, 528 (1973).
11) H. Wolf and D. Mathias, *J. Phys. Chem.*, **77**, 2081 (1973).
12) M. Chao, E. Schempp, and R. D. Rosenstein, *Acta Crystallogr., Sect. B*, **31**, 2922 (1975).

Catalytic Activity of Highly Dispersed Palladium. II. X-Ray Photoelectron Spectroscopic and Thermal Desorption Studies of the Effects of ZrO_2 Added to α-Alumina-supported Palladium

Bu Yong LEE,* Yasunobu INOUE, and Iwao YASUMORI

Department of Chemistry, Tokyo Institute of Technology, Ookayama, Meguro-ku, Tokyo 152

(Received May 1, 1981)

The effects of ZrO_2 upon the catalytic properties of α-alumina-supported palladium for the hydrogenation of gaseous cyclohexene were studied by means of detailed kinetic analysis, thermal desorption (TD), and X-ray photoelectron spectroscopy (XPS). The catalysts, with ZrO_2 added in amounts ranging from 0.1 to 45 in Zr/Pd ratio, were characterized by CO chemisorption and X-ray diffraction. The addition of ZrO_2 at the Zr/Pd ratio of 0.5 enhanced the turn-over frequency of the hydrogenation by a factor of 7 and changed the hydrogen order of the reaction from 1.0 to 0.75 and the cyclohexene order from 0 to 0.6. The reaction with D_2 exhibited deuterium-distribution patterns similar to those for the reaction on the ZrO_2-supported Pd catalysts. The hydrogenation pathway on the ZrO_2-added catalyst was described by an associative mechanism in which the slow step was a surface reaction between a cyclohexyl radical and a hydrogen atom. In the thermal desorption spectra, the addition of ZrO_2 caused a broadening of the adsorbed hydrogen peak as well as a shift of the dissolved hydrogen peak toward a lower temperature. The desorption of cyclohexene from Pd/α-Al_2O_3 catalysts underwent a disproportionation to produce benzene around 318 K and cyclohexane at 368 K, whereas the latter peak shifted by 70 K to the lower-temperature side upon the addition of ZrO_2. The XPS study showed that the presence of ZrO_2 provided Pd metal atoms in a negatively-charged state. The support effect was discussed on the basis of the interaction between Pd metal atoms and ZrO_2 oxide.

In recent research in heterogeneous catalysis by supported-metal catalysts, it has been recognized that the catalytic and adsorptive properties of metals loaded depend not only on the characteristics of their geometrical structures, but also on the nature of the underlying supports.[1-5] In the first paper of this series,[6] we have reported that the turn-over frequency of the cyclohexene hydrogenation is larger by one order of magnitude for the ZrO_2-supported Pd catalysts than for the α-alumina-supported Pd and Pd black catalysts. The kinetic behavior of the hydrogenation is also different, and it was proposed that there existed a considerable interaction between the dispersed Pd and ZrO_2 surfaces. For a better understanding of this phenomenon, quantitative information on the interaction between the metal and oxide is needed, and thus it is of interest to employ catalysts in which Pd and ZrO_2 were loaded in different ratios on an inert carrier of α-alumina.

The present study aims at comparing the effect of the ZrO_2 codispersed with Pd to the effects of the ZrO_2 support and at revealing how the catalytic properties vary as a function of the atomic ratio of Zr/Pd. Mechanistic analysis based on the detailed kinetics using D_2 as a tracer was applied to the hydrogenation of gaseous cyclohexene over catalysts with different Zr/Pd ratios. Further, the thermal desorption study was undertaken in order to examine the influence of ZrO_2 upon the adsorbed states of hydrogen and cyclohexene.

In an effort to reveal the change in electronic structures which might be induced through the metal-oxide interaction, X-ray photoelectron spectroscopy (XPS) was employed. The controllable atomic ratio of Zr/Pd in the present system makes this XPS analysis more effective than the previous system of Pd supported on ZrO_2, in which the tail of a large Zr 3d peak interfered with an accurate determination of the Pd 3d levels. The geometric structure of Pd metal in the presence of ZrO_2 was characterized by X-ray diffraction and CO chemisorption methods.

Experimental

The procedure of preparing the catalysts, α-alumina-supported Pd and ZrO_2, and the chemical reagents used were the same as those employed previously[6] except for the use of mixed solutions of palladium and zirconyl nitrates. The concentration of palladium was adjusted to maintain a 2.1 wt% of α-alumina for each of the catalysts, while the atomic ratio of Zr/Pd was increased from 0.1 to 45. Prior to the kinetic run, the catalysts were treated with 20 Torr of oxygen (1 Torr=133.3 Pa) at 523 K, reduced with 20 Torr of hydrogen, and then evacuated at the same temperature. The kinetic behavior of the reaction was examined in the temperature range of 283—323 K, using reactants in the pressure range of 10—40 Torr. The apparatus, procedure, and reactant used have been described elsewhere.[6] The crystallite size and the percentage exposed of the dispersed catalysts were determined by means of the CO chemisorption and X-ray diffraction in manners similar to those employed in the previous study.[6]

The X-ray photoelectron spectra were recorded at room temperature on a Hewlett-Packard 5950A ESCA spectrometer with monochromatized Al $K\alpha$ excitation. Each catalyst sample was pressed in the form of pellets, mounted on a recessed quartz plate, and transferred into the XPS preparation chamber, where it was subjected to "*in situ*" treatment similar to the activation used in the kinetic study except for relatively lower pressures of oxygen and hydrogen (≈5 Torr). The background pressure during photoemission measurement was below 3×10^{-9} Torr. The charging shift was compensated for, or at least minimized, by showering low-energy electron by the use of a flood gun. The binding energies of Al $2s_{1/2}$= 119.1 eV and C 1s=284.8 eV were taken as reference.

The thermal desorption spectra were recorded by using a high-vacuum apparatus pumped at such a high speed that the rate of desorption was proportional to the partial pressure

of the desorbing species.[7] This apparatus was equipped with an ionization gauge to monitor the change in the total pressure, and with a quadrupole mass spectrometer, Mitsubishi MF-T_2M, for the analysis of the desorbed molecules. After being subjected to the pretreatments, the catalyst samples were exposed to different pressures of hydrogen or cyclohexene at various temperatures. The temperature of the catalysts was raised at a rate of 13 K min^{-1} by the use of an outside electric furnace, and was monitored with a Pt-Pt/13%Rh thermocouple which was directly brought into contact with the samples.

Results

Figure 1 shows the variation in the catalytic activity, V_g, as a function of the Zr/Pd ratio. The initial activity, 0.88×10^{21} molecule $min^{-1}g\text{-}Pd^{-1}$, for the 2.1 wt% Pd/α-Al_2O_3 catalyst increased markedly with the addition of ZrO_2 up to a Zr/Pd ratio of 0.5, slowed to a gradual increase, and then reached a stationary value, 4.3×10^{22}, at a ratio of Zr/Pd=45. This activity is in substantial agreement with that for the 2.1 wt% Pd/ZrO_2 catalyst. No catalytic hydrogenation proceeded on the alumina and ZrO_2 under the same conditions. The variations in the pressure and temperature dependence of the hydrogenation rate were systematically examined for the catalysts with different Zr/Pd ratios; the kinetic parameters thus obtained are summarized in Table 1. By the addition of ZrO_2 at a Zr/Pd ratio of 0.5, the reaction order with respect to the hydrogen pressure, P_h, decreased from 1.0 to 0.75, whereas the order with respect to the cyclohexene pressure, P_e, increased from 0 to 0.60. Above this ratio, no significant change was observed, and it should be noted that the values obtained were almost the same as those for the ZrO_2-supported Pd catalysts.[6] There was a similar trend in the variation in the activation energy, E_a, with the addition of the ZrO_2 component.

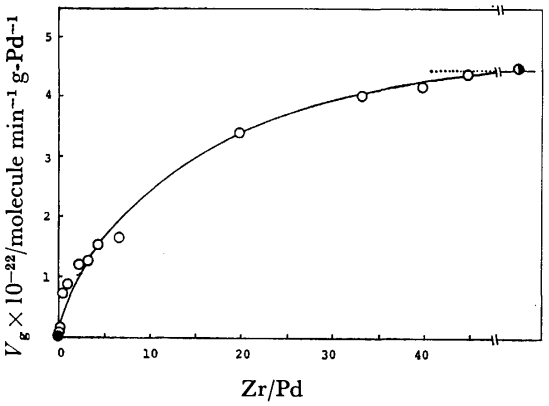

Fig. 1. Variation in catalytic activity, V_g, with Zr/Pd ratio.
P_h=40 Torr, P_e=40 Torr, reaction temperature: 301 K.
●: 2.1 wt% Pd/α-Al_2O_3, ○: ZrO_2-added 2.1 wt% Pd/α-Al_2O_3, ◑: 2.1 wt% Pd/ZrO_2.

Table 1 also shows the results of the characterization of ZrO_2-added Pd catalysts by the CO chemisorption and X-ray line broadening methods, together with the turn-over frequency of the reaction rate, N_t. The percentage exposed, D_{CO}, gradually rose with the increase in the amount of ZrO_2, *e.g.*, by a factor of 1.4 at Zr/Pd=0.5 and of 2.3 at Zr/Pd=2.5, whereas a marked rise in N_t's occurred around the ratio of Zr/Pd=0.3—0.5. Both values converged with those for the 2.1 wt% Pd/ZrO_2 catalyst at Zr/Pd ratios larger than 45.

Table 2 shows the deuterium distributions in the reaction of cyclohexene with D_2 or with an equimolar mixture of H_2+D_2 at 301 K over a catalyst with a Zr/Pd ratio of 0.5. In the case of the former reaction, the cyclohexane product exhibited wide deuterium distributions, ranging from D_0 to D_5, whereas there

Table 1. Characterization of ZrO_2-added Pd/α-Al_2O_3 catalysts and kinetic parameters of cyclohexene hydrogenation

Pd wt%	Ratio of Zr/Pd	V_g[a] molecule / min g-Pd	CO[b] molecule / g-Pd	D_{CO}/%[c]	D_X/%[d]	N_t / s^{-1}	Reaction order[e] m	n	Activation energy[f] E_a / kJ mol^{-1}
2.1	0.0	0.88×10^{21}	1.30×10^{20}	2.2	2.5	0.10	1.00	0.10	38.5
	0.1	2.23	1.37	2.4	1.5	0.27	0.90	0.20	36.7
	0.3	2.79	1.49	2.6	2.1	0.32	0.78	0.33	42.3
	0.5	7.02	1.69	3.0	—	0.69	0.75	0.60	46.3
	1.0	8.61	2.09	3.7	2.8	0.70	0.75	0.63	46.1
	2.5	12.0	2.83	5.0	—	0.71	0.78	0.60	48.1
	3.3	12.3	—	—	—	—	0.76	0.60	47.6
	4.3	15.1	3.49	6.2	—	0.72	0.72	0.60	51.5
	6.5	16.3	—	—	—	—	0.70	0.60	46.1
	20.0	34.2	—	—	—	—	0.77	0.60	51.5
	34.0	40.0	5.25	9.3	—	1.06	0.70	0.60	50.3
	40.0	41.2	—	—	—	—	0.76	0.66	53.3
	45.0	43.3	5.37	9.6	10.1	1.33	0.72	0.67	49.4
2.1 wt%Pd/ZrO_2[g]		44.5	5.71	10.1	9.7	1.35	0.70	0.60	46.1

a) P_h: 40 Torr, P_e: 40 Torr; Reaction temperature: 301 K. b) Saturated adsorption at 301 K. c) Percentage exposed(%) evaluated on the assumption of one CO admolecule on each Pd atom. d) Percentage exposed from X-ray line broadening. e) $V=k\,P_h^m\cdot P_e^n$. f) Temperature range: 283—323 K, ±1.4 kJ mol^{-1}. g) Ref. 6.

also existed exchanged cyclohexene ranging up to D_4. Considerable amounts of HD and H_2 were produced in the gas phase, but the value of K, defined as P_{HD}^2/P_hP_D, remained at 1.3—1.4. The latter reaction with a mixture of H_2 and D_2 gave rise to K=1.4—2.5. These values apparently deviated from that for equilibrium at this reaction temperature, indicating that no equilibrium among H_2, HD, and D_2 in the gas phase was established. It should be noted that the deuterium distributions noted here resembled those obtained for the ZrO_2-supported Pd catalyst rather than those of the α-alumina-supported one.[6] From the above-mentioned variations in N_t, kinetic parameters, and deuterium distribution patterns, one can see that the addition of Zr atoms (as ZrO_2), when its concentration attained about a half of that of Pd atoms, caused an almost complete change in the catalytic properties of the Pd metal.

Table 2. Deuterium distribution in the reaction of cyclohexene with deuterium

Catalyst		2.1 wt%Pd+ZrO_2/α-Al_2O_3 (Zr/Pd=0.5)				
		$D_2+C_6H_{10}$[a]			$D_2+H_2+C_6H_{10}$[b]	
Conversion	(%)	7	10	17	7	17
Cyclohexane	D_0	13	21	17	39	35
	D_1	27	29	32	42	45
	D_2	25	19	25	14	17
	D_3	15	13	13	3	3
	D_4	12	11	9	2	0
	D_5	8	7	4	0	0
	D_6—D_{12}	0	0	0	0	0
Cyclohexene	D_0	87	82	83	93	81
	D_1	6	8	3	3	11
	D_2	2	5	3	2	4
	D_3	2	5	3	2	3
	D_4	2	0	3	0	1
	D_5	1	0	3	0	0
	D_6	0	0	2	0	0
	D_7—D_{10}	0	0	0	0	0
H_2		2	3	4	31	29
HD		15	18	20	37	44
D_2		83	79	76	32	27

Reaction temperature: 301 K; a) $P_D=P_e=40$ Torr, b) $P_h=P_D=20$ Torr, $P_e=40$ Torr.

Figure 2 shows the X-ray photoelectron spectra in the Pd 3d region. Palladium supported on α-alumina gave the peaks due to Pd $3d_{5/2}$ and $3d_{3/2}$ levels at 335.2 and 340.6 eV respectively. As for the ZrO_2-added catalysts, these peaks shifted to 335.0 and 340.5 eV at Zr/Pd=0.5, and to 334.8 and 340.2 eV at Zr/Pd=2.5, whereas little change was observed with the Zr 3d level. Table 3 lists the binding-energy values.

Figure 3 illustrates the thermal desorption spectra of hydrogen. The desorption from α-alumina-supported Pd catalysts provided three peaks, at α(273 K), β_1(363—383 K), and β_2(460 K). The initial adsorption gave rise to the β_2-peak, and further adsorption developed the β_1-peak. With an increase in the amount of hydrogen

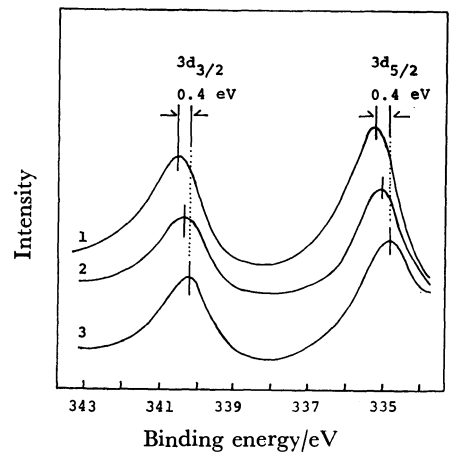

Fig. 2. X-Ray photoelectron spectra in Pd 3d region. 1: 2.1 wt% Pd/α-Al_2O_3, 2: ZrO_2-added 2.1 wt% Pd/α-Al_2O_3(Zr/Pd=0.5), 3: ZrO_2-added 2.1 wt% Pd/α-Al_2O_3(Zr/Pd=2.5).

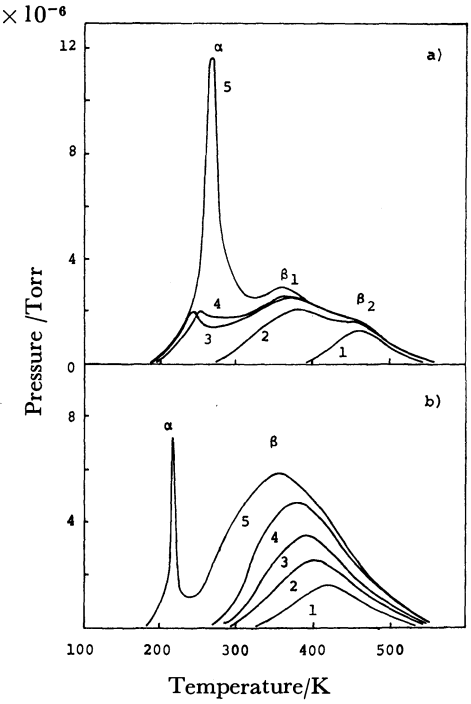

Fig. 3. Thermal desorption spectra of hydrogen.
a) 2.1 wt% Pd/α-Al_2O_3 catalyst exposed to hydrogen at 298 K and cooled to 78 K.
Pressure of hydrogen;
1), 2): below 1×10^{-2}, 3): 3.5×10^{-2}, 4): 7×10^{-2}, and 5): 1.8×10^{-1} Torr.
b) ZrO_2-added 2.1 wt% Pd/α-Al_2O_3 catalyst (Zr/Pd=0.5) under the same conditions as a).
1), 3): below 1×10^{-2}, 4): $\approx1\times10^{-2}$, and 5): 7×10^{-2} Torr.

adsorbed, the β_1-peak shifted to the lower-temperature side by 20 K. After the saturation of the β peaks, the very sharp α-peak began to appear and thereafter grew. In the case of the ZrO_2-added Pd catalyst (Zr/Pd=0.5), the desorption spectra of hydrogen resulted in a broad β peak at 363—413 K, the peak maximum of which shifted to the lower-temperature side with the amount

TABLE 3. BINDING ENERGIES OF Pd 3d AND Zr 3d PEAKS[a]

Catalysts	Pd		Zr	
	$3d_{5/2}$	$3d_{3/2}$	$3d_{5/2}$	$3d_{3/2}$
$Pd/\alpha\text{-}Al_2O_3$	335.2 eV	340.6 eV	—	—
$Pd+ZrO_2/\alpha\text{-}Al_2O_3$ (1 : 0.5)	335.0	340.5	182.0	184.3
$Pd+ZrO_2/\alpha\text{-}Al_2O_3$ (1 : 2.5)	334.8	340.2	181.9	184.3

Accuracy of the values: ±0.15 eV.

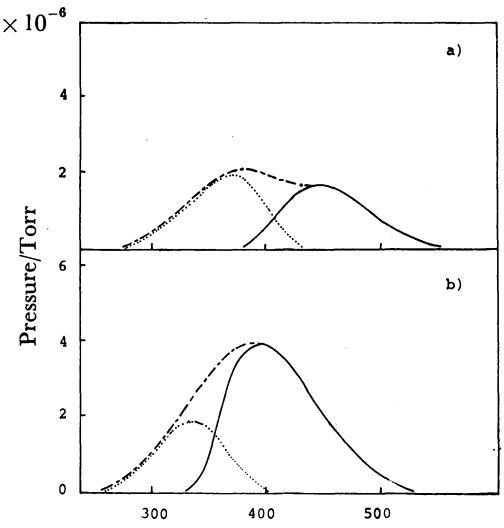

Fig. 4. Thermal desorption spectra of hydrogen contacted with cyclohexene at 195 K. a): 2.1 wt% $Pd/\alpha\text{-}Al_2O_3$, b): ZrO_2-added 2.1 wt% $Pd/\alpha\text{-}Al_2O_3$ (Zr/Pd= 0.5). Dashed line (—·—·): before the contact with cyclohexene, Solid line (——): after the contact, dotted line (····): removed hydrogen by reaction. In these experiment, desorbing hydrocarbon species were trapped off before entering the mass spectrometer.

of hydrogen adsorbed, whereas the narrower α-peak appeared at 223 K. The TD spectra of hydrogen from the ZrO_2-supported Pd surface were analogous to those for the ZrO_2-added Pd catalyst, except for the appearance of the α-peak at 190 K. Only a small peak of hydrogen was observed around 220 K from α-alumina-supported ZrO_2 without Pd metals.

In order to examine the reactivity of the adsorbed hydrogen, the surface with β-hydrogen was exposed to cyclohexene; as is shown in Fig. 4, the desorption spectra of hydrogen from the $Pd/\alpha\text{-}Al_2O_3$ catalyst resulted in the near disappearance of the β_1-peak, without any significant change in the β_2-peak, whereas those from the ZrO_2-added catalysts lacked the portion on the lower-temperature side of the peak.

The desorption spectra of cyclohexene from the $Pd/\alpha\text{-}Al_2O_3$ surface provided a peak of benzene around 318 K, together with a peak of cyclohexane at 368 K (Fig. 5). In the case of the ZrO_2-added catalyst (Zr/Pd= 0.5), the benzene peak appeared at almost the same temperature, 313 K, while the cyclohexane peak shifted to a temperature lower by 70 K. No peak due to

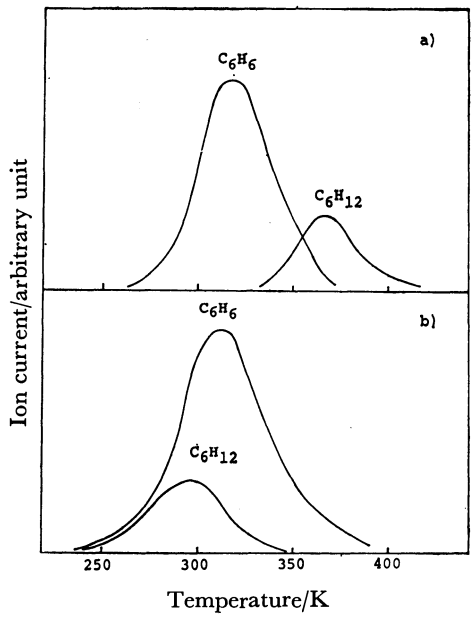

Fig. 5. Thermal desorption spectra of preadsorbed cyclohexene.
a): 2.1 wt% $Pd/\alpha\text{-}Al_2O_3$, b): ZrO_2-added 2.1 wt% $Pd/\alpha\text{-}Al_2O_3$ catalyst (Zr/Pd=0.5). Adsorption temperature: 195 K.

cyclohexene was observed in either catalyst. When hydrogen was preadsorbed, followed by the adsorption of cyclohexene, the resulting desorption spectra exhibited only a cyclohexane peak at 320 K for $Pd/\alpha\text{-}Al_2O_3$ and one at 308 K for the ZrO_2-added catalysts.

Discussion

The present study showed remarkable effects of ZrO_2 upon the catalytic activity of Pd dispersed on α-alumina, and also revealed that the characteristic modification is achieved by a concentration of Zr at 0.5 as the Zr/Pd ratio, since the N_t value was increased significantly; also, the kinetic parameters became almost the same as those for the hydrogenation over Pd/ZrO_2 catalysts. The deuterium distributions also exhibited a characteristic pattern similar to those for ZrO_2-supported Pd catalysts, *i.e.*, a wide deuterium exchange in cyclohexane, but less exchange in cyclohexene, as well as a composition of gaseous hydrogen isotopes far from equilibrium. Therefore, we are able to describe the ZrO_2-affected catalytic hydrogenation by the associative mechanism which was employed in the same reaction on the ZrO_2-supported catalysts:[6]

$$H_2(g) \underset{k_{-1}}{\overset{k_1}{\rightleftharpoons}} 2H(a), \quad (1)$$

$$C_6H_{10}(g) \underset{k_{-2}}{\overset{k_2}{\rightleftharpoons}} C_6H_{10}(a), \quad (2)$$

$$H(a) + C_6H_{10}(a) \underset{k_{-3}}{\overset{k_3}{\rightleftharpoons}} C_6H_{101}(a), \quad (3)$$

$$H(a) + C_6H_{11}(a) \xrightarrow[k_4]{} C_6H_{12}(g), \quad (4)$$

where k_i and k_{-i} denote, respectively, the rate constants of the forward and reverse reactions at the ith step. The formation of highly-exchanged cyclohexanes allows us

to assume that Step 3 is in pseudo-equilibrium. In addition to this assumption, the employment of the steady-state approximation on the concentrations of hydrogen atom, cyclohexene, and the cyclohexyl intermediate leads to the following rate equation:[6]

$$V_g = \frac{2k_1k_4K_2K_3P_hP_e}{[(1+K_2P_e)\sqrt{2k_{-1}+k_4K_2K_3P_e}+(1+K_2K_3P_e)\sqrt{2k_1P_h}]^2}, \quad (5)$$

where $K_i=k_i/k_{-i}$.

Equation 5 is transformed into:

$$\sqrt{\frac{P_h}{V_g}} = \sqrt{\frac{1}{2k_1k_4K_2K_3P_e}}[\sqrt{2k_1P_h}(1+K_2K_3P_e) + (1+K_2P_e)\times\sqrt{2k_{-1}+k_4K_2K_3P_e}], \quad (6)$$

or;

$$\sqrt{\frac{P_e}{V_g}} = \sqrt{\frac{1}{k_4K_1K_2K_3P_h}}[1+\sqrt{K_1P_h} + (1+K_3\sqrt{K_1P_h}+\frac{k_4K_3}{4k_{-1}})K_2P_e], \quad (7)$$

in an approximate form. Figure 6 shows the plots of the $\sqrt{P_e/V_g}$ term *vs.* P_e, and of the $\sqrt{P_h/V_g}$ term *vs.* $\sqrt{P_h}$, for the catalysts with Zr/Pd=0.5 and 1.0 respectively. The good linear relationships verify the validity of the equation, and hence the mechanism proposed.

By analogy with the previous results on the thermal desorption of hydrogen from Pd powder,[7] Pd wire,[8] and Pd/activated carbon,[9] the β_1 and β_2 peaks from the α-alumina-supported Pd catalysts were associated with the adsorbed hydrogen, whereas the α-peak was assigned to the dissolved hydrogen. Judging from the reactivity with cyclohexene, one can reasonably consider that the β_1-hydrogen species is responsible for the hydrogenation. The shift of this peak toward the lower-temperature side with the amount of hydrogen is indicative of a second-order desorption, and hence of the dissociated state of the hydrogen. This supports the aforementioned reaction mechanism.[6] As to the reactivity and dissociated state, similar situations hold for the β-hydrogen on the ZrO_2-added catalyst. Although the separation between β_1 and β_2 peaks is difficult in this case, it is not unreasonable to assume, by taking the reactivity with cyclohexene into account, that the hydrogen located on the lower-temperature side of the β peak is associated with the β_1-state, as is shown by the dotted line in Fig. 4, and that the remaining peak corresponds to the β_2-state. In this classification, there is a tendency for the β_1 and β_2 hydrogens on the ZrO_2-added catalysts to be desorbed at slightly lower temperatures than those on α-alumina-supported Pd catalysts. An other feature of the ZrO_2 effect was the shift of the α peak due to the dissolved hydrogen to a lower temperature. As is shown in Table 4, the temperature of each peak maximum was lowered with an increase in the Zr/Pd ratio. These results suggest that the dissolved hydrogen became unstable with the addition of ZrO_2, in accordance with a weakening of the adsorption bond of hydrogen. Such unstability is partly ascribable to the increase in D_{CO}, *i.e.*, the crystallite-size effect, but the main reason appears to be the changes in the electronic states of dispersed Pd metals.

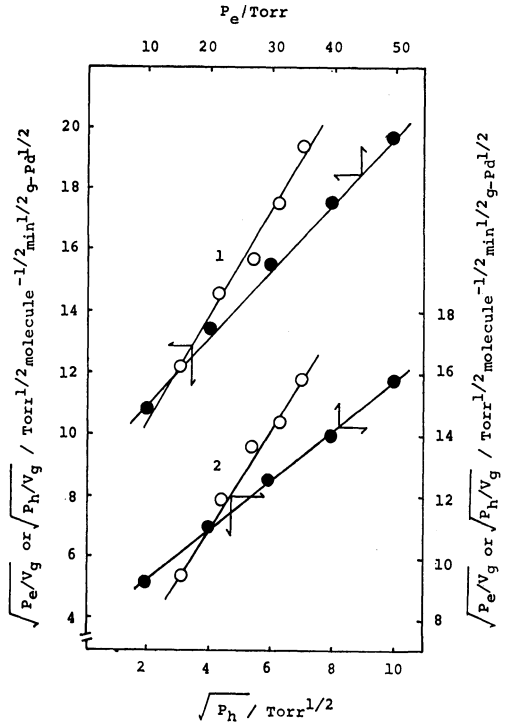

Fig. 6. Rate-partial pressure relationships for cyclohexene hydrogenation on ZrO_2-added 2.1 wt% Pd/α-Al_2O_3 catalysts.
○: $\sqrt{P_h/V_g}$ *vs.* $\sqrt{P_h}$, ●: $\sqrt{P_e/V_g}$ *vs.* P_e.
1): Zr/Pd=0.5, 2): Zr/Pd=2.5.

Table 4. Variation in the peak temperature of α-hydrogen with the Zr/Pd ratio

	2.1 wt% Pd+ZrO_2/α-Al_2O_3					2.1 wt% Pd/ZrO_2
Zr/Pd ratio	0	0.1	0.3	0.5	2.5	
Peak temperature/K	273	253	238	223	190	190

The present XPS study has revealed that the Pd 3d line shifts to a lower binding energy upon the addition of ZrO_2. Provided the contribution of a relaxation effect to the photoemission process is not significantly changed by the presence of the ZrO_2 component, it follows that this shift reflects an increased electron density around surface Pd metal atoms as a consequence of electron transfer from the oxide to Pd metal atoms. According to the DV Xα-calculation of the electronic state for H–Pd_6 and H–Ni_6 clusters,[10] a hydrogen atom on the Pd cluster is slightly negative, in contrast to largely-negative hydrogen on the Ni cluster, and the formation of a stable hydride phase in the Pd–H system is attributable to covalency in bonding between hydrogen and Pd metal atoms. Therefore, it can reasonably be concluded that the transfer of an electron to the Pd metal observed in the present system makes the adsorbed and dissolved hydrogen unstable.

A possible mechanism of benzene and cyclohexane formation during the thermal desorption of cyclohexene is:

$$C_6H_{10}(a) \longrightarrow C_6H_6 + 4H(a), \quad (8)$$

$$C_6H_{10}(a) + 2H(a) \longrightarrow C_6H_{12}, \quad (9)$$

where Step 9 is regarded as being a combination of Steps 3 and 4. The low-temperature shift of cyclohexane, together with the TD result that the cyclohexene adsorbed on the hydrogen-covered surface was desorbed as cyclohexane at a lower temperature in the presence of ZrO_2, suggests that the total energy level of the adsorbed hydrocarbon species including the cyclohexene and/or the cyclohexyl radical becomes higher in the case of the ZrO_2-added Pd catalyst surface. This view is in line with the fact that the apparent activation energy with reference to the energy level of gaseous reactants became higher for the reaction on the ZrO_2-added Pd catalyst than on the Pd/α-Al_2O_3 catalyst. Thus, it may be concluded that the variations in the reaction orders with ZrO_2 addition are mainly to be contributed to the much weakened adsorption of hydrocarbon species compared to that of hydrogen.

The support effects were also observed for TiO_2, the oxide of Group IV_a metals; nickel deposited on this oxide exhibited a stable and high catalytic activity for the methanation reaction of CO.[11] A recent systematic study using XPS, UPS, LEED, and AES[12] revealed that the nickel atoms at the Ni/TiO_2(110) interface are negatively charged as a result of electron transfer through Ni-O^{2-} interaction, which is responsible for the enhanced backdonation of electrons to the $2\pi^*$ orbital of the adsorbed CO molecule, thereby facilitating the dissociation of CO. The negatively-charged state of platinum was also observed to exist on the $SrTiO_3$(100) surface.[13] The SCF Xα-scattered wave calculation for a Pt atom on the $(TiO_6)^{8-}$ cluster[14] showed that the ability of the Pt atom to chemisorb hydrogen was lost when there was a strong interaction between Pt and Ti atoms, whereas the importance of metal-oxygen interaction and the role of the resulting electronic structure in breaking the hydrogen bond were suggested in the Ru/SiO_2 system.[15]

The present TD spectra of hydrogen showed that the chemisorption of hydrogen was not severely suppressed in the presence of ZrO_2. In our IR study of CO adsorbed on silica-supported Pd surfaces, the absorption bands characteristic of the C–O stretching vibration shifted to a frequency lower by 65 cm^{-1} when ZrO_2 was added at the Zr/Pd ratio of 0.5;[16] this shift is evidently ascribable to the enhanced backdonation to the $2\pi^*$ orbital of CO, which was similar to that observed in the above-mentioned Ni–TiO_2 system. From these findings, therefore, it seems reasonable at present to assume that the interfacial interaction between Pd and ZrO_2 occurs through the Pd–O bond, although we need more essential understanding from the theoretical point of view.

The present ZrO_2-added Pd catalysts allow us to consider two structural models. One is that Pd metal and ZrO_2 oxide particles grow almost independently on the alumina surface and can interact each other through the particle-to-particle interface; this requires a long-range interaction for ZrO_2 to exert its effect. Another model is that the Pd metal is mainly deposited on ZrO_2 oxide over α-Al_2O_3. The latter model is more plausible, since the preferential interaction between Pd and ZrO_2 components can be expected, as is revealed by XPS, and since the catalytic properties of the ZrO_2-added Pd catalysts were substantially the same as those of the ZrO_2-supported Pd catalysts. Furthermore, it seems more reasonable to consider that Pd-metal clusters grow on ZrO_2 with a specific structure so as to increase the interfacial boundary-area with the ZrO_2 component than to assume the long-range interaction of the former model.

In order to verify the validity of these models, we have to await precise analysis, *e.g.*, using the EXAFS technique,[17] which will be able to provide information on the composition and microscopic local structure around each of the atoms in these solid mixtures.

References

1) G. M. Schwab, *Adv. Catal.*, **27**, 1 (1976).
2) G. J. Den Otter and F. M. Dautzenberg, *J. Catal.*, **53**, 116 (1978).
3) S. J. Tauster, S. C. Fung, and R. L. Garten, *J. Am. Chem. Soc.*, **100**, 170 (1978).
4) M. A. Vannice and R. L. Garten, *J. Catal.*, **56**, 236 (1979).
5) D. J. C. Yates, L. L. Murrell, and E. B. Prestridge, *J. Catal.*, **57**, 41 (1979).
6) B. Y. Lee, Y. Inoue, and I. Yasumori, *Bull. Chem. Soc. Jpn.*, **54**, 13 (1981).
7) Y. Inoue, I. Kojima, S. Moriki, and I. Yasumori, *Proc. 6th Int. Congr. Catal.*, **1**, 139 (1976).
8) A. W. Aldag and L. D. Schmidt, *J. Catal.*, **22**, 260 (1971).
9) J. A. Konvalinka and J. J. F. Scholten, *J. Catal.*, **48**, 374 (1977).
10) H. Adachi, S. Imoto, T. Tanabe, and M. Tsukada, *J. Phys. Soc. Jpn.*, **44**, 1039 (1978); T. Tanabe, H. Adachi, and S. Imoto, *Jpn. J. Appl. Phys.*, **17**, 49 (1978).
11) M. A. Vannice, *J. Catal.*, **44**, 152 (1976); *Catal. Rev. Sci. Eng.*, **14**, 153 (1976).
12) C. C. Kao, S. C. Tsai, M. K. Bahl, and Y. W. Chung, *Surf. Sci.*, **95**, 1 (1980).
13) Y. W. Chung and W. B. Weissbard, *Phys. Rev. B*, **20**, 3456 (1979); M. K. Bahl, S. C. Tsai, and Y. W. Chung, *Phys. Rev. B*, **21**, 1344 (1980).
14) J. A. Horsley, *J. Am. Chem. Soc.*, **101**, 2870 (1979).
15) K. H. Johnson, A. C. Balazs, and H. J. Kolari, *Surf. Sci*, **72**, 737 (1978).
16) B. Y. Lee, Y. Inoue, and I. Yasumori, unpublished.
17) G. H. Via, J. H. Sinfelt, and F. W. Lytle, *J. Chem. Phys.*, **71**, 690 (1979); R. B. Greegor, and F. W. Lytle, *J. Catal.*, **63**, 476 (1980).

  Bull. Chem. Soc. Jpn., 54, 3717—3722 (1981)

Solid-Liquid and Liquid-Liquid Phase Equilibria in the Symmetrical Tetraalkylammonium Halide-Water Systems

Haruo NAKAYAMA

Department of Chemistry, Faculty of Engineering, Yokohama National University, Tokiwadai, Hodogaya-ku, Yokohama 240

(Received May 11, 1981)

Solid-liquid and liquid-liquid phase diagrams of the binary R_4NX–water (R=n-C_3H_7—n-C_6H_{13} and i-C_5H_{11}; X=F, Cl, Br, and I) systems were determined in the temperature range between −20 °C and +80 °C. These diagrams showed (1) the formation of a clathrate-like hydrate for four salts $(n\text{-}C_5H_{11})_4NF$, $(n\text{-}C_5H_{11})_4NCl$, $(i\text{-}C_5H_{11})_4NBr$, and $(i\text{-}C_5H_{11})_4NI$; (2) a phase separation into two liquid phases in the systems of $(n\text{-}C_5H_{11})_4NBr$, $(i\text{-}C_5H_{11})_4NBr$, $(n\text{-}C_6H_{13})_4NCl$, and $(n\text{-}C_6H_{13})_4NBr$; (3) that the solubility (in water at a definite temperature) of a series of the salts did not show a systematic change with respect to either the alkyl-chain length or the kind of anion; and (4) that the salt which gave the maximum solubility in water at 25 °C was $(n\text{-}C_5H_{11})_4NCl$ for chloride, $(n\text{-}C_4H_9)_4NBr$ for bromide, and $(C_2H_5)_4NI$ for iodide, respectively. The effect of anions on the solubilities of a series of salts having the same cation was examined. It was found that the ratio m_{Cl}/m_I at 25 °C became as high as 22800 for the tetrapentylammonium salts. Phase diagrams for the bolaform salt $[(n\text{-}C_4H_9)_3N(CH_2)_6N(n\text{-}C_4H_9)_3]X_2$–water systems are also presented.

Though it is well known that the solubilities of symmetrical tetraalkylammonium halides in water are generally high except for iodides, accurate numerical values have been reported only for a limited number of salts[1] and even among the existing data some discrepancies are seen. Our studies on the formation of clathrate hydrates of quaternary ammonium halides[2-4] have found that the solubilities of these salts in water depend sensitively on the temperature, since the phenomena such as the formation of clathrate hydrate and/or the phase separation into two liquids are often observed.

Thus, it would be important to know an accurate phase diagram for the binary mixture of these salts with water before various properties of its aqueous solution are examined. So far as the author knows, no complete phase diagrams for the symmetrical tetraalkylammonium halide–water systems have so far been examined, except for tetrabutylammonium bromide,[5] tetrabutylammonium iodide,[6] and tetrapentylammonium iodide.[6] For the latter two iodides the solubilities in water have been measured at various temperatures (2—43 °C). In this paper we are reporting the complete phase diagrams of the R_4NX (R=n-C_3H_7, n-C_4H_9, n-C_5H_{11}, i-C_5H_{11}, and n-C_6H_{13}; X=F, Cl, Br, and I)–water systems, together with those of the $[(n\text{-}C_4H_9)_3N(CH_2)_6N(n\text{-}C_4H_9)_3]X_2$–water systems.

Experimental

Materials. All the iodides R_4NI (R=n-C_3H_7, n-C_4H_9, n-C_5H_{11}, i-C_5H_{11}, and n-C_6H_{13}) were synthesized by reacting trialkylamines with the corresponding alkyl iodide in ethyl acetate and were purified by recrystallization either from ethyl acetate or ethyl acetate–acetone mixture.[2] These iodides were confirmed by their NMR spectra. Other halides were obtained by neutralizing each hydroxide solution with its corresponding acid HX (X=F, Cl, or Br). The hydroxide solution was prepared by reacting iodide with freshly prepared silver hydroxide in water with vigorous shaking, followed by filtration in a CO_2-free atomsphere.[3] A series of salts $(n\text{-}C_4H_9)_4NX$ and $(i\text{-}C_5H_{11})_4NX$ (X=F, Cl, and Br) was purified by separating out the solids in the form of clathrate hydrates from the above neutralized solutions by cooling. Anhydrous $(n\text{-}C_5H_{11})_4NBr$ was purified by recrystallization from water. Other salts could not be purified either because of high solubility in water or because of two-liquid phase separation. It was observed that three fluorides $(n\text{-}C_4H_9)_4NF$, $(n\text{-}C_5H_{11})_4NF$, and $(n\text{-}C_6H_{13})_4NF$ gradually decomposed when their aqueous solutions were concentrated by evaporation of water. Melting points are summarized in Table 1. Figures in parentheses represent the water content (wt%) of the sample. These salts are somewhat hygroscopic.

Table 1. Melting points (°C) of symmetrical tetraalkylammonium halides R_4NX

R	X		
	Cl	Br	I
n-C_3H_7	143—145 (1.6) [a]	293—295 (0.1)	>290 (0.1)
n-C_4H_9	70—74 (3.5)	99—100 (0.9)	145—147 (0.1)
n-C_5H_{11}	—	99—100 (1.1)	134—135 (0.2)
i-C_5H_{11}	67—68 (1.5)	131—132 (0.7)	146—147 (0.1)
n-C_6H_{13}	—	81—83 (5.3)	103—104 (0.8)

a) Figures in parentheses represent the water content (wt%).

Measurements and Analyses. Phase diagrams for the systems containing all the fluorides and the salts R_4NX having R=n-C_3H_7, n-C_4H_9, i-C_5H_{11} and X=Cl and Br were determined in the following manner. A sample solution (about 1.0—1.5 g) was prepared by weighing out water and a concentrated mother solution; it then was sealed in a small glass ampoule. The concentrations of the mother solutions were determined either by measuring the water content using the Karl Fischer titration method on a MK-AII apparatus (Kyoto Electronics Manufacturing Co.) or by a standard KNCS titration method (the Volhard method).[7]

Each ampoule was gradually cooled until the solid phase appeared and was annealed for at least 24 h at a temperature several degrees lower than the temperature at which the solid phase completely dissolved. After that, the ampoule was slowly warmed (at the rate of about 0.5 °C per hour) with vigorous shaking in a constant temperature bath and the temperature at which the solid phase completely disappeared was accurately determined.

All the phase diagrams of the iodide-water systems were determined by measuring their solubilities in water at various temperatures. In a measuring cell (3 cm diameter and 10 cm high) immersed in a constant temperature bath, the iodide solid was saturated in 10—20 cm^3 of water by vigorous mixing with a magnetic stirrer for 2—10 h. Then a given amount of each saturated solution was withdrawn and was analyzed by the KNCS titration method.

The phase diagrams of $(n\text{-}C_5H_{11})_4NBr$, $(n\text{-}C_6H_{13})_4NCl$, and $(n\text{-}C_6H_{13})_4NBr$ systems, in which a liquid-liquid phase separation occurred, were determined either by an ampoule method or by a solubility measurement. In the former method, the temperature at which the phase separation occurred was measured when an aqueous solution, sealed in an ampoule, was gradually heated. In the latter method, the respective concentrations of the two liquid phases which were in equilibrium with each other at a given temperature were determined by the KNCS titration method.

Results

Tetrapropylammonium Halide–Water Systems. Figure 1 shows the phase diagrams of the tetrapropylammonium halide-water systems. The logarithm of the concentration expressed in mole fraction (X) is plotted against the reciprocal of the absolute temperature. For comparison, the temperature expressed in ordinary Celsius scale is shown on the upper side of the figure. This figure indicates a typical behavior of symmetrical lower quaternary ammonium salts; high solubilities for fluoride, chloride, and bromide and relatively low solubility for iodide. At 25 °C, for example, X's of the chloride and the bromide were 0.255 and 0.162, which correspond to 80.8 and 74.1 wt%, respectively. On the other hand, X was only 0.011 (16.2 wt%) for iodide, though this iodide was the most soluble among the iodides investigated in this study.

In the concentration range between X=0.05 and 0.15, no solid phase appeared, except for the iodide, from the solutions which were kept at −30 °C for two months. Thus, the phase diagrams in this region remain uncertain.

Tetrabutylammonium Halide–Water Systems. The solid-liquid phase diagrams for $(n\text{-}C_4H_9)_4NX$–water systems are shown in Fig. 2 in the same manner as in Fig. 1. The phase diagram for the bromide is in fairly

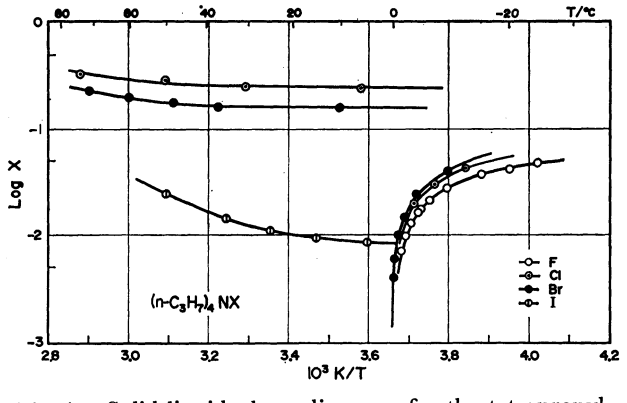

Fig. 1. Solid-liquid phase diagrams for the tetrapropylammonium halide–water systems.

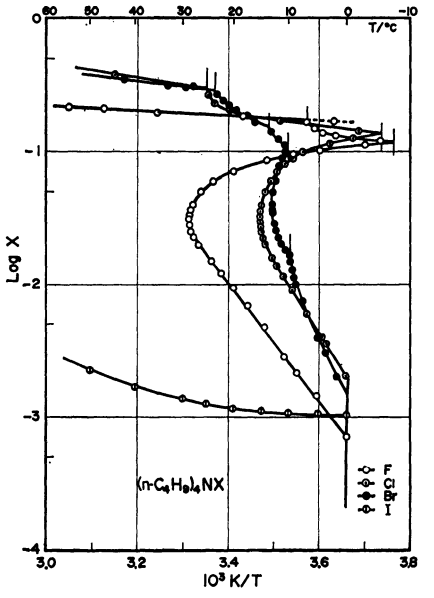

Fig. 2. Solid-liquid phase diagrams for the tetrabutylammonium halide–water systems.

good agreement with the one reported by Diadin *et al.*[5] At temperatures higher than about 30 °C, these phase diagrams also exhibit a similar trend to that in Fig. 1; low solubility for the iodide and high solubilities for the other salts. However, at lower temperatures, the phase diagrams, except for that of iodide, become fairly complicated because of the formation of clathrate-like hydrates[2,5,8,9] and other lower hydrates. The congruent melting point and its composition is 28.3 °C, X=0.032 for the fluoride, 15.0 °C, X=0.032 for the chloride, and 12.9 °C, X=0.040 for the bromide, respectively. These X values correspond to the hydrates $(n\text{-}C_4H_9)_4NF\cdot 30H_2O$, $(n\text{-}C_4H_9)_4NCl\cdot 30H_2O$, and $(n\text{-}C_4H_9)_4NBr\cdot 24H_2O$. For the bromide hydrate two more incongruent melting points were recognized at 9.8 °C (X=0.0168) and at 12.4 °C (X=0.033), although the composition of each hydrate is not known. Diadin *et al.*[5] have reported three incongruent melting points at 9.5, 11.6—11.7, and 12.2 °C and a congruent melting point at 12.36 °C which is slightly different from our result (12.9 °C). A slight discrepancy in a melting point of a clathrate hydrate is often observed.[10,11]

It is interesting to note that the composition of the eutectic points of the clathrate hydrate–ice system are very low (X=0.00075 for the fluoride, 0.0019 for the chloride, and 0.0014 for the bromide). This means that the solubilities of these salts are quite low at temperatures slightly higher than the eutectic point and steeply increase with increasing temperature.

The composition of the other solid phases formed in the concentration ranges of X=0.118—0.168 for the fluoride, X=0.134—0.282 for the chloride, and X=0.106—0.275 for the bromide were not known because the solutions in this concentration ranges, which were highly viscous, were supercooled so easily that ordinary thermal analysis could not be applied. Diadin *et al.*[5] have reported two solid phases $(n\text{-}C_4H_9)_4NBr\cdot 3H_2O$ and $(n\text{-}C_4H_9)_4NBr\cdot 2H_2O$.

The solubility of the iodide is about 10 per cent higher than that reported by Franks and Clarke[6] over the temperature range examined and the minimum in the log X *vs.* T^{-1} curve exists near at 5 °C instead of 12.6 °C.[6]

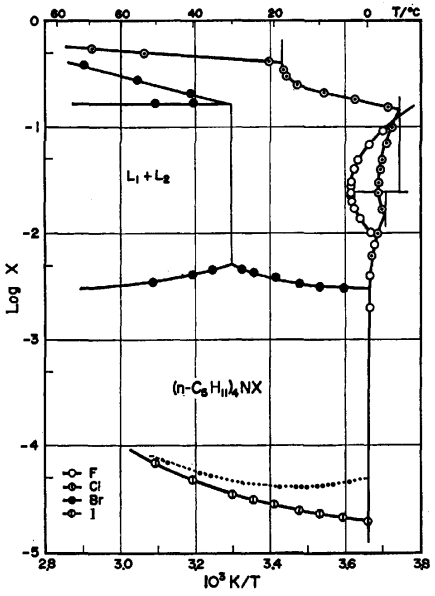

Fig. 3. Solid-liquid and liquid-liquid phase diagrams for the tetrapentylammonium halide-water systems. Dotted line indicates the solubility data for the iodide taken from the Ref. 6.

Tetrapentylammonium Halide–Water Systems. The solid-liquid and liquid-liquid phase diagrams for the $(n\text{-}C_5H_{11})_4NX$–water systems are shown in Fig. 3. For the fluoride and chloride systems, there exist fairly unstable congruent melting points (3.6 °C and −2.3 °C) indicating the formation of clathrate-like hydrates. The peak composition of both hydrates lies around $X=$ 0.025, which corresponds to a hydrate of hydration number 39. The formation of clathrate hydrates of tetrapentylammonium salts has not been reported so far. It is interesting to note that three fairly unstable hydrates can only be formed in the narrowly-limited concentration range of $X\simeq 0.01$—0.1, in striking contrast to the case of tetrabutylammonium (Fig. 2) and tetraisopentylammonium (given later, Fig. 4) salt hydrates.

In the bromide system, phase separation into two liquids occurs above 30.4 °C. The concentration of both phases were, at 50 °C for example, 6.78 wt% in the water-rich phase and 80.92 wt% in the salt-rich phase. Below 30.4 °C the solid phase, which seems to be anhydrous, is in equilibrium with a relatively dilute solution of about 8 wt% or less. This indicates that the solubility of the bromide below 30.4 °C is about a hundredth of that of the chloride.

The solid-liquid equilibrium curve for the iodide is not in agreement with that reported by Franks and Clarke;[6] their curve is shown in Fig. 3 by a dotted line. The observed solubilities were about 1.4 times lower at 25 °C and about 2 times lower at 5 °C than the reported values. Furthermore, our data did not show the existence of a minimum around 16 °C.[6]

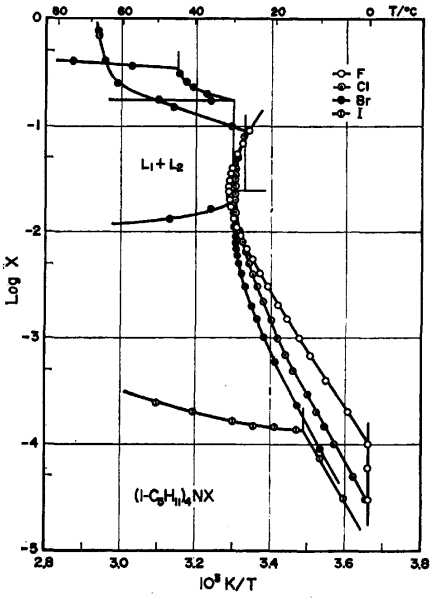

Fig. 4. Solid-liquid and liquid-liquid phase diagrams for the tetraisopentylammonium halide–water systems.

Tetraisopentylammonium Halide–Water Systems. The phase diagrams for the tetraisopentylammonium halide–water systems are given in Fig. 4. The striking feature in this figure is that the formation of clathrate hydrates occurs over a very wide concentration range. In the fluoride system, clathrate hydrate occurs from solutions greater than $X=1\times10^{-4}$ (0.176 wt%), and the solubility of the hydrate steeply increases with increasing temperature. The congruent melting point of the hydrate is 31.5 °C and its X is 0.025, which corresponds to the hydration number of 39. These values are in fairly good agreement with those reported earlier (31.2 °C and about 40).[9] The phase diagrams in the concentrated regions are somewhat uncertain because a solution more concentrated than about $X=0.1$ (66 wt%) gradually decomposes even at room temperature.

The phase diagram of the chloride system exhibits almost the same behavior as that of the fluoride. The formation of clathrate hydrate begins from a solution as low as $X=3\times10^{-5}$ (0.0556 wt%). The melting point and the composition of the hydrate is 29.6 °C and $X=$ 0.025, which corresponds to the same hydration number 39 as that of the fluoride. These values are also in good agreement with those already reported (29.8 °C and hydration number 38.3).[9] The chloride solution was stable even at very high concentrations. The solid phase which appears from the solution greater than $X=0.088$ (eutectic composition at 26.9 °C) seems to be anhydrous.

The phase diagram of the bromide system also indicates the formation of a clathrate hydrate. The clathrate hydrate formation of $(i\text{-}C_5H_{11})_4NBr$ has not been reported so far. However, the congruent melting point and the composition of it could not be determined because of the occurrence of liquid-liquid phase separa-

tion at 30.1 °C. The amount of water in the solid separated from a solution (X=0.005) which had been kept at 10 °C was determined by the Karl Fischer titration method. The mean hydration number was 54.1 for the initial wet sample, and was 36.4 and 0.4 for the solid which had been kept at about 10 °C and allowed to stand in contact with air for 3 h and 48 h, respectively. These results indicate that the solid which is in equilibrium with an aqueous solution at low temperatures has a large amount of water, characteristic of a clathrate hydrate, and the solid kept standing in air gradually loses its water with time owing to an efflorescence. This is a characteristic often found for the clathrate hydrates of quaternary ammonium salts.[2]

The solid phase which appears in the concentration region of X=0.17—0.34 seems to be either a mono hydrate or an anhydrous salt which has a different crystal structure from that of the solid which is stable at temperatures higher than 44.5 °C.

The similarity of the log X *vs.* T^{-1} curve at low temperatures for the iodide system to those of the other systems indicates that iodide also can form a clathrate-like hydrate in the temperature range between an eutectic point (near 0 °C) and an incongruent melting point (13.3 °C). Analogous water analyses for the solid phase separated from its solution phase at 10 °C showed that the mean hydration number was 75.6 for the wet solid sample just after filtration, and 38.9 and 0.18 for the sample which had been kept standing in contact with air for 2 d and 5 d, respectively. These results, just as in the case of the above bromide systems, also suggest that the solid phase which separates out from its solution phase at temperatures lower than 13.3 °C is a clathrate-like hydrate.

The solubility of anhydrous iodide in water is about 4—5 times larger than that of tetrapentylammonium iodide (Fig. 3) at an identical temperature.

Tetrahexylammonium Halide–Water Systems. Phase diagrams for the tetrahexylammonium halide–water systems are shown in Fig. 5. No line indicating the formation of clathrate hydrate is present in this figure. It should be noted that not only in the bromide system but also in the chloride system liquid-liquid phase separation occurs over a wide temperature range. The two liquid phases existed up to at least 100 °C.

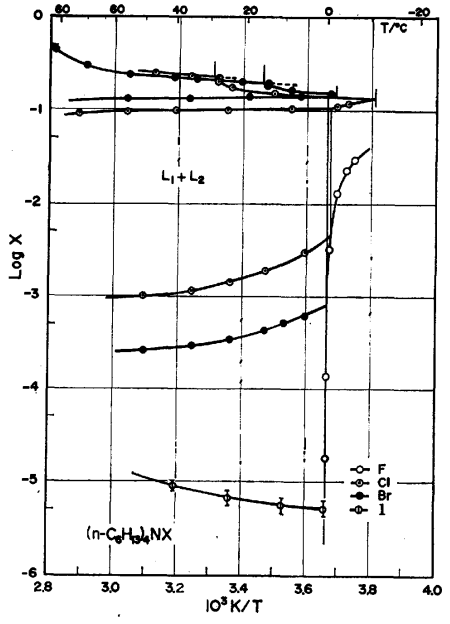

Fig. 5. Solid-liquid and liquid-liquid phase diagrams for the tetrahexylammonium halide–water systems.

In the fluoride system only the ice appeared from the solution of $X<0.03$. From the solutions greater than X=0.03 no solid phase could be formed when cooled at −30 °C for 10 d.

The chloride system shows an eutectic point (at −10.5 °C) between ice and a hydrate, with a hydration number less than 3 and an incongruent melting point at 29.6 °C. The bromide system also has similar points at −1.6 °C and 15.7 °C. The solubility of the iodide was so low that the values obtained would have errors of the order of 10—15 per cent.

Discussion

The Formation of Clathrate Hydrates. Although the formation of clathrate hydrates of $(n\text{-}C_4H_9)_4NX$ (X=F, Cl, and Br)[2,4,8,9,13] and of $(i\text{-}C_5H_{11})_4NX$ (X=F and Cl)[9,12] has already been known, it was newly found in this experiment that other four salts, $(n\text{-}C_5H_{11})_4NF$, $(n\text{-}C_5H_{11})_4NCl$, $(i\text{-}C_5H_{11})_4NBr$, and $(i\text{-}C_5H_{11})_4NI$, could also form a similar type of hydrates.

The two tetrapentylammonium salt hydrates have relatively low melting points (3.6 °C and −2.3 °C), as mentioned earlier. The unstableness of these hydrates may be due to the fact that a pentyl group is somewhat too long[2] to be accomodated stably within a hydrogen-bonded water cage such as a tetrakai- or pentakaidecahedron. Judging from the hydration number of 39, the crystal structure of these hydrates is presumed to resemble that of a tetraisopentylammonium fluoride hydrate[12] (hydration number 39) rather than that of tetrabutylammonium fluoride hydrate[13] (hydration number 30).

Although an accurate hydration number of the $(i\text{-}C_5H_{11})_4NBr$ and of the $(i\text{-}C_5H_{11})_4NI$ hydrates cannot be determined owing to the absence of congruent melting points, it may be assumed to be around 39 taking into consideration: (1) the similarity of log X *vs.* T^{-1} curves at temperatures lower than each incongruent melting point to those of the other fluoride and bromide systems and (2) the above mentioned results of water analyses for the solid separated from its aqueous solution. However, for the bromide hydrate, there is a possibility that some hydrates which have a slightly different hydration number are formed, as in the case of $(n\text{-}C_4H_9)_4NBr$ hydrate, since its log X *vs.* T^{-1} curve becomes almost vertical to the T^{-1} axis at temperatures 29.7—29.9 °C.

The formation of a clathrate hydrate of any other quaternary ammonium iodides has not been reported so far. The fact that $(i\text{-}C_5H_{11})_4NI$ can actually form such a hydrate manifests that the lattice distortion arising from the presence of a large iodide anion can be overcome by the ability of the isopentyl group to stabilize the surrounding hydrogen-bonded water frameworks.[2]

Furthermore, it should be noted that, at temperatures higher than the incongruent point (13.3 °C), the iodide hydrate decomposes into an anhydrous solid and a dilute aqueous solution (around 0.3 wt%). This property would be appropriate to an application of the salt such as the purification of saline water through a cyclic process of the formation and the decomposition of the hydrate.

Solubilities of Tetraalkylammonium Halides in Water. These results clearly show the solubilities of symmetrical tetraalkylammonium halides in water at a definite temperature are affected not only by the type of alkyl chain of the cation and the type of the gegen ion but also by such phenomena as the formation of a clathrate-like hydrate and the separation into two liquid phases. The solubilities of R_4NX in water at 25 °C, which are obtained from the diagrams, are summarized in Table 2, together with the values taken from some recent references.

Table 2. Solubilities of symmetrical tetraalkylammonium halides (R_4NX) in water at 25 °C(in molality)

R	X			
	F	Cl	Br	I
CH_3	—	*ca.* 19.1[1]	6.3±0.2[14]	0.2715[15]
C_2H_5	—	*ca.* 9.5[1]	15.0±0.2[14]	1.75[16]
n-C_3H_7	Extremely high	19.00	10.73 (10.4±0.2[14])	0.6255
n-C_4H_9	12.52 (0.93)[a]	20.53	21.48	0.0679 (0.0622[6])[b]
n-C_5H_{11}	—	40.20	0.2318	0.0018 (0.0025[6])[b]
n-C_6H_{13}	—	0.088[c]	0.019[c]	0.0004

a) Solid phase is a clathrate hydrate. b) At 26 °C. c) Values for water-rich phase in two-liquid phase systems.

For a series of salts having the same alkyl chain, the solubilities decrease with changing X in the order Cl, Br, and I, with the exception of $(C_2H_5)_4NBr$ and $(n\text{-}C_4H_9)_4NBr$. However, the solubilities of a group of salts having the same anion do not show a monotonous change with increasing its alkyl-chain length. Eventually, the alkyl chain which gives the maximum solubility is reduced to *n*-C_5H_{11} for the chloride, *n*-C_4H_9 for the bromide, and C_2H_5 for the iodide.

The approximate values of the solubility ratios for salts with different anions are shown in Table 3. It is interesting to note that, among these figures, relatively high values are seen for tetrabutylammonium salts (except for m_{Cl}/m_{Br}) and tetrapentylammonium salts. The ratio m_{Cl}/m_I for the $(n\text{-}C_5H_{11})_4NX$ salts is exceptionally high, as a result of very high solubility of the chloride and very low solubility of the iodide (Table 2). These high values will give a suitable condition for the separation of one halide anion from another through, for example, the distribution equilibrium between an aqueous phase and an organic phase. It was observed that, when a 0.08 *m* NaI aqueous solution was equilibrated at 25 °C with an equal volume of chloroform after addition of $(n\text{-}C_4H_9)_4NCl$ in amounts equimolar with NaI, 90.4 percent of the I^- ion which had been originally present in the aqueous phase was transferred into the chloroform phase in the form of $(n\text{-}C_4H_9)_4NI$ which is sparingly soluble in water (Table 2) and very soluble in chloroform (67.8 wt% at 25 °C). A more extensive study of the distribution equilibrium is under way and will appear in near future.

Table 3. The solubility ratios (in water at 25 °C) for symmetrical tetraalkylammonium halides (R_4NX) having different anions

R	m_{Cl}/m_{Br}	m_{Cl}/m_I	m_{Br}/m_I
CH_3	3.0	70	23
C_2H_5	0.6	5	8
n-C_3H_7	1.8	30	17
n-C_4H_9	1.0	302	316
n-C_5H_{11}	173	22800	132

Appendix

Phase Diagrams of Bolaform Salt $[(n\text{-}C_4H_9)_3N(CH_2)_6N(n\text{-}C_4H_9)_3]X_2$*-Water Systems.* The formation of clathrate hydrates of this series of salts (except for iodide) has already been reported.[4] The entire phase diagrams of the binary mixture of this type of salts with water have also been determined in this study and are shown in Fig. 6. These diagrams are similar to those of the $(n\text{-}C_4H_9)_4NX$–water systems (Fig. 2).

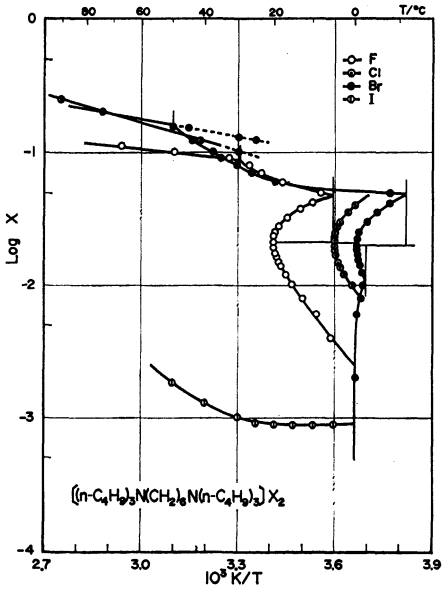

Fig. 6. Solid-liquid phase diagrams for the $[(n\text{-}C_4H_9)_3N(CH_2)_6N(n\text{-}C_4H_9)_3X_2$–water systems.

References

1) W.-Y. Wen, "Water and Aqueous Solutions," ed by R. A. Horne, John Wiley and Sons, Inc., New York (1971), p. 617.

2) H. Nakayama and K. Watanabe, *Bull. Chem. Soc. Jpn.*, **49**, 1254 (1976).

3) H. Nakayama and K. Watanabe, *Bull. Chem. Soc. Jpn.*, **51**, 2518 (1978).

4) H. Nakayama, *Bull. Chem. Soc. Jpn.*, **52**, 52 (1979).

5) I. A. Diadin, I. I. Iakovlyev, I. V. Bondariuk, L. S. Aladko, and L. S. Zyelyenina, *Dokl. Akad. Nauk SSSR*, **203**, 1068 (1972).
6) F. Franks and D. L. Clarke, *J. Phys. Chem.*, **71**, 1155 (1967).
7) F. P. Treadwell and W. T. Hall, "Analytical Chemistry," John Wiley, New York (1963), Vol. 2.
8) D. L. Fowler, W. V. Loebenstein, D. B. Pall, and C. A. Kraus, *J. Am. Chem. Soc.*, **62**, 1140 (1940).
9) R. McMullan and G. A. Jeffrey, *J. Chem. Phys.*, **31**, 1231 (1959).
10) H. Nakayama and M. Hashimoto, *Bull. Chem. Soc. Jpn.*, **53**, 2427 (1980).
11) S. R. Gough and D. W. Davidson, *Can. J. Chem.*, **49**, 2691 (1971).
12) D. Feil and G. A. Jeffrey, *J. Chem. Phys.*, **35**, 1863 (1961).
13) R. K. McMullan, M. Bonamico, and G. A. Jeffrey, *J. Chem. Phys.*, **39**, 3295 (1963).
14) J. A. Burns and W. F. Furter, *Adv. Chem. Ser.*, **155**, 99 (1976).
15) B. J. Levin, *Aust. J. Chem.*, **18**, 1161 (1965).
16) C. J. Peddle and W. E. S. Turner, *J. Chem. Soc.*, **103**, 1202 (1913).

Electrochemical Properties of Ferrocenophanes. I. Voltammetric Studies on the Oxidation of Mono-, Di-, and Tri-bridged Ferrocenophanes in Acetonitrile

Tateaki OGATA,* Kazuo OIKAWA, Tadashi FUJISAWA, Shunsuke MOTOYAMA,†
Taeko IZUMI,† Akira KASAHARA,† and Nobuyuki TANAKA††

Department of Environmental Chemistry, Yamagata Technical College, Jonan, Yonezawa 992
†*Department of Applied Chemistry, Faculty of Engineering, Yamagata University, Jonan, Yonezawa 992*
††*Department of Chemistry, Faculty of Science, Tohoku University, Aramaki, Sendai 980*

(Received May 18, 1981)

Electrode reactions of mono-, di- and tri-bridged ferrocenophanes ([3]Fcp, [4]Fcp, [3][3]Fcp, [4][3]Fcp, [4][4]Fcp, [3][3][3]Fcp, [4][4][3]Fcp and [4][4][4]Fcp) in acetonitrile were investigated by direct current polarography, pulse polarography, and cyclic voltammetry. The oxidation of these compounds proceeds reversibly as a one-electron process. The linear relationship between the half-wave potential and the number of methylene groups was obtained for ferrocene and ferrocenophanes other than [3][3]Fcp and [3][3][3]Fcp. The Taft substituent constants of trimethylene and tetramethylene groups were estimated.

Electrochemical properties of ferrocene and substituted ferrocenes have been studied by many authors.[1,2] These studies have revealed that the oxidation of ferrocene and its derivatives proceeds reversibly as a one-electron process in nonaqueous solutions. Their reversible oxidation potentials change in ways dependent on the substituent: the oxidation potential of the derivatives with the electron donating substituents, such as alkyl groups, is lower than that of ferrocene. Such substituent effects have been discussed through the examination of the relation between the oxidation potential and some substituent constant, for example, the Taft substituent constant (σ^*). Thus, Hoh, McEwen, and Kleinberg[3] have reported the following experimental equation:

$$(E_{1/4} \text{ vs. aq SCE})/\text{V} = 0.0978\,\Sigma\sigma^* - 0.1374, \qquad (1)$$

where $E_{1/4}$ is the chronopotentiometric quarter-wave potential in acetonitrile and $\Sigma\sigma^*$ is the summation of Taft substituent constants. This equation is applicable to ferrocene and nineteen mono- and disubstituted ferrocenes.

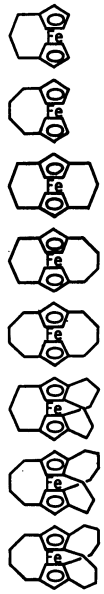

[3](1,1')ferrocenophane ([3]Fcp)
[4](1,1')ferrocenophane ([4]Fcp)
[3](1,1')[3](3,3')ferrocenophane ([3][3]Fcp)
[4](1,1')[3](3,3')ferrocenophane ([4][3]Fcp)
[4](1,1')[4](3,3')ferrocenophane ([4][4]Fcp)
[3](1,1')[3](2,2')[3](4,4')ferrocenophane ([3][3][3]Fcp)
[4](1,1')[4](4,4')[3](2,2')ferrocenophane ([4][4][3]Fcp)
[4](1,1')[4](2,2')[4](4,4")ferrocenophane ([4][4][4]Fcp)

Fig. 1. Structures and names of ferrocenophanes used in this study. Abbreviation is given in parenthesis.

Recently, many ferrocenophanes have become increasingly important in the organometallic chemistry. However, the electrode reactions and the substituent effects, as mentioned above, still remain open to investigation. Therefore, the electrode reactions of the eight ferrocenophanes shown in Fig. 1 have been investigated by direct current polarography, pulse polarography, and cyclic voltammetry in acetonitrile. The results are reported here. Furthermore, the substituent effects on the oxidation potentials of ferrocenophanes are discussed.

Experimental

Acetonitrile (Wako Chemical Co.) was purified by the method proposed by Coetzee.[4] Ferrocenophanes used in this study were prepared according to the methods given in the literature,[5–9] and identified by the elemental analysis and the measurements of NMR and IR spectra. Tetraethylammonium perchlorate (TEAP) was prepared and dried by the usual method.[10] Ferrocene (Eastman Kodak Co.) and other chemicals were of guaranteed reagent grade and used without further purification.

Direct current (d.c.) polarograms, pulse polarograms, and cyclic voltammograms were recorded with a PAR Model 174A polarographic analyzer equipped with a Rikadenki Model RW-11 x-y recorder and a potential scanner made in this laboratory at Yamagata University. All the measurements were carried out at 25 °C under a dry nitrogen atmosphere by use of a three electrode system consisting of a working electrode (dropping mercury electrode for d.c. and pulse polargraphy, and spherical platinum electrode for cyclic voltammetry), a coiled platinum wire counter electrode, and an aqueous saturated calomel electrode (aq SCE) as a reference electrode. The dropping mercury electrode used had a flow rate of 1.02 mg s^{-1} in acetonitrile at open circuit. Drop time for pulse polarography was controlled to 5 s with the drop timer attached to the Model 174A. The pretreatment of the platinum working electrode (approximately 1 mm in diameter) prior to measurements was to apply a cycling potential (between −0.3 V and 1.1 V *vs.* aq SCE) to the electrode in an aqueous solution of 0.1 mol dm^{-3} sulfuric acid. This electrode was washed with distilled water, dried, and then used in the measurements. For electrolytic contact

of aq SCE, an agar salt bridge with 1 mol dm^{-3} aqueous sodium chloride solution was inserted into one compartment of the electrolytic cell. The half cells in the electrolytic cell were interconnected through a sintered glass disk. All the test solutions contained 0.2 mol dm^{-3} TEAP as a supporting electrolyte.

Results and Discussion

Electrode Reactions of Ferrocenophanes. Ferrocenophanes used here gave one d.c. polarographic oxidation wave in acetonitrile containing 0.2 mol dm^{-3} TEAP as a supporting electrolyte. The limiting current of the wave was found to be diffusion-controlled. The diffusion coefficients at 25 °C calculated from the Ilkovic equation by assuming $n=1$ are given in Table 1. The diffusion coefficient of ferrocene obtained in this study is also given in Table 1. From the result that the values of diffusion coefficients of ferrocenophanes were nearly equal to that of ferrocene, the electrode reaction of each ferrocenophane at the mercury electrode was concluded to be a one-electron process. Table 1 also gives the experimental results for the d.c. polarographic half-wave potential, $E_{1/2}$, and the d.c. polarographic slope, $\Delta E(=E_{3/4}-E_{1/4})$, as conventional criteria of reversibility. The values of ΔE indicate that the oxidation step of ferrocenophanes is a reversible one-electron process.

TABLE 1. D. C. AND PULSE POLAORGRAPHIC DATA IN ACETONITRILE CONTAINING 0.2 mol dm^{-3} TEAP AT 25 °C

Compound[a]	$E_{1/2}$ *vs.* aq SCE / V	ΔE / mV	D[b] / 10^{-5} cm^2 s^{-1}	$\lvert I_{1c}/I_{1a}\rvert$
Ferrocene	0.365	56	3.8	0.89
[3]Fcp	0.300	57	3.3	0.99
[4]Fcp	0.279	56	3.3	0.98
[3][3]Fcp	0.291	56	2.9	1.03
[4][3]Fcp	0.202	58	2.6	1.03
[4][4]Fcp	0.196	56	2.8	1.02
[3][3][3]Fcp	0.292	57	2.6	1.03
[4][4][3]Fcp	0.119	57	2.5	1.03
[4][4][4]Fcp	0.103	55	2.5	1.01

a) Concentration of each compound is 1 mmol dm^{-3}.
b) Diffusion coefficient.

In order to investigate the reversibility of the electrode reactions of the above compounds more exactly, pulse polarograms were obtained by use of the dropping mercury electrode with a drop time of 5 s. Typical pulse polarograms obtained for [4]Fcp, [4][4]Fcp, and [4][4][4]Fcp are shown in Fig. 2. In the case of a reversible oxidation process, the current-potential curve for anodic potential scan coincides with that for cathodic one, and the magnitude of the limiting current ratio for cathodic to anodic scan, $|I_{1c}/I_{1a}|$, closely approximates unity.[11] The values of $|I_{1c}/I_{1a}|$ in last column of Table 1 indicate that the electrode reactions of ferrocenophanes are reversible.

Cyclic voltammograms of these compounds were measured by using a spherical platinum electrode at scan rates of 10 to 500 mV s^{-1}. In the region, −0.2 to 1.0 V *vs.* aq SCE, only one anodic and one cathodic

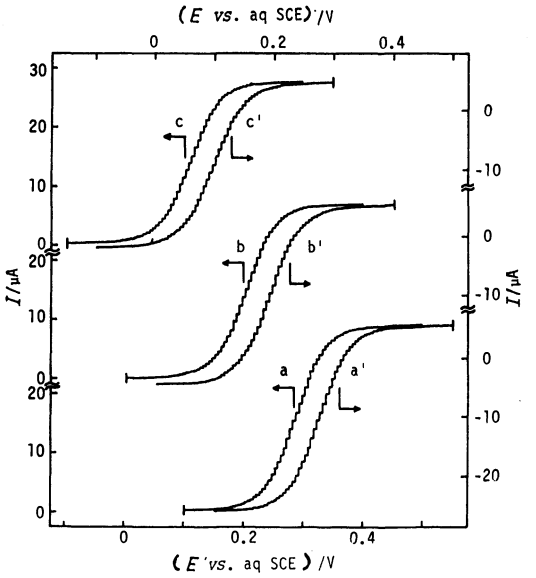

Fig. 2. Pulse polarograms of [4]Fcp (a, a'), [4][4]Fcp (b, b'), and [4][4][4]Fcp (c, c') in acetonitrile containing 0.2 mol dm^{-3} TEAP at 25 °C. Concentration of each compound is 1 mmol dm^{-3}. Curves a, b, and c are by anodic scan, and a', b', and c', cathodic scan.

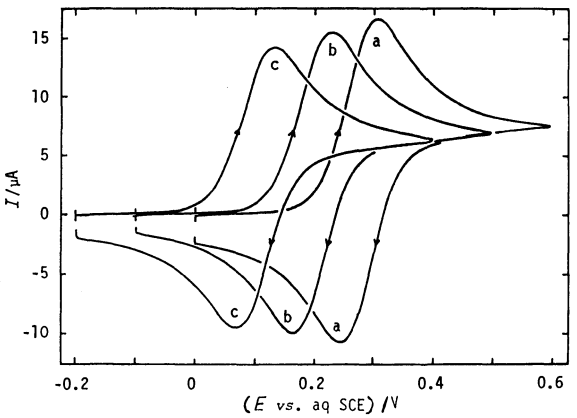

Fig. 3. Cyclic voltammograms of [4]Fcp (a), [4][4]Fcp (b), and [4][4][4]Fcp (c) in acetonitrile containing 0.2 mol dm^{-3} TEAP at 25 °C. Concentration of each compound is 1 mmol dm^{-3}.

current peak were observed. Typical cyclic voltammograms of [4]Fcp, [4][4]Fcp, and [4][4][4]Fcp are shown in Fig. 3. The cyclic voltammetric data at a scan rate of 100 mV s^{-1} for the formal potential, $E_f(=(E_{pa}+E_{pc})/2$, calculated from anodic peak potential, E_{pa}, and cathodic one, E_{pc}), the anodic-cathodic peak separation, $\Delta E_p(=E_{pa}-E_{pc})$, the anodic peak current, I_{pa}, the cathodic peak current, I_{pc}, and the cathodic to anodic peak current ratio, $|I_{pc}/I_{pa}|$, are given in Table 2. The values of I_{pa} of ferrocenophanes almost agree with the value of ferrocene, indicating that the electrode reaction of ferrocenophanes at the platinum electrode is a one-electron oxidation process. In addition, the values of ΔE_p and $|I_{pc}/I_{pa}|$ indicate that the electrode reactions of these compounds are reversible.

From all the results described above, it is concluded

Table 2. Cyclic voltammetric data in acetonitrile containing 0.2 mol dm^{-3} TEAP at 25 °C

Compound[a)]	E_f *vs.* aq SCE / V	ΔE_p / mV	I_{pa} / μA	$-I_{pc}$ / μA	$\lvert I_{pc}/I_{pa}\rvert$
Ferrocene	0.363	65	17.1	17.6	1.03
[3]Fcp	0.297	61	16.3	16.4	1.01
[4]Fcp	0.276	65	16.4	16.8	1.02
[3][3]Fcp	0.286	63	15.0	15.6	1.04
[4][3]Fcp	0.206	63	14.8	15.4	1.04
[4][4]Fcp	0.196	61	15.1	15.7	1.04
[3][3][3]Fcp	0.293	60	14.7	15.3	1.04
[4][4][3]Fcp	0.114	62	14.6	14.8	1.01
[4][4][4]Fcp	0.100	64	13.9	14.2	1.02

a) Concentration of each compound is 1 mmol dm^{-3}.

that the electrode reactions of ferrocenophanes used here correspond to a simple reversible one-electron oxidation from the neutral compound to its mono cation in acetonitrile at both mercury and platinum electrodes. As seen in Tables 1 and 2, the values of $E_{1/2}$ and E_f are almost the same. For this reason, the $E_{1/2}$ values are used when the substituent effects on the oxidation potential are discussed below.

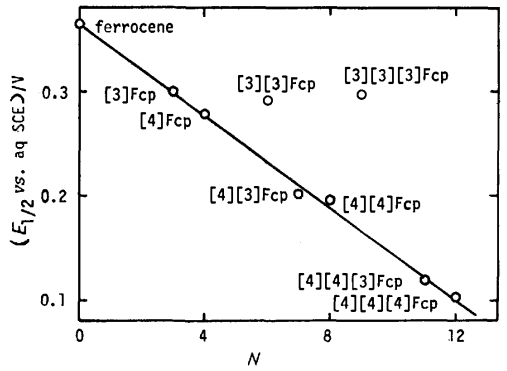

Fig. 4. Half-wave potential, $E_{1/2}$, *vs.* the number of methylene groups, N. Solid line represents Eq. 2.

Substituent Effects on the Oxidation Potential. As seen in Table 1, the $E_{1/2}$ values of ferrocenophanes are lower than the value of ferrocene and generally become more negative with an increase in the number of methylene groups. In Fig. 4, there is shown a plot of the $E_{1/2}$ value *vs.* the number of methylene groups. A linear relationship was observed for ferrocene and ferrocenophanes, except for [3][3]Fcp and [3][3][3]Fcp. The equation of the regression line for this relationship is

$$(E_{1/2}\ vs.\ \text{aq SCE})/\text{V} = -0.0221N + 0.3654 \qquad (2)$$

with a correlation coefficient of −0.9986, where N is the number of methylene groups. This result indicates that the additivity is established between the $E_{1/2}$ value and the number of methylene groups. For example, the $E_{1/2}$ of [4]Fcp is 0.086 V lower than that of ferrocene, and addition of a second tetramethylene group, as in [4][4]Fcp, lowers $E_{1/2}$ by 0.169 V, nearly twice the value found between [4]Fcp and ferrocene. A similar additive effect has been observed in the case of mono- and disubstituted ferrocenes, such as ethylferrocene and 1,1′-diethylferrocene.[12] Therefore, the linear relationship given by Eq. 2 supports the suggestion that the bridge of trimethylene and tetramethylene groups gives rise to few metal-ring distortions in ferrocenophanes, except for [3][3]Fcp and [3][3][3]Fcp. The $E_{1/2}$ values of [3][3]Fcp and [3][3][3]Fcp are more positive than the values expected from Eq. 2. The deviation from this linearity is presumed to be due to steric effects, that is, to metal-ring bond distortions. The distortions in these two compounds can be confirmed by making a molecular model. On the basis of molecular models of [3][3]Fcp and [3][3][3]Fcp, the compression of the metal-ring bond needed to accommodate the bridge was found to be remarkable. Ferrocenophanes except for these two compounds, however, can keep enough distance between ferrocene rings at the normal distance of 332 pm.

The linear relationship between the $E_{1/2}$ and the number of methylene groups suggests that trimethylene and tetramethylene groups have a certain substituent constant. As described above, Eq. 1 is established for many substituted ferrocenes. This equation enables us to estimate the Taft substituent constant, σ^*, of trimethylene and tetramethylene groups. In the case of a reversible electrode reaction, the chronopotentiometric quarter-wave potential, $E_{1/4}$, is equal to the d.c. polarographic half-wave potential, $E_{1/2}$. Furthermore, from the $E_{1/2}$ value of ferrocene obtained in this study, Eq. 1 can be rewritten as follows:

$$(E_{1/2}\ vs.\ \text{aq SCE})/\text{V} = 0.0978\,\Sigma\sigma^* - 0.1142, \qquad (3)$$

where $\Sigma\sigma^*$ is the total of Taft substituent constants. When the $E_{1/2}$ values of 0.300 V for [3]Fcp and 0.279 V for [4]Fcp are substituted for $E_{1/2}$ in Eq. 3, the $\Sigma\sigma^*$ values of [3]Fcp and [4]Fcp are calculated to be 4.24 and 4.02, respectively. Then, the σ^* values of trimethylene and tetramethylene groups (σ^*_3 and σ^*_4) are obtained to be 0.32 and 0.10, respectively (σ^*_3 or $\sigma^*_4 = \Sigma\sigma^* - 8\sigma^*_H$). The $\Sigma\sigma^*$ values of di- and tribridged ferrocenophanes are calculated by using these values of σ^*_3 and σ^*_4: for example, $\Sigma\sigma^*$ value of [4][3]Fcp is 3.36 by the sum of $6\sigma^*_H$, σ^*_3, and σ^*_4. The results of the calculation are given in Table 3. The plot of $E_{1/2}$ *vs.* $\Sigma\sigma^*$ is shown in Fig. 5. The solid line in Fig. 5 represents Eq. 3. In the case of [4][3]Fcp, [4][4]Fcp, [4][4][3]Fcp, and [4][4][4]Fcp, which have the linear relationship between the $E_{1/2}$ and the number of methylene groups and have little metal-ring bond

Table 3. Total Taft substituent constant ($\Sigma\sigma^*$) of ferrocene and ferrocenophanes

Compound	$\Sigma\sigma^*$
Ferrocene	4.90 ($10\sigma^*_H$)
[3]Fcp	4.24 ($8\sigma^*_H+\sigma^*_3$)
[4]Fcp	4.02 ($8\sigma^*_H+\sigma^*_4$)
[3][3]Fcp	3.58 ($6\sigma^*_H+2\sigma^*_3$)
[4][3]Fcp	3.36 ($6\sigma^*_H+\sigma^*_4+\sigma^*_3$)
[4][4]Fcp	3.14 ($6\sigma^*_H+2\sigma^*_4$)
[3][3][3]Fcp	2.92 ($4\sigma^*_H+3\sigma^*_3$)
[4][4][3]Fcp	2.48 ($4\sigma^*_H+2\sigma^*_4+\sigma^*_3$)
[4][4][4]Fcp	2.26 ($4\sigma^*_H+3\sigma^*_4$)

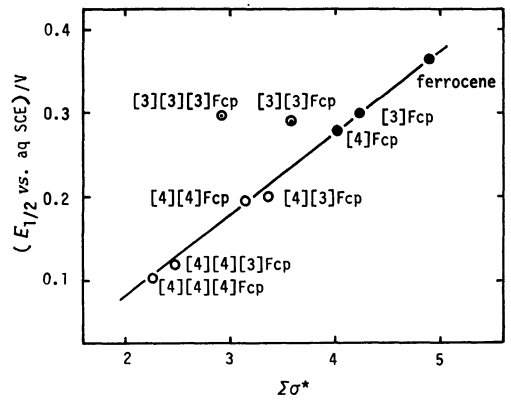

Fig. 5. Half-wave potential, $E_{1/2}$, *vs.* total Taft substituent constant, $\sum\sigma^*$. Solid line represents Eq. 3.

distortions, the points (open circles) are on the solid line. Therefore, the values of σ^*_3 and σ^*_4 obtained by assuming that Eq. 1 or Eq. 3 are valid for [3]Fcp and [4]Fcp seem to be reasonable. If so, the electronic effects of substituents for ferrocenophanes other than [3][3]Fcp and [3][3][3]Fcp are transmitted to the reaction center, *i.e.*, iron atom, through an inductive mechanism.

Since the ferrocenophanes studied here undergo a simple electrode reaction, it is expected that these compounds can be used as a "standard" for electrochemical studies. Application of ferrocenophanes to a reference redox system is now being investigated in many solvents.

References

1) C. K. Mann and K. K. Barnes, "Electrochemical Reactions in Nonaqueous Systems," Marcel Dekker, New York (1970), p. 418.

2) G. J. Janz and R. P. T. Tomkins, "Nonaqueous Electrolytes Handbook," Vol. 2, Academic Press, New York (1978), p. 611.

3) G. L. K. Hoh, W. E. McEwen, and J. Kleinberg, *J. Am. Chem. Soc.*, **83**, 3949 (1961).

4) J. F. Coetzee, *Pure Appl. Chem.*, **25**, 305 (1971).

5) K. L. Rinehart, Jr., R. T. Curby, D. H. Gustafson, K. G. Harrison, R. E. Bozak, and D. E. Bublitz, *J. Am. Chem. Soc.*, **84**, 3263 (1962).

6) M. Rosenblum, A. K. Banerjee, N. Danieli, R. W. Fish, and V. Schlatter, *J. Am. Chem. Soc.*, **85**, 316 (1963).

7) K. L. Rinehart, Jr., D. E. Bublitz, and D. H. Gustafson, *J. Am. Chem. Soc.*, **85**, 970 (1963).

8) M. Hisatome, T. Sakamoto, and K. Yamakawa, *J. Organomet. Chem.*, **107**, 87 (1976).

9) M. Hisatome, N. Watanabe, T. Sakamoto, and K. Yamakawa, *J. Organomet. Chem.*, **125**, 79 (1977).

10) I. M. Kolthoff and J. F. Coetzee, *J. Am. Chem. Soc.*, **70**, 870 (1957).

11) K. B. Oldham and E. P. Parry, *Anal. Chem.*, **42**, 229 (1970).

12) T. Kuwana, D. E. Bublitz, and G. Hoh, *J. Am. Chem. Soc.*, **82**, 5811 (1960).

The Solvent Extraction of Alkali Metal Picrates by Benzo-15-crown-5

Yasuyuki TAKEDA,* Yoshimasa WADA, and Shizuo FUJIWARA
Department of Chemistry, Faculty of Science, Chiba University, Yayoi-chō, Chiba 260
(Received August 14, 1981)

Benzo-15-crown-5 (B15C5) extracted alkali metal picrates (MA) into benzene by forming M(B15C5)A or $M(B15C5)_2A$ complexes and moreover, in the presence of tributyl phosphate (B), B15C5 extracted rubidium and caesium picrates by forming M(B15C5)BA complexes. The extractability sequences of the M(B15C5)A, $M(B15C5)_2A$, and M(B15C5)BA complexes are $Na^+>K^+>Rb^+>Li^+>Cs^+$, $K^+>Rb^+>Cs^+$, and $Rb^+>Cs^+$ respectively. The extraction equilibrium constants for these complexes have been determined at 25 °C, and the synergistic formation constants of the $M(B15C5)_2A$ and M(B15C5)BA complexes in the benzene solution have been calculated. The synergistic effects for the alkali metal ions for the B15C5 system were compared with those for the 15C5 system.

The solvent extractions of alkali metal ions with various crown ethers have been widely studied.[1] In the previous papers,[2,3] it was reported that 15-crown-5 (15C5) extracted alkali metal picrates (MA) into benzene by forming M(15C5)A or $M(15C5)_2A$ complexes and moreover, in the presence of tributyl phosphate (B), 15C5 extracted rubidium and caesium picrates by forming M(15C5)BA complexes.

In this paper, the solvent extraction of alkali metal picrates has been investigated between benzene and water at 25 °C in the presence of benzo-15-crown-5 (B15C5) or both B15C5 and B in order to compare with the case of 15C5. The synergistic formation constants of the $M(B15C5)_2A$ and M(B15C5)BA complexes in the benzene solution have been calculated.

Experimental

Materials. B15C5 and analytical-grade B were obtained from Merck Japan Ltd. and Wako-Pure Chemicals, Ltd. respectively. B15C5 was dissolved in heptane, and filtered while hot. Then it was recrystallized from heptane three times and, before use, dried at 40 °C in a vacuum oven. B was used without further purification. The concentrations of the alkali metal hydroxides and picric acid solutions were determined by means of acid and basic titrations respectively. Analytical-grade benzene was washed twice with distilled water.

Procedure. All the experiments were carried out at 25±0.2 °C. The experimental procedures were the same as those described in the previous papers.[3,4]

The Distribution Coefficient of B15C5. Most of the procedures were similar to those in the previous paper.[5] The average value of the distribution coefficient is 20.

Results

When an aqueous phase of an alkali metal ion (M^+) and a picrate ion (A^-), and a benzene phase of a crown ether (L) or both B and L are equilibrated, the equilibrium constants may be defined by the following equations:

$$K_{ex}(ML_mA) = [ML_mA]_o[H^+]/[M^+][L]_o^m[HA]_o \quad (1)$$

$$K_{ex}(MLBA) = [MLBA]_o[H^+]/[M^+][L]_o[B]_o[HA]_o \quad (2)$$

$$K_{D,L} = [L]_o/[L] \quad (3)$$

$$K_{ML} = [ML^+]/[M^+][L] \quad (4)$$

$$K'_{ex} = [MLA]_o/[ML^+][A^-] \quad (5)$$

$$K_{ex}(HA) = [HA]_o/[H^+][A^-], \quad (6)$$

where the subscript "o" means organic and the lack of a subscript refers to the aqueous phase. Thus, $K_{ex}(MLA)$ can be written as follows:

$$K_{ex}(MLA) = K_{ML}K'_{ex}/K_{D,L}K_{ex}(HA). \quad (7)$$

The $K_{ex}(HA)$ value was spectrophotometrically determined to be 247.

When the benzene phase contains only B15C5, the distribution ratio of the alkali metal may be represented by

$$D = [ML_mA]_o/[M^+]. \quad (8)$$

In the case of $m=1$, Eq. 8 becomes

$$D = K_{ex}(MLA)K_{ex}(HA)[L]_o[A^-]. \quad (9)$$

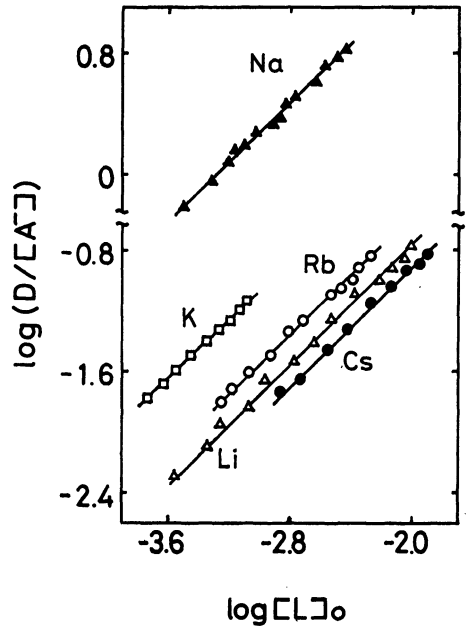

Fig. 1. Plots of $\log(D/[A^-])$ *vs.* $\log[L]_o$ for the MLA system.

The $\log(D/[A^-])$ *vs.* $\log[L]_o$ plot in Fig. 1 shows a linear relationship with a slope of 1 in every case, indicating that B15C5 forms the 1 : 1 complex with the alkali metal ion. The values of $[L]_o$ and $[A^-]$ in Eq. 9 were calculated by means of Eqs. 10 and 11 respectively:

$$[L]_o = ([L]_t - [MLA]_o)/(1 + K_{D,L}^{-1}), \quad (10)$$

$$[A^-] = ([HA]_t - [MLA]_o)/\{1 + (K_{HA} + K_{ex}(HA))[H^+]\}, \quad (11)$$

where the subscript "t" denotes the total concentration and K_{HA} is the association constant of picric acid ($K_{HA}=1.9_5$[6]). In the case of $m=2$, Eq. 8 becomes

$$D = K_{ex}(ML_2A)K_{ex}(HA)[L]_o^2[A^-]. \quad (12)$$

The log $(D/[A^-])$ *vs.* log $[L]_o$ plot in Fig. 2 shows a straight line with a slope of 2 in each case, indicating that B15C5 forms the 2 : 1 complex with the alkali metal ion. The values of $[L]_o$ and $[A^-]$ in Eq. 12 were calculated from Eqs. 13 and 14 respectively:

$$[L]_o = ([L]_t - 2[ML_2A]_o)/(1 + K_{D,L}^{-1}), \quad (13)$$

$$[A^-] = [HA]_t - [ML_2A]_o. \quad (14)$$

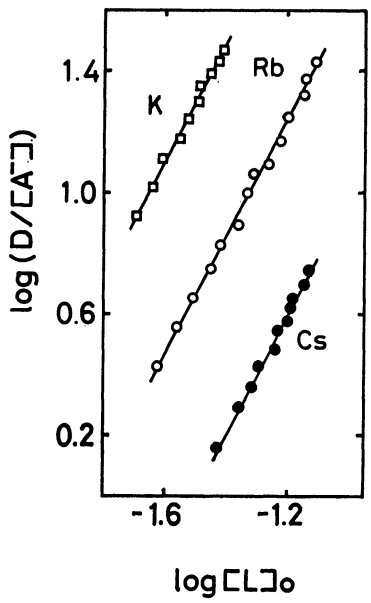

Fig. 2. Plots of $\log(D/[A^-])$ *vs.* $\log[L]_o$ for the ML_2A system.

When the benzene phase contains both B15C5 and B, D may be represented by

$$D = [MLBA]_o/[M^+]. \quad (15)$$

The substitution of Eqs. 2 and 6 into Eq. 15 gives

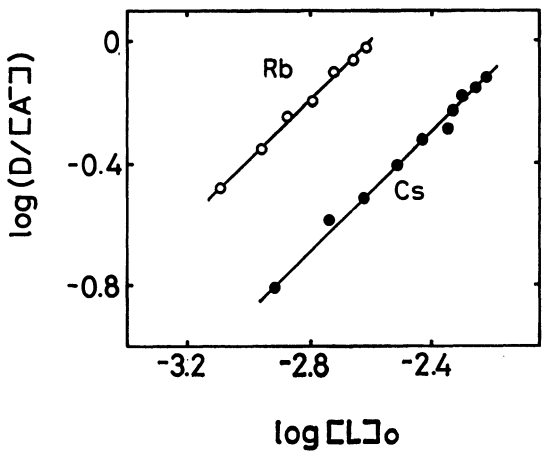

Fig. 3. Plots of $\log(D/[A^-])$ *vs.* $\log[L]_o$ for the MLBA system.

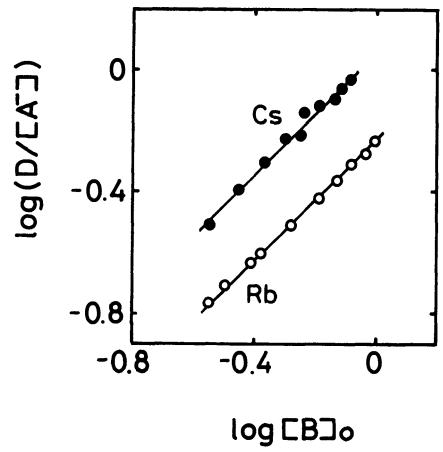

Fig. 4. Plots of $\log(D/[A^-])$ *vs.* $\log[B]_o$ for the MLBA system.

$$D = K_{ex}(MLBA)K_{ex}(HA)[L]_o[B]_o[A^-]. \quad (16)$$

The log $(D/[A^-])$ *vs.* log $[L]_o$ and log $[B]_o$ plots are given in Figs. 3 and 4 respectively. It may be seen from Figs. 3 and 4 that, in each case, the plots of both Rb and Cs have a slope of 1. Thus, the Kex(MLBA) in this work can be described by Eq. 2. The value of $[B]_o$ in Eq. 16 was supposed to be approximately equal to that of $[B]_t$ under the present experimental conditions, and those of $[L]_o$ and $[A^-]$ were calculated from Eqs. 17 and 18 respectively:

$$[L]_o = ([L]_t - [MLBA]_o)/(1 + K_{D,L}^{-1}), \quad (17)$$

$$[A^-] = [HA]_t - [MLBA]_o. \quad (18)$$

The extraction equilibrium constants obtained from these experiments are listed in Table 1, together with those from the literature.

TABLE 1. EXTRACTION EQUILIBRIUM CONSTANTS AT 25 °C

		15C5[2]	B15C5
$K_{D,L}$		0.15_6	20
log K_{ex} (MLA)	Li^+	−1.10	−1.13
	Na^+	1.51	0.90
	K^+	0.19	−0.46
	Rb^+	−0.25	−0.95
	Cs^+	−0.49	−1.31
log K_{ex} (MLBA)	Rb^+	0.56	0.37
	Cs^+	0.19	−0.15
log K_{ex} (ML_2A)	K^+	—	1.91
	Rb^+	2.15	1.22
	Cs^+	1.48	0.41
log ($K_{ML}K'_{ex}$)	Li^+	0.49	2.56
	Na^+	3.10	4.59
	K^+	1.78	3.23
	Rb^+	1.34	2.74
	Cs^+	1.10	2.38

Discussion

The $K_{D,L}$ value of B15C5, which is more bulky than 15C5, is much larger than that of 15C5.

The logK_{ex}(MLA) series for B15C5 and 15C5 are given by $Na^+>K^+>Rb^+>Li^+>Cs^+$ and $Na^+>K^+>$

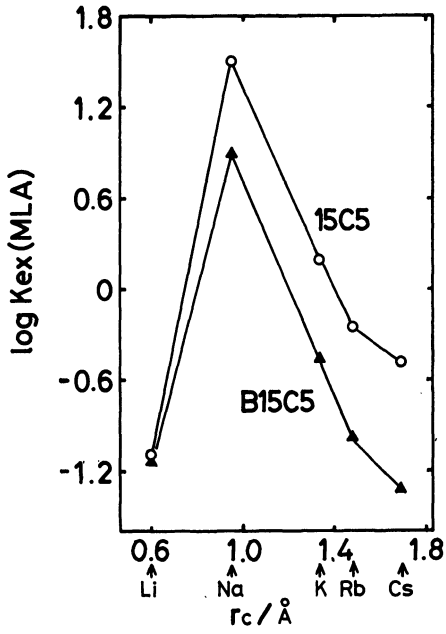

Fig. 5. Plots of log K_{ex}(MLA) *vs.* crystal ionic radii, r_c, of alkali metals for the B15C5 and 15C5 systems.
▲: B15C5, ○: 15C5.

$Rb^+ > Cs^+ > Li^+$ respectively (Table 1). The selectivity tendency of B15C5 (cavity radius: 0.85—1.1 Å[7]) for the alkali metal ions is not much different from that of 15C5 and agrees with the size-fit concept (Fig. 5). A possible explanation for the difference in the sequences of Li^+ and Cs^+ is as follows. The extractability of the crown ether complex with the univalent metal picrate depends on the interaction of the univalent metal ion trapped in the crown ether cavity with water molecules.[8] Since, for the alkali metal ion in the cavity, the interaction of the lithium ion with water molecules seems to be the strongest of all the alkali metal ions, the hindrance for the hydration of the B15C5 complex by the benzo group attached to 15C5 may be much more effective for the case of Li^+ compared to Cs^+. Thus, in the case of B15C5, Li^+ is more extractable than Cs^+. The following data may support the above discussion, though they have been obtained in the nitrobenzene–water system. The numbers of water molecules coextracted with the Li^+–15C5, Li^+–B15C5, Cs^+–15C5, and Cs^+–B15C5 complexes into the nitrobenzene phase are 2.0, 1.4, 0.2, and 0.4 respectively.[9] For the lithium complex, the number of water molecules decreases remarkably on moving from 15C5 to B15C5, while, for the caesium complex, it increases only slightly.

Equation 7 shows that $K_{D,L}$, K_{ML}, and K'_{ex} are important factors which determine the magnitude of K_{ex}(MLA) for the same alkali metal ion and different crown ethers. Although the log ($K_{ML}K'_{ex}$) sequence of B15C5 and 15C5 for the same alkali metal ion is B15C5>15C5, the log K_{ex}(MLA) value of B15C5 for Li^+ is nearly equal to that of 15C5 and that of B15C5 for the other alkali metal ion is smaller than that of 15C5. This is entirely attributed to the much greater $K_{D,L}$ value of B15C5 compared to 15C5 (Table 1). The basicity of the aromatic ether oxygen atom is lower than that of the aliphatic one. Since B15C5 has two aromatic ether oxygen atoms, the B15C5 complex with the same alkali metal ion may be more unstable than the 15C5 complex. The B15C5 complex with the same alkali metal ion may be more extractable than the 15C5 complex because of its larger size compared to 15C5. The log ($K_{ML}K'_{ex}$) value of B15C5 for the same alkali metal ion is larger than that of 15C5 (Table 1). It thus appears that the log ($K_{ML}K'_{ex}$) sequence of B15C5 and 15C5 depends completely on the K'_{ex} sequence. By way of example, in the case of K^+, the log K_{ML} values of B15C5 and 15C5 are 0.38[10] and 0.74,[11] and the log K'_{ex} values are 2.85 and 1.04,[2] respectively.

For the MLA, MLBA, and ML_2A systems, Rb^+ is more extractable than Cs^+, and, for the B15C5–ML_2A system, K^+ is the most extractable (Table 1). In the cases of the MLA, MLBA, and ML_2A systems, the difference in the extractabilities of Rb^+ and Cs^+ increases in going from 15C5 to B15C5.

When MLA undergoes further complex formation with B and L in the organic phase, the equilibria can be described as Eqs. 19 and 20 respectively:

$$MLA_o + B_o \rightleftharpoons MLBA_o,$$

$$K_{MLBA,o} = K_{ex}(MLBA)/K_{ex}(MLA) = [MLBA]_o/[MLA]_o[B]_o, \quad (19)$$

$$MLA_o + L_o \rightleftharpoons ML_2A_o,$$

$$K_{ML_2A,o} = K_{ex}(ML_2A)/K_{ex}(MLA) = [ML_2A]_o/[MLA]_o[L]_o, \quad (20)$$

where $K_{MLBA,o}$ and $K_{ML_2A,o}$ are the formation constants for the MLBA and the ML_2A complexes in a benzene solution respectively; they are summarized in Table 2.

Table 2. Complex-formation constants for synergistic reactions in a benzene solution at 25 °C

		K^+	Rb^+	Cs^+
log $K_{MLBA,o}$	15C5[3]	—	0.81	0.68
	B15C5	—	1.32	1.16
log $K_{ML_2A,o}$	15C5[3]	—	2.40	1.97
	B15C5	2.37	2.17	1.72

The log $K_{ML_2A,o}$ values of B15C5 for K^+ and Rb^+ are approximately identical with those in the literature[10] (K^+: 2.65 and Rb^+: 1.97 in 70 wt% CH_3OH in H_2O, K^+: 2.6 in 80 wt% CH_3OH in H_2O).

It is interesting that, in the benzene solution, both the B15C5 and 15C5 complexes with CsA accept a B molecule, while the 2-thenoyltrifluoroacetone complex with Cs^+ (Cs(TTA)) accepts two B molecules.[12] This may be largely due to that HTTA is a chelating acid, while B15C5 and 15C5 are neutral ligands.

As can be seen from Table 2, for every crown ether system, the smaller the size of the alkali metal ion is, the larger is the complex-formation constant. For the MLBA system, this may reflect the higher charge density of Rb^+ compared to Cs^+. For the ML_2A system, this is presumably attributable to both the charge density of the cation and the accommodation of the cation into the crown ether cavity.

Since B15C5 has two aromatic ether oxygen atoms, the electron density in the B15C5 cavity may be lower than that in the 15C5 cavity. Thus, the apparent charge density of the exposed part of the alkali metal ion trapped in the crown ether cavity seems higher for the case of B15C5 compared to 15C5. Consequently, this may be the reason why, in each case of Rb^+ and Cs^+, the log $K_{MLBA,O}$ value of B15C5 is larger than that of 15C5 (Table 2). In each case of Rb^+ and Cs^+, the log $K_{ML_iA,O}$ value of B15C5 is smaller than that of 15C5. This is probably due to two aromatic ether oxygen atoms of B15C5.

The fact that the crown ether has much more donor oxygen atoms than B may be the reason why, for both B15C5 and 15C5, the log $K_{ML_iA,O}$ value of the same alkali metal ion is larger than the log $K_{MLBA,O}$ value (Table 2).

References

1) I. M. Kolthoff, *Anal. Chem.*, **51**, 1R (1979).
2) Y. Takeda and H. Gotō, *Bull. Chem. Soc. Jpn.*, **52**, 1920 (1979).
3) Y. Takeda, *Bull. Chem. Soc. Jpn.*, **54**, 526 (1981).
4) Y. Takeda, *Bull. Chem. Soc. Jpn.*, **53**, 2393 (1980).
5) Y. Takeda, *Bull. Chem. Soc. Jpn.*, **52**, 2501 (1979).
6) "Dissociation Constants of Organic Acids in Aqueous Solution," ed by G. Kortün, W. Vogel, and K. Andrussov, Butterworths, London (1961).
7) C. J. Pedersen and H. K. Frensdorff, *Angew. Chem. Int. Ed.*, **11**, 16 (1972).
8) Y. Takeda and F. Takahashi, *Bull. Chem. Soc. Jpn.*, **53**, 1167 (1980).
9) T. Iwachido, M. Minami, M. Kimura, A. Sadakane, M. Kawasaki, and K. Tōei, *Bull. Chem. Soc. Jpn.*, **53**, 703 (1980).
10) R. M. Izatt, R. E. Terry, D. P. Nelson, Y. Chan, D. J. Eatough, J. S. Bradshaw, L. D. Hansen, and J. J. Christensen, *J. Am. Chem. Soc.*, **98**, 7626 (1976).
11) R. M. Izatt, R. E. Terry, B. L. Haymore, L. D. Hansen, N. K. Dalley, A. G. Avondet, and J. J. Christensen, *J. Am. Chem. Soc.*, **98**, 7620 (1976).
12) T. V. Healy, *J. Inorg. Nucl. Chem.*, **30**, 1025 (1968).

The Crystal Structure of *cis*-Diammine(orotinato)platinum(II)

Takaaki Solin, Kazuko Matsumoto,* and Keiichiro Fuwa

Department of Chemistry, Faculty of Science, The University of Tokyo, Hongo, Bunkyo-ku, Tokyo 113

(Received December 15, 1980)

From the reaction of *cis*-$[Pt(NH_3)_2(H_2O)_2]$ with orotic acid, yellow needle crystals, green needle crystals, and dark-blue microcrystalline crystals were obtained. The results of elemental analyses, the IR absorption spectra, and X-ray Weissenberg photographs showed that the yellow and green needles are identical, whereas the dark-blue microcrystalline compound exhibits slight difference in the elemental analyses and IR spectra. Green needle crystals of *cis*-diammine(orotinato)platinum(II), *cis*-$[Pt(NH_3)_2(C_5H_2N_2O_4)]$, were subjected to X-ray single crystal analysis. The crystals belong to the monoclinic system, with the space group $P2_1/c$, and the cell dimensions are $a=7.468(5)$, $b=7.537(3)$, $c=15.618(9)$ Å, and $\beta=107.90(7)°$, with $Z=4$. The structure was solved by the heavy-atom method and refined to the final R value of 0.0567 for 1918 non-zero reflections. The complex is almost planar, and the platinum atom is coordinated by the orotic acid at N1 and carboxylic oxygen, forming a five-membered chelate ring. The structure of the pyrimidine ring of the orotic acid is compared with free and coordinated uracil and thymine. No definite explanation for the color difference was obtained.

Since the discovery of the antitumor activity of *cis*-diamminedichloroplatinum(II) by Rosenberg *et al.*,[1,2] considerable interest has been focused on this class of square-planar *cis*-diammineplatinum(II) complexes. The mechanism of the antitumor action has been supposed to be the complex formation between *cis*-diammineplatinum(II) compounds and purine or pyrimidine bases of DNA.[3] These bases have several possible coordinating sites, and many investigations have been carried out into the structures of the platinum complexes with purine or pyrimidine bases.[4-16] Among these complexes, the so-called "platinum-pyrimidine blues" are of special interest from the viewpoint of not only the mechanism of the complex formation between *cis*-diammineplatinum and pyrimidines, but also the anomalously deep blue color and the high antitumor activity of the complexes.[17] As for their structures in the solid and solution states, as well as their chemical properties, however, only a little knowledge has thus far been obtained. Although Lippard *et al.* reported the structure of platinum α-pyridon blue,[18,19] there are still a large number of other platinum pyrimidine blues whose formulas and structures are unknown. In the present paper, we wish to report on the crystal structure of the reaction product between *cis*-diammineplatinum and one of the uracil derivatives, orotic acid. We obtained three compounds, yellow needles, green needles and blue microcrystals, from the reaction solution. The green needle crystals were subjected to X-ray diffraction analysis in order to elucidate the structural relations among the three and to discuss whether there are structural changes in the pyrimidine ring of orotic acid due to coordination to a platinum atom.

Experimental

Preparation. The *cis*-diammineplatinum(II) hydrolysis product was prepared from 1 mmol of *cis*-$[Pt(NH_3)_2Cl_2]$ and 2 mmol of $AgNO_3$ in 10 ml of water in the dark. After removing the AgCl by centrifugation and filtration, an equivalent amount of orotic acid in a minimum amount hot water was added; this resulted in the decrease of the pH of the solution to 1—2. On standing at room temperature for 1 d, the solution yielded green needle crystals. If the solution was adjusted to pH 6—7 with NaOH and left to stand for 1 d, it yielded yellow needles. After the filtration of these green or yellow compounds, a small quantity of dark-blue microcrystals precipitated from the filtrate after 2—3 d. Found: Yellow needles; C, 15.35; H, 2.16; N, 14.48; Pt, 50.7%. Green needles; C, 15.38, H, 2.18; N, 14.70; Pt, 49.5%. Dark-blue microcrystals; C, 14.93; H, 2.21; N, 14.27; Pt, 53.0%. Calcd for $[Pt(NH_3)_2(C_5H_2N_2O_4)]$: C, 15.67; H, 2.10; N, 14.62; Pt, 50.91%. Although the results of elemental analyses for yellow and green needles are identical within the limits of experimental error, the platinum content of the dark-blue compound significantly differs from that of the yellow and green needles. Moreover, the IR spectra of the three compounds are very similar to one another; the yellow and green needles give the same spectra, whereas that of the dark-blue compounds shows only a slight difference. The latter has three more absorption peaks, at 545 (w), 660 (w), and 1100 (w) cm^{-1}, than those of yellow and green compounds. These findings suggest that the three compounds have very similar structures. In the present study, the crystal structure of the green compound was investigated by means of X-ray diffraction.

Data Collection. A crystal of 0.15 mm × 0.05 mm × 0.25 mm was used for intensity measurements; the cell dimensions were obtained from twelve 2θ values measured on a diffractometer. The crystal data for *cis*-$[Pt(NH_3)_2(C_5H_2N_2O_4)]$ are: monoclinic $P2_1/c$, $a=7.468$ (5), $b=7.537$ (3), $c=15.618$ (9) Å, $\beta=107.90$ (7)°, $M.W.=383.2$, $Z=4$, $D_x=3.04$ g cm^{-3}, $\mu=176.4$ cm^{-1} for Mo $K\alpha$. The intensity measurements were performed on a Philips four-circle diffractometer with graphite-monochromated Mo $K\alpha$ radiation. The ω-2θ scan mode was employed at the scan rate of 1° min^{-1} in 2θ, and the reflections were measured up to 60° in 2θ. Three reference reflections monitored periodically showed no significant intensity loss during the course of the data collection. The data were corrected for Lorentz and polarization effects, and a total of 1918 reflections with $|F_o| \geqq 3\sigma(|F_o|)$ were used for structural analysis.

Solution and Refinement of the Structure. The structure was solved by the heavy-atom method. The platinum atom was located from a three-dimensional Patterson map, while all the remaining non-hydrogen atoms were located from the successive Fourier systheses. Although a difference synthesis was calculated at the final stage of the analysis, the hydrogen atoms were not located. The positional and anisotropic temperature factors were refined by the blockdiagonal least-squares method to the final R factor of 0.0567. All the atomic

Table 1. Final positional parameters ($\times 10^4$) and isotropic temperature factors($\times 10^2$), with their estimated standard deviations in parentheses

	x	y	z	B_{eq}/Å^2
Pt	2987(1)	1995(1)	4065(1)	168(2)
C2	1544(24)	−1693(22)	4266(10)	191(25)
C4	1503(23)	−2926(25)	5731(10)	197(23)
C5	2394(24)	−1310(24)	6120(11)	214(27)
C6	2783(23)	−57(22)	5586(10)	172(23)
C7	3704(24)	1661(22)	5964(10)	181(25)
N1	2310(18)	−184(19)	4647(8)	167(20)
N3	1085(21)	−3012(22)	4791(9)	206(21)
N4	2102(22)	1064(22)	2774(8)	200(22)
N5	3693(20)	4320(18)	3588(9)	197(22)
O2	1161(20)	−2030(20)	3442(8)	247(20)
O4	1059(20)	−4178(18)	6123(8)	237(20)
O5	3924(18)	2857(18)	5380(7)	206(18)
O6	4308(20)	1934(20)	6777(7)	234(19)

scattering factors used were taken from Ref. 20, while the correction of the effect of the anomalous dispersion for platinum was based on Ref. 21. The final atomic coordinates and thermal parameters are given in Table 1.

Results and Discussion

The bond lengths and angles within the molecule are listed in Table 2, while the molecular structure and the numbering scheme are depicted in Fig. 1. Orotic acid coordinates to the platinum atom by chelating with deprotonated N1 and carboxylic O5 atoms to form a five-membered ring. It is of interest where, in uracil or its derivatives, is the coordinating site to platinum atoms and how much the bond lengths and angles within the pyrimidine ring are changed by coordination. Although

Table 2. Bond lengths and angles within the molecule, with their estimated standard deviations in parentheses

	l/Å		l/Å
Pt–N1	2.012(28)	C5–C6	1.349(28)
N4	2.039(31)	C6–N1	1.402(21)
N5	2.049(16)	C2–O2	1.255(20)
O5	2.055(14)	C4–O4	1.226(27)
N1–C2	1.329(27)	C6–C7	1.499(30)
C2–N3	1.397(27)	C7–O5	1.328(24)
N3–C4	1.405(21)	C7–O6	1.228(19)
C4–C5	1.430(31)		
	ϕ/°		ϕ/°
N4–Pt–N5	88.4(5)	C6–N1–C2	117.5(14)
N5–Pt–N1	96.5(5)	N1–C2–O2	124.3(16)
N1–Pt–O5	82.3(5)	O2–C2–N3	116.0(15)
O5–Pt–N4	92.8(5)	N3–C4–O4	118.6(15)
Pt–N1–C2	129.1(11)	O4–C4–C5	127.2(15)
Pt–N1–C6	113.3(10)	C5–C6–C7	121.4(15)
N1–C2–N3	119.7(14)	N1–C6–C7	114.1(14)
C2–N3–C4	124.4(14)	C6–C7–O6	122.1(15)
N3–C4–C5	114.1(15)	C6–C7–O5	117.0(13)
C4–C5–C6	119.6(16)	C7–O5–Pt	113.2(10)
C5–C6–N1	124.4(15)	O5–C7–O6	120.9(15)

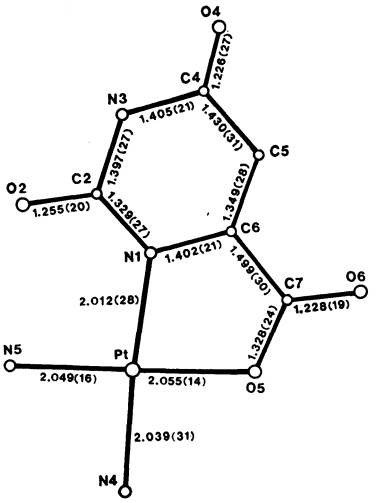

Fig. 1. The molecular structure and the numbering scheme for *cis*-[$Pt(NH_3)_2(C_5H_2N_2O_4)$].

uracil or thymine deprotonates first at the N3 site, and although the pK_a value is 9.5 for both uracil and thymine,[22] most of the platinum complexes so far investigated by X-ray diffraction or NMR show that coordination takes place at N1.[4] One exception is the triammineplatinum uracil complex, [$Pt(NH_3)_3(C_4H_3N_2O_2)$]NO_3, where the platinum atom is considered, on the basis of the NMR spectra, to be coordinated by uracil at N3.[5] In the present complex, the coordination at N1 is much more favored due to the chelate formation.

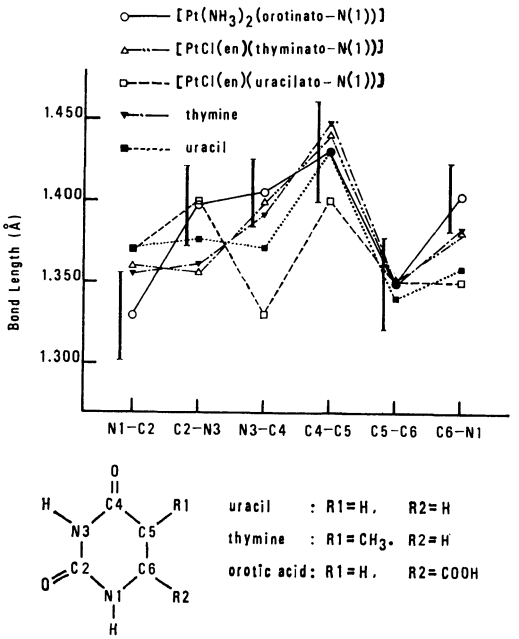

Fig. 2. Comparison of C–C and C–N bond lengths in pyrimidine rings of [$Pt(NH_3)_2$(orotinato-N(1))], [PtCl(en)(thyminato-N(1))], [PtCl(en)(uracilato-N(1))], thymine and uracil. Standard deviations in [$Pt(NH_3)_2$(orotinato-N(1))] are shown with error bars and those of other complexes are in the range one tenth to half of those in [$Pt(NH_3)_2$(orotinato-N(1))].

A comparison of the structures of free and coordinating orotic acid would give valuable information on the change in the electronic structure due to the coordination. However, as no X-ray investigation of free orotic acid has thus far been reported, a comparison with thymine and uracil was carried out. The C–C and C–N bond lengths in thymine,[23] uracil,[24] the platinum thymine complex,[4] the platinum uracil complex,[4] and orotic acid in the present compound are compared in Fig. 2. The corresponding C–C and C–N bond lengths are significantly different from uracil to thymine; these differences were satisfactorily explained by Gerdil[23] in terms of the canonical structures. The C–C and C–N bond lengths of free and coordinating thymine are considered to be identical with each other, whereas the C2–N3, N3–C4, and C4–C5 bond lengths of uracil are slightly different from those of the coordinating uracil. The bond lengths of coordinating orotic acid are different from both uracil and thymine; the N1–C2 distance of orotic acid is significantly shorter than that of uracil or thymine, whereas the C6–N1 distance of orotic acid is longer than that of uracil or thymine. This is explained by the electron flow from the C2–O2 to the N1–C2 bond and from the C6–N1 to the C6–C7 bond, a flow which is aroused by the electrophilic carboxyl group substituted at C6. The comparison of the C=O distances shows that most differences are within the standard deviations and that, therefore, no significant differences are observed. As for the bond angles of the ring nitrogens, C6–N1–C2 (117.5(14)°) is significantly smaller than C2–N3–C4 (124.4(14)°). This fact is consistent with Singh's report[25] that the nitrogen valence angle with an extraannular hydrogen atom is 125±3°, whereas that without any attachment is 116±3°. The coordination of the N1 to the platinum atom does not seem to affect the nitrogen valence angle, since C6–N1–C2 is essentially the same as the valence angle for the nitrogen without any hydrogen attachment. Similarly the two kinds of nitrogen valence angles are also observed in the platinum–uracil complex, (H_5O_2)-$[PtCl(en)(C_4H_3N_2O_2)]Cl$, and the platinum–thymine complex, $[PtCl(en)(C_5H_5N_2O_2)]$.[4]

All the atoms in the molecule are almost coplanar, and the dihedral angle between the best least-squares plane of Pt, N1, N4, N5, and O5, and that of the

Table 3. The best least-squares planes and the deviations of each atom (Å)

Best plane calcd from all the atoms

$-0.91149X+0.39487Y-0.11516Z+0.40060=0.0$

Pt, 0.045(18); N1, 0.011(22); N3, 0.042(24); N4, 0.128(23); N5, 0.026(24); O2, −0.076(23); O4, 0.068(23); O5, 0.013(22); O6, −0.151(23); C2, −0.018(25); C4, 0.033(25); C5, 0.011(25); C6, −0.023(25); C7, −0.038(25).

Best plane calcd from pyrimidine ring

$-0.90314X+0.41168Y-0.12188Z+0.47151=0.0$

N1, 0.029(15); N3, 0.015(17); C2, −0.019(19); C4, −0.004(19); C5, −0.005(19); C6, −0.013(18).

Best plane calcd from Pt, N1, N4, N5, O5

$-0.92308X+0.36910Y-0.10814Z+0.35706=0.0$

Pt, 0.002 (12); N1, 0.025(18); N4, 0.026(19); N5, −0.012 (20); O5, −0.034(18).

The coordinate system is:

X(Å)$=ax+cz(\cos\beta)$

$Y=by$

$Z=cz(\sin\beta)$

Table 4. Possible hydrogen bond distances and angles in $[Pt(NH_3)_2(C_5H_2N_2O_4)]$, with their estimated standard deviations in parentheses

	l/Å		
N3···O4^{i}	2.771(37)		
N4···O5^{ii}	2.921(36)		
O6^{iii}	3.145(24)		
N5···O2	2.733(42)		
O2^{iv}	2.960(38)		
O6^{iii}	2.999(35)		
	ϕ/°		ϕ/°
C4–N3–O4^{i}	118.8(11)	N5–O2–C2	102.4(11)
C2–N3–O4^{i}	116.7(10)	N5–O2–N5^{v}	115.3(6)
Pt–N4–O5^{ii}	127.2(6)	C2–O2–N5^{v}	129.8(11)
Pt–N4–O6^{iii}	101.5(6)	C4–O4–N3^{i}	122.2(12)
O5^{ii}–N4–O6^{iii}	118.9(6)	Pt–O5–N4^{ii}	138.0(7)
Pt–N5–O2	87.6(6)	Pt–O5–C7	113.2(10)
Pt–N5–O2^{iv}	114.8(7)	C7–O5–N4^{ii}	107.4(10)
Pt–N5–O6^{iii}	106.1(7)	C7–O6–N5^{vi}	122.4(12)
O2–N5–O2^{iv}	113.7(7)	C7–O6–N4^{vi}	140.4(12)
O2–N5–O6^{iii}	151.0(8)	N4^{vi}–O6–N5^{vi}	55.2(5)*
O2^{iv}–N5–O6^{iii}	84.1(5)		

Symmetry code

i	$-x$,	$-1.0-y$,	$1.0-z$
ii	$1.0-x$,	$1.0-y$,	$1.0-z$
iii	x,	$0.5-y$,	$-0.5+z$
iv	$-x$,	$0.5+y$,	$0.5-z$
v	$-x$,	$-0.5+y$,	$0.5-z$
vi	x,	$0.5-y$,	$0.5+z$

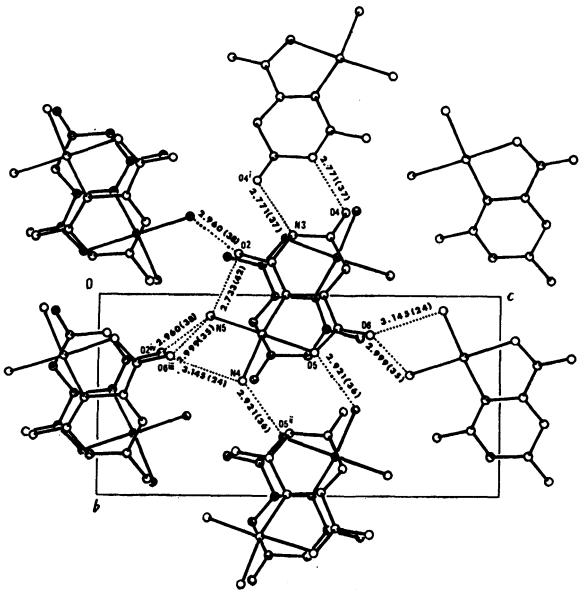

Fig. 3. Projection of the structure of *cis*-$[Pt(NH_3)_2(C_5H_2N_2O_4)]$ down the a axis showing part of the hydrogen bonding scheme and their lengths.

pyrimidine ring is 2.81°. The best least-squares planes calculated from all the atoms, the pyrimidine ring and Pt, N1, N4, N5, and O5, are shown in Table 3.

The molecules are hydrogen-bonded to each other; the possible hydrogen bond distances and angles are listed in Table 4 and are shown in Fig. 3. Using the expected coordinates for hydrogen atoms, the donor-hydrogen atom-acceptor angles were calculated. They are between 145.6° and 172.7°, satisfactory for hydrogen-bondings. The only angle which is marked with an asterisk is small; in this case, the hydrogen atom may shift greatly from the donor-acceptor line.

Although the present work has been undertaken in order to elucidate the structural relations among the three complexes, yellow needles, green needles, and dark-blue microcrystals, preliminary Weissenberg photographs show that the yellow and green needles are structurally identical. Since the dark-blue microcrystals are too small for X-ray single-crystal analysis, only the green needle crystals were subjected to X-ray intensity measurement. There is no definite explanation for the color difference at present, but after the X-ray diffraction analysis had been completed, a close microscopic examination of the crystals showed that the yellow and green needles seem to differ only in their habit of crystal growth; that is, they are identical complexes actually, but seem slightly different in color because of the difference in crystal growth. Otherwise, although the results of ESCA showed no difference, a slight difference in the oxidation states of the platinum atoms, which cannot be detected with ESCA, might exist between the yellow and green needles. It has been reported that platinum α-pyridon blue contains platinum atoms of the formal oxidation state, 2.25.[19] The shortest platinum-platinum distance in the present complex is 4.601(1) Å. A comparison of the platinum-platinum distances with those of other complexes, *cis*-diammine-platinum α-pyridon blue: 2.7745(4) and 2.8770(5) Å,[19] and Magnus' green salts: 3.25—3.46 Å,[26] shows that the platinum-platinum distance of the present complex is much longer, and there seems to be no interaction between adjacent platinum atoms.

This work has been suported by a grant for the development of anti-cancer medicines (No. 23665) from the Japanese Ministry of Health and Welfare.

References

1) B. Rosenberg, L. VanCamp, and T. Krigas, *Nature*, **205**, 698 (1965).
2) B. Rosenberg, L. VanCamp, J. E. Trosko, and V. H. Mansour, *Nature*, **222**, 384 (1969).
3) "Recent Results in Cancer Research-48," ed by T. A. Connors and J. J. Roberts, Springer-Verlag, New York (1974).
4) R. Faggiani, B. Lippert, and C. J. L. Lock, *Inorg. Chem.*, **19**, 295 (1980).
5) K. Inagaki and Y. Kidani, *Bioinorg. Chem.*, **9**, 157 (1978).
6) R. E. Cramer, P. L. Dahlstrom, M. J. T. Seu, T. Norton, and M. Kashiwagi, *Inorg. Chem.*, **19**, 148 (1980).
7) L. G. Marzilli and P. Chalilpoyil, *J. Am. Chem. Soc.*, **102**, 873 (1980).
8) R. E. Cramer and P. L. Dahlstrom, *J. Am. Chem. Soc.*, **101**, 3679 (1979).
9) S. Louie and R. Bau, *J. Am. Chem. Soc.*, **99**, 3874 (1977).
10) R. W. Gellert and R. Bau, *J. Am. Chem. Soc.*, **97**, 7379 (1975).
11) L. G. Marzilli, P. Chalipoyil, C. C. Chiang, and T. J. Kistenmacher, *J. Am. Chem. Soc.*, **102**, 2480 (1980).
12) S. Mansy, B. Rosenberg, and A. J. Thomson, *J. Am. Chem. Soc.*, **95**, 1633 (1973).
13) P. Kong and T. Theophanides, *Inorg. Chem.*, **13**, 1167 (1974).
14) I. A. G. Roos, A. J. Thomson, and S. Mansy, *J. Am. Chem. Soc.*, **96**, 6484 (1974).
15) W. M. Scovell and T. O'Connor, *J. Am. Chem. Soc.*, **99**, 120 (1977).
16) P. Kong and T. Theophanides, *Inorg. Chem.*, **13**, 1981 (1974).
17) J. P. Davidson, P. J. Faber, R. G. Fischer, Jr., S. Mansy, H. J. Peresie, B. Rosenberg, and L. VanCamp, *Cancer Chemother. Rep.*, **59**, 287 (1975).
18) J. K. Barton, H. N. Rabinowitz, D. J. Szalda, and S. J. Lippard, *J. Am. Chem. Soc.*, **99**, 2827 (1977).
19) J. K. Barton, D. J. Szalda, H. N. Rabinowitz, J. V. Waszczak, and S. J. Lippard, *J. Am. Chem. Soc.*, **101**, 1434 (1979).
20) "International Tables for X-Ray Crystallography," Kynoch Press, Birmingham (1974), Vol. IV.
21) D. T. Cromer, *Acta Crystallogr.*, **18**, 17 (1965).
22) M. Ikehara, "Kakusan," Asakura Shoten (1979).
23) R. Gerdil, *Acta Crystallogr.*, **14**, 333 (1961).
24) R. F. Stewart and L. H. Jensen, *Acta Crystallogr.*, **23**, 1101 (1967).
25) C. Singh, *Acta Crystallogr.*, **19**, 861 (1965).
26) J. R. Miller, *J. Chem. Soc.*, **1965**, 713.

  Bull. Chem. Soc. Jpn., 54, 3735—3738 (1981)

Mössbauer Spectroscopic Study of Potassium Borosilicate Glasses at Low Temperatures

Tetsuaki NISHIDA,* Toshiharu HIRAI, and Yoshimasa TAKASHIMA

Department of Chemistry, Faculty of Science, Kyushu University 33, Hakozaki, Higashiku, Fukuoka 812

(Received January 26, 1981)

The Mössbauer technique at the liquid nitrogen temperature (78 K) was applied to the estimation of non-bridging oxygens in FeO_4, BO_4, and SiO_4 units in potassium borosilicate glasses. Mössbauer spectra consist of a quadrupole doublet and a hyperfine structure due to Fe^{3+} ions with tetrahedral symmetry. The hyperfine structure is attributed to a relaxation effect because magnetic susceptibility measurements revealed the glasses to be paramagnetic in the temperature range 78—295 K. A linear decrease in the absorption area and a similar decrease in the internal magnetic field for the hyperfine structure were observed with an increase in the alkali content of glasses. The decrease is ascribed to a formation of non-bridging oxygen at the site adjacent to iron, because the mean life-time of the internal magnetic field produced by 3d-electrons of iron is considered to decrease with increasing thermal vibration of the iron and neighboring oxygens. Fractions of non-bridging oxygens obtained from the reduction rate of the absorption area of hyperfine structure are in good agreement with earlier results for borate glasses with the same K_2O/B_2O_3 ratios, in the alkali region of 8—20 mol% where the borosilicate glasses are essentially considered to be borate glasses diluted with SiO_2.

NMR studies by Yun and Bray[1] reported on each fraction of BO_3 and BO_4 units in various borate or borosilicate glasses, where the fraction of BO_4 unit proved to increase linearly with the alkali content of glasses in the low alkali region. Mössbauer technique was also applied to studying the structure of borate glasses,[2-7] and a formation of non-bridging oxygen (NBO) was suggested to start at an alkali content of 20 mol%. The fraction of NBO in the oxygens constituting BO_4 or FeO_4 units was also estimated from a Mössbauer study of γ-ray irradiated borate glasses,[6] and from a study at low temperatures.[7] A Mössbauer study of potassium borosilicate glasses[8] suggested the formation of NBO to start at an alkali content of 8 mol% in the case of borosilicate glasses with an SiO_2/B_2O_3 ratio of 2.0. It was also considered that the fraction of NBO in borosilicate glasses is increased as a result of the substitution of B_2O_3 for SiO_2.

The present study was performed to estimate the fraction of NBO in potassium borosilicate glasses by using the Mössbauer technique at low temperatures.

Experimental

Potassium borosilicate glasses denoted by the formula $x\,K_2O\cdot(100-x)(B_2O_3,\ SiO_2)\cdot 0.33\,Fe_2O_3$ were prepared by melting mixtures of weighed quantities of K_2CO_3, H_3BO_3, SiO_2, and Fe_2O_3 of guaranteed reagent grade. As for the iron(III) oxide, an enriched isotopic species $^{57}Fe_2O_3$ (^{57}Fe= 90.24%) was used for the preparation. The value of x was changed from 12 to 40, and the molar ratio of SiO_2 to B_2O_3 was so chosen as to be 2.0. Each mixture in a platinum crucible was melted at 1300 °C for 3 h in an electric muffle furnace. The melt was sometimes stirred to be made homogeneous, and was quenched by steeping the platinum crucible into cold water in a beaker. Amorphous structure of almost colorless and transparent glasses was confirmed by X-ray diffractometry. All the glass samples were preserved in a desiccator to protect them from the atmospheric moisture.

Mössbauer measurements were performed by the constant acceleration method at room (295 K), Dry Ice (196 K), and liquid nitrogen (78 K) temperatures. Cobalt-57 (5 mCi) diffused into a palladium foil was used as the source, and the velocity of the spectrometer was calibrated using a pure iron foil enriched with iron-57. The iron foil was used as a reference for isomer shift values. All the spectra were fitted to Lorenzian line shape by computer calculations.

Results and Discussion

Mössbauer spectra for the potassium borosilicate glass with an alkali content of 12 mol% are shown in Fig. 1. All the Mössbauer spectra at room and Dry Ice temperatures consist of a quadrupole doublet (qd) due to the Fe^{3+} ions with tetrahedral symmetry,[2-12] together with a marked wing shape of base line. Isomer shift values of the quadrupole doublet are consistent with the corresponding values of the borosilicate glasses containing 7 mol% Fe_2O_3.[8] Mössbauer spectra for the borosilicate glasses containing 0.33 mol% Fe_2O_3 can, therefore, be analyzed in the same way as for the borosilicate glasses containing 7 mol% Fe_2O_3, although each of the spectra has a wing shape of base line. This is also the case for the Mössbauer spectra at the liquid nitrogen temperature, *i.e.*, the isomer shift values of the quadrupole doublet are well consistent with the corresponding values of the borosilicate glasses containing 7 mol% Fe_2O_3.

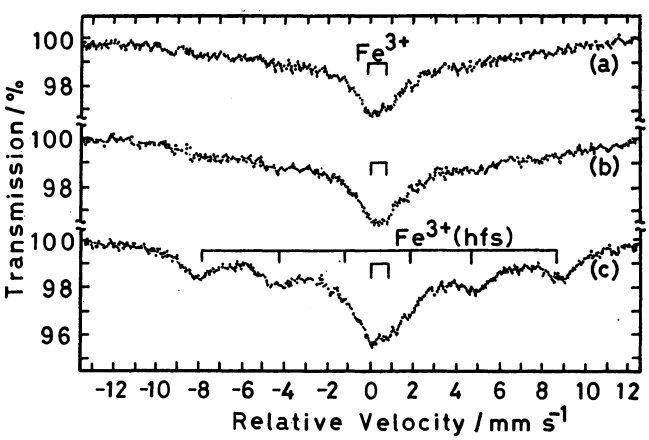

Fig. 1. Mössbauer spectra for the potassium borosilicate glass with an alkali content of 12 mol%.
(a): 295 K, (b): 196 K, (c): 78 K.

Mössbauer spectra at the liquid nitrogen temperature are, therefore, analyzed into a quadrupole doublet and six absorptions of hyperfine structure (hfs). The hfs suggests that the ^{57}Fe nuclei are in the magnetic field and that the mean lifetime of the internal magnetic field is at least of the order of nuclear Larmor precession time. Magnetic susceptibility measurements were then performed to confirm the hfs to be due to a paramagnetic relaxation effect and not due to a magnetic transition or magnetic impurities in the glasses. The data is shown in Fig. 2, which proves the borosilicate glasses to be paramagnetic in the temperature range 78—295 K where the hfs and/or the marked wing shape of base line were observed.

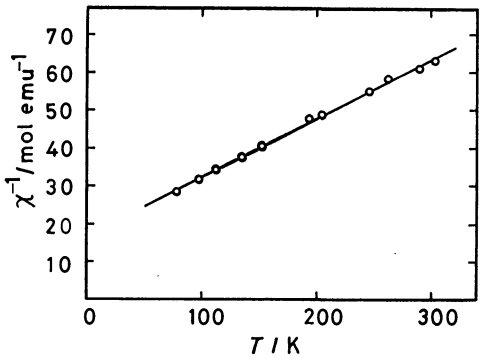

Fig. 2. Magnetic susceptibility measurements of the potassium borosilicate glass with an alkali content of 12 mol%.

TABLE 1. MÖSSBAUER PARAMETERS FOR THE POTASSIUM BOROSILICATE GLASSES AT 78 K

X[a] mol%	Species	δ[b] mm s^{-1}	Δ[c] mm s^{-1}	Γ[d] mm s^{-1}	A[e] %
12	Fe^{3+}(qd)	0.41	0.89	0.73	32.1
12	Fe^{3+}(hfs)	0.39	−0.14	0.77	67.9
15	Fe^{3+}(qd)	0.38	0.61	0.70	37.4
15	Fe^{3+}(hfs)	0.37	−0.07	0.67	62.6
20	Fe^{3+}(qd)	0.36	0.75	1.03	37.9
20	Fe^{3+}(hfs)	0.33	−0.12	0.96	62.1
25	Fe^{3+}(qd)	0.30	0.68	0.85	39.4
25	Fe^{3+}(hfs)	0.35	−0.07	0.57	60.6
30	Fe^{3+}(qd)	0.30	0.65	0.78	42.0
30	Fe^{3+}(hfs)	0.32	−0.03	0.69	58.0
40	Fe^{3+}(qd)	0.32	0.80	0.86	43.3
40	Fe^{3+}(hfs)	0.34	−0.06	0.64	56.7

a) Alkali content. b) Isomer shift. c) Quadrupole splitting. d) Line width (FWHM). e) Absorption area.

The Mössbauer parameters obtained at the liquid nitrogen temperature are summarized in Table 1. The experimental error including the one from computer calculation is estimated to be ± 0.02 mm s^{-1} or more for the isomer shift, since the spectrum is less sharp than the one for the corresponding borosilicate glass containing 7 mol% Fe_2O_3.[8] In the latter case, the error was estimated to be ± 0.01 mm s^{-1}, and the spectrum consists only of a quadrupole doublet free from the relaxation effect. Errors are also estimated to be ± 0.02 mm s^{-1} for the quadrupole splitting and the line width and ± 0.1% for the absorption area. All the isomer shift values for the Fe^{3+} ions with tetrahedral symmetry are increased because of the decreased second-order Doppler effect at lower temperatures. Table 1 also demonstrates that isomer shift values decrease with increasing alkali content of the glasses, as in the case of borosilicate glasses containing 7 mol% Fe_2O_3[8] measured at room temperature. A continuous decrease in isomer shift with increasing alkali content has already been attributed to a formation of NBO in borate[2-5,7] or borosilicate[8] glasses. The decrease in isomer shift indicates an increased s-electron density at iron nucleus as a result of the formation of NBO at the site adjacent to the iron. The increase in s-electron density can be explained by the increased overlap of the 4s-orbital of iron with the 2*p*-orbital of NBO, followed by the transfer of electron from the NBO to the iron. The electron transfer has also been confirmed by the reduction of Fe^{3+} to Fe^{2+} in borate glasses irradiated with γ-rays.[4,6] The increased s-electron density is also explained by the decreased screening effect of s-electrons by p-electrons, because more electrons (3/4 of which are considered to be p-electron) in the sp^3 hybrid orbital will be attracted to the NBO than to the bridging oxygens. The decrease in isomer shift in borosilicate glasses is thus attributed to a formation of NBO at sites adjacent to iron, boron, and silicon in FeO_4, BO_4, and SiO_4 units, respectively.

The quadrupole splitting values for the quadrupole doublet are also consistent with results for Fe^{3+} ions with tetrahedral symmetry in glasses.[2-12] The negative sign of the quadrupole splitting values for the hfs demonstrates that the direction of the electric field gradient tensor is parallel to the xy plane of the network structure. The very small quadrupole splitting values for the hfs suggest that the direction of the electric field gradient tensor is also the same as that of the internal magnetic field. The small quadrupole splitting may be observed probably because the direction of the internal magnetic field depends upon the relaxation time of 3d-electrons, and therefore upon the measuring temperature. It is, therefore, assumed that the magnitude of the quadrupole splitting for the hfs would become as large as the corresponding value for the quadrupole doublet, at much lower temperatures. All the line width (FWHM) values are also characteristic of the absorptions for irons in glasses,[2-12] and are a little increased because of a relaxation effect.

Figures 3 and 4 show changes of the absorption area and the internal magnetic field for the hfs, respectively. The internal magnetic field was obtained by comparing the distance between the outermost absorptions of the hfs with the corresponding distance of a pure iron foil with an internal magnetic field of 330 kOe at room temperature. It is obvious from Figs. 3 and 4 that there occurs a distinct change of glass structure at the alkali region of 16—18 mol%, because all the glasses were prepared so that the iron content should be equal to each other (0.33 mol%), and because all the spectra were measured at the same temperature (78 K). These results are consistent with the NMR results by Yun and Bray[1] that the borosilicate glasses are essentially

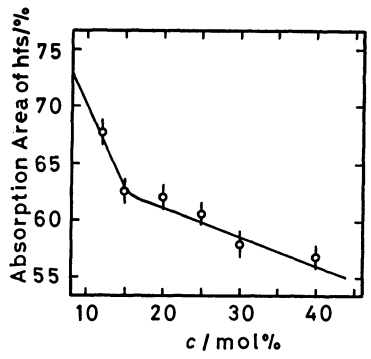

Fig. 3. Mössbauer absorption area of hyperfine structure (hfs) at 78 K plotted against the alkali content of potassium borosilicate glasses.

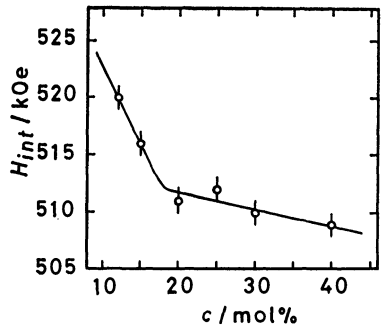

Fig. 4. Internal magnetic field for hyperfine structure (hfs) at 78 K plotted against the alkali content of potassium borosilicate glasses.

considered to be borate glasses diluted with SiO_2 in the alkali region lower than 18 mol%. The additional alkali oxide molecules will therefore be attracted to BO_3 units to form BO_4 units with and without NBO in the alkali region of 8—18 mol%. Formation of BO_4 unit with only bridging oxygens is assumed to occur in the alkali region lower than 8 mol%. In the alkali region higher than 18 mol%, the additional alkali oxide will also be attracted to SiO_4 units to form NBO. The decreasing absorption area of hfs (Fig. 3) can therefore be correlated with the fraction of NBO in FeO_4 units, and also with the fraction in BO_4 and SiO_4 units because all the irons are considered to be present at the substitutional site of boron or silicon. The decrease in the absorption area of hfs is well explained by taking account of the thermal vibration at a certain temperature, *e.g.*, 78 K. The thermal vibration of oxygen is considered to be more frequent in the case of NBO as compared with bridging oxygen, because the former is bonded with only one network former such as iron, boron, or silicon and the latter is bonded with two atoms of network formers.[7] It is, therefore, considered that the thermal vibration of iron is also more frequent in the case of the iron bonded with NBO. Therefore, the internal magnetic field produced by 3d-electrons of iron[7] is considered to be closely correlated with the fraction of NBO in FeO_4 units, because the mean lifetime of the internal magnetic field will be reduced with increasing thermal vibration, *i.e.*, with increasing NBO fraction. The reduction rate of the absorption area for the hfs, therefore, seems to be useful for the estimation of NBO fraction at the site adjacent to iron, because the paramagnetic hfs (relaxation spectrum) is observed as a result of the interaction of the Mössbauer nuclei (^{57}Fe) with the internal magnetic field produced by 3d-electrons of the irons.[7] Fractions of NBO at individual alkali concentrations are summarized in Table 2, where the absorption areas of the hfs at 8 and 10 mol% were obtained by extrapolation of the straight line shown in Fig. 3. The absorption area at the alkali content of 35 mol% was obtained by interpolation of the straight line of Fig. 3. Each of the NBO fractions was obtained by dividing the decreased absorption area by the absorption area at the alkali content of 8 mol% (*i.e.*, 73.0%) where the formation of NBO is considered to start.[8] All the fractions of NBO seem to be reasonable, because the values in the alkali region lower than 20 mol% are consistent, within the experimental error, with earlier results for potassium borate glasses[6,7] having the same K_2O/B_2O_3 ratios as in the borosilicate glasses. The borosilicate glasses are, therefore, considered to be borate glasses diluted with SiO_2 in the alkali region lower than 18 mol%, as described above. The present method seems to be very useful for the estimation of NBO in borate or borosilicate glasses. It is expected that the absorption area for the hfs increases with decreasing iron content of the glasses, and also with a decrease in the measuring temperature. The experimental error for the calculation of absorption area will be reduced with increasing hfs, because the spectral analysis of the innermost peaks is somewhat uncertain in the case of partially relaxed spectra. The fractions of NBO obtained in the present study, however, are considered to be reasonable because each of them was obtained from the relative absorption area of hfs and not from the absolute absorption area of hfs.

Table 2. Estimation of non-bridging oxygens in potassium borosilicate glasses

X[a] / mol %	Absorption area of hfs/%	Fraction[b] of NBO/%
8	73.0	0
10	70.2	3.8±1.9
15	63.0	13.7±1.9
20	61.2	16.1±1.9
25	59.8	18.1±2.0
30	58.6	19.7±2.0
35	57.3	21.5±2.0
40	56.0	23.3±2.0

a) Alkali content. b) Estimated from the decrease in the absorption area of hfs.

The authors are grateful to Dr. Shuji Emori of Saga University for his kind help in the magnetic susceptibility measurements of the glass samples. They are also grateful to Dr. Yusuke Nakayama of Ehime University for his kind suggestions in the computer analyses of the Mössbauer spectra. The present work was partially supported by a Grant-in-Aid for Scientific Research No. 347036 from the Ministry of Education, Science and Culture.

References

1) Y. H. Yun and P. J. Bray, *J. Non-Cryst. Solids*, **27**, 363 (1978).
2) S. S. Sekhon and R. Kamal, *J. Non-Cryst. Solids*, **33**, 169 (1979).
3) T. Nishida and Y. Takashima, *J. Non-Cryst. Solids*, **37**, 37 (1980).
4) T. Nishida, Y. Takashima, and Y. Nakayama, *J. Solid State Chem.*, **33**, 141 (1980).
5) T. Nishida, T. Hirai, and Y. Takashima, *Radiochem. Radioanal. Lett.*, **42**, 189 (1980).
6) T. Nishida, T. Shiotsuki, and Y. Takashima, *J. Non-Cryst. Solids*, **41**, 161 (1980).
7) T. Nishida, T. Hirai, and Y. Takashima, *J. Non-Cryst. Solids*, **43**, 221 (1981).
8) T. Nishida, T. Hirai, and Y. Takashima, *Phys. Chem. Glasses*, **22**, 94 (1981).
9) C. R. Kurkjian and E. A. Sigety, *Phys. Chem. Glasses*, **9**, 73 (1968).
10) M. F. Taragin and J. C. Eisenstein, *J. Non-Cryst. Solids*, **3**, 311 (1970).
11) R. R. Bukrey, P. F. Kenealy, G. B. Beard, and H. O. Hooper, *Phys. Rev. B*, **9**, 1052 (1974).
12) S. S. Sekhon and R. Kamal, *J. Non-Cryst. Solids*, **28**, 189, (1978).

Kinetic Studies of the Electron Transfer Reactions in Iron(II) and Iron(III) Systems. XI. Electron Transfer Reaction between Aquairon(II) and Tris(1,10-phenanthroline)iron(III) in Water Mixed with Methanol, Ethanol, 1-Propanol, and Ethylene Glycol

Goro WADA,* Kumiko TAKAHASHI, and Masako ISOBE
Department of Chemistry, Faculty of Science, Nara Women's University, Nara 630
(Received January 29, 1981)

The electron transfer reaction $Fe^{2+}_{aq}+Fe(phen)_3^{3+}\rightarrow Fe^{3+}_{aq}+Fe(phen)_3^{2+}$ has been investigated in order to find out the influence of the dielectric nature of media on the reaction rates, by the method of stopped-flow spectrophotometry. As the reaction media, were used aqueous mixtures with various alcohols, such as methanol, ethanol, 1-propanol, and ethylene glycol at their various mole fractions x. The second-order rate constant k grows larger approximately linearly with the increase in x, in a sequence: methanol<ethylene glycol<ethanol<1-propanol. When ln k is plotted against D^{-1} (the reciprocal dielectric constant), all points come together on a single straight line with a positive slope, indifferent to the kinds of the alcohols used. This fact suggests that the reaction proceeds through three successive elementary processes, $Fe^{2+}_{aq}+Fe(phen)_3^{3+}\xrightarrow{i}[Fe(H_2O)_6^{2+}\cdot Fe(phen)_3^{3+}]\xrightarrow{ii}[Fe(H_2O)_6^{3+}\cdot Fe(phen)_3^{2+}]\xrightarrow{iii}Fe^{3+}_{aq}+Fe(phen)_3^{2+}$, in which Process i is the formation of an outer-sphere ion-pair between two reacting ions, Process ii the intramolecular electron transfer in the intermediate complex, and Process iii the separation of the ion-pair into the product ions, the last being the rate-determining step. The reaction scheme is compared with that of the reaction $Fe^{2+}_{aq}+Fe(OH)^{2+}\rightarrow Fe(OH)^{2+}+Fe^{2+}_{aq}$, where the first step of the ion-pair formation is rate-determining.

The electron transfer reactions between iron(II) and iron(III) species in various media have been investigated extensively since the study of Silverman and Dodson.[1] The kinetics of the electron transfer reactions are now roughly divided into two main categories; the inner-sphere and outer-sphere mechanisms, the latter including the hydrogen-atom transfer mechanism. The oxidation reaction of aquairon(II) by tris(1,10-phenanthroline)-iron(III) was first studied by Sutin and Gordon[2,3] by applying a flow method, and was found to proceed *via* the outer-sphere mechanism, with a rate constant $k=3.7\times10^4$ M^{-1} s^{-1} in a 0.5 M perchloric acid media at 25 °C (M=mol dm^{-3}).

In the present study, this reaction was again adopted in order to see which of the two processes, the ionic association process between the two reacting ions or the ionic dissociation process of the associated ion-pair into the two leaving ions, is the rate-determining step in the overall outer-sphere electron transfer. For this purpose, aqueous media mixed with a number of alcohols such as methanol, ethanol, 1-propanol, and ethylene glycol were used with diversely different dielectric constants according to the kinds and the mixing ratios of alcohols. A part of the results have been preliminarily reported elsewhere.[4]

The reaction under consideration is as follows:

$$Fe^{2+}_{aq} + Fe(phen)_3^{3+} = Fe^{3+}_{aq} + Fe(phen)_3^{2+}. \quad (1)$$

Since the standard redox potentials of $Fe^{3+}_{aq}/Fe^{2+}_{aq}$ and $Fe(phen)_3^{3+}/Fe(phen)_3^{2+}$ are 0.76 V and 1.14 V respectively, the equilibrium constant of Reaction 1 is calculated to be $K_a=2.69\times10^6$ at 25 °C. Therefore, the rate of the backward reaction can be ignored in the course of the kinetic measurements. The reaction rate is consequently expressed by an equation

$$v = k[Fe^{2+}_{aq}][Fe(phen)_3^{3+}] \quad (2)$$

with a second-order rate constant k. Under a condition of excess $[Fe^{2+}_{aq}]$ over $[Fe(phen)_3^{3+}]$, the rate can be measured as an apparent pseudo-first-order reaction.

$$v = k'[Fe(phen)_3^{3+}] \quad (3)$$
$$k' = k[Fe^{2+}_{aq}]$$

Experimental

Materials. *$Fe(ClO_4)_2$*: Iron wire of 99.99% purity was dissolved in 3 M perchloric acid and the solution was concentrated under a reduced pressure at 60 °C. The precipitated crystals were washed by ether to remove the occluded acid and dried completely in vaccum.

$[Fe(phen)_3](ClO_4)_3$: Crystals of $[Fe(phen)_3]Cl_2$ were precipitated by adding an appropriate amount of NaCl crystals to a solution containing iron(II) perchlorate and 1,10-phenanthroline with the concentration of the latter slightly excess over the molar ratio 1 : 3. A solution of $[Fe(phen)_3]Cl_2$ in 1 M sulfuric acid was gradually added with PbO_2 powder to oxidize $Fe(phen)_3^{2+}$ ion to $Fe(phen)_3^{3+}$ ion, and after filtering the solution to remove the deposited $PbSO_4$ and the excess PbO_2, crystals of $NaClO_4$ were added to the solution to precipitate the crystals of $[Fe(phen)_3](ClO_4)_3$, which were then filtered out, washed by ether, and dried in a vacuum. The crystals of 1,10-phenanthroline were a commercial reagent and were used without further purification.

Water: Water was purified by double distillation after being deionized through ion-exchange resin.

Alcohols: The alcohols used in the present study were methanol, ethanol, 1-propanol, and ethylene glycol. The first three of the above alcohols were distilled under ordinary atmospheric pressure and the last one under reduced one.

Procedure. Kinetic measurements were carried out by use of a Yanagimoto stopped-flow spectrophotometer Model SPS-1 with a thermostated equipment. The reaction was initiated by mixing two solutions containing Fe^{2+}_{aq} and $Fe(phen)_3^{3+}$ ions respectively. The reaction rate was traced by observing the diminution of transmittance due to the production of $Fe(phen)_3^{2+}$ ion at 510 nm, which was recorded on a memoriscope. The temperature was always kept at

25 °C unless otherwise noted and the ionic strength of the reaction solution was adjusted at 1.0 M with $NaClO_4$.

The apparent pseudo-first-order rate constant k' was evaluated from the slope of a straight line obtained by plotting the values of the left-hand side in the following equation *vs.* reaction time t,

$$\ln([Fe(phen)_3^{3+}]_o - [Fe(phen)_3^{2+}]) = -k't + \ln[Fe(phen)_3^{3+}]_o \quad (4)$$

where $[Fe(phen)_3^{3+}]_o$ is the initial concentration of $Fe(phen)_3^{3+}$ ion at $t=0$. An example of the linearity for a reaction run is shown in Fig. 1. For each mole fraction of alcohols x in water, rate measurements were generally performed about ten times, changing the initial concentrations in ranges of $[Fe^{2+}]_o$ $(0.6—5.0)\times10^{-3}$ M and $[Fe(phen)_3^{3+}]_o$ $(0.5—10.0)\times10^{-5}$ M, the values of k being averaged.

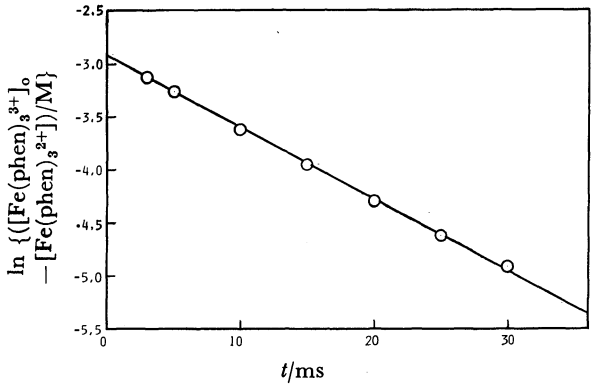

Fig. 1. Plots of $\ln([Fe(phen)_3^{3+}]_o-[Fe(phen)_3^{2+}])$ *vs.* t at $[Fe^{2+}]_o=8.47\times10^{-4}$ M, $[Fe(phen)_3^{3+}]_o=9.28\times10^{-6}$ M, $[HClO_4]=0.05$ M, $\mu=0.1$ M, and 25 °C, in a mixed solvent of water and methanol at $x_{MeOH}=0.225$.

Results and Discussion

Figure 2 shows the variation of k according to the increase in the mole fractions of alcohols. Within the lower mole fractions $x<0.1$, k grows up approximately linearly with the increase in x with steeper slopes in an order, methanol<ethylene glycol<ethanol<1-propanol; namely, it seems that the more the number of the carbon atoms in the monohydric alcohols and the less the number of OH groups in the alcohols with two carbon atoms, the more accelerated is k with the increase in x. In other words, the hydrophobicity of alkyl groups looks like to make the electron transfer reaction occur faster, while the hydrophilicity of OH group shows a trend to behave unfavorably to the reaction.

When the logarithms of k are plotted against the reciprocals of the dielectric constants of the mixed solvents[5] as are depicted in Fig. 3, they come altogether on an approximately single straight line with a positive slope indifferent to the kinds of the alcohols adopted.

$$\frac{d\ln k}{d D^{-1}} > 0 \quad (5)$$

This fact indicates that the reaction is largely controlled by the dielectric constants of the media, although the molecular and structural features of alcohols have been seen to partly affect the reaction rates to some

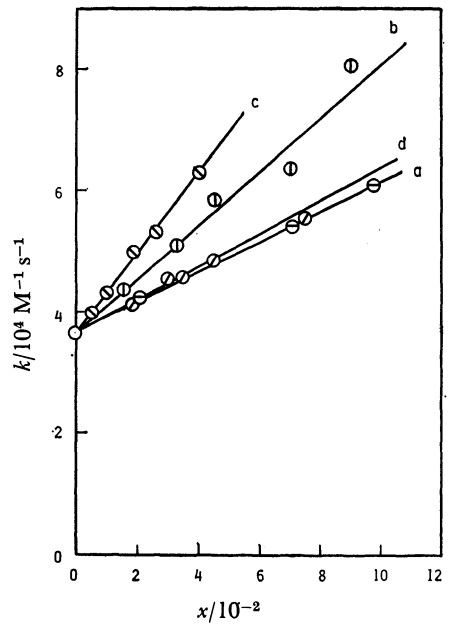

Fig. 2. Variation of k *vs.* mole fraction of alcohol x.
a(⊖): Methanol, b(◑): ethanol, c(⊘): 1-propanol, d(⊘): ethylene glycol.

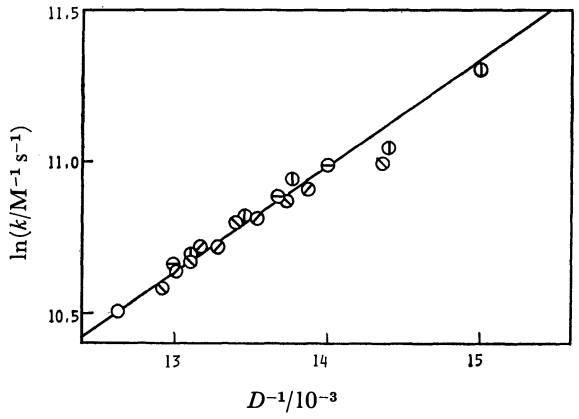

Fig. 3. Plots of $\ln k$ *vs.* D^{-1} in mixed solvents of water and alcohols.
○: Pure water, ⊖: water+methanol, ◑: water+ethanol, ⊘: water+1-propanol, ⊘: water+ethylene glycol.

extent as mentioned above. Thus, the linearity in Fig. 3 can be interpreted by a hypothesis that an electrostatic interaction between the two reacting species plays an important role in the rate-determining step as shown below.

Now, let us consider the mechanism of Reaction 1 as taking place *via* three successive elementary processes.

$$Fe_{aq}^{2+} + Fe(phen)_3^{3+} \rightleftharpoons [Fe(H_2O)_6^{2+}.\ Fe(phen)_3^{3+}] \quad (i)$$

$$[Fe(H_2O)_6^{2+}.\ Fe(phen)_3^{3+}] \rightleftharpoons [Fe(H_2O)_6^{3+}.Fe(phen)_3^{2+}] \quad (ii)$$

$$[Fe(H_2O)_6^{3+}.\ Fe(phen)_3^{2+}] \longrightarrow Fe_{aq}^{3+} + Fe(phen)_3^{2+} \quad (iii)$$

Process i is a step in which an outer-sphere ion-pair formation occurs with a pre-equilibrium constant K_i, Process ii is an intramolecular electron transfer process

with an equilibrium constant K_{ii}, and Process iii is a separation process of the ion-pair into two leaving ions.

When the rate constants of the forward reactions of Processes i, ii, and iii are denoted by k_i, k_{ii}, and k_{iii} and those of the reverse reactions of Processes i and ii by k_i' and k_{ii}' respectively, the apparent second-order rate constant k is expressed by the following relation, derived by virtue of the steady-state method considering both $[Fe(H_2O)_6^{2+}\cdot Fe(phen)_3^{3+}]$ and $[Fe(H_2O)_6^{3+}\cdot Fe(phen)_3^{2+}]$ as reaction intermediates.

$$k = \frac{k_i k_{ii} k_{iii}}{k_i' k_{ii}' + k_i' k_{iii} + k_{ii} k_{iii}} \tag{6}$$

For the three limiting cases, the relation can be simplified as follows:

If $k_{ii}k_{iii} \gg (k_{ii}' + k_{iii})k_i'$

$$k = k_i, \tag{7}$$

if $k_i'k_{iii} \gg k_i'k_{ii}' + k_{ii}k_{iii}$,

$$k = K_i k_{ii}, \tag{8}$$

and if $k_i'k_{ii}' \gg (k_i' + k_{ii})k_{iii}$,

$$k = K_i K_{ii} k_{iii}. \tag{9}$$

Each of these three cases corresponds to that in which Process i, ii, or iii is rate-determining, respectively.

If the overall rate of Reaction 1 were actually controlled by Process i, the dielectric dependence of k_i would be shown by the Scatchard relation,[6,7]

$$\ln k_i = \ln k_i^\circ - \frac{z_A z_B e^2}{kTd_i D}, \tag{10}$$

where D is the dielectric constant of the mixed solvents, k the Boltzmann constant, d_i the internuclear distance between Fe(II) and Fe(III) in the outer-sphere ion-pair formed in Process i, k_i° the imaginary k_i at $D=\infty$, and Z_A and Z_B the numbers of electric charges on the respective reacting ions, *viz.* $Z_A=2$ and $Z_B=3$ in the present case. According to Eq. 10, the linearity of the plot of $\ln k$ *vs.* D^{-1} should have a negative slope, this expectation being against the observed fact shown in Fig. 3. Therefore, the assumption that Process i is the rate-determining step is not probable.

Next, if Process ii were rate-determining, $\ln k$ would vary dependently upon D as follows.

$$\frac{d\ln k}{d\,D^{-1}} = \frac{d\ln K_i}{d\,D^{-1}} + \frac{d\ln k_{ii}}{d\,D^{-1}} \tag{11}$$

Since Process ii is an intramolecular electron transfer, the rate would not be seriously affected by D, and consequently, $d\ln k_{ii}/d\,D^{-1}$ would be approximately equal to zero. But $d\ln K_i/d\,D^{-1}$ would have a negative value with a similar reason to the case in Eq. 10. Therefore, $d\ln k/d\,D^{-1}$ should be negative, this being also contrary to the experimental result.

Finally, the case that Process iii is rate-determining must be considered. By differentiating Eq. 9 with respect to D^{-1}, the following relation is given.

$$\frac{d\ln k}{d\,D^{-1}} = \frac{d\ln K_i}{d\,D^{-1}} + \frac{d\ln K_{ii}}{d\,D^{-1}} + \frac{d\ln k_{iii}}{d\,D^{-1}} \tag{12}$$

Since Processes i and iii are the process of ionic association and ionic separation respectively, the following three relations will be established.

$$\frac{d\ln K_i}{d\,D^{-1}} = -\frac{z_A z_B e^2}{kTd_i} < 0 \tag{13}$$

$$\frac{d\ln K_{ii}}{d\,D^{-1}} \fallingdotseq 0 \tag{14}$$

$$\frac{d\ln k_{iii}}{d\,D^{-1}} = \frac{z_C z_D e^2}{kTd_{iii}} > 0 \tag{15}$$

The symbols appearing in Eq. 15 are similar to those described above, with $Z_C=3$ and $Z_D=2$ in this case. Since $Z_AZ_B=Z_CZ_D=6$, Eq. 12 becomes

$$\frac{d\ln k}{d\,D^{-1}} = \frac{6e^2}{kT}\cdot\frac{d_i - d_{iii}}{d_i d_{iii}} > 0. \tag{16}$$

The bond lengths $d(Fe^{II}\text{–}O)$ and $d(Fe^{III}\text{–}O)$ in aquairon complexes to be taken are 2.21 Å and 2.05 Å respectively,[8] and $d(Fe^{II}\text{–}N)$ in $Fe(phen)_3^{2+}$ ion would be shorter than $d(Fe^{III}\text{–}N)$ in $Fe(phen)_3^{3+}$ ion due to the stronger bonding by back donation in the former complex. Accordingly, $d_i(Fe^{II}\text{–}O,\ Fe^{III}\text{–}N)$ will be larger than $d_{iii}(Fe^{III}\text{–}O,\ Fe^{II}\text{–}N)$, resulting in a positive value in Eq. 16, being consistent with the experimental fact in Fig. 3 and Eq. 5.† This indicates that the absolute value of the electrostatic repulsive energy required to form an ion-pair between ions with the same sign in Process i is smaller than that liberated to dissociate the ion-pair in Process iii. Therefore, it may be reasonably recognized that the rate-determining step of Reaction 1 must be Process iii. Evidence for an initial association, as an example, has been known also in reactions of plastocyanin with some inorganic complexes.[10]

As far as the mole fractions of alcohols are lower than 0.1, the obvious preferential solvation of alcohol molecules would not occur around iron(III) ion[11] and, therefore, the structure of the intermediate ion-pair may be commonly available throughout this range of mole fractions. Since the second-order rate constant for the water exchange in $Fe(H_2O)_6^{3+}$ ion is $k=2.8\times10^2$ $M^{-1}\,s^{-1}$ [12,13] and $Fe(phen)_3^{2+}$ ion is substitution-inert, the intermediate outer-sphere ion-pair is considered to be probable.

A contrasting instance to Reaction 1 has been found in the electron transfer reaction in mixed solvents of water and alcohols at various mole fractions,[14]

$$Fe_{aq}^{2+} + Fe(OH)^{2+} \longrightarrow Fe(OH)^{2+} + Fe_{aq}^{2+} \tag{17}$$

in which case the plot of logarithms of the rate constants shows a good linear relationship with D^{-1} with a negative slope, instead of having a positive slope as in the case of Reaction 1. This fact suggests that the first step must be rate-determining, where the two reacting ions encounter to each other in Reaction 17 with the rate constant $k=k_i$ as a typical instance as is shown in Eq. 7. On this viewpoint, the trend how the dielectric

† According to the numerical calculation from the slope of the straight line in Eq. 16, the values of d_i and d_{iii} can not be strictly decided, but only roughly estimated. Although sets of $d_i=14.0$ Å and $d_{iii}=6.2$ Å, $d_i=12.0$ Å and $d_{iii}=5.7$ Å, $d_i=10.0$ Å and $d_{iii}=5.2$ Å, etc. are numerically derived, any of them may not be probable, as compared with the dimension of the complexes.[9] This discrepancy may mostly be caused by the dielectric saturation phenomenon in the direct vicinity aroud ions.

constants of the reaction media exhibit an influence on the reaction rate looks like to offer a nice tool as a method for distinguishing the rate-determining step among some successive elementary processes in the electron transfer reactions.

The activation enthalpy and the activation entropy of Reaction 1 in a mixed solvent $x_{MeOH}=0.16$ were found to be $\Delta H^*=-0.4\pm0.8$ kJ mol^{-1} and $\Delta S^*=-160$ J K^{-1} mol^{-1} by measuring the reaction rates at 14, 25, 33, and 40 °C. These values are in good accordance with those $\Delta H^*=3.2\pm0.8$ kJ mol^{-1} and $\Delta S^*=-155$ J K^{-1} mol^{-1} measured in pure water by Sutin and Gordon.[2] Cramer and Meyer[15] pointed out that the very small or even slightly negative values of ΔH^* in the oxidation reactions of Fe^{2+}_{aq} by polypyridine complexes of iron(III) and ruthenium(III) suggest the possibility of occurrence of multiple paths in the electron transfer reactions. This idea may also prevail for the reactions in the mixed solvents of alcohols, and may support the reaction mechanism proposed above. They also indicate[15] that the reaction is "non-Marcus" because calculated values for the Fe(II)–Fe(III) polypyridine self-exchange rates are too low approximately by 10^5 [16,17] as expected from the observed rate constant k_{11} for Fe^{2+}_{aq}–Fe^{3+}_{aq} reaction[1,14] and the one k_{12} for the reaction under consideration, according to the Marcus relations which are shown in the followings, the symbols being the same as usual.[18]

$$k_{12} = (k_{11}k_{22}K_{12}f)^{1/2} \tag{18}$$

$$\ln f = \frac{(\ln K_{12})^2}{4\ln(k_{11}k_{22}/z^2)} \tag{19}$$

The reason for the dissatisfaction to the Marcus theory is not only due to the existence of the multiple paths throughout the electron transfer reaction as Cramer and Meyer noticed, but also because of the fact that the reaction Fe^{2+}_{aq}–Fe^{3+}_{aq} does not go through an outer-sphere mechanism in a strictly narrow sense of the word, but through a hydrogen-atom-transfer mechanism.[14] Therefore, k_{11} should not actually satisfy the value expected from the Marcus theory, as a matter of course.

References

Part X of this series: G. Wada and A. Kawauchi, *Bull. Chem. Soc. Jpn.*, **53**, 3023 (1980).

1) J. Silverman and R. W. Dodson, *J. Phys. Chem.*, **56**, 846 (1952).

2) N. Sutin and B. M. Gordon, *J. Am. Chem. Soc.*, **83**, 70 (1961).

3) M. H. Ford-Smith and N. Sutin, *J. Am. Chem. Soc.*, **83**, 1830 (1961).

4) M. Kimura and G. Wada, *Inorg. Chem.*, **17**, 2239 (1978).

5) G. Åkerlöf, *J. Am. Chem. Soc.*, **54**, 4125 (1932).

6) G. Scatchard, *Chem. Rev.*, **10**, 229 (1932).

7) E. S. Amis, "Solvent Effects on Reaction Rates and Mechanisms," Academic Press, New York (1966), Chap. 1.

8) F. Basolo and R. G. Pearson, "Mechanisms of Inorganic Reactions," John Wiley, New York (1967), p. 458. In crystals, the bond length Fe^{III}–O in $Fe(H_2O)_6^{3+}$ is 1.986 Å, which is 0.14 Å shorter than that of Fe^{II}–O in $Fe(H_2O)_6^{2+}$ (N. J. Hair and J. K. Beattie, *Inorg. Chem.*, **16**, 245 (1977)).

9) J.-M. Lucie, D. R. Stranks, and J. Burgess, *J. Chem. Soc., Dalton Trans.*, **1975**, 245.

10) M. G. Segal and A. G. Sykes, *J. Chem. Soc. Chem. Commun.*, **1977**, 764.

11) G. Wada, C. Ito, and K. Horie, *J. Electrochem. Soc. Jpn.*, **28**, 58 (1960).

12) R. E. Connick and E. D. Stover, *J. Phys. Chem.*, **65**, 2075 (1961).

13) D. Seewald and N. Sutin, *Inorg. Chem.*, **2**, 643 (1963).

14) G. Wada, Y. Ohta, S. Hayashida, H. Sugino, T. Mizui, and Y. Aihara, *Bull. Chem. Soc. Jpn.*, **53**, 1278 (1980).

15) J. L. Cramer and T. J. Meyer, *Inorg. Chem.*, **13**, 1250 (1974).

16) J. N. Braddock and T. J. Meyer, *J. Am. Chem. Soc.*, **95**, 3158 (1973).

17) G. Dulz and N. Sutin, *Inorg. Chem.*, **2**, 917 (1963).

18) R. A. Marcus, *J. Phys. Chem.*, **67**, 853 (1963).

Reactions of Manganese(III) Schiff Base Complexes with Superoxide Ion in Dimethyl Sulfoxide

Takayuki MATSUSHITA* and Toshiyuki SHONO

Department of Applied Chemistry, Faculty of Engineering, Osaka University, Yamadaoka, Suita, Osaka 565

(Received February 17, 1981)

The reactions of the chloromanganese(III) complexes of the Schiff bases derived from salicylaldehydes or β-diketones and diamines or monoamines with superoxide ion, O_2^-, in dimethyl sulfoxide were investigated. The complexes were found to react to give either the oxygenated Mn Schiff base complexes or the reduced Mn(II) Schiff base complexes. The difference in the reactivity toward O_2^- was correlated to the polarographic half-wave potentials corresponding to the reduction of Mn(III) to Mn(II) of the complexes. Some oxygenated complexes were isolated and characterized.

Manganese complexes have been of interest in connection with the biological redox processes including catalytic disproportionation of superoxide ion, O_2^-. Examples are the manganese-containing superoxide dismutases (Mn–SOD) and the oxygen evolving photosystem II in green plants.[1] In the Mn–SOD process, a manganese ion may exist in the oxidation state of +III.[2,3] Recently, McAdam *et al.* have reported that the reaction of the Mn–SOD with O_2^- depends on a ratio of O_2^- concentration to the enzyme and that at high ratios (>15) it can not be explained by the simple two-step mechanism proposed for the Cu–SOD. Thus, they have postulated a kinetic model including a form of the enzyme, E_C, as follows:

$$E_A + O_2^- \longrightarrow E_B + O_2$$

$$E_B + O_2^- \xrightarrow{2H^+} E_A + H_2O_2$$

$$E_B + O_2^- \longrightarrow E_C$$

$$E_C \longrightarrow E_A,$$

where E_A represents a native oxidized enzyme, E_B a reduced enzyme, and E_C an enzyme unreactive toward O_2^-.[4]

Howie *et al.* have reported that the reaction of the manganese(II) and -(III) 8-quinolinol complexes with O_2^- in dimethyl sulfoxide (DMSO) can be considered as a redox model for the Mn–SOD.[5] Valentine *et al.* have found that Mn^{III}(tpp)Cl reacts with O_2^- in DMSO to give Mn^{II}(tpp); here tpp denotes tetraphenylporphyrin dianion.[6] Recently, Stein *et al.* have reported that Mn^{III}(cydta)$^-$ and Mn^{III}(edta)$^-$ react with O_2^- in DMSO to give Mn^{II}(cydta)$^{2-}$ and Mn^{II}(edta)$^{2-}$, respectively, where H_4cydta and H_4edta denote 1,2-cyclohexanediamine-*N,N,N',N'*-tetraacetic acid and ethylenediaminetetraacetic acid, respectively.[7]

In this paper we report on the reactions of a series of the chloromanganese(III) Schiff base complexes (Fig. 1) with O_2^- in DMSO.

Experimental

Preparation of Chloromanganese(III) Schiff Base Complexes. All the chloromanganese(III) Schiff base complexes were prepared by the following method, adapted from the literature.[8,9]

Chloro[N,N'-*bis*(*2-benzoyl-1-methylethylidene*)*ethylenediaminato*]-*manganese(III)*, *Mn(bzacen)Cl.* To a dichloromethane (50 cm³)-methanol (50 cm³) solution of *N,N'*-bis(2-benzoyl-1-methylethylidene)ethylenediamine (3.47 g), manganese(III) acetate dihydrate, $Mn(CH_3COO)_3 \cdot 2H_2O$ (2.68 g), was added. The mixture was allowed to stand at 40 °C for 30 min, and then lithium chloride (0.6 g) was added. After having been

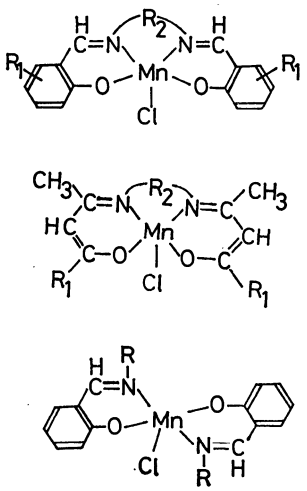

R_1	R_2	L
H	CH_2CH_2	salen
5-CH_3	CH_2CH_2	5-Mesalen
5-Br	CH_2CH_2	5-Brasalen
5-NO_2	CH_2CH_2	5-NO_2salen
5,6-Benzo	CH_2CH_2	5,6-Benzosalen
3-OCH_3	CH_2CH_2	3-MeOsalen
H	C_6H_4	salphen
H	C_6H_{10}	salchxn
H	$CH(CH_3)CH_2$	salpln
CH_3	CH_2CH_2	acacen
C_6H_5	CH_2CH_2	bzacen
CH_3	$CH(CH_3)CH_2$	acacpln
C_6H_5	$CH(CH_3)CH_2$	bzacpln

R	L'
C_3H_7	*N*-Prsai
C_4H_9	*N*-Busai
C_6H_{11}	*N*-c-Hxsai

Fig. 1. Manganese(III) Schiff base complexes studied.

TABLE 1. ELEMENTAL ANALYSES AND MAGNETIC MOMENTS OF MANGANESE(III) COMPLEXES

Complex	Found (%)				Calcd (%)				μ_{eff}[a]
	C	H	N	Mn	C	H	N	Mn	BM
Mn(acacen)Cl·$(H_2O)_{0.5}$	44.81	5.95	8.71	16.92	45.02	5.72	8.97	17.08	4.96
Mn(acacpln)Cl·$(H_2O)_{0.3}$	46.98	6.22	8.51	16.40	46.93	6.21	8.42	16.51	4.77
Mn(bzacen)Cl	60.20	4.91	6.23	12.35	60.49	5.08	6.41	12.58	4.91
Mn(bzacpln)Cl	61.75	5.60	6.08	12.02	61.27	5.37	6.21	12.19	4.81
Mn(5,6-Benzosalen)Cl	62.84	3.96	5.93	11.89	63.10	3.97	6.13	12.03	4.97

a) Measured at room temperature.

stirred for 1 h, the solution was concentrated to *ca.* 20 cm^3 under reduced pressure. Ether (200 cm^3) was then added to precipitate brown solids. They were collected on a glass filter, washed with small volumes of water, 2-propanol, and then ether, and then dried *in vacuo*. They were recrystallized from dichloromethane. The yield was *ca.* 60%. The analytical data and the magnetic moments of some manganese(III) complexes are given in Table 1.

Isolation of Oxygenated Complexes. *[Mn(salen)]$_2O_2$, Complex 1 and [Mn(salen)O]$_n$, Complex 2.* To a DMSO solution of Mn(salen)Cl·H_2O (0.7 g) and 18-crown-6 ether (0.5 g), potassium superoxide, KO_2 (0.15 g) was added in a nitrogen atmosphere at room temperature. After having been stirred for 2 h, the solution was evaporated to remove DMSO under reduced pressure. The reddish brown solids which separated were collected on a glass filter, washed with water, methanol, and then ether, and then dried *in vacuo*. The solids were extracted with dichloromethane (500 cm^3). The dichloromethane solution was evaporated under reduced pressure to give reddish brown needles, complex **1**, which was identified to be [Mn(salen)]$_2O_2$ by the infrared spectrum and the magnetic susceptibilities. On the other hand, the insoluble product in dichloromethane was identified to be [Mn(salen)O]$_n$, complex **2**. The yields of complexes **1** and **2** were 0.21 and 0.43 g, respectively. When the reaction of Mn(salen)Cl·H_2O with KO_2 in DMSO was carried out in the absence of 18-crown-6 ether, the yields of complexes **1** and **2** were 0.03 and 0.50 g, respectively.

The oxygenated manganese complexes, Mn(salchxn)O·H_2O and Mn(5,6-benzosalen)O·H_2O were obtained by the reactions of the corresponding chloromaganese(III) complexes with KO_2 in DMSO and benzene, respectively. These complexes were reddish brown powders and were insoluble in common organic solvents. Therefore, further purification could not be performed. Mn(salchxn)O·H_2O: Found: C, 58.70; H, 4.98; N, 6.98; Mn, 13.23%. Calcd for Mn($C_{20}H_{22}N_2O_4$): C, 58.69; H, 5.42; N, 6.84; Mn, 13.42%. IR: 650 and 618 cm^{-1} (νMn–O). Magnetic moment at room temperature: 1.89 BM. Mn(5,6-Benzosalen)O·H_2O: Found: C, 63.93; H, 3.99; N, 6.23; Mn, 12.25%. Calcd for Mn($C_{24}H_{20}N_2O_4$): C, 63.31; H, 4.43; N, 6.15; Mn, 12.06%. IR: 653 and 603 cm^{-1} (νMn–O). Magnetic moment at room temperature: 2.90 BM.

[Mn(bzacen)O]·$(CH_2Cl_2)_{0.3}$: To a benzene solution (200 cm^3) containing Mn(bzacen)Cl (0.7 g) and 18-crown-6 ether (0.5 g), KO_2 (0.15 g) was added in a nitrogen atmosphere. The solution turned the color from brown to reddish brown gradually on stirring for 2 h. The mixture was filtered and the filtrate was evaporated under reduced pressure. The precipitated solids were collected on a filter, washed with small volumes of water and methanol and then thoroughly with ether, and then dried *in vacuo*. On recrystallization from dichloromethane, reddish brown needles were obtained. The yield was *ca.* 0.2 g. The complex is soluble in dichloromethane and slightly soluble in DMSO. Found: C, 60.07; H, 5.16; N, 6.10; Mn, 12.39%. Calcd for Mn($C_{22}H_{22}N_2O_3$)·(CH_2Cl_2)$_{0.3}$: C, 60.48; H, 5.14; N, 6.33; Mn, 12.40%. IR: 650 cm^{-1} (νMn–O). Magnetic moment at room temperature: 2.55 BM.

The oxygenated complex, Mn(bzacpln)O·$(CH_2Cl_2)_{0.4}$ was obtained in a similar manner. Found: C, 60.45; H, 5.25; N, 6.02; Mn, 11.84%. Calcd for Mn($C_{23}H_{24}N_2O_3$)(CH_2Cl_2)$_{0.4}$: C, 60.40; H, 5.37; N, 6.02; Mn, 11.81%. IR: 644 cm^{-1} (νMn–O). Magnetic moment at room temperature: 1.87 BM.

Reagents. All reagents were of reagent grade. Potassium superoxide, KO_2, was purchased from Alfa products Inc. (Above 96.5%). Dimethyl sulfoxide was distilled twice under reduced pressure prior to use. Benzene was distilled over sodium. Acetonitrile was refluxed over diphosphorus pentaoxide and distilled twice prior to use. Dichloromethane was distilled over calcium chloride.

Preparation of DMSO Solution of KO_2. A DMSO solution of KO_2 (*ca.* 10^{-2} M, 1 M = 1 mol dm^{-3}) was prepared by dissolving KO_2 (18.7 mg) into DMSO (25 cm^3) in the presence of 18-crown-6 ether (0.1 g). The O_2^- concentration of the solution was determined by spectrophotometry.[10]

Measurements. The UV, V, and NIR spectra were recorded on Hitachi EPS-3 and Hitachi 340 recording spectrophotometers. The IR spectra in the 4000—650 and 700—250 cm^{-1} regions were recorded on a Hitachi 215 and on a Hitachi EPI-L grating spectrophotometer, respectively. Polarograms were obtained by using a Yanagimoto p-8 polarograph. A dropping mercury electrode and a mercury pool were used as the working and the reference electrode, respectively; this avoided any effect of water on the reaction systems that would occur if a saturated calomel electrode was used. Tetrabutylammonium perchlorate, $(Bu)_4NClO_4$, was used as the supporting electrolyte and Triton-X 100 as the maximum suppressor. Magnetic susceptibilities were measured by a Gouy method at room temperature. The reactions of the manganese(III) complexes with O_2^- were carried out under nitrogen atmosphere.

Results and Discussion

It is supposed that in the native Mn–SOD the nitrogen and/or oxygen atoms of the amino acid residues of the proteins are coordinated with manganese ions, although the details of coordination structure have not yet been clarified. Recently, the manganese ion in the native Mn–SOD has been found to be in the oxidation state +III.[2,3] The reactions of the manganese(III) Schiff base complexes with O_2^- investigated here afford information in connection with the catalytic disproportionation of O_2^- by the Mn–SOD.

Visible Absorption Spectra. Figure 2 shows the

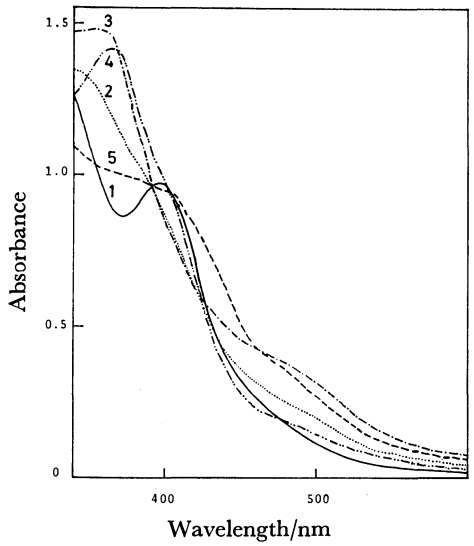

Fig. 2. Spectral changes of a DMSO solution of Mn(salen)Cl·H_2O, 2×10^{-4} M, caused by the addition of KO_2.
1): No addition, 2): $[KO_2]/[complex]=2$, 3): 4, 4): 6, 5): after passing O_2 through the solution shown by curve 4. Cell length: 1 cm.

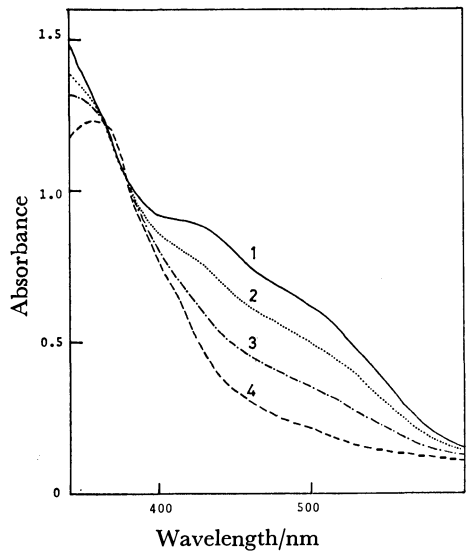

Fig. 3. Spectral changes of a DMSO solution of [Mn(salen)]$_2O_2$, 8×10^{-5} M, caused by the addition of KO_2.
1): No addition, 2): $[KO_2]/[complex]=3$, 3): 6, 4): 10. Cell length: 1 cm.

spectral changes of Mn(salen)Cl·H_2O in the DMSO solution caused by the addition of KO_2 in different molar ratios. The spectra changed remarkably, showing an isosbestic point at 390 nm. And a broad absorption band which appeared for the first time around 480 nm increased in intensity on the addition of KO_2 up to $[KO_2]/[complex]=4$; further amounts of KO_2 caused an decrease in the intensity and the appearance of an absorption band at 364 nm. These spectral changes can be interpreted as follows. The absorption band around 480 nm may be due to the formation of the oxygenated complex. This is supported by the fact that the oxygenated complex, [Mn(salen)]$_2O_2$, obtained by the reaction of Mn^{II}(salen) with molecular oxygen in DMSO is characterized by an intense absorption band in the same region.[11] The spectral changes observed on the further addition of KO_2 are considered to be due to a reaction of the oxygenated complex formed in solution with an excess amount of O_2^- to yield the manganese(II) complex, Mn^{II}(salen). This is confirmed by the facts that the absorption spectrum shown by curve 4 is in agreement with that of Mn^{II}(salen) in DMSO, and that by introducing molecular oxygen (O_2) into this solution it comes to show an absorption curve similar to that of the oxygenated complex, [Mn(salen)]$_2O_2$; this complex again reacts with O_2^-, showing similar spectral changes, as seen in Fig. 3.

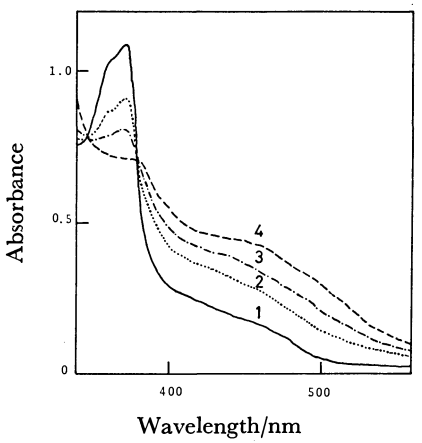

Fig. 4. Spectral changes of a DMSO solution of Mn(acacpln)Cl·$(H_2O)_{0.3}$, 2×10^{-4} M, caused by the addition of KO_2.
1): No addition, 2): $[KO_2]/[complex]=1.5$, 3): 2, 4): 2.5. Cell length: 1 cm.

Figure 4 shows the spectral changes for the complex Mn(acacpln)Cl by the addition of KO_2. These are similar to those observed for the complex Mn(salen)Cl·H_2O. This indicates that the oxygenation of Mn(acacpln)Cl occurs because of the reaction with O_2^-.

Figure 5 shows the spectral changes for the complex Mn(5-NO_2salen)Cl. Unlike the above two complexes, the intensity of the weak absorption band around 500 nm decreases with increasing intensity of a new absorption band at 402 nm. The final absorption curve shown by curve 4 in Fig. 5 is coincident with that of Mn^{II}(5-NO_2salen) in DMSO. This indicates that Mn(5-NO_2salen)Cl is reduced with O_2^- to form the manganese(II) complex. The spectral changes for the complex Mn^{III}(3-MeOsalen)Cl·H_2O are shown in Fig. 6. We previously reported that Mn^{II}(3-MeOsalen)·H_2O was readily oxidized by O_2 in common organic solvents to give the oxidized complex.[11] It is clearly evidenced in Fig. 6 that Mn^{III}(3-MeOsalen)Cl·H_2O is reduced with O_2^- to the manganese(II) complex. Bubbling O_2 into the solution including $[KO_2]/[complex]=3$ and showing absorption curve 4 results in the change of the absorption

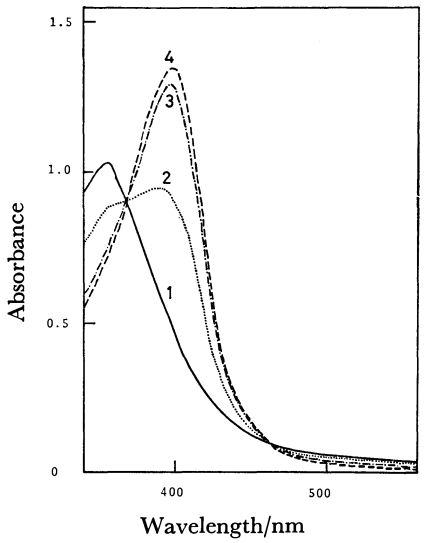

Fig. 5. Spectral changes of a DMSO solution of Mn(5-NO_2salen)Cl, 4×10^{-5} M, caused by the addition of KO_2.
1): No addition, 2): $[KO_2]/[complex]=1$, 3): 2, 4): 3. Cell length: 1 cm.

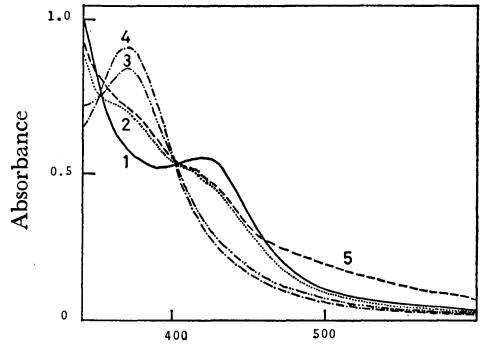

Fig. 6. Spectral changes of a DMSO solution of Mn(3-MeOsalen)Cl·H_2O, 1.0×10^{-4} M, caused by the addition of KO_2.
1): No addition, 2): $[KO_2]/[complex]=1$, 3): 2, 4): 3, 5): after passing O_2 through the solution shown by curve 4. Cell length: 1 cm.

to curve 5, which is quite like that observed in the reaction of Mn^{II}(3-MeOsalen)·H_2O with O_2 in DMSO.

Polarograms. The polarograms of the manganese(III) complexes show one cathodic wave around −0.2 V and one- or two-step cathodic waves in the −1.5——2.0 V range. The polarogram of Mn(5-NO_2salen)Cl in DMSO is shown by curve 1 in Fig. 7. The first cathodic wave can be assigned to the reduction of Mn(III) to Mn(II) and the second and third waves may involve the reductions of the coordinated Schiff base ligand.[12,13] An addition of KO_2 to the solution of the complex ($[KO_2]/[complex]=2$) caused a decrease in the height of the first cathodic wave and the appearance of a new cathodic wave at a half-wave potential of −0.6 V. With increasing amounts of KO_2, the wave height of the former decreased and that of the latter increased. The above new cathodic wave can be easily assigned to the

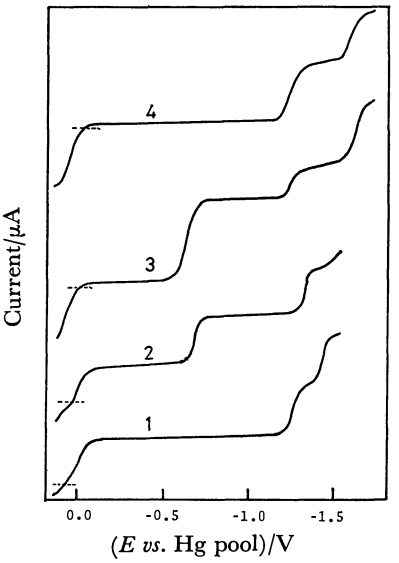

Fig. 7. Changes in polarograms during the reaction of Mn(5-NO_2salen)Cl, 2×10^{-4} M, with KO_2 in DMSO.
1): No addition of KO_2, 2): $[KO_2]/[complex]=2$, 3): 4, 4): after passing N_2 through the solution shown by curve 3.

reduction of free O_2 in the solution, because the half-wave potential is nearly equal to that observed for dissolved O_2 and the wave would disappear readily if nitrogen gas was passed through the solution. The solution obtained after passing nitrogen gas has a polarogram which resembles that of Mn^{II}(5-NO_2salen). These results indicate that Mn(5-NO_2salen)Cl is reduced with O_2^- to yield the manganese(II) complex and O_2, $Mn^{III}L^+ + O_2^- \rightarrow Mn^{II}L + O_2$, where L denotes 5-$NO_2$-salen. This is consistent with the results observed in the absorption spectral changes.

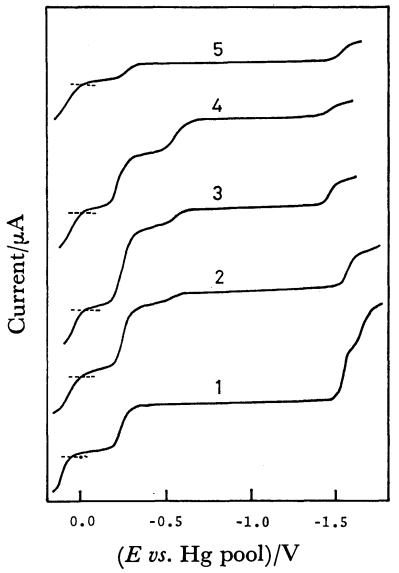

Fig. 8. Changes in polarograms during the reaction of Mn(bzacen)Cl, 2×10^{-4} M, with KO_2 in DMSO.
1): No addition of KO_2, 2): $[KO_2]/[complex]=1$, 3): 2, 4): 4, 5): after passing N_2 through the solution shown by curve 4.

The polarogram of Mn(bzacen)Cl shown in Fig. 8 exhibits three cathodic waves at the half-wave potentials of −0.3, −1.6, and −1.8 V. The first cathodic wave is due to the reduction of Mn(III) to Mn(II). By the addition of KO_2, the cathodic wave due to free O_2 barely appeared in the solution composed with $[KO_2]/[complex]=2$, though the wave height around −0.3 V was observed to increase. Further addition of KO_2 ($[KO_2]/[complex]=4$) caused a decrease in this wave height and an increase in the wave height due to free O_2. The polarogram obtained after passing nitrogen gas through the solution (shown by curve 4 in Fig. 8) exhibits only a small wave height at −0.3 V; this may be due to the residue of the manganese(III) complex. From these polarographic observation, the reaction of Mn(bzacen)Cl with O_2^- can be explained as follows. The increase in the wave height at −0.3 V observed at the molar ratio change from 1 to 2 may be caused by the formation of the oxygenated complex, hence the cathodic wave due to O_2 is slightly observed. At the molar ratio of 4 the oxygenated complex reacts with O_2^- to give the manganese(II) complex and O_2.

Reactivity toward O_2^-. In view of the reactivity toward O_2^- observed in the spectral and polarographic behavior, the chloromanganese(III) Schiff base complexes investigated here can be classified into two types: one involving the complexes which form the oxygenated complex in the solution containing KO_2 in the molar ratio of $[KO_2]/[complex]<2$—3, and the other involving the complexes which are only reduced to the corresponding manganese(II) complexes with the evolution of molecular oxygen. These results are summarized in Table 2, along with the half-wave potentials for the reduction of Mn(III) to Mn(II). The reactivity toward O_2^- is clearly correlated with the reduction potentials of the complexes. That is, the complexes having more negative potentials than that of Mn(salen)Cl·H_2O form the oxygenated complexes, whereas the complexes having more positive potentials than that of Mn(salpln)-Cl are reduced to the manganese(II) complexes.

Table 2. Reduction potentials of manganese(III) complexes and reactivity toward O_2^-

Complex	$-E_{1/2}$[a] *vs.* Hg pool V Mn(III)→Mn(II)	Reactivity toward O_2^-
Mn(acacen)Cl·$(H_2O)_{0.5}$	0.39	Oxygenation
Mn(acacpln)Cl·$(H_2O)_{0.3}$	0.33	Oxygenation
Mn(bzacen)Cl	0.32	Oxygenation
Mn(bzacpln)Cl	0.30	Oxygenation
Mn(salchxn)Cl	0.21	Oxygenation
Mn(5-Mesalen)Cl	0.20	Oxygenation
Mn(5,6-Benzosalen)Cl	0.19	Oxygenation
Mn(salen)Cl·H_2O	0.19	Oxygenation
Mn(salpln)Cl	0.18	Reduction
Mn(3-MeOsalen)Cl·H_2O	0.15	Reduction
Mn(5-Brsalen)Cl	0.15	Reduction
Mn(salphen)Cl	0.08	Reduction
Mn(5-NO_2salen)Cl	0.03	Reduction
Mn(*N*-Busai)$_2$Cl	0.02	Reduction
Mn(*N*-Prsai)$_2$Cl	0.02	Reduction
Mn(*N*-c-Hxsai)$_2$Cl	0.00	Reduction

a) Measured in acetonitrile containing 0.1 mol dm^{-3} $(Bu)_4NClO_4$ at 25 °C.

Isolation and Characterization of the Oxygenated Complexes. Several oxygenated manganese complexes were isolated by the reactions of chloromanganese(III) Schiff base complexes with KO_2 in DMSO or benzene. In the case of Mn(salen)Cl·H_2O, two types of the oxygenated complexes, $[Mn(salen)]_2O_2$ and $[Mn(salen)O]_n$, were isolated. The former complex shows an intense broad absorption band around 480 nm. In the IR spectrum the former complex shows a strong band assignable to the Mn–O stretching vibration at 645 cm^{-1}, while the latter, which is insoluble in common organic solvents, shows two strong bands due to the Mn–O stretching vibrations at 665 and 605 cm^{-1}. The effective magnetic moments of $[Mn(salen)]_2O_2$ and $[Mn(salen)O]_n$ were 2.16 and 2.04 BM, respectively. These values are lower than the spin-only one which is expected for a complex with the d^4 or d^3 high-spin configuration; they may be caused by the antiferromagnetic interactions observed for the complexes where the manganese atoms are probably linked by the oxygen atoms: Mn^{III}–O_2–Mn^{III} and $-[Mn^{IV}-O]-_n$.[11]

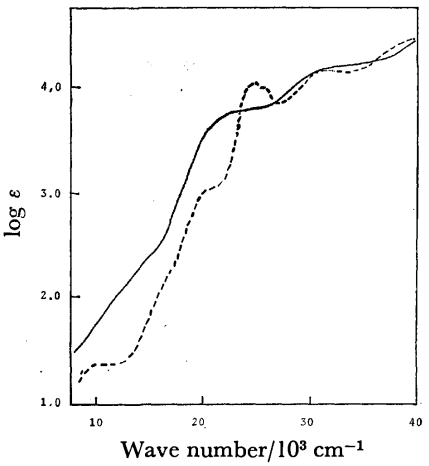

Fig. 9. Electronic spectra.
——: Mn(bzacen)O·$(CH_2Cl_2)_{0.3}$ in dichloromethane,
------: Mn(bzacen)Cl in DMSO.

The other oxygenated manganese complexes obtained in this work also show lower magnetic moments. The IR spectra of the oxygenated complexes, Mn(salchxn)O and Mn(5,6-Benzosalen)O, which are insoluble in common organic solvents, show two strong bands in the 700—600 cm^{-1} region. Therefore, these complexes may have a structure similar to that of $[Mn(salen)O]_n$. On the other hand, the IR spectra of the oxygenated complexes, Mn(bzacen)O and Mn(bzacpln)O, which are soluble in dichloromethane show one strong band in the 700—600 cm^{-1} region. Moreover, the electronic spectrum of Mn(bzacen)O in dichloromethane shows an intense absorption band around 500 nm, as shown in Fig. 9. These results suggest that the oxygenated complexes may have a structure similar to that of

$[Mn(salen)]_2O_2$. Since the manganese(II) complexes with the Schiff bases derived from β-diketones and diamines have not been isolated due to the instabilities, there has been no attempt to prepare their oxygenated complexes by reacting them with O_2.

Among the oxygenated manganese-Schiff base complexes, the compounds with such unitary groups as oxo (Mn=O), μ-oxo (Mn–O–Mn), catena-μ-oxo ($\{Mn–O\}_n$), μ-peroxo (Mn–O–O–Mn), and di-μ-oxo (Mn$\begin{smallmatrix}\diagup O \diagdown \\ \diagdown O \diagup\end{smallmatrix}$Mn) have so far been reported.[1b] However, these structures have been determined only by the elemental analyses and the conventional physicochemical measurements, with the exception of the oxygenated product of Mn^{II}-(salpn)·H_2O. This has been revealed by X-ray structural analysis to be a di-μ-hydroxo structure (Mn$\begin{smallmatrix}\diagup OH \diagdown \\ \diagdown OH \diagup\end{smallmatrix}$Mn), where salpn$H_2$ denotes *N*,*N*′-disalicylidene-1,3-propanediamine.[14]

The reactivity of KO_2 with the present manganese(III) complexes will open a new route for synthesis and will provide a method of characterization for the oxygenated complexes.

References

1) a) G. D. Lawrence and D. T. Sawyer, *Coord. Chem. Rev.*, **27**, 173 (1978); b) W. M. Coleman and L. T. Taylor, *ibid.*, **32**, 1 (1980).

2) J. A. Fee, E. R. Shapiro, and T. H. Moss, *J. Biol. Chem.*, **251**, 6157 (1976).

3) J. J. Villafranca, F. J. Yost, Jr., and I. Fridovich, *J. Biol. Chem.*, **249**, 3532 (1974).

4) a) M. E. McAdam, R. A. Fox, F. Lavelle, and E. M. Fielden, *Biochem. J.*, **165**, 71 (1977); b) M. E. McAdam, F. Lavelle, R. A. Fox, and E. M. Fielden, *ibid.*, **165**, 81 (1977).

5) J. K. Howie and D. T. Sawyer, *J. Am. Chem. Soc.*, **98**, 6698 (1976).

6) J. S. Valentine and A. E. Quinn, *Inorg. Chem.*, **15**, 1997 (1976).

7) J. Stein, J. P. Fackler, Jr., G. J. McClune, J. A. Fee, and L. T. Chan. *Inorg. Chem.*, **18**, 3511 (1979).

8) L. J. Boucher and V. W. Day, *Inorg. Chem.*, **16**, 1360 (1977).

9) L. J. Boucher, *J. Inorg. Nucl. Chem.*, **36**, 531 (1974).

10) S. Kim, R. DiCosimo, and J. S. Filippo, Jr., *Anal. Chem.*, **51**, 679 (1979).

11) T. Matsushita, T. Yarino, I. Masuda, T. Shono, and K. Shinra, *Bull. Chem. Soc. Jpn.*, **46**, 1712 (1973).

12) W. M. Coleman, R. R. Goehring, L. T. Taylor, J. G. Mason, and R. K. Boggess, *J. Am. Chem. Soc.*, **101**, 2311 (1979).

13) R. K. Boggess, J. M. Hughes, W. M. Coleman, and L. T. Taylor, *Inorg. Chim. Acta*, **38**, 183 (1980).

14) H. S. Maslen and T. N. Waters, *J. Chem. Soc., Chem. Commun.*, **1973**, 760.

Equilibrium and Structure of Deprotonated Bis(glycylglycinato)-copper(II) in Aqueous Solution

Noriyuki NAKASUKA,* Kenya MAKIMURA, and Hiroko KAJIURA†

Laboratory of Analytical Chemistry, Faculty of Science, Nagoya University, Chikusa-ku, Nagoya 464

(Received February 27, 1981)

Potentiometric titration was carried out at 25.0±0.1 °C and at an ionic strength of 1.00 mol dm^{-3} in sodium perchlorate for a system of copper(II)–dipeptide(A)–a second ligand(B) in an aqueous solution to obtain the formation constants of mixed ligand complexes $Cu_pH_qA_rB_s$. A was glycylglycine or glycinamide, and B was ethylamine or 2-aminoethanol. The structure of $CuH_{-1}A_2$ in solution is discussed. It was found that the ligand A acts as a unidentate ligand and the other deprotonated $H_{-1}A$ as a terdentate one for the most part; only about 2% of this complex are in a bidentate-bidentate form.

Glycylglycine, one of the simplest peptides, gives rise to several metal complexes in an aqueous solution, and serves as a model compound for the complexation reactions of polypeptides and even of proteins. Thermodynamic equilibria of copper(II)–glycylglycine complexes have been studied rather extensively,[1-4] and the existence of species such as CuA, CuHA, $CuH_{-1}A$, $CuH_{-2}A$, and $CuH_{-1}A_2$ has been reported (HA represents a glycylglycine molecule). Strandberg *et al.* have elucidated by crystallographic studies the structure of the diaquaglycylglycinatocopper(II) hydrate ($CuH_{-1}A$), in which the peptide NH proton is released; they found that the ligand acts as a terdentate one.[5] For $CuH_{-1}A_2$, however, two possible structures are expected, so it is of interest to discuss the equilibrium data.

Experimental

Reagents. Glycylglycine and glycinamide hydrochloride were used as received (Tokyo Kasei Kogyo Co., G. R.).

Ethylamine hydrochloride and 2-aminoethanol were obtained from Wako Pure Chemical Ind. Ltd. The former was recrystallized from water and dried *in vacuo* at 60 °C, while the latter was vacuum distilled over sodium hydroxide.

Copper(II) perchlorate: Copper(II) carbonate was prepared by mixing copper(II) chloride (Wako Pure Chemical Ind. Ltd., G. R.) with a solution of sodium carbonate. Perchloric acid was added in small excess to the washed copper carbonate and copper perchlorate was then crystallized from the solution.

Sodium perchlorate: Commercial sodium perchlorate (Merck, *pro analysi*) was recrystallized from water. A concentrated solution was analyzed gravimetrically after heating the solution gently in a platinum crucible on a hot plate to dryness. This simple method gives very reproducible and accurate results.

Potentiometry. Measurement of potential was made with a digital pH/mV meter(Orion, model 801) using a glass electrode (Metrohm EA 109) and a reference calomel electrode (Metrohm EA 404), which contained an internal solution of sodium chloride. Each measurement was accurate to 0.2 mV. Titrations were carried out in double-walled glass cell thermostated at 25±0.1 °C under nitrogen presaturated with water vapor. A Metrohm piston burette was used for addition of 1.140 M†† sodium hydroxide solution. The ionic strength of each solution was adjusted to 1.00 M in sodium perchlorate.

Results

Determination of Stability Constants. Complex formation of copper(II) ion (M) with a complexing agent (A) and a second ligand (B) is represented in general by the following expression:

$$pM + qH + rA + sB \rightleftharpoons M_pH_qA_rB_s, \quad (1)$$

where charges are omitted for simplicity. The formation constant β_{pqrs} is defined as follows:

$$\beta_{pqrs} = [M_pH_qA_rB_s]/m^ph^qa^rb^s, \quad (2)$$

where m, h, a, and b refer to the concentrations of the free metal ion, proton, and free A and B ligands, respectively. When B is absent from the system, only β_{par} is defined.

Table 1. Experimental conditions for the measurement of formation constants

1) Protonation constants		
No.	$10^2\ C_{ligand}$/M	Ligand
I	1.088	Glycylglycine
II	1.694	Glycinamide
III-1, III-2	1.113, 2.197	Ethylamine
IV	1.170	2-Aminoethanol

2) Glycinamide complexes		
No.	$10^2\ C_A$/M	$10\ C_M$/M
V-1	1.778	0.7054
V-2	1.449	1.033

3) Glycylglycine complexes			
No.	$10^3\ C_A$/M[a]	$10^3\ C_M$/M	$10^2\ C_B$/M
VI-1	3.727	3.299	
VI-2	8.565	4.124	
VI-3	8.698	4.124	
VI-4	12.69	4.124	
VI-5	5.159	4.124	
VI-6	8.707	8.248	
VI-7	8.704	2.062	
VII-1[b]	4.127	3.299	1.024
VII-2[b]	4.977	4.124	2.100
VII-3[b]	4.348	4.124	4.184
VIII[c]	4.284	4.124	1.247

a) A: Glycylglycine. b) B: Ethylamine. c) B: 2-Aminoethanol.

† Present address: National Institute for Basic Biology, National Center for Biological Sciences, Myodaiji, Okazaki 444.

†† Throughout this paper: 1 M=1 mol dm^{-3}.

TABLE 2. FORMATION CONSTANTS β_{pqrs} ($c^{\circ}=1$ mol dm^{-3}, 25.0±0.1 °C, $\mu=1$ ($NaClO_4$)).

1) Protonation constants

Ligand	*pqr*	log β_{pqrs}
Glycylglycine	011	8.21±0.05
	021	11.46±0.08
Glycinamide	011	8.208±0.003
Ethylamine	011	11.04±0.10
2-Aminoethanol	011	9.77±0.05

2) Glycinamide complexes

pqr	log β_{pqrs}
101	5.53±0.03
102	10.00±0.05
1$\bar{1}$2	2.72±0.05
1$\bar{2}$2	−5.75±0.08

3) Glycylglycine complexes

pqrs	log β_{pqrs}	B
101	5.54±0.05	
1$\bar{1}$1	1.31±0.05	
1$\bar{2}$1	−7.99±0.10	
1$\bar{1}$2	4.50±0.05	
1$\bar{1}$11	4.71±0.08	2-Aminoethanol
1$\bar{1}$11	4.9±0.2	Ethylamine

Lefebvre's method (Méthode de la surface potentiométrique)[6] provided compositions of species present as well as approximate values of the corresponding formation constants. These values were further refined by using a least-squares technique with the data $\bar{q}$ (average number of protons bound per mole of constituent A and B)[4] on an electronic computer FACOM 230-75 at the Computation Center of Nagoya University. A Fortran program QPOL (R.-P. Martin, Universite Claude Bernard, Lyon I) was used for this calculation after certain modifications by the present authors. Experimental conditions and the results of calculation are summarized in Tables 1 and 2.

Table 2 shows a remarkable similarity between the protonation constants as well as between the complex formations of CuA for glycylglycine and glycinamide. These similarities indicate that the terminal nitrogen atoms in these ligands have the same basicity.

The values in this work for glycinamide are somewhat larger than those obtained by Dorigatti and Billo;[7] this may be accounted for in terms of different ionic media (0.10 M in $NaClO_4$). The results obtained for glycylglycine are essentially the same as those obtained by Martin *et al.*[4]

Discussion

There are two possible structures for the complex $CuH_{-1}A_2$, as shown in Fig. 1. In the first case, one peptide coordinates to the central ion as a terdentate ligand, while the other works as a unidentate: this is termed type (3,1). This type of crystal structure has already been found for a copper(II)–glycylglycine–imidazole complex.[8]

In the second complex, each ligand coordinates as a bidentate one, although the donor atoms are different.

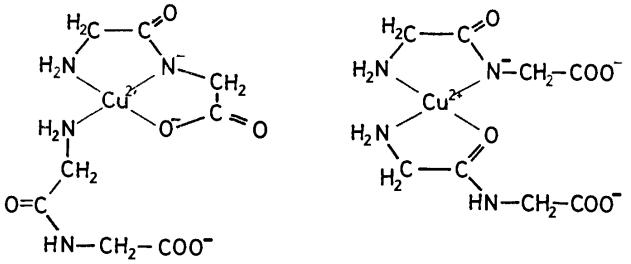

type(3,1) type(2,2)

Fig. 1. Possible structures for bis(glycylglycinato) copper (II) $CuH_{-1}A_2$.

Therefore this is referred to as type (2,2). The principal point of interest is which predominates in an aqueous solution.

For the first type of complex, a unidentate glycylglycine A may be designated as N, because the donor atom must be the amino nitrogen. Then formation of a complex of type (3,1), $Cu_{-1}AN$, is formulated as follows:

$$CuH_{-1}A + N \overset{K^{N}_{CuH_{-1}AN}}{\rightleftharpoons} CuH_{-1}AN. \quad (3)$$

The formation constant of mixed ligand complexes has been discussed by many authors. Here the formulation of Tanaka[9] is applied, since the interactions between donor atoms are very important in this case.

$$\log K^{N}_{CuH_{-1}AN} = \log K^{N}_{CuN} + \Delta \log K_{os} + \Sigma\delta_{ij}x_i(H_{-1}A)x_j(N), \quad (4)$$

$$\Delta \log K_{os} = \log K_{os}(CuH_{-1}A, N) - \log K_{os}(Cu, N), \quad (5)$$

where K^{N}_{CuN} is the formation constant of CuN, δ_{ij} the effect of the donor atom i in the ligand $H_{-1}A$ on the donor atom j in the ligand N (mainly a repulsion term, $\delta_{NO}=-0.26$ and $\delta_{NN}=-0.35$, and x_i or x_j is the number of the donor atoms i or j in each ligand. K_{os} denotes the formation constant of an outer sphere complex, but with amino acids and their related ligands log K_{os} may be assumed to be negligible.[9]

The data for K^{N}_{CuN} is not available and therefore the formation constant of copper(II)–ammine complex is substituted for it.[10]

$$\log K^{N}_{CuH_{-1}AN} = 4.197 + 0 - 0.97 = 3.24, \quad (6)$$

$$\beta_{1\bar{1}2}(3, 1) = \frac{[CuH_{-1}A_2]}{[CuH_{-1}A][N]} \frac{[CuH_{-1}A]\,h}{m\,a} = K^{N}_{CuH_{-1}AN} \cdot \beta_{1\bar{1}1}, \quad (7)$$

$$\log \beta_{1\bar{1}2}(3,^{6}1) = 3.24 + 1.31 = 4.55. \quad (7')$$

The observed value 4.50 for log $\beta_{1\bar{1}2}$ is in good accord with the above value calculated. 2-Aminoethanol and ethylamine act only as a unidentate ligand; the formation constants of their mixed ligand complexes (log $\beta_{1\bar{1}11}$) correspond unambiguously to that of type (3,1). The experimental values of 4.71 (2-aminoethanol) and 4.9 (ethylamine) compare with the theoretical ones. Koltun *et al.* have reported the formation constant of the imidazole complex, from which log $\beta_{1\bar{1}11}$ is calculated to be 4.91 (ionic strength=0.075 M, 25 °C).[2] The terdentate nature in this complex is well established

in a solid state.[8] These findings suggest predominance of the complex of type (3,1) in solution. A similar calculation for type (2,2) is also interesting.

The structure of $CuH_{-1}A$ has been determined by the X-ray method.[5] The majority of the deprotonated ligands may play the role of terdentate ligands also in solution (ε form).

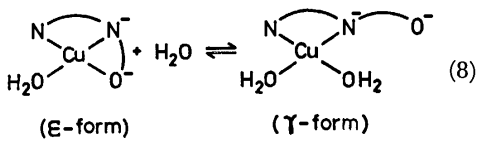

(8)

Nevertheless, there may exist a complex in which the peptide acts as bidentate ligand, though in a very small amount; this type of complex is named γ form. In fact Nakahara *et al.* have prepared dipotassium bis-(glycylglycinato)cuprate(II),[11] whose structure has been determined.[12] The primary coordination around the central ion is approximately square, and two ligands bond to the copper ion through the amino and peptide nitrogen atoms alone, that is, in a γ form.

The thermodynamic constant for the equilibrium between γ and ε is not available, so we consider the complexation reactions of ethylenediamine monoacetic acid (EDMA, potentially terdentate) with copper(II).[13] The equilibrium between γ and ε forms in the EDMA complex is written as follows:

$$R = \frac{[\varepsilon]}{[\gamma]} = \frac{[\mathrm{Cu(edma)}]}{[\mathrm{Cu(edma)'}]} = \frac{[\mathrm{Cu(edma)}]}{m[\mathrm{edma}]} \frac{m[\mathrm{edma}]}{[\mathrm{Cu(edma)'}]}. \quad (9)$$

Cu(edma)' represents a complex in which EDMA is attached to copper(II) ion as a bidentate ligand, with the ethylenediamine nitrogen atoms being donor ones. Thus the formation constant of this complex may be approximated by the Cu–ethylenediamine complex ($\beta_{\mathrm{Cu(en)}}$).[14]

$$R = \beta_{\mathrm{Cu(edma)}}/\beta_{\mathrm{Cu(en)}} = 10^{2.82} \quad (10)$$

This ratio R may be substituted for the equilibrium constant for Reaction 8 of the dipeptide complexes. The validity of this assumption is also confirmed by the following argument on the deprotonation of copper chelates:

$$\mathrm{CuA} \rightleftharpoons \mathrm{CuH_{-1}A'} + \mathrm{H}, \quad (11)$$

where $CuH_{-1}A'$ denotes the deprotonated copper complex of glycylglycine in γ form.

$$K_1 = \frac{[\mathrm{CuH_{-1}A'}]\,h}{[\mathrm{CuA}]} = \frac{[\varepsilon]\,h}{[\mathrm{CuA}]} \frac{[\gamma]}{[\varepsilon]} = \beta_{111}/(\beta_{101}R) = 10^{-7.05}. \quad (12)$$

For glycinamide, corresponding data are not available, but this equilibrium constant K_1, may be approximated by that of the deprotonation of CuA_2 giving rise to $CuH_{-1}A_2$, neglecting some effects resulting from the other ligand A.

$$K_2 = \frac{[\mathrm{CuH_{-1}A_2}]h}{[\mathrm{CuA_2}]} = \beta_{1\bar{1}2}/\beta_{102} = 10^{2.72}\,10^{-10.00} = 10^{-7.28} \fallingdotseq K_1. \quad (13)$$

The equality of K_1 to K_2 justifies experimentally the validity of the R value, because this ratio is used in calculating K_1, while K_2 is derived from the experimental data. Thus the formation constant of the glycylglycine complex of type (2,2) is rewritten as:

$$\beta_{1\bar{1}2}(2,2) = \frac{[\mathrm{CuH_{-1}A_2}]h}{m\,a} = \frac{[\mathrm{CuH_{-1}A'}]}{[\mathrm{CuH_{-1}A}]} \frac{[\mathrm{CuH_{-1}A}]h}{m\,a} \frac{[\mathrm{CuH_{-1}A_2}]}{[\mathrm{CuH_{-1}A'}]\,a} = R^{-1}\beta_{1\bar{1}1}K^{\mathrm{A}}_{\mathrm{CuH_{-1}A'A}}. \quad (14)$$

Application of the formulation from Tanaka[9] gives:

$$\log K^{\mathrm{A}}_{\mathrm{CuH_{-1}A'A}} = \log K^{\mathrm{A}}_{\mathrm{CuA}} + \log K_{\mathrm{os}} + \Sigma\delta_{ij}x_i(\mathrm{H_{-1}A})x_j(\mathrm{A}) = 5.54 + 0 - 1.22 = 4.32. \quad (15)$$

Then we have

$$\log \beta_{1\bar{1}2}(2,2) = -2.82 + 1.31 + 4.32 = 2.81. \quad (16)$$

This calculated value is about two orders of magnitude less than the observed one, while it is in good agreement with the experimental one for glycinamide ($\log \beta_{1\bar{1}2} = 2.72$). Since this amide complex can take only the geometry of type (2,2), as evident from Fig. 2, the agreement is a fair indication of the validity of such an approach.

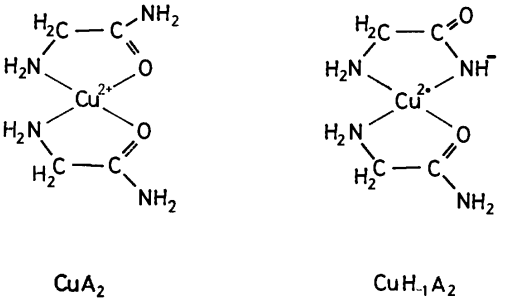

Fig. 2. Structures of bis(glycinamide) copper(II) complexes.

For the mixed ligand complex $CuH_{-1}AB$ which includes glycine as B, a similar calculation shows that $\log \beta_{1\bar{1}1}(3,1) = 4.55$ and that $\log \beta_{1\bar{1}1}(2,2) = 5.35$, while the observed value is 5.255.[4] Thus, glycine and the deprotonated dipeptide both chelate on the basal plane as bidentate ligands, in contrast to the situation in the $CuH_{-1}A_2$ complex. This may result from the much greater ability of glycine to chelate a metal ion compared with the dipeptide interacting with the non-deprotonated CONH group.

On the other hand, glycine is supposed to coordinate with an apical position in its mixed ligand copper(II) complexes with substituted iminodiacetic acids or diethylenetriamine, because its formation constants are considerably greater than those for its esters.[15,16]

For a dipeptide, however, coordination *via* carbonyl oxygen is generally very weak (type (3,1)), and its terminal carboxylate cannot interact with the apical position without considerable strain, according to the Dreiding Stereomodel (type (2,2)). Therefore the apical coordination will be unimportant in the case of

glycylglycinato copper(II) complexes, which probably account for the good agreement between the observed and calculated formation constants as shown above.

In brief, the glycylglycine complex $CuH_{-1}A_2$ of type (3,1) predominates in an aqueous solution, while about 2% of them are still present in the form of type (2,2), since $\beta(2,2)/\beta(3,1) = 1.8 \times 10^{-2}$. This conclusion supports the proposal by Gergely and Nagypál,[17] apart from the question of the apical interaction.

The authors are greatly indebted to Prof. M. Tanaka, Nagoya University, for helpful discussions as well as for continuing encouragement in performing this investigation, and also to Mr. T. Noda, Nagoya University, for technical assistance in improvement of the glassware apparatus.

This research was financially supported in part by a Grant-in-Aid for Scientific Research No. 554184 from the Ministry of Education, Science and Culture.

References

1) H. Dobbie and W. O. Kermack, *Biochem. J.*, **59**, 246 (1955).
2) W. L. Koltun, M. Fried, and F. R. N. Gurd, *J. Am. Chem. Soc.*, **82**, 233 (1960).
3) M. K. Kim and A. E. Martell, *Biochemistry*, **3**, 1169 (1964).
4) R.-P. Martin, L. Mosoni, and B. Sarkar, *J. Biol. Chem.*, **246**, 5944 (1971).
5) B. Strandberg, I. Lindqvist, and R. Rosenstein, *Z. Kristallogr.*, **116**, 266 (1961).
6) J. Lefebvre, *J. Chim. Phys.*, **54**, 553 (1957).
7) T. F. Dorigatti and E. J. Billo, *J. Inorg. Nucl. Chem.*, **37**, 1515 (1975); H. Sigel, *Angew. Chem.*, **80**, 124 (1968).
8) J. D. Bell, H. C. Freeman, and A. M. Wood, *J. Chem. Soc., Chem. Commun.*, **1969**, 1441.
9) M. Tanaka, *J. Inorg. Nucl. Chem.*, **36**, 151 (1974).
10) M. Bonnet, Ph. D. Thesis, Université Claude Bernard, Lyon, France, 1971.
11) Y. Nakao, K. Sakurai, and A. Nakahara, *Bull. Chem. Soc. Jpn.*, **39**, 1608 (1966).
12) A. Sugihara, T. Ashida, Y. Sasada, and M. Kakudo, *Acta Crystallogr., Sect. B*, **24**, 203 (1968).
13) Y. Fujii and M. Kodama, *Bull. Chem. Soc. Jpn.*, **42**, 3172 (1969).
14) R. Näsänen and M. Koskinen, *Acta Chem. Scand.*, **18**, 1337 (1964).
15) B. E. Leach and R. J. Angelici, *Inorg. Chem.*, **8**, 907 (1969).
16) R. J. Angelici and J. W. Allison, *Inorg. Chem.*, **10**, 2238 (1971).
17) A. Gergely and I. Nagypál, *J. Chem. Soc., Dalton Trans.*, **1977**, 1104.

The Complex Formation of the Copper(II) Ion with Ethylenediaminetetraacetic Acid and *N*-(2-Hydroxyethyl)ethylenediamine-*N*,*N*′,*N*′-triacetic Acid

Shuichiro YAMAGUCHI, Noboru OYAMA,† Kazuo IKEDA,†† and Hiroaki MATSUDA*

Department of Electronic Chemistry, Graduate School at Nagatsuta, Tokyo Institute of Technology, Nagatsuta, Midori-ku, Yokohama 227

(Received March 20, 1981)

The complex formation of the Cu(II) ion with ethylenediaminetetraacetic acid (EDTA) and *N*-(2-hydroxyethyl)ethylenediamine-*N*,*N*′,*N*′-triacetic acid (HEDTA) has been studied potentiometrically and polarographically over the wide pH range from 1 to 11 in aqueous solutions containing 1.0 mol dm^{-1} $NaClO_4$ at 25.0 °C. Both the emf data obtained by potentiometric titrations and the pH-dependence of reversible half-wave potentials were explained in terms of the formation of the following complex species: for the Cu–EDTA complexes, CuL^{2-} ($\log\beta_{101}=17.28\pm0.04$), $CuHL^{-}$ ($\log\beta_{111}=20.15\pm0.04$), CuH_2L ($\log\beta_{121}=22.73\pm0.04$), CuH_3L^{+} ($\log\beta_{131}=24.12\pm0.04$), and $CuH_{-1}L^{3-}$ ($\log\beta_{1-11}=6.83\pm0.05$); for the Cu–HEDTA complexes, CuL^{-} ($\log\beta_{101}=16.30\pm0.05$), CuHL ($\log\beta_{111}=18.76\pm0.04$), CuH_2L^{+} ($\log\beta_{121}=19.85\pm0.04$) and $CuH_{-1}L^{2-}$ ($\log\beta_{1-11}=6.35\pm0.05$), where $\beta_{pqr}=[Cu_pH_qL_r]/[Cu^{2+}]^p[H^+]^q[L]^r$, and where L denotes the unprotonated molecule of EDTA or HEDTA.

The complex-formation reaction of the Cu(II) ion with ethylenediaminetetraacetic acid (EDTA) and *N*-(2-hydroxyethyl)ethylenediamine-*N*,*N*′,*N*′-triacetic acid (HEDTA) has been studied by a number of workers, and the formation constants of unprotonated and monoprotonated species have been reported.[1,2] The formation constants of the diprotonated Cu(II)–EDTA complex have been reported only by Gorelova *et al.*[3] Interest has also been shown in the problem of determining the protonation schemes of the coordinated ligands and structures of metal complexes by using infrared spectrometry,[4-6] NMR spectrometry[4,7-10] and other methods.[11-14] Nuttall and Stalker[15] have recently proposed, from measurements of the Raman spectra, that protons in protonated Cu(II)–EDTA complexes are located at the oxygen atoms of the ligand carboxyl groups.

In our previous papers[16,17] we have found that a number of protonated complex species of the MH_qL type ($q=1,2,3$ for the EDTA complex and $q=1,2$ for the HEDTA complex) are formed in an acidic solution containing Cd(II) and Pb(II) ions. Therefore, it seemed it would be interesting to see if Cu(II)-complexes with EDTA and HEDTA form a series of protonated species in an acidic solution. The examination of complex-formation equilibria was performed by potentiometric titration measurements, polarographic method, and visible-spectrum measurements over the wide pH range from 1.0 to 11.0.

Symbols

h	Concentration of hydrogen ions at equilibrium.
m	Concentration of metal ions at equilibrium.
H	Analytical excess of hydrogen ions in a test solution.
c_{Cu}	Total concentration of Cu(II) ions.
L	Ethylenediaminetetraacetate anion ($edta^{4-}$) or *N*-(2-Hydroxyethyl)ethylenediamine-*N*,*N*′,*N*′-triacetate anion ($hedta^{3-}$).
c_L	Total concentration of L.
l	Concentration of free L.
$\bar{X}$	Degree of neutralization of H_4L for EDTA or H_3L for HEDTA: $(-H+[H]-[OH])/c_L$.
p	Number of metal atoms bound to the complex.
q	Number of protons bound to the complex; $q<0$ corresponds to the formation of a deprotonated complex.
r	Number of ligands bound to the complex.
β_{pqr}	Equilibrium constant for the reaction: $pM+qH+rL=M_pH_qL_r$.
[ ]	Concentration.
D_{Cu}	Diffusion coefficient of the aqua Cu(II) ion.
D	Average diffusion coefficient of all complex species present.[18]
$(E_{1/2})_{Cu}$	Reversible half-wave potential of the aqua Cu(II) ion.
$(E_{1/2}^r)_{rev}$	Reversible half-wave potential of the Cu(II)–EDTA or –HEDTA system.
R	Gas constant.
T	Thermodynamic temperature.
F	Faraday constant.

All ionic charges are omitted for the sake of convenience.

Experimental

Reagents. *Disodium ethylenediaminetetraacetate* (reagent grade, Dojindo Lab.) was recrystallized twice, dried, and then stored in a desiccator over silica gel. *N-(2-Hydroxyethyl)ethylenediamine-N,N′,N′-triacetic acid* (Dojindo Lab.) was recrystallized from distilled water and dried under a reduced pressure. *Copper(II) perchlorate* was prepared by dissolving $CuCO_3$ in an $HClO_4$ solution and purified by recrystallizing it three times from distilled water. The $CuCO_3$ used was precipitated from a $Cu(NO_3)_2$ solution with Na_2CO_3 and then thoroughly decanted. The stock solution contained a small amount of $HClO_4$ to prevent the hydrolysis of the Cu(II) ion. The concentration of excess $HClO_4$ in the solution was determined from the location of the end point of neutralization by means of a Gran-plot. The concentration of Cu(II) ions in the stock solution was determined by electrogravimetry. *Sodium perchlorate*, *sodium hydroxide*, and *perchloric acid* stock solutions were prepared by the methods described previously.[16] A copper-amalgam was prepared by the electrolysis of a copper sulfate

† Present address: Department of Applied Chemistry for Resources, Tokyo University of Agriculture and Technology, Koganei, Tokyo 184.

†† Present address: Technical Education Center of Tokyo Metropolis, 2-1-45, Horinouchi, Suginami-ku, Tokyo 166.

solution with a Metrohm model E 211 A coulometer. The metal content of the amalgam was about 1 wt%. The oxidation of the amalgam was prevented by preparing and storing it in a nitrogen atmosphere. All the other chemicals were prepared and purified by the methods described previously.[16]

Potentiometric Measurements. The measurements were carried out in a paraffin oil thermostat at (25.00±0.02) °C by using glass and copper-amalgam electrodes. Emf measurements of electrodes were carried out with essentially the same method as has been described previously.[16] The potential of the amalgam electrode became constant after 5—15 min within an accuracy of ±0.02 mV in the pH range of 1.0—2.5 and within an accuracy of ±0.05 mV in that of 2.5—4.0. At pH values above 4.0 the potential was slightly unstable, and it required 1 h to attain a constant value within an accuracy of ±0.1 mV at pH values up to 10.0. The emf of the glass electrode cell became constant after about 5 min and was determined within an accuracy of 0.1 mV over the pH range of 1.0—11.0. The perchlorate concentration was kept constant at 1.0 mol dm^{-3} in all runs. The apparatus and the experimental procedures used for potentiometric titrations have been described previously.[16]

Polarographic Measurements. The polarographic apparatus used was described previously.[18] No buffer was added to the test solution, because the ligands present in a large excess relative to Cu(II) ions have a large buffer capacity in the pH ranges below 3.5 and from 5.5 to 10.5 for both HEDTA and EDTA, and because the polarographic wave-form may be affected by the presence of an acetate buffer in the pH range from 3.5 to 5.5. The hydrogen-ion concentration of the test solution was varied and measured before and after the recording of each polarogram.[16] The difference between the pH values ($-\log h$) obtained before and after recording was less than 0.01 pH unit. No maximum suppressor was added, since no polarographic maximum appeared at pH values above 1. The test solution was deaerated for at least 30 min with argon gas before each measurement.

Spectrophotometric Measurements. The ultraviolet and visible absorption spectra were measured by using a Hitachi Model 200-10 Spectrophotometer at room temperature (25±1 °C).

Results

Determination of the Composition and the Formation Constants of Cu(II)-EDTA and -HEDTA Complexes by Potentiometric Titrations. The titration curves shown in Figs. 1 and 2 result when the experiments were carried out under the conditions where the c_{Cu}/c_L ratio was 1/2, 1/4, 1/6, or 1/8 and where c_{Cu} was changed from 1 to 10 mmol dm^{-3}. Both c_{Cu} and c_L were kept practically constant for each run. The difference in neutralization degree between EDTA or HEDTA solutions with and without Cu(II) ions reveals that protons were released from the ligand by the complex formation, even at pH 1.3.

As has been described previously,[16,17] since any possibility of the formation of polynuclear or polyligand complexes may be disregarded when the solution contains an excess of EDTA and HEDTA ligands relative to the Cu(II) ion, we can use the same procedure for data analysis as that employed for Cd(II)- and Pb(II)-complexes with EDTA and HEDTA.[16,17] We assume that the complex formation proceeds:

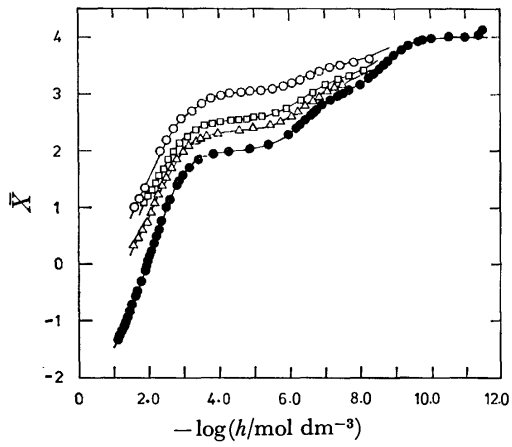

Fig. 1. Degrees of neutralization, $\bar{X}$, of EDTA solutions for the Cu(II)–EDTA system.
●: $c_{Cu}=0.0$ mol dm^{-3}, $c_L=0.02500$ mol dm^{-3}, ○: $c_{Cu}=0.006221$ mol dm^{-3}, $c_L=0.011985$ mol dm^{-3}, □: $c_{Cu}=0.001107$ mol dm^{-3}, $c_L=0.003987$ mol dm^{-3}, △: $c_{Cu}=0.001075$ mol dm^{-3}, $c_L=0.005998$ mol dm^{-3}. Solid lines are the values of $\bar{X}$ calculated by the use of the formation constants given in Table 1.

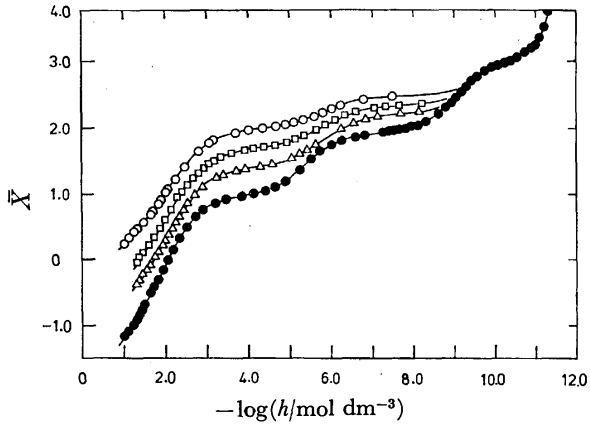

Fig. 2. Degrees of neutralization, $\bar{X}$, of HEDTA solutions for the Cu(II)–HEDTA system.
●: $c_{Cu}=0.0$ mol dm^{-3}, $c_L=0.02500$ mol dm^{-3}, ○: $c_{Cu}=0.01010$ mol dm^{-3}, $c_L=0.02020$ mol dm^{-3}, □: $c_{Cu}=0.004970$ mol dm^{-3}, $c_L=0.02000$ mol dm^{-3}, △: $c_{Cu}=0.002500$ mol dm^{-3}, $c_L=0.02000$ mol dm^{-3}. Solid lines are the values of $\bar{X}$ calculated by the use of the formation constants given in Table 1.

$$Cu^{2+} + qH^+ + L^{z-} = CuH_qL^{(2+q-z)+} \quad (1)$$

from which the following relationships are obtained:

$$c_{Cu} = m + \sum_{q=-1}^{Q}[CuH_qL] \quad (2)$$

$$c_L = l + \sum_{n=1}^{N}[H_nL] + \sum_{q=-1}^{Q}[CuH_qL]. \quad (3)$$

The combination of Eqs. 2 and 3 leads to:

$$l = (c_L - c_{Cu} + m)/(1 + \sum_{n=1}^{N}\beta_{0n1}h^n), \quad (4)$$

where l can be calculated by using the protonation constants of the ligands obtained previously.[16,17] A function, $F_0(h)$, is defined as:

$$F_0(h) = (c_{Cu}-m)/ml = \sum_{q=-1}^{Q}[CuH_qL]/ml = \sum_{q=-1}^{Q}\beta_{1q1}h^q \quad (5)$$

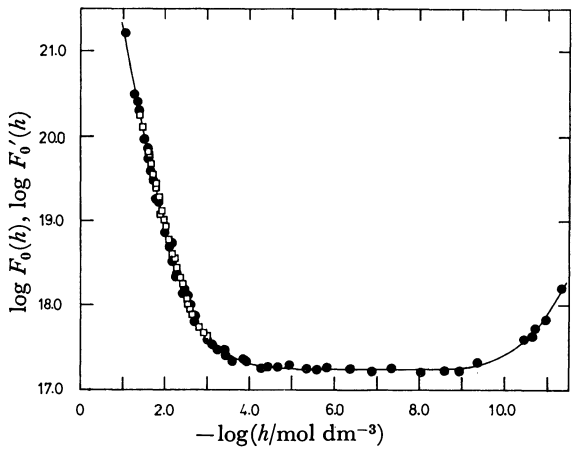

Fig. 3. Plots of log $F_0(h)$ and log $F_0'(h)$ against $-\log h$ for Cu(II)–EDTA system. Solid line is the best fit curve calculated by Eqs. 5 and 9.
□: log $F_0(h)$, ●: log $F_0'(h)$.

The plots of log $F_0(h)$ against $-\log h$ for the EDTA system fall into a single curve regardless of the variations in c_{Cu} and c_L (Fig. 3), and the assumption that no polynuclear and polyligand complexes are formed in an acidic solution is confirmed to be reasonable. The formation constant, β_{1q1}, was calculated from the $F_0(h)$ *vs.* h curve by means of a generalized least-squares method.[16] The method was applied to make the error-squares sum, $\sum\{\log F_0 - \log F_{0,calcd}\}^2$, a minimum for the set of the formation constants over the pH range of 1.0—7.0, where $F_{0,calcd}$ denotes the value of F_0 calculated for a particular set of formation constants. The values of the formation constants of all the complex species present are given in Table 1. In addition to the normal complex, CuL^{2-}, a series of protonated complexes, such as $CuHL^-$, CuH_2L^0, and CuH_3L^+, were detected. No information has yet been published on the formation of the triprotonated species.

Table 1. Formation constants of Cu(II)–EDTA and–HEDTA complexes in 1.0 mol dm^{-3} $NaClO_4$ solution at 25 °C

	Potentiometry	Polarography	Spectrophotometry
Cu(II)–EDTA system			
log β_{1-11}	—	6.83±0.05	5.5±0.1
log β_{101}	17.22±0.10	17.28±0.04	—
log β_{111}	20.15±0.04	20.13±0.06	—
log β_{121}	22.73±0.04	22.88±0.04	—
log β_{131}	24.12±0.04	24.15±0.04	—
Cu(II)–HEDTA system			
log β_{1-11}	—	6.35±0.05	5.2±0.1
log β_{101}	16.12±0.10	16.30±0.05	—
log β_{111}	18.85±0.05	18.76±0.04	—
log β_{121}	19.86±0.04	19.85±0.04	—

The same analytical method as was used for the EDTA system was used to determine the formation constants for the HEDTA system. Figure 4 demonstrates that the plots of log $F_0(h)$ against $-\log h$ in the HEDTA system give a single curve. From the analysis of the curve, we found that the normal complex, CuL^-,

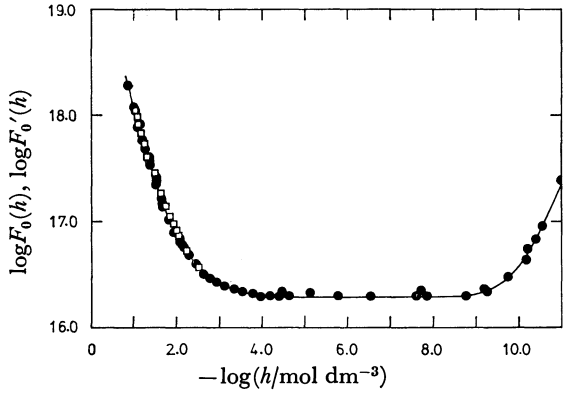

Fig. 4. Plots of log $F_0(h)$ and log $F_0'(h)$ against $-\log h$ for Cu(II)–HEDTA system. Solid line is the best fit curve calculated by Eqs. 5 and 9.
□: log $F_0(h)$, ●: log $F_0'(h)$.

as well as two protonated complexes, CuHL and CuH_2L^+, are formed. The formation constant of the diprotonated species was obtained for the first time in the Cu–HEDTA system. The solid curve in Fig. 4 represents the curve calculated from the final values of the formation constants which are summarized in Table 1.

Above pH 4.0, the emf's of the amalgam electrodes became unstable for both systems, and the values of log $F_0(h)$ in Figs. 3 and 4 were somewhat scattered around the best-fit curve. This may be due to the contamination of amalgam surfaces by a small amount of oxygen dissolved in solution. Thus, we may expect to obtain correct information on complex-formation reactions above pH 4 by means of polarographic measurements.

Determination of the Formation Constants by Polarography. Single well-defined waves with diffusion-controlled limiting currents were observed for the Cu(II)–EDTA and –HEDTA systems in the pH range from 1.0 to

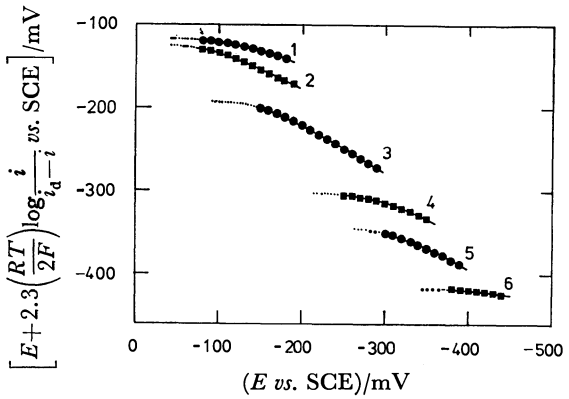

Fig. 5. Typical examples of the plots of $E+2.3\,(RT/2F)\cdot\log[i/(i_d-i)]$ *vs.* E for determination of reversible half-wave potentials. $c_{Cu}=0.00040$ mol dm^{-3}.
●: Cu(II)–EDTA system. $c_L=0.0080$ mol dm^{-3}. Values of $-\log(h/\text{mol dm}^{-3})$: (1) 2.12, (3) 3.73, (5) 6.11.
■: Cu(II)–HEDTA system. $c_L=0.0200$ mol dm^{-3}. Values of $-\log(h/\text{mol dm}^{-3})$: (2) 2.70, (4) 6.05, (6) 10.19.

11.0. The log-plot analysis of the current-potential curves demonstrates that the waves correspond to the quasi-reversible, two-electron reduction. For the quasi-reversible wave we can determine the reversible half-wave potential by using the extrapolation methods.[19,20] Figure 5 shows typical examples of the $[E+2.3(RT/2F)\times \log\{i/(i_d-i)\}]$ *vs.* E plots, where E denotes the potential of the dropping mercury electrode, i the current corresponding to E, and i_d the limiting diffusion current. The reversible half-wave potentials were determined as the limiting constant values of $[E+2.3(RT/2F)\log\{i/(i_d-i)\}]$ at sufficiently positive potentials.[19]

Consider the electrode reaction, symbolically designated by:

$$\left\{\begin{array}{l}\mathrm{CuH_QL^{(2+Q-z)+}}\\ \quad\vdots\\ \quad\downarrow\uparrow\\ \mathrm{CuH_qL^{(2+q-z)+}}\\ \quad\vdots\\ \quad\downarrow\uparrow\\ \mathrm{CuL^{(2-z)+}}\\ \quad\downarrow\uparrow\\ \mathrm{CuH_{-1}L^{(1-z)+}}\end{array}\right\} + 2e(\mathrm{Hg}) \rightleftharpoons$$

$$\mathrm{Cu\,(Hg)} + \left\{\begin{array}{l}\mathrm{H_NL^{(N-z)+}}\\ \quad\vdots\\ \quad\downarrow\uparrow\\ \mathrm{H_nL^{(n-z)+}}\\ \quad\vdots\\ \quad\downarrow\uparrow\\ \mathrm{L^{-z}}\end{array}\right\}. \qquad (6)$$

The reversible half-wave potential can then be expressed by:[18]

$$(E_{1/2})_{\mathrm{rev}} = (E^{\mathrm{r}}_{1/2})_{\mathrm{Cu}} - \frac{RT}{2F}\ln\sqrt{\frac{D}{D_{\mathrm{Cu}}}} - \frac{RT}{2F}\ln[1+(\sum_{q=-1}^{Q}\beta_{1q1}h^q)l]. \qquad (7)$$

Equation 7 can be rewritten as:

$$\left\{\sqrt{\frac{D_{\mathrm{Cu}}}{D}}\exp\left\{\left(\frac{2F}{RT}\right)[(E^{\mathrm{r}}_{1/2})_{\mathrm{Cu}} - (E_{1/2})_{\mathrm{rev}}]\right\} - 1\right\}/l = \sum_{q=-1}^{Q}\beta_{1q1}h^q. \qquad (8)$$

The left-hand side of Eq. 8 is the experimentally accessible quantity and is here written as $F_0'(h)$. Thus,

$$F_0'(h) = \sum_{q=-1}^{Q}\beta_{1q1}h^q, \qquad (9)$$

which is identical to the $F_0(h)$ function defined by Eq. 5.

The plots of $\log F_0'(h)$ against $-\log h$ are shown in Figs. 3 and 4 for the systems of EDTA and HEDTA respectively. In each system, a single curve was obtained for both functions, $F_0(h)$ and $F_0'(h)$, and only small differences between the formation constants determined from these two functions were observed.

In the EDTA system, the triprotonated complex, CuH_3L^+, was also detected by polarography. In the pH range of 4.0—9.5, the values of the $\log F_0'(h)$ function were constant, and we can consider that the Cu(II) ion is present predominantly as the normal complex, CuL^{2-}, in a solution containing an excess EDTA. The values of the $\log F_0'(h)$ function begin to increase above pH 10.0 (Fig. 3), indicating the formation of hydroxo complexes. The $F_0'(h)$ function is proportional to h^{-1} in the range above pH 10.0, and the product $[F_0'(h)-\beta_{101}]\times h$ yields a constant value. This behavior of $F_0'(h)$ can be understood in terms of the formation of only one deprotonated complex, $CuH_{-1}L^{3-}$, which is probably the same as the hydroxo complex $Cu(OH)L^{3-}$, reported previously.[3] The formation constant of the hydroxo complex was determined by the curve-fitting method; it is given in Table 1.

In the HEDTA system, all of the complex species, CuL^-, $CuHL^0$, and CuH_2L^+, being found potentiometrically, were also detected by the polarographic method. Above pH 9.0, the values of the $\log F_0'(h)$ function began to increase, indicating the formation of deprotonated species, $CuH_{-1}L^{2-}$. The formation constants of these four species were determined by the analysis of the $F_0'(h)$ *vs.* h curve; they are given in Table 1.

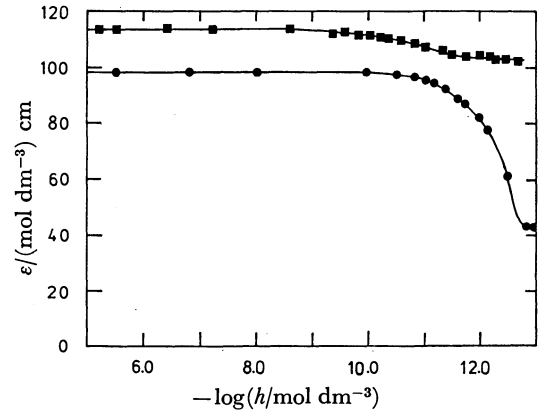

Fig. 6. Variations of the molar absorbances with $-\log h$ at the absorption maxima of Cu(II)–EDTA (●) and Cu(II)–HEDTA (■) solutions.

Spectrophotometric Measurements. In order to obtain further information on the formation of deprotonated species, measurements of the absorption spectra were carried out in the alkaline region. For the EDTA system, the hydroxo complex formation was also observed by spectrophotometry. Figure 6 demonstrates the intensity change in the absorption maximum (at 740 nm) with $-\log h$, from which the formation of the $Cu(OH)L^{3-}$ species was confirmed to be as previously reported by Bhat and Krishnamurthy.[13] On the other hand, the intensity change in the absorption maximum (at 710 nm) with $-\log h$ for the HEDTA system in the pH range of 9.5—12 is not so large (Fig. 6), though two isosbestic points were observed at 600 and 835 nm. This fact proves that two species, the normal complex, CuL^- and only one deprotonated complex, $CuH_{-1}L^{-2}$, are formed in the pH range from 9.5 to 12.

As can be seen from Table 1, the values of the formation constants obtained by spectrophotometry are different from those obtained by polarography. The reason for this discrepancy is not clear at present.

Discussion

The step-by-step protonation constants for protonated complexes of the $CuH_{q-1}L$ type may be defined as $K_H^{CuH_qL} = [CuH_qL]/[CuH_{q-1}L][H] = \beta_{1q1}/\beta_{1(q-1)1}$. The values of log $K_H^{CuH_qL}$ for the EDTA complexes are 2.87, 2.58, and 1.39 for $q=1,2$, and 3 respectively, while those of the HEDTA complexes are 2.46 and 1.09 for $q=1$ and 2 respectively. These values are close to the values of log $K_H^{H_nL}$=log $\{[H_nL]/[H_{n-1}L][H]\}$ with $n=3,4$, and 5 of the corresponding ligands,[17] which are the step-by-step protonation constants for the carboxyl groups of the EDTA and HEDTA ligands. Thus, as has been reported previously[16,17] for the systems of the Cd(II)- and Pd(II)–HEDTA and -EDTA complexes, we may conclude that the protonation of the complexes occurs on the carboxyl groups with the cleavage of Cu(II)–oxygen bonds within the complexes, while the strong Cu(II)–nitrogen bonds remain unaltered.

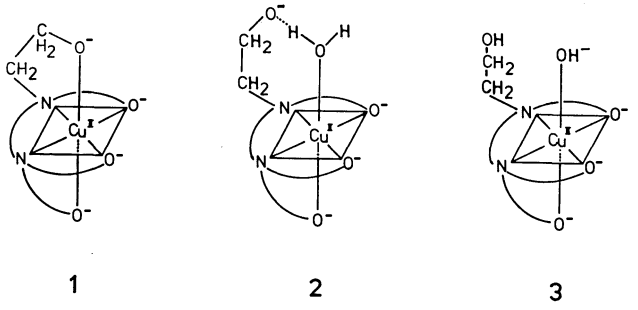

Fig. 7. Possible structures for the deprotonated species of Cu(II)–HEDTA complex.

We define the deprotonation constant of the $CuH_{-1}L$ species as $K_{H_{-1}}^{CuH_{-1}L}=\{[CuH_{-1}L][H]/[CuL]\}$. Then, we obtain log $K_{H_{-1}}^{CuH_{-1}L}=-10.45$ and -9.95 for the EDTA and HEDTA systems respectively. Thus, the values of the deprotonation constant are shown to be almost the same for the EDTA and HEDTA systems. However, Fig. 6 indicates that the intensity changes in the absorption maxima with $-\log h$ in the pH range from 10 to 11.5 are large for the EDTA system, but not for the HEDTA system. The observed result may be attributable to the difference between the deprotonation reaction schemes of the EDTA and HEDTA complexes. The large intensity change in the absorption maximum for the EDTA complex is possibly caused by the deprotonation of the water molecule coordinated to the Cu(II) ion, and the resulting species is a hydroxo complex. On the other hand, three possible reaction schemes for the HEDTA complex may be considered on the basis of the pentadentate coordination of the HEDTA ligand to the Cu(II) ion at the state of the normal complex, as is shown in Fig. 7: (1) the hydroxyethyl group in the ligand releases a proton, and the resulting ethyl alcoholate coordinates to the Cu(II) ion directly; (2) the hydroxyethyl group releases a proton to form a hydrogen bond with the water molecule coordinated to the Cu(II) ion, or (3) the deprotonation occurs from the water molecule coordinated to Cu(II), and the hydroxyethyl group gives no interaction for the hydrolysis reaction. The observed absorption spectra seem to support the reaction scheme (2), since the Cu(II) ion was not subjected to any strong interaction with the deprotonation of the complex.

The degree of neutralization, $\bar{X}$, of H_3hedta exceeds 3.0 at pH values above 11.0, but that of H_4edta remains constant (4.0), although the emf of the glass electrode cell becomes uncertain in such a high pH region. Therefore, it may be considered that the reaction of the hydroxyethyl group of HEDTA to ethylalcolate starts at this pH in the HEDTA solution containing no Cu(II) ion. The adoption of the reaction scheme (2) depicted in Fig. 7 means that the coordination of HEDTA to the Cu(II) ion accelerates the deprotonation of the hydroxyethyl group, since the deprotonation reaction of the Cu(II)–HEDTA complex starts at pH 9.5. The acceleration of the deprotonation process of 2-aminoethanol by its coordination to the metal ion has been reported for the $[Co(NH_2CH_2CH_2NH_2)_2(NH_2CH_2CH_2OH)]^{3+}$ complex.[21]

The authors wish to express their thanks to Drs. H. Ogino and K. Ogino, Tohoku University, for their stimulating discussion on the formation of deprotonated species. The present work was partially supported by a Grand-in-Aid for Scientific Research No. 247065 from the Ministry of Education, Science and Culture.

References

1) L. G. Sillen and A. E. Martell, "Stability Constants of Metal-Ion Complexes," Chemical Society, London (1964), Supplement No. 1, (1971).
2) D. D. Perrin, "Stability Constants of Metal-Ion Complexes, Part B, Organic Ligands," IUPAC Chemical Data Series No. 22, Pergamon Press, Oxford (1979).
3) R. I. Gorelova, V. A. Babich, and I. P. Gorelov, *Zh. Neorg. Khim.*, **16**, 1873 (1971).
4) D. Chapman, D. R. Lloyd, and R. H. Prince, *J. Chem. Soc.*, **1963**, 3645.
5) N. Nakamoto, Y. Morimoto, and A. E. Martell, *J. Am. Chem. Soc.*, **85**, 309 (1963).
6) D. T. Sawyer and J. E. Tackett, *J. Am. Chem. Soc.*, **85**, 314 (1963).
7) R. J. Kula, D. T. Sawyer, S. I. Chan, and C. M. Finley, *J. Am. Chem. Soc.*, **85**, 2930 (1963).
8) J. L. Sudmeier and C. N. Reilley, *Anal. Chem.*, **36**, 1698 (1964).
9) L. E. Erickson, D. C. Young, F. F. L. Ho, S. R. Watkins, J. B. Terrill, and C. N. Reilley, *Inorg. Chem.*, **10**, 441 (1971).
10) D. S. Everhast and R. F. Evilia, *Inorg. Chem.*, **14**, 2755 (1975).
11) W. C. E. Higginson, *J. Chem. Soc.*, **1962**, 2761.
12) A. P. Brunetti, G. H. Nancollas, and P. N. Smigh, *J. Am. Chem. Soc.*, **91**, 4680 (1969).
13) T. R. Bhat and M. Krishnamurthy, *J. Inorg. Nucl. Chem.*, **25**, 1147 (1963).
14) R. G. Wilkins and R. E. Yellin, *J. Am. Chem. Soc.*, **89**, 5946 (1967).
15) R. H. Nuttall and D. M. Stalker, *Inorg. Nucl. Chem. Lett.*, **12**, 639 (1976).
16) N. Oyama, T. Shirato, H. Matsuda, and H. Ohtaki, *Bull. Chem. Soc. Jpn.*, **49**, 3047 (1976).
17) N. Oyama, H. Matsuda, and H. Ohtaki, *Bull. Chem. Soc. Jpn.*, **50**, 409 (1977).

18) N. Oyama and H. Matsuda, *J. Electroanal. Chem.*, **78** 89 (1977).
19) H. Matsuda, Y. Ayabe, and K. Adachi, *Ber. Bunsenges. Phys. Chem.*, **67**, 593 (1963); H. Matsuda, *Tokyo Kogyo Shikensho Hokoku*, **61**, 315 (1966).
20) R. Tamamushi and N. Tanaka, *Z. Phys. Chem.* (*Frankfurt*), **39**, 117 (1963).
21) K. Ogino and H. Seki, *Bull. Chem. Soc. Jpn.*, **54**, 719 (1981).

The Formation of Molybdenum Disulfide by the Reaction between Molybdenum Trioxde and Sulfur Dioxide in the Presence of Carbon

Akimasa YAJIMA, Ryoko MATSUZAKI, Motonori EGUCHI, and Yuzo SAEKI*

Research Laboratory of Resources Utilization, Tokyo Institute of Technology, 4259, Nagatsuta-cho, Midori-ku, Yokohama 227

(Received March 27, 1981)

The reaction products obtained by heating a mixture of MoO_3 and carbon in a SO_2 stream at various temperatures were examined. The possible reactions during the above process were also studied. Further, thermodynamical consideration was made of the formation of MoS_2. When a mixture of MoO_3 and carbon was heated in a SO_2 stream, MoO_2 was formed above 400 °C. At 500—550 °C, the formation of a small amount of Mo_4O_{11} was also observed. Above 700 °C, the formation of MoS_2 in addition to MoO_2 was observed, and MoS_2 alone was obtained at 1000 °C. Sulfur was obtained outside the heating zone throughout the temperature range in this experiment. The process of the formation of MoS_2 by the reaction between MoO_3 and SO_2 in the presence of carbon can be represented as follows: The reaction between carbon and SO_2 occurs at first to form sulfur. Above *ca.* 400 °C, the reductions of MoO_3 with carbon and with sulfur occur to form MoO_2. Above *ca.* 700 °C, MoS_2 is formed by the reaction between MoO_2 and sulfur, which are formed by the above reactions.

As sulfidizing agents for synthesizing molybdenum disulfide (MoS_2), hydrogen sulfide and sulfur have been well known. But there has been no report on the chemical process for synthesizing MoS_2 from molybdenum trioxide (MoO_3) using sulfur dioxide (SO_2) as a sulfidizing agent. It is not only interesting from the viewpoint of the synthesis of the sulfide itself, but also important for the development of SO_2 utilization, to obtain knowledge of the above chemical process.

In this work, the reaction products between MoO_3 and SO_2 in the presence of carbon at various temperatures were examined. In order to elucidate the reaction process between MoO_3 and SO_2 in the presence of carbon, the reactions of MoO_3 with carbon and of MoO_3 with gaseous sulfur in a SO_2 stream were examined. Also, the reactions of MoO_2, formed during the reaction process between MoO_3 and SO_2 in the presence of carbon, with carbon and of MoO_2 with gaseous sulfur in a SO_2 stream were examined. Further, thermodynamical consideration was made of the formation of MoS_2.

Experimental

The MoO_3 used was prepared by the thermal decomposition of the guaranteed reagent ammonium paramolybdate at 600 °C. The carbon was prepared by the thermal decomposition of the guaranteed reagent D-glucose. The above materials were used as powders under 150 mesh. Gaseous SO_2 was dried by passing it through concd H_2SO_4 and over P_2O_5.

A mixture of MoO_3 and carbon at a specified ratio in a quartz boat (length: 72 mm, width: 16 mm, depth: 9 mm) was placed in a transparent quartz reaction tube (inner diameter: 28 mm, length: 1000 mm). Gaseous SO_2 was then introduced into the reaction tube. The sample part was positioned in the middle of the tubular electric furnace (heating length: 300 mm) maintained at a specified temperature for 1 h. The temperature of the sample part was controlled within ± 2 °C. After heating, the sample was held at 100 °C for 1 h in an argon stream in order to release the adsorbed SO_2 on unreacted carbon.[1] The reactions of MoO_3 with carbon in an argon stream, of MoO_3 with gaseous sulfur in a SO_2 stream, of MoO_2 with carbon in an argon stream, and of MoO_2 with gaseous sulfur in a SO_2 stream were examined in a similar manner.

The X-ray analysis of the sample was performed with an X-ray powder diffractometer equipped with a proportional counter using Ni filtered Cu radiation. The thermogravimetry (TG) was performed by using a thermal balance with a quartz helix. The sensitivity of the quartz helix used was approximately 72 mm/g, and the heating rate of 2.5 °C/min was employed.

The molybdenum content in the sample was determined gravimetrically as $PbMoO_4$ after the fusion of the sample with a mixture of Na_2CO_3 and K_2CO_3. The sulfur content in the sample was determined gravimetrically as $BaSO_4$ after decomposing the sample with HNO_3 and $KClO_3$.

Results and Discussion

Reaction Products between Molybdenum Trioxide and Sulfur Dioxide in the Presence of Carbon. The TG of MoO_3 (0.3 g) in a SO_2 stream at a flow-rate of 50 cm^3/min was carried out. The heating temperature of the sample was limited to below 700 °C, since MoO_3 vaporized above this temperature. No weight change was observed, and the sample after the heating was found to be unreacted MoO_3 by X-ray analysis.[2] These results indicate that MoO_3 does not react with SO_2.

The reaction between MoO_3 and SO_2 in the presence of carbon was then examined. First, the products obtained by heating a mixture of 2.00 g of MoO_3 and 1.20 g of carbon at various temperatures for 1 h in a SO_2 stream at a flow-rate of 100 cm^3/min were examined. The results are shown in Table 1, together with the weight changes in the samples. The sample in the boat was identified by X-ray analysis.[2-5]

The formation of MoO_2 was observed above 400 °C, and a small amount of Mo_4O_{11} in addition to MoO_2 was also observed at 500—550 °C. The formation of MoS_2 was observed at 700 °C. A small amount of sulfur was obtained outside the heating zone throughout the temperature range in this experiment. The slight increase in the sample weight at 350—400 °C was due to the adsorption of the sulfur formed by the reaction on the unreacted carbon.[1]

In addition to the above observations, it was observed

TABLE 1. PRODUCTS OBTAINED BY HEATING A MIXTURE OF MoO_3 AND CARBON IN A SO_2 STREAM AT VARIOUS TEMPERATURES

Temp °C	Weight change/%	Sample in the boat	Amount of sulfur obtained outside the heating zone/g
350	+0.1	MoO_3	Trace
400	+0.1	$MoO_3>>MoO_2$	Trace
450	−0.1	$MoO_3>>MoO_2$	Trace
500	−4.7	$MoO_2>MoO_3>Mo_4O_{11}$	Trace
550	−7.2	$MoO_2>>MoO_3>Mo_4O_{11}$	Trace
600	−8.8	MoO_2	0.00_5
650	−8.9	MoO_2	0.03
700	−7.8	$MoO_2>>MoS_2$	0.09

that a small amount of unreacted MoO_3 vaporized and deposited outside the heating zone at 700 °C. As seen from Table 1, all the MoO_3 used was converted to non-volatile MoO_2 above 600 °C. The reactions at temperatures above 800 °C were examined by using a mixture of MoO_2 and carbon. When a mixture of 2.00 g of MoO_2 and 1.20 g of carbon was heated in a SO_2 stream (100 cm^3/min) at 800 °C for 1 h, unreacted carbon was not observed in the sample obtained after the heating. This result is considered to be due to the fact that the reaction between carbon and SO_2 proceeds markedly.[1] Based on the results of preliminary experiments on the suitable amount of carbon to be mixed, the products obtained by heating a mixture of 2.00 g of MoO_2 and 5.00 g of carbon in a SO_2 stream (100 cm^3/min) at various temperatures above 800 °C for 1 h were examined. The mixture of MoO_2 and carbon was prepared by adding fresh carbon to a mixture of MoO_2 and carbon, obtained by the reduction of MoO_3 with carbon at 700 °C. The results are shown in Table 2.

TABLE 2. PRODUCTS OBTAINED BY HEATING A MIXTURE OF MoO_2 AND CARBON IN A SO_2 STREAM AT VARIOUS TEMPERATURES

Temp °C	Weight loss/%	Sample in the boat	Amount of sulfur obtained outside the heating zone/g
800	34.3	$MoO_2\approx MoS_2$	3.90
900	54.0	$MoS_2>MoO_2$	4.86
950	57.6	$MoS_2>MoO_2$	5.04
1000	64.2	MoS_2	5.66

Chemical analysis of the sample obtained at 1000 °C showed it to contain 59.8% Mo and 39.9% S. Chemical analysis also proved that sulfur was not adsorbed on the unreacted carbon at 1000 °C. From these results, the sulfur was found to be due to the sulfide formed. The atomic ratio of Mo : S in the sample was calculated to be $1 : 2.0_0$. The results indicated that all the MoO_2 used was sulfidized to MoS_2 at 1000 °C.

Reaction Process between Molybdenum Trioxide and Sulfur Dioxide in the Presence of Carbon. To elucidate the reaction process between MoO_3 and SO_2 in the presence of carbon, the following experiments were carried out under conditions similar to those described above.

Reaction between MoO_3 and Carbon: The products formed by heating a mixture of MoO_3 (2.00 g) and carbon (1.20 g) at various temperatures in an argon stream (100 cm^3/min) for 1 h were examined. The results are shown in Table 3.

TABLE 3. EXPERIMENTAL RESULTS FOR THE REACTION BETWEEN MoO_3 AND CARBON IN AN ARGON STREAM

Temp °C	Weight loss/%	Sample in the boat
350	—	MoO_3
400	0.2	$MoO_3>>MoO_2$
450	0.9	$MoO_3>>MoO_2$
500	5.2	$MoO_2>MoO_3$
600	9.7	$MoO_2>>MoO_3$
700	9.7	MoO_2

These results indicate that the reduction of MoO_3 with carbon to form MoO_2 proceeds above about 400 °C.

Reaction between MoO_3 and Sulfur in a SO_2 Stream: As seen from Table 1, when the mixture of MoO_3 and carbon was heated in a SO_2 stream, sulfur was formed. The reaction between carbon and SO_2 occurs even at 350 °C to form sulfur and this reaction proceeds markedly above about 700 °C, as reported by the present authors.[1] Therefore, the reaction between MoO_3 and gaseous sulfur was examined in a SO_2 stream.

MoO_3 (2.00 g) was heated in a stream of SO_2 (100 cm^3/min) containing a specified amount of gaseous sulfur at various temperatures for 1 h. The amounts of sulfur introduced at various temperatures were controlled so as to be the same as those obtained by heating 1.20 g of carbon in a stream of SO_2 at a flow-rate of 100 cm^3/min for 1 h: the amounts were 0.01 g for the experiments below 550 °C, 0.03 g at 600 °C, 0.09 g at 650 °C, and 0.25 g at 700 °C.[1] The results are shown in Table 4.

These results and the fact that MoO_3 does not react with SO_2 as described before show that the reaction between MoO_3 and gaseous sulfur proceeds above about 400 °C and that MoO_3 was reduced to MoO_2.

TABLE 4. PRODUCTS OBTAINED BY HEATING MoO_3 IN A STREAM OF SO_2 CONTAINING GASEOUS SULFUR

Temp °C	Weight loss/%	Sample in the boat
350	—	MoO_3
400	0.2	$MoO_3>>MoO_2$
450	0.3	$MoO_3>>MoO_2$
500	0.5	$MoO_3>>MoO_2>Mo_9O_{26}$, Mo_4O_{11}
550	0.7	$MoO_3>>MoO_2>Mo_9O_{26}$, Mo_4O_{11}
600	1.0	$MoO_3>MoO_2>Mo_9O_{26}>Mo_4O_{11}$
650	4.2	$MoO_3>MoO_2>Mo_9O_{26}>>Mo_4O_{11}$
700	8.2	$MoO_2>>MoO_3>Mo_9O_{26}$, Mo_4O_{11}

These experimental results showed that the MoO_2 formed by heating a mixture of MoO_3 and carbon in a SO_2 stream (Table 1) was formed by the reductions of MoO_3 with carbon and with sulfur. As seen from Table 1, the formation of a small amount of Mo_4O_{11} in addition to MoO_2 was observed at 500—550 °C. As seen from Table 3, no formation of any intermediate oxide was observed in the reaction between MoO_3 and carbon. As seen from Table 4, however, the formation of intermediate oxides (Mo_4O_{11},[4] Mo_9O_{26}[6]) in addition to MoO_2 was observed during the reaction between MoO_3 and sulfur. It has been reported that on heating a mixture of MoO_3 and a sufficient amount of carbon in an argon stream, no intermediate oxide is formed.[7] These facts suggested that the Mo_4O_{11} formed by heating a mixture of MoO_3 and carbon in a SO_2 stream was due to the reduction of MoO_3 with sulfur.

Formation Reaction of MoS_2 from MoO_2: As mentioned before, when a mixture of MoO_3 and carbon was heated in a SO_2 stream, MoS_2 was formed above about 700 °C. Above this temperature, MoO_3 was reduced to MoO_2. Therefore, the reactions of MoO_2 with carbon in an argon stream and of MoO_2 with gaseous sulfur in a SO_2 stream were examined.

The products formed by heating a mixture of MoO_2 (2.00 g) and carbon (5.00 g) at various temperatures for 1 h in an argon stream (100 cm^3/min) were examined. The results are shown in Table 5.

Table 5. Experimental results for the reaction between MoO_2 and carbon in an argon stream

Temp °C	Weight loss/%	Sample in the boat
700	—	MoO_2
750	0.7	$MoO_2 >> Mo_2C > Mo$
800	2.0	$MoO_2 > Mo_2C > Mo$
900	7.6	$Mo_2C > MoO_2 > Mo$
1000	11.3	$Mo_2C > Mo$

The results indicate that the reaction between MoO_2 and carbon proceeds above about 750 °C to form molybdenum[8] and dimolybdenum carbide (Mo_2C).[9] The Mo_2C was considered to be due to the reaction between the molybdenum formed and the carbon.[7]

The products formed by heating MoO_2 (2.00 g) in a stream of SO_2 (100 cm^3/min) containing a specified amount of gaseous sulfur at various temperatures for 1 h were examined. The MoO_2 used was prepared by the hydrogen reduction of MoO_3 at 600 °C,[10] because the reduction of MoO_3 with carbon gave a mixture of MoO_2 and unreacted carbon, as described in the previous paragraph.

Prior to this experiment, the amounts of sulfur formed by heating 5.00 g of carbon at various temperatures for 1 h in a SO_2 stream at a flow-rate of 100 cm^3/min were examined.[1] Based on the experimental results, the amounts of sulfur introduced at various temperatures were controlled to be 0.43 g for the experiment at 650 °C, 0.81 g at 700 °C, 4.79 g at 800 °C, 5.46 g at 900 °C, and 6.59 g at 1000 °C. The experimental results are shown in Table 6. These results indicate that the

Table 6. Products obtained by heating MoO_2 in a stream of SO_2 containing gaseous sulfur

Temp °C	Weight gain/%	Sample in the boat
650	—	MoO_2
700	4.2	$MoO_2 > MoS_2$
800	10.8	$MoO_2 \approx MoS_2$
900	17.6	$MoS_2 > MoO_2$
1000	22.9	$MoS_2 >> MoO_2$

reaction between MoO_2 and gaseous sulfur proceeds above about 700 °C to form MoS_2.

As shown in Table 5, on heating a mixture of MoO_2 and carbon in an argon stream, MoO_2 was reduced to molybdenum, and Mo_2C was also formed. Thermodynamical consideration was made on the Mo–S–C–O system, in order to discuss whether MoO_2 was converted to MoS_2 *via* molybdenum or without molybdenum formation. The chemical potential diagrams for the Mo–S–C–O system were constructed in a manner similar to that described by Yazawa[11] on the basis of the available thermodynamic data[12] and phase relations.[13] As an example, the digram at 1000 °C is shown in Fig. 1. The broken line shows the oxygen and sulfur potentials in the gas phase formed by the reaction between carbon and SO_2, depending on the carbon content in the gas phase. The activity of carbon is unity at the dot mark. In these calculations, CO, CO_2, O_2, COS, CS_2, SO_2, SO_3, S_2, S_4, S_6, and S_8 were assumed to be gaseous products between carbon and SO_2.

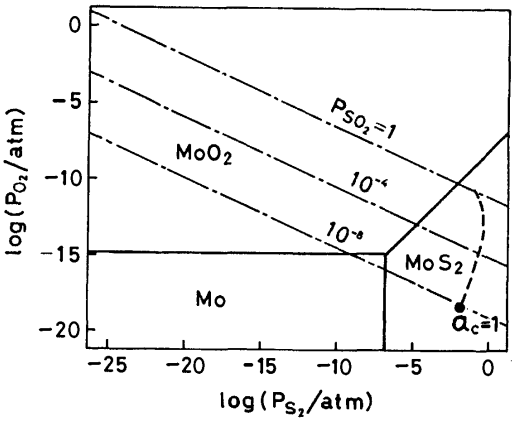

Fig. 1. Chemical potential diagram for the Mo–S–C–O system at 1000 °C.

The results shown in Fig. 1 indicate that MoO_2 is converted to MoS_2 *via* molybdenum under a low pressure of SO_2 below *ca.* 10^{-7} atm, and that MoO_2 is converted to MoS_2 without molybdenum formation under a higher partial pressure of SO_2. Considering the experimental conditions in this work, the results in Fig. 1 show that MoS_2 is formed from MoO_2 without any formation of molybdenum.

The process of formation of MoS_2 by the reaction between MoO_3 and SO_2 in the presence of carbon can be represented as follows: On heating a mixture of MoO_3 and carbon in a SO_2 stream, the reaction between

carbon and SO_2 occurs at first to form sulfur. Above about 400 °C, the reductions of MoO_3 with carbon and with sulfur occur to form MoO_2. Above about 700 °C, MoS_2 is formed by the reaction between MoO_2 and sulfur, which are formed by the above reactions.

The present work was partially supported by a Grant-in-Aid for Scientific Research No. 555306 from the Ministry of Education, Science and Culture.

References

1) H. Araki, Y. H. Ryoo, M. Eguchi, R. Matsuzaki, and Y. Saeki, *Bull. Chem. Soc. Jpn.*, **53**, 2271 (1980).
2) ASTM X-Ray Powder Data File, 5-508.
3) ASTM X-Ray Powder Data File, 5-452.
4) ASTM X-Ray Powder Data File, 5-337.
5) JCPDS Powder Data File, 24-513.
6) JCPDS Powder Diffraction File, 12-753.
7) A. J. Hegedüs and J. Neugebauer, *Z. Anorg. Allg. Chem.* **305**, 216 (1960).
8) ASTM X-Ray Powder Data File, 4-809.
9) JCPDS Powder Diffraction File, 11-680.
10) M. J. Kennedy and S. C. Bevan, *J. Less-Common Metals*, **36**, 23 (1974).
11) A. Yazawa, *Metall. Trans.*, **10B**, 307 (1979).
12) O. Kubaschewski, E. Ll. Evans, and C. B. Alcock, "Metallurgical Thermochemistry," 4th ed, Pergamon Press, (1967); I. Barin and O. Knacke, "Thermochemical Properties of Inorganic Substances," Springer-Verlag (1973); I. Barin, O. Knacke, and O. Kubaschewski, "Thermochemical Properties of Inorganic Substances, Supplement," Springer-Verlag (1977).
13) B. Phillips and L. L. Y. Chang, *Trans. Metall. Soc. AIME*, **233**, 1433 (1965).

Selective Extraction Spectrophotometric Determination of Iron by Utilizing the Peculiar Absorption of Iron(II)-2-(2-Thiazolylazo)-5-dimethylaminophenol Complex

Kazumasa UEDA,* Yasushi KIYOTA, and Yoshikazu YAMAMOTO

Department of Industrial Chemistry, Faculty of Technology, Kanazawa University, Kodatsuno, Kanazawa 920

(Received April 3, 1981)

Thiazolylazo compounds react with iron(II) to form brownish complexes, which show a characteristic absorption in near-infrared region. These compounds possess the hydroxyl group in the *o*-position next to the azo group. Among them, iron(II)-2-(2-thiazolylazo)-5-dimethylaminophenol complex has the absorption maximum at 760 nm in chloroform; the optimum pH for iron extraction lies between 8.2—10.0. Beer's law holds up to 2.0 $\mu g\ cm^{-3}$ of iron and the molar absorption coefficient is $2.70\times10^4\ dm^3\ mol^{-1}\ cm^{-1}$. The composition and the extraction constant of the complex are estimated to be Fe: TAM=1 : 2 and $\log K_{ex}=-4.20\pm0.04$, respectively. Since the present method utilizes the specific absorption of the iron(II)-TAM complex, the presence of many ions is tolerable, especially of 3d type metals. The method was applied to the determination of traces of iron dissolved in river and sea waters with satisfactory results.

Many azo compounds containing a hetero ring are useful as analytical reagents.[1,2] Above all, thiazolylazo derivatives are especially attractive, because their complexing properties are often specific.[3,4] In previous papers, the authors reported highly selective spectrophotometric methods for the determination of iron with 4-(2-thiazolylazo)resorcinol[5] and 2-(2-thiazolylazo)-4-methylphenol[6] by utilizing the specific absorption of iron(II) complexes in the near-infrared region. The homolog 2-(2-thiazolylazo)-5-dimethylaminophenol (TAM) has been applied for the determination of specific metals, such as uranium,[7] vanadium,[8] niobium,[9] bismuth,[10] yttrium,[11] nickel,[12] titanium,[13] zirconium,[14] and thorium.[15] We investigated the color reaction of TAM with iron(II) and recognized that iron(II)-TAM complex also showed a characteristic absorption at 760 nm. It is rarely the case that a metal complex possesses the absorption maximum in this infrared region. In this research, the fundamental conditions for the selective extraction spectrophotometric determination of traces of iron were investigated. We also prepared eleven (thiazolylazo)phenol and naphthol derivatives in order to elucidate these absorption features and obtained some information about the substituent effect of the chelate ligand and the nature of iron(II) complex.

Experimental

Reagents. Thiazolylazo compounds were synthesized by the diazotization of 2-aminothiazole (or 2-amino-4-methylthiazole and 2-aminobenzothiazole) with nitrous acid and the subsequent coupling with phenols (or naphthols) at 0 °C.[4,16,17] Phenols used were resorcinol, 4-chlororesorcinol, orcinol, *m*-methoxyphenol, *m*-dimethylaminophenol, *p*-methoxyphenol, *p*-chlorophenol, 2,4-dimethylphenol, and pyrocatechol; naphthols were 2-naphthol and 2-naphthol-3,6-disulfonic acid. The products were purified by repeated crystallization with ethanol or re-precipitation with dilute hydrochloric acid and were identified by elementary analyses. TAR, TAM, TAC, and TAN were commercially available and were used without further purification. The standard iron(II) solution was prepared by dissolving ammonium iron(II) sulfate hexahydrate in deionized distilled water. The solution was acidified to pH 1 by sulfuric acid and was standardized by permanganometry. A 0.05% TAM solution was prepared by dissolving the Dotite TAM in ethanol. A fresh 0.1% ascorbic acid solution was prepared every three days. All the other chemicals used were of guaranteed reagent quality.

Apparatus. A sample solution was prepared in a 50 cm^3 graduated centrifuge tube with a glass-stopper; the solution was shaken in an Iwaki-KM type reciprocating shaker. A Kubota K-80 type centrifuge with 5000 min^{-1}. was used for phase separation. A Hitachi-Horiba model M-5 pH meter equipped with a combined glass electrode was used for pH measurements. Absorption spectra and absorbance were measured with a Hitachi 124 recording spectrophotometer and a Hitachi-Perkin Elmer 139 spectrophotometer using 10-mm quartz cells.

Standard Procedure. Transfer the sample solution containing up to 20 μg of iron into a centrifuge tube. Add 1 cm^3 of 0.1% ascorbic acid and 2 cm^3 of 0.05% TAM solutions, and adjust the pH to 9.0 with 5 cm^3 of 1 mol dm^{-3} ammonia buffer solution. Dilute the solution to 20 cm^3 and shake it with 10 cm^3 of chloroform for 5 min. After centrifugal separation, transfer the extract into an absorption cell, and measure the absorbance at 760 nm against the reagent blank.

Results and Discussion

Complexing Properties of Thiazolylazo Compounds with Iron(II). Table 1 shows the complexing properties of (thiazolylazo)phenols and naphthols with iron(II). Thiazolylazo compounds react with iron(II) to form brownish complexes from the weakly acidic to the alkaline region, which have the characteristic absorption maxima beyond 700 nm. The compounds have the phenolic hydroxyl group in the *o*-position next to the azo group; TAPC, possessing this group in the *m*- and *p*-position, shows different absorption features. The bathochromic shift of these absorption maxima is promoted by the resonance effect of the substituent group in the *p*-position to the *o*-hydroxyl group for phenols and of the naphthalene ring for naphthols. TAR, TARCl, and TAM show higher molar absorptivities than TAC, TAMP, and TACl. The difference would come from the inductive and the resonance effects of the substituent in the *m*- and *p*-position to the *o*-hydroxyl group. The derivatives possessing resorcinol

TABLE 1. COMPLEXING PROPERTIES OF THIAZOLYLAZO COMPOUNDS WITH IRON(II)

Systematic name (abbreviation)	λ_{max} / nm	ε / $dm^3\ mol^{-1}\ cm^{-1}$	pH	Solvent
4-(2-Thiazolylazo)resorcinol (TAR)[5]	730	2.90×10^4	8.9—10.3	Water
4-(2-Thiazolylazo)-6-chlororesorcinol (TARCl)	740	2.90×10^4	9.2—10.5	Water
4-(4-Methyl-2-thiazolylazo)resorcinol (MeTAR)	737	2.45×10^4	9.0—10.0	Water
4-(2-Thiazolylazo)orcinol (TAO)	742	2.02×10^4	9.0	Water
2-(2-Thiazolylazo)-5-methoxyphenol (TAMR)	720	1.59×10^4	8.0— 9.0	Water
2-(2-Thiazolylazo)-5-dimethylaminophenol (TAM)	760	2.70×10^4	8.2—10.0	Chloroform
2-(4-Methyl-2-thiazolylazo)-5-dimethylaminophenol (MeTAM)	765	2.71×10^4	5.5— 9.0	Chloroform
2-(2-Thiazolylazo)-4-methylphenol (TAC)[6]	762	1.37×10^4	4.8—10.2	Chloroform
2-(2-Thiazolylazo)-4-methoxyphenol (TAMP)	784	1.57×10^4	5.0— 9.0	Chloroform
2-(2-Thiazolylazo)-4-chlorophenol (TACl)	757	1.36×10^4	5.8— 8.5	Chloroform
2-(2-Thiazolylazo)-4,6-dimethylphenol (TACMe)	762	9.38×10^3	5.5— 7.5	Chloroform
4-(2-Thiazolylazo)pyrocatechol (TAPC)	590	3.43×10^4	6.5	Water
1-(2-Thiazolylazo)-2-naphthol (TAN)	786	1.89×10^4	3.5—10.0	Chloroform
1-(4-Methyl-2-thiazolylazo)-2-naphthol (MeTAN)	790	4.03×10^3	5.0—10.0	Chloroform
1-(2-Thiazolylazo)-2-naphthol-6-sulfonic acid (TAN6S)	761	4.19×10^3	4.8— 8.5	Water

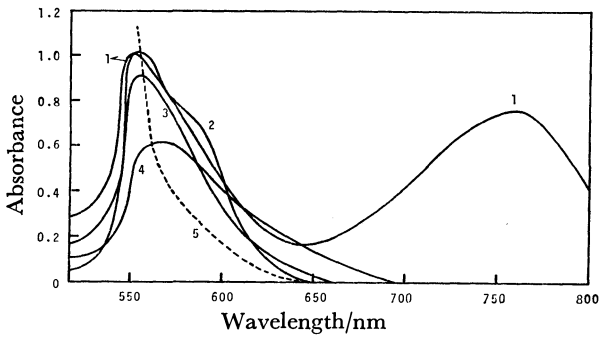

Fig. 1. Absorption spectra of TAM complexes.
pH: 9.0, 0.05% TAM: 2 cm^3, 0.1% ascorbic acid: 1 cm^3. 1: Fe (15 μg), 2: Ni (10 μg), 3: Cu (10 μg), 4: Co (10 μg), 5: reagent blank.

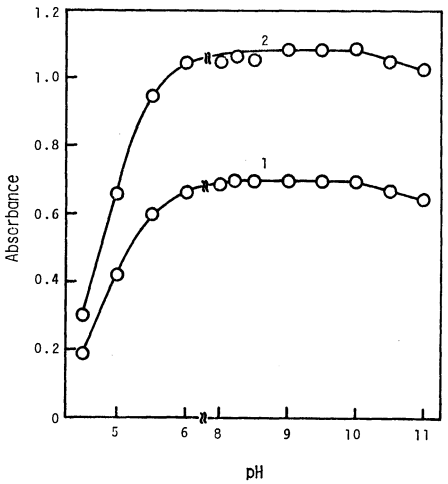

Fig. 2. Effect of pH.
Fe: 15 μg, 0.05% TAM: 2 cm^3, 0.1% ascorbic acid: 1 cm^3. 1: 760 nm, 2: 550 nm.

ring show higher molar absorptivities, but naphthols give lower ones. The effect of the substituent group in the thiazole ring is not so noticeable.

Absorption Spectra. The iron(II) complexes of thiazolylazo compounds usually have two or three absorption maxima. Fig. 1 shows the absorption spectra of 3d type metal–TAM complexes extracted into chloroform. The iron(II) complex has two maxima at 550 nm and 760 nm, while the other 3d type metal complexes have only one maximum near 550 nm. We could not observe any other metal–TAM complex which showed an absorption maximum over 700 nm, hence this maximum at 760 nm is thought to be the characteristic absorption for iron(II). It is not an easy matter to assign these characteristic absorption bands clearly. The configuration of iron(II) complex may differ from those of the other 3d type metal complexes, or thiazole sulfur atom might follow the peculiar behavior on the complexation. But there is some evidence that TAN forms an octahedrally configurated inner complex with iron(II),[18] which is just the same as those of $[Ni^{II}(TAN)_2]$,[19] $[Zn^{II}(TAN)_2]$, and $[Co^{III}(TAN)_2]^+$,[20] and thiazole sulfur atoms never participate in the coordination. The iron(II)–TAN complex also shows the specific absorption at 786 nm in chloroform. Even if iron(II)–TAM complex would take the same configuration as those of the other 3d type metal complexes, its characteristic absorption is thought to be caused by the $t_{2g}\rightarrow\pi^*$ transition of the iron's 3d electrons.[21] As the TAM blank shows no absorption above 650 nm, one might expect the enhancement of the accuracy for the determination of iron.

Effect of pH. The effect of pH on the extraction of iron(II)–TAM complex was examined, as shown in Fig. 2. The extract shows a constant absorbance over the pH range from 8.2 to 10.0. A decrease of the absorbance in the acidic region is attributable to the incomplete formation of the iron(II)–TAM complex, owing to the protonation of the thiazole nitrogen atom.[4]

Choice of Buffering Agent. The iron complex is stable even in relatively higher concentration of ammonia solution, and a constant absorbance is obtained by adding from 2 to 10 cm^3 of 1 mol dm^{-3} ammonia buffer solution. The use of diethylbarbiturate and borax buffer reduces the absorbance, moreover, reproducible absorbances were not obtained. Taking into account the masking effect, 5 cm^3 of 1 mol dm^{-3} ammonia buffer solution was used.

Effect of TAM Concentration. A constant absorbance was obtained by adding from 0.4 to 5.0 cm^3 of 0.05% TAM solution for 15 μg of iron. Though 2 cm^3 of 0.05% TAM solution was used in practice, the amount corresponds 14.5 times excess to that of iron, calculating in molar ratio. If the consumption of TAM is noticeable owing to the coexistence of other metal ions in some sample, further addition of TAM may be allowed, because the absorbance of the reagent blank is negligible.

Effect of Reducing Agent. The iron(III)-TAM complex shows a weak color ($\varepsilon=1.30\times10^3$ at 760 nm); the rate of complexation reaction is slow. But the reaction of iron(II) with TAM is completed almost in a moment, so it is necessary to fix the oxidation number of iron to iron(II). The effect of addition of ascorbic acid and hydroxylamine hydrochloride was examined, but no significant differences were found. In this work, ascorbic acid was used and a constant absorbance was obtained by adding from 1 to 10 cm^3 of 0.1% ascorbic acid. As ascorbic acid forms a 2 : 1 complex with iron(II),[22] it may act as an assistant chelating agent as well as a reducing agent.

Organic Solvent. The chelate was effectively extracted into such hydrocarbons as carbon disulfide ($\varepsilon=2.75\times10^4$, 779 nm), dichloromethane, 1,2-dichloroethane, trichloroethylene, and aromatic hydrocarbons such as benzene (2.72×10^4, 769 nm), toluene, xylene (2.37×10^4, 769 nm), and chlorobenzene. The other ketones and esters show low absorbance, as compared with chloroform, and MIBK destroys the chelate during the extraction. Chloroform was used in practice, because of its fine phase separation and ease of use.

Composition of Iron(II)-TAM Complex. The result obtained by the continuous variation method is shown in Fig. 3; from this it can be confirmed that iron(II) forms a 1 : 2 complex with TAM. As thiazolylazo derivatives generally act as tridentate ligands,[23] this complex will be an inner complex of the six-coordinate octahedral type,[18] and supplementary ligands such as hydroxyl group, ascorbic acid and ammonia would not part icipate in the complex system.

Extraction Equilibrium of Iron(II)-TAM Complex. When $pK_2(8.65)>pH>pK_1(3.13)$,[24] most of the TAM is present in chloroform, and the iron(II) complex formed is also readily extracted into the organic phase. If auxiliary ligands would not participate in the chelate, the following extraction equilibrium can be considered:

$$M + 2HR_{(o)} \rightleftarrows MR_{2(o)}\,2H^+,\quad K_{ex}=\frac{[MR_2]_o[H^+]^2}{[M][HR]_o^2},\quad (1)$$

where M, R, and K_{ex} denote the iron ion, TAM, and the extraction constant, respectively, and the subscript o refers to the organic phase. From Eqs. 1 and 2 can be derived:

$$\log K'_{ex}=\log\frac{[MR_2]_o}{[M][HR]_o^2}=\log K_{ex}+2pH. \quad (2)$$

The value of $\log K'_{ex}$ can be calculated by the measurement of the absorbance. The results are shown in Fig. 4. The plots of $\log K'_{ex}$ against pH show a good linearity, and the slope is 2.0, which indicates that Eqs. 1 and 2 are reasonable. The calculated value of $\log K_{ex}$ is -4.20 ± 0.04. The extractabilities of 3d type metal complexes of TAM were also examined, and the order of the half extraction pH was Cu(4.8)<Ni(5.3)<Fe(5.5)<Co(6.4)<Zn(7.5). Nickel, cobalt, and zinc complexes showed smaller slopes than iron's. These facts indicate that auxiliary ligands may participate in the chelate systems or the rates of the complexation with TAM are slow except iron.

Calibration Curve. A calibration curve was made under the optimum conditions. The curve obeys Beer's law up to 20 μg of iron per 10 cm^3 of chloroform. The optimum concentration range for the accurate determination of iron evaluated by Ringbom's method[25] is 0.3 to 1.2 ppm of iron, corresponding to absorbance values of 0.2 to 0.8 unit. The molar absorption coefficient and Sandell's sensitivity index for $\log I_0/I=0.001$ are 2.70×10^4 $dm^3\,mol^{-1}\,cm^{-1}$ and 2.07×10^{-3}

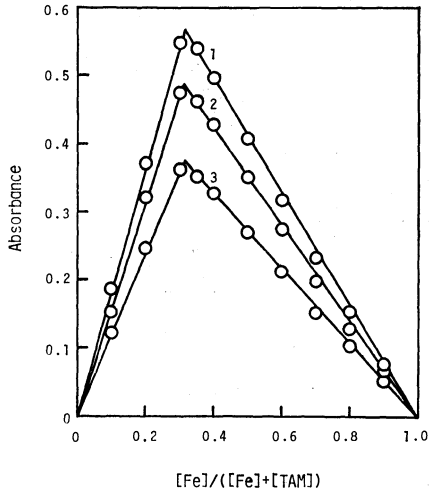

Fig. 3. Continuous variation method.
[Fe]+[TAM]=7.892×10^{-5} mol dm^{-3}, pH: 9.0. 1: 760 nm, 2: 740 nm, 3: 720 nm.

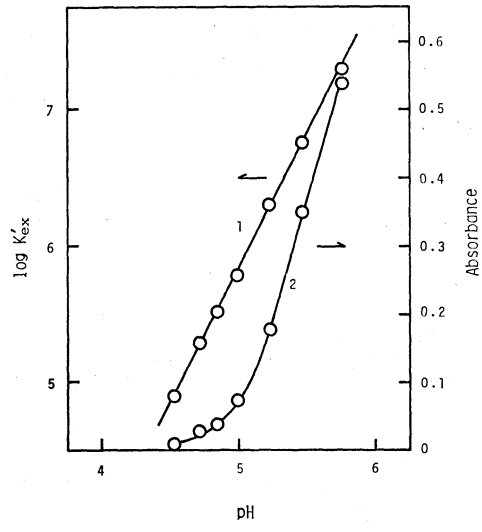

Fig. 4. The plots of $\log K'_{ex}$ and absorbance *vs.* pH at 760 nm.
[Fe]=2.686×10^{-5} mol dm^{-3}, [TAM]=4.124×10^{-4} mol dm^{-3}, μ=0.1 (KCl). 1: $\log K'_{ex}$ *vs.* pH, 2: absorbance *vs.* pH.

TABLE 2. EFFECT OF CATIONS

Cations added	Tolerance limit(ppm)
Li(I), Na(I), K(I)	30000
As(V), Mo(VI), W(VI), Ca(II)	1000
Mg(II), Sr(II), Ba(II), Cu(II),[a] V(V), Cr(III), Bi(III), Se(IV), Th(IV), Ga(III), Ge(IV), Ag(I)	500
Zn(II), Hg(II), Al(III), Sn(II), Sb(III), Rh(IV), Tl(III)	100
Mn(II), Pd(II), Pb (II), U(VI), Au(III), Ti(IV), Zr(IV), Hf(VI), Ce(III)	50
Ni(II)[b]	30
Cd(II), Co(II),[b] Pt(IV), Ru(III), In(III)	20
Cu(II), Ni(II), Co(II)	8

Iron taken: 1.5 ppm. a) and b): Ten cm^3 of 2% thiosemicarbazide and three cm^3 of 1 % dimethylglyoxime solutions were added, respectively.

TABLE 3. EFFECT OF ANIONS

Anions added	Tolerance limit(ppm)
Cl^-, Br^-, I^-, NO_3^-, SO_4^{2-}, SCN^-, Acetate	50000
F^-, CO_3^{2-}, Thiosemicarbazide, Thiourea	20000
Tartrate	10000
Oxalate	3000
Dimethylglyoxime	3000
Citrate	1000

Iron taken: 1.5 ppm.

TABLE 4. DETERMINATION OF IRON IN SYNTHETIC SEA WATER

Iron added (μg)	Iron found (μg)	Error (%)
5.00	5.11[a]	2.2
10.00	10.05	0.5
15.00	15.29	1.9
20.00	20.16	0.8

a) The values obtained were averages of 5 determinations.

TABLE 5. DETERMINATION OF IRON IN NATURAL WATER

Sample	Sample volume cm^3	Iron content ppm
Sair iver		
Uchikawa	100	0.026(0.023)[a]
Okuwa	100	0.034(0.035)
Kamikiku	100	0.027(0.024)
Mikage	100	0.025(0.025)
Outfall	100	0.143(0.140)
Kanazawa port	500	0.012(0.015)
Kanaiwa breakwater	500	0.026(0.028)

a) The values obtained by A.A.S. are shown in parentheses.

μg cm^{-2}, respectively, which is more sensitive than the most common reagents,[26] such as 1,10-phenanthroline, 4,7-dihydroxy-1,10-phenanthroline, 2,2′-bipyridine, 2,4,6-tri(2-pyridyl)-1,3,5-triazine, and 1-(2-pyridylazo)-2-naphthol. The variation coefficient of the absorbance for 1.50 ppm of iron is 0.67%; this was determined by ten measurements.

Effect of Diverse Ions. Thiazolylazo dyes generally give similar colored complexes, especially with some of transition metals. That is a disadvantage from the practical viewpoint. As the present method utilizes the specific absorption of iron(II)–TAM complex, the selectivity is significantly elevated. The effect of diverse ions are summarized in Table 2 for cations and in Table 3 for anions, where the tolerance limit is set to ±5% for iron recovery. Iron can be determined in the presence above 20 ppm each of 41 metal ions, where vanadium, bismuth, thorium, uranium, titanium, and zirconium, whose spectrophotometric determinations have already been developed, are tolerable even in large amounts. 3d type metals form colored complexes, but copper can be effectively masked by thiosemicarbazide and nickel, and cobalt by dimethylglyoxime. Since concentrations of these ions in most natural waters are usually low, their interferences are almost negligible. Among the anions tested, acetate, tartrate, thiourea, and citrate can also serve as masking agents.

Determination of Iron in River and Sea Waters. In order to apply the present method to natural waters, we determined iron first in synthetic sea waters.[27] Sea water usually contains 10 ppb order of iron.[28] So known amounts of iron were added to synthetic sea waters as shown in Table 4. The results show that the present method is applicable to sea waters within 3% errors. Table 5 shows the results of determinations in the Sai river from the upper stream to the down stream and in sea waters near river ports. These values agreed well with those obtained by atomic absorption spectrometry. For sea waters, the following procedure is recommended. Take an aliquot of sample solution which is filtered off immediately after sampling. Add 2 cm^3 of concd hydrochloric acid and concentrate the solution to 100 cm^3 on the water bath. Add 1 cm^3 of 0.1% ascorbic acid and 5 cm^3 of 10% sodium acetate solutions, and neutralize by ammonia solution. Transfer the solution into a 200 cm^3 separatory funnel, and determine iron according to the standard procedure. For river waters, filtrates were directly used without preconcentration.

References

1) R. G. Anderson and G. Nickless, *Analyst*, **92**, 207 (1967).
2) S. Shibata, *Bunseki Kagaku*, **21**, 551 (1972).
3) H. Wada, *Bunseki Kagaku*, **21**, 543 (1972).
4) H. R. Hovind, *Analyst*, **100**, 769 (1975).
5) K. Ueda and Y. Yamamoto, *Nippon Kagaku Kaishi*, **1980**, 1713.
6) K. Ueda, S. Sakamoto, and Y. Yamamoto, *Nippon Kagaku Kaishi*, **1981**, 1111.
7) E. Soerensen, *Acta. Chem. Scand.*, **14**, 965 (1960).
8) C. Tsurumi, M. Ota, and K. Furuya, *Bunseki Kagaku*, **22**, 1597 (1973).
9) C. Tsurumi, H. Mitsuhashi, K. Furuya, and K. Fujimura, *Bunseki Kagaku*, **23**, 143 (1974).
10) C.Tsurumi and K. Furuya, *Bunseki Kagaku*, **24**, 566 (1975).
11) C. Tsurumi and K. Furuya, *Nippon Kagaku Kaishi*, **1975**, 1738.
12) H. Ishii and H. Watanabe, *Bunseki Kagaku*, **26**, 86 (1977).
13) C. Tsurumi and K. Furuya, *Bunseki Kagaku*, **26**, 149

(1977).
14) C. Tsurumi, *Bunseki Kagaku*, **26**, 260 (1977).
15) C. Tsurumi, K. Furuya, and H. Kamada, *Bunseki Kagaku*, **28**, 754 (1979).
16) A. Kawase, *Bunseki Kagaku*, **11**, 621 (1962).
17) G. Nakagawa and H. Wada, *Nippon Kagaku Zasshi*, **85**, 202 (1964).
18) M. Kurahashi and A. Kawase, *Bull. Chem. Soc. Jpn.*, **49**, 1419 (1976).
19) M. Kurahashi, *Bull. Chem. Soc. Jpn.*, **47**, 2067 (1974).
20) A. Kawase, *Bunseki*, **11**, 816 (1978).
21) K. Yamazaki and H. Yamadera, "Mukikagaku Zensho, Bekkan, Sakutai (Jo)," Maruzen, Tokyo (1977), p. 117.
22) J. Maslowska and A. Owczarek, *Chem. Anal.*, **23**, 825 (1978).
23) A. Kawase, *Bunseki Kagaku*, **13**, 553 (1964).
24) J. Minczewski and K. Kasiura, *Chem. Anal.*, **10**, 21 (1965).
25) G. H. Ayres, *Anal. Chem.*, **21**, 652 (1949).
26) "Muki Oyohishokubunseki," Kyoritsu Shuppan, Tokyo (1974), No. 2, p. 324.
27) JIS K 2510 (1980).
28) "Shiryō Chōsei," ed by Nippon Bunseki Kagakukai, Maruzen, Tokyo (1978), p. 393.

Kinetics of Ligand Substitution Reactions in Trimalonatovanadium(III)

Yasuhisa IKEDA, Sumio SOYA, Hiroshi TOMIYASU, and Hiroshi FUKUTOMI*

Research Laboratory for Nuclear Reactors, Tokyo Institute of Technology, O-okayama, Meguro-ku, Tokyo 152

(Received April 22, 1981)

The kinetics of ligand substitution reactions in trimalonatovanadium(III), $V(mal)_3^{3-}$, with various multidentate ligands, malonate (MAL), ethylenediaminetetraacetate (EDTA), and nitrilotriacetate (NTA) have been studied. The rate constant of the malonate exchange in $V(mal)_3^{3-}$ was obtained from the NMR line-broadening method to be $k_{ex}=50\ s^{-1}$ at 70 °C. The rate of EDTA substitution depends on the entering EDTA species. The values of second order rate constants are $k_{21}=0.04\ M^{-1}\ s^{-1}$ (1 M=1 mol dm^{-3}) for H_2edta as an entering ligand and $k_{22}=0.25\ M^{-1}\ s^{-1}$ for H_3edta at 25 °C. The NTA substitution is reversible under the experimental conditions studied. The apparent rate constants of the forward and backward reactions are $k_3=1.3\times10^{-2}\ M^{-1}\ s^{-1}$ and $k_{-3}=2.0\times10^{-3}\ M^{-1}\ s^{-1}$ at pH 3.5 and 25 °C, respectively. The univalent H_2nta is found to be the only entering ligand.

In spite of numerous investigations on the kinetics of ligand substitutions of various transition metal complexes, sufficient data are not available on vanadium(III) complexes.[1-7] Among vanadium species, ligand substitution reactions have been most extensively studied for oxovanadium(IV)[8-16] and it has been found that the rates depend largely on the properties of entering ligands. Similar substitution processes can be expected for V(III) complexes by considering the electronic configurations of these complexes.

In the present paper, a detailed analysis of the kinetics of ligand substitution reactions for V(III) complexes will be presented for the following reactions.[17]

$$V(mal)_3^{3-} + MAL \rightleftarrows V(mal)_3^{3-} + MAL \quad (1)$$

$$V(mal)_3^{3-} + EDTA \longrightarrow V(edta)^- + 3MAL \quad (2)$$

$$V(mal)_3^{3-} + NTA \rightleftarrows V(nta)(mal)^{2-} + 2MAL \quad (3)$$

Experimental

Vanadium(III) perchlorate solutions were prepared by electrolytic reduction of VO^{2+} in 1.0 M $HClO_4$ at a mercury cathode under an atmosphere of nitrogen. The preparation of VO^{2+} perchlorate was described elsewhere,[11] The concentration of V(III) solutions was determined by titration with standard permanganate. Since V(III) perchlorate is very easily oxidized to VO^{2+}, the preparation of V(III) was carried out just before kinetic experiments. Reagent grade malonic acid (Wako Pure Chemical Ind. Ltd.) was recrystallized twice from distilled water and dried under reduced pressure. Sodium perchlerate was prepared as described earlier.[11] Analytical grade EDTA and NTA were used without further purification. The NMR measurements were carried out on a JEOL JNM-4H-100 spectrometer. The spectrophotometric and kinetic measurements for the EDTA and NTA substitution reactions were made by using a Shimadzu MPS-50 spectrophotometer. The pH was obtained by measurement with a Hitachi-Horiba Model F-7SS pH meter. The ionic strength was kept at 2.5 by the addition of $NaClO_4$ throughout the kinetic experiments.

Results and Discussion

Absorption Spectra of V(III) Complexes. The absorption spectra of various V(III) complexes, $V(H_2O)_6^{3+}$, $V(mal)_3^{3-}$, $V(nta)(mal)^{2-}$, and $V(edta)^-$, are shown in Fig. 1. The main absorption bands, which appear at about 420 and 590 nm for $V(H_2O)_6^{3+}$, are slightly shifted in $V(mal)_3^{3-}$. However, $V(mal)_3^{3-}$ has much larger extinction coefficients than $V(H_2O)_6^{3+}$ in both bands, so that the assignment of the bands to the aqua or malonato complexes can be made from the spectra. The spectra of $V(edta)^-$ and $V(nta)(mal)^{2-}$ are much different from those of $V(H_2O)_6^{3+}$ and $V(mal)_3^{3-}$. Therefore, the rates of ligand substitution between these complex species can be determined from the changes in absorbance.

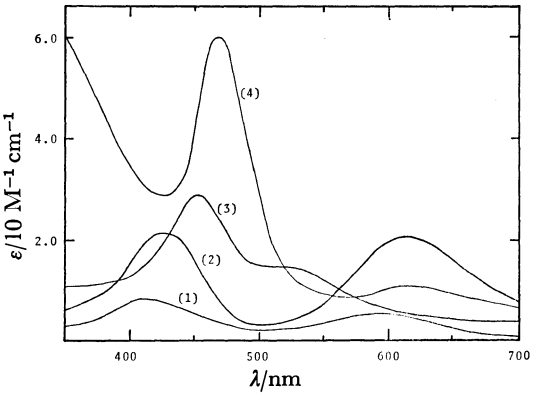

Fig. 1. Absorption spectra of various vanadium(III) complexes: (1): $V(H_2O)_6^{3+}$, (2): $V(mal)_3^{3-}$, (3): V-(edta)$^-$, (4): $V(nta)(mal)^{2-}$.

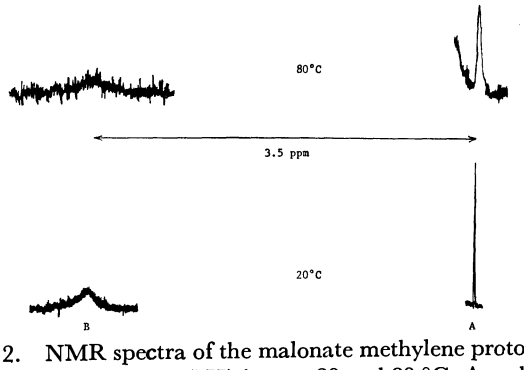

Fig. 2. NMR spectra of the malonate methylene protons in the presence of V(III) ions at 20 and 80 °C: A and B correspond to the methylene protons of bulk malonate and coordinated malonate, respectively.

NMR Measurements in $V(mal)_3^{3-}$ Solutions. The NMR measurements of the methylene protons of malonic acid were made in the presence of V(III) ions and two peaks of the malonate methylene protons were observed as shown in Fig. 2. The downfield and upfield signals are assigned to the coordinated malonate

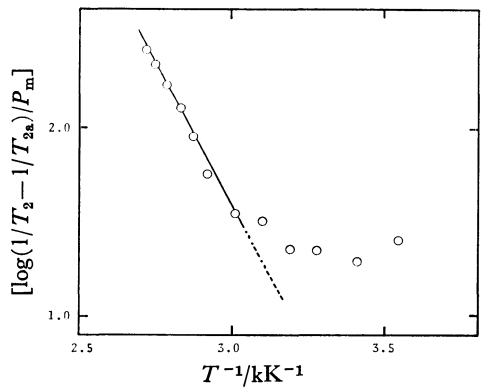

Fig. 3. A plot of $\log((1/T_2-1/T_{2a})/P_m)$ *vs.* $1/T$ for methylene protons of malonic acid in V(III) solution. [V(III)]=0.075 M, $[MAL]_T$=1.0 M, and pH=3.75.

and bulk malonate, respectively. The earlier work on ^{17}O NMR measurements of H_2O in the presence of $V(H_2O)_6^{3+}$ observed a similar splitting of the H_2O signal.[1)]

The signal of the coordinated malonate protons is broad at room temperature because of the direct interaction with the paramagnetic V(III) ion, while that of bulk malonate is very sharp. Figure 2 shows that these malonate signals become broad as the temperature increases above 80 °C. This suggests that the line widths are affected by a chemical exchange between bulk malonate and the coordinated malonate. In order to examine the line broadening in detail, the expression $\log(1/T_2-1/T_{2a})$, where T_2 is the transverse relaxation time of the bulk malonate protons in the presence of V(III) ion and T_{2a} is the transverse relaxation time in the absence of V(III) ion, was plotted against the reciprocal temperature as shown in Fig. 3. The plot gives a straight line with a negative slope. The deviation from the straight line in the region below 50 °C corresponds to the so-called region I.[18,19)] Therefore, it may be concluded that the relaxation process is controlled by a chemical exchange[18)] and the mean life-time of a ligand in the first coordination sphere of V(III) ion, τ_m, is expressed by the equation

$$1/T_2 - 1/T_{2a} = P_m/\tau_m, \quad (4)$$

where P_m is approximated by the Eq. 5 in a dilute solution.

$$P_m = n[\text{complex}]/[\text{total ligand}], \quad (5)$$

where n is the number of coordinated ligands and assumed to be 3 in the present case. The first order rate constants of the malonate exchange in $V(mal)_3^{3-}$, $k_{ex}=1/\tau_m$, are listed in Table 1 for a variety of pH values. Since the NMR measurements were carried out at high temperatures above 70 °C, it was very hard to maintain the V(III) solution and the instrument at constant condition. Consequently, the errors in k_{ex} values are estimated at approximately 20% and it is concluded that k_{ex} does not depend on pH within experimental errors. In the EDTA and NTA substitution reactions, which will be mentioned later, the rates were found to be first order with respect to entering ligands. Although the dependence of the exchange rate on malonate concentrations was not tested, it may be also expected for the malonate exchange that the rate is first order to entering malonate ion, which exists principally in the Hmal or mal form in solution. However, the concentration of Hmal is much larger than that of mal over the pH range studied so that Hmal should play an important role as an entering ligand. In addition, Hmal appears to be more reactive as an entering ligand compared with mal because it is favorable for coming close to the negatively charged complex ion, $V(mal)_3^{3-}$. The values of second order rate constant calculated from the expression, $k_1=k_{ex}/[Hmal]$, are listed in Table 1, which shows that k_1 changes only slightly with pH values. The activation parameters for the malonate exchange obtained from Fig. 3, are summarized in Table 6.

Substitution by EDTA. The substitution of the coordinated malonate by EDTA can be written by Eq. 2. The rate law which consists with the experimental results is expressed by the equation:

$$-d[V(mal)_3^{3-}]/dt = k_2[V(mal)_3^{3-}][EDTA]_T, \quad (6)$$

where $[EDTA]_T$ indicates the total concentartion of EDTA at $t=0$. The rate constant, k_2, was calculated by a least squares method. The values of k_2 obtained at various EDTA concentrations were constant within the experimental errors (Table 2). The pH dependence of k_2 is shown in Table 3 together with the apparent first order rate constant, k_{2f} defined by $k_{2f}=k_2[EDTA]_T$. Since H_3edta and H_2edta are major species in the pH region studied, two substitution processes by H_2edta (k_{21} path) and H_3edta (k_{22} path) are considered leading to the following rate equation:

$$R_2 = k_{21}[V(mal)_3^{3-}][H_2edta] + k_{22}[V(mal)_3^{3-}][H_3edta]. \quad (7)$$

Hence k_{2f} can be given by Eq. 8.

Table 1. Rate constants of the malonate exchange in $V(mal)_3^{3-}$ at 70 °C

pH	k_{ex} / s^{-1}	k_1 / $M^{-1}s^{-1}$
2.89	44	81
2.95	44	77
2.99	40	67
3.40	57	72
3.75	50	56
3.99	50	54

The concentrations of the MAL species were calculated by using the following pK values; $pK_1=5.78$ and $pK_2=2.82$.[22)]

Table 2. Values of second order rate constants of the EDTA substitution reaction at various EDTA concentrations

pH	$[EDTA]_T$ / M	k_2 / $M^{-1}s^{-1}$
3.66	0.049	0.083
3.65	0.075	0.082
3.67	0.100	0.073
3.67	0.125	0.078
3.68	0.150	0.079
		Average 0.079±0.003

[V(III)]=0.0127 M, $[MAL]_T$=1.0 M and 26 °C.

Table 3. pH dependence on the rate of the EDTA substitution reaction

pH	k_2 / $M^{-1}\,s^{-1}$	k_{2f} / $10^{-3}\,s^{-1}$
2.62	0.142	3.98
2.86	0.109	3.05
3.25	0.078	2.18
3.59	0.066	1.85
4.00	0.053	1.48
4.80	0.042	1.18

[V(III)]=0.0127 M, $[EDTA]_T=2.8\times10^{-2}$ M, $[MAL]_T$ = 1.0 M at 25 °C. The concentrations of EDTA species were calculated by using the following pK values, pK_1= 10.26, pK_2=6.16, pK_3=2.67, pK_4=1.99.[23]

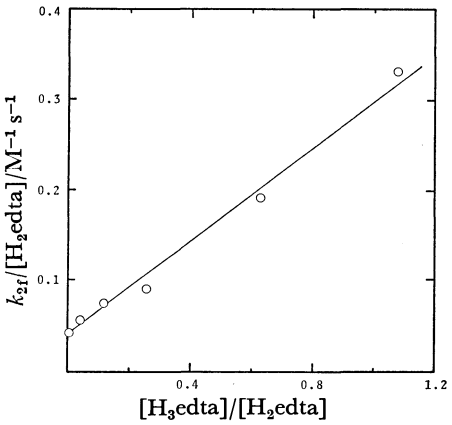

Fig. 4. A plot of $k_{2f}/[H_2edta]$ *vs.* $[H_3edta]/[H_2edta]$ in the substitution reaction of the coordinated malonate by EDTA.

$$k_{2f} = k_{21}[H_2edta] + k_{22}[H_3edta] \quad (8)$$

As shown in Fig. 4, the plot of $k_{2f}/[H_2edta]$ *vs.* $[H_3edta]/[H_2edta]$ is linear and it proves Eq. 8 to be valid. The intercept and the slope of the straight line yield k_{21}=0.04 $M^{-1}\,s^{-1}$ and k_{22}=0.25 $M^{-1}\,s^{-1}$, respectively. The activation parameters obtained from the measurements at temperatures ranging from 20 to 40 °C were summarized in Table 6.

Substitution by NTA. The substitution of the coordinated malonate by NTA can be described by Eq. 3. The V(nta)(mal)$^{2-}$ complex, though its structure is not known, seems to have an octahedral structure. The following explanation will give the stoichiometric evidence for Reaction 3.

Under the experimental conditions studied, Reaction 3 was reversible and the rate equation is

$$-d[V(mal)_3^{3-}]/dt = k_3[V(mal)_3^{3-}][NTA]_T - k_{-3}[V(nta)(mal)^{2-}][MAL]_T. \quad (9)$$

The values of the forward and backward rate constants, k_3 and k_{-3}, were calculated by the least squares method. A typical least squares fit to experimental data is shown in Fig. 5. The results are listed in Table 4 for a variety of $[NTA]_T$ and $[MAL]_T$ values. The pH dependence of the substitution rates is shown in Table 5.

At infinite time, $-d[V(mal)_3^{3-}]/dt=0$, which leads to

$$[V(nta)(mal)^{2-}][MAL]_T/([V(mal)_3^{3-}][NTA]_T) = k_3/k_{-3}. \quad (10)$$

On the other hand, the equilibrium constant, K, of the

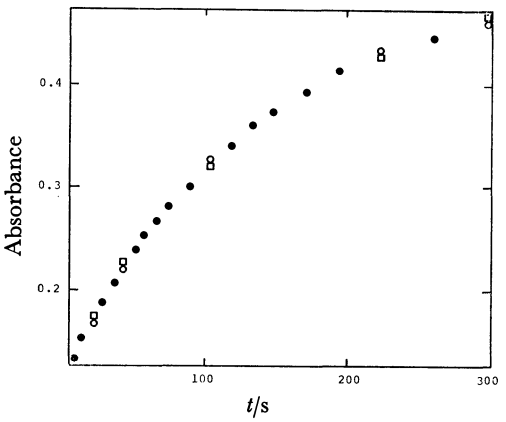

Fig. 5. The variation of absorbance with time in the substitution reaction of the coordinated malonate by NTA.
□: Experimental, ○: calculated. Closed circles indicate the points where the values of □ in accord with those of ○.

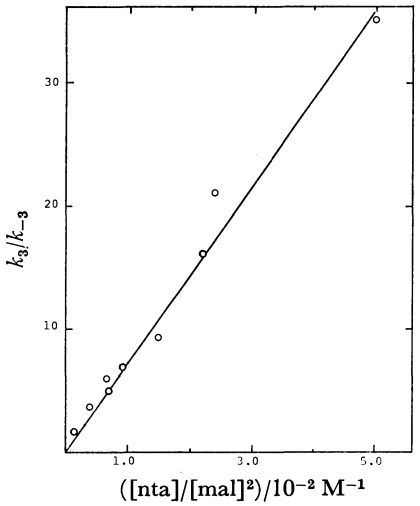

Fig. 6. A plot of k_3/k_{-3} *vs.* $[nta]/[mal]^2$ in the substitution reaction of the coordinated malonate by NTA.

Table 4. Rate constants of the NTA substitution reaction for various $[MAL]_T$ and $[NTA]_T$ at 25 °C

pH	$[MAL]_T$ / M	$[NAT]_T$ / M	k_3 / $10^{-2}\,M^{-1}\,s^{-1}$	k_{-3} / $10^{-3}\,M^{-1}\,s^{-1}$
3.53	1.061	0.146	1.26	2.3
3.50	1.033	0.146	1.30	2.0
3.59	0.884	0.146	1.06	2.4
3.47	0.778	0.146	1.36	2.2
3.47	0.707	0.146	1.72	2.5
3.40	1.167	0.0732	1.31	2.8
3.40	1.167	0.110	1.36	2.5
3.44	1.167	0.146	1.43	2.5

Eq. 3 is

$$[V(nta)(mal)^{2-}][mal]^2/([V(mal)_3^{3-}][nta]) = K. \quad (11)$$

From Eqs. 10 and 11

$$k_3/k_{-3} = K[MAL]_T[nta]/([NTA]_T[mal]^2). \quad (12)$$

If the stoichiometry in Eq. 3 is correct, a plot of k_3/k_{-3} *vs.* $[nta]/[mal]^2$ should be linear. The equilibrium constant

Table 5. pH dependence on the rate of the NTA substitution reaction

pH	k_3 / 10^{-2} M^{-1} s^{-1}	k_{-3} / 10^{-3} M^{-1} s^{-1}	k_{3f} / 10^{-3} s^{-1}
2.95	7.08	2.0	10.3
3.15	4.19	2.0	6.12
3.18	4.38	2.7	6.39
3.31	2.62	2.8	3.83
3.47	1.72	2.5	2.51
3.57	1.01	1.7	1.47
3.77	0.64	1.7	0.93
4.18	0.32	1.9	0.47

[V(III)]=0.00429 M, $[MAL]_T$=0.707 M, $[NTA]_T$=0.146 M, at 25 °C. The concentrations of the NTA species were calculated by using the following pK values; pK_1=9.73, pK_2=2.49, pK_3=1.89.[23]

is obtained from the slope in Fig. 6 to be 1.5×10^2 M. Hence it is confirmed that V(nta)(mal)$^{2-}$ is the most reasonable species for the product of the substitution of the coordinated malonate by NTA.

In comparison with the EDTA substitution reaction, the mechanism seems to be more complicated for the NTA substitution. A plot of k_{3f}/[Hnta] *vs.* [H_2nta]/[Hnta], where k_{3f} is the first order rate constant for Reaction 3, does not give a straight line, while the corresponding plot for the EDTA substitution was linear as shown in Fig. 4. Considering these results, we estimate the following substitution scheme for the NTA substitution. The initial step is a reversible substitution process between V(mal)$_3^{3-}$ (I) and the intermediate complex V(mal)$_2$(NTA) (II), whose charge can not be determined, followed by the chelation of NTA.

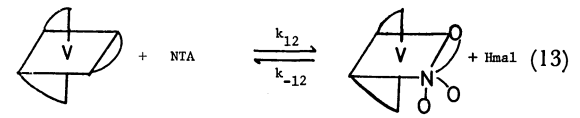

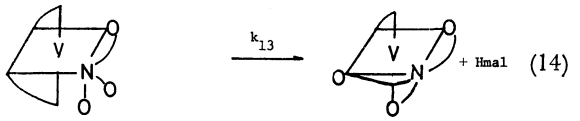

where NTA is supposed to be Hnta or H_2nta. In the intermediate complex (II), NTA, which is primarily a quadridentate ligand, coordinates to V(III) as a bidentate. Such a complex is presumed to be unstable compared with the complexes (I) and (III). On the basis of the above assumption, a steady state approximation for the complex (II) leads to the following rate law:

$$R_3 = k_{12}k_{13}[V(mal)_3^{3-}][NTA]/(k_{-12}[Hmal]+k_{13}). \quad (15)$$

The backward rate of Reaction 13 (k_{-12} path) is supposed to be as fast as that of Reaction 1, because both processes are the substitution of bidentate ligands by Hmal. Since the rate constant of the malonate exchange (1) is

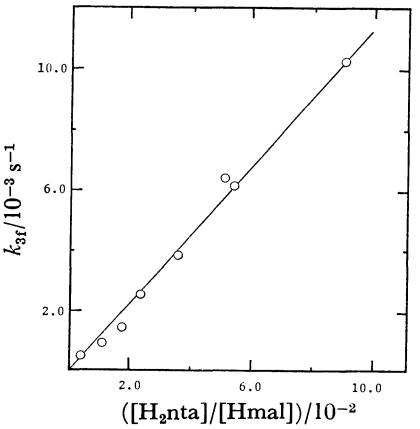

Fig. 7. A plot of k_{3f} *vs.* [H_2nta]/[Hmal] in the substitution reaction of the coordinated malonate by NTA.

Table 6. Activation parameters for the substitution reactions in V(mal)$_3^{3-}$

Reaction	$\Delta H^{\neq}$ / kJ mol^{-1}	$\Delta S^{\neq}$ / J mol^{-1} K^{-1}
Malonate exchange (Reaction 1)	54.8[a]	−50.2[a]
EDTA substitution (Reaction 2)	42.3±1.7	−119±5
NTA substitution (k_3 path in Reaction 3)	67.4±3.8	−44±13

a) The errors in these values are estimated at approximately 20%.

3.5 s^{-1} at 25 °C, which is about hundred times greater than that of the NTA substitution (3), it may be assumed that k_{-12}[Hmal] is relatively larger than k_{13}. If k_{-12}[Hmal]$\gg k_{13}$ is assumed, Eq. 15 becomes

$$R_3 = k_{12}k_{13}[V(mal)_3^{3-}][NTA]/k_{-12}[Hmal], \quad (16)$$

or

$$k_{3f} = k_{12}k_{13}[NTA]/k_{-12}[Hmal]. \quad (17)$$

The plot of k_{3f} as a function of [H_2nta]/[Hmal] is linear (Fig. 7) and this fact supports that the reaction mechanism described above is reasonable. It is also found that only H_2nta of NTA species acts as an entering ligand because the intercept in Fig. 7 is approximately zero. Recently, Tanaka *et al.* reported the existence and reactivity of the protonated species, H_4nta.[20] However, H_4nta will not play the important role, since the concentration of H_4nta (10^{-5}—10^{-7} M) is much lower than those of H_2nta and Hnta in the pH region studied.

The activation parameters were obtained from the measurements at temperatures ranging from 20 to 40 °C. The results were summarized in Table 6.

Conclusion

We conclude that the ligand substitution reactions in V(mal)$_3^{3-}$ proceed *via* an A mechanism.[21] These results are consistent with those of earlier studies.[2,3] Larger negative values of activation entropies as shown in Table 6 may support the A mechanism.

It is of particular interest that univalent anions are markedly reactive as the entering ligand in substitution

reactions compared with other multivalent ions. This is quite reasonable because a mutual repulsion between the univalent anion and trivalent complex anion, $V(mal)_3^{3-}$, is supposed to be much smaller than that between $V(mal)_3^{3-}$ and multivalent anions.

In the earlier study dealing with the malonate exchange in $VO(mal)_2^{2-}$, it was suggested that the reaction would proceed *via* acid catalysis,[12] where the second order rate constants for $VO(mal)_2^{2-}$ and $Hmal^-$ increased more than fivefold when pH changed from 2.30 to 4.05. From the present study, however, we conclude that the acid effect is very small or nearly negligible. In the case of the EDTA substitution reaction, it can not be determined whether the pH dependence of the rate constant is due to the acid catalysis or the concentration dependence of the entering ligand, if only H_2edta is assumed to be active as an entering ligand. However, such an assumption seems unlikely, because H_2edta should be more inactive than H_3edta to $V(mal)_3^{3-}$ owing to the electric repulsion. In fact, the linear relationship between the substitution rate and the hydrogen ion concentration was not obtained in the NTA substitution reaction. As shown in Table 1, the second order rate constant of the malonate exchange in $V(mal)_3^{3-}$ increases slightly with increasing hydrogen ion concentrations. However, it may be hard to conclude whether the exchange rate is slightly accelerated by acid or not, because unlike the malonate exchange reaction in $VO(mal)_2^{2-}$ the pH dependence of the rate constant is too small by considering large experimental errors in NMR measurements.

The authors wish to thank Professor Gilbert Gordon of Miami University for his helpful discussions.

References

1) A. E. Chemelnick and D. Fiat, *J. Magn. Reson.*, **8**, 325 (1972).
2) B. R. Baker, N. Sutin, and T. J. Welch, *Inorg. Chem.*, **6**, 1948 (1967).
3) W. Kruse and D. Thusius, *Inorg. Chem.*, **7**, 464 (1968).
4) J. H. Espenson and J. R. Pladziewicz, *Inorg. Chem.*, **9**, 1380 (1970).
5) C. H. Langford and F. M. Chung, *Can. J. Chem.*, **48**, 2969 (1970).
6) A. J. C. Nixon and D. R. Eaton, *Can. J. Chem.*, **56**, 1005 (1978).
7) A. J. C. Nixon and D. R. Eaton, *Can. J. Chem.*, **56**, 1012 (1978).
8) K. Wüthrich and R. E. Connick, *Inorg. Chem.*, **6**, 583 (1967).
9) J. Reuben and D. Fiat, *Inorg. Chem.*, **6**, 597 (1967).
10) K. Wüthrich and R. E. Connick, *Inorg. Chem.*, **7**, 1337 (1968).
11) H. Tomiyasu, K. Dreyer, and G. Gordon, *Inorg. Chem.*, **11**, 2409 (1972).
12) H. Tomiyasu, S. Itoh, and S. Tagami, *Bull. Chem. Soc. Jpn.*, **47**, 2843 (1974).
13) H. Tomiyasu and G. Gordon, *Inorg. Chem.*, **15**, 870 (1976).
14) M. Nishizawa and K. Saito, *Bull. Chem. Soc. Jpn.*, **51**, 483 (1978).
15) M. Nishizawa and K. Saito, *Inorg. Chem.*, **17**, 3676 (1978).
16) M. Nishizawa and K. Saito, *Inorg. Chem.*, **19**, 2284 (1980).
17) For the convenience, malonate and bimalonate ions will be expressed as mal and Hmal, respectively. Corresponding species of ethylenediaminetetraacetic acid will be expressed as edta, Hedta, H_2edta, and H_3edta. Similarly, nitrilotriacetic acid species will be abbreviated as nta, Hnta, and H_2nta. The charge on these species will be omitted. Abbreviations, MAL, EDTA, and NTA, will be used for the system including all nonprotonated and protonated species of malonic acid, ethylenediaminetetraacetic acid, and nitrilotriacetic acid, respectively.
18) T. J. Swift and R. E. Connick, *J. Chem. Phys.*, **37**, 307 (1962).
19) T. R. Stengle and C. H. Langford, *Coord. Chem. Rev.*, **2**, 349 (1967).
20) S. Yamada, J. Nagase, S. Funahashi, and M. Tanaka, *J. Inorg. Nucl. Chem.*, **38**, 617 (1976).
21) C. H. Langford and H. B. Gray, "Ligand Substitution Processes," Benjamin, London (1974).
22) S. Itoh, H. Tomiyasu, and H. Ohtaki, *Bull. Chem. Soc. Jpn.*, **46**, 2238 (1973).
23) L. G. Sillén and A. E. Martell, "Stability Constants of Metal-Ion Complexes," Special Publication No. 17, (1964); Supplement No. 1, Special Publication No. 25, (1971), The Chemical Society, London.

Ternary α-Amino Acid-Palladium(II) Complexes with Ligand-Ligand Hydrogen Bonding

Akira ODANI and Osamu YAMAUCHI*

Faculty of Pharmaceutical Sciences, Kanazawa University, Takaramachi, Kanazawa 920

(Received May 1, 1981)

Histidinate(His)-containing ternary α-amino acid–palladium(II) complexes have been studied by synthetic and spectroscopic methods. The following complexes with imidazolate (im), L- and D-His, L-asparaginate (L-Asn), and L-glutaminate (L-Gln) have been isolated as crystals: $[Pd(im)_2]\cdot 0.5H_2O$; [Pd(L-His)(D-His)]·H_2O; [Pd(L-Asn)-(L-His)]·$2H_2O$; [Pd(L-Gln)(L-His)]·$2H_2O$. The ternary systems involving palladium(II), L-His, and an amino acid L-AA with an OH or a $CONH_2$ group (AA=Asn, Gln, serinate, threoninate, or homoserinate) exhibit absorption maxima at 300—311 nm with ε 310—440 and negative and positive circular dichroism (CD) peaks at 307—328 nm and ≈300 nm, respectively. ^{13}C and ^1H NMR spectra gave the amounts of the *cis* and *trans* isomers of Pd(His)-(AA) in solution and confirmed that Pd(His)(AA) has an N_3O donor set in the coordination plane. Whereas the CD magnitude additivity holds for the ternary systems Pd(L-His)(B) with B=glycinate, L-alaninate, or L-valinate and the systems with L-histidine methyl ester (L-HisOMe) and L-AA, Pd(L-HisOMe)(L-AA), the magnitudes for Pd(L-His)(L-AA) deviate significantly from those estimated on the basis of the additivity. The CD magnitude anomaly as well as the geometrical and rotational isomer populations calculated from the ^1H NMR spectra establishes the existence of the ligand-ligand interaction between the carboxylato group of His and the hydroxyl or amido group of AA in solution.

With the recognition of the importance of non-covalent interactions in biological processes,[1] weak intramolecular interactions between coordinated ligands have recently attracted considerable attention. Intramolecular aromatic ring stacking between 2,2′-bipyridine, 1,10-phenanthroline, or tryptophan and the base moiety of nucleosides or nucleotides in the ternary complexes of copper(II), zinc(II), *etc.* has been detected in solution[2–9] and revealed by X-ray analysis of a crystalline copper(II) complex.[10] Electrostatic ligand-ligand interactions in the ternary α-amino acid–copper-(II) complexes have received substantial experimental support,[11–14] and the recent NMR spectroscopic study provides conclusive evidence for their existence in the corresponding palladium(II) complexes.[15] On the other hand, histidinate(His)-containing ternary amino acid–copper(II) complexes with asparaginate (Asn), glutaminate (Gln), citrullinate, serinate (Ser), homoserinate (Hmser), or threoninate (Thr) (abbreviated as AA hereafter) have been inferred to involve hydrogen bonding between the carboxylato group of His and the polar side group of AA.[16] Preferential crystallization of Cu(L-Asn)(L-His) from the solution containing Cu(II), L-Asn, and DL-His in the ratio of 1 : 1 : 1.5 has led to nearly complete optical resolution of histidine,[16,17] which is in support of the stereoselectivity due to the interaction. The molecular structures of [Cu(L-Asn)(L-His)(H_2O)]·$3H_2O$ and [Cu(L-Asn)(L-His)] disclosed by X-ray analysis[18] exhibit difference in the side chain conformation of L-Asn, indicating the side chain flexibility and its accessibility to the histidine carboxylato group axially coordinated to copper(II). Probably because hydrogen bonds are too weak in aqueous solution to affect the stability constants, however, analysis of the solution equilibria in water[16] and in 20% dioxane–water[19] failed to show any effects of the bonding.

As an extention of the studies on copper(II) complexes, we now carried out synthetic and spectroscopic investigations of the corresponding histidinate- and cysteate-($CySO_3H$)-containing ternary palladium(II) systems in order to obtain convincing information on the ligand-ligand interaction in the ternary systems Pd(His)(AA) in solution.

Experimental

Materials. DL-Histidine methyl ester dihydrochloride was prepared according to the literature.[20] L-1-Methylhistidine, L-histidine methyl ester dihydrochloride, and D- and DL-histidine hydrochloride were purchased from Sigma. All the other amino acids were obtained from Nakarai. Disodium hexachloropalladate(II) and palladium(II) chloride were from Mitsuwa and Kishida, respectively. The deuterated solvents, D_2O, CD_3OD, and DCl in D_2O were obtained from Merck. The chemicals used were of highest grade available.

Syntheses. *[Pd(L-His)(D-His)]·H_2O*: To a solution of palladium(II) chloride (0.36 g, 2.0 mmol) in 2 M HCl (2 ml; 1 M=1 mol dm^{-3}) was added an aqueous solution of DL-histidine hydrochloride (0.84 g, 4.0 mmol), and the pH of the mixture was adjusted at 6—7 with aqueous NaOH. Colorless crystals were collected and recrystallized from water. Found: C, 33.16; H, 4.23; N, 19.97%. Calcd for $C_{12}H_{16}N_6O_4Pd\cdot H_2O$: C, 33.31; H, 4.19; N, 19.42%.

[Pd(im)$_2$]·0.5H_2O: An aqueous solution of imidazole (0.27 g, 4.0 mmol) was added to a solution of palladium(II) chloride (0.36 g, 2.0 mmol) in 2 M HCl (2 ml). The pH of the resulting mixture was adjusted at ≈7 with aqueous NaOH, when almost colorless crystals separated. Found: C, 28.64; H, 2.77; N, 22.15%. Calcd for $C_6H_6N_4Pd\cdot 0.5H_2O$: C, 28.88; H, 2.83; N, 22.45%.

[Pd(L-Gln)(L-His)]·2H_2O: Palladium(II) chloride (0.36 g 2.0 mmol) in 2 M HCl (2 ml) was mixed with aqueous solutions of L-histidine hydrochloride (0.42 g, 2.0 mmol) and L-glutamine (0.59 g, 4.0 mmol), and the pH of the resulting solution was adjusted at 5—6 with aqueous NaOH. The solution was then concentrated *in vacuo* to a small volume at room temperature and kept in a refrigerator for a few days to give yellowish crystals after removal of slightly soluble Pd(L-Gln)$_2$. Found: C, 29.46; H, 4.65; N, 15.85%. Calcd for $C_{11}H_{17}N_5O_5Pd\cdot 2H_2O$: C, 29.91; H, 4.79; N, 15.85%.

[Pd(L-Asn)(L-His)]·2H_2O: The complex was prepared in the manner described for Pd(L-Gln)(L-His). Found: C,

28.62; H, 4.09; N, 16.65%. Calcd for $C_{10}H_{15}N_5O_5Pd \cdot 2H_2O$: C, 28.08; H, 4.48; N, 16.37%.

Instruments. Absorption spectra were recorded in the range 230—430 nm on a Union Giken SM-401 high sensitivity recording spectrophotometer. CD spectra were measured in the range 260—420 nm with a JASCO MOE-1 spectropolarimeter. ^1H NMR spectra at 90 MHz were obtained at 34 °C with a Hitachi R-22 NMR spectrometer equipped with a Hitachi A 1600A signal averaging analyzer internally locked and a Hitachi R-900 Fourier transform NMR spectrometer (90 MHz). ^{13}C NMR spectra at 22.63 MHz were recorded at 34 °C on a Hitachi R-900 Fourier transform spectrometer with D-lock and digital resolution of 0.02 ppm. The probe temperature was measured with a thermocouple.

Spectral Measurements. Absorption and CD Spectra: Absorption and CD spectra were measured at room temperature for the systems involving Pd(II), His, and AA in the ratio of 1 : 1 : 1 at pH 6.5—7.0 at a Pd(II) concentration of 1×10^{-3}—2×10^{-3} M. The samples were prepared from disodium tetrachloropalladate(II) freshly dissolved in water and 0.02 M aqueous solutions of amino acids, the pH values being adjusted with aqueous NaOH (0.05 M) and hydrochloric acid (0.01 M).

NMR Spectra. The samples were prepared in deuterated solvents (pD 5—7) in the manner described above. The palladium(II) concentrations were *ca.* 0.04—0.2 M for ^1H and 0.1—1.0 M for ^{13}C NMR spectral measurements. All carbon chemical shifts were measured relative to dioxane as an internal reference.

Results

Syntheses. Isolation of the crystalline binary copper(II) complex of L-histidine has been a challenge to a number of investigators, and only the *meso* complex, Cu(L-His)(D-His), has been successfully crystallized and analyzed crystallographically.[21] With palladium(II), the corresponding *meso* complex was obtained as crystals, whereas the active complex was obtained as a gelatinous precipitate just as the platinum(II) complex.[22] As regards the ternary complexes, only Pd(L-Asn)(L-His) and Pd(L-Gln)(L-His) were isolated as crystals by using Pd(II), His, and AA in the ratio of 1 : 1 : 2. The ternary complexes with Ser, Thr, and Hmser could not be obtained as analytically pure crystals probably owing to contamination with the binary complexes $Pd(AA)_2$, and are in contrast with the corresponding copper(II) complexes which have been isolated as crystals in previous studies.[16,17]

Spectral Properties. Absorption and CD Spectra: At neutral pH the ternary systems Pd(L-His)(L-AA) exhibit an absorption band centered at 300—311 nm with ε 310—440, whose pattern appears to involve a shoulder and a peak ascribable to $Pd(L\text{-}His)_2$ and $Pd(L\text{-}AA)_2$, respectively (Table 1). The CD spectra of the Pd(L-His)(L-AA) systems have a negative maximum at 307—328 nm with a positive shoulder at $\approx$300 nm and sometimes a weak positive peak at $\approx$380 nm. In the absence of ligand-ligand interactions within complex molecules, the CD magnitude additivity has been shown to hold for the copper(II) and palladium(II) complexes with two amino acids[11,12,15] or a peptide with two or three amino acid residues,[23,24] where the magnitudes, $\Delta\varepsilon_{calcd}$, can be estimated by summing up the experimental magnitude assigned to each molecule or residue of the amino acids constituting the systems. Thus, for ternary palladium(II) systems with amino acids L-A and L-B devoid of interacting side groups, Pd(L-A)(L-B), $\Delta\varepsilon_{calcd}$ given by Eq. 1 corresponds well with the observed value:[15]

$$\Delta\varepsilon_{calcd} = \frac{1}{2}(\Delta\varepsilon_{Pd(L\text{-}A)_2} + \Delta\varepsilon_{Pd(L\text{-}B)_2}), \quad (1)$$

where $\Delta\varepsilon_{Pd(L\text{-}A)_2}$ and $\Delta\varepsilon_{Pd(L\text{-}B)_2}$ refer to the magnitudes exhibited by the binary complexes $Pd(L\text{-}A)_2$ and $Pd(L\text{-}B)_2$, respectively. Because the ligand fields are supposedly different in the histidinate-containing systems from those of the systems with the other amino acids owing to the imidazole ring, we used Eq. 2 for Pd(L-His)(L-AA):

$$\Delta\varepsilon_{calcd} = \Delta\varepsilon_{Pd(DL\text{-}His)(L\text{-}AA)} + \Delta\varepsilon_{Pd(L\text{-}His)(DL\text{-}AA)}. \quad (2)$$

The estimated values given by Eq. 2 are in good agreement with the experimental ones for the systems with glycinate (Gly), L-alaninate (L-Ala), or L-valinate (L-Val) in place of L-AA (Table 1). On the other hand, polar side chains of Ser, Thr, Hmser, Asn, and Gln affect the magnitudes, decreasing the relative magnitudes $\Delta\varepsilon/\Delta\varepsilon_{calcd}$. This is reminiscent of the magnitude anomaly due to the electrostatic ligand-ligand interaction in the ternary copper(II) and palladium(II) systems with an acidic and a protonated basic amino acid and related systems,[11-13,15] and serves as an indication

Table 1. Absorption and CD spectral data for L-His-containing ternary systems

System	pH	Absorption spectrum		CD spectrum		Relative magnitude[a]
		λ_{max} / nm	ε	λ_{max} / nm	$\Delta\varepsilon$	$\Delta\varepsilon/\Delta\varepsilon_{calcd}$
Pd(L-His)(Gly)	7.1	305	310	328	−0.15	1.00
Pd(L-His)(L-Ala)	7.1	311	380	324	−0.10	0.93
Pd(L-His)(L-Val)	7.0	305	420	319	−0.47	0.96
Pd(L-His)(L-Ser)	6.9	305	410	321	−0.11	0.58
Pd(L-His)(L-Thr)	7.1	306	400	315	−0.29	0.90
Pd(L-His)(L-Hmser)	7.1	305	430	323	−0.10	0.64
Pd(L-His)(L-Asn)	6.8	300	400	307	−0.12	0.64
Pd(L-His)(L-Gln)	7.0	305	430	325	−0.15	0.74

a) Calculated according to Eq. 2. The $\Delta\varepsilon$ values were measured at λ_{max} of Pd(L-His)(L-AA).

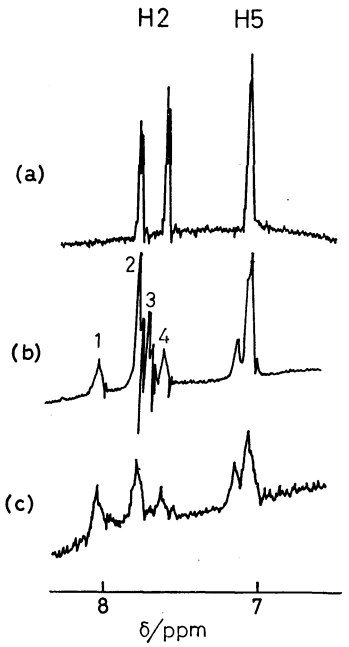

Fig. 1. ^{1}H NMR spectra of the imidazole moiety at pD 5.0 in the systems Pd(L-His)$_2$ (a), Pd(Dmgly)(L-His) (b), and Pd(Gly)(L-His) (c). The numbered signals in (b) correspond to *cis*-Pd(Gly)(L-His) (1), *cis*-Pd(L-His)$_2$ (2), *trans*-Pd(Gly)(L-His) (3), and *trans*-Pd(L-His)$_2$ (4), the geometry referring to the amino groups.

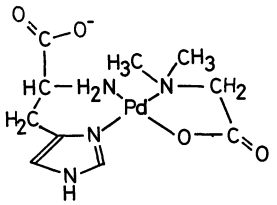

Fig. 2. Preferred coordination structure of Pd(Dmgly)-(L-His).

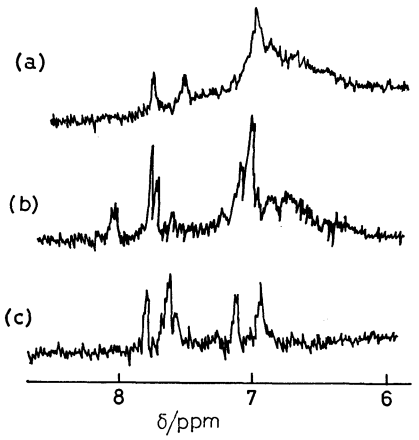

Fig. 3. ^{1}H NMR spectra of the imidazole moiety at pD >7 in the systems 1 : 1.33 Pd(II)-L-His (a), Pd(L-Ala)(L-His) (b), and Pd(L-Ala)(L-1-methylhistidinate) (c).

of side chain interactions between the carboxylato group of L-His and the hydroxyl or amido group of L-AA in the present cases.

NMR Spectra: The signal assignments were made on the basis of the substituent effects, the peak areas, and the chemical shifts observed for the amino acids in the absence of palladium(II).[25] The ^{1}H NMR spectra of Pd(L-His)$_2$ and Pd(Histam)$_2$ (Histam=histamine) show two separate peaks of the C^2 proton of the imidazole nucleus (Fig. 1). The signals exhibit splittings due to coupling with the C^5 proton. Since the imidazolyl groups contained in *cis*-Pt(L-His)$_2$[22] and *cis*-Pd(imH)$_2$Cl$_2$[26] (imH=imidazole) have been reported to give the corresponding peaks at lower fields than those observed for the *trans* forms, the signals at lower fields for Pd(L-His)$_2$ and Pd(Histam)$_2$ are also assigned to the *cis* isomers. In this connection, the spectrum of the ternary system containing *N,N*-dimethylglycinate (Dmgly), Pd(Dmgly)(L-His), shows only the lower field peak of the imidazole moiety in contrast to the two peaks in Pd(Gly)(L-His) (Fig. 1). The difference is probably attributed to the steric repulsion between the C^2 proton and the methyl groups in Pd(Dmgly)(L-His) and may thus point to the structure involving a *cis* arrangement with respect to the amine nitrogens (Fig. 2). Binary complexes of amino acids with the glycinate-like coordination exhibit spectra apparently due to single 1 : 2 species, indicating that the interconversion between geometrical isomers is fast as compared with the NMR time scale. The ternary systems with L-Ala, on the other hand, have four peaks of the C^2 proton, and those which are unaffected by the presence of L-AA can be assigned to *cis*- and *trans*-Pd(L-His)$_2$ involved in the system Pd(L-His)(L-AA) in solution.

At the Pd(II)/L-His ratios of >0.5 at pD 7.0, the binary system gives additional broad peaks at δ 6—8, which are also detected in the spectra of the ternary systems at pD>7 (Fig. 3). Since the ternary system involving L-1-methylhistidinate and L-Ala does not show such broad peaks, they may be associated with the coordination to palladium(II) of the deprotonated pyrrole nitrogen of His, such as is observed with Pd(im)$_2$ where both imidazole nitrogens are coordinated.

The ^{13}C chemical shift differences between free and coordinated amino acids at constant pD, shown in Table 2, reveal that coordination to Pd(II) causes downfield shifts of 11 ppm at the carbonyl carbon of L-Ala and L-Thr and 3 ppm at that of L-His. The imidazole moiety suffers larger irregular shifts indicative of its coordination. The ^{1}H NMR spectral pattern exhibited by the methyl group of L-Ala in Pd(L- or D-His)(L-Ala) corresponds well with that in Pd(Histam)-(L-Ala), while the patterns of all the protons of L-Hmser undergo changes on going from Pd(Histam)(L-Hmser) to Pd(L-His)(L-Hmser) and Pd(D-His)(L-Hmser), suggesting the side chain conformational changes of L-Hmser (Fig. 4). Glutamate involved in place of His in the ternary systems show different patterns of the β- and γ-CH$_2$ groups; Glu in the system Pd(D-Glu)(L-Thr) suffers considerable spectral changes while that in Pd(L-Glu)(L-Thr) shows patterns which are slightly different from those of Pd(L-Glu)$_2$ and Pd(L-Glu)-(L-Ala).

Discussion

Palladium(II)–Amino Acid Bonding Modes. The

TABLE 2. ^{13}C COMPLEX SHIFTS OF BINARY AND TERNARY SYSTEMS[a]

System	Assignment[b]	Complex shifts/ppm									
		L-His[c]						L-Ala or L-Thr			
		C=O	α-C	β-C	C^2	C^4	C^5	C=O	α-C	β-C	CH_3
Pd(L-His)$_2$	*cis*	3.3	−1.1	4.1	2.4	5.2	−3.5				
	trans	3.3	−1.1	4.7	2.7	5.5	−3.5				
Pd(L-His)(L-Ala)		3.0	−0.4	3.0	1.4	4.6	−3.5	11.0	4.3		2.9
Pd(L-His)(L-Thr)		3.0	−0.4	3.0	1.5	4.4	−3.5	11.3	3.5	1.6	−0.9

a) In ppm downfield at pD 5.0. Complex shifts are defined as the chemical shift differences between the complexed and free amino acids. b) Complex shifts of the peaks assigned to *cis* and *trans* isomers in the system Pd(L-His)$_2$. c) The carbons C^2, C^4, and C^5 refer to those of the imidazole nucleus.

TABLE 3. ABSORPTION AND CD SPECTRAL DATA FOR L-HisOMe-CONTAINING TERNARY SYSTEMS

System	pH	Absorption spectrum		CD spectrum		Relative magnitude[a] $\Delta\varepsilon/\Delta\varepsilon_{calcd}$
		λ_{max}/nm	ε	λ_{max}/nm	$\Delta\varepsilon$	
Pd(L-HisOMe)(L-Ala)	6.7	304	340	345	−0.042	1.00
Pd(L-HisOMe)(L-Val)	5.0	306	320	324	−0.31	0.98
Pd(L-HisOMe)(L-Ser)	6.9	305	360	343	−0.003	1.0
Pd(L-HisOMe)(L-Thr)	6.7	305	360	371	0.030	1.00
Pd(L-HisOMe)(L-Hmser)	7.0	304	370	339	−0.042	1.00
Pd(L-HisOMe)(L-Gln)	7.0	304	370	336	−0.084	1.04

a) $\Delta\varepsilon_{calcd}=\Delta\varepsilon_{Pd(L\text{-}HisOMe)(DL\text{-}AA)}+\Delta\varepsilon_{Pd(DL\text{-}HisOMe)(L\text{-}AA)}$. The values were measured at λ_{max} of Pd(L-HisOMe)(L-AA).

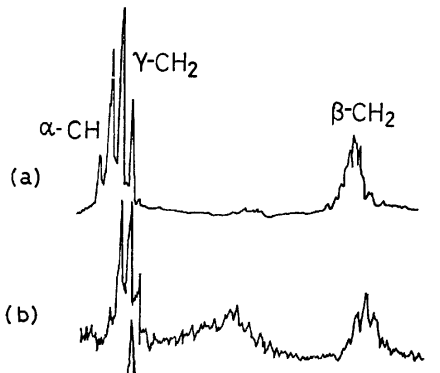

Fig. 4. ^1H NMR signal patterns of homoserinate at pD 7.0 in the systems Pd(Histam)(L-Hmser) (a), Pd(L-His)-(L-Hmser) (b), and Pd(D-His)(L-Hmser) (c).

^{13}C NMR complex shifts found in the Pd(L-His)$_2$ system indicate that His coordinates to palladium(II) through the amine and imidazole nitrogens, while the glycinate-like coordination in Pd(L-AA)$_2$ is confirmed by the absorption and CD spectra[23] as well as the ^{13}C complex shifts (Table 2).[15] The spectral data also show that the ternary complexes, Pd(His)(AA), have an N_3O donor set that corresponds with the set in Cu(L-His)-(L-Thr)[27] and Cu(L-Asn)(L-His)[18] disclosed by X-ray analysis. In solution the geometrical isomers of Pd(His)$_2$ and Pd(Histam)$_2$ exist in approximately the same amounts, and this suggests that the two imidazole rings in the *cis* isomers are slightly distorted from the coordination plane in analogy with the arrangements in *trans*-Pd(Histam)$_2$Cl$_2$[28] and *trans*-Cu(L-His)(D-His),[21] since the steric repulsion between the C^2 protons of the two imidazoles in the *cis* position should otherwise be considerable and tend to favor the *trans* isomers greatly.

Intramolecular Hydrogen Bonding in Ternary Complexes. His-containing Systems: Ligand-ligand interactions between the side chains in ternary copper(II) and palladium(II) complexes have been found to give rise to CD magnitude anomaly in the d-d region due to increased asymmetry.[11-13,15] The L-His-containing ternary palladium(II) complexes with L-AA (AA=Ser, Thr, Hmser, Asn, or Gln) exhibit this anomaly in the $d_{xy}\rightarrow d_{x^2-y^2}$ transition,[15] which is considered to indicate the structural changes in the xy-plane. Direct evidence establishing that the carboxylato group of His is essential for the CD magnitude anomaly is provided by the CD spectra of the systems containing L-histidine methyl ester (L-HisOMe) instead of L-His, Pd(L-HisOMe)-(L-AA), where participation of the carboxylato group in the ligand-ligand interaction is blocked by esterification and as a consequence the relative magnitudes are expectedly close to unity (Table 3). Whereas the signals due to the methyl group of L-Ala in Pd(L-Ala)-(L- or D-His) remain the same as in Pd(L-Ala)(Histam), the presence of the carboxylato group of His in the ternary systems Pd(L-Gln)(L- or D-His) and Pd(L- or D-His)(L-Hmser) affects the ^1H NMR spectral patterns of L-Gln and L-Hmser, respectively. This implies the conformational changes of the amino acid side chains and possibly the effects of the ligand-ligand interaction

Table 4. Fractions of *cis*-isomers in ternary systems[a]

System	Temp °C	$r_{L\text{-His}}$[b]	$r_{L\text{-His}}$[c]	$\frac{r_{L\text{-His}}}{r_{D\text{-His}}}$
1 : 1 : 1 Pd(II)–His–L-Ala	34	0.33	0.35	0.9
1 : 1 : 2 Pd(II)–His–L-Ala	34	0.35	0.34	1.0
1 : 1 : 1 Pd(II)–His–L-Thr	34	0.18	0.13	1.4
1 : 1 : 2 Pd(II)–His–L-Thr	34	0.24	0.16	1.5
1 : 1 : 2 Pd(II)–His–L-Ala	8	0.33	0.32	1.0
1 : 1 : 2 Pd(II)–His–L-Thr	8	0.20	0.16	1.3
1 : 1 : 1 Pd(II)–His–L-Gln	8	0.40	0.24	1.7

a) The fraction is defined as the ratio of the *cis* isomer to the total isomers in the system. b) The fractions for the L-Hi-scontaining systems. c) The fractions for the D-His-containing systems.

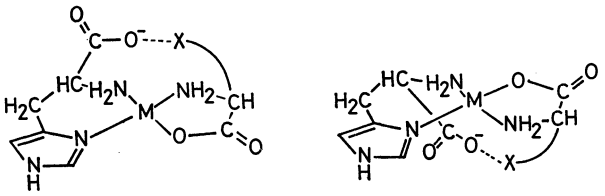

Fig. 5. Geometrical isomers expected from steric requirements for ligand-ligand interactions.

on the species distribution in the ternary systems. That such an interaction is intramolecular rather than intermolecular is reasonably deduced from the fact that the NMR spectral patterns and relative CD magnitudes are indifferent to concentrations of the samples.

The side chain interaction should also affect the distribution of geometrical isomers in the ternary systems as estimated from the peak areas of the C^2 proton signals of the imidazole moiety assigned to each isomer. Table 4 shows that, although the fractions of the *cis* isomers $r_{L\text{-His}}$ and $r_{D\text{-His}}$ in Pd(L-Ala)(L-His) and Pd(L-Ala)(D-His), respectively, are almost identical, those in Pd(L-His)(L-AA) and Pd(D-His)(L-AA) (AA= Thr or Gln) slightly differ from each other, the difference

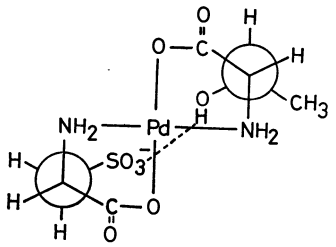

Fig. 6. Conformations of α-amino acids in Pd(L-$CySO_3H$)(L-Thr) with a ligand-ligand interaction.

being more clearly seen from the ratios of *cis* isomer contents in both systems. As shown previously for copper(II) complexes, the intramolecular ligand-ligand interaction requires *cis* arrangements of the NH_2 groups in Pd(L-His)(L-AA) and *trans* arrangements in Pd(D-His)(L-AA) (Fig. 5). In the palladium(II) systems investigated, the *cis* isomer contents in Pd(L-His)(L-AA) are greater than those in Pd(D-His)(L-AA), but the isomers that do not allow the ligand-ligand interaction still predominate, indicating that the stabilization due to the interaction is minimal in aqueous media.

Cysteate-containing Systems: The conformation of a coordinated α-amino acid is represented by the weighted average of three staggered rotational isomers, whose populations can be estimated by using the coupling constants between the protons on the α- and β-carbons and the constants for *trans* and vicinal couplings evaluated for α-amino acids by Pachler[30] and Martin.[31] The ligand-ligand interaction expected between the side chains of L-cysteate, which offers an SO_3^- group instead of the COO^- group of His, and L-Thr in Pd(L-$CySO_3H$)(L-Thr) requires that each amino acid assumes the conformation depicted in Fig. 6. In this connection, we reported in a previous communication[32] that the fractional population of L-$CySO_3H$ assuming the conformation shown in Fig. 6 increases with temperature decrease in 50% CD_3OD, which was taken as evidence for the presence of the hydrogen bond-type ligand-ligand interaction in solution. The abnormal CD magnitude of Pd(L-$CySO_3H$)(L-Thr) in 75% aqueous dioxane as compared with the magnitude of Pd(L-$CySO_3H$)(L-Ala) is also in line with the above conclu-

Table 5. Absorption and CD spectral data for L-$CySO_3H$-containing ternary systems

System	Solvent	pH	Absorption spectrum λ_{max} nm	Absorption spectrum ε	CD spectrum λ_{max} nm	CD spectrum $\Delta\varepsilon$	Relative magnitude[a] $\Delta\varepsilon/\Delta\varepsilon_{calcd}$
Pd(L-$CySO_3H$)(L-Ala)	H_2O	6.6	304	330	344	0.32	0.99
					303	−0.76	0.99
	75% aq dioxane	8.2			347	0.33	0.96
					307	−0.65	0.99
Pd(L-$CySO_3H$)(L-Thr)	H_2O	6.4	319	320	353	0.37	0.94
					311	−1.45	1.00
	75% aq dioxane	7.9			353	0.40	0.87
					309	−1.32	0.96
Pd(L-Ala)(L-Thr)	75% aq dioxane	7.7			353	0.34	1.06
					310	−0.88	1.03

a) $\Delta\varepsilon_{calcd}=1/2(\Delta\varepsilon_{Pd(L\text{-}CySO_3H)_2}+\Delta\varepsilon_{Pd(L\text{-}AA)_2})$. The $\Delta\varepsilon$ values were measured at λ_{max} of Pd(L-$CySO_3H$)(L-AA).

sion (Table 5). The system involving L-lysinate (L-Lys) in place of L-Thr exhibits greater deviation from the CD magnitude additivity and greater increase with temperature decrease of the population of the rotamer of L-$CySO_3H$ shown in Fig. 6,[15] demonstrating that the electrostatic interaction between the ε-NH_3^+ group of L-Lys and the SO_3^- group of L-$CySO_3H$ is more effective than the hydrogen bonding. Involvement of the negatively charged group in the interaction is further supported by the ^1H NMR signal pattern of Glu in Pd(L- or D-Glu)(L-Thr).

Comparison with the Copper(II) Systems. On the basis of synthetic and spectroscopic studies, histidinate-containing ternary copper(II) systems with AA have been inferred to involve an intramolecular hydrogen bond around the central copper(II) ion.[16] Since both copper(II) and palladium(II) form essentially planar complexes with α-amino acids except ornithinate in the same mode of coordination, the present conclusion on the ligand-ligand interaction in the palladium(II) complexes, reached from the CD and NMR studies, most probably holds for the corresponding copper(II) systems and substantiates our previous interpretation[16] of the preferential formation of Cu(L-His)(L-AA) (AA= Asn, Gln, and Thr) in human blood plasma.[33,34] The complex species Cu(L-His)(L-AA) should meet the requirement for copper(II) transport across biological membranes, because hydrogen bonding is more effective in such hydrophobic regions and may have a ligand-discriminating ability. The hydrogen bonded cyclic structure has been elucidated by X-ray analysis for the silver(I) and other metal complexes of an antibiotic monensin,[35] whose ring structures are best suited for the transport.

Interestingly, very recent X-ray structural analysis of [Cu(L-Ala)(L-His)(H_2O)]·$3H_2O$ shows that L-His coordinates to copper(II) through the amino and imidazole nitrogens with the carboxylato group axially bound to a neighboring copper(II).[36] This is in contrast with the modes of coordination found in Cu(L-His)(L-Thr)[27] and Cu(L-Asn)(L-His),[18] where the carboxylato group of His occupies an apical position within the same molecule. The difference in coordination has been attributed to slightly higher basicity of the carboxylato group of L-Ala as compared with that of L-Thr and of L-Asn and resulting lower electronegativity of copper(II).[36] Considering that the difference in the acid dissociation constants ($<$0.3 log unit) does not seem to be large enough to warrant such a structural difference, however, we are inclined to ascribe it to the absence of the intramolecular ligand-ligand interaction in Cu(L-Ala)(L-His).

We are grateful to Professor Yoshio Sasaki, Osaka University, for helpful comments and encouragement. This work was supported by a Grant-in-Aid for Scientific Research from the Ministry of Education, Science and Culture, to which our thanks are due.

References

1) E. Frieden, *J. Chem. Educ.*, **52**, 754 (1975).
2) H. Sigel, *Angew. Chem. Int. Ed. Engl.*, **14**, 394 (1975).
3) H. Sigel and C. F. Naumann, *J. Am. Chem. Soc.*, **98**, 730 (1976).
4) P. Chaudhuri and H. Sigel, *J. Am. Chem. Soc.*, **99**, 3142 (1977).
5) Y. Fukuda, P. R. Mitchell, and H. Sigel, *Helv. Chim. Acta*, **61**, 638 (1978).
6) P. R. Mitchell and H. Sigel, *J. Am. Chem. Soc.*, **100**, 1564 (1978).
7) P. R. Mitchell, B. Prijs, and H. Sigel, *Helv. Chim. Acta*, **62**, 1723 (1979).
8) J. B. Orenberg, B. E. Fischer, and H. Sigel, *J. Inorg. Nucl. Chem.*, **42**, 785 (1980).
9) K. H. Scheller, F. Hofstetter, P. R. Mitchell, B. Prijs, and H. Sigel, *J. Am. Chem. Soc.*, **103**, 247 (1981).
10) K. Aoki, *J. Am. Chem. Soc.*, **100**, 7106 (1978).
11) O. Yamauchi, Y. Nakao, and A. Nakahara, *Bull. Chem. Soc. Jpn.*, **48**, 2572 (1975).
12) T. Sakurai, O. Yamauchi, and A. Nakahara, *Bull. Chem. Soc. Jpn.*, **49**, 169 (1976).
13) T. Sakurai, O. Yamauchi, and A. Nakahara, *Bull. Chem. Soc. Jpn.*, **49**, 1579 (1976).
14) T. Sakurai, O. Yamauchi, and A. Nakahara, *J. Chem. Soc., Chem. Commun.*, **1976**, 553; O. Yamauchi, T. Sakurai, and A. Nakahara, *Bull. Chem. Soc. Jpn.*, **50**, 1776 (1977).
15) O. Yamauchi and A. Odani, *J. Am. Chem. Soc.*, **103**, 391 (1981).
16) O. Yamauchi, T. Sakurai, and A. Nakahara, *J. Am. Chem. Soc.*, **101**, 4164 (1979).
17) T. Sakurai, O. Yamauchi, and A. Nakahara, *J. Chem. Soc., Chem. Commun.*, **1977**, 718.
18) T. Ono, H. Shimanouchi, Y. Sasada, T. Sakurai, O. Yamauchi, and A. Nakahara, *Bull. Chem. Soc. Jpn.*, **52**, 2229 (1979).
19) O. Yamauchi, T. Takaba, and T. Sakurai, *Bull. Chem. Soc. Jpn.*, **53**, 106 (1980); correction, *ibid.*, **53**, 836 (1980).
20) N. C. Davis, *J. Biol. Chem.*, **223**, 935 (1956).
21) N. Camerman, J. K. Fawcett, T. P. A. Kruck, B. Sarkar, and A. Camerman, *J. Am. Chem. Soc.*, **100**, 2690 (1978).
22) L. E. Erickson, J. W. McDonald, J. K. Howie, and R. P. Clow, *J. Am. Chem. Soc.*, **90**, 6371 (1968).
23) E. W. Wilson, Jr., and R. B. Martin, *Inorg. Chem.*, **9**, 528 (1970).
24) J. M. Tsangaris and R. B. Martin, *J. Am. Chem. Soc.*, **92**, 4255 (1970); R. B. Martin, "Metal Ions in Biological Systems," ed by H. Sigel, Marcel Dekker, New York (1974), Vol. 1, p. 129.
25) M. H. Freedman, J. R. Lyerla, Jr., I. M. Chaiken, and J. S. Cohen, *Eur. J. Biochem.*, **32**, 215 (1973); D. H. Sachs, A. N. Schechter, and J. S. Cohen, *J. Biol. Chem.*, **246**, 6576 (1971); H. L. Surprenant, J. E. Sarneski, R. R. Key, J. T. Byrd, and C. N. Reilley, *J. Magn. Reson.*, **40**, 231 (1980).
26) C. G. Van Kralingen, J. K. De Ridder, and J. Reedijk, *Inorg. Chim. Acta*, **36**, 69 (1979).
27) H. C. Freeman, J. M. Guss, M. J. Healy, R.-P. Martin, C. E. Nockolds, and B. Sarkar, *Chem. Commun.*, **1969**, 225.
28) F. Dahan, *Acta Crystallogr., Sect. B*, **32**, 2472 (1976).
29) H. Ishizuka, T. Yamamoto, Y. Arata, and S. Fujiwara, *Bull. Chem. Soc. Jpn.*, **46**, 468 (1973); A. Allain, M. Kubiak, B. Jezowska-Trzebiatowska, H. Kozłowski, and T. Głowiak, *Inorg. Chim. Acta*, **46**, 127 (1980).
30) K. G. R. Pachler, *Spectrochim. Acta*, **20**, 581 (1964).
31) R. B. Martin, *J. Phys. Chem.*, **83**, 2404 (1979); P. I. Vestues and R. B. Martin, *J. Am. Chem. Soc.*, **102**, 7906 (1980).
32) A. Odani and O. Yamauchi, *Inorg. Chim. Acta*, **46**, L63 (1980).

33) B. Sarkar and T. P. A. Kruck, "The Biochemistry of Copper," ed by J. Peisach, P. Aisen, and W. E. Blumberg, Academic Press, New York and London (1966), p. 183.
34) P. Z. Neumann and A. Sass-Kortsak, *J. Clin. Invest.*, **46**, 646 (1967).
35) M. Pinkerton and L. K. Steinrauf, *J. Mol. Biol.*, **49**, 533 (1970); W. L. Duax, G. D. Smith, and P. D. Strong, *J. Am. Chem. Soc.*, **102**, 6725 (1980).
36) T. Ono and Y. Sasada, *Bull. Chem. Soc. Jpn.*, **54**, 90 (1981).

Solubility Diagrams of Cobalt(III) Complexes Containing Amino Acid. I. Spontaneous Resolution of Tetraammine-(valinato or leucinato)cobalt(III) Salts

Kazuaki YAMANARI,* Shigeru NAITO, and Yoichi SHIMURA
Department of Chemistry, Faculty of Science, Osaka University, Toyonaka, Osaka 560
(Received May 11, 1981)

The binary and ternary solubility phase diagrams of the racemic and optically active complexes, $[Co(val)(NH_3)_4]X_2$ and $[Co(leu)(NH_3)_4]X_2$ ($X=(1/2)SO_4^{2-}$, Cl^-, Br^-, and I^-), were determined in water. Spontaneous resolution was found for $[Co(DL\text{-}val)(NH_3)_4]X_2$ ($X=Cl^-$ and Br^-) at 5—55 °C and for $[Co(DL\text{-}leu)(NH_3)_4]SO_4$ at 30—55 °C, the latter of which has been shown to crystallize as both a racemic compound (below 30 °C) and a conglomerate (above 30 °C).

A variety of metal complexes containing racemic amino acid have been prepared, but in most of the cases it remains unknown whether the complex is a racemic mixture (conglomerate) or a racemic compound (double salt between enantiomers), because no solubility isotherm has been reported for the system of such amino acid complexes.

The present paper deals with the binary and ternary solubility diagrams of cobalt(III) complexes, $[Co(L\text{- or }DL\text{-val})(NH_3)_4]X_2$ and $[Co(L\text{- or }DL\text{-leu})(NH_3)_4]X_2$, where val and leu denote a valinate and a leucinate ligand, respectively, and X stands for a univalent anion of Cl^-, Br^-, I^-, or $(1/2)SO_4^{2-}$. The tetraammine type complexes have the only chirality based on that of amino acid.[1] In the case of spontaneous resolution of such a complex, optical resolution of amino acid is realized in each of crystals. Therefore, if an effective recovery route from the metal complex is established, this procedure will be applicable to optical resolution of amino acid. Few reports have been published for the utilization of metal chelate compounds for the optical resolution of racemic amino acids.[2]

Experimental

Materials. *$[Co(L\text{-}val)(NH_3)_4]SO_4\cdot H_2O$*: The complex was prepared from $[Co(H_2O)(NH_3)_5](ClO_4)_3$ and L-valine according to the method of Yasui *et al.*[3] and separated on a column of SP-Sephadex C-25 (Na^+ form) by elution of 0.15 mol dm^{-3} Na_2SO_4. The orange red eluate was evaporated to give the desired crystals, which were recrystallized from water at 50 °C. Found: C, 16.82; H, 6.76; N, 19.75%. Calcd for $[Co(L\text{-val})(NH_3)_4]SO_4\cdot H_2O=C_5H_{24}N_5O_7SCo$: C, 16.81; H, 6.77; N, 19.60%.

$[Co(DL\text{-}val)(NH_3)_4]SO_4\cdot 2H_2O$: This cymplex was prepared by the same procedure as described above except for the use of DL-valine instead of L-valine. Found: C, 16.17; H, 6.83; N, 18.76%. Calcd for $[Co(DL\text{-val})(NH_3)_4]SO_4\cdot 2H_2O=C_5H_{26}N_5O_8SCo$: C, 16.00; H, 6.98; N, 18.66%.

$[Co(L\text{-}val)(NH_3)_4]X_2$ ($X=Cl$, Br, and I): The above sulfate salt of L-valinato complex was converted into the desired salts by ion exchangers (Dowex 50W-X2 for Cl^- or Br^- form; QAE-Sephadex A-25 for I^- form). Found for chloride salt: C, 19.18; H, 7.05; N, 22.27%. Calcd for $[Co(L\text{-val})(NH_3)_4]Cl_2=C_5H_{22}N_5O_2Cl_2Co$: C, 19.12; H, 7.06; N, 22.29%. Found for bromide salt: C, 15.02; H, 5.52; N, 17.35%. Calcd for $[Co(L\text{-val})(NH_3)_4]Br_2=C_5H_{22}N_5O_2Br_2Co$: C, 14.90; H, 5.50; N, 17.37%. Found for iodide salt: C, 12.18; H, 4.48; N, 13.94%. Calcd for $[Co(L\text{-val})(NH_3)_4]I_2=C_5H_{22}N_5O_2I_2Co$: C, 12.08; H, 4.46; N, 14.09%.

$[Co(DL\text{-}val)(NH_3)_4]X_2\cdot nH_2O$ ($X=Cl$, Br, and I): These complexes were prepared by the same method as that for the corresponding L-valinato complexes. Found for chloride salt: C, 19.13; H, 7.01; N, 22.18%. Calcd for $[Co(DL\text{-val})(NH_3)_4]Cl_2=C_5H_{22}N_5O_2Cl_2Co$: C, 19.12; H, 7.06; N, 22.29%. Found for bromide salt: C, 14.82; H, 5.50; N, 17.27%. Calcd for $[Co(DL\text{-val})(NH_3)_4]Br_2=C_5H_{22}N_5O_2Br_2Co$: C, 14.90; H, 5.50; N, 17.37%. Found for iodide salt: C, 11.89; H, 4.65; N, 13.52%. Calcd for $[Co(DL\text{-val})(NH_3)_4]I_2\cdot 0.5H_2O=C_5H_{23}N_5O_{2.5}I_2Co$: C, 11.87; H, 4.58; N, 13.84%.

$[Co(L\text{-}leu)(NH_3)_4]SO_4$ and $[Co(DL\text{-}leu)(NH_3)_4]SO_4\cdot 2H_2O$: These complexes were prepared by the same method as that for $[Co(L\text{-val})(NH_3)_4]SO_4$ with the use of L-leucine or DL-leucine instead of L-valine. Found for L-leucinato complex: C, 20.16; H, 6.82; N, 19.61%. Calcd for $[Co(L\text{-leu})(NH_3)_4]SO_4=C_6H_{24}N_5O_6SCo$: C, 20.40; H, 6.85; N, 19.82%. Found for DL-leucinato complex: C, 17.96; H, 7.20; N, 17.41%. Calcd for $[Co(DL\text{-leu})(NH_3)_4]SO_4\cdot 2H_2O=C_6H_{28}N_5O_8SCo$: C, 18.06; H, 7.34; N, 17.58%.

$[Co(L\text{-}leu)(NH_3)_4]X_2\cdot H_2O$ and $[Co(DL\text{-}leu)(NH_3)_4]X_2\cdot H_2O$ ($X=Cl$, Br, and I): These complexes were prepared from the corresponding sulfate salt by the ion exchangers described above. Found for chloride of L-leucinato complex: C, 20.65; H, 7.44; N, 20.01%. Calcd for $[Co(L\text{-leu})(NH_3)_4]Cl_2\cdot H_2O=C_6H_{26}N_5O_3Cl_2Co$: C, 20.82; H, 7.57; N, 20.23%. Found for bromide of L-leucinato one: C, 16.55; H, 5.98; N, 16.02%. Calcd for $[Co(L\text{-leu})(NH_3)_4]Br_2\cdot H_2O=C_6H_{26}N_5O_3Br_2Co$: C, 16.56; H, 6.02; N, 16.10%. Found for iodide of L-leucinato one: C, 13.63; H, 4.96; N, 13.35%. Calcd for $[Co(L\text{-leu})(NH_3)_4]I_2\cdot H_2O=C_6H_{26}N_5O_3I_2Co$: C, 13.62; H, 4.95; N, 13.24%. Found for chloride of DL-leucinato one: C, 20.89; H, 7.43; N, 19.90%. Calcd for $[Co(DL\text{-leu})(NH_3)_4]Cl_2\cdot H_2O=C_6H_{26}N_5O_3Cl_2Co$: C, 20.82; H, 7.57; N, 20.23%. Found for bromide of DL-leucinato one: C, 16.47; H, 5.95; N, 15.97%. Calcd for $[Co(DL\text{-leu})(NH_3)_4]Br_2\cdot H_2O=C_6H_{26}N_5O_3Br_2Co$: C, 16.56; H, 6.02; N, 16.10%. Found for iodide of DL-leucinato one: C, 13.66; H, 4.96; N, 13.37%. Calcd for $[Co(DL\text{-leu})(NH_3)_4]I_2\cdot H_2O=C_6H_{26}N_5O_3I_2Co$: C, 13.62; H, 4.95; N, 13.24%.

Measurements. Solubility in water was determined according to the previously reported method.[4] The absorption and CD maximum values which were used for the calculations of concentrations of complexes in solutions are summarized in Table 1. The solid phases were identified from elemental analyses, absorption, CD, and infrared spectra. Optical densities were measured with a JASCO UVIDEC-1 spectrophotometer, CD with a JASCO MOE-1 spectropolarimeter, and infrared spectra with a JASCO DS-402G spectrophotometer.

Table 1. Absorption and CD maximum values used for calculation of solubility[a)]

Complex salt	$\varepsilon(\lambda_{max})$	$\Delta\varepsilon(\lambda_{max})$
$[Co(L\text{-val})(NH_3)_4]SO_4$	83.48 (495)	−0.426 (462)
$[Co(DL\text{-val})(NH_3)_4]SO_4$	83.48 (495)	
$[Co(L\text{-val})(NH_3)_4]Cl_2$	81.98 (495)	−0.418 (462)
$[Co(DL\text{-val})(NH_3)_4]Cl_2$	81.98 (495)	
$[Co(L\text{-val})(NH_3)_4]Br_2$	82.88 (495)	−0.405 (462)
$[Co(DL\text{-val})(NH_3)_4]Br_2$	82.88 (495)	
$[Co(L\text{-val})(NH_3)_4]I_2$	72.91 (495)	−0.366 (462)
$[Co(DL\text{-val})(NH_3)_4]I_2$	72.90 (495)	
$[Co(L\text{-leu})(NH_3)_4]SO_4$	82.30 (492)	−0.326 (459)
$[Co(DL\text{-leu})(NH_3)_4]SO_4$	82.28 (492)	
$[Co(L\text{-leu})(NH_3)_4]Cl_2$	81.33 (492)	−0.329 (459)
$[Co(DL\text{-leu})(NH_3)_4]Cl_2$	81.33 (492)	
$[Co(L\text{-leu})(NH_3)_4]Br_2$	81.95 (492)	−0.319 (459)
$[Co(DL\text{-leu})(NH_3)_4]Br_2$	81.95 (492)	
$[Co(L\text{-leu})(NH_3)_4]I_2$	82.36 (492)	−0.327 (459)
$[Co(DL\text{-leu})(NH_3)_4]I_2$	82.37 (492)	

a) The ε and λ (in parentheses) values are given in the unit of $mol^{-1}\,dm^3\,cm^{-1}$ and nm, respectively.

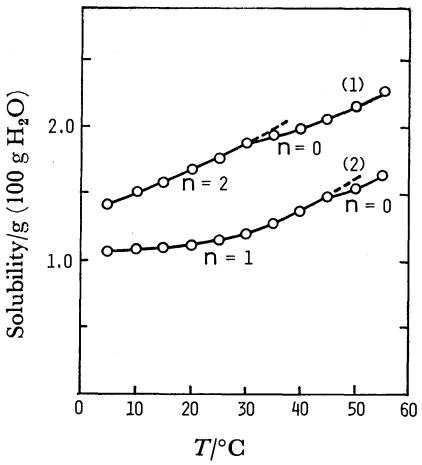

Fig. 1. Solubility curves of $[Co(L\text{-val})(NH_3)_4]SO_4\cdot nH_2O$ (1) and $[Co(DL\text{-val})(NH_3)_4]SO_4\cdot nH_2O$ (2).

Results and Discussion

The binary solubility data are given in Table 2 and Figs. 1, 3, and 5, and the ternary data in Tables 3 and 4 as well as in Figs. 2, 4, and 6—8. In the triangular isotherms the top part (H_2O corner) is enlarged for the sake of convenience and the tie lines are omitted.

The Valinato Complexes. The solubility curves of sulfate salt are shown in Fig. 1. The L-complex shows an inflection at 30 °C, at which the solid phase changes from dihydrate to anhydrate. A similar inflection appears at 45 °C for the DL-complex, corresponding to the transition from monohydrate to anhydrate. Since the solubility of L-complex is larger than that of DL-complex at 5—55 °C, the sulfate salt is not spontaneously resolvable.[5)] The ternary isotherm at 25 °C shows the formation of racemic compound $[Co(L\text{-val})(NH_3)_4][Co(D\text{-val})(NH_3)_4](SO_4)_2\cdot 4H_2O = [Co(DL\text{-val})(NH_3)_4]SO_4\cdot 2H_2O$ (Fig. 2).[4)]

The solubility curves of bromide salt are shown in Fig. 3. The solubility ratio of DL-complex/L-complex is 1.46 at 5 °C and 1.40 at 55 °C. For a spontaneously resolvable 1 : 2 electrolyte, the ratio must be larger than $2^{1/3}=1.26$.[5)] Therefore, the bromide salt is spontaneously resolvable. The ternary solubility isotherm at 25 °C (Fig. 4) shows the only one invariant point. This fact confirms that the two enantiomers form a racemic mixture in the solid state. The racemate of free valine does not form a racemic mixture. This is the first example, in which the complexation of amino acid enabled the spontaneous resolution. The chloride salt shows a similar solubility relationship to the bromide salt, the ratio of DL-complex/L-complex being 1.30 at 5 °C and 1.28 at 55 °C. A crystal, which precipitated out of the racemic solution, showed the same CD

Table 2. Solubility of the complex salts
(Grams of anhydrous salt in 100 g of water.)

T/°C	No. of complex salt[a)]																		
	1	2	3	4	5	6	7	8	9	10	11	12	13	14	15	16	17	18	19
5	1.42		1.07		12.6	16.4	7.00	10.2	3.62	1.19	1.47	4.37		147	66.1	6.90	6.32	1.76	1.68
10	1.50		1.08		13.8	18.0	7.75	11.2	4.59	2.12	1.49	4.59		153	73.5	7.90	7.21	2.07	1.95
15	1.58		1.10		15.0	19.5	8.60	12.5	5.71	3.05	1.53	4.87		162	81.2	9.07	8.34	2.46	2.36
20	1.68		1.12		16.4	21.3	9.71	14.1	6.83	4.28	1.59	5.19		172	90.5	10.4	9.64	2.86	2.77
25	1.77		1.15		17.7	23.0	11.2	16.3	8.17	5.56	1.63	5.56		184	99.8	11.9	11.0	3.40	3.26
30		1.88	1.20		19.2	25.0	12.5	18.2	9.79	6.99	1.68	5.93		195	112	13.5	12.4	3.95	3.82
35		1.93	1.27		20.5	26.7	14.0	20.4	11.6	8.38	1.74		6.27			15.4	14.1	4.61	4.46
40		1.99	1.37		22.7	29.2	15.7	22.8	13.4	9.98	1.78		6.75			17.6	16.0	5.37	5.20
45		2.05		1.47	24.0	31.2	17.5	25.5	15.4	11.6	1.85		7.10			20.0	18.3	6.25	6.07
50		2.14		1.53	25.6	33.4	19.6	28.0	17.7	13.6	1.92		7.68			22.7	20.7	7.21	7.01
55		2.26		1.63	27.6	35.4	21.9	30.6	20.3	16.0	2.00		8.29			25.7	23.3	8.25	8.02

a) **1**: $[Co(L\text{-val})(NH_3)_4]SO_4\cdot H_2O$, **2**: $[Co(L\text{-val})(NH_3)_4]SO_4$, **3**: $[Co(DL\text{-val})(NH_3)_4]SO_4\cdot 2H_2O$, **4**: $[Co(DL\text{-val})(NH_3)_4]SO_4$, **5**: $[Co(L\text{-val})(NH_3)_4]Cl_2$, **6**: $[Co(DL\text{-val})(NH_3)_4]Cl_2$, **7**: $[Co(L\text{-val})(NH_3)_4]Br_2$, **8**: $[Co(DL\text{-val})(NH_3)_4]Br_2$, **9**: $[Co(L\text{-val})(NH_3)_4]I_2$, **10**: $[Co(DL\text{-val})(NH_3)_4]I_2\cdot 0.5H_2O$, **11**: $[Co(L\text{-leu})(NH_3)_4]SO_4$, **12**: $[Co(DL\text{-leu})(NH_3)_4]SO_4\cdot 2.5H_2O$, **13**: $[Co(DL\text{-leu})(NH_3)_4]SO_4$, **14**: $[Co(L\text{-leu})(NH_3)_4]Cl_2\cdot H_2O$, **15**: $[Co(DL\text{-leu})(NH_3)_4]Cl_2\cdot H_2O$, **16**: $[Co(L\text{-leu})(NH_3)_4]Br_2\cdot H_2O$, **17**: $[Co(DL\text{-leu})(NH_3)_4]Br_2\cdot H_2O$, **18**: $[Co(L\text{-leu})(NH_3)_4]I_2\cdot H_2O$, and **19**: $[Co(DL\text{-leu})(NH_3)_4]I_2\cdot H_2O$.

TABLE 3. SOLUBILITY IN THE TERNARY SYSTEMS, H_2O–[Co(L-val)$(NH_3)_4$]X_2–[Co(D-val)$(NH_3)_4$]X_2
Solubility is given in weight % of anhydrous salt. Abbreviations: [Co(L-val)$(NH_3)_4$]$X_2\cdot nH_2O$=[L]$X_2\cdot nH_2O$, [Co(D-val)$(NH_3)_4$]$X_2\cdot nH_2O$=[D]$X_2\cdot nH_2O$, and [Co(DL-val)$(NH_3)_4$]$X_2\cdot nH_2O$=[DL]$X_2\cdot nH_2O$.

X	Liquid phase composition (wt%)		Solid phase
	[L]X_2	[D]X_2	
(1/2)SO_4	1.70	0	[L]$SO_4\cdot H_2O$
(25 °C)	1.69	0.05	[L]$SO_4\cdot H_2O$
	1.68	0.16	[L]$SO_4\cdot H_2O$
	1.68	0.22	[L]$SO_4\cdot H_2O$
	1.69	0.23	[L]$SO_4\cdot H_2O$+[DL]$SO_4\cdot 2H_2O$
	1.65	0.24	[DL]$SO_4\cdot 2H_2O$
	1.55	0.24	[DL]$SO_4\cdot 2H_2O$
	1.37	0.26	[DL]$SO_4\cdot 2H_2O$
	1.20	0.28	[DL]$SO_4\cdot 2H_2O$
	1.10	0.31	[DL]$SO_4\cdot 2H_2O$
	0.96	0.35	[DL]$SO_4\cdot 2H_2O$
	0.89	0.38	[DL]$SO_4\cdot 2H_2O$
	0.74	0.45	[DL]$SO_4\cdot 2H_2O$
	0.66	0.50	[DL]$SO_4\cdot 2H_2O$
	0.60	0.55	[DL]$SO_4\cdot 2H_2O$
	0.57	0.57	[DL]$SO_4\cdot 2H_2O$
Br	10.1	0	[L]Br_2
(25 °C)	10.0	0.15	[L]Br_2
	9.87	0.35	[L]Br_2
	9.66	0.72	[L]Br_2
	9.32	1.38	[L]Br_2
	9.01	2.01	[L]Br_2
	8.55	2.98	[L]Br_2
	8.32	3.72	[L]Br_2
	7.71	5.08	[L]Br_2
	7.46	5.85	[L]Br_2
	7.17	6.69	[L]Br_2
	7.09	6.95	[L]Br_2
	7.11	7.11	[L]Br_2+[D]Br_2
I	7.55	0	[L]I_2
(25 °C)	7.64	0.41	[L]I_2+[DL]$I_2\cdot 0.5H_2O$
	7.36	0.52	[DL]$I_2\cdot 0.5H_2O$
	6.86	0.53	[DL]$I_2\cdot 0.5H_2O$
	6.15	0.62	[DL]$I_2\cdot 0.5H_2O$
	5.53	0.89	[DL]$I_2\cdot 0.5H_2O$
	4.76	1.15	[DL]$I_2\cdot 0.5H_2O$
	4.25	1.42	[DL]$I_2\cdot 0.5H_2O$
	3.56	1.80	[DL]$I_2\cdot 0.5H_2O$
	3.43	2.09	[DL]$I_2\cdot 0.5H_2O$
	2.78	2.52	[DL]$I_2\cdot 0.5H_2O$
	2.64	2.64	[DL]$I_2\cdot 0.5H_2O$

spectra as that of the active complex.

With the iodide salt, the active complex (0.5-hydrate) is more soluble than the anhydrous racemate. No optical rotation was observed for the crystals out of the racemic solution. The result was confirmed by the ternary isotherm at 25 °C which indicates the existence of a racemic compound [Co(L-val)$(NH_3)_4$][Co(D-val)-$(NH_3)_4$]I_4=[Co(DL-val)$(NH_3)_4$]I_2 (Tables 2 and 3).

The Leucinato Complexes. The solubility curves of

TABLE 4. SOLUBILITY IN THE TERNARY SYSTEMS, H_2O–[Co(L-leu)$(NH_3)_4$]X_2–[Co(D-leu)$(NH_3)_4$]X_2
Solubility is given in weight % of anhydrous salt. Abbreviations: [Co(L-leu)$(NH_3)_4$]$X_2\cdot nH_2O$=[L]$X_2\cdot nH_2O$, [Co(D-leu)$(NH_3)_4$]$X_2\cdot nH_2O$=[D]$X_2\cdot nH_2O$, and [Co(DL-leu)$(NH_3)_4$]$X_2\cdot nH_2O$=[DL]$X_2\cdot nH_2O$.

X	Liquid phase composition (wt%)		Solid phase
	[L]X_2	[D]X_2	
(1/2)SO_4	1.57	0	[L]SO_4
(25 °C)	1.58	0.07	[L]SO_4
	1.58	0.21	[L]SO_4
	1.60	0.46	[L]SO_4
	1.62	0.60	[L]SO_4
	1.67	0.93	[L]SO_4
	1.69	1.15	[L]SO_4
	1.73	1.24	[L]SO_4
	1.75	1.37	[L]SO_4
	1.83	1.54	[L]SO_4
	1.87	1.64	[L]SO_4
	1.94	1.80	[L]SO_4
	2.06	1.95	[L]SO_4
	2.14	2.06	[L]SO_4
	2.25	2.18	[L]SO_4
	2.33	2.29	[L]SO_4
	2.42	2.38	[L]SO_4
	2.51	2.43	[L]SO_4+[DL]$SO_4\cdot 2.5H_2O$
	2.47	2.47	[DL]$SO_4\cdot 2.5H_2O$
(1/2)SO_4	1.74	0	[L]SO_4
(35 °C)	1.72	0.08	[L]SO_4
	1.71	0.21	[L]SO_4
	1.74	0.27	[L]SO_4
	1.72	0.42	[L]SO_4
	1.74	0.51	[L]SO_4
	1.75	0.70	[L]SO_4
	1.78	0.86	[L]SO_4
	1.82	0.98	[L]SO_4
	1.87	1.14	[L]SO_4
	1.92	1.33	[L]SO_4
	1.99	1.55	[L]SO_4
	2.06	1.78	[L]SO_4
	2.10	1.89	[L]SO_4
	2.11	1.96	[L]SO_4
	2.19	2.06	[L]SO_4
	2.29	2.20	[L]SO_4
	2.38	2.32	[L]SO_4
	2.52	2.52	[L]SO_4+[D]SO_4
Br	10.6	0	[L]$Br_2\cdot H_2O$
(25 °C)	10.6	0.1	[L]$Br_2\cdot H_2O$+[DL]$Br_2\cdot H_2O$
	10.3	0.3	[DL]$Br_2\cdot H_2O$
	9.91	0.60	[DL]$Br_2\cdot H_2O$
	9.51	0.91	[DL]$Br_2\cdot H_2O$
	8.62	1.65	[DL]$Br_2\cdot H_2O$
	7.75	2.38	[DL]$Br_2\cdot H_2O$
	7.91	3.14	[DL]$Br_2\cdot H_2O$
	6.54	3.47	[DL]$Br_2\cdot H_2O$
	6.04	3.94	[DL]$Br_2\cdot H_2O$
	5.47	4.45	[DL]$Br_2\cdot H_2O$
	4.94	4.94	[DL]$Br_2\cdot H_2O$

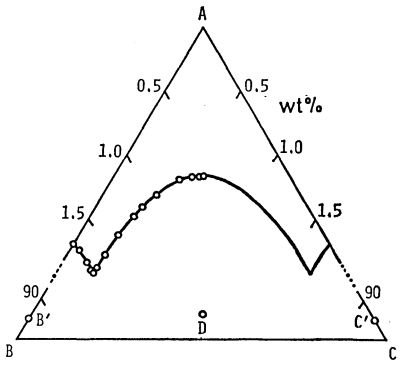

Fig. 2. Solubility isotherm of the system H_2O(A)–[Co(L-val)$(NH_3)_4]SO_4$(B)–[Co(D-val)$(NH_3)_4]SO_4$(C) at 25 °C. The solid phase B′ or C′ is monohydrate of B or C, respectively, and D [Co(DL-val)$(NH_3)_4]SO_4\cdot 2H_2O$.

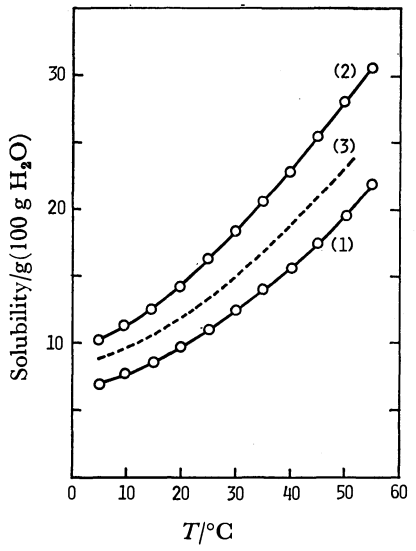

Fig. 3. Solubility curves of [Co(L-val)$(NH_3)_4]Br_2$(1), [Co(DL-val)$(NH_3)_4]Br_2$(2), and calculated curve (3) : (1)$\times \sqrt[3]{2}$.

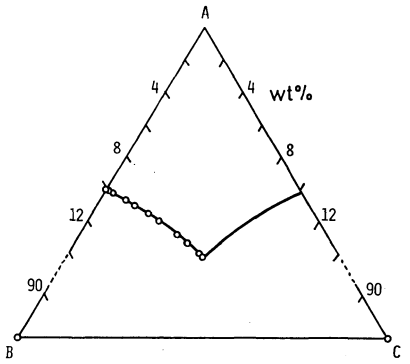

Fig. 4. Solubility isotherm of the system H_2O(A)–[Co(L-val)$(NH_3)_4]Br_2$(B)–[Co(D-val)$(NH_3)_4]Br_2$(C) at 25 °C.

[Co(L-leu)$(NH_3)_4]SO_4$ and [Co(DL-leu)$(NH_3)_4]SO_4$ are shown in Fig. 5. The solubility ratio of DL-complex/L-complex is 2.97 at 5 °C and 4.15 at 55 °C which goes well beyond $2^{1/2}=1.41$ expected for 1 : 1 electrolyte.[5] The racemate shows an inflection at *ca.* 30 °C where the solid phase changes from 2.5-hydrate (below 30 °C)

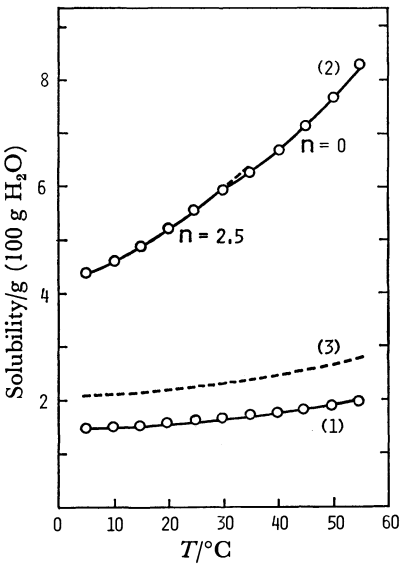

Fig. 5. Solubility curves of [Co(L-leu)$(NH_3)_4]SO_4$(1), [Co(DL-leu)$(NH_3)_4]SO_4\cdot nH_2O$(2), and calculated curve(3) : (1)$\times\sqrt{2}$.

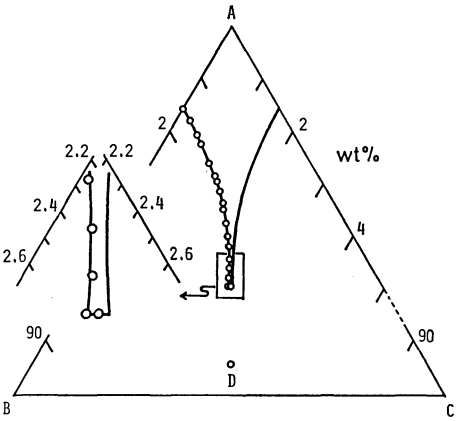

Fig. 6. Solubility isotherm of the system H_2O(A)–[Co(L-leu)$(NH_3)_4]SO_4$(B)–[Co(D-leu)$(NH_3)_4]SO_4$(C) at 20 °C.
The solid phase D is [Co(DL-leu)$(NH_3)_4]SO_4\cdot 2.5H_2O$.

to anhydrate. On the other hand, the anhydrous active complex shows no solid phase change at 5—55 °C. If the racemate forms a racemic mixture, the racemate and the pure enantiomer must have the same composition and crystal structure. Therefore, spontaneous resolution seems to be possible at temperatures higher than 30 °C in this case. The ternary isotherm at 20 °C reveals the formation of racemic compound [Co(L-leu)$(NH_3)_4$]-[Co(D-leu)$(NH_3)_4](SO_4)_2\cdot 5H_2O$= [Co(DL-leu)$(NH_3)_4$]-$SO_4\cdot 2.5H_2O$, though the region for this compound is significantly narrow as compared with those of the pure enantiomers (Fig. 6). The infrared spectra also indicate that the solid crystallized out of racemic solution at 20 °C is different from the optically active complex. As is shown in Fig. 7, the region of the racemic compound disappears at 35 °C and the only invariant point exists in the ternary isotherm. Thus, the racemic sulfate [Co(DL-leu)$(NH_3)_4]SO_4$ crystallizes as both the racemic compound (below 30 °C) and the conglomerate (above 30 °C).

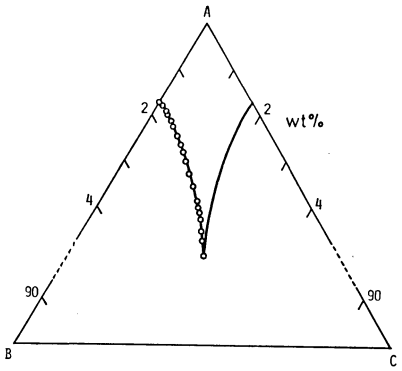

Fig. 7. Solubility isotherm of the system H_2O(A)–[Co(L-leu)$(NH_3)_4$]SO_4(B)–[Co(D-leu)$(NH_3)_4$]SO_4(C) at 35 °C.

The solubility ratio DL-complex/L-complex at temperatures of 5—30 °C goes well beyond $2^{1/2}=1.41$ (Fig. 5), but spontaneous resolution did not occur in this sulfate salt. This fact may be explained in relation to the characteristics of SO_4^{2-} ion, which has been reported to have a strong tendency to associate with various ammine or amine cobalt(III) complexes.[6] The ion-pair formation affects the activity coefficients of the complexes to a great extent and causes the apparent large solubility ratio.

All the halide salts of leucinato complexes are monohydrate regardless of whether it is racemate or active form. The solubility of racemate is lower than that of the corresponding active form, no spontaneous resolution being observed. Figure 8 shows the ternary isotherm of [Co(leu)$(NH_3)_4$]Br_2 at 25 °C. The extremely flat curve of the racemic compound is spread over a wide region and the region of pure enantiomers are much suppressed.

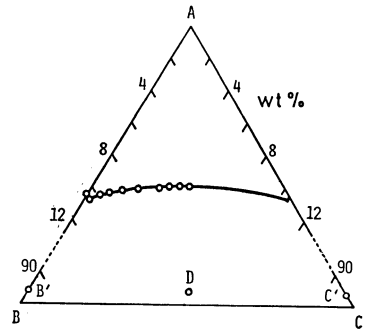

Fig. 8. Solubility isotherm of the system H_2O(A)–[Co(L-leu)$(NH_3)_4$]Br_2(B)–[Co(D-leu)$(NH_3)_4$]Br_2(C) at 20 °C. The solid phase B′ or C′ is monohydrate of B or C, respectively, and D [Co(DL-leu)$(NH_3)_4$]$Br_2\cdot H_2O$.

References

1) Y. Shimura, *Bull. Chem. Soc. Jpn.*, **31**, 315 (1958).

2) A. D. Gott and J. C. Bailar, *J. Am. Chem. Soc.*, **74**, 4820 (1952); B. D. Sarma and J. C. Bailar, *ibid.*, **78**, 895 (1956); K. Harada and S. W. Fox, *Nature*, **194**, 768 (1962); M. Shibata, Y. Fujita, M. Naito, and K. Hori, *Bull. Chem. Soc. Jpn.*, **36**, 485 (1963).

3) T. Yasui, J. Hidaka, and Y. Shimura, *Bull. Chem. Soc. Jpn.*, **39**, 2417 (1966).

4) Y. Shimura and K. Tsutsui, *Bull. Chem. Soc. Jpn.*, **50**, 145 (1977).

5) K. Yamanari, J. Hidaka, and Y. Shimura, *Bull. Chem. Soc. Jpn.*, **46**, 3724 (1973).

6) L. G. Sillen and A. E. Martell, "Stability Constants of Metal-Ion Complexes," Chemical Society, London (1964, 1971).

Multiple Paths for Photo-methylation and -methoxylation of Methyl 2-Pyridinecarboxylate in Methanol

Toru SUGIYAMA, Toshikazu FURIHATA, Kyoko TAKAGI, Michitsugu SATO, Shinya AKIYAMA, Gen P. SATÔ, and Akira SUGIMORI*

Department of Chemistry, Faculty of Science and Technology, Sophia University, Kioi-cho 7-1, Chiyoda-ku, Tokyo 102

(Received September 12, 1980)

UV-irradiation of methyl 2-pyridinecarboxylate in methanol in the absence of added acid brings about methylation at the 5-position *via* the excitation of C=O of the ester group, while in the presence of added acid the 4-position of the pyridine ring is methylated. In the presence of sulfuric acid methoxylation *via* an excimer is dominant over methylation. In the presence of hydrochloric acid methylation *via* chlorine atoms becomes dominant.

Pyridinecarboxylic acids and their derivatives show a variety of photoreactions. In alcoholic solutions they undergo photochemical decarboxylation, alkylation, hydroxyalkylation, and alkoxylation.[1-4] The features of the photoreactions of the derivatives of pyridinecarboxylic acids are: 1) the photoreactivities are sensitive to the reaction conditions (the nature of the solvents, the concentration of the substrate, the added acids, the concentration of the added acid, and the additives), 2) the same products can be derived from the different excited states, and 3) the simultaneous contribution of several types of excited states.

Previously we reported the detailed analyses of the photoreactions of 3-pyridinecarboxylic ester in alcoholic solutions.[2] We report here the analysis of the photoreactions of 2-pyridinecarboxylic ester in alcohol.[5]

Results and Discussion

Similar to 3-pyridinecarboxylic ester, methyl 2-pyridinecarboxylate (**1**) undergoes the substitution of the ring hydrogen by alkyl or alkoxyl group derived from the solvent alcohol upon the UV-irradiation of **1** in the presence of sulfuric or hydrochloric acid.

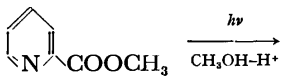

(1)

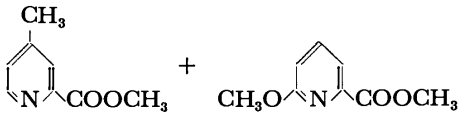

(2) (3)

The photo-methylation and -methoxylation of **1** are dependent on the reaction conditions: 1) concentration of the substrate, 2) added acid, and 3) additives.

In Figs. 1 and 2 are shown the dependencies of the photoreactions and the molar absorption coefficient of **1** on the concentration of the added acid at 10^{-3} mol dm^{-3} of **1**. The change in the molar absorption coefficient corresponds to the protonation and the deprotonation of the pyridine derivatives. The dependence of the efficiency of the photoreactions on the acid concentration correlates well with the dependence of the molar absorption coefficient on the acid concentration. This suggests that the photo-methylation and -methoxylation occur effectively, when the substrate is protonated.

In the photoreaction of **1** in methanol in the presence of H_2SO_4, the methoxylation at the 6-position is dominant and the methylation occurs in a low yield (Fig. 1). However, the methylation is promoted by hydrochloric acid, especially at its higher concentrations (Fig. 2). The addition of lithium chloride increases the yield for the methylation as is shown in Table 1. Analogous promotion of the methylation and depression of the methoxylation have been observed in the photoreaction of methyl 3-pyridinecarboxylate, for which a mechanism involving the electron transfer from chloride ion to the substrate has been proposed.[2] In the photoreaction of **1** in the presence of chloride ion, a similar mechanism should operate.

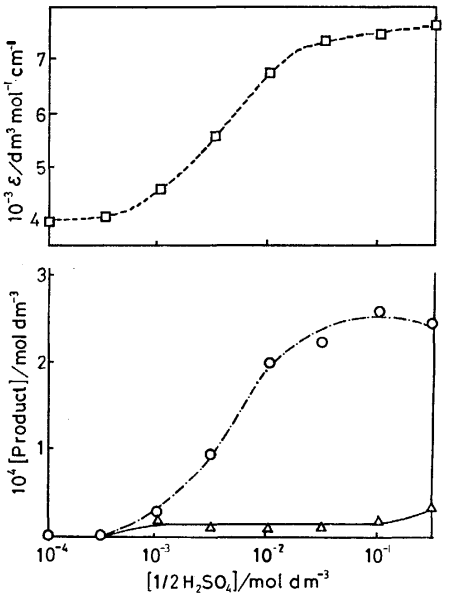

Fig. 1. Dependences of the photoreaction and the molar absorption coefficient of **1** upon the concentration of added H_2SO_4.
[**1**] = 1×10^{-3} mol dm^{-3}, irradiation time, 10 min.
—△—: Yield of **2**, ---○---: yield of **3**, ----□----: molar absorption coefficient.

The most characteristic nature of the photo-methoxylation of **1** is its concentration dependence (Fig. 3). The concentration dependence suggests the participation of a dimer species of the substrate in the photo-methoxylation.

A mechanism involving an excimer can be postulated (Scheme 1). In this Scheme, **A** and **B** represent the products of other processes than the alkoxylation.

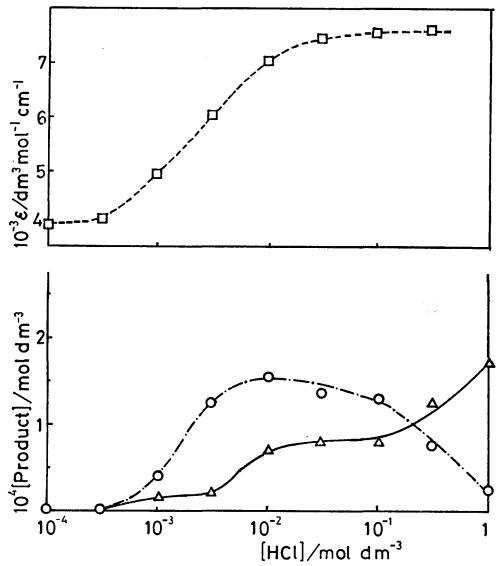

Fig. 2. Dependences of the photoreaction and the molar absorption coefficient of **1** upon the concentration of added HCl.
[**1**]$=1\times10^{-3}$ mol dm^{-3}; irradiation time, 10 min.
—△—: Yield of **2**, ···○···: yield of **3**, ----□----: molar absorption coefficient.

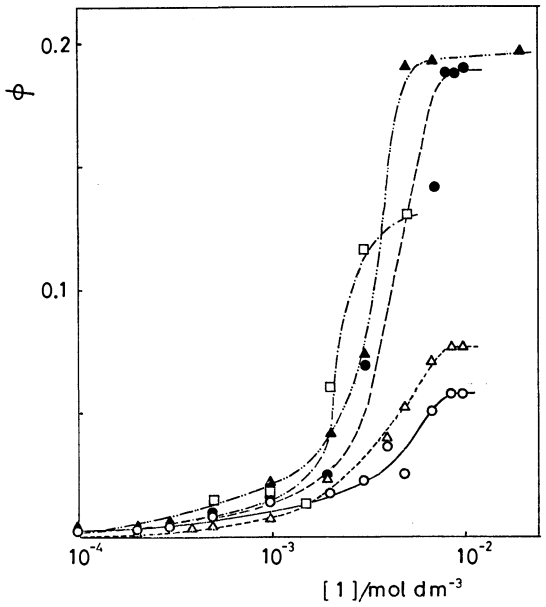

Fig. 3. Dependence of the quantum yield of photomethoxylation on the concentration of **1** at various temperatures.
[H_2SO_4]$=5\times10^{-2}$ mol dm^{-3}.
—○—: at 11 °C, ----△----: at 17.5 °C, ···□···: at 27 °C, ---●---: at 32 °C, ····▲····: at 40 °C.

The mechanism gives the following kinetic relationship:

$$1/\phi_3 = \frac{k_3[CH_3OH]+k_4+k_5}{k_3[CH_3OH]} + \frac{(k_{-1}+k_{-5})(k_{-2}+k_3[CH_3OH]+k_4+k_5)}{k_2k_3[CH_3OH]\,[\mathbf{1}]},$$

where ϕ_3 is the quantum yield of the methoxylation product *via* an excimer. The concentration of methanol

$$\mathbf{1} \underset{k_{-1}}{\overset{h\nu}{\rightleftharpoons}} \mathbf{1}^*$$

$$\mathbf{1}^* + \mathbf{1} \underset{k_{-2}}{\overset{k_2}{\rightleftharpoons}} (\mathbf{1}-\mathbf{1})^* \text{ (an excimer)}$$

$$(\mathbf{1}-\mathbf{1})^* + CH_3OH \xrightarrow{k_3} \mathbf{3}$$

$$(\mathbf{1}-\mathbf{1})^* \xrightarrow{k_4} 2\,\mathbf{1}$$

$$(\mathbf{1}-\mathbf{1})^* \xrightarrow{k_5} \mathbf{A}$$

$$\mathbf{1}^* \xrightarrow{k_6} \mathbf{B}$$

Scheme 1.

TABLE 1. EFFECT OF LITHIUM CHLORIDE ON THE PHOTOREACTION OF **1**
[**1**]$=1\times10^{-3}$ mol dm^{-3}; irradiation time, 10 min.

[HCl] / mol dm^{-3}	[LiCl] / mol dm^{-3}	Alkoxylation [**3**] / 10^{-5} mol dm^{-3}	Alkylation [**2**] / 10^{-5} mol dm^{-3}
10^{-3}	—	3.6	1.9
10^{-3}	1	0.5	5.5
3×10^{-3}	—	23	5
3×10^{-3}	1	2	14

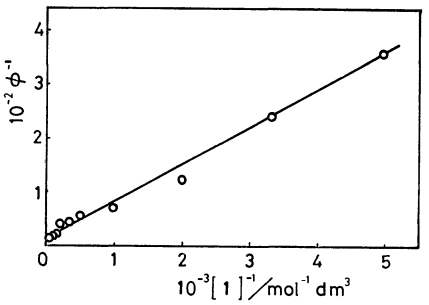

Fig. 4. Relation between the reciprocal of the quantum yields for the photomethoxylation at 40 °C and the reciprocal of the concentration of **1**.

is constant in the experimental conditions.

The plot of $1/\phi_3$ against $1/[\mathbf{1}]$ for the photo-methoxylation at 11 °C resulted in a straight line (Fig. 4) as predicted by the above equation and the mechanism *via* an excimer is thus kinetically supported.[6]

Since **1** is not fluorescent at any concentration even at the liquid nitrogen temperature, no direct evidence for the excimer has been obtained. However, the excimers of quinoline and isoquinoline have been established on the basis of the emission spectra.[7] These facts support the mechanism *via* an excimer.

The effects of additives for the photo-methylation are different from those for the photo-methoxylation. Because the additives absorb the 254 nm light competitively with the substrate, the effects of additives were analyzed by means of an index A, the relative quantum yield calculated on the basis of the light absorbed by the substrate,

$$A = Y/L$$

$$Y = \frac{\text{Yield in the presence of additive}}{\text{Yield in the absence of additive}}$$

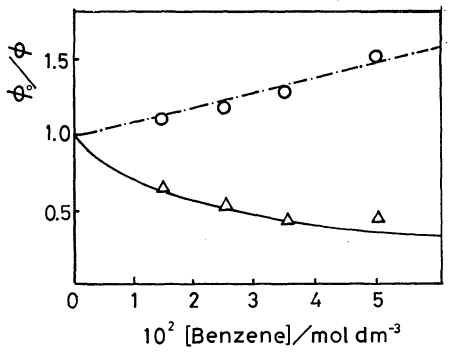

Fig. 5. Effect of benzene on the photoreaction of **1** in methanol acidified with H_2SO_4.
[**1**]$=1\times10^{-3}$ mol dm^{-3}, [H_2SO_4]$=5\times10^{-2}$ mol dm^{-3}.
—△—: **2**, ---○---: **3**.

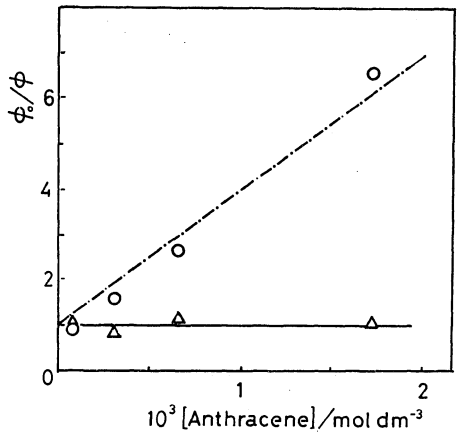

Fig. 6. Effect of anthracene on the photoreaction of **1** in methanol acidified with H_2SO_4.
[**1**]$=1\times10^{-3}$ mol dm^{-3}, [H_2SO_4]$=5\times10^{-2}$ mol dm^{-3}.
—△—: **2**, ---○---: **3**.

$$L=\frac{\varepsilon_1 c_1}{\varepsilon_1 c_1+\varepsilon_Q c_Q}$$
$$=\{\text{Light absorbed by substrate (1)}\}/\{\text{Light absorbed by substrate (1)}+\text{Light absorbed by additive(Q)}\},$$

where ε_1 and ε_Q are the molar absorption coefficients of the substrate and the additive at 254 nm, respectively. Symbols c_1 and c_Q are the concentrations of the substrate and the additive.

$A>1$ means that the additive promotes the reaction and $A<1$ means that the additive inhibits it. A^{-1} corresponds to ϕ_0/ϕ in the Stern-Volmer equation for the quenching experiment.

As is shown in Figs. 5 and 6, the methoxylation is inhibited to a smaller extent by benzene and to a larger extent by anthracene. Benzene, which has a high triplet energy value (E_T, 352 kJ mol^{-1}), is an inhibitor, although the effect is small. As reported earlier,[8] acetophenone has no effect on the photo-methoxylation. These facts suggest that the photo-methoxylation does not originate from a triplet state.

The additives may quench either an excited monomer or an excited dimer. The fact that the inhibition by anthracene was observed only for methoxylation and not for methylation suggests that the inhibition occurs not in the process of an excited monomer but in the process of an excited dimer.

The inhibition by benzene and anthracene can be explained by the electron transfer quenching by aromatic hydrocarbons:[9] anthracene with the lower ionization potential (I_p=7.43 eV[10]) causes greater inhibition ($k_q\tau$=300 dm^3 mol^{-1}) than benzene (I_p=9.245 eV,[10] $k_q\tau$=10 dm^3 mol^{-1}) with the higher ionization potential. (Here k_q is the rate constant for bimolecular quenching and τ is the lifetime of an excited species.) The results are similar to those reported by Caldwell *et al.*,[9] who investigated extensively the electron transfer quenching for excimers and exciplexes. Concerning the photo-methoxylation peculiar effects of additives were observed:[8] the photo-methoxylation is promoted specifically by 4-substituted pyridines. The promotion is explained by the exciplex formation between **1** and the 4-substituted pyridine.

The photo-methylation at the 4-position in the presence of added acid is promoted by benzene. Anthracene has no effect on the reaction. However, a detailed study on the excited state responsible for the formation of **2** could not be done, because methylation is only a very minor reaction.

The UV-irradiation of **1** in methanol in the absence of added acid gives a methylation product. In this case methylation occurs at the 5-position and the efficiency for the methylation at the 5-position is much lower than that at the 4-position in the presence of acid.

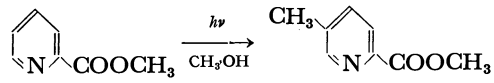

(**4**)

With pyridine derivatives photoreactions occur normally at α- and γ-positions.[11] For the unusual alkylation at the β-position, the participation of the ester group should be taken into consideration. The hydrogen abstraction by the excited C=O of the ester group (or the electron transfer followed by proton transfer) has been reported for some aromatic esters.[12] Thus, the following mechanism is conceivable for the photo-methylation at the 5-position.

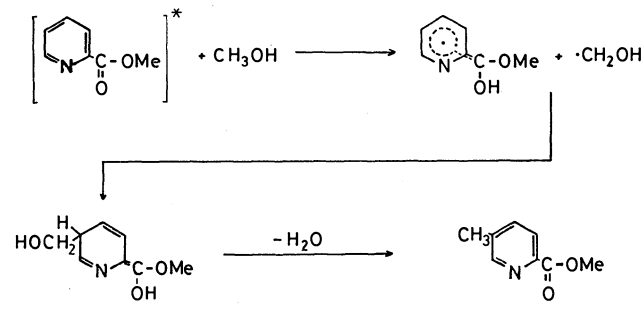

The effects of additives on the photo-methylation in the absence of added acids (Table 2) suggest that a triplet state is responsible for the methylation at the 5-position: the additives with higher triplet energies, benzene (E_T=352 kJ mol^{-1}) and naphthalene (E_T= 255 kJ mol^{-1}), promote the photo-methylation, anthracene (E_T=178 kJ mol^{-1}) has no effect, and oxygen inhibits the reaction.

Table 2. Effects of additives on the formation of **4** in the absence of added acid
[**1**] = 1×10^{-3} mol dm^{-3}; irradiation time, 20 min.

Additive	[Additive] / mol dm^{-3}	L[a]	Y[a]	A[a]
Benzene	5.0×10^{-3}	0.87	1.05	1.21
	5.0×10^{-2}	0.40	0.87	2.18
Naphthalene	2.2×10^{-3}	0.84	1.10	1.31
	1.1×10^{-2}	0.50	2.41	4.82
Anthracene	3.9×10^{-5}	0.41	0.39	0.96
	1.6×10^{-4}	0.15	0.15	1.00
Oxygen	saturated	1.00	0.0	0.0

a) See text for the definition of L, Y and A.

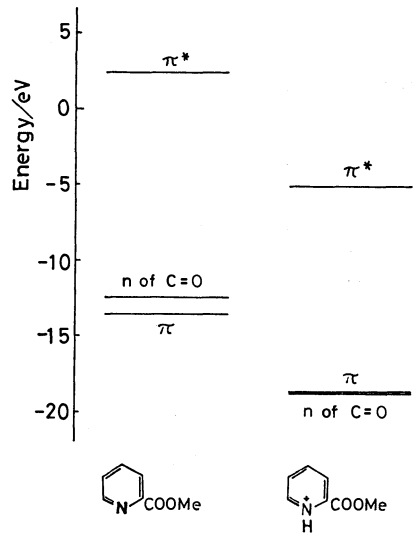

Fig. 7. Electronic state of **1**.

The participation of the n-π^* state of the C=O in the ester group is supported by the consideration of the electronic states calculated by means of CNDO/2.[13] The results are shown in Fig. 7. For the free base form of **1**, the highest occupied orbital is assigned to the non-bonding orbital at C=O. On the other hand, for the pyridinium form π-orbital is the highest occupied orbital. This result can explain that the n-π^* excited state is preferably formed in the irradiation of the free base form of **1**, whereas the π-π^* excited state is populated in the photoreaction of the pyridinium form of **1**.

The photoreactions of methyl 2-pyridinecarboxylate, thus, can be summarized in Scheme 2.

Experimental

Materials. Commercial methyl 2-pyridinecarboxylate (**1**) (GR grade reagent of Tokyo Kasei Co.) was purified by vacuum distillation; bp 105—108 °C/7 mmHg. (1 mmHg≈ 133.322 Pa.) Anthracene (standard reagent for elementa analysis made by E. Merck Co.) was used for the quenching experiment.

UV-irradiation. The solutions of **1** containing mineral acid, and the additive if necessary, were deaerated by bubbling nitrogen or argon for 40 min before irradiation. The solutions were irradiated with a low pressure mercury lamp in a merry-go-round type irradiation apparatus which was set in a thermostat. Irradiation was carried out at 20 °C except in the experiment for temperature dependence.

Isolation and Identification of Products. After the irradiation the solution was concentrated under reduced pressure and neutralized with sodium hydrogencarbonate when the mineral acid was present. The products were extracted repeatedly with dichloromethane and were separated by means of TLC (plate, GF_{254} (Type 60) of E. Merck Co.; developing solvent, ethyl acetate–dichloromethane 1 : 1 v/v)

Methyl 4-methyl-2-pyridinecarboxylate (**2**), methyl 5-methyl-2-pyridinecarboxylate (**4**), and methyl 6-methoxy-2-pyridinecarboxylate (**3**) were identified by the accordance of their NMR spectra with those reported by Deady *et al.*[14]

Determination of the Yields of Products. The yields of the photoproducts were determined by the UV-spectrophotometric method or by the gas-chromatographic method. For the determination of the quantum yields for the photo-methoxylated product (data for Figs. 3 and 4) the spectrophotometric method was applied using the characteristic absorption of **3** at 287 nm. Actinometry was carried out by using potassium trioxalatoferrate(III). In other cases, the yields of the products were determined by means of GLC (column, 2 m column of PEG 20M (10%) on Celite 545 or 2 m column of Triton OS-15 (15%) on Uniport B; column temperature, 160—170 °C).

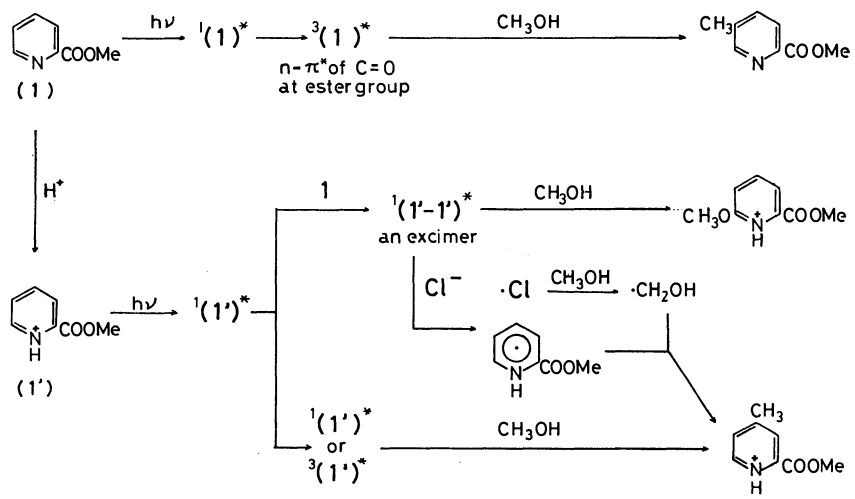

Scheme 2.

The authors are grategul to Professor L. W. Deady of La Trobe University in Australia for sending us the spectral data of pyridinecarboxylic acid derivatives.

References

1) F. Takeuchi, T. Sugiyama, T. Fujimori, K. Seki, Y. Harada, and A. Sugimori, *Bull. Chem. Soc. Jpn.*, **47**, 1245 (1974).

2) A. Sugimori, E. Tobita, Y. Kumagai, and G. P. Satô, *Bull. Chem. Soc. Jpn.*, **54**, 1761 (1981).

3) H. Kurokawa, T. Furihata, F. Takeuchi, and A. Sugimori, *Tetrahedron Lett.*, **1973**, 2623.

4) T. Furihata and A. Sugimori, *J. Chem. Soc., Chem. Commun.*, **1975**, 241.

5) A part of this work has been reported preliminarily: a) T. Sugiyama, T. Furihata, Y. Edamoto, R. Hasegawa, G. P. Satô, and A. Sugimori, *Tetrahedron Lett.*, **1974**, 4339; b) T. Sugiyama, E. Tobita, K. Takagi, M. Sato, Y. Kumagai, G. P. Satô, and A. Sugimori, *Chem. Lett.*, **1980**, 131.

6) The following mechanism *via* the excitation of a dimer formed in the ground state could explain the concentration dependence in Fig. 3 qualitatively.

$$2\,\mathbf{1} \overset{K}{\rightleftharpoons} (\mathbf{1}-\mathbf{1})$$

$$(\mathbf{1}-\mathbf{1}) \xrightarrow{h\nu} (\mathbf{1}-\mathbf{1})^*$$

$$\mathbf{1} \underset{k_{-1}}{\overset{h\nu}{\rightleftharpoons}} \mathbf{1}^*$$

$$(\mathbf{1}-\mathbf{1})^* + CH_3OH \xrightarrow{k_3} \mathbf{3}$$

$$(\mathbf{1}-\mathbf{1})^* \xrightarrow{k_4} 2\,\mathbf{1}$$

$$(\mathbf{1}-\mathbf{1})^* \xrightarrow{k_5} \mathbf{A}$$ (Product of the side reaction from $(\mathbf{1}-\mathbf{1})^*$)

$$\mathbf{1}^* \xrightarrow{k_6} \mathbf{B}$$ (Product of the side reaction from $\mathbf{1}^*$)

This mechanism, however, leads to the following expression for ϕ_3, the quantum yield of **3**:

$$1/\phi_3 = \left(\frac{k_3[CH_3OH]+k_4+k_5}{4K\,k_3[CH_3OH]}\right)\left\{\frac{1}{c}+4K+\left(\frac{1}{c^2}+8K\frac{1}{c}\right)^{1/2}\right\},$$

where $c=[\mathbf{1}]+[(\mathbf{1}-\mathbf{1})]$. This expression is based on the assumption that the molar absorption coefficient of $(\mathbf{1}-\mathbf{1})$ is twice that of **1**. Evidently the above mechanism is not compatible with the observed linear dependence of $1/\phi_3$ on $1/c$ (Fig. 4). The fact that the UV-spectra of **1** at higher concentrations, where photo-methoxylation occurs effectively, are identical with those at much lower concentrations is consitent with the view that $(\mathbf{1}-\mathbf{1})$ plays no important role.

7) R. P. Blaunstein and K. S. Gant, *Photochem. Photobiol.*, **18**, 347 (1973).

8) Y. Miyazawa, R. Hasegawa, E. Tobita, T. Furihata, T. Sugiyama, and A. Sugimori, *Chem. Lett.*, **1977**, 1155.

9) R. A. Caldwell, D. Creed, D. C. DeMarco, L. A. Melton, H. Ohta, and P. H. Wine, *J. Am. Chem. Soc.*, **102**, 2369 (1980).

10) S. L. Murov, "Handbook of Photochemistry," Marcel Dekker, New York (1973), p. 199.

11) D. G. Whitten, "Photoreduction and Photoaddition Reactions of Heterocyclic Compounds," ed by O. Buchardt, John Wiley and Sons, New York (1976), Chap. 8, pp. 524—573.

12) K. Fukui, K. Senda, Y. Shigemitsu, and Y. Odaira, *J. Org. Chem.*, **37**, 3176 (1972).

13) Electronic states of methyl 2-pyridinecarboxylate were calculated using the CNDO/2 program (Q. C. P. E. 141) prepared by Pople, Beveridge, and Dobosh and arranged by Kihara, Fujikawa, and Aoyama.

14) L. W. Deady, P. M. Harrison, and R. D. Topson, *Org. Magn. Reson.*, **7**, 41 (1975); L. W. Deady, private communication.

The Interaction between α-Helical Poly-L-lysine and Thyroxine as Measured by Circular Dichroism

Nobuo OKABE,* Mariko OKAMURA, Ryoji TOKUOKA, and Ken-ichi TOMITA
Faculty of Pharmaceutical Sciences, Osaka University, Suita, Osaka 565
(Received October 24, 1980)

The interaction between α-helical poly-L-lysine (poly(L-Lys)) and the thyroid hormone, L-thyroxine (L-T_4), was investigated at pH 11 by means of circular dichroism (CD) measurements in the wavelength region of 200—380 nm. At least four CD bands were induced near 235, 250, 290, and 343 nm. This indicates that these induced Cotton effects occurred as the result of the binding of L-T_4 to poly(L-Lys), probably due to the electrostatic interaction. The wavelengths of the induced CD bands corresponded to those of the UV absorption bands of L-T_4 in the poly(L-Lys) : L-T_4 mixture, although small red-shifts of the CD bands were observed at the shortest and the longest wavelengths (235 nm and 343 nm). These CD bands might be interpreted by the fixed intramolecular orientation around an asymmetric α-carbon atom of the bound L-T_4 or by the intermolecular interaction between the peptide backbone of poly(L-Lys) and the bound L-T_4.

In previous papers,[2-4] the interaction between bovine serum albumin (BSA) or human serum albumin (HSA) and a thyroid hormone, L-thyroxine (L-T_4, Fig. 1), was investigated by means of CD measurements. The negative CD band was induced at the longest UV absorption maximum of L-T_4, suggesting a specific interaction between proteins and L-T_4. However, the binding mechanism has remained obscure. For this reason, as a model study to obtain much information about the binding mechanism of L-T_4 to a protein, the interaction between α-helical poly-L-lysine and L-T_4 was investigated by means of the CD method at pH 11. This synthetic polypeptide was chosen as a suitable model compound for this study because the lysine residue plays an important role in the binding of L-T_4 to human serum albumin;[5] the residue also sometimes appears either at the surface or at the helical region of globular proteins.

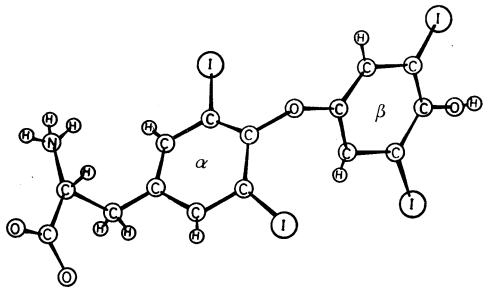

Fig. 1. Perspective drawing of L-T_4 molecule determined by X-ray analysis (Ref. 1). The dihedral angle between the planes of the α-ring and β-ring and the interring C–O–C angle are 79° and 120°±3°, respectively.

Experimental

Materials. Poly-L-lysine HBr (poly(L-Lys)) with a molecular weight of 46500 and a degree of polymerization (DP) of 222 (Lot No. LY-185) was purchased from Miles-Yeda, Ltd., U.S.A., and L-thyroxine sodium salt (L-T_4), from Nakarai Chemicals Co., Kyoto, Japan.

Procedure. Poly(L-Lys) was dissolved in distilled and deionized water, and the pH was adjusted to 11 by adding 1 mol dm^{-3} of NaOH. About 3×10^{-3} mol dm^{-3} of L-T_4 was dissolved in 0.01 mol dm^{-3} of the NaOH solution to serve as a stock solution. To prepared the mixture of poly(L-Lys) and L-T_4, a small amount of L-T_4 was gradually added to 2 cm^3 of the poly(L-Lys) solution under continuous stirring until the appropriate molar ratio was reached. The pH change in the poly(L-Lys) solution upon the addition of L-T_4 was negligible under those experimental conditions. The CD measurements were carried out on a JASCO J-40A spectropolarimeter equipped with a data-processor system, J-DPZ, at the wavelength region of 200—380 nm. CD cells with light-path lengths of 1 and 10 mm were used for the measurement in the wavelength regions of 200—260 nm and 260—380 nm respectively. The optical rotatory dispersion (ORD) measurements were performed with a JASCO J-20 spectropolarimeter. A cell with a light-path length of 2 mm was used in the wavelentgth region of 210—300 nm. The ultraviolet (UV) absorption spectra were obtained with a Hitachi 323 recording spectrophotometer. The pH adjustment was done by means of a Hitachi Horiba D-5 pH meter. The CD ellipticity and the ORD rotation were represented as a unit of degree cm^2 $decimol^{-1}$ on the basis of the concentration of the lysine residues of poly(L-Lys) or L-T_4. All the measurements except one noted in the text were carried out at 22 °C.

Results and Discussion

Figure 2 shows the absorption spectra of L-T_4 in a 30% ethanol aqueous solution at various pH values. The peak around 300 nm (pH 3.2) was shifted to 330 nm with an increase in its height in the alkaline solution (pH 11.7), although a small shoulder remained at 290 nm. The isosbestic points appeared at 285 nm and 308 nm. This peak-height increment at 330 nm is due to the dissociation of the phenolic hydroxyl group of the β-ring of L-T_4 (Fig. 1). The pK value of this group was calculated as 6.32, coincident well with the values of 6.2 and/or 6.7 reported by Steiner[6] and Gemmill[7] respectively. This indicates that the hydroxyl group completely dissociates at pH 11. It is well known that poly(L-Lys) takes a α-helical conformation in the aqueous solution at pH 11. The ε-amino groups of poly(L-Lys) may be not completely uncharged at pH 11, since the pK of these groups is 10.8.[9] This suggests that the negatively charged hydroxyl and carboxyl groups of L-T_4 at pH 11 cause electrostatic interaction with some positively charged ε-amino groups of poly(L-Lys). The binding of L-T_4 to the helical poly(L-Lys) may induce some optical activities to arise from L-T_4, although a

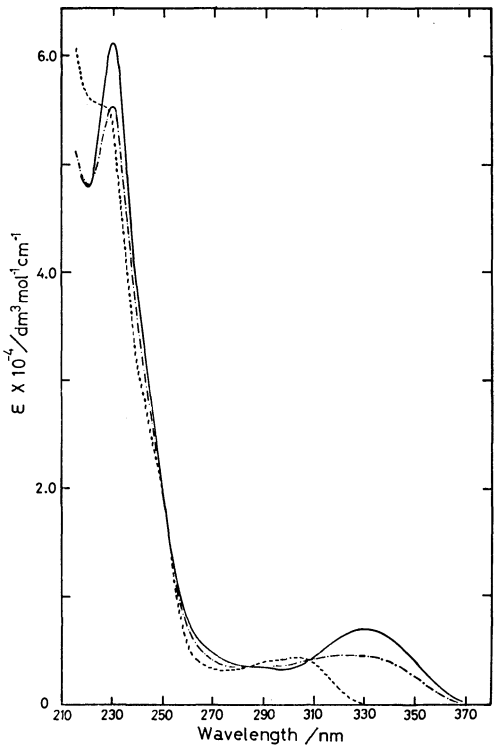

Fig. 2. The ultraviolet absorption spectra of L-T_4 as a function of pH in 30% ethanol aqueous solution. Curves are at pH 11.7 (——); at pH 6.6 (—·—); at pH 3.2 (------). L-T_4 concentration was 4.28×10^{-5} mol dm^{-3}. Temperature was 24 °C.

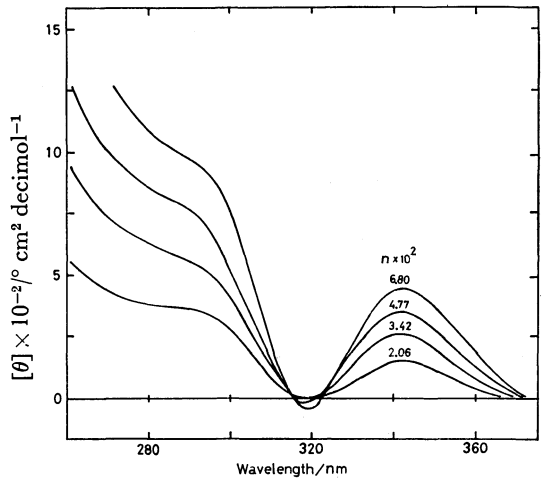

Fig. 3. CD spectra of poly(L-Lys): L-T_4 at pH 11. The ratios of the L-T_4 molecules to lysine residues of poly(L-Lys), n, are cited in the figure. Poly(L-Lys) concentration was kept at 5.31×10^{-6} mol dm^{-3}. The residue ellipticity was calculated on the basis of poly(L-Lys) concentration (DP=222).

free L-T_4 has no detectable optical activity in the wavelength region of 200—400 nm, even at a high concentration of 10^{-4} mol dm^{-3} (these data are not shown here). Therefore, the CD spectra of the poly(L-Lys) : L-T_4 system was measured in the wavelength region of 200—400 nm at pH 11 with a variation in the n ratio, which is defined as the ratio of L-T_4 molecules to the lysine residues of poly(L-Lys).

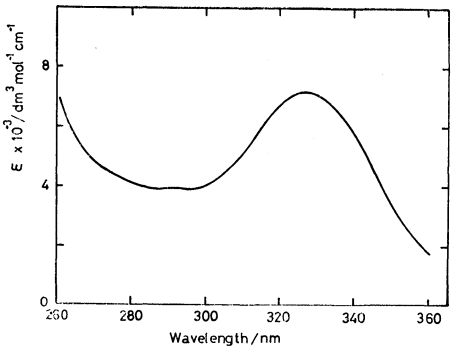

Fig. 4. The ultraviolet absorption spectra of poly(L-Lys): L-T_4 at pH 11.0. The spectra were the same for the ratios of L-T_4 molecules to lysine residues of poly(L-Lys) between 2.58×10^{-2} and 7.75×10^{-2}. Poly(L-Lys) concentration was kept at 5.31×10^{-6} mol dm^{-3}.

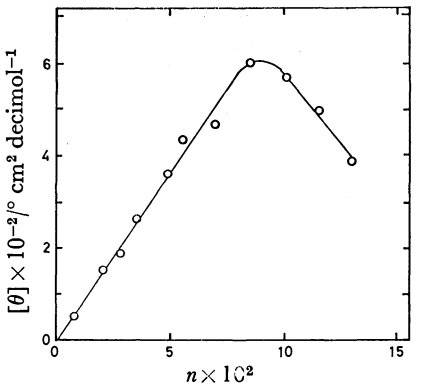

Fig. 5. Plot of the ellipticities of poly(L-Lys): L-T_4 at 343 nm against the ratio of the L-T_4 molecules to lysine residues of poly(L-Lys), n, and pH 11.0. Poly(L-Lys) concentration was kept at 5.31×10^{-6} mol dm^{-3}. The residue ellipticity was calculated on the basis of poly(L-Lys) concentration (DP=222).

The CD spectra and the absorption spectra of the poly(L-Lys) : L-T_4 mixture at various n values in the wavelength region of 260—380 nm are shown in Figs. 3 and 4 respectively. The positive CD bands with a peak near 343 nm and a shoulder around 270—300 nm were induced. The peak near 343 nm showed a red-shift by about 13 nm from the longest absorption maximum at 330 nm. The residue ellipticities at 343 nm are plotted against n in Fig. 5. They increased linearly with the increase in n up to about $n=9\times10^{-2}$, but thereafter they decreased. At n values of over 9×10^{-2} it was impossible to obtain reliable CD data because of the appreciable turbidity in the sample solution due to the aggregation of the poly(L-Lys) : L-T_4 complex. These results suggest the binding of L-T_4 to poly(L-Lys). The aggregation of poly(L-Lys) : L-T_4 might be a result of the neutralization of positively charged ε-amino groups of poly(L-Lys) by the binding of negatively charged hydroxyl and carboxyl groups of L-T_4, followed by an increase in the hydrophobic interaction between poly(L-Lys) : L-T_4 complexes.

The effect of L-T_4 binding on the helical poly(L-Lys) was also investigated by measuring CD and ORD in the far-ultraviolet region, 200—260 nm for CD and 210—

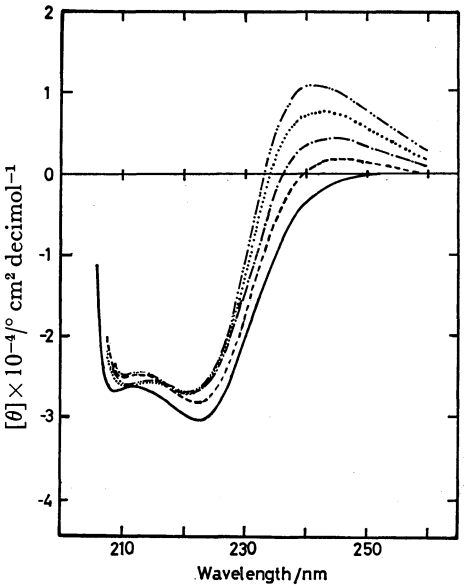

Fig. 6. The far ultraviolet CD spectra of poly(L-Lys): L-T_4 at pH 11.0. The ratios of the L-T_4 molecule to lysine residues of poly (L-Lys) mol are, poly(L-Lys) alone, (——); 2.25×10^{-2}, (------); 4.50×10^{-2}, (—·—); 6.75×10^{-2}, (·····); 9.00×10^{-2}, (-··-). Poly(L-Lys) concentration was kept at 6.13×10^{-6} mol dm^{-3}. The residue ellipticity was calculated on the basis of poly-(L-Lys) concentration (DP=222).

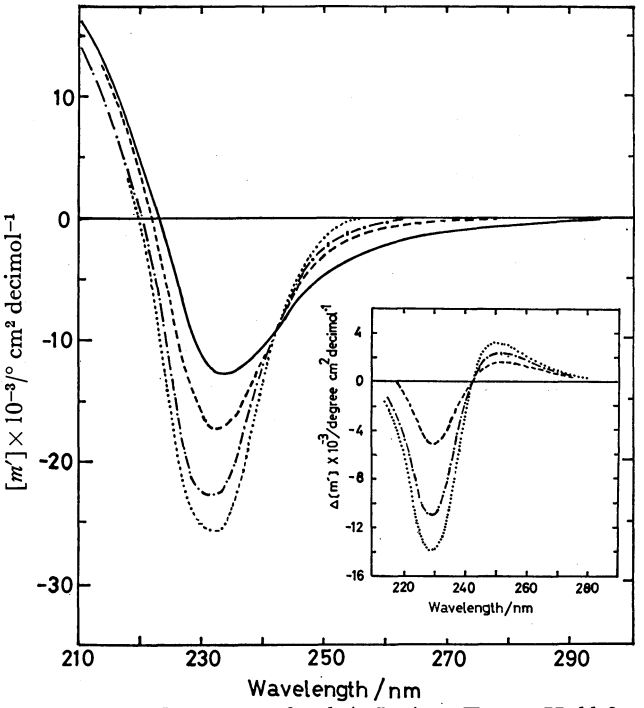

Fig. 7. ORD spectra of poly(L-Lys): L-T_4 at pH 11.0. The ratios of the L-T_4 molecules to lysine residues of poly(L-Lys) are, poly(L-Lys) alone, (——); 2.25×10^{-2}, (----); 4.50×10^{-2}, (-·-); 6.75×10^{-2}, (·····). Poly(L-Lys) concentration was kept at 6.50×10^{-6} mol dm^{-3}. The residue rotation was calculated on the basis of poly(L-Lys) concentration (DP=222). The difference rotation is also shown in the same figure.

300 nm for ORD. Figure 6 shows the CD spectra of poly(L-Lys) in the presence of various amounts of L-T_4. The CD spectrum of a free poly(L-Lys) at pH 11 is characteristic of the α-helical conformation, having the CD maxima both at 208 nm and 222 nm; these maxima are assigned to the π-π^* and n-π^* transitions of the peptide groups respectively, as has been reported by Greenfield and Fasman.[8] The percent helix of poly-(L-Lys) was calculated by means of the equation:[8]

$$\%\ \text{helix} = ([\theta]_{208}-4000)/(33000-4000), \quad (1)$$

where $[\theta]_{208}$ is the residue ellipticities at 208 nm. The helix content of poly(L-Lys) in the absence of L-T_4 was 78%. In the presence of L-T_4, a new CD band appeared at around 240 nm, although the characteristic CD bands at 208 nm and 222 nm still remained. Figure 7 shows the ORD spectra of poly(L-Lys) in the presence of various amounts of L-T_4. The ORD spectrum of a free poly(L-Lys) is characteristic of the α-helical conformation, as has been reported by Davidson *et al.*[10] The negative ORD band of poly(L-Lys) increased at 233 nm, and decreased around 250 nm, in the presence of L-T_4. The difference rotation, $\Delta[m']$, was obtained by subtracting the residue rotation of a free poly(L-Lys) from that of a poly(L-Lys) : L-T_4 mixture according to the following equation and inserted into Fig. 7:

$$\Delta[m'] = [m'](\text{poly(L-Lys)}:\text{L-}T_4) - [m'](\text{poly(L-Lys)}). \quad (2)$$

The difference ORD curves show a positive Cotton effect around 240 nm. These results of both CD and ORD measurements suggest that the Cotton effect observed in the 230—250 nm region was induced by L-T_4 bound to poly(L-Lys). From the data in Fig. 6, the difference ellipticity, $\Delta[\theta]$, was calculated in the same manner as in Eq. 2 by means of the following equation, and $\Delta[\theta]$ at 235 nm was plotted against n in Fig. 8:

$$\Delta[\theta] = [\theta](\text{poly(L-Lys)}:\text{L-}T_4) - [\theta](\text{poly(L-Lys)}). \quad (3)$$

It increased linearly with the increase of n up to about $n=9\times10^{-2}$, as was observed at 343 nm (Fig. 5). This indicates that the induced optical activity at around 235 nm as well as that at 343 nm is attributable to the binding of L-T_4 to poly(L-Lys). In this study, therefore, assuming that no conformational changes in the α-helical poly(L-Lys) were induced by the binding of L-T_4 at low n values, the difference CD spectrum was obtained by using Eq. 3 from the CD spectra measured at the same concentration of poly(L-Lys) at the wavelength region of 200—380 nm, while the difference molar ellipticity for L-T_4 was calculated on the basis of the L-T_4 concentration. The difference CD spectrum at $n=2.25\times10^{-2}$ (Fig. 9(a)) had a large positive peak near 235 nm, a small one at 343 nm, and two shoulders around 250 nm and 290 nm. The UV absorption spectra of the L-T_4 and poly(L-Lys) : L-T_4 mixture were also measured at the same n value ($n=2.25\times10^{-2}$) (Fig. 9(b)). In the case of the poly(L-Lys) : L-T_4 mixture, the UV maximum at 228 nm decreased and a new shoulder appeared near 250 nm, and the small peaks at both 290 nm and 330 nm increased as compared with a free L-T_4. The molar extinction coefficient of 7.25×10^3 at 330 nm for L-T_4 in the poly(L-Lys) : L-T_4 system is slightly larger than the values of 6.27×10^3

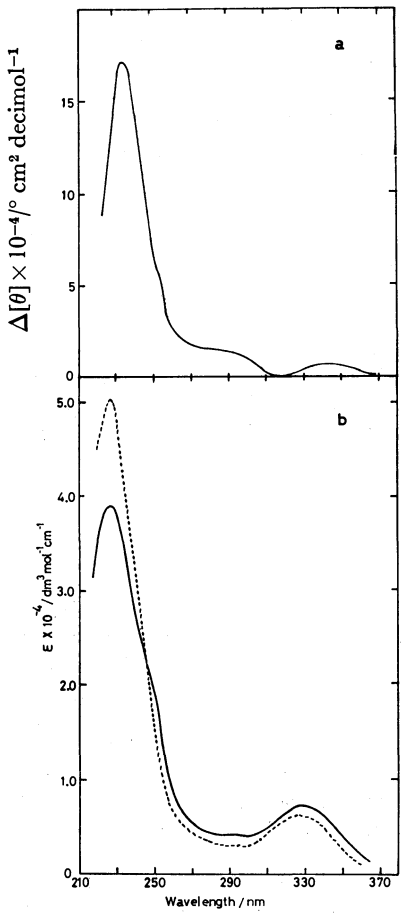

Fig. 9. (a): Difference CD spectrum of poly(L-Lys): L-T_4 obtained by subtracting the CD spectrum of poly(L-Lys) alone from that of poly(L-Lys): L-T_4. The concentration of poly(L-Lys) and L-T_4 were 1.13×10^{-5} mol dm^{-3} and 5.67×10^{-5} mol dm^{-3}, respectively. pH was 11.0. The difference ellipticity was calculated on the basis of L-T_4 concentration.
(b): The ultraviolet absorption spectra of poly(L-Lys): L-T_4, (——) and L-T_4, (……) at pH 11.0. The concentration of poly(L-Lys) and L-T_4 were 1.03×10^{-5} mol dm^{-3} and 5.10×10^{-5} mol dm^{-3}, respectively.

for the free L-T_4 at 325 nm, which is in good agreement with the 6.21×10^3 at 325 nm reported by Gemmill.[7] The induced CD bands appearing in the poly(L-Lys) : L-T_4 complex (Fig. 9(a)) coincided with the corresponding absorption maxima (Fig. 9(b)) except for the small red-shifts at 235 nm and 343 nm.

The induced CD bands observed in this study may be interpreted by the following mechanisms: (1) a certain fixed intramolecular orientation between the carboxyl group and the aromatic ring of L-T_4 occurs upon binding to poly(L-Lys), and (2) intermolecular interaction occurs between the peptide backbone of poly-

(L-Lys) (-C(=O)-N(H)-) and the bound L-T_4. At present, however, it is unclear why the CD maxima at the shortest and the longest wavelengths (235 nm and 343 nm) shifted to wavelengths a little longer from their UV absorption maxima at 230 nm and 330 nm.

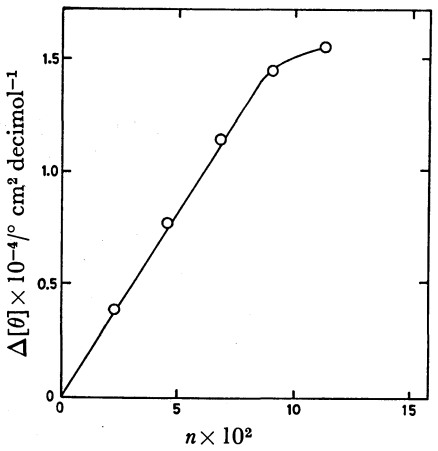

Fig. 8. Plot of the difference ellipticities of poly(L-Lys): L-T_4 at 235 nm against n and pH 11. Poly(L-Lys) concentration was kept at 6.13×10^{-6} mol dm^{-3}. The difference ellipticity was calculated on the basis of poly(L-Lys) concentration (DP=222).

Conclusion

The possibility of the binding of the thyroid hormone, L-T_4, to the α-helical poly(L-Lys) was strongly suggested by the facts that optical activity arising from L-T_4 was newly induced by mixing L-T_4 with α-helical poly-(L-Lys) at pH 11 and that the induced ellipticity increased linearly with an increase in the ratio of L-T_4 molecules to lysine residues of poly(L-Lys). The results of this study suggest that L-T_4 may bind to the helical region of non-specific proteins as well as of specific ones for L-T_4 containing lysine residues in their α-helical regions. The CD peaks observed in this study seem to be usable in investigating the interaction between L-T_4 and specific or non-specific proteins for L-T_4 or other synthetic polypeptides by means of CD measurements.

References

1) N. Camerman and A. Camerman, *Proc. Natl. Acad. Sci. U.S.A.*, **69**, 2130 (1972).
2) N. Okabe, N. Manabe, R. Tokuoka, and K. Tomita, *J. Biochem.*, **77**, 181 (1975).
3) N. Okabe, N. Manabe, R. Tokuoka, and K. Tomita, *J. Biochem.*, **80**, 455 (1976).
4) R. Tokuoka, N. Okabe, and K. Tomita, *J. Biochem.*, **87**, 1729 (1980).
5) S. Y. Cheng, H. J. Cahman, M. Wilchek, and R. N. Ferguson, *Biochemistry*, **14**, 4132 (1975).
6) R. F. Steiner, J. Roth, and J. Robbins, *J. Biol. Chem.*, **241**, 560 (1966).
7) G. L. Gemmill, *Arch. Biochem. Biophys.*, **54**, 359 (1955).
8) N. Greenfield and G. D. Fasman, *Biochemistry*, **8**, 4108 (1969).
9) J. T. Edsall and J. Wyman, "Biophysical Chemistry," Academic Press, New York, N. Y. (1958), Vol. I, p. 465.
10) B. Davidson, N. Tooney, and G. D. Fasman, *Biochem. Biophys. Res. Commun.*, **23**, 156 (1966).

Bovine Serum Albumin Coordinated Iron-Sulfur Cluster as a Hydrogenase Model†

Ichiro OKURA,* Satoshi NAKAMURA, and Masatoshi KOBAYASHI
Department of Chemical Engineering, Tokyo Institute of Technology, Meguro-ku, Tokyo 152
(Received January 24, 1981)

The bovine serum albumin coordinated Fe_4S_4-cluster, which had hydrogenase activity, was synthesized. Its physical and chemical characteristics were then compared with those of natural hydrogenase. Though the affinities of hydrogenase and the albumin-coordinated Fe_4S_4-cluster for the substrate, methyl viologen, were similar, the hydrogenase activity for hydrogen evolution was 10^5 times greater than the cluster. Two types of Fe_4S_4-clusters, coordinated by the fragments of the cleaved albumin obtained by treatment with cyanogen bromide, were synthesized, and their hydrogenase activities were compared. The activity with the iron–sulfur cluster incorporated in the fragment with MW 40000 was much higher than that of the one incorporated in the fragment with MW 20000. The amino acid arrangement to form the active site was discussed on the analogy of the other iron-sulfur proteins.

The core structures of iron-sulfur proteins have been studied extensively, and the physicochemical investigations have conclusively established that iron-sulfur proteins have at least three fundamental types of central cores: $Fe(S\text{–}Cys)_4$, $Fe_2S_2(S\text{–}Cys)_4$, and $Fe_4S_4(S\text{–}Cys)_4$.[2]

Holm *et al.*[3–11] have reported the synthesis of the tetranuclear cluster complexes $[Fe_4S_4(SR)_4]^{2-}$ and binuclear cluster complexes $[Fe_2S_2(SR)_4]^{2-}$ (R=alkyl or aryl), whose structure and properties demonstrate them to be a close representation of the central cores of iron–sulfur proteins, and have developed the core-extrusion method for the identification of active sites in native iron-sulfur proteins. Rabinowitz *et al.*[12–14] have also applied the method to the preparation and isolation of apoprotein of ferredoxin from *Clostridium pasteurianum*, and have reconstituted ferredoxin by the addition of iron(II) ions, sodium sulfide, and 2-mercaptoethanol. This procedure, which has considerable utility, is now being applied to other iron-sulfur proteins.[15–17]

Recently we found,[18–21] by the extrusion and reconstitution techniques mentioned above, that the hydrogenase from *Desulfovibrio vulgaris* contained two Fe_4S_4-type clusters per enzyme molecule; we also found[18,20] two active sites per enzyme molecule by kinetics and an inhibition method with mercury(II) chloride. The presence of three Fe_4S_4-type clusters has been established in the case of the hydrogenases from *Desulfovibrio gigas*[22] and *Clostridium pasteurianum*,[11] which contain 12 iron atoms and 12 labile sulfur atoms per molecule. Generally, hydrogenase is regarded as an iron-sulfur protein with Fe_4S_4-type clusters. Although the Fe_4S_4-cluster alone does not have the hydrogenase activity,[23] the Fe_4S_4-clusters synthesized in the presence of apo-hydrogenase has the catalytic activity.[21] Therefore, the Fe_4S_4-cluster and also the environment of the Fe_4S_4-cluster within the protein, such as apo-hydrogenae, play important roles in the hydrogenae activity.

In this paper we wish to describe the development of a hydrogen-evolution system which combines the Fe_4S_4-cluster and some protein, and to compare the characteristics of the artificial and natural hydrogenase.

† Part of this paper has been published as a preliminary communication in *J. Mol. Catal.*[1]

Experimental

Materials. The methyl viologen (1,1′-dimethyl-4,4′-bipyridinium dichloride) and trypsin were purchased from the Tokyo Kasei Kogyo Co. and ICN Pharmaceuticals Inc. respectively. The bovine serum albumin, α-chymotrypsinogen-A, and lysozyme were products of the Sigma Chemicals Co. The other chemicals, obtained from the Wako Pure Chemicals Co., were the best commercial grades available. All solutions were degassed and stored under nitrogen. The nitrogen gas was purified by passage through a copper column at 200 °C.

The copolymer of styrene and *p*-vinylphenylmethanethiol was synthesized according to the procedure of Okawara *et al.*[24]

Hydrogenase from the *Desulfovibrio vulgaris* (Miyazaki type, which has kindly been provided by Professor T. Yagi of Shizuoka Univ.) was purified according to the procedure of Yagi *et al.*[25,26]

Measurement of Hydrogenase Activity. The hydrogenase activity was measured under anaerobic conditions. The hydrogenase activities of the iron-sulfur proteins were determined by the rate of hydrogen evolution from reduced methyl viologen at 30 °C and pH 7.0. The evolved hydrogen was analyzed by gas chromatography on a 2 m×0.5 mm active carbon column (Gasukuro Kogyo Co.) with a nitrogen carrier. The reaction mixture (8.5 ml) consisted of 4.0 ml of the iron-sulfur protein solution with the 7.73×10^{-7} M Fe_4S_4-cluster described in "Synthesis of Iron-Sulfur Clusters," 1.96 μmol of methyl viologen, and 5 mg of $Na_2S_2O_4$ in 4.5 ml of a 0.02 M phosphate buffer (pH 7.0).

Synthesis of Iron–Sulfur Clusters. The $[Fe_4S_4(SR)_4]^{2-}$ complexes (R=phenyl or *t*-butyl) were prepared by the procedure of Holm *et al.*[4] The synthesis of other iron-sulfur clusters was carried out under a nitrogen atmosphere as follows. To a stirred solution of thiol or protein with mercapto ligands (4×10^{-5} mol) in 4 ml of H_2O containing 0.01 M iron(II) chloride, 2 ml of aq Na_2S (0.02 M) were added; the mixture thereupon turned dark brown in each case and was incubated at 30 °C for 30 min. The solution was then centrifuged (20000 g×30 min) to remove fine black precipitate, which may be iron(II) sulfate.

Cleavage of Bovine Serum Albumin. Albumin was cleaved according to the method of King and Spencer.[27] To 12.2 ml of a formic acid (75%) solution containing 26.4 μmol of albumin, we added a solution of cyanogen bromide (2.31 mmol) in 36 ml of formic acid, after which the solution was stirred for 20 h at room temperature. Then the solution was

placed in a Sephadex G-75 column (2.2 cm × 140 cm) and eluted with the 0.02 M Tris–HCl buffer (pH 7.0; to compare the hydrogenase activity, this pH value was employed, for this value was suitable for the hydrogenase). The eluted solution was then concentrated by ultrafiltration with an UM-2 Diaflo membrane.

Results and Discussion

Preparation and Properties of Bovine Serum Albumin Coordinated Iron–Sulfur Cluster. The method used for the preparation of the albumin cluster was a modification of those of Suzuki and Kimura[28] and Lovenberg and McCarthy.[29] The preparation was carried out under a nitrogen atmosphere as follows: eighty milligrams of albumin was dissolved in 6 ml of water containing 6.7 mM iron(II) chloride or ammonium iron(II) sulfate. 2-Mercaptoethanol (0.4 ml) was then added, followed by 2 ml of aq Na_2S (0.02 M).

In order to separate the albumin-cluster from the excess reagents, the solution containing the albumin-cluster was placed in a Sephadex G-50 column (5 cm × 23 cm) with 0.02 M Tris–HCl (pH 7.0) containing 0.08 M NaCl as an eluting buffer. The eluting solution was monitored by means of the absorption bands for proteins and iron–sulfur clusters; the results are shown in Fig. 1. Albumin came out at the elution position peak A. As the eluting solution has the absorption band at 420 nm which is attributable to the iron–sulfur clusters, and also a molecular weight corresponding to albumin, the product is not a crude mixture of albumin and the iron–sulfur cluster, but the iron–sulfur clusters incorporated in albumin. The solution was dark brown, and iron(II) sulfide as a by-product may also be incorporated in the protein. Although the eluting solution corresponding to Peak A was centrifuged at 20000 g for 60 min to remove the black precipitate, it was not separated from the protein completely. The iron–sulfur clusters incorporated in albumin were not synthesized by the reaction of the preformed iron–sulfur cluster and albumin. Therefore, the iron(II) sulfide concomitant in the iron-sulfur incorporated in albumin was not avoided by this method. The specific absorption coefficients, 35600 $M^{-1}\,cm^{-1}$ at 280 nm and 14000 $M^{-1}\,cm^{-1}$ at 420 nm,[28] were used to estimate the concentrations of protein and iron–sulfur clusters respectively. The B peak also has ultraviolet and visible absorption bands which seem to be due to an excess of the 2-mercaptoethanol reagent and the synthesized $Fe_4S_4(S\text{–}CH_2CH_2OH)_4$ dianion respectively.

When the solution of the iron–sulfur cluster incorporated in albumin (albumin-cluster; the spectrum is shown in Fig. 2, Curve a) was incubated under a hydrogen atmosphere at 30 °C, the spectrum of the solution changed as is shown in Fig. 2, Curve b. When exposed in air, the spectrum returned to its original shape. A similar spectrum change has been observed[26] in the reduction of hydrogenase from *Desulfovibrio vulgaris* by hydrogen. In this case, however, cytochrome C_3 is needed as an electron-acceptor. When excess 2-mercaptoethanol is added to the albumin-cluster solution for the identification of the core types, the obtained absorption spectrum (λ_{max}=410 nm) of the resulting solution resembled that of the synthesized $Fe_4S_4(S\text{–}CH_2CH_2OH)_4$ dianion, as is shown in Fig. 2, Curve c. From the above results, the iron–sulfur clusters incorporated in albumin seem to be Fe_4S_4-type clusters, but another possibility still remains that the corresponding Fe_2S_2-clusters were rapidly converted to the Fe_4S_4-clusters.

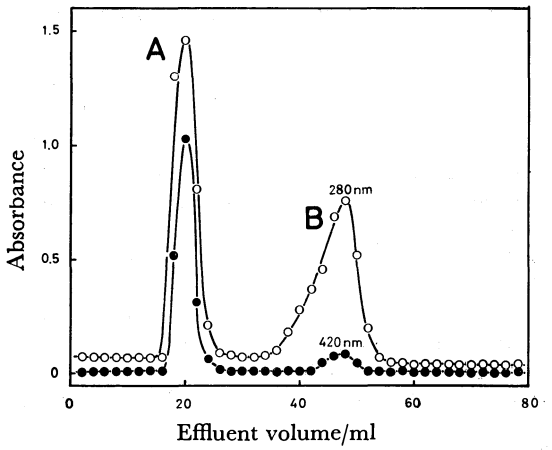

Fig. 1. Elution patterns of the albumin-cluster from a Sephadex G-50 column.

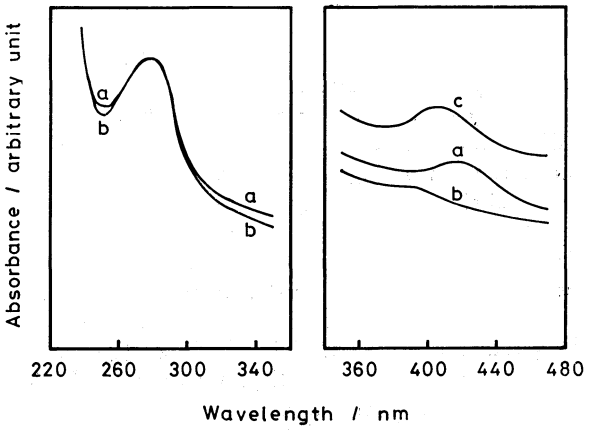

Fig. 2. Absorption spectra of the albumin-cluster.
a: Albumin-cluster, b: Albumin-cluster is incubated under hydrogen for 24 h, c: Mixture of albumin-cluster and 2-mercaptoethanol.

We lack the extinction coefficient data for the spectrum required for a quantitative analysis of the $Fe_4S_4(S\text{–}CH_2CH_2OH)_4$ dianion. However, it is clear that the Fe_4S_4-cluster is the dominant product.

Synthesis of Various Iron–Sulfur Clusters. The method used for the preparation of the iron–sulfur clusters with various mercapto ligands was the same as that used for the albumin-clusters. Though a number of Fe_4S_4 cores are synthesized in the presence of some thiols, SH-containing polymer, and natural proteins containing cysteinyl residues instead of apo-hydrogenase, an estimation has not been made whether each product is a crude mixture of protein and the iron–sulfur cluster or the iron–sulfur cluster incorporated in a compound as a ligand. As is evident from Table 1, no cluster complex but the albumin-coordinated Fe_4S_4-cluster can catalyze the hydrogen-evolution reaction from reduced methyl

Table 1. Catalytic activities of synthesized iron–sulfur clusters

Ligand	Solvent[a)]	Activity (mol-H_2/min/mol-Catal.)
2-Methyl-2-propanethiol	DMF/H_2O	0
Thiophenol	HMPA/H_2O	0
2-Mercaptoethanol	H_2O	0
Dithiothreitol	H_2O	0
Glutathione	H_2O	0
L-Cysteine	H_2O	0
Copolymer of styrene and *p*-vinylphenylmethanethiol	DMSO/H_2O	0
Bovine serum albumin	H_2O	9.62×10^{-3}
Lysozyme	H_2O	Trace
α-Chymotrypsinogen	H_2O	0
Papain	H_2O	0

a) DMF: *N*,*N*-Dimethylformamide; HMPA: hexamethylphosphoric triamide; DMSO: dimethyl sulfoxide.

viologen, although its activity is lower than that of the actual enzyme, hydrogenase.

Specificity for Electron Carriers and Kinetics. When the albumin-cluster was added to a solution of dithionite-reduced methyl viologen, hydrogen evolved under the same conditions of hydrogenase-activity measurement. Various redox carriers were tested to see if they would replace methyl viologen and mediate the electron transfer to the albumin-cluster from dithionite. The electron-carrier specificities for albumin-cluster and hydrogenases are compared in Table 2. The albumin-cluster was specific for methyl viologen and nicotinamide–adenine dinucleotide.

The time course showed that the amount of hydrogen evolved from reduced methyl viologen increased linearly with the time. It is reasonable to assume that the iron–sulfur cluster in the albumin-cluster (which has not been separated from iron(II) sulfide) has a central role in hydrogen evolution, because it has been confirmed experimentally that iron(II) sulfide has no activity for hydrogen evolution. With a 44-h reaction time, the molar ratio (the turnover number) of the evolved hydrogen for the iron–sulfur cluster was 18.[1)] This means that the albumin-cluster behaves as a catalyst. Though the stability of the albumin cluster was not examined, it seems fairly stable in the long term because it was still intact after a 44-h reaction.

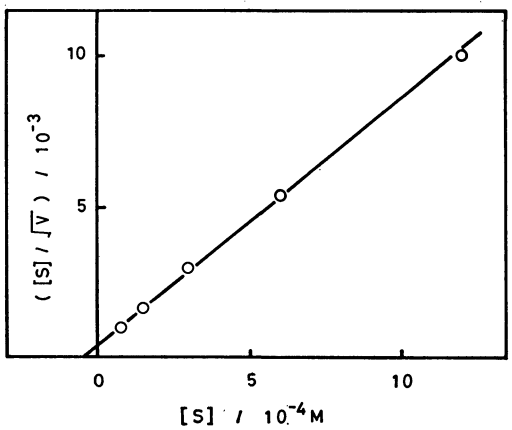

Fig. 3. Relation between $[S]/\sqrt{V}$ and [S].

The initial rate of hydrogen evolution increased with the methyl viologen concentration until it finally reached a constant value. In the case of the hydrogenase, the rate of hydrogen evolution from reduced methyl viologen was expressed as follows:[20,30)]

$$V=\frac{kK^2[S]^2}{(1+K[S])^2},$$

or

$$\frac{[S]}{\sqrt{V}}=\frac{[S]}{\sqrt{k}}+\frac{1}{\sqrt{k}K},$$

where k and K are constants and where [S] is the concentration of methyl viologen. In the case of the albumin-cluster, a good linear relation was also obtained between $[S]/\sqrt{V}$ and [S], as is shown in Fig. 3. Although the $[S]/V$ *vs.* [S] plot on the basis of the first-order kinetic equation:

$$V=\frac{kK[S]}{1+K[S]}$$

was also tried, there were some deviations. The albumin-cluster may also catalyze hydrogen evolution by the same mechanism as that of the hydrogenase. From the slope and the intercept, the equilibrium constant, K, and the rate constant, k, for hydrogen evolution from

Table 2. Electron-carrier specificity in H_2 evolution by the hydrogenase from *Desulfovibrio vulgaris* and the albumin-cluster

Electron carrier	Concentration M	Activity (mol-H_2/min/mol-Catal.)	
		Hydrogenase	Albumin-cluster
Cytochrome C_3	5.94×10^{-7}	245	0
Flavin monoculeotide	2.45×10^{-4}	Trace	0
Nicotinamide–adenine dinucleotide	1.61×10^{-4}	13	4.54×10^{-3}
Coenzyme II	1.72×10^{-4}	0	0
Methyl viologen	2.48×10^{-4}	1770	9.62×10^{-3}
Methylene Blue	1.96×10^{-4}	0	0
Neutral Red	2.03×10^{-4}	47	0
Safranine T	2.07×10^{-4}	40	0
Phenosafranine	1.91×10^{-4}	34	Trace
Potassium hexacyanoferrate(III)	2.01×10^{-4}	0	0

reduced methyl viologen at 30 °C were calculated as follows:

Catalyst	K / M^{-1}	k / min^{-1}
Hydrogenase	8.8×10^{3}	2.3×10^{3}
Albumin-cluster	1.9×10^{4}	1.5×10^{-2}

Judging from the K values, the affinity of the albumin-cluster for methyl viologen seems to be similar to that of the hydrogenase. The k value of hydrogenase, however, was 10^5 times greater than that of the albumin-cluster.

Effect of Mercury(II) Chloride. As has been reported earlier[15,20] some heavy metals, mercury, copper, and silver, strongly inhibit the activity of the hydrogenase, even though their concentrations are low in comparison with that of the hydrogenase. Although the albumin-cluster was inhibited in the presence of mercury(II) chloride, as is shown in Table 3, it was less inhibited than the hydrogenase at the same concentration. Mercury atoms are exchangeable with the iron atoms in the hydrogenase,[20] and the inhibition of the hydrogenase by mercury(II) chloride is a result of the exchange between mercury and iron. Although the inhibition by metal ions is explained by the binding of these ions to the thiolate sulfurs, the inhibition of the albumin-cluster by mercury(II) chloride may be caused by the exchange between mercury and iron, just as in the case of the hydrogenase.

Cleaved Bovine Serum Albumin Coordinated Iron–Sulfur Clusters. Though the Fe_4S_4-cluster of the albumin-cluster combines cysteine residues of albumin, none of the cysteine residues (there are 35 cysteine residues per albumin molecule[31]) participate in the cluster formation, for the concentration of the synthesized clusters is low compared to that of the cysteine residues. To determine the situation needed for the hydrogenase model, the hydrogenase activities were measured with Fe_4S_4-clusters with cleaved albumin as ligands.

The cyanogen bromide cleavage of albumin between two amino acid residues, 183 (Met) and 184 (Arg), gives two peptides with molecular weights of 40000 and 20000.[27] A chromatogram of the formic acid solution containing albumin and cyanogen bromide obtained by means of a Sephadex G-75 column is shown in Fig. 4. Fragment 1 is the original albumin, while Fragments 2 and 3 are examples of cleaved albumin with molecular weights of 40000 and 20000 respectively. The reagents to produce the Fe_4S_4-cluster, iron(II) chloride, 2-mercaptoethanol, and Na_2S, were added to a solution containing the protein corresponding to Fragment 2 or 3, and then the mixture was placed in a Sephadex G-50 column to remove the excess reagents as well as to produce albumin-cluster synthesis. As is shown in Table 4, the activity of the iron-sulfur cluster incorporated in Fragment 2 was much higher than that of the one incorporated in Fragment 3.

Table 3. Inhibition by mercury(II) chloride

Hg^{2+}/Cluster (M/M)	% Activity[a]	
	Hydrogenase	Albumin-cluster
0	100	100
5	82	100
20	42	100
50	0	53
100	—	0

a) Samples were preincubated with $HgCl_2$ for 24 h at 4 °C. Methyl viologen: 2.31×10^{-4} M.

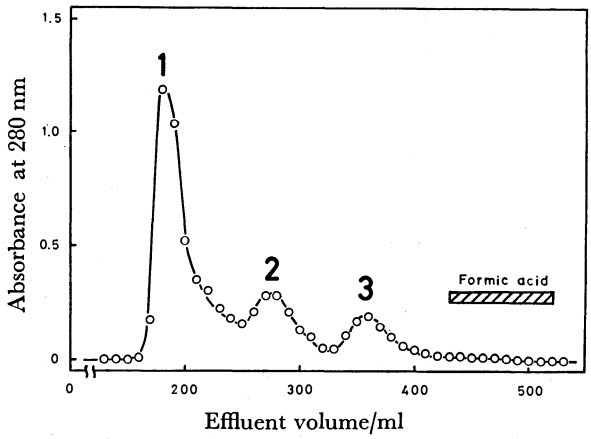

Fig. 4. Separation of cyanogen bromide fragments of albumin on a Sephadex G-75 column.

In albumin, two cysteine residues are adjacent to each other except for the two cysteine residues 276 and 280, where three other amino-acid residues are incorporated between them. This part belongs to Fragment 2 in the cleaved albumin, and there is no other remarkable difference in geometrical arrangement between Fragments 2 and 3. Judging from the chelate structures of other iron–sulfur proteins determined by X-ray diffraction studies,[2] the following two situations in amino acid sequence seem to be required for Fe_4S_4-cluster formation: the existence of four cysteine residues as ligands close to each other, and the presence of two, three, or four other amino acids between the cysteine residues. As Fragment 2 contains the portion of the 263—287 residues which satisfies the situation, the iron-sulfur cluster will be incorporated at this portion of Fragment 2. The concentration of the iron-sulfur cluster is comparable with that of Fragment 2 protein.

Table 4. Hydrogenase activities with some clusters[a]

Protein source	Protein concentration / M	Cluster concentration / M	Activity (mol-H_2/min/mol-cluster)
Albumin whole chain	3.74×10^{-6}	7.73×10^{-7}	7.75×10^{-3}
Fragment 2	1.86×10^{-6}	1.34×10^{-6}	4.84×10^{-3}
Fragment 3	3.42×10^{-6}	2.46×10^{-6}	5.70×10^{-4}

a) See text for reaction conditions.

This means that only one cluster is formed per protein molecule.

After all, not only the proper distance between two cysteine residues which is suitable for the formation of the Fe_4S_4-core in the albumin molecule, but also the proper amino acid residues near the active-site core seem to be required for the hydrogenase activity.

We wish to express our appreciation to Professor Tominaga Keii for his stimulating and helpful discussions.

References

1) I. Okura, S. Nakamura, and K. Nakamura, *J. Mol. Catal.*, **6**, 71 (1979).
2) R. H. Holm and J. A. Ibers, "Iron-Sulfur Proteins," ed by W. Lovenberg, Academic Press, New York (1977), Vol. 3, p. 206 and the references cited therein.
3) T. Herskovitz, B. A. Averill, R. H. Holm, J. A. Ibers, W. H. Phillips, and J. F. Weiher, *Proc. Natl. Acad. Sci. U.S.A.*, **69**, 2437 (1972).
4) J. J. Mayerle, S. E. Denmark, B. V. De Pamphilis, J. A. Ibers, and R. H. Holm, *J. Am. Chem. Soc.*, **97**, 1032 (1975).
5) B. A. Averill, T. Herskovitz, R. H. Holm, and J. A. Ibers, *J. Am. Chem. Soc.*, **95**, 3523 (1973).
6) J. J. Mayerle, R. B. Frankel, R. H. Holm, J. A. Ibers, W. D. Phillips, and J. F. Weiher, *Proc. Natl. Acad. Sci. U.S.A.*, **70**, 2429 (1973).
7) M. A. Borik, L. Que, Jr., and R. H. Holm, *J. Am. Chem. Soc.*, **96**, 285 (1974).
8) B. V. DePamphilis, B. A. Averill, T. Herskovitz, L. Que, Jr., and R. H. Holm, *J. Am. Chem. Soc.*, **96**, 4159 (1974).
9) L. Que, Jr., M. A. Borik, J. A. Ibers, and R. H. Holm, *J. Am. Chem. Soc.*, **96**, 4168 (1974).
10) L. Que, Jr., R. H. Holm, and L. E. Mortenson, *J. Am. Chem. Soc.*, **97**, 463 (1975).
11) W. O. Gillum, L. E. Mortenson, and R. H. Holm, *J. Am. Chem. Soc.*, **99**, 584 (1977).
12) W. B. Lovenberg, B. Buchanan, and J. C. Rabinowitz, *J. Biol. Chem.*, **238**, 3899 (1963).
13) R. Malkin and J. C. Rabinowitz, *Biochem. Biophys. Res. Commun.*, **23**, 822 (1966).
14) J. Hong and J. C. Rabinowitz, *Biochem. Biophys. Res. Commun.*, **29**, 246 (1967).
15) E. Bayer, D. Josef, P. Krauss, H. Hagenmaier, A. Roder, and A. Trebst, *Biochim. Biophys. Acta*, **143**, 435 (1967).
16) K. Suzuki, *Biochemistry*, **6**, 1335 (1967).
17) J. M. C. Tribris, M. J. Namtvedt, and I. C. Gunsalus, *Biochem. Biophys. Res. Commun.*, **30**, 323 (1968).
18) I. Okura, K. Nakamura, and T. Keii, *J. Mol. Catal.*, **4**, 453 (1978).
19) I. Okura, K. Nakamura, and S. Nakamura, *J. Mol. Catal.*, **6**, 307 (1979).
20) I. Okura, K. Nakamura, and S. Nakamura, *J. Mol. Catal.*, **6**, 311 (1979).
21) I. Okura, K. Nakamura, and S. Nakamura, *J. Mol. Catal.*, **6**, 299 (1979).
22) E. C. Hatchikian, M. Bruschi, and L. LeGall, *Biochem. Biophys. Res. Commun.*, **82**, 451 (1978).
23) M. W. W. Adams, S. G. Reeves, D. O. Hall, G. Christou, B. Ridge, and H. N. Rydon, *Biochem. Biophys. Res. Commun.*, **79**, 1184 (1977).
24) M. Okawara, T. Nakagawa, and E. Imoto, *Kogyo Kagaku Kaishi*, **60**, 73 (1957).
25) T. Yagi, *J. Biochem.*, **68**, 649 (1970).
26) T. Yagi, K. Kimura, H. Daidoji, F. Sakai, S. Tamura, and H. Inokuchi, *J. Biochem.*, **79**, 661 (1976).
27) T. P. King and M. Spencer, *J. Biol. Chem.*, **245**, 6134 (1970).
28) K. Suzuki and T. Kimura, *Biochem. Biophys. Res. Commun.*, **28**, 514 (1967).
29) K. W. Lovenberg and K. McCarthy, *Biochem. Biophys. Res. Commun.*, **30**, 453 (1968).
30) I. Okura, S. Nakamura, and K. Nakamura, *J. Mol. Catal.*, **5**, 315 (1979).
31) T. Peters, Jr., "Plasma Proteins," ed by F. W. Putnam, Academic Press, New York (1975), Vol. 1, p. 133.

Application of the Water-gas Shift Reaction. I. Hydrogenation and Hydroformylation Reactions of Olefins with Carbon Monoxide and Water Catalyzed by Rhodium Phosphine Complexes

Tamon OKANO,* Teruyuki KOBAYASHI, Hisatoshi KONISHI, and Jitsuo KIJI*

Department of Environmental Chemistry and Technology, Faculty of Engineering, Tottori University, Tottori 680

(Received February 12, 1981)

The hydrogenation of methyl crotonate with CO and H_2O is efficiently catalyzed by $RhH_2(O_2COH)[P(i\text{-}Pr)_3]_2$ or $[RhCl(C_7H_8)]_2/P(i\text{-}Pr)_3/n\text{-}BuLi$ (C_7H_8=norbornadiene). Both catalyst precursors are shown to form the same active species; *trans*-$Rh(OH)(CO)[P(i\text{-}Pr)_3]_2$. The catalytic activity of the system ($[RhCl(C_7H_8)]_2$/phosphine/*n*-BuLi) increases with increase of the basicity of the phosphine ligands (phosphine=$P(i\text{-}Pr)_3>P(n\text{-}Bu)_3>PPh(i\text{-}Pr)_2>PPh_2(i\text{-}Pr)>PPh_3$). This reaction is also applicable to the hydrogenation of the C=C bond of electron-withdrawing olefins and the C=O bond of ketones and aldehydes. Interestingly, the catalysis for the C=C bond, to which less electron-withdrawing groups are attached, gives dominantly aldehydes due to hydroformylation. The mechanism is also discussed.

The water-gas shift reaction (Eq. 1) attracts our attention from a viewpoint of the use of coal as a hydrogen source. Recently, many studies have been reported on the shift reaction using homogeneous catalysts,[1-4] which are active even at such a low temperature as the boiling point of water. The catalysis generates such a reactive reducing species that hydrogenation[5] and hydroformylation[6,7] of olefins, reduction of nitrobenzenes,[8,9] and α-methylation of ketones[10] and *N*-methylation of amines[11] with formaldehyde have been carried out in homogeneous phase without using molecular hydrogen.

$$CO + H_2O \longrightarrow CO_2 + H_2 \quad (1)$$

To date, metal carbonyls combined with base[1,5,6,8-11] or acid[2] have habitually been used for the shift reaction as well as the organic reactions, while these catalyst systems are perturbed by side reactions such as aldol condensation, hydrolysis, isomerization of double bond, *etc.* One of our authors has reported that homogeneous rhodium phosphine complexes possess high catalytic activities for the shift reaction in an essentially neutral solution.[4] Though few reports have appeared on the catalysis of phosphine complexes for Eq. 1, phosphine complexes are, in general, more active than metal carbonyls in the homogeneous catalytic hydrogenations and hydroformylation reactions.

Aiming at application of the water-gas shift reaction to the organic reactions, we employed the homogeneous rhodium phosphine complexes as the catalyst. The present paper deals with the hydrogenation and the hydroformylation of olefins using carbon monoxide and water in place of molecular hydrogen.

Table 1. Hydrogenation of methylcrotonate with CO and H_2O catalyzed by triphenylphosphine complexes of group VIII[a]

Catalyst precursor	Yield/% of methyl butyrate[b]
$RhH(CO)(PPh_3)_3$	90
$RhCl(PPh_3)_3$	66
$RuH_2(PPh_3)_4$	53
$CoH(N_2)(PPh_3)_3$	28
$Pd(PPh_3)_4$	23

a) Conditions ; catalyst precursor=0.2 mmol, methyl crotonate=20 mmol, H_2O=100 mmol, P_{CO}=50 atm, 150 °C, 20 h. b) Based on methyl crotonate added.

Results and Discussion

Catalytic Activity of Group VIII Metal Complexes. Because it is easily hydrogenated and hydroformylated, methyl crotonate was used as a typical substrate to survey the catalytic activities of different Group VIII metal complexes of triphenylphosphine. The results are shown in Table 1. The catalytic activity increased in the order; Rh>Ru>Co≫Pd. Among them the halide-free rhodium complex, $RhH(CO)(PPh_3)_3$ (**1**), was found to be most active. Methyl butyrate was

Table 2. Effect of phosphine ligands in the catalyst system of $[RhCl(C_7H_8)]_2$/Phosphine/*n*-BuLi[a]

Phosphine	$CH_3CH=CHCOOCH_3$			CO_2[b]	A/(A+B+C)	B/(B+C)
	$CH_3CH_2CH_2$-$COOCH_3$[b] A	$CH_3CH(CHO)$-CH_2COOCH_3[b] B	$CH_3CH_2CH(CHO)$-$COOCH_3$[b] C			
PPh_3	15	≈0	≈0	8	1	—
$PPh_2(i\text{-}Pr)$	46	0.9	0.1	47	0.98	0.9
$PPh(i\text{-}Pr)_2$	55	2.6	0.5	59	0.95	0.8
$P(n\text{-}Bu)_3$	60	0	≈0	63	1	—
$P(i\text{-}Pr)_3$	72	4.8	4.3	82	0.87	0.5

a) Conditions; catalyst ($[RhCl(C_7H_8)]_2$=0.05 mmol, phosphine=0.2 mmol, *n*-BuLi=0.25 mmol), methyl crotonate=20 mmol, H_2O=50 mmol, P_{CO}=15 atm, THF=6.5 ml, 115 °C, 20 h. b) The yields/% are based on methyl crotonate used.

Table 3. Activities of various catalyst precursors and effect of CO pressure in the hydrogenation of methyl crotonate with CO and H_2O[a]

Catalyst precursor[b]	CO (atm)[c]	Products (%)[d]				B/(A+B+C)	B/(B+C)
		CO_2	$CH_3CH_2CH_2$-$COOCH_3$ A	$CH_3CH(CHO)$-CH_2COOCH_3 B	CH_3CH_2CH-$(CHO)COOCH_3$ C		
$[RhCl(C_7H_8)]_2$/L/*n*-BuLi	15	82	72	4.8	4.3	0.88	0.53
$RhH_2(O_2COH)L_2$	15	102	91	4.2	3.9	0.91	0.52
$[Rh(CO)L_2]_2(CO_3)$[e]	15		86	7.3	6.6	0.86	0.53
$RhH_2(O_2COH)L_2$[f]	7.5	40	49	4.5	3.0	0.87	0.40
$RhH_2(O_2COH)L_2$[f]	15	65	58	8.5	3.0	0.83	0.74
$RhH_2(O_2COH)L_2$[f]	30	83	53	29	1.5	0.63	0.95
$RhH_2(O_2COH)L_2$[f]	60	30	25	14	0.5	0.63	0.97

a) Conditions; catalyst precursor=0.1 mmol, methyl crotonate=20 mmol, H_2O=50 mmol, THF=6.5 ml, 115 °C, 20 h. b) L=P(*i*-Pr)$_3$. c) Initial pressure. d) Based on methyl crotonate used. e) Catalyst precursor=0.05 mmol. f) At 95 °C.

formed in a 90% yield. Thus, the halide-free rhodium complexes were used hereafter in the present study to widen the scope of the application of the water-gas shift reaction to the organic reactions.

Little is known about the synthetic method for the hydrido rhodium(I) complexes of various phosphines, which are expected as the effective catalyst precursor. Therefore, the effects of the phosphine ligands were examined using a catalyst precursor prepared *in situ* by the reaction of $[RhCl(C_7H_8)]_2$ with *n*-BuLi in the presence of phosphine, which affords the hydrido complex (*vide infra*). The results are summarized in Table 2. By successive replacement of the phenyl groups on the phosphorus of triphenylphosphine by alkyl groups, the catalytic activity for the hydrogenation increased in the order; P(*i*-Pr)$_3$>PPh(*i*-Pr)$_2$>PPh$_2$(*i*-Pr)>PPh$_3$. The replacement by the isopropyl group makes the phosphine more electron-donating and bulky.[12] The activity of the system using P(*n*-Bu)$_3$, which is less bulky than any other ligands examined, was close to that using PPh(*i*-Pr)$_2$. In general, ligand effects may be separated into electronic and steric factors. According to Tolman,[13] the infrared CO stretching frequencies of Ni(CO)$_3$L (L=P(*n*-Bu)$_3$ and PPh(*i*-Pr)$_2$), which reflect the electronic donor-acceptor property of L, are 2060.3 and 2062.4 cm^{-1}, respectively. Both are estimated to be similar in electronic nature. Consequently, the above results suggest that the electronic factor of the auxiliary ligand is more dominant than the steric factor over the greater part of the catalytic activity for the hydrogenation.

In some cases, small amounts of aldehydes were formed by hydroformylation. Their yields increased in the order similar to that of the hydrogenation product, but no appreciable amounts of aldehydes were formed in the case of P(*n*-Bu)$_3$. A plausible interpretation of the fact is described later. From these results, P(*i*-Pr)$_3$ was one of the most effective auxiliary ligands.

Catalyst Precursor. When a THF solution containing $[RhCl(C_7H_8)]_2$, P(*i*-Pr)$_3$, and *n*-BuLi was treated with H_2O and CO_2 (1 atm), a dihydrido hydrogencarbonato complex, $RhH_2(O_2COH)[P(i\text{-}Pr)_3]_2$ (**2**), was obtained. This complex is known to be formed also *via* the oxidative addition of H_2O and CO_2 to $RhH[P(i\text{-}Pr)_3]_3$ or *trans*-$RhH(N_2)[P(i\text{-}Pr)_3]_2$.[14] It has also been reported that *trans*-$RhH(N_2)[PPh(t\text{-}Bu)_2]_2$ is isolated from the reaction mixture of $[RhCl(CH_2{=}CH_2)_2]_2$ with *n*-BuLi in the presence of the phosphine under an atmosphere of nitrogen.[15] These facts indicate that the reaction of $[RhCl(C_7H_8)]_2$ with *n*-BuLi in the presence of phosphine presents a general method to provide the halide-free hydrido phosphine complexes. The dihydrido hydrogencarbonato complex (**2**) is known to react readily with CO to give a carbonyl carbonato complex, $\{Rh(CO)[P(i\text{-}Pr)_3]_2\}_2(CO_3)$ (**3**).[14] Since large amounts of CO, H_2O, and CO_2 are present in the catalytic system, the three catalyst precursors, $[RhCl(C_7H_8)]_2$/P(*i*-Pr)$_3$/*n*-BuLi, **2**, and **3**, shown in Table 3 must form the same active species. The reaction mixture catalyzed by **2** was treated with $NaBPh_4$ in the

$$[RhCl(C_7H_8)]_2 + P(i\text{-}Pr)_3 + n\text{-BuLi} \longrightarrow [\text{rhodium(I) hydride}] \xrightarrow{H_2O,\ CO_2} RhH_2(O_2COH)[P(i\text{-}Pr)_3]_2 \quad \mathbf{2}$$

presence of pyridine to give a cationic complex, {*trans*-Rh(CO)(pyridine)[P(*i*-Pr)$_3$]$_2$}BPh$_4$ (**5**), which is known to be formed by a similar treatment of **3**.[4] This fact suggests that the hydroxo complex, *trans*-Rh(OH)(CO)-[P(*i*-Pr)$_3$]$_2$ (**4**), plays an important role in the catalysis, because **4** in pyridine is known to be in equilibrium with a solvated ion pair complex which produces **5** by an anion exchange with BPh_4^-.[4]

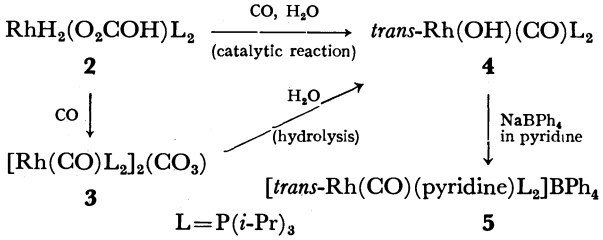

Scheme 1.

Hydrogenation and Hydroformylation of Various Olefins. The reactions of electron-withdrawing and -donating olefins are summarized in Table 4. The hydrogenation of the electron-withdrawing olefins occurred exclusively, except for methyl crotonate. On the contrary, the hydroformylation of styrene occurred in preference to

Table 4. Hydrogenation and hydroformylation with CO and H_2O catalyzed by $RhH_2(O_2COH)[P(i\text{-}Pr)_3]_2$[a]

Substrate	Product	Yield/%[b]
CH_2=CHCN	CH_3CH_2CN	≈100
CH_2=$CHCONH_2$	$CH_3CH_2CONH_2$	86
CH_3CH=$CHCOOCH_3$	$CH_3CH_2CH_2COOCH_3$	91
	$CH_3CH(CHO)CH_2COOCH_3$	4
	$CH_3CH_2CH(CHO)COOCH_3$	4
PhCH=$CHCOOCH_3$	$PhCH_2CH_2COOCH_3$	93
$(CH_3)_2C$=$CHCOCH_3$	$(CH_3)_2CHCH_2COCH_3$	92
	$(CH_3)_2CHCH_2CH(OH)CH_3$	2
PhCH=CHCHO	$PhCH_2CH_2CHO$	99
Cyclohexanone[c]	Cyclohexanol	95
$PhCOCH_3$[c]	$PhCH(OH)CH_3$	68
PhCHO[c]	$PhCH_2OH$	92
$PhNO_2$[d]	$PhNH_2$	95
PhCN[d]	$PhCH_2NH_2$	2
PhCH=CH_2	$PhCH_2CH_2CHO$	57
	$PhCH(CHO)CH_3$	23
	$PhCH_2CH_3$	16
p-$CH_3OC_6H_4CH$=CH_2	*p*-$CH_3OC_6H_4CH_2CH_2CHO$	44
	p-$CH_3OC_6H_4CH(CHO)CH_3$	30
	p-$CH_3OC_6H_4CH_2CH_3$	18
$Ph(CH_3)C$=CH_2	$PhCH(CH_3)CH_2CHO$	80
	$PhC(CH_3)_2CHO$	5
$CH_3(CH_2)_3CH$=CH_2	$CH_3(CH_2)_3CH_2CH_2CHO$	42
	$CH_3(CH_2)_3CH(CHO)CH_3$	35
cyclo-C_8H_{14}	*cyclo*-$C_8H_{15}CHO$	54

a) Conditions; $RhH_2(O_2COH)[P(i\text{-}Pr)_3]_2$=0.1 mmol, substrate=20 mmol, H_2O=50 mmol, P_{CO}=15 atm, THF=6.5 ml, 115 °C, 20 h. b) Based on the substrate used. c) At 150 °C. d) At 165 °C.

hydrogenation. α-Methylstyrene and alkenes gave only the corresponding aldehydes. It is well known that hydrogenation incidental to the hydroformylation with CO and H_2 becomes dominant in the reaction of electron-withdrawing olefins such as α,β-unsaturated aldehydes and ketones,[16] or under conditions of higher H_2/CO ratio.[17] The hydrogen pressure during the reaction of electron-withdrawing olefins is, however, estimated to be very low, because the amount of molecular hydrogen is, at the highest, equal to that of CO_2 produced by the water-gas shift reaction. For example, the yield of CO_2 shown in Table 3 is almost equal to the total yield of organic products. Actually, in the course of the reaction of methyl crotonate (at a 71% conversion), the partial pressure of hydrogen observed was *ca.* 0.09 atm, meaning the H_2/CO ratio to be 0.01. These facts suggest that the hydrogenation of electron-withdrawing olefins occurred at least to a great extent with CO and H_2O as the reducing agent, without intermediate generation of molecular hydrogen. The fitting mechanism is discussed below.

Hydrogenation of carbonyl groups was somewhat difficult. Ketones and aldehydes were reduced only above 150 °C. Namely, α,β-unsaturated carbonyl compounds afforded selectively the corresponding saturated ketones and aldehydes at 115 °C, and at 150 °C the corresponding alcohols were obtained. Nitrobenzene could also be reduced to aniline quantitatively at 165 °C, but the phenyl ring remained unchanged.

Effects of CO and H_2 Pressure. The rate and the product distribution of this reaction strongly depended upon the pressure of CO (Table 3). The maximum conversion of methyl crotonate was attained at 30 atm of the initial CO pressure, and the selectivity to the hydrogenation was decreased with increasing the CO pressure up to 30 atm because of the enhanced rate of the hydroformylation. The insertion of CO into the alkyl-rhodium bond, which is involved in an intermediate, seems to be favored at a moderate pressure. Under higher pressure of CO, however, both the hydrogenation and the hydroformylation were inhibited. The reduced activities are probably ascribed to the decrease in coordinative unsaturated species by the coordination of CO.[18]

To inquire how the addition of molecular hydrogen exerts action on this hydrogenation, methyl crotonate (40 mmol) was reduced in a THF solution containing D_2O (100 mmol) under H_2 (40.6 mmol) and CO (40.6 mmol). After the reaction, the gas phase in the autoclave was a mixture of CO_2 (8.5 mmol), H_2, HD, and D_2 (total 9.3 mmol), and CO (30.2 mmol). Methyl butyrate (38 mmol) was formed. The sum of the amounts of CO_2 formed and H_2 consumed is in good agreement with the yield of methyl butyrate. The result is a consequence of the fact that side reactions are negligible. Therefore, at the highest 21% (CO_2 formed (8.5 mmol)/[H_2 consumed (31.3 mmol)+CO_2 formed]) of the hydrogenation would occur with CO and D_2O rather than H_2 as the reducing agent. However, the

TABLE 5. DEUTERIUM CONTENT OF THE PRODUCTS OF THE HYDROGENATION AND THE HYDROFORMYLATION WITH CO, D_2O, AND H_2[a]

Source of methyl butyrate[c]	Deuterium content (atm-%)[b]	
	α-CH	β-CH
Methyl crotonate CO (15 atm)/D_2O/H_2 (15 atm)	78	41
Methyl crotonate CO(1 atm)/D_2O/H_2 (15 atm)	70	15
Methyl butyrate CO(15 atm)/D_2O/H_2 (15 atm)	<5	<5
Source of β-phenylpropanal[d]	-CHO α-CH	β-CH
α-Methylstyrene CO(15 atm)/D_2O/H_2 (15 atm)	22 6	19

a) Conditions ; $RhH_2(O_2COH)[P(i\text{-}Pr)_3]_2 = 0.2$ mmol, $D_2O = 100$ mmol, THF = 6.5 ml, 115 °C. b) The values show deuterium contents out of the hydrogen and deuterium incorporated. c) For 7.5 h. d) For 1 h.

^{1}H-NMR analysis of the formed methyl butyrate showed 59% incorporation of deuterium. Its contents at the 2- and 3-positions were 78 and 41 atom-%,

$$CH_3CH{=}CHCOOCH_3 \xrightarrow{CO,\ D_2O,\ H_2} CH_3{-}CH_{1.59}D_{0.41}{-}CH_{1.22}D_{0.78}{-}COOCH_3$$

respectively. In a separated experiment, it was confirmed that theH-D exchange reaction of methyl butyrate with D_2O does not occur under these conditions. Another possibility of H-D exchange proceeding through alkylrhodium intermediates (**8a** and **8b**), *i.e.*, a half hydrogenated state, *via* metal hydride addition and elimination[19] (see Scheme 3, **4**⇌**6**⇌**7**⇌**8**) is excluded for the following reason. If this exchange were sufficiently fast, the deuterium contents at the 2- and 3-positions would be closely similar, and would not be effected by the amount of CO (*vide infra*). Therefore, the facts that the amount of deuterium incorporated into methyl butyrate is larger than that of CO_2 formed and that the deuterium content at the 2-position is higher than that at the 3-position rationalize the following assumption; D_2O itself participates in the hydrogenation to a considerable extent without generating D_2 and CO_2, and the hydrogen (deuterium) added to the 2-carbon atom comes dominantly from the water even under a pressure of H_2 (see Cycle B in Scheme 3). The nature of this hydrogenation process is discussed below in more detail.

A similar reaction of methyl crotonate with D_2O and H_2 under a low pressure of CO (1 atm, 2.7 mmol) also gave deuterated methyl butyrate (80% yield), of which deuterium content at the 2- and 3-positions was 70 and 15 atom-%, respectively. Interestingly, lowering CO pressure decreased the deuterium content at the 3-position more markedly than that at the 2-position. The result indicates that the reaction of methyl crotonate with CO–D_2O–H_2 includes the hydrogenations with CO–D_2O (Cycle A) and with D_2O–H_2 (Cycle B), which give methyl butyrate-2,3-d_2 and -2-d, respectively.

The addition of molecular hydrogen extremely accelerated the hydroformylation of α-methylstyrene with CO and D_2O, and a conversion of 68% was reached within 1 h at 115 °C. At the time, the yield of CO_2 was 4.5% based on α-methylstyrene converted. 3-Phenylbutanol, which was formed in a 67% yield, contained 22, 6, and 19 atom-% of deuterium at the 1, 2, and 3-positions, respectively. From the fact that the deuterium contents at the 1- and 3-positions are equal within experimental errors, the incorporated deuterium seems to come from D_2 and HD generated by H-D exchange reactions.[20]

Reaction Mechanism. The hydrogenation with CO and H_2O occurs in two stages; (*i*) formation of a reducing species by a reaction of the catalyst with CO and H_2O, and (*ii*) hydrogenation of olefin with the reducing species. The catalysis in the former stage (*i*) is explained by the same mechanism as the water-gas shift reaction catalyzed by **2**,[4] because both the hydrogenation and the shift reaction were ascertained to contain the hydroxo complex (**4**) as one of the active key intermediates. The precise reaction pathway for the formation of a hydrido complex, *trans*-$RhH(CO)[P(i\text{-}Pr)_3]_2$ (**6**), and molecular hydrogen, in which **4** plays an important role, has been reported elsewhere.[4]

The hydrido complex (**6**) thus formed is a homologue of the active species of $RhH(CO)(PPh_3)_3$ (**1**) which is widely used as catalyst, not only for hydrogenation but also for hydroformylation. Therefore, complex **6** is most

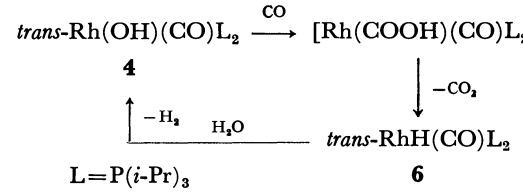

Scheme 2.

suitable for the key intermediate in the latter stage (*ii*). The possible routes for the hydrogenation of methyl crotonate are shown in Scheme 3. In the hydrogenation and the hydroformylation using CO and H_2O, an σ-alkylrhodium intermediate formed by the insertion of olefin into the rhodium hydrido bond of the 16 valence-electron complex (**6**) is most probable. The hydrogenation following Cycles A and B involves the oxidative addition of H_2O followed by the reductive elimination of methyl butyrate to give **4**. The resultant complex is converted into **6** with CO in a similar manner to the water-gas shift reaction (Cycle A, Steps 1 and 3). Cycle C represents the same mechanism as the usual hydrogenation with molecular hydrogen. The mechanism for this hydrogenation with CO and H_2O is well represented by Cycle A from the following reasons. Methyl butyrate and CO_2 are formed in similar yields in the hydrogenation of methyl crotonate (see Table 3); the partial pressure of H_2 is very low during this reaction, therefore there is no appreciable amount of H_2 involved in Steps 2 and 7. Cycle B is not important unless a large amount of H_2 is present, but it is appropriate to illustrate the fact that the amount of deuterium in methyl butyrate formed by the hydrogenation with CO, D_2O, and H_2 is larger than that of CO_2 formed. Undoutedly, all the results indicate that Cycle C is not important.

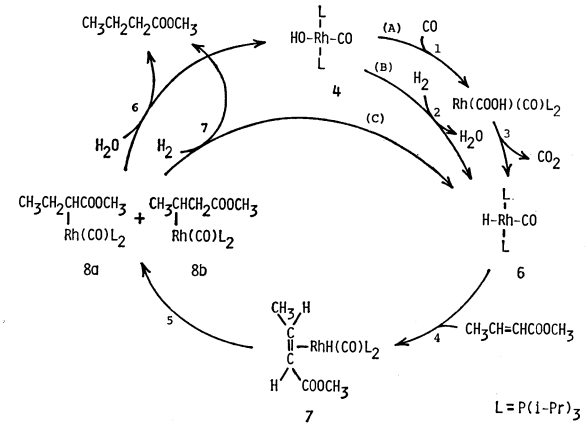

Scheme 3. Possible mechanisms for the hydrogenation of methyl crotonate with CO and H_2O.

Between the two possible types of σ-alkylrhodium intermediate, the 2-metalated one is predominant in the reaction of electron-withdrawing olefins. This conclusion is based on the following evidence; (*i*) the reaction of methyl crotonate with CO, D_2O, and H_2 gives mainly methyl butyrate-2-*d*, and (*ii*) electron-withdrawing olefins are hydrogenated, whereas electron-donating olefins are hydroformylated. The above view is in accord with the previous reports based on the isomer distribution of the conventional hydroformylation products catalyzed by **1**.[21] The stability of the 2-metalated species is ascribed to the electronic effect of the substituent on the rhodium-bearing carbon atom, because the substituent is able to accept the excess charge on the rhodium induced by the electron-donating trialkylphosphine ligands. Consequently, using more electron-donating phosphines as the ligand, the 2-metalated species is expected to be more dominant. In fact, this expectation is consistent with the observation that the formylation at the 2-position prevails in the reaction of methyl crotonate, using $P(i\text{-}Pr)_3$ as the auxiliary ligand (Table 2).

The more strongly the phosphine is electron-donating, the more the catalytic activities are increased for hydrogenation as well as hydroformylation (Table 2). The enhancement of both rates is explicable in terms of the facilitated oxidative addition reactions of H_2O and H_2 toward the σ-alkyl and acyl intermediates, respectively. Similar ligand effects have been known in various oxidative addition reactions, and are ascribed to the elevated electron density on the metal caused by the donating ligands. For example, the oxidative additions of H_2[22] and H_2O[23] toward rhodium(I) and platinum(0) complexes are accelerated by the coordination of donating phosphines.

It is not clear why the electron-donating and -withdrawing olefins give the respective products selectively, because a number of factors are involved. One plausible explanation is as follows. The modification of the catalyst with donating phosphines causes the activity for the hydroformylation to increase more markedly than that for the hydrogenation (Table 2). The coordination of the donating phosphines increases the electronic density on the rhodium. The equilibrium between alkyl and acyl complexes under the pressure of CO, which has well been established,[18] is displaced to the acyl species by the coordination, because the acyl ligand is capable of accepting the excess charge from the rhodium. This displacement tends to facilitate the hydroformylation. This explanation is supported by the facts that an acyl complex from oxidative addition to $RhCl(CO)(PPh_3)_2$ have not yet been successful and that the addition of acyl bromide to more nucleophilic $RhBr(CO)(PPhEt_2)_2$ was reported to give stable $RhBr_2(CH_3CO)(CO)(PPhEt_2)_2$.[24] Similarly, it is explainable that the electronic property of the substituent of olefins has a large effect on the selectivity. When the substituent is electron-donating, the equilibrium is displaced more markedly to the acyl species than in the case of electron-withdrawing olefins. The α-metalated alkyl complexes formed from electron-withdrawing olefins are considered to be stabilized by its electron-withdrawing group at the α-position, but those from electron-donating olefins are never. This view is also consistent with the observations that the reaction of **1** with $CF_2=CF_2$ gives a stable insertion product, $CHF_2CF_2Rh(CO)(PPh_3)_2$, in which the insertion of CO no longer takes place, and that $CH_2=CH_2$ does not give the corresponding stable alkyl complex but the acyl one.[25]

Exceptional is the function of $P(n\text{-}Bu)_3$, which is strongly electron-donating but less bulky than $P(i\text{-}Pr)_3$. The alkyl ligand of the key intermediate has a larger cone angle than the corresponding acyl ligand.[12] Therefore, the steric repulsion between the alkyl moiety and the bulky triisopropylphosphine, which has displaces the equilibrium, is more evident. When using less bulky $P(n\text{-}Bu)_3$ as the ligand, however, the steric repulsion appears not to be important. Thus, the alkyl intermediate is relatively stable and subjected to hydrolysis to give the hydrogenation product.

Experimental

All reactions and manipulations were carried out under a nitrogen atmosphere. All organic compounds were purified by distillation or recrystallization under a nitrogen atmosphere before use. Literature methods were employed for preparations of $RhH(CO)(PPh_3)_3$,[26] $RhCl(PPh_3)_3$,[27] $RuH_2(PPh_3)_4$,[28] $CoH(N_2)(PPh_3)_3$,[29] $Pd(PPh_3)_4$,[30] $PPh_2(i\text{-}Pr)$,[31] $PPh(i\text{-}Pr)_2$,[32] $P(i\text{-}Pr)_3$,[33] $[RhCl(C_7H_8)]_2$,[34] $RhH_2(O_2COH)[P(i\text{-}Pr)_3]_2$,[14] and $\{Rh(CO)[P(i\text{-}Pr)_3]_2\}_2(CO_3)$.[14] The ^{1}H-NMR and IR spectra were recorded on a Varian T-60-A spectrometer and a JASCO IRA-1 spectrometer, respectively.

Catalytic Hydrogenation and Hydroformylation. The following procedure is illustrative. To a 65 ml stainless steel autoclave containing a THF solution (6.5 ml) of $RhH_2(O_2COH)[P(i\text{-}Pr)_3]_2$ (**2**) (48.7 mg, 0.1 mmol) were added H_2O (0.9 g, 50 mmol), methyl crotonate (2.0 g, 20 mmol), and CO (15 atm, 40.6 mmol) in that order. After heating at 115 °C for 20 h, the autoclave was cooled to room temperature. The GLC analysis of the gaseous products (on a column, active carbon, 3 m; at 50 °C; carrier gas, H_2) using nitrogen as an internal calibrant showed the presence of CO_2 (19.5 mmol, 98% based on methyl crotonate) and CO (19 mmol). The GLC analysis of the solution (on a column, PEG 20M, 2 m; at 110 °C; carrier gas, H_2) employing naphthalene as an internal standard showed the formation of $CH_3CH_2CH_2COOCH_3$ (1.87 g, 91%), $CH_3CH(CHO)CH_2COOCH_3$ (0.11

g, 4.2%), and $CH_3CH_2CH(CHO)COOCH_3$ (0.1 g, 3.9%).

The other catalytic reaction experiments were carried out according to similar procedures. The amount of H_2 formed was determined by GLC (on a column, molecular sieve 5A, 3 m; at 80 °C; carrier gas, Ar). The catalyst solution from $[RhCl(C_7H_8)]_2$ was prepared in the following manner. A hexane solution of *n*-BuLi (0.15 ml, 0.25 mmol) was slowly added to a mixture of $[RhCl(C_7H_8)]_2$ (23.1 mg, 0.05 mmol) and phosphine (0.2 mmol) in THF (6.5 ml), and the stirring was continued for 30 min. This freshly prepared pale brown solution was used immediately.

Preparation of $RhH_2(O_2COH)[P(i\text{-}Pr)_3]_2$ (2). To a catalyst solution, which was prepared from a mixture of $[RhCl(C_7H_8)]_2$ (46.1 mg, 0.1 mmol), $P(i\text{-}Pr)_3$ (96 mg, 0.6 mmol), and *n*-BuLi (0.6 mmol in 0.36 ml of hexane) in THF (2 ml) with stirring at room temperature for 30 min, was added H_2O (0.25 g, 14 mmol). The resultant brown mixture was stirred under an atmosphere of CO_2 at room temperature for 1 h. The IR spectrum of the concentrated residue showed the formation of a mixture of **2** (ν_{Rh-H} 2140, 2120; $\nu_{C=O}$ 1590 cm^{-1}) and $\{Rh(CO)[P(i\text{-}Pr)_3]_2\}_2(CO_3)$ (**3**) ($\nu_{C\equiv O}$ 1930; $\nu_{C=O}$ 1530 cm^{-1}). The residue was recrystallized from toluene to give colorless crystals of **2** (20 mg, 21%)

Isolation of $\{trans\text{-}Rh(CO)(pyridine)[P(i\text{-}Pr)_3]_2\}BPh_4$ (5) from the Reaction Mixture. A solution from the hydrogenation reaction of methyl crotonate catalyzed by **2** (48.7 mg, 0.1 mmol) was concentrated under reduced pressure, and the oily residue was redissolved in pyridine (5 ml). After addition of $NaBPh_4$ (34.7 mg, 0.1 mmol), the brown solution was stirred at room temperature for 10 min. The mixture was concentrated to dryness, and the solid residue was recrystallized from THF–toluene to give $\{trans\text{-}Rh(CO)(pyridine)[P(i\text{-}Pr)_3]_2\}BPh_4 \cdot 2toluene$ as pale yellow crystals (45 mg, 45%), mp 150 °C dec, $\nu_{C\equiv O}$ 1985 cm^{-1}.

Hydrogenation of Methyl Crotonate with CO, D_2O, and H_2. To a 65 ml autoclave containing a mixture of **2** (97.3 mg, 0.2 mmol, methyl crotonate (4.0 g, 40 mmol), and D_2O (2.0 g,100 mmol) in THF (6.5 ml) were charged CO (15 atm, 40.6 mmol) and H_2 (15 atm, 40.6 mmol), successively. After heating at 115 °C for 7.5 h, the autoclave was cooled to room temperature. The pressure inside the autoclave was 18 atm. The GLC analysis of the gas phase showed the presence of CO_2 (8.5 mmol, 3.1 atm), H_2, HD, and D_2 (total 9.3 mmol, 3.5 atm) and CO (30.1 mmol ,11.3 atm). The GLC analysis of the solution showed the formation of methyl butyrate 3.88 g, 95%). The methyl butyrate was collected into a cold trap under reduced pressure, and purified by distillation. The ^1H-NMR showed the 2-CH_2 (δ 2.2, m), 3-CH_2 (δ 1.62, m), CH_3C (δ 0.95, t), and CH_3O proton signals (δ 3.63, s) in a corrected relative intensity of 1.22 : 1.59 : 3 : 3. The incorporated deuterium contents calculated from these values were 78 and 41% at 2- and 3-positions, respectively.

Hydroformylation of α-Methylstyrene with CO, D_2O, and H_2. In a 65 ml autoclave pressured with CO (15 atm, 40.6 mmol) and H_2 (15 atm, 40.6 mmol), a mixture of **2** (97.3 mg, 0.2 mmol), α-methylstyrene (4.72 g, 40 mmol), and D_2O (2.0 g, 100 mmol) in THF (6.5 ml) was heated at 115 °C for 1 h. The gas phase (2.5 atm) was analyzed by GLC, and shown to contain CO_2 (1.4 mmol, 0.5 atm), H_2, HD, and D_2 (total 0.5 mmol, 0.2 atm), and CO (4.9 mmol, 1.8 atm). The ^1H-NMR spectrum of 3-phenylbutanal purified by preparative GLC showed to contain 22, 6, and 19% of deuterium at the 1-, 2-, and 3-positions, respectively.

The authors wish to express their thanks to Professor Sei Otsuka and Associate Professor Toshikatsu Yoshida of Osaka University for their helpful discussions and suggestions. The present work was partially supported by a Grant-in-Aid for Scientific Research No. 575545 from the Ministry of Education, Science and Culture.

References

1) A. D. King, Jr., R. B. King, and D. B. Yang, *J. Am. Chem. Soc.*, **102**, 1028 (1980); A. D. King, R. B. King, and D. B. Yang, *J. Chem. Soc., Chem. Commun.*, **1980**, 529; C. Ungermann, V. Landis, S. A. Moya, H. Cohen, H. Walker, R. G. Peason, R. G. Rinker, and P. C. Ford, *J. Am. Chem. Soc.*, **101**, 5922, (1979); R. B. King, C. C. Frazier, R. M. Hanes, and A. D. King, Jr., *ibid.*, **100**, 2925 (1978); R. M. Raine, R. G. Rinker, and P. C. Ford, *ibid.*, **99**, 252 (1977).

2) E. C. Baker, D. E. Hendriksen, and R. Eisenberg, *J. Am. Chem. Soc.*, **102**, 1020 (1980); P. C. Ford, R. G. Rinker, C. Ungermann, R. M. Laine, V. Landis, and S. A. Moya, *ibid.*, **100**, 4595 (1978); C.-H. Cheng and R. Eisenberg, *ibid.*, **100**, 5968 (1978); C.-H. Cheng, D. E. Hendriksen, and R. Eisenberg, *ibid.*, **99**, 2791 (1977).

3) T. Yoshida, Y. Ueda, and S. Otsuka, *J. Am. Chem. Soc.*, **100**, 4941 (1978).

4) T. Yoshida, T. Okano, and S. Otsuka, *J. Am. Chem. Soc.*, **102**, 5966 (1980); T. Yoshida, T. Okano, Y. Ueda, and S. Otsuka, *J. Am. Chem. Soc.*, **103**, 3411 (1981).

5) T. Kitamura, T. Joh, and N. Hagihara, *Chem. Lett.*, **1975**, 203; T. Kitamura, N. Sakamoto, and T. Joh, *ibid.*, **1973**, 379.

6) R. M. Laine, *J. Am. Chem. Soc.*, **100**, 6451 (1978); H. Kang, C. Mauldin, T. Cole, W. Slegeir, K. Cann, and R. Pettit, *ibid.*, **99**, 8323 (1977).

7) K. Murata, A. Matsuda, K. Bando, and Y. Sugi, *J. Chem. Soc., Chem. Commun.*, **1979**, 785.

8) R. C. Ryan, G. M. Wilemon, M. P. Dalsanto, and C. U. Pittman, Jr., *J. Mol. Cat.*, **5**, 319 (1979); K. Cann, T. Cole, W. Slegeir, and R. Pettit, *J. Am. Chem. Soc.*, **100**, 3969 (1978); A. F. M. Iqbal, *Tetrahedron Lett.*, **1971**. 3385.

9) Y. Watanabe, N. Suzuki, S. C. Shim, M. Yamamoto, T. Mitsuda, and Y. Takegami, *Chem. Lett.*, **1980**, 429.

10) Y. Watanabe, K. Takatsuki, and Y. Takegami, *Tetrahedron Lett.*, **1978**, 3369; Y. Watanabe, Y. Shimizu, K. Takatsuki, and Y. Takegami, *Chem. Lett.*, **1978**, 215.

11) Y. Sugi, A. Matsuda, K. Bando, and Murata, *Chem. Lett.*, **1979**, 363; Y. Watanabe, M. Yamamoto, T. Mitsudo, and Y. Takegami, *Tetrahedron Lett.*, **1978**, 1289.

12) C. A. Tolman, *Chem. Rev.*, **77**, 313 (1977); C. A. Tolman, *J. Am. Chem. Soc.*, **92**, 2956 (1970).

13) C. A. Tolman, *J. Am. Chem. Soc.*, **92**, 2953 (1970).

14) T. Yoshida, D. L. Thorn, T. Okano, J. A. Ibers, and S. Otsuka, *J. Am. Chem. Soc.*, **101**, 4212 (1979).

15) T. Yoshida, T. Okano, D. L. Thorn, T. H. Tulip, S. Otsuka, and J. A. Ibers, *J. Organomet. Chem.*, **181**, 183 (1979).

16) For example, see B. Heil and L. Markó, *Magy. Kem. Lapja*, **23**, 669 (1968); *Chem. Abstr.*, **70**, 56861 (1968); B. Fell and W. Rupilius, *Tetrahedron Lett.*, **1969**, 2721; J. Falbe and N. Huppes, *Brennstoff-Chem.*, **48**, 248 (1971).

17) C. K. Brown and G. Wilkinson, *J. Chem. Soc., A*, **1970**, 2753.

18) P. Pino, F. Piacenti, and M. Bianchi, "Reactions of Carbon Monoxide and Hydrogen with Olefinic Substrates," in "Organic Syntheses *via* Metal Carbonyls," ed by I. Wender and P. Pino, J. Wiley and Sons, New York, N. Y. (1977).

19) J. F. Harrod and A. J. Chalk, *J. Am. Chem. Soc.*, **88**, 3491 (1966).

20) A similar H-D exchange reaction catalyzed by rhodium

complexes is known. See T. Yoshida, T. Okano, K. Saito, and S. Otsuka, *Inorg. Chim. Acta*, **44**, L135 (1980).
21) C. U. Pittman, Jr., W. D. Honnick, and J.J. Yang, *J. Org. Chem.*, **45**, 684 (1980), and references therein.
22) J. Chatt and S. A. Butter, *J. Chem. Soc., Chem. Commun.*, **1967**, 501; C, A. Tolman, P. Z. Meakin, D. L. Lindner, and J. P. Jesson, *J. Am. Chem. Soc.*, **96**, 2762 (1974); T. Yohisda and S. Otsuka, *ibid.*, **99**, 2134 (1977).
23) T. Yoshida, T. Matsuda, T. Okano, T. Kitani, and S. Otsuka, *J. Am. Chem. Soc.*, **101**, 2027 (1979); T. Yoshida, T. Okano, K. Saito, and S. Otsuka, *Inorg. Chim. Acta*, **44**, L135 (1980).
24) J. Chatt and B. L. Shaw, *J. Chem. Soc., A*, **1966**, 1437.
25) G. Yagupsky, C. K. Brown, and G. Wilkinson, *J. Chem. Soc., A*, **1970**, 1392.
26) D. Evans, G. Yagupsky, and G. Wilkinson, *J. Chem. Soc., A*, **1968**, 2660.
27) J. A. Osborn and G. Wilkinson, *Inorg. Synth.*, **10**, 67 (1967).
28) R. O. Harris, N. K. Hota, L. Sandavoy, and J. M. C. Yuen, *J. Organomet. Chem.*, **54**, 259 (1973).
29) A. Sacco and M. Rossi, *Inorg. Synth.*, **12**, 18 (1970).
30) D. R. Coulson, *Inorg. Synth.*, **13**, 121 (1972).
31) W. Kuchen and H. Buchwald, *Chem. Ber.*, **92**, 227 (1959).
32) E. Fluck and J. Lorenz, *Z. Naturforsch., Teil B*, **22**, 1095 (1967).
33) A. H. Cowly and M. W. Taylor, *J. Am. Chem. Soc.*, **91**, 2915 (1969).
34) E. W. Abel, M. A. Bennett, and G. Wilkinson, *J. Chem. Soc.*, **1959**, 3178.

Dimerization of Tryptophan Derivatives in Trifluoroacetic Acid[1)]

Kazunari HASHIZUME and Yasutsugu SHIMONISHI*
Institute for Protein Research, Osaka University, Yamada-kami, Suita, Osaka 565
(Received February 23, 1981)

Side-products are formed when Ac–Trp–OMe, Ac–Gly–Trp–OMe, or Ac–Trp–Trp–OMe is stored in trifluoroacetic acid. Two products from each of Ac–Trp–OMe and Ac–Gly–Trp–OMe and one product from Ac–Trp–Trp–OMe are isolated by the column chromatography on silica gel and confirmed for homogeneity by the high-performance liquid chromatography. As confirmed by ^{1}H-NMR and mass spectral analyses, they have dimerized structures through the α-carbon to α′-carbon binding of two indole rings. One of the two products from each of Ac–Trp–OMe and Ac–Gly–Trp–OMe is the *trans*-isomer(s) and the other the *cis*-isomer(s). Only a *trans*-isomer(s) is obtained from Ac–Trp–Trp–OMe.

The acid-labile indole moiety in the tryptophan residue is responsible for several side-reactions under acidic conditions used for peptide synthesis. One type of reactions is an oxidation of the indole ring; Theodolopoulos and Fruton[2)] reported a possible formation of "β-oxindolylalanine" in a treatment of *N*-(benzyloxycarbonyl)tryptophan peptide with hydrogen bromide in acetic acid, however this has not yet been proved. Another type of reactions is a substitution in the indole ring by a cation derived from a protecting group: Concerning this type, Alakhov *et al.*[3)] first pointed out that when *N*-(*t*-butyloxycarbonyl)tryptophan peptide acids or *t*-butyl esters are treated with TFA, a *t*-butyl cation, released from the protecting peptides, is introduced onto the indole ring in the tryptophan residue. Subsequently, this was confirmed by Wünsch *et al.*,[4)] who isolated a side product having been butylated at the NH group of the indole ring in the tryptophan residue. This substitution is reported also to occur at positions 2, 5, and 7 of the indole rings.[4,5)] A third type of reactions is an intra- or intermolecular substitution of the indole ring; Uphaus *et al.*[6)] isolated an α-carboline derivative formed through an intramolecular cyclization in a solution of acetyl-DL-tryptophan in TFA, but in low yield. Recently,[7)] one of the authors and others isolated from a solution of Ac–Trp–OMe in TFA or HF a product having a dimerized structure in which the α-position of one indole ring binds with the α′-position of the other indole ring which is reduced simultaneously to an indoline, as shown in Fig. 1.

In this work, we isolated another product which is also formed when Ac–Trp–OMe is kept in TFA and determined its structure on the basis of ^{1}H-NMR and mass spectra. The spectral analysis suggests that the new product is a steric isomer of the compound previously isolated. We found also that when tryptophan-peptides (Ac–Gly–Trp–OMe and Ac–Trp–Trp–OMe) are stored in TFA under the same conditions as with Ac–Trp–OMe, side-products similar to those from Ac–Trp–OMe in structure are formed.

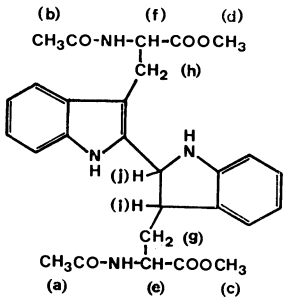

Fig. 1. Dimerized structure of Ac–Trp–OMe.

Results and Discussion

Isolation of Reaction Products. After keeping Ac–Trp–OMe in TFA, we detected two compounds with lower mobility than the starting compound on a TLC plate with a concentration zone (Fig. 2). These compounds gave yellow spots on being stained with the Ehrlich reagent. Previously,[7)] these two compounds could not be separated from each other on a TLC plate with no concentration zone, and only one of them could be isolated on crystallization. In the present work we found that the previously isolated compound corresponds to the compound with the lower R_f value on the TLC plate with a concentration zone, which finding encouraged us to isolate the other compound. For isolation of this compound, a solution of Ac–Trp–OMe in TFA was subjected to a chromatography on a silica-gel

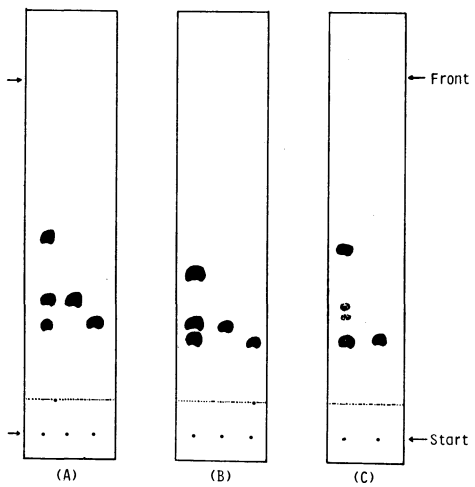

Fig. 2. TLC of products in TFA and isolated materials on silica gel 60 with a concentration zone (Merck Art. 11845). (A) Ac–Trp–OMe (from left, reaction mixture, compounds **1B** and **1A**), (B) Ac–Gly–Trp–OMe (from left, reaction mixture, compounds **2B** and **2A**) and (C) Ac–Trp–Trp–OMe (from left, reaction mixture and compound **3**). Solvent system: (A) and (C), CH_3CN–$CHCl_3$ (2 : 1), (B) CH_3CN–$CHCl_3$–MeOH (60 : 30 : 5). Staining with Ehrlich reagent.

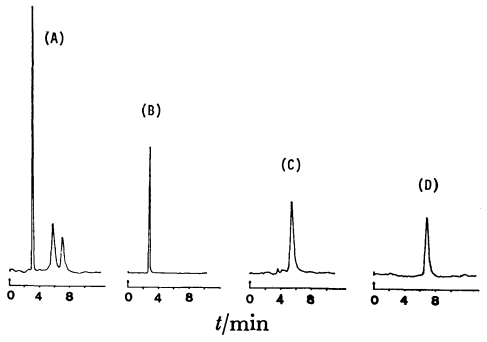

Fig. 3. Elution profiles at 280 nm of reaction mixture of Ac–Trp–OMe in TFA and isolated materials by HPLC on a μ-porasil column (0.39 cm × 30 cm). Solvent: CH_3CN–$CHCl_3$ (2 : 1). Flow rate: 1 ml/min. (A) reaction mixture, (B) starting material (Ac–Trp–OMe), (C) compound **1B**, and (D) compound **1A**.

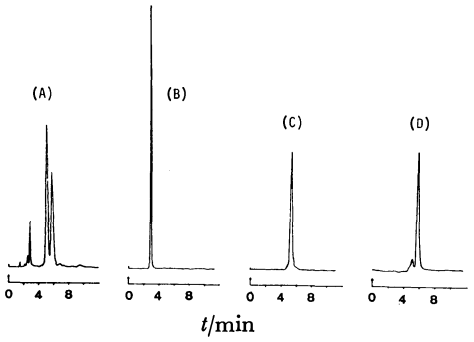

Fig. 4. Elution profiles at 280 nm of reaction mixture of Ac–Gly–Trp–OMe in TFA and isolated materials by HPLC on a μ-porasil column (0.39 cm × 30 cm). Solvent: CH_3CN–$CHCl_3$–MeOH (60 : 30 : 5). Flow rate: 1 ml/min. (A) reaction mixture ,(B) starting material (Ac–Gly–Trp–OMe), (C) compound **2B**, and (D) compound **2A**.

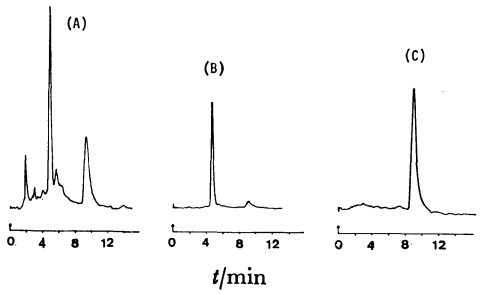

Fig. 5. Elution profiles at 280 nm of a reaction mixture of Ac–Trp–Trp–OMe in TFA and the isolated product by HPLC on a μ-porasil column (0.39 cm × 30 cm) in a solvent mixture of CH_3CN and $CHCl_3$ (2 : 1). Flow rate: 1 ml/min. (A) reaction mixture, (B) starting material (Ac–Trp–Trp–OMe), and (C) compound **3**.

column with a mixture of CH_3CN and $CHCl_3$ (v/v, 2/1). The first compound eluted was the starting compound, and the last compound eluted was identified as the compound previously isolated (denoted as compound **1A**). A compound (denoted as **1B**) eluted between the starting compound and compound **1A** was isolated; the purity of **1B** had been examined by a high-performance liquid chromatography (HPLC) using the same solvent

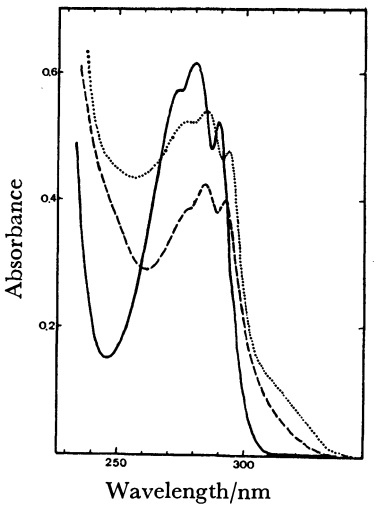

Fig. 6. UV absorption spectra of Ac–Trp–OMe (——), compounds **1A** and **1B** isolated from a solution of Ac–Trp–OMe in TFA (——), and compound **3** isolated from a solution of Ac–Trp–Trp–OMe in TFA (·····) in EtOH.

system as for the preparative chromatography on silica gel to be found homogeneous on HPLC (Fig. 3).

After storage of solutions of tryptophan-peptides (Ac–Gly–Trp–OMe and Ac–Trp–Trp–OMe) in TFA under the same conditions as for Ac–Trp–OMe, TLC indicated presence of new compounds forming yellow spots when stained with the Ehrlich reagent, in addition to the starting compound, as illustrated in Fig. 2. The products from Ac–Gly–Trp–OMe were isolated by chromatography on a silica-gel column using a mixture of CH_3CN, $CHCl_3$, and MeOH (60/30/5) as eluting solvent. Two compounds (denoted as **2A** and **2B**) were eluted separately after the starting compound, and their purities were examined by HPLC (Fig. 4). From a solution of Ac–Trp–Trp–OMe in TFA, we could isolate only one product which was eluted more slowly than the starting peptide from a silica-gel column with a mixture of CH_3CN and $CHCl_3$ (v/v, 2/1) as solvent. Profiles of the reaction mixture and the isolated compound (denoted as compound **3**) on HPLC are shown in Fig. 5.

Structural Determination of Side-products. An elemental analysis showed that compound **1B** has the same composition as the starting compound and also as compound **1A** previously isolated. The mass spectrum of this compound showed a molecular ion at m/z=520, which is twice the m/z value of the starting compound but the same as that of compound **1A**. The UV absorption spectrum also was the same as that of compound **1A**, as shown in Fig. 6. The ^{1}H-NMR spectra of compound **1B** in DMSO-d_6 with and without D_2O suggest the presence of both one indole ring and one indoline ring in the molecule (Fig. 7), as in compound **1A**,[7] although the chemical shifts are slightly different from those of compound **1A**. The chemical shifts were assigned by the decoupling technique described in Ref. 7. These results suggest that compounds **1A** and **1B** are steric isomers associated with the asymmetric α- and β-carbons on the newly formed indoline rings

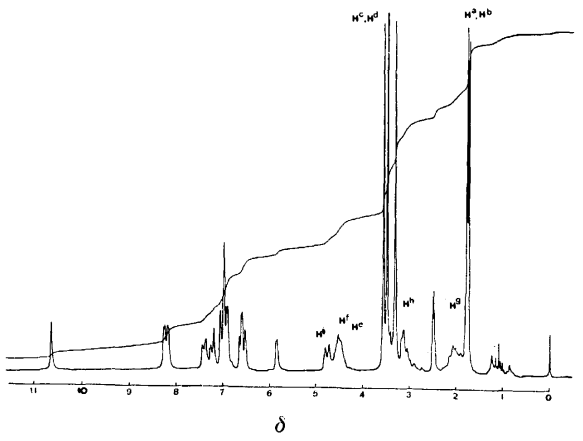

Fig. 7. ^{1}H-NMR spectrum of compound **1B** in DMSO-d_6 at 100 MHz.

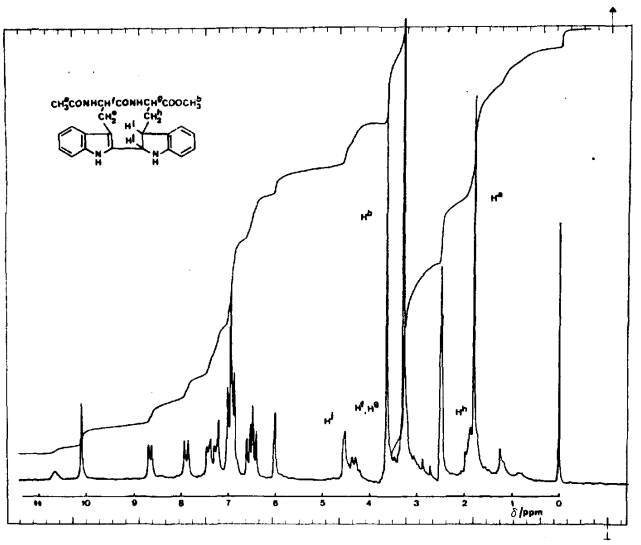

Fig. 8. ^{1}H-NMR spectrum of compound **3** in DMSO-d_6 at 100 MHz.

TABLE 1. COUPLING CONSTANTS (Hz) BETWEEN α-CH AND β-CH IN INDOLINE RINGS

Starting compound	Product	In DMSO-d_6 (+D_2O)	In DMSO-d_6 (+DCl)
Ac-Trp-OMe	**1A**	9.34	8.97
	1B	8.14	8.42
Ac-Gly-Trp-OMe	**2A**	9.33	0.08
	2B	8.79	8.80
Ac-Trp-Trp-OMe	**3**	3.28	3.03
Indoline[8]		J_{trans}=8.43	J_{trans}=6.63
		J_{cis}=8.43	J_{cis}=8.99

because the coupling constant between α-CH (i) and β-CH (j) of the indoline ring in compound **1B** is different from that of compound **1A**, as will be described later.

The two compounds **2A** and **2B** isolated from a solution of Ac-Gly-Trp-OMe in TFA gave analytical values similar to those of the starting peptide, but the molecular ions in their field-desorption mass spectra were at m/z=634, which is twice the value of that of the starting peptide. Their ^{1}H-NMR and UV absorption spectra are similar to those of compounds **1A** and **1B**, respectively, isolated from Ac-Trp-OMe. These results indicate that the compounds isolated from a solution of Ac-Gly-Trp-OMe in TFA have dimerized structures similar to those of the dimerized compounds from Ac-Trp-OMe, and further that they are steric isomers to each other because the coupling constants between α-CH and β-CH on the newly formedinidoline ring are different from each other, similarly to the above-mentioned case with compounds **1A** and **1B**.

The compound isolated from the solution of Ac-Trp-Trp-OMe in TFA was subjected to a field-desorption mass spectrometric analysis and found to have a molecular weight corresponding to m/z=446, the same as that of the starting peptide; an elemental analysis on this compound gave analytical results similar to those on the starting peptide. However, its UV absorption spectrum is different from that of the starting peptide, but similar to those of compounds **1A** and **1B**, as illustrated in Fig. 6. Furthermore, only one NH proton in the indole ring and one NH proton of the indoline ring are observed on the ^{1}H-NMR spectrum, as shown in Fig. 8. These results suggest that in this compound the two indole rings are joined together not intermolecularly but intramolecularly, as shown in Fig. 8.

It is known that protonation of the indoline NH will cause the coupling constant between the α-CH and β-CH of indoline ring increase in the case of *cis*-conformation and to decrease in the case of *trans*-conformation.[8] The coupling constant between α-CH (i) and β-CH (j) in compound **1A** decreased by addition of DCl in DMSO-d_6, while that of compound **1B** increased, as shown in Table 1; such phenomena were observed also in compounds **2A** and **2B**. Also, an addition of DCl to a solution of compound **3** in DMSO-d_6 decreased the coupling constant between α-CH and β-CH of the indoline ring. These facts suggest that compounds **1A**, **2A**, and **3** obtained from Ac-Trp-OMe, Ac-Gly-Trp-OMe, and Ac-Trp-Trp-OMe, respectively, have the *trans*-conformation, while compounds **1B** and **2B** isolated from Ac-Trp-OMe and Ac-Gly-Trp-OMe, respectively, have the *cis*-conformation. These results are summarized in Table 1.

Change in Quantity of Side-products with Time. An HPLC elution profile of a reaction product from Ac-Trp-OMe in TFA is shown in Fig. 3. It is clear that compounds **1A** and **1B** are completely separated not only from the starting compound but also from each other, so that they can be used as a standard for their quantitative determination for a mixture on HPLC. When Ac-Trp-OMe was stored in TFA, besides compounds **1A** and **1B** some fluorescence material, which would not move on a thin layer chromatogram, was formed in too small an amount. Therefore, the amount of the products was calculated by taking the sum of the amounts of the unreacted compound, compounds **1A** and **1B** as 100%. When Ac-Trp-OMe was dissolved in TFA, immediately concentrated under reduced pressure, extracted with ethyl acetate, applied to a column of HPLC, the unreacted compound amounted to 91.4% of the starting reactant, and the percentages of compounds **1A** and **1B** were 2% and 6.6%, respectively, as measured by the method described above.

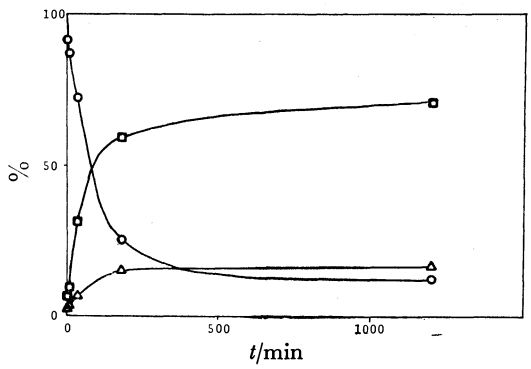

Fig. 9. Relative rate of decrease of Ac-Trp-OMe (—○—) and yields of compounds **1A** (—□—) and **1B** (—△—) in TFA. Values are averages for triplicate measurements.

As illustrated in Fig. 9, a 3-h storage in TFA at 20 °C caused the amount of the reactant to decrease rapidly to less than 25% of the starting reactant. On the other hand, the formation of compound **1A** surprisingly proceeded to more than 60%, but this compound could not be recovered preparatively in a similar yield; the formation of compound **1B** amounted to about 15%. These results suggest either that **1A** will be formed sterically with more advantage or that it is sterically more stable than **1B**. The isolated compounds **1A** and **1B** were stable at room temperature when stored in TFA. Therefore, it seems likely that the dimerized compounds are formed by an irreversible reaction from the starting monomer.

Experimental

All melting points were measured by the capillary method and are given as uncorrected values. TLC was performed on silica gel 60 (Merck Art. 11845) with a concentration zone using the following solvent systems (volume ratios): $CHCl_3$–acetone (2 : 1), $CHCl_3$–CH_3CN (4 : 1), and $CHCl_3$–MeOH–AcOH (95 : 5 : 5). HPLC was performed on a Toyosoda high speed liquid chromatograph HLC-803 and/or a Shimadzu HPLC LC-3A equipped with a data processor, Chromatopac C-R1A. Optical rotations were determined with a Perkin-Elmer Model 241 polarimeter. UV-absorption spectra were measured by using a Hitachi spectrometer type-124, equipped with a recording attachment. ^{1}H-NMR spectra were recorded on a JEOL PFT-100 pulse Fourier transform NMR spectrometer, locked on deuterium and equipped with an FT-1A pulse control system. Chemical shifts were measured relative to an internal reference, tetramethylsilane. Mass spectra were recorded with a second-order double focusing mass spectrometer[9] with a mono field-desorption ion source, equipped with a data processor (JEOL JMA-2000 mass data analysis system).

Ac–Trp–OMe. Ac–Trp–OH (17.4 g) was dissolved in MeOH (300 ml) and mixed with an ethereal solution of diazomethane in an ice–water bath under stirring. The solution was concentrated to dryness under reduced pressure. The residue was recrystallized from ethanol and hexane: wt 14.6 g (79.0%); mp 153—154 °C (lit,[10] 151 °C); $[\alpha]_D^{25}$ +13.2° (*c* 1.0, MeOH) (lit,[10] +13.2°); MS, *m/z*, 260 (M^+); ^{1}H-NMR [DMSO-d_6], CH_3CO δ=1.78 (3H, s), β-CH_2 ≈3.14 (2H, m), OCH_3 3.57 (3H, s), α-CH ≈4.59 (1H, t-d), aromatic CH ≈7.55 (5H, m), amide NH ≈8.32 (1H, d), and indole NH 10.82 (1H, s).

Found: C, 64.87; H, 6.16; N, 10.90%. Calcd for $C_{14}H_{16}O_3N_2$: C, 64.60; H, 6.20; N, 10.76%.

Ac–Gly–Trp–OMe. Z–Gly–Trp–OMe (3.39 g) was dissolved in MeOH (100 ml) and hydrogenated over a palladium–charcoal catalyst under atmospheric pressure. The catalyst was filtered off and the filtrate was concentrated under reduced pressure to a syrupy residue, which was dissolved in DMF (50 ml). The solution was stirred with Ac–ONp (2.8 g) at room temperature for 1 d, and then concentrated to an oil under reduced pressure. The oil was purified on a column (3 cm × 60 cm) of silica gel using a mixture of ethyl acetate and benzene (v/v, 1/1) as elution solvent. Fractions containing the compound were collected and concentrated to a syrup under reduced pressure. The syrupy material was solidified in ethyl acetate and hexane: wt 0.69 g (27%); mp 178 °C; $[\alpha]_D^{24.5}$ +14.0° (*c* 1.0, MeOH); MS, *m/z*, 317 (M^+); ^{1}H-NMR [DMSO-d_6], CH_3CO δ=1.82 (3H, s), β-CH_2 (Trp) ≈3.13 (2H, m), OCH_3 3.55 (3H, s), α-CH_2(Gly) ≈3.70 (2H, d), α-CH(Trp) ≈4.53 (1H, m), aromatic CH ≈7.49 (5H, m), amide NH(Gly) ≈7.99 (1H, t), amide NH(Trp) ≈8.21 (1H, d), and indole NH 10.82 (1H, s).

Found: C, 60.67; H, 5.97; N, 13.37%. Calcd for $C_{16}H_{19}O_4N_3$: C, 60.55; H, 6.04; N, 13.24%.

Ac–Trp–Trp–OMe. Z–Trp–Trp–OMe[11] (4.11 g) was dissolved in MeOH (80 ml) and hydrogenated over a palladium–charcoal catalyst under reduced pressure. The catalyst was filtered off and the filtrate was concentrated to a syrup under reduced pressure. The syrup was dissolved with Ac–ONp (2.8 g) in DMF (50 ml), stirred for a day at room temperature and concentrated to an oil under reduced pressure. The oil was purified on a column (3 cm × 60 cm) of silica gel using a mixture of benzene and ethyl acetate (v/v, 1/1) as eluting solvent. Fractions containing the compound were pooled and concentrated under reduced pressure to a syrupy material, which was triturated in ethyl acetate and hexane: wt 1.21 g (35.5%); mp 78 °C; MS, *m/z*, 466 (M^+); ^{1}H-NMR [DMSO-d_6], CH_3CO δ=1.74 (3H, s), β-CH_2 ≈3.14 (2H × 2, m), OCH_3 3.54 (3H, s), α-CH ≈4.55 (1H × 2, m), aromatic CH ≈7.60 (5H × 2, m), amide NH ≈7.98 (1H, d) and ≈8.36 (1H, d), and indole NH 10.74 (1H, s) and 10.83 (1H, s).

Found: C. 68.01; H, 5.95; N, 12.31%. Calcd for $C_{25}H_{26}O_4N_4$: C, 67.25; H, 5.87; N, 12.55%.

*Compounds **1A** and **1B** from Ac–Trp–OMe.* Ac–Trp–OMe (1.00 g) was dissolved in TFA (10 ml). The solution was kept for 3 h at room temperature in a brown glass vessel to exclude light and then concentrated to dryness under reduced pressure. The residue was dissolved in ethyl acetate, washed with 5% aq $NaHCO_3$ and water and then dried over anhydrous Na_2SO_4. The dried solution was concentrated to a pale yellow solid under reduced pressure. **1A** was crystallized from EtOH and ether and collected to wt *ca.* 280 mg. The filtrate was concentrated to dryness under reduced pressure. The residue was subjected to chromatography in a brown glass column (3 cm × 60 cm) of silica gel 60 suspended in $CHCl_3$, in such a way that the sample was dissolved in $CHCl_3$, charged on the column, washed with a mixture of CH_3CN and $CHCl_3$ (v/v, 1/4) and then eluted with CH_3CN and $CHCl_3$ (v/v, 2/1). Fractions containing compound **1B** were pooled and concentrated to dryness under reduced pressure. The residue was recrystallized from ethyl acetate and hexane: wt *ca.* 50 mg.

*Compound **1A**:* Mp 218 °C; MS, *m/z*, 520 (M^+); ^{1}H-NMR [DMSO-d_6], CH_3CO δ=1.55 (3H, s), and 1.79 (3H, s) β-CH_2

(g) ≈2.16 (2H, m), β-CH_2(h) ≈3.18 (2H, q), OCH_3 3.49 (3H, s) and 3.53 (3H, s), indoline 3-CH(i) concealed under OCH_3, α-CH(e) ≈4.32 (1H, m), α-CH(f) ≈4.60 (1H, m), indoline 2-CH(j) ≈4.73 (1H, d-d), indoline NH 5.97 (1H, d), aromatic CH ≈7.50 (8H, m), amide NH ≈8.23 (1H, d) and ≈8.39 (1H, d), and indole NH 10.88 (1H, s).

Found: C, 64.37; H, 6.15; N, 10.99%. Calcd for $C_{28}H_{32}O_6N_4$: C, 64.60; H, 6.20; N, 10.76%.

Compound ***1B***: Mp 215 °C; MS, *m/z*, 520 (M^+); ^{1}H-NMR (Fig. 7).

Found: C, 64.23; H, 6.23; N, 10.73%. Calcd for $C_{28}H_{32}O_6N_4$: C, 64.60; H, 6.20; N, 10.76%.

Compounds ***2A*** *and* ***2B*** *from Ac–Gly–Trp–OMe.* Ac–Gly–Trp–OMe (1.22 g) was dissolved in TFA (10 ml) and kept under the conditions used for Ac–Trp–OMe. The solution was concentrated to dryness under reduced pressure. The residue was dissolved in CH_2Cl_2, washed with 5% aq $NaHCO_3$ and water and then dried over anhydrous Na_2SO_4. The dried solution was concentrated to a solid under reduced pressure. The solid was dissolved in $CHCl_3$, applied to silica gel 60 in $CHCl_3$ in a brown glass column (3 cm × 60 cm) and washed with a mixture (50 ml) of $CHCl_3$ and CH_3CN (v/v, 2/1). Materials were eluted with a mixture of CH_3CN, $CHCl_3$, and MeOH (v/v/v, 60/30/5). The starting material was eluted first, followed by compounds **2B** and **2A**. Fractions containing compounds **2A** and **2B** were separately pooled and concentrated to dryness under reduced pressure. The residues were collected with ethyl acetate and hexane: wt **2A**, *ca.* 20 mg; **2B**, *ca.* 70 mg.

Compound ***2A***: Mp 152 °C; MS, *m/z*, 634 (M^+); ^{1}H-NMR [DMSO-d_6], CH_3CO δ=1.80 (3H×2, s), β-CH_2(Ind) ≈2.07 (2H, m), β-CH_2(Trp) ≈3.10 (2H, d), OCH_3 3.46 (3H, s) and 3.50 (3H, s), α-CH_2(Gly) ≈3.61 (2H, d) and ≈3.67 (2H, d), indoline 3-CH concealed under OCH_3, α-CH (Ind) ≈4.27 (1H, m), α-CH(Trp) ≈4.60 (1H, m), indoline 2-CH ≈4.77 (1H, d-d), indoline NH 5.91 (1H, s (broad)), aromatic CH ≈7.45 (8H, m), amide NH(Gly) ≈7.76 (1H, t) and ≈7.92 (1H, t), amide NH (Trp and Ind) 8.24 (1H, d) and 8.32 (1H, d), and indole NH 10.80 (1H, s).

Found: C, 60.74; H, 6.27; N, 12.83%. Calcd for $C_{32}H_{38}O_8N_6$: C, 60.55; H, 6.04; N, 13.24%.

Compound ***2B***: Mp 151 °C; MS, *m/z*, 634 (M^+); ^{1}H-NMR [DMSO-d_6], CH_3CO δ=1.80 (3H×2, s), β-CH_2(Ind) ≈2.18 (2H, m), β-CH_2(Trp) concealed under OCH_3, OCH_3 3.27 (3H×2, s), indoline 3-CH concealed under 3.40—3.50, α-CH_2 (Gly) ≈3.66 (2H×2, d), α-CH(Trp and Ind) ≈4.53 (1H×2, m), indoline 2-CH ≈4.86 (1H, d-d), indoline NH 5.92 (1H, s (broad)), aromatic CH ≈7.38 (8H, m), amide NH(Gly) ≈7.85 (1H, t) and ≈7.90 (1H, t), amide NH (Trp and Ind) ≈8.24 (1H, d) and ≈8.31 (1H, d), and indole NH 10.70 (1H, s).

Found: C, 60.41; H, 6.21; N, 12.85%. Calcd for $C_{32}H_{38}O_8N_6$: C, 60.55; H, 6.04; N, 13.24%.

Compound ***3*** *from Ac–Trp–Trp–OMe.* Ac–Trp–Trp–OMe(800 mg) was dissolved in TFA (10 ml) and treated under conditions similar to those for Ac–Trp–OMe. The extracted reaction mixture was subjected to chromatography on silica gel in $CHCl_3$ in a brown glass column (3 cm × 60 cm). Materials were eluted successively with CH_3CN and $CHCl_3$ (v/v, 1/2) and CH_3CN and $CHCl_3$ (v/v, 2/1). Fractions containing compound **3** were collected and concentrated under reduced pressure to an oil, which was triturated in ethyl acetate and hexane: wt 46 mg; mp 118 °C; MS, *m/z*, 446 (M^+); ^{1}H-NMR (Fig. 8).

Found: C, 66.92; H, 6.01; N, 12.18%. Calcd for $C_{22}H_{26}O_4N_4$: C, 67.25; H, 5.87; N, 12.55%.

References

1) Part of this work was presented at the 17th Symposium on Peptide Chemistry; K, Hashizume and Y. Shimonishi, "Peptide Chemistry 1979," Proceedings of the 17th Symposium on Peptide Chemistry, ed by H. Yonehara, Protein Research Foundation, Minoh, Osaka (1980), p. 77. The abbreviations used in this paper are those recommended by IUPAC-IUB: *J. Biol. Chem.*, **247**, 977 (1972). Additional abbreviations: TFA, trifluoroacetic acid; DMF, *N,N*-dimethylformamide; DMSO, dimethyl sulfoxide; Np, *p*-nitrophenyl; Ind, 3-(3-indolinyl)alanine; TLC, thin-layer chromatography; HPLC, high-performance liquid chromatography.

2) D. M. Theodoropoulos and J. S. Fruton, *Biochemistry*, **1**, 933 (1962).

3) Yu. B. Alakhov, A. A. Kiryushkin, V. M. Lipkin, and G. W. A. Milne, *J. Chem. Soc., Chem. Commun.*, **1970**, 406.

4) E. Wünsch, E. Jaeger, L. Kisfaludy, and M. Löw, *Angew. Chem.*, **80**, 330 (1977); E. Jaeger, P. Thamm, S. Knof, E. Wünsch, M. Löw, and L. Kisfaludy, *Hoppe-Seyler's Z. Physiol. Chem.*, **359**, 1617 (1978); E. Jaeger, P. Thamm, S. Knof, and E. Wünsch, *ibid.*, **359**, 1629 (1978); M. Löw, L. Kisfaludy, E. Jaeger, P. Thamm, S. Knof, and E. Wünsch, *ibid.*, **359**, 1637 (1978); M. Löw, L. Kisfaludy, and P. Sohar, *ibid.*, **359**, 1643 (1978).

5) H. Ogawa, T. Sasaki, H. Irie, and H. Yajima, *Chem. Pharm. Bull.*, **26**, 3144 (1978).

6) R. A. Uphaus, L. I. Grossweiner, J. J. Katz, and K. D. Kopple, *Science*, **129**, 641 (1959).

7) Y. Omori, Y. Matsuda, S. Aimoto, Y. Shimonishi, and M. Yamamoto, *Chem. Lett.*, **1976**, 805.

8) W. A. Thomas, "Annual Review of NMR Spectroscopy, I," ed by E. F. Mooney, Academic Press (1968), p. 73.

9) H. Matsuda, *Atomic Masses Fundam. Constants*, **5**, 185 (1976).

10) H. Zahn and K. Mella, *Hoppe-Seyler's Z. Physiol. Chem.*, **344**, 75 (1966).

11) S. Terashima, M. Wagatsume, and S. Yamada, *Tetrahedron*, **29**, 1487 (1973).

α,β-Unsaturated Carboxylic Acid Derivatives. XXI. A Novel Synthesis of α-Dehydroamino Acid Derivatives by the Arbusov Reaction of α-Phosphoranylideneamino-2-alkenoates[1]

Chung-gi SHIN,* Yasuchika YONEZAWA, Kazuhiro WATANABE, and Juji YOSHIMURA†

Laboratory of Organic Chemistry, Faculty of Technology, Kanagawa University, Rokkakubashi, Kanagawa-ku, Yokohama 221

†*Laboratory of Chemistry for Natural Products, Faculty of Science, Tokyo Institute of Technology, Nagatsuta, Midori-ku, Yokohama 227*

(Received February 28, 1981)

The reaction of ethyl 2-azido-2-alkenoate with organic tervalent phosphorus reagent gave the corresponding 2-phosphoranylideneamino derivative as an stable intermediate. This transformed gradually at room temperature, or immediately on a silica-gel column to give the corresponding 2-phosphinylamino derivative in a good yield. The Arbusov reaction of the intermediate which occurred during the transformation was found to be applicable for the other azido olefins. The formation mechanism and the configurational determination of the new products are discussed.

In connection with the synthesis of α-dehydroamino acid (DHA), which is an important constituent or precursor in the versatile cyclic peptide antibiotics, the development of the synthetic methods for DHA has been of interest and several routes have been investigated by us.[2-6]

So far, no report has been appeared on the synthesis of DHA N-protected with phosphinyl group except for our earlier paper,[7] whereas the diphenylphosphinyl (Dpp) group was utilized recently as an useful N-protecting group for α-amino acid and peptide.[8,9]

In the present paper, we wish to report a preparative route for DHA N-protected with a few kinds of phosphinyl groups by the reaction of ethyl 2-azido-2-alkenoate (**1**) with organic tervalent phosphorus reagents by two steps. Furthermore, the attempt to employ a similar reaction of *t*-butyl 3-azido-2-acetylamino-2-alkenoate (**8**) with triethyl phosphite was successful in giving the corresponding β-N-phosphinyl-DHA derivative.

Results and Discussion

Reaction of 1 with Tervalent Phosphorus Reagent. The reaction of (*Z*)-isomer of **1** (**a**; R=CH_3, **b**; R=C_2H_5, **c**; R=*n*-C_3H_7, **d**; R=*i*-C_3H_7, **e**; R=C_6H_5) with equimolar triphenylphosphine as a typical organic tervalent phosphorus reagent in dry benzene under nitrogen gas at room temperature was readily carried out to give colorless crystals or a syrup, which was identified as ethyl 2-triphenylphosphoranylideneamino-2-alkenoate (**2**), obtained in *ca.* 80% yield. The compound **2** thus obtained was found to be a very stable, even though it was heated for a long time or treated with an acid or a base.

In a similar manner, the reaction of **1** with triethyl phosphite also proceeded smoothly to give a colorless viscous oil, which was identified as 2-triethoxyphosphoranylideneamino-2-alkenoate (**3**), in *ca.* 81% yield. However, the syrupy product **3** isolated purely by the vacuum distillation was found to change gradually into a yellowish solid substance at room temperature during about a month. The colorless crystals obtained in *ca.* 87% yield from **3** were characterized to be ethyl 2-diethoxyphosphinylamino-2-alkenoate (**4**). Interestingly, when the chromatogram of **3** was developed through a silica-gel column using benzene initially and then a mixture of benzene–ethyl acetate (6 : 1 v/v) as the eluent, the compound **3** immediately transformed to give **4** in a fairly good yield. Since the transformation of **3** to **4** was further promoted in the presence of water, it was found that **3** reacted with water to give **4**. As a result, the desired new DHA N-protected with phosphinyl group was first synthesized.

Furthermore, in order to ascertain and generalize the preparative route for the DHA N-protected with phosphinyl group from **1**, a similar reaction of **1** with ethyl diphenylphosphinite was also performed to obtain ethyl 2-ethoxydiphenylphosphoranylideneamino-2-alkenoate (**5**) as a colorless syrup in an almost quantitative yield. Subsequently, the treatment of **5** on a silica-gel column was worked up similarly to give the expected ethyl 2-diphenylphosphinylamino-2-alkenoate (**6**) as colorless needles in *ca.* 74% yield. Furthermore, in order to remove the Dpp N-protecting group, when ethyl 2-diphenylphosphinylamino-2-butenoate (**6a**) was treated with trifluoroacetic acid at room temperature for 2 h, ethyl 2-trifluoroacetylamino-2-butenoate (**7a**) was readily obtained in 75% yield. The structure of **7a** was determined by the independent preparation from ethyl (*Z*)-2-amino-2-butenoate and trifluoroacetic anhydride. Since Breitholle and Stammer[10] reported the removal of N-trifluoroacetyl group in DHA and dehydropeptide (DHP) with amine, the Dpp group was found to be a useful N-protecting group for DHA and DHP, although two-step treatments were required.

In order to confirm the structure and the configuration of **2**—**5**, and **6** thus obtained, the independent preparation of **4** was performed. The reaction of (*Z*)-isomer of ethyl 2-amino-2-alkenoate with diethyl phosphorochloridate by the usual method proceeded to give colorless crystals, whose properties were in complete agreement with **4** prepared from (*Z*)-**1** and triethyl phosphite *via* **3**. As a result, the geometric structure of **4** and **6** could be easily determined to be (*Z*)-isomerism. Accordingly, the configurational structure of **2**, **3**, and **5** was also assigned to be (*Z*)-geometry. On the other hand, the attempt to obtain another independent

preparation of **4** by the direct condensation of α-oxo carboxylic acid ester with diethyl phosphoramidate by the method reported previously[6] was unsuccessful, because of the lability and the decomposition of the phosphoramidate in acidic conditions.

The structure and configuration confirmed above were further supported by the results of the following spectroscopic analyses and by the studies on the formation mechanism.

In the IR spectrum of **2**, **3**, and **5**, the characteristic absorption bands of ester carbonyl, carbon-carbon double bond, and =P–O–CH_2– groups appear at 1722—1700 (strong), 1630—1590 (medium), and 1050—1035 (in **3** and **5**, strong) cm^{-1} regions respectively. On the other hand, in that of **4** and **6**, the stretching absorption bands of NH and >P=O groups newly appear at 3170—3070 (medium) and 1290—1240 (strong) cm^{-1} regions, along with the appearance of ethoxycarbonyl and C=C bands at 1730—1710 and 1660—1625 cm^{-1} regions, respectively.

On the other hand, the NMR spectra of **2**—**5**, and **6**, clearly showed the long range coupling between β-olefinic, γ-methylene protons, and phosphorus atoms. As summarized in Tables 1 and 2, the olefinic proton signals of **2**, **3**, and **5** shifted at δ 6.70—5.95 ($J_{3,4}$= 6.8—9.2 Hz), whereas those of **4** and **6** resonated at lower magnetic field (at δ 7.23—6.02) with the comparatively larger coupling constant ($J_{3,4}$=7.0—11.4 Hz). On the other hand, the coupling constants between β-olefinic proton and phosphorus in **4** and **6** were found to be smaller ($J_{3,P}$=1.8—2.6 Hz) than the constants ($J_{3,P}$=2.9—4.5 Hz) in **2**, **3**, and **5**. Similarly, the long range coupling between γ-methylene protons and phosphorus ($J_{4,P}$=2.5—3.0 Hz) was also observed, as listed in Tables 1 and 2. Moreover, in the NMR and IR spectra of **4** and **6**, the appearance of NH groups at δ 5.50—4.70 and at *ca.* 3100 cm^{-1} respectively indicates unambiguously the transformation of the phosphoranylideneamino into the phosphinylamino group.

The above results suggest the following formation mechanism of **4** and **6**: the Arbusov reaction of the intermediates **3** and **5** with water occurred to give **4** and **6** respectively, along with the yielding of ethanol, which could be detected by gas chromatography. This process is illustrated in Scheme 1.

The yields, physical constants, and NMR spectral data of **2**—**5**, and **6** are summarized in Tables 1 and 2.

Reaction of 8 with Triethyl Phosphite. In order to apply extensively to the various azido olefins, β-azido olefin was subjected to the reaction with triethyl phosphite.

As in the case of **1**, *t*-butyl 2-acetylamino-3-azido-2-alkenoate (**8**: **a**; R=CH_3, **b**; R=C_2H_5), derived by the reaction of *t*-butyl 2-(*N*-bromoacetylamino)-2-alkenoate with sodium azide, with the successive substitution and the subsequent 1,3-shift,[11] was treated with triethyl phosphite to give a pale yellowish syrup in a fairly good yield. Interestingly, the syrupy products thus obtained were found to have a satisfactory elemental analysis for the corresponding β-phosphinylamino derivative (**10**), not the expected β-phosphoranylideneamino derivative (**9**). Furthermore, the above structural identification

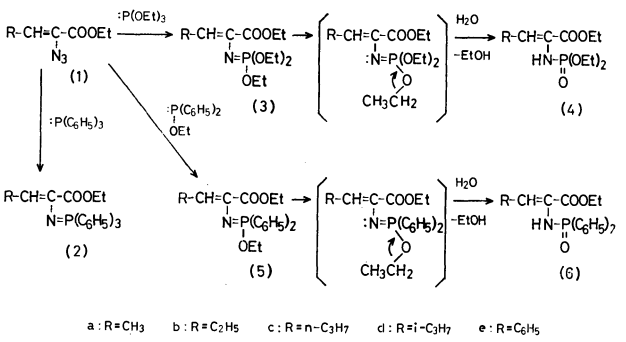

Scheme 1.

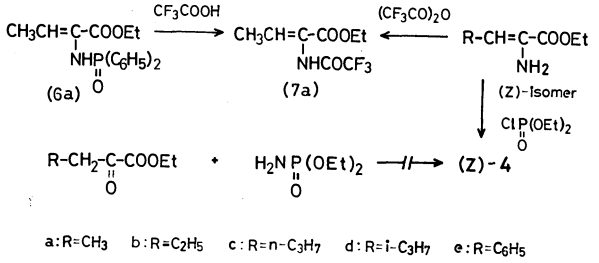

Scheme 2.

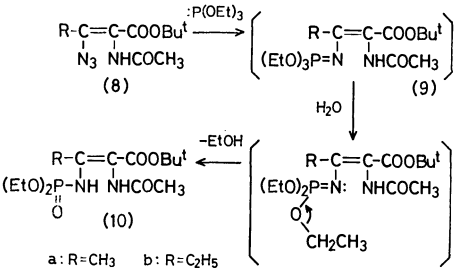

Scheme 3.

was exactly supported by the IR and NMR spectral data as follows. The appearance of the absorption band at 3260—3200 cm^{-1} and that of the chemical shift resonating at δ 6.83—6.70 regions as a broad singlet due to NH and the presence of >P=O at 1260 cm^{-1} as a strong absorption indicates unambiguously the formation of an α,β-unsaturated α,β-diamino derivative, which was identified as *t*-butyl 2-acetylamino-3-diethoxyphosphinylamino-2-alkenoate, obtained in *ca.* 78% yield.

The above results show that the formation mechanism of **10** was the following: the one-pot reaction of **8** with triethyl phosphite took place to give the unstable intermediate **9**, then the following Arbusov reaction with water during the treatment process gave **10**, as is illustrated in Scheme 3.

Experimental

All the melting and boiling points are uncorrected. The IR spectra were recorded with a Hitachi EPI-G3 Spectrometer. The NMR spectra were measured with a JNM-PS-100 Spectrometer (Japan Electron Laboratory Co. Ltd.), using tetramethylsilane as the internal standard.

Preparation of 2. Into a solution of (*Z*)-**1** (50 mmol) in dry benzene (50 ml) under nitrogen gas we stirred triphenyl-

Table 1. Ethyl (*Z*)-2-phosphoranylideneamino-2-alkenoate (**2**, **3**, and **5**)

Compd No.	Yield %	Bp/°C[mmHg] (Mp/°C)[a]	Formula	Found (Calcd) (%) C	H	N	NMR spectrum, δ in $CDCl_3$ Olefinic proton (J_{Hz})	γ-Proton (J_{Hz})
2a	72	(101—102)	$C_{24}H_{24}NO_2P$	74.12 (74.04	6.21 6.17	3.56 3.60)	6.04dt (3.0) (7.0)	
2b	87	syrup	$C_{25}H_{26}NO_2P$	74.56 (74.44	6.58 6.45	3.25 3.47)	5.95dt (2.9) (6.9)	
2c	91	syrup	$C_{26}H_{28}NO_2P$	74.88 (74.82	6.98 6.71	3.28 3.36)	5.98dt (3.0) (8.3)	
2d	68	(71—72)	$C_{26}H_{28}NO_2P$	74.92 (74.82	6.81 6.71	3.34 3.36)	5.82dd (3.0) (8.3)	
2e	85	(141—142)	$C_{29}H_{26}NO_2P$	77.20 (77.16	7.49 7.47	3.05 3.10)	6.78d (6.8)	
3a	83	105—107/[0.5]	$C_{12}H_{24}NO_5P$	49.81 (49.14	8.71 8.25	4.21 4.78)	5.99dq (4.0) (6.9)	1.79dd (3.0) (6.9)
3b	63	111—115/[0.5]	$C_{13}H_{26}NO_5P$	51.15 (50.80	8.84 8.53	4.71 4.56	5.92dt (4.1) (7.0)	2.29dq (2.7) (7.0)
3c	92	113—115/[0.5]	$C_{14}H_{28}NO_5P$	52.45 (52.32	8.85 8.78	4.41 4.36)	5.93dt (4.1) (7.0)	2.28dq (2.7) (7.0)
3d	75	115—119/[0.5]	$C_{14}H_{28}NO_5P$	52.39 (52.32	8.82 8.82	4.39 4.39)	5.77dt (4.5) (8.3)	2.97m
3e	89	syrup	$C_{17}H_{26}NO_5P$	57.95 (57.95	7.03 7.03	3.58 3.58)	6.70d (8.0)	7.12—7.36m (C_6H_5+H)
5a	91	syrup	$C_{20}H_{24}NO_3P$	67.33 (67.21	6.76 6.77	3.68 3.92)	6.18dq (4.0) (7.0)	2.02dd (2.5) (7.0)
5b	90	syrup	$C_{21}H_{26}NO_3P$	67.85 (67.91	7.00 7.06	3.91 3.77)	6.08dt (4.0) (7.2)	2.56dq (2.5) (7.2)
5c	89	syrup	$C_{22}H_{28}NO_3P$	69.05 (68.55	7.09 7.32	3.48 3.64)	6.10dt (4.0) (7.2)	2.52dq (2.5) (7.2)
5d	90	syrup	$C_{22}H_{28}NO_3P$	68.79 (68.55	7.38 7.32	3.49 3.64)	5.94dd (4.5) (9.2)	3.24m
5e	85	syrup	$C_{25}H_{26}NO_3P$	71.52 (71.58	6.29 6.25	3.31 3.34)	6.80d (6.8)	7.16—8.20 (C_6H_5+H)

a) Colorless needles from cyclohexane.

Table 2. Ethyl (*Z*)-2-phosphinylamino-2-alkenoates (**4** and **6**)

Compd No.	Yield/% A[a]	B[b]	Mp/°C[c]	Formula	Found (Calcd) (%) C	H	N	NMR spectrum, δ in $CDCl_3$ Olefinic proton (J_{Hz})	γ-Proton(J_{Hz})	NH(J_{Hz})
4a	87	81	47—48	$C_{10}H_{20}NO_5P$	45.22 (45.22	7.63 7.63	5.25 5.24)	6.50dq (2.6) (7.0)	1.92dd (2.6) (7.0)	4.78
4b	86	81	30—31	$C_{11}H_{22}NO_5P$	47.39 (47.30	7.91 7.94	5.11 5.02)	6.37dt (2.6) (7.0)	2.42dq (2.6) (7.0)	4.80
4c	81	76	46—47	$C_{12}H_{24}NO_5P$	49.20 (49.14	8.21 8.25	4.77 4.78)	6.42dt (2.6) (7.0)	2.39dq (2.6) (7.0)	4.78
4d	88	71	40—42	$C_{12}H_{24}NO_5P$	49.11 (49.14	8.28 8.25	4.71 4.78)	6.19dd (2.5) (10.0)	3.06m	4.70
4e	91		70—71	$C_{15}H_{22}NO_5P$	55.01 (55.04	6.75 6.78	4.32 4.28)	7.23s	7.36—7.77m (C_6H_5+H)	4.80
6a	70		121—122	$C_{18}H_{20}NO_3P$	65.69 (65.64	6.05 6.12	4.22 4.25)	6.36dq (2.1) (8.0)	1.84d (8.0)	5.50d (8.0)
6b	77		85—85.5	$C_{19}H_{22}NO_3P$	66.41 (66.46	6.45 6.46	4.03 4.08)	6.24dt (2.0) (8.0)	2.40qu (8.0)	5.50d (8.0)
6c	68		97—98	$C_{20}H_{24}NO_3P$	67.28 (67.21	6.79 6.77	3.85 3.92)	6.20dt (2.0) (8.0)	2.34q (8.0)	5.48d (8.0)
6d	65		106—107	$C_{20}H_{24}NO_3P$	67.23 (67.21	6.71 6.77	3.81 3.92)	6.02dd (1.8) (11.4)	3.32m	5.41d (8.6)
6e	89		168—169	$C_{23}H_{22}NO_3P$	70.69 (70.62	5.73 5.67	3.66 3.58)	7.00s	7.18—7.78m (C_6H_5+H)	5.38d (6.0)

a) From **3** and **5**. b) From ethyl (*Z*)-2-amino-2-alkenoate and $ClP(O)(OEt)_2$. c) Colorless needles from cyclohexane.

phosphine (50 mmol), portion by portion, under cooling. After the resulting solution had been stirred at room temperature for 1 h, the benzene was evaporated under reduced pressure to give a colorless syrup or a semi-solid residue, in which the latter was crystallized in petroleum ether (20 ml). The collected crystals were recrystallized from cyclohexane to give colorless needles.

Preparation of ***3***. A solution of equimolar (*Z*)-**1** (50 mmol) and triethyl phosphite in dry benzene was worked up similarly to give an oily residue, which was distilled under reduced pressure to give a colorless viscous oil.

Preparation of ***5***. A solution of equimolar (*Z*)-**1** (50 mmol) and ethyl diphenylphosphinite in dry benzene was worked up similarly for 3 h to give a colorless syrup.

Preparation of ***4***. *From* ***3***. *By Standing*: When viscous oil (**3**) was allowed to stand at room temperature for about a month, the oil gradually crystallized to give a yellowish solid substance. The collected solid was recrystallized from hexane or cyclohexane to give colorless needles.

On a Silica-gel Column. The compound **3** (50 mmol) was chromatographed on a silica-gel column using benzene (150 ml) intially and then a mixture of benzene–ethyl acetate (6 : 1 v/v) as the eluent. The fraction solution obtained was evaporated under reduced pressure to give colorless crystals.

From Ethyl (Z)-2-Amino-2-alkenoate and $ClP(O)(EtO)_2$. Into a solution of the enamine (20 mmol) and pyridine (30 mmol) in dry diethyl ether (30 ml) we stirred diethyl phosphorochloridate (25 mmol), drop by drop, at room temperature. After the resulting solution had been stirred at room temperature for 5 h, ether (50 ml) was further added to the reaction solution and then the resultant solution was washed with 1 M HCl†† and with water three times. The ether layer was dried over anhydrous Na_2SO_4 and then concentrated to give a residual product. The residue was purified on a silica-gel column using ehter as the eluent to give colorless needles, which was in agreement with **4** obtained above. Yield *ca.* 80%.

Preparation of ***6***. In a similar manner to that in the case of **4**, compound **5** was chromatographed on a silica-gel column using a mixture of benzene and ethyl acetate (4 : 1 v/v) as the eluent. The fraction obtained was condensed under reduced pressure to give crude residual crystals, which were collected by filtration and then recrystallized from cyclohexane to give **6** as colorless needles.

Preparation of ***7a***. *From* ***6a*** *and* CF_3COOH: A solution of **6a** (10 mmol) in trifluoroacetic acid (5 ml) was stirred at room temperature for 2 h and the reaction solution was concentrated under reduced pressure. The residual oil obtained was distilled to give a colorless oil, bp 67—68 °C/1.5 mmHg,††† yield 75.2%. IR (KBr): 3280 (NH), 1720 (COOEt), 1660 (C=C) cm^{-1}. NMR ($CDCl_3$): δ 8.64bs (NH), 7.07q (3-H, J=7.4 Hz), 1.82 d (4-H, J=7.5 Hz). Found: C, 43.05; H, 4.36; N, 6.11%. Calcd for $C_8H_{10}NO_3F_3$: C, 42.67; H, 4.44; N, 6.22%.

From Ethyl (Z)-2-Amino-2-butenoate and $(CF_3CO)_2O$. Into a solution of the enamine (20 mmol) and pyridine (30 mmol) in dry diethyl ether (20 ml) was added trifluoroacetic anhydride (30 mmol), with stirring, drop by drop under cooling and then the stirring was continued at room temperature for 2 h. After a further addition of ether (20 ml), the resulting solution was washed with water four times and dried ove anhydrous $MgSO_4$. After removal of ether, the residual oil obtained was distilled to give a colorless oil, yield 85.0%.

Preparation of ***10a***. Into a solution of **8a** (4.2 mmol) in dry benzene (10 ml) we stirred triethyl phosphite (4.2 mmol), drop by drop, at 0 °C. After the resulting solution had been stirred at 0 °C for 3 h, the reaction solution was concentrated under reduced pressure to give a residual syrup. The crude syrup obtained was purified on a silica-gel column using a mixture of benzene–acetone (5 : 1 v/v) as the eluent. The fraction was condensed under reduced pressure to give **10a** as a pale yellow syrup, yield 81%. IR (KBr): 3260 (NH), 1700 ($COOBu^t$), 1670 (NHCO, C=C), 1260 (>P=O), 1040 (=P–O–CH_2–) cm^{-1}. NMR ($CDCl_3$): δ 6.70 s (NH), 2.14 s ($COCH_3$), 2.06 s (γ-protons). Found: C, 50.58; H, 8.15; N, 8.16%. Calcd for $C_{14}H_{27}N_2O_5P$: C, 50.30; H, 8.08; N, 8.38%.

Preparation of ***10b***. In a similar manner, the treatment of **8b** with triethyl phosphite was worked up to give **10b** as a pale yellow syrup, yield 74%. IR (KBr): 3200 (NH), 1705 ($COOBu^t$), 1675 (NHCO, C=C), 1260 (>P=O), 1040 (=P–O–CH_2–) cm^{-1}. NMR ($CDCl_3$): δ 6.83 s (NH), 2.78 q (γ-protons, J=8.0 Hz), 2.11 s ($COCH_3$). Found: C, 51.98; H, 8.56; N, 7.91%. Calcd for $C_{15}H_{29}N_2O_5P$: C, 51.72; H, 8.33; N, 8.05%.

†† 1 M=1 mol dm^{-3}. ††† 1 mmHg≈133.3322 Pa.

References

1) Part XX: C, Shin, Y. Sato, M. Hayakawa, M. Kondo, and J. Yoshimura, *Heterocycles*, **16**, 1573 (1981).

2) C. Shin, M. Masaki, and M. Ohta, *J. Org. Chem.*, **32**, 1860 (1967).

3) C. Shin, M. Masaki, and M. Ohta, *Bull. Chem. Soc. Jpn.*, **44**, 1657 (1971).

4) C. Shin, K. Nanjo, E. Ando, and J. Yoshimura, *Bull. Chem. Soc. Jpn.*, **47**, 3109 (1974).

5) C. Shin, Y. Yonezawa, K. Unoki, and J. Yoshimura, *Bull. Chem. Soc. Jpn.*, **52**, 1657 (1979).

6) Y. Yonezawa, C. Shin, Y. Ono, and J. Yoshimura, *Bull. Chem. Soc. Jpn.*, **53**, 2905 (1980).

7) Y. Yonezawa, C. Shin, M. Kiyohara, and J. Yoshimura, *Tetrahedron Lett.*, **1979**, 3851.

8) M. Ueki and S. Ikeda, *Chem. Lett.*, **1976**, 827.

9) G. W. Kenner, G. A. Moore, and R. Ramage, *Tetrahedron Lett.*, **1976**, 3623.

10) E. G. Breitholle and C. H. Stammer, *J. Org. Chem.*, **41**, 1344 (1976).

11) C. Shin, K. Nanjo, T. Nishino, Y. Sato, and J. Yoshimura, *Bull. Chem. Soc. Jpn.*, **48**, 2492 (1975).

Synthesis and Properties of *S,S*-Diaryl Thymidine Phosphorodithioates[1)]

Mitsuo SEKINE, Ken HAMAOKI, and Tsujiaki HATA*

Department of Life Chemistry, Tokyo Institute of Technology, Nagatsuta, Midori-ku, Yokohama 227

(Received April 10, 1981)

Appropriately protected or unprotected *S,S*-diphenyl thymidine 3′- or 5′-phosphorodithioates and *S,S*-bis(4-methoxyphenyl) thymidine 3′- or 5′-phosphorodithioates were successfully prepared by the reaction of the thymidine derivatives with cyclohexylammonium *S,S*-diaryl phosphorodithioates in the presence of 2,4,6-triisopropylbenzenesulfonyl chloride (TPS). Stabilities of the thymidylic compounds under acidic or alkaline conditions were described in detail. Several methods for the deprotection of one or both arylthio groups under neutral conditions were also described in connection with the synthesis of oligothymidylates. By the use of the bis(4-methoxyphenylthio)-phosphoryl group, di- and tri-thymidylates were synthesized in high yields.

With the recent remarkable developments of the so-called "phosphotriester method" in oligonucleotide synthesis, the conventional methods for phosphorylation have been reconsidered by introducing new synthetic procedures.[2)] Recently, more considerable attention has been turned to phosphorylating agents which made the phosphotriester products separable by column chromatography on silica gel.[2)]

A few years ago, we described methods for the synthesis of nucleoside *S*-phenyl phosphorothioates by the reaction of nucleotide with a combined reagent of diphenyl disulfide and tributylphosphine[3)] and alternatively by the reaction of nucleoside phosphites with diphenyl disulfide in the presence of a silylating agent *via* highly reactive "nucleoside silyl phosphite" intermediates.[4)] The phenylthio group has been demonstrated as a useful phosphate protecting group in oligonucleotide synthesis.[5)]

In this paper, we wish to report a general method for the synthesis of oligonucleotides by use of *S,S*-diaryl phosphorodithioates as phosphorylating agents for introduction of a 5′-terminal phosphate and promising features of the arylthio groups as "activatable" protecting groups.[6)]

Results and Discussion

In an early work, we showed that *S*-phenyl phosphorodithioate (**1**) could be obtained quantitatively by the reaction of phosphonic acid with diphenyl disulfide in the presence of a trimethylsilylating agent.[4)] However, **1** was too unstable to use as a phosphorylating agent since **1** decomposed rapidly to release benzenethiol in dry pyridine even at room temperature. On the other hand, phosphorothioates of diester-type (*O,S*-phosphorothioates) are known to be rather stable compared with those of monoester-type.[7)] The fact led us to prepare, a new type of compound, *S,S*-diphenyl phosphorodithioate (**2a**) not only to enhance the stability as the phosphorylating agent but also to facilitate the separation of the phosphorylated products by chromatography on silica gel.

By extending the preparative method of **1**, a convenient synthesis of **2a** was performed: When phosphinic acid with further lower oxidation state than phosphonic acid was allowed to react with 2.1 equiv. of diphenyl disulfide in the presence of each 2.1 equiv. of triethylamine and trimethylsilyl chloride in dry tetrahydrofuran (THF) for 20 h at room temperature, **2a** was obtained as the cyclohexylammonium salt in 83% yield. Cyclohexylammonium *S,S*-bis(4-methoxyphenyl) phosphorodithioate (**2b**) was similarly prepared in 85% yield. Both **2a** and **2b** were found to be quite stable compared with **1** under acidic or alkaline conditions such as 80% acetic acid or 0.1 M (1 M=1 mol dm^{-3}) NaOH at room temperature for several weeks.

An improved method for the preparation of **2a** and **2b** in relatively large scale was established in this laboratory.[8)]

The new phosphorylating agents, **2a** and **2b**, were successfully applied to the synthesis of *S,S*-diaryl nucleoside phosphorodithioates (**3**) by condensing **2a** or **2b** with the corresponding nucleosides in the presence of 2,4,6-triisopropylbenzenesulfonyl chloride (TPS). These results are summarized in Table 1. In these reactions, it is noted that all reactions proceeded cleanly without brownish coloration, which was observed often in the case of coupling reactions using TPS in dry pyridine, to give the phosphorylated products in high yields and that the crystalline cyclohexylammonium salt of **2a** could be used without exchange to the pyridinium salt for the phosphorylation by employing two hold TPS. When **2a** was pre-activated by TPS in order to avoid sulfonylation of 5′-hydroxyl groups of nucleosides by TPS, the 2—5% formation of *S,S*-diphenyl phosphorodithiocychlohexylamidate was always accompanied. However, the by-product could be easily separated from *S,S*-diphenyl nucleoside phosphorodithioates since it was

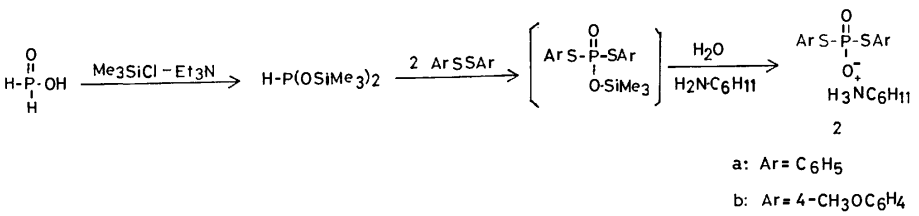

Scheme 1.

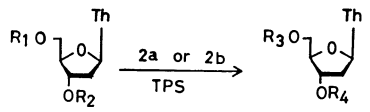

3: Ar = C_6H_5
17: Ar = 4-$CH_3OC_6H_4$

	R_3	R_4
a:	$(ArS)_2P(O)$	Ac
b:	Tr	$(ArS)_2P(O)$
c:	MMTr	$(ArS)_2P(O)$
d:	$(ArS)_2P(O)$	$(ArS)_2P(O)$
e:	$(ArS)_2P(O)$	H
f:	H	$(ArS)_2P(O)$

Tr=trityl
MMTr=monomethoxytrityl

Scheme 2.

eluted with only dichloromethane by silica-gel column chromatography.

The phenylthio group of **3** was found to be quite stable either in dry or aqueous pyridine and also in 80% acetic acid at room temperature for several days. In addition, when **3a** was refluxed in methanol, ethanol, or 2-propanol for 1 h, **3a** was recovered quantitatively and no transesterification between the dithioester and alcohols was observed. The conditions for the selective removal of one and two phenylthio groups and the relationship with other protecting groups are illustrated in Scheme 3.

When **3c** was treated with 80% acetic acid at room temperature for 6 h, **3f** was isolated in 94% yield. Under these conditions the loss of the phenylthio group was essentially negligible. Whenever **3c** was heated in 80% acetic acid at 100 °C for 1 h, **3f** could be also obtained in 91% yield. In this case, 3% of *S*-phenyl thymidine 3′-phosphorothioate (**4**) was formed by losing one of two phenylthio groups from **3f**. Treatment of **3c** with 0.2 M NaOH–dioxane (1 : 1, v/v) at room temperature for 15 min gave 5′-*O*-monomethoxytrityl-thymidine *S*-phenyl 3′-phosphorothioate (**5**) quantitatively.

Van Boom[9] and Pfleiderer[10] have recently reported that, when dinucleotide derivatives bearing an aryloxy group in internucleotidic phosphate and an unprotected hydroxyl at the 3′- or 5′-position were treated with NaOH to remove one of two phenoxy groups, the 3′–5′ isomerization of phosphoryl group was accompanied to some extent depending upon the conditions. Therefore, in the case of alkaline treatment of **3e** or **3f** which has an unprotected hydroxyl at the 3′-or 5′-position, the above-mentioned problem should be taken into account.

When **3e** was treated with 0.2 M NaOH–dioxane (1 : 1, v/v) at room temperature for 15 min, two new

TABLE 1. YIELDS AND ELEMENTAL ANALYSIS OF *S,S*-DIARYL THYMIDINE PHOSPHORODITHIOATE DERIVATIVES (**3** AND **17**)

Compound	Yield/%	Formula	Calcd (%)			Found (%)		
			C	H	N	C	H	N
3a	92	$C_{24}H_{25}O_7N_2PS_2$	52.55	4.59	5.11	52.34	4.61	4.93
3b	96	$C_{41}H_{37}O_6N_2PS_2$	65.76	4.98	3.74	66.08	5.45	3.42
3c	95	$C_{42}H_{39}O_7N_2PS_2$	64.77	5.05	3.60	64.81	5.07	3.51
3d	88	$C_{34}H_{32}O_7N_2P_2S_4$	52.98	4.18	3.63	53.34	4.32	3.56
3e	66	$C_{22}H_{23}O_6N_2PS_2$	52.17	4.58	5.53	51.68	4.77	5.20
3f	—	$C_{22}H_{23}O_6N_2PS_2$	52.17	4.58	5.53	52.41	4.50	5.43
17a	95	$C_{26}H_{29}O_9N_2PS_2$	51.31	4.80	4.60	51.89	4.54	4.47
17c	93	$C_{44}H_{43}O_9N_2PS_2$	62.99	5.17	3.34	63.26	5.49	3.15
17e	71	$C_{24}H_{27}O_8N_2PS_2$	50.88	4.80	4.94	50.20	4.85	4.93
17f	—	$C_{24}H_{27}O_8N_2PS_2$	50.88	4.80	4.94	50.77	4.97	4.78

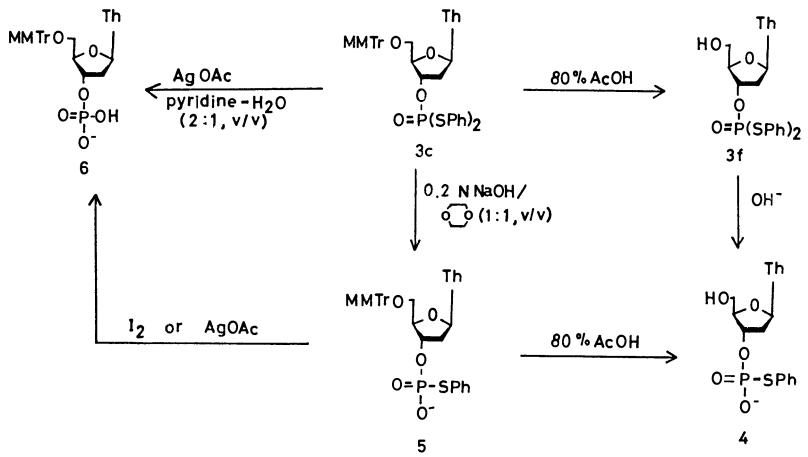

Scheme 3.

Table 2. ^{1}H-NMR spectra of phosphorylated products **3** and **17**

Compound	$C_{1'}H$	$C_{2'}Ha$ $C_{2'}Hb$	$C_{3'}H$	$C_{4'}H$	$C_{5'}Ha$ $C_{5'}Hb$	CH_3	C=CH	Others
3a	6.37(dd) $J_{1'-2'a}$=9.0 $J_{1'-2'b}$=6.0	2.03—2.63(m)	5.21(dd) $J_{2'-3'}$=6.9 $J_{3'-4'}$=2.1	4.24(m)	4.51(m)	1.90(s)	7.28(s)	2.16 (3H, s, OC(O)CH_3), 7.14—7.74 (10H, m, ArH), 9.41 (1H, br. s, NH)
3b	6.40(t) J=5.5	2.35 (m)	5.39(m)	4.04(m)	3.36(m)	1.40(s)	—	7.00—7.73 (26H, m, C=CH and ArH), 9.47 (1H, br. s, NH)
3c	6.42(t) J=7.2	2.32(t) J=3.7	5.33(m)	4.05(m)	3.38(m)	1.39(s)	—	6.85 (2H, d, J=8.4, ArH), 7.09—7.79 (23H, m, C=CH and ArH), 9.49 (1H,br. s, NH)
3d	6.32(dd) $J_{1'-2'a}$=6.7 $J_{1'-2'b}$=5.4	2.03—2.63(m)	4.15(m)	4.24 ———	4.55(m)	1.87(s)	—	7.23—7.73 (11H, m, C=CH and ArH), 9.32 (1H, br. s, NH)
3e	6.53(t) J=6.0	1.90—2.53(m)	4.23— 4.77(m)	4.17(m)	4.23—4.77(m)	1.83(s)	7.26(s)	7.08—7.67 (10H, m, ArH), 9.33 (1H, br. s, NH)
3f	6.22(t) J=7.0	2.31(m)	5.35(m)	4.04(m)	3.73(m)	1.88	7.31(s)	2.16 (1H, s, OH), 7.18—7.75 (10H, m, ArH), 9.48 (1H, br. s, NH)
17a	6.41(dd) $J_{1'-2'a}$=9.0 $J_{1'-2'b}$=6.0	2.03—2.50(m)	5.23(dd) $J_{3'-4'}$=2.0 $J_{2'-3'}$=6.0	4.24(dd) $J_{3'-4'}$=2.0 $J_{4'-5'}$=2.8	4.50(dd) $J_{4'-5'}$=2.0 J_{P-H}=7.0	1.90(s)	7.37(s)	2.14 (3H, s, OC(O)CH_3), 6.87 (2H, d, J=8.4, ArH), 7.55 (2H, dd, J=8.4, J=2.0, ArH), 9.46 (1H, br. s, NH)
17c	6.38(t) J=7.0	2.37(m)	5.36(m)	4.10(m)	3.38(m)	1.40(s)	—	3.77 (6H, s, OCH_3), 6.85 (4H, d, J=8.8, ArH), 6.93 (2H, d, J=8.8, ArH),7.10—7.64 (17H, m, C=CH and ArH)
17e	6.38(t) J=6.5	2.07—2.50(m)	4.31— 4.63(m)	4.18(m)	4.31—4.63(m)	1.84	7.30(s)	3.84 (6H, s, OCH_3), 6.89 (2H, d, J=8.4, ArH), 7.45 (4H, dd, J=8.4, J_{P-H}=2.1, PS-C=CH), 9.39 (1H, br. s, NH)
17f	6.21(t) J=7.0	2.35(m)	5.32(m)	4.08(m)	4.08(m)	1.90	7.35(s)	3.83 (6H, s, OCH_3), 6.96 (4H, d, J=9.0, O-C=CH), 7.56 (4H, dd, J=9.0, J_{P-H}=2.0, S-C=CH), 9.49 (1H, br. s, NH)

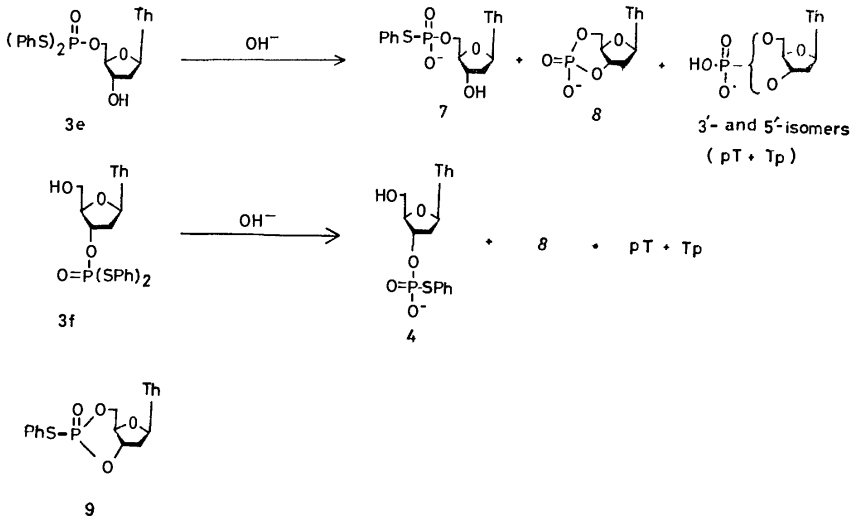

Scheme 4.

spots of R_f 0.53 and 0.20 (Solvent I) were observed other than the major spot which showed the R_f value corresponding to *S*-phenyl thymidine 5'-phosphorothioate (**7**) on TLC. The nucleotidic substance of R_f 0.53 was determined as thymidine 3',5'-cyclic phosphate (**8**) by comparison with the authentic sample. The yield of **8** was estimated to be 12% spectroscopically. The other minor spot was identified with thymidine 3'-or 5'-phosphate formed in 1% yield.

Since it is known that the 3'–5' isomerization of phosphoryl group occurs through a cyclic triester intermediate,[9] if the 3'–5' isomerization occurs during the alkaline treatment of **3e**, thymidine 3',5'-cyclic phosphate derived from thymidine *S*-phenyl 3',5'-cyclic phosphorothioate (**9**) by further alkaline hydrolysis of **9** should be expected as a by-product. Our result indicated that during this alkaline treatment the cyclization reaction along with elimination of one of two phenylthio groups took place at least to the extent of 12%. It is possible that, *S*-phenyl thymidine 3'-phosphorothioate (**4**) might be produced from **9**, if the bond of P–O of **9** at the 5'-position was competitively hydrolyzed with cleavage of the ester bond of P–O at the 3'-position or with cleavage of P–S bond of **9**. Therefore, the nucleotidic material corresponding to **7**, which was estimated to be formed in 87% yield, was further confirmed whether it contained TpSPh (**4**), although it was not separated from PhSpT (**7**) by paper chromatography and electrophoresis.

In a previous paper,[4] we reported that pure PhSpT (**7**) was obtained from thymidine 5'-phosphite by the silylation in the presence of 1.1 equiv. of diphenyl disulfide in quantitative yield. It was found that this pure **7** was completely degraded by snake venom phosphodiesterase in Tris buffer (pH 8). On the other

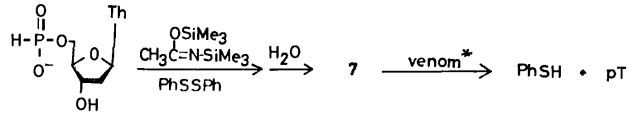

* *Venom phosphodiesterase*

Scheme 5.

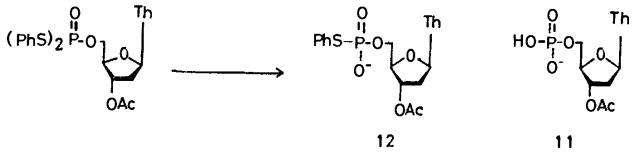

Scheme 6.

hand, **4** was found to be resistant to the same enzyme. The results are of interest in connection with the report by Nussbaum and Cook that *S*-ethyl thymidine 5'-phosphorothiate (**10**) served as a substrate of snake venom phosphodiesterase.[7]

On the basis of this finding, the nucleotidic substance obtained by alkaline treatment from **3e** was incubated at pH 8 with snake venom phosphodiesterase for 1 h. The nucleotidic substance was degraded in more than 99.3% to give thymidine 5'-phosphate as the sole degraded product. This result indicates that the P–S bond predominantly cleaved on hydrolysis of **9**. Therefore, it is concluded that the 3'–5' isomerization of hydroxy(phenylthio)phosphoryl group is essentially negligible in alkaline treatment of **3e**.

Similarly, treatment of **3f** with 0.2 M NaOH–dioxane (1 : 1, v/v) for 15 min gave a main product of R_f 0.71, **8**, and thymidine 3'- or 5'-phosphate in 76, 21, and 3% yields, respectively. When the product of R_f 0.71 was incubated with snake venom phosphodiesterase, the nucleotidic material remained unchanged and recovered in more than 97%.

This result shows that the 3'–5' isomerization was not observed in the case of **3f**.

Next, complete removal of both phenylthio groups by one-step from **3a** was examined. In spite of facile transformation of S-phenyl nucleoside phosphorothioates to nucleotides by the action of aqueous iodine,[3,4] **3a** was found to be extremely stable toward oxidizing agents such as iodine, sodium periodate, iodosobenzene, hydrogen peroxide, *N*-chlorosuccinimide, and *N*-bromosuccinimide. Removal of both phenylthio groups by use of transition metal salts was examined, since it was expected that sulfur atom has a strong affinity for

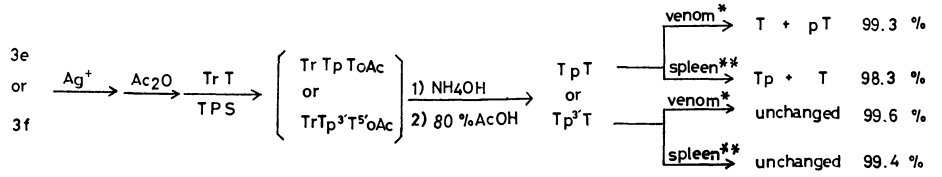

*Venom phosphodiesterase **Spleen phosphodiesterase

Scheme 7.

the transition metals such as copper, mercury, and silver. Copper(I) chloride, copper(II) chloride, copper-(II) acetylacetonate, copper(II) acetate, mercury(II) acetate, mercury(II) chloride, silver acetate, and silver nitrate were examined. The former three copper salts were not effective. For example, the use of 16 molar equiv. of copper(II) acetylacetonate in pyridine–water (2 : 1, v/v) at room temperature for 24 h gave only 3'-*O*-acetylthymidine *S*-phenyl 5'-phosphorothioate (**12**) in a poor yield. Among the mercury salts, mercury(II) acetate was not effective, but treatment of **3a** with 16 equiv. of mercury(II) chloride at room temperature for 16 h gave **11** quantitatively. On the other hand, two silver salts showed almost the same results as mercury-(II) chloride. From the three effective metal salts, silver acetate was finally chosen as an effective and mild agent for removal of both phenylthio groups. The details of one-step removal of both phenylthio groups from **3a** are summarized in Table 3. This deblocking reaction was carried out at room temperature for 16 h using 16 molar equiv. of silver acetate in pyridine–water (2 : 1, v/v). After the deblocking reaction was completed, the excess of silver acetate, disilver salt of nucleotide, and AgSPh could be converted to the mixture of acetic acid, pyridinium salt of nucleotide, and benzenethiol, respectively, by bubbling hydrogen sulfide with the formation of insoluble silver sulfide which could be easily separated off by centrifugation or filtration. Thus, from **3a**, **3b**, **3c**, and **3d**, the corresponding deblocked nucleotides (**11a**, **11b**, **11c**, and **11d**) were obtained by paper chromatography in 99, 97, 96, and 95 yields, respectively. The use of cation exchange resin (DIAION SK IB, pyridinium form) was also useful for removal of silver ions. In this case, AgSPh was not converted sufficiently to benzenethiol. However, it could be filtered off with the resin.

Table 3. Deprotection of arylthio groups from phosphorylated compounds (**3**)

Phosphorylated compound	Conditions		Product (%)	
	AgOAc (equiv.)	Time h	pT	ArSpT
$(PhS)_2$pT	4	3	46	9
	6	3	55	20
	8	3	55	46
	8	18	97	0
	16	3	80	15
	16	18	100	0
$(PhS)_2$pTOAc	16	18	99 (pTOAc)	0 (PhSpTOAc)
$(4\text{-}CH_3OC_6H_4S)_2$pT	16	18	87	10
	20	18	98	0
MMTrTp$(SPh)_2$	16	18	96 (MMTrTp)	0 (MMTr-TpSPh)

Furthermore, in these silver ion-catalyzed hydrolysis reactions, the 3'–5' isomerization of phosphoryl group was also examined by taking **3e** and **3f**. Each mononucleotidic substance corresponding to pT or Tp obtained by treatment of **3e** or **3f** with silver acetate in aqueous pyridine as described above was acetylated with acetic anhydride in pyridine followed by condensation with 5'-*O*-tritylthymidine in the presence of TPS. Consequently, trityl containing dinucleotide corresponding to TrTpTOAc or TrTp$^{3'}$T$^{5'}$OAc was obtained. The dinucleotide derivatives were deprotected by successive treatment with concentrated ammonium hydroxide and with 80% acetic acid to afford unprotected dinucleotides corresponding to TpT and Tp$^{3'}$T. The dinucleotidic substance (90.1 OD) originally derived from **3e** was degraded by snake venom phosphodiesterase in more than 99.3% to give T (45.4 OD) and pT (47.4 OD) in the ratio of 1.00 : 0.96 and by spleen phosphodiesterase in more than 98.3% to give Tp (42.8 OD) and T (46.2 OD) in the ratio of 1.00 : 1.08. On the other hand, the dinucleotidic substance derived from **3f** was recovered in more than 99.6 and 99.4% yields, respectively, when it was incubated with snake venom phosphodiesterase and with spleen phosphodiesterase under the same conditions. The results indicate clearly that the 3'–5' isomerization of phosphoryl group does not take place during the silver ion-catalyzed hydrolysis in the case of **3e** and **3f**. No isomerization was also suggested from the fact that thymidine 3',5'-cyclic phosphate (**8**) could not be detected.

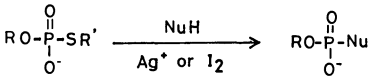

Scheme 8.

It has been well known that a diester type of phosphorothioates represented as RS–P(O)(OR')O$^-$ can be activated oxidatively on sulfur atom by oxidizing agents such as iodine and sodium metaperiodate to produce a metaphosphate derivative, R'OP(O)=O, which in turn reacts with various nucleophiles to afford the corresponding phosphorylated products. This reaction has been utilized for the synthesis of nucleoside di- and tri-phosphates by Nussbaum.[7] Furthermore, it has recently been reported that unsymmetrical α,γ-dinucleosides triphosphates could be obtained in good

yields by activating the phenylthio group of P¹-*S*-phenyl P²-ribonucleoside 5′-pyrophosphorothioates in the presence of silver salts.[6]

Therefore, conversion of phosphorodithioates to phosphoromonothioates under milder conditions should be required.

In connection with our previous results in oligonucleotide synthesis *via* the phosphotriester method where the phenylthio group was used as an internucleotidic phosphate protecting group,[5] we have found that one of two phenylthio groups can be removed selectively from bis(phenylthio)phosphoryl group under very mild conditions.

In order to introduce a phosphite group (p_3) into 3′-hydroxyl of **3e** for the preparation of $(PhS)_2pTp_3$ (**13**), **3e** was treated with 4 equiv. of phosphonic acid in the presence of TPS in dry pyridine for 24 h according to the procedure reported early. However, **13** could not be obtained but a product (**14**: $PhSpTp_3$) leaving one of two phenylthio groups was obtained as the main product. The formation of **14** might be explained as a result of elimination of one phenylthio group from the expected compound (**13**) by the catalytic action of phosphonic acid. Consequently, the independent reaction of **3a** with 4 equiv. of phosphonic acid under the same conditions was tested. When **3a** was treated with 4 equiv. of phosphonic acid in dry pyridine at room temperature for 24 h, *S*-phenyl 3′-*O*-acetylthymidine 5′-phosphorothioate (**12**) was obtained quantitatively. The reaction was keenly specific because acetyl group could not be removed at all under the same conditions. It was also found that under the conditions monomethoxytrityl group and trityl group were stable as indicated in the following experiment. When **3c** was treated with 6 equiv. of phosphonic acid in dry pyridine for 20 h, TLC showed a negligible loss of monomethoxytrityl group, and *S*-phenyl 5′-*O*-monomethoxytritylthymidine 3′-phosphorothioate (**5**) was obtained in 86% yield. In comparison with phosphonic acid, phosphates, such as 2,2,2-trichloroethyl phosphate, made only negligible effect on such deblocking reaction.

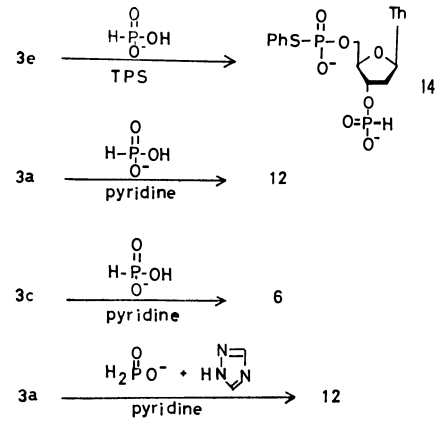

Scheme 9.

In order to extend the catalyst we examined to use phosphinic acid ($pK_a=1.1$)[11] which has a little smaller pK_a value than phosphonic acid ($pK_{a_1}=1.3$).[11] It was found that phosphinic acid is much more soluble in pyridine than phosphonic acid and that the velocity of the deprotection was considerably accelerated for the dearylthioation compared with phosphonic acid: When **3a** was treated with 1.2 equiv. of phosphinic acid in dry pyridine, **3a** disappeared completely after 10 h and **12** was formed in 97% yield along with 3′-*O*-acetylthymidine-5′-phosphate and the corresponding pyrophosphate derivative. Furthermore, an effect of addition of 1,2,4-triazole was tried for the deblocking reaction. The compound, **3a**, was treated with 1.2 equiv. each of phosphinic acid and 1,2,4-triazole at room temperature. The deblocking reaction occured only in 61% yield after 3 h. For the complete deprotection, it took about one day. Although the addition of 1,2,4-triazole reduced the reaction velocity, the deblocking reaction proceeded selectively and gave **12** in quantitative yield without any visible by-products.

Next, the synthesis of protected dithymidine diphosphate derivatives was examined by using **3e** as the 5′-terminal nucleotide component. Compound **3e** was

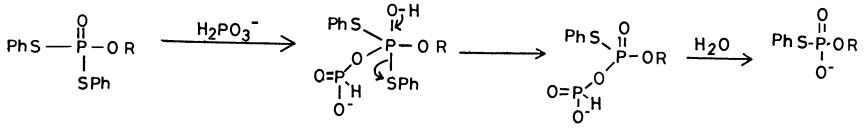

Scheme 10.

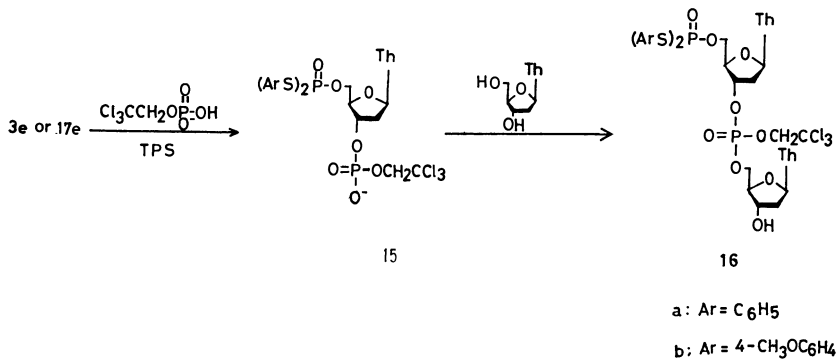

Scheme 11.

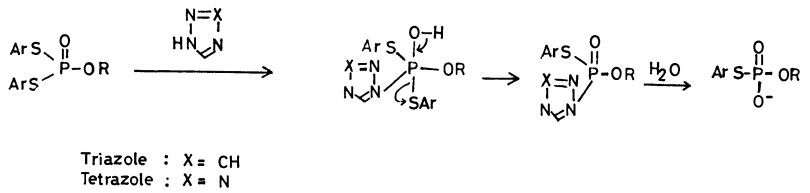

Scheme 12.

phosphorylated with 2,2,2-trichloroethyl phosphate[12] in the presence of TPS and then condensed with thymidine by use of 1-(*p*-nitrobenzenesulfonyl)-1*H*-1,2,4-triazole (NBST).[13] However, the desired dinucleotide (**16a**) was obtained unexpectedly in a lower yield of 44% than expected. In this reaction, a partial dephenylthioation was observed during the second coupling reaction. Such deprotection could be hardly observed during the phosphorylation step using 2,2,2-trichloroethylphosphate and TPS or the condensation step of introducing the bis(phenylthio)phosphoryl group into nucleoside hydroxyls using TPS. The above remarkable difference seemed to be attributed to the kind of condensing agent. The lower yield of **16a** by use of NBST was considered as a result of nucleophilic attack of 1,2,4-triazole to phosphorus of the phosphorodithioate followed by elimination of benzenethiol to give a phosphotriazole intermediate. During the phosphorylation 1,2,4-triazole accumulates up to at least equimolar amount. The phosphotriazole is easily hydrolyzed during work-up of the reaction mixture to form the deblocked product. This catalytic effect of triazole was also confirmed by the following experiment. By treatment of **3a** in the presence of one equiv. of 1,2,4-triazole in dry pyridine at room temperature for 72 h, **12** was formed in 31% yield. In the case of imidazole, **12** was found in 67% yield under the same conditions. On the other hand, tetrazole gave **12** only in 4% yield. Thus, it was concluded that the catalytic effect of these azoles on the undesirable deprotection of the phenylthio group decreases in the following order: imidazole>triazole<tetrazole. The powerful catalytic effect of imidazole might be utilized for the selective removal of the phenylthio group from the bis(phenylthio)phosphoryl group as well as that of phosphonic acid or phosphinic acid described precedingly. In fact, **12** was obtained in 96% yield by treatment with 10 equiv. of imidazole for 28 h. The details of the selective deprotection are summarized in Table 4.

The above results indicate that arenesulfonyl imidazales should not be used condensing agents for phosphorylation of nucleotides having bis(phenylthio)-phosphoryl group. Accordingly, TPS was used for the formation of internucleotidic bond and **16a** was obtained in 92% yield. In this case, the monomethoxytritylation after the condensation was performed so as to remove the by-product of the 3′–3′ isomer.[14]

Since neutral condensing agents such as NBST, 1-(2,4,6-triisopropylbenzenesulfonyl)-1*H*-tetrazole (TPSTe), and 1-(8-quinolinesulfonyl)-1*H*-tetrazole (QSTe) have become apparently more desirable than TPS in several aspects as reported in a number of labolatories,[15–21] our efforts were focused on the exploration of protecting groups more stable towards the above-mentioned azoles. In conclusion, it was found that 4-methoxyphenylthio group having an electron-donating group on benzenethiol was sufficiently stable.

Table 4. Treatment of **3a** and **17a** with imidazole, 1,2,4-triazole, and tetrazole

Azole	$(ArS)_2$pTOAc Ar	Ratio of Azole/$(ArS)_2$pTOAc	Pyridine–H_2O (ml)	(ml)	Time h	Product[a] (%) ArSpTOAc	pTOAc
Imidazole	$(PhS)_2$pTOAc	10	1.0	—	6	63	0
		10	1.0	—	28	96	1
		10	1.0	0.1	6	81	5
		1	0.2	—	72	67	3
1,2,4-Triazole		10	1.0	—	6	4	0
		10	1.0	—	72	21	0
		1	0.2	—	72	31	1
Tetrazole		10	1.0	—	6	<1	0
		10	1.0	—	72	5	0
		1	0.2	—	72	4	0
Imidazole	$(4\text{-}CH_3OC_6H_4S)_2$pTOAc	10	10	—	72	0	0
		10	1.0	—	72	4	0
		1	0.2	—	72	14	0
1,2,4-Triazole		1	0.2	—	72	2	0
Tetrazole		10	1.0	—	72	0	0
		1	0.2	—	72	0	0

a) The yields of PhSpTOAc and 4-$CH_3OC_6H_4$SpToAc were calculated by using ε values of PhSpT [λ_{max} 267 mm (ε 8.6×10^3)] and 4-$CH_3OC_6H_4$SpT [λ_{max} 267 mm (ε 9.2×10^3)].

The introduction of bis(4-methoxyphenylthio)phosphoryl group into hydroxyls of nucleosides could be readily carried out as well as that of the bis(phenylthio)phosphoryl group as shown in Table 1. The promising feature of 4-methoxyphenylthio group is demonstrated in the following experiment: When 3'-*O*-acetylthymidine *S*,*S*-di(4-methoxyphenyl) 5'-phosphorodithioate (**17a**) was treated with one equiv. of 1,2,4-triazole in pyridine at room temperature for 72 h, only 2% of the corresponding deprotected product (**18**) was formed. Therefore, the deprotection reaction can be suppressed within 1% under the usual conditions using NBST in coupling reactions. In fact, when *S*,*S*-di(4-methoxyphenyl) thymidine 5'-phosphorodithioate (**17a**) was phosphorylated with 2,2,2-trichloroethyl phosphate by use of TPS and successively condensed with thymidine by employing NBST followed by the monomethoxytritylation of the mixture, the corresponding dithymidine diphosphate derivative (**16b**) was obtaind in 90% yield. In a similar manner, the corresponding trithymidylate, (4-$CH_3OC_6H_4S)_2$pTp(tc)Tp(tc)T, was obtained in 82% yield from **16b**.

Removal of Protecting Groups from the Oligomers. Selective removal of one of two phenylthio or two 4-methoxyphenylthio groups from **16a** or **16b** was also carried out by using 0.2 M NaOH–dioxane (1 : 1, v/v) at room temperature for 20 min or by phosphonic acid in pyridine containing a small amount of water at room temperature for 24 h. The product, PhSpTp(tc)T, or 4-$CH_3OC_6H_4$SpTp(tc)T was easily converted to pTp(tc)T by treatment with iodine in aqueous pyridine. This two-step procedure for removal of both arylthio groups is efficient for obtaining pTp(tc)T in high yields. When zinc/acetylacetone in DMF–pyridine[22] was employed for removal of 2,2,2-trichloroethyl group of **16a**, the phenylthio groups were together removed and pTpT was obtained by one-step treatment in 71% yield. It seems to be plausible that the active $ZnCl^+$ formed along with 1,2-dichloroethylene serves as an activating reagent of the phenylthio group to liberate ZnCl(SPh) or $Zn(SPh)_2$. In order to remove 2,2,2-trichloroethyl group selectively, benzenethiol was added as a scavenger of $ZnCl^+$. Contrary to our expectation, pTpT was obtained in 84% yield from **16a**. Under the same conditions, pTpT was obtained in 35% yield from **16b** and the desired product, $(4\text{-}CH_3OC_6H_4S)_2$-pTpT, was obtained in 34% yield.

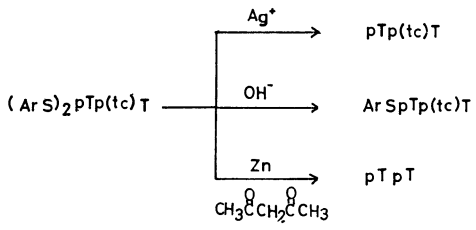

Scheme 13.

Removal of both phenylthio or both 4-methoxyphenylthio groups from the fully protected dinucleotide (**16a**) or (**16b**) was carried out as follows: Treatment of **16a** or **16b** with 16 equiv. of silver acetate in pyridine–water (2 : 1, v/v) at room temperature for 16 h or 18 h gave the deprotected dinucleotide pTp(tc)T in 98 or 97% yield. The successive treatment of the deprotected dinucleotide with zinc powder in DMF–pyridine (2 : 1, v/v) in the presence of acetylacetone gave pTpT in quantitative yield. On the other hand, treatment of $(4\text{-}CH_3OC_6H_4S)_2$pTp(tc)Tp(tc)T with 20 equiv. of silver acetate in aqueous pyridine followed by zinc/acetylacetone in DMF–pyridine gave pTpTpT in 97% yield.

Experimental

Proton magnetic resonance spectra were recorded at 60 Hz on a Varian A-60 spectrometer. Infrared spectra were obtained on a Hitachi 124 spectrophotometer. Melting points were taken on a Fisher-Johns melting point block. Reagent grade pyridine was distilled by addition of *p*-toluenesulfonyl chloride and stored over calcium hydride for several weeks. Paper chromatography was performed using the descending technique on Toyo Roshi No. 51 or Whatman 3 MM paper. The solvent systems used for paper chromatography were: isopropyl alcohol–concentrated ammonium hydroxide–water (7: 1: 2, v/v) (Solvent I); ethyl alcohol–1 M ammonium acetate (pH 7.5) (7: 3, v/v) (Solvent II); butyl alcohol–water (84: 16, v/v) (Solvent III). Paper electrophoresis was carried out on Toyo Roshi No. 51A (15 cm × 60 cm) impregnated with the solvents described by Markham[23] and 1200 V for 1.5 h (buffer I) or at 1500 V for 1.5 h (buffer II) using an apparatus similar to that described by Markham and Smith;[23] buffer I, 0.05 M potassium phosphate (pH 8.0); buffer II, 0.05 M potassium phosphate (pH 6.0). For separation of appropriately protected nucleotide derivatives of triester-type, silica gel (C-200) purchased from Wako Chemical Co. was used. The eluent was monitored by thin layer chromatography using pre-coated plates of silica-gel 60 F-254 purchased from Merck Chemical Co. The yields of water-soluble nucleotidic products were estimated spectrophotometrically after elution of the bands from paper chromatograms. Absorbances were determined with a Hitachi spectrophotometer by the absorbancy for a blank cut from the paper adjacent to the product spot. Snake venom and calf spleen phosphodiesterases were purchased from Boehringer Mannheim Co.

S,S-*Diphenyl Phosphorodithioate (2a).* Sodium Phosphinate (5.30 g, 50 mmol) was converted to pyridinium salt by passing the aqueous solution through DIAION SK 1B (Mitsubishi Kasei Kogyo Co., pyridinium form). Elution was performed with 500 ml of water. The eluent was evaporated and the residue was dried by repeated coevaporations with pyridine. The resulting white solid was mixed with diphenyl disulfide (22.89 g, 105 mmol) and dissolved in 400 ml of dry tetrahydrofuran (THF). Trimethylsilyl chloride (13.1 ml, 105 mmol) and triethylamine (14.8 ml, 105 mmol, were added dropwise to the THF solution at 0 °C. After the addition the mixture was warmed to room temperature and stirred for 20 h. A precipitate of triethylamine hydrochloride was filtered off and the filtrate was evaporated to dryness. The residue was treated with 2 M hydrochloric acid (200 ml) and extracted with dichloromethane (CH_2Cl_2) (4 × 100 ml). The extracts were combined and evaporated to dryness. The residue was dissolved in chloroform (200 ml) and treated with cyclohexylamine (5.73 ml, 50 mmol). The solvent was removed *in vacuo* to give an oily material which solidified after washing with three 50 ml portions of hexane. The solid was recrystallized from water containing a small ammount of THF to afford 15.8 g (83%) of **2a**: mp 177—

179 °C; IR(KBr) 3040, 2950, 1629, 1580, 1523, 1476, 1388, 1220, 1210, 1052 cm^{-1}; NMR (DMSO-d_6–CD_3OD, 1: 1, v/v) δ 1.00—1.57 (5H, m, protons of cyclohexane ring), 1.57—2.11 (5H, m, protons of cyclohexane ring), 2.86 (1H) m, CH–N), 7.29 (3H, m, ArH), 7.56 (2H, m, ArH).

Found: C, 56.71; H, 6.47; N, 3.75; S, 16.52%. Calcd for $C_{18}H_{24}O_2S_2NP$: C, 56.67; H, 6.34; N, 3.67; S, 16.81%.

S,S-*Bis(4-methoxyphenyl)phosphorodithioate.* The title compound (18.8 g, 85%) was prepared according to the same procedure as described above by using bis(4-methoxyphenyl) disulfide (29.2 g, 105 mmol); mp 174—175 °C; IR(KBr) 3050, 2920, 2830, 1588, 1535, 1488, 1450, 1390, 1282, 1238, 1210, 1175, 1050, 1028 cm^{-1}.NMR (DMSO-(DMSO-d_6–CD_3OD, 1: 1, v/v) 1.00—1.64 (m, 5H, protons of cyclohexane ring), 1.64—2.32 (m. 5H, protons of cyclohexane ring), 2.90 (m, 1H, CH–N), 3.82 (s, 6H, OCH_3), 6.89 (d, 4H, J=9.0 Hz, ArH), 7.58 (d, 4H, J=9.0 Hz, ArH).

Found: C, 54.42; H, 6.44; N, 3.12; S, 14.73%. Calcd for $C_{20}H_{28}O_4NS_2P$: C, 54.40; H, 6.39; N, 3.17; S, 14.52%.

Introduction of S,S-*Diaryl Phosphorodithioyl Group into Appropriately Protected Nucleosides. Typical Procedure A) 3'-O-Acethylthymidine* S,S-*Diphenyl 5'-Phosphorodithioate (3a)*: TPS 727 mg (2.4 mmol) was added to **2a** (458 mg, 1.2 mmol) in dry pyridine (2.0 ml) and it was kept at room temperature for 30 min. 3'-O-Acethylthymidine[19] (284 mg, 1 mmol), was added. The mixture was stirred at room temperature for 20 h. The solution was diluted with CH_2Cl_2 (20 ml) and then water (20 ml) was added. The aqueous layer was further treated with CH_2Cl_2 (3×20 ml) and the organic layers were combined and dried over Na_2SO_4. The solution was concentrated *in vacuo* to dryness. The last traces of pyridine was removed by coevaporation with toluene (3× 10 ml). The residue was treated with ethyl acetate (20 ml) whereupon pyridinium salt of 2,4,6,triisopropylbenzenesulfonic acid was separated. The white precipitate was filtered off and washed with cold ethyl acetate (10 ml). The filtrate and washings were combined, dried over Na_2SO_4, and evaporated to a gum. The residue was dissolved in a small amount of benzene and applied to a column on silica gel (20 g). Elution with benzene–ethyl acetate (1: 2, v/v) gave 505 mg (92%) of **3a** as a white foam:

B) S,S-*Diaryl Thymidine 5'-Phosphorodithioates (3d and 17d)*: Compound **2a** (2.1 g, 5.5 mmol) was coevaporated with dry pyridine (3×5 ml) and dissolved in dry pyridine (10 ml). To the solution was added TPS (3.33 g, 11 mmol). The mixture was stirred at room temperature for 1 h and then well pulverized thymidine (1.21 g, 5.0 mmol) was added. After stirring at room temperature for 22 h, the mixture was diluted with chloroform (40 ml) and then water (40 ml) was added. The organic layer was collected and the aqueous layer was further extracted with chloroform (3×10 ml). The organic extracts were combined, dried over Na_2SO_4, evaporated to dryness, and coevaporated with toluene (10 ml). The residue was treated with ethyl acetate (100 ml) and a white precipitate was filtered off. The filtrate was evaporated *in vacuo* and dissolved in dry pyridine after repeated evaporations with dry pyridine (3×5 ml). To the solution was added monomethoxytrityl chloride (577 mg, 2.0 mmol). After stirring at room temperature for 15 h, the mixture was diluted with chloroform (50 ml) and then water (50 ml) was added. The aqueous layer was further extracted with chloroform (2×10 ml) and the organic extracts were combined and dried over Na_2SO_4. The solution was evaporated to dryness *in vacuo*, coevaporated with CH_2Cl_2–toluene (3×5 ml), and the residue chromatographed on silica gel with THF (5: 1, v/v) to afford **3d** (3.34 g, 66%) as a white foam.

Removal of Monomethoxytrityl Group from 3c. S,S-*Diphenyl Thymidine 3'-Phosphorodithioate (3f)*: Compound **3c** (779 mg, 1 mmol) was dissolved in 80% acetic acid (50 ml) and the solution was kept at room temperature for 6 h. The mixture was evaporated to dryness *in vacuo*, and coevaporated with pyridine (5 ml) and then with toluene (3×5 ml). The residue was chromatographed on silica gel with CH_2Cl_2–methanol to give **3e** (477 mg, 94%): UV_{max} (MeOH) 256 nm (ε 14×10^3), UV_{min} (MeOH) 245 nm (ε 13.5×10^3). The data of its elemental analysis and ^{1}H-NMR spectrum are shown in Tables 1 and 2.

Conversion of 3c to 5: To a solution of **3c** (389.5 mg, 0.5 mmol) in dioxane (12 ml) was added 0.2 M NaOH (11 ml) with stirring. The mixture was kept at room temperature for 15 min and then neutralized through a column (1 cm×27 cm) of DIAION SK 1B (NH_4^+ form). The column was washed with dioxane–water (2: 1, v/v, 60 ml), and the eluent and washings were combined and concentrated to *ca.* 20 ml. The aqueous solution was extracted with hexane (3×20 ml) for removal of benzenethiol and then passed through a column (1 cm×27 cm) of DIAION SK 1B (Na^+ form). The column was eluted with dioxane–water (2: 1, v/v, 200 ml) and the eluent was concentrated to *ca.* 20 ml. The solution was extracted with CH_2Cl_2 (3×20 ml) by addition of a few milliliters of saturated sodium chloride. The organic layer was dried over Na_2SO_4, concentrated to 5 ml, and poured into hexane (100 ml). A white precipitate was collected and dried over P_4O_{10} *in vacuo* to give sodium salt (310 mg, 81%) of **5**: UV_{max} (H_2O) 266 nm (ε 10.4×10^3), UV_{min} (H_2O) 255 nm (ε 9.5×10^3), UV_{sh} (H_2O), 232 nm (ε 1.9×10^3).

Found: C, 56.56; H, 5.10; N, 3.52%. Calcd for $C_{36}H_{34}NO_8PSNa\cdot 3H_2O$: C, 56.69; H, 5.29; N, 3.67%.

Conversion of 5 to 4: The sodium salt of **6** (140.7 mg, 0.2 mmol) obtained in the above experiment was treated with 80% acetic acid (10 ml) at room temperature for 6 h. Then water (20 ml) was added and the aqueous solution was extracted with CH_2Cl_2 (3×20 ml). The aqueous solution was evaporated and lyophilized to give a hygroscopic sodium salt (87 mg, 100%) of **4**: UV_{max} (H_2O) 266 nm (ε 9.2×10^3), 245 nm (ε 7.6×10^3), UV_{min} (H_2O) 249 nm (7.6×10^3), 230 nm (ε 6.2×10^3).

Found: C, 40.50; H, 4.41; N, 5.6%. Calcd for $C_{16}H_{18}O_7N_2PSNa\cdot 2H_2O$: C, 40.68; H, 4.70; N, 5.93%.

Alkaline Treatment of 3e and 3f and Enzymatic Assay of the Resulting Diesters: To a solution of **3e** (93 mg, 0.184 mmol) in dioxane (4.4 ml) was added 0.2 M NaOH (4.4 ml) with stirring. After being stirred at room temperature for 15 min, the solution was passed through a column (1 cm×2 cm) of DIAION SK 1B (NH_4^+ form) and the elution was performed with dioxane–water (1: 1, v/v, 60 ml). The eluent was concentrated to *ca.* 10 ml, and extracted with ether (3×10 ml) for removal of benzenethiol. The aqueous solution was concentrated and applied to Whatman 3MM paper developed with Solvent I to afford **7** (R_f 0.72, 87%), **8** (R_f 0.53, 12%), and pT (+Tp) (R_f 0.20, 1%).

A similar treatment of **3f** gave **4** (R_f 0.71, 76%), **8** (R_f 0.47, 21%), and Tp (+pT) (R_f 0.18, 3%).

The ammonium salt (138 OD) of **7**, obtained from **3e** in the above experiment, was incubated with snake venom phosphodiesterase (70 μg) in Tris buffer (pH 8, 1.4 ml) at 37 °C for 1 h. After incubation the mixture was treated with pyridine (1 ml) and chromatographed on Whatman 3MM paper developed with Solvent I to give pT (R_f 0.20, 130 OD) as the sole nucleotidic material.

In a similar manner, the ammonium salt (143 OD) of **4**, obtained by alkaline treatment of **3f**, was incubated under the same conditions. The paper chromatography showed unchanged **4** (138 OD) and Tp (R_f 0.20, 2 OD).

Enzymatic Assay of the Authentic Samples (7 and 4): The ammonium salt (112 OD) of **7**, obtained from thymidine 5′-phosphite, was incubated with snake venom phosphodiesterase (66 μg) in Tris buffer (pH 8.0, 1.32 ml) at 37 °C for 1 h. One tenth of the incubation mixture was treated with pyridine (0.1 ml) and analyzed with paper electrophoresis (pH 8.0), which showed a single band of pT (12.5 OD).

The ammonium salt (76.1 OD) of **4**, obtained by treatment of **5** with 80% acetic acid in the previous experiment, was incubated with snake venom phosphodiesterase (38 μg) in Tris buffer (pH 8, 0.76 ml) at 37 °C. After 1, 6, and 20 h, 0.1 ml aliquots of the incubation mixture were analyzed with paper electrophoresis (pH 8.0), and the bands corresponding to pT were eluted with water, and the yields of pT were spectroscopically calculated to be 1.5% (1 h), 7% (6 h), and 11% (20 h), respectively. These results showed that this enzyme is essentially resistant to TpSPh within 1 h but degrades it gradually to Tp and benzenethiol for prolonged incubation.

One-step Removal of Both Phenylthio Groups from Bis(phenylthio)-phosphoryl Group. Typical Procedure A): To a solution of silver acetate (97 mg, 0.58 mmol) in pyridine–water (2 : 1, v/v, 3 ml) was added **3a** (20.0 mg, 36.5 μmol) and the homogeneous solution was vigorously stirred at room temperature. The solution turned gradually to a suspension. After being stirred for 18 h, the suspension was bubbled with hydrogen sulfide gas until a clear supernatant solution had been obtained. The precipitate was removed by centrifugation (or sometime by filtration) and washed with water (2×5 ml). The supernatant and washings were concentrated to *ca.* 2—3 ml and chromatographed on Whatman 3MM paper developed with solvent II to give a single band of R_f 0.20. Elution of the band with water afforded pTOAc (315 OD, 99%).

B): To a solution of **3c** (77.9 mg. 0.1 mmol) in pyridine (5 ml) was added water (2.5 ml) and then silver acetate (267 mg, 1.6 mmol). The resulting solution was stirred vigorously at room temperature for 18 h and then bubbled with hydrogen sulfide gas at 0 °C until a clear supernatant solution had been obtained. The resulting suspension was evaporated *in vacuo* to remove excess hydrogen sulfide and then diluted with pyridine–water (2 : 1, v/v, 10 ml). The black precipitate was removed by centrifugation, and the supernatant and washings with pyridine–water (2 : 1, v/v, 3×2 ml) were combined, evaporated, and chromatographed on Whatman 3MM paper developed with Solvent I. A band of R_f 0.45 was eluted with water to give MMTrTp (37.1 OD, 96%).

Treatment of 3e and 3f with Silver Acetate in Aqueous Pyridine. In the Case of 3e: To a solution of **3e** (33.9 mg, 0.767 mmol) in pyridine (3.9 ml) was added water (1.9 ml) and then silver acetate (205 mg, 1.23 mmol). The mixture was stirred vigorously at room temperature for 16 h. The resulting suspension was bubbled with hydrogen sulfide gas until a clear supernatant had been obtained. The precipitate of silver sulfide was centrifuged and the supernatant solution was decanted. The precipitate was washed with pyridine–water (2 : 1, v/v, 2×3 ml), and the supernatant and washings were collected and then evaporated to dryness. The residue was dried by repeated evaporations with dry pyridine (4×3 ml) and treated with acetic anhydride (0.22 ml) in dry pyridine (0.77 ml) at room temperature for 12 h. Then ice–water (20 ml) was added and the mixture was extracted with chloroform (3×20 ml). The aqueous layer was evaporated to dryness and a benzene adduct of TrT (35.9 mg, 0.064 mmol) was mixed. The mixture was dried by repeated evaporations with dry pyridine (4×3 ml) and treated with TPS (46.5 mg, 0.15 mmol) in dry pyridine (0.8 ml) at room temperature for 3 h. Then the mixture was quenched with water (20 ml) and extracted with chloroform (3×10 ml). The organic extracts were collected, evaporated to dryness *in vacuo*, and treated with 80% acetic acid (10 ml) at 100 °C for 20 min. After removal of the solvent *in vacuo*, the residue was treated with concd NH_4OH–MeOH (1 : 1, v/v, 20 ml) at room temperature for 10 h. Then the mixture was evaporated to dryness and chromatographed on Whatman 3MM paper developed with Solvent I. A band of R_f 0.43 corresponding to TpT was eluted with water to give a nucleotidic material of 194 OD.

In a similar manner, a nucleotidic material (203 OD) corresponding to Tp$^{3'}$T was obtained from **3f** (40.5 mg, 0.08 mmol) *via* TrTp$^{3'}$T$^{5'}$ OAc.

Enzymatic Assay of the Dithymidine Monophosphate Derivatives Obtained in the Above Experiments. A): TpT (90.1 OD, 4.92 mol) obtained from **3e** was incubated with snake venom phosphodiesterase (50 μg) in 0.1 M Tris buffer (pH 8, 1.0 ml) at 37°C for 12 h. After addition of pyridine (1 ml), the mixture was chromatographed on Whatman 3MM paper developed with Solvent I to give T (45.4 OD, 96.1%) and pT (47.4 OD, 100%).

The same substrate (90.1 OD, 4.92 mol) was incubated with spleen phosphodiesterase (140 μg) in 0.05 M NH_4OAc (1.0 ml) at 37 °C for 8 h. Paper chromatography of the mixture gave T (46.2 OD, 98%) and Tp (42.8 OD, 90%). In the above two enzymatic assays, the band corresponding to the original substrate was eluted with water and its recovery was spectroscopically calculated and estimated to be 0.71% (0.64 OD) and 1.7% (1.5 OD), respectively. B) Tp$^{3'}$T (90.7 OD, 4.96 μmol) obtained from **3f** was incubated with snake venom phosphodiesterase and spleen phosphodiesterase under the same conditions as described in the above enzymatic assays. In both cases, the bands corresponding to the substrate unchanged and pT (or Tp) were cut and eluted with water. The recovery of Tp$^{3'}$T was 100% (91 OD) and 98.6% (87 OD), respectively, after treatment with snake venom and spleen phosphodiesterases. pT and Tp eluted were estimated to be less than 0.3% (0.16 OD) and 0.6% (0.36 OD).

Reaction of 3e with Phosphonic Acid in the Presence of p-Toluenesulfonyltriazole. To a solution of phosphonic acid (0.124 mmol) in pyridine–water (9 : 1, v/v, 1 ml) added **3e** (15.7 mg, 0.02 mmol). The mixture was rendered anhydrous by repeated evaporations with pyridine (5×4 ml) and treated with 1-(*p*-toluenesulfonyl)-1*H*-triazole (27.4 mg, 0.124 mmol) in dry pyridine (0.5 ml) at room temperature for 24 h. Then the mixture was quenched with water (10 ml) and extracted with CH_2Cl_2 (3×10 ml). The organic layer was analyzed by TLC ("Avicel" plate, Funakoshi Co.), which showed no significant spots containing phosphate group indicating that the Hanes-Isherwood test (spray) was negative. TLC of the aqueous layer showed a main product of R_f 0.49 (Solvent I) which was formed almost quantitatively. The spot did not change when concd NH_4OH was added to an aliquot of the aqueous layer. When one third of the aqueous layer was dried by repeated evaporations with dry pyridine (4×1 ml) and treated with 2,2′-dipyridyl disulfide (4.4 mg, 0.02 mmol) in the presence of *N,O*-bis(trimethylsilyl)acetamide (0.1 ml) in dry pyridine (0,2 ml) at room temperature for 2 h, the spot changed to a new one of R_f 0.23 (Solvent I) or 0.39 (Solvent III) corresponding ot PhSpTp. The spot was also converted to a new spot of R_f 0.84 (Solvent I) when one third of the aqueous layer was treated with diphenyl disulfide in place of 2,2′-dipyridyl disulfide. The spot of R_f 0.84 was identical with PhSpTpSPh obtained by treatment of **3d** (29 mg, 0.038 mmol) with 0.2 M NaOH–dioxane (1 : 1, v/v, 8 ml) at room temperature for 15 min. Treatment of PhSpTpSPh

with 20 equiv. of iodine in pyridine–water (2 : 1, v/v) gave pTp of R_f 0.05 (Solvent I). The changes in the above transformations of the product of R_f 0.23 were also followed by paper electrophoresis. The data are shown as follows: PhSpTp$_3$: Rm (pH 8.0, relative to pT) 0.94; PhSpTp: 1.10; PhSpTpSPh: 0.82; pTp: 1.18. These results suggested that the initial product from the reaction of **3e** with phosphonic acid was PhSpTp$_3$.

*Selective Removal of One Phenylthio Group from **3a** by Using Phosphonic acid.* By dissolving phosphonic acid (2.05 g, 25 mmol) in THF using 25 ml measuring flask, 1 M solution of phosphonic acid was prepared. The standard solution of 2.4 ml was taken, evaporated, and dried by repeated evaporations with dry pyridine (3×1 ml). To the pyridinium phosphonate was added **3a** (27.4 mg, 0.05 mmol) in dry pyridine (*ca.* 0.5 ml). The weight of the mixture was 537 mg. Aliquots from the reaction mixture after 0.5, 1, 7, 11, and 21 h were taken out, weighed, and applied to paper electrophoresis (pH 6.0) at 1500 V for 1 h. A band of Rm 0.8 (to pT) was eluted with 0.1 M phosphate buffer (pH 7.0) and the yield was estimated by UV spectrophotometer.

*Conversion of **3c** to **5** by Use of Phosphonic Acid.* The pyridinium salt (2.4 mmol) of phosphonic acid and **3c** (312 mg, 0.4 mmol) were mixed, dried by repeated evaporations using dry pyridine (4×1 ml) and finally dissolved in dry pyridine (4 ml). After being stirred at 30 °C for 15 h, the solution was treated with CH_2Cl_2 (20 ml) and water (20 ml). The aqueous solution was further extracted with CH_2Cl_2 (3×10 ml). The CH_2Cl_2 extracts were combined dried over Na_2SO_4, concentrated to *ca.* 2 ml, and poured into hexane (50 ml). A white precipitate was collected and dried over P_4O_5 *in vacuo* for 12 h to give the free acid of **5** (236 mg, 86%). The product was almost homogeneous on TLC [R_f 0.42 (silica gel plate), Solvent III].

Synthesis of (PhS)$_2$pTp(tc)T. Pyridinium salt (0.6 mmol) of 2,2,2-trichloroethyl phosphate and **3e** (203.1 mg, 0.5 mmol) were mixed, dried by repeated coevaporations with dry pyridine (4×3 ml), and treated with TPS (379 mg, 1.25 mmol) in dry pyridine (2.5 ml) at room temperature for 20 h. Then CH_2Cl_2 (20 ml) and water (20 ml) were added. The aqueous layer was extracted with CH_2Cl_2 (3×10 ml). The CH_2Cl_2 extracts were combined, dried over Na_2SO_4, and evaporated to dryness, and then thymidine (183 mg, 0.75 mmol) was added. The mixture was rendered anhydrous by repeated coevaporations with dry pyridine (4×4 ml), dissolved in dry pyridine (1.0 ml), and finally treated with *p*-nitrobenzenesulfonyl 1,2,4-triazole (153 mg, 0.6 mmol) at room temperature for 24 h. Then CH_2Cl_2 (20 ml) and water (20 ml) were added to the solution. The aqueous layer was further extracted with CH_2Cl_2 (3×10 ml) and the extracts were combined and evaporated to dryness after dryning over Na_2SO_4. The residue was evaporated with toluene (3×4 ml) to remove the last traces of pyridine and chromatographed on silica gel with CH_2Cl_2–methanol to give the title compound (209 mg, 44%): NMR ($CDCl_3$) δ 1.81 (3H, s, C=C–CH_3), 1.90 (3H, C=CH_3), 2.13—2.67 (4H, 2'H), 4.44 (2H, m, 4'H), 4.24—4.70 (5H, m, OH and 5'H), 4.70 (2H, d, J_{P-H}=7 Hz, Cl_3CCH_2–O–P), 5.00—5.47 (2H, m, 3'H), 6.33 (2H, m, 1'H), 7.20—7.73 (12H, m, ArH and)H): UV_{max} (MeOH) 261 nm (ε 21.4×10^3), UV_{min} (MeOH) 241 nm (ε 16.6×10^3).

Found: C, 43.32; H, 3.95; N, 5.87%. Calcd for $C_{34}H_{37}O_{13}N_4S_2P_2Cl_3$: C, 43.35; H, 3.96; N, 5.95%.

Similarly, the use of TPS (303 mg, 1 mmol) in the second coupling reaction gave (PhS)$_2$pTp(tc)T (433 mg, 92%). This compound was further treated with monomethoxytrityl chloride (308 mg, 1 mmol) in dry pyridine (10 ml) for 6 h in order to remove the 3'–3' isomer. After the usual workup, pure (PhS)$_2$pTp(tc)T (400 mg) was obtained by chromatography. For further transformation or deprotection, this purified material was used.

*Treatment of **3a** or **17a** with Imidazole, 1,2,4-Ttriazole, and Tetrazole. General Procedure*: To a solution of **3a** or **17a** in dry pyridine was added an appropriate azole. The reaction conditions and the results are summarized in Table 4. The total weight of the reaction mixture was measured and 10—20 mg aliquots of the mixture after the times described in Table 4 were taken to be analyzed by paper electrophoresis.

*Synthesis of (4-$CH_3OC_6H_4S$)$_2$pT(tc)T (**16b**).* Pyridinium salt (513 mg, 1.2 mmol) of 2,2,2-trichloroethyl phosphate was dried by repeated evaporations with dry pyridine (4×5 ml) and finally dissolved in dry pyridine (5 ml). TPS (727 mg, 2.4 mmol) was added to the mixture and the solution was stirred at room temperature for 21 h. Then CH_2Cl_2 (30 ml) and water (30 ml) were added. The organic layer and further extracts with CH_2Cl_2 (3×10 ml) from the aqueous layer were combined, dried over Na_2SO_4, and concentrated to dryness. The residue was rendered anhydrous by repeated evaporations with dry pyridine (5×4 ml) and treated with NBST (509 mg, 2 mmol) in dry pyridine (1 ml) for 1 h. Then well pulverized thymidine (363 mg, 1.5 mmol) was added to the mixture. The mixture was stirred at room temperature for 26 h. Then CH_2Cl_2 (30 ml) and water (30 ml) were added and the organic layer was collected, and then the aqueous solution was further extracted CH_2Cl_2 (3×10 ml). The organic extracts were combined, dried over Na_2SO_4, and concentrated to dryness. The residue was coevaporated with toluene (4×4 ml), and chromatographed on silica gel with CH_2Cl_2–methanol to afford **16b** (902 mg, 90%). The crude product containing the 3'–3' isomer was further treated with monomethoxytrityl chloride (308 mg, 1 mmol) in pyridine (10 ml) at room temperature for 6 h to remove the 3'–3' isomer and the purified material (798 mg) was used for further transformation and deprotection: NMR($CDCl_3$) δ 1.82 (6H, m, CH_3), 2.00—2.50 (4H, m, 2'H), 3.75 (6H, OCH_3), 4.00—4.27 (2H, m, 4'H), 4.27—4.57 (5H, m, CHOH and 5'H), 4.60 (2H, d, J_{P-H}=7 Hz, Cl_3CCH_2O–P), 4.90—5.32 (1H, m, CH–O–PS), 6.08—6.56 (2H, m, 1'H), 6.85 (4H, d, J=8.4 Hz, ArH), 7.24 (2H, s, C=CH), 7.58 (4H, dd, J=2 Hz, J=8.4 Hz, ArH); UV_{max} (MeOH) 257 nm (ε 35.7×10^3), UV_{min} (MeOH) 225 nm (ε 18.6×10^3).

Found: C, 43.52; H, 4.19; N, 5.61%. Calcd for $C_{36}H_{41}O_{15}N_4Cl_3P_2S_2$: C, 43.15; H, 4.12; N, 5.59%.

*Deprotection of the Fully Protected Dithymidine Diphosphates (**16a**) and (**16b**).* The protected dinuclotide, **16a**, (7.9 mg, 8.4 μmol) was treated with silver acetate (22,4 mg, 0.134 mmol) in pyridine–water (2 : 1, v/v, 0.8 ml) at room temperature for 16 h. Then the mixture was bubbled with hydrogen sulfide gas at 0 °C until a clear supernatant had been obtained, and the suspension was sucked by aspirator for a few minutes for removal of excess hydrogen sulfide. The black precipitate was removed off centrifugation by and washed with pyridine–water (2×2 ml). The supernatant and washings were combined and evaporated to dryness *in vacuo*. The residue was dissolved in DMF–pyridine (2: 1, v/v, 0.8 ml). The analysis of the solution with paper electrophoresis (pH 6.0) showed a single spot of Rm 0.50 (relative to pT) corresponding to pTp(tc)T (151 OD, 98%). To the DMF–pyridine solution was added zinc powder (50 mg) and acetylacetone (0.08 ml) and the mixture was stirred vigorously at room temperature for 8 h. Then water (5 ml) and DIAION SK 1B (NH_4^+ form, 5 ml) were added with stirring. The supernatant was passed through a column (1 cm×5 cm) of DIAION SK 1B (NH_4^+ form) and the resin was washed with concd NH_4OH–water (1 : 1, v/v, 30 ml). The eleuent was evaporated and

chromatographed on Whatman 3MM developed with Solvent II. A band of R_f 0.18 was eluted with water to give pTpT (150 OD, 98%). b) In a similar manner, pTpT (250 OD, 99.5%) was obtained from **16b** (11.27 μmol). In this case, 20 equiv. of silver acetate was used and the time for complete removal of 4-methoxyphenylthio group was 18 h.

Conversion of $(PhS)_2$pTp(tc)T to PhSpTp(tc)T. A): $(PhS)_2$pTp(tc)T (7.3 mg, 7.74 μmol) was treated with 0.2 M NaOH–dioxane (1 : 1 (v/v), 0.2 ml) at room temperature for 20 min. Then DIAION SK 1B (NH_4^+ form, 1 ml) was added to the mixture and the supernatant was analyzed by paper electrophoresis and paper chromatography. The electrophoresis showed a single spot of Rm 0.51 (relative to pT, pH 6.0) corresponding to PhSpTp(tc)T [$UV_{max}(H_2O)$ 266 nm, UV_{min} (H_2O) 236 nm, $UV_{sh}(H_2O)$ 250 nm] which appreared at R_f 0.77 (Solvent I) in paper chromatography.

B): $(PhS)_2$pTp(tc)T (7.3 mg, 7.74 μmol) was mixed with pyridinium salt of phosphonic acid (0.046 mmol) and dissolved in pyridine–water (19 : 1, v/v, 0.2 ml). The solution was kept with stirring at 30 °C for 2 d. Paper chromatography and paper electrophoresis of the solution showed the same product as described in the above experiment the yield was nearly quantitative.

Conversion of PhSpTp(tc)T to pTp(tc)T. PhSpTp(tc)T obtained by alkaline treatment of $(PhS)_2$pTp(tc) was dissolved in pyridine–water (2 : 1, v/v, 1 ml) and iodine (392 mg, 1.55 mmol) was added with continuous stirring. The mixture was stirred at room temperature for 30 min and then 1 M sodium sulfite was added until the color of iodine had disappeared. The clear solution was diluted with pyridine (5 ml) and the resulting salt (mainly Na_2SO_4) was filtered off and washed with pyridine–water (5 : 1, v/v, 5 ml). The filtrate and washings were combined, concentrated, and analyzed with paper chromatography. A single spot of pTp(tc)T (R_f 0.18 (Solvent II), 121 OD, 90%) was obtained.

*Conversion of $(4\text{-}CH_3OC_6H_4S)_2$pTp(tc)T (**16b**) to 4-$CH_3OC_6H_4$SpTp(tc)T.* To a solution of **16b** (5.8 mg, 5.8 μmol) in dioxane (0.2 ml) was added 0.2 M NaOH (0.2 ml). After being stirred at room temperature for 20 min, the solution was passed through a column (1 cm × 1 cm) of DIAION SK 1B (pyridinium form) and the resin was washed with pyridine–water (1 : 1, v/v, 10 ml). The eluent was concentrated to *ca.* 4 ml. The weight of the condensed solution was 3.94 g. One gram of the solution was analyzed with paper electrophoresis to afford three spots of Rm 0.57, 0.85, and 1,22 (relative to pT, pH 6.0). The fast running spot was estimated to be pTpT or TpTp (2.2 OD, 8.4%). The middle spot may be cyclic dithymidine diphosphate derivative, $\overline{|\text{pTpT}|}$ (2.2 OD, 8.2%). The slowest moving spot was 4-$MeOC_6H_4$SpTp(tc)T (22.0 OD, 83%, $UV_{max}(H_2O)$ 264 nm, 241 nm; UV_{min} (H_2O) 252 nm, 231 nm).

*One-step Conversion of **16a** to pTpT.* To a solution of **16a** (9.4 mg, 0.01 mmol) in DMF–pyridine (2 : 1, v/v, 0.7 ml) were added acetylacetone (0.07 ml) and zinc powder (0.5 mmol). The mixture was vigorously stirred at room temperature for 8 h. After being passed through a column (1 cm × 3 cm) of DIAION SK 1B (NH_4^+ form), the mixture was analyzed by paper electrophoresis. Compounds pTpT and $(PhS)_2$pTpT were formed in 61 and 22% yields, respectively. Some alternative conditions for the deprotection with zinc-acetylacetone are summarized in Table 4.

Synthesis of $(4\text{-}CH_3OC_6H_4S)_2$pTp(tc)Tp(tc)T. A mixture of **16b** (501.6 mg, 0.5 mmol) and 2,2,2-trichloroethyl phosphate (126.3 mg, 0.55 mmol) was rendered anhydrous by repeated evaporations with dry pyridine (4 × 3 ml) and finally dissolved in dry pyridine (5 ml). To the solution was added TPS (333.6 mg, 1.1 mmol) and the mixture was stirred at room temperature for 2 d. Then CH_2Cl_2 (20 ml) and water (20 ml) were added. The aqueous solution was extracted with CH_2Cl_2 (3 × 10 ml). The organic extracts were combined and concentrated to dryness. The residue was mixed with well pulverized thymidine (145.3 mg, 0.6 mmol). The mixture was rendered anhydrous by repeated evaporations with dry pyridine (4 × 4 ml) and dissolved in dry pyridine (3.0 ml). It was treated with NBST (280 mg, 1.1 mmol) at room temperature for 2 d. Then CH_2Cl_2 (20 ml) and water (20 ml) were added. The aqueous layer was extracted with CH_2Cl_2 (3 × 10 ml), and the organic extracts were combined and concentrated and dried by repeated coevaporation with dry pyridine (3 × 4 ml). The residue was finally dissolved in dry pyridine (3 ml) and allowed to react with monomethoxytrityl chloride (154 mg, 0.5 mmol) at room temperature for 6 h. Then the mixture was extracted by addition of CH_2Cl_2 (20 ml) and water (20 ml). The aqueous layer was extracted with CH_2Cl_2 (2 × 10 ml) and the organic extracts were combined, dried over Na_2SO_4, and concentrated to dryness. The residue was coevaporated with toluene (3 × 5 ml) and chromatographed on silica gel with CH_2Cl_2–methanol to afford the title compound (593 mg, 82%).

Deprotection of $(4\text{-}CH_3OC_6H_4S)_2$pTp(tc)Tp(tc)T. To a solution of $(4\text{-}CH_3OC_6H_4S)_2$pTp(tc)Tp(tc)T (28.8 mg, 0.02 mmol) in pyridine–water (2 : 1, (v/v), 2.5 ml) was added silver acetate (66.8 mg, 0.4 mmol). The mixture was stirred vigorously at room temperature for 24 h. The resulting suspension was bublled with hydrogen sulfide gas until a clear supernatant had been obtained at 0 °C (*ca.* 5 min). The black precipitate was removed off by centrifugation and washed with pyridine–water (2 : 1, v/v, 2 × 2 ml). The supernatant and washing were combined and evaporated to dryness. The residue was dissolved in DMF–pyridine (1 : 1, v/v, 1 ml). To the solution was added acetylacetone (0.4 ml) and then zinc powder (80 mg). The mixture was stirred at room temperature for 3 h. Then water (4 ml) was added and the solution was passed through a column (1 cm × 5 cm) of DIAION SK 1B (NH_4^+ form). The resin was washed with water (30 ml). The eluent and washings were combined, concentrated to *ca.* 2 ml, and chromatographed on Whatman 3MM paper to afford pTpTpT (470 OD, 97%) which appeared at the position of 9.6 cm from the starting point after development by *i*-PrOH–concd NH_4OH–H_2O (6 : 1 : 3, v/v/v) for 3 d.

Enzymatic Assay of pTpTpT. Compound pTpTpT (85 OD) obtained in the above experiment was incubated with snake venom phosphodiesterase (40 μg) in 0.1 M Tris buffer (pH 8, 1 ml) at 37 °C for 18 h. After addition of pyridine (1 ml) the mixture was analyzed by paper chromatography using Whatman 3MM paper to give pT (91 OD) as a single degradation product.

References

1) A preliminary report appeared as a communication: M. Sekine, K. Hamaoki, and T. Hata, *J. Org. Chem.*, **44**, 2325 (1979).

2) For recent reviews on oligonucleotide Synthesis see V. Amarnath and A. D. Broom, *Chem. Rev.*, **77**, 183 (1977); C. B. Reese, *Tetrahedron*, **34**, 3143 (1978,); M. Ikehara, E. Ohtsuka, and A. F. Markham, *Adv. Carbohyd. Chem. Biochem.*, **36**, 135 (1978).

3) T. Hata and M. Sekine, *Chem. Lett.*, **1974**, 837.

4) T. Hata and M. Sekine, *J. Am. Chem. Soc.*, **96**, 7363 (1974).

5) M. Sekine and T. Hata, *Tetrahedron Lett.*, **1975**, 1711.

6) I. Nakagawa, S. Konya, S. Ohtani, and T. Hata,

Synthesis, **1980**, 556.

7) A. L. Nussbaum and R. Tiberi, *J. Am. Chem. Soc.*, **87**, 2513 (1965); A. F. Cook, M. J. Holman, and A. L. Nussbaum, *J. Am. Chem. Soc.*, **91**, 1522 (1969); A. F. Cook, M. J. Holman, and A. L. Nussbaum, *ibid.*, **91**, 6479 (1969); A. F. Cook, *ibid.*, **92**, 190 (1970); A. F. Cook, E. P. Heimer, M. J. Holman, D. T. Maichuk, and A. L. Nussbaum, *ibid.*, **94**, 1334 (1972); E. P. Heimer, M. Ahmad, S. Roy, A. Ramel, and A. L. Nussbaum, *ibid.*, **94**, 1707 (1972); E. P. Heimer, M. Ahmad, and A. L. Nussbaum, *Biochem. Biophys. Res. Commun.*, **48**, 348 (1972); M. S. Poonian, E. F. Nowoswiat, L. Tobios, and A. L. Nussbaum, *Bioorg. Chem.*, **2**, 322 (1973); S. Åkerfeldt, *Srensk Kem. Tidsky.*, **75**, 231 (1963); S. Åkerfeldt, *Acta Chem. Scand.*, **16**, 1897 (1962).

8) T. Hata, K. Yamaguchi, S. Honda, and I. Nakagawa, *Chem. Lett.*, **1978**, 507.

9) J. H. van Boom, P. M. J. Burgers, P. H. van Deursen, and J. F. M. de Rooy, and C. B. Reese, *Chem. Commun.*, **1976**, 167.

10) H. Rokos, A. Myles, W. Hutzenlaub, and W. Pfleiderer, *Chem. Ber.*, **108**, 2872 (1975).

11) J. Emsley and D. Hall, "The Chemistry of Phosphorus," Harper and Row Ltd. London (1976), p. 307.

12) F. Eekstein and I. Rizk, *Angew. Chem.*, **79**, 939 (1967).

13) N. Katagiri, K. Itakura, and S. A. Narang, *J. Am. Chem. Soc.*, **97**, 7332 (1975).

14) R. L. Letsinger and K. K. Ogilvie, *J. Am. Chem. Soc.*, **91**, 3350 (1969).

15) J. Stawinski, T. Hozumi, and S. A. Narang, *Can. J. Chem.*, **54**, 670 (1976); K. Miyoshi and K. Itakura, *Tetrahedron Lett.*, **1979**, 3635; J. Stawinski, T. Hozumi, S. A. Narang, C. P. Bahl, and R. Wu, *Nucleic Acids Res.*, **4**, 353 (1977).

16) A. K. Sood and S. A. Narang, *Nucleic Acids Res.*, **4**, 2757 (1977); W. L. Sung, H. M. Hsiung, R. Brousseau, J. Michniewicz, R. Wu, and S. A. Narang, *Nucleic Acids Res.*, **7**, 2199 (1979).

17) J. H. van Boom, P. M. J. Burgers, *Tetrahedron Lett.*, **1976**, 4875; J. H. van Boom, P. M. J. Burgers, G. van der Marel, C. H. M. Verdegaal, and G. Wille, *Nucleic Acids Res.*, **4**, 1047 (1977); F. M. De Rooij, G. Wille-Hazeleger, P. H. van Deuresen, J. Serdijn, and J. H. van Boom, *Recl. Trav. Chim. Pays-Bas*, **98**, 537 (1979).

18) C. B. Reese, R. C. Titmas, and L. Yau, *Tetrahedron Lett.*, **1978**, 2727; J. B. Chattopadhyaya and C. B. Reese, *Tetrahedron Lett.*, **1979**, 5059; S. S. Jones, B. Rayner, C. B. Reese, A. Ubasawa, and M. Ubasawa, *Tetrahedron*, **36**, 3075 (1980); J. B. Chattopadhyaya and C. B. Reese, *Nucleic Acids Res.*, **8**, 2039 (1980).

19) G. R. Gough, K. J. Collier, H. L. Weith, and P. T. Gilham, *Nucleic Acids Res.*, **7**, 1955 (1979).

20) H. Takaku, M. Yoshida, M. Kato, and T. Hata, *Chem. Lett.*, **1979**, 811.

21) J. Engels, *Tetrahedron Lett.*, **21**, 4339 (1980).

22) R. W. Adamiak, E. B. K. Grzeskowiak, R. Kierzek, A. Kraszewski, W. T. Markiewicz, J. Stawinski, and M. Wiewiorowski, *Nucleic Acids Res.*, **4**, 2321 (1977).

23) R. Markham and J. D. Smith, *Biochem. J.*, **52**, 552 (1952).

Synthesis of Macrocyclic [*n.n.n*](1,3,5)Cyclophane Polylactones

Masayuki KANISHI, Jun-ichi KUNIZAKI, Junji INANAGA, and Masaru YAMAGUCHI*
Department of Chemistry, Faculty of Science, Kyushu University, Higashi-ku, Fukuoka 812
(Received April 10, 1981)

A series of new macrocyclic cyclophane polylactones has been synthesized by one-step condensation of the appropriate tri(acid chloride)s and triols using the silver cyanide-promoted esterification procedure.

A remarkable development of the chemistry of crown ethers and cryptands has promoted the synthesis of various types of macrocyclic diolides or tetraolides.[1] However, they have so far been essentially confined to monocyclic compounds in respect to the macrocyclic polyolide rings and no bicyclic analogues[2] have been reported, probably because of the lack of powerful lactonization methods suitable for this purpose.[3] Most of the hitherto reported polyolides have been prepared by the reaction between di(acid chloride)s and diols[4] in varied yields depending on the ease of cyclization of substrates. However, a simple extension of the method to the synthesis of macrobicyclic analogues from tri(acid chloride)s and triols does not seem to be very promising because of the highly unfavorable entropy factors in the dual cyclizations.

Recently, silver cyanide has been found to promote the esterification reaction between acid chlorides and alcohols to a high extent and several strongly hindered esters have been synthesized by this method.[5] In this report is demonstrated the applicability of the method to the synthesis of macrocyclic cyclophane polylactones (**3a**—**f** and **5**) which seem to be otherwise difficultly accessible by one-step procedure.

Starting Materials. 1,3,5-Benzenetrimethanol (**2a**) was prepared by lithium aluminum hydride reduction of triethyl 1,3,5-benzenetricarboxylate according to the literature.[6] Conversion of **2a** into α,α′,α″-trichloromesitylene by the reported procedure[6] followed by the treatment of the latter with potassium cyanide under the presence of phase-transfer catalyst[7] gave 1,3,5-benzenetriacetonitrile which was then hydrolyzed to give known 1,3,5-benzenetriacetic acid[8] in good overall yield. Conversion of the triacetic acid to the corresponding tri(acid chloride) (**1a**)[6] or to 1,3,5-benzenetriethanol (**2b**)[6] and transformation of α,α′,α″-trichloromesitylene to 1,3,5-benzenetripropionic acid[6] or to 1,3,5-benzenetripropanol (**2c**)[9] were carried out by the reported procedures. 1,3,5-Benzenetripropionyl trichloride (**1b**) was prepared from the corresponding triacid in a similar way to **1a**. Treatment of 1,3,5-benzenetricarbonyl trichloride with mono(tetrahydropyranyl) ether[10] of 2,2′-oxydiethanol gave **4a** which on hydrolysis with 1 mol dm^{-3} hydrochloric acid gave **4b** in 48% yield from the tri(acid chloride). Treatment of **1a** with a large excess of 2,2′-oxydiethanol in dichloromethane gave **4c** in 61% yield.

Synthesis of Cyclophanes. Condensations of the tri(acid chlorides)s (**1a** or **1b**) and the triols (**2a**, **2b**, **2c**, or **4c**) were carried out under high-dilution conditions in the presence of silver cyanide in refluxing benzene, xylene, or acetonitrile, giving the cyclophanes (**3a**—**f** and **5**) in 3.6—20.4% yields. They are summarized in Table 1. In an experiment carried out for comparison, reaction of **1b** with **2a** in refluxing pyridine under the similar high-dilution conditions in the absence of silver cyanide gave **3d** in only 3% yield. In experiments with the combination of 1,3,5-benzenetricarbonyl trichloride and **2a** or **4b**, no monomeric products were isolated. Properties of the cyclophanes obtained are listed in

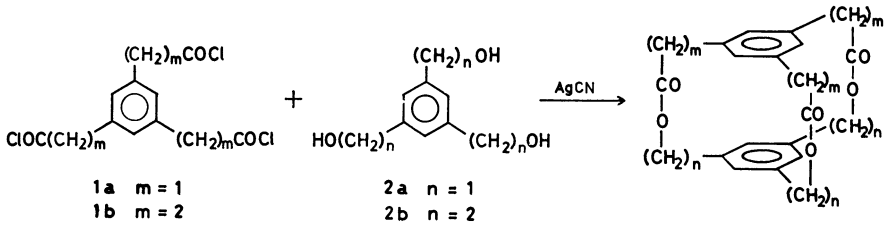

1a m = 1
1b m = 2

2a n = 1
2b n = 2
2c n = 3

3a m = n = 1
3b m = 1, n = 2
3c m = 1, n = 3
3d m = 2, n = 1
3e m = n = 2
3f m = 2, n = 3

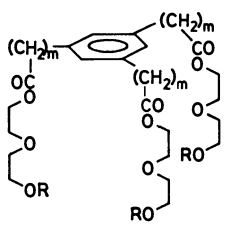

4a R = THP, m = 0
4b R = H, m = 0
4c R = H, m = 1

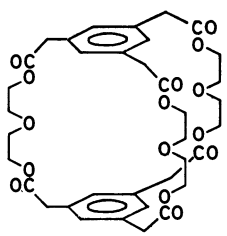

5

Table 1. Isolated yield of cyclophanes

Acid chloride	Alcohol	Solvent[a]	Time of addition/h	Product[b]	Mp/°C	Isolated yield/%
1a	**2a**	Benzene	25	**3a**	>305	6.8
1a	**2b**	Benzene	21	**3b**	244	3.9
1a	**2c**	Xylene	26	**3c**	177.5	3.6
1b	**2a**	Benzene	20	**3d**	267	20.4
1b	**2a**	Pyridine	20	**3d**		3.0[c]
1b	**2b**	Benzene	26	**3e**	220	6.0
1b	**2c**	Acetonitrile	9.5	**3f**	190	6.1
1a	**4c**	Xylene	34	**5**	132	13.6

a) Triols were dissolved in a small amount of acetonitrile and then diluted with the solvent given in the Table. b) Each product gave a distinctive molecular ion peak as a monomer in MS spectrum. c) The experiment was carried out in 1 mmol scale without the addition of silver cyanide.

Table 2. Spectral properties of cyclophanes

Compound	UV/nm (ε)	IR[a]/cm^{-1}	^{1}H NMR			
			Aromatic[b]	$-CH_2-COO-$	$-CH_2-OCO-$	Other protons
3a	268(405)	1732	7.04, 6.83	3.32(s)	4.97(s)	
3b	266(767)	1730	6.79, 6.66	3.40(s)	4.42 (t, J=6.0 Hz)	2.82 (t, J=6.0 Hz)
3c	266(533)	1720	7.12, 6.50	3.42(s)	4.16 (t, J=5.9 Hz)	1.65—2.20(m), 2.47(t, J=7.0 Hz)
3d	266(455)	1732	7.24, 6.67	2.73(br. s)[c]	4.94(s)	
3e	263(459)	1724	6.77, 6.71	2.25—2.55(m)	4.03—4.29(m)	2.60—2.93(m)
3f	266(578)	1718	6.73, 6.70	2.10—2.93(m)[d]	4.10(t, J=6.0 Hz)	1.60—2.07(m)
5	265(376)	1720	7.14	3.54(s)	4.08—4.32(m)[e]	

a) ν_{CO}. b) All singlet. c) The signal was overlapped with the neighboring methylene protons α to the benzene ring. d) The signal indistinguishably overlapped with the methylene protons α to the two benzene rings. e) The signal indistinguishably overlapped with other protons of ethylene bridges.

Table 2.

Aromatic protons of these cyclophanes resonated in NMR spectra at the upper field by *ca.* 0.1—0.3 ppm than those of open chain models (the trimethyl esters or triacetates of the corresponding triacids or triols, respectively), as a trend usually observed in cyclophanes. The C=O stretching vibrations of the cyclophanes with shorter bridges (**3a**, **3b**, and **3d**) appeared at the higher wavenumber positions by *ca.* 10 cm^{-1} than those with longer bridges (**3c**, **3e**, **3f**, and **5**) implying the presence of some strain in the former compounds. However, UV absorptions which appeared at almost the same positions as those of open chain models (266 nm) indicated that the strain, if any, is not appreciable. The UV spectra did not change after the addition of tetracyanoethylene.

Recrystallization of the cyclophanes (**3a—f**) from benzene, ethyl acetate, or acetonitrile did not give any adducts with the solvent molecule.

Though the open chain triol (**4b**) gave a crystalline 1 : 1 adduct with KSCN, the cyclized **5** did not form the isolable adduct. Further examination of **5** on complexation with metal salts such as KSCN, LiSCN, NaSCN, Cs_2CO_3, $MgSO_4$, $AgNO_3$, $CuSO_4$, and NH_4Cl by 2,4,6-trinitrophenol method[11] also gave negative results.

Experimental

Melting points or boiling points were uncorrected. UV spectra (Hitachi 200-10) were recorded in dichloromethane solutions. IR spectra (Hitachi R-215) were obtained in potassium bromide pellets. ^{1}H NMR spectra (Hitachi R-20B) were taken in deuteriochloroform solutions. Mass spectra (Hitachi RMU-6MG) were recorded with a direct-inlet system operating at 70 eV. Solvents were purified and dried by the standard methods.

1,3,5-Benzenetrimethanol (2a). Mp 77 °C (lit,[6] 77 °C), 95%.[12]

1,3,5-Benzenetriacetonitrile. α,α′,α″-Trichloromesitylene[6] (4 g, 18 mmol) was added dropwise to a mixture of potassium cyanide (6 g, 122 mmol) and 18-crown-6 (690 mg, 2.7 mmol)[7] in acetonitrile at room temperature and the mixture was stirred for 6 days. The reaction was followed by TLC. The mixture was filtered and the precipitate was extracted with dichloromethane. The combined filtrate and extract were concentrated and the residue was chromatographed on a silica-gel column from benzene–ethyl acetate (9 : 1). The early fractions contained the practically pure trinitrile (2.8 g, 80%) which was recrystallized from a mixture of benzene and petroleum ether. Mp 123—125 °C. NMR; δ 3.80 (s, 6H), 7.33 (s, 3H): IR; 2220, 1870, 1600, 1420, 1390 cm^{-1}. Found: C, 73.74; H, 4.74; N, 21.46%. Calcd for $C_{12}H_9N_3$: C, 73.83; H, 4.65; N, 21.53%.

1,3,5-Benzenetriacetic Acid. 1,3,5-Benzenetriacetonitrile (1.45 g, 7.46 mmol) was dissolved in a mixture of concentrated sulfuric acid (2.2 ml) and water (2.5 ml) and the solution was refluxed for 5 h. The cooled mixture was diluted with water (5 ml) and extracted with ether. Evaporation of ether gave

a colorless solid which was recrystallized from acetic acid to give 1,3,5-benzenetriacetic acid [1.85 g (98%), mp 208—209 °C (lit,[8] 215—216 °C)].

*1,3,5-Benzenetripropionyl Trichloride (**1b**).* It was prepared from 1,3,5-benzenetripropionic acid (294 mg, 1 mmol) by refluxing with excess thionyl chloride (1 ml) in benzene (1 ml) for 4 h. Colorless needles, mp 59—60 °C (from pentane). NMR; δ 6.94 (s, 3H).

*Tris(tetrahydropyranyloxyethoxyethyl) 1,3,5-Benzenetricarboxylate (**4a**).* Pyridine (16 ml) was added to an ice-cooled solution of 1,3,5-benzenetricarbonyl trichloride (5.2 g) and tetrahydropyranyloxyethoxyethanol (11.7 g)[10] in dry benzene under stirring. After stirring overnight at room temperature, the mixture was filtered and concentrated. Hydrochloric acid (0.1 mol dm^{-3}, 140 ml) was added to the residue and the mixture was extracted with ether. The extract was washed with water, aqueous sodium hydrogencarbonate, and water, and dried over sodium sulfate. Evaporation residue was separated by TLC on silica-gel (acetone–benzene, 1 : 4) giving **4a** as a viscous oil, 11.8 g (83%). IR; 2900, 1720, 1240, 740 cm^{-1}: NMR; δ 8.86 (s, 3H), 4.6 (m, 9H), 3.75 (m, 24H), 1.65 (m, 18H). Found: C, 59.18; H, 7.40%. Calcd for $C_{36}H_{54}O_{15}$: C, 59.48; H, 7.49%.

*Tris(hydroxyethoxyethyl) 1,3,5-Benzenetricarboxylate (**4b**).* **4a** (4 g, 5.5 mmol) was stirred in a mixture of hydrochloric acid (1 mol dm^{-3}, 36 ml) and THF (25 ml) at room temperature for 12 h. Sodium hydrogencarbonate (3.4 g) was added and the mixture was extracted with petroleum ether. The aqueous layer was evaporated and the residue was extracted with dioxane. TLC (silica-gel, dioxane–petroleum ether 5 : 2) of the evaporation residue of the extract gave **4b** as a viscous oil[13] (1.51 g, 58%).[9] NMR; δ 8.88 (s, 3H), 4.85 (m, 6H), 3.75 (m, 18H), 3.14 (s, 3H).

Evaporation of a solution of **4b** (32.4 mg, 0.068 mmol) and KSCN (9 mg, 0.093 mmol) in acetone (1 ml) followed by treatment of the residue with ethyl acetate gave an adduct which melted at 85—86 °C (recrystallized from acetone–ethyl acetate). IR; 3500—3200, 2050, 1720, 1240, 740 cm^{-1}. Found: C, 45.96; H, 5.22; N, 2.49%. Calcd for $C_{21}H_{30}O_{12}\cdot$ KSCN: C, 46.23; H, 5.29; N, 2.45%.

*Tris(hydroxyethoxyethyl) 1,3,5-Benzenetriacetate (**4c**).* A solution of **1b** (140 mg) in dichloromethane (8 ml) was added dropwise to a stirred solution of 2,2′-oxydiethanol (13.3 ml), pyridine (0.17 ml) and dichloromethane (10 ml) under ice-cooling. After stirring overnight, the mixture was refluxed for 5 h. Solvent and excess 2,2′-oxydiethanol were then removed under vacuum as thoroughly as possible. The residue was separated by TLC (Merck, kieselgel 60HF$_{254}$, silanisiert; water–acetonitrile 2 : 1) giving **4c** as a viscous oil[13] (148 mg, 61.3%). NMR; δ 7.15 (s, 3H), 4.3 (m, 6H), 3.65 (m, 24H), 2.5 (s, 3H). The triol did not give an isolable KSCN adduct.

*Cyclophanes (**3a**—**f**, **5**).* Cyclophanes were prepared by essentially the same procedure as exemplified below for **3a**.

A solution of **2a** (168 mg, 1 mmol) in a mixture of acetonitrile (50 ml) and dry benzene (400 ml), and a solution of **1b** (308 mg, 1 mmol) in dry benzene (450 ml) were added dropwise at the same rate to a stirred suspension of silver cyanide (10 g, 75 mmol) in refluxing benzene (100 ml) over a period of 25 h. The mixture was cooled, filtered, and concentrated. The residue was separated by TLC (silica-gel, benzene–ethyl acetate 4 : 1). The residue of the corresponding zone was recrystallized from ethyl acetate to give **3a** (25 mg, 6.8%) as colorless prisms, mp>305 °C. Mass; 366 (M$^+$), 294, 278, 234, 219.

CH-Analyses of these cyclophanes are given in Table 3.

Table 3. CH-analysis of cyclophanes

Compound (Formula)	Found (%)		Calcd (%)	
	C	H	C	H
3a ($C_{21}H_{18}O_6$)	68.62	4.99	68.84	4.98
3b ($C_{24}H_{24}O_6$)	70.33	6.06	70.57	5.92
3c ($C_{27}H_{30}O_6$)	71.73	6.79	71.98	6.71
3d ($C_{24}H_{24}O_6$)	70.32	5.91	70.57	5.92
3e ($C_{27}H_{30}O_6$)	71.90	6.75	71.98	6.71
3f ($C_{30}H_{36}O_6$)	72.95	7.30	73.14	7.37
5 ($C_{36}H_{42}O_{15}$)	60.41	5.97	60.49	5.92

This work was partially supported by a Grant-in-Aid for Encouragement of Young Scientist (No. 174174).

References

1) A recent review: J. S. Bradshaw, G. E. Maas, R. M. Izatt, and J. J. Christensen, *Chem. Rev.*, **79**, 37 (1979).

2) Not a few macrobicyclic cryptands with bridgehead nitrogen atoms [A review: J. M. Lehn, *Acc. Chem. Res.*, **11**, 49 (1978)] and bridgehead carbon atoms [for example; A. C. Coxon and J. F. Stoddart, *J. Chem. Soc., Perkin Trans. 1*, **1977**, 767] have been known. Two porphyrin derivatives having macrotricyclic tetraolide structure have been prepared by means of porphyrin-ring-formation reaction [J. Almog, J. E. Baldwin, R. L. Dyer, and M. Peters, *J. Am. Chem. Soc.*, **97**, 226 (1975); N. E. Kagan, D. Mauzerall, and R. B. Merrifield, *J. Am. Chem. Soc.*, **99**, 5484 (1977)]. Various carbopolycylic cyclophanes are also known [for example; A. J. Hubert, *J. Chem. Soc., C*, **1967**, 6, 11; H. E. Högberg, B. Thulin, and O. Wennerström, *Tetrahedron Lett.*, **1977**, 931]. Most of these compounds have been prepared by stepwise cyclizations.

3) Several mild and fairly rapid esterification methods have recently been developed in connection with the synthesis of natural macrolides [K. C. Nicolaou, *Tetrahedron*, **33**, 683 (1977); T. G. Back, *ibid.*, **33**, 3041 (1977); E. Haslam, *ibid.*, **36**, 2409 (1980)]. However, when sensitive functionalities do not exist in the molecule, the use of acyl halides still remains as one of the most effective carboxylic acid-activation.

4) Recently, activation of the hydroxyl group by dibutyltin oxide has been developed and some macrocyclic tetraolide have been synthesized (A. Shanzer and N. Mayer-Shochet, *J. Chem. Soc., Chem. Commun.*, **1980**, 176; A. Shanzer and E. Barman, *ibid.*, **1980**, 259). Reaction of carboxylates and alkyl halides has also been used for the synthesis of this class of compounds (Ref. 1) and the use of caesium carboxylates has recently been recommended [O. Piepers and R. M. Kellogg, *J. Chem. Soc., Chem. Commun.*, **1978**, 383].

5) S. Takimoto, J. Inanaga, T. Katsuki, and M. Yamaguchi, *Bull. Chem. Soc. Jpn.*, **49**, 2335 (1976).

6) W. P. Cochrane, P. L. Pauson, and T. S. Stevens, *J. Chem. Soc., C*, **1968**, 630.

7) F. L. Cook, C. W. Bowers, and C. L. Liotta, *J. Org. Chem.*, **39**, 3416 (1974).

8) M. S. Newman and H. S. Lowrie, *J. Am. Chem. Soc.*, **76**, 6196 (1954).

9) F. Effenberger and W. Kurtz, *Chem. Ber.*, **106**, 511 (1973).

10) C. Quivoron and J. Neel, *J. Chim. Phys.*, **63**, 1210 (1966).

11) H. K. Frensdorff, *J. Am. Chem. Soc.*, **93** 4684 (1971).

12) As **2a** was very soluble in water, the isolation procedure

was modified as described below. The ethereal reduction mixture was cooled and after the addition of a calculated amount of water, excess Dry Ice was added to the mixture. The mixture was then filtered and the precipitate was washed well with ethanol. The filtrate and the wash were combined and concentrated to a white solid. Sublimation [140 °C (bath temp), 133 Pa] gave **2a** in 95% yield.

13) The removal of a small amount of contaminating water was difficult and the sample gave a low carbon value by *ca.* 1% in CH-analysis.

Restricted Rotation Involving the Tetrahedral Carbon. XL. Barriers to Rotation of 9-(1-Methyl-2-propenyl)triptycenes[1)]

Hiromi KIKUCHI, Shiro HATAKEYAMA, Gaku YAMAMOTO, and Michinori ŌKI*
Department of Chemistry, Faculty of Science, The University of Tokyo, Bunkyo-ku, Tokyo 113
(Received June 20, 1981)

9-(1-Methyl-2-propenyl)triptycenes were prepared by addition of substituted benzynes to 9-(1-methyl-2-propenyl)anthracene or Dields-Alder addition of *p*-benzoquinone to the anthracene followed by enolization and methylation. The crystals of these compounds were pure or enriched isomers of the possible rotamers but the rotational barriers were too low to obtain every possible isomer in a pure state at room temperature. The barriers to rotation were obtained by both classical and dynamic NMR methods. These values were almost the same when the peri-substituent was either a chloro or a bromo but were definitely lower when the peri-substituent was a methyl or a methoxyl.

Although stable rotamers of 9-*t*-alkyltriptycenes were isolated at room temperature,[2)] the same has not been possible for any organic compound which carries a *s*-alkyl group. We have reported in a previous paper[1)] that triptycenes which carry a *s*-alkyl group give one of the possible rotamers as crystalline materials but due to their low barriers to rotation it is not possible to isolate another. Thus it has become necessary to carry out a series of experiments which reveal the effect of substituents on the rotational barriers in order to search a model which gives a high enough barrier to rotation for isolation of rotamers at room temperature.

Introduction of a π-system to a tertiary carbon in the 9-position of triptycene definitely lowers the barrier to rotation about the C_9–C_{subst} bond.[3)] However, it is also pointed out that, since the barrier to rotation is the difference in free energies between the ground state and the transition state of rotation, a large substituent is not necessarily raising the barrier to rotation and sometimes it even lowers the barrier.[4,5)] Since it is not known what will be the effect of a π-system on the barrier to rotation in the *s*-alkyl series, we have wished to start the investigation of this series by putting a vinyl group instead of a methyl of an isopropyl group.

The compounds in question were prepared in the following ways. A Grignard reaction of anthrone with *trans*-2-butenylmagnesium chloride afforded 9-(1-methyl-2-propenyl)-9,10-dihydro-9-anthrol which was dehydrated to give 9-(1-methyl-2-propenyl)anthracene (**1**). The anthracene was treated with benzynes to give triptycenes (**2**, **3**, and **4**). Treatment of the anthracene with *p*-benzoquinone followed by enolization and subsequent methylation gave 1,4-dimethoxy-9-(1-methyl-2-propenyl)triptycene (**5**).

This paper presents the results of the investigation and discusses the effects of substituents on the barrier to rotation.

Experimental

9-(1-Methyl-2-propenyl)anthracene (1). A Grignard reagent was prepared by adding 22 g (0.24 mol) of *trans*-1-chloro-2-butene in ether to a mixture of 7 g (0.29 mol) of magnesium and 50 mL of ether during a period of 2 h. Anthrone (38 g or 0.29 mol) was added in small portions to the Grignard solution and the reaction mixture was decomposed with aqueous ammonium chloride. The organic layer was treated in the usual manner to afford 9-(1-methyl-2-propenyl)-9,10-dihydro-9-anthrol. This crude product in chloroform was treated with concentrated hydrochloric acid at room temperature for 1 h. The mixture was washed, dried, and evaporated. The desired product, mp 44—46 °C, was obtained in 27% yield after chromatography on silica gel with the use of hexane as an eluent. Found: C, 93.31; H, 6.73%. Calcd for $C_{18}H_{16}$: C, 93.06; H, 6.94%. ^{1}H NMR ($CDCl_3$,

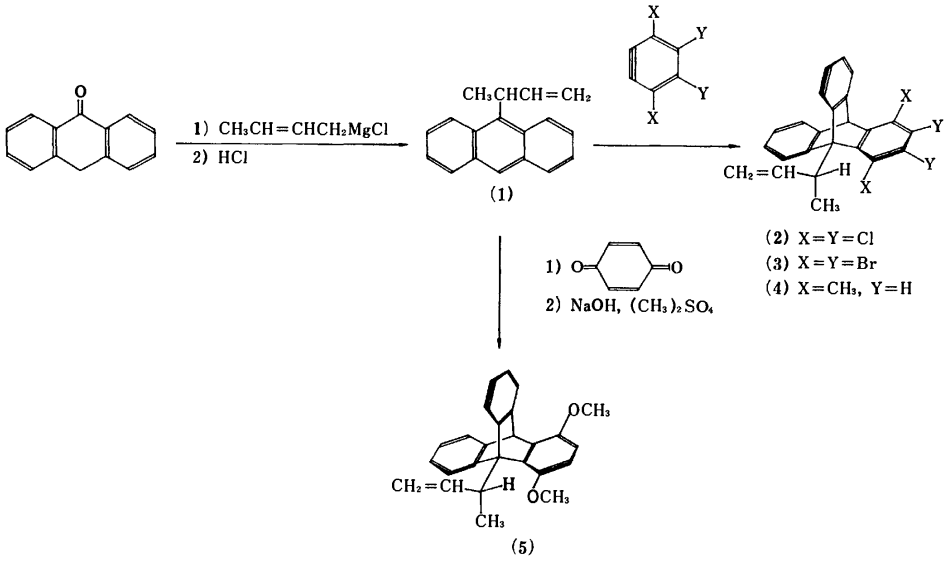

δ): 1.75 (3H, d, J=7 Hz), 5.00 (1H, m), 5.11 (1H, m), 5.28 (1H, m), 6.41 (1H, m), 8.34 (1H, s), 7.2—8.6 (8H, m).

1,2,3,4-Tetrachloro-9-(1-methyl-2-propenyl)triptycene (2). To a boiling solution of 1.9 g (8 mmol) of 9-(1-methyl-2-propenyl)-anthracene and 1 mL of isopentyl nitrite in 30 mL of dichloromethane, was added 4.1 g (14 mmol) of tetrachloroanthranilic acid[6] in 10 mL of acetone in 30 min. The solution was evoporated and the residue was purified by chromatography on silica gel (hexane). Recrystallization of the product from hexane–acetone afforded 0.9 g (25%) of the desired material, mp 191—196 °C. Found: C, 64.88; H, 3.48%. Calcd for $C_{24}H_{16}Cl_4$: C, 64.60; H, 3.62%. High resolution MS gave M^+ peaks at *m/e* 444.0021, 445.9965, 447.9941, and 449.9940, whereas calculation requires *m/e* 444.0002, 445.9973, 447.9943, and 449.9914. The relative intensities of these peaks were in good agreement with those calculated from the natural abundance of ^{35}Cl and ^{37}Cl. ^1H NMR ($CDCl_3$, δ) of the crystals, immediately after dissolution in chloroform-*d* at room temperature indicated that the crystals contained 3 : 1 *ap* and $\pm sc$ conformations. The intensities of the signals changed as time elapsed and the following signals were observed for the rotamers. *ap*: 1.98 (3H, d, J=6.7 Hz), 4.7—5.7 (3H, m), 5.94 (1H, s), 6.2—6.7 (1H, m), 6.9—7.9 (8H, m). $\pm sc$: 1.85 (3H, d, J=6.7 Hz), 4.7—5.7 (3H, m), 5.94 (1H, s), 6.2—6.7 (1H, m), 6.9—7.9 (8H, m).

1,2,3,4-Tetrabromo-9-(1-methyl-2-propenyl)triptycene (3), mp 235—240 °C, was similarly prepared from **1** and tetrabromoanthranilic acid[7] in 23% yield. Found: C, 46.19; H, 2.59%. Calcd for $C_{24}H_{16}Br_4$: C, 46.20; H, 2.58%. High resolution MS showed M^+ peaks at *m/e* 619.8008, 621.7984, 623.7924, 625.7906, and 627.7876, whereas calculation requires *m/e* 619.7987, 621.7967, 623.7947, 625.7927, and 627.7908. The intensities of the observed peaks agreed well with those calculated from the natural abundance of ^{79}Br and ^{81}Br. ^1H NMR ($CDCl_3$, δ) of the crystals, immediately after dissolution in chloroform-*d* at room temperature, indicated that the crystals contained 3 : 1 *ap* and $\pm sc$ conformations. The intensities of the signals changed as time elapsed and the following signals were observed for the rotamers. *ap*: 1.97 (3H, d, J=6.6 Hz), 4.9—5.7 (3H, m), 6.01 (1H, s), 6.1—6.7 (1H, m), 6.8—7.9 (8H, m). $\pm sc$: 1.83 (3H, d, J=6.6 Hz), 4.9—5.7 (3H, m), 6.01 (1H, s), 6.1—6.7 (1H, m), 6.8—7.9 (8H, m).

1,4-Dimethyl-9-(1-methyl-2-propenyl)triptycene (4), mp 140—141 °C, was prepared from **1** and 3,6-dimethylanthranilic acid[8] as above. The yield was 9%. Found: C, 93.11; H, 7.39%. Calcd for $C_{26}H_{24}$: C, 92.81; H, 7.19%. A ^1H NMR spectrum obtained at −25 °C immediately after dissolving the sample of crystalline **4** in chloroform-*d* at −25 °C indicated that the compound was consisted of pure *sc* forms. However, another ^1H NMR spectrum recorded at room temperature immediately after dissolving the crystals of **4** in chloroform-*d* showed that the equilibrium between the conformers had been already reached. The following data were obtained. $\pm sc$: 1.98 (3H, d, J=6.7 Hz), 2.44 (3H, s), 2.58 (3H, s), 4.26—4.70 (1H, m), 5.07—5.67 (2H, m), 5.53 (1H, s), 6.32—7.84 (11H, m).

1,4-Dimethoxy-9-(1-methyl-2-propenyl)triptycene (5). A mixture of 1 g (4 mmol) of 9-(1-methyl-2-propenyl)anthracene and 0.47 g (4 mmol) of *p*-benzoquinone in 30 mL of toluene was heated under reflux for 4 h. After cooling, crystals were collected and washed with ethanol to give 0.91 g (63%) of the adduct. ^1H NMR ($CDCl_3$, δ): 1.93 (2/3 3H, d, J=7 Hz), 1.70 (1/3 3H, d, J=7 Hz), 2.9—3.4 (2H, m), 3.4—3.8 (1H, m), 4.58 (1H, d, J=2 Hz), 5.1—5.7 (2H, m), 5.98 (2H, s), 6.07—6.57 (1H, m), 6.96—7.85 (8H, m).

To the crude adduct (2.7 mmol) in 50 mL of dioxane was added 0.43 g (10.8 mmol) of sodium hydroxide in 5 mL of water and the mixture was stirred with 0.68 g (5.4 mmol) of dimethyl sulfate for 2 d. The mixture was diluted with water and extracted with benzene. The benzene layer was washed with aqueous ammonium chloride and then with water, and dried over magnesium sulfate. After evaporation, the residue was recrystallized from hexane–ethanol to give a pure product, mp 203—204 °C, in 26% yield. Found: C, 84.99; H, 6.50%. Calcd for $C_{26}H_{24}O_2$: C, 84.75; H, 6.56%. ^1H NMR spectrum ($CDCl_3$, δ) of the crystals, immediately after dissolution in chlorofom-*d* at −25 °C, indicated that the compound was a mixture of 8 : 1 *ap* and $\pm sc$ isomers. The intensities of the signals changed rather rapidly and the equilibrium was attained within 30 min at room temperature. We conclude that the crystals obtained here were consisted of almost pure *ap* forms. The following assignments were made. *ap*: 1.90 (3H, d, J=6.7 Hz), 3.70 (3H, s), 3.76 (3H, s), 4.42—4.83 (1H, m), 4.97—5.65 (2H, m), 5.81 (1H, s), 6.35—7.86 (9H, m), 6.50 (2H, s). $\pm sc$: 1.88 (3H, d, J=6.7 Hz), 3.60 (3H, s), 3.74 (3H, s), 4.42—4.83 (1H, m), 4.97—5.65 (2H, m), 5.81 (1H, s), 6.35—7.86 (9H, m), 6.46 (2H, s).

Measurements of Spectra. The ^1H NMR spectra were obtained on a Hitachi R-20B spectrometer operating at 60 MHz or a Varian EM 390 spectrometer operating at 90 MHz. Both were equipped with a temperature variation accessory. The temperature was read by a thermocouple. High resolution mass spectra were obtained on a JEOL JMS-D300 instrument.

Kinetic Measurements. Samples were dissolved in chloroform-*d* placed in NMR sample tubes at low temperature to make up ca. 25 mg per 0.5 mL solutions. The sample tube was placed in an NMR probe of which temperature was set at a given one and the methyl signals were scanned every 30 s. In practice, the inner signal of the methyl doublet due to the $\pm sc$ form overlapped with the outer signal of that due to the *ap* form. Therefore it was necessary to calibrate the intensities of the signals due to $\pm sc$ and *ap* forms to obtain the populations. This was performed by simulating the spectra by computation. Namely, the intensity ratios of inner and outer signals due to *ap* and $\pm sc$ forms were calculated by the dynamic NMR program by putting the chemical shift difference and the coupling constant. This gave the intensity ratio of the inner signal due to the *ap* form and the outer signal due to the $\pm sc$, 0.92, if the populations were the same. This ratio was used throughout the calculation for calibration.

Dynamic NMR Method. The NMR measurements were carried out with *o*-dichlorobenzene solutions. The spectra of the methyl part were simulated by computation with the use of modified Binsch program.[9] The chemical shift difference drifted according to temperatures. Thus the tendency at lower temperatures was extrapolated to afford the chemical shift difference at a given temperature where the line shape could not afford the exact difference directly. The coupling constant was assumed to be constant throughout the temperature range examined. The chemical shift of the methine proton was determined by searching that which gave the sharpest signal due to the methyl protons on irradiation of the former. T_2 was determined by a trial-and-error method to give the best fit of the calculated spectra with the observed at low temperatures. Populations of the rotamers were taken as constant and those in chloroform-*d* were diverted. This is because both are relatively nonpolar solvents and the population ratios in chloroform-*d* was constant throughout the temperature range. The best rates of exchange were obtained by visual fitting of the calculated spectra with the

observed.

Representative rates (s^{-1}) of isomerization (*ap*→*sc*) and temperature (°C) in parentheses are given below.

2: 10.1 (161.9), 11.7 (167.0), 16.8 (172.4), 20.5 (176.4), 23.0 (178.0).

3: 3.1 (150.9), 7.1 (166.3), 8.8 (169.2), 13.7 (176.0), 15.9 (180.0).

4: 2.7 (125.3), 4.0 (129.5), 5.3 (134.1), 8.1 (140.8), 11.3 (146.2), 13.7 (148.9).

5: 3.2 (127.4), 4.6 (132.9), 9.1 (143.7), 9.4 (146.9).

Coalescence temperatures were obtained with the sample solutions used for the dynamic NMR study. Since the populations of the rotamers were not equal, the determination of the coalescence may involve some errors.[10]

Acquisition of Kinetic Parameters. The rate constants of the isomerization in the classical method were obtained by assuming the first order reversible reactions. They were obtained as follows:

2: 3.72×10^{-5} (20.5), 1.34×10^{-4} (31.1), 2.54×10^{-4} (36.0), 4.38×10^{-4} (42.8), 8.57×10^{-4} (46.8).

3: 6.31×10^{-5} (26.7), 2.73×10^{-4} (35.1), 3.24×10^{-4} (39.1), 6.68×10^{-4} (44.0).

where the unit is s^{-1} and the numericals in parentheses are temperatures in °C. Equilibrium constant ($\pm sc/ap$) of **2** was 0.81 throughout the temperature range examined. Equilibrium constant ($\pm sc/ap$) of **3** was also constant at 0.88 over the temperature range. **4** and **5** gave the equilibrium constants at ambient temperature as 1.52 and 0.72, respectively.

The rate constants, which were obtained by the classical or the dynamic NMR method were put into the Eyring equation to obtain the enthalpy and the entropy of activation.

The rates of isomerization (*ap*→*sc*) and the free energies of activation at the coalescence temperature were obtained by the following equations.[11] The chemical shift difference ($\Delta\delta$) was obtained as described above.

$$k_c = \frac{\pi}{\sqrt{2}}\Delta\delta$$

$$k_c = \frac{k_B}{h}T_c e^{-\frac{\Delta G^{\ddagger}}{RT}}$$

Results and Discussion

Assignment of Conformations. The naming of the conformations of these compounds poses problems again,[12] because it contains a chiral center. Due to the presence of a chiral center, enantiomers of the $-sc$ and *ap* forms shown in the scheme are possible and $+sc$ form may be confused with **6** because it is another $+sc$ conformation. However, in practice, we observe the existence of only two rotational isomers by ^{1}H NMR. Thus we may assume that a conformation (**6** or its enantiomer) in which a methyl and a vinyl group flank the peri-substituent does not exist because of the steric repulsions as were in other cases:[13] we may forget the conformation **6** in the following discussion. From the above grounds, we wish to name the conformation on the left side of the equilibrium equation and its enantiomer as $\pm sc$ for the simplicity of discussion in this paper. Accordingly, the conformation on the right of the equation and its enantiomer are called *ap*.

Assignment of conformations is not an easy task. A distinct difference in ^{1}H NMR spectra is seen with the chemical shifts of methyl signals but the data themselves give no definite information. We wish to assign a conformation which gives rise to a higher field methyl signal to $\pm sc$ and that which gives a lower field methyl signal to *ap* tentatively. It is reasonable if we consider the van der Waals shifts because the methyl flanking the peri-substituent should suffer the steric compression which tends to give the chemical shifts at lower fields. A small difference in chemical shifts of the methyls in compound **5** relative to others lends support to this assignment because a smaller compression should cause a smaller down field shift.

Kinetics by the Classical Method. The rates of rotation in 1,2,3,4-tetrahalo compounds (**2** and **3**) were conveniently measured at about room temperature but those of 1,4-dimethyl (**4**) and 1,4-dimethoxy (**5**) compound were too large to obtain reliable data at ambient temperatures. Thus the classical method for determining the rates of rotation was abandoned for the latter two compounds.

The rate constants of rotation of **2** and **3** given in the Experimental part afforded the following data. **2** gave

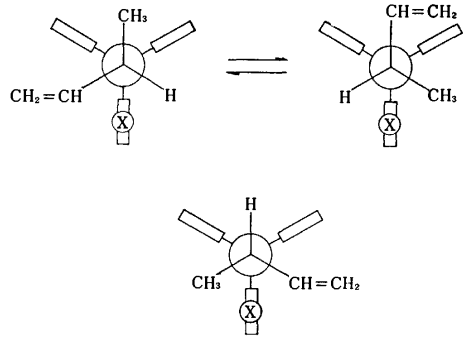

(6)

Table 1. Activation parameters for rotation (*ap sc*) of 9-(1-methyl-2-propenyl)triptycenes obtained by dynamic NMR method

Substituent	$\Delta H^{\ddagger}$ kcal mol^{-1}	$\Delta S^{\ddagger}$ e. u.	$\Delta G_c^{\ddagger a)}$ kcal mol^{-1}	$\Delta G_c^{\ddagger b)}$ kcal mol^{-1}	T_c °C	$K^{c)}$ (sc/ap)
1,2,3,4-Cl_4	19.0±2.0	−11.2±4.6	24.0	24.3	176.2	0.81
1,2,3,4-Br_4	21.0±1.2	−7.4±2.7	24.3	24.2	176.0	0.88
1,4-$(CH_3O)_2$	18.5±2.5	−10.7±6.1	22.9	22.7	140.7	0.72
1,4-$(CH_3)_2$	21.5±0.8	−3.2±1.9	22.8	22.3	137.2	1.52

a) Free energies of activation at the coalescence temperature calculated by using $\Delta H^{\ddagger}$ and $\Delta S^{\ddagger}$. b) Free energies of activation at the coalescence temperature calculated by using the temperature and the chemical shift difference. c) The equilibrium constants were independent of temperature in the range of 20—50 °C.

$\Delta H^{\ddagger}$ 21.0±1.4 kcal/mol (1 cal=4.18 J) and $\Delta S^{\ddagger}$ −7.2± 4.5 e. u. (1 e. u.=4.18 J K^{-1} mol^{-1}). Using these values, $\Delta G^{\ddagger}_{298}$ and $\Delta G^{\ddagger}_{449.5}$ were calculated as 23.1 and 24.3 kcal/mol. **3** gave $\Delta H^{\ddagger}$ 24.5±4.6 kcal/mol and $\Delta S^{\ddagger}$ 4.3±15.0 e. u. Using these values, $\Delta G^{\ddagger}_{298}$ and $\Delta G^{\ddagger}_{449.2}$ were obtained as 23.2 and 22.6 kcal/mol respectively.

The results suggest that the barriers to rotation in compounds **2** and **3** are about the same but are definitely larger than those of **4** and **5**. At any rate, the barriers in these compounds are not high enough for the isolation of rotamers at room temperature. Thus attempt at isolating rotamers of these compounds was abandoned, although the crystalline forms of **4** and **5** were almost pure rotamers and those of **2** and **3** showed some enrichment.

Dynamic NMR Studies. Results obtained by the total line shape analyses of ^{1}H NMR spectra together with those of coalescence temperature method are listed in Table 1. The free energies of activation for rotation, calculated by using $\Delta H^{\ddagger}$'s and $\Delta S^{\ddagger}$'s which were obtained by total line shape analyses, agreed reasonably well with those which were calculated by the T_c's and $\Delta\delta$'s. As was pointed out in the Experimental section, the reading of the coalescence temperatures might involve some errors because of the different populations of the two rotamers. Considering these limitations, we conclude the agreement is satisfactory. It is also worthy to note that the free energies of activation for rotation at 298 K (22.3 and 23.2 kcal/mol for **2** and **3** respectively) calculated with the use of $\Delta H^{\ddagger}$'s and $\Delta S^{\ddagger}$'s from the total line shape analyses agree quite closely with those (23.1 and 23.2 kcal/mol for **2** and **3** respectively) obtained from $\Delta H^{\ddagger}$'s and $\Delta S^{\ddagger}$'s from the classical method, although the enthalpies and entropies of activation themselves seemed to differ to some extent.

Among compounds examined here, the tetrahalo derivatives (**2** and **3**) gave the maximum barriers to rotation and 1,4-dimethoxy and 1,4-dimethyl derivatives gave lower barriers. For the 1,4-dimethoxy compound (**5**), it is a reasonable outcome since the effective size of the methoxyl group is much smaller than those of chloro and bromo groups. However, since the van der Waals radius of the methyl group (2.0 Å) is known to be larger than those of the chloro (1.80 Å) and the bromo (1.95 Å) group, the results deserve mention here. The facts that compounds carrying a methyl group in a peri-position of the triptycene skeleton show lower barriers to rotation than those carrying a halogen at the same place have been noted from time to time.[13,14] We have ascribed this phenomenon to the possible gear effect: since a methyl group is a three-toothed gear, its effective size could be smaller than a chloro or a bromo group in a congested state. This postulate was questioned by Mislow *et al.*[15] because, in 1,2,3,4-tetrahalotriptycenes, the buttressing effect is present, whereas it is absent in 1,4-dimethyltriptycenes. However, since we have been able to show that the buttressing effect of the 2-substituent in this system acts to lower the barrier to rotation of a 9-substituent when the latter is tertiary,[5] the buttressing effect does not seem to be a cause for the lower barriers of the 1-methyl compounds, at least, in the 9-*s*-alkyl series.

This is clearly shown when we carefully examine the barriers to rotation of the compounds reported here and 9-(2-methoxy-1-methylethyl)triptycenes reported in a previous paper.[1] In both cases, 1-methoxy compounds show lower barriers to rotation than 1-chloro compounds but the barriers of the latter compounds are almost the same with 1-bromo compounds: this indicates that the barriers to rotation of triptycenes carrying a *s*-alkyl group at the bridgehead become maximum when the peri-substituent is a chloro or a bromo group. A series of 9-isopropyltriptycenes showed the same tendency.[1,13] Being a larger group than a bromo, the methyl group in 1-position may cause a lower barrier as was the case of *t*-alkyltriptycenes. The maximum barrier is achieved in *t*-alkyltriptycenes when the peri-substituent is a fluoro or a methoxyl[4] and we realize that the substituent which gives the maximum barrier to rotation in *s*-alkyl series shifted to a larger size. This must be a reflection of a fact that, being a smaller group than a *t*-alkyl, the *s*-alkyl group in 9-position of triptycene gives less crowdedness in the ground state and the highest barrier is manifested when the peri-substituent is bulkier. Thus the exact cause for the low barrier of the methyl compounds is not yet known. It is obvious that we must take the crowdedness in the ground state into account.

Comparison of the barriers to rotation of the compounds examined here with those of 9-(2-methoxy-1-methylethyl)triptycenes reveals that both exhibit almost the same height if the peri-substituent is the same. Since the van der Waals half-thickness of the π-system (1.70 Å) is known to be smaller than the van der Waals radius (2.0 Å) of the methyl, of the methoxymethyl and the vinyl groups which we compare here, the latter must be smaller in an effective size. We take the results again that they reflect the stabilities of the ground states of the 9-(1-methyl-1-propenyl) series because in the transition state for rotation of this series the free energy is thought to be less increased relative to those of 9-(2-methoxy-1-methylethyl) series.

Conformational Equilibriums. Comparing the conformational equilibrium constants of the compounds examined here, we immediately notice that the stable conformation switches from *ap* to ±*sc* when we go from compounds **2**, **3**, and **5** to compound **4** if our assignment of the conformation is correct. Since we have assigned the conformations by considering the van der Waals shifts of the methyl signals in ^{1}H NMR spectra and have not been able to provide further evidence, we may have to discuss the cause of the switch in conformational equilibriums with great care. However, it is tempting to consider that in these congested systems a weak interaction which is otherwise not detected can be found:[16] there could be a weak attractive interaction, which stabilizes the *ap* conformation in spite of the fact that a methyl group is larger than a π-system, between a methyl group and a group bearing a lone-pair of electrons. Such possibilities are suggested by Zushi *et al.*[17]

We wish to acknowledge receipt of a Grant-in-Aid for Scientific Research of the Ministry of Education, from which the cost of this wrok has been defrayed.

References

1) For Part XXXIX see, M. Suzuki, G. Yamamoto, H. Kikuchi, and M. Ōki, *Bull. Chem. Soc. Jpn.*, **54**, 2883 (1981).
2) G. Yamamoto and M. Ōki, *J. Chem. Soc., Chem. Commun.*, **1974**, 67; *Bull. Chem. Soc. Jpn.*, **48**, 3686 (1975).
3) S. Otsuka, T. Mitsuhashi, and M. Ōki, *Bull. Chem. Soc. Jpn.*, **52**, 3663 (1979); S. Otsuka, G. Yamamoto, T. Mitsuhashi, and M. Ōki, *ibid.*, **53**, 2095 (1980).
4) G. Yamamoto, M. Suzuki, and M. Ōki, *Angew. Chem. Int. Ed. Engl.*, **20**, 607 (1981).
5) G. Yamamoto, M. Suzuki, and M. Ōki, *Chem. Lett.*, **1980**, 1523.
6) V. Villiger and L. Blangey, *Ber.*, **42**, 3549 (1909).
7) H. Heaney, K. G. Mason, and J. M. Stechley, *J. Chem. Soc.*, **1971**, 567.
8) S. Gronowitz and G. Hansen, *Arkiv. Kemi.*, **27**, 145 (1967).
9) G. Binsch, *Topics in Stereochemistry*, **3**, 97 (1968).
10) A. Jaeschke, G. Munsch, H. G. Schmid, H. Friebolin, and A. Mannschreek, *J. Mol. Spectrosc.*, **31**, 14 (1969).
11) J. A. Pople, W. G. Schneider, and H. J. Bernstein, "High Resolution Nuclear Magnetic Resonance," McGraw-Hill, New York (1959), pp. 218—224.
12) T. Mori and M. Ōki, *Bull. Chem. Soc. Jpn.*, **54**, 1199 (1981).
13) F. Suzuki, M. Ōki, and H. Nakanishi, *Bull. Chem. Soc. Jpn.*, **47**, 3114 (1974).
14) M. Nakamura, M. Ōki, H. Nakanishi, and O. Yamamoto, *Bull. Chem. Soc. Jpn.*, **47**, 2415 (1974).
15) W. D. Hounshell, L. D. Iroff, D. J. Iverson, R. J. Wroczynski, and K. Mislow, *Isr. J. Chem.*, **20**, 65 (1980).
16) G. Izumi, G. Yamamoto, and M. Ōki, *Chem. Lett.*, **1980**, 969 and papers cited therein.
17) S. Zushi, Y. Kodama, K. Nishihata, K. Umemura, M. Nishio, J. Uzawa, and M. Hirota, *Bull. Chem. Soc. Jpn.*, **53**, 3631 (1980) and papers cited therein.

Syntheses of Recyclized Macrolide Antibiotics and Related Derivatives from Mycaminosyltylonolide

Akihiro TANAKA, Azuma WATANABE, Reiko KOBAYASHI, Tsutomu TSUCHIYA,* and Sumio UMEZAWA

Institute of Bioorganic Chemistry, 1614 Ida, Nakahara-ku, Kawasaki 211

(Received June 30, 1981)

Mycaminosyltylonolide diethyl acetal was, after reduction of the 9-keto group, hydrolyzed, and the seco-acids obtained were recyclized to give new 16-membered (9*R*)- and (9*S*)-hydroxy macrolide derivatives, in which the 23-hydroxyl group of the starting substance was incorporated into the macrolactone ring. Selective oxidation of the (9*S*)-hydroxy derivative (**15**) with DDQ gave the keto compound (**18**). Removal of the acetal-protecting groups gave a new macrolide (**19**), which is antibacterial. Several other *O*-acetyl derivatives were also prepared and their antibacterial activities were measured. By the ^{1}H- and ^{13}C-NMR spectroscopies of 3,23-di-*O*-acetyl-mycaminosyltylonolide diethyl acetal by varying the temperature, the presence of two rotamers was clarified.

Mycaminosyltylonolide[1] (**1**) easily obtained by acidic hydrolysis of tylosin,[2] a typical 16-membered macrolide antibiotic, has fairly strong antibacterial activity, inspite of the relatively simple structure. Since structurally related demycarosyljosamycin[3] obtained by acidic hydrolysis of josamycin,[4] and demycarosylcarbomycin B,[5] both having mycaminosylmacrolactone structure, have much weaker antibacterial activity, the activity of **1** will partially be ascribable to the structure of the macrolactone portion, tylonolide. In this paper, we describe a new mycaminosylmacrolactone (**19**) obtained by recyclizing the 23-hydroxyl group of the seco-acid of **1** to the carboxylic acid to form a 16-membered lactone.

Synthesis of the new mycaminosylmacrolactone was started from mycaminosyltylonolide diethyl acetal (**2**) prepared from **1**. To protect the C-8 position from epimerization during the synthesis, the carbonyl at C-9 of **2** was reduced with sodium borohydride following the procedure by Masamune *et al.*,[6] to give two 9-hydroxy derivatives. The configurations at C-9 of the faster- (**6**) and the slower-moving derivatives (**7**) were decided from the studies of their ^{1}H-NMR spectra. Since structurally related macrolide, josamycin (leucomycin A_3) (9*R* epimer) and 9-epi-josamycin (9*S* epimer) show, in their ^{1}H-NMR spectra,[7] the coupling constants of $J_{9,10}$ 9.0 and 4.0 Hz, respectively, **6** ($J_{9,10}$ 8.0 Hz) and **7** ($J_{9,10}$ 4.5 Hz) could reasonably be assigned as 9*R*- and 9*S*-isomers. Removal of the acetal protecting groups of **6** and **7** by treatment in acidic aqueous acetonitrile gave the corresponding aldehyde derivatives (**8** and **9**) in high yields. Again the $J_{9,10}$ of **8** and **9** were shown to be 8 and 4 Hz, respectively. The deblocking of the acetal-protecting groups is necessary in order to have antibacterial derivatives.

Ring-opening of the macrolactone portion of the mixture of **6** and **7** to 15-hydroxy carboxylic acids (**10**, **11**) (seco-acids) was performed by treating the mixture with sodium hydroxide in aqueous methanol. The completion of the opening was verified by the lack, in the ^{1}H-NMR spectrum, of the H-15 proton signals near δ 4—5. The structures were also confirmed by the formation of the corresponding esters (**12**, **13**).

Recyclization of **10** and **11** was carried out by applying the double activation method developed by Corey *et al.*[8] Treatment of the mixture (**10**, **11**) with 2,2′-dipyridyl disulfide and triphenylphosphine according to Mukaiyama *et al.*[9] gave intermediary active esters,

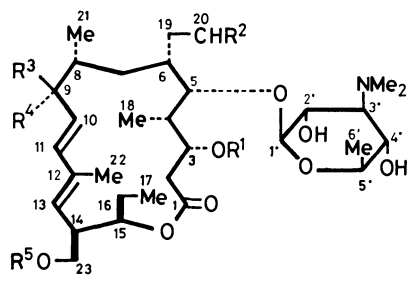

	R^1	R^2	R^3	R^4	R^5
1	H	=O	=O		H
2	H	$(OEt)_2$	=O		H
3	Ac	$(OEt)_2$	=O		Ac
4	Ac	=O	=O		Ac
5	Ac	=O	=O		H
6	H	$(OEt)_2$	H	OH	H
7	H	$(OEt)_2$	OH	H	H
8	H	=O	H	OH	H
9	H	=O	OH	H	H

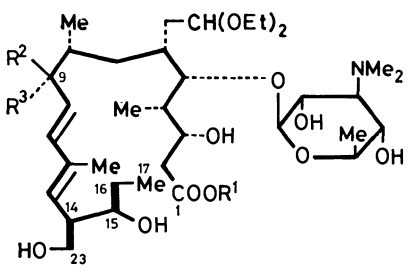

	R^1	R^2	R^3
10	H	H	OH
11	H	OH	H
12, 13	Me	H	OH
	Me	OH	H

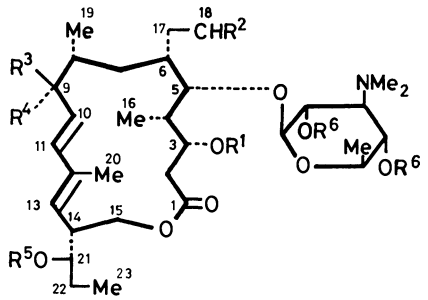

	R^1	R^2	R^3	R^4	R^5	R^6
14	H	$(OEt)_2$	H	OH	H	H
15	H	$(OEt)_2$	OH	H	H	H
16	H	=O	H	OH	H	H
17	H	=O	OH	H	H	H
18	H	$(OEt)_2$	=O		H	H
19	H	=O	=O		H	H
20	Ac	$(OEt)_2$	=O		Ac	Ac
21	Ac	$(OEt)_2$	=O		Ac	H
22	Ac	=O	=O		Ac	H

which were then diluted (0.003—0.006 M) with toluene and heated (80 °C, 24 h) to give a mixture of recyclized products (**14** and **15**) in 17% yield (after purification). Similar treatment of the acids (**10**, **11**) with bis(4-*t*-butyl-1-isopropyl-2-imidazolyl)disulfide[10] and triphenylphosphine followed by dilution with toluene and heating as described above gave the better yields of **14** (*R*-isomer, 11.7%) and **15** (*S*-isomer, 11.7%), the total yield being 26%. Recyclization by the method of Masamune *et al.*[11] was unsuccessful in this case. The structures of **14** and **15** were proved by the ^{1}H-NMR (250 MHz) studies. The H-14 proton resonance (multiplet, δ 3.19 for **12** and δ 3.29 for **13**), which was clearly discernable from other signals by the presence of coupling with the olefin proton at C-13, could be correlated, by the decoupling method, to the resonance of the CH_2 protons (H-15a,b) at δ 4—4.4 (δ 4.20 and 4.29 for **14**; δ 4.07 and 4.38 for **15**). The low-field resonances of the C-15 methylene protons as compared with those of C-23 methylene protons ($\delta \approx 3.7$) of **1** and **5** indicated that the methylenes of **14** and **15** should be bonded to a carboxyl group. The methylenes in question should originate from the 23-methylenes of **10** and **11**, because all the free hydroxyl groups (at C-3, 15,2′, and 4′) other than that at C-23 are bonded to a methine group, respectively. In the above reaction, formation of condensation products formed by linking the carboxylic acid groups with the secondary hydroxyl groups above-mentioned, or formed by intermolecular condensation should be considered, however, none of them were isolated. The fact that **14** and **15** were not the intermolecular-condensation products was verified from the physicochemical properties of **14**, **15** and other derivatives as described later. It is, therefore, concluded that ring closure occurred principally at the primary hydroxyl groups to form 16-membered lactones. It should be noted that this is the first successful macrolide recyclization of seco-acids bearing a sugar portion.

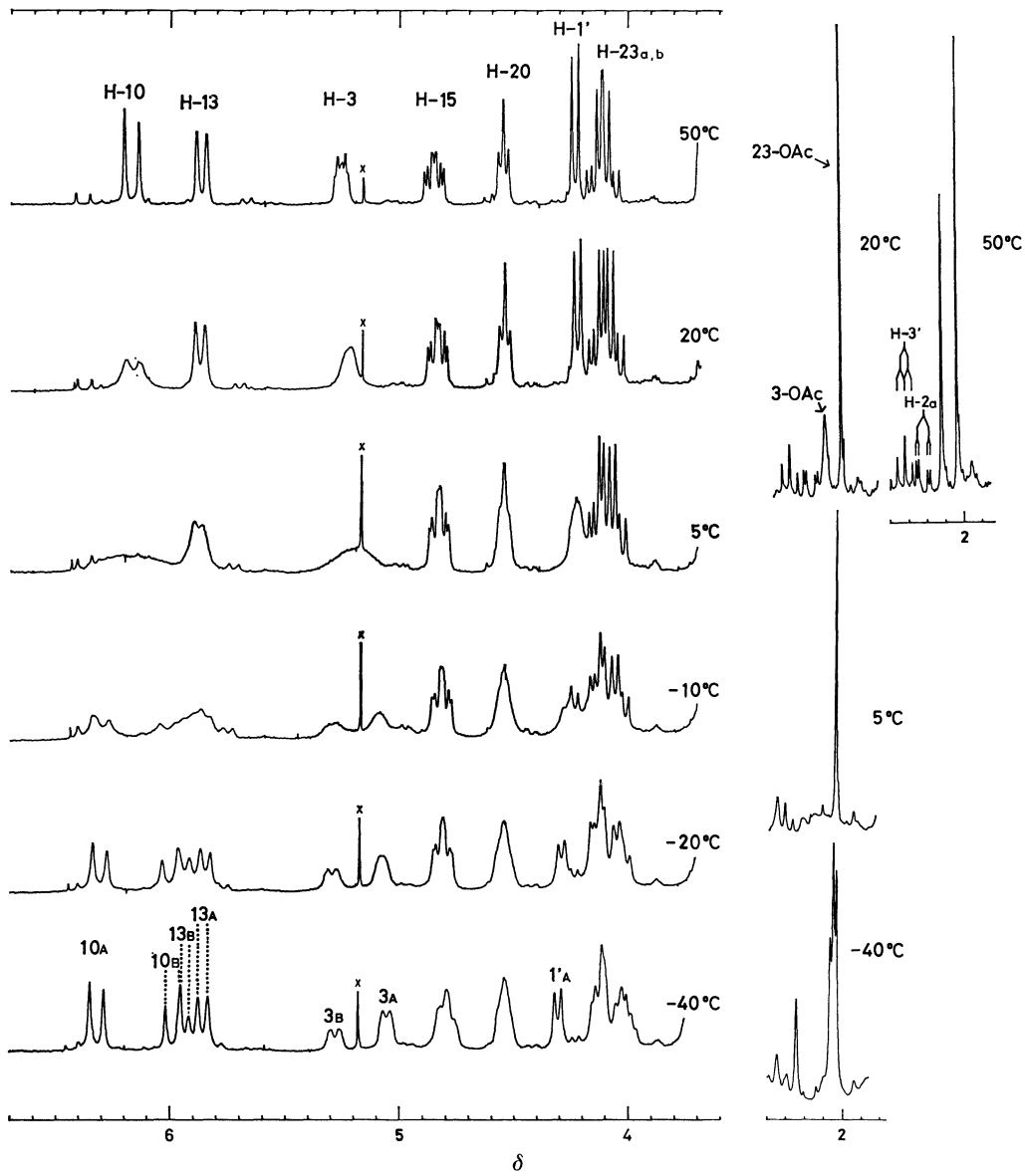

Fig. 1. Partial ^{1}H-NMR spectra of **3** in $CDCl_3$ at several temperatures. Letters of A and B indicate the signals caused by the rotamors. Impurity signals are denoted by x.

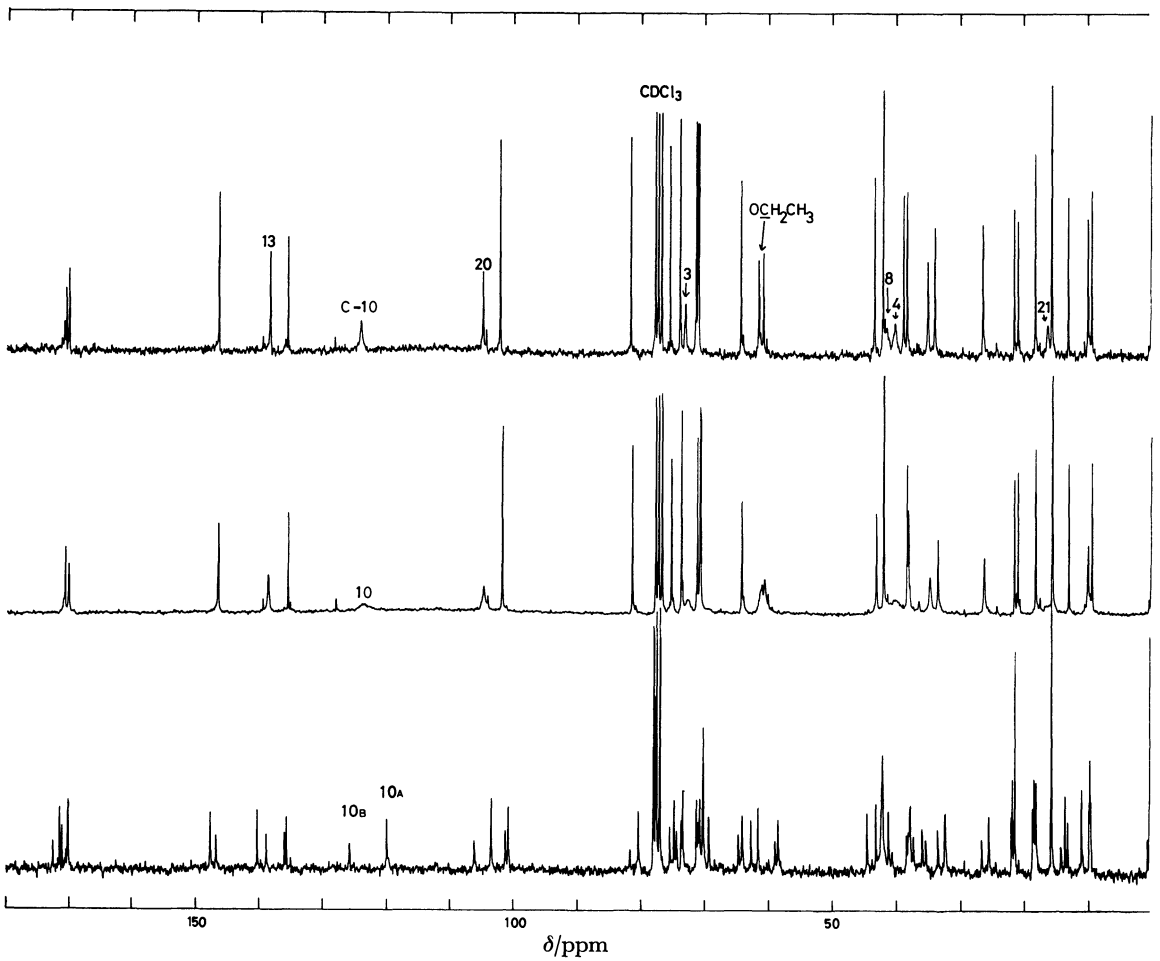

Fig. 2. ^{13}C-NMR spectra of **3** in $CDCl_3$ at several temperatures (at 50, 20, and −40 °C from the upper).

Table 1. Minimal inhibitory concentration (mcg/ml) of the products

	1	**4**	**5**	**8**	**9**	**16**	**19**	**22**	Demycarosyl josamycin
Staph. aureus 209P	1.56	0.39	3.12	25	50	>100	12.5	6.25	100
Sarcina lutea PCI 1001	0.2	<0.2	0.39	3.12	3.12	50	0.78	6.25	12.5
B. subtilis B-558	12.5	0.78	50	50	100	>100	50	12.5	50
E. coli NIHJ	12.5	25	25	100	100	>100	>100	>100	>100
Kl. pneumoniae PCI 602	6.25	12.5	100	100	25	>100	100	>100	>100
Sh. dysenteriae TS 11910	0.78	0.78	3.12	3.12	12.5	50	3.12	6.25	25
Sal. enteritidis 1891	3.12	6.25	6.25	6.25	25	>100	6.25	12.5	50

Deacetalation of **14** gave (9*R*)-9-hydroxy compound (**16**) which is a recyclized congener of bioactive **8**. Deacetalation of **15**, however, failed to give the corresponding (9*S*)-9-hydroxy compound (**17**) owing to the difficulty of isolation of **17** from the reaction mixture.

Selective oxidation at C-9 of **14** and **15** was next performed. Oxidizing agents usually used for macrolides were, for example, active manganese dioxide[6,12] in dichloromethane, aluminium isopropoxide–cyclohexanone in toluene[13] (Oppenauer method), pyridinium chlorochromate in dichloromethane,[14] chromium trioxide in hexamethylphosphoric triamide[15] and acetic anhydride–dimethyl sulfoxide. These reagents, however, when applied to **14** and **15**, gave poor yields of the desired 9-keto derivatives possibly owing to the simultaneously occurring nonselective oxidation of the hydroxyl, dimethylamino, and olefinic groups. One successful case was met, however, when 2,3-dichloro-5,6-dicyano-*p*-benzoquinone[16] (DDQ) was used. This reagent had been reported[17] to convert allylic alcohols to the corresponding unsaturated aldehydes or ketones. Treatment of **15** (9*S* isomer) with DDQ in tetrahydrofuran gave 9-keto compound (**18**) in 47% yield. Use of benzene as solvent, which is usually used in this kind of reaction, was found to be unsuccessful. The structure of **18** was confirmed by the IR, mass, and ^{1}H-NMR spectroscopy. In the ^{1}H-NMR spectrum, no signal assignable to H-9 was observed, and H-10 olefin proton appeared as a doublet indicating again that H-9 was lacked. Similar oxidation of the 9*R* isomer (**14**), however, gave **18** in only 2.5% yield with an unresolved product mainly produced, indicating that the oxidation

(hydrogen abstraction) pathway is highly dependent on the stereo-specificity. Deacetalation of **18** gave **19** which is the recyclized congener of **1**.

Several acetyl derivatives were further prepared in order to confirm the structure of **18** and to test their antibacterial activities. Acetylation of **18** gave 3,21,2′,4′-tetra-*O*-acetyl derivative (**20**), which on treatment with methanol (*vide supra*) gave 3,21-di-*O*-acetyl derivative (**21**). Deacetalation of **21** gave 3,21-di-*O*-acetyl derivative (**22**) of **19**.

Antibacterial spectra of the compounds having the aldehyde free were shown in Table 1. Comparison of the data of **19** and **1**, and **22** and **4** (*vide infra*) shows that the recyclized products have antibacterial activity lower than the mother compounds. It should be noted, however, that the recyclized compounds, except **16**, show stronger activities than that of demycarosyl-josamycin which is closely related to **19**.

Several acetyl derivatives of **1** were also prepared as reference compounds for biological test. Mycaminosyl-tylonolide diethyl acetal (**2**) was treated with acetic anhydride in pyridine to give 3,23,2′,4′-tetra-*O*-acetyl derivative, which, on treatment with methanol,[18] gave 3,23-di-*O*-acetyl derivative (**3**), showing that the 2′- and 4′-*O*-acetyl groups were selectively removed. Acidic hydrolysis of **3** in aqueous acetonitrile gave deacetalated 3,23-di-*O*-acetyl derivative (**4**). Acidic hydrolysis of **3** in slightly stronger conditions gave 3-*O*-acetyl derivative (**5**).

Here we describe the conformational feature of **3** detected by ^{1}H-NMR spectroscopy by varying the temperature (see Fig. 1). At 50 °C in chloroform-*d*, all proton signals appeared as sharp lines, and at lower temperatures, they gradually broadened. Among them, the singlet of 3-*O*-acetyl (δ 2.12) showed rapid broadening; the ratio of the height of the acetyl signal for that of 23-*O*-acetyl (δ 2.03) changed as follows: 0.66 (at 50 °C), 0.42 (44 °C), 0.34 (34 °C), 0.14 (20 °C). At 0 °C the 3-*O*-acetyl signal melted away not to be detectable. At −10 °C, the acetyl peak at δ 2.08 (*ca.* 4.5H in strength) still kept sharp line, but a broadened peak (*ca.* 1.5H) newly appeared at δ 2.26. At −20 °C the latter peak sharpened a little, and at −40 °C all peaks assignable to acetyls appeared as four sharp singlets at δ 2.09 (major), 2.10 (major), 2.12 (minor), and 2.29 (minor, *ca.* 1.2H). The H-3 signals (δ 5.23) also behaved similarly. The sharp multiplet (apparently double triplets of $J_{2b,3}$ 8.5 Hz, $J_{2a,3} \simeq J_{3,4} \simeq 4$ Hz) at 50 °C gradually broadened at lower temperatures, and at 20 °C it became a broadened singlet. At 0 °C it melted away (δ 5.0—5.4). At that temperature, the following signals still kept sharp lines or slightly broadened: methyls of 17, 21, 22, 6′; 23-*O*-acetyl, dimethylamino, $-OCH_2C\underline{H}_3$; methylenes of 16, 23; methines of 15 and 3′. At −10 °C, line-resharpening of all signals began, and H-3 signals were separated into two broadened singlets at δ 5.13 and 5.33 (*ca.* 1 : 1 in strength), which, at lower temperatures, gradually sharpened to become two doublets (J 7.5 and 9 Hz) in the strength of *ca.* 1.2 : 1 (−20 °C), 1.5 : 1 (−40 °C), and 2 : 1 (−55 °C) without substantial change in the shift-values. Other signals separated into two parts were those of H-10 (eminent below −10 °C), -11 (below −20 °C), -13 (below −20 °C), 18-methyl (below −20 °C), and H-1′ (−20 °C). Other signals which showed great broadening at low temperatures were the peaks of H-4 (broadening began at 34 °C, and at 0 °C, melted away), H-10 (broadening began at 20 °C), H-2a and -2b (broadening began both at 10 °C and melted away at 0 °C), 18-methyl (broadening began at 10 °C), and possibly H-7.

Above data can be summarized as follows: 1) line-broadening occurred not at a time, the signals of H-3, 3-*O*-acetyl, H-4, and H-10 being first broadened, then those of 18-methyl, H-2a, and -2b followed, 2) the signals at C-15, 16, 17, 21, 23, 3′, 6′, of $(OCH_2C\underline{H}_3)_2$, 23-*O*-acetyl, and $N(CH_3)_2$ resisted to the broadening, and 3) at low temperatures, the signals of H-3, 10, 11, 13, and 3-*O*-acetyl separated into two parts with varying the strength-ratio with the temperatures.

These data disclosed the conformational feature of **3** dissolved in chloroform-*d*. First, it is concluded, from 3), that **3** will have two rotational isomers on the NMR time scale, and at 55 °C, for example, they show faster interconversion to give a clear spectrum. The situation is typically shown by the fact that the J values relating

Table 2. The ^{13}C-NMR chemical shifts of **1**, **3**, and **4** in $CDCl_3$ (in ppm downfield from TMS)

	1 (at 20 °C)	**3** (at 50 °C)	**4** (at 20 °C)
C-1	173.85	170.08	170.20
C-2	39.54	38.09	37.78
C-3	67.8(v. br)	72.79(small)	68.60(small)
C-4	47.14	39.94(v. br)	43.33(small)
C-5	81.15(br)	81.47	80.66
C-6	31.96(br)	38.61	33.01
C-7	32.75(br)	33.77[a]	33.01
C-8	40.42(br)	41.14(v. br)	40.17
C-9	203.61	204.40	203.56
C-10	118.72(br)	123.91(br)	120.35(small)
C-11	148.14	146.36	147.77
C-12	135.65	135.41	135.63
C-13	142.10	138.31	139.64
C-14	44.61	43.05	42.99
C-15	75.10	75.20	74.64
C-16	25.52	26.24	25.80
C-17	8.98	9.24	9.22
C-18	9.68	9.80	10.25
C-19	43.75	34.82[a]	44.21
C-20	203.02	104.62	202.36
C-21	17.35	16.03(br)	17.19
C-22	13.06	12.86	13.05
C-23	62.73	64.20	63.98
$OCO\underline{C}H_3$		20.67, 21.31	20.80, 21.27
$O\underline{C}OCH_3$		170.53, 170.78	170.80, 170.94
$OCH_2\underline{C}H_3$		15.43	
$O\underline{C}H_2CH_3$		60.64, 61.39	
C-1′	104.03	101.90	104.20
C-2′	70.90	70.70	71.15
C-3′	70.16	70.87	70.22
C-4′	70.90	71.16	70.88
C-5′	73.32	73.67	73.58
C-6′	17.81	18.01	17.84
NMe_2	41.68	41.77	41.75

a) May be interconvertible.

to H-2a, 2b, 3, and 4 is changed at the temperatures above and below 5 °C. The coalescence point is estimated to be near 5 °C, the (high) value being unexpected for the macrolide derivative. From 2) and 3) it is suggested that the origin of the energy barrier for the interconversion between the rotamers might be principally created by the steric crowd of the substituents between C-3—C-8 including 3-*O*-acetyl. The diene portion will come near to the above portion (C-3—C-8) and be influenced by the above rotational changes. The positions remote from the above portion (C-3—C-8) will not much be influenced, keeping always similar spectral environments.

Above conclusions were basically confirmed by the ^{13}C-NMR spectroscopy. The spectra of **3** measured at various temperatures are shown in Fig. 2. Signal assignments (see Table 2) were made on the basis of the comparison of the spectrum with that of tylosin[19] and also by off-resonance method as well as by selective proton decouplings (see Experimental). In the spectrum, the signals of ^{13}C-3, 4, 8, and 10 appeared, even at 50 °C, as low and broadened peaks. At 20 °C, the signals of ^{13}C-18 (slight), 16 (slight), 19, O$\underline{C}$H$_2$CH$_3$, 20, 13, and 9 were additionally broadened. At −40 °C, most of the carbon signals split into doublets of unequal intensities. These results indicate again that **3** has two major rotational isomers.

Experimental

General. Melting points were determined on a Kofler block and are uncorrected. Optical rotations were measured with a Perkin-Elmer 241 polarimeter. Thin-layer chromatography (TLC) was carried out on Wakogel B5 silica gel with detection by spraying with sulfuric acid, followed by slight heating. Column chromatography was performed on Kiesel gel 60, 230—400 mesh (E. Merck). UV spectra were recorded with a Hitachi 200-10 spectrometer, and IR spectra, with a Hitachi 255 grating spectrometer. ^{1}H-NMR spectra were recorded at 90 MHz with a Varian EM-390 spectrometer, or at 250 MHz in the FT mode using a Bruker WM 250 spectrometer at 20 °C unless otherwise stated. ^{13}C-NMR spectra were recorded in the FT mode with a Bruker WM 250 spectrometer operating at 62.9 MHz.

^{1}H-NMR(in CDCl$_3$ at 250 MHz) of **1**: δ 0.95 [3H t, Me(17)], 1.02 [3H d, Me(18)], 1.22 [3H d, Me(21)], 1.27 [3H d, Me(6′)], 1.83 [3H very narrow m; apparently s, Me(22)], 1.96 (1H d, $J_{2a,2b}$ 15 Hz, H-2a), 2.36 (1H t, J 10 Hz, H-3′), 2.50 (6H s, NMe$_2$), 2.53 (1H dd, $J_{2b,3}$ 10 Hz, H-2b), 2.6 (1H m, H-8), 2.9 (H-14), 3.06 (1H t, $J\simeq$9.3 Hz, H-4′), 3.26 (1H m, H-5′), 3.47 (1H dd, $J_{1',2'}$ 7.5 Hz, $J_{2',3'}$ 10.5 Hz, H-2′), 3.73 (1H, H-5), 3.75 (2H d, J 5 Hz, H-23a,b), 3.85 (1H br d, $J\simeq$10 Hz, H-3), 4.25 (1H d, H-1′), 4.95 (1H dt, $J_{14,15}=J_{15,16a}\simeq$9 Hz, $J_{15,16b}$ 2.5 Hz, H-15), 5.92 (1H slightly br, d, $J_{13,14}$ 10 Hz, H-13), 6.30 (1H d, J 15 Hz, H-10), 7.34 (1H d, H-11), 9.70 (1H s, CHO).

Irradiation at δ 1.65 (H-4, 16a, and possibly one of H-7a, 7b) caused the triplet of H-17 and the doublet of H-18 to collapse to a doublet and a singlet, respectively; at the same time, signals both at δ 1.88 (H-16b) and of H-5 to change. Irradiation at δ 2.6 (H-2b, -8) collapsed the doublets of H-2a, -3, and -21 to singlets respectively; the signals near δ 1.5 (H-7a,7b) also changed. Irradiation at δ 2.9 (H-14 and -19?) caused the doublet of H-23, the doublet of H-13, and the double triplets of H-15 to collapse to a singlet, a singlet, and a doublet, respectively.

^{13}C-NMR (in CDCl$_3$ at 20 °C). (s, d, and t cited in the parenthesis are the splitting pattern in the off-resonance). Carbon- 17, 18, 22, 21, 6′, 16(t), 6(d), 7(t), 2(t), 8(d), NMe$_2$, 19(t), 5(d), 1′(d), 10(d), 12(s), 13(d), 11(d), 1(s), 20(d), 9(s) (see Table 2.) were assigned on the bassi of the comparison of the shift-values with those of tylosin[19] as well as by off-resonance method. Carbon-23 can be assigned by the off-resonance method (appeared as a triplet) as well as by the appearance at an up-field shift (62.73 ppm) in comparison to the shift (68.2 ppm) of C-23 of tylosin, the shift being in accord with the removal of the glycoside linkage from tylosin. On H-3′ proton irradiation, C-3′ appeared as a singlet; the splitting spaces of the signals (each doublet) of C-4′, 2′ and 5′, 3 and 15 became wider in this order, which were proportional to the order of the $\Delta\delta$ value of the protons (H-4′, 2′, 5′, 3, and 15) from the δ value of H-3′. This observation assisted the carbon assignments in question. Distinction between C-4 and -14 was performed by the H-14 proton irradiation.

Mycaminosyltylonolide Diethyl Acetal (2). A solution of **1** (825 mg) in dry ethanol (8.3 ml) containing anhydrous *p*-toluenesulfonic acid (360 mg) was kept at room temperature for 20 min. After addition of triethylamine (0.3 ml), the solution was concentrated and the residue was dissolved in chloroform. The solution was washed with saturated aqueous sodium hydrogencarbonate and water, dried over sodium sulfate and concentrated to give a solid. Recrystallization from acetone solution by adding hexane gave needles, 852 mg (92%), mp 193—195 °C, $[\alpha]_D^{25}$ +14° (*c* 1, chloroform); UV λ_{max} (MeOH) 283 nm (log ε 4.40).

Found: C, 62.29; H, 8.95; N, 2.13%. Calcd for $C_{35}H_{61}NO_{11}$: C, 62.57; H, 9.15; N, 2.08%.

3,23-Di-O-acetylmycaminosyltylonolide Diethyl Acetal (3). Treatment of **2** (992 mg) in pyridine (10 ml) with acetic anhydride (2.5 ml) at 50 °C for 2 d gave 3,23,2′,4′-tetra-*O*-acetyl derivative, which gave, on TLC with benzene–acetone (5 : 1), a spot of R_f 0.35. The crude derivative was dissolved in methanol and the solution was kept at 50 °C overnight to give an amorphous solid of **3**, 1.05 g (94%); R_f 0.5 on TLC with chloroform–methanol (7 : 1) (the tetraacetyl intermediate: R_f 0.95), $[\alpha]_D^{25}$ +3° (*c* 1, chloroform).

Found: C, 62.15; H, 8.59; N, 1.88%. Calcd for $C_{39}H_{65}NO_{13}$: C, 61.97; H, 8.64; N, 1.85%.

^{1}H-NMR (in CDCl$_3$ at 250 MHz) (at 50 °C): δ 0.93 [3H t, Me(17)], 1.03 [3H d, Me(18)], 1.15 [3H d, Me(21)], 1.15—1.24 [6H, (OCH$_2$C$\underline{H}_3$)$_2$], 1.31 [3H d, Me(6′)], $\simeq$1.35—1.5 (H-19a), $\simeq$1.37—1.52 (H-7), 1.61 (1H m, H-16a), $\simeq$1.75 (H-4), $\approx$1.8 (H-16b), 1.81 [3H s, Me(22)], $\approx$2.0 (H-6, 19b), 2.03 (3H, s, 23-*O*-Ac), 2.12 (3H s, 3-*O*-Ac), 2.22 (1H dd, $J_{2a,3}$ 3.3 Hz, $J_{2a,2b}$ 15 Hz, H-2a), 2.32 (1H t, H-3′), 2.51 (6H s, NMe$_2$), 2.57 (1H dd, $J_{2b,3}$ 8.5 Hz, H-2b), 2.95—3.07 (3H, H-8, 14, 4′), 3.29 (1H m, H-5′), 3.44—3.55 [(OC$\underline{H}_2$CH$_3$)$_2$], 3.59 (1H dd, H-2′) $\approx$3.67 (H-5); 4.08 (1H dd with the lower-field half being intense, $J_{14,23a}$ 6.5 Hz, $J_{23a,23b}$ 11.5 Hz, H-23a), 4.14 (1H dd with the higher-field half being intense, $J_{14,23b}$ 5 Hz, H-23b), 4.23 (1H d, $J_{1',2'}$ 7.5 Hz, H-1′), 4.54 (1H apparent t, H-20), 4.84 (1H ddd, H-15), 5.25 (1H m, H-3), 5.86 (1H d, $J_{13,14}$ 10 Hz, H-13), 6.17 (1H d, J 15.5 Hz, H-10), 7.25 (1H d, H-11).

Irradiation of 17-methyl collapsed the multiplet of H-16a to double doublets ($J_{15,16a}$ 9.5, $J_{16a,16b}$ 15 Hz), and the signals between δ 1.77—1.86 (H-16b) changed. Irradiation at δ 1.82 (H-16b and 4) caused the triplet of H-17, the multiplet of H-15, the multiplet of H-3 and the doublet of CH$_3$ (18) to collapse to a doublet, double doublets ($J_{14,15}$ and 9.5 Hz), double doublets, and a singlet, respectively; the signals of

H-16a also changed although they were biased by the near-by irradiation. Irradiation at δ 3.0 (H-8, 14, and 4′) collapsed the doublet of Me(21) to a singlet, the multiplet of H-23a, -23b to an AB quartet, the doublet of H-13 to a singlet, and the multiplet of H-15 to double doublets; the signals of H-5′ and -3′ also changed to the form as expected. Irradiation of H-3 caused the signals of H-2a, -2b to collapse to an AB quartet and the signals near δ 1.75 (H-4) to change. Irradiation at δ 3.67 (H-5) caused the signals of H-4 to change. Irradiation at δ 1.95 (H-6, 19b) caused the signals between δ 1.35—1.53 (H-7, 19b) to simplify, and the triplet of H-20 to a doublet. To confirm the signal assignments, the positions of H-15, 20, and 1′ were also irradiated.

At −20 °C: 18-Methyl separated into two incomplete doublets at δ 1.01 and 1.10. H-1′ separated into two, the bigger half being appeared at δ 4.33 (J 7.5 Hz). H-13 gave two doublets (each $J\simeq$10 Hz) at δ 5.88 and 5.97. H-10 gave two doublets (each $J\simeq$15 Hz) at δ 6.03 and 6.34. H-11 gave apparent triplet at δ 7.34.

At −40 °C: 18-Methyl gave two doublets at δ 1.01 (J 6.3 Hz) and 1.12 (J 5 Hz). The bigger signals of H-1′ appeared at δ 4.35 ($\simeq$0.6H d, J 7.5 Hz). H-3 gave two slightly broaened doublets at δ 5.09 ($\simeq$0.6H, $J\simeq$7.5 Hz) and 5.33 ($\simeq$0.4H, $J\simeq$10 Hz). H-13 gave two sharp doublets (J 10 Hz) at δ 5.90 ($\simeq$0.6H) and 5.98 ($\simeq$0.4H). H-10 gave two sharp doublets (J 15.5 Hz) at δ 6.03 ($\simeq$0.4H) and 6.37 ($\simeq$0.6H).

^{13}C-NMR (in $CDCl_3$ at 50 °C). Carbon-17, 18, 22, ($\underline{C}H_3$-CH_2O-)$_2$(q, each), 21, 6′, ($\underline{C}H_3CO_2$–)$_2$, 16(t), NMe_2(q), 14(d), ($CH_3\underline{C}H_2O$–)$_2$ (t, each), 23, 5, 1′, 20(d), 10, 12, 13, 11, 1, ($CH_3\underline{C}O_2$–)$_2$, 9(s) (see Table 2) were assigned on the basis of the comparison of the shift-values with those of **4** as well as by the off-resonance. The carbons ranging between 30—45 ppm (C-2, 4, 6, 7, 8, 14, and 19) could be classified into two groups of methylene (C-2, 7, 19) and methine (C-4, 6, 8, 14) by the method of off-resonance. By the proton irradiation at δ 1.3, C-2(d) could be distinguished from C-7(s) and 19(s). By the H-14(16 and 22) proton irradiation, C-4(s) and C-6 (narrow d) could be distinguished from C-8 and 14. The above assignments were also confirmed by the proton irradiations of H-6 and of 14(8 and 4′). By the latter irradiation, also, assignments of carbons (between 70—76 ppm) of 4′(s), 5′(very narrow d), 2′(narrow d), 3′(d), 15 and 3(wide d, each) were made. The above assignments were substantiated by the observation that the $^1J_{C-H}$ values in question came roughly in the range of similar magnitudes (by gated decoupling method). Carbon-3 was decided by the H-3 proton irradiation.

3,23-Di-O-acetylmycaminosyltylonolide (4). A solution of **3** (100 mg) in a mixture of acetonitrile (2 ml) and 0.1 M aqueous hydrochloric acid (2 ml) was kept at room temperature for 1 h. After addition of sodium hydrogencarbonate (34 mg) and water (4 ml), the reaction mixture was extracted with chloroform. The crude product obtained was purified by chromatography on a short column of silica gel with chloroform–methanol (7 : 1) to give an amorphous solid of **4**, 86 mg (96%), $[\alpha]_D^{25}$ +19° (c 0.7, chloroform).

Found: C, 61.83; H, 8.35; N, 2.32%. Calcd for $C_{35}H_{55}NO_{12}$: C, 61.66; H, 8.13; N, 2.05%.

^{1}H-NMR (in $CDCl_3$ at 250 MHz): δ 0.94 [3H t, Me(17)], 1.09 [3H d, Me(18)], 1.23 [3H d, Me(21)], 1.27 [3H d, Me(6′)], 1.83 [3H s, Me(22)], 1.78—1.92 (H-4, 16b), 2.05 (3H s, 23-*O*-Ac), 2.15 (3H s, 3-*O*-Ac), 2.35 (1H t, H-3′), 2.50 (6H s, NMe_2), 2.64 (1H dd, H-2), 2.98—3.1 (H-14), 3.07 (1H t, H-4′), 3.27 (1H dd, H-5′), 3.48 (1H dd, H-2′), 3.57 (1H d, H-5), 4.09 (1H dd, H-23a), 4.16 (1H dd, H-23b), 4.21 (1H d, H-1′), 4.82 (1H ddd, H-15), 5.18 (1H unresolved d, $J\simeq$10 Hz, H-3), 5.90 (1H d, H-13), 6.30 (1H d, H-10), 7.43 (1H d, H-11), 9.65 (1H s, CHO). Above assignments were confirmed by the decoupling method.

^{13}C-NMR (in $CDCl_3$ at 20 °C). Carbon-17, 18, 22, 21, 6′, ($\underline{C}H_3CO_2$–)$_2$ (q, each), 16(t), 6, 7, 2(t), 8(d), NMe_2, 19(t), 23(t), 3(d), 5′, 15, 5, 1′, 10, 12, 13, 11, 1, ($CH_3\underline{C}O_2$–)$_2$ (s, each), 20(d), 9(s) (see Table 2.) were assigned on the basis of the comparison of the shift-values with those of **1** as well as by the off-resonance method. Carbon-15 was confirmed by the H-15 proton irradiation. Distinction between C-4 and -14 was performed by the H-14 proton irradiation. Distinction between C-2′, 3′, and 4′ was performed by the H-4′ proton irradiation, whereupon C-4′ appeared as a singlet, and C-2′ and 3′ as a doublet, respectively, but the peak space of the latter doublet was wider than that of the former one (see the similar statement of ^{13}C-NMR of **3**). Since $^1J_{C2'-H2'}$ and $^1J_{C3'-H3'}$ were observed to be almost equal (by the gated decoupling technique), assignments of C-2′ and 3′ by the above space-method will be resonable.

3-O-Acetylmycaminosyltylonolide (5). An aqueous solution (3.5 ml) of **3** (69 mg) and *p*-toluenesulfonic acid monohydrate (26 mg) was kept at 65 °C for 20 h. After addition of sodium hydrogencarbonate (20 mg), the reaction mixture was extracted with chloroform. The crude product obtained showed, on TLC with chloroform–methanol-28% aqueous ammonia (10 : 1 : 0.1), three spots of R_f 0.4 (slight **3**), 0.3 (major, **5**), and 0.22 (slight, 23-*O*-acetyl derivative?). Silica-gel column chromatography with chloroform–methanol–28% aqueous ammonia (20 : 1 : 0.1) gave an amorphous solid of **5**, 30 mg (51%), $[\alpha]_D^{18}$ +15° (c 1, chloroform).

Found: C, 62.17; H, 8.46; N, 2.18%. Calcd for $C_{33}H_{53}NO_{11}$: C, 61.95; H, 8.35; N, 2.19%.

^{1}H-NMR (in $CDCl_3$ at 250 MHz): δ 1.85 [3H s, Me(22)], 2.15 (3H s, 3-*O*-Ac), 2.50 (6H s, NMe_2), 3.66 (1H dd, $J_{14,23a}$ 7 Hz, $J_{23a,23b}$ 11.5 Hz, H-23a), 3.73 (1H dd, $J_{14,23b}$ 5 Hz, H-23b), 4.21 (1H d, H-1′), 4.80 (1H m, H-15), 5.20 (1H unresolved d, $J\simeq$11 Hz, H-3), 5.93 (1H d, H-13), 6.29 (1H d, H-10), 7.41 (1H d, H-11), 9.65 (1H s, CHO).

Irradiation at δ 2.93 (H-14) collapsed the signals of H-23a, 23b to an AB quartet, and the doublet of H-13 to a singlet.

(9R)-9-Deoxo-9-hydroxy- (6) and (9S)-9-Deoxo-9-hydroxymycaminosyltylonolide Diethyl Acetal (7). To an ice-cold solution of **2** (567 mg) in methanol (5.7 ml) was added sodium borohydride (96 mg) and the solution was kept in the cold for 3 h. On TLC with chloroform–methanol–28% aqueous ammonia (12 : 1 : 0.1), the reaction mixture showed spots of R_f 0.37 (**6**), 0.33 (**7**) (the color-intense was equal), and 0.3 (very slight), the spot of **2** (R_f 0.4) being disappeared. After concentration, the residue was extracted with chloroform and the solution was washed with water, dried, and concentrated. Column chromatography of the residue with chloroform–methanol–28% aqueous ammonia (15 : 1 : 0.1) gave amorphous solids of **6** (73 mg, 13%), **7** (86 mg, 15%) and the mixture of the two (383 mg, 67%).

6: $[\alpha]_D$ +38° (c 1, chloroform); UV λ_{max} (MeOH) 237 nm (log ε 4.57).

Found: C, 62.11; H, 9.20; N, 2.08%. Calcd for $C_{35}H_{63}NO_{11}$: C, 62.38; H, 9.42; N, 2.08%.

^{1}H-NMR (in $CDCl_3$ at 250 MHz): δ 1.78 [3H s, Me(22)], 2.51 (6H s, NMe_2), 4.28 (1H broadened d; at 50 °C: sharp dd, $J_{8,9}$ 2.5 Hz, $J_{9,10}$ 8.0 Hz, H-9), 4.34 (1H d, H-1′), 4.65 (1H unresolved m; at 50°C, sharp dd, J 4 and 6.5 Hz, H-20), 4.89 (1H dt, H-15), 5.24 (1H d, J 10 Hz, H-13), 5.76 (1H dd, $J_{10,11}$ 15.5 Hz, H-10), 6.15 [1H br ($\simeq$6.0—6.3) s; at 50 °C, sharp d, J 15.5 Hz, H-11].

Irradiation (at 50 °C) of H-10 collapsed the signals of H-9

and H-11 to a small doublet, and a singlet, respectively. Irradiation (at 50 °C) at δ 1.9 (H-8) collapsed the double doublets of H-9 to a doublet (J 8 Hz).

7: $[\alpha]_D^{25}$ +37° (*c* 1, chloroform); UV λ_{max} (MeOH) 237 nm (log ε 4.41).

Found: C, 62.56; H, 9.27; N, 2.16%.

^{1}H-NMR (in $CDCl_3$ at 250 MHz): δ 1.78 (3H s, Me(22)), 2.51 (6H s, NMe_2), 4.32 (1H d, H-1′), 4.61 (H-20), 4.90 (H-15), 5.29 (1H d, J 10 Hz, H-13), 5.95 (1H br ($\simeq$5.85—6.1) s; at 50 °C: sharp dd, $J_{9,10}$ 4.5 Hz, $J_{10,11}$ 15.5 Hz, H-10), 6.47 (1H d, H-11). Signals of H-1′, -20, -15, -13, and -11 slightly sharpened at 50 °C.

Irradiation (at 50 °C) of H-10 collapsed the doublet of H-11 to a singlet. Irradiation (at 50 °C) at δ 3.92 (H-9) collapsed the double doublets of H-10 to a doublet.

*9-Deoxo-9(R)-hydroxy- (**8**) and 9-Deoxo-9(S)-hydroxy-mycaminosyltylonolide (**9**).* To a solution of **6** or **8** (40 mg, 0.06 mmol) in acetonitrile (1.2 ml) was added 0.1 M aqueous hydrochloric acid (1.2 ml) and the solution was kept at room temperature for 1 h. After addition of aqueous saturated sodium hydrogencarbonate (1.2 ml), the mixture was extracted with chloroform. The organic solution was washed thoroughly with water, dried over sodium sulfate, and concentrated. The residue was chromatographed on a short column of silica gel with chloroform–methanol–28% aqueous ammonia (10 : 1 : 0.1) to remove the slightly remained starting material to give an amorphous solid of **8** (30.5 mg, 86%) or **9** (31.5 mg, 88%).

8: $[\alpha]_D^{25}$ +44° (*c* 0.5, chloroform). ^{1}H-NMR ($CDCl_3$): δ 4.23 (1H dd, $J_{8,9}$ $\simeq$2 Hz, $J_{9,10}$ 8 Hz, H-9), 4.94 (1H dt, H-15), 5.33 (1H d, $J_{13,14}$ 10 Hz, H-13), 5.78 (1H dd, H-10), 6.25 (1H d, $J_{10,11}$ 16 Hz, H-11), 9.86 (1H s, H-20).

Found: C, 62.28; H, 9.01; N, 2.26%. Calcd for $C_{31}H_{53}NO_{10}$: C, 62.08; H, 8.91; N, 2.34%.

9: $[\alpha]_D^{25}$ +34° (*c* 0.5, chloroform). ^{1}H-NMR ($CDCl_3$): δ 4.95 (1H dt, H-15), 5.37 (1H d, H-13), 5.96 (1H dd, $J_{9,10}$ 4 Hz, $J_{10,11}$ 16 Hz, H-10), 6.57 (1H d, H-11), 9.80 (1H s, H-20).

Found: C, 61.99; H, 8.86; N, 2.24%. Calcd for $C_{31}H_{53}NO_{10}$: C, 62.08; H, 8.91; N, 2.34%.

*Basic Hydrolysis of the Mixture of **6** and **7** (to Give **10** and **11**).* To a solution of a mixture of **6** and **7** (4.95 g) in methanol (92 ml) was added 0.4 M aqueous sodium hydroxide (92 ml) and the mixture was heated at 50 °C for 5 h. Addition of 1 M aqueous hydrochloric acid (37 ml) followed by concentration to $\approx$80 ml gave precipitates of sodium chloride, which was filtered and washed with methanol. The filtrate and the washings combined were concentrated, filtered from sodium chloride further precipitated, and the concentrate was chromatographed on a column of Sephadex LH-20 (pretreated with methanol) with methanol to give a mixture of sodium chloride-free products (**10**, **11**), 4.56 g (91%).

*Esterification of **10** and **11** (to Give **12** and **13**).* To a solution of a mixture of **10** and **11** (142 mg) in dry tetrahydrofuran (1.4 ml) was added bis(4-*t*-butyl-1-isopropyl-2-imidazolyl) disulfide (124 mg) and triphenylphosphine (82 mg) under argon atmosphere and the mixture was kept at room temperature for 5 min. Methanol (14 ml) was added and the solution was kept overnight at room temperature. The products obtained were chromatographed with chloroform–methanol–28% aqueous ammonia (9 : 1 : 0.1) to give a mixture of **12** and **13**, 78.5 mg (53%). The mixture was further chromatographed (8 g of silica gel) in a similar manner to give **11** (R_f 0.32 on TLC with chloroform–methanol–28% aqueous ammonia = 10 : 1 : 0.1), 10.9 mg, and **12** (R_f 0.28), 15.4 mg, and the mixture of the two.

11: $[\alpha]_D^{21}$ −4° (*c* 0.5, chloroform); *m/e* 705 (M^+), 659. Found: C, 61.08; H, 9.41; N, 2.00%. Calcd for $C_{36}H_{67}NO_{12}$: C, 61.25; H, 9.57; N, 1.98%.

^{1}H-NMR ($CDCl_3$): δ 3.72 (3H s, CO_2Me).

12: $[\alpha]_D^{21}$ −10° (*c* 0.5, chloroform): *m/e* 659. Found: C, 61.16; H, 9.34; N, 2.13%.

^{1}H-NMR ($CDCl_3$): δ 3.72 (3H s, CO_2Me).

*Cyclization of **10** and **11** (to Give **14** and **15**).* *Method A*: To a solution of a mixture of **10** and **11** (30.6 mg, 0.044 mmol) in dry tetrahydrofuran (0.6 ml) was added, under argon atmosphere, 2,2′-dipyridyl disulfide (14.6 mg, 0.066 mmol) and triphenylphosphine (17.4 mg, 0.063 mmol) and the mixture was kept at room temperature for 30 min. Concentration gave a residue, which was dissolved in dry toluene (16 ml) and the solution was heated at 80 °C for 24 h. The reaction mixture showed, on TLC, two spots of R_f 0.25 (**14**) and 0.28 (**15**) (with 10 : 1 : 0.1 chloroform–methanol–28% aqueous ammonia) accompanied by tailing zones of R_f 0—0.18 and 0.34—0.45. The solution was concentrated and the residue was dissolved in chloroform. The solution was washed with water, dried over sodium sulfate, and concentrated. The residue was chromatographed on a silica-gel column (6 g) with chloroform–methanol–28% aqueous ammonia (12 : 1 : 0.1) to give a mixture of **14** and **15**, 5.1 mg (17%).

Method B: To a solution of a mixture of **10** and **11** (4.56 g, 6.59 mmol) in dry tetrahydrofuran (90 ml) was added bis-(4-*t*-butyl-1-isopropyl-2-imidazolyl) disulfide (3.91 g, 9.88 mmol) and triphenylphosphine (2.60 g, 9.88 mmol) under arogon atmosphere and the mixture was kept at room temperature for 5 min. The reaction mixture showed, on TLC with 6 : 1 chloroform–methanol, spots of R_f 0.3 (active ester) and 0 (hydrolyzed products of the active esters?). Concentration gave a residue, which was dissolved in toluene (1140 ml) and the solution was heated at 80 °C for 24 h. The TLC pattern of the reaction mixture was substantially the same with that obtained by "Method A". Similar work-up as described in "Method A" gave an amorphous powder, which was chromatographed on a silica-gel column (Wakogel C-200, 450 g) with chloroform–methanol–28% ammonia (10 : 1 : 0.1) to give **14** (0.52 g, 11.7%), **15** (0.52 g, 11.7%), and a mixture of **14** and **15** (0.10 g, 2.3%).

14: $[\alpha]_D^{25}$ −6° (*c* 0.5, chloroform): UV λ_{max} (MeOH) 236 nm (log ε 4.26); IR(KBr): 1640, 1730 cm^{-1}.

Found: C, 62.44; H, 9.19; N, 2.18%. Calcd for $C_{35}H_{63}NO_{11}$: C, 62.38; H, 9.42; N, 2.08%.

^{1}H-NMR (in $CDCl_3$ at 250 MHz): 0.96 [3H d, Me(19 or 16)], 0.98 [3H t, Me(23)], 1.13 [3H d, Me(16 or 19)], 1.19 and 1.21 [each 3H t, $OCH_2C\underline{H}_3)_2$], 1.32 [3H d, Me(6′)], 1.78 [3H d, $J\simeq$1 Hz, Me(20)], 2.26 (1H dd, $J_{2a,2b}$ 14 Hz, $J_{2a,3}$ 4 Hz, H-2a), 2.37 (1H dd, $J_{2b,3}$ 7.5 Hz, H-2b), 2.38 (1H t, H-3′), 2.50 (6H s, NMe_2), 3.02 (1H t, H-4′), 3.19 (1H m, H-14), 3.35 (1H dd, H-5′), 4.2 (1H t, $J_{14,15a}=J_{15a,15b}$ 10.5 Hz, H-15a), 4.29 (1H dd, $J_{14,15b}$ 6 Hz, H-15_b), 4.32 (1H d, J 7.5 Hz, H-1′), 4.62 (1H unresolved t, H-18), 5.38 (1H slightly br d, $J_{13,14}$ 10 Hz, H-13), 5.55 (1H dd, $J_{9,10}$ 9 Hz, $J_{10,11}$ 15 Hz, H-10), 6.18 (1H sharp d, H-11).

Irradiation of H-14 caused the signals of H-15a, -15b to collapse to an AB quartet, the doublet of H-13 to a singlet. Irradiation at δ 3.58 (includes H-9) collapsed the signals of H-10 to a doublet. Irradiation at δ 1.45 [includes H-22 and -4(or 8)] collapsed the triplet of Me(23) and the doublet at δ 1.13 to singlets. Irradiation at δ 1.67 (H-8 or 4) collapsed the doublet at δ 0.96 to a singlet. Irradiation of H-5′ collapsed the doublet of Me(6′) and the triplet of H-4′ to a singlet and a doublet, respectively.

15: $[\alpha]_D^{25}$ −4° (*c* 0.5, chloroform); UV λ_{max} (MeOH)

236 nm (log ε 4.23); IR(KBr): 1640, 1730 cm^{-1}.

Found: C, 62.07; H, 9.20; N, 2.07%. Calcd for $C_{35}H_{63}NO_{11}$: C, 62.38; H, 9.42; H, 2.08%.

^{1}H-NMR (in $CDCl_3$ at 250 MHz): δ 0.94 [3H d, Me(19 or 16)], 0.98 [3H t, Me(23)], 1.18 [3H d, Me(16 or 19)], 1.18 and 1.19 [each 3H t, $(OCH_2C\underline{H}_3)_2$], 1.31 [3H d, Me(6')], 1.76 [3H d, $J\simeq1$ Hz, Me(20)], 2.21 (1H dd, $J_{2a,2b}$ 14 Hz, $J_{2a,3}$ 4 Hz, H-2a), 2.34 (1H dd, $J_{2b,3}$ 9.5 Hz, H-2b), 2.38 (1H t, H-3'), 2.50 (6H s, NMe_2), 3.01 (1H t, H-4'), 3.29 (1H m, H-14), 3.34 (1H dd, H-5'), 4.07 (1H t, $J_{14,15a}=J_{15a,15b}$ 10.5 Hz, H-15), 4.29 (1H d, H-1'), 4.37 (1H ,H-9), 4.38 (1H dd, $J_{14,15b}$ 6 Hz, H-15b), 4.61 (1H dd, J 4 and 7.5 Hz, H-18), 5.35 (1H slightly br d, $J_{13,14}$ 10 Hz, H-13), 5.67 (1H dd, $J_{9,10}$ 3.5 Hz, $J_{10,11}$ 15.5 Hz, H-10), 6.34 (1H dd, $J_{9,11}\simeq1.5$ Hz, H-11).

Irradiation of H-14 caused the signals of H-15a and -15b to collapse to two doublets, and the doublet of H-13 to a singlet. Irradiation of H-9 collapsed the double doublets of H-10 and those of H-11 to a doublet, respectively, to form an AB quartet.

Deacetalation of ***14*** *(to Give* ***16****).* To a solution of **14** (46.6 mg) in acetonitrile (1.4 ml) was added gradually 0.1 M aqueous hydrochloric acid (1.4 ml) and the mixture was kept at room temperature for 1 h. After addition of aqueous saturated sodium hydrogencarbonate (1.5 ml), the mixture was extracted with chloroform. The chloroform-soluble products were chromatographed with silica gel with chloroform–methanol–28% aqueous ammonia (9 : 1 : 0.1) to give an amorphous solid of **16**, 32.3 mg (78%), $[\alpha]_D^{25}$ −12° (*c* 0.5, chloroform), UV λ_{max} (MeOH) 236 nm (log ε 4.34).

Found: C, 61.83; H, 8.81; N, 2.07%. Calcd for $C_{31}H_{53}NO_{10}$: C, 62.08; H, 8.91; N, 2.34%.

^{1}H-NMR ($CDCl_3$): δ 5.43 (1H d, H-13), 5.50 (1H dd, H-10), 6.21 (1H d, H-11), 9.81 (1H s, –CHO); $J_{9,10}$ 9, $J_{10,11}$ 16, $J_{13,14}$ 10 Hz.

Oxidation of ***15*** *(to Give* ***18****).* To an ice-cold solution of **15** (73.1 mg) in tetrahydrofuran (1.5 ml) was added DDQ (49.3 mg) and the solution was kept at room temperature for 1 h. The solution showed, on TLC with chloroform–methanol–28% aqueous ammonia (10 : 1 : 0.1), spots of R_f 0.4 (**18**), 0.33 (**15**), 0.1 and 0. Concentration gave a residue which was charged on a silica-gel column (7 g) and the column was washed with ethyl acetate (350 ml). DDQ and the reduced compound of DDQ were eluted. The developing solvent was then changed to chloroform–methanol–28% aqueous ammonia (12 : 1 : 0.1) to elute **18** to give a pale-brown solid (59.5 mg). The methanol solution of the solid was decolorized with charcoal and, after evaporation, the residue was chromatographed with chloroform–methanol–28% aqueous ammonia (15 : 1 : 0.1) to give a colorless solid of **18**, 34.4 mg (47%); recrystallization from acetone–hexane gave plates, mp 165—168 °C, $[\alpha]_D^{18}$ +16° (*c* 0.5, chloroform); UV λ_{max} (MeOH) 284 nm (log ε 4.32); IR(KBr): 1590, 1680, 1730 cm^{-1}; *m/e* 671 (M^+).

Found: C, 61.56; H, 9.06; N, 2.01%. Calcd for $C_{35}H_{61}NO_{11}\cdot1/2\ H_2O$: C, 61.74; H, 9.18; N, 2.06%.

^{1}H-NMR (in $CDCl_3$ at 250 MHz): δ 1.83 (3H d, $J\simeq1$ Hz, Me(20)], 2.50 (6H s, NMe_2), 4.18 (1H t, H-15a), 4.30 (1H d, H-1'), 4.46 (1H dd, H-15b), 4.66 (1H m, H-18), 5.85 (1H d, H-13), 6.35 (1H d, H-10), 7.17 (1H d, H-11); $J_{10,11}$ 15, $J_{13,14}$ 11, $J_{14,15a}$ 10, $J_{14,15b}$ 6.5, $J_{15a,15b}$ 10 Hz.

Deacetalation of ***18*** *(to Give* ***19****).* Compound **18** was treated similarly as described for **16** to give crude **19** in *ca.* 80% yield (the purity was estimated to be *ca.* 90%). Repeated column-chromatography gave no pure product. On TLC with chloroform–methanol–28% aqueous ammonia (10 : 1 : 0.1), it gave the spots of R_f 0.3 (**19**) and 0.24 (slight).

^{1}H-NMR (in $CDCl_3$ at 250 MHz; peaks for **19** were only cited): δ 4.24 (1H d, H-1'), 4.27 (1H dd, H-15b), 4.48 (1H t, H-15a), 5.88 (1H d, H-13), 6.21 (1H d, H-10), 7.18 (1H d, H-11), 9.80 (1H s, –CHO); $J_{10,11}$ 15.5, $J_{13,14}$ 10.5, $J_{14,15a}$ 10, $J_{14,15b}$ 6, $J_{15a,15b}$ 10 Hz.

*3,21,2',4'-Tetra-*O*-acetyl Derivative (***20***) of* ***18****.* A solution of **18** (82.9 mg) in pyridine (0.8 ml) containing acetic anhydride (0.21 ml) was kept at 50 °C for 2 d. Usual work-up gave amorphous solid of **20**, 92 mg (89%), $[\alpha]_D^{22}$ +65° (*c* 1, chloroform).

Found: C, 61.72; H, 8.12; N, 1.75%. Calcd for $C_{43}H_{69}NO_{15}$: C, 61.48; H, 8.28; N, 1.67%.

^{1}H-NMR ($CDCl_3$): δ 1.90, 2.05, 2.10 and 2.15 (each 3H s, Ac).

*3,21-Di-*O*-acetyl Derivative (***21***) of* ***18****.* A methanol solution (2.0 ml) of **20** (41.6 mg) was kept at 50 °C overnight. Evaporation gave a residue, which was chromatographed on a silica-gel column with chloroform–methanol–28% aqueous ammonia (25 : 1 : 0.1) to give an amorphous solid, 37.2 mg (99%), $[\alpha]_D^{23}$ +61° (*c* 1, chloroform): TLC: R_f 0.32 (*cf.* **17**: R_f 1) (20 : 1 : 0.1 chloroform–methanol–28% aqueous ammonia).

Found: C, 61.68; H, 8.50; N, 1.76%. Calcd for $C_{39}H_{65}NO_{13}$: C, 61.97; H, 8.64; N, 1.85%.

^{1}H-NMR (in $CDCl_3$ at 250 MHz): δ 0.89 (3H t, H-23), 1.10 [3H d, J 7 Hz, Me(16)], 1.11—1.24 [9H, Me(19) and $(OCH_2C\underline{H}_3)_2$], 1.31 [3H d, Me(6')], 1.57 (2H m, H-22), 1.92 [3H very narrow m, Me(20)], 2.04 and 2.11 (each 3H s, 3- and 21-*O*-Ac), 2.37 (1H t, J 10 Hz, H-3'), 2.51 (6H s, NMe_2), 3.04 (1H t, $J\simeq10$ Hz, H-4'), 3.12 (1H m, H-14), 3.30 (1H m, H-5'), 3.55 (1H dd, H-2'), 3.94 (1H dd, $J_{14,15a}$ 5 Hz, $J_{15a,15b}$ 10.5 Hz, H-15a), 4.29 (1H d, $J_{1',2'}$ 7.5 Hz, H-1'), 4.48 (1H t, J 10 Hz, H-15b), 4.59 (1H dd, J 3.7 and 7.5 Hz, H-18), 4.86 (1H br m, H-3), 4.96 (1H m, H-21), 5.77 (1H slightly br d, $J_{13,14}$ 10 Hz, H-13), 6.40 (1H sharp d, $J_{10,11}$ 15.5 Hz, H-10), 7.16 (1H slightly br d, H-11).

Irradiation of H-14 collapsed the doublet of H-13 to a singlet, the quartet of H-15a and the triplet of H-15b to an AB quartet in total, and the multiplet of H-21 to a quartet. Irradiation at δ 1.57 (H-22a,b) collapsed the triplet of H-23 to a singlet.

Deacetalation of ***21*** *(to Give* ***22****).* Treatment of **21** similarly as described for **16** gave an amorphous solid of **22** in 79% yield, $[\alpha]_D^{22}$ +61° (*c* 1, chloroform).

Found: C, 61.67; H, 8.12; N, 1.98%. Calcd for $C_{35}H_{55}NO_{12}$: C, 61.66; H, 8.13; N, 2.05%.

We are grateful to Professor Hamao Umezawa of Institute of Microbial Chemistry for his support and encouragement. We also wish to thank Mr. Saburo Nakada, Department of Applied Chemistry, Keio University, for the microanalysis, and Dr. Masa Hamada of Institute of Microbial Chemistry, for the bioassay. Thanks are also due to Miss Miyako Igarashi of our Institute for her helpful assistance to make the manuscript.

References

1) R. B. Morin and M. Gorman, *Tetrahedron Lett.*, **1964** 2339.

2) J. M. McGuire, W. S. Boniece, C. E. Higgens, M. M. Hoehn, W. M. Stark, J. Westhead, and R. N. Wolfe, *Antibiot. Chemoth.* **11**, 320 (1961).

3) S. Ōmura, M. Katagiri, H. Ogura, and T. Hata, *Chem.*

Pharm. Bull., **16**, 1181 (1968).
4) T. Osono, Y. Oka, S. Watanabe, Y. Numazaki, K. Moriyama, H. Ishida, K. Suzaki, Y. Okami, and H. Umezawa, *J. Antibiot.*, **20**(A), 173 (1967).
5) S. Rakhit and K. Singh, *J. Antibiot.*, **27**, 221 (1974).
6) S. Masamune, Y. Hayase, W. K. Chan, and R. L. Sobczak, *J. Am. Chem. Soc.*, **98**, 7874 (1976).
7) L. A. Freiberg, R. S. Egan, and W. H. Washburn, *J. Org. Chem.*, **39**, 2474 (1974).
8) E. J. Corey and K. C. Nicolaou, *J. Am. Chem. Soc.*, **96**, 5614 (1974).
9) T. Mukaiyama, R. Matsueda, and M. Suzuki, *Tetrahedron Lett.*, **1970**, 1901; T. Mukaiyama, T. Matsueda, and H. Maruyama, *Bull. Chem. Soc. Jpn.*, **43**, 1271 (1970).
10) E. J. Corey and D. H. Brunelle, *Tetrahedron Lett.*, **1976**. 3409.
11) S. Masamune, S. Kamata, J. Diakur, Y. Sugihara, and G. S. Bates, *Can. J. Chem.*, **53**, 3693 (1975).
12) S. Ōmura, M. Katagiri, H. Ogura, and T. Hata, *Chem. Pharm. Bull.*, **16**, 1181 (1968).
13) A. Nakagawa, K. Suzuki, K. Iwasaki, K. Kaji, S. Ōmura, A. Jakubowski, and M. Tishler, *Chem. Pharm. Bull.*, **24**, 1749 (1976).
14) E. J. Corey and J. W. Suggs, *Tetrahedron Lett.*, **1975**, 2647; E. J. Corey and G. Schmidt, *ibid.*, **1979**, 399.
15) K. Tatsuta, Y. Amemiya, S. Maniwa, and M. Kinoshita, *Tetrahedron Lett.*, **1980**, 2837.
16) D. Walker and J. D. Hiebert, *Chem. Rev.*, **67**, 153 (1967).
17) E. A. Braude, R. P. Linstead and K. R. Wooldridge, *J. Chem. Soc.*, **1956**, 3070.
18) A. A. Nagel and L. A. Vincent, *J. Org. Chem.*, **44**, 2050 (1979).
19) S. Ōmura, A. Nakagawa, A. Neszmélyi, S. D. Gero, A-M. Sepulchre, F. Piriou, and G. Lukacs, *J. Am. Chem. Soc.*, **97**, 4001 (1975).

Studies on the Behavior of Natural Surfactant at the Oil-Water Interface. II. Behavior of Natural Surfactant at the Oil-Water Interface

Keizo OGINO,* Hitoshi YAMAUCHI, and Yoshinori UENO

Faculty of Science and Technology, Science University of Tokyo, Yamazaki Noda, Chiba 278

(Received January 20, 1981)

The behavior of natural surfactants was studied at an oil-water interface by measurement of the interfacial tension and the observation of the oil-water interface. Lecithin was used as an oil-soluble substance and sodium cholate was used as a water-soluble substance; *n*-paraffin, corn oil, unsaturated fatty acid and fatty alcohol were used as an oil phase. The reduction of interfacial tension was greatest in a dodecane–sodium cholate solution system, but the minimum interfacial tension was observed in an oleic acid–sodium cholate solution system. Spontaneous emulsification occurred in the oil phase when oleic acid was left in contact with sodium cholate solution. The most remarkable change was found in the system of oleic acid in contact with sodium cholate solution, in which crystal of cholic acid were formed at the interface.

At the oil-water inferface, various interfacial phenomena occur when the oil containing oil-soluble substance is allowed to contact the water containing water-soluble substance. Manabe and Okuyama[1] have reported that there are many natural surfactants, especially in living body.

We have studied the molecular interactions at the interface of oil/water systems with various kinds of additives with respect to the tendency of spontaneous emulsification,[2-4] and the behavior of natural surfactants, lecithin and cholesterol, at the oil-water interface.[5]

In this work, lecithin and sodium cholate were used as oil-soluble and water-soluble natural surfactants, respectively. Lecithin is an important constituent of biological membranes and has been used widely in field such as the food industry as an excellent emulsifier.[6-8] Sodium cholate to be used is one of the bile salts. Bile salts are necessary for absorption of oil-soluble vitamins such as Vitamin A, D, E, and K.[9-11] Further, it is known that cholesterol is solubilized by a lecithin-bile salt micelle.[12]

In the present investigation, the behavior of natural surfactants at the oil-water interface was studied by the measurements of interfacial tension; the interfacial products were observed by a polarizing microscope.

Experimental

Materials. *Natural Surfactants*: Lecithin from soybean, the so-called asolecithin (Associated Concentrates Inc.) of commercial grade containing 95—98% lipid, was used. Sodium cholate (Tokyo Kasei Ind. Ltd.) of reagent grade was used without further purification.

Oil Phase: Dodecane (Nikko petrochemical Co.), Corn oil (Ajinomoto Co.), *cis*-9-octadecenoic acid (oleic acid) and *cis*-9-octadecen-1-ol (oleyl alcohol) (Tokyo Kasei Co.) of a commercial grade were used without purification.

Water Phase: Double distilled and deionized water with an indicated resistivity of 18.0 megohm/cm was used.

Apparatus. The interfacial tension was measured by a Wilhelmy-type surface-tensiometer (Shimadzu Surface Tensiometer ST-1) and interfacial products were observed by a polarizing microscope with crossed nicols (Nippon Kogaku S-PO).

Procedure. Lecithin and sodium cholate were dissolved in oil and water, respectively, and the interfacial tension was measured at various concentrations of the solutes at 30 °C. These measurements were made 30, 50, and 15 min after the contact of oil and water phases in the case of dodecane and *cis*-9-octadecenoic acid, corn oil and *cis*-9-octadecen-1-ol, respectively. It was confirmed that the equilibria at these interfaces were reached after the times mentioned above.

Results and Discussion

The Lowering of Interfacial Tension. Figure 1 shows the effect of concentration of sodium cholate on the interfacial tension at the oil-water interface. As is shown, the interfacial tension decreased with increasing concentration of sodium cholate. In particular, the reduction of interfacial tension was the greatest in dodecane–sodium cholate solution system, but the minimum interfacial tension was observed in *cis*-9-octadecenoic acid–sodium cholate solution system, being about 1.7 dyn†/cm at higher concentration of sodium cholate. The interfacial tension of *cis*-9-octadecenoic acid–sodium cholate solution system was lower than *cis*-9-octadecen-1-ol. This may be due to a stronger

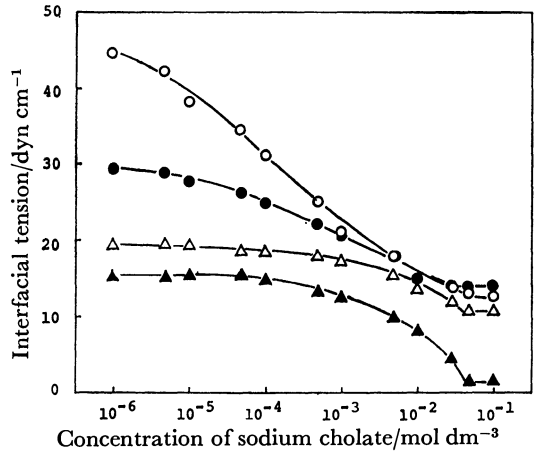

Fig. 1. The effect of sodium cholate on the interfacial tention of oil-water interface.
○: Dodecane, ●: corn oil, △: *cis*-9-octadecen-1-ol, ▲: *cis*-9-octadecenoic acid.

† Throughout this paper 1 dyn = 10^{-5} N.

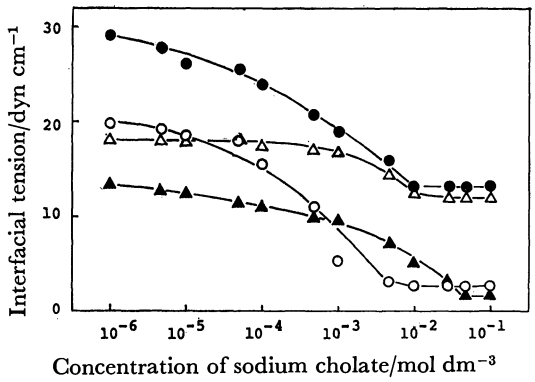

Fig. 2. The effect of sodium cholate on the interfacial tention of oil containing lecithin (2×10^{-3} wt%)-water interface.
○: Dodecane, ●: corn oil, △: *cis*-9-octadecen-1-ol, ▲: *cis*-9-octadecenoic acid.

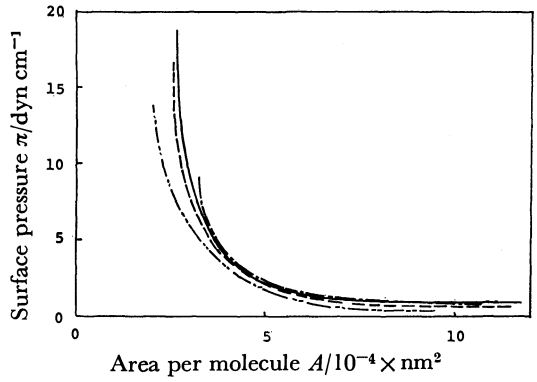

Fig. 3. π-A curves for various oils.
——: Dodecane, ------: corn oil, –·–: *cis*-9-octadecen-1-ol, –···–: *cis*-9-octadecenoic acid.

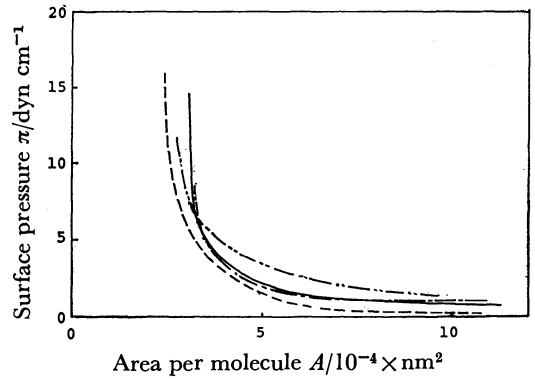

Fig. 4. π-A curves for various oils containing lecithin (2×10^{-3} wt%).
——: Dodecane, ------: corn oil, –·–: *cis*-9-octadecen-1-ol, –···–: *cis*-9-octadecenoic acid.

interaction between the carboxyl group of *cis*-9-octadecenoic acid and cholate ions than between *cis*-9-octadecen-1-ol and cholate ions.

Figure 2 shows the effect of the concentration of sodium cholate on the interfacial tension at the oil (containing 2×10^{-3} wt% lecithin)-water interface. As can be seen, the interfacial tension showed similar results to that of Fig. 1 except for dodecane, the interfacial tension of which was considerably lowered by the addition of a low concentration of lecithin. From the results, it was confirmed that lecithin affected most strongly the interfacial tension of dodecane–water.

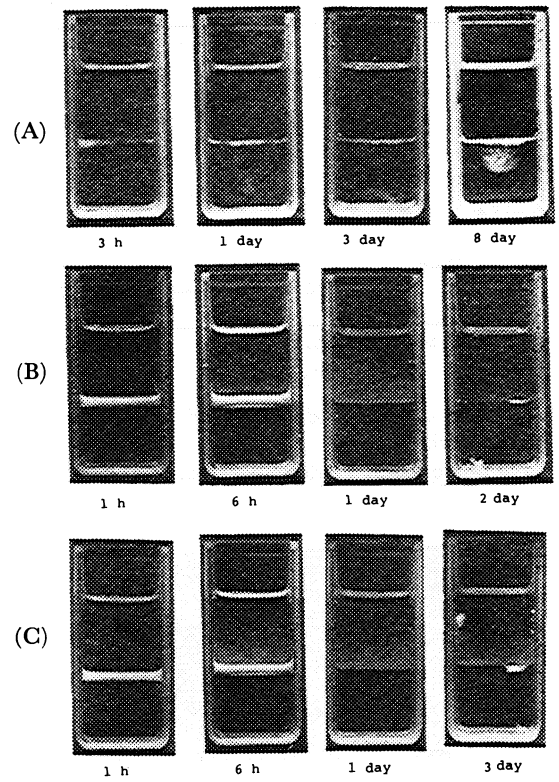

Fig. 5. The progress of spontaneous emulsification with time.
Water phase: sodium cholate 1×10^{-1} mol dm^{-3}.
Oil phase: (A) corn oil+lecithin 5×10^{-2} wt%. (B) *cis*-9-octadecenoic acid. (C) *cis*-9-octadecenoic acid+lecithin 1×10^{-2} wt%.

Figures 3 and 4 show the surface pressure (π)-area (A) curves calculated from Figs. 1 and 2 using the Gibbs equation. It is evident that the area is greatly decreased with increasing cholate ions at low surface pressure. This means that the molecules are tightly packed at higher surface pressure, the compressibility of the film being small.

Spontaneous Emulsification and Interfacial Product. Figure 5 shows the state when oils were left to stand in contact with sodium cholate solution. When corn oil containing lecithin was left in contact with aqueous solution, spontaneous emulsification occurred in the water phase.[5] However, no distinct change was recognized by the use of corn oil without lecithin. Further, the spontaneous emulsification was also observed when corn oil containing lecithin was left in contact with distilled water. From these results, it is found that lecithin affects the spontaneous emulsification when corn oil is used as the oil phase.

On the contrary, spontaneous emulsification occurred in the oil phase and the crystals were deposited at the oil-water interface when *cis*-9-octadecenoic acid was left in contact with sodium cholate solution. A similar change was also observed when *cis*-9-octadecenoic acid containing lecithin was used as the oil phase. However

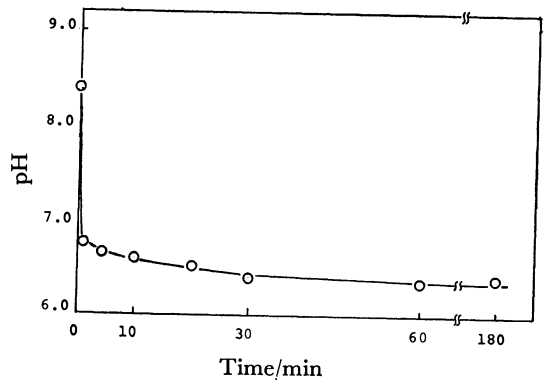

Fig. 6. The time dependence of pH of water phase in contact with oil phase.
Oil phase: *cis*-9-octadecenoic acid.
Water phase: sodium cholate 1×10^{-1} mol dm^{-3}.

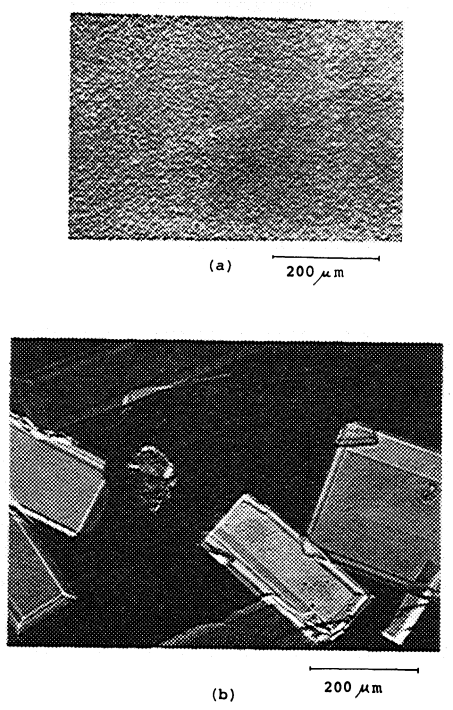

Fig. 7. The products formed at the oil-water interface.
(a) Thin milky film. Oil phase: dodecane+lecithin 1×10^{-2} wt%. Water phase: sodium cholate 1×10^{-1} mol dm^{-3}.
(b) Plate crystals. Oil phase: *cis*-9-octadecenoic acid +lecithin 2×10^{-2} wt%. Water phase: sodium cholate 1×10^{-1} mol dm^{-3}.

both spontaneous emulsification and crystal deposit were not observed when *cis*-9-octadecenoic acid containing lecithin was left in contact with water.[5] From these results, it is found that sodium cholate affects spontaneous emulsification when *cis*-9-octadecenoic acid is used as the oil phase.

Figure 6 shows the change of pH of the aqueous phase with time when *cis*-9-octadecenoic acid was left in contact with sodium cholate solution. It is clear from this figure that the initial pH of the water phase decreased rapidly with time. It seems that sodium ions of the water phase reacted with *cis*-9-octadecenoic acid, hydrogen ions of the water phase increased and some of the cholate ions transferred to the oil phase with the hydrogen ions. The results indicate that spontaneous emulsification or crystal deposit occur in the oil phase. Davies *et al.* showed that the spontaneous emulsification was caused by one or more of the following possibilities:[13,14] i) The instability of the interface due to a non-uniform diffusion of the components of the phases across the interface, which disturbs the interface violently enough to form droplets of the adjacent bulk phase. ii) An accompanying diffusion of oil and an additive into water, which results in a dilution of the additive by the water, leaving oil droplets to form an emulsion. iii) The temporary appearance of a negative interfacial tension which causes an enlargement of the interface area.

Schulman *et al.*[15,16] have shown that spontaneous emulsification occurs when a complex is formed between an oil-soluble substance and a water-soluble surfactant at the oil-water interface. The spontaneous emulsification of oil containing lecithin in contact with sodium cholate solution is attributed to the formation on liquid crystal of lecithin or to the formation of mixed micelle consisting of lecithin and sodium cholate.

Figure 7 shows photographs of the interfacial products. The thin milky film formed at the dodecane-sodium cholate solution interface is shown in Fig. 7-a. The plate crystals deposited at the *cis*-9-octadecenoic acid–sodium cholate solution interface are shown in Fig. 7-b. Crystals were obtained a few days after the oil and water phase came into contact at sodium cholate concentrations above 5×10^{-2} mol dm^{-3}. This crystal was identified to be a single crystal of cholic acid by the measurement of the melting point, IR spectroscopy and X-ray diffraction.

Similar results were obtained when (9*Z*,12*Z*)-9,12-octadecadienoic acid (linoleic acid) was used as the oil phase and were not obtained when *cis*-9-octadecen-1-ol was used. As mentioned above, it seems that the hydrogen ions of *cis*-9-octadecenoic acid, (9*Z*,12*Z*)-9,12-octadecadienoic acid and cholate ion in water affect the formation of this single crystal.

References

1) T. Manabe and N. Okuyama, *Yukagaku*, **26**, 578 (1977).
2) K. Ogino and M. Ota, *Yukagaku*, **23**, 28 (1974).
3) K. Ogino and M. Ota, *Bull. Chem. Soc. Jpn.*, **49**, 1187 (1976).
4) K. Ogino and H. Umetsu, *Bull. Chem. Soc. Jpn.*, **51**, 1543 (1974).
5) K. Ogino and M. Onishi, *J. Colloid Interface Sci.*, **83**, 18 (1981).
6) J. Stanly, "Soybeans and Soybean Products," ed by K. S. Markley, Interscience Publishers, New York (1951), Vol. II, p. 593.
7) S. Ota, *Yukagaku*, **19**, 792 (1970).
8) S. Sato and A. Nishioka, *Yukagaku*, **28**, 773 (1979).
9) A. F. Hofmann, *Biochem. Biophys. Acta*, **70**, 306 (1960).
10) A. F. Hofmann, *Biochem. J.*, **89**, 57 (1963).
11) M. C. Carey and D. M. Small, *Arch. Int. Med.*, **130**, 506 (1972).
12) N. A. Mazer, R. F. Kwasnic, M. C. Carey, and G. B. Bendenk, "Micellization, Solubilization and Microemulsions,"

ed by K. L. Mittal, Plenum Press, New York (1977), Vol. 1, p. 383.
13) J. T. Davies and E. K. Rideal, "Interfacial Phenomena of Natural Surfactant," Academic Press, New York and London (1963), pp. 360—377.
14) J. T. Davies and D. A. Haydon, *Proc. 2nd Int. Congr. Surface Activety*, **1**, 417 (1957).
15) J. H. Schulman and E. G. Cockbain, *Trans. Faraday Soc.*, **36**, 651 (1940).
16) A. E. Alexander and J. H. Schulman, *Trans. Faraday Soc.*, **36**, 960 (1940).

Cyclic Voltammetry of Aromatic Amine *N*-Oxides in Nonaqueous Solvents and the Stability of the Free Radicals Produced[1)]

Hiroshi MIYAZAKI, Yoshio MATSUHISA,† and Tanekazu KUBOTA*,†

Shionogi Research Laboratories, Shionogi and Co., Ltd., 5-12-4, Fukushima-ku, Osaka 553

†*Gifu College of Pharmacy, 6-1, Mitahora-higashi 5-chome, Gifu 502*

(Received January 27, 1981)

Cyclic voltammograms of aromatic amine *N*-oxides were recorded in nonaqueous solvents at various sweep rates less than 10 V/s. The measurement was carried out for both cathodic and anodic sweeps, and the sweep rate for obtaining a good cyclic voltammogram was correlated with the wave height of the a.c. polarogram in the reduction and oxidation processes, respectively. A good correlation was found between the sweep rate and the wave height in both the reduction and oxidation processes. This confirmed that the two values serve as good measures of the stability of the anion or cation free radical produced by the electrode reaction of the aromatic amine *N*-oxides. The data were also examined by comparison with results from an electron spin resonance study. Finally, the temperature effect on the cyclic voltammogram of pyridine *N*-oxide was investigated in detail.

The study of cyclic voltammetry (CV) of aromatic amine *N*-oxides was carried out in nonaqueous solvents to compare the results with those of our previous polarographic and electron spin resonance (ESR) investigations on the same compounds.[2-7)] The results of these CV studies are considered to be good measures of the reversibility of the electrode reaction[8)] and were expected to display good correlation with the previous results mentioned above.

Experimental

The CV measurement was made using a combination of a Yanagimoto Applied Potential Sweep Unit Model PE-21-TB2SS, a Yanagimoto polarograph P8-AP, a Hitachi Synchroscope Model V-104, and a Riken Denshi XY-Recorder Model D-51P to obtain a cyclic voltammogram at a sweep rate of 0.0017—10 V/s. As working electrodes, a PAR Model 9323 hanging mercury drop electrode (HMDE), a hanging mercury electrode (HME), and a platinum disk electrode (PDE: 2 mm in diameter) were used. All the measurements of samples, except for pyridine *N*-oxide (PNO: *vide infra*) were done at 25±0.1 °C by using the so called three-electrode-technique, a saturated calomel electrode (SCE) being employed as a reference electrode except for the low temperature measurement. The solvents used were *N*,*N*-dimethylformamide (DMF) and CH_3CN containing 0.1 mol dm^{-3} tetrapropylammonium perchlorate (TPAP) as the supporting electrolyte.

The cathodic sweep cyclic voltammogram of PNO was measured in the temperature range between 23.5 °C and −40

Table 1. Polarographic, cyclic voltammetric, and electron spin resonance (ESR) data of aromatic amine *N*-oxides in reduction and oxidation processes

Compound	Reduction[a)]							Oxidation[b)]						
	Polarography[c)]		Cyclic voltammetry[d,h)]				ESR[e)]	Polarography[f)]		Cyclic voltammetry[g,h)]				ESR[e)]
	$(-E^{red}_{1/2}$ *vs.* SCE)/V	$I_{a.c.}/\mu$ mol m^{-3}	$(-E_{p,f}$ *vs.* SCE)/V	$(-E_{p,b}$ *vs.* SCE)/V	$(-E^{red}_{1/2}$ *vs.* SCE)/V	Sweep rate[i)]/V s^{-1}		$(E^{oxd}_{1/2}$ *vs.* SCE)/V	$I_{a.c.}/\mu$ mol m^{-3}	$(-E_{p,f}$ *vs.* SCE)/V	$(-E_{p,b}$ *vs.* SCE)/V	$(E^{oxd}_{1/2}$ *vs.* SCE)/V	Sweep rate[i)]/V s^{-1}	
Phenazine 5,10-dioxide	0.833	306	0.849	0.785	0.817	≈1×10^{-3}	Yes	1.344	400	1.374	1.30	1.337	1.12×10^{-2}	Yes
Phenazine 5-oxide	0.972	348	0.983	0.922	0.953	≈1×10^{-3}	Yes	1.745	78	—	—	—	>10	No
Acridine 10-oxide	1.300	180	1.361	1.262	1.312	—	Yes	1.280	137	1.30	1.238	1.269	≈0.1	Yes
Quinoxaline 1,4-dioxide	1.241	293	1.236	1.171	1.204	<1×10^{-3}	Yes	1.598	335	1.619	1.492	1.556	0.18	Yes*
Quinoxaline 1-oxide	1.419	315	1.427	1.344	1.386	<1×10^{-3}	Yes	1.971	—	—	—	—	>10	No
Quinoline 1-oxide	1.809	317	1.859	1.736	1.798	≈1×10^{-3}	Yes	1.537	59	—	—	—	>10	No
Isoquinoline 2-oxide	1.946	231	1.918	1.839	1.879	0.4	Yes*	1.600	51	—	—	—	>10	No
Pyrazine 1,4-dioxide	1.616	306	1.659	1.566	1.613	0.025	Yes	1.741	331	1.788	1.685	1.737	≈0.3	Yes*
Pyrazine 1-oxide	1.837	325	1.859	1.773	1.816	<1×10^{-3}	Yes	2.312	55	—	—	—	>10	No
Pyridine 1-oxide	2.297	106	—	—	—	>10	Yes*	1.802	90	—	—	—	>10	No
4-(dimethylamino)-pyridine 1-oxide	—	—	—	—	—	—	—	0.759	145	0.820	0.744	0.782	4	Yes

a) Data in DMF. b) Data in CH_3CN. c) Obtained with DME, and taken from Refs. 2, 3, 4, and 5. d) Obtained with HMDE. e) Taken from Refs. 2, 3, and 6. Here "Yes" means that the ESR spectra due to the anion or cation free radicals were recorded at room temperature. However, the free radicals of several *N*-oxides were obtained only at below 0 °C; in such a case the asterisk is put on "Yes" as superscript. f) Obtained with PDE at 600 r.p.m., and taken from Ref. 5. g) Obtained with PDE. h) The equation, $E_{1/2}=(E_{p,f}+E_{p,b})/2$, was used to determine the half-wave potential. Each value of $E_{p,f}$ and $E_{p,b}$ is for the CV curves at the sweep rate where the backward sweep wave becomes evident. See text for details. i) This is the value corresponding to the $(i_{p,b}/i_{p,f})=0.5$. See text for details.

°C.[10] A platinum wire was employed instead of the SCE, since the SCE can not be used at the lower temperatures.[9] HME was employed as a working electrode, the solvent being DMF containing TPAP. Note here that, since the PNO anion radical is unstable at room temperature (*vide infra*), checking the reversibility of the electrode process at the lower temperature was the most important problem for PNO.

The aromatic amine *N*-oxides used here, listed in Table 1, are the same ones previously studied with polarographic and ESR techniques.[2-7]

Results and Discussion

For the analyses of CV curves, the following methods were applied. The peak current of the backward sweep was measured by the switching potential current (SPC) method reported by Nicholson.[11-12] The value of the half-wave potential $E_{1/2}$ was cyclovoltammetrically determined by the equation $E_{1/2}=(E_{p.f}+E_{p.b})/2$, which is in principle applicable to the reversible redox system.[13] Here, $E_{p.f}$ and $E_{p.b}$ are the forward and the backward peak potentials, respectively. This equation gave $E_{1/2}$ values almost independent of the sweep rate and compatible with those determined polarographically. In the case of the cathodic sweep, generally speaking, the CV curves recorded in DMF with HMDE were almost the same as those obtained with PDE, and the difference is not remarkable. The CV data recorded with HMDE are given in Table 1, which also lists the other experimental results and, as references, our previously reported data. In the cathodic sweep cyclic voltammograms of the *N*-oxides in DMF the backward sweep waves were always observed for all the samples, except for PNO, at room temperature and at a sweep rate less than 10 V/s. Comparison with previous ESR and polarographic studies of the *N*-oxides[2-7], clearly shows that this backward sweep wave is due to the oxidation process of the anion radical produced by the cathodic sweep. The sweep rate to obtain the backward sweep wave would be related to the stability of the anion radical. In the case of PNO, we could not observe the backward sweep wave at room temperature even when the sweep rate is increased to 10 V/s, as shown in Fig. 1a. However, when the voltammogram was recorded at −30 °C and at a moderate sweep rate, the backward sweep wave was clearly observed, as is seen in Fig. 1b.[14] Since our previous study indicated that the ESR spectrum of the PNO anion radical was clearly obtained at about −50 °C by employing the electrochemical technique,[2] the above backward sweep wave must be due to the oxidation process of the PNO anion radical, in agreement with the ESR study.

Next we would consider the anodic sweep cyclic voltammogram in CH_3CN. Only four of the aromatic amine *N*-oxides studied here showed the backward sweep wave under the present experimental conditions (see Table 1). A typical compound, phenazine 5,10-dioxide, shows a clear backward sweep wave even at 0.1 V/s. This agrees with observations by other workers.[15] The cyclic voltammogram of quinoxaline 1,4-dioxide (Fig. 2) showed no clear backward sweep wave at the rate 0.1 V/s, but the curve is obviously observed at 2 V/s. The cation radical of this *N*-oxide

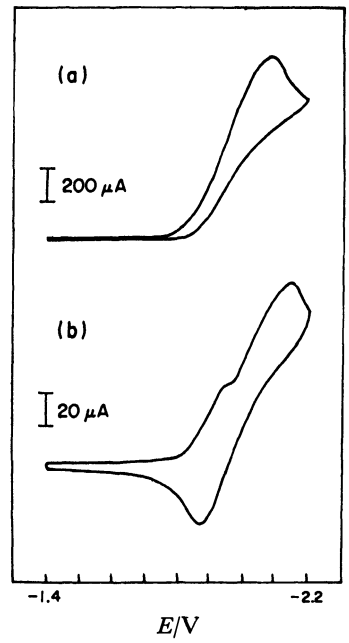

Fig. 1. Cyclic voltammograms of pyridine *N*-oxide (2.51×10^{-3} mol dm^{-3}) in DMF containing 0.1 mol dm^{-3} TPAP. Sweep rate and temperature were, respectively, 10 V/s and 23.5 °C for (a), and 8 V/s and −30 °C for (b). The electrode system was HME and platinum wire, the latter being used instead of SCE (see text).

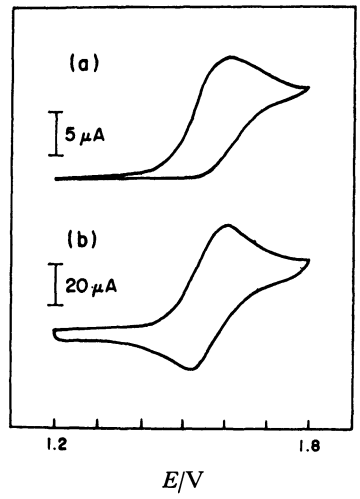

Fig. 2. Cyclic voltammograms of quinoxaline 1,4-dioxide (8.02×10^{-4} mol dm^{-3}) in CH_3CN containing 0.1 mol dm^{-3} TPAP at 25 °C. Sweep rate was 0.1 V/s and 2 V/s for (a) and (b), respectively. Reference electrode was SCE.

is unstable compared with that of phenazine 5,10-dioxide. In the case of pyrazine 1,4-dioxide, the cation radical was more unstable and therefore the backward sweep wave required a higher sweep rate. These observations agreed well with the results derived from our ESR study of cation radicals.[6]

Based on the discussion mentioned hitherto the sweep rate of the cyclic voltammogram should be closely correlated with the life time of the anion or cation free radical produced by the electrode reaction. Alternative-

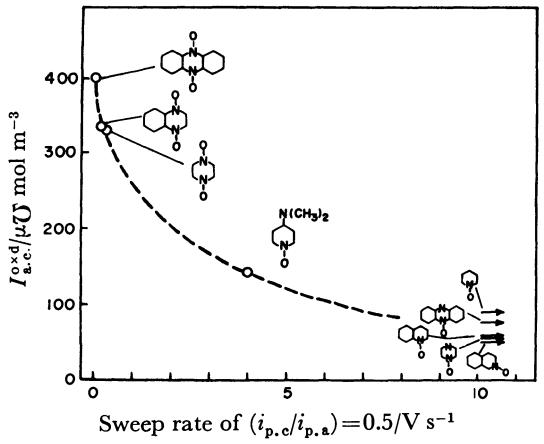

Fig. 3. Relationship between the wave height of the a.c. polarograms and the sweep rate at $(i_{p.c}/i_{p.a})=0.5$ of the cyclic voltammograms in the oxidation process of aromatic amine *N*-oxides in CH_3CN. The backward sweep wave was not observed for the compounds designated by arrows.

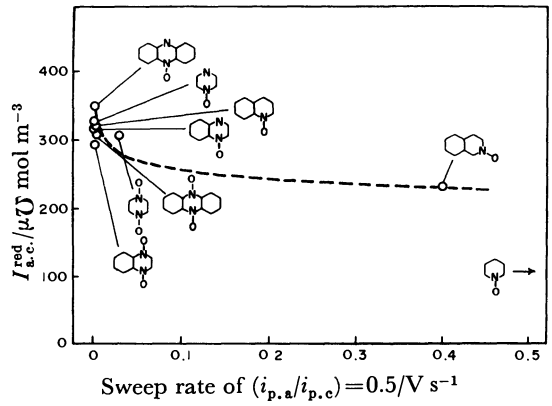

Fig. 4. Relationship between the wave height of the a.c. polarograms and the sweep rate at $(i_{p.a}/i_{p.c})=0.5$ of the cyclic voltammograms on the reduction process of aromatic amine *N*-oxides in DMF. See text on the pyridine *N*-oxide, the backward sweep wave of which was not observed at room temperature.

ly many reports support the fact that the wave height of an a.c. polarogram is a good measure of the reversibility of the electrode reaction.[16] Accordingly, the correlation between the sweep rate of the cyclic voltammograms and the wave height of a.c. polarograms was examined for the *N*-oxides studied. As a sweep rate of the former, the value of $(i_{p.b}/i_{p.f})=0.5$ was conveniently chosen (see Table 1), since the half wave height of a backward sweep against the forward sweep wave height would be considered to be related to the life time of the free radical.[8c] This value was obtained by plotting the $i_{p.b}/i_{p.f}$ value to the sweep rate, where $i_{p.b}$ and $i_{p.f}$ are the peak height of the backward and the forward sweep waves, respectively. The wave heights of a.c. polarograms, reported in our previous papers,[2-5] were obtained under the same experimental conditions and with the same compounds as those employed here. The data are cited in Table 1. In Figs. 3 and 4 the above correlation was illustrated. Figure 3 indicates that the wave height $I^{oxd}_{a.c}$ of the a.c. polarograms for oxidation and the sweep rate value at $(i_{p.c}/i_{p.a})=0.5$ have a good correlation with each other and that the larger the $I^{oxd}_{a.c}$ value and the smaller the sweep rate value, the more stable is the cation radical. The ESR spectra of the cation radicals of the three *N,N'*-dioxides and the 4-(dimethylamino)pyridine 1-oxide shown in Fig. 3 were successfully measured (*vide supra*).[6] As seen in Fig. 4, a correlation of the $I^{red}_{a.c}$ (wave height of a.c. polarogram for reduction) to the sweep rate value at the $(i_{p.a}/i_{p.c})=0.5$ was also obtained, although the relation was somewhat ambiguous compared with the case of Fig. 3. This is due to the high stability of the anion radicals of the *N*-oxides[2-5] as discussed hitherto, so that the $I^{red}_{a.c}$ values are rather large and the sweep rate values defined above are also small. From the results shown in Figs. 3 and 4, we may say that the potential sweep rate for yielding a cyclic voltammogram with a good backward sweep wave is a good measure for checking the reversibility of the electrode reaction of the aromatic amine *N*-oxides in nonaqueous solvents, and that a good correlation exists between the potential sweep rate and the wave height of a.c. polarograms or the stability of the free radicals of the *N*-oxides as studied by the ESR technique.

References

1) Most of this work was done at the Shionogi Research Laboratories where T. K. studied until March 31, 1980.

2) T. Kubota, K. Nishikida, H. Miyazaki, K. Iwatani, and Y. Ōishi, *J. Am. Chem. Soc.*, **90**, 5080 (1968).

3) T. Kubota, Y. Ōishi, K. Nishikida, and H. Miyazaki, *Bull. Chem. Soc. Jpn.*, **43**, 1622 (1970).

4) H. Miyazaki and T. Kubota, *Bull. Chem. Soc. Jpn.*, **44**, 279 (1971).

5) H. Miyazaki, T. Kubota, and M. Yamakawa, *Bull. Chem. Soc. Jpn.*, **45**, 780 (1972).

6) K. Nishikida, T. Kubota, H. Miyazaki, and S. Sakata, *J. Magn. Reson.*, **7**, 260 (1972).

7) T. Kubota, H. Miyazaki, M. Yamakawa, K. Ezumi, and Y. Yamamoto, *Bull. Chem. Soc. Jpn.*, **52**, 1588 (1979).

8) a) R. N. Adams, "Electrochemistry at Solid Electrodes," Marcel Dekker, New York and Basel (1969), Chap. 5; b) T. Takamura, *Denki Kagaku*, **39**, 445 (1971); c) K. B. Wiberg and T. P. Lewis, *J. Am. Chem. Soc.*, **92**, 7154 (1970).

9) This was a recommendation (private communication) of Professor Masanori Sato of Kyoto University of Industrial Arts and Textile Fibers. Also, our experiments indicated that the CV curves could be recorded with no difficulty with platinum reference electrode, although the peak potentials could not be accurately determined.

10) The melting point of mercury is −38.89 °C, thus CV measurement at temperatures below −40 °C was not tried.

11) R. S. Nicholson, *Anal. Chem.*, **38**, 1406 (1966).

12) Using ferrocene as the standard (0.1 mol dm^{-3} TPAP/CH_3CN, Pt electrode) we compared the SPC technique with the conventional holding method.[8a,b] The result indicated that the former method is better than the latter, and it always leads to the 1.00 for the value of (backward sweep peak current$=i_{p.b}$)/(forward sweep peak current$=i_{p.f}$) despite of the selection of switching potentials. The value of $(i_{p.b}/i_{p.f})$ is calculated by the equation: $(i_{p.b}/i_{p.f})=(i^{\circ}_{p.b}/i^{\circ}_{p.f})+0.485\times(i^{\circ}_{sp}/i^{\circ}_{p.f})+0.086$. The i°_{sp} is the current at the switching potential. Here superscript zero means the current measured

from the galvanometer zero line, so that $i_{p,f}=i^{\circ}_{p,f}$.

13) S. F. Nelsen, V. Peacock, and G. R. Weisman, *J. Am. Chem. Soc.*, **98**, 5269 (1976).

14) In this case, a pre-wave was always accompanied by the main forward wave, as Fig. 1b shows. The origin of this pre-wave is not clear at the present, but perhaps it may be due to the adsorption phenomena of PNO to the HME surface at lower temperature, as was seen in the cyclic voltammogram of pyridine.[8c)]

15) a) A. Stüwe, M. W. Schäfer, and H. Baumgärtel, *Ber. Bunsenges. Phys. Chem.*, **78**, 309 (1974); b) M. W. Schäfer and H. Baumgärtel, *ibid.*, **78**, 317 (1974); c) A. Stüwe and H. Baumgärtel, *ibid.*, **78**, 320 (1974).

16) See, for example, T. Fujinaga and K. Izutsu, "Bunseki Kagaku II," in "Shin Jikken Kagaku Koza," ed by the Chemical Society of Japan, Maruzen, Tokyo (1977), Vol. 9, p. 389.

An Optical Absorption Study of Trapped Electrons in γ-Irradiated 3-Methylhexane–2,2,4-Trimethylpentane–2,2-Dimethylbutane Mixture Glasses at 77 K

Toyoaki KIMURA,* Naoyuki OGAWA, and Kenji FUEKI

Department of Synthetic Chemistry, Faculty of Engineering, Nagoya University, Chikusa-ku, Nagoya 464

(Received June 8, 1981)

An optical absorption study was made on trapped electrons in γ-irradiated 3-methylhexane–2,2,4-trimethylpentane–2,2-dimethylbutane glasses at 77 K. The absorption maximum of trapped electron spectra shifts to longer wavelengths and the trapped electron yield decreases with decreasing 3-methylhexane concentration. The observed spectral shifts were interpreted through a semicontinuum model calculation.

Excess electrons generated by ionizing radiation in polar and nonpolar matrices have been extensively studied by various experimental methods. Studies on electron mobilities in nonpolar hydrocarbon liquids have revealed that electron mobilities range over three orders of magnitude depending on the hydrocarbon liquids,[1] which reflects the strength of interaction between an excess electron and the medium. Measurements of the quasi-free electron state energy V_0 have also shown that the V_0 value differs considerably among hydrocarbons in the liquid state[2,3] as well as in the glassy state.[4] On the basis of the results from these two types of experiment, hydrocarbons can roughly be classified into two types: type I in which electron mobilities are high (>10 cm^2 V^{-1} s^{-1}) and the V_0 values are low, and type II in which electron mobilities are low (<1 cm^2 V^{-1} s^{-1}) and the V_0 values are high. It is well known that excess electrons in the type I hydrocarbons are not localized, whereas those in the type II hydrocarbons are localized. On the other hand, it is known that optical absorption spectra of trapped electrons (e_t^-) in hydrocarbon glasses at 77 K are similar to each other.[5] This may be due to the fact that hydrocarbon matrices studied so far belong to type II. Thus, it is of interest to investigate how the optical absorption spectrum of e_t^- would change if we could choose as matrices the hydrocarbons which do not belong to type II. Values of V_0 of the type I hydrocarbons, 2,2,4-trimethylpentane (224TMP) and 2,2-dimethylbutane (22DMB), and the type II hydrocarbons at 77 and 295 K are listed in the upper, middle and bottom portions in Table 1, respectively. The electron mobilities ($10 \gtrsim \mu_e \gtrsim 1$ cm^2 V^{-1} s^{-1}) and V_0 values in 224TMP and 22DMB lie between those in the type I hydrocarbons and those in the type II hydrocarbons. We have found that a mixture of 224TMP and 22DMB makes a clear glass at 77 K. We report here absorption spectra and yields of e_t^- in the mixed systems of 3-methylhexane(3MHx)–224TMP–22DMB. We used a mixture of 224TMP and 22DMB in 1 : 1 volume ratio (at room temperature), which will be designated as (224TMP–22DMB) in what follows.

TABLE 1. QUASI-FREE ELECTRON STATE ENERGIES IN SOME HYDROCARBONS

	V_0 at 77 K/eV	V_0 at 295 K/eV
Neopentane	0.33[a]	−0.38[c]
224TMP	0.57[a]	−0.17[c]
22DMB	0.59[a]	−0.26[c]
Hexane	0.98[a]	0.1[c]
MCH	1.00[a]	0.08[d]
3MP	0.86[b]	0.01[c]

a) Ref. 4. b) Ref. 4. Value estimated relative to V_0 of MCH. c) Ref. 2 a). d) Ref. 2 b).

Experimental

3-Methylhexane (Tokyo Kasei, extra pure) and 2,2,4-trimethylpentane and 2,2-dimethylbutane (Tokyo Kagaku Seiki, standard pure) were degassed and then purified *in vacuo* three times using molecular sieves 13X which were heated at 550 K *in vacuo* for 12 h before use. The hydrocarbons were taken into a volumetric flask *in vacuo*, and vacuum distilled into optical cells. Samples were sealed off a vacuum line. The optical cells were made of Suprasil quartz and the optical path length was ≈2 mm. γ-Irradiation was made with ^{60}Co γ-rays to a dose of 1.0×10^5 rad. Optical absorption spectra were taken on a Hitachi 323 spectrophotometer. γ-Irradiation and optical absorption measurements were carried out at 77 K.

Results and Discussion

Optical Absorption Spectra. No optical absorption was observable for the γ-irradiated (224TMP–22DMB) samples in the wavelength range from 340 to 2000 nm over the dose range from 0.1 to 1.8 M rad. Thus, it is concluded that electrons cannot be stably trapped in the (224TMP–22DMB) glass at 77 K. The optical absorption spectrum of e_t^- in a 3MHx–(224TMP–22DMB) mixture glass has an absorption maximum at a wavelength longer than that in neat 3MHx glass. The e_t^- spectrum in a 0.5 electron fraction (e.f.) 3MHx–

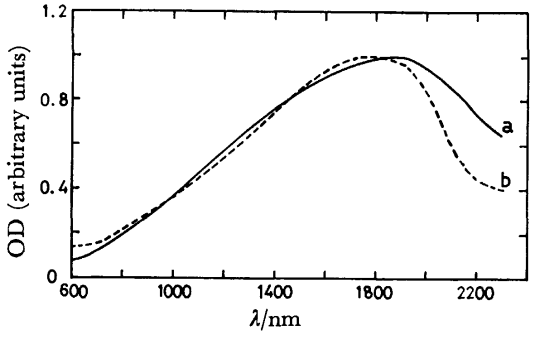

Fig. 1. Optical absorption spectrum of e_t^- in (a) 0.5 e.f. 3MHx–(224TMP–22DMB) and (b) 3MHx.

Table 2. Comparison of the observed wavelengths at the absorption maxima and the calculated wavelengths of the 1s→2p transition in 3MHx–(224TMP–22DMB) systems

[3MHx], e.f.	λ_{max}(obsd)/nm	$\lambda_{1s\rightarrow 2p}$(calcd)/nm
0.2	—	2030
0.4	1950	1780
0.5	1900	1720
0.6	1880	1670
0.8	1800	1570
1.0	1780	1500

(224TMP–22DMB) glass is shown in Fig. 1 together with that in neat 3MHx. Both spectra in Fig. 1 are normalized to the same peak height. It is seen in Fig. 1 that the spectrum in 0.5 e.f. 3MHx–(224TMP–22DMB) system has λ_{max} at 1900 nm (curve a), whereas that in neat 3MHx has λ_{max} at 1780 nm (curve b), and that the half-width of spectrum a is somewhat wider than that of spectrum b. The values of λ_{max} for e_t^- in 3MHx–(224TMP–22DMB) systems are listed in Table 2 as a function of e.f. of 3MHx.

Semicontinuum Model Calculation of the Optical Transition. In the present calculation we assumed four 3MHx molecules in a first solvation layer, which were arranged in such a way that the center of e_t^- and the midpoints of each C–C bond in the main chain of 3MHx lie on a straight line. The medium beyond the first solvation layer was treated as a continuous dielectric medium. The total energy for the ith state is given by Eq. 1,

$$E_t(i) = E_k(i) + E_e^s(i) + E_m^s(i) + E_e^l(i) + E_m^l(i) + E_q(i) + E_v + E_{HH}, \quad (1)$$

where E_K is the kinetic energy of the excess electron; E_e^s and E_m^s are short-range electronic and medium rearrangement energies, respectively; E_e^l and E_m^l are long-range electronic and medium rearrangement energies, respectively; E_q is the short-range repulsive interaction energy between the excess electron and the medium electrons; E_V is the energy required to form a cavity in the medium; and E_{HH} is the repulsive interaction energy between the hydrogen atoms in the different methyl groups nearest to the center of the cavity in which the electron is localized. Detailed expressions for each term in Eq. 1 are given in Ref. 6. The 1s→2p transition energy is then calculated using hydrogenic 1s and 2p wave-functions as Eq. 2. The physical parameters for the mixtures, A_{mix}, were estimated assuming a simple relation, $A_{mix}=\sum_i \chi_i A_i$, where χ_i and A_i are the mole fraction and the physical parameter value for hydrocarbon component i, respectively. The V_0 values for 224TMP and 22DMB were taken from Table 1. The V_0 value for 3MHx at 77 K is not available. Since V_0 values for the type II hydrocarbons at 77 K in Table 1 are close to 1.0 eV although it is somewhat lower for 3MP, we have assumed that V_0 for 3MHx is 1.0 eV at 77 K. Using these V_0 values the short-range repulsive interaction between the excess electron and the medium electrons was incorporated in the calculation. The values of 1s→2p transition energy in wavelength units are listed in Table 2. The calculated $\lambda_{1s\rightarrow 2p}$ is in semiquantitative agreement with the observed λ_{max}. The calculation accounts for a red shift in λ_{max} of e_t^- in 3MHx–(224TMP–22DMB) systems with decreasing concentration of 3MHx. This trend is unchanged even if different molecular arrangements in the first solvation layer are assumed. Such a shift is ascribed to the lower V_0 values for (224TMP–22DMB) compared with that for 3MHx.

$$h\nu_{1s\rightarrow 2p} = E_t(2p) - E_t(1s) \quad (2)$$

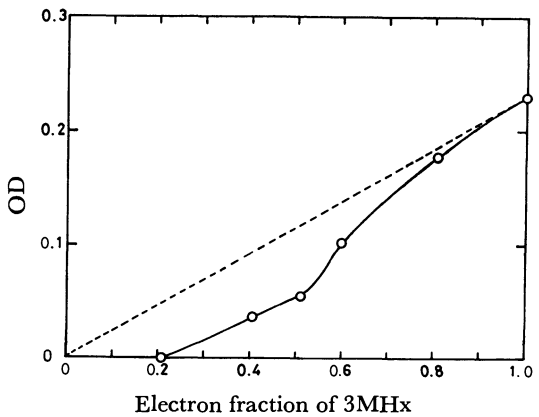

Fig. 2. Optical densities of e_t^- in 3MHx–(224TMP–22DMB) systems *vs.* electron fraction of 3MHx.

The Yield of Trapped Electrons. Trapped electrons in 3MHx decay quite slowly at 77 K. In 3MHx–(224TMP–22DMB)systems the decay rate of e_t^- increases with decreasing 3MHx concentration. Taking the decay into consideration, the optical density of e_t^- immediately after the 10 min γ-irradiation, normalized to the 1 mm optical path length, is shown in Fig. 2 as a function of e.f. of 3MHx. It can be seen from Fig. 2 that the optical densities of e_t^- in 3MHx–(224TMP–22DMB) systems are lower than those expected from a linear relationship (dashed line) between OD of e_t^- and e.f. of 3MHx, especially at lower concentrations, and that e_t^- is not observable for $\lesssim$0.2 e.f. 3MHx. The V_0 value for 0.2 e.f. 3MHx–(224TMP–22DMB) system in which no e_t^- is observable is calculated to be 0.67 eV. Then, we are tempted to say that electrons cannot be trapped in the glassy hydrocarbon matrices whose V_0 is lower than $\approx$0.67 eV.

The viscosity of 3MHx–(224TMP–22DMB) systems probably decreases with decreasing 3MHx concentration, which reflects on the decay rate of e_t^-. Thus, we cannot exclude the possibility that e_t^- has decayed out completely for low 3MHx concentrations before the optical measurements are made. Taking the case of 0.5 e.f. 3MHx–(224TMP–22DMB) system as an example, only 14% correction for the e_t^- decay is required for the observed OD at the shortest time to obtain OD at time zero**, whereas the observed e_t^- yield is about a half of that expected from a simple mixture law. Further, we note that the decay of e_t^- does not occur over an hour in 0.2 e.f. 1-propanol–(224TMP–

** Since the correction for e_t^- decay was made by extrapolation of data points from steady-state experiments, the resulting initial OD or e_t^- yield should not be taken as identical to that obtained by pulse radiolysis measurements.

22DMB) system.[7] These observations indicate that the matrix viscosity alone is insufficient for the interpretation of decrease in the e_t^- yield. The decrease in the e_t^- yield at lower 3MHx concentrations mentioned above may probably be explained in terms of lower V_0 and viscosity of (224TMP–22DMB). It should be pointed out that both lower values of V_0 and viscosity arise from a larger free volume in the medium.[8]

The present work was partially supported by the Nagoya University Computation Center.

References

1) A. Hummel and W. F. Schmidt, *Radiat. Res. Rev.*, **5**, 199 (1974).
2) a) R. A. Holroyd and R. L. Russell, *J. Phys. Chem.*, **78**, 2128 (1974); b) R. A. Holroyd, *J. Chem. Phys.*, **57**, 3007 (1972).
3) W. Tauchert, H. Jungblut, and W. F. Schmidt, *Can. J. Chem.*, **55**, 1860 (1977).
4) D. Grand and A. Bernas, *J. Phys. Chem.*, **81**, 1209 (1977).
5) H. Hase, T. Higashimura, and M. Ogasawara, *Chem. Phys. Lett.*, **16**, 214 (1972).
6) T. Kimura, K. Fueki, P. A. Narayana, and L. Kevan, *Can. J. Chem.*, **55**, 1940 (1977).
7) T. Kimura, S. Fukuda, and K. Fueki, unpublished results.
8) R. A. Holroyd, S. Tames, and A. Kennedy, *J. Phys. Chem.*, **79**, 2857 (1975).

Prediction of Adsorption Isotherms of Organic Compounds from Water on Activated Carbons. II.[1] Relative Adsorbabilities of Elements

Ikuo ABE,* Katsumi HAYASHI, and Mutsuo KITAGAWA**
Osaka Municipal Technical Research Institute, Ogimachi, Kita-ku, Osaka 530
***Society for Activated Carbon Research, Ogimachi, Kita-ku, Osaka 530*
(Received April 27, 1981)

Synopsis. In order to predict the adsorbability of organic compounds out of water onto activated carbon, the contribution of individual atoms to the adsorbability is calculated. The contribution of the carbon atom is positive, that of nitrogen and oxygen atoms is negative, and that of the hydrogen atom is very small.

Adsorption onto activated carbon provides a technique for purification of municipal and industrial wastewaters. In the design of such water purification facilities, equilibrium adsorption information is required. To reduce experimental work, it is desirable to predict the adsorbability of organic compounds.

In a previous paper,[2] the partition coefficients (α) of 93 organic compounds between the solution and the adsorbed phases at an infinite dilution have been calculated and correlated with the molecular weight (MW). Further details of the relationship between $\log \alpha$ and MW are illustrated in Fig. 1. For 52 aliphatic monofunctional compounds, a good linear relationship has been obtained, with a high correlation coefficient (r). Furthermore, the standard deviation (s), the t-value in the Student test, and the over-all goodness of fit expressed by means of the F-value indicate that the relationship is statistically significant. The adsorbability of the multifunctional compounds is lower than that of the monofunctional compounds. This result suggests that the adsorbability of oxygen and nitrogen atoms constituting the functional group is lower than that of the carbon atom. The over-all correlation coefficient is low for this reason.

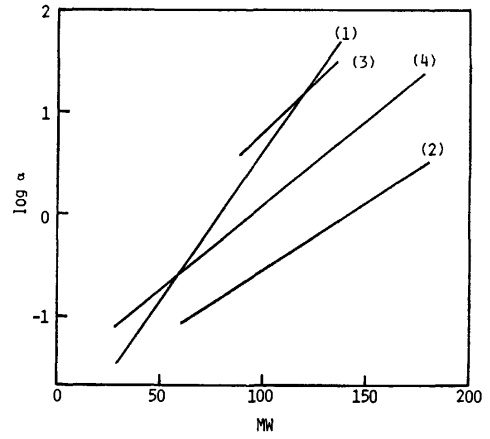

Fig. 1. Relationship between $\log \alpha$ and molecular weight (MW).
(1): Aliphatic monofunctional compounds,
$n=52$, $r=0.9512$, $s=0.2635$, $F=475.0$***, $t=21.79$***.
(2): Aliphatic multifunctional compounds,
$n=27$, $r=0.6459$, $s=0.5614$, $F=17.89$***, $t=4.230$***.
(3): Aromatic compounds,
$n=14$, $r=0.6024$, $s=0.4263$, $F=6.834$*, $t=2.614$*.
(4): All compounds,
$n=93$, $r=0.6051$, $s=0.6867$, $F=52.58$***, $t=7.251$***.
Significance level: *<0.05, **<0.01, ***<0.001.

The relationship between adsorbability and molecular weight can be expressed by the following equation:

$$\log \alpha = aMW + b = a(12N_C + 1N_H + 14N_N + 16N_O + \cdots) + b, \quad (1)$$

where N_C, N_H, N_N, and N_O are the number of carbon, hydrogen, nitrogen, and oxygen atoms, respectively, in a molecule, and a and b are constants. Equation 1 assumes that the individual atoms contribute to the adsorbability of the molecule by the relative magnitude of atomic weight.

In order to estimate the exact contribution of the individual atoms to the adsorbability, the a coefficients in Eq. 2 have been calculated by multiple regression analysis. The relative magnitude of these coefficients is a measure of the contribution to the adsorbability.

$$\log \alpha = a_C N_C + a_H N_H + a_N N_N + a_O N_O + \cdots + b. \quad (2)$$

The data of 91 compounds, excluding two halogenated compounds, have been processed by a SHARP PC-7300 computer, and Eq. 3 has been derived. Table 1 shows

Table 1. Squared correlation matrix for independent variables in Eq. 3

	N_C	N_H	N_N	N_O
N_C	1.000			
N_H	0.458	1.000		
N_N	0.005	0.011	1.000	
N_O	0.013	0.084	0.122	1.000

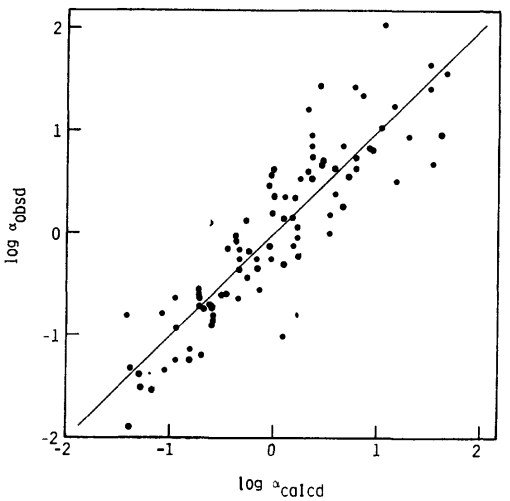

Fig. 2. Relationship between $\log \alpha$ observed and $\log \alpha$ calculated using Eq. 3.
$\log \alpha_{obsd} = 0.9998 \log \alpha_{calcd} - 0.0002$,
$n=91$, $r=0.8803$, $s=0.4090$, $F=306.3$***, $t=17.50$***.

$$\log \alpha = 0.4370N_C - 0.04465N_H - 0.2050N_N - 0.1302N_O - 1.501 \quad (3)$$

(n=91, r=0.8803, s=0.4161, F=74.01***, $t(N_C)$=13.60***, $t(N_H)$=−2.659**, $t(N_N)$=−2.104*, $t(N_O)$=−2.490*)

the squared correlation matrix for degree of collinearity between the variables used in Eq. 3.

A comparison of the coefficients in Eq. 3 yields the following conclusions. The presence of carbon atom in a molecule increases the adsorbability of the molecule. Nitrogen and oxygen atoms decrease the adsorbability. The contribution of hydrogen atom is much smaller than those of the other atoms.

Figure 2 shows the relationship between log α observed and log α calculated using Eq. 3. For the same 91 compounds, the relation between log α and the molecular weight is expressed by Eq. 4:

$$\log \alpha = 0.01639MW - 1.558. \quad (4)$$

(n=91, r=0.6050, s=0.6864, F=51.39***, t=7.169***)

These results indicate that Eq. 3 provide a better approximation than Eq. 4. The adsorbability of many compounds can be predicted from the molecular formula alone.

References

1) Part I: I. Abe, K. Hayashi, and M. Kitagawa, *Bull. Chem. Soc. Jpn.*, **54**, 2819 (1981).

2) I. Abe, K. Hayashi, M. Kitagawa, and T. Urahata, *Bull. Chem. Soc. Jpn.*, **53**, 1199 (1980).

Metachromatic Absorption Spectra of Spin-labeled Mono- and Diaminoacridine Dyes Bound to Synthetic Polyelectrolytes[1]

Kiwamu YAMAOKA,* Takumi MATSUDA, and Tsuyoshi MURAKAMI
Faculty of Science, Hiroshima University, Higashisenda-machi, Naka-ku, Hiroshima 730
(Received April 16, 1981)

Synopsis. Interactions between nitroxide spin-labeled dyes (Acridine Orange, Proflavine, and 9-aminoacridinium chloride) and poly(*p*-styrenesulfonate), polyphosphate, and polyacrylate were studied by measuring visible absorption spectra in aqueous solutions. The bound-dye spectra and equilibrium constants were determined by the principal-component-analysis method. The metachromatic behavior of dye–polymer complexes was clarified.

Previous reports have shown that acridine dyes labeled with stable nitroxides can be utilized in the study of dye–polymer interactions by two independent methods of ESR and optical absorption.[2] Molecular dynamics of spin-labeled dyes bound to various polyelectrolytes were clarified by analyzing ESR signals of spin moieties.[2,3] The characteristics of absorption spectra of newly synthesized spin-labeled and other related dyes were compared to determine the effect of attaching the labels.[4] For full utilization of these dyes as ESR-optical double probes, their spectral behavior should be assessed quantitatively in the presence of various polymers under diverse conditions.

In this Note, the metachromatic behavior of three spin-labeled acridine dyes toward three polyelectrolytes with different charged-groups will be reported. By applying the principal-component-analysis (PCA) method to the measured absorption spectra of each dye–polymer combination, the spectrum and the fraction of the bound-dye species were evaluated, together with the apparent equilibrium constant. For each polyelectrolyte, the bound-dye spectra are similar to those of the corresponding unlabeled or mother dyes, indicating that the metachromatic tendency is well preserved.

Experimental

Materials. Spin-labeled dyes were all described in detail previously: monopyrrolidinylated Proflavine (slPF),[2–4] monopiperidylated Acridine Orange (slAO),[2,3] and a spin-labeled 9-aminoacridinium chloride (slAA).[2,3,5] Their structural formulas are shown in Fig. 1. A 3-acetamido derivative of Proflavine (AcPF), for which R_1=–$NHCOCH_3$,[4] was used as the reference for slPF. Sodium salts of poly(*p*-styrenesulfonate) (NaPSS), polyphosphate (NaPP), and polyacrylate (NaPA) were also described elsewhere.[6,7]

Measurements and the Procedure for Data Analysis. Absorption spectra were measured at 25 °C as before.[4,6] A salt-free dye solution was titrated by the dropwise addition of a salt-free polymer solution in an absorption cell with a Gilson micropipet.[1] The molar absorption coefficients, ε, are defined both for dye–polymer solution and for the bound-dye species in the same manner as before.[6,7] A series of titration spectra for a given dye–polymer system were analyzed by the extended PCA procedure.[6–8]

Results and Discussion

Pure Spectra of Bound-dye Species and Equilibrium Constants.

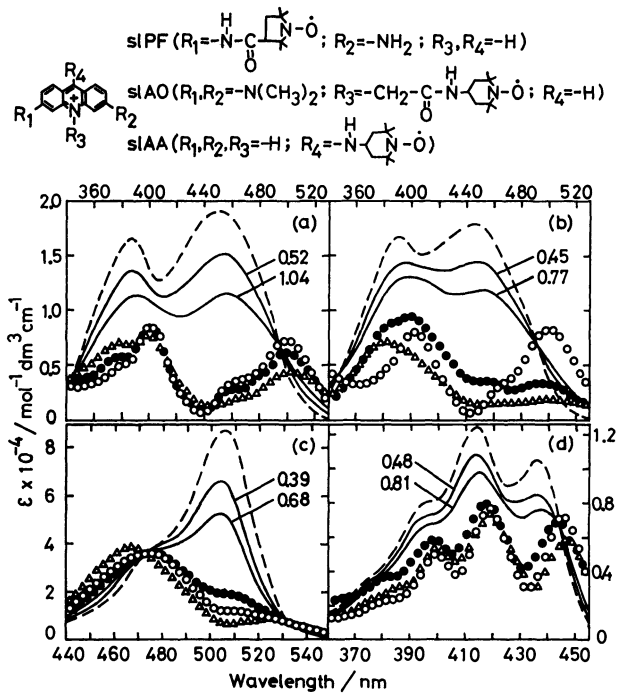

Fig. 1. Structural formulas of dyes and the bound-dye spectra extracted from the series of titration spectra of dye–polymer systems. (a) slPF, (b) AcPF, (c) slAO, and (d) slAA. Polymers bound by each dye are (○) NaPSS, (△) NaPP, and (●) NaPA. Broken lines are the spectra of dyes in the absence of polymers. Solid lines are typical spectra of the respective dye–NaPSS solutions, for which *P*/*D* values are indicated.

Figure 1 shows typical absorption spectra of each of four dyes in the presence and the absence of polyanions. For each dye–polymer system, five to nine titration spectra were measured at a neutral pH over a low *P*/*D* range (0 to 1—2), where *P* and *D* are the concentrations of a polymer in monomer unit and of a dye, respectively.[6] Only a few observed spectra were drawn here, since the details are the same as those reported previously.[6,7] The number of light-absorbing, independent species, *i.e.*, *components*, in each dye–polymer solution was concluded to be two, a free and a bound dye species, by comparing the eigenvalues of the correlation matrix.[6–8] In order to apply the extended PCA procedure to each dye–polymer combination, therefore, use was made of the binding scheme with the apparent equilibrium constant K and the adjustable parameter α: $K=[DP^*]/[D][P]^{\alpha}$. The notations are all the same as before.[6–8] Estimated values of K and α are given in Table 1.

The visible spectra of slPF and AcPF show two absorption bands (Figs. 1a and b) as a result of acylamination, differing from those of PF and Trypaflavine (TF).[2,4] The monosubstituted slPF and AcPF bind

Table 1. The apparent equilibrium constants, K and K', and the parameter α for dye–polymer combinations at 25 °C

		slPF (23.3)[a]	AcPF (20.6)	slAO (5.42)	slAA (37.6)
NaPSS	α	1.3	1.1	1.3	1.2
	K	1.6×10^{6}	2.1×10^{5}	5.0×10^{7}	3.6×10^{5}
	K'[b]	5.6×10^{4}	6.8×10^{4}	9.6×10^{5}	4.2×10^{4}
NaPP	α	1.7	1.3	1.5	1.3
	K	2.4×10^{8}	9.8×10^{6}	1.2×10^{8}	3.9×10^{5}
	K'	8.6×10^{4}	2.8×10^{5}	2.1×10^{5}	1.6×10^{4}
NaPA	α	1.1	0.9	1.4	0.9
	K	4.1×10^{4}	9.2×10^{6}	1.2×10^{7}	9.0×10^{2}
	K'	1.4×10^{4}	2.8×10^{4}	8.3×10^{4}	2.5×10^{3}

a) Values in parentheses are the initial concentrations of the respective dyes in μmol/dm³. b) $K'=K[\mathrm{P}]^{\alpha-1}$ calculated at $P/D=1$.

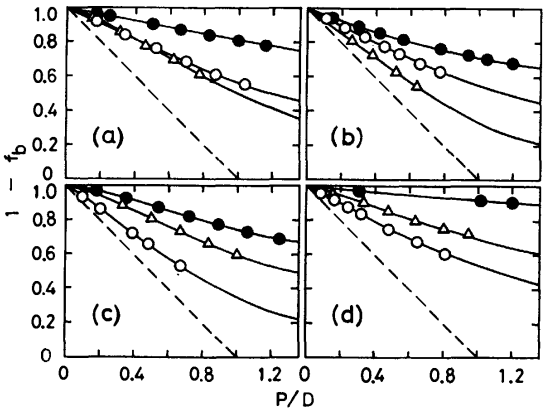

Fig. 2. The P/D dependence of the fraction of free-dye species remaining in the dye–polymer solution, $1-f_b$. (a) slPF, (b) AcPF, (c) slAO, and (d) slAA. The values obtained directly from the t matrix[6–8] are shown by the respective symbols which are the same as in Fig. 1. Solid lines are the binding curves which were calculated with values of K and α in Table 1.[6,7] Dashed lines indicate the relationship: $(1-f_b)=1-(D^b/P)(P/D)$, for which $D^b/P=1$, where D^b is the concentration of a dye species actually bound to the polymer site in solution.

to each of three polyanions, whose functional groups are phosphate, sulfonate, and carboxylate, giving rise to the bound-dye spectra, which resemble each other but differ from those obtained for symmetric TF.[6] Except for the case of AcPF–NaPP, each of the two bands of the bound-slPF or -AcPF spectrum is bathochromic and hypochromic relative to the corresponding band of the spectrum of free slPF or AcPF, showing a possible vibrational structure with energy separations of 1400—1650 cm^{-1};[9] the bound-dye spectra generally show neither hypsochromism nor a new *metachromasy band*, both of which are characteristic of a symmetric 3,6-diaminoacridine dye.[6] The bound-dye spectra of slAO (Fig. 1c) are typically metachromatic, showing the hypochromic effect with new broad bands—one on the longer and the other on the shorter wavelength side of the spectrum of free slAO.[6,10,11] The bound-dye spectra of slAA (Fig. 1d) are associated with a marked hypochromism and a modest bathochromic shift but without any metachromasy band; they are very similar to those of the unlabeled 9-aminoacridinium–polyanion systems reported previously.[7]

Fractions of Bound-dye Species. The fraction of bound-dye species in each solution, f_b, was calculated with values of K and α in Table 1.[6–8] The results are shown in Fig. 2, where the fraction of free-dye species remaining in solution, $1-f_b$, is plotted against P/D. Curvatures of the $(1-f_b)$ *vs.* P/D curves are mostly convex in the initial P/D range, corresponding to values of α larger than unity.[6,7] It is convenient to compare the values of $(1-f_b)$ at $P/D=1$, where equimolar amounts of a dye and a polyanion are present in solution. Spin-labeling lowers the fraction of bound-dye species slightly for slPF but considerably for slAA; the substitution of a label to the amino group may be responsible.[12] Polyacrylate shows a weak affinity toward each spin-labeled dye ($f_b<30\%$ at $P/D=1$) in a way similar to that noted for other dyes;[6,7] this is probably due to the weak acid nature of the side chain.

In conclusion, the spectra of spin-labeled acridine dyes bound to three representative polyanions are very similar to the bound-dye spectra of the corresponding nonlabeled dyes in the low P/D range and, therefore, these labeled dyes can be used for elucidation of metachromasy by the ESR and other magnetic methods.

References

1) Part IX of *Metachromasy*. For the preceding paper of this series: K. Yamaoka and M. Takatsuki, *Bull. Chem. Soc. Jpn.*, **54**, 923 (1981).

2) K. Yamaoka and S. Noji, *Chem. Lett.*, **1976**, 1351, 1355; **1977**, 449; **1979**, 1123.

3) S. Noji and K. Yamaoka, *J. Sci. Hiroshima Univ., Ser. A*, **44**, 101 (1980).

4) K. Yamaoka, S. Noji, and M. Yoshida, *Bull. Chem. Soc. Jpn.*, **54**, 31 (1981).

5) B. K. Sinha, R. L. Cysyk, D. B. Millar, and C. F. Chignell, *J. Med. Chem.*, **19**, 994 (1976).

6) K. Yamaoka and M. Takatsuki, *Bull. Chem. Soc. Jpn.*, **51**, 3182 (1978).

7) K. Yamaoka, M. Takatsuki, and K. Nakata, *Bull. Chem. Soc. Jpn.*, **53**, 3165 (1980).

8) M. Takatsuki and K. Yamaoka, *J. Sci. Hiroshima Univ., Ser. A*, **40**, 387 (1976).

9) Y. Matsuoka and K. Yamaoka, *Bull. Chem. Soc. Jpn.*, **53**, 2146 (1980).

10) M. Miura and Y. Kubota, *Bull. Chem. Soc. Jpn.*, **40**, 466 (1967).

11) V. Vitagliano, L. Costantino, and A. Zagari, *J. Phys. Chem.*, **77**, 204 (1973).

12) A. Albert, "The Acridines," St. Martin's Press, New York, N. Y. (1966), Chap. 10.

The Crystal Structure of Dibromobis(iminodiacetamide)palladium(II)

Masao SEKIZAKI

College of Liberal Arts, Kanazawa University, Marunouchi, Kanazawa 920

(Received April 22, 1981)

Synopsis. The crystals are triclinic, $P\bar{1}$. R is 0.047 for 1617 independent non-zero reflections. The complex has a centrosymmetric square-planar coordination, with two imino nitrogen and two bromine atoms in *trans* positions.

Iminodiacetamide, $HN(CH_2CONH_2)_2$ (abbreviation, $idaaH_2$), acts as a terdentate ligand to the copper(II)[1] and nickel(II)[2] atoms through one imino nitrogen and two amide oxygen atoms. However, the molecular structures of these two complexes are different, as is shown in Fig. 1. If some other transition metals are used, complexes with different structures can be expected. With this expectation, the palladium(II) complex has been prepared and its crystal structure has been analysed.

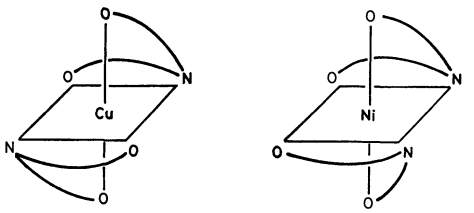

Fig. 1. The structures of $[Cu(idaaH_2)_2]^{2+}$ and $[Ni(idaaH_2)_2]^{2+}$.

Experimental

Preparation of the Complex. Palladium metal powder (0.5 g) was dissolved in an excess amount of a hot conc HBr–HNO_3 mixture (3 : 1 in volume). To this solution, an aqueous solution of 0.2 g of the ligand prepared by a method previously reported[1] was added. The mixture was then kept at pH 2—3 by the use of an HBr or KOH solution, after which it was slowly cooled to room temperature until yellowish-brown plate crystals precipitated.

Measurement of Intensity Data. A crystal with dimensions of 0.1 mm × 0.1 mm × 0.1 mm was selected. The intensities were measured up to $2\theta=60°$ on a Philips PW1100 four-circle diffractometer with Mo $K\alpha$ radiation monochromated by a graphite plate (θ-2θ scan). The 1617 independent reflections with $|F|>3\sigma$ were used with no corrections for absorption and extinction effects ($\mu r=0.3$).

Analytical and Crystal Data. Found: C, 17.92; H, 3.15; N, 15.49%. Calcd for $C_8H_{18}N_6O_4PdBr_2$: C, 18.18; H, 3.43; N, 15.90 %. F. W.=528.50. Triclinic, $a=9.694(2)$, $b=7.434(2)$, $c=6.505(2)$ Å, $\alpha=88.51(4)$, $\beta=101.34(4)$, $\gamma=71.50(2)°$. $U=434(1)$ Å^3. $D_x=2.02$ g/cm^3. $Z=1$. Space group $P\bar{1}$. $\mu=59.3$ cm^{-1} (Mo $K\alpha$ radiation, $\lambda=0.7107$ Å).

Determination and Refinement of the Structure. The structure was determined by means of a heavy-atom method. The block-diagonal least-squares refinement was carried out with the weights of 1.0 for $|F_o|>1.3$ and 0.5 for the others. The positional parameters of all the hydrogen atoms obtained by means of a D-Fourier synthesis were refined with the isotropic temperature factors of 4.0 Å^2. The final R was 0.047. The atomic scattering factors were taken from Ref. 3, together with the anomalous scattering factors, f', of the palladium and bromide ions. A FACOM M-160 computer at the Data Processing Center of Kanazawa University and a FACOM M-200 computer at the Computation Center of Nagoya University were used. The final atomic parameters are listed in Table 1.†

TABLE 1. THE FINAL ATOMIC PARAMETERS WITH ESTIMATED STANDARD DEVIATIONS IN PARENTHESES ($\times 10^3$ FOR H's; $\times 10^4$ FOR OTHERS)

Atom	x	y	z	B_{eq}/Å^2 [5]
Pd	0	0	0	1.58(01)
Br	221(02)	−2463(02)	2653(02)	2.83(02)
N(1)	4069(12)	−2626(10)	−1440(13)	3.29(13)
O(1)	4059(07)	−3415(08)	1876(09)	2.28(08)
C(1)	3773(09)	−2207(10)	395(13)	1.96(10)
C(2)	3145(09)	−104(11)	685(13)	2.08(10)
N(3)	1912(07)	266(09)	1772(10)	1.83(08)
C(4)	1640(10)	2140(12)	2693(13)	2.40(10)
C(5)	2930(09)	2030(11)	4506(12)	2.05(10)
N(5)	3369(10)	3564(11)	4672(14)	3.45(12)
O(5)	3524(08)	590(09)	5717(10)	2.69(09)
Ha(N1)	441(10)	−391(10)	−183(10)	
Hb(N1)	420(10)	−214(10)	−224(10)	
Ha(C2)	396(10)	24(10)	158(10)	
Hb(C2)	252(10)	68(10)	−79(10)	
H(N3)	223(10)	−51(10)	270(10)	
Ha(C4)	132(10)	317(10)	162(10)	
Hb(C4)	63(10)	234(10)	312(10)	
Ha(N5)	414(10)	355(10)	576(10)	
Hb(N5)	222(10)	529(10)	344(10)	

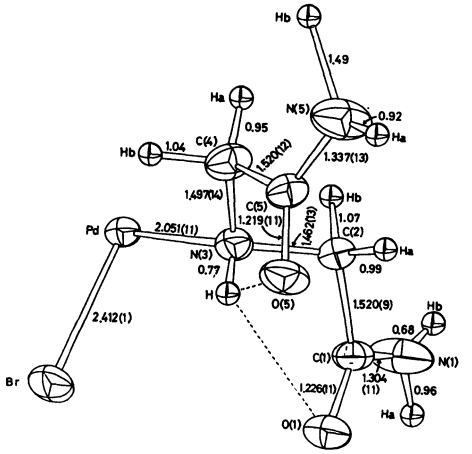

Fig. 2. Structure of the asymmetric unit with the bond lengths (l/Å) and the e.s.d.'s.
Thermal ellipsoids are drawn at 50% probability level.[4] Hydrogen atoms are drawn as spheres with a diameter of 0.2 Å.

† A table of the anisotropic temperature factors and a list of the observed and calculated structure amplitudes have been deposited with the Chemical Society of Japan (Document No. 8154).

Table 2. Bond angles (φ/°)

Br–Pd–N(3)	87.3(3)	C(2)–C(1)–O(1)	120.3(7)
Pd–N(3)–C(2)	114.3(7)	N(1)–C(1)–O(1)	123.0(8)
Pd–N(3)–C(4)	112.3(7)	N(3)–C(4)–C(5)	110.0(8)
C(2)–N(3)–C(4)	110.8(9)	C(4)–C(5)–N(5)	116.8(8)
C(1)–C(2)–N(3)	111.2(7)	C(4)–C(5)–O(5)	120.3(8)
C(2)–C(1)–N(1)	120.3(7)	N(5)–C(5)–O(5)	122.9(9)

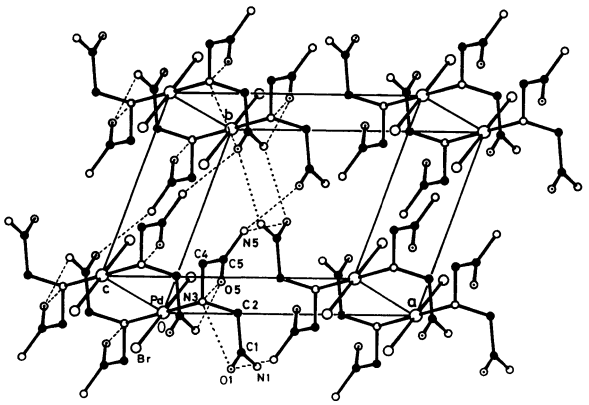

Fig. 3. Crystal structure. Dashed lines exhibit hydrogen bonds.

Description of the Structure

The molecular structure is shown in Fig. 2, along with the bond lengths. The bond angles are listed in Table 2.

The complex is square-planar, with the central atom lying on a center of symmetry of the triclinic unit cell. The bromide ions coordinate in *trans* positions of the square-plane so as to form a non-ionic complex. Each of the iminodiacetamide molecules acts as a unidentate ligand through the imino nitrogen atom; the two amide groups are uncoordinated. This coordination mode of the ligand molecule is different from that for the copper(II)[1] or nickel(II)[2] complex (Fig. 1). Details of the differences will be discussed elsewhere in comparison with other metal–iminodiacetamide complexes.

Table 3. Hydrogen bonds (l/Å)

D —— H···A[a]				D–H	H–A	D–A
N(3)(x,y,z)H	O(1)(	x,	y, z)	0.77	2.47	2.86
N(3)(x,y,z)H	O(5)(	x,	y, z)	0.77	2.42	2.79
N(1)(x,y,z)Ha	O(1)(1−x,	−1−y,	$-z$)	0.96	2.08	2.98
N(1)(x,y,z)Hb	O(5)(	x,	y, −1+z)	0.68	2.24	2.83
N(5)(x,y,z)Ha	O(1)(1−x,	$-y$,	1−z)	0.92	2.06	2.98
N(5)(x,y,z)Hb	O(1)(	x,	1+y, z)	1.49	2.62	3.17
N(5)(x,y,z)Hb	Br (	x,	1+y, z)	1.49	2.08	3.50

a) D, hydrogen donor; A, hydrogen acceptor.

The crystal structure is shown in Fig. 3. The hydrogen bonds are shown in this figure and also in Table 3.

The amide groups turn their oxygen atoms to the palladium atom, and a bifurcated intramolecular hydrogen bond is formed with the imino nitrogen atom, as is shown in Fig. 2 by dashed lines. The two amide nitrogen atoms approach the oxygen atoms of the neighboring molecules to form intermolecular hydrogen bonds in the directions of [1$\bar{1}$0], [100], [010], and [001]. The three-dimensional network is, thus, completed by these N–O-type hydrogen bonds. No contacts shorter than 3.5 Å are, however, observed around the bromine atom.

The author is grateful to Professor Seiji Sugiura of Kanazawa University for the use of the diffractometer.

References

1) M. Sekizaki, *Bull. Chem. Soc. Jpn.*, **47**, 1447 (1974).
2) M. Sekizaki, *Acta Crystallogr., Sect. B*, **32**, 1568 (1976).
3) "International Tables for X-Ray Crystallography," Kynoch Press, Birmingham (1974), Vol. IV.
4) C. K. Johnson, Oak Ridge National Laboratory Report ORNL-3794 (1965); K. Sasaki, "ORTEP-II(NUNICS)," Library Program of the Computation Center of Nagoya University.
5) W. C. Hamilton, *Acta Crystallogr.*, **12**, 609 (1959).

The Action of Boron Trifiuoride on Aromatic Nitrile Oxides

Shinsaku SHIRAISHI,* Tadashi SHIGEMOTO, Masatoshi MIYAHARA, and Shojiro OGAWA
Institute of Industrial Science, The University of Tokyo, Roppongi, Minato-ku, Tokyo 106
(Received July 14, 1980)

Synopsis. The action of boron trifluoride etherate on stable aromatic nitrile oxides effected the isomerization of nitrile oxides into isocyanates competitively with their dimerization to 1,4,2,5-dioxadiazines and/or (1,2,4-oxadiazol-4-io) oxytrifluoroborates. Quenching the reaction with methanol at an earlier stage of the reaction gave methyl benzohydroximate. The reacion was interpreted in terms of the initial coordination of BF_3 with the nitrile-oxide-oxygen atom.

We found the catalytic isomerization of stable aromatic nitrile oxides (NO, **1**) into isocyanates with some Lewis acids. Morrocchi and his co-workers reported the reaction of 2,4,6-trimethylbenzonitrile oxide (**1b**) with BF_3 forming 3,5-bis-(2,4,6-trimethylphenyl)-1,2,4-oxadiazol-4-io]oxytrifluoroborate (**5b**) and 3,6-bis(2,4,6-trimethylphenyl)-1,4,2,5-dioxadiazine (**4b**),[1] but they did not mention the formation of isocyanate. No catalytic isomerization of nitrile oxides has been reported except that with sulfur dioxide, which has been established to proceed *via* a 1,3-dipolar cycloadduct.[2] Here we report the multiplicity of the action of boron trifluoride on stable nitrile oxides.

Results and Discussion

An equimolar reaction of 2,3,5,6-tetramethylbenzonitrile oxides (**1a**) with $BF_3 \cdot OEt_2$ in refluxing dichloromethane gave 2,3,5,6-tetramethylphenylisocyanate (**2a**) in 55% yield. The treatment of the reaction mixture with methanol improved the recovery of **2a** up to 78% as methyl 2,3,5,6-tetramethylphenylcarbamate (**3a**). Various Lewis acids were also found to effect the isomerization of NO (Table 1), though in unsatisfactory yields because of the formation of a sticky mass. The reaction with $BF_3 \cdot OEt_2$ was rather clean, though, and so a detailed investigation was conducted on it (Table 2). The products varied with the reaction conditions employed. In the reaction in dichloromethane, **3a** was obtained as the sole isolable product, but in benzene, 2,4-bis-(2,3,5,6-tetramethylphenyl)-1,4,2,5-dioxadiazine (**4a**) was obtained along with **3a**. In toluene or xylene, a small amount of [3,5-bis(2,3,5,6-tetramethylphenyl)-1,2,4-oxadiazol-4-io]oxytrifluoroborate (**5a**) was obtained in aditdion to **3a** and **4a**. On the contrary, **5a** was the main product in ether, accompanied by a small amount of **3a**. In diisopropyl ether, the three products were obtained in comparable yields. It is noteworthy that the formation of **5a** was favorable compared with that of **4a** in a more polar solvent and that of **4a** in a less polar one. Table 2 also shows that the molar ratio of BF_3/NO influences on the products composition in the reactions in benzene or ether. Morrocchi *et al.* reported the reaction of **1b** with gaseous BF_3 or $BF_3 \cdot OEt_2$ forming **4b** and **5b**.[1] They suggested that **4b** was formed by the bimolecular cyclization of BF_3 coordinated NO. This speculation seems inconsistent with our experimental

TABLE 1. YIELD OF THE URETHANE IN THE REACTION OF THE NITRILE OXIDE WITH VARIOUS LEWIS ACIDS

Nitrile oxide	Lewis acid	Product	Yield/%
1a	$BF_3 \cdot OEt_2$	**3a**	78
1a	$TiCl_4$	**3a**	55
1a	$SnCl_4$	**3a**	43
1a	BBr_3	**3a**	25
1b	$BF_3 \cdot OEt_2$	**3b**	72
1b	$SnCl_4$	**3b**	22

In refluxing dichloromethane. for 2 h Lewis acid/**1** = 1.

TABLE 2. YIELDS OF THE URETHANE (**3a**), THE DIOXADIAZINE (**4a**) AND THE OXADIAZOLIOOXYTRIFLUOROBORATE(**5a**) IN THE REACTION OF THE NITRILE OXIDE (**1a**) WITH BF_3OEt_2 IN VARIOUS SOLVENTS AT 25°C

Solvent	Molar ratio BF_3/**1a**	Yield/%		
		3a	**4a**	**5a**
Dichloromethane	1.0	80	0	0
	0.50	81	0	0
Benzene	2.0	38	29	0
	1.0	37	43	0
	0.55	33	47	0
	0.40	29	44	0
	0.20	28	49	0
Toluene	1.0	38	26	5
	0.50	33	33	3
Xylene	1.0	39	40	3
	0.50	39	38	1
Diisopropyl ether	1.0	31	0	25
	0.50	33	10	25
Ether	1.0	10	0	59
	0.75	9	0	65
	0.50	7	0	57[a]
	0.38	7	0	39[b]
	0.20	0	0	27[c]

a) A small amount of **9a** was also obtained. b) Unreacted **1a** and **9a** were recovered in 19 and 15% yields respec tively. c) **9a** and **1a** were also recovered in 36 and 16% yields respectively.

results. If it were the case, **4a** should be formed favorablly at a higher BF_3/NO ratio, but our result was the opposite as seen in the reactions in benzene. Furthermore, when the reaction was quenched with methanol soon after the addition of $BF_3 \cdot OEt_2$ in the solution of **1b**, methyl 2,4,6-trimethylbenzohydroximate (**9b**) was obtained in a moderate yield in the reaction in either benzene or ether. **9b** was obtained by Grundmann and Frommeld[3] by the methanolysis of **1b** with sulfuric acid. The result implies that the reaction proceeds through the initial coordination of BF_3 with the NO oxygen atom. A subsequent reaction of the free NO with the BF_3-coordinated one (**6**) is considered to afford **4** and **5**. At this stage, two conformers, **7** and **8**, are conceivable for the intermediate; **8** is more stable in polar solvents, and **7** in less polar ones. **7** and **8** may lead to **4** and **5** respectively.

The treatment of **4a** with $BF_3 \cdot OEt_2$ in benzene and subsequently with methanol gave **3a** in 75% yield, but in ether no change was observed. Nor was change observed in diisopropyl ether, where the treatment of **1a** with BF_3 gave **3a** as well **4a** and **5a**. Furthermore, **5a** was confirmed not to be affected by $BF_3 \cdot OEt_2$ in either benzene or ether. This indicates that no interconversion between **2a**, **4a**, and **5a** in the ethereal solvents takes place and that the unimolecular rearrangement fo **6** may be a route to **2** except in benzene, where

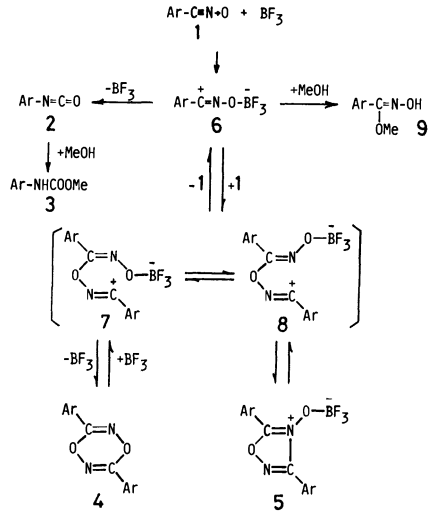

1~9 : Ar = a) 2,3,5,6-$(CH_3)_4C_6H$, b) 2,4,6-$(CH_3)_3C_6H_2$

Scheme 1.

a route *via* **4** cannot be definitely ruled out.

The reaction of **1a** with $BF_3 \cdot OEt_2$ in anisole gave *p*-methoxybenz-2,3,5,6-tetramethylanilide (**10a**) in 68% yield. This may be formed by a Friedel-Crafts reaction of the isocyanate formed with anisole.[4]

Experimental

The melting points are uncorrected. The column chromatography was conducted on silica gel (Waco-gel C-200) with chloroform as the eluent. The IR and ^1H NMR were measured in a KBr disk and in $CDCl_3$ respectively.

Materials. The nitrile oxides (**1a**) and (**1b**) were prepared according to Grundmann and Richter's procedure.[5] The Lewis acids were distilled under nitrogen before use. The solvents were purified and dried by usual methods.

Reactions of **1a** *with* $BF_3 \cdot OEt_2$. *In Dichloromethane*: Into a solution of **1a** (351 mg, 2.0 mmol) in dichloromethane (50 ml) $BF_3 \cdot OEt_2$ (250 μl, 2.0 mmol) was added. The solution was then heated to reflux for 2 h. The subsequent evaporation of the solvent gave an oil, which was treated with column chromatography to give 192 mg (55%) of **2a**, mp 24—25 °C. IR(neat): 2200 cm^{-1} (N=C=O). Treating it with methanol at room temperature (r.t.) overnight gave 224 mg (99%) of **3a**: mp 156—157 °C. IR: 3920 (NH), 1720 cm^{-1} (C=O). ^1H-NMR: δ 2.15 (6H, s, Me), 2.26 (6H, s, Me), 3.75 (3H, s, OMe), 6.96 (1H, s, ArH). Found: C, 69.40; H, 8.38, N, 6.89%; M^+, 207.1294. Calcd for $C_{12}H_{17}NO_2$: C, 69.54; H, 8.27; N, 6.76%, M^+, 207.1258.

The addition of methanol (10 ml) to the reaction mixture after the reaction and subsequently letting it stand at r.t. overnight gave **3a** in 78% yield on column chromatography. This methanol treatment was applied to all the working-up steps hereafter for the full recovery of the **2** in the form of **3**.

Reactions with the other Lewis acids and working-up were conducted similarly. The results are summarized in Table **1**.

In Benzene: A solution of **1a** (1.0 mmol) and $BF_3 \cdot OEt_2$ (1.0 mmol) in benzene (20 ml) was allowed to stand at 25 °C for 3 d under nitrogen. After methanol treatment of the reaction mixture without separating a solid precipitate a precipitate was taken by filtration (67 mg). The filtrate was evaporated to give an oil, column chlomatography of which gave 9 mg of the same solid as was separated above from an earlie elute, **4a**; mp 195—198 °C (from methanol). The total yield was 43%. From the later elute, 76 mg (37%) of **3a** were obtained. **4a**: IR: 2860—3000, 1635, 1615, 1590, 1460, 1330, 1025, 820 cm^{-1}. ^1HNMR: δ 2.26 (12H, s, Me), 2.33 (12H, s, Me), 7.06 (2H, s, ArH). Found: C, 75.41; H, 7.74; N, 7.89%; M^+, 350.1954. Calcd for $C_{22}H_{26}N_2O_2$: C, 75.40; H, 7.48; N, 7.99%; M^+, 350.1993.

In Ether: A solution of **1a** (2.0 mmol) and $BF_3 \cdot OEt_2$ (0.40 mmol) in ether (20 ml) was kept at 25 °C for 3 d. The white needles of **5a** which precipitated were collected by filtration, 113 mg (27%); mp 203—205 °C (from benzene–pet. ether). Methanol treatment of the filtrate and working-up with column chromatography gave 55 mg (16%) of **1a** and 150 mg (36%) of **9a** mp 198—200 °C. Neither **3a** nor **4a** was obtained. **5a**: IR: 2840—3000, 1580, 1050, 860 cm^{-1}. ^1H NMR: δ 2.18 (6H, s, Me), 2.20 (6H, s, Me), 2.32 (12H, s, Me), 7.19 (1H, s, ArH), 7.26 (1H, s, ArH). Found: C, 62.95; H, 6.23; N, 6.56%. Calcd for $C_{22}H_{26}BF_3N_2O_2$: C, 63.17; H, 6.27; N, 6.70%. **9a**: IR: 3200—4000 (OH), 1650 cm^{-1}(C=N). ^1H NMR: δ 2.18 (6H, s, Me), 2.23 (6H, s, Me), 3.74 (3H, s, OMe), 7.00 (1H, s, ArH), 7.90 (1H, broad,OH). Found: C, 69.54; H, 8.34; N, 6.83%; M^+, 207.1257. Calcd for $C_{12}H_{17}NO_2$: C, 69.54; H, 8.27; N, 6.76%; M^+, 207.1258.

The reaction in toluene, xylene, or diisopropyl ether was conducted and worked-up in almost the same manner.

In Anisole: The reaction was conducted using 1 mmol each of **1a** and $BF_3 \cdot OEt_2$ in 10 ml of anisole at r.t. for 3 d. Methanol treatment and solvent evaporation gave an oil, the trituration of which with ether and subsequent filtration gave 123 mg of *p*-methoxybenz-2,3,5,6-tetramethylanilide (**10a**). From the filtrate, 16 mg (9%) of **4a** and 71 mg of **10a** were obtained on column chromatography. The total yield of **10a** was 68%. **10a**, mp 225—227 °C (from benzene–pet. ether): IR: 3285 (NH), 2840—3020, 1630 cm^{-1} (C=O). ^1H NMR: δ 2.11 (6H s, Me), 2.21(6H, s,Me), 3.28 (3H,s, OMe), 6.84(1H, s,ArH), 6.92 (2H, d, ArH), 7.35 (1H, broad, NH), 7.83 (2H, d, ArH). Found: C, 75.84, H, 7.40; N, 4.55%; M^+, 283.1581. Calcd for $C_{18}H_{21}NO_2$: C, 76.30, H, 7.47; N, 4.94; M^+, 283.1571.

Quenching with Methanol. Ten minutes after the addition of $BF_3 \cdot OEt_2$ (0.5 mmol) to a solution of **1b** (161 mg, 1.0 mmol) in ether (50 ml), methanol (5 ml) was added to the solution. The mixture was kept standing at r.t. for 3 d. The subsequent solvent evaporation and column chromatography gave 13 mg (8%) of **1b** and 116 mg (60%) of **9b**; mp 140—141 °C (lit,[3] 140—141 °C). A similar reaction in benzene gave 4% of **1b**, 14% of **4b** (mp 171—174 °C (lit,[1] 172—173 °C)), and 54% of **9b**.

A similar reaction of **1a** in ether afforded 74% of **9a** as the sole isolable product.

Reaction of **4a** *with* $BF_3 \cdot OEt_2$. A solution of **4a** (88 mg, 0.25 mmol) and $BF_3 \cdot OEt_2$ (65 μl, 0.50 mmol) in benzene (20 ml) was let stand at 25 °C for 3 d. The subsequent methanol treatment of the solution and evaporation of the solvent gave a solid, which afforded 12 mg (14%) of **4a** and 78 mg (75%) of **3a** on column chromatography. A similar treatment of **4a** in ether or diisopropyl ether only resulted in no change.

References

1) S. Morrocchi, A. Ricca, A. Selva, and A. Zanarotti, *Gazz. Chim. Ital.*, **99**, 165 (1965).

2) G. Trickes and H. Meier, *Angew. Chem.*, **89**, 637 (1977).

3) C. Grundmann and H-D. Frommeld, *J. Org. Chem.*, **31**, 157 (1966).

4) F. Effenberger, R. Gleiter, L. Heider, and R. Niess, *Chem. Ber.*, **101**, 502 (1968).

5) C. Grundmann and R. Richter, *J. Org. Chem.*, **33**, 476 (1968).

Solid Phase Synthesis of Crystalline Protected Penta-L-tryptophan Methyl Esters

Masaaki UEKI,* Shigeru IKEDA, and Takashi HANDA

Department of Applied Chemistry, Science University of Tokyo, 1-3 Kagurazaka, Shinjuku-ku, Tokyo 162

(Received December 26, 1980)

Synopsis. Solid phase syntheses of protected tryptophan homo-oligomers were accomplished by utilizing dimethylphosphinothioyl(Mpt) group as an N^{α}-amino protecting group which was removed by treatment with triphenylphosphine dihydrochloride. By measurements of the ultraviolet and fluorescence spectra it was ascertained that no modification on the tryptophan indole ring had occurred during these syntheses.

Studies on conformation of tryptophan containing peptides have restriction because of difficulty in synthesizing pure model peptides. The usual synthesis by the use of *t*-butoxycarbonyl (Boc) group as an N^{α}-amino protecting group is not applicable to the synthesis of tryptophan containing peptides without special care because *t*-butylation of the tryptophan indole ring easily occurs during deprotection by trifluoroacetic acid.[1] Occurrence of modification of the indole nucleus can be most conveniently detected by fluorescence spectrum measurement.[2]

Recently we reported that the diphenylphosphinothioyl (Ppt) group was useful for the synthesis of tryptophan containing peptides because Ppt–Cl, a by-product formed in the deprotection step, did not modify the indole ring.[3,4] Lately dimethylphosphinothioyl (Mpt) group was found to be much more easily removable than the Ppt group and especially suitable for solid phase synthesis as shown in the synthesis of Leu^5-enkephalin and its D-Ala^2 analog.[5] In this work solid phase synthesis of tryptophan oligomers by use of Mpt-tryptophan was tried.

The *N*-Mpt group can be removed by the hydrogen chloride reagents used generally in peptide synthesis. As an especially effective reagent for the removal of the Mpt group, hydrogen chloride absorbed in a solution of triphenyl phosphine (TPP) in dichloromethane is recommended. TPP is added; firstly because it can suppress the acidity of HCl through the salt formation with TPP (pK_a 2.3 in 80% ethanol)[6] and secondly because it makes it possible to prepare a storable dichloromethane solution of HCl of practically useful concentration. The effectiveness of the acidity control of HCl by TPP was made clear by comparison of deprotection rates of Boc- and Mpt-di-L-tryptophan methyl esters in the presence or absence of TPP. The results are summerized in Table 1. The rate of removal of the Boc group which needs sufficient proton concentration was markedly lowered by the addition of TPP. On the other hand the removal rate of the Mpt group was affected only slightly.

Table 1. Deprotection rate of R–L-Trp–L-Trp–OCH_3

Reagent	R=Mpt k/h^{-1}	R=Boc k/h^{-1}
0.1 M HCl/CH_2Cl_2	1.90	2.40
0.1 M HCl (0.1 M TPP)/CH_2Cl_2	1.65	0.027

The stability of tryptophan during the course of deprotection of the Mpt group was ascertained by measuring the per cent recovery of tryptophan with an amino acid analyzer. When Mpt-L-tryptophan was deprotected by treating with 0.2 M† HCl (0.2 M TPP)/CH_2Cl_2 a clear colorless solution resulted to give 98% recovery of tryptophan. No ninhydrin-positive spot other than tryptophan was detected by silica gel thin layer chromatography.

Solid phase syntheses of protected penta-L-tryptophan methyl esters were performed on the automatically programmed Beckman model 990 peptide synthesizer.

Table 2. Properties of protected tryptophanhomo-oligomers

Compound	Mp/°C	$[\alpha]_D^{25}$(deg)	Found (Calcd)(%) C	H	N
Mpt-L-Trp-OCH_3	108—109	−2.4 (*c* 1, methanol)	54.31 (54.20)	6.50 (6.12)	9.05 (9.02)
Mpt-(L-Trp)$_2$-OCH_3	153—154	−47.6 (*c* 0.5, methanol)	60.84 (60.47)	6.03 (5.89)	11.35 (11.28)
Mpt-(L-Trp)$_3$-OCH_3	amorphous	−66.8 (*c* 0.5, methanol)	63.21 (63.33)	5.96 (5.76)	12.23 (12.31)
Mpt-(L-Trp)$_4$-OCH_3	amorphous	−65.6 (*c* 0.5, methanol)	63.52 (63.67)[a]	5.87 (5.75)[a]	12.27 (12.63)[a]
Mpt-(L-Trp)$_5$-OCH_3	151—154	−65.0 (*c* 0.5, methanol)	65.11 (64.91)[b]	5.56 (5.73)[b]	13.13 (13.05)[b]
Ac-(L-Trp)$_5$-OCH_3	233—236 (dec)	−33.1 (*c* 0.6, DMF)	67.70 (68.08)[c]	5.58 (5.71)[c]	13.81 (13.69)[c]
Boc-(L-Trp)$_5$-OCH_3	211—213 (dec)	−51.0 (*c* 0.5, methanol)	68.71 (68.91)	5.93 (5.88)	13.04 (13.17)

a) Calcd for $C_{47}H_{49}N_8O_5PS \cdot H_2O$. b) Calcd for $C_{58}H_{59}N_{10}O_6PS \cdot H_2O$. c) Calcd for $C_{58}H_{56}N_{10}O_7 \cdot H_2O$.

† 1 M=1 mol dm^{-3}.

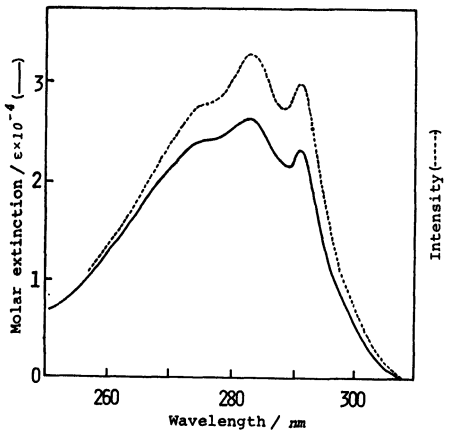

Fig. 1. a) UV spectrum of **1**(——) in methanol. b)Fluorescences excitation spectrum of **1** (emmission at 340 nm) (------) in methanol.

N^{α}-Mpt-penta-L-tryptophan methyl ester (**1**) was separated from the resin support by transesterification.[7] The crude product was purified by gel chromatography on Sephadex LH-20 and recrystallization from ethanol. Pure **1** was obtained in 60% yield as colorless crystals.

In order to know the effect of *N*-terminal group N^{α}-Boc-penta-L-tryptophan methyl ester (**2**) was also synthesized by coupling tetra-L-tryptophan resin with Boc-L-tryptophan. Compound **2** was obtained in 66% yield after the same processes of isolation and purification used in the synthesis of the Mpt derivative. The N^{α}-acetyl (Ac) derivative was obtained in 66% yield by treating unprotected penta-L-tryptophan resin with acetic anhydride and triethylamine.

Among the three types of protected-penta-L-tryptophan methyl esters the Mpt derivative showed the highest solubility in organic solvents such as methanol.

N^{α}-Mpt-tri- and tetra-L-tryptophan methyl esters were synthesized according to the same solid phase procedures. N^{α}-Mpt-mono- and di-L-tryptophan methyl esters were obtained by a liquid phase method. The physical properties and elemental analysis data of all the synthetic peptides are summarized in Table 2.

Chemical purity was checked by high performance liquid chromatography by adopting an ODS support and a linear (0 to 3%) methanol–chloroform gradient for elution. Each peptide appeared as a single peak.

Purity of the peptide **1** was further ascertained by measurements of the ultraviolet and fluorescence spectra. The UV spectrum (Fig. 1a) showed the typical curve of tryptophan with λ_{max} at 283 nm; also the fluorescence excitation spectrum (Fig. 1b) gave the same pattern as the UV spectrum. From these results it was ascertained that no modification on the tryptophan indole ring had occurred during the synthesis. Boc- and Ac-derivatives also showed high purity.

The relationships between the spectroscopic properties and the conformation of these synthetic peptides are now being studied and the results will be published in due course.

Experimental

N^{α}-*Dimethylphosphinothioyl-penta-*L-*Tryptophan Methyl Ester (Mpt-*L-*Trp-*L-*Trp-*L-*Trp-*L-*Trp-*L-*Trp-*L-*Trp-*OCH_3*) (**1**).* Chloromethylated copoly(styrene-1% divinylbenzene) resin (0.96 mmol Cl/g, Wako Pure Chemicals Ind., Ltd.) was esterified with N^{α}-Mpt-L-tryptophan by the caesium salt method.[8] The amino acid content of the resin was obtained as 0.56 mmol/g by Dorman method.[9] One gram of the ester resin was placed in the reaction vessel of the Beckman model 990 peptide synthesizer. Mpt group was removed by treating twice for each 30 min with 0.2 M HCl (0.2 M TPP)/CH_2Cl_2. After neutralization with 10% triethylamine in dichloromethane, couplings were mediated with the oxidation-reduction condensation[10] using tris(*p*-methoxyphenyl)phosphine and 2,2′-dithiodipyridine. After four cycles of these procedures N^{α}-Mpt-penta-L-tryptophan was cleaved from the resin support as its methyl ester by treating it five times with 1 M triethylamine in methanol for each 12 h. All the filtrates and methanol washings were combined and evaporated *in vacuo*. The residue was washed with water and dried to give a slightly yellow solid containing minor impurity when analyzed on silica gel by thin layer chromatography; 0.611 g. The solid was dissolved in a small volume of methanol and applied to a Sephadex LH-20 (1.9 cm × 100 cm) column. Methanol eluate (flow rate-1 ml/min) was monitored by UV spectrophotometry at 254 nm and collected as 5 ml fractions. The fractions containing a single component, when detected on silica gel thin layer chromatography, were combined and evaporated to give colorless crystals of **1**; 0.414 g. An analytically pure sample was obtained by recrystallization from ethanol; 0.354 g (60% calculated from N^{α}-Mpt-L-tryptophan resin).

References

1) E. Wünsch, E. Jaeger, L. Kisfaludy, and M. Low, *Angew. Chem.*, **89**, 330 (1977).
2) E. Jaeger, P. Thamm, I. Schmidt, S. Knof, L. Moroder, and E. Wunsch, *Hoppe-Seyler's Z. Phys. Chem.*, **359**. 155 (1978).
3) M. Ueki and S. Ikeda, *Chem. Lett.*, **1977**, 869.
4) S. Ikeda, F. Tonegawa, E. Shikano, K. Shinozaki, and M. Ueki, *Bull. Chem. Soc. Jpn.*, **52**, 1431 (1979).
5) M. Ueki, T. Inazu, and S. Ikeda, *Bull. Chem. Soc. Jpn.*, **52**, 2424 (1979).
6) H. Goetz and A. Sidhu, *Justus Lieblgs Ann. Chem.*, **682**, 71 (1965).
7) H. C. Beyerman, H. Hindriks, and E. W. B. de Leer, *J. Chem. Soc., Chem. Commun.*, **1968**, 1668.
8) B. F. Gisin, *Helv. Chim. Acta*, **56**, 1476 (1973).
9) L. C. Dorman, *Tetrahedron Lett.*, **1969**, 2319.
10) T.Mukaiyama, R.Matsueda, and M. Suzuki, *Tetrahedron Lett.*, **1970**, 1901.

Abnormal $LiAlH_4$ Reduction of 4,4-Diphenyl-3-cyano-2-methyl-2-pyrrolin-5-one

Sadatoshi AKABORI,* Kazue TAKAHASHI, Michiko OHTOMI, and Yohko SAKAMOTO

Department of Chemistry, Faculty of Science, Toho University, Funabashi, Chiba 274

(Received January 29, 1981)

Synopsis. The reduction of 4,4-diphenyl-3-cyano-2-methyl-2-pyrrolin-5-one with lithium aluminum hydride yields three unexpected reduction products, together with the usual product.

We have recently reported[1] that benzoins can be converted into 4,4-diaryl-3-cyano-2-methyl-2-pyrrolin-5-ones in good yields by a reaction with sodio-3-iminobutanenitrile in THF.

We now wish to report our results on the reduction of 4,4-diphenyl-3-cyano-2-methyl-2-pyrrolin-5-one (**1**) with $LiAlH_4$. Thus, **1** was treated with an excess of $LiAlH_4$ under anhydrous conditions, in THF. The expected compound (**2**) was formed in a minute amount; 3,3-diphenyl-4-cyano-5-methyl-2-pyrrolidinone (**3**) was a major product, along with **4** and **5** in about 5 and 3% yields respectively.

The molecular formula of **2** was deduced to be $C_{18}H_{16}N_2$ by means of the mass spectrum (M^+, *m/e* 260) and the elemental analysis. The IR spectrum of **2** displayed a strong NH absorption at 3300 cm^{-1} and C≡N at 2190 cm^{-1}. However, the IR spectrum lacked bands arising from the carbonyl group. Furthermore, in the ^1H NMR spectrum of **2**, the resonance for the methylene group appeared at δ 4.02 (s, 2H) as a sharp singlet, in addition to a singlet (3H, CH_3) at δ 2.00, a broad singlet (1H, NH) at δ 4.45, and a multiplet (10H, aromatic protons) at δ 7.27. All these results can be accommodated in the **2** structure. The molecular formula of **3** was deduced to be $C_{18}H_{16}N_2O$ by means of the mass spectrum (M^+, *m/e* 276) and by elemental analysis. The ^1H NMR spectrum of **3** showed the signal of methyl (δ 1.35, d, J=5 Hz) and two methine (δ 3.75, m, and 4.20, d, J=8 Hz) groups, in addition to a broad singlet (1H, NH) at δ 8.74 and a multiplet (10H, aromatic protons) at δ 7.30, which could be assigned to two phenyl groups. Decoupling experiments revealed that the multiplet observed at δ 3.57 is coupled to a proton at δ 4.20 with J=8 Hz and also to a methyl proton at δ 1.35 with J=5 Hz, showing the presence of the CH_3–CH–CH– moiety. The presence of the carbonyl group was supported by the appearance of the characteristic carbonyl absorption at 1720 cm^{-1} in the IR spectrum. From these facts, the structure of **3** was assigned. The molecular formula of **4** was deduced to be $C_{18}H_{18}N_2O$ by means of the mass spectrum (M^+, *m/e* 278) and by the elemental analysis. The ^1H NMR spectrum of **4** showed the signals of methyl (δ 0.69), methylene (δ 1.52), and methine (δ 4.42) groups, in addition to two NH protons as a broad singlet at δ 6.95 and δ 8.05 and phenyl protons as a multiplet at δ 7.38. Decoupling experiments revealed that the multiplet protons observed at δ 1.52 are coupled to the methyl protons at δ 0.69 with J=7 Hz, and also to a methylene proton at δ 4.42 with J=7 Hz, showing the presence of a $-CHCH_2CH_3$ moiety. Irradiation at δ 1.52 changed the triplet at δ 0.69 into a singlet and the triplet at δ 4.42 into a singlet. Its IR spectrum exhibited absorption bands at 3300 (NH), 1770, and 1700 cm^{-1}. These absorptions suggested the presence of a –CO–NH–C(=NH)– moiety. All these results can be accommodated in the **4** structure. The molecular formula of **5** was also deduced to be $C_{18}H_{17}NO_2$ by means of the mass spectrum (M^+, *m/e* 279) and the elemental analysis. Compound **5** showed IR absorption bands at 3200, 1780, 1715, and 1500 cm^{-1}. These absorptions suggested the presence of a –CO–NH–CO– moiety. From these facts, the structure of **5** was assigned.

It is known[2] that an amide, on reduction with $LiAlH_4$, is converted in a good yield into a corresponding amine. For example, in THF at 65 °C, 5,5-dimethyl-2-pyrrolidinone is reduced to 2,2-dimethylpyrrolidine in a 67—79% yield. However, the similar reaction of **1** failed to give 3,3-diphenyl-4-cyano-5-methyl-2,3-dihydropyrrole (**2**) as a main product. The considerable difficulty in the reduction of the carbonyl group may be explained by the steric hindrance given by the adjacent two phenyl groups. It is interesting to note that $LiAlH_4$ reduces the double bond of **1**,[4] in spite of the fact that it does not reduce ethylenic or acetylenic hydrocarbons.[3] The formation of **4** can be explained by the process initiated by the cleavage of the N–C_5 bond of **3** and the attack of the nitrogen anion[5] on the carbon atom of the cyano group, followed by the addition of a proton at the C=N$^-$ group. Additionally, the hydrolysis of **4** affords **5**. With the proper control of the amount of $LiAlH_4$, *N,N*-disubstituted amide is known[5] to be susceptible to the cleavage of the –CO–NH– bond. However, the formation of an amine and an aldehyde on the reduction of an amide is induced by the addition of the hydride anion to the carbonyl. The present reduction differs from this type of cleavage in that the C–N bond is directly attacked by the hydride. In support of this explanation, two compound, **4** and **5**,[7] were obtained, in 13 and 8% yields respectively, by the reduction of **3** with $LiAlH_4$ in THF.

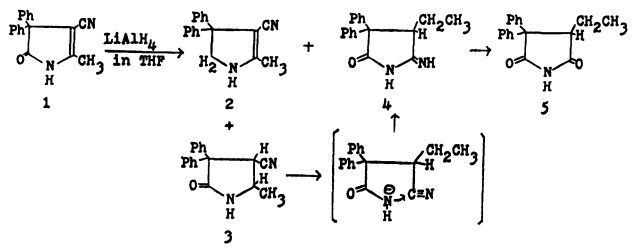

Experimental

All the melting points are uncorrected. The infrared spectra were measured on a JASCO IRA-2 Diffraction Grating

Infrared Spectrometer. The NMR spectra were determined on a JNM-4H-100 spectrometer instrument, using TMS as the internal reference. The MS spectra were taken by using a JEOL-JMS-OlSG-2 mass spectrometer.

Materials. 4,4-Diphenyl-3-cyano-2-methyl-2-pyrrolin-5-one was prepared according to the procedure described in a previous paper.[1] Lithium aluminum hydride was used without further purification. The solvents were purified by distillation.

*Reduction of **1** with Lithium Aluminum Hydride in THF.* A solution of 2.74 g (10 mmol) of **1** in 150 ml of THF was added, over a period of 2 h, to a stirred suspension of an excess of lithium aluminum hydride (1.52 g, 40 mmol) in 150 ml of THF at reflux under an atmosphere of nitrogen. After careful decomposition with cold water, the solution was concentrated to *ca.* 80 ml. To a solution this obtained we added 10% hydrochloric acid (30 ml). The mixture was allowed to stand overnight to give yellowish solids. The precipitated solids were filtered off and recrystallized from ethyl acetate–hexane to give **3** (78%); mp 224—226 °C. Found: C, 78.11; H, 5.99; N, 10.20%. Calcd for $C_{18}H_{16}N_2O$: C, 78.23; H, 5.86; N, 10.14%. MS 276 (M^+). IR (KBr) 3290 (NH), 2200 (C≡N), 1720 (C=O) cm^{-1}. ^1H NMR (DMSO-d_6) δ 1.35 (d, J=5 Hz, 3H, CH_3), 3.75 (m, 1H, CH), 4.20 (d, J=8 Hz, 1H, CH), 7.30 (m, 10H, aromatic H), 8.74 (bs, 1H, NH). The evaporation of the mother-liquor at room temperature, after the separation of the **3**, gave a solid residue which was fractionally recrystallized from hexane containing a small amount of ethyl acetate to give **2** (3%); mp 115—116 °C. Found: C, 82.69; H, 6.31; N, 10.56%, Calcd for $C_{18}H_{16}N_2$: C, 83.04; H, 6.20; N, 10.74%. MS 260 (M^+). IR(KBr) 3300 (NH), 2190 (C≡N), 1600 cm^{-1}. ^1H NMR($CDCl_3$) δ 2.00 (s, 3H,CH_3), 4.02 (s, 2H, CH_2), 4.45 (s, 1H, NH), 7.27 (s, 10H, aromatic H). The mother-liquors, after isolation of **2**, were evaporated at room temperature to give the crude **5**. The recrystallization of the crude material from ethanol give pure **5** (3%); mp 134—136 °C. Found: C, 77.48; H, 6.13; N, 4.98%, Calcd for $C_{18}H_{17}NO_2$: C, 77.48; H, 6.13; N, 5.01%. MS 279 (M^+). IR (KBr) 3200 (NH), 1780, 1715 cm^{-1}. ^1H NMR (DMSO-d_6) δ 0.92 (t, J=5 Hz, 3H, CH_3), 1.15 (m, 2H, CH_2), 3.65 (t, J=6 Hz, 1H, CH), 7.25 (m, 10H, aromatic H), 9.13 (bs, 1H, NH).

*Isolation of **4** from the Reduction Mixture of **1** with $LiAlH_4$ in THF.* The reduction was carried out in the same manner used the above reaction. After careful decomposition with water, the solution was concentrated to *ca.* 80 ml. The aqueous solution was extracted with ether; the ether extract was washed with water, dried over anhydrous $MgSO_4$, and filtered. After the removal of the solvent and several recrystallizations from ethyl acetate–hexane, we obtained 0.692 g of **3**. The aqueous solution was allowed to stand at room temperature until crystallization occurred. The recrystallization of the filtered solid product from ethanol gave **4** as colorless crystals in 5% yields; mp 289—291 °C. Found: C, 77.52; H, 6.58; N, 10.05%. Calcd for $C_{18}H_{18}N_2O$: C, 77.67; H, 6.58; N, 10.05%. MS 278 (M^+). IR (KBr) 3300 (NH), 1770, 1700 cm^{-1}. ^1H NMR (DMSO-d_6) δ 0.69 (t, J=7 Hz, 3H, CH_3), 1.52 (m, 2H, CH_2), 4.42 (t, J=7 Hz, 1H, CH), 7.38 (bs, 10H, aromatic H), 6.95 (bs, 1H, NH), 8.05 (bs, 1H, NH).

*Reduction of **3** with Lithium Aluminum Hydride in THF.* A solution of 1.38 g (5 mmol) of **3** in 70 ml of THF was stirres, over a period of 2 h, into a suspension of an excess of $LiAlH_4$ (0.76 g, 20 mmol) in 70 ml of THF at reflux under an atmosphere of nitrogen. After careful decomposition with cold water, the volume of the solution was concentrated to *ca.* 35 ml. To the solution thus obtained we added 10% hydrochloric acid (13 ml). The mixture was allowed to stand overnight to give a yellowish, unreacted material as a solid. The solids were filtered off and recrystallized from ethyl acetate–hexane to give pure **3** (0.75 g). The evaporation of the mother-liquor at room temperature, after the separation of the **3**, gave a solid residue which was fractionally recrystallized from ethyl acetate–hexane to give **4** (13%); mp 289—291 °C. The mother-liquors, after the isolation of **4** were evaporated at room temperature to give the crude **5**. The recrystallization of the crude material from ethanol give pure **5** (8%); mp 134—136 °C.

The authors wish to thank Mr Mitsuo Takayama, Department of Pharmacology, Toho University, for the measurements of the mass spectra.

References

1) S. Akabori, M. Ohtomi, K. Takahashi, Y. Sakamoto, and Y. Ichinohe, *Synthesis*, **1980**, 900.

2) R. B. Moffet, *Org. Synth.*, Coll. Vol. 4, 355 (1963).

3) L. F. Fieser and M. Fieser, "Reagents for Organic Synthesis," John Wiley and Sons (1967), Vol. 1, p. 592.

4) It is known that an α,β-unsaturated alcohol affords a complex with $LiAlH_4$ which, on decomposition with water, affords saturated alcohol; R. F. Nystrom and W. G. Brown, *J. Am. Chem. Soc.*, **69**, 2548 (1947); **70**, 3738 (1948); R. T. Gilsdorf and F. F. Nord, *J. Org. Chem.*, **15**, 807 (1956). It is also known that the lithium aluminum hydride reduction of the double bond of α,β-unsaturated ketone gave the corresponding saturated ketone; T. G. Halsall and M. Moyle, *J. Chem. Soc.*, **1960**, 1324; T. Anthonsen, P. H. McCabe, R. McCrindle, and R. D. H. Murray, *J. Chem. Soc., Chem. Commum.*, **1966**, 740.

5) F. Baumann, B. Bienert, G. Rasch, H. Vollmann, and W. Wolf, *Angew. Chem.*, **68**, 133 (1956).

6) F. Weygand and R. Mitau, *Chem. Ber.*, **89**, 301 (1955).

7) Compound **5** was also obtained in a 58% yield by the hydrolysis of **4** with dilute hydrochloric acid.

Acid-induced Ring-opening of 2′-Substituted Spiro[anthracene-9(10H), 1′-cyclopropan]-10-ones

Kiyoichi HIRAKAWA* and Hajime SATO

Department of Chemistry, Faculty of Textile Science and Technology, Shinshu University, Ueda, Nagano 386

(Received February 6, 1981)

Synopsis. The title compounds (**1**) reacted under acidic conditions to give cyclopropane ring-opened products. In these reactions of **1** bearing methyl-, phenyl-, chloro-, bromo-, and acetoxy-substituents, the cyclopropane ring opened from the more substituted side.

We have previously investigated the reactions of spiro keto compounds.[1,2] In these investigations, it has been found that phenyl-substituted spiro[anthracene-9(10*H*),1′-cyclopropan]-10-ones undergo thermal rearrangement with ring expansion to aceanthrylen-6(2*H*)-ones, whereas a simple cyclopropane-opening, involving the formation of the hydroxy-carbonium ion (*e.g.* **2**) as an intermediate, is observed in the acid-induced reaction. We have further examined the cyclopropane-opening reactions of 2′-substituted spiro[anthracene-9(10*H*),1′-cyclopropan]-10-ones **1** under acidic conditions and their utilization in the preparations of substituted anthracenes.

Results and Discussion

The spiro anthrones **1a**—**c** and **g** were prepared by previously known procedures.[3] The spiro anthrones **1d**—**f** were obtained in 66, 45, and 53% yields, respectively, by irradiation of 10-diazoanthrone (**3**) in the presence of an appropriate olefin.

As was observed in the previous work, the expected products **4** and **5** in the reaction with acidic reagent (HZ) were too unstable to be isolated.[1] Therefore, the acid-induced reactions were carried out in acetic anhydride in the presence of a small amount of mineral acid to convert **4** and **5** to isolable **6** and **7**. Treatment of **1a**, **b**, and **f** with acetic anhydride–sulfuric acid gave **8a** (86%), **b** (81%), and **f** (33%), respectively.[4] The structures of products were assigned as **8** rather than $AcOC_{14}H_8CHRCH_2OAc$, cyclopropane ring-opening from the less substituted side, by their ^1H NMR spectral data: *e.g.* the assignment of **8b** is based on its absorption for methylene and methine hydrogens at δ 3.74 (center, m) and 5.27 (m), respectively; these values are normal compared with those estimated from the absorption which was found in **8a**. The structure $AcOC_{14}H_8CHMeCH_2OAc$ should exhibit methylene absorption near δ 4.12—4.56 (for CH_2CH_2OAc of **8a**), and the observed methine absorption at δ 5.27 is too far downfield to support this claim. The similar acid-induced reactions of 2′-halogenosubstituted spiro anthrones **1d** and **e** afforded 10-acetoxy-9-(formylmethyl)anthracene (**9**) (14—17%) and **8f** (34—35%). The anthracene **9** was identified on the basis of its spectral data and chemical behavior, *i.e.* the reaction of **9** with acetic anhydride in the presence of sulfuric acid led to **8f**. The formation of **9** may be accounted for by the formation of the anthracenes **7d** and **e** followed by elimination of acyl halide.[5] On the other hand, the reaction of **1g** bearing such strongly electron-withdrawing groups as CN gave a complex mixture.

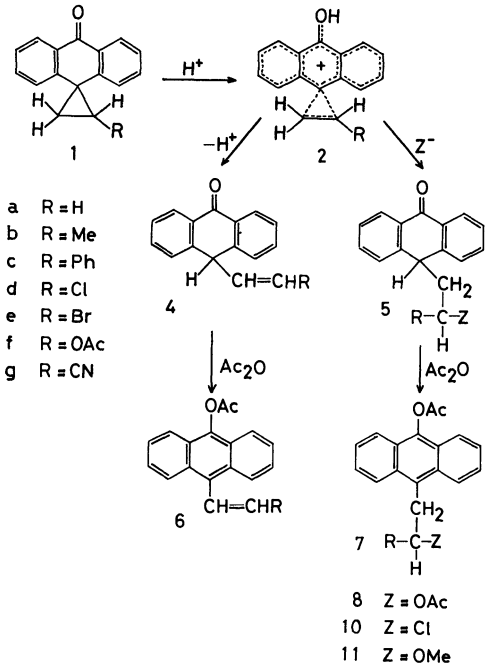

The reactions of **1a**, **b**, **d**, and **e** with acetic anhydride-hydrochloric acid yielded **10a** (78%), **b** (75%), **d** (71%), and **e** (69%), respectively, as the major products, together with **8a** (4%), **b** (5%), **9** (10%), and **9** (9%), respectively, as the minor products. The structural assignments of **10** are based on their ^1H NMR spectral data. The predominant formation of **10** is compatible with the common observation that a chloride ion is more nucleophilic than an acetate ion.[6] Under similar conditions, the spiro anthrones **1c** and **f** afforded a complex product mixture, and **1g** gave no products.

The ring-opening of **1** with hydrochloric acid in methanol were further examined. As mentioned above, the products of the type **5** (Z=Cl or OMe) were too unstable to be isolated, so that they were isolated after acetylation. The reactions of **1a** and **b** gave **10a** (70%) and **b** (65%), respectively. In the similar treatment of **1c**, the anthracene **11c**, which resulted from the solvolysis of **5c** (Z=Cl) in methanol, was obtained in a 69% yield. The similar treatment of **1d**, **e**, and **g** with methanolic hydrochloric acid gave no product.

The spiro anthrone system is intriguing in that the protonation of the carbonyl oxygen may lead to a hydroxy-carbonium ion **2** which is conceivably bridged.[7] The direction of the cyclopropane-opening is consistent with the expectation that the relative stability of the incipient cationic centers will be a controlling factor.

Experimental

Preparations of 2'-Substituted Spiro[anthracene-9(10H),1'-cyclopropan]-10-ones **1**. ***1d***: A solution of 10-diazoanthrone (**3**)[8] (3.30 g, 15 mmol) in benzene (300 ml) was saturated with vinyl chloride, and the resulting mixture was then irradiated at 5 °C with a 100 W high pressure mercury lamp through a Pyrex filter until TLC showed the absence of **3** (*ca.* 12 h). The solvent and unchanged vinyl chloride were removed under reduced pressure; then the residue was chromatographed on silica gel (benzene as eluant). The first eluate gave **1d** as colorless needles (2.52 g, 66%), mp 122—123 °C.

1e: The product from photoreaction of **3** (3.30 g, 15 mmol) with vinyl bromide (32.1 g, 0.3 mol) in benzene (300 ml) under nitrogen was chromatographed to give **1e** as colorless needles (2.02 g, 45%), mp 134—135 °C.

1f: A similar photoreaction of **3** (3.30 g, 15 mmol) and vinyl acetate (28.8 g, 0.3 mol) in benzene (300 ml) gave **1f** as colorless microcrystals (2.21 g, 53%), mp 94—95 °C.

The spectral and analytical data of **1d**—**f** are consistent with the proposed structures.

Reaction of **1** *with Acetic Anhydride–Sulfuric Acid.* A solution of a spiro anthrone **1** (2—3 mmol) in acetic anhydride (30 ml) containing sulfuric acid (0.5 ml) was allowed to stand at room temperature (10 h). After TLC showed the absence of the starting material, the mixture was poured into water. The precipitate was worked up by recrystallization or chromatography. Spectral and analytical data of the products are given below.

8a: Yellow needles (from benzene); mp 157 °C; IR (KBr disc) 1768 and 1750 cm^{-1} (CO); ^1H NMR ($CDCl_3$) δ 2.20 (3H, s), 2.51 (3H, s), 3.58—4.02 (2H, a part of A_2B_2), 4.12—4.56 (2H, a part of A_2B_2), and 7.15—8.95 (8H, m); MS *m/e* 332 (M^+). Found: C, 74.60; H, 5.68%. Calcd for $C_{20}H_{18}O_4$: C, 74.52; H, 5.63%.

8b: Yellow microcrystals (from benzene–hexane); mp 130—131 °C; IR 1778 and 1746 cm^{-1} (CO); ^1H NMR δ 1.13 (3H, d, J=6.5 Hz), 1.93 (3H, s), 2.50 (3H, s), 3.63 and 3.84 (1H each, AB part of ABX, J_{AB}=13.5, J_{AX}=8,2, J_{BX}=5.7 Hz), 5.27 (1H, m), and 7.25—8.58 (8H, m); MS *m/e* 336 (M^+). Found: C, 74.94; H, 6.00%. Calcd for $C_{21}H_{20}O_4$: C, 74.98; H, 5.99%.

8f: Yellow microcrystals (from benzene–hexane); mp 185—186 °C; IR 1760 cm^{-1} (CO); ^1H NMR δ 1.90 (6H, s), 2.62 (3H, s), 4.10 (2H, d, J=6.0 Hz), 7.12 (1H, t, J=6.0 Hz), and 7.40—8.65 (8H, m); MS *m/e* 380 (M^+). Found: C, 69.33; H, 5.38%. Calcd for $C_{22}H_{20}O_6$: C, 69.46; H, 5.30%.

9: Yellow microcrystals (from benzene); mp 198—200 °C; IR 1755 and 1726 cm^{-1} (CO); ^1H NMR δ 2.66 (3H, s), 4.65 2H, d, J=2.1 Hz), 7.35—8.35 (8H, m), and 9.83 (1H, t, J=2.1 Hz); MS *m/e* 278 (M^+). Found: C, 77.51; H, 5.12% Calcd for $C_{18}H_{14}O_3$: C, 77.68; H, 5.07%.

Reactions of **1** *with Acetic Anhydride–Hydrochloric Acid.* The procedure was identical with that described above, except that hydrochloric acid (1 ml) was used instead of sulfuric acid. The products were isolated by chromatography, followed by recrystallization from benzene–hexane. The characterization data of products are given below.

10a: Pale yellow needles; mp 206—207 °C; IR 1765 cm^{-1} (CO); ^1H NMR δ 2.58 (3H, s), 3.52—4.22 (4H, m), and 7.25—8.40 (8H, m); MS *m/e* 300/298 (M^+). Found: C, 72.46; H, 5.10; Cl, 11.76%. Calcd for $C_{18}H_{15}O_2Cl$: C, 72.35; H, 5.06; Cl, 11.87%.

10b: Pale yellow needles; mp 173 °C; IR 1768 cm^{-1} (CO); ^1H NMR δ 1.44 (3H, d, J=6.5 Hz), 2.55 (3H, s), 3.64—4.78 (3H, m), and 7.25—8.42 (8H, m); MS *m/e* 314/312 (M^+). Found: C, 72.85; H, 5.61; Cl, 11.22%. Calcd for $C_{19}H_{17}O_2Cl$: C, 72.96; H, 5.48; Cl, 11.33%.

10d: Pale yellow needles; mp 192—193 °C.

10e: Yellow needles; mp 195—196 °C.

Reactions of **1** *with Methanol–Hydrochloric Acid.* A solution of **1** (2—3 mmol) in methanol containing hydrochloric acid (1 ml) was refluxed under nitrogen for 1 h. The solvent was removed under reduced pressure. After the usual acetylation using acetic anhydride, the products were purified by recrystallization or chromatography.

11c: Yellow needles (from benzene–hexane); mp 160 °C; IR 1755 cm^{-1} (CO); ^1H NMR δ 2.56 (3H, s), 3.06 (3H, s), 3.55—4.65 (3H, m), and 7.15—8.35 (8H, m); MS *m/e* 370 (M^+). Found: C, 81.05; H, 5.95%. Calcd for $C_{25}H_{22}O_3$: C, 81.05; H, 5.99%.

References

1) K. Hirakawa and T. Nosaka, *J. Chem. Soc., Perkin Trans. 1*, **1980**, 2835.

2) K. Hirakawa, T. Ito, Y. Okubo, and S. Nakazawa, *J. Org. Chem.*, **45**, 1668 (1980); K. Hirakawa, T. Toki, K. Yamazaki, and S. Nakazawa, *J. Chem. Soc., Perkin Trans. 1*, **1980**, 1944.

3) A. Mustafa and M. K. Hilmy, *J. Chem. Soc.*, **1952**, 1434; G. Gauguis and G. Reverdy, *Tetrahedron Lett.*, **1968**, 1085; J. C. Fleming and H. Shechter, *J. Org. Chem.*, **34**, 3962 (1969).

4) The reaction of **1c** is shown in Ref. 1.

5) R. Adams and E. H. Vollweiler, *J. Am. Chem. Soc.*, **40**, 1732 (1918); H. E. French and R. Adams, *ibid.*, **43**, 651 (1921); L. H. Ulich and R. Adams, *ibid.*, **43** 660 (1921).

6) J. Hine, "Physical Organic Chemistry," 2nd ed, McGraw-Hill, New York (1962), Chap. 7.

7) L. E. Eberson and S. Winstein, *J. Am. Chem. Soc.*, **87**, 3506 (1965); J. W. Pavlik and N. Filipescu, *J. Chem. Soc., Chem. Commun.*, **1970**, 765; L. H. Schwartz, R. V. Flor, and V. P. Gullo, *J. Org. Chem.*, **39**, 219 (1974).

8) M. Regitz, *Chem. Ber.*, **94**, 2742 (1964).

A Short-step Synthesis of 4-Hydroxyproline

Junko HARA, Yoshinobu INOUYE,* and Hiroshi KAKISAWA
Department of Chemistry, The University of Tsukuba, Sakura-mura, Niihari-gun, Ibaraki 305

(Received March 23, 1981)

Synopsis. The reaction of *N*-benzyl-, *N*-diphenylmethyl-, or *N*-(1-phenylpropyl)-α-methoxycarbonylmethanimine *N*-oxide newly prepared with acrylaldehyde in benzene, followed by hydrogenolysis over palladium hydroxide and by acid hydrolysis, gave 4-hydroxyprolines.

After Leuchs synthesis[1] of 4-hydroxyprolines *via* a α-bromo-δ-chloro-γ-valerolactone, many procedures have been reported: one was a variant of the Leuchs method involving a α,δ-disubstituted γ-valerolactone intermediate,[2] others was a methods using a 2-amino-4-pentenoic acid derivative,[3] and the rest were along different routes.[4,5] All of these were based on the stepwise introduction of two asymmetric centers; the ratios of allohydroxyproline (**6**) to hydroxyproline (**5**) were near one. The predominant production of **6** was recognized in some cases,[2c,2e,4] but the overall yields were not high due to the rather long reaction sequences.

We wish to report here a new short-step synthesis of 4-hydroxyprolines (**5** and **6**). The method is comprised of 1,3-dipolar cycloaddition of *N*-alkyl-α-methoxycarbonylmethanimine *N*-oxide (**1**)[6] with acrylaldehyde, followed by the cleavage of the N–O bond and recyclization between the nitrogen and the aldehyde group to give a pyrrolidine ring. Two asymmetric centers can be introduced simultaneously at the stage of the cycloaddition.

The nitrones [**1**: **a**; *N*-benzyl-, **b**; *N*-diphenylmethyl-, and **c**; *N*-(1-phenylpropyl)-α-methoxycarbonylmethanimine *N*-oxides] were prepared according to the previous procedure.[6] NMR spectra of **1** showed the presence of both *E*- and *Z*-isomers.

The reaction of **1a** (E/Z=1.6) with acrylaldehyde in benzene for 24 h gave a mixture of two isomeric isoxazolidines (**2a** and **3a**; **2a**/**3a**=1.6); the structures were assigned by the comparison of their NMR spectra and pseudocontact shifts (0.057 equiv. of Eu-FOD) with those of the related compound.[6] The mixture thus obtained was subjected to the catalytic hydrogenolysis and the resulted crude ester **4** was hydrolyzed to give a mixture of **6** and **5** (**6**/**5**=1.61) in a 46% yield based on **1a**.

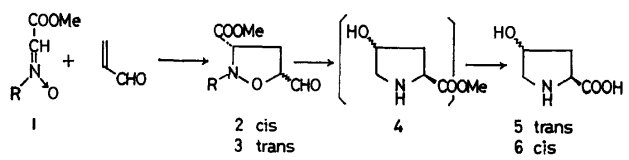

1 — 2 cis, 3 trans — 4 — 5 trans, 6 cis

a: R = $C_6H_5CH_2$ b: R = $(C_6H_5)_2CH$ c: R = $C_6H_5(C_2H_5)CH$

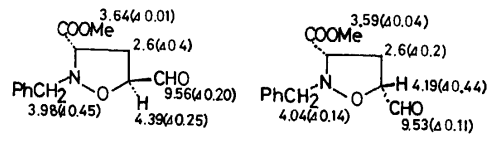

2a 3a

Table 1. The ratio of allo-Hyp(**6**)/Hyp(**5**) and yield in variation of nitrone and reaction type

		Nitrone		
		1a	**1b**	**1c**
Type I	**6**/**5**	1.61	3.66	1.43
	Yield/%	46	56	55
Type II	**6**/**5**	1.87	5.90	1.23
	Yield/%	32	71	65

When **1b** (E/Z=1.1) was used, a mixture of **6** and **5** (**6**/**5**=3.66) was obtained in a 56% yield.

The above results show that the E/Z ratio in $CDCl_3$ had not necessarily reflected on the ratio of **6**/**5**. This led to the finding[7] that nitrones (**1**), though they exist in a *Z*-form in a crystalline state, exhibit a novel *E*-*Z* equilibrium in a solution. Therefore, two types of reactions were performed in order to clarify the synthetic utility of the present method. In type I, the crystalline *Z*-nitrone was added to a solution of acrylaldehyde in benzene, while in type II, acrylaldehyde was added to a equilibrium mixture of *E*- and *Z*-nitrones in benzene.

The results are summarized in Table 1. The **6**/**5** ratio was the highest when **1b** was subjected to the type II condition. Stereoselectivity (**6**/**5**=5.90) and overall yield (71%) for the production of **5** and **6** are superior to hitherto reported procedures.[2-5] On the other hand, the stereoselective production of **5** was not specified in the present method.

Experimental

All the melting points are uncorrected. The IR spectra were recorded with a Hitachi 215 grating spectrophotometer and the NMR spectra were measured with a JEOL MH-100 spectrophotometer, using TMS as the internal standard. The amino acid chromatograms were taken on a Dionex D-500 Mark II analyzer using a column of DC-6A (1.75φ× 480 mm) at 41 °C with an elution buffer Li-A (pH 2.75).

Preparation of Nitrones. Nitrones (**1a**, **1b**, and **1c**) were prepared by condensation of methyl glyoxylate with a corresponding *N*-alkylhydroxylamine.

1a: Mp 90—92 °C (colorless prisms from benzene); ν(KBr): 1727, 1570, 1220, and 1205 sh cm^{-1}; δ ($CDCl_3$, E/Z=1.6): 7.6—7.1 (m, C_6H_5 and =CH), 5.70 (s, N–CH_2– of *E*-form), 4.98 (s, N–CH_2– of *Z*-form), 3.77 (s, $COOCH_3$, *Z*), and 3.78 (s, $COOCH_3$, *E*); E/Z=3.3 (C_6D_6). Found: C, 61.87; H, 5.65; N, 7.18%. Calcd for $C_{10}H_{11}NO_3$: C, 62.16; H, 5.65; N, 7.24%.

1b: Mp 131.5—132.5 °C (colorless needles from benzene); ν (KBr): 1725, 1700, 1550 br, 1215, and 1205 cm^{-1}; δ ($CDCl_3$, E/Z=1.1): 8.2 (s, =CH, *E*), 7.5—7.2 (m), 6.28 (s, N–CH, *Z*), and 3.71 (s, $COOCH_3$, *E*+*Z*); E/Z=1.7 (C_6D_6). Found: C, 71.50; H, 5.52; N, 5.13%. Calcd for $C_{16}H_{15}NO_3$: C, 71.36; H, 5.61; N, 5.20%.

1c: Mp 72.5—74.5 °C (colorless prisms which formed slowly from benzene); ν (KBr): 1730, 1550 br, 1220 sh, 1210,

and 1170 cm^{-1}; δ ($CDCl_3$, E/Z=0.95): 7.7—7.2 (m, C_6H_5 and =CH), 6.86 (dd, J=10 and 6 Hz, N-CH, Z), 4.83 (dd, J=10 and 6 Hz, N-CH, E), 3.84 (s, $COOCH_3$, E), 3.80 (s, $COOCH_3$, Z), 2.7—1.9 (m, $C\underline{H}_2CH_3$, $E+Z$), 0.97 (t, J=7 Hz, $CH_2C\underline{H}_3$, Z), and 0.94 (t, J=7 Hz, $CH_2C\underline{H}_3$, E); E/Z= 1.9 (C_6D_6). Found: C, 65.13; H, 6.78; N, 6.31%. Calcd for $C_{12}H_{15}NO_3$: C, 65.14; H, 6.83; N, 6.33%.

Preparation of **6** *and* **5**. Typical procedures of both types were as follows:

Type I: To a solution of acryladehyde (1.5 mmol) in benzene (4 ml), was added **1a** (0.5 mmol), in one portion. The mixture was stirred at room temperature for 24 h. The removal of benzene and the excess of acryladehyde *in vacuo* at 25 °C gave an oily mixture of **2a** and **3a** (100%, **2a**/**3a**= 1.6). Without further purification, the mixture thus obtained was dissolved in methanol (20 ml) and then hydrogenated over palladium hydroxide (85 mg) under a hydrogen atmos phere (3 atm) for 24 h, After removal of the catalyst, the filtrate was concentrated to give **4** (127 mg), which was subsequently refluxed with 1 mol dm^{-3} HCl (5 ml) for 4.5 h. After decolorizing with activated carbon, the solution was concentrated to give pale yellow crystals (103 mg). The ratio of stereoisomers and the yield from **1a** were determined by amino acid analysis (**6**/**5**=1.61, yield 46%).

Type II: A solution of **1b** (0.26 mmol) in benzene (5 ml) was left at room temperature for 3 h. To the solution was added acrylaldehyde (0.8 mmol) in one portion and the mixture was stirred at room temperature for 24 h. The removal of benzene and excess of acryladehyde *in vacuo* at 25 °C gave a colorless oily mixture of **2b** and **3b** (100%, **2b**/**3b**=4.4). The mixture of **2b** and **3b** (87 mg) was subjected to catalytic hydrogenolysis and acid hydrolysis under similar conditions as in Type I, giving a crystalline mixture of **6** and **5** (**6**/**5**=5.90, yield 71% from **1b**).

In the case of **1a** or **1c**, the solution in benzene was left for 3 h or 2 d, respectively, before the addition of acryladehyde.

We are deeply indebted to Dr. Chikahiko Eguchi, Central Research Laboratories, Ajinomoto Co., Inc., for a gift of allohydroxyproline.

References

1) H. Leuchs, *Chem. Ber.*, **35**, 2660 (1902).

2) a) E. Fisher and A. Krämer, *Chem. Ber.*, **41**, 2728 (1908); b) H. Leuchs, M. Giua, and J. F. Brewster, *ibid.*, **45**, 1960 (1912); c) W. Traube, R. Johow, and W. Tepohl, ibid, **56**, 1861 (1923); d) V. Feofilakov and A. Onishchenko, *C. R. Acad. Sci. SSR*, **20**, 133 (1938); *Chem. Abstr.*, **33**, 1725[1] (1939); e) H. McIlwain and G. M. Richardson, *Biochem. J.*, **33**, 44 (1939); f) J. Capkova-Jirku, J. V. Kostir, and M. Vondracek, *Chem. Listy*, **44**, 19 (1950); *Chem. Abstr.*, **45**, 8004i (1951); g) R. Gaudry and C. Godin, *J. Am. Chem. Soc.*, **76**, 139 (1954); h) B. Witkop and T. Beiler, *idid.*, **78**, 2882 (1956); i) C. Eguchi and A. Kakuta, *Bull. Chem. Soc. Jpn.*, **47**, 1704 (1974).

3) a) E. Hammarsten, *C. R. Trav. Lab. Carlsberg*, **11**, 233 (1916); *Chem. Abstr.*, **10**, 3064 (1916); b) R. Gaudry, L. Berlinguet, A. Langis, and G. Paris, *Can. J. Chem.*, **34**, 502 (1956); c) T. Wieland and U. Wintermeyer, *Chem. Ber.*, **90**, 1721 (1957); d) N. Izumiya and B. Witkop, *J. Am. Chem. Soc.*, **85**, 1935 (1963); e) Y. K. Lee and T. Kaneko, *Bull. Chem. Soc. Jpn.*, **46**, 2924 (1973).

4) R. Kuhn and G. Osswald, *Chem. Ber.*, **89**, 1423 (1956).

5) S. G. Ramaswamy and E. Adams, *J. Org. Chem.*, **42**, 3440 (1977).

6) Y. Inouye, Y. Watanabe, S. Takahashi, and H. Kakisawa, *Bull. Chem. Soc. Jpn.*, **52**, 3763 (1979).

7) Y. Inouye, J. Hara, and H. Kakisawa, *Chem. Lett.*, **1980**, 1407.

Stereochemical Behavior of 1-Methoxycyclopropyl Radical in Hunsdiecker Reaction[1]

Teiichi Ando,* Takashi Ishihara, Akira Yamashita, and Masahiro Matsumoto

Department of Industrial Chemistry, Faculty of Engineering, Kyoto University, Sakyo-ku, Kyoto 606

(Received March 23, 1981)

Synopsis. The Hunsdiecker reaction of Ag (*E*)- and (*Z*)-2,2-dichloro-1-methoxy-3-methylcyclopropanecarboxylates with bromine in CCl_4 at 0 and 77 °C occurs with substantial inversion of configuration, suggesting that the 1-methoxycyclopropyl radical is configurationally less stable than the 1-fluorocyclopropyl or the 1-methoxyvinyl radical.

Recent studies[2] have established that the configurational stability, or the energy barrier for inversion, of 1-substituted cyclopropyl radicals is strongly affected by the nature of the 1-substituent; best known is the effect of 1-fluorine stabilizing the pyramidal configuration of the cyclopropyl radical, which is much more powerful than that of 1-chlorine.

As compared with the configurational stability of 1-halo radicals, that of the 1-methoxy radical has only scarcely been investigated, probably because of the difficulty of its generation. In fact, no reports on this subject have appeared so far in the literature except the one by Walborsky *et al.*[2b,c]

The stereochemistry of the Hunsdiecker reaction of Ag salts of some 1-methoxy- and 1-fluorocyclopropanecarboxylic acids has now been examined to learn the effect of the 1-methoxyl substituent on the stereochemical stability of cyclopropyl radicals.

Results and Discussion

The Hunsdiecker reaction of Ag salts of (*Z*)-2,2-dichloro-1-methoxy- (**1a**), (*E*)-2,2-dichloro-1-methoxy- (**2a**), and (*Z*)-2,2-dichloro-1-fluoro-3-methylcyclopropanecarboxylic acids (**1b**) was effected in the presence of bromine in CCl_4, to give the corresponding bromocyclopropane as an isomeric mixture (Scheme and Table 1). The structures of these bromocyclopropanes were determined from their ^1H[3] and/or ^{13}C NMR spectra.[4]

The reaction of methoxy acids **1a** and **2a** occurred with substantial inversion of configuration even at 0 °C. The stereospecificity was completely lost at 77 °C; the isomer ratios of the product are equal irrespective of the stereochemistry of the starting acid. This indicates that isomeric 1-methoxycyclopropyl radicals are configurationally rather unstable, inverting their configuration at a rate comparable to their bromine abstraction at 0 °C and at a rate faster than the latter at 77 °C.

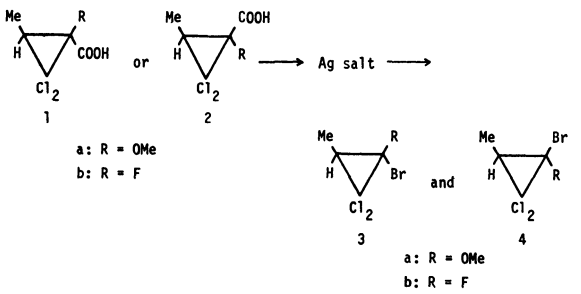

Table 1. Hunsdiecker reaction of acids **1** and **2**

Acid	Temp °C	Time h	Yield %	Isomer ratio retn : invn
1a	0	1.5	54	58 : 42
	0	2.0	76	56 : 44
	77	1.5	53	41 : 59
	77	2.0	59	39 : 61
2a	0	2.0	—	68 : 32
	0	3.0	71	69 : 31
	77	0.5	—	61 : 39
	77	1.0	62	62 : 38
1b	20	1.5	—	90 : 10
	20	2.5	59	91 : 9
	77	2.0	69	81 : 19
	77	3.0	—	82 : 18

In discussing the effect of the 1-methoxyl substituent from the above facts, the presence of two 2-chlorine atoms in this system must be taken into account, because they can more or less destabilize the pyramidal configuration of cyclopropyl radicals. Such an effect of electronegative 2-substituents was suggested theoretically by Dewar *et al.*[6] and demonstrated experimentally in our previous work.[7]

The Hunsdiecker reaction of Ag salt of **1b** was conducted in this connection; the reaction took place with high (but not complete) stereospecificity at room temperature, and the degree of inversion increased at 77 °C (Table 1). Evidently, the configurational stability of the 1-fluorocyclopropyl radical is lowered to such an extent that its inversion of configuration competes with its bromine abstraction, in spite of the presence of 1-fluorine.

These findings, as combined with the extremely high configurational stability of 2-hetero-unsubstituted 1-fluorocyclopropyl radicals observed in the previous work,[2] strongly suggest the existence of the 2-chlorine effect in the 1-methoxy radicals as well as in the 1-fluoro radical.[8] The data in Table 1 also show that the 1-methoxy radical is configurationally less stable than the 1-fluoro radical, *i.e.*, that the 1-methoxyl substituent is less powerful than the 1-fluoro in stabilizing the pyramidal configuration of cyclopropyl radicals.

The behavior of 1-methoxycyclopropyl radicals described herein is in sharp contrast with that of (*E*)- and (*Z*)-1-methoxy-1-propenyl radicals.[9] This difference can be explained in terms of the difference in *s*-character of the odd-electron orbital between the cyclopropyl and the vinyl systems, though the above-cited 2-chlorine effect may play a minor role. It is to be noted that similar differences have been observed between the 1-chlorocyclopropyl[2] and the 1-chlorovinyl radicals.[10]

Experimental[11]

Methyl (E)-2-Methoxy-2-butenoate. Methyl *trans*-2-methylglycidate was treated with *p*-toluenesulfonic acid to form 2-hydroxy-3-(*p*-tolylsulfonyloxy)butanoate (100%), which was then methylated with methyl iodide/Ag_2O (97%). Treatment of the resulting 2-methoxy-3-(*p*-tolylsulfonyloxy)-butanoate with KOH in methanol, followed by acidification, gave an isomeric mixture of (*E*)- and (*Z*)-2-methoxy-2-butenoic acid (*E*/*Z*=85/15). Recrystallization from hexane gave pure (*E*)-acid, mp 44.5—45.5 °C (65%), which was converted to the methyl ester by the usual method (82%), bp 62—63 °C/16 mmHg. IR (film) 1724, 1644, 1207, 1164, 1105, 1026 cm^{-1}; ^1H NMR δ 1.93 (d, J=7.4 Hz, 3H), 3.50 (s, 3H), 3.70 (s, 3H), 5.14 (q, J=7.4 Hz, 1H); MS *m/e* (%) 130 (M^+, 68), 55 (100).

Methyl (Z)-2-Methoxy- and (Z)-2-Fluoro-2-butenoates were prepared according to the method of Owen[12] and of Bergmann *et al.*,[13] respectively. Attempts to prepare the (*E*)-fluoro acid or its ester in our hands were unsuccessful.

*1-Substituted 2,2-Dichloro-3-methylcyclopropanecarboxylic Acids (**1a**, **2a**, and **1b**)* were prepared by addition of dichlorocarbene to the corresponding methyl 2-substituted-2-butenoate followed by hydrolysis. The reaction conditions were similar to those described in our previous paper.[14]

1a: 37% yield; mp 75—76 °C; IR (KBr) 3000, 1708, 1292, 1258, 1040 cm^{-1}; ^1H NMR δ 1.29 (d, J=6.6 Hz, 3H), 2.43 (q, J=6.6 Hz, 1H), 3.76 (s, 3H), 12.24 (s, 1H); ^{13}C NMR δ 7.9 (Me on ring).

Found: C, 36.30; H, 4.11; Cl, 35.47%.

2a: 37% yield; mp 52.5—53.5 °C; IR (KBr) 3030, 1706, 1301, 1158, 1075 cm^{-1}; ^1H NMR δ 1.43 (d, J=6.6 Hz, 3H), 2.03 (q, J=6.6 Hz, 1H), 3.61 (s, 3H), 12.14 (s, 1H); ^{13}C NMR δ 9.7 (Me on ring).

Found: C, 36.29; H, 4.22%. Calcd for $C_6H_8O_3Cl_2$: C, 36.21; H, 4.05; Cl, 35.63%.

1b: 33% yield; mp 42—43 °C; IR (KBr) 3000, 1720, 1250, 1180, 1000 cm^{-1}; ^1H NMR δ 1.37 (d, J=6.6 Hz, 3H), 2.53 (dq, J=6.6 and 7.8 Hz, 1H), 11.16 (s, 1H); ^{13}C NMR δ 7.4 (J_{CF}=6.0 Hz, Me on ring).

Found: C, 31.82; H, 2.57; Cl, 38.04; F, 10.16%. Calcd for $C_5H_5O_2Cl_2F$: C, 32.11; H, 2.70; Cl, 37.92; F. 10.16%.

*Hunsdiecker Reaction of **1a**, **2a**, and **1b**.* To a suspension, which had been maintained at a specified temperature, of Ag salt (5 mmol) in dry CCl_4 (10 ml) was rapidly added 1.2 equiv. of bromine in dry CCl_4 (10 ml). After a specified period, inorganic silver salt was removed by filtration and was washed with a small amount of CCl_4. The filtrate was concentrated below 30 °C. The isomer ratios in the products were measured by GLC before distillation.

3a** and **4a: Bp 78—79 °C/15 mmHg; IR (film) 2960, 1043, 780, 765 cm^{-1}; ^1H NMR **3a**: δ 1.30 (d, J=6.6 Hz, 3H), 2.12 (q, J=6.6 Hz, 1H), 3.54 (s, 3H), **4a**: δ 1.25 (d, J=6.6 Hz, 3H), 1.84 (q, J=6.6 Hz, 1H), 3.54 (s, 3H); ^{13}C NMR **3a**: δ 8.1 (Me on ring), **4a**: δ 13.3 (Me on ring); MS *m/e* (%) 232 (M^+, 1), 199 (100).

3b** and **4b: Bp 52—53 °C/23 mmHg; IR (film) 2940, 1096, 996, 898, 862 cm^{-1}; ^1H NMR **3b**: δ 1.35 (d, J=6.6 Hz, 3H), 2.03 (dq, J=6.6 and 7.2 Hz, 1H), **4b**: δ 1.33 (dd, J=6.6 and 1.6 Hz, 3H), 2.06 (dq, J=6.6 and 19.8 Hz, 1H); ^{13}C NMR **3b**: δ 7.9 (J_{CF}=5.2 Hz, Me on ring), **4b**: δ 12.7 (J_{CF}=0 Hz, Me on ring); MS *m/e* (%) no parent to 220, 141 (100).

References

1) For preliminary communication of this work, T. Ando, A. Yamashita, M. Matsumoto, T. Ishihara, and H. Yamanaka, *Chem. Lett.*, **1973**, 1133.

2) a) T. Ishihara, K. Hayashi, T. Ando, and H. Yamanaka, *J. Org. Chem.*, **40**, 3264 (1975); b) H. M. Walborsky and P. C. Collins, *ibid.*, **41**, 940 (1976); c) H. M. Walborsky, *Tetrahedron*, **37**, 1625 (1981), and references cited therein.

3) K. L. Williamson, Y.-F. Li Hsu, F. H. Hall, S. Swager, and M. S. Coulter, *J. Am. Chem. Soc.*, **90**, 6717 (1968).

4) The relative chemical shifts for the methyl carbon, which can experience the well-documented γ-gauche effect,[5] were used for structural determination of **3** and **4**. The observation of C–F couplings in **3b** and **4b** made a straightforward assignment possible.

5) N. K. Wilson and J. B. Stothers, *Top. Stereochem.*, **8**, 1 (1974), and references cited therein.

6) R. C. Bingham and M. J. S. Dewar, *J. Am. Chem. Soc.*, **95**, 7180, 7182 (1973).

7) T. Ishihara, E. Ohtani, and T. Ando, *J. Chem. Soc. Chem. Commun.*, **1975**, 367.

8) An attempt to get direct evidence for the presence of the 2-chlorine effect failed; the Hunsdiecker reaction of (*Z*)- and (*E*)-2,2-dideuterio-1-methoxy-3-methylcyclopropanecarboxylic acids, prepared by reduction of **1a** and **2a** with tributyltin deuteride, resulted in ring opening.

9) M. S. Liu, S. Soloway, D. K. Wedegaertner, and J. A. Kampmeier, *J. Am. Chem. Soc.*, **93**, 3809 (1971).

10) L. A. Singer and N. P. Kong, *J. Am. Chem. Soc.*, **89**, 5251 (1967).

11) IR spectra were taken on a Shimadzu JR-400 infrared spectrometer. Varian EM-360 and CFT 20 spectrometers were used to measure ^1H (CCl_4) and ^{13}C NMR ($CDCl_3$) spectra, respectively.

12) L. N. Owen, *J. Chem. Soc.*, **1945**, 385.

13) E. D. Bergmann and I. Shahak, *J. Chem. Soc.*, **1961**, 4033.

14) A. Yamashita, T. Ishihara, M. Matsumoto, and T. Ando, *Mem. Fac. Eng., Kyoto Univ.*, **37**, 1 (1975).

The Synthesis of 2,5-Dialkylcyclopentanones from Aliphatic Aldehydes and Formaldehyde

Yoshihisa WATANABE,* Fukashi SAKAMOTO, Sang Chul SHIM, and Take-aki MITSUDO
Department of Hydrocarbon Chemistry, Kyoto University, Sakyo-ku, Kyoto 606
(Received April 8, 1981)

Synopsis. Aliphatic aldehydes react with formaldehyde in the presence of dimethylamine hydrochloride at 200 °C to form 2,5-dialkylcyclopentanones in moderate yields. Propanal, butanal, and pentanal give 2,5-dimethyl-, 2,5-diethyl-, and 2,5-dipropylcyclopentanone respectively, but ethanal gives only a tarry material.

A large variety of methods are available for building up the cyclopentanone and cyclopentenone ring.[1-9] In the course of our study of the α-methylation of ketones,[10] we have found a novel method for the preparation of cyclopentanone derivatives by treating aliphatic aldehydes with formaldehyde in the presence of a secondary amine hydrochloride. The combination of straight chain aliphatic aldehydes with formaldehyde in the present method represents a unique pathway to the formation of the cyclopentanone ring.

Experimental

Reagent. The propanal and butanal were distilled and dried over Na_2SO_4. The other reagents were commercial products. Formaldehyde(guaranteed reagent 35% Wako Chemicals Co.,) was used.

Reaction Procedure. An autoclave with a 100-ml capacity, made of stainless steel and equipped with a magnetic stirrer, was used in each run. Forty mmol of aliphatic aldehyde, 35% aqueous formaldehyde (40—80 mmol as formaldehyde), 20 ml of a solvent, and 20—40 mmol of dimethylamine hydrochloride were put into it. After the replacement of the argon in the autoclave, it was kept at 200 °C by electrical heating for 4 h. The products, such as 2,5-dimethyl-, 2,5-diethyl-, 2,5-dipropyl-, and 2,5-dipentylcyclopentanone, were isolated by distillation or column chromatography. They were characterized by their IR, ^1H, ^{13}C-NMR, and mass spectra, and by elemental analysis. The 2,5-dimethylcyclopentanone formed was identified by a comparison of its mp, IR, and ^1H and the ^{13}C-NMR spectra of its 2,4-dinitrophenylhydrazone derivative with those of an authentic sample. GLC analysis was made using internal standards: a column (0.3 cmϕ × 3 m) packed with PEG 20M 10%.

2,5-Diethylcyclopentanone (**1b**); bp 71—76 °C/17 Torr (1 Torr = 133.3 Pa). Found as 2,4-dinitrophenylhydrazone, mp 113—115 °C: C, 56.01; H, 6.24; N, 17.48; O, 20.25%. Calcd for $C_{15}H_{20}N_4O_4$: C, 56.24; H, 6.29; N, 17.48; O, 19.98%. 2,5-Dipropylcyclopentanone (**1c**); bp, 89—92 °C/8 Torr. Found as semicarbazone, mp, 168—170 °C: C, 63.69; H, 10.36; N, 18.56%. Calcd for $C_{12}H_{23}N_3O$: C, 63.96; H, 10.29; N, 18.65%. 2,5-Dibutylcyclopentanone (**1d**); bp 86—92 °C/4 Torr. Found as semicarbazone, mp 118—120 °C: C, 65.80; H, 10.72; N, 16.12%. Calcd for $C_{14}H_{27}N_3O$: C, 66.34; H, 10.74; N, 16.31%. 2,4-Dipentylcyclopentanone (**1e**) was chromatographed on silica gel (3 cm × 30 cm), using benzene as an eluent. A light yellow liquid was obtained.[12]

Analytical Procedure. The infrared spectra were measured on a Hitachi model 215 grating spectrophotometer. The ^1H-NMR spectra were obtained at 60 MHz with a JEOL JNM-60, at 100 MHz with a JEOL JNM-100, and at 220 MHz with a Varian model HR-220 NMR spectrometer. The ^{13}C-NMR spectra were obtained at 25.05 MHz with a JEOL pulsed Fourier transform spectrometer model FX-100. Samples were dissolved in $CDCl_3$ and the chemical shift values were expressed in δ-values (ppm) relative to Me_4Si as an internal standard. The mass spectra were recorded on a JMS-O1SG mass spectrometer.

Results and Discussion

Two molecules of aldehydes reacted with one molecule of formaldehyde in the presence of dimethylamine hydrochloride to form 2,5-dialkylcyclopentanones in moderate yields. The results are summarized in the Tables. Each of the C_3—C_7 aldehydes with a straight chain structure, such as propanal, butanal, pentanal, hexanal, and heptanal, gives the corresponding 2,5-

Table 1. Synthesis of 2,5-dialkylcyclopentanones from aliphatic aldehydes and formaldehyde[a]

Run	Aldehyde	Substituted cyclopentanone	Yield/%
1	Ethanal	Tarry material	
2	Propanal	2,5-Dimethyl-(**1a**)	16[b]
3	Butanal	2,5-Diethyl-(**1b**)	22[b]
4	Pentanal	2,5-Dipropyl-(**1c**)	26[c]
5	Hexanal	2,5-Dibutyl-(**1d**)	19[c]
6	Heptanal	2,5-Dipentyl-(**1e**)	21[c]
7[d]	Butanal	None	≈0

a) Aldehyde 40 mmol, $NH(CH_3)_2 \cdot HCl$ 40 mmol, HCHO, 80 mmol, 200 °C, 4 h, dioxane 20 ml, HCOOH 20 mmol. b) Determined by GLC. Based on the amount of aldehyde used. c) Isolated yield. d) Without $NH(CH_3)_2 \cdot HCl$.

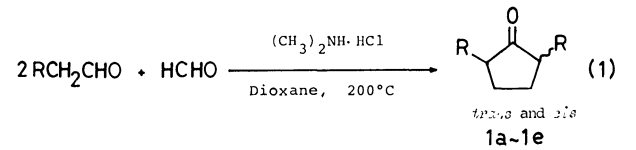

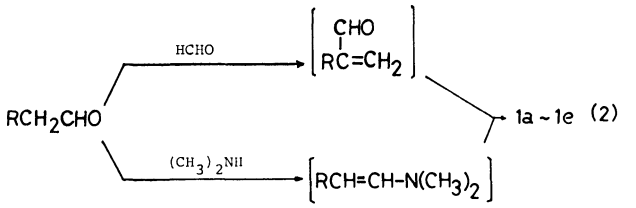

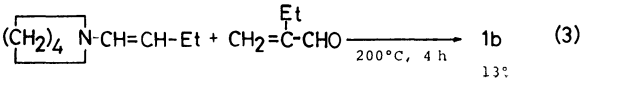

Table 2. Spectroscopic data of 2,5-dialkylcyclopentanones

^{13}C-NMR (ppm from TMS)

		IR $\nu_{C=O}$/cm^{-1}	M$^+$	C=O	CH	CH_2 (in ring)	CH_2 (side chain)			CH_3
1b	*trans*	1740	140	222.2	51.0	27.0	23.0			11.7
	cis			222.8	49.9	26.2	23.1			12.0
1c	*trans*	1740	168	222.2	49.3	27.7	32.3	20.7		14.0
	cis			222.6	48.2	26.8	32.4	20.8		
1d	*trans*	1740	196	223.0	49.4	27.7	29.8	29.6	22.7	13.9
	cis			223.6	48.3	26.7				
1e	*trans*	1740	224	222.5	49.5	27.7	31.8	30.0	27.1 22.5	14.0
	cis				(48.4)	(26.8)				

dialkylcyclopentanone. Ethanal failed to give cyclopentanone, but provided only a tarry material. The amine salt is necessary for this ring formation (see Run 7).

The ^{13}C-NMR spectra of the products from butanal, pentanal, hexanal, and heptanal exhibited two sets of peaks with different intensities, assignable to *trans*- and *cis*-2,5-dialkylcyclopentanone.[11] The *trans* isomers predominate in **1b**, **1c**, and **1d**, and the *trans* to *cis* mole ratios are estimated to be about 2 : 1 from the height of peaks of ^{13}C-NMR spectra. With **1e**, the *trans* isomer highly predominates, and only a trace of the *cis* isomer is formed.

Though the mechanism of this reaction is not yet clear, the following two condensates are considered to be the reaction intermediates: the 2-alkylpropenal derived by the reaction of the aldehyde with formaldehyde, and an enamine (Eq. 2). 2,5-Dialkylcyclopentanones may be derived from these condensates *via* several steps. This consideration may be supported by the fact that the reaction between 2-ethylpropenal and 1-(1-pyrrolidinyl)-1-butene at 200 °C for 4 h gave 2,5-diethylcyclopentanone in a 13% yield, while 2-alkylpropenals were readily formed under the conditions used.

References

1) P. S. Pinkey, *Org. Synth.*, Coll. Vol. 2, 116 (1943).
2) J. F. Thorpe and G. A. R. Kon, *Org. Synth.*, Coll. Vol. 1, 192 (1941).
3) L. Rand, W. Wagner, P. O. Warner, and L. R. Kovac, *J. Org. Chem.*, **27**, 1034 (1962).
4) B. Fell, W. Side, and F. Asinger, *Tetrahedron Lett.*, **1968**, 1003.
5) R. F. Heck, *J. Am. Chem. Soc.*, **85**, 3116 (1963).
6) R. C. Cookson and S. A. Smith, *J. Chem. Soc., Chem. Commun.*, **1979**, 145.
7) G. P. Chiusoli, *Bull. Soc. Chim. Fr.*, **1969**, 1139.
8) R. Noyori, K. Yokoyama, and Y. Hayakawa, *J. Am. Chem. Soc.*, **95**, 2722 (1973).
9) H. Sakurai, A. Shirahata, and A. Hosomi, *Angew. Chem.*, **91**, 178 (1979).
10) Y. Watanabe, Y. Shimizu, K. Takatsuki, and Y. Takegami, *Chem. Lett.*, **1978**, 215.
11) J. B. Stothers and C. T. Tan, *Can. J. Chem.*, **52**, 308 (1974).
12) Although **1e** could not be isolated in an analytically pure form and failed to give its semicarbazone and 2,4-dinitrophenylhydrzaone, it was identified on the basis of its spectral data.

The Formation of a Propellane by the Oxidation of Biphenylene with Manganese(III) Acetate

Kazu KUROSAWA* and John F. W. McOMIE**

Department of Chemistry, Faculty of Science, Kumamoto University, Kurokami 2-39-1, Kumamoto 860
***School of Chemistry, The University, Bristol, Cantock's Close, Bristol BS8 1TS, England*

(Received April 24, 1981)

Synopsis. The reaction of biphenylene with manganese (III) acetate gave 2-acetoxybiphenylene, 2-formylbiphenylene, 2-(acetoxymethyl)biphenylene, and 7-oxa-10,11-benzotricyclo[4.3.2.0]undeca-2,4,10-trien-8-one. The reaction pathways are discussed.

Although a number of investigation of the reactions of biphenylene have been reported, the reaction of manganese(III) acetate with this compound was not known. In connection with our previous investigations of the radical reactions of manganese(III) acetate with various aromatic compounds,[1,2] the reaction of biphenylene with manganese(III) acetate was examined. The reaction of biphenylene with manganese(III) acetate in a molar ratio of 1 : 4 in boiling acetic acid containing 8 equivalents of acetic anhydride gave three products, **2**, **3**, and **4** (Table 1, Entry 2). Compounds **2** and **3** were found to be 2-acetoxybiphenylene and 2-formylbiphenylene respectively by studying their ^{1}H-NMR and IR spectra. The ^{1}H-NMR spectrum of Compound **4** in CCl_4 indicated the presence of an acetoxymethyl group [δ=2.00 (3H, s) and δ=4.80 (2H, s)] and seven aromatic protons centered at δ=6.65. The IR spectrum exhibited a carbonyl absorption at 1738 cm^{-1}. When **4** was oxidized with manganese(III) acetate, 2-formylbiphenylene (**3**) was obtained. Therefore, the structure of **4** was proved to be 2-(acetoxymethyl)biphenylene (Scheme 1). When the reaction was conducted in acetic acid containing a large amount of acetic anhydride, it gave **4** and **5** (Entry 3). The yield of **4** was much improved at the expense of the yields of **2** and **3**, and the maximum yield was obtained when the molar ratio was 1 : 4 (Entry 3). The structure of **5** was also elucidated by means of the study of its ^{1}H-NMR spectrum, which showed the presence of an AB system (δ=2.74 and 2.97 with a J value of 18.0 Hz), vinylic protons [δ= 5.8—6.5 (4H, m)], and aromatic protons centered at δ=7.35 (4H, m). Its IR spectrum showed a carbonyl absorption at 1775 cm^{-1} characteristic of five-membered lactone. These spectral properties suggested that the structure is 7-oxa-10,11-benzotricyclo[4.3.2.0]-undeca-2,4,10-trien-8-one. The ^{13}C-NMR of **5** further

TABLE 1. OXIDATION OF BIPHENYLENE WITH MANGANESE (III) ACETATE IN ACETIC ACID CONTAINING ACETIC ANHYDRIDE AT THE REFLUX TEMPERATURE

Entry	Molar ratio of substrate : oxidant : Ac_2O	Time / min	Recovered substrate (%)	Product(yield/%)[a] 2	3	4	5
1	1 : 2 : 100	6	35			18	7
2	1 : 4 : 8	60	34	7	6	7	
3	1 : 4 : 100	9	26			23	10
4	1 : 6 : 100	9	12			12	5

a) Yields are based on the substrate used.

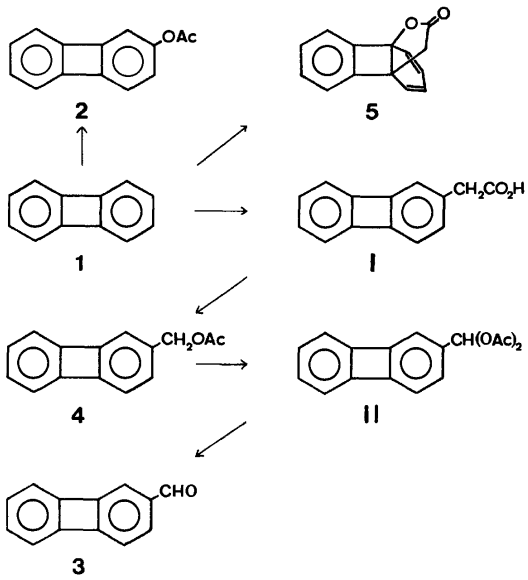

Scheme. 1.

confirmed the structure. The data are shown in the experimental part.

It is well known that there are two reaction mechanisms operative in the manganese(III) acetate oxidation. One is the electron-transfer mechanism, which operates in the oxidation of aromatic compounds having ionization potentials below 8 eV.[3,4] The other is the free-radical mechanism, which operates in the reaction of compounds having higher ionization potentials.[4] Both mechanisms can compete in the reaction of some aromatic compounds under certain reaction conditions.[4] The free-radical mechanism predominates under anhydrous conditions and at high temperatures. It seems reasonable to assume that **2** was derived *via* the electron-transfer mechanism, by analogy to the oxidation of 2-methylnaphthalene, which gave 1-acetoxy-2-methylnaphthalene,[4] whereas the other products were formed *via* the free-radical mechanism. The fact that the acetoxymethyl group in **4** is located at the (2) position is in harmony with the results of the phenylation reaction of biphenylene, where 2-phenylbiphenylene is the major product, together with a minor quantity of 1-phenylbiphenylene.[5] It should be pointed out that there was no precedent for the formation of a lactone from an aromatic substrate in the oxidation by manganese(III) acetate. Interestingly, the lactone is a propellane and a derivative of the ring system (A), but it cannot isomerize to benzocyclooctene (B) (Fig. 1). Several reactions are known in which X-Y reagents add to biphenylene, and the product is nearly always a derivative of (B), as is shown in the reactions of biphenylene with nitric acid and acetic anhydride,[6] and with bromine,[7] and in the reaction of methoxybi-

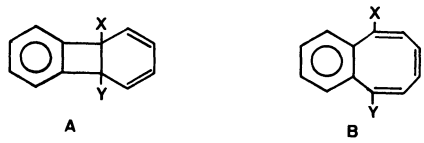

Fig. 1.

phenylene with bromine.[8] The formation of the acetoxymethyl group *via* the carboxymethyl group (I) in the oxidation by manganese(III) acetate has been well established,[4] and the further oxidation of **4** gave 2-(diacetoxymethyl)biphenylene (II), which yielded **3** on hydrolysis during the work-up procedure (Scheme 1).

Experimental

The ^{1}H-NMR spectra were recorded with a Hitachi R-24 NMR spectrometer, with TMS as the internal standard, while the proton-decoupled ^{13}C-FT NMR spectrum was measured at 22.5 MHz on a JEOL FX 90Q spectrometer (pulse width, 24 μs; spectral width 5000 Hz; data points, 8000; acquisition time 920 ms) in a 5-mm tube at 28 °C, using TMS as the internal reference. The IR spectra were taken for the chloroform solution on a JASCO IRA-1 grating spectrometer. The UV spectra were recorded for the methanol solution with a Hitachi EPS-3T spectrophotometer. The melting points were determined on a Yanagimoto micro-melting-point apparatus and were not corrected.

Oxidiation of Biphenylene with Manganese(III) Acetate. A typical procedure for the oxidation of biphenylene with manganese(III) acetate was as follows. A mixture of biphenylene[9] (2 mmol), manganese(III) acetate dihydrate,[3] acetic acid (20 ml), and acetic anhydride was heated under reflux for the time shown in the table until the color of the Mn(III) ion disappeared. Water (150 ml) was then added to the reaction mixture, and the solution was kept at room temperature overnight. The reaction mixture was extracted with benzene twice (30 ml of each portion), and then the benzene was removed *in vacuo*. The resulting semi-solid was separated on TLC, using chloroform as the developing solvent.

2-Acetoxybiphenylene (2): Mp 91—92 °C (light petroleum) (lit,[10] mp 91—92 °C); UV λ_{max} (ε) 245 (27900), 252 (46900), 330 (2980), 335_{sh} (3350), 344 (6270), 347_{sh} (5960), and 365 nm (8500); ^{1}H-NMR ($CDCl_3$) δ=2.23 (3H, s, OAc) and 6.2—6.9 (7H, m, aromatic).

2-Formylbiphenylene (3): Mp 80—81 °C (light petroleum) (lit,[11] mp 78—79 °C); IR 1700, 2720, and 2810 cm^{-1}; ^{1}H-NMR ($CDCl_3$) δ=6.5—7.5 (7H, m, aromatic) and 9.61 (1H, s, CHO).

2-(Acetoxymethyl)biphenylene (4): Mp 63—64 °C (EtOH); IR 1738 cm^{-1} (OAc); UV λ_{max} (ε) 245.5 (28300), 254 (55000), 329.5_{sh} (2750), 335_{sh} (2910), 345.5 (5900), 347.5 (5660), 352.5_{sh} (4050), and 365 nm (8900). Found: C, 80.30; H, 5.32%. Calcd for $C_{15}H_{12}O_2$: C, 80.33; H, 5.39%.

7-Oxa-10,11-benzotricyclo[4.3.2.0]undeca-2,4,10-trien-8-one (5): Mp 125 °C (CCl_4); IR 1775 cm^{-1} (γ-lactone); UV λ_{max} (ε) 221_{sh} (3960), 228_{sh} (3120), 258_{sh} (1410), 264_{sh} (1860), 269.5 (2130), 276 (2050), and 285_{sh} (723); ^{13}C-NMR δ= 39.709 (–CH_2–), 51.736 (–C–CH_2–), 84.837 (–C–O–), 121.080, 121.242, 121.513, 122.380, 124.059, 128.989, 129.260, 131.373 (four vinylic =CH– and four aromatic =CH–), 146.650 (=C–), 146.975 (=C–), and 175.308 (>C=O). Found: C, 79.86; H, 4.81%. Calcd for $C_{14}H_{10}O_2$: C, 79.98; 4.79%.

Oxidation of 2-(Acetoxymethyl)biphenylene (4) with Manganese(III) Acetate. A mixture of **2** (45 mg), manganese (III) acetate dihydrate (107 mg), acetic acid (2 ml), and acetic anhydride (0.1 ml) was heated under reflux for 20 min. The reaction mixture was diluted with water (20 ml) and then extracted with benzene. After the removal of the benzene *in vacuo*, the resulting mixture was separated on TLC, using benzene as the developing solvent, to give **3** (10 mg, 28%) and also unchanged **4** (15.6 mg, 35%) identical with authentic samples.

Oxidation of 2-(Acetoxymethyl)biphenylene (4) with Manganese(IV) Oxide. A mixture of **2** (45 mg), manganese (IV) oxide (1 g), and anhydrous diethyl ether (50 ml) was stirred at room temperature for 48 h. After the manganese (IV) oxide has been removed by filtration, the ethereal solution was concentrated and the resulting product was purified on TLC, using benzene as the developing solvent, to give **3** (20 mg, 56%).

References

1) K. Kurosawa and H. Harada, *Bull. Chem. Soc. Jpn.*, **52**, 2386 (1979).
2) H. Nishino, Ms. D. Thesis, Kumamoto University (1981).
3) P. J. Andrulis, Jr., M. J. S. Dewar, R. Dietz, and R. L. Hunt, *J. Am. Chem. Soc.*, **88**, 5473 (1966).
4) E. I Heiba, R. M. Dessau, and W. J. Koehl, Jr., *J. Am. Chem. Soc.*, **91**, 138 (1969).
5) S. C. Dickerman, W. M. Feigenbaum, M. Fryd, N. Milstein, G. B. Vermont, I. Zimmerman, and J. F. W. McOmie, *J. Am. Chem. Soc.*, **95**, 4624 (1973).
6) J. W. Barton and K. E. Whitaker, *J. Chem. Soc., C*, **1968**, 1663.
7) J. W. Barton and K. E. Whitaker, *J. Chem. Soc., C*, **1968**, 28.
8) H. Kidokoro, M. Sato, and S. Ebine, *Abstracts of the 5th Joint Meeting of Basic Organic Chemistry*, 235 (1980).
9) F. M. Logullo, A. H. Seitz, and L. Friedman, *Org. Synth.*, Coll. Vol. 5, 54 (1973).
10) J. M. Blatchly, D. V. Gardner, and J. F. W. McOmie, *J. Chem. Soc., C*, **1967**, 272.
11) J. F. W. McOmie and S. D. Thatte, *J. Chem. Soc.*, **1962**, 5298.

Synthesis of Amphiphilic Porphyrins

Shigeru TAKAGI, Takeshi YAMAMURA,* Masayuki NAKAJIMA, Koji ISHIGURO, Yuji KAWANISHI, Shigeru NIHOJIMA, Hiroo TSUCHIYA, Taro SAITO, and Yukiyoshi SASAKI

Department of Chemistry, and Research Centre for Spectrochemistry, Faculty of Science, The University of Tokyo, Hongo, Bunkyo-ku, Tokyo 113

(Received June 1, 1981)

Synopsis. A water soluble surfactant porphyrin 5,10,15-tris(1-methylpyridinium-4-yl)-20-[4-(octadecyloxy)phenyl]-21*H*, 23*H*-porphine triiodide and its metal complexes have been synthesized and characterized.

Recently, several surfactant porphyrins have been reported in relation to the simulation of the intricate functions of chlorophylls in photosynthetic membranes.[1-3]

We report here the synthesis of 5,10,15-tris(1-methylpyridinium-4-yl)-20-[4-(octadecyloxy)phenyl]-21*H*,-23*H*-porphine triiodide and its metal complexes which are amphiphilic.

Experimental

*Preparation of 5,10,15-Tris(4-pyridyl)-20-[4-(octadecyloxy)-phenyl]-21*H, *23*H*-porphine (Abbreviated as H_2TPyStPP).* A starting compound, *p*-(octadecyloxy)benzaldehyde, was prepared in the following manner according to the literature method.[4] *p*-Hydroxybenzaldehyde (48.8 g, 0.4 mol) and octadecyl iodide (243.2 g, 1.7 mol) in cyclohexane (320 cm³) were heated under reflux for 3 h. The reaction mixture was cooled to room temperature and extracted with diethyl ether (300 cm³). The ether was evaporated and the residue was distilled under high vacuum (250 °C, 0.03 Pa) to give the product (25.6 g, 17.1%).

p-(Octadecyloxy)benzaldehyde (21.2 g, 0.057 mol), 4-pyridinecarbaldehyde (18.2 g, 0.17 mol), and pyrrole (15.2 g, 0.23 mol) in propionic acid (1000 cm³) were heated under reflux for 2 h. Propionic acid was removed by distillation to give a mixture of porphyrins having one to three octadecyloxyphenyl and three to one pyridyl groups. Tetrakis(octadecyloxyphenyl)- and tetrapyridylporphine were not produced. The crude mixture was dissolved in chloroform and chromatographed on alumina columns (Merck 70—230 mesh, grade 2—3, 5 cm×50 cm) with chloroform as an eluent. Mono-, bis-, and tris(octadecyloxyphenyl) porphyrins eluted first and the other by-products tended to be adsorbed on alumina. Similar procedures were repeated three times and the mixture of the three porphyrins was obtained. When the mixture was again chromatographed using half the flow rate of chloroform, three bands were separated and the slowest elute was the solution of the target compound. Chloroform was evaporated to give the mono(octadecyloxyphenyl) porphyrin. Yield 6.5 g (12.8% based on *p*-(octadecyloxyphenyl)benzaldehyde). Found C, 79.21; H, 7.45; N, 10.67%. Calcd for $C_{59}H_{63}N_7 \cdot 1/2H_2O$: C, 79.16; H, 7.21; N, 10.95%. Vis ($CHCl_3$) 418 (ε 369000), 483 (sh), 514 (17500), 550 (6910), 580 (5490), and 646 nm (3100).

Preparation of [Zn(TPyStPP)]. H_2TPyStPP (0.5 g, 0.56 mmol) and $Zn(CH_3COO)_2 \cdot 2H_2O$ (0.25 g, 1.1 mmol) in acetic acid (50 cm³) were heated under reflux for 1 h. Acetic acid was removed by distillation to give a solid product. The zinc porphyrin was isolated by using alumina column (Merck, 70—230 mesh, grade 2—3, 2 cm×30 cm) chromatography with a mixture of chloroform and methanol (8 : 2) as an eluent. Yield 0.48 g (90%). Found: C, 74.77; H, 6.63; N, 10.25%. Calcd for $C_{59}H_{61}N_7OZn$: C, 74.63; H, 6.48; N, 10.33%. Vis (DMSO) 317 (ε 19200), 406 (sh), 428 (512000), 516 (sh), 560 (20600), and 599 nm (7380).

Preparation of [Co(TPyStPP)] and [Mn(OH)(TPyStPP)]. The cobalt and manganese complexes were prepared from H_2TPyStPP and $Co(CH_3COO)_2 \cdot 4H_2O$ or $Mn(CH_3COO)_2 \cdot 4H_2O$ by similar procedures to those for the preparation of the zinc porphyrin. In the case of the cobalt complex, tetrahydrofuran was used as an eluent of the chromatography. [Co(TPyStPP)]: Yield 85%. Found: C, 73.11; H, 6.59; N, 9.51%. Calcd for $C_{59}H_{61}CoN_7O \cdot 3/2H_2O$: C, 73.05;H, 6.65; N, 10.11%. Vis ($CHCl_3$–CH_3OH (1 : 1)) 328 (ε14800), 432 (141000), 546 (8970), and 592 nm (sh).

[*Mn(OH)(TPyStPP)*]: Yield 85%. Found: C, 74.08; H, 6.56; N, 10.00%. Calcd for $C_{59}H_{62}MnN_7O_2$: C, 74.12; H, 6.54; N, 10.25%. Vis (DMSO) 372 (ε 41900), 394 (44000), 463 (143000), 512 (7140), 565 (12200), 600 (8170), and 762 nm (1140).

Preparation of [Mg(TPyStPP)]. The magnesium complex was prepared according to the method of Eschenmoser.[5] The preparation was carried out in nitrogen atmosphere. Magnesium turnings (1.5 g, 62 mmol) and ethyl iodide (5 cm³, 62 mmol) were treated in diethyl ether (80 cm³) to give ethyl Grignard (C_2H_5MgI) reagent. 3,5-Di-*t*-butyl-4-hydroxytoluene (1.5 g, 11 mmol) was treated with the Grignard solution (8 cm³, 5.8 mmol), and H_2TPyStPP (0.5 g, 0.56 mmol) in dichloromethane (40 cm³) was added dropwise to the reaction mixture in 30 min. The solution was kept for 16 h at room temperature and water (500 cm³) was added. After the mixture was well shaken in a separatory funnel, the dichloromethane layer was separated. Dichloromethane was removed and the residue was dried *in vacuo*. The magnesium porphyrin was isolated by alumina column chromatography using $CHCl_3$–CH_2OH (8 : 2) as an eluent. Yield 0.36 g (70% based on H_2TPyStPP). Found: C, 77.54; H, 6.80; N, 10.48%. Calcd for $C_{59}H_{61}N_7MgO \cdot 1/2H_2O$: C, 77.24; H, 6.81; N, 10.69%. Vis (DMF) 314 (ε 21200), 404 (sh), 425 (570000), 520 (sh), and 563 nm (20100).

N-*Methylation of [Mg(TPyStPP)].* [Mg(TPyStPP)] (0.5 g, 0.54 mmol) and methyl iodide (7.8 g, 55 mmol) in mixed solvents of chloroform, methanol, and tetrahydrofuran (1 : 1 : 1) (300 cm³) were heated under reflux in nitrogen atmosphere for 5 h. The solvents were removed by distillation and the solid product was dried *in vacuo*. The *N*-methylated porphyrin was purified by column chromatography using alumina (Merck, 70—230 mesh, grade 4) columns and $CHCl_3$–CH_3OH (8 : 2) as an eluent. Yield 0.73 g (90%). Found: C, 49.72; H, 5.22; N, 6.37%. Calcd for $C_{62}H_{70}I_3MgN_7O \cdot 9H_2O$: C, 49.76; H, 5.93; N, 6.55%. Vis ($CHCl_3$–CH_3OH (1 : 1)) 328 (ε 14800), 432 (141000), 546 (8970), and 592 nm (sh).

N-*Methylation of H_2TPyStPP and [M(TPyStPP)] (M=Zn, Co, and Mn).* The porphyrins were treated with methyl iodide in mixed solvents of chloroform, methanol, and tetrahydrofuran (1 : 1 : 1) in a similar manner to the *N*-methylation of magnesium porphyrin. In the case of the cobalt

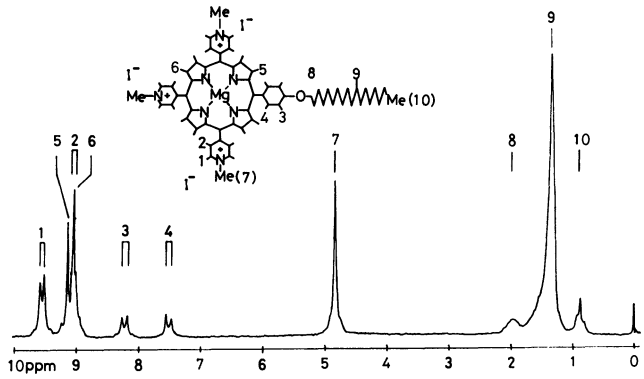

Fig. 1. ^{1}H-NMR Spectrum of 5,10,15-tris(1-methylpyridinium-4-yl)-20-[4-(octadecyloxy)phenyl]porphinatomagnesium(II) triiodide (dimethyl sulfoxide-d_6 solution, TMS internal reference, 100 MHz).

complex, a mixture of chloroform, methanol, and pyridine was used as an eluent.

5,10,15-Tris(1-methylpyridinium-4-yl)-20-[4-(octadecy)loxyphenyl]-21H,23H-porphine Triiodide (Abbreviated as $H_2TMePyStPPI_3$): Yield 50%. Found :C, 56.67; H, 5.66; N, 7.47%. Calcd for $C_{62}H_{72}I_3N_7O$: C, 56.76; H, 5.53; N, 7.18%. Vis (DMSO) 422 (ε 230000), 515 (15000), 552 (6800), 584 (5200), and 645 nm (3100).

[Zn(TMePyStPP)]I_3: Yield 80%. Found: C, 50.60; H, 5.06; N, 6.21%. Calcd for $C_{62}H_{70}I_3N_7OZn\cdot 6H_2O$: C, 50.20; H, 5.57; N, 6.61%. Vis (H_2O) 437 (ε 127000), 568 (16200), and 614 nm (9160).

[Co(TMePyStPP)]I_3: Yield 85%. Found: C, 54.67; H, 5.15; N, 7.19%. Calcd for $C_{62}H_{70}CoI_3N_7O$: C, 54.40; H, 5.15; N, 7.16%. Vis (H_2O) 332 (ε 12700), 439 (58700), 554 (8920), and 610 nm (sh).

[Mn(OH)(TMePyStPP)]I_3: Yield 50%. Found: C, 52.77; H, 5.20; N, 6.73%. Calcd for $C_{62}H_{71}I_3MnN_7O_2\cdot 2H_2O$: C, 52.52; H, 5.33; N, 6.91%. Vis (H_2O) 400 (ε 44700), 464 (111000), 563 (12900), 680 (1920), and 774 nm (1970).

Results and Discussion

All the *N*-methylated porphyrins are soluble in polar organic solvents such as *N,N*-dimethylformamide, dimethyl sulfoxide, tetrahydrofuran, methanol, chloroform, *etc.* They are soluble also in water due to the hydrophilic 1-methylpyridinium-4-yl groups forming presumably normal micelle colloid solutions. In a preliminary experiment to check the colloid formation in water, loss of porphyrins was not observed after passing the solution through a Sephadex G-50 column, indicating that they dissolve in water as high molecular weight aggregates. Because of the water solubility, they can be readily incorporated into pre-formed vesicles of phospholipids by immersing them in aqueous solutions of the porphyrins to give interesting asymmetrical vesicles[6] which are convenient systems for the study of the role of electron mediators in the photo-induced electron transport *via* the lipid membranes.[7–10]

References

1) T. Yamamura, *Chem. Lett.*, **1977**, 773.
2) Y. Okuno, W. E. Ford, and M. Calvin, *Synthesis*, **1980**, 537.
3) T. Matsuo, K. Itoh, K. Takuma, K. Hashimoto, and T. Nagamura, *Chem. Lett.*, **1980**, 1009.
4) G. W. Gray and B. Jones, *J. Chem. Soc.*, **1954**, 1467.
5) H.-P. Isering, E. Zass, K. Smith, H. Falk, L.-L. Luiser, and A. Eschenmoser, *Helv. Chim. Acta*, **58**, 2357 (1975).
6) T. Katagi, T. Yamamura, T. Saito, and Y. Sasaki, *Chem. Lett.*, **1981**, 1451.
7) T. Katagi, T. Yamamura, T. Saito, and Y. Sasaki, *Chem. Lett.*, **1981**, 503.
8) W. E. Ford, J. W. Otovos, and M. Calvin, *Proc. Natl. Acad. Sci. U.S.A.*, **76**, 3590 (1979).
9) K. Kurihara, N. Sukigara, and Y. Toyoshima, *Biochem. Biophys. Acta*, **547**, 117 (1979).
10) Y. Sudo, T. Kawashima, and F. Toda, *Chem. Lett.*, **1980**, 355.

Ring-opening Polymerization of Tetrahydrofuran Initiated by the 2-Norbornyl Cation Generated from *exo*-2-Norbornyl Tosylate in the Presence of Lithium Perchlorate

Ken'ichi TAKEUCHI, Yukari KATO, and Kunio OKAMOTO*

Department of Hydrocarbon Chemistry, Faculty of Engineering, Kyoto University, Sakyo-ku, Kyoto 606

(Received June 26, 1981)

Synopsis. *exo*-2-Norbornyl tosylate initiates ring-opening polymerization of THF in the presence of lithium perchlorate. The deuterium scrambling of *exo*-2-norbornyl-*exo*-3-*d* tosylate indicates the S_N1 nature of the initiation mechanism.

The S_N2 type initiation of the ring-opening polymerization of THF has been extensively studied by Saegusa and his coworkers by use of superacid esters as initiator.[1] On the other hand, the mechanism of initiation by carbocation is not straightforward. Some stable carbocations such as triphenylmethyl[2] and tropylium[3] ions initiate the polymerization, but the actual initiator is believed to be a proton which is expelled from the 2-oxacyclopentyl cation, generated by the hydride-abstraction of THF by the stable carbocations.[2] In contrast, acyl[4] and polystyryl[5] cations react with THF to form oxonium ions at the initiation step (Eq. 1).

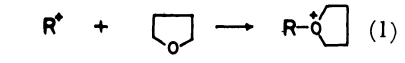

(1)

Recently we reported that the ionization of *exo*-2-norbornyl tosylate (**1**) in THF is dramatically promoted by added lithium perchlorate ($LiClO_4$).[6] Although it has been well known that $LiClO_4$ promotes ionization of organic substrates in ethereal solvents,[7-9] the fate of the carbocations produced in such reactions has not necessarily been clarified. Here we report that the 2-norbornyl cation thus generated initiates the polymerization of THF following Eq. 1, providing a clear example of S_N1 type initiation.

Results and Discussion

*Time-course and Products in the Reactions of **1** in THF in the Presence of Lithium Perchlorate.* In the absence of $LiClO_4$ the tosylate **1** is stable in THF even heated to 50 °C for 24 h. However, the addition of $LiClO_4$ causes the formation of the species which is easily saponified on titration with aqueous sodium hydroxide.

When the reaction of **1** (0.0981 M, 1 M = 1 mol dm^{-3}) in the presence of $LiClO_4$ (0.2984 M) in THF at 50.0 °C is followed titrimetrically, it obeys first-order kinetics ($k_1 = 2.24 \times 10^{-5}$ s^{-1}) until 20% reaction and then slows down, eventually leveling off at 10 h reaction with liberation of acid in 43% on titration. From the reaction mixture was isolated viscous liquid (46% on THF) which solidified on standing. The ^1H and ^{13}C NMR spectra of the polymers indicated that they were produced from THF *via* ring-opening polymerization and that they contained the *exo*-2-norbornyl and tosyl moieties (see Experimental). Integration of ^{13}C NMR signals for the norbornyl and tetramethylene groups indicated that the average degree of polymerization was *ca.* 60, which approximately agreed with the value calculated from the weight of polymers and the amount of the initiator **1**. A GLPC analysis of the reaction mixture prior to isolation of polymers revealed that none of nortricyclene, norbornene, or norbornane were formed, suggesting that the acid titrated was not a free acid arising from possible elimination reactions. Furthermore, saponification of the polymers in 90% ethanol with added sodium hydroxide indicated that 56% of the initial TsO- group was incorporated in the polymers.

These findings strongly indicate that the initiation occurs following an S_N1 mechanism, *i.e.*, ionization of **1** followed by the attack of THF to the produced 2-norbornyl cation. The *exo*-configuration of the terminal 2-norbornyl group indicates that the attack of THF to the norbornyl cation occurs from *exo* side, which is generally the case in S_N1 solvolyses of **1**.[10,11] Presumably, the

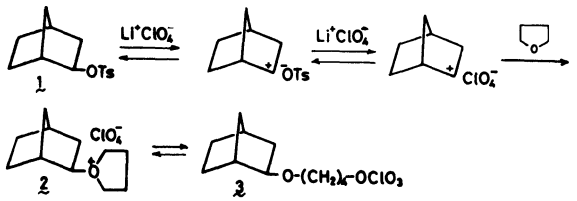

first formed oxonium ion **2** and the propagating oxonium ion are in equilibrium with their corresponding ester forms (*e.g.* **3**),[1b] and these four species are easily hydrolyzed during titration. The results of the NMR analysis and the saponification experiment indicate the formation of terminated species **4**.

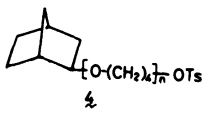

*Deuterium Scrambling in the Reclaimed Tosylate **1**.* Further evidence for ionization of **1** in THF containing $LiClO_4$ was obtained by examining *d*-scrambling of *exo*-2-norbornyl-*exo*-3-*d* tosylate (**1**-3-*d*). When **1**-3-*d* (0.100 M) was heated in THF with added $LiClO_4$ (0.307 M) for 38 min at 50.0 °C, the reclaimed tosylate was found to be a mixture of **1**-3-*d* (87%) and **1**-7-*d* (13%) by examining the *d*-contents at the 3- and 7-positions with ^{13}C NMR. This indicates that the Wagner-Meerwein rearrangement occurs through ionization under the reaction conditions, which is also generally observed in S_N1 solvolyses of **1**.[10]

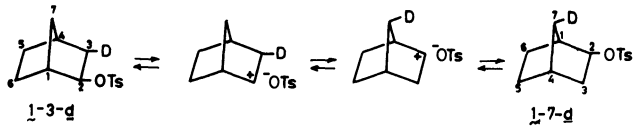

Experimental

Materials. THF was distilled from $LiAlH_4$ just before use. Lithium perchlorate ($LiClO_4 \cdot 3H_2O$) was dehydrated at 160 °C and 4 Torr.† The tosylates **1** and **1**-3-*d* were prepared as described previously.[12]

Polymerization of THF and Analysis of Polymers. A solution of **1** (0.0981 M) and $LiClO_4$ (0.2984 M) in THF (1.000 cm^3) was heated in a sealed tube under nitrogen at 50 °C for 87 h. The viscous solution was worked up in the usual manner to give a pale brown viscous liquid (0.409 g) which solidified on standing: ^1H NMR ($CDCl_3$, 60 MHz) $\delta=1.57$ (br. t, $J=4$ Hz) and 3.40 (br, t, $J=4$ Hz); ^{13}C NMR ($CDCl_3$, 25 MHz) $\delta=24.3$ (C-6), 28.3 (C-5), 34.5 (C-7), 34.8 (C-4), 39.3 (C-3), 40.0 (C-1), and 82.0 (C-2) for the norbornyl group, 26.2 and 70.0 for the tetramethylene groups, and 21.3 (CH_3), 127.5, and 129.5 for the tosyl group. The ^{13}C NMR data for the norbornyl group agree well with those for *exo*-2-(4-phenoxybutoxy)norbornane.[6] Saponification of the polymers (0.4086 g) in 10.00 cm^3 90% ethanol containing NaOH (0.00965 M) at 100 °C in sealed tubes for 1 h showed liberation of acid corresponding to 56% of the original tosylate, which was invariant on prolonged saponification time.

Deuterium Scrambling. A solution containing **1**-3-*d* (1.071 g, 0.1002 M) and $LiClO_4$ (1.633 g, 0.3069 M) in THF (40.0 cm^3) was heated to 50.0 °C for 38 min under nitrogen in a sealed tube, and the unchanged tosylate was recovered in the usual manner (0.160 g). The deuterium distribution was determined by the integration of ^{13}C NMR ($CDCl_3$, 25 MHz) signals as previously reported.[12]

Rate Measurements. The reaction was conducted under nitrogen in sealed tubes. Aliquots were titrated in acetone with 0.01 M NaOH by using Lacmoid as indicator.

† 1 Torr=133.322 Pa.

References

1) For leading references, see; a) S. Kobayashi, H. Danda, and T. Saegusa, *Bull. Chem. Soc. Jpn.*, **46**, 3214 (1973); b) S. Kobayashi, H. Danda, and T. Saegusa, *Macromolecules*, **7**, 415 (1974); c) S. Kobayashi, K. Morikawa, and T. Saegusa, *ibid.*, **8**, 386 (1975).

2) M. P. Dreyfuss, J. C. Westfahl, and P. Dreyfuss, *Macromolecules*, **1**, 437 (1968).

3) C. E. H. Bawn, C. Fitzsimmons, and A. Ledwith, *Proc. Chem. Soc.*, **1964**, 391.

4) R. Wegler and R. Schmitz-Josten, "Methoden der organischen Chemie," ed by E. Müller, Georg Thieme Verlag, Stuttgart (1963), Vol. 14-2, p. 557.

5) F. J. Burgess, A. V. Cunliffe, J. R. MacCallumm, and D. H. Richards, *Polymer*, **18**, 719, 726 (1977); F. J. Burgess, A. V. Cunliffe, J. V. Dawkins, and D. H. Richards, *ibid.*, **18**, 733 (1977).

6) K. Takeuchi, Y. Kato, T. Moriyama, and K. Okamoto, *Chem. Lett.*, **1981**, 935.

7) For a review, see; J. E. Gordon, "The Organic Chemistry of Electrolyte Solutions," Wiley-Interscience, New York (1975), Chap. 1.

8) S. Winstein, S. Smith, and D. Darwish, *J. Am. Chem. Soc.*, **81**, 5511 (1959); S. Winstein, E. C. Friedrich, and S. Smith, *ibid.*, **86**, 305 (1964).

9) Y. Pocker and D. L. Ellsworth, *J. Am. Chem. Soc.*, **99**, 2284 (1977), and their previous papers cited therein.

10) For a review, see; H. C. Brown, "Nonclassical Ion Problem," Plenum Press, New York (1977).

11) The structural formulas in the form of a "classical" ion are tentatively employed for convenience.

12) S. Saito, T. Moriwake, K. Takeuchi, and K. Okamoto, *Bull. Chem. Soc. Jpn.*, **51**, 2634 (1978).

Sand Separated from Athabasca Tar Sand (Canada) by Solvent Extraction

Ryoichi Yoshida,*[1] Takeshi Okutani, Katsuyoshi Shimokawa, Yasuko Ikawa,**
Yousuke Maekawa, Kohei Kodaira,** and Yuji Yoshida
Government Industrial Development Laboratory, Hokkaido, Sapporo 061-01
***Department of Applied Chemistry, School of Engineering, Hokkaido University, Sapporo 060*
(Received June 3, 1981)

Synopsis. The nature of the sand separated from Athabasca tar sand (Canada) by solvent extraction was examined. The existence of α-SiO_2 was confirmed by X-ray analysis. By DTA-TG determination, the occurrence of displacive transformation from low quartz to high quartz at 573±1 °C was proved, this coincides with the results obtained by means of X-ray analysis.

The amount of synthetic crude oil extractible from Athabasca tar sand is estimated to be roughly comparable with the total recoverable oil reserves in the Middle East.[2] However, an inorganic matter, sand, constitutes 87—89 wt % of the tar sand.[3] Consequently, if the tar sand is used as a source of petroleum in the near future, the treatment and/or utilization of the sand will be of great importance.

Hereby reported are the results of an examination of the nature of the sand separated from Athabasca tar sand by solvent extraction.

Experimental

Preparation. The procedure and apparatus employed for the extraction were the same as those used previously.[3]

Measurements. The benzene-insoluble residue (sand) was observed under an optical microscope. X-ray fluorescence analysis and X-ray powder diffraction were carried out on the sand. Simultaneous DTA-TG determination was carried out with a sample weight of 61.7 mg at a heating rate of 10 °C min^{-1}.

Results and Discussion

Athabasca tar sand was extracted with hexane and benzene in steps.[3] The yield of the sand (benzene-insoluble matter) was 87.6—88.5 wt.%, which is almost equal to the ash content of tar sand, 87.2 wt.%, as determined by a high-temperature ashing technique (815 °C).

The color of the sand after solvent extraction was brownish white, but it proved to be transparent upon washing with water. The optical micrograph of the sands is shown in Fig. 1. The maximum diameter of sands is 400 μm, while a typical diameter is 100—150 μm.

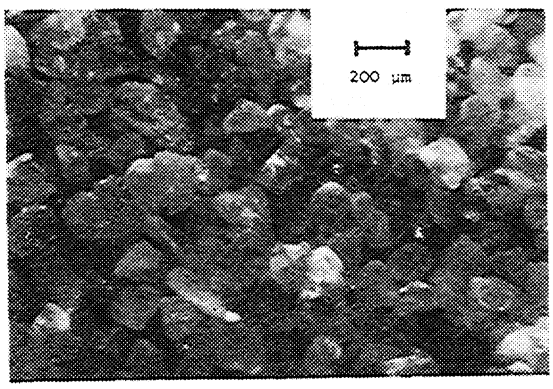

Fig. 1. The sands after washing with water.

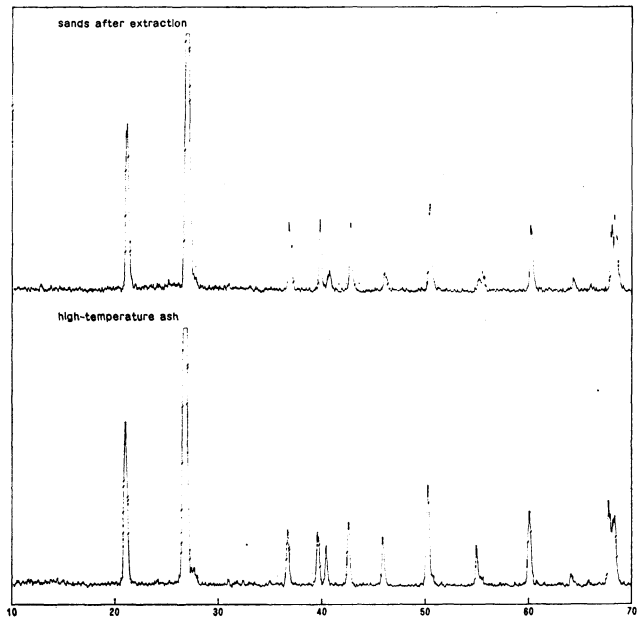

2θ (Cu Kα)
Fig. 2. X-Ray powder diffraction profiles of the sand and the high-temperature ash.

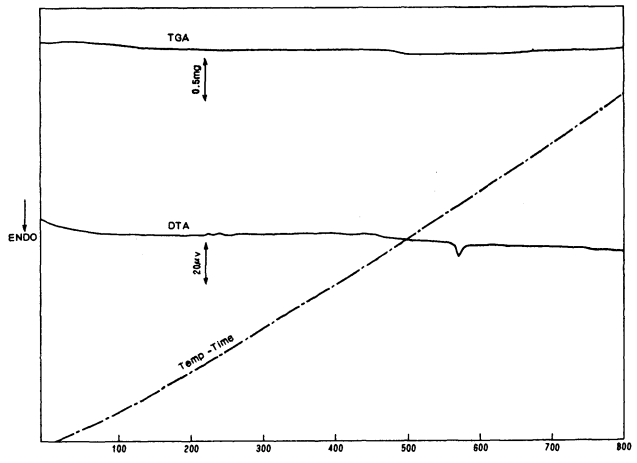

Temperature/°C
Fig. 3. DTA-TG profile up to 800 °C of the sand.

The X-ray powder diffraction profiles of the sand and the high-temperature ash are shown in Fig. 2. All the peaks in both profiles were identified as those of α-SiO_2.

A DTA-TG profile of the sand up to 800 °C is shown in Fig. 3. The weight decrease up to 800 °C is 0.2 wt.%. An endothermic peak at 573±1 °C was observed, which corresponds to the displacive transformation from low quartz to high quartz. This result coincides with that obtained by X-ray analysis.

X-Ray fluorescence analysis of the sand shows that the principal constituting elements are Si and Al. Zn, Cu, K, Fe, Ni, Ti, Ca, and Cl are present as minor or trace elements. Therefore, the existence of other unknown components such as aluminates can be estimated.

The authors are grateful to Professor D. M. Bodily of the University of Utah for his helpful discussion.

References

1) Visiting fellow at the Coal Research Institute, Hokkaido University.

2) N. Berkowitz and J. G. Speight, *Fuel*, **54**, 138 (1975).

3) R. Yoshida, T. Yoshida, Y. Ikawa, T. Okutani, Y. Hirama, Y. Nakata, S. Yokoyama, M. Makabe, and Y. Hasegawa, *Bull. Chem. Soc. Jpn.*, **52**, 1464 (1979).